The Mössbauer Effect in Ethyltin Halides and Related Compounds

Noriyuki WATANABE and Eiji NIKI

Department of Industrial Chemistry, Faculty of Engineering, The University of Tokyo, Hongo, Tokyo

(Received September 12, 1970)

The Mössbauer spectra for ethyltin halides and related compounds (Et_4Sn, SnX_4 (X=Cl,Br, I), Et_3SnX, Et_2SnX_2 (X=Cl, Br, I), $EtSnI_3$) were obtained. The replacement of ethyl groups by halogen atoms made the isomer shifts more positive relative to the tetraethyltin precursor. These results may be explained in terms of the rehybridization theory that the *s*-character of a central atom tends to concentrate in orbitals directed toward electropositive substituents. A suggestion that the compounds of $RSnX_3$ type show smaller quadrupole splittings than the R_3SnX compounds is made and discussed in terms of the rehybridization in the orbitals of the tin atom and in terms of bond ionicity.

The ^{119}Sn-Mössbauer parameters in organotin compounds provide some useful information about the nature of the chemical bond formed by the tin atom. Among them, the isomer shift depends on the *s*-electron density at the tin nucleus. Changes in the electron density at the tin nucleus arise primarily through changes in the valence 5*s*-electrons, but other valence 5*p*- and 5*d*-electrons can shield 5*s*-electrons from the tin nucleus.[1a] An increase in the isomer shift corresponds to an increase in the *s*-electron density at the tin nucleus.[1b] Alkyl- and aryltin halides show positive isomer shifts compared to the corresponding tetraalkyl- and tetraaryltin.[1a,2-5] These findings on isomer shifts cannot be interpreted only in terms of polarization due to the electronegativity of the bonding halogen atoms. Stöckler and Sano have made a plausible suggestion that the tin *d*-orbital electron donated to the halogen atom may antishield the tin nucleus from the *s*-electron.[4] In the present study, similar results for ethyltin halides were obtained. Further, diethyltin dihalides showed an obvious dependence of the isomer shift on the halogen atoms. These results may be interpreted in terms of both the rehybridization of tin valence orbitals and the polarization due to the bonding halogen atoms. Very large quadrupole splittings were observed for triethyltin halides and diethyltin dihalides, whereas for ethyltin triiodide the splitting was drastically reduced. The fact that the compounds of $RSnX_3$ type (X=halogen or pseudohalogen, R=alkyl or aryl group) show smaller quadrupole splittings than the R_3SnX compounds will be discussed in terms of the rehybridization in the valence orbitals of the tin atom and in terms of bond ionicity.

Experimental

The compounds used in the present study were prepared by published procedures.[6,7] All of the triethyltin halides and ethyltin triiodide were purified by fractional distillation at a reduced pressure. The diethyltin dihalides were washed with ether and dried at a reduced pressure. The elemental analyses of C and H gave almost completely satisfactory results. The ^{119m}Sn-Mössbauer spectra were taken using a constant acceleration electromagnetic driver previously reported on.[8] The source was $Pd^{119m}Sn$, containing about 0.2 mCi ^{119m}Sn. The source was operated at room temperature, while the absorbers were cooled with liquid nitrogen in a cryostat previously reported on.[8] The velocity scale has been calibrated by the isomer shifts of β-Sn and SnO_2. The isomer shifts of β-Sn and SnO_2 are +1.11 and −1.58 mm/sec respectively with respect to $Pd^{119m}Sn$.

Results and Discussion

The Mössbauer parameters for ethyltin halides and related compounds are presented in Table 1. The Mössbauer spectra of Et_4Sn, Et_3SnCl, and Et_2SnCl_2 are shown in Fig. 1. The dependences of the isomer shifts on halogen atoms bonding to tin and on their number are shown in Fig. 2. Parish and Platt reported the quadrupole splittings of Et_nSnX_{4-n} (n=1, 2, 3, X=Cl, Br, I), with the exception of $EtSnI_3$ but their results do not agree with ours.[9] On the other hand, Bryuchova *et al.* presented quadrupole splittings and

TABLE 1. MÖSSBAUER PARAMETERS FOR TIN HALIDES

Compounds[a]	I.S.(*vs.*$Pd^{119m}Sn$)[b]	Q.S.[b]
Et_4Sn	−0.15 mm/sec	0 mm/sec
$SnCl_4$	−0.70[c]	0
Et_3SnCl	+0.11	3.84
Et_2SnCl_2	+0.20	3.78
$SnBr_4$	−0.40	0
Et_3SnBr	+0.14	3.42
Et_2SnBr_2	+0.23	3.48
SnI_4	+0.05	0
Et_3SnI	+0.09	3.09
Et_2SnI_2	+0.32	3.24
$EtSnI_3$	+0.18	1.77

a) Et=C_2H_5, b) ±0.03 mm/sec c) Ref. 19.

1) a) V. I. Goldanskii, V. V. Khrapov, O. Y. Okhlobystin, and V. Y. Rochev, "Chemical Application of Mössbauer Spectroscopy," ed. by V. I. Goldanskii and R. H. Herber, Academic Press, New York and London (1968), p. 336. b) See the editor's note in this reference, p. 320.
2) M. Cordey-Hayes, *J. Inorg. Nucl. Chem.*, **26**, 2306 (1964).
3) M. Cordey-Hayes, R. D. Peacock, and M. Vucelic, *ibid.*, **29**, 1177 (1967).
4) H. A. Stöckler and H. Sano, *Trans. Faraday Soc.*, **64**, 577 (1968).
5) R. V. Parish and R. H. Platt, Chem. Commun., **1968**, 1118.
6) "Mukikagakuzensho XII-I-I Tin," Maruzen, Tokyo, (1963), pp. 368, 379.
7) "Yuki Kinzoku Handbook," Asakura shoten, Tokyo, (1967), p. 463.
8) N. Watanabe and E. Niki, This Bulletin, **43**, 3034 (1970).
9) R. V. Parish and R. H. Platt, *J. Chem. Soc.*, **A**, **1969**, 2145.

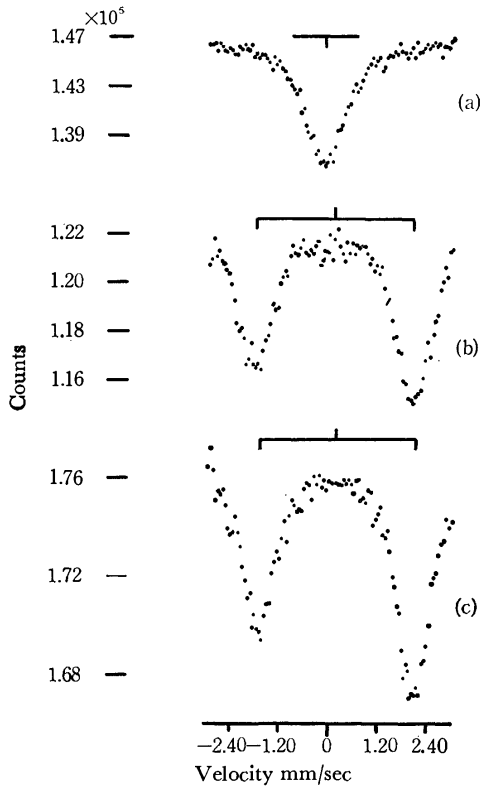

Fig. 1. Mössbauer spectra of Et_4Sn (a), Et_3SnCl (b) and Et_2SnCl_2 (c).

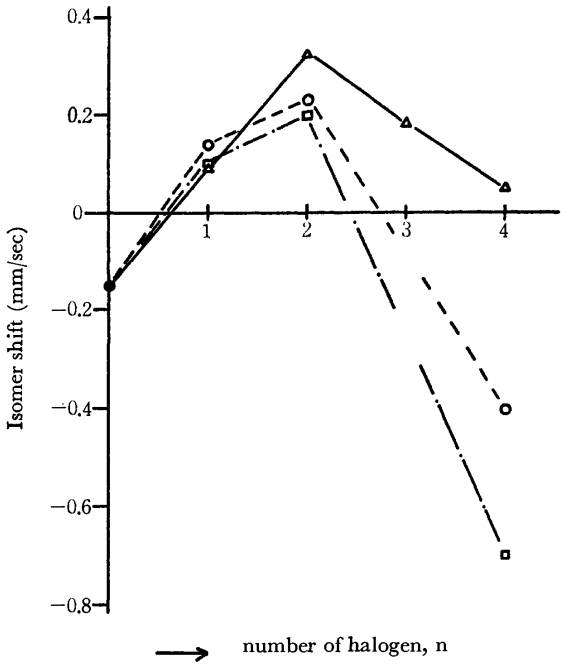

Fig. 2. Dependences of the isomer shifts on number of halogen substituents in ethyltin halides, $Et_{4-n}SnX_n$.
X=I; △, Br; ○, Cl; □, Et_4Sn; ●

isomer shifts consistent with our results for Et_3SnBr and Et_2SnI_2; that is, they reported that Et_3SnBr and Et_2SnI_2 showed the quadrupole splittings of 3.45 and 3.21 mm/sec and isomer shifts of −0.48 and −0.33 mm/sec relative to α–Sn, which could be converted to shifts of +0.12 and +0.27 mm/sec respectively relative to PdSn.[10]

Isomer Shift. Ethyltin halides showed more positive isomer shifts than did tetraethyltin. The isomer shifts in dihalides were more positive than those in monohalides. These results indicate that the *s*-electron density at the tin nucleus increase with an increase in the isomer shifts; $Et_4Sn < Et_3SnX < Et_2SnX_2$. Similar results for alkyl- and aryltin halides have been reported.[2-5] It may seem that the electron-withdrawing abilities of halogen atoms should decrease the 5*s*-electron density at the tin nucleus. Moreover, the 5*p*-electrons, which can shield 5*s*-electrons from the tin nucleus, may be decreased in the same way, but the decrease in the 5*p*-electron cannot compensate for the decrease in the 5*s*-electron density at the tin nucleus.[11] Hence, these results on isomer shifts cannot be interpreted only in terms of polarization due to the electronegativity of the halogen atoms. Stöckler and Sano have interpreted these results in terms of the deshielding by the tin *d*-orbital participated in $d\pi$–$p\pi$ bonding with halogen atoms.[4] However, the way in which the *d*-electron deshields the *s*-electron from the tin nucleus is ambiguous. Devooght *et al.* suggested that all the halides, with the exception of trimethyltin halides, could be tetracoordinated monomers.[12] The far-infrared spectra obtained in this study for ethyltin halides with neat samples sandwiched between CsI plates or nujol mulls showed the same Sn–C stretching frequencies as that in a previously-reported cyclohexane solution, in which ethyltin halides were tetrahedral monomers.[13] Bent proposed the following theory on the basis of the effects of the orbital hybridization and the electronegative substituents on the bond angles, bond lengths, and other physical properties.[14] He mentioned that the *s*-character of a central atom tends to be concentrated in orbitals directed toward electropositive substituents. This rule can explain our findings on the isomer shifts. That is, the *s*-character in tin valence orbitals is concentrated in the orbitals toward the more electropositive ethyl groups (in general, alkyl groups), while the *p*-character is concentrated in the orbitals directed to the electronegative halogen atoms. Moreover, the bonds directed to halogen atoms are more ionic due to their electronegativity. The increased ionicity in an orbital with a predominant *p*-character leads to an increase in the *s*-electron density at the tin nucleus due to decreased shielding by the *p*-electron. For triethyltin halides, the dependence of the isomer shifts on the bonding halogen atoms is not evident. However, it is obvious for diethyltin dihalides, in the case of which it coincides with the order of halogen electronegativity. Therefore, it may be assumed that the rehybridization effect is predominant

10) E. V. Bryuchova, G. K. Semin, V. I. Goldanskii, and V. V. Khrapov, Chem. Commun., **1968**, 491.
11) S. L. Ruby and G. M. Kalvious, *Phys. Rev.*, **159**, 239 (1967); J. K. Less and P. A. Flinn, *J. Chem. Phys.*, **48**, 882 (1968).
12) J. Devooght, M. Gielen, and S. Lejeune, *J. Organometal. Chem.*, **21**, 333 (1970).
13) R. J. H. Clark, A. G. Davies, and R. J. Ruddephat, *J. Chem. Soc.*, A, **1968**, 1828.
14) H. A. Bent, *J. Inorg. Nucl. Chem.*, **19**, 43 (1961); *Chem. Rev.*, **61**, 275 (1961).

for triethyltin halides, while, for diethyltin dihalides, the polarization effect due to the electronegativity of halogen atoms is comparable to the rehybridization effect.

Quadrupole Splitting. The quadrupole splittings for mono- and dihalides increased in the order; iodides<bromides<chlorides. These results are consistent with the observations previously published.[2-5,9,10] The splitting of ethyltin triiodide was drastically reduced. Similar results for trihalides have been reported in several pairs of compounds. Stöckler and Sano reported that the splittings for $(C_6H_5)_3SnCl$ and $C_6H_5SnCl_3$ were 2.46 and 1.80 mm/sec respectively, while for $(CH_3)_3SnBr$ and CH_3SnBr_3 they were 3.28 and 1.91 mm/sec respectively.[4] Moreover, Gassenheimer and Herber reported similar results for alkyltin pseudohalides[15] (for $(C_4H_9)_3SnSCN$ and $C_4H_9Sn(SCN)_3$, 3.88 and 1.46 mm/sec, respectively). Consequently, it seems to be a general rule that the compounds of the $RSnX_3$ type (X=halogen or pseudohalogen, R=alkyl or aryl group) show smaller quadrupole splittings than the compounds of the R_3SnX type in cases where these compounds are monomeric. This can be understood if we consider the field gradient at the tin nucleus in the following model. From the fact previously mentioned, we assume a C_{3v} symmetry around the tin atom for $RSnX_3$. The four valence hybrid orbitals of the tin atom are as follows;

$$\begin{aligned}
\varphi_1 &= C_R\varphi_s + (1-C_R^2)^{1/2}\varphi_{p(z)} \\
\varphi_2 &= C_X\varphi_s + (1-C_X^2)^{1/2}(\varphi_{p(z)}\cos\alpha - \varphi_{p(x)}\sin\alpha) \\
\varphi_3 &= C_X\varphi_s + (1-C_X^2)^{1/2}(\varphi_{p(z)}\cos\alpha + \frac{1}{2}\varphi_{p(x)}\sin\alpha \\
&\quad - \frac{\sqrt{3}}{2}\varphi_{p(y)}\sin\alpha) \\
\varphi_4 &= C_X\varphi_s + (1-C_X^2)^{1/2}(\varphi_{p(z)}\cos\alpha + \frac{1}{2}\varphi_{p(x)}\sin\alpha \\
&\quad + \frac{\sqrt{3}}{2}\varphi_{p(y)}\sin\alpha) \qquad (1)
\end{aligned}$$

where α is the angle between the direction of the tin-carbon bond (z axis) and that of the tin-halogen bonds, where φ_s and φ_p are the tin valence $5s$ and $5p$ orbitals, and where C_X and C_R are the s-character of the hybrid orbitals directed to alkyl group and to the halogen atoms respectively. From the orthogonality of φ_1 with φ_2, we obtain;

$$\cos^2\alpha = \frac{C_R^2C_X^2}{(1-C_R^2)(1-C_X^2)} \qquad (2)$$

and from the orthogonality of φ_3 with φ_4, we obtain;

$$C_X^2 = \frac{1-3\cos^2\alpha}{3\sin^2\alpha} \qquad (3)$$

The four molecular orbitals are;

$$\begin{aligned}
\psi_1 &= \frac{\varphi_1 + i_R\varphi_R}{(1+i_R^2)^{1/2}} \\
\psi_j &= \frac{\varphi_j + i_X\varphi_X}{(1+i_X^2)^{1/2}}, \quad j = 2, 3, 4 \qquad (4)
\end{aligned}$$

where φ_R and φ_X are the valence atomic orbitals of carbon and halogen, and where i_R and i_X are their characters in the appropriate molecular orbitals.

The field gradient, $(V_{zz})_j$, due to electrons in the molecular orbital, ψ_j, is given by the expectation value of the field gradient operator, H_q ($H_q = \frac{3\cos^2\theta-1}{r^3}$);

$$(V_{zz})_j = 2\langle\psi_j|H_q|\psi_j\rangle \qquad (5)$$

The contribution of ψ_1 is;

$$(V_{zz})_1 = 2\frac{1-C_R^2}{1+i_R^2}V_{p(z)} \qquad (6)$$

where $V_{p(z)} = \langle\varphi_{p(z)}|H_q|\varphi_{p(z)}\rangle$ and $\langle\varphi_s|H_q|\varphi_{p(z)}\rangle = 0$, neglecting the two-center integral, $\langle\varphi_R|H_q|\varphi_R\rangle$, $\langle\varphi_{p(z)}|H_q|\varphi_R\rangle$, *etc.* as too small.

The contribution of $p(z)$ electrons in the molecular orbitals, ψ_2, ψ_3, and ψ_4, is;

$$\sum_{j=2}^{4}(V_{zz})_j = 6\frac{1-C_X^2}{1+i_X^2}V_{p(z)}\cos^2\alpha \qquad (7)$$

Moreover, the contributions of the $p(x)$ and $p(y)$ electrons in ψ_2, ψ_3, and ψ_4 are;

$$\sum_{j=2}^{4}(V_{xx})_j = 3\frac{1-C_X^2}{1+i_X^2}V_{p(x)}\sin^2\alpha \qquad (8)$$

and;

$$\sum_{j=2}^{4}(V_{yy})_j = 3\frac{1-C_X^2}{1+i_X^2}V_{p(y)}\sin^2\alpha \qquad (9)$$

where $V_{p(x)} = \langle\varphi_{p(x)}|H_q|\varphi_{p(x)}\rangle$, *etc.*

If it is assumed that all of the $5p_x$, $5p_y$, and $5p_z$ orbitals have the same radial functions, the next equation is obtained:

$$V_{p(x)} = V_{p(y)} = -\frac{1}{2}V_{p(z)} \qquad (10)$$

Consequently, the total field gradient, V_{zz}, is:

$$V_{zz} = 2V_{p(z)}\left[\frac{1-C_R^2}{1+i_R^2} + 3\frac{1-C_X^2}{1+i_X^2}\left(\frac{3\cos^2\alpha-1}{2}\right)\right]$$

By introducing (2) and (3) into the above equation, we obtain:

$$\begin{aligned}
V_{zz} &= V_{p(z)}[(1-C_R^2)(1+I_R) - (1-C_R^2)(1+I_X)] \\
&= (1-C_R^2)(I_R-I_X)V_{p(z)} \qquad (11)
\end{aligned}$$

where the bond ionic characters, I_X and I_R, are expressed as:

$$I_X = \frac{1-i_X^2}{1+i_X^2}, \quad I_R = \frac{1-i_R^2}{1+i_R^2}. \quad (I_X<0,\ I_R>0,\ |I_X|>|I_R|)$$

An analogus calculation for R_3SnX yields:

$$V_{zz}(R_3SnX) = (1-C_X'^2)(I_X'-I_R')V_{p(z)} \qquad (12)$$

where C'_X is the coefficient included in one of the tin valence orbitals for R_3SnX, ($\varphi'_1 = C'_X\varphi_s + (1-C'_X{}^2)^{1/2}\varphi_{p(z)}$) and where I'_X and I'_R are the bond ionic characters for R_3SnX ($I'_X<0$, $I'_R>0$, $|I'_X|>|I'_R|$).

By combining (11) with (12), we obtain:

$$\frac{V_{zz}(RSnX_3)}{V_{zz}(R_3SnX)} = -\frac{(1-C_R^2)(I_X-I_R)}{(1-C_X'^2)(I_X'-I_R')} \qquad (13)$$

Since the rehybridization theory can be applied to $RSnX_3$ as well as to R_3SnX, it may be assumed that $C_R^2 > 1/4$ for $RSnX_3$ and $C_X'^2 < 1/4$ for R_3SnX. (This is exactly what Bent's rehybridization theory predicts.)

15) B. Gassenheimer and R. H. Herber, *Inorg. Chem.*, **8**, 1120 (1969).

Moreover, it is reasonable that we consider $|I'_X|>|I_X|$. For example, this consideration may be supported by the fact that the replacement of hydrogen by the more electronegative chlorine for chloromethanes, CH_nCl_{4-n}, makes the C–Cl bond less ionic.[16] As more direct evidence, we find, from the n.q.r. data for $(n\text{-}C_4H_9)_n\text{-}SnCl_{4-n}$ (n=0, 1, 2), that the replacement of chlorine atoms by buthyl groups leads to an increase in the ionic character in the Sn–Cl bond.[17] Other support is found in the recent calculation of orbital populations in aryltin chlorides.[18] Moreover, since I_R and I'_R are small compared to I_X and I'_X, $(I_X-I_R)/(I'_X-I'_R)\fallingdotseq I_X/I'_X$.[18] Therefore, it can be concluded that $|V_{zz}(RSnX_3)|<|V_{zz}(R_3SnX)|$ and that the more electronegative the substituents, X, the larger the field gradient, V_{zz}, for R_3SnX.

16) R. Livingston, *J. Phys. Chem.*, **57**, 496 (1953).
17) E. D. Swiger and J. D. Graybeal, *J. Amer. Chem. Soc.*, **87**, 1464 (1965).
18) D. E. Williams and C. W. Kocher, *J. Chem. Phys.*, **52**, 1480 (1970).
19) J. Philip, M. A. Mullins, and C. Curran, *Inorg. Chem.*, **7**. 1895 (1968).

BULLETIN OF THE CHEMICAL SOCIETY OF JAPAN, VOL. 45, 4—7(1972)

The X-Ray Emission Spectra of the Compounds of Third-period Elements. II. The *K* Spectra of Phosphorus in Compounds

Yoshihito TAKAHASHI

Government Industrial Development Laboratory, Hokkaido Higashi-Tsukisamu, Sapporo

(Received February 5, 1971)

On sixteen compounds of phosphorus, the wavelength shifts of the $K\alpha_{1,2}$ lines and the fine structures of the $K\beta$ band of the phosphorus emission spectra were measured. For the oxygen compounds, the relationship between the intensity ratio of the $K\beta'$ line and the energy shift of the $K\alpha_{1,2}$ lines was found to be expressed by a straight line similar to that found for sulfur and chlorine compounds. In the spectra of the oxyacids and their salts, the intensity ratio of the satellite line which is observed between the $K\beta_1$ and $K\beta'$ lines is proportional to the number of the hydroxyl groups in a molecule. The appearance of this line seems to be attributable to the covalent bond between a third-period atom and a non-ionized atom. In the $K\beta$ spectrum of triphenyl phosphite, the strong satellite line at the highest energy site seems to have a nature similar to those found in sulfite, chlorate, and phosphorus trichloride.

Previously, we have studied the nature of the satellite line $K\beta'$ which is observed on the longer-wavelength side of the $K\beta_1$ line of sulfur and chlorine in many kinds of oxygen compounds, and have found that the relationship between the ratio of the integral intensity of the $K\beta'$ line to the total intensity of the $K\beta$ line (we call it the intensity ratio of the $K\beta'$ line) and the energy shift of $K\alpha_{1,2}$ lines (it relates to the effective charges of the atom in a molecule[1,2]) can be expressed by straight line similar to those for the oxygen compounds of both sulfur and chlorine. From these facts, it has been suggested that the appearance of the $K\beta'$ line is due to the transfer of valence electrons from the third-period atom to the bonded oxygen atoms in the molecule, and that its intensity is related to the nature of the ligand atoms rather than to the kind of third-period atom.[3,4]

In order to check the general truth of these facts as regards all the third-period elements, the P$K\beta$ spectra of various phosphorus compounds have been measured. Although the data on the P$K\alpha_{1,2}$ lines have been already reported by Yao and Holst,[5] and more recently by Nikolaev *et al.*,[6] new measurements are now made for several compounds.

Experimental

The spectra were measured on the same apparatus as that descrived in a previous work.[4] A flat germanium analyzing crystal ((111) plane, $2d$: 6.53272 Å) was also used. The wavelength values of the P$K\alpha_{1,2}$ lines on each compound were measured, using the fourth-order reflection of the Cu$K\alpha_1$ line (corresponding to 6.16200 Å) as the standard; they were then converted to the value of the energy shift from the value of red phosphorus. The spectra of P$K\beta$ were obtained using the step-by-step method as in the previous work. However, in the case of phosphorus trichloride, in order to avoid the oxydation of the material during the measurements, the spectrum was obtained by the chart-recording method (one running time was 12 min), and the average of the three runs was taken. The background was measured at the 5.90 Å position. The separation of the $K\beta$ spectrum into several component peaks was attempted, taking the P$K\beta_1$ peak of anhydrous sodium phosphate as the standard shape.

1) C. A. Coulson and C. Zauli, *Mol. Phys.*, **6**, 525 (1963).
2) W. S. Urusov, *Dokl. Akad. Nauk SSSR*, **166**, 660 (1966).
3) Y. Takahashi and K. Yabe, This Bulletin, **42**, 3064 (1969),
4) Y. Takahashi, *ibid.*, **44**, 587 (1971).
5) T. C. Yao and J. J. Holst, *Spectrochim. Acta*, **23B**, 19 (1967).
6) A. V. Nikolaev, L. N. Mazalov, A. P. Sadovskii, V. V. Murachtanov, E. A. Gal'tsova, T. I. Gujavina, and N. I. Yakovleva, *Dokl. Akad. Nauk SSSR*, **189**, 784 (1969).

Results and Discussion

The P$K\beta$ spectra measured are shown in Fig. 1. We named the component peaks as is shown in Fig. 1, *i.e.*, A($K\beta'$), B, C($K\beta_1$), C', and D, counting from the longer-wavelength side. The structure of the spectrum of red phosphorus was so complicated that the separation into component peaks was not attempted for this substance. The characteristic values of the $K\alpha_{1,2}$ and $K\beta$ lines for each compound are summarized in Table 1.

Table 1. Characteristic values of the $K\alpha_{1,2}$ and $K\beta$ lines measured for various compounds of phosphorus

	$K\alpha_{1,2}$		$K\beta$, λ(Å)			Intensity ratio (%)				
	λ(Å)	⊿E(eV)	A	C	D	A	B	C	C'	D
P_4(red)	6.15837			5.7940						
Na_3PO_4	5595	0.79	5.8370	5.7990		0.26		0.74		
Na_2HPO_4	5605	0.76	8365	7985		0.26	0.08	0.66		
NaH_2PO_4	5592	0.80	8380	7985		0.25	0.14	0.57	0.04	
H_3PO_4	5595	0.79	8380	7990		0.24	0.27	0.34	0.15	
$Na_4P_2O_7$	5595	0.79	8365	7980		0.28	0.08	0.62	0.02	
$(NaPO_3)_3$	5585	0.82	8375	7990		0.24	0.17	0.38	0.21	
$(P_2O_5)_2$	5585	0.82	8380	8050		0.21	0.13	0.33	0.33	
$(\phi O)_3PO$	5624	0.70	8400	8095	5.781	0.18	0.13	0.34	0.30	0.05
PCl_5	5655	0.59	8195	7955	781	0.25	0.10	0.61		0.04
Na_2HPO_3	5637	0.66	8375	7995		0.22	0.06	0.68	0.04	
H_3PO_3	5650	0.59	8395	8010		0.20	0.14	0.49	0.17	
$(\phi O)_3P$	5672	0.54	8430	8090	786	0.10	0.10	0.21	0.30	0.29
PCl_3	5710	0.41	8205	7970	785	0.16	0.04	0.61		0.19
NaH_2PO_2	5690	0.48	8930	8000		0.18	0.08	0.68	0.06	
H_3PO_2	5701	0.45	8400	8005		0.11	B' (0.16 / 0.03)	0.57	0.13	
Error (2σ)		±0.07	±0.0010	±0.0010		±0.02	±0.03	±0.03	±0.03	±0.03

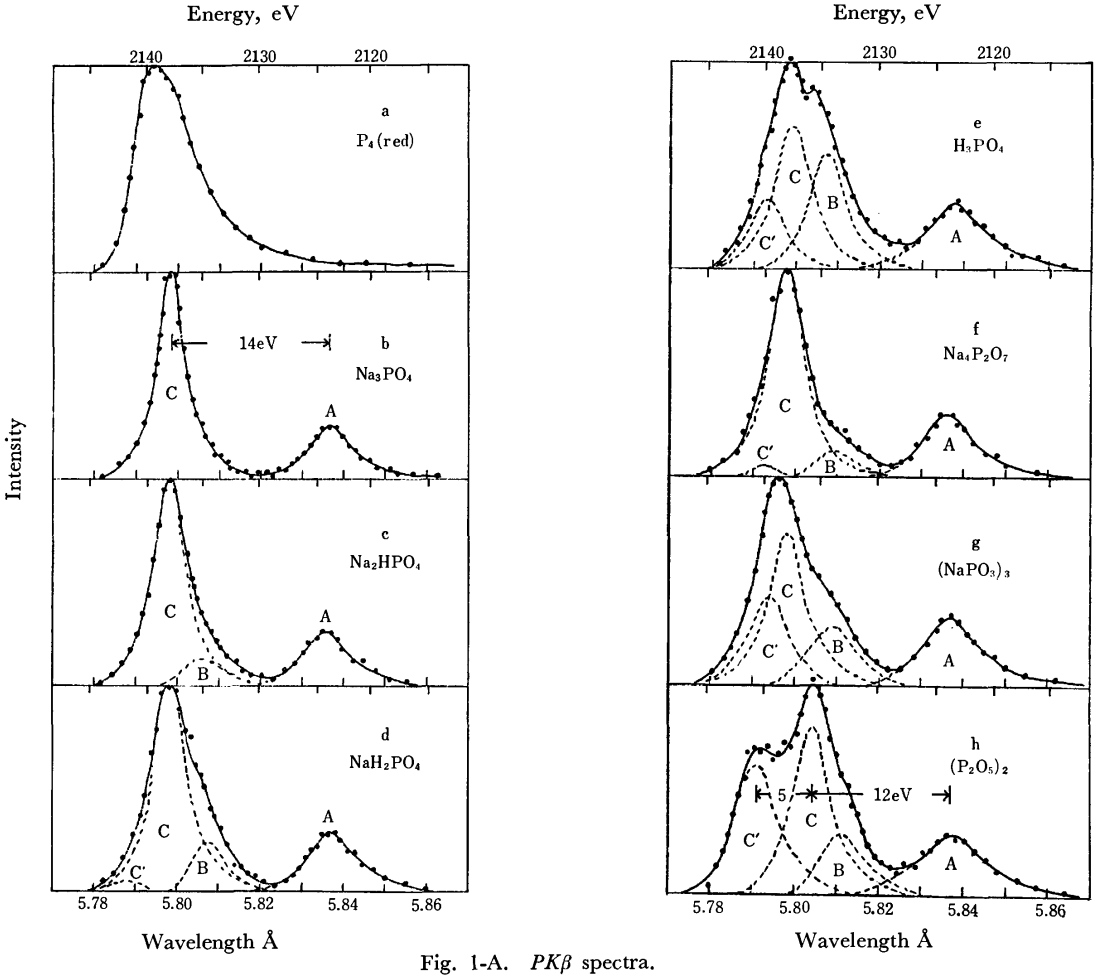

Fig. 1-A. $PK\beta$ spectra.

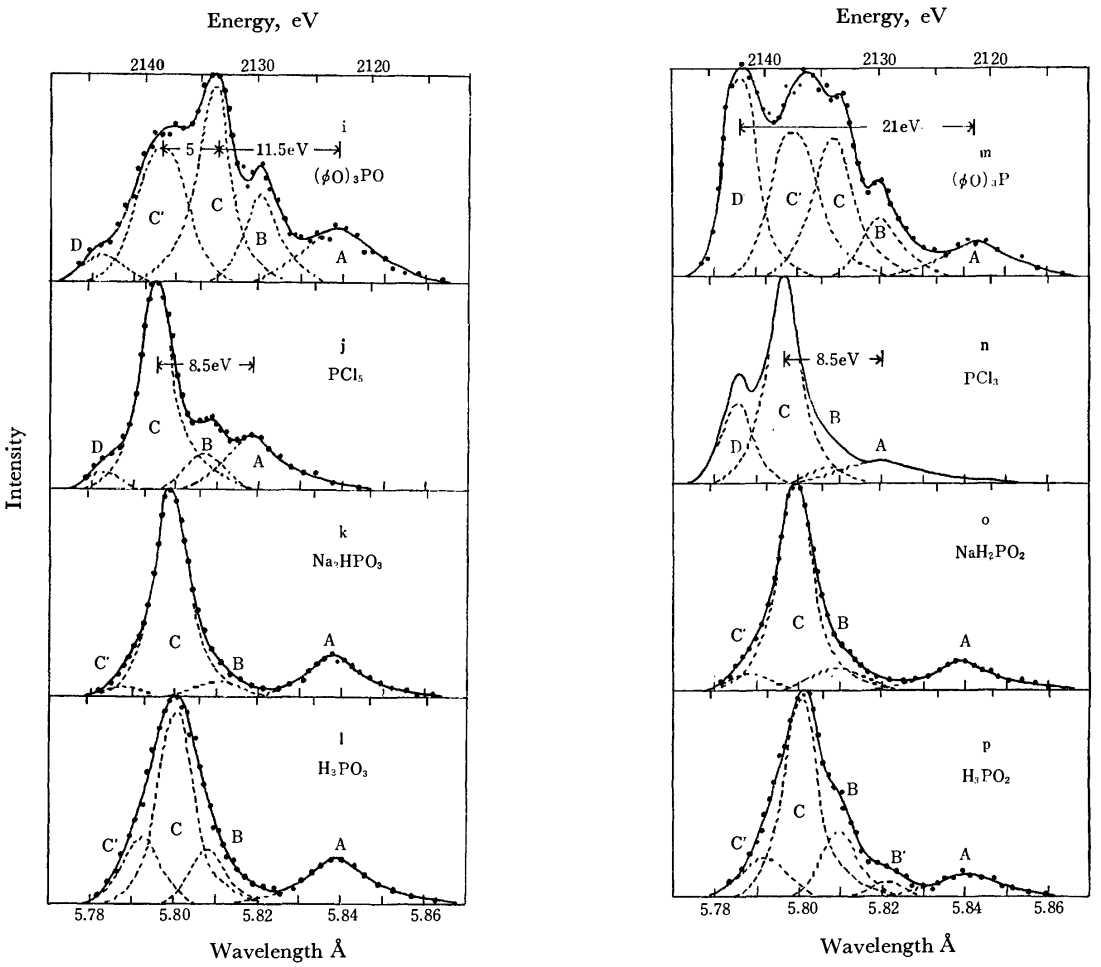

Fig. 1-B. P$K\beta$ spectra.

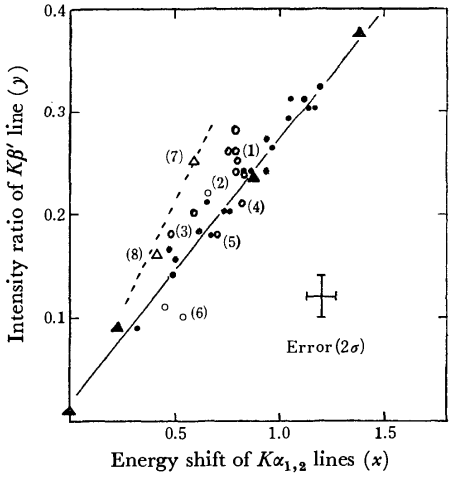

Fig. 2. The relationship between the intensity ration of $K\beta'$ line and the energy shift of $K\alpha_{1,2}$ lines.
○: oxygen-compound of phosphorus (P$K\beta$), (1) Na_3PO_4, (2) Na_2HPO_3, (3) NaH_2PO_2, (4) $(P_2O_5)_2$, (5) $(\phi O)_3PO$, (6) $(\phi O)_3P$.
△: chloride of phosphorus (P$K\beta$), (7) PCl_5, (8) PCl_3.
●: oxygen-compound of sulfur (S$K\beta$)
▲: oxygen-compound of chlorine (Cl$K\beta$)
——: regression line relating to the oxygen-compounds of sulfur and chlorine, $y=0.25x+0.02$.
------: anticipated line relating to the compounds of chlorine ligand.

The relationship between the $K\beta'$ intensity ratio and the energy shift of the $K\alpha_{1,2}$ lines found in the oxygen compounds and chlorides of phosphorus (mark ○ and △, respectively) is shown in Fig. 2. Although the points for the oxygen compounds are scattered in some extent, it may be concluded that they lie on a straight line similar to that found in the oxygen compounds of sulfur and chlorine. To speak more exactly, the points for the oxysalts of phosphorus drop on the upper side of the line, while those for the molecular oxygen compounds (phosphorus pentoxide P_2O_5, triphenyl phosphate $(\phi O)_3PO$, *etc.*) lie on the lower side. The points for phosphorus pentachloride and phosphorus trichloride deviate much from the line (mark △). It might be presumed that the latter points lie on another line, having a larger gradient. From this fact, it seems that the gradient of the line in the Fig. 2 is related not to the kind of third-period atom in the molecule, but to the kind of ligand atom.

In the $K\beta$ spectra of the oxygen compounds of sulfur and chlorine, and in those of the oxysalts of phosphorus, the energy difference between A and C was measured to be about 14 eV. However, in the case of the molecular oxygen compounds of phosphorus (P_2O_5, $(\phi O)_3PO$, *etc.*), the energy difference between A and C is about 12 eV, and there is a strong C' peak separated about 5 eV from the C peak on the higher-energy side. On the other hand, in the $K\beta$ spectra of the chlorides

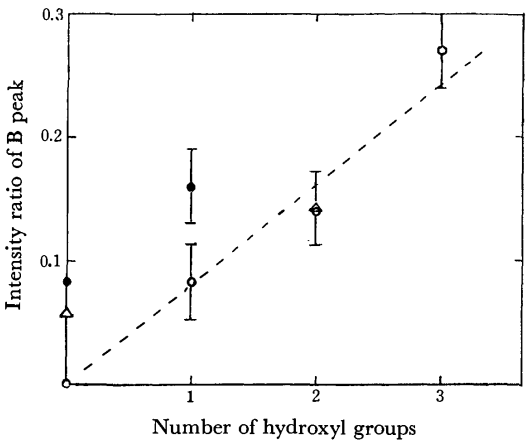

Fig. 3. The relationship between the intensity ratio of B peak and the number of hydroxyl groups in the oxyacids and their salts.
○: phosphoric acid (sodium salt)
△: phosphorous acid (sodium salt)
●: hypophosphorous acid (sodium salt)
We supposed that hypophosphorous acid was monobasic, in this Figure. We did not adupt the B′ peak, but adupted only the B peak on the intensity ratio of hypophosphorous acid.

of phosphorus, the energy differece between A and C was about 8.5 eV. The difference in these two cases may be compared with the difference in the gradients of the two lines in Fig. 2.

As in the case of the sulfur compounds, in which the B peak is observed in the $K\beta$ spectrum of such molecular compounds as dimethyl sulfone and the N,N-derivative of sulfoneamide,[3] the B peak is also observed in the molecular compounds of phosphorus, such as phosphorus pentoxide, triphenyl phosphate, and phosphorus pentachloride. In addition, in the oxysalts and oxyacids of phosphorus, the intensity of the B peak is proportional to the number of hydroxyl groups in the molecule.[7] In the spectrum of anhydrous sodium phosphate, which does not have a hydroxyl group, the B peak is, as expected, not observed. This relationship is shown in Fig. 3. Considering the position of the points for phosphite and hypophosphite in the figure, it seems that the P–H bond of these compounds slightly affects the appearance of the B peak. The appearance of the B peak seems to be attributable to the covalent bond between a third-period atom and a non-ionized atom, such as P–OH, P–OC, and P–OP. On sodium pyrophosphate, $[^{=}O_3P\text{–}O\text{–}PO_3^{=}]\cdot 4Na^+$, which involves only one such covalent bond per phosphorus atom, the B peak intensity ratio is close to the value in disodium hydrogenphosphate, and while on sodium metaphosphate, $^{-}O_2P\langle^{O\text{–}PO_2^{-}}_{O\text{–}PO_2^{-}}\rangle O\cdot 3Na^+$, which has two such covalent bonds per phosphorus atom, the ratio is close to the value in sodium dihydrogenphosphate. Further, on phosphorus pentoxide (dimer), in which there are one and a half such covalent bonds per phosphorus atom, the value of the ratio is conformable to the number of the covalent bond (see Table 1).

The D peak, as has been mentioned in a previous work, was markedly observed in the S$K\beta$ spectra of sulfite and sulfoxides and in the Cl$K\beta$ spectrum of chlorate.[3,4] As for the phosphorus compounds, a remarkable D peak is also observed in the spectrum of phosphorus trichloride. Generally, it seems that the remarkable D peak is observed in the $K\beta$ spectrum of the compound in which the third-period atom has one lone pair, such as $SO_3^{=}$, ClO_3^{-}, SF_4,[9] and PCl_3. The phosphorus atom of triphenyl phosphite $(\phi O)_3P$ also has one lone pair, so the appearance of the remarkable D peak in the spectrum can be anticipated. The D peak in the $K\beta$ spectrum measured (Fig. 1m) seems to correspond to the D peak of the sulfite or the phosphorus trichloride in view of the position and the intensity of the peak. That is, the peak appears in nearly the same position as the D peak of the phosphorus trichloride, and the peak separation between A and D in the spectrum of Fig. 1m, about 21 eV, corresponds to that between A and D for the sulfite, 21 eV, and to that for the chlorate, 20 eV. The intensity ratios of the D peak to the total $K\beta$ line in these compounds (0.29, 0.19, and 0.14 for triphenyl phosphite, phosphorus trichloride, and sodium sulfite, respectively) are larger than in other compounds.

The C′ peak is observed in the spectra of phosphorus pentoxide, triphenyl phosphate, and triphenyl phosphite. This peak can be distinguished from the D peak as a result of the difference in the position of the C′ peak (5.790—5.800 Å) from that of the D peak (5.783—5.787 Å). For example, in the spectrum of triphenyl phosphite, both D and C′ peaks are observed, and they can be distinguished, as is shown in Fig. 1m.

7) To make the matter clearer, the chemical structures of these oxyacides are shown below:

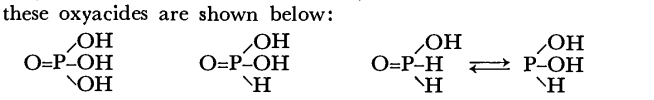

phosphoric acid, (tribasic) phosphorous acid, (dibasic) hypophosphorous acid, (monobasic)

in which dibasic inorganic hypophosphites are not present.[8]

8) "Mellor's Comprehensive Treatise on Inorganic and Theoretical Chemistry," Vol. VIII, (1962), p. 873.

9) In the S$K\beta$ spectrum of sulfur tetrafluoride, the intensity ratio of the D peak is 0.13, the peak separation between the D and C peaks is 7.2 eV, and that between the C and A peaks is 18.5 eV.[10]

10) Y. Takahashi, (unpublished data).

Spectra of Anions in Pure Iodine Melt and Iodine Solution Containing Tellurium

Kazuhiko ICHIKAWA and Mitsuo SHIMOJI

Department of Chemistry, Faculty of Science, Hokkaido University, Sapporo

(Received February 27, 1971)

The absorption spectra in the ultraviolet and visible region were measured as a function of the temperature for pure molten I_2 and for I_2+Te solutions. The two peaks found at about 305 and 370 mμ can be attributed to the I_3^- ion. These peaks increase with the addition of Te indicating an increase in the concentration of the I_3^- ion. This result is consistent with the previous interpretation of the conductivity of molten I_2 containing Te. The ionization potential of I_3^- can be estimated to be about 3.1 eV on the basis of a cyclic analysis using the model of Stein and Treinin which was developed for anion spectra in aqueous solutions. The temperature shift of the absorption energy can also be interpreted in terms of the same model. The heat change for the $I_2(g)+I(g)=I_3(g)$ reaction is estimated as -48.0 kcal·mol^{-1}.

In a previous paper[1] we have described our finding on the electrical conductivity of molten I_2+Te solutions, and pointed out that, in the I_2-rich region, the triiodide ion, I_3^-, probably resulting from some chemical reactions, may contribute largely to the electrical conduction.

This paper will report on the absorption spectra of the same solutions in the ultraviolet and visible regions. The experimental results confirm the presence of the I_3^- ion in these solutions and are discussed in terms of the theory given by Platzman and Franck[2] and modified by Stein and Treinin[3] for anion spectra in aqueous solutions.

Experimental

Materials. The tellurium used was 99.9999% pure. Guaranteed reagent-grade I_2 was dried at room temperature under a vacuum in order to remove the surface water and was purified by sublimation *in vacuo* at about 50°C.

Apparatus and Procedure. The absorption spectra in the ultraviolet and visible regions (230—700 mμ) were measured for the pure I_2 liquid and I_2+Te solutions. Measurements of diffuse reflectance spectra were carried out with a Beckman DK-2A ratio recording spectro-photometer. The quartz-drum-cell containing the sample, in which a fine powder phase was made of the guaranteed reagent-grade aluminum oxide, was sealed off under a vacuum. The observed temperature range was limited to below 200°C because of the limited temperature-supporting capacity of this spectrometer. The diffuse reflectance obtained for a given wavelengh was transformed to the optical density in arbitary units by means of the Kubelka-Munk equation.[4]

Results

The absorption bands of the I_2+Te solutions at several concentrations and temperatures are plotted in Fig. 1. All the absorption spectra show two peaks with a charactristic spacing at about 305 and 370 mμ. Their optical densities increase with the addition of Te,

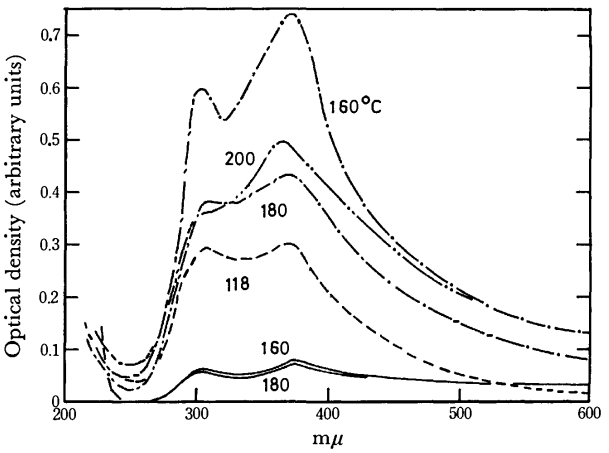

Fig. 1. Absorption spectra of I_2+Te solutions at various temperatures (——: pure, - - - -: I_2+2 at.% Te, —·—: I_2+4 at.% Te, and ——·——: I_2+40 at.% Te).

TABLE 1. ABSORPTION BANDS OF TRIIODIDE ANION (10^4 cm^{-1})

150°C		Room temperature		
I_2	I_2+4 at.%Te	KI crystal +I_2[7]	CsI_3 in water[5]	KI+I_2 in water[6]
3.260	3.295	3.454	3.478	3.478
2.699	2.722	2.821	2.846	2.846

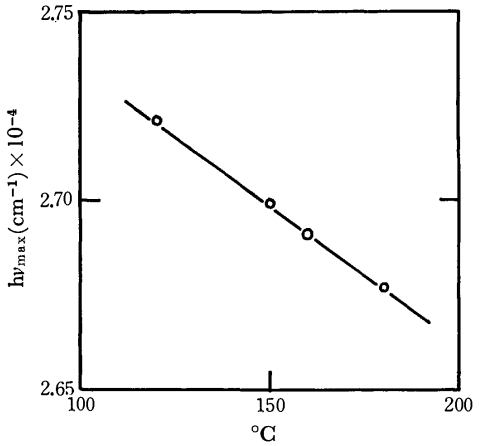

Fig. 2. $h\nu_{max}$ of molten iodine at various temperatures.

1) K. Ichikawa, T. Ōkubo, and M. Shimoji, *Trans. Faraday Soc.*, **67**, 1426 (1971).
2) R. Platzman and J. Franck, *Z. Physik*, **138**, 411 (1954).
3) G. Stein and A. Treinin, *Trans. Faraday Soc.*, **55**, 1086 and 1091 (1959).
4) *E.g.*, R. J. H. Clark, *J. Chem. Educ.*, **41**, 488 (1964).

although the wavelengths of the peaks are almost unchanged. Above about 150°C the optical density decreases and the band width increases with the temperature. Table 1 shows the two absorption maxima in the molten I_2 and I_2+4 at.% Te systems at 150°C. The energy separation between these two band maxima is very small, with a range of only about 0.6×10^4 cm^{-1}. In Fig. 2 the temperature dependence of the $h\nu_{max}$ of the longer wavelength band in the pure I_2 liquid is recorded. The straight line gives $dh\nu_{max}/dT=-7.3$ cm^{-1} deg^{-1}.

Discussion

In our previous work,[1] the considerable increase in the conductivity of molten I_2, upon the addition of 0.1—4 at.% Te was interpreted in terms of a charge-transport mechanism, and the formation of the triiodide ion I_3^-, resulting from the $I_2+I^-\longrightarrow I_3^-$ reaction, was suggested. The existence of the I_3^- ion is now confirmed by the absorption maxima found at 305 and 370 mμ, as is shown in Fig. 1 and Table 1, in which the other data for the CsI_3,[5] $KI+I_2$[6] aqueous solutions and the $KI+I_2$[7] solid solutions are also cited. The two peaks of the absorption spectra suggest a doublet splitting of some kind in the electronic states of the I_3 molecule.

The magnitude of $h\nu_{max}$ and its temperature shift, $dh\nu_{max}/dT$, obtained here will be discussed using the theory of Stein and Treinin,[3] which accounts for the anion spectra in aqueous solutions in terms of the charge-transfer-to-solvent mechanism.[2,3,8-10] Since the solvent structure in their theory is approximated only by a dielectric continuum with a static dielectric constant, D_s, the formula proposed by them may be used for systems other than the aqueous solution. Thus, the absorption energy of the solvated I_3^- ion may be written, using Stein and Treinin's notation, by:

$$h\nu_{max}=E_x-L_x+\frac{e^2}{r_0}\left(\frac{1}{2}+\frac{1}{2D_{op}}-\frac{1}{D_s}\right)-\frac{e^2}{2\bar{R}_e}\left(1-\frac{1}{D_{op}}\right)-\left(\frac{\pi^2me^4}{2h^2}\right)\left(\frac{1}{D_{op}}-\frac{1}{D_s}\right)^2 \quad (1)$$

The value of the apparent radius, r_o, of the cavity in the continuous medium can be determined from the relation $r_o\cong\alpha r_c$,[3] where r_c is the crystallographic radius and where α is a constant with a value of about 1.275. The value of r_c for I_3^- is taken as 3.51 Å from the crystallographic data of CsI_3,[11] by using the method of Gray and Waddington[12] for the calculation of the effective radius of N_3^-. The energy change associated with the non-thermodynamic dissolution of the I_3 molecule, $-L_x$, is roughly taken as $-3\Delta H_e/2$ by considering the dispersion forces. Here, ΔH_e[13] is the heat of evaporation of liquid I_2. The average distance of the excited electron from the center, $\bar{R}_e$, is calculated using the hydrogen-like wave function in the Coulomb force field due to the effective charge of the Landau type.

Table 2. Ionization potential E_x of I_3 evaluated by means of eq. (1) energies in 10^4 cm^{-1}

	150°C molten I_2	Room temperature		
		aq. CsI_3	aq. $KI+I_2$	crystal $KI+I_2$
E_x	2.41	2.60	2.60	2.60
D_{op}	2.73	1.78	1.78	2.69
D_s	13.0	78.5	78.5	4.94
L_x	0.607	0.483	0.483	0.758

The values of the optical dielectric constant D_{op} and those of D_s for the liquids are referred to "Gmelins Handbuch der anorganischen Chemie" **8**, Jod, Verlag Chemie, Berlin (1933) p. 85, 649. and **5**, Sauerstoff, Verlag, Weinheim, (1963) p. 1550, 1591, and those for the crystal are taken from N. F. Mott and R. W. Gurney, "Electronic Processes in Ionic Crystals," Clarendon Press, Oxford (1940), p. 12.

No data have been obtained so far for the value of the ionization potential of the I_3^- ion, E_x. Therefore, the value shown in Table 2 is evaluated on the basis of Eq. (1) using the experimental $h\nu_{max}$ values. Similar calculations were also made for CsI_3 and $KI+I_2$ aqueous solutions and for the KI crystal containing I_2, where it is assumed that the values of $-L_x$ are 3/2 of the heats[13,14] of solution of I_2 into the respective solvents. The calculated E_x values in Table 2 are almost constant, ranging only $(2.4-2.6)\times10^4 cm^{-1}$, despite the differences in the parameters of the respective solvents.

No quantitative calculations have been performed for the I_2+Te solutions, because no observed values of D_s in this system are available. The resemblance in the positions of the absorption maxima reported in Fig. 1 and Table 1, however, suggests the applicability of the same model for the extremely I_2-rich melts. In other words, the parameter values (for r_o, D_s, D_{op}, L_x, *etc.*) in the molten I_2 containing a small amount of Te below 4 at.% may not be very different from those in pure I_2. Further, the increase in the optical densities of the peaks (Fig. 1) upon the addition of Te and the decrease upon the raising of the temperature indicate an increase in the concentration of the I_3^- ion. These facts are consistent with the conclusion in the conductivity work[1] that the enthalpy change in the I_3^- formation must be negative, because the I_3^- concentration decreases with an increase in the temperature in these I_2-rich liquids.

Theoretically, the temperature shift can be written by a differentiation of Eq. (1) with respect to the temperature. The contribution from the temperature change in D_s and D_{op} is, at most, -1 $cm^{-1}deg^{-1}$, which is much smaller than the experimental value of -7.3

5) F. L. Gilbert, R. R. Gosdstein, and T. M. Loury, *J. Chem. Soc.*, 1092 (1931).
6) L. I. Katzin, *J. Chem. Phys.*, **23**, 2055 (1955).
7) E. Mollowo, quoted in H. N. Hersh, *Phys. Rev.*, **105**, 1410 (1957).
8) M. Smith and M. C. R. Symons, *Trans. Faraday Soc.*, **54**, 338 and 346 (1958).
9) M. J. Blandamer and M. F. Fox, *Chem. Rev.*, **70**, 59 (1970).
10) A. Maruyama, M. Shimoji, and K. Niwa, This Bulletin, **34**, 1234 (1961).
11) H. A. Tasman and K. H. Boswijk, *Acta. Cryst.*, **8**, 59 (1955).
12) P. Gray and T. C. Waddington, *Proc. Roy. Soc. A*, **235**, 481 (1956).
13) *E.g.*, O. Kubaschewski and E. LL. Evans, "Metallurgical Thermochemistry", Pergamon Press, Oxford (1958).
14) "Selected Values of Chem. Thermody. Property," Technical Note 270—3, National Bur. Stand. (1968).

$cm^{-1}deg^{-1}$. The term of dL_x/dT can be calculated from the value of the heat capacity of the I_3^- ion in the excited state, $C_p(I_3(I_2)_n^-)$. The heat-capacity effect in the gaseous state practically vanishes[10] in these cyclic calculations, for its effect appears in the processes of both the ion removal and the radical solvation (*e.g.*, in the terms of E_1 and E_2 in Eq. (6) in the paper of Stein and Treinin,[3] from which Eq. (1) in this paper is obtained). $C_p(I_3(I_2)_n^-)$ is roughly taken as 3/2 of the heat capacity of the I_2 molecule in the liquid state. dr_o/dT is evaluated from the $\alpha dr_c/dT$ relation using the density data.[15] Thus, for pure I_2 the calculated $dh\nu_{max}/dT$ value of $-8.7\ cm^{-1}deg^{-1}$ is in fair agreement with the experimental value of $-7.3\ cm^{-1}deg^{-1}$ (Fig. 2). This temperature shift may also be interpreted alternatively in terms of the vibrational effect[10] of the solvated molecules.

In a simpler model, proposed by Smith and Symons,[8] the temperature effect is explained by considering only the change in the excited state, which is approximated as a state of a free particle in a spherical box. Adopting $E_x=2.41\ cm^{-1}deg^{-1}$ from Table 2 and $h\nu_{max}=26990\ cm^{-1}$, we get 10.2 Å for the radius, r_o*, of the spherical box in their model. However, such a free-electron-like behaviour in the box may be difficult to correlate with any physical property of the ion, as was pointed out by Stein and Treinin.[3]

The heat of formation of triiodide molecules in the gaseous state has not previously been reported. However, the heat of reaction, $\Delta H_r(I_3^-(aq))$, for the equilibrium in aqueous solutions[16]:

$$I_2(aq) + I^-(aq) \rightleftharpoons I_3^-(aq) \qquad (2)$$

has been well investigated, and the heats[14] of hydration of the iodine molecule and ion, *i.e.*, $\Delta H_h(I_2)$ and $\Delta H_h(I^-)$, are konwn. Further, the ionization potential of the I^- ion, $E_x(I^-)$,[9] has been established, the heat of hydration of the I_3^- ion can be estimated theoretically by means of Born's equation,[17] and the semiempirical value of the ionization potential of the I_3^- ion, $E_x(I_3^-)$, is shown in Table 2 of this paper. Thus, if we use $\Delta H_r(I_3^-(aq))=-4.7\ kcal\cdot mol^{-1}$, $\Delta H_h(I_2)=-9.5$, $\Delta H_h(I)=-72.1$, $\Delta H_h(I_3^-)=-39.3$, $E_x(I^-)=72.5$, and $E_x(I_3^-)=71.5$, the heat of reaction, $\Delta H_r(I_3(g))$, for the reaction:

$$I_2(g) + I(g) = I_3(g) \qquad (3)$$

can be given by $-48.0\ kcal\cdot mol^{-1}$. This calculated result suggests that the I_3 molecule is stable in the gaseous phase, as is observed in the mass spectra.[17]

We are indebted to Professor Y. Matsunaga, in whose laboratory the measurements of the absorption spectra were made. We also wish to thank Professors K. Ohno and Y. Matsunaga for their helpful discussions. One of us (K.I.) is grateful for a grant from the Sakkokai Foundation.

15) K. Saito, K. Ichikawa, and M. Shimoji, This Bulletin, **41**, 1104 (1968).

16) G. Jones and B. B. Kaplan, *J. Amer. Chem. Soc.*, **50**, 1845 (1928).

17) *E.g.*, H. O. Pritchard, *Chem. Rev.*, **52**, 529 (1953).

A MO-theoretical Study of the Catalytic Activity of Onium Compounds in the Liquid-phase Oxidation

Katsutoshi OHKUBO and Hirokazu KANAEDA

Department of Synthetic Chemistry, Kumamoto University, Kurokami-machi, Kumamoto

(Received March 3, 1971)

A theoretical study with the extended Hückel method augmented by *d*-orbitals was undertaken in order to elucidate the relation between the electronic structures of various onium compounds and their catalytic activities in the liquid-phase oxidation of hydrocarbons. There were several findings. Firstly, the differences in the catalytic activities of the carbonium, ammonium, and oxonium compounds are ascribed to those in the AO populations of the p_z-orbitals on their central atoms. Secondly, the distinguished activities of sulfonium and phosphonium compounds were well explained by the partially-occupied sulfur or phosphorus 3*d*-orbitals, in which the d_{xz} (or d_{yz}) orbital is utilized most effectively for the interaction with the $(1\pi_g)_z$–orbital of O_2. Finally, the relatively low activities of arsonium and telluronium compounds are ascribed to the vacant and diffused 4*d* or 5*d* orbitals, while the appreciable activity of the selenonium compound is caused by the partial electron-occupancy of the $4d_{xz}$ (or $4d_{yz}$) orbital of the central selenium.

The catalyst in the liquid-phase oxidation of hydrocarbons has been widely investigated from the viewpoints of both theory and technology. Among several oxidation catalysts, such as transition metal compounds[1] (including chelates[2] and complexes[3]) and halogen compounds[4] (involving ammonium salts[5]), ammonium salt-catalysts exhibit some especially interesting features in their catalytic behavior because they show little activity for the promotion of the oxidation reaction, even though the ammonium cation possesses the counter anion of perchlorate[5] or tetrafluoroborate,[6] and also because the difference in the substituents attached to the central nitrogen has an influence upon the catalytic activity. Our own previous studies[7,8] of the catalytic activities of several onium compounds demonstrated that the activity was affected directly by the differences in the onium central atoms and immediately by those in the structures of the counter anions and the substituents. That is, sulfonium and phosphonium salts involving the lower vacant 3*d*-orbitals (strictly speaking, the partially-occupied 3*d*-ones) were found most effective, and it was shown that the larger the alkyl group attached to the central atom, the higher the catalytic activity. As for the counter anions, phosphate, sulfate, *etc.* are more active than halides. These experimental phenomena are directly connected with the catalytic activation of molecular oxygen, as was suggested by our spectroscopic[9] and theoretical[10,11] investigations concerning the possible interaction between the catalyst and O_2.

In this paper, we will attempt to clarify the correlation between the electronic structures of onium compounds and their catalytic activities in the liquid-phase oxidation of hydrocarbons, such as cumene and α-pinene. For example, the catalytic activity of several onium tetrafluoroborates has been found to be in approximately the following order: carbonium<ammonium<oxonium, silyl<phosphonium≃sulfonium, arsonium≃telluronium<selenonium. Extended Hückel molecular orbital (EHMO) calculations were performed on these onium compounds.

Method of Calculation

The extended Hückel method (EHMO) proposed by Hoffmann[12] was adopted to the calculations of $(CH_3)_3CCl$, $(CH_3)_4NCl$, $(CH_3)_3OCl$, $(CH_3)_3SiCl$, $(CH_3)_4PCl$, $(CH_3)_3SCl$, $(CH_3)_4AsCl$, $(CH_3)_3SeCl$, and $(CH_3)_3TeCl$. Methyl derivatives of onium compounds were taken for mathematical convenience. The geometries used for the calculations are illustrated in the figures of this paper.

The orbital exponents and the Coulomb integrals ($H_{\mu\mu}$) were supplied by Clementi[13] and Jaffè,[14,15] respectively. Especially, the $H_{\mu\mu}$ value of the oxygen 2*p*-orbital was obtained from the atomic ground-state ionization potential[14] ($H_{\mu\mu}$(O 2*p*)$=-13.61$ eV). The $H_{\mu\mu}$ values of the *d*-orbitals of S, P, As, Se, and Te were -7.00,[16] -6.53, -5.00, -4.00, and -4.00 eV respectively. The resonance integrals ($H_{\mu\nu}$) were evaluated by the Wolfsberg-Helmholtz approximation[17]:

$$H_{\mu\nu} = 0.875(H_{\mu\mu}+H_{\nu\nu})S_{\mu\nu}$$

1) For instance, J. A. Barnard and D. S. Mitchell, *J. Catal.*, **12**, 386 (1968); W. F. Brill, *Ind. Eng. Chem.*, **52**, 837 (1960), and the references cited therein.

2) L. H. Vogt, Jr., *Chem. Rev.*, **63**, 269 (1963), and the references cited therein.

3) L. Vaska, *Science*, **140**, 809 (1963); S. Otsuka, A. Nakamura, and T. Tatsuno, *Chem. Commun.*, **1967**, 836, *etc.*

4) W. G. Toland, *Ind. Eng. Chem.*, **50**, 1386 (1958); D. A. S. Ravens, *Trans. Faraday Soc.*, **55**, 1768 (1959).

5) H. Bredereck, A. Wagner, R. Blascke, C. Demetriades, and K. G. Kottenhahn, *Chem. Ber.*, **92**, 2628 (1959).

6) K. Kanai, K. Ohkubo, H. Kitano, and K. Fukui, *Bull. Japan Petrol. Inst.*, **7**, 52 (1965).

7) K. Ohkubo and T. Yamabe, *ibid.*, **12**, 130 (1970).

8) K. Fukui, K. Ohkubo, and T. Yamabe, This Bulletin, **42**, 312 (1969).

9) K. Ohkubo and T. Yamabe, *J. Org. Chem.*, **36**, 3149 (1971).

10) K. Ohkubo and T. Yamabe, This Bulletin, **44**, 1183 (1971).

11) K. Ohkubo, *Tetrahedron Lett.*, **1971**, 2571, 2897.

12) R. Hoffmann, *J. Chem. Phys.*, **39**, 1397 (1963); **40**, 2474 (1964).

13) E. Clementi and D. L. Raimondi, ibid., **38**, 2686 (1963).

14) J. Hinze and H. H. Jaffè, *J. Amer. Chem. Soc.*, **84**, 540 (1962).

15) J. Hinze and H. H. Jaffè, *J. Phys. Chem.*, **67**, 1501 (1963).

16) T. Jordan, H. W. Smith, L. L. Lohr, Jr., and W. N. Lipscomb, *J. Amer. Chem. Soc.*, **85**, 846 (1963).

17) M. Wolfsberg and L. Helmholtz, *J. Chem. Phys.*, **20**, 837 (1952).

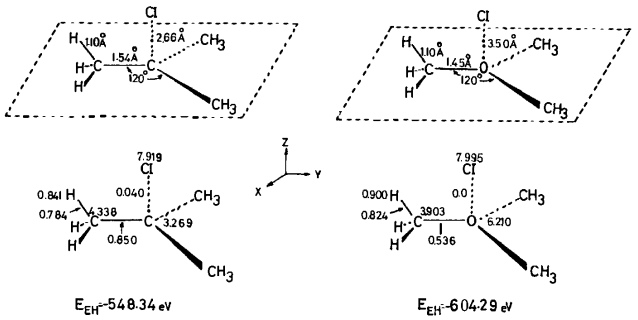

Fig. 1. Valence electron distributions and total energies of $(CH_3)_3CCl$ and $(CH_3)_3OCl$.

where $S_{\mu\nu}$ is the overlap integral between AOs.

The wave-function contours were calculated on the basis of the Slater AO functions.[18]

Results and Discussion

Electronic Structures of Second-row Onium Compounds. It is necessary at first to assume the molecular structures of carbonium, ammonium, and oxonium compounds under the present experimental conditions. In view of the propeller-like D_3 symmetry of the triphenylcarbonium cation[19] and the ionic property of these compounds, it is plausible to assume planar C_{3v} structures for the trimethylcarbonium and trimethyloxonium cations.[20] On the basis of the above discussion, the EHMO calculations were performed for $(CH_3)_3CCl$ and $(CH_3)_3OCl$ at the ionic distances of C–Cl and O–Cl (2.66 and 3.5 Å respectively). The valence-electron distributions of the above compounds are shown in Fig. 1. In regard to the structure of $(CH_3)_4NCl$, two representative configurations can be considered: one of them takes the C_{4v} symmetry of the ammonium cation, while the other takes the T_d symmetry. The two distinct electronic structures of $(CH_3)_4NCl$ are indicated in Fig. 2.

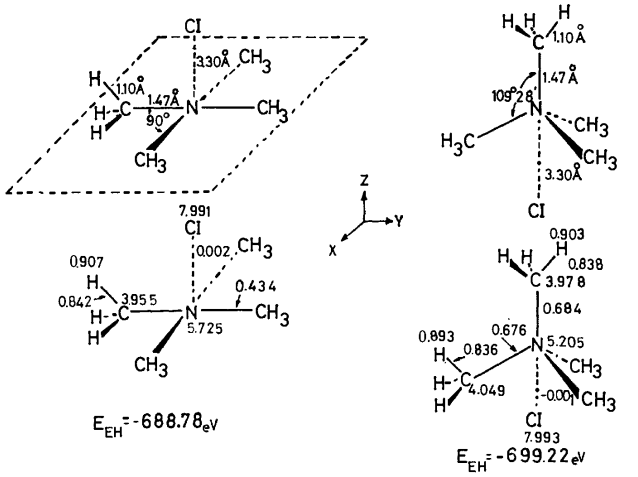

Fig. 2. Valence electron distributions and total energies of the two representative structures of $(CH_3)_4NCl$.

The catalytic activities of the second-row onium compounds were not remarkable as compared with sulfonium and phosphonium compounds. This may be ascribed to their inoic character, which reflects the small or negative overlap population between the cation and the anion (see M_{A-Cl} in Table 1), considering that the considerable covalency of the bond between the cation and the anion contributes directly to the partial electron-occupation of the lowest unoccupied (LU) central-atom orbital, which can then be utilized for the interaction with the $1\pi_g$-orbitals of O_2.

It is necessary here to discuss the order of the activity, carbonium<ammonium<oxonium, in hydrocarbon oxidations. In the case of carbonium and oxonium catalysts, the interaction between the catalyst and the $(1\pi_g)_z$-orbital of O_2 takes place in the direction of the p_z-orbital of the central atom from the opposite side of the counter anion, since, in such a mode of interaction, an overlapping of the orbitals but no steric hindrance can be expected. The above discussions lead to an assumption that the partially-occupied carbon p_z-orbital (the LU orbital of $(CH_3)_3CCl$) and the nonbonding oxygen p_z-orbital (the highest occupied (HO) orbital of $(CH_3)_3OCl$) play an important role in the interaction with the $(1\pi_g)_z$-orbital of O_2. That is, the AO population of the HO level on the p_z-orbital of the central atom ($N_{HO}(Z_A)$) is closely related to the catalytic activity, because the activity results from the electron-donor property of the onium cation.[8] In the case of the ammonium catalyst, the interaction between the p_z-orbital of the ammonium cation and the $(1\pi_g)_z$-orbital of O_2 is sterically hindered to some extent by the substituents attached to the central nitrogen. The values of $N_{HO}(Z_A)$ and the AO population of the central atom ($N(Z_A)$) are listed in Table 1. The order of the above values is in agreement with the catalytic activity as defined by the maximum reaction rate (R_{max}).

Electronic Structures of Third-row Onium Compounds. The EHMO calculations were carried out on the electronic structures of onium compounds possessing third row-atoms, *i.e.*, silyl, phosphonium, and sulfonium compounds. The silyl compound was taken as a com-

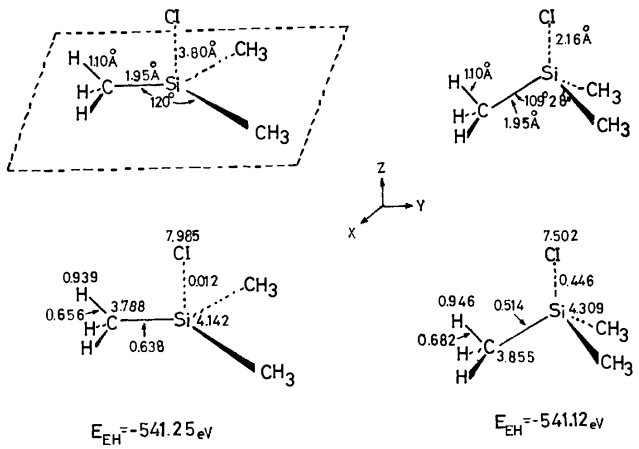

Fig. 3. Valence electron distributions and total energies of the two distinct $(CH_3)_3SiCl$.

18) J. C. Slater, *Phys. Rev.*, **36**, 57 (1930).

19) D. W. A. Sharp and N. Sheppard, *J. Chem. Soc.*, **1957**, 674.

20) The ASMO SCF calculations on $(CH_3)_3SCl$[9] have found that the planar C_{3v} symmetry of the sulfonium cation was most stable energetically. This may support the planar C_{3v} symmetry of the oxonium cation.

TABLE 1. RELATION BETWEEN THE ELECTRONIC STRUCTURES OF SECOND ROW ONIUM COMPOUNDS AND THE CATALYTIC ACTIVITIES

Onium chloride R_3ACl or R_4ACl		A–Cl (Å)	M_A [a]	M_{A-Cl} [b]	$N(Z_A)$ [c]	$N_{HO}(Z_A)$ [c]	Orbital energy (eV) HO	Orbital energy (eV) LU	$R_{max} \times 10^4$ [d] (mol/l sec)	
$(CH_3)_3C$		2.66	3.27	0.039	0.296	0.0018	−12.79	−9.19	0.26[a]	0.52[b]
$(CH_3)_4N$	T_d	3.30	5.20	−0.001	1.267 (1.263[e])	0.0444 (0.0[e])	−13.11	0.45	0.34[a]	0.74[b]
	C_{3v}	3.30	5.73	0.002	1.957	−0.0	−10.42	−3.88		
$(CH_3)_3O$		3.50	6.201	0.0	1.981	0.357	−11.74	−1.34	0.67[a]	0.82[b]

a) Atom population of the central atom. b) Overlap population between the cation and the anion. c) AO populations of the p_z-orbital of the central atom and that at the HO MO ($N_{HO}(Z_A)$). d) R_{max} values were obtained from cumene (a) and α-pinene (b) oxidations at 85°C, respectively. e) Values are those of p_x and p_y.

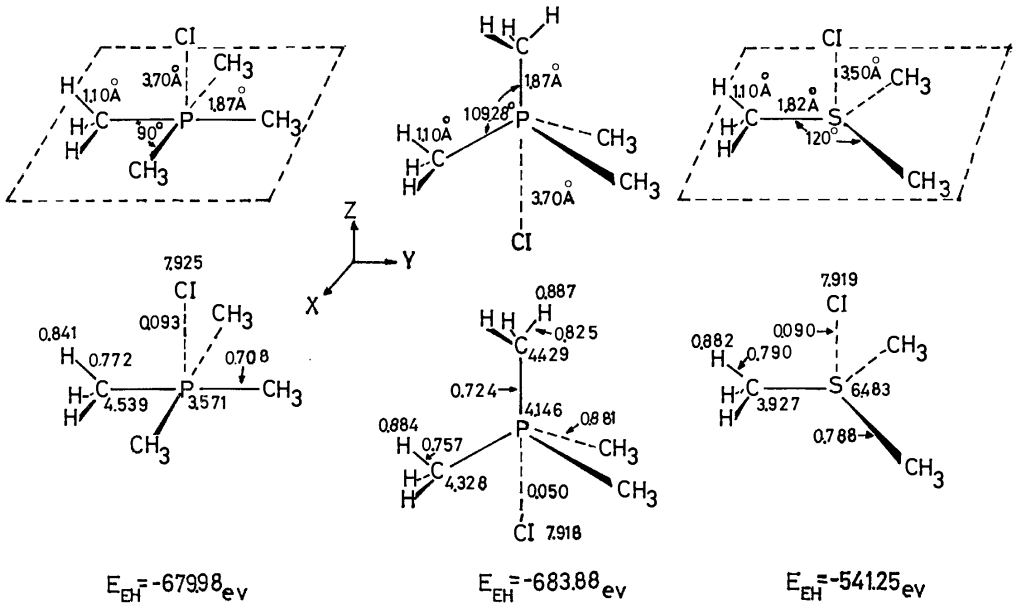

Fig. 4. Electronic structures of $(CH_3)_4PCl$ and $(CH_3)_3SCl$.

parison. As to the molecular structure of the sulfonium compound, the planar C_{3v} symmetrical sulfonium cation gave the most stable configuration of the trimethylsulfonium compounds.[20] The structures of silyl and phosphonium compounds have, however, thus far remained obscure. There are two possible representative configurations for each of the cations, silyl and phosphonium: for the former, one is the planar C_{3v} symmetrical silyl cation and the other is the C_{3v} symmetrical silyl compound,[21] while for the latter, the one is the C_{4v} symmetrical phosphonium ion and the other is the T_d symmetry of the phosphonium compound. Figures 3 and 4 show the configurations of these compounds and the electronic structures, together with the total energies (E_{EH}). $(CH_3)_3SiCl$ would take the C_{3v} symmetry, although the Si–Cl bond may be lengthened to some extent in hydrocarbons involving such polar oxidation

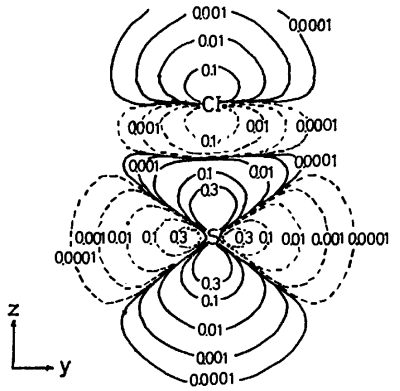

Fig. 5. Orbital contour of $(CH_3)_3SCl$ at the LU MO. (the solid and broken lines stand for the positive and the negative MO signs respectively.)

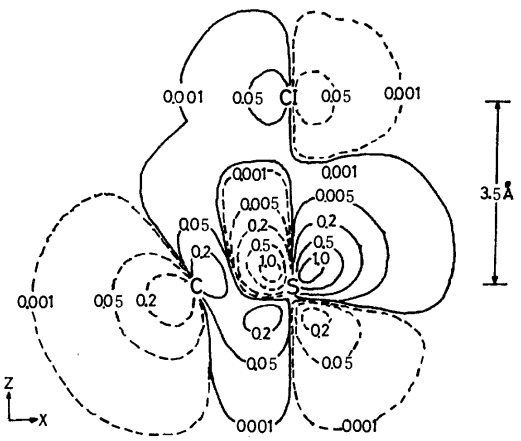

Fig. 6. Orbital contour of $(CH_3)_3SCl$ at the LU+1 MO.

21) E. Newman, J. K. O'Loane, S. R. Polo, and M. K. Wilson, *J. Chem. Phys.*, **25**, 855 (1956).

TABLE 2. RELATION BETWEEN ELECTRONIC STRUCTURES OF THIRD ROW ONIUM COMPOUNDS AND THE CATALYTIC ACTIVITIES

Onium chloride R_3ACl or R_4ACl		A–Cl (Å)	N_A			N_d					$R_{max} \times 10^4$ (mol/l sec)
			p_z	p_y	p_x	d_{xz}	d_{yz}	d_{xy}	$d_{x^2-y^2}$	d_{z^2}	
$(CH_3)_3Si$	C_{3v}	3.80	0.161	1.410	1.411						0.75[b]
$(CH_3)_3SiCl$	C_{3v}	2.16	0.308	1.423	1.423						
$(CH_3)_4P$	C_4	3.70	0.453	0.833	0.833	0.137	0.137	0.056	−0.067	0.032	0.89[b]
	T_d	3.70	0.883	0.885	0.828	0.122	0.144	0.105	0.031	0.021	
$(CH_3)_3S$	C_{3v}	3.50	1.981	0.992	0.992	0.142	0.142	0.092	0.092	0.068	1.12[a] 0.97[b]

R_{max} indicates the maximum oxidation reaction rates in cumene (a) and α-pinene (b) at 85°C.

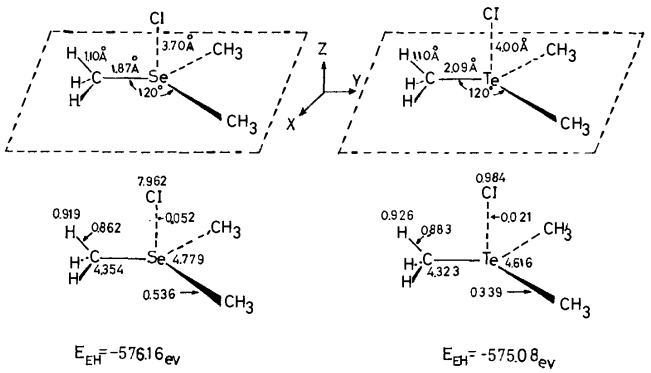

Fig. 7. Electronic structures of $(CH_3)_3SeCl$ and $(CH_3)_3TeCl$ in two distinct configurations.

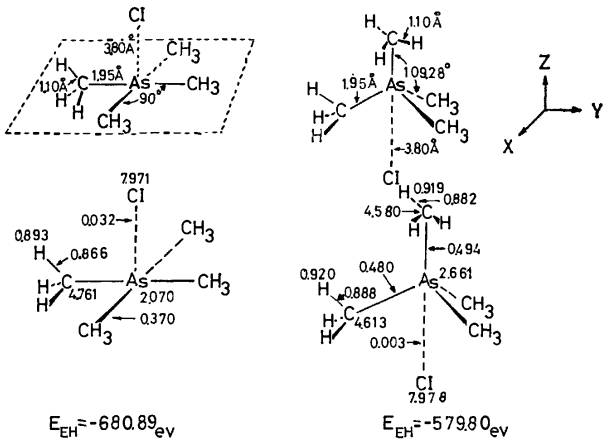

Fig. 8. Electronic structure of $(CH_3)_4AsCl$ in two distinct configurations.

products as alcohols and hydroperoxides.

Among the onium compounds utilized for the liquid-phase oxidation catalysts, phosphonium and sulfonium compounds exhibit the most remarkable activity. The extraordinary activities of these compounds are due to the catalytic activation of molecular oxygen by means of their partially occupied *d*-orbitals, in which the d_{xz} or the d_{yz} is the most preferable orbital for the interaction with the $(1\pi_g)_x$-orbital of O_2.[10,11] Moreover, the mode of the interaction has been discussed in detail in Refs. 8, 10, and 11. This partial occupancy of the sulfur or phsophorus *d*-orbitals is not only due to the somewhat covalent nature of the bond between the onium cation and the counter anion, but also to the *d*–π interactions between the carbon *p*-orbitals of the substituents and the *d*-orbitals. Some aspects of these features mentioned above can be explained by the orbital contours of $(CH_3)_3SCl$ illustrated in Figs. 5 and 6.

In conclusion, the order of the catalytic activity, silyl<phosphonium<sulfonium, can be well explained by the small AO population of the p_z-orbital of the silyl compound and the almost identical AO populations of the *d*-orbitals (indicated by N_d in Table 2) of phosphonium and sulfonium compounds. It is necessary here to mention that, in the case of the sulfonium compound, the nonbonding sulfur p_z-orbital at the HO MO may contribute to some extent to the increase in the electron-donor property of the compound, while the nonbonding or electron-rich *p*-orbitals can not be expected in the case of the phosphonium compound.

Electronic Structures of Fourth- or Fifth-row Onium Compounds. The onium compounds discussed in this section are arsonium, selenonium, and telluronium compounds. In regard to the structures of selenonium and telluronium compounds, they would take the planar C_{3v} symmetrical cations much like the sulfonium compound. On the other hand, two distinct structures can be considered for the arsonium compound; one takes the C_{4v} symmetrical ligand plane of the arsonium ion, while the other takes the T_d symmetrical arsonium ion. Perhaps, the latter configuration is more plausible. The

TABLE 3. RELATION BETWEEN ELECTRONIC STRUCTURES OF FOURTH AND FIFTH ROWS ONIUM COMPOUNDS AND THE CATALYTIC ACTIVITIES

Onium Chloride R_3ACl or R_4ACl		A–Cl (Å)	N_A			N_d					$R_{max} \times 10^4$ (mol/l sec)
			p_z	p_x	p_y	d_{xz}	d_{yz}	d_{xy}	$d_{x^2-y^2}$	d_{z^2}	
$(CH_3)_4As$	C_4	3.80	0.427	0.784	0.784	−0.042	−0.042	−0.186	−0.517	−0.0647	0.22
	T_d	3.80	0.806	0.837	0.790	−0.125	−0.096	−0.119	−0.185	−0.202	
$(CH_3)_3Se$	C_{3v}	3.70	1.989	0.836	0.836	0.020	0.200	−0.111	−0.111	−0.008	1.04
$(CH_3)_3Te$	C_{3v}	4.00	1.991	0.804	0.806	−0.024	−0.024	−0.168	−0.174	−0.043	0.45

R_{max} stands for the maximum reaction rate in the cumene oxidation at 85°C.

valence electron distributions of $(CH_3)_3SeCl$, $(CH_3)_3TeCl$, and $(CH_3)_4AsCl$ are shown in Figs. 7 and 8.

The relatively low catalytic activities of these compounds as compared with sulfonium and phosphonium compounds may be attributed to the diffused $4d$ or $5d$ orbitals of the central atoms. Especially, the arsonium compound and the telluronium compound indicate negative N_d values for the AO populations of their d-orbitals. On the other hand, the appreciable activity of the selenonium compound results from the partial-occupied selenium d_{xz} or d_{yz} orbital. The order of the activity, arsonium$\simeq$telluronium$<$selenonium, can be well explained by that of the N_d values indicated in Table 3.

The molecular structures of the onium compounds discussed in this paper will be treated in more detail in a succeeding report.

Most of the calculations were carried out on FACOM 230.60 computer at the Computer Center of Kyushu University, but some of them were done at the Computer Center of Kyoto University.

BULLETIN OF THE CHEMICAL SOCIETY OF JAPAN, VOL. 45, 15—19(1972)

Measurements of the Vapor and Dissociation Pressures of Potassium Sulfate and Carbonate at High Temperatures

Tetsuo KOSUGI

Hitachi Research Laboratory, Hitachi Ltd., Kuji-Machi, Hitachi, Ibaraki

(Received March 8, 1971)

The dissociation reactions of potassium sulfate and potassium carbonate were determined using a quadrupole-type mass spectrometer with a Knudsen-cell-type ion source. The vapor and dissociation pressures of potassium sulfate and the dissociation pressure of potassium carbonate were obtained, by the use of the Knudsen effusion method at temperatures from 900 to 1700°K, as follows:

$$\log P = -1.253 \times 10^4\left(\frac{1}{T}\right) + 7.724 \quad (K_2SO_4)$$

$$\log P_d = -3.275 \times 10^4\left(\frac{1}{T}\right) + 20.83 \quad (K_2SO_4)$$

$$\log P_d = -1.135 \times 10^4\left(\frac{1}{T}\right) + 9.257 \quad (K_2CO_3)$$

The equilibrium constants of the dissociation reaction were estimated from the above data and from those of Kröger and Stratmann:[1]

$$\log K_p = -6.94 \times 10^4\left(\frac{1}{T}\right) + 38.8 \quad (K_2SO_4)$$

$$\log K_p = -1.38 \times 10^4\left(\frac{1}{T}\right) + 9.80 \quad (K_2CO_3)$$

An easily ionizable material (seed) must be added to the combustion products of fuels to achieve a sufficient degree of ionization of the gases in a magneto-hydrodynamic (MHD) generator. The problem of seed recovery in open-cycle MHD power plants is of critical importance for the successful economic realization of MHD power generation. In general, the seed used for open-cycle MHD power generation is a potassium compound. Hart *et al.*[2] suggested that the potassium compounds which were contained in exhaust gases from the MHD generator were potassium sulfate and potassium carbonate when a sulfur-contained fuel was used.

Unfortunately, the physical and chemical properties of the potassium compounds are not yet clear because of their strong reactivity at high temperatures. Therefore, a seed-recovering technique has not been established.

This paper will give experimental data on the dissociation reactions and some thermodynamic constants of potassium sulfate and potassium carbonate at high temperatures.

Experimental

Mass Spectrometric Studies. Apparatus: Details of the mass spectrometer used have been described in a previous paper.[3] The Knudsen cell, made of Pt-5%Rh alloy, was heated with a tantalum heater. The temperature of the cell was measured with a calibrated Pt/Pt-13%Rh thermocouple at the bottom of the cell.

The vapor effusing from the Knudsen cell entered directly into the ionization chamber, which was mounted on top of

1) C. Kröger and J. Stratmann, *Glastech. Ber.*, **34**, 311 (1961).

2) A. B. Hart, G. C. Gradner, W. D. Halstead, J. W. Laxton, and D. Tidy, "International Symposium on Magnetohydrodynamic Electrical Power Generation," Paris (1964), No. 89.

3) T. Kosugi, *Kogyo Kagaku Zasshi*, **73**, 148 (1970).

the analyzer tube. In the ionization chamber, neutral atoms and molecules were bombarded with electrons of controlled energy and thus ionized. A secondary electron multiplier was used for ion detection. The out-put of this multiplier was amplified and recorded.

Materials: A special grade of potassium compound was used. Impurities in the powder were checked by means of emission spectroscopy. The results of qualitative analysis showed a trace of Na and no evidence of As, Ca, Mg, Pt, Fe, Al, Sn, Ag, Cu, and Pb. Further sample purification was not carried out.

Preparation of the Sample: The method of sample preparation was the same as given in a previous paper.[3]

After preparation, the cell was cooled to below 50°C. Then, the ion intensity of each dissociaton product was measured by means of the mass spectrometer at each experimental temperature. Then peaks at masses 32, 39, 48, 64, and 94 were attributed to O_2^+, K^+, SO^+, SO_2^+, and K_2O^+ respectively for the potassium sulfate on the basis of the detected mass number and the atomic construction of the sulfate. On the other hand, the peaks at masses 12, 16, 28, 39, 44, and 94 for the carbonate were associated with C^+, O^+, $CO,^+$ K^+, CO_2^+, and K_2O^+ respectively. Throughout these experiments, no potassium-oxygen compounds other than K_2O were observed. SO_3 was also not observed from the potassium sulfate.

The product $(I_x^+ \cdot T)$ is proportional to the partial pressure of the species x,[4] where I_x^+ is the measured ion intensity. Thus, the thermal dissociation reaction was discussed on the basis of the relation between $\log(I_x^+ \cdot T)$ and $1/T$. The vapor and dissociation pressures were measured independently of the results of the mass-spectrometric studies.

The values of $\log(I_x^+ \cdot T)$ *vs.* $1/T$ are shown in Fig. 1 for the sulfate and in Fig. 2 for the carbonate.

As is obvious from Fig. 1, the chemical species marked O_2^+, SO_2^+, and K_2O^+ showed the same temperature dependency. In the case of the carbonate, CO^+, K^+, CO_2^+, and K_2O^+ exhibited similar slopes, as is shown in Fig. 2.

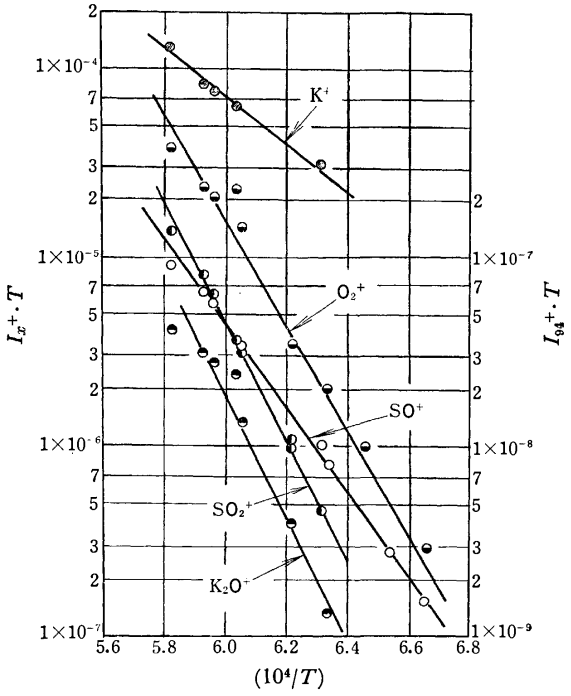

Fig. 1. Plots of $I_x^+ \cdot T$ *vs.* $1/T$ for thermal dissociation products of potassium sulfate.

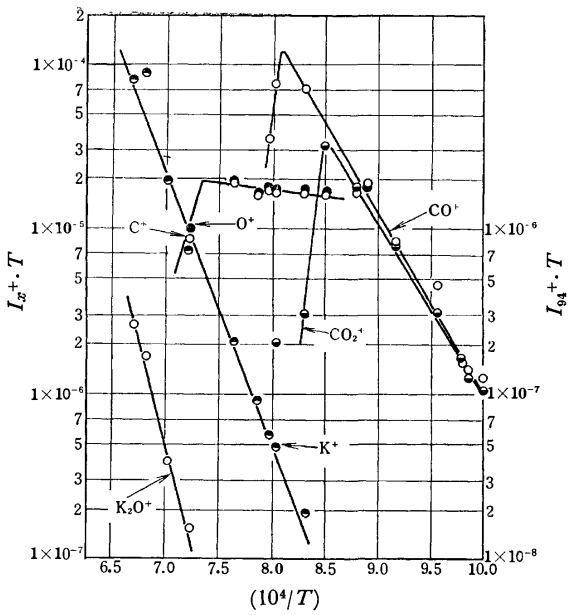

Fig. 2. Plots of $I_x^+ \cdot T$ *vs.* $1/T$ for thermal dissociation products of potassium carbonate.
(x=molecular weight)

It should be noted that the thermal dissociation reaction of the carbonate is effected completely below 1,250°K and that the temperature dependencies of C^+, and O^+ are very slight.

Effusion-rate Measurements by Knudsen Method. The cell was made of Pt-5%Rh alloy; the orifice diameter was 0.5 mm, and the thickness of the orifice was 0.25 mm. The inner diameter of the cell was 9.5 mm.

The effusion weight of the sample was calculated as the weight change in the cell before and after each run, because the evaporation rate of the platinum was very small (*ca.* 1×10^{-11} g/cm²/sec at 1,700°K).[5] The cell weight was measured to be about 0.01 mg by means of a semi-micro-balance.

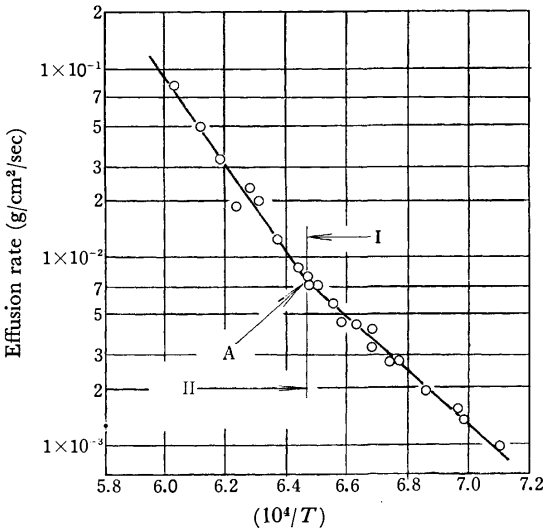

Fig. 3. Plots of effusion rate *vs.* $1/T$ of K_2SO_4.

4) D. White, K. S. Seshadri, and D. F. Dever, *J. Chem. Phys.*, **39**, 2463 (1963).

5) H. A. Jones, I. Langmuir, and D. H. J. Mackey, *Phys. Rev.*, **30**, 201 (1927). See T. Okada and R. Goto, "Hakkinzoku to Kogyoteki Riyo," Sangyo Tosho, Tokyo (1956), p. 91.

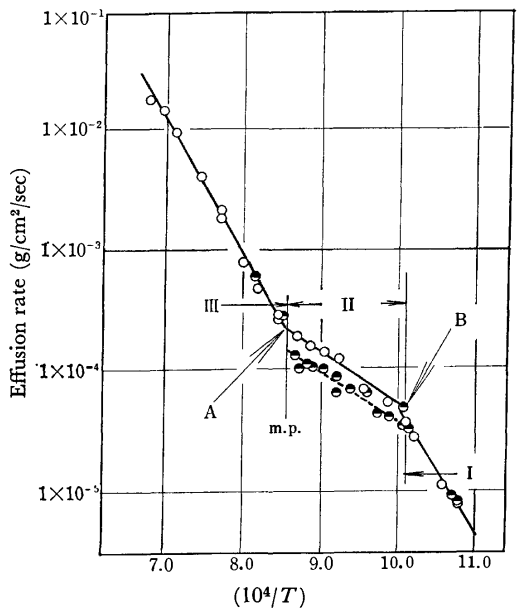

Fig. 4. Plots of effusion rate *vs.* $1/T$ of K_2CO_3.

In the precise calculation of the effusion rate, the orifice area change caused by the thermal expansion of the cell material must be calibrated. However, as the thermal expansion of platinum at 1,700°K is about 1.5%,[6] the orifice-area change was disregarded and a value measured at room temperature was used in this experiment. The preparations of the samples and cell were described previously.[7,8]

The effusion rates of the sulfate and carbonate are plotted in Figs. 3 and 4 as log G *vs.* $1/T$ where G is the effusion rate. It was obvious that the effusion rate of the sulfate showed a temperature-dependency change at Point A and that the slope of the curve in the higher temperature region (II) was larger than that in the lower temperature region (I).

The effusion-rate change of the carbonate was very complicated compared with that of the sulfate. The effusion rate was changed by the maximum degassing temperature in the (II) region indicated in Fig. 4.

Discussion

Thermal Dissociation Reaction of the Samples. The detected species will be generated by several reactions for example, as primary thermal dissociation reaction products of the sample, consecutive reaction products of the above primary reaction products might be detected. Therefore, it is impossible to conclude that all the detected species are generated from the primary dissociation reaction of the sample or that those species indicating larger ion intensities were the primary dissociation products.

Thus, the identification of the primary dissociation products was made by a comparison of the heats of formation of all the species in this study.

Now, let us assume the following primary dissociation reaction:

$$ABC \longrightarrow A + B + C \qquad (1)$$

In this reaction, the heat of formation of A, B, and C species must be equal to the heat of dissociation of the starting material, ABC. Therefore, the slopes of the relations of $\log(I_A^+ \cdot T)$, $\log(I_B^+ \cdot T)$, and $\log(I_C^+ \cdot T)$ *vs.* $1/T$ should be equal. From this point of view, chemical species as O_2, SO_2, and K_2O were assumed to be the primary dissociation products of potassium sulfate (from Fig. 1).

Then, the dissociation reaction of the sulfate can be estimated as:

$$K_2SO_4 \longrightarrow K_2O + SO_2 + \frac{1}{2}O_2 \qquad (2)$$

Regarding the carbonate the species which have the same slope in Fig. 2 are K, K_2O, CO, and CO_2. Of these, the potassium atoms indicate the same temperature dependency as was observed for the sulfate shown in Fig. 5. In addition, the heat of formation of the potassium atom is very close to that of the K_2O molecules, from the following reaction:

$$2K + \frac{1}{2}O_2 \longrightarrow K_2O \qquad (3)$$

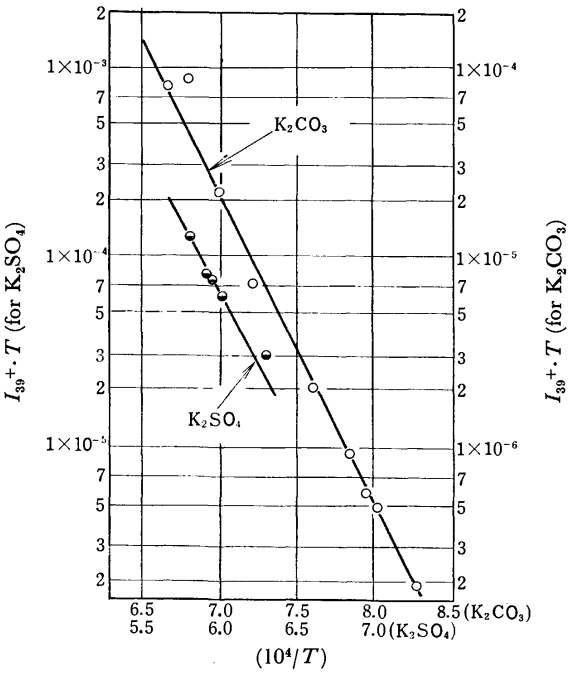

Fig. 5. Plots of $I_{39}^+ \cdot T$ *vs.* $1/T$ for K^+ in K_2SO_4 and K_2CO_3.

Therefore, it can be considered that the potassium atoms are produced by thermal dissociation of the potassium oxide in the two samples. On the basis of the above discussion and the mass balance between the starting material and the dissociation products, the thermal dissociation reaction of the carbonate was estimated as follows:

$$K_2CO_3 \longrightarrow K_2O + CO_2 \qquad (4)$$

Recently, a mass spectrometric study of the dissociation reaction of alkali metal compounds was reported by Ficalora *et al.*[9] They proposed the following dissociation reaction for the sulfate on the basis of a com-

6) J. W. Edwards, R. Speiser, and H. L. Johnston, *J. Appl. Phys.*, **22**, 424 (1951).
7) T. Kosugi, *Kogyo Kagaku Zasshi*, **70**, 2089 (1967).
8) T. Kosugi, *ibid.*, **71**, 1581 (1968).
9) P. U. Ficalora, O. M. Uy, D. W. Muenow, and J. L. Margrave, *J. Amer. Ceram. Soc.*, **51**, 574 (1968).

parison of the measured ion intensities:

$$K_2SO_4 \longrightarrow 2K + SO_2 + O_2 \quad (5)$$

In this study, however, the heat of formation of a potassium atom was different from that of the SO_2 and O_2 molecules shown in Fig. 1. This implies that the potassium atom differs from the SO_2 and O_2 molecules in its formation mechanism. The generation mechanism of a potassium atom should, then, be considered as a dissociation product of K_2O molecules as has been described above.

Kellogg[10] proposed that the dissociation reaction of sodium sulfate porceeded as:

$$Na_2SO_4 \longrightarrow Na_2O + SO_3 \quad (6)$$

However, it is difficult to consider that the dissociation reaction of potassium sulfate proceeds in that way for the following two reasons:

1) Sulfur trioxide was not detected in this study. In addition, it is considered, from the above description, that sulfur dioxide might be one of the true primary dissociation products.

2) It was estimated, on the basis of a previous report,[11] that sulfur trioxide was not stable in this experimental temperature range, and that only sulfur dioxide was present.

On the basis of the above considerations, Eqs. (5) and (6) can be said not to be adequate for indicating the dissociation mechanism of potassium sulfate.

Vapor and Dissociation Pressures. Potassium Sulfate: The relationship of log G *vs.* $1/T$ should be linear if the dissociation reaction is not observed. The experimental results for the sulfate, however, show a change in the slope at Point A (*ca.* 1,555°K) in Fig. 3. The slope is steeper in the higher-tempearture region. It is estimated that the main effused species are changed near Point A; *i.e.*, the primary dissociation products are only detected by the mass spectrometer above 1,555°K.

Therefore, it is assumed that the measured G value consists of two components: the K_2SO_4 molecules (G_1) and all the dissociation products (G_2). Thus, we assumed the measured G value to be:

$$G = G_1 + G_2 \quad (7)$$

where:

$$\log G_1 = -A\left(\frac{1}{T}\right) + B$$

$$\log G_2 = -C\left(\frac{1}{T}\right) + D$$

$$G_2 = G_3 + G_4 + G_5$$

$$G_1 = G(K_2SO_4)$$

$$G_3 = G(K_2O)$$

$$G_4 = G(SO_2)$$

$$G_5 = G(O_2)$$

A, B, C, D: constants

These constants were calculated by least-means-square method from the measured G values using a computor (HITAC-5020F). The resulting values were 1.220×10^4 for A, 5.638 for B, 3.245×10^4 for C, and 18.36 for D. The vapor pressure equation derived from G_1 using the Knudsen equation[12] for the sulfate is, then:

$$\log P = -1.253\times10^4\left(\frac{1}{T}\right) + 7.724 \text{ (Torr)} \quad (8)$$

The average heat of vaporization in the experimental temperature range is estimated to be 57.3 ± 8.6 kcal/mol, and the entropy of vaporization at the melting point (1,342°K) is estimated to be 42.7 ± 6.4 e.u. from the extrapolation of the vapor-pressure equation.

The vapor-pressure data measured in this experiment were in good agreement with the data of Nettleton *et al.*[13] obtained from the evaporation-rate measurement of a droplet of the sulfate melted under several atmospheric conditions. However, they disagree with the data reported by Kröger and Stratmann.[1]

The dissociation pressure of the sulfate was estimated by using the G_2 values and the ideal gas equation; it can be represented by the following equation:

$$\log P_d = -3.275\times10^4\left(\frac{1}{T}\right) + 20.83 \text{ (Torr)} \quad (9)$$

The average heat of dissociation was 150 ± 22.5 kcal/mol. The vapor and dissociation pressures are shown in Fig. 6, together with the published data.

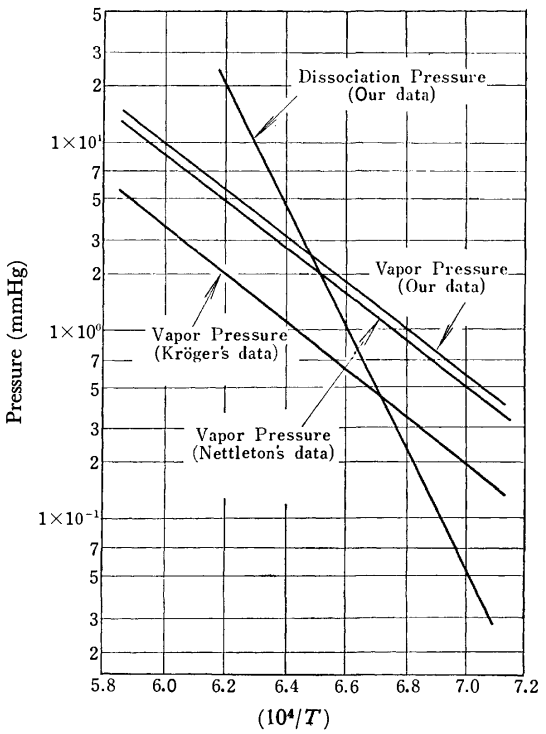

Fig. 6. Vapor and dissociation pressure of K_2SO_4.

Potassium Carbonate: From the results of the mass-spectrometric study and Wöhler's report,[14] it should be considered that the major effusing vapors are dissociation products of the sample throughout the experimental-temperature range.

10) H. H. Kellogg, *Trans. Met. Soc.*, AIMT **230**, 1622 (1964).
11) F. Hals, L. Keefe, and A. E. Bindari, An ASME publication 64-WA/ENER-5 (1964).
12) A. N. Nesmeyanov, Edited by Gray, "Vapor Pressure of the Chemical Elements," Elsevier Publishing Company (1963).
13) M. A. Nettleton and E. Raask, *J. Appl. Chem.*, **17**, 18 (1967).
14) L. Wöhler, *Z. Elektrochem.*, **11**, 836 (1905).

From a previous discussion,[8] it can be considered that the slope in the (I) region of Fig. 4 depends mainly on the activation energy of Eq. (4).

Then, the true effusion rate of the primary dissociation products of the carbonate was calculated from the measured effusion rate at the lowest experimental temperature (925°K) and the temperature dependency of the CO_2 molecule obtained from the mass-spectrometric experiment.

The relationship of the effusion rate and the temperature, assuming that there was no reaction between the sample vapor and the cell, was:

$$\log G = -1.105 \times 10^4\left(\frac{1}{T}\right) + 6.989 \qquad (10)$$

where:

$$G = G(K_2O) + G(CO_2)$$

Thus, the dissociation pressure of the carbonate was estimated to be:

$$\log P_d = -1.135 \times 10^4\left(\frac{1}{T}\right) + 9.257 \text{ (Torr)} \qquad (11)$$

using the method described for the sulfate. The average heat of dissociation in the experimental temperature range was found to be 51.9 ± 8.1 kcal/mol. The dissociation pressure is shown in Fig. 7 along with the data reported by Kröger and Stratmann,[1] measured by the same method as the present data, and the data of Howarth and Turner,[15] measured by the static method. All the data agree well.

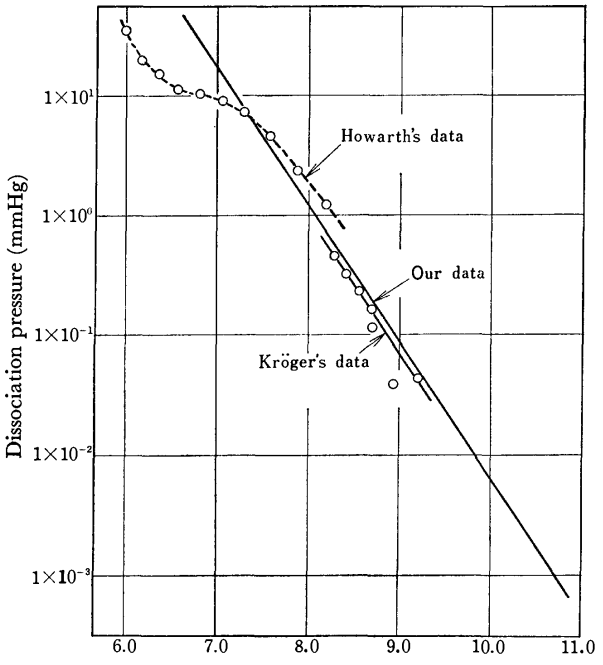

Fig. 7. Dissociation pressure of K_2CO_3.

Equilibrium Constants of The Dissociation Reaction. From the above discussion, the equilibrium constants of the two samples can be said to be:

$$K_p(K_2SO_4) = P(K_2O)\cdot P(SO_2)\cdot P(O_2)^{1/2}\cdot P(K_2SO_4)^{-1} \qquad (12)$$

$$K_p(K_2CO_3) = P(K_2O)\cdot P(CO_2)\cdot P(K_2CO_3)^{-1} \qquad (13)$$

For the sulfate, the relation between the measured dissociation pressure and the partial pressure of each dissociation product is:

$$P_d = P(K_2O) + P(SO_2) + P(O_2) \qquad (14)$$

Therefore, $K_p(K_2SO_4)$ is expressed as follows, using the measured vapor and dissociation pressures:

$$\log K_p(K_2SO_4) = -6.94 \times 10^4\left(\frac{1}{T}\right) + 38.8 \text{ (atm}^{1.5}\text{)} \qquad (15)$$

$K_p(K_2CO_3)$ can be calculated by the same method; however, vapor pressure of the carbonate could not be obtained in the present work. Consequently, the vapor-pressure data of Kröger and Stratmann[1] were used for $P(K_2CO_3)$. The following relation was thus estimated:

$$\log K_p(K_2CO_3) = -1.38 \times 10^4\left(\frac{1}{T}\right) + 9.80 \text{ (atm)} \qquad (16)$$

Both relations are shown in Fig. 8.

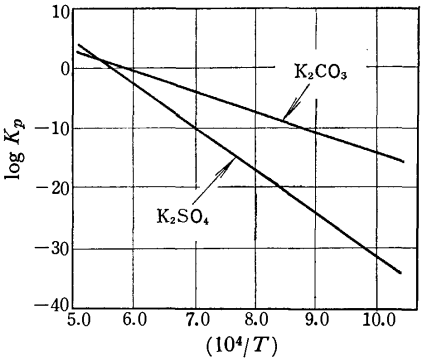

Fig. 8. Equilibrium constants of dissociation reaction.

A part of this work was sponsored by the Ministry of International Trade and Industry of Japan.

The useful suggestions of Dr. K. Shinriki and Dr. N. Kawashima of this laboratory are greatly appreciated.

15) J. T. Howarth and W. E. S. Turner, *J. Soc. Glass Tech.*, **15**, 360 (1931).

Studies of Rare Earth Oxyfluorides in the High-temperature Region

Koichi NIIHARA and Seishi YAJIMA

The Research Institute for Iron, Steel and Other Metals, Tohoku University, Sendai

(Received March 29, 1971)

The behavior of the rhombohedral LnOF and the tetragonal $Ln_4O_3F_6$ at high temperatures was investigated by differential thermal analysis and the high-temperature X-ray diffraction technique. In the case of the rare earth oxyfluorides, LnOF (Ln=La, Pr, Nd, Sm, Eu, Gd, Tb, Dy, Ho, Er, Tm, Yb, Lu, and Y), the high-temperature transition rhombohedral⇄cubic was observed by means of DTA and a high-temperature X-ray camera. The heat of transformation from rhombohedral to cubic was obtained by means of DTA. The transition temperatures and the heat of transformation, ΔH, shift to higher temperatures and to greater values respectively as the atomic numbers of the rare earth elements increase, although there are some anomalies. One endothermic peak was observed for the rare earth oxyfluorides, $Ln_4O_3F_6$, from Sm to Lu. On the other hand, no peak was observed up to 1300°C for La, Pr, Nd, and Y. The behavior of the peak temperature of DTA against the atomic number for $Ln_4O_3F_6$ is similar to that for LnF_3; this indicates a transformation from an orthorhombic to a hexagonal structure.

In the system of LnF_3–Ln_2O_3, three forms of rare earth oxyfluorides have been reported.[1-9] The relations between these rhombohedral, tetragonal and cubic forms have not, however, been known at all. According to our previous study[10] of the rare earth oxyfluorides (Sm through Lu), the rhombohedral pahses, LnOF, have the stoichiometric composition and the tetragonal phases, $Ln_4O_3F_6$, have the comparatively large nonstoichiometric composition range. The third cubic phases, with a fluorite-type structure, were observed in the SmOF–$Sm_4O_3F_6$ region after quenching from a high temperature, but in the other system the cubic phases were not identified by a similar procedure. The variety of structures reported for the rare earth oxyfluorides suggests that a study of the structures at high temperatures would be fluitful. In particular, based on Zachariasen's structure analysis[3] employing the order-disorder of the anion, it was hoped that the order-to-disorder transition could be observed by means of the high-temperature X-ray technique. In this paper, the behavior of the rhombohedral LnOF and the tetragonal $Ln_4O_3F_6$ at high temperatures was investigated by means of differential thermal analysis and the high-temperature X-ray technique.

Experimental

Materials. Many rare earth oxides[11] (La_2O_3, Pr_6O_{11}, Nd_2O_3, Sm_2O_3, Eu_2O_3, Gd_2O_3, Tb_4O_7, Dy_2O_3, Ho_2O_3, Er_2O_3, Tm_2O_3, Yb_2O_3, Lu_2O_3, and Y_2O_3) were separated from a crude rare eath mixture in this laboratory by the ion-exchange method, using the EDTA solution as the solvent. The rare earth oxides obtained by this method were >99.9% pure.

The anhydrous lanthanon trifluorides, LaF_3 through LuF_3, were prepared as has previously been described.[10]

The rare earth metals[12] were prepared by the calcium reduction of LnF_3 according to the following reaction:

$$2LnF_3 + 3Ca = 2Ln + 3CaF_2$$

The metals obtained by this method were >99.5% pure.

Sample Preparation. All the rhombohedral LnOF and tetragonal $Ln_4O_3F_6$ rare earth oxyfluorides, except for Pr and Tb, were prepared as has previously been described.[10] In the cases of Pr and Tb, the oxyfluorides were prepared by the hydrolic heating of the fluorides in an atmosphere with a relatively high humidity, or by the following chemical reactions:

$$3Pr_6O_{11} + 11PrF_3 + 4Pr = 33PrOF \quad (1)$$

$$3Pr_6O_{11} + 22PrF_3 + 4Pr = 11Pr_4O_3F_6 \quad (2)$$

$$3Tb_4O_7 + 7TbF_3 + 2Tb = 21TbOF \quad (3)$$

$$3Tb_4O_7 + 14TbF_3 + 2Tb = 7Tb_4O_3F_6 \quad (4)$$

The mixture of oxide, metal, and fluoride, weighed in a stoichiometric composition, was melted in a platinum boat. The chemical analyses were performed by igniting to the oxide.

High-temperature X-ray Diffraction. High-temperature X-ray diffraction patterns were obtained by means of a Rigaku Denki high-temperature X-ray diffraction camera mounted a X-ray diffractometer. The mounted samples were placed in the camera, which was then evacuated. The pressure at the inlet in the camera was found to be less than 5×10^{-4} mmHg, but either oxidation or hydrolysis occurred when samples were heated above 800—1000°C. Because of this problem, the high-temperature phases of the tetragonal oxyfluorides, $Ln_4O_3F_6$, were not identified.

Differential Thermal Analysis. The DTA apparatus consisted of a platinum-wound furnace, a sample chamber, and a microvolt recorder. The sample holder consisted of a 25-mm-diameter nickel rod, in which two symmetrical, 7.9-mm-diameter, 19.2-mm-deep sample wells were drilled. The rare earth oxyfluoride placed in a platinum sample chamber with the same geometry as the sample wells was

1) W. Klemm and H. Klein, *Z. Anorg. Chem.*, **248**, 167 (1941).
2) W. Finkelnburg and A. Stein, *J. Chem. Phys.*, **18**, 1296 (1950).
3) W. H. Zachariasen, *Acta Crystallogr.*, **4**, 231 (1951).
4) F. Hund, *Z. Anorg. Allg. Chem.*, **265**, 62 (1951).
5) L. Mazza and A. Landelli, *Chem. Abst.*, **47**, 4194a (1953).
6) N. C. Baenziger, J. R. Holder, G. E. Knudsen, and A. I. Popov, *J. Amer. Chem. Soc.*, **76**, 4734 (1954).
7) A. I. Popov and G. E. Knudsen, *J. Amer. Chem. Soc.*, **76**, 3921 (1954).
8) F. Hund, *Z. Anorg. Allg. Chem.*, **273**, 312 (1953).
9) L. R. Batsanova and G. E. Kustova, *Russ. J. Inorg. Chem.*, **9**, 181 (1964).
10) K. Niihara and S. Yajima, This Bulletin, **44**, 643 (1971).
11) S. Yajima, K. Sasaki, and S. Konno, *Kogyo Kagaku Zasshi*, **72**, 1213 (1969).
12) F. H. Spedding and A. H. Daane, "The Rare Earth," Wiley, New York (1961), p. 102.

Table 1. The lattice parameter of the rhombohedral LnOF and the tetragonal LnOF of Pr, Tb, and Lu

Ln in LnOF and $Ln_4O_3F_6$	Lattice parameter			
	LnOF		$Ln_4O_3F_6$	
	a in Å	α in degree	a in Å	c in Å
Pr	7.018±0.002	33.05±0.05	5.710±0.004	5.758±0.003
Tb	6.751±0.004	33.09±0.03	5.575±0.003	5.491±0.003
Lu	6.536±0.002	33.05±0.02	5.482±0.002	5.308±0.003

placed in one well, and Al_2O_3 in the other.

The standard conditions for each DTA run were a 950—1000-mg portion of the sample and a heating rate of 2.5°C/min in a vacuum or in an inert gas atmosphere. The Pt-Pt·Rh thermocouples were used for the temperature measurement. The calibration data indicate an error of ±3°C at 600°C.

The DTA apparatus was calibrated for the heat-of-transformation studies by the use of compounds with a known heat of decomposition or transformation in a temperature range not far from that under study. The calibration compounds were $CuSO_4 \cdot 5H_2O$, SiO_2, and $BaCO_3$. The heat of transformation obtained could be reproduced to within ±7%.

Experimental Results

Sample Preparation. The X-ray diffraction data showed that all of the rhombohedral LnOF and tetragonal $Ln_4O_3F_6$ rare earth oxyfluorides, except for Ce and Pm, from La to Lu had an isostructure with the previously-reported rhombohedral and tetragonal forms[10] respectively. The results of chemical analyses and the lattice parameters for Pr, Tb, and Lu are summarized in Table 1 and Table 2. The preparation of Pr and Tb oxyfluorides by the hydrolysis technique resulted in mixed products of the rhombohedral and tetragonal oxyfluorides. In general, hydrolysis was found to be unsatisfactory since the extent to which the reaction proceeded could not be controlled.

Table 2. Metal content of LnOF and $Ln_4O_3F_6$ for Pr, Tb, and Lu

Ln in LnOF and $Ln_4O_3F_6$	LnOF		$Ln_4O_3F_6$	
	obsd%	calcd%	obsd%	calcd%
Pr	79.55	80.10	77.50	77.65
Tb	81.42	81.95	79.24	79.69
Lu	83.31	83.33	81.05	81.20

High-temperature X-ray Diffraction. In the case of the LnOF (Ln=La, Pr, Nd, Sm, Eu, Gd, Tb, Dy, Ho, Er, Tm, Yb, Lu, and Y) rare earth oxyfluorides, the high-temperature rhombohedral⇄cubic transition was observed by the high-temperature X-ray camera. It was found, from the relative-intensity measurements of the X-ray diffraction, that the high-temperature phase had a fluorite-type structure and that the rhombohedral⇄cubic transition was reversible. The X-ray patterns of LaOF at 25, 450, and 550°C are shown in Fig. 1. The lattice parameters of LaOF and NdOF were determined over the temperature range of 25—700°C. It can be seen from Fig. 2 that the unit cell volume varied continiously with the temperature in the regions of the rhombohedral and cubic forms respectively, and that it increased abruptly at the transition temperatures. The extrapolated values of the volume differences of the two phases at the transition temperature are 0.80 Å^3 and 0.65 Å^3 for LaOF and NdOF respectively.

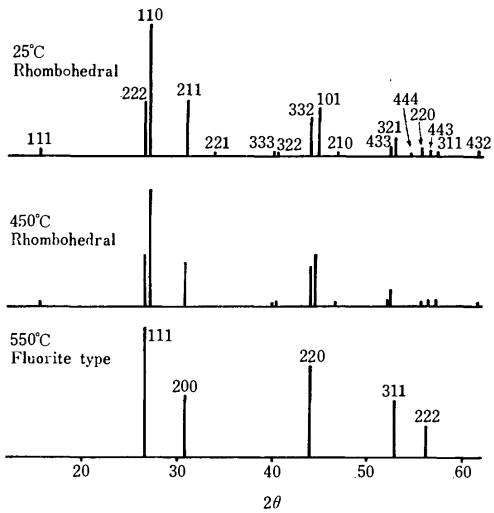

Fig. 1. X-ray patterns of LaOF at 25, 450, and 550°C by high-temperature camera.

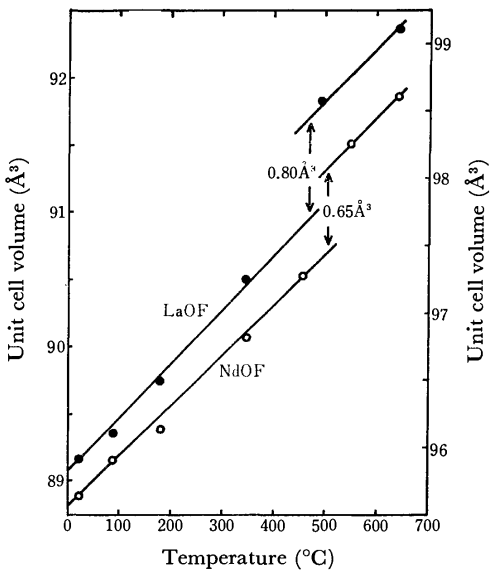

Fig. 2. Thermal expantion of LaOF and NdOF by high-temperature camera. Half cell volume for the fluorite type structure. The scale on the right is NdOF, that on the left for LaOF.

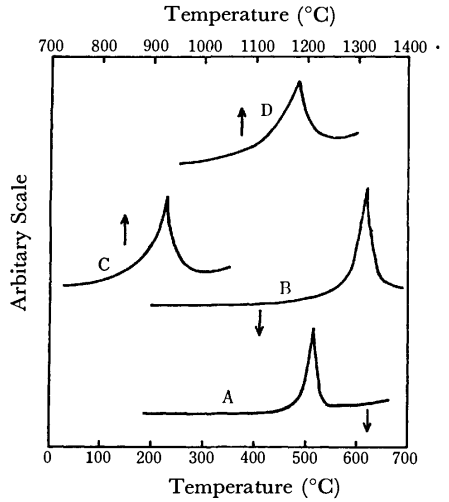

Fig. 3. DTA curves of rare earth oxyfluorides.
A: LaOF B: GdOF C: $Gd_4O_3F_6$ D: $Er_4O_3F_6$

Differential Thermal Analysis. Differential thermal analyses (DTA) were made of both the rhombohedral LnOF and the tetragonal $Ln_4O_3F_6$ of the rare earth oxyfluorides of La through Lu. In the cases of the rhombohedral oxyfluorides, the DTA curves exhibited one endothermic peak up to 1250°C. Since all of the DTA curves were quite similar to each other, only two of them are reproduced in Fig. 3. It can be seen from Fig. 1—3 that the endothermic peak temperatures of DTA correspond to the transition temperatures of rhombohedral⇄cubic. From these results, it can be concluded that all of the LnOF rare earth oxyfluorides transform from the rhombohedral structure to the fluorite-type structure. In Table 3 we list the temperatures of the DTA peaks for the rhombohedral oxyfluorides. The DTA peaks against the atomic numbers are plotted in Fig. 4. As may be shown from Fig. 4, the peak temperatures shift to higher temperature as the atomic numbers increase, that is, as the ionic radii of the rare earth ion decrease, although there are several anomalies.

TABLE 3. DIFFERENTIAL THERMAL ANALYSIS PEAK TEMPERATURE FOR LnOF AND LnOF. ALL AT 2.5°C/min HEATING RATE

Ln in LnOF and $Ln_4O_3F_6$	Peak temperature (°C)	
	LnOF	$Ln_4O_3F_6$
La	505	—
Ce	—	—
Pr	460	—
Nd	515	—
Pm	—	—
Sm	530	553
Eu	495	733
Gd	613	914
Tb	544	892
Dy	579	1049
Ho	590	1098
Er	595	1178
Tm	545	1180
Yb	566	1155
Lu	580	1120
Y	560	—

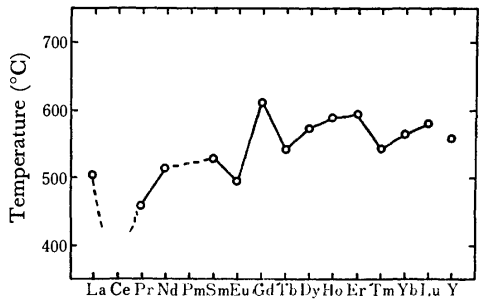

Fig. 4. DTA peak temperature of rare earth oxyfluorides LnOF as a function of atomic number.

The DTA results for the $Ln_4O_3F_6$ oxyfluorides are summarized in Table 3. One endothermic peak was observed for Sm, Eu, Gd, Tb, Dy, Ho, Er, Tm, Yb, and Lu, but no peak was observed at all up to 1250°C for La, Pr, Nd, and Y. Two of these DTA curves are reproduced in Fig. 3. The variation in the DTA-peak temperature for the $Ln_4O_3F_6$ oxyfluorides are plotted as a function of the atomic number of the rare earth element in Fig. 5. The efforts to identify the high-temperature phase of the tetragonal oxyfluorides, $Ln_4O_3F_6$, using the high-temperature X-ray technique beyond the DTA peak temperatures were not successful because of the oxidation of samples and the inaccuracy of the diffraction patterns. The high-temperature phases could not be observed by quenching techniques, either.

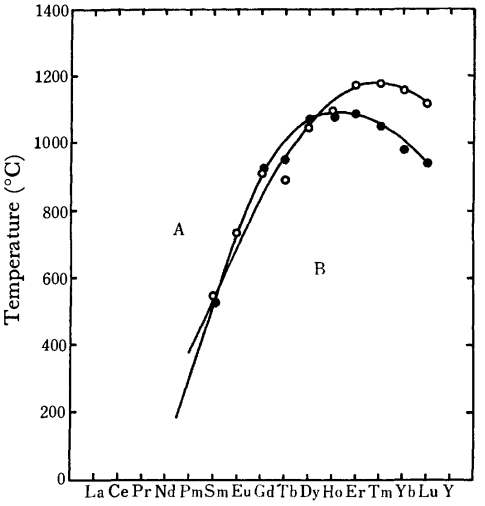

Fig. 5. DTA peak temperature of rare earth oxyfluoride $Ln_4O_3F_6$ as a function of atomic number.
(●: The transition temperature of orthorhombic to hexagonal LnF_3 as a function of atomic number)

The Heat of Transformation from Rhombohedral to Cubic Structure for LnOF. Under specific experimental conditions, DTA can be used to determine the heat of transformation by the integration of the differential curve peak. From the theories of Speil[13] and others[14,15] the area of curve peak is:

$$\text{peak area} = \int_{t_1}^{t_2} \theta dt = \frac{\Delta HM}{g\lambda}$$

13) S. Speil, L. H. Berkelkamer, and J. A. Pask, *U. S. Bur. Min. Tech. Paper*, 664 (1954).
14) M. J. Vold, *Analyst. Chem.*, **21**, 683 (1949).
15) S. L. Boersma, *J. Amer. Ceram. Soc.*, **38**, 281 (1955).

where t_1 and t_2 are the temperature limits of the peak, θ is the differential temperature, ΔH is the heat of transformation, M is the mass of the reactive sample present, λ is the thermal conductivity of sample, and g is a constant dependent on the furnace and sample-holder geometry. In practice, the apparatus is calibrated by studying the reaction of known thermal effects. In this manner, the constants, g and λ, are evaluated. Table 4 gives the heat of transformation from rhombohedral to cubic for LnOF and the values of the ionic radii. The heat of transformation, ΔH, is plotted as a function of the atomic number of the rare earth element in Fig. 6. As is shown by Fig. 6, ΔH shifted to higher values as the atomic number of the rare earth ion increased, although there were several anomalies.

Table 4. Heat of transformation of rare earth oxyfluorides LnOF from rhombohedral structure to fluorite structure.

Ln in LnOF	Ln^{3+} radii	ΔH(kcal/mol)
La	1.061	2.65
Ce	1.034	—
Pr	1.013	1.89
Nd	0.995	3.25
Pm	(0.979)	—
Sm	0.964	2.83
Eu	0.950	3.40
Gd	0.938	3.25
Tb	0.923	1.91
Dy	0.908	3.25
Ho	0.894	3.22
Er	0.881	3.71
Tm	0.869	3.53
Yb	0.854	3.60
Lu	0.848	3.70
Y	0.88	2.76

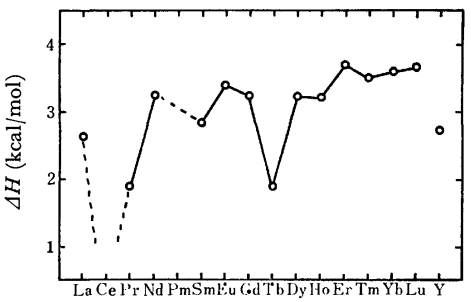

Fig. 6. Heat of transformation of rhombohedral to cubic LnOF as a function of atomic number.

Discussion

All of the rare earth oxyfluorides, LnOF, were observed to be transformed from a rhombohedral to a fluorite-type structure in the temperature region of 450—600°C. It is considered that this transition is due to the order-disorder of the anion: the rhombohedral oxyfluorides,[3] LnOF, result from a complete ordering of the oxygen and fluorine atoms into a distinct site in the unit cell, while the fluorite-type phase results from a statistical distribution of oxygen and fluorine. The transition temperature observed in thermal analyses do not follow the smooth trend so characteristic of lanthanide compounds. However, the phase-transition temperatures in $LnNbO_4$ and $LnTaO_4$ increase as the ionic radii decrease at first and then become relatively constant beyond Gd.[16] The data presented in this paper seem to show a similar phenomenon.

The heat of transformation from a rhombohedral to a fluorite-type structure is 1.8—3.8 kcal/mol. On the other hand, the heats of transformation of cubic to monoclinic Eu_2O_3[17] and of cubic to hexagonal Pr_2O_3[17] are about 4.3 and 1.0 kcal/mol respectively. It can be seen that the values of the heat of transformation from a rhombohedral to a fluorite-type structure are as large as those of the heat of transformation of rare earth sesquioxides, Ln_2O_3. The ΔH of rhombohedral to cubic LnOF shifts to higher values as the atomic number of the rare earth ion increases, although there are some anomalies. This trend is the same as that for the heat of decomposition of rare-earth sulphate and oxysulphate.[18] The ΔH for Pr and Tb is much lower than the other values. A possible explanation of the anomalies for Pr and Tb is that PrOF and TbOF form a solid solution with either oxides or the fluorides. As has previously been reported,[10] all the rhombohedral phases, LnOF, except for Pr and Tb have a stoichiometric composition, and no nonstoichiometric composition range exists in any of the systems. The method of preparing PrOF and TbOF is different from that of other rare earth oxyfluorides. In this method, the stoichiometry of PrOF and TbOF could not be determined by metal analyses alone because the oxides of Pr and Tb have a comparatively large nonstoichiometric composition range at high temperatures,[19] although the oxides of all the rare earths except Pr and Tb have the stoichiometric composition $LnO_{1.500}$.[20] The ions of Pr and Tb are comparatively easy to convert into tetravalent ions relative to other rare earth ions. Judging from this fact, it is possible that the rhombohedral phase for Pr and Tb may be stable for nonstoichiometries, $LnO_{1\pm x}F_{1\pm y}$, and that a small variation in stoichiometry could effect a large change in the transformation of rhombohedral to cubic LnOF.

The efforts to determine the cause of an endothermic peak $Ln_4O_3F_6$ from Sm to Lu were unsuccessful. As is shown in Fig. 5, the variation in the peak temperature of DTA against the atomic number is quite similar to that of the transition temperature of rare earth trifluorides from orthorhombic to hexagonal LnF_3.[21] It is reasonable to consider that the crystal structures are different between the A region and the B region. This point is still open to question, though, and further work is called for.

16) V. S. Stubican, *J. Amer. Ceram. Soc.*, **47**, 55 (1964).
17) M. M. Factor and R. Hanks, *J. Inorg. Nucl. Chem.*, **31**, 1649 (1969).
18) M. W. Nathans and W. W. Wendlandt, *ibid.*, **24**, 869 (1962).
19) G. Brauer, "Progress in the Science and Technology of Rare Earths," Vol. 1, ed. by L. Eyring, Pergamon, Oxford (1966), p. 152.
20) G. Brauer, "Progress in the Sience and Technology of Rare Earth," Vol. 3, ed. by L. Eyring, Pergamon, Oxford (1966), p. 447.
21) F. H. Spedding and A. H. Daane, "The Rare Earths," Wiley, New York (1961), p. 78.

The Kinetics and Mechanism of the Photo-oxidation of *N,N'*-Diphenyl-*p*-phenylenediamine. Electron-transfer from the Upper Excited Singlet State to Oxygen

Haruo SHIZUKA, Yasuyoshi SAWAGURI, and Toshifumi MORITA

Department of Chemistry, Gunma University, Kiryu, Gunma

(Received April 26, 1971)

The photo-oxidation of *N,N'*-diphenyl-*p*-phenylenediamine (DPPD) has been studied spectrophotometrically. The quantum yield for the diimine formation, Φ, in aerated cyclohexane at 2537 Å and 20°C did not change with variations of the irradiation time, the concentration of DPPD, or the light intensity. However, the Φ values increased, as did the decrease in the fluorescence quantum yields, as the excitation energies increased. The dissolved oxygen had the optimum concentration (1.2×10^{-4}M), giving the maximum value of Φ in aerated cyclohexane at 2537 Å, and none of the product, the diimine, was obtained in the degassed system. When about 0.13M of ethanol or methanol was added to aerated cyclohexane, the maximum value of Φ was measured, and the addition of a highly-polar solvent, acetonitrile or H_2O, decreased regularly in Φ. On the basis of these results, it can be said that the photo-oxidation of DPPD originates from the Franck-Condon state of the upper excited singlet state, $^1(RH_2)_n$. It seems that, in the primary processes of the reaction, the electron transfers take place from the Franck-Condon state of $^1(RH_2)_n$ directly to the oxygen molecule ($^3\sum_g^-$) and to the solvent, resulting in a trapped electron which immediately jumps into the oxygen molecule. Then, the $(RH_2)^+O_2^-$ ion pair may be formed, and subsequently the intermediate, $(RH_2)^+O_2^-$, may be converted to the product or the starting materials. The dissolved oxygen and the polar solvents are responsible for the electron-transfer processes, but they deactivate the ion pair, resulting in the decrease in Φ.

It is known that aromatic amine derivatives give rise photochemically to many interesting reactions, such as photoionization, photocyclization, rearrangement, photo-oxidation, and decomposition.

The photoionizations of aromatic amines can be classified as follows: (1) The photo-ionization in a polar solvent *via* the singlet exciplex formed by the interaction between the lowest excited singlet state of the amines (the electron donor) and the ground state of the electron acceptor, or *vice versa*, was originally shown by Leonhardt and Weller.[1] Similar results for organic donor-acceptor systems have been reported by Tsubomura *et al.*[2,3] and by Koizumi *et al.*[4,5] The exciplex formation has been extensively studied by Mataga *et al.*[6–10] and by Weller *et al.*[11,12] (2) The photo-ionization in a rigid matrix at the temperature of nitrogen by a two-step excitation *via* the lowest triplet states of the amines has been well accomplished by several workers[2,13–16] since the pioneering work of Lewis and Lipkin.[17] The photo-ionization in fluid media by the two-step excitation *via* the lowest triplet states has also been studied by means of a flash technique.[2,18–20] (3) It has been reported by Potashnik *et al.* that the photo-ionization may occur through a CT triplet state of an electron-donor-acceptor pair in a polar matrix.[21] (4) Of course, the direct photo-ionization is induced by excitation energies larger than those of the ionization potentials of the molecules.

The photocyclization of diphenylamines has been preliminarily reported by Bowen and Eland,[22] and by Linschitz *et al.*[23] The reaction mechanism of the photocyclization of diphenylamines has been kinetically studied by Shizuka *et al.*[24]: the photo-cyclization of

1) H. Leonhardt and A. Weller, *Z. Phys. Chem., N. F.*, **29**, 277 (1961): *Ber. Bunsenges. Phys. Chem.*, **67**, 791 (1963).
2) Y. Nakato, N. Yamamoto, and H. Tsubomura, This Bulletin, **40**, 2480 (1967).
3) K. Kawai, N. Yamamoto, and H. Tsubomura, *ibid.*, **42**, 369 (1969).
4) K. Kaneta and M. Koizumi, *ibid.*, **40**, 2254 (1967).
5) H. Yamashita, H. Kokubun, and M. Koizumi, *ibid.*, **41**, 2312 (1968).
6) N. Mataga, K. Ezumi, and K. Takahashi, *Z. Phys. Chem., N. F.*, **44**, 250 (1965).
7) N. Mataga, T. Okada, and H. Oohari, This Bulletin, **39**, 2563 (1966).
8) N. Mataga, T. Okada, and N. Yamamoto, *Chem. Phys. Lett.*, **1**, 119 (1967).
9) N. Mataga and O. Tanimoto, *Theor. Chim. Acta*, **15**, 111 (1969).
10) T. Okada, H. Oohari, and N. Mataga, This Bulletin, **43**, 2750 (1970).
11) H. Knibbe, K. Röllig, F. P. Schäffer, and A. Weller, *J. Chem. Phys.*, **47**, 1184 (1967).
12) H. Knibbe, D. Rehm, and A. Weller, *Ber. Bunsenges. Phys. Chem.*, **72**, 257 (1968).
13) K. D. Cadogan and A. C. Albrecht, *J. Chem. Phys.*, **43**, 2550 (1965).
14) G. E. Johnson and A. C. Albrecht, *ibid.*, **44**, 3162 (1966); *ibid.*, **44**, 3179 (1966).
15) J. Joussot-Dubien and R. Lesclaux, *Compt. Rend.*, **258**, 4260 (1964).
16) W. A. Gibbons, G. Porter, and M. I. Savadatti, *Nature*, **206**, 1355 (1965).
17) G. N. Lewis and D. Lipkin, *J. Amer. Chem. Soc.*, **64**, 2801 (1942).
18) E. J. Land, G. Porter, and E. Strachan, *Trans. Faraday Soc.*, **57**, 1885 (1961).
19) N. Yamamoto, Y. Nakato, and H. Tsubomura, This Bulletin, **39**, 2603 (1966).
20) K. Kawai, N. Yamamoto, and H. Tsubomura, *ibid.*, **43**, 2266 (1970).
21) R. Potashnik, M. Ottolenghi, and R. Bensasson, *J. Phys. Chem.*, **73**, 1912 (1969).
22) E. J. Bowen and J. H. D. Eland, *Proc. Chem. Soc.* (London), 202 (1963).
23) K. H. Grellmann, G. M. Sherman, and H. Linschitz, *J. Amer. Chem. Soc.*, **85**, 1881 (1963). H. Linschitz and K. H. Grellmann, *ibid.*, **86**, 303 (1964).
24) H. Shizuka, Y. Takayama, I. Tanaka, and T. Morita, *ibid.*, **92**, 7270 (1970); H. Shizuka, Y. Takayama, T. Morita, S. Matsumoto, and I. Tanaka, *ibid.*, **93**, 5987 (1971).

diphenylamines originates from the lowest triplet state, and subsequently the triplet transient leads to the formation of the intermediate, M (11,12-dihydrocarbazole, whose two central hydrogens are in the *cis*-configuration), competing with the triplet deactivation processes; then M converts to the corresponding carbazoles, with and without oxygen, or to the ground state of the original substance.

The photo-Fries rearrangements of benzene derivatives (acetanilide, phenylacetate, *N*-acetyl diphenylamine, *N*-acetyl carbazole, *etc.*) in the liquid phase occur *via* the predissociative intersystem crossing $^3\sigma_0$-(N–C)←$S_1(\pi\pi^*)(^1B_2)$ or $^3\sigma_0$(O–C)←$S_1(\pi\pi^*)(^1B_2)$, thus forming the pair radicals; these radicals recombine efficiently in a solvent cage into the original substance and *ortho*- and *para*-isomers, as has been studied by Shizuka *et al.*[25] In general, the predissociation of the benzene derivative occurs at a β-bond *via* the $^1B_2$ state.[25] The photolysis of hydrazobenzene[26] also occurs *via* the predissociative intersystem crossing $^3\sigma_0$(N–H)←$S_1(\pi\pi^*)$, involving the β-bond fission of the benzene derivative and subsequent disproportionation between *N,N'*-diphenylhydrazyl radicals, giving, as products, azobenzene and the starting material. If oxygen is dissolved in the system, the radical intermediate reacts with oxygen, thus forming azobenzene and the HO_2 radical. A similar photo-decomposition of acetanilide in the vapor phase may occur *via* the predissociation at the β-bond, as has been reported by Shizuka and Tanaka.[27]

Recently, the flash photolysis of aniline derivatives in various solutions has been studied by Hori, Itoi, and Tsubomura.[28] The initial yield of the cation formed in an oxygenated solution is proportional to the intensity of the flash light, indicating that the photo-ionization is a one-photon process; they suggested that the charge-transfer states are formed between the aromatics and the oxygen molecule, either by direct excitation or *via* the interaction of excited anilines and the ground state of oxygen, and the charge-transfer states then lead to the solvated cations and anions in highly-polar solvents.

The photo-oxdiation of *N,N'*-diphenyl-*p*-phenylenediamine (DPPD) has been predicted by Linschitz *et al.*[29] However, little mechanistic work has yet been reported. In addition to the photochemical processes described above, several processes in the photo-oxidation of DPPD have been considered: the reaction of the lowest excited singlet state of DPPD with the ground state of oxygen ($^3\Sigma_g^-$), the reaction of the ground state of DPPD with the singlet oxygen ($^1\Delta_g$),[30] and an electron transfer from the upper excited singlet state of DPPD to the ground state of oxygen. Furthermore, it is unknown whether or not the photochemical reaction of DPPD is accompanied by a photocyclization similar to that of diphenylamine.

This paper will report in some detail on the kinetics and mechanism of the photo-oxidation of DPPD.

Experimental

Materials. The *N,N'*-Diphenyl-*p*-phenylenediamine (DPPD) and *N*-cyclohexyl-*N'*-phenyl-*p*-phenylenediamine (CPPD) were Seiko Chem. Co., Ltd., reagent-grade products and were purified by repeated recrystallizations from ethanol and from ligroin respectively. The corresponding diimines, prepared by the chromic-acid oxidation of DPPD or CPPD in glacial acetic acid,[31] were recrystallized several times from ethanol and cyclohexane. The photoproducts were identified by UV and IR spectroscopy and by thin-layer chromatography. The cyclohexane was a Tokyo Kasei Co. G.R.-grade product; it was purified by passing it through a silica-gel column and by distillation. The acetonitrile was a Tokyo Kasei Co. G.R.-grade product; it was dried over calcium chloride, refluxed repeatedly over phosphorus pentoxide until no color appeared on the oxide, distilled into freshly-fused potassium carbonate, distilled from it, and finally fractionally distilled.[32] The ethanol and methanol were Kanto Chemical Co. G.R.-grade products and were used without further purification.

Light Source and Actinometry. A low-pressure mercury resonance lamp with a Vycor glass filter was used as the 2537 Å radiation source, while a xenon lamp (an Ushio 150 W UXL-150D-SS), equipped with a diffraction grating, was used as the 2400—3200 Å range radiation source. The diffraction grating admitted only a narrow band of light wavelengths (±70 Å). Actinometry was carried out using a ferric oxalate solution.[33] The fluorescence quantum yields of DPPD and CPPD were obtained by comparison with the relative fluorescence intensity of naphthalene, whose fluorescence quantum yield is 0.21 in ethanol.[34]

Degassing Procedure and Measurement of the Oxygen Concentration. The solution was thoroughly degassed on a high-vacuum line by the freeze-pump-thaw method. The concentration of dissolved oxygen was adjusted by flushing with nitrogen at room temperature, and was determined by the method of Munck and Scott.[35]

Analysis. The amounts of the photoproducts (diimines) were determined spectrometrically. The ultraviolet and visible absorption spectra were measured by Hitachi 139 and 124 spectrophotometers. The fluorescence and phosphorescence spectra were taken with a Hitachi MPF-2A fluorescence spectrophotometer. The μ-second flash apparatus was an ordinary one.

25) H. Shizuka and I. Tanaka, This Bulletin, **41**, 2343 (1968). H. Shizuka, *ibid.*, **42**, 52 (1969); **42**, 57 (1969). H. Shizuka, T. Morita, Y. Mori, and I. Tanaka, *ibid.*, **42**, 1831 (1969). H. Shizuka, M. Kato, T. Ochiai, K. Matsui, and T. Morita, *ibid.*, **43**, 67 (1970).

26) H. Shizuka, H. Kayoiji, and T. Morita, *Mol. Photochem.*,**2**, 165 (1970).

27) H. Shizuka and I. Tanaka, This Bulletin, **42**, 909 (1969).

28) M. Hori, H. Itoi, and H. Tsubomura, *ibid.*, **43**, 3765 (1970).

29) H. Linschitz, M. Ottolenghi, and R. Bensasson, *J. Amer. Chem. Soc.*, **89**, 4592 (1967).

30) *E.g.* B. Stevens and B. E. Algar, *J. Phys. Chem.*, **72**, 3468 (1968); **73**, 1711 (1969); **74**, 3029 (1970). W. Fenical, D. R. Kearns, and P. Radlick, *J. Amer. Chem. Soc.*, **91**, 3396 (1969). W. S. Gleason, A. D. Broadbent, E. Whittle, and J. N. Pitts, Jr., *ibid.*, **92**, 2068 (1970).

31) J. Picard, *Ber.*, **46**, 1853 (1913).

32) A. Weissberger, E. S. Proskauer, J. A. Riddick, and E. E. Toops, Jr., "Organic Solvents", Interscience Publishers, Inc., New York, (1955), p. 435.

33) C. G. Hatchard and C. A. Parker, *Proc. Roy. Soc.*, (London), **A235**, 518 (1956).

34) C. A. Parker and T. A. Joyce, *Trans. Faraday Soc.*, **62**, 2785 (1966).

35) A. U. Munck and J. F. Scott, *Nature*, **177**, 587 (1956). The molar extinction coefficient of contact CT band between cyclohexane and oxygen was 109 $l mol^{-1} cm^{-1}$ at 220 nm.

Method of Calculation

The π electronic structure of DPPD was studied by the variable β, γ procedure of the semiempirical SCF–MO method in combination with singly-excited CI calculation. The parameters were taken to be as was proposed by Nishimoto and Forster.[36] The one-center repulsion integrals, $\gamma_{\mu\mu}$, were estimated from the corresponding valence-state ionization potentials (I_μ) and electron affinities (A_μ) by the Pariser-Parr approximation.[37] The values of I_μ and A_μ were found in the paper of Hinze and Jaffé.[38] The two-center electron-repulsion integrals, $\gamma_{\mu\nu}$, were estimated by the use of the Nishimoto-Mataga approximation.[39] The corresponding bond-order (P)/bond-length (r) relations[36] are $r_{CC}(\text{Å}) = 1.517 - 0.180P$ for C–C bonds and $r_{CN}(\text{Å}) = 1.451 - 0.180P$ for C–N bonds. The two-center core-resonance integrals, $\beta_{\mu\nu}$, were evaluated by the Nishimoto-Forster approximation.[36] The geometries of DPPD were assumed to be as follows:

Geometries of DPPD

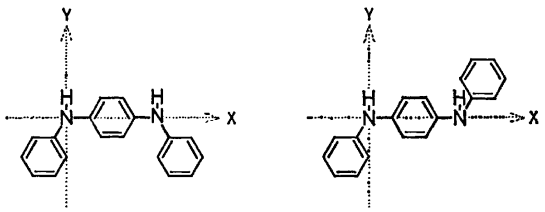

cis-form. *trans*-form.

The C–C and C–N bond lengths were assumed to be 1.39 and 1.38 Å respectively. All the bond angles were assumed to be 120°. The computation was carried out by means of a HITAC 5020E located at the Computer Center, The University of Tokyo.

Results

(1) Absorption and Emission Spectra. In order to study the behavior of DPPD in electronically-excited states, the absorption and emission spectra of DPPD were measured. Figure 1 shows the absorption and emission spectra of DPPD. Several quantities for the electronically-excited states of DPPD and those calcu-

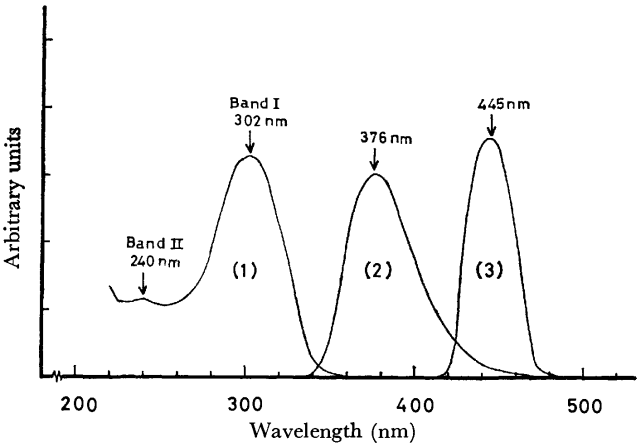

Fig. 1. Absorption and emission spectra of DPPD: (1) absorption spectrum in cyclohexane at 20°C, (2) fluorescence spectrum by the excitation of the 2537 Å light in cyclohexane at 20°C, (3) phosphorescence spectrum by the excitation of the 3000 Å light in methylcyclohexane at 77°K.

Table 1. Several quantities for the electronically excited states of DPPD

Substance	Excited state	Transition energy eV		Transition moment		Oscillator strength	
		Obsd	Calcd	X	Y	Obsd	Calcd
DPPD *cis*-form	Singlet	4.11	4.135	0.000	−0.273		0.027
−309.7794eV[a]		(Band I)	4.444	−0.451	0.000		0.079
			4.451	0.000	−0.067		0.002
			4.607	1.233	0.000	0.576	0.613
			5.269	0.000	1.040	0.298	0.499
		5.17	5.556	0.099	0.000		0.005
		(Band II)	5.781	−0.610	0.000		0.188
			5.784	0.000	−0.021		0.000
	Triplet	2.81	2.659				
DPPD *trans*-form	Singlet	4.11	4.145	0.055	0.334		0.041
−309.7802eV[a]		(Band I)	4.429	0.429	−0.010		0.071
			4.449	0.000	0.000		0.000
			4.611	−1.262	−0.737	0.576	0.862
			5.234	0.000	0.000		0.000
		5.17	5.627	−0.458	−0.553	0.298	0.254
		(Band II)	5.783	−0.562	0.178		0.176
			5.791	0.000	0.000		0.000
	Triplet	2.81	2.533				

Where a denotes total π electonic energy, and the values of the $^1(RH_2)_\pi \leftarrow RH_2$ and $^3(RH_2) \leftarrow RH_2$ transition energies are estimated by those of absorption and phosphorescence spectra respectively.

36) K. Nishimoto and L. S. Forster, *Theor. Chim. Acta*, **3**, 407 (1965); **4**, 155 (1966).
37) R. Pariser and P. G. Parr, *J. Chem. Phys.*, **21**, 767 (1953).
38) J. Hinze and H. H. Jaffé, *J. Amer. Chem. Soc.*, **84**, 540 (1962).
39) K. Nishimoto and N. Mataga, *Z. Phys. Chem.*, **12**, 335 (1957); **13**, 140 (1957).

lated by the semiempirical SCF–MO–CI method are summarized in Table 1. In the case of CPPD, similar results were obtained.

(2) Quantum Yields for the Diimine Formations. Aerated solutions of DPPD and CPPD are stable at room temperature for several hours. Therefore, the amounts of the corresponding diimines produced by thermal reactions can be neglected.

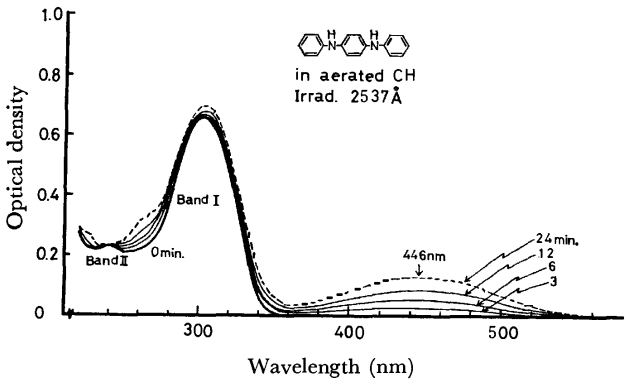

Fig. 2. Spectral change of DPPD in aerated cyclohexane upon irradiation with the 2537 Å light. Numbers refer to time at measurement in minutes.

The spectrum of the aerated cyclohexane solution of DPPD changed upon irradiation with the 2537 Å light, as is shown in Fig. 2. A new band with a maximum at 446 nm appeared; the spectral change showed the formation of *N,N'*-diphenyl-*p*-quinonediimine (DPI). The photoproduct was separated by column chromatography and was identified by UV and IR spectroscopy and by thin-layer chromatography. The photo-oxidation of CPPD also occurred in aerated cyclohexane. However, no photochemical diimine formation was observed in the degassed system in either case, and no photocyclization such as that of diphenylamines took place in the photochemical reactions of DPPD and CPPD. Table 2 shows the molar extinction coefficients of the diimines.

Table 2. The molar extinction coefficients of the diimines

Substance	Solvent	λ_{max} nm	$\varepsilon_{max}(\times 10^{-4})$ $l\,mol^{-1}cm^{-1}$
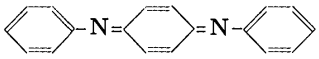 (DPI)	CH	304	2.83
		446	0.63
	EtOH	304	2.71
		443	0.67
(CPI)	CH	296	2.84
		428	0.30

Where CH and EtOH denote cyclohexane and ethanol respectively, and, where CPI denotes *N*-cyclohexyl-*N'*-phenyl-*p*-quinonediimine.

The quantum yields for the product formation (Φ^{λ}) were measured spectrophotometrically. Figure 3 shows the quantum yields for DPI formation under various conditions at 2537 Å. The quantum yields in aerated cyclohexane did not change with any variations in the

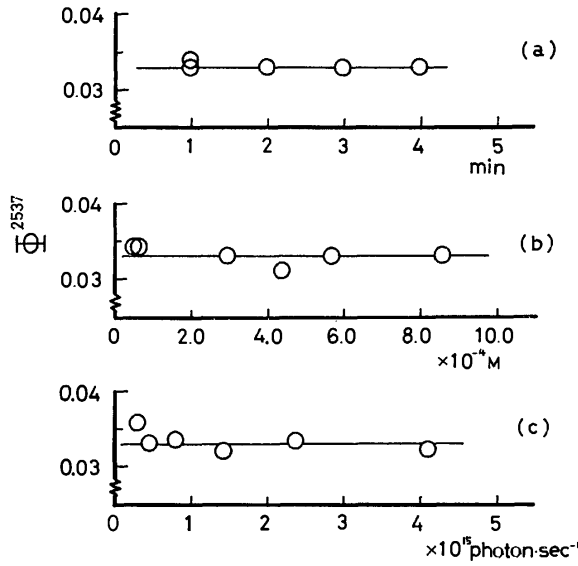

Fig. 3. Dependence of quantum yields for DPPD in cyclohexane solutions at 2537 Å and 20°C: (a) on irradiation time with initial concentration of 5.6×10^{-4}M, (b) on concentration, (c) on light intensity.

irradiation time, the concentration of DPPD, or the light intensity. However, the effects of the excitation wavelength, dissolved oxygen, and polar solvents on Φ^{λ} were measured. Similar results were obtained in the case of CPPD. The quantum yields (Φ_0^{2537}) of DPPD and CPPD in aerated cyclohexane at 2537 Å and 20°C were 0.033 and 0.041 respectively.

(3) Effects of the Excitation Wavelength on the Quantum Yields for the Product Formation (Φ^{λ}) and on the Fluorescence Quantum Yields ($\Phi^{\lambda}{}_f$). The dependence of the excitation wavelength (3200—2400 Å) on Φ^{λ} and $\Phi^{\lambda}{}_f$ in aerated cyclohexane at 20°C was measured using a xenon lamp with a diffraction grating filter. The results are shown in Fig. 4. The Φ^{λ} values increased as a function of the excitation energy. In contrast, the $\Phi^{\lambda}{}_f$ values decreased gradually as the excitation energy increased. The $\Phi^{\lambda}{}_f$ values became constant in the 3000—3200 Å range, where scarcely any photo-oxidation took place.

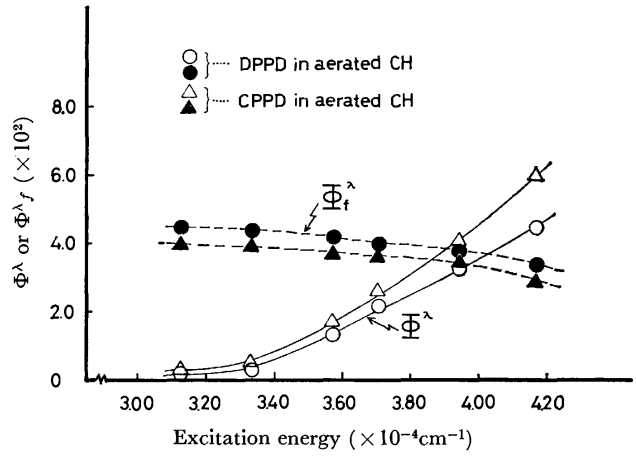

Fig. 4. Dependence of quantum yields Φ^{λ} for the diimine formation and of fluorescence quantum yields $\Phi^{\lambda}{}_f$ on excitation energy in aerated cyclohexane at 20°C.
○: Φ^{λ} of DPPD ●: $\Phi^{\lambda}{}_f$ of DPPD
△: Φ^{λ} of CPPD ▲: $\Phi^{\lambda}{}_f$ of CPPD

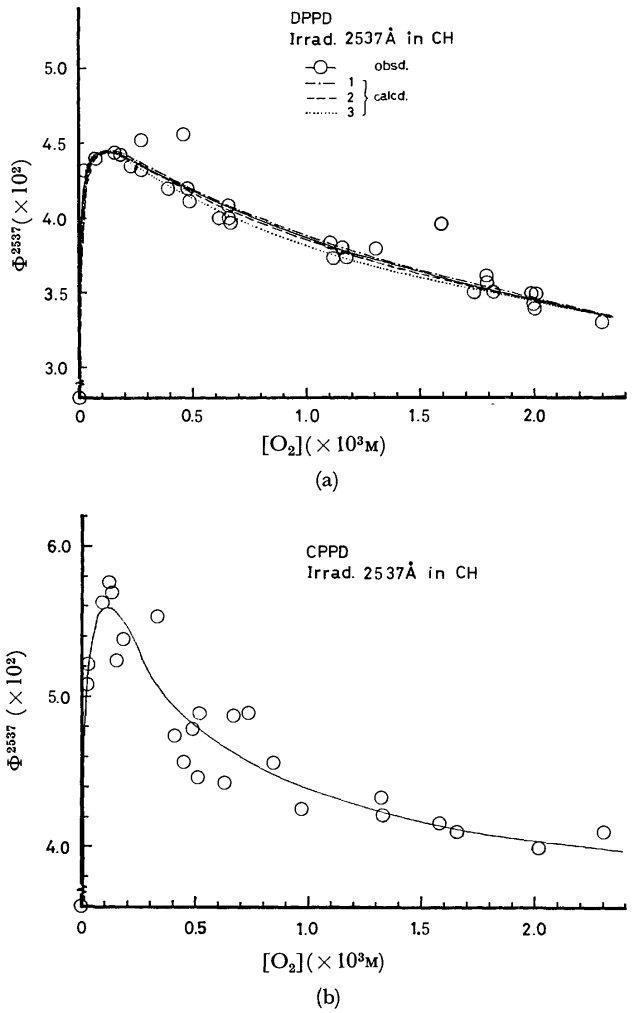

Fig. 5. Dependence of quantum yields Φ^{2537} on oxygen dissolved in cyclohexane at 2537 Å and 20°C: (a) for DPPD; -○- observed values, (1)—(3) calculated values. See Table 4. (b) for CPPD; -○- observed values.

(4) Effect of Dissolved Oxygen on Φ^{2537}. The dependence of dissolved oxygen on Φ^{2537} in cyclohexane at 2537 Å and 20°C was measured by the method described above. The results are shown in Fig. 5(a) and (b). The Φ^{2537}_{max} value of DPPD (0.044) was measured at $[O_2]=1.2\times10^{-4}$M. This shows that the dissolved oxygen has the optimum concentration (1.2×10^{-4}M), giving the maximum value of Φ^{2537} in the photo-oxidation of DPPD. The oxygen effect on the Φ^{2537} of DPPD was in good accordance with the simulation calculated kinetically, as will be discussed later. Similar experimental results were obtained in the case of CPPD, as is shown in Fig. 5(b).

(5) Effects of the Addition of Polar Solvents on Φ^{2537}. The effects of polar solvents on Φ^{2537} in the aerated system at 2537 Å and 20°C were measured. The mixed solvents used were prepared by the addition of a small amount of polar solvents to cyclohexane, except in the case of H_2O. The polar solvents used were ethanol, methanol, acetonitrile, and H_2O. Figure 6 shows the dependence of the relative quantum yields ($\Phi^{2537}/\Phi^{2537}_0$) on the addition of polar solvents to cyclohexane in the aerated system at 2537 Å and 20°C. The photo-oxidation of DPPD was considerably affected by the addition of a small amount of polar solvents to cyclohexane. When about 0.13M of ethanol or methanol was added to cyclohexane, the maximum value of $(\Phi^{2537}/\Phi^{2537}_0)_{max}$ was measured.

In the cyclohexane and ethanol system, the addition of ethanol increased the Φ^{λ} values; the values then decreased gradually, passing through the maximum value ($\Phi^{2537}_{max}=0.050$) at [EtOH]=0.13M. However, the addition of a highly polar solvent, acetonitrile or H_2O, immediately decreased those values, as is shown in Fig. 6.

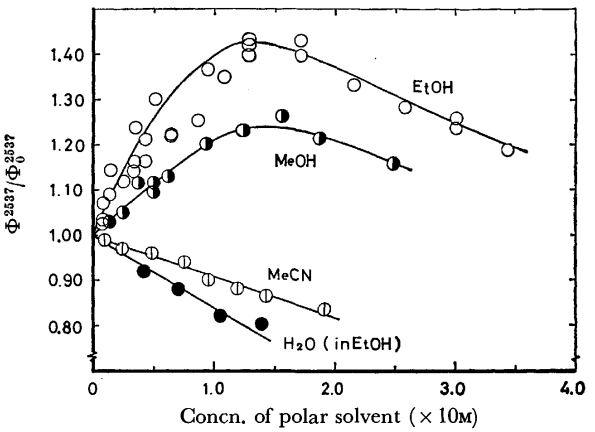

Fig. 6. Effects of the addition of polar solvents on Φ^{2537} for DPPD at 2537 Å and 20°C, where EtOH, MeOH, and MeCN denote ethanol, methanol, and acetonitrile. A small amounts of polar solvents, except H_2O, added to aerated cyclohexane, and in the case of H_2O the aerated EtOH solution was used.

Figure 7 shows the excitation-wavelength effect on the Φ^{λ} of DPPD in the mixed solvent (cyclohexane and ethanol). At every excitation wavelength, similar results were obtained, as is shown in Fig. 7.

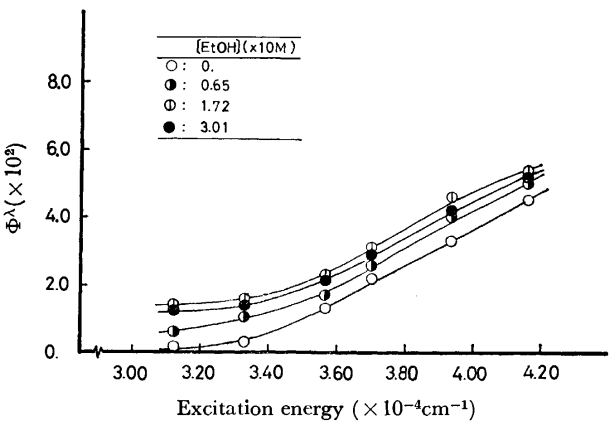

Fig. 7. Dependence of quantum yield Φ^{λ} for DPPD on excitation energy in the mixed solutions of cyclohexane and ethanol.

On the other hand, no intermediate of the photo-oxidation in aerated and degassed cyclohexane or in ethanol was observed by a μ-second flash technique.

Discussion

The results on the excitation-wavelength, dissolved-oxygen, and polar-solvent effects on the quantum yields

of the reaction and the fluorescence can be accounted for by the following schemes:

$$RH_2 + h\nu \xrightarrow{I_a} {}^1(RH_2)_n \quad (0)$$

$${}^1(RH_2)_n \xrightarrow{k_1} {}^1(RH_2)_1 \quad (1)$$

$${}^1(RH_2)_n + O_2 \xrightarrow{k_2'} RH_2^+ \cdots O_2^- \xrightarrow{k_2'} (RH_2)^+O_2^- \quad (2)$$

$${}^1(RH_2)_n + CH \xrightarrow{k_3'} RH_2^+ + e_{solv}^{CH} \xrightarrow{k_{3e}[O_2]}$$

$$\downarrow k_{3q}$$

$$RH_2 + CH$$

$$RH_2^+ + O_2^- + CH \xrightarrow{k_{3p}} (RH_2)^+O_2^- + CH \quad (3)$$

$${}^1(RH_2)_n + EtOH \xrightarrow{k_4'} RH_2^+ + e_{solv}^{EtOH} \xrightarrow{k_{4e}[O_2]}$$

$$\downarrow k_{4q}$$

$$RH_2 + EtOH$$

$$RH_2^+ + O_2^- + EtOH \xrightarrow{k_{4p}} (RH_2)^+O_2^- + EtOH \quad (4)$$

$$(RH_2)^+O_2^- \xrightarrow{k_5} R + (H_2O_2) \quad (5)$$

$$(RH_2)^+O_2^- \xrightarrow{k_6} RH_2 + O_2 \quad (6)$$

$$(RH_2)^+O_2^- + O_2 \xrightarrow{k_7} RH_2 + 2O_2 \quad (7)$$

$$(RH_2)^+O_2^- + EtOH \xrightarrow{k_8} RH_2 + O_2 + EtOH \quad (8)$$

$${}^1(RH_2)_1 \xrightarrow{k_s} RH_2 \quad (9)$$

$${}^1(RH_2)_1 \xrightarrow{k_f} RH_2 + h\nu_f \quad (10)$$

$${}^1(RH_2)_1 \xrightarrow{k_{isc}} {}^3(RH_2) \quad (11)$$

$${}^1(RH_2)_1 + O_2 \xrightarrow{k_d} RH_2 + O_2 \quad (12)$$

$${}^3(RH_2) \xrightarrow{k_t} RH_2 \quad (13)$$

$${}^3(RH_2) \xrightarrow{k_p} RH_2 + h\nu_p \quad (14)$$

$${}^3(RH_2) + O_2 \xrightarrow{k_d} RH_2 + O_2 \quad (15)$$

where RH_2, ${}^1(RH_2)_1$, ${}^1(RH_2)_n$, and ${}^3(RH_2)$ are the ground state, the lowest excited singlet state, the upper excited singlet state, and the lowest triplet state of *p*-phenylenediamines (DPPD and CPPD) respectively, where R is the diimine, where f and p denote the fluorescence and the phosphorescence respectively, where e_{solv}^{CH} and e_{solv}^{EtOH} denote solvated electrons trapped by CH and by EtOH respectively, where CH and EtOH are cyclohexane and ethanol respectively, and where λ denotes the excitation wavelength.

The effects of the excitation wavelength on Φ^λ and $\Phi^\lambda{}_f$ show that the photo-oxidation of *p*-phenylenediamines originates from the upper excited singlet state, ${}^1(RH_2)_n$. Furthermore, it seems, considering the continuously increasing and decreasing of Φ^λ and $\Phi^\lambda{}_f$ shown in Fig. 4, that the primary processes of the reaction occur from the Franck-Condon state of the upper excited singlet state. Thus, the primary processes of the reaction have very high rate constants, $\sim 10^{11}$ sec^{-1}; the rate constants of the processes should be comparable

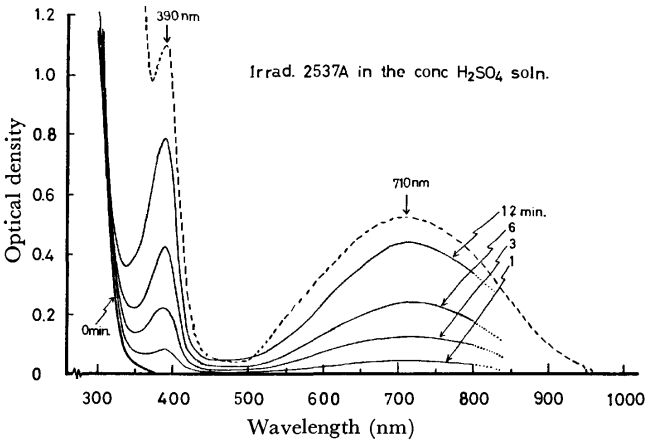

Fig. 8. The spectral change of DPPD upon irradiation with the 2537 Å light in the mixed solution of ethanol and H_2SO_4 in proportions 2 : 1 at 20°C. Numbers refer to time at measurement in minutes. The broken line denote the absorption spectrum for the cation radical RH_2^+ as has been reported by Linschitz *et al.*[29,40]

to those of the internal conversion, ${}^1(RH_2)_n \rightarrow {}^1(RH_2)_1$, whose rate constants are of the order of 10^{12}—10^{13} sec^{-1}. These processes can be accounted for by the ionization processes; one is the long-range electron-transfer process from ${}^1(RH_2)_n$ to the ground state of $O_2({}^3\Sigma_g^-)$, while the other is the electron-transfer process from ${}^1(RH_2)_n$ to the solvent. Polar solvents such as ethanol promote the latter process, since the electron-trapping ability in a polar solvent is larger than that in a nonpolar solvent.[2,14] In addition to this, the polar solvents dissolve the intermediate in the reaction, resulting in a decrease in Φ^{2537} as shown in Fig. 6. Therefore, it seems that the intermediate is an ion pair $(RH_2)^+O_2^-$ formed by the processes described in Eqs. (2)—(4). This assumption is supported by the fact that the spectrum of DPPD in the concd. H_2SO_4 solution at 2537 Å and 20°C was the same as that of the corresponding cation radical, as is shown in Fig. 8. The UV-V absorption spectrum of the DPPD cation radical has been reported by Linschitz *et al.*[29,40] The ESR absorption spectrum of the cation radical in acetic acid has also been measured.[40] In an acidic solution, the cation radical is very stable. Of course, in a highly polar solvent, no ion pair $(RH_2)^+O_2^-$ is formed because of the high dielectric constant. The photoionization processes in the photo-oxidation of DPPD and CPPD differ from that of the Weller-type ionization.[1] The Weller-type photoionization occurs through the exciplex $(DA)^*$ formed by the interaction between the lowest excited singlet state of the donor and the ground state of the acceptor, or *vice versa*, in a highly polar solvent. The electron transfer between oxygen and aromatic anilines *via* the exciplex formation has been proposed by Hori, Itoi, and Tsubomura;[28] they have also shown that the photoionization is mainly a single-photonic process. In the present work, the electron transfer occurs from the Franck-Condon state of the upper excited state ${}^1(RH_2)_n$. Since Φ^{2537} is not dependent

40) H. Linschitz, J. Rennert, and T. M. Korn, *J. Amer. Chem. Soc.*, **76**, 5839 (1954).

on the light intensity (Fig. 3(c)), the photoionization is a single-photonic process.

The possibility of a predissociative β-bond fission (N–H bond), such as that of hydrazobenzene,[26] can be disregarded, since the reactive state of DPPD was not the lowest excited singlet state, but the upper excited singlet state, since the Φ^{2537} values did not depend on the light intensity, and since no diimine formation was observed in the degassed system. The possibility that complex formation between DPPD and O_2 in the ground states is responsible for this photo-oxidation was shown to be unlikely by the fact that the spectral intensities and the positions of the aerated solution were identical with those of the degassed solution.

From the steady-state approximation, the following equations are obtained:

$$\frac{d[(RH_2)^+O_2^-]}{dt} = k_2^\lambda[^1(RH_2)_n][O_2] + (k_{3p}+k_{4p})[RH_2^+][O_2^-] - (k_5+k_6+_7[O_2] + k_8[EtOH])[(RH_2)^+O_2^-] = 0 \quad (16)$$

$$[(RH_2)^+O_2^-] = \frac{k_2^\lambda[^1(RH_2)_n][O_2]+(k_{3p}+k_{4p})[RH_2^+][O_2^-]}{k_5+k_6+k_7[O_2]+k_8[EtOH]} \quad (16')$$

$$\Phi^\lambda = \frac{d[R]/dt}{I_a} = \frac{k_5[(RH_2)^+O_2^-]}{I_a} = \left\{\frac{k_2^\lambda[O_2]+\frac{k_3^\lambda[CH]k_{3e}[O_2]}{k_{3e}[O_2]+k_{3q}[RH_2^+]}+\frac{k_4^\lambda[EtOH]k_{4e}[O_2]}{k_{4e}[O_2]+k_{4q}[RH_2^+]}}{k_1+k_2^\lambda[O_2]+k_3^\lambda[CH]+k_4^\lambda[EtOH]}\right\} \times \frac{k_5}{k_5+k_6+k_7[O_2]+k_8[EtOH]} \quad (17)$$

where:

$$[^1(RH_2)_n] = \frac{I_a}{k_1+k_2^\lambda[O_2]+k_3^\lambda[CH]+k_4^\lambda[EtOH]}$$

$$[RH_2^+] = \frac{\{k_3^\lambda[CH]+k_4^\lambda[EtOH]\}[^1(RH_2)_n]}{k_{3q}[e_{solv}^{CH}]+k_{4q}[e_{solv}^{EtOH}]+(k_{3p}+k_{4p})[O_2^-]}$$

$$[O_2^-] = \frac{\{k_{3e}[e_{solv}^{CH}]+k_{4e}[e_{solv}^{EtOH}]\}[O_2]}{(k_{3p}+k_{4p})[RH_2^+]}$$

$$[e_{solv}^{CH}] = \frac{k_3^\lambda[CH][^1(RH_2)_n]}{k_{3e}[O_2]+k_{3q}[RH_2^+]}$$

and

$$[e_{solv}^{EtOH}] = \frac{k_4^\lambda[EtOH][^1(RH_2)_n]}{k_{4e}[O_2]+k_{4q}[RH_2^+]}$$

If [EtOH]=0, Eq. (17′) is derived from Eq. (17).

$$\Phi^\lambda = \left\{\frac{k_2^\lambda[O_2]+\frac{k_3^\lambda[CH]k_{3e}[O_2]}{k_{3e}[O_2]+k_{3q}[RH_2^+]}}{k_1+k_2^\lambda[O_2]+k_3^\lambda[CH]}\right\}\frac{k_5}{k_5+k_6+k_7[O_2]} = \left\{\frac{a^\lambda[O_2]+\frac{b^\lambda c[O_2]}{c[O_2]+1}}{1+a^\lambda[O_2]+b^\lambda}\right\}\frac{1}{1+d+e[O_2]} \quad (17')$$

where:

$$a^\lambda = \frac{k_2^\lambda}{k_1}, \quad b^\lambda = \frac{k_3^\lambda}{k_1}[CH], \quad c = \frac{k_{3e}}{k_{3q}[RH_2^+]}$$

$$d = \frac{k_6}{k_5}, \text{ and } e = \frac{k_7}{k_5}$$

On the other hand, the fluorescence quantum yield, Φ^λ_f, is given by:

$$\Phi_f^\lambda = \frac{k_1}{k_1+k_2^\lambda[O_2]+k_3^\lambda[CH]}\cdot\frac{k_f}{k_s+k_f+k_{isc}+k_d[O_2]} \quad (18)$$

Scarcely any photo-oxidation of DPPD occurred upon irradiation with the 3200 Å light, as is shown in Fig. 4. Therefore, Eq. (19) holds approximately:

$$\Phi_f^{3200} = \frac{k_f}{k_s+k_f+k_{isc}+k_d[O_2]} \quad (19)$$

where $k_1 \gg k_2^{3200}+k_3^{3200}[CH]$. The relative fluorescence quantum yield, $\Phi_f^{3200}/\Phi^\lambda_f$, is obtained from Eqs. (18) and (19):

$$\frac{\Phi_f^{3200}}{\Phi_f^\lambda} = 1+\frac{k_2^\lambda[O_2]+k_3^\lambda[CH]}{k_1} = 1+a^\lambda[O_2]+b^\lambda \quad (20)$$

where $[O_2]=2.3\times10^{-3}$M.[24] The $\Phi_f^{3200}/\Phi^\lambda_f$ values are listed in Table 3.

Table 3. The $\Phi_f^{3200}/\Phi_f^\lambda$ values of DPPD in aerated cyclohexane

Excitation wavelength Å	Excitation energy eV	$\Phi^\lambda\times10^2$	$\Phi_f^{3200}/\Phi_f^\lambda$
2400	5.17	4.5	1.33
2537	4.88	3.3	1.19_3
2700	4.59	2.2	1.12
2800	4.43	1.33	1.07
3000	4.13	0.28	1.02
3200	3.87	0.18	1.00

The following values can be estimated:

$$a^{2537}[O_2]+b^{2537} = 0.19_3 \quad (21)$$

where $[O_2]=2.3\times10^{-3}$M. Then, the simulation of Φ^{2537} as a function of $[O_2]$ was carried out using Eqs. (17′) and (21).

The (Φ^{2537}_{calcd}) values of DPPD are in accordance with those obtained experimentally, as is shown in Fig. 5(a). The appropriate values of the a^{2537}, b^{2537}, c, d, and e parameters are listed in Table 4. From the results of the calculations, the two rates, $k_2^{2537}[O_2]$ and $k_3^{2537}[CH]$, in the electron-transfer processes (Eqs. (2) and (3)) can be said to be nearly equivalent in aerated cyclohexane, where $[O_2]=2.3\times10^{-3}$M, and at 2537 Å, because the $(2.3\times10^{-3}a^{2537})/b^{2537}$ ratio is approximately equal to unity.

Table 4. The appropriate values of the parameters

No. of plot in Fig. 5 (a)	$a^{2537}\times10^{-1}$	$b^{2537}\times10$	$c\times10^{-5}$	d	$e\times10^{-3}$
1	3.35	1.16	3.00	1.22	1.12
2	4.20	0.96_5	3.00	0.86_5	1.28
3	5.04	0.77	3.00	0.51_1	1.44

Thus, Eq. (22) is obtained:

$$k_2^{2537} = 4\times10^3 k_3^{2537} \quad (22)$$

If n molecules of oxygen are randomly distributed around a DPPD molecule in a certain volume, V, the radius ($\bar{r}$) between the DPPD molecule and the nearest-neighbor oxygen molecule can be evaluated by the following equation, derived by Yamamoto, Nakato, and

Tsubomura:[41]

$$\bar{r} = (V/2\pi n)^{1/3}$$

or
$$\bar{r} = 6.42[O_2]^{-1/3}\text{Å} \quad (23)$$

The calculated $\bar{r}$ value is 49 Å in aerated cyclohexane ($[O_2]=2.3\times10^{-3}$M) at 2537 Å and 20°C. The large $\bar{r}$ value shows the long-range electron transfer from the Franck-Condon state of the $^1(RH_2)_n$ state to dissolved oxygen. The rate constant of the long-range electron transfer, k_2^{2537}, is very much larger than that of the electron transfer to the solvent (cyclohexane), as is shown in Eq. (22).

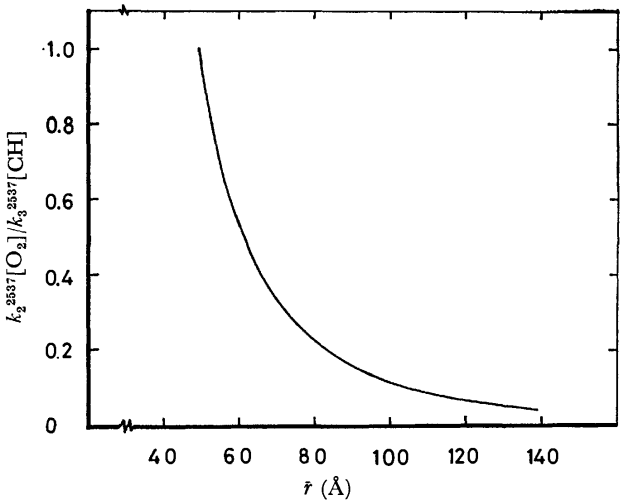

Fig. 9. The ratio k_2^{2537} $[O_2]/k_3^{2537}[CH]$ as a function of $\bar{r}$.

The plot of the $k_2^{2537}[O_2]/k_3^{2537}[CH]$ ratio as a function of $\bar{r}$ is shown in Fig. 9. It can be understood that the $k_2^{2537}[O_2]/k_3^{2537}[CH]$ values significantly decrease as the $\bar{r}$ values increase. The dissolved oxygen in cyclohexane acts as an electron-trapping center in the primary processes of the photo-oxidation and also deactivates the intermediate $(RH_2)^+O_2^-$, as is shown in Eq. (7). In the electron-transfer processes from $^1(RH_2)_n$ to the solvents, it may be assumed that the $^1(RH_2)_n$ species ejects an electron to the solvents and that subsequently the electron is trapped by the dissolved oxygen, as is shown in Eqs. (3) and (4). Scarcely any photooxidation of DPPD in aerated cyclohexane occurred upon irradiation with the 3200 Å light, which corresponds to the shoulder of the absorption Band I in Fig. 1. The absorption Band I is comprised of several singlet-singlet transitions, as is shown in Table 1, where the calculated data for the *cis*-form are almost the same as those for the *trans*-form. Although the reactive state can not be assigned exactly, the photo-ionization processes described above apparently take place from the upper excited singlet state, $^1(RH_2)_n$. In the secondary processes of the reaction, it seems that the $(RH_2)^+O_2^-$ ion pair is converted to the corresponding diimine (Eq. (5)). This transformation probably involves an intramolecular proton transfer process:

$$(RH_2)^+O_2^- \longrightarrow (RH)(HO_2) \longrightarrow R + H_2O_2 \quad (24)$$

The H_2O_2 formation was identified by iodometry.

Finally, a schematic energy diagram of the photooxidation of DPPD and CPPD is shown in Fig. 10. The detailed reaction schemes can be written as in Eqs. (0)—(15).

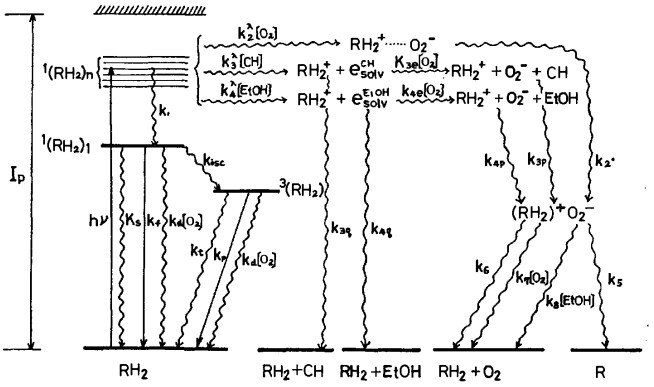

Fig. 10. Schematic energy state diagram for the photooxidation of DPPD.

The authors wish to thank Professors Ikuzo Tanaka and Yuji Mori of the Tokyo Institute of Technology for their very helpful discussions of this paper.

41) N. Yamamoto, Y. Nakato, and H. Tsubomura, This Bulletin, **40**, 451 (1967).

Calculation of Infrared Band Intensities of Various Chlorinated Ethanes

Kazutoshi TANABE and Shinnosuke SAËKI

Government Chemical Industrial Research Institute of Tokyo, Honmachi, Shibuyaku, Tokyo

(Received May 8, 1971)

Infrared absorption intensities of fundamental bands of three molecular species, CH_3CCl_3, CD_3CCl_3 in the vapor phase, and C_2Cl_6 in dilute solution in carbon disulfide have been measured. From the intensity data of four kinds of chlorinated ethanes C_2H_6, C_2D_6, CH_3CCl_3, CD_3CCl_3, the least number of common intensity parameters has been determined using the least squares method. Intensities of C_2Cl_6 calculated using the determined values of intensity parameters have been compared with the observed intensities in solution. It has proved that for almost all electro-optical parameters, it is possible to determine values commonly applicable to various chlorinated ethanes, while for μ_{CH} and $\delta\mu_{CH}/\delta r_{CH}$, it is not possible to find commonly applicable values, as in the case of chlorinated methanes.

In our previous paper,[1] infrared band intensity data of thirteen kinds of chlorinated methanes, from methane to carbon tetrachloride, were interpreted in terms of common intensity parameters as few as possible. The least squares method was applied to determine values of those parameters to obtain the best fit between observed and calculated intensities. As a result, for most of the electro-optical parameters, values commonly applicable to all chlorinated methanes could be determined, while for the two parameters μ_{CH} and $\delta\mu_{CH}/\delta r_{CH}$, it was not possible to find commonly applicable values.

In this study, in order to examine whether similar trends are also found in other cases, the molecular series of chlorinated ethane have been investigated, using the same technique as in the previous study. Molecular species treated in this study are C_2H_6, C_2D_6; CH_3CCl_3, CD_3CCl_3; C_2Cl_6, all having three-fold symmetry axis.

As compared with the case of chlorinated methanes, the treatment of ethane series requires many more electro-optical parameters in calculation. For example, several parameters associated with C–C bonds such as μ_{CC} or $\delta\mu_{CC}/\delta r_{CC}$ have to be taken into account, from the intensity expression based on the theory. Consequently, computative process is more complex and more time-consuming. However, it is of much interest to examine how the values of parameters change from chlorinated methanes to ethanes.

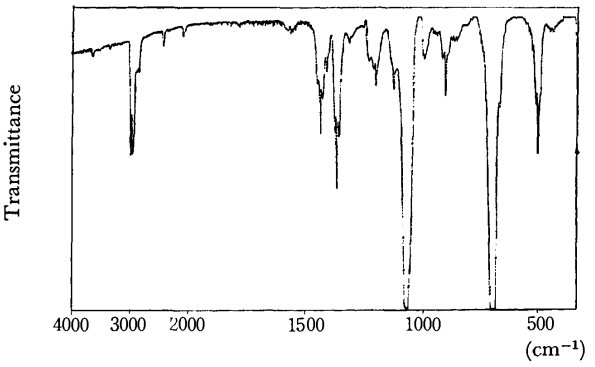

Fig. 1. Vapor phase spectrum of CH_3CCl_3.

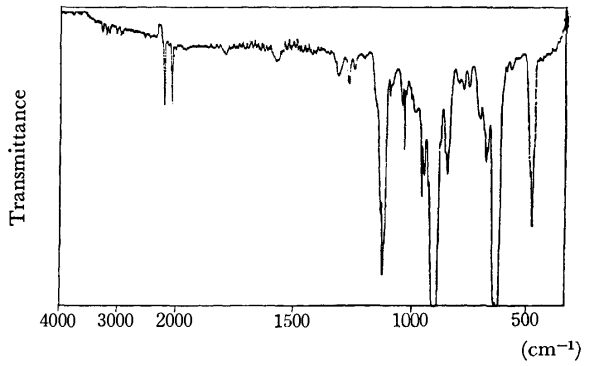

Fig. 2. Vapor phase spectrum of CD_3CCl_3.

Experimental

Infrared absorption intensities of fundamental bands of three molecular species CH_3CCl_3, CD_3CCl_3 in the vapor phase and C_2Cl_6 in dilute carbon disulfide solution were measured in a range 4000—600 cm^{-1} using a Perkin-Elmer Model 421 grating spectrophotometer combined with a digital data recorder.[2] Intensities for bands below 600 cm^{-1} were roughly estimated by inspection from observed spectra measured using Perkin-Elmer Model 225 and 180 spectrophotometers. Deuterated methyl chloroform CD_3CCl_3, supplied from Merk Sharp & Dohm of Canada Limited, was used without further purification. Observed spectra of CH_3CCl_3 and CD_3CCl_3 in the vapor phase are shown in Figs. 1 and 2. Methods and instrumental conditions were almost the same as described in the previous papers.[1,3]

Results and Discussion

In order to estimate the absolute band intensity, and to obtain the **L**-matrix necessary for computing the band intensity, the assignment of fundamental bands has to be determined definitely. Concerning the ethane species, C_2H_6 and C_2D_6, the frequency and intensity data are all obtained from literatures[4-13]

1) K. Tanabe and S. Saëki, *Spectrochim. Acta*, **26A**, 1469 (1970).
2) K. Tanabe, S. Saëki, and M. Mizuno, *Japan Analyst*, **18**, 1347 (1969).
3) S. Saëki and K. Tanabe, *Spectrochim. Acta*, **25A**, 1325 (1969).
4) F. Stitt, *J. Chem. Phys.*, **7**, 297 (1939).
5) A. M. Thorndike, *J. Chem. Phys.*, **15**, 868 (1947).
6) L. F. Smith, *ibid.*, **17**, 139 (1949).
7) G. E. Hansen and D. M. Dennison, *ibid.*, **20**, 313 (1952).
8) J. Romanko, T. Feldman, and H. L. Welsh, *Can. J. Chem.*, **33**, 588 (1955).
9) I. M. Nyquist, I. M. Mills, W. B. Person, and B. Crawford, *J. Chem. Phys.*, **26**, 552 (1957).
10) D. W. Lepard, D. M. C. Sweeney, and H. L. Welsh, *Can. J. Chem.*, **40**, 1567 (1962).
11) J. L. Duncan, *Spectrochim. Acta*, **20**, 1197 (1964).
12) D. W. Lepard, D. E. Shaw, and H. L. Welsh, *Can. J. Chem.*, **44**, 2353 (1966).
13) D. E. Shaw and H. L. Welsh, *ibid.*, **45**, 3823 (1967).

Table 1. Frequencies and intensities of ethane

Species		ν_{obsd} [a]	A_{obsd} [b]
CH_3CH_3			
A_{1g}	1	2954	—
	2	1388	—
	3	995	—
A_{1u}	4	289	—
A_{2u}	5	2954	4780±280
	6	1379	400± 40
E_u	7	2996	12320±370
	8	1486	1340±130
	9	820	610± 10
E_g	10	2969	—
	11	1460	—
	12	1190	—
CD_3CD_3			
A_{1g}	1	2100	—
	2	1155	—
	3	843	—
A_{1u}	4	200	—
A_{2u}	5	2095	2420±140
	6	1077	290± 30
E_u	7	2236	6440±360
	8	1081	910± 90
	9	594	330± 20
E_g	10	2225	—
	11	1055	—
	12	970	—

a) ν_{obsd} (cm^{-1}) taken from Refs. 4—13.
b) A_{obsd} ($l \cdot mol^{-1} \cdot cm^{-2}$) from Ref. 9.

where band assignments are correctly made. These data are summarized in Table 1.

As for methyl chloroform CH_3CCl_3, several authors reported frequency data and made a tentative assignment of fundamental bands. The observed bands are considered to be correctly assigned therein, except for the C–C stretching vibration. To this mode, diffrent frequencies, 1075,[14] 1068,[15] 1012,[16] 1007,[17] 977,[18] 867,[19] and 714 cm^{-1},[20] were assigned by different authors. The last two values seem inappropriately low as compared with the C–C stretching frequencies in similar molecules: 995 in C_2H_6, 972 in CH_3CH_2Cl, 1052 in *trans*-CH_2ClCH_2Cl, 1027 in *gauche*-CH_2ClCH_2Cl, and 975 in C_2Cl_6. In particular, the band at 714 cm^{-1} should be assigned to the C–Cl degenerate stretching mode.

The vapor phase spectrum observed in the region 1500—400 cm^{-1} is shown in Fig. 3. The strongest band at 1100—1070 cm^{-1} shows a very complex band envelope, which is undoubtedly assigned to the CH_3 rocking vibration (species E). On the other hand, the C–C stretching mode is expected to show a P, Q, R

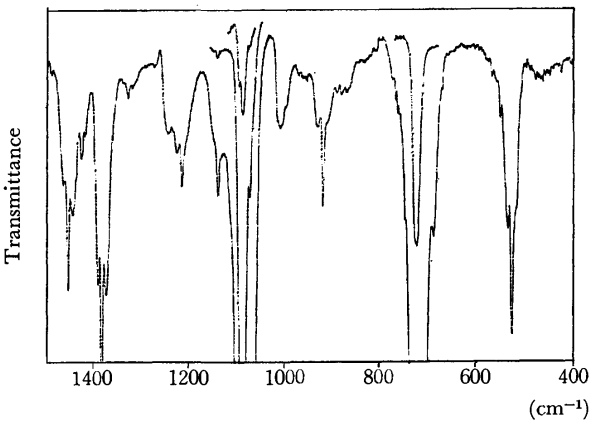

Fig. 3. Vapor phase spectrum of CH_3CCl_3 in a region 1500—400 cm^{-1}.

band envelope similar to the CH_3 symmetric stretching (at 2951 cm^{-1}) or symmetric deformation band (at 1386 cm^{-1}) of the same symmetry species A_1. Although no observed band may be assigned to the C–C stretching mode with certainty, the band observed at about 1010 cm^{-1} has been tentatively assigned to this mode, after Cleveland *et al.* (1012 cm^{-1}),[16] or Karplus and Halford (1007 cm^{-1}).[17]

As for deuterated methyl chloroform CD_3CCl_3, no previous data on vibrational frequencies and intensities have been reported. Most of fundamental bands for this molecule have been assigned by referring to those of CH_3CCl_3, or taking into account band profiles observed in the vapor phase. The C–C stretching frequency could not be determined in like manner, hence its band has been assigned by referring to the frequency product rule for the isotopic species CH_3CCl_3 and CD_3CCl_3, as given in Table 2. Although there may be some ambiguity in assigning the fundamental frequencies only on the basis of observed spectrum, the observed values listed in Table 3 have been adopted as the tentative assignment. Taking into account the fact that not the harmonic frequencies but the observed frequencies are employed for the product rule in Table 2, the observed values listed are considred to satisfy the rule, hence the band assignment for these species might be correctly made.

Table 2. Frequency product rule for CH_3CCl_3 and CD_3CCl_3

	Theoretical	Observed
A_1	$\left(\frac{m_H^2 \times M_D}{m_D^2 \times M_H}\right)^{1/2} = 0.5060$	$\prod_{i=1}^{5} \frac{\nu_{obsd}^i(D)}{\nu_{obsd}^i(H)} = 0.5233$
E	$\left(\frac{m_H^3 \times M_D \times I_D}{m_D^3 \times M_H \times I_H}\right)^{1/2} = 0.3725$	$\prod_{i=7}^{12} \frac{\nu_{obsd}^i(D)}{\nu_{obsd}^i(H)} = 0.3812$

m: atomic weight, m_H=1.0078, m_D=2.0141
M: molecular weight, M_H =133.405, M_D =136.424
I : moment of inertia, I_H=213.175, I_D=229.075.

The calculation of normal vibrations, necessary for determining the **L**-matrix to evaluate the band intensity as well as for confirming the above band assignment, has been carried out using the local symmetry force field (LSFF). Force constants based on this field, being considered to be mutually transferable among

14) D. C. Smith and G. F. Brown, *J. Chem. Phys.*, **20**, 473 (1952).
15) G. Allen and H. J. Bernstein, *Can. J. Chem.*, **32**, 2124 (1954).
16) M. Z. El-Sabban, A. G. Meister, and F. F. Cleveland, *J. Chem. Phys.*, **19**, 855 (1951).
17) R. Karplus and R. S. Halford, *ibid.*, **18**, 910 (1950).
18) T. R. Rubin, B. H. Levedahl, and D. M. Yost, *J. Amer. Chem. Soc.*, **66**, 279 (1944).
19) P. Venkateswarlu, *J. Chem. Phys.*, **19**, 298 (1951).
20) G. F. Hull Jr., *ibid.*, **3**, 534 (1935).

TABLE 3. OBSERVED AND CALCULATED NORMAL FREQUENCIES (cm^{-1})

Species	A		E	
	ν_{obsd}	ν_{calcd}	ν_{obsd}	ν_{calcd}
CH_3CH_3	2954	2951	2996	3001
	1388	1395	1486	1476
	995	1005	820	823
	2954	2953	2969	2971
	1379	1399	1460	1455
			1190	1188
CD_3CD_3	2100	2140	2236	2237
	1155	1155	1081	1063
			594	594
	2095	2127	2225	2230
	1077	1065	1055	1033
			970	948
CH_3CCl_3	2951	2945	3013	3002
	1386	1383	1455	1499
	1010	1006	1088	1090
	526	524	724	721
	344	333	303	319
			239	234
CD_3CCl_3	2146	2122	2264	2255
	1140	1120	1045	1077
	950	920	925	924
	510	507	660	652
	330	327	300	306
			220	218
CCl_3CCl_3	978	998	780	783
	432	432	278	280
	169	170	115	116
	679	683	858	862
	375	387	341	332
			224	211

the chlorinated ethanes treated here, have been determined using the least squares method from fifty-five observed frequencies. Calculated normal frequencies are given in Table 3, compared with the observed values, and the converged values of the LSFF constants are in Table 4, where asterisks indicate the constants fixed at zero in the least squares calculation.

Agreement between calculated and observed frequencies is satisfactory on the whole, and the converged values of the LSFF constants seem appropriate. The frequencies assigned tentatively for the C–C stretching vibration of methyl chloroforms CH_3CCl_3 and CD_3CCl_3 are represented with the above LSFF constants to a reasonable extent, thus the above band assignment could be considered acceptable.

Infrared band intensities of fundamental bands of three molecular species CH_3CCl_3, CD_3CCl_3, and C_2Cl_6, estimated on the basis of such band assignment, are listed in Table 5. The intensity sum rule proposed by Crawford[21] gives the results shown in the same table. It can be deduced from this result that these intensity data are reliable and accurate for calculation.

For computing the band intensity of chlorinated ethanes, parameters other than those used for chlorinated

21) B. Crawford Jr., *J. Chem. Phys.*, **20**, 977 (1952).

TABLE 4. CONVERGED VALUES AND THEIR DEVIATIONS OF THE LSFF CONSTANTS (md/Å, md, or md·Å)

f(CC)	4.52 (0.08)	f(ds)	4.71 (0.05)
f(ss)	4.99 (0.02)	f(dd)	0.58 (0.03)
f(sd)	0.57 (0.01)	f(dr)	0.68 (0.03)
f(ss,sd)	0.00*	f(ds,dd)	0.09 (0.10)
f(ss,CC)	0.00*	f(ds, dr)	0.00*
f(sd, CC)	−0.31 (0.01)	f(dd, dr)	−0.01 (0.04)
f(ss, ss)	−0.01 (0.04)	f(ds, ds)	−0.06 (0·01)
f(sd, sd)	0.02 (0.01)	f(dd, dd)	−0.01 (0.01)
		f(dr, dr)	0.13 (0.01)
f(SS)	4.52 (0.05)	f(DS)	2.33 (0.46)
f(SD)	1.09 (0.05)	f(DD)	2.10 (0.58)
f(SS, SD)	0.67 (0.05)	f(DR)	0.80 (0.10)
f(SS, CC)	0.00*	f(DS, DD)	0.00*
f(SD, CC)	−0.91 (0.05)	f(DS, DR)	0.69 (0.15)
f(SS, SS)	0.00*	f(DD, DR)	0.00*
f(SD, SD)	−0.03 (0.05)	f(DS, DS)	0.55 (0.14)
		f(DD, DD)	0.00*
		f(DR, DR)	−0.17 (0.07)
f(ss, SS)	0.00*	f(ds, DS)	−1.23 (0.20)
f(sd, SD)	0.06 (0.10)	f(dd, DD)	0.00*
		f(dr, DR)	0.07 (0.02)

SS : symmetric stretching SD : symmetric deformation
DS : degenerate stretching DD: degenerate deformation
DR: degenerate rocking

Small and capital letters are referred to the LSFF coordinates for the C–H and the C–Cl bonds, respectively.

Asterisks indicate the force constants fixed at zero in the least squares calculation.

TABLE 5. OBSERVED INTENSITIES AND THEIR SUM RULE

Species			ν_{obsd} (cm^{-1})	A_{obsd} $\left(\frac{l}{mol\cdot cm^2}\right)$	$\frac{A_{obsd}}{\nu^2_{obsd}}\times 10^3$
CH_3CCl_3	A_1	1	2951	550± 50	
		2	1386	770± 30	
		3	1010	260± 20	6.99±0.36
		4	526	800± 100	
		5	344	400± 50	
	E	7	3013	660± 30	
		8	1455	750± 70	
		9	1088	10000±1000	43.7±2.7
		10	724	17500±1400	
		11	303	50± 20	
		12	239	50± 20	
CD_3CCl_3	A_1	1	2146	150± 50	
		2	1145	1500± 300	
		3	950	50± 40	7.06±0.92
		4	510	800± 100	
		5	330	300± 100	
	E	7	2264	200± 50	
		8	1045	170± 50	
		9	925	14500±1000	41.1±1.6
		10	660	9500±700	
		11	300	100± 50	
		12	220	50± 20	
C_2Cl_6	A_{2u}	5	679	4000± 300	
		6	375	100± 50	
	E_u	7	780	39400±3500	
		8	278	100± 50	
		9	115	(100)	

A_{obsd} in CH_3CCl_3, CD_3CCl_3 is in the vapor phase, and A_{obsd} in C_2Cl_6 is in dilute solution of carbon disulfide.

methanes have to be introduced into the calculation based on the valence-optical theory.[22,23] These parameters are for example, the ones associated with the C–C bond, such as μ_{CC}, or $\delta\mu_{CC}/\delta r_{CC}$. Furthermore, if parameters due to the long-range methyl-methyl group interaction such as $\delta\mu_{CH}/\delta r_{CH}$ (where μ_{CH} and r_{CH} are attached to different carbon atoms, respectively) are taken into account, the total number of the electro-optical parameters becomes too large as compared with the number of available intensity data. In order to determine values for intensity parameters from the observed data, reduction of the unknown parameters is necessary, and for this purpose, those parameters which might be expected to have rather small values, such as the above $\delta\mu_{CH}/\delta r_{CH}$, are neglected.

Intensity parameters determined in calculation based on these considerations are twenty-four as follows:

(a) for C–H bond; μ_{CH}, $\delta\mu_{CH}/\delta r_{CH}$, $\delta\mu_{CH}/\delta r'_{CH}$, $\delta\mu_{CH}/\delta r_{CC}$, $\delta\mu_{CH}/\delta\alpha_{HCH}$, $\delta\mu_{CH}/\delta\alpha'_{HCH}$, $\alpha\mu_{CH}/\delta\alpha_{HCC}$, $\alpha\mu_{CH}/\delta\alpha'_{HCC}$,

(b) for C–Cl bond; μ_{CCl}, $\delta\mu_{CCl}/\delta r_{CCl}$, $\delta\mu_{CCl}/\delta r'_{CCl}$, $\delta\mu_{CCl}/\delta r_{CC}$, $\delta\mu_{CCl}/\delta\alpha_{ClCCl}$, $\delta\mu_{CCl}/\delta\alpha'_{ClCCl}$,, $\delta\mu_{CCl}/\delta\alpha_{ClCC}$, $\delta\mu_{CCl}/\delta\alpha'_{ClCC}$,

(c) for C–C bond; μ_{CC}, $\delta\mu_{CC}/\delta r_{CC}$, $\delta\mu_{CC}/\delta r_{CH}$, $\delta\mu_{CC}/\delta r_{CCl}$, $\delta\mu_{CC}/\alpha_{HCH}$, $\delta\mu_{CC}/\delta\alpha_{HCC}$, $\delta\mu_{CC}/\delta\alpha_{ClCCl}$, $\delta\mu_{CC}/\delta r_{ClCC}$.

These twenty-four parameters have been adjusted using the least squares method from the thirty-three data, that is, the thirty-two intensity data of C_2H_6, C_2D_6, CH_3CCl_3, CD_3CCl_3, and the permanent dipole moment of the methyl chloroform molecule.[24] The computative process is the same as in the previous papers, and the molecular constants used are given in Table 6.

Taleb 6. Molecular constants

	CH_3CH_3 CD_3CD_3	CH_3CCl_3 CD_3CCl_3	C_2Cl_6
C–H	1.1068	1.09	
C–Cl		1.76	1.763
C–C	1.5324	1.54	1.499
∠HCH	107°55′	109°28′	
∠ClCCl		109°	108°14′

Bond lengths are in (Å).

Because of the sign ambiguity inherent in intensity studies, several converged sets of intensity parameters are obtained, as in our previous cases. Although it is desirable to repeat the least squares calculation by changing the starting values of parameters in various ways to find out the most acceptable set with the smallest residual, such repetative computations are time-consuming and could not be carried out. Hence, first, the parameters were classified into the following three groups: (1) these common to chlorinated methanes, (2) those considered to be less important and to have small values, and (3) those considered to be more important and to have significant values. And as the starting values of the parameters, the values already determined were adopted for the first group, zero values were assumed for the second group, and various with changes of signs were tested for the third group. After more than fifteen starting sets of parameters have been tested, several sets have been obtained for converged values of the least squares calculation, and the set with the smallest residual among those has been considered to be most acceptable.

Table 7. Calculated intensities (l mol^{-1} cm^{-2})

Species		i	A_{obsd}	A_{calcd} (I)	A_{calcd} (II)	Mode
CH_3CH_3	A_{1u}	5	4780	4690	4696	CH_3 ss
		6	400	447	445	CH_3 sd
	E_u	7	12320	1420	12266	CH_3 ds
		8	1340	648	1495	CH_3 dd
		9	610	611	611	CH_3 dr
CD_3CD_3	A_{1u}	5	2420	2459	2462	CD_3 ss
		6	290	243	242	CD_3 sd
	E_u	7	6440	762	6547	CD_3 ds
		8	910	318	811	CD_3 dd
		9	330	327	325	CD_3 dr
CH_3CCl_3	A_1	1	550	411	411	CH_3 ss
		2	770	760	760	CH_3 sd
		3	260	265	265	CC
		4	800	860	863	CCl_3 SS
		5	400	399	395	CCl_3 SD
	E	7	660	827	667	CH_3 ds
		8	750	953	737	CH_3 dd
		9	10000	2653	6741	CH_3 dr
		10	17500	12081	15233	CCl_3 DS
		11	50	280	17	CCl_3 DD
		12	50	403	26	CCl_3 DR
CD_3CCl_3	A_1	1	150	362	362	CD_3 ss
		2	1500	487	488	CD_3 sd
		3	50	42	42	CC
		4	800	728	731	CCl_3 SS
		5	300	348	345	CCl_3 SD
	E	7	200	196	244	CD_3 ds
		8	170	397	127	CD_3 dd
		9	14500	7446	13804	CD_3 dr
		10	9500	8304	8413	CCl_3 DS
		11	100	70	190	CCl_3 DD
		12	50	134	36	CCl_3 DR
CCl_3CCl_3[a]	A_{1u}	5	(4000)	4000	3972	CCl_3 SS
		6	(100)	100	98	CCl_3 SD
	E_u	7	(39400)	45496	47375	CCl_3 DS
		8	(100)	10	27	CCl_3 DD
		9	(100)	64	287	CCl_3 DR
$\mu(CH_3CCl_3)$	(Debye)		1.78	1.78	1.78	
Residual				1416	93	

a) For C_2Cl_6, A_{obsd} is measured in solution of carbon disulfide, and should not be compared directly with A_{calcd}.

Band intensities thus calculated in terms of twenty-four parameters (Calcd I) are listed in Table 7, compared with the observed values, where intensities of C_2Cl_6 have been calculated using the determined values of parameters as described above. Agreement between calculated and observed values is satisfactory on the whole, but considerable disagreement is found in several bands,

22) L. A. Gribov and E. M. Popov, *Opt. Spectry.*, **12**, 304 (1962).
23) L. A. Gribov, "Intensity Theory for Infrared Spectra of Polyatomic Molecules," Consultants Bureau (1964).
24) R. H. Wiswall and C. P. Smyth, *J. Chem. Phys.*, **9**, 356 (1941).

This is the same situation as in the case of the chlorinated methanes reported in our previous paper.[1] That is, intensities for bands associated with the C–Cl bonds are well represented in terms of the above parameters, while in some bands associated with the C–H or C–D bonds, the calculated intensities are very much lower than the observed values. The disagreement in the CH_3 or CD_3 degenerate stretching in ethanes and rocking bands in methyl chloroforms is especially remarkable.

In order to revise such deficiency, it will be necessary to adjust some parameters separately for each molecules. In the case of chlorinated methanes treated in our previous paper,[1] similar disagreements in calculated intensities of some bands were encountered, and in order to get over such difficulties, two parameters μ_{CH} and $\delta\mu_{CH}/\delta r_{CH}$ were separately adjusted for each molecule. As a result, it has been proved that these two parameters may really be effective and sensitive in interpreting the observed intensities. And it has also been found that the adjustment of parameters other than μ_{CH} or $\delta\mu_{CH}/\delta r_{CH}$ was not effective for the satisfactory explanation of observed intensities. Therefore, in order to fit the calculated intensities of the $CH_3(CD_3)$ degenerate rocking bands of CH_3CCl_3 (CD_3CCl_3) to the observed values, it is considered effective to assign different values to μ_{CH} for ethanes and methyl chloroforms, and in order to resolve large discrepancies in the $CH_3(CD_3)$ degenerate stretching band intensities of ethanes, it is considered effective to assign different values to $\delta\mu_{CH}/\delta r_{CH}$. It may be considered less effective to adjust other parameters for resolving the discrepancies in intensities.

Hence, next calculation based on these considerations has been carried out using the least squares method to adjust the twenty-six parameters, of which μ_{CH} and $\delta\mu_{CH}/\delta r_{CH}$ are assumed to take different values for ethanes and methyl chloroforms (Calcd II). The calculated intensities are given in Table 7, compared with the observed values and the calculated values obtained in Calcd I. It is seen that the agreement is much improved and large discrepancies in the CH_3 (CD_3) degenerate stretching and rocking band intensities are successfully resolved in this calculation. The value 93 of the residual, sum of weighted deviations, in Calcd II is much smaller than the value 1416 in Calcd I. This shows that the average difference between observed and calculated intensities in Calcd II is about twice as large as the experimental errors of the intensity measurement.

As mentioned in Experimental, since the vapor phase spectrum of C_2Cl_6 was not observed because of its very low pressure, the band intensities were measured in solution of carbon disulfide. Therefore, the calculated intensities for C_2Cl_6 listed in Table 7 correspond to the intensities to be measured in the vapor phase, and should not be compared with the intensities observed in solution which are also shown in parentheses in Table 7 only as the information.

In Table 8, converged values and their standard deviations in most acceptable sets are given for intensity parameters for Calcd I and II. Parameters with asterisks in the table are fixed at zero in the least squares calculation. Among these parameters, μ_{CC} may probably have some finite value especially in the case of CH_3CCl_3. However, its value can by no means be determined here because too many parameters are taken in this case. Therefore the values determined for the other parameters should be considered to be valid only under the postulation of negligence of μ_{CC}. Although this is indeed a very disagreable ambiguity, this is inevitable at the present stage of such intensity studies. In the treatment of many other molecules, it will be probable to obtain experimental facts which give us a clearer knowlegde about μ_{CC}.

TABLE 8. CONVERGED VALUES AND THEIR DEVIATIONS OF INTENSITY PARAMETERS (D, or D/Å)

Parameter	Calcd (I)	Calcd (II)
μ_{CH} (C_2H_6)	0.28 (0.04)	0.35 (0.02)
μ_{CH} (CH_3CCl_3)		0.49 (0.05)
μ_{CCl}	−1.47 (0.05)	−0.93 (0.98)
$\mu_{CC}(CH_3CCl_3)$	0.00*	0.00*
$\delta\mu_{CH}/\delta r_{CH}$ (C_2H_6)	0.57 (0.06)	0.88 (0.01)
$\delta\mu_{CH}/\delta r_{CH}$ (CH_3CCl_3)		0.28 (0.04)
$\delta\mu_{CH}/\delta r'_{CH}$	0.33 (0.03)	0.17 (0.01)
$\delta\mu_{CH}/\delta r_{CC}$	0.00*	0.00*
$\delta\mu_{CH}/\delta\alpha_{HCH}$	0.27 (0.06)	0.38 (0.02)
$\delta\mu_{CH}/\delta\alpha'_{HCH}$	0.00*	0.00*
$\delta\mu_{CH}/\delta\alpha_{HCC}$	−0.00 (0.03)	0.04 (0.01)
$\delta\mu_{CH}/\delta\alpha'_{HCC}$	0.00*	0.00*
$\delta\mu_{CCl}/\delta r_{CCl}$	−2.33 (0.30)	−2.28 (0.25)
$\delta\mu_{CCl}/\delta r'_{CCl}$	−0.16 (0.22)	−0.19 (0.20)
$\delta\mu_{CCl}/\delta r_{CC}$	0.00*	0.00*
$\delta\mu_{CCl}/\delta\alpha_{ClCCl}$	1.36 (0.46)	1.85 (0.66)
$\delta\mu_{CCl}/\delta\alpha'_{ClCCl}$	0.00*	0.00*
$\delta\mu_{CCl}/\delta\alpha_{ClCC}$	0.70 (0.67)	1.24 (0.39)
$\delta\mu_{CCl}/\delta\alpha'_{ClCC}$	1.97 (0.39)	1.50 (0.65)
$\delta\mu_{CC}/\delta r_{CC}$	0.86 (0.10)	0.86 (0.09)
$\delta\mu_{CC}/\delta r_{CH}$	−0.18 (0.04)	0.02 (0.04)
$\delta\mu_{CC}/\delta r_{CCl}$	−0.15 (0.22)	−0.15 (0.22)
$\delta\mu_{CC}/\delta\alpha_{HCH}$	0.00*	0.00*
$\delta\mu_{CC}/\delta\alpha_{HCC}$	0.20 (0.02)	0.06 (0.04)
$\delta\mu_{CC}/\delta\alpha_{ClCCl}$	0.00*	−0.00 (0.00)
$\delta\mu_{CC}/\delta\alpha_{ClCC}$	0.30 (0.20)	0.33 (0.21)

Asterisks indicate the parameters fixed at zero in the least squares calculation.

It can be deduced that in Calcd II, a slight difference in converged values for μ_{CH} of ethanes and of methyl chloroforms is found but this is the very reason for the successful explanation of the CH_3 (CD_3) degenerate rocking band intensities in these molecules. That is, μ_{CH} is a very sensitive parameter to interpret the band intensity, and consequently, it has proved that it is not possible to find out a value commonly applicable to ethanes and methyl chloroforms for this parameter.

A similar situation is also found in the derivative $\delta\mu_{CH}/\delta r_{CH}$. The fact that some difference in $\delta\mu_{CH}/\delta r_{CH}$ for ethane and methyl chloroform obtained in Calcd II is quite similar to the chlorinated methanes,[1] hence, assigning different values to this parameter for each molecule is necessary for a successful explanation of the CH_3 (CD_3) degenerate stretching band intensities of these molecules.

Some comment has to be made here with respect to the significance of the converged values of the intensity parameters as listed in Table 8. As mentioned in our previous papers[1,3] as well as pointed out by Gribov himself,[25] the valence-optical theory used here has an essential disadvantage which seems to be almost fatal. Too many electro-optical parameters have to be taken into account, and furthermore, due to the fact that they always appear in forms of linear combinations in intensity expressions, individual value of each parameter can not be determined. This is attributed to an assumption that a molecular dipole moment is decomposed as a vector sum of bond dipole moments, in interpreting the band intensity data in terms of intensity parameters.

If one takes a viewpoint in which significant or meaningful quantities are derived from the infrared intensity data, such decomposition is certainly broken down, and one relies upon the treatment as in the serial works by Crawford and his collaborators. In their treatment, the infrared intensity data are interpreted in terms of parameters which are derivatives of the molecular dipole moment with respect to various symmetry coordinates. However, analyses in their studies are restricted within different isotopic species of a certain molecule, and infrared intensity data of various molecules can not be interpreted with their approach. Because the intensity parameters used in their analysis are chracteristic of a molecule as a whole and cannot be transferred among various molecules since both μ and S_i in $(\delta\mu/\delta S_i)$ (where μ is a molecular dipole moment and S_i is the i-th molecular symmetry coordinate) are quantities inherent to a framework of a molecule as a whole.

If one attempts to interpret the intensity data of different molecules in terms of the least number of common parameters, such parameters have to be associated with the bond property. Because the conception of "bond" is most natural and general for chemists in considering some properties of various kinds of different molecular species. In the classical "bond moment hypothesis" used in the previous infrared studies, all bond moments are assumed to depend only on the variation of their own bond lengths. On this basis, many calculations have been carried out for bond moments and their derivatives with respect to the stretching of their bonds, using the experimental results of the band intensities. However, with this approximation, it was very often encountered that different sets of values were obtained for bond moments and/or bond derivatives from sets of the band intensities belonging to different symmetry species, and that the vector sum of bond moments was not equal to the total permanent dipole of the molecule. This fact suggests that this approximation is too rough to explain the observed intensities.

Taking into account the dependence of a bond dipole on the variation of its neighboring internal coordinates, Gribov *et al.* pointed out the necessity of introducing the moment derivatives with respect to some neighboring internal coordinates. This improvement is quite reasonable from the viewpoint of the necessary variation in electron distribution with the displacements of atoms in vibration. This valence-optical theory is an extension of the classical bond moment hypothesis which is designated as the zero-order approximation of the valence-optical theory according to Gribov. That is, in addition μ_i and $\delta\mu_i/\delta r_i$ determined in the classical theory, more electro-optical parameters $\delta\mu_i/\delta r_j$ and $\delta\mu_i/\delta\alpha_{jkl}$ are to be determined using the observed band intensity data. As mentioned above, those parameters cannot be obtained individually, but merely their linear combinations can be determined from the intensity calculations as a disadvantage of this theory.

The form of the linear combinations in which the parameters take part, is dependent on the framework of the molecule as a whole, and is different from molecule to molecule. Hence, if the assumption that the electro-optical parameters may take the same values independent of the molecular species is accepted, some of the parameters are to be determined by solving simultaneous equations of linear combinations of the parameters. Values thus determined for the parameters are qualified to explain the observed intensity data of various different molecules. The converged values given in Table 8 implies such significance, although they still depend on values at which undeterminable parameters should be fixed. Since no unambiguous answer can be given to the question which parameters among several undeterminable parameters should be fixed at what values, it is reasonable to fix less important parameters at zero, using some chemical intuition or taking into account the potential energy matrix element.[1,3] Therefore it is concluded that the converged values in Table 8 are necessary and sufficient to interpret the infrared intensity data of ethanes and methyl chloroforms. And, even though the above parameters μ_{CH} and $\delta\mu_{CH}/\delta r_{CH}$ may also be linearly combined with some other parameters and only values of those linear combinations may be determined definitely, it is considered to be very probable that these two parameters may really be effective and sensitive in interpreting the band intensity data, as was already experienced in the case of chlorinated methanes.[1]

For several parameters common to the chlorinated methanes and ethanes, results are summarized in Table 9. This shows clearly the above conclusion that in

Table 9. Parameters common to chlorinated methanes and ethanes (D, or D/Å)

Species	μ_{CH}	$\frac{\delta\mu_{CH}}{\delta r_{CH}}$	μ_{CCl}	$\frac{\delta\mu_{CCl}}{\delta r_{CCl}}$
CH_4	0.95	0.54		
CH_3Cl	0.59	0.34		
CH_2Cl_2	0.13	0.10	−1.32	−2.86
$CHCl_3$	0.09	−0.06		
CCl_4				
C_2H_6	0.35	0.88		
CH_3CCl_3	0.49	0.28	−0.93	−2.28
C_2Cl_6				

Results for chlorinated methanes are taken from Set (A) in Table 9 of Ref. 1, and for ethanes, from Calcd II in Table 8 of this paper.

25) L. A. Gribov, *Opt. Spectry.*, **25**, 53 (1968).

order to explain the band intensity data of various chlorinated ethanes as well as methanes in terms of as few common intensity parameters as possible,, most parameters may take common values transferable to various molecular species, but it is not possible to find out commonly applicable values for the two parameters μ_{CH} and $\delta\mu_{CH}/\delta r_{CH}$ for the various chlorinated methanes and ethanes. Furthermore, this may suggest that bond properties in the C–H bonds in these molecules vary from one to another much more than in C–Cl bonds. These conclusions might be confirmed by the quantum-chemical approach such as the CNDO techniques.

BULLETIN OF THE CHEMICAL SOCIETY OF JAPAN, VOL. 45, 38—42(1972)

Study of Grinding Reaction of the System of Fine Particle Silica and Basic Zinc Carbonate by X-Ray Silicon K-Emission Band Spectra[1]

Muneyuki MOTOYAMA and Genzo HASHIZUME
Industrial Research Institute of Hyogo Pref., Suma-ku, Kobe

(Received May 17,1971)

Usefulness of X-ray emission spectrometry was demonstrated in a study of the grinding reaction of the system of fine particle silica and basic zinc carbonate. Si$K\alpha$ bands of the ground mixtures shifted toward the lower energy side relative to that of the fine particle silica, whearas Si$K\beta$ bands toward the opposite side. These band shifts were regarded as a measure of the reaction progress. The Si$K\beta$ band shift was shown more distinctly than the $K\alpha$ band shift and explained as come from a decrease in the *s*-character of the bond caused by the chemical bonding of the zinc atom with the fine particle silica. The $K\beta$ band shift was also correlated with the destabilization energy relative to the fine particle silica after C. G. Dodd and G. L. Glen. The band shifts indicated that the final product of this grinding reaction was amorphous zinc silicate-like compound. The correspondence of the X-ray band shifts with the infrared spectral shifts was also shown.

Solid structures of materials are distorted by a mechanical treatment such as grinding, rolling, or crushing.[2] This sort of structural distortions gives samples physicochemical activities and, when mixtures of more than two chemicals are subjected to such a mechanical treatment, chemical reactions occur in some cases.[3] The chemical state of each species in the ground mixture is not easily known. It can hardly be measured whether some species become chemically bounded or not.

X-Ray emission and absorption spectra originate in electronic process, so that, to a first approximation, they are not affected by physical states and reflect electronic structures of materials. Many studies have been made of the chemical effects on the X-ray spectra, particularly for third-period elements such as magnesium, aluminum, and silicon.[4] This paper describes an experimental application of X-ray emission spectra to studying amorphous ground mixtures of fine particle silica and basic zinc carbonate. A correspondence of the X-ray method with infrared spectroscopic method is also shown.

Experimental

Materials and Grinding Procedure. Basic zinc carbonate was used in commercial grade. The samples of fine particle silica named Nipsil VN-3, Carplex #1120 and Aerosil were obtained from Nihon Silica Co. Ltd., Shionogi Seiyaku Co. Ltd., and Degussa Inc., respectively. Some properties of these kinds of silica were shown in Table 1. Amorphous zinc silicate was obtained from Kantoo Chemical Co., Ltd. Crystalline zinc silicate was prepared by heating amorphous zinc silicate for two hours at 950°C in an electric furnace. A mixture of 3 g of the basic zinc carbonate and 2 g of the fine particle silica was dry-ground in an automatic mortor for a desired time. The grinding process was monitored with the X-ray diffraction diagram of basic zinc carbonate in the ground mixture.

TABLE 1. SOME PROPERTIES OF FINE PARTICLE SILICA

Fine particle silica	Particle size Å	Specific surface area m^2/g	pH
Nipsil VN-3	160	240	6.2
Carplex #1120	100	110	10.5
Aerosil	200	200	4.0

Apparatus and Measurements. A Rigakudenki Geigerflex fluorescent X-ray spectrometer equipped with a type D9C constant potential X-ray generator and with a type KG5 goniometer was used for the X-ray emission measurements.

1) Study on the Grinding Effect on the Mixtures. II. Part I of this series: G. Hashizume and K. Amita, *Kogyo Kagaku Zasshi*, **71**, 1379 (1968).

2) H. Takahashi and K. Tsutsumi, This Bulletin, **40**, 7 (1967); I. Motooka, G. Hashizume, and M. Kobayashi, *J. Phys. Chem.*, **73**, 3012 (1969); I. Motooka, *Dissertation*, Osaka Univ. (1969); G. B. Alexander, *J. Phys. Chem.*, **61**, (1957); H. Takahashi, This Bulletin, **31**, 275 (1958); *ibid.*, 235, 245, 252 (1959).

3) F. M. Acampora, A. S. Tompa, and N. O. Smith, *J. Chem. Phys.*, **24**, 1104 (1956); R. Rasch, *Ber. Deut. Keram. Ges.*, **40**, 635 (1963); G. Hashizume, *Dissertation*, Osaka City Univ. (1963).

4) D. M. Koffman and S. H. Moll, *Advance X-ray Anal.*, **9**, 323 (1966); E. W. White and G. V. Gibbs, *Amer. Mineral.*, **54**, 931 (1969); N. D. Savchenko, P. V. Gel, and V. P. Tsvetkov, *Ukr. Fiz. Zh.*, **15**, 835 (1970); C. G. Dodd and G. L. Glen, *J. Appl. Phys.*, **39**, 5377 (1968); G. Widch, "Soft X-Ray Band Spectra and the Electronic Structure of Metals and Materials," ed. by D. J. Fabian, Academic Press, London and New York (1968); D. W. Fischer and W. L. Baun, *Advance X-Ray Anal.*, **10**, 374 (1966).

The chromium target of Philips PW2164 X-ray tube operated at 50 kV and 40 mA was used for the excitation. The silicon K-emission spectra were analyzed with a flat crystal of EDDT cut for its (020) plane ($2d$=8.808 Å). The detector was a cylindrical gas flow proportional counter with a 2 μ thick polypropyrene film, where counting gas was a 90% argon-10% methane mixture and a voltage of 1920 V was applied. A pulse height analyzer was used for improving peak-to-background ratios. The X-Ray chamber was kept vacuum of less than 10^{-2} mmHg during the measurements. Two Soller collimators were used. Each of the entrance collimator of 100 mm long and the receiving collimator of 30 mm long had a 0.15 mm vane spacing. The band profiles of the silicon K-emission spectra were measured by counting X-ray intensities at every 1/100° (2θ) for $K\alpha$ and 5/100° (2θ) for $K\beta$ band. Instrumental drifts including that by a temperature change were monitored by measuring a standard fine particle silica for every five samples.

The X-ray diffraction diagrams were recorded with a Geigerflex X-ray diffractometer. Nickel-filtered copper $K\alpha$ line excited at 40 kV and 10 mA was used with a scanning speed of 1° (2θ) per min, a divergence slit of 1°, and a receiving slit of 3 mm.

Infrared spectra were measured with a spectrometer type DS-403G (Japan Spectroscopic Co., Ltd.) equipped with grating monochrometers. The ground products were suspended in liquid paraffin and held between two potassium bromide plates for the measurements.

Results

The X-ray diffraction diagrams of the ground mixtures are shown in Fig. 1 in which diffraction peaks corresponded to those for basic zinc carbonate. The crystalline structure of the basic zinc carbonate seems distorted with an increase of grinding time, and the ground mixture becomes wholly amorphous after about 300 hours' grinding. In the early stages of the grinding treatment, however, the intensities of the diffraction peak at 35.9° (2θ) increase as shown in Fig. 2. But it is not evident that these changes of the diffraction diagrams are correlated with some grinding reactions. The X-ray diffraction diagrams may not give further information about any grinding reactions.

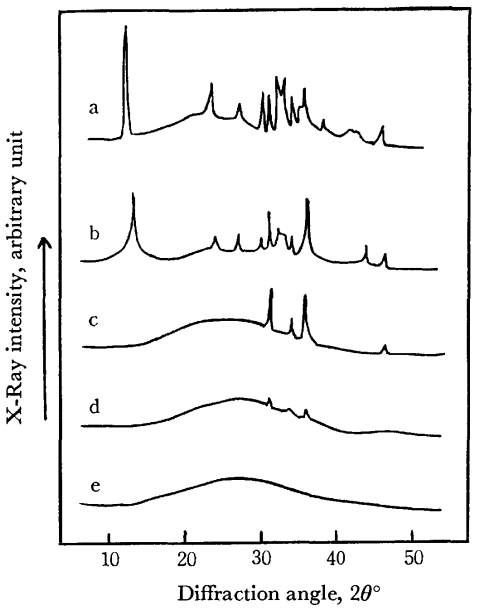

Fig. 1. X-ray diffraction diagrams of the ground mixtures of the fine particle silica and the basic zinc carbonate. Diagrams from a to e correspond to the grinding times for 0, 24, 90, 300, and 600 hr, respectively.

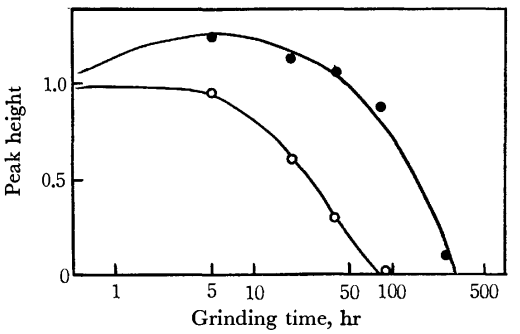

Fig. 2. Variation of diffraction peaks with the grinding time. The peak heights are the relative value to a non-treated mixture of the fine particle silica and the basic zinc carbonate.
●: Peak at 35.9° (2θ)
○: Peak at 12.4° (2θ)

X-Ray Emission Spectra. The Si K-emission spectra of the fine particle silica and the zinc silicate are shown in Fig. 3. In these spectra, both the $K\alpha$ and the $K\beta$ bands are normalized in such a way that each maximum is made as taking a uint intensity. When compared with those for the fine particle silica, the $K\alpha$ band of the zinc silicate shifts toward the lower energy side, whearas the $K\beta$ band toward the higher energy side. Any differences among the K-emission spectra of Nipsil VN-3, Aerosil and, Carplex # 1120 were not observed in this experiment. A satellite band, $K\beta'$, at the lower energy side of the main $K\beta$ band also shifted, but its intensity was too weak to be studied. Although the $K\alpha$ band was also accompanied by some satellite bands, the resolving power of the instrument was not satisfactory and it was difficult to determine their pre-

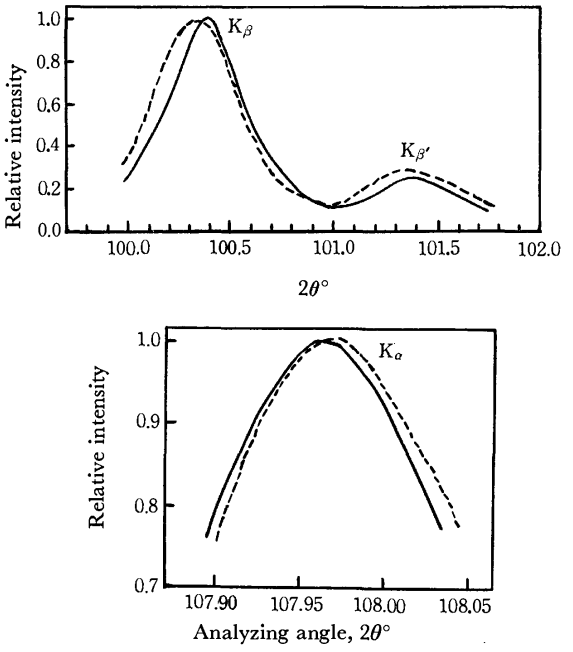

Fig. 3. Silicon K-emission spectra: Solid and dashed lines show spectra of fine particle silica and zinc silicate, respectively. The peak heights are normalized.

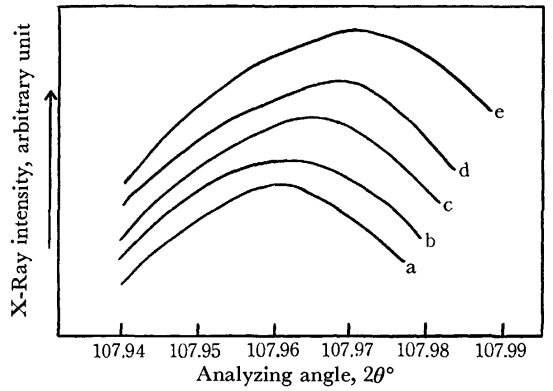

Fig. 4. Variation of Si$K\alpha$ bands of the ground mixtures of the fine particle silica and the basic zinc carbonate with the grinding treatment. Spectra from a to e correspond to the grinding times of 0, 46, 93, 160, and 610 hr, respectively.

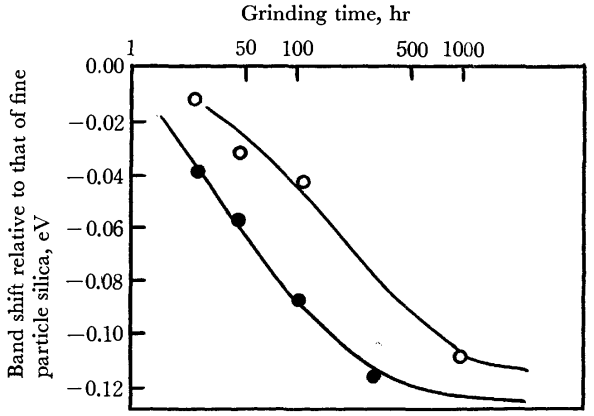

Fig. 5. Si$K\alpha$ band shifts with the grinding treatment
●: System of Nipsil VN-3 or Aerosil and basic zinc carbonate
○: System of Carplex #1120 and basic zinc carbonate

cise band profiles and positions. Therefore, only the main $K\alpha$ and $K\beta$ bands were used for the present study.

The $K\alpha$ bands of the ground mixtures measured at the various stages of the grinding treatment are shown in Fig. 4 in which the peak maxima are illustrated. The shifts of the $K\alpha$ band of the ground mixture from that of the fine particle silica are expressed in electron volts and plotted against the grinding time as shown in

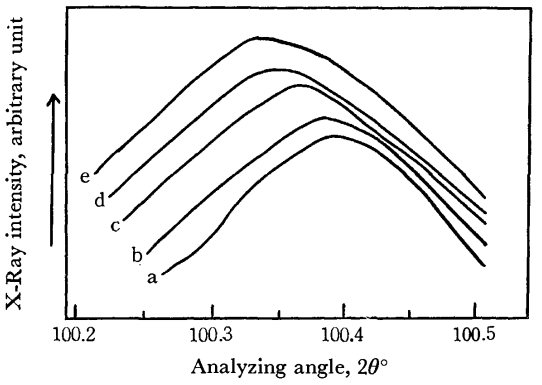

Fig. 6. Variation of Si$K\beta$ bands of the ground mixtures of the fine particle silica and the basic zinc carbonate with the grinding treatment. Spectra from a to e correspond to the grinding time of 0, 46, 93, 160, and 610 hr, respectively.

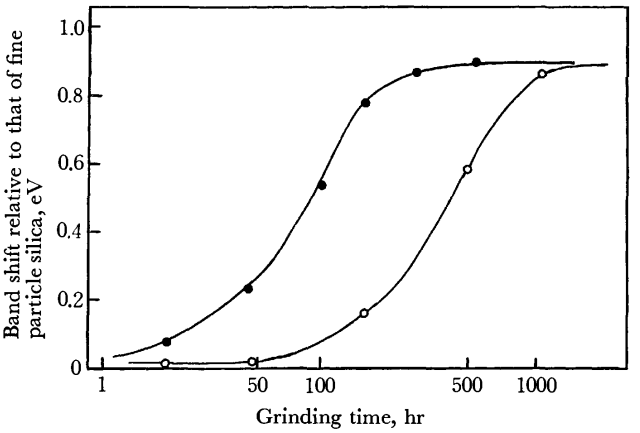

Fig. 7. Si$K\beta$ band shifts with the grinding treatment.
●: System of Nipsil VN-3 or Aerosil and basic zinc carbonate
○: System of Carplex #1120 and basic zinc carbonate

Fig. 5. The $K\alpha$ band shifts are not so large that each electron volt value plotted lacks accuracy. However, a distinct difference can be seen in the reactivities of Nipsil VN-3 or Aerosil and Carplex #1120. This fact would become more evident in the measurement of the Si$K\beta$ bands showing relatively large spectral shifts.

Figure 6 shows the Si$K\beta$ bands of the ground mixtures near the peak maxima measured at the various stages of the grinding treatment. A plot of the spectral shifts against the grinding time is also shown in Fig. 7 in which the $K\beta$ band shifts are increased about one order of magnitude compared with the $K\alpha$ band shifts. Figure 7 indicates that the grinding reaction of Nipsil VN-3 or Aerosil with the basic zinc carbonate proceeds for about 300 hr. Thereafter, the rates of this reaction become very small and finally not appreciable after about 500 hr. On the other hand, Carplex #1120 reacts quite late as the final state is obtained with more than 1,000 hr of the grinding treatment.

Infrared Spectra. Infrared spectrometry also provided useful information about the grinding reaction. This is demonstrated in Fig. 8. With increasing the grinding time, the stretching absorption band of Si–O

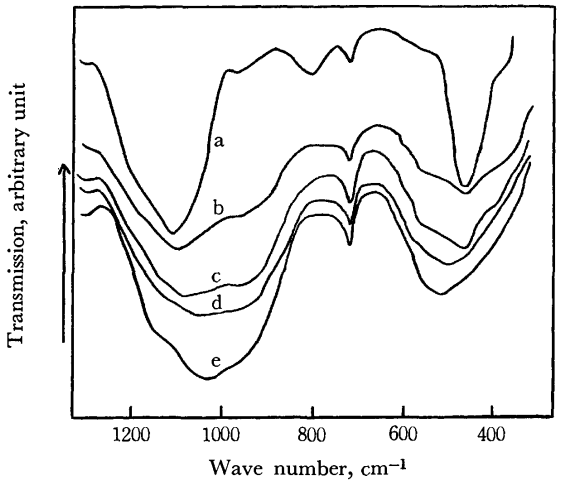

Fig. 8. Infrared spectra of the ground mixtures of the fine particle silica and the basic zinc carbonate. Spectra from a to e correspond to the grinding time of 0, 46, 93, 166, and 610 hr, respectively.

bond shifts toward the lower energy side and the bending one toward the opposite side. Although this figure represents the reaction system of Nipsil VN-3 and the basic zinc carbonate, the same was true for the case of the other samples of the fine particle silica.

Discussion

White and Gibbs found a correlation between the mean Si–O bond lengths of various silicate minerals and their Si$K\beta$ band shifts from the Si$K\beta$ band of quartz.[5] They used quartz as a standard sample for the determination of wavelength shifts, whereas fine particle silica was used for the same purpose in the present measurement. However no differences in wavelength of the Si$K\beta$ bands were observed between the fine particle silica and quartz in the present measurement, so that values of Si$K\beta$ band shifts in their report may be regarded as in the same scale as in the present study.

Thus the variation of the mean Si–O bond length can be correlated with the time of the grinding treatment as shown in Fig. 9, in which their data were adopted in such a way that the linear correlation coefficient should be 0.85.[5] The mean Si–O bond length is also correlated with the mean coordination number of oxygen as reported by Brown and Gibbs.[6] The increase in the oxygen coordination number corresponds to the less s-character in a bond as a result of the withdrawal of the electrons on oxygen when zinc atom comes to make a chemical bond with silica.

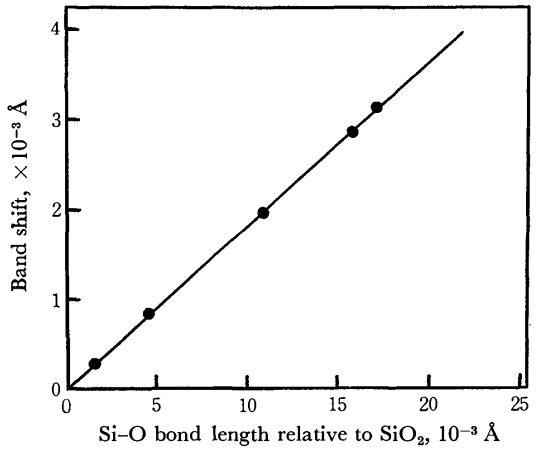

Fig. 9. Relation between Si$K\beta$ band shifts and Si–O bond lengths of the ground mixtures of the fine particle silica and the basic zinc carbonate. A correlation coefficient is 0.85 after White and Gibbs.[5]

The situation is also reflected in the infrared absorption spectra, because an increase in the oxygen coordination number causes a variation in O–Si–O bond angle. The bending absorption bands shift toward the higher energy side with increasing the grinding time in Fig. 8. If the zinc atoms are, in fact, chemically bound with the oxygen atoms in silica, the shifts in the infrared absorption bands may be compared with those in the Si$K\beta$ X-ray bands. Although the infrared absorption band in Fig. 8 is composed of more than two single bands, its absorption position in wave number was, for convenience, graphically determined as shown in Fig. 10. Figure 11 is a plot of the shifts in the bending absorption bands relative to the fine particle silica against those of the Si$K\beta$ bands. A linear relationship is evident between the two spectroscopic measurements. This suggests that these variations in the individual spectrum result from the same chemical effects as mentioned above.

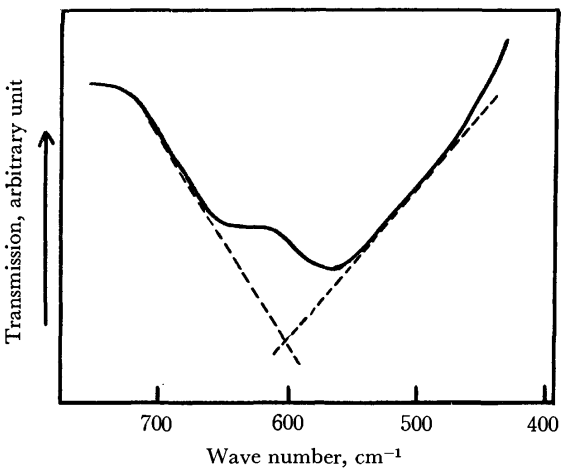

Fig. 10. Graphical method for the determination of infrared band position. Wave number at which two dashed lines intersect is adopted, for convenience, as a band position.

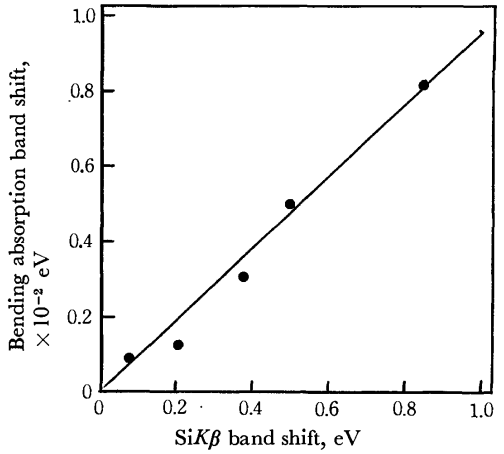

Fig. 11. Relation between X-ray Si$K\beta$ band shifts and infrared bending absorption band shifts relative to that of fine particle silica.

Cauchois[7] and Fischer[8] assumed the Si$K\beta$ bands of the oxides of magnesium, aluminum, and silicon to be due to the crossover transitions which originate from the anion or oxygen and terminate in the metal ion. Their assumption gives a relatively easy interpretation of the influence of zinc atoms on the Si–O bond. As the zinc atoms come to make chemical bonds with the oxygen atoms which are nearly tetrahedrally coordinated around the silicon atom, the Si–O bond will

5) E. W. White and G. V. Gibbs, *Amer. Mineral.*, **52**, 985 (1967).

6) G. E. Brown and G. V. Gibbs, *ibid.*, **54**, 1528 (1969).

7) Y. Cauchois, "Soft X-Ray Band Spectra and the Electronic Structure of Metals and Materials," ed. by D. J. Fabian, Academic Press, London and New York (1968).

8) D. W. Fischer, *Advance X-Ray Anal.* **14**, 159 (1970).

become more ionic. This increase in ionic character corresponds to a decrease in the *s*-character of Si–O bond, which causes the Si$K\beta$ bands to shift toward the higher energy side. The interpretation of the $K\alpha$ band shifts are perhaps more complicated because the band shifts are so small that only a slight change in the 1*s* orbital of silicon influences the band shifts.

TABLE 2. DESTABILIZATION OF Si–O BOND BY GRINDING TREATMENT

Grinding time hr	Si$K\beta$ band shift[a)]	Destabilization energy[a)]	
	-10^{-4} Å	eV	kcal/mol
0	0	—	—
19	3.0	0.08	1.8
46	8.4	0.23	5.3
93	19.7	0.54	12.4
160	28.6	0.78	17.9
280	31.5	0.86	19.8
610	33.0	0.90	20.7
Amorphous zinc silicate	33.0	0.90	20.7
Crystalline zinc silicate	37.5	1.02	23.5

a) Relative to Nipsil VN-3 or Aerosil

Another estimation was given by Dodd and Glen[9] that the Si–O bond is stable in the structure of α-quartz, the Si$K\beta$ band of which appears in the lowest energy position of all the silicate structures. Thus the Si$K\beta$ band shift of a certain silicate toward the higher energy side from that of α-quartz is a measure of the degree of Si–O bond destabilization relative to the Si–O bond of α-quartz. This estimation is readily accepted as a measure of the grinding reaction process, because it is not difficult to consider that the ground products are in metastable higher energy states in the sense of chemical bonding. The destabilizations of the ground mixtures relative to the fine particle silica were thus calculated from the X-ray shifts in Table 2 together with those of the synthetic amorphous zinc silicate and the crystalline zinc silicate. This table indicates that the final state in the ground product may result in amorphous zinc silicate and further reaction does not occur by the more grinding treatment. This phenomenon discriminates the grinding reaction or, more generally, the mechanical treatment from the ordinary thermal reaction in which the entire rearrangement of each species take place and the final crystalline product is

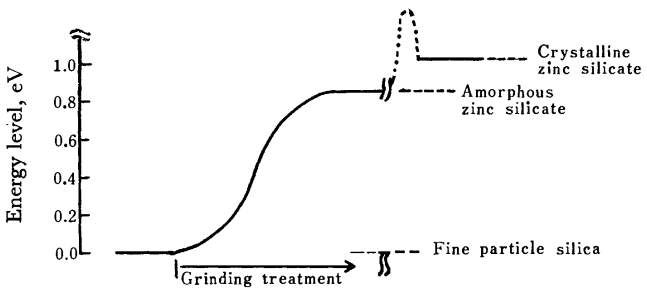

Fig. 12. Schematic illustration of the destabilization of the Si–O bond in fine particle silica.

9) C. G. Dodd and G. L. Glen, *Amer. Mineral.*, **54**, 1299 (1969).

TABLE 3. HALF WIDTH OF Si$K\beta$ BAND OF GROUND MIXTURE

Grinding time hr	Half width[a)]	
	Å	eV
0	0.0225	6.03
19	0.0250	6.79
46	0.0271	7.35
160	0.0271	7.35
610	0.0281	7.62
Amorphous zinc silicate	0.0278	7.54
Crystalline zinc silicate	0.0263	7.15

a) The precision of the measured values should be taken as better than two significant figures, although three are reported in this column.

obtained. This is summarized schematically in Fig. 12.

Further information is obtained with the changes of the Si$K\beta$ band width which are shown in Table 3. The half widths of the crystalline and amorphous zinc silicate are broader than that of the fine particle silica. However, the Si$K\beta$ band widths of the ground mixtures rapidly approach to that of the amorphous zinc silicate whose width is broader furthermore than that of the crystalline zinc silicate. It is notable that, even in the early stages of the grinding reaction, considerable band broadening occurs. On the other hand, considerable band shifts can not be seen in these stages as indicated in Fig. 5 and Fig. 7. Thus even in the early stages of the grinding treatment, chemical reaction may occur to a considerable extent, and with increasing the grinding time, the reaction more thoroughly. Hence the grinding reaction in the early stages of the treatment differs merely in the extent and not in the quality from that of the last stage of the treatment. The Si$K\alpha$ bands did not show so distinct a change in the band widths as seen in the $K\beta$ bands.

Roughly speaking, the changes in the X-ray diffraction diagram correspond to the progress in the grinding reaction described by means of Si*K*-emission spectral shifts in the cases of Nipsil VN-3 and Aerosil but not in the case of Carplex #1120. The surface acidity is critical to the difference of the reactivities of these three kinds of fine particle silica, as seen from Table 1.

Conclusion

The X-ray Si*K* spectra gave useful information about the grinding reaction in which the products are usually amorphous. The $K\beta$ band shifts changed depending on the grinding time which caused the corresponding decrease in the *s*-character in the Si–O bonds. The band shifts indicated that the final product in the reaction between the fine particle silica and the basic zinc carbonate was amorphous zinc silicate-like compound which was in a metastable higher energy state relative to the fine particle silica. The infrared spectra also provided useful information about this reaction but the X-ray spectroscopic method was superior to the former because the latter gave direct reflections of electronic structures.

Re-absorption Effect of Charge-Transfer Fluorescence by the Excited Electron Donor-Acceptor Complex

Hiroshi MASUHARA and Noboru MATAGA

Department of Chemistry, Faculty of Engineering Science, Osaka University, Toyonaka, Osaka

(Received May 19, 1971)

It has been shown that excited electron donor-acceptor (EDA) complexes of *s*-tetracyanobenzene (TCNB) with benzene or toluene can be produced quite densely when excited with a giant pulse laser and that there arises a remarkable re-absorption of the charge-transfer (CT) fluorescence by the excited EDA complexes. We have investigated in detail the re-absorption effect by examining the dependence of the CT fluorescence spectra on the direction of observation, the decay function of the fluorescence, the effect of the concentration of solution as well as the effect of the exciting light intensity on it. The excited singlet-singlet (S_n←S_1) absorption spectra have been obtained by analyzing the re-absorption effect. Since the CT fluorescence spectra are broad and have no structure, the fluorescence can work as a good light source for the absorption spectral measurement.

The nsec flash photolysis has been made possible by using a giant pulse laser as an exciting light source. The absorption spectra of short-lived transient species such as excited singlet state of aromatic molecules produced by excitation with the laser in solution have been determined with some intense flash lamps of short duration. Novak and Windsor used laser-induced sparks in O_2 and Xe gases as spectroflashes and an image-converter camera as a detection apparatus.[1] Porter and Topp used some scintillators as a spectroflash.[2] On the other hand, there are some difficulties in the kinetic analysis of processes in nsec time region. As an example, strong fluorescence spectra caused by the laser excitation often overlap the absorption bands of excited singlet states and the signal to noise ratio in the photoelectric measurement is rather large. Such difficulties have been removed to some extent by applying a Xe flash lamp[2] or a pulsed Xe lamp as a monitoring light source.[3,4]

Recently, we have found a characteristic hollow in time-resolved fluorescence spectra of EDA complexes of TCNB, which is due to the re-absorption of CT fluorescence by excited complex. The S_n←S_1 absorption spectra of TCNB-benzene and TCNB-toluene complexes have been obtained by analyzing the re-absorption.[5] Since the CT fluorescence spectra of TCNB complexes are rather broad and have no structure, the fluorescence can work as a good light source for the absorption spectral measurement. In the present paper, results of investigations concerning the dependence of the CT fluorescence on the direction of observation, fluorescence decay function, effect of the solute concentration as well as the effect of exciting light intensity on the re-absorption of CT fluorescence, will be reported and a theoretical estimation of the re-absorption effect will be given.

Experimental

We used a Q-switched ruby laser (Japan Electron Optics, JLR-02A) with an output of *ca.* 1.5 J. An exciting light pulse of 347 nm was produced through the ADP frequency doubler with conversion efficiency of *ca.* 8%. The output of a 347 nm pulse was measured with a ballistic thermopile TRG model 100 (HADRON). Fluorescence spectra and fluorescence decay curves were observed with a Nalumi R21 spectrograph and an RCA 1P28 photomultiplier. A Tektronix 585 A synchroscope was triggered by a signal from a Hewlett-Packard 5082-4220 photodiode which receives a scattered laser pulse. Fluorescence was observed from the side of the cuvett opposite the laser excitation (rear observation) as well as from a direction perpendicular to the excitation (side observation). The ordinary fluorescence measurement was made with an Aminco-Bowman spectrophotofluorometer. All the chemicals were the same as used before.[5] Solutions were degassed carefully by the usual method.

Results and Discussion

Since the population of the excited EDA complex in the case of laser excitation is much larger than that in ordinary spectrophotometric measurement, there arises strong re-absorption of the CT fluorescence by the excited complex. The following features of the CT fluorescence were found in the case of TCNB-benzene and TCNB-toluene complexes.[5,6] (1) A characteristic hollow appears at about 460 nm in the time-resolved fluorescence spectra at an earlier stage of decay (0—50 nsec). It can be obtained by plotting the fluorescence intensities at various stages of decay. (2) At about 460 nm, the decay curve of the fluorescence is not exponential but has a peculiar shape, while the decay curves are nearly exponential at other wavelengths. Time-resolved fluorescence spectra and typical decay curves are shown in Figs. 1 and 2. They can be ascribed to re-absorption of CT fluorescence by the high density excited state produced by the laser excitation. We have carried out a quantitative estimation of the re-absorption effect as follows.[7]

Spatial Distribution of Excited EDA Complexes. The

1) J. R. Novak and M. W. Windsor, *Proc. Roy. Soc. A*, **308**, 95 (1968).

2) G. Porter and M. R. Topp, *ibid.*, **315**, 163 (1970).

3) R. Mcneil, J. T. Richards, and J. K. Thomas, *J. Phys. Chem.*, **74**, 2290 (1970).

4) C. R. Goldschmidt, M. Ottolenghi, and G. Stein, *Israel J. Chem.*, **8**, 29 (1970).

5) H. Masuhara and N. Mataga, *Chem. Phys. Letters*, **6**, 608 (1970).

6) H. Masuhara and N. Mataga, "The Electronic Structure of the Electron Donor-Acceptor Complex in its Lowest Excited Singlet State," *Z. Physik. Chem. N. F.*, in press.; The 24 th Annual Meeting of the Chemical Society of Japan, Osaka, 1971.

7) In relation to the S_n←S_1 absorption spectra of TCNB complexes, only the final Eqs. (5), (6), (9), (10) were given without any detailed account in Ref. 5.

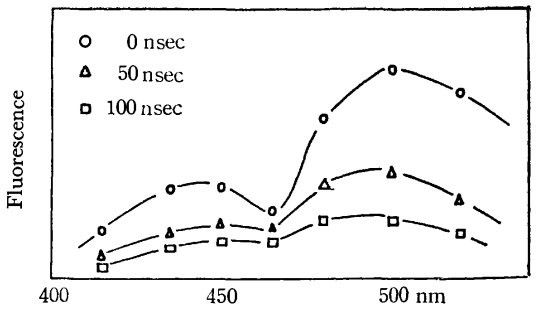

Fig. 1. The time-resolved fluorescence spectra of TCNB-benzene complex in the case of rear observation. $\varepsilon_{g\lambda}c_g=0.8$. In the present paper (Figs. 1, 5, and 7), 0 nsec is used to indicate the time when the concentration of excited complex is the maximum (taken from Ref. 6).

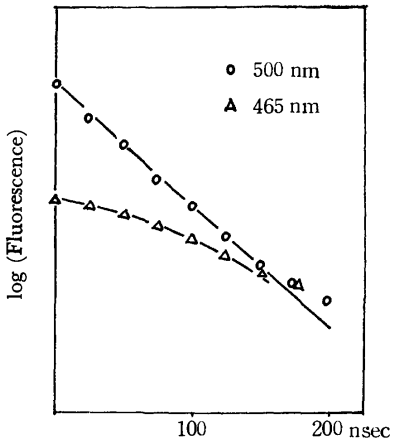

Fig. 2. Observed (○, △) and calculated (——) fluorescence decay curves of TCNB-benzene complex in the case of rear observation. $\varepsilon_{g\lambda}c_g=0.8$ (taken from Ref. 6).

distribution of fluorescent EDA complexes is expected to be proportional to $\Phi_{\lambda 0}10^{-\varepsilon_{g\lambda}c_g x}$, where $\Phi_{\lambda 0}$ is the intensity of 347 nm pulse which is exciting exclusively the CT band of TCNB complexes; x is the distance from the front face of the cell in cm; $\varepsilon_{g\lambda}$ and c_g are the molar extinction coefficient at 347 nm and the concentration of EDA complex in the ground state, respectively. In the present work $\varepsilon_{g\lambda}c_g$ is *ca.* 1.0. However, a deviation of distribution from $\Phi_{\lambda 0}10^{-\varepsilon_g c_{g\lambda} x}$ can be expected, since the high intensity excitation often leads to saturation of absorption in the front part of the sample. We have examined this question by photographing the fluorescing sample cell from a direction perpendicular to the excitation.[8] The obtained film blackening is given in Fig. 3, which shows an approximate linear relation between log I(flourescence intensity) and x. Consequently, it is appropriate to assume that the distribution of the excited EDA complex is proportional to $\Phi_{\lambda 0}10^{-\varepsilon_{g\lambda}c_g x}$.

The distribution of the re-absorbing EDA complex is of course the same as that of the fluorescent EDA complex. The concentration of the excited complex in M, c_e, is given by

8) The authors wish to express their thanks to Prof. Shunji Kato of Osaka University for his helpful discussion on this problem.

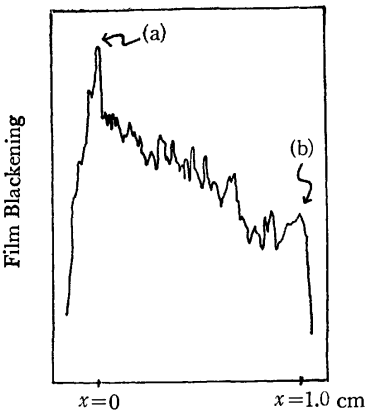

Fig. 3. Film blackening due to the fluorescing sample cell. TCNB-toluene system. $\varepsilon_{g\lambda}c_g=1.67$.
(a) Front. (b) Back.

$$c_e(x) = s\Phi_{\lambda 0}10^{-\varepsilon_{g\lambda}c_g x} \quad (1)$$

where s is a proportionality constant.

Dependence of Fluorescence on the Direction of Observation. In the case of rear observation, since differential fluorescence intensity I_x emitted from the thin layer between x and $x+dx$ can be re-absorbed by the thin layer between y and $y+dy$, the following equation can be obtained.

$$dI_x = -\mu(y)I_x dy \quad (2)$$

where y is the distance from x to the back of the cell in cm and $\mu(y)$ is the absorption coefficient at y. A schematic model for the present analysis is shown in

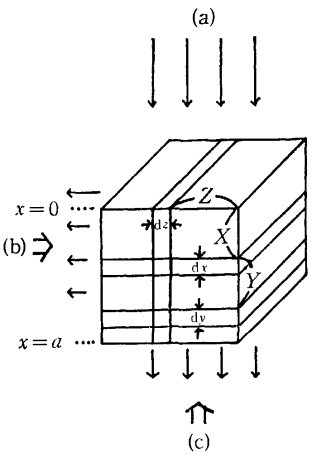

Fig. 4. A schematic model for analysis of the re-absorption of CT fluorescence by excited complex itself.
(a) excitation (b) side observation (c) rear observation.

Fig. 4. Although μ is independent of y in the usual treatment, it is a function of y in the present case and can be written as

$$\mu(y) = \varepsilon_{e\lambda'}c_e(x+y) = \varepsilon_{e\lambda'}s\Phi_{\lambda 0}10^{-\varepsilon_{g\lambda}c_g x}10^{-\varepsilon_{g\lambda}c_g y} \quad (3)$$

where $\varepsilon_{e\lambda'}$ is the molar extinction coefficient of the $S_n \leftarrow S_1$ band at λ' (the wavelength at which the fluorescence is observed). Putting Eq. (3) into Eq. (2) and integrating Eq. (2) with respect to y, the differential fluorescence intensity I_x observed at the back of the cell is given as follows.

$$I_x(y=a-x) =$$
$$10^{-\varepsilon_{g\lambda}c_g x}10^{\log q}10^{\varepsilon_{e\lambda'}s\Phi_{\lambda 0}(10^{-\varepsilon_{g\lambda}c_g a}-10^{-\varepsilon_{g\lambda}c_g x})/\varepsilon_{g\lambda}c_g} \quad (4)$$
$$Q = \rho\Omega\Phi_{\lambda 0}F_\lambda(\lambda')\varepsilon_{g\lambda}c_g/4\pi n^2$$

where ρ, Ω, $F_\lambda(\lambda')$, and n represent reflective index on the surface of the cell, solid angle in which the fluorescence is observed, fluorescence quantum yield observed in the wavelength range $\lambda'\sim\lambda'+d\lambda'$, and refractive index of solvent, respectively. Since we are observing the sum of the differential fluorescence intensities, I_x must be integrated with respect to x from 0 to a. Consequently the fluorescence intensity at λ' in the side opposite the excitation is given as follows.

$$d\Phi'(\lambda') = \int_0^a I_x dx d\lambda'$$
$$= \rho\Omega F_\lambda(\lambda')\varepsilon_{g\lambda}c_g(1-10^{\varepsilon_{e\lambda'}s\Phi_{\lambda 0}(10^{-\varepsilon_{g\lambda}c_g a}-1)/\varepsilon_{g\lambda}c_g})$$
$$\times d\lambda'/4\pi n^2\varepsilon_{e\lambda'}s \quad (5)$$

For notation in these equations, we refer to Förster's treatment.[9] When the excitation intensity $\Phi_{\lambda 0}$ is weak, Eq. (5) is reduced to the usual Eq. (6).[9]

$$d\Phi'(\lambda') = \rho\Omega\Phi_{\lambda 0}F_\lambda(\lambda')(1-10^{-\varepsilon_{g\lambda}c_g a})d\lambda'/4\pi n^2 \quad (6)$$

In the present case, the excitation intensity $\Phi_{\lambda 0}$ is determined to be *ca.* 1.7×10^{17} photons,[10] $\varepsilon_{g\lambda}c_g$ is adjusted to be 1.0, a is 1 cm, and s is calculated to be 2×10^{-21}, assuming the re-absorption extinction coefficient of $S_n\leftarrow S_1$ band at 462 nm $\varepsilon_{e\lambda'}$ to be 10^4. The re-absorption of several tens % of the fluorescence at 460 nm is expected from the estimation by Eqs. (5) and (6) with these values. It is in good agreement with our result.

In the case of side observation, the differential fluorescence intensity I_x can be re-absorbed in the layer between z and $z+dz$. Thus, we have

$$dI_x = -\varepsilon_{e\lambda'}c_e(x)I_x dz \quad (7)$$

The equation is in the same form as the usual Lambert-Beer equation. The fluorescence intensity in the case of side observation is given as follows.

$$d\Phi'(\lambda', x) =$$
$$\rho\Omega F_\lambda(\lambda')\varepsilon_{g\lambda}c_g(1-10^{-a\varepsilon_{e\lambda'}s\Phi_{\lambda 0}10^{-\varepsilon_{g\lambda}c_g x}})d\lambda'/4\pi n^2\varepsilon_{e\lambda'}s \quad (8)$$

where one should note the x-dependence of the fluorescence intensity. Numerical estimation by means of Eq. (8) indicates that at $x\sim0$ cm a re-absorption of several tens % of fluorescence arises as in the case of rear observation, while no appreciable re-absorption effect will be observed at $x\sim1.0$ cm. The results shown in Fig. 5 are in good agreement with this numerical estimation.

9) Th. Förster, "Fluoreszenz Organischer Verbindungen," Vandenhaeck und Ruprecht, Götingen, 1951. p. 35.

10) In Ref. 5 effective excitation intensity $\Phi_{\lambda 0}$ was assumed to be 10^{16} photons per pulse. However, no change of the results in Ref. 5 is required since there was a numerical mistake in calculating s, which cancelled out an error in value. There arises some ambiguity in estimating effective concentration of the excited EDA complex, which is required for calculating s, since the distribution of the excited complex is not uniform. In the present work s was obtained assuming the concentration of the excited complex as $(1.7\times10^{17}/\pi r^2\times a\times6.03\times10^{23})\times10^{-x}$M, where r is an effective diameter of a 347 nm pulse.

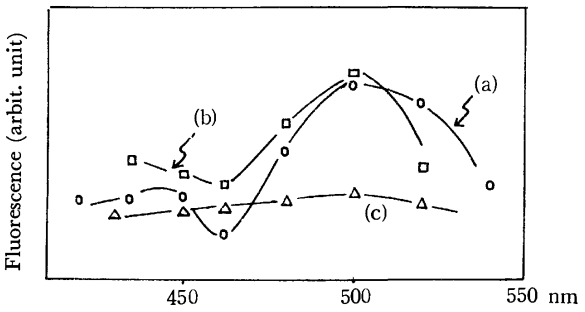

Fig. 5. The fluorescence spectra of TCNB-benzene system (t$\sim$0 nsec) obtained in the case of side observation. $\varepsilon_{g\lambda}c_g=0.8$.
(a) $x\sim0$ cm (b) $x\sim0.5$ cm (c) $x\sim1.0$ cm

Fluorescence Decay Function.[11] Since the coefficients of re-absorption as well as fluorescence follow the exponential decay, the following can be easily derived in the case of rear observation:

$$d\Phi'(\lambda', t) =$$
$$\rho\Omega F_{\lambda 0}(\lambda')\varepsilon_{g\lambda}c_g(1-10^{\varepsilon_{e\lambda'}s_0\Phi_{\lambda 0}e^{-t/\tau}(10^{-\varepsilon_{g\lambda}c_g a}-1)/\varepsilon_{g\lambda}c_g})$$
$$\times d\lambda'/4\pi n^2\varepsilon_{e\lambda'}s_0 \quad (9)$$

where τ is fluorescence lifetime, and $F_{\lambda 0}$ and s_0 satisfy the following equations, respectively.

$$F_\lambda = F_{\lambda 0}e^{-t/\tau}$$
$$s = s_0 e^{-t/\tau} \quad (10)$$

The simulated curves obtained by means of Eq. (9), using the value of lifetime obtained from the fluorescence decay at 500 nm, are given in Fig. 2. One can see a good agreement between experimental and simulated curves. In the case of side observation at $x\sim0$ cm the same nonexponential decay of the fluorescence at λ' as indicated by Eq. (9) is expected, while little deviation of fluorescence decay from the exponential function will occur at $x\sim1.0$ cm. As shown in Fig. 6, the simulated curves can reproduce the experimental ones satisfactorily.

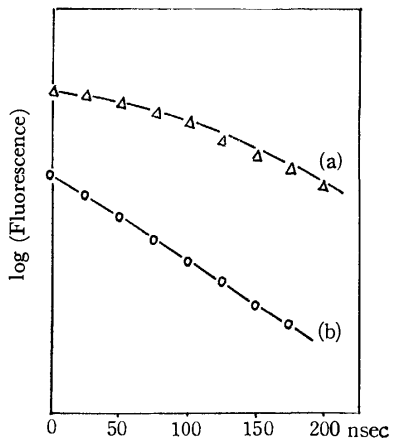

Fig. 6. Observed (○, △) and calculated (——) fluorescence decay curves of TCNB-benzene system at 465 nm in the case of side observation. $\varepsilon_{g\lambda}c_g=0.8$.
(a) $x\sim0$ cm (b) $x\sim1.0$ cm

11) The effect of absorption by excited singlet state as well as triplet state on fluorescence decay function was mentioned in Ref. 2.

Effect of the Concentration of Solution on Re-absorption. Since the CT fluorescence is re-absorbed by the excited EDA complex the characteristic hollow in the fluorescence spectra as well as the nonexponential decay of fluorescence might not be observable under low concentration of the excited complex. The excitation of a low concentration solution of the EDA complex with a laser pulse of moderate intensity as well as low intensity excitation of a solution of mederate concentration will produce excited EDA complexes of rather low concentration. A comparison of the time-resolved fluorescence spectra between solutions of moderate and low concentrations is given in Fig. 7, where the excitation light intensity was moderate and side observation was performed. A characteristic hollow is observed only in the case of rather high concentration solution.

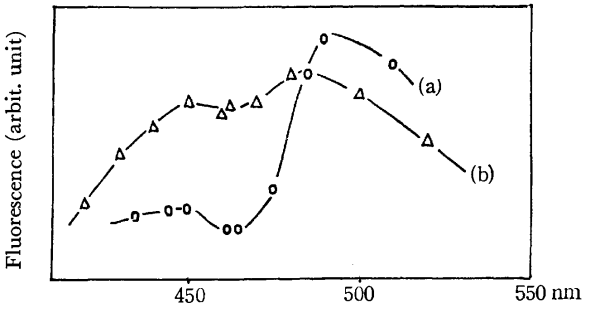

Fig. 7. Concentration dependence of the re-absorption effect in the case of the TCNB-toluene complex. ($t\sim0$ nsec)
(a) $\varepsilon_{g\lambda}c_g=1.67$. (b) $\varepsilon_{g\lambda}c_g=0.16$.

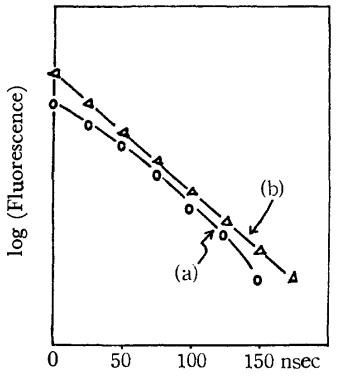

Fig. 8. Effect of the excitation light intensity on the re-absorption. TCNB-benzene system, $\varepsilon_{g\lambda}c_g=0.8$.
Intensity; (a) normal laser excitation (b) 0.3% of the normal value.

Effect of Exciting Light Intensity on Re-absorption. The excitation intensity was varied by neutral filters composed of wire gauzes. The dependence of decay function at 462 nm on the exciting light intensity is given in Fig. 8. When the exciting light intensity was reduced to 0.3% of the normal value (1.7×10^{17} photons/pulse), the observed fluorescence decay was almost exponential.

The $S_n\leftarrow S_1$ Absorption Spectra. From the above results, it is confirmed that a characteristic hollow in the fluorescence spectra of earlier stage of decay and the nonexponential decay at about 460 nm are due to the re-absorption of the fluorescence by the excited singlet state of the EDA complex. Consequently, we can obtain the $S_n\leftarrow S_1$ absorption spectra by comparing the fluorescence spectra observed by an Aminco-Bowman spectrophotofluorometer and those observed by laser excitation. The result in the case of TCNB-benzene complex is given in Fig. 9. For the absorption spectral measurement of the excited complex, the fluorescent light can work as a good light source, the duration of which is the same as the lifetime of the objective transient. Thus, it is concluded that this method is useful for obtaining $S_n\leftarrow S_1$ absorption spectra.

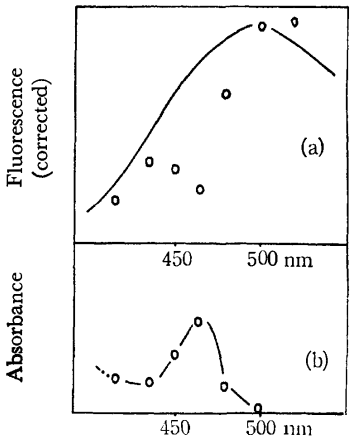

Fig. 9. Fluorescence spectra and $S_n\leftarrow S_1$ absorption spectra of TCNB-benzene complex. $\varepsilon_{g\lambda}c_g=0.8$ (taken from Ref. 6).
(a) Fluorescence spectra measured by laser excitation (○) and by Aminco-Bowman spectrophotofluorometer (—).
(b) $S_n\leftarrow S_1$ absorption spectra.

The conditions necessary for the absorption spectral measurement by this method might be as follows; (1) The optical density at λ can be adjusted to be *ca.* 1.0. (2) The fluorescence and the $S_n\leftarrow S_1$ absorption spectra overlap each other to some extent. (3) The fluorescence lifetime is in the same order as the duration of an exciting pulse, although in order to identify the lifetime of the re-absorbing species with that of the fluorescent one the lifetime of fluorescence must be longer than the duration of the 347 nm pulse. We have a few critical experimental results concerning the above conditions. We have studied the $S_n\leftarrow S_1$ spectra of TCNB-mesitylene complex by the present re-absorption method. However, no appreciable re-absorption was observed, but we were able to measure the $S_n\leftarrow S_1$ spectra of this complex by the nsec flash photolysis method.[6,12] Since the fluorescence lifetime is 43 nsec,[13] which satisfies the condition (3), no observation by the present re-absorption method can be ascribed to the poor overlapping between fluroescence and the $S_n\leftarrow S_1$ absorption spectra. Concerning condition (3), the fluorescence lifetime of TCNB-benzene complex was adjusted by saturating the solution with air. The re-absorption of CT fluorescence was observed in the case

12) H. Masuhara and N. Mataga, The Symposium on Molecular Structures, Kyoto, 1971.
13) T. Kobayashi, K. Yoshihara, and S. Nagakura, The Symposium on EDA Complexes, Osaka, 1970, Preprint.

of this complex, where the shape of the fluorescence light pulse was almost the same as that of the exciting pulse and the apparent lifetime was several nsec. Thus, condition (3) is valid.[14]

Related Problems. When the re-absorption of CT fluorescence by the excited complex itself occurs, higher excited states of the complex will be produced. The rate equation for these processes can be written as

$$\frac{dE}{dt} = -aE - fE + \beta cE^* \tag{11}$$

$$\frac{dE^*}{dt} = \alpha fE - cE^* \tag{12}$$

where E and E^* are concentrations of fluorescent and higher excited states, a and c represent the rate constants of the unimolecular decay of E and E^*, respectively, and f is the rate constant of the re-absorption of CT fluorescence. The notations α and β are the yields of corresponding processes. Since f is proportincal to E, these equations are similar to those used in analyzing the lifetime shortening of exciplexes through bimolecular interaction.[15] In this paper the higher excited state is assumed to return to the fluorescent state through radiationless degradation. Problems on the higher excited states of TCNB complexes as well as those on the interactions of excited complexes through re-absorption of CT fluorescence by the excited complex will be solved with progress of laser experiments.

The authors thank Mr. N. Tsujino for his assistance in the experimental work.

14) The $S_n \leftarrow S_1$ spectra of 1,12-benzperylene-*N*,*N*-dimethylaniline heteroexcimer have been observed in this laboratory. This heteroexcimer is an another good example which satisfies conditions (1)—(3).

15) H. Masuhara and N. Mataga, *Chem. Phys. Letters*, **7**, 417 (1970).

BULLETIN OF THE CHEMICAL SOCIETY OF JAPAN, VOL. 45, 47—51(1972)

Acidic Property and Catalytic Activity of TiO_2·ZnO

Kozo Tanabe, Chijiko Ishiya, Isao Matsuzaki, Ichiro Ichikawa, and Hideshi Hattori
Department of Chemistry, Faculty of Science, Hokkaido University, Sapporo
(Received May 21, 1971)

A new type of mixed metal oxide TiO_2·ZnO was prepared by either heterogeneous or homogeneous co-precipitation and the acidic property was measured by *n*-butylamine titration and by observation of infrared spectra of adsorbed pyridine. It was found that TiO_2·ZnO containing about 7 or 57% of ZnO shows a very large acid amount of 0.5—0.9 mmol/g and a fairly high acid strength of $H_0 \leqq -3$, the acid sites being both Brönsted and Lewis type and the acid sites of high strength created by heterogeneous precipitation. The catalytic activity and selectivity of TiO_2·ZnO were found very high for the hydration reaction of ethylene. The catalyst was active also for the alkylation of phenol by methanol and gave only monoalkylated products.

Metal oxides such as SiO_2·Al_2O_3, SiO_2·MgO, SiO_2·ZrO_2, Al_2O_3·B_2O_3, and Al_2O_3·MgO are known to be solid acid catalysts, each of which contains either SiO_2 or Al_2O_3, both essential constituents of natural clay minerals. The oxides have been extensively used as useful catalysts for various acid-catalyzed reactions in the field of petroleum chemistry. However, not much work has been done on other combinations of oxides, which might show surface acidity and catalytic acitvity, and we have initiated a systematic study on mixed metal oxides which do not contain any clay mineral component. The present paper reports the acidic property and catalytic activity of TiO_2·ZnO, a new combination of metal oxides. Each of TiO_2 and ZnO was previously reported to have only weak acidic property,[1,2] but the combination shows large acid amount and high acid strength as well as high catalytic activity.

1) K. Tanabe and M. Katayama, *J. Res. Inst. Catalysis, Hokkaido Univ.*, **7**, 106 (1959).
2) K. Tanabe and T. Yamaguchi, *ibid.*, **11**, 179 (1964).

Experimental

Preparation of Catalysts. Titanium oxide, zinc oxide, and TiO_2·ZnO of various compositons were prepared respectively by heating titanic acid, zinc hydroxide and the mixtures in air at 200—500° for 3 hr. Titanic acid, zinc oxide and their mixtures were prepared as follows.

1) Titanic Acid; 62.6 m*l* of $TiCl_4$ was dissolved into 120 m*l* of distilled water cooled by ice. To this was added 240 m*l* of distilled water in which 3 m*l* of concd. HCl and 156 g of $(NH_4)_2SO_4$ had been dissolved. The solution was boiled on a water bath for 1 hr and 110 m*l* of 28% ammonia water was added to form the precipitate of titanic acid H_4TiO_4, pH of the solution being 6.67. After the solution had been heated further for 1 hr, the precipitate was filtered off and washed thoroughly with distilled water until no anions of chloride and sulfate were detected in the washing. The precipitate was dried at 90° for 1—2 days.

2) Zinc Hydroxide: A precipitate was formed by adding 56 m*l* of 28% ammonia water into 100 m*l* of water containing 46.9 g of $ZnCl_2$, the final pH of the solution being found to be 6.27. The precipitate was washed and dried as in 1).

Table 1. Conditions for preparation of co-precipitated mixtures 2 and 3

	Co-precipitated mixture 2	Co-precipitated mixture 3
Solution I	137 g $ZnCl_2$ dissolved in 100 m*l* H_2O	261 g $ZnCl_2$ dissolved in 100 m*l* H_2O
Solution II	4 m*l* conc. HCl+210 g $(NH_4)_2SO_4$ in 322 m*l* H_2O	0.4 m*l* conc. HCl+21.0 g $(NH_4)_2SO_4$ in 32 m*l* H_2O
Solution III	84 m*l* $TiCl_4$ in 161 m*l* cooled H_2O	8.4 m*l* $TiCl_4$ in 16.1 m*l* cooled H_2O
Aqueous NH_3	198 m*l*	270 m*l*
Final pH	6.02	7.04

3) Co-precipitated Mixtures 1,2,3,4, and 5 of Titanic Acids and Zinc Hydroxides: Co-precipitated mixture 1 was prepared as follows. 14.0 g of $ZnCl_2$ was dissolved in 30 m*l* of water. 398 g of $(NH_4)_2SO_4$ and 7.6 m*l* of concd. HCl were dissolved in 600 m*l* of water. These were added to 160 m*l* of a solution prepared by dissolving $TiCl_4$ in 306 m*l* of water cooled by ice. The solution was heated on a water bath for 1 hr and 337 m*l* of 28% ammonia water was added to form co-precipitates of the mixture, the final pH of the solution being 7.08. After the solution was heated further for 1 hr, the precipitate was filtered off and washed thoroughly with distilled water until no anions of chloride and sulfate were detected in the washing. It was then dried at 90° for 1—2 days. Weight% of ZnO in the calcined mixture was calculated to be 6.7.

Co-precipitated mixtures 2 and 3 were prepared by adding 28% ammonia water to mixtures of solutions I, II, and III heated on a water bath for 1 hr (see Table 1), and by treating the co-precipitated mixture in a similar way to that for 1. Weight % of ZnO in 2 and 3 was 57.4 and 96.2, respectively.

Co-precipitated mixture 4 was prepared as follows. A cooled solution prepared by dissolving 10 m*l* concd. HCl and 150 g of $(NH_4)_2SO_4$ in 300 m*l* H_2O was added to a cooled mixture of two solutions, one 15.07 g $ZnCl_2$ in 50 m*l* H_2O and the other 69 m*l* $TiCl_4$ in 132 m*l* H_2O. After stirring 150 m*l* of ammonia was added and the solution was then treated in a similar way to that for 1. The final pH of the solution was 7.3. Weight % of ZnO was 15.2.

In the preparation of co-precipitated mixtures 1—3, two thirds of the added ammonia was poured at once and the remaining portion dropwise until the pH of the solution became approximately 7. For 4, all the ammonia was added gradually. The concentration of ammonium hydroxide ion differs locally during the formation of precipitates, *i.e.*, precipitates are formed in a heterogeneous concentration of hydroxide ion. Co-precipitated mixture 5 was prepared by homogeneous precipitation using urea instead of ammonia.[3] By this method, precipitates are formed from homogeneous solution of hydroxide ion, since urea decomposes to give ammonium hydroxide at elevated temperatures according to the formulas.

$$(NH_2)_2CO + H_2O \rightleftharpoons 2NH_3 + CO_2$$
$$NH_3 + H_2O \rightleftharpoons NH_4OH$$

Two solutions, one prepared by dissolving 26.9 m*l* $TiCl_4$ in 51 m*l* H_2O, and the other 5.3 g $ZnCl_2$ in 25 m*l* H_2O, were put into a 5 *l* beaker and the solution was diluted with water to make the volume 5 *l*. 97.2 g of urea was then added and the solution was stirred, the pH being 2. When the solution was heated at 95—98°C for 10—20 min, a fine colloidal and elastic precipitate was formed gradually. The solution was heated further for 2—3 hr until the pH of the solution became approximately 7. The precipitate was filtered off, washed with water until no anions of chloride and sulfate were detected in the washing and then dried at 120—150°C for 1—2 days. The weight % of ZnO was 13.9. All reagents used were of guaranteed grade from Wako Pure Chemical Co.

X-Ray Diffraction. The powder pattern of each specimen was obtained with an X-ray diffractometer ADG-301 DIFF PET, Toshiba electric Co. with filtered Cu$K\alpha$ radiation. The specimen was scanned between 10 and 65° (2θ).

Measurement of Surface Area and Acidic Property. Surface areas of TiO_2, ZnO, and No. 1 and 3 samples of TiO_2·ZnO which were calcined at 200—500° were determined by applying the BET method to the adsorption isotherm of nitrogen at −196°.

The acid amounts and strengths of catalysts were measured by titrating the 100—200 mesh powder suspended in benzene with 0.1N *n*-butylamine benzene solution, using neutral red ($pK_a=6.8$), methyl red (4.8), 4-phenylazo-1-naphthylamine (4.0), *p*-dimethylaminoazobenzene (3.3), benzeneazodiphenylamine (1.5), dicinnamalacetone (−3.0) or benzalacetophenone (−5.6) as indicators.

The Brönsted and Lewis acidity was determined by observing the infrared spectra of pyridine adsorbed on catalyst surface. The catalyst was heat-treated in a glass tube at various temperatures for 3 hr in air and the glass tube was sealed off. Immediately after the tube had been opened, it was connected to a vacuum apparatus and evacuated to 10^{-5} mmHg for 30 min at room temperature. Pyridine (about 2 mmHg) was then introduced and adsorbed for 10 min. After removing the excess of pyridine by evacuating at 100°C for 30 min, 3 mg of the sample was mixed with 200 mg of KBr powder and pressed into tablets of 12 mm diameter using a pressure of approximately 40000 psi. The spectrum in the 1400—1600 cm^{-1} region was measured using a Hitachi EPI-2 infrared spectrophotometer.

Measurement of Catalytic Activity. Hydration of ethylene was carried out by circulating a mixture of ethylene and water vapor (molar ratio:20) through 2 g of TiO_2·ZnO catalyst at 200°C. The ethanol formed was analyzed with a gas chromatograph using a column of silicon DC 550 on celite.

Alkylation of phenol by methanol was carried out by means of the usual flow method at 400°C. The products were analyzed by a gas chromatograph using a column of polyethylene glycol on celite.

Results and Discussion

Acidic Properties and Structures. Acid amounts at various acid strengths of TiO_2, ZnO, and samples 1—3 of TiO_2·ZnO calcined at various temperatures are given in Tables 2 and 3. Titanium oxides calcined at 400—500°C and zinc oxide at 400°C showed an acid strength of $H_0 \leqq +1.5$, which was never observed in their commercial products calcined at any temperature.[1,2] The effects of ZnO content on the acidities of TiO_2·ZnO calcined at 300 and 400°C are shown in Figs. 1 and

3) H. H. Willard and N. K. Tang, *J. Amer. Chem. Soc.*, **59**, 1190 (1937).

Table 2. Acidic property of TiO_2 and ZnO

	Calcination temp., °C	Acid amount, mmol/g					
		$H_0 \leqq$ 6.0	$H_0 \leqq$ 4.8	$H_0 \leqq$ 4.0	$H_0 \leqq$ 3.3	$H_0 \leqq$ 1.5	$H_0 \leqq$ −3
TiO_2	300	—	0.056	—	0.029	0	
	400	—	0.056	—	0.038	0.028	0
	500	—	0.061	—	0.058	0.032	0
	600	—	0.037	—	0.017	0	
ZnO	200	0.37	0.29	0.005	0		
	300	2.07	1.71	—	0.15	0	
	400	2.29	1.81	—	0.52	0.22	0
	500	0.024	0.018	—	0.017	0	

Table 3. Acidic property of TiO_2·ZnO

No. of sample (wt % of ZnO)	Calcination temp., °C	Acid amount, mmol/g				
		$H_0 \leqq$ 4.8	$H_0 \leqq$ 3.3	$H_0 \leqq$ 1.5	$H_0 \leqq$ −3	$H_0 \leqq$ −5.6
No. 1 (7)	200	0.76	0.86	0.83	0.73	0.5—0.4[a]
	300	0.95	1.04	1.04	0.92	
	400	0.64	0.70	0.65	0.57	
	500	0.56	0.59	0.58	0.54	
No. 2 (57)	200	0.39	0.89	0.89	0.84	
	300	0.42	0.93	0.90	0.85	
	400	0.24	0.57	0.53	0.48	
	500	0.28	0.68	0.63	0.50	
No. 3 (96)	200	0.48	0.02	0		
	300	0.95	0.34	0.003	0	
	400	1.72	1.44	1.42	0	
	500	1.35	1.24	1.07	0	

a) End point of titration was not clear. Anthraquinone of $pK_a = -8.2$ did not show its acidic color on the surface.

we see that the acid amounts at various acid strengths become large when TiO_2·ZnO contains about 7 or 57% of ZnO. The acidities of the mixed oxides containing about 96% of ZnO are small when they are calcined at 300°C, but their acid amounts at $H_0 \leqq 3.3$ and 1.5 increase greatly when calcined at 400°C. In both cases of Figs. 1 and 2, fairly strong acid sites of $H_0 \leqq -3.0$ appear only when about 7 or 57% of ZnO is contained in the catalyst. This fact and a comparison of the specific surface areas of TiO_2·ZnO containing

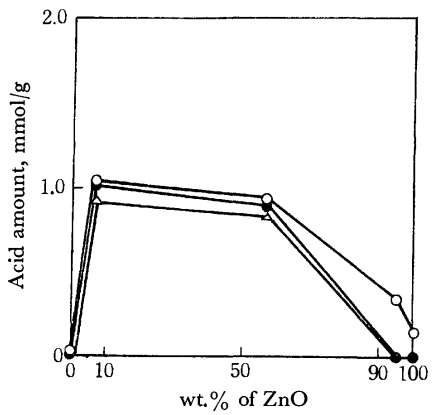

Fig. 1. Acid amounts at various acid strengths of TiO_2·ZnO calcined at 300°C *vs.* wt% of ZnO.
(-○-): $H_0 \leqq 3.3$, (-●-): $H_0 \leqq 1.5$, (-△-): $H_0 \leqq -3.0$

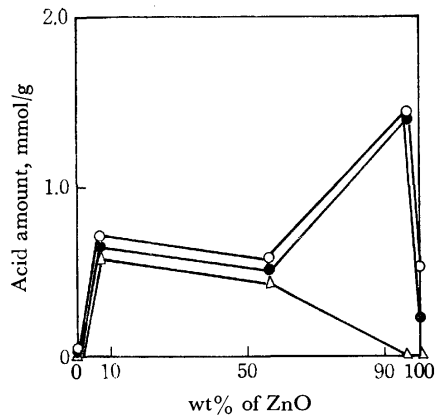

Fig. 2. Acid amounts at various acid strengths of TiO_2·ZnO calcined at 400°C *vs.* wt% of ZnO.
(-○-): $H_0 \leqq 3.3$, (-●-): $H_0 \leqq 1.5$, (-△-): $H_0 \leqq -3.0$

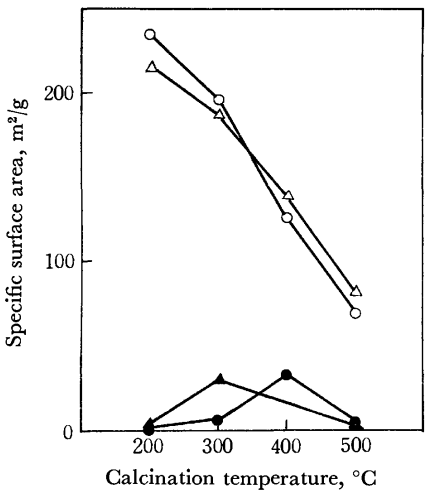

Fig. 3. Change in surface area of TiO_2 (-△-), ZnO (-▲-) sample 1 (-○-), and sample 3 (-●-) on calcination temperature.

7% of ZnO with those of TiO_2 alone (Fig. 3) indicate that the observed large amount and high strength of acid sites of TiO_2·ZnO are not due to the increase of specific surface area. Since the actual amount of surface acid in a given H_0 range is given by the difference between acid amounts at pK_a's of the two indicators bracketing that H_0 range, it may be said that the characteristic of acidity distribution of TiO_2·ZnO containing about 7 or 57% of ZnO calcined at 200—500°C is a fairly large acid amount in the range of acid strength, $H_0 \leqq -3.0$ (in some cases, $H_0 \leqq -5.6$), and of TiO_2·ZnO containing about 96% of ZnO calcined at above 400°C is a very large acid amount in the range of acid strength, $-3.0 < H_0 \leqq 1.5$ (Figs. 1—2 and Table 3).

The effects of calcination temperature on the acidities are given in Tables 2 and 3. The maximum acid amount of sample 1 was observed when calcined at 300°C and that of 3 at 400°C. The acidity change in 2 is shown in Fig. 4. It should be noted that methyl red behaves anomalously on the surface of TiO_2·ZnO (57% ZnO); the acid amounts measured by using methyl red of $pK_a = 4.8$ were found in all cases to be

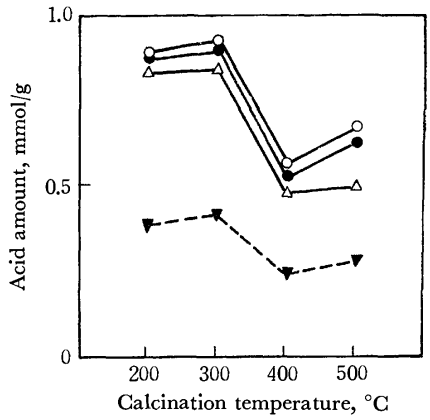

Fig. 4. Dependence of acid amount of sample 2 on temperature.
(-○-): $H_o \leqq 3.3$, (-●-): $H_o \leqq 1.5$, (-△-): $H_o \leqq -3.0$, (-▼--): $H_o \leqq 4.8$

lower than those measured by indicators having lower values of pK_a, as is shown by a dotted line in Fig. 4.

The acidity of 4 containing 15% of ZnO prepared by a slightly modified method is compared with that of 5 containing the same amount of ZnO prepared by using urea where acid amount was plotted against acid strength (Fig. 5). The acid strength of 4 is higher than that of 5, the latter having no acid sites of $H_0 \leqq -3.0$. However, the acid amount in the range of $-3 < H_0 \leqq 6.8$ is found much larger in 5 than in 4, about 0.6 mmol/g and 0.02 mmol/g, respectively. Thus, it might be said that the heterogeneous precipitation method using aqueous ammonia creates strong acid and the homogeneous method using urea relatively weak acid sites.

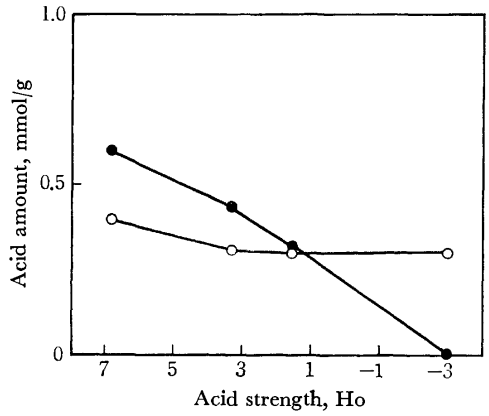

Fig. 5. Comparison of acidic property of TiO_2·ZnO prepared by heterogeneous precipitation method sample 4 (-○-) with that by homogeneous precipitation method sample 5 (-●-).

The infrared spectra of pyridine adsorbed on TiO_2·ZnO and samples 1 and 3 of TiO_2·ZnO calcined at 200—500°C are shown in Figs. 6 and 7. Since it is known that the band of coordinately bonded pyridine appears at 1445—1460 cm^{-1} on the surface of various solid acids, and that of pyridinium ion at around 1530—1540 cm,[-1 4-8] the band near 1540 cm^{-1} in Fig. 6

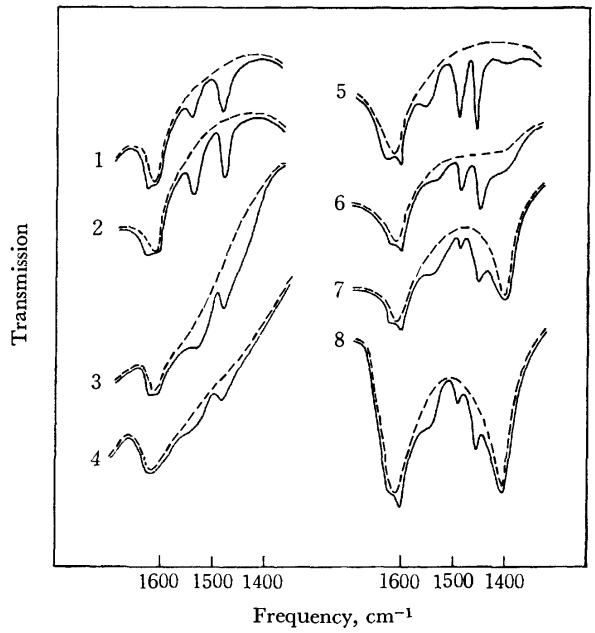

Fig. 6. Infrared spectra of pyridine adsorbed on TiO_2 (1—4) and sample 1 (5—8) calcined at various temperatures. Calcined temperatures are 500 (1,5), 400 (2,6), 300 (3,7), and 200°C (4,8)

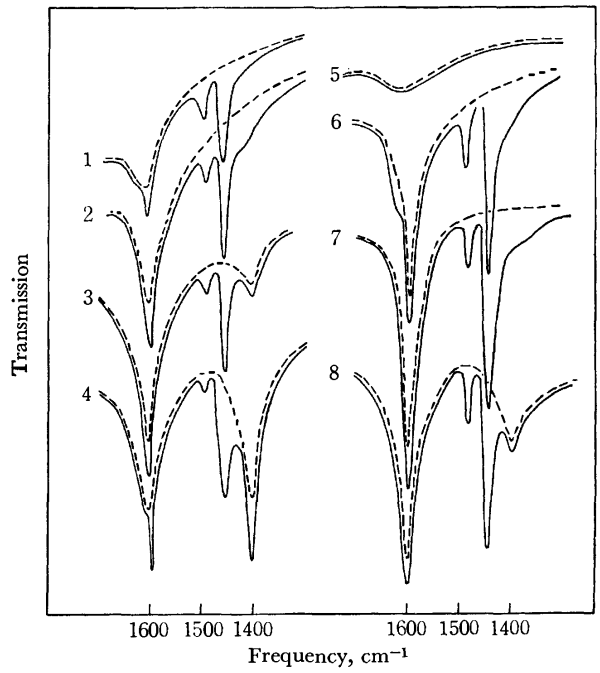

Fig. 7. Infrared spectra of pyridine adsorbed on sample 3 (1—4) and ZnO (5—8) calcined at various temperatures. Calcined temperatures are 500 (1,5), 400 (2,6), 300 (3,7), and 200°C (4,8)

has been assigned to the band due to pyridinium ion formed on Brönsted acid site and that at 1450 cm^{-1} in Figs. 6 and 7 due to coordinately bonded pyridine on Lewis acid site. Thus, TiO_2 has only Brönsted acid

4) E. P. Parry, *J. Catalysis*, **2**, 371 (1963).
5) M. R. Basila, T. R. Kantner, and K. H. Rhee, *J. Phys. Chem.*, **68**, 3197 (1964).
6) J. W. Ward, *J. Catalysis*, **9**, 225 (1967).
7) B. V. Liengme and W. K. Hall, *Trans. Faraday Soc.*, **62**, 3229 (1966).
8) H. Hattori and T. Shiba, *J. Catalysis*, **12**, 111 (1968).

sites and ZnO only Lewis acid sites, though the latter disappear when calcined at 500°C. Sample 1 of TiO_2·ZnO has both Brönsted and Lewis acid sites, while 3 has only Lewis acid sites. The Lewis acid sites of both samples do exist even when calcined at 500°C.

The band at 1485 cm^{-1} appears commonly on both Brönsted and Lewis acid sites. The bands near 1600 cm^{-1} observed in all samples before adsorption of pyridine are considered due to the adsorbed water molecules and/or coordinately bonded ammonia which are retained even after calcination. The bands near 1400 cm^{-1} observed in 1 and 3 and ZnO calcined below 400, 300, and 200°C, respectively, are those of the ammonium ion retained after calcination at relatively low temperature. The infrared spectra of ammonium sulfate used for the preparation of oxides give only the band at 1400 cm^{-1}, but TiO_2 prepared by using ammonium sulfate shows no band. This indicates that ammonium sulfate is not retained on the surface and therefore does not cause the observed acidic property.

A survey of the structure of TiO_2·ZnO by X-ray diffraction shows that sample 2 is entirely amorphous. Sample 1 showed only a pattern of the rutile type and sample 3 only a pattern of hexagonal ZnO, no pattern of the spinel structure being found. However, the structure of acid sites of TiO_2·ZnO is not clear at present.

Catalytic Activity. Since TiO_2·ZnO containing about 7% of ZnO (sample 1) was found to show fairly high acidity, its catalytic activity was tested for the hydration reaction of ethylene and the alkylation of phenol with methanol which are known to be catalyzed by the usual solid acids. Hydration reaction of ethylene over sample 1 of TiO_2·ZnO calcined at 400°C, was carried out at 200°C. The result is shown in Fig. 8, where the catalytic activities of nickel sulfate calcined at 300°C[9] and phosphoric acid mounted on celite[9] for the reaction under the same reaction conditions are also shown for comparison. The activity of the new TiO_2·ZnO catalyst is higher than that of nickel sulfate and solid phosphoric acid which are well-known catalysts for olefin hydration. Since the acid strength of acid sites effective for ethylene hydration is reported to be $H_0 \leqq -3$ in the case of various metal sulfate catalysts,[9] the observed high activity of TiO_2·ZnO catalyst is considered to be due to the fact that the catalyst has a large acid amount at $H_0 \leqq -3$ as shown in Table 3.

9) M. Nitta, I. Isa, I. Matsuzaki, and K. Tanabe, *J. Japan Petroleum Inst.*, **14**, 779 (1971).

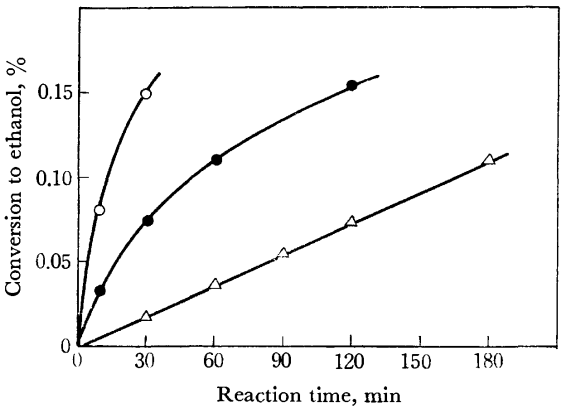

Fig. 8. Hydration of ethylene catalyzed by solid acids.
(-○-) Catalyst: 2 g of sample 1 calcined at 400°C, Reaction temp.: 200°C
(-●-) Catalyst: 2 g of $NiSO_4$ calcined at 300°C, Reaction temp.: 220°C
(-△-) Catalyst: 17 g of H_3PO_4 on celite, Reaction temp.: 220°C

The selectivity of this catalyst was also high, only ethyl alcohol being formed, although diethyl ether or acetaldehyde is usually formed when the catalysts of high acid strength ($H_0 \leqq -8.2$) such as SiO_2·Al_2O_3 and Al_2O_3·B_2O_3 are used.[9]

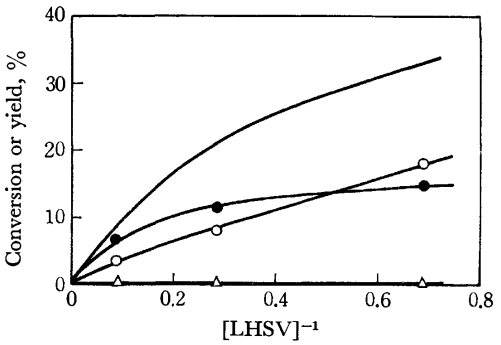

Fig. 9. Alkylation of phenol by methanol catalyzed by TiO_2·ZnO.
Reaction temp.: 400°C, total conversion (——), yield of *o*-cresol (-●-), *m*- and *p*-cresol (-○-), anisol (-△-)

The activity and selectivity of sample 1 of TiO_2·ZnO for alkylation of phenol with methanol are shown in Fig. 9. The conversion was about 33% at $LHSV^{-1}$ 0.7 and only monoalkylated phenols were obtained. The cause of selectivity and reaction kinetics are being studied in comparison with various known acidic catalysts.

Gas-Phase Charge-Transfer Complexation of Carbonyl Cyanide as Acceptor

Takayuki FUENO and Yoshiro YONEZAWA

Department of Chemistry, Faculty of Engineering Science, Osaka University, Toyonaka, Osaka

(Received May 27, 1971)

Charge-transfer complexations of carbonyl cyanide with furan, tetrahydrofuran, diethyl ether, and their sulfur homologs have been investigated in gaseous phase at temperatures 22—82°C. Thermodynamic data showed that the complexations are enthalpy-controlled in the temperature range studied and that the complexes formed from *n*-donors are fairly strongly bound. Both the transition and bonding energies could be interpreted in terms of the usual two-state resonance model. It has been deduced that the spatial arrangements of the components do not greatly differ for the various donors studied, despite the difference in precise nature of the bondings involved.

Intermolecular interactions leading to the formation of "charge-transfer (CT)" complexes have been attracting increasing interests of both physical and organic chemists.[1] Studies have recently been conducted in gaseous phase, which have served to disclose the role of solvents in the CT complexations formerly observed in condensed phases. The gas-phase CT complexations studied so far include those with iodine,[2-8] sulfur dioxide,[9] tetracyanoethylene,[6,10,11] and carbonyl cyanide[12,13] as electron acceptor.

From a particular interest in the role of molecular complexation in the kinetics of some gas-phase reactions,[14,15] we investigated the bonding character of the gas-phase CT complexes of carbonyl cyanide, $(CN)_2CO$. This compound was chosen as acceptor because of relative unfamiliarity with respect to its structure and reactivity. The donor compounds here investigated are furan, tetrahydrofuran, diethyl ether and their sulfur homologs, *i.e.*, a series of C_2XC_2-type compounds with X=O or S. Carbonyl cyanide, being highly electron-deficient at its carbonyl carbon atom, gives fairly strong complexes with some of the donor molecules studied. Nonetheless, it has been found that the usual assumption of weak complexation is still valid for characterizing the present CT interaction systems.

Experimental

Materials. Carbonyl cyanide was synthesized from tetracyanoethylene according to the method of Linn, Webster, and Benson.[16] It was distilled under reduced pressure in an all-glass apparatus and stored in a reservoir which was screened from sunlight and cooled with Dry Ice-methanol.

Furan, thiophene, tetrahydrofuran, tetrahydrothiophene, diethyl ether, and diethyl sulfide were all purchased and purified by drying and distillation.

Apparatus and Procedure. The apparatus used is diagrammatically shown in Fig. 1. The absorption cell made of cylindrical quartz is 2 cm in diameter and 10 cm in light-path length. The side arm of the absorption cell has a sampling part for donors and two capillary parts, S_1 and S_2, for sealing off. The volumes of the absorption cell and of the glass tube between sealing-off points were measured before the absorption cell was connected with the vacuum line. The sampling part for donors consists of a glass tube stoppered with silicone gum and tightened with stainless steel fittings having a hole for a microinjector. The whole apparatus maintained vacuum under 10^{-3} mmHg.

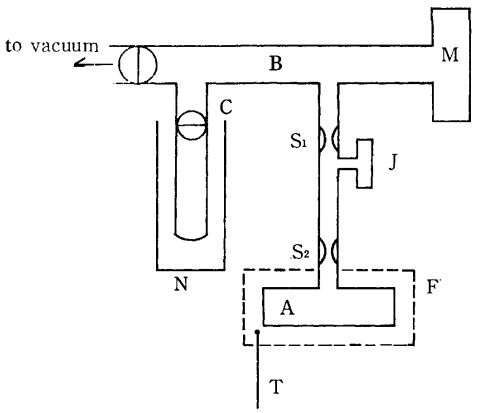

Fig. 1. Apparatus used for the gas-phase complexation measurements.
A, absorption cell; B, auxiliary tube; C, reservoir; M, oil manometer; F, electric heater; J, sampling part; T, thermocouple; N, liquid N_2 vessel; and S_1, S_2, seal-off parts

Gaseous mixtures of carbonyl cyanide and donor were prepared by the following method. The carbonyl cyanide vapor was metered into the evacuated absorption cell, using an oil manometer. The absorption cell was sealed off at capillary point S_1 from the vacuum line. While carbonyl cyanide in the absorption cell was condensed in the cell cooled with Dry Ice-methanol, liquid donor was introduced into the sampling part by use of a 25-μl microinjector. The cell was then sealed off at capillary point S_2. The concentration of carbonyl cyanide was calculated from its vapor

1) *E.g.*, G. Briegleb, "Electronen Donator-Acceptor Komplexe," Springer Verlag, Berlin, (1961).
2) F. T. Lang and R. L. Strong, *J. Amer. Chem. Soc.*, **87**, 2345 (1965).
3) M. Goodenow and M. Tamres, *J. Chem. Phys.*, **43**, 3393 (1965).
4) M. Tamres and J. M. Goodenow, *J. Phys. Chem.*, **71**, 1982 (1967).
5) E. Ginns and R. L. Strong, *ibid.*, **71**, 3059 (1967).
6) M. Kroll, *J. Amer. Chem. Soc.*, **90**, 1097 (1968).
7) W. K. Duerksen and M. Tamres, *ibid.*, **90**, 1397 (1968).
8) M. Tamres and J. Grundnes, *ibid.*, **93**, 801 (1971).
9) J. Grundnes and S. D. Christian, *ibid.*, **90**, 2239 (1968).
10) M. Kroll and M. L. Ginter, *J. Phys. Chem.*, **69**, 3671 (1965).
11) J. Aihara, M. Tsuda, and H. Inokuchi, This Bulletin, **40**, 2446 (1967).
12) J. Prochorow, *J. Chem. Phys.*, **43**, 3394 (1965).
13) J. Prochorow and A. Tramer, *ibid.*, **44**, 4545 (1966).
14) D. L. Bunker and N. Davidson, *J. Amer. Chem. Soc.*, **80**, 5090 (1958).
15) R. L. Strong and J. Perano, *ibid.*, **89**, 2535 (1967).
16) W. J. Linn, O. W. Webster, and R. E. Benson, *ibid.*, **87**, 3651 (1965).

pressure and the predetermined cell volume, assuming that the vapor is an ideal gas. Concentrations of donor vapors were also calculated from the weight of the liquid samples and cell volume. The absorption cell was covered with a heat jacket whose temperature was read with a thermocouple. Spectral measurements were carried out at varying temperatures between 22 and 82°C.

Absorption spectra of gaseous mixtures were recorded on a Shimadzu-MPS-50L spectrophotometer. The spectrophotometric equation which can be applied to this study is[17]

$$\frac{c_a c_b}{d-d_0} = \left(c_a + c_b - \frac{d-d_0}{\varepsilon-\varepsilon_0}\right)\frac{1}{\varepsilon-\varepsilon_0} + \frac{1}{K_c(\varepsilon-\varepsilon_0)} \quad (1)$$

where c_a and c_b are the initial concentrations of carbonyl cyanide and donor, respectively; ε and d_0 are the extinction coefficients of the complex and free carbonyl cyanide, respectively; d is the absorbance per unit length; d_0 is $\varepsilon_0 c_a$; and K_c is the equilibrium constant of complex formation. c_a was varied from 1.1 to 2.3 mM, and c_a from 1.4 to 9.3 mM.

In evaluating ε and K_c from Eq. (1), we adopted the method of Lang.[18] An approximate value of ε was obtained by solving an appropriate pair of simultaneous equations based on Eq. (1). The values of $c_a c_b/(d-d_0)$ obtained from measurements at various c_a and c_b were then plotted against the values of $c_a+c_b-(d-d_0)/(\varepsilon-\varepsilon_0)$. From the slope calculated by the least squares method, a better value of ε was obtained. The procedure was repeated until the resulting value of ε coincided with the assumed. Usually, two iterations sufficed for the present purpose. The values of K_c at various temperatures were calculated from Eq. (1) by use of the ε value finally obtained. In the temperature range studied, ε of each complex did not vary appreciably with temperature.

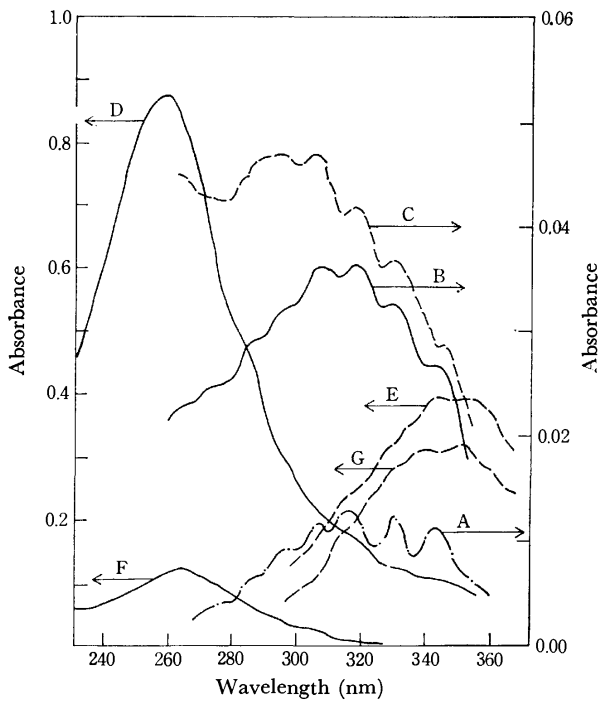

Fig. 2. Absorption spectra of the gas-phase CT complexes of $(CN)_2CO$ at 62°C.
A, $(CN)_2CO$ (1.50 mM) alone
B, $(CN)_2CO$ (1.80 mM) +furan (6.88 mM)
C, $(CN)_2CO$ (2.00 mM) +thiophene (6.30 mM)
D, $(CN)_2CO$ (1.64 mM) +tetrahydrofuran (4.17 mM)
E*, $(CN)_2CO$ (1.58 mM) +tetrahydrothiophene (2.11 mM)
F, $(CN)_2CO$ (1.39 mM) +diethyl ether (8.02 mM)
G, $(CN)_2CO$ (2.24 mM) +diethyl sulfide (4.02 mM)
* Measured at 72°C

Results

Figure 2 shows the absorption spectra of gaseous CT complexes of carbonyl cyanide with a series of donors at 62°C. The intensities of absorption increased (decreased) with the lowering (rising) in temperature and were essentially reproducible at temperatures between 22 and 82°C. This indicates that the complexes can exist in equilibrium with the free donor (D) and acceptor (A) species. Above 90°C, however, the absorbance in the shorter-wavelength region tended to show a gradual decrease with the elapsing time, indicating the occurrence of an irreversible reaction.

Prochorow *et al.*[19] investigated the absorption spectrum of carbonyl cyanide in both gaseous phase and

Table 1. Spectral and thermodynamic data of the gas-phase CT complexes of $(CN)_2CO$

Donor	λ_{max} nm	ε $M^{-1}cm^{-1}$	K_c[a] M^{-1}	$-\Delta H°$[a] kcal mol^{-1}	$-\Delta S°$[a] e.u.	I_D eV
Furan	315	20	16.1±2.5	2.6±1.0	2.5±1.5	9.0[b]
Thiophene	295	20	30.6±3.5	6.0±2.2	11.8±2.1	9.0[b]
Tetrahydrofuran	260	100	322±100	8.2±1.3	13.8±6.1	10.1[c]
Tetrahydrothiophene	345	40	8020±500	14.3±4.4	26.2±6.2	8.6[d]
Diethyl ether	262	30	39.3±1.0	4.4±0.5	6.1±2.7	9.7[e]
Diethyl sulfide	350	50	740±250	16.8±2.8	38.4±4.5	8.3[f]

a) At 52°C. The uncertainties indicate the probable errors.
b) W. C. Price and A. D. Walsh, *Proc. Roy. Soc.* (London), **A179**, 201 (1941).
c) J. Hissel, *Bull. Soc. Roy. Sci. Liége*, **21**, 457 (1952) [F. H. Field and J. L. Franklin, "Electron Impact Phenomena," Academic Press, Inc., New York, N. Y. (1957), p. 283].
d) E. J. Gallegos and R. W. Kiser, *J. Phys. Chem.*, **66**, 136 (1962).
e) J. D. Morrison and A. J. C. Nicholson, *J. Chem. Phys.*, **20**, 1021 (1952).
f) Calculated from $I_D = AP - D_{C\text{-}S}$, where AP (11.15 eV) is the appearance potential of $C_2H_5S^+$ from $(C_2H_5)_2S$ [J. L. Franklin and H. E. Lumpkin, *J. Amer. Chem. Soc.*, **74**, 1023 (1952)] and where $D_{C\text{-}S}$ (2.83 eV) is the C-S bond energy [J. D. Roberts and M. C. Caserio, "Basic Principles of Organic Chemistry," W. A. Benjamin, Inc., New York, N. Y. (1965), p. 77].

17) N. J. Rose and R. S. Drago, *J. Amer. Chem. Soc.*, **81**, 6138 (1959).
18) R. P. Lang, *ibid.*, **84**, 1185 (1962).
19) J. Prochorow, A. Tramer, and K. L. Wierzchowski, *J. Mol. Spectrosc.*, **19**, 45 (1966).

n-hexane solution and attributed the weak absorption with vibrational structure appearing in the 260—400 nm region to the symmetry forbidden n-π^* transition of the carbonyl group. The extinction coefficient at the absorption maximum $\lambda_{max}=330$ nm was reported to be 3.0 $M^{-1}cm^{-1}$. The vibrational structure of carbonyl cyanide remains clearly in the CT complexes with furan (Fu) and thiophene (Th). It is also discernible in the complexes with tetrahydrothiophene (THT) and diethyl sulfide (DES), but absent in the tetrahydrofuran (THF) and diethyl ether (DEE) complexes.

Table 1 summarizes the spectral and thermodynamic data of the CT complexes observed. Prochorow and Tramer[13] have already reported that the gaseous CT complex of carbonyl cyanide with DEE has $\lambda_{max}=$ 262 nm, $\varepsilon\simeq65$ $M^{-1}cm^{-1}$ and $K_c\simeq45$ M^{-1} at an unspecified temperature. The ε value we obtained is about half as great as theirs, but the K_c values observed in both studies are in rough accord with each other.

Figure 3 gives a plot of the wavenumbers of the CT band maxima, $\bar{\nu}_{max}$, against the ionization potentials I_D of donor compounds. For the sake of reference, the points for benzene, toluene, and *p*-xylene[13] have been included. The points including those of the benzene derivatives fit approximately the simple theoretical formula[20,21]

$$h c\bar{\nu}_{max} = I_D - C_1 + \frac{C_2}{I_D - C_1} \qquad (2)$$

with $C_1=5.7$ eV and $C_2=2.5$ $(eV)^2$.

Inspection of the equilibrium data given in Table 1 indicates that the K_c values of saturated donors are appreciably greater than those of unsaturated donors. The K_c values of the sulfur compounds are uniformly greater than those of the corresponding oxygen homologs. The results are in agreement with those found for the gas-phase CT complexes of iodine as acceptor.[2,4,6] The CT complexations here observed may be characterized by the relatively large equilibrium constants K_c for some donors and the correspondingly large enthalpy change of complexation, $-\Delta H°$.

In Fig. 4, the observed values of $\Delta H°$ are plotted against the values of $\Delta S°$. Although errors inherent to these thermodynamic quantities are too large to permit any quantitative considerations, it does appear that an extrathermodynamic relationship[22] holds between the $\Delta H°$ and $\Delta S°$ values observed. The "isokinetic" temperature as determined from the slope is *ca.* 435°K. The results indicate that the relative complexation abilities of the series of donor compounds here investigated are enthalpy-controlled in the temperature range studied.

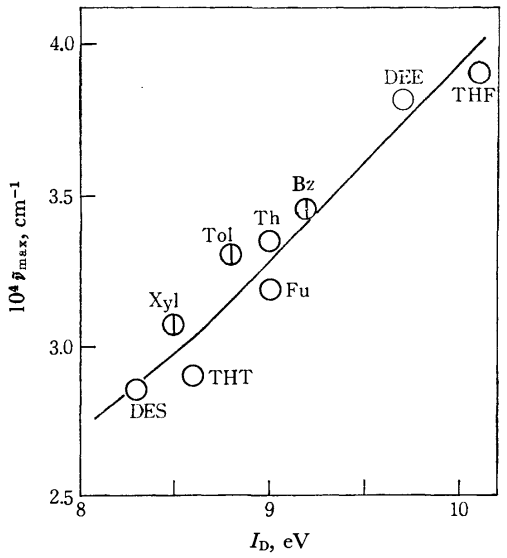

Fig. 3. Plots of the wavenumber of the CT band maxima *vs.* the ionization potential of donors.
Fu, furan; Th, thiophene; THF, tetrahydrofuran; THT, tetrahydrothiophene; DEE, diethyl ether; DES, diethyl sulfide; Bz, benzene[13]; Tol, toluene[13]; Xyl, *p*-xylene[13]

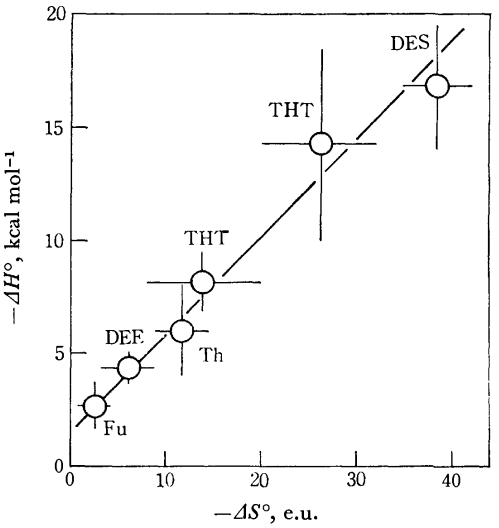

Fig. 4. Plots of $\Delta H°$ *vs.* $\Delta S°$.
The vertical and horizontal lines drawn on the circles indicate the ranges of the probable errors. For the symbols appended, see Fig. 3.

Discussion

The observed dependence of $\bar{\nu}_{max}$ on I_D (Fig. 3) confirms that the absorption bands in question are essentially due to the intermolecular charge transfer transitions. The constants C_1 and C_2 appearing in Eq. (2) are given by[20,21]

$$C_1 = E_A - E_C + W_0 \qquad (3)$$

and

$$C_2 = 2\beta^2 \qquad (4)$$

where E_A is the electron affinity of the acceptor; E_c is the Coulombic energy involved in the ionic state, D^+A^-; W_0 is the van der Waals interaction energy of the no-bond state, DA; and β is the exchange interaction between the two extreme states.

If the simple two-state resonance model, on which

20) G. Briegleb and J. Czekalla, *Z. Elektrochem.*, **63**, 6 (1959).
21) S. H. Hastings, J. L. Franklin, J. C. Schiller, and F. A. Matsen, *J. Amer. Chem. Soc.*, **75**, 2900 (1953).
22) J. E. Leffler and E. Grundwald, "Rates and Equilibria of Organic Reactions," John Wiley, New York, N .Y. (1963), Chapter 9.

Eq. (2) is based, is also an adequate description of the bondings in the present complexations, then the binding energy should be given approximately by just a half the second term of Eq. (2)[23]:

$$\Delta E_R = C_2/2(I_D - C_1) \quad (5)$$

Substitution of the spectroscopically determined values of C_1=5.7 eV and C_2=2.5(eV)^2 into Eq. (5) gives ΔE_R=8.7(Fu), 8.7(Th), 6.6(THF), 9.9(THT), 7.2 (DEE), and 11.1(DES) kcal mol^{-1}. Although the values of ΔE_R thus calculated are all in order-of-magnitude agreement with the observed heats of complexation (Table 1), one can hardly see any quantitative correlation between these two sets of data.

One possible reason for the absence of correlation between ΔE_R and $\Delta H°$ might be sought in the premise that the C_1 and C_2 values can be assumed to be constant for the different types of donor compounds. Some of the donors studied in this work are unsaturated compounds which should fall in the category of the so-called π-donors (Fu and Th), while others are saturated n-donors (THF, THT, DEE, and DES). There is no justification for expecting the bonding characters of these two types of donors in complexes to be nearly the same.

In order to find logical consistency, we have solved Eqs. (2) and (5) simultaneously with respect to C_1 and C_2. The results are listed in Table 2.

Table 2. Values of C_1 and C_2[a]

Donor	C_1, eV	C_2, (eV)^2
Furan	5.3	1.0
Thiophene	5.3	1.9
Tetrahydrofuran	6.0	2.9
Tetrahydrothiophene	6.2	2.9
Diethyl ether	5.3	1.7
Diethyl sulfide	6.2	3.0

a) Calculated from the experimental vaules of ν_{max} and $\Delta H°$ through Eqs. (2) and (5).

Although no quantitative significance should be attached to the C_1 and C_2 values thus derived, it is worth noting that the π-donors take C_1=5.3 eV and C_2=1.4 (eV)^2 on the average, while three n-donors (THF, THT, and DES) possess values centered on C_1=6.1 eV and C_2=2.9 (eV)^2. The case of DEE is apparently closer to the π-donor case, which might be accidental. The values C_1=5.7 eV and C_2=2.5 (eV)^2 obtained from Fig. 3 should be taken merely as the averages of these individual values.

That the n-donors have greater values of C_1 and C_2 than the π-donors can best be reconciled by assuming that the former are complexed with $(CN)_2CO$ at an intermolecular distance somewhat shorter than in the case of the latter. In the present π-donor complexes it is likely that the component molecules are located on two parallel planes as in most π-donor-π-acceptor complexes. Taking the interplanar distance in our π-donor complexes to be the same (3.50 Å) as in crystalline naphthalene-TCNE[24] and assuming the W_0 to be negligibly small, we obtain E_A=1.2 eV for $(CN)_2CO$. This value of E_A in turn gives the intermolecular distance of *ca.* 3.0 Å for the n-donor-$(CN)_2$-CO complexes, a not unreasonable distance.

The constant C_2=2.9 (eV)^2 reduced for the present n-donor-$(CN)_2CO$ interactions is perhaps the greatest of the values hithero recorded.[1] For such a large C_2 value, the usual assumption of weak complexes would no longer be reliable, and thus both Eqs. (2) and (5) would need to be modified accordingly. Nevertheless, in view of the approximate nature of the present treatment, we may be satisfied for the present with such semiquantitative arguments as presented above on the basis of the assumption of weak complexation.

Discussion so far has been based on the assumption that charge transfer is the only cause of intermolecular bonding energies. However, Dewar and Thompson[25] argued that charge transfer is not generally the main factor responsible for the intermolecular bondings in donor-acceptor complexes. Lippert, Hanna, and Trotter[26] theoretically demonstrated that the Coulombic, induction, dispersion, charge-transfer, and exchange-repulsion energies all contribute to the total binding energies of the aromatic-TCNE as well as aromatic-halogen complexes.

Charge transfer spectra certainly provide no direct evidence for dominancy of the role of charge transfer in intermolecular bondings. Nonetheless, cases do exist in which the relative complexation abilities of donors can be interpreted in terms of charge transfer alone.[27,28] We thus consider the simple charge-transfer description to be useful in certain cases, occasionally providing good estimates of the bonding energies. Implicit in this view is the fact that the charge-transfer energy can be in line with the total bonding energy for structurally analogous complexes. If the contribution of the various other stabilizing factors happens to be counterbalanced by the intermolecular exchange repulsion, the role of charge transfer may even be regarded as a dominant factor of the bondings.

Despite the above complexity of the bonding character, the observed thermodynamics of complexation manifests a simple feature. The isokinetic relationship holding between $\Delta H°$ and $\Delta S°$ would imply an apparent thermodynamic uniformity of the complexation, irrespective of the precise nature of the bondings involved. This may not be quite a fortuitous result, if the spatial arrangements of the components are similar (*i.e.*, all parallel planes) for the various donors studied.

23) Both Eqs. (2) and (5) may be considered to be correct, only if $2C_2/(I_D-C_1)^2$ is small enough as compared with unity. For the sake of simplicity, we assume that this requirement is fulfilled here.

24) O. Hassel and K. Strømme, *Acta Chem. Scand.*, **12**, 1146 (1958); **13**, 178 (1959).

25) M. J S. Dewar and C. C. Thompson, Jr., *Tetrahedron*, Supplement No. 7, 97 (1966).

26) J. L. Lippert, M. W. Hanna, and P. J. Trotter, *J. Amer. Chem. Soc.*, **91**, 4035 (1969).

27) R. L. Flurry, Jr., *J. Phys. Chem.*, **69**, 1927 (1965).

28) W. C. Herndon and J. Feuer, *J. Amer. Chem. Soc.*, **90**, 5914 (1968).

ESR Investigation of Copper Ions on Several Kinds of Cation Exchange Resins

Kayoko UMEZAWA and Takeo YAMABE
Institute of Industrial Science, The University of Tokyo, Roppongi, Minato-ku, Tokyo
(Received June 1, 1971)

Copper ions on several kinds of cation exchange resins were investigated by means of ESR spectroscopy. It was found that the motion of copper ions is restricted in the network of the ion exchange resin, and that the mobility of copper ions is closely connected with the chemical interaction of the copper ions with the fixed ionic groups of the resins. The mobility of copper ions is in the order of; on the sulfonic group>on the phosphonic group>on the carboxylic group>on the iminodiacetate group. This sequence is the reverse of the selectivity for the copper ion. The effect of the water molecules involved in ion exchange resins is also considered, and the copper species on each ion exchange resin are assumed.

It is interesting to investigate the physico-chemical properties of hydrated ion-exchange resin by NMR, ESR, and IR measurements, because it can be considered as a concentrated electrolyte solution. Studying the behavior of ion-exchange resin may also be helpful in making clear the behavior of a concentrated electrolyte solution.

With this in view, Zundel *et al.*[1] investigated in detail by infrared measurements the water molecules involved in ion exchange resins, and several recent reports have been concerned with the water molecules in ion exchange resins, which were investigated by the NMR technique.[2]

However, only a few studies using ESR measurements have been reported.[3] By ESR measurements, although the measurable ions are limited in such substances as Cu(II), Mn(II), VO(II), and Fe(III), the behavior of ions on ion exchange resin can be directly observed instead of the water molecules.

In this paper, we will describe the results of the investigation of copper ions on several kinds of cation exchange resins by ESR measurements. The bonding of copper ions with fixed ionic groups, the mobility of the copper ions, and the effect of water molecules will be discussed. It will be concluded that the mobility of copper ions with fixed ionic groups, and that water molecules also influence the mobility of copper ions and the bonding of copper ions when copper ions are exchanged on ion exchange resin of either the sulfonic- or phosphonic-acid type.

Experimental

Materials. Cation exchange resins used were as follows, Dowex 50W X-2, 4, 8, and 16(sulfonic-acid-type cation exchange resin), Amberlite IRC 50(carboxylic-acid-type cation exchange resin), and Dowex A-1 (chelating ion-exchange resin containing an iminodiacetate group). These ion exchange resins were conditioned by the usual method.

Preparation of Samples. Wet ion exchange resin/10 m*l*, Na form was equilibrated with 20 m*l* of a copper nitrate solution of 10^{-3} mol/*l* for 24 hr, then it was collected by filtration, washed thoroughly with distilled water, and kept in a desiccator in which the relative humidity was 100%.

Measurements. A Japan Electron Optics Co., Ltd. ESR spectrometer model JES. ME 3X was used at room temperature or at 77°K. The modulation frequency was 100 kHz, and the modulation width was 5 gauss.

Results and Discussion

The ESR line shape of copper ions on each ion exchange resin showed a well-resolved spectrum at 77°K, suggesting that the copper ions were homogeneously dispersed. Moreover, at room temperature, the ESR line consists of an asymmetric single line or a line consisting of $g_{//}$ and $g_{\perp}$ components. This suggests that the motion of copper ions was affected. It was found that the motion of copper ions was affected by the fixed ionic groups and also by the amount of water in the ion exchange resins.

(1-1) The Influence of the Amount of Water in the Ion Exchange Resins on the Motion of Copper Ions. Figure 1 shows the influence of the amount of water in Dowex 50 W on the ESR line shape of copper ions. The ESR spectrum shows an asymmetric single line, not a symmetric one, when the ion exchange resin is full of water. With the decrease in the amount of water in the ion exchange resin, the ESR spectra show $g_{//}$ and $A_{//}$ components. The change in these spectra is very similar to that in the spectra of copper ions obtained by Kneubühl[4] in glycerin. He discussed the influence of the viscosity of the solvent on the motion of copper ions and showed that the increase in viscosity causes a slower Brownian motion, resulting in the ESR spectra with $g_{//}$ and $A_{//}$ components of copper ions. This suggests that the decrease in the amount of water in ion exchange resin causes a slower Brownian motion of copper ions on ion exchange resin. In other words, the decrease in the amount of water from the network of the ion exchange resin results in an increase in the microscopic viscosity and a large correlation time, τ_c.

Figure 2 shows the effect of the DVB (divinylbenzene) content in the resin on the Brownian motion. It shows

1) G. Zundel, "Hydration and Intermolecular Interaction", Academic Press, 1969, and literature cited in.

2) for example, a) J. E. Gordon, *J. Phys. Chem.*, **66**, 1150 (1962); b) R. W. Creekmore and C. N. Reilley, *Anal. Chem.*, **42**, 570 (1970); c) L. S. Frankel, *Anal. Chem.*, **42**, 1638 (1970).

3) a) R. J. Faber and M. T. Rogers, *J. Amer. Chem. Soc.*, **81**, 1849 (1959). b) C. Heitner-Wirguin and R. Cohen, *J. Phys. Chem.*, **71**, 2556 (1967). c) C. Heitner-Wirguin, and R. Cohen, *Inorg. Chim. Acta*, 3: 4, 647 (1969).

4) F. K. Kneubühl, *J. Chem. Phys.*, **33**, 1074 (1964).

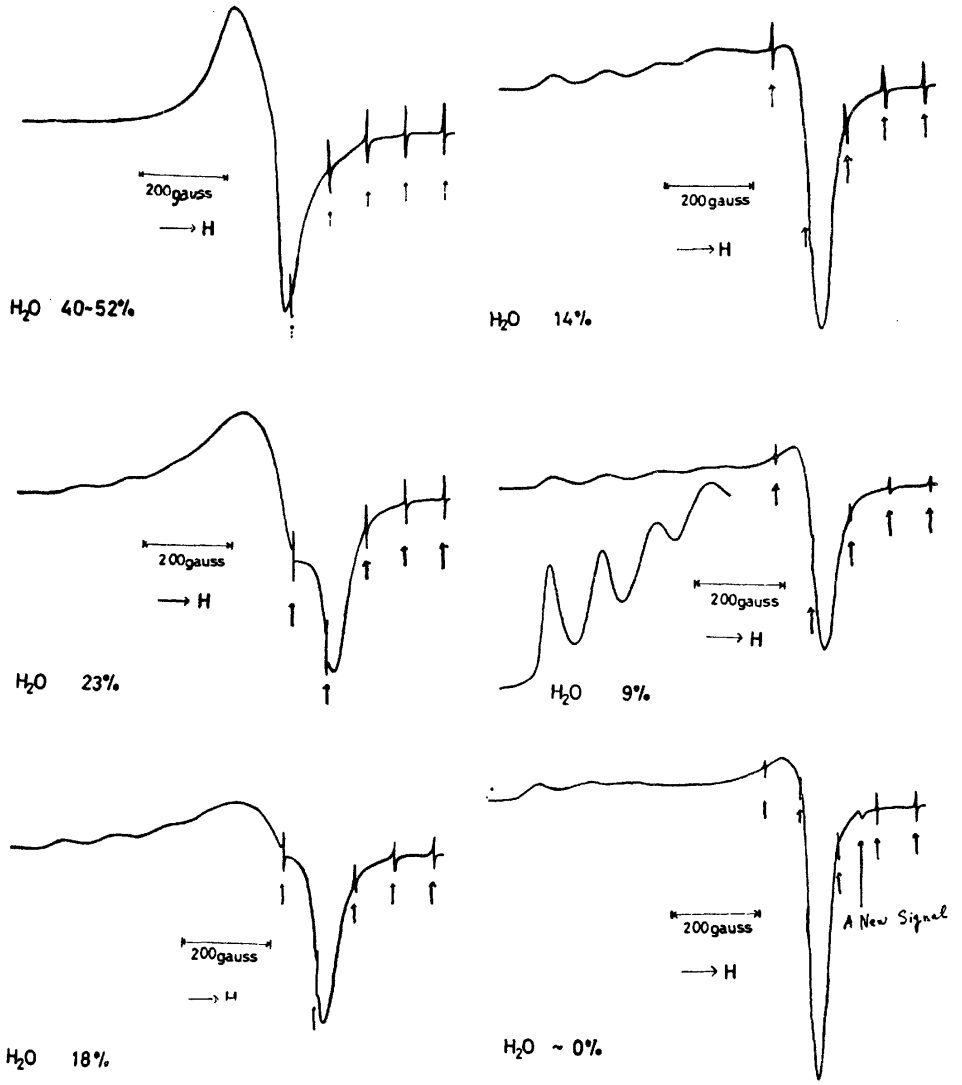

Fig. 1. ESR spectra of copper ions sorbed on Dowex 50W X-8, containing various amount of water. The arrows show the absorption signal of Mn^{2+} as standard.

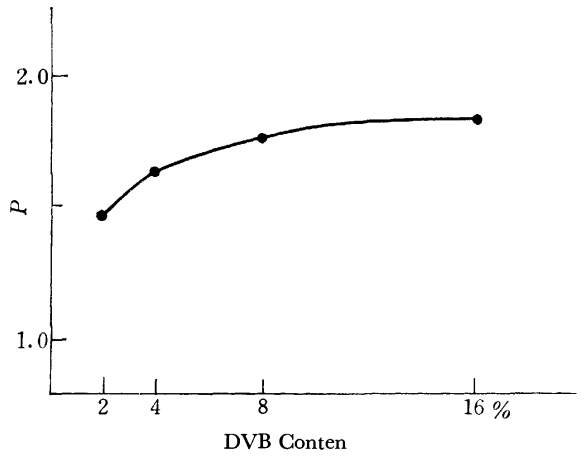

Fig. 2. Influence of DVB content on the motion of copper ion sorbed on Dowex 50W.

that the Brownian motion becomes slower with the increase in the DVB content. P indicates the ratio of the half maximum line width in the lower magnetic field to that in the higher magnetic field.[5] When P is equal to unity, the movement of copper ions is as fast as in an aqueous solution, while when P is larger than unity, the movement is slower than in an aqueous solution. The amount of copper ions sorbed was about 0.02 mmol/m*l* ion exchange resin. In this concentration range, the influence of dipolar interaction or electron exchange interaction is negligible. There are several points to be considered with regard to the effects of the increase in DVB content—the decrease in the amount of water in the ion exchange resin per unit of volume or per unit of weight, the increase in the number of sulfonic groups per unit of volume, and the decrease in the average pore diameter of the network. This last effect, however, seems to have little influence on the motion of copper ions, since the average pore diameter is about 16.9 Å for the ion exchange resin containing 15% of DVB,[6] this value is sufficiently large for the

5) S. Fujiwara, S. Katsumata, and T. Seki, *J. Phys. Chem.*, **71**, 115 (1967).
6) M. Senō and T. Yamabe, This Bulletin **37**, 754 (1965).

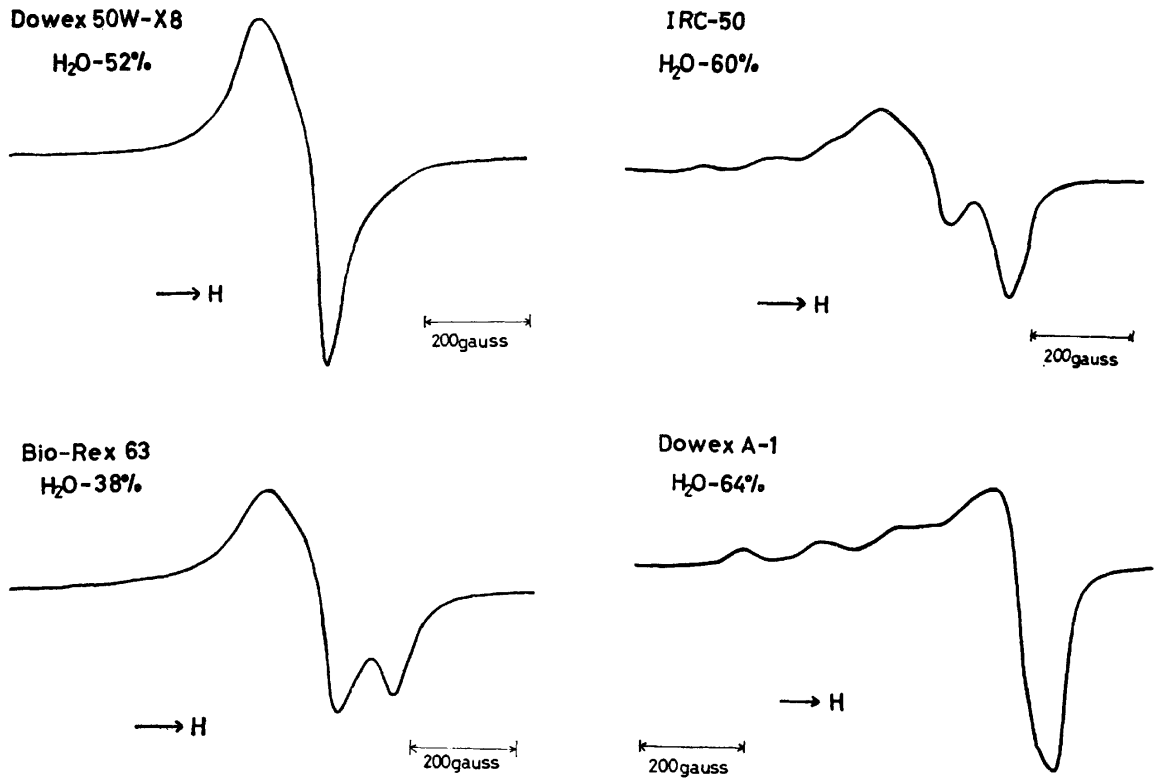

Fig. 3. ESR spectra of copper ions sorbed on various kinds of ion exchange resins at room temperature. The arrows show the absorption signal of Mn^{2+} as standard.

copper ion radius. On the other hand, the other two factors are important, because the decrease in the amount of water is responsible for the slow Brownian motion of copper ions mentioned above, and because the increase in the number of sulfonic groups causes the increase in the amount of counter ions per unit of weight or per unit of volume of the ion exchange resins. The latter results in the decrease in the number of water molecules per cation; therefore, the copper ions are tightly attached to the sulfonic groups. A similar result was obtained by Creekmore and Reilley.[2b] They observed line broadening of the NMR spectra of Na^+ on Dowex 50 W.

(1-2) Influence of Fixed Ionic Groups on the Motion of Copper Ions on Ion Exchange Resins. Figure 3 shows the line shape of the copper ion on various ion exchange resins, which were equilibrated with a relative humidity of 100% at room temperature. The amount of copper ions sorbed was about 0.02 mmol/m*l* ion exchange resin. As can be seen from the figure, the motion of copper ions sorbed is affected more strongly by the kind of fixed ionic group than by the amount of water in the resin. For example, Dowex A-1, containing about 64% of water, shows $g_{//}$ and $A_{//}$ components in its ESR spectrum, suggesting a very slow motion, while Dowex 50W, containing about 52% of water, shows an asymmetric single line spectrum and no $g_{//}$ and $A_{//}$ components. From this comparison, it can be said that the mobility of copper ions decreases in the order of; on the sulfonic group>on the phosphonic group>on the carboxylic group>on the iminodiacetate group. This sequence is the reverse of the selectivity of copper ions. In other words, the stronger the chemical interaction of a fixed ionic group with copper ions, the slower the Brownian motion of the copper ions. This will be discussed in detail in the following section (2). In the higher concentration region of copper ions, we also observed the influence of the difference in the mobility of copper ions on the ESR line shape. In the iminodiacetate group, the line shape changed little except for a little line broadening, even in the higher concentration region of copper ions, while in sulfonic groups P approached to unity with increase in the copper ion concentration, as

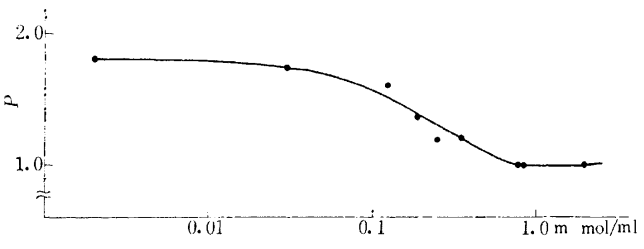

Fig. 4. Concentration dependence of copper ions on P.

is shown in Fig. 4. This difference can be interpreted as follows. As the mobility of copper ions on sulfonic groups is less restricted in the network of ion exchange resin, copper ions can interact with each other by collision in the higher concentration region of copper ions. Therefore, the asymmetry due to a slow Brownian motion in the lower concentration region is averaged out by such strong interaction as electron exchange, resulting in a symmetric single line of the ESR spectrum.

Furthermore, a narrowing of the line width was observed. When P is equal to unity, the line width, ΔH_{pp}, was 110 gauss a value which was consistent with that reported as the exchange narrowed line width by Fujiwara and Hayashi.[7] On the other hand, in iminodiacetate groups, the mobility of copper ions is too restricted for copper ions to move around; therefore, an increase in copper ions only causes dipolar interaction, resulting in line broadening.

Table 1.

Ion Exchange resin	$g_{//}$	$g_{\perp}$	$A_{//}$ $\times 10^{-4}$ cm^{-1}	*d–d* band maxima
Dowex 50W (hydrated)	2.408	2.087	135	~800mμ
(dehydrated)[a]	2.438	2.09	114	——
Bio-Rex 63 (hydrated)	2.381	2.08	134	~800mμ
(dehydrated)[a]	2.419	2.08	113	——
Amberlite IRC 50 (hydrated)	2.338	2.07	145	~690mμ
(dehydrated)[a]	2.323	2.066	146	——
Doxew A-1 (hydrated)	2.275	2.07	151	~710mμ
(dehydrated)[a]	2.282	2.074	149	——
Copperacetatemonohydrate[b]	2.344	2.053 2.093	80	
Zinc-doped Copperacetate-monohydrate[c]	2.344	2.052 2.082	147	

All *g*- and *A*-values were obtained at 77°K and amount of copper ion sorbed was about 0.02 mmol/m*l* ion exchange resin.

a) ion exchange resin was dehydrated in vacumm at 10^{-3} mmHg for 24 hr at room temperature, at 50°C and at 100°C, but it was not observed the influence of dehydration temperature on *g*- and *A*-values.

b) see Ref. 10.

c) see Ref. 11.

(2) Copper Species on Each Ion Exchange Resin. Table 1 shows the *d–d* band absorption maxima and the *g*- and *A*-values of copper ions on hydrated ion exchange resins and on dehydrated ones. The values for hydrated ion exchange resins agree well with those obtained by Cohen and Heitner-Wirguin.[3c] They assumed that the copper species on hydrated Dowex 50W was $[Cu(H_2O)_6]^{2+}$ on the bases of a comparison of the *g*-values and *d–d* band absorption maxima of the aqueous solution of $[Cu(H_2O)_6]^{2+}$ with those of copper ions on Dowex 50W.[3b] However, as can be seen from Table 1, the *g*-values increased and the $A_{//}$ value decreased when Dowex 50W was dehydrated in a vacuum at 10^{-3} mmHg for 24 hr.[8] These changes may be due to a decrease in the coordination number of the water molecules around the copper ions. In Table 2, there are listed the *g*- and *A*-values of copper ions in H_2O-ethyleneglycol, those of copper *p*-toluenesulfonic acid in H_2O and those of copper polystyrene sulfonic acid in H_2O; almost all were the same and coincided well with those of copper ions on hydrated Dowex 50W. In the media of sulfuric acid, however, the *g*-vaulues of copper ions increased slightly and the *A*-value decreased with the increase in the coordination of sulfuric acid. This can be interpreted as being due to the decrease in the number of water molecules around copper ions as a result of dehydration by sulfuric acid. This tendency of change in *g*- and *A*-values was consistent with the results on copper ions on hydrated and dehydrated Dowex 50W. Similar results were obtained by Zundel and Murr[9] by studying the infrared spectra. They concluded that, when the resin was hydrated, the copper ion was $[Cu(H_2O)_6]^{2+}$, and that when it was dehydrated, the copper ions was $[Cu(H_2O)_4]^{2+}$. It is difficult to estimate the coordination number of water molecules from the ESR data, but it seems reasonable, in view of the Jahn-Teller effect, to assume that the coordination number of water molecules decreases from six to four upon dehydration. As is well known, as a result of the Jahn-Teller effect one copper ion interacts with four ligands more strongly than with the other two ligands. Therefore, two among six water molecules coordinated with the copper ion are rather easily dehydrated. Similarly, copper ions on Bio-Rex 63 are $[Cu(H_2O)_6]^{2+}$ when hydrated and $[Cu(H_2O_4)]^{2+}$ when dehydrated. These results suggest that the sulfonic and phosphonic groups interact with copper ions only by means of electro-static force. Moreover the difference in the mobility of copper ions may be due to the difference in the charge number of the fixed ionic groups. The sulfonic group is one minus ion, while the phosphonic group can be two minus.

Table 2. *g*- AND *A*-VALUES OF COPPER ION VARIOUS FROZEN SOLUTION AT 77°K

	Volume Ratio of Solvent	$g_{//}$	$g_{\perp}$	$A_{//}$ $\times 10^{4}$ cm^{-1}
$Cu(NO_3)_2$/water-ethyl-eneglycol	1:5	2.406	2.084	133
$Cu(NO_3)_2$-*p*-toluenesulfonic acid/water		2.383	2.091	133
$Cu(NO_3)_2$-polystyrenesulfonic acid/water		2.413	2.085	133
$Cu(NO_3)$/water-sulfuric acid	5:1	2.40	2.08	145
	1:5	2.44	2.10	123
	1:10	2.48	2.10	104
	1:500	2.48	2.10	98

Concentration of copper ion was about 10^{-3} mol/*l*.

The *g*- and *A*-values of copper ions on Amberlite IRC 50, which were not influenced by dehydration, suggest a strong interaction of copper ions with the carboxylic group. The form of the copper species can be assumed to be $[Cu(OOC\text{–}R)_2]_2$, $(H_2O)_4Cu\langle^{OOC\text{–}R}_{OOC\text{–}R}$, or $R\text{–}C\langle^{O}_{O}\ Cu\ ^{O}_{O}\rangle C\text{–}R$. Cohen and Heitner-Wirguin found a strong IR absorption at 1650 cm^{-1} and attributed it to COO–M groups; they also found broad absorption maxima usually found for octahedral copper carboxylates, at 14300 cm^{-1}. They proposed the second form for copper species on IRC 50.[3c] However, the data obtained by them strongly suggest that copper ions form chelate bonding with carboxylic groups, but

7) S. Fujiwara and H. Hayashi, *J. Chem. Phys.*, **43**, 23 (1965).

8) A new ESR signal always appeared at about 3360 gauss; the same magnetic field as in the absorption of DPPH, after the dehydration of the ion exchange resin. This will be reported elsewhere in more detail.

9) G. Zundel and A. Murr, *Z. Phys. Chem.*, **54**, 59 (1967).

give weak evidence of coordination by four water molecules. We propose the last form for it for the following reasons. First, it should be noted that copper ions on the carboxylic group exists as a monomer, not a dimer, which is the first form, although copper ions generally form a dimer with acetic acid and other fatty acids. The *g*- and *A*-values have already been obtained for copper acetate monohydrate,[10] which is a dimer form, and zinc-doped copper acetate monohydrate,[11] X-ray-[12] or γ-ray-[13] irradiated copper acetate monohydrate, which are monomer forms.[14] Moreover, the ESR spectrum of copper ions on the carboxylic group showed only a doublet spectrum and the *g*- and *A*-values are consitent with those of the monomer form, Second, no influence of dehydration on *g*- and *A*-values was observed, and these was a restricted motion of copper ions; these facts suggest that water molecules have little influence on the bonding or mobility of copper ions. If one copper ion is surrounded by four water molecules as Cohen *et al.* proposed, the copper ion is mobile, as are copper ions on the sulfonic group, by the rapid exchange of water molecules from coordination sphere to the outer sphere; furthermore, two of the water molecules around the copper ion are unstable upon dehydration, and the dehydration will cause a change in the *g*- and *A*-values. As has been mentioned above, however, the *g*- and *A*-values changed little upon dehydration. Therefore, the second form can be ruled out; only the $R\text{–}C\langle^{O}_{O}\,Cu\,^{O}_{O}\rangle C\text{–}R$ model can well explain these results.

The copper ion on Dowex A-1 was discussed in detail by Cohen and Heitner-Wirguin;[3c] they assumed that the iminodiacetate group acts as a trivalent ligand when the copper ion is sorbed from a neutral solution. Considering the coincidence of our *g*- and *A*-values with those obtained by them, the small influence of the dehydration on the *g*- and *A*-values, the very slow motion of the copper ion, our results agree well with theirs.

One of the authors (K. U.) wishes to thank Dr. Shinsaku Shiraishi and Mr. Nobuharu Takai in this Institute and Dr. Tomi Sugimoto for their many helpful discussions and suggestions.

10) K. D. Bowers and J. Owen, *Rept. Progr. Phys.*, **18**, 304 (1955).
11) G. F. Kokoszka, H. C. Allen, Jr., and G. Gordon, *J. Chem. Phys.*, **42**, 3693 (1965).
12) A. Kawamori, *Bull. Am. Phys. Soc. Ser.* II, **14**, 599 (1969).
13) U. Sakaguchi, Y. Arata, and S. Fujiwara, *J. Chem. Phys.*, **53**, 464 (1970).
14) Strictly speaking, copper acetate monohydrate does not change its dimer form upon X-ray or γ-ray irradiation or by dopetion by zinc ions. However, the elctronic exchange interaction between copper ions disappears and the elctronic behavior of the copper ion is that of a monomer.

BULLETIN OF THE CHEMICAL SOCIETY OF JAPAN, VOL. 45, 60—63(1972)

Electron Spin Resonance Studies of Bis(acetylacetonato)copper(II) Adsorbed on X-Type Zeolite. I. Interaction with Ammonia and Aniline

Yoshio YAMADA*

Department of Chemistry, Faculty of Science, Hiroshima University, Higashisenda-machi, Hiroshima

(Received June 7, 1971)

The interaction of bis(acetylacetonato)copper(II) ($Cu(acac)_2$) adsorbed on X-type zeolite of the sodium form and on silica gel with ammonia and aniline was investigated by ESR. The magnetic and bonding parameters for $Cu(acac)_2$ on the surfaces indicate that the axial-ligand field about the copper on the surfaces is similar to that in a toluene solution. This finding implies that the copper in $Cu(acac)_2$ does not interact strongly with these surfaces. However, it was deduced from the change in the spectrum at higher temperatures that the quasi-π-electrons in $Cu(acac)_2$ interact with the electrostatic field arising from the cations on the zeolite. When ammonia or aniline was introduced, the bonding characters of the complex altered significantly. It was found, from the variation in the parameters, that the axial-ligand field about the complex strengthens and that an adduct is formed. Furthermore, a spectral line at $g=2.004$, which was observed only for $Cu(acac)_2$ on the zeolite in the presence of aniline, was considered to be due to a cation radical formed by an electron transfer from the aniline to the complex.

The ESR spectra of copper(II) complexes have been measured in the liquid and frozen solution states by several authors.[1-5] However, very little work has been done as yet on the complexes in the adsorbed state.[6,7] If a copper complex is adsorbed on a solid surface, it can be expected that the interaction of the complex with the surface will alter the bonding character of the complex.

In this paper, the stability of bis(acetylacetonato)-copper(II) in the adsorbed state and the effect of am-

* Present address: National Research Institute for Pollution and Resources, Kawaguchi, Saitama, Japan.

1) D. Kivelson and R. Neiman, *J. Chem. Phys.*, **35**, 149 (1961).
2) H. R. Gersmann and J. D. Swalen, *ibid.*, **36**, 3221 (1962).
3) H. A. Kuska, M. T. Rogers, and R. E. Drullinger, *J. Phys. Chem.*, **71**, 109 (1967).
4) V. C. Swett and E. P. Dudek, *ibid.*, **72**, 1224 (1968).
5) K.-E. Falk, E. Ivanova, B. Roos, and T. Vänngard, *Inorg. Chem.*, **9**, 556 (1970).
6) E. V. Kavalerova, V. B. Golubev, and V. B. Evdokimov, *Zh. Fiz. Khim.*, **37**, 226 (1963).
7) Y. Yamada, A. Hasegawa, and M. Miura, This Bulletin, **43**, 2661 (1970).

monia or aniline on the adsorbed complex are studied in order to estimate the variation in the bonding character of the complex and in order to examine the interaction with the surface. In the following paper, the reaction of the complex with pyridine will be described on the basis of the interaction with the surface. The purpose of these works is to obtain information on the characteristic reactions taking place on the surface and on the structure of the complex formed on it. In this connection, these studies may contribute to our understanding of heterogeneous catalytic reactions involving complexes.

Experimental

Materials. An X-type zeolite of the sodium form (Linde Lot No. 1380019, Molecular Sieve 13X powder) free from any binder and silica gel was used as the adsorbent. The method of preparation of silica gel has already been described in a preceding paper.[8] The bis(acetylacetonato)-copper(II)($Cu(acac)_2$) was prepared according to the method in the literature[9] and was purified by recrystallization from chloroform. The ammonia and aniline were repeatedly distilled under a vacuum prior to use. The former was synthesized by the ordinary method, while the latter was obtained commercially.

Procedures. The zeolite was heated in a vacuum for 5 hr at 500°C. The amount of $Cu(acac)_2$ (0.88 mg in 1 m*l* of chloroform per 0.25 g of the zeolite) was adjusted so that all of the complex molecules entered the cages of the zeolite in the ratio of one molecule to *ca.* 20 cages. The chloroform solution of $Cu(acac)_2$ was introduced to the zeolite through a breakable seal. Note should be taken of the procedure that the zeolite was cooled before the introduction of the solution in order to prevent the $Cu(acac)_2$ from decomposing by the heat of adsorption. After the chloroform had been eliminated under a vacuum, the complex adsorbed on the zeolite was exposed, at room temperature, to ammonia at a pressure of 100 Torr or to aniline vapor, and then the ESR spectra were measured with a Japan Electron Optics Laboratory JES-3BS-X type ESR spectrometer, equipped with a 100kc field-modulation unit. The g value was determined by comparison with the value for DPPH, 2.0036.

Results and Discussion

The ESR spectrum of $Cu(acac)_2$ adsorbed on the X-type zeolite is shown in Fig. 1 (a). It can be considered, from the well-resolved lines of this spectrum, that the complex molecules are sufficiently remote from one another. When a Molecular Sieve 3A was used as the adsorbent, only a broad singlet spectrum was observed. The absence of structure seems to be ascribable to the dipole-dipole interaction among the complex molecules. From the difference between these spectra, the complex molecules may be deduced to be included in the cages of the X-type zeolite.

If the complex takes a structure with a completely axial symmetry, the spectrum at the perpendicular g component ($g_\perp$) should consist of four lines as a result

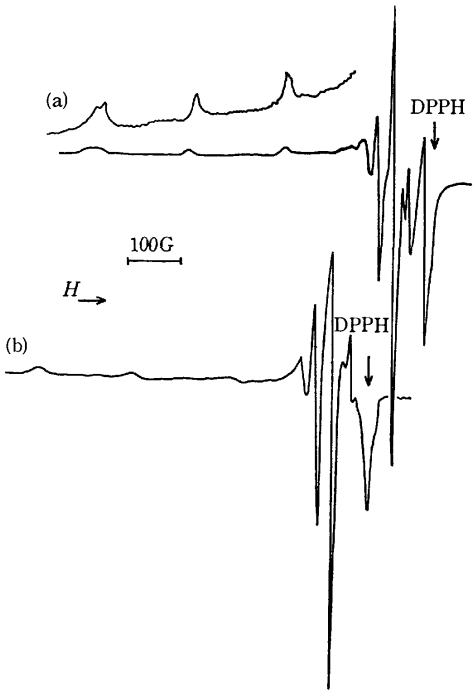

Fig. 1. ESR spectra of $Cu(acac)_2$ (a) on NaX zeolite and (b) on silica gel at 77°K.

of the coupling between an electron spin and a nuclear moment ($I=3/2$) of copper, neglecting the isotope of its nucleus.[10] However, a few unexpected peaks, which had also been observed in the frozen solution,[2] were found, as can be seen in Fig. 1 (a). Recently, these extra peaks have been analyzed on the basis of a theoretical consideration.[11] According to this theory, the observed peaks seem to be due not only to the separation of $g_\perp$ components, g_x and g_y, because of the deviation from axial symmetry, but also to angular anomalies and to transitions with $m_I>0$ caused by electric quadrupole effects.

When the complex was adsorbed on silica gel, a spectrum similar to that on the zeolite was observed

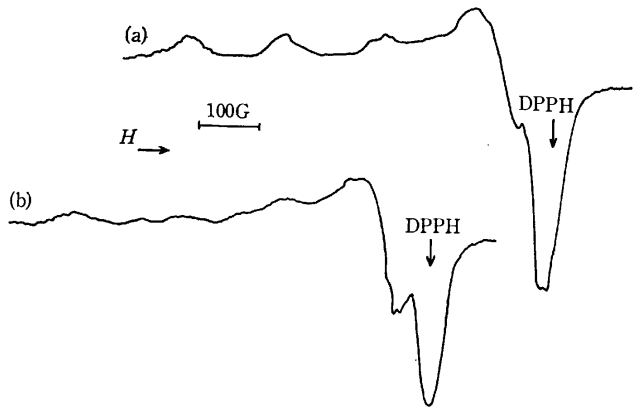

Fig. 2. Spectra of $Cu(acac)_2$ (a) on NaX zeolite and (b) on silica gel in the presence of ammonia (100 Torr) at 77°K.

8) M. Miura, A. Hasegawa, and Y. Yamada, *ibid.*, **41**, 1320 (1968).

9) M. M. Jones, *J. Amer. Chem. Soc.*, **81**, 3188 (1959).

10) The maximum separation due to copper nuclei (^{63}Cu and ^{65}Cu) is about 2—3 gauss at the $g_\perp$ component.

11) L. D. Rollmann and S. I. Chan, *J. Chem. Phys.*, **50**, 3416 (1969).

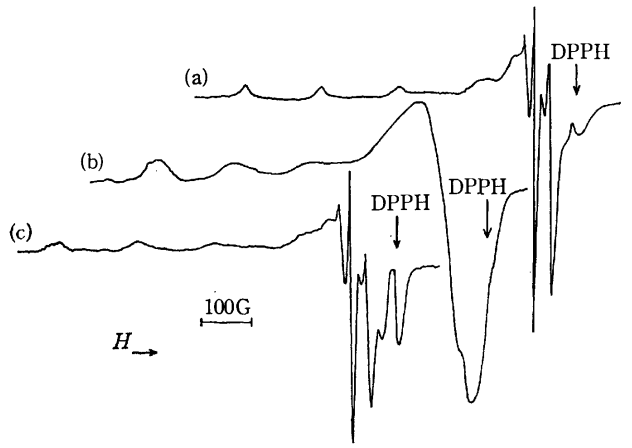

Fig. 3. Spectra of $Cu(acac)_2$ (a) on NaX zeolite (b) on silica gel in the presence of aniline at 77°K, and (c) 77°K after sample (a) was left for a few days at room temperature.

(Fig. 1 (b)). The extra peaks in the $g_\perp$ region are not clearly discernible, as may be seen in Fig. 1 (b), because of the linewidth broadening. The spectra shown in Figs. 2 (a) and (b) were obtained when ammonia was introduced, at a pressure of 100 Torr, to $Cu(acac)_2$ on the zeolite and the silica gel respectively, and then the samples were heated at 80°C. The original spectrum was replaced by an ill-resolved one in each case. On the other hand, the well-resolved spectrum shown in Fig. 3 (a) appeared on the exposure of the $Cu(acac)_2$ on the zeolite to aniline vapor. A weak singlet at $g=2.004$ behaved differently from the other signals in the variation of the temperature and the microwave power. A detailed discussion of the singlet will be presented later. The magnetic parameters determined from these spectra are listed in Table 1, along with those from the spectrum of $Cu(acac)_2$ in a toluene solution.[12]

In order to discuss the nature of the copper-ligand bonding in terms of these experimental parameters, the bonding parameters were calculated by a molecular orbital theory.[1,13] That is, α^2, which is a measure of the covalency of in-plane σ-bonding between a copper $3d$ orbital and the ligand orbitals, can be written in the

Table 1. Magnetic parameters

	$g_{\parallel}$	$g_\perp$	$\lvert A_{\parallel}\rvert \times 10^4 cm^{-1}$	$\lvert A_\perp\rvert \times 10^4 cm^{-1}$
$Cu(acac)_2$ in $C_6H_5CH_3$[a]	2.246	2.062	197	15
$Cu(acac)_2$ on SiO_2	2.253	2.055	195	28
$Cu(acac)_2$ on zeolite	2.264	2.043	190	31
$Cu(acac)_2$ on SiO_2–NH_3	2.240	2.029	193	—[b]
$Cu(acac)_2$ on zeolite–NH_3	2.268	2.034	183	—[b]
$Cu(acac)_2$ on SiO_2–$C_6H_5NH_2$	2.301	2.031	160	—[b]
$Cu(acac)_2$ on zeolite–$C_6H_5NH_2$	2.300	2.054	165	23

a) Ref. 12
b) These values were not obtained.

12) S. Antosik, N. M. D. Brown, A. A. McConnell, and A. L. Porte, *J. Chem. Soc.*, A, **1969**, 545.
13) A. H. Maki and B. R. McGarvey, *J. Chem. Phys.*, **29**, 31 (1958).

first approximation:

$$A_{\parallel} = P\left[-\alpha^2\left(\frac{4}{7}+\kappa_0\right)+(g_{\parallel}-2.002)+\frac{3}{7}(g_\perp-2.002)+0.04\right] \quad (1)$$

where $P=0.036$ cm^{-1} and where κ_0 is the Fermi contact term for the free cupric ion and is nearly equal to 0.43, according to Kivelson and Neiman.[1]

The value of β_1^2, which is a measure of the covalency of the in-plane π-bonding, was evaluated from the equation:

$$g_{\parallel} - 2.002 = -8\rho[\alpha\beta_1 - \alpha'\beta_1 S - \alpha'(1-\beta_1^2)^{1/2}T(n)/2] \quad (2)$$

where $\rho=\lambda_0\alpha\beta_1/\Delta E_{xy}$ and where $T(n)$ has the value of 0.220 for the β-keto enolate chelates. The spin-orbit coupling constant for the free cupric ion, λ_0, is -828 cm^{-1}. On account of the difficulty in observing the absorption spectra, the energy difference between E_{xy} and $E_{x^2-y^2}$ is approximately set as the constant value of 15000 cm^{-1}. The normalization of the in-plane σ-bonding orbital yields:

$$\alpha^2 + \alpha'^2 - 2\alpha\alpha' S = 1, \quad (3)$$

where S, the overlap integral, is equal to 0.076 for the β-keto enolate complexes. By the use of Eqs. (1), (2), and (3), the values of the bonding parameters, that is, α^2, β_1^2, and α'^2, were calculated; the results are summarized in Table 2.

Table 2. Bonding parameters

	α^2	α'^2	β_1^2
$Cu(acac)_2$ in $C_6H_5CH_3$	0.82	0.25	0.73
$Cu(acac)_2$ on SiO_2	0.86	0.21	0.72
$Cu(acac)_2$ on zeolite	0.85	0.22	0.75
$Cu(acac)_2$ on SiO_2–NH_3	0.83	0.24	0.71
$Cu(acac)_2$ on zeolite–NH_3	0.83	0.24	0.79
$Cu(acac)_2$ on SiO_2–$C_6H_5NH_2$	0.80	0.27	0.91
$Cu(acac)_2$ on zeolite–$C_6H_5NH_2$	0.82	0.25	0.89

Prior to the consideration of the bonding character, the stability of the complex on the surfaces was examined. The intensity of the spectrum of $Cu(acac)_2$ adsorbed on the zeolite gradually decreased and the linewidth became broader as the temperature was raised. The spectrum disappeared near 90°C. The broadening of the spectral lines can be explained in terms of the decomposition of the complex; the cupric ion thus produced interacts more strongly with the surface than that in the complex does. On the other hand, a small decrease in the intensity was observed up to *ca.* 200°C for $Cu(acac)_2$ on silica gel. It, therefore, may be considered that the especially active sites on the zeolite play an important role in the decomposition of the complex. Abramov *et al.*[14] studied the IR spectra of benzene adsorbed on zeolites and interpreted the various shifts of some bands in the IR spectra as being caused by the interaction of the π-electron of the benzene molecule with the electrostatic field of the cations on the walls of the cavities in the zeolites. An

14) V. N. Abramov, A. V. Kiselev, and V. I. Lygin, *Zh. Fiz. Khim.*, **37**, 1156 (1963).

essentially similar interaction can be expected for the quasi-π-electrons in $Cu(acac)_2$ adsorbed on the zeolite. As can be seen in Table 2, the in-plane π-bonding for $Cu(acac)_2$ on the zeolite is somewhat more ionic than that for the complex on silica gel. This may be interpreted as follows: the symmetry of the complex lowers slightly as a result of the interaction of the quasi-π-electrons in the complex with the electrostatic field from the cations on the zeolite, and the copper atom is no longer coplanar to the four chelating oxygen atoms.

It is well known that the magnetic parameters of copper complexes depend largely upon the kind of solvent.[12] This arises from the differences in the basicity of the solvent molecules, one or two of which coordinate to the complex along the axis normal to the molecular plane. When apical ligands coordinate to the cupric ion, *i.e.*, when the axial-ligand field strengthens, the values of $g_{//}$ increase, while those of $|A_{//}|$ decrease.[5,15] On the basis of this rule and the results shown in Table 1, the axial field can be said to be weak in the adsorbed state as well as in a toluene solution, where none of the solvent molecules coordinates to the complex as an apical ligand.[12] Consequently, it seems reasonable to consider that the copper atom in the complex does not interact strongly with the surface.

When ammonia or aniline is introduced to $Cu(acac)_2$ on the zeolite or silica gel, the $g_{//}$ value increases and the $|A_{//}|$ value decreases, except for $Cu(acac)_2$ on silica gel in the presence of ammonia. According to the above rule, these facts may indicate that the adsorbed molecule coordinates as an apical ligand. Since such basic molecules have a strong donating ability, their equatorial coordination should be weakened by back-donation, resulting in an increase in α^2. Nevertheless, this phenomenon was not seen on the introduction of ammonia or aniline. This unexpected result may be attributable to the use of the Fermi contact term, κ_0, as a constant in the calculations. It has been indicated[16] that the axial coordination of the electron-donating molecule increases the charge density in the 4*s* orbital, thereby reducing the promotion of the unpaired electron to the 4*s* orbital and causing a decrease in κ_0. Hence, this conflict can be removed in terms of the decrease in κ_0. From the above discussion, it can be concluded that the introduction of aniline or ammonia to $Cu(acac)_2$ on the zeolite, and that of aniline to $Cu(acac)_2$ on silica gel, bring about the axial-ligand field, leading to the formation of the adduct, though the circumstances of the complex are not clear for the system of $Cu(acac)_2$-ammonia on silica gel. Furthermore, when we take into account the finding that the copper atom in the complex interacts more strongly with ammonia or aniline than with the surface, it seems likely that the complex has such a structure that the copper atom is located above the plane containing the four chelating oxygen atoms. These oxygen atoms may interact with the surface hydroxy groups.

When $Cu(acac)_2$ adsorbed on the zeolite in the presence of aniline was allowed to stand for a few days at room temperature, the spectral line at $g=2.004$ in Fig. 3 (a) grew considerably, whereas the other lines arising from the complex slightly decayed (Fig. 3 (c)). The saturation curves for microwave power of the former line and of the latter lines were recorded according to the methods described by Bloembergen and Wang.[17] It was found from the curves that the former line easily saturates with microwave power. These results suggest that there is a possibility of the formation of a cation radical by the electron transfer from aniline to $Cu(acac)_2$. The ionization potential of aniline, which was measured by the photoionization method, is 7.7 eV.[18] This value is quite low.

When the temperature of the system was raised, the intensity of the signal due to the cation radical increased remarkably and became constant near 130°C. From the increase in the radical concentration, it may be deduced that the mixing of the lone-pair orbital with an orbital of the copper atom occurs to a greater extent as a result of the strong interaction between the copper atom and the aniline molecule at elevated temperatures, and that it accelerates the electron transfer. The formation of radical was observed in the solution containing aniline.

The effect of the zeolite on aniline in the absence of $Cu(acac)_2$ was examined in an additional experiment. When aniline was adsorbed on the zeolite, a weak line, probably due to the cation radical, was observed at the same position as above, but its intensity did not increase at higher temperatures. It can be concluded from these facts that the cation radical formed in the system of $Cu(acac)_2$-aniline on the zeolite arises mainly from the electron transfer and partly from some other mechanism.

The author wishes to express his hearty thanks to Professor Masaji Miura and Dr. Akinori Hasegawa for their valuable discussions and encouragement throughout this work.

15) H. Yokoi, M. Sai, and T. Isobe, This Bulletin, **42**, 2232 (1969).
16) B. R. McGarvey, *J. Phys. Chem.*, **71**, 51 (1967).
17) N. Bloembergen and S. Wang, *Phys. Rev.*, **93**, 72 (1954).
18) K. Watanabe, *J. Chem. Phys.*, **26**, 542 (1957).

Electron Spin Resonance Studies of Bis(acetylacetonato)copper(II) Adsorbed on X-Type Zeolite. II. The Substitution Reaction of Ligands with Pyridine

Yoshio YAMADA*

Department of Chemistry, Faculty of Science, Hiroshima University, Higashisenda-machi, Hiroshima

(Received June 7, 1971)

The interaction of bis(acetylacetonato)copper(II) ($Cu(acac)_2$) adsorbed on X-type zeolite of the sodium form with pyridine was investigated by means of ESR. When a pyridine vapor was introduced to $Cu(acac)_2$ on the zeolite, the spectral lines of the perpendicular g component for $Cu(acac)_2$ were replaced by those consisting of a superhyperfine structure, which arises from the ligand nitrogen atoms. The observed spectrum was assigned to $[Cu(pyridine)_4]^{2+}$. Such a characteristic substitution reaction of $Cu(acac)_2$ with pyridine was not, however, observed on silica gel nor in ordinary solvents. It is pointed out, on the basis of these results and of the considerations described in a preceding paper, that the reaction involves the following mechanism: the interaction of quasi-π-electrons in $Cu(acac)_2$ with an electrostatic field originating from the cation on the zeolite lowers the stability of $Cu(acac)_2$, and the complex is attacked by two adsorbed pyridine molecules and two pyridinium ions which are formed by the combination with protons on acid sites, resulting in the substitution reaction. In addition, $[Cu(pyridine)_4]^{2+}$ was produced on other cation-exchanged zeolites and silica-alumina. The substitution reaction was also found when α-, β-, or γ-picoline was used instead of pyridine.

The interaction of adsorbed bis(acetylacetonato)-copper(II) ($Cu(acac)_2$) with the surface and the effect of ammonia and aniline on the complex were studied in the preceding paper (hereafter to be designated as part I). With regard to the interaction with pyridine, we[1] have recently reported that a ligand-substitution reaction occurs on the introduction of pyridine to $Cu(acac)_2$ adsorbed on the zeolite. Yokoi *et al.*[2] have found a substitution reaction with pyridine in the solution of bis(ethylacetoacetato)copper(II) or bis(salicylaldehydrato)copper(II). They have pointed out, however, that $Cu(acac)_2$ brings about no substitution reaction with pyridine in a chloroform solution. It is known, with respect to $Cu(acac)_2$ and other copper(II) β-diketone chelate complexes, that some heterocyclic bases coordinate to the complex as one or two apical ligands in ordinary solvents, such as chloroform or toluene, and that an adduct is formed.[2-6] Therefore, in order to explain the difference between the reactivity of the complex on the surface and that in solution, a reaction mechanism is proposed on the basis of the influence of the surface, and, at the same time, the assignment attempted in the short communication[1] is reconsidered in the present work.

Experimental

The X-type zeolite of the sodium form (NaX zeolite) is the same as that used in part I. The cation-exchanged zeolites, NH_4X (NH_4X may not be a precise representation, because ammonia gas is released from NH_4X zeolite by the evacuation at 500°C and protons are considered to be present on the surface.), LiX, and CaX, were prepared from the original NaX zeolite by the conventional method.[7] The amount of the sodium ion exchanged was determined by means of atomic-absorption spectroscopy. The percentage of the exchanged cation was 96.1, 86.0, or 94.4 for NH_4X, LiX, or CaX respectively. Silica-alumina (alumina content *ca.* 40%) was synthesized from ethyl orthosilicate and aluminum isopropoxide. GR-grade pyridine was further purified by distillation under a vacuum. The IR spectra were obtained using a Hitachi EPI-S2 spectrophotometer. The preparation of the other samples and the procedure of the measurements have been described in part I.

Results and Discussion

The Formation of $[Cu(pyridine)_4]^{2+}$ on NaX Zeolite. When $Cu(acac)_2$ adsorbed on NaX zeolite was exposed to pyridine vapor at room temperature, the spectrum presented in Fig. 1 (a) was observed. This spectrum differs remarkably at the perpendicular g component ($g_\perp$) from that due to $Cu(acac)_2$ on the zeolite, which has been shown in Fig. 1 (a) of part I. The variation in the spectrum suggests the conversion of $Cu(acac)_2$ into another complex. When the sample was allowed to stand for a few days at room temperature, the relative intensities of the spectral lines at the $g_\perp$ component changed slightly. However, as can be seen from Figs. 1 (a) and (b), they altered considerably after the sample had been heated at 100°C and the excess pyridine had been removed. These results show that the formation of the new complex is slow at room temperature, but is accelerated by heating. The spectrum in Fig. 1 (b) consists of many lines with a coupling constant of 16 gauss; this value was determined from the splitting between lines at the central part of the $g_\perp$ component. Figure 1 (c) shows a K-band spectrum in the $g_\perp$ region, which is remarkably broad in contrast to that at the

* Present address: National Research Institute for Pollution and Resources, Kawaguchi, Saitama, Japan.

1) Y. Yamada, A. Hasegawa, and M. Miura, This Bulletin, **43**, 2661 (1970).

2) H. Yokoi, M. Sai, and T. Isobe, *ibid.*, **43**, 1078 (1970).

3) H. A. Kuska, M. T. Rogers, and R. E. Drullinger, *J. Phys. Chem.*, **71**, 109 (1967).

4) D. P. Graddon, *Nature*, **183**, 1610 (1959).

5) D. P. Graddon and E. C. Watton, *J. Inorg. Nucl. Chem.*, **21**, 49 (1961).

6) A. F. Garito and B. B. Wayland, *J. Amer. Chem. Soc.*, **91**, 866 (1969).

7) T. I. Barry and L. A. Lay, *J. Phys. Chem. Solids*, **27**, 1821 (1966).

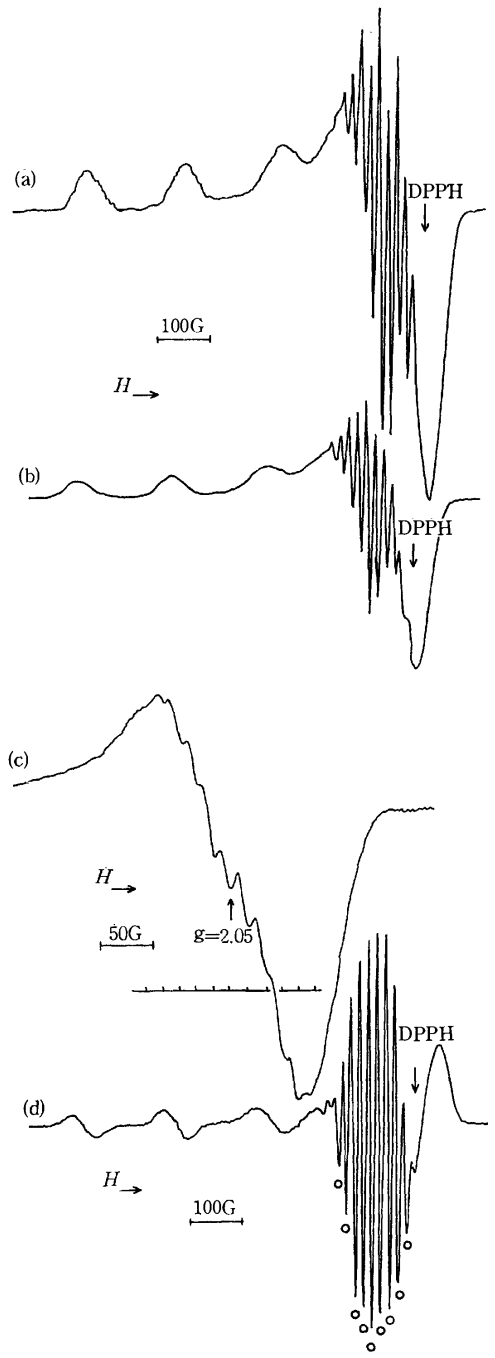

Fig. 1. (a) ESR spectrum of $Cu(acac)_2$ on NaX zeolite in the presence of pyridine at 77°K, (b) spectrum measured at 77°K, after sample (a) was heated at 100°C and excess pyridine was removed, (c) K-band spectrum of sample (a) at 77°K, and (d) second derivative X-band spectrum of sample (b) at 77°K.

X-band. Nevertheless, the observed spectrum consists of lines with a nearly equal splitting of about 16 gauss. Therefore, the separation of $g_\perp$ components, g_x and g_y, due to the deviation from axial symmetry can be disregarded and the value of the coupling constant determined from the X-band spectrum is confirmed.

The superhyperfine (shf) structure arising from the coupling with the nitrogen nucleus of pyridine contributes to the observed spectral lines at the $g_{//}$ component. Therefore, the shf structure should be observed on each of the four lines constituting the parallel hyperfine (hf) structure from the copper atom. Unfortunately, the resolved shf structure in the $g_{//}$ region could not be found, even on the second derivative spectrum (Fig. 1 (d)), but the linewidth of the individual hf structure showed a considerable broadening compared with that for $Cu(acac)_2$ on the zeolite. In a short communication,[1] it has been concluded, on the basis of the 11 lines observed at the $g_\perp$ component, that two of the four oxygen atoms originally coordinating to the cupric ion are replaced by two pyridine molecules. However, an ambiguity remains in this assignment, because the complexity of the spectrum caused by angular anomalies,[8] the electric quadrupole interaction of copper, and the isotope of copper makes it difficult to determine exactly the number of the lines at the $g_\perp$ component. In addition, the number of the lines depends not only on the number of pyridine molecules coordinating to the cupric ion, but also on the ratio of the splitting constant of the copper nucleus to that of the ligand nitrogen nucleus. Since the isotropic hf structure was not observed for this system, it was impossible to determine the perpendicular hf coupling constant of the copper nucleus. Thus, no assignment for the complex can be made. However, the second derivative spectrum shown in Fig. 1 (d) is similar to that for a complex formed in the pyridine - chloroform solution of $CuCl_2$ at 77°K.[9] Moreover, the values of the magnetic parameters obtained from the spectrum of Fig. 1 (b), *i.e.*, $A_{//}$ and $g_{//}$, correspond to those for the complex, in which four pyridine molecules coordinate to the cupric ion in a methanol solution.[10] The intensities of the nine lines at the central part shown in Fig. 1(d) are remarkably stronger than those of the other parts. These lines are represented by circles.

Gersmann and Swalen[9] have reported that the value of the perpendicular hf coupling constant from the copper nucleus is negligibly small in the spectrum observed for $CuCl_2$ in pyridine - chloroform. The same result has also been obtained for $[Cu(pyridine)_4]^{2+}$ in methanol.[10] Hence, assuming that these results can be applied in the present case, the nine intense peaks may be considered to be due only to a shf structure arising from the coupling with four equivalent nitrogen atoms, whereas the weak remaining peaks in the $g_\perp$ region may originate from angular anomalies,[8] the transition with $m_I > 0$ due to the electric quadrupole interaction, and the isotopes of copper. These results and considerations lead to the conclusion that the four chelating oxygens of $Cu(acac)_2$ on the zeolite are replaced by four pyridine molecules after the introduction of pyridine, resulting in the formation of a new complex, $[Cu(pyridine)_4]^{2+}$. The substitution reaction was also suggested by the IR measurements; the absorption band at 1580 cm^{-1} for $Cu(acac)_2$ on the zeolite, which has been assigned to the stretching of chelating carbonyl groups,[11] disappears with the adsorption of pyridine.

8) L. D. Rollmann and S. I. Chan, *J. Chem. Phys.*, **50**, 3416 (1966).
9) H. R. Gersmann and J. D. Swalen, *ibid.*, **36**, 3221 (1962).
10) K. Takimoto, A. Hasegawa, and M. Miura, unpublished results.
11) R. L. Belford, A. E. Martell, and M. Calvin, *J. Inorg. Nucl. Chem.*, **2**, 11 (1956).

TABLE 1. MAGNETIC AND BONDING PARAMETERS OF THE COPMLEXES ON SILICA GEL AND NaX ZEOLITE

	$\lvert A_{//}\rvert \times 10^4\text{cm}^{-1}$	$\lvert A_{\perp}\rvert \times 10^4\text{cm}^{-1}$	$g_{//}$	$g_{\perp}$	α^2	α'^2	β_1^2
$Cu(acac)_2/SiO_2$	195	28	2.253	2.055	0.86	0.21	0.72
$Cu(acac)_2$-pyridine/SiO_2	166	43	2.311	2.050	0.83	0.24	0.90
$Cu(acac)_2$/NaX zeolite	190	31	2.264	2.043	0.85	0.22	0.75
$[Cu(pyridine)_4]^{2+}$/NaX zeolite	196	—	2.254	2.052	0.86	0.22	0.74

The values of the magnetic parameters determined from the spectra of Fig. 1 (b) and of the bonding parameters, calculated using Eqs. (1), (2), and (3) of part I, are listed in Table 1. The observed $|A_{//}|$ value of $[Cu(pyridine)_4]^{2+}$ on the zeolite is larger than that of $Cu(acac)_2$. The result can be explained in terms of the fact that the strong coordination of pyridine along the equatorial axis accompanies an increase in covalent character, that is, the promotion of the unpaired electron to the 4*s* copper orbital, and brings about a positive contribution to the $|A|$ value.[12,13] A similar result has been obtained in the case of copper phthalocyanine[14] or copper tetraphenylporphine,[15] in which the cupric ion is coordinated with four ligand nitrogen atoms. The in-plane σ-bonding of these complexes is known to be highly covalent. Thus, $[Cu(pyridine)_4]^{2+}$ is considered to exhibit a considerably covalent character in the copper-nitrogen σ-bonding. However, an unexpected increase in α^2 was obtained (Table 1). This can be interpreted as being caused by the fact that a constant value of κ_0 is used in the calculation of α^2, as has been described in part I.

On the other hand, the value of α'^2 can also be evaluated from the observed shf coupling constant of the nitrogen atoms, independent of the hf coupling constant due to the copper nucleus. The relations between α'^2 and the shf coupling constants are expressed by the following two formulas:[16]

$$A_{//}^{N} = \left(\frac{\alpha'}{4}\right)^2 (2\gamma\beta_0\beta_N)\left[-\frac{8\pi}{9}|\rho_s(0)|^2 + \frac{8}{15}\langle r_p^{-3}\rangle\right] \quad (1)$$

$$A_{\perp}^{N} = \left(\frac{\alpha'}{4}\right)^2 (2\gamma\beta_0\beta_N)\left[-\frac{8\pi}{9}|\rho_s(0)|^2 - \frac{1}{15}\langle r_p^{-3}\rangle\right] \quad (2)$$

where $A_{//}^{N}$ and $A_{\perp}^{N}$ are the shf coupling constants in the directions of the N–Cu–N axis and perpendicular to it respectively, where $|\rho_s(0)|^2$ is the 2*s* electron density at the nitrogen nucleus; r_p, the radius of the 2*p* nitrogen orbital; γ, the gyromagnetic ratio of the ^{14}N nucleus, being set as 0.4036; β_0, the Bohr magneton, and β_N, the nuclear magneton. Maki and McGarvey[16] have calculated $|\rho_s(0)|^2 = 33.4\times10^{24}\text{cm}^{-3}$ for the 2*s* function and $\langle r_p^{-3}\rangle = 21.1\times10^{24}\text{cm}^{-3}$ for the 2*p* function. By the substitution of the parallel shf coupling constant observed at the $g_{\perp}$ component of the copper, $A_{//}^{N} = 15.3\times10^{-4}\text{cm}^{-1}$, into Eq. (1), $\alpha'^2 = 0.40$ was obtained. Even if the experimental errors are taken into account, this value is still considerably different from that calculated from α^2. This deviation seems to be responsible for the overestimation of α^2 described above. The large parallel shf coupling constant indicates that the copper-nitrogen bond is strong and highly covalent. This result is consistent with that derived from the hf coupling constant of the copper atom.

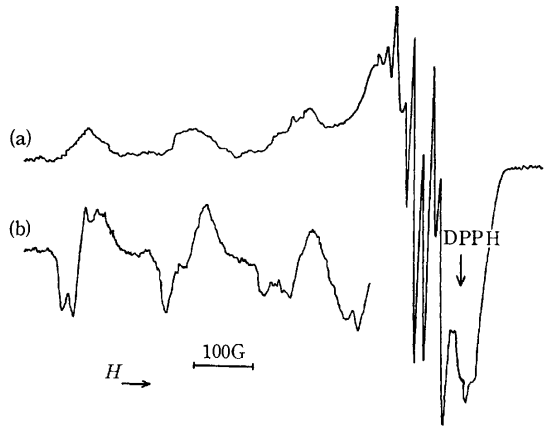

Fig. 2. (a) First and (b) second derivative spectra of $Cu(acac)_2$ on NaX zeolite in the presence of γ-picoline, measured at 77°K after the sample was heated at 80°C.

The Substitution of $Cu(acac)_2$ on the Zeolite with Picoline. When α-, β-, or γ-picoline was used instead of pyridine, the spectra obtained were similar to that observed in the case of pyridine. Figure 2 (a) shows a typical spectrum. The shf structure due to $[Cu(picoline)_4]^{2+}$ is also seen on this spectrum, but the intensity ratio of each peak is irregular. The second derivative spectrum in the $g_{//}$ region of Fig. 2 (a) was measured (Fig. 2 (b)). By taking into account the finding that two sets of hf structure are observed in the $g_{//}$ region, two species of the complex are thought to be formed on the zeolite. Hence, it may be deduced that the irregularity is caused by the superposition of the spectra due to the two molecular species. The stability of these complexes lowers in the sequence of γ-, β-, α-picoline; the intensity of the spectrum decreases near 110, 130, and 140°C for the complexes of $[Cu(\alpha\text{-picoline})_4]^{2+}$, $[Cu(\beta\text{-picoline})_4]^{2+}$, and $[Cu(\gamma\text{-picoline})_4]^{2+}$ respectively. On the other hand, $[Cu(pyridine)_4]^{2+}$ is stable even at 150°C. From these results, the stability of these complexes may be considered to be responsible for the differences in the structure arising from the position of the methyl group and in the interaction with the surface.

The Interaction of $Cu(acac)_2$ with Pyridine on the Various Surfaces. Figures 3, 4, and 5 show the spectra recorded after the introduction of pyridine to $Cu(acac)_2$

12) H. A. Kuska and M. T. Rogers, *J. Chem. Phys.*, **43**, 1744 (1965).
13) B. R. McGarvey, *J. Phys. Chem.*, **71**, 51 (1967).
14) S. E. Harrison and J. M. Assour, *J. Chem. Phys.*, **40**, 365 (1964).
15) J. M. Assour, *ibid.*, **43**, 2477 (1965).
16) A. H. Maki and B. R. McGarvey, *ibid.*, **29**, 35 (1958).

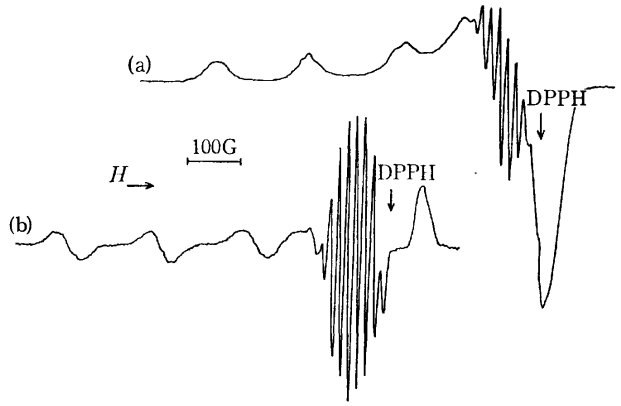

Fig. 3. (a) First and (b) second derivative spectra of $[Cu(pyridine)_4]^{2+}$ on LiX zeolite at 77°K.

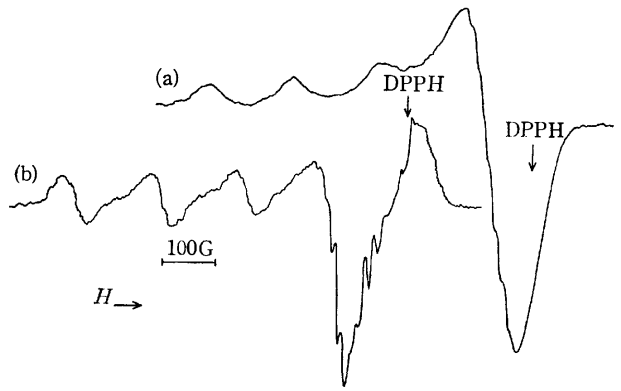

Fig. 4. (a) First and (b) second derivative spectra of $[Cu(pyridine)_4]^{2+}$ on NH_4X zeolite at 77°K.

adsorbed on LiX, NH_4X, and CaX zeolites respectively. In the case of LiX zeolite, the shf structure in the $g_\perp$ region is discernible in the first derivative spectrum. On the other hand, for the complex on NH_4X or CaX zeolite, the structure is hardly observed in the first derivative because of the linewidth broadening, but it becomes appreciable in the second derivative (Figs. 4 (b) and 5 (b)). All of these spectra have the same shf coupling constant in the $g_\perp$ region as that for the spectrum of $[Cu(pyridine)_4]^{2+}$ on NaX zeolite. Therefore, $[Cu(pyridine)_4]^{2+}$ must be produced also on these zeolites. Moreover, not only on these zeolites, but on

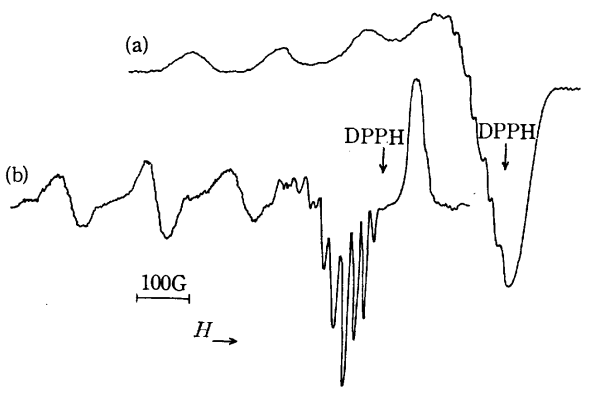

Fig. 5. (a) First and (b) second derivative spectra of $[Cu(pyridine)_4]^{2+}$ on CaX zeolite at 77°K.

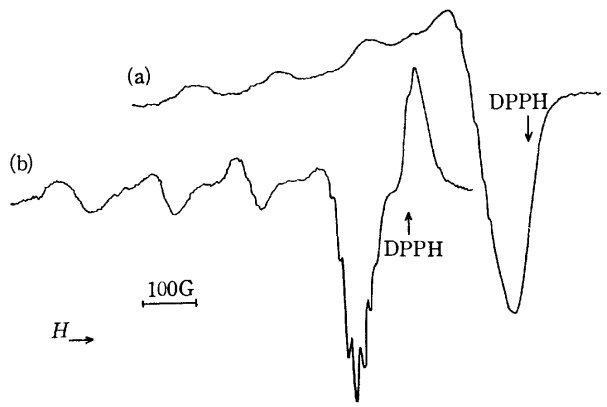

Fig. 6. (a) First and (b) second derivative spectra of $[Cu(pyridine)_4]^{2+}$ on silica-alumina at 77°K.

silica-alumina, the formation of $[Cu(pyridine)_4]^{2+}$ can be recognized from the second derivative spectrum in Fig. 6 (b).

When $Cu(acac)_2$ on silica gel was exposed to pyridine vapor, a spectrum which is remarkably different from that of $[Cu(pyridine)_4]^{2+}$ formed on NaX zeolite appeared, as can be seen in Fig. 7. The magnetic and bonding parameters determined from the spectrum in

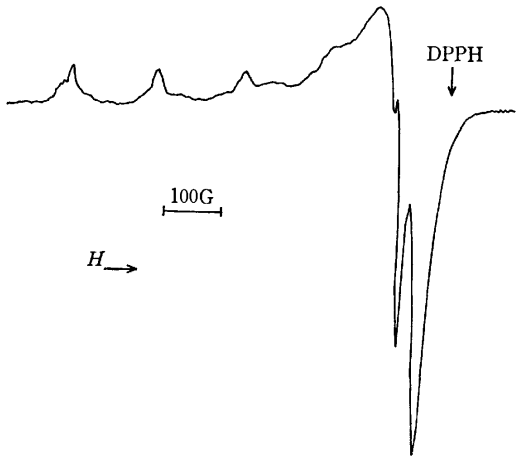

Fig. 7. Spectrum of $Cu(acac)_2$ on silica gel in the presence of pyridine at 77°K.

Fig. 7 are summarized in Table 1. The value of $|A_{//}|$ decreases, but the value of $g_{//}$ increases, in striking contrast to the variation in the parameters of the spectrum observed on NaX zeolite. This means that an adduct is formed, as has been described in part I. Therefore, it can be concluded that such a substitution reaction as observed on the zeolites does not occur on silica gel. This conclusion is predictable from the findings presented in part I; since $Cu(acac)_2$ on silica gel is stable even at 180°C, it is considered that the interaction of quasi-π-electrons in $Cu(acac)_2$ with the surface is weak.

The Mechanism for the Formation of $[Cu(pyridine)_4]^{2+}$. Though the characteristic substitution reaction was not observed in ordinary solvents,[1] the coordination of pyridine along the molecular plane was found in the solution of ethanol - water at pH$\leqq$3. It has already been reported that the following reaction takes place in the

aqueous ethanol solution at a low pH:[17]

$$Cu(acac)_2 + H^+ \rightleftarrows [Cu(acac)]^+ + \text{acetylacetone}$$

Accordingly, the proton may participate also in the substitution reaction on NaX zeolite.

As has been described in part I, the magnetic parameters of the complex on the zeolite are similar to those in toluene. In addition, an IR absorption band due to the stretching of the chelating carbonyl group is observed for $Cu(acac)_2$ on zeolite. Therefore, it is unnecessary to consider that, before the introduction of pyridine, $Cu(acac)_2$ dissociates into Cu^{2+} and two acetylacetone molecules through interaction with NaX zeolite.

Ward[18] has shown, by means of the IR spectra, that NaX zeolite dehydrated fully at 500°C has no detectable Brönsted and Lewis acids, while Watanabe and Habgood[19] have detected the Brönsted acid sites by heating the zeolite under a vacuum at temperatures between 150 and 200°C. Since chloroform contains a trace amount of water,[20] there is a further possibility that the water associated with cation-deficient centers produces the Brönsted-acid sites. Hence, it is thought that the Brönsted-acid sites combine with the adsorbed pyridine molecules to form pyridinium ions. On the other hand, as has been described in part I, the quasi-π-electrons in $Cu(acac)_2$ interact with the electrostatic field of the cations on zeolites and the complex becomes unstable. Consequently, it can be concluded that two pyridine molecules and two pyridinium ions attack the unstable complex and substitute themselves for the acetylacetone molecules.

When the zeolite was exposed to pyridine vapor and $Cu(acac)_2$ was then adsorbed on the zeolite, only a faint, broad singlet spectrum was observed, showing that the substitution reaction did not occur. This may be due to the facts that the acid sites are poisoned by the pyridine molecules and that the electrostatic field from the sites is screened. From the results, it seems reasonable to consider that the stability of the complex is not lowered significantly because the interaction of the complex with the zeolite is weakened by the preadsorption of pyridine.

In conclusion, the substitution of the ligands in $Cu(acac)_2$ with pyridine molecules was found to occur on various zeolites and silica-alumina, but not on silica gel and in ordinary solvents. The complex formed on the zeolites and silica-alumina was identified as $[Cu(pyridine)_4]^{2+}$ on the basis of the various results and considerations. This reaction was interpreted in terms of both the instabilization of $Cu(acac)_2$ caused by the interaction of the quasi-π-electrons in $Cu(acac)_2$ with the electrostatic field of the cations on zeolites, and the attack of two pyridine molecules and two pyridinium ions. Such a substitution reaction was also observed on NaX zeolite using α-, β-, or γ-picoline instead of pyridine, though the complexes produced were less stable than $[Cu(pyridine)_4]^{2+}$.

The author wishes to express his hearty thanks to Professor Masaji Miura and Dr. Akinori Hasegawa of Hiroshima University for their valuable discussions. Special thanks are also due to Assistant Professor Koichi Itoh of Osaka University for his generous permission to use the ESR spectrometer with a K-band.

17) A. H. I. Ben-Bassat and G. Frydman-Kupfer, *Bull. Soc. Chim. Fr.*, **1963**, 2284.
18) J. W. Ward, *J. Catal.*, **14**, 365 (1969).
19) Y. Watanabe and H. W. Habgood, *J. Phys. Chem.*, **72**, 3066 (1968).
20) It was impossible to eliminate completely a trace amount of water from the chloroform.

The Dehydrogenation of Amines by Molten Metal Catalysts[1]

Kiyohisa Okano, Yasuo Saito, and Yoshisada Ogino
Department of Chemical Engineering, Faculty of Engineering, Tohoku University, Aramaki Aoba, Sendai
(Received June 7, 1971)

In order to investigate the catalytic activity of molten metal, experiments were carried out using the dehydrogenation of *n*-butylamine, benzylamine, and cyclohexylamine as test reactions. The molten zinc catalyst was thus found to show specially high activities and selectivities in all test reactions. The activity of the molten gallium catalyst for the dehydrogenation of *n*-butylamine was also considerable. However, the selectivity of this catalyst was somewhat lower than that of the molten zinc catalyst, and considerable amounts of dibutylamine were produced at lower reaction temperatures. The other molten metals were found to be almost inactive. That is, Pb, Cd, Sn, and Bi were inactive, while Tl and In were only slightly active.

The present authors have undertaken a systematic study of the catalysis of liquid metals and have found that some liquid metals, such as zinc and indium, efficiently dehydrogenate methanol,[2] *n*-butanol,[3] *iso*-butanol,[3] and *sec*-butanol.[3] Further studies of the dehydrogenation of the other alcohols, including cyclohexanol and benzyl alcohol, are now proceeding.

Although the details of the mechanism of the catalysis by the liquid metal have not yet been clarified, it is assumed that the interaction between lone-pair electrons around the oxygen atom of alcohol causes the dehydrogenation of alcohol. By extending this idea, it can be expected that the dehydrogenation of amine is catalyzed by the liquid metal. The present work has been undertaken to confirm this expectation.

Experimental

Catalysts. The liquid zinc (Zn-L) was mainly used as a catalyst in the present work. However, in some cases, other liquid metals, *i.e.* In-L, Tl-L, Ga-L, Pb-L, Cd-L, and Bi-L, were also examined.

Reactants. The *n*-butylamine, benzylamine, and cyclohexylamine were obtained commercially. They were of the highest quality among the available reagents.

Activity Test. The method of the activity test was similar to that described in previous papers.[2,3] The reaction products were analyzed mainly by gas chromatography, but the results were supplemented by chemical analysis and by infrared spectroscopic analysis.

Results and Discussion

Dehydrogenation of n-*Butylamine.* According to the experimental results, Zn-L and Ga-L showed considerably high catalytic activities for the dehydrogenation of *n*-butylamine. The activities of In-L and Tl-L were too low to be measured accurately, and Pb-L, Sn-L, Cd-L, and Bi-L were inactive. Therefore, only the details of the activities of Zn-L and Ga-L will be presented below.

Catalytic Activity of Zn-L for the Dehydrogenation of n-*Butylamine.* The experimental results showed that the catalytic activity of Zn-L persisted for a long period (more than 10 hr). The gaseous products were mainly hydrogen, and the contents of methane, ethane, and ethylene were very small. The main liquid product was *n*-butyronitrile (II). In addition to the main product, a small amount of a liquid by-product was also detected on the gas-chromatographic chart. The retention time of this peak agreed with that of the product of the following reaction[4]:

$$CH_3CH_2CH_2CH_2NH_2 + CH_3CH_2CH_2CHO \longrightarrow CH_3CH_2CH_2CH{=}N{-}CH_2CH_2CH_2CH_3 + H_2O$$

Thus, the by-product was identified as Schiff's base, *i.e.* $CH_3CH_2CH_2CH{=}N{-}CH_2CH_2CH_2CH_3$ (III). The infrared spectra shown in Fig. 1 support this view. The absorption peak appearing at 1660 cm^{-1} indicates the presence of a $-\overset{|}{C}{=}N-$ group.

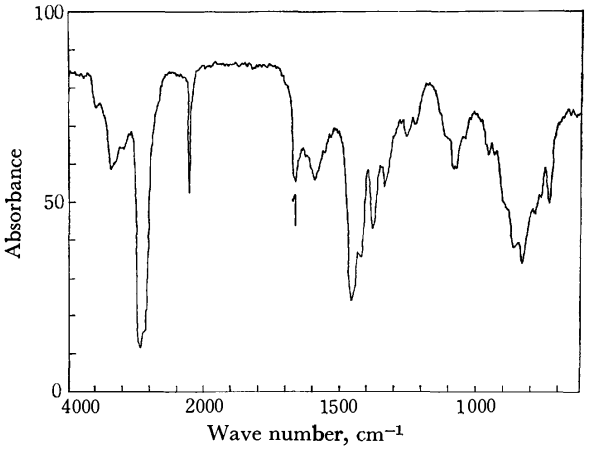

Fig. 1. Infrared spectra of the liquid products obtained by dehydrogenating *n*-butylamine in the presence of the Zn-L catalyst.

1) Studies on Catalysis by Molten Metal. III.

2) Y. Saito, A. Miyamoto, and Y. Ogino, *Kogyo Kagaku Zasshi*, **74**, No. 8, 1521 (1971).

3) K. Kashiwadate, Y. Saito, A. Miyamoto, and Y. Ogino, This Bulletin, **44**, 3004 (1971).

4) The procedures for obtaining Schiff's base (III) (*i.e. N*-butyliden-*n*-butylamine) by a reaction such as that described in the text had been reported by K. N. Campbell *et al.* (*J. Amer. Chem. Soc.*, **66**, 82 (1944)), and by C. W. C. Stein *et al.* (*ibid.*, **64**, 2569 (1942)). In the present research, the products of this reaction was distilled in a nitrogen stream. The isolated material showed a definite boiling point of 142—143°C, which agreed well with the literature values of 141—145°C. Therefore, the isolated material may be identified as *N*-butylidene-*n*-butylamine and may be used as a standard material for the gas-chromatographic analysis, which was carried out under the following conditions: column; 20% PEG20M+10% KOH on cellite 2.25 m, carrier gas; He 8.10 ml/min, temperature; 80°C.

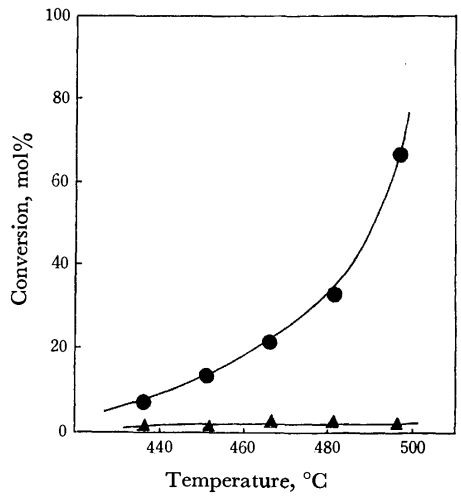

Fig. 2. The temperature dependency of the catalytic activity of Zn-L for the dehydrogenation of *n*-butylamine:
—●— conversion to *n*-butyronitrile, —▲— conversion to Schiff's base. (Zn 70 g, Feed 0.089 mol/hr).

The conversion-*vs*-temperature relation is shown in Fig. 2. As can be seen in this figure, the conversion of *n*-butylamine to *n*-butyronitrile increased steeply with the increase in the reaction temperature, whereas the conversion to Schiff's base increased only a little.

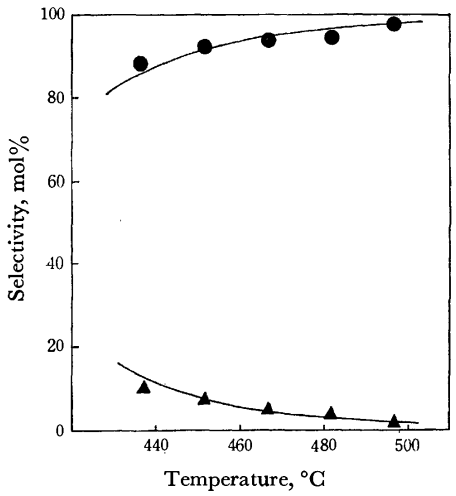

Fig. 3. The temperature dependency of the selectivity of the Zn-L catalyst in the dehydrogenation of *n*-butylamine:
—●— for *n*-butyronitrile, —▲— for Schiff's base. (Zn 70 g, Feed 0.089 mol/hr).

The selectivity-*vs*-temperature relation is shown in Fig. 3. It can be seen in this figure that, with an increase in the reaction temperature, the selectivity for the formation of *n*-butyronitrile increased, while the selectivity for the formation of Schiff's base decreased. Further, it must be noted that the selectivity of the Zn-L catalyst for the formation of nitrile was generally high and that an especially high selectivity (~100%) was obtainable at high reaction temperatures (~500°C).

According to Dolgow,[5] Schiff's base can be regarded as an intermediate product in the catalytic hydrogenation of nitrile. Therefore, the same base may be produced by the reverse reaction, *i.e.*, the dehydrogenation of amine. Presumably, the primary product of the dehydrogenation would be aldimine, *i.e.*, $CH_3CH_2CH_2CH{=}NH$ (I), which is unstable and which can easily be subjected to further dehydrogenation to form nitrile (II). In addition, the aldimine (I) may react with *n*-butylamine to form Schiff's base in the following way:

$$\underset{\text{I}}{CH_3CH_2CH_2CH{=}NH} + CH_3CH_2CH_2CH_2NH_2 \longrightarrow \underset{\text{III}}{CH_3CH_2CH_2CH{=}N\text{-}CH_2CH_2CH_2CH_3} + NH_3$$

Thus, the over-all reaction scheme for the Zn-L catalyzed dehydrogenation of *n*-butylamine may be expressed as follows:

$$n\text{-butylamine} \xrightarrow[\text{Zn-L}]{-H_2} \text{aldimine (I)} \xrightarrow[\text{Zn-L}]{-H_2} n\text{-butyronitrile (II)}$$

$$\text{aldimine (I)} \xrightarrow[\text{Zn-L}]{+n\text{-butylamine}} \text{Schiff's base (III)} + \text{ammonia}$$

According to this reaction scheme (the parallel formation of II and III), when the total conversion of *n*-butylamine reaches zero, the concentrations of both II and III should be extraporated to values which are larger than 0% and smaller than 100%. As can be seen in Fig. 4, the experimental results supported this expectation. If II is consecutively formed *via* III the concentration of II should be extraporated to 0% and the concentration of III should be extraporated to 100%.

Catalytic Activity of Ga-L for the Dehydrogenation of Butylamine. As can be seen in Fig. 5, Ga-L showed a persistent activity for the dehydrogenation of *n*-butylamine. As in the dehydrogenation by the Zn-L catalyst, the main gaseous product was hydrogen, but very small amounts of methane, ethane, and ethylene were also

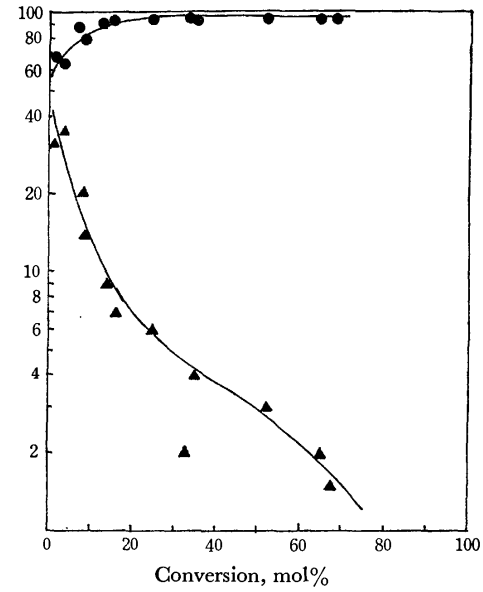

Fig. 4. Relations between the total conversion and the selectivities of the Zn-L catalyst for the formation of *n*-butyronitrile (-●-) and for the formation of Schiff's base (-▲-). (Zn 70 g, Feed 0.089 mol/hr).

5) B. N. Dolgow, "Die Katalyse in der organischen Chemie" VEB Deutscher Verlag der Wissenschaften (1963), p. 285.

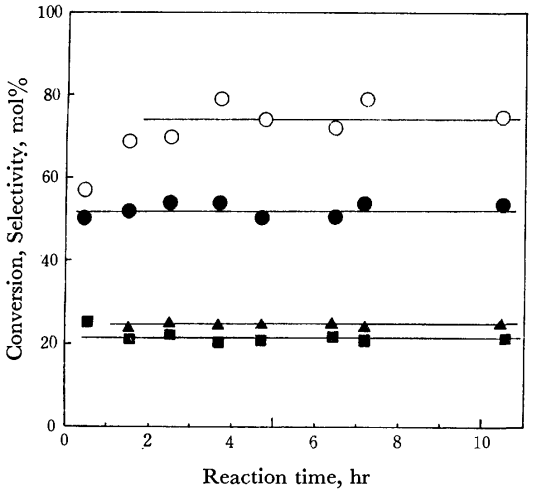

Fig. 5. Relations between the reaction time and the activity of the Ga-L catalyst for the dehydrogenation of *n*-butylamine: -○- total conversion, -●- selectivity for *n*-butyronitrile, -▲- selectivity for dibutylamine, -■- selectivity for Schiff's base. (Ga 40 g, Feed 0.089 mol/hr, Temperature 500°C).

produced. On the other hand, the liquid product[6] contained considerable amounts of dibutylamine, $(CH_3CH_2CH_2CH)_2NH$ (IV), in addition to *n*-butyronitrile (II) and Schiff's base (III).

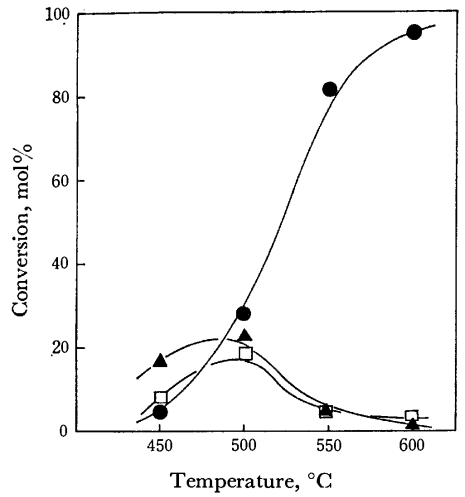

Fig. 6. The temperature dependency of the catalytic activity of the Ga-L catalyst: -●- conversion to *n*-butyronitrile, -▲- conversion to dibutylamine, -□- conversion to Schiff's base. (Ga 40 g, Feed 0.089 mol/hr).

The temperature dependency of the catalytic activity of Ga-L is given in Fig. 6. At lower reaction temperatures, the conversion to nitrile (II) was rather low and the conversion to Schiff's base (III) or the conversion to dibutylamine (IV) was found to be high. However, the conversion to nitrile (II) increased steeply with the increase in the reaction temperature, whereas the conversion both to Schiff's base (III) and to dibutylamine (IV) decreased markedly with the increase in the reaction temperature. Thus, the selectivity for the formation of *n*-butyronitrile (II) increased steeply with the increase in the reaction temperature and reached ~95% at a temperature of 600°C.

As can be seen in Fig. 6, the curve which expresses the relation between the reaction temperature and the conversion of *n*-butylamine to Schiff's base (III) is nearly parallel with the curve which expresses the relation between the reaction temperature and the conversion to dibutylamine (IV). This means that the formation of III is intimately related to the formation of IV. Further information about this point was obtained by plotting each of the fractions, III/III+IV and IV/III+IV, against the conversion of *n*-butylamine to III+IV. As can be seen in Fig. 7, th eIII/III+IV fraction approaches unity, while the IV/III+IV fraction approaches zero, as the conversion is reduced to zero. These facts indicate that IV is formed consecutively from III.

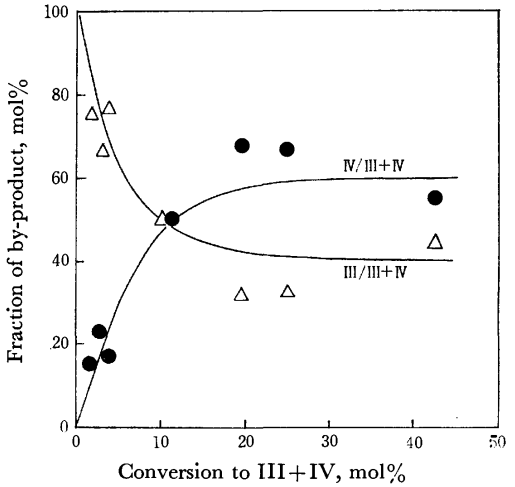

Fig. 7. Relations between the conversion of *n*-butylamine to by-products (dibutylamine and Schiff's base) and the respective fraction of each component in the by-products obtained in the presence of the Ga-L catalyst: -△- fraction of Schiff's base, -●- fraction of dibutylamine. (Ga 40 g, Feed 0.089 mol/hr).

The above-mentioned features of the Ga-L-catalyzed dehydrogenation of *n*-butylamine are somewhat different from those of the Zn-L-catalyzed dehydrogenation, which were described in the previous section; the following reaction scheme[7] seems to be applicable to the Ga-L-catalyzed dehydrogenation:

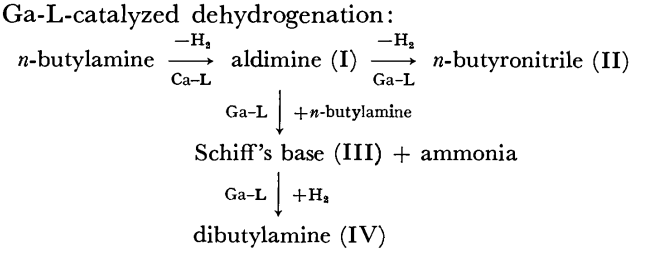

6) Ammonia was also detected, in addition to negligibly small amounts of ethylamine, diethylamine, *n*-propylamine, dipropylamine, acetonitrile, propionitrile, and acrylonitrile. These materials were also found in the products obtained by the use of the Zn–L catalyst.

7) W. S. Brey *et al.* (*Ind. Eng. Chem.*, **51**, 1031 (1959)) dehydrogenated butylamines by using an alumina catalyst and obtained dibutylamine, *N*-butylidenbutylamine, and some other compounds. They proposed a reaction scheme. However, because of the complicated product distribution, their reaction scheme was more complex than the present one.

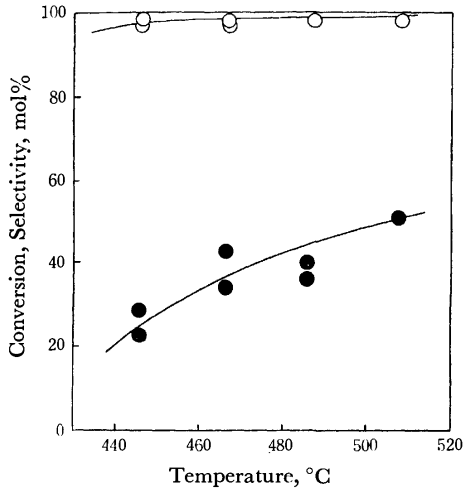

Fig. 8. The temperature dependencies of the catalytic activity and the selectivity of the Zn-L catalyst for the dehydrogenation of benzylamine: -●- total conversion, -○- selectivity for the formation of benzonitrile. (Zn 50 g, Feed 0.068 mol/hr).

Dehydrogenation of Benzylamine. In the dehydrogenation of benzylamine, only Zn-L was used as a catalyst. As can be seen in Fig. 8, Zn-L showed catalytic activity in the dehydrogenation of benzylamine. The reaction products were mainly hydrogen and benzonitrile, and the selectivity of the dehydrogenation was nearly 100% under the present experimental conditions. Thus, the over-all reaction may be expressed simply by:

$$C_6H_5CH_2NH_2 \xrightarrow{\text{Zn-L}} C_6H_5CN + 2H_2$$

Dehydrogenation of Cyclohexylamine. Also in this reaction, only Zn-L was used as a catalyst. According to the experimental results, cyclohexylamine decomposed and evolved hydrogen and ammonia, together with very small amounts of cyclohexene, cyclohexane, and a trace of unidentified compound. The mole ratio of hydrogen to ammonia was nearly 1 : 1. Further, the liquid products gave the infrared spectra shown in Fig. 9. This figure shows the presence of the $-\overset{|}{C}=N-$ group in the the liquid products.

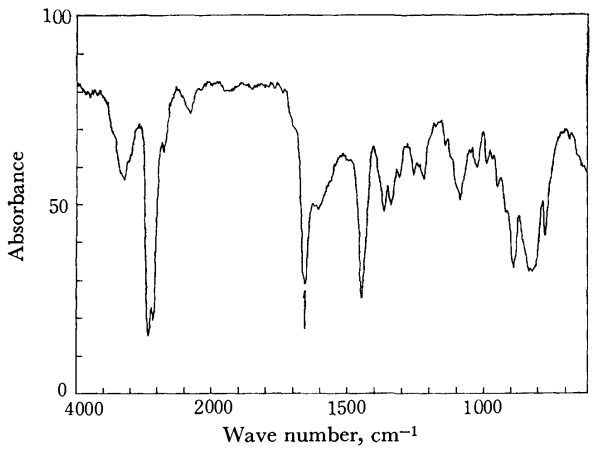

Fig. 9. Infrared spectra of the liquid products obtained by dehydrogenating cyclohexylamine in the presence of the Zn-L catalyst.

Thus, it was suspected that the dehydrogenation product (V) was *N*-cyclohexylidencyclohexylamine, which had been obtained by Pasek *et al.*[8] in the cyclohexylamine decomposition over alumina. To confirm this suspicion, *N*-cyclohexylidencyclohexylamine was prepared by the procedure reported by Pasek *et al.*[8] and properties of this compound were compared with those of the dehydrogenation product. That is, the reaction product (V′) of the following reaction:

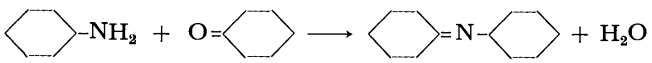

was isolated by means of distillation in a nitrogen stream at a pressure of 20 mmHg. Further, the dehydrogenation product (V) was also isolated by distillation. Then, the properties of V′ and V were compared. The results were as follows; i) both V′ and V crystallized at a given temperature of 26°C and boiled at 132°C (20 mmHg), and ii) the gas-chromatographic retention time[9] of V agreed well with that of V′. These facts indicate that the dehydrogenation product (V) is *N*-cyclohexylidencyclohexylamine. Considering these facts, the over-all reaction may be expressed as follows;

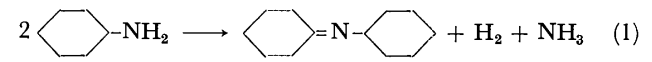

(1)

In the present work, the reaction (1) was assumed to be the main reaction and the conversion of cyclohexylamine was calculated on the base of this scheme. The results are given in Fig. 10.

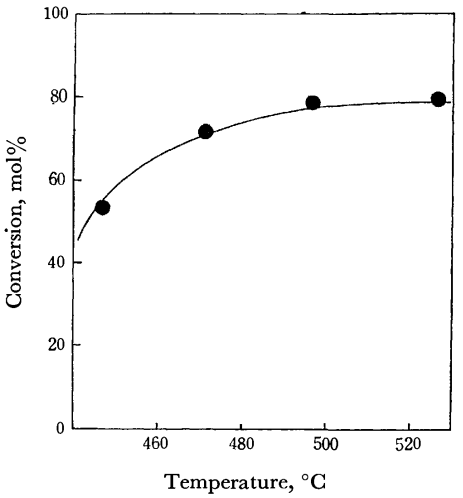

Fig. 10. The temperature dependency of the catalytic activity of the Zn-L catalyst for the dehydrogenation of cyclohexylamine. (Zn 50 g, Feed 0.072 mol/hr).

Presumably, the primary reaction is a dehydrogenation of cyclohexylamine to ketimine, *i.e.*, $C_6H_{10}NH$ (VI). However, because of the high reactivity of this compound, a further reaction between this compound and cyclohexylamine occurs. Therefore, it is not unlikely that the compound (VI) was not detected.

8) J. Pasek, J. Tyrpekl, and M. Machova, *Collect. Czech. Chem. Commun.*, **31**, 4108 (1966).

9) Except for the temperature (135°C), the conditions of the gas-chromatographic analysis were identical with those described in the foot note of the previous section.

Summary

The present work has demonstrated that some liquid metals catalyze the dehydrogenation of amine. Especially, the high activity and the high selectivity of the Zn–L catalyst must be noted. The dehydrogenation of amine by solid catalysts has been said to be difficult,[5] and it has been considered that specially-prepared catalysts[10] are necessary for the selective dehydrogenation of amine. On the contrary, the liquid metal catalysts can be prepared without difficulty. Therefore, the use of the liquid-metal catalyst seems to give a useful tool not only for a scientific study of the dehydrogenation of amine, but also for the industrial dehydrogenation of amine.

10) G. Zuby, C. E. Johonson, and T. D. Nevitt, U. S. 2849478 (1958).

BULLETIN OF THE CHEMICAL SOCIETY OF JAPAN, VOL. 45, 73—77(1972)

Interaction between Phenothiazine Triplet State with Several Electron Acceptors

Teiki IWAOKA, Hiroshi KOKUBUN, and Masao KOIZUMI
Department of Chemistry, Faculty of Science, Tohoku University, Katahira, Sendai

(Received June 14, 1971)

As an extension of the previous paper (This Bulletin, **44**, 341 (1971)) which proposed the formation of a certain charge transfer complex between triplet phenothiazine (PTH^T) and oxygen or dimethylisophthalate, the similar donor-acceptor interaction has been studied between PTH^T and several other acceptors such as dimethylterephthalate (DMTP), nitrobenzene, dinitrobenzene, and terephthalonitrile in deaerated ethanol solutions. In case of DMTP, studies have been made also in cyclohexane. It has been established that all the acceptors except nitrobenzene attack PTH^T with the diffusion controlled rate constant and that in ethanol they give rise to free radical ions and/or solvent shared ion-pair. In cyclohexane, however, no transient species other than triplet has been detected.

Donor and acceptor interaction in the singlet excited state of aromatic compounds has been studied extensively since the discovery of exciplex by Leonhardt and Weller.[1] But very few researches have been reported on the analogous phenomena related with the triplet states of aromatic compounds. As far as we know, Beens and Weller's work[2] on the formation of C-T complex between the triplet state of pyrene and terephthalonitrile, is the only one so far reported. One reason why such investigations are few may be due to the higher ionization potential of the triplet state as compared with that of the singlet excited state, which makes it difficult for such an interaction to occur specifically in the triplet state but not in the ground state. It is expected that for the interaction analogous to the exciplex formation to occur in the triplet state, the ionization potential of donor should be very low or the singlet and triplet energy difference is small. Indeed it has been reported that in some dyestuffs for which S*- and T-levels are close with each other, reactions such as $D^T+D \longrightarrow D^+ + D^-$ or $D^+ + O_2 \longrightarrow D^+ \cdots O_2^-$ really occur.[3]

In the previous paper,[4] we have found that the triplet state of phenothiazine (PTH) with a low ionization potential of 6.9 eV[5] interacts with weak electron acceptors such as oxygen and dimethylisophthalate and forms transiently a certain type of C-T complex. In case of oxygen, an ultimate product was a neutral radical of PTH while the initial compounds were recovered in case of dimethylisophthalate. This paper reports the interaction of triplet PTH with several other electron acceptors.

Experimental

Materials. Dimethylterephthalate was recrystallized three times from G. R. grade ethanol. Nitrobenzene of G. R. grade from Wako Junyaku was used without further purification. *p*-Dinitrobenzene was recrystallized twice from G. R. grade ethanol. Terephthalonitrile was recrystallized from methanol and was sublimed *in vacuo*. Cyclohexane of E. P. grade of Wako Junyaku was shaken with the mixture of fuming sulfuric acid and conc. sulfuric acid (1:1) six times, washed with the aqueous solution of potassium permanganate and then shaken with the aqueous NaOH solution three times. After being washed with water five times, it was kept in contact with metallic sodium for one day and then distilled over sodium metal renewed.

Procedures. Apparatus and procedures for the flash experiment are the usual ones employed in our laboratory. A suitable combination of filters (plate glass, Toshiba-glass filters, UVD-25, VB-40, VB-48, PV-43, *etc.*) was used in the flash apparatus in order to excite only phenothiazine.

1) H. Leonhardt and A. Weller, *Ber. Bunsenges. Physik. Chem.*, **61**, 791 (1963).
2) H. Beens and A. Weller, "Molecular Luminescence," Benjamin Inc. (1969), p. 203.
3) T. Ohno, S. Kato, and M. Koizumi, This Bulletin, **39**, 232 (1966); Y. Usui and M. Koizumi, *ibid.*, **40**, 1041 (1967). L. Lindqvist, *Arkiv Kemi*, **16**, 79 (1960).
4) T. Iwaoka, H. Kokubun, and M. Koizumi, This Bulletin, **44**, 341 (1971).
5) A. Falton and L. E. Lyons, *Aust. J. Chem.*, **21**, 873 (1968).

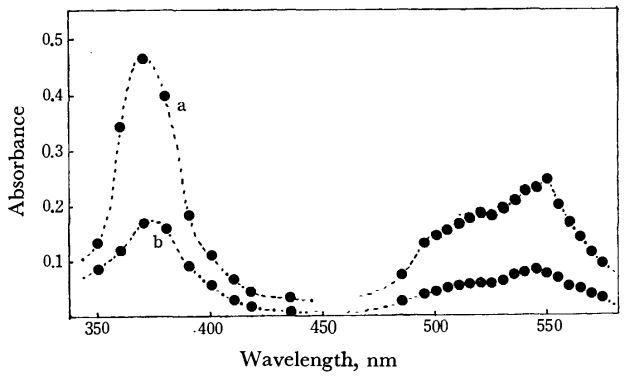

Fig. 1. Transient absorption spectra obtained upon flashing the degassed ethanol solutions of PTH-DMTP;
[PTH]=8.0×10^{-5}M, [DMTP]=1×10^{-4}M
a, immediately after flashing
b, 300 μsec after flashing

Results and Discussion

Interaction between PTH^T and Dimethylterephthalate (DMTP). The electron affinity of DMPT is expected to be a little larger than that of dimethylisophthalate. Figure 1 shows the transient spectrum when the degassed ethanol solution of DMTP (1×10^{-4}M) and PTH (8×10^{-5}M) is flashed. The spectrum resembels that of DMTP radical anion produced when the tetrahydrofuran solution of DMTP is treated with sodium.[6] A little swell in the region 500~520 nm might be due to the PTH cation which should be produced simultaneously. It may be due to the small absorbance that the radical cation is not clearly discerned. The spectrum in Fig. 1 strongly suggests that contrary to dimethylisophthalate, the free radical ion or solvent-shared ion-pair is produced in this system. The decay of the absorbance at 550 nm is of the first order with the same rate constant independent of the DMTP concentration at least when the concentration is lower than 1.0×10^{-5}M. However in case that [DMTP] is 2.5×10^{-5}M or 1.0×10^{-4}M, the early part of the decay is appreciably larger though the latter part decays almost with the same rate constant as that in the lower concentration of DMTP. Table 1 gives the decay constants for the later stage at various DMTP concentrations. Figure 2 shows the change of absorbance with time at different DMTP concentrations. In spite of such situations in the decay curves, the transient spectra in the early and later stages practically coincide, which suggest strongly the coexistence of the free radical ions and the solvent-shared ion-pair. It is reasonable that the latter decays as the first order while the former does in the second order, and the second order decay becomes negligible as the concentration of free ion becomes low.

Table 1. First order decay constants (at the later stage) of the intermediate at various DMTP concentrations (sec^{-1})

[DMTP]	Wavelength, nm		
	380	555	470
1×10^{-4}	3.1×10^{3}	2.2×10^{3}	
2.5×10^{-5}		2.6×10^{3}	2.9×10^{3}
1.0×10^{-5}		2.3×10^{3}	
5.0×10^{-6}	2.6×10^{3}	2.8×10^{3}	2.8×10^{3}
2.5×10^{-6}		2.5×10^{3}	
7.0×10^{-7}		3.1×10^{3}	

6) T. Kowata and M. Koizumi, This Bulletin, **42**, 3352 (1969).

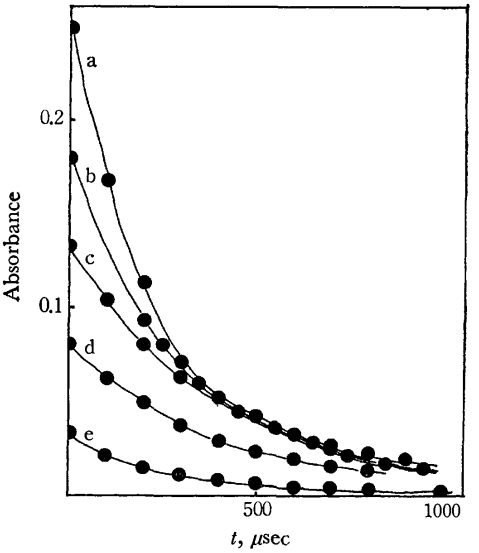

Fig. 2. Change of transient absorption with time at different DMTP concentrations observed at 550 nm.
[PTH]=8.0×10^{-5}M
DMTP concentartion is as follows:
a, 1.0×10^{-4}M b, 2.5×10^{-5}M c, 1.0×10^{-5}M
d, 2.5×10^{-6}M e, 7.5×10^{-7}M

Figure 3 shows the decay of T–T absorption and the rise of absorption at 550 nm. It is clearly seen that these processes occur simultaneously, and this suggests that the 550 nm species is mainly produced from the interaction of triplet PTH and DMTP. Figure 4 gives the decay constant of PTH^T as a function of [DMTP]. From the slope, the rate constant for PTH^T+DMTP $\xrightarrow{k_1}$ is evaluated as $1.4\times10^{9}M^{-1}sec^{-1}$. Figure 5 shows the absorbance at 550 nm immediately after flashing, which is the measure of the yield of transient species, plotted against [DMTP].

Assuming the following scheme

$$^3PTH + DMTP \xrightarrow{k_r} (PTH^+\cdots DMTP^-)$$

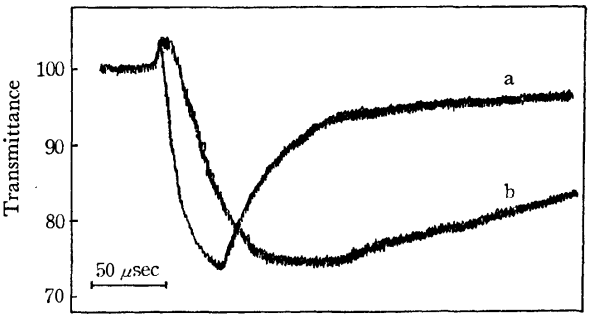

Fig. 3. Change in the transmittance at 470 nm and 550 nm on oscilloscope.
a, 470 nm b, 550 nm

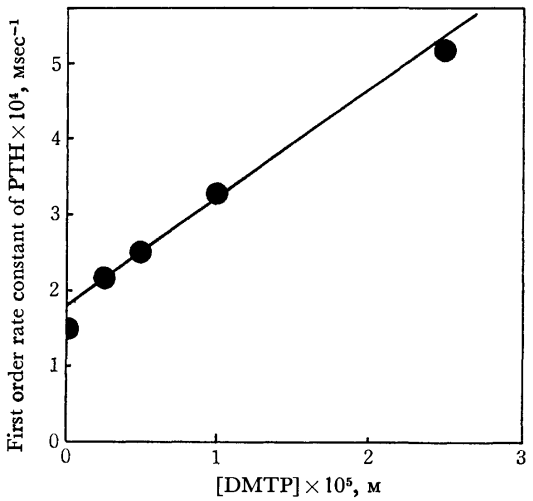

Fig. 4. Dependence of the apparent first order rate constant of phenothiazine triplet state upon the concentration of dimethylterephthalate.
[PTH]=8.0×10⁻⁵M

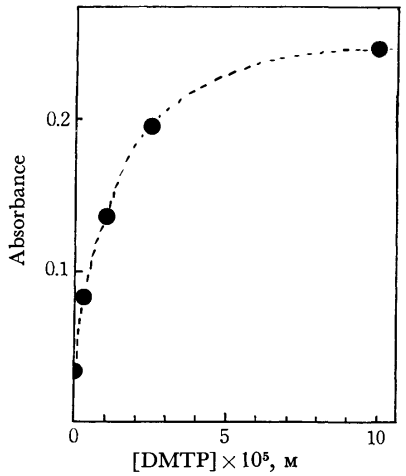

Fig. 5. Plot of the absorbance at 550 nm, immediately after flashing against [DMTP].

$$^3\text{PTH} + \text{DMTP} \xrightarrow{k_q} \text{PTH} + \text{DMTP}$$

$$^3\text{PTH} \xrightarrow{k_d} \text{PTH}$$

and by taking into account the constancy of [PTH] and the flash intensity, the following relation can easily be derived.

$$[\text{PTH}^+\cdots\text{DMTP}^-] = [^3\text{PTH}] \times \frac{k_r[\text{DMTP}]}{k_d + (k_r + k_q)[\text{DMTP}]}$$

If the above scheme holds, the plot $1/[\text{PTH}^+\cdots\text{DMTP}^-]$ *vs.* $1/[\text{DMTP}]$ should be linear. Figure 6 shows that this holds very satisfactorily.

In case of cyclohexane used as a nonpolar solvent, no transient spectrum other than T–T absorption is observable. The decay of T–T absorption increases with the increase in [DMTP] as shown in Fig. 7. From this plot, the rate constant k_1 for $^3\text{PTH}+\text{DMTP} \xrightarrow[\text{in } C_6H_{12}]{k_1}$ is evaluated as $k_1 = 1.3\times10^9\,\text{M}^{-1}\text{sec}^{-1}$.

Interaction of Nitrobenzene and p-*Dinitrobenzene with PTH*^{T}. The addition of 1×10^{-4}M of nitrobenzene

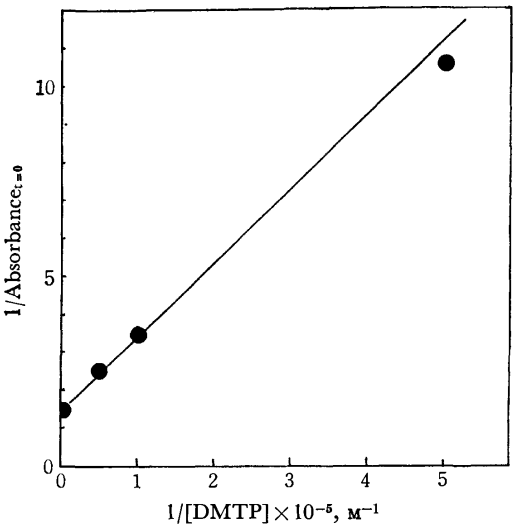

Fig. 6. Plot of 1/Absorbance (at 550nm)$_{t=0}$ against 1/[DMTP].
[PTH]=8.0×10⁻⁵M

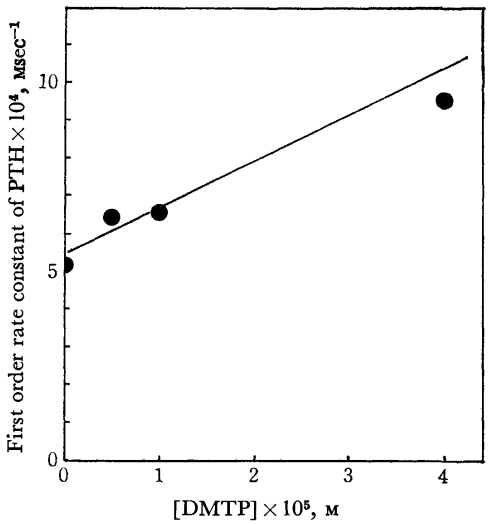

Fig. 7. Dependence of the decay rate of phenothiazine triplet state upon the concentration of dimethylterephthalate in cyclohexane. [PTH]=8.0×10⁻⁵M

(NB) to the deaerated ethanol solution of PTH did not affect the yield of T–T absorption of PTH appreciably. There was no other transient species detected. The decay constant of PTH^T was $4—5\times10^4\,\text{M}^{-1}\text{sec}^{-1}$ as compared with 1.5×10^4 in the absence of NB. Hence the rate constant k_1 for $\text{PTH}^T+\text{NB}\longrightarrow\text{PTH}+\text{NB}$ is estimated to be $\lesssim10^8\,\text{M}^{-1}\text{sec}^{-1}$.

In case of 10^{-2}M *p*-dinitrobenzene (DNB), the strongest acceptor in our experiment,[7] no T–T absorption was observed and the transient spectrum perhaps due to radical cation (PTH^+) was observed in addition to the absorption of radical anion (DNB^-). For 10^{-6}M—10^{-5}M DBN, only the absorption of anion

7) Electron affinity of DNB is estimated to be about 1.7 eV according to R. Foster and P. Hanson, *Biochem. Biophys. Acta*, **112**, 482 (1966). Judging from the absorption spectrum, it is plausible that C-T complex is formed already in the ground state.

radical (DNB^-) was obtained as shown in Fig. 8.[8] It decays according to second order from initial to final, which suggests its existence as free radical anion. Figure 9 shows the dependence of triplet decay upon the DNB concentration. The rate constant k_r for $PTH^T + DNB \xrightarrow{k_r}$ was estimated to be $1.7 \times 10^9 M^{-1}sec$. Dependence of the absorption of DNB anion radical at 630 nm on the concentration of triplet PTH clearly showed the formation of the former by the reaction between DNB and PTH^T.

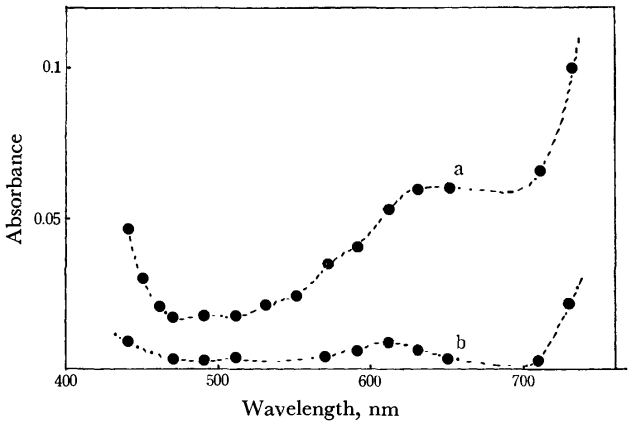

Fig. 8. Transient absorption spectra obtained upon flashing the degassed ethanol solutions of PTH-DNB.
[PTH] $=8.0 \times 10^{-5}$ M, [DNB] $=3 \times 10^{-5}$ M
a, immediately after flashing
b, 8 msec after flashing[7]

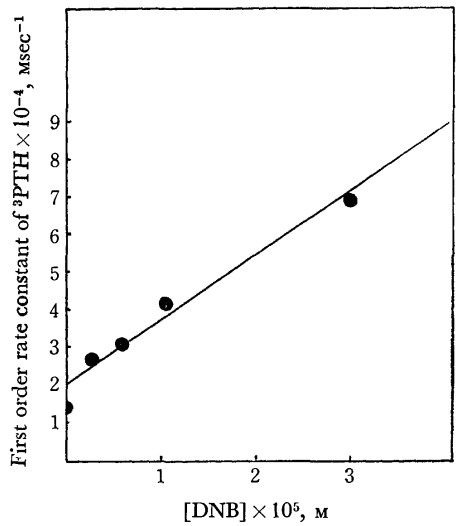

Fig. 9. Dependence of the apparent first order rate constant of phenothiazine triplet state upon the concentration of dinitrobenzene. [PTH] $=8.0 \times 10^{-5}$ M

Interaction of Terephthalonitrile (TPN) with PTH^T. Figure 10 shows the transient spectra of ethanol solutions of 1×10^{-5} M PTH containing TPN of two different concentrations. A short-lived absorption at

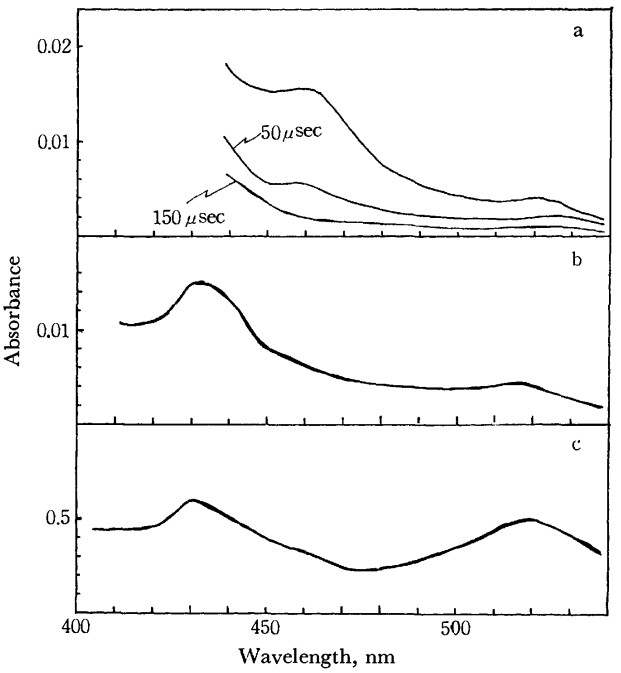

Fig. 10. Transient absorption spectra obtained upon flashing the degassed ethanol solutions of PTH-TPN.
[PTH] $=8.0 \times 10^{-5}$ M
a, [TPN] $=1.0 \times 10^{-5}$ M b, [TPN] $=1.0 \times 10^{-4}$ M
c, Spectrum of the anion radical of terephthalonitrile in tetrahydrofuran.[9]

450—460 nm in Fig. 10a is due without doubt to T–T absorption. In case [TPN] is 1.0×10^{-4} M, T–T absorption does not appear, as shown in Fig. 10b. Figure 10c is the spectrum of $TPN^{\cdot -}$ in tetrahydrofuran obtained by sodium-treatment, as reported by Ishitani and Nagakura.[9] The relative peak height at 430 nm in Fig. 10b is appreciably larger than in Fig. 10c. This suggests the superposition of another species in this region.[10] It was really found that the decay at

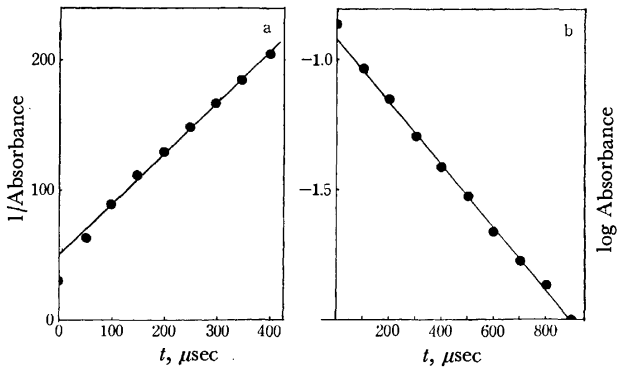

Fig. 11. Second order decay at 520 nm (free TPN^-) and first order decay at 430 nm ($PTH^+ - TPN^-$).
a, 520 nm b, 430 nm

8) According to the referee's unpublished result, the absorption spectrum of DNB radical anion has no peak at ~610 nm clearly seen on curve b. In fact there is no sign of its existence on curve a. The 610 nm peak might be due to some unknown by-product produced secondarily from DNB radical anion.

9) A. Ishitani and S. Nagakura, *Theor. Chim. Acta*, **4**, 236 (1966).

10) According to the referee, TPN radical anion has no absorption in the wavelength region longer than 500 nm only having a peak at ~430 nm; he attributes the peak at 520 nm reported in Ref. 9 to some unknown by-product. If this is true, the peak in question observed in Fig. 10b may be due to the phenothiazine radical cation.

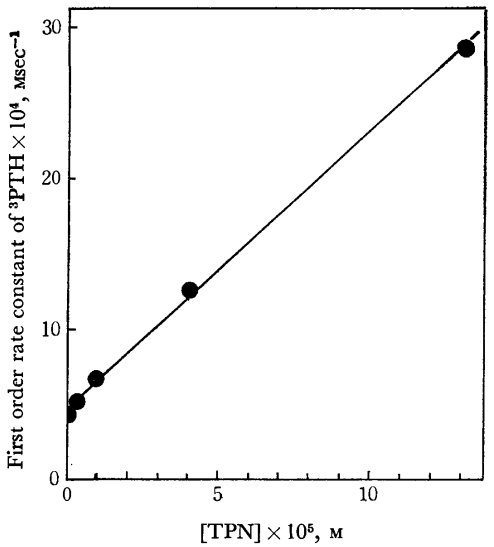

Fig. 12. Dependence of the apparent first order rate constant of phenothiazine triplet state upon the concentration of terephthalonitrile; [PTH] $=8.0 \times 10^{-5}$M.

520 nm in Fig. 10b is of second order as indicated in Fig. 11a and the peak may be attributed to the free TPN^-. The decay at 430 nm on the other hand, obeys the first order as shown in Fig. 11b, and is independent of [TPN]. It is reasonable to consider that free radical ion and the solvent shared ion-pair are produced simultaneously and decay rather independently with each other.

As shown in Fig. 12, the decay of T–T absorption is linearly related with [TPN], and from the slope the rate constant for $PTH^T + TPN \longrightarrow$ is evaluated as $2.0 \times 10^9 M^{-1}sec^{-1}$.

General Discussion. Although the results of the present investigation are still preliminary, we can draw some conclusions from them. First, the electron acceptors with the values of electron affinity larger than 0.7—0.9 eV quench the triplet PTH with almost the rate constant controlled by diffusion irrespective of the solvent polarity. Secondly, the molecular mechanism for triplet quenching is not the T–T energy transfer, because the T-levels of all the present acceptors are higher than that of PTH. It is due, as verified in the present investigation, to various types of donor-acceptor interaction.

In non-polar solvents no transient species other than triplet are observable. Perhaps transient species produced has too short a life time as to be captured by the ordinary flash technique. In polar solvents formations of C-T complex, ion-pair, and the free ions depend on the electron affinity of the acceptor and on the solvent polarity. However, the detailed feature of these donor-acceptor interaction in the triplet state phenothiazine awaits further systematic studies.

Thanks are due to the referee's presentation of his unpublished absorption spectra of DNB and TPN radical anions.

BULLETIN OF THE CHEMICAL SOCIETY OF JAPAN, VOL. 45, 77—81(1972)

Transient Species Obtained by the Flash Photolysis of Chloranil in Various Solutions

Kiyoshi KAWAI,* Yasuhiko SHIROTA,** Hiroshi TSUBOMURA,*** and Hiroshi MIKAWA**

Department of Chemistry, Faculty of Engineering Science, Osaka University, Toyonaka, Osaka

(Received June 17, 1971)

Transient absorption spectra have been obtained by the flash photolysis of chloranil in various organic solvents. In trichlorotrifluoroethane, two T-T′ absorption systems of chloranil were obtained with well-resolved vibrational structures. In tetrahydrofuran, on the other hand, absorption spectra mostly consist of semiquinone radical formed by the hydrogen abstraction from solvent. In benzene and in acetone, the first T-T′ absorption system was much more diffuse and was accompanied by a weak, broad absorption at longer wavelength ($\lambda >$ 550 nm) which might be assigned to a charge transfer absorption from triplet chloranil as acceptor and the solvent molecule as donor. In acetone and in methanol, it has also been found that there is an equilibrium between semiquinone radical and semiquinone anion.

Porter and his co-workers obtained transient absorption spectra by the flash photolysis of quinones and assigned them to semiquinone radicals, semiquinone anions, and relatively short-lived triplet quinones (quinones in the lowest triplet state).[1] Recently, Kemp and Porter[2] illuminated a degassed ethanol solution of chloranil with a nitrogen laser and obtained the transient absorption spectrum of triplet chloranil with a maximum at about 500 nm. The triplet chloranil is expected to have a larger electron affinity than in

* Present address: Central Research Laboratory, Sumitomo Chem. Co., Ltd., Takatsuki, Osaka.

** Department of Chemical Technology, Faculty of Engineering, Osaka University, Suita, Osaka.

*** To whom requests for reprints of this paper should be made.

1) N. K. Bridge and G. Porter, *Proc. Roy. Soc.* (London), **A244**, 259, 276 (1958).

2) D. R. Kemp and G. Porter, *Chem. Commun.*, **1969**, 1029.

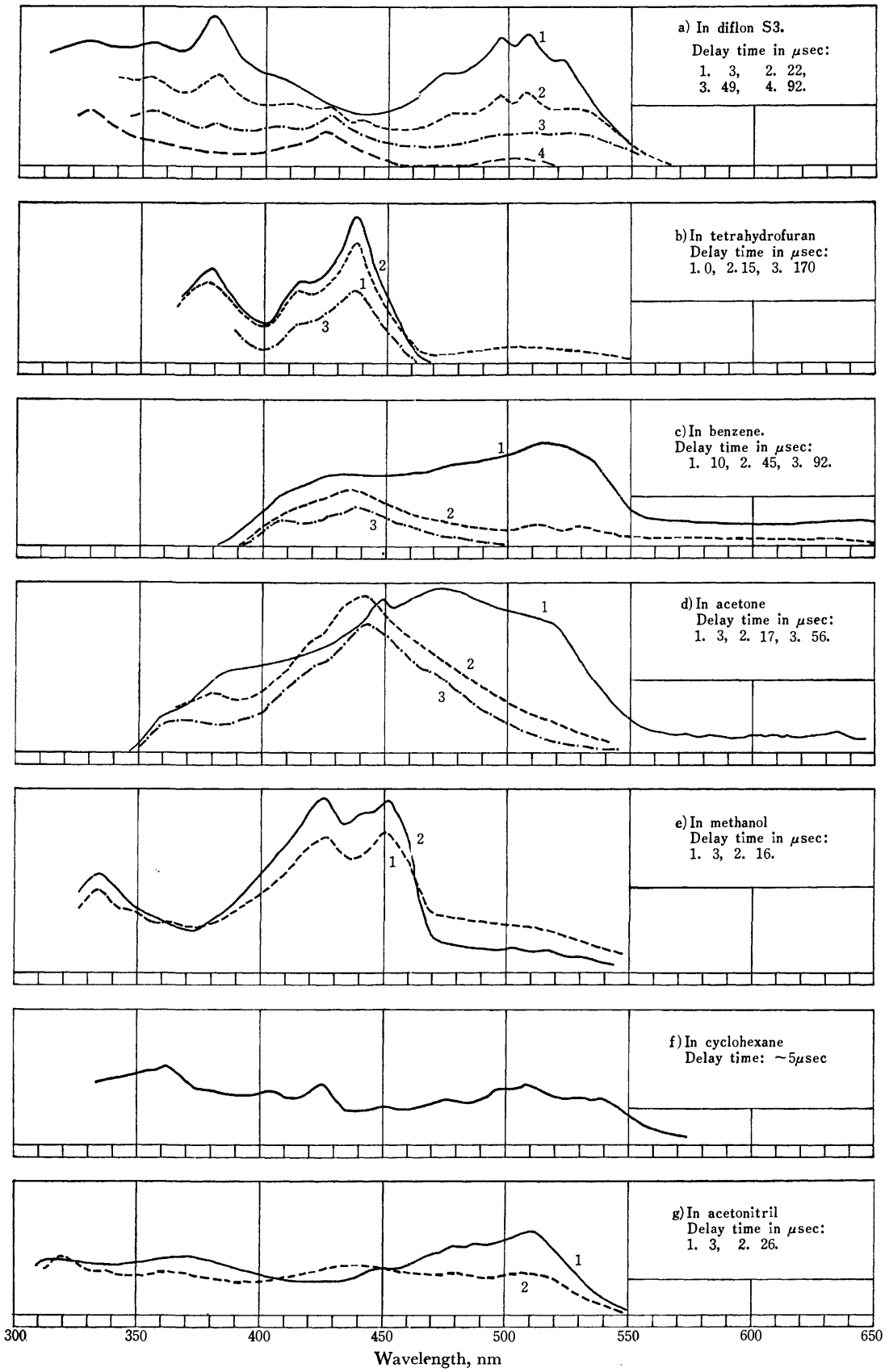

Fig. 1. Absorption spectra of transient species obtained by the flash photolysis of chloranil in various solvents.

the ground state, and might have specific interactions with solvents having electron-donating properties. We have carried out detailed investigations on the T-T′ spectra of chloranil using various solvents in order to obtain evidence on any such donor-acceptor interactions, and also on the chemical properties of semiquinones formed photo-chemically.

Experimental

Materials. Chloranil was purified by recrystallization from benzene, passing through a calcium carbonate column, and further recrystallization from benzene. Trichlorotrifluoroethane (Diflon S3), a commercial product from Daikin Kogyo Co., Ltd. and which may be a mixture of isomers, was shaken with sulfuric acid, neutralized, dried with calcium chloride and distilled with a Widmer column. Acetone was refluxed with potassium permanganate for half a day, dried with calcium sulfate and distilled. Tetrahydrofuran was refluxed overnight with potassium hydroxide, distilled, refluxed with sodium wire again and then distilled. Benzene was shaken with sulfuric acid, neutralized, dried with calcium chloride, refluxed with sodium wire and then distilled with a Widmer column. Methanol was refluxed overnight on sodium wire and then distilled. Acetonitrile was purified by passing through an alumina column, refluxed with calcium hydride and then distilled.

Methods. Concentrations of the solutions of chloranil used in the experiment were mostly in the range $1—3\times 10^{-4}$M. Solutions were bubbled with highly purified nitrogen gas so as to purge dissolved oxygen, and then poured in a cylindrical silica cell 1.5 cm in diameter and 20 cm in length. The apparatus used for the flash spectroscopic measurements is mostly the same as that described in an earlier paper.[3]

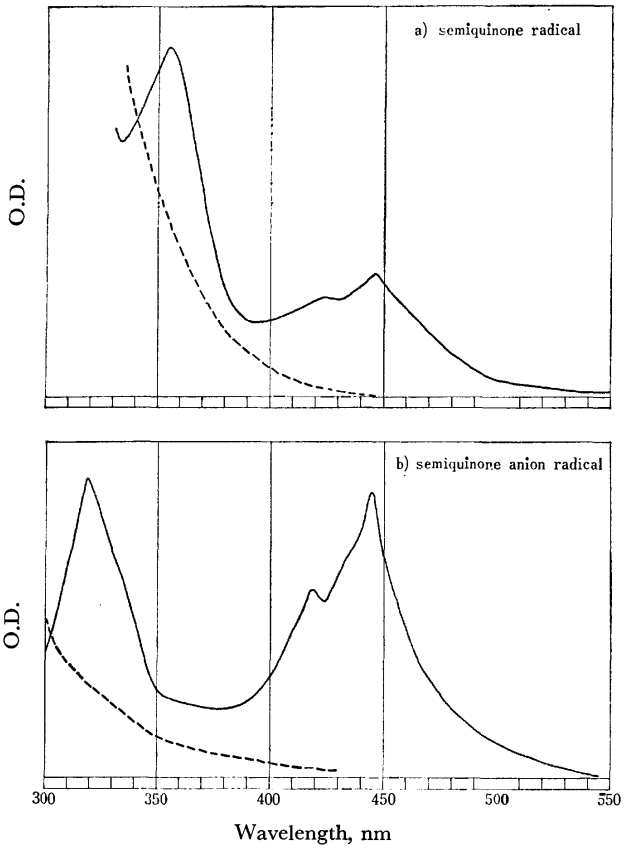

Fig. 2. Absorption spectra of the semiquinone radical and semiquinone anion chemically produced from chloranil.
a) ------ Absorption of chloranil in α-methyltetrahydrofuran at 77°K.
—— The same, after irradiation with a high pressure mercury lamp.
b) ------ Absorption of chloranil in degassed tetrahydrofuran.
—— The same, after contact with sodium-potassium alloy.

Results

The transient spectra obtained by the flash photolysis of chloranil in various solvents are shown in Fig. 1, a)—g). For the sake of comparison, the spectrum of semiquinone radical obtained by the photolysis of chloranil in an α-methyltetrahydrofuran matrix at 77°K is shown in Fig. 2 a), and that of the semiquinone anion obtained by the reduction of chloranil in tetrahydrofuran with sodium-potassium alloy in Fig. 2 b).

The spectra obtained in trichlorotrifluoroethane (Diflon S3) is shown in Fig. 1 a). The solvent was used for the purpose of obtaining pure T-T′ absorption spectrum of chloranil, for it was expected to be inert to excited chloranil, especially with the hydrogen-abstraction reaction. There is a band system at around 500 nm with four apparent vibrational sub-bands at 522, 507, 497, and 473 nm, and a second eminent one with a principal maximum at 379 nm. Both these two systems may be assigned to the T-T′ transitions of chloranil, since they could not be detected in the solution saturated with oxygen. The general characteristics of the first 500 nm system coincide also with those of the T-T′ spectrum reported by Kemp and Porter in an ethanol solution, though the resolution in their spectrum is a little poorer than ours. They did not measure the T-T′ spectrum in the region below 450 nm, while our results give the second system lying below 400 nm. We have also determined the life time of the triplet state (decay of these bands) to be *ca.* 30 μsec.

Besides these T-T′ absorptions, a minor transient band centered at 425 nm was obtained which persists for a longer time than the triplet state. The spectrum is like that of the semiquinone radical mentioned later, and is tentatively assigned to a radical () formed by the abstraction of chlorine atom from the solvent.

The spectra obtained in tetrahydrofuran is shown in Fig. 1 b). The main feature at around 430 nm is quite like that of the first band-system of the semiquinone radical (Fig. 2 a)), though the former is shifted to the blue by about 10 nm. The semiquinone anion radical has a similar band system at the same region. However, the semiquinone radical has a band at 357 nm, while semiquinone anion lacks it. The presence of a band at around 375 nm in the spectra of Fig. 1 b) seems to indicate that the semiquinone radical is the main product formed by flash photolysis. This is also in harmony with the fact that the α-hydrogen of tetrahydrofuran is easily abstracted.[4]

3) N. Yamamoto, Y. Nakato, and H. Tsubomura, This Bulletin, **39**, 2603 (1966).

The weak absorption appearing in the 500 nm region is ascribable to the T-T′ absorption. The absorption decays in a few microseconds, indicating a rapid hydrogen abstraction in the triplet state. It was also found that the semiquinone radical was formed even in an aerated tetrahydrofuran solution (containing oxygen). This indicates that the hydrogen abstraction occurs at least partly at the singlet excited state of chloranil. In aerated ethanol, no semiquinone radical was formed.

The spectra obtained from the flash photolysis of benzene solutions in the range $\lambda>320$ nm are shown in Fig. 1 c). At the delay time of 10 μsec, a broad spectrum was obtained with the principal peak at 516 nm, which is assigned to the first T-T′ system. It decays quickly, and another system ascribable to the semiquinone radical appears at a longer delay time. It is generally believed difficult to abstract a hydrogen atom from benzene. However, our present results have revealed that a hydrogen abstraction can occur from benzene.[5] It is to be noted that the T-T′ spectrum in the case of benzene solution is much more broad and structureless than that in Diflon S3. There is also a broad, weak absorption beyond 550 nm, which decays at nearly the same rate as the triplet state. Transient spectra obtained for a number of solutions containing both benzene and Diflon S3 (Fig. 3) show that the absorption intensity in the 550 to 650 nm region, relative to that of the first T-T′ system, increases obviously with the increase in the benzene content. This seems to indicate strongly that a new absorption system is found which arises from the interaction of benzene and triplet chloranil.

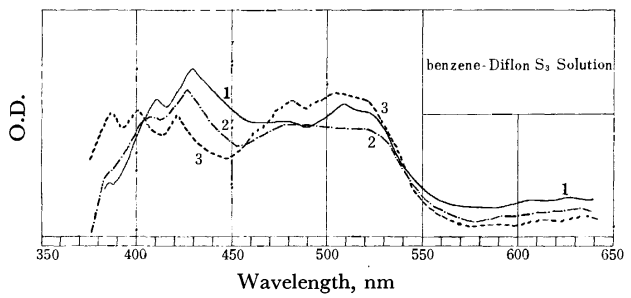

Fig. 3. Absorption spectra of transient species obtained by the flash photolysis of chloranil in a mixture of trichlorotrifluoroethane (Diflon S3) and benzene, at a delay time of 15 μsec. The volume ratio, Diflon S3/benzene for each curve, is given below:
1) 3/7 2) 7/3 3) 9/1

The transient spectra obtained for the acetone solutions is shown in Fig. 1 d). In this case, the flash excitation was carried out in the region $\lambda>330$ nm by use of a combination filter system composed of a glass plate and an aqueous solution of sodium nitrate. Absorption in the region 450—550 nm appearing at the delay time of 3 μsec fades out mostly at 17 μsec and a new system appears at about 440 nm. The former (450—550 nm) may be assigned to the T-T′ spectrum of chloranil from its wavelength and decay time, while the latter does not exactly fit into the spectrum of either semiquinone radical or semiquinone anion but can be explained by assuming that the two species are mixed, indicating that the semiquinone radical formed in the first place by the flash undergoes ionic dissociation and is in the following acid-base equilibrium in acetone.

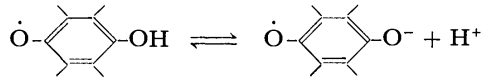

The situation is quite similar to the photolysis product of hydroquinone in neutral or acid solutions.[6] In the acetone solution, a broad absorption is also found beyond 550 nm, which may most probably be interpreted as an absorption arising from the interaction between triplet chloranil and acetone similar to the case of benzene solutions.

In methanol, the transient spectra (Fig. 1e)) can be interpreted as an assembly of the T-T′ absorption and the absorption by semiquinone radical and semiquinone anion. The bands at 426 and 451 nm decay in the first order kinetics with different decay constants.

The transient spectra obtained in cyclohexane showed bands ascribable to the T-T′ and the semiquinone radical absorption (Fig. 1 f)). Those in acetonitrile show the T-T′ absorption and the absorption mostly ascribable to the semiquinone radical (Fig. 1 g)).

The peak wavelengths of the transient spectra obtained in various solvents and their assignments are summarized in Table 1.

TABLE 1. THE PEAK WAVELENGTHS OF TRANSIENT ABSORPTION SPECTRA OBTAINED BY THE FLASH PHOTOLYSIS OF CHLORANIL IN VARIOUS SOLVENTS IN nm

Transient Species	Triplet Chloranil	Semiquinone Radical	Semiquinone Anion
Diflon S3	522, 507, 497, 473; 410, 379	425	
Cyclohexane	539, 507, 495, 474	425, 403	
Benzene	516	436, 408	
THF	~500	437, 415, 377	
Acetone	520, 503; 471	(441, 420, 365)[a]	
Methanol	~500	426	451
Acetonitril	510, 487, 479; 372	(440, 319)[a]	

a) Strongly overlapped.

Discussion

From the results, a considerable influence of solvents can be seen on the first T-T′ system in various solvents, especially in such electron-donating solvents as benzene and acetone. In these solvents, the first T-T′ system is much more diffuse than others. It is of particular interest that there are broad absorptions in the range $\lambda>$ 550 nm, which seem to be charge transfer bands with the solvent molecule as donor and triplet chloranil as

4) It is suggested that the discrepancy between the peak wavelength of the first band system in Fig. 2 a) and that in Fig. 1 b) may be attributed to differences in solvent and temperature.

5) Rubin *et al.* reported a hydrogen abstraction reaction from benzene by excited phenanthraquinone. M. B. Rubin and Z. Neuwirth-Weiss, *Chem. Commun.*, **1968**, 1607.

6) K. Kimura, K. Yoshinaga, and H. Tsubomura, *J. Phys. Chem.*, **71**, 4485 (1967).

acceptor. Quite independently, Briegleb and Schuster recently reported a few cases of absorption spectra of triplet pyromellitic dianhydride at 77°K showing similar bands and assigned them to charge transfer absorption from solvent to triplet pyromellitic dianhydride.[7]

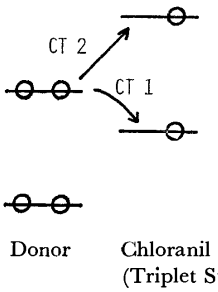

Fig. 4. Diagram indicating charge transfer between donor and triplet chloranil.

It is a delicate problem to determined whether the lowest triplet state of chloranil is (n-π^*) or (π-π^*). Shcheglova *et al.* found an emission spectrum from chloranil in a hexane (9 vol)-toluene (1 vol) solution and concluded that it arises from the lowest triplet (π-π^*) state at 17200 cm^{-1} above the ground state,[8] where π and π^* are the highest filled and lowest vacant π-MO, respectively. Thus, a charge transfer can occur from the highest filled MO of the donor (solvent) to the π-MO of chloranil, leading to a charge transfer band at very long wavelength regions (CT 1 in Fig. 4). The transition energy for a charge transfer absorption can be given approximately by the equation

$$h\nu_{CT} = I_D - E_A - e^2/r_{DA} + \Delta, \quad (1)$$

where I_D and E_A are the ionization energy of donor and the electron affinity of acceptor, r_{DA} is the distance between donor and acceptor, and Δ is a term collecting all other minor contributions. For an ordinary benzene-chloranil complex, the charge transfer band has $\lambda_{max}=$ 335 nm, which corresponds to $h\nu_{CT}$ of 3.7 eV.[9] The electron affinity of chloranil in the lowest triplet state can be given by

$$E_A{}^T = E_A + W_T - W_G$$

where W_T and W_G are the energies of the triplet and ground state, respectively. Using the value derived by Shcheglova (17200 cm^{-1}=2.1 eV), we obtain for the complex between benzene and triplet chloranil

$$h\nu'_{CT} = I_D - E_A - (W_T - W_G) - e^2/r_{DA} + \Delta, \quad (2)$$

If it is assumed that r_{DA} and Δ are the same for both complexes, then from (1) and (2), we obtain

$$h\nu'_{CT} = 1.6\ eV \equiv 780\ nm.$$

This value seems to be in harmony with our experimental result, especially when one takes account of the resonance splitting between the upper and lower states which seems to be somewhat larger than the splitting for the ordinary chloranil-benzene complex. But further investigations seem to be necessary for the elucidation of the nature of the lowest triplet state of chloranil, and the weak, long-wavelength absorption found in the present work.

7) G. Briegleb and H. Schuster, *Angew. Chem. (Intern. Ed.)*, **9**, 369 (1970).

8) N. A. Shcheglova, D. N. Shigorin, G. G. Yakobson, and L. Sh. Tushishuili, *Zh. Fiz. Khim.*, **43**(**8**), 1984 (1969).

9) C. Briegleb and J. Czekalla, *Z. Physik. Chem. N. F.*, **24**, 37 (1960); *Z. Elektrochem.*, **58**, 249 (1954).

Partial Pressures of Strontium and Strontium Oxide over Strontium Oxide Heated on Platinum

Mitsuru ASANO, Yutaka YAMAMOTO, Noriaki SASAKI, and Kenji KUBO

Institute of Atomic Energy, Kyoto University, Uji, Kyoto

(Received June 18, 1971)

A quadrupole mass filter was used to determine the partial pressures of Sr(g) and SrO(g) over strontium oxide heated on a platinum-ribbon filament. The ion currents of $^{88}Sr^+$ and $^{88}Sr^{16}O^+$ were measured while the filament temperature was continuously increasing at a heating rate of about 14°C/min; the calculations of the partial pressures were carried out by the integral method for Sr(g) and by the sensitivity-calibration method for SrO(g). The data are represented by:

$$\log P_{Sr(g)}(\text{atm}) = 6.633 - \frac{2.536\times 10^4}{T}$$

in the temperature range of 1643—1851°K, and by:

$$\log P_{SrO(g)}(\text{atm}) = 6.707 - \frac{2.793\times 10^4}{T}$$

in the 1747—1850°K range. From the values of the partial pressures, the dissociation energy of strontium oxide was determined to be $D_0°(SrO)=96.2\pm 0.9$ kcal/mol by the third-law treatment and $D_0°(SrO)=102\pm 5$ kcal/mol by the second-law treatment.

Many studies have been carried out on the nature of vapor species from strontium oxide heated on various materials, such as platinum,[1-3] tungsten,[4-5] molybdenum,[4] and alumina.[7] Using mass-spectrometric techniques, Aldrich,[1] Bickel and Holroyd,[2] and Pelchowitch[3] have observed that, in the strontium oxide-platinum system, the main vaporization products are free strontium atom, plus small amounts of the strontium oxide molecules, and that no reactions occur between strontium oxide and platinum. However, the partial pressures of Sr(g) and SrO(g) could not be determined, since no sensitivity calibration of their mass spectrometers was done. Drowart *et al.*[4,5] have measured the relative ion intensities of the vapor products produced by the reactions of alkaline earth oxides with a tungsten Knudsen cell or molybdenum cell, and determined the dissociation energy of alkaline earth oxides and the stabilities of the gaseous tungstates, tungstites, molybdates, and molybdites of alkaline earths. Recently, the present authors[6] measured the partial pressures of Sr(g), SrO(g), $SrWO_4$(g), and $SrWO_3$(g) over the solid products produced by the reactions between strontium oxide and a tungsten-ribbon filament. Porter *et al.*[7] also measured the partial pressure of SrO(g) in equilibrium with the solid placed in an alumina Knudsen cell only at the temperature of 2100°K.

Hitherto, the vapor pressure over strontium oxide heated on a platinum filament have all[8,9] been determined on the assumption that SrO(g) is the only gaseous species, although experimental evidence to justify this assumption has never been published.

In the present work, a quadrupole mass filter was used to determine the partial pressures of Sr(g) and SrO(g) over strontium oxide heated on a platinum-ribbon filament. The ion currents of $^{88}Sr^+$ and $^{88}Sr^{16}O^+$ were measured while the filament temperature was continuously increasing at a constant rate; the partial pressures were calculated by the integral method for Sr(g) and by the sensitivity-calibration method for SrO(g). Moreover, from the values of the partial pressures, the dissociation energy of strontium oxide was determined by third-law and second-law treatments.

In a conventional integral method,[10] the ion currents are ordinarily measured at a fixed temperature or by varying the temperature step by step for a proper interval, while in the present work the currents were measured under the above conditions, since the measurements were carried out with a very small sample.

The vaporization of strontium oxide supported on various materials is of interest in the physics and chemistry concerned with the phenomena of the thermal emissions of electrons and ions.

Experimental

The platinum-ribbon filament used to hold the strontium oxide was 0.75 mm wide and 0.025 mm thick (H. Cross. Co.) and was kept straight with the aid of a tungsten spring, even at high temperatures.

Strontium nitrate was used to prepare strontium oxide on the filament. Reagent-grade strontium nitrate was

1) L. T. Aldrich, *J. Appl. Phys.*, **22**, 1168 (1951).
2) P. W. Bickel and L. V. Holroyd, *J. Chem. Phys.*, **22**, 1793 (1954).
3) I. Pelchowitch, *Chem. Abstr.*, **48**, 7963f (1954); *Phillips Research Repts.*, **9**, 42 (1954).
4) J. Drowart, G. Exsteen, and G. Verhaegen, *Trans. Faraday Soc.*, **60**, 1920 (1964).
5) G. Verhaegen, R. Colin, G. Exsteen, and J. Drowart, *ibid.*, **61**, 1372 (1965).
6) Y. Yamamoto, M. Asano, N. Sasaki, and K. Kubo, *Meeting of the Mass Spectroscopy Society of Japan*, Tokyo, May, 1970.
7) R. F. Porter, W. A. Chupka, and M. G. Inghram, *J. Chem. Phys.*, **23**, 1374 (1955).
8) G. E. Moore, H. W. Allison, and J. D. Struthers, *J. Chem Phys.*, **18**, 1572 (1950).
9) A. Claassen and C. F. Veenemans, *Z. Phys.*, **80**, 342 (1933).
10) R. T. Grimley, "The Characterization of High-Temperature Vapors," ed. by J. L. Margrave, John Wiley and Sons, New York (1967), p. 193.

purified by the carbonate method and was crystallized out from a nitrate solution. Using a micro syringe, 1 μl of strontium nitrate solution containing 20.30 μg of strontium was placed on the central part of the filament for a length of about 3 mm and dried under an infrared lamp. After it had then been set in a vacuum chamber, the filament was slowly heated by an externally-programmed DC power supply driven by a motor of an adjustable speed; the strontium nitrate was thus thermally decomposed to strontium oxide. Then, the filament was further heated at a rate of about 14°C/min, and the partial pressures of the gaseous species vaporized from the strontium oxide on the platinum filament were measured by means of a NEVA NAG 510H quadrupole mass filter equipped with a secondary electron multiplier.

A collimated gaseous beam originating from strontium oxide was ionized in an ionization chamber by low-energy electrons (13 eV), so the fragmentation of SrO(g) to Sr^+ and O was assumed to be negligible.

The filament holder was devised so as to move back and forth; this mechanism was used as a shutter.

A schematic diagram of the arrangement of the experimental apparatus is shown in Fig. 1.

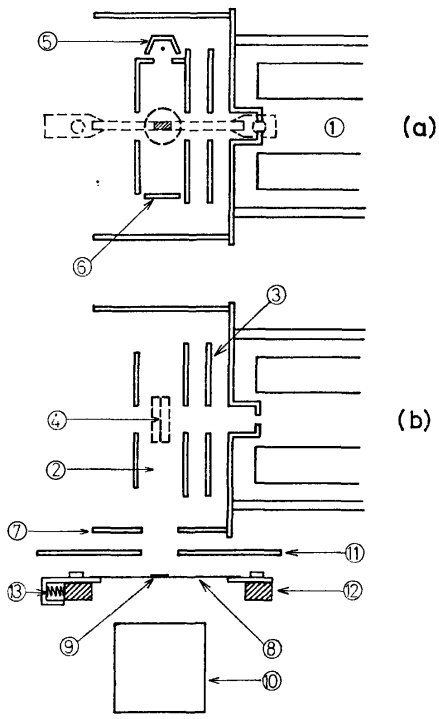

Fig. 1. Schematic diagram of the arrangement of experimental apparatus.
(a) Upper view and (b) side view.
1) quadrupole mass analyser 2) ionization chamber 3) ion focusing plate 4) filament for electron emission 5) electron repeller 6) electron trap 7) beam collimator 8) platinum ribbon filament 9) sample 10) prism 11) shield 12) filament holder 13) spring

The filament temperature was measured with a Leed and Northrup 8632C optical pyrometer by sighting the back side of the filament, on which strontium oxide was applied, through a prism; the readings were corrected for the emissivity of the platinum filament and the transmission coefficients of the prism and the glass window of the vacuum chamber. If an appreciable thermal gradient existed throughout the sample, the results might be seriously in error. Under the present conditions, however, the error seems to be negligible because of the very small sample.

The background pressure in a vacuum chamber was maintained at less than 2×10^{-8} Torr with an ion pump during all the experiments.

The basic data of the present work are the ion-current measurements of $^{88}Sr^+$ and $^{88}Sr^{16}O^+$ made with a continuosly-increasing temperature at a heating rate of about 14°C/min. The upper temperature limit was dictated by the amount of the sample, and the lower limit, by the ion-detection ability of the mass filter.

The resolution of a quadrupole mass filter varies automatically throughout mass scanning, so that the sensitivity varies with the mass number. The mass filter used in this study was designed to maintain a constant relation between sensitivity and resolution. Consequently, for a given resolution, the ion current is quantitatively proportional to the number of ionizable gaseous atoms. To obtain this relation, the ion currents of the M/e=28, 44, 71, 85, and 109 peaks were measured as a function of the resolution. The resolution is here defined as $M/\Delta M$, where M is the mass number and where ΔM is the half-width of the ion peak in amu. The relations for the five ion species are shown in Fig. 2, where the slopes are constant. In the present work, the resolution was kept high enough to measure the ion currents of Sr^+ and SrO^+, usually higher than 130.

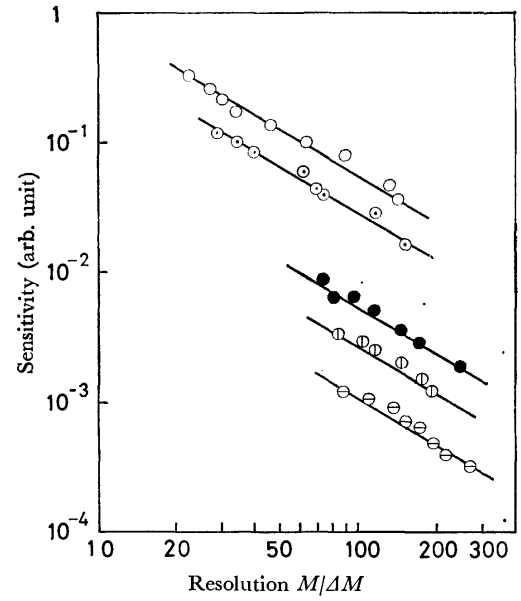

Fig. 2. Relation between sensitivity and resolution. M/e= 28 ⊙, 44 ○, 71 ●, 85 ◑, and 109 ⊖.

The background ions of the same mass number as the interesting species resulted from the residual gases in a vacuum chamber. However, the effect of the background was practically negligible at higher temperatures, since the ion intensities of Sr^+ and SrO^+ were much greater than the residual gas ions.

Method for Determining Partial Pressures

The determination of the vapor pressures of solid materials with a mass spectrometer has been carried out by two methods, namely, the sensitivity-calibration method[10–12] and the integral method.[10,11] In the

11) W. A. Chupka and M. G. Inghram, *J. Phys. Chem.*, **59**, 100 (1955).
12) J. Drowart, G. DeMaria, R. P. Burns, and M. G. Inghram, *J. Chem. Phys.*, **32**, 1366 (1960).

latter method, a known amount of sample is completely vaporized out and the ion intensity is integrated over the period of time required to vaporize the entire sample. Knowing the whole amount of sample vaporized and making use of the vaporization equation, the vapor pressure of the sample is calculated. The modified integral method was used to calculate the partial pressure of Sr(g).

The total number of gaseous atoms (or molecules), z_{tot}, vaporized from the sample is given by:

$$z_{tot} = a\int_0^{t_{end}} z\mathrm{d}t \tag{1}$$

where z is the number of gaseous atoms vaporized per unit of time per unit of area, where a is the vaporization area, and where t_{end} is the time after which the sample is completely vaporized out. The ion current, I^+, is given by the following relation:

$$I^+ = C\frac{(E-I)\sigma\gamma S_1 S_2}{\bar{v}}z \tag{2}$$

where C is the factor for instrument geometry, E is the energy of the impact electron, I is the ionization potential of the element (or compound), σ is the maximum ionization cross section of the gaseous species, γ is the isotopic abundance ratio for the ionized gaseous species, S_1 is the efficiency of the electron multiplier, S_2 is the sensitivity of the mass filter, and $\bar{v}$ is the average velocity of the gaseous atoms.

From Eqs. (1) and (2), the following equation is obtained:

$$z_{tot} = \frac{a}{C(E-I)\sigma\gamma S_1 S_2}\int_0^{t_{end}} I^+\bar{v}\mathrm{d}t \tag{3}$$

Since, in the present work, the ion currents are measured with a continuously increasing temperature at a constant rate, the $\bar{v}$ is given as a function of the time:

$$\bar{v} = \sqrt{\frac{8RT_t}{\pi M}} \tag{4}$$

where $\boldsymbol{R}$ is the gas constant and where T_t is the sample temperature at time t. Substituting for $\bar{v}$, Eq. (3) becomes:

$$z_{tot} = K\int_0^{t_{end}} I^+\sqrt{T_t}\mathrm{d}t \tag{5}$$

where:

$$K = \frac{a}{C(E-I)\sigma\gamma S_1 S_2}\sqrt{\frac{8R}{\pi M}}$$

Similarly, the number of gaseous atoms, $z_{\Delta t}$, vaporized in the time interval between t_1 and t_2, during which the temperature increases from T_1 to T_2, is given by:

$$z_{\Delta t} = K\int_{t_1}^{t_2} I^+\sqrt{T_t}\mathrm{d}t \tag{6}$$

Taking the ratio of Eqs. (5) and (6):

$$\frac{z_{\Delta t}}{z_{tot}} = \frac{W_{\Delta t}}{W_{tot}} = \frac{\int_{t_1}^{t_2} I^+\sqrt{T_t}\mathrm{d}t}{\int_0^{t_{end}} I^+\sqrt{T_t}\mathrm{d}t} \tag{7}$$

where W_{tot} is the whole amount of the sample and where $W_{\Delta t}$ is the amount vaporized in the time interval $\Delta t = t_2 - t_1$. The graphical integrals in Eq. (7) are shown in Fig. 3, where the experimental data for only the Sr^+ ion current are given against the time, together with the temperature. The whole area under the curve of $I^+\sqrt{T_t}$ corresponds to W_{tot}, and the oblique line part area, to $W_{\Delta t}$. Consequently, the rate of the vaporization of atoms vaporized per unit of time per unit of area, m, is obtained from the following equation:

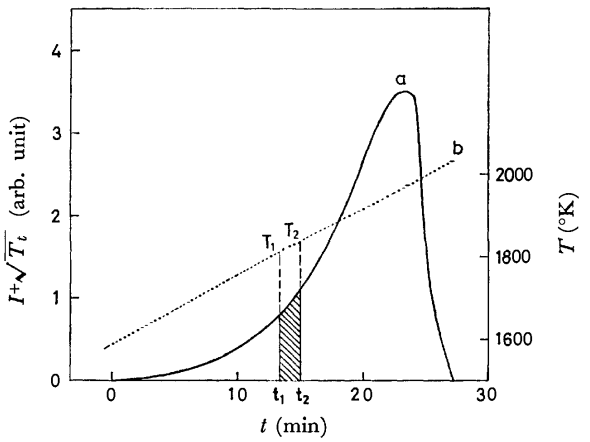

Fig. 3. Graphical representation for the integrals in Eq. (7).
(a) $I_{Sr}{}^+\sqrt{T}$ and (b) temperature.
Whole area under the curve (a) is corresponded to the integral of the denominator and oblique line part area to the numerator in Eq. (7).

$$m = \frac{W_{\Delta t}}{a\Delta t} = \frac{W_{tot}}{a\Delta t}\frac{\text{oblique-line part of Fig. 3}}{\text{whole area of Fig. 3}} \tag{8}$$

For the vaporization from an open surface, the vapor pressure, P, at the average temperature of $\bar{T}=(T_1+T_2)/2$ in the time interval of Δt can be calculated by the Langmuir equation[13]:

$$P = m\sqrt{\frac{2\pi R\bar{T}}{M}} \tag{9}$$

assuming the vaporization coefficient to be unity. Then, for a series of time intervals, the vapor pressures are successively calculated in the same manner, until the amount of sample decreases and the rate of vaporization does not give the pressure corresponding to the temperature.

When a vaporization occurs in only one vapor species the above procedure can be applied to the measurement of the vapor pressure without any correction. In the case of the vaporization of strontium oxide on the platinum filament, however, the strontium-containing vapors consists of a predominant amount of Sr(g) and a small amounts of SrO(g), as is shown in Fig. 4, where the experimental data for the Sr^+ and SrO^+ ion currents from their vapors are given. Consequently, in the present work the SrO^+ ion current was first converted into an imaginary strontium ion current, $I^+_{Sr}(imag)$, which was equivalent to I^+_{SrO}; then, by using the sum of the actual and the imaginary strontium ion currents, $I^+_{Sr}(sum)=I^+_{Sr}+I^+_{Sr}(imag)$, the integral of the denominator in Eq. (7) was carried out. In this case, Eqs. (8) and (9) become:

13) L. Langmuir, *Phys. Rev.*, **2**, 329 (1913).

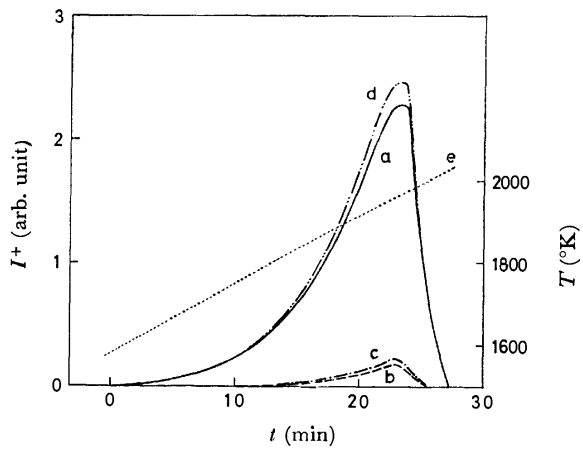

Fig. 4. Experimental data for I^+_{Sr} and I^+_{SrO} against time, together with I^+_{Sr} (imag) and I^+_{Sr}(sum).
(a) —— I^+_{Sr}, (b) ---- I^+_{SrO}, (c) -·- I^+_{Sr} (imag) equivalent to I^+_{SrO}, (d) —·— I^+_{Sr} (sum)$=I^+_{Sr}+I^+_{Sr}$ (imag), and (e) ------ temperature.

$$m_{Sr} = \frac{W_{Sr} \text{ in SrO}}{a\Delta t} \frac{\int_{t_1}^{t_2} I^+_{Sr}\sqrt{T_t}\,dt}{\int_0^{t_{end}} I^+_{Sr}(\text{sum})\sqrt{T_t}\,dt} \tag{10}$$

and:

$$P_{Sr} = m_{Sr}\sqrt{\frac{2\pi RT}{M_{Sr}}} \tag{11}$$

respectively. The values of I^+_{Sr} (imag) and I^+_{Sr} (sum) are also shown in Fig. 4.

The conversion of I^+_{SrO} into I^+_{Sr} (imag) was carried out as follows. When SrO(g) is vaporized from strontium oxide, the current of the strontium oxide ion is given from Eq. (2):

$$I^+_{SrO} = C\frac{(E-I_{SrO})\sigma_{SrO}\gamma_{SrO}S_{1SrO}S_{2SrO}}{\bar{v}_{SrO}}z_{SrO}$$

$$= k\frac{(E-I_{SrO})\sigma_{SrO}\gamma_{SrO}S_{1SrO}S_{2SrO}\sqrt{M_{SrO}}}{\sqrt{T}}z_{SrO} \tag{12}$$

where $k=C\sqrt{\pi/8R}$.
Similarly, for the imaginary strontium ion:

$$I^+_{Sr}(\text{imag}) = k\frac{(E-I_{Sr})\sigma_{Sr}\gamma_{Sr}S_{1Sr}S_{2Sr}\sqrt{M_{Sr}}}{\sqrt{T}}z_{Sr}(\text{imag}) \tag{13}$$

Now, if the $^{88}Sr^+$ and $^{88}Sr^{16}O^+$ are measured, the following relations hold:

$$z_{SrO} = z_{Sr}(\text{imag}) \tag{14}$$

and:

$$\gamma_{SrO} = \gamma_{Sr} \tag{15}$$

Consequently, from Eqs. (12) and (13):

$$I^+_{Sr}(\text{imag}) = \frac{(E-I_{Sr})\sigma_{Sr}S_{1Sr}S_{2Sr}\sqrt{M_{Sr}}}{(E-I_{SrO})\sigma_{SrO}S_{1SrO}S_{2SrO}\sqrt{M_{SrO}}}I^+_{SrO} \tag{16}$$

That is, the amount of I^+_{SrO} at a given temperature can be converted into the I^+_{Sr}(imag) using Eq. (16).

For the calculation of the partial pressure of SrO(g), the sensitivity-calibration method was employed. Here, the partial pressure of Sr(g) was used as a reference; that is:

$$P_{SrO} = \frac{I^+_{SrO}(E-I_{Sr})\sigma_{Sr}S_{1Sr}S_{2Sr}T_{SrO}}{I^+_{Sr}(E-I_{SrO})\sigma_{SrO}S_{1SrO}S_{2SrO}T_{Sr}}P_{Sr} \tag{17}$$

In the mass-spectrometric Knudsen effusion technique, silver has been widely used as a reference material, since silver vaporizes almost entirely in the form of monoatomic gases and the vapor pressure is well known. However, in the present condition of free vaporization from an open surface, it is difficult to use an outer reference such as silver.

The values of the ionization potentials for strontium and strontium oxide were taken from Drowart[4] to be $I_{Sr}=5.7$ and $I_{SrO}=6.1$ eV, while the relative maximum ionization cross section for strontium was taken from Mann[14] to be $\sigma_{Sr}=8.88$ and the cross section for strontium oxide was obtained, by summing the values for the constituent atoms, as $\sigma_{SrO}=10.19$. The efficiency of the electron multiplier for the mass dependence, S_1, was corrected by a factor of the reciprocal of the square root of the mass number, taking into account the so-called mass effect.[15] Moreover, the sensitivity of the mass filter, varying with the resolution, S_2, was corrected from the constant slope of the lines in Fig. 2. As the time interval, Δt, 1 min was taken for all calculations.

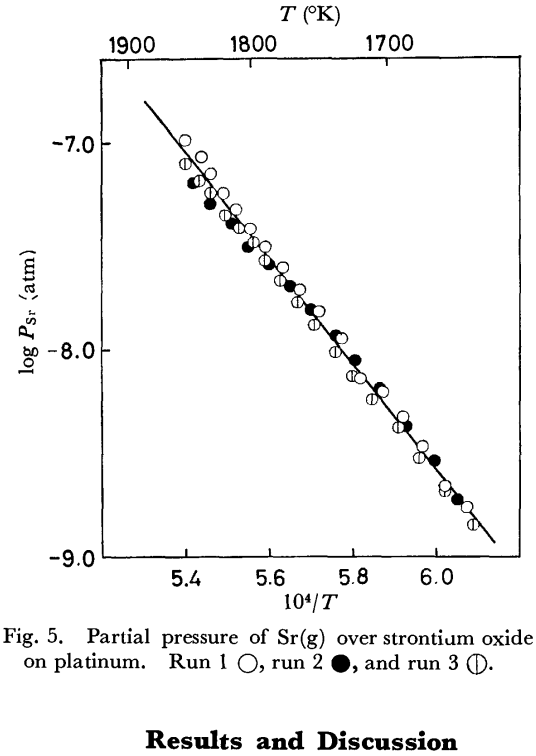

Fig. 5. Partial pressure of Sr(g) over strontium oxide heated on platinum. Run 1 ○, run 2 ●, and run 3 ⓘ.

Results and Discussion

1. Partial Pressure of Sr(g). The partial pressures of Sr(g) over strontium oxide heated on a platinum filament are shown in Fig. 5. The line drawn by the least-squares treatment of the data follows this equation:

$$\log P_{Sr}(\text{atm}) = 6.633 - \frac{2.536\times10^4}{T} \tag{18}$$

in the temperature range of 1643—1851°K. Moreover, from the slope of the line the heat of the vaporization of Sr(g)[16] was calculated to be 116 ± 2 kcal/mol at the

14) J. B. Mann, *J. Chem. Phys.*, **40**, 1646 (1967).
15) W. Ploch and W. Walcher, *Rev. Sci. Instrum.*, **22**, 1028 (1951).
16) This value corresponds to the partial molar enthalpy of the vaporization of Sr(g) from SrO(g).

experimental temperatures. Here, the uncertainty is the standard deviation for the least-squares fit.

As will be described later, the partial pressure of Sr(g) is more than an order of magnitude greater than that of SrO(g). Consequently, it may be observed that the total vapor pressures over strontium oxide obtained by Moore *et al.*,[8] and by Claassen and Veenemans,[9] assuming SrO(g) to be the only gaseous species, are approximately equivalent to the partial pressure of Sr(g) if the consideration of a factor of $\sqrt{M_{Sr}/M_{SrO}}$ is made for their values. The agreement between the observed partial pressure of Sr(g) and their total vapor pressures is extremely good.

In the experiments of Moore *et al.* and of Claassen and Veenemans, the vaporization took place in sealed-off tubes, so the Sr(g) vaporized from the heated sample to the cold collector wall could readily recombine with the released oxygen. Thus, even though strontium oxide was found in the collected products on the wall, the calculations should be carried out for each vapor species of Sr(g) and SrO(g) by the aid of mass analysis.

Bickel and Holroyd[2] have described that the temperature dependence of the Sr^+ ion current is at first seemingly irreproducible. However, the sample passes through a series of changes as the temperature is cycled, and eventually equilibrium conditions are reached on the platinum filament, where reproducible data can be obtained. They have also determined the heat of the vaporization of Sr(g) from the slopes of the lines obtained by plotting the log Sr^+ ion current against the reciprocal of the temperature; they found it to be 164 kcal/mol in the initial state, and 60 kcal/mol for the higher-temperature range and 138 kcal/mol for the lower in the final state. However, Aldrich[1] has observed that the vaporization process of strontium oxide heated on platinum is reproducible without any particular care, and from similar plots of his data he obtained the heat of the vaporization of Sr(g) as 144 kcal/mol over the full temperature range investigated. In the present work, where the measurements were carried out with a continuously increasing temperature, the Sr^+ and SrO^+ ion currents were satisfactorily reproducible in all runs.

Further, the heat of the vaporization of SrO(g) has been obtained by Moore *et al.*, from their data on the total vapor pressure, to be 126.6 kcal/mol, while Blewett,[17] from the data of Claassen and Veenemans,[9] found it to be 117 kcal/mol. Again, these values are approximately equivalent to the value for Sr(g). The agreement of the heats of the vaporization of Sr(g) determined by many workers is poor.

2. Partial Pressure of SrO(g). The partial pressures of SrO(g) vaporized congruently from strontium oxide on platinum are shown in Fig. 6. The line represents the least-squares fit of the data of three runs and is given by the following equation:

$$\log P_{SrO}(\text{atm}) = 6.707 - \frac{2.793\times10^4}{T} \qquad (19)$$

in the temperature range of 1747—1850°K. Moreover, the heat of the vaporization of SrO(g) was calculated to be 128±2 kcal/mol at the experimental temperatures.

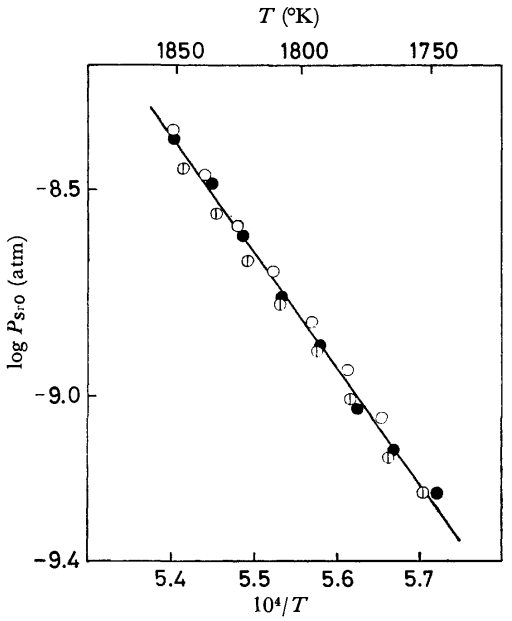

Fig. 6. Partial pressure of SrO(g) over strontium oxide heated on platinum. Run 1 ○, run 2 ●, and run 3 ⦶.

Here again, the uncertainty given is the standard deviation for the least-squares fit.

The measurements for the vapor pressure and for the heat of vaporization of SrO(g) have been carried out by Porter *et al.*[7] only at the temperature of 2100°K, using a mass-spectrometric Knudsen effusion method with an alumina cell. The vapor pressure of 2.5×10^{-7} atm for SrO(g), obtained by extrapolating the line in Fig. 6 to 2100°K, may be seen to be in conflict with the value of 3.8×10^{-8} atm estimated by Porter *et al.* at this temperature; also, the heat of vaporization, 135±3 kcal/mol, corrected to 298°K, is in poor agreement with their value of 155.1 kcal/mol at 298°K. These discrepancies seem to be due to the difference in the supporting materials for strontium oxide and/or the uncertainty as to their experimental error for the single measurement at 2100°K.

The reactions between strontium oxide and platinum have been studied thermodynamically by Moore *et al.*[8] Their results indicate that strontium oxide and platinum do not react in such a manner as to form free Sr(g), and at the same time they do not produce any compounds containing strontium and platinum. In the present work, no high-mass compounds resulting from a reaction between strontium oxide and platinum were detected, although some Pt^+ ions were observed at the highest temperature.

3. Dissociation Energy of Strontium Oxide. For the experimental determination of the dissociation energy of strontium oxide, it is necessary to measure the partial pressures of Sr(g), SrO(g), and oxygen in the present system. The mass spectra of O^+ and O_2^+ ions exhibited a more indistinct shutter effect than those of the Sr^+ and SrO^+ ions did, so the partial pressure of oxygen was calculated from the following relation:

$$P_O(\text{atm}) = \sqrt{\frac{M_O}{M_{Sr}}}P_{Sr}(\text{atm}) = 0.4273P_{Sr}(\text{atm}) \qquad (20)$$

assuming that the oxygen atoms were vaporized by an

17) J. P. Blewett, *J. Appl. Phys.*, **10**, 668 (1939).

equivalent amount of Sr(g) at a given temperature. If oxygen molecules are assumed to be in equilibrium with Sr(g) and SrO(g), half of the dissociation energy of the oxygen molecule must be considered in the calculations.

The free-energy function for SrO(g) was calculated from the usual statistical mechanical equations[18] by using the data of the vibration frequency of strontium oxide, $\omega=653.5\ cm^{-1}$ [19]; the interatomic distance, $r=1.921$ Å[19], and the electronic states, $^3\Sigma$ and $^3\Pi$, lying about $10870\ cm^{-1}$ above the ground state, $X^1\Sigma$.[4] The values calculated are $-(G_T^\circ-H_0^\circ)/T=60.4$(1500°K), 60.9 (1600°K), 61.4(1700°K), 61.9(1800°K), 62.4(1900°K), and 62.8(2000°K) in cal/mol deg respectively. The free-energy functions for Sr(g) and O(g) were taken from Margrave.[20]

By combining the free-energy functions of SrO(g), Sr(g), and O(g) with the free-energy change for the following reaction:

$$SrO(g) = Sr(g) + O(g) \qquad (21)$$

the dissociation energy was calculated to be $D_0^\circ(SrO)=96.2\pm0.9$ kcal/mol. Moreover, a least-squares fit to the second-law treatment for the equilibrium constant of the same reaction gave $D_{1800}^\circ(SrO)=103\pm5$ kcal/mol, which became $D_0^\circ(SrO)=102\pm5$ kcal/mol when corrected to 0°K by using the heat capacities of SrO(g), Sr(g), and O(g). Here, the heat capacity of SrO(g) was calculated by the use of the kinetic theory.[21]

In general, the analysis of the data by third-law treatment is considered superior to that using the second law because each data point is independent of the other.

The dissociation energy of strontium oxide has been determined by various methods, that is, mass-spectrometric measurements by the Langmuir method and the Knudsen effusion method, total vapor-pressure measurements, spectrometric measurements, and theoretical calculations. In Table 1, the values determined in this work are shown together with the literature values. The values obtained by the present mass-spectrometric Langmuir method agree, within the limits of experimental error, with those obtained by the Knudsen method except for the low value reported by Porter *et al.*,[7] As for this low value, Drowart *et al.*[4] have explained it by saying that SrO(g) vaporized from an alumina Knudsen cell, thus leading to the formation of a compound, $(SrO)_{1\text{-}4}Al_2O_3$ in the condensed phase; they derived $D_0^\circ(SrO)=105$ kcal/mol by adding the heat of the formation of the $SrO\cdot Al_2O_3$ compound, -19 kcal/mol, to the value obtained by Porter *et al.* However, it is less easy to explain the low value calculated from the data for all the gas-phase reactions of Eq. (21), since this equilibrium should be independent of the solid-phase composition.

Table 1. Summary of the values of D_0°(SrO), kcal/mol

Method	D_0°(SrO)	Ref.
Mass spectrometry(Langmuir)	96.2 ± 0.9[a]	This work
	$102\ \pm5$[b]	This work
Mass spectrometry(Knudsen)	$102\ \pm5$[a]	4
Mass spectrometry(Knudsen)	92.2 ± 6[a]	22
Mass spectrometry(Knudsen)	83.6 ± 5[a]	7
Total vapor pressure(Langmuir)	110.4 ± 3.5[c]	23
Spectrometry	$111\ \pm3$	24
Spectrometry	94.7 ± 1.4	25
Spectrometry	99	26
Spectrometry	106	27
Spectrometry	120	28
Theory	$102\ \pm10$[d]	29
Theory	59[e]	30
	43[f]	30

a) Third law treatment.
b) Second law treatment.
c) Calculation from the data of Ref. 8.
d) Ion model.
e) Internuclear potential function with three parameters, *i.e.*, equilibrium bond distance, force constant, and anharmonicity constant.
f) Internuclear potential function with five parameters, *i.e.*, in addition to above three parameters, vibrational-rotational coupling constant and one constant of 1.065.

As may be seen in Table 1, the values obtained by the spectrometric method[24-28] are systematically higher than those obtained by the mass-spectrometric method. This discrepancy is presumably due to the uncertainties of the measurements of the flame temperature and its gradient by the spectrometric method, and the defference in principle between the spectrometric and the thermochemical values.

The value calculated by the ionic model[29] is in fair agreement with those experimental determined, whereas the values obtained by the internuclear potential functions[30] deviate markedly from the other values.

The authors wish to express their thanks to Professor S. Magari of the Institute of Atomic Energy, Kyoto University, for his valuable suggestions and discussions.

18) G. N. Lewis and M. Randall, "Thermodynamics," revised by K. S. Pitzer and L. Brewer, McGraw-Hill Book Co., New York (1961), p. 419.
19) G. Herzburg, "Molecular Spectra and Molecular Structure I. Spectra of Diatomic Molecules," D. Van Nostrand Co., Princeton (1961), p. 575.
20) J. L. Margrave, "Physicochemical Measurements at High Temperatures," ed. by J. O'M. Bockris, J. L. White, and J. D. Mackenzie, Butterworths Scientific Pub., London (1959), p. 353.
21) Ref. 18, p. 53.
22) R. Colin, P. Goldfinger, and M. Jeunehomme, *Trans. Faraday Soc.*, **60**, 306 (1964).
23) G. Drummond and R. F. Barrow, *ibid.*, **47**, 1275 (1951).
24) I. V. Veits and L. V. Gurvich, *Chem. Abstr.*, **52**, 9727e (1958); *Zh. Fiz. Khim.*, **31**, 2306 (1957).
25) P. J. Kalff, Tj. Hollander, and C. Th. J. Alkemade, *J. Chem. Phys.*, **43**, 2299 (1965).
26) B. V. L'Vov, *Chem. Abstr.*, **54**, 20467a (1960); *Inzhner. Fiz. Zh., Akad. Nauk Belorus, S. S. S. R.*, **2**, 44 (1959).
27) A. Lagergvist and L. Huldt, *Z. Naturforsch.*, **A9**, 991 (1954).
28) L. Huldt and A. Lagergvist, *Chem. Abstr.*, **45**, 404c (1951); *Ark. Fys.*, **2**, 333 (1951).
29) M. S. Chandrasekharaiah, *J. Phys. Chem.*, **68**, 2020 (1964).
30) E. R. Lippincott, D. Steele, and P. Caldwell, *J. Chem. Phys.*, **35**, 123 (1961).

Viscous Properties of Liquid Oligotrifluorochloroethylene

Naosato Yoshida and Shuichi Hamada

Department of Chemistry, Faculty of Science, Science University of Tokyo, Kagurazaka, Shinjuku-ku, Tokyo

(Received June 18, 1971)

The viscosities of fractionated liquid oligotrifluorochloroethylene were measured in the molecular-weight range from 820 to 2100 at temperatures ranging from 40 to 120°C. While the relationships between log η and log M_n were regarded as being approximately linear in the molecular-weight range smaller than 1090, and their slopes were much larger than unity, a considerable deviation from the approximately linear relationship was observed in the molecular-weight range larger than 1090. The temperature dependence of the viscosities was well explained in terms of the WLF equation under the present experimental conditions. The large slope in the range of the linear relationship may be caused because the reciprocals of the free-volume fractions, $1/f$, increase remarkably with an increase in the molecular-weight. The free-volume per cubic centimeter, F, contributed by chain-ends increased abruptly with an increase in the molecular-weight in the range smaller than about 1200.

In a previous paper,[1] it was reported that the slope of the log η-log M_n relationship for oligotrifluorochloroethylene was much larger than unity in the molecular-weight range from 820 to 1090; a similar behavior in oligostyrene and oligoisobutylene has also been reported by Fox and Flory[2,3] and by Uchida and Hata.[4]

In this work, the dependence of the viscosity on the molecular-weight will be discussed in connection with the free-volume.

Experimental

Materials. Daifloil's No. 20, 50, 100, and 200, which were obtained from the Daikin Kogyo Company, were used as the samples of oligotrifluorochloroethylene. The acetone-soluble part was fractionated in the manner described in our previous paper,[1] while the acetone-insoluble part was fractionated according to whether it was soluble or insoluble in benzene or carbon tetrachloride. The number-average molecular-weight of the oligotrifluorochloroethylene thus fractionated was estimated by cryoscopic and ebullioscopic methods, using benzene and carbon tetrachloride respectively as the solvents.

Procedure. The melting point, T_m, of the sample crystallized was estimated by a dilatometric method. Beforehand, a rough melting point, T_m', of the sample was estimated by a capillary method in order to obtain the crystallization temperature of the sample fractionated. A suitable amount of the sample was crystallized in a container of the dilatometer by allowing it to stand for about 30 hr at a temperature of $(7/9)\,T_m'$. The samples were considered to crystallize sufficiently, since sharp X-ray patterns were observed even with samples obtained by quenching. The sample thus crystallized was sealed in a dilatometer containing mercury. The dilatometer was kept at $T_m' - 20°$ for 30 min to establish a thermal equilibriun, and then it was heated slowly at a heating rate of 0.05°C/min. The melting point was estimated graphically from the specific volume-temperature relationship.

The viscosities and the densities of the liquid samples were measured with an Ubbelohde-type viscometer and a dilatometer respectively in the manner described in a previous paper;[1] they were determined at given temperatures in the range from 40 to 120°C with an accuracy of ± 0.01°C in thermostated baths filled with water or silicone oil.

Results

Melting Points of Oligotrifluorochloroethylene. Table 1 shows the melting points of the samples fractionated in the molecular-weight range from 1200 to 3800.

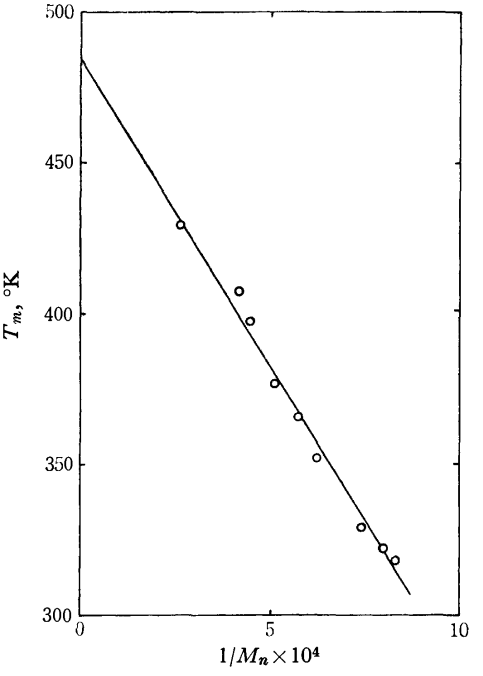

Fig. 1. Relationship between T_m and $1/M_n$.

Table 1. Melting points of oligotrifluorochloroethylene

M_n	1200	1250	1350	1600	1750	1950	2250	2400	3800
T_m, °K	317	321	328	351	365	376	397	407	429

Figure 1 shows the relationship between the melting point, T_m, and the reciprocal of the number-average molecular-weight, $1/M_n$. The linear relationship between T_m and $1/M_n$ can be expressed as follows:

$$T_m = 485 - 2.10 \times 10^5/M_n \qquad (1)$$

1) N. Yoshida, S. Hamada, and T. Shirai, This Bulletin, **42**, 3131 (1969).
2) T. G. Fox and P. J. Flory, *J. Chem. Phys.*, **55**, 221 (1951).
3) T. G. Fox and P. J. Flory, *J. Polym. Sci.*, **13**, 315 (1954).
4) Y. Uchida and T. Hata, Preprint of the 13th Annual Meeting of Soc. Polymer Sci., Japan, 222 (1964).

Table 2. Viscosities of oligotrifluorochloroethylene

M_n	Viscosities η, poise								
	40°C	50°C	60°C	70°C	80°C	90°C	100°C	110°C	120°C
820	6.39	2.93	1.51	0.855	0.521				
860	10.78	4.71	2.33	1.26	0.730	0.451			
870	18.81	6.68	3.16	1.64	0.916	0.547			
890		9.16	4.23	2.15	1.19	0.698			
1010		29.53	12.28	5.68	2.99	1.63			
1030			16.60	7.59	3.77	2.01	1.14		
1050			21.21	9.49	4.63	2.43	1.36		
1070			23.20	10.39	5.05	2.64	1.47		
1090			26.23	11.66	5.64	2.93	1.62		
1200				24.94	11.20	5.44	2.83		
1600					49.25	22.55	11.14		
2100							23.88	12.20	6.60

The melting point, T_m^0, of a high-polymeric trifluorochloroethylene is expected to be 485°K from the linear relationship. This value is nearly equal to that of polytrifluorochloroethylene, 497°K, as reported by Hoffman and Weeks.[5,6]

Viscosities of Oligotrifluorochloroethylene. The viscosities of the liquid samples fractionated are given in Table 2.

Though the results in the molecular-weight range smaller than 1090 have been reported in the previous paper,[1] they were reexamined for this work.

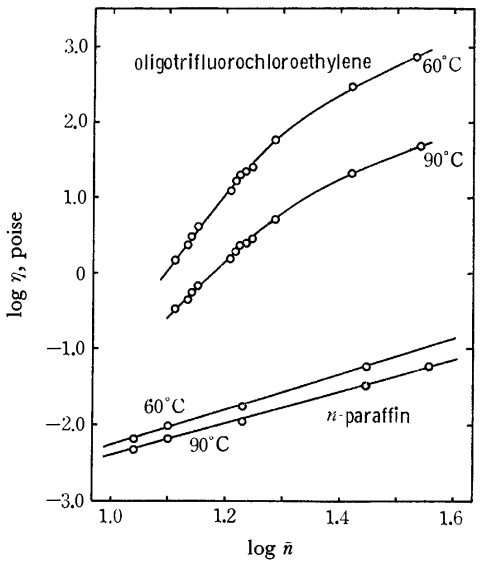

Fig. 2. Chain-length dependence of viscosity.
(The viscosity values for oligotrifluorochloroethylene in the molecular-weight range larger than 1200 at 60°C, and those in the molecular-weights of 820 and 2100 at 90°C were calculated by using WLF equation, respectively.)

Figure 2 shows the relationships between log $\bar{n}$ and log η at 60 and 90°C in the chain-length range from 12.8 to 34.8; the chain-length, $\bar{n}$, shows the number of carbon atoms in the skeleton of oligotrifluorochloroethylene and *n*-paraffin molecules. An expression, $\bar{n}$, was taken in order to compare the dependence of the viscosities of oligotrifluorochloroethylene on the chain-length with those for *n*-paraffin. While an approximately linear relationship was obtained between log η and log $\bar{n}$, *i.e.*, between log η and log M_n, in the molecular-weight range smaller than 1090, as was reported in the previous paper,[1] the linear relationship did not hold in the molecular-weight range larger than 1090. On the contrary, in the case of *n*-paraffin[7,8] log η varied linearly with log$\bar{n}$ in the chain-length range from 5 to 64 (the molecular-weight range from 72.15 to 899.68). The slopes of the linear part were much larger than those found in the usual lower-molecular-weight chain polymers, and they rose remarkably with an increase in the temperature.[1]

Temperature Dependence of Viscosities. The shift factor, a_T, based on an arbitrary fixed temperature, T_0, obeyed well the WLF equation,[9] reported in the previous paper.[1] From the linear relationship between $(T-T_0)/\log a_T$ and $(T-T_0)$, the WLF parameters, C_1^0 and C_2^0, were estimated in the molecular-weight range from 820 to 2100. Table 3 shows C_1^0 and C_2^0 at the fixed temperature of 70°C and their products, $C_1^0C_2^0$.

The apparent activation energy, E_a, for the viscous flow was estimated from the following equation:[6]

Table 3. Values of C_1^0, C_2^0, and $C_1^0C_2^0$ at 70°C

M_n	C_1^0	C_2^0	$C_1^0C_2^0$
820	3.50	146.2	511.9
860	4.13	158.8	655.8
870	4.55	164.6	749.7
890	4.61	161.8	744.8
1010	5.76	180.1	1037.1
1030	5.95	179.9	1069.7
1050	6.09	179.7	1094.9
1070	6.27	184.3	1155.6
1090	6.34	185.0	1173.2
1200	7.03	187.1	1314.7
1600	7.51	185.4	1392.0
2100	7.70	179.9	1385.6

5) J. D. Hoffman and J. J. Weeks, *J. Res. Nat. Bur. Stand.*, **60**, 465 (1958).
6) J. D. Hoffman and J. J. Weeks, *J. Chem. Phys.*, **37**, 1723 (1962).
7) A. K. Doolittle, *J. Appl. Phys.*, **22**, 1471 (1951).
8) A. K. Doolittle, *ibid.*, **23**, 236 (1952).
9) M. L. Williams, R. F. Landel, and J. D. Ferry, *J. Amer. Chem. Soc.*, **77**, 3701 (1955).

$$E_a = 2.303C_1^0C_2^0RT^2/(C_2^0+T-T_0)^2 - RT + \alpha RT^2 \quad (2)$$

where R and α are the gas constant and the thermal-expansion coefficient of the liquid sample respectively.

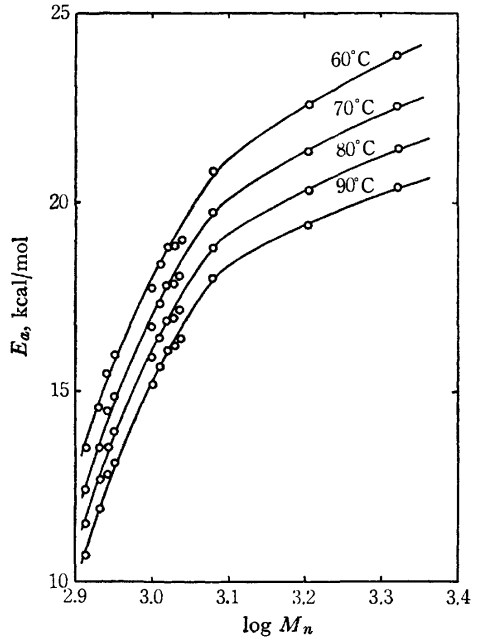

Fig. 3. Dependence of apparent activation energy for viscous flow on log M_n.

Figure 3 shows the dependence of E_a on log M_n. Though the values of E_a increased with an increase in the molecular-weight, they were quite large in comparison with those found in the usual lower-molecular-weight oligomers without branched chains.[10]

Discussion

According to Doolittle,[7,11] the viscosity is related to free-volume fraction by the following equation:

$$\ln \eta = \ln P + Q(1/f_T) \quad (3)$$

where P and Q are empirical constants; where f_T is the free-volume fraction at T, and where the parameter, Q, is regarded as being approximately unity.[12] The reciprocal of the free-volume fraction, $1/f_T$, at a given temperature, T, was calculated from the following equation in conjunction with the WLF equation:

$$1/f_T = 2.303C_1^0C_2^0/(C_2^0+T-T_0) \quad (4)$$

The dependence of $1/f_T$ on the molecular-weight, M_n, and the number of carbon atoms, $\bar{n}$, in the skeletons of oligotrifluorochloroethylene and n-paraffin molecules at given temperatures is shown in Fig. 4. The parameters, C_1^0 and C_2^0, for n-paraffin were estimated from the results reported by Doolittle[7] by the manner used in the case of oligotrifluorochloroethylene. The reciprocal of the free-volume fraction, $1/f_T$, varied considerably with $\bar{n}$ in the case of oligotrifluorochloroethylene; this is in contrast with the case of n-paraffin, as is shown

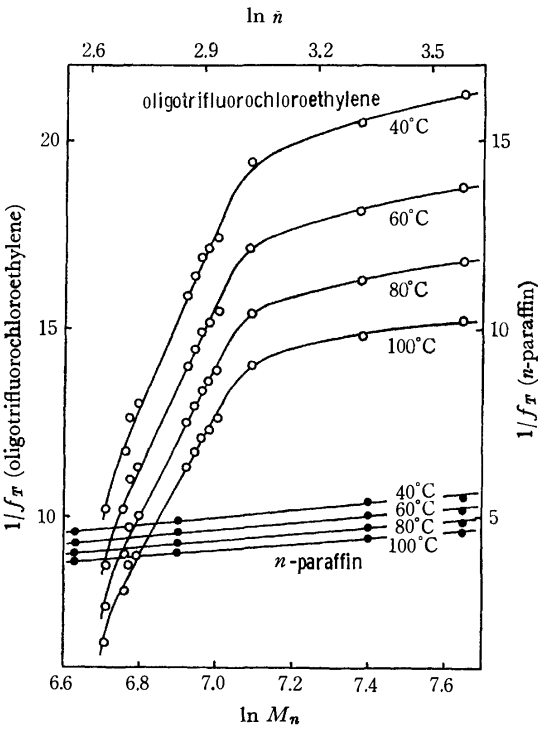

Fig. 4. Relationship between ln M_n and $1/f_T$.

in Fig. 4. While linear relationships between $1/f_T$ and log M_n were obtained in the molecular-weight range from 860 to 1200, considerable deviations from the linear relationships were observed in the molecular-weight range larger than 1200. In the molecular-weight range from 860 to 1200, the relationship between $1/f_T$ and ln M_n is expressed as follows:

$$1/f_T = \ln h + k \ln M_n \quad (5)$$

The slopes, k, were much larger than unity, and they decreased with an increase in the temperature, as is shown in Table 4.

Table 4. Slopes, k, of the linear relationship

Temp., °C	40	60	80	100
k	23.8	22.0	20.0	18.8

The free-volume fraction, f_T, at T is expressed by the following equation:

$$f_T = f_g + \alpha_f(T-T_g) \quad (6)$$

where f_g is the free-volume fraction at T_g, and α_f, its thermal-expansion coefficient. The thermal-expansion coefficient, α_f, of the free-volume fraction is expressed as $1/2.303C_1^0C_2^0$. Figure 5 shows the relationships between α_f and $\bar{n}$ for oligotrifluorochloroethylene and n-paraffin. The α_f values of oligotrifluorochloethylene increased remarkably as the $\bar{n}$ values decreased in the range of $\bar{n}$ smaller than approximately 20; they reached a constant value, 3×10^{-4}°C^{-1}, above an $\bar{n}$ value of 20, though the α_f values for n-paraffin scarcely changed at all.

The glass-transition temperatures, T_g, of the fractionated oligotrifluorochloroethylenes were deduced from their melting points, because the measurement of the glass-transition temperature was difficult because of a tendency toward easy crystallization. The ratio be-

10) H. Schott, *J. Appl. Polym. Sci.*, **6**, S29 (1962).
11) A. K. Doolittle and D. B. Doolittle, *J. Appl. Phys.*, **28**, 901 (1957).
12) F. Bueche, *J. Chem. Phys.*, **24**, 418 (1956).

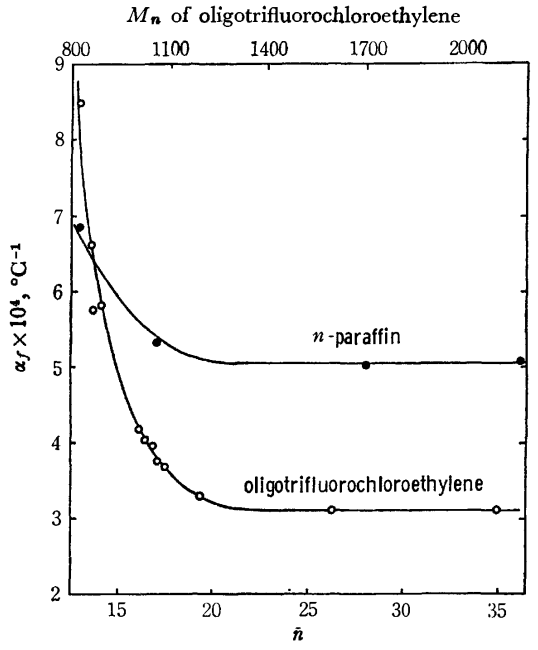

Fig. 5. Relationship between α_f and $\bar{n}$.

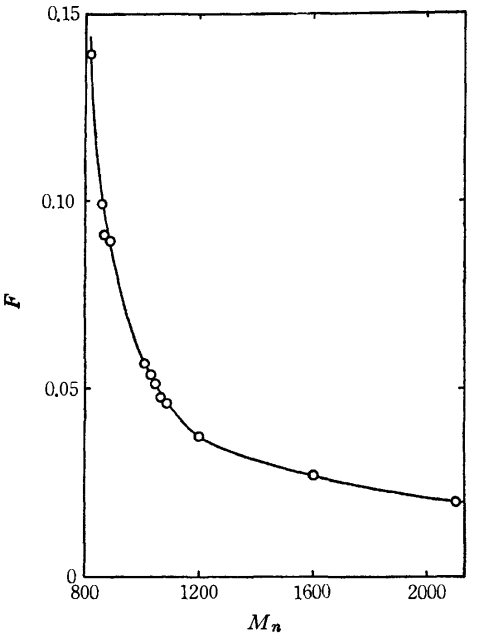

Fig. 6. Relationship between chain-end free volume per cc, F, and M_n at 52°C.

tween the glass-transition temperature and the melting point, T_g/T_m, for polytrifluorochloroethylene was reported to be 0.654 by Hoffman and Weeks.[5,6] This ratio was nearly equal to the value, 0.667, found in usual asymmetric polymers.[13] By the use of this value, 0.667, found in usual asymmetric polymers.[13] By the use of this value in the oligomer range, the relationship between the T_g and the M_n of oligotrifluorochloroethylene can be expressed from the relationship of $T_g/T_m=0.654$ and Eq. (1) as follows:

$$T_g = 317 - 1.37 \times 10^5/M_n \quad (7)$$

Thus, the glass-transition temperature, T_g, of oligotrifluorochloroethylene is considered to rise remarkably as the molecular-weight increases in the oligomer range.

Accordingly, the free-volume fraction, f_T, in the molecular-weight range below 1200 ($\bar{n}=20$) is considered to vary remarkably with the effects of both an abrupt decrease in α_f and a remarkable rise in T_g with an increase in the molecular-weight. The free-volume fractions, f_T, were related only to the variation in T_g depending on the molecular-weight above 1200, because the thermal-expansion coefficient, α_f, of the free-volume was nearly constant.

Bueche[14] pointed out that the chain-ends of the polymer would contribute a certain amount to the total free-volume of the system, because each chain-end would necessarily possess more free-volume than that of a continuous chain. If the free-volume contributed by a chain-end is designated as θ, the total amount of free-volume per cubic centimeter, F, contributed by chain-ends can be expressed as follows:

$$F = \theta(2\rho N/M_n) \quad (8)$$

where ρ is the polymer density, and N, the Avogadro number. Further, the glass-transition temperature, T_g, in relation to the free-volume contributed by chain-ends, was expressed as follows:

$$T_g = T_g^0 - (2\rho N\theta/\alpha_f)(1/M_n) \quad (9)$$

where T_g^0 is the glass-transition temperature of high-polymeric polymer. From Eqs. (7) and (9), the F and the θ values for polytrifluorochloroethylene are given by the following equations:

$$F = 1.37 \times 10^5\alpha_f/M_n \quad (10)$$

$$\theta = 1.37 \times 10^5\alpha_f/2\rho N \quad (11)$$

where α_f is the function of the molecular-weight, as is shown in Fig. 5.

Table 5. Free volume, θ, contributed by a chain-end, Å^3

M_n	θ	M_n	θ
820	51	1050	24
860	40	1070	23
870	35	1090	22
890	35	1200	20
1010	25	1600	19
1030	24	2100	19

Table 5 shows the free-volume, θ, contributed by a chain-end in the molecular-weight range from 820 to 2100 at 52°C (the glass-transition temperature of polytrifluorochloroethylene[5,6]), when ρ is regarded as approximately 1.9. The θ values decreased with an increase in the molecular-weight up to about 1200.

Figure 6 shows the relationship between the free-volume, F, contributed by chain-ends and the molecular-weight at 52°C. The F value increased abruptly with a decrease in the molecular-weight below about 1200.

13) R. G. Reaman, *J. Polym. Sci.*, **9**, 470 (1952).
14) F. Bueche, "Physical Properties of Polymers," Interscience Publishers, New York (1962), p. 113.

The Microwave Spectrum of Dimethyl Sulfone

Shuji SAITO and Fumio MAKINO
Sagami Chemical Research Center, Sagamihara, Kanagawa
(Received June 24, 1971)

The microwave spectra of normal and ^{13}C-isotopic species of dimethyl sulfone have been investigated, and the rotational constants of both species have been determined. The following r_0-structural parameters have been determined: r(C–S)$=1.777\pm0.006$ Å, r(S–O)$=1.431\pm0.004$ Å, $\angle$CSC$=103°17'\pm10'$, and $\angle$OSO$=121°1'\pm15'$, assuming that r(C–H)$=1.091$ Å and $\angle$HCH$=109°34'$. The variations in the structural parameters among the related alkyl sulfides, alkyl sulfoxides, and alkyl sulfones have been discussed. The dipole moment has been determined to be $\mu=4.432\pm0.041$ D along the b axis. This value is consistent with the results of a bond-moment calculation based on the dipole moment of dimethyl sulfoxide.

Recently, ethylene episulfone, $(CH_2)_2SO_2$[1], has been subjected to a microwave spectroscopic study; we have found an r_0 structure characterized by a long C–C bond (1.590 Å) and rather short C–S bonds (1.731 Å). These distinct features have been considered to arise from the ring strain. Dimethyl sulfone, $(CH_3)_2SO_2$, may be a typical molecule with no ring strain, corresponding to ethylene episulfone. In fact, the structural comparison mentioned above was made with reference to the structure of dimethyl sulfone, which was determined by X-ray crystallography, not by microwave spectroscopy. Sands[2] reported that r(C–S) $=1.78$Å, a little shorter than the distance of the normal single C–S bond, r(S–O)$=1.44$ Å, $\angle$CSC$=103°$, and $\angle$OSO$=117.9°$, slightly smaller than the $\angle$OSO angle for the normal sulfone group. To make the situation clear, it may be desirable to compare the structure of ethylene episulfone with those of simple alkyl sulfones as accurately determined by microwave spectroscopy. Feairheller and Katon[3] observed the infrared and Raman spectra for dimethyl sulfone with detailed frequency assignments; they pointed out that this molecule is roughly an accidental spherical top. A normal-coordinate analysis of dimethyl sulfone was carried out by Carter, Freeman, and Henshall.[4] There have been a few reports on the dipole moment for this molecule as studied by the dielectric-constant method.[5–7]

In this paper we wish to report the results of the determination of the molecular structural parameters and the dipole moment for dimethyl sulfone from its microwave spectrum.

Experimental

The dimethyl sulfone sample used was obtained from the Tokyo Kasei Kogyo Co. A ^{13}C-enriched sample (6 at. % of ^{13}C) was prepared by oxidizing ^{13}C-enriched dimethyl sulfide with potassium permanganate.[8] The enriched dimethyl sulfide was formed by the reaction[9] of sodium sulfide on methyl iodide enriched to about 6 at. % of ^{13}C. The spectra were observed with a 110-kHz Stark-modulation microwave spectrometer.[10] As the vapor pressure of dimethyl sulfone was about 0.02 mmHg at about 20°C, all the measurements were carried out at room temperature. A high-precision dc-voltage power supply (Fluke, Model 415B) was used in the Stark-effect measurements.

TABLE 1. ROTATIONAL TRANSITIONS OF NORMAL DIMETHYL SULFONE (MHz)[a]

Transition	ν_{obs}[b]	$\nu_{obs}-\nu_{calc}$[d]
$2_{02}\leftarrow1_{11}$	16576.64	−0.07
$2_{12}\leftarrow1_{01}$	17169.78	0.25
$2_{21}\leftarrow1_{10}$	18091.48	−0.11
$2_{20}\leftarrow1_{11}$	18235.73	0.11
$3_{03}\leftarrow2_{12}$	25071.70[c]	−0.15
$3_{13}\leftarrow2_{02}$	25475.84	0.14
$3_{22}\leftarrow2_{11}$	26445.73[c]	−0.11
$3_{21}\leftarrow2_{12}$	26922.32[c]	0.09
$3_{31}\leftarrow2_{20}$	27415.78	−0.20
$3_{30}\leftarrow2_{21}$	27445.40	0.11
$4_{13}\leftarrow3_{22}$	33194.18	−0.54
$4_{04}\leftarrow3_{13}$	33529.75	−0.30
$4_{14}\leftarrow3_{03}$	33765.00	0.05
$4_{23}\leftarrow3_{12}$	34738.66	−0.28
$4_{22}\leftarrow3_{13}$	35772.55	−0.19
$4_{32}\leftarrow3_{21}$	35835.07	−0.17
$4_{31}\leftarrow3_{22}$	35981.21	0.08
$4_{41}\leftarrow3_{30}$	36705.33	−0.03
$4_{40}\leftarrow3_{31}$	36709.35	−0.02
$5_{14}\leftarrow4_{23}$	41832.38	−1.09
$5_{05}\leftarrow4_{14}$	41946.27	−0.39
$5_{15}\leftarrow4_{04}$	42065.75	−0.43
$5_{24}\leftarrow4_{13}$	42980.98	−0.26
$5_{33}\leftarrow4_{22}$	44179.05	−0.35
$5_{32}\leftarrow4_{23}$	44598.87	−0.23
$5_{42}\leftarrow4_{31}$	45171.33	−0.23
$5_{41}\leftarrow4_{32}$	45199.40	−0.27

a) First ten transitions were used in least squares fit.
b) Accuracy better than ±0.1 MHz, unless otherwise indicated.
c) ±0.2 MHz.
d) Calculated frequencies were obtained using rotational constants in Table 3.

1) Y. Nakano, S. Saito, and Y. Morino, This Bulletin, **43**, 368 (1970).
2) D. E. Sands, *Z. Kristallogr.*, **119**, 245 (1963).
3) W. R. Feairheller, Jr., and J. E. Katon, *Spectrochim. Acta*, **20**, 1099 (1964).
4) J. H. Carter, J. M. Freeman, and T. Henshall, *J. Mol. Spectrosc.*, **22**, 18 (1967).
5) H. Lumbroso and R. Passerini, *Bull. Soc. Chim. Fr.*, **1955**, 1179.
6) M. J. Aroney, L. R. Fisher, and R. J. W. Le Fèvre, *J. Chem. Soc.*, **1963**, 4450.
7) C. W. N. Cumper, J. F. Read, and A. I. Vogel, *ibid.*, **1965**, 5323.
8) T. B. Douglas, *J. Amer. Chem. Soc.*, **68**, 1072 (1946).
9) D. S. Tarbell and C. Weaver, *ibid.*, **63**, 2939 (1941).
10) S. Saito, This Bulletin, **42**, 663 (1969).

Microwave Spectrum

Most of the measurements were made using a recorder, because the spectral lines were all weak. The assignment of the spectral lines for the normal species was performed by observing the Stark effect on each transition. The frequencies of the observed transitions are listed in Table 1. The rotational constants for the normal species were determined by a least-squares fitting of the lowest ten transitions. The centrifugal distortion effect was discarded in the analysis, because only low-J transitions were observed. Although the ^{13}C-enriched sample was used, it was difficult to assign the spectral lines of the ^{13}C species. This is because the expected frequency regions for low-J transitions of the ^{13}C species were densely covered with other strong lines. Observation had to be made very carefully of the Stark effect for each candidate line and of its relative intensity in the natural sample and in the ^{13}C-enriched sample. A simple relation between the moments of inertia, $\Delta I=I_c-(I_a+I_b)$, was also helpful for the assignment, because it remains essentially unchanged for the isotopic substitution of the atoms in the CSC plane. Ten observed transitions of the ^{13}C species are listed in Table 2. Most of them were used to calculate the rotational constants. The observed rotational constants and moments of inertia are given in Table 3. The three rotational constants thus obtained differ from one another only by a few hundred megahertz, so the dimethyl sulfone molecule is a nearly accidental spherical-top, as has been pointed out by Feairheller and Katon.[3] Table 3 also shows that the ΔI's for the normal species and the ^{13}C species agree very well. This indicates that the effect of zero-point vibrations can be disregarded.

Table 2. Observed rotational transitions of ^{13}C-enriched dimethyl sulfone (MHz)

Transition	ν_{obs}[a]	$\nu_{obs}-\nu_{calc}$[c]
$2_{12}\leftarrow 1_{01}$	16846.45	−0.30
$3_{03}\leftarrow 2_{12}$	24504.85	−0.21
$3_{13}\leftarrow 2_{02}$	24950.96	−0.13
$3_{22}\leftarrow 2_{11}$	26058.90	0.10
$4_{13}\leftarrow 3_{22}$	32427.73[b]	−0.86
$4_{14}\leftarrow 3_{03}$	33036.88	−0.19
$4_{23}\leftarrow 3_{12}$	34147.74	0.53
$4_{22}\leftarrow 3_{13}$	35376.13	0.03
$4_{32}\leftarrow 3_{21}$	35401.52[b]	0.02
$4_{41}\leftarrow 3_{30}$	36394.31	−0.19

a) Accuracy better than ±0.2 MHz.
b) Not included in least squares fit.
c) Calculated frequencies were obtained using rotational constants in Table 3.

Table 3. Rotational constants (MHz) and moments of inertia (amuÅ^2)[a] for dimethyl sulfone

	Normal species	^{13}C-species
A	4638.15±0.02	4606.03±0.05
B	4295.44±0.02	4219.71±0.05
C	4177.13±0.02	4080.24±0.05
I_a	108.961±0.0006	109.721±0.0015
I_b	117.654±0.0006	119.766±0.0015
I_c	120.987±0.0006	123.859±0.0015
ΔI	−105.628	−105.627

a) Conversion factor $=5.05376\times10^5$ amuÅ^2 MHz for amu based on the ^{12}C scale.
b) $\Delta I=I_c-(I_a+I_b)$.

Dipole Moment

The second-order Stark effect was measured for six transitions, as is shown in Table 4. The electrode spacing was calibrated using the $J=1\leftarrow0$ transition of OCS.[11] From the Stark coefficients, the dipole moment along the b axis was determined to be 4.432± 0.041 D, where the error quoted was 2.5 times the standard deviation. This value is in agreement with the values ($\mu=4.25$—4.26 D) obtained by the dielectric-constant measurements.[5-7]

Table 4. Stark coefficients and dipole moments of dimethyl sulfone

Transition		$\Delta\nu/E^2_{obs}$[a]	μ_{obs}(D)
$2_{20}-1_{11}$	$M=1$	2.536×10^{-4}	4.484
$3_{03}-2_{12}$	$M=1$	-0.6268×10^{-4}	4.411
$3_{30}-2_{21}$	$M=1$	-0.6665×10^{-4}	4.439
$3_{30}-2_{21}$	$M=2$	-2.483×10^{-4}	4.455
$3_{31}-2_{20}$	$M=1$	-1.571×10^{-4}	4.436
$3_{31}-2_{20}$	$M=2$	-6.083×10^{-4}	4.367
$\mu=\mu_b=4.432\pm0.041$D[b]			

a) Values in MHz (V/cm)$^{-2}$.
b) Error is 2.5 times the standard deviation.

Structure

Dimethyl sulfone has six independent structural parameters. Among them, it is hard to determine the two parameters related to methyl groups without information on the deuterated species. As has been discussed in the cases of ethylene episulfoxide[10] and ethylene episulfone[1], it may be reasonable to assume that the structure of the methyl groups for dimethyl sulfone is the same as that of dimethyl sulfide[12]: r(C–H) $=1.091$ Å and $\angle$HCH$=109°34'$. The remaining four structural parameters, the C–S and S–O bond distances and the $\angle$CSC and $\angle$OSO bond angles, were determined by fitting to the three moments of inertia for the normal species and I_a for the ^{13}C species; this choice of moments of inertia was found to be the most suitable for determining the four structural parameters. The results are

Table 5. r_0 structure of dimethyl sulfone

r(C–S)	1.777±0.006Å
r(S–O)	1.431±0.004Å
$\angle$CSC	103°17′±10′
$\angle$OSO	121°1′ ±15′
Assumed parameters[a]	
r(C–H)	1.091Å
$\angle$HCH	109°34′

a) Ref. 12.

11) J. S. Muenter, *J. Chem. Phys.*, **48**, 4544 (1968).
12) L. Pierce and M. Hayashi, *ibid.*, **35**, 479 (1961).

Table 6. Observed and calculated moments of inertia (amuÅ^2)

	Observed	$I_{obs}-I_{calc}$ [a]
Normal species		
I_a	108.961	0.000
I_b	117.654	0.000
I_c	120.987	0.000
^{13}C species		
I_a	109.721	0.000
I_b	119.766	−0.001
I_c	123.859	0.001

a) Based on the structure given in Table 5.

given in Table 5. The uncertainties estimated are due to the experimental uncertainties of the rotational constants and the assumption regarding the methyl groups. The moments of inertia for dimethyl sulfone are calculated using the structure thus obtained; they are compared with the observed values in Table 6. The agreement between them is good.

Discussion

As the comparison in Table 7 shows, the structure of dimethyl sulfone obtained by Sands[2] is in good agreement with our results except for the value of the ∠OSO angle. The ∠OSO angle of 121°1′ which was obtained by this work seems quite reasonable for the ∠OSO angle of alkyl sulfone compounds.

Table 7. C–S and S–O bond distances (Å) and ∠CSC and ∠OSO angles in various compounds

Molecule		r(C–S)	r(S–O)	∠CSC	∠OSO
$(CH_3)_2SO_2$ [a]	r_o	1.777	1.431	103°17′	121°1′
$(CH_3)_2SO_2$ [b]	X	1.78	1.44	103°	117.9°
$(CH_3)_2S$ [c]	r_s	1.802	—	98°52′	—
$(CH_2)_2S$ [d]	r_o	1.819	—	48°25′	—
$(CH_3)_2SO$ [e]	r_s	1.799	1.485	96°34′	—
$(CH_2)_2SO$ [f]	r_o	1.822	1.483	48°46′	—
$(CH_2)_2SO_2$ [g]	r_o	1.731	1.439	54°40′	121°26′
$(CH_3CH_2)_2SO_2$ [h]	X	1.73[j]	1.42_5[k]	55°24′	120°24′
SO_2 [i]	r_e	—	1.4307_6	—	119°19.8′

a) This work. b) Ref. 2. c) Ref. 12. d) Ref. 14.
e) Ref. 13. f) Ref. 10. g) Ref. 1.
h) R. Desiderato and R. L. Sass, *Acta Crystallogr.*, **23**, 430 (1967).
i) S. Saito, *J. Mol. Spectrosc.*, **30**, 1 (1969).
j) The mean value of 1.72 Å and 1.74 Å.
k) The mean value of 1.41 Å and 1.44 Å.

For the purpose of comparison, the four main structural parameters of several related compounds are also listed in Table 7. The C–S bond of dimethyl sulfone is shorter than those of dimethyl sulfide[12] and dimethyl sulfoxide.[13] On the other hand, the C–S bond of ethylene episulfone[1] is distinctly shorter than that of dimethyl sulfone, but, contrary to the case of ethylene episulfone, the C–S bonds of other ring compounds, ethylene episulfide[14] and ethylene episulfoxide,[10] are slightly longer than those of the corresponding compounds, dimethyl sulfide and dimethyl sulfoxide respectively. The former fact means that the sulfone group has a strong electron withdrawing force, resulting in the decrease of the C–S bond distances. The latter fact suggests that the ring strain has some effect on the structures of ring compounds. The behavior of the ring strain can be understood by comparing the ∠CSC bond angles listed in Table 7. The ∠CSC angle of dimethyl sulfone is appreciably wider than those of dimethyl sulfide and dimethyl sulfoxide, so the corresponding ring compound, ethylene episulfone, suffers from severe ring strain. The unusually short C–S bonds of ethylene episulfone may be formed by the combined effects of the weakened long C–C bond and the migration of electrons from the C–C bond to the C–S bonds caused by the strong electron-withdrawing force of the sulfone group. The variation in the ∠CSC bond angle among alkyl sulfides, alkyl sulfoxides, and alkyl sulfones can be explained by the degree of the *s*-character of the C–S bond, which itself depends on the oxidation state of the sulfur atom. However, another point remains to be discussed why the C–S bond distances of ethylene episulfide and ethylene episulfoxide increase slightly, contrary to the case of ethylene episulfone. It is difficult to say why this is so, but it may be said that both the ring strain and the electron-withdrawing force around the sulfur atom in ethylene episulfide and ethylene episulfoxide are so weak that the ring-structures depend on a balance between the two forces. It must be noted that the S–O bond distance and the ∠OSO bond angle of the sulfone group are nearly constant, regardless of the structure of the alkyl group.

Finally, it is interesting to divide the dipole moment of dimethyl sulfone into the C–S and S–O bond moments. When the C–S and S–O bond moments are assumed to be 1.47 D and 2.70 D respectively, values which are derived from the moment of dimethyl sulfoxide,[13] the dipole moment of dimethyl sulfone can be estimated to be 4.47 D. This agrees with the observed value, 4.432 D, given in Table 4. In the same way, the dipole moment of ethylene episulfone can be calculated to be 4.36 D by using the C–S and S–O bond moments of ethylene episulfoxide.[10] The observed value for ethylene episulfone is 4.41 D.[1]

The authors would like to thank Professor Yonezo Morino for his helpful discussions.

13) W. Feder, H. Dreizler, H. D. Rudolph, and V. Typke, *Z. Naturforsch.*, **A, 24**, 266 (1962).

14) G. L. Cunningham, Jr., A. W. Boyd, R. J. Myers, and D. W. Gwinn, *J. Chem. Phys.*, **19**, 676 (1951).

Low-Frequency Raman Spectra and Phase Transition of the 1,2-Dichloroethane Crystal

Akira OZORA, Tsugito NAKAGAWA, and Mitsuo ITO
Department of Chemistry, Faculty of Science, Tohoku University, Sendai
(Received July 1, 1971)

In order to study the phase transition of 1,2-dichloroethane crystal at 177°K, the low-frequency Raman spectra were measured at various temperatures, and normal coordinate analysis was carried out. It was found that the phase transition is of rotational type in which the librational motion of the molecule about the axis passing through two chlorine atoms of the molecule changes into a nearly free rotation about the same axis.

Introduction

It is well-known that 1,2-dichloroethane in gas and liquid phases consists of two rotational isomers of *gauche*- and *trans*-forms, but only the *trans*-form is stable in the solid.

The 1,2-dichloroethane crystal has a phase transition at 177°K, on which a number of investigations have been made. According to the X-ray diffraction studies by Lipscomb *et al.*[1,2] both high[1] and low temperature phases[2] (hereafter referred to as crystals I and II, respectively) are monoclinic, the space group C_{2h}^5-$P2_1/c$ with two molecules in a unit cell, and have very similar cell dimensions. The positions of the carbon atoms could readily be identified for crystal II, but not for crystal I. The chlorine atoms were located at nearly the same positions in both phases (Table 1). They concluded that a nearly free rotational motion of the molecule about the axis passing through the two chlorine atoms takes place in crystal I.

TABLE 1. CRYSTAL STRUCTURES OF 1,2-DICHLOROETHANE

Crystal I	Crystal II
monoclinic	monoclinic
$Z=2$	$Z=2$
$C_{2h}^5-P2_1/c$	$C_{2h}^5-P2_1/c$
$a=5.04$ Å	$a=4.66$ Å
$b=5.56$ Å	$b=5.42$ Å
$c=8.00$ Å	$c=7.88$ Å
$\beta=109°30'$	$\beta=103°30'$
x(C)=—	x(C)=0.099
y(C)=—	y(C)=0.003
z(C)=—	z(C)=0.094
x(Cl)=0.303	x(Cl)=0.318
y(Cl)=0.279	y(Cl)=0.278
z(Cl)=0.074	z(Cl)=0.084
at 223°K	at 133°K

In this paper, we report a new evidence available from the low-frequency Raman spectra supporting Lipscomb's conclusion about the nature of the transition.

Experimental

1,2-Dichloroethane was obtained from Junsei Pure Chemical Co., and distilled twice in a vacuum. The Raman spectra were obtained with a Narumi model 750Z-1200 double monochromator. The 6328Å line from He-Ne gas laser was used as an exciting light. An S-20 photomultiplier followed by a photon counting system was employed for detection of the spectra. The optical arrangement for laser Raman measurements is the same as described previously.[3] Temperature control of the sample was made by regulating flow speed of dry nitrogen gas cooled with liqudid nitrogen. Accuracy of temperature was estimated to be ±3°C.

Results

From the crystal structure of 1,2-dichloroethane,nine optical active lattice vibrations are expected, of which three are of translational lattice modes ($2A_u+B_u$) active only in the infrared spectrum. The remaining six are of rotational lattice modes ($3A_g+3B_g$) active only in the Raman spectrum.

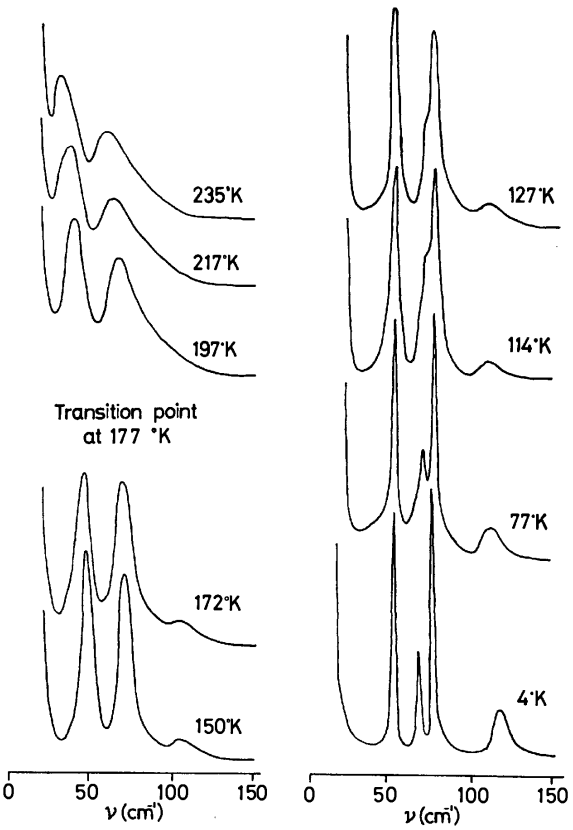

Fig. 1. Lattice vibrational Raman spectra of the 1,2-dichloroethane crystal at various temperatures.

1) M. E. Milberg and W. N. Lipscomb, *Acta Cryst.*, **4**, 369 (1951).

2) T. B. Reed and W. N. Lipscomb, *ibid.*, **6**, 45 (1953); W. N. Lipscomb and F. E. Wang, *ibid.*, **14**, 1100 (1961).

3) M. Suzuki, T. Yokoyama, and M. Ito, *Spectrochim. Acta*, **24**, 1091 (1968).

Table 2. Observed raman frequencies of the lattice vibrations of the 1,2-dichloroethane crystal (cm^{-1})

Crystal I			Crystal II					
235°K	217°K	197°K	172°K	150°K	127°K	114°K	77°K	4.2°K
33	37	40	47	49	51	52	54	56
			—	—	—	72	74	74
62	65	69	72	74	76	77	79	80
			101	107	109	112	117	121

The Raman spectra of the lattice vibrational region at various temperatures between 4.2°K and 235°K are shown in Fig. 1, and the observed frequencies are summarized in Table 2. Four Raman lines were observed in crystal II, although some bands were not resolved at high temperatures.

The highest frequency line at 110 cm^{-1} is probably due to A_g rotational lattice mode around the axis of the least moment of inertia of the molecule nearly coinciding with the direction connecting the two chlorine atoms of the molecule. Weak intensity of this line may be explained by this assignment as a result of small anisotropy of the molecular polarizability around the Cl–Cl axis. Fairly strong intensities and low frequencies of the other lines suggest that they are assigned to rotational modes around the molecular axes perpendicular to the Cl–Cl axis. We assigned tentatively the strong lines at 52 and 77 cm^{-1} at 114°K to the A_g mode and the weaker line at 72 cm^{-1} to the B_g mode.

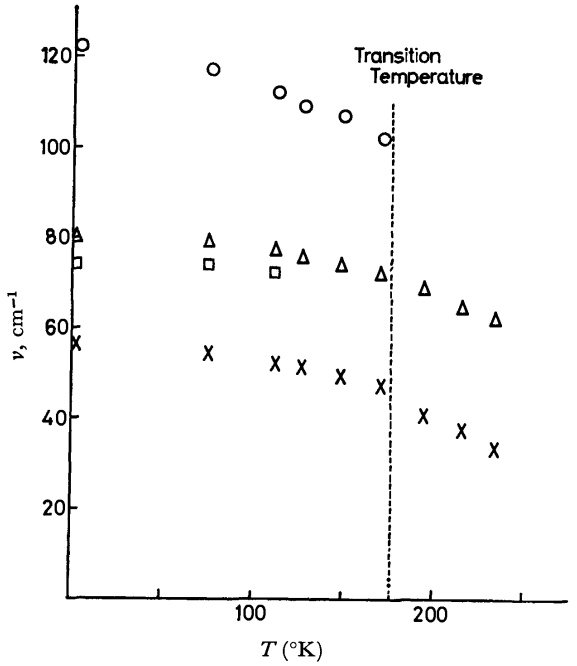

Fig. 2. Effects of temperature on frequencies of lattice vibrational Raman lines.

It should be emphasized that existence of the weak band at 110 cm^{-1} was clearly recongnized even at a temperature just below transition point. However, the weak band is hardly seen as soon as it is transformed into crystal I, while good correspondence is observed for the other lines between the two phases. Figure 2 shows the effect of temperature on the Raman frequencies. The effect is rather large for the highest frequency Raman line of 110 cm^{-1} and it amounts to 20 cm^{-1} between 4.2°K and 172°K as compared with about 10 cm^{-1} for the other lines. We see that smooth curves can be drawn for the Raman lines commonly observed in both phases with no discontinuity at transition point. On the other hand, width of these lines shows discontinuity at transition point as seen in Fig. 3, where the line widths are plotted against temperatures.

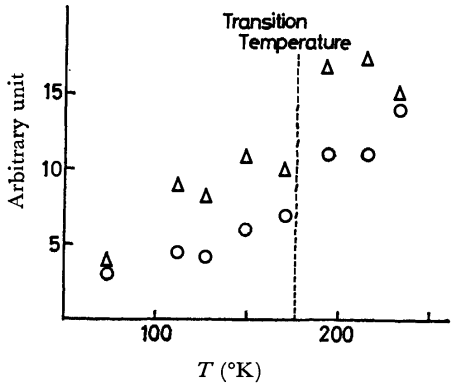

Fig. 3. Effects of temperature on widths of lattice vibrational Raman lines (Plots are given for the Raman lines commonly observed in crystals I and II at about 70 cm^{-1} (△) and 50 cm^{-1} (○)).

Normal Coordinate Calculation

The normal coordinate calculation of the lattice vibrations was carried out for crystal II according to the GF matrix method developed by Shimanouchi *et al.*[4,5] in a rigid body approximation. The approximation may be valid for the Raman active lattice vibrations of the *g* species, since the lowest frequency intramolecular vibration of the *g* species of the molecule which may interact with the *g* lattice vibrations comes out at about 300 cm^{-1} and is well separated from the highest frequency lattice vibrations. The fact that the lowest frequency intramolecular vibration varies within 3 cm^{-1} in the transformation from liquid to the crystal[6] also supports the approximation.

The crystal structure of 1,2-dichloroethane at 133°K is shown in Fig. 4. The positions of hydrogen atoms were located by assuming the C–H distance of 1.08 Å and the ∠CCH and ∠HCH of 109°28′. The principal axes of the moment of inertia of the molecule are also shown in Fig. 4. U and V axes lie in the ClCCCl plane

4) T. Shimanouchi, M. Tsuboi, and T. Miyazawa, *J. Chem. Phys.*, **35**, 1597 (1961).
5) T. Shimanouchi and I. Harada, *ibid.*, **40**, 2651 (1964).
6) S. Mizushima and Y. Morino, *Proc. Ind. Acad. Sci.*, **8**, 315 (1938).

Table 3. Parameters of atom-atom potentials

		C–C	H–H	Cl–Cl	C–H	C–Cl	H–Cl
Williams (Set I)	*A*	51.76	2.81	180.50	6.54	96.66	22.52
	B	3.60	3.74	3.65	3.67	3.63	3.70
	C	37.19	2.50	129.99	9.66	69.53	18.03
Kitaigorodsky (Set II)	*A*	28.19	28.19	180.50	28.19	71.33	71.33
	B	3.60	4.86	3.65	4.12	3.63	4.26
	C	24.03	3.64	129.99	9.83	55.89	21.75
Bartell-Crowell (Set III)	*A*	27.20	4.58	180.50	11.17	70.07	28.75
	B	3.55	4.08	3.65	3.81	3.60	3.87
	C	23.90	3.42	129.99	9.04	55.74	21.08
Dashevsky (Set IV)	*A*	26.19	6.31	159.07	12.86	64.54	31.69
	B	3.52	4.64	3.52	4.08	3.52	4.08
	C	32.93	1.49	201.44	7.00	81.44	17.31

A, in unit of 10^{-10} erg, *B*, in unit of $Å^{-1}$, *C*, in unit of 10^{-12} erg $Å^6$

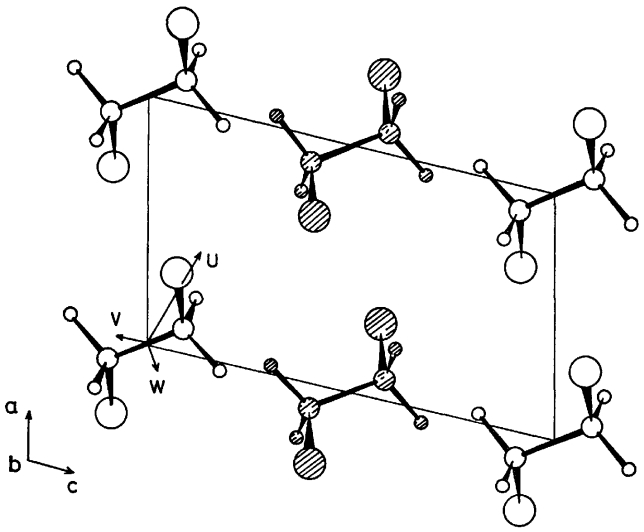

Fig. 4. The crystal structure of 1,2-dichloroethane at 133°K. The shaded molecules are located upward or downward by half a translation of *b*.

and the U axis makes an angle of 1°24′ with the line connecting the two chlorine atoms. The W axis is perpendicular to the U and V axes and coincides with the C_2 symmetry axis of the molecule.

For the intermolecular potential, we assumed the atom-atom interaction potential in the form

$$V(r) = A \exp(-Br) - Cr^{-6},$$

where r is the interatomic distance and A, B, C are constants characteristic of the type of atom pair. Usefulness of this type of potential in calculation of the lattice vibrations of molecular crystals was demonstrated on many occasions.[7]

Three sets of constants proposed by Williams, Kitaigorodsky and Bartell-Crowell[8] for the three types of atom pairs, C–C, C–H, and H–H (hereafter referred to sets I, II, and III, respectively) were used to calculate the lattice frequencies in combination with the Cl–Cl potential obtained by Hill.[9] The set of constants proposed by Dashevsky[10] was also used (hereafter it is referred to set IV). The four sets of constants are listed in Table 3. The constants for C–Cl and H–Cl were taken as geometric mean of the corresponding pairs of identical atoms for A and C, and as arithmetic mean for B.

The atom-atom interactions were assumed for all the atom pairs whose interatomic distances are less than 5.0, 4.0, 5.5, 4.5, 5.0, and 5.0 Å for C–C, H–H, Cl–Cl, C–H, C–Cl, and H–Cl, respectively Further inclusion of the atom pairs beyond these limits have

Table 4. Observed and calculated frequencies of lattice vibrations for the 133°K structure (cm^{-1})

		Set I	Set II	Set III	Set IV	Obsd[a]	Vibrational modes
A_g	ν_1	188	149	155	109	109	85%Ru, 5%Rv, 10%Rw
	ν_2	114	101	102	87	76	14%Ru, 48%Rv, 38%Rw
	ν_3	64	57	60	58	51	47%Rv, 53%Rw
B_g	ν_6	169	127	140	99	—	88%Ru, 12%Rv
	ν_7	92	83	85	77	71	2%Rv, 98%Rw
	ν_8	80	67	71	60	—	85%Rv, 15%Rw
A_u	ν_4	133	116	118	98	—	25%Tu, 75%Tv
	ν_5	102	89	90	71	—	25%Tu, 5%Tv, 70%Tw
B_u	ν_9	78	69	69	53	—	50%Tu, 20%Tv, 30%Tw

a) Extrapolated to 133°K from Table 2.

7) D. A. Oliver and S. H. Walmsley, *Mol. Phys.*, **17**, 617 (1969).
8) Cited in Ref. 7.
9) T. L. Hill, *J. Chem. Phys.*, **16**, 399 (1948).
10) P. G. Dashevsky, U. T. Steruchukof, and S. A. Akappayan, *J. Struct. Chem. USSR*, **7**, 594 (1966).

little effect on the calculated frequencies.

The calculated frequencies obtained with the four sets of potentials are given in Table 4, together with the observed frequencies. It is seen that the Dashevsky's potential (set IV) shows fairly good agreement between the observed and calculated frequencies, while the other sets give higher calculated frequencies. The 1,2-dichloroethane crystal involves fairly short Cl–Cl and Cl–H distances, and slight changes in their interatomic potentials have a large effect on the calculated frequencies. When the force constants for these two atom pairs are compared, it was found that the force constant-interatomic distance curves for Cl–H differ a great deal between set IV and the other sets especially in the short distance range, while the Cl–Cl curves are very similar to each other. The difference in the Cl–H curves must be ascribed to difference in the H–H potentials, since we assumed the parameters for Cl–H to be geometric and arithmetic means of the Cl–Cl and H–H parameters. The force constant curves for H–H are compared in Fig. 5. It is seen that the curve obtained from Dashevsky's potential differs considerably from the others. This is probably the principal reason for the difference in the calculated frequencies between set IV and the others[11].

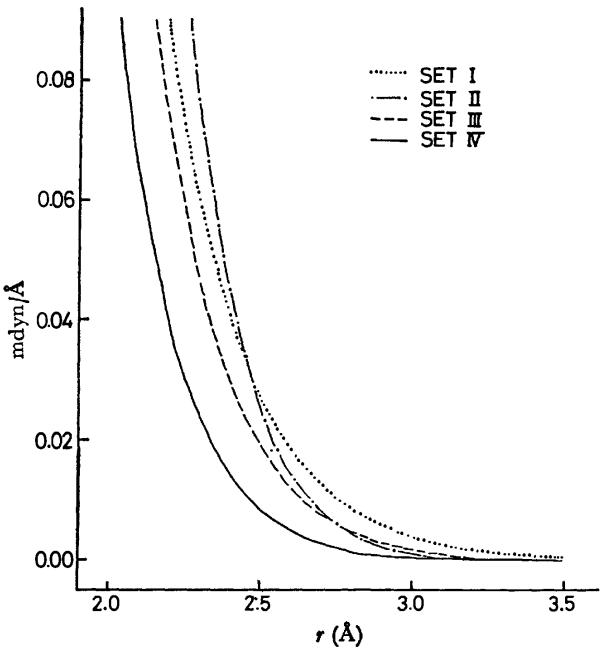

Fig. 5. Force constant curves for H–H.

In the last column of Table 4, approximate vibrational modes calculated with Dashevsky's potential are given. It is noted that the highest frequency vibrations $\nu_1(A_g)$ and $\nu_6(B_g)$ may be described approximately as due to rotational oscillations around the U axis. The situation is the same also in the vibrational modes obtained with other potentials.

Nature of the Phase Transition

Main differences between the Raman spectra of crystals I and II may be summarized as follows: the $\nu_1(A_g)$ line of 110 cm^{-1}, which is weak but distinctly observed in crystal II, is hardly recognized in crystal I, and the widths of all the Raman lines change abruptly at transition temperature.

On the other hand, normal coordinate calculation showed that $\nu_1(A_g)$ (and also $\nu_6(B_g)$) of crystal II is mainly due to the rotational oscillation around the U axis, which almost coincides with the line connecting the two chlorine atoms of the molecule.

The results strongly suggest that the phase transition of the 1,2-dichloroethane crystal at 177°K is a transition in which the rotational oscillational motion about the Cl–Cl axis of the molecule changes into a nearly free rotational motion about the same axis and *vice versa*, supporting the conclusion obtained by Lipscomb *et al.* from their X-ray studies. The $\nu_1(A_g)$ line of crystal II is stilll broad even at 4.2°K, and its band width increases with increase of temperature more rapidly than that of other lines. This implies that the molecular rotational oscillation about the U axis is fairly easy even at very low temperatures, and the oscillational amplitude rapidly increases up to the transition point where a nearly free rotation of the molecule takes place.

11) In the calculation of lattice vibrations of naphthalene and anthracene crystals, the observed frequencies are fairly well reproduced with the potentials given by Kitaigorodsky and Bartell-Crowell, while considerably lower and higher frequencies are calculated with the potentials given by Dashevsky and Williams, respectively.

Exact Classical-Mechanical Calculation of the Translational-Vibrational Energy Transfer of Energized Anharmonic Diatomic Molecules

Okitsugu KAJIMOTO and Takayuki FUENO

Department of Chemistry, Faculty of Engineering Science, Osaka University, Toyonaka, Osaka

(Received July 2, 1971)

The exact classical-mechanical calculation of the translational-vibrational energy transfer of diatomic molecules was extended to collisions between inert gas and anharmonic oscillator of varying initial vibrational energy. The systems investigated were H_2–He, N_2–Ar, and I_2–Ar. It was found that, at lower vibrational levels, the transitions in both upward and downward directions become more efficient with an increase in the initial vibrational energy of molecules. In a high vibrational energy region, however, vibrational deactivation reaches a maximum and then diminishes as the initial vibrational energy approaches the dissociation threshold. The results illuminate the essence of a "bottleneck" to vibrational energy flow involved in the activation process of bimolecular dissociation of diatomic molecules.

Several workers[1-9] have developed theories on the kinetics of diatomic molecules (and the three-body atomic recombination as the reverse reaction) coupled with molecular vibrational relaxation. Their theories all show that dissociation kinetics should receive a sizable draw-back effect from the limited rates of vibrational activation of molecules, the overall reaction being a process proceeding under vibrational non-equilibrium. Details of the non-equilibrium kinetics should essentially be subject to the vibrational transition probabilities of reacting molecules in their collisions with heat-bath molecules.

However, it is an extremely cumbersome problem to evaluate such probabilities for an anharmonic oscillator energized up to its dissociation threshold. In this high-energy region, the vibrational levels are in general not only densely spaced but also poorly definable because of the coupling between vibrational and rotational degrees of freedom. This constitutes an unsurmountable obstacle to an otherwise successful adaption of the concept of vibrational ladder climbing to the overall kinetics of bimolecular dissociations.

One way to overcome the difficulty is to consider the reaction in question as a process of energy flow, by assuming the vibrational energy to be indiscrete. In principle, the diffusion theory presented by Keck and Carrier[10] and the energy-band theory proposed by Rice[11] are both along this line. In this work we treat the average vibrational energy, $\Delta\varepsilon$, which could be gained or lost by Morse oscillators of arbitrary internal energy on their single collision with an inert gas molecule.

It should be noted that the vibrational energy increment, when calculated for an oscillator of relatively low internal energy, should be related, in its classical limit, to the quantum-mechanical vibrational transition probability, P_{ij}, through $P_{ij}=\Delta\varepsilon/(\varepsilon_i-\varepsilon_j)$, where ε_i and ε_j are the energies of the discrete vibrational levels i and j, respectively. Although a number of theoretical procedures (classical, semiclassical or quantum) have been given for such calculations in the literature,[12] any procedure assuming complete separability between the translational and vibrational motions is of little use for our purpose. Separability is justifiable only when the maximum displacement of an oscillating atom from its equilibrium position is considered to be sufficiently small compared with the range size of interaction between the atom and an incident sphere, which is certainly not the case for an energized anharmonic oscillator. Benson and Berend[13] were the first to calculate the $0\rightarrow1$ transition probabilities of diatoms under *mutual* interaction with the incident atom during a collision; exact collision trajectories were obtained by numerical integration of the classical equations of motion for the colinear system. An analogous "exact" classical-mechanical procedure has been used by Kelley and Wolfsberg[14] in order to calculate the energy transferred between harmonic oscillators and inert atoms. A quantum-mechanical version of these "exact" treatments was presented by Secrest and Johnson,[15] who calculated several lower-level transition probabilities of diatoms as a function of incident energy.

In the present paper, we have adopted the exact classical-mechanical procedure to calculate the energy transfer of Morse oscillators as a function of the initial vibrational energy of oscillators as well as the initial relative translational energy of the collision system. The main part of this paper will be bisected. The first half deals with the transition probabilities between lower vibrational levels. The exact quantum-mechanical results of Secrest and Johnson are used as a

1) E. W. Montroll and K. E. Shuler, *J. Chem. Phys.*, **26**, 454 (1957); *Advances Chem. Phys.*, **1**, 361 (1958).
2) E. V. Stupochenko and A. I. Osipov, *J. Fiz. Khim.*, **33**, 1526 (1959).
3) H. O. Pritchard, *J. Phys. Chem.*, **65**, 504 (1961).
4) O. K. Rice, *ibid.*, **65**, 1972 (1961); **67**, 1733 (1963).
5) S. W. Benson and T. Fueno, *J. Chem. Phys.*, **36**, 1597 (1962).
6) H. J. Kolker, *ibid.*, **44**, 582 (1966).
7) H. J. Kolker, *Z. Naturforsch.*, **23a**, 1102 (1968).
8) V. A. LoDato, D. L. S. McElwain, and H. O. Pritchard, *J. Amer. Chem. Soc.*, **91**, 7688 (1969).
9) D. L. S. McElwain and H. O. Pritchard, *ibid.*, **91**, 7693 (1969).
10) J. Keck and G. Carrier, *J. Chem. Phys.*, **43**, 2284 (1965).
11) O. K. Rice, "Statistical Mechanics, Thermodynamics and Kinetics," Freeman and Co., San Francisco, Calif. (1967), Chapter 19.
12) For review, see D. Rapp and T. Kassel, *Chem. Rev.*, **69**, 61 (1969).
13) S. W. Benson and G. C. Berend, *J. Chem. Phys.*, **44**, 470 (1966).
14) J. D. Kelley and M. Wolfsberg, *ibid.*, **44**, 324 (1966).
15) D. Secrest and B. R. Johnson, *ibid.*, **45**, 4556 (1966).

standard for comparison. The latter half deals with the energy transfer of energized anharmonic oscillators. Some important features of the mechanism of bimolecular dissociation of diatomic molecules are shown by comparison of the resulting energy transfer with that of harmonic oscillators.

Method of Calculation

The calculation is based on the classical colinear collision model. The coordinate system is as defined in Fig. 1; a Morse-type molecule BC is struck by an atom A.

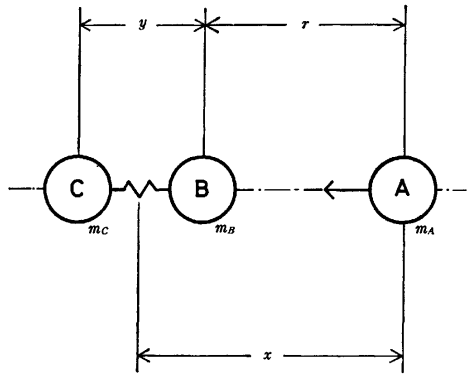

Fig. 1. The colinear collision model and its coordinate system.

The potential of the Morse oscillator is defined by

$$U(y) = D\{\exp[-a(y-y_e)]-1\}^2 \quad (1)$$

The potential acting between the colliding atoms A and B is assumed to be given by the Lennard-Jones 6—12 function:

$$V(r) = 4D_L[(r_L/r)^{12}-(r_L/r)^6] \quad (2)$$

where

$$r = x - ym_C/(m_B+m_C) \quad (3)$$

and m_B and m_C are the masses of atoms B and C respectively. In addition to the above potentials, the harmonic potentials and exponential repulsion potentials were also used for $U(y)$ and $V(r)$, whenever appropriate.

$$U(y) = \frac{1}{2}k(y-y_e)^2 \quad (4)$$

$$V(r) = A\exp(-r/L) \quad (5)$$

The total Hamiltonian of the collision system is expressed by

$$H = \frac{p_x^2}{2m} + \frac{p_y^2}{2\mu} + U(y) + V(x,y) \quad (6)$$

where p_x and p_y denote the momenta with respect to the ordinate variables x and y, respectively, and m and μ are the reduced masses of the collision system and the oscillator, respectively.

$$m = m_A(m_B+m_C)/(m_A+m_B+m_C) \quad (7)$$

$$\mu = m_Bm_C/(m_B+m_C) \quad (8)$$

Hamilton's equations of motion were solved numerically on a digital computer (NEAC 2200) with the aid of the Runge-Kutta-Gill procedure. The initial position of an incoming atom was so selected as to be large enough to render the initial interaction potential $V(x,y)$ negligibly small. The same criterion was applied for terminating the computations. The time step used for integration was 0.5×10^{-16} sec, which proved to be sufficiently small to warrant energy conservation.

For a given vibrational energy ε of the oscillator and a given translational energy E of the incident atom, the energy increment $\Delta\varepsilon$ of the oscillator was calculated as the function of the initial phase angle ϕ of the oscillator. Each initial phase was determined by dividing the period of oscillation into equal time increments. The corresponding initial bond length and momentum were calculated by use of the analytical solution of the internal motion of the Morse oscillator.[16] $\Delta\varepsilon$ was directly evaluated from the difference between the vibrational energies of the oscillator before and after the collision. The $\Delta\varepsilon$ values thus obtained were smooth functions of ϕ, as shown in Fig. 2.

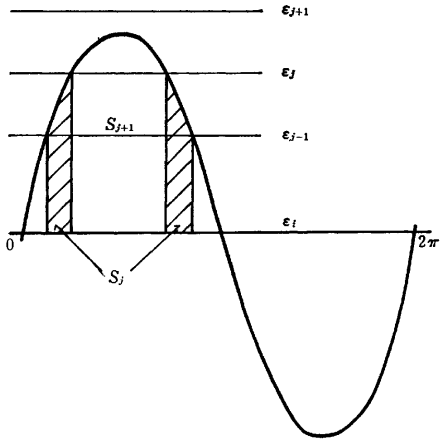

Fig. 2. Definitions of $\Delta\varepsilon_{i\to j}$ and the exact classical transition probability $P_{i\to j}$.

The average energy gain of the oscillator on a collision can be evaluated simply by integrating the $\Delta\varepsilon(E, \varepsilon, \phi)$ over the region where it is positive, and by dividing the results by 2π.

$$\Delta\varepsilon_{act}(E,\varepsilon) = \frac{1}{2\pi}\int_{\Delta\varepsilon>0}\Delta\varepsilon(E,\varepsilon,\phi)\mathrm{d}\phi \quad (9)$$

Likewise, the average energy loss, $\Delta\varepsilon_{deact}$, can be derived from $\Delta\varepsilon(E, \varepsilon, \phi)$ in the region where $\Delta\varepsilon<0$.

In cases where the initial vibrational energy is not very large, Eq. (9) should be related with the quantum-mechanical transition probability. Suppose the collision energy is relatively low, so that the maximum value of $\Delta\varepsilon(E, \varepsilon, \phi)$ for fixed E and ε is small compared with the energy difference between adjacent vibrational levels. The average energy gain of the oscillator which was initially at the i-th level, can then be expressed by

$$\Delta\varepsilon_{i\to i+1}(E) = \frac{1}{2\pi}\int_{\Delta\varepsilon>0}\Delta\varepsilon(E,\varepsilon_i,\phi)\mathrm{d}\phi \quad (10)$$

The transition probability $P_{i\to i+1}(E)$ can be defined as $\Delta\varepsilon_{i\to i+1}(E)$ divided by the energy difference be-

16) N. B. Slater, *Nature*, **180**, 1352 (1957).

tween the i-th and the $(i+1)$-th levels, *viz.*,

$$P_{i\to i+1}(E) = \Delta\varepsilon_{i\to i+1}(E)/(\varepsilon_{i+1}-\varepsilon_i) \qquad (11)$$

$P_{i\to i-1}(E)$ can be obtained through an analogous procedure, except that $\Delta\varepsilon_{i\to i-1}(E)$ is calculated from $\Delta\varepsilon(E, \varepsilon, \phi)$ in the region where $\Delta\varepsilon<0$.

On the high-energy collisions, however, the computed energy gain or loss exceeds the energy difference between adjacent levels (see Fig. 2), so that $\Delta\varepsilon_{i\to j}(E)$ should be properly defined so as to include the jumps over more than one quantum. The main problem is how $\Delta\varepsilon$ should be related with these various quantum jumps.

We here propose a working hypothesis that $\Delta\varepsilon$ can be partitioned into various $\Delta\varepsilon_{i\to j}$'s according to the relevant range of phase angles. That is, just as the activation and deactivation were discriminated according to the range of the phase angles which rendered the calculated $\Delta\varepsilon$ positive or negative, the various quantum jumps are considered to be properly characterized by the phase angle ranges which make such multi-step jumps possible on a single collision. Equation (10) can then be extended into a more general form

$$\Delta\varepsilon_{i\to j}(E) = \frac{1}{2\pi}\int_{\varepsilon_j-\varepsilon_i>\Delta\varepsilon>\varepsilon_{j-1}-\varepsilon_i} \Delta\varepsilon(E, \varepsilon_i, \phi)\mathrm{d}\phi \qquad (12)$$

where $j=i+1, i+2,\cdots\cdots$. For deactivation, the corresponding expression will be as follows:

$$\Delta\varepsilon_{i\to j}(E) = \frac{1}{2\pi}\int_{\varepsilon_{j+1}-\varepsilon_i>\Delta\varepsilon>\varepsilon_j-\varepsilon_i} \Delta\varepsilon(E, \varepsilon_i, \phi)\mathrm{d}\phi \qquad (13)$$

where $j=i-1, i-2,\cdots\cdots$. The transition probabilities are given by

$$P_{i\to j}(E) = \Delta\varepsilon_{i\to j}(E)/(\varepsilon_j-\varepsilon_i) \qquad (14)$$

for either of the activation and deactivation processes. Plausibility of the above hypothesis can only be judged from its outcomings given in the following section.

Vibrational Transitions at Lower Levels

Before discussing the characteristic behavior of the energy transfer of energized molecules, we examine the reliability of the transition probabilities derived for lower levels. Let us compare the exact classical transition probabilities with those obtained by the approximate methods and by the exact quantum-mechanical calculations. In their exact quantum-mechanical theory, Secrest and Johnson[15] assumed a harmonic oscillator model struck by an atom through an exponential repulsion potential. In order to facilitate comparison, we have used the same collision model and potential parameters. Other approximate probabilities based on the classical,[17] semiclassical,[18] and quantum (distorted wave)[19] methods were also evaluated for the same model. The collision systems studied were H_2–He, N_2–Ar, and I_2–Ar. Both the intramolecular and intermolecular potential parameters used are listed in Table 1.

Table 1. Parameters for the harmonic-exponential-repulsion potential models

System	Harmonic potential[a]		Collision potential[b]
	k, 10^4g/sec^2	y_e, Å	L, Å
H_2–He	57.494	0.7413	0.1576
N_2–Ar	229.43	1.0975	0.2041
I_2–Ar	17.202	2.667	0.2400

a) $U(y)=1/2\,k(y-y_e)^2$. k was evaluated from ω_e by use of the equation $k=(2\pi c\omega_e)^2\mu$, where c is the velocity of light and μ is the reduced mass of the oscillator. ω_e was taken from G. Herzberg, "Molecular Spectra and Molecular Structure I. Spectra of Diatomic Molecules," van Nostrand Reinhold Co., New York (1950).

b) $V(r)=A\exp(-r/L)$. A was taken to be equal to the initial translational energy E. L is evaluated from collision diameter σ by use of the equation $L=\sigma_{A\text{-}B}/17.5$ (K. F. Herzfeld and T. A. Litovitz, "Absorption and Dispersion of Ultrasonic Waves," Academic Press, New York (1959)). σ was taken from J. O. Hirschfelder *et al.*, "Molecular Theory of Gases and Liquids," Wiley, New York (1967).

H_2–He system. The values of $P_{0\to1}(E)$ calculated by the various methods as the functions of the initial translational energy of the incident atom are compared in Fig. 3. The approximate classical-, semicalssical-, and quantum-mechanical solutions all give $P_{0\to1}$ values exceeding unity at energetic collisions, whereas both the exact solutions give values which seem reasonable. The latter two solutions are in essential agreement with each other. In the lower collision energy region, however, the exact classical results are somewhat greater than those of the quantum-mechanical calculations.

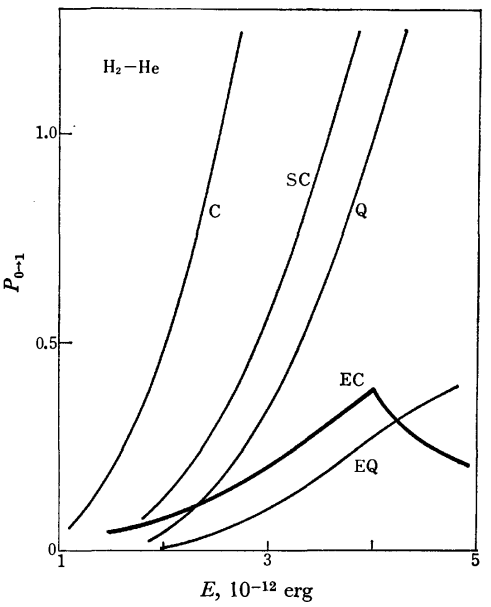

Fig. 3. The 0→1 transition probability of a harmonic H_2 molecule on its collision with an He atom as a function of incident energy.
C, classical[17]; SC, semiclassical[18]; Q, quantum(DW)[19]; EC, exact classical; EQ, exact quantum[15]

The exact classical probabilities calculated for several upward transitions are shown in Fig. 4, and the exact quantum-mechanical results obtained for the same transitions in Fig. 5. A comparison of Figs. 4 and 5

17) D. Rapp, *J. Chem. Phys.*, **32**, 735 (1960).
18) D. Rapp and T. E. Sharp, *ibid.*, **38**, 2641 (1963); **43**, 1233 (1965).
19) J. D. Jackson and N. F. Mott, *Proc. Roy. Soc.* (London), **A137**, 703 (1932).

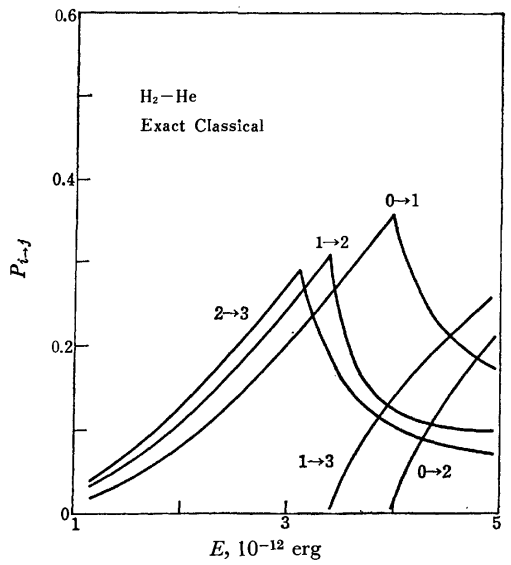

Fig. 4. Exact classical transition probabilities of a harmonic H_2 molecule colliding with a He atom as functions of incident energy.

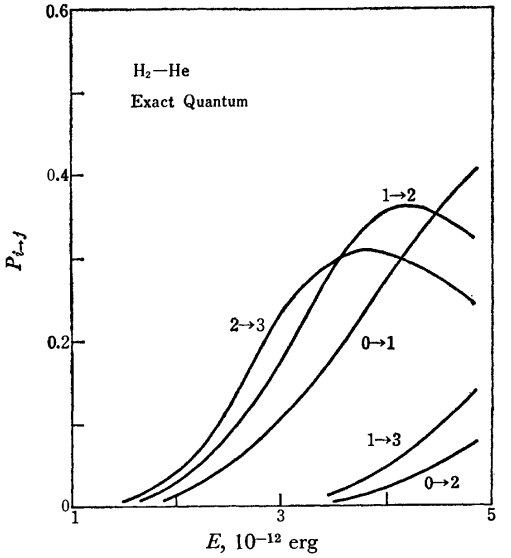

Fig. 5. Exact quantum transition probabilities of a harmonic H_2 molecule colliding with an He atom as functions of incident energy.

TABLE 2. DETAILED BALANCINGS OF THE $P_{i\to j}$ VALUES CALCULATED FOR THE H_2–He SYSTEM

Method	Transition probability	
	$P_{0\to1}$ ($E=3.0\times10^{-12}$ erg)	$P_{1\to0}$ ($E=2.17\times10^{-12}$ erg)
Semiclassical	0.60	0.19
Quantum(DW)	0.35	0.35
Exact Quantum	0.11	0.11
Exact Classical	0.20	0.20
	$P_{1\to2}$ ($E=3.0\times10^{-12}$ erg)	$P_{2\to1}$ ($E=2.22\times10^{-12}$ erg)
Semiclassical	1.21	0.41
Quantum(DW)	0.70	0.70
Exact Quantum	0.18	0.18
Exact Classical	0.29	0.30

a) $\varepsilon_1-\varepsilon_0=0.83\times10^{-12}$erg
b) $\varepsilon_2-\varepsilon_1=0.78\times10^{-12}$erg

shows that the general features of the numerical results reached from the two methods agree fairly well.

One criterion for testing the soundness of the theoretical procedure can be brought about from the microscopic reversibility relationship, which demands that $P_{1\to0}$ at an incident energy E be equal to $P_{0\to1}$ at the energy $E+(\varepsilon_1-\varepsilon_0)$. Table 2 presents a part of such tests. The exact classical method is seen to be at least as good as the quantum-mechanical methods.

N_2–Ar system. The $P_{0\to1}(E)$ values calculated by the various methods are shown in Fig. 6. Here also, the results of the exact quantum-mechanical calculations and those of exact classical calculations closely resemble each other. Although the approximate theories again give too high values of $P_{0\to1}(E)$ for energetic collisions, the differences between the approximate and exact calculations are not as great as those in the case of the H_2–He system, provided the probabilities are compared in the range of ε between 2×10^{-12} and 4×10^{-12}erg.

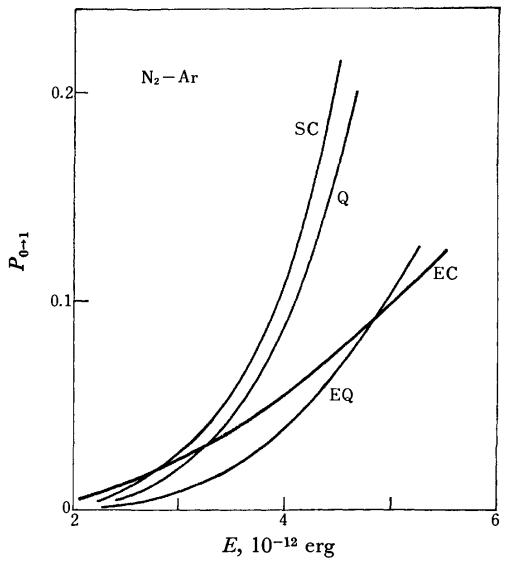

Fig. 6. The 0→1 transition probability of a harmonic N_2 molecule on its collision with an Ar atom as a function of incident energy.
SC, semiclassical[18]; Q, quantum(DW)[19]; EC, exact classical; EQ, exact quantum[15]

The calculations showed that the 1→2 and 2→3 transition probabilities are nearly two- and threefold the 0→1 probability, respectively. This is to be expected, since nitrogen is recognized as the least anharmonic oscillator, to which the well-known Landau-Teller formula,[20] $P_{i\to i+1}=(i+1)P_{0\to1}$, could be applied at lower levels.

I_2–Ar system. Iodine molecules have a very shallow potential and a small vibrational quantum, and the transition probabilities are relatively great even at lower vibrational levels. The first excited vibrational level of iodine molecule lies only 0.035×10^{-12}erg above the ground state. Comparing this value with 0.04×10^{-12}erg, the RT value at 300°K, one may expect that the 0→1 transition probability will be large

20) L. Landau and E. Teller, *Physik. Z. Sowjet Union*, **11**, 18 (1937).

even at room temperature. This in turn implies that at higher temperatures the multi-quantum transition might be more efficient than the 0→1 transition. As an example, the average energy transferred at the collision of $E=0.87\times10^{-12}$erg (the corresponding temperature being as high as 5000°K) is about 0.2×10^{-12}erg, which corresponds to the 0→6 transition.

Several transition probabilities calculated for the I_2–Ar system by the exact classical method are shown in Fig. 7. It may be seen that the 0→1 transition probability reaches its maximum at a collision energy of 0.3×10^{-12}erg and then gradually decreases. The 0→2 transition becomes significant around this energy, attains its maximum at 0.4×10^{-12}erg, and then is replaced by the 0→3 transition.

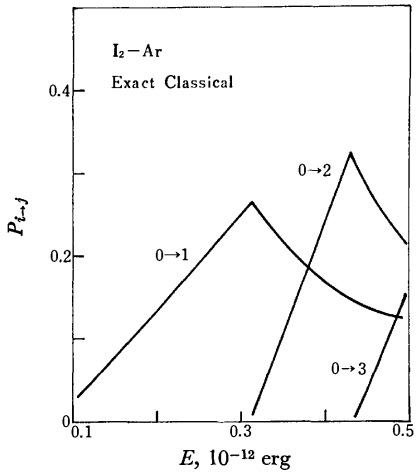

Fig. 7. Exact classical transition probabilities of a harmonic I_2 molecule colliding with an Ar atom as functions of incident energy.

In the case of iodine molecule, one significant transition from a given level is liable to be replaced quickly by another as the incident energy increases. Moreover, the level spacings are so dense that the transition probabilities of each level lose their meaning. Therefore, $\Delta\varepsilon$ will be a more convenient measure of the energy transfer even in the room temperature region.

Energy Transfer in the Higher Vibrational Energy Region

We have extended the exact classical-mechanical calculations to the energy transfer of vibrationally activated diatomic molecules. The collision system consists of a Morse oscillator and an atom interacting with it through the Lennard-Jones potential, a collision model which is more realistic for energized molecules. The systems investigated are H_2–He and I_2–Ar. Various potential parameters used are summarized in Table 3. A harmonic oscillator model was also used for the sake of comparison. Both oscillator models lead to the same results only at lower vibrational levels.

H_2–He system. As an illustrative example, typical trajectories of an atom and a Morse oscillator are shown in Fig. 8. The solid lines represent the motions of an oscillator initially at the 12-th vibrational level

Table 3. Parameters for the Morse-Lennard-Jones potential models

System	Morse Potential[a]			Collision Potential[b]	
	D, 10^{-12} erg	a, Å^{-1}	y_e, Å	D_L, 10^{-12} erg	r_L, Å
H_2–He	7.602	2.284	0.7413	0.002633	2.759
N_2-Ar	15.88	2.452	1.0975	0.01357	3.576
I_2–Ar	2.495	1.546	2.667	0.0465	4.20

a) $U(y)=D\{\exp[-a(y-y_e)]-1\}^2$. Parameters were taken from G. Herzberg, "Molecular Spectra and Molecular Structure I. Spectra of Diatomic Molecules," van Nostrand Reinhold Co., New York (1950).

b) $V(r)=4D_L[(r_L/r)^{12}-(r_L/r^6)]$. Parameters were taken from J. O. Hirschfelder *et al.*, "Molecular Theory of Gases and Liquids," Wiley, New York (1967).

and of an atom colliding with the incident energy of 0.5×10^{-12}erg (the corresponding temperature being *ca.* 3620°K). The trajectories of an atom and an oscillator initially at the ground vibrational level are given by broken lines. The amplitude of the energized oscillator is so large, about 1.5 Å at the 12-th level, which is 8 times greater than that of the ground state oscillator, that the assumption $|\Delta y|\ll L$ used in the approximation does not hold. The time duration for the maximum extension is much more prolonged in the energized H_2, thus facilitating its excitation on collision. These facts clearly indicate the necessity of adopting exact treatments, if reliable results are to be obtained for energized diatomic molecules.

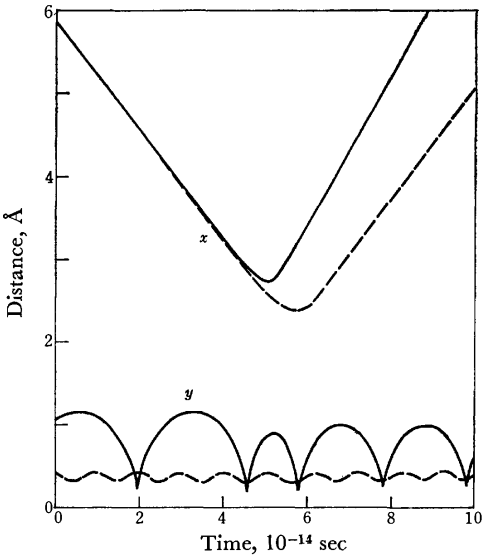

Fig. 8. Trajectories for collisions between a Morse H_2 molecule and an He atom with the incident energy fixed at 0.5×10^{-12} erg.
The initial vibrational levels of H_2 are the 0th (------) and the 12th (——).

The phase-averaged $\Delta\varepsilon$ is calculated for each level for various collision energies ranging from 0.51×10^{-12} to 5.62×10^{-12}erg. Figure 9 shows the results obtained for $E=2.02\times10^{-12}$erg. For the E value chosen, the energy transferred in either of the upward and downward directions increases at first with the level height, and the downward transitions tend to dominate over

the upward transitions, except for the 0-th level. Above the 9-th level, however, the energy transferred downward gradually decreases with the level height, until it becomes overshadowed by that for the upward transition, which is capable of leading to dissociation. The higher levels must then be kept depopulated below their thermal-equilibrium populations during the course of overall dissociation reaction.

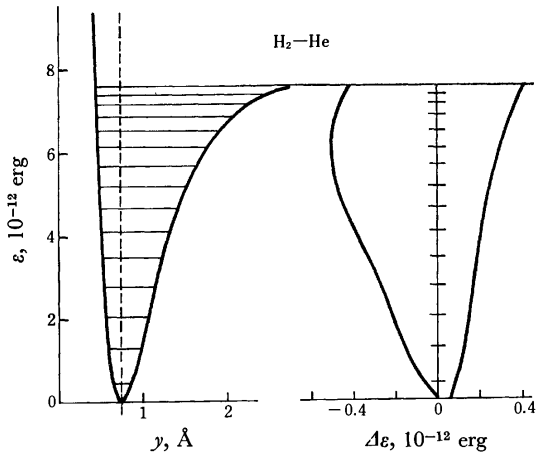

Fig. 9. The average energy change of a Morse H_2 molecule in collision with an He atom as a function of initial vibrational energy. The incident energy is fixed at 2.02×10^{-12} erg.

I_2–Ar system. Dependence of the vibrational energy increment $\Delta\varepsilon$ on the initial vibrational energy of the oscillator is shown in Fig. 10. The features of energy transfer are similar to those noted for the H_2–He system. Occurrence of the maximal deactivation in the vicinity of the threshold region is even more marked than in the H_2–He system.

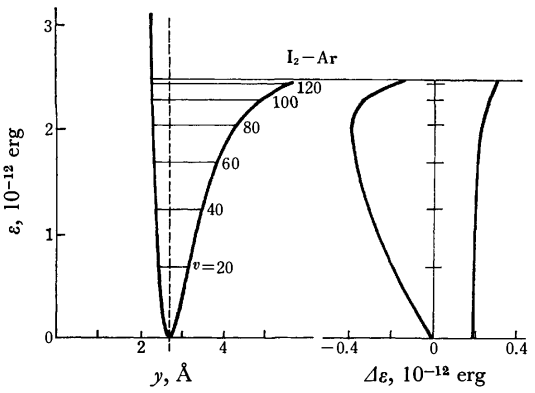

Fig. 10. The average energy change of a Morse I_2 molecule in collision with an Ar atom as a function of initial vibrational energy. The incident energy is fixed at 0.87×10^{-12} erg.

For the sake of comparison, calculations were also carried out for the hypothetical harmonic iodine molecule colliding with an argon atom of $E=0.87\times10^{-12}$erg. The results are shown in Fig. 11, where it is apparent that no such maximal efficiency for deactivation shows up; the deactivation becomes more efficient monotonously with an increase in the initial vibrational energy, and always exceeds the efficiency of activation except in the very low vibrational energy region.

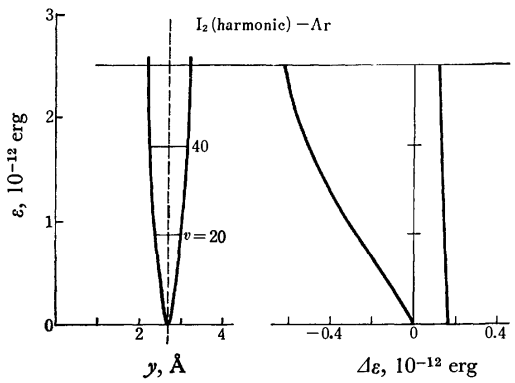

Fig. 11. The average energy change of a harmonic I_2 molecule in collision with an Ar atom as a function of initial vibrational energy. The incident energy is fixed at 0.87×10^{-12} erg.

The effects of the variation of the Morse parameter a on the energy transfer were also examined for a fixed collision energy of $E=0.87\times10^{-12}$erg. The results are shown in Fig. 12. The a values chosen were 1.0 and 3.0 which should be compared with the most plausible value 1.546 for the I_2–Ar system. A larger a corresponds to a greater anharmonicity.[21] The main feature of the results for a large a is the decrease in efficiency of the upward transitions for molecules of low vibrational energy together with the uniform diminution in efficiency of the downward transitions. The former would act to retard the activation of stable molecules, while the latter would accelerate the dissociation of vibrationally excited molecules to continuum. The net result is

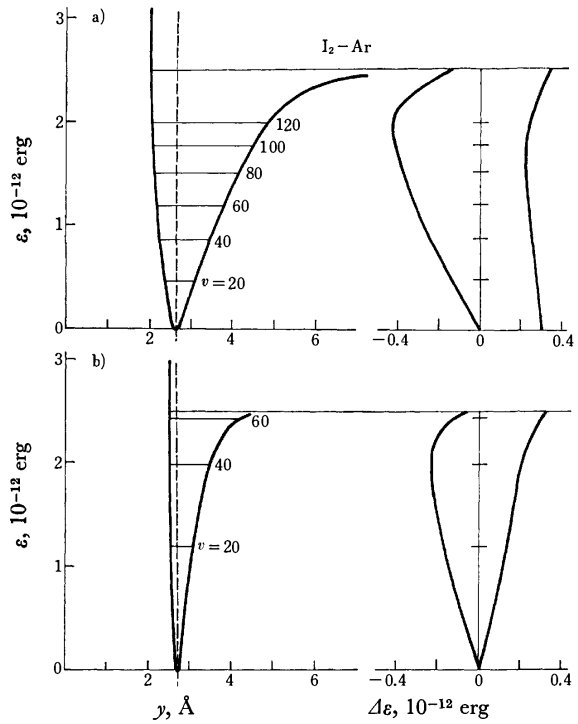

Fig. 12. Effects of the vibrational anharmonicity on the energy change of I_2 in collision with Ar.
a) $a=1.0$ Å; b) $a=3.0$ Å

21) This can be readily verified by expanding the Morse potential function with respect to $(y-y_e)$:

$$D\{\exp[-a(y-y_e)]-1\}^2 = Da^2(y-y_e)^2 \times[1-a(y-y_e)+(7/12)a^2(y-y_e)^2+\cdots]$$

that the depopulation of energized molecules will be more conspicuous for diatoms of greater vibrational anharmonicity.

Discussion

From the results we conclude that Morse oscillators are subjected to a maximal extent of vibrational deactivation in the region just beneath the dissociation threshold. The conclusion has an important bearing on the dissociation-recombination kinetics of diatomic molecules in inert gas.

In dissociation, the molecules energized up to the threshold would tend to get excited still more or dissociated on a collision with a heat-bath molecule, whereas the molecules of low internal energy would be provided with far less opportunity of getting excited. As a result, the energized molecules would be kept depopulated below their thermal distribution, thus effecting a considerable lowering in dissociation rate. This is exactly what we have as an image for the non-equilibrium kinetics of dissociation processes.[3] The region of the maximal deactivation efficiency can then be taken as a "bottleneck" to a normal upward flow of vibrational energy.

By the same token, the highly energized molecules formed by recombination of atoms would be over-populated on one hand, and would still retain a good deal of chance to get redissociated on the other. Once the energized molecules have passed through the bottleneck, they are all subjected to deactivation to stable molecules. The net effect is again a lowering in the rate of downward flow because of the presence of the bottleneck, if it is not too narrow. This could be regarded as a physical basis of the steady-flow assumption[5] which was invoked in order to account for the kinetics of the molecular recombinations of iodine and bromine atoms. However, if the bottleneck is very narrow because of a great anharmonicity of the molecule formed, it will play a critical role in controlling the rate of energy flow. The steady-state assumption will then be considerably in error, and the net rate will be decreased anomalously as in the case of fluorine.[22]

We have not attempted to consider the energy increments averaged over the thermal distribution of collision energies, E. Neither was the energy flow considered explicitly in relation with the reaction rates. Nevertheless, the $\Delta\varepsilon(E, \varepsilon)$ calculated for energized molecules is useful for understanding the kinetic feature of dissociation and recombination. The presence of a bottleneck in these reactions (viewed as energy flow phenomena) can be visualized more clearly than ever before, from an inspection of $\Delta\varepsilon(E, \varepsilon)$ calculated for anharmonic diatomic molecules.

22) D. J. Seery, *J. Phys. Chem.*, **70**, 1684 (1966).

BULLETIN OF THE CHEMICAL SOCIETY OF JAPAN, VOL. 45, 105—109(1972)

The Physical Properties of the Anion Radical Salts Derived from 3,5,3′,5′-Tetrachloro-4,4′-diphenoquinone and 3,5,3′,5′-Tetrabromo-4,4′-diphenoquinone[1]

Yôichi IIDA

Department of Chemistry, Faculty of Science, Hokkaido University, Sapporo

(Received July 3, 1971)

The anion radical salts derived from 3,5,3′,5′-tetrachloro-4,4′-diphenoquinone and 3,5,3′,5′-tetrabromo-4,4′-diphenoquinone were prepared. The absorption spectra in solution and the solid-state spectra were examined in order to study the solid-state properties characteristic of the anion radical salts. The measurements of the static magnetic susceptibilities and the electrical resistivities were also useful for this purpose. These physical properties were found to be based on the charge-transfer interaction between the anion radical molecules. It was suggested that, in these solid anion radical salts, the anion radical molecules might be stacked by a unique face-to-face arrangement in groups of two or an infinite number of molecular systems.

The solid-state properties of the anion radical salts of various halogen-substituted *p*-benzoquinones have been reported in a previous paper.[2] The present paper will describe some anion radical salts of the halogen-substituted 4,4′-diphenoquinones with diamagnetic counter cations (see Fig. 1). The electron spin resonance (ESR) spectra of these crystalline salts have already been examined by Matsunaga.[3]

In general, solid ion radical salts have been a matter of great interest, because the ion radical molecules form, in themselves, a plane-to-plane stacking into columns so as to make a large overlap between their half-filled molecular orbitals.[4] In this case, any individual radi-

1) This work was presented at the 21st Annual Meeting of the Chemical Society of Japan, Osaka (1968).

2) Y. Iida, This Bulletin, **43**, 2772 (1970).

3) Y. Matsunaga, *Canad. J. Chem.*, **38**, 1172 (1960).

4) G. R. Anderson and C. J. Fritchie, Jr., Second National Meeting, Society for Applied Spectroscopy, San Diego, October, 14, Paper 111 (1963); C. J. Fritchie, Jr., *Acta Crystallogr.*, **20**, 892 (1966); C. J. Fritchie, Jr., and P. Arthur, Jr., *ibid.*, **21**, 139 (1966); P. Goldstein, K. Seff, and K.N. Trueblood, *ibid.*, **B24**, 778 (1968); J. Tanaka and N. Sakabe, *ibid.*, **B24**, 1345 (1968); H. Kobayashi, Y. Ohashi, F. Marumo, and Y. Saito, *ibid.*, **B26**, 459 (1970).

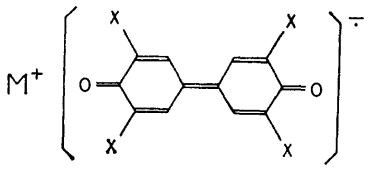

(a); X=Cl, (b); X=Br

Fig. 1. The anion radical salts of (a) 3,5,3′,5′-tetrachloro-4,4′-diphenoquinone (TCDQ) and (b) 3,5,3′,5′-tetrabromo-4,4′-diphenoquinone (TBDQ). M^+ represents a diamagnetic counter cation.

cal molecule interacts through charge transfer most strongly with one or two other radicals. Much knowledge concerning the mutual charge-transfer interaction has been accumulated by measuring the solid-state spectra, the magnetic susceptibilities, and the electrical conductivities.[5-11] The purpose of the present paper is to apply these physical methods to the anion radical salts derived from 3,5,3′,5′-tetrachloro-4,4′-diphenoquinone (TCDQ) and 3,5,3′,5′-tetrabromo-4,4′-diphenoquinone (TBDQ). We shall examine how the charge-transfer interaction between the anion radicals contributes to the solid-state properties of these anion radical salts. The properties of these compounds are interesting in comparison with those previously-investigated properties of the halogen-substituted *p*-benzoquinone anion radical salts.[2]

Materials

3,5,3′,5′-Tetrachlorobiphenyl-4,4′-diol was made by the chlorination of biphenyl-4,4′-diol (Eastman Kodak Co., white-label grade) suspended in acetic acid, while 3,5,3′,5′-tetrabromobiphenyl-4,4′-diol was similarly made by the bromination of biphenyl-4,4′-diol.[12] The TCDQ and TBDQ[13] were obtained by the oxidation of 3,5,3′,5′-tetrachlorobiphenyl-4,4′-diol and 3,5,3′,5′-tetrabromobiphenyl-4,4′-diol respectively with fuming nitric acid.[12] They were purified by treating them with chloroform.

The following four anion radical salts were prepared according to the method of Matsunaga[14]: Na^+ $TCDQ^{\cdot-}$, K^+ $TCDQ^{\cdot-}$, Na^+ $TBDQ^{\cdot-}$, and K^+ $TBDQ^{\cdot-}$. In this method, the anion radical salts were made by the one-electron reduction of the corresponding quinones with alkali metal iodides in an acetone solution.

The Absorption Spectra in Solution

In order to characterize the solid-state spectra of these anion radical salts, it will be necessary to compare them with the absorption spectra of the salts dissolved in solution; therefore, we will examine the spectra in this section. The absorption spectra in solution were measured at room temperature, using a Beckman DK-2A spectrophotometer at concentration of the order of 10^{-5} mol/*l*. Since the anion radical salts are soluble only with difficulty in an acetone solution, it was difficult to determine the values for the molar extinction coefficients.

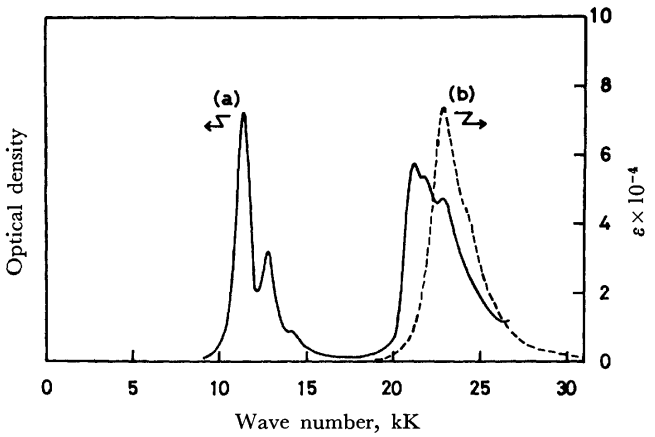

Fig. 2. The absorption spectra of (a) Na^+ $TCDQ^{\cdot-}$ in acetone solution and of (b) neutral TCDQ in ethylene dichloride solution.

The TCDQ Anion Radical Salts. The aborption spectrum of Na^+ $TCDQ^{\cdot-}$ in an acetone solution is reproduced in Fig. 2, together with that of neutral TCDQ in an ethylene dichloride solution. The absorption spectrum of neutral TCDQ has an absorption peak at 23.0 kK with the molar extinction coefficient of 7.33×10^4 and a shoulder around 24.2 kK, while that of the anion radical salt has low-energy absorption peaks at 11.4 kK, 12.9 kK, and 14.2 kK, and a high-energy band with some vibrational structures at 21.2 kK, 21.8 kK, and 22.9 kK. This anion radical salt in solution appears greenish yellow, and it is quite stable at room temperature. The spectrum is not changed when the counter cation of the salt is replaced by the potassium cation. Since the concentration is so dilute, the salt seems to be completely dissociated in the solution. The spectrum obtained is that of the anion radical

5) W. J. Siemons, P. E. Bierstedt, and R. G. Kepler, *J. Chem. Phys.*, **39**, 3523 (1963).
6) R. G. Kepler, *ibid.*, **39**, 3528 (1963).
7) Y. Iida and Y. Matsunaga, This Bulletin, **41**, 2615 (1968).
8) Y. Iida, *ibid.*, **42**, 71, 637 (1969).
9) Y. Iida, *ibid.*, **44**, 663 (1971).
10) Y. Iida, *ibid.*, **44**, 1777 (1971).
11) J. Tanaka and M. Mizuno, *ibid.*, **42**, 1841 (1969).
12) L. M. Jackman, "Advances in Organic Chemistry," Vol. II ed. by R. A. Raphael, E. C. Taylor, and H. Wynberg, Interscience Publishers, New York (1960) p. 329.
13) Generally speaking, stable anion radicals are made from strong electron-acceptor molecules. Both TCDQ and TBDQ molecules are strong electron acceptors. In order to investigate their electron-accepting properties, the charge-transfer complexes of TCDQ and TBDQ with such donors as aromatic hydrocarbons were examined in an ethylene dichloride solution. The absorption spectra of the complexes were measured at room temperature. The complex of pyrene with TCDQ showed the maximum position of the charge-transfer band at 14.2 kK, while the complex of pyrene with TBDQ showed it at 13.6 kK. Let us compare these results with the charge-transfer absorption of the pyrene-7,7,8,8-tetracyanoquinodimethane complex, where the absorption maximum of the first charge-transfer band has been reported to be located at 13.7 kK. For a common donor, the variation of the charge-transfer energies of the complexes arises mostly from the difference in the electron affinities of the acceptors. Therefore, if the value of 1.7 eV for the electron affinity of 7,7,8,8-tetracyanoquinodimethane is chosen as a reference, the electron affinities of TCDQ and TBDQ can be estimated to be 1.6_4 eV and 1.7_1 eV respectively. See Y. Iida, This Bulletin, **44**, 1430 (1971); G. Briegleb, *Angew. Chem.*, **76**, 326 (1964).
14) Y. Matsunaga, *Nippon Kagaku Zasshi*, **89**, 905 (1968).

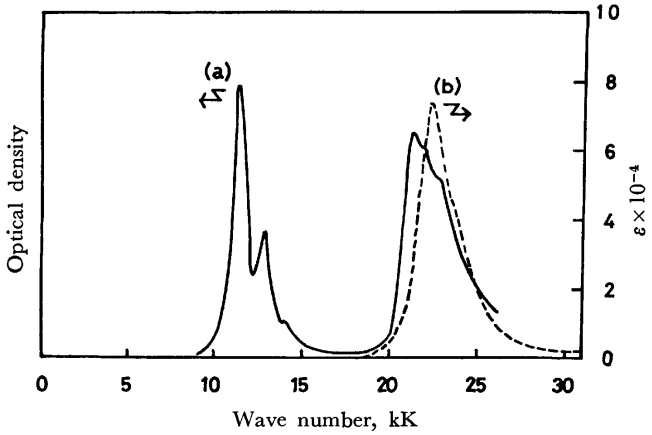

Fig. 3. The absorption spectra of (a) Na^+ $TBDQ^-$ in acetone solution and of (b) neutral TBDQ in ethylene dichloride solution.

monomer,[15] because the counter cations of the salts are simple alkali metal cations.

The TBDQ Anion Radical Salts. The absorption spectrum of Na^+ $TBDQ^-$ in an acetone solution is given in Fig. 3, together with that of neutral TBDQ in an ethylene dichloride solution. The absorption spectrum of neutral TBDQ has an absorption peak at 22.4 kK with the molar extinction coefficient of 7.40×10^4, and a shoulder around 23.5 kK, while that of the anion radical salt has low-energy absorption peaks at 11.4 kK, 12.9 kK, and 14.2 kK, and a high-energy band with some vibrational structures at 21.3 kK, 21.8 kK, and 22.9 kK.[15] The spectroscopic features of Na^+ $TBDQ^-$ were found to be very similar to those for Na^+ $TCDQ^-$. Therefore, it can be said that the electronic states of the 4,4′-diphenoquinone anion radicals are scarcely affected even though the chlorine substituents are replaced by the bromine substituents.

The Solid-State Spectra

In general, it is interesting to examine the solid-state spectra of ion radical salts if the charge-transfer interaction between the ion radicals takes place in the solid state. In this case, the solid-state spectra are known to be different from the monomer spectra of the ion radicals in solution and to show the intermolecular charge-transfer band in the low-energy region.[2,7-11] In this section, we will apply this method to the solid TCDQ and TBDQ anion radical salts by measuring the diffuse reflection spectra.

The diffuse reflection spectra were recorded on a Beckman DK-2A spectroreflectometer in the range from 4.0 kK to 30.8 kK at room temperature. In order to avoid cation exchange between the salt and the diluent, the sodium salts were ground and diluted with sodium chloride, while the potassium salts were similarly treated with potassium bromide. The solid-state spectra were then obtained by plotting the diffuse reflection spectra using the Kubelka-Munk equation, $f(R)=(1-R)^2/2R$, in which R is the reflectance.

The TCDQ Anion Radical Salts. These crystalline anion radical salts are dark blue and are quite stable at room temperature. The solid-state spectrum of Na^+ $TCDQ^-$ (Fig. 4, Curve a) shows a low-energy band at 6.6 kK and high-energy bands at 15.5 kK and 26.2 kK.[16] Theses pectroscopic features were found to be quite different from those of the monomer spectrum of the TCDQ anion radical in solution. The band at 6.6 kK appears in the low-energy region, where the anion radical monomer does not absorb. This band is broad without vibrational structures, and the intensity is strong. It cannot be assigned to the charge-transfer transition from the anion radical to the counter cation, since its maximum position is scarcely shifted when the counter cation of the salt is replaced (see below). Although, at present, no experimental data on the charge-transfer absorption in the dimer of the anion radicals are available for purposes of comparison, the low-energy band at 6.6 kK seems to be attributable to the charge-transfer transition between the anion radicals in the solid state. In this case, the TCDQ anion radicals will be stacked closely enough together for the half-filled molecular orbitals to make a large overlap, and the π-π transitions of the monomer will be much perturbed in the field of the other anion radicals. This is shown as appreciable blue-shifts of the high-energy bands at 15.5 kK and 26.2 kK for the solid-state spectrum of Na^+ $TCDQ^-$, compared to the monomer absorptions of the TCDQ anion radical at 11.4 kK and 21.2 kK respectively.

The solid-state spectrum of K^+ $TCDQ^-$ (Fig. 4, Curve b) shows a low-energy band at 6.7 kK and high-energy bands at 15.3 kK and 25.4 kK. The locations and the intensities of these bands were found to coincide well with those for Na^+ $TCDQ^-$. Therefore, the situation of the solid state of K^+ $TCDQ^-$ seems to be

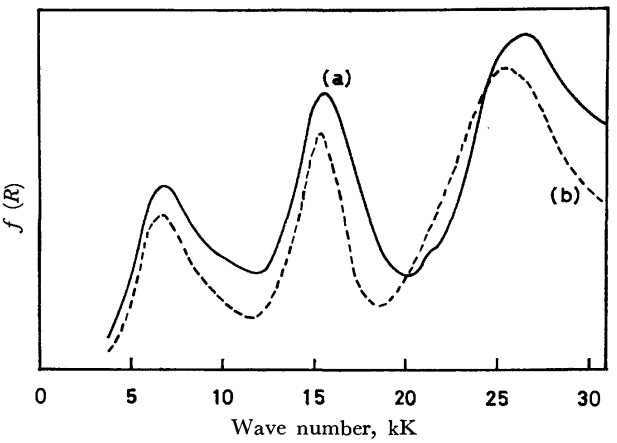

Fig. 4. The solid-state spectra of (a) Na^+ $TCDQ^-$ and (b) K^+ $TCDQ^-$.

15) The monomer spectrum of the 4,4′-diphenoquinone anion radical was found to be very similar to that of the benzidine cation radical. Concerning the π-electron systems, the 4,4′-diphenoquinone anion radical seems to be, in spite of the opposite electric charge, isoelectronic to the benzidine cation radical. See H. Matsusaka and K. Suzuki, paper presented at the 19th Annual Meeting of the Chemical Society of Japan, Tokyo, April, 1966.

16) The monomer spectrum and also the solid-state spectrum of the 4,4′-diphenoquinone anion radical salt were found to be very similar to those of the cation radical salt of benzidine bromide, respectively. The solid-state spectrum of the benzidine bromide shows a low-energy charge-transfer band at 6.7 kK and high-energy bands at 15.6 kK and 26.0 kK. See Refs. 7 and 15.

very analogous to that of Na^+ $TCDQ^{\cdot-}$.

The TBDQ Anion Radical Salts. These crystalline anion radical salts are also dark blue and are quite stable at room temperature. The solid-state spectrum of Na^+ $TBDQ^{\cdot-}$ (Fig. 5, Curve a) is composed of a low-energy band at 6.5 kK and high-energy bands at 15.1 kK and 25.5 kK.[16] These spectroscopic features were again found to be quite different from those of the monomer spectrum of the TBDQ anion radical in solution, but they were very similar to those of the solid-state spectrum of Na^+ $TCDQ^{\cdot-}$. Therefore, the low-energy band at 6.5 kK can also be assigned to the charge-transfer transition between the anion radicals in the solid state, while the high-energy bands at 15.1 kK and 25.5 kK can be assigned to the shifted bands of the monomer absorptions at 11.4 kK and 21.3 kK respectively. The electronic structures of the solid 4,4'-diphenoquinone anion radical salts are scarcely affected even though the chlorine substituents are replaced by the bromine substituents.

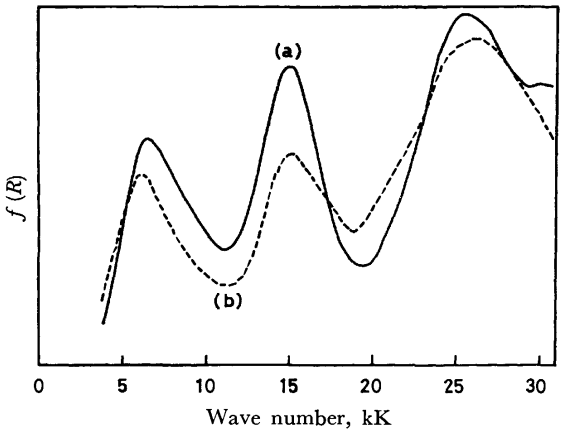

Fig. 5. The solid-state spectra of (a) Na^+ $TBDQ^{\cdot-}$ and (b) K^+ $TBDQ^{\cdot-}$.

K^+ $TBDQ^{\cdot-}$ gives a solid-state spectrum (Fig. 5, Curve b) comprising a low-energy charge-transfer band at 6.2 kK and high-energy bands at 15.2 kK and 25.8 kK. The locations and the intensities of these bands are coincident with those for the corresponding bands in Na^+ $TBDQ^{\cdot-}$. Therefore, the charge-transfer interactions in these two solid substances appear to be very much alike in manner.

The Magnetic Susceptibilities

It has been well established that the charge-transfer interaction between the ion radicals leads to a marked decrease in the paramagnetic susceptibilities of the ion-radical salts.[2,6-9]. The charge-transfer interaction is known to stabilize the antiferromagnetic state where the spins associated with the ion radicals are antiparallel. Hence, we will attempt to measure the static magnetic susceptibilities for the TCDQ and TBDQ anion radical salts.

The magnetic susceptibilities of the anion radical salts and the neutral TCDQ and TBDQ were measured by the Gouy method. All the measurements were made at room temperature under an atmospheric pressure. The susceptibility balance was calibrated by referring to distilled oxygen-free water, for which the susceptibility was taken to be -0.720×10^{-6} emu/g at room temperature.

Na^+ $TCDQ^{\cdot-}$. Although the TCDQ anion radical molecule possesses an unpaired electron, the magnetic susceptibility of Na^+ $TCDQ^{\cdot-}$ at 18°C was found to be diamagnetic. Its value was experimentally determined to be $-(143\pm3)\times10^{-6}$ emu/mol, while the value for the neutral TCDQ was determined to be $-(142\pm1)\times10^{-6}$ emu/mol. The value for the neutral TCDQ was used for the diamagnetic susceptibility of its anion radical, since the skeleton of the neutral TCDQ is very similar to that of its anion radical. By making the correction for the diamagnetism of the counter cation, the diamagnetic susceptibility of Na^+ $TCDQ^{\cdot-}$ was estimated to be $-(147\pm1)\times10^{-6}$ emu/mol. The paramagnetic susceptibility of Na^+ $TCDQ^{\cdot-}$ was evaluated by subtracting the diamagnetic susceptibility from the observed magnetic susceptibility. The paramagnetic susceptibility was thus determined to be as small as $(4\pm4)\times10^{-6}$ emu/mol; this value corresponds only to $(0.3\pm0.3)\%$ of the free-spin paramagnetism. This marked disappearance of the paramagnetism can be understood in terms of the antiferromagnetic spin exchange interaction between the unpaired electrons on the TCDQ anion radicals. Although it is not clear, at present, whether the spin exchange interaction can be described by the singlet-triplet model or by the linear chain Heisenberg model, the antiferromagnetic spin exchange interaction in this salt seems to be as large as 0.1—0.2 eV. At any rate, it is certain that the charge-transfer interaction between the anion radicals makes a significant contribution to the antiferromagnetic spin exchange interaction.

Na^+ $TBDQ^{\cdot-}$. The magnetic susceptibility of Na^+ $TBDQ^{\cdot-}$ at 18 °C was also found to be diamagnetic. Its value was experimentally determined to be $-(155\pm2)\times10^{-6}$ emu/mol, while the value for neutral TBDQ was determined to be $-(174\pm1)\times10^{-6}$ emu/mol. In a way similar to the case of Na^+ $TCDQ^{\cdot-}$, the paramagnetic susceptibility of Na^+ $TBDQ^{\cdot-}$ was estimated to be $(24\pm3)\times10^{-6}$ emu/mol by subtracting the diamagnetic susceptibility of $-(179\pm1)\times10^{-6}$ emu/mol. The magnitude of this paramagnetic susceptibility, although it is rather larger than that of Na^+ $TCDQ^{\cdot-}$, is much less than that of the free-spin paramagnetism. Except for a slight decrease in the antiferromagnetic spin-exchange interaction in Na^+ $TBDQ^{\cdot-}$, the magnetic state of Na^+ $TBDQ^{\cdot-}$ appears to be similar to that of Na^+ $TCDQ^{\cdot-}$.

The Semiconductivities

Among the organic semiconductors, ion radical salts are known to exhibit particularly high electrical conductivities.[5] These electrical properties are based on a unique face-to-face stacking of the ion radical molecules in the solid state.[4] In this respect, it seemed that it would be interesting to examine the semiconductive properties of the TCDQ and TBDQ anion radical salts.

The electrical resistivity and its variation when the

temperature ranged from 15 °C to 90°C were measured with the DC method. The anion radical salts have been available only as small crystals, excluding the possibility of single-crystal measurements. Hence, the measurements were performed with the sample powder under a compression of 5.4×10^2 kg per cm^2 between stainless steel electrodes in a Teflon cylinder.

For all of these compounds, a good linear relationship was obtained when the logarithm of the resistivity was plotted against the reciprocal of the absolute temperature. Therefore, the resistivity (ρ) was described by:

$$\rho = \rho_0 \exp(E/kT), \quad (1)$$

where E is the activation energy for conduction. For the TCDQ and TBDQ anion radical salts, the data on the specific resistivity at room temperature and the value of E are collected in Table 1. Table 1 shows that these values are scarcely affected when the substituents of the anion radicals or the counter cations now under investigation are replaced.

Table 1. The electrical resistivity data on the TCDQ and TBDQ anion radical salts

Compound	ρ at 20°C (Ωcm)	E[a)] (eV)
Na^+TCDQ^-	2.0×10^4	0.24
K^+TCDQ^-	3.3×10^4	0.24
Na^+TBDQ^-	3.2×10^3	0.22
K^+TBDQ^-	8.7×10^4	0.27

a) The activation energy for conduction.

These anion radical salts were found to be highly conductive. This implies the arrangement of a face-to-face stacking of the anion radical molecules in these solid salts. It is interesting to see that the specific resistivities of these anion radical salts are as low as those of the 7,7,8,8-tetracyanoquinodimethane (TCNQ) anion radical salts, in which the specific resistivities of Na^+ $TCNQ^-$ and K^+ $TCNQ^-$ have been reported to be 1×10^5 Ω cm and 1×10^4 Ω cm respectively at room temperature.[5)]

Discussion

The above-mentioned characteristics in the solid-state spectra, the magnetic susceptibilities, and the electrical resistivities clearly indicate that the strong charge-transfer interaction between the anion radical molecules takes place in the TCDQ and TBDQ anion radical salts. Therefore, the anion radical molecules are expected to form, in themselves, a place-to-plane stacking into columns so as to make a large overlap between their half-filled molecular orbitals; this feature of the crystal structure has also been found in a number of other ion radical salts.[4)] The charge-transfer absorption characteristic of the solid-state spectra should be ascribed to the transition of the $<\cdots Q^-Q^-Q^-Q^-\cdots>$ $\rightarrow<\cdots Q^-Q^0Q^2-Q^-\cdots>$ type, where Q^- denotes a 4,4′-diphenoquinone anion radical molecule. However, a question still remains whether the intermolecular interaction is to be described predominantly by pair-by-pair or by a linear chain column composed of an infinite number of anion radical molecules. In the former case, the interaction is approximately confined to the dimer of the anion radicals, while, in the latter case, one individual anion radical interacts equally strongly with two others. In this respect, a further study of the X-ray diffraction will be required to determine by which arrangement the TCDQ and TBDQ anion radicals are stacked in the present solid salts.

Finally, we have to compare the results on the TCDQ and TBDQ anion radical salts with those previously determined for the anion radical salts of various halogen-substituted *p*-benzoquinones.[2)] The charge-transfer interaction in the halogen-substituted *p*-benzoquinone anion radical salts is largely affected not only by the kinds of the halogen substituents in the anion radical molecules, but also by the species of the counter cations. In the case of the potassium cation, the interaction of the salt is markedly decreased compared to that of the sodium salt. Moreover, the charge-transfer interaction is decreased when the substituted chlorine for the anion radical molecule is replaced by bromine. In contrast to these halogen-substituted *p*-benzoquinone anion radical salts, it is noteworthy that the manner of the charge-transfer interaction in the TCDQ and TBDQ anion radical salts does not depend practically on the kinds of the halogen substituents in the anion radical molecules or on the species of the counter cations now under investigation.

The Photochemical Decomposition of Ethylamine as Studied by Means of the Electron Spin Resonance

Yashige KOTAKE, Mitsuo ONO, and Keiji KUWATA

Department of Chemistry, Faculty of Science, Osaka University, Toyonaka, Osaka

(Received July 5, 1971)

The photochemical decomposition of ethylamine at low temperatures was studied using ultra-violet light of various wavelengths (120—400 nm), and the photochemical reactions were examined. The initial stage of the decomposition is the release of the hydrogen atom by far ultra-violet light. As the decomposition proceeds, the effective wavelengths for the succeeding reactions become longer. The final products of the decomposition are the methyl radical and other diamagnetic species. The effects of the matrix and the counter ion on the reaction are also discussed.

In the field of radiation chemistry, alkylamines have been investigated intensively as hole-trap reagents.[1] Because most alkylamines have their optical absorption peaks in the far ultra-violet (FUV) region, the peaks being assigned as n-σ^* excitations, photochemical study by direct photolysis with FUV light is difficult. Wood *et al.* reported that, upon X-ray irradiation, many alkylamines decompose into π-radicals with the structure of $RCHNH_2$.[2-4] This π-radical converts into the $RCH{=}\dot{N}$ radical after a short UV-irradiation.

Richerzhagen and Volman[5] irradiated ethylamine in an adamantane matrix with mercury resonance lines (184, 253 nm). Both X-ray and UV studies indicate complex reactions, however, and the mechanism of its decompositions is not clear. Also, the effective wavelength of the radiation has not been specified.

By selecting the light source well, the primary and succeeding processes of the decomposition can be observed selectively. The control of the matrix is also informative for the study of the reaction mechanism.

In this study, the photochemical decomposition of ethylamine was investigated by means of selective illumination. The primary process of the photochemical decomposition of ethylamine was the elimination of an α proton, much as in the case of X-ray irradiation. The primary process was affected strongly by its counter ion and the state of the matrix.

Experimental

Materials. The ethylamine used was obtained by the dehydration of 70% aqueous solution by potassium hydroxide. An especially purified sample was obtained by the neutralization and dehydration by KOH of an aqueous solution of ethylamine hydrochloride of a guaranteed grade.

Aqueous solutions of different concentrations were prepared by the volumetric dilution of pure ethylamine. The amino group was deuterated by the exchange reaction of heavy water with the ethylamine in the solution.

Irradiation. FUV light from a hydrogen (~120 nm) or a mercury (~180 nm) discharge lamp which was excited by microwave discharge was irradiated in the sample through a LiF window *in vacuo*. The apparatus for the irradiation has been reported elsewhere.[6] The sample was deposited on the outside of the quartz coldfinger cooled with liquid nitrogen and was thought to be amorphous.

UV light and near UV light from a 1-kW high-pressure mercury arc were irradiated using Toshiba UVD-1B and UVD-25 filters respectively. Samples were placed in quartz or spectrosil tubes, evacuated several times, and then irradiated at the temperature of liquid nitrogen. These samples, when cooled to 77°K, became polycrystalline.

Temperatures higher than −150°C were obtained by mixing isopentane and liquid nitrogen and by putting the irradiated samples into the mush.

Results and Discussion

FUV Irradiation. Amorphous pure ethylamine, which consists of FUV (120—180 nm) irradiated for 1 hr, gives the ESR spectrum shown in Fig. 1A.

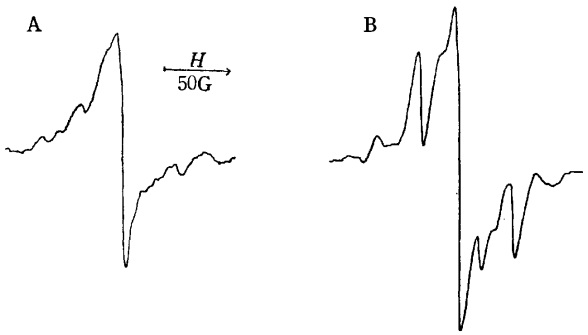

Fig. 1. A: ESR spectrum of FUV irradiated ethylamine at 77°K. B: UV (240 nm) re-irradiated to A.

This unresolved spectrum, which spreads over 70 gauss, is assigned to the $CH_3\dot{C}HNH_2$ radical. Wood and Lloyd[4] identified the $CH_3\dot{C}HNH_2$ radical by the X-ray irradiation of ethylamine in an adamantane matrix and obtained $a_{H\alpha}=15.3$, $a_{H\beta}=20.2$, $a_{HN}=4.9$, and $a_N=4.9$ gauss. The envelope of the spectrum is consistent with these assignments. The poor resolution of the spectrum may be attributed to the fact that the sample is amorphous and that other radicals may also exist. The poor resolution also prevented the detection of the deuterium substitution effect of amino hydrogen.

1) I. D. Eubanks, *Atom. Energy Rev.*, **7**, 49 (1969).

2) D. E. Wood, R. V. Lloyd, and D. W. Pratt, *J. Amer. Chem. Soc.*, **92**, 4115 (1970).

3) D. E. Wood and R. R. V. Lloyd, *J. Chem. Phys.*, **52**, 3840 (1970).

4) D. E. Wood and R. V. Lloyd, *J. Chem. Phys.*, **53**, 3932 (1970).

5) T. Richerzhagen and D. H. Volman, *J. Amer. Chem. Soc.*, **93**, 2062 (1971).

6) K. Kuwata, Y. Kotake, K. Inada, and M. Ono, to be published in *J. Phys. Chem.*

UV Irradiation. By the subsequent irradiation of UV light (~240 nm) for 2 or 3 min, the FUV-irradiated sample gave another radical, the spectrum of which is shown in Fig. 1B. This spectrum shows, in addition to the spectrum of the CH_3CHNH_2 radical, a comparatively sharp doublet with a separation of 79 gauss. By further irradiation by UV light the methyl radical was also produced.

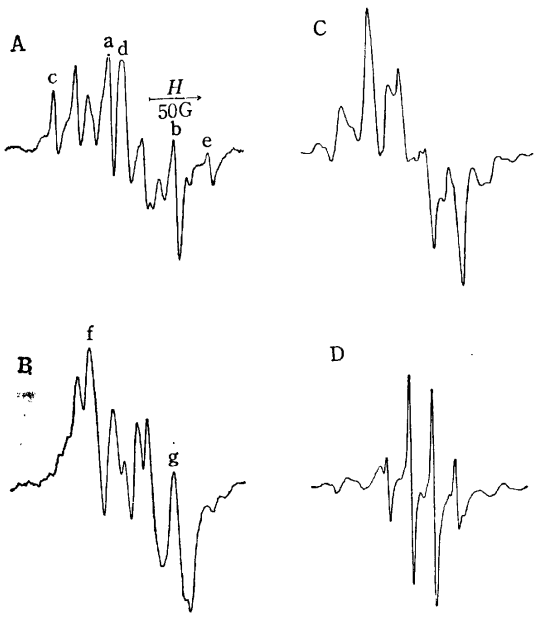

Fig. 2. ESR spectra of UV (240 nm) irradiated ethylamine at 77°K. A: 100% B: added trace of water C: 75 vol % aqueous solution D: 30 vol% aqueous solution.

Aqueous Solution of Ethylamine. The ESR spectra of several kinds of aqueous solutions of ethylamine observed after a 1 hr irradiation of UV light (240—400 nm) are shown in Fig. 2. In concentrated ethylamine solutions, the spectra show complex features (Fig. 2A), indicating the conversion of the primarily-produced radicals. However, the most striking feature of this spectrum is the sharp 64G doublet, marked a, b, and the 87G triplet of the methylene imino radical,[7,8]

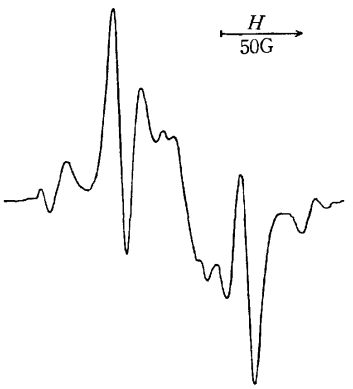

Fig. 3. ESR spectrum of UV (240 nm) irradiated ethylamine 75 vol % aqueous solution at 77°K which is observed at −150°C ($CH_3\dot{C}H{=}\dot{N}$ radical).

marked c, d, and e. Also another unidentified radical exists in this spectrum. By irradiating UV light, ethylamine containing a trace of water gives the spectrum shown in Fig. 2B. Instead of the 64G sharp doublet peak, the 79G sharp doublet peaks are revealed (f, g). By increasing the amount of water, a methyl radical was observed with the 79G doublet (Fig. 2C, 2D).

The spectra shown in Fig. 2C changed to Fig. 3 when the sample was warmed to −150°C. At this temperature, the methyl radical disappeared, and only the radical which shows the 79G doublet survived. This radical may be assigned to the ethylidenimino (CH_3-$CH{=}\dot{N}$) radical. Many investigators[2-5,9,10] have observed this radical in the solid and liquid phases, and it has an isotropic hydrogen splitting of 79—80 gauss. In this study, the radical shown in Fig. 3 shows no deuterium-substitution effect of amino hydrogen. This 79-gauss doublet agrees with the radical produced by the UV irradiation following the FUV irradiation of ethylamine.

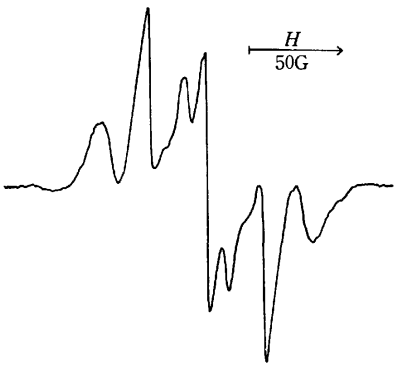

Fig. 4. ESR spectrum of UV (240 nm) irradiated ethylamine hydrochloride at 77°K ($\dot{C}H_2CH_2NH_3^+Cl^-$ radical).

Ethylamine Hydrochloride. Ethylamine hydrochloride gives the spectrum shown in Fig. 4 upon irradiation with UV light longer than 240 nm at 77°K. In the spectra of Fig. 4, the splitting of both side lines is 64G; this coincides with the a and b lines of Fig. 2A. This spectrum is very similar to the spectrum obtained for FUV- and UV-irradiated *n*-propanol.[6] In the case of *n*-propanol, this was assigned to the CH_2–CH_2–CH_2–OH radical, while the radical from irradiated ethylamine hydrochloride can be assigned to the CH_2–CH_2–NH_3^+–Cl^- radical. Taniguchi *et al.*[11] observed this radical in the flow system of an aqueous solution of ethylamine with hydrogen peroxide and $TiCl_3$, and they reported $a_{H\alpha}=26.6$, $a_{H\beta}=22.7$, and $a_N=5.1$ gauss. These coupling constants satisfactorily explain the spectrum of Fig. 4.

Mechanism of Decomposition. The radical species generated by the photolysis show absorption maxima of progressively longer wavelengths as the decomposition proceeds. Ethylamine has its optical absorption peak in the far ultraviolet region; CH_3CHNH_2, at 240—400 nm, and $CH_3C\dot{H}{=}N$, at wavelengths longer than

7) E. L. Cochran, F. J. Adrian, and V. A. Bowers, *J. Chem. Phys.*, **36**, 1938 (1962).
8) M. Kamachi, K. Kuwata, and S. Murahashi, *J. Phys. Chem.*, **75**, 164 (1971).
9) P. Svejda and D. H. Volman, *ibid.*, **74**, 1872 (1970).
10) P. Neta and R. W. Fessenden, *ibid.*, **74**, 3362 (1970).
11) H. Taniguchi, K. Fukui, S. Ohnishi, H. Hatano, H. Hasegawa, and T. Maruyama, *ibid.*, **72**, 1926 (1968).

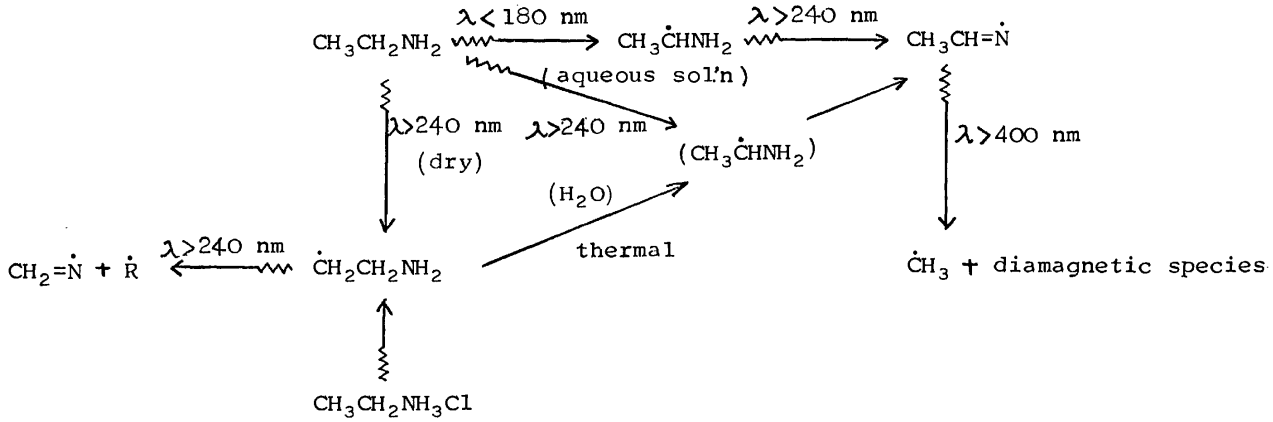

Fig. 5. Photochemical reaction scheme of ethylamine.

400 nm. The ethylidenimino radical decomposes into the methyl radical and other diamagnetic species upon irradiation with light longer than 400 nm. This fact indicates that the precursor of the methyl radical formed in the aqueous solution of less than a 75 vol % of ethylamine is the ethylidenimino radical.

Wood *et al.*[2] reported that several alkylamines gave no ESR signal upon UV irradiation unless the sample had previously been X-ray irradiated. Though alkylamines have their optical absorption peaks in the FUV region, they usually gave tailing absorptions in the UV region, and prolonged irradiation gives products with poor quantum yields. All the features of the photochemical reaction sequence are shown in Fig. 5.

The slightly different primary product for each sample may be attributed to the difference in the trapping states of the radicals. In addition, in the case of ethylamine hydrochloride the strong counter ion of chlorine may interfere with the secondary photochemical decompositions. The role of the water molecule seems to be mainly to affect the rigidity of the matrix. Also, it isolates the amine molecule and promotes the unimolecular decomposition. The dependence of the matrix state on the amount of water is exemplified by the result that the methyl radical in an ethylamine aqueous solution of less than 30% disappeared at about −100°C, while in a 75% solution it disappeared at −150°C.

Molecular Vibrations and Force Fields of Alkyl Sulfides. II. Infrared Spectra of $CH_3S(CH_2S)_nCH_3$ ($n=0-3$)

Masaru OHSAKU, Yuji SHIRO,* and Hiromu MURATA

Department of Chemistry, Faculty of Science, Hiroshima University, Higashisenda-machi, Hiroshima
**Shinonome Branch School, Faculty of Education, Hiroshima University, Shinonome-3-chome, Hiroshima*

(Received July 12, 1971)

Infrared spectra recorded in the liquid and solid states of dimethyl sulfide, CH_3SCH_3, bis(methylthio)methane, $CH_3SCH_2SCH_3$, bis(methylthiomethyl) sulfide, $CH_3SCH_2SCH_2SCH_3$, and bis[(methylthio)methylthio]methane, $CH_3SCH_2SCH_2SCH_2SCH_3$, are reported. For the $CH_3SCH_2SCH_3$ species, the gaseous spectra were also recorded. For these molecules, the observed bands were assigned to the fundamental modes of the vibrations with reference to those of reported analogous-structure molecules. The existence of the rotational isomers of the last three compounds was postulated. The regularity of the wave number of the fundamentals obtained and the intensity change in some of the bands for this series of compounds were discussed. The frequency shift in the liquid-solid phase transition was also described for a few bands.

The vibrational analysis of dimethyl sulfide, CH_3SCH_3, has been reported elsewhere.[1-4] For bis(methylthio)methane, $CH_3SCH_2SCH_3$, and bis(methylthiomethyl) sulfide, $CH_3SCH_2SCH_2SCH_3$, Welti and Whittaker[5] have reported an infrared treatment. Complete assignments, however, were not made. For bis[(methylthio)methylthio]methane, $CH_3SCH_2SCH_2SCH_2SCH_3$, we have not found any vibrational treatment reported up to 1970. In the first paper of this series,[4] we determined the molecular force fields of dimethyl sulfide. However, we could not obtain complete experimental results with the low-resolution instrument we used. Therefore, we recorded the spectra of dimethyl sulfide a new. On the molecular series of $CH_3S(CH_2S)_nCH_3$ ($n=0-3$), some correlations may exist between those vibrational spectra and the degree of n. Rotational isomerism is also expected in the molecular species of $n=1-3$. From this point of view, we have investigated the infrared spectra of this series: $CH_3S(CH_2S)_nCH_3$ ($n=0-3$). This paper will treat the vibrational interpretation of polythiomethylene.

Experimental

Materials. The dimethyl sulfide was commercially obtained (Tokyo Kasei Co., Tokyo) and distilled in a vacuum over phosphorus pentoxide before use. The other materials used in the infrared recording were prepared according to the method reported by Fehér and Vogelbruch.[6]

Bis(methylthio)methane
found bp 149—150°C/760 mmHg, 44°C/14 mmHg; purity (above 99%)
lit.[5-6] bp 148—150°C/760 mmHg, 45°C/14 mmHg

Bis(methylthiomethyl) Sulfide
found bp 106°C/5 mmHg; purity (above 98%)
lit.[5-6] bp 100—103°C/3.5 mmHg, 113°C/13 mmHg

Bis[(methylthio)methylthio]methane
found bp ~135°C/1—2 mmHg, mp 17.0°C; purity (above 90%)
lit.[6] bp 117.5°C/0.7 mmHg, mp 17.2°C

The purity of all the samples was estimated by means of gas chromatography. The infrared spectra were measured in the liquid and solid states in the range of 4000—200 cm^{-1} with a Perkin-Elmer Model 621 Spectrophotometer equipped with KBr and CsI cells. The liquid spectra of dimethyl sulfide were recorded at a temperature slightly above its melting point. The other materials were recorded at room temperature (*ca.* 22°C). For the $CH_3S(CH_2S)_nCH_3$ ($n=1-3$) series the infrared spectra in CS_2 and CH_3NO_2 solutions were also recorded (1400—600 cm^{-1}). The solid spectra were obtained with a conventional cell which was cooled by liquid nitrogen. The spectrum of the solid film was recorded before and after annealing near the melting point. The gaseous spectra of $CH_3SCH_2SCH_3$ were also investigated in the 850—600 cm^{-1} region at temperatures of 26—129°C. The wave numbers thus obtained were calibrated by the use of bands of indene and polystyrene. The frequency of the obtained spectra has measured with an estimated accuracy of ± 1 cm^{-1} at 2000—400 cm^{-1} and with an accuracy of ± 2 cm^{-1} at 4000—2000 cm^{-1}; the accuracy of the 400—200 cm^{-1} region may be within 5 cm^{-1}. The $\sim$ sign in Tables 2—4 shows that the wave number of its band was poorly estimated.

Vibrational Assignment

The assignments of the observed bands were made on the basis of those of dimethyl sulfide,[1-4] monochloromethyl methyl sulfide,[7] (methylthio)methanethiol,[8] polymethylene disulfide,[9] and 1,3,5-trithiane.[10]

Dimethyl Sulfide. The assignments are summarized in Table 1. The annealed spectra are more finely resolved than the liquid spectra. We compared the spectra of liquid and solid states, and found that a new band, which was not observed in the liquid spectra, appeared in the C–H stretching, CH_3 degenerate deformation, and CH_3 rocking regions, in the solid state.

1) D. W. Scott and J. P. McCullough, *J. Amer. Chem. Soc.*, **80**, 3554 (1958).
2) J. P. Perchard, M. T. Forel, and M. L. Josien, *J. Chim. Phys.*, **61**, 645 (1964).
3) J. R. Allkins and P. J. Hendra, *Spectrochim. Acta*, **22**, 2075 (1966).
4) Y. Shiro, M. Ohsaku, M. Hayashi, and H. Murata, This Bulletin, **43**, 609 (1970).
5) D. Welti and D. Whittaker, *J. Chem. Soc.*, **1962**, 4372.
6) F. Fehér and K. Vogelbruch, *Chem. Ber.*, **91**, 996 (1958).
7) M. Hayashi, *Nippon Kagaku Zasshi*, **80**, 1073 (1959).
8) M. Ohsaku, Y. Shiro, and H. Murata, unpublished work.
9) M. Hayashi, Y. Shiro, and H. Murata, This Bulletin, **39**, 1857 (1966).
10) M. Ohsaku and H. Murata, *J. Sci. Hiroshima Univ.*, A-II, **33**, 179 (1969).

Table 1. Infrared frequencies (cm^{-1}) and assignments of dimethyl sulfide[a)]

Liquid	Solid		Assignment
	Unannealed	Annealed	
	2986 sh, vw	2986 w	C–H str (A_2)
2982 m	2979 m	2979 m	C–H str
2965 s	2965 s	2965 s	C–H str
2915 s	2915 vs	2917 vs	C–H str
2901 sh, m	2901 sh, m	2903 sh, m	C–H str
2855 m, br	2858 m, br	2860 m, br	$2\times CH_3$ deg or C–H str
2830 m	2830 m	2830 s	C–H str or $2\times CH_3$ deg
1451 sh, w	1448 m	1448 s	CH_3 deg def
1429 vs	1432 sh, m	1432 m	CH_3 deg def
	1427 sh, w	1428 w	CH_3 deg def (A_2)
1421 sh, s	1421 vs	1421 vs	CH_3 deg def
1329 vvw	1331 m	1331 m	CH_3 sym def
1307 m	1305 m	1303 m	CH_3 sym def
1038 s	1039 vs	1039 vs	CH_3 rock
984 s	985 vs	985 vs	CH_3 rock
	951 vw	952 w	CH_3 rock (A_2)
909 w	910 w	910 w	CH_3 rock
742 vw	743 w	744 w	C–S str
691 m	692 s	693 s	C–S str
275 vw	275 vw	275 vw	skel def

s, strong, m, medium, w, weak, v, very, sh, shoulder, br, broad.

a) Above 3000 cm^{-1} and 2800—1500 cm^{-1} regions are omitted.

Dimethyl sulfide has a C_{2v} symmetry. However, if the site symmetry of C_{2v} does not remain in the solid state, the forbidden bands may appear. Moreover, one each of C–H stretching, CH_3 degenerate deformation, CH_3 rocking, and torsional vibrations belong to the A_2 species. In the spectral region we treated, the former three bands are expected. This sufficiently coincident with the observed result that only three bands belonging to the A_2 vibrations appeared in the solid state, in addition to the bands in the liquid state. The obtained wave numbers closely agreed with the calculated wave number of the previous normal coordinate treatment.[4)] Thus, these observations lead to the findings that the site symmetry of the dimethyl sulfide molecule changes to C_2 or C_s in the solid state and that the new bands can be assigned to the A_2 mode. In the spectra obtained in the solid state, unannealed or annealed, seven bands were observed in the 2900 cm^{-1} region. Among these bands the overtone bands of the CH_3 degenerate deformation vibrations may be confused; they are hardly distinguishable from each other. In the annealed spectra around 1400 cm^{-1}, we obtained four bands, at 1448, 1432, 1428, and 1421 cm^{-1}. Among these bands, the band at 1428 cm^{-1} is assigned to the CH_3 degenerate deformation vibration of the A_2 species. In the region around 1300 cm^{-1}, two bands were obtained finely in the solid film. In our previous paper,[4)] we considered that these CH_3 symmetrical deformation bands overlapped each other with a low resolution of the spectrometer. For the CH_3 rocking region, we obtained three bands in the liquid, and four bands in the solid, film. The band at 952 cm^{-1} appeared only in the solid film. This band corresponds well to the band (960—950 cm^{-1}) obtained from the Pd and Pt complex of dimethyl sulfide.[11)] As for the weak band obtained at 909 cm^{-1} (liquid), we previously identified it as an impurity band. Scott and El-Sabban treated[12)] the normal coordinate treatment and identified it as the sum-combination of the A_2 torsional and B_1 C–S stretching vibrations. Allkins and Hendra treated[3)] the vibrational spectra of CH_3XCH_3 spectral series (X=S, Se, and Te) and identified it as the fundamental. If the band around 900 cm^{-1} of CH_3SCH_3 is the sum-combination, the sum-combination for CH_3SeCH_3 and CH_3TeCH_3 would not be observed in this region. However, in the expected region, the corresponding band due to the fundamental was reported.[3)] Thus, the band around 900 cm^{-1} is not to be considered as a sum-combination, but can be assigned to a rocking fundamental. For the C–S stretching region, a couple of the bands were obtained, at 744 and 693 cm^{-1}, in the annealed state. Below 400 cm^{-1} the skeletal deformation bands can be expected. The weak band at 275 cm^{-1} may be assigned to the skeletal deformation vibration.

Bis(methylthio)methane. The obtained infrared data of bis(methylthio)methane are summarized in Table 2. The annealed spectra are well resolved in the C–H stretching, CH_3 degenerate deformation, and CH_3 rocking regions. The bands around 2950 cm^{-1} may due to the C–H stretching vibrations. In this region the overtone bands of the CH_3 degenerate deformation fundamentals may be present. As for the CH_3 degenerate deformation, the bands obtained around 1430 cm^{-1} may be assigned. For the region 1400—1100 cm^{-1}, the CH_2 bending, CH_3 symmetrical deformation, CH_2 wagging, and the CH_2 twisting vibrations are expected. The medium band obtained at 1387 cm^{-1} and the very strong band at 1203 cm^{-1} in the liquid spectra separate into two components upon crystallization. This splitting may be attributed to the crystal field effect or to the imperfection annealing. Around 960 cm^{-1} two bands appeared in the liquid state and three bands in the crystalline state. The liquid-solid phase transition shift of this region is fairly large. The bands obtained in this region may be due to the CH_3 rocking vibrations. A rather puzzling feature of the spectra is the infrared band of a weak intensity at 874 cm^{-1}. It seems too high for a CH_2 rocking fundamental and too low for a CH_3 rocking fundamental; we can not explain reasonably. For the C–S stretching region, 760—600 cm^{-1}, we observed seven bands, including three shoulder bands, in the liquid state. This molecule has four C–S stretching vibrational freedom for one conformation. Actually, in the solid state, four bands appeared. For the skeletal deformation region, 400—200 cm^{-1}, we obtained nine very weak and fairly broad bands in the liquid state.

11) J. R. Allkins and P. J. Hendra, *Spectrochim. Acta*, **24A**, 1305 (1968).

12) D. W. Scott and M. Z. El-Sabban, *J. Mol. Spectrosc.*, **30**, 317 (1969).

TABLE 2. INFRARED FREQUENCIES (cm^{-1}) AND ASSIGNMENTS OF BIS(METHYLTHIO)METHANE[a)]

Liquid	CS_2 soln	CH_3NO_2 soln	Solid		Assignment
			Unannealed	Annealed	
2985 sh, m			2985 sh, m	2985 sh, w	C–H str
				2977 sh, w	C–H str
2975 s			2971 m	2969 m	C–H str
2955 sh, w			2955 sh, w	2958 m	C–H str
2914 vs			2914 s	2910 s	C–H str
				2881 w	C–H str
2857 m			2856 w	2851 w	C–H str or 2×CH_3 deg
2832 m			2825 w	2821 w	C–H str or 2×CH_3 deg
1441 sh, vw			1441 sh, w	1441 sh, w	CH_3 deg def
1435 vs			1435 s	1436 s	CH_3 deg def
			1422 sh, w	1421 sh, w	CH_3 deg def
1423 vs			1418 s	1417 s	CH_3 deg def
1387 m	1385 m		1390 sh, w 1382 m	1391 m 1385 sh, w	CH_2 bend
1327 sh, vw	1327 sh, vw		—	1325 vw	
1318 m	1318 m		1316 w	1311 m	CH_3 sym def
			1306 sh, vw	—	CH_3 sym def
1203 vs	1205 vs	1207 vs	1205 s	1218 m 1210 s	CH_2 wag
1163 sh, vw	1164 sh, vvw		—	—	
1155 w	1153 w		1161 m	1166 m	CH_2 twist
1124 vw	1123 vw		—	—	
986 s	985 s	988 s	988 s	995 vs	CH_3 rock
959 s	958 s	961 s	959 s	960 m 952 s	CH_3 rock
(874 w)	(874 w)		(876 w)	(874 vw)	?
824 sh, w	825 sh, w	825 sh, vw	—	—	
806 s	806 s	807 m	807 m	808 s	CH_2 rock
758 sh, m	757 sh, m	760 sh, m	—	—	
746 vs	746 vs	748 vs	747 vs	747 vs	C–S str
724 w	724 w	724 w	726 w	725 w	C–S str
705 sh, vw	705 sh, vw	706 sh, w	—	—	
694 vs	694 vs		694 vs	693 vs	C–S str
669 sh, vw	669 sh, vw		—	—	
649 w	649 w		651 w	653 w	C–S str
~360 sh, vvw			—	—	
~350 sh, vvw			—	—	
340 vw, br			339 vw	341 vw	skel def
321 sh, vvw			314 w	314 w	
303 vvw, br			305 sh, vw	305 sh, vw	
~270 sh, vvw			~270 vvw	—	
~265 vvw, br			~260 vvw	—	
~235 vvw, br			~235 vvw	~235 vvw	skel def
216 vvw, br			~220 vvw	~220 vvw	

s, strong, m, medium, w, weak, v, very, sh, shoulder, br, broad.
The sign, —, shows the band which disappears in the solid state.
a) Above 3000 cm^{-1} and 2800—1500 cm^{-1} regions are omitted.

Bis(methylthiomethyl) Sulfide. The obtained spectra of an annealed film of bis(methylthiomethyl) sulfide were well resolved. The infrared data we obtained are summarized in Table 3. The molecule has two methylene groups and six C–S bonds. The obtained spectra of bis(methylthiomethyl) sulfide are more complicated than those of bis(methylthio)methane. However, the spectral features in the 3000—1300 cm^{-1} region are similar to those of bis(methylthio)methane. The bands which appeared around the 1200 and 1150 cm^{-1} regions are to be assigned to the CH_2 wagging and twisting vibrations respectively. As for the CH_3 rocking region, two bands appeared in the liquid state. In the crystalline state, three sharp bands were obtained, at 969, 961, and 955 cm^{-1}. To the CH_2 rocking vibrations, two bands at 844 and 780 cm^{-1} in the solid state are assigned. The bands around 700 cm^{-1} may due to the C–S stretching vibrations. In this region, seven bands, including three shoulder bands, appeared in the liquid state. In the crystalline film, five bands of them are retained, their intensities changed. In the region 400—200 cm^{-1}, the skeletal deformation vibrations

Table 3. Infrared frequencies (cm^{-1}) and assignments of bis(methylthiomethyl) sulfide[a)]

Liquid	CS_2 soln	CH_3NO_2 soln	Solid		Assignment
			Unannealed	Annealed	
2985 sh, w			2983 sh, w	2981 w	C–H str
2973 m			2970 m	2973 m	C–H str
2963 sh, w			2957 sh, w	2954 w	C–H str
2915 vs			2914 s	2914 s	C–H str
2854 w			2853 w	2853 w	C–H str or $2\times CH_3$ deg
2830 w			2825 w	2815 w	C–H str or $2\times CH_3$ deg
1441 sh, w			1439 sh, w	1439 sh, s	CH_3 deg def
1435 s			1435 s	1434 s	CH_3 deg def
1423 s			1422 sh, w	1416 sh, m	CH_3 deg def
1420 sh, w			1419 s	1410 s	CH_3 deg def
1395 w			—	—	CH_2 bend
1379 s	1379 s		1378 s	1381 m 1372 s	CH_2 bend
1327 sh, vw			—	—	CH_3 sym def
1317 w	1316 m		1314 w 1307 sh, vw	1312 w 1306 vw	CH_3 sym def
1218 w	1216 m	1221 m	1220 w	1219 m	CH_2 wag
1193 vs	1190vs	1195 vs	1191 s	1193 s	CH_2 wag
1165 sh, w	1163 sh, w		1171 w	1167 w	CH_2 twist
1132 w	1131 m	1134 m	1135 m	1133 m	CH_2 twist
1119 sh, vw	1120 sh, vw		—	—	
974 s	974 s	975 s	978 s	969 s	CH_3 rock
961 s	959 s	961 s	961 m	961 s 955 m	CH_3 rock
855 sh, vw			—	—	
841 w	841 w	841 w	844 w	844 m	CH_2 rock
834 w	832 w	832 w	—	—	
820 sh, vw			—	—	
778 s	779 s	778 s	778 s	780 m	CH_2 rock
754 sh, w	753 sh, w	754 sh, w	—	—	
742 vs	741 vs	742 vs	743 vs	746 s 736 s	C–S str C–S str
712 m	711 m	712 s	714 s	711 w	C–S str
700 s	698 s	699 s	699 vs	695 vs	C–S str
690 sh, vw			—	—	
661 w	660 w		661 m	657 s	C–S str
645 sh, vw	645 sh, vw		647 vw	—	
365 sh, vw			—	—	
350 vvw			355 vvw	—	
~340 sh, vvw			—	—	
331 vw			331 vw	339 vw	skel def
315 sh, vvw			—	318 vw	
305 sh, vvw			305 vvvw	—	
277 vvw			~275 vvw	275 vvw	skel def ?
259 sh, vvw			~260 vvw	—	
254 sh, vvw			—	—	
244 w			250 vw	247 w	skel def

s, strong, m, medium, w, weak, v, very, sh, shoulder, br, braod.
The sign, —, shows the band which disappears in the solid state.
a) Above 3000 cm^{-1} and 2800—1500 cm^{-1} regions are omitted.

would appear. We obtained ten bands in the liquid state.

Bis[(methylthio)methylthio]methane. The infrared data of bis[(methylthio)methylthio]methane we obtained are summarized in Table 4. In this molecule, there are two methyl and three methylene groups, and eight C–S bonds. The infrared spectra of bis[(methylthio)methylthio]methane we obtained are similar to those of bis(methylthiomethyl) sulfide without any CH_2 deformation region. The spectra in the C–H stretching region are not well resolved. The spectra in the CH_3 degenerate deformation region are, however, well resolved in the solid state. The spectral features of this region are similar to those in the same region of dimethyl sulfide. The bands around 1200 cm^{-1} and 1150 cm^{-1} can be assigned to the CH_2 wagging and

Table 4. Infrared frequencies (cm^{-1}) and assignments of bis[(methylthio)methylthio]methane[a)]

Liquid	CS_2 soln	CH_3NO_2 soln	Solid		Assignment
			Unannealed	Annealed	
2984 sh, m			2985 sh, vw	2985 sh, vw	C–H str
2967 m			2965 m	2965 m	C–H str
2912 vs			2907 m	2906 m	C–H str
2854 w			2854 vw	2854 vw	C–H str or 2 × CH_3 deg
2826 w			2824 vw	2824 vw	C–H str or 2 × CH_3 deg
			1444 sh, m	1446 m	CH_3 deg def
1438 sh, s			1438 sh, m	1441 sh, m	CH_3 deg def
1434 s			1430 s	1431 vs	CH_3 deg def
1422 s			1418 m	1418 m	CH_3 deg def
1401 sh, w			—	—	
1394 sh, m			1378 m	1379 s	CH_2 bend
1378 s	1377 s		1369 vs	1369 vs	CH_2 bend
			1354 sh, vw	1355 w	CH_2 bend
1316 w	1316 w	1318 w	1329 vw 1310 vw	1332 w 1311 vw	CH_3 sym def CH_3 sym def
1223 sh, w	1222 sh, w	1223 sh, w	1220 w	1220 w	CH_2 wag
1205 sh, w	1205 sh, w	1205 sh, w	—	—	
1199 sh, s	1198 sh, s		1204 m	1204 m	CH_2 wag
1188 vs	1186 vs	1191 vs	1182 m	1182 m	CH_2 wag
1171 sh, w	1171 sh, w	1168 sh, w	1172 sh, w	1173 sh, w	CH_2 twist
1145 w	1144 w	1147 w	1152 w	1153 w	CH_2 twist
1125 w	1124 w	1123 w	1126 w	1126 w	CH_2 twist
971 s	971 s	973 s	973 vs	974 vs	CH_3 rock
960 sh, s	958 s	961 sh, s	957 sh, w	957 sh, w	CH_3 rock
858 w	859 w	860 w	864 s	866 s	CH_2 rock
820 w	819 w	819 w	811 w	811 w	CH_2 rock
785 w	785 w	786 w	—	—	
763 s	763 s	764 s	759 m	760 m	CH_2 rock
740 vs	740 vs	740 vs	742 s	742 s	C–S str
731 sh, s	728 s	729 sh, s	729 s	729 s	C–S str
712 sh, vw	712 sh, w		—	—	
700 vs	699 vs	698 vs	699 vs	701 vs	C–S str
687 sh, w	687 sh, w		—	—	
663 w	663 w		663 s	665 s	C–S str
651 sh, vw	650 sh, vw		652 w	654 w	C–S str
~640 sh, vw	~640 sh, vw		—	—	
360 sh, vvw			—	—	
338 vvw, br			326 w, br	331 w, br	skel def
305 vvw, br			—	—	
272 sh, vvw			274 w	275 w	skel def
265 vw			266 sh, w	269 sh, w	
235 vvw, br			~240 vvvw	235 vvvw	
217 vvw, br			~220 vvw	~220 vvvvw	

s, strong, m, medium, w, weak, v, very, sh, shoulder, br, broad.
The sign, —, shows the band which disappears in the solid state.
a) Above 3000 cm^{-1} and 2800—1500 cm^{-1} regions are omitted.

twisting vibrations respectively. The bands obtained around 970 cm^{-1} may be due to the rocking vibrations of the terminal CH_3 groups. The strong shoulder band of the liquid state at 960 cm^{-1} decreases in its intensity in the solid state. Three bands of the CH_2 rocking vibrations are expected for this molecule. Actually, four bands appeared in the liquid state, at 858, 820, 785, and at 763 cm^{-1}, and in the annealed film, three bands appeared, at 866, 811 and at 760 cm^{-1}. The C–S stretching vibrations are obtained around 700 cm^{-1}. We obtained eight bands in the liquid state (740, 731, 712, 700, 687, 663, 651, and 640 cm^{-1}) and five bands in the crystalline state (742, 729, 701, 665, and 654 cm^{-1}). In the region 400—200 cm^{-1}, seven bands appeared in the liquid state.

Discussion

The existence of the rotational isomer of the series of the compounds discussed above may be investigated by means of studying the spectra in the region of the CH_2 rocking, C–S stretching, and the skeletal deformation

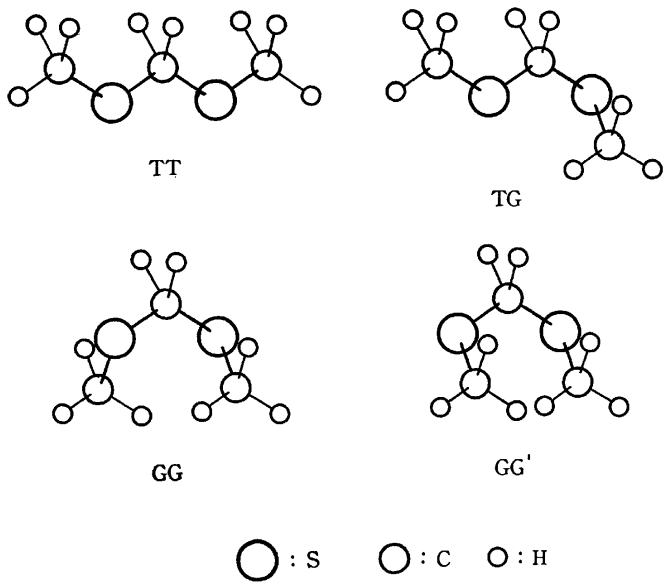

Fig. 1. Structures and conformations of bis(methylthio)methane.
T=*Trans*, G=*Gauche*.

vibrations. Among these vibrations, the ones which were sufficiently covered in the spectral range we treated are the CH_2 rocking and C–S stretching vibrations. On bis(methylthio)methane, one CH_2 rocking and four C–S stretching bands can be expected. Actually, two CH_2 rocking and seven C–S stretching bands appeared in the liquid-state spectra. In bis(methylthiomethyl) sulfide, two CH_2 rocking and six C–S stretching bands can be expected. We obtained five CH_2 rocking and eight C–S stretching bands in the liquid spectra. In the case of bis[(methylthio)methylthio]methane, treatment is above only with difficulty. In this molecule, three CH_2 rocking and eight C–S stretching vibrations can be expected; we observed four CH_2 rocking and eight C–S stretching bands in the liquid state.

On bis(methylthio)methane, four conformations (TT, TG, GG, and GG') may be supposed on theoretical, as is shown in Fig. 1. We revealed the existence of the rotational isomers by means of a comparison between the spectra of the liquid and solid states, since some bands of the liquid spectra disappeared in the solid state. Moreover, in order to confirm the existence of the rotational isomers, we attempted to investigate the temperature dependence of the band intensity of the gaseous state in the 850—600 cm^{-1} region on $CH_3SCH_2SCH_3$. The wave numbers of the gaseous bands we obtained are summarized in Table 5, together with the corresponding wave numbers of the liquid and solid spectra. From the gaseous envelopes obtained at different temperatures, we found that the intensity change was not large enough to determine the energy differences between and/or among the rotational isomers. Therefore, in order to observe the wave number change due to the rotational angles, we have made a normal coordiante treatment of $CH_3SCH_2SCH_3$ with four conformations: TT, TG, GG, and GG', using the Urey-Bradley force field. The details of the normal coordinate treatment will be reported in a separate paper.[13]

Table 5. Infrared frequencies of the gaseous bands with their corresponding liquid and solid bands, and assignments of bis(methylthio)methane (850—600 cm^{-1})

Solid	Liquid	Gaseous	Assignment
808	806	812 sh, w 805 w 798 sh, w	CH_2 rock
—	758	762 sh, w 759 m	C–S str
747	746	753 m 747 m 740 sh, m	C–S str
725	724	720 vvw	C–S str
—	705	705 w	C–S str
693	694	698 w 691 w 687 sh, w	C–S str
—	669	669 vw	C–S str
653	649	647 vvw	C–S str

Table 6. Observed and calculated frequencies (cm^{-1}) of bis(methylthio)methane in the C–S stretching region

Obsd	Calcd			
	TT	TG	GG	GG'
758[a)]	756	757		753
746	741		750	
724		732	739	730
705[a)]	709	702		
694			689	693
669[a)]	660			
649		643	625	627

a) Not appeared in the solid state.

13) M. Ohsaku, Y. Shiro, and H. Murata, to be published.

The computed wave numbers of the C–S stretching vibrations are listed in Table 6. As is shown in Table 6, the calculated wave number changes with the skeletal conformations. The bands which disappeared in the solid state may be identified as fundamentals. Among the four conformations, the GG′ form might have a higher energy than the other forms. Therefore, three conformations remain: TT, TG, and GG. We, at present, can not venture to decide how many conformations (two or three) may exist in the liquid or gaseous state with stability. However, from only these data, we can not deny that these three conformations coexist in either the liquid or gaseous state. In the solid state, this molecule may have one conformation. In the case of bis(methylthiomethyl) sulfide and bis-[(methylthio)methylthio]methane, a large number of conformations can be expected. The situation is difficult in studying the longer molecules. The difficulty

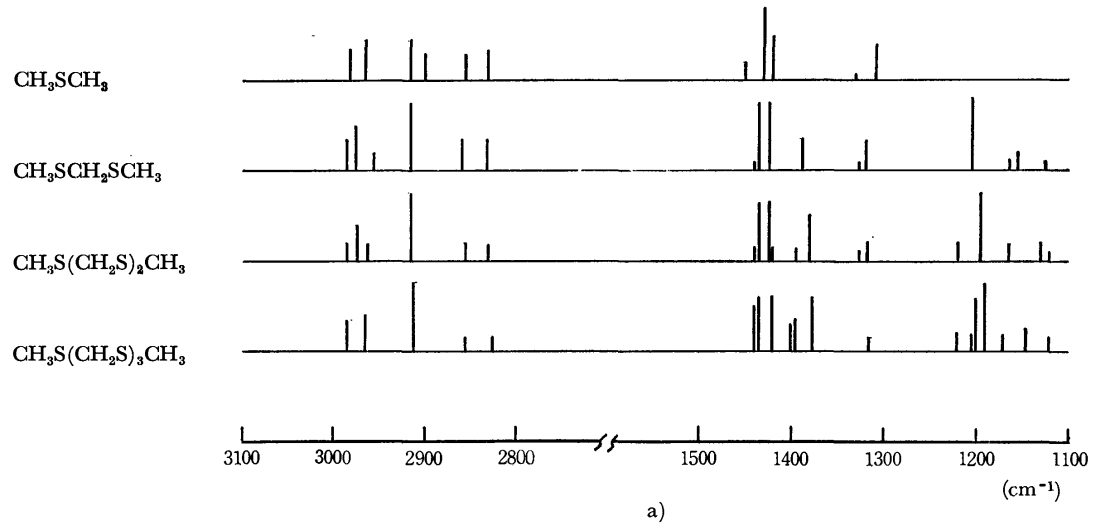

a)

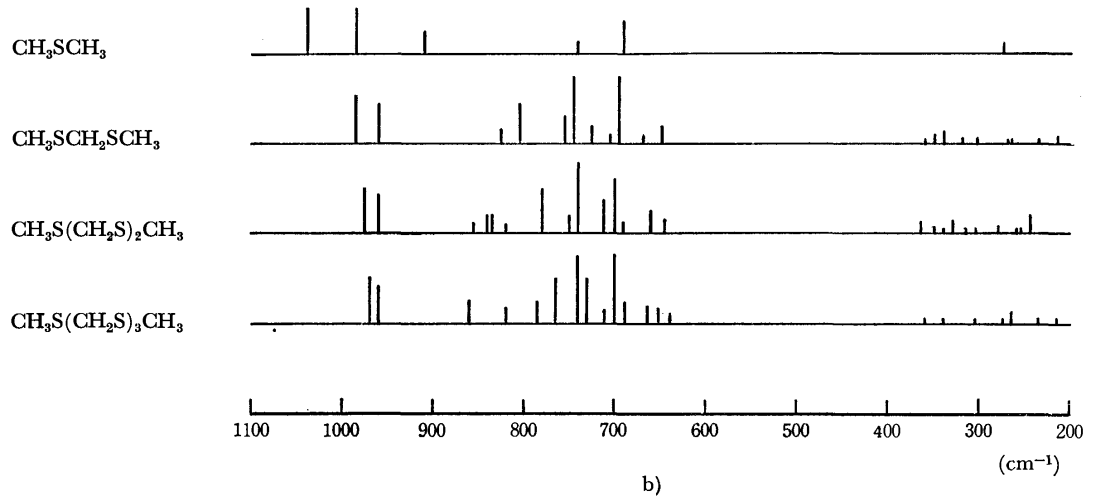

b)

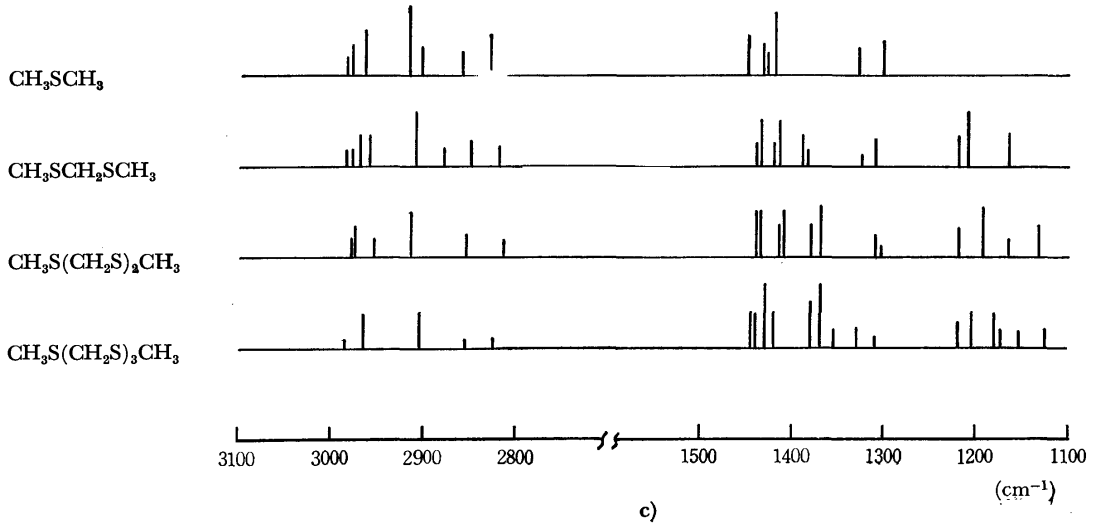

c)

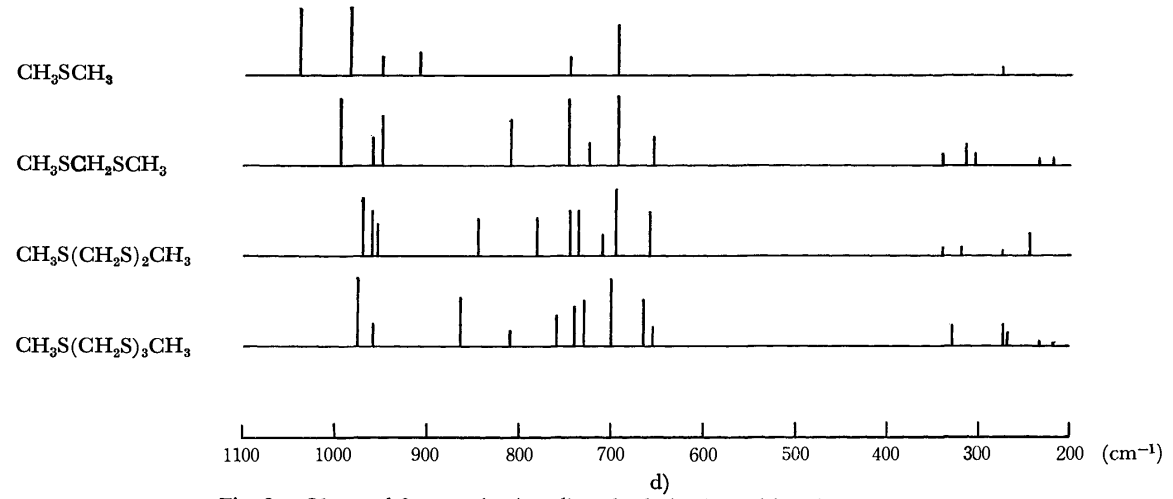

Fig. 2. Observed frequencies (cm^{-1}) and relative intensities of $CH_3S(CH_2S)_nCH_3$ (n=0—3).
a) 3000—1100 cm^{-1} (Liquid) b) 1100—200 cm^{-1} (Liquid)
c) 3000—1100 cm^{-1} (Annealed) d) 1100—200 cm^{-1} (Annealed)

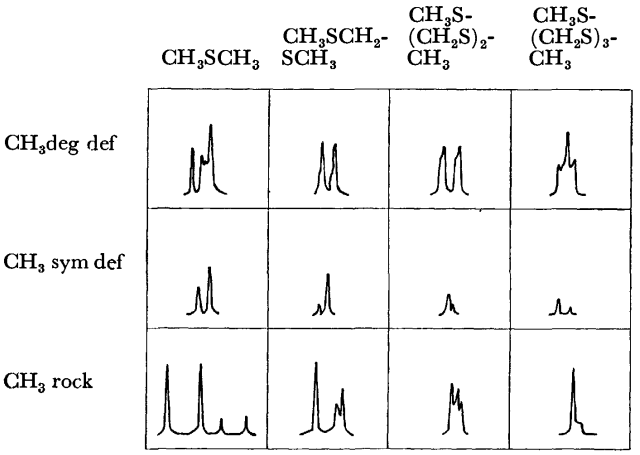

Fig. 3. Infrared band shapes of terminal CH_3 groups (Annealed): $CH_3S(CH_2S)_nCH_3$ (n=0—3).

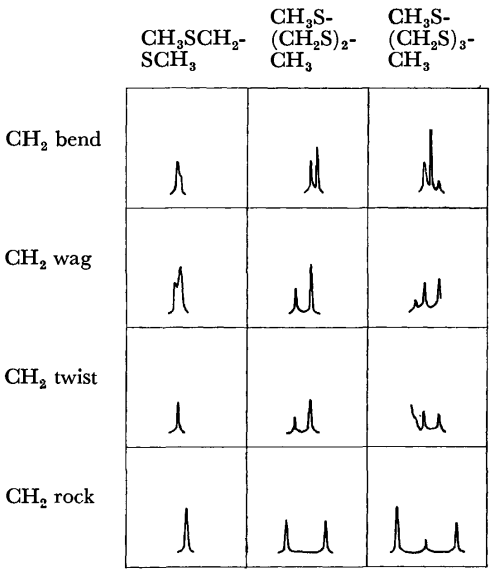

Fig. 4. Infrared band shapes of internal CH_2 groups (Annealed): $CH_3S(CH_2S)_nCH_3$ (n=1—3).

in the recognition of the rotational isomer will be reported separately in connection with the normal coordinate treatment of this series of compounds.

The observed frequencies for the spectral series studied, $CH_3S(CH_2S)_nCH_3$ (n=0—3), are graphically summarized in Fig. 2. Figures 3 and 4 show the band shapes thus obtained in relation to the CH_3 and CH_2 groups (annealed). Tables 7 and 8 show the infrared frequencies of the terminal CH_3 groups and the internal CH_2 groups obtained in the crystalline state. The C–H stretching region shows no definite tendency in either the liquid or solid state. The frequency of the CH_3 degenerate deformation and the CH_3 symmetrical deformation bands obtained in the liquid state changes little from dimethyl sulfide to bis[(methylthio)methylthio]methane. However, the frequency obtained in the annealed state shows a little irregularity. The spacing of two CH_3 symmetrical deformation bands also shows a little irregularity. The CH_2 bending, wagging, and the twisting vibrations constantly shifted to a lower frequency region with increase in the molecular chain length. The frequency difference among CH_3 rocking bands becomes small hyperbolically with an increase in the chain length. This shows that the intramolecular interaction of methyl groups between the two ends rapidly decreases with an increase in the chain length. We observed the CH_2 rocking vibrations in the wider range around 800 cm^{-1}. It is interesting that, in the annealed spectra, the central band at 811 cm^{-1} of bis-[(methylthio)methylthio]methane has nearly the same frequency of that of bis(methylthio)methane (808 cm^{-1}), and that the spacings between their bands and their side bands are nearly the same width on both sides (55 and 51 cm^{-1}). For the C–S stretching region, the bands obtained are gradually complicated with an increase in the molecular chain. However, a couple of more intense bands appeared at nearly the same wave number in any case; that is, in the liquid spectra the intense bands were 742 and 691 cm^{-1}, 746 and 694 cm^{-1}, 742 and 700 cm^{-1}, and 740 and 700 cm^{-1} for dimethyl sulfide, bis(methylthio)methane, bis-(methylthiomethyl) sulfide, and for bis[(methylthio)-

Table 7. Infrared frequencies (cm^{-1}) of terminal CH_3 groups (annealed): $CH_3S(CH_2S)_nCH_3$ (n=0—3)

	n=0	n=1	n=2	n=3
CH_3 deg def	1448 (16) 1432 (4) 1428 (7) 1421	1441 (5) 1436 (15) 1421 (4) 1417	1439 (5) 1434 (18) 1416 (6) 1410	1446 (5) 1441 (10) 1431 (13) 1418
CH_3 sym def	1331 (28) 1303	1325 (14) 1311	1312 (6) 1306	1332 (21) 1311
CH_3 rock	1039 (54) 985 (33) 952 (42) 910	995 (35) 960 (8) 952	969 (8) 961 (6) 955	974 (17) 957

Figures in parentheses show the difference between adjacent bands.

Table 8. Infrared frequencies (cm^{-1}) of internal CH_2 groups (annealed): $CH_3S(CH_2S)_nCH_3$ (n=1—3)

	n=1	n=2	n=3
CH_2 bend	1391 1385	1381 (9) 1372	1379 (10) 1369 (14) 1355
CH_2 wag	1218 1210	1219 (26) 1193	1220 (16) 1204 (22) 1182
CH_2 twist	1166	1167 (34) 1133	1173 (20) 1153 (27) 1126
CH_2 rock	808	844 (64) 780	866 (55) 811 (51) 760

Figures in parentheses show the difference between adjacent bands.

methylthio]methane respectively.

The intensities of various fundamentals are of interest. That is, the intensities of fundamentals arising from CH_3 groups, *i.e.*, the CH_3 degenerate deformation, CH_3 symmetrical deformation, and the CH_3 rocking fundamentals, decrease, while on the other hand, the intensities of the fundamentals arising from CH_2 groups, *i.e.*, the CH_2 bending, CH_2 wagging, CH_2 twisting, and the CH_2 rocking fundamentals, increase with an increase in the chain length.

The relations of the obtained wave numbers will be discussed in detail by the aid of the normal coordinate treatment analysis. The results of the normal coordinate treatment of the molecules described in this paper will be reported separately.[13]

Conclusion

The infrared spectra of the $CH_3S(CH_2S)_nCH_3$ (n=0—3) series obtained in the liquid and solid states have been assigned. For the last three molecules, the rotational isomer can be expected. On the $CH_3SCH_2SCH_3$ molecular species, the existence of more than two conformations was confirmed in the liquid or gaseous states by two procedures: a) a comparison between the liquid and solid spectra, and b) a normal coordinate treatment. Moreover, in the solid state, the species $CH_3SCH_2SCH_3$ would be one conformation. We tried to ascertain the temperature dependence of the gaseous envelopes. However, the differences by which to determine the energy difference based on the rotational isomer were not obtained. It seems that some regularities stay in the fundamentals of this series thus obtained: $CH_3S(CH_2S)_nCH_3$ (n=0—3).

The authors wish to express their gratitude to Assistant Professor Michiro Hayashi of Hiroshima University for his encouragement throughout this work. One of the authors (M. O.) is largely indebted to the foundation of the Kumura Syogakukai (Teijin Co., Tokyo).

Charge-transfer Interaction and Chemical Reaction. IV. Reactions of *para*-Substituted Derivatives of Aniline with Chloranil

Takashi NOGAMI,* Keitaro YOSHIHARA,** and Saburo NAGAKURA

The Institute for Solid State Physics, The University of Tokyo, Roppongi, Minato, Tokyo

(Received July 20, 1971)

Interactions of chloranil with *p*-phenylenediamine, *N,N*-dimethyl-*p*-phenylenediamine, and *N,N,N',N'*-tetramethyl-*p*-phenylenediamine were studied by measuring visible and ultraviolet absorption spectra at various temperatures between 77°K and 300°K. In an ether-isopropyl alcohol (3:1) mixed solvent, the *p*-phenylenediamine- and *N,N*-dimethyl-*p*-phenylenediamine-chloranil systems were led to the substitution reaction through the outer complex and the ionic species as reaction intermediates. In ethyl ether, the *p*-phenylenediamine- and *N,N*-dimethyl-*p*-phenylenediamine-chloranil systems were found to yield the inner complex and the substituted species through the outer complex, respectively. In the *N,N,N',N'*-tetramethyl-*p*-phenylenediamine-chloranil system, the inner complex was found to be formed *via* a clustering of the outer complexes.

The interactions between aromatic amines and chloranil were found to be classified into the following three types: (a) the charge-transfer (outer or inner) complex is formed between an electron donor and an acceptor and no further reaction proceeds; (b) the substitution reaction occurs through the outer and inner complexes; (c) the substitution reaction occurs through the outer complex and ionic species. The difference in the reactivities between *meta*-substituted derivatives of aniline and *ortho*- and *para*-substituted ones was explained by taking the π-electron density on the amino group into account.

In previous papers of this series,[1] the reactions of several aromatic amines with chloranil were studied from the viewpoint of charge-transfer interaction. Detailed studies were made of the reactions of chloranil with aniline,[1a] 1,3,5-triaminobenzene,[1b] and *m*-phenylenediamine.[1d] In these three systems, the substitution reactions were found to occur through the outer and inner complexes as the reaction intermediates. A detailed kinetic study was made of the third case by measuring the formation and decay curves of the inner complexes, and the potential energy curves of the reactions were determined experimentally. Substitution reactions of a similar mechanism were found to occur for the systems including chloranil and several *meta*-substituted derivatives of aniline (*m*-anisidine, *m*-aminophenol, *N,N*-dimethyl-*m*-phenylenediamine, *N,N,N',N'*-tetramethyl-*m*-phenylenediamine, and 1-methyl-2,4,6-triaminobenzene).

On the other hand, another type of reactions were found for systems containing *ortho*- or *para*-substituted derivatives of aniline and chloranil. The main purposes of the present study are to clarify the mechanism for the interaction of chloranil with *p*-substituted anilines and to obtain information on the effect of the position of the substituted group upon the reaction mechanism. For these purposes, we took *p*-phenylenediamine (PD), *N,N*-dimethyl-*p*-phenylenediamine (DMPD), and *N,N,N',N'*-tetramethyl-*p*-phenylenediamine (TMPD) as electron donors. Furthermore, the classification of the reactions between chloranil and various aromatic amines is described on the basis of the π-electron density on the amino group by comparing the *meta*-substituted derivatives of aniline with *ortho*- and *para*-substituted ones.

Experimental

Materials. PD, DMPD, and TMPD were purified by vacuum sublimation. Chloranil was purified by repeated recrystallizations from acetone.

Measurements. A Cary recording spectrophotometer model 14 M was used for the measurements of electronic absorption spectra, a quartz cell with a 1-cm light path length being used. The donor and acceptor solutions, which were separately prepared, were mixed with each other immediately before the absorption measurements at low temperatures. For the measurements at low temperatures, a sample cell was immersed in a quartz dewar vessel designed for the spectroscopic measurements and was cooled with cold nitrogen gas. The temperature was regulated by nitrogen-flow velocity.

Results and Discussion

Reaction of PD with Chloranil. We studied the interaction of chloranil with PD, DMPD, and TMPD using ethyl ether and ether-isopropyl alcohol (3:1) as solvents. First of all, let us describe the results for the PD-chloranil system in ethyl ether.

After mixing the ethyl ether solutions of PD and chloranil at a low temperature (the concentrations of PD and chloranil in the final solution were 6.7×10^{-4}M and 3.3×10^{-4}M, respectively), the change in the absorption spectra was measured. The 785 and 390 nm bands assigned to the outer complex[2] appear at first and decrease in intensity with increasing temperature. After the solution was kept at room temperature for a few hours, a blue species gradually precipitated. The absorption spectra of the precipitate, which was mea-

* Present address: Department of Chemical Technology, Faculty of Engineering, Osaka University, Yamada-kami, Suita, Osaka.

** Present address: The Institute of Physical and Chemical Research, Wako, Saitama.

1) (a) T. Nogami, K. Yoshihara, H. Hosoya, and S. Nagakura, *J. Phys. Chem.*, **73**, 2670 (1969); (b) T. Yamaoka and S. Nagakura, This Bulletin, **43**, 355 (1970); (c) T. Nogami, K. Yoshihara, and S. Nagakura, *ibid.*, **44**, 295 (1971); (d) T. Nogami, T. Yamaoka, K. Yoshihara, and S. Nagakura, *ibid.*, **44**, 380 (1971).

2) This assignment was made from the relation between the peak position of the charge-transfer absorptions observed with the chloranil complexes and the ionization potentials of several electron donors.

sured by coating the powdered sample on a glass plate by a stainless steel spatula,[3] were found to consist of the absorption bands of the 2:1 (PD: chloranil) complex (380, 590, and 670 nm) plus the charge-transfer absorption band of the 1:1 complex (850 nm).[4] The elemental analysis data of the precipitate show that it is a mixture of about 90% of the 2:1 complex and about 10% of the 1:1 complex. These two complexes show an ESR signal.[4] This indicates the formation of ion pair type complexes which may be denoted by inner complexes. From the above-mentioned experimental facts, the reaction mechanism of the system under consideration may be represented as follows:

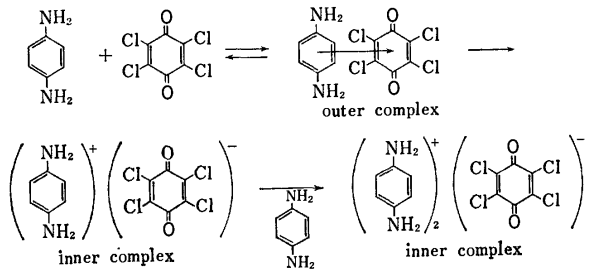

Next, let us turn to the PD-chloranil system in an ether-isopropyl alcohol (3:1) mixed solvent. After mixing the solutions of PD and chloranil in the mixed solvent (the concentrations of PD and chloranil in the final solution were 6.7×10^{-4}M and 3.3×10^{-4}M, respectively) at 193°K, the temperature dependence of the absorption spectrum was measured; the results are shown in Fig. 1. At first, the absorption bands of the outer complex appear; then they decrease in intensity with the increasing temperature. With the decrease in the bands due to the outer complex, new bands due to the PD cation monomer (500 and 465 nm) and dimer (605 nm)[5] appear with the isosbestic points at 430 and 640 nm. This fact shows that the outer complex directly converts into the cation monomer and dimer.

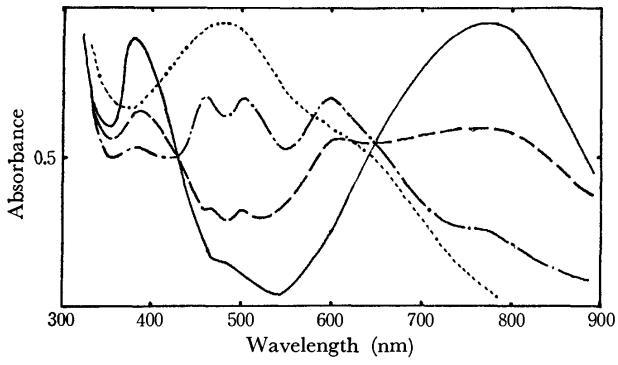

Fig. 1. The absorption spectra of the PD—chloranil system in an ethyl ether-isopropyl alcohol (3:1) mixed solvent; [PD]$=6.7\times10^{-4}$M, [chloranil]$=3.3\times10^{-4}$M.
—— The absorption spectrum measured immediately after mixing at 193°K; the spectrum of the outer complex.
– – – The absorption spectra measured at 225°K; the spectra of the outer complex and of the PD cation monomer and dimer.
– • – The absorption spectra measured at 235°K; the spectra of the PD cation monomer and dimer.
····· The absorption spectrum measured at room temperature; the spectrum of the final reaction product.

The ionic specimens do not cause succeeding reactions at temperatures lower than 230°K. When the solution is recooled from 230°K to 193°K, the absorption bands of the outer complex and cation dimer always increase in intensity and those of the cation monomer disappear. However, the outer complex bands do not completely recover the initial absorbance at 193°K.

The absorption bands due to the chloranil anion (426 and 455 nm)[6] can not be detected, probably because the concentration of the chloranil anion is rather low and its absorption band may be covered by those of the outer complex, the PD cation monomer, and a final reaction product.

By raising the temperatures of the solution to room temperature, the absorption bands due to the outer complex and to the PD cation monomer and dimer disappear in a few minutes; thereafter, those due to the final reaction product (460 and 630 nm) gradually increase the intensity for a few hours. The elemental analysis of the reaction product corresponds to $C_{18}H_{14}Cl_2N_4O_2$[7] and indicates that it is 2,5-dichloro-3,6-di-*p*-aminoanilino-*p*-benzoquinone.

In order to clarify whether the PD cation monomer and dimer exist as reaction intermediates in the main reaction path or only in the side reaction, the time dependences of the absorption spectra of the PD cation and final reaction product were measured in the temperature range from −15°C to 0°C[8]; the result is shown in Fig. 2. The absorption band of the PD cation at 450—500 nm is covered by that of the final reaction product; therefore, the vibrational structure of the former band is smeared out with the latter band as the reaction proceeds. From Fig. 2, we can obtain[9]

3) T. Sakata and S. Nagakura, This Bulletin, **42**, 1497 (1969).

4) Dr. Sakata in our laboratory obtained the 2:1 complex (PD: chloranil) by adding PD to the 1:1 CT complex in ethanol. The 1:1 complex was prepared by mixing the benzene solutions of PD and chloranil.

5) K. Kimura, H. Yamada, and H. Tsubomura, *J. Chem. Phys.*, **48**, 440 (1968).

6) R. Foster and T. J. Thomson, *Trans. Faraday Soc.*, **58**, 860 (1962).

7) The PD—chloranil system in ethyl ether-isopropyl alcohol (3:1) mixed solvent. Found: C, 54.16; H, 4.21; Cl, 17.58; N, 15.81%. Calcd for $C_{18}H_{14}Cl_2N_4O_2$: C, 55.52; H, 3.59; Cl, 18.25; N, 14.39%. The DMPD—chloranil system in ethyl ether. Found: C, 58.43; H, 5.00; Cl, 16.28; N, 12.07%. Calcd for $C_{22}H_{22}Cl_2N_4O_2$: C, 59.32; H, 4.94; Cl, 15.95; N, 12.58%. The DMPD—chloranil system in ethyl ether-isopropyl alcohol (3:1) mixed solvent. Found: C, 59.24; H, 4.88; Cl, 15.56; N, 12.55%. Calcd for $C_{22}H_{22}Cl_2N_4O_2$: C, 59.32; H, 4.94; Cl, 15.95; N, 12.58%. The agreement between the found and the calculated is not good for the PD—chlornail system in the mixed solvent. The discrepancy may be due to the difficulty in removing the 1:1 substitution product and other impurities and also to their hygroscopic property. We tried to separate each product by chromatography and other methods, but we did not succeed mainly because of very small solubility of the precipitate.

8) Because of the difficulty of keeping the temperature constant, we measured the absorption spectra without controlling the temperature.

9) The absorption intensities at 630 and 500 nm were measured at some time intervals determined by the wavelength scanning speed. Since the reaction is rather fast, we can not ignore the absorption intensity change which occurs during the intervals. Therefore, in the analysis of the experimental results, we made a suitable correction for this change.

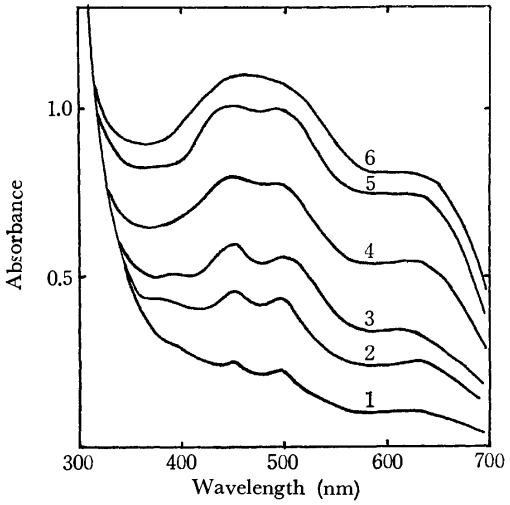

Fig. 2. The time dependence of the absorption spectrum of the PD—chloranil system in an ether-isopropyl alcohol (3: 1) mixed solvent; [PD]$=5.0\times10^{-4}$M, [chloranil]$=2.5\times10^{-4}$M. Curves 1, 2, 3, 4, 5, and 6 are, respectively, the spectrum measured at 3, 7, 11, 19, 40, and 73 min after the mixing of the donor and acceptor solutions at -15°C. The temperature increased gradually from -15 to 0°C during the measurements.

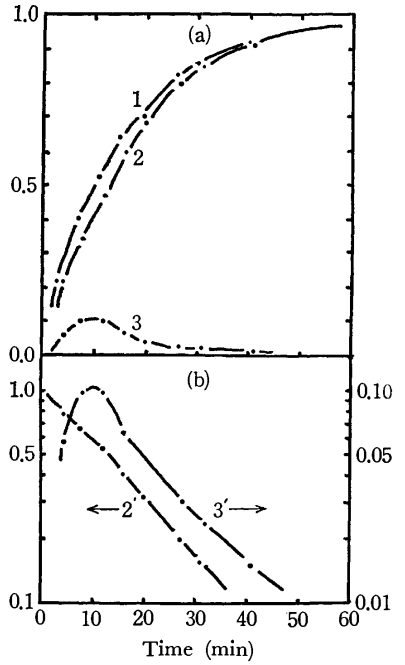

Fig. 3. The time dependence of the absorption intensities of the PD cation and the reaction product derived from the curves shown in Fig. 2. (a); the ordinate is I_{500}/I_{500}^{max}, I_{630}/I_{630}^{max}, and $I_{500}/I_{500}^{max}-I_{630}/I_{630}^{max}$ for curves 1, 2, and 3, respectively: (b); the ordinate is $(I_{630}^{max}-I_{630})/I_{630}^{max}$ and $I_{500}/I_{500}^{max}-I_{630}/I_{630}^{max}$ for curves 2′ and 3′, respectively. The left- and right-hand side ordinates are concerned with curves 2′ and 3′, respectively.

the time dependences of the absorption intensities at 500 and 630 nm (I_{500}/I_{500}^{max} and I_{630}/I_{630}^{max}, respectively), as shown in Fig. 3[10]. Here, I_{500} and I_{630} denote the absorption intensities at 500 and 630 nm, respectively; the superscript "max" means that the corresponding quantity is the value at the final stage of the reaction.

I_{500} is concerned with both the PD cation and the reaction product, but I_{630} with only the reaction product.[10] Therefore, we can obtain an information about the time dependence of the absorption intensity of the PD cation by calculating the $I_{500}/I_{500}^{max}-I_{630}/I_{630}^{max}$ value at each time. Curves 1, 2, and 3 in Fig. 3(a) represent the time dependences of the values, I_{500}/I_{500}^{max}, I_{630}/I_{630}^{max}, and $I_{500}/I_{500}^{max}-I_{630}/I_{630}^{max}$, respectively. In Fig. 3(b), the time dependence of $[I_{630}^{max}-I_{630}]/I_{630}^{max}$ is compared with that of $[I_{500}/I_{500}^{max}-I_{630}/I_{630}^{max}]$. The two curves in Fig. 3(b) are almost parallel to each other after 15 min. This means that the decreasing rate of the PD cation is almost equal to the increasing rate of the reaction product. Therefore, the PD cation undoubtedly takes part in the main reaction path as an intermediate and plays an important role in the reaction of PD with chloranil in an ether-isopropyl alcohol (3: 1) mixed solvent. Although the details of the mechanism are not clear, it seems probable that the reaction proceeds through the interaction between the chloranil anion and the PD cation (or its dimer).

Reaction of DMPD with Chloranil. The ether solution containing DMPD and chloranil shows absorption bands due to the outer complex at 815 and 390 nm[2] at 193°K. With the increasing temperature, the intensities of these bands decrease and absorption bands due to a final reaction product which appear at 460 and 670 nm increase in intensity. The elemental analysis of the reaction product corresponds to $C_{22}H_{22}Cl_2N_4O_2$,[7] indicating that it is 2,5-dichloro-3,6-di-*p*-dimethylaminoanilino-*p*-benzoquinone. The infrared absorption measurements also support this identification.[11] No reaction intermediate could be detected between the outer complex and the final reaction product. Two reaction mechanisms are conceivable in this solvent, *i.e.*, a substitution reaction through the outer and inner (σ) complexes and one through the outer complex and ionic species. If the former is the case, the reaction mechanism of the system under consideration is phenomenologically similar to that of the aniline-chloranil system[1a] in the sense that we can not detect spectrophotometrically the inner complex through which the reaction may be expected to proceed. From only the above experimental facts, we can not conclude which of these two reactions actually occurs.

In an ether-isopropyl alcohol (3: 1) mixed solvent, the reaction of DMPD with chloranil is similar to that of the PD-chloranil system in the same solvent because, in both systems, the substitution reaction occurs through the outer complex and such ionic species as the donor cation, which exists in an equilibrium between the monomer and the dimer. Figure 4 shows the change in the absorption spectrum with the progress of the reaction of DMPD with chloranil. The cation dimer and monomer have absorption maxima at 670 nm and at 523 and 570 nm,[5] respectively. The final reaction product which has absorption bands at 460 and 670 nm was identified as 2,5-dichloro-3,6-di-*p*-dimethylaminoanilino-*p*-benzoquinone by an elemental analysis.[7] The absorption bands due to ionic species

10) The temperature is high enough to disregard the absorption due to the PD cation dimer at 605 nm.

11) One band of the N-H stretching mode was observed at 3180 cm^{-1}.

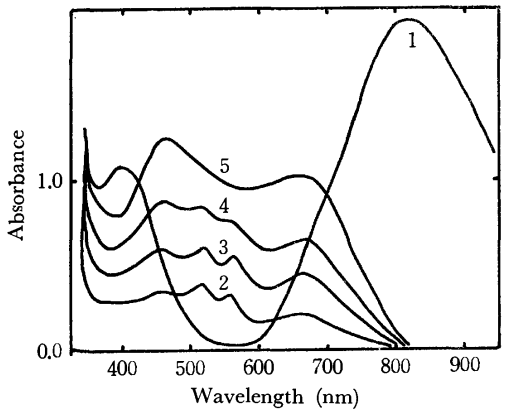

Fig. 4. The absorption spectra of the DMPD-chloranil system in an ether-isopropyl alcohol (3: 1) mixed solvent; [DMPD] $=5.0\times10^{-4}$M, [chloranil] $=2.5\times10^{-4}$M. Curve 1, is the absorption spectrum measured at 198°K; the spectrum of the outer complex. Curves 2, 3, 4, and 5 are the spectra measured at 17, 28, 45, and 129 min after the mixing at 253°K. During the measurements, the temperature increased from 253 to 273°K.

disappear almost completely at room temperature a few minutes after the mixing and those due to the final reaction product gradually increase. No reaction intermediate was found between the ionic species and the final reaction product.

Interaction of TMPD with Chloranil. The temperature and concentration dependencies of this system were investigated by studying the electronic absorption spectra in an ethyl ether-isopropyl alcohol (3: 1) mixed solvent. The system showed two different kinds of complexes. One of them is greenish yellow and exhibits an absorption peak at 830 nm. This band was identified by Foster and Thomson as the CT band of the outer complex.[6] The other is reddish-brown and

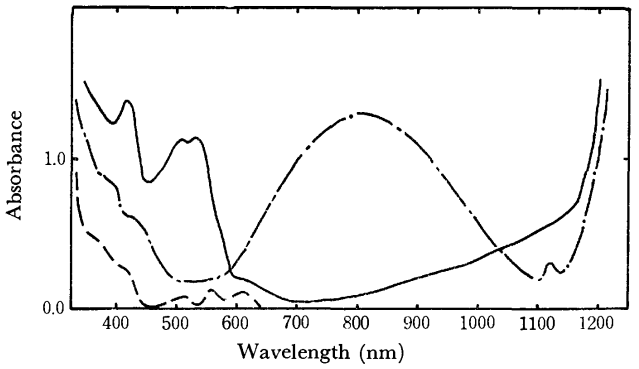

Fig. 5. The absorption spectra of the TMPD—chloranil system in an ethyl ether-isopropyl alcohol (3: 1) mixed solvent; [TMPD] $=1.25\times10^{-4}$M, [chloranil] $=1.0\times10^{-3}$M.
- - - The absorption spectrum measured at room temperature; the spectrum of TMPD cation superposed on the spectra of the component molecules.
- • - The absorption spectrum measured at 77°K; the spectrum of the outer complex.
—— The absorption spectrum measured at 193°K after once having lowered to 77°K; the spectrum of the inner complex. The 1100 nm band is very broad and appears as a shoulder of a strong band due to solvent molecules.

Table 1. Concentration and temperature dependencies of the CT complex formations between TMPD and chloranil in an ethyl ether-isopropyl alcohol (3:1) mixed solvent

[D]\[A]	2	1	1/2	1/4	7/40	1/40
16	A	A	B	C	C	C
8		B				
2	B					
1		C	C			
1/2	C					
9/40					D	D
1/5				D		
7/40	D	D	D			E
3/20				E	E	
1/8						
1/10	E	E	E			

a) [A] denotes the concentration of chloranil in the unit of 10^{-3} M.
b) [D] denotes the concentration of TMPD in the unit of 10^{-3} M.

has absorption peaks at 1100, 635, 520, and 434 nm. The 1100 nm band corresponds to a reverse CT band ($D\cdot A\leftarrow D^+A^-$) of the inner (ion-pair or ionic EDA) complex observed by Sato, Kinoshita, Sano, and Akamatu for the solid TMPD-chloranil complex.[12]

We studied the behaviors of these two specimens in solutions of various concentrations of the components by measuring their absorption spectra at room temperature, 193°K, and 77°K; as an example, the temperature dependence of the spectrum observed with the solution consisting of 1.25×10^{-4}M TMPD and 1.0×10^{-3}M chloranil is shown in Fig. 5.[13] The results obtained for the solutions containing various concentrations of the components are classified and tabulated in Table 1. In this table, A,B,C,D, and E denote the following phenomena: A: Immediately after mixing the TMPD and chloranil solutions at room temperature, the outer complex is formed and is gradually converted into the inner complex which precipitates as a reddish-brown crystal. At this stage, the outer and inner complexes coexist in the solution. B: The solution is green at room temperature because of the outer complex formation. The inner-complex formation starts by lowering the temperature of the solution to 193°K and the solution turns reddish-brown without a precipitate. The solution becomes green again by raising its temperature. C: Only the outer complex is formed in the temperature range from room temperature to 193°K, and the inner-complex formation starts at 77°K. D: The component molecules which are almost completely free at room temperature start to form the outer complex at 193°K. This pro-

12) Y. Sato, M. Kinoshita, M. Sano, and H. Akamatu, This Bulletin, **43**, 2370 (1970).
13) The concentrations of D and A in this solution correspond to class D in the classification of Table 1.

cess is reversible. By raising the solution temperature to 193°K after having once lowered it to 77°K, the inner complex is formed. By raising the temperature further, the solution returns to the initial stage at room temperature. E: Only the outer complex is formed in the range from 193°K to 77°K; the inner complex is not formed.

The present results of the outer-complex formation are reasonable and can be explained by the equilibrium-shift toward the outer-complex formation caused by the lowering of the temperature. The results concerning the inner complex, though rather complicated, suggest that its formation can not occur unless the outer-complex concentration exceeds some limited value. This seems to show that the inner-complex formation needs environmental cooperation, in particular, that there must be a clustering of donor-acceptor pairs before the inner-complex formation begins.[14] In this connection, phenomenon D is particularly interesting as showing the following color cycle with the temperature:

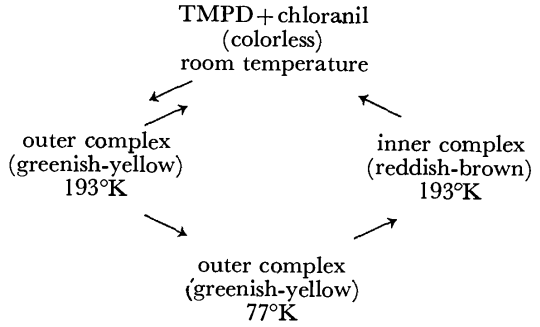

The colorless solution at room temperature turns greenish-yellow at 193°K; the color becomes deeper by decreasing the temperature to 77°K. The solution changes from greenish-yellow to reddish-brown by raising the temperature from 77°K to 193°K.[15] By raising further the temperature, the solution returns to the initial colorless state. The color cycle occurs regardless of the lowering and raising rates of the temperature and can be repeated many times.

In order to investigate the process from the outer complex to the inner complex, we measured the change in the scattering light intensity with the time, using a He–Ne gas laser as the light source. After keeping a cell containing the solution of TMPD and chloranil in the mixed solvent (the concentrations of TMPD and chloranil were 1.25×10^{-4}M and 5.0×10^{-4}M, respectively, corresponding to D in Table 1) to 77°K, we set it in a dewar vessel designed for the optical measurement and started the measurement of the scattering light intensity as soon as possible.

The inner complex is formed as the temperature of the solution is raised by acetone of room temperature surrounding the cell in the dewar vessel; thereafter, it dissociates into its component molecules. Corresponding to the change in the inner-complex concentration

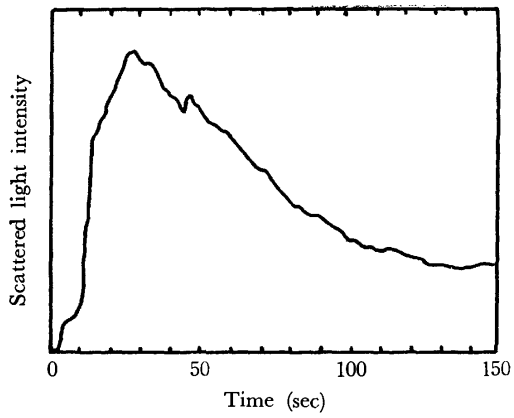

Fig. 6. The time dependence of the scattered light intensity measured for the solution containing TMPD and chloranil in an ethyl ether-isopropyl alcohol (3: 1) mixed solvent, [TMPD]$=1.25\times10^{-4}$M, [chloranil]$=5.0\times10^{-4}$M. With the rapid temperature rising from 77°K to room temperature, the scattered light intensity increases and decreases corresponding to the formation and decay of the inner complex, respectively.

with the time, the scattering light intensity changes, as is shown in Fig. 6. Briefly speaking, the time-change of the scattering light intensity shown in this figure is parallel to that of the concentration of the inner complex. This seems to support the view that the clustering of the outer complexes is related to the formation of the inner complex.[16] As pointed out by Mulliken,[17] a potential barrier between the outer and inner complexes may be expected to decrease with the increase in the polarity of the environment caused by the clustering.

A similar phenomenon was observed when we used ethyl ether as the solvent instead of an ethyl ether-isopropyl alcohol (3: 1) mixed solvent. Furthermore, both solvents are not enough polar to dissociate the inner complex between TMPD and chloranil into the ions, although the system is known to ionize in such a polar solvent as a chloroform-ethanol (1: 1) mixed solvent.[18]

Classification of Interactions of Aromatic Amines with Chloranil. On the basis of the results described in previous papers[1a–1d] and in the present paper, the interactions of various aromatic amines with chloranil in ethyl ether and in an ethyl ether-isopropyl alcohol (3: 1) mixed solvent can be classified as in Table 2. In this classification, the interactions are briefly divided into three classes, (a), (b), and (c), and each of the first two is further divided into two subclasses.

(a) The charge-transfer complex is stable and no further reaction proceeds. This class is divided further into two subclasses.

(a1) Only the outer complex is formed.

$$D + A \rightleftarrows D\cdot A$$

(An example of D in this subclass is diphenylamine)

14) Mulliken presented a similar view for the formation of NH_4^+ Cl^- crystal from NH_3+HCl gases (R. S. Mulliken, *J. Phys. Chem.* **56**, 801 (1952)).

15) This process is irreversible.

16) The details of the light-scattering experiment will be published in a forthcoming paper.

17) R.S. Mulliken, *J. Phys. Chem.*, **56**, 801 (1952).

18) I. Isenberg and S. L. Baird, *J. Amer. Chem. Soc.*. **84**, 3803 (1962).

Table 2. Ionization potentials of aromatic amines, maximum wavelengths of CT absorptions of their complexes with chloranil, and their chemical reactivities with chloranil

Amine	I_p[a] (eV)	λ_{CT} (nm)	Classification of reaction
Diphenylamine	7.1	655	a1
Aniline	7.69[b]	556	b1
o-Toluidine	7.7	555	b1
m-Toluidine	7.50[b]	555	b1
p-Toluidine	7.4	600	b1
o-Anisidine	7.6	568	—
m-Anisidine	7.6	567	b2
p-Anisidine	7.3	616	—
o-Aminophenol	7.6	567	—
m-Aminophenol	7.5	580	b2
p-Aminophenol	7.5	578	—
o-PD[c]	6.9	710	c
m-PD	7.0	680	b2
p-PD	6.8	785	a2, c[d]
1,3,5-Triaminobenzene	7.1	660	b2
1-Methyl-2,4,6-triaminobenzene	7.0	680	b2
N,N-dimethylaniline[e]	7.2	650	c
N,N-dimethyl-*m*-phenylenediamine	7.0	680	b2
DMPD	6.5	815	b1 or c, c[f]
N,N,N',N'-tetramethyl-*m*-phenylenediamine	—	g)	b2
TMPD	6.5	830	a2

a) Estimated from the absorption peak positions of the corresponding outer complexes with chloranil except for aniline and *m*-toluidine.
b) F. I. Vilesov, *Soviet Phys. Usp.*, **6**, 888 (1964).
c) In the *o*-phenylenediamine–chloranil system, the outer complex was found to produce some ionic species as reaction intermediates, although the ionic species and the final reaction product are not yet identified.
d) The a2 and c were found in ethyl ether and in an ethyl ether-isopropyl alcohol (3:1) mixed solvent, respectively.
e) In *N,N*-dimethylaniline–chloranil system, the outer complex ionizes into the *N,N*-dimethylaniline cation and the chloranil anion, and thereafter, the cation produces crystal violet as a final product in acetonitrile. J. W. Eastman, G. Engelsma, and M. Calvin, *J. Amer. Chem. Soc.*, **84**, 1339 (1962). Similar reaction processes were found by us in ethyl ether or in an ethyl ether-isopropyl alcohol (3:1) mixed solvent.
f) The b1 or c and c were found in ethyl ether and in an ethyl ether-isopropyl alcohol (3:1) mixed solvent, respectively.
g) The absorption spectrum of the outer complex has not been measured.

(a2) Both outer and inner complexes are formed.

$$D + A \rightleftarrows D\cdot A \longrightarrow D^+A^-$$

(An example of D in this subclass is TMPD)

(b) The substitution reaction proceeds through the outer and inner complexes.

$$D + A \rightleftarrows D\cdot A \longrightarrow D^+A^- \cdots \longrightarrow P$$

This class is also phenomenologically divided into two subclasses.

(b1) The inner complex is too unstable to be observed by electronic absorption measurements. Aniline is an example of D in this subclass.[1a]

(b2) The inner complex can be observed by electronic absorption measurements. *m*-Phenylenediamine is an example of D in this subclass.[1d]

(c) The reaction proceeds through the outer complex and the ionic species as the reaction intermediates.

$$D + A \rightleftarrows D\cdot A \longrightarrow D^+ \text{ (or } D_2^{2+}) + A^- \cdots \longrightarrow P$$

(An example of D in this class is PD in an ethyl ether-isopropyl alcohol (3:1) mixed solvent)[19]

In the above classification, D, A, D·A, D^+A^-, D^+, D_2^{2+}, A^-, and P represent aromatic amine, chloranil, the outer complex, the inner complex, the aromatic amine cation, its dimer, the chloranil anion, and the final product, respectively.

Stability of the Inner Complex. In a previous paper[1d], we pointed out that there exists a parallel relationship between the electron-donating abilities of the *meta*-substituent groups in *meta*-derivatives of aniline and the stabilities of their inner complexes with chloranil. For instance, the inner complex formed between *m*-phenylenediamine and chloranil exists about two hours at room temperature, while the complex with *m*-anisidine lasts only a few seconds. The inner complex can not be observed for the system including chloranil and toluidine which has a weaker electron-donating substituent at the *meta*-position than does *m*-anisidine. This fact was explained[1d] on the basis of the reasonable expectation that the nonbonding electron density on the nitrogen atom of the amino group increases with the electron-donating ability of the *meta*-substituent. From the same point of view, we shall consider the difference in stability between the inner complexes of chloranil with *meta*-substituted anilines and *ortho*- or *para*-substituted anilines.

From Table 2 we can deduce the general tendency that aniline derivatives having the electron-donating substituent(s) at the *meta*-position can form such stable inner complexes as can be detected spectroscopically as intermediates in the substitution reactions. As is clearly seen from the following figure in which the electron-density increments on the carbon atoms at the *ortho*- and *para*-positions of the substituent group (s= X or NH_2) are designated by δ^-_{os} and δ^-_{ps}, respectively, in the case of the *meta*-substituted derivatives of aniline, both the amino group and the *meta*-substituent group act to increase the π-electron densities on the three carbon atoms (*ortho* and *para* carbon atoms) by their electron migration effect, while in the case of *ortho*- and *para*-substituted derivatives of aniline, the π-electron densities on all six carbon atoms increase almost equally

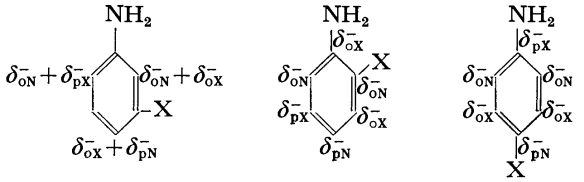

by the same effect. This means that, in the former case, the electron migration effect of the amino group

19) The contribution of A^- to this type of reaction is not certain.

is hindered to a greater extent by that of the *meta*-substituent group; therefore, the nonbonding electron density on the amino group is greater than in the latter case. Since the electron-donating ability of aromatic amines in the case of the inner-complex formation may be considered to increase with an increase in the nonbonding electron density on the nitrogen atom of the amino group, the *meta*-substituted derivatives of aniline may be expected to form more stable inner complexes with chloranil than do the *ortho*- and *para*-substituted derivatives.

The ionization potentials (I_p's) of the aromatic amines used as electron donors and the observed peak positions, (λ_{CT}), of the CT bands of the corresponding outer complexes with chloranil are also tabulated in Table 2. Neither the I_p's nor the λ_{CT}'s exhibit any tendency characteristic of the aniline derivatives with an electron-donating substituent(s) at the *meta*-position of the amino group. This may be reasonable, because they are mainly connected with the donor ability of the π-electrons on the benzene ring, while the inner-complex formation is connected with that of the nonbonding electrons of the amino group.

We should like to express our sincere gratitude to Dr. Tomihiko Ohsawa, The Institute of Physical and Chemical Research and Dr. Nobuharu Takai, The Institute of Industrial Science, The University of Tokyo, for their help in the purification of the reaction products.

BULLETIN OF THE CHEMICAL SOCIETY OF JAPAN, VOL. 45, 128—132(1972)

The Infrared Spectra and the Antiferroelectric Phase Transition of Copper Formate Tetrahydrate

Jiro HIRAISHI*

Department of Chemistry, Faculty of Science, The University of Tokyo, Hongo, Tokyo

(Received July 23, 1971)

The infrared spectra of copper formate tetrahydrate are measured in the frequency region from 4000 to 24 cm^{-1} at various temperatures. This compound is known to undergo an antiferroelectric phase transition at −37.7°C. The bands due to the librational and translational modes of the crystalline water molecules in the antiferroelectric phase are quite different from those in the paraelectric phase, while no appreciable differences between the spectra in the two phases are observed for other bands. Those facts agree with the results obtained by the crystallographic study, which show that the ordering of the orientation of the water molecules occurs at the phase transition. The similarity of the librational and the translational modes of the water molecules to those of ice is also discussed.

Solid copper formate tetrahydrate, $Cu(HCOO)_2 \cdot 4H_2O$, undergoes an antiferroelectric phase transition at −37.7°C, and the transition temperature shifts to −27.7°C, when the crystalline water is deuterated.[1-3] The crystal structure of the paraelectric phase (above the transition temperature) was determined by means of X-ray diffraction by Kiriyama, Ibamoto, and Matsuo[4] and by means of neutron diffraction by Okada, Cromer, and Almodovar[5]; they found the space group of the crystal to be $P2_1/a$—C_{2h}^5, with two formula units per unit cell. The crystal consists of alternative layers, one of copper formate and one of crystalline water, parallel to the *ab* plane. The orientation of the crystalline water molecules is disordered; this disorder is similar to that observed in ice.[5] Okada *et al.* suggested that a two-dimensional ordering of the orientation of the water molecules occurs at the phase transition. Turberfield[6] studied the crystal structure of $Cu(HCOO)_2 \cdot 4D_2O$ by means of neutron diffraction at temperatures ranging from 4.2 to 253°K and concluded that the ordering process at the transition temperature involves a cell doubling along the *c* axis. The ordered structure of the crystalline water molecules in the antiferroelectric phase was studied by means of deuteron magnetic resonance by Soda and Chiba.[7,3] They proposed that the ordered layer of the water molecules has a 2-fold screw axis symmetry. The corresponding space group is $P2_1/n$. The structures of the copper formate and of the disordered and ordered water molecules layers are shown in Figs. 1 and 2 respectively.

The infrared spectra of the compound were measured by Kuroda and Kubo.[9] They analyzed the bands due to the copper formate layer, assuming a planar model of the space group $P4/mbm$—D_{4h}^5. The librational modes of the crystalline water molecules were observed in the frequency region from 800 to 500 cm^{-1} [9]. The translational modes of the water molecules, expected to

* Present address: Government Chemical Industrial Research Institute, Tokyo, Honmachi, Shibuya, Tokyo.

1) H. Kiriyama, This Bulletin **35**, 1199 (1962).
2) K. Okada, *Phys. Rev. Lett.*, **15**, 252 (1965).
3) K. Okada and H. Sugie, *J. Phys. Soc. Japan*, **25**, 1128 (1968).
4) R. Kiriyama, H. Ibamoto, and K. Matsuo, *Acta Crystallogr.*, **7**, 482 (1954).
5) K. Okada, M. I. Kay, D. T. Cromer, and I. Almodovar, *J. Chem. Phys.*, **44**, 1648 (1966).
6) K. C. Turberfield, *Solid State Commun.*, **5**, 887 (1967).
7) G. Soda and T. Chiba, *J. Chem. Phys.*, **48**, 4328 (1968).
8) G. Soda and T. Chiba, *J. Phys. Soc. Japan*, **26**, 249 (1969).
9) Y. Kuroda and M. Kubo, *Sepectrochim. Acta*, **23A**, 2779 (1967).

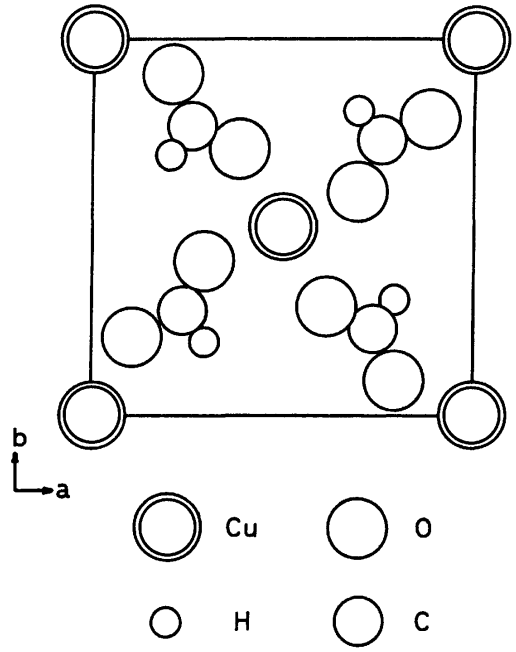

Fig. 1. Structure of the copper formate layer.[5]

appear in the frequency region lower than 350 cm^{-1}, were not yet measured. They assigned the CH stretching, the CO_2 asymmetric stretching, the CO_2 symmetric stretching, the CH in-plane and the CH out-of-plane bending, and the CO_2 scissoring vibrations to the bands at 2910, 1562, 1384, 1366, 1050, and 834 cm^{-1} respectively. In the present work, the infrared spectra of the solid in the frequency region from 4000 to 24 cm^{-1} are measured at various temperatures, as the librational and the translational modes of the water molecules are expected to give some information about the phase transition. The spectrum above 1000 cm^{-1} is not discussed in the present paper, because our results do not differ from those obtained by Kuroda and Kubo.[9]

Experimental

The sample was prepared by the method reported by Okada *et al.*[5] Single crystals grown from an aqueous solution were crushed to prepare Nujol mull for the infrared absorption measurements. The crystalline water was deuterated by keeping the powdered sample in a desiccator with heavy water for a few weeks. As the compound reacts with potassium bromide, plates of Ge, KRS-5, and polyethylene were used for the measurement of the spectra. The infrared spectra were usually recorded on JASCO model 402-G (from 4000 to 400 cm^{-1}), Hitachi model EPI-L (from 700 to 200 cm^{-1}), and Hitachi model FIS-1 (from 500 to 60 cm^{-1}) grating spectrophotometers. A Hitachi model FIS-21 single-beam grating spectrophotometer of the Cryogenic Center, University of Tokyo, was also used for the measurement in the frequency region from 180 to 24 cm^{-1}. The temperature was measured with a copper constantan thermocouple, which was inserted into the plates through a small hole. The temperatures shown in the figures were measured within an accuracy of $\pm 2°K$ for the measurement of the frequency region of the librational modes and within an accuracy of $\pm 1°K$ for the measurement of the frequency region of the translational modes.

Results and Discussion

(1) Temperature Dependency of the Spectra. The infrared spectra in the frequency region from 1000 to

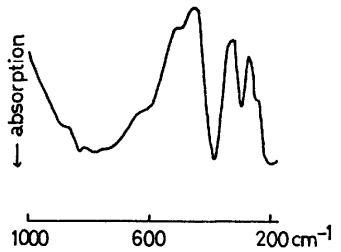

Fig. 3. Infrared spectra in the frequency region from 1000 to 180 cm^{-1} of $Cu(HCOO)_2 \cdot 4H_2O$ at room temperature.

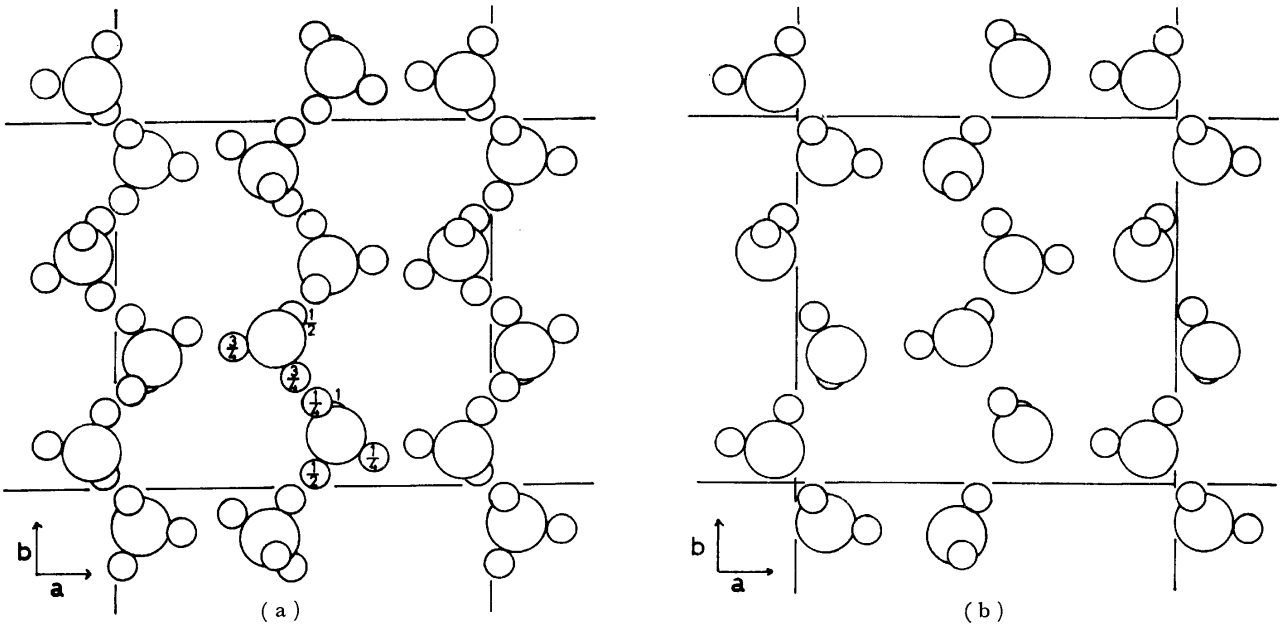

Fig. 2. Structure of the H_2O layers (a) in the paraelectric phase[5] and (b) in the antiferroelectric phases.[8] The large and the small circles represent the oxygen and the hydrogen atoms of water molecules, respectively. The number on small circles indicates the statistical weight of each hydrogen atom.

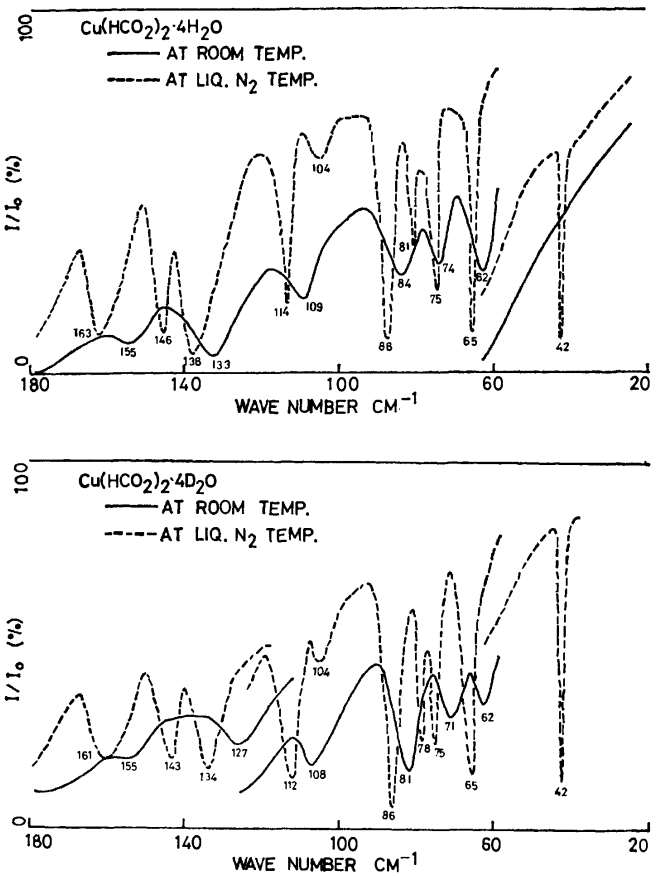

Fig. 4. Far infrared spectra in the frequency region from 180 to 24 cm^{-1} of $Cu(HCOO)_2 \cdot 4H_2O$ and $Cu(HCOO)_2 \cdot 4D_2O$ (70—80% of the crystalline water is deuterated) at room and liquid nitrogen temperatures.

180 cm^{-1} of $Cu(HCOO)_2 \cdot 4H_2O$ are shown in Fig. 3. The spectra below 180 cm^{-1} at room temperature and the temperature of liquid nitrogen for $Cu(HCOO)_2 \cdot 4H_2O$ and $Cu(HCOO)_2 \cdot 4D_2O$ are also shown in Fig. 4. The spectra at low temperatures in the frequency region from 700 to 450 cm^{-1} and below 180 cm^{-1} are quite different from those at room temperature. Spectral change in the librational and the translational modes of crystalline water upon temperature depression has been observed for several salts, such as $CuCl_2 \cdot 2H_2O$[10] and $Li_2SO_4 \cdot H_2O$,[11] although no phase-transition phenomenon has been reported for these compounds. In order to confirm that the spectral change observed in copper formate tetrahydrate arises from the antiferroelectric phase transition, the spectra were recorded at various temperatures in the frequency region from 700 to 450 cm^{-1} and from 90 to 60 cm^{-1}. The results, shown in Figs. 5 and 6, indicate that the spectral change occurs at the transition temperature. The discontinuity in the spectra with the temperature depression found in the bands due to the translational and the librational modes of the crystalline water molecules (see the later discussion of the assignment) is not found in the bands due to the formate group and the H_2O stretching and the bending vibrations. These

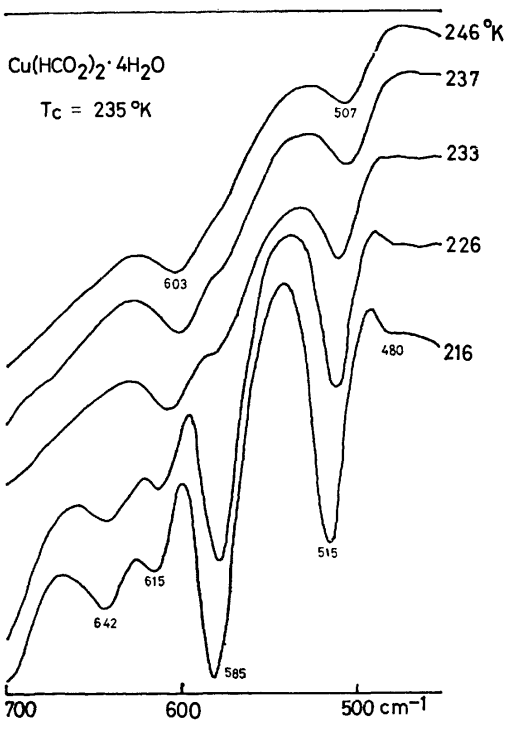

Fig. 5. Temperature dependency of the bands due to the H_2O librational modes (measured in cooling process).

10) K. Fukushima, This Bulletin, **44**, 372 (1971).

11) S. Meshizuka and H. Takahashi, Preceedings of the 24th Annual Meeting of Chemical Society of Japan, **1**, 229 (1971).

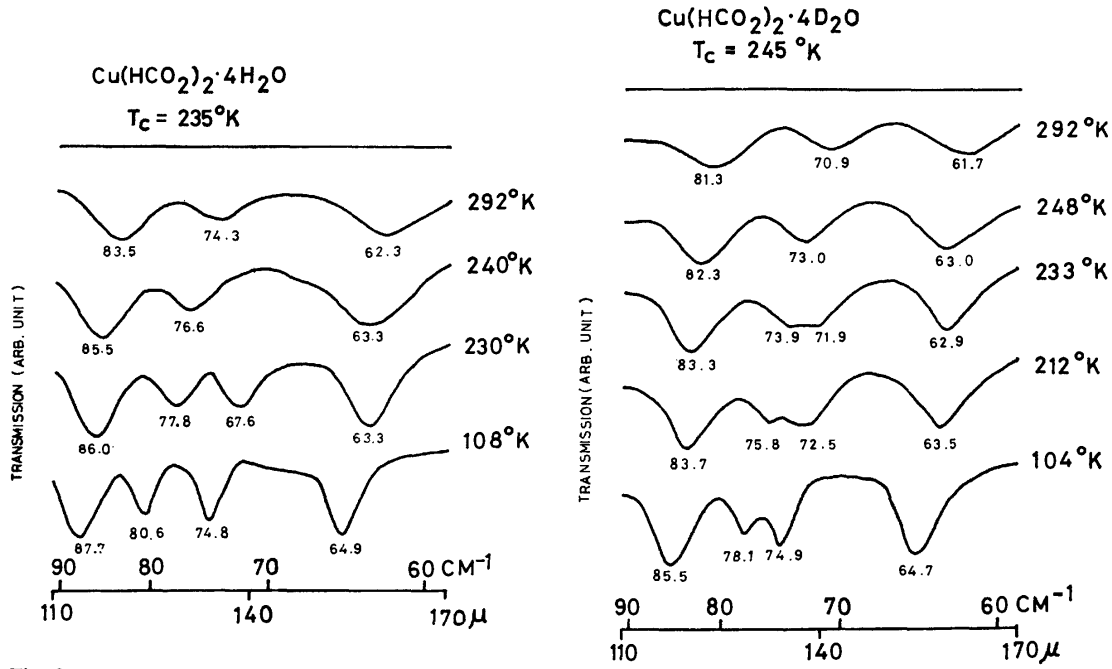

Fig. 6. Temperature dependency of the bands in the frequency region of the H_2O and D_2O translational modes.

facts agree with the finding obtained by other methods—that the crystalline water molecules are connected with the antiferroelectric phase transition.

(2) The Librational Modes of the Crystalline Water Molecules. The broad band covering the frequency region from 900 to 450 cm^{-1} in Fig. 3 was assigned to the H_2O librational modes by Kuroda and Kubo.[9] This assignment was confirmed by the deuteration of the crystalline water, on which the broad band shifted to the lower frequency region around 550 cm^{-1} and left the CO_2 scissoring vibration band at 834 cm^{-1}. The disordered structure of the crystalline water in the paraelectric phase, shown in Fig. 2a, is somewhat similar to that found in ice.[5] The infrared and Raman spectra of ice were measured by Whalley *et al.*[12] The librational bands of ice I, which has an disordered structure, form a broad band covering the frequency region from 1000 to 400 cm^{-1}, while those of ice II and III give a good deal of a fine structure below 700 cm^{-1}. They explained that this fine structure arose from the ordering of the hydrogen atoms in ice II and III because of the disappearance of the fine structure in partially-deuterated ice II or III. The librational band of ice I is similar to that of the crystalline water of the formate in the paraelectric phase; those of ice II and III are also similar to that of the formate in the antiferroelectric phase. The spectra of the librational modes of the partially-deuterated crystalline water molecules of the formate below the transition temperature do not give such a fine structure as is observed for the ordinary water molecules of the formate. These facts indicate that the transition from the paraelectric to the antiferroelectric phase involves the ordering of the orientation of the crystalline water molecules, as was pointed out by a crystallographic study.[5]

(3) The Spectra below 400 cm^{-1}. The vibrations which are expected to appear below 400 cm^{-1} can be classified into three groups. The first group, A, includes the vibrations due to the copper formate layer, except for the intramolecular vibrations of the HCO_2 group and three acoustic modes of the layer. In the paraelectric phase, these vibrations are classified as $6a_g+8a_u+6b_g+7b_u$; that is, fifteen vibrations are infrared active. The second group, B, includes the translational modes of the crystalline water molecules, except for three acoustic modes of each layer. There are 42 modes ($11a_g+10b_g+11a_u+10b_u$) in the antiferroelectric phase. The rest of the vibrations (Group C) are due to the acoustic modes of each layer. There are three modes for the paraelectric phase (a_u+2b_u) and nine for the antiferroelectric phase ($a_g+3a_u+2b_g+3b_u$), except for three acoustic modes of the crystal.

The number of the bands observed below 400 cm^{-1} is much less than expected. It is not the purpose of the present paper to assign all the observed bands. We may say, at least, that most of the bands below 180 cm^{-1} can be assigned to the vibrations of group B, because the translational vibrations of water molecules in ice are located in this frequency region,[12] and that most of the bands below 180 cm^{-1} of the formate shift more or less to the lower frequency region on the deuteration of the crystalline water molecules, as is shown in Fig. 4. The following discussion may explain the difference between the spectra below 180 cm^{-1} in the para- and the antiferroelectric phases. Whalley and Bertie discussed the vibrational spectra of orientationally-disordered crystals.[12a] Their conclusion was that all the translational lattice vibrations of the orientationally-disordered crystal can be active in both the Raman and infrared spectra. They analyzed the translational vibrations of ice I,[12b] considering that the features in the

12) a) J. E. Bertie and E. Whalley, *J. Chem. Phys.*, **40**, 1637, 1646 (1964). b) *ibid.*, **46**, 1271, 1264 (1967). c) M. J. Taylor and E. Whalley, *ibid.*, **40**, 1660 (1964). d) J. E. Bertie, H. J. Labbe, and E. Whalley, *ibid.*, **49**, 775 (1968).

infrared spectrum correspond to similar features in the density of states of the lattice vibrations. The far infrared spectra of ice I show a very broad band with a sharp maximum at 229.2 cm^{-1} and several shoulder bands, while the spectra of ice II show sharp maxima at 237.1, 186.4, 151.4, 136.1, and 106.5 cm^{-1}, plus a few shoulder bands.[12d] Makita and Seo measured the dielectric constant of the formate and reported the relaxation time to be 10^{-6}—10^{-7} sec,[13] which is much larger than the period of the translational lattice vibrations of the crystalline water molecules (10^{-11}—10^{-12} sec). That is, the orientation of the water molecules of the formate is disordered during the period of the translational lattice vibrations of the water molecules. Accordingly, all of the translational lattice vibrations, not only with the wave vector $k\sim0$, but also with $k\neq0$, are infrared active in the paraelectric phase. In the antiferroelectric phase, the structure is ordered and the ordinary selection rule of the symmetry C_{2h} holds for the infrared absorption.

Figure 7 shows the vibrational modes of Group C. The interatomic distances of Cu–O_W (2.38 Å) and H_W–O_F (1.88 Å) are about the same as the distances of Cu–O_F (2.00 Å) and the H_W–O_W hydrogen bond (1.72—1.90 Å) respectively,[5] where O_W, H_W, and O_F represent the oxygen and hydrogen atoms of the water molecule and the oxygen atom of the formate group respectively. This indicates that the interaction between the copper formate and the crystalline water layers are similar to the interaction between the copper and the formate group, or to that between the water molecules, so that the bands due to the vibrations, ν_b and ν_e in Fig. 7 can be expected not to appear below

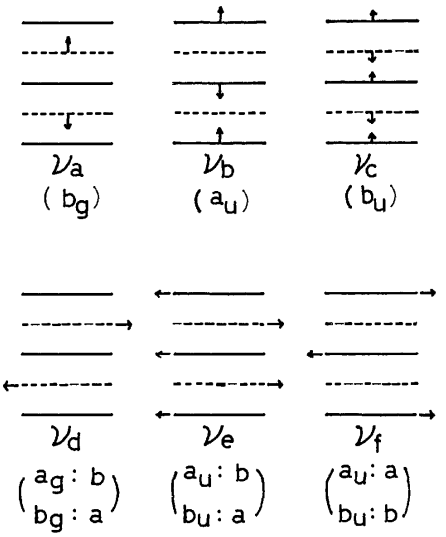

Fig. 7. Vibrations due to the acoustic modes of each layer in the antiferroelectric phase. Bravais unit cell consists of four layers, two of copper formate layer (solid line) and two of H_2O layer (dashed line). Symmetry species of each vibration is given in parenthesis. a_g: b represents that symmetry species of the vibration, the displacement coordinate of which is along b axis, is a_g.

100 cm^{-1}. The bands due to ν_e and ν_f are expected to have lowest frequency. ν_f is active in the antiferroelectric phase, but inactive in the paraelectric phase, because the wave vector of the vibration is zero in the former phase, but π in the latter phase. It can be concluded from the above considerations that the band at 42 cm^{-1}, which appears only in the antiferroelectric phase, may be assigned to ν_f, and the band at 62 cm^{-1} to ν_e.

13) Y. Makita and I. Seo, *J. Chem. Phys.*, **51**, 3058 (1969).

Heat Capacity of Ammonium Chloride between 8 and 300 K

Hideaki CHIHARA and Minoru NAKAMURA*

Department of Chemistry, Faculty of Science, Osaka University, Toyonaka

(Received August 16, 1971)

Heat capacity of NH_4Cl was measured between 8 and 300 K with an adiabatic calorimeter. The low-temperature limit of the Debye temperature is 352 K and its high-temperature limit in the harmonic approximation is 285 K. The λ transition point T_λ is 242.502±0.004 K with the heat of transition 1168 J mol^{-1} and the entropy of transition 5.00 JK^{-1} mol^{-1}. It is very close to the first-order transition. From the analysis of the heat capacity between 242 and 300 K, an extra contribution to the heat capacity that amounts to 11.5 JK^{-1} mol^{-1} at 300 K is extracted and explained by a simple model which assumes an additional type of order-disorder in the arrangment of NH_4 ions above T_λ. The energy difference between the parallel and the antiparallel pairs of NH_4 ions is estimated to be 1.46 kJ mol^{-1} from the low-temperature tail of the heat capacity anomaly near T_λ.

Ammonium chloride undergoes a diffuse phase transition at 242.5 K (hereafter designated by T_λ) and an abrupt phase transition at 457.6 K (hereafter designated by T_c). Detailed experimental and theoretical investigations[1] have been made concerning the lower phase transition at T_λ.[2-8] It is generally agreed that this transition is associated with disordering of ammonium ions between two possible orientations. Such mechanism has been established by experiments on the neutron diffraction[9] and infrared absorption[2,3] on single crystals of NH_4Cl as well as ND_4Cl.

Heat capacity measurements have been reported by many investigators[10-13] particularly below room temperature and they are fully analyzed in the paper by Sakamoto.[8] The earlier measurements, however, were not sufficiently closely spaced to reveal the shape of the heat capacity anomaly in the vicinity of T_λ. We have undertaken the precision measurements of the heat capacity between 8 and 300 K using an adiabatic calorimeter and found the results suggesting that T_λ is merely the starting point of the higher temperature transition at T_c.

Experimental

Material. Ammonium chloride (Yashima Chemicals Co., stated purity 99.9%) was recrystallized from aqueous solution and purified further by vacuum sublimation.

Calorimeter. The cryostat and calorimeter used for the present study is a modification of the one described earlier.[14] To employ larger amount of specimen, the larger calorimeter vessel (gold) and the larger adiabatic shield were newly machined, the refrigerant container being the same as before. Helium exchange gas was used to aid in the attainment of the equilibrium within the calorimeter, its amount corresponding to less than 1 Torr at room temperature. The correction to the solid heat capacities due to dissociative vaporization of NH_4Cl in the calorimeter was negligibly small even at room temperature.[15]

Temperature scales. The working thermometer above 11 K was a Leeds & Northrup platinum thermometer calibrated at the U. S. National Bureau of Standards; This was based on 1948 International Temperature Scales. A carbon resistor (Allen-Bradley, 1/8 W, 10Ω at room temperature) was used for the region below 11 K. It was calibrated by comparison with the platinum thermometer *in situ* at five different temperatures between 11 and 21 K. The results of comparison were fitted to the Clement-Quinell formula in the form

$$\log R + \frac{K}{\log R} = A + \frac{B}{T} \qquad (1)$$

for the purpose of extrapolation below 11 K. The calibration was carried out immediately after each series of measurements. The primary heat capacity values reported in the present paper are based on this temperature scale.

Since there was no fixed points below 11 K, the resulting temperature scale may be in error below about 6 K. After the experiments were concluded, the carbon scale was reexamined by comparing the carbon resistance with ^4He vapor pressure at 4.2 K in addition to the five comparisons above 11 K. The carbon scale was found to depend to a small extent on whether or not the fixed point at 4.2 K was included in the determination of the constants in Eq. (1). Further, an additional term, $C/(\log R)^2$, on the left-hand side of Eq. (1) improved the fitting of the equation. The probable error in the heat capacity values that arises from this type of uncertainty in the temperature scale were estimated to be about 10% at 4.0 K, 7.5% at 5 K, 2.5% at 6 K, 1.7% at 7 K, and 0.3% at 10 K in the present case. In view of rather large uncertainties below 8 K, the measured points below 8 K will be omitted from Table 1.

* Present address: Hitachi, Ltd., Hitachi city, Ibaraki-ken, Japan.

1) Since the number of papers on ammonium chloride is very large, only more recent references are given here which will lead one to earlier papers.

2) N. E. Schumaker and C. W. Garland, *J. Chem. Phys.*, **53**, 392 (1970).
3) E. L. Wagner and D. F. Hornig, *ibid.*, **18**, 296 (1950).
4) C. C. Stephenson, R. W. Blue, and J. W. Stout, *ibid.*, **20**, 1046 (1952).
5) H. C. Teh and B. N. Brockhouse, *Phys. Rev.*, **B3**, 2733 (1971).
6) D. E. Woessner and B. S. Snoden, Jr., *J. Phys. Chem.*, **71**, 952 (1967).
7) T. Nagamiya, *Proc. Phys.-Math. Soc. Japan*, **24**, 137 (1942).
8) Y. Sakamoto, *J. Sci. Hiroshima Univ.* **A18**, 95 (1954).
9) H. A. Levy and S. W. Peterson, *Phys. Rev.*, **83**, 1270 (1951); **86**, 766 (1952).
10) F. Simon, *Ann. Phys.*, **68**, 241 (1922).
11) F. Simon, Cl. v. Simson, and M. Ruhemann, *Z. Physik. Chem.*, **A129**, 339 (1927).
12) W. T. Ziegler and C. E. Messer, *J. Amer. Chem. Soc.*, **63**, 2694 (1941).
13) C. C. Stephenson, private communication.
14) T. Shinoda, H. Chihara, and S. Seki, *J. Phys. Soc. Japan*, **19**, 1637 (1964).
15) H. Wagner and K. Neumann, *Z. Physik. Chem., N. F.*, **28**, 51 (1961).

TABLE 1. MOLAR HEAT CAPACITIES OF AMMONIUM CHLORIDE
Weight of specimen 37.3304 g. Molecular weight 53.49. 1948 International Temperature Scales.

T/K	C_p/JK^{-1} mol^{-1}	T/K	C_p/JK^{-1} mol^{-1}
Series I		99.950	37.91
12.394	0.2339		
14.253	0.3883	Series V	
15.590	0.5305	101.802	38.49
16.605	0.6514	104.227	39.29
17.498	0.7858	106.812	40.14
18.312	0.9297	109.421	41.06
19.080	1.074	111.852	41.92
19.821	1.222	114.378	42.78
20.602	1.400	116.998	43.60
21.465	1.625	119.577	44.47
22.463	1.884	122.121	45.25
23.586	2.214	124.701	46.11
24.840	2.607	127.318	46.94
26.223	3.087	129.902	47.70
27.709	3.638	132.453	48.45
29.143	4.226		
30.588	4.853	Series VI	
32.134	5.556	8.12	0.0573
33.778	6.360	9.02	0.0803
35.453	7.222	9.97	0.104
37.116	8.071	10.91	0.145
38.758	8.929	11.79	0.192
40.630	9.920	12.619	0.2397
42.668	11.037		
44.407	12.012	Series VII	
		134.480	49.08
Series II		137.179	49.87
46.198	13.02	139.845	50.67
47.980	13.97	142.479	51.46
49.826	14.98	145.083	52.22
51.700	16.02	147.659	52.93
53.569	17.11		
		Series VIII	
Series III		149.941	53.47
53.539	17.05	152.573	54.39
55.536	18.13	155.377	55.15
57.482	19.15	158.236	55.94
59.516	20.20	161.055	56.78
61.617	21.24	163.855	57.49
		166.628	58.32
Series IV		169.372	59.12
61.754	21.29	172.094	59.87
63.853	22.33	174.791	60.63
66.063	23.45	177.565	61.38
68.390	24.61	180.418	62.47
70.689	25.64	183.236	63.55
72.942	26.68	186.146	64.52
75.181	27.61	189.153	65.48
77.463	28.73		
79.854	29.85	Series IX	
82.299	30.92	191.360	66.27
84.854	32.02	194.509	67.40
87.490	33.15	197.612	68.58
90.062	34.14	200.677	69.71
92.573	35.06	203.706	71.09
95.032	36.07	206.687	72.34
97.481	36.99	209.622	73.93

Table 1. Continued

T/K	C_p/JK^{-1} mol^{-1}
212.509	75.44
215.345	77.07
218.133	78.95
220.869	81.25
Series X	
222.942	82.89
225.044	85.02
226.590	86.48
228.112	88.37
229.607	90.54
231.073	92.76
232.509	95.35
233.910	98.58
Series XI	
(Transition region, run 1)	
234.895	101.1
236.219	105.5
237.497	110.7
238.715	119.0
239.853	130.8
240.881	144.6
241.502	179.2
241.765	205.8
241.995	246.3
242.181	328.4
242.311	569
242.395	786
242.454	1251
242.497	1372
242.547	954
242.672	275.7
242.935	144.7
243.307	112.5
243.741	97.78
244.213	90.50
244.836	85.94
245.604	83.05
246.518	81.42
247.593	80.33
Series XII	
(Transition region, run 2. Continuous heating)	
Series XIII	
248.661	80.08
250.254	79.66
252.381	79.58
256.117	79.70
260.601	80.08
264.156	80.46
268.267	80.96
272.350	81.46
276.213	82.13
280.232	82.72
284.450	83.30
288.861	84.10
293.238	84.64
297.581	85.35
301.890	85.94

Results

Measured values of the heat capacity are given in Table 1 and the smoothed values at rounded temperatures in Table 2. Curvature corrections were not applied, but may be computed from Table 1 since each series is result of continuous measurements. In the transition region, the temperature was constant at worst to within 5/10000 K when equilibrium has been reached and the smallest temperature rise in a single heating was about 2/100 K; the maximum error in $E/\Delta T$ that comes from the smallness of ΔT was therefore about 5%.

The present results are compared in Fig. 1 with previously published results of Simon,[10] Simon, Simson, and Ruhemann,[11] and Ziegler and Messer.[12] More recent unpublished measurements by Stephenson[13] above 19 K agree more satisfactorily with the present measurements. Fractional deviations from our smoothed values are compared in Table 3.

The temperature T_λ was determined from the point of maximum slope in the enthalpy *vs.* temperature graph as 242.502±0.004 K. The heat of transition was evaluated by estimating 'normal' heat capacity curve as indicated in Fig. 1. It was 1168 J mol^{-1} and the corresponding entropy of transition was 5.00 JK^{-1} mol^{-1} or 0.601 R where R is the gas constant. Table 4 is the comparison of different measurements.

Table 2. Molar heat capacities of ammonium chloride at rounded temperatures

T/K	C_p/JK^{-1} mol^{-1}	T/K	C_p/JK^{-1} mol^{-1}
8	0.0548	130	47.74
9	0.0782	140	50.75
10	0.1088	150	53.60
12	0.2046	160	56.40
14	0.3594	170	59.20
16	0.5766	180	62.26
18	0.8719	190	65.81
20	1.269	200	69.45
25	2.659	210	74.06
30	4.581	220	80.42
35	6.975	230	91.13
40	9.590	240	130.29
50	15.07	250	79.71
60	20.48	260	80.04
70	25.36	270	81.21
80	29.90	280	82.63
90	34.11	290	84.14
100	37.88	298.15	85.40
110	41.41	300	85.69
120	44.56		

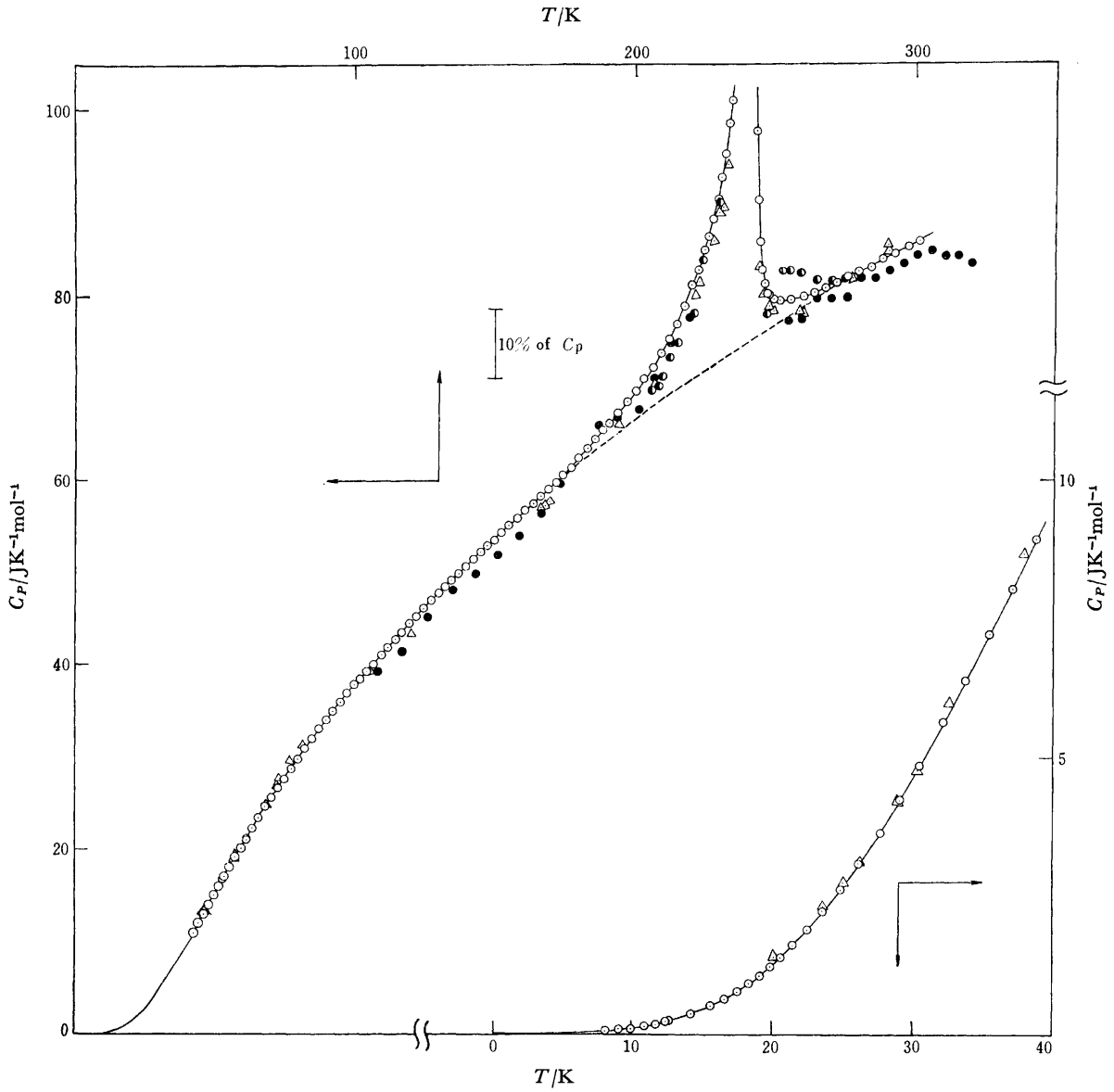

Fig. 1. Molar heat capacities of ammonium chloride; ○ present results, △ Simon,[10] ◐ Simon *et al.*,[11] ● Ziegler *et al.* [12]

TABLE 3. PERCENT DEVIATIONS FROM THE PRESENT MEASUREMENTS

Author	Deviation (%)			
	T=50K	100K	200K	300K
Simon[10,11]	+1.6	−0.7	−1.8	+2.0
Ziegler[12]	—	−2.8	−1.2	−2.0
Stephenson[13]	−0.8	−0.8	−0.9	−0.7

TABLE 4. COMPARISON OF THE TRANSITION TEMPERATURE AND THE HEAT OF TRANSITION

	T_λ/K	ΔH_λ/J mol^{-1}
Simon[10]	242.65	1490
Klug and Johnson[22]	242.61±0.10	—
Ziegler and Messer[12]	242.55±0.15	1117
This research	242.502±0.004	1168

Conversion of C_p to C_v

One of the crucial procedure in the analysis of experimental heat capacities is the conversion of C_p to C_v. Very rarely, reliable values of thermal expansion coefficient and isothermal compressibility are available over a sufficiently wide temperature range. We plotted available data of the molar volume on a large graph paper and found that the data by Staveley *et al.*[16] Lawson,[17] Hüllsmann-Biltz,[18] and Vegard-Hillesund[19] are mutually consistent below T_λ whereas those by Dinichert[20] and Adenstadt[21] deviate con-

16) D. G. Thomas and L. A. K. Staveley, *J. Chem. Soc.*, **1951**, 1420.
17) A. W. Lawson, *Phys. Rev.*, **57**, 417 (1940).
18) O. Hüllsmann and W. Biltz, *Z. anorg. allg. Chem.*, **219**, 357 (1934).
19) L. Vegard and S. Hillesund, *Avhandl. Norske Videnskaps-Akad. Oslo*, **1**, *Mat. Naturv. Kl.* No. 8 (1942).
20) P. Dinichert, *Helv. Phys. Acta*, **15**, 462 (1942).
21) H. Adenstadt, *Ann. Physik*, [5] **26**, 69 (1936).

siderably in the opposite directions. We then adopted the temperature of 150 K as the reference temperature to fix C_p–C_v because the effect of the transition is barely seen at this temperature.

The adiabatic compressibility χ_S at 150 K was calculated from an extrapolation of Garland's values on c_{11} and c_{44} and it was converted to the isothermal compressibility χ_T by using the formula

$$\chi_T = \chi_S + (V\alpha^2 T/C_p) \quad (2)$$

where V is the molar volume, α the volume expansion coefficient, and T the absolute temperature. The reference values at 150 K were thus $V=33.806$ cm^3 mol^{-1}, $\alpha=1.005\times10^{-4}$K^{-1}, $C_p=53.58$JK^{-1}mol^{-1}, $\chi_S=3.8596\times10^{-7}$ cm^{-2} N^{-1}, and $\chi_T=3.9551\times10^{-7}$ cm^{2}N^{-1}. These values give

$$C_p - C_v = \frac{V\alpha^2 T}{\chi_T} = 1.294\text{JK}^{-1}\text{mol}^{-1}$$

at 150 K. Because few experimental determinations have been reported of α and χ below 150 K, an approximate formula

$$C_p - C_v = AC_p^2 T \quad (3)$$

was applied below 150 K, where the value of A was fixed as 3.004×10^{-6} mol J^{-1} so as to reproduce the correction at 150 K. Between 150 and 230 K, we adopted Lawson's length data[17] and normalized them so that they become consistent with the molar volume at 273.2 K (34.826 cm^3), thus estimating the values of α which are shown in Fig. 2. χ_S was derived from the measured elastic constants.[23] Above T_λ, Sakamoto's calculated values[8] of α and Garland's χ_S values were used to obtain the C_p–C_v correction. The results of such computations and the estimated C_v values are listed in Table 5.

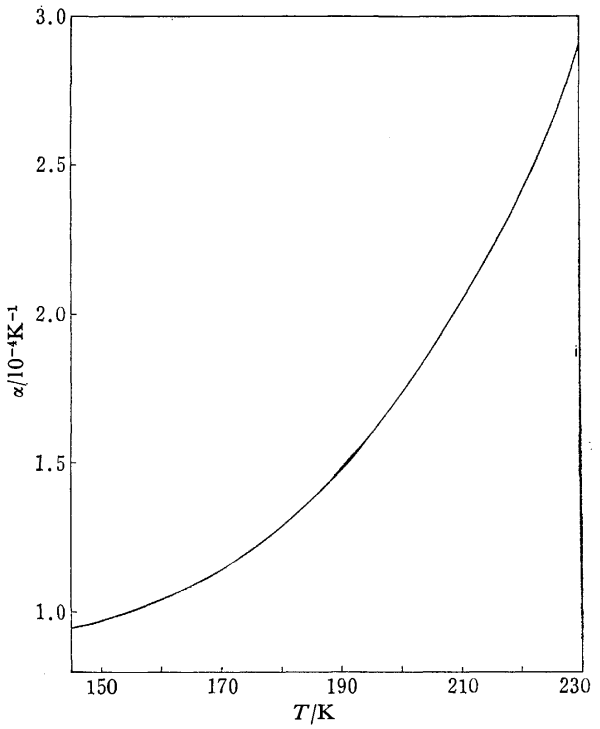

Fig. 2. Thermal expansion coefficient of ammonium chloride used for the evaluation of C_p-C_v.

Table 5. Estimates of the C_p–C_v correction and the C_v values derived therefrom (in JK^{-1} mol^{-1})

T/K	C_p–C_v	C_v	T/K	C_p–C_v	C_v
40	0.013	9.577	200	4.757	64.71
60	0.075	20.41	220	9.046	67.46
80	0.213	29.69	250	3.360	76.36
100	0.431	37.45	260	3.184	76.83
120	0.715	43.85	270	3.523	77.67
140	1.084	49.65	280	3.996	78.65
160	1.464	54.95	290	4.531	79.59
180	2.427	59.84	300	5.272	80.41

Low-temperature Heat Capacities

The low-temperature C_v was converted to the equivalent Debye temperature Θ_D^C for six degrees of freedom per unit cell after the contributions[2,3] of the intra-ionic vibrations at 1403 cm^{-1} (triply degenerate) and 1683 cm^{-1} (doubly degenerate) and of librations of ammonium ions at 391 cm^{-1} (triply degenerate, below T_λ) have been subtracted from C_v. The plot of Θ_D^C *vs* temperature (Fig. 3) shows a shallow minimum around

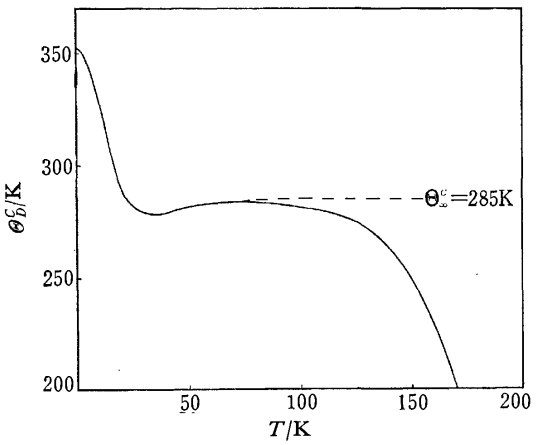

Fig. 3. Equivalent Debye temperature of ammonium chloride based on C_v for $6N$ degrees of freedom.

35 K with Θ_D^C (min)=279 K. The Debye temperature at the high temperature limit in the harmonic approximation was estimated to be Θ_∞^C=285 K corresponding to the Debye cut-off frequency of 198 cm^{-1} or 5.9×10^{12} Hz. This cut-off frequency is in good agreement with that obtained from the analysis of coherent inelastic scattering results for ND_4Cl.[24] The cut-off frequency is not affected by the deuterium substitution. The limiting low-temperature Θ_0 was obtained from the plot of C_vT^{-3} against T^2 at 352 ± 6 K.

High-temperature Heat Capacities

Inspection of Fig. 3 shows that Θ_D^C tends to decrease above 100 K. Because the intra-ionic and the libra-

22) H. P. Klug and W. W. Johnson, *J. Amer. Chem. Soc.*, **59**, 2061 (1937).

23) C. W. Garland and R. Renard, *J. Chem. Phys.* **44**, 1130 (1966).

24) E. R. Cowley, *Phys. Rev.* **B3**, 2743 (1971).

tional contributions in the harmonic approximation have been subtracted from C_v which was used in deriving Θ_D^C, the descending trend of Θ_D^C must be due either to onset of the phase transition and/or to some anharmonic effect.

To visualize the behavior near T_λ, the 'rotational' part of C_v, defined by

$$C_R = C_v - C_i - C_D(285\,\mathrm{K}) \tag{4}$$

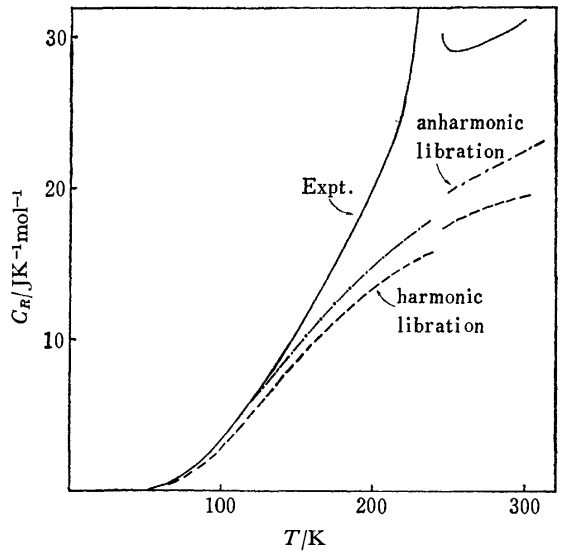

Fig. 4. Rotational contribution to the molar heat capacity.

was calculated, were C_i is the heat capacity due to intra-ionic vibrations and C_D (285 K) is the Debye heat capacity corresopnding to Θ_∞^C. The results are shown in Fig. 4. In the same figure, a curve is drawn that corresponds to the harmonic libration of NH_4^+ ions (391 cm^{-1} for $T<T_\lambda$ and 359 cm^{-1} for $T>T_\lambda$). The use of Einstein heat capacity for the libration mode may be justified by the flatness of the dispersion relation observed by the inelastic neutron scattering experiments.[5] It is apparent that the harmonic libration model can account for C_R only up to about 130 K where C_R begins to curl up rapidly. Such deviation may be taken as indicating on-set of the order-disorder transition, but what seems to be abnormal is the large discrepancy between C_R and the harmonic librational heat capacity above T_λ which amounts to as great as 11.5 J K^{-1} mol^{-1}. The existence of this extra heat capacity was already pointed out by Sakamoto[8] although his estimate was somewhat smaller (8.95 J K^{-1} mol^{-1} at 298.15 K) than ours. We shall now examine some possibilities that could account for the extra contribution.

a) Anharmonic Librations. Woessner and Snoden[6] derived a value of 19.7 kJ mol^{-1} ($T<200$ K and $T<T_\lambda$) for the activation energy of the reorientation of ammonium ions from their measurements of the NMR spin-lattice relaxation time. Since the activation energy is only eight times as large as the average thermal energy of a single ammonium ion at 300 K, the anharmonic contribution to the librational heat capacity could be significant.

If we assume the potential energy of an ammonium ion of the form

$$V(\phi) = \frac{1}{2}V_0(1-\cos n\phi)$$
$$= c\phi^2 + f\phi^4 + \cdots \tag{5}$$

where V_0 is the barrier height and ϕ is the angle of rotation, the anharmonic Einstein heat capacity then becomes[25]

$$\frac{c_v}{R} = \frac{c_v^h}{R} - \frac{3}{2}\frac{fRT}{c^2} + \cdots \tag{6}$$

Equation (6) is also plotted in Fig. 4 by the dot-dash curve. It still falls short of the C_R values. The situation is almost the same if we use Eq. (5) and calculate the heat capacity of a triply degenerate hindered rotor with the help of Pitzer-Gwinn's tables.[26] Recently, Garland and Weiner[27] introduced a more anharmonic potential function that can account for the optical spectra.[1] However, the use of their energy level scheme (with $\omega=391$ cm^{-1} and $x=29$ cm^{-1}) gave too small a heat capacity, only 16.6 J K^{-1} mol^{-1} to be compared with 19.6 J K^{-1} mol^{-1} obtained at 300 K in the harmonic approximation.

b) Subsidiary Minima in the Potential Energy. At the upper transition point (T_c), NH_4Cl is transformed into NaCl type of structure probably because the reorientation rate of NH_4 cations becomes progressively larger at higher temperatures, finally reaching a point where the molecular field an NH_4 cation sees is made effectively spherical. The shape of the heat capacity curve near T_c is such that the heat capacity drops abruptly at T_c by as much as about 22.5 J K^{-1} mol^{-1} (5.38 cal K^{-1} mol^{-1}). If the transition were simply associated with the change from reorientation to nearly free rotation of NH_4 cations, the heat capacity drop would be about $^3/_2 R$ or 12.5 J K^{-1} mol^{-1}, about half of the decrease found experimentally. The sum of contributions 76 J K^{-1} mol^{-1}, Debye lattice heat capacity 25 J K^{-1} mol^{-1}, C_p—C_v correction *ca.* 30, rotation of NH_4 cations 12.5, and internal vibrations of NH_4 8.6, roughly account for the observed heat capacity, *ca.* 81 J K^{-1} mol^{-1}, immediately above T_c. The fact that the distance (3.27 Å) between the nearest N and Cl atoms is equal to the sum (3.29 Å) of the ionic radii also suggests that ammonium ions undergo almost free rotation above T_c. This in turn will indicate that there must be some extra contribution to the heat capacity below T_c. Therefore, the observed heat capacity contains such extra persistently between T_λ and T_c.

To interpret the extra contribution to the heat capacity we shall assume a simple model in which ammonium ions can assume additional type of disorder other than the one that is responsible for the transition at T_λ. Below T_λ the NH_4 cations are rather rigidly held in one of the two possible orientations but as the complete disorder is attained immediately above T_λ,

25) A. J. E. Foreman and A. B. Lidiard, *Phil. Mag.* **8**, 97, (1963).
26) K. S. Pitzer, 'Quantum Chemistry', Prentice Hall, New York (1953).
27) C. W. Garland and B. B. Weiner, *J. Chem. Phys.*, **53**, 1609 (1970).

the ions will execute a kind of rattling motion as a result of frequent reorientational motion. The lowest potential barrier over which an NH_4 ion can reverse its orientation will be such that the ion is rotated through about 60° around one of its N–H bond (threefold axis) and then 60° around the axis perpendicular to the bond. The first type of rotation will lead the ion to a shallow minimum of the potential energy—here, three hydrogen bonds are broken but they are replaced by electrostatic attraction between hydrogen and chloride ions. At such an intermediate orientation, the remaining N–H···Cl⁻ hydrogen bond will become shortened giving rise to eightfold position of the N atom, slightly displaced from (½½½) toward one of the eight neighboring chloride ions. If we now assume that those subsidiary eight minima have energy ε relative to the principal minima, we shall obtain a Schottky type anomaly in the heat capacity, *i.e.*

$$C_{\mathrm{Sch}} = \frac{N\varepsilon^2}{kT^2}\frac{g_0}{g_1}\frac{\exp(\varepsilon/kT)}{[1+(g_0/g_1)\exp(\varepsilon/kT)]^2} \qquad (7)$$

where $g_0=2$ and $g_1=8$ for the model proposed. Equation (7) is plotted in Fig. 5 for $g_0/g_1=1/4$, $\varepsilon=7.5$ kJ mol^{-1}. The maximum of C_{Sch} was fixed at 300 K as Sakamoto's analysis suggested the existence of a broad maximum here. At 300 K, Eq. (7) gives 10.36 J K^{-1} mol^{-1} whereas the experimental extra heat capacity is 11.50 J K^{-1} mol^{-1} if we assume harmonic librational modes or 8.57 J K^{-1} mol^{-1} if we assume Eq. (5) for the potential energy function. The agreement with Eq. (5) appears satisfactory in the absence of reliable estimates for the anharmonicity. Our measurements of the heat capacity did not extend beyond 300 K and therefore Eq. (5) would not deserve more detailed fitting at present. However, the existence of large extra heat capacities between T_λ and T_c is beyond doubt and they must be associated with some additional degrees of freedom in the crystal. We have proposed a possible interpretation here which may have consequences in other properties of NH_4Cl at high temperatures, *e.g.* inelastic neutron scattering, Raman spectra, and dielectric dispersion.

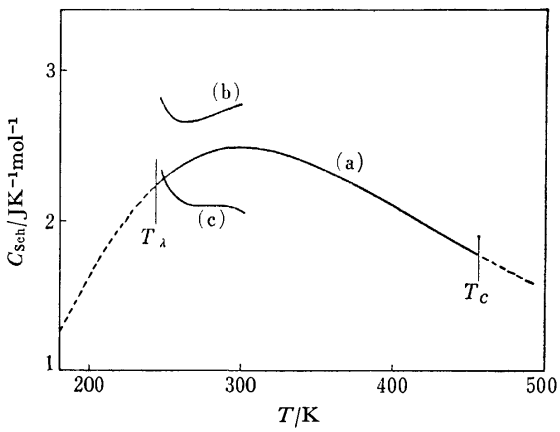

Fig. 5. Schottky heat capacity [Eq. (7)]. Comparison with 'experimental' estimates of the anomalous heat capacity above T_λ. Curve a: theoretical calculation for $g_0/g_1=1/4$, $\varepsilon=7.5$ kJ mol^{-1}, Curve b: estimate based on the harmonic libration model, Curve c: estimate based on the anharmonic libration model.

A similar type of anomaly was reported[28] in the case of stoichiometric AgI, in which case positional disorder of Ag cations were assumed to explain an anomalously large heat capacity after it has transformed to the α form at 150°C.

Anomaly Associated with the λ Transition

Garland and Schumaker[29] confirmed a good correlation between the intensity of the 1444 cm^{-1} infrared band and the anomalous part of the heat capacity using Stephenson's unpublished results. Since our results agree satisfactorily with Stephenson's heat capacities, we shall not attempt to repeat the analysis but merely point out that the transition is very close to the first order transition as may be inferred from Series XI, Table 1.

The Energy to Reorient an NH_4 ion in the Ordered Matrix

It is possible to estimate the energy required to rotate an NH_4^+ ion through 180° from the low temperature tail of the λ transition. Assuming that the number of NH_4^+ in the wrong orientation n is very small compared with the total number of the ions N, we have

$$\frac{n}{N} = \exp(s/k)\exp(-\varepsilon/kT) \qquad (8)$$

where ε is such energy and the anomalous heat capacity ΔC is given by

$$\Delta C = \frac{1}{T^2}\cdot\frac{\varepsilon^2}{k}e^{s/k}e^{-\varepsilon/kT} \qquad (9)$$

in an analogous way to the case of vacancy formation.[30]

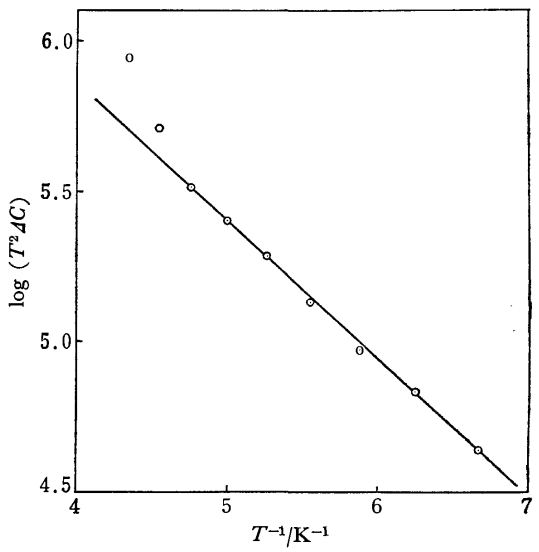

Fig. 6. Evaluation of the energy to reorient an NH_4 cation in almost perfectly ordered lattice.

28) C. M. Perrott and N. H. Fletcher, *J. Chem. Phys.* **48**, 2143, 2681 (1968).
29) C. W. Garland and N. E. Schumaker, *J. Phys. Chem. Solids*, **28**, 799 (1967).
30) R. H. Beaumont, H. Chihara, and J. A. Morrison, *Proc. Phys. Soc.* (London), **78**, 1462 (1961).

ΔC was evaluated as the difference between C_R and C_{lfb} in Fig. 4 and a plot is made of log $(T^2\Delta C)$ *versus* $1/T$ in Fig. 6. A good straight line is obtained between 150 and 210 K, the slope of which gives $\varepsilon=8.77$ kJ mol^{-1}. The deviation of the points for 220 and 230 K is due to rapid increase of the heat capacity in the transition region. Eq. (8) then reads

$$\frac{n}{N} = 5.32 \exp(-1055/T) \tag{10}$$

which leads to a value of $n/N=0.035$ at 210 K. The magnitude of ε (8.77 kJ mol^{-1}) corresponds to the difference in energy between six parallel pairs and six antiparallel pairs; the energy difference between one parallel and one antiparallel pair is then 1.46 kJ mol^{-1}, about 3/4 of kT_λ (=2.02 kJ mol^{-1}).

The authors would like to thank Mr. Tooru Atake for assistance during the measurements. They also express gratitude to Professor Stephenson of Massachusetts Institute of Technology for sending them his unpublished heat capacity values. Discussions with Dr. Nobuo Nakamura of Osaka University were very fruitful to whom their thanks are due.

BULLETIN OF THE CHEMICAL SOCIETY OF JAPAN, VOL. 45, 140—145(1972)

Polarographic Catalytic Waves of Titanium(IV) Chelates of EDTA and Related Compounds

Hiroko KANEKO and Takeo OZAWA
Electrotechnical Laboratory, Tanashi, Tokyo
(Received July 29, 1970)

In the presence of the chlorate ion, the electrode reaction of the various titanium(IV)-chelates is followed by a cyclic process, *i.e.*, an electrochemical reduction of electroactive species generated continuously by coupled chemical oxidation. The reaction rate constant of the regeneration is determined from the ratio of the limiting current observed by the DC polarographic method in the presence of the chlorate ion to that determined without it, and it is calculated using Koutecky's equation. The complex-forming agent decreases the wave height of the catalytic waves of titanium(IV) chelates, and a clear dependency of the height of the catalytic waves on the dissociation constants of the titanium chelates is found. The catalytic wave heights of the titanium(IV) chelates decrease in the order of oxalic acid, NTA, EDTA-OH, EDTA, and CyDTA; the dependency on the stability seems to be the reverse. The logarithm of the dissociation constant is in a linear relation with the logarithm of the catalytic current. The mechanism is discussed on the basis of the above-mentioned facts.

The reduction of titanium(IV) in the presence of the chlorate ion is an example of the type of behavior in which the original depolarizer is regenerated by the reaction of the primary product with a certain component of the solution. These catalytic waves of titanium(IV) in various solutions were investigated.[1-3] The DC polarographic behaviors of the titanium(IV) ion in an ethylenediamine tetraacetate(EDTA)s olution[4] and in a cyclohexanediamine *N,N,N',N'*-tetraacetate(CyDTA) solution[5] have already been investigated, and the compositions and stability constants of titanium(IV) complexes and the mechanism of the electrode reaction have been determined.

Though it is supposed that, in the presence of a chelating agent, the regeneration rate of titanium(IV) might become considerably slow, no investigation of it has yet been reported. In the present paper, the effects of these EDTA-like agents on the regeneration of titanium(IV) by the chlorate ion are investigated, and the rate constants of the regeneration reactions of some titanium(IV) chelates are calculated by the use of Koutecky's equation.[6] The complex-forming agent decreases the wave height of the catalytic wave of the titanium(IV) chelate, and a clear dependency of the height of the catalytic waves on the dissociation constants of titanium chelates is found.

Experimental

Reagents. All the solutions used were prepared from analytical reagent-grade chemicals. Titanium metal (spongy one) was dissolved in dilute sulfuric acid and oxidized by a small amount of dilute warm nitric acid, after which the solution was standardized by visual chelatometric titration with EDTA as the titrant. The solutions of the complex-forming reagents, EDTA, CyDTA, *N*-(2-hydroxyethyl)-ethylenediamine *N,N',N'*-triacetic acid (EDTA-OH), nitrilo-triacetic acid (NTA), and oxalic acid (OX), were prepared from commercial analytical-grade chemicals and were standardized by visual titration with a zinc solution and with a Eriochrome Black T solution as the indicator.

Apparatus. Polarographic current-voltage cruves were

1) J. Koryta and J. Tenygl, *Collect. Czech. Chem. Commun.*, **19**, 839 (1954).
2) A. Blazek and J. Koryta, *ibid.*, **18**, 326 (1953).
3) K. Tanaka, K. Morinaga, and K. Nakano, *Nippon Kagaku Zasshi*, **90**, 478 (1969).
4) R. L. Pecsok and E. F. Maverick, *J. Amer. Chem. Soc.*, **76**, 358 (1954).
5) H. Kaneko and K. Kaneko, The Preprint of the symposium on complex salts, Dec. 6 1966, Tokyo.
6) J. Koutecky, *Collect. Czech. Chem. Commun.*, **18**, 311 (1953).

obtained with a Yanagimoto P8 series polarograph, model P8-DPR. A three-electrode system is utilized in this instrument, and the potentials are measured at intervals of a few seconds with an electrodehammer which also dislodges the mercury drop. The capillary employed for the DME measurements had a capillary constant ($m^{2/3}t^{1/6}$) of 1.14 in 0.1 mol/*l* sulfuric acid (open circuit), where m is the flow of electrode mercury per second and where t is the drop time.

The pH of the solution was measured immediately after the measurements of the current-voltage curve by means of a Toa HM-5A pH meter equipped with a glass electrode.

Procedure. The measurements were carried out in solutions containing 0.96 mmol/*l* of titanium(IV), 0.1 mol/*l* of oxalic aicd, and 0.05 mol/*l* of potassium chlorate; the concentrations of chelating agents in the solutions were 5, 10, 20, and 50 mmol/*l*. All the solutions were de-aerated with nitrogen gas for 10 min before the polarogram was obtained. During the course of the measurement, a nitrogen atmosphere was maintained over the solution in the cell. The temperature of the solutions was kept at 25.0°C within a variation of ±0.1°C by using a thermostat. The polarogram of the above-mentioned solution was recorded after recording the wave of the solution of the same composition without potassium chlorate.

Results

The rate constants, k, of the regeneration reactions of some titanium chelates are calculated as follows:

$$\begin{array}{ccc} \text{Ti (IV)} + e & \longrightarrow & \text{Ti (III)} \\ \uparrow & & \downarrow \\ \overbrace{\text{ClO}_3^-} & & \overbrace{k} \end{array} \qquad (1)$$

In the case of $i_l/i_d > 2.5$ and $i_l \ll {}_x i_d$, the equation for the total limiting current can be derived from the approximate expression of Koutecky:[6]

$$i_l/i_d = 1 + 0.815\sqrt{kCt} \qquad (2)$$

where i_l and i_d indicate the kinetic current of the catalytic reaction and the diffusion current respectively; where i_t is the sum of i_l and i_d; k, the rate constant of the regeneration reaction of titanium(IV); C, the concentration of the oxidizer; ${}_x i_d$, the hypothetical diffusion current which would be observed for the reduction of all the chlorate ions, and t, the drop time. Equation (2) holds only when the complex-forming agent and the oxidizer exist in a large excess over the titanium(IV) in the solution. In the case of $i_l/i_d > 2.5$, if the relation betwen i_l/i_d and $C^{1/2}$ is linear, the rate of the catalytic reaction of the regeneration of titanium(IV) is rapid and the decrease in the concentration of the oxidizer can be neglected.

When i_l/i_d is plotted against the square root of the concentration of the chlorate ion, the rate constant, k, of the regeneration reaction of titanium(IV) can be obtained from the slopes of these linear plots, provided that the polarographic waves of titanium chelate in the solution without the chlorate ion can be observed. Actually, the polarographic waves of titanium chelates in the solution without the chlorate ion are observed with solutions containing 20 mmol/*l* of EDTA, EDTA-OH, and CyDTA, 50 mmol/*l* of NTA, and 0.1 mol/*l* of oxalic acid respectively at pH 1.

In Fig. 1, the wave height divided by the root of h_0 is plotted against the mercury height, where h_0 is the mercury height corrected for back pressure. It can be inferred that the limiting current of titanium chelate in the solution without the chlorate ion is the diffusion current. This inference is also derived from the temperature coefficient (1.4%/°C) of the wave of the EDTA-OH titanium-chelate (Fig. 9).

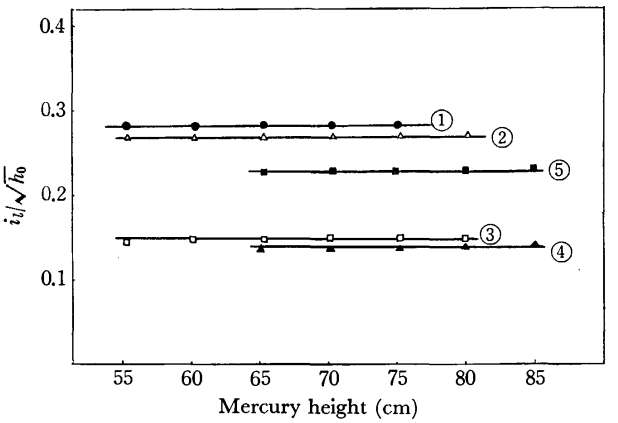

Fig. 1. The effect of mercury height on the diffusion current. 1, OX; 2, NTA; 3, EDTA-OH; 4, EDTA; 5, CyDTA.

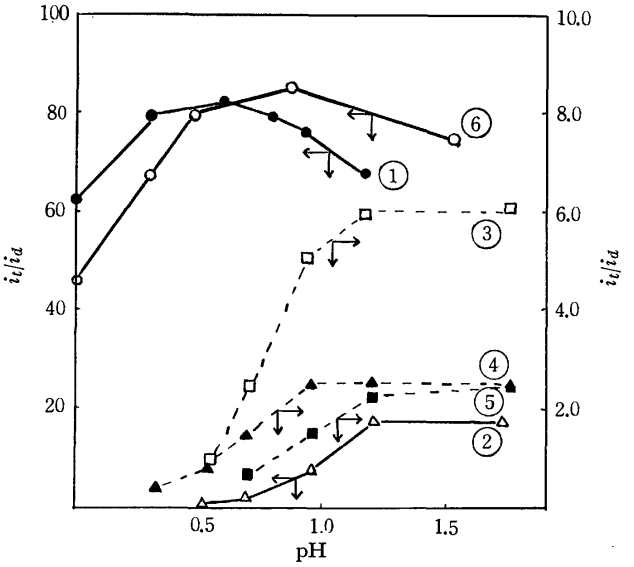

Fig. 2. The effect of pH on i_l/i_d. 1, OX; 2, NTA; 3, EDTA-OH; 4, EDTA; 5, CyDTA; 6, nothing.

Then, the dependencies of the i_l/i_d ratio on the pH of the solution and on the concentration of the chelating agents were observed. In Fig. 2, the dependencies of the i_l/i_d ratio on the pH are shown, where the concentration of the chelating agents is 5 mmol/*l*, except for oxalic acid and NTA, whose concentrations are 0.1 and 0.02 mol/*l*. As is shown in Fig. 2, the dependency is negligible in the range of pH larger than 1.2, except for the solution containing oxalic acid and that without any chelating agent. The large variations observed in the latter cases seem to be due to the low stabilities of the complexes. All the measurements hereafter are made by controlling pH within an accuracy of ±0.1. The effect of the pH on the half-wave potential of the catalytic wave is shown in Fig. 3.

The effect of the concentration of the chelating

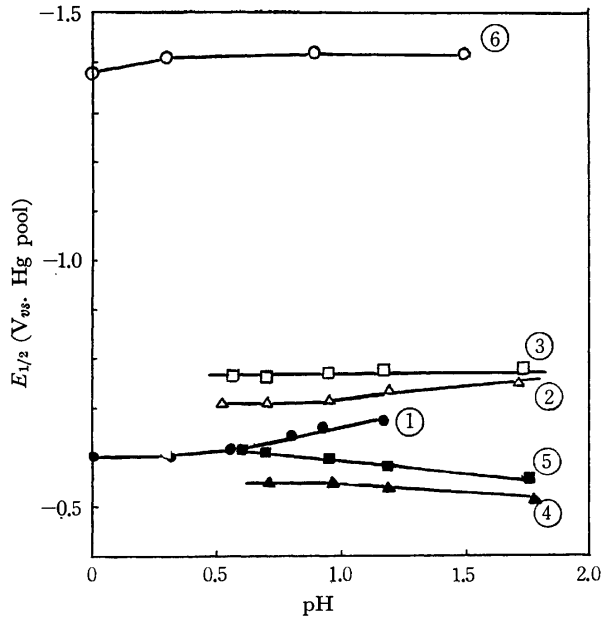

Fig. 3. Effect of pH on half-wave potential. 1, OX; 2, NTA; 3, EDTA-OH; 4, EDTA; 5, CyDTA; 6, nothing.

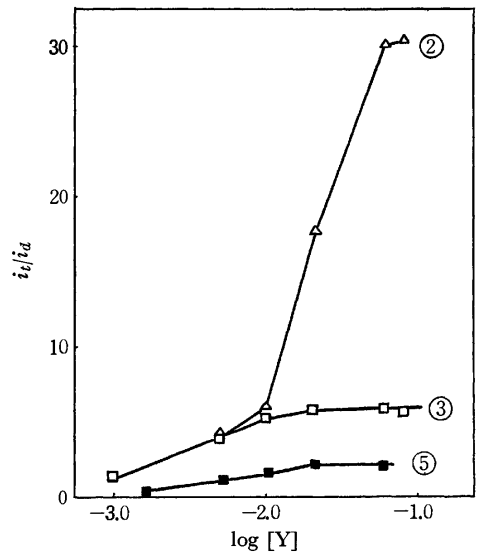

Fig. 4. The effect of the concentration of chelating agents, [Y], on i_l/i_d. 2, OX; 3, EDTA-OH; 5, CyDTA.

agents is shown in Fig. 4, where the concentration of titanium(IV) is 0.94 mmol/*l* and where that of chlorate is 0.05 mol/*l*. At concentrations higher than 0.01 mol/*l*, the dependency of the i_l/i_d ratio on the concentration is low for EDTA-OH and CyDTA; the dependency for EDTA might be similar because its properties are similar to those of CyDTA, while a large dependency is found for the solution containing NTA, where the dependency seems to be negligible for the range higher than 0.05 mol/*l* and where the precipitation is found in the NTA solution in the range over 0.07 mol/*l*. This large dependency might be caused by the co-existence of the complex ion containing a single NTA molecule and that complex ions containing NTA molecules. The second wave found for the NTA chelate mentioned below is presumably other evidence of this. Hereafter, the concentration of NTA will be controlled at 0.05 mol/*l*, and that of oxalic acid at 0.1 mol/*l*.

The diffusion current of the titanium(IV)-EDTA-OH chelate solution increases as the temperature increases, and its temperature coefficient is 1.4%/°C. However, the catalytic current is in a nonlinear relationship with the temperature (Fig. 5).

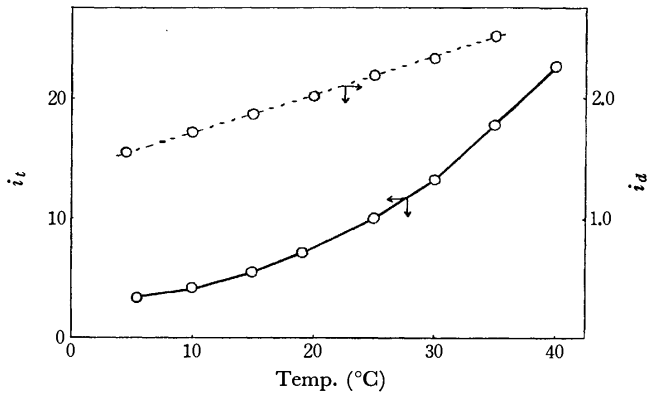

Fig. 5. The effect of the temperature on the diffusion current and the catalytic current of titanium-EDTA-OH complex.

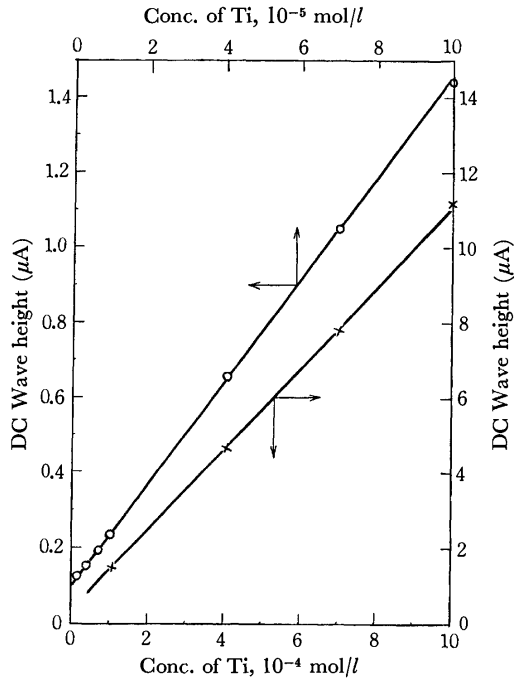

Fig. 6. Calibration curves of the catalytic wave of titanium-EDTA-OH chelate.
pH: 1.2, EDTA-OH: 0.02M, $KClO_3$: 0.05M.

As is shown in Fig. 6, a linear relationship is found between the concentration of titanium(IV)-EDTA-OH and their catalytic current in the presence of 0.05 mol/*l* potassium chlorate over the range from 1×10^{-6} mol/*l*, to 1×10^{-3} mol/*l* of titanium(IV).

In Fig. 7, the values of i_l/i_d at the drop time of 3.0 sec and at pH 1.0 ± 0.1 are plotted against the square root of the concentration of the total chlorate ion. The catalytic wave height of titanium chelates decreases in the order of oxalic acid, NTA, EDTA-OH, EDTA, and CyDTA. Straight lines can be drawn through

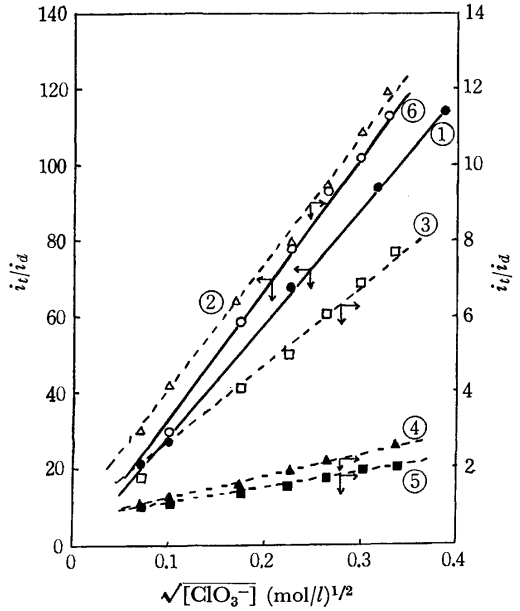

Fig. 7. The catalytic current of the titanium-chelate ion.
1, OX; 2, NTA; 3, EDTA-OH; 4, EDTA; 5, CyDTA; 6, nothing.
Ti: 0.86 mM, pH: 1.0±0.1.

the plots, as is seen in Fig. 7, and the intercepts are 1; these facts are in accordance with Eq. (2). The rate constant of the regeneration can be obtained, since $(i_l/i_d-1)/0.815\sqrt{Ct}$ equals $\sqrt{k}$. The rate constants thus obtained are shown in Figs. 8A and 8B, where the variations in the rate constant with *the drop time* and with *the concentation of the oxidizer* are shown. Here the rate constants, k, in the case of the regeneration of EDTA-Ti(IV) and CyDTA-Ti(IV) are the apparent ones, because the values of i_l/i_d are less than 2.5. As is clearly seen in these figures, there is no variation; these results are in good agreement with Eq. (2). The average values are tabulated in Table 1. For the solution of the titanium-NTA complex, two catalytic waves are observed; the first one is shown in Figs. 7 and 8 and is tabulated in Table 1. Since the values of i_l/h_0 against the mercury height for

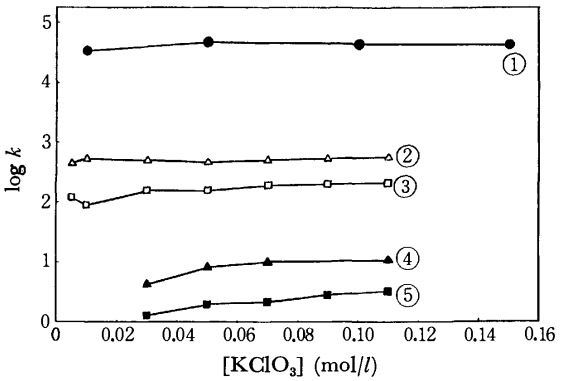

Fig. 8. (A) Relation of log k to the concentration of oxidizer, C.
1, OX; 2, NTA; 3, EDTA-OH; 4, EDTA; 5, CyDTA
Ti: 0.96 mM, H_2SO_4: 0.1M, $KClO_3$: 0.05M.

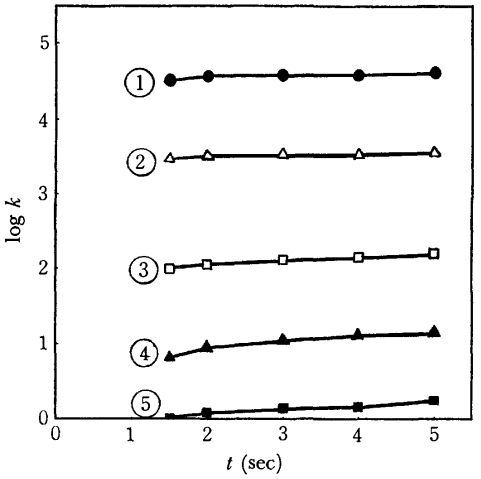

Fig. 8. (B) Relation of log k of drop time t.
1, OX; 2, NTA; 3, EDTA-OH; 4, EDTA; 5, CyDTA
Ti: 0.96 mM, H_2SO_4: 0.1M, t:3.0 sec.

the catalytic wave of 0.96 mmol/l titanium(IV) in 0.1 mol/l sulfuric acid and 0.05 mol/l of potassium chlorate are constant, this wave seems to be controlled by the diffusion of the chlorate ion and to be actually due to the reduction of chlorate ions, catalyzed by the

Table 1. Polarographic and catalytic waves of titanium chelates and the rate constant of the regeneration of titanium(IV) chelates.

Chelating agents	i_d(μA)	$E_{1/2}$V *vs.* SCE	$i_l^{a)}$(μA)	i_l/i_d	$E_{1/2}$V *vs.* SCE	K l/mol·sec
Nothing	2.05	−0.82	171	82.5	−1.26	6×10^4
0.1M OX	2.15	−0.13	162	74.5	−0.32	4.0×10^4
0.1M OX	2.58	−0.30	163.5	62.4	−0.33	
20 mM NTA	1.07	−0.27	21.0	17.5	−0.46	3.3×10^3
50 mM NTA	1.58	−0.27	30.9	18.6	−0.45	
20 mM EDTA-OH	1.83	−0.34	10.5	4.25	−0.47	1.5×10^2
50 mM EDTA-OH	2.14	−0.35	9.9	3.62	−0.48	
20 mM EDTA	2.16	−0.27	4.5	2.5	−0.29	
20 mM CyDTA	1.80	−0.22	2.7	1.1	−0.23	

Ti: 0.96 mM/l, H_2SO_4: 0.1M/l
a) $KClO_3$: 0.05M, pH: 1.0±0.1.
b) In the case of the regeneration reaction of EDTA-titanium chelate and CyDTA-titanium chelate, i_l/i_d is less than 2.5, and the values calculated as the regeneration rate from Eq. (2) are empty.

presence of titanium(IV) ions. Therefore, the rate constant in this case, in Table 1, is the apparent rate constant of the regeneration of titanium(IV), and it seems that the actual rate is more rapid than the apparent one.

On the other hand, the value of k obtained, using 0.1 mol/l of oxalate, 0.2 mol/l of sulfuric acid, 10^{-3} mol/l of titanium chloride, and 0.008—0.256 mol/l of potassium chlorate solutions, by Koryta[7] is 5.3×10^4 l/mol·sec, and that obtained, using 0.2 mol/l of oxalate, 3.36 mmol/l of the titanium(IV) ion, and 0.06—0.08 mol/l of potassium chlorate solutions, by Smith,[8] are both 2.5×10^4 l/mol·sec. Tanaka *et al.*[3] obtained 2.1×10^4 l/mol·sec using 0.2 mol/l of oxalate, 1×10^{-3} mol/l of the titanium(IV) ion, and 0.07—0.15 mol/l of sodium chlorate solutions at pH 1.07. The value of k in titanium(IV)-oxalic acid obtained by the present authors is in good agreement with the value obtained by Koryta, though his values are generally somewhat greater than our values, and with those obtained by Smith and by Tanaka *et al.*, though their values are somewhat less than our value. The difference might be caused by the difference in pH and the concentration of the oxalate, as may be seen in Fig. 2.

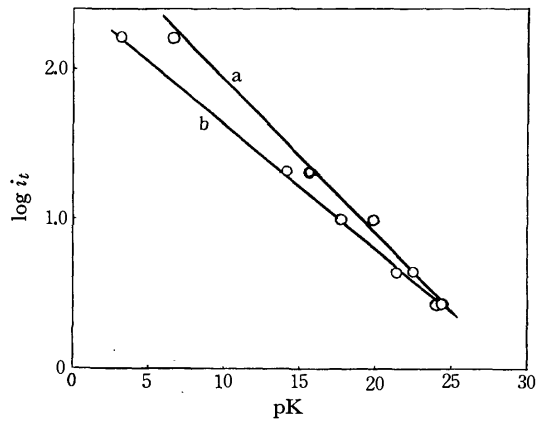

Fig. 9. Relation of log i_t to pK_4 or pK_3 of the titanium chelates. a is the relation to pK_4 and b to pK_3.
Ti: 0.86 mM, pH: 1.0±0.1, $KClO_3$: 0.05M.
OX: 0.1M, NTA, EDTA-OH: 0.05M, EDTA, CyDTA: 0.02M.

Discussion

As is shown in Figs. 7, 8, and Table 1, the values of i_t/i_d vary according to the kind of chelating agent, and they seem to be in an order the reverse of that of the dependency on the stability of the titanium chelates. In Fig. 9, the i_t values of various titanium (Ti-CyDTA, Ti-EDTA, Ti-EDTA-OH, Ti-NTA, and Ti-OX) are plotted against the logarithms of their stability constants, where the stability constants of titanium-oxalic acid reported by Babco *et al.*,[9] of titanium-EDTA reported by Pecsok *et al.*,[4] of titanium-CyDTA and titanium-EDTA-OH to be reported elsewhere soon by one of the present authors,[5,10] and of titanium-NTA obtained by the same procedure are used. There is a linear relationship between the logarithms of the reciprocal of the dissociation constants and those of catalytic currents of the chelates. The following empirical equation is obtained, by the method of the least squares, between the current and the stability constant of the titanium(III) complex, pK_3.

$$\log i_t = \text{const.} - 0.08\text{p}K_3 \qquad (3)$$

A similar clear linear dependency of the catalytic current on the dissociation constant of the complex of titanium(IV), pK_4, is also found; the empirical equation obtained by the same procedure is as follows.

$$\log i_t = \text{const.} - 0.1\text{p}K_4 \qquad (4)$$

On the other hand, a more simple relationship can be found between the rate constant of the regeneration tabulated in Table 1 and the logarithum of the ratio of the dissociation constant of the titanium(IV) complex to that of the titanium(III) complex; *i.e.*, k is proportional to the logarithms of the ratio of the dissociation constant over the pH range from 1.2 to 1.8 except in the case of oxalic acid. This is shown in Fig. 10(a), as is the empirical equation obtained by using all plots;

$$\log k = -0.1 + 1.4\log K_4/K_3 \qquad (5)$$

where K_4 and K_3 are the dissociation constant of the titanium(IV) complex and that of the titanium(III) complex respectively. Here, the rate constants, k, in the case of the regeneration of EDTA-Ti(IV) and CyDTA-Ti(IV) are the apparent ones because these values of i_t/i_d are less than 2.5.

Thus, the problem to be solved is which one of these three empirical equations is the fundamental one. The confusion is caused by the facts that i_t is roughly proportional to i_t/i_d and that log K_4/K_3 is also in a

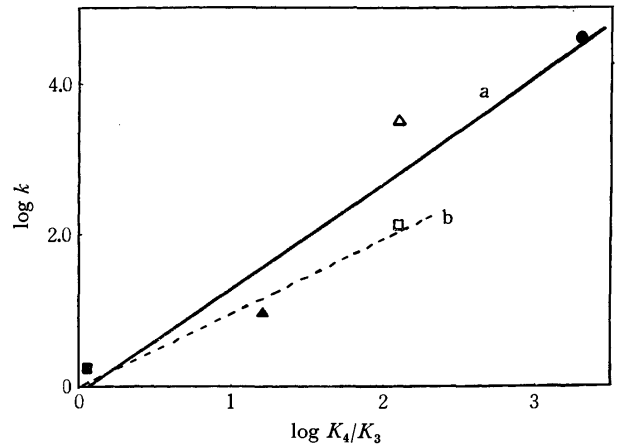

Fig. 10. Relation between the rate of the regeneration and the ratio of dissociation constants of titanium(IV) chelates to titanium(III) chelates.

7) J. Koryta, *Collect. Czech. Chem. Commun.*, **20**, 1125 (1955).
8) D. Smith, *Anal. Chem.*, **35**, 610 (1963).
9) A. K. Babco and L. I. Dubovenko, *Zh. Neorg. Khim.*, **4**, 372 (1959). L. G. Sillén and A. E. Martell, "Stability constants of Metal ion complexes," The Chemical Society, London (1964), pp. 362, 640.
10) The stability constants of the 1:1 chelates of Ti(III)-EDTA-OH, Ti(III)-CyDTA, Ti(III)-NTA, TiO(II)-EDTA-OH, TiO(II)-CyDTA, and TiO(II)-NTA at pH 1.5±0.1 obtained by one of the present authors are 17.7, 23.8, 13.6, 19.7, 24.3, and 15.4, respectively.

roughly linear relation with pK_4 or pK_3. If Eq. (3) is the true fundamental equation, the mechanism that titanium(III) ions formed by the dissociation of the titanium(III)-chelates are oxidized by the chlorate ions is supported, because the rate of oxidation may depend directly on the concentration of the titanium(III) ion, which in turn depends on the rate of dissociation of the complex, if the dissociation is a rate-determining process, or which, in turn, depends on the stability constant of the complex, if the oxidation is a rate-determining one. This type of effect of the complex is widely observed.[11] However, there are some difficulties in explaining the exponent of 0.08 and the relation of i_t and pK_3. Besides, since the rates of the dissociation of some metal complexes of EDTA and CyDTA are low, they should be in relation not with the stability constants, but with the dissociation rates. The mechanism seems to be implausible.

If the mechanism by which the titanium(III)-chelate complexes are directly oxidized by the chlorate ions is the true mechanism:

$$\begin{array}{l} \text{Ti(III)-Y} + \text{Oxid.} \longrightarrow \text{Oxid.} \cdots \text{Ti} \cdots \text{Y} \\ \qquad\qquad\qquad\qquad\qquad\quad \downarrow \\ \text{Ti(IV)-Y} + \text{Red.} \longleftarrow \text{Red.} \cdots \text{Ti} \cdots \text{Y} \end{array} \qquad (6)$$

Equation (5) is directly related to the rule of the linear free energy relation (LFER, Brönsted-Horiuchi-Polanyi-Hammett's rule),[12] since $\log K_4/K_3$ is the difference in the free energies of the product and the reactant of regeneration. As may be seen in Figs. 2 and 4, i_t/i_d depends on the pH and on the concentration of the chelating agents. Hence, the rate constants are also dependent on these parameters. However, except the case of oxalate, the rate constants in Fig. 10 are obtained in the range where i_t/i_d is scarcely dependent on these parameters and where only a single type of complex exists for each chelating agent.[5] On the other hand, it seems that two or more types of complexes, *e.g.*, the complexes with the chelating agent and one with other components of the solution, can exist in the region where i_t/i_d depends on the parameters; therefore, $\log K_4/K_3$ is not equal to the difference in the free energies of the product and the reactant of the regeneration. The scattering of the data in Fig. 10 is caused partly by these effects. As has been mentioned above, since two waves are observed for the NTA complex, there is a possibility of the coexistence of two different type of complexes. The first wave may be due to the complex of titanium with a single molecule of NTA, while K_3 and K_4 are apparent equilibrium constants among two more types of complexes. Therefore, there are some questions of including the plot of the NTA complex, and also of including the plot of the oxalate complex for the reason mentioned above. If we omit their two plots, a less-scattered relation can be obtained, as is shown by Line(b) in Fig. 10(b), and the empirical equation is:

$$\log k = -0.05 + 1.0 \log K_4/K_3 \qquad (7)$$

The relation is very clear and simple, the mechanism is in accordance with the postulation of Vlcek,[13] and a similar mechanism has also been reported for other complexes.[14] However, K_4 is not the dissociation constant of the titanim(IV) complex but that of the titanyl complex. The process of the oxidation of the titanium(III) complex consists of the process of the oxidation of the titanium(III) ion and the hydrolysis of the titanium(IV) ion to the titanyl ion, and the rate of oxidation observed may be that of the titanium(III) complex to the titanyl complex.

Since the reactions are complicated, no conclusion supported by clear, direct evidence can be obtained, but the mechanism would be elucidated if similar reactions were observed for other ion-complexes.

11) A. E. Martell and M. Calvin, "Chemistry of the metal chelate compounds," Prentice-Hall, Englewood Cliffs (1956).

12) J. O. Edwards, "Inorganic Reaction Mechanisms," W. A. Benjamin Inc., New York (1964).

13) A. A. Vlcek, "Progress in Inorganic Chemistry," Vol. 5, ed. by F. A. Cotton, Interscience Publishers, New York, London, Sydny (1967) p. 326.

14) M. Anbar, "Mechanisms of Inorganic Reactions; Advances in chemistry series 49," (1965), pp. 131, 137.

Electric Conduction and Density of Condensed Phosphoric Acids and Their Mixtures with Sulfuric Acid

Akitane AKIYAMA, Tsuyoshi SUZUKI, and Takashi SAJI

Department of Electrochemistry, Tokyo Institute of Technology, Meguro-ku, Tokyo

(Received January 22, 1971)

The electrolytic conductivities and densities of condensed phosphoric acids have been measured in the P_2O_5 concentration range from 55% to 80% at 55.0, 70.0, and 90.0°C. Assuming the proton jump mechanism through the hydrogen bond network of H_2O and H_3PO_4, the molar conductance was calculated and found to be constant in the P_2O_5 concentration range between 60% and 76%. The investigation has been extended to the mixtures of condensed phosphoric acids and concentrated sulfuric acid. The complex formation of $[H_4PO_4^+ \cdot HSO_4^-]$ and $[H_3O^+ \cdot HSO_4^-]$ has been suggested in the mixture.

The physical and chemical characteristics of condensed phosphoric acid (abbreviated as CPA) have been studied by a number of investigators.[1] However, the mechanism of the electric conduction in CPA still remains unclarified. The conduction should be closely related to the physico-chemical structure of CPA. This paper deals with the relation between the electric conduction and physico-chemical structure of CPA in relation concentrated sulfuric acid and its mixtures with CPA.

Studies have been made on the density[2-6] and electric conduction[7,8] of CPA, but the results do not coincide. The discrepancy can be ascribed to the difference in experimental procedures. Since the chemical composition and purity of an electrolyte affect density and conduction, the so-called "reorganization" of CPA[9] cannot be overlooked. The effect of reorganization of CPA on density and electrolytic conductivity has not so far been investigated except for anhydrous orthophosphoric acid[14,16] and we have therefore, examined it first. The measurements of electrolytic conductivity and density were undertaken over a wide range of P_2O_5 concentrations.

Some interesting information on the relation between the physico-chemical structure and electric conduction of CPA has been obtained by means of the concept of "molar conductance."

Experimental

The two conductivity cells used in this work were the same type as the one designed by Jones for precision measurements.[12] The electrodes were flat platinum disks (15 mm in diameter) not platinized, since a platinized platinum electrode undergoes corrosion in CPA. The cell constants were 4.72 and 11.97 cm^{-1}. The cell was placed in a constant temperature bath containing silicone oil. The measurements were carried out at 55, 70, and 90°C ±0.02°C. The curve, linear extrapolation to the infinite frequency of the measured resistance *versus* (frequency)$^{1/2}$, was constructed. The resistance at the infinite frequency can be considered to be free from impedance caused by electrode reactions.

The density measurement was carried out by weighing a calibrated silica cylinder (11.6 mm in diameter and 57 mm in length). The silica cylinder was suspended with a thin platinum wire from one end of an analytical balance and submerged in a liquid to be tested.

CPA was prepared as follows.

(1) Reagent grade phosphorus pentoxide was sublimated in iron pipes[10] in an oxygen atmosphere at 800°C in order to remove organic impurities and lower phosphorus oxides such as PO_2, P_2O_3, and P_4O_6.

(2) The purified P_2O_5 was then dissolved in reagent grade phosphoric acid by heating in a glassy carbon beaker.

(3) The concentration of CPA was determined by means of potentiometric titration.[11]

Results

Crystalline orthophosphoric acid is regarded to be H_3PO_4.[13] Upon fusion, a small portion of H_3PO_4 is converted into pyrophosphoric acid by self-dehydration and a part becomes triphosphoric acid. This process is called reorganization. The reorganization of orthophosphoric acid has been found to be accompanied by a decrease in conductance.[14] Crystalline phosphoric acid prepared by fractional freezing method[15] was reexamined first. It was melted just before the experiment and the conductivity was measured at 55, 70, and 90°C as a function of time. The conductivity decreased with time and reached a steady value, which can be considered to be the conductivity of the equilibrated mixture of $H_{n+2}P_nO_{3n+1}$ (n=0, 1, 2,···). The time required to reach the equilibrated CPA was about one hour at 90°C and about 30 hours at 55°C.

1) J. R. Van Wazer, "Phosphorus and its Compounds," (Interscience Pub. Inc., New York), Vol. 1, chap. 12 (1958). p. 717.
2) J. H. Lum, J. E. Malowan, and C. B. Durgin, *Chem. and Met. Eng.*, **44**, 726 (1937).
3) M. M. Striplin, D. Mcknight, and G. H. Megar, *Agricult. and Food Chem.*, **6**, 298 (1958).
4) E. J. Griffith, Ref. 1, p. 771.
5) D. E. Person and R. M. Stone, *J. Amer. Chem. Soc.*, **83**, 1715 (1961).
6) S. Ohashi and H. Sugatani, This Bulletin, **33**, 1286 (1960).
7) G. P. Kakoolin and I. G. Fedorrchenko, *Zhur. Neorg. Khim.*, **7**, 2485 (1962).
8) I. G. Fedorrchenko, G. P. Kakoolin, and Z. V. Kondratchenko, *ibid.*, **10**, 1945 (1965).
9) J. R. Van Wazer, Ref. 1, p. 747.
10) G. I. Finch and R. Fraser, *J. Chem. Soc.*, **129**, 117 (1926).
11) L. M. Kolthoff and P. J. Elving, "Treatise on Analytical Chemistry," Vol. 5, Interscience Pub. Inc., New York (1961), Part 2, p. 346.
12) G. Jones and G. M. Bollinger., *J. Amer. Chem. Soc.*, **53**, 1207 (1931).
13) A. Simon and G. Schulze, *Z. Anorg. Allgem. Chem.*, **242**, 313 (1939).
14) R. A. Manson, *J. Phys. Chem.*, **69**, 1761 (1965).
15) A. Simon and M. Weist, *ibid.*, **268**, 302 (1952).

The rate of self-hydration or dehydration is so high at a high temperature that CPA heat-treated at 200°C for one hour can be regarded as an equilibrated mixture of $H_{n+2}P_nO_{3n+1}$ (n=0, 1, 2, ···). The mixture was quenched in to a refrigerator and transferred into the conductivity cell. The conductivity of quenched CPA was then measured as a function of time at 55, 70, and 90°C. No change in the conductance was observed, that is, no change in the composition of CPA could be detected. It might be assumed from the result that the equilibrium constants of the self-hydration and dehydration reactions in a CPA were independent of temperature within experimental accuracy. All CPA's used in the following experiments were heat treated at 200°C for one hour.

The electrolytic conductivities *versus* P_2O_5 concentration are shown in Fig. 1. The conductivity decayed linearly with increasing concentration down to about 72% and then a rapid decrease was observed. The P_2O_5 concentration of 72% corresponds to the stoichiometrically pure orthophosphoric acid. This result coincides with those reported by other workers.[8,6]

The densities *versus* P_2O_5 concentration are shown in Fig. 2. Tye results agreed with those reported by Ferr.[4]

CPA can be considered to be a mixture of H_2O, H_3PO_4 $H_4P_2O_7$,···$H_{n+2}P_nO_{3n+1}$ in the concentration range used in this experiment. In order to introduce the concept of "molar conductance," it was assumed first that the main conducting components in the CPA are H_2O and H_3PO_4 and that both H_2O and H_3PO_4 behave as equally effective species for the electric

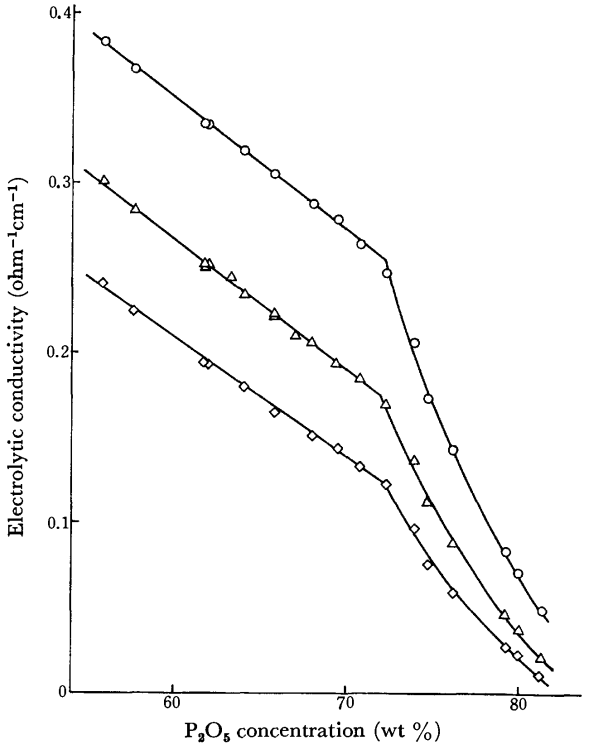

Fig. 1. Electrolytic conductivity of CPA.
Temp: 55°C (◇), 70°C (△), and 90°C (○).

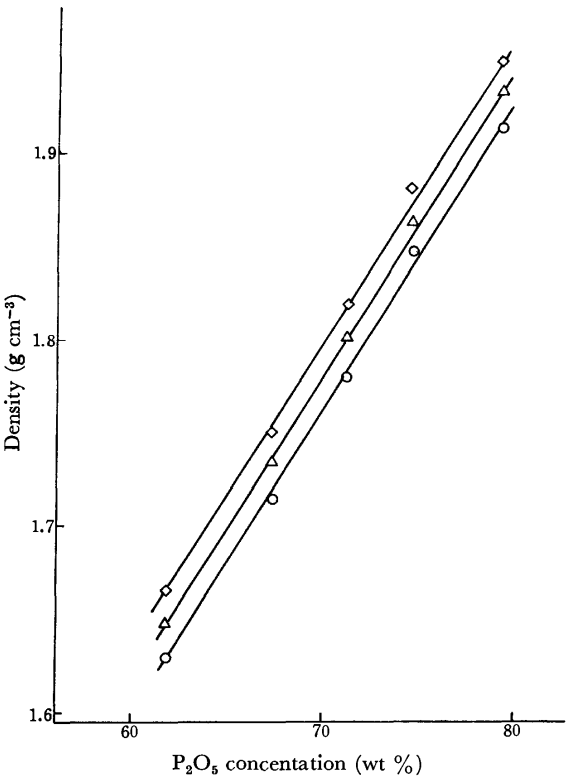

Fig. 2. Density of CPA. Temp.: 55°C (◇), 70°C (△), and 90°C (○).

conduction of CPA. The molar conductance (Λ) of CPA, therefore, can be calculated from electrolytic conductivity (κ) and the density (ρ) by means of the following equation:

$$\Lambda = \kappa\sum\chi_i M_i/\rho(\chi_{H_2O}+\chi_{H_3PO_4}) \quad (1)$$

where χ_i is the mole fraction of the ith component of the molecular weight of M_i and χ_{H_2O} and $\chi_{H_3PO_4}$ are the

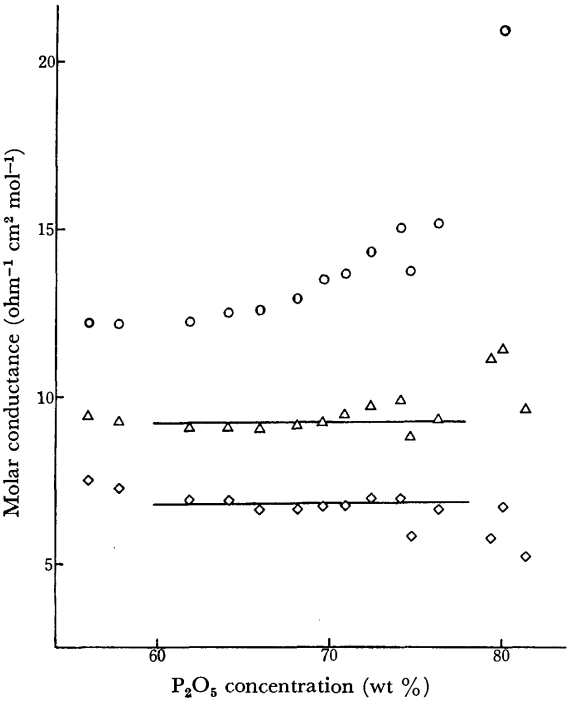

Fig. 3. Molar conductance of CPA.
Temp: 55°C (◇), 70°C (△), and 90°C (○).

16) N. N. Greenwood and A. Thompson, *J. Chem. Soc.*, **1959**, 3485.

mole fractions of H_2O and H_3PO_4, respectively. They are given from the analytical data by Huhti and Gartaganis.[17] The calculated molar conductances are plotted against the P_2O_5 concentration in Fig. 3. It was noted that the molar conductances of CPA at 55 and 70°C are constant in the concentration range between 60% and 76%.

Concentrated sulfuric acid was mixed with CPA's of 61.8, 66.8, 70.8, 74.8, and 79.3%, respectively. The electrolytic conductivities of the five mixtures at 55°C are plotted in Fig. 4 against the weight percentages of CPA's, and the densities in Fig. 5. Measurements were carried out at 70 and 90°C. The results were very similar to those for 55°C. It was noted that the electrolytic conductivities of mixtures were far from additive as compared to those of CPA and H_2SO_4.

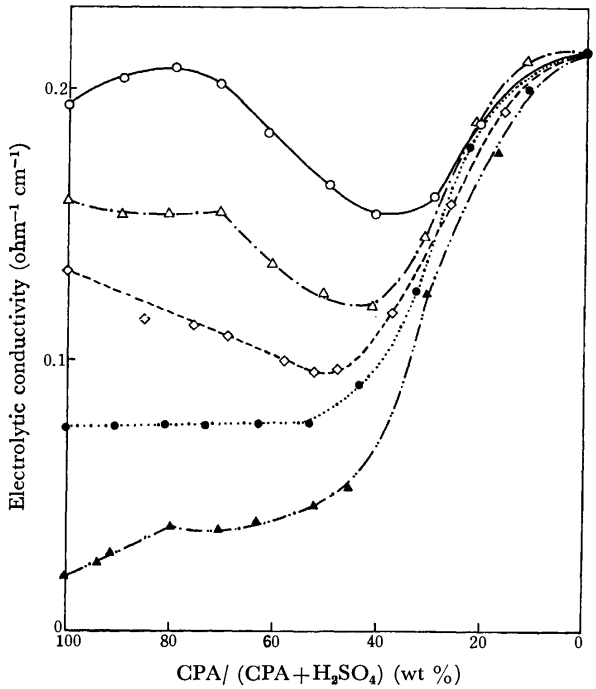

Fig. 4. Electrolytic conductivity of CPA-H_2SO_4 mixtures. 100% CPA's are of P_2O_5 concentrations of 61.8% (○), 66.8% (△), 70.8% (◇), 74.8% (●), and 79.3% (▲).

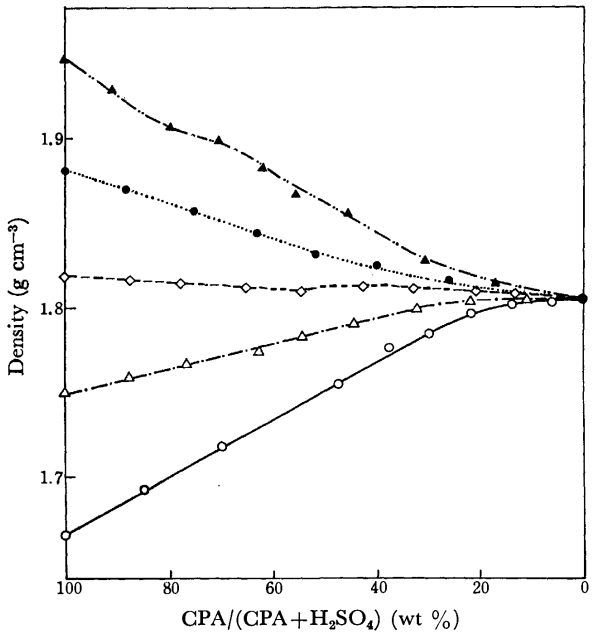

Fig. 5. Density of CPA-H_2SO_4 mixtures. Symbols are same as Fig. 4.

The molar conductance of CPA-H_2SO_4 mixture was introduced in a similar way to that of CPA. H_2O and H_3PO_4 as well as H_2SO_4 are assumed to be conducting components, and they behave as equally effective species on the electric conduction. Then, Eq. (1) becomes

$$\Lambda = \kappa\sum\chi_i M_i/\rho(\chi_{H_2O}+\chi_{H_3PO_4}+\chi_{H_2SO_4}) \quad (2)$$

The molar conductances of mixtures at 55°C are plotted in Fig. 6 against the molar composition rate R which is represented by

$$R = (\chi_{H_2O}+\chi_{H_3PO_4})/(\chi_{H_2O}+\chi_{H_3PO_4}+\chi_{H_2SO_4}) \quad (3)$$

The 79.3% CPA mixture was excluded in the figure since the discrepancy from the straight line in Fig. 3 was so remarkable that the assumption on the electric conduction of CPA does not hold for CPA of high P_2O_5 concentrations. It is particularly noteworthy in Fig. 6 that a minimum was observed at the R value of 0.5.

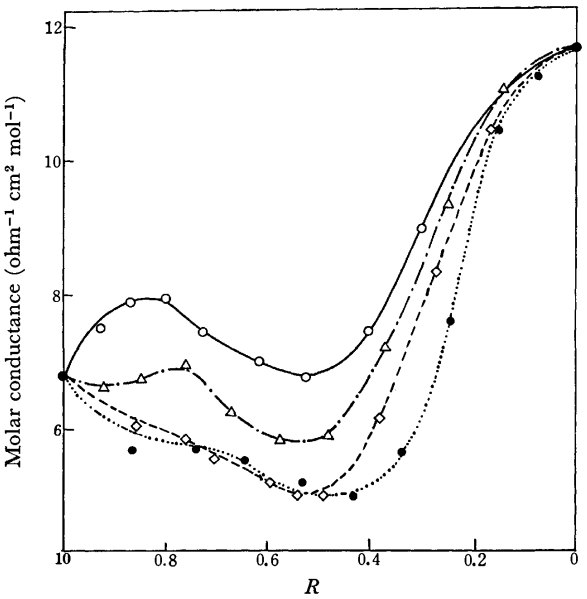

Fig. 6. Molar conductance of CPA-H_2SO_4 mixtures. Symbols are same as Fig. 4.

Discussion

CPA: The mechanism of electric conduction in condensed phosphoric acid as well as in anhydrous sulfuric acid has been investigated.[16,18] It was confirmed that the characteristic features of these acids are the self-dissociation into ionic products and their ability to conduct electricity by proton-jump. There are a number of ionic species in CPA such as H_3O^+,

17) A. L. Huhti and P. A. Gartaganis, *Can. J. Chem.*, **34**, 785 (1956).

18) N. N. Greenwood and A. Thompson, *J. Chem. Soc.*, **1959**, 3475.

$H_4PO_4^+$, $H_2PO_4^-$, $H_3P_2O_7^-$. Greenwood and Thompson[16] assumed that $H_2PO_4^-$ was the only conductive species with proton-jumps. They explained that the sharp drop in κ at about 72% P_2O_5 was due predominantly to the decrease in the concentration of anomalously conductive $H_2PO_4^-$ ions. All the previous discussions on the conduction mechanism of concentrated acids were based on an ion which has a high mobility by proton-switch conduction. In this investigation, however, the electrolytic conductivity and density data of CPA are handled on the basis of the length of hydrogen bond networks along which protons can be transferred; it was assumed that the hydrogen bond network leading to a high proton conductivity in CPA was constructed by H_2O and H_3PO_4. The "molar conductance" term which is defined by Eq. (1) has been introduced. When Λ was plotted against the cencentration of CPA, Λ at 55° and 70°C could be considered to be constant in the concentration range from 60% to 76% P_2O_5 (Fig. 3). This might indicated that our assumption of Eq. (1) is reasonable; the electric conduction of CPA (60%—76% P_2O_5) occurs by proton-jumps through the hydrogen bonds of H_2PO_4 and H_2O, and by the following rotation of these molecules. The constant value of Λ also seems to show that both H_2O and H_3PO_4 bahave as equally effective species on electrical conduction. Condensed phosphoric acids of higher molecular weights such as pyrophosphoric acid and triphosphoric acid do not play important roles in the conduction of CPA in this concentration range because the massiveness inhibits the rotation of molecule after a proton-jump. The discrepancy of Λ's from a streight line at 90°C can be attributed to the additional contribution of pyrophosphoric acid to the conduction, since it seems that the rotation of a massive molecule becomes more favorable at higher temperatures. The discrepancy of Λ's from straight lines at low P_2O_5 concentrations of CPA can be assumed to be due to the ionic conduction by hydrated H^+ and ionized phosphoric acids.

We assumed that H_2O as well as H_3PO_4 is electrical conductive species, whereas Greenwood *et al.*[16] concluded that H_3O^+ could not be considered as conductive species since H_3O^+ was unlikely to take part in the hydrogen bonded structure of CPA. The conclusion by Greenwood was made by the analogy of the behavior of H_3O^+ in sulfuric acid. The structure of CPA, however, is considered to be a more complicated hydrogen bridge system containing mobile protons as current-carrying species. The Raman spectroscopy and other physico-chemical properties of anhydrous H_3PO_4 were studied by Simon and his co-workers.[13,15] It was suggested that there are free mobile protons which are not located at a fixed PO_4 group. Mobile protons were also found within the hydrogen bonded structure of water and ice by Eigen and Mayer.[19] It seems, therefore, to be reasonable to assume that H_2O is a conductive species in CPA.

It is interesting that the molar conductance of CPA does not depend upon the ratio of H_2O to H_3PO_4. This shows either that the number of mobile protons as well as mobility do not change with the change of the ratio of H_2O to H_3PO_4, or that the increase of mobility and the decrease of number mobile protons occur at the same rate with the change in the concentration of CPA. This is still an open question.

The reorganization rate of orthophosphoric acid could be calculated by use of the assumption. Suppose α mol% of orthophosphoric acid is converted into pyrophosphoric acid. The electrolytic conductivity of pure orthophosphoric acid (κ_0), which is the initial conductivity, changes to conductivity (κ_0) of the reorganized phosphoric acid mixture according to the equation

$$\kappa_e = \kappa_0(1-\alpha/100). \quad (4)$$

The reorganization rate calculated by this equation was 6.6 mol% at 70°C, and coincided with 6.38 mol% obtained by means of paper chromatography.[17]

CPA-H_2SO_4 Mixtures: The idea of the hydrogen bond network of H_2O and H_3PO_4 assumed for CPA is extended for CPA-H_2SO_4 mixtures. Upon calculation of the molar conductance for the mixtures, it was assumed that H_2SO_4 plays a part in the network of H_2O and H_3PO_4 as an equally effective species of conduction. Variation of the molar conductance in Fig. 6 show that the mixture is complicated. The complication also could be predicted from the that the electrolytic conductivity was far from the additivity of that of CPA and H_2SO_4. Reorganization of CPA by the addition of H_2SO_4 can not be neglected; however, in following discussion, the mole fractions of H_2O, H_3PO_4, and H_2SO_4 are calculated by assuming that no reorganization reaction of CPA occurs upon mixing with H_2SO_4. The most interesting result is that there exists a minimum in the molar conductance for R value of 0.5, where the molar ratio of $[H_2O+H_3PO_4]$ to $[H_2SO_4]$ was unity, as seen in Fig. 6. The minimum suggests the complex formation between H_3PO_4 and H_2SO_4 as well as between H_2O and H_2SO_4, such as $[H_4PO_4^+ \cdot HSO_4^-]$ and $[H_3O^+ \cdot HSO_4^-]$. It seems to be reasonable to assume such complex formation because H_2SO_4 has been found to be a strong mono-protonic acid in CPA.[20] It can be concluded that the length of hydrogen bonding reduced by complex formation, resulting in a decrease in the molar conductance of pure CPA or pure H_2SO_4 by mixing.

The ionic conduction plays a role in the electric conduction of a CPA of low P_2O_5 concentration. The addition of H_2SO_4 into a CPA of low concentration caused the increase in the molar conductance up to the R value of 0.8. This can be explained by the increase of conductive ions by mixing H_2SO_4 with CPA of low concentration.

An inflection point exists in the electrolytic conductivity curve and the density curve at a high P_2O_5 concentration CPA of 79.3%. The weight % of CPA at the inflection was 80% for the electrolytic conductivity curve and 70% for the density curve. The mechanism of electric conduction in the pure CPA of 79.3% is still unknown.

19) M. Eigen and L. D. Mayer, "Structure of Electrolytic Solutions," ed. W. J. Hamer, John Willy & Sons, Inc., New York, (1959), p. 64.

20) R. A. Munson, *J. Phys. Chem.*, **68**, 3374 (1964).

Copper(I) Perchlorate Complexes of Allyl, 2-Methylallyl and *cis*- and *trans*-2-Butenyl Alcohols[1]

Yoshio ISHINO,[2] Tetsuya OGURA, Kenichiro NODA,* Tsuneaki HIRASHIMA,* and Osamu MANABE*

Department of Chemistry, Faculty of Science, Osaka City University, Sumiyoshi-ku, Osaka

**The Osaka Municipal Technical Research Institute, Kitaku, Osaka*

(Received June 5, 1971)

[Cu(allyl alcohol)(H_2O)]ClO_4 (abb. Cu(all)$(H_2O)ClO_4$), [Cu(allyl alcohol)$_2(H_2O)$]ClO_4 (abb. Cu(all)$_2$-$(H_2O)ClO_4$), [Cu(2-methylallyl alcohol)(H_2O)]ClO_4 (abb. Cu(meth)$(H_2O)ClO_4$) and [Cu(*cis*- and *trans*-2-butenyl alcohol)$_2$ (H_2O)]ClO_4 (abb. Cu(*cis*-and *trans*- but$_2$ $(H_2O)ClO_4$) were synthesized. It was shown by means of equivalent conductance that Cu(all)$(H_2O)ClO_4$ is a strong electrolyte of uni-uni valent in acetone. The molecular weight of Cu(all)$(H_2O)ClO_4$ obtained from measurements of the direct vapor-pressure depression of acetone showed that the complex is monomeric. The C=C stretching band of the allylic alcohol shifts by about 100 cm^{-1} to the lower frequency side upon coordination. The chemical shifts of the vinyl protons in these complexes shift by about 0.5—1 ppm to the higher frequency side than those of free alcohols. It was concluded that the allylic alcohol coordinates to the copper atom through both the double bond and the oxygen atom. The equilibrium constant corresponding to Cu(*trans*-but)$^+_2(H_2O)ClO_4$+2*cis*-2-butenyl alcohol=Cu(*cis*-but)$^+_2(H_2O)ClO_4$+2*trans*-2-butenyl alcohol in 2-butenyl alcohol was estimated to be 9.82 at 25°C and the enthalpy change was estimated to be −3.13 kcal/mol.

Manahan[3] found that two potentials corresponding to Cu(II)=Cu(I)+e and Cu(I)=Cu(0)+e are observed in aqueous solutions containing allyl alcohol. However only one potential corresponding to Cu(II)=Cu(0)+2e is observed in the absence of allyl alcohol. Further data concerning the dependence of the reduction potential on the concentrations of copper(II) and allyl alcohol were explained on the basis of the formation of the copper(I)-allyl alcohol complex with a mole ratio of one to one and with a formation constant of $5.02\times10^4 mol^{-1}\,l$. The isolation of the complex, however, has not been successful.

Previously we synthesized crystalline complexes of allyl alcohol[4] and some related compounds[5,6] with copper(I) chloride. It was then established that allyl alcohol coordinates to the copper(I) atom with both the double bond and the oxygen atom, and that this complex is a dimer with a double chloro bridge. However, the dissociation vapor pressures of these complexes are fairly large and they easily decompose to the original unsaturated ligands and copper(I) chloride. From the fact that one of the decomposition products, copper(I) chloride, is stabilized by the chloro bridges with the formation of a tetrahedral configuration, this instability is presumably enhanced by the high donating power and by the bridging potential of the chloride ligand. Now we have synthesized the copper(I) perchlorate-allylic alcohol complexes with molar ratios of one to one and one to two with expectation of obtaining stable complexes, but the former was rather explosive.

Experimental

Materials. The copper(II) perchlorate hexahydrate was prepared from copper(II) hydroxide and a 60% aqueous solution of perchloric acid and was recrystallized from ethyl acetate. The allyl alcohol, 2-methylallyl alcohol and 2-butenyl alcohol were used after distillation. The acetone used for the measurements of the molecular weight and the electric conductance was purified in the usual manner[7] and distilled *in vacuo*.

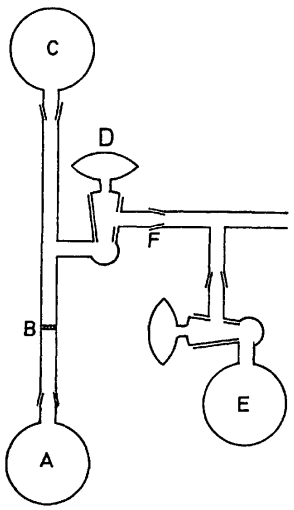

Fig. 1. The ampoule system for the synthesis of the copper(I) perchlorate complexes with allylic alcohols.

Synthesis of Cu(all)$(H_2O)ClO_4$. The ampoule system employed for the synthesis of the complex is illustrated in Fig. 1. Copper(II) perchlorate hexahydrate (100—200 mg), copper metal and a stirring bar were placed in an ampoule A. Allyl alcohol was then transferred from another ampoule E and the stopcock D was closed. The solution was stirred magnetically till the blue color of copper(II) faded and it became colorless. Then the apparatus was inverted at the taper joint F so that the solution could be filtered through the

1) This paper was presented at 22nd Annual Meeting of the Chemical Society of Japan, Tokyo, April, 1969.

2) Present address: The Osaka Municipal Technical Research Institute.

3) S. E. Manahan, *Inorg. Chem.*, **5**, 482 (1966).

4) T. Ogura, N. Furuno, and S. Kawaguchi, This Bulletin, **40**, 1171 (1967).

5) S. Kawaguchi and T. Ogura, *Inorg. Chem.*, **5**, 944 (1966).

6) T. Ogura, T. Hamachi, and S. Kawaguchi, This Bulletin, **41**, 892 (1968).

7) A. Weissberger and E. S. Proskauer; J. A. Riddick and E. E. Toops, Jr., "Organic Solvents," 2nd ed., Interscience Publishers, New York (1955), p. 379.

sintered glass B into yet another ampoule C. The solvent was then transferred into E by vacuum distillation. In the course of the transfer of the alcohol, colorless crystals were formed. The complex was obtained as a white powder by further drying.

After the complex was weighed, the ligand was freed by the addition of aqueous ammonium chloride. All the allyl alcohols were collected together with the water by the vacuum distillation of the aqueous solution. It was determined by means of gas chromatographic and IR assay that the volatile materials were composed of water and allyl alcohol. The quantity of allyl alcohol was determined by bromination as has been described previously.[4] The nonvolatile material was dissolved in aqueous ammonia and analyzed for copper electrolytically and for the perchlorate ion as a nitron adduct.

Found: Cu, 26.1; C_3H_6O, 24.7; ClO_4, 41.7%. Calcd for $Cu(C_3H_6O)(H_2O)ClO_4$: Cu, 26.6; C_3H_6O, 24.7; ClO_4, 41.7%. Further, the water was detected in the IR spectra and the mole ratio of water to allyl alcohol was estimated to be unity on the basis of the NMR assay.

Synthesis of $Cu(all)_2(H_2O)ClO_4$. A small quantity of allyl alcohol was distilled into the ampoule C containing $Cu(all)(H_2O)ClO_4$, and then the complex was dissolved completely (Fig. 1). The excess of alcohol was distilled back to the E ampoule by means of a difference of temperature of between 20.5°C (the mp of acetophenone) and 0°C, the complex was thus obtained as colorless and transparent crystals. When the temperature of the ampoule C was higher by several degrees, the complex was decomposed to $Cu(all)(H_2O)ClO_4$; when it was lower by several degrees, the complex was not dried because of its high solubility in allyl alcohol. The complex was analyzed as has been described above.

Found: Cu, 21.5; C_3H_6O, 40.0; ClO_4, 34.8%. Calcd for $Cu(C_3H_6O)_2(H_2O)ClO_4$: Cu, 21.4; C_3H_6O, 39.2; ClO_4, 33.4%.

Synthesis of $Cu(meth)(H_2O)ClO_4$ and $Cu(but)_2(H_2O)ClO_4$. $Cu(meth)(H_2O)ClO_4$ was synthesized and analyzed much as in case of $Cu(all)(H_2O)ClO_4$.

Found: Cu, 25.3; C_4H_8O, 28.5; ClO_4, 40.6%. Calcd for $Cu(C_4H_8O)(H_2O)ClO_4$: Cu, 25.3; C_4H_8O, 28.5; ClO_4; 39.3%. The presence of the 1:2 complex of 2-methyl-allyl alcohol was suggested on the basis of the IR spectra, but its isolation was difficult.

$Cu(but)_2(H_2O)ClO_4$ was obtained and analyzed much as in the case of $Cu(all)(H_2O)ClO_4$.

Found: Cu, 20.5; C_4H_8O, 44.3; ClO_4, 31.2%. Calcd for $Cu(C_4H_8O)_2(H_2O)ClO_4$: Cu, 19.0; C_4H_8O, 44.4; ClO_4, 30.6%. We failed to obtained the one to one 2-butenyl alcohol complex.

Equivalent Conductance. The equivalent conductance of $Cu(all)(H_2O)ClO_4$ in acetone was measured at 25.0°C with a cell modified only enough to make it possible to operate it in a vacuum using the Yanagimoto conductivity outfit, Model MY-7. The results are listed in Table 1.

Table 1. Equivalent conductances of $Cu(all)(H_2O)ClO_4$ in acetone (at 25.0°C)

Concn. $\left(\frac{\text{formal}}{\text{kg acetone}}\right)$	Equivalent conductance
0.1055	39.6
0.05174	71.6
0.02745	107.9
0.02003	118.3

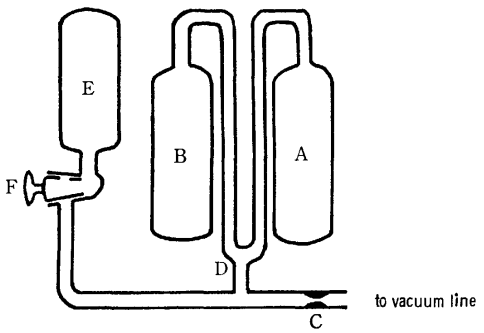

Fig. 2. The apparatus used for the direct measurements of depressions of vapor pressures.

Molecular Weight Measurement. The molecular weight of $Cu(all)(H_2O)ClO_4$ was determined by direct measurements of the vapor-pressure depressions of acetone. The apparatus used is illustrated in Fig. 2. The complex was prepared and dried completely in the A ampoule. Carefully degassed acetone was transferred from the vacuum line to A and B at the same time and the apparatus was sealed off at C. Mercury charged in E was transferred to D through the stopcock F. The difference in the vapor pressure between the pure solvent and the acetone solution of the complex was measured at a constant temperature by the U-type mercury manometer formed at D. The value of Dreisbach[8] was referred to be estimating the vapor pressures of acetone in this study. The estimated values are in good agreement with our measurement; for instance, the 263 mmHg measured at 28.5°C agrees with the 263 mmHg evaluated from Ref. 8. The results are listed in Table 2.

Table 2. The data to obtain the molecular weight of $Cu(all)(H_2O)ClO_4$ in acetone

	Sample 1	Sample 2	
Concn. (wt. %)	2.92	3.01	
Temp. (°C)	28.8	25.7	30.0
Depression of vapor press. (mmHg)	3.05	2.60	3.29
Vapor press. of acetone (mmHg)[a]	266	209	279
Mol. wt.	151	145	153
	average 150		

a) Evaluated from $\log P = 7.19038 - 1233.4/(t-230)$

Gas Chromatography. The *cis*- and *trans*-isomers of 2-butenyl alcohol were separated by the use of gas chromatography under the following conditions: PEG 1500/siliconized Celite; temperature, 110°C; column, 4.5 mm in od × 3.5 m; carrier gas, hydrogen, 30 ml/min. The ratio of the isomers was evaluated from the average value of five measurements.

IR Spectra. The infrared absorption spectra were measured with a Hitachi infrared spectrophotometer EPI-2. The sprctra of $Cu(all)_2(H_2O)ClO_4$ and $Cu(but)_2(H_2O)ClO_4$ were measured by the use of both a sodium chloride cell and a polyethylene film, since these complexes easily exchange the anion. All the samples were prepared in nitrogen atmospheres.

NMR Spectra. The samples for NMR measurements were prepared in the vacuum system and the spectra were measured with a 60 MHz spectrometer, model JNM 3H60 of the Japan Electron Optics Laboratory, Ltd.

8) R. R. Dreisbach and R. A. Martin, *Ind. Eng. Chem.*, **41**, 2875 (1949).

Results and Discussion

The present investigation has been undertaken to synthesize stable complexes of allylic alcohols with copper(I) perchlorate; however the complexes obtained were slightly unstable. For instance, when a methanol solution of Cu(all)$(H_2O)ClO_4$ was kept standing at room temperature it became turbid forming copper(I) oxide within a few days. The decomposition rate of the complex increased markedly upon heating. The solid complex heated under a vacuum exploded at around 200°C. A further accidental explosion occurred when it was treated with a spatula of stainless steel in a nitrogen atmosphere.

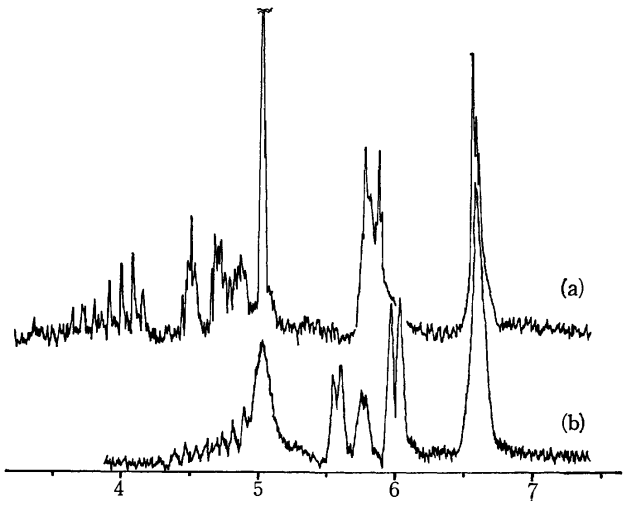

Fig. 3. The NMR spectra of allyl alcohol (a) and Cu(all)-ClO_4 (b) in CD_3OD. The quintet lines around 6.6 τ are signals of CHD_2OD.

Table 3. The NMR spectra of allylic alcohols and their complexes with copper(I) perchlorate[a] (τ value in CD_3OD)

	R_1	R_2	R_3	CH_2	OH
Allyl alcohol	4.1m	(4.53 4.90 4.73)		5.85d	5.05
Cu(all)$(H_2O)ClO_4$	4.9m	(5.59 5.83m 5.64)		6.03d	5.07
2-Methylallyl alchohol	8.28	(5.02	5.46)	6.02	5.10
Cu(meth)$(H_2O)ClO_4$	8.25	(5.46	5.59)	6.04	5.05
cis-2-Butenyl alcohol			8.30m	5.81	5.10
Cu(*cis*-but)$_2$-$(H_2O)ClO_4$			8.29m	5.91d	5.10
trans-2-Butenyl alcohol	4.3m	8.30m	4.3m	6.04	5.10
Cu(*trans*-but)$_2$-$(H_2O)ClO_4$	4.8m	8.33d	4.8m	6.06	5.06

d; doublet, m; multiplet.

a) R_n's are based on $R_2\diagdown\ \diagup R_1$ C=C $R_3\diagup\ \diagdown CH_2OH$

Cu(all)$(H_2O)ClO_4$ and Cu(meth)$(H_2O)ClO_4$. The NMR spectra of allyl alcohol and its complex are shown in Fig. 3. Table 3 shows the data of the NMR spectra of allylic alcohols and their complexes.

The spectra of allyl groups are very complex.[9] The NMR spectra of the complex of allylic alcohol are also so complex that the chemical shifts and coupling constants of the vinyl protons were difficult to determine. However, it is clear that the chemical shifts of the protons attached to the saturated carbons are affected little by coordination, and that the chemical shifts of the vinyl protons shifted by 0.5—1 ppm to a higher field. These shifts can be explained as being mostly due to a decrease in the double bond character upon coordination, and the small shift of methylene protons to a higher field is consistent with the decrease in the electron density of the double bond.

It is found that the intensity ratio of $(OH+R_1)$: (R_2+R_3): CH_3 of Cu(all)$(H_2O)ClO_4$ is 4:2:2; this is consistent with the composition obtained from elementary analysis, $Cu(CH_2=CHCH_2OH)(H_2O)ClO_4$. A similar intensity ratio was observed in the case of the 2-methylallyl alcohol complex.

The NMR spectra of neat 2-methylallyl alcohol are essentially the same as those of 2-methylallyl alcohol in deuterated methanol solutions. Because the OH proton signal overlaps with one of the vinyl proton signals, the NMR spectra of 2-methylallyl alcohol was used to distinguish between the absorptions of the OH group and the vinyl proton.

Table 4. The C=C stretching bands of allylic alcohols and their complexes with copper(I) perchlorate

	ν(C=C) cm^{-1}
Allyl alcohol	1646
Cu(all)$(H_2O)ClO_4$	1538
Cu(all)$_2(H_2O)ClO_4$	1537
2-Methylallyl alcohol	1657
Cu(meth)$(H_2O)ClO_4$	1579
trans-2-Butenyl alcohol	1673
Cu(*trans*-but)$_2(H_2O)ClO_4$	1558
cis-Butenyl alcohol	1654
Cu(*cis*-but)$_2(H_2O)ClO_4$	1540

The frequencies of the C=C stretching bands of both the free and the coordinated allylic alcohols are listed in Table 4. The IR spectra of the complexes with allylic alcohols closely resemble those of copper(II) perchlorate and free alcohols except for the C=C stretching bands. The C=C stretching bands of the ligands are shifted by about 110 cm^{-1} to the lower frequency side by coordination. This shift indicates a decrease in the electron density of the double bond and is consistent with the decrease in shielding observed in the NMR spectra. The shift in the copper(I) perchlorate complex is considerably larger than that in the copper(I) chloride complex (95 cm^{-1}) and suggests a stronger coordination as expected.

It has been reported[10] that the Cl-O stretching

9) L. M. Jackman, "Application of Nuclear Magnetic Rsonance Spectroscopy in Organic Chemistry," Pergamon Press, London (1959).

10) B. J. Hathaway and A. E. Underhill. *J. Chem. Soc.*, **1961**, 3091.

absorption of the perchlorate ion at around 1100 cm^{-1} is split into three or four peaks and is shifted to the lower frequency side by coordination. No absorption bands of the complexes in this region split and differ from those of copper(II) perchlorate hexahydrate.

The equivalent conductances of the one to one complex of allyl alcohol listed in Table 1 were plotted against the roots of the concentrations and the conductance at an infinite dilution, 195, was obtained by extrapolation. This value is close to those of lithium halides and potassium iodide in acetone[11] suggesting that the complex is a strong electrolyte of uni-uni valent.

The equivalent conductance at 25.7°C of a 30.1% solution of $Cu(all)(H_2O)ClO_4$ in acetone was found to be 40. This value is quite small as compared with the conductance at an infinite dilution, showing a small activity coefficient together with the presence of nondissociated species at this concentration. As Table 2 shows, the molecular weight of the complex in acetone is about 150. Because the formula weight of the complex in acetone is 237, the molecular weight of the completely dissociated complex is 119. From this fact, it can be concluded that the complex is monomeric and that the somewhat large molecular weight may be due to the presence of the undissociated complex in acetone.

It is difficult to obtain direct evidence showing the coordination of the oxygen atom of allylic alcohols to the copper atom. We failed to isolate similar complexes with alkene such as ethylene, propene and butenes. This failure suggests that the coordination ability of simple monoolefins is too weak for them to form stable complexes and that the allylic alcohol chelates to copper(I) *via* both the double bond and oxygen atom.

There is some evidence of coordination of the water to the copper(I) ion. Firstly, as has been described above, $Cu(all)(H_2O)ClO_4$ dissolved in alcohols or ketones forms Cu(I) oxide slowly. This implies that the dissociation constant of the proton of the water molecule coordinated to the copper(I) ion is larger than that of free water. Secondly, at room temperature the water molecule can not be removed under a vacuum of 10^{-3} mmHg. Furthermore, the complex does not lose its water molecule on treatment with 2,2-dimethoxypropane. It seems that the water is removed before an explosion.

$Cu(all)_2(H_2O)ClO_4$ and $Cu(but)_2(H_2O)ClO_4$. The NMR spectrum of $Cu(all)_2(H_2O)ClO_4$ could not be measured because it dissociates rapidly into the one to one complex and allyl alcohol in solution.

The NMR data of the complex of 2-butenyl alcohol are listed in Table 3. As Fig. 4 shows, commercial 2-butenyl alcohol is composed of *cis*- and *trans*-isomers in a ratio of about one to three. The complex prepared from the commercial alcohol, however, had nearly the same amounts of the *cis*- and *trans*-isomers. The vinyl protons of both isomers shift to the lower frequency side by about 0.5 ppm from the parent vinyl proton upon coordination; the intensity ratio of the protons is consistent with the $[Cu(C_4H_8O)_2(H_2O)]ClO_4$ composition (Fig. 4 and Table 3).

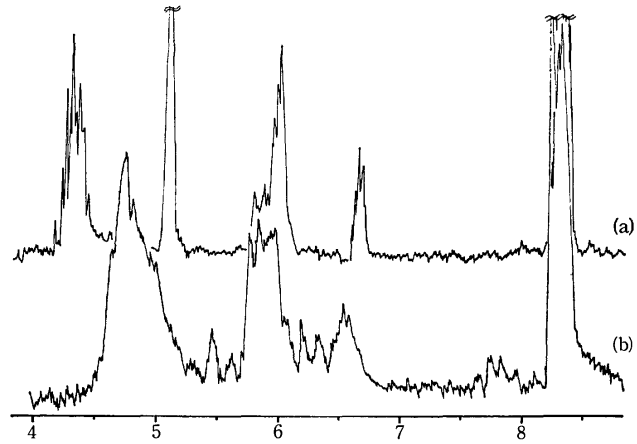

Fig. 4. The NMR spectra of commercial 2-butenyl alcohol and $Cu(but)_2ClO_4$ (b) in CD_3OD.

The IR spectra of the one to two complexes are similar to those of the one to one complexes (Table 4), and they show no absorption due to the free double bond. Therefore, both double bonds may coordinate to copper(I). The oxygen atoms of alcohols may coordinate to copper(I) just as in $Cu(all)(H_2O)ClO_4$. It is not clear from the present data whether the water molecule coordinates or not.

*The Equilibrium between the Cu(*cis*-but)$_2(H_2O)ClO_4$ and Cu(*trans*-but)$_2(H_2O)ClO_4$.* As has been described above, the mole ratio of *cis*-isomers to *trans*-isomers in the complex is greater than that in the original alcohol. Copper(I) chloride is soluble in 2-butenyl alcohol, suggesting the formation of a copper(I) chloride-2-butenyl alcohol complex similar to the copper(I) chloride-allyl alcohol complex.[4] When 2-butenyl alcohol was added to an excess of powdered copper(I) chloride and was then collected by vacuum distillation, it was found that the early fractions were rich in the *trans*-isomer while the later fractions were rich in the *cis*-isomer. These facts show that the *cis*-2-butenyl alcohol coordinates more easily to copper(I) chloride than does the *trans*-alcohol. On the basis of these findings, we tried to evaluate the difference in the stabilities of the complexes of these isomers.

It is known that the vapor pressure of *trans*-butene is rather close to that of the *cis*-isomer. For instance, the vapor pressures of the former and the latter at 0°C are 660 and 730 mmHg respectively.[12] The smallness of the difference may reflect the isomers of 2-butenyl alcohol. In fact, when 2-butenyl alcohol was collected by vacuum distillation, no difference in the composition of the isomers was found between the early and the final fractions. It was confirmed that the complex does not catalyze the isomerization of 2-butenyl alcohol.

Now the following equilibrium and equilibrium constant can be assumed:

$$2C + CuT_2(H_2O)^+ = 2T + CuC_2(H_2O)^+ \quad (1)$$

11) L. G. Savedoff, *J. Amer. Chem. Soc.*, **88**, 664 (1966).

12) D. R. Stull, *Ind. Eng. Chem.*, **39**, 517 (1947).

$$K = \frac{[T]^2[CuC_2(H_2O)^+]}{[C]^2[CuT_2(H_2O)^+]} \quad (2)$$

where C and T represent *cis*- and *trans*-2-butenyl alcohol respectively. It was ascertained that all the copper(II) used is reduced to the copper(I) complexes. The α_0 and α fraction are defined by:

$$\alpha_0 = [T]_0/[C]_0 \quad (3)$$

$$\alpha = [T]/[C] \quad (4)$$

where $[T]_0$ and $[C]_0$ are the concentrations of *trans*- and *cis*-2-butenyl alcohol respectively before the preparation of the complex, while [T] and [C] are those of *trans*- and *cis*-2-butenyl alcohol after the preparation of the complex. The following relations are obtained:

$$[C]_t = [C] + 2[CuC_2(H_2O)^+] \quad (5)$$

$$[T]_t = [T] + 2[CuT_2(H_2O)^+] \quad (6)$$

$$[Cu]_t = [CuC_2(H_2O)^+] + [CuT_2(H_2O)^+] \quad (7)$$

where the subcript "t" represents the total concentration of each species. The β fraction is defined by Eq. (8). Equation (9) then results, since no isomerization occurs.

$$\beta = [C]_t/[C]_0 \quad (8)$$

$$[T]_t/[T]_0 = \beta \quad (9)$$

The following relations are derived from Eqs. (3)—(9):

$$[CuC_2(H_2O)^+] = \{2[Cu]_t + (\alpha-\alpha_0)\beta[C]_0\}/2(\alpha+1) \quad (10)$$

$$[CuT_2(H_2O)^+] = \{2\alpha[Cu]_t + (\alpha-\alpha_0)\beta[C]_0\}/2(\alpha+1) \quad (11)$$

Substitution in Eq. (2) results in:

$$K = \alpha^2\{2[Cu]_t + (\alpha-\alpha_0)\beta[C]_0\}/\{2\alpha[Cu]_t - (\alpha-\alpha_0)\beta[C]_0\} \quad (12)$$

If the ratio of *cis*-2-butenyl alcohol to the *trans*-isomer in the vapor phase is equal to that in the liquid phase, α and α_0 should be the ratio of the isomers of the starting 2-butenyl alcohol measured in the vapor phase and after the preparation of the complex respectively.[13]

In this experiment, we prepared the copper(I) complex in pure 2-butenyl alcohol and collected small portions of the solvent ($\sim$10 μl) by vacuum distillation in order to determine α_0 and α. The results are listed in Table 5.

The temperature dependence of the equilibrium constant was determined. Figure 5 shows the plot of log$K$ *versus* $1/T$. The enthalpy change corresponding to Eq. (1) was evaluated as -3.13 kcal/mol from the gradient.

Muhs and Weiss[14] determined the equilibrium constants of silver-olefin complexes by the use of ethylene glycol solutions of silver nitrate as the liquid phase of gas chromatographic column. These reactions are expressed by:

$$\text{olefin} + AgNO_3 = \text{olefin}\cdot AgNO_3$$

In the case of 2-butene, the ratio of the equilibrium constants of *cis*- and *trans*- is 3.9 at 40°C. The ratios of most olefins fall around 4. These values must be squared in order to be compared with the present data. The value of K at 40°C is estimated to be 7.1 by the extrapolation of the straight line in Fig. 5. The value for copper(I) is rather similar to that of silver(I) though the former is smaller. The stability of *cis*-2-butenyl alcohol compared to that of the *trans*-isomer may be attributed to the relief of the inner strain of the *cis*-isomer by coordination.

Table 5. The equilibrium constant for the reaction of Eq.(1)[a] (at 30.1°C)

Concn. (mol/kg sol)		*trans*-Isomer / *cis*-Isomer	Equilibrium constant, K
2-Butenyl alcohol	Cu(I)	at vapor phase	
6.13	2.44	4.25	8.00
7.67	1.94	3.85	8.27
8.69	1.61	3.53	7.95
9.40	1.39	3.38	8.03
			av. 8.06

a) The ratio of *trans*- to *cis*-isomer of starting 2-butenyl alcohol is 2.53.

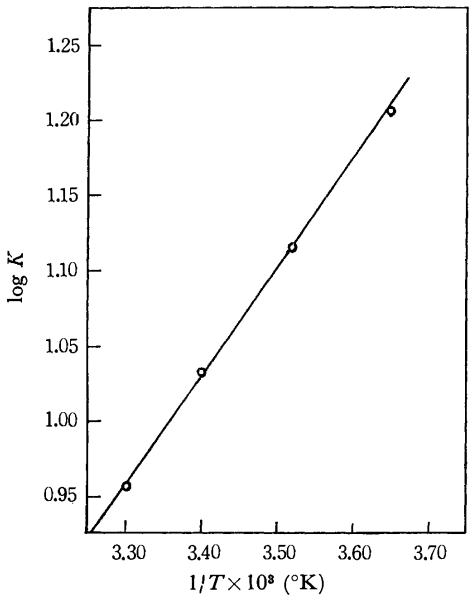

Fig. 5. The temperature dependencies of the formation constant, K.

The authors wish to thank Professor Shinichi Kawaguchi of Osaka City University for his valuable advice and encouragement.

13) Here we assumed that the fractions, α_0 and α, in liquid phase are equal to those of gas phase. However, if the *trans*- and *cis*-2-butenyl alcohol have their vapor pressures, Pt and Pc, respectively, and obey Raoult's law, then α_0 and α in Eq. (12) are represented as $(Pt/Pc)\alpha_0$(gas) and $(Pt/Pc)\alpha$(gas), respectively, where α_0(gas) and α(gas) are the fractions in gas phase corresponding to them in liquid phase.

14) M. A. Muhs and F. T. Weiss, *J. Amer. Chem. Soc.*, **84**, 4697 (1962).

Reactions of Tris(acetylacetonato)manganese(III) and Bis(acetylacetonato)-manganese(II) with Ethylenediamine and Other Primary Amines

Yoshinori NISHIKAWA, Yukio NAKAMURA, and Shinichi KAWAGUCHI*

Department of Chemistry, Faculty of Science, Osaka City University, Sumiyoshi-ku, Osaka

(Received June 10, 1971)

Tris(acetylacetonato)manganese(III) reacts with ethylenediamine (L_2) and other primary amines (L) in organic solvents at room temperature producing $Mn(acac)_2L_2$. The same Mn(II) complexes were also prepared quantitatively by reactions of $Mn(acac)_2(H_2O)_2$ with amines. Besides the usual hexa-coordinate monomeric complex, allylamine gave a dimeric compound $[Mn(acac)_2(CH_2=CHCH_2NH_2)]_2$, which is the first example of the binuclear manganese(II) complex of acetylacetone. The stoichiometry of the redox reaction between $Mn(acac)_3$ and ethylenediamine was established and discussed in connection with the initiation mechanism of vinyl polymerization.

In previous papers, reactions of acetylacetone chelates of copper(II),[1] beryllium,[2] and aluminum[3] with bromine in dichloromethane have been reported to result in different kind of products. Similar reactions of the corresponding cobalt(III),[4] cobalt(II),[5] nickel(II),[6] manganese(III), and manganese(II) complexes are now under investigation. In the course of these studies it was noticed that primary alkylamines react with tris(acetylacetonato)manganese(III) producing amine adducts of bis(acetylacetonato)manganese(II). The same compounds have also been derived from the latter manganese(II) chelate by direct reactions with the corresponding amines.

Dwyer and Sargeson[7] synthesized bis(acetylacetonato)diamminemanganese(II) and similar adducts of 2,2′-bipyridine and 1,10-phenanthroline either by substitution reactions between bases and sodium tris(acetylacetonato)manganate(II), or by direct addition reactions between bases and bis(acetylacetonato)manganese(II). Graddon and Mockler[8] also prepared mono- and bis-adducts of pyridine derivatives with the manganese(II) chelate by reactions of bis(acetylacetonato)diaquomanganese(II) with the heterocyclic bases. However, corresponding alkyl amine adducts have not been reported as yet.[9]

As to the redox reactions, tris(acetylacetonato)manganese(III) has been reduced by phenylhydrazine[10] and 2,6-xylenol[11] but has not been reduced by biguanide,[12] picolinic acid or 8-hydroxyquinoline.[13] The present paper reports on the redox reactions between tris(acetylacetonato)manganese(III) and several aliphatic amines, and also on the characterization of manganese(II) complexes produced.

Experimental

Materials. Tris(acetylacetonato)manganese(III),[14] bis(acetylacetonato)manganese(II)[15] and bis(acetylacetonato)-diaquomanganese(II)[15] were synthesized by the methods of Charles (Found for $Mn(C_5H_7O_2)_3$: Mn, 15.59; C, 51.15; H, 5.98%. Found for $Mn(C_5H_7O_2)_2$: Mn, 21.85; C, 47.21; H, 5.58%. Found for $Mn(C_5H_7O_2)(H_2O)_2$: Mn, 19.09; C, 41.68; H, 6.29%). Bis(acetylacetone)ethylenediimine was also prepared according to the literature[16] and recrystallized twice from water (Found: C, 64.39; H, 9.02; N, 12.54%).

Methallylamine was prepared by ammonolysis of methallyl chloride.[17] In an autoclave 96 m*l* of methallyl chloride (1 mol), 500 g of 28% aqueous ammonia (8 mol) and 140 g of ammonium chloride (2.5 mol) were allowed to react at 80—90°C for about 30 min under a pressure of 10 kg/cm^2. Then an aqueous solution of 160 g of sodium hydroxide was added to the mixture and methallylamine was extracted with ether and purified by fractional distillation. Found: C, 66.41; H, 12.63%. *trans*-Crotylamine was also synthesized according to the similar method. Found: C, 67.07; H, 12.81%.

Commercial ethylenediamine, propylamine and allylamine were distilled over metallic sodium. Allylamine was allowed in advance to stand over potassium hydroxide for one day in the cold. Diethyl ether was dried with calcium chloride and distilled over sodium. Benzene and *N,N*-dimethylformamide (DMF) were also purified by the standard methods.[18]

Redox reactions. The reaction between ethylenediamine and tris(acetylacetonato)manganese(III) was performed in a

* To whom communications should be addressed.

1) Y. Nakamura and S. Kawaguchi, This Bulletin, **38**, 954 (1965); T. Ogura, Y. Kojima, Y. Nakamura, and S. Kawaguchi, *ibid.*, **38**, 1468 (1965).

2) Y. Nakamura and S. Kawaguchi, *ibid.*, **40**, 1179 (1967).

3) Y. Nakamura, M. Hirata, and S. Kawaguchi, *ibid.*, **40**, 2572 (1967).

4) Y. Nakamura, M. Gotani, and S. Kawaguchi, *ibid.*, in press.

5) Y. Nakamura, N. Kanehisa, and S. Kawaguchi, *ibid.*, in press.

6) Y. Nakamura, K. Noda, and S. Kawaguchi, 14th Symposium on the Chemistry of Metal Coordination Compounds, Fukuoka, Nov., 1964.

7) F. P. Dwyer and A. M. Sargeson, *J. Proc. Roy. Soc. N. S. W.*, **90**, 29 (1956).

8) D. P. Graddon and G. M. Mockler, *Aust. J. Chem.*, **17**, 1119 (1964).

9) D. P. Graddon, *Coord. Chem. Rev.*, **4**, 1 (1969).

10) B. Emmert and O. Schneider, *Ber.*, **69**, 1316 (1936).

11) T. Shono, K. Yamanoi, T. Matsushita, and K. Shinra, *Kogyo Kagaku Zasshi*, **70**, 2062 (1967).

12) M. M. Ray, J. N. Adhya, D. Biswas, and S. N. Poddar, *Aust. J. Chem.*, **19**, 881 (1966).

13) M. M. Ray, J. N. Adhya, D. Biswas, and S. N. Poddar, *Aust. J. Chem.*, **19**, 1737 (1966).

14) R. G. Charles, "Inorganic Syntheses," **7**, 183 (1963).

15) R. G. Charles, *ibid.*, **6**, 164 (1970).

16) P. J. McCarthy, R. J. Hovey, K. Ueno, and A. E. Martell, *J. Amer. Chem. Soc.*, **77**, 5820 (1955).

17) M. Tamele, C. J. Ott, K. E. Marple, and G. Hearne, *Ind. Eng. Chem.*, **33**, 115 (1941).

18) J. A. Riddick and E. E. Toops, Jr., "Organic Solvents," 2nd ed., Vol. 7 of "Technique of Organic Chemistry," ed. by A. Weissberger, Interscience Publishers, New York (1955).

three-necked flask equipped with a burette and a glass tube containing calcium chloride. To an ethereal solution of the manganese(III) complex (*ca.* 0.3 g) was added dropwise an ethereal solution of three times as many moles of ethylenediamine with magnetic stirring. Agitation was continued further after mixing of reactant solutions was finished. After about half an hour a precipitate of ivory color began to separate, but it took about one week before intense black-brown color of the starting solution disappeared indicating completion of the reaction. Then the precipitate was filtered and submitted to the elemental analysis. The filtrate was divided into three portions and contents of acetylacetone, ethylenediamine and total nitrogen were determined.

Analyses. Manganese content in each solid sample was determined gravimetrically as the sulfate after decomposition of the compound with nitric acid.

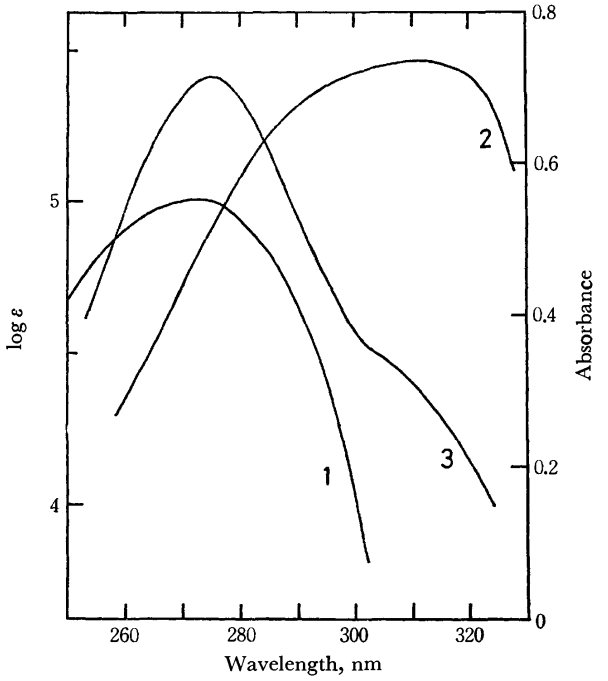

Fig. 1. Ultraviolet absorption spectra of acetylacetone (curve 1, left ordinate), bis(acetylacetone)ethylenediimine (curve 2, left ordinate), and a filtrate from the redox reaction between tris (acetylacetonato)manganese(III) and ethylenediamine (curve 3, right ordinate) in ether.

The filtrate from the above redox reaction contained the liberated acetylacetone, the excess ethylenediamine, produced bis(acetylacetone)ethylenediimine, and the decomposition products of ethylenediamine. The ultraviolet absorption spectrum of this solution is shown in Fig. 1 together with those of acetylacetone and bis(acetylacetone)ethylenediimine. Ethylenediamine does not absorb light in this region and its decomposition products may not either. Thus the absorption spectrum of the solution was analysed on the assumption that it is due to acetylacetone and bis(acetylacetone)ethylenediimine, and the total amount of acetylacetone freed in this redox reaction was determined.

Another aliquot of the filtrate solution was acidified with dilute sulfuric acid and freed of solvent under reduced pressure. The residue was dissolved in water and neutralized with a dilute solution of sodium hydroxide. An aqueous solution of sodium rhodizonate was added in excess to this solution producing a violet precipitate of one to one salt of ethylenediamine with rhodizonic acid. The gravimetric determination of ethylenediamine by this method was tested in advance employing a known amount of the amine, and the accuracy was proved to be more than 99%.

The third aliquot of the filtrate solution was placed in a 500 m*l* Kjeldahl flask, to which potassium sulfate (10 g), selenium (0.2 g) and concentrated sulfuric acid (25—30 m*l*) were added. The mixture was carefully heated by an infrared irradiation to vaporize ether almost completely, and then the total nitrogen content was measured according to the usual Kjeldahl method.

Syntheses of Mixed Complexes of Manganese(II). To prevent oxidation of manganese(II) the following preparations were all performed in an atmosphere of nitrogen employing deoxygenated solvents.

Bis(acetylacetonato)ethylenediaminemanganese(II): Two methods were employed. (i) About 3 g of tris(acetylacetonato)manganese(III) was dissolved in DMF, to which a DMF solution of three times as many moles of ethylenediamine was added. After about 30 min an ivory precipitate began to separate, which was recrystallized from DMF resulting in pale yellow crystals: mp around 150°C (dec). Found: Mn, 17.55; C, 45.83; H, 7.08; N, 8.63%. Calcd for Mn(acac)$_2$en=$C_{12}H_{22}O_4N_2Mn$: Mn, 17.54; C, 46.00; H, 7.09; N, 8.94%.

(ii) Bis(acetylacetonato)diaquomanganese(II) was allowed to react with an equimolar amount of ethylenediamine in DMF. A pale yellow precipitate appeared at once in an almost quantitative yield, and was recrystallized from DMF. Found: M, 17.51; C, 46.10; H, 7.14; N, 9.15%.

Thus, the same compound was obtained in these two types of reactions as evidenced by results of the elemental anaysis and infrared spectra. The corresponding complex containing deuterated ethylenediamine was prepared by the following method. Ethylenediamine-d_4 was prepared by repeated fractional distillations from heavy water solutions and characterized by means of NMR spectra. To a solution of 0.3 g of anhydrous bis(acetylacetonato)manganese(II) in 10 m*l* of DMF containing a few drops of heavy water was added ten drops of ethylenediamine-d_4 and allowed to react for a while with frequent shaking. Bis(acetylacetonato)(ethylenediamine-d_4)manganese(II) was produced as a pale yellow precipitate, filtered and washed with DMF containing a small quantity of heavy water.

Bis(acetylacetonato)bis(allylamine)manganese(II): This compound was also prepared by the following two methods. (i) About 2 g of tris(acetylacetonato)manganese(III) was dissolved in 200 m*l* of ether, to which more than ten times as many moles of allylamine was added. A precipitate began to appear after a while, but the mixture was stirred for one or two days. Pale yellow needles were obtained after recrystallization from ether. Found: Mn, 15.11; C, 52.16; H, 7.57; N, 7.98%. Calcd for Mn(acac)$_2$(CH_2=$CHCH_2NH_2$)$_2$ = $C_{16}H_{28}O_4N_2Mn$: Mn, 14.96: C, 52.31; H, 7.68; N, 7.63%. If about six times as many moles of allylamine is employed, a mixture of bis- and mono-adducts of allylamine with bis(acetylacetonato)manganese(II) is obtained.

(ii) An ethereal solution of twice as many moles of allylamine was added to a suspension of bis(acetylacetonato)diaquomanganese(II) (3 g) in ether. Immediately appeared a pale yellow fuzzy precipitate, which was recrystallized from ether. Found: C, 52.12; H, 7.63; N, 7.30%. Infrared spectra of this specimen were identical with those of the product from the above redox reaction.

Bis(acetylacetonato)allylaminemanganese(II): When an ethereal solution of equimolar allylamine was added to an ethereal suspension of bis(acetylacetonato)diaquomanganese(II) (2.5 g), a fuzzy precipitate appeared at first, but changed gradually to a powder. Pale yellow crystals were obtained

by recrystallization from ether. Found: C, 50.25; H, 6.86; N, 4.10%. Calcd for $Mn(acac)_2(CH_2{=}CHCH_2NH_2)$ = $C_{13}H_{21}O_4NMn$: C, 50.33; H, 6.82; N, 4.51%.

Bis(acetylacetonato)bis(propylamine)manganese(II): The reaction between tris(acetylacetonato)manganese(III) and propylamine in ether gave pale yellow needles. Found: Mn, 15.09; C, 51.64; H, 8.62; N, 7.45%. Calcd for $Mn(acac)_2(C_3H_7NH_2)_2 = C_{16}H_{32}O_4N_2Mn$: Mn, 14.79; C, 51.75; H, 8.69; N, 7.54%. The same complex was also produced by the reaction of propylamine with bis(acetylacetonato)-diaquomanganese(II) in ether. Found: Mn, 14.97; C, 51.71; H, 8.63; N, 7.50%. Even when an equimolar amount of propylamine was allowed to react with the manganese(II) complex, the one to one adduct was not produced but the bis(amine)-adduct was obtained exclusively.

Bis(acetylacetonato)bis(methallylamine)manganese(II) was prepared by the reaction of bis(acetylacetonato)diaquomanganese(II) with methallylamine in ether in the mole ratio of one to two and recrystallized from ether. Found: Mn, 13.91; C, 54.55; H, 8.23; N, 7.25%. Calcd for $Mn(acac)_2(CH_2{=}C(CH_3)CH_2NH_2)_2 = C_{18}H_{32}O_4N_2Mn$: Mn, 13.89; C, 54.68; H, 8.16; N, 7.08%.

*Bis(acetylacetonato)bis(*trans*-crotylamine)manganese(II)* was also prepared in a similar reaction. Found: Mn, 13.71; C, 54.80; H, 8.20, N, 7.07%. Either of these allylic amines did not give the mono(amine)-adduct even in reactions at the reactants mole ratio of one to one.

Measurements. Ultraviolet absorption spectra were measured by means of a Hitachi spectrophotometer model EPS-2. Infrared absorption spectra in the 4000—650 cm^{-1} region were measured with a Hitachi infrared spectrophotometer EPI-2, and those in 700—200 cm^{-1} with a Hitachi grating infrared spectrophotometer EPI-L. Magnetic susceptibilities were measured at room temperature by the Gouy method with a Shimadzu magnetic balance employing hexaamminechromium(III) chloride as a reference substance. Diamagnetic corrections were calculated from Pascal's constants. Thermogravimetric analysis was performed using a thermo-spring-balance C-282 of Hamada Denki Seisakusho, Ltd. under reduced pressure. The rate of temperature elevation was fixed at 30°C/hr for the ethylenediamine complex and at 20°C/hr for allylamine and propylamine complexes. Molecular weight was determined by the cryoscopic method in benzene in a deaerated vessel to prevent oxidation of the manganese(II) complexes and also with a vapor-pressure osmometer of Toa electronics, Ltd. employing ether as a solvent and tris(acetylacetonato)aluminum as a reference substance.

Results

Properties of Bis(acetylacetonato)ethylenediaminemanganese-(II). A novel mixed ligand complex bis(acetylacetonato)ethylenediaminemanganese(II) was prepared either by a redox reaction between tris(acetylacetonato)manganese(III) and ethylenediamine, or by a substitution reaction of bis(acetylacetonato)diaquomanganese(II) with the amine. Infrared absorption spectra of the compound in the higher frequency region are composed of those due to the acetylacetonate ligand and also those due to coordinated ethylenediamine. Characteristic bands due to the diamine ligand are listed in Table 1 which were assigned by reference to literatures[19] and also to the deuteration effects. As

Table 1. Characteristic infrared bands of the diamine group in bis(acetylacetonato)ethylenediamine-manganese(II) and the corresponding ethylenediamine-d_4 complex

$Mn(acac)_2$en	$Mn(acac)_2$(en-d_4)	ν_{NH2}/ν_{ND2}	Assignment
3278 m	2422 w	1.35	NH_2 stretch
3195 m	2340 w	1.36	
~1600[a]	1187 w	1.35	NH_2 scissor
1317 m	1000 m	1.32	NH_2 wag
1120 m	868 m	1.29	
1096 sh	860 sh	1.28	NH_2 twist
1014 s			
762 m	580	1.31	NH_2 rock

a) This band is obscured by the intense absorption of the acetylacetonate ligand.

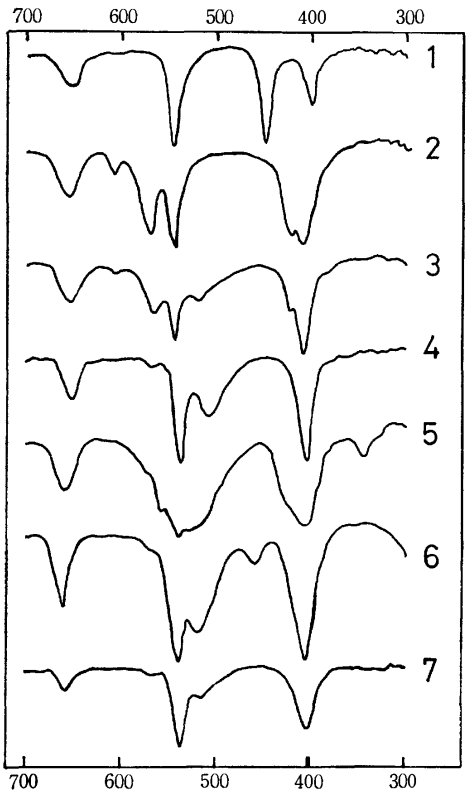

Fig. 2. Infrared spectra in the 700—300 cm^{-1} region of bis(acetylacetonato)manganese(II) and amine adducts in Nujol mull: 1, $Mn(acac)_2$; 2, mono(allylamine)-adduct; 3, bis(allylamine)-adduct; 4, bis(propylamine)-adduct; 5, bis(methallylamine)-adduct; 6, bis (*trans*-crotylamine)-adduct; 7, ethylenediamine-adduct.

shown in Fig. 2, infrared absorption spectrum of bis(acetylacetonato)manganese(II) in the 700—300 cm^{-1} region consists of a broad band around 650 cm^{-1} and three strong peaks at 543, 449, and 399 cm^{-1}. Dismukes, Jones, and Bailar interpreted the spectrum in terms of coupling of metal-oxygen vibrational modes with three low-frequency vibrational modes of the acetylacetonate anion.[20] The strong peak at 449 cm^{-1} was not ob-

19) D. B. Powell and N. Sheppard, *Spectrochim. Acta*, **17**, 68 (1961); G. W. Watt and D. S. Klett, *Inorg. Chem.*, **5**, 1278 (1966).

20) J. P. Dismukes, L. H. Jones, and J. C. Bailar, Jr., *J. Phys. Chem.*, **65**, 792 (1961).

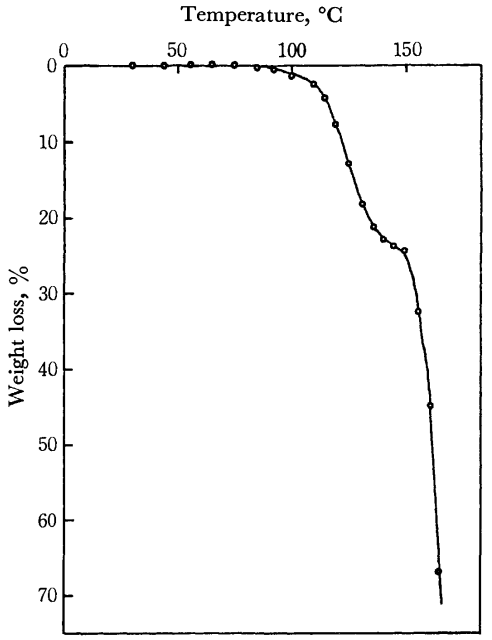

Fig. 3. Thermogravimetric analysis of bis(acetylacetonato)-ethylenediaminemanganese(II) *in vacuo*. The rate of temperature elevation was fixed at 30°C/hr.

served in the spectrum of the ethylenediamine adduct. It may be due to the structural change from trimeric $Mn(acac)_2$[8] to monomeric $Mn(acac)_2en$. Weak bands at 572 and 516 cm^{-1} in the latter spectrum may be assigned to the metal-nitrogen stretching.

Thermogravimetric analysis, as shown in Fig. 3, indicates that bis(acetylacetonato)ethylenediaminemanganese(II) begins to decompose at around 95°C liberating ethylenediamine, which was trapped at −78°C. The ethylenediamine was transformed to the hydrochloride and identified by the elemental analysis and infrared spectra.[21] Sudden decrease of weight at temperatures above 150°C is due to sublimation of the decomposition residue, which was identified as bis-(acetylacetonato)manganese(II) by the elemental analysis and infrared spectra. The weight loss below 150°C amounts to 24% exceeding the calculated value of 19.2% for the ethylenediamine content in this adduct. This discrepancy seems to be caused by partial sublimation of the residual bis-chelate. When a sample was kept at 100°C *in vacuo*, the weight decreased more slowly and reached a constant weight after 6 hr. The weight loss in this case was 22.0% and still higher than the calculated ethylenediamine content.

Molecular weight of $Mn(acac)_2en$ could not be measured on account of insolubility in ether, benzene, and other solvents suitable for the measurement, but it could be presumed to be monomeric from analogy with the bis(allylamine)-adduct which will shortly be described. Magnetic moment of this compound was determined to be 6.08 B.M. by the Gouy method at room temperature. This value is so close to the value of 5.91 B.M. estimated by the spin-only equation that high-spin octahedral configuration of manganese(II) may be proposed for this compound.

21) D. B. Powell, *Spectrochim. Acta*, **16**, 241 (1960); J. Bellanato, *ibid.*, **16**, 1344 (1960).

Other Primary Amine Adducts with Bis(acetylacetonato)manganese(II). Bis(acetylacetonato)bis(amine)manganese(II) complexes were also prepared by the two types of reactions just as in the case of the ethylenediamine adduct. The 1 : 1 amine adduct was obtained only in a 1 : 1 reaction between bis(acetylacetonato)manganese-(II) and allylamine. Even when other primary amines such as propylamine, methallylamine and *trans*-crotylamine were allowed to react with $Mn(acac)_2$ in the mole ratio of one to one, the bis(amine)-adducts were produced exclusively.

TABLE 2. THE NH STRETCHING AND NH_2 BENDING FREQUENCIES OF SEVERAL PRIMARY AMINES AND THEIR ADDUCTS WITH BIS(ACETYLACETONATO)MANGANESE(II) TOGETHER WITH THE C=C STRETCHING FREQUENCIES OF ALLYLIC COMPOUNDS

Compound[a)]	$\nu(NH_2)$	$\delta(NH_2)$	ν(C=C)
Ethylenediamine, en	3370 m 3280 m	1592 m, br	
$Mn(acac)_2en$	3278 m 3195 m	~1600	
Propylamine, $PrNH_2$	3385 m 3298 m	1590 m, br	
$Mn(acac)_2(PrNH_2)_2$	3280 w 3200 w, sh	1558 m, sh	
Allylamine, $AllNH_2$	3380 m 3290 m	1595 w, br	1642 m
$Mn(acac)_2(AllNH_2)$	3340 w 3240 w 3160 w	1553 m, sh	1638 w
$Mn(acac)_2(AllNH_2)_2$	3270 w 3200 w, sh	1555 m, sh	1640 w
Methallylamine, $MethallNH_2$	3390 s 3310 s 3190 sh	1595 m, br	1645 m
$Mn(acac)_2(MethallNH_2)_2$	3350 sh 3300 s 3260 m, br	1595 m, br	1645 w
trans-Crotylamine, $CrotNH_2$	3380 m 3300 m 3190 sh	1585 m, br	1655 sh
$Mn(acac)_2(CrotNH_2)_2$	3310 m 3200 w	1600 (?)	1655 sh

a) Free amines as neat liquid and metal complexes in Nujol.

Table 2 summarizes infrared frequencies of NH stretching and NH_2 bending vibrations of these primary amines and their adducts, and those of C=C stretching in allylic amines. The NH stretching frequencies of amine adducts are shifted remarkably to the lower frequency side indicating coordination of amine groups to the metal. Close resemblance of infrared spectra in the lower frequency region as shown in Fig. 2 suggests that the bis-adducts of primary monoamines take the *cis* configuration as is the case for the ethylenediamine adduct. The C=C stretching frequencies of adducts of allylamine and its derivatives show no appreciable shifts from those of free ligands implying non-participation of the C=C group in coordination.

Magnetic moments of allylamine, bis-allylamine and bis-propylamine adducts are 5.97, 6.08, and 6.14 B.M.,

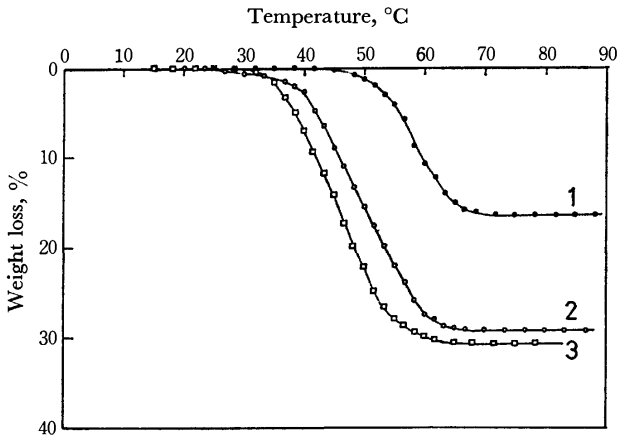

Fig. 4. Thermogravimetric curves for decompositions of amine adducts with bis(acetylacetonato)manganese(II). Curve 1, mono(allylamine)-adduct; curve 2, bis(allylamine)-adduct; curve 3, bis(propylamine)-adduct.

Table 3. Results of thermogravimetric analysis of amine adducts with bis(acetylacetonato)-manganese(II)

Compound	Beginning of decomposition (°C)	Weight loss (%)	Calcd amine content (%)
$Mn(acac)_2en$	95	22.0	19.2
$Mn(acac)_2(AllNH_2)$	45	16.4	18.4
$Mn(acac)_2(AllNH_2)_2$	25	29.1	31.1
$Mn(acac)_2(PrNH_2)_2$	30	30.7	31.8

respectively, indicating that they are all high-spin complexes. Results of thermogravimetric analysis of these compounds are shown in Fig. 4 and Table 3. Allylamine and propylamine adducts decomposed at much lower temperatures than the ethylenediamine adduct did. Thus the weight became constant below 70°C in each case since sublimation of the decomposition residue did not start at these lower temperatures even *in vacuo*.

The volatile product was identified as the free amine, and the decomposition residue as bis(acetylacetonato)-manganese(II) in either case. The observed weight loss in these compounds is close to the calculated amine content, respectively. The higher temperature of decomposition of the ethylenediamine complex seems to reflect its higher thermodynamic stability, compared with bis-adducts of monoamines. However, the trend is independent of the negative shift observed for the N–H stretching frequencies, and might be understood in terms of the entropy effect in the diamine chelate.

The decomposition pressure of the bis(allylamine) complex is higher than that of its mono-adduct and the former compound changes to the latter by prolonged evacuation even at room temperature. The results of molecular weight determination shown in Table 4 indicate that the bis(allylamine) complex is monomeric both in benzene and ether, but the mono(allylamine) complex is dimeric in ether. The latter compound is less soluble in benzene and did not allow the cryoscopic measurement.

Table 4. Molecular weights of allylamine adducts with bis(acetylacetonato)manganese(II)

Compound	Calcd	Found in benzene[a)]	Found in ether[b)]
$Mn(acac)_2(AllNH_2)$	310		580
$Mn(acac)_2(AllNH_2)_2$	367	350	350

a) Cryoscopy
b) Vapor pressure osmometry

Stoichiometry of the Redox Reaction between Tris(acetylacetonato)manganese(III) and Ethylenediamine. A precipitate formed by the reaction between tris(acetylacetonato)manganese(III) and ethylenediamine was identified as bis(acetylacetonato)ethylenediaminemanganese(II) by the elemental analysis and infrared spectra. Since this compound is insoluble in ether at all, the filtrate could be used for the analysis of the excess ethylenediamine, total nitrogen, and liberated acetylacetone as described in the Experimental section.

Table 5. Products of a reaction between tris-(acetylacetonato)manganese(III) and ethylenediamine in ether

	No. of mols	Mol ratio
Reactants employed:		
$Mn(acac)_3$	8.31×10^{-4}	1
ethylenediamine	24.93×10^{-4}	3
Ppt. produced:		
$Mn(acac)_2en$	8.47×10^{-4}	1.02
Contained in the filtrate:		
acetylacetone	6.32×10^{-4}	
bis(acac)ethylenediimine	1.01×10^{-4}	
total acetylacetone	8.34×10^{-4}	1.00
total ethylenediamine	9.30×10^{-4}	1.12
total nitrogen	27.8×10^{-4} g·atom	

As summarized in Table 5 the manganese(II) complex was produced quantitatively. Liberated acetylacetone was also equimolar to the complex, indicating that no appreciable decomposition of the acetylacetonate ligand occurred in this redox reaction. Since 2.493 mmol of ethylenediamine was employed and 0.847 mmol was found as coordinated in the Mn(II) complex, the remaining 1.646 mmol might be expected to exist in the solution. However only 0.930 mmol of ethylenediamine was found in the filtrate existing both as the free diamine and the diimine. Thus 0.716 mmol of the amine must be considered to have been decomposed. Total nitrogen contained in the filtrate was not 2×1.646 mg·atom but only 2.78 mg·atom. These results suggest that ethylenediamine was consumed in reducing Mn(III) to Mn(II). Oxidized products of the amine have not yet been characterized, but some volatile product(s) corresponding to 0.51 mg·atom of nitrogen must have escaped from the reaction mixture during a long period reaction. Thus the over-all redox reaction between tris(acetylacetonato)manganese-(III) and ethylenediamine can be represented by the following equation.

$$Mn(acac)_3 + 2en = Mn(acac)_2en + acacH + \text{decomposition products of en} \quad (1)$$

Discussion

Bis(acetylacetonato)bis(allylamine)manganese(II) was ascertained to be monomeric in benzene and ether. Molecular weights of other bis(monoamine) and ethylenediamine complexes have not been determined, but it may be presumed by analogy that they are all monomeric six-coordinate complexes. Allylamine is quite specific in forming the 1:1 adduct which is dimeric in ether and in crystals, too.[22] It is worth noting that the mono-allylamine-adduct is more stable than the bis(allylamine)-adduct while similar mono-adducts of propyl-, methallyl-, and crotyl-amines can not be obtained.

Graddon and Mockler[8] found that 1:1 adducts of pyridine and 4-methylpyridine with bis(acetylacetonato)-manganese(II) are both monomeric in benzene and proposed five-coordinate structures for these complexes. On the contrary the present 1:1 adduct of allylamine is dimeric and a six-coordinate structure must be considered. As evidenced by the IR data, the ethylenic group of allylamine is not involved in coordination to the metal, and the amine molecule acts as a unidentate ligand. Thus the acetylacetonate groups are considered to take the role of bridging ligands as depicted in Fig. 5. This structure is analogous to that given to dimeric bis(acetylacetonato)aquocobalt(II) by Cotton and Elder,[23] and is the first example of the dimeric manganese(II) complex containing acetylacetonate groups as bridging ligands. It is not certain at the present stage of investigation why propylamine and other monoamines can not assume similar structures, but will be clarified by the X-ray studies now in progress.[22]

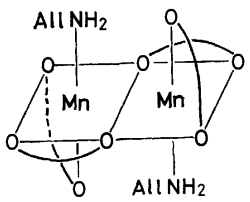

Fig. 5. A proposed structure of dimeric bis(acetylacetonato)-allylaminemanganese(II).

Tris(acetylacetonato)manganese(III) is known as one of the most effective initiators of free-radical polymerization of vinyl monomers.[24] Recently Bamford and Ferrar found that propylenediamine and other donor additives stimulate the radical initiation quite markedly in the polymerizations of styrene, methyl methacrylate and acrylonitrile initiated by Mn(acac)$_3$.[25] The first step of the redox reaction must be coordination of an amine molecule to the manganese(III) metal in such a fashion as represented by Eq. (2), since the outer-sphere electron transfer seems

$$Mn^{III}(acac)_3 + en \longrightarrow (acac)_2Mn^{III}\langle^{acac}_{en} \quad (2)$$

less probable. Succeeding steps may be either (3) or (5). If an electron is transferred from the coordinated

$$(acac)_2Mn^{III}\langle^{acac}_{en} \longrightarrow Mn^{II}(acac)_2 + C_5H_8O_2 + (en-H)\cdot \quad (3)$$

$$Mn^{II}(acac)_2 + en \xrightarrow{fast} Mn^{II}(acac)_2en \quad (4)$$

$$(acac)_2Mn^{III}\langle^{acac}_{en} \longrightarrow Mn^{II}(acac)_2en + C_5H_7O_2\cdot \quad (5)$$

$$C_5H_7O_2\cdot + en \xrightarrow{fast} C_5H_8O_2 + (en-H)\cdot \quad (6)$$

amine to the metal and the acetylacetonate anion dissociates as a molecule abstracting a proton from neighboring ethylenediamine, there will result the deprotonated ethylenediamine radical (Eq. 3). The product Mn(acac)$_2$ is labile and will add an excess molecule of ethylenediamine quite easily (4) as shown in this paper. On the other hand if an electron is delivered by an acetylacetonate ligand, an acetylacetone radical will be produced (5).

Uehara *et al.*[26] reported that pyridine, α,α'-lutidine, and piperidine accelerated polymerization of styrene, methyl methacrylate, and vinyl acetate initiated by Mn(acac)$_3$, and that polystyrene prepared in the Mn(acac)$_3$-py system showed the carbonyl stretching band at round 1700 cm^{-1} but no absorption due to the pyridine ring. By means of tracer experiments Bamford and Ferrar[27] also disclosed that in the vinyl polymerization initiated by Mn(acac)$_3$ and propylenediamine or dimethyl sulfoxide, each growing radical carried one acetylacetonate residue, but fragments derived from the additives were incorporated in the polymer only to a minor extent. These results indicate unequivocally that the process (5) occurred in the main. As described already acetylacetone molecules are recovered quantitatively in the reaction between Mn(acac)$_3$ and ethylenediamine in the absence of vinyl monomers. The succeeding step (6) must proceed rapidly in advance to spontaneous degradation of the acetylacetone radical.

A grant given to Nakamura by Fuji Photo Film Co., Ltd. is gratefully acknowledged. The authors also thank Mr. J. Gohda for the elemental analyses.

22) S. Koda, S.Ooi, H. Kuroya, Y. Nishikawa, Y. Nakamura, and S. Kawaguchi, *Inorg. Nucl. Chem. Lett.*, in press.
23) F. A. Cotton and R. C. Elder, *Inorg. Chem.*, **5**, 423 (1966).
24) E. G. Kastning, H. Naarmann, H. Reis, and C. Berding, *Angew. Chem.*, **77**, 313 (1965); C. H. Bamford and D. J. Lind, *Chem. and Ind.* (London), **1965**, 1627; *Chem. Commun.*, **1966**, 792; *Proc. Roy. Soc.*, **A302**, 145 (1968); Y. Nishikawa and T. Otsu, *Kogyo Kagaku Zasshi*, **72**, 751 (1969).
25) C. H. Bamford and A. N. Ferrar, *Chem. Commun.*, **1970**, 315.
26) K. Uehara, Y. Kataoka, M. Tanaka, and N. Murata, *Kogyo Kagaku Zasshi*, **72**, 754 (1969).
27) C. H. Bamford and A. N. Ferrar, *Proc. Roy. Soc.* (London), **A321**, 425 (1971).

Studies of Mixed Cyano Cobalt(III) Complexes. IV.[1] Preparation and Characterization of *trans*(O,X)-[Co(X)(aminoacidato)(diethylenetriamine)]$^+$ Complexes with X=CN^-, NO_2^-, or Cl^-

Kuwako OHKAWA, Junnosuke FUJITA,* and Yoichi SHIMURA**

Department of Applied Chemistry, Faculty of Engineering, Tokushima University, Tokushima

**Department of Chemistry, Faculty of Science, Tohoku University, Sendai*

***Department of Chemistry, Faculty of Science, Osaka University, Toyonaka, Osaka*

(Received June 18, 1971)

A series of new kinds of mixed cobalt(III) complexes, *trans*(O,X)-[Co(X)(aminoacidato)(diethylenetriamine)]Y, have been prepared and characterized by visible and ultraviolet, circular dichroism, and proton magnetic resonance spectroscopy for X=CN^-, NO_2^-, and Cl^-; aminoacid=glycine, α-aminoisobutyric acid, L-alanine, L-valine, L-threonine, and L-proline; and Y=Br^-, Cl^-, or ClO_4^-. The proton magnetic resonance spectra of the cyano mixed complexes show the existence of new conformational isomers, *endo* and *exo* forms, which concern the ligand CN^- and the hydrogen atom attached to the central nitrogen atom of the meridionally coordinated diethylenetriamine ligand.

In the course of preparative studies of mixed cyano cobalt(III) complexes,[1-3] we have obtained a group of new cyano-diethylenetriamine cobalt(III) complexes with various aminoacids, including optically active ones.[4] In order to characterize these complexes, we have also prepared analogous complexes in which cyanide ion is replaced by a chloride or a nitrite ion. This paper reports the preparation of such complexes and their structures as determined by visible and ultraviolet, circular dichroism, and proton magnetic resonance spectroscopy. A short communication was given on the existence of a couple of novel isomers of the new cyano-diethylenetriamine cobalt(III) complex ion.[5]

Experimental

Ligands and Starting Materials. Diethylenetriamine, glycine, α-aminoisobutyric acid, L-alanine, L-proline, L-valine, and L-threonine were obtained from Wako Pure Chemicals, and used without further purification.

$[Co(NO_2)_3dien]$,[6] $[CoCl_3dien]$,[6] and *trans*-$[Co(CN)(SO_3)(NH_3)_4]$[7] were prepared according to the methods described in literature.

Preparation of the Complexes. All *trans*(O,X)-monoacido-aminoacidato-diethylenetriamine-cobalt(III) complexes (X=CN^-, NO_2^-, or Cl^-) were prepared as follows.

Method 1) *trans*-$[Co(CN)(SO_3)(NH_3)_4] \xrightarrow{dien}$ an intermediate complex (not isolated) $\xrightarrow{concd.\ HBr}$ $Co(CN)(OH_2)(dien)Br_2 \xrightarrow{amH,\ NaOH}$ *trans*(O, CN)-$[Co(CN)(am)(dien)]^+$ (in water)

Method 2) *trans*(O, Cl)-$[Co(Cl)(am)(dien)]^+ \xrightarrow{KCN}$ *trans*(O,CN)-$[Co(CN)(am)(dien)]^+$ (in DMSO)

Method 3) $[CoCl_3dien] \xrightarrow{amH,\ NaOH}$ *trans*(O, Cl)-$[Co(Cl)(am)(dien)]^+$ (in water)

Method 4) $[CoCl_3dien] \xrightarrow{amH,\ NaOH,\ NaNO_2}$ *trans*(O, NO_2)-$[Co(NO_2)(am)(dien)]^+$ (in water)

Method 5) $[Co(NO_2)_3dien] \xrightarrow{amH,\ NaOH}$ *trans*(O, NO_2)-$[Co(NO_2)(am)(dien)]^+$ (in water)

trans*(O,CN)-[Co(CN)(gly)(dien)]*$Br\cdot 3H_2O$. *Method 1*: To a suspension of 35 g of *trans*-$[Co(CN)(SO_3)(NH_3)_4]\cdot 2H_2O$ in 250 m*l* of water was added 15.5 g of diethylenetriamine. Upon heating at 70—80°C for 2 hr with occasional stirring, the starting complex dissolved nearly completely with evolution of ammonia gas. The resulting brown solution was filtered, and the filtrate was concentrated to about 60 m*l* at 60°C under reduced pressure. The sticky solution was treated wtih 100 m*l* of concd. hydrobromic acid, cooled in an ice bath overnight and filtered. The brown solution was warmed at 75°C for about 4 hr until the color turned deep red and was then filtered. To the filtrate was added 400 m*l* of water and an appropriate amount of methanol and acetone. A crude complex, precipitated on cooling was filtered off, washed with methanol, air-dried and recrystallized from water by adding methanol and acetone. Elemental analysis showed the composition $Co(CN)(OH_2)(dien)Br_2$.

Found: C, 16.13; H, 4.81; N, 15.53%. Calcd for $C_5H_{15}N_4OCoBr_2$: C, 16.41; H, 4.13; N, 15.31%. The complex turns from pale rose to testaceous by storing in a vacuum desiccator or by heating. Such a color change might be due to the dehydration of coordinated water followed by the anation of bromide ion. Further study was not made.

To a warm aqueous solution (50—60°C, 50 m*l*) containing 7.3 g of $Co(CN)(OH_2)(dien)Br_2$ was added slowly an aqueous solution (50 m*l*) containing 1.5 g of glycine and 0.56 g of sodium hydroxide. The solution was warmed at 75°C with occasional stirring until the color changed from dark red

1) Part III of this series: K. Ohkawa, J. Hidaka, and Y. Shimura, This Bulletin, **40**, 2830 (1967).

2) K. Ohkawa, J. Fujita, and Y. Shimura, This Bulletin, **38**, 66 (1965).

3) K. Ohkawa, J. Hidaka, and Y. Shimura, *ibid.*, **39**, 1715 (1966).

4) Abbreviations: dien, diethylenetriamine: amH, aminoacid; gly, glycinate ion; L-ala, L-alaninate ion; L-pro, L-prolinate ion; L-val, L-valinate ion; L-thr, L-threoninate ion; α-aibut, α-aminoisobutyrate ion.

5) K. Ohkawa, S. Yano, and J. Fujita, This Bulletin, **41**, 2224 (1968).

6) B. Bosnich and F. P. Dwyer, *Aust. J. Chem.*, **19**, 2045 (1966); P. H. Crayton and T. A. Mattern, *J. Inorg. Nucl. Chem.*, **13**, 248 (1960); *Inorg. Synth.*, **7**, 207 (1963).

7) H. Siebert, *Z. Anorg. Chem.*, **327**, 63 (1964).

to yellow brown, and then concentrated to about 15 m*l* at about 60°C and cooled. Orange yellow crystalline powder precipitated was filtered off, washed with methanol and air-dried. The aqueous solution of this product was passed through a column (3×30 cm) containing cation exchange resin Dowex 50W-X8 in hydrogen ion form. The column was washed with water and the adsorbed yellow band was eluted with 4% aqueous solution of lithium bromide. The desired complex was eluted first, followed by $[Co(CN)(glyH)_2(dien)]^{2+}$. Each fraction was checked by its visible absorption spectrum. The fractions containing the desired complex were collected and concentrated at 60°C under reduced pressure. A yellow complex, *trans*(O,CN)-$[Co(CN)(gly)(dien)]Br\cdot 3H_2O$ was precipitated by adding methanol, filtered off, washed with water-methanol and methanol and air-dried. The complex was recrystallized from water by adding methanol.

An orange complex $[Co(CN)(glyH)_2(dien)]Br_2\cdot 3H_2O$ was obtained from the fractions eluted later.

Found: C, 20.26; H, 5.46; N, 15.72%. Calcd for $C_9H_{29}N_6O_7CoBr_2$: C, 19.57; H, 5.29; N, 15.22%. The complex which contains two neutral unidentate glycine is less soluble in water than *trans*(O,CN)-$[Co(CN)(gly)(dien)]Br\cdot 3H_2O$.

Method 2: Four grams of *trans*(O,Cl)-$[Co(Cl)(gly)(dien)]ClO_4$ was ground thoroughly and suspended in 30 m*l* of dimethylsulfoxide (DMSO) with mechanical stirring, and 1 g of potassium cyanide was added. The color of the solution changed from reddish violet to orange and a yellowish orange product precipitated. This was filtered off as rapidly as possible and was dissolved in 0.47% hydrobromic acid. The solution was poured on a column containing cation exchange resin Dowex 50W-X8 in hydrogen ion form. The column was washed with water and the adsorbed band was eluted with an aqueous solution containing 20 m*l* of 47% hydrobromic acid and 30 g of lithium bromide in 1000 m*l* of water. A pure complex was obtained from the eluate by the same way as in Method 1.

trans*(O,CN)*-$[Co(CN)(am)(dien)]Br\cdot xH_2O$ (am=α-aibut, L-ala, L-pro, L-val, and L-thr)

The complexes were prepared by Method 1) as for the glycine complex using α-aibutH, L-alaH, L-proH, L-valH and L-thrH instead of glyH.

trans*(O,Cl)*-$[Co(Cl)(gly)(dien)]ClO_4$. *Method 3*: An aqueous solution (30 m*l*) containing 1.5 g of glycine and 0.56 g of sodium hydroxide was added to a suspension of 5.4 g of $[CoCl_3dien]$ in 30 m*l* of warm water (40°C) with mechanical stirring. This was warmed at 65°C until the $[CoCl_3dien]$ dissolved nearly completely, and then filtered. The filtrate was passed through a column containing the same kind of resin as in Method 1. By elution with 3% aqueous solution of sodium perchlorate, the column gave many bands with different colors. The desired complex was obtained from the brownish-violet band eluted first. The brownish-violet eluate was concentrated at 50°C under reduced pressure and cooled. Pure crystals precipitated were filtered off, washed with ice water, water-methanol and methanol, and air-dried.

trans*(O,Cl)*-$[Co(Cl)(am)(dien)]ClO_4\cdot xH_2O$ (am=L-ala, L-pro, L-val, and L-thr)

The complexes were obtained from $[CoCl_3dien]$ and L-alaH, L-proH, L-valH, and L-thrH by Method 3) as for the glycinato complex.

trans*(O,NO$_2$)*-$[Co(NO_2)(gly)(dien)]Cl\cdot H_2O$ *Method 4*: A mixture containing 5.4 g of $[CoCl_3dien]$, 1.5 g of glycine and 0.56 g of sodium hydroxide in 50 ml of water was warmed at 50°C for an hour, and filtered. 1.3 g of sodium nitrite was added to the filtrate and the resulting solution was concentrated to about 25 m*l* at 80°C, filtered and cooled. Brownish-yellow crystals were precipitated by adding 10 m*l* of concd. hydrochloric acid under cooling in an ice bath. They were filtered off, washed with ice water, water-methanol and methanol, and air-dried. The complex was recrystallized from hot water or water-methanol.

Method 5: The complex was also prepared from $[Co(NO_2)_3dien]$ (3.8 g), glycine (1.5 g), sodium hydroxide (0.56 g) and a small amount of activated charcoal, using a method similar to Method 4.

trans*(O,NO$_2$)*-$[Co(NO_2)(am)(dien)]Cl\cdot xH_2O$ (am=α-aibut, L-ala, L-val, L-pro, and L-thr)

The complexes were prepared from $[CoCl_3dien]$ or $[Co(NO_2)_3dien]$ and α-aibutH, L-alaH, L-proH, L-valH, and L-thrH according to the method for the glycinato complex.

Table 1. Chemical analysis of the complexes

Complexes	C, %		H, %		N, %	
	Found	Calcd	Found	Calcd	Found	Calcd
trans(O,CN)-$[Co(CN)(gly)(dien)]Br\cdot 3H_2O$[a]	21.18	21.22	5.61	5.85	17.94	17.68
trans(O,CN)-$[Co(CN)(gly)(dien)]Br\cdot 3H_2O$[b]	21.10	21.22	5.62	5.85	17.65	17.68
trans(O,CN)-$[Co(CN)(α\text{-aibut})(dien)]Br\cdot 2H_2O$[a]	26.41	26.61	6.18	6.20	17.31	17.24
trans(O,CN)-$[Co(CN)(L\text{-ala})(dien)]Br\cdot 2H_2O$[a]	24.49	24.50	5.68	5.91	17.66	17.86
trans(O,CN)-$[Co(CN)(L\text{-pro})(dien)]Br\cdot 2H_2O$[a]	28.38	28.72	6.01	6.03	16.71	16.75
trans(O,CN)-$[Co(CN)(L\text{-val})(dien)]Br$[a]	31.12	31.27	6.33	6.04	18.24	18.23
trans(O,CN)-$[Co(CN)(L\text{-thr})(dien)]Br\cdot 2H_2O$[a]	25.98	25.61	6.06	5.97	15.78	16.59
trans(O,NO$_2$)-$[Co(NO_2)(gly)(dien)]Cl\cdot H_2O$	21.46	21.47	5.77	5.71	20.75	20.87
trans(O,NO$_2$)-$[Co(NO_2)(α\text{-aibut})(dien)]Cl\cdot 2H_2O$	25.10	25.17	6.37	6.60	18.28	18.35
trans(O,NO$_2$)-$[Co(NO_2)(L\text{-ala})(dien)]Cl\cdot H_2O$	24.19	24.05	6.46	6.05	19.83	20.03
trans(O,NO$_2$)-$[Co(NO_2)(L\text{-pro})(dien)]Cl\cdot H_2O$	28.62	28.77	6.08	6.17	18.58	18.64
trans(O,NO$_2$)-$[Co(NO_2)(L\text{-val})(dien)]Cl\cdot H_2O$	28.71	28.62	6.68	6.67	18.32	18.54
trans(O,NO$_2$)-$[Co(NO_2)(L\text{-thr})(dien)]Cl\cdot 2H_2O$	24.17	24.16	6.36	6.34	17.57	17.61
trans(O,Cl)-$[Co(Cl)(gly)(dien)]ClO_4$	19.42	19.42	4.64	4.62	15.08	15.10
trans(O,Cl)-$[Co(Cl)(L\text{-ala})(dien)]ClO_4\cdot H_2O$	20.82	20.86	5.29	5.25	14.09	13.90
trans(O,Cl)-$[Co(Cl)(L\text{-pro})(dien)]ClO_4$	26.25	26.29	5.12	5.15	13.79	13.63
trans(O,Cl)-$[Co(Cl)(L\text{-val})(dien)]ClO_4$	26.12	26.17	5.59	5.61	13.78	13.56
trans(O,Cl)-$[Co(Cl)(L\text{-thr})(dien)]ClO_4$	23.12	23.15	5.12	5.10	13.72	13.50

a) Prepared according to Method 1. b) Prepared according to Method 2.

Results of the chemical analyses of all the new complexes are given in Table 1.

Measurements. Visible and ultraviolet absorption spectra were obtained with a Beckman DU spectrophotometer and a Hitachi EPS-3 recording spectrophotometer. The circular dichroism (CD) curves were recorded with a Model ORD/UV-5 spectrophotometer of Japan Spectroscopic Co. Proton magnetic resonance (PMR) spectra were obtained with a Varian A-60 spectrometer in deuterium oxide, with sodium tetramethylsilane (NaTMS) as an internal reference. All spectral measurements were carried out at room tempertaure.

Results and Discussion

Configuration of the Complexes. As Fig. 1 shows, the first absorption bands of the cyano complexes exhibit no sign of splitting and the absorption curves have a pattern very similar to those of *trans*(O,CN)-[Co(OH$_2$)(CN)en$_2$]$^{2+}$ and *trans*(O,CN)-[Co(OH)(CN)-en$_2$]$^+$ reported in the previous paper.[1] The chloro complexes, on the other hand, give the first absorption bands split into two components at *ca.* 18000 and *ca.* 22000 cm^{-1}. Such a splitting is expected for only the complex in which chloride ion takes the position *trans* to the oxygen atom of amino-acidato group. The *trans*(O,Cl) structure of the chloro complex has been confirmed by a recent X-ray analysis on the [Co(Cl)-(gly)(dien)]ClO$_4$.[8] We thus conclude that all the cyano and chloro complexes we prepared have the structure of *trans*(O,X) type (X=CN$^-$ or Cl$^-$). The data of absorption spectra are summarized in Table 2.

The absorption spectra of the nitro complexes provide no definite information on the structure, but their CD curves are very similar to those of the cyano complexes as is seen in Fig. 2. Thus, it is concluded that the nitro complexes also take the *trans*(O,NO$_2$) structure. This conclusion has been confirmed by X-ray analysis on *trans*(O,NO$_2$)-[Co(NO$_2$)(gly)(dien)]Cl·H$_2$O.[9]

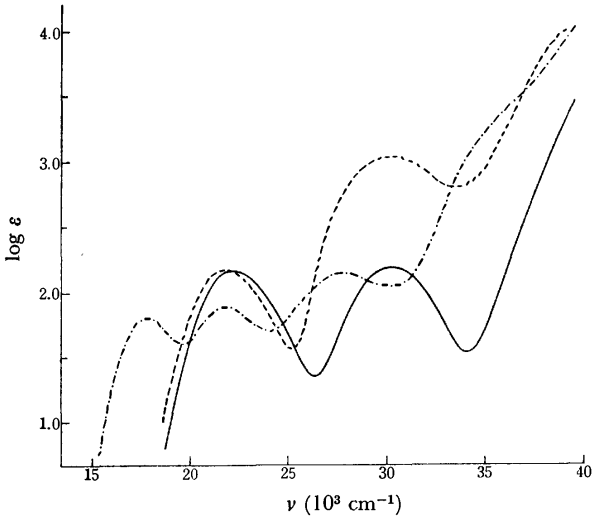

Fig. 1. Absorption spectra of *trans*(O,X)-[Co(X)(gly)(dien)]$^+$ ions in water:
—— CN$^-$, - - - NO$_2^-$, —·— Cl$^-$

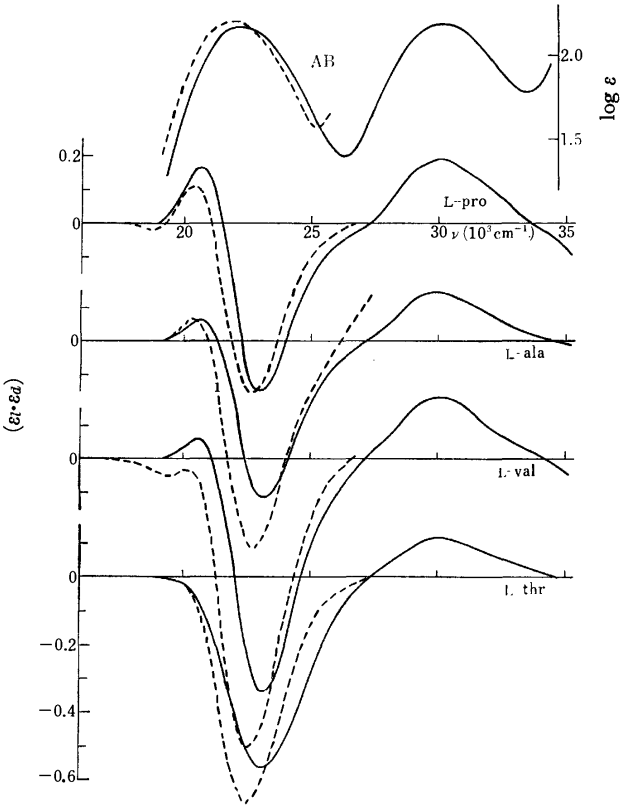

Fig. 2. Absorption(AB) and CD curves of *trans*(O,X)-[Co(X)-(L-am)(dien)]$^+$ ions in water:
—— CN$^-$, - - - NO$_2^-$.

PMR spectra of the complexes in deuterium oxide also support the *trans*(O,X) structure (X=CN$^-$, Cl$^-$, and NO$_2^-$). In the deuterium oxide solutions, hydrogen atoms of the amino groups were deuterated rapidly. Legg and Cooke[10] reported that the ethylene signals of dien coordinated meridionally in Co(III) complexes showed a rather sharp peak in the 181—187 cps region (60 MHz), while those of facially coordinated dien gave broad and complicated peaks in the 156—190 cps region. As Fig. 3 and Table 3 show, the present complexes exhibit sharp signals characteristic of the meridionally coordinated dien in the 179—186 cps region.

Further evidence for the *trans*(O,X) structure can be seen in the CD spectra of the complexes in the region of the first absorption band. Since the complex *trans*-(O,X)-[Co(X)(L-am)(dien)]$^+$, has no configurational chirality around the cobalt(III) ion, the CD in the region of the *d–d* transitions can be brought about by the vicinal effect of the coordinated L-amino-acidato group. Figure 2 shows the CD spectra of the cyano and nitro complexes in the region of the first and second absorption bands. The pattern and magnitude of these CD curves correspond to those of the complexes of the type [Co(NH$_3$)$_4$(L-am)]$^{2+}$,[11] indicating that the present dien complexes have no configurational chirality. This in turn suggests that the dien group in the

8) S. Yamaguchi and S. Ooi, private communication (1970).

9) S. Yamaguchi and S. Ooi, private communication (1969).

10) J. I. Legg and D. W. Cooke, *Inorg. Chem.*, **5**, 594 (1966).

11) T. Yasui, J. Hidaka, and Y. Shimura, This Bulletin, **39**, 2417 (1966).

Table 2. Absorption and circular dichroism data of *trans*(O,X)-[Co(X)(am)(dien)]$^+$ ions in the *d-d* absorption band region[a)]

Complexes	I-Band		II-Band	
	ν^{AB}_{max} (log ε)	ν^{CD}_{ext} ($\varepsilon_l - \varepsilon_d$)	ν^{AB}_{max} (log ε)	ν^{CD}_{ext} ($\varepsilon_l - \varepsilon_d$)
(CN)(L-ala)[c)]	22.1 (2.15)	20.7 ($+0.06_4$) 23.2 (-0.47)	30.2 (2.16)	29.9 ($+0.14_6$)
(CN)(L-pro)[c)]	22.1 (2.12)	20.6 ($+0.16_1$) 23.1 (-0.50)	30.1 (2.19)	30.1 ($+0.19$)
(CN)(L-val)[c)]	22.2 (2.10)	20.6 ($+0.05_7$) 23.2 (-0.69_7)	30.1 (2.12)	30.1 ($+0.18_2$)
(CN)(L-thr)[c)]	22.2 (2.16)	*ca.* 22 sh 23.2 (-0.55_5)	30.1 (2.19)	29.9 ($+0.13$)
(CN)(gly)[c)]	22.2 (2.16)		30.2 (2.19)	
(CN)(gly)[d)]	22.2 (2.16)		30.2 (2.19)	
(CN)(α-aibut)[c)]	22.3 (2.15)		30.3 (2.17)	
(NO_2)(L-ala)	21.7 (2.20)	20.4 ($+0.07$) 22.7 (-0.51)		
(NO_2)(L-pro)	21.6 (2.21)	20.4 ($+0.10_2$) 22.7 (-0.50)		
(NO_2)(L-val)	21.7 (2.19)	19.4 (-0.04_8) 22.6 (-0.84_8)		
(NO_2)(L-thr)	21.9 (2.20)	*ca.* 22 sh 22.6 (-0.67)		
(NO_2)(gly)	21.7 (2.17)			
(NO_2)(α-aibut)	21.8 (2.20)			
(Cl)(L-ala)	18.0 (1.83) 21.9 (1.91)	17.3 ($+0.05_3$) 22.1 (-0.28_6)	27.8 (2.15)	28.0 (-0.14)
(Cl)(L-pro)	17.8 (1.79) 21.6 (1.93)	18.1 ($+0.54$) 21.9 (-0.44_2)	27.2 (2.17)	25.3 ($+0.13_7$) 28.0 (-0.18)
(Cl)(L-val)	18.1 (1.81) 21.9 (1.94)	16.9 (-0.03_8) 22.2 (-0.37_7)	28.2 (2.20)	27.9 (-0.12_7)
(Cl)(L-thr)	18.0 (1.79) 21.8 (1.93)	18.3 (-0.09_4) 22.2 (-0.27)	*ca.* 28 (2.25)	28.0 (-0.09_8)
(Cl)(gly)	17.9 (1.79) 21.8 (1.88)		27.7 (2.14)	

a) The frequencies are given in 10^3 cm^{-1}.
b) Complexes are abbreviated to (X) (am).
c) Prepared from [Co(CN)(SO_3)(NH_3)$_4$] according to Method 1.
d) Prepared from *trans*(O,Cl)-[Co(Cl)(gly)(dien)]$^+$ according to Method 2.

Table 3. Resonance frequency assignments[a)] and integration values from the PMR spectra (60 MHz) of *trans*(O,X)-[Co(X)(am)(dien)]$^+$ dissolved in D_2O

Complexes[d)]	$-CH_3$		$>NCH_2CH_2NH_2$		$-CH_2-$	
	Res. freq. cps	No. of H's	Res. freq.[b)] cps	No. of H's	Res. freq. cps	No. of H's
(CN)(gly)[e)]			179.5	8.0	210.5 213.5	2.0
(CN)(gly)[f)]			179	8.3	210.0	1.7
(Cl)(gly)			185	8.1	216.3	1.9
(NO_2)(gly)			186	8.1	213.4	1.9
(CN)(L-ala)[e)]	86.5[c)] 87.5[c)]	3.2	180.0	7.8	221.0	1.0
(Cl)(L-ala)	85.0[c)]	2.7	182.5	8.4	219.5	0.9
(NO_2)(L-ala)	87.5[c)]	2.5	183.9	8.6	218.5	0.8
(CN)(α-aibut)[e)]	84.2 86.0	5.7	179.2	8.3		
(NO_2)(α-aibut)	87.5	5.7	186	8.3		

a) All frequencies on low-field side of NaTMS (internal reference).
b) The center of rather broad peaks.
c) The center of -CH_3 doublet.
d) Complexes are abbreviated to (X) (am).
e) Prepared from [Co(CN)(SO_3)(NH_3)$_4$] according to Method 1.
f) Prepared from *trans* (O, Cl)-[Co(Cl)(gly)(dien)]$^+$ according to Method 2.

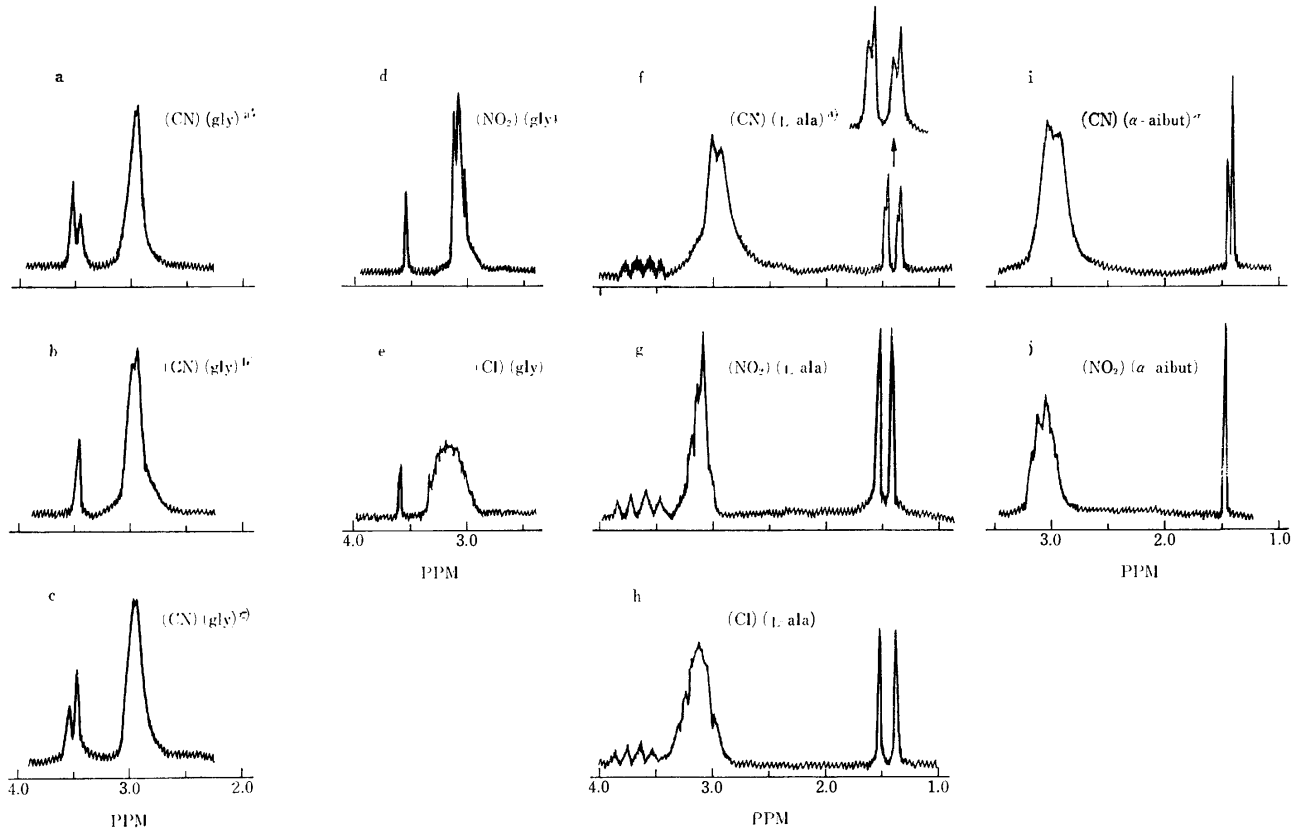

Fig. 3. The PMR spectra (60 MHz) of *trans*(O,X)-[Co(X)(am)(dien)]$^+$ in D_2O. NaTMS was used as an internal reference.
a) Samples prepared according to Method 1: Mixture of *endo* and *exo*(CN,NH) forms.
b) *endo* (CN,NH) form prepared from *endo*(Cl,NH) complex according to Method 2: see text.
c) Sample b isomerized to a mixture of *endo* and *exo*(CN,NH) forms: see text.

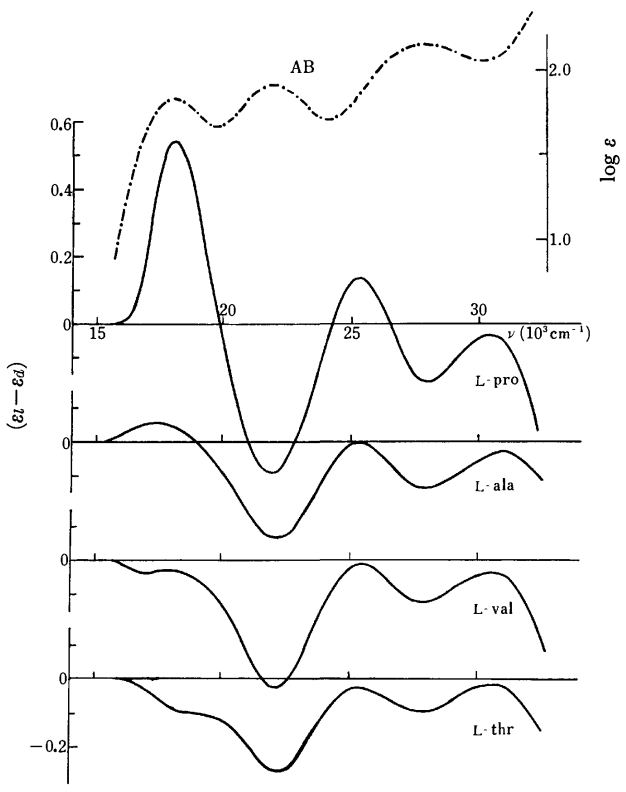

Fig. 4. Absorption (AB) and CD curves of *trans*(O,Cl)-[Co(Cl)(L-am)(dien)]$^+$ ions in water.

present complexes takes a meridional coordination.

Figure 4 shows that the chloro complexes give CD curves differing somewhat from those of the cyano or nitro complexes in the region of the *d–d* absorption bands. Such a difference may be attributed to the larger splitting of the first absorption band of the chloro complex than those of the cyano or nitro complex.[1)]

Conformational Isomerism. As Fig. 3-a shows, *trans*(O,CN)-[Co(CN)(gly)(dien)]$^+$, prepared from [Co(CN)$(SO_3)(NH_3)_4$] by Method 1, gives two kinds of methylene signals due to the glycinato chelate at 210.5 and 213.5 cps. Similarly, *trans*(O,CN)-[Co(CN)(L-ala)-(dien)]$^+$ and *trans*(O,CN)-[Co(CN)(α-aibut)(dien)]$^+$ show two kinds of methyl signals at 86.5 and 87.5, and at 84.2 and 86.0 cps, respectively (Fig. 3-f and 3-i). On the other hand, the corresponding chloro (Fig. 3-e) and nitro (Fig. 3-d) complexes show only one kind of methylene or methyl signal due to the amino-acidato chelate.

The appearance of the two kinds of methylene or methyl signals in the cyano-aminoacidato complexes can be attributed to the existence of two isomers such as shown in Fig. 5. We refer to them as *endo*(X,NH) form and *exo*(X,NH) form in this paper. Such an isomerism is originated from a puckering structure of the dien group and produces a remarkable difference in the direction of the hydrogen atom attached to the central nitrogen atom of dien. As Fig. 5 shows, the direction of this hydrogen atom of the *endo*(X,NH)

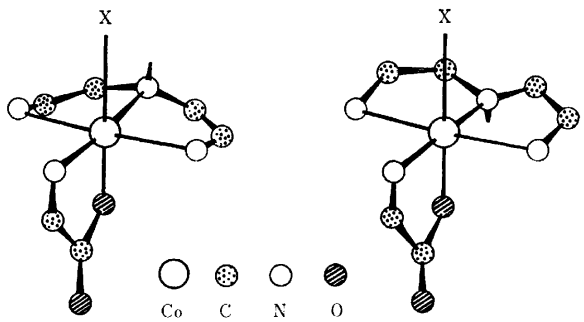

endo (X, NH) form *exo* (X, NH) form

Fig. 5. Two isomers of *trans*(O,X)-[Co(X)(gly)(dien)]$^+$.

isomer is toward the ligand X, while that of the *exo*-(X,NH) isomer toward the oxygen atom of amino-acidato chelate.

In order to confirm the existence of such isomers, we prepared another sample of *trans*(O,CN)-[Co(CN)(gly)-(dien)]$^+$ from *trans*(O,Cl)-[Co(Cl)(gly)(dien)]$^+$, which gave only one methylene signal in its PMR spectrum, according to Method 2. The cyano complex thus prepared gives an identical electronic absorption spectrum with that of the sample prepared from *trans*-[Co-(CN)$(SO_3)(NH_3)_4$], but its PMR spectrum exhibits only one methylene signal. As Fig. 3-b shows, this signal coincides with one of the two signals observed for the sample prepared by Method 1. The result strongly supports the existence of two stable isomers of *endo* and *exo* forms, in the cyano complex. It is not possible to correlate the chemical shift of methylene or methyl signal with the structure of these isomers at present. However, the complexes *trans*(O,Cl)-[Co(Cl)(gly)(dien)]ClO_4[8] and *trans*(O,NO_2)-[Co(NO_2)-(gly)(dien)]$Cl\cdot H_2O$[9] were determined to have the *endo* form by X-ray analysis. Consequently, the *trans*-(O,CN)-[Co(CN)(gly)(dien)]$^+$ prepared from the *trans*-(O,Cl)-[Co(Cl)(gly)(dien)]$^+$ can be assigned to the *endo*(CN,NH) form, since complete isomerization to the *exo* form during synthesis from the *endo* form seems to be very unlikely. The methylene signal of this cyano complex coincides with the higher field component of the doublet observed for the mixture of two cyano isomers prepared from [Co(CN)$(SO_3)(NH_3)_4$].

The isomerization reaction between the *endo* and the *exo* isomers is expected to take place relatively easily in an alkaline solution, since the reaction may involve deprotonation of the secondary amine of the dien group. In fact, the *trans*(O,CN)-[Co(CN)(gly)(dien)]$^+$ which gave only one methylene signal showed two kinds of methylene signals on being treated with aqueous hydroxide (pH 10, 60°C, 6 hr), as shown in Fig. 3-c.

The present isomerism would be attributed to the coordination of X on either of the non-equivalent sides of the N_4 plane involving the puckered rings of dien.[5] Hence, this kind of isomerism can not be substantiated in such complexes as [Co$(NO_2)_3$(dien)],[12] in which both sides of the N_4 plane are occupied by the same NO_2^- ions.

A similar isomerism was found by Gainsford and House[13] for [Co(Cl)(en)(dien)]$^{2+}$ (en=ethylenediamine).

The authors wish to express their thanks to Prof. Kazuo Saito, Tohoku University, for his encouragement throughout this work.

12) Y. Kushi, K. Watanabe, and H. Kuroya, This Bulletin, **40**, 2985 (1967).

13) A. R. Gainsford and D. A. House, *Inorg. Chim. Acta*, **3**, 367 (1969).

Rapid Solvent Extraction and Direct Spectrophotometric Determination of Lead(II) with 1,1,1-Trifluoro-4-(2-thienyl)-4-mercaptobut-3-en-2-one

S. B. Akki and S. M. Khopkar

Department of Chemistry, Indian Institute of Technology, Bombay-76, India

(Received April 19, 1971)

The thio derivative of 2-thenoyltrifluoroacetone 1,1,1-trifluoro-4-(2-thienyl)-4-mercaptobut-3-en-2-one (STTA) is used for the simultaneous extraction and direct colorimetric determination of lead. About 100 μg of lead is quantitatively extracted, at pH 6.5, with 10 m*l* of 0.0020M STTA-CCl_4 as a bright orange colored complex, which can be measured spectrophotometrically at 480 nm. The system conforms to Beer's law over the concentration range of 1—40 μg/m*l* of lead(II). The color of the complex is stable for 60 hr. Lead can be quantitatively extracted and determined in the presence of a number of ions. The method is made selective by using some sequestering agents and carrying out selective extractions with mesityl oxide. The procedure is found to be suitable for the analysis of lead in gun metal and solder.

Thiothenoyltrifluoroacetone (1,1,1-trifluoro-4-(2-thienyl)-4-meracptobut-3-en-2-one) was used for the solvent extraction of several transition elements.[1] Lead also forms bright orange colored complex with this reagent around pH 6.5 which can be measured spectrophotometrically at 480 nm. The above reagent shall for the sake of brevity be assigned the symbol STTA indicating that it is a monosulphur substituted derivative of thenoyltrifluoroacetone commonly known as TTA. It has structural formula as:

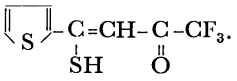

The various β-diketones used as extractants for lead are acetylacetone,[2] benzoylacetone, dibenzoylmethane,[3] and thenoyltrifluoroacetone.[4] Extraction with acetylacetone was not quantitative, while that with dibenzoylmethane or benzoylacetone was possible only in alkaline media. Extraction with thenoyltrifluoroacetone needed high reagent anion concentration. Several other chelating agents[5] such as oxine, oximes, cupferron, azonaphthols, dithizone, neutral organophosphorus compounds were used for the extraction of lead to little advantage.

The method proposed by us is simple and rapid, and it affords clean-cut separation of lead from other ions. The method is sensitive and applicable at tracer concentrations. It is also found to be applicable to the analysis of lead in alloys such as gun metal or solder.

Experimental

Apparatus and Reagents. A type Cϕ4 quartz spectrophotometer with 10 mm matched cells; Cambridge pH meter; Wrist action flask shaker. 1,1,1-Trifluoro-4-(2-thienyl)-4-mercaptobut-3-en-2-one (STTA) was synthesised from 2-thenoyltrifluoroacetone (Fluka, A. G.) by the procedure of Berg and Reed.[6] About 0.0020M reagent in carbon tetrachloride was utilised. The reagent was always preserved in a refrigerator.

A stock solution of lead nitrate was prepared by dissolving about 1.6 g of lead nitrate (May and Baker, England) in 1 *l* of distilled water containing 0.01% nitric acid. The solution was standardised gravimetrically as the chromate[7] and was found to contain 1 mg of lead per m*l*. The dilute solution containing 100 μg/m*l* of lead was prepared by ten fold dilution.

A buffer solution of pH 6.5 was prepared by dissolving 77 g of ammonium acetate in water, acidified with acetic acid to pH 6.5, and diluted to 1 *l*.

General Procedure. An aliquot of lead nitrate solution (containing about 100 μg of lead) was taken. It was treated with 10 m*l* of buffer solution of pH 6.5 and then diluted with water to 25 m*l*. For the study of extraction as a function of pH, the buffer solution was not added except when pH 6.5 was required. In such cases the pH of lead nitrate solution was adjusted to the desired value with 0.01N nitric acid and 0.01N ammonium hydroxide, the pH meter being used and then the solution was diluted as above. For the study of the effect of diverse ions, the solution containing the foreign ion under investigation was added prior to the buffer solution. The aqueous solution was then transferred into a 250 m*l* separatory funnel. It was extracted for 10 min, on a wrist action flask shaker, with 10 m*l* of 0.0020M STTA solution in carbon tetrachloride. The solution was allowed to settle and separate into two layers. The bright orange colored organic phase was withdrawn in a 10 m*l* volumetric flask. It was then measured at 480 nm against the reagent blank. The amount of lead was then computed from the calibration curve.

Results and Discussion

Absorption Curve. The absorption spectrum of a solution of lead(II)-STTA complex (lead$=4.33\times10^{-4}$M) extracted at pH 6.5 is illustrated in Fig. 1; the reagent blank being used as a reference solution. The spectrum of the reagent blank against carbon tetrachloride is also given. The bright orange lead(II) chelate solution shows maximum difference in absorbance, between itself and the reagent blank at 480 nm.

1) V. M. Shinde and S. M. Khopkar, *Chem. Ind.*, **1967**, 1785.
2) A. Krishen and H. Freiser, *Anal. Chem.*, **29**, 288 (1957).
3) J. Stary and E. Hladky, *Anal. Chim. Acta*, **28**, 227 (1963).
4) F. Hagemann, *J. Amer. Chem. Soc.*, **72**, 768 (1950).
5) A. K. De, S. M. Khopkar, and R. A. Chalmers, "Solvent Extraction of Metals," Van Nostrand Reinhold Co., London (1970).
6) E. W. Berg and K. P. Reed, *Anal. Chim. Acta*, **36**, 372 (1966).
7) A. I. Vogel, "The Text Book of Quantitative Inorganic Analysis," 3rd Ed. Longmans and Green, (1968), p. 484.

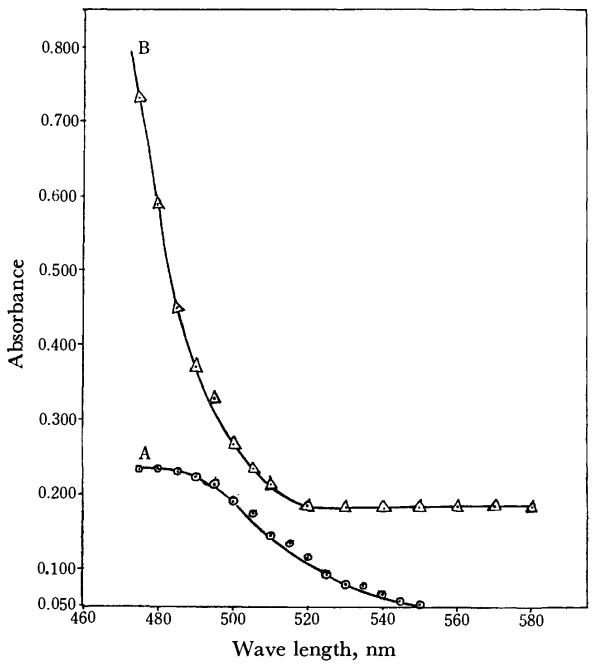

Fig. 1. Absorption spectra of (A) lead(II) thiothenoyltrifluoroacetone in carbon tetrachloride *vs.* reagent blank and (B) reagent blank *vs.* carbon tetrachloride.
Pb(II) 4.83×10^{-4}M, STTA=1×10^{-3}M, pH=6.5.

Table 1. Extraction of lead(II)-STTA complex as a function of pH
Pb(II)=100 μg; 0.0020M STTA-CCl_4

pH	Extraction (%E)	Distribution ratio (D)
0.5	10.6	0.30
1.0	10.6	0.30
1.5	10.6	0.30
2.0	14.8	0.44
2.5	19.1	0.59
3.0	23.4	0.76
3.5	23.4	0.76
4.0	29.8	1.06
4.5	29.8	1.06
5.0	63.8	4.41
5.5	74.5	7.31
6.0	93.6	36.56
6.1	95.0	47.50
6.2	97.9	116.50
6.3	97.9	116.50
6.4	100.0	∞
6.5	100.0	∞
6.6	100.0	∞
6.7	97.9	116.50
6.8	85.1	14.17
6.9	85.1	14.17
7.0	85.1	14.17
7.5	85.1	14.17
8.0	85.1	14.17
8.5	63.8	4.41
9.0	48.9	2.40

The curve steadily falls and the absorbance of the complex becomes negligible beyond 600 nm. The reagent blank itself has strong absorbance till 460 nm and falls beyond this wavelength. Thus all the absorbance measurements were performed at 480 nm. The absorptivity at 480 nm is 4.803×10^2, calculated on the basis of lead content of 4.83×10^{-4}M, with an absorbance of 0.235 at 480 nm, when 1 cm cell was used.

Extraction as a Function of pH. The liquid-liquid extraction behaviour of lead(II)-STTA system was studied in the pH range of 0.5—9.0. The extraction is quantitative at pH of 6.4—6.6 (Table 1, Fig. 3). Beyond this pH the extraction decreases and becomes negligible at pH 9.0. Therefore, all extractions were carried out at pH 6.5 using the acetate buffer to facilitate rapid quantitative extractions.

Table 2. Applicability of Beer's law

Lead (II) taken, μg	Absorbance		
	475 nm	480 nm	490 nm
10	0.055	0.065	0.060
25	0.110	0.110	0.095
50	0.135	0.135	0.120
100	0.235	0.235	0.225
150	0.300	0.310	0.275
200	0.375	0.375	0.350
250	0.460	0.460	0.420
300	0.550	0.560	0.510
400	0.650	0.650	0.600

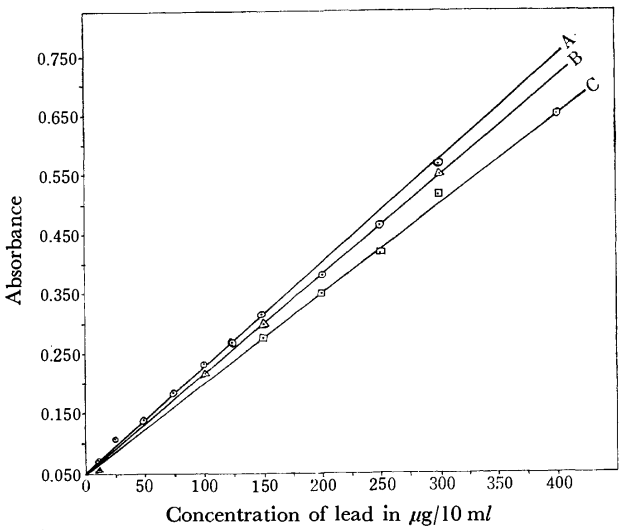

Fig. 2. Beer's law curve. pH=6.5
A=480 nm, B=475 nm, C=490 nm

Beer's Law Curve. Different amounts of lead(II) were taken and extracted at pH 6.5 as above. Their corresponding absorbances were measured at various wavelengths, *viz.* 475, 480, and 490 nm, to observe how colored system holds in the Beer's law (Table 2, Fig. 2). The Pb(II)-STTA system conforms to Beer's law over the concentration range of 1—40 μg of lead per m*l* at 480 nm.

Stability of Coloration. The absorbance of Pb(II)-STTA complex was measured at intervals of 0, 0.5, 1, 2, 3, 6, 12, 24, 48, 60, 72, and 96 hr. The absorbance is stable up to 60 hr, beyond which it undergoes about

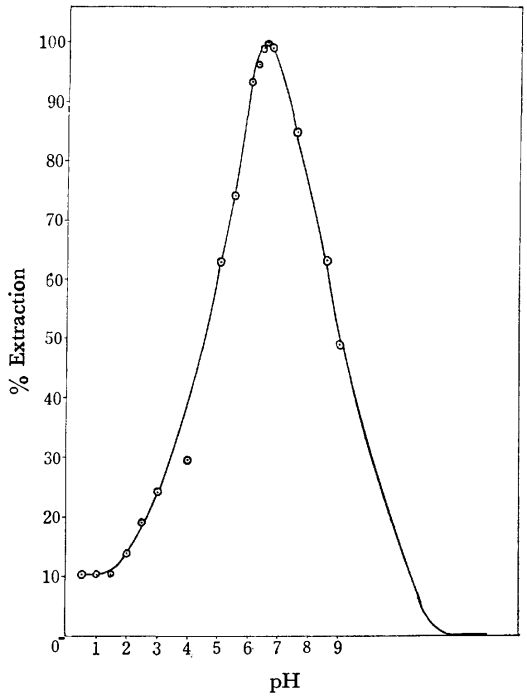

Fig. 3. Extraction as the function of pH.

4% decomposition. It is recommended therefore to measure the absorbance of the complex within 60 hr of extraction.

Reagent Concentration. With other factors being constant, the concentration of STTA was varied from 5.0×10^{-4}M to 2.0×10^{-3}M. The results in Table 3 indicate that the optimum reagent concentration is 10 m*l* of 2.0×10^{-3}M. Similarly, the absorbance is essentially constant with higher reagent concentration *e.g.* 3.0×10^{-3}M or 4.0×10^{-3}M. Extraction is incomplete with dilute solution of the reagent *viz.* 5.0×10^{-4}M, 1.0×10^{-3}M. The variation in volume of 2.0×10^{-3}M reagent showed that 10 m*l* of this reagent is quite adequate for quantitative extraction of lead.

Table 3. Effect of reagent concentration
(100 μg of Pb(II) after extraction with 0.0020 M STTA-CCl_4 at pH 6.5 gives an absorbance of 0.235±0.010 in 10 m*l* of solution.)

STTA concentration (M) $\times 10^{-3}$	STTA added (m*l*)	Absorbance at 480 nm
0.5	10	0.120
1.0	10	0.180
1.5	10	0.230
2.0	10	0.235
3.0	10	0.245
4.0	10	0.245
2.0	15	0.190
2.0	7.5	0.185
2.0	5.0	0.185

Diverse Ions. The effect of the presence of several ions on the extraction behaviour of lead was studied (Table 4). The tolerance limit was set at the amount required to cause ±2.0% error in the lead recovery. It was observed that the alkaline earths, alkali metals, fluoride, tartrate, ascorbate etc. are tolerated in the ratio of 1: 50; while thallium(III), aluminium, beryllium, arsenite, cyanide, sulphite, thiocyanate, malonate, citrate are tolerated in the ratio of 1: 10. Some elements form characteristic colored complexes with the reagent and show interferences. They are mercury, cadmium, palladium, noble metals, cobalt, nickel, and

Table 4. Effect of diverse ions
Pb(II) = 100 μg; pH=6.5; STTA=0.0020M

Foreign ions	Added as	Tolerance limit μg
Tl^{3+}	$Tl(NO_3)_3$	1000
Cu^{2+}	$CuSO_4\cdot5H_2O$	250
Sb^{3+}	$SbCl_3\cdot3H_2O$	250[a]
Bi^{3+}	$Bi(NO_3)_3\cdot5H_2O$	None
Sn^{2+}	$SnCl_2\cdot2H_2O$	None
Pt^{4+}	$H_2PtCl_6\cdot xH_2O$	75
Rh^{3+}	$RhCl_3\cdot3H_2O$	250[a]
Fe^{3+}	$FeCl_3\cdot6H_2O$	250[c]
Cr^{3+}	$Cr_2(SO_4)_3\cdot18H_2O$	100[c]
Al^{3+}	$Al(NO_3)_3\cdot9H_2O$	1000[b]
Zn^{2+}	$Zn(NO_3)_2\cdot4H_2O$	250[c]
Mn^{2+}	$MnCl_2\cdot4H_2O$	100[b]
Th^{4+}	$Th(NO_3)_4\cdot4H_2O$	250[a]
Zr^{4+}	$Zr(NO_3)_4$	100[a]
$Mo_7O_{24}^{6-}$	$(NH_4)_6Mo_7O_{24}\cdot12H_2O$	100[c]
U^{6+}	$UO_2(NO_3)_6\cdot6H_2O$	100
VO_3^-	NH_4VO_3	250[c]
Be^{2+}	$Be(NO_3)_2$	1000
Ti^{4+}	$Ti(SO_4)_2$	None
Re^{7+}	$KReO_4$	100[c]
Ge^{4+}	$GeCl_4$	100[b]
Ca^{2+}	$Ca(NO_3)_2\cdot4H_2O$	5000
Sr^{2+}	$SrCl_2\cdot6H_2O$	5000
Ba^{2+}	$BaCl_2\cdot2H_2O$	5000
Mg^{2+}	$MgSO_4\cdot7H_2O$	5000
Li^+	LiCl	5000
Rb^+	RbCl	5000
Cs^+	CsCl	5000
WO_4^{2-}	Na_2WO_4	100
AsO_3^{2-}	Na_2AsO_3	1000
TeO_3^{2-}	Na_2TeO_3	None
SeO_3^{2-}	Na_2SeO_3	200
F^-	NaF	5000
CN^-	KCN	1000
$EDTA^{4-}$	EDTA (disodium salt)	None
$S_2O_3^{2-}$	$Na_2S_2O_3\cdot5H_2O$	250
Br^-	NaBr	500
SO_3^{2-}	Na_2SO_3	2500
NO_2^-	$NaNO_2$	5000
SCN^-	KSCN	2500
$C_2O_4^{2-}$	$H_2C_2O_4\cdot2H_2O$	None
$Malon^{2-}$	Malonic acid	2500
$Tart^{3-}$	Tartaric acid	5000
Cit^{3-}	Citric acid	1000
$Ascorb^-$	Ascorbic acid	5000

Masked with (a) citric acid; (b) sodium fluoride; (c) selective extraction with pure mesityl oxide for Fe, at 3.5M HCl; Cr, from 1M HCl containing 2.5M KCl; Mo, form 1M HCl and 8M LiCl; V, from 6M HCl and Re, from 1M HCl and KCl.[5]

cerium. However, the interference of ions such as antimony, rhodium, and thorium can be eliminated by using masking agents, while alkali fluoride can mask interferences due to aluminium, manganese and germanium. In addition, the process of selective extraction[5] with mesityl oxide (4-methyl-3-pentene-2-one) can eliminate interferences due to iron(III), chromium(III), molybdenum(VI), vanadium(V), and rhenium(VI), (Table 4). The interference due to copper or zinc can be similarly removed by prior extraction with acetylacetone,[3,8] or with 8-hydroxyquinoline-chloroform,[9,10] respectively.

Separation of Lead from Gun Metal. 0.692 g of gun metal was dissolved in concentrated nitric acid. Tin was removed as metastannic acid and it was determined gravimetrically. The filtrate was evaporated to dryness. The residue was dissolved in water and made up to 1 *l*. One milliliter of the diluted solution was then taken and adjusted to pH 2.5, and extracted with (10 $\times$5) m*l* of 0.1 M acetylacetone-benzene solution to remove copper.[3,8] The aqueous phase was then adjusted to pH 4.5 and extracted with (10$\times$3) m*l* of 0.01 M oxine-chloroform to remove zinc.[9,10] Finally the aqueous phase containing lead was taken and mixed with 10 m*l* of acetate buffer of pH 6.5, and extracted with 10 m*l* of 0.0020 M STTA in carbon tetrachloride. The bright orange colored Pb(II)-STTA complex was measured spectrophotometrically at 480 nm. The percentage of lead was found to be 4.90, 4.98, and 4.96 as against 5.0%.

Separation of Lead from Solder. About 0.5 g of the solder was dissolved in minimum volume of concentrated nitric acid. Tin was then removed as the insoluble residue of metastannic acid. The filtrate was evaporated to dryness, extracted with water and made up to 1 *l*. Two milliliters of this diluted solution was taken and mixed with 5% citric acid to complex antimony. Then 10 m*l* of buffer solution (pH 6.5) was added, and lead was extracted with 10 m*l* of 0.0020 M STTA-carbon tetrachloride and measured at 480 nm. The percentage of lead was found to be 58.2, 59.3, and 60% as against 59.5%.

Recommended Procedure and Precision. Take an aliquot of the solution containing 10—400 μg of lead in a separatory funnel. Add 10 m*l* of buffer solution of pH 6.5 to and shake it for 10 min with 10 m*l* of 0.0020 M STTA-carbon tetrachloride solution. Allow the layers to settle. Separate the aqueous layer into the beaker and organic layer into 10 m*l* volumetric flask. Then measure the absorbance of bright orange colored lead-(II)-STTA complex at 480 nm against the reagent blank. Calculate the lead concentration from the calibration curve.

In six runs with 100 μg of lead(II) the absorbance found was 0.235$\pm$0.010. The standard deviation was $\pm$1.2%.

Table 5. Accuracy data

Lead taken μg	Absorbance at 480 mμ	Lead found μg	% Error
30	0.115	30	0
40	0.125	41	2.0
60	0.170	62	3.3
110	0.250	112	2.0
175	0.360	175	0
275	0.525	273	3.5
		Av. Error = $\pm$1.8%	

Different amounts of lead(II) were taken and determined by the recommended procedure. The results (Table 5) are accurate to within $\pm$1.8%. Thus the proposed method has fairly good precision and accuracy within $\pm$1.8%. The total operation for each run requires only 25—30 min. The sensitivity of the method by Sandell's definition is 0.5 μg/cm^2 per m*l* of solution.

8) A. Krishen and H. Freiser, *Anal. Chem.*, **31**, 923 (1959).
9) J. Stary, *Anal. Chim. Acta*, **28**, 132 (1963).
10) F. C. Chou, Q. Fernando, and H. Freiser, *Anal. Chem.*, **37**, 361 (1965).

The Preparation of Bis(dimethylglyoximato)nitrosylcobalt(II) and its Conversion into the Nitro Complex

Motonori TAMAKI, Isao MASUDA, and Koichiro SHINRA

Department of Applied Chemistry, Faculty of Engineering, Osaka University, Yamada-kami, Suita

(Received June 21, 1971)

The preparation of diamagnetic $Co^{II}(dmgH)_2NO$ (dmgH=dimethylglyoximato monoanion) is reported. The complex shows the IR absorption band of NO at 1641 cm^{-1}, indicating a neutral NO ligand in the complex. The IR and electronic spectra are consistent with the structure of the penta-coordinate, the square-pyramidal configuration of the complex. In the presence of oxygen and water, the complex is oxidized rapidly ($NO \rightarrow NO_2^-$, $Co(II) \rightarrow Co(III)$) and converted into $Co^{III}(dmgH)_2NO_2 \cdot OH_2$. During the reaction, a complex formulated as $[Co^{II}(dmgH)_2NO \cdot OH_2][Co^{III}(dmgH)_2NO_2] \cdot 2H_2O$ is obtained. It is considered that, in the complex, the Co(II) is bound with the Co(III) through a NO bridge. The assignments of the IR spectra have been made using ^{15}NO and $^{15}NO_2$.

Thus far, many transition metal nitrosyl complexes have been prepared.[1] The low-spin Co(II) complexes with square-planar configurations are known to bind NO, thus forming diamagnetic, penta-coordinate Co(II) complexes with square-pyramidal configurations, such as CoAE(NO), CoSalen(NO), and $Co(dtc)_2(NO)$.[2,3] Recently, Schrauzer and Windgassen isolated planar $Co(dmgH)_2$,[2,4] with a magnetic moment of 1.70 B.M.

In this paper, the preparation and properties of $Co^{II}(dmgH)_2NO$ will be described. Of the transition-metal nitrosyl complexes with the same type of structure, the present complex is anomalous in that it is oxidized easily to form the nitro-Co(III) complex, $Co^{III}(dmgH)_2NO_2 \cdot OH_2$.

Experimental

Preparation of the Complexes. Bis(dimethylglyoximato)-nitrosylcobalt(II), $Co^{II}(dmgH)_2NO$; Complex I: a) $Co(CH_3COO)_2 \cdot 4H_2O$ (2.5 g) was dissolved in 30 m*l* of methanol, and the solution was saturated with NO at 0°C. Into this solution we stirred, drop by drop, dimethylglyoxime (2.3 g) suspended in 60 m*l* of ethanol. Bubbling NO into the solution for about 2 hours resulted in the precipitation of a black compound. The NO dissolved in the solution was driven off by nitrogen, then the precipitates were collected on a filter and washed with a small amount of water under a nitrogen stream. Three grams of a black, crystalline complex, I, were thus obtained.

Found: Co, 18.30; C, 29.91; H, 4.77; N, 21.69%. Calcd for $CoC_8H_{14}N_5O_5$: Co, 18.46; C, 30.10; H, 4.43; N, 21.95%. The same complex was obtained in a similar way in an acetone solution.

b) One gram of $Co(dmgH)_2$[3] was dissolved in 80 m*l* of methanol, and then NO was bubbled into the solution for about one hour with ice cooling, by which time the solution turned a brownish-black. After the remaining NO had been expelled with nitrogen, the solution was concentrated to 20 m*l* *in vacuo* at 50°C, thus leaving a crystalline precipitate of a brownish-black color. Yield: 0.5 g. The complex was proved to be identical with the complex I by a study of its IR spectral data.

Complex II: One gram of the complex I was quickly dissolved in 1 *l* of ether at room temperature, then the undissolved complex was filtered off. When the complex stood in air for a few minutes, yellowish-brown needles (complex II) were precipitated. Yield: 0.7 g.

Found: Co, 16.60; C, 27.08; H, 4.82; N, 19.51%. Calcd for $Co_2C_{16}H_{34}N_{10}O_{14}$: Co, 16.64; C, 27.12; H, 4.85; N, 19.78%. The complex II is soluble in methanol, tetrahydrofuran, and acetonitrile, but it is, unlike the complex I, sparingly soluble in benzene and insoluble in chloroform and ether.

The complex II was also obtained from a dichloromethane solution. One gram of the complex I was dissolved in 200 m*l* of dichloromethane, after which the solution was allowed to stand in air for about 24 hours (the solution had been concentrated to about 50 m*l*). Yellowish-brown needles, 0.7 g were thus separated. Elementary analysis and IR spectrum indicated the compound to be identical with the complex II obtained from ether solution.

Found: Co, 16.70; C, 27.22; H, 4.81; N, 19.84%. Calcd for $Co_2C_{16}H_{34}N_{10}O_{14}$: Co, 16.64: C, 27.12; H, 4.85; N, 19.78%.

Bis(dimethylglyoximato)nitroaquocobalt(III), $Co^{III}(dmgH)_2NO_2 \cdot OH_2$. One gram of the complex II was dissolved in a mixture of 150 m*l* of acetone and 10 m*l* of water. The solution was refluxed at 70—80°C for 10 hours, and then evaporated to 10 m*l* *in vacuo* to leave a brown precipitate (complex III). Yield: 0.8 g. This complex could be recrystallized from acetone.

Found: Co, 16.65; C, 27.34; H, 4.54; N, 20.00%. Calcd for $CoC_8H_{16}N_5O_7$: Co, 16.68; C, 27.20; H. 4.58; N, 19.83%. The complex III is soluble in methanol and acetonitrile, but insoluble in chloroform, ether, and benzene. The molecular weight, determined in an acetonitrile solution at 37°C by means of a Vapor Pressure Osmometer, was 341, corresponding to the value of 353 calculated on the basis of the above formula.

The complex III was also separated from an acetone solution of the complex II when it stood in air for two days.

The results of elementary analysis and the IR and UV spectral data agreed with those obtained for the same com-

1) For a comprehensive survey on transition metal nitrosyl complexes, see B. F. G. Johnson and J. A. McCleverty, *Progr. Inorg. Chem.*, **7**, 277 (1966).

2) The following abbreviations are used in the present paper. dmgH: dimethylglyoximato monoanion, AE: bis(acetylacetone)-ethylenediiminato dianion, BE: bis(benzoylacetone)ethylenediiminato dianion, Salen: bis(salicylaldehyde)ethylenediiminato dianion, and dtc: *N,N*-dimethyldithiocarbamato monoanion.

3) a) M. Tamaki, I. Masuda, and K. Shinra, This Bulletin, **42**, 2858 (1969). b) A. Earnshaw, P. C. Hewlett, and L. F. Larkwortly, *J. Chem. Soc.*, **1965**, 4718. c) F. A. Miller and C. H. Wilkins, *Anal. Chem.*, **24**, 1253 (1952); R. L. Carlin, F. Canziani, and W. K. Bratton, *J. Inorg. Nucl. Chem.*, **26**, 898 (1964).

4) G. N. Schrauzer and R. J. Windgassen, *Chem. Ber.*, **99**, 602 (1966).

pound prepared by Tschugaeff.[5]

^{15}NO-, and $^{15}NO_2$-Substituted Complexes. The (^{15}NO)-complex I was synthesized similarly by using ^{15}NO, generated from $K^{15}NO_3$ (97%).[6] The (^{15}NO)($^{15}NO_2$)-complex II and the ($^{15}NO_2$)-complex III were obtained from the (^{15}NO)-complex I. (^{15}NO)-complex I; Found: C, 29.01; H, 4.58; N, 21.92%. Calcd: C, 30.01; H, 4.42; N, 22.18%.

(^{15}NO)($^{15}NO_2$)-complex II; Found: C, 26.84; H, 4.38; N, 19.02%. Calcd: C, 27.12; H, 4.85; N, 19.78%.

($^{15}NO_2$)-complex III; Found: C, 27.33; H, 4.57; N, 19.91%. Calcd: C, 27.13; H, 4.56; N, 20.05%.

Measurements. The IR spectra were measured in Nujol or in hexachlorobutadiene, with a Hitachi 225 grating spectrometer for the 4000—200 cm^{-1} region and a JASCO IR-G spectrometer for the 4000—400 cm^{-1} region. The thermogravimetric analysis was carried out by using a Rigaku-denki thermobalance at a heating rate of 2°C/min under a nitrogen stream. The magnetic susceptibilities were measured at room temperature by the Gouy method. A nickel chloride solution was used as the calibrant. The electronic absorption spectra were obtained with a Hitachi EPS-3 spectrophotometer.

Results and Discussion

Complex I. The elementary analysis shows that the complex I has a composition corresponding to $Co(dmgH)_2NO$. The physical and chemical data, to be discussed below, agree with a structure where NO is bound axially to the central metal ion of the planar $Co^{II}(dmgH)_2$. As is seen in the IR spectrum in Fig. 1, $Co(dmgH)_2NO$ shows an absorption band at 1641 cm^{-1} which can be assigned to the NO stretching frequency.[7] The NO band observed in this region has been discussed as an indication of the neutral NO ligand in the complexes.[3a] Upon replacing the NO ligand with ^{15}NO, this band shifts to 1615 cm^{-1} (Fig. 1 and Table 1). Besides the above band, the bands at 575 cm^{-1} and 540 cm^{-1} are also observed to shift slightly to lower wave numbers. The IR spectral feature of $Co(dmgH)_2NO$ in the 1600—700 cm^{-1} region resembles that of the planar, metal complexes including dimethylglyoximato, such as $Ni^{II}(dmgH)_2$,[8] $Cu^{II}(dmgH)_2$,[9] and $[Co^{III}(dmgH)_2LL'](L,L'=Cl$ and/or $NH_3)$.[9]

The electronic absorption spectrum of the complex measured in a chloroform solution is presented in Fig. 2. The spectrum shows an absorption band at 20×10^3 cm^{-1} with $\log\varepsilon \fallingdotseq 2.8$. This band may be com-

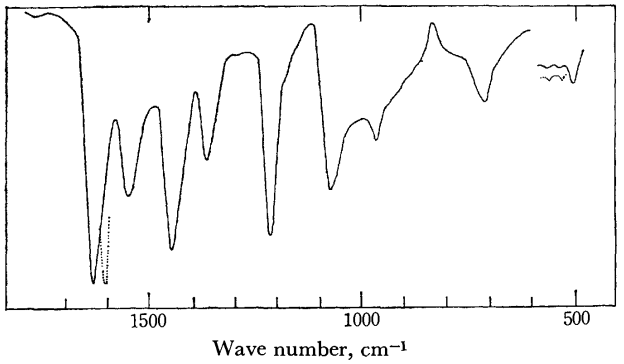

Fig. 1. IR spectra of $Co^{II}(dmgH)_2NO$ (——) and $Co(dmgH)_2$-(^{15}NO) (·····) in Nujol.

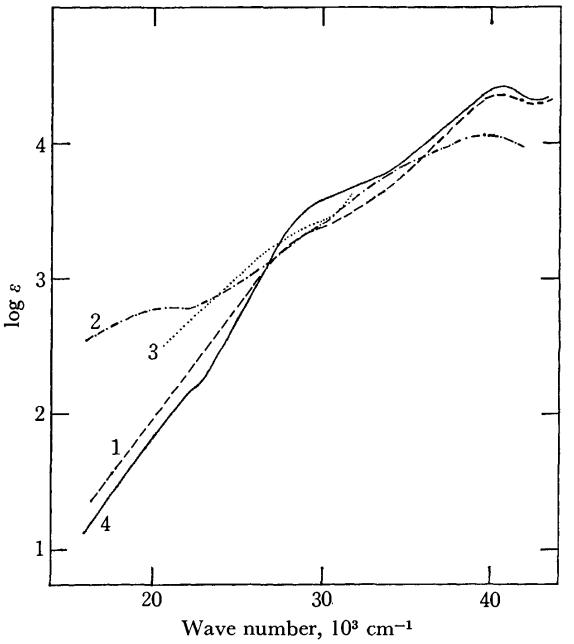

Fig. 2. Electronic spectra.
$Co^{II}(dmgH)_2NO$; curve 1 (– – –) in water, curve 2 (– · –) in $CHCl_3$, and curve 3 (·····) in deaerated water. Co^{III}-$(dmgH)_2NO_2\cdot OH_2$; curve 4 (——) in water.

Table 1. Characteristic frequencies in the IR spectra[a] (cm^{-1})

	ν(NO)	$\nu_{as}(NO_2)$	$\nu_s(NO_2)$	δ(ONO)	$\rho_w(NO_2)$
Complex I:					
$Co^{II}(dmgH)_2NO$	1641				
$Co^{II}(dmgH)_2(^{15}NO)$	1615				
Complex II:					
$[Co^{II}(dmgH)_2NO\cdot OH_2][Co^{III}(dmgH)_2NO_2]\cdot 2H_2O$	1628	1453	1322	820	618
$[Co^{II}(dmgH)_2(^{15}NO)\cdot OH_2][Co^{III}(dmgH)_2(^{15}NO_2)]\cdot 2H_2O$	1600	1415	1301	812	603
Complex III:					
$Co^{III}(dmgH)_2NO_2\cdot OH_2$		1453	1321	819	618
$Co^{III}(dmgH)_2(^{15}NO_2)\cdot OH_2$		1416	1300	812	604

a) Obtained in Nujol and hexachlorobutadienes mulls at room temperature.

5) L. Tschugaeff, *Chem. Ber.*, **41**, 2226 (1908).
6) E. Miki, T. Ishimori, H. Yamatera, and H. Okuno, *Nippon Kagaku Zasshi*, **87**, 703 (1966).
7) J. Lewis, R. J. Irving, and G. Wilkinson, *J. Inorg. Nucl. Chem.*, **7**, 32 (1958); W. P. Griffith, J. Lewis, and G. Wilkinson, *ibid.*, **7**, 38 (1958).
8) R. Bling and D. Hadzi, *J. Chem. Soc.*, **1958**, 4536.
9) A. Bigotto, G. Costa, V. Galasso, and G. De. Alti, *Spectrochim. Acta*, **26A**, 1939 (1970).

parable to the band which has been taken as an indication of the square-pyramidal configuration of the complex, as in the cases of CoAE(NO),[3a] CoSalen(NO),[3a] or RCoSalen (R=C_2H_5 and C_6H_5),[10] though the assignment of these transitions has not yet been clarified. The diamagnetic property of the present complex is consistent with the above spectral data, both IR and electronic. Thus, this evidence has led us to propose a square-pyramidal configuration for the $Co(dmgH)_2NO$ complex.

As has been described in the Experimental part, $Co(dmgH)_2NO$ is easily converted into the complex III, which can be formulated as $Co(dmgH)_2NO_2\cdot OH_2$. The molecular weight, 341, determined in acetonitrile, is consistent with this formula. The electronic spectra in an aqueous solution and the IR spectrum are identical with those of $Co^{III}(dmgH)_2NO_2\cdot OH_2$,[11] which has been synthesized by Tschugaeff[5] in a different way. Four IR absorption bands, which are characteristic of the nitro group in the complexes,[12] $\nu_{as}(NO_2)$, $\nu_s(NO_2)$, $\delta(ONO)$, and $\rho_w(NO_2)$ are assigned for the complex III at 1453, 1321, 819, and 618 cm^{-1} respectively (Fig. 3 and Table 1). The above assignments have been confirmed by the shifts of the bands to a lower frequency upon replacing the $^{15}NO_2$. It is worth noticing that the band for $\rho_w(NO_2)$ can clearly be assigned by ($^{15}NO_2$)-substitution indicating that the NO_2 group coordinates through nitrogen.[13]

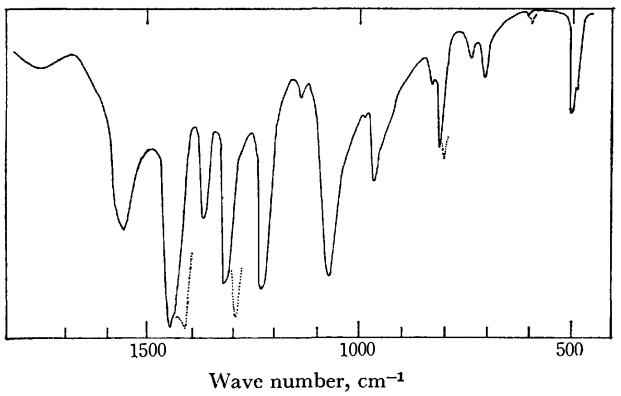

Fig. 3. IR spectra of $Co^{III}(dmgH)_2NO_2\cdot OH_2$ (——) and $Co^{III}(dmgH)_2$ ($^{15}NO_2$)$\cdot OH_2$ (·····) in Nujol.

Conversion of NO into NO_2^-. It has been extensively studied how, in a series of six-coordinate Co(III) complexes including the NO_2 ligand, such as $[Co^{III}(NH_3)_5NO_2]Cl_2$, NO_2 exists as ONO^- in an alkaline solution and as NO_2^- in an acid solution.[14] This isomerization proceeds reversibly depending on the pH of the solution. As for the NO^+ ligand, it has been found, in the case of $[Fe^{II}(CN)_5NO]^{2+}$, that the NO^+ ligand is converted into ONO^- in an alkaline solution.[15,16] Recently, Godwin and Meyer reported the NO^+ ligand of $[Ru^{II}(bipy)_2(NO)X]^{2+}$ (X=Cl, Br) reacts with the hydroxide ion in an aqueous solution to form NO_2^-.[17] As far as the neutral NO ligand is concerned, no report has been presented dealing with the conversion of NO into ONO^- or NO_2^-, though many of the nitrosyl complexes have been synthesized where NO has been considered to be formally neutral.[3,18]

As has been described in the Experimental section, $Co^{II}(dmgH)_2NO$ (I) is very unstable in water and is rapidly oxidized to $Co^{III}(dmgH)_2NO_2\cdot OH_2$(III). As may be seen in Fig. 2, the electronic spectrum of the complex I in an aqueous solution (curve 1) is quite different from that in chloroform (curve 2), but it is very close to the spectrum of the complex III in water (curve 4). These spectral data are thought to show that the conversion of the complex I into III takes place almost quantitatively. An oxygen-free, aqueous solution which was prepared by using a high vacuum line showed no absorption band at around 20×10^3 cm^{-1}. Upon exposing this solution to air, the solution came to show an absorption curve which is similar to the curve 1.

It may be said, from the above results, that, in an oxygen-free, aqueous solution, the complex I no longer preserves its penta-coordinate configuration and that both water and oxygen are consumed in the conversion reaction of the complex I to III.

Table 2. The ν(NO) of the nitrosyl complexes (cm^{-1})

	a (in Nujol mull)	*b* (in CH_2Cl_2)	*b*−*a*
$Co(dmgH)_2NO$	1641	1705	64
$Co(dmgH)_2(^{15}NO)$	1615	1680	65
CoSalen(NO)	1624	1666	42
CoAE(NO)	1654	1650	−4
CoBE(NO)	1635	1653	18

An aqueous solution of the complex I shows acid: pH =4.35 for 2×10^{-3} M, implying that the conversion reaction includes the addition of the OH^- anion to the NO ligand, as in the case of the reaction of $[Fe^{II}(CN)_5NO]^{2+}$ forming $[Fe^{II}(CN)_5ONO]^{4+}$ in an alkaline solution.[15] As may be seen from Table 2, the NO stretching frequency of the complex I observed at 1641 cm^{-1} in Nujol shifts to 1705 cm^{-1} in CH_2Cl_2 solution; this shift is considerably larger than those observed for other nitrosyl complexes with similar structures. These data are considered to reflect a larger polarization, as $(Co^{II})^{\delta-}$—$(N=O)^{\delta+}$ in the present complex, which may facilitate the OH^- addition, as is shown in Scheme (I).

$$(Co^{II})^{\delta-}-(NO)^{\delta+} + OH^- \longrightarrow \left[Co^{II}-N\begin{matrix}O\\ \diagdown OH\end{matrix}\right]^- \longrightarrow Co^{III}-NO_2 + H^+ \qquad (I)$$

10) G. Costa, G. Mestroni, and L. Stefani, *J. Organometal. Chem.*, **7**, 493 (1967).
11) A. Nakahara, This Bulletin, **27**, 560 (1954); **28**, 207 (1955).
12) I. Nakagawa, T. Shimanouchi, and K. Yamazaki, *Inorg. Chem.*, **3**, 772 (1964); I. Nakagawa and T. Shimanouchi, *Spectrochim. Acta*, **23A**, 2099 (1967); K. Nakamoto, "Infrared Spectra of Inorganic and Coordination Compounds," John Wiley & Sons, New York and London (1962), p. 155.
13) K. Nakamoto, J. Fuzita, and H. Murata, *J. Amer. Chem. Soc.*, **80**, 4817 (1958).
14) F. Basolo and R. G. Pearson, "Mechanisms of Inorganic Reactions," 2nd Ed. John Wiley & Sons, New York (1967), p. 291.
15) J. Masek and H. Wendt, *Inorg. Chim. Acta*, **3**, 455 (1969).
16) K. A. Hofmann, *Z. Anorg. Allg. Chem.*, **11**, 279 (1896); F. Hölzl and K. Rokitansky, *Monatsh. Chem.*, **56**, 90 (1930).
17) J. B. Godwin and T. J. Meyer, *Inorg. Chem.*, **10**, 471 (1971).
18) C. A. Reed and W. R. Roper, *J. Chem. Soc., A*, **1970**, 3054.

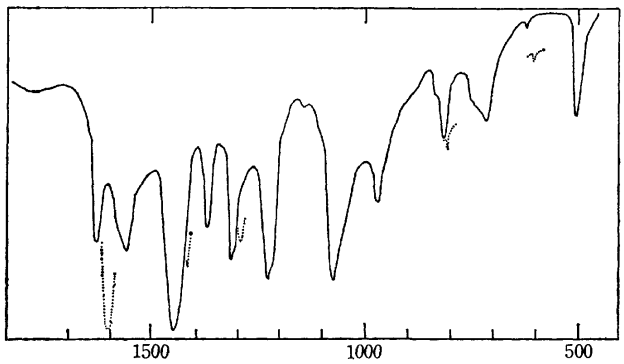

Fig. 4. IR spectra of $[Co^{II}(dmgH)_2NO\cdot OH_2]$ $[Co^{III}(dmgH)_2NO_2]\cdot 2H_2O$ (——) and $[Co^{II}(dmgH)_2(^{15}NO)\cdot OH_2][Co^{III}(dmgH)_2(^{15}NO_2)]\cdot 2H_2O$ (·····) in Nujol.

Complex II. This compound was separated as a crystalline precipitate during the conversion of the complex I into the complex III in an ether solution. The complex II is diamagnetic, and the results of elementary analysis are in fair agreement with the $Co_2(dmgH)_4NO\cdot NO_2\cdot 3H_2O$ composition. In the thermogravimetric analysis curve for the complex II, the weight loss of about 8.5% observed between 145—165°C is thought to correspond to the loss of three water molecules in the complex. Unlike the complex I, the complex II is insoluble in chloroform and ether. The complex exhibits the characteristic bands for both NO_2 and NO, as may be seen in Fig. 4 and Table 1. Each of the four bands for NO_2 is observed at almost the same frequency as for the complex III; the NO band is found to be slightly shifted to a lower frequency than in the complex I. These facts can hardly be understood without proposing that both the NO_2 and NO groups are involved in the complex. Thus, the structure of the complex II seems to include either a Co—Co bond or an NO bridge. The possible formation of a Co—Co bond by the interaction between Co(II) complexes with a low-spin d^7 configuration has been reported for $[Co^{II}(dmgH)_2B]_2$ where B is pyridine, aquo or triphenylphosphine.[4, 19] However, in the case of a diamagnetic complex such as $Co(dmgH)_2NO$, it is difficult to expect a similar Co—Co bond. With respect to the complexes with bridging NO, it has been reported that the NO band is observed at about 1500 cm^{-1} for $(C_5H_5)_3Mn(NO)_3$ and $[C_5H_5Cr(NO)_2]_2$.[20] The fact that the present complex shows the NO band at 1628 cm^{-1}, only slightly shifted to a lower frequency than that (1641 cm^{-1}) of the complex I, does not indicate clearly the existence of a bridging NO group. A very weak interaction through the NO group may be supposed to take place in the complex II.

19) F. A. Cotton, *Accounts Chem. Res.*, **2**, 240 (1969).
20) R. B. King and M. B. Bisnette, *Inorg. Chem.*, **3**, 791 (1964).

BULLETIN OF THE CHEMICAL SOCIETY OF JAPAN, VOL. 45, 174—178(1972)

Thermal Properties of Copper(II) Chelates of Some 1,5-Alkylpentane-2,4-diones[1)]

Isao YOSHIDA, Yoshitsugu OONO, Hiroshi KOBAYASHI, and Keihei UENO
Department of Organic Synthesis, Faculty of Engineering, Kyushu University, Fukuoka

(Received June 26, 1971)

Thermally stable and low melting copper(II) chelates of β-diketones have been synthesized as follows; bis(heptane-2,4-dionato)copper(II), mp 172°C; bis(nonane-4,6-dionato)copper(II), mp 162°C; bis(5-ethylheptane-2,4-dionato)copper(II), mp 72°C; bis(3-ethylnonane-4,6-dionato)copper(II), mp 50°C; bis(3,7-diethylnonane-4,6-dionato)copper(II), mp 58°C. Their thermal characteristics including enthalpy and entropy of fusion, have been discussed in relation with the molecular structure of the copper chelates.

In relation to our research project on the application of zone-melting technique to the systems containing metal chelate compounds,[2-6)] we have been interested in the metal chelates which melt at relatively low temperature without decomposition. It has been known that the introduction of alkyl groups on 1 and/or 5 positions of 2,4-pentanedione results in the lowering of melting point of the corresponding metal chelates.[7-10)] However, no systematic investigation on this respect have been appeared in literatures. This paper is to report on the results of the investigation on the thermal properties of copper(II) chelates of 1-

1) Contribution No. 250 from the Department of Organic Synthesis, Kyushu University.

2) K. Ueno, H. Kaneko, and N. Fujimoto, *Talanta*, **11**, 1371 (1964).

3) K. Ueno, H. Kaneko, and Y. Watanabe, *Microchemical J.*, **10**, 244 (1966).

4) H. Kaneko and K. Ueno, *Talanta*, **13**, 1525 (1966).

5) H. Kaneko, H. Kobayashi, and K. Ueno, *ibid.*, **14**, 1403 (1967).

6) H. Kaneko, H. Kanagawa, H. Kobayashi, and K. Ueno, *ibid.*, **14**, 1411 (1967).

7) H. Gilman, R. G. Jones, E. Bindschadler, D. Blume, G. Karmas, G. A. Martin, Jr., J. F. Nobis, J. R. Thirtle, H. L. Yale, and F. A. Yoeman, *J. Amer. Chem. Soc.*, **78**, 2790 (1956).

8) J. T. Adams and C. R. Hauser, *ibid.*, **66**, 1220 (1944).

9) G. S. Hammond, D. C. Nonhebel, and Chin. Hau. S. WU, *Inorg. Chem.*. **2**, 73 (1963).

10) B. O. Linn and C. R. Hauser, *J. Amer. Chem. Soc.*, **78**, 6066 (1956).

and/or 5-ethyl-substituted 2,4-pentanedione.

The ligands chosen in this study are heptane-2,4-dione (Etacac), nonane-4,6-dione (EtacacEt), 5-ethylheptane-2,4-dione (Et_2acac), 3-ethylnonane-4,6-dione (Et_2acacEt), 3,7-diethylnonane-4,6-dione (Et_2acacEt_2). The measurements of absorption spectra in visible as well as infrared region, the differential thermal analyses, the differential scanning calorimetric analyses, and the determination of melting point and molecular volume have been carried out on the 1:2 copper(II) chelates of the above ligands, and the relationship between the structure of the chelates and their thermal properties was discussed.

Experimental

Syntheses of Ligands. The ligands except Et_2acacEt and Et_2acac have been reported in the literatures, and they were synthesized by the condensation of corresponding ketone and ester in the presence of sodium amide. The ligands obtained were; Etacac (bp 67.5—70°C/20 mmHg),[11] EtacacEt (bp 101—102°C/20 mmHg),[8] and Et_2acacEt_2 (81—82°C/1.8—1.9 mmHg).[12]

The new ligands, Et_2acac and Et_2acacEt, were also synthesized in a similar manner to those described above, from 3-ethyl-2-pentanone and ethyl acetate for Et_2acac, and from 2-pentanone and phenyl 2-ethylbutyrate for Et_2acacEt. While the former was separated as pure ligand (bp 77°C/10 mmHg), the latter was not obtained as a pure form from the reaction mixture, and therefore the reaction product was directly converted into copper(II) chelate, which was eventually purified as copper chelate.

All these ligands were characterized in the form of copper(II) chelates by elemental analyses as shown in Table 1.

Preparation of Copper(II) Chelates. The copper(II) chelates of acac, Etacac, and EtacacEt were easily prepared by shaking stoichiometric amount of aqueous cupric acetate and the ligand, and the precipitated chelate was recrystallized from ethanol.

The copper(II) chelate of Et_2acac was prepared by the similar manner to the above procedure, but was obtained as dark violet oily product which crystallized after standing for a few hours. It was recrystallized from 80% ethanol to afford blue sticks. The chelate of Et_2acacEt_2, which was prepared by the similar manner, was also a dark violet oily product which slowly crystallized during 24 hours. If the ligand was not pure enough, the crystallization could hardly be observed. The crude chelate was recrystallized from 90% ethanol to afford blue sticks.

The copper(II) chelate of Et_2acacEt was prepared from the crude ligand and aqueous cupric acetate as described in the previous section. The crude copper chelate, which was obtained as a blue green oily product, was extracted with hexane. The hexane solution was washed successively with water and a saturated sodium bicarbonate solution. After evaporating hexane, blue oily residue was kept standing in a dish to afford a violet crystalline mass which was eventually purified by repeated precipitation from ethanol solution with water. No condition and solvent for the recrystallization of this chelate could be found.

The molecular formula and the analytical data of the chelates are summarized in Table 1.

Table 1. The molecular formula and the analytical results of the copper(II) chelates investigated

Chelate	Molecular formula	Elemental analysis Found C%	Found H%	Calcd C%	Calcd H%
$Cu(acac)_2$	$C_{10}H_{14}O_4Cu$	45.89	5.63	45.91	5.35
$Cu(Etacac)_2$	$C_{14}H_{22}O_4Cu$	52.90	6.99	52.90	6.98
$Cu(EtacacEt)_2$	$C_{18}H_{30}O_4Cu$	57.82	8.17	57.81	8.09
$Cu(Et_2acac)_2$	$C_{18}H_{30}O_4Cu$	57.83	8.23	57.81	8.09
$Cu(Et_2acacEt)_2$	$C_{22}H_{38}O_4Cu$	61.21	8.89	61.44	8.91
$Cu(Et_2acac Et_2)_2$	$C_{26}H_{46}O_4Cu$	64.12	9.65	64.23	9.54

Apparatus and Procedure. Melting points were observed on a micro-hot-stage with a Yanagimoto micro melting point apparatus (model MP-S2) which was calibrated with a standard sample.

Densities of the copper(II) chelate were determined by the standard procedure using a 3—4 m*l* picnometer. The volume of immersion liquid displaced by a known weight of a finely powdered solid chelate was measured at 25±0.1°C. The molecular volume was then calculated by deviding the molecular weight by density. The result is summarized in Table 2.

The heat of fusion was determined with a Perkin-Elmer Model DSC-18 differential scanning calorimeter. The differential thermal analysis was carried out on a Rigakudenki Thermoflex-8001 with a 3—5 mg sample sealed in an aluminum capsule at a heating rate of 3°C/min, using alumina as a reference, either in air or in nitrogen atmosphere.

The thermodynamic characteristics of the copper(II) chelates are summarized in Table 3.

The infrared spectra were measured with a JASCO Model DS-403G grating spectrophotometer on the samples in KBr pellet, and the absorption spectra in visible region were measured with a Hitachi Model 124 recording spectrophotometer.

Results and discussion

DTA Study. In order to evaluate the thermal stability of the copper chelates, the differential thermal analysis (DTA) was carried out on the samples in air as well as in nitrogen atmosphere. The results are given in Fig. 1. The DTA curves except for $Cu(acac)_2$, are characterized with a sharp endothermic peak A. The endothermic peak (A) temperature was found to be in good agreement with the melting point of the respective copper chelate which was determined by the micro-hot-stage method (Table 3).

The repeated DTA measurement on the same sample up to the temperature 15°C above the melting point of the chelate, did not show any change of the endothermic temperature. This implies that the peak is not due to the decomposition, but purely due to the fusing process. This was also confirmed by the comparison of the infrared spectra of the samples before and after the DTA run, which were found to be exactly superimposable.

The samples of $Cu(Etacac)_2$, $Cu(Et_2acacEt)_2$, and $Cu(Et_2acacEt_2)_2$ did not show any change in the

11) R. Levine, J. A. Conroy, J. T. Adams, and C. R. Hauser, *J. Amer. Chem. Soc.*, **67**, 1510 (1945).

12) E. H. Man, F. W. Swamer, and C. R. Hauser, *ibid.*, **73**, 901 (1951).

endothermic peak area and peak temperature as well as the sample weight during the repeated runs. On the other hand, $Cu(Etacac)_2$ decreased its sample weight and the peak area. The change can be ascribed to the slow sublimation or vaporization of the sample during the heating process.

As to $Cu(Et_2acac)_2$, a single endothermic peak at 71°C splitted into two peaks at 65°C and 70°C after the first run, however the sample weight and peak area remained constant during the repeated runs. As the twin peaks did not change after the second run, this may be related with a kind of phase transition accompanied with the fusing process.

The endothermic peak B at higher temperature in nitrogen atmosphere is related with the decomposition of the samples, while the complicated exothermic peaks in air at the same temperature range being related with the oxidative decomposition of the samples.

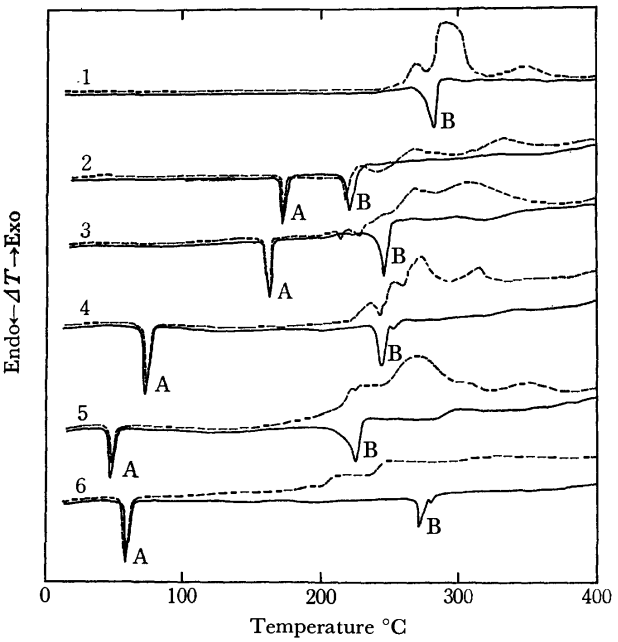

Fig. 1. DTA curves of the copper (II) chelates heated in nitrogen atmosphere (——) and in air (·····).
1. $Cu(acac)_2$ 2. $Cu(Etacac)_2$ 3. $Cu(EtacacEt)_2$
4. $Cu(Et_2acac)_2$ 5. $Cu(Et_2acacEt)_2$ 6. $Cu(Et_2acacEt_2)_2$

The thermal stability of copper chelates, roughly estimated by the decomposition peak temperature, increases in the order of $Cu(Et_2acacEt)_2 < Cu(Etacac)_2 < Cu(Et_2acac)_2 < Cu(EtacacEt)_2 < Cu(Et_2acacEt_2)_2 < Cu(acac)_2$. In general, the copper chelates of the symmetric ligands are more stable than those of the unsymmetric ligands, and the melting point becomes lower with increasing number of terminal ethyl groups on the ligand. Thus, the temperature range where the molten chelate is stable, is widest for $Cu(Et_2acacEt_2)_2$ and becomes narrower in the order of $Cu(Et_2acacEt)_2$, $Cu(Et_2acac)_2$, $Cu(EtacacEt)_2$, and $Cu(Etacac)_2$. Finally, the chelate of non-ethylated ligand, $Cu(acac)_2$, can not exist as molten state.

Spectral Study. As shwon in Table 4, the infrared absorption bands due to the stretching mode of C=C and C=O bonds in the chelate ring do not shift significantly from one chelate to another. The result suggests that the introduction of ethyl groups on 1 and/or 5 positions of pentane-2,4-dione does not affect appreciablly the bond strengths in the chelate ring of bis(pentane-2,4-dionato)copper(II).

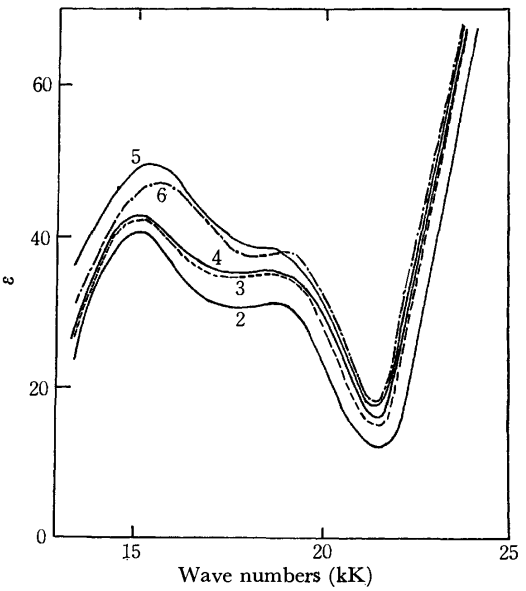

Fig. 2. Visible absorption spectra of copper(II) chelates in carbon tetrachloride at room temperature.
2. $Cu(Etacac)_2$ 3. $Cu(EtacacEt)_2$ 4. $Cu(Et_2acac)_2$
5. $Cu(Et_2acacEt)_2$ 6. $Cu(Et_2acacEt_2)_2$

The visible absorption spectra of the copper chelates in carbon tetrachloride are shown in Fig. 2. The spectra are characterized with two peaks at about 15000 cm^{-1} and 17500 cm^{-1} which shift very little with the kind of ligand, and the spectra are very similar to that of bis(pentane-2,4-dionato)copper(II) which is known to take a tetra-coordinate square planar structure. The similarity of visible absorption spectra regardless of the kind of ligands indicates that the introduction of ethyl groups on the terminal methyl carbon of the ligands does not cause any intramolecular steric hindrance which may results in the change in the symmetry of square planar coordination structute. The construction of molecular model also proved that the terminal ethyl groups did not cause any steric repulsion between the opposing two ligands in the chelate molecule. Furthermore, the molecular model suggested that the terminal ethyl groups fixed into rather restricted spaces with least steric interaction with the chelate ring, so that the ethyl groups could not rotate freely but extend above or below the *x-y* plane of the copper chelate.

The molecular volume of the chelate increases with the increasing number of ethyl groups introduced into the ligand as shown on the fourth column in Table 2. However, the increase of molecular volume per ethyl group increases as the complexity of the chelated ligand increases as indicated on the fifth column of Table 2. This tendency may be attributed to the mutual interaction of ethyl groups, as the increment should be unchanged if there is no interaction between the ethyl groups. As to the question of whether the interaction of ethyl groups is intramolecular one or

Table 2. Molecular volumes of copper(II) chelates

Copper chelate	Immersion liquid	Density d^{25}	Molecular volume V_M cm³/mol	Increase of molecular volume[a] ΔV_M cm³/mol	Increase of ΔV_M per ethyl group[b] cm³/mol
$Cu(acac)_2$	*n*-hexane	1.57	166.7	—	—
$Cu(Etacac)_2$	*n*-hexane	1.42	223.9	57.2	28.5
$Cu(EtacacEt)_2$	water-methanol	1.27	294.5	127.8	32.0
$Cu(Et_2acac)_2$	water-methanol	1.26	296.8	130.1	32.5
$Cu(Et_2acacEt_2)_2$	water-methanol	1.08	450.2	283.5	35.3

a) Increase of molecular volume of listed chelate from that of $Cu(acac)_2$.
b) Increase of molecular volume divided by the total number of ethyl groups introduced in the chelate molecule.

Table 3. Thermodynamic characteristics of copper(II) chelates

Copper chelate	Melting point °C	Melting point (T_f) °K	Enthalpy of fusion (ΔH_f) (kcal·mol⁻¹)	Entropy of fusion (ΔS_f)[a] (e.u.)
$Cu(acac)_2$	263 (283)	536 (decomp.)	—	—
$Cu(Etacac)_2$	172 (170)	445	9.5	21.4
$Cu(EtacacEt)_2$	162 (162)	435	9.1	20.9
$Cu(Et_2acac)_2$	72 (71)	345	7.8	22.6
$Cu(Et_2acacEt)_2$	50 (45)	323	~6	~18.5
$Cu(Et_2acacEt_2)_2$	58 (57)	331	5.2	15.6

a) $\Delta S_f = \Delta H_f / T_f$
b) The values in parentheses were determined by the DTA study.

Table 4. Characteristic infrared absorption bands of the copper chelates

Copper chelate	Wave number of the band (cm⁻¹)					
	$-CH_3$	$-CH_2-$				
	ν_{C-H}	ν_{C-H} (as)	ν_{C-H} (s)	$\nu_{C=C}$	$\nu_{C=O}$	
$Cu(acac)_2$	2969	—	—	1580	1554	1525
$Cu(Etacac)_2$	2966	2936	2876	1575	1552	1519
$Cu(EtacacEt)_2$	2966	2936	2876	1574	1549	1521
$Cu(Et_2acac)_2$	2968	2937	2879	1577	1552	1518
$Cu(Et_2acacEt)_2$	2966	2935	2876	1573	—	1518
$Cu(Et_2acacEt_2)_2$	2968	2938	2879	1576	—	1525

Table 5. Contribution of additional ethyl groups to the molecular volume

Difference in V_M between			ΔV_M/Ethyl group	Contribution from additional ethyl groups
$Cu(acac)_2$	$-Cu(Etacac)_2$	57.2	28.5	7.0
$Cu(Etacac)_2$	$-Cu(EtacacEt)_2$	70.6	35.5	
$Cu(acac)_2$	$-Cu(Et_2acac)_2$	130.1	32.5	5.8
$Cu(Et_2acac)_2$	$-Cu(Et_2acacEt_2)_2$	153.4	38.3	
$Cu(acac)_2$	$-Cu(EtacacEt)_2$	127.8	32.0	6.8
$Cu(EtacacEt)_2$	$-Cu(Et_2acacEt_2)_2$	155.7	38.8	

intermolecular one, the latter seems to be true from the following observations. First, there operates no steric interaction between the terminal ethyl groups within the ligand molecule or of opposing two ligands in the copper(II) chelate, as proved by the molecular model. Secondly, the extent of the contribution of additional ethyl groups to the increase of molecular volume of less complicated ligands remains almost the same as visualized in Table 5. If the interaction between the ethyl groups within the same ligand does exist, the value on the last column in Table 5 should increase with increasing degree of interaction. Additionally, molecular volume of $Cu(EtacacEt)_2$ and of $Cu(Et_2acac)_2$ are nearly equal (Table 2).

It has been shown that the visible absorption spectra of bis(pentane-2,4-dionato)copper(II) in chloroform (15000 cm⁻¹ and 18000 cm⁻¹) changed into single band in pyridine (15200 cm⁻¹). According to Ortolano,[13] of the two absorption bands in chloroform, a band at 18000 cm⁻¹ is assigned to a transition of d_{xy}—d_{z^2}. When the chelate is dissolved in a strongly coordinating solvent such as pyridine, this band receives a bathochromic and hypsochromic change and emerges into the parent band resulting in a broad band at 15200 cm⁻¹ region, the reason for which is explained as the coordination of pyridine molecule to the central copper ion along the *z*-axis.

The similar spectral change was observed on the copper chelates investigated in this study, when they were dissolved in pyridine and in 2,6-lutidine. The results are summarized in Table 6. In contrast to

Table 6. Characteristic visible absorption bands of copper(II) chelates in various solvents

Copper chelate	Absorption bands in (cm⁻¹)				
	Chloroform	Carbon tetrachloride	2,6-Lutidine	Pyridine	$\Delta\nu$[a]
$Cu(acac)_2$	15300 17800	—	—	15200	—
$Cu(Etacac)_2$	15200 —	15200 18500	15200	15400	200
$Cu(EtacacEt)_2$	15200 ~18200	15100 18500	15100	15400	300
$Cu(Et_2acac)_2$	15200 18300	15100 18500	15000	15300	300
$Cu(Et_2acacEt)_2$	15200 18500	15100 18600	14900	15300	400
$Cu(Et_2acacEt_2)_2$	15200 18600	15100 18700	14500	15300	800

a) Difference of wave numbers between the absorption maxima in pyridine and in 2,6-lutidine.

13) L. L. Funck and T. R. Ortolano, *Inorg. Chem.*, **7**, 567 (1968).

the spectra in pyridine, where the frequency of absorption maxima remained almost unchanged for all chelates, those in 2,6-lutidine were broader in band width and showed rather wide variation in the frequencies. The latter spectra may be understood to be an intermediate stage of coordination of solvent molecule to the copper(II) ion, where the band due to d_{xy}—d_{z^2} transition does not completely emerge into the parent band, resulting in the broadening and the apparent bathochromic shift of the parent band. If it is the case, the extent of bathochromic shift of a bond near 15300 cm^{-1} in 2,6-lutidine from that in pyridine, can be used as a measure of estimating the intensity of interaction between the solvent molecules and the chelated copper(II) ion. In other words, the greater is the shift of the band between the two solvents, the weaker is the coordination of solvent molecules to the chelated copper(II) ion. As shown in Table 6, the order of decreasing intensity of interaction between 2,6-lutidine and the copper ion is $Cu(Etacac)_2 > Cu(EtacacEt) > Cu(Et_2acac)_2 > Cu(Et_2acacEt)_2 > Cu(Et_2acacEt_2)_2$. This order is in accordance with the shielding effect of ethyl groups introduced on 1- and/or 5-carbon of pentane-2,4-dione, if one assume that the terminal ethyl groups extend above or below of the *xy* plane of copper(II) chelate as discussed above.

Refering to the thermodynamic characteristics on the fusion of copper(II) chelates, it is noticed that the melting point of the chelate is dependent upon ΔH_f term rather than ΔS_f term. The monotonous decrease of the enthalpy of fusion with the increasing number of terminal ethyl groups introduced on the ligand, is understood to be due to the increase of intermolecular distance as suggested by the molecular volume, and also due to the increasing shielding effect by the terminal ethyl groups.

It is also noticed that ΔS_f decreases as ΔH_f decreases with an exception of $Cu(Et_2acac)_2$. Such parallel change of ΔS_f and ΔH_f can be often found in a series of hydrocarbon compounds. The change of entropy of fusion may be explained mainly in terms of the difference in crystal structure, if one remined that the structure of the chelate ring is found to be almost the same for all ligands and that the terminal ethyl groups are conceivably fixed in rather restricted spaces. Thus the difference of ΔS_f can be understood to be mainly due to the difference in ordering of the chelate molecules in the crystalline state.

As to the copper chelates of unsymmetric ligands, there is a possibility that the solid chelate is a mixture of *cis*- and *trans*-isomers, which may result in the lowering of melting point, lower than the expected value for one of the isomers. This effect must be most prominent for $Cu(Et_2acac)_2$, because the ligand is most unsymmetric. Thus, values of the thermodynamic parameters for $Cu(Et_2acac)_2$ do not fit in the general tendency of those of other chelates.

As discussed above, the melting point of bis(pentane-2,4-dionato)copper(II) lowers with the increasing number of ethyl groups introduced on 1- and/or 5-position. Although the result can be discussed semiquantitatively by the spectroscopic evidences as well as the thermodynamic data, the crystal structure data are needed for the more quantitative discussion of the melting point of these metal chelates.

DSC measurements were carried out by courtesy of Professors T. Oyama and K. Takamizawa, to whom the authors are thankful. They are also grateful to the Ministry of Education for a grant-in-aid for scientific research.

Isomerism of the Metal Complexes containing Multidentate Ligands. I. Geometric and Optical Isomers of the Bis(diethylenetriamine)-cobalt(III) Ion[1]

Yuzo Yoshikawa and Kazuo Yamasaki

Department of Chemistry, Faculty of Science, Nagoya University, Chikusa-ku, Nagoya

(Received July 15, 1971)

Three possible isomers of bis(diethylenetriamine)cobalt(III) halide were isolated by column chromatography on ion-exchange cellulose and Sephadex, and the *mer*- and *u-facial* isomers were completely resolved by column chromatography on SE-Sephadex. These isomers were studied by electronic, infrared, and PMR spectroscopy, and the absolute configuration of the *u-facial* isomer was assigned on the basis of the circular dichroism spectrum.

The cobalt(III) complex of diethylenetriamine (abbreviated as dien), $[Co(dien)_2]X_3$, was first described by Mann[2] in 1934. Later Brigando *et al.*[3] and also Schmidtke[4] measured the absorption spectrum in the visible and ultraviolet regions, and Basolo *et al.*[5] determined the rate of proton exchange of this complex. These authors, however, did not refer to the possible isomers of this complex, and it is not certain which isomer was used for these investigations. The complex, $[Co(dien)_2]X_3$ can exist in three geometric isomers, as is shown in Fig. 1; the isomerism has been discussed by several authors,[6–10] but the isomers have never been isolated and characterized. In a previous paper[11] we have reported the resolution of one of the isomers of this complex by column chromatography on P-cellulose. The details of the isolation and characterization of all three isomers will be described in the present paper.

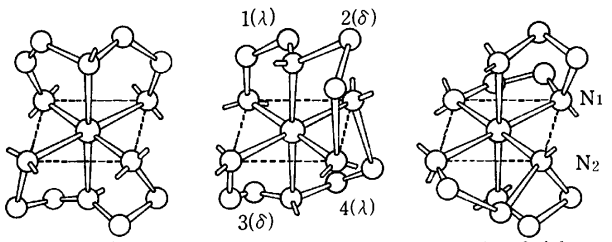

(a) *s-facial* (b) *mer* (c) *u-facial*

Fig. 1. Three geometric isomers of $[Co(dien)_2]^{3+}$. The hydrogen atoms of the $-CH_2-$ groups are not shown. The figure 1 (c) represents the configuration of the $(+)_{589}$-*u-facial* isomer. The configuration of $(+)_{589}$-$[Co(penten)]^{3+}$ is the same with 1(c), the N_1 and N_2 atoms being linked by an ethylene group.

Experimental

1.1. Measurements. All the measurements were carried out at 25°C. The electronic absorption, optical rotatory dispersion (ORD), and circular dichroism (CD) spectra were measured by means of a JASCO ORD/UV-5 and a JASCO J-20 spectrometer, using quartz cells 1, 5, and 10 mm thick. The intensities of the ORD and CD spectra were checked using those of $(+)_{589}$-$[Co(en)_3]Br_3 \cdot H_2O$, $[M]^{25}_{589} = 602°$,[12] and $\Delta\varepsilon_{490} = +1.89$[13,14] as references. The infrared spectrum (4000—650 cm^{-1}) was measured with a JASCO-402G infrared spectrophotometer by using Nujol and hexachlorobutadiene mulls, and the far-infrared spectrum (700—200 cm^{-1}), with a Hitachi EPI-L spectrophotometer by using Nujol mulls. The PMR spectrum in deuterated dimethylsulfoxide was determined using a JEOL model C-60H spectrometer with tetramethylsilane(TMS) as the reference, the concentration used being 20 wt%.

1.2. Ligand. Commercially-available diethylenetriamine was further purified by vacuum distillation.

1.3. Synthesis of the Isomers. The complex was prepared as mixtures of isomers by the following four methods.

Method A: Cooled diethylenetriamine (7.7 g) was dissolved in 30 m*l* of cold water, and to this solution 14 g of $K_3[Co(CO_3)_3] \cdot 3H_2O$[15] was added in small portions with vigorous stirring. The mixture was kept at 0—3°C during the reaction for about one hour. One gram of active charcoal was then added and stirring was continued for 5 hr. After the solution had been kept at 0°C overnight, 100 m*l* of ice water and then 25 m*l* of concentrated hydrobromic acid were slowly added under cooling (5—10°C). After the evolution of carbon dioxide, the active charcoal was filtered off and the filtrate was evaporated to half the volume. The crystallized yellowish needles were filtered, recrystallized from water, washed with aqueous ethanol (1:1), and dried in air. The yield of the complex bromide, which was named the isomer A, was about 1 g. The above reaction mixture contained three isomers, and the formation ratio was found to be: *s-facial*: *u-facial*: *mer* = 16:25:59 by separation on an SE-Sephadex column and by subsequent spectrophotometric determination (*cf.* 1.4).

1) A part of the present investigation was published as a preliminary report: F. R. Keene, G. H. Searle, Y. Yoshikawa, A. Imai, and K. Yamasaki, *Chem. Commun.*, **1970**, 784.

2) F. G. Mann, *J. Chem. Soc.*, **1934**, 466.

3) P. Job and J. Brigando, *Compt. rend.*, **210**, 438 (1940); **236**, 708 (1953); J. Brigando, *Bull. Soc. Chim. Fr.*, **1957**, 211, 221.

4) H. H. Schmidtke, *Z. physik. Chem.*, **38**, 170 (1963).

5) F. Basolo, J. W. Palmer, and R. G. Pearson, *J. Amer. Chem. Soc.*, **82**, 1073 (1960).

6) W. C. Fernelius and B. E. Bryant, *ibid.*, **75**, 1735 (1953).

7) P. H. Crayton and J. A. Mattern, *J. Inorg. Nucl. Chem.*, **13**, 248 (1960).

8) A. M. Sargeson, "Chelating Agents and Metal Chelates," Academic Press, New York (1964), p. 183.

9) G. G. Schlessinger, "Werner Centennial," American Chemical Society (1967), p. 565.

10) A. M. Sargeson and G. H. Searle, *Inorg. Chem.*, **6**, 787 (1967).

11) Y. Yoshikawa and K. Yamasaki, *Inorg. Nucl. Chem. Lett.*, **4**, 697 (1968).

12) A. Werner, *Ber.*, **45**, 127 (1912).

13) A. J. McCaffery and S. F. Mason, *Mol. Phys.*, **6**, 359 (1963).

14) J. H. Dunlop, R. D. Gillard, and G. Wilkinson, *J. Chem. Soc.*, **1964**, 3160.

15) M. Mori, M. Shibata, E. Kyuno, and T. Adachi, This Bulletin, **29**, 883 (1956); M. Shibata, M. Mori, and E. Kyuno, *Inorg. Chem.*, **3**, 1573 (1964).

Method B: To 50 g of $[CoBr(NH_3)_5]Br_2$ suspended in 400 m*l* of water, 2 g of active charcoal was added, and then 30 g of diethylenetriamine was slowly added in about one hour. Ammonia was evolved, and then the stirring was continued for 24 more hours at 25°C. The charcoal was then filtered off, and the filtrate was evaporated to half its volume under reduced pressure. Large amounts of ethanol and diethyl ether were then added until the precipitation was complete. The yellowish-brown powder thus obtained was filtered and washed several times with 1-butanol and once with diethyl ether, and then dried in air. The yield was 65.5 g. This product is a mixture of three isomers with the formation ratio of *s-facial: u-facial: mer*=7:30:63, which was determined by separation on an SE-Sephadex column as has been described above.

Method C: A mixture of isomers was also obtained by adding diethylenetriamine to a cobalt chloride solution in the presence of active charcoal and by then oxidizing the reaction mixture with air or hydrogen peroxide. This method gave almost the same results as the method B.

Method D: To 2 m*l* of diethylenetriamine, 0.8 g of finely ground *mer*-$[CoCl_3(dien)]$[7] was added. The mixture was well triturated for about 20 min in an ice-bath, and then the the excess diethylenetriamine was thoroughly washed away with 1-butanol. The remaining solid was dissolved in a small amount of water, and the isomers were separated by column chromatography as has been described in 1.4. The product obtained contained only the *u-facial* and *mer* isomers in the ratio of 8:92. This preparative method is not an equilibrium one, but was used for confirming the configurational assignment of the *mer* (the isomer C).

1.4. Separation of the Isomers. Since the separation of three isomers by the conventional fractional crystallization technique was unsatisfactory and laborious, a chromatographic method using ion-exchange Sephadex[16] and cellulose was developed. The SE-Sephadex used was a product of Pharmacia, Sweden, with a particle size of 40—120 μ and an ion-exchange capacity of 2.3 ± 0.3 meq/g. A mixture of the isomers obtained by one of the above methods, A, B, C, or D, was poured on an SE-Sephadex column (diameter, 3.0 cm; length, 120 cm) and eluted with a 0.15 M sodium $(+)_{589}$-tartrate solution at the rate of 1.2—1.4 m*l* per minute. Three completely-separated bands were thus obtained. The fastest moving complex was named A; the middle one, B, and the slowest one, C. The isomer A is the same as the one which is least soluble among the products obtained by the method A. Three isomers, A, B, and C, were found by experiments to be described in the later sections, to be *s-facial*, *u-facial*, and *mer* isomers respectively. Eluted fractions of the isomer B were optically active, indicating a partial resolution. Consequently, the isomer B was identified as the *u-facial* isomer. An example of the separation experiment is shown in Fig. 2.

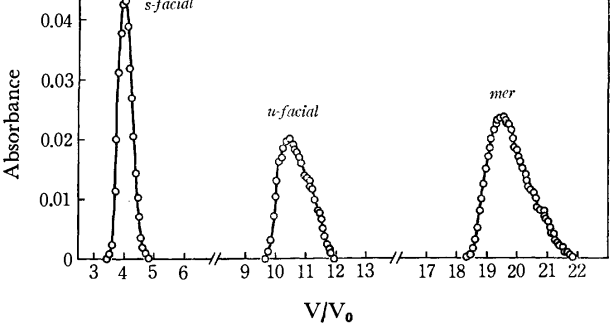

Fig. 2. Elution curves of an equimolecular (0.02 mmol) mixture of three isomers of $[Co(dien)_2]^{3+}$. Eluent: 0.15M sodium $(+)_{589}$-tartrate solution. The horizontal axis shows the volume ratio of the effluent *versus* the bed volume of the column.

The isomers could also be separated on a P-cellulose column (100 cm long), using 1-butanol saturated with water as the solvent, and a mixture of 1-butanol, concentrated hydrochloric acid, and water in a ratio of 200:15:15 as the eluent. First, the *mer*, then *s-facial*, and lastly *u-facial* isomers were eluted. Each isomer was back-extracted into the water phase, which was then evaporated to dryness. The chlorides thus obtained were recrystallized from water, washed quickly with an equal mixture of water and ethanol, and then dried in air.

The bromides of the *mer* and *u-facial* isomers were prepared by passing the respective chlorides through an ion-exchange resion column of the bromide form. The *s-facial* bromide was obtained as the least soluble isomer by the method A. The *mer* iodide was obtained by converting the chloride on an ion-exchange resin column of the iodide form. The *u-facial* and *s-facial* iodides were precipitated when potassium iodide was added to solutions of the *u-facial* and *s-facial* chlorides respectively.

1.5. Resolution of the u-Facial *and* Mer *Isomers.* The chromatographic method using SE-Sephadex described in 1.4 was also applied, with minor modifications, to the complete resolution of the *u-facial* and *mer* isomers. When eluted by a sodium $(+)_{589}$-tartrate solution, the adsorbed *u-facial* isomer was not clearly separated into two bands, but the initial and last several fractions indicated an almost complete resolution. The use of a 0.3 M sodium antimony $(+)_{589}$-tartrate solution instead of a sodium $(+)_{589}$-tartrate solution caused the two bands corresponding to $(+)_{589}$ and $(-)_{589}$ antipodes to be completely separated in the column. The fast-moving band corresponds to the $(+)_{589}$-antipode with the CD value of $\Delta\varepsilon_{502}=+0.98$ and the molar rotation of $[M]_{589}=+211°$ (*cf.* Fig. 3). The optically-active complexes, both $(+)_{589}$ and $(-)_{589}$, have the same chemical composition, $[Co(dien)_2]\cdot Cl_3\cdot H_2O$, while the racemic complex has two moles of water of crystallization.

The resolution of the *mer* isomer was first carried out by Searle and Keene[17] by the conventional fractional crystallization of the diastereoisomers. The chromatographic method used in the resolution of the *u-facial* isomer has been successfully applied by us to the resolution of the *mer* isomer as well. The *mer* isomer adsorbed on a column of SE-Sephadex was eluted by a 0.3 M sodium antimony $(+)_{589}$-tartrate solution. First $(+)_{589}$ and then $(-)_{589}$ antipodes were eluted with complete separation. The effluents thus obtained were diluted five times, and then they were again adsorbed on columns of SE-Sephadex. After the columns had been washed with 0.01 N hydrochloric acid, each antipode was eluted with 1 N NaCl containing 0.01 N HCl. To the effluents, potassium hexacyanocobaltate(III) was added. The sparingly soluble yellowish crystals thus obtained were suspended in 0.01 N HCl with an ion-exchange resin (Dowex 1X8) in the chloride form. After the solution had been stirred for 2 hours, the resin was filtered off. The filtrate which contained the optically-active chloride was again

16) Y. Yoshikawa and K. Yamasaki, *Inorg. Nucl. Chem. Lett.*, **6**, 523 (1970).

17) F. R. Keene, G. H. Searle, and S. F. Mason, *Chem. Commun.*, **1970**, 893.

passed through a column of Dowex (chloride form) to ensure its conversion into the chloride, and then it was evaporated to dryness. The resulting chloride was dissolved in water and precipitated by adding ethanol. The rotation observed for $(+)_{589}$-*mer*-$[Co(dien)_2]Cl_3$ has its maximum at 484 mμ with the value of $[M]_{589}=-658°$ (*cf* Fig. 4). The half-time of the racemization of the aqueous solution is about 4 weeks at room temperature.

Results and Discussion

2.1. Chemical Compositions. The three isomers have the chemical compositions shown in Table 1; they have been characterized by a study of their infrared, electronic, and PMR spectra.

Table 1. Chemical composition of the isomers

Complex	Elemental analyses (Calcd value)			
	Co	Halogen	N	H_2O
s-facial $[Co(dien)_2]Cl_3\cdot H_2O$	15.05 (15.12)	27.08 (27.30)	—	4.58% (4.62)
$[Co(dien)_2]Br_3$	11.58 (11.67)	47.41 (47.47)	16.70 (16.64)	
$[Co(dien)_2]I_3$	9.29 (9.12)	58.93 (58.94)	— —	
u-facial $[Co(dien)_2]Cl_3\cdot 2H_2O$[a]	14.38 (14.46)	25.88 (26.09)	—	8.78 (8.84)
$[Co(dien)_2]Br_3\cdot H_2O$	11.25 (11.27)	45.87 (45.87)	16.29 (16.07)	3.53 (3.44)
$[Co(dien)_2]I_3\cdot H_2O$	8.91 (8.88)	57.27 (57.33)	— —	2.60 (2.71)
mer $[Co(dien)_2]Cl_3\cdot 2\frac{1}{2}H_2O$	14.03 (14.14)	25.13 (25.53)	— —	10.81 (10.81)
$[Co(dien)_2]Br_3\cdot 2H_2O$	10.74 (10.89)	44.07 (44.31)	15.65 (15.53)	7.10 (6.67)
$[Co(dien)_2]I_3\cdot \frac{1}{2}H_2O$	8.94 (9.00)	58.25 (58.39)	— —	1.17 (1.38)

a) Optically active antipodes, both $(+)_{589}$ and $(-)_{589}$, have one mol of water of crystallization.

The isomer B has been proved to have the *u-facial* structure by its resolution into optical antipodes. The *mer* isomer is also resolvable, but its optical activity is less stable than that of the *u-facial* isomer.[17] The *s-facial* isomer cannot be resolved because it has a center of symmetry. The X-ray crystal analysis of *s-facial*-$[Co(dien)_2]Br_3$ has recently been carried out by Saito *et al.* This complex cation has a center of symmetry with an approximate C_{2h} symmetry.[18]

The distinction between *mer* and *s-facial* isomers was made by studying the PMR spectrum. The preparative method D also afforded additional evidence for the meridional structure of the isomer C.

2.2. Circular Dichroism Spectrum. The structure of the two complex ions, $[Co(dien)_2]^{3+}$ and $[Co(penten)]^{3+}$, are closely related; they are different only in that a fifth chelate ring joining the two secondary nitrogen atoms is present in the latter (*cf.* Fig. 1). Therefore, the absolute configuration of $[Co(penten)]^{3+}$ may give a clue to the elucidation of that of the *u-facial*-$[Co(dien)_2]^{3+}$. The X-ray crystal analysis of $(+)_{589}$-$[Co(en)_3]^{3+}$ [19] and $(+)_{589}$-$[Co(penten)]^{3+}$ [20] showed that both ions have the same *Λ* configuration in terms of the IUPAC nomenclature.[21] The absolute configuration of the latter ion has also been assigned on the basis of the stereospecificity of the methylated penten.[22]

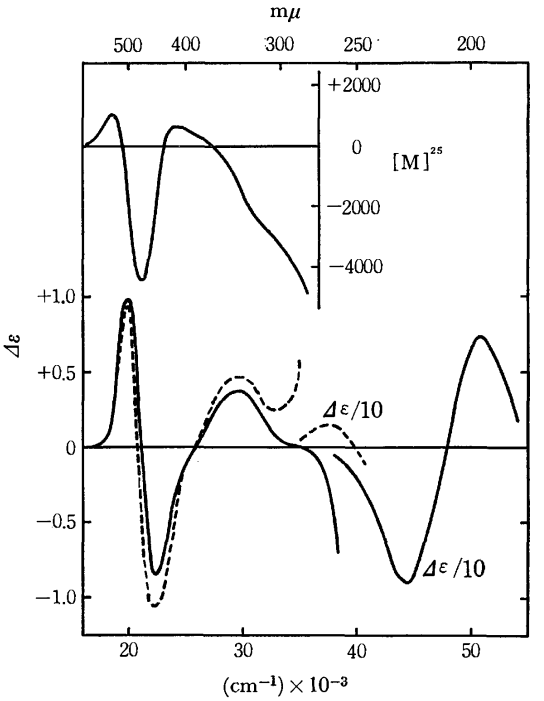

Fig. 3. Optical rotatory dispersion (upper curve) and circular dichroism (lower curve) spectra of $(+)_{589}$-*u-facial* $[Co(dien)_2]Cl_3$;——in water and·····in 0.2M Na_2SeO_3.

The relationship between the absolute configuration and the CD spectrum of $(+)_{589}$-$[Co(en)_3]^{3+}$ has been well established. This complex has a major positive band and a minor negative band at a lower and a higher frequency in the region of the octahedral $^1A_{1g}\rightarrow T^1_{1g}$ absorption, the area of these CD bands being diminished and enhanced respectively by the addition of selenite or phosphate ions.[23,24] The same relationship holds also for $(+)_{589}$-$[Co(penten)]^{3+}$.[22] The ORD and CD curves of $(+)_{589}$-*u-facial*-$[Co(dien)_2]^{3+}$ are shown in Fig. 3. The CD spectrum shows a lower-energy positive ($\Delta\varepsilon=+0.98$, 19900 cm^{-1}) and a higher-energy negative ($\Delta\varepsilon=-0.84$, 22500 cm^{-1}) component in the region of the first ligand-field band. Further, another positive component ($\Delta\varepsilon=+0.37$, 29900 cm^{-1}) exists in the region of the second band, and intense negative and positive components ($\Delta\varepsilon=-9.0$, 44400 cm^{-1} and $\Delta\varepsilon=+7.4$, 50700 cm^{-1}) in the region of the charge-transfer band. Since the sign and magnitude of the

18) Y. Saito, private communication.

19) Y. Saito, K. Nakatsu, M. Shiro, and H. Kuroya, *Acta Crystallogr.*, **8**, 729 (1955); This Bulletin, **30**, 158, 795 (1957).

20) A. Muto, F. Marumo, and Y. Saito, *Inorg. Nucl. Chem. Lett.*, **5**, 85 (1969); *Acta Crystallogr.*, **B26**, 226 (1970).

21) *IUPAC Information Bull.*, No. 33, 68 (1968); *Inorg. Chem.*, **7**, 1 (1970).

22) Y. Yoshikawa, E. Fujii, and K. Yamasaki, *Proc. Japan Acad.*, **43**, 495 (1967), and the references cited therein; J. R. Golgogy and C. J. Hawkins, *Chem. Commun.*, **1966**, 873.

23) H. L. Smith and B. E. Douglas, *J. Amer. Chem. Soc.*, **86**, 3885 (1964); *Inorg. Chem.*, **5**, 784 (1966).

24) S. F. Mason and B. J. Norman, *Proc. Chem. Soc.*, **1964**, 339; *J. Chem. Soc., A*, **1966**, 307.

CD bands of $(+)_{589}$-*u-facial*-$[Co(dien)_2]^{3+}$ are similar to those of $(+)_{589}$-$[Co(en)_3]^{3+}$ and $(+)_{589}$-$[Co(penten)]^{3+}$, it may be concluded that these three complexes have the same absolute configuration, *Λ*, those of the dien and penten complexes being shown in Fig. 1.

Further, from a consideration of the sign of the CD band in the charge-transfer region,[25] each five-membered chelate ring can be presumed to have the conformation shown in Fig. 1. The X-ray determination of the absolute configuration of the $(+)_{589}$-*u-facial*-$[Co(dien)_2]^{3+}$ is now under way by Prof. Y. Saito, University of Tokyo. Both the ring-pairing method[26] and the octant rule[27] support the absolute configuration proposed here.

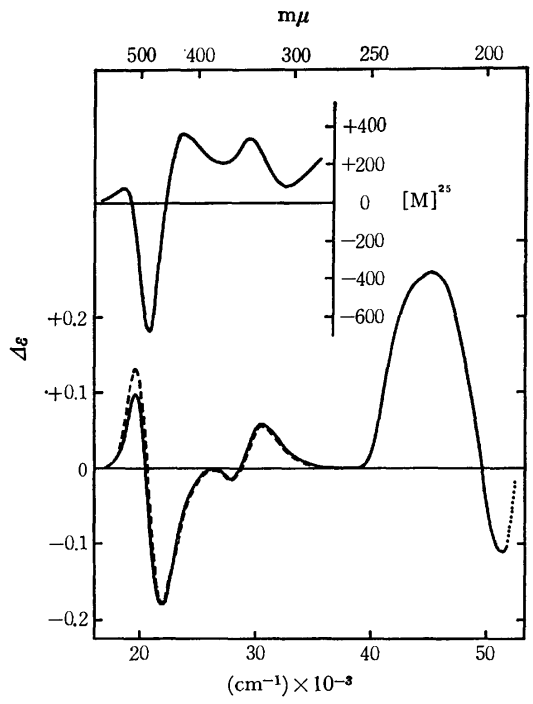

Fig. 4. Optical rotatory dispersion (upper curve) and circular dichroism (lower curve) spectra of $(+)_{589}$-*mer*-$[Co(dien)_2]Cl_3$; ——in water and ·····in 0.2M Na_2SO_4.

In Fig. 4 the ORD and CD curves of the $(+)_{589}$-*mer*-$[Co(dien)_2]Cl_3$ are shown. The CD spectrum has peaks split into two in the regions of the $^1A_{1g} \rightarrow {}^1T_{1g}$ ($\Delta\varepsilon = +0.096$, 19500 cm^{-1}; $\Delta\varepsilon = -0.181$, 21900 cm^{-1}) and $^1A_{1g} \rightarrow {}^1T_{2g}$ ($\Delta\varepsilon = -0.014$, 27800 cm^{-1}; $\Delta\varepsilon = +0.057$, 30700 cm^{-1}) transitions; these are much less intense than those of the $(+)_{589}$-*u-facial* isomer. In the charge-transfer region, a CD peak with a weak intensity is observed. The $(-)_{589}$-antipode shows an identical CD spectrum with the opposite sign. In 0.2 M sodium sulfate, the intensity of the lower-energy band in the first absorption region is enhanced, while the other peaks are affected very little. Sodium sulfate is used because sodium selenite commonly used accelerates the racemization because of the increase in the pH. The optically-active *mer* isomer is stable only in the pH region lower than 6.

In the structure of the *mer* isomer shown in Fig. 1, both the skew chelate pairs, 1,3 and 2,4 have the *Λ* (*δ*, *λ*) configuration, while the pairs, 2,3 and 1,4 have the *Λ*(*δ*, *δ*) and *Λ*(*λ*, *λ*) configurations respectively. This isomer, therfore, has, as a whole, an equal number of *Λ* and *Λ* configurations, and *δ* and *λ* conformations. Thus, the dissymmetric effects seem to be cancelled out. Nevertheless, CD peaks, though very weak, are observed; they may be due to the integration of the three different configuraions and conformations mentioned above.

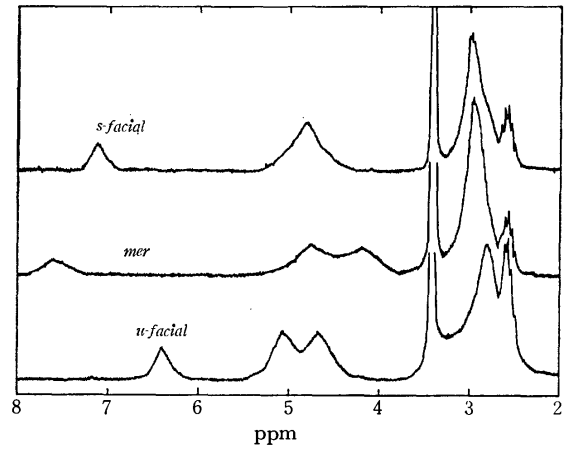

Fig. 5. PMR spectra of *s-facial* (curve 1,) *mer*(curve 2) and *u-facial* (curve 3) isomers of $[Co(dien)_2]I_3$ in deuterated DMSO.

2.3. *PMR Spectrum.* Figure 5 shows the PMR spectra of the three isomers taken in deuterated dimethylsulfoxide. The isomer A shows broad signals at *δ* 4.80 and 7.12 (intensity ratio 4: 1); the isomer C at *δ* 4.18, 4.75, and 7.60 (intensity ratio 2: 2: 1), and the isomer B, at *δ* 4.68, 5.08, and 6.40 (intensity ratio 2: 2: 1). From the intensities, the siganls at *δ* 4.0—5.5 are assigned to the protons in NH_2 groups, and those in the lower field, to the protons in NH groups, both of which are broadened by the quadrupole relaxation of the ^{14}N nucleus.[28]

The signal at *δ* 3.4 is due to water remaining in the solution, and that at *δ* 2.5—2.6, to residual CH_3 groups in the deuterated solvent. Further, the signals of methylene groups appear at *δ* 2.7—3.0. As is clear from the structures shown in Fig. 1 the NH_2 signals for the *mer* and *u-facial* isomers should be split into two, while only one signal can be expected for the *s-facial* isomer.

In the *s-facial* isomer, the NH_2 groups are equivalent, while the other two isomers have unequivalent sets of two NH_2 groups. The observed results agree with the expectation, and so the isomer A is identified as *s-facial*. The signal due to two equivalent NH groups of the *u-facial* isomer should be in the highest field because the two central nitrogen atoms may be displaced from the

25) K. Ogino, K. Murano, and J. Fujita, *Inorg. Nucl. Chem. Lett.*, **4**, 351 (1968).
26) J. I. Legg and B. E. Douglas, *J. Amer. Chem. Soc.*, **88**, 2967 (1966).
27) C. J. Hawkins and E. Larsen, *Acta Chem. Scand.*, **19**, 185 (1965).
28) J. A. Pople, *Mol. Phys.*, **1**, 168 (1958).

octahedral positions by large non-bonded interactions around them, while that of the *mer* isomer should be in the lowest fields (*cf.* 2.4). On the basis of these results, the isomer A, B, and C are identified as *s-facial*, *u-facial*, and *mer* respectively. Yoneda *et al.*[29] reported the PMR spectrum of $[Co(dien)_2]Cl_3$ in trifluoroacetic acid without referring to the isomerism. Judging from the reported spectrum, their sample seems to be the *mer* isomer.

2.4. Electronic Absorption Spectrum. The absorption spectra of the three isomers in the region 18000—52500 cm^{-1} are shown in Table 2 and Fig. 6. By stereochemistry the *mer* isomer is more distorted from a regular octahedron than the other two. Consequently, it may reasonably be concluded that the distortion of the ligand molecule makes the Co–N(secondary) bond length shorter than the Co–N(primary) bond length, and that two terminal nitrogen(primary) atoms are considerably displaced from the apices of a regular octahedron. This expected difference in bond lengths has been found by X-rays for several complexes, as shown in Table 3.

Table 2. Absorption spectra

Complex	First band $^1A_{1g} \rightarrow {}^1T_{1g}$	Second band $^1A_{1g} \rightarrow {}^1T_{2g}$	CT band N(σ) $\rightarrow e_g(\sigma^*)$	CT band (halide ion)
s-facial $[Co(dien)_2]Cl_3$	21800 (66.5)	30000 (61.0)	47400cm^{-1} (21700)	
u-facial	21500 (93.0)	29700 (88.5)	46300 (22600)	
mer	21600 (146)	29300 (107)	44400 (21200)	
s-facial $[Co(dien)_2]Br_3$	21800 (66.5)	30000 (60.5)	~45500sh (21100)	51000 (50300)
u-facial	21500 (93.4)	29800 (89.2)	~45500sh (23500)	51000 (47400)
mer	21600 (141)	29300 (106)	~44400sh (22900)	51300 (45500)
s-facial $[Co(dien)_2]I_3$	21800 (69.6)	31000sh (101)	44600[a] (58800)	51300 (58900)
u-facial	21500 (94.5)	30200 (121)	44600[a] (61900)	51300 (54100)
mer	21600 (140)	29900 (136)	44400[a] (64300)	51500 (50000)

Figures in the parentheses are molar extinction coefficients.
sh: shoulder, CT: charge transfer.
a) The band due to iodide ion is superposed on this CT band.

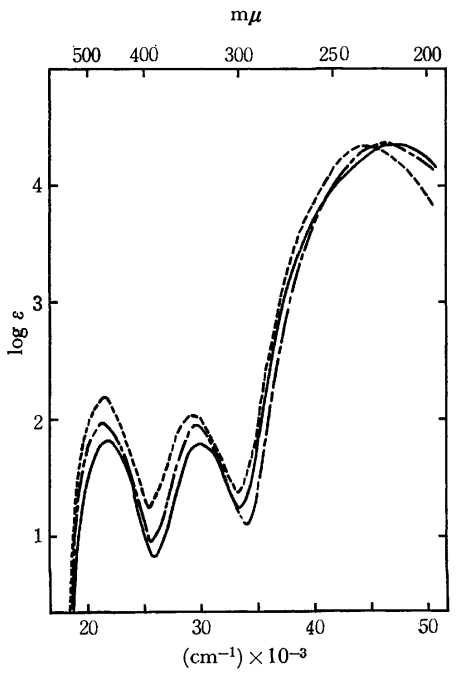

Fig. 6. Absorption spectra of three isomers of $[Co(dien)_2]Cl_3$ in water; —— *s-facial*, ····· *mer* and -·-*u-facial*.

Table 3

Complex	M-NH	M-NH_2	Ref.
mer-$[Co(NO_2)gly(dien)]Cl \cdot H_2O$	1.91Å	1.94Å	30
mer-$[CoCl(gly)(dien)]ClO_4$	1.94	1.99	30
mer-$[Ni(dien)_2]Cl_2 \cdot H_2O$	2.05	2.16	31

If the conformational structure (δ,λ) of each chelate ring is not taken into consideration, the *s-facial* isomer can be said to have a center of symmetry,[18] while the other two have none, and the structures of the latter two may deviate considerably from an octahedron. This expectation agrees with the intensity of the *d–d* absorption bands shown in Table 2. On the other hand, the first ligand field bands, which are observed at 21800, 21600, and 21500 cm^{-1} for *s-facial*, *mer*, and *u-facial* isomers respectively, reveal that the ligand field is highest for the *s-facial* isomer and lowest for the *u-facial* isomer. In spite of the strained structure, the *mer* isomer has a higher ligand field than the *u-facial* isomer. Presumably it contributes to this result that the Co–N(secondary) bond in the *mer* isomer is appreciably stronger than the others. The above result is consistent with the PMR results.

By comparing the absorption bands reported by Brigando[3] and Schmidtke[4] with those of the present investigation, we find that the sample used by Brigando seems to be a mixture of the *mer* and *u-facial* isomers, while that of the latter investigator is the *mer* isomer.

2.5. Infrared Spectra. Recently Schmidtke and Garthoff[32] studied in detail the infrared spectra of the geometric isomers of mono(diethylenetriamine)

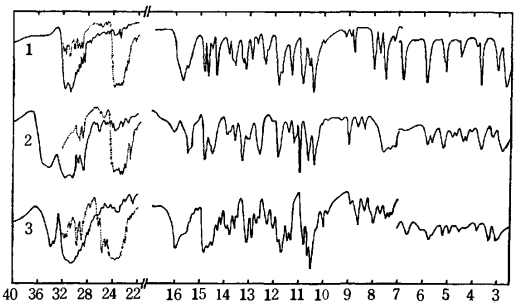

Fig. 7. Infrared spectra of *s-facial* (curve 1), *mer* (curve 2), and *u-facial* (curve 3) isomers of $[Co(dien)_2]Br_3$. ····· deuterated complexes.

29) H. Yoneda and Y. Morimoto, This Bulletin, **39**, 2180 (1966).

30) H. Kuroya, private communication.

31) P. Paoletti, S. Biagini, and M. Cannas, *Chem. Commun.*, **1969**, 513.

32) H. H. Schmidtke and D. Garthoff, *Inorg. Chim. Acta*, **2**, 357 (1968).

complexes of Rh(III), Cr(III), and Co(III), and concluded that the *facial* and *meridional* isomers can be distinguished by different spectral features. Buckingham and Jones[33] have also studied the infrared spectra of isomers of diacido(triethylenetetramine)cobalt(III) complexes. On the basis of these results, and also of those of ethylenediamine complexes, the infrared spectra of $[Co(dien)_2]Br_3$ are assigned. The spectra in the region 4000—300 cm^{-1} are shown in Fig. 7.

In all three isomers the NH stretching vibrations observed at 3200—3000 cm^{-1} shift to 2400—2250 cm^{-1} on deuteration, with the ratio of $\nu_{NH}/\nu_{ND}=1.33$—1.34. The frequency of these vibrations is highest for the *u-facial*, medium for the *mer*, and lowest for the *s-facial* isomers. For the *mer* isomer, a medium strong band appears at 2848 cm^{-1} and this shifts to 2128 cm^{-1} on deuteration ($\nu_{NH}/\nu_{ND}=1.35$), while the other two show only very weak bands in this region. Therefore, this band may be characteristic of the *mer* isomer, and it can tentatively be assigned to the NH stretching vibration of the secondary amine.

The absorption bands at 1610—1550 cm^{-1} shift on deuteration to 1220—1150 cm^{-1} with the ratio of $\nu_{NH}/\nu_{ND}=1.32$—1.36; therefore, they are identified as antisymmetric NH_2 bending vibrations. The *mer* isomer showed a larger splitting in the same region; it may be due to the two unequivalent NH_2 groups. In the region lower than 600 cm^{-1}, the bands due to ring deformation and those related to the Co–N bonds coupled with them are observed. Generally the *s-facial* isomer shows fewer and sharper bands than the other two, as is to be expected from its higher symmetrical structure.

A near-infrared band of HDO was used to study the kinetics of proton exchange[34] in these three isomers; it was found that the NH group exchanged protons faster than the NH_2 group of the ligand and that, further, the rate of the exchange of the NH group of the *mer* isomer is largest among the three isomers.[35] This fact is consistent with the position of the NH signal of the *mer* isomer in the lowest magnetic field (*cf.* 2.3).

The authors appreciate the experimental contribution of Mr. A. Imai in the early stage of the present investigation. A part of the expenses was met by a Grant-in-Aid of the Ministry of Education.

33) D. A. Buckingham and D. Jones, *Inorg. Chem.*, **4**, 1378 (1965).
34) H. Yamatera and M. Fujita, This Bulletin, **42**, 3043 (1969).
35) H. Yamatera, private communication.

The Analytical Application of Sulfur Analogues of β-Diketones. I. The Extraction Spectrophotometric Determination of Cobalt(II) with 1,1,1-trifluoro-4-(2-thienyl)-4-mercaptobut-3-en-2-one (STTA)

Takaharu HONJYO and Toshiyasu KIBA

Department of Chemistry, Faculty of Science, Kanazawa University, Kanazawa, Ishikawa Prefecture

(Received July 26, 1971)

The solvent extraction of cobalt(II) with 1,1,1-trifluoro-4-(2-thienyl)-4-mercaptobut-3-en-2-one (abbreviated as STTA) in cyclohexane has been investigated, and a new spectrophotometric method for the determination of minute amounts of cobalt has been developed on the basis of the results obtained in the extraction study. When a sample solution the pH of which had been adjusted to 6.0—6.5 with hydrochloric acid or sodium hydroxide solution was shaken with a 10^{-3}M STTA organic solution, the extraction of cobalt(II) proceeded rapidly and quantitatively. The amount of cobalt up to 8 ppm in the final organic phase could be determined by measuring the absorbance at 480 or 490 nm against the reagent blank. All other interferring ions, such as Hg(II), Cu(II), Ni(II), Pb(II), Zn(II), and Fe(III), extractable together with cobalt(II) could be stripped out of the organic phase by shaking it with 1—12M hydrochloric acid, while cobalt remained in the organic phase as it was. After this treatment, the organic phase was shaken with an aqueous buffer solution of pH 9—11; thereby, the excess of the reagent was released to a great extent from the organic phase into the aqueous solution. The cobalt-STTA chelate was then the only one existing in the organic phase; therefore, the sensitivity and the selectivity of the method increased so much that a few ppb of cobalt(II) could be determined precisely by measuring the absorbance of the final organic phase at 360 nm against the reagent blank. In this work, the apparent mole ratio of STTA to cobalt in the complex formation was estimated to be 4: 1, and the molar absorption coefficients of the chelate in cyclohexane were found to be 4970000 (at 360 nm), 13200 (at 450 nm), 6500 (at 480 nm), and 5500 (at 490 nm) respectively. Anions, such as oxalate and citrate, as well as EDTA interfered with this extraction. By the recommended procedure, cobalt of a few ppb in an analytical-grade reagent of nickel nitrate hexahydrate could be determined.

Thenoyltrifluoroacetone (abbreviated as TTA) is a well-known chelating agent useful for the solvent extraction and for the colorimetric determination of various metal ions.[1] One of its substituents, monothiothenoyltrifluoroacetone (1,1,1-trifluoro-4-(2-thienyl)-4-mercaptobut-3-en-2-one, abbreviated as STTA), in which one oxygen atom of TTA is replaced with sulfur, has stimulated the interest of many investigators because of its chemical and physical behaviors. Because of the difficulty of its preparation, however, this attractive reagent has not been extensively investigated. However various monometric monothio-derivatives of β-diketones have appeared in the past seven years thanks to the efforts of Chaston *et al.*,[2,3] Uhlemann and Müller,[4] Berg and Reed,[5] and Yokoyama, *et al.*,[6] and many energetic investigations of the coordinative properties of the metal chelates are now under way. Among these reagents, STTA has been found to form its chelates with transition elements, each of them having a specific color and the attribute of being extracted with organic solvents.[5,7,8] Taking advantage of this behavior, the extraction spectrophotometric determination of copper,[9] palladium,[10] and mercury,[11,12] with STTA and the use of the isotope-dilution method for mercury[13] with monothio-dibenzoylmethane have been tried. Nevertheless, the chemical properties of monothio-derivatives of β-diketones and their metal chelates have not yet been reported in detail. The present authors aimed to investigate the extraction behavior of STTA chelates of various metals, and, as a first step, attempted to prepare the STTA reagent by their own method, based on the report by Berg and Reed.[5] After preliminary experiments, the STTA was found to react with the divalent cobalt ion to form a complex of extreme stability. The present paper will describe the extraction-spectrophotometric method for the determination of cobalt with STTA in cyclohexane. The method seems to be more sensitive and selective for cobalt than other methods consisting of synergistic solvent extraction and spectrophotometry, *i.e.*, with benzoyltrifluoroacetone in the presence of tri-*n*-octylphosphine oxide.[14]

Experimental

Apparatus. The visible and ultraviolet absorption spectra were obtained with a Hitachi EPU-2A type spectro-

1) J. Starly, "The Solvent Extraction of Metal Chelates," Pergamon, London, 1964, p. 70.
2) S. H. H. Chaston, S. E. Livingstone, T. N. Lockyer, V. A. Pickles, and J. S. Shannon, *Aust. J. Chem.*, **18**, 673 (1965).
3) S. H. H. Chaston and S. E. Livingstone, *Proc. Chem. Soc.* (London), **1964**, 111.
4) E. Uhlemann and H. Müller, *Angew. Chem.*, **77**, 172 (1965).
5) E. W. Berg and K. P. Reed, *Anal. Chim. Acta*, **36**, 372 (1966).
6) A. Yokoyama, S. Kawanishi, M. Chikuma, and H. Tanaka, *Chem. Pharm. Bull.* (Tokyo), **15**, 540 (1967).
7) V. M. Shinde and S. M. Khopkar, *Chem. Ind.*, **1967**, 1785.
8) E. Uhlemann and H. Müller, *Z. Chem.*, **8** (5), 185 (1968).
9) V. M. Shinde and S. M. Khopkar, *Anal. Chem.*, **41**, 342 (1969).
10) A. U. Rangneckar and S. M. Khopkar, *Chem. Ind.* (London), **10**, 293 (1969).
11) H. Hashitani and K. Katsuyama, *Bunseki Kagaku*, **19**, 355 (1970).
12) K. Itsuki and H. Komuro, *ibid.*, **19**, 1214 (1970).
13) H. Tanaka, N. Nakanishi, Y. Sugiura, and A. Yokoyama, *ibid.*, **17**, 1428 (1968).
14) T. Shigematsu and T. Honjyo, *ibid.*, **18**, 68 (1969).

photometer with 1-cm quartz cells. Radioactivity counting was done with a Kobe Kogyo NaI (Tl) well-type scintillation counter, Model PS-400, connected to a transistorized scaler, Model SA-250. A Hitachi-Horiba glass electrode pH meter, Model M-3, was employed for the pH measurement. A Iwaki shaking machine, type KM, was used for the agitation of the aqueous and organic phases in the solvent extraction. The melting point of the prepared STTA was measured with a Yanagimoto Micro Melting-point Apparatus, Model MP-J2. The infrared absorption spectra were obtained by the nujol method with a Japan Spectroscopic Infrared Spectrophotometer, Model DS 301.

Materials. A stock solution of cobalt(II) was prepared by dissolving a definite amount of cobalt(II) chloride hexahydrate of a guaranteed grade in distilled water, and it was standardized by EDTA titration, using MX as an indicator.[15] The concentration of the solution was estimated to be 0.97×10^{-3} M. The STTA was synthesized in the authors' laboratory by the following procedure, which was based on the method reported by Berg and Reed: the starting substance, TTA, was first stored in a desiccator containing silica gel in order to dry it satisfactorily. Anhydrous ethanol was prepared by adding 5 g of metallic sodium to 500 m*l* of commercial-reagent-grade ethanol (99.5%), by heating it under reflux for 5 to 8 hr, and by then distilling the alcohol. Hydrogen sulfide gas from a steel bomb (from Seitetsu Kagaku Co.) was introduced into a washing bottle containing distilled water dried through a glass tube containing anhydrous calcium chloride, and thereafter passed into the reaction vessel. Hydrogen chloride gas was generated by dropping concentrated sulfuric acid onto solid sodium chloride of a suitable amount in a distillation flask under occasional heating; the gas evolved was introduced from the outlet tube of the flask into a washing bottle containing concentrated hydrochloric acid, and then into another one containing concentrated sulfuric acid. After having been dried well, the hydrogen chloride gas was also passed into the reaction vessel. The dehydration of these three materials, ethanol, hydrogen sulfide, and hydrogen chloride, might lead a worker to a successful synthesis of STTA. This vital part of the process has, however, not been described, not even by Berg and Reed;[5] therefore, if one works according to their procedure, the result might fail. The synthesis in this work was done by a method modified by the present authors as follows. Into a 500-m*l* flask with four necks, 5 to 10 g of TTA and 150 to 200 m*l* of the dehydrated ethanol were put through the large central neck of the flask, and then the vessel was cooled to 0°C in an ice bath. The dried hydrogen chloride gas was introduced through the first slender neck into the vessel in order to saturate the gas in it. The dried hydrogen sulfide gas was then passed through the second slender neck into the reaction vessel for 3 to 4 hr under occasional shaking. Here the third slender neck was useful for letting the gases out under slow suction. The content of the vessel began to turn dark red even after the passing of hydrogen sulfide gas for only about thirty minutes, but the passing of the gas was continued for 3 to 4 more hr in order to complete the reaction. The dark red solution thus obtained was poured over ice in a beaker; the red precipitate of STTA began gradually to appear as the ice melted. The product was separated from the solution by filtration, washed with an appropriate amount of water and dried by sucking the air through the filter and finally on the silica gel in a desiccator. The dried substance was submitted to its recrystallization from the dehydrated ethanol and further purified by repeating the recrystallization twice or thrice. The purified STTA was sealed in a brown-colored bottle in a nitrogen atmosphere and stored in a refrigerator kept at 5°C. The reagent when stored in this manner was quite stable during the storage for as long a time as two years or more, but once it was placed in the air, it slowly turned dark by oxidation. The synthesis was repeated seven times; all were successful when the described procedure was followed exactly. The STTA purified by the recrystallization from dehydrated ethanol showed a melting point of 60—70°C, but the material insufficiently purified or incompletely dried showed a melting point lower than that. The STTA in cyclohexane showed its absorption maximum at 365 nm and a molar absorption coefficient of 1.90×10^{4}. The characteristic absorption frequencies and their assignments were as follows: 1623 (ref. 1612,[3] 1620[5]) ν (C=O); 1260 (ref. 1260,[3] 1258[5]) μ (C=S); 817 (ref. 817,[3] 819[5]) μ (C=S)+δ(C–H). The stock solution of STTA prepared by dissolving the reagent in cyclohexane so as to be 10^{-3}—10^{-2} M was stored in a brown-colored bottle placed in a refrigerator to avoid its decomposition before use. A dilute reagent solution has a yellow color, and the concentrated solution, a red color. The concentration of the reagent was checked from time to time by measuring the absorbance at 350—450 nm. The cyclohexane was purified by distillation, and the chloroform, by washing it successively with a dilute sodium hydroxide solution, water, dilute hydrochloric acid, and three portions of water, and by finally distilling it. Thenoyltrifluoroacetone of a guaranteed reagent grade was purchased from the Dojindo Research Laboratory Co., Ltd., and was used as a starting substance for the synthesis of STTA after drying the commercial reagent in a desiccator containing silica gel. All the other reagents were of a reagent grade and were employed without further purification.

Procedure. An aqueous solution containing cobalt(II) ions was made to have 0.1 M acetic acid (in the acidic region) or 0.1 M boric acid (in the basic region), and its pH was adjusted to a desired value. Ten milliliters of this solution and 10 m*l* of 10^{-3} M STTA in cyclohexane were put together in a 30-m*l* glass-stoppered centrifuge tube and agitated by means of a mechanical shaker for 15—30 min at room temperature (25—29°C). After the separation of the two phases by centrifugation, the amount of cobalt(II) in the cyclohexane was determined by measuring the absorbance at 480 or 490 nm. The extractability of cobalt(II) was also determined by using a ^{60}Co tracer and by counting the radioactivity in both phases with a NaI (Tl) scintillation counter. The pH of the aqueous phase was checked again after each extraction.

Results and Discussion

Absorption Spectra. The absorption spectra of STTA in cyclohexane and those of the extracted cobalt(II)-STTA chelate are shown in Fig. 1. The absorption curve of the chelate has its maximum at 450 nm, but the absorbance of the reagent blank is remarkably large around this wavelength. The measurement of the absorbance of the chelate was, therefore, performed at 480 or 490 nm.

Effect of pH. The effect of the pH on the extractability of cobalt(II) of 10^{-4}M with 10^{-3} M STTA in cyclohexane was examined; the results are shown in Fig. 2 in terms of the absorbance of the chelate. A complete and quantitative extraction is found to be accomplished in the pH region between 5.5 and 7.5. The decrease in the distribution in the basic region may be due to

15) K. Ueno, "Chelatometric Titration" (in Japanese), Nankodo, Tokyo, 1967, p. 243.

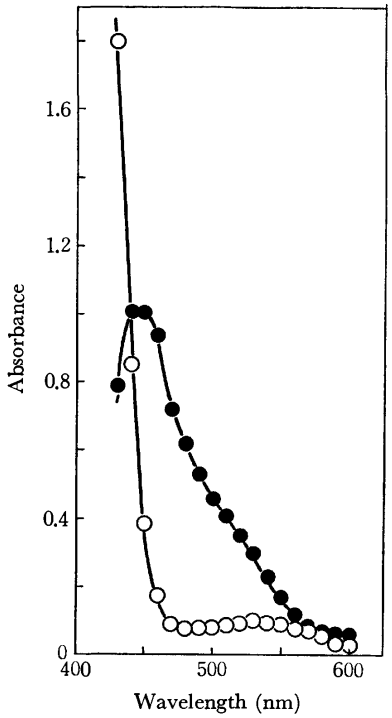

Fig. 1. Absorption spectra of STTA and cobalt-STTA in cyclohexane.
Aqueous phase: 10 m*l* of 0.97×10^{-4}M Co(II) solution of pH 6.0.
Organic phase: 10 m*l* of 10^{-3}M STTA-cyclohexane.
Shaking time: 30 min.

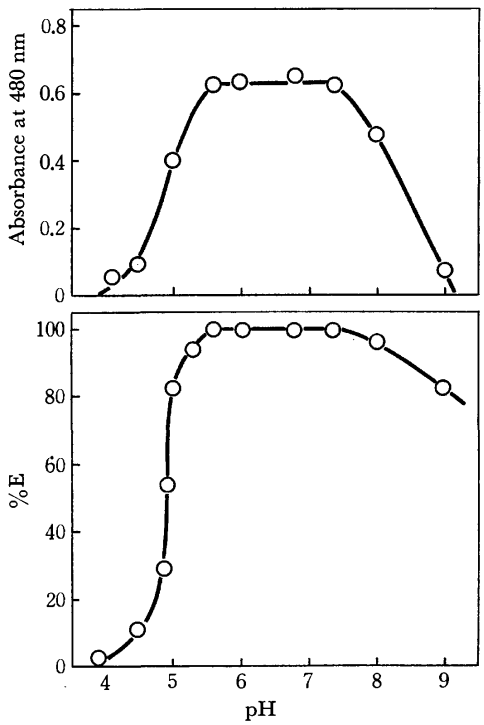

Fig. 2. Dependence of pH on the extraction of Co-STTA in cyclohexane.
Aqueous phase: 10 m*l* of 0.97×10^{-4}M Co(II) solution.
Organic phase: 10 m*l* of 10^{-3}M STTA-cyclohexane.
Shaking time: 30 min.

the increasing solubility of STTA into the aqueous phase, since a yellow color appears in the aqueous beyond pH 6.0. This gradually turns yellowish red with an increase in the pH, while the original color of the reagent in the organic phase fades little by little. Some yellow deposit of an unknown composition is observed in the aqueous phase at pH 9.0.

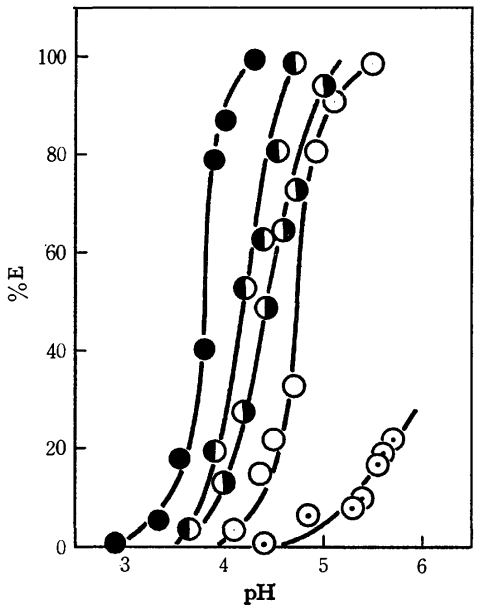

Fig. 3. Extraction of cobalt(II) with STTA in various solvents.
Aqueous phase: 10 m*l* of solution containing only radioactive tracer.
Organic phase: 10 m*l* of 10^{-3}M STTA-solvent.
Shaking time: 10 min.
—●— cyclohexane, —◐— carbon tetrachloride,
—◑— methyl isobutyl ketone, —○— benzene,
—⊙— chloroform.

Effect of Organic Solvents. STTA was dissolved in various organic solvents to make various 10^{-3}M STTA solutions, and the extraction of ^{60}Co in concetrations lower than 10^{-10}M was performed with these organic solutions. Among cyclohexane, benzene, carbon tetrachloride, chloroform, and methyl isobutyl ketone, cyclohexane was found to be the most excellent solvent to extract cobalt in the lower pH region, as can be seen in Fig. 3. In the lower pH region, hydroxo-complexes of many metals are not formed; therefore, serious interference can be avoided spontaneously. This is the reason for our preferring cyclohexane as a solvent in this study. The distribution of cobalt from a 10^{-4}M solution was found to be somewhat lower than that of radioactive cobalt in a trace amount. This might be attributed to the decrease in the effective concentration of STTA in the organic phase caused by the consumption of the reagent during the chelate formation and also to the time-lag needed to reach the extraction equilibrium.

Effect of the Reagent Concentration. The extraction of cobalt from a 10^{-4}M aqueous solution with cyclohexane containing STTA of varying concentrations was done; the absorbance of the organic phase is given in Fig. 4 in terms of the initial concentration of STTA in cyclohexane. The results show that it is enough to keep the

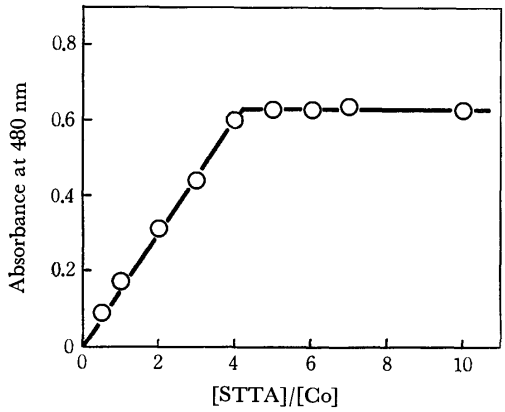

Fig. 4. Effect of the concentration of STTA in cyclohexane.
Aqueous phase: 10 m*l* of 0.97×10^{-4}M Co(II) solution of pH 6.5.
Organic phase: 10 m*l* of cyclohexane containing various amounts of STTA.
Shaking time: 30 min.

concentration of STTA four times that of cobalt in order to achieve the quantitative extraction of the metal.

Effect of Shaking Time. The extractability of 10^{-4}M cobalt with 10^{-3}M STTA in cyclohexane at pH 6.0 is given in Fig. 5 as a function of the shaking time. The quantitative result is attained in about ten minutes of shaking.

Effect of the Volume of the Aqueous Solution. When the volume of the organic phase of 10^{-3}M STTA in cyclohexane was kept at 10 m*l*, when that of the aqueous phase was varied from 10 m*l* to 100 m*l*, and when the absorbance of the organic phase was measured at 480 nm after every extraction, almost the same absorbance was obtained in each case, as is shown in Fig. 6. Therefore, the volume of the initial aqueous solution seems to have no effect on the extraction recovery of cobalt, even at a ten-fold volume of the organic phase.

Stability of the Extracted Chelate. By measuring the absorbance of the cobalt-STTA chelate in cyclohexane at 480 nm at long intervals, the brown color

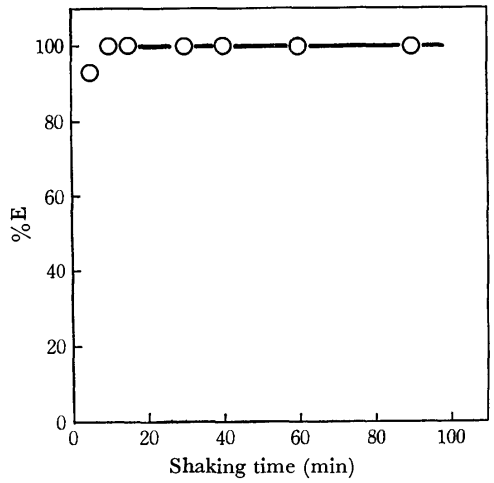

Fig. 5. Effect of shaking time.
Aqueous phase: 10 m*l* of 0.97×10^{-4}M Co(II) solution of pH 5.9.
Organic phase: 10 m*l* of 10^{-3}M STTA-cyclohexane.

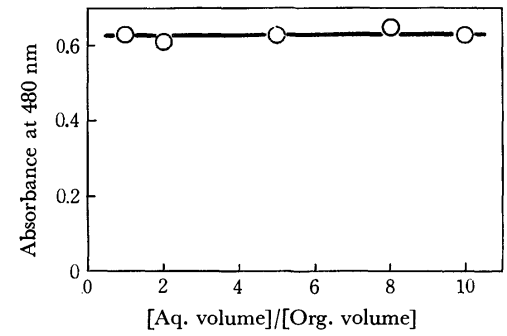

Fig. 6. Effect of the volume of the aqueous phase.
Aqueous phase: varying volume containing 0.97×10^{-3}m mol Co(II) of pH 6.0.
Organic phase: 10 m*l* of 10^{-3}M STTA-cyclohexane.
Shaking time: 30 min.

of the chelate was found to be quite stable; it showed no change in the absorbance for several weeks. The extraction was carried out in natural daylight and also in the dark, but no differences in the distribution as in the absorbance could be found between the two cases.

Back-extraction of the Chelate from the Organic Phase. The back-extraction of the extracted chelate was attempted by shaking the organic phase with hydrochloric acid of from 1 to 12M for thirty minutes. It was found that the back-extraction of cobalt did not occur at all. On the other hand, when the organic phase was shaken with an aqueous buffer solution of pH 9.0—11.0, the excess of the STTA reagent was almost entirely transferred into the aqueous solution, leaving only the cobalt-STTA in the organic phase. Thus, by the above two treatments, other interferring ions could be stripped out and the excess of the STTA be back-washed from the organic phase; therefore, the spectrophotometric determination of cobalt might be more sensitive and selective. This can be readily seen in Fig. 7, in which the absorbance of the organic phase after shaking with aqueous solutions of varying pH values, one at 480 nm when cobalt-STTA is present and another at 440 nm when only STTA is present, are shown together for the sake of comparison. The

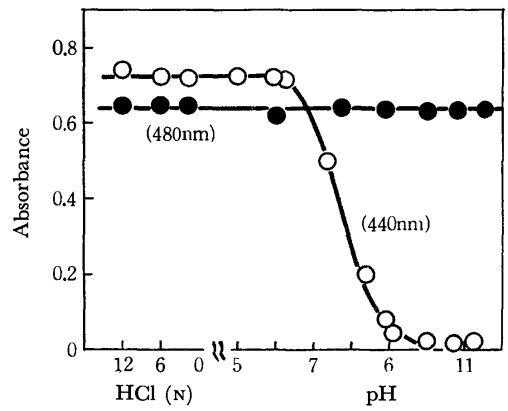

Fig. 7. Back-washing of STTA and Co-STTA with an aqueous solution of different pH/acidity.
Aqueous phase: 10 m*l*. Organic phase: 10 m*l* containing 10^{-2}m mol STTA and 0.97×10^{-3}m mol Co(II).
Shaking time: 30 min.

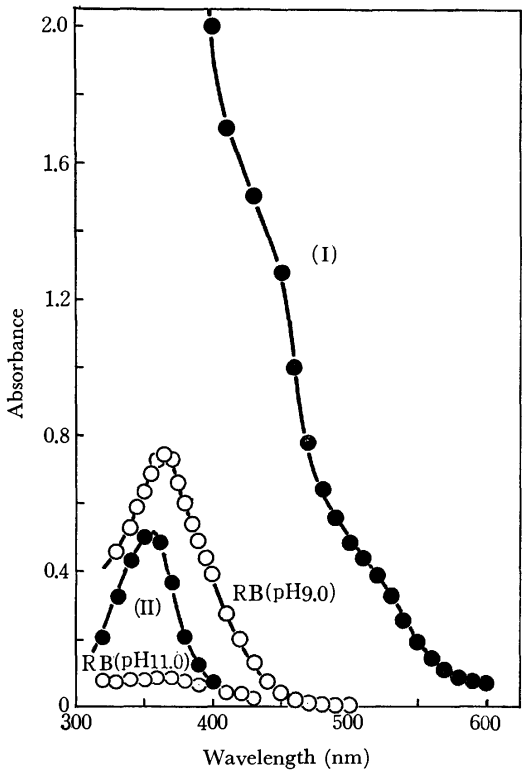

Fig. 8. Absorption spectra of STTA and Co-STTA in cyclohexane after back-washing of the organic phase prepared as in Fig. 1, (I) with a solution of pH 9.0 and (II) with that of pH 11.0. Organic phase: 10 m*l* of (I) 0.97×10^{-4}M Co-STTA and of (II) 0.97×10^{-7}M Co-STTA, both containing the excess of the STTA;
Aqueous phase 10 m*l*. Shaking time: 30 min.
—●— Co-STTA, —○— reagent blank.

STTA in the organic phase is found to begin to transfer itself into the aqueous phase at pH 6.0; it completely dissolves into the aqueous solution of pH above 9.5. On the other hand, the cobalt-STTA remains in the organic phase, as before. The absorbance of this cobalt-STTA could keep its value constant for at least several hours. The absorption spectra of the cobalt-STTA chelate remaining in the organic phase after back-washing with an aqueous solution of pH 9 and pH 11 are shown in Fig. 8, in which the reagent blank is found to have remarkably decreased, particularly at pH 11, without any effect on the STTA chelate. Thus, when the uncombined STTA was removed from the organic phase, the quantitative determination of cobalt could be extended to the order of ppb in the final organic phase.

Recommended Procedure and Working Curve. From the experimental results described above, a useful procedure for cobalt could be developed as follows. From 10 to 100 m*l* of an aqueous sample solution, the pH of which had been adjusted at 6.0—6.5 with 0.1M acetic acid and 0.1M sodium hydroxide, was put in a 30—300 m*l* glass-stoppered centrifuge tube or separating funnel, and 10 m*l* of 10^{-3}M STTA cyclohexane solution was then added into the vessel. The content was agitated by a mechanical shaker for 15 to 30 min at room temperature (25—29°C). After

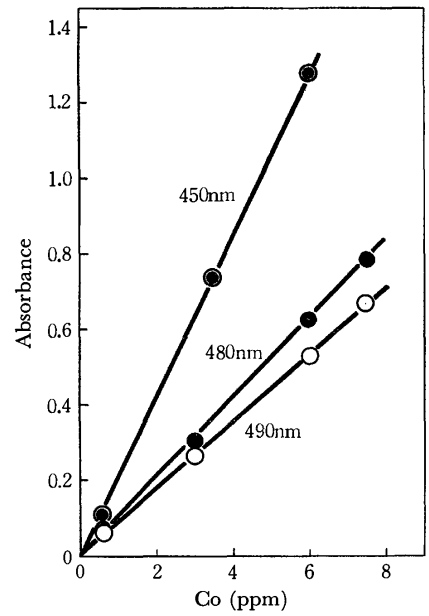

Fig. 9. Working curves for cobalt(II) at different wavelength.
Aqueous phase: 10 m*l* of pH 6.0.
Organic phase: 10 m*l* of 10^{-3}M STTA-cyclohexane.
Shaking time: 15—30 min.

the lower aqueous phase had been separated off, the remaining organic phase was shaken again with 1M hydrochloric acid and then with a buffer solution of pH 9.0—11.0. After centrifugation, the organic phase was taken out to determine its absorbance at 450, 480, or 490 nm arbitrarily against the reagent blank. The analytical working curves prepared at each wavelength are shown in Fig. 9, in which it is found that Beer's law is obeyed up to 8 ppm of cobalt in the final organic solution and in which the molar absorption coefficients are found to be 13200 (at 450 nm), 6500 (at 480 nm), and 5500 (at 490 nm).

Effect of Diverse Ions. The effect of foreign ions on the determination of cobalt according to the above procedure is noted in individual cases in Table 1. Mercury(II), Pb(II), Cu(II), Ni(II), Zn(II), and Fe(III) could form their extractable, colored complexes with STTA and, therefore, interfered with the spectrophotometric detemination of cobalt(II) if they could not be removed from the organic phase. However, when the organic phase containing the chelates of these metals was shaken with hydrochloric acid of 1.0—12M for thirty minutes, all these ions other than cobalt could be readily back-extracted into the acid. This fact was examined by the tracer method and by the colorimetric method to make sure that the separation was complete. On the other hand, these metal ions existing in the original sample solution consume the STTA reagent, being competitive with the formation of cobalt-STTA, and therefore hinder the extraction of the latter. When a large amount of these other ions are present a larger amount of the reagent should be employed to permit the complete extraction of all the metal ions. The back-extraction with hydrochloric acid could remove all the metal ions other than cobalt from the organic phase; this process seemed indispensable for the purpose. Strange to say, the cobalt-

Table 1. Effect of foreign ions on the absorbance of Co–STTA in cyclohexane

Ion coexisting in aq. phase	Taken μg/10ml	Absorbance of org. phase		Absorbance after back-washing with 1.0M HCl		Remark
		480 nm	490 nm	480 nm	490 nm	
none	—	0.620	0.535			
Ag(I)	6000	0.605	0.515			oxide ppt.
Pb(II)	6000	0.705	0.585	0.625	0.528	
	600	0.670	0.568			
	60	0.630	0.540			
Hg(II)	6000	0.642	0.548	0.635	0.545	
	600	0.635	0.545			
	60	0.632	0.535			
Cu(II)	6000	1.40	1.08	0.215	0.170	
	600	0.970	0.818	0.350	0.330	
	60	0.665	0.570			
Ni(II)	6000	2.02	1.75	0.362	0.315	
	600	1.22	0.975	0.340	0.322	
	60	0.690	0.590			
Mn(II)	6000	0.625	0.540			
Sr(II)	6000	0.628	0.535			
Zn(II)	6000	0.655	0.555	0.595	0.510	
	600	0.648	0.555	0.350	0.330	
Cd(II)	600	0.632	0.545			
	60	0.623	0.538			
Mg(II)	6000	0.630	0.540			
Fe(III)	6000	1.32	1.19	0.620	0.532	
	600	0.980	0.880			
	60	0.640	0.555			
Cr(III)	6000	0.615	0.520			
Bi(III)	6000	0.860	0.665			hydroxide ppt.
Al(III)	6000	0.565	0.478			hydroxide ppt.
Cl^-	60000	0.620	0.532			
CH_3COO^-	60000	0.630	0.540			
SO_4^{2-}	60000	0.618	0.530			
$C_2O_4^{2-}$	60000	0.410	0.350			
PO_4^{3-}	60000	0.620	0.530			
BO_3^{3-}	60000	0.638	0.555			
Cit^{3-}	60000	0.522	0.445			
$EDTA^{4-}$	60000	0.040	0.050			
NO_3^-	60000	0.622	0.538			

In each case 57.2 μg of cobalt(II) was taken in 10 ml of the aqueous solution of pH 6.0—6.5 and extracted with 10 ml of 10^{-3} M STTA-cyclohexane.

STTA chelate was scarcely back-extracted from cyclohexane, even with 1—12M hydrochloric acid, 70% perchloric acid, and 18M sulfuric acid as well as an aqueous buffer solution of pH 9—13, each after one hour's shaking. The chelate could, however, be back-extracted to the extent about 15% with 1.0M sodium hydroxide after thirty minutes' shaking and to the extent about 10% and 90% under shaking with concentrated nitric acid for thirty and sixty minutes respectively. With concentrated sulfuric acid, all the cobalt was transferred immediately from the organic phase into the acid accompanying the decomposition of the organic matter.

Some Aspects of the Nature of Co-STTA. As has been described above, the cobalt-STTA once formed in the extraction system is remarkably stable. At pH 6.5, all of the cobalt in the aqueous solution was extracted into the organic phase (as is shown in Fig. 2), while a small amount of the STTA reagent was back-extracted into the aqueous phase under the same contitions (as is shown in Fig. 7). The absorbance of the extracted cobalt-STTA was examined in terms of the mole ratio of STTA to cobalt; the absorbance was found to become constant in the region above the 4:1 ratio, as is shown in Fig. 4. This confirms that the apparent mole ratio of STTA to cobalt in the complex formation was 4:1. Similar investigations have been done for Co(II)-1-nitroso-2-naphthol,[16,17] Co(II)-dithizone,[18,19] and Co(II)-monothio-dibenzoylmethane.[6,20]

16) R. Paulais, *Bull. Soc. Chim. Fr.*, **1951**, 206.
17) N. Suzuki and H. Yoshida, *Nippon Kagaku Zasshi*, **80**, 1008 (1959).
18) J. F. Duncan and F. G. Thomas, *J. Inorg. Nucl. Chem.*, **4**, 376 (1957).
19) J. F. Duncan and F. G. Thomas, *J. Chem. Soc.*, **1960**, 2814.
20) E. Uhlemann and H. Müller, *Anal. Chim. Acta*, **41**, 311 (1968).

In all cases involving the present study, it may be assumed that the original cobalt could no longer be present as divalent, but must be trivalent or something else after its chelate formation. A detailed report concerning the composition of this stable cobalt-STTA will be presented in the near future.

Table 2. Recovery of cobalt(II) in the presence of nickel

Co(II), taken in 10 m*l* mmol	Ni(II), taken in 10 m*l* mmol	Recovery of Co(II) %
1.94×10^{-3}	1.0×10^{-3}	98.0
0.97×10^{-3}	1.0×10^{-3}	98.4
0.97×10^{-4}	1.0×10^{-3}	97.8
trace ($<10^{-9}$)	1.0×10^{-3}	97.4

Table 3. Determination of cobalt in nickel nitrate reagent

$Ni(NO_3)_2$ solution prepared M	Taken m*l*	Absorbance of Co-STTA at 360 nm	Recovery by ^{60}Co tracer %	Cobalt, found M $\times10^{-7}$	Cobalt, found %
1.0×10^{-4}	10.00	0.412	96.9	0.855	0.088
1.0×10^{-4}	10.00	0.375	97.6	0.778	0.080
1.0×10^{-4}	10.00	0.420	98.0	0.871	0.088

Application of the Recommended Method. The extraction spectrophotometric procedure for cobalt recommended by the present authours will find extensive application for various purposes. First of all, the method has been applied to the determination of a minute amount of cobalt in a nickel nitrate reagent of the guaranteed analytical grade. The recovery of cobalt was ascertained at the same time by employing a radioactive tracer, $^{60}Co(<10^{-10}M)$; it was found to be 97.4—98.4% from an aqueous solution of $10^{-4}M$ nickel(II). The results obtained are shown in Table 2, while the practical analysis of a trace amount of cobalt in nickel nitrate of an analytical grade gives the data shown in Table 3. In the latter case, the recovery of cobalt was checked by using ^{60}Co in order to confirm the spectrophotometric data. In this case, when a minute amount of cobalt is to be determined, the absorbance of cobalt-STTA at 360 nm is preferred. As is shown in Fig. 8, when the organic phase was back-washed with a solution of pH 11.0, the proper absorption spectra of cobalt-STTA appeared distinctly since the reagent blank was reduced to an almost indetectable value. Therefore, as little as 5.89 ppb of cobalt(II) in a sample aqueous solution could be determined by using a 10 m*l* of the initial solution and by measuring the absorbance of the final organic phase as being 0.482, corresponding to $0.97\times10^{-7}M$ Co-STTA. The molar absorption coefficient of Co-STTA was found to be 4970000 at 360 nm. In the determination of a trace amount of cobalt in the nickel nitrate reagent, a working curve was prepared at 360 nm for cobalt of 0.6 to 60 ppb in the final organic phase; each measured absorbance was adopted to this working curve, and the amount of cobalt was evaluated. The results after three experiments are shown in Table 3; the standard deviation is also estimated to be 0.004%.

A part of the expense for the experiment has been defrayed from a grant given by the Ministry of Education, to which the authors' thanks are due.

Substituent Effect of Dipole and Dipolarophile in the Reaction of Nitrones with *N*-(Substituted phenyl)maleimides

Yosio IWAKURA, Keikichi UNO, Suck-Ju HONG, and Tatsuhiko HONGU

Department of Synthetic Chemistry, Faculty of Engineering, Tokyo University, Bunkyo-ku, Tokyo

(Received May 4, 1971)

The reactions of *C*-(*p*-substituted phenyl)-*N*-(*p*-substituted phenyl)nitrones with *N*-(*p*-substituted phenyl)maleimides were carried out in THF to give both *trans*- and *cis*-isoxazolidines. The formation ratios of *trans*- to *cis*-isoxazolidines (I_T/I_C) were determined by the NMR spectra of the cycloadduct mixtures. Though the values of I_T/I_C varied with the electronic characters of the substituents, R_1, R_2, and R_3, they were always found to be larger than unity.

In an earlier paper[1] from this laboratory we have reported on the configuration of the cycloadduct of nitrone with *N*-phenylmaleimide. In order to investigate the substituent effect of dipole and dipolarophile in the reactions of nitrones and *N*-phenylmaleimides, we have studied the reactions of nitrones having the substituents R_1 in *C*-phenyl and R_2 in *N*-phenyl groups both at the *p*-positions, with *N*-phenylmaleimide having the substituent R_3 at the *p*-position. We have found that the ratios of *trans*- to *cis*-isoxazolidines in the

TABLE 1. THE MELTING POINTS, ANALYTICAL DATA, AND RATIOS, I_T/I_C, OF *trans*- TO *cis*-ISOXAZOLIDINES

Run No.	R_1	R_2	R_3	Mp[a] °C	Anal (Calcd), % C	H	N	I_T/I_C
1-A[1]	H	H	H	197—199 (*cis*)	—	—	—	1.7
				153—155 (*trans*)	—	—	—	
1-B	H	H	NO_2	213—214	66.61	4.14	10.22	2.1
				194—195.5	66.50	4.18	10.19	
					(66.50	4.13	10.21)	
1-C	H	H	OCH_3	215	71.90	4.99	6.96	1.5
				191—192	71.99	4.98	6.90	
					(71.98	5.03	7.00)	
2-A	NO_2	H	H	226—228 (decomp.)	66.67	4.33	10.26	2.6
				204—207 (decomp.)	66.57	4.13	10.17	
					(66.50	4.13	10.12)	
2-B	OCH_3	H	H	193—195	72.20	5.09	7.23	1.4
				148—150	71.66	5.08	7.22	
					(71.98	5.03	7.00)	
3-A	H	CH_3	H	188—189	75.00	5.24	7.16	2.9
				170—171	74.76	5.26	7.14	
					(74.94	5.24	7.29)	
3-B	H	CH_3	NO_2	—	—	—	—	3.0
3-C	H	CH_3	OCH_3	207—208	72.41	5.36	6.63	2.4
				179	72.32	5.36	6.66	
					(72.45	5.35	6.76)	
4-A	H	*t*-Bu	H	196—197.5	76.28	6.14	6.28	2.5
				166—167	75.77	6.09	6.63	
					(76.03	6.15	6.57)	
4-B	H	*t*-Bu	NO_2	198—199	68.20	5.33	8.91	3.9
				180—182	68.13	5.43	8.91	
					(68.78	5.34	8.92)	
4-C	H	*t*-Bu	OCH_3	195—196	74.36	6.24	6.22	2.1
				179—181	73.27	6.25	6.32	
					(73.66	6.18	6.14)	
5-A	H	Cl	H	175—176 (*trans*)	68.76	4.76	6.83	3.1
					(68.23	4.23	6.92)	
5-B	H	Cl	NO_2	158—159 (*trans*)	62.00	3.91	9.35	1.6
					(61.43	3.58	9.56)	
5-C	H	Cl	OCH_3	—	—	—	—	3.6

a) Upper line for *cis*-isomer, lower line for *trans*-isomer.

1) Y. Iwakura, K. Uno, and T. Hongu, This Bulletin, **42**, 2282 (1969).

cycloadduct mixtures varied with the electronic character of the substituents, R_1, R_2, and R_3. The ratios of *trans*- to *cis*-isoxazolidines were determined directly by the NMR spectra of the cycloadduct mixtures. Detailed results are described in the present paper.

Results and Discussion

The reactions of *C*-phenyl-*N*-(*p*-substituted phenyl) nitrones with *N*-(*p*-substituted phenyl)maleimides were carried out in anhydrous THF to give cycloadducts in quantitative yields. In agreement with earlier work,[1] the formations of *trans*- and *cis*-isoxazolidines were observed. The melting points and analytical data of *trans*- and *cis*-isoxazolidines obtained are summarized in Table 1 with the ratios of *trans*- to *cis*-isoxazolidines in the cycloadduct mixtures.

The NMR spectra of the cycloadduct mixture (run 4-B) obtained without any purification are shown in Fig. 1. Signals of each isomers were assigned as shown in the figure according to the previous paper.[1]

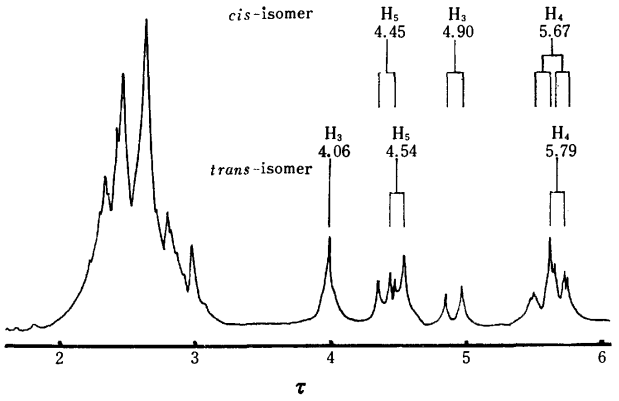

Fig. 1. The NMR spectra of cycloadduct mixture (run 4-B) in DMSO-d_6.

As shown in Fig. 1, proton signals at *C*-3 of isoxazolidine rings appear to be a singlet and doublet according to *trans*- and *cis*-isoxazolidines, respectively, without any overlap. Accordingly, the ratio of *trans*- to *cis*-isoxazolidines (I_T/I_C) can be directly obtained from the NMR spectral comparison, and the values of I_T/I_C thus obtained are summarized in Table 1.

The value of I_T/I_C for every 1,3-dipolar cycloaddition reaction was found to be >1, indicating that the formation of *trans*-isoxazolidine is more favorable than *cis*-isomer. Assuming the reaction of nitrone with *N*-phenylmaleimide by one step mechanism,[2] $I_T/I_C>1$ reveals that addition reaction of nitrone with *N*-phenylmaleimide would proceed favorably through the above transition state as shown in Scheme 1.

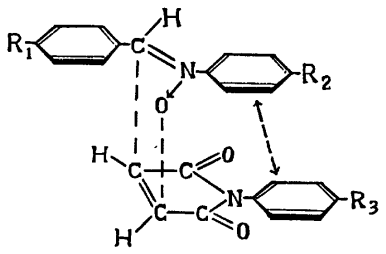

Scheme 1

For establishing such a favorable transition state of the addition reaction in the present investigation, it is necessary that the dipole moments of both reaction species, dipole and dipolarophile, should orient to the arrow-signed direction as shown in Scheme 2.

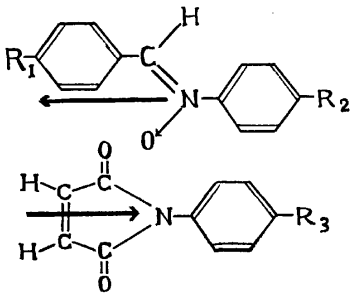

Scheme 2

If the substituent R_1 of nitrone is an electron withdrawing group, the greater dipole moment is anticipated, *i.e.*, the formation of *trans*-isoxazolidine would be predominant. Eventually higher value of I_T/I_C is obtained.

Figure 2 shows the relation between the electronic characters of R_1 and the values of I_T/I_C from Table 1. An approximately linear relation appeared to exist between the Hammett σ value of R_1 and the value of log I_T/I_C. Increasing the negativities of the substituents R_1, the greater values of I_T/I_C were obtained. Such experimental facts seem to support strongly above mentioned assumptions.

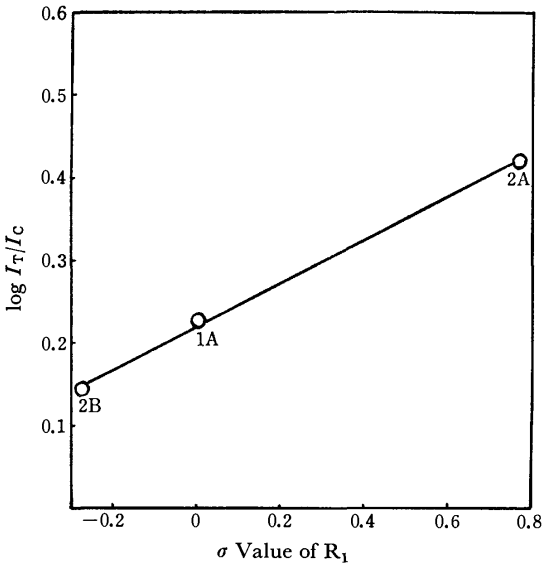

Fig. 2. The relation between the Hammett σ value of R_1 and the log I_T/I_C.
R_2=H; R_3=H.

The magnitudes of dipole moments of *N*-phenylmaleimides may depend on the electronic characters of R_3 in *p*-substituted *N*-phenylmaleimides. There are also fairly good relationships between the Hammett σ values and the values of log I_T/I_C as shown in Fig. 3.

In the series of the substitutents (R_2=H, CH_3, and

2) R. Huisgen, *J. Org. Chem.*, **33**, 2291 (1968).

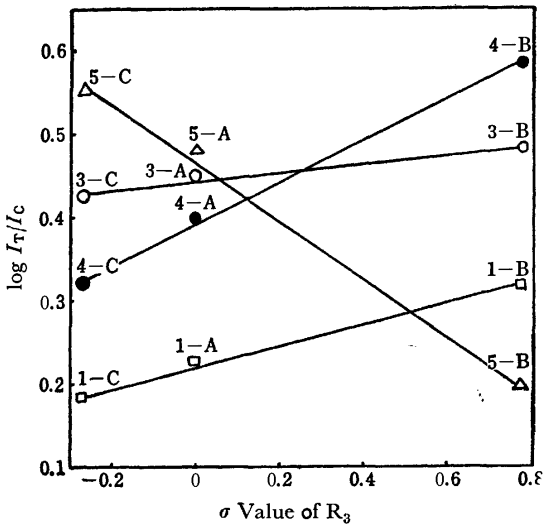

Fig. 3. The relation between the Hammett γ values of R_3 and the log I_T/I_C.
R_1=H; R_2: △=Cl, ○=CH_3, ●=*t*-Bu, □=H.

t-Bu) on *N*-phenyl group of nitrone, the greater electronegativities of the substituents, the greater values of I_T/I_C were obtained. These results may also appear to be consistent with that the dipole-dipole interaction between dipole and dipolarophile would influence on the formation ratios of *trans*- to *cis*-isoxazolidines. But when R_2 is Cl, the results are reversed, *i.e.*, with increase in the electro-negativities of R_3, the smaller values of I_T/I_C were obtained.

If the above mentioned assumptions are reasonable, we may draw a conclusion tentatively that the dipole moment of nitrone having the substituent, R_2=Cl, should orient to the reverse direction to those of nitrones having the substituents, R_2=H, CH_3, and *t*-Bu. Considering that Cl is an electron-withdrawing group, such a possible dipole orientation of a nitrone having Cl as R_2 can not be denied. We can point out one more additional possible consideration as an influencing factor on the configurations of *trans*- and *cis*-isoxazolidines in the present work. As shown in Scheme 1, at the transition state in 1,3-dipolar cycloaddition of nitrone with *N*-phenylmaleimide *N*-phenyl group of nitrone exists near enough to *N*-phenyl group of *N*-phenylmaleimide. In this event, the affinity between *N*-phenyl group of nitrone and *N*-phenyl group of *N*-phenylmaleimide may affect on the values of I_T/I_C. This explanation is in accordance with the fact that $I_T/I_C>1$ was always obtained as shown in Table 1. The τ values of the protons of *N*-phenyl group of nitrone having Cl as R_2, shifted to lower values than those of other nitrones as shown in Table 2. Such a fact may indicate clearly that the electron density of *N*-phenyl group of nitrone having Cl as R_2, is being much lowered. Accordingly, the affinity between *N*-phenyl group of *N*-phenylmaleimide having electron-donating R_3 and *N*-phenyl group of nitrone would exert to give the results as indicated in Fig. 3.

The relations between the Hammett σ values of R_2 and the values of log I_T/I_C are shown in Fig. 4.

In the series of the reaction of nitrone with *N*-phenylmaleimide having NO_2 as R_3, the greater electro-

TABLE 2. THE CHEMICAL SHIFTS OF *N*-PHENYL PROTONS OF NITRONES, R_1–C(H)=N(O)–R_2, IN DMSO-d_6

R_1	R_2	Position of protons		
		-CH=	A	B
H	H	2.00	1.91	2.50
H	CH_3	1.54	2.16	2.66
H	*t*-Bu	1.68	2.28	2.68
H	Cl	1.46	2.01	2.39

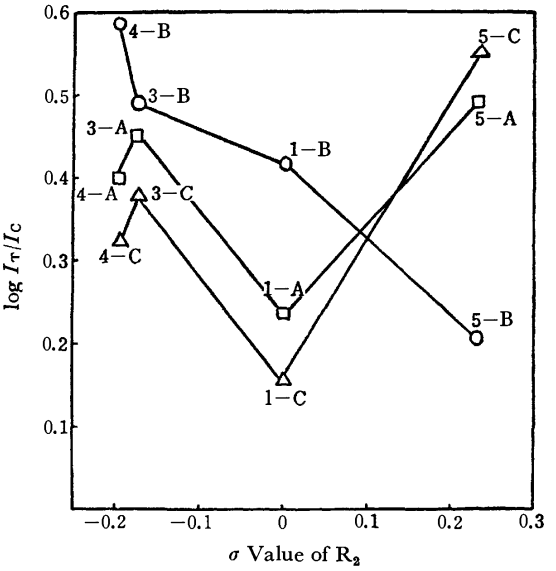

Fig. 4. The relation between the Hammett σ values of R_2 and the log I_T/I_C.
R_1=H; R_3: □=H, ○=NO_2, △=OCH_3

negativities of R_2, the greater values of I_T/I_C were obtained but not linearly. But as shown in Fig. 4, in the case of R_2=H and CH_3, the results obtained were different, *i.e.*, nitrone having no substituent on *N*-phenyl group gave the smallest value of I_T/I_C. Nitrones having either electron donating or withdrawing group on *N*-phenyl group gave the greater values of I_T/I_C.

As we have already pointed out on the explanations of Figs. 2 and 3, the value of I_T/I_C may be influenced by following two factors: (1) dipole orientation of the dipole and dipolarophile; (2) affinity between *N*-phenyl group of nitrone and *N*-phenyl group of *N*-phenylmaleimide. When affinity between *N*-phenyl group on nitrone and *N*-phenyl group of *N*-phenylmaleimide is small, (1) will be a main factor governing the value of I_T/I_C. The results shown in Fig. 4 may not be inconsistent with this explanation. In Fig. 4, if the Hammett σ value of R_2 is positive, (2) might be assumed as a governing factor for the I_T/I_C, but if the σ value of R_2 is negative, (1) will become important. When (1) is a predominant factor governing the value of I_T/I_C, *p*-substituent of *N*-phenyl group of nitrone would come near to *N*-phenyl group of phenylmaleimide. It will be reasonably explained that the decrease of the value of I_T/I_C, in the case of *t*-Bu, is due to the steric hindrance of bulky group.

We have proceeded explanations on the results obtained in the present work, on the basis of one step addition mechanism. Further studies are under progress.

Experimental

Materials. A typical example of *C*-phenyl-*N*-(*p*-*t*-butylphenyl)nitrone was prepared in the following manner. Nitration of *t*-butylbenzene was carried out by the procedure of Ketcham.[3] The oily product, *p*-nitro-*t*-butylbenzene was obtained in 80% yield (bp, 108.5—110°C/5 mmHg), identified by the IR spectrum. Then *p*-nitro-*t*-butylbenzene was reduced to hydroxylamine by zinc dust in 65% yield by the usual manner, mp 89.5—90°C.

Found: C, 72.57; H, 8.89; N, 8.32%.

Calcd for $C_{10}H_{15}ON$: C, 72.69; H, 9.15; N, 8.48%.

The mixture of equimolar amounts of *p*-*t*-butylphenylhydroxylamine and benzaldehyde in ethanol was refluxed for three hrs. Recrystallization three times from *n*-hexane afforded white needles, *C*-phenyl-*N*-(*p*-*t*-butylphenyl)-nitrone (mp, 117—119°C) in 71% yield.

Found: C, 80.31; H, 7.39; N, 5.40%.

Calcd for $C_{17}H_{19}ON$: C, 80.57; H, 7.56; N, 5.53%.

Other nitrones, were prepared in over 70% yields by the procedure of Wheeler *et al.*[4] Their melting points were as follows: R_1=H, R_2=H, 112—113°C (lit, 114°C);[4] R_1=H, R_2=CH_3, 123°C (lit. 123°C);[4] R_1=H, R_2=Cl, 174—175°C (lit, 174°C)[5], 181°C)[4]. *N*-phenylmaleimides, R_3, were synthesized by the procedure of Searle.[6] Their melting points were as follows: R_3=H, 90—91°C (lit, 90—91°C);[6] R_3=NO_2, 167°C (lit, 167—168°C);[6] R_3=OCH_3, 146°C. The last product was a new compound and gave following analytical data.

Found: C, 64.98; H, 4.46; N, 6.89%. Calcd for $C_{11}H_9O_3N$: C, 65.69; H, 4.46; N, 6.89%.

NMR Spectra. The NMR spectra were measured in DMSO-d_6 solution (concentration: about 10% solution of the sample by weight) at room temperature with Japan Electron Optics C-60 spectrometer (60 MHz). Tetramethylsilane was used as an internal reference.

3) R. Ketcham, R. Cavestri, and D. Jambotkar, *J. Org. Chem.*, **28**, 2139 (1963).

4) O. H. Wheeler and P. H. Gore, *J. Amer. Chem. Soc.*, **78**, 3363 (1956).

5) K. Kubota, M. Yamakawa, and Y. Mori, This Bulletin, **36**, 1552 (1963).

6) N. E. Searle, U. S. 2444536 (1948).

BULLETIN OF THE CHEMICAL SOCIETY OF JAPAN, VOL. 45, 195—198(1972)

The Synthesis and Asymmetric Adsorption of an Optically-active Basic Polymer Starting from L-Proline

Tetsushi YAMASHITA

Department of Chemistry, Faculty of Science, Osaka City University, Sumiyoshi-ku, Osaka

(Received April 9, 1971)

N-Prolyl-*p*-aminostyrene was synthesized by the reaction of *N*-carboxy-L-proline anhydride with *p*-aminostyrene phosphate. This optically-active basic monomer was then copolymerized wtih *N*,*N*′-bis(*p*-vinylphenyl)-adipamide to give a basic polymer. Similar basic polymers were also obtained, starting from other α-amino acids, through this procedure. Of these polymers, the polymer involving L-proline was used for the chromatographic resolution of the phthalamidic acid derivatives of DL-phenylalanine, DL-valine, and DL-phenylglycine. The polymer resolved partially DL-*N*-(*o*-carboxybenzoyl)phenylalanine.

There have been many reports[1-5] concerning the use of synthetic optically-active basic polymers as adsorbents for the chromatographic resolution of racemates.

Most such polymers have been synthesized by the method in which an optically-active group is introduced into an optically-inactive "reactive polymer"[6] (*e.g.*, chloromethylated polystyrene[2-5] and polymethacroyl chloride[1]).

On the other hand, we[7] previously reported several optically-active basic polymers synthesized by a different method, which involves either the hydrazinolysis or hydrogenolysis of the neutral copolymers composed of *N*-(*N*-phthaloyl or *N*-tosyl-α-amino acyl)-*p*-aminostyrene and *N*,*N*′-diacroylhexamethylenediamine. However, this synthetic method has two limitations.

The first limitation is that this method cannot be applied to imino acids or to the α-amino acids with *s*-alkyl, acetoxyl, and/or indole groups. The second one is the difficulty of removing completely the *N*-blocking group from the polymer; the optimum yield of the dephthalization of the polymer upon treatment with hydrazine hydrate was below 60%.

This article will describe the procedure of synthesizing directly the optically-active basic monomers by

1) N. Grubhofer and L. Schleith, *Z. Phys. Chem.*, **296**, 262 (1954).
2) S. Tsuboyama and M. Yanagita, *Sci. Pap. Inst. Phys. Chem. Res.*, **53**, 245 (1959).
3) H. Suda and R. Oda, *Kanazawa Daigaku Kiyo*, **2**, 215 (1960).
4) J. A. Lott and W. Rieman, *J. Org. Chem.*, **31**, 561 (1966).
5) G. Maneck and W. Lamer, *Naturwissenschaften*, **52**, 539 (1965); **54**, 140 (1967).
6) G. W. Roberts and D. H. Haigh, *J. Org. Chem.*, **27**, 3375 (1962).
7) N. Nakamura, T. Yamashita, and T. Uemura, *Nippon Kagaku Zasshi*, **88**, 1238 (1967).

the use of several *N*-carboxy-α-amino acid anhydrides and *p*-aminostyrene phosphate.

Wessley and John[8] reported a synthetic procedure of α-amino acid anilides in which aniline picrate was allowed to react with some *N*-carboxy-α-amino acid anhydrides (Eq. (1)).

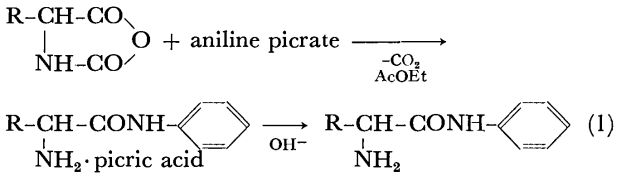

(1)

In this reaction, they nicely utilized the difference between the pK_a's of aniline and the resulting anilide, the former being an aromatic amine, and the latter, aliphatic. The picric acid formed a salt with the anilide, whose pK_a is higher than that of the aniline. The salt formation also prevented any further reaction between the still-remaining *N*-carboxy-α-amino acid anhydride and the resulting anilide.

If *N*-carboxy-α-amino acid anhydride is allowed to react with a similar salt of *p*-aminostyrene in lieu of aniline, *N*-(α-amino acyl)-*p*-aminostyrene should be obtained as an optically-active basic monomer.

The synthesis of the monomer was attempted with several salts of *p*-aminostyrene with acids of different pK_a's.

When the salt of a weak acid, such as acetic acid or formic acid, was used, the amine formed was not stabilized as a salt, but it attacked successively the unreacted *N*-carboxy-α-amino acid anhydrides to give only a polyamide. *p*-Aminostyrene hydrochloride polymerized itself, to poly-*p*-aminostyrene, while the salt of *p*-toluenesulfonic acid gave a small amount of the monomer, accompanied mostly by complex by-products.

When the phosphate or picrate was allowed to react with *N*-carboxy-α-amino acid anhydride, the synthesis of the monomer was successful, especially in the former case (Eq. (2)).

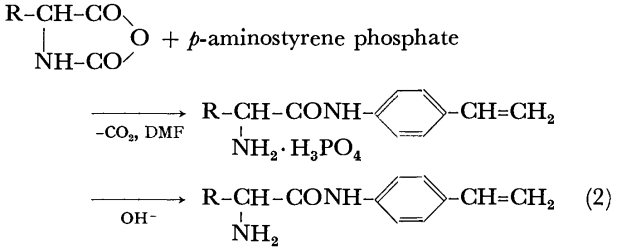

(2)

Table 1 shows the physical data on the monomers synthesized by the above procedure.

Table 1. Monomers derived from α-amino acids

Monomers started from	Mp (°C)	$[\alpha]_D$	Yield (%)
Cystine	171—172	−10(THF)	50
Proline	100—102	−62(AcOEt)	50
Tryptophan	115	−68(AcOEt)	84
O-acetyl-Tyrosine	125—150	−77(AcOEt)	45
Methionine	Oil	−55($CHCl_3$)	76

8) F. Wessley and M. John, *Monatsch. Chem.*, **48**, 1 (1927).

In order to obtain an insoluble basic polymer suitable as a chromatographic sorbent, the monomers were copolymerized with some crosslinking agents [divinyl benzene, *N*,*N*′-diacroylhexamethylenediamine,[7] *N*,*N*′-bis(*p*-vinylphenyl)adipamide].

N,*N*′-bis(*p*-vinylphenyl)adipamide was found to be especially useful among these crosslinking agents.

The homogeneous copolymerization of monomer with *N*,*N*′-bis(*p*-vinylphenyl)adipamide was performed, by the use of azo-bis-isobutyronitrile as an initiator, in tetrahydrofuran under refluxing conditions.

Of these polymers, the polymer from L-proline was subjected to hydrolysis in order to examine whether or not racemization occurred during the synthesis. The crude proline obtained after hydrolysis was purified as the picrate. No apparent racemization was detectable from the observed value of the optical rotation of the proline freed from the picrate with aniline.[9]

The chromatographic resolutions of phthalamidic acid derivatives of DL-phenylalanine, DL-valine, and DL-phenylglycine by means of this proline polymer were attempted. As eluent solvents, 10^{-3}, 10^{-4}, and 10^{-5}N aqueous ammonia were used successively.

When DL-*N*-(*o*-carboxybenzoyl)phenylalanine was eluted chromatographically with 10^{-5}N aqueous ammonia, the observed value of the specific rotation for the first fraction was $[\alpha]_D = -18°$ (optical purity, 33%).

The results of the resolution of DL-*N*-(*o*-carboxybenzoyl)phenylalanine eluted with 10^{-4}N aqueous ammonia are given in detail in Table 2.

Table 2. Result of resolution of ammonium salt of DL-*N*-(*o*-carboxybenzoyl)phenylalanine with proline polymer

Fraction No.	Weight (mg)	*c*	α_D	$[\alpha]_D$(°)	α_{546}	$[\alpha]_{546}$(°)
1	13.5	0.45	−0.070	−15	−0.090	−20
2	51.0	1.70	−0.086	− 5	−0.123	− 7
3	21.0	0.70	0	0	0	0
4—14	29.0	0.96	+0.040	+ 4	+0.046	+ 5
15—34	21.0	0.70	+0.042	+ 6	+0.045	+ 6
35—74	3.0	0.10	+0.010	+10	+0.012	+12
last fraction	45.0	1.50	+0.105	+ 7	+0.120	+ 8

In the case of the elution of DL-*N*-(*o*-carboxybenzoyl)-valine with 10^{-4}N aqueous ammonia, the fraction at the earliest stage of the elution showed only an unreliable, low specific rotation.

As was indicated in the previous paper[10] concerning acidic polymers, the substrate involving a benzyl group was more efficiently resolved than that with an isopropyl group in the corresponding moiety of the molecule.

The parallel result in the present study seems quite interesting.

DL-*N*-(*o*-carboxybenzoyl)phenylglycine was less stable than the two above-mentioned substrates under the basic condition; it was, however, found that this sub-

9) G. J. Cox and H. King, *J. Biol. Chem.*, **84**, 533 (1929).

10) T. Yamashita and N. Nakamura, This Bulletin, **43**, 1809 (1970).

strate unfortunately suffered from hydrolysis during the elution despite the expected resolution.

In the optical resolution of the racemates of amino acids, amino acid derivatives, and mandelic acid by means of synthetic optically-active polymers[5,6,10,11] derived from the starting materials of the L-configuration, it has been reported that these polymers are apt to adsorb the substrates of the L-configuration more strongly than those of the D-configuration.

In the present work, the *N*-(*o*-carboxybenzoyl)-phenylalanine of the L-configuration was also more adsorptive, on the L-polymer, than that of the D-configuration.

However, further experimentation and consideration are necessary to explain this observation fully.

Experimental

The Synthesis of p-*Aminostyrene Phosphate.* When 98% phosphoric acid (23 g) in ethanol (35 m*l*) was added to an ether solution of *p*-aminostyrene[12] obtained by the reduction of *p*-nitrostyrene[13] (34 g) with an aluminum amalgam, a white solid salt separated. The solid was collected on a filter, washed with ethanol and ether, and dried in a vacuum desiccator. Yield, 72%. mp 138—140°C.

The salt in a sealed tube was stable for a long period in a refrigerator.

The Syntheses of N-*Carboxy-α-amino Acid Anhydrides.* All of the *N*-carboxy-α-amino acid anhydrides except that of L-cystine[14] were prepared by the phosgenation procedure.[15-18]

The Synthesis of the L-*Proline Monomer.* *p*-Aminostyrene phosphate (0.1 mol) was dissolved, in small portions, in a solution of *N*-carboxy-L-proline anhydride (0.1 mol) in anhydrous dimethylformamide; the evolution of CO_2 gas thus occurred. The solution was then allowed to stand for 2—3 days at room temperature. The end point of the reaction was confirmed by the absence of the spot of *p*-aminostyrene on a silica-gel thin-layer chromatogram [benzene-ethyl formate-methanol (5:4:1) and 95% ethanol-28% aqueous ammonia (4:1) as solvents.]

The dimethylformamide was distilled off from the solution under reduced pressure below 40°C. The residue was decomposed with aqueous sodium bicarbonate, and then extracted with chloroform or ethyl acetate. The extract was washed with water, dried over anhydrous sodium sulfate, and evaporated to dryness under reduced pressure.

The *N*-prolyl-*p*-aminostyrene was recrystallized from ethyl acetate-petroleum ether to give needles; mp 100—102°C, $[\alpha]_D^{20}$ −62° (*c* 0.5, AcOEt). IR (cm^{-1}): 3200—3400 (NH amide and amine), 1670 (C=O), 990, 910 (–CH=CH_2), 835 (*p*-substitution). Found: C, 72.60; H, 7.31; N, 12.80%. Calcd for $C_{13}H_{16}N_2O$: C, 72.19; H, 7.46; N, 12.95%.

The monomers starting from some other α-amino acids were prepared by procedures similar to that desribed above.

The Synthesis of N,N′-*Bis(*p-*vinyl phenyl)adipamide.* Adipic acid dichloride[19] (0.05 mol) was added, under external cooling with ice water, to an ether solution of *p*-aminostyrene (0.1 mol) and pyridine (0.1 mol) to separate a white, solid material. After standing overnight at room temperature, the solid was collected on a filter, washed with water and ethanol, and then dried in a vaccum desiccator. The *N,N′*-bis(*p*-vinylphenyl)adipamide was recrystallized from ethanol or tetrahydrofuran. Yield, 75%. mp 240°C dec.. IR (cm^{-1}): 3350 (NH), 1655 (C=O), 990, 905 (–CH=CH_2), 840 (*p*-substitution). Found: C, 75.64; H, 7.26; N, 7.65%. Calcd for $C_{22}H_{24}N_2O_2$: C, 75.83; H, 6.94; N, 8.04%.

Copolymerization. A mixture of *N*-prolyl-*p*-aminostyrene (0.01 mol) and *N,N′*-bis(*p*-vinylphenyl)adipamide (0.01 mol) in anhydrous tetrahydrofuran (100—120 m*l*) was stirred, after the addition of a small amount of azo-bis-isobutyronitrile, under reflux for 30—40 hr. The copolymer precipitated as a white powder; it was filtered and then washed thoroughly with dimethylformamide, methanol, and tetrahydrofuran successively. Yield, 60%.

The copolymers containing α-amino acids other than L-cystine were also obtained by procedures similar to that described above. The cystine monomer was polymerized in anhydrous benzene without the addition of any cross-linking agent. The exchange capacities of these polymers, determined by using 0.1 N hydrochloric acid, were as follows: proline, 1.5 *meq*/g; tryptophan, 1.0 *meq*/g; methionine, 0.72 *meq*/g; cystine, 3.64 *meq*/g.

Isolation of Proline from the Hydrolysates of the Polymer Starting from L-*Proline.* The proline copolymer was hydrolyzed and proline was isolated according to the ordinary procedure[9,20] for the isolation of L-proline from protein hydrolysates. The polymer was boiled in 5 N hydrochloric acid for 10 hr under reflux and filtered. The filtrate was decolorized with charcoal and evaporated *in vacuo* to dryness. Picric acid was added to the residue dissolved in ethanol, and the resulting picrate was recrystallized from water. mp 150°C. Free proline was isolated from the picrate after decomposition with aniline by the usual method.[9] mp 219—221°C dec. (from ethanol-ether). $[\alpha]_D^{20}$ −84.5° (*c* 1, in water). Lit,[20] $[\alpha]_D^{20}$ −86° in water.

The Syntheses of Substrates. The substrates were obtained by the ordinary method,[21] in which *N*-phthaloyl-α-amino acids were treated with aqueous alkali.

DL-*N*-(*o*-carboxybenzoyl)phenylalanine, mp 180—182°C. $[\alpha]_D$ +67°, $[\alpha]_{546}$ +80° (*c* 1, 0.5N aqueous ammonia) in L-form. The ammonium salt of the L-configuration, mp 178—182°C. $[\alpha]_D$ +56° (*c* 0.51, 10^{-4}N aqueous ammonia), +54° (*c* 0.52, 10^{-5} N aqueous ammonia).

DL-*N*-(*o*-carboxybenzoyl)valine, mp 164—166°C. $[\alpha]_D$ +12°, $[\alpha]_{546}$ +12° (*c* 1, 0.1 N aqueous ammonia) in L-form.

DL-*N*-(*o*-carboxybenzoyl)phenylglycine,[21] mp 185—188°C. $[\alpha]_D$ +101 (*c* 2, acetone) in L-form.

The ammonium salt of DL-*N*-(*o*-carboxybenzoyl)phenylalanine was prepared by the addition of tetrahydrofuran or acetone to a solution of the acid in aqueous ammonia. The ammonium salts of the other acids failed to crystallize.

Column Chromatography. A proline copolymer (45 g) suspended in a sufficient volume of water was poured into a column (2 cm in diameter; 150 cm in length; the final length

11) H. Suda, Y. Hosono, Y. Hosokawa, and T. Seto, *Kogyo Kagaku Zasshi*, **73**, 1250 (1970).
12) J. H. Boner and H. Alul, *J. Amer. Chem. Soc.*, **81**, 2136 (1959).
13) M. M. Koton, Yu. V. Mittin, and F. S. Florinski, *Zh. Obshch. Khim*, **25**, 1469 (1955).
14) J. L. Bailey, *Nature*, **164**, 889 (1949); *J. Chem. Soc.*, **1950**, 3461.
15) A. C. Farthing, *J. Chem. Soc.*, **1950**, 3213.
16) E. Datchornik, M. Sela, and E. Katchalski, *J. Amer. Chem. Soc.*, **76**, 299 (1954).
17) J. Kurz, G. D. Fasman, A. Berger, and E. Katchalski, *ibid*, **80**, 393 (1958).
18) J. Honzyl and J. Rudinger, *Collect. Czech. Chem. Commun.*, **20**, 1190 (1955).
19) R. Meyer, *Ann. Chem.*, **347**, 49 (1906).
20) M. Bergman, *J. Biol. Chem.*, **110**, 471 (1935).
21) A. Mc Kenzie, *J. Chem. Soc.*, **1928**, 646.

of the packed polymer was *ca.* 80 cm). The ammonium salt of DL-*N*-(*o*-carboxybenzoyl)phenylalanine (200 mg), dissolved in *ca.* 10 m*l* of 10^{-4} N aqueous ammonia, was adsorbed on the upper zone of the sorbent; then was eluted with the same solvent at room temperature. The flow rate of the solvent was *ca.* 6 m*l*/hr under atmospheric pressure; 12.50 m*l* portions of the eluent were collected automatically. Each of the eluents showed only a single spot on a silica-gel thin-layer chromatogram, the R_f value being in agreement with that of authentic *N*-(*o*-carboxy-benzoyl)phenylalanine. Acetic acid-*n*-butanol-water (1:1:1), 95% ethanol-28% aqueous ammonia(4:1), and benzene-ethyl formate-methanol (5:4:1) were used as the solvents. The concentration of the substrate in each fraction was estimated by UV absorption by using a Hitachi EPS-2-photometer. When the observed concentration was too low to determine the optical rotation, 10—30 consecutive fractions were combined and concentrated under reduced pressure. The last fraction was eluted with 0.1 N aqueous ammonia. The optical rotation of the evaporated residue was determined in 10^{-4}N aqueous ammonia by means of a Rex-automatic polarimeter. The chromatographic resolution of the other two racemates were also carried out by a procedure similar to that described above.

BULLETIN OF THE CHEMICAL SOCIETY OF JAPAN, VOL. 45, 198—202(1972)

The Syntheses and Reactions of Sulfenyl-substituted Sulfonium Ylides

Yosio HAYASI and Hitosi NOZAKI

Department of Industrial Chemistry, Kyoto University, Yoshida, Kyoto

(Received April 24, 1971)

Unstable dimethylsulfonium (phenylthio)methylide (**2**) is prepared in a THF solution from the corresponding sulfonium salt by treating it with *n*-butyllithium. Sulfenyl-substituted stable phenacylides **6a** and **6b** are obtained in three ways. The ylide **6a** decomposes at 120°C in benzene to give (E)-**9**, the dimer of benzoyl(phenylthio)carbene. In contrast, the heating of **6a** in ethanol affords ethanolysis products (**11**, **12**) and ethyl benzoate. The alkylation of **6a** and **6b** with trimethyl- and triethyloxonium fluoroborate gives the vinylsulfonium salt **13**. The ylide **2** reacts with (Z)- and (E)-1,2-dibenzoylethylene and with diethyl fumarate to give cyclopropanes, **15** and **16** respectively.

Sulfonium ylides are often stabilized by the introduction of an electron-withdrawing group or groups on the ylide carbon, such groups as COR, COOR, and SO_2R.[1] Herewith we report on the syntheses and reactions of sulfenyl-substituted sulfonium ylides,[2] as no precedent of this class has yet appeared. The sulfenyl group should effectively delocalize the negative charge by using a 3*d* orbital of the sulfur atom.[3] Incidentally, the cleavage of the ylide bond gave rise to sulfenylcarbenes, whose behavior was also investigated.[5]

Dimethylsulfonium (phenylthio)methylide (**2**) was obtained as a solution in tetrahydrofuran (THF) upon the treatment of the sulfonium salt **1** with *n*-butyllithium. The solution was stable at lower temperatures, as after 1 hr of standing at −20°C **2** was reconverted quantitatively into the sulfonium salt **1** by the addition of hydrogen bromide. The concentration of the ylide solution under reduced pressure below room temperature afforded (Z)-1,2-bis(phenylthio)ethylene (**3a**, 27% yield) and its (E) isomer (**3b**, 43% yield).

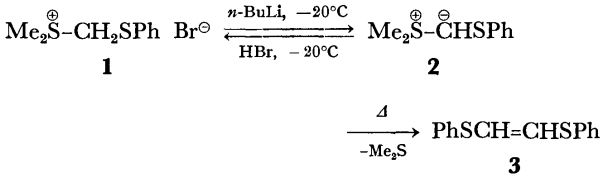

When dimethyl sulfide was allowed to react with phenacyl bromides **4a** and **4b**, two sulfonium salts, **5a** and **5b** respectively, were obtained as highly hygroscopic crystals. The treatment of **5a** and **5b** with sodium hydride in THF gave two crystalline ylides, **6a** and **6b** respectively.

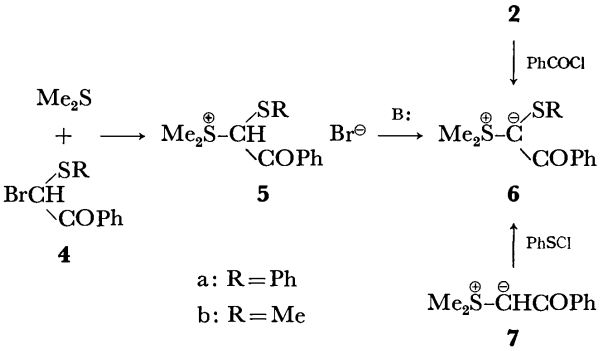

The ylide **6a** was also obtained by two alternative methods: the treatment of dimethylsulfonium phe-

1) H. Nozaki, M. Takaku, Y. Hayasi, and K. Kondo, *Tetrahedron*, **24**, 6563 (1968) and the references cited therein.

2) Communicated in part: Y. Hayasi, M. Takaku, and H. Nozaki, *Tetrahedron Lett.*, **1969**, 3179.

3) For the sulfenyl-substituted phosphonium ylides, see Ref. 4.

4) a) G. Wittig and M. Schlosser, *Chem. Ber.*, **94**, 1373 (1961); b) T. Mukaiyama, S. Fukuyama, and T. Kumamoto, *Tetrahedron Lett.*, **1968**, 3787.

5) For the sulfenylcarbenes, see Ref. 6. No acylsulfenylcarbene has previously been reported, as far as the authors are aware.

6) W. Kirmse, "Carbene Chemistry," Academic Press, New York, N. Y. (1964), p. 109.

nacylide (**7**)[7] with benzenesulfenyl chloride, and that of **2** with benzoyl chloride. The "ylide carbonyl" IR band of **6a** and **6b** appeared in the same region as that of **7**, whereas the UV absorption experienced a blue shift of *ca.* 20 nm upon the introduction of the sulfenyl group into **7** (see Experimental section). Apparently the sulfenyl group delocalizes the ylide negative charge by utilization of the 3*d* orbital of the sulfur atom.[8]

In contrast to the reaction of the ylide **7**, that of two mole equivalents of methylphenylsulfonium phenacylide (**8**)[9] with benzenesulfenyl chloride gave a complex mixture, which consisted of (E)-1,2-dibenzoyl-1,2-bis(phenylthio)ethylene (**9**, 13%), thioanisole (122%), α-chloroacetophenone (50%), and (E)-1,2,3-tribenzoylcyclopropane (**10**, 20%), plus a remainder of unknown substances.

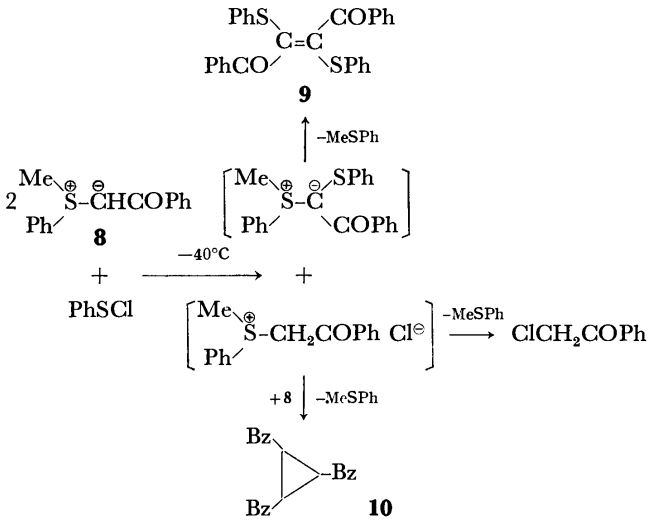

The ylides **6a** and **6b** have been found to serve as precursors of benzoyl(phenylthio)carbene.[10] The ylide **6a** was stable in boiling benzene, but decomposition took place at 120°C to yield (E)-1,2-dibenzoyl-1,2-bis(phenylthio)ethylene (**9**). The analytical and spectral data supported the constitution given, while the (E)-configuration was deduced on the basis of its IR spectrum, which showed a conjugated carbonyl absorption band at 1665 cm^{-1}.[11]

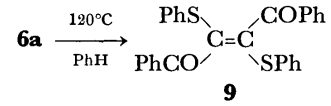

The prolonged heating of **6a** in boiling ethanol afforded α-ethoxy-α-(phenylthio)acetophenone (**11**, 23%), ethyl benzoate (19%), and phenylthiomethyl ethyl ether (**12**, 12%). The olefin **9** and the compound originating from the Wolff rearrangement of benzoyl(phenylthio)carbene could not be detected. A possible scheme of the reaction is shown below:

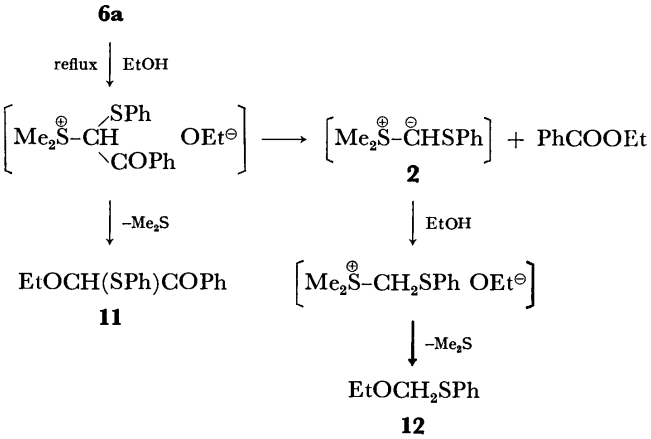

The photolytic decomposition of **6a** was carried out in some solvents, but no single product was isolated.

The treatment of the ylides **6a** and **6b** with trimethyl- and triethyloxonium tetrafluoroborate resulted in O-alkylation, giving vinylsulfonium salts, **13** (Table 1), instead of an S-alkylated product. The oily sulfonium tetrafluoroborates (**13a**: R=Ph, R′=Me and **13c**: R=R′=Me) were converted to crystalline tetraphenylborates (**14a** and **14c**) by treatment with sodium tetraphenylborate. The structure of these vinylsulfonium salts was confirmed by the results of analyses and by the spectral data. Especially, the NMR spectrum of **14c** showed three peaks of methyl protons at δ 2.07 (–SMe), 2.83 (>S⊕–Me), and 3.50 (O–Me) ppm; they supported the structure of **14** and, therefore, that of **13**:

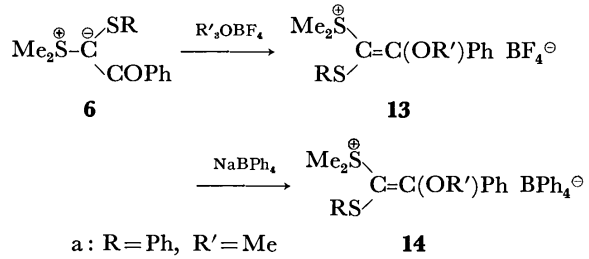

a: R=Ph, R′=Me
b: R=Ph, R′=Et
c: R=R′=Me

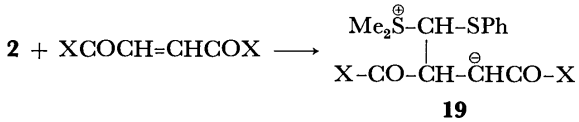

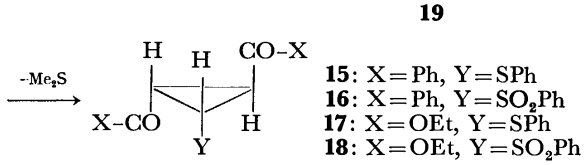

15: X=Ph, Y=SPh
16: X=Ph, Y=SO_2Ph
17: X=OEt, Y=SPh
18: X=OEt, Y=SO_2Ph

7) a) B. M. Trost, *J. Amer. Chem. Soc.*, **89**, 138 (1967); b) A. W. Johnson and R. T. Amel, *Tetrahedron Lett.*, **1966**, 819; c) K. W. Ratts and A. N. Yao, *J. Org. Chem.*, **31**, 1185 (1966).

8) The same explanation has been given in the case of sulfonium sulfonyl-substituted phenacylides. See Ref. 1.

9) H. Nozaki, M. Takaku, and K. Kondo, *Tetrahedron*, **22**, 2145 (1966).

10) A. W. Johnson, "Ylid Chemistry," Academic Press, New York, N. Y. (1966).

11) W. Lüttke and H. Hermann studied the IR and UV spectra of 3,4-bis(methylthio)-3-hexene-2,5-dione, 3,4-bis(phenylthio)-3-hexene-2,5-dione, and related compounds in order to make a definite configurational assignment of these sulfenylsubstituted olefins on the basis of the spectral data. See Ref. 12). In a private communication they advised the authors of having deduced the (E)-configuration of **9** from the IR spectral data. The authors are grateful for their courtesy.

12) a) W. Lüttke, H. Hermann, and M. Klessinger, *Angew. Chem., Int. Ed. Engl.*, **5**, 598 (1966); b) H. Hermann and W. Lüttke, *Chem. Ber.*, **101**, 1708 (1968); c) H. Hermann and W. Lüttke, *ibid.*, **101**, 1715 (1968).

Table 1. Mps and spectral data of novel vinylsulfonium salts **13** and **14**

Compd.	R	R′	mp °C	IR(KBr) cm^{-1}	NMR δ ppm (relative intensity, multiplicity)
14a	Ph	Me	143—145	1542, 1304, 1125	2.63 (s, 6H), 3.65 (s, 3H), 6.7—7.6 (m, 30H)[a]
13b	Ph	Et	89— 94	1554, 1313, 1110, 1050	1.36 (t, 3H), 2.89 (s, 6H), 4.03 (q, 2H), 7.1—7.7 (m, 10H)[a]
14b	Ph	Et	165—167	1565, 1290, 1130, 1110	1.35 (t, 3H), 2.89 (s, 6H), 4.03 (q, 2H), 7.1—7.7 (m, 30H)[b]
14c	Me	Me	174—175	1568, 1300, 1125	2.07 (s, 3H), 2.83 (s, 6H), 3.50 (s, 3H), 6.7—7.6 (m, 25H)[c]

a) In acetone-d_6 solution with TMS as a reference.
b) In $CDCl_3$ solution with TMS as a reference.
c) In DMSO-d_6 solution with sodium 3-(trimethylsilyl)propanesulfonate as a reference.

In view of the well known reaction[13] of dimethylsulfonium methylide with electron-deficient olefins or carbonyl compounds, we have examined the possible reactions of **2** with such substrates. However, benzophenone failed to react with **2** at −20°C, whereas both benzaldehyde and *p*-nitrobenzaldehyde actually reacted with **2** to afford a very complex mixture which could not be characterized.

When (E)-1,2-dibenzoylethylene was allowed to react with **2** in THF, *r*-1,*t*-2-dibenzoyl-*t*-3-(phenylthio)-cyclopropane (**15**) was obtained in a 27% yield as the sole product. The assignment of the indicated configuration is based on the NMR spectral data of the corresponding sulfone, **16** (see Experimental section).

The reaction of **2** with (Z)-1,2-dibenzoylethylene gave the same stereoisomer, **15**, in a 53% yield. Analogously, the treatment of **2** with diethyl fumarate afforded diethyl *t*-3-(phenylthio)-*r*-1,*t*-2-cyclopropanedicarboxylate (**17**) in a 51% yield; its oxidation led to the sulfone **18**. The given configuration was also based on the NMR spectral data, in which the ethyl protons were obviously nonequivalent. The preference for the (E) configuration of **15** and **17** may be ascribed to the intermediacy of the betaines, **19**.

Expectedly, the ylide **6a** did not react with (E)-1,2-dibenzoylethylene and diethyl maleate under reflux in THF.

Experimental

All the melting and boiling points are uncorrected. The microanalyses were performed at the Elemental Analyses Center of Kyoto University. The NMR spectra were taken with JEOL C-60H and Varian ME-100 spectrometers, and the chemical shifts are reported in δ values relative to the TMS internal standard unless otherwise stated. The abbreviations s, t, q, and m refer to singlet, triplet, quartet, and multiplet respectively. The UV absorption spectra were taken in 95% EtOH on a Shimadzu MPS-50L spectrometer.

Preparation of Dimethyl(phenylthiomethyl)sulfonium Bromide (1). A solution of bromomethyl phenyl sulfide[14] (7.0 g, 34.4 mmol) and dimethyl sulfide (2.6 g, 42.0 mmol) in dry acetone (50 m*l*) was stirred at 0°C for 24 hr. The resulting precipitates were collected by filtration, washed with dry acetone, and dried in a vacuum desiccator to afford very hygroscopic crystalline solids **1** (8.0 g, 88%); mp 69—70°C (dec.). NMR (DMSO-d_6): 3.12 (s, 6H), 5.41 (s, 2H), 7.2—7.9 (m, 5H). Found: C, 40.7; H, 5.0%. Calcd for $C_9H_{13}BrS_2$: C, 40.8; H, 4.9%.

Preparation of Dimethylsulfonium (Phenylthio)methylide (2). To a suspension of **1** (2.65 g, 10.0 mmol) in THF (150 m*l*), a solution of *n*-butyllithium (10 mmol) in *n*-hexane (14.7 m*l*) was added in one portion at −20°C under nitrogen, after which the mixture was stirred for five min. Thus we obtained a pale yellow solution of dimethylsulfonium (phenylthio)-methylide (**2**). After standing for 1 hr at −20°C, the solution was treated with HBr gas. The resulting precipitates melted at 69—70°C (mixed mp 69°C) and showed an IR spectrum identical with that of an authentic sample of **1**.

The Decomposition of Dimethylsulfonium (Phenylthio)methylide (2). The solution of **2** in THF (50 m*l*), prepared by the treatment of **1** (2.65 g, 10.0 mmol) with a solution of *n*-butyllithium (10.0 mmol) in hexane (14.7 m*l*) at −20°C, was allowed to warm up to room temperature. The reaction mixture was then concentrated under reduced pressure at 0—5°C to afford a crude oil, which was submitted to chromatography on an alumina column with *n*-hexane. The initial eluate was (E)-1,2-*bis*(phenylthio)ethylene (**3b**, 0.52 g, 43%); mp 61—62°C (from EtOH) (lit.[15] mp 62°C). IR (KBr): 924 cm^{-1}; NMR (CCl_4): 6.44 (s, 2H), 7.0—7.4 (m, 10H). The second one was (Z)-1,2-bis(phenylthio)ethylene (**3a**; 0.33 g, 27%): mp 30.5—31°C (lit,[15] mp 31.5°C). NMR (CCl_4): 6.41 (s, 2H), 7.0—7.4 (m, 10H).

α-Bromo-α-(phenylthio)acetophenone (4a)[16] was prepared by the treatment of α-(phenylthio)acetophenone with bromine in the presence of a catalytic amount of aluminum chloride in dry ether at 0°C.

Preparation of Dimethyl[α-(phenylthio)phenacyl]sulfonium Bromide (5a). A solution of **4a** (20 g, 66 mmol) and an excess of dimethyl sulfide in dry acetone was stirred at 0°C for 5 hr. The resulting precipitates were filtered, washed with dry acetone, and dried over P_2O_5 in a vacuum desiccator to afford hygroscopic crystals **5a** (19 g, 78%), mp 76—78°C (dec.). IR (Nujol): 1675, 1290 cm^{-1}; NMR ($CDCl_3$): 2.07 (s, 6H), 6.42 (s, 1H), 7.2—8.1 (m, 10H). Found: C, 52.3; H, 4.7%. Calcd for $C_{16}H_{17}BrOS_2$: C, 52.0; H, 4.6%.

Preparation of Dimethyl[α-(methylthio)phenacyl]sufonium Bromide (5b). To a solution of α-(methylthio)acetophenone (8.3 g, 50 mmol) in dry benzene (200 m*l*) under nitrogen, we added sodium hydride (2.4 g, a 50% dispersion in mineral oil, 50 mmol) in one portion at 0°C. After the evolution of hydrogen gas had ceased, bromine (8.0 g, 50 mmol) was

13) E. J. Corey and M. Chaykovsky, *J. Amer. Chem. Soc.*, **87**, 1353 (1965).
14) H. Böhme, H. Fischer, and R. Frank, *Ann. Chem.*, **563**, 54 (1949).
15) a) W. E. Truce and R. J. McManimie, *J. Amer. Chem. Soc.*, **76**, 5745 (1954); b) W. E. Parham and J. Heberling, *ibid.*, **77**, 1175 (1955).
16) W. Groebel, *Chem. Ber.*, **92**, 2887 (1959).

added dropwise to the reaction mixture at the same temperature. The mixture was stirred for an additional 5 min and then filtered in order to remove the NaBr. After an excess of dimethyl sulfide had been added to this filtrate, the mixture was stirred at 0°C for 5 hr. The resulting precipitates were filtered, washed with dry acetone, and dried over P_2O_5 under reduced pressure to afford hygroscopic salt **5b** (11.0 g, 72%), mp 92—93°C (dec.); this product was subjected to the following reaction without further purification. IR (Nujol): 1673, 1278 cm^{-1}; NMR ($CDCl_3$): 2.14 (s, 3H), 2.33 (s, 6H), 6.44 (s, 1H), 7.2—8.1 (m, 5H). Found: C, 42.6; H, 4.7%. Calcd for $C_{11}H_{15}BrOS_2$: C, 43.0; H, 4.9%.

Preparation of Dimethylsulfonium α-(Phenylthio)phenacylide (6a). (a) To a solution of **5a** (17.0 g, 46 mmol) in THF (250 m*l*) cooled with an ice-water bath, we added NaH (2.2 g, 50% dispersion in mineral oil, 46 mmol) in one portion. The reaction mixture was stirred until the evolution of hydrogen had subsided. Filtration followed by concentration gave a crystalline solid substance, which was recrystallized from benzene to afford **6a** (11.0 g, 85%), mp 135—136°C. IR (KBr): 1530, 1335 cm^{-1}; λ_{max}^{EtOH} 247 (log ε 4.07), 282 (3.84) nm; NMR ($CDCl_3$): 2.64 (s, 6H), 7.1—7.9 (m, 10H). Found: C, 67.0; H, 5.5%. Calcd for $C_{16}H_{16}OS_2$: C, 66.6; H, 5.6%.

(b) To a solution of **7** (18.0 g, 100 mmol) in THF (300 m*l*), we added, drop by drop, a solution of benzenesulfenyl chloride (7.2 g, 50 mmol) in THF (50 m*l*) under nitrogen at −20°C. After being stirred for an additional 4 hr at the same temperature, the reaction mixture was allowed to warm to room temperature, diluted with water, and extracted with $CHCl_3$. The extract was dried ($MgSO_4$) and concentrated *in vacuo*. The residual solid was recrystallized from benzene to afford **6a** (12.5 g, 87%), mp and mixed mp 135—136°C. Its identity was further confirmed by a study of its IR spectrum.

(c) To a solution of **2** in THF (150 m*l*), prepared by the treatment of **1** (2.65 g, 10.0 mmol) with *n*-BuLi, we added, drop by drop, a solution of benzoyl chloride (0.70 g, 5.0 mmol) in THF (5 m*l*) under nitrogen at −20°C. After being stirred for an additional hour, the reaction mixture was allowed to warm up to room temperature under stirring. Work-up then afforded **6a** (1.00 g, 72%); mp and mixed mp 135—136°C.

Preparation of Dimethylsulfonium α-(Methylthio)phenacylide (6b). A mixture of **5b** (10.0 g, 32.6 mmol) and NaH (1.56 g, 50% dispersion in mineral oil, 32.6 mmol) in THF (250 m*l*) was stirred at 0°C under nitrogen for 5 hr. The reaction mixture was then filtered, and the filtrate was concentrated under reduced pressure. The recrystallization of the residue from petroleum ether (bp 30—50°C) and THF (1:1) afforded **6b** (6.1 g, 83%); mp 85—86°C. IR (KBr): 1485, 1340 cm^{-1}; λ_{max}^{EtOH} 280 (log ε 3.83); NMR ($CDCl_3$): 1.96 (s, 3H), 2.66 (s, 6H), 7.1—7.9 (m, 5H). The compound decomposed slowly on standing at room temperature on exposure to air. Found: C, 58.1; H, 6.4%. Calcd for $C_{11}H_{14}OS_2$: C, 58.4; H, 6.2%.

Reaction of Methylphenylsulfonium Phenacylide (8) with Benzenesulfenyl Chloride. A solution of benzenesulfenyl chloride (2.89 g, 20 mmol) in THF (30 m*l*) was added to a solution of **8** (9.68 g, 40 mmol) in THF (250 m*l*) at −40°C under nitrogen. The mixture was stirred for an additional 8 hr at the same temperature and then filtered. The filtrate was concentrated, and the residual oil was chromatographed on a Florisil column. Elution with hexane gave thioanisole (3.03 g, 122%) and α-chloroacetophenone (1.54 g, 50%). Elution with benzene gave **9** (1.16 g, 13%), mp and mixed mp 173.5—174°C. Final elution with chloroform yielded (E)-1,2,3-tribenzoylcyclopropane (**10**, 1.30 g, 20%), mp and mixed mp 213—214°C.[17]

Thermolysis of 6a in Benzene. A solution of **6a** (2.2 g, 7.8 mmol) in dry benzene (100 m*l*) was heated in a sealed glass tube at 120°C for 3 hr. After the solvent had been removed, the residue was chromatographed (silica gel, benzene) to afford **9** (0.34 g, 10%), mp 173.5—174°C (from benzene). λ_{max}^{EtOH} 212 (log ε 4.63), 256 (4.52) nm; IR (KBr): 1665, 1240 cm^{-1}; NMR ($CDCl_3$): 7.0—8.0 (m). The parent peak in the mass spectrum was observed at *m/e* 452. Found: C, 74.6; H, 4.4%. Calcd for $C_{28}H_{20}O_2S_2$: C, 74.3; H, 4.5%.

Thermolysis of 6a in Ethanol. A solution of **6a** (1.1 g, 3.9 mmol) in 100% EtOH (100 m*l*) was heated to reflux for 22 hr. After the evaporation of the solvent, ether was added to the residual oil (0.83 g). The resulting precipitates were collected and found to be **6a** (0.14 g). The filtrate was concentrated, and the residual oil was subjected to chromatography on a silica gel column. Elution with hexane gave phenylthiomethyl ethyl ether (**12**, 0.08 g, 12%), which was found to be identical with an independently synthesized specimen upon a comparison of their IR and NMR spectra and retention times on glc. Elution with hexane and benzene (2:1) gave ethyl benzoate (0.11 g, 19%). A final elution with benzene gave α-ethoxy-α-(phenylthio)acetophenone (**11**) as an oil (0.24 g, 23%). IR (neat): 1693, 1274, 1098 cm^{-1}; NMR ($CDCl_3$): 1.32 (t, 3H, $J_{AX}=J_{BX}=$ 7.2 Hz), 3.70 (1H, $J_{AB}=9.0$ Hz, $J_{AX}=7.2$ Hz), 4.07 (1H, $J_{AB}=9.0$ Hz, $J_{BX}=7.2$ Hz), 5.40 (s, 1H), 7.1—8.1 (m, 10H). Found: C, 70.7; H, 5.8%. Calcd for $C_{16}H_{16}O_2S$: C, 70.6; H, 5.9%.

Preparation of Phenylthiomethyl Ethyl Ether (12). An authentic sample was prepared as follows. To an EtOH (150 m*l*) solution of sodium thiophenoxide prepared from thiophenol (29.0 g, 26.4 mmol) and an equivalent amount of sodium (6.1 g, 26.4 mmol), we added, drop by drop, chloromethyl ethyl ether (25.0 g, 26.4 mmol) at 0°C. The reaction mixture was then extracted with ether. The removal of the solvent *in vacuo*, followed by distillation at 114—125°C/15 mmHg, afforded a mixture of **12** and chloromethyl ethyl ether (45:55). Purification by preparative glc (10% SE 30 on Chromosorb W) yielded **12**. IR (neat): 1077 cm^{-1}; NMR (CCl_4): 1.20 (t, 3H), 3.62 (q, 2H), 4.92 (s, 2H), 7.0—7.6 (m, 5H). Found: C, 64.5; H, 7.2%. Calcd for $C_9H_{12}OS$: C, 64.3; H, 7.2%.

Photolysis of 6a. A solution of **6a** (3.0 g, 10.5 mmol) in 100% EtOH (350 m*l*) was irradiated by means of a 200-W high-pressure mercury arc (Pyrex filter) for 30 hr. Crystalline precipitates were then collected and found to be sulfur (0.42 g). The evaporation of the solvent afforded an intractable oil.

Reaction of 6a with Trimethyloxonium Tetrafluoroborate. A mixture of **6a** (1.7 g, 5.9 mmol) and trimethyloxonium tetrafluoroborate (1.3 g, 8.8 mmol) in dry CH_2Cl_2 (20 m*l*) was stirred at room temperature under nitrogen for 24 hr. After the evaporation of the solvent, the residual oil was washed with ether to afford **13a** as an insoluble oil (1.47 g). The crude oil was taken up in deionized water (20 m*l*) and treated with sodium tetraphenylborate (1.6 g, 4.7 mmol) to precipitate **14a** (0.97 g, 33%); mp 143—145°C (dec.) (from acetone-water). Found: C, 78.8; H, 5.9%. Calcd for $C_{41}H_{39}BOS_2$: C, 79.1; H, 6.0%.

Reaction of 6a with Triethyloxonium Tetrafluoroborate. A mixture of **6a** (1.0 g, 3.5 mmol) and triethyloxonium tetrafluoroborate (1.0 g, 5.3 mmol) in CH_2Cl_2 (20 m*l*) was stirred at room tempeature for 24 hr. The evaporation residue was then dissolved in ethanol; the subsequent cautious addition of ether to the solution at 0°C resulted in the precipita-

17) G. Maier, *ibid.*, **95**, 611 (1962).

tion of pure crystals of **13b** (0.79 g, 56%); mp 89—94°C (dec.). Found: C, 53.5; H, 5.2%. Calcd for $C_{18}H_{21}BF_4OS_2$: C, 53.5; H, 5.2%.

The treatment of **13b** (0.28 g, 0.7 mmol) with sodium tetraphenylborate (0.24 g, 0.7 mmol) in deionized water (10 m*l*) afforded **14b** (0.41 g, 92%); mp 165—167°C (from acetone-water). Found: C, 79.3; H, 6.7%. Calcd for $C_{42}H_{41}BOS_2$: C, 79.2; H, 6.5%.

*Reaction of **6b** with Trimethyloxonium Tetrafluoroborate.* A mixture of **6b** (2.26 g, 10.0 mmol) and trimethyloxonium tetrafluoroborate (1.48 g, 10.0 mmol) in CH_2Cl_2 (20 m*l*) was stirred at 0°C for 20 hr. Work-up then afforded **13c** as an oil (2.15 g). The treatment of the crude oil with sodium tetraphenylborate (2.36 g, 6.9 mmol) in a mixture of CH_2Cl_2 (40 m*l*) and water (30 m*l*) afforded a crystalline solid, **14c** (1.72 g, 31%); mp 174—175°C (from acetone-water). Found: C, 77.2; H, 6.6%. Calcd for $C_{36}H_{37}BOS_2$: C, 77.1; H, 6.7%.

*Reaction of **2** with (E)-1,2-Dibenzoylethylene.* To a solution of **2** in THF (150 m*l*), prepared by the treatment of **1** (2.65 g, 10.0 mmol) with *n*-butyllithium at −20°C, we added, drop by drop, solution of (E)-1,2-dibenzoylethylene (2.30 g, 9.7 mmol) in THF (50 m*l*). After being stirred for an additional hour at the same temperaure, the reaction mixture was allowed to warm up to room temperature; it was then diluted with water and extracted with chloroform. The chloroform solution was dried ($MgSO_4$) and concentrated, and the residual oil was chromatographed on a silica gel column. Elution with a mixture of benzene and hexane (3:1) afforded *r*-1, *t*-2-dibenzoyl-*t*-3-(phenylthio)-cyclopropane (**15**, 0.96 g, 27%); mp 113.5—114°C (from PhH-hexane). IR (KBr): 1660, 1336, 1208, 1010 cm^{-1}; NMR (CCl_4): 3.40—3.76 (m, 3H), 6.9—8.0 (m, 15H). Found: C, 76.8; H, 5.2%. Calcd for $C_{23}H_{18}O_2S$: C, 77.1; H, 5.1%.

*Reaction of **2** with (Z)-1,2-Dibenzoylethylene.* To a solution of **2** in THF (150 m*l*), prepared by the treatment of **1** (1.92 g, 7.3 mmol) and *n*-BuLi (7.3 mmol) at −50°C under nitrogen, we added, drop by drop, a solution of (Z)-1,2-dibenzoylethylene (1.52 g, 6.4 mmol) in THF (40 m*l*). After being stirred for an additional hour at the same temperature, the reaction mixture was allowed to warm up to room temperature. Work-up then afforded **15** (1.21 g, 53%) (mp and mixed mp 113.5—114°C), which was identical with the above sample.

*Oxidation of **15**.* A solution of **15** (0.09 g, 0.3 mmol) and 30% H_2O_2 (*ca.* 5 m*l*) in AcOH (10 m*l*) was stirred at room temperature for 4 days. The reaction mixture was then diluted with water, neutralized with aqueous $NaHCO_3$ and extracted with $CHCl_3$. After drying ($MgSO_4$), the solution was concentrated to afford *r*-1,*t*-2-dibenzoyl-*t*-3-phenylsulfonylcyclopropane (**16**, 0.10 g, 100%); mp 188—189°C (from benzene). IR (KBr): 1676, 1318, 1270, 1220, 1151 cm^{-1}; NMR ($CDCl_3$): 3.47 (q, 1H, J_{AC}=6.0 Hz, J_{AB}=10.2 Hz), 3.81 (q, 1H, J_{BC}=6.0 Hz, J_{AB}=10.2 Hz), 4.42 (t, 1H, J_{AC}=J_{BC}=6.0 Hz), 7.1—8.2 (m, 15H). Found: C, 70.9; H, 4.8%. Calcd for $C_{23}H_{18}O_4S$: C, 70.8; H, 4.7%.

*Reaction of **2** with Diethyl Fumarate.* To a solution of **2** in THF (150 m*l*), prepared from **1** (2.65 g, 10.0 mmol) and *n*-BuLi (10.0 mmol) at −20°C under nitrogen, we added, drop by drop, a solution of diethyl fumarate (1.55 g, 9.0 mmol) in THF (15 m*l*). After the reaction mixture had then been stirred for 1 hr at the same temperature, it was allowed to warm up to room temperature. Work-up then afforded diethyl *t*-3-(phenylthio)-*r*-1,*t*-2-cyclopropanedicarboxylate (**17**, 1.34 g, 51%); bp 125—126°C/0.05 mmHg. An analytically-pure sample was obtained by preparative GLC (30% High Vacuum Silicone Grease on Celite 535, 220°C). IR (neat): 1729, 1328, 1255, 1172, 1025 cm^{-1}; NMR (CCl_4): 1.15 (t, 3H), 1.31 (t, 3H), 2.30—3.10 (m, 3H), 3.98 (q, 2H), 4.08 (q, 2H), 6.8—7.3 (m, 5H). Found: C, 61.5; H, 6.3%. Calcd for: $C_{15}H_{18}O_4S$: C, 61.2; H, 6.2%.

*Oxidation of **17**.* A solution of **17** (0.31 g, 1.1 mmol) and 30% H_2O_2 (*ca.* 15 m*l*) was heated at 70°C for 12 hr with stirring. Subsequent work-up and chromatography (silica gel column, benzene) afforded diethyl *t*-3-phenylsulfonyl-*r*-1,*t*-2-cyclopropanedicarboxylate (**18**, 0.32 g, 90%) as an oil. This oil solidified on standing at room temperature for several months, mp 60—61.5°C. IR (neat): 1730, 1370, 1320, 1265, 1180, 1150, 1019, 1030 cm^{-1}; NMR (CCl_4): 1.30 (t, 3H), 1.33 (t, 3H), 2.43—3.10 (m, 3H), 4.16 (q, 2H), 4.23 (q, 2H), 7.2—8.0 (m, 5H). Found: C, 54.9; H, 5.6%. Calcd for $C_{15}H_{18}O_6S$: C, 55.2; H, 5.6%.

*Attempted Reaction of **6a** with (E)-1,2-Dibenzoylethylene and Diethyl Fumarate.* A solution of **6a** (1.2 g, 4.3 mmol) and (E)-1,2-dibenzoylethylene (1.0 g, 4.3 mmol) in THF (100 m*l*) was heated under reflux for 6 hr. A work-up then resulted in a complete recovery of the starting materials. The similar treatment of **6a** (1.44 g, 5.0 mmol) and diethyl maleate (0.86 g, 5.0 mmol) also resulted in a complete recovery of the starting materials.

The authors are grateful to Professor K. Sisido for his generous help and to Toray Science Foundation for its financial support. They are also thankful to the Ministry of Education, Japanese Government, for a Scientific Research Grant-in-aid.

C-C Bond Fission in Carboxamides. Kinetic Studies on Alkaline Hydrolysis of Substituted α-Nitroisobutyranilides

Hiroteru SAYO, Hidenobu OHOMORI, Tsuneji UMEDA, and Masaichiro MASUI

Faculty of Pharmaceutical Sciences, Osaka University, Toyonaka, Osaka-fu

(Received May 4, 1971)

Alkaline hydrolysis of substituted α-nitroisobutyranilides, trichloroacetanilide and trifluoroacetanilide was studied kinetically at various hydroxyl ion concentrations in 10% aqueous dioxane. The formation of phenylcarbamate ion as an intermediate was confirmed on hydrolysis of the α-nitroisobutyranilides and trichloroacetanilide but not trifluoroacetanilide. All the substituted α-nitroisobutyranilides except the *p*-nitro derivative were found to undergo C–C bond fission exclusively. Trichloroacetanilide and the *p*-nitro derivative of α-nitroisobutyranilide underwent both C–C and C–N bond fission. The mechanism of C–C bond fission in the hydrolysis of α-nitroisobutyranilides was explained on the basis of the solvent isotope effect as a fast reversible addition of a hydroxyl ion followed by a rate-determining decomposition of the tetrahedral addition intermediate to form a phenylcarbamate ion and a carbanion.

Alkaline hydrolysis of anilides containing strongly electron attracting groups in the acylic part of the molecule has been studied extensively by many workers, but the only reaction pathway so far proposed is C–N bond fission to give carboxylate anion and aniline as primary products.

The only exception to this pathway is that deduced from the brief description of Eriksson and Holst[1] of a distinct odour of phenyl isocyanide and formation of chloride ion during the alkaline hydrolysis of trichloroacetanilide, but these authors did not discuss the origin of these compounds.

Previously we found an unusual C–C bond fission besides the usual C–N bond fission during studies on alkaline hydrolysis of α-nitroisobutyramide[2] and trichloroacetanilide,[3] and showed the origin of phenyl isocyanide and chloride ion in the latter case.

The present work was on alkaline hydrolysis of substituted α-nitroisobutyranilides to examine C–C bond fission in the alkaline hydrolysis of carboxamides. Use of substituted anilides facilitated studies on the effect of structural change on the hydrolysis and provided much information on the mechanism of the reaction.

Experimental

Materials. α-Nitroisobutyranilides were prepared by condensation of α-nitroisobutyryl chloride, obtained by a known method,[4] with appropriate anilines in dichloromethane at 0°C in the presence of potassium carbonate. They were recrystallized from appropriate solvents. The results of analyses are shown in Table 1. Trichloroacetanilide[5] and trifluoroacetanilide[6] were prepared by a known method and gave the expected analytical values. Deuterium oxide (99.75% D_2O) and NaOD (in 99.75% D_2O) were obtained from Merck and Co., Inc. The inorganic compounds used were of reagent grade.

Apparatus. Spectroscopic measurements were carried out with a Shimadzu, type QV-50, spectrophotometer. A Metrohm pH-meter, type E-300B, with a combined electrode was used for pH measurements.

Kinetic Measurements. Kinetic measurements were made spectrophotometrically at 50±0.02°C in 10% (V/V) aqueous dioxane unless otherwise specified. The ionic strength of the reaction mixture was adjusted to 0.9 by addition of potassium chloride except for $[OH^-]>0.9$M. The initial concentration of anilides was in the range 10^{-3} to 10^{-4}M. The concentration of sodium hydroxide was estimated with sulfamic acid. In a typical run, a volume of about 85 m*l* of sodium hydroxide solution, with the desired amount of potassium chloride, was put into a 100 m*l* volumetric flask and warmed to 50±0.02°C in a water bath. A volume of 10 m*l* of anilide in dioxane and the necessary amount of sodium hydroxide solution to make up the volume, both at 50°C, were added to the flask. The resulting mixture was quickly shaken, and then stood in the bath. At appropriate intervals 0.50 m*l* of the solution was pippetted into 5 m*l* of 1N HCl and the absorbance due to unreacted anilide was measured. The rate constant of the reaction was obtained graphically using the usual pseudo-first order kinetic treatment. The absorption maxima of the anilides used are shown in Table 1. With the *m*-nitro derivative, the absorption of *m*-nitroaniline overlaps that of the anilide in acidic solution, so the above method was not applicable. Hence *m*-nitroaniline was converted into its diazonium salt in 1N-HCl solution, and the absorption of this salt at 540 mμ was followed. *m*-Nitrophenylcarbamic acid was rapidly converted into *m*-nitroaniline under these condition and hence the amount of diazonium salt observed corresponded to the sum of the amounts of aniline and phenylcarbamic acid present in the reaction mixture.

Phenylcarbamate ion in the reaction mixture was separated and determined by the method of Christenson.[7] The rate of decomposition of phenylcarbamate ion (k_6 in Table 4) was measured with phenyl isocyanate.

Acid Dissociation Constants. pK_a values for the α-nitroisobutyranilides were determined from the change in the absorbance with pH. Stock solutions of an anilide were mixed with appropriate buffers and the absorbances of the anilide in its undissociated form were measured at its λ_{max} shown in Table 1. Error due to the time lapse between mixing and reading the absorbance was corrected by extrapolation of values to zero time.

1) S. O. Eriksson and C. Holst, *Acta Chem. Scand.*, **20**, 1892 (1966).
2) M. Masui, H. Sayo, H. Ohmori, and T. Minami, *Chem. Commun.*, **1969**, 404.
3) M. Masui, H. Ohmori, H. Sayo, and Y. Umeda, *Chem. Pharm. Bull.* (Tokyo), **19**, 1508 (1971).
4) L. W. Kissinger and H. E. Ungnade, *J. Org. Chem.*, **24**, 1244 (1959).
5) E. Votocek and J. Buroda, *Ber.*, **48**, 1002 (1915).
6) E. J. Bourne, *J. Chem. Soc.*, **1952**, 4014.
7) I. Christenson, *Acta Chem. Scand.*, **18**, 904 (1964).

Table 1. Melting points, analytical results and absorption maxima of α-nitroisobutyranilides, $Me_2C(NO_2)CONHC_6H_4X$

X	mp, °C	Calcd. %			Found, %			λ_{max}, mμ
		C	H	N	C	H	N	
p-OMe	73 — 74	55.45	5.92	11.76	55.46	5.86	11.90	239
p-Me	115 —116	59.45	6.35	12.60	59.62	6.25	12.63	238
m-Me	107 —108	59.45	6.35	12.60	59.56	6.23	12.45	237
H	104 —105	57.68	5.81	13.46	57.89	5.80	13.63	235
p-Cl	121 —122.5	49.48	4.57	11.55	49.63	4.84	11.46	242
m-Cl	134.5—136	49.48	4.57	11.55	49.42	4.52	11.47	240
m-NO_2	135 —136	47.43	4.38	16.60	47.41	4.37	16.67	235
p-NO_2	137.5—139	47.43	4.38	16.60	47.14	4.26	16.45	304

Results

Hydrolysis of Substituted α-Nitroisobutyranilides. The rate of hydrolysis of all α-nitroisobutyranilides used was first-order in the anilide at constant hydroxyl ion concentration. The final products were 2-nitropropane aci-ion, substituted aniline and carbonate ion. The observed pseudo-first-order rate constant, k_{obs}, approaches a limiting value with increase in hydroxyl ion concentration, as shown in Fig. 1 and Table 2. These limiting values, k_{limit}, are also summarized in Table 2. A similar phenomenon was observed by Erikson and Holst on hydrolysis of trichloro- and trifluoroacetanilide.[1] The effect of the initial concentration on k_{obs} was examined with concentrations of 2×10^{-4} to 8×10^{-4}M of unsubstituted α-nitroisobutyranilide at a hydroxyl ion concentration of 0.9M and μ=0.9: no effect was observed. Change in ionic strength between 0.9 and 3.6 had no effect on k_{obs} for hydrolysis of the same anilide at a hydroxyl ion concentration of 0.9M. Substituted phenylcarbamate ion was detected by the method of Christenson[7] in the reaction mixture during the hydrolysis, and its concentration increased with time, up to a maximum, and then decreased slowly towards zero at infinite time. A typical example of the hydrolysis of unsubstituted α-nitroisobutyranilide is shown in Fig. 2. The time when the phenylcarbamate ion reaches its maximum concentration is given in Table 3, as t_{max}, with the relative concentration of phenylcarbamate ion at this time. The maximum concentration of phenylcarbamate ion increased with the concentration of hydroxyl ion.

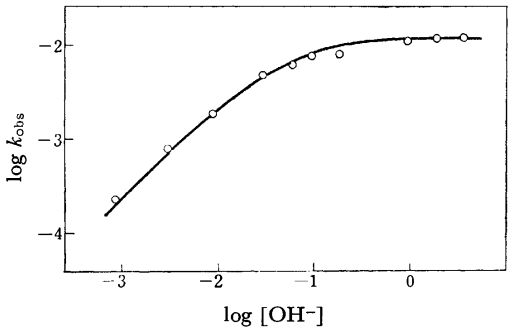

Fig. 1. Plot of log k_{obs} against log [OH⁻] in the alkaline hydrolysis of α-nitroisobutyranilide. The line is calculated from Eq. (16) and parameter values in Table 2.

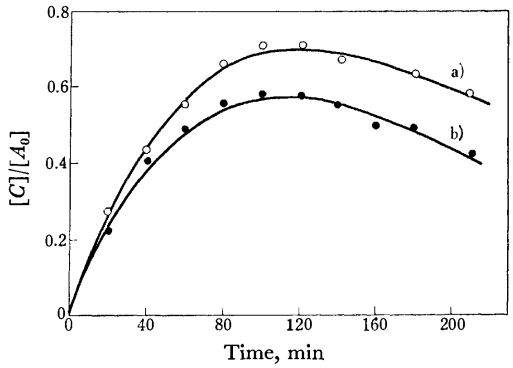

Fig. 2. Time-dependences of the concentration of phenylcarbamate ion during hydolysis of α-nitroisobutyranilide.
a) [OH⁻]=1.8M, b) [OH⁻]=0.9M

Table 2. Pseudo-first-order rate constants, k_{obs}, and limiting values of k_{obs}, k_{limit}, for the hydrolysis and dissociation constants of anilides, $RCONHC_6H_4X$, at 50°C

	[OH⁻], M[a]	R	$Me_2C(NO_2)$								CCl_3	CF_3
		X	*p*-OMe	*p*-Me	*m*-Me	H	*p*-Cl	*m*-Cl	*m*-NO_2	*p*-NO_2	H	H
10^3k_{obs}, min^{-1}	3.6		12.8			11.9						
	1.8		10.4	12.4	12.4	11.6	9.36	7.74	7.29	8.75		
	0.9		9.6	10.1	12.3	10.8	8.26	6.93	7.57	8.54	117	291
	0.09		4.1	4.86	7.13	7.11	5.57	3.92	6.67		93	230
	0.009		1.77	1.48	2.41	1.84	2.35	3.00	3.57	7.95	17	63.2
	0.0027		0.32	0.54	0.67	0.77	1.64	1.74	1.99			
	0.0009		0.11	0.17	0.17	0.21	0.37	0.75	1.15	6.28		
10^3k_{limit}, min^{-1}			14.0	13.0	12.4	12.0	9.5	7.8	7.6	8.8		
pK_a			12.1	12.0	12.0	11.8	11.6	11.4	11.0	10.3	9.98[b]	9.51[b]

a) μ=0.9 except for [OH⁻]>0.9 M, containing 10% (v/v) dioxane. b) Data from Ref. 1 at 25°C

Table 3. Values of t_{max}, $[C]_{max}/[A_0]$ and $(k_{obs}-\lambda)$ for the hydrolysis of anilides at 50°C, $\mu=0.9$

R	X	$[OH^-]$ M	t_{max} obsd. min	t_{max} calcd. min	$[C]_{max}/[A_0]$[a]	$10^3\times(k_{obs}-\lambda)$ min^{-1}
$Me_2C(NO_2)$	*p*-OMe	0.9	100		0.79	0
	p-Me	0.9	100		0.34	0
	m-Me	0.9	90		0.64	0
	H	1.8	120	150	0.71	0
		0.9	110	118	0.58	0
		0.09	100	108	0.43	0
		0.009	80	90	0.08	0
	p-Cl	0.9	140		0.67	0
	m-Cl	0.9	150		0.60	0
	m-NO_2	0.009	200		0.30	0
	p-NO_2	0.9	140		0.17	5.14
		0.009	130		0.26	2.54
CCl_3	H	0.9	27	26	0.40	60
		0.09	27	25	0.30	60
		0.009	40	42	0.09	10.5

a) $[C]_{max}$ represents the concentration of phenylcarbamate ion at $t=t_{max}$; $[A_0]$ is the initial concentration of total anilide.

Acid Dissociation Constants. The acid dissociation constants of α-nitroisobutyranilides are summarized in Table 2. A plot of the acid dissociation constants for substituted α-nitroisobutyranilides against the Hammett σ values was linear with $\rho=+1.19$ (figure not shown). With the *p*-nitro derivative, use of the σ^- value fitted the line better.

Decomposition of Phenylcarbamate Ion. In aqueous alkaline solution phenyl isocyanate is rapidly transformed to phenylcarbamate ion, and the latter decomposes gradually to give aniline and carbonate ion.[7,8] The rate of the decarboxylation reaction was measured at 50—70°C. The pseudo-first-order rate constants are summarized in Table 4.

Table 4. Pseudo-first-order rate constants for the decomposition of phenylcarbamate ion k_6 at 50°C

$[OH^-]$, M[a]	1.9	0.9	0.18	0.09	0.009
10^3k_6, min^{-1}	3.31	6.50	8.56	11.8	35.0

a) $\mu=0.9$ except for $[OH^-]>0.9$ M, containing 10% (v/v) dioxane.

Hydrolysis of Trichloro- and Trifluoroacetanilide. Table 2 also shows data for the hydrolysis of trichloro- and trifluoroacetanilide. The rates obtained at 25°C are in fairly good agreement with those reported previously.[1] A considerable amount of phenylcarbamate ion was obtained on hydrolysis of trichloroacetanilide, and the amount increased to a maximum as in the case of α-nitroisobutyranilides (Table 3). Thus it seems that the reaction pathway for the hydrolysis of trichloroacetanilide is comparable to that of α-nitroisobutyranilides. However, with trifluoroacetanilide, the concentration of phenylcarbamate ion was very low during the run and so no maximum was observed.

8) E. Mohr, *J. Prakt. Chem.*, [2] **73**, 177 (1906); C. Naegeli, A. Tyabji, L. Conrad, and F. Litwan, *Helv. Chim. Acta*, **21**, 1100 (1938).

Table 5. Rate constants k_{obs} and activation parameters for the hydrolysis of anilides $RCONHC_6H_5$, $[OH^-]=0.9$M, $\mu=0.9$

Temp. (°C)		R: $Me_2C(NO_2)$	CCl_3	CF_3
10^3k_{obs}, min^{-1}	25		10.0	33.7
	35		27.0	85.0
	50	10.8	117	291
	60	28.7		
	70	80.6		
E_a, kcal/mol		21.8	18.9	16.4
$\Delta S^{\neq}$, e.u.		−10.5	−14.7	−20.5

The rate of aniline formation was essentially the same as that of disappearance of anilide. The results suggest that a C–C bond fission similar to that with trichloroacetanilide scarcely occurs during hydrolysis of trifluoroacetanilide.

Activation Parameters. The activation parameters for the hydrolysis of α-nitroisobutyranilide, trichloroacetanilide and trifluoroacetanilide are shown in Table 5. They were obtained at a hydroxyl ion concentration of 0.9M, where the observed pseudo-first-order rate constant is very close to its limiting value, k_{limit}.

Solvent Isotope Effect. Solvent isotope effects on the hydrolysis of α-nitroisobutyranilide, trichloroacetanilide and trifluoroacetanilide were examined at a hydroxyl ion concentration of 1.8M, where $k_{obs}=k_{limit}$ was valid for each of these compound. The $k_{obs}(H)/k_{obs}(D)$ ratio was 1.10 ± 0.07 for α-nitroisobutyranilide, 1.33 ± 0.06 for trifluoroacetanilide and 1.39 ± 0.04 for trichloroacetanilide.

Discussion

Formation of phenylcarbamate ion as an intermediate and other results suggest the following reaction pathway for the hydrolysis of α-nitroisobutyranilides:

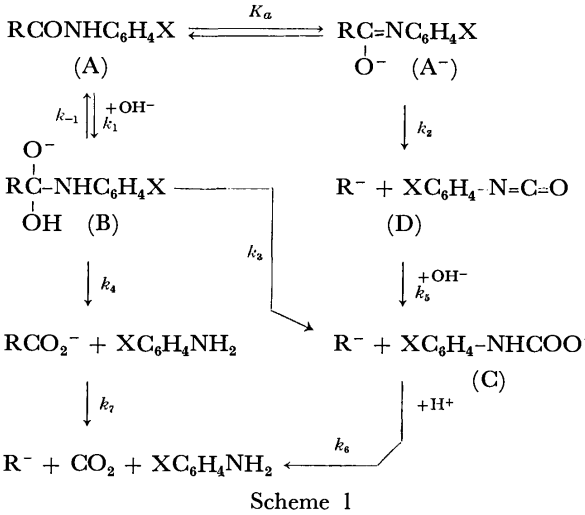

Scheme 1

(The possibility that step k_3 involves a term catalyzed by hydroxyl ion cannot be excluded at this point.

This will be discussed later.) A similar step to that involving formation of phenyl isocyanate (D) as an intermediate has been demonstrated in the hydrolysis of carbamic acid esters.[7] Assuming that B is in a steady state, the observed pseudo-first-order rate constant (k_{obs}) for the disappearance of total anilide is given by Eq. (1).

$$k_{obs} = \frac{K_w}{K_a+a_H}\left(\frac{k_1k_3}{k_{-1}+k_3+k_4} + \frac{k_1k_4}{k_{-1}+k_3+k_4}\right) + \frac{k_2K_a}{K_a+a_H} \quad (1)$$

where K_a is the dissociation constant defined in Eq. (2), K_w is the ionic product of water, and a_H is the activity of hydronium ion.

$$K_a = \frac{[A^-]a_H}{[A]} \quad (2)$$

The conversion of phenyl isocyanate into phenylcarbamate ion has been reported to be very rapid in alkaline solution,[7,8] and hence D can also be considered to be in a steady-state. The rate of the change in C is given by Eq. (3).

$$\frac{d[C]}{dt} = \lambda[A_0]e^{-k_{obs}t} - k_6[C], \quad (3)$$

where $$\lambda = \frac{K_w}{K_a+a_H}\cdot\frac{k_1k_3}{k_{-1}+k_3+k_4} + \frac{k_2K_a}{K_a+a_H} \quad (4)$$

and $[A_0]$ is the initial concentration of total anilide, so that

$$[C] = \frac{\lambda[A_0]}{k_{obs}-k_6}(e^{-k_6t}-e^{-k_{obs}t}). \quad (5)$$

We now define t_{max} as the time for C to reach its maximum concentration, and $[C]_{max}$ as the concentration of C at this time. When $t=t_{max}$, then $d[C]/dt=0$ is valid. Substituting [C] from equation (5) in equation (3) and solving about t_{max} gives Eq. (6).

$$t_{max} = \frac{\ln k_{obs} - \ln k_6}{k_{obs}-k_6} \quad (6)$$

The t_{max} calculated in Table 3 was obtained using experimental values of k_{obs} (Table 2), k_6, measured separately (Table 4),[9] and Eq. (6). The good agreement between the observed and calculated values substantiates the above equations.

From Eq. (3)

$$\lambda[A_0]e^{-k_{obs}\cdot t_{max}} - k_6[C]_{max} = 0$$

$$\lambda = k_6\frac{[C]_{max}}{[A_0]}e^{k_{obs}\cdot t_{max}} \quad (7)$$

Thus the value of λ can be calculated from experimental values. By subtracting Eq. (4) from Eq. (1), we obtain Eq. (8).

$$k_{obs} - \lambda = \frac{K_w}{K_a+a_H}\cdot\frac{k_1k_4}{k_{-1}+k_3+k_4}. \quad (8)$$

As shown in Table 3, the values of $k_{obs}-\lambda$ for the substituted α-nitroisobutyranilides are essentially zero within the limits of experimental error except with the *p*-nitro derivative. This strongly suggests that the hydrolysis of these compounds proceeds exclusively through pathways involving phenylcarbamate ion as an intermediate, that is, k_1 or k_4 is negligible. If $k_4\simeq 0$, Eq. (1) can be reduced to Eq. (9). (As will be discussed later, the experimental results obtained were not explained successfully when $k_1\simeq 0$).

$$k_{obs} = \frac{K_w}{K_a+a_H}\frac{k_1k_3}{k_{-1}+k_3} + \frac{k_2K_a}{K_a+a_H} \quad (9)$$

From Eq. (9)

$$\frac{k_1k_3K_w}{k_{-1}+k_3} + k_2K_a = k_{obs}(K_a+a_H) \quad (9')$$

Table 6. Values of $k_{obs}(K_a+a_H)$ for the hydrolysis of α-nitroisobutyranilide at various hydroxyl ion concentrations at 50°C

$[OH^-]$, M	3.6	1.8	0.9	0.09	0.054	0.009	0.0009
$10^{14}k_{obs}(K_a+a_H)$, M·min^{-1}	1.90	1.88	1.80	1.77	1.84	1.97	1.95

As shown in Table 6, the value of $k_{obs}(K_a+a_H)$ does not change with hydroxyl ion concentration within the limits of experimental error, and hence the left hand side of Eq. (9') can also be regarded as constant. Since mechanistically k_1, k_{-1}, and k_2 should be constants, two possibilities may be considered. First, k_3 does not contain a term dependent on hydroxyl ion concentration; that is, k_3 is also a constant. If this is not the case, $k_3 \gg k_{-1}$ should be true to make the term constant. In Eq. (9) the first term represents the rate constant for disappearance of total anilide through the tetrahedral intermediate (B), and the second term that for disappearance through phenyl isocyanate (D). It is difficult to decide which step is predominant, but solvent isotope effects should afford a clue to this problem. Tobias and Kézdy have reported a method for determining whether carbanions are intermediates in the hydrolysis of esters with labile α protons.[10] This method would be applicable in the present case.

In the pH region where $K_a \gg a_H$ Eq. (9) can be simplified to Eq. (10).

$$k_{obs} = k_{limit} = \frac{K_w}{K_a}\cdot\frac{k_1k_3}{k_{-1}+k_3} + k_2 \quad (10)$$

If only step k_2 is operative,

$$k_{obs} = k_2$$

Since no proton transfer is involved in this step, it is expected that $k_{obs}^{H_2O}/k_{obs}^{D_2O}=1$.[10] On the other hand, if step k_3 is actually operative, the observed isotope effect should be

$$k_{obs}^{H_2O}/k_{obs}^{D_2O} = (k^{H_2O}/k^{D_2O})(K_w^{H_2O}/K_w^{D_2O})(K_a^{D_2O}/K_a^{H_2O}), \quad (11)$$

where $k=k_1k_3/(k_{-1}+k_3)$.

The values of $K_w^{H_2O}/K_w^{D_2O}$ and $K_a^{H_2O}/K_a^{D_2O}$ at 50°C were estimated by the method of Swain, Kuhn and Schowen[11] to be 5.8 and 3.05, respectively. The

9) k_6 is the pseudo-first-order rate constant for the decomposition of phenylcarbamic acid and varies with hydroxyl ion concentration in a complicated manner. No further investigation was carried out, since the absence of information on the detailed nature of k_6 would not affect the conclusion.

10) P. S. Tobias and F. J. Kézdy, *J. Amer. Chem. Soc.*, **91**, 5171 (1969).

11) C. G. Swain, D. A. Kuhn, and R. L. Schowen, *ibid.*, **87**, 1553 (1965).

value of $K_w^{H_2O}/K_w^{D_2O}$ at 25°C estimated by the same method is 6.75, which is in good agreement with the reported value of 6.67 ($K_w^{D_2O}/K_w^{H_2O}=0.15$).[12] This seems to substantiate the above assumptions. Using these values and Eq. (11), we get

$$k_{obs}^{H_2O}/k_{obs}^{D_2O} = 1.9(k_1^{H_2O}/k_1^{D_2O}) \quad (12)$$

where $k_3 \gg k_{-1}$, and another Eq. (13) where $k_{-1} \gg k_3$.

$$k_{obs}^{H_2O}/k_{obs}^{D_2O} = 1.9\times(k_1k_3/k_{-1})^{H_2O}/(k_1k_3/k_{-1})^{D_2O} \quad (13)$$

It has been reported that an inverse isotope effect is involved in a process in which hydroxyl ion attacks a carbon atom, and the expected maximum isotope effect in such a process should be 1.7^{-1}.[13] Equation (12) is, then

$$k_{obs}^{H_2O}/k_{obs}^{D_2O} = 1.9/1.7^{\beta} \quad (14)$$

where β represents the degree of bond formation in the transition state, that is $0 \leqq \beta \leqq 1$.[11] As discussed above step k_3 does not involve a term catalyzed by hydroxyl ion when Eq. (13) holds, and hence no solvent isotope effect is expected as in step k_2. Thus Eq. (13) becomes

$$k_{obs}^{H_2O}/k_{obs}^{D_2O} = 1.9/1.7 \fallingdotseq 1.12 \quad (15)$$

The observed solvent isotope effects were 1.33 and 1.39 for trifluoroacetanilide and trichloroacetanilide, respectively. On hydrolysis of these two anilides, at the lyoxide ion concentration used in this study the attack of hydroxyl ion on the anilide was shown to be rate-determining.[1] The observed values are in the range expected from Eq. (14). In the hydrolysis of trichloroacetanilide, therefore, the possibility of phenylcarbamate ion being produced through step k_2 seems unlikely. If it is not the case, the observed solvent effect should be smaller than that for trifluoroacetanilide, because more than one third of the whole reaction proceeds through phenylcarbamate ion.

The solvent isotope effect observed in the hydrolysis of α-nitroisobutyranilide at a lyoxide ion concentration of 1.8M was 1.10, which is very close to the value expected from Eq. (15). The results strongly suggest that the hydrolysis of α-nitroisobutyranilide mainly proceeds through the tetrahedral addition intermediate (B), and the rate of decomposition of this intermediate to phenylcarbamate ion is slower than that of liberation of hydroxyl ion to give the original anilide, that is, $k_{-1} \gg k_3$.

The value of activation entropy, $\Delta S^{\ddagger} = -10.5$ eu., also seems to support this view. In the hydrolysis of carbamic acid esters, those hydrolyzed *via* a reaction pathway with an isocyanate intermediate like step k_2 in Scheme 1, have positive $\Delta S^{\ddagger}$ values, and those having negative $\Delta S^{\ddagger}$ values have been stated to be hydrolyzed *via* a tetrahedral addition intermediate.[7] The $\Delta S^{\ddagger}$ values of several of the latter esters are less negative than that of α-nitroisobutyranilide. If step k_2 in Scheme 1 actually operates in the hydrolysis of α-nitroisobutyranilide, the value of $\Delta S^{\ddagger}$ should be positive. The possibility that the reaction occurs *via* both pathways, k_2 and k_3, is not completely eliminated, but it seems extremely likely that step k_2 is not the main pathway.

From the above discussion Eq. (9) may be reduced to Eq. (16).

$$k_{obs} = \frac{K_w}{K_a + a_H} \cdot \frac{k_1k_3}{k_{-1}}. \quad (16)$$

Using the values of k_{limit} (Table 2), K_a (Table 2), and K_w, the value of k_1k_3/k_{-1} is calculated to be 0.347 min^{-1} for the hydrolysis of α-nitroisobutyranilide. The solid line in Fig. 1 is calculated from Eq. (16) and these values. This calculated line agrees well with the observed rate constants.

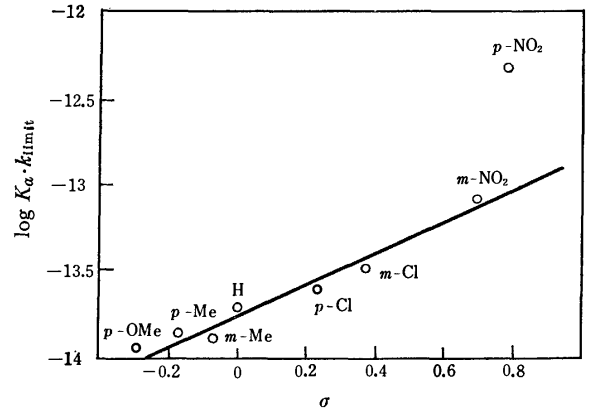

Fig. 3. Plot of $k_{limit} \cdot K_a$ against σ.

A plot of the value $k_1k_3K_w/k_{-1}$ ($=k_{limit} \cdot K_a$) for the substituted α-nitroisobutyranilides against Hammett σ values was essentially linear with $\rho=0.83$ (Fig. 3) except for the *p*-nitro derivative. The upward deviation observed with this anilide was reduced when the σ^- value was used. However, it is doubtful whether this treatment is adequate in the present case. Since the value of $k_{obs}-\lambda$ for the *p*-nitro derivative (Table 3) is more than half that of k_{obs} at 0.9M hydroxyl ion concentration, a considerable amount of C–N bond fission, that is normal hydrolysis, occurs in the hydrolysis. This fact seems compatible with the observed deviation in Fig. 3. In the hydrolysis of substituted acetanilide, the *p*-nitro derivative reacts appreciably faster than the rate predicted from the rates observed with other anilides, and thus a new mechanism was introduced to interpret the hydrolysis of anilides with strongly electron withdrawing substituents on the phenyl ring.[14] The C–N bond in the *p*-nitro derivative of α-nitroisobutyranilide must be activated by the *p*-nitro group more than that in other derivatives, and hence normal hydrolysis becomes possible to some extent.

It is interesting to compare the results obtained with trifluoroacetanilide, trichloroacetanilide and α-nitroisobutyranilide. In the hydrolysis of the trifluoro-derivative, no C–C bond fission was observed, that is the reaction was normal. With the trichloro-derivative, the ratio of C–C bond fission to C–N bond fission is more than one third. With the α-nitroisobutyr-deriv-

12) R. P. Bell, "The Proton in Chemistry," Cornell University Press, Ithaca, N. Y., (1959).

13) R. L. Schowen, H. Jayaraman, L. Kershner, and G. W. Zuorick, *J. Amer. Chem. Soc.*, **88**, 4008 (1966).

14) R. M. Pollack and M. L. Bender, *ibid.*, **92**, 7190 (1970).

TABLE 7. ACTIVATION ENERGIES FOR DECARBOXYLATION OF CARBOXYLIC ACIDS RCO_2H

R	Solvent	E_a, kcal/mol	Ref.
CF_3	Ethylene glycol	42.0	16
CCl_3	Ethylene glycol	31.6	16
CCl_3	Ethyl alcohol	31.0	17
CCl_3	Water	36.3	17, 18
CBr_3	Water	33.0	18
$Me_2C(NO_2)$	Water	22.5	19

atives, the reaction proceeds exclusively through C–C bond fission except with the *p*-nitro-derivative. A similar phenomenon was observed in studies on the formation of a tetrahedral addition intermediate of ethyl acetate derivatives.[15] The addition compound from ethyl trichloroacetate was found to decompose *via* C–C bond fission to give ethyl carbonate, whereas that from ethyl trifluoroacetate did not.

The value of activation energy for the decarboxylation of the carboxylic acids shown in Table 7 are interesting. The order of facility of C–C bond fission coincides with that observed in the present study. It seems clear from the above considerations that C–C bond fission increases with stability of the carbanion formed.

15) M. L. Bender, *J. Amer. Chem. Soc.*, **75**, 5986 (1953).

16) I. Auerbach, F. H. Verhoek, and A. L. Henne, *ibid.*, **72**, 299 (1950).

17) F. H. Verhoek, *ibid.*, **56**, 571 (1934); G. A. Hall, Jr. and F. H. Verhoek, *ibid.*, **69**, 613 (1947).

18) P. Johnson and E. A. Moelwyn-Hughes, *Proc. Roy. Soc., Ser. A*, **175**, 118 (1940).

19) K. J. Pedersen, *J. Phys. Chem.*, **38**, 559 (1934).

BULLETIN OF THE CHEMICAL SOCIETY OF JAPAN, VOL. 45, 208—213 (1972)

Studies of the Synthesis of Furan Compounds. XXVI.[1] The Reaction of 5-Nitro-2-furimidoylhydrazine with Acid Anhydrides[2]

Ichiro HIRAO, Yasuhiko KATO, and Hiromichi TATEISHI

Laboratory of Organic Synthesis, Department of Chemical Engineering, Kyushu Institute of Technology, Tobata-ku, Kita-kyushu

(Received May 10, 1971)

Reactions between 5-nitro-2-furimidoylhydrazine (I) and acetic or propionic anhydride (or the corresponding acids) under various conditions afforded 5-methyl- (II) and 5-ethyl-2-(5-nitro-2-furyl)-1,3,4-oxadiazole (IV) and 5-methyl- (III), 5-ethyl- (IX), 1-acetyl-5-methyl- (VII), 1-propionyl-5-ethyl- (VIII), 1-propionyl-5-methyl- (X), and 1-acetyl-5-ethyl-3-(5-nitro-2-furyl)-1,2,4-triazole (XI) respectively. The treatment of I with acetic and propionic anhydride in refluxing benzene or tetrahydrofuran gave 1-acetyl- (V) and 1-propionyl-2-(5-nitro-2-furimidoyl)-hydrazine (VI) respectively. Compounds, VII, VIII, X, and XI were also prepared by the cyclization of V with propionic anhydride and by that of VI with acetic anhydride in dioxane. The structures of the products were discussed on the basis of the spectral data.

In continuation of our previous report on the preparation of several 5-nitro-2-furyl-heterocycles by the cyclization of 5-nitro-2-furimidoylhydrazine (I) with bifunctional compounds,[3] this paper will deal with the preparation of acyl (or without acyl)-(5-nitro-2-furyl)-5-alkyl-1,2,4-triazoles by the reaction of I with acid anhydries under various reaction conditions, and with the determination of the position of the acyl group in the triazole nucleus on the basis of the reactions of the acyl derivatives of I with acetic and propionic anhydrides.

Results and Discussion

Atkinson and Polya reported the synthesis of 1-methyl (or phenyl)-3-phenyl-1,2,4-triazole by the reaction of the corresponding 1-substituted 2-benzimidoylhydrazine with formic acid,[4] while Atkinson *et al.* reported that of 3-amino-5-alkyl (or aryl)-1,2,4-triazoles from an aminoguanidine salt and the appropriate organic acid in the presence of a small amount of nitric acid.[5] In a similar manner, when I was heated in glacial acetic acid, two products, II and III, were obtained. Compound II was identified as the 2-(5-nitro-2-furyl)-5-methyl-1,3,4-oxadiazole by an admixture-test and by a comparison of its IR spectrum with that of an authentic specimen,[3] while III was confirmed to be 3-(5-nitro-2-furyl)-5-methyl-1,2,4-triazole on the basis of the analytical and spectral data. The similar treatment of I with propionic acid afforded only one product, 2-(5-nitro-2-furyl)-5-ethyl-1,3,4-oxadiazole (IV) (Scheme 1).

1-Acetyl-(V) and 1-propionyl-2-(5-nitro-2-furimidoyl)-

1) Part XXV of this series; I. Hirao and Y. Kato, This Bulletin, **44**, 3136 (1971).

2) Presented at the 24th Annual Meeting of the Chemical Soceity of Japan, Osaka, April, 1971.

3) I. Hirao, Y. Kato, T. Hayakawa, and H. Tateishi, This Bulletin, **44**, 780 (1971).

4) M. R. Atkinson and J. B. Polya, *J. Chem. Soc.*, **1953**, 1471; **1954**, 3319.

5) M. R. Atkinson, A. A. Komzak, E. A. Parkes, and J. B. Polya, *ibid.*, **1954**, 4508.

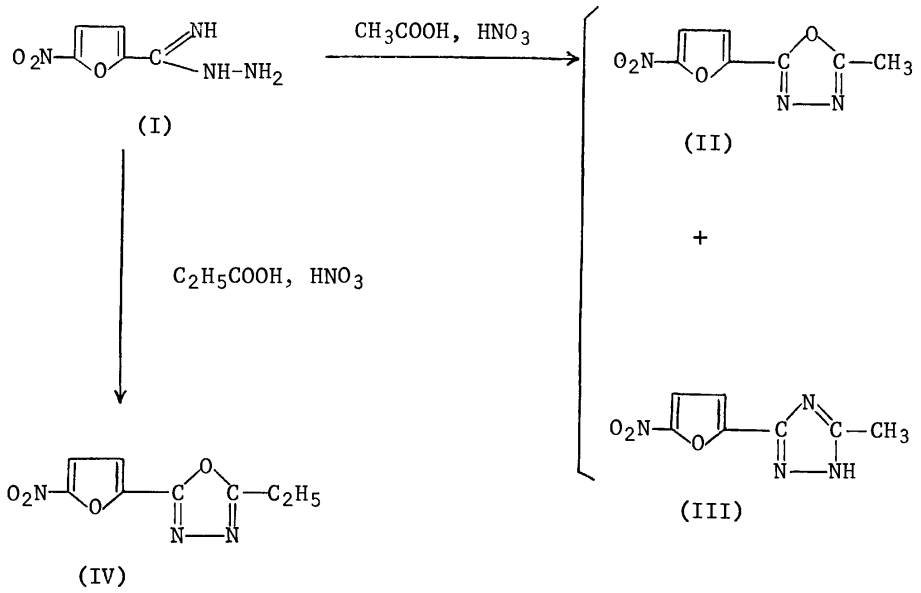

Scheme 1

hydrazine (VI) were obtained by treating I with acetic and propionic anhydrides respectively in refluxing benzene or tetrahydrofuran. However, I afforded 1-acetyl-3-(5-nitro-2-furyl)-5-methyl-1,2,4-triazole (VII) and 1-propionyl-3-(5-nitro-2-furyl)-5-ethyl-1,2,4-triazole (VIII) when heated in large excesses of acetic and propionic anhydride respectively. Compounds VII and VIII were similarly obtained from, respectively, V and acetic anhydride, and VI and propionic anhydride.

When heated in water, VII afforded III, and VIII provided 3-(5-nitro-2-furyl)-5-ethyl-1,2,4-triazole (IX),

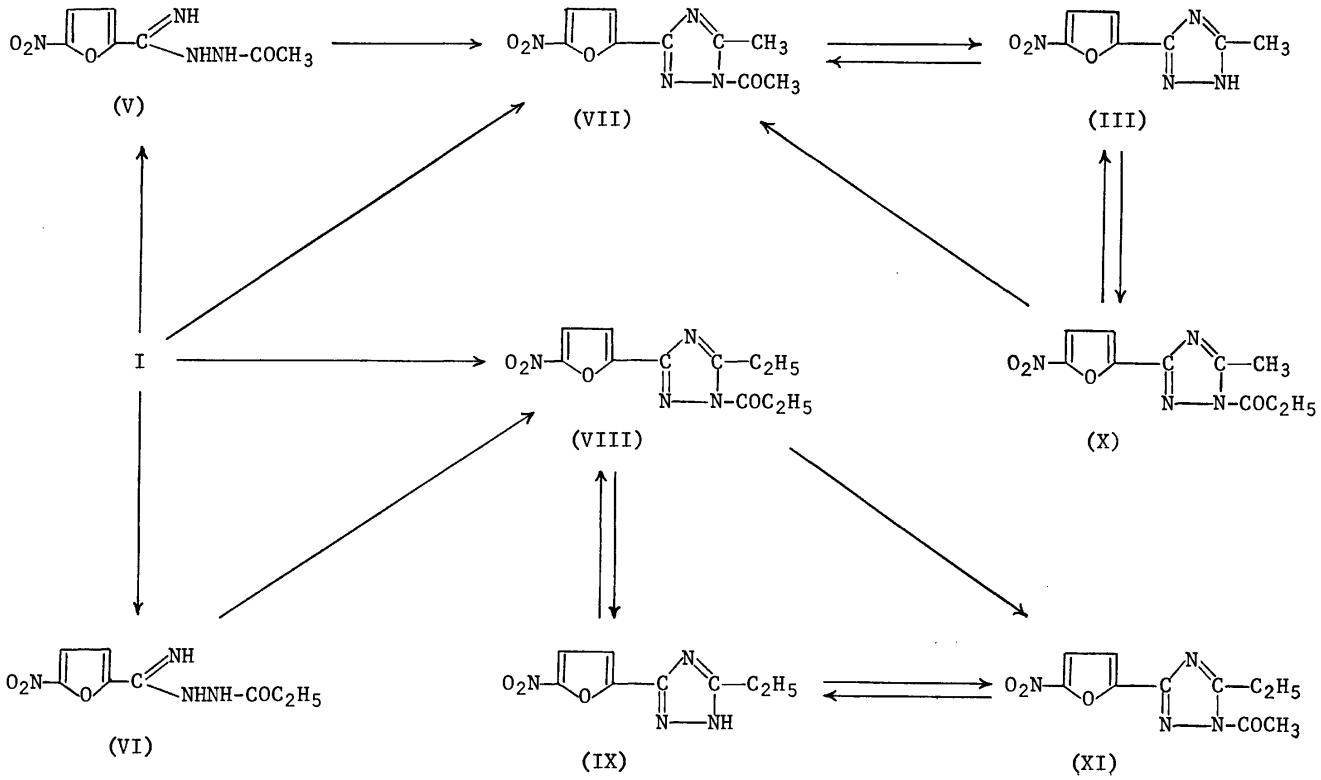

Scheme 2

TABLE 1. NMR DATA OF III, VII, VIII, IX, X, AND XI. (δ value, at 60 MHz)

	III	IX	VII	VIII	X		XI	
	in DMSO-d_6[a]				in DMSO-d_6	in CCl_3COOH[b]	in DMSO-d_6	in CCl_3COOH
Furan ring 4-H	7.76 (1H, d, J=4.0 Hz)	7.72 (1H, d, J=4.0 Hz)	7.71 (1H, d, J=4.0 Hz)	7.84 (1H, d, J=4.0 Hz)	7.81 (1H, d, J=4.0 Hz)	7.23[c] (2H, s)	7.81 (1H, d, J=4.0 Hz)	7.23[c] (2H, s)
Furan ring 3-H	7.19 (1H, d, J=4.0 Hz)	7.17 (1H, d, J=4.0 Hz)	7.35 (1H, d, J=4.0 Hz)	7.44 (1H, d, J=4.0 Hz)	7.42 (1H, d, J=4.0 Hz)		7.42 (1H, d, J=4.0 Hz)	
$\overset{\|\|}{C}-CH_3$	2.46 (3H, s)		2.74[d] (6H, s)		2.74 (3H, s)	2.62 (3H, s)		
$-CO-CH_3$							2.74 (3H, s)	1.86 (3H, s)
$\overset{\|\|}{C}-CH_2-\overset{\|}{C}-$		2.80 (2H, q, J=7.5 Hz)		3.19 (2H, q, J=7.5 Hz)			3.15 (2H, q, J=7.5 Hz)	2.94 (2H, q, J=7.5 Hz)
$\overset{\|\|}{C}-\overset{\|}{C}-CH_3$		1.30 (3H, t, J=7.5 Hz)		1.37 (3H, t, J=7.5 Hz)			1.33 (3H, t, J=7.5 Hz)	1.16 (3H, t, J=7.5 Hz)
$-CO-CH_2-\overset{\|}{C}-$				3.22 (2H, q, J=7.5 Hz)	3.18 (2H, q, J=7.5 Hz)	2.14 (2H, q, J=7.5 Hz)		
$-CO-\overset{\|}{C}-CH_3$				1.23 (3H, t, J=7.5 Hz)	1.19 (3H, t, J=7.5 Hz)	0.82 (3H, t, J=7.5 Hz)		

a) TMS was used as the internal standard. b) HMDS was used as the internal standard. c) Two protons of the furan ring were overlapped and showed a singlet. d) The CH_3 and $COCH_3$ protons appeared the same field and formed a singlet.

both in almost quantitative yields. III was reverted to VII by heating it in acetic anhydride, and IX, to VIII in propionic anhydride. 1-Propionyl-5-methyl- (X) and 1-acetyl-5-ethyl-3-(5-nitro-2-furyl)-1,2,4-triazole (XI) were obtained by the treatment of III with hot propionic anhydride, and by the treatment of IX with hot acetic anhydride, whereas X and XI reverted to III and IX respectively upon heating with water. Furthermore, X was converted into VII, and also VIII into XI, by heating them with acetic anhydride. These results show that the acyl group on a nitrogen of the triazole nucleus could be replaced easily be an acyl group of the acid anhydride employed (Scheme 2).

The IR spectra showed a characteristic wide ammonium absorption in the 3010—2550 cm^{-1} region for III, and in the 3150—2800 cm^{-1} region for IX. This fact, as has been discussed previously,[3] suggests that both III and IX contribute to an intermolecular association because of the hydrogen transfer between two adjacent molecules. Neither the spectrum of III nor that of IX showed the C=O stretching absorption which was observed at 1680 cm^{-1} in the spectra of compounds V and VI. In the finger-print region, III had a sharp band at 1058 cm^{-1} due to a methyl rocking vibration, and IX contained three absorptions, at 1062, 1048, and 842 cm^{-1}. The 1048 cm^{-1} band is assigned to the CH_3 rocking vibration, and the 1062 and 842 cm^{-1} bands to the C–H wagging motion of the $-C_2H_5$ group.

On comparing the IR spectra of the four acyl compounds (VII, VIII, X, and XI), all of them were found to show a strong absorption band, VII at 1736, VIII at 1738, X at 1759, and XI at 1754 cm^{-1} due to the C=O stretching vibration. The weak to medium bands due to the C–H stretching motion in VII, VIII, X, and XI appeared in the 3000—2800 cm^{-1} region. In the finger-print regions, the band assignable to the CH_3 rocking mode in VII was observed at 1091 cm^{-1} and also in X at 1089 cm^{-1}. In the compound VIII, the 1084, 1060, and 828 cm^{-1} bands, and in XI, the 1085, 1060, and 830 cm^{-1}, bands might be assignable much as in the mother compound, IX. Two strong bands and a weak one appeared at 962, 646, and 727 cm^{-1} respectively in VII; the corresponding ones at 962, 646, and 723 cm^{-1} in XI were assigned to a $-COCH_3$ group introduced, while the bands due to the $-COC_2H_5$ motion in VIII are observed as a weak band at 964 cm^{-1} and a strong one at 943 cm^{-1}, while those in X are observed at 965 and 943 cm^{-1}.

The NMR spectra in DMSO-d_6 supported the structures of III, VII, VIII, IX, X, and XI presented above. As is shown in Table 1, the chemical shifts of the ring methyl or methylene protons of VII, VIII, X, and XI shifted to a lower magnetic field than those of III or IX upon the introduction of an acetyl or propionyl group. This indicates that the acyl group may be introduced into the vicinal nitrogen atom next to the existing alkyl group. The NMR spectra of X and XI in DMSO-d_6 were different from those in trichloroacetic acid (Table 1). Both the acetyl protons and the methylene protons of a propionyl group are more subject to the solvent effect than are the methyl and methylene protons attached to the triazole ring, and their chemical shifts shifted to a higher magnetic field. The C_4-proton of the furan nucleus was very subject to the solvent effect and revealed the signal together, with that of the C_3-ptoton

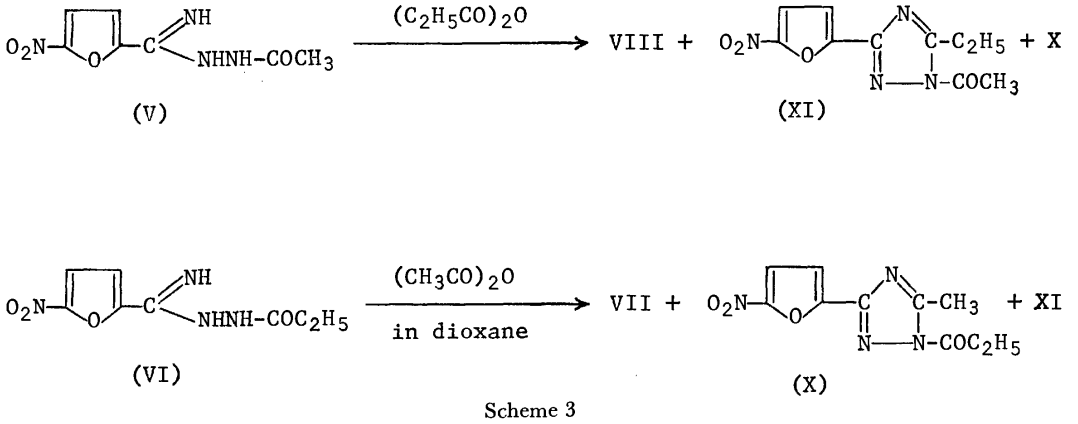

Scheme 3

at 7.23 ppm of hexamethyldisiloxane (HMDS); accordingly, the signals were observed as a singlet.

On the treatment of VI with a large excess of acetic anhydride in dioxane at 95—100°C for 1 hr, a mixed product was obtained. The components were successfully resolved by treating the mixture with hot ligroin. The ligroin-insoluble part was confirmed to be VII on the basis of the analytical and spectral data. From the ligroin solution, a crystalline powder (XII) (mp 103—105°C) was obtained. The results of an elemental analysis of XII was in good accordance with the calculated value for $C_{10}H_{10}N_4O_4$ (X or XI). Subsequent crystallization from ligroin raised the melting point to 112—114°C, but the results of the elemental analysis were unchanged. In addition, the IR spectrum of XII did not agree with that of X or XI, and it had bands at 980, 955, 725, and 645 cm^{-1}, indicating the presence of both acetyl and propionyl groups. The NMR spectrum as is shown in Fig. 1a, revealed signals at (δ from TMS in DMSO-d_6) 1.26 (q, J=7.5 Hz), 2.74 (s), *ca.* 2.95—3.35 (m), 7.42 (d, J=4.0 Hz), and 7.80 (d, J=4.0 Hz), with relative intensities of 3:3:2:1:1. However, when measured in trichloroacetic acid, the NMR spectrum (Fig. 2b) varied remarkably and showed signals at (δ from HMDS) 0.82 (t, J=7.5 Hz), 1.16 (t, J=7.5 Hz), 1.86 (s), 2.15 (q, J=7.5 Hz), 2.62 (s), 2.94 (q, J=7.5 Hz) and 7.23 (s) (the signal intensity ratio; 0.58: 0.93: 0.92: 0.40: 0.58: 0.62: 1). Considering these data, it was concluded that XII was obviously a mixture of X and XI, and that the component ratio (X:XI) was 39:61 (on the basis of the NMR intensity ratio).

The similar treatment of V with propionic anhydride also produced three compounds, VIII, X, and XI, in the proportion of 1: 0.8: 0.6.

A modern representation of the structure of 1,2,4-triazole takes cognizance of the imino hydrogen atom not being attached to any of the nitrogen atoms, but rather existing as a charged atom closely bound by a negatively-charged triazole nucleus stabilized by resonance.[6] The substitution reaction upon the imino

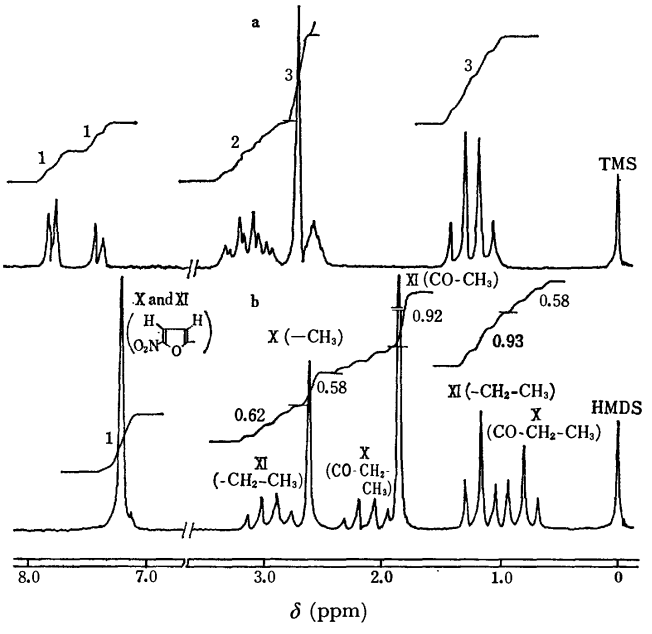

Fig. 1. NMR spectra of XII (mixture of X and XI).
a: measured in DMSO-d_6 at 24°C
b: measured in CCl_3COOH at 70°C

nitrogen of triazole could, then, give three isomeric *N*-substituted derivatives (1-, 2-, and 4-substituted derivatives). In this investigation, none of the isomeric acetyl or propionyl derivatives were isolated, but only a sort of product was obtained in each type of derivative. It is very difficult to determine the position of an acyl group substituted on the triazole nucleus, fortunately, however, we could confirm the formation of XI from the reaction of V with propionic anhydride and from that of X from VI and acetic anhydride by studying the NMR spectra. Consequently, it seems reasonable to conclude that the position of the introduced acyl group of VII, VIII, X, and XI is the vicinal nitrogen atom, far from the 5-nitro-2-furyl group, as has been discussed above.

Experimental

All the melting and decomposition points are uncorrected. The elemental analyses were performed on a Yanagimoto C. H. N. Corder, MT-2 type. The infrared absorption spectra (IR) were measured in potassium bromide discs on a Hitachi grating infrared spectrophotometer, Model EPI-G3.

6) K. T. Potts, *Chem. Rev.*, **61**, 87 (1961). The π-electron densities for 1,2,4-triazole were published in the following literature: a) L. E. Orgel, T. L. Cottrell, W. Dick, and L. E. Sutton, *Trans. Faraday Soc.*, **47**, 113 (1951). b) M. R. Atkinson and J. B. Polya, *J. Chem. Soc.*, **1954**, 3319. c) S. Basu, *Proc. Natl. Inst. Sci. India*, **21A**, 173 (1955).

The nuclear magnetic resonance spectra (NMR) were determined by means of a Nihon-Denshi NMR spectrometer, JNM C-60HL (60 MHz). The spectra were measured in DMSO-d_6 at 24°C with tetramethylsilane (TMS) as the internal standard, and in trichloroacetic acid at 70°C with hexamethyldisiloxane (HMDS) as the internal standard; the chemical shifts are expressed in δ-values.

2-(5-Nitro-2-furyl)-5-methyl-1,3,4-oxadiazole (II) and 3-(5-Nitro-2-furyl)-5-methyl-1,2,4-triazole (III). 5-Nitro-2-furimidoylhydrazine[7] (I) (3 g, 17.6 mmol), glacial acetic acid (50 m*l*), and nitric acid (5 drops) were heated under reflux for 2 hr. After cooling, water (100 m*l*) was added and the mixture was extracted with ether (500 m*l*). The ether extracts were washed with water and dried over anhydrous sodium sulfate. After the concentration of the extracts, the residue was treated with hot benzene (50 m*l*) and the insoluble product was filtered off while hot. Thus, the crude material of III was obtained as an ochreous powder; mp 232—234°C; 0.7 g. Recrystallization from water gave yellow needles; mp 243—244°C. The yield was 0.6 g (17.5%).

Found: C, 43.05; H, 2.95; N, 28.55%. Calcd for $C_7H_6N_4O_3$ (III): C, 43.29; H, 3.09; N, 28.86%.

On cooling of the benzene filtrate, a yellow-ochre powder (0.5 g) was obtained; mp 138—148°C. Crystallization from ethanol afforded pale yellow needles; mp 153—154°C. Yield, 0.3 g (8.7%).

Found: C, 43.54; H, 2.35; N, 21.92%. Calcd for $C_7H_5N_3O_4$ (II): C, 43.07; H, 2.56; N, 21.53%.

This product was identified as the 1,3,4-oxadiazole (II) by an admixture-test and by a comparison of the IR spectrum with that of an authentic specimen.[3]

2-(5-Nitro-2-furyl)-5-ethyl-1,3,4-oxadiazole (IV). A mixture of I (1 g, 5.8 mmol), propionic acid (20 m*l*), and nitric acid (3 drops) was refluxed for 2 hr. Work-up as above afforded 0.3 g (24.4%) of IV, mp 182—183°C, as yellow needles (recrystallized from benzene-ligroin).

Found: C, 46.30; H, 3.36; N, 20.20%. Calcd for $C_8H_7N_3O_4$: C, 45.93; H, 3.35; N, 20.10%.

1-Acetyl- (V) or 1-Propionyl-2-(5-nitro-2-furimidoyl)hydrazine (VI). Acetic or propionic anhydride (each 20 mmol) was added slowly to a stirred solution of I (3.4 g, 20 mmol) in 100 m*l* of benzene (or 70 m*l* of tetrahydrofuran). The mixture was then stirred vigorously at room temperature for 1 hr. After cooling, the product was filtered and recrystallized from methanol. V; orange-yellow cylinders; mp 211—212°C decomp. Yield, 3.96 g (93.3%).

Found: C, 39.98; H, 3.73; N, 26.74%. Calcd for $C_7H_8N_4O_4$ (V): C, 39.62; H, 3.77; N, 26.42%.

VI; orange-yellow needles; mp 216—217°C decomp. Yield, 4.18 g (92.5%).

Found: C, 42.82; H, 4.48; N, 24.77%. Calcd for $C_8H_{10}N_4O_4$ (VI): C, 42.47; H, 4.42; N, 24.78%.

If the recrystallization was achieved from water, V was obtained as its semi-hydrate of yellow needles; mp 210°C.

Found: C, 38.52; H, 4.11; N, 25.31%. Calcd for $C_7H_8N_4O_4 \cdot \frac{1}{2}H_2O$: C, 38.01; H, 4.07; N, 25.34%.

1-Acetyl-3-(5-nitro-2-furyl)-5-methyl-1,2,4-triazole (VII).

From I and Acetic Anhydride: A solution of I (3.4 g, 20 mmol) in 50 m*l* of acetic anhydride was stirred at room temperature for 1 hr and then heated under reflux for an additional hour. On cooling, the separated product was collected and washed with benzene to afford 3.4 g (72%) of VII (mp 210—213°C) as pale yellow needles. Recrystallization from acetone gave pale yellow needles; mp 211—212°C.

Found: C, 45.73; H, 3.39; N, 23.72%. Calcd for $C_9H_8N_4O_4$: C, 45.76; H, 3.39; N, 23.73%.

From V and Acetic Anhydride: A mixture of V (2.12 g, 10 mmol) and acetic anhydride (30 m*l*) was refluxed for 1 hr. Subsequent work-up as above afforded 1.85 g (78.4%) of pale yellow needles. Mp 211—212°C; undepressed upon admixture with a sample prepared by the above method.

From the Acetylation of III: Compound III (1.94 g, 10 mmol) was covered with acetic anhydride (20 m*l*) and heated under reflux for 1 hr. The excess acid anhydride was then removed *in vacuo*, and the residue was recrystallized from acetone to give 1.9 g (80%) of VII as pale yellow needles, mp 210—211°C. This product was found to be identical with VII by a mixed-melting-point determination and by a comparison of the IR spectrum with that of an authentic sample.

1-Propionyl-3-(5-nitro-2-furyl)-5-ethyl-1,2,4-triazole (VIII).

From I and Propionic Anhydride: This was prepared in the same way as was VII, but using propionic anhydride (50 m*l*). The resulting solution was taken to dryness *in vacuo*, and the residue was crystallized from ligroin to give 2.9 g (55%) of VIII as pale brown granules; mp 78—79°C.

Found: C, 49.75; H, 4.48; N, 20.92%. Calcd for $C_{11}H_{12}N_4O_4$: C, 50.00; H, 4.54; N, 21.21%.

From VI and Propionic Anhydride: VI (2.26 g, 10 mmol) and propionic anhydride (20 m*l*) were heated together under reflux for 1 hr. The excess acid anhydride was removed *in vacuo*, and the oily residue was solidified by cooling, washed with ether, and then dried. Thus, 1.8 g of the crude product were obtained; mp 69—72°C. Subsequent recrystallization from ligroin gave 1.46 g (55.3%) of pale yellow granules; mp 78—79°C. This product was found to be identical with VIII by a mixed-melting-point determination.

From the Acylation of IX with Propionic Anhydride: The procedure outlined above for VII was followed using IX (2.08 g, 10 mmol) and propionic anhydride (20 m*l*). A work-up as above afforded 1.85 g (70%) of pale brown granules melting at 80—81°C. The product was shown to be the same as above by a study of its IR spectrum and by its failure to depress the melting point when mixed with a sample prepared by the above method.

1-Propionyl-3-(5-nitro-2-furyl)-5-methyl-1,2,4-triazole (X).

The procedure outlined above for VII was employed using III (0.97 g, 5 mmol) and propionic anhydride (25 m*l*). Work-up as above gave 1.03 g (82.3%) of pale yellow cylinders; mp 148—149°C (from ligroin).

Found: C, 48.12; H, 4.08; N, 22.62%. Calcd for $C_{10}H_{10}N_4O_4$: C, 48.00; H, 4.00; N, 22.40%.

1-Acetyl-3-(5-nitro-2-furyl)-5-ethyl-1,2,4-triazole (XI).

The procedure outlined above for VII was followed using IX (1.04 g, 5 mmol) and acetic anhydride (40 m*l*). A work-up as above then afforded 1.09 g (87.6%) of XI as pale yellow needles which melted at 119°C.

Found: C, 48.11; H, 4.11; N, 22.29%. Calcd for $C_{10}H_{10}N_4O_4$: C, 48.00; H, 4.00; N, 22.40%.

Hydrolyses of VII, VIII, X, and XI. Five mmol of acyl-triazole (VII, VIII, X, or XI) were heated in 100 m*l* of water under reflux for 1 hr. On cooling, the hydrolyzed product (III or IX) was separated as pale yellow needles; the needles were filtered, washed with a small amount of cold water, and then dried. The yield were almost quantitative. Recrystallization was achieved from water when the purity was unsatisfactory. IX; pale yellow needles; mp 179—181°C.

Found: C, 46.45; H, 3.80; N, 26.67%. Calcd for $C_8H_8N_4O_3$ (IX): C, 46.15; H, 3.85; N, 26.95%.

Reaction of VIII or X with Acetic Anhydride. Acetic anhydride (30 m*l*) and the propionyl-triazole VIII (or X)

7) Y. Kato and I. Hirao, *Bull. Kyushu Inst. Technol.*, No. 15, 57 (1965).

(5 mmol) were heated together under reflux for 1 hr. On cooling or concentration, a crude product was obtained; it was then recrystallized from ligroin (acetone) to afford pure XI (or VII) in a 66% (69%) yield.

Reaction of VI with Acetic Anhydride in Dioxane. A mixture of VI (2.26 g, 10 mmol), acetic anhydride (10.2 g, 0.1 mol), and dioxane (50 m*l*) was heated at 100°C for 1 hr. The solvent and acid anhydride were removed *in vacuo*, and the residue was heated in ligroin (100 m*l*) under reflux. The insoluble material was filtered while hot and recrystallized from acetone to afford VII as pale yellow needles, which melted at 211—212°C and which weighed 0.4 g (17%). This was identical in its IR spectrum with an authentic sample of VII.

On the concentration of the mother filtrate, a light yellow, crystalline product was obtained. Mp 103—105°C; the yield was 1.35 g.

Found: C, 48.34; H, 3.71; N, 22.73%. Calcd for $C_{10}H_{10}N_4O_4$ (X and XI): C, 48.00; H, 4.00; N, 22.40%.

Recrystallization from ligroin raised the melting point to 112—114°C, but the value of the elemental analysis was unchanged. This product was identified as a mixture of X and XI by a study of its IR and NMR spectra. However, the resolution of X and XI could not be achieved by solvents or solvent pairs. The compound ratio (X: XI) was determined to be 39: 61 on the basis of the NMR intensity ratio of the methyl and acetyl proton (in CCl_3COOH).

Reaction of V with Propionic Anhydride. A mixture of V (2.12 g, 10 mmol) and propionic anhydride (20 m*l*) was heated under reflux for 1 hr. A work-up as above afforded 0.65 g of pale yellow crystals (mp 108—110°C) as the first precipitate from the ligroin solution.

Found: C, 48.36; H, 4.12; N, 22.41%. Calcd for $C_{10}H_{10}N_4O_4$ (X and XI): C, 48.00; H, 4.00; N, 22.40%.

This substance was confirmed to be a mixture of X and XI on the basis of its IR and NMR spectra. The compound ratio was determined to be X: XI=8: 5 by the NMR method, using trichloroacetic acid as the solvent.

The ligroin filtrate was concentrated *in vacuo*, and the residue was crystallized from petroleum ether to give 0.53 g (20%) of VIII as pale yellow granules; mp 79—80°C. The melting point of this compound was not depressed upon admixture with an authentic sample of VIII.

The authors are indebted to Mr. T. Hayakawa and Mr. T. Shiraishi for their help in the experimental work.

BULLETIN OF THE CHEMICAL SOCIETY OF JAPAN, VOL. 45, 213—215(1972)

Syntheses of 1,2-Dithiole Derivatives[1]

Akiko CHINONE, Kozo INOUYE, and Masaki OHTA

Department of Chemistry, Faculty of Science, Tokyo Institute of Technology, Ookayama, Meguro-ku, Tokyo

(Received May 21, 1971)

Sulfurization of 1,3-diarylpropanetrione (**1**) with hydrogen sulfide and hydrogen chloride afforded a mixture of 4-hydroxy-3,5-diaryl-1,2-dithiolium chlorides (**3**) and 3,5-diaryl-1,2-dithiolium chlorides (**4**). Treatment of a mixture of **3a** and **4a** with triethylamine in alcohol gave anhydro-4-hydroxy-3,5-diphenyl-1,2-dithiolium hydroxide (**5a**) and the 4-substituted product (**6**). Sulfurization of dibenzoyldibromomethane yielded 3,5-diphenyl-1,2-dithiolium bromide. Reactions of **5a** with picric acid and acetic anhydride in the presence of perchloric acid were carried out.

Sulfurization of 1,3-diphenylpropanetrione (**1a**) with hydrogen sulfide and hydrogen chloride in a mixture of chloroform and ethanol afforded a crude product, from which a mesoionic compound **5a** (anhydro-4-hydroxy-3,5-diphenyl-1,2-dithiolium hydroxide) was obtained by treatment with triethylamine.[2] Schönberg[3] reported recently that the reaction of potassium ethyl xanthogenate with 1,1,3,3-tetrabromo-1,3-diphenylacetone gave the same compound as **5a** which is regarded as a valence isomer of 1,3-diphenylpropane-1,3-dithione-2-one (**2**). In this report, we wish to describe our results on the sulfurization products in detail. Further examination of the crude sulfurization product of **1a** revealed that the product was composed of two components, **3a** and **4a**. Since the mixture was not separable by recrystallization and detection by tlc was unsuccessful, the mixture was subjected to further reaction without separation. Structures of **3a** and **4a** were confirmed as stable perchlorates **7** and **8** by treating the mixture with perchloric acid or silver perchlorate. They were identical with those reported by Schönberg[3] and Leaver.[4] Dehydrohalogenation of the mixture with triethylamine in ethanol afforded a mixture of a mesoionic compound **5a** and 3-ethoxy-3,5-diphenyl-1,2-dithiole (**6a**). The latter was prepared by the reaction of 3,5-diphenyl-1,2-dithiolium perchlorate with sodium ethoxide.[5] 3-Methoxy derivative (**6b**) was obtained when the mixture was treated with triethylamine in methanol. When the mixture was treated with pyridine in methanol, **5a** and unreacted **4a** were obtained. This result shows that **4a** is convertible to **6** only in the presence of a strong

1) Studies of mesoionic compounds. XXXVI. Part XXXV: Y. Huseya, A. Chinone, and M. Ohta, This Bulletin, **44**, 1667 (1971).
2) K. Inouye, S. Sato, and M. Ohta, *ibid.*, **43**, 1911 (1970).
3) A. Schönberg and E. Frese, *Chem. Ber.*, **103**, 3885 (1970).
4) D. Leaver and W. A. H. Robertson, *Proc. Chem. Soc.*, **1960**, 252.
5) D. Leaver, D. M. McKinnon, and W. A. H. Robertson, *J. Chem. Soc.*, **1965**, 32.

base. In a similar way, sulfurization of 1-(*p*-methoxyphenyl)-3-phenylpropanetrione (**1b**) gave two products, **3b** and **4b**. As in the case of sulfurization of **1a**, **3b**, and **4b** could not be separated by recrystallization. Treatment of the mixture of **3b** and **4b** with triethylamine in methanol gave a mesoionic compound **5b**, but the methoxy-substituted product corresponding to **6** was not isolated. The IR spectrum of **5b** was similar to that of **5a** in the region 1500—1400 cm^{-1} due to the CO group and dithiole ring. In UV spectra of **5b**, a hypsochromic shift was observed as in the case of **5a**,[3] as shown below.

UV SPECTRA OF **5b**

Solvent	λ_{max}(mμ)	log ε
Benzene	586	4.12
Pyridine	574	4.38
DMF	574	4.36
Acetonitrile	558	4.11

Sulfurization of 1-methyl-3-phenylpropanetrione did not afford the aimed product. Under the same conditions, dibenzoyldibromomethane was subjected to sulfurization to give 3,5-diphenyl-1,2-dithiolium bromide, which was converted into perchlorate **8** by treating with silver perchlorate.

The mechanism for the formation of **3** and **4** from **1** could be explained *via* a chlorohydrin intermediate and the reduction with hydrogen sulfide during the course of the reaction.

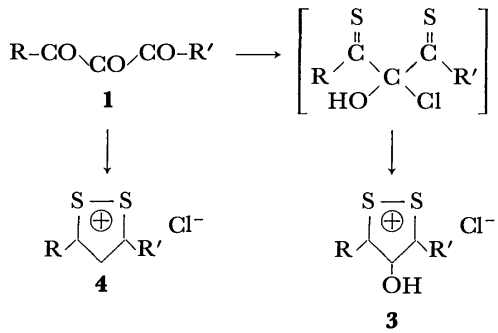

The reaction of 1,2-dithiolium salts without hydroxyl group at its 4-position has been extensively studied.[4-6] It is known that the 3- and 5-positions of 1,2-dithiole show high reactivity toward nucleophilic reagents.[5,6] Treatment of **5a** with acetic anhydride and perchloric acid yielded the *O*-acetyl derivative **9**, which showed an absorption peak at 1790cm^{-1} due to the C=O group in its IR spectrum. This is consistent with the fact that the CO bond of **5a** is highly polarized as shown in its IR spectrum, in which the CO group showed absorption peak at 1495 cm^{-1}. Methylation of **5a** with methyl iodide was not successful and resulted in the recovery of the starting material. The picrate of **5a** was obtained by treatment with picric acid. Reaction of **5a** with aniline gave a product which was recrystallized from ethanol to give dark blue needles with a mp of 168—170° C. The results of elementary analysis and molecular weight measurement (304 in DMF) indicate that the molecular formula is $C_{21}H_{15}SN$. It was assumed to be 3,4,5-triphenylisothiazole from its IR spectrum and NMR spectrum. Reaction of **5a** with dry ammonia in refluxing methanol afforded a product which was recrystallized from benzene or ligroin to give colorless needles with a mp of 102—105°C, $C_{15}H_{11}NSO$, which is most likely to be 4-hydroxy-3,5-diphenylisothiazole from its elementary analysis and spectral data. Reaction of **5a** with a dipolarophile such as dimethyl acetylenedicarboxylate, tolane or phenyl isocyanate did not give the adduct and resulted in the recovery of the starting material.

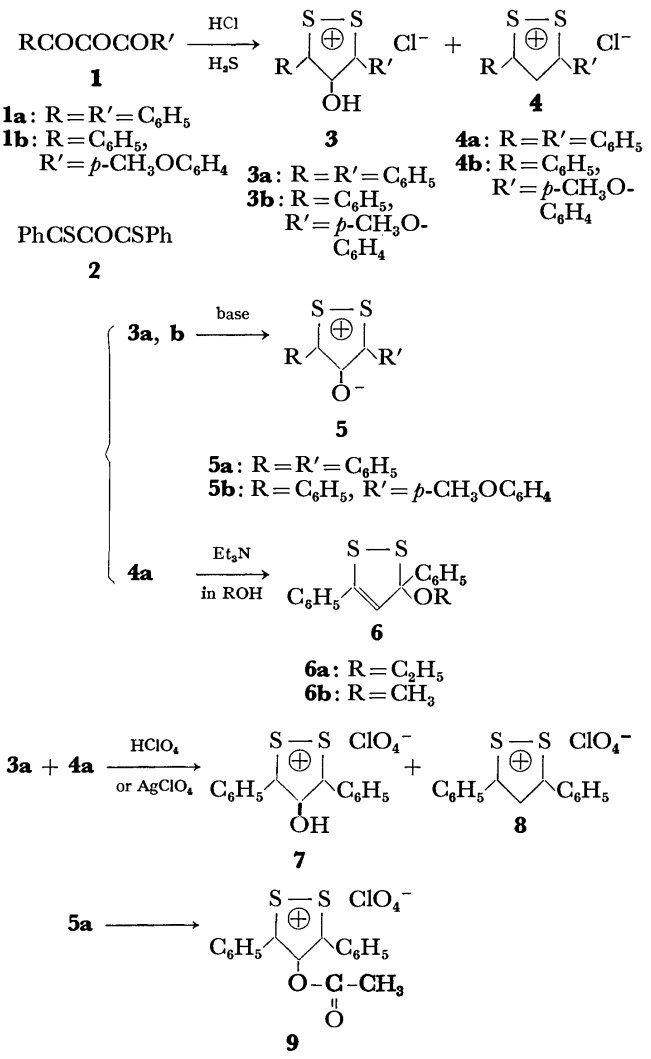

Experimental

Sulfurization of 1,3-Diphenylpropanetrione. To a solution of 100 g of 1,3-diphenylpropanetrione in 200 m*l* of chloroform, 1400 m*l* of ethanol was added. Into the solution, dry hydrogen chloride and hydrogen sulfide were bubbled for 1.5 hr under ice cooling, and then hydrogen sulfide was bubbled at room temperature for further 5.5 hr. During the course of bubbling, the color of the solution turned from yellow to reddish brown. After the solution was kept to stand for 2 days at room temperature, precipitates contaminated with sulfur were filtered off and the filtrate was concentrated *in vacuo* at 40—50°C. Ether was added to the residue to give a crude mixture of **3a** and **4a**. When the mixture was re-

6) G. Duguay and H. Quiniou, *Bull. Soc. Chim. Fr.*, **1970**, 1918.

crystallized from acetonitrile, two forms of crystal separated out, silky crystals melting at about 200°C (dec.) and needles melting at about 110°C (dec.). We could not find a suitable solvent for fractional crystallization.

Sulfurization of 1-(p-Methoxyphenyl)-3-phenylpropanetrione. Dry hydrogen chloride was bubbled into 90 m*l* of methanol under ice cooling until the volume of the methanol solution became 110 m*l*, to which a solution of 1-(*p*-methoxyphenyl)-3-phenylpropanetrione (5g) in 20 m*l* of chloroform was added. Dry hydrogen sulfide was bubbled into the solution for 3.5 hr with stirring under ice cooling. After the solution was kept to stand for 2 days at room temperature, precipitates were filtered off and the filtrate was concentrated *in vacuo* at 40—45°C. Ether was added to the residue to give a mixture of **3b** and **4b**, which partially melted at about 120°C (dec.) and 190°C (dec.), but the mixture could not be separated analytically pure by recrystallization.

Sulfurization of Dibenzoyldibromomethane. Dibenzoyldibromomethane was dissolved in 50 m*l* of chloroform, to which 300 m*l* of ethanol was added. Dry hydrogen chloride and hydrogen sulfide were bubbled into the solution for 2 hr at room temperature with stirring. After the solution was kept to stand for 2 days at room temperature, percipitates containing sulfur were filtered off and filtrate was concentrated *in vacuo* at 40—50°C. Recrystallization from ethanol afforded reddish yellow needles with a mp of 190—200°C, yield 5 g (54%). Although the value of elementary analysis was not satisfactory, the structure of this product was assigned to be 3,5-diphenyl-1,2-dithiolium bromide by treatment with silver perchlorate to give the perchlorate **8**.

Reaction of Sulfurization Products with Base. i) To a solution of a mixture (57 g) of **3a** and **4a** in 500 m*l* of ethanol, 19 g of triethylamine was added dropwise. After being stirred for 1 hr, precipitates were collected (filtrate was treated as described in ii)), washed with ether repeatedly, and recrystallized from acetic acid, DMF, or pyridine to give dark brown needles with a mp of 240—241°C (dec.), yield 21 g (41%).

Found: C, 66.48; H, 3.89; S, 23.40%. Calcd for $C_{15}H_{10}OS_2$: C, 66.67; H, 3.73; S, 23.68%.

ii) The filtrate obtained as described in i) was concentrated in a vacuum. The residue was washed with water and recrystallized from acetonitrile to give 3-ethoxy-3,5-diphenyl-1,2-dithiole, yield 15 g (29%), as pale yellow needles with a mp of 68—69°C.

iii) To a solution of a mixture (22 g) of **3a** and **4a** in methanol was added 7 g of triethylamine, and precipitates were filtered off and washed with ether, and the ether and filtrate were combined and concentrated *in vacuo*. The residue was washed with ether and recrystallized from methanol to give **6b** as yellow needles with a mp of 83—84°C, yield 9 g (42%).

Found: C, 63.52; H, 4.64; S, 21.90%. Calcd for $C_{16}H_{14}O_2S_2$: C, 63.52; H, 4.64; S, 21.20%. VU: λ_{max}^{MeOH} mμ(log ε) 227 (4.18), 345 (2.55). NMR: τ($CDCl_3$) 2.40—2.82 (m, 10H), 4.10 (s, 1H), 6.49 (s, 3H).

Reaction of 5a with Acetic anhydride in the Presence of Perchloric Acid. To a solution of 0.27 g of **5a** in acetic anhydride, 0.3 g of 70% perchloric acid was added dropwise with stirring under ice cooling. Ether was added to the reaction mixture to give orange crystals, which were recrystallized from methanol yielding **9** as orange needles with a mp of 174—176°C; yield 0.38 g (92%).

Found: C, 49.41; H, 3.41; S, 15.50%. Calcd for $C_{17}H_{13}O_6S_2Cl$: C, 49.45; H, 3.15; S, 15.52%.

Picrate of 5a. A mixture of picric acid and **5a** (0.13 g) in benzene was stirred at room temperature for 30 min. Precipitates were collected and recrystallized from methanol to give the picrate of **5a** as orange plate with a mp of 245—246°C.

Found: C, 50.73; H, 2.71; N, 8.45; S, 12.76%. Calcd for $C_{21}H_{13}N_3O_8S_2$: C, 50.50; H, 2.61; N, 8.42; S, 12.83%. IR: 3500—3200, 1560, 1440—1400, 1350 cm^{-1}.

Reaction of 5a with Aniline. After treating 0.35 g of **5a** in 30 m*l* of refluxing aniline for 3 hr, excess aniline was removed by filtration and methanol was added to the residue. Precipitates were collected and recrystallized from ethanol to give dark blue needles with a mp of 168—170°C, yield 0.36 g (88%).

Found: C, 80.78; H, 4.01; N, 4.41; S, 9.99%. Calcd for $C_{21}H_{15}SN$: C, 80.51; H, 4.79; N, 4.47; S, 10.22%.

Reaction of 5a with Ammonia. Ammonia was bubbled into a refluxing solution of **5a** (1.0 g) in 60 m*l* of methanol for 1.5 hr. After cooling, precipitates were filtered off and the filtrate was concentrated to give a crude product. Recrystallization from benzene or ligroin afforded colorless needles with a mp of 102—105°C.

Fould: C, 71.29; H, 4.57; N, 5.75; S, 12.40%. Calcd for $C_{15}H_{11}NSO$: C, 71.15; H, 4.35; N, 5.53; S, 12.65%.

Hydrogenation and Hydrogenolysis. XIV.[1] The Hydrogenation of Ethyl *p*-Tolyl Ether over Platinum Metal Catalysts[2]

Shigeo NISHIMURA, Masayoshi URAMOTO, and Tetsuo WATANABE

Department of Industrial Chemistry, Tokyo University of Agriculture and Technology, Koganei-shi, Tokyo

(Received May 28, 1971)

The hydrogenation of ethyl *p*-tolyl ether (**1**) in ethanol has been studied with five unsupported platinum metals as catalysts, mainly with the purpose of estimating the yields of ethyl 4-methyl-1-cyclohexenyl ether (**2**) formed as intermediate. Except for ruthenium catalyst, the hydrogenation of **1** in ethanol was accompanied by the formation of acetal **3**, ketone **4** and alcohol **5** which seem to be related to the formation of **2**. The amounts of **2** and the related compounds which were desorbed from the catalyst surface have been estimated to be 32—33% for Ru, 32—34% for Rh, 72—76% for Pd, 3.7% for Ir and 4.7% for Pt, by application of both kinetic and extrapolation methods. A good agreement was obtained between the results from the two methods. The proportion of hydrogenolysis increased for the catalyst metals in the order Pd$<$Ru$\ll$Rh$<$Ir$<$Pt. With platinum catalyst a noticeable amount of toluene was formed along with methylcyclohexane. The hydrogenation of ethyl 4-methyl-3-cyclohexenyl ether (**6**), one of the other intermediates of the hydrogenation of **1**, has also been studied in ethanol. Hydrogenolysis occurred extensively with palladium and rhodium catalysts, but much less with ruthenium, iridium and platinum catalysts. The hydrogenation route of **1** and its relation to hydrogenolysis and stereochemistry of hydrogenation of **1** are discussed with reference to the formation and hydrogenation of its intermediates.

The study of catalytic hydrogenation of aromatic compounds with reference to formation of their hydrogenation intermediates has been the subject of recent investigations.[3-6] The stereochemistry of hydrogenation of aromatic compounds has been discussed on the basis of the results of the hydrogenation of their intermediates.[3,4b-d] In most cases, the amount of intermediates detectable during the course of hydrogenation is rather small, which makes it difficult to estimate the real yields of the intermediates formed on the catalyst surface and to interpret the course of hydrogenation quantitatively.[3] However, in some cases, the rate of hydrogenation of intermediates is low and these might accumulate in considerable amount during the course of hydrogenation, as with phenols,[4] where the intermediate cyclohexanones are usually hydrogenated rather slowly and the estimation of the yields of the ketones can be made quantitatively.[4d,7] In other cases, the intermediates formed on the catalyst surface are transformed into the derivatives which are hydrogenated only slowly, or they may give products which differ from those resulting from the simple hydrogenation of parent aromatic compounds. Such cases are known, for example, in the hydrogenation of aniline in acetic acid over some platinum metals where considerable amounts of *N*-phenylcyclohexylamine accumulate as intermediate[5] and in the hydrogenation of benzene with platinum or rhodium catalyst in the presence of hydrogen fluoride where the formation of phenylcyclohexane became as much as 25% by weight of the hydrogenation products.[6]

We carried out the hydrogenation of ethyl *p*-tolyl ether (**1**) in ethanol over five platinum metals. The main purpose was to estimate the yields of the enol ether **2** formed as the intermediate, the hydrogenation of which was also studied in detail and reported in the preceding paper.[1] The hydrogenation of **1** in ethanol is accompanied by the formation of the acetal **3** which probably results from the addition of ethanol to the enol ether **2** formed on the catalyst surface. The extent of the acetal formation might depend on the nature of catalyst metals.[1] Since the rate of hydrogenation of the acetal is always lower than that of the enol ether, its formation may be advantageous for an estimation of the yield of the enol ether intermediate. The hydrogenation was studied at 25 or 50°C under the atmospheric pressure of hydrogen. The hydrogenation of ethyl 4-methyl-3-cyclohexenyl ether (**6**) was also studied, since **6** may be one of the other intermediates which are susceptible to desorption from the catalyst surface on hydrogenation of **1**. It is also of interest to observe the behavior of **6**, a homoallyl ether, towards hydrogenolysis.

Experimental

Materials. Ethyl *p*-tolyl ether (**1**) was prepared according to the procedure of Vogel[8] by the reaction of ethyl iodide with sodium *p*-methylphenoxide in absolute ethanol. Bp 82°C/17 mmHg.

Ethyl 4-methyl-3-cyclohexenyl ether (**6**) was prepared by the dehydration with iodine of 4-ethoxy-1-methyl-1-cyclohex-

1) Part XIII: S. Nishimura, M. Katagiri, T. Watanabe, and M. Uramoto, This Bulletin, **44**, 166 (1971).

2) Presented partly at the 25th Symposium on Catalysis, Fukuoka, October, 1969.

3) a) S. Siegel, G. V. Smith, B. Dmuchovsky, D. Dubbel, and W. Halpern, *J. Amer. Chem. Soc.*, **84**, 3136 (1962). b) F. Hartog and P. Zwietering, *J. Catal.*, **2**, 79 (1963). c) H. Yamamoto, H. Horiguchi, K. Noda, and T. Kwan, *Chem. Pharm. Bull.* (Tokyo), **15**, 752, 1129 (1967). d) A. W. Weitkamp, *Advan. Catal.*, **19**, 360 (1968). e) S. Nishimura, F. Mochizuki, and S. Kobayakawa, This Bulletin, **43**, 1919 (1970).

4) a) H. A. Smith and B. L. Stump, *J. Amer. Chem. Soc.*, **83**, 2739 (1961). b) P. N. Rylander and D. R. Steele, *Engelhard Ind. Tech. Bull.*, **3**, 125 (1965). c) F. Zymalkowsky and G. Strippel, *Arch. Pharm.*, **297**, 727 (1964). d) Y. Takagi, S. Nishimura, and K. Hirota, *J. Catal.*, **12**, 214 (1967); This Bulletin, **43**, 1846 (1970).

5) K. Ikedate, T. Suzuki, and S. Suzuki, *Nippon Kagaku Zasshi*, **88**, 972 (1967); *ibid.*, **89**, 90 (1968); K. Ikedate and S. Suzuki, *ibid.*, **90**, 92 (1969).

6) B. F. Dannels and A. F. Shepard, *J. Catal.*, **15**, 106 (1969).

7) F. Coussemant and J. C. Jungers, *Bull. Soc. Chim. Belges*, **59**, 295 (1950).

8) A. I. Vogel, *J. Chem. Soc.*, **1948**, 616.

Table 1. Hydrogenation of ethyl *p*-tolyl ether (**1**) with ruthenium catalyst in ethanol[a)]

Reac. time (hr)	Composition of reaction mixture, mol %									*cis*/*trans* ratio of **7**	Selectivity for formation of **2** and related compounds[b)] (mol %)
	1	**2**	**3**	**4**	**5**	**6**	**7**	**8**	**9**		
0.08	90.0	3.1	—	—	—	0.6	5.8	—	0.6	6.3	31.0
0.22	68.0	8.8	0.1	—	—	0.8	20.0	—	2.3	4.9	27.8
0.37	52.8	11.1	0.1	—	—	0.7	32.3	—	3.0	4.8	23.7
0.55	44.4	11.6	0.1	—	—	0.6	39.0	—	4.3	4.0	21.0
0.77	32.6	11.8	0.2	—	—	0.5	49.2	—	5.8	3.7	17.8
1.25	17.8	9.4	0.2	—	—	0.3	64.9	—	7.5	3.3	
3.78	0.0	0.0	0.2	—	—	0.0	90.2	—	9.6	2.9	

a) **1** (0.2 m*l*) was hydrogenated in 10 m*l* ethanol with 25 mg of ruthenium catalyst at 25°C under the atmospheric pressure of hydrogen.
b) Given by 100×mol (**2**+**3**+**4**+**5**)/mol (100−1).

anol which was obtained by the addition of methylmagnesium iodide to 4-ethoxycyclohexanone. Bp 170°C; n_D^{20} 1.4530. The structure of **6** was confirmed by the NMR spectrum obtained on a JNM-C-60HL spectrometer (Japan Electron Optics Laboratory, Co.) at 60 MHz: τ 4.75 (1H, m, vinyl proton), 6.52 (2H, q, $OC\underline{H}_2CH_3$), 6.30—6.75 (1H, m, C$\underline{H}$ adjacent to oxygen), 7.5—8.5 (6H, broad m, saturated ring protons other than at C-1), 8.36 (3H, s, 4-$C\underline{H}_3$), 8.82 (3H, t, $OCH_2C\underline{H}_3$).

Catalysts. Unsupported ruthenium, rhodium, palladium, iridium and platinum catalysts were prepared by the methods descibed in the preceding paper.[1)]

Solvent. The S. S. G. ethanol of the Wako Pure Chemical Industries was further dehydrated by refluxing with sodium metal and diethyl phthalate.[9)]

Hydrogenation. The substrate (0.2 m*l*) was hydrogenated as usual with 25—50 mg of the catalyst in 10 m*l* ethanol at 25 or 50°C under the atmospheric pressure of hydrogen. The catalyst was shaken with hydrogen for about 10 min before the addition of the substrate.

Analysis of Reaction Mixture. The reaction mixture was taken into a microsyringe through a silicone rubber stopper during the course of hydrogenation and subjected to gas chromatography. For most analyses a column of 10% PEG 20M on Chromosorb W (3 mm×3.75 m) was used at the temperature programmed in 2°C/min for 36—100°C and in 4°C/min for 100—160°C. Under these conditions, the peaks of unsaturated ethers **2** and **6** were not separated. Since in most cases the amount of **6** in the reaction mixture was extremely small, the peak corresponding to **2** and **6** was regarded to be that of **2**. When separation of **2** and **6** was needed, a column consisting of PEG 20M and Apiezon L was used. However, complete separation of the reaction mixture was also difficult even with this column. Accordingly, a complete analysis of the reaction mixture was carried out by superposing the two gas chromatograms obtained using the two columns described above.

Results

*Hydrogenation of **1** with Ruthenium Catalyst.* Table 1 shows the change in composition of the reaction mixture during the hydrogenation of **1** with ruthenium catalyst in ethanol at 25°C. A noteworthy feature of the ruthenium-catalyzed hydrogenation is that the enol ether **2**, formed as intermediate, is hydrogenated to saturated ether **7** with little formation of acetal **3**. This result was not unexpected as addition of ethanol to **2** occurred only very slowly during the hydrogenation of **2** with ruthenium catalyst in ethanol.[1)] In Fig. 1 the varying amounts of **2** and **3** during the course of hydrogenation are plotted *versus* the conversion of **1**. The maximum amount was 12.0% at 67.4% conversion of **1**. The amount of intermediates desorbed from the catalyst surface can be calculated by means of the following equation (deduced on the reaction scheme shown below)[10)] to be 32.6% [f=0.326 in Eq. (1)].[11)]

$$C_B = \frac{f}{K-1}(C_A - C_A^K) \qquad (1)$$

C_A: concentration of aromatic compound A when the initial concentration of A is unity.
C_B: concentration of intermediate B when the initial concentration of A is unity.
f: fraction of A that leaves the catalyst surface as B during hydrogenation.
K: a constant which depends on the relative reactivity of A and B.

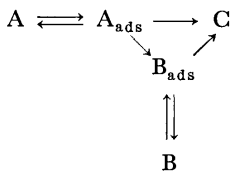

The amount can also be obtained by extrapolating the varying selectivity for formation of **2** and **3** during

9) L. F. Fieser, "Experiments in Organic Chemistry," 3rd Ed., Heath and Company, Boston (1955), p. 285.

10) Equation (1) is obtained by assuming that the hydrogenation is of first order and the function of hydrogen is the same, for A and B. For the derivation, see Ref. 7 which deals with the case where A is all transformed into C through the intermediate B and the establishment of adsorption-desorption equilibria is fast. It was shown by de Boer and van der Borg that Eq. (1) is also widely applicable to other cases [J. H. de Boer and R. J. A. M. van der Borg, *Actes Congr. Intern. Catal.*, 2e, *Paris*, 1960, p. 919 (Editions Technip, Paris, 1961)].

11) Approximate values of f and K can be obtained from the maximum concentration of B, $(C_B)_{max}$, and the corresponding concentration of A, $(C_A)_m$, using the following relations obtained by differentiating Eq. (1) with respect to C_A and putting the resulting expression equal to zero:

$$(C_A)_m = K^{1/1-K};\ (C_B)_{max} = f \times K^{K/1-K}$$

The values of f and K thus obtained were corrected graphically to represent the experimental results better throughout the course of hydrogenation.

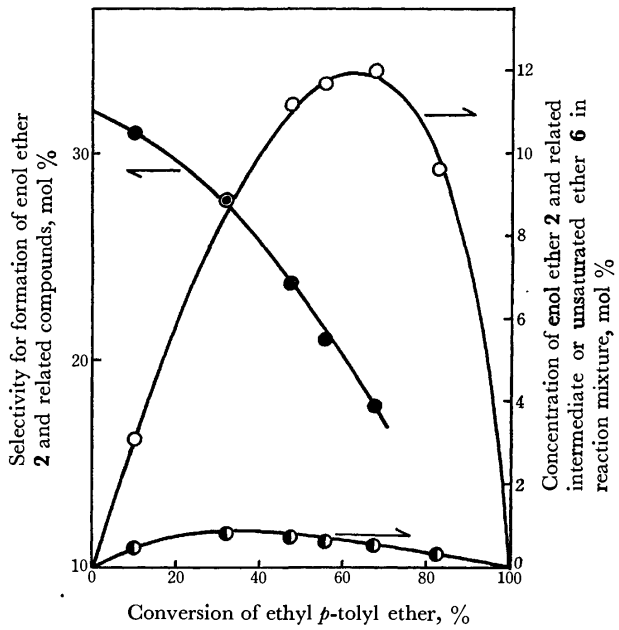

Fig. 1. Hydrogenation of ethyl *p*-tolyl ether with ruthenium catalyst in ethanol at 25°C and the atmospheric pressure of hydrogen.
● : Selectivity for formation of enol ether **2** and related compound (see Table 1).
○ : Concentration of enol ether **2** and related intermediate in the reaction mixture. The full line shows the theoretical curve given by Eq. (1) when $K=1.0$ and $f=0.326$.
◐ : Concentration of unsaturated ether **6** in reaction mixture. The full line shows the theoretical curve given by Eq. (1) when $K=5.0$ and $f=0.060$.

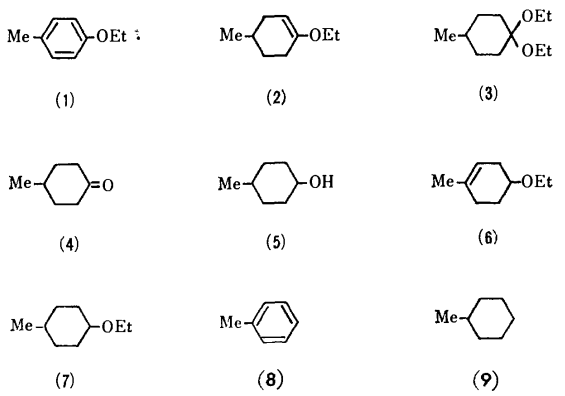

hydrogenation to the initiation, as also shown in Fig. 1. By this method we obtain a 32% yield of **2** and **3** which is in excellent accord with the value obtained above by the kinetic method. Detectable amounts of the intermediate **6** were very small, the maximum amount being only 0.8% in 32% conversion of **1** (see Fig. 1). Application of Eq. (1) to the change in the amount of **6** during hydrogenation gives the amount of **6** which leaves the catalyst surface to be 6%. The *cis/trans* ratio of saturated ether **7** formed decreases during the course of hydrogenation from 6.3 at an initial stage to 2.9 at an almost complete hydrogenation. The degree of hydrogenolysis is rather small with ruthenium catalyst (9.6%), but somewhat greater than that with palladium catalyst.

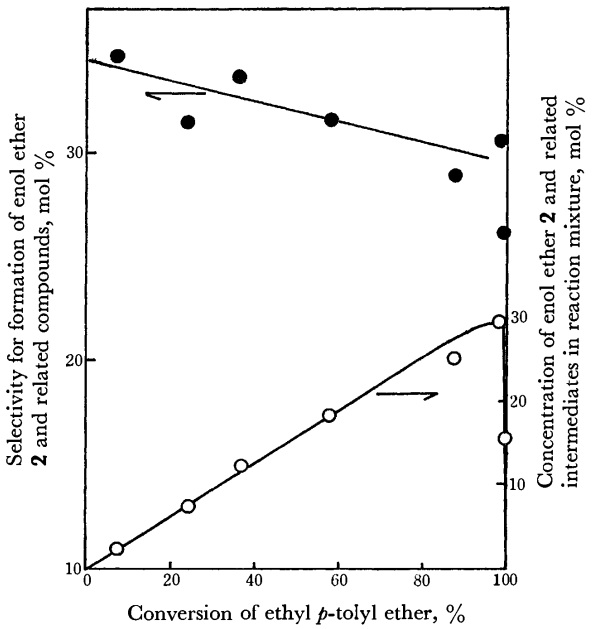

Fig. 2. Hydrogenation of ethyl *p*-tolyl ether with rhodium catalyst in ethanol at 25°C and the atmospheric pressure of hydrogen.
● : Selectivity for formation of enol ether **2** and related compounds (see footnote b in Table 1).
○ : Concentration of enol ether and related intermediates in reaction mixture. The full line shows the theoretical curve given by Eq. (1) when $K=0.02$ and $f=0.32$.

Table 2. Hydrogenation of ethyl *p*-tolyl ether(**1**) with rhodium catalyst in ethanol[a)]

Reac. time (hr)	Composition of reaction mixture, mol %[b)]									*cis/trans* ratio of **7**	Selectivity for formation of **2** and related compounds[c)] (mol %)
	1	**2**	**3**	**4**	**5**	**6**	**7**	**8**	**9**		
0.12	92.5	0.9	1.4	0.3	—	—	1.5	—	3.4	21.0	34.7
0.28	75.8	1.0	5.2	1.4	—	—	5.7	—	10.9	19.3	31.4
0.67	63.2	0.7	9.0	2.7	—	—	9.2	—	15.2	14.9	33.7
1.2	41.9	1.2	13.0	4.0	0.1	—	13.6	—	26.2	12.8	31.5
1.5	12.2	1.6	18.0	5.5	0.3	—	20.1	—	42.3	11.8	28.9
1.9	0.7	2.1	20.8	6.7	0.8	—	24.4	—	44.5	11.3	30.6
2.5	0.0	0.5	6.0	1.6	17.8	—	26.3	—	48.0	9.8	25.9

a) **1** (0.2 m*l*) was hydrogenated in 10 m*l* ethanol with 25 mg of rhodium catalyst at 25°C under the atmospheric pressure of hydrogen.
b) The amount of **6** was very small and included in **2** because of incomplete separation on gas chromatography (see Experimental).
c) See footnote b, Table 1.

TABLE 3. HYDROGENATION OF ETHYL *p*-TOLYL ETHER(**1**) WITH PALLADIUM CATALYST IN ETHANOL[a)]

Reac. time (hr)	Composition of reaction mixture, mol %[b)]									*cis/trans* ratio of **7**	Selectivity for formation of **2** and related compounds[c)] (mol %)
	1	**2**	**3**	**4**	**5**	**6**	**7**	**8**	**9**		
0.7	95.9	0.3	1.5	1.1	0.1	—	1.0	—	0.3	8.6	73.2
1.4	90.0	0.6	3.7	2.1	0.1	—	2.7	—	0.8	7.3	65.0
2.4	82.8	0.8	4.6	3.6	0.1	—	7.1	—	1.0	11.0	52.9
3.4	78.8	0.9	4.6	4.6	0.1	—	9.4	—	1.6	9.4	48.1
5.4	64.8	1.1	4.9	6.2	0.1	—	20.6	—	2.3	11.2	34.9
6.4	59.3	1.0	5.0	6.5	0.1	—	25.4	—	2.7	11.4	27.7
7.6	54.1	1.1	4.8	6.2	0.1	—	30.8	—	2.9	12.2	
9.2	44.0	0.9	4.4	5.5	0.1	—	41.6	—	3.3	14.1	
10.9	36.2	0.6	4.1	5.2	0.1	—	50.4	—	3.4	14.2	

a) **1** (0.2 m*l*) was hydrogenated in 10 m*l* ethanol with 50 mg of palladium catalyst at 50°C under the atmospheric pressure of hydrogen.
b) See footnote b, Table 2.
c) See footnote b, Table 1.

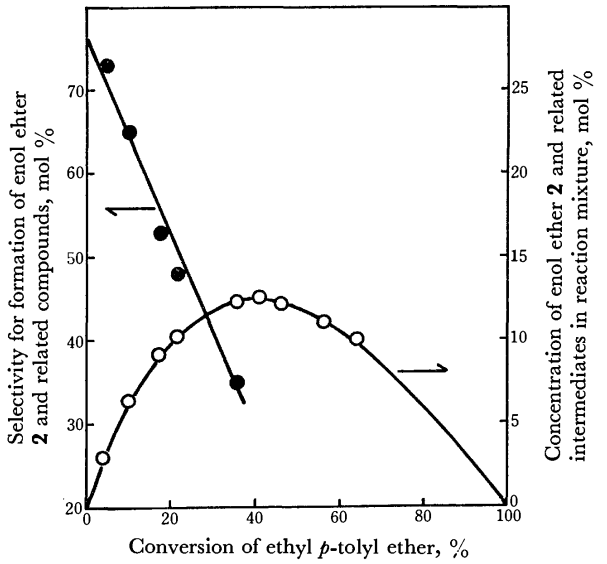

Fig. 3. Hydrogenation of ethyl *p*-tolyl ether with palladium catalyst in ethanol at 50°C and the atmospheric pressure of hydrogen.
● : Selectivity for formation of enol ether and related compounds (see footnote b, Table 1).
○ : Concentration of enol ether **2** and related intermediates in reaction mixture. The full line shows the theoretical curve given by Eq. (1) when $K=3.5$ and $f=0.72$.

Hydrogenation of **1** *with Rhodium Catalyst.* Table 2 indicates the change in composition of the reaction mixture during hydrogenation of **1** with rhodium catalyst in ethanol at 25°C. It is seen that the intermediates accumulate mostly as acetal **3** along with small amounts of enol ether **2** and ketone **4**. The ketone **4** probably is the product of the hydrolysis of **2** or **3** during hydrogenation, in spite of the fact that carefully dehydrated solvent was used. It is noteworthy that **2**, **3**, and **4** formed are scarcely hydrogenated during the hydrogenation of **1** and their sum increases almost linearly with the conversion of **1** (Fig. 2). By assuming that **3** and **4** were all formed through **2** which was produced on the catalyst surface, the amount of **2** which left the catalyst surface as itself or its derivatives can be calculated to be 32% by means of Eq. (1) (Fig. 2). Application of the extrapolation method gives a 34% yield of **2** and related compounds, as also shown in Fig. 2. When the amount of unreacted **1** approaches almost zero, hydrogenation of the accumulated intermediates seems to begin and the main product is the alcohol **5**, as indicated by a definite increase of **5** over saturated ether **7** and methylcyclohexane (Table 2).[12] The *cis/trans* ratio of **7** formed is very high at the initial stage, but decreases to about 10 towards the end of hydrogenation. Hydrogenolysis occurs rather extensively with rhodium catalyst (about 45% at 58.1% conversion of **1**) and constitutes the most important hydrogenation pathway of **1**.

Hydrogenation of **1** *with Palladium Catalyst.* **1** was hydrogenated at 50°C in ethanol, the results being shown in Table 3. The main intermediates are acetal **3** and ketone **4** and they are hydrogenated further to give ether **7** as the major product. Change in the sum of **2**, **3**, and **4** during hydrogenation is shown in Fig. 3. The amount of **2** and the related intermediates which left the catalyst surface was estimated to be 72% by the kinetic method. The value of 76% was obtained for that amount by the extrapolation method (Fig. 3). Alcohol **5** was formed only slightly with palladium catalyst although the ketone was produced in considerable amount during the course of hydrogenation. This might be due to the fact that with palladium catalyst in ethanol ketone **3** is hydrogenated mostly to give **7**, rather than alcohol **5**.[13] The *cis/trans* ratio of ether **7** formed is about 8 at initial stages of hydrogenation and then increases gradually to about 14 towards later stages. It is to be noted that the yield of *cis*-ether is the greatest with palladium catalyst among the platinum metals investigated. Another noteworthy feature of the palladium-catalyzed hydrogenation is that hydrogenolysis occurred only to the extent of 5.3% which is smaller than any of those obtained by the other platinum metals.

12) The alcohol was also the main product of hydrogenation of acetal **3** with rhodium catalyst in ethanol.[1)]
13) S. Nishimura, T. Itaya, and M. Shiota, *Chem. Commun.*, **1967**, 422.

TABLE 4. HYDROGENATION OF ETHYL *p*-TOLYL ETHER(**1**) WITH IRIDIUM CATALYST IN ETHANOL[a)]

Reac. time (hr)	Composition of reaction mixture, mol %[b)]									*cis*/*trans* ratio of **7**	Selectivity for formation of **2** and related compounds (mol %)[c)]
	1	**2**	**3**	**4**	**5**	**6**	**7**	**8**	**9**		
0.2	90.9	0.1	0.1	—	0.1	—	3.8	—	5.0	10.1	3.3
1.2	74.6	0.1	0.4	—	0.1	—	10.9	0.7	13.3	7.9	2.4
2.1	64.6	0.1	0.4	—	0.2	—	13.9	1.1	19.7	8.0	2.5
4.7	52.5	—	0.4	—	0.4	—	20.8	0.7	25.3	7.6	1.7
8.3	45.9	—	0.2	—	0.6	—	21.4	0.7	31.3	6.4	1.5

a) **1** (0.2 m*l*) was hydrogenated in 10 m*l* ethanol with 50 mg of iridium catalyst at 50°C under the atmospheric pressure of hydrogen.
b) See footnote b, Table 2.
c) See footnote b, Table 1.

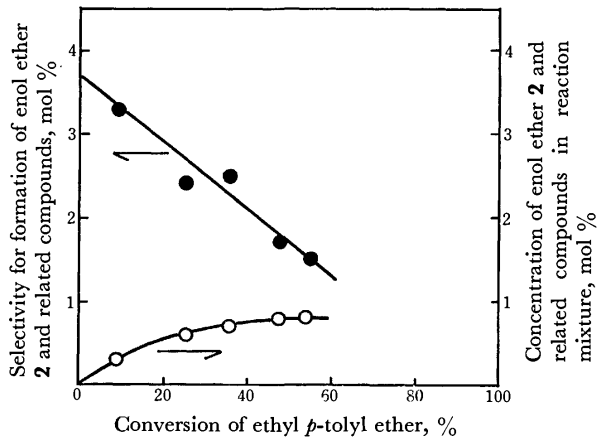

Fig. 4. Hydrogenation of ethyl *p*-tolyl ether with iridium catalyst in ethanol at 50°C and the atmospheric pressure of hydrogen.
● : Selectivity for formation of enol ether **2** and related compounds (see footnote b, Table 1).
○ : Concentration of enol ether **2** and related compounds in the reaction mixture.

Hydrogenation of ***1*** *with Iridium Catalyst.* Table 4 shows the results of the hydrogenation of **1** in ethanol at 50°C with iridium as a catalyst. The iridium-catalyzed hydrogenation is characteristic in that the detectable amount of **2**, **3**, **4**, and **5** is extremely small, their sum being less than 1% at maximum. The amount of **2** and related compounds was estimated to be 3.7% by the extrapolation method as shown in Fig. 4. The *cis*/*trans* ratio of **7** formed decreases slightly during hydrogenation from about 10 to 6.4. Hydrogenolysis occurred more extensively than with rhodium (59% at 54.1% conversion of **1**) and a small amount of toluene (1.1% at 35.4% conversion of **1**) was formed along with methylcyclohexane.

Hydrogenation of ***1*** *with Platinum Catalyst.* The results of the hydrogenation of **1** in ethanol at 50°C

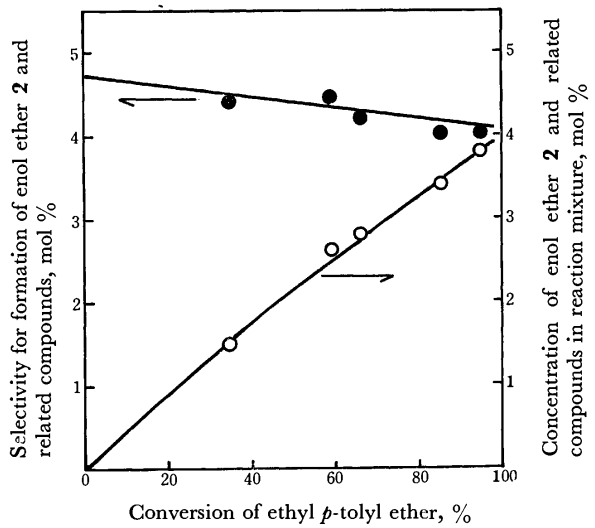

Fig. 5. Hydrogenation of ethyl *p*-tolyl ether with platinum catalyst in ethanol at 50°C and the atmospheric pressure of hydrogen.
● : Selectivity for formation of enol ether **2** and related compounds (see footnote b, Table 1).
○ : Concentration of enol ether **2** and related compounds in the reaction mixture.

TABLE 5. HYDROGENATION OF ETHYL *p*-TOLYL ETHER(**1**) WITH PLATINUM CATALYST IN ETHANOL[a)]

Reac. time (hr)	Composition of reaction mixture, mol %[b)]									*cis*/*trans* ratio of **7**	Selectivity for formation of **2** and related compounds[c)] (mol %)
	1	**2**	**3**	**4**	**5**	**6**	**7**	**8**	**9**		
1.9	65.7	0.1	1.2	0.2	—	—	11.7	2.9	18.1	8.5	4.4
3.5	41.2	0.2	2.0	0.4	—	—	20.0	3.7	32.5	8.5	4.4
4.5	33.8	0.2	2.3	0.3	—	—	23.5	3.8	36.0	8.8	4.2
7.3	14.7	0.1	3.0	0.3	—	—	27.9	2.7	51.3	8.9	4.0
10.3	5.2	0.1	3.5	0.2	—	—	31.1	1.8	58.2	9.9	4.0

a) **1** (0.2 m*l*) was hydrogenated in 10 m*l* ethanol with 30 mg of platinum catalyst at 50°C under the atmospheric pressure of hydrogen.
b) See footnote b, Table 2.
c) See footnote b, Table 1.

Table 6. Hydrogenation of ethyl 4-methyl-3-cyclohexenyl ether (**6**) with platinum metal catalysts[a]

Catalyst	Amount (mg)	Reac. time (hr)	Reac. temp. (°C)	Composition of reac. mixture, mol %				*cis*/*trans* ratio of **7**	Proportion of hydrogenolysis[b] (mol %)
				6	**7**	**8**	**9**		
Ruthenium	25	1.0	25	0.0	97.0	—	3.0	3.0	3.0
Rhodium	25	1.0	25	0.0	76.4	—	23.6	4.0	23.6
Palladium	30	1.9	50	27.3	27.2	4.0	41.5	2.0	62.6
Iridium	25	1.7	50	0.0	96.1	0.2	3.7	4.4	3.9
Platinum	10	1.0	50	0.0	93.0	0.6	6.5	5.2	7.1

a) **6** (0.2 m*l*) was hydrogenated in 10 m*l* ethanol under the atmospheric pressure of hydrogen.
b) Given by mol 100 × mol(**8**+**9**)/mol(**7**+**8**+**9**)

are given in Table 5. The formation of acetal **3** and related compounds is small, although they are hydrogenated only with difficulty and increases almost linearly with hydrogenation. The amount of **2** and the related compounds was estimated to be 4.7% by the extrapolation method as shown in Fig. 5. The *cis*/*trans* ratio of ether **7** formed was 9.9 near the end of hydrogenation and it did not vary much during hydrogenation. It is noticeable that of the platinum metals investigated hydrogenolysis occurred to the greatest extent with platinum (about 63%). The platinum-catalyzed hydrogenation is also characteristic in that a noticeable amount of toluene is formed along with methylcyclohexane (about 4% at 72.5% conversion) and the toluene formed is hydrogenated rather slowly in the presence of **1**.[14] By applying Eq. (1) to the change in the amount of toluene during hydrogenation, the amount which left the surface was estimated to be 9.5% [f=0.095, K=0.9 in Eq. (1)].

Hydrogenation of **6** *with Platinum Metal Catalysts.* Table 6 summarizes the results of the hydrogenation of **6** in ethanol with the five platinum metals as catalysts. It is seen that hydrogenolysis occurs rather extensively with palladium and rhodium catalysts, but not so with ruthenium, iridium and platinum catalysts. In general, the *cis*-ether is formed in larger amounts than the *trans*-ether.[15]

Discussion

It is seen that the results of estimation of enol ether **2** and related compounds by the kinetic and extrapolation methods were in good agreement. Thus the amount of enol ether and related compounds which leaves the catalyst surface during hydrogenation has been estimated to be 32—33% for ruthenium, 32—34% for rhodium, 72—76% for palladium, 3.7% for iridium and 4.7% for platinum. If we assume that acetal, ketone and alcohol are all formed through enol ether **2**, the values obtained above are considered to show the amount of **2** which left the catalyst surface. Since it is not certain whether these values indicate the real yields of the enol ether intermediate formed on the catalyst surface, they might be considered to be the minimum values of the amount of the intermediate formed in hydrogenation of **1**.[17]

Table 7. Amount of enol ether or ketone intermediate which leaves the catalyst surface during the course of hydrogenation of ethyl *p*-tolyl ether or *p*-cresol

Catalyst	Amount of the intermediate, mol %	
	Enol ether in hydrogenation of ethyl *p*-tolyl ether	Ketone in hydrogenation of *p*-cresol[a]
Ru	33,[b] 32[c]	60[b]
Rh	32,[b] 34[c]	54[b]
Pd	72,[b] 76[c]	100[b]
Ir	— 3.7[c]	20[b]
Pt	— 4.7[c]	—[d]

a) Data from Ref. 4d and Y. Takagi, *Sci. Pap. Inst. Phys. Chem. Res.* (Tokyo), **64**, 39 (1970).
b) Estimated by kinetic method.
c) Estimated by extrapolation method.
d) Not estimated accurately. The maximum amount of ketone detected was only 2—2.5%.

When the present results are compared with those obtained previously on the ketone intermediate formed in hydrogenation of *p*-cresol (Table 7), it is obvious that there exists a common tendency in the selectivity of the catalyst metals for the formation of the intermediates, although the yield of enol ether is always smaller than that of ketone over the same metal. Thus, the palladium-catalyzed hydrogenation of **1** proceeds to a greater part through enol ether as intermediate, and *p*-cresol is hydrogenated quantitatively *via* the ketone intermediate over the same metal. Ruthenium and rhodium catalysts are very similar in the way they give nearly the same yield of enol ether or ketone in hydrogenation of **1** or *p*-cresol. Both iridium and platinum catalysts are characteristic in that detectable amounts of the intermediates are small in hydrogenation.

The extent of hydrogenolysis also depends on the nature of the catalyst metals and increases in the order

14) Formation of toluene in as much as 21% was observed in hydrogenation of ethyl *m*-tolyl ether with platinum catalyst under the same conditions as for the hydrogenation of **1** (the results presented at the 23rd Annual Meeting of the Chemical Society of Japan, Tokyo, April, 1970).

15) It should be noted that 1,4-dimethylcyclohexene is reported to give the product of much smaller *cis*/*trans* ratios (1.56, 0.39, 1.33 for Rh, Pd, Pt catalysts, respectively, in acetic acid at 25°C and 1 atm).[16]

16) A. S. Hussey, T. A. Schenach, and R. H. Baker, *J. Org. Chem.*, **33**, 3258 (1968).

17) Acetal formation is adventageous for the estimation of enol ether formed on the catalyst surface. As an example, the largest amount of enol ether **2** during hydrogenation was only 1.2% at 35.4% conversion on hydrogenation of **1** with rhodium catalyst in *t*-butyl alcohol in which an acetal is not formed.

Pd<Ru≪Rh<Ir<Pt. The very small amount of hydrogenolysis observed with palladium catalyst suggests that the yields of the allyl and homoallyl ether intermediates are also small, because these ethers are expected to be susceptible to extensive hydrogenolysis in further hydrogenation when produced on the catalyst surface (Table 6). This is in line with the fact that the enol ether intermediate is formed in a large yield, since enol ether is known to be hydrogenolyzed only to a slight extent with palladium catalyst.[1] The hydrogenation of **1** over palladium catalyst is fairly stereospecific, the *cis*-ether being formed in a selectivity of 93%. This result may also be related to the production of enol ether or acetal in large yield since they are known to give the saturated ether of a high *cis*/*trans* ratio.[1,18] Thus, it is suggested that the predominant hydrogenation route of ethyl *p*-tolyl ether over palladium catalyst will be the one shown in Scheme 1. The selective hydrogenation of the dihydro intermediate **10** to the enol ether **2** can be expected from similar examples.[19]

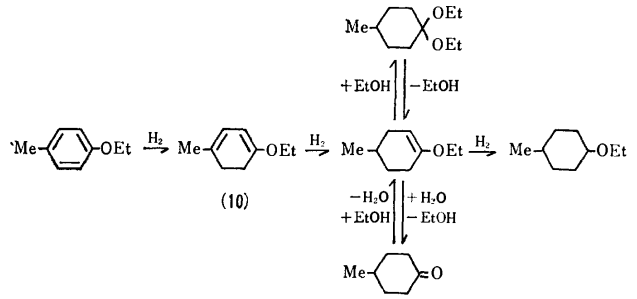

Scheme 1. Hydrogenation pathway of ethyl *p*-tolyl ether with palladium catalyst in ethanol.

It is of interest that the selectivity of ruthenium and rhodium catalysts for the formation of the enol ether intermediate is similar, and its estimated yield is very close to the value 33.3% based on the assumption that all tetrahydro derivatives of **1** are formed in equal probability. This assumption was proposed by Siegel and his coworkers[3a] for an explanation of the results of stereochemistry of the hydrogenation of isomeric xylenes with platinum catalyst. If the other two tetrahydro intermediates, the allyl and homoallyl ethers (**11** and **6**), are also produced equally in 33.3% yield according to the above assumption and the allyl ether is assumed to be hydrogenolyzed completely over rhodium catalyst, we can calculate the amount of hydrogenolysis which will occur in hydrogenation of **1**, using the value in Table 6 for the homoallyl ether. Thus the proportion of hydrogenolysis over rhodium catalyst may be evaluated to be 41.2% as shown in Scheme 2. It is seen that the value obtained experimentally (45%) is fairly close to the calculated one. Over ruthenium

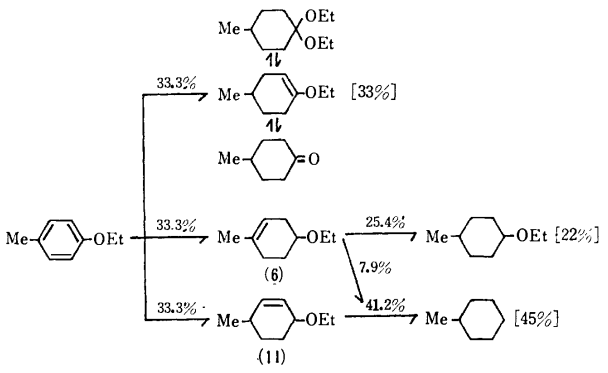

Scheme 2. Hydrogenation pathways of ethyl *p*-tolyl ether over rhodium catalyst in ethanol: figures in parentheses indicate the observed composition of the reaction mixture.

catalyst, the hydrogenation pathways leading to the tetrahydro derivatives may be similar to those given in Scheme 2. The small amount of hydrogenolysis over this catalyst will probably be due to its poor activity towards the hydrogenolysis of the allyl and homoallyl ethers.

The large extent of hydrogenolysis taking place with iridium and platinum catalysts must result from the formation of the allyl and enol ether intermediates, because the homoallyl ether **6** is hydrogenolyzed only to a small extent over these metals (see Table 6). With platinum the hydrogenolysis of **1** to give toluene is also responsible for the extensive hydrogenolysis. It was shown that enol ether **2** is extensively hydrogenolyzed with platinum catalyst in ethanol.[1] Since **1** is also considered to be an enol type ether, this type of hydrogenolysis is also expected to occur according to the mechanism suggested for the hydrogenolysis of **2** as shown in Scheme 3.[1] On the other hand, the saturated ether **7** formed with platinum catalyst on hydrogenation of **1** may be supposed to be formed mostly through the homoallyl ether intermediate.

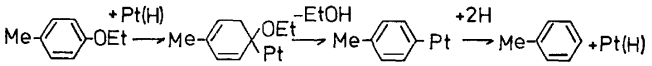

Scheme 3. Hydrogenolysis of ethyl *p*-tolyl ether with platinum catalyst.

With respect to the stereochemistry of hydrogenation of **1**, the fairly high stereospecificity of palladium catalyst has been discussed. Among the other platinum metals, rhodium and platinum catalysts also give the saturated ether of rather high *cis*/*trans* ratio, as compared with the hydrogenation of *p*-xylene.[20] This is probably due to the fact that homoallyl ether **6** gives the saturated *cis* isomer in much greater yield than does 1,4-dimethylcyclohexene in the hydrogenation with these catalysts.[21] A lower yield of saturated *cis*-ether with ruthenium catalyst can also be explained in relation to the stereochemistry of hydrogenation of the intermediate unsaturated ethers, since both **2** and **6** give a saturated ether of rather small *cis*/*trans* ratio (1.45 for **2** and 3.0 for **6**).

18) Hydrogenation of ethyl *m*-tolyl ether in ethanol with palladium catalyst gives *trans*-ether predominantly. Similarly, 3-methylcyclohexanone diethyl acetal as well as the enol ethers derived from it also give the *trans*-ether predominantly under the same conditions (the results partly presented at the 23rd Annual Meeting of the Chemical Society of Japan, Tokyo, April, 1970).

19) a) J. M. Bell, R. Garrett, V. A. Jones, and D. G. Kubler, *J. Org. Chem.*, **32**, 1307 (1967). b) W. S. Johnson, *J. Amer. Chem. Soc.*, **78**, 6278 (1956).

20) Hydrogenation of *p*-xylene with rhodium and platinum catalysts in isopropyl alcohol at 25°C under 1 atm gave the product of *cis*/*trans* ratio 2.4 and 2.3, respectively (unpublished results). *Cf.* also Ref. 3a.

21) See Ref. 15 and Table 6.

Phytosterols and Triterpenes in the Roots of the "Kidney Bean" (*Phaseolus vulgaris* L.)[1]

Nobukatsu KATSUI, Hajime MATSUE, Tomohiko HIRATA, and Tadashi MASAMUNE
Department of Chemistry, Faculty of Science, Hokkaido University, Sapporo

(Received May 20, 1971)

In connection with the studies of hatching substances for soybean cyst nematodes, the neutral fraction of the roots of the "kidney bean" (*Phaseolus vulgaris* L.) has been examined. It was found that phytosterols and triterpenes exist in the roots of plants.

Recently the hatching of eggs and larval emergence from the soybean cyst nematode (*Heterodera glycines*) has been found to be stimulated by root diffusates of several host plants.[2] Among the host plants, soybean (*Glycine Max* Merrill) has been studied extensively and reported to contain γ-sitoserol (clionasterol), stigmasterol, and soyasapogenols-A~E[3,4] as its neutral components. On the other hand, root diffusates of the "kidney bean" (*Phaseolus vulgaris* L.) are known to be more active for the hatching,[2] but no paper on the components of this plant seems to have been published. Accordingly, in connection with studies on the relevant hatching substances, we have examined the neutral fraction of the "kidney bean".

The dried powdered roots of the "kidney bean" were percolated with water and then extracted with methanol, after removal of the aqueous solution which was active for the hatching. The methanol extracts were subjected to column and thin layer chromatography as well as fractional recrystallization to isolate and identify triterpenes and phytosterols. The results deserve some comment.

(1) Compound II, $C_{32}H_{48}O_5$, was presumed to be a 21-dehydro derivative of I on the basis of mass, IR, and NMR spectra. In fact, compound I was transformed *via* its acetonide to 21-dehydrosoyasapogenol-B,

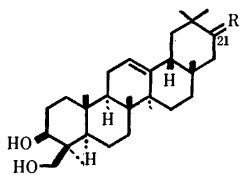

I R=-----OH, -H
II R=O

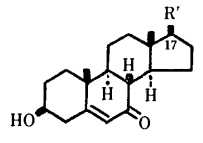

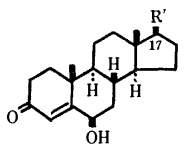

IV R′=R¹
V R′=R²

VI R =R¹
VII R′=R²

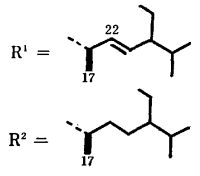

Table 1. Triterpenes and phytosterols[a] in the roots of the "kidney bean"

	Compound	Mp (°C)	Yield (%)	$[\alpha]_D$	Ref.
I	Soyasapogenol-B[b]	259—261	0.005	+89°	3
II	Soyasapogenol-E	249—250	0.0013	+34°	4
III	Stigmast-5-en-3β-ol (β-sitosterol)	141—142	0.003		
IV	Stigmasta-5,22-dien-3β-ol-7-one	160—162[c]	0.00024	−78°	5, 6a
V	Stigmast-5-en-3β-ol-7-one	128—130[c]	0.00012	−85°	7
VI	Stigmasta-4,22-dien-6β-ol-3-one	210—212[d]	0.00014	+ 8°	
VII	Stigmast-4-en-6β-ol-3-one	211—213[d]	0.00014	+29°	

a) For nomenclature, see, *J. Org. Chem.*, **34**, 1517 (1969).
b) The authors are indebted to Professors C. Djerassi and O. Jeger for their kind donation of the sample.
c) These compounds have been obtained by synthesis (Ref. 5—7), but do not appear to have been isolated from natural sources.
d) New compounds.

1) Part I of Constituents from the "Kindney Bean."
2) M. Tsutsumi and K. Sakurai, *Rev. Plant Protec. Rec.*, **2**, 128 (1962).
3) a) E. Ochiai, K. Tsuda, and S. Kitagawa, *Ber.*, **70**, 2083 (1936). b) A. Meyer, O. Jeger, and L. Ruzicka, *Helv. Chim. Acta*, **33**, 672, 687, 1835 (1950). c) H. G. Smith and F. S. Spring, *Tetrahedron*, **4**, 111 (1958).
4) D. Willner, B. Gestetner, D. Lavie, Y. Birk, and A. Bondi, *J. Chem. Soc.*, **1964**, 5884.
5) O. Linsert, *Z. Phys. Chem.*, **241**, 125 (1936).
6) It is known that steroids with Δ^5-3-ol structure are partially oxidized by passing oxygen into the colloidal suspension to give those with Δ^5-3,7-diol and/or Δ^5-3-ol-7-one. However, no examples of the formation of steroids with Δ^4-6β-ol-3-one structure under the conditions have been reported. *Cf.* a) S. Bergstrom and O. Wintersteiner, *J. Biol. Chem.*, **141**, 597 (1941); b) S. Bergstrom, *ibid.*, **145**, 327 (1942).
7) W. Wunderlich, *Z. Phys. Chem.*, **241**, 116 (1936).

mp 247—248°C and $[\alpha]_D+32°$, which was identical with II. As a compound corresponding to the above structure, Willner *et al.*[4] obtained a triterpene, soyasapogenol-E, from soybean. While their compound is amorphous and its crystalline derivatives, acetonide and diacetate, differ slightly from ours in physical constants, we consider that II should be assigned soyasapogenol-E.

(2) Occurrence of phytosterols IV, V, VI, and VII is a noticeable fact in the sense that these compounds appear to have been isolated newly from natural source. The latter two compounds, hitherto unknown, involve 6β-hydroxy-Δ^4-3-ketone structure, and the former two contain a ketonic group at C_7.[8] In view of the fact that no detectable amount of stigmast-5-en-3β-ol (VIII, stigmasterol) could be found, it would be certain that these four sterols, at least IV and VI, are not artifacts formed by air oxidation[6] or microbiological oxidation[9] during the course of isolation.

Experimental

The melting points are uncorrected. The optical rotations, UV and IR spectra were measured in chloroform, 99% ethanol, and Nujol, respectively, unless otherwise stated. The NMR spectra were recorded at 60 and/or 100 MHz in deuterochloroform, TMS being used as an internal standard, unless otherwise stated. The abbreviations "s, d, t, q, br, and m" in the NMR spectra denote "singlet, doublet, triplet, quartet, broad, and multiplet," respectively. Thin layer chromatography (tlc) was carried out on silica gel (Merck G), using benzene-ether 5: 1 (solvent A) or chloroform-ether 1: 1 (B). Column chromatography was carried out over silica gel (Mallinckrodt A.R. 100 mesh).

Extraction of Roots of the "Kidney Bean" (Phaseolus vulugaris L.). The dried, powdered roots (22 kg) were percolated with water (3×100 *l*) and, after removal of the aqueous solution, extracted with methanol (2×125 *l*). The extracts were concentrated to about 20 *l in vacuo* and extracted continuously with chloroform to give resinous material (124 g), which was treated with *n*-hexane. The hexane-insoluble materials (97 g) were redissolved in chloroform and washed with 2N sodium hydroxide solution and then 1N hydrochloric acid. The neutral substances (16 g) thus obtained were chromatographed over a mixture of silica gel (250 g) and celite (100 g), using *n*-hexane, benzene, chloroform, and ether, successively. Elution with benzene gave an oily, complex mixture (3.3 g, probably esters), which was not examined further. Elution with chloroform afforded phytosterols (2.2 g) and a mixture of ketones (4.4 g), and that with ether crude soyasapogenol-B (4.3 g).

β-Sitosterol (III). The phytosterol mixture was crystallized from methanol to give crude β-sitosterol (0.90 g), mp 126—130°C, which on recrystallization from methanol afforded III (0.54 g), colorless plates, mp 141—142°C in pure state.

The mother liquors were treated with bromine to check the presence of stigmasterol (VIII), but no crystalline substance corresponding to its tetrabromide[10] was obtained.

Soyasapogenol-B (I). The crude soyasapogenol-B was recrystallized repeatedly from methanol to give I (1.1 g), mp 253—254°C, in pure state, which gave green color by the Lieberman-Burchards test. This was recrystallized from methanol to yield an analytical sample (0.99 g), mp 259—261°C and $[\alpha]_D+89°$ (*cf.* Ref. 3c); mass, *m/e* 458 (M^+), 234 (base peak, IX), 224 (X), and 219 (IX−Me);[11] IR, ν_{max} 3300, 1388, 1379, and 845 cm^{-1}; NMR (deuteropyridine), δ 0.99, 1.08, and 1.23 (each 3H, s), 1.28 (6H, s), 1.56 (3H, s), and 3.73 (3H, br m). This compound was identical (mixed mp, tlc, mass, IR, and NMR spectra) with authentic specimens donated by Professors C. Djerassi[12] and O. Jeger.[3b]

Found: C, 78.36; H, 10.94%. Calcd for $C_{30}H_{50}O_3$: C, 78.55; H, 10.99%.

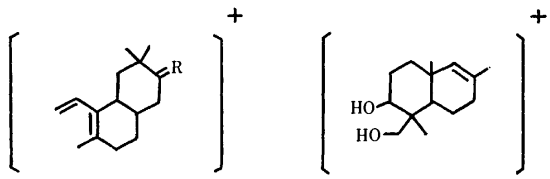

IX R=OH, H
XI R=O

X

Compound I (51 mg) was acetylated with acetic anhydride (1 m*l*) and pyridine (1 m*l*) at room temperature for 24 hr to give the triacetate (Ia, 55 mg), colorless prisms, mp 176—177°C from methanol and $[\alpha]_D+80°$ (*cf.* Ref. 3c); mass, *m/e* 584 (M^+), 276 and 261; IR, ν_{max} 1724 cm^{-1}; NMR, δ 0.83 and 0.91 (each 3H, s), 1.00 (9H, s), 1.04 and 1.16 (each 3H, s), 2.03 (6H, s, OAc), 2.06 (3H, s, OAc), 4.14 and 4.38 (each 1H, ABq $J=12$ Hz, CH_2OAc), 4.62 (2H, br m, 2 CH-OAc) and 5.25 (1H, br t $J=4.5$ Hz, H at C_{12}) (*cf.* Ref. 13).

Found: C, 74.02; H, 9.40%. Calcd for $C_{36}H_{56}O_6$: C, 73.90; H, 9.65%.

Soyasapogenol-E (II). The mixture of ketones was rechromatographed over a mixture of silica gel (80 g) and celite (20 g) using chloroform as solvent, and separated into four fractions. The first fraction gave a brown-red oil (1.3 g, probably esters), which was not examined further. The second yielded a mixture of ketones (0.97 g), which was submitted to separation. The next fraction afforded crude soyasapogenol-E (1.7 g), and the last fraction was proved to contain I (0.17 g) as a main component by tlc (solvent B).

Crude soyasapogenol-E was recrystallized from methanol to give colorless needles (260 mg), mp 233—234°C, which on recrystallizations from methanol afforded an analytical sample of II (80 mg), mp 249—250°C (amorphous[4]) and $[\alpha]_D+34°$; mass,[11] *m/e* 456 (M^+) and 232 (base peak, XI); IR, ν_{max} 1705 cm^{-1}; NMR, δ 0.86, 0.89, and 0.92 (each 3H, s), 0.98 (6H, s), 1.20 and 1.23 (each 3H, s), 3.36 (2H, br CH_2-OH), 4.33 (1H, br CHOH), and 5.29 (1H, br H at C_{12}) (*cf.* Ref. 4).

Found: C, 78.93; H, 10.76%. Calcd for $C_{30}H_{48}O_3$: C, 78.89; H, 10.51%.

The second crops (70 mg), obtained from the mother liquor on recrystallizations of II, gave the diacetate (IIa, 50 mg),

8) Tremulone and antheridiol have been reported as the only natural sterols containing a ketonic group at C_7;
a) R. A. Abramovitch and R. G. Micetich, *Can. J. Chem.*, **40**, 2017 (1962); b) J. A. Edwards, J. S. Mills, J. Sundeen, and J. H. Fried, *J. Amer. Chem. Soc.*, **91**, 1248 (1969).

9) Ch. Tamm, *Angew. Chem.*, **74**, 225 (1962).

10) A. Windaus and A. Hauth, *Ber.*, **39**, 4378 (1906).

11) *Cf.*, H. Budzikiewicz, J. M. Wilson, and C. Djerassi, *J. Amer. Chem. Soc.*, **85**, 3688 (1963).

12) E. D. Walter, E. M. Bickoff, C. R. Thompson, C. H. Robinson, and C. Djerassi, *ibid.*, **77**, 4936 (1955).

13) M. Shamma, R. E. Glick, and R. O. Mumma, *J. Org. Chem.*, **27**, 4512 (1962).

mp 243—244°C and $[\alpha]_D$+21° (*cf.* Ref. 4); mass, *m/e* 540 (M^+) and 232; IR, ν_{max} 1706, 1740, and 1745 cm^{-1} (*cf.* Ref. 4); NMR, δ 0.87 (3H, s), 0.98, 0.99, and 1.01 (total 15H, each s), 1.20 (3H, s), 2.01 and 2.03 (each 3H, s, OAc), 4.16 and 4.32 (each 1H, ABq J=12 Hz, CH_2OAc), 4.52 (1H, dd J= 7.5 and 2.5 Hz, CHOAc), and 5.26 (1H, br d J= 5 Hz, H at C_{12}) (*cf.* Ref. 4). Compound IIa was reconverted into II by hydrolysis under the same conditions as those[4] reported.

Found: C, 75.08; H, 9.72%. Calcd for $C_{34}H_{52}O_5$: C, 75.51; H, 9.69%.

Soyasapogenol-B (I, 786 mg) dissolved in a 4: 1 mixture (10 m*l*) of chloroform and ether was passed through a column of silica gel (Wakogel Q-23), freshly washed successively with methanol, acetone, and *n*-hexane, using *n*-hexane containing 8% acetone. The eluate was recrystallized from methanol to give the acetonide (Ib, 500 mg), mp 177—178°C and $[\alpha]_D$+111° (*cf.* Ref. 3c); IR, ν_{max} 3430, 1150, 1100, 1080, 1052, and 1025 cm^{-1}; NMR, δ 0.88, 0.90, 0.99, 1.03, 1.11, 1.15, 1.20, 1.35, and 1.40 (each 3H, s), 3.35 (2H, br), 4.03 (1H, br d J=10 Hz), and 5.25 (1H, br).

Compound Ib (450 mg) in pyridine (10 m*l*) was oxidized with chromic anhydride (530 mg) in pyridine (4 m*l*) at room temperature for 20 hr under stirring. The product was treated with water and ether, and the ether solution afforded amorphous keto-acetonide (495 mg). This was converted into crystalline glycol on heating with methanol, which was recrystallized from methanol to give II (300 mg), mp 246—248°C and $[\alpha]_D$+32°. This compound and its diacetate, mp 243—244°C and $[\alpha]_D$+24°, were identical with the corresponding natural specimens.

Stigmasta-5,22-dien-3β-ol-7-one (IV) and Stigmast-5-en-3β-ol-7-one (V). A mixture of ketones (970 mg), the second fraction obtained on rechromatography, was triturated with methanol to give crystalline material (340 mg), which was separated into two fractions (150 and 65 mg) by preparative tlc (chloroform: ether 3 : 1). Recrystallization of the former from ethanol afforded crystal A (IV and V, 80 mg), and that of the latter crystal B (VI and VII, 50 mg), each showing a single spot on tlc (solvent A).

Crystal A had mp 144—146°C and $[\alpha]_D$−80°; mass, *m/e* 428 (M^+), 426 (M^+), 410, 408, 396, 383, 314, 287 (base peak, XII), and 174 (XIII);[14] UV, λ_{max} 238 mμ (ε 16000); IR, ν_{max} 3360 and 1675 cm^{-1}; NMR, δ 0.69 (s, 18-Me), 0.74, 0.78, 0.84, 0.88, 0.96, and 1.07 (each sharp), 1.19 (s, 19-Me), 3.58 (1H, br CH–OH), 5.06 (*ca.* 1.5H, br W_H=12 Hz, 2H at C_{22} and C_{23}), and 5.64 (1H, s, H at C_6).

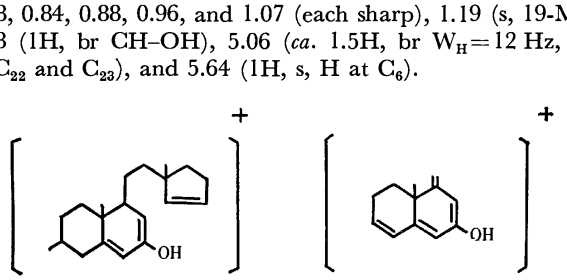

XII XIII

XIV XII−H_2O

Crystal A (50 mg) was converted into the acetate, which on preparative tlc (benzene: chloroform 2 : 1) followed by trituration with acetone afforded a sample (35 mg) showing a single spot, mp 176—179°C and $[\alpha]_D$−102°; mass, *m/e* 410 (M^+–AcOH), 408 (M^+–AcOH), 396, 365, and 269 (base peak, XIV) and 174; UV, λ_{max} 238 mμ (ε 15000); IR, ν_{max} 1740 and 1670 cm^{-1}; NMR, δ 0.68 (3H, s, 18-Me), 0.75, 0.79, 0.86, 0.89, 0.97, and 1.08 (each sharp), 1.18 (3H, s, 19-Me), 2.00 (3H, s, OAc), 4.68 (1H, br CH-OAc), 5.08 (1.3H, t J=6 Hz, 2H at C_{22} and C_{23}), and 5.68 (1H, s, H at C_6).

Attempted purifications of crystal A [preparative tlc over silica gel (benzene: *n*-hexane 1: 1), over silica gel containing silver nitrate, or over alumina or bromination followed by debromination] failed and only repeated recrystallization from methanol effected isolation of IV (10 mg from 80 mg of A) in pure state, which had mp 138—140°C and, after drying, 160—162°C and $[\alpha]_D$−78°; mass, *m/e* 426 (M^+), 408, 383, 287 (XII), and 269 (XIV); UV, λ_{max} 238 mμ (ε 16000); IR, ν_{max} 3360 and 1675 cm^{-1}; NMR, δ 0.69 (s, 18-Me), 0.83 (t J=7 Hz, 29-Me), 0.83 (d J=6 Hz, 26- and 27-Me), 1.00 (d J=7 Hz, 21-Me), 1.19 (s, 19-Me), 3.60 (1H, br CH–OH), 5.08 (2H, br t J=5 Hz, 2H at C_{22} and C_{23}), and 5.65 (1H, s, H at C_6). This compound was identified as IV by direct comparison with an authentic sample.

Found: C, 81.54; H, 10.84%. Calcd for $C_{29}H_{46}O_2$: C, 81.63; H, 10.87%.

A 2: 1 mixture of synthetic samples IV and V had mp 144—146°C and $[\alpha]_D$−81°, and that of the respective acetates mp 176—179°C and $[\alpha]_D$−101°. The former and the latter mixtures revealed mass, UV, IR, and NMR spectra, superimposable over the corresponding spectra of crystal A and its acetate, respectively.

Stigmasterol acetate (VIIIa) and β-sitosterol acetate (IIIa) were oxidized[8a] to give the respective 7-oxo derivatives (IVa), mp 183—184°C (*cf.* Refs. 5 and 6a) and $[\alpha]_D$−103° (*cf.* Ref. 6a); mass, *m/e* 408, 365, 297, and 269 (base peak); UV, λ_{max} 238 mμ (ε 15000); IR, ν_{max} 1740 and 1670 cm^{-1}; NMR, δ 0.69 (3H, s, 19-Me), 0.83 (t J=7 Hz, 29-Me), 0.83 (d J= 7 Hz, 26- and 27-Me), 1.02 (d J=7 Hz, 21-Me), 1.21 (s, 19-Me), 2.02 (3H, s, OAc), 4.63 (1H, br CH–OAc), 5.02 (2H, br t J=5.5 Hz, 2H at C_{22} and C_{23}), and 5.61 (1H, s, H at C_6), and (Va), mp 174—176°C and $[\alpha]_D$−95° (*cf.* Ref. 7); mass, *m/e* 410, 396, and 174 (base peak); UV, λ_{max} 238 mμ (ε 15000); IR, ν_{max} 1740 and 1670 cm^{-1}; NMR, δ 0.69 (3H, s, 18-Me), 0.86 (d J=6 Hz, 21-, 26-, and 27-Me), 0.88 (t J= 7 Hz, 29-Me), 1.22 (s, 19-Me), 2.06 (3H, s, OAc), 4.67 (1H, br CH–OAc), and 5.70 (1H, s, H at C_6).

The resulting 7-oxo-compounds (IVa and Va) were saponified[6a] to yield the respective alcohols IV and V. Compound IV had mp 138—140°C (from methanol) and mp 158—160°C (after drying at 90°C) (154°C[5] and 130—135°C[6a]) and showed $[\alpha]_D$−78° (−113°[5]). Compound V had mp 128—130°C and $[\alpha]_D$−85° (144—145°C and −116°[7]); mass, *m/e* 428, 410, 396, and 174 (base peak); UV, λ_{max} 238 mμ (ε 16000); IR, ν_{max} 3380 and 1675 cm^{-1}; NMR, δ 0.68 (3H, s, 18-Me), 0.82 (d J=6 Hz, 21-, 26-, and 27-Me), 0.85 (t J=7 Hz, 29-Me), 1.19 (s, 19-Me), 3.63 (1H, br CH–OH), and 5.70 (1H, s, H at C_6).

Stigmasta-4,22-dien-6β-ol-3-one (VI) and Stigmast-4-en-6β-ol-3-one (VII). Crystal B (50 mg) had mp 210—213°C and $[\alpha]_D$+16°; mass, *m/e* 428 (M^+) and 426 (M^+); UV, λ_{max} 238 mμ (ε 16000); IR, ν_{max} 3400, 1680, 1035, and 1010 cm^{-1}; NMR, δ 0.76 (s, 18-Me), 0.81, 0.84, 0.87, 0.91, 0.98, and 1.09 (each sharp), 1.39 (3H, s, 19-Me), 4.34 (1H, br s W_H=5 Hz, CH–OH), 5.12 (1H, br t J=5 Hz, 2H at C_{22} and C_{23}), and 5.80 (1H, s, H at C_4). This crysatal resisted further purification.

Treatment of crystal B (43 mg) with acetic anhydride (0.4 m*l*) and pyridine (0.4 m*l*) gave its acetate, amorphous, showing $[\alpha]_D$+21°; mass, *m/e* 470, 468, 428, 426, and 149 (base peak); UV, λ_{max} 237 mμ (ε 15000); IR, ν_{max} 1740 and 1680 cm^{-1}; NMR, δ 0.76 (s, 18-Me), 0.84, 0.88, 0.90, 0.98, and 1.09 (each sharp), 1.28 (3H, s, 19-Me), 2.02 (3H,

14) S. Sasaki, "Interpretation of Mass Spectra," Hirokawa Publishing Co., Tokyo (1965), p. 172.

s, OAc), 5.09 (1H, br t J=5 Hz, 2H at C_{22} and C_{23}), 5.40 (1H, br t J=3 Hz, CH–OAc), and 5.91 (1H, s, H at C_4) (*cf.*, NMR spectrum[15] of cholest-4-en-6β-ol-3-one).

These spectral data suggest crystal B to be a 1:1 mixture of VI and VII. In fact, a 1:1 mixture of synthetic samples of VI and VII, had mp 209—212°C and $[\alpha]_D$+15°, and the corresponding acetate, amorphous, showed $[\alpha]_D$+23°. These synthetic alcohol and acetate mixtures exhibited the mass, UV, IR, and NMR spectra superimposable over the corresponding spectra of crystal B and its acetate, respectively.

Preparation of VI and VII. To a solution of stigmasterol (VIII, 2.40 g) in benzene (11 m*l*) and acetic acid (10 m*l*) was added sodium bichromate (1.5 g as hydrate) in acetic acid (5 m*l*) at room temperature (*cf.* Ref. 16). The mixture was stirred at room temperature overnight and, after addition of ethanol (*ca.* 10 m*l*), diluted with water (50 m*l*), and then extracted with ether (50 m*l*). The ether solution was washed with a 5% sodium bicarbonate solution and then with water, dried and evaporated to leave amorphous residue. This was purified by chromatography over silica gel (100 g), using a 10:1 mixture of chloroform and ether, and it gave a crude sample of VI (1.1 g), mp 198—203°C, showing a single spot on tlc. Recrystallization from ethanol afforded a pure sample, mp 210—212°C and $[\alpha]_D$+8°; mass, *m/e* 426; UV, λ_{max} 238 mμ (ε 16000); IR, ν_{max} 1680 and 1620 cm^{-1}; NMR, δ 0.77 (3H, s, 18-Me), 1.39 (s, 19-Me), 4.33 (1H, br s W_H=6 Hz, CH–OH), 5.11 (2H, br t J=5 Hz, 2H at C_{22} and C_{23}), and 5.79 (1H, s, H at C_4).

Found: C, 81.25; H, 10.99%. Calcd for $C_{29}H_{46}O_2$; C, 81.63; H, 10.84%.

Compound VI was converted into the acetate (VIa), mp 107—109°C (from *n*-hexane) and $[\alpha]_D$+16°; mass, *m/e* 468, 426, and 149 (base peak); UV, λ_{max} 238 mμ (ε 15,000); IR, ν_{max} 1740, 1680, and 1620 cm^{-1}; NMR, δ 0.77 (3H, s, 18-Me), 1.29 (s, 19-Me), 2.02 (3H, s, OAc), 5.12 (2H, br t J=5 Hz, 2H at C_{22} and C_{23}), 5.40 (1H, br s W_H=5 Hz, CH–OAc), and 5.90 (1H, s, H at C_4).

Found: C, 79.50; H, 10.15%. Calcd for $C_{31}H_{48}O_3$; C, 79.43; H, 10.32%.

Compound VII (1.49 g) was likewise obtained from β-sitosterol (III, 2.2 g) in crude state and had mp 188—194°C. Recrystallization from ethanol gave a pure sample, mp 211—213°C and $[\alpha]_D$+29°; mass, *m/e* 428; UV, λ_{max} 238 mμ (ε 16000); IR, ν_{max} 1680 and 1620 cm^{-1}; NMR, δ 0.76 (3H, s, 18-Me), 1.39 (s, 19-Me), 4.31 (1H, br s W_H=6 Hz, CH–OH), and 5.79 (1H, s, H at C_4).

Found: C, 81.48; H, 11.37%. Calcd for $C_{29}H_{48}O_2$: C, 81.25; H, 11.29%.

An acetate (VIIa) of VII was obtained only in amorphous state and showed $[\alpha]_D$+27°; mass, *m/e* 470, 428, and 149; UV, λ_{max} 238 mμ (ε 15000); IR, ν_{max} 1740, 1680, and 1620 cm^{-1}, NMR, δ 0.77 (3H, s, 18-Me), 1.29 (s, 19-Me), 2.02 (3H, s, OAc), 5.39 (1H, br s W_H=5 Hz, CH–OAc), and 5.90 (1H, s, H at C_4).

Found: C, 79.35; H, 10.50%. Calcd for $C_{31}H_{50}O_3$: C, 79.10; H, 10.71%.

15) K. Tori and K. Kuriyama, *Chem. Ind.*, **1963**, 1525.
16) L. F. Fieser, *J. Amer. Chem. Soc.*, **75**, 4377 (1953).

BULLETIN OF THE CHEMICAL SOCIETY OF JAPAN, VOL. 45, 226—229(1972)

The Syntheses of 5-Azidotropolones and Their Electrophilic, Nucleophilic, and Thermal Reactions[1]

Takashi TODA, Hiroshi HORINO, and Tetsuo NOZOE
Department of Chemistry, Faculty of Science, Tohoku University, Katahiracho-ni-chome, Sendai

(Received June 2, 1971)

Several 5-azidotropolones were synthesized by the reaction of sodium azide with tropolone diazonium salts which has been prepared from the corresponding 5-aminotropolones. Most of the 5-azidotropolones thus obtained were stable except for the 4-alkyl derivatives. Their electrophilic substitution reactions took place at their 3- and 7-positions, and also their hydroxyl groups behaved like those of other tropolones. 5-Azidotropolone methyl ether did not react with aromatic amines, but it did with aliphatic amines and guanidine to give 2-aminotropone derivatives and 1,3-diazaazulene derivative. The thermolysis of 5-azidotropolone and its methyl ether afforded 5-aminotropolone and its methyl ether respectively; however, 5-azido-4-phenyltropolone gave indolo[3,2-*d*]tropolone.

Recently, organic azido-compounds have been investigated by many researchers because of their interesting properties.[2] However, azido derivatives of tropolones have not been known until recently; only 2-, 3-, and 4-azidotropones[3–5] and 2-azido-5-nitrotropone[6] have been synthesized, and their properties have been investigated very recently.

Azidotropolones are expected to form nitrene intermediates by photolysis or thermolysis, or by the formation of heterocyclic troponoid compounds and other

1) Presented at the 18th annual meeting of the Chemical Society of Japan, Osaka, April, 1965; preliminarily communicated to *Tetrahedron Lett.*, **1967**, 5349.

2) L. Horner and A. Christmann, *Angew. Chem.*, **75**, 707 (1963); R. Huisgen, *ibid.*, **75**, 604, 743 (1963); R. A. Abramovitch and B. A. Daves, *Chem. Rev.*, **64**, 149 (1964); D. Liever, R. L. Minnis, and C. N. Rao, *ibid.*, **65**, 377 (1965); G. Labbe, *ibid.*, **69**, 345 (1969).

3) J. D. Hobson and J. R. Malpass, *Chem. Commun.*, **1966**, 141; *J. Chem. Soc., C*, **1967**, 1645.

4) J. D. Hobson, M. M. Holly, and J. R. Malpass, *Chem. Commun.*, **1968**, 764.

5) J. D. Hobson and J. R. Malpass, *J. Chem. Soc., C*, **1969**, 1499.

6) S. Takenaka and S. Seto, *Sci. Rep. Res. Inst., Tohoku Univ., Ser. A*, **21**, 97 (1969).

interesting properties in the case of the azido groups. This prompted us to investigate azidotropolones; in this report, we will present our findings on the syntheses, chemical properties, and thermolysis of 5-azidotropolones.

Azidotropones were synthesized from hydrazinotropone with sodium nitrite or from halotropones with sodium azide.[3-6] However, the synthesis of hydrazino derivatives of tropolones and the direct replacement of halogen derivatives of tropolone by sodium azide were difficult. On the other hand, the reaction of sodium azide with diazonium salts of 5-aminotropolones[7] afforded the corresponding azidotropolones in fairly good yields.

The structure of those compounds was established as follows; the azido compound (IIa) obtained from 5-aminotropolone (I) shows strong absorption bands at 3280 cm^{-1} (tropolones' OH group),[8] at 2130 cm^{-1} (N_3),[9] and at 870 and 851 cm^{-1} (two adjacent hydrogens of troplones).[8] The catalytic reduction of IIa gave 5-aminotropolone in a good yield. Therefore, IIa is 5-azidotropolone.

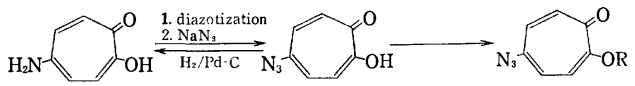

I IIa IIIa: R=Ac
b: R=Me
c: R=Ts

Also, IIa gave a sodium salt, a copper complex, and an acetate (IIIa), a methyl ether (IIIb), and a tosylate (IIIc). These properties are parallel with those of other tropolones.

Other 5-azidotropolones, possessing different functional groups at the 3- and 4-positions on the tropolone nucleus, were synthesized by an analogous method; they are shown in Table 1. These azido compounds show spectral properties analogous with those of IIa; however, the introduction of azido groups did not cause any special change in their spectral properties.

As a typical electrophilic substitution reaction, the bromination of IIa was investigated. The bromination of IIa and IIb gave the same 3,7-dibromo derivative (IVa), while 5-azido-3-phenyltropolone (IId) gave the corresponding 7-bromo derivative. Unlike the cases of the electrophilic reactions of phenyl azides,[10] the results showed that this substitution occurred at the 3- and 7-positions, just as in other 5-substituted tropolones and that the azido group did not affect the direction of the brominations.

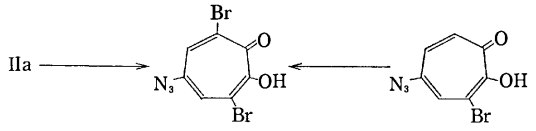

IVa IIb

2-Amino-5-azidotropone derivatives, (Va) and (Vb), and 2-amino-6-azido-1,3-diazaazulene (VI) were obtained by the reaction of IIIb with aliphatic amines and with guanidine respectively. The properties of IIIb are parallel with those of tropolone methyl ethers.[11] However, no reactions with aromatic amines occurred; presumably, the electron-releasing effect of the azido group[10] and the weak nucleophilicity of the aromatic amines[12] are responsible for this. It is interesting that 5-azidotropolone is stable toward amines, though 2-azido-5-nitrotropone gives 2-aminotropone derivatives by its direct displacement of the azido group with amines.[6]

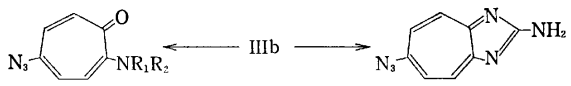

Va: R_1=Et, R_2=H
b: R_1=R_2=Et VI

Although 2-azidotropones are thermaly unstable and readily loose nitrogen to form ring-cleavage substances, all the 5-azidotropolones except 4-alkyl derivatives are fairly stable entities.

However, when IIa and its methyl ether IIIb were heated in ethylene glycol, 5-aminotropolone and its methyl ether[13] were obtained in 50 and 25% yields respectively; also some intractable resinous substances were formed.

It is known that decomposition of azido compounds in protic solvents affords the corresponding amino compounds, but the yields are rather poor.[2] The reason for the fairly good yield of 5-aminotropolone is as follows; the tropolonyl nitrene formed during the thermolysis has the resonance formula represented below. The nitrene intermediate is stabilized by the contribution of those resonances and lives rather stably until the formation of 5-aminotropolone by hydrogen abstraction from the solvent.

Benzenoid azido compounds, which possess good substituents at the ortho-position of the azido group,

TABLE 1

	R_1	R_2	mp °C (dec)	ν_{KBr} cm^{-1}
IIa	H	H	140	2130
IIb	Br	H	117	2140
IIc	Me	H	100	2130
IId	Ph	H	115	2120
IIe	H	Ph	122	2110, 2140
IIf	H	Me	135	2130
IIg	H	i-Pr	109	2080

7) T. Nozoe, Y. Kitahara, K. Yamane, and A. Yoshikoshi, *Proc. Japan Acad.*, **27**, 18 (1951); T. Nozoe, Y. Kitahara, and K. Doi, *ibid.*, **27**, 156 (1951).

8) Y. Ikegami, Kagaku no Ryoiki Special Issue. Infrared Spectra No. 8, Nanko-Do, Tokyo (1958), p. 33.

9) L. J. Bellamy, "Infra-red Spectra of Complex Molecules," 2nd ed., Methuen, London (1958), p. 273,

10) A. S. Smith and J. H. Hall, *J. Amer. Chem. Soc.*, **84**, 480 (1964).

11) T. Nozoe, K. Takase, and H. Matsumura, "Dai Yuki Kagaku," Vol. 13, ed. by M. Kotake, Asakura Shoten, Tokyo (1960), p. 178.

12) L. F. Bunnett and R. E. Zahler, *Chem. Rev.*, **49**, 273 (1951)

13) T. Toda, T. Nishino, K. Sasaki, and T. Mukai, *Nippon Kagaku Zasshi*, **91**, 475 (1970).

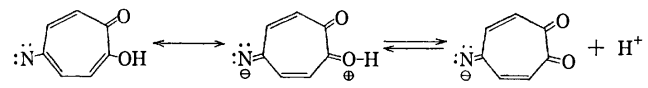

and aliphatic azido compounds, which possess suitable chains, afford five- or six-membered hetero-cyclic compounds.[2] The thermolysis of 5-azido-4-phenyltropolone in ethylene glycol gave an acidic substance in a 50% yield. The IR and UV spectra of this compound are similar to those of indolo[2,3-*d*]tropone.[14] Thus, the structure of VIIa can be said to be indolo[3,2-*d*]tropolone (9-hydroxycycloheptatrieno[*b*]indol-8(5*H*)-one). The spectral evidence of its diacetate (VIIb), methyl ether (VIIc), and an acetate of VIIc (VIId) also support this conclusion.

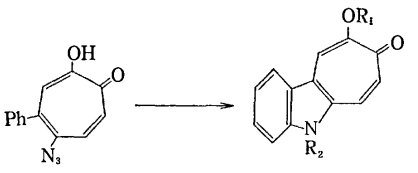

IIe

VIIa: $R_1=R_2=H$
b: $R_1=R_2=Ac$
c: $R_1=Me$, $R_2=H$
d: $R_1=Me$, $R_2=Ac$

4-Alkyl-5-azidotropolones (IIf and IIg) are very unstable and could not be obtained in an analytically pure state. This unstability and the formation of complex tarry substances of 4-alkyl-5-azidotropolones suggest that hydrogens of alkyl groups, especially those of the isopropyl group, are abstracted by azido groups, which form nitrene intermediates. The alkyl radicals formed gave complex resultants by means of intra- or inter-molecular reactions. However, no clear substances were obtained.

Experimental[15]

5-Azidotropolone (IIa). A solution of 5.0 g of 5-amino-tropolone I in 150 m*l* of 6N sulfuric acid was treated with 2.77 g of sodium nitrite in 25 m*l* of water. The resulting solution was stirred, drop by drop, into a solution of 2.84 g of sodium azide in 20 m*l* of water at −6——9°C. After the mixture had been allowed to stand overnight at room temperature, 5.53 g of the brown precipitates (IIa) were collected and recystallized from ethanol; mp 140°C (dec.). The residue was extracted with ethyl acetate and dried, and the solvent was removed to afford 0.03 g of the additional IIa.

Found: C, 52.04; H, 3.18; N, 25.44%. Calcd for $C_7H_5O_2N_3$: C, 52.07; H, 2.42; N, 25.10%. λ_{max}^{MeOH}, mμ (log ε); 242 (4.20), 355 (3.49), 425 (3.54 sh).

5-Azido-3-bromotropolone (IIb). A solution of 200 mg of 5-amino-3-bromotropolone in a mixture of 4 m*l* of dioxane and 1 m*l* of 18N sulfuric acid was treated with a solution of sodium nitrite in 0.3 m*l* of water. After standing for 20 min, the resulting solution was stirred, drop by drop, into an aqueous solution of 73 m*l* of sodium azide at −5——8°C. It was then allowed to stand at room temperature for about 5 hr. Subsequent dilution with 30 m*l* of water gave a precipitate, which was then collected and recrystallized from ethanol to yield 112 mg of IIb; mp 117°C (dec.).

Found: C, 34.73; H, 1.63; N, 17.35%. Calcd for $C_7H_4O_2N_3Br$: C, 35.32; H, 1.92; N, 16.80%. λ_{max}^{MeOH}, mμ (log ε); 260 (4.22), 351 (4.07), 410 (3.62 sh).

The following substituted 5-azidotropolones were prepared in the same way as above. The data of the analyses and some physical properties are as follows.

5-Azido-3-methyltropolone (IIc). Mp 100°C, from methanol.

Found: C, 54.21; H, 4.08; N, 23.47%. Calcd for $C_8H_7O_2N_3$: C, 54.23; H, 3.98; N, 23.72%. $\lambda_{m\mu}^{MeOH}$, mμ (log ε); 242 (4.23), 345 (4.07).

5-Azido-3-phenyltropolone (IId). Mp 115°C (dec.), from methanol.

Found: C, 65.49; H, 3.71; N, 16.93%. Calcd for $C_{13}H_9O_2N_3$; C, 65.26; H, 3.79; N, 17.57%. λ_{max}^{MeOH}, mμ (log ε); 229 (4.11), 256 (4.05), 285 (3.98), 356 (3.90), 405 (3.70).

5-Azido-4-phenyltropolone (IIe). Mp 122°C (dec.), from methanol.

Found: C, 65.44; H, 3.97; N, 16.93%. Calcd for $C_{13}H_9O_2N_3$: C, 65.26; H, 3.79; N, 17.57%. λ_{max}^{MeOH}, mμ (log ε) 229 (4.15), 267 (4.21), 356 (4.18), 402 (3.85).

5-Azido-4-methyltropolone (IIf). Mp 135°C (dec.). λ_{max}^{MeOH} mμ (log ε), 228 (4.15), 346 (4.03).

5-Azido-4-isopropyltropolone (IIg). Mp 109°C (dec.).

5-Azizo-2-acetoxytropone (IIIa). One hundred mg of 5-azidotropolone IIa were allowed to stand overnight in a solution of pyridine (1.5 m*l*) and acetic anhydride (1.5 m*l*). Subsequent heating on a water bath for 10 min and evaporation *in vacuo* produced 117 mg of IIIa; mp 117°C (dec.), recrystallized from ethanol.

Found: C, 52.68; H, 3.44; N, 20.48%. Calcd for $C_9H_7O_3N_3$: C, 52.89; H, 3.43; N, 20.68%. ν(KBr); 2130 cm^{-1}.

5-Azido-2-methoxytropone (IIIb). An ethereal solution of diazomethane was added, drop by drop, to 90 mg of IIa dissolved in a cold mixture of 20 m*l* of ethyl acetate and 8 m*l* of ether until there was no coloration by a ferric chloride test. After it had then stood overnight, the solution was evaporated to dryness *in vacuo* thus giving 170 mg of yellow IIIb; mp 110°C (dec), recrystallized from a mixture of benzene and cyclohexane.

Found: C, 54.66; H, 3.85; N, 23.36%. Calcd for $C_8H_7O_2N_3$: C, 54.85; H, 3.88; N, 23.06%. λ_{max}^{MeOH}, mμ (log ε); 226 (4.17), 343 (4.15), ν(KBr); 2130 cm^{-1}.

5-Azido-2-tosyloxytropone (IIIc). To a solution of 100 mg of IIa in 1.5 m*l* of pyridine, 100 mg of *p*-toluenesulfonyl chloride was added at once, upon which the reaction occurred exothermically. After the mixture had stood for a night, further addition of 140 mg of the reagent led to a negative ferric chloride test. The solution was then poured into 30 m*l* of water and acidified succesively with 6N hydrochloric acid to yield 140 mg of IIIc; mp 136°C (dec), recrystallized from ethanol.

Found: C, 53.28; H, 3.68; N, 12.80%. Calcd for $C_{14}H_{11}O_4N_3$: C, 53.00; H, 3.50; N, 12.25%. ν (KBr); 2130 cm^{-1}.

5-Azido-3,7-dibromotropolone (IVa). *1) Bromination of IIa*: Into a solution of 100 mg of IIa and 110 mg of sodium acetate in 2 m*l* of acetic acid, 220 mg of bromine in 0.3 m*l* of acetic acid was stirred for 12 min. The product was collected and filtered to give 160 mg of IVa, which was recrystallized from ethanol; mp 119°C (dec.). The residue was concentrated under reduced presure without heating to yield 41 mg of the additional IVa. The filtrate was diluted with water and then extracted with chloroform; this procedure afforded 40 mg of a paste after the evaporation of the solvent. The paste was chromatographed over a paper treated with phosphoric acid; this showed only one spot, the same as IVa.

Found: C, 26.16; H, 1.35; N, 12.75%. Calcd for $C_7H_3O_2N_3Br_2$: C, 26.19; H, 0.94; N, 13.09%. λ_{max}^{MeOH}, mμ (log ε);

14) J. Shin, D. Sc. thesis of Tohoku University, March, 1958.
15) All the melting points are uncorrected.

264 (4.27), 355 (3.90), 420 (3.43), 456 (3.36).

2) Bromination of IIb: An acetic acid solution of 80 mg of bromine was added to a mixture of 100 mg of IIb and 40 mg of sodium acetate in 2 m*l* of acetic acid. The solution was then treated as above. This gave 87 mg of IVa, which showed no melting-point depression on admixture with the product obtained in 1); also, their IR spectra are superimposable.

5-Azido-7-bromo-3-phenyltropolone (IVb). IVb was prepared in the way described above and recrystallized from ethanol; mp 117.5°C (dec.).

Found: C, 49.58; H, 2.78; N, 12.83%. Calcd for $C_{13}H_8O_2N_3Br$: C, 49.10; H, 2.53; N, 13.21%. ν (KBr); 3235, 2140, 2105 cm^{-1}.

Catalytic Reduction of IIa. A solution of IIa (100 mg) in 30 m*l* of ethyl acetate was shaken with 30 mg of 10 per cent palladium on carbon in a hydrogen atomosphere. The catalyst was then removed, and the filtrate was concentrated to give 73 mg of yellow crystals. Recrystallization from a mixture of benzene and ethyl acetate made its mp 181°C; it was identified as 5-aminotropolone by a mixed-melting-point determination with an authentic sample.

Reaction of IIIb with Aromatic Amines. 1) A mixture of 100 mg of IIIb and 100 mg of *o*-phenylenediamine dissolved in 4 m*l* of absolute ethanol was heated to reflux for 2 hr. It was then evaporated to yield 84 mg of IIIb; mp 105—107°C, identified by thin-layer chromatography and admixture with the starting material.

2) A mixture of 100 mg of IIIb and 64 mg of *p*-toluidine in absolute ethanol was boiled for 2 hr. The same treatment as above gave 85 mg of IIIb; mp 109—110°C.

5-Azido-2-ethylaminotropone (Va). A solution of 200 mg of IIIb was dissolved in a mixture of 3 m*l* of ethanol and a 70% aqueous solution of monoethylamine. After standing for two days, the solution was diluted with water, neutralized with 2N hydrochloric acid, and then extracted with ethyl acetate to give 180 mg of a red oil. Treatment of it with 230 mg of picric acid in ethanol afforded 365 mg of yellow crystals which was recrystallized from ethanol; mp 128—129°C (dec.).

Found: C, 43.13; H, 3.02; N, 23.47%. Calcd for $C_{15}H_{13}O_8N_7$: C, 42.97; H, 3.12; N, 23.39%. ν (KBr); 2100 cm^{-1}.

5-Azido-2-diethylaminotropone (Vb). Two hundred mg of IIIb were dissolved in a mixture of 1 m*l* of diethylamine and 2 m*l* of absolute ethanol. After having stood overnight, the solution was evaporated; water was added, and then it was acidified with 2N hydrochloric acid. It was extracted with ethyl acetate, evaporated, and then chromatographed over silica gel to give a reddish oil (56 mg) and the recovered IIIb (180 mg). λ_{max}^{MeOH}, mμ; 255, 382, 437. ν (KBr); 2130 cm^{-1}.

A picrate of this oil was obtained by treatment with an alcoholic solution of picric acid; mp 112—113°C (dec.), from ethanol.

Found: N, 21.92%. Calcd for $C_{17}H_{17}O_8N_7$: N, 21.90%. ν (KBr); 2100 cm^{-1}.

2-Amino-6-azido-1,3-diazaazulene (VI). To a solution of guanidine hydrochloride (142 mg) and sodium (35 mg) in absolute ethanol (2 m*l*), IIIb (220 mg) was added and it was stirred for a night. The yellow precipitate thus formed (132 mg) was collected and recrystallized from ethanol. No clear melting point was observed, but it decomposed gradually.

Found: C, 51.45; H, 3.63; N, 44.50%. Calcd for $C_8H_6N_6$: C, 51.61; H, 3.25; N, 45.14%. λ_{max}^{MeOH}, mμ (log ε); 224 (4.19), 253 (4.25), 376 (3.87). ν (KBr); 3050, 2120, 1675, 844, 826 cm^{-1}.

Thermolysis of 5-Azidotropolone. A suspension of IIa (500 mg) in ethylene glycol (5 m*l*) was heated under a nitrogen atomosphere. It became a solution at about 105°C and bubbled at 115—130°C. After gas evolution had ceased, the solvent was removed by suction and the residue was extracted with hot ethanol. The evaporation of this solution and recrystallization from benzene gave 126 mg of yellow crystals (mp 179—180°C), which were identified with I by a mixed-melting-point determinations with an authentic sample. The subsequent treatment of this filtrate with a saturated alcoholic solution of picric acid gave 90 mg (mp 226°C (dec.)) of 5-aminotropolone picrate.[16]

Thermolysis of 5-Azido-2-methoxytropone. A suspension of IIb (300 mg) in ethylene glycol (3 m*l*) was heated under a nitrogen atmosphere. The nitrogen gas began to bubble about at 115—125°C. The solution was then concentrated under reduced pressure and extracted with hot methanol to afford 70 mg of a yellow oil, which was then crystallized with a saturated alcoholic solution of picric acid; mp 220°C, from ethanol. This picrate was identified with 5-amino-2-methoxytropone picrate[13] by a mixed-melting-point determination with an authentic sample.

Thermolysis of 5-Azido-4-phenyltropolone. A solution of IIe (350 mg) in ethylene glycol (4 m*l*) was heated under a nitrogen atmosphere. It bubbled at 115—120°C. After gas evolution had ceased, the solution was poured into 20 m*l* of water and then extracted with chloroform; this procedure afforded 150 mg of yellow crystals of indolo[3,2-*d*]tropolone (VIIa). Recrystallization from ethanol made its mp 240—241°C (dec.).

Found: C, 74.02; H, 4.64. N, 6.42%. Calcd for $C_{13}H_9O_2N$: C, 73.92; H, 4.30; N, 6.63%. λ_{max}^{MeOH}, mμ (log ε); 243 (4.44), 260 (4.10 sh), 300 (4.24 sh), 325 (5.55), 364 (4.04 sh), 405 (3.96), 426 (3.98). ν (KBr); 3080, 840, 773, 746 cm^{-1}.

Methyl Ether (VIIb) of VIIa. A solution of VIIa (200 mg) in methanol (16 m*l*) was treated with ethereal diazomethane cooled in an ice-bath. After it has been allowed to stand for 8 hr, yellow needles which precipitated were collected and recystallized from ethanol; mp 266—267°C.

Found: C, 73.92; H, 5.10; N, 5.62%. Calcd for $C_{14}H_{11}O_2N$: C, 74.65; H, 4.92; N, 6.22%. λ_{max}^{MeOH}, mμ (log ε); 241 (4.37), 254 (4.23 sh), 325 (4.45), 363 (4.02), 309 (3.97), 417 (3.95). ν (KBr); 3095, 1625 cm^{-1}.

N,O-*Diacetate (VIIc) of VIIa.* A solution of VIIa (50 mg) and acetic anhydride (0.3 m*l*) in pyridine (0.7 m*l*) was refluxed for 5 min. The solution was then poured into water to afford colorless crystals (50 mg) ,which were recrystallized from ethanol; mp 203°C.

Found: C, 69.40; H, 4.64; N, 4.71%. Calcd for $C_{17}H_{13}O_4N$: C, 69.14; H, 4.44; N, 4.74%. λ_{max}^{MeOH}, mμ (log ε); 235 (4.42), 324 (4.38), 348 (4.22 sh), 380 (4.48). ν (KBr); 1765, 1701 cm^{-1}.

N-*Acetyl Methyl Ether (VIId) of VIIa.* A solution of VIIa (55 mg) and acetic anhydride (0.4 m*l*) in pyridine (0.8 m*l*) was heated on a water bath for 30 min and then refluxed for 1 min. The solution was poured into water, neutralized with 2N hydrochloric acid, and extracted with chloroform. The extract was concentrated to yield a yellow powder (56 mg), which was recrystallized from ethanol; mp 206—207°C.

Found: C, 71.27; H, 5.07; N, 5.41%. Calcd for $C_{16}H_{13}O_3N$: C, 71.90; H, 4.90; N, 5.24%. λ_{max}^{MeOH}, mμ; 240, 256, 325, 378, 397. ν (KBr); 1670 cm^{-1}.

16) T. Nozoe, K. Takase, and H. Matsumura, "Dai Yuki Kagaku," Vol. 13, ed. by M. Kotake, Asakura Shoten, Tokyo (1960), p. 337.

Palladium-catalyzed Exchange of Allylic Groups of Ethers and Esters with Active Hydrogen Compounds. II.[1]

Kuniyuki TAKAHASHI, Akihisa MIYAKE, and Go HATA
Basic Research Laboratory, Toray Industries, Inc., Tebiro, Kamakura
(Received June 4, 1971)

The allylic compounds (I), R^1–O–R (R=allylic groups, R^1=Ph, Me, $PhCH_2$, MeCO), react with active-hydrogen compounds such as phenols, alcohols, carboxylic acids, primary and secondary amines and active methylene compounds, to give allylic derivatives of the active-hydrogen compounds by an intermolecular exchange of the allylic groups of I with the atom to which the active hydrogens are bonded in the presence of palladium catalysts. Allyl and substituted-allyl ethers are more reactive than the corresponding carboxylates. In the reactions of methyl and benzyl ethers, it is necessary to add phenol to obtain the exchange products in fairly good yields. Bis(triphenylphosphine)palladium chloride plus sodium phenoxide, palladium acetate plus triphenylphosphine, and zerovalent palladium complexes such as tetrakis(triphenylphosphine)palladium and (maleic anhydride)bis(triphenylphosphine)palladium are effective catalysts.

It has been reported that the vinyl group of ethers and esters exchanges with various active-hydrogen compounds such as phenols, alcohols and carboxylic acids in the presence of mercury salts[2,3] or palladium salts.[4] Mercury acetate also catalyzes the exchange of an allyl group of allyl ethers with a hydroxyl group of alcohols.[5] Sabel and his coworkers have reported[4] on the exchange reaction of an allyl group between allyl acetate and propionic acid by $PdCl_2$·NaCl-$CH_3CH_2CO_2Na$ catalyst system.

Recently a new type of palladium catalyzed dimerization of 1,3-dienes completed by the addition of active-hydrogen compounds such as alcohols, phenols, amines, carboxylic acids and active methylene compounds, has been found.[6-9] Smutny found[10] that the palladium complexes, which catalyzed the reaction of phenol with butadiene to the formation of 1-phenoxy-2,7-octadiene, degradated the resulting ether to phenol and 1,3,7-octatriene. The degradation reaction seems to proceed through an allylic intermediate by the insertion of the palladium atom to the C–O bond of the ether. If such an intermediate exists, the intermediate is expected to react with active-hydrogen compounds to afford 2,7-octadienyl derivatives of the corresponding active-hydrogen compounds. In fact, the reaction of 1-phenoxy-2,7-octadiene with methyl acetoacetate gave the expected products. A further research has led to the finding that allylic compounds (I) react with active-hydrogen compounds in the same way

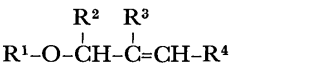

I

R^1=Ph, CH_3, $PhCH_2$, CH_3CO
R^2=H, $CH_2CH_2CH_2CH{=}CH_2$
R^3=H, CH_3
R^4=H, CH_3, $CH_2CH_2CH_2CH{=}CH_2$

to give allylic derivatives of the active hydrogen compounds by the intermolecular exchange of the allylic groups of the allylic compounds to the atom to which the active-hydrogen is bonded. This type of reaction is applied to alcohols, phenols, carboxylic acids, and primary and secondary amines. The same type of exchange reactions of allylic group has been reported independently by Atkins and his coworkers.[11] We reported a part of these reactions in a preliminary communication.[1] The present paper describes the reactions in detail.

An active and easily available catalyst is prepared by mixing dichlorobis(triphenylphosphine)palladium (II) and sodium phenoxide. The combination of palladium acetate and triphenylphosphine, and zerovalent palladium phosphine complexes such as tetrakis(triphenylphosphine)palladium(0) and (maleic anhydride)bis(triphenylphosphine)palladium(0) are also effective catalysts. Platinum catalysts such as the combination of dichlorobis(triphenylphosphine)platinum(II) and sodium phenoxide, and tetrakis(triphenylphosphine)platinum(0) also showed catalytic activity, but the activity of the platinum catalysts was smaller than that of palladium catalysts. It is noted that all of the catalysts are also effective for the dimerization reaction of 1,3-dienes in the presence of active hydrogen compounds.[6-9] The reactions proceeded as shown in the following equation. Only small amounts of the branched products(III) were normally observed.

The reaction products were confirmed by elemental analysis, molecular weight measurement, and IR and NMR spectral measurement or by comparison with authentic samples.[6-10]

1) G. Hata, K. Takahashi, and A. Miyake, *Chem. Commun.*, **1970**, 1392.
2) G. Slinckx and G. Smets, *Tetrahedron*, **22**, 3163 (1966).
3) H. Hopff and M. A. Osman, *ibid.*, **24**, 2205 (1968).
4) A. Sabel, J. Smidt, R. Jira, and H. Prigge, *Chem. Ber.*, **102**, 2939 (1969).
5) W. H. Watanabe, L. E. Conlon, and J. C. H. Hwa, *J. Org. Chem*, **23**, 1966 (1958).
6) S. Takahashi, T. Shibano, and N. Hagihara, *Tetrahedron Lett.*, **1967**, 2451.
7) S. Takahashi, T. Shibano, and N. Hagihara, This Bulletin, **41**, 454 (1968).
8) E. J. Smutny, *J. Amer. Chem. Soc.*, **89**, 6793 (1968).
9) G. Hata, K. Takahashi, and A. Miyake, *Chem. Ind* (London), **1969**, 1836.
10) E. J. Smutny and H. Chung, Preprint of Symposium on Homogeneous Catalystic Reactions Involving Palladium, ACS Mineapolis Meeting, 1969, B112.
11) K. E. Atkins, W. E. Walker, and R. M. Manyik, *Tetrahedron Lett.*, **1970**, 3821.

TABLE 1. REACTION OF ALLYL AND SUBSTITUTED-ALLYL COMPOUNDS WITH ACTIVE-HYDROGEN COMPOUNDS[a)]

Phenoxy compound mol	Active hydrogen compound mol	Catalyst mol	Time hr	Product[c)] and Yield[d)] %
$PhOCH_2CH=CH(CH_2)_3CH=CH_2$ 0.05	$CH_3COCH_2CO_2CH_3$ 0.1	$PdCl_2(Ph_3P)_2$–PhONa 0.05 0.5	2	X–$CH(COCH_3)CO_2CH_3$ 84 X_2–$C(COCH_3)CO_2CH_3$ 7
$PhOCH_2CH=CH_2$ 0.1	$CH_3COCH_2CO_2CH_3$ 0.05	$PdCl_2(Ph_3P)_2$–PhONa 0.05 0.5	8.5	$CH_2=CHCH_2CH(COCH_3)CO_2CH_3$ 18 $(CH_2=CHCH_2)_2C(COCH_3)CO_2CH_3$ 47
$PhOCH_2CH=CH_2$ 0.08	$CH_3COCH_2CO_2CH_3$ 0.08	$PdCl_2(Ph_3As)_2$–PhONa 0.1 0.5	1	$CH_2=CHCH_2CH(COCH_3)CO_2CH_3$ 6 $(CH_2=CHCH_2)_2C(COCH_3)CO_2CH_3$ 13
$PhOCH_2CH=CH_2$ 0.05	$(C_2H_5)_2NH$ 0.1	$PdCl_2(Ph_3P)_2$–PhONa 0.1 0.5	1	$CH_2=CHCH_2N(C_2H_5)_2$ 100
$PhOCH_2CH=CH_2$ 0.05	$(C_2H_5)_2NH$ 0.1	$Pd(Ph_3P)_2$ 0.1	1	$CH_2=CHCH_2N(C_2H_5)_2$ 100
$PhOCH_2C(CH_3)=CH_2$ 0.05	$(C_2H_5)_2NH$ 0.1	$PdCl_2(Ph_3P)_2$–PhONa 0.1 0.5	1	$CH_2=C(CH_3)CH_2N(C_2H_5)_2$ 89
$PhOCH_2CH=CHCH_3$ 0.05	$(C_2H_5)_2NH$ 0.1	$PdCl_2(Ph_3P)_2$–PhONa 0.1 0.5	1	$CH_3CH=CHCH_2N(C_2H_5)_2$ 92
$PhOCH_2CH=CH_2$ 0.05	t-$C_4H_9NH_2$ 0.1	$PdCl_2(Ph_3P)_2$–PhONa 0.2 1.0	1 1	$CH_2=CHCH_2NH$-t-C_4H_9 89 $(CH_2=CHCH_2)_2N$-t-C_4H_9 4
$PhOCH_2CH=CH_2$ 0.1	0.05	$PdCl_2(Ph_3P)_2$–PhONa 0.1 1.0	1	$CH_2=CHCH_2$ $CH_2CH=CH_2$ 33
$PhOCH_2CH=CH(CH_2)_3CH=CH_2$ 0.05	cyclo–$C_6H_{11}NH_2$ 0.1	$PdCl_2(Ph_3P)_2$–PhONa 0.1 1.0	2	X–NH–cyclo–C_6H_{11} 69
$PhOCH_2CH=CH(CH_2)_3CH=CH_2$ 0.05	$PhNH_2$ 0.1	$PdCl_2(Ph_3P)_2$–PhONa 0.05 0.5	1	X–NHPh 84
$PhOCH_2CH=CH_2$ 0.025	p-$CH_3C_6H_4OH$ 0.025	$PdCl_2(Ph_2P)_2$–PhONa 0.05 0.5	3	$CH_2=CHCH_2OC_6H_4$-p-CH_3 41
$PhOCH_2CH=CH_2$ 0.025	p-ClC_6H_4OH 0.025	$PdCl_2(Ph_3P)_2$–PhONa 0.05 0.5	3	$CH_2=CHCH_2OC_6H_4$-p-Cl 26
$PhOC_8H_{13}$[b)] 0.025	$PhCH_2OH$ 0.05	$PdCl_2(Ph_3P)_2$–PhONa 0.05 0.5	2	X–OCH_2Ph 59 Y–OCH_2Ph 2 1,3,7-OT 20
$PhOC_8H_{13}$[b)] 0.05	CH_3COOH 0.1	$Pd(OCOCH_3)_2$–Ph_3P 0.1 0.25	24	X–$OCOCH_3$ 32 Y–$OCOCH_2$ 6 1,3,7-OT 5
$PhOC_8H_{13}$[b)] 0.05	CH_3COOH 0.1	$Pd(OCOCH_3)_2$–Ph_3P 0.1 0.25 in 10 ml DMF	24	X–$OCOCH_3$ 40 Y–$OCOCH_3$ 16 1,3,7-OT trace
$PhOC_8H_{13}$[b)] 0.05	PhCOOH 0.1	$Pd(OCOCH_3)_2$–Ph_3P 0.1 0.25 in 10 ml DMF	24	X–OCOPh 42 Y–OCOPh 18 1,3,7-OT trace

a) All reactions were carried out at 85°C.
b) A mixture of 1-phenoxy-2,7-octadiene (92%) and 3-phenoxy-1,7-octadiene (8%)
c) X=CH_2=$CH(CH_2)_3CH$=$CHCH_2$-, Y=CH_2=$CH(CH_2)_3CH(CH$=$CH_2)$-, 1,3,7-OT=CH_2=$CHCH$=$CHCH_2CH_2CH$=CH_2
d) Based on the phenoxyl compound employed.

$$I + R^5\text{-}H \longrightarrow R^5\text{-}CH(R^2)\text{-}C(R^3)=CH\text{-}R^4 + R^5\text{-}CH(R^4)\text{-}C(R^3)=CH\text{-}R^2$$

II III

	R^2	R^3	R^4	R^5
IIa	— H	H	$-(CH_2)_3CH=CH_2$	$CH_3COCHCO_2CH_3$
IIb	— H	H	$-(CH_2)_3CH=CH_2$	$CH_3COC(C_8H_{13})CO_2CH_3$
IIc	— H	H	H	$CH_3COCHCO_2CH_3$
IId	— H	H	H	$CH_3COC(C_3H_5)CO_2CH_3$
IIe	— H	H	$-(CH_2)_3CH=CH_2$	cyclo-C_6H_{11}-NH-
IIf	— H	H	$-(CH_2)_3CH=CH_2$	PhNH-
IIg	— H	CH_3	H	$(C_2H_5)_2N$-
IIh	— H	H	H	*p*-Cl-C_6H_4O-
IIi	— H	H	H	*p*-CH_3-C_6H_4O-
IIj IIIj	H	H	$-(CH_2)_3CH=CH_2$	CH_3O-
IIk IIIk	H	H	$-(CH_2)_3CH=CH_2$	$PhCH_2O$-
III	— H	H	H	$PhCH_2O$-
IIm IIIm	H	H	$-(CH_2)_3CH=CH_2$	CH_3COO
IIn IIIn	H	H	$-(CH_2)_3CH=CH_2$	PhCOO

C_8H_{13}=$-CH_2CH=CH(CH_2)_3CH=CH_2$, C_3H_5=$-CH_2CH=CH_2$

Reaction of Allyl and Substituted-allyl Phenoxide. The reaction of methyl acetoacetate with 1-phenoxy-2,7-octadiene in the presence of dichlorobis(triphenylphosphine)palladium(II) and sodium phenoxide at 85°C gave methyl 2-acetyl-4,9-decadienoate(IIa) and methyl 2-acetyl-2-(2,7-octadienyl)-4,9-decadienoate (IIb), in 84 and 7% yields, respectively, besides phenol. These products are also formed by the reaction of methyl acetoacetate with 1,3-butadiene in the presence of the palladium catalyst.[9]

1-phenoxy-2-propene similarly reacted with methyl acetoacetate in the presence of $PdCl_2(Ph_3P)_2$ and sodium phenoxide to give methyl 4-acetyl-4-pentenoate (IIc) and methyl 2-acetyl-2-allyl-4-pentenoate(IId) in 18 and 47% yields, respectively. The catalytic activity of the combination of $PdCl_2(Ph_3As)_2$ and sodium phenoxide is slightly smaller than that of $PdCl_2(Ph_3P)_2$ and sodium phenoxide.

Allyl and substituted-allyl phenoxide also reacted with substituted phenols, alcohols, amines and carboxylic acids in the presence of the palladium or platinum catalyst to give corresponding allylic derivatives. Results of the reactions of allyl and substituted allyl phenoxide with active hydrogen compounds are summarized in Table 1.

In the reactions of 1-phenoxy-2,7-octadiene with amines, neither branched products, 1-vinyl-5-hexenylamines, nor 1,3,7-octatriene were detected. The formation of diallylpiperadine could be confirmed in the reaction of 1-phenoxy-2-propene with piperadine. In the reaction of 1-phenoxy-2,7-octadiene with cyclohexylamine and aniline, *N*-(2,7-octadienyl)-cyclohexylamine and -aniline, (IIe) and (IIf), were formed.

The reaction of 1-phenoxy-2-propene with *p*-chlorophenol and with *p*-cresol afforded the corresponding exchange products (IIh) and (IIi) in 26 and 41% yields, respectively. The reaction mixture of 1-phenoxy-2-propene and *p*-cresol was confirmed to consist of 1-phenoxy-2-propene, *p*-cresol, 1-(*p*-methylphenoxyl)-2-propene (IIi) and phenol as expected, while in the reaction mixture of 1-phenoxy-2-propene and *p*-chlorophenol an unidentified product was observed besides four expected components.

Results of the reactions of alcohols with phenoxyoctadienes consisting of 1-phenoxy-2,7-octadiene(92%) and 3-phenoxy-1,7-octadiene(8%) in the presence of dichlorobis(triphenylphosphine)palladium(II) and sodium phenoxide are summarized in Table 2. The reaction of methanol with the phenoxyoctadienes gave a mixture of IIj(93%) and IIIj(7%) in an 89% yield. Formation of a small amount of 1,3,7-octatriene was observed. The reactivity of methanol was much

Table 2. Reactions of phenoxyoctadiene[a] with alcohols

Alcohol[b]	Catalyst mmol	Temp. °C	Time hr	Conv.[c] %	Products, %[d] $-O-CH_2CH=CH(CH_2)_3-CH=CH_2$	Products, %[d] $-O-CH(CH=CH_2)(CH_2)_3-CH=CH_2$	Products, %[d] 1,3,7-Octatriene
CH_3OH	$PdCl_2(Ph_3P)_2$–PhONa 0.05 0.5	60	3	100	83	6	6
C_2H_5OH	$PdCl_2(Ph_3P)_2$–PhONa 0.05 0.5	60	3	70	35	—	17
iso-C_3H_7OH	$PdCl_2(Ph_3P)_2$–PhONa 0.05 0.5	60	3	20	—	—	13
$PhCH_2OH$	$PdCl_2(Ph_3P)_2$–PhONa 0.05 0.5	85	1.5	90	57	2	28
$PhCH_2OH$	$Pd(Ph_3P)_4$ 0.05	85	2.5	100	24	11	41
$PhCH_2OH$	$Pd(OCOCH_3)_2$–Ph_3P 0.05 0.1	85	2.5	76	52	2	11
$PhCH_2OH$	$PdCl_2$ — PhONa 0.05 0.5	85	2.5	0	—	—	—
$PhCH_2OH$	$Pt(Ph_3P)_4$ 0.05	85	2.5	89	19	15	44
$PhCH_2OH$	$PtCl_2(Ph_3P)_2$–PhONa 0.05 0.5	85	2.5	93	43	10	25

a) 5.05 g (0.025 mol) of a mixture of 1-phenoxy-2,7-octadiene (92%) and 3-phenoxy-1,7-octadiene (8%).
b) 0.05 mol. c) Conversion of phenoxyoctadiene. d) Based on phenoxyoctadiene.

TABLE 3. REACTION OF PHENOXYOCTADIENE WITH BENZYL ALCOHOL[a)]

Time min	Reaction products,[b)] g				
	1,3,7-Octatriene	$PhOCH_2CH=CHC_5H_9$	$PhOCH(CH=CH_2)C_5H_9$	$PhCH_2OCH_2CH=CH_3CH_9$	$PhCH_2OCH-(CH=CH_2)C_5H_9$
0	0	4.65	0.40	0	0
10	0.97	2.34	0.56	0.42	0.03
30	0.80	1.14	0.44	1.40	0.07
90	0.78	0.39	0.16	3.16	0.11

a) Reaction conditions: $PdCl_2(Ph_3P)_2$ 0.05 mmol, PhONa 0.5 mmol, Phenoxyoctadiene 5.05 g (0.025 mol) and benzyl alcohol 0.05 mol, 85°C

b) C_5H_9=$-CH_2CH_2CH_2CH=CH_2$

greater than that of ethanol, isopropyl alcohol and benzyl alcohol. The reaction of isopropyl alcohol gave only 1,3,7-octatriene in a 13% yield. It seems that the acidity of alcohol has a large effect on the reactivity. A similar tendency has been observed in the dimerization of 1,3-butadiene in the alcohols by the palladium catalyst.[7)]

The reaction of the phenoxyoctadienes with benzyl alcohol by the $PdCl_2(Ph_3P)_2$-PhONa catalyst was studied as a function of time. The result is shown in Table 3. The products, IIk and IIIk, were formed in 58 and 2% yields, respectively. This shows that the ratio of 3-phenoxy-1,7-octadiene to 1-phenoxy-2,7-octadiene changed from 0.09 to 0.24 in ten minutes after the beginning of the reaction with the formation of 1,3,7-octatriene. This indicates the rearrangement of 1-phenoxy-2,7-octadiene to 3-phenoxy-1,7-octadiene with the catalyst. The initial formation of 1,3,7-octatriene was rapid. However, the amount of the triene decreased gradually. The decrease seems to be due to the consumption of 1,3,7-octatriene for the formation of its adducts by the reaction of the triene with benzyl alcohol. Vpc showed an unidentified peak near that of 1-benzyloxy-2,7-octadiene.

Results of the reactions of benzyl alcohol with phenoxyoctadiene by several palladium and platinum catalysts are shown in Table 2. Platinum catalysts and a mixture of palladium acetate and triphenylphosphine are also effective, but a combination of palladium chloride and sodium phenoxide did not show any catalytic activity. Apparently, the reaction by tetrakistriphenylphosphine complexes of Pd(0) and Pt(0) gives a larger amount of 1,3,7-octatriene than bistriphenylphosphine complexes of Pd(II) and Pt(II), and the reaction by the platinum catalysts affords a much larger amount of the branched product (IIIk) than the palladium catalysts. The allyl group of 1-phenoxy-2-propene also migrated to benzyl alcohol in the presence of $PdCl_2(Ph_3P)_2$ and sodium phenoxide to give 1-benzyloxy-2-propene (III) in an 82% yield.

The reaction of the phenoxyoctadienes consisting of 1-phenoxy-2,7-octadiene(92%) and 3-phenoxy-1,7-octadiene(8%), with acetic acid in the presence of palladium acetate and triphenylphosphine proceeded to give octadienyl acetate(IIm) and (IIIm) in 32 and 6% yields based on the phenoxyoctadienes, respectively, and a small amount of 1,3,7-octatriene. The reaction in dimethylformamide as a solvent proceeded more smoothly to give IIm and IIIm in 40 and 16% yields, respectively.

Easy fission of the allylic carbon-oxygen bond is shown by the reversibility of the above reaction. It is interesting to note that the reverse reaction using a 74:26 mixture of IIm and IIIm resulted in a predominant formation of 1-phenoxy-2,7-octadiene (ratio of the linear to the branched 97:3).

$$PhOCH_2CH=CH(CH_2)_3CH=CH_2 \underset{PhOH}{\overset{CH_3COOH}{\rightleftharpoons}} CH_3CO_2CH_2CH=CHCH_2CH_2CH_2CH=CH_2 \quad \text{IIm}$$

$$+ CH_3CO_2CH(CH=CH_2)CH_2CH_2CH_2CH=CH_2 \quad \text{IIIm}$$

Benzoic acid reacted similarly with the phenoxyoctadienes in the presence of palladium acetate and triphenylphosphine to afford a 70:30 mixture of octadienyl benzoate (IIn) and (IIIn) in a 60% yield.

Reaction of Allyl and Substituted-allyl Alkoxides. 1-Phenoxy-2,7-octadiene reacts readily with active hydrogen compounds in the presence of palladium catalysts to give 2,7-octadienyl derivatives of the active hydrogen compounds. However, 1-alkoxy-2,7-octadienes such as 1-methoxy-2,7-octadiene and 1-benzyloxy-2,7-octadiene did not react with amines and active methylene compounds under similar conditions. It was found, however, that the alkoxyoctadienes react with phenol to give 1-phenoxy-2,7-octadiene and alcohols, and that the reaction is reversible although the equilibrium exists between the alkoxyoctadienes and phenol. The reaction of the benzyloxyoctadienes(a 97:3 mixture of IIk and IIIk) with phenol by the $PdCl_2(Ph_3P)_2$-sodium phenoxide catalyst gave an 86:14 mixture of 1-phenoxy-2,7-octadiene and 3-phenoxy-1,7-octadiene in a 7% yield. The reaction of methoxyoctadienes with phenol afforded phenoxyoctadienes in a 3% yield.

The results suggest that the presence of phenol makes it possible for the reaction of the alkoxyoctadienes with amines and active methylene compounds to give the corresponding octadienyl derivatives of the active hydrogen compounds through the two successive exchanges of the octadienyl group, as shown by the following equation.

$$R'\text{-}O\text{-}C_8H_{13} + Ph\text{-}OH \rightleftharpoons PhO\text{-}C_8H_{13} + R'\text{-}OH$$
$$PhO\text{-}C_8H_{13} + R''\text{-}H \longrightarrow R''\text{-}C_8H_{13} + PhOH$$

$R'=CH_3$, $C_6H_5CH_2$
R''-H = active hydrogen compounds
C_8H_{13} = 2,7-octadienyl group

TABLE 4. REACTION OF ALLYL AND SUBSTITUTED-ALLYL ALKOXIDES WITH ACTIVE HYDROGEN COMPOUNDS

Alkoxy compound mol	Active hydrogen compound mol	Catalyst[c] mmol $PdCl_2(Ph_3P)_2$-	PhONa	Temp. °C	Time hr	Product	Yield[d] %
$PhCH_2OC_8H_{13}$[a] 0.05	$CH_3COCH_2CO_2CH_3$ 0.1	0.1	1.0	85	18	$CH_2=CH(CH_2)_3CH=CHCH_2$-$CH(COCH_3)CO_2CH_3$	46
$CH_3OC_8H_{13}$[b] 0.05	$CH_3COCH_2CO_2CH_3$ 0.1	0.1	1.0	85	16	$CH_2=CH(CH_2)_3CH=CHCH_2$-$CH(COCH_3)CO_2CH_3$	74
$PhCH_2OCH_2CH=CH_2$ 0.025	$CH_3COCH_2CO_2CH_3$ 0.05	0.05	0.5	85	15	$CH_2=CHCH_2CH(COCH_3)$-CO_2CH_3	42
						$(CH_2=CHCH_2)_2C(COCH_3)$-CO_2CH_3	4
$PhCH_2OC_8H_{13}$ 0.05	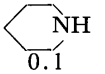 0.1	0.1	1.0	80	40	$CH_2=CH(CH_2)_3CH=CHCH_2$	78
$CH_3OC_8H_{13}$ 0.05	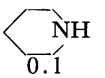 0.1	0.1	1.0	85	24	$CH_2=CH(CH_2)_3CH=CHCH_2$	57
$CH_2=CHCH_2OCH_2CH=$ $CH(CH_2)_3$–$CH=CH_2$ 0.025	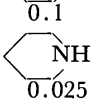 0.025	0.05	0.5	95	36	$CH_2=CH(CH_2)_3CH=CHCH_2$	12
						$CH_2=CHCH_2$	24

a) A mixture of 1-benzyloxy-2,7-octadiene (97%) and 3-benzyloxy-1,7-octadiene (3%)
b) A mixture of 1-methoxy-2,7-octadiene (99%) and 3-methoxy-1,7-octadiene (1%)
c) The reaction was carried out in the presence of an equivalent amount of phenol to that of the active hydrogen compounds.
d) Based on the alkoxy compounds

TABLE 5. REACTION OF ALLYL AND SUBSTITUTED-ALLYL CARBOXYLATES WITH ACTIVE-HYDROGEN COMPOUNDS

Carboxylate[a]	Active hydrogen Compound[c]	Catalyst mmol $PdCl_2(Ph_3P)_2$-	PhONa	Temp. °C	Time hr	Product[f]	Yield[g] %
$CH_3CO_2C_8H_{13}$[b]	$CH_3CH_2CO_2H$	0.05[d]	0.2[e]	85	15	$CH_3CH_2CO_2X$	37
						$CH_3CH_2CO_2Y$	13
						1,3,7-OT	trace
$CH_3CO_2C_8H_{13}$	$PhCO_2H$	0.05[d]	0.2[c]	85	15	$PhCO_2X$	27
						$PhCO_2Y$	16
						1,3,7-OT	12
$CH_3CO_2C_8H_{13}$*1	PhOH*2	0.1	1.0	85	24	PhOX	27
						PhOY	1
						1,3,7-OT	24
$CH_3CO_2CH_2CH=CH_2$	PhOH	0.05	0.5	85	17	$PhOCH_2CH=CH_2$	14
$CH_3CO_2CH_2CH=CH_2$	$PhCH_2OH$	0.05	0.5	70	20	$PhCH_2OCH_2CH=CH_2$	10
$CH_3CO_2C_8H_{13}$	$PhCH_2OH$	0.05	0.5	85	24	$PhCH_2OX$	19
$CH_3CO_2C_8H_{13}$	CH_3OH	0.05	0.5	70	18	CH_3OX	7
$CH_3CO_2CH_2CH=CH_2$	$CH_3COCH_2CO_2CH_3$	0.05	0.5	85	20	$CH_2=CHCH_2CH(COCH_3)$-CO_2CH_3	17
$CH_3CO_2C_8H_{13}$	$CH_3COCH_2CO_2CH_3$	0.05	0.5	85	20	X–$CH(COCH_3)CO_2CH_3$	15
$CH_3CO_2C_8H_{13}$	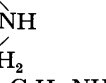	0.05	0.5	85	1		93
$CH_3CO_2C_8H_{13}$	$PhNH_2$	0.05	0.5	85	1	PhNH–X	89
$CH_3CO_2C_8H_{13}$	cyclo-$C_6H_{11}NH_2$	0.05	0.5	100	1	cyclo-C_6H_{11}NH–X	31
$CH_3CO_2CH_2CH=CH_2$	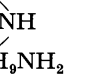	0.05	0.5	85	1		90
$CH_3CO_2CH_2CH=CH_2$	t-$C_4H_9NH_2$	0.05	0.5	85	1	t-$C_4H_9NHCH_2CH=CH_2$	46

a) 0.025 mol except *1 (0.05 mol)
b) Octadienyl acetate ($CH_3CO_2C_8H_{13}$) was a mixture of 2,7-octadienyl acetate (74%) and 1-vinyl-5-hexenyl acetate (26%).
c) 0.05 mol except *2 (0.1 mol)
d) $Pd(OAc)_2$
e) Ph_3P
f) $X=CH_2=(CH_2)_3CH=CHCH_2$-, $Y=CH_2=CH(CH_2)_3CH(CH=CH_2)$-, 1,3,7-OT = $CH_2=CHCH=CHCH_2CH_2CH=CH_2$
g) Based on the allyl or substituted-allyl carboxylate employed.

TABLE 6. PHYSICAL AND ANALYTICAL DATA OF THE PRODUCTS

Product[a]	Bp °C/mmHg	n_D^{25}	Empirical formula	Calcd C (%)	Calcd H (%)	Calcd N (%)	Calcd Mol wt	Found C (%)	Found H (%)	Found N (%)	Found Mol wt
$(C_2H_5)_2NCH_2CH=CH_2$	112	1.4186	$C_7H_{15}N$	74.27	13.36	12.37	113	74.05	13.34	12.29	113[c]
$(C_2H_5)_2NCH_2CH=CHCH_3$	135	1.4298	$C_8H_{17}N$	75.52	13.47	11.01	127	75.32	13.47	11.07	127[c]
$(C_2H_5)_2NCH_2C(CH_3)=CH_2$	123.5	1.4208	$C_8H_{17}N$	75.52	13.47	11.01	127	75.64	13.57	11.01	127[c]
t-$C_4H_9NHCH_2CH=CH_2$	107.5	1.4162	$C_7H_{15}N$	74.27	13.36	12.37	113	74.06	13.45	12.50	113[c]
t-$C_4H_9N(CH_2CH=CH_2)_2$	164	1.4428	$C_{10}H_{19}N$	78.36	12.50	9.14	153	78.27	12.51	9.29	153[c]
$CH_2=CHCH_2$-(N,N)-NCH_2-$CH=CH_2$	200	1.4748	$C_{10}H_{18}N_2$	72.24	10.91	16.85	166	71.95	10.84	16.70	166[c]
cyclo-C_6H_{11}-NH-X	117—118/2	1.4813	$C_{14}H_{25}N$	81.09	12.15	6.76	205	81.06	12.18	6.49	207
$CH_2=CHCH_2CH(COCH_3)$-CO_2CH_3	188	1.4398	$C_8H_{12}O_3$	61.52	7.75		156	61.31	8.02		156[c]
$(CH_2=CHCH_2)_2C(COCH_3)$-CO_2CH_3	131/38	1.4576	$C_{11}H_{16}O_3$	67.32	8.27		196	67.66	8.27		196
p-$CH_3C_6H_4OCH_2CH=CH_2$	95/12	1.5163	$C_{10}H_{12}O$	81.04	8.16		148	81.04	7.93		153
p-$ClC_6H_4OCH_2CH=CH_2$	107/12	1.5342	C_9H_9OCl	64.11	5.38	21.03[b]	167	64.30	5.63	20.75[b]	172
$PhCH_2O$-X	126—129/3	1.5050	$C_{15}H_{20}O$	83.28	9.32		216	83.26	9.33		212
$PhCH_2O$-Y	102—104/1.8	1.4990	$C_{15}H_{20}O$	83.28	9.32		216	82.91	9.08		216
PhCOO-X	143—144/5	1.5136	$C_{15}H_{18}O_2$	78.23	7.88		230	78.34	7.99		226
PhCOO-Y	79/0.1	1.5081	$C_{15}H_{18}O_2$	78.23	7.88		230	77.83	8.03		222
CH_3CH_2COO-X	80—84/5[d]	1.4481	$C_{11}H_{18}O_2$	72.49	9.96		182	72.46	9.71		186
CH_3CH_2COO-Y		1.4370	$C_{11}H_{18}O_2$	72.49	9.96		182	72.37	9.71		185
$PhCH_2OCH_2CH=CH_2$	87—88/10	1.5079	$C_{10}H_{12}O$	81.04	8.16		148	80.89	8.12		154
N-$CH_2CH=CH_2$	62/50	1.4608	$C_8H_{15}N$	76.73	12.08	11.19	125	76.41	12.28	11.03	125[c]

a) X=CH_2=$CH(CH_2)_3CH$=$CHCH_2$-, Y=CH_2=$CH(CH_2)_3CH(CH$=$CH)$-,
b) Cl
c) Determined by mass spectroscopy. The other quantities were measured by vapor pressure osmometry.
d) Mixture of linear and branched compounds.

The reaction of the benzyloxyoctadiene with piperidine in the presence of phenol and a palladium catalyst gave the expected octadienyl piperidine. The reaction is applicable to 1-alkoxy-2-alkenes. The reaction of 1-benzyloxy-2-propene with methyl acetoacetate in the presence of the palladium catalyst and phenol afforded methyl 2-acetyl-4-pentenoate and methyl 2-acetyl-2-(2-propenyl)-4-pentenoate. The results are summarized in Table 4. The reaction was much slower than that of 1-phenoxy-2-propene with methyl acetoacetate.

The reaction of 1-(2-propenyloxy)-2,7-octadiene with piperidine proceeded to give two products, *N*-(2,7-octadienyl)piperidine and *N*-(2-propenyl)piperidine, in 12 and 24% yields, respectively, which shows that the reactivity of the propenyl group is larger than that of the octadienyl group.

Reaction of Allyl and Substituted-allyl Carboxylates. As described, 2,7-octadienyl acetate and benzoate react with phenol in the presence of the palladium catalysts to afford 1-phenoxy-2,7-octadiene. The same type of reaction occurred between 2-propenyl acetate and active hydrogen compounds such as phenol, carboxylic acids, alcohols, amines and active methylene compounds. Results of the reactions of allyl and substituted-allyl carboxylates with the active hydrogen compounds are summarized in Table 5. The reactions proceed usually much more slowly than those of 1-phenoxy-2-propene and its derivatives, but the reaction with amines proceeds at a moderate rate.

Experimental

Reagents. $PdCl_2(Ph_3P)_2$,[12] $PdCl_2(Ph_3As)_2$,[13] $Pd(OAc)_2$,[14] $Pd(Ph_3P)_4$,[12] $Pd(Ph_3P)_2$(maleic anhydride),[15] $PtCl_2(Ph_3P)_2$[16] and $Pt(Ph_3P)_4$[16] were prepared by previously reported methods.

Methyl acetoacetate, 2-propenyl acetate and all the phenols, alcohols, amines and carboxylic acids were purified by distillation. 1-Phenoxy-2,7-octadiene,[8] 1-alkoxy-2,7-octadienes[7] and 2,7-octadienyl carboxylates[17] were prepared by the reaction of 1,3-butadiene with phenol, alcohols and carboxylic acids, respectively, in the presence of the palladium catalyst. 1-Phenoxy-2-propene,[18] 1-phenoxy-2-methyl-2-propene[18] and 1-phenoxy-2-butene[18] were prepared by the reactions of phenol with allyl chloride, methallyl chloride and crotyl chloride, respectively, in the presence of potassium carbonate. 1-Benzyloxy-2-propene was prepared by the reaction of benzyl alcohol with 1-phenoxy-2-propene in the presence of $PdCl_2(Ph_3P)_2$ and sodium phenoxide. All the reactions were carried out under argon atmosphere.

Reaction of 1-Phenoxy-2-propene with Methyl Acetoacetate. A

12) L. Malatesta and M. Angolleta, *J. Chem. Soc.*, **1957**, 1186.
13) J. L. Burmeister and F. Basolo, *Inorg. Chem.*, **3**, 1587 (1964).
14) T. Matsuda, T. Mitsuyasu, and Y. Nakamura, *Kogyo Kagaku Zasshi*, **72**, 1751 (1969).
15) P. Fitton and J. E. Mckeon, *Chem. Commun.*, **1968**, 4.
16) L. Malatesta and C. Cariells, *J. Chem. Soc.*, **1958**, 2323.
17) S. Hattori, H. Munakata, T. Suzuki, and N. Imaki, Netherland 6816008 (1969).
18) W. M. Iaver and W. F. Filbert, *J. Amer. Chem. Soc.*, **58**, 1388 (1936).

mixture of 0.05 mol of methyl acetoacetate, 0.1 mol of 1-phenoxy-2-propene, 0.05 mmol of $PdCl_2(Ph_3P)_2$ and 0.5 mmol of sodium phenoxide was stirred at 85° for 8.5 hr under argon atmosphere. The reaction mixture was subjected to distillation and the ratio of the products was determined by vpc. The product consisted of IIc(2.8 g, 18%) and IId(4.6 g, 47%). The yields were calculated on the basis of 1-phenoxy-2-propene. IIc, IR(neat)cm^{-1}: 1745 and 1722(keto ester), 1646, 995 and 922(–CH=CH_2). NMR(CCl_4) τ: 7.86(s, CH_3CO–), 7.47(t, J=7.0 Hz, =C–CH–C), 6.50(t, J=7.0 Hz, C–CH–CO), 6.34(s, CH_3O–) and 4.06—5.05(m, olefinic protons). IId, IR(neat)cm^{-1}: 1744 and 1714(keto ester), 1644, 993 and 921(CH_2=CH–). NMR(CCl_4)τ: 7.97(s, CH_3CO–), 7.46 (d, J=7.0 Hz, =C–CH_2–C), 6.34(s, CH_3O) and 4.22—5.03 (m, olefinic protons).

Reaction of 1-Phenoxy-2,7-octadiene with Cyclohexylamine. A mixture of 0.05 mol of 1-phenoxy-2,7-octadiene, 0.1 mol of cyclohexylamine, 0.1 mmol of $PdCl_2(Ph_3P)_2$ and 1.0 mmol of sodium phenoxide was stirred at 85° for 2 hr to give IIe (10.4 g, 69%). IR(neat)cm^{-1}: 1644, 991 and 911(CH_2=CH–), 968(*trans*-CH=CH–). NMR(CCl_4) τ: 9.24(s, –NH), 7.5—8.9(m, –$(CH_2)_3$– and cyclo-C_6H_{11}), 6.84(d, J=4.0 Hz, N–CH_2–C=) and 4.01—5.12(m, olefinic protons).

Reaction of 1-Phenoxy-2-methyl-2-propene with Diethylamine. A mixture of 0.05 mol of 1-phenoxy-2-methyl-2-propene, 0.1 mol of diethylamine, 0.1 mmol of $PdCl_2(Ph_3P)_2$ and 0.5 mmol of sodium phenoxide was stirred at 85° in a 100 m*l* autoclave for 1 hr to give *N*-(2-methyl-2-propenyl)diethylamine (5.6 g, 89%). IR(neat)cm^{-1}: 1654 and 893(CH_2=C<), NMR(CCl_4) τ: 9.03(t, J=7.0 Hz, CH_3–C–N–), 8.30 (s, CH_3–C=), 7.53(q, J=7.0 Hz, C–CH_2–N–), 7.14(s, –N–CH_2–C=) and 5.18—5.25(C=CH_2).

Reaction of 1-Phenoxy-2-propene with p-*Cresol.* A mixture of 0.025 mol of 1-phenoxy-2-propene, 0.025 mol of *p*-cresol, 0.05 mmol of $PdCl_2(Ph_3P)_2$ and 0.5 mmol of sodium phenoxide was stirred at 85°C for 3 hr to afford IIi(1.5 g, 41%). Unreacted 1-phenyl-2-propene(1.3 g, 40%) was recovered.

Reaction of Phenoxyoctadiene with Benzyl Alcohol. A mixture of 0.025 mol of the phenoxyoctadiene(92% 1-phenoxy-2,7-octadiene and 8% 3-phenoxy-1,7-octadiene), 0.05 mol of benzyl alcohol and 0.05 mmol of $Pd(Ph_3P)_4$ was stirred at 85°C for 2.5 hr to give 1,3,7-octatriene(1.1 g, 41%), IIk(1.3 g, 24%) and IIIk(0.6 g, 11%). IIk IR(neat)cm^{-1}: 1666 and 1640 (C=C), 991 and 908(–CH=CH_2) and 970(*trans* –CH=CH–). NMR(CCl_4) τ: 7.8—8.7(6H, m, =C–$CH_2CH_2CH_2$–C=), 6.13 (2H, d, J=5.5 Hz, –O–CH_2–C=), 5.58(2H, s, Ph–CH_2–O–), 4.0—5.2(5H, m, olefinic protons) and 2.67(5H, s, C_6H_5–). IIIk IR(neat)cm^{-1}: 1644, 991, 922, and 915(CH_2=CH–). NMR(CCl_4) τ: 7.8—8.7(6H, m, –$CH_2CH_2CH_2$–C=), 6.3(1H, m, –O–CH), 5.67 and 5.33(2H, two d, J=12.0 Hz, C_6H_5–CH_2–O–), 3.9—5.4(6H, m, olefinic protons) and 2.67(5H, s, C_6H_5–).

Reaction of Phenoxyoctadiene with Benzoic Acid. A mixture of 0.05 mol of the phenoxyoctadienes(92% 1-phenoxy-2,7-octadiene and 8% 3-phenoxy-1,7-octadiene), 0.1 mol of benzoic acid, 0.1 mmol of $Pd(OAc)_2$, 0.25 mmol of triphenylphosphine and 10 m*l* of dimethylformamide was stirred at 85°C for 24 hr. The product consisted of IIn(4.9 g, 42%), IIIn(2.1 g, 18%) and a trace amount of 1,3,7-octatriene. The unreacted phenoxyoctadienes(3.8 g) were recovered. IIn, IR(neat)cm^{-1}: 1720(ester), 1672 and 966(*trans* –CH=CH–), 1643, 988, and 907(CH_2=CH–). NMR(CCl_4) τ: 8.25—8.75 (2H, m, –CH_2–C–C=), 7.70—8.15(4H, m, =C–CH_2–C–CH_2–C=), 5.28(2H, d, J=6.5 Hz, –O–CH_2–) and 3.9—5.25(5H, m, olefinic protons). IIIn, IR(neat)cm^{-1}: 1720(ester), 1644, 990, 922(sh), and 916(CH_2=CH–). NMR(CCl_4) τ: 7.7—8.8 (6H, m, –$CH_2CH_2CH_2$–) and 3.85—5.25(7H, m, –O–CH– and olefinic protons).

Reaction of 1-Methoxy-2,7-octadiene with Methyl Acetoacetate. A mixture of 0.05 mol of 1-methoxy-2,7-octadiene, 0.1 mol of methyl acetoacetate, 0.1 mmol of $PdCl_2(Ph_3P)_2$, 1.0 mmol of sodium phenoxide and 0.05 mol of phenol was stirred at 85°C for 16 hr to give IIa in a 74% yield. IR(neat)cm^{-1}: 1748 and 1724(>C=O), 1644(C=C), 992 and 911(–CH=CH_2) and 971(*trans* –CH=CH–). NMR(CCl_4) τ: 8.61(2H, m, –C–CH_2–C–), 8.04(4H, m, =C–CH_2–C–CH_2–C=), 7.88(3H, s, –CO–CH_3), 7.55(2H, t, J=7.0 Hz, =C–CH_2–C–CO=), 6.51 (1H, t, J=7.0 Hz, –C–CH–CO–), 6.34(3H, s, –O–CH_3) and 3.98—5.16(5H, m, olefinic protons).

Reaction of 1-(2-Propenyloxy)-2,7-octadiene with Piperidine. A mixture of 0.025 mol of 1-(2-propenyloxy)-2,7-octadiene, 0.05 mol of piperidine, 0.1 mol of $PdCl_2(Ph_3P)_2$, 1.0 mmol of sodium phenoxide and 0.025 mol of phenol was stirred at 85°C for 20 hr and at 110°C for 16 hr. The product consisted of *N*-(2,7-octadienyl)piperidine(0.6 g, 12%) and *N*-(allyl)piperidine(0.75 g, 24%). *N*-(Allyl)piperidine showed the following spectral characteristics. IR(neat)cm^{-1}: 1643, 993, and 915(CH_2=CH–). NMR(CCl_4) τ: 8.52 and 7.70(protons of piperidine ring), 7.13(2H, d, J=7.0 Hz, N–CH_2–) and 3.8—5.1(3H, m, olefinic protons).

Reaction of Octadienyl Acetate with Propionic Acid. A mixture of 0.025 mmol of octadienyl acetate(74% 2,7-octadienyl acetate and 26% 1-vinyl-5-hexenyl acetate), 0.05 mol of propionic acid, 0.05 mmol of $Pd(OAc)_2$, 0.2 mmol of triphenylphosphine and 5 m*l* of dimethylformamide was stirred at 85°C for 15 hr. The product consisted of 1,7-octadienyl propionate(1.7 g, 37%), 1-vinyl-5-hexenyl propionate(0.6 g, 13%) and a trace amount of 1,3,7-octatriene.

Reaction of Octadienyl Acetate with Aniline. A mixture of 0.025 mol of the octadienyl acetate(74% 2,7-octadienyl acetate and 26% 1-vinyl-5-hexenyl acetate), 0.05 mol of aniline, 0.05 mmol of $PdCl_2(Ph_3P)_2$ and 0.5 mmol of sodium phenoxide was stirred at 85°C for 1 hr. To the reaction mixture 10 m*l* of water was added, and the organic layer was extracted with ether to give *N*-(2,7-octadienyl)aniline (4.5 g, 89%).

Studies of Benzoylsulfene. V.[1] The Reaction of Benzoylsulfene with Enamines

Otohiko TSUGE, Sumio IWANAMI, and Shigeru HAGIO[2]
Research Institute of Industrial Science, Kyushu University, Hakozaki, Fukuoka
(Received June 9, 1971)

The reaction of benzoylmethanesulfonyl chloride with enamines derived from cyclohexanone in the presence of triethylamine has been studied. The chloride reacted with 1-(1-morpholino)- and 1-(1-piperidino)cyclohexene in the presence of triethylamine, affording the corresponding acyclic sulfones. On the other hand, the reaction of the chloride with 1-(1-pyrrolidinyl)cyclohexene gave 2-benzoylmethanesulfonylcyclohexanone and 2,3-dibenzoyl-2,3,4,5,6,7-hexahydrothianaphthene 1,1-dioxide. The latter compound, whose structure corresponded to the compound derived from the 2:1 adduct of benzoylsulfene and the enamine with the elimination of sulfur dioxide and pyrrolidine, reacted with hydrazine hydrate to give 1,4-diphenyl-5*a*,6,7,8,9,9*a*-hexahydrothianaphtheno[2,3-*d*]-pyridazine, which was then transformed into 3,4,6-triphenylpyridazine.

In general, sulfenes ($RCH{=}SO_2$) generated *in situ* from aliphatic sulfonyl chlorides and triethylamine (NEt_3) react with enamines derived from aldehydes and cyclic ketones to give four-membered cyclic sulfones. Examples are the additions of methanesulfonyl chloride to 2-methyl-1-pyrrolidinyl-1-propene[3] and 1-(1-morpholino)cyclohexene[4] in the presence of NEt_3, which gave the corresponding thiethane 1,1-dioxides.

However, the study concerning the reaction of benzoylmethanesulfonyl chloride (I) with an enamine in the presence of NEt_3 has not been extended beyond that of Opitz,[5] who reported that the reaction of benzoylsulfene ($PhCOCH{=}SO_2$), generated from I and NEt_3, with 2-methyl-1-pyrrolidinyl-1-propene gave the four-membered cyclic sulfone, whose structure corresponded to the (2+2) cycloadduct of benzoylsulfene to the enamine.

$$\underset{\text{I}}{PhCOCH_2SO_2Cl} \xrightarrow[NEt_3]{-HCl} [PhCOCH{=}SO_2]$$

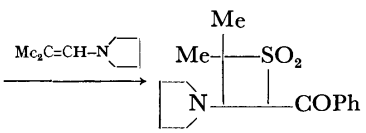

In previous papers, the reactions of I with anils[6] and carbodiimides[7] in the presence of NEt_3 were investigated and it was found that the corresponding (4+2) and/or (2+2) cycloadducts of benzoylsulfene to the C=N bond were formed. These facts indicate that benzoylsulfene is more reactive than usual sulfenes ($RCH{=}SO_2$) and that, in the cycloaddition reaction benzoylsulfene behaves as a 1,2- or 1,4-dipole.

We plan to develop the cycloaddition reactions of benzoylsulfene with various compounds. In the present paper we wish to report on the reaction of benzoylsulfene with enamines derived from cyclohexanone, which unexpectedly led to the formation of acyclic sulfones and an abnormal product.

Results and Discussion

The reaction of benzoylmethanesulfonyl chloride (I) with equimolar amounts of 1-(1-morpholino)cyclohexene (IIa) and NEt_3 in dioxane at room temperature for 1.5 hr gave a crystalline compound, IIIa, mp 135°C (decomp.), in a 61% yield, besides triethylammonium chloride in a quantitative yield. The results of elemental analysis and the molecular weight (M^+ *m/e* 349) of IIIa were consistent with the expected 1:1 adduct of benzoylsulfene and IIa. The IR spectrum of IIIa exhibited characteristic bands ascribed to the $\nu_{C=O}$ and $\nu_{C=C}$ at 1685 and 1640 cm^{-1} respectively. On the other hand, the NMR spectrum in deuteriochloroform ($CDCl_3$) showed signals at τ 5.5 (1H, $\geqslant$C<u>H</u>, multiplet), 5.13 and 4.63 (each 1H, $-SO_2-C\underline{H}_2-COPh$, doublet, J= 15 Hz), and 4.56 (1H, =C<u>H</u>–, triplet, J=3.7 Hz), besides signals of cyclohexenyl- and morpholino-methylene protons and of phenyl protons.

On the basis of these spectral data and the following chemical transformations, it seems reasonable to conclude that IIIa is 6-benzoylmethanesulfonyl-1-(1-morpholino)cyclohexene.

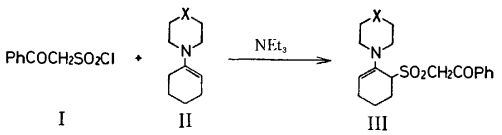

I II III

a: X=O, b: X=CH_2

The hydrolysis of IIIa with dilute hydrochloric acid gave 2-benzoylmethanesulfonylcyclohexanone (IV), mp 103°C (decomp.), in an almost quantitative yield; its structure was confirmed by the spectral studies as well as by the elemental analysis. Furthermore, IIIa reacted with I in the presence of NEt_3 to afford 1,3-di(benzoylmethanesulfonyl)-2-(1-morpholino)cyclohexene (V), mp 152.5—153°C (decomp.), which was subsequently hydrolyzed to 2,6-di(benzoylmethanesulfonyl)-cyclohexanone (VI), mp 141—142°C, in a 37% yield. The structures of V and VI were established on the basis of the spectral studies and of the elemental analyses.

1) Part IV in this series: O. Tsuge and S. Iwanami, This Bulletin, **44**, 2750 (1971).
2) Present address: Sanyo Kasei Co., Ltd., Kyoto-shi.
3) G. Opitz and H. Adolph, *Angew. Chem.*, **74**, 77 (1962).
4) G. Stork and I. Borowitz, *J. Amer. Chem. Soc.*, **84**, 313 (1962).
5) G. Opitz, *Angew. Chem.*, **79**, 162 (1967).
6) O. Tsuge and S. Iwanami, This Bulletin, **43**, 3543 (1970).
7) O. Tsuge and S. Iwanami, *Nippon Kagaku Zasshi*, **92**, 448 (1971).

The mass spectrum of IIIa was also in harmony with the proposed structure.

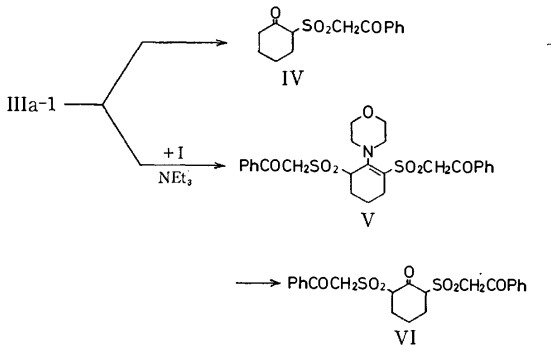

A similar reaction of I with 1-(1-piperidino)cyclohexene (IIb) in the presence of NEt_3 gave 6-benzoylmethanesulfonyl-1-(1-piperidino)cyclohexene (IIIb), mp 151°C (decomp.), in a 61% yield.

On the other hand, I reacted with 1-(1-pyrrolidinyl)-cyclohexene (IIc) under similar conditions to give IV and a novel product, VII, mp 183°C (decomp.), in 11 and 22% yields respectively.

The compound VII was assumed, as a result of the spectral studies and the elemental analysis as well as the chemical transformations, to be 2,3,4,5,6,7-hexahydro-2,3-dibenzoylthianaphthene 1,1-dioxide. The molecular formula ($C_{22}H_{20}O_4S$) of VII was in agreement with that of the compound derived from a 2:1 adduct of benzoylsulfene and IIc upon the elimination of sulfur dioxide and pyrrolidine. It is obvious that VII contains two benzoyl groups in the molecule, because the hydrolysis of VII with methanolic sodium hydroxide afforded two moles of benzoic acid per mole of VII, and the IR spectrum of VII showed characteristic bands at 1670 ($\nu_{C=O}$), 1300 and 1130 cm^{-1} (ν_{SO_2}). In the mass spectrum, the parent ion peak (M^+) appeared at *m/e* 380, together with major peaks at *m/e* 316 (M^+-SO_2), 211 (316^+-PhCO), 106 (211^+-PhCO) and 105 ($PhCO^+$).

The NMR spectrum of VII is illustrated in Fig. 1. As is shown in Fig. 1, two methine protons appeared at τ 4.48 (1H, doublet with J=5.5 Hz) and 4.20 (1H, multiplet, changed to a doublet with J=5.5 Hz when irradiated at τ 7.6 (2H, quasi-equatorial protons at the 4- and 7-positions)) respectively.

Furthermore, VII reacted with hydrazine hydrate to give 1,4-diphenyl-5*a*,6,7,8,9,9*a*-hexahydrothianaphtheno[2,3-*d*]pyridazine (VIII), mp 198°C (decomp.), in a quantitative yield. The structure of VIII was confirmed by the spectral studies and elemental analysis as well as by the chemical transformation. The NMR spectrum of VIII in $CDCl_3$ showed a multiplet (2H, two methine protons) at τ 6.35; this fact seems to exclude the possibility of an alternate structure, VIII', for VIII.

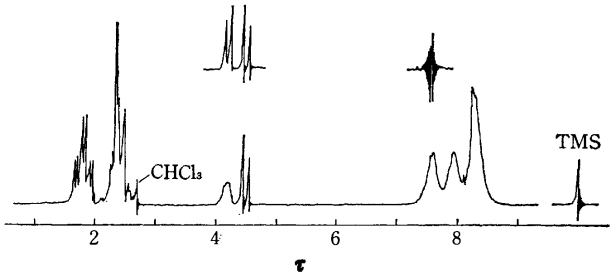

Fig. 1. NMR spectrum of VII in $CDCl_3$.

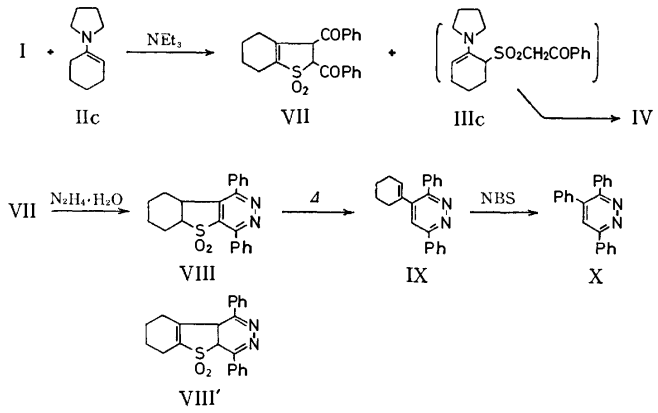

The thermal decomposition of VIII at 210°C gave 4-(1-cyclohexenyl)-3,6-diphenylpyridazine (IX), mp 160°C, whose structure was established by the spectral studies and by the transformation to 3,4,6-triphenylpyridazine (X) in a 33% yield. The treatment of IX with *N*-bromosuccinimide in carbon tetrachloride afforded X, mp 176°C (lit,[8] mp 176—177.5°C), which was identical with an authentic sample prepared by the reported method.[8]

Incidentally, the formation of IV in the reaction of I with IIc may be illustrated by the hydrolysis of the initially-formed 6-benzoylmethanesulfonyl-1-(1-pyrrolydinyl)cyclohexene (IIIc).

It is known that, in the reaction of sulfonyl chlorides with enamines in the presence of NEt_3, the formation of acyclic sulfones is favored by increasing the substitution at the α-carbon of the sulfonyl chloride and also of the enamine.[9] Recently, Looker[10] found that the additions of methanesulfonyl and arenesulfonyl chlorides to 1,3-diphenyl-2-(1-pyrrolidinyl)propene in the presence of NEt_3 gave the corresponding acyclic sulfones, and suggested that the acyclic sulfones were formed by the ring opening of the initially-formed cyclic sulfones.

The reaction of methanesulfonyl chloride with IIa gave the four-membered cyclic sulfones, as was mentioned at the beginning of this paper, while phenylmethanesulfonyl chloride reacted with IIc to afford, on hydrolysis, 2-phenylmethanesulfonylcyclohexanone, which was assumed to be derived from 1-phenylmethanesulfonyl-2-(1-pyrrolidinyl)cyclohexene.[10]

It is, then, of interest to form acyclic sulfones III and/or the hexahydrothianaphthene VII *via* the reaction of benzoylsulfene with II.

Although the exact course of the reaction of benzoylsulfene with II is not clear, the formation of the betaine intermediate by a two-step sequence (the formation of a betaine intermediate, followed by proton transfer)

8) R. A. Carboni and R. V. Lindsey, Jr., *J. Amer. Chem. Soc.*, **81**, 4342 (1959).

9) A. G. Cook, "Enamines: Synthesis, Structure, and Reactions," Marcel Dekker, New York and London (1969), p. 115.

10) J. J. Looker, *J. Org. Chem.*, **31**, 2973 (1966).

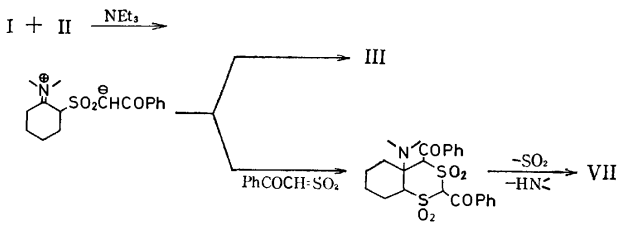

seems more reasonable than that through the ring opening of a cyclic sulfone. On the other hand, the formation of VII may be explained if the further addition of benzoylsulfene to the betaine intermediate and the subsequent elimination of both sulfur dioxide and pyrrolidine are assumed.

Experimental

All the melting points are uncorrected. The IR spectra were measured in KBr disks, while the NMR spectra were recorded on a 60 MHz Hitachi R-20 NMR spectrometer, using TMS as the internal reference. The mass spectra were obtained on a Hitachi RMS-4 mass spectrometer, using a direct inlet and an ionization energy of 70 eV.

Materials. Benzoylmethanesulfonyl chloride (I), mp 88°C (lit,[11] mp 87.5—88.2°C), was prepared according to the method of Truce and Vriesen.[11] 1-(1-Morpholino)- (IIa), bp 105—107°C/10 mmHg (lit,[12] bp 113—114°C/12 mmHg), 1-(1-piperidino)- (IIb), bp 107—109°C/13 mmHg (lit,[13] bp 108.5/12 mmHg) and 1-(1-pyrrolidinyl)cyclohexene (IIc), bp 87—88°C/3 mmHg (lit,[13] bp 110—111°C/12 mmHg) were prepared from cyclohexanone and the corresponding amines.

Reaction of I with IIa in the Presence of NEt_3. To a solution of 1.7 g (0.01 mol) of IIa and 1.0 g (0.01 mol) of NEt_3 in 10 m*l* of dioxane, a solution of 2.2 g (0.01 mol) of I in 40 m*l* of dioxane was added, drop by drop, at room temperature over a period of 30 min while the mixture was being stirred. After the reaction mixture had been stirred at the same temperature for 1 hr, triethylammonium chloride precipitated in a quantitative yield was removed by filtration. The filtrate was evaporated *in vacuo* to leave a residue, which was crystallized on trituration with methanol. Recrystallization from methanol gave 6-benzoylmethanesulfonyl-1-(1-morpholino)cyclohexene (IIIa) mp 135°C (decomp.), as colorless prisms. Yield, 2.2 g (61%).

Found: C, 61.90; H, 6.73; N, 3.97%. Calcd for $C_{18}H_{23}O_4NS$: C, 61.88; H, 6.64; N, 4.01%.

NMR ($CDCl_3$): τ 6.7—8.4 (10H, C<u>H</u>$_2$ in cyclohexenyl ring and –C<u>H</u>$_2$–N–C<u>H</u>$_2$–, multiplet), 6.38 (4H, –C<u>H</u>$_2$–O–C<u>H</u>$_2$–, triplet), 5.5 (1H, >C<u>H</u>, multiplet), 5.13, 4.63 (each 1H, –SO_2–C<u>H</u>$_2$–COPh, doublet, J=15 Hz), 4.56 (1H, =C<u>H</u>–, triplet, J=3.7 Hz), 2.3—2.55 (3H, 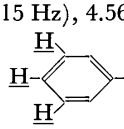 , multiplet), 1.8—2.1 (2H, 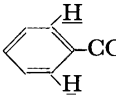 , multiplet). Mass: *m/e* 349 (M^+), 285 (M^+–SO_2), 268 (285$^+$–OH), 180 (285$^+$–PhCO), 167 (285$^+$–PhCOCH), 166, 165, 164, 163, 120 ($PhCOCH_3^+$), 105 ($PhCO^+$), 86 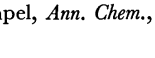 , 77 (Ph^+).

A similar reaction of I with IIb in the presence of NEt_3 gave 6-benzoylmethanesulfonyl-1-(1-piperidino)cyclohexene (IIIb), mp 151°C (decomp.), as colorless prisms in a 61% yield.

Found: C, 65.68; H, 7.50; N, 4.00%. Calcd for $C_{19}H_{25}O_3NS$: C, 65.69; H, 7.25; N, 4.03%.

IR: cm^{-1} 1685 ($\nu_{C=O}$), 1640 ($\nu_{C=C}$), 1300, 1115 (ν_{SO_2}). NMR ($CDCl_3$): τ 6.1—8.9 (16H, C<u>H</u>$_2$ in rings, multiplet), 5.5 (1H, >CH, multiplet), 4.8—5.3 (2H, –SO_2–C<u>H</u>$_2$–COPh, multiplet), 4.6 (1H, =C<u>H</u>–, broad triplet), 2.3—2.6 (3H, 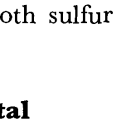 , multiplet), 1.8—2.0 (2H, , multiplet). Mass: *m/e* 347 (M^+), 283 (M^+–SO_2), 178 (283$^+$–PhCO), 165 (283$^+$–PhCOCH), 164, 163, 120 ($PhCOCH_3^+$), 105 ($PhCO^+$), 84 , 77 (Ph^+).

Hydrolysis of IIIa. After a suspension of 100 mg of IIIa in 6 m*l* of 1N aqueous hydrochloric acid had been stirred at room temperature for 1 hr, the crystals were collected by filtration, washed with water, and then dried; yield, 75 mg (93%). Recrystallization from methanol gave 2-benzoylmethanesulfonylcyclohexanone (IV), mp 103°C (decomp.), as colorless prisms.

Found: C, 59.95; H, 5.82%. Calcd for $C_{14}H_{16}O_4S$: C, 59.99; H, 5.75%. IR: cm^{-1} 1710, 1680 ($\nu_{C=O}$). NMR ($CDCl_3$): τ 7.2—8.4 (8H, CH_2 in cyclohexanone ring, multiplet), 5.55 (1H, >CH, double doublet, J=6 and 8 Hz), 1.9—2.6 (5H, phenyl protons, multiplet). Mass: *m/e* 280 (M^+), 216 (M^+–SO_2), 215, 188 (216$^+$–CO), 161 (M^+–$PhCOCH_2$), 120 ($PhCOCH_3^+$), 105 ($PhCO^+$), 77 (Ph^+).

Similarly, 100 mg of IIIb were hydrolyzed with hydrochloric acid to afford 74 mg (92%) of IV.

Reaction of IIIa with I in the Presence of NEt_3. To a stirred solution of 2.2 g of IIIa and 0.6 g of NEt_3 in 20 m*l* of dioxane, a solution of 1.4 g of I in 30 m*l* of dioxane was added, drop by drop, at room temperature over a period of 30 min. After the reaction mixture had been stirred at the same temperature for 30 min, triethylammonium chloride (0.85 g, 96%) was removed by filtration. The filtrate was evaporated *in vacuo* to leave a residue, from which IIIa (1.1 g, 48%) was separated when it was treated with 10 m*l* of methanol. The methanol filtrate was allowed to stand overnight to afford 1.1 g (37%) of 1,3-di(benzoylmethanesulfonyl)-2-(1-morpholino)cyclohexene (V), which, on recrystallization from methanol, gave colorless prisms, mp 152.5—153°C (decomp.).

Found: C, 58.93; H, 5.76; N, 2.93%. Calcd for $C_{26}H_{29}O_7NS_2$: C, 58.75; H, 5.50; N, 2.63%. IR: cm^{-1} 1680 ($\nu_{C=O}$), 1610 ($\nu_{C=C}$), 1300, 1120 (ν_{SO_2}). NMR ($CDCl_3$): τ 6.0—8.5 (14H, C<u>H</u>$_2$ in cyclohexenyl and morpholino ring, multiplet), 5.18, 5.32 (each 1H, –SO_2–C<u>H</u>$_2$–COPh, doublet, J=17.5 Hz), 4.70, 5.11 (each 1H, –SO_2–C<u>H</u>$_2$–COPh, doublet, J=14.5 Hz), 5.10 (1H, >CH, multiplet), 1.8—2.6 (10H, phenyl protons, multiplet). Mass: *m/e* 349 (M^+–$PhCOCH{=}SO_2$).

Hydrolysis of V. A suspension of 0.3 g of V in 15 m*l* of methanol was refluxed with 0.5 m*l* of concentrated hydrochloric acid for 3 hr. The reaction mixture was then evaporated *in vacuo* to leave crystals, which, on recrystallization from a benzene-petroleum benzine (bp 45—60°C) mixture, gave 0.23 g (95%) of 2,6-di(benzoylmethanesulfonyl)cyclohexanone (VI), mp 141—142°C, as colorless prisms.

Found: C, 56.99; H, 4.54%. Calcd for $C_{22}H_{22}O_7S_2$: C,

11) W. E. Truce and C. W. Vriesen, *J. Amer. Chem. Soc.*, **75**. 2525 (1953).

12) R. Dulon, E. Elikik, and A. Veillard, *Bull. Soc. Chim. Fr.* **1960**, 967.

13) G. Opitz and E. Tempel, *Ann. Chem.*, **699**, 74 (1966).

57.14; H, 4.80%. IR: cm^{-1} 1712 ($\nu_{C=O}$), 1680 ($\nu_{C=O}$), 1310, 1125 (ν_{SO_2}). NMR ($CDCl_3$): τ 7.0—8.2 (6H, $C\underline{H}_2$ in cyclohexanone ring, multiplet), 5.3 (2H, $\geq C\underline{H}$, multiplet), 5.05 (4H, $-SO_2-C\underline{H}_2-COPh$, singlet), 1.9—2.7 (10H, phenyl protons, multiplet).

Reaction of I with IIc in the Presence of NEt_3. The reaction of 2.2 g of I with 1.5 g of IIc in the presence of 1.0 g of NEt_3 in dioxane was carried out in a manner similar to that used in the reaction of IIa, and then triethylammonium chloride was removed by filtration. The filtrate was evaporated *in vacuo* to leave a residue, which was crystallized on trituration with methanol. Filtration and recrystallization from methanol gave 0.37 g (22%) of 2,3-dibenzoyl-2,3,4,5,6,7-hexahydrothianaphthene 1,1-dioxide (VII), mp 183°C (decomp.), as colorless needles.

Found: C, 69.47; H, 5.36%. Calcd for $C_{22}H_{20}O_4S$: C, 69.46; H, 5.30%.

The compound IV was obtained from the filtrate; yield, 0.3 g (11%).

Hydrolysis of VII. A solution of 0.4 g of VII in 30 m*l* of methanol was stirred with 1 m*l* of 1N aqueous sodium hydroxide at room temperature for 12 hr. The reaction mixture was evaporated *in vacuo*, and then a residue was extracted with benzene and water. The water extract was neutralized with hydrochloric acid, giving 0.21 g of benzoic acid, while from the benzene-extract an unidentified substance was obtained in a trace amount.

1,4-Diphenyl-5a,6,7,8,9,9a-hexahydrothianaphtheno[2,3-d]pyridazine (VIII). After a solution of 0.11 g of VII in 30 m*l* of methanol had been stirred with three drops of 80% hydrazine hydrate at room temperature for 3 hr, filtration afforded yellow crystals. Recrystallization from methanol gave 90 mg (83%) of VIII, mp 198°C (decomp.), as yellow needles.

Found: C, 69.95; H, 5.42; N, 7.38%. Calcd for $C_{22}H_{20}O_2N_2S$: C, 70.20; H, 5.36; N, 7.44%. IR: cm^{-1} 1312, 1135 (ν_{SO_2}). Mass: *m/e* 376 (M^+), 312 (M^+-SO_2).

Thermal Decomposition of VIII. After the thermal decomposition of 350 mg of VIII had been carried out at 210°C for 10 min, the product was extracted with hot ligroin (bp 60—85°C). The ligroin-extract was evaporated *in vacuo* to leave a residue, which, on recrystallization from benzene, gave 4-(1-cyclohexenyl)-3,6-diphenylpyridazine (IX), mp 160°C, as yellow prisms. Yield, 96 mg (33%).

Found: C, 84.40; H, 6.29; N, 8.71%. Calcd for $C_{22}H_{20}N_2$: C, 84.58; H, 6.45; N, 8.97%. NMR ($CDCl_3$): τ 7.5—8.7 (8H, $C\underline{H}_2$, multiplet), 4.0 (1H, $=C\underline{H}-$, multiplet), 1.6—2.8 (11H, phenyl protons, multiplet). Mass: *m/e* 312 (M^+), 308 (M^+-2H_2), 283 (M^+-N_2-H).

3,4,6-Triphenylpyridazine (X). A mixture of 200 mg of IX and 200 mg of *N*-bromosuccinimide in 100 m*l* of carbon tetrachloride was refluxed with a trace amount of benzoyl peroxide for 20 hr. After the reaction mixture had been concentrated *in vacuo*, the precipitated crystals were washed with a dilute aqueous sodium hydrogensulfide solution and then water. The insoluble substance was chromatographed on silica gel, using chloroform as the eluent, to afford 30 mg (15%) of crystals. Recrystallization from ethanol gave colorless prisms of X, mp 176°C (lit,[8] mp 176—177.5°C), which was identical with an authentic sample prepared by the reported method.[8]

BULLETIN OF THE CHEMICAL SOCIETY OF JAPAN, VOL. 45, 240—245(1972)

Stereochemical Studies of Monoterpene Compounds. XIII.[1] The Conformational Analysis of the Acetyl Group of 4-Methyl-10-nor-8-oxomenthols by Circular Dichroism

Takayuki Suga and Satoru Watanabe

Department of Chemistry, Faculty of Science, Hiroshima University, Higahisenda-machi, Hiroshima

(Received June 14, 1971)

The conformational analysis of the acetyl group of a stereoisomeric pair of 4-methyl-10-nor-8-oxomenthols was made by means of the temperature-dependent circular dichroism. (1R:3S:4R)-(+)-4-Methyl-10-nor-8-oxoneomenthol (**1**) exhibited a double-humped Cotton effect at a low temperature. This phenomenon seems to indicate the existence of a conformational equilibrium among **1b**, **1c**, and **1d**, but not **1a**. On the other hand (1R:3R:4R)-(−)-4-methyl-10-nor-8-oxomenthol (**3**) exhibited an inversion in the sign of the Cotton effect when the solvent and the temperature were changed. This phenomenon was interpreted in terms of the conformational equilibrium among **3a**, **3b**, and **3c**. These phenomena were interpreted in terms of the competition of the steric factor and the intramolecular hydrogen bonding.

The temperature-dependent circular dichroism (CD) has been found useful for investigating the rotational conformation of the 17-acetyl group of 20-ketosteroids.[2-4] We have previously studied[5] the rotational conformation of the acetyl group of an epimeric pair of 10-nor-8-oxomenthols. In order now to investigate the influence of the C-4 methyl group on the conformation of the acetyl group, the conformational analysis of (1R: 3S: 4R)-(+)-4-methyl-10-nor-8-oxoneomenthol (**1**), (1R: 3R: 4R)-(−)-4-methyl-10-nor-8-oxomenthol

1) Paper XII of this series: T. Hitata and T. Suga, This Bulletin, under the contribution (71173).

2) G. Snatzke and E. Schwinum, *Tetrahedron*, **22**, 761 (1966).

3) K. M. Wellman and C. Djerassi, *J. Amer. Chem. Soc.*, **87**, 60 (1965).

4) G. Snatzke, "Optical Rotatory Dispersion and Circular Dichroism in Organic Chemistry," Heyden and Son Ltd., London (1967), p. 335.

5) T. Suga, T. Shishibori, and T. Matsuura, This Bulletin, **41**, 1175 (1968).

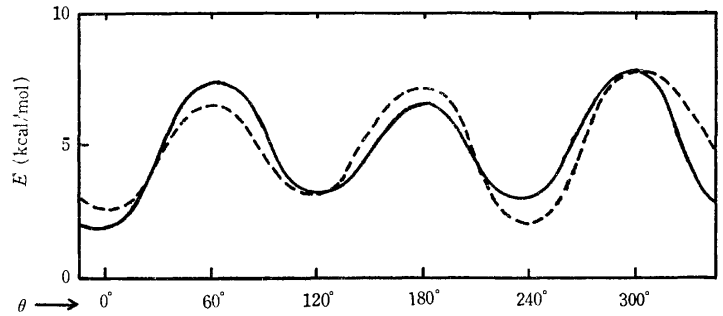

Compd.	The sign of Cotton effect predicted											
1	±	+	+	+	+	+	−	−	−	−	−	−
3	+	+	+	+	+	±	−	−	−	−	−	+

Fig. 1. Conformational energy calculated for the rotational conformation of the acetyl group of the compounds **1** and **3** as a function of θ: - - - for **1** and —— for **3**, and the sign of the Cotton effect for each conformation.

(**3**), and their acetates, (**2**) and (**4**), was undertaken by means of the solvent- and temperature-dependent circular dichroisms.

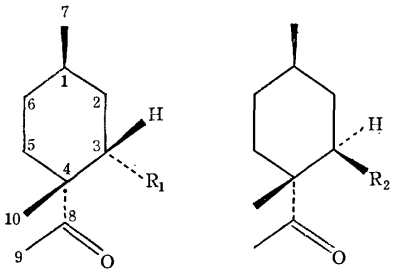

1: R_1=OH
2: R_1=OAc

3: R_2=OH
4: R_2=OAc

Results and Discussion

4-Methyl-10-nor-8-oxomenthols (**1**) and (**3**) were prepared from (1R : 3S : 4S)-(+)-4-methylneoisopulegol and (1R : 3R : 4S)-(−)-4-methylisopulegol respectively by ozonization. The configuration of the isopulegol derivatives was assigned according to Brewster's benzoate rule.[6] Thus, the configuration of the-4-methyl-10-nor-8-oxomenthols was determined to be as is shown by **1** and **3**.

Throughout the following discussion of the conformational analysis, the conformation of the C-4 acetyl group has been assumed to be equatorial for the following reasons: (a) the compounds, **1** and **3**, with equatorial acetyl group are energetically more stable by 0.5 and 2.0 kcal/mol respectively than the axial isomers on the basis of the $-\Delta G^\circ$ value,[7] although the stabilization energy of the hydrogen bonding is not involved in this value. (b) The nuclear magnetic resonance spectra indicated the C-3 proton of compounds **1** and **3** in carbon tetrachloride to be equatorial and axial respectively. (c) The C-4 acetyl group of the acetates, **2** and **4**, was proved to be equatorial

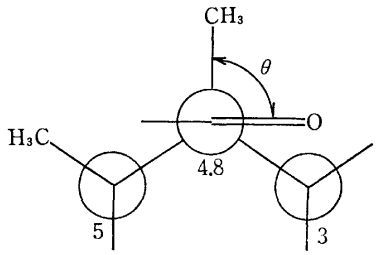

5

by studying the nuclear mangnetic resonance spectrum.

As is shown in Fig. 1, the conformational energy of the acetyl group of compounds **1** and **3** around the C(4)—C(8) bond was estimated by using the energy functions given for our previous calculation of 10-nor-8-oxomenthols,[5] where θ corresponds to a dihedral angle of the Newman projection (5). The sign of the Cotton effect shown was predicted by an examination of the model[8] for each conformer, according to the octant rule.[9] The conformers with θ=120, 240, or 360° may be preferred to both compounds, **1** and **3**. This is supported by the speculation[10,11] that the carbonyl group would eclipse the C–C bond in its equilibrium position. In the calculation of the energy, the energy function of the intramolecular hydrogen bonding between the hydroxyl and the carbonyl groups has not been considered. However, the energy of hydrogen bonding should affect the preference of the rotational conformation of the acetyl group. The **1b** and **3b** conformers may be stabilized by hydrogen bonding. However, if intramolecular hydrogen bonding is obstructed by such a factor as polar solvents, the electrostatic interaction between the hydroxyl lone-pair electrons and the carbonyl π and/or lone-pair electrons may destabilize the bonded conformers, (**1b**) and (**3b**). This would, then, cause the occurence

6) J. H. Brewster, *Tetrahedron*, **13**, 106 (1961); J. H. Brewster, *J. Amer. Chem. Soc.*, **81**, 5475, 5483, 5493 (1959).

7) N. L. Allinger and E. L. Eliel, "Topics in Stereochemistry, Vol. 1," Interscience Publishers, New York (1968), p. 199.

8) Examined by "Dreiding Stereomodels," W. Buchi Manufacture of Glass Apparatus Flwail, Switzerland.

9) W. Moffit, R. B. Woodward, A. Moscowitz, W. Klyne, and C. Djerassi, *J. Amer. Chem. Soc.*, **83**, 4013 (1961).

10) D. M. Piatak and E. Caspi, *Tetrahedron*, **24**, 2899 (1968).

11) A. A. Bother-By, C. Naar-Colin, and H. Günsther, *J. Amer. Chem. Soc.*, **84**, 2748 (1962).

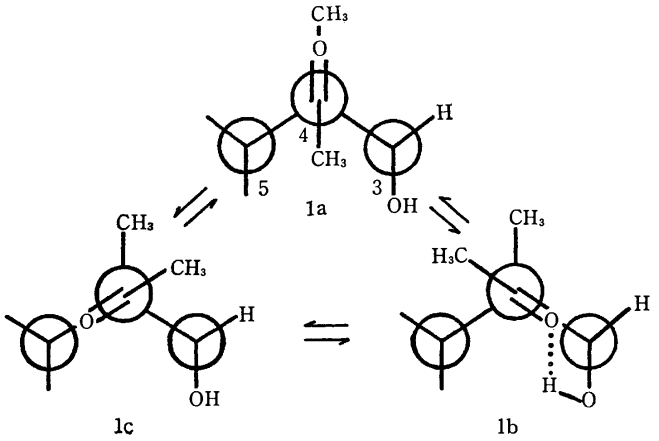

Chart 1. Possible preferred conformation of the acetyl group of (1R:3S:4R)-(+)-4-methyl-10-nor-8-oxoneomenthol (**1**) as viewed from C-8 to C-4.

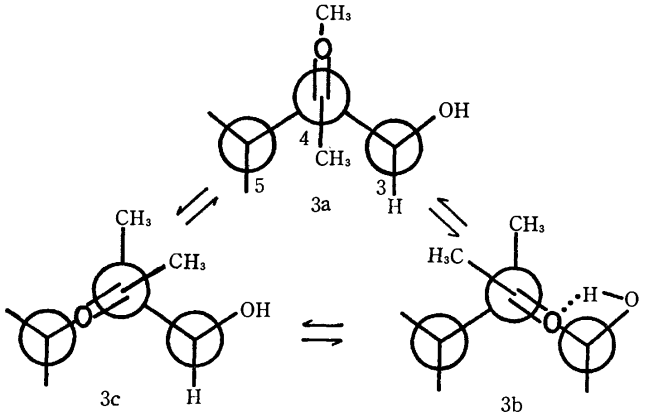

Chart 2. Possible preferred conformation of the acetyl group of (1R:3R:4R)-(−)-4-methyl-10-nor-8-oxomenthol (**3**) as viewed from C-8 to C-4.

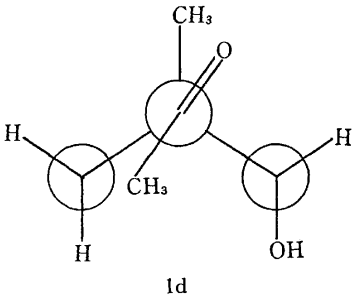

1d

of unstable conformers, (**1a**) and (**1c**), and (**3a**) and (**3c**). According to the octant rule,[9] the **1b**, **3a**, and **3b** conformers should exhibit a positive Cotton effect, while the (**1c**) and (**3c**) conformers should exhibit a negative one. On the other hand, the **1a** conformer may not show any Cotton effect at all.

(1R : 3S : 4R)-(+)-4-Methyl-10-nor-8-oxoneomenthol (1). The CD curves of the compound (**1**) showed a positive Cotton effect regardless of the solvent polarity (Fig. 2), although the maximum position and the molecular ellipticity exhibited a remarkable difference when the solvent was changed from a nonpolar to a polar one. The weak positive Cotton effect in the polar solvents may be attributable to the **1d** conformer rather than to **1a**, while the strong one in the nonpolar

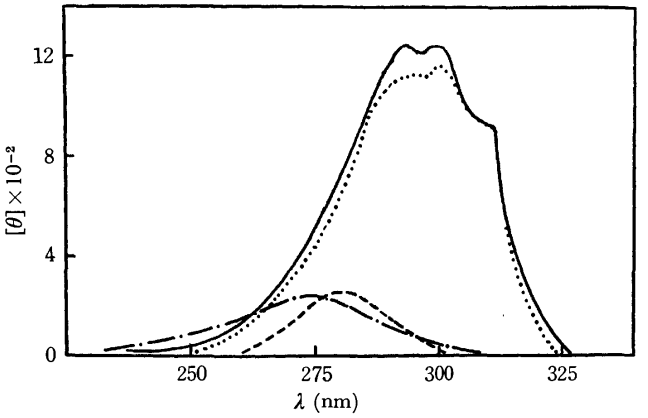

Fig. 2. CD curves of (1R:3S:4R)-(+)-4-methyl-10-nor-8-oxoneomenthol (**1**) in selected solvents at +25°C: ····· in CCl_4, —— in isooctane, —·— in MeOH, and - - - in DMSO.

media may be attributable to the bonded conformer (**1b**). The attribution of this weak positive Cotton effect to the **1d** conformer in place of the **1a** conformer may here be justified by the apperance of the positively-rotating conformer (**1d**) as a result of the interaction between the hydroxyl and the methyl groups in the **1a** conformer. The intramolecularly-hydrogen-bonded conformer (**1b**) is preferred in the nonpolar solvents, whereas the nonbonded conformer (**1d**) is preferred in the polar ones. This was supported by the infrared spectrum in the carbon tetrachloride solution, which exhibited a free hydroxyl band at 3623 cm^{-1} (ε=28), along with two peaks, at 3580 (ε=32) and 3535 cm^{-1} (ε=20), due to the interacted hydroxyl group[12] between the π-electrons of the carbonyl and the hydroxyl groups and between the lone-pair electrons of the hydroxyl groups and the carbonyl oxygen respectively.

The variable-temperature CD curves of the compound (**1**) in EPA (Fig. 3) showed a double-humped Cotton effect at −192°C. The positions of the re-

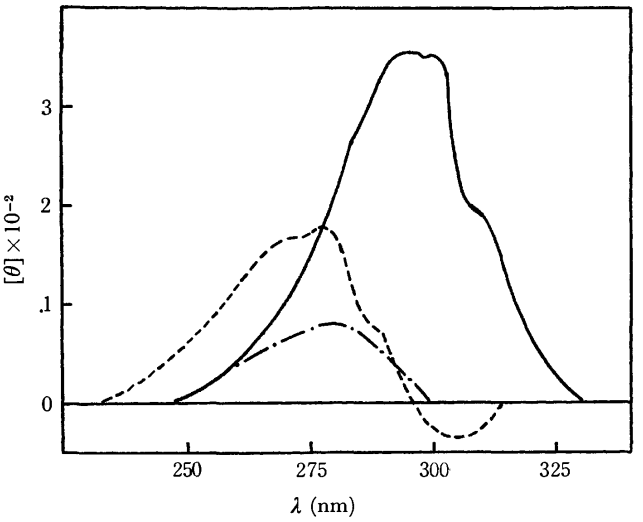

Fig. 3. CD curves of (1R:3S:4R)-(+)-4-methyl-10-nor-8-oxoneomenthol (**1**) in EPA: —— at +25°C, —·— at −74°C, and ····· at −192°C.

12) T. Shishibori, *J. Sci. Hiroshima Univ., Ser. A-II*, **32**, 125 (1968).

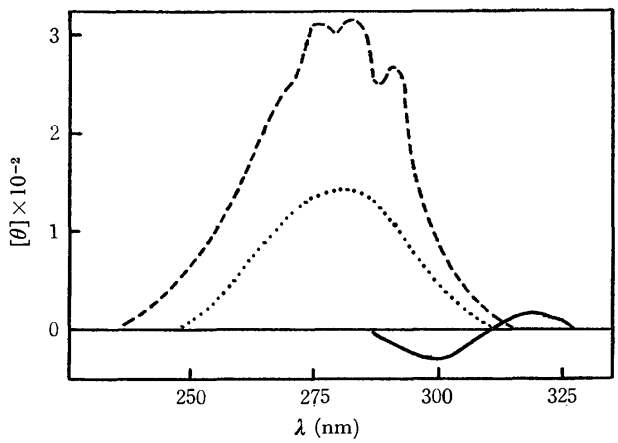

Fig. 4. CD curves of (1R:3S:4R)-(+)-4-methyl-10-nor-8-oxomenthyl acetate (**2**) in EPA: —— at +25°C, ····· at −127°C, and - - - at −190°C.

spective extremes differ by nearly 25 nm. The positive maximum observed at the same position as in the case of other polar solvents at room temperature was attributed to the **1d** conformer, whereas the negative one was attributed the **1a** conformer. The strong positive maximum at 25°C contrasted with that at −192°C, showing the similarity to the position in the case of nonpolar solvents at 25°C, but the rotational strength was slightly weakened. This positive Cotton effect curve implied a preference for the **1b** conformer at 25°C in EPA. A similar phenomenon was also observed in the variable-temperature CD curves in the MI solvent. Consequently, these results, together with the conformational energy in Fig. 1, seem to indicate the existence of a conformational equilibrium among **1b**, **1c**, and **1d**. The positively-rotating hydrogen-bonded conformer (**1b**) is preferred at room temperature, whereas the nonbonded conformers (**1c**) and (**1d**) are preferred at low temperatures. On the other hand, the acetate (**2**) in EPA exhibited only the positive Cotton effect at −190°C (Fig. 4), in contrast with the parent compound (**1**) under the same conditions. The replacement of the hydroxyl group with the acetoxy one made the positively-rotating conformation (**2a**) preferred at low temperatures because of the increase in the electrostatic interaction between the acetoxy and the carbonyl groups. At low temperatures, the frozen staggerd conformation[3] (**2b**) may be considered to prescribe the orientation of the lone-pair electrons of this group. Accordingly, the **2a** conformation with about θ=0—30° would be preferred because of the strengthened interaction due to the orientation of the electrons.

(1R : 3R : 4R)-(−)-4-Methyl-10-nor-8-oxomenthol (3). The CD curves of the oxomenthol (**3**) exhibited a

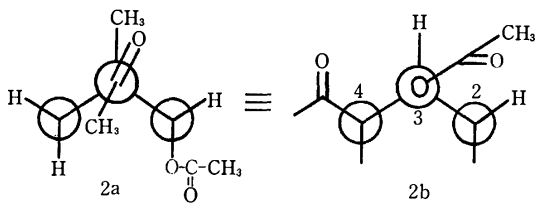

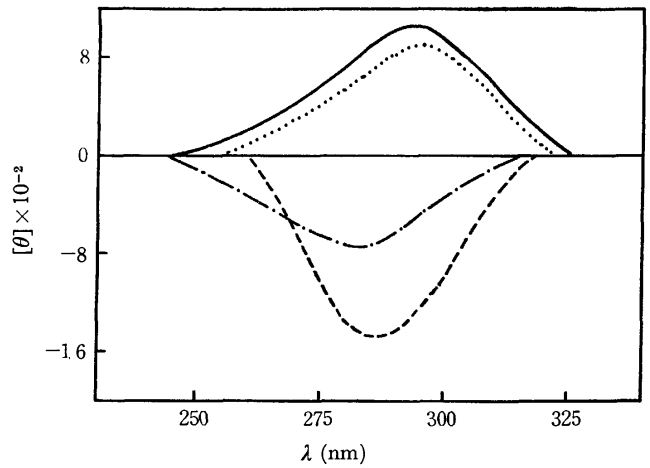

Fig. 5. CD curves of (1R:3R:4R)-(−)-4-methyl-10-nor-8-oxomenthol (**3**) in selected solvents at +25°C: ····· in CCl_4, —— in isooctane, —·— in MeOH, and - - - in DMSO.

positive Cotton effect in isooctane and carbon tetrachloride, and a negative one in methanol and dimethyl sulfoxide (Fig. 5). Such an inversion of the sign of the Cotton effect upon the change of the solvent can be ascribed to the conformational alteration of the acetyl group among **3a**, **3b**, and **3c**. For the compound **3**, the **3a** conformer with θ=0° may be expected because of the absence of the steric interaction between the methyl (of the acetyl group) and the hydroxyl groups; this is in contrast with the **1a** conformer to be expected for the compound **1**. In a nonpolar medium at a room temperature, the positively-rotating conformer (**3b**) with θ=120° is implied to be dominant because of the stabilizing intramolecular hydrogen bonding. This is further supported by the infrared spectrum, which exhibited a weak free hydroxyl band at 3620cm^{-1} (ε=21), along with two peaks at 3575 (ε=35) and 3530 cm^{-1} (ε=20) due to the intramolecularly-interacting hydroxyl group between π-electrons of the carbonyl and the hydroxyl groups and between lone-pair electrons of the hydroxyl group and the carbonyl oxygen respectively. In polar solvents at room temperature, the negatively-rotating conformer (**3c**) with θ=240° is interpreted as preferred becasue of the losses of the stabilization energy due to hydrogen bonding and, consequently, because of the destabilizing electrostatic repulsion between the carbonyl and the hydroxyl groups. This idea is supported by the solvent- and temperature-dependent CD curves of the acetate (**4**), which inherently possesses no ability of intramolecular hydrogen bonding but which does possess the ability to have an electrostatic repulsion between the carbonyl and the acetoxy groups. The CD curves of the acetate exhibited only a negative Cotton effect in both nonpolar and polar solvents. The rotational strength of the Cotton effect increased exceedingly in proportion as the temperature was lowered from −74 to −190°C in EPA. Accordingly, the acetate (**4**) exists predominantly in a negatively-rotating and energetically-favorable conformation, with θ=about 240°.

The CD curves of the compound (**3**) in EPA at low temperatures (at −74 and −180°C) exhibited a

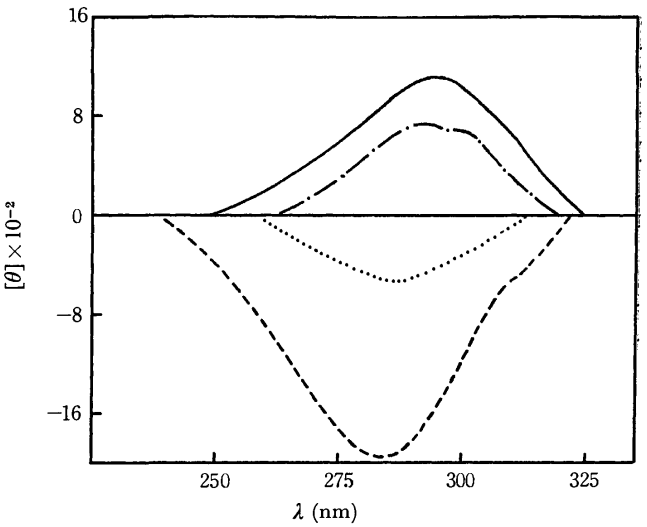

Fig. 6. CD curves of (1R:3S:4R)-(−)-4-methyl-10-nor-8-oxomenthol (**3**) in MI: —— at +25°C, −·− at −74°C, ····· at −127°C, and − − − at −186°C.

strong negative Cotton effect, in contrast with the curve at 25°C, whereas the curves in MI showed a positive Cotton effect at 25 and −74°C and a negative one at lower temperatures, as is shown in Fig. 6. This inversion in the sign of the Cotton effect with the change in the temperature is very similar to the phenomenon observed upon changing the solvent. The inversion of the sign was interpreted as an indication of the increase in the nonbonded conformer at the sacrifice of the bonded conformer with a lowering of the temperature. Thus, at lower temperatures in both polar and nonpolar media, the **3c** conformer, with $\theta=240°$, should be preferred. Our interpretation of such phenomena of the compound (**3**) can be understood after due consideration of the explanation given of the CD curve of 2-oxo-1-*p*-menthanol,[13] which exhibits such an inversion of the sign from a positive Cotton effect to a negative one at lower temperatures. The decrease in the rotational strength for the positive CD curves of the compound (**3**) in decalin at both higher and lower temperatures suggested also that the hydrogen-bonded conformer (**3b**) would be diminished with an increase in the population of the nonbonded conformers by being kept out of room temperature.

Thus, it was concluded that the presence of the C-4 methyl group remarkably alters the conformational preference of the acetyl side-chain of 4-methyl-10-nor-8-oxomenthols in comparison with that of 10-nor-8-oxomenthols.[5] The presence of the C-4 methyl group decreases the population of the conformer when $\theta=180°$, whereas the absence of this group increases the conformer when $\theta=150$—$210°$. These results were very consistent with a prediction judging from the calculated energy function.

Experimental

Measurements. The CD curves were measured on a Japan Spectroscopic Co., Ltd., automatically-recording spectropolarimeter, Model ORD/UV-5, equipped with a circular dichroism attachment. The low- and high-temperature CD curves were obtained by the use of the same spectrometer, using low- and high-temperature CD cells designed and constructed by the present authors. The EPA solvent was composed of ether-isopentane-ethanol in the ratio of 5: 5: 2 by volume. The MI solvent was composed of methylcyclohexane-isopentane in the ratio of 1: 3 by volume.

The IR spectra in the hydroxyl-stretching region were measured with a Perkin-Elmer Model 621 Grating Infrared spectrometer at 25°C. A sodium chloride absorption cell (10 mm long) was used; the concentration of the solution was 0.005 mol/*l*.

(1R: 3S: 4S)-(+)-4-Methylneoisopulegol and (1R: 3R: 4S)-(−)-4-Methylisopulegol. (−)-Methylisopulegone (bp 69—70°C/8 mmHg; n_D^{25} 1.4682; d_4^{25} 0.9231; $[\alpha]_D^{25}-139.18°$ (neat); the semicarbazone derivative, mp 201—202°C) was synthesized by the methylation of (+)-pulegone (81—82°C/5 mmHg; n_D^{25} 1.4843; d_4^{25} 0.9303; $[\alpha]_D^{25}+23°$ (neat)) following the method in the literature,[14] and then it was reduced with lithium alminum hydride in dry ether to two isomeric alcohols. The configuration of the alcohols was identified as (1R: 3S: 4S)-(+)-4-methyl-neoisopulegol, 62.0—63.0°C/3 mmHg; n_D^{25} 1.4735; d_4^{25} 0.9204; $[\alpha]_D^{25}+54.32°$ (neat); the 3,5-dinitrobenzoate derivative, mp 142—143°C, $[\alpha]_D^{25}+59.24°$ (*c* 0.00211, $CHCl_3$), and (1R: 3R: 4S)-(−)-4-methylisopulegol, 63.0—64.5°C/3 mmHg; n_D^{25} 1.4776; d_4^{25} 0.9192; $[\alpha]_D^{25}-1.67°$ (neat); the 3,5-dinitrobenzoate derivative, mp 107°C, $[\alpha]_D^{25}-29.66°$ (*c* 0.00236, $CHCl_3$), by applying Brewster's benzoate rule.

(1R: 3S: 4R)-(+)-4-Methyl-10-nor-8-oxoneomenthol (1). The ozonization of (1R: 3S: 4S)-(+)-4-methyl-neoisopulegol gave (1R: 3S: 4R)-(+)-4-methyl-10-nor-8-oxoneomenthol (**1**): mp 69.5°C; $[\alpha]_D^{25}+57.46°$ (*c* 0.1514, MeOH); NMR ($CDCl_3$), >CH–C<u>H</u>$_3$ 0.92 ppm (doublet, $J=6.0$ Hz, 3H), –C–CH_3 1.15 (singlet, 3H), O=C–CH_3 2.15 (singlet, 3H), >C<u>H</u>–OH 4.0 (broad singlet, 1H), >CH–O<u>H</u> 2.79 (broad singlet, 1H); ν_{max}^{Nujol} 3503 cm^{-1} (OH), 1690 (C=O), 1352 ($-COCH_3$); λ_{max}^{MeOH} 282 nm ($\varepsilon=30.32$), $\lambda_{max}^{Isooctane}$ 288 (32.94); mass spectrum, *m/e* 170 (M^+); CD (max) in decalin (*c* 0.154): $[\theta]_{295}^{+150°}$ +549, $[\theta]_{292}^{+74°}$ +922, $[\theta]_{301}^{+25°}$ +922, $[\theta]_{293}^{+25°}$ +1093, $[\theta]_{300}^{+25°}$ +1111, $[\theta]_{293}^{-74°}$ +634, $[\theta]_{301}^{-74°}$ +617, $[\theta]_{324}^{-74°}$ −137, MI (*c* 0.15): $[\theta]_{293}^{+25°}$ +1350, $[\theta]_{301}^{+25°}$ +1350, $[\theta]_{295}^{-74°}$ +901, $[\theta]_{300}^{-74°}$ +801, $[\theta]_{270}^{-192°}$ +313, $[\theta]_{297}^{-192°}$ −128.

The acetate (2): The acetylation of (**1**) with acetic anhydride in the presence of pyridine afforded the acetate (**2**): mp 60.5°C; $[\alpha]_D^{25}+66.96°$ (*c* 0.134, MeOH); NMR (CCl_4) >CH–C<u>H</u>$_3$ 0.89 ppm (doublet, $J=5.5$ Hz, 3H), –$\underset{|}{C}$–CH_3 1.09 (singlet, 3H), O=$\underset{|}{C}$–CH_3 1.92 and 1.96 (each singlet, 6H), >CH–O– 5.09 (singlet, 1H); ν_{max}^{Nujol} 1730, 1374 cm^{-1} (acetate), 1708 (C=O), 1350 (methyl ketone); λ_{max}^{MeOH} 280 nm ($\varepsilon=31.55$), $\lambda_{max}^{isooctane}$ 281 (31.29); CD (max) in CCl_4 (*c* 0.4362): $[\theta]_{292}^{+25°}$ −92, in MeOH (*c* 0.4544): $[\theta]_{282}^{+25°}$ −20, $[\theta]_{315}^{+25°}$ +22, in isooctane (*c* 0.4018): $[\theta]_{300}^{+25°}$ −48.

(1R: 3R: 4R)-(−)-4-Methyl-10-nor-8-oxomenthol (3). The ozonization of (1R: 3R: 4S)-(−)-4-methylisopulegol gave (1R: 3R: 4R)-(−)-4-methyl-10-nor-8-oxomenthol (**3**): bp 83.0°C/0.5 mmHg; $[\alpha]_D^{25}-30.77°$ (*c* 0.156, MeOH); n_D^{25} 1.4682; NMR ($CDCl_3$) >CH–C<u>H</u>$_3$ 0.94 ppm (doublet, $J=5.5$ Hz, 3H), –$\underset{|}{C}$–CH_3 1.16 (singlet, 3H), O=$\underset{|}{C}$–CH_3 2.16 (singlet, 3H), >C<u>H</u>–OH 3.98 (double doublet, $J_{vic}=3.0$ and 11.0 Hz, 1H), –CH–O<u>H</u> 2.90 (singlet, 1H); $\nu_{max}^{liq.}$ 3490 cm^{-1} (OH), 1690 (C=O), 1350 ($-COCH_3$); λ_{max}^{MeOH} 284 nm ($\varepsilon=27.35$), $\lambda_{max}^{isooctane}$ 287 (25.54); mass spectrum, *m/e* 170 (M^+);

13) K. M. Wellman, W. S. Briggs, and C. Djerassi, *J. Amer. Chem. Soc.*, **87**, 73 (1965).

12) M. V. Kulkarni, E. V. Kulkarni, E. J. Eisenbraun, and M. M. Marsh, *J. Org. Chem.*, **33**, 1661 (1967).

CD (max) in EPA (c 0.143): $[\theta]^{+25°}_{280}$ −667, $[\theta]^{-74°}_{280}$ −1687, $[\theta]^{-186°}_{280}$ −1820, $[\theta]^{-186°}_{287}$ −2040, in decalin (c 0.164): $[\theta]^{+155°}_{295}$ +726, $[\theta]^{+25°}_{293}$ +1026, $[\theta]^{-74°}_{292}$ +644, $[\theta]^{-74°}_{300}$ +596.

The Acetate (4). The acetylation of (**3**) in the same manner as above gave the acetate (**4**): mp 35°C; $[\alpha]^{25}_{D}$ −27.54° (c 0.138, MeOH); NMR (CCl_4), >CH–C$\underline{H}_3$ 0.96 ppm (doublet, J=5.5 Hz, 3H), –$\overset{|}{\underset{|}{C}}$–$CH_3$ 1.13 (singlet, 3H), O=$\overset{|}{C}$–CH_3 1.90 and 2.03 (each singlet, 6H), >CH–O– 5.08 (double doublet, J_{vic}=3.0 and 11.0 Hz, 1H); ν^{Nujol}_{max} 1730, 1375 cm^{-1} (acetate), 1698 (C=O), 1367 (methyl ketone); λ^{MeOH}_{max} 285 nm (ε=33.27), $\lambda^{isooctane}_{max}$ 285 (29.71); CD (max) in CCl_4 (c 0.13): $[\theta]^{+25°}_{290}$ −585, in isooctane (c 0.132): $[\theta]^{+25°}_{290}$ −606, in dioxane (c 0.133): $[\theta]^{+25°}_{292}$ −333, in EPA (c 0.114): $[\theta]^{+25°}_{290}$ −67, $[\theta]^{-74°}_{290}$ −87, $[\theta]^{-190°}_{292}$ −1996, $[\theta]^{-190°}_{302}$ −1641, $[\theta]^{-190°}_{312}$ −710.

The authors wish to thank Dr. Motoichi Indō of Takasago Perfumery Co., Ltd., Tokyo, for his gift of pulegone.

BULLETIN OF THE CHEMICAL SOCIETY OF JAPAN, VOL. 45, 245—247(1972)

Studies on Nucleosides and Nucleotides. II. Selective Acylation of 5′-Hydroxyl Group of Thymidine[1]

Oyo MITSUNOBU, Junji KIMURA, and Yoshiyuki FUJISAWA

Department of Chemistry, College of Science and Engineering, Aoyama Gakuin University, Megurisawa-cho, Setagaya-ku, Tokyo

(Received June 15, 1971)

Treatment of thymidine and either acetic acid or benzoic acid with diethyl azodicarboxylate (**1**) and triphenylphosphine (**2**) in dioxane afforded 5′-*O*-acetyl or 5′-*O*-benzoylthymidine along with a trace of 3′,5′-di-*O*-acylated product. When thymidine and benzoic acid or *p*-substituted benzoic acids were allowed to react with **1** and **2** in hexamethylphosphoric triamide(HMPA), the corresponding 5′-*O*-aroylthymidines were selectively obtained. The aroyl groups having electron-withdrawing substituents were much more readily removed than those having electron-releasing groups under mild alkaline conditions.

For the chemical synthesis of nucleotides and oligonucleotides, the hydroxyl groups of sugar moiety should be appropriately protected prior to phosphorylation. Of many blocking groups examined so far, triarylmethyl groups have been widely used because they can be introduced predominantly to 5′-hydroxyl group of nucleosides and removed under acidic conditions. It is known, however, that alkali-labile protecting groups are superior to acid-labile ones for the synthesis of oligonucleotides.[2] Thus acyl groups are used as alkali-labile groups for the protection of the hydroxyl functions as well as amino functions. There are few reports, however, of the selective acylation of 5′-hydroxyl groups of nucleosides.

In a previous paper,[3] we have reported that the 5′-hydroxyl groups of thymidine and uridine were predominantly phosphorylated by means of dibenzyl hydrogen phosphate, diethyl azodicarboxylate (**1**) and triphenylphosphine (**2**). It is of interest to apply this procedure to the selective acylation of 5′-hydroxyl groups of nucleosides.

Acylation of Thymidine. Thymidine was allowed to react with equimolar amounts of acetic acid, **1** and **2** in dioxane at 60°C for 3 hr. The thymidine remaining insoluble disappeared as the reaction proceeded and 5′-*O*-acetylthymidine was isolated in a 55.2% yield by silica gel column chromatography.[4] Differing from the case of phosphorylation of thymidine, a trace of 3′,5′-di-*O*-acetylthymidine was also isolated. Similarly, the reaction of thymidine with benzoic acid, **1** and **2** led to the formation of 5′-*O*-benzoylthymidine in isolated yield of 78.0%. A trace of 3′,5′-di-*O*-benzoylthymidine was also formed.

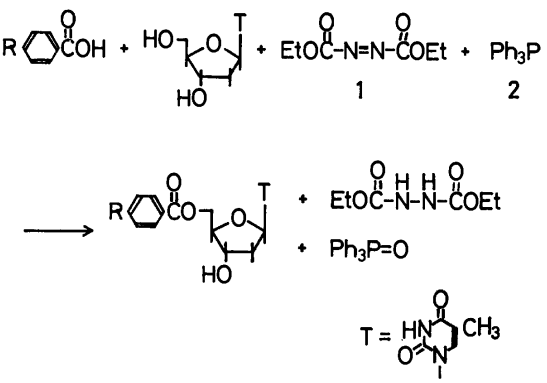

Since thymidine was found to be sufficiently soluble in hexamethylphosphoric triamide (HMPA), further experiment was carried out using HMPA as the solvent. When a solution of thymidine and **2** in HMPA was

1) Presented at the 24th meeting of the Chemical Society of Japan (April, 1971). Part I: O. Mitsunobu, K. Kato, and J. Kimura, *J. Amer. Chem. Soc.*, **91**, 6510 (1969).

2) a) M. Smith, D. H. Rammler, I. H. Goldberg, and H. G. Khorana, *J. Amer. Chem. Soc.*, **84**, 430 (1962). b) D. H. Rammler and H. G. Khorana, *ibid.*, **84**, 3112 (1962). c) H. Schaller, G. Weimann, B. Lerch, and H. G. Khorana, *ibid.*, **85**, 3821 (1963). d) M. W. Moon, S. Nishimura, and H. G. Khorana, *Biochemistry*, **5**, 937 (1966). e) B. E. Griffin, M. Jarman, and C. B. Reese, *Tetrahedron*, **24**, 639 (1968) and refs. therein.

3) O. Mitsunobu, K. Kato, and J. Kimura, *J. Amer. Chem. Soc.*, **91**, 6510 (1969).

4) No attempt was made to obtain the optimum yield.

Table 1. Preparation of 5′-*O*-aroylthymidines

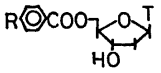

R	Yield[a] %	Mp °C	R_f[b]	Anal. C% Calcd	Anal. C% Found	Anal. H% Calcd	Anal. H% Found	Recovered thymidine %
NO_2	84.6	182[c]	0.89	52.17	52.59	4.38	4.38	10.8
CN	79.5	168—170	0.82	58.22	58.28	4.61	4.50	20.0
H	74.0	171—172	0.84	58.96	58.72	5.20	5.09	25.0
OCH_3	65.5	176—177	0.85	57.44	57.48	5.35	5.42	33.5
CH_3	65.0	202	0.87	59.99	59.88	5.59	5.13	34.5

a) The yield was calculated by paper chromatography.
b) Solvent system; *n*-butanol-0.1 N HCl=5:1 R_f value of thymidine was 0.57.
c) Lit. mp 180—181°C.[7b]

treated with benzoic acid and **1** at room temperature, 5′-*O*-benzoylthymidine was formed in yield of 74.0% and 25.0% of thymidine was recovered as determined by paper chromatography. It is noteworthy that no 3′,5′-di-*O*-benzoylthymidine could be detected by thin layer chromatography (tlc) of the reaction mixture. By a similar way, 5′-*O*-*p*-nitrobenzoyl-, 5′-*O*-*p*-cyanobenzoyl-, 5′-*O*-*p*-methoxybenzoyl- and 5′-*O*-*p*-toluylthymidine were obtained. The results are summarized in Table 1.

As shown in Table 1, benzoic acid derivatives having electron-withdrawing groups gave higher yields of the corresponding 5′-*O*-aroylthymidines than those having electron-releasing groups. 5′-*O*-Aroylthymidine could be isolated by silica gel column chromatography.

Thymidine is soluble in HMPA, while triphenylphosphine oxide formed precipitated nearly quantitatively and could be readily removed by filtration. Although HMPA is known to form complexes with protic acids,[5] no disturbing influence on the present reaction was observed. HMPA is, therefore, a suitable solvent for the present purpose in spite of its high boiling point.

Generally, acid chlorides, acid anhydrides or aryl carboxylates react with 5′-hydroxyl group as well as 3′(2′)-hydroxyl group of nucleosides to give both 5′-*O*-acylated and 3′(2′),5′-poly-*O*-acylated compounds.[6,7] As an example, *p*-nitrobenzoylation of unprotected thymidine (5 mmol) by means of *p*-nitrobenzoyl chloride (5.5 mmol) in pyridine resulted in the formation of 5′-*O*-*p*-nitrobenzoylthymidine (55%) and 3′,5′-di-*O*-*p*-nitrobenzoylthymidine (18%).[8] Thus, the present method might be convenient for the selective formation of 5′-*O*-aroylthymidine.

Table 2. Properties of UV absorbance for 5′-*O*-aroylthymidines

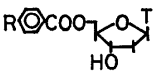

R	$\varepsilon \times 10^{-4}$	λ_{max} (mμ)
NO_2	1.77	265
CN	2.24	242
H	0.884	270
OCH_3	2.46	265
CH_3	2.10	246

Acylation of alcohols by means of carboxylic acids, **1** and **2** may proceed through quaternary phosphonium salts, **3** and **4**, *e.g.*, may involve activation of alcohols rather than carboxylic acids.[9] Acylating and carboxylating reagents having bulky groups predominantly gave corresponding 5′-*O*-protected nucleosides.[10] Thus, it would be reasonable to postulate that the selective formation of 5′-*O*-aroylthymidines by the present method is due to steric hindrance of three phenyl groups around the positively charged phosphorus atom in the intermediate **3**.[3]

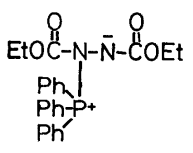

3

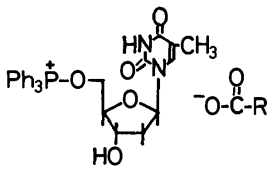

4

Dearoylation of 5′-O-Aroylthymidine. The 5′-*O*-aroylthymidines were treated with methanolic ammonia (saturated at room temperature) at 35°C and the reactions were monitored by paper chromatog-

5) H. Normant, *Angew. Chem.*, **79**, 1029 (1967).
6) P. T. Gilham and H. G. Khorana, *J. Amer. Chem. Soc.*, **80**, 6212 (1958). b) C. Kresze, E. Lodemann, and A. Wacker, *Z. Naturforsch.*, **B22**, 285 (1967); *Chem. Abstr.*, **67**, 117177n (1967).
7) T. Sasaki and Y. Mizuno reported that acylation of cytidine with an equimolar amount of acetic anhydride at refluxing temperature in dry pyridine afforded predominantly N^4-acetylcytidine which on further treatment with acetic anhydride in pyridine predominantly gave N^4, 5′-*O*-diacetyl-cytidine. On the other hand, treatment of cytidine with glacial acetic acid in the absence of pyridine gave 3′(or 2′),5′-*di*-*O*-acetylcytidine and 5′-*O*-acetylcytidine. *Chem. Pharm. Bull.*, **15**, 894 (1967).
8) K. E. Pfitzner and J. G. Moffat, *J. Amer. Chem. Soc.*, **87**, 5661 (1965).
9) O. Mitsunobu and M. Yamada, This Bulletin, **40**, 2380 (1967). b) O. Mitsunobu and M. Eguchi, *ibid.*, in press.
10) a) G. Weimann and H. G. Khorana, *J. Amer. Chem. Soc.*, **84**, 4329 (1962). b) K. Gerzon and D. Kau, *J. Med. Chem.*, **10**, 189 (1967); *Chem. Abstr.*, **66**, 74881x (1967). c) K. K. Ogilvie and R. L. Letsinger, *J. Org. Chem.*, **32**, 2365 (1967).

raphy. As expected,[11] the nature of the *p*-substituents affected the rate of solvolysis; the aroyl groups having electron-withdrawing substituents were much more readily removed than those having electron-releasing groups. The time(hr) required for the complete dearoylation was as follows: *p*-NO_2, 1.0; *p*-CN, 1.5; H, 8.0; *p*-CH_3O, 22; *p*-CH_3, 23.

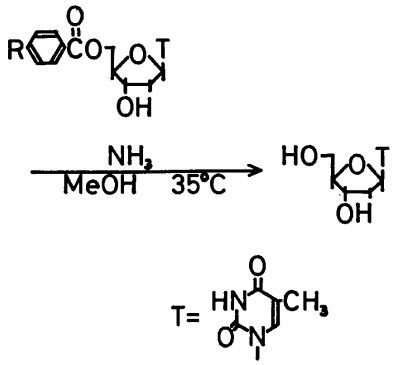

The results indicate that the acylation of thymidine by means of carboxylic acids, **1** and **2** provides a convenient and selective method available for the preparation of 5′-*O*-acylthymidines.

Experimental

Methods. Paper chromatography was carried out by the ascending technique using Toyoroshi No. 51A paper. The solvent used was *n*-butanol-2NHCl (5: 1). The R_f values of different compounds are listed in Table 1. Estimation of the yields of 5′-*O*-aroylthymidines formed by the reaction in HMPA was carried out spectrophotometrically after elution of spots from paper chromatograms. The spots and appropriate blank areas of the paper were eluted after it was cut into small pieces by soaking in 0.1N hydrochloric acid for 1 day at 37°C in sealed vessels, the contents of the vessels being shaken occasionally. The extracts were measured by a Hitachi EPS-3T recording spectrometer.

Thin layer chromatographic plates were prepared using silica gel PF_{254} (E. Merck) and developed with $CHCl_3$: CH_3CN=1: 1. Silica gel (Wakogel C-300) was used for column chromatography.

Commercial thymidine was dried at 80—90°C over phosphorus pentoxide. Diethyl azodicarboxylate[12] and *p*-toluic acid[13] were prepared by known procedures. Other commercial reagents and solvents were purified and dried by ordinary procedures.

11) On alkaline hydrolysis of 5′-*O*-acyl-2′,3′-isopropylidenuridine, the order of reactivity is $CF_3CO>CCl_3CO>CH_2ClCO>CH_3CO$. F. Cramer, H. P. Bär, H. J. Phaese, W. Sänger, K. H. Scheit, G. Schneider, and J. Tennigkeit, *Tetrahedron Lett.*, **1963**, 1039.

12) J. C. Kauer, "Organic Syntheses," Coll. Vol. IV, p. 411.

13) W. F. Tuley and C. S. Marvel, "Organic Syntheses," Coll. Vol. III, p. 822.

Preparation of 5′-O-Acetylthymidine. Acetic acid (180 mg, 3×10^{-3} mol) and diethyl azodicarboxylate (522 mg, 3×10^{-3} mol) in dioxane (5 m*l*) were added to a mixture of thymidine (726 mg, 3×10^{-3} mol) and triphenylphosphine (786 mg, 3×10^{-3} mol) in dioxane (5 m*l*) at 60°C under stirring. Stirring was continued for 3 hr and the solution was concentrated. The residue was applied to silica gel column (3.2×70 cm). Elution with ethyl acetate afforded diethyl hydrazodicarboxylate in the first fraction, a trace of 3′,5′-di-*O*-acetylthymidine in the next fraction and 5′-*O*-acetylthymidine in the third fraction. 5′-*O*-Acetylthymidine was obtained by evaporating and crystallizing the residue from ethyl acetate, 55.2% (470 mg). It melted at 153—154°C (lit,[6a] mp 150°C). Found: C, 50.67; H, 5.72; N, 10.34%. Calcd for $C_{12}H_{16}N_2O_4$: C, 50.70; H, 5.63; N, 9.86%.

Similarly, the reaction of benzoic acid (366 mg, 3×10^{-3} mol) with equimolar amounts of thymidine, diethyl azodicarboxylate and triphenylphosphine was carried out in dioxane. Elution with acetonitrile afforded a trace of 3′,5′-di-*O*- benzoylthymidine (mp 154—156°C: Found: C, 63.41; H, 5.02; N, 6.03%. Calcd for $C_{24}H_{22}N_2O_7$: C, 64.00; H, 4.89; N, 6.22%) and a 75.1% (780 mg) yield of 5′-*O*-benzoylthymidine, mp 171—172°C recrystallized from benzene-ethyl acetate. Found: C, 58.72; H, 5.09; N, 8.23%. Calcd for $C_{17}H_{18}N_2O_6$: C, 58.96; H, 5.20; N, 8.09%.

Preparation of 5′-O-Aroylthymidines. General Procedure. A mixture of triphenylphosphine (1×10^{-3} mol) and thymidine (1×10^{-3} mol) in HMPA (1 m*l*) was stirred with exclusion of moisture and a solution of carboxylic acid (1×10^{-3} mol) and diethyl azodicarboxylate (1×10^{-3} mol) in HMPA (1 m*l*) was added over a period of 1 hr at room temperature. Stirring was continued for 5 hr and the mixture was then kept standing overnight at room temperature. After removal of triphenylphosphine oxide (nearly quantitative yield) by filtration, the filtrate was concentrated to a sirup under reduced pressure. The residue was dissolved in dry methanol and the solution was adjusted to exactly 100 m*l* to determine the amounts of the 5′-*O*-aroylthymidine formed and the thymidine unreacted by means of paper chromatography. Methanol was then removed and the residue was chromatographed over silica gel to isolate the product. Elemental analyses and physical properties of 5′-*O*-aroylthymidines thus isolated are summarized in Table 2.

Isolation of 5′-O-p-Methoxybenzoylthymidine. The residue obtained by the removal of methanol was applied to silica gel column (2.2 cm×50 cm), and eluted with a mixture of chloroform-acetonitrile (1: 1) giving a 54.5% yield of 5′-*O*-*p*-methoxybenzoylthymidine. This was purified by recrystallization from methanol.

Solvolysis of 5′-O-Aroylthymidine. 5′-*O*-Aroylthymidine (30 mg) was dissolved in methanolic ammonia (10 m*l*, saturated at room temperature) and stirred at 35°C. The reaction was monitored by paper chromatography and tlc. Time required for the 5′-*O*-aroylthymidines to disappear was as follows; 5′-*O*-*p*-nitrobenzoylthymidine, 1.0; 5′-*O*-*p*-cyanobenzoylthymidine, 1.5; 5′-*O*-benzoylthymidine, 8.0; 5′-*O*-*p*-methoxybenzoylthymidine, 22; 5′-*O*-*p*-toluylthymidine, 23 hr.

The Reaction of Hydrosilanes with Chlorosilanes in the Presence of Grignard Reagents. A New Method of Silicon-Silicon Bond Formation

Akira Hosomi and Hideki Sakurai
Department of Chemistry, Faculty of Science, Tohoku University, Sendai
(Received June 15, 1971)

A new method has been developed for the formation of a silicon-silicon bond. Hydrosilanes having at least one phenyl or one trimethylsilyl group on a silicon atom were subjected to reaction with chlorosilanes to give unsymmetrically substituted disilanes in the presence of secondary or tertiary Grignard reagent which was inert to both chlorosilanes and hydrosilanes. The method was extended to the preparation of benzyl, allyl, and alkylsilanes.

Chemistry of organopolysilanes has recently become a subject of growing interest.[1] In investigations of organopolysilanes, it is frequently desirable to prepare unsymmetrically substituted organodisilane compounds. For this the Wurtz-type condensation between the two different kinds of halosilanes may be employed. However, it does not necessarily give the desired compound selectively unless one of the two halosilanes makes a stable silylalkali metal bond.[2]

It was reported that cyclohexylmagnesium bromide was also effective for the condensation of halosilanes.[3] A silyl Grignard reagent, "Ph_3Si–MgX", formed by the interaction between triphenylchlorosilane and cyclohexylmagnesium bromide was assumed as an intermediate. This was further coupled with another chlorosilane to form a new silicon-silicon bond. The presence of magnesium metal gave rise to more favorable results.[4] Some symmetrically substituted disilanes have been also obtained by the action of magnesium metal upon chlorosilanes[5] where an intermediacy of the "Si–MgX" compound formed directly from magnesium and the chlorosilane was presumed.

We have investigated the reaction of various hydrosilanes with sterically hindered Grignard reagents, such as isopropylmagnesium chloride in tetrahydrofuran (THF), primarily in the hope of preparing a stable silyl Grignard reagent. Although the convincing evidence of its formation was not available, some unsymmetrically substituted disilanes were obtained in good yield by adding chlorosilane to the reaction mixture.

Results and Discussion

An appropriate hydrosilane was added to a solution of Grignard reagent from *sec*- or *tert*-alkyl halides in THF and was heated to reflux. Trimethylchlorosilane was then added to the reaction mixture and the mixture was heated to reflux under nitrogen. After work-up, an unsymmetrically substituted disilane was obtained as a result of the condensation between hydrosilane and chlorosilane. The products were identified by comparing their retention times on gas chromatography and IR and NMR spectra with those of authentic samples.

$$\equiv Si^1\text{–}H + \equiv Si^2\text{–}Cl \xrightarrow{RMgX} \equiv Si^1\text{–}Si^2\equiv + MgXCl + RH$$

It has been shown that the introduction of an alkyl group into silicon took place in the reaction of hydrosilanes with Grignard reagents derived from primary alkyl halides,[6] and thus the sterically hindered Grignard reagent formed from *sec*- or *tert*-alkyl halides was employed. It has been also established that *sec*- or *tert*-Grignard reagents give no substitution product in the reaction with trialkylchlorosilanes.[7]

The results are summarized in Table 1. It is interesting to note that the presence of an aromatic or an organosilyl group on silicon in a hydrosilane is apparently necessary for the condensation, just as in the formation of "silyl Grignard reagents,"[3,5] or silyl alkali metal compounds[2] from chlorosilanes. These groups may play a role in the stabilization of the negative charge, which would develop on the silicon atom of "silyl Grignard reagents." If hydrosilanes were converted into chlorosilanes under the present reaction conditions, the reaction may be trivial, since coupling of chlorosilanes by means of Grignard reagents is known. However, the fact that no such conversion of hydrides into chlorides really occurred was verified by several control experiments; for example, after a hydrosilane was heated at reflux with the starting alkyl halide or chlorosilane in the presence of magnesium metal, magnesium salts, or alkyl Grignard reagents, no traces of the corresponding chlorosilane could be detected.

The yields are independent of the presence of magnesium in the reaction mixture. However, the effect of solvent is very significant. Thus, although disilanes were not obtained in diethyl ether, the reaction took

1) a) H. Sakurai, *Yuki Gosei Kagaku Kyokai Shi*, **25**, 555, 642 (1967). b) H. Gilman, W. H. Atwell, and F. K. Cartledge, *Advan. Organometal. Chem.*, **4**, 1 (1968). c) M. Kumada and K. Tamao, *ibid.*, **6**, 19 (1968). d) M. Kumada, *Pure Appl. Chem.*, **13**, 167 (1966).

2) C. Eaborn, "Organosilicon Compounds," Butterworth, London (1960), p. 351—366.

3) T. G. Selin and R. West, *Tetrahedron*, **5**, 97 (1959).

4) G. Scott and J. Meyer, *Z. Anorg. Allgem. Chem.*, **313**, 107 (1961).

5) a) W. Stendel and H. Gilman, *J. Amer. Chem. Soc.*, **82**, 403 6129 (1960). b) H. J. S. Winkler and H. Gilman, *J. Org. Chem.*, **26**, 1265 (1961).

6) a) M. C. Harvey, W. H. Nebergall, and J. S. Peake, *J. Amer. Chem. Soc.*, **79**, 1437 (1957). b) H. Gilman and E. A. Zuech, *ibid.*, **79**, 4560 (1957). c) H. Gilman and R. A. Tomasi, *ibid.*, **81**, 137 (1959). d) H. Gilman and E. A. Zuech., *ibid.*, **81**, 5925 (1959). e) H. Gilman, E. A. Zuech, and W. Stendel, *J. Org. Chem.*, **27**, 1836 (1962).

7) L. H. Sommer, D. L. Bailey, J. R. Gould, and F. C. Whitmore, *J. Amer. Chem. Soc.*, **76**, 801 (1954).

Table 1. Condensation of hydrosilane with halides in the presence of alkyl Grignard reagent (RMgX) in THF

Exp. No.	R-X	Hydrosilane	Chlorosilane or halide	Product	Yield (%)[a]
1[b]	*t*-BuCl	Ph_2SiH_2	Me_3SiCl	$Ph_2(H)Si-SiMe_3$	0
2	*t*-BuCl	Ph_2SiH_2	Me_3SiCl	$Ph_2(H)Si-SiMe_3$	22 (6)[c]
3	*t*-BuCl	Ph_2MeSiH	Me_3SiCl	$Ph_2MeSi-SiMe_3$	(trace)
4	*t*-BuCl	Ph_3SiH	Me_3SiCl	$Ph_3Si-SiMe_3$[b]	(trace)
5	*Cyclo*-$C_6H_{11}Cl$	Ph_2SiH_2	Me_3SiCl	$Ph_2(H)Si-SiMe_3$	(3)[d]
6[e]	*Cyclo*-$C_6H_{11}Cl$	Ph_2MeSiH	Me_3SiCl	$Ph_2MeSi-SiMe_3$	62 (25)
7	*i*-PrBr	Ph_3SiH	Me_3SiCl	$Ph_3Si-SiMe_3$	68 (6)
8	*i*-PrCl	Ph_3SiH	Me_3SiCl	$Ph_3Si-SiMe_3$	73 (29)
9	*i*-PrCl	Ph_2MeSiH	Me_3SiCl	$Ph_2MeSi-SiMe_3$	86 (50)
10	*i*-PrCl	Me_5Si_2H	Me_3SiCl	$Me_5Si_2-SiMe_3$	(14)[d]
11	*i*-PrCl	$PhCH_2Me_2SiH$	Me_3SiCl	$PhCH_2Me_2Si-SiMe_3$	0
12	*i*-PrCl	Ph_2MeSiH	$PhCH_2Cl$	$Ph_2MeSi-CH_2Ph$	76 (28)
13	*i*-PrCl	$PhMe_2SiH$	$PhCH_2Cl$	$PhMe_2Si-CH_2Ph$	57 (11)
14	*i*-PrCl	Ph_2MeSiH	$CH_2=CHCH_2Cl$	$Ph_2MeSi-CH_2CH=CH_2$	(trace)
15	*i*-PrCl	Ph_2MeSiH	MeI	$Ph_2MeSi-Me$	(19)[d]
16	*i*-PrCl	Ph_2MeSiH	*n*-BuI	$Ph_2MeSi-Bu-n$	(13)[d]

a) Excess amount of Grignard reagents and halides were used, yields being based on the amount of hydrosilanes.
b) in Et_2O. c) The conversion is shown in parentheses.
d) Yields were not determined, although the products were separated and identified.

Table 2. NMR data of some organosilicon compounds

a b c d	τ values				
	a	b	c	d	e
$(CH_3)_3Si-Si(C_6H_5)_3$	9.79(s)	2.47—2.77(m)			
$(CH_3)_3Si-Si(C_6H_5)_2(H)$	9.72(s)	2.39—2.90(m)	5.24(s)		
$(CH_3)_3Si-Si(C_6H_5)_2(CH_3)$	9.85(s)	2.37—2.93(m)	9.41(s)		
$(CH_3)_3Si-Si(C_6H_5)\ (CH_3)_2$	9.95(s)	2.49—2.86(m)	9.67(s)		
$[(CH_3)_3Si]_2-Si(CH_3)_2$	10.00(s)	10.02(s)			
$(CH_3)_3Si-Si(CH_3)_2\ (CH_2-C_6H_5)$	9.99(s)	9.96(s)	7.89(s)	2.83—3.33(m)	
a b c d e					
$(CH_3)\ (C_6H_5)_2Si(CH_2-CH=CH_2)$	9.75(s)	2.39—2.82(m)	8.37(d)	3.88—4.59(m)	4.97—5.39(m)
$(CH_3)_2(C_6H_5)\ Si(CH_2-C_6H_5)$	9.55(s)	2.47—3.27(m)	7.40(s)		
$(CH_3)_2(C_6H_5)_2Si$	9.48(s)	2.38—2.88(m)			
$(CH_3)\ (C_6H_5)_2Si(C_4H_9-n)$	9.48(s)	2.27—2.82(m)	8.27—9.27(m)		

place smoothly in more basic solvents such as hexamethylphosphoramide (HMPA) or especially in THF. However, the formation of δ-hydroxybutylsilane due to the cleavage of THF by magnesium salts[5a,8] causes the lowering of the yields, competing with the condensation between Si–H and Si–Cl.

It would be of interest to assume the intermediacy of the "silyl Grignard reagent" in this reaction. However, hydrolysis with deuterium oxide after heating hydrosilanes and Grignard reagent in THF gave no deuterium-containing product.

The reaction was extended to the preparation of benzyl, allyl, and alkylsilanes.

$$Ph_nMe_{3-n}SiH + RX + i\text{-}PrMgCl \longrightarrow Ph_nMe_{3-n}SiR + MgXCl + C_3H_8$$

$$RX = PhCH_2Cl,\ CH_2=CHCH_2Cl,\ MeI,\ n\text{-}BuI$$

Results are shown in Table 1. All the products were separated by preparative GLC and identified by NMR. NMR data are given in Table 2.

8) D. Wittenberg, D. Aoki, and H. Gilman, *ibid.*, **80**, 5933 (1958).

Experimental

Alkyl chlorides were prepared from the corresponding alcohols by known methods. Triphenylsilane, diphenylsilane, and pentamethyldisilane were prepared by reduction with lithium aluminum hydride of the corresponding chlorosilanes. Diphenylmethylsilane was prepared by partial phenylation of methyldichlorosilane with phenylmagnesium chloride. All physical constants and GLC analyses confirmed the purity of the materials.

Typical Runs of Condensation. a) The Reaction of Diphenylmethylsilane with Trimethylchlorosilane: From a dropping funnel diphenylmethylsilane (2.5 g, 0.0125 mol) was added to the Grignard reagent prepared from isopropyl chloride (15.7 g, 0.20 mol) and magnesium (4.8 g, 0.20 mol) in THF in a three-necked flask. After refluxing for one hour, trimethylchlorosilane (22 g, 0.20 mol) was added to this solution, and additional refluxing was continued for 10 hr. By GLC analysis of the reaction mixture 1,1-diphenyltetramethyldisilane (1.32 g, 0.0049 mol) and diphenylmethylsilane (1.04 g, 0.0052 mol) were detected. After hydrolysis, however, an additional product identified to be δ-hydroxybutyldiphenylmethylsilane (0.44 g, 0.0016 mol), was obtained. It had n_D^{20}

1.5685 (lit,[8] 1.5693, 1.5688). These products were separated by preparative glc and characterized by IR and NMR spectra and by the known physical constants.

b) The Reaction of Diphenylmethylsilane with Benzylchloride: By means of essentially the same procedure, diphenylmethylbenzylsilane (1.00 g, 0.00344 mol), mp 64°C was obtained from diphenylmethylsilane (2.5 g, 0.0125 mol) and benzyl chloride (2.50 g, 0.020 mol). The product was separated by glc.

An Attempt of Detection of a Silyl Grignard Reagent. In a three-necked flask were refluxed isopropylmagnesium chloride and diphenylmethylsilane for 20 hr in THF. After quenching with deuterium oxide, the product was separated by preparative glc. The silicon-deuterium bond in the compound could not be characterized by IR, NMR or mass spectra.

An Attempted Redistribution between Diphenylmethylsilane and Trimethylchlorosilane Catalyzed by Magnesium Bromide. Diphenylmethylsilane (2.5 g, 0.0125 mol) was heated with stirring in THF for 6 hr in the presence of magnesium bromide prepared *in situ* from magnesium (3.6 g, 0.15 mol) and 1,2-dibromoethane (9.4 g, 0.0125 mol). Diphenylmethylbromosilane was not detected by careful examination by glc. Trimethylchlorosilane (10.8 g, 0.1 mol) was then added to the mixture, which was heated for 4 hr. glc examination revealed that neither diphenylmethylchlorosilane nor 1,1-diphenyltetramethyldisilane was formed.

We are indebted to Tokyo Shibaura Electric Co., Ltd., for a gift of chlorosilanes.

BULLETIN OF THE CHEMICAL SOCIETY OF JAPAN, VOL. 45, 250—255(1972)

Ring Expansion through a 1,3-Acyl Rearrangement. Reactions of Cyclic Sulfonium Ylides with Acetylenic Compounds[1]

Moriaki HIGO, Takeshi SAKASHITA, Minoru TOYODA, and Teruaki MUKAIYAMA

Laboratory of Organic Chemistry, Tokyo Institute of Technology, Ookayama, Meguro-ku, Tokyo

(Received June 17, 1971)

Ring expansion of cyclic sulfonium ylides with acetylenic compounds was investigated. It was found that a six-membered cyclic sulfonium ylide (I) gave eight-membered ring expansion products (IIIa—e) in high yields under mild conditions on treatment with acetylenic compounds (IIa—e) in dimethyl sulfoxide. In a similar manner, the reactions of five- and seven-membered cyclic sulfonium ylides with II afforded ring expansion products (XIa) and (IXa—c). The ring expansion was considered to proceed through an intramolecular 1,3-acylrearrangement. It was found that, when the reaction of I and IIa was carried out in benzene, an intermediate bicyclic sulfonium betaine (VIIa) was obtained as yellow precipitates. The properties and reactions of VIIa were investigated. It was shown that the ring expansion product IIIa gave cyclooctenone derivatives (XIIa—c) by the reaction with some nucleophiles. IIIa was found to give diene esters (XIII, R=acyl) and diene ethers (XIII, R=alkyl) upon reaction with acyl and alkyl halides.

It was found[2] that 3,4-furandicarboxylic acid derivatives were produced by the reactions of sulfonium ylides with dimethyl acetylenedicarboxylate through a 1,3-acyl rearrangement.

This paper deals with a new ring expansion of cyclic sulfonium ylides by two carbon atoms[3] by the reactions with acetylenic compounds through an intramolecular 1,3-acyl rearrangement.

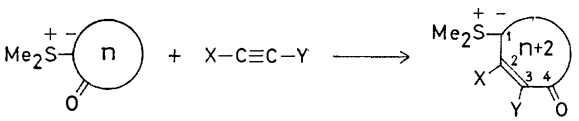

(I) (n=6) (II) (III) (n=6)
(VIII) (n=7) (IX) (n=7)
(X) (n=5) (XI) (n=5)

When a six-membered cyclic sulfonium ylide, *i.e.*, dimethylsulfonium-2-oxocyclohexylide (I) was treated with dimethyl acetylenedicarboxylate (IIa) in dimethyl sulfoxide (DMSO), an exothermic reaction soon took place and a ring expansion product, dimethylsulfonium-2,3-dicarbomethoxy-4-oxo-2-cyclooctenylide (IIIa) was obtained in quantitative yield. The IR spectrum of IIIa showed strong absorptions at 1726, 1627, and 1528 cm^{-1}. The absorption at 1726 cm^{-1} can be attributed to the unsaturated ester carbonyl and those at 1627 and 1528 cm^{-1} to the ester and ketone carbonyl, respectively, both conjugated with the ylide carbanion.[2,4,5] Based upon IR, NMR, and UV spectra, IIIa was found to have the structure of a sulfonium ylide stabilized by a conjugated system.[2,4] The ylide IIIa gave a sulfonium salt (IVa) with 2,4,6-trinitrobenzenesulfonic acid (TNBS-H) in quantitative yield.

The NMR spectrum of IVa showed a low field peak

1) Preliminary report, T. Mukaiyama, and M. Higo, *Tetrahedron Lett.*, **1970**, 5297.

2) M. Higo and T. Mukaiyama, *ibid.*, **1970**, 2565.

3) C. D. Gutsche and D. Redmore, "Carbocyclic Ring Expansion Reactions," Academic Press, New York and London, (1968), p. 161.

4) (a) C. Kaiser, B. M. Trost, J. Beeson, and J. Weinstock, *J. Org. Chem.*, **30**, 3972 (1965); (b) J. Ide and Y. Kishida, *Tetrahedron Lett.*, **1966**, 1787.

5) (a) B. M. Trost, *J. Amer. Chem. Soc.*, **89**, 138 (1967); (b) G. B. Payne, *J. Org. Chem.*, **33**, 3517 (1968).

TABLE 1. RING EXPANSION OF THE SIX-MEMBERED CYCLIC SULFONIUM YLIDE (I) WITH ACETYLENIC COMPOUNDS (II)

	X	Y	III			III·TNBS-H (IV)						
			Yield (%)	Mp (°C)[a]	IR, $\nu_{C=O}$ (cm^{-1})	Mp (°C)[a]	NMR δ (ppm)[b]		*Anal.* (%) C	H	N	S
a	CO_2Me	CO_2Me	100	166.5—167.5	1726, 1627, 1528	202.0	12.80	Found	40.40	4.21	7.13	10.66
								Calcd	40.47	3.92	7.08	10.78
b	Ph	CO_2Et	55	137.0—139.0	1655, 1500,	201.0	13.02	Found	48.06	4.61	6.91	10.48
								Calcd	48.00	4.35	6.72	10.23
c	Ph	COPh	82	165.0—166.0	1534, 1512,	211.0	16.25	Found	53.16	4.23	6.42	9.70
								Calcd	52.97	4.14	6.39	9.73
d	COPh	COPh	52	136.0—138.0	1652, 1528, 1500	196.5	9.16	Found	52.49	4.19	6.39	9.56
								Calcd	52.55	3.94	6.13	9.34
e	H	CO_2Me	33[c]	c)	c)	183.0	13.00	Found	40.65	4.04	8.00	12.11
								Calcd	40.38	3.95	7.85	11.95

a) Decomposition point.
b) Chemical shift of an enolated proton[6] (in DMSO-d_6).
c) Isolated as 2,4,6-trinitrobenzenesulfonate.

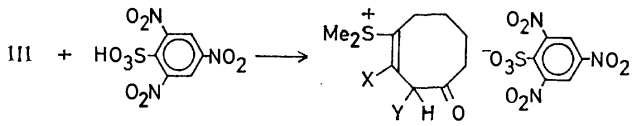

TNBS-H (IV)

at δ=12.80 attributable to a partially enolated α-proton[6] in the β-keto ester system. It is thus obvious that IVa exists in the form of a vinylsulfonium salt rather than that of an allylsulfonium salt.

The structure of IIIa, the ring expansion product, was firmly supported by the fact that IIIa was desulfurized by Raney nickel to afford 2,3-dicarbomethoxy-4-oxocyclooctene (V) in 50% yield, identical with an authentic sample.[7]

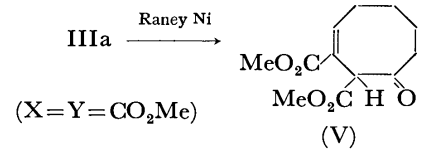

(V)

In a similar manner, when ethyl phenylpropiolate (IIb), benzoylphenylacetylene (IIc), dibenzoylacetylene (IId), and methyl propiolate (IIe) were treated with I, the corresponding ring expansion compounds (IIIb—e) were obtained in good yields. Similarly, IIIb—e afforded TNBS salts (IVb—e). In the cases of asymmetric acetylenes IIb,c,e, the NMR spectra of IVb,c,e, indicate that more electron attracting groups, *i.e.*, carboalkoxy and benzoyl groups, are attached to C_3 of III. The reaction of I with phenylacetylene, however, did not occur even after prolonged stirring for several days at room temperature. The results are summarized in Table 1.

It is reasonable to consider that the reaction of I with II proceeds through an intermediate betaine (VI), which is transformed into III by way of the intramolecular 1,3-migration of the acyl group.[8] The chemical driving force of the reaction is probably due to the enhanced stability of III over I gained from the extended conjugation formed by acyl migration. Perhaps severe steric interaction prevented further cyclization of III to a bicyclofuran ring by means of intramolecular nucleophilic displacement accompanied with elimination of dimethyl sulfide.

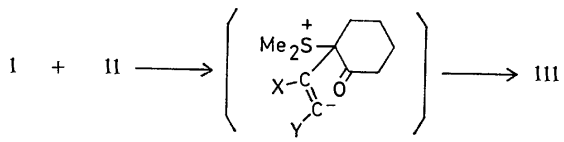

(VI)

In order to elucidate acyl migration mechanism, the effect of the solvents in the reaction of I with IIa was investigated. Solvents such as *N*,*N*-dimethylformamide (DMF), acetonitrile and tetrahydrofuran (THF) also afforded IIIa in 24, 55, and 25% yields, respectively. The results indicate that DMSO is the most suitable as solvent for the reaction. On the other hand, when the reaction of I and IIa was carried out in benzene, IIIa was not formed and yellow precipitates were obtained. The precipitates melted at 90—100°C, resolidified above this temperature and decomposed at 165°C. It was also found that the precipitates were easily transformed into IIIa by heating at 90°C for several minutes or merely dissolving into polar solvents, even into chloroform. Their limited solubility in benzene and facile

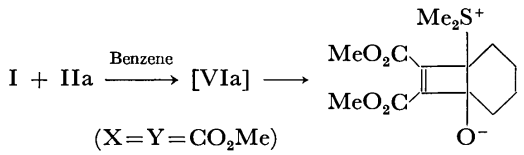

(VIIa)

6) L. A. Paquette and R. W. Begland, *J. Amer. Chem. Soc.*, **88**, 4685 (1966).
7) K. C. Brannock, R. D. Burpitt, V. W. Goodlett, and J. G. Thweatt, *J. Org. Chem.*, **28**, 1464 (1963).
8) For reports on 1,3-acyl migrations from carbon to carbon, see a) N. Inamoto, N. Iwata, and O. Shimamura, *Chem. & Ind.*, **1959**, 47 ; b) N. H. Bromham, *ibid.*, **1959**, 258; c) H. Nozaki, M. Takaku, and Y. Hayashi, *Tetrahedron Lett.*, **1967**, 2303; d) E. Baggiolini, K. Schaffner, and O. Jeger, *Chem. Commun.*, **1969**, 1103.

TABLE 2. RING EXPANSION OF THE SEVEN-MEMBERED CYCLIC SULFONIUM YLIDE (VIII) WITH ACETYLENIC COMPOUNDS (II)

	X	Y	IX Yield (%)	IX Mp (°C)[a]	IX IR, $\nu_{C=O}$ (cm^{-1})	IX·TNBS–H Mp (°C)[a]	IX·TNBS–H NMR δ (ppm)[b]		Anal. (%) C	H	N	S
a	CO_2Me	CO_2Me	87	100	1710, 1657, 1510	209.0	12.60	Found	41.23	4.04	6.80	10.81
								Calcd	41.52	4.15	6.92	10.54
b	Ph	CO_2Et	35	132	1650, 1515,	211.5	12.68	Found	49.13	4.78	6.71	9.72
								Calcd	48.83	4.57	6.57	10.01
c	Ph	COPh	53	105	1546, 1490	213.5	c)	Found	53.79	4.59	6.22	9.42
								Calcd	53.65	4.35	6.26	9.53

a) Decomposition point.
b) Chemical shift of an enolated proton[6] (in DMSO-d_6).
c) Not observed.

conversion into IIIa in polar solvents precluded measurements of NMR and UV spectra. In view of the above facts, however, it seems most reasonable to assume that the precipitates are a bicyclic sulfonium betaine having [4.2.0]bicyclooctene structure (VIIa), a valence isomer of IIIa.

VIIa ⟶ IIIa

In order to have further proof for the structure VIIa, prevention of a facile ring opening of VIIa, which might be caused by electron migration from the oxygen anion to the bicyclo ring system, was attempted by means of alkylation[9] of the anion. However, alkylation of VIIa with triethyloxonium fluoborate resulted in the ring opening and the product was the same as that formed from IIIa and the alkylating reagent.

It was established that the ring expansion of a seven-membered cyclic sulfonium ylide, dimethylsulfonium-2-oxocycloheptylide (VIII) also occurred upon reaction with IIa giving dimethylsulfonium-2,3-dicarbomethoxy-4-oxo-2-cyclononenylide (IXa) in 87% yield.

Similarly, the reactions of VIII with IIb,c afforded the ring expansion products (IXb,c) in good yields under mild conditions. The results are listed in Table 2.

In the case of a five-membered cyclic sulfonium ylide (X), X was prepared *in situ* from the corresponding sulfonium salt on treatment with *n*-butyllithium because of an unsuccessful isolation of X. X was immediately allowed to react with IIa to afford a ring expansion product (XIa) in 52% yield.

The ring expansion of eight- and twelve-membered cyclic sulfonium ylides, however, has not yet been successful.

The reactions of the ring expansion product IIIa were investigated with the expectation that IIIa, being a reactive sulfonium ylide, would become a potential synthetic intermediate.

It was shown that IIIa gave cyclooctenone derivatives (XIIa—c) by displacement reactions with some nucleophiles accompanied with elimination of dimethyl sulfide. When IIIa was allowed to react with benzenethiol, 1-phenylthio-2,3-dicarbomethoxy-4-oxocyclooctene (XIIa) was obtained in 80% yield with evolution of dimethyl sulfide. The structural assignment was made on the basis of elemental analysis and IR and NMR[6] spectra.

In a similar manner, cyclooctenone derivatives (XIIb—d) were obtained in excellent yields when IIIa was allowed to react with ethanethiol, hydrogen cyanide or methanol. The results are shown in Table 3.

IIIa + R–H $\xrightarrow{-Me_2S}$ 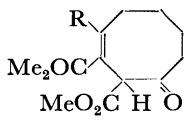

(XII)

On the other hand, the reactions of IIIa with several

TABLE 3. REACTIONS OF THE RING EXPANSION PRODUCT (IIIa) WITH NUCLEOPHILES

	Nucleophile	Reaction conditions Solvent	Temp.	Time (hr)	Product, XII R	Yield (%)	Mp (°C)	NMR δ (ppm)[a]	Anal. (%)	C	H	N	S
a	PhSH	Benzene	RT	33	PhS	80	118.5—119.5	12.66	Found	62.07	5.99		9.46
									Calcd	62.06	5.79		9.19
b	EtSH	Benzene	RT	19	EtS	95	68.3—69.8	b)	Found	56.03	6.88		10.47
									Calcd	55.99	6.71		10.66
c	HCN	Benzene	RT	48	NC	60	154.5—155.5	12.87	Found	59.13	5.97	5.24	
									Calcd	58.86	5.70	5.28	
d	MeOH	MeOH	65°C	9	MeO	90	105.0	12.68	Found	58.04	6.87		
									Calcd	57.77	6.71		

a) Chemical shift of an enolated proton[6] (in $CDCl_3$).
b) Not measured.

9) S. H. Smallcombe, R. J. Holland, R. H. Fish, and M. C. Caserio, *Tetrahedron Lett.*, **1968**, 5987.

Table 4. Reactions of the ring expansion product (IIIa) with electrophiles

	Electrophile	Reaction conditions			Product, XIII					
		Solvent	Temp.	Time (day)	R	Yield (%)	Mp (°C)		Anal. (%) C	H	S
a	PhCOCl	Benzene	RT	1	PhCO	68	138.5—139.5	Found	61.53	5.84	8.43
								Calcd	61.53	5.68	8.20
b	MeCOCl	Benzene	RT	2	MeCO	59	96.5—98.0	Found	54.99	6.19	9.80
								Calcd	54.87	6.14	9.75
c	MeI	MeI	50°C	0.4	Me	74	118.0—119.0	Found	55.87	6.96	10.62
								Calcd	55.99	6.71	10.66
d	$PhCH_2Br$	DMSO	RT	1.5	$PhCH_2$	23	127.5—128.5	Found	64.10	6.71	8.36
								Calcd	63.82	6.43	8.50

active methylene compounds, such as acetylacetone and ethyl malonate, in various solvents resulted only in the formation of 1-methylthio-2,3-dicarbomethoxy-4-oxocyclooctene (XII, R=MeS) in 23—74% yields.

The reactions of IIIa with electrophilic reagents were also investigated. It was found that IIIa gave diene esters (XIII, R=acyl) and diene ethers (XIII, R=alkyl) on treatment with acyl and alkyl halides. Acylation and alkylation were found to occur exclusively on the oxygen atom.[10] The results are recorded in Table 4.

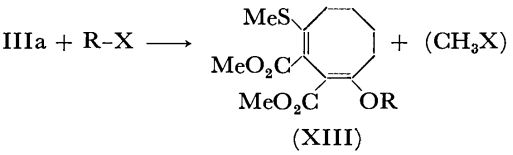

(XIII)

It should be noted that the reactions of cyclic sulfonium ylides I, VIII and X with II in DMSO afforded the ring expansion (by two carbon atoms) products III, IX, and XI through the 1,3-acyl rearrangement in high yields under extremely mild conditions. The cyclic sulfonium ylide III, having a reactive sulfonium group, was found to be an important intermediate for the syntheses of various cyclooctane derivatives with cyclohexanone as a starting material.

Experimental

All the experiments were carried out in atmosphere of nitrogen. Melting points are uncorrected. NMR spectra were measured in $CDCl_3$ unless otherwise stated with tetramethylsilane as internal standard.

Preparation of Cyclic Stable Sulfonium Ylides. Dimethylsulfonium-2-oxocyclohexylide (I) was newly prepared from dimethyl-2-oxocyclohexylsulfonium fluoborate in 80% yield by the action of aqueous sodium hydroxide in a mixture of chloroform and saturated aqueous potassium carbonate.

In a similar manner, seven-, eight-, and twelve-membered cyclic stable sulfonium ylides were obtained in good yields from the corresponding fluoborate or methylsulfate. The cyclic ylides gave sulfonium salts with 2,4,6-trinitrobenzenesulfonic acid (TNBS-H)[11] in quantitative yields. The results are listed in Table 5.

Reaction of Dimethylsulfonium-2-oxocyclohexylide (I) with Dimethyl Acetylenedicarboxylate (IIa)[12] *in Dimethyl Sulfoxide (DMSO).* When a solution of IIa (1.42 g, 10 mmol) in 15 m*l* of dry DMSO was added dropwise to a solution of I (1.58 g, 10 mmol) in DMSO with stirring at 18°C, an exothermic reaction soon took place and yellow precipitates of dimethylsulfonium-2,3-dicarbomethoxy-4-oxo-2-cyclooctenylide (IIIa) were deposited. After being stirred for an hour, IIIa was filtered and washed well with dry benzene. Dilution of the filtrate with 1 *l* of dry ether gave additional 0.99 g of IIIa. The total yield was 2.99 g (100%). Mp 166.5—167.5°C (dec). IR (KBr): 1726, 1627, 1528 (C=O) and 1575 (C=C) cm^{-1}. NMR (DMSO-d_6): δ 1.3—2.3 (8H, m, C_4H_8), 2.94 (6H, s, $Me_2\overset{+}{S}$), 3.33 (3H, s, MeOCO) and 3.64 (3H, s, MeOCO) ppm. UV: λ_{max}^{EtOH} 280 (ε 9,800) and 368 (ε 4,900) mμ.

In a similar manner, reactions of I with ethyl phenylpropiolate (IIb),[13] benzoylphenylacetylene (IIc),[14] dibenzoylacetylene (IId),[15] and methyl propiolate (IIe)[16] afforded the corresponding ring expansion compounds (IIIb—e). The yields and the properties are summarized in Table 1.

Reaction of IIIa with 2,4,6-Trinitrobenzenesulfonic Acid (TNBS-H). An equimolar amount of TNBS-H was added to a solution of IIIa in methanol at room temperature and dimethyl-2,3-dicarbomethoxy-4-oxo-1-cyclooctenylsulfonium 2,4,6-trinitrobenzenesulfonate (IVa) was obtained instantly in quantitative yield. Mp 202.0°C (dec) (recrystallized from methanol).

Similarly, reactions of IIIb—e with TNBS-H afforded the corresponding 2,4,6-trinitrobenzenesulfonates (IVb—e) quantitatively. The results are also shown in Table 1.

Desulfurization of IIIa with Raney Nickel. A mixture of IIIa (0.87 g, 2.9 mmol) and large excess of Raney nickel (W-4)[17] in 20 m*l* of water and 15 m*l* of ethanol was heated at 90—100°C for 8.5 hr. After removal of precipitates from the hot reaction mixture by centrifugal separation, the solution was evaporated to give 2,3-dicarbomethoxy-4-oxocyclooctene (V), 0.35 g (50%), mp 75.0—76.0°C (purified by sublimation). Found: C, 59.69; H, 6.90%. Calcd for $C_{12}H_{16}O_5$: C, 59.99; H, 6.71%. The melting point was not depressed by admixture with an authentic sample prepared by the method of Brannock *et al.*[7] The IR spectra of both samples are identical.

10) E. Winterfeldt and H. J. Dillinger, *Chem. Ber.*, **99**, 1558 (1966).
11) D. J. Pettitt and G. K. Helmkamp, *J. Org. Chem.*, **29**, 2702 (1964).
12) E. H. Huntress, T. E. Lesslie, and J. Bornstein, "Organic Syntheses," Coll. Vol. 4, p. 329 (1963).
13) T. W. Abbott, *ibid.*, Vol. 12, 60 (1932).
14) J. V. Nef, *Ann.*, **308**, 276 (1899).
15) R. E. Lutz and W. R. Smithey, Jr., *J. Org. Chem.*, **16**, 51 (1951).
16) V. Wolf, *Chem. Ber.*, **86**, 735 (1953).
17) G. R. Pettit and E. E. van Tamelen, "Organic Reactions," Vol. 12, p. 406 (1962).

TABLE 5. PROPERTIES OF DIMETHYLSULFONIUM-2-OXOCYCLOALKYLIDES AND 2,4,6-TRINITROBENZENESULFONATES

n	X[a]	Cyclic Ylide		TNBS–H Salt[c]					
		Mp (°C)	IR, $\nu_{C=O}$ (cm^{-1})	Mp (°C)[b]		*Anal.* (%) C	H	N	S
5	TNBS[c]	d)	d)	180	Found	35.52	3.72	9.90	14.63
					Calcd	35.70	3.43	9.61	14.64
6	BF_4	107	1535	198	Found	37.28	3.90	9.16	14.43
					Calcd	37.26	3.80	9.31	14.19
7	BF_4	106	1530	203	Found	38.57	3.95	9.18	13.98
					Calcd	38.73	4.11	9.03	13.75
8	$MeSO_4$	82	1516	195	Found	40.25	4.69	9.03	13.43
					Calcd	40.09	4.41	8.77	13.14
12[e]	$MeSO_4$	80	1505	182	Found	46.07	5.60	7.52	11.48
					Calcd	45.89	5.69	7.65	11.65

a) Anion of starting salt. b) Decomposition point. c) 2,4,6-Trinitrobenzenesulfonate.
d) Not isolated. e) Methylethylsulfonium-2-oxocyclododecylide.

Reaction of I with IIa in Benzene. *1) Isolation of Bicyclic Sulfonium Betaine (VIIa)*: A solution of IIa (0.71 g, 5 mmol) in 15 m*l* of dry benzene was added over a period of 25 min at 10°C to a suspension of I (0.79 g, 5 mmol) in 30 m*l* of dry benzene. After stirring for 2 hr, the resulting bright yellow precipitates (VIIa), 0.93 g (62%), were filtered, washed and dried at reduced pressure. IR (KBr): 1710, 1677, and 1532 cm^{-1}. VIIa melted at 90—100°C, resolidified above this temperature and decomposed at 165°C. When VIIa was heated at 90°C for several minutes, its IR spectrum became identical with that of IIIa.

2) Alkylation of VIIa with Triethyloxonium Fluoborate.[18] When VIIa was allowed to react with triethyloxonium fluoborate at room temperature for 6 hr, dimethyl-2,3-dicarbomethoxy-4-ethoxy-1,3-cyclooctadienylsulfonium fluoborate was produced in quantitative yield. Mp 147—148°C (Methanol). Found: C, 45.92; H, 5.88; S, 7.94%. Calcd for $C_{16}H_{25}BF_4O_5S$: C, 46.17; H, 6.06: S, 7.69%. IR (KBr): 1727, 1709, 1681, and 1590 cm^{-1}. NMR: δ 1.43 (3H, t, Me–CH_2, J=4.5 Hz), 1.9—2.8 (8H, m, C_4H_8), 3.13 (6H, s, $Me_2\overset{+}{S}$), 3.65 (3H, s, MeOCO), 3.78 (3H, s, MeOCO), and 6.20 (2H, q, Me–CH_2–O, J=4.5 Hz) ppm.

The same sulfonium fluoborate was obtained by the reaction of IIIa with triethyloxonium fluoborate.

Reaction of Dimethylsulfonium-2-oxocycloheptylide (VIII) with II. When VIII was treated with IIa—c in DMSO in the same manner as described above for the reaction between I and II, the corresponding ring expansion products (IXa—c) were obtained. Reactions of IXa—c with TNBS-H gave 2,4,6-trinitrobenzenesulfonates (IXa—c·TNBS-H) in quantitative yields. The results are listed in Table 2.

Reaction of Dimethylsulfonium-2-oxocyclopentylide (X) with IIa. To a solution of dimethyl-2-oxocyclopentylsulfonium 2,4,6-trinitrobenzenesulfonate[19] (2.19 g, 5 mmol) and IIa (0.71 g, 5 mmol) in 10 m*l* of dry DMSO, a solution of *n*-butyllithium (5 mmol) in 6 m*l* of *n*-hexane was added *via* hypodermic syringe over a period of an hour with occasional cooling. After stirring for 2 hr, TNBS-H (5 mmol) was added to the reaction mixture. Addition of methanol gave crystalline dimethyl-2,3-dicarbomethoxy-4-oxo-1-cycloheptenylsulfonium 2,4,6-trinitrobenzenesulfonate (XIa·TNBS-H), mp 194°C (dec) (methanol), in 52% yield. Found: C, 39.34; H, 3.80; N, 7.44; S, 10.79%. Calcd for $C_{19}H_{21}N_3O_{14}S_2$: C, 39.38; H, 3.63; N, 7.25; S, 11.05%.

Reaction of IIIa with Benzenethiol. When a mixture of IIIa (0.300 g, 1 mmol) and benzenethiol (0.110 g, 1 mmol) in 15 m*l* of dry benzene was stirred at room temperature, the crystals of IIIa gradually disappeared to give an almost clear solution after 6 hr. Stirring was continued overnight and the solvent was removed under reduced pressure. The resulting viscous oil was chromatographed over silica gel. Elution with ether-petroleum ether (1: 1) gave 1-phenylthio-2,3-dicarbomethoxy-4-oxocyclooctene (XIIa), mp 118.5—119.5°C (*n*-hexane), in 80% yield. Further elution with the same mixture afforded 1-methylthio-2,3-dicarbomethoxy-4-oxocyclooctene (XII, R=MeS) in 18% yield.

In a similar way, reactions of IIIa with ethanethiol, hydrogen cyanide and methanol gave 1-substituted-4-oxocyclooctene derivatives(XIIc—d) in high yields without concomitant formation of XII(R=MeS). In the case of hydrogen cyanide, the reaction was carried out with twofold excess of hydrogen cyanide generated *in situ* from potassium cyanide and acetic acid. The yields, melting points, NMR spectra and analytical values of XIIa—d are shown in Table 3.

Reaction of IIIa with Acetylacetone. A solution of IIIa (0.300 g, 1 mmol) and acetylacetone (0.100 g, 1 mmol) in 10 m*l* of dry DMSO was heated at 90—100°C for 18 hr. The reaction mixture was poured into ice-water and worked up with ether to give a semi-crystalline viscous oil which was chromatographed over silica gel. Elution with methylene chloride afforded 1-methylthio-2,3-dicarbomethoxy-4-oxocyclooctene (XII, R=MeS) in 23% yield, mp 124—125°C (*n*- or *c*-hexane). Found: C, 54.69; H, 6.47; S, 11.10%. Calcd for $C_{13}H_{18}O_5S$: C, 54.54; H, 6.34; S, 11.18%. IR (KBr): 1703, 1650, 1618, and 1553 cm^{-1}. NMR: δ 1.2—2.85 (8H, m, C_4H_8), 3.37 (3H, s, MeS), 3.68 (3H, s, MeOCO), 3.70 (3H, s, MeOCO), and 12.67 (1H, s, CO–CH–CO_2Me) ppm.

Similarly, reactions of IIIa with diethyl malonate, malononitrile, ethyl acetoacetate, dibenzoylmethane and trifluoroacetylacetone in various solvents such as DMSO, DMF, acetonitrile, methylene chloride, THF, dioxane or benzene also gave XII (R=MeS) in 23—74% yields.

Reaction of IIIa with Benzoyl Chloride. When a mixture of I (0.310 g, 1.03 mmol) and benzoyl chloride (0.149 g, 1.05 mmol) in 15 m*l* of dry benzene was stirred at room temperature, the yellow crystals of IIIa gradually disappeared. After being stirred overnight, the solvent was evaporated to give a viscous oil which was chromatographed over silica gel. 1-Methylthio-2,3-dicarbomethoxy-4-benzoyloxy-1,3-cyclooctadiene (XIIIa), mp 138.5—139.5°C, was obtained in 68%

18) H. Meerwein, "Methoden der Organischen Chemie," Vol. 6 (III), p. 336.

19) The sulfonium salt was prepared from dimethyl sulfide, 2-bromocyclopentanone and silver 2,4,6-trinitrobenzenesulfonate.[11]

yield by elution with ether-petroleum ether (2: 3). NMR (DMSO-d_6): δ 1.1—2.9 (8H, m, C_4H_8), 2.40 (3H, s, MeS), 3.42 (3H, s, MeOCO), 3.47 (3H, s, MeOCO) and 7.4—8.1 (5H, m, C_6H_5) ppm.

In a similar way, the reactions of IIIa with acetyl chloride, methyl iodide and benzyl bromide afforded the corresponding diene ester (XIIIb) and diene ethers (XIIIc, d). The results are recorded in Table 4.

BULLETIN OF THE CHEMICAL SOCIETY OF JAPAN, VOL. 45, 255—258(1972)

Structure and Reactivity of Organic Ions in Gas-Phase Radiolysis. III. The Benzenonium Ions Formed by the Reactions of CH_5^+ and $C_2H_5^+$ Ions from Methane with *o*-Xylene[1]

Yukio YAMAMOTO, Setsuo TAKAMUKU, and Hiroshi SAKURAI

The Radiation Laboratory, The Institute of Scientific and Industrial Research, Osaka University, Suita, Osaka

(Received June 18, 1971)

The gas-phase radiolysis of mixtures of *o*-xylene and excess methane has been studied at room temperature as a function of methane pressure and the added NO and NH_3 in order to investigate the reactions of CH_5^+ and $C_2H_5^+$ ions from methane with *o*-xylene. It has been suggested that the proton transfers from these ions to *o*-xylene result in the isomerization to *m*-xylene *via* an intermediate σ complex, dimethylbenzenonium ion, and that a part of the $C_2H_5^+$ ions is added to *o*-xylene leading to the formation of two isomers of dimethylethylbenzene. The proposed mechanism of the methane-sensitized isomerization of *o*-xylene to *meta* isomer has been supported by the observation that both *m*-xylene-d_0 and *m*-xylene-d_1 were formed in the radiolysis of a mixture of *o*-xylene and methane-d_4. The isotope effect (k_H/k_D) on the proton loss from the dimethylbenzenonium ion was roughly estimated to be 1.8 ± 0.4. Group migration of intermediate σ complexes was discussed.

In previous studies,[2-5] it was reported that, in the gas-phase radiolysis of toluene, ethylbenzene, and *m*-xylene, $C_7H_7^+$ ions,[6] formed from these alkylbenzenes, react with the parent alkylbenzene molecules to produce the corresponding benzylated alkylbenzenes, alkyldiphenylmethanes.[7] The products predominantly consisted of such isomers as are benzylated at a *meta* position to the resident alkyl groups. It has also been reported that, in the gas-phase radiolysis of a mixture of propane with benzene or toluene, the isopropylation of the aromatics by $C_3H_7^+$ ions from propane was observed, and in the case of toluene the isopropylation occurred mainly at a *meta* position at higher pressures of toluene.[1] Attention was paid to the mechanism of these electrophilic aromatic substitution reactions in the gas phase in order to explain the observed isomer distribution of the products, which is in contrast to that known in analogous liquid-phase reactions such as the Friedel-Crafts reactions.[8] We have proposed a mechanism involving an isomerization process of intermediate σ complexes, benzenonium ions,[1,3] where R_1 and R_2 show the resident

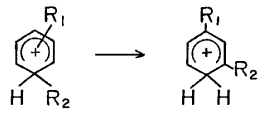

I II

and attacking alkyl groups, respectively. Thus, it has been suggested that the primarily formed complex I easily isomerizes to the more stable one II, which is most effectively stabilized by the inductive effect of alkyl groups, since in the gas phase it exists as a free ion with a certain internal energy. We have extended the study of this type of reaction, which proceeds through benzenonium ion intermediate, especially in order to investigate its intramolecular rearrangement.

In the high pressure mass spectrometry of methane, it has been reported that the major product ions at higher pressures are CH_5^+ and $C_2H_5^+$ ions, which comprise approximately 90% of the total ionization.[9] The ions are unreactive with methane but highly reactive with some kinds of additives such as ammonia, water, and aromatic hydrocarbons.[10,11] Munson and Field reported that these ions react with several aromatic hydrocarbons to yield predominantly protonated aromatic ions along with a relatively small amount of ethyl ion adducts.[11] The present investigation deals with the reactions of these benzenonium ions expected to

1) Part II; S. Takamuku, K. Iseda, and H. Sakurai, *J. Amer. Chem. Soc.*, **93**, 2420 (1971).
2) Y. Yamamoto, S. Takamuku, and H. Sakurai, *ibid.*, **91**, 7192 (1969).
3) Y. Yamamoto, S. Takamuku, and H. Sakurai, *J. Phys. Chem.*, **74**, 3325 (1970).
4) Y. Yamamoto, S. Takamuku, and H. Sakurai, This Bulletin, **44**, 574 (1971).
5) Y. Yamamoto, S. Takamuku, and H. Sakurai, *ibid.*, **44**, 2104 (1971).
6) This ion is known to be the most abundant ion in the mass spectra of toluene, ethylbenzene, and xylenes (see Ref. 17).
7) The analogous product formation was observed in the gas-phase radiolyses of *o*- and *p*-xylenes, and the results will be published.
8) See for example, C. C. Price, "Organic Reactions," Vol. 3, John Wiley & Sons, Inc., New York, N. Y. (1964), p. 1.
9) F. H. Field and M. S. B. Munson, *J. Amer. Chem. Soc.*, **87**, 3289 (1965).
10) M. S. B. Munson and F. H. Field, *ibid.*, **87**, 4242 (1965).
11) M. S. B. Munson and F. H. Field, *ibid.*, **89**, 1047 (1967).

be also formed in the gas-phase radiolysis of mixtures of *o*-xylene and excess methane.

Experimental

Materials. *o*-Xylene obtained from Wako Pure Chem. Indust. Co. was purified by the usual method. After distillation using a 1 m column packed with stainless helices, the purity determined gas chromatographically by means of flame-ionization detection was more than 99.9%. The purified *o*-xylene was dried over sodium, degassed, and stored in a high vacuum line. Methane-h_4 and methane-d_4, obtained from Takachiho Shoji Co. and Merck and Dohme of Canada, respectively, were also stored in the vacuum line, after several trap-to-trap distillations. These samples were thoroughly dried by passing through sodium mirrors prior to use. Ammonia and nitric oxide, both obtained from Takachiho Shoji Co., were also purified by several trap-to-trap distillations.

Procedures. Experimental procedures were almost the same as those reported previously.[1] Irradiation was carried out in Pyrex cylinders approximately 120 m*l* in volume with γ rays from a 5000 Ci ^{60}Co source at room temperature. The dose rate and the dose were 3.7×10^{15} eV/hr·μmol and 2.6×10^{17} eV/μmol, respectively, for *o*-xylene. The products were analyzed by gas chromatography using a combination of Bentone 34 (3 m) and Apiezon L (3 m) and a flame-ionization detector. The column temperatures were 100 and 140°C for the products with retention times less and more than that of *o*-xylene, respectively. The isotopic distribution of *m*-xylene formed in the radiolysis of a mixture of *o*-xylene and methane-d_4 was determined using a directly coupled gas chromatograph-mass spectrometer (Hitachi RMS-4 mass spectrometer) at an ionizing potential of 80 eV.

Results and Discussion

All the radiolysis experiments were performed at the same pressure of *o*-xylene, 3.3 ± 0.2 mmHg. The *G* values were calculated on the basis of the energy absorbed by *o*-xylene. The *G* values of the products of the gas-phase radiolysis of a mixture of *o*-xylene and methane in the presence and absence of a radical scavenger, nitric oxide, together with those of the radiolysis of pure *o*-xylene are presented in Table 1.[12] The dependence of the product yields on methane pressure is shown in Figs. 1 and 2. When excess methane was added to *o*-xylene, the *G* values of *m*-xylene, *o*-ethyltoluene, and 1,2,3- and 1,2,4-trimethylbenzenes appreciably increased, and 1,2-dimethyl-3-ethylbenzene and 1,2-dimethyl-4-ethylbenzene were newly formed. The yields of these products increased with increasing methane pressure. Among these products, *o*-ethyltoluene and two isomers of trimethylbenzene were appreciably reduced by the addition of NO (Table 1). Thus, it is suggested that these products are mainly formed by the reactions of radicals from methane with *o*-xylene as follows.

$$R\cdot + (CH_3)_2C_6H_4 \longrightarrow RH + CH_3C_6H_4CH_2\cdot \quad (1)$$

$$CH_3C_6H_4CH_2\cdot + CH_3\cdot \longrightarrow CH_3C_6H_4CH_2CH_3 \quad (2)$$

$$CH_3\cdot + (CH_3)_2C_6H_4 \longrightarrow (CH_3)_3C_6H_3 + H \quad (3)$$

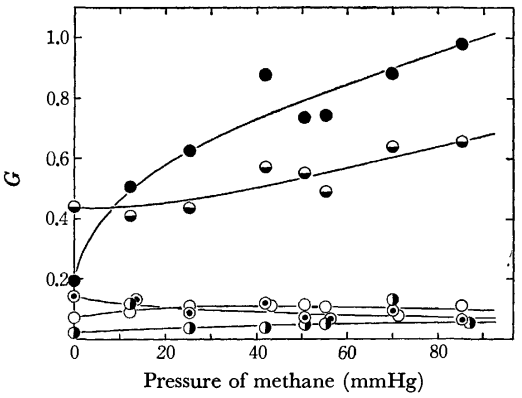

Fig. 1. Dependence of the *G* values on methane pressure (1): ⊙, Benzene; ◒, Toluene; ◑, Ethylbenzene; ○, *p*-Xylene; ●, *m*-Xylene.

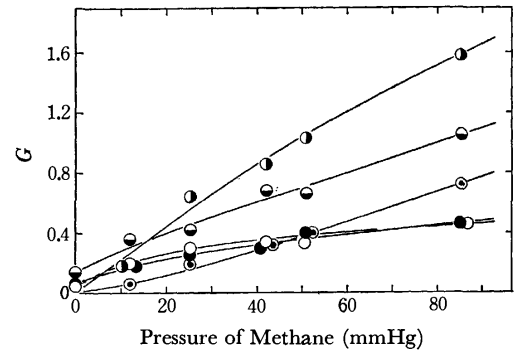

Fig. 2. Dependence of the *G* values on methane pressure (2): ◒, *o*-Ethyltoluene; ●, 1,2,3-Trimethylbenzene; ○, 1,2,4-Trimethylbenzene; ⊙, 1,2-Dimethyl-3-ethyl-benzene; ◑, 1, 2-Dimethyl-4-ethylbenzene.

Table 1. The *G* values of products in gas-phase radiolyses of pure *o*-xylene and *o*-xylene-methane mixture

Product	Pure *o*-xylene	*o*-Xylene-methane mixture	
	o-Xylene, 3.3 mmHg		
		Methane, 51.0 mmHg	
			with NO[a]
Benzene	0.14	0.07	0.08
Toluene	0.44	0.55	0.34
Ethylbenzene	0.02	0.05	0.02
p-Xylene	0.07	0.11	0.11
m-Xylene	0.19	0.73	0.61
o-Ethyltoluene	0.14	0.66	0.01
1,2,3-Trimethylbenzene	0.06	0.40	0.07
1,2,4-Trimethylbenzene	0.04	0.33	0.14
1,2-Dimethyl-3-ethylbenzene	0	0.40	0.51
1,2-Dimethyl-4-ethylbenzene	0	1.03	1.18

a) The mol ratio of added NO to methane was about 0.07.

12) In a previous study of the gas-phase radiolysis of pure *o*-xylene, it was reported that benzocyclobutene is also formed with a *G* value of 0.08 at a *o*-xylene pressure of 4.7 mmHg [K. E. Wilzbach and L. Kaplan, *Advances in Chemistry Series*, No. 82, American Chemical Society, Washington, D. C., (1968), p. 134]. However, the yield of this product could not be determined under the analytical conditions of this study. The yields of other liquid products in these studies are in good agreement with each other.

where R· shows any radical or a hydrogen atom formed from methane. On the other hand, *m*-xylene and two isomers of dimethylethylbenzene were not so much affected by the added NO, indicating that the methane-sensitized isomerization and ethylation of *o*-xylene are nonradical processes.

It might be expected that the major ionic reactions in the primary process of the gas-phase radiolysis of mixtures of *o*-xylene and excess methane are the proton transfer from the CH_5^+ and $C_2H_5^+$ ions and the addition of the $C_2H_5^+$ ions to *o*-xylene as follows.

$$CH_4 \xrightarrow{\sim\sim} CH_5^+, C_2H_5^+ \qquad (4)$$

$$CH_5^+ \text{ (or } C_2H_5^+) + \text{C}_8\text{H}_{10} \longrightarrow \text{C}_8\text{H}_{11}^+ + CH_4 \text{ (or } C_2H_4) \qquad (5)$$

IIIa

$$C_2H_5^+ + \text{C}_8\text{H}_{10} \longrightarrow \text{C}_{10}\text{H}_{15}^+ \qquad (6)$$

IVa

In solution chemistry it is known that the acid-catalyzed isomerization of *o*-xylene results in the exclusive formation of *m*-xylene.[13] Such a result is similar to that of the methane-sensitized isomerization of *o*-xylene. Thus, the methane-sensitized isomerization might be attributed to an acid-catalyzed reaction where the CH_5^+ and $C_2H_5^+$ ions act as Brønsted acids to *o*-xylene. Ethylation of *o*-xylene might also be considered to be an electrophilic substitution reaction by the $C_2H_5^+$ ions analogous to the benzylation and isopropylation of aromatics.[1-5]

It has been reported that the CH_5^+ and $C_2H_5^+$ ions from methane are highly reactive with NH_3 though unreactive with NO[10]

$$CH_5^+ \text{ (or } C_2H_5^+) + NH_3 \longrightarrow NH_4^+ + CH_4 \text{ (or } C_2H_4) \qquad (7)$$

Thus, it may be expected that a competition would occur between reactions (5) and (6) and reaction (7)

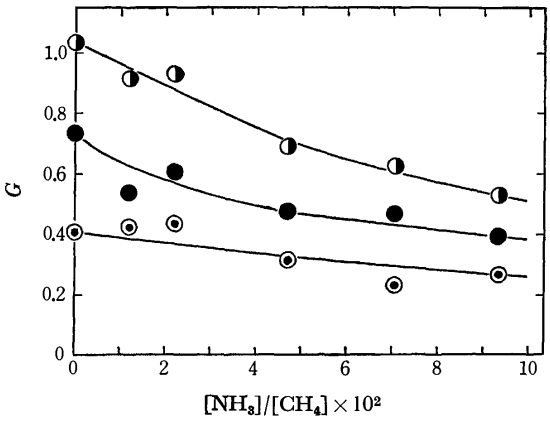

Fig. 3. Effect of added NH_3: ●, *m*-Xylene; ⊙, 1,2-Dimethyl-3-ethylbenzene; ◑, 1,2-Dimethyl-4-ethylbenzene.

13) H. C. Brown and H. Jungk, *J. Amer. Chem. Soc.*, **77**, 5579 (1955).

in the *o*-xylene-methane-NH_3 system. The effect of added NH_3 on the yields of *m*-xylene and two isomers of dimethylethylbenzene was studied from this point of view at a methane pressure of 51.1 mmHg, and the result is shown in Fig. 3. It was observed that the *G* values of these products decreased apparently with increasing NH_3 concentration, while those of *o*-ethyltoluene and two isomers of trimethylbenzene, formed by radical reactions, were not appreciably affected by the added NH_3. Thus, it seems reasonable to conclude that the methane-sensitized isomerization and ethylation of *o*-xylene are initiated by reactions (5) and (6), respectively, and the subsequent reactions may be considered to be as follows.

IIIa → IIIb → IIIc

IIIc → IIId $\xrightarrow{-H^+}$ m-Xylene

IVa → IVb or IVc

IVb or IVc $\xrightarrow{-H^+}$ Dimethylethylbenzene

where the primarily formed intermediate σ complexes IIIa and IVa have certain excess internal energies because of the exothermicities of reactions (5) and (6), and are easily isomerized to the more stable σ complexes IIId and IVb or IVc, respectively. The mechanisms are identical with those of the acid-catalyzed isomerization of *o*-xylene in solution and of the benzylation and isopropylation of aromatics in gas-phase radiolysis.[1,3] The loss of a proton from the intermediate σ complexes to produce the neutral products may be considered to be due to the proton transfer from these complexes to *o*-xylene molecules or to other species with higher proton affinities existing in the radiolytic system.[1,3]

As is shown in Figs. 1 and 2, the dependence of the *m*-xylene yield on methane pressure differed from those of two isomers of dimethylethylbenzene; the sensitization effect on the formation of *m*-xylene was appreciably reduced at higher pressures of methane, while the yields of dimethylethylbenzenes increased almost linearly with methane pressure. Such a deviation of the plot of the *m*-xylene yield against methane pressure from linearity could be explained by a selective consumption of the CH_5^+ ions by the radiolysis products from methane; it has been reported that in the high pressure mass spectrometry of methane containing a small amount of ethane, which is the most abundant hydrocarbon product in the gas-phase radiolysis of methane,[14] the

14) See for example, K. Yang and P. J. Manno, *ibid.*, **81**, 3507 (1959).

CH_5^+ ions rapidly decrease with increasing pressure, while the $C_2H_5^+$ ions somewhat increase.[15]

The activation energy of the acid-catalyzed isomerization of *o*-xylene in solution has been estimated to be 22.8 kcal/mol;[13] it may be considered that the analogous reaction in the gas phase requires the same order of activation energy. The reaction heats of the protonation of benzene by the CH_5^+ and $C_2H_5^+$ ions have been calculated to be -32 and $+3$ kcal/mol, respectively,[11] although those for *o*-xylene are not known. Since the methyl inductive effect would result in a higher proton affinity of *o*-xylene than that of benzene, the protonation of *o*-xylene by the CH_5^+ ion may be considered to be exothermic with more than 32 kcal/mol. Thus, it seems also correct to conclude that the protonation of *o*-xylene by the CH_5^+ ions results in the isomerization to *m*-xylene; the overall reaction is exothermic. However, it is not at present possible to decide whether the $C_2H_5^+$ ions contribute to the isomerization of *o*-xylene as well as the CH_5^+ ions or not.

In these experiments of the gas-phase radiolysis of mixtures of *o*-xylene and methane, 1,3-dimethyl-5-ethylbenzene was not detected. This indicates that the migration of the resident methyl groups of *o*-xylene does not occur in the transition state of the ethylation of *o*-xylene by the $C_2H_5^+$ ions, in spite of the fact that it gives the most stable σ complex of the dimethylethylbenzenonium ions as follows.

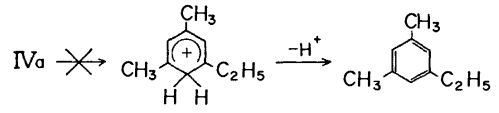

This finding could probably be explained in terms of the activation energy of the methyl migration and the excess internal energy of the intermediate complex IVa.

In order to obtain further information about the mechanism of the methane-sensitized isomerization in gas-phase radiolysis, the radiolysis of a mixture of *o*-xylene and methane-d_4 was examined at a methane-d_4 pressure of 51.4 mmHg, and the mass spectrum of the produced *m*-xylene was measured and compared with that of authentic *m*-xylene-d_0, both of which are shown in Fig. 4. The *G* value of *m*-xylene in this experiment was 0.81, and no difference in the product formation was observed between the experiments using methane-d_0 and methane-d_4. The mass spectra shown in Fig. 4 indicate that both *m*-xylene-d_1 and *m*-xylene-d_0 were formed in the radiolysis of the mixture of *o*-xylene and methane-d_4.[16] The mechanism proposed above is supported by this result; the deuterium ion transfer from the CD_5^+ and $C_2D_5^+$ ions to *o*-xylene yields the benzenonium ion containing a deuterium atom which, after the methyl migration, loses a proton or a deuterium ion to give *m*-xylene-d_1 or *m*-xylene-d_0, respectively. The ratio of *m*-xylene-d_1 to *m*-xylene-d_0 was calculated to be 2.0 ± 0.2 from the relative intensities of the ions with mass 91, 92, and 93 of these mass spectra. The calculation was based on the assumption that the *m*-xylene-d_1, which contains the deuterium in the aromatic ring, yields the mass 91 and 92 ions with the relative yields of 11 and 89%, respectively.[17] An estimation of the isotope effect (k_H/k_D) on the proton loss from the intermediate σ complex IIId is possible on the basis of the following assumptions: (a) In the radiolysis of the mixture of *o*-xylene and methane-d_4, *m*-xylene is formed by the direct energy absorption of *o*-xylene with the same *G* value as in the direct radiolysis of *o*-xylene, 0.19 (Table 1). (b) The increase of *m*-xylene by the addition of methane-d_4 to *o*-xylene is exclusively attributed to the reactions of the CD_5^+ and $C_2D_5^+$ ions with *o*-xylene. (c) In the transition state of the methane-sensitized isomerization of *o*-xylene, a rapid hydrogen migration occurs around a ring of the intermediate σ complex, and the deuterium is statistically distributed among the five possible positions attached to the ring carbons before the loss of a proton or a deuterium ion.[18] The value of k_H/k_D obtained in this way was 1.8 ± 0.4.

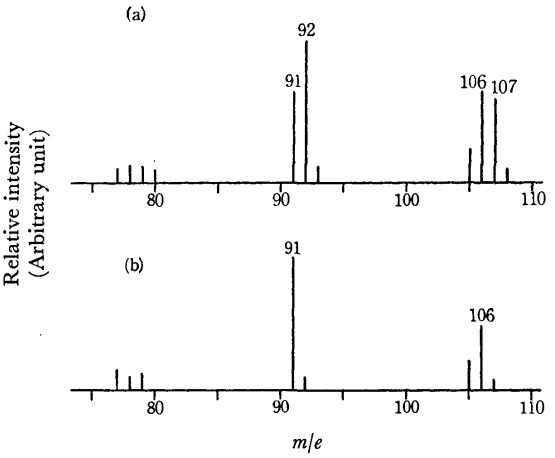

Fig. 4. Partial mass spectra of (a) the *m*-xylene formed in the gas-phase radiolysis of an *o*-xylene-CD_4 mixture and (b) authentic *m*-xylene-d_0.

The most interesting result obtained in this study is that the ionic species formed from methane by γ irradiations react with *o*-xylene to produce *m*-xylene *via* an intermediate σ complex, and this reaction is identical with the acid-catalyzed isomerization of *o*-xylene in solution. This conclusion was strongly supported by the isotopic distribution of the *m*-xylene, formed in the gas-phase radiolysis of a mixture of *o*-xylene and methane-d_4.

We wish to thank Mr. Tamotsu Yamamoto and Mr. Tomikazu Sawai in the Radiation Laboratory for assistance in the γ irradiations.

15) M. S. B. Munson and F. H. Field, *J. Amer. Chem. Soc.*, **87**, 3294 (1965).

16) The mass spectra indicate that no other *m*-xylene containing more than one deuterium atom was formed; the *m*-xylene-d_1 was not formed by a hydrogen-deuterium exchange reaction on the produced *m*-xylene-d_0.

17) H. M. Grubb and S. Meyerson, "Mass Spectrometry of Organic Ions," ed. by F. W. McLafferty, Academic Press, New York (1963), p. 453.

18) This assumption seems to be reasonable on the basis of the following reports: a) Rapid hydrogen migration around the ring of benzenonium ions has been observed in acidic solutions of aromatic hydrocarbons. See for example, G. A. Olah, R. H. Schlosberg, D. P. Kelly, and Gh. D. Mateescu, *J. Amer. Chem. Soc.*, **92**, 2546 (1970). b) In the high pressure mass spectrometry of methane containing a small amount of 1-methyl-4-isopropylbenzene, the result has been accounted for by rapid hydrogen migration (see Ref. 11).

Linear Conjugated Systems Bearing Aromatic Terminal Groups. VI. Syntheses and Electronic Spectra of 6,6′-Dichrysenylpoly-ynes

Shuzo AKIYAMA and Masazumi NAKAGAWA

Department of Chemistry, Faculty of Science, Osaka University, Toyonaka, Osaka

(Received June 18, 1971)

6,6′-Dichrysenylpoly-ynes (I_n, $n=1$—6) have been synthesized and their electronic spectra were measured. It was found that the bathochromic shifts of the longest-wavelength absorption peaks (λ_{max}) along with an increase in the number of acetylenic bond (n) were proportional to $n^{1.6}$ ($\lambda_{max}=5.8\,n^{1.6}+394$ nm).

In previous papers we reported that new linear relationships between the longest-wavelength absorption maxima (λ_{max}) and the xth power of the number of acetylenic bond (n) [$\lambda_{max} \infty n^x$] hold in various kinds of diarylpoly-ynes (II_n[1], III_n[2], IV_n[3], V_n[3], VI_n[4], VII_n[4], and $VIII_n$[4]) (Fig. 1). It was shown that the value of x is dependent on the nature of terminal groups as well as on the position of linking of polyacetylene chain.

In order to get further information on the role of aromatic terminal groups in the photoexcitation of diarylpoly-ynes, 6,6′-dichrysenylpoly-ynes (I_n) have been synthesized. The present paper deals with the syntheses and spectral regularity of I_n.

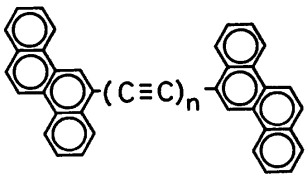

I_n
$n=1, 2, 3, 4, 5, 6$.

Syntheses. The synthesis of 6,6′-dichrysenylacet-

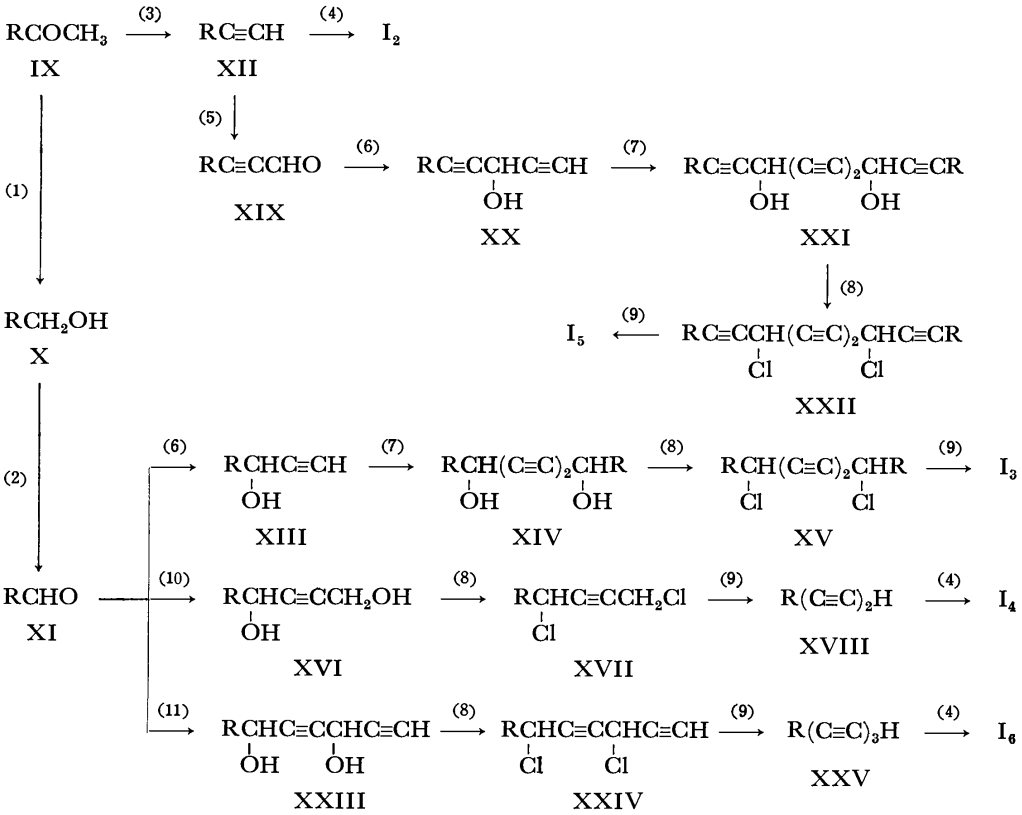

R = 6-chrysenyl

(1) i. NaOCl, ii. methanol-H_2SO_4, iii. $LiAlH_4$; (2) pyridine-CrO_3; (3) i. PCl_5, ii. $NaNH_2$/liq. NH_3; (4) $Cu(OAc)_2 \cdot H_2O$/pyridine; (5) i. *iso*-C_3H_7MgBr/THF, ii. DMF, iii. *dil.* H_2SO_4; (6) HC≡CMgBr/THF; (7) CuCl-NH_4Cl-O_2; (8) $SOCl_2$-pyridine/THF; (9) $NaNH_2$/liq. NH_3; (10) BrMgC≡CCH$_2$OMgBr; (11) BrMgC≡CCH(OMgBr)C≡CH/THF.
DMF = dimethylformamide. THF = tetrahydrofuran.

Scheme 1. Syntheses of 6,6-dichrysenylpoly-ynes (I_n)

1) S. Akiyama and M. Nakagawa, This Bulletin, **40**, 340 (1967).
2) S. Akiyama and M. Nakagawa, *ibid.*, **43**, 3561 (1970).
3) K. Nakasuji, S. Akiyama, K. Akashi, and M. Nakagawa, *ibid.*, **43**, 3576 (1970).
4) S. Akiyama and M. Nakagawa, *ibid.*, **44**, 2237 (1971).

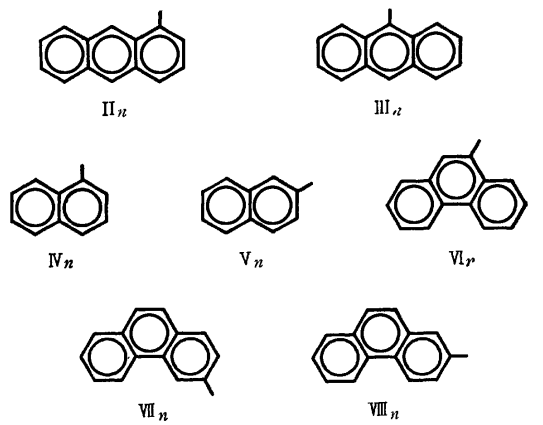

Fig. 1. The terminal groups (R) of diarylpoly-ynes [R(C≡C)$_n$R].

ylene (I_1) by means of an intramolecular Wittig reaction has been reported[5] together with other diarylacetylenes.

Acetyl-[6] and formyl derivatives (IX and XI) were used as starting materials for the syntheses of 6,6′-dichrysenylpoly-ynes (I_n, n=2—6). 6-Chrysenecarboxaldehyde (XI) was obtained in a good yield by chromium trioxide-pyridine oxidation of hydroxymethyl derivative (X).[7] The reaction sequence adapted for the preparation of I_n is a general method which had been established to be useful for the syntheses of various types of diarylpoly-ynes.[1-4]

6,6′-Dichrysenylpoly-ynes (I_1—I_6) were found to be fairly stable. It was observed that I_n is less soluble in common organic solvents as compared with other diarylpoly-ynes. I_2 and I_6 in particular were found to be the least soluble materials. Upon recrystallization from toluene, the solvent persistently incorporated into the crystals of diacetylene (I_2) and tetraacetylene (I_4), and the solvent of crystallization of I_4 (1 mol) could not be removed *in vacuo* even at elevated temperature.

The color of crystals, decomposition points and IR absorptions due to $\nu_{C\equiv C}$ are summarized in Table 1. The highest wave number of $\nu_{C\equiv C}$ was observed in the spectrum of tetraacetylene (I_4), as in the case of II$_n$[1], diphenyl- and dimethylpoly-ynes.[8] Like other series

Table 1. Physical properties of I_n

n	Color of crystals	Decomposition point (°C)	$\nu_{C\equiv C}$ (cm^{-1})
1	light yellow	>330	—
2	yellow	>330	—
3	deep yellow	*ca.* 295	2185
4	deep yellow	*ca.* 250	2190
5	orange	*ca.* 230	2170
6	orange red	*ca.* 150	2150

a) The crystals (I_4) contain 1 mol of toluene as solvent of crystallization.

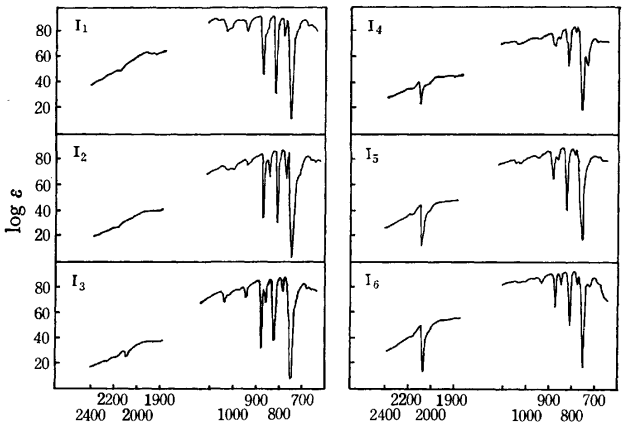

Fig. 2. IR spectra of 6,6′-dichrysenylpoly-ynes (I_n). Measurements were performed by KBr-disk method except for I_6. The spectrum of I_6 was obtained by Nujol-mull method. The sample of I_4 contains 1 mol of toluene as a solvent of crystallization.

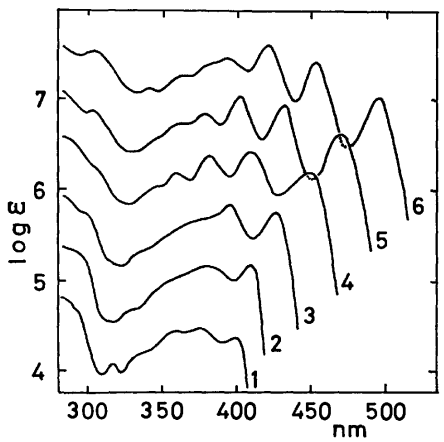

Fig. 3. Absorption curves of 6,6′-dichrysenylpoly-ynes (I_n) in toluene. The curves, with the exception of I_1 at the bottom, have been displaced upward on the ordinate axis by 0.5 log ε unit increments from the curve immediately below.

Table 2. Electronic spectral data of 6,6-dichrysenylpoly-ynes (I_n)

n	Absorption maxima, λ (in nm) and log ε (in parentheses) in toluene								
1	284.5 (4.911)	316 (4.159)	357 (4.508)	377 (4.535)	400 (4.452)				
2	283.5 (4.885)	379 (4.670)	411 (4.668)						
3	284 (4.925)	297.5 (4.776)	377 (4.677)	396 (4.834)	428 (4.759)				
4	283.5 (5.119)	358 (4.705)	381 (4.889)	407 (4.927)	449 (4.696)				
5	283 (5.064)	305 (4.952)	362 (4.715)	378 (4.854)	402 (4.869)	431 (4.955)	471 (4.631)		
6	283.5 (5.039)	302.5 (5.067)	340 (4.626)	363 (4.767)	392 (4.938)	421 (5.087)	453 (4.903)	495 (4.530)	

5) S. Akiyama and M. Nakagawa, This Bulletin, **44**, 2231 (1971).
6) W. Carruthers, *J. Chem. Soc.*, **1953**, 3486.
7) M. J. S. Dewar and R. J. Sampson, *ibid.*, **1957**, 2946.
8) C. L. Cook, E. R. H. Jones, and M. C. Whiting, *J. Chem, Soc.*, **1952**, 2883; M. Yamaguchi and Y. Hayashi, "Infrared Spectroscopy, No. 9" (Special issue of Kagaku no Ryoiki, No. 40), Nankodo Tokyo (1960).

of diarylpoly-ynes, the absorption intensities of the most intense peaks in $\nu_{C\equiv C}$ bands seem to increase with the increase in the length of poly-yne chain. The IR spectra of I_n are shown in Fig. 2.

Electronic Spectra. The absorption curves and electronic spectral data of I_n are shown in Fig. 3 and Table 2. The L_b band of chrysene could not be observed in the spectra of I_n, due presumably to its coalescence with the L_a band which is shifted to a longer wavelength by interaction with polyacetylenic chromophore.

Chrysene can be regarded as benzophenanthrene. Thus, the 6-position in chrysene corresponds to either 3- or 9-position of phenanthrene. Actually, 6,6′-dichrysenylpoly-ynes (I_n) exhibit closely related electronic spectra with those of 3,3′- and 9,9′-diphenanthrylpoly-ynes.[4] The characteristic of the spectrum of chrysene could not be observed even in the spectra of a lower member of I_n just as in the case of diphenanthrylpoly-ynes. Like the spectra of other diarylpoly-ynes, the pronounced vibrational fine structure in the long-wavelength absorption band exhibits characteristic features of the spectra of I_n. The magnitude of red shift of the longest-wavelength maximum (λ_{max}) increases gradually with an increase in the number of n (11, 17, 21, 22, and 24 nm).

Table 3. Spacing of vibrational fine structure

n	1	2	3	4	5	6
Spacing (cm^{-1})	—	2050	1890	2300	1970	1870

As is shown in Table 3, the highest wave number of spacing between the longest-wavelength vibrational subband and the next longest-wavelength one was observed in the spectrum of tetraacetylene (I_4), which corresponds to the fact that the highest wave number of $\nu_{C\equiv C}$ is also observed in I_4.[9]

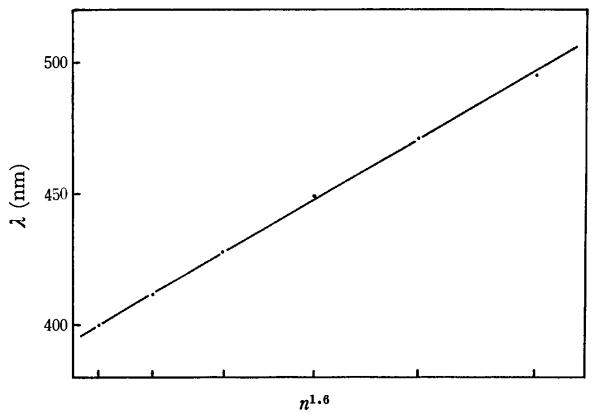

Fig. 4. Linear relationship between λ and $n.^{1.6}$

The plots of longest-wavelength absorption maxima (λ_{max}) against $n^{1.6}$ gave an excellent straight line as illustrated in Fig. 4. The linear relationship could be expressed by the following empirical formula:[10]

$$\lambda_{max} = 5.8n^{1.6} + 394 \text{ nm (in toluene)}.$$

The observed and calculated values of λ_{max} are listed in Table 4.

Table 4. Observed and calculated values of λ_{max} (nm)

n	1	2	3	4	5	6
Found	400	411	428	449	471	495
Calcd	400	412	428	447	470	496
$\Delta\lambda$	0	−1	0	+2	+1	−1

Experimental

All melting points are uncorrected. The electronic spectra were obtained on a Hitachi EPS-3T Spectrophotometer at room temperature. The infrared spectra were measured with a Hitachi EPI-2 Infrared Spectrophotometer by KBr-disk method. Evaporation of solvent and concentration of solution were performed under reduced pressure.

6-Chrysenecarboxaldehyde (XI). A solution of X (14.30 g, 0.056 mol)[7] in pyridine (120 m*l*) was added to a chilled solution of chromium trioxide (18.0 g, 0.18 mol) in pyridine (250 m*l*). The mixture was shaken in an ice-salt bath for 30 min, and then for 45 min at room temperature. The reaction mixture was poured into water (2 *l*). The resulting precipitate was filtered, washed with water and dried to give a brown powder. The powder was extracted with benzene (500 m*l*) using a Soxhlet type extractor. The extract was passed through a short column of alumina (15 g). Concentration of the filtrate (up to *ca.* 30 m*l*) gave faint yellow cubes (12.30 g, 86%, mp 164—166°C). Recrystallization of this material three times from benzene gave analytical sample with mp 165—166°C.

Found: C, 88.91; H, 4.66%. Calcd for $C_{19}H_{12}O$: C, 89.04; H, 4.72%. IR: 1690 (C=O) cm^{-1}.

6-Ethynylchrysene (XII). Chlorination of 6-Acetylchrysene (XI): A mixture of 6-acetylchrysene (XI, 27.0 g, 0.1 mol),[6] phosphorus pentachloride (22.9 g, 0.11 mol) and benzene (150 m*l*) was refluxed for 75 min. The volatile material was removed under reduced pressure and the residue was placed for several hours in an evacuated desiccator containing potassium hydroxide. Light brown crystalline mass obtained was subjected to the subsequent reaction.

Dehydrochlorination of the Chloride: The crude chloride in tetrahydrofuran (100 m*l*) was added over a period of 20 min at −70°C to a suspension of sodium amide (from sodium, 9.2 g, 0.4 g-atom) in liquid ammonia (500 m*l*). After 3 hr the ammonia was allowed to evaporate, and then a saturated solution of ammonium chloride was added to the reaction mixture. The organic solvent was distilled off and the residue was collected by filtration and washed with water. The benzene extract of the residue (800 m*l*) was passed through a short column of alumina (80 g). Concentration of the filtrate resulted in yellow cubes, mp 176—178°C (dec.), 24.0 g (96%). A solution of the crude crystals in petroleum ether (bp 60—80°C) was passed through a thin layer of alumina. Crystals obtained by concentrating the filtrate were recrystallized from methanol to afford colorless cubes (mp 182°C (dec.)), which gave yellow silver and yellow cuprous acetylides.

Found: C, 94.89; H, 4.79%. Calcd for $C_{20}H_{12}$: C, 95.21; H, 4.79%. UV: $\lambda_{max}^{benzene}$ (log ε) 282 (4.97), 301.5 (3.93), 315 (4.10), 329 (4.33), 344 (4.35) nm. IR: 3280 (≡CH) cm^{-1}.

6,6′-Dichrysenyldiacetylene (I_2). A mixture of 6-ethynyl-

9) Detailed discussion on the spacing and the $\nu_{C\equiv C}$ will be given elsewhere.

10) The linear relationship between λ_{max} and n^x in various diaryl-poly-ynes could be explained in terms of HMO based on a modified bond-alternation approximation.

chrysene (XII, 0.070 g, 0.28 mmol), cupric acetate monohydrate (0.70 g), pyridine (20 ml) and methanol (5 ml) was stirred for 2 hr at 50°C. The reaction mixture was cooled. The insoluble material was collected by filtration and washed with methanol and water successively, yielding light yeollw fine crystals in a quantitative yield (dec. p>330°C). This was recrystallized from toluene to give yellow cubes (dec. p>330°C). Elemental analysis of the cryatals revealed that the substance contained solvent of crystallization, which could be removed by heating the crystals at 100°C for several hr under reduced pressure (2×10^{-3} mmHg).

Found: C, 95.35; H, 4.52%. Calcd for $C_{40}H_{22}$: C, 95.59; H, 4.41%.

6-Chrysenyl-2-propyn-1-ol (XIII). A solution of 6-formylchrysene (XI, 6.15 g, 0.024 mol) in tetrahydrofuran (200 ml) was added to an ice-cooled solution of ethynylmagnesium bromide (from magnesium, 1.80 g, 0.075 g-atom and ethyl bromide, 8.20 g, 0.075 mol) in tetrahydrofuran (35 ml). After having been stirred overnight at room temperature, the reaction mixture was decomposed by adding a saturated ammonium chloride solution. The organic layer was separated, and dried. Concentration of the solution (up to *ca.* 10 ml) gave an oily material, which was mixed with benzene (20 ml). Crystals deposited on warming the mixture were washed with a small amount of benzene to yield light brown fine crystals, mp 170—173°C, 5.98 g (88%).

Found: 89.15; H, 5.03%. Calcd for $C_{21}H_{14}O$: C, 89.33; H, 5.00%. IR: 3100—3400 (O–H), 3290 (≡CH), 1060 (C–O) cm^{-1}.

1,6-Di(6-chrysenyl)-1,6-dihydroxy-2,4-hexadiyne (XIV). A mixture of 6-chrysenyl-2-propyn-1-ol (XIII, 3.00 g, 0.011 mol), cuprous chloride (1.4 g), ammonium chloride (1.0 g) and acetone-methanol (1: 1, 80 ml) was vigorously stirred at room temperature under an atmosphere of oxygen at a slightly elevated pressure. After being stirred overnight, the precipitate deposited was collected by filtration and dissolved in tetrahydrofuran. Insoluble material was removed by filtration and the filtrate was passed through a short column of alumina (8 g). The crystals, 1.62 g (54%), obtained by evaporating the solvent were recrystallized from dioxane to give faint yellow needles (dec. p *ca.* 160°C). Elemental analysis indicates that the crystals contain 1 mol of dioxane as a solvent of crystallization.

Found: C, 84.96; H, 5.14%. Calcd for $C_{42}H_{26}O_2\cdot C_4H_8O_2$: C, 84.90; H, 5.27%. IR: 3600—3100 (O–H), 1065 (C–O) cm^{-1}.

6,6'-Dichrysenyltriacetylene (I_3). *Formation of XV*: A solution of thionyl chloride (0.21 g, 1.8 mmol) and pyridine (0.14 g, 1.8 mmol) in tetrahydrofuran (5 ml) was added to a solution of glycol (XIV, 0.337 g, 0.6 mmol) in tetrahydrofuran (15 ml) over a period of 15 min at −20°C, and the mixture was then shaken for 30 min. The reaction mixture containing chloride (XV) was subjected to the following reaction without isolation.

Dehydrochlorination of dichloride (XV): To a vigorously stirred suspension of sodium amide (from sodium, 0.46 g, 0.02 g-atom) in liquid ammonia (90 ml), the solution of dichloride (XV) was added in one portion at −70°C. After 30 min, ammonium chloride (2.5 g) was added and the ammonia was allowed to evaporate. After the organic solvent had been removed, a small amount of water was added to the residue. The insoluble material was collected and washed successively with water, a small amount of ethanol and benzene, and then dissolved in hot toluene (350 ml). The hot solution was passed through a short column of alumina (13 g). On cooling the filtrate to room temperature, I_3 crystallized out as yellow needles (dec. p *ca.* 295°C, 0.147 g, 47%). Analytical specimen was prepared by recrystallization from toluene.

Found: C, 95.94; H, 4.20%. Calcd for $C_{42}H_{22}$: C, 95.79; H, 4.21%.

1-(6-Chrysenyl)-2-butyn-1,4-diol (XVI). A solution of aldehyde (XI, 5.1 g, 0.02 mol) in tetrahydrofuran (200 ml) was added to an ice-cooled solution of Grignard derivative of propargyl alcohol in tetrahydrofuran (70 ml), which had been prepared from magnesium, 2.88 g, 0.12 g-atom, ethyl bromide, 13.1 g, 0.12 mol and propargyl alcohol, 3.36 g, 0.06 mol. The mixture was allowed to stand overnight, then a saturated aqueous solution of ammonium chloride was added to the reaction mixture. The organic layer separated was dried and concentrated. The residue was treated with a small amount of hot benzene to cause crystallization. The crystals (mp 193—197°C, 5.54 g, 89%) were recrystallized from ethanol-benzene to give colorless fine crystals (mp 197—198°C).

Found: C, 84.27; H, 5.19%. Calcd for $C_{22}H_{16}O_2$: C, 84.59; H, 5.16%. IR: 3600—3100 (O–H), 1040—1000 (C–O) cm^{-1}.

6-Butadiynylchrysene (XVIII). *Preparation of XVII*: A solution of thionyl chloride (3.22 g, 0.027 mol) in tetrahydrofuran (10 ml) was added over a period of 15 min to a solution of glycol (XIV, 2.00 g, 6.4 mmol) and pyridine (2.13 g, 0.027 mol) in tetrahydrofuran (40 ml) at −10°C. After the mixture had been stirred for further 2 hr at room temperature, crushed ice was added, and extraction was carried out with benzene (100 ml). The extract was washed with an aqueous solution of sodium hydrogen carbonate, and dried. The solvent was removed to yield an oily material which solidified on standing.

Dehydrochlorination of dichloride (XVII): The crude XVII in tetrahydrofuran (15 ml) was treated with sodium amide (from sodium, 1.0 g, 0.44 g-atom) in liquid ammonia (100 ml) for 1 hr at −70°C. The reaction mixture was worked up as usual. The product was repeatedly digested with petroleum ether (bp 60—80°C, total 600 ml). The filtrate obtained by passing the extract through a thin layer of alumina (3.5 g) was concentrated to yield XVIII as faint yellow crystals, 1.138 g (34%). The butadiynyl compound (XVIII) was found to be extremely unstable, and readily turned into an insoluble deep green substance. XVIII gave orange-yellow silver and deep yellow cuprous acetylides.

UV: $\lambda_{max}^{\text{petroleum ether}}$ 357 (L_a), 375 (L_b) nm.

6,6'-Dichrysenyltetraacetylene (I_4). The yellow crystalline powder (0.180 g, 50%) obtained by the cupric acetate oxidation [cupric acetate monohydrate (2.5 g), methanol (5 ml) and pyridine (50 ml), 1 hr at 50°C] of XVIII (0.360 g, 1.3 mmol) was digested with boiling toluene (350 ml). The hot extract was percolated through a short column of alumina (10 g). On standing the filtrate, I_4 containing 1 mol of solvent of crystallization was obtained as deep yellow fine needles (dec. p *ca.* 250°C, 0.096 g, 27%). It was found that the solvent could not be removed upon heating to 60°C for 24 hr under reduced pressure (2×10^{-3} mmHg).

Found: C, 95.38; H, 4.62%. Calcd for $C_{44}H_{22}\cdot C_7H_8$: C, 95.30; H, 4.70%.

3-(6-Chrysenyl)-prop-2-ynal (XIX). To an ice-cooled solution of isopropylmagnesium bromide (from magnesium, 1.92 g, 0.08 g-atom and isopropyl bromide, 10.8 g, 0.088 mol) in tetrahydrofuran (50 ml) was added, over a period of 15 min, a solution of 6-ethynylchrysene (XII, 10.08 g, 0.04 mol) in the same solvent (250 ml) under stirring. The mixture was refluxed for 1 hr, and dimethylformamide (18 ml) was added under cooling with an ice-salt bath. After the mixture had been stirred for 4 hr at 30°C, 5% sulfuric acid (600 ml) was

added under vigorous agitation, after which benzene (500 m*l*) was added and then stirring was continued overnight. The mixture was extracted with benzene (500 m*l*). The extract was washed with a saturated solution of sodium hydrogen carbonate, and dried. The solvent was removed to afford yellow crystals. The crystals were washed with a small amount of benzene-cyclohexane (1: 1), thus yielding light orange-yellow needles (8.11 g, 72%). This was recrystallized twice from benzene-cyclohexane (1: 1) to yield XIX as orange-yellow needles, mp 160—161°C (dec.).

Found: C, 89.70; H, 4.36%. Calcd for $C_{21}H_{12}O$: C, 89.98; H, 4.32%. IR: 2830, 2730 (CHO), 2175 (C≡C), 1655 (C=O) cm^{-1}.

1-(6-Chrysenyl)-1,4-pentadiyn-3-ol (XX). The reaction of ethynylmagnesium bromide with XIX (5.60 g, 0.02 mol) according to the procedure used for XIII afforded XX as yellow fine crystals, mp *ca.* 140°C (dec.), 3.51 g (62%). This substance was recrystallized twice from ethyl acetate to yield pure XX, mp 152—154°C (dec.).

Found: C, 89.68; H, 4.56%. Calcd for $C_{23}H_{14}O$: C, 90.17; H, 4.61%. IR: 3600—3100 (OH), 3300 (≡CH), 2220, 2100 (C≡C), 1023 (C–O) cm^{-1}.

6,6'-Dichrysenylpentaacetylene (I_5). Oxidative Coupling of Chrysenylpentadiynol (XX): The product obtained by the Glaser reaction [cuprous chloride (1.00 g), ammonium chloride (0.90 g), methanol (80 m*l*) and oxygen] of XX (2.50 g, 8.2 mmol) was dissolved in tetrahydrofuran (100 m*l*). The solution was percolated through a thin layer of alumina (3 g). Concentration of the filtrate afforded a viscous brown oil which crystallized on treatment with a small amount of benzene (0.90 g, 36%). Repeated recrystallization of this substance from tetrahydrofuran or dioxane gave slightly impure material whose IR spectrum was in accord with that expected for XXI.

Chlorination of XXI: According to the procedure used in the preparation of XV, glycol (XXI, 0.305 g, 0.5 mmol) was treated with a solution of thionyl chloride at −30°C. The reaction mixture containing XXII was immediately subjected to the following reaction.

Dehydrochlorination of XXII: Dehydrochlorination of XXII with sodium amide (from sodium, 0.20 g, 8.4 mg-atom) was performed according to the method used for I_3. I_5 was obtained as light orange fine needles (dec. p *ca.* 230°C, 31 mg, 11% based on crude XXI). The second crop of I_5 (15 mg, 5%) was obtained from the mother liquor.

Found: C, 96.05; H, 3.82%. Calcd for $C_{46}H_{22}$: C, 96.14; H, 3.86%.

1-(6-Chrysenyl)-2,5-hexadiyn-1,4-diol (XXIII). A solution of 6-formylchrysene (XI, 6.15 g, 0.024 mol) in tetrahydrofuran (200 m*l*) was added to a stirred and ice-cooled solution of the Grignard derivative of 2,4-pentadiyn-3-ol[11] (from alcohol, 2.65 g, 0.033 mol and ethylmagnesium bromide in tetrahydrofuran, 100 m*l*). The mixture was stirred overnight at room temperature. The reaction mixture was hydrolyzed by the addition of a saturated solution of ammonium chloride. The aqueous layer was extracted with benzene. Viscous oily material obtained by concentration of the combined organic layer was warmed with benzene (30 m*l*) to cause crystallization. The crude material was recrystallized from ethyl acetate-benzene to afford light brown powder (4.50 g, 56%). This was used without further purification in the subsequent reaction. A small portion of the crude material was dissolved in dioxane and passed through a thin layer of alumina. The crystals obtained by concentrating the filtrate were redissolved in ethyl acetate and chromatographed on alumina to result in pure XXIII as colorless needles, mp 197—199°C (dec.).

Found: C, 85.19; H, 4.75%. Calcd for $C_{24}H_{16}O_2$: C, 85.69; H, 4.79%.

The second crop obtained from the mother liquor was colorless needles, mp 165—170°C. (Found: C, 85.40; H, 4.83%). The two stereoisomeric kinds of crystal gave almost the same IR spectra. IR: 3600—3100 (O–H), 3300 (≡CH), 2100 (C≡C), 1035 (C–O) cm^{-1}.

6-Chrysenyltriacetylene (XXV). Chlorination of XXIII: According to the procedure used for XVII, XIII (2.02 g, 6 mmol) in a mixture of tetrahydrofuran (30 m*l*) and pyridine (1.42 g, 18 mmol) was converted into XXIV on treatment with thionyl chloride (2.14 g, 18 mmol) in tetrahydrofuran (5 m*l*) at −15°C. Crude XXIV obtained as a brown oily material was used without further purification in the subsequent reaction.

Dehydrochlorination of XXIV. The procedure used for XVII was applied to XXIV. Since the triacetylene (XXV, Faint yellow fine needles, UV: $\lambda_{max}^{petroleum\ ether}$ 379 nm) was found to be extremely unstable, a petroleum ether solution was used in the following reaction.

6,6'-Dichrysenylhexaacetylene (I_6). A mixture of the solution of triacetylene (XXV), cupric acetate monohydrate (2.0 g) and pyridine (50 m*l*) was concentrated to *ca.* 30 m*l* *in vacuo* and pyridine (50 m*l*) and methanol (5 m*l*) were added. Stirring was continued overnight at room temperature. The insoluble material was collected and washed with ethanol and then with water. Crude hexaacetylene (I_6), thus obtained, brick red crystalline powder (0.440 g, 24% based on diol, XXIII), was digested with hot toluene (350 m*l*), and the hot extract was percolated through a short column of alumina (7 g). Pure I_6, orange-red needles, dec. p. *ca.* 150°C was obtained on standing the filtrate.

Found: C, 96.17; H, 3.77%. Calcd for $C_{48}H_{22}$: C, 96.30; H, 3.70%.

11) E. R. H. Jones, L. Skatteböl, and M. C. Whiting, *J. Chem. Soc.*, **1956**, 4765.

Modified Clemmensen Reductions of Keto Groups to Methylene Groups

Masaaki TODA, Mikio HAYASHI, Yoshimasa HIRATA, and Shosuke YAMAMURA*

Chemical Institute, Nagoya University, Chikusa-ku, Nagoya

**Faculty of Pharmacy, Meijo University, Showa-ku, Nagoya*

(Received June 24, 1971)

A modified Clemmensen reduction is described for the conversion of keto-groups into methylene groups by using active zinc powder in common organic solvents and acetic anhydride saturated with hydrogen chloride; the scope and limitations of these new reduction systems are also discussed.[1]

In a previous paper,[2] we reported a useful method for the conversion of isolated keto-groups into methylene groups using active zinc powder in acetic anhydride saturated with hydrogen chloride under very mild conditions (0°C, 2—6 hr). Furthermore, it has been suggested that the easy reductions of keto-groups to methylene groups are attributable to the formation of an acyl cation from acetic anhydride and hydrogen chloride, and that the acetoxyorganozinc compound is a likely intermediate (I). In fact, the treatment of the β-diketone (II) with Zn–Ac_2O–HCl has been known to afford the corresponding diacetoxycyclopropane (III) in a high yield.[3] However, attempts to reduce cholestan-3-one to cholestane with active zinc powder in Ac_2O-*p*-TsOH (or BF_3 etherate) under various conditions proved unsuccessful.

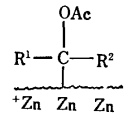

(I)

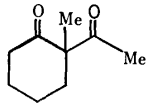

(II)

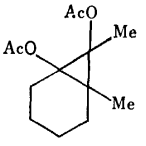

(III)

In the above experiments we were able to do such zinc reductions by using common organic solvents saturated with hydrogen chloride instead of acetic anhydride. When treated with active zinc powder in diethyl ether saturated with hydrogen chloride (0°C, 1 hr), cholestan-3-one afforded the corresponding reduction product, cholestane, in a high yield. Other solvents were also used; the results, summarized in Table 1, indicate that diethyl ether is much better for the modified Clemmensen reduction than the other solvents. These zinc reductions, which must be carried out under anhydrous conditions, take place more easily than the usual Clemmensen reduction. The mechanism of the former seems, however, to be essentially the same as that of the Clemmensen reduction.[4]

In view of the high reactivity of these reduction systems (Zn–HCl–Ac_2O (or Et_2O)), zinc reductions of α-substituted, α,β-unsaturated, and aryl ketones were carried out (Table 2).

TABLE 1. ZINC REDUCTIONS IN COMMON ORGANIC SOLVENTS SATURATED WITH HYDROGEN CHLORIDE

Ketone	Solvent	Product	Yield (%)
Cholestan-3-one	Ac_2O	Cholestane	87[a]
	Et_2O	Cholestane	89[b]
	Tetrahydrofuran	Cholestane	44[b]
	Benzene	Cholestane	64[b]
		3-Chlorocholestane	21
	n-Hexane	Cholestane	57[b]
		3-Chlorocholestane	8
Androstan-3,17-dione	Ac_2O	Androstane	66[c]
		17β-Acetoxyandrostane	26
	Et_2O	Androstane	75[b]

a) At 0°C for 2 hr. b) At 0°C for 1 hr. c) At 0°C for 6 hr.

TABLE 2. ZINC REDUCTIONS OF α-SUBSTITUTED, α,β-UNSATURATED, AND ARYL KETONES

Ketone	Product	Yield (%)
2α-Bromocholestan-3-one	Cholestane	86[a], 85[b]
	3-Acetoxycholest-2-ene	8[a]
α-Acetoxycholestan-3-one[c]	Cholestane	90[a], 79[b]
	Enol acetates	2[a],[d]
3β,5α-Diacetoxy-7α-bromocholestan-6-one	3β-Acetoxycholestane	73[e]
3β,17α-Diacetoxypregn-5-en-20-one	3β-Acetoxypregn-5-ene	62[e]
Cholest-1-en-3-one	Cholestane	30—32[a], 88[b]
	3-Acetoxycholest-2-ene	24—10[a]
	Cholestan-3-one	30—40[a]
Cholest-4-en-3-one	Cholestane	48[b]
	Coprostane	40[b]
Methyl β-benzoyl propionate	Methyl γ-phenyl butyrate	45[a], 41[b]
Indanone	Indane	22[a], 42[b]

a) In acetic anhydride saturated with HCl (0°C, 2 hr).
b) In diethyl ether saturated with HCl (0°C, 1 hr).
c) A mixture of 2α- and 4α-acetoxycholestan-3-ones (1:1).
d) A mixture of 3-acetoxycholest-2 and 3-enes.
e) In acetic anhydride saturated with HCl (0°C, 6 hr).

In particular, the reductions of α-halo- and α-acetoxy-oxo-steroids with active zinc powder in diethyl ether saturated with hydrogen chloride are expected to afford the following reduction products: an olefin (IV), an acetate (or halide) (V), and a completely reduced compound (VI). In the case of the (Zn–Ac_2O–HCl) reduction system, two more reduction products (VII and

1) Preliminary communications: S. Yamamura, *Chem. Commun.*, **1968**, 1494; M. Toda, Y. Hirata, and S. Yamamura, *ibid.*, **1969**, 919.
2) S. Yamamura and Y. Hirata, *J. Chem. Soc., C*, **1968**, 2887.
3) T. J. Curphey, C. W. Amelotti, T. P. Layloff, R. L. McCartney, and J. H. Williams, *J. Amer. Chem. Soc.*, **91**. 2817 (1969).
4) H. O. House, "Modern Synthetic Reactions," Benjamin, New York (1965), p. 58; J.G. St. C. Buchanan and P. D. Woodgate, *Quart. Rev.* (London), **23**, 522 (1969).

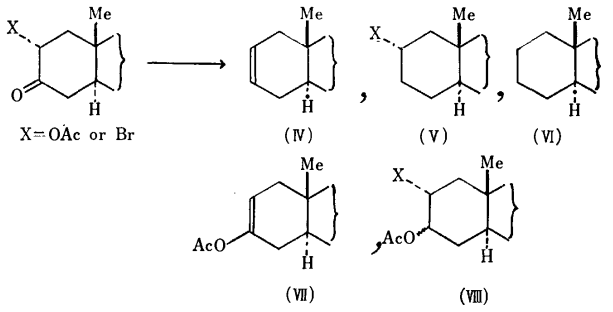

VIII) are expected in addition to the three above compounds (IV, V, and VI). In our experiments, modified Clemmensen reductions of α-acetoxy and α-halo-cholestan-3-one afforded a mixture of cholestane (86—90%) and 3-acetoxycholest-2-ene (2—8%) with Zn–Ac_2O–HCl, and only cholestane (79—85%) with Zn–Et_2O–HCl. In these reactions, the first step is probably the same as in usual zinc reductions in acetic acid or aqueous mineral acid leading to the formation of an enolate anion. Therefore, the ketonization of the enolate anion and the subsequent protonation take place much faster than an attack of the acyl cation on the oxygen atom of the enolate anion.[5] The resulting cholestan-3-one is converted into cholestane as usual. In the cases of α,β-unsaturated ketones, results considerably different from those obtained with the α-substituted ketones were obtained. When treated with active zinc powder in acetic anhydride saturated with hydrogen chloride, cholest-1-en-3-one gave a mixture of three reduction products (cholestane (32—30%), 3-acetoxycholest-2-ene (24—10%) and cholestan-3-one (30—40%)). The completely reduced product, cholestane, is probably formed through the cyclopropoxide or enolate anion. Furthermore, both cholestan-3-one and 3-acetoxycholest-2-ene (VII) may be derived from an intermediate of the corresponding acetoxycyclopropane structure (IX), an intermediate which seems to be converted into cholestan-3-one in the course of isolation. Recently, Elphimoff-Felkin and Sarda[6] have reported that the α,β-unsaturated ketones with a phenyl group afford the corresponding acetoxycyclopropanes when treated with Zn–Ac_2O–HCl. Accordingly, it can be expected that the completely reduced product can be obtained in a high yield by using active zinc powder in diethyl ether saturated with hydrogen chloride. In fact, the reduction of cholest-1-en-3-one to cholestane was successfully achieved by the use of the above-mentioned reduction system under mild conditions. Cholest-4-en-3-one was also converted into a mixture of cholestane and coprostane in a high yield. Zinc reductions of aryl ketones were also carried out under the same conditions.[7] However, these reductions are not always better in yields than usual Clemmensen reductions of aryl ketones except under mild conditions (0°C, 1 hr), since undesirable dimerization reactions seem to take place between two anion radical intermediates, which are much more stabilized by the aryl group than is the anion radical from such an isolated ketone as cholestan-3-one.

Experimental

The melting points were determined on a micro hot-stage. The infrared spectra were recorded in KBr or film with a JASCO IR-S spectrophotometer.

Preparation of Active Zinc Powder. Commercial zinc powder (Kishida Chemical Co., *ca.* 300 mesh) was activated by washing it well with 2% hydrochloric acid according to a previously-described procedure (see Ref. 2). The zinc powder thus obtained was used immediately.

General Procedure for the Zinc Reduction. Cholestan-3-one was dissolved in diethyl ether saturated with hydrogen chloride at 0°C, and then active zinc powder was slowly stirred into the resulting solution. After being stirred at 0°C for 1 hr, the reaction mixture was poured into large amounts of ice water. Then, the aqueous solution was made basic with sodium carbonate and extracted thoroughly with diethyl ether. The extracts were dried over anhydrous Na_2SO_4; the solvent was then removed under reduced pressure to give a pale yellow oil, which was chromatographed on silica gel (Mallinckrodt, 100 mesh) (25 g) and eluted with benzene to afford colorless crystals of cholestane (mp 77.5—79°C). The yields of cholestane varied with the quantity of zinc powder, as the chart shows below.

Cholestan-3-one (mg)	Zn (g)	Et_2O (m*l*)	Yield (%)
500	5.0	75	89
500	1.25	12.5	84
500	0.50	10	85
500	0.25	10	56

According to the above-mentioned procedure or the previously-reported procedure,[2] zinc reductions of α-substituted, α,β-unsaturated and aryl ketones were carried out (see Tables 1 and 2); the reduction products were carefully separated by

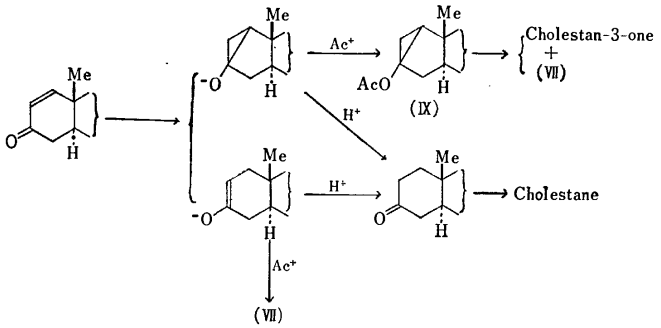

5) The enol acetate (VII) is stable for the (Zn-Ac_2O-HCl) reduction system.

6) M. I. Elphimoff-Felkin and P. Sarda, *Tetrahedron Lett.*, **1969**, 3045.

7) The reaction mixture spontaneously turned brown when active zinc powder was added to the solution.

silica-gel chromatography (Mallinckrodt, 100 mesh), using benzene as the eluant, except for a mixture of cholestane and coprostane.[8] When experiments were carried out in a large scale, the reduction procedure was further modified as follows.

In a 500-m*l*, three-necked, round-bottomed flask fitted with a sealed mechanical stirrer, a gas inlet tube, and a Y-tube fitted with a low-temperature thermometer and a calcium chloride tube, we placed 250 m*l* of dry diethyl ether which had been cooled in a dry ice-acetone bath to −10——15°C; then dry hydrogen chloride gas was bubbled in with slow stirring. After about 45 min, 10 g of cholestan-3-one were dissolved, with stirring, in the above solution below −15°C. To the ethereal solution we then added 12.3 g of activated zinc powder at about −20°C over a period of 2—3 min, and then the temperature of the reaction solution was elevated to −5°C. Stirring was continued for 2 hr, keeping the reaction temperature between 0——4°C. Finally, the reaction mixture was cooled to −15°C, slowly poured into large amounts of ice, and then worked-up as usual to give 8.2—8.9 g of cholestane. mp 78—79°C.

All the reduction products were found to be identical with the known compounds by a study of their mps, IR, and mass spectra.

8) The relative ratio of the two reduction products was determined by studying their peak areas on a gas-liquid chromatogram (SE-30 (5%); 250°C, N_2; flame-ionized detector).

The authors are grateful to Professor T. Goto, Nagoya University, for providing some α-acetoxy-oxosteroids.

BULLETIN OF THE CHEMICAL SOCIETY OF JAPAN, VOL. 45, 266—268(1972)

The Epoxidation of Homoallylic Alcohols and the Formation of Sesquiterpene Diols

Shosuke YAMAMURA, Masanobu IGUCHI, Masatake NIWA, and Yoshimasa HIRATA*

Faculty of Pharmacy, Meijo University, Showa-ku, Nagoya

**Chemical Institute, Nagoya University, Chikusa-ku, Nagoya*

(Received June 24, 1971)

The epoxidation of homoallylic alcohols was effected with *m*-chloroperbenzoic acid in ether, and the resulting epoxides were reduced with lithium aluminum hydride to the corresponding diols. Particularly in the cases of calameone and isocalamendiol, the exocyclic double bond at the C_3-position was attacked by the peroxy-acid from the side opposite to the axial hydroxyl group at the C_5-position.

In the course of structural studies of calameone (I), a sesquiterpen-diol isolated from *Acorus calamus* L. (Japanese name "Shyobu"), we obtained some interesting results.

In the cases of homoallylic alcohols generally, a peroxy-acid attacks the double bond from the same side as the hydroxyl group.[1] On the other hand, the double bond can be attacked by the same reagent from the opposite side when a methoxyl group is used instead of the hydroxyl group in the same system.[1] In fact, the dehydrated compound (II), which had been obtained from isocalamendiol (III),[2] was treated with *m*-chloroperbenzoic acid and then reduced with lithium aluminum hydride to afford a mixture of calameone (I) and a new isomer (IV), the structure of which was proposed on the basis of a reaction mechanism analogous to that of calameone (I).[1,3] We could further make a configurational isomer (V) at the C_3-position as follows. When treated with *m*-chloroperbenzoic acid in ether, isocalamendiol (III) did not give a β-epoxide (VI), but an α-isomer (VII), in a 98% yield. Furthermore, the dehydration of VII was effected with $POCl_3$-pyridine to give, in a 48% yield, a dehydrated epoxide (VIII). Finally, the reduction of VIII with lithium aluminum hydride afforded the new diol (V), the structure of which was elucidated by a comparison of the NMR spectra of these four sesquiterpen-diols (see Table 1). In the NMR spectra of the compounds

TABLE 1. NMR SIGNALS OF SESQUITERPEN-DIOLS

Compound	*i*-Pr	$-\dot{C}Me-OH$	$-\dot{C}=CH_2$
Calameone	δ 0.90 (6H, d, J=6.8 Hz)	δ 1.13 (3H, s)	δ 4.80 (1H, br.s)
			4.89 (1H, br.s)
Isocalamendiol (III)	0.90 (3H, d, J=7.0 Hz)	1.22 (3H, s)	4.80 (1H, br.s)
	0.93 (3H, d, J=7.0 Hz)		4.89 (1H, br.s)
Compound (IV)	0.93 (6H, d, J=6.5 Hz)	1.12 (3H, s)	4.68—5.00 (2H, br.m)
Compound (V)	0.88 (3H, d, J=6.9 Hz)	1.21 (3H, s)	4.77 (1H, br.s)
	0.91 (3H, d, J=6.9 Hz)		4.95 (1H, br.s)

1) H. B. Henbest, *Proc. Chem. Soc.*, **1963**, 159.

2) M. Iguchi, A. Nishiyama, H. Koyama, S. Yamamura, and Y. Hirata, *Tetrahedron Lett.*, **1969**, 3729.

3) M. Iguchi, A. Nishiyama, M. Niwa, S. Yamamura, and Y. Hirata, *Chem. Commun.*, **1970**, 1323.

(III and V) with an axial methyl group, the methyl singlets were observed at δ 1.21—1.22 in a magnetic field lower than those of the other two compounds (I and IV) by *ca.* 0.1 ppm. Accordingly, it is clear that the peroxy-acid attacked the double bond in III from the side opposite to the hydroxyl group at the C_5-position. This result does not agree with that of the usual epoxidation in homoallylic alcohols.

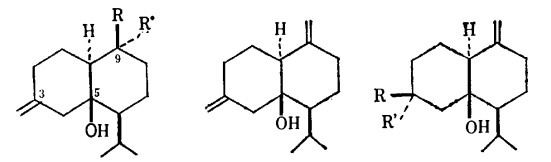

(I) R=OH, R'=Me
(III) R=Me, R'=OH

(II)

(IV) R=OH, R'=Me
(V) R=Me, R'=OH

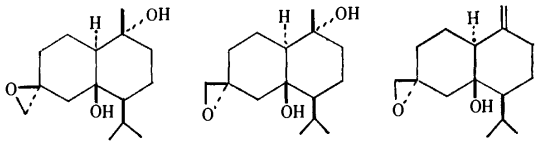

(VI) (VII) (VIII)

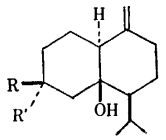

(IX) R=H, R'=Me
(X) R=Me, R'=H

We made further experiments using three different compounds (I, IX, and X), which had already been synthesized from isocalamendiol (III).[2,3] The epoxidation of the (IX) compound, which has an equatorial methyl group at the C_3-position, with *m*-chloroperbenzoic acid gave the expected β-epoxide (XI) in a 76% yield; this substance has then reduced with lithium aluminum hydride to afford a known compound (XII).[3] In the case of the (X) compound, which has an axial methyl group at the C_3-position, we can expect the formation of an α-epoxide analogous to that of isocalamendiol (III). However, the treatment of X with the same peroxy-acid gave a β-isomer (XIII) in an 88% yield; this isomer was also reduced with lithium aluminum hydride to afford a known compound (XIV).[3] On the other hand, in the case of calameone (I), an α-epoxide (XV) was obtained in an almost quantitative yield; its structure was determined by a comparison of the NMR spectra of five epoxides (VII, VIII, XI, XIII, and XV) (see Table 2): the NMR signal of XV, which can be attributed to the methylene protons on the epoxide-ring, is very similar to those of compounds VII and VIII in its chemical shift as well as its coupling constant.

The present studies indicate that such a peroxy-acid as *m*-chloroperbenzoic acid attacks the double bond,

Table 2. NMR signals of several epoxides

Compound	Methylene-protons on the epoxide-ring
VII	δ 2.60 (2H, s)
VIII	2.60 (2H, s)
XI	2.38 (1H, d, J=4.3 Hz), 2.81 (1H, d, J=4.3 Hz)
XIII	2.37 (1H, d, J=4.2 Hz), 2.83 (1H, d, J=4.2 Hz)
XV	2.63 (2H, s)

as usual, from the same side as the hydroxyl group in homoallylic alcohols which are not sterically hindered (in II and IX), whereas different results have been obtained in the cases of calameone (I) and isocalamendiol (III), as has been described above. Probably, interaction between the peroxy-acid and the homoallylic hydroxyl group at the C_5-position can be prevented by the axial tertiary methyl group at the C_9-position (in III). In the case of I, such an interaction may also be sterically hindered by the 9β-hydroxyl group or prevented by the formation of hydrogen bonding between the two axial hydroxyl groups at the C_5 and C_9-positions. Finally, the epoxidation of the compound (X), which has an axial secondary methyl group at the C_3-position, did not afford the expected α-epoxide, but the β-epoxide (XIII). Probably, the axial secondary methyl group at the C_3-position is easily moved from the normal position so as not to interrupt such an interaction between the peroxy-acid and the hydroxyl group, as compared with the case of the tertiary methyl group in III.

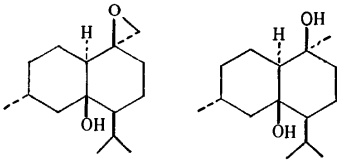

(XI) (XII)

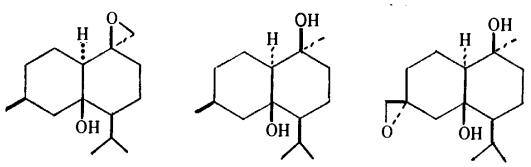

(XIII) (XIV) (XV)

Experimental

All the melting-points are uncorrected. The IR spectra were recorded on a Hitachi-215 spectrophotometer. The NMR spectra were taken on Varian A-60 and Nihondenshi JNM-60H (60 MHz) spectrometers, using $CDCl_3$ as the solvent, unless otherwise stated. Only prominent peaks are cited. The chemical shifts are given in ppm relative to the internal TMS. The coupling constants are given in Hz (s: singlet; d: doublet; t: triplet; q: quartet; m: multiplet). The mass spectra were obtained on a Hitachi RMU-6D mass spectrometer operating with an ionization energy of 70 eV. Column chromatography was carried out on neutral alumina

(Katayama Co. Ltd., 150—250 mesh).

Epoxidation of Isocalamendiol (III). A solution of isocalamendiol (810 mg) and *m*-chloroperbenzoic acid (705 mg) in abs. ether (30 m*l*) was heated under reflux for 3 hr and then cooled to room temp. After the decomposition of the excess peroxy-acid with 10% aq. Na_2SO_3 (10 m*l*), the ethereal solution was washed with 5% aq. $NaHCO_3$ (5 m*l*×2) and then satu. aq. NaCl, and dried over Na_2SO_4. The subsequent removal of the solvent gave white crystals (835 mg). Recrystallization from *n*-hexane gave white needles; mp 100—101°C; ν_{max}^{KBr} 3520 and 3400 cm^{-1}; δ 0.90 (6H, d, J=6.3 Hz), 1.29 (3H, s) and 2.60 ppm (2H, s); *m/e* 236 (M^+-18) (Found: C, 70.70; H, 10.31%. $C_{15}H_{26}O_3$ requires: C, 70.83; H, 10.3 %).

Dehydration of Epoxy-isocalamendiol (VII). Into a solution of epoxy-isocalamendiol (296 mg) in abs. pyridine (10 m*l*), we slowly stirred a solution of $POCl_3$ (1 m*l*) in abs. pyridine (3 m*l*) at − 16°C. The reaction solution was further stirred for 30 min, and then at 15°C for 2 hr. The reaction solution was then poured into large amounts of ice and extracted with ether. The ether extract was washed well with satu. aq. NaCl and dried over anhydrous Na_2SO_4. The subsequent removal of the solvent gave a pale brown oil, which was chromatographed on alumina (7 g) and eluted with pet. ether-ether (1: 1) to leave a colorless oil (175 mg). This oil was dissolved in *n*-hexane and then allowed to stand at 0°C to give 135 mg of white crystals; mp 61.5—62.5°C (from *n*-hexane); ν_{max}^{KBr} 3560, 3450 br., 1642, 895, and 885 cm^{-1}; δ 0.87 (3H, d, J=6.8 Hz), 0.90 (3H, d, J=6.8 Hz), 2.60 (2H, s), 4.68 (1H, br. s), and 4.90 ppm (1H, br. s); *m/e* 236 (M^+) (Found: C, 76.22; H, 10.56%. $C_{15}H_{24}O_2$ requires: C, 76.22; H, 10.24%).

Reduction of Dehydrated Epoxide (VIII) with Lithium Aluminum Hydride. Lithium aluminum hydride (10 mg) was added to a solution of dehydrated epoxide (130 mg) in abs. ether (20 m*l*), and then the mixture was stirred at room temp. for 2 hr. After the decomposition of the excess lithium aluminum hydride with satu. aq. ether, the reaction solution was washed with 20% aq. potassium sodium tartarate. The ether solution was washed with satu. aq. NaCl and then dried over anhydrous Na_2SO_4. The subsequent removal of the solvent gave 130 mg of white crystals; mp 112.5—114°C (from *n*-hexane); ν_{max}^{KBr} 3450 sh., 3380 br., 3090, 1650, and 895 cm^{-1}; δ 0.88 (3H, d, J=6.9 Hz), 0.91 (3H, d, J=6.9 Hz), 1.21 (3H, s), 4.77 (1H, br. s), and 4.95 ppm (1H, br. s); *m/e* 238 (M^+) (Found: C, 75.90; H, 10.97%. $C_{15}H_{26}O_2$ requires: C, 75.58; H, 11.00%).

Epoxidation of the Equatorial Sec. Methyl Olefin (IX). A solution of IX (102 mg) and *m*-chloroperbenzoic acid (95 mg) in abs. ether (8 m*l*) was heated under reflux for 3 hr; then it was worked up as usual to give a white solid, which was chromatographed on alumina (2.5 g) and eluted with pet. ether-ether (3: 1) to afford 83 mg of white crystals; mp 91.5—92.5°C (from *n*-hexane); ν_{max}^{KBr} 3570 cm^{-1}; δ 0.88 (3H, d, J=6.0 Hz), 0.92 (3H, d, J=6.9 Hz), 0.93 (3H, d, J=6.9 Hz), 2.38 (1H, d, J=4.3 Hz), and 2.81 ppm (1H, d, J=4.3 Hz); *m/e* 238 (M^+) (Found: C, 75.21; H, 11.15%. $C_{15}H_{26}O_2$ requires: C, 75.58; H, 11.00%).

Reduction of the Epoxide (XI) with Lithium Aluminum Hydride. Lithium aluminum hydride (4 mg) was stirred into a solution of the epoxide (49 mg). The reaction solution was stirred at room temp. for 2 hr and then worked up as usual to give 49 mg of white crystals (mp 133—134°C (from *n*-hexane)) which were completely identical with an authentic sample of dihydrocalameone (XII) (mp and IR spectrum).

Epoxidation of the Axial Sec. Methyl Olefin (X). A solution of X (340 mg) and *m*-chloroperbenzoic acid (320 mg) in abs. ether (10 m*l*) was refluxed for 3 hr and then worked up as usual to give a colorless oil, which was chromatographed on alumina (8.5 g) and eluted with pet. ether-ether (2: 1) to give 322 mg of white crystals; mp 61—62.5°C (from *n*-hexane); ν_{max}^{KBr} 3580 and 3450 br. cm^{-1}; δ 0.90 (3H, d, J=6.9 Hz), 0.94 (3H, d, J=6.9 Hz), 1.13 (3H, d, J=7.0 Hz), 2.37 (1H, d, J=4.2 Hz), and 2.83 ppm (1H, d, J=4.2 Hz); *m/e* 238 (M^+) (Found: C, 75.30; H, 11.21%. $C_{15}H_{26}O_2$ requires: C, 75.58; H, 11.00%).

Reduction of the Epoxide (XIII) with Lithium Aluminum Hydride. Lithium aluminium hydride (10 mg) was stirred into a solution of XIII (77 mg) in abs. ehter (10 m*l*). The reaction solution was further stirred at room temp. for 2 hr and then worked up as usual to give 100 mg of white needles, mp 123—124°C (from *n*-hexane), which were completely identical with an authentic sample of the isomer (XIV) of dihydrocalameone (mp and IR spectrum).

Epoxidation of Calameone (I). A solution of calameone (68 mg) and *m*-chloroperbenzoic acid (60 mg) in abs. ether (5 m*l*) was heated under reflux for 3 hr and then worked up as usual to give a crystalline solid; this solid was then chromatographed on neutral alumina (1.5 g) and eluted with chloroform to give 65 mg of white crystals; mp 96—98°C (from *n*-hexane); ν_{max}^{KBr} 3370 br. cm^{-1}; δ 0.91 (6H, d, J=6.8 Hz), 1.16 (3H, s), 1.63 (2H, s), 3.12 (1H, s, OH), and 4.44 ppm (1H, s, OH); *m/e* 254 (M^+) (Found: C, 70.78; H, 10.45%. $C_{15}H_{26}O_3$ requires: C, 70.83; H, 10.30%).

The authors wish to thank Miss E. Naoi, Meijo University, for the elemental analysis.

Syntheses of Benzo[5,6]cyclohept[1,2-*b*]indol-6-ones

Kameji YAMANE and Kunihide FUJIMORI

Department of Chemistry, Faculty of Science, Shinshu University, Matsumoto

(Received June 25, 1971)

The monoarylhydrazones(IIa—c) of benzocycloheptene-5,6-dione (I) underwent Fischer indolization to form 11,12-dihydrobenzo[5,6]cyclohept[1,2-*b*]indol-6-ones (IIIa—c). The treatment of IIIa—c with *N*-bromosuccinimide gave the benzoindolotropone derivatives (Va—c). Va, Vc, and VI afforded a dibromo compound (VII) on treatment with bromine in acetic acid.

Previous investigations in this area have dealt almost exclusively with syntheses of indolotropones[1] and indolotropolones.[2-4] The present paper will report on the syntheses of benzotropone derivatives fused with the indole ring.

Results and Discussion

When benzocycloheptene-5,6-dione (I) was treated in ethanol or acetic acid with an equivalent amount of phenylhydrazine, hydrochloride of *p*-tolylhydrazine, or *p*-bromophenylhydrazine, monoarylhydrazones (IIa—c) were obtained. IIa—c underwent Fischer indolization in acetic acid in the presence of zinc chloride or concd. hydrochloric acid to form 11,12-dihydrobenzo[5,6]cyclohept[1,2-*b*]indol-6-ones (IIIa—c). IIIa and IIIb were also prepared by the reaction of I with phenyl- or *p*-tolylhydrazine hydrochloride in acetic acid.

The dione (I) or monophenylhydrazone (IIa) gave IV, the phenylhydrazone of IIIa, on treatment with an excess of phenylhydrazine in acetic acid, but IIIa did not give the compound (IV). It can be presumed that bisphenylhydrazone was first formed, and that the Fischer indolization occurred smoothly under these conditions, although the bisphenylhydrazone could not be isloated.

The treatment of IIIa—c with *N*-bromosuccinimide resulted in dehydrogenation, thus formed the benzoindolotropone derivatives (Va—c) in good yields; however, the treatment of IIIa with bromine in acetic acid gave the monobromo compound (IIIc). The reaction of IIIa with two or three molar equivalents of *N*-bromosuccinimide afforded the monobromo compound (VI), which is isomeric with Vc.

The bromination of Va in acetic acid gave the dibromo compound (VII), which was also prepared by the reaction of Vc or VI with bromine in acetic acid.

Furthermore, the *N*-benzyl derivative was obtained by the reaction of IIIa with benzyl chloride.

The ultraviolet spectra of Va—c and VI were more complex than those of IIIa—c.

The infrared spectra of Va—c and VI showed olefinic C–H stretching absorption at 3100—3000 cm^{-1}. In contrast with IIIa—c, Va—c, and VI indicated the absence of paraffinic C–H stretching absorption bands in the 3000—2800 cm^{-1} region. The N–H and C=O stretching absorption bands of Va—c and VI appeared

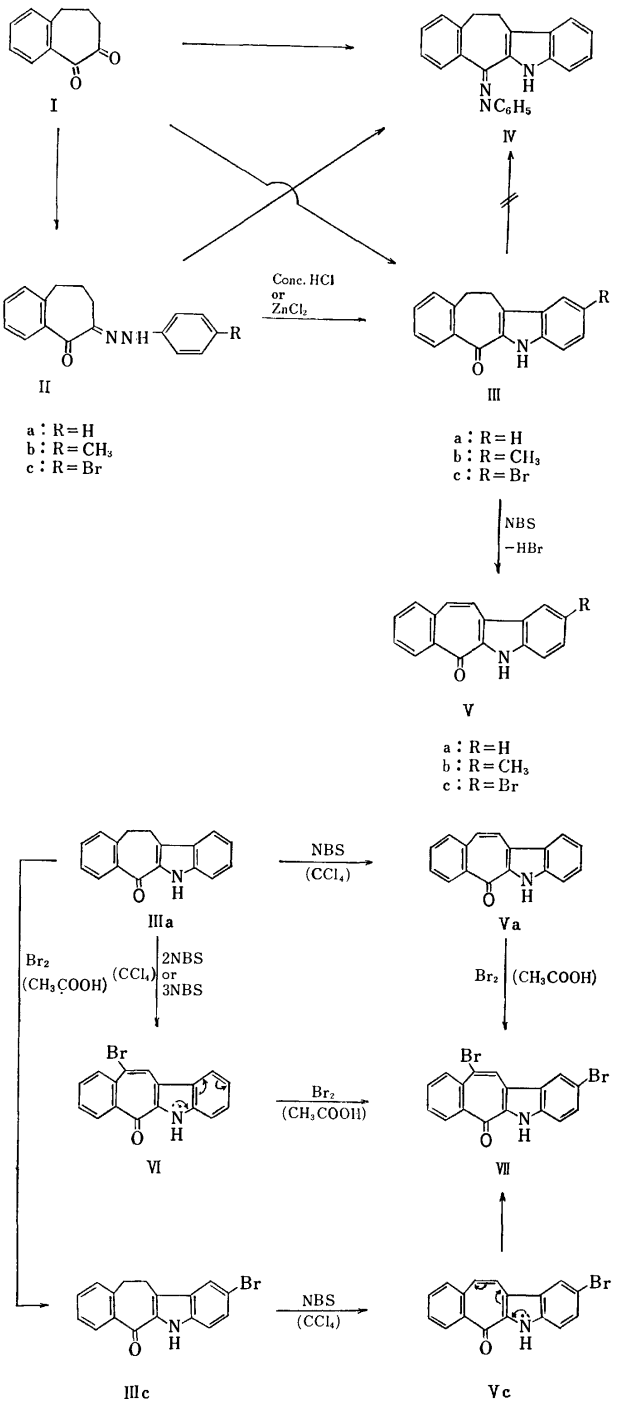

1) T. Nozoe, Y. Kitahara, and J. Shin, unpublished works.
2) M. Mühlstädt and W. Treibs, *Ann.*, **608**, 38 (1957).
3) T. Nozoe, H. Horino, and T. Toda, *Tetrahedron Lett.*, **1967**, 5349.
4) M. Mühlstädt and H. Lichtmann, *J. Prakt. Chem.*, **312**, 466 (1970).

in regions about 60—65 cm^{-1} and 60—62 cm^{-1} lower than those of IIIa—c respectively. It can, therefore, be concluded that Va—c and VI are the dehydro products of IIIa—c.

As Va—c and VI were only slightly soluble in common organic solvents, the NMR spectra could not be measured. In the NMR spectra of III, four methylene protons appeared as a singlet at τ 6.7.

Experimental

All the melting points were determined in a liquid bath and are uncorrected. The IR spectra were run as KBr tablets on a Hitachi Model EPI-G spectrophotometer. The UV absorption spectra were measured in ethanol on a Hitachi spectrophotometer Model 124. The NMR measurements were carried out on a JEOL Model JNM-4H-100 spectrometer in deuterochloroform as the solvent, with tetramethylsilane as the internal standard.

Benzocycloheptene-5,6-dione Monophenylhydrazone (IIa). *a)* A mixture of I (0.5 g) and phenylhydrazine (0.3 g) in ethanol (6 m*l*) was refluxed for 2 hr on a water bath. After cooling, the separated crystalline material was collected and recrystallized from ethanol as orange needles (0.3 g, 39%); mp 111—112°C. Found: C, 77.24; H, 6.11; N, 10.61%. Calcd for $C_{17}H_{16}ON_2$: C, 77.24; H, 6.14; N, 10.60%.

b) The reaction of I with an equivalent amount of phenylhydrazine in acetic acid afforded orange needles, mp 111°C, which are also obtained when using 2.5 molar amounts of phenylhydrazine in *n*-butyl alcohol; these needles showed no depression in mp on mixed fusion with monophenylhydrazone (IIa).

*Benzocycloheptene-5,6-dione Mono-*p*-tolylhydrazone (IIb).* A mixture of I, *p*-tolylhydrazine hydrochloride, and sodium acetate in ethanol was treated by a method similar to that described above. Orange needles (44%); mp 160—161°C. Found: C, 77.39; H, 6.42; N, 10.08%. Calcd for $C_{18}H_{18}ON_2$: C, 77.68; H, 6.51; N, 10.06%.

*Benzocycloheptene-5,6-dione Mono-*p*-bromophenylhydrazone (IIc).* This was obtained by a method similar to that used for IIb; it was recrystallized from ethanol to give orange yellow needles (54%); mp 160—161°C. Found: C, 59.68; H, 4.38; N, 8.19%. Calcd for $C_{17}H_{15}ON_2Br$: C, 59.48; H, 4.41; N, 8.16%.

*11,12-Dihydrobenzo[5,6]cyclohept[1,2-*b*]indol-6-one (IIIa).* *a)* To a solution of IIa (0.5 g) in acetic acid (15 m*l*) we added zinc chloride (0.4 g) or concd. hydrochloric acid (a few m*l*); the mixture was then refluxed for 4 hr in an oil bath. After cooling, the reaction mixture was diluted with water, and the resulting material was collected and recrystallized from ethanol to give yellow needles (0.45 g, 96%); mp 185—186°C. IR(KBr): ν NH 3305 cm^{-1}, ν conjugated C=O 1612 cm^{-1}, 1586 cm^{-1}. UV: λ_{max} (EtOH): 253 mμ (log ε 4.15), 338 mμ (log ε 4.32). NMR (in $CDCl_3$): τ 1.8—3.0 (multiplet, 8H), τ 6.74 (singlet, 4H). Found: C, 82.58; H, 5.31; N, 5.99%. Calcd for $C_{17}H_{13}ON$: C, 82.57; H, 5.30; N, 5.67%.

b) A suspension of I (0.5 g) and phenylhydrazine hydrochloride (0.5 g) in acetic acid (5 m*l*) was refluxed for 3 hr in an oil bath. After cooling, the reaction mixture was diluted with water, and the resulting material was collected and recrystallized from ethanol to give yellow needles (0.43 g, 61%); mp 185—186°C.

*2-Methyl-11,12-dihydrobenzo[5,6]cyclohept[1,2-*b*]indol-6-one (IIIb).* *a)* A mixture of IIb (0.12 g), zinc chloride (0.4 g), and acetic acid (6 m*l*) was treated as in IIIa a). Yellow needles (0.09 g, 82%); mp 174—176°C.

b) A mixture of I (0.5 g), *p*-tolylhydrazine hydrochloride (0.46 g), and acetic acid (5 m*l*) was treated as in IIIa. Yellow needles (0.47 g, 63%); mp 174—175°C. IR(KBr): ν NH 3306 cm^{-1}, ν conjugated C=O 1611 cm^{-1}, 1590 cm^{-1}. UV: λ_{max} (EtOH): 254 mμ (log ε 4.18), 345 mμ (log ε 4.37). NMR (in $CDCl_3$) τ 1.8—3.0 (multiplet, 7H), τ 6.76 (singlet, 4H), τ 7.53 (singlet, 3H). Found: C, 82.75; H, 5.70; N, 5.48%. Calcd for $C_{18}H_{15}ON$: C, 83.05; H, 5.82; N, 5.38%.

*2-Bromo-11,12-dihydrobenzo[5,6]cyclohept[1,2-*b*]indol-6-one (IIIc).* *a)* A mixture of IIc (0.3 g), zinc chloride (0.6 g), and acetic acid (10 m*l*) was treated by a method similar to that described above. Light yellow needles from ethanol (0.25 g, 86%); mp<230°C. UV: λ_{max} (EtOH): 257 mμ (log ε 4.06), 336 mμ (log ε 4.32). IR(KBr): νNH 3310 cm^{-1}, ν conjugated C=O 1613 cm^{-1}, 1585 cm^{-1}. Found: C, 62.59; H, 3.67; N, 4.11%. Calcd for $C_{17}H_{12}ONBr$: C, 62.59; H, 3.71; N, 4.30%.

b) Into a solution of IIIa (0.2 g) in acetic acid (35 m*l*), bromine (0.16 g) in acetic acid (5 m*l*) was stirred; the mixture was then stirred for 3 hr at room temperature. The separated material was collected by filtration and recrystallized from acetic aicd as yellow micro needles (0.23 g, 88%); mp>230°C. The needles were found to be identical with the product which was obtained by Method a).

Phenylhydrazone of IIIa (IV). *a)* A mixture of I (0.5 g) and phenylhydrazine (1.25 g) in acetic acid (10 m*l*) was refluxed for 4 hr. After cooling, the separated material was recrystallized from ethanol as yellow micro needles (0.43 g, 44%); mp 237—238°C. IR(KBr): νNH 3390 cm^{-1}, 3340 cm^{-1}. Found: C, 81.87; H, 5.62; N, 12.66%. Calcd for $C_{23}H_{19}N_3$: C, 81.87; H, 5.68; N, 12.45%.

b) A mixture of IIa (0.2 g) and phenylhydrazine (0.12 g) in acetitic acid (6 m*l*) was refluxed for 3 hr. After cooling, the separated material was recrystallized from ethanol as yellow micro needles (0.14 g, 54%); mp 237—238°C. Their mp was not depressed on admixture with IV, which was obtained by Method a).

*Benzo[5,6]cyclohept[1,2-*b*]indol-6-one (Va).* To a solution of IIIa (0.3 g) in carbon tetrachloride (30 m*l*), NBS (0.22 g) and benzoyl peroxide (0.06 g) were added; then the mixture was refluxed for 3 hr on a water bath. After cooling, the separated material was collected by filtration. The treatment of this with a small amount of chloroform gave an insoluble material which was then recrystallized from acetic acid as yellow micro needles (0.3 g, *ca.* 100%); mp >270°C. IR(KBr): νNH 3243 cm^{-1}, ν conjugated C=O 1581 cm^{-1} (medium), 1558 cm^{-1} (strong), 1533 cm^{-1} (shoulder). UV: λ_{max} (EtOH): 233 mμ (log ε 4.41), 295 mμ (log ε 4.53), 327 mμ (log ε 4.29). Found: C, 83.55; H, 4.34; N, 5.85%. Calcd for $C_{17}H_{11}ON$: C, 83.24; H, 4.52; N, 5.71%.

*2-Methylbenzo[5,6]cyclohept[1,2-*b*]indol-6-one (Vb).* A mixture of IIIb (0.15 g), NBS (0.10 g), benzoyl peroxide (0.06 g), and carbon tetrachloride (30 m*l*) was treated as in the case of Va. Yellow needles from chloroform (0.11 g, 81%); mp>270°C. IR(KBr): νNH 3251 cm^{-1}, ν conjugated C=O 1582 cm^{-1} (medium), 1550 cm^{-1} (strong), 1532 cm^{-1} (shoulder). UV: λ_{max} (EtOH): 235 mμ (log ε 4.46), 296 mμ (log ε 4.56), 336 mμ (log ε 4.36). Found: C, 83.38; H, 4.96; N, 5.40%. Calcd for $C_{18}H_{13}ON$: C, 83.37; H, 5.05; N, 5.40%.

*2-Bromobenzo[5,6]cyclohept[1,2-*b*]indol-6-one (Vc).* This was prepared from IIIc (0.2 g), NBS (0.13 g), benzoyl peroxide (0.04 g), and carbon tetrachloride (40 m*l*) by a method similar to that used for Vb. Yellow micro needles (0.18 g, 90%); mp >270°C. IR(KBr): νNH 3262 cm^{-1}, ν conjugated C=O 1575 cm^{-1} (medium), 1555 cm^{-1} (strong), 1533 cm^{-1}

(weak). UV: λ_{max} (EtOH): 252 mμ (log ε 4.40), 284 mμ (log ε 4.57), 328 mμ (log ε 4.38). Found: C, 63.33; H, 3.03; N, 4.30%. Calcd for $C_{17}H_{10}ONBr$: C, 62.98; H, 3.11; N, 4.32%.

Bromo Compound (VI). To a solution of IIIa (0.2 g) in carbon tetrachloride (20 m*l*), NBS (0.30 g) and benzoyl peroxide (0.06 g) were added, and then the mixture was refluxed for 3 hr on a water bath. After cooling, the separated material was collected by filtration. This was dissolved in chloroform and purified by passing through a silica gel column. The eluate gave yellow needles (0.12 g, 46%); mp >270°C. IR(KBr): νNH 3254 cm^{-1}, ν conjugated C=O 1581 cm^{-1} (shoulder), 1559 cm^{-1} (strong), 1551 cm^{-1} (shoulder). UV: λ_{max} (EtOH): 237 mμ (log ε 4.34), 299 mμ (log ε 4.43), 332 mμ (log ε 4.31). Found: C, 62.99; H, 2.94; N, 4.16%. Calcd for $C_{17}H_{10}ONBr$: C, 62.98; H, 3.11; N, 4.32%.

Dibromo Compound (VII). *a)* Into a solution of Va (0.1 g) in acetic acid (25 m*l*), bromine (0.15 g) in acetic acid (5 m*l*) was stirred, and then the mixture was stirred for 3 hr at room temperature. The separated material was collected by filtration and recystallized from acetic acid as yellow micro needles (0.14 g, 85%); mp >270°C. IR(KBr): νNH 3249 cm^{-1}, ν conjugated C=O 1601 cm^{-1} (weak), 1571 cm^{-1} (shoulder), 1560 cm^{-1} (strong), 1541 cm^{-1} (shoulder). Found: C, 50.76; H, 2.25; N, 3.67%. Calcd for $C_{17}H_9ONBr_2$: C, 50.76; H, 2.25; N, 3.48%.

b) This was prepared from VI (0.1 g) and bromine (0.1 g) in acetic acid (160 m*l*) by a method similar to that used for VII a). Yellow micro needles (0.1 g, 83%); mp >270°C. This showed an infrared spectrum identical with that of VII a).

c) A mixture of Vc (0.05 g), bromine (0.05 g), and acetic acid (150 m*l*) was treated as in the case of VII a). Yellow micro needles (0.06 g, *ca.* 100%); mp >270°C. This showed an infrared spectrum identical with that of VII a).

N-*Benzyl Derivative (VIII).* A mixture of IIa (0.15 g) and potassium (0.02 g) in dry toluene (10 m*l*) was stirred for 10 hr at room temperature. The unreacted potassium was filtered off. Benzyl chloride (0.10 g) was added to the filtrate, and the mixture was refluxed for 3 hr in an oil bath. After the reaction mixture had then cooled, we added water to it. After the insoluble material had been removed by filtration, the toluene layer was dried and the solvent was evaporated. The residue was dissolved in benzene and purified by passing it through an alumina column. Yellow needles from ethanol (trace); mp 131—131.5°C. IR(KBr): ν conjugated C=O 1618 cm^{-1} (strong), 1588 cm^{-1} (medium). Found: C, 85.59; H, 5.76; N, 4.00%. Calcd for $C_{22}H_{19}ON$: C, 85.43; H, 5.68; N, 4.15%.

The authors wish to express their thanks to Professor Emeritus Tetsuo Nozoe of Tohoku University for his kind guidance and to Mr. Hidekichi Nakajima for his cooperation in this work.

BULLETIN OF THE CHEMICAL SOCIETY OF JAPAN, VOL. 45, 271—274(1972)

The Kinetics and Mechanism of the Reactions of *N*-Sulfinylanilines with Formic Acid

Fukiko YAMADA, Tomihiro NISHIYAMA, and Toshiharu EMI

Department of Applied Chemistry, Faculty of Engineering, Kansai University, Senriyama, Suita, Osaka

(Received August 9, 1971)

We have examined the kinetics of the reactions between *N*-sulfinylanilines and formic acid. The reactions follow this rate equation; rate=k[R–C_6H_4–NSO][HCOOH]. The kinetic runs were made over a wide temperature range (40—90°C) in order to obtain the values of the activation energy. The values for the reactions of *N*-sulfinylaniline, *N*-sulfinyl-*p*-toluidine, and *N*-sulfinyl-*p*-chloroaniline with formic acid are 14.6, 15.1, and 10.1 kcal/mol respectively. The reaction mechanism is discussed by means of their NMR spectral data.

In 1932, Carré and Libermann reported that carboxylic acids react with *N*-sulfinylaniline to form the corresponding anilides:[1]

$$C_6H_5NSO + RCOOH \longrightarrow C_6H_5NHCOR + SO_2$$

Recently, Smith and King re-examined the above reaction.[2] They presented the possibility that a trace of either thionyl chloride, or hydrogen chloride, or traces of both, might be present as an impurity in *N*-sulfinylaniline and that one of these impurities might have been acting as the catalyst. In consequence, the following mechanism was postulated by them;

$$C_6H_5NSO + 3HCl \longrightarrow C_6H_5NH_2 \cdot HCl + SOCl_2$$

$$RCOOH + SOCl_2 \longrightarrow RCOCl + SO_2 + HCl$$

$$C_6H_5NH_2 \cdot HCl + RCOCl \longrightarrow C_6H_5NHCOR + 2HCl$$

They concluded that the steps involved in the reaction of *N*-sulfinylaniline with carboxylic acids are correctly described by the above sequence, in which both aniline hydrochloride and thionyl chloride are intermediates. The reaction was shown to require the presence of hydrogen chloride.

On the other hand, some recent reports from this laboratory have described the reactions of *N*-sulfinylanilines with alkene oxides[3,4] and the general structures of the reaction products, the oxathiazolidines, as determined by means of their NMR[4] and mass spec-

1) P. Carre' and D. Libermann, *C. R. Acad. Sci. Paris.*, **194**, 2218 (1932).

2) W. T. Smith and G. G. King, *J. Org. Chem.*, **24**, 976 (1959).

3) F. Yamada, T. Nishiyama, M. Kinugasa, and M. Nakatani, This Bulletin, **43**, 3611 (1970).

4) T. Nishiyama and F. Yamada, *ibid.*, **44**, 3073 (1971).

tra.[5] In these circumstances, it became of interest to study the reactivity of *N*-sulfinylanilines in relation to formic acid. The present paper is concerned with the kinetics of the reactions of *N*-sulfinylanilines with formic acid carried out in the absence of the catalysts, that is, in the absence of both hydrogen chloride and thionyl chloride. The reaction mechanism is also discussed.

Experimental

Measurements. All the melting points are uncorrected. The NMR spectra were obtained at 60 MHz with a Japan Electron Optics Model JNM 3H-60 spectrometer at room temperature. The chemical shifts are reported in ppm downfield from the internal TMS (δ). A constant-temperature bath was employed; it was equipped with an immersion heating element that afforded a temperature control of ± 0.1°C.

Materials. *N*-Sulfinylaniline, *N*-sulfinyl-*p*-toluidine, and *N*-sulfinyl-*p*-chloroaniline were prepared and purified by the reported method.[6] No hydrogen chloride or thionyl chloride was left in the *N*-sulfinylanilines. These facts were confirmed by using both gas chromatography and the NMR method. The formic acid was of an analytical grade and was dried for several days over anhydrous copper sulfate and filtered, after which the filtrate was distilled under reduced pressure.

Kinetic Procedure. In a 3-necked, 30-m*l* flask equipped with a gas inlet and output tubes and an addition funnel, we placed *N*-sulfinylaniline (0.05 mol). In a typical second-order run, about a twofold excess of formic acid was added rapidly to start the reaction. The flask was swirled in order to mix the reactants and was then kept at a constant temperature. A constant flow of dry nitrogen gas was introduced into the reaction mixture throughout the reaction (2.0—4.5 *l*/hr). Nitrogen was passed through the reaction flask to sweep the sulfur dioxide evolved into 80 m*l* of water in the absorption bulbs; at the end of a sufficient period, 5 or 10 min, the bulbs were disconnected and exchanged for other bulbs using a three-way stopcock. In each run, a 10-m*l* portion was withdrawn from the aqueous solution; we then added a known excess of an iodine solution (0.1N) and determined the amount of the excess by back titration with standard sodium thiosulfate. The rate of sulfur dioxide's release was obtained by this method. The conversion of *N*-sulfinylaniline based on the initial concentration can, therefore, be obtained by means of the measurement of the sulfur dioxide evolved. The rate constants given in the table are the averages of two or more determinations.

Reaction-products Criterion. The crystals were obtained in almost quantitative yields by the reactions of *N*-sulfinylanilines with formic acid and did not show any melting-point depression when the products were mixed with authentic samples of the corresponding *p*-substituted formanilides; formanilide, mp and mmp 46.0—47.5°C; *N*-*p*-tolylformamide, 50.0—50.4°C, and *N*-*p*-chlorophenylformamide, 99.0—99.8°C. The analytical results of these compounds coincided with those of the authentic compounds.

Results and Discussion

The rate of the reaction of *N*-sulfinylanilines with formic acid was followed by the iodine titration of the sulfur dioxide evolved. The results gave good second-order rate constants for all the runs, and the points obtained fell on good straight lines (Fig. 1):

$$\text{rate} = k[\text{R-C}_6\text{H}_4\text{-NSO}][\text{HCOOH}]$$

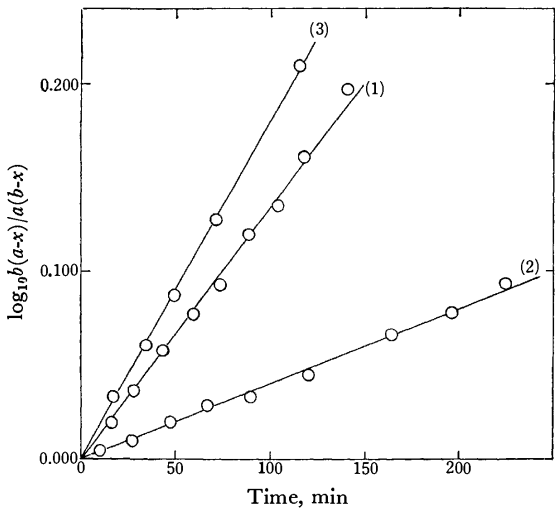

Fig. 1. The second-order plots for the reaction of *N*-sulfinylanilines with formic acid at 60°C. *a* and *b* are the initial concentrations of formic acid and *N*-sulfinylanilines, respectively.
(1) *N*-sulfinylaniline, 5.03 mol/*l*; formic acid, 13.03 mol/*l*. conversion 48.4%.
(2) *N*-sulfinyl-*p*-toluidine, 5.98 mol/*l*; formic acid, 10.86 mol/*l*. conversion 34.7%.
(3) *N*-sulfinyl-*p*-chloroaniline, 5.17 mol/*l*; formic acid, 10.92 mol/*l*. conversion 54.0%.

TABLE 1. THE RATE CONSTANTS AND THE VALUES OF THE ACTIVATION ENERGY FOR THE REACTION OF *N*-SULFINYLANILINES WITH FORMIC ACID

Temp. C°	*N*-Sulfinylaniline $k\times10^4$, *l*/mol·min	*N*-Sulfinyl-*p*-toluidine $k\times10^4$, *l*/mol·min	*N*-Sulfinyl-*p*-chloroaniline $k\times10^4$, *l*/mol·min
40	—	—	2.9
50	1.5	0.9	4.8
60	3.6	1.8	7.2
70	7.3	4.0	12.3
80	12.2	6.6	—
90	16.1	9.4	—
E, kcal/mol	14.6	15.1	10.1

Table 1 shows the rate constants of the reactions of *N*-sulfinylanilines with formic acid at various temperatures, along with the values of the activation energy as evaluated from the slopes of the Arrhenius plots. The data given in Table 1 clearly indicate that *N*-sulfinyl-*p*-chloroaniline reacted faster with formic acid than did *N*-sulfinylaniline, as expected, and also faster than *N*-sulfinyl-*p*-toluidine. The reaction is facilitated by the introduction of an electron-attracting substituent into the phenyl group, but is retarded by that of an electron-releasing substituent.

Observation of the Reaction Process using NMR. The spectrum of *N*-sulfinylaniline in carbon tetrachloride exhibits the two-proton and three-proton multiplets due to the ring proton in the regions of 7.93—8.10 and 7.45—7.58 ppm respectively (Fig. 2). In the reaction

5) F. Yamada, T. Nishiyama, Y. Fujimoto, and M. Kinugasa, *ibid.*, **44**, 1152 (1971).
6) A. Michaelis and R. Herz, *Ber.*, **23**, 3480 (1890).

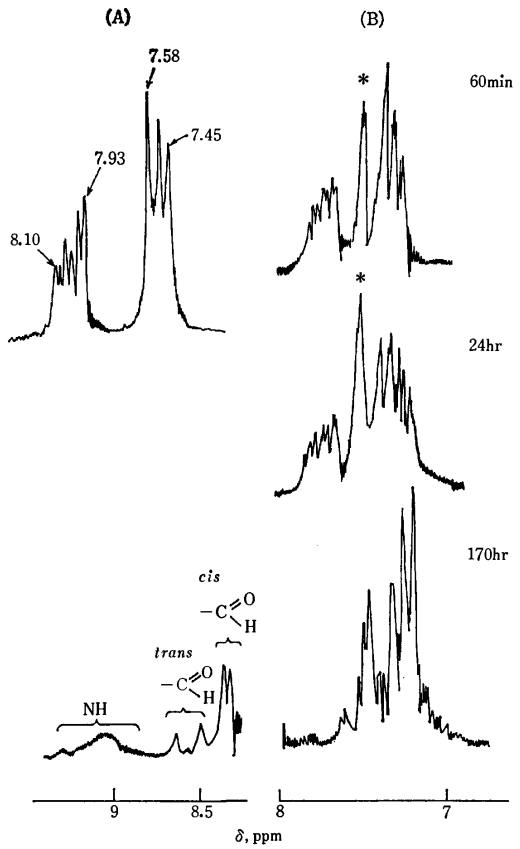

Fig. 2. The NMR spectrum of *N*-sulfinylaniline in CCl_4 (A) and changes of the NMR spectra with reaction time (B). Asterisks indicate the peak at 7.73 ppm.

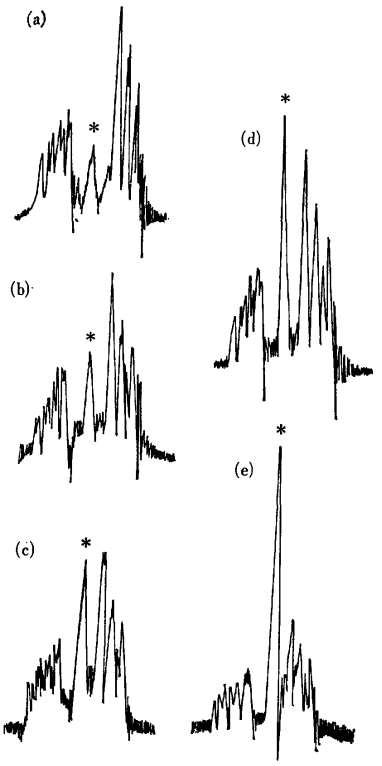

Fig. 3. The NMR signals of the ring protons of the reaction mixtures of *N*-sulfinylaniline with formic acid under various concentrations at 40°C for 60 min, molar ratios of *N*-sulfinylaniline to formic acid; (a) 1:4.3, (b) 1:5.5, (c) 1:7.6, (d) 1:11.1, and (e) 1:17.6. The spectra are not necessarily on exactly the same scale. Asterisks indicate the peak at 7.73 ppm.

of a fivefold excess of formic acid with *N*-sulfinylaniline at 25°C, a new single peak immediately appears at 7.73 ppm (60 min). After the mixture has stood 24 hr, the peak was intensified. These signals changed with the reaction time. Of these signals, the three-proton signal changed most remarkably as a result of the overlapping of the ring-proton signal of the reaction product. The peak at 7.73 ppm increased and then decreased gradually. When the reaction was over, the two-proton signal disappeared; these NMR signals were changed to those of formanilide (170 hr).

Figure 3 shows the NMR spectra of the reaction mixtures at different concentrations. After a mixture has stood for 60 min at 40°C, the peak at 7.73 ppm shows various intensities. This fact indicates that the intensive changes at the 7.73 ppm peak depend on the molar ratios of *N*-sulfinylaniline to formic acid under these experimental conditions.

Table 2. Chemical shifts in different solvents (1.70 mmol/ml)

Compound	Solvent	Chemical shifts, δ, ppm					
		Ring proton				New peak	Methyl
N-Sulfinyl-aniline	HCOOH	7.49—8.08				7.73	—
	CCl_4	7.45—8.10				—	—
N-Sulfinyl-*p*-toluidine	HCOOH	7.28	7.41	7.80	7.93	7.54	2.47
	CCl_4	7.22	7.35	7.84	7.97	—	2.62
N-Sulfinyl-*p*-chloroaniline	HCOOH	7.41	7.57	7.84	8.00	7.70	—
	CCl_4	7.40	7.55	7.87	8.02	—	—

The chemical shifts of *N*-sulfinylanilines in both formic acid and carbon tetrachloride are shown in Table 2. No new peak, such as the peak at 7.73 ppm, was observed in the carbon tetrachloride solutions. Peaks at 7.73, 7.54, and 7.70 ppm could, however, be observed in the formic acid solutions.

Probable Mechanism. The results presented above indicate that the reactions proceed by the following pathway:

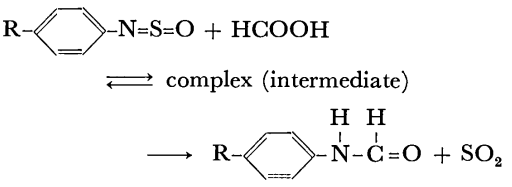

The reaction is initiated by the interaction between a sulfur atom of the –N=S=O group and a carbonyl oxygen of formic acid. Thus, the molecules can form a 1:1 complex; this step is probably rate-determining and is followed by the step yielding anilides and sulfur dioxide. The rates of the reactions in the 40—90°C temperature range showed a second-order dependence on the concentrations of the reactants. When *N*-sulfinylanilines react with more than fourfold excesses of formic acid or at low temperatures, below 40°C, new peaks were observed in their NMR spectra (in Table 2). It can, therefore, be suggested that the peaks indicate the existence of the intermediate in each reaction,

The new chemical shifts appeared as a result of the formation of the intermediates. The NMR spectrum of aniline formate in formic acid shows a single peak at 7.53 ppm, a slightly higher shift than that of the above intermediates. Aniline formate is also well-known as an intermediate of the reaction of aniline with formic acid.

There are ample examples in the literature to show that *N*-sulfinyl compounds form four-membered intermediates *via* the cycloaddition of the reactants. For example, Kresze and Albrecht[7,8] reported that the reactions of *N*-sulfinyl compounds with carbonyl compounds were transformations analogous to a Wittig reaction in which the carbonyl oxygen is replaced by the R–N= or RSO_2–N= group and the sulfur dioxide is eliminated. On the other hand, we have easily prepared the 2-oxo-3-aryl-1,2,3-oxathiazolidines, that is, five-membered heterocyclic compounds, by the cycloadditions of *N*-sulfinylanilines to alkene oxides.[3,4] From these facts, the four-membered ring structure seems to be less stable than the five-membered ring structure. In these circumstances, we propose a four or six-membered heterocyclic structure as an intermediate as follows:

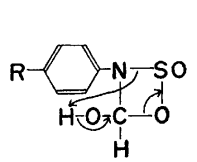

four-membered intermediate

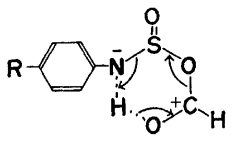

six-membered intermediate

At the present time, the four-membered ring-activated complex and the six-membered ring-activated complex are entirely compatible with the above experimental data.

7) R. Albrecht, G. Kresze, and B. Mlakar, *Chem. Ber.*, **97**, 483 (1964).

8) G. Kresze and R. Albrecht, *Angew. Chem.*, **74**, 782 (1962).

BULLETIN OF THE CHEMICAL SOCIETY OF JAPAN, VOL. 45, 274—279(1972)

The Reaction between Hydrocarbon and Hydrogen Sulfide in Silent Electrical Discharge. I. The Reaction of Ethylene or Propylene with Hydrogen Sulfide

Yoshiharu NISHIMURA[1] and Kazuaki KAWAMOTO

Institute of Commodities, Faculty of Economics, Kagawa University, Takamatsu

(Received August 6, 1971)

In order to examine the possibility of the direct introduction of the sulfhydryl radical into ethylene or propylene and that of the telomerization by means of a silent discharge, the mixture of ethylene or propylene and hydrogen sulfide was discharged in an ozonizer. (1) With ethylene and hydrogen sulfide, the main products were ethyl mercaptan, *n*-butyl mercaptan, and ethylene dithioglycol. Besides these compounds, the reaction products were confirmed to be diethyl sulfide, *s*-butyl, *n*-hexyl, *n*-propyl, and isopropyl mercaptans, and gaseous products. (2) With propylene and hydrogen sulfide, on the other hand, *n*-propyl mercaptan, di-*n*-propyl sulfide, isopropyl mercaptan, and 1,2-propylene dithioglycol were obtained as the main products. Besides these compounds, there were diisopropyl sulfide, ethyl and *n*-butyl mercaptans, 4-methyl-1-pentene, 2,3-dimethylbutane, 1,5-hexadiene, 2-methylpentane, 1-hexene, *n*-hexane, and gaseous products. The maximum yield of the liquid products was obtained when ethylene or propylene and hydrogen sulfide were mixed in approximately the ratio of 1:1. Judging from the relative concentration of each compound in the reaction products, it may be said that vinyl, ethyl, and sulfhydryl radicals in the reaction system of ethylene and hydrogen sulfide, and 2-methylvinyl, isopropenyl, propyl, allyl, isopropyl, and sulfhydryl radicals in the reaction system of propylene and hydrogen sulfide, are the main intermediates.

The oxidation of hydrocarbons by a silent electrical discharge has been studied by Sugino *et al.*[2] and by Tsutsumi *et al.*[3]

In previous papers,[4] the reaction between hydrocarbon (cyclohexane, ethylene, and propylene) and hydrogen cyanide in a silent discharge was studied. When a mixed gas of ethylene and hydrogen cyanide was discharged in an ozonizer under atmospheric pressure, acrylonitrile could be prepared in one step. Besides this compound, the formation of telomers, such as ethyl, *n*-butyl, and *n*-hexyl cyanides, was also observed. Moreover, the reactions of ethylene with 2-propanol and with carboxylic acid under a silent dis-

1) Present address: Department of Chemistry, Faculty of Education, Kagawa University, Takamatsu.

2) K. Sugino and E. Inoue, This Bulletin, **24**, 93 (1951); K. Sugino and E. Inoue, *Nippon Kagaku Zasshi*, **75**, 10, 617 (1954); E. Inoue, *J. Electrochem. Soc. Jap.*, **22**, 668 (1954); E. Inoue, *ibid.*, **23**, 18, 76, 403, 452, 574, 648 (1955); E. Inoue and K. Sugino, *ibid.*, **24**, 33 (1956); K. Sugino, E. Inoue, K. Shirai, T. Koseki, and T. Gomi, *Nippon Kagaku Zasshi*, **86**, 114 (1965).

3) N. Sonoda, S. Yamamoto, K. Okumura, S. Noda, and S. Tsutsumi, "Oxidation of Organic Compounds," Vol. II, Advances in Chemistry Series 76, American Chemical Society, Washington (1968), pp. 352—362.

4) K. Kawamoto, N. Sonoda, and S. Tsutsumi, This Bulletin, **41**, 1376 (1968); K. Kawamoto, *ibid.*, **41**, 2161 (1968); K. Kawamoto and Y. Nishimura, *ibid.*, **42**, 1105 (1969).

charge have been reported by Hiraki.[5]

The direct synthesis of mercaptan and sulfide from olefin and hydrogen sulfide has been reported by many investigators. Vaughan and Rust[6] found that the photo-chemical addition of hydrogen sulfide to olefinic bonds took place very readily, giving mixtures of the corresponding mercaptans and sulfides. The radiation-induced addition of hydrogen sulfide to propylene to give *n*-propyl mercaptan and di-*n*-propyl sulfide has been investigated by Sugimoto *et al.*[7] The X-ray initiated free-radical addition of hydrogen sulfide to fluoroethylenes has been reported by Harris and Stacey.[8]

Losanitsch[9] reported that when a mixture of ethylene and hydrogen sulfide was subjected to a silent electrical discharge, ethyl mercaptan and the polymer of thioaldehyde ($(C_2H_4S)_6$) were obtained. However, no detailed study of the reaction of propylene with hydrogen sulfide under a silent discharge has yet been reported.

The present study was undertaken to find out whether the mercaptan and the sulfide are obtained by the reaction of ethylene or propylene with hydrogen sulfide under a silent discharge, to check whether or not a telomerization occurs under the present reaction conditions, and, at the same time to ascertain the mechanism of this reaction. In this research, the silent discharge was carried out in a Siemen ozonizer for 6 hr, using a voltage of 12 kilovolts. The direct introduction of a sulfhydryl radical into hydrocarbon was observed.

Experimental

Materials. The ethylene and propylene were purchased from the Nihon Sekiyu Kagaku Co., Ltd. (Kawasaki) and the Takachiho Chemicals Co. (Tokyo) respectively, and the hydrogen sulfide, from the Seitetsu Chemicals Co. (Osaka). These materials were used without further purification. No impurity was found in these reagents by gas-chromatographic analysis. (Columns of activated charcoal, acetonylacetone, dimethylsulfolane, and silica gel were used.)

Apparatus. The silent discharge reactor system used in this study is shown in Fig. 1. (1) Helium, hydrogen sulfide, and ethylene or propylene coming from the bomb were passed over calcium chloride (A). (2) The molar ratios of the ethylene or propylene and the hydrogen sulfide were roughly determined by means of a manometer (B), and the quantitative analysis of the mixed gas in this experiment was performed by gas chromatography. (A column of silica gel was used.) (3) The reservoirs (C) were filled with a mixture of ethylene or propylene and hydrogen sulfide. (4) The mixed gas was circulated by means of a pump (D) at the rate of 2 *l*/min. (5) The outside (a) of the discharge tube (E) was filled with water, and the inner tube (b), with a 3% $CuSO_4$ solution. (6) The discharge tube (E) used was a Pyrex tube 45 cm in effective length, 3.5 cm in outside diameter, and with a space gap of 0.25 cm. (7) The electrical energy was supplied by a 15-kV transformer (F).

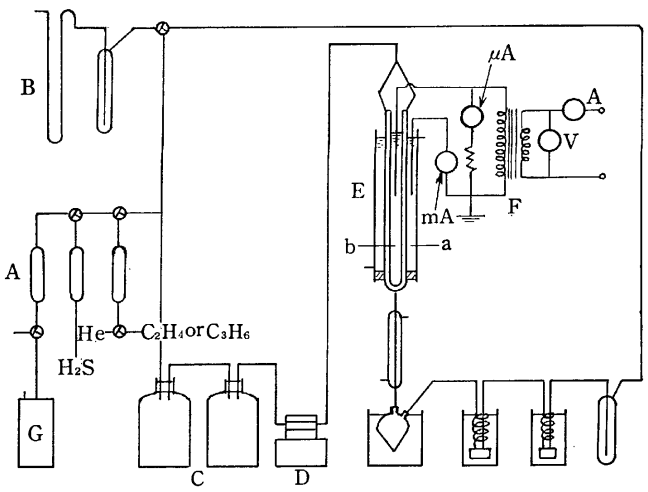

Fig. 1. Apparatus.

Procedure. In order to exclude the oxygen, the pressure in the system was reduced by means of a vacuum pump (G), and the oxygen was completely replaced by helium. In the presence of a small quantity of air, a great deal of a tarry yellow deposit was formed on the glass wall. A mixture of ethylene or propylene and hydrogen sulfide, at the molar ratio shown in Tables 1 and 3, was then put into the system. The volume of the system was 49.0 *l*. The mixed gas was made homogeneous by using a pump (D) for 30 min and was then passed through the discharge tube at a regular velocity of 2 *l*/min for the period of the reaction. A current of 60 cycles was passed through a voltage regulator; the voltage was stepped up by a transformer to give the required value. The products coming out of the discharge tube were condensed by passing them through a condenser; then they were collected by being passed through two traps cooled to −45°C by acetone-dry ice. The liquid products were analyzed by the method described below, while the non-condensable gases were analyzed by gas chromatography at intervals of 20 min. The pressure in the system during the period of the reaction was measured at intervals of 20 min.

Identification and Analysis of the Reaction Products. The liquid products obtained by the reaction between ethylene or propylene and hydrogen sulfide were identified by comparing their retention times on the gas chromatogram with those of authentic samples. (Columns of tricresyl phosphate, dinonyl phthalate, and Silicone DC-550 were used.) In addition, the reaction products were fractionally distilled, and the constituents of the fraction were identified by observing the formation of the derivatives.[10] Ethyl mercaptan was obtained in a fraction boiling at 33—36°C. From this fraction, 2,4-dinitrophenyl thioether, mp 114—115°C, and the 3,5-dinitrobenzoyl thioester, mp 61—62°C were obtained. The fraction boiling at 90—93°C was confirmed to consist mainly of diethyl sulfide by transforming it into the diethyl sulfone,[11] mp 73—74°C. Furthermore, the infrared spectrum of this fraction agreed with that of the authentic diethyl sulfide. *n*-Butyl mercaptan, obtained as a fraction boiling at 96—100°C, was converted into its 2,4-dinitrophenyl thioether and the 3,5-dinitrobenzoyl thioester, the melting points of the derivatives being 65—66°C and 48—49°C respectively. The ethylene dithioglycol was obtained in a fraction boiling at 144—146°C. Upon gas-chromatographic analysis, this frac-

5) T. Hiraki, *ibid.*, **42**, 1981, 2993, 3216 (1969).
6) W. E. Vaughan and F. F. Rust, *J. Org. Chem.*, **7**, 472 (1942).
7) K. Sugimoto, W. Ando, and S. Oae, This Bulletin, **37**, 365 (1964).
8) J. F. Harris, Jr., and F. W. Stacey, *J. Amer. Chem. Soc.*, **85**, 749 (1963).
9) S. M. Losanitsch, *Ber.*, **40**, 4656 (1907).
10) R. W. Bost, J. O. Turner, and R. D. Norton, *J. Amer. Chem. Soc.*, **54**, 1985 (1932); E. Wertheim, *ibid.*, **51**, 3662 (1929).
11) E. O. Beckmann, *J. Prakt. Chem.*, (2), **17**, 439 (1878).

tion showed the same retention time as that of authentic ethylene dithioglycol. The infrared spectrum of this fraction agreed with that of the authentic specimen.

The liquid products obtained by the reaction between propylene and hydrogen sulfide were identified by the following method. The fraction boiling at 56—60°C consisted of isopropyl mercaptan, which was identified by transforming it into the 2,4-dinitrophenyl thioether, mp 94—94.5°C, and the 3,5-dinitrobenzoyl thioester, mp 83—84°C. *n*-Propyl mercaptan was present in a fraction boiling at 65—68°C. From this fraction, the 2,4-dinitrophenyl thioether, mp 80—81°C, and the 3,5-dinitrobenzoyl thioester, mp 51—52°C were obtained. Di-*n*-propyl sulfide, obtained as a fraction boiling at 140—143°C, and 1,2-propylene dithioglycol (bp 148—154°C) showed the same retention times on the gas chromatogram as those of the authentic reagents, furthermore, the infrared spectra of these fractions agreed with those of the authentic specimens. The liquid hydrocarbon products listed in Table 4 were identified by the use of squalane, *β,β'*-oxydipropionitrile, tricresyl phosphate, and dimethylsulfolane columns.

These derivatives showed no depression of their melting points when mixed with authentic specimens. The gaseous products, obtained by the reaction between ethylene or propylene and hydrogen sulfide, were also analyzed by gas chromatography. (Columns of activated charcoal, tricresyl phosphate, a mixture of molecular sieve 13 X and hexamethylphosphoramide, acetonylacetone, and dimethylsulfolane were used.) The gaseous products could not be determined quantitatively. The quantitative analysis of the liquid products in this experiment was performed by gas chromatography.

Results and Discussion

The results obtained by running ethylene with hydrogen sulfide in an ozonizer under the conditions described in Table 1 are summarized in Table 2. Further, by running propylene with hydrogen sulfide under the conditions listed in Table 3, a large number of compounds were obtained. The compositions of those compounds which have been identified are summarized in Table 4. The percentage of the compounds shown in these tables does not necessarily represent the maximum yield, but is an average of three experiments under constant operating conditions. However, the fluctuation in the yields of the compounds obtained in repeated experiments was less than 1 per cent. A small amount of air was found to reduce the liquid products.

TABLE 1. THE REACTION BETWEEN ETHYLENE AND HYDROGEN SULFIDE IN SILENT ELECTRICAL DISCHARGE
(Experimental conditions)

Experiment No.	1	2	3	4	5
Second. voltage (kV)	12	12	12	12	12
Second. current (mA)	1.9	2.0	2.1	2.1	2.2
Temp. of discharge tube (°C)					
Inside	17—39	20—49	20—52	19—49	16—47
Outside	17—32	20—42	20—45	19—41	16—40
Discharge time (hr)	6	6	6	6	6
Materials used (*l*)					
Ethylene	40.8	35.0	27.2	19.6	14.0
Hydrogen sulfide	8.2	14.0	21.8	29.4	35.0
Molar ratio (C_2H_4/H_2S)	4.9	2.5	1.3	0.7	0.4

TABLE 2. THE REACTION BETWEEN ETHYLENE AND HYDROGEN SULFIDE IN SILENT ELECTRICAL DISCHARGE
(Experimental results)

Experiment No.	1	2	3	4	5
Liquid product collected (g)	1.43	4.92	8.54	7.00	4.74
Conversion efficiency[a] (%)	2.3	7.6	12.7	10.1	6.7
Composition of liquid reaction products[b] (%)					
Ethyl mercaptan	62.1	62.6	62.7	61.6	60.8
n-Butyl mercaptan	18.3	13.0	7.5	3.5	3.2
s-Butyl mercaptan	0.4	0.3	0.2	0.1	0.1
Ethylene dithioglycol	3.1	9.2	15.6	24.2	25.2
Diethyl sulfide	3.1	2.8	2.4	1.7	1.2
n-Propyl mercaptan	4.5	4.3	4.1	3.9	3.9
Isopropyl mercaptan	0.9	0.6	0.5	0.5	0.4
n-Hexyl mercaptan	T	T	T	T	T
Unidentified product	7.6	7.2	7.0	4.5	5.2

T: Trace
a) The conversion efficiency was given by (grams of reaction product/grams of materials (ethylene+hydrogen sulfide) used) × 100.
b) The yields of each compound produced were given by (grams of each compound/grams of total reaction product) × 100.

TABLE 3. THE REACTION BETWEEN PROPYLENE AND HYDROGEN SULFIDE IN SILENT ELECTRICAL DISCHARGE
(Experimental conditions)

Experiment No.	6	7	8	9
Second. voltage (kV)	12	12	12	12
Second. current (mA)	1.9	1.9	1.9	2.0
Temp. of discharge tube (°C)				
Inside	19—44	14—45	15—46	18—46
Outside	19—39	14—40	15—40	18—41
Discharge time (hr)	6	6	6	6
Materials used (*l*)				
Propylene	37.7	28.0	21.3	16.3
Hydrogen sulfide	11.3	21.0	27.7	32.7
Molar ratio (C_3H_6/H_2S)	3.3	1.3	0.8	0.5

TABLE 4. THE REACTION BETWEEN PROPYLENE AND HYDROGEN SULFIDE IN SILENT ELECTRICAL DISCHARGE
(Experimental results)

Experiment No.	6	7	8	9
Liquid product collected (g)	4.18	6.20	6.93	6.08
Conversion efficiency (%)	4.8	7.3	8.4	7.6
Composition of liquid reaction products (%)				
n-Propyl mercaptan	49.4	57.5	56.5	48.3
Isopropyl mercaptan	10.2	12.2	11.3	10.4
Di-*n*-propyl sulfide	14.8	5.7	3.9	2.8
Diisopropyl sulfide	4.2	1.8	1.2	0.8
1,2-propylene dithioglycol	3.6	5.8	10.9	20.4
Ethyl mercaptan	3.0	2.0	1.2	0.7
n-Butyl mercaptan	0.6	0.7	0.3	0.2
4-Methyl-1-pentene	0.3	0.2	0.1	0.1
2,3-Dimethylbutane	0.2	0.1	0.1	T
1,5-Hexadiene	0.1	0.1	T	T
2-Methylpentane	0.1	T	T	T
1-Hexene	T	T	T	T
n-Hexane	T	T	T	T
Unidentified product	13.5	13.9	14.5	16.3

Air apparently acts as a free radical scavenger to retard this chain reaction. The gaseous products given by the reaction of ethylene and hydrogen sulfide consisted of hydrogen, methane, ethane, acetylene, propane, propylene, *n*-butane, 1-butene, and 1,3-butadiene. In the cases of propylene and hydrogen sulfide, the gaseous products were found to be hydrogen, methane, ethane, ethylene, acetylene, propane, methylacetylene, and allene.

Influence of the Molar Ratio of Ethylene to Hydrogen Sulfide on the Yield. In order to check the molar-ratio effects on the discharge reaction of ethylene and hydrogen sulfide, the reaction was carried out with various ratios of the ethylene to the hydrogen sulfide, as is shown in Table 1. As may be seen from Table 2, the yield of the reaction product depends upon the molar ratio of the ethylene and the hydrogen sulfide; the maximum yield of liquid products was obtained when they were mixed in the ratio of approximately 1 : 1. However, the distribution of the products depends on the molar ratio of the reactants as follows: (1) The yield of ethylene dithioglycol increased at high ratios of hydrogen sulfide to ethylene. (2) On the other hand, the *n*-butyl mercaptan and diethyl sulfide decreased with an increase in the ratio of hydrogen sulfide to ethylene. (3) The yield of ethyl mercaptan, though the molar ratio of ethylene and hydrogen sulfide changed, was approximately constant. Ethyl, *n*-butyl, and *n*-hexyl mercaptans seem to be formed by the telomerization between ethylene and hydrogen sulfide. However, the formation of *n*-octyl mercaptan (1 : 4 telomer) and one-to-five or more products could not be observed by gas-chromatographic analysis. The total pressure in the reaction system was measured at intervals of 20 min; the results are shown in Fig. 2.

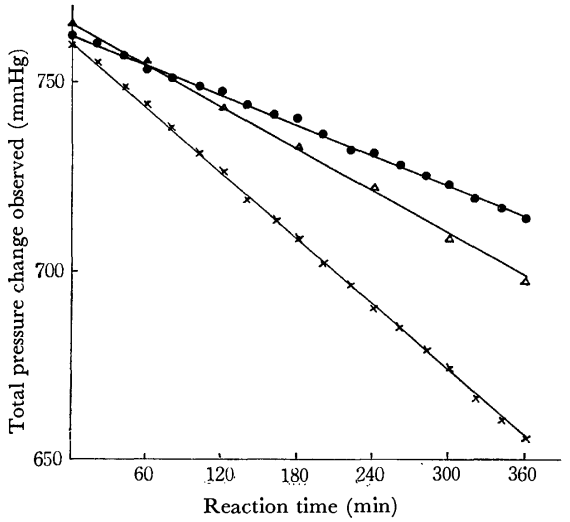

● : Experiment No. 1 △ : Experiment No. 5
× : Experiment No. 3

Fig. 2. Relation between total pressure in reaction system and time of reaction. (Reactants: C_2H_4 and H_2S)

As may be seen from this graph, the total pressure decreased linearly with the progress of the reaction time, in spite of the molar ratios of ethylene and hydrogen sulfide. A proportional relation was found between the velocity of the reduced pressure in the reaction system and the yield of the reaction product; that is, it has been found that increasing the velocity of the reduced pressure increases the amount of the reaction product. In addition, the ratio of the consumption of ethylene to hydrogen sulfide was found, from gas analysis, to be kept constant during the period of the reaction.

The Reaction between Propylene and Hydrogen Sulfide. When a mixture of propylene and hydrogen sulfide was allowed to react in a silent discharge, a large number of products (summarized in Table 4) were obtained. As is shown in Table 4, the conversion efficiency (grams of reaction product per grams of propylene and hydrogen sulfide used $\times 100$) depends upon the ratio of propylene to hydrogen sulfide; it has been found that the maximum yield of the liquid product was obtained when the mixed components of the reactant were approximately in the ratio of 1 : 1, that, in the 1 : 1 ratio, the addition products, such as *n*-propyl mercaptan and isopropyl mercaptan, were obtained in high yileds, while such sulfides as di-*n*-propyl sulfide and diisopropyl sulfide decreased with an increase in the ratio of hydrogen sulfide to propylene, and that, on the other hand, the yield of 1,2-propylene dithioglycol increased at high ratios of hydrogen sulfide to propylene. The formation of allyl mercaptan could not be observed by gas-chromatographic analysis. The yield of *n*-propyl mercaptan was higher than that of isopropyl mercaptan. Therefore, the addition followed an anti-Markownikoff rule. This rule was observed in both the photo-chemical addition[6] and the radiation-induced addition[7] of hydrogen sulfide to propylene. The nature of the discharge-induced addition appears to be similar to that of these additions. Figure 3 shows how the total pressure in the reaction system changes during the period of the silent discharge. In the cases of propylene and hydrogen sulfide, the same results as in the case of ethylene were obtained.

The Mechanism of the Formation of the Main Products Obtained by the Reaction of Ethylene and Hydrogen Sulfide.

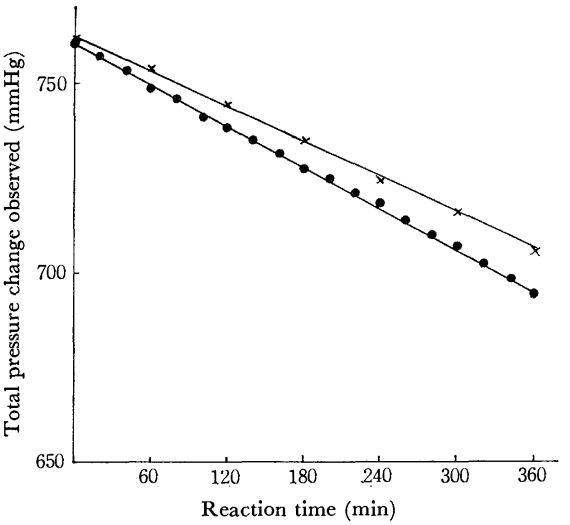

● : Experiment No. 8
× : Experiment No. 9

Fig. 3. Relation between total pressure in reaction system and time of reaction. (Reactants: C_3H_6 and H_2S)

It was reported by Egloff *et al.*[12] that the radical from ethylene in the electrical discharge was a vinyl radical, and that it was produced by breaking a carbon-hydrogen bond. Tsutsumi[13] reported that the vinyl radical was obtained by two molecular processes,[14] as is shown below. One of the present authors reported that the formation of acrylonitrile by the reaction of ethylene with hydrogen cyanide in the silent discharge may be observed by a combination of the vinyl radical and the cyano radical.[4] It has been reported by Hiraki[5] that the formation of the methyl vinyl ketone by a reaction between ethylene and methyl acetate in a silent discharge may be due to the combination of the vinyl radical and acetyl radical. Gorden and Ausloos[15] reported that the vacuum-ultraviolet photolysis of ethylene led essentially to three types of processes, as is indicated below.[16]

The mechanism of the formation of ethyl mercaptan, *n*-butyl mercaptan, ethyl dithioglycol, and diethyl sulfide by the reaction of ethylene with hydrogen sulfide may be represented as follows: The first step is the vibrational excitation of the ethylene molecule and the hydrogen sulfide molecule by electron impact,[17] while the second step consists of both (1) the reaction of the excited ethylene molecule with a normal ethylene molecule to give the vinyl radical and the ethyl radical,[14] and(2) the decomposition of the excited molecules to give the vinyl radical, the sulfhydryl radical, and the hydrogen atom. Ethyl mercaptan may be formed by three paths: (1) the combination of the ethyl radical (obtained by two molecular processes) and the sulfhydryl radical, (2) the reaction of the sulfhydryl radical with ethylene, and then the addition of a hydrogen atom to the $\dot{C}H_2$-CH_2SH radical so formed, and (3) the formation of vinylthiol[18] or ethylene sulfide[19] by the combination of the vinyl radical and the sulfhydryl radical, and then the addition of hydrogen atoms to the compounds thus obtained. The formation of acetylene, 1,3-butadiene, and 1-butene may show the existence of the vinyl radical. Further, it seems that ethane, *n*-butane, and 1-butene are obtained by the use of the ethyl radical. The formation of *n*-butyl mercaptan may be presented as follows:

$$CH_2{=}CH_2 + \cdot SH \longrightarrow \dot{C}H_2{-}CH_2SH$$

$$CH_2{=}\dot{C}H + \cdot SH \longrightarrow CH_2{-}CH_2 \quad (\text{S bridge})$$

$$CH_2{-}CH_2\ (\text{S bridge}) + H_2S \longrightarrow \dot{C}H_2{-}CH_2SH + \cdot SH$$

$$\dot{C}H_2{-}CH_2SH + C_2H_4 \longrightarrow \dot{C}H_2{-}(CH_2)_3SH$$

$$\dot{C}H_2{-}(CH_2)_3SH + H_2S \longrightarrow CH_3{-}(CH_2)_3SH + \cdot SH$$

Ethyl dithioglycol may be formed by the addition of the sulfhydryl radical to the $\dot{C}H_2$–CH_2SH radical. The formation of diethyl sulfide may proceed by two paths: (1) the reaction between vinylthiol or ethylene sulfide and the hydrogen atom, the addition of the $CH_3CH_2S\cdot$ radical thus obtained to ethylene and then the reaction of the $CH_3CH_2SCH_2\dot{C}H_2$ radical and the hydrogen atom, and (2) the reaction of the ethyl mercaptan, once formed, with ethylene to give the diethyl sulfide.[20]

The Mechanism of the Formation of the Main Products Obtained by the Reaction of Propylene and Hydrogen Sulfide. The formation of the main products obtained by the reaction of propylene and hydrogen sulfide in a silent discharge is thought to proceed by a mechanism similar to that proposed for the reaction between ethylene and hydrogen sulfide. The process consists of both (1) the reaction of the excited propylene molecule with a normal propylene molecule to give 2-methylvinyl, isopropenyl, allyl, propyl, and isopropyl radicals,[21] and (2) the decomposition of the excited propylene or hydrogen sulfide to give 2-methylvinyl, isopropenyl, allyl,

12) C. L. Thomas, C. Egloff, and J. C. Morell, *Chem. Rev.*, **28**, 1 (1941).

13) S. Tsutsumi, *Kagaku Kogyo*, **16**, 623 (1965).

14) $CH_2{=}CH_2 + e^* \longrightarrow CH_2{=}CH_2^* + e$
$CH_2{=}CH_2^* + CH_2{=}CH_2 \longrightarrow CH_2{=}\dot{C}H + CH_3\dot{C}H_2$

15) R. Gorden, Jr., and P. Ausloos, *J. Chem. Phys.*, **47**, 1799 (1967).

16) $C_2H_4^* \longrightarrow C_2H_2 + H_2$
$C_2H_4^* \longrightarrow C_2H_3 + H$
$C_2H_4^* \longrightarrow C_2H_2 + 2H$

17) Although ion-molecular process are possible in some electron-impact reactions, in the present case this process does not seem to be the main path, judging from the results presented by Devins *et al.*, Inoue,[2] and Egloff *et al.*[12] The present reaction is presumed to be mostly a radical reaction. (J.C. Devins and M. Burton, *J. Amer. Chem. Soc.*, **76**, 2618 (1954).)

18) Stacey *et al.* reported the preparation of vinylthiols by the X-ray-initiated addition of hydrogen sulfide to mono- and disubstituted acetylenes at room temperature, and it has been reported by Oae that vinylthiol is more stable than thioaldehyde. (F. W. Stacey and J. F. Harris, Jr., *J. Amer. Chem. Soc.*, **85**, 963 (1963); S. Oae, "Chemistry of Organic Sulfur Compounds," Kagakudojin, Kyoto (1968), p. 103.)Strausz *et al.* found that irradiation by a medium-pressure mercury arc lamp of mixtures of hydrogen sulfide and acetylene or methylacetylene in quartz reaction cells at −78° C gave good yields of vinyl mercaptan and 2-methylvinyl mercaptan respectively. (O. P. Strausz, T. Hikida, and H. E. Gunning, *Can. J. Chem.*, **43** (3), 717 (1965).)

19) It was reported by Strausz *et al.* that, when a photo-chemical reaction between ethylene or propylene and carbonyl sulfide was carried out, the corresponding vinylthiols, such as vinyl mercaptan, methylvinyl mercaptan, and propenethiol, and the corresponding cyclic compounds, such as ethylene sulfide, and propylene sulfide, were formed. Furthermore, they reported that the following steps must be considered for the primary reaction:

$$S(^1D) + \text{olefin} \longrightarrow \begin{cases} [C{-}C]^{**} \ (\text{S bridge}) \\ [C{=}C{-}SH]^{**} \\ S(^3P) + \text{olefin}^* \\ [C{=}C{-}CH_2{-}SH]^{**} \end{cases}$$

(O. P. Strausz and H. E. Gunning, *J. Amer. Chem. Soc.*, **84**, 4080 (1962); H. A. Wiebe, A. R. Knight, O. P. Strausz, and H. E. Gunning, *ibid.*, **87**, 1443 (1965).)

20) The free radical addition of thiols to olefin under irradiation with gamma rays has been investigated by Fontijn and Spinks, and by Araki. They found that the corresponding sulfides were formed as the main products. (A. Fontijn and J. W. J. Spinks, *Can. J. Chem.*, **35**, 1384, 1397, 1410 (1957); K. Araki, *Nippon Kagaku Zasshi*, **81**, 807 (1960).) It has been reported by Bach that the processes induced by the discharge reaction are similar to those induced by radiolysis. (N. Bach, *Chem. Eng. Progr.*, **51**, 478 (1955).)

21) $CH_2{=}CH{-}CH_3 + e^* \longrightarrow C_3H_6^* + e$
$C_3H_6^* + CH_2{=}CH{-}CH_3 \longrightarrow$

$$\begin{cases} \dot{C}H{=}CH{-}CH_3 \\ CH_2{=}\dot{C}{-}CH_3 \\ CH_2{=}CH{-}CH_2\cdot \end{cases} + \begin{cases} CH_3{-}CH_2{-}CH_2\cdot \\ CH_3{-}\dot{C}H{-}CH_3 \end{cases}$$

and sulfhydryl radicals, and a hydrogen atom.[22] The formation of *n*-propyl mercaptan may be represented by the same mechanism as the formation of ethyl mercaptan in the case of ethylene. In the case of the reaction between propylene and hydrogen sulfide, vinylthiols ($CH_3CH{=}CHSH$ and $CH_3C(SH){=}CH_2$) or propylene sulfide ($CH_3{-}CH\overset{S}{\diagdown\!\diagup}CH_2$) may be formed by the combination of the 2-methylvinyl radical or the isopropenyl radical and the sulfhydryl radical.

Isopropyl mercaptan may be formed by two paths: (1) A hydrogen atom adds preferentially to the terminal carbon atom of propylene to form the isopropyl radical,[23] and the radical thus produced yields isopropyl mercaptan. (2) This compound is obtained by the addition of hydrogen atoms to vinylthiols or propylene sulfide.

The dimeric products, such as 4-methyl-1-pentene, 2,3-dimethylbutane, 2-methylpentane, 1,5-hexadiene, 1-hexene, and *n*-hexane, may be formed by a recombination reactions between propyl, isopropyl, and allyl radicals.

22) $C_3H_6^* \longrightarrow \begin{cases} \dot{C}H{=}CH{-}CH_3 \\ CH_2{=}\dot{C}{-}CH_3 \\ CH_2{=}CH{-}CH_2\bullet \end{cases} + \bullet H$

$H_2S^* \longrightarrow \bullet SH + \bullet H$

23) Moore reported that, when the mercury-photosensitized hydrogenation of propylene was carried out over a range of temperatures from 30 to 200°C, a hydrogen atom was added to the terminal carbon atom of propylene to form the isopropyl radical. (W. J. Moore, *J. Chem. Phys.*, **16**, 916 (1948).)

NOTES

BULLETIN OF THE CHEMICAL SOCIETY OF JAPAN, VOL. 45, 280—281(1972)

The Mass Spectra of *N,N'*-Diarylpiperazines

Fukiko YAMADA, Yasuyoshi FUJIMOTO, and Tomihiro NISHIYAMA

Department of Applied Chemistry, Faculty of Engineering, Kansai University, Senriyama, Suita, Osaka

(Received January 6, 1971)

In a previous paper, we reported on the preparation of *N,N'*-diarylpiperazines, which have a substituent, a *p*-methyl or *p*-chloro group, on the benzene ring.[1] Mass spectrometric data will now be reported for *N,N'*-diphenylpiperazine (I, R=H), *N,N'*-di-*p*-tolylpiperazine (II, R=CH_3), and *N,N'*-di-*p*-chlorophenylpiperazine (III, R=Cl). By the use of metastable-ion measurements, the major fragmentation pathways of the three compounds, I, II, and III, have been deduced.

The mass spectral data of the compounds are shown

Table 1. Mass spectral data of the compounds, I, II, and III

Compound I			Compound II			Compound III		
m/e	Ion composition[a]	Rel. int. (%)	*m/e*	Ion composition	Rel. int. (%)	*m/e*	Ion composition	Rel. int. (%)
238	$C_{16}H_{18}N_2$	79	266	$C_{18}H_{22}N_2$	89	306	$C_{16}H_{16}N_2Cl_2$	57
223	$C_{15}H_{15}N_2$	14	251	$C_{17}H_{19}N_2$	26	291	$C_{15}H_{13}N_2Cl_2$	3
196	$C_{14}H_{14}N$	10	224	$C_{16}H_{18}N$	13	264	$C_{14}H_{12}NCl_2$	6
132	$C_9H_{10}N$	40	146	$C_{10}H_{12}N$	49	166	C_9H_9NCl	39
119	C_8H_9N	21	133	$C_9H_{11}N$	29	153	C_8H_8NCl	12
105	C_7H_7N	100	119	C_8H_9N	100	139	C_7H_6NCl	100
104	C_7H_6N	39	118	C_8H_8N	34	138	C_7H_5NCl	41
91	C_7H_7	19	105	C_8H_9	23	125	C_7H_6Cl	16
78	C_6H_6	11	92	C_7H_8	23	111	C_6H_4Cl	26
77	C_6H_5	53	91	C_7H_7	60			

a) The high-resolution mass spectra of these compounds gave correct composition of all ions mentioned in the table, within the error of ±5 millimass units.

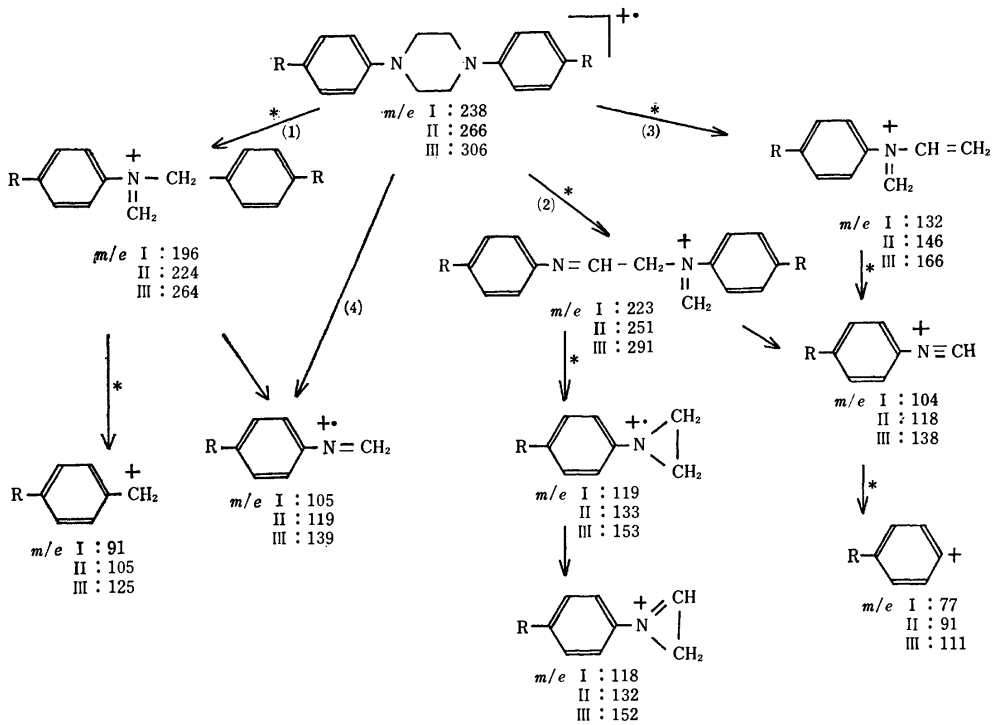

* Asterisks denote the processes for which metastable transitions were observed.

Scheme 1. The major fragmentation paths of the compounds.

1) F. Yamada, T. Nishiyama, M. Kinugasa, and M. Nakatani, This Bulletin, **43**, 3611 (1970).

in Table 1, while the major fragmentation paths are shown in Scheme 1.

The molecualr ions produce a prominent peak and are usually the second most abundant ion in the spectra of the compounds. The base peaks are at masses 105, 119, and 139 respectively, and are due to $R-C_6H_4N-CH_2^{+}\cdot$. These ions result from the elimination of the $R-C_6H_4\dot{C}H_2$ radical from the intermediate ion, $(R-C_6H_4)_2\overset{+}{N}CH_2CH_2$, (Path 1 in Scheme 1) or from the retro-Diels-Alder decomposition of the molecular ion (Path 4). This decomposition will be a dominating process in the formation of the $R-C_6H_4\overset{+\cdot}{N}CH_2$ ion:

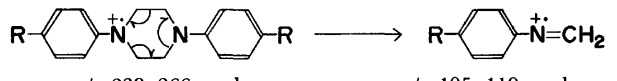

m/e 238, 266, and 306 → *m/e* 105, 119, and 139

In the case of Compound I, the metastable transition indicates that the above ion can also be formed by another route, one which involves the loss of C_2H_2 from the $C_9H_9N^{+}\cdot$ ion with the mass of 131. Thus, the fragmentation pathways of I are rather more complex than those of II and III. However, all three compounds, I, II, and III, give very similar pathways, as is shown in Scheme 1.

The metastable transitions and exact mass measurements indicate the following results.

Path (1), Giving m/e 196, 224, and 264. These fragments are generated directly from the molecular ion by the loss of a C_2H_4N radical. The probable fragmentation mechanism is indicated by the following diagram:

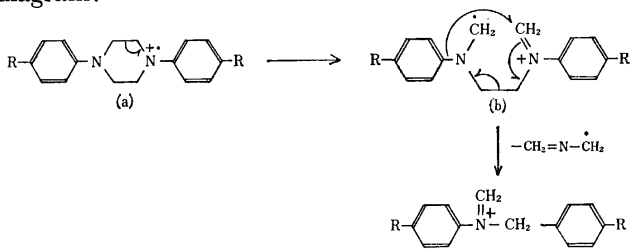

m/e 196, 224, and 264

The ring cleavage of the molecular ion as in **a** and the subsequent rearrangement with the transfer of the *N*-bonded aryl group, as is shown in **b**, afforded the fragment ion.

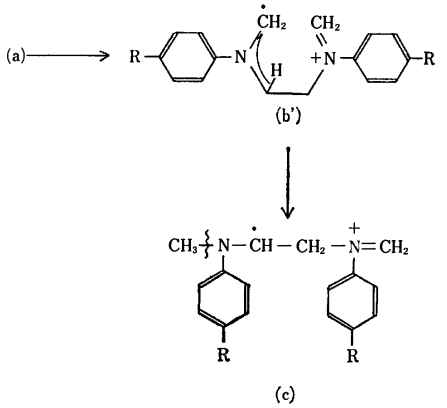

Path (2), Giving m/e 223, 251, and 291. These ions are produced from the molecular ion by the loss of the respective methyl radicals.

The rearrangement with the transfer of a hydrogen atom, as is shown in **b'**, followed by the loss of the species from **c**, gives the fragment ions.

The ions at the masses of 119, 133, and 153 can be formed by the loss of the $R-C_6H_4NCH$ radical from *m/e* 223, 251, and 291 respectively, while the ions at *m/e* 104, 118, and 138 may also be formed by the expulsion of the $R-C_6H_4NC_2H_4$ fragment from the same point of origin. It is thought that this fragmentation process is due to a one- or two-electron shift, as is shown below:

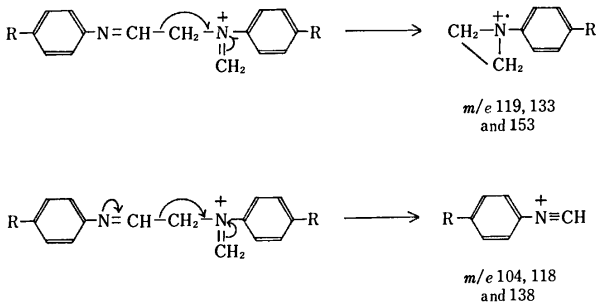

m/e 119, 133 and 153

m/e 104, 118 and 138

Path (3), Giving m/e 132, 146, and 166. These ions are produced by the loss of the $R-C_6H_4NCH_3$ radicals from the respective molecular ions.

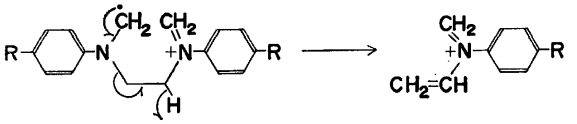

m/e 132, 146, and 166

As has been described above, in the mass spectra of the three compounds, I, II, and III, there are four principal modes of fragmentation of the molecular ion:

(1) Aryl rearrangement (Path 1)
(2) Loss of a methyl radical (Path 2)
(3) Loss of a $R-C_6H_4NCH_3$ radical (Path 3), and
(4) retro-Dieles-Alder decomposition (Path 4).

This fragmentation behavior of the compounds resembles that of piperazine and its derivatives,[2] but the M−1 ions were not observed, as expected, in the *N,N'*-diarylpiperazines.

Experimental

The high-resolution mass spectra were obtained with a Japan Electron Optics Co., Ltd., JMS-O1SG mass spectrometer. Accurate mass values were obtained from the photoplate by means of a JMA-1C Automatic Data analyzer. The metastable-ion transitions were determined by scanning the accelerating voltage, as has been described in the literature.[3]

2) H. Budzikiewicz, C. Djerassi, and D. H. Williams, "Mass Spectrometry of Organic Compounds," Holden-Day, San Francisco (1967), p. 321.

3) J. H. Futrell, K. R. Ryan, and L. W. Sieck, *J. Chem. Phys.*, **43**, 1832 (1965).

BULLETIN OF THE CHEMICAL SOCIETY OF JAPAN, VOL. 45, 282—283(1972)

The Formation Constants of Some Metal Thiobenzoato- and Thioacetato-Complexes in Dioxane-Water Solvent

Akira OUCHI, Toshio TAKEUCHI, Yoshiaki TAKAHASHI, and Mitsuhisa NAKATANI

Department of Chemistry, College of General Education, The University of Tokyo, Komaba, Meguro-ku, Tokyo

(Received January 27, 1971)

Recently the metal complexes of sulfur-containing ligands have been actively studied and many papers have been published. However, only a few data about their stability in the solution state have been obtained because of their low solubilities in water or their instabilities in a solution due to solvolytic decomposition.

Monothiocarboxylic acid is one of the most interesting sulfur-containing ligands, and solid metal complexes of monothio-benzoic acid have recently been synthesized and investigated by several authors.[1-3] Although they are insoluble in water, some of them are soluble in a 60% dioxane-water solution. Therefore, it seemed that it would be interesting to obtain their formation constant data.

The nickel(II), cobalt(II), manganese(II), zinc(II), and iron(II) complexes of thiobenzoic acid as well as thioacetic acid were investigated. When the copper(II) salt was mixed with the thiocarboxylic acid, an insoluble copper(I) complex has precipitated immediately. In the run using cadmium(II) salt, the equilibrium was not obtained even after it had stood 2 hr; after that turbidity was observed in the solution. Consequently, the formation constants of neither copper(II) nor cadmium(II) complexes were obtained.

Experimental

Materials. The 1,4-dioxane was a G. R. reagent of the Wako Chemical Co., Ltd., and was used after being purified according to the directions of Riddich and Toops.[4] The thiobenzoic acid and thioacetic acid used were G. R. reagents of the Tokyo Kasei Chemical Co., Ltd., while the other chemicals used were G. R. reagents of the Wako Chemical Co., Ltd.; they were used without any further purification.

General Procedure. The techniques employed were those of Calvin.[5] A Toa Denpa Co. model HA-5A pH meter, a glass electrode, and a saturated calomel electrode were used. All the measurements were made at 30.0±0.1°C. Each run was repeated 4 times, and the average values were used for the calculations.

The Measurement of the Acid-dissociation Constants. 30 ml of dioxane, 5 mmol of potassium nitrate, and 1 mmol of thiocarboxylic acid were diluted to 50 ml with water.[6] The sample was titrated with a 1.000N sodium hydroxide standard aqueous solution. From the reading of the pH meter of the half-neutralized point (B), the pK_D (where K_D is the acid dissociation constant) was obtained by the Uitert's equation, $pK_D=B+(\log U_H^0+\log 1/\gamma)$ (where U_H is a conversion factor obtained by the diagram of the authors).[7]

The Measurement of Formation Constants of the Complexes. 30 ml of dioxane, 4 mmol of potassium nitrate, 1 mmol of nitric acid, 0.1 mmol of metal nitrate (the sulfate was used in the cases of iron(II) salt), and 1 mmol of the ligand were mixed and diluted to 50 ml with water. The sample solution was left in a thermostat bath more than 3 hr in order to attain the equilibrium state. The titration of the sample was done over a 6 hr period after the dissociation in order to avoid the effect of the decomposition of the solute.

No precipitation was found during the ($n<2$) process. The calculation of the formation constants was done as has been described by Calvin,[5] Uitert,[7-9] and Goldberg.[10]

Results and Discussion

A typical run of the data and the results of the calculation are shown in Table 1. The acid dissociation constants obtained and the formation constants of their complexes are shown in Table 2.

Generally, the thiobenzoates are slightly more stable than the thioacetates of the corresponding metals.

TABLE 1. TITRATION OF 60% DIOXANE-WATER SOLUTION OF NICKEL NITRATE (2.00×10^{-2}M), THIOBENZIOC ACID (2.00×10^{-2}M), POTASSIUM NITRATE (8.00×10^{-3}M), AND NITRIC ACID (2.00×10^{-3}M) WITH STANDARD AQUEOUS SOLUTION OF SODIUM HYDROXIDE (1.00N)

NaOH (ml)	B	$\bar{n}$	p(Ch$^-$)
1.050	3.96	0.54	4.30
1.100	4.20	1.00	4.09
1.150	4.40	1.44	3.91
1.200	4.65	1.91	3.69

B: Reading of the pH meter standardized with aqueous buffer.
(Ch$^-$): Mole concentration of the monovalent chelate anion Ch$^-$.
$\bar{n}$: The number of the coordinated ligand molecules per one metal ion.

1) V. V. Savant, J. Gopalakrishnan, and C. C. Patel, *Inorg. Chem.*, **9**, 748 (1970).
2) G. A. Melson, N. P. Crawford, and B. J. Geddes, *ibid.*, **9**, 1123 (1970).
3) G. A. Melson, P. T. Greene, and R. F. Bryan, *ibid.*, **9**, 1116 (1970).
4) J. A. Riddich and E. E. Toops, Jr., "Organic Solvents," 2nd Ed., Interscience Publ., London (1955), p. 371.
5) M. Calvin and K. W. Wilson, *J. Amer. Chem. Soc.*, **67**, 2003 (1945).
6) As the sample was titrated with a sodium hydroxide aqueous solution, each calculation was carried out using the U_H^0 (conversion factors) and values of each dioxane concentration, assuming that the total volume was obtained by the addition of the two. In these regions, the difference of $(U_H^0+\log 1/\gamma)$ per 1% difference in the dioxane concentration is about 0.02. In Table 2, the concentration of dioxane is abbreviated to 60%, even though the precise values at 60% are expected to be in the range of ±0.02.
7) L. G. V. Uitert and W. C. Fernelius, *J. Amer. Chem. Soc.*, **76**, 5887 (1954).
8) L. G. V. Uitert and C. G. Haas, *ibid.*, **75**, 451 (1953).
9) L. G. V. Uitert, C. G. Haas, W. C. Fernelius, and B. E. Douglas, *ibid.*, **75**, 455 (1953).
10) D. E. Goldberg, *J. Chem. Educ.*, **40**, 341 (1963).

Table 2. The dissociation constants and the formation constants of metal complexes of thiobenzoic acid and thioacetic acid in 60% dioxane[6] at 30°C

	Thiobenzoic acid		Thioacetic acid	
	$\log K_1$	$\log K_2$	$\log K_1$	$\log K_2$
H	-7.3_4		-7.6_1	
Mn(II)	4.1	3.5	4.1	3.5
Fe(II)	4.3	3.8	4.2	3.8
Co(II)	4.3	3.9	4.0	3.5
Ni(II)	4.3	3.9	4.1	3.6
Zn(II)	5.4	4.5	4.8	4.1

The formation constants of manganese(II), iron(II), nickel(II), and cobalt(II) were almost all the same, but that of the zinc(II) complex was a little higher, when the ligand acid was the same. According to Savant,[1] in the nickel(II) and zinc(II) complexes of thiobenzoic acid, the ligand acts as the bidentate and coordinates to the central metal *via* oxygen as well as *via* the sulfur atom of the ligand. Although the complexes of some of the metals used in this experiment have not yet been obtained in the solid state, they are expected to be in almost a very similar form in the solution. These complexes may be solvetad by dioxane, as in the case of pyridine adduct shown by Melson.[2] In the calculations, however, it is assumed that the thiocarboxylic acid will coordinate far more strongly than dioxane. According to Yamasaki,[11] the formation constants of nickel(II) and zinc(II) benzoate in an aqueous solution are slmost the same. On the other hand, Yamasaki,[12] Leussing,[13] and Freiser[14] have reported that zinc(II) makes a more stable complex than does nickel(II) when the ligand bonds to the central metal with charged sulfur.

Therefore, from these results, it seems that the sulfur atom of the thiocarboxylato complexes of these metals is likely to bond to the central metal even in a solution.

The authors wish to thank Professor Yukichi Yoshino and their colleagues for their helpful discussions.

11) M. Yasuda, K. Yamasaki, and H. Ohtaki, This Bulletin, **33**, 1067 (1960).
12) K. Suzuki and K. Yamasaki, *J. Inorg. Nucl. Chem.*, **24**, 1093 (1962).
13) D. L. Leussig, *J. Amer. Chem. Soc.*, **80**, 4180 (1958).
14) G. E. Shevy, H. Freiser, and Q. Fernando, *ibid.*, **81**, 2611 (1959).

BULLETIN OF THE CHEMICAL SOCIETY OF JAPAN, VOL. 45, 283—285(1972)

An NMR Study of Metal Complexes Containing Acetylacetone and Related Compounds. II. The Preparation and Structure of Mixed Cobalt(III) Complexes Containing Acetylacetone and Amino Acids

Yuki Fujii and Toshio Ejiri

Department of Chemistry, Ibaraki University, Bunkyo-cho, Mito, Ibaraki

(Received May 7, 1971)

Many reports have been published on the NMR spectra of tris-type β-diketonatocobalt(III) complexes.[1-3] Recently, bis-type acetylacetonatocobalt(III) complexes have also been prepared. Their NMR spectra have been studied and their geometrical isomers assigned.[4-8]

In this paper, we will report the preparations of mixed cobalt(III) complexes containing one molecule of the acetylacetone anion and two molecules of the amino acid anion, and will discuss the relation between the structures of mono-type acetylacetonatocobalt(III) complexes and their NMR spectra.

1) R. C. Fay and T. S. Piper, *J. Amer. Chem. Soc.*, **84**, 2023 (1962); **85**, 500 (1963).
2) R. C. Fay and T. S. Piper, *Inorg. Chem.*, **3**, 875 (1964).
3) J. P. Collman and J. Y. Sun, *ibid.*, **4**, 1273 (1965).
4) L. J. Boucher and J. C. Bailar, Jr, *J. Inorg. Nucl. Chem.*, **27**, 1093 (1765).
5) R. D. Archer and B. P. Cotsoradis, *Inorg. Chem.*, **4**, 1584 (1965).
6) B. P. Cotsoradis and R. D. Archer, *ibid.*, **6**, 800 (1967).
7) R. J. York. W. D. Bonds, Jr., B. P. Cotsoradis, and R. D. Archer, *ibid.*, **8**, 789 (1969).
8) L. J. Boucher and N. G. Paeg, *ibid.*, **9**, 418 (1970).

Experimental

Preparation of the Complexes. *1)* cis(N)cis(O)-*Bisglycinatoacetylacetonatocobalt(III) Monohydrate*, cis(N) cis (O)-[*Co(gly)$_2$(acac)*]·H_2O *(I)*: Sodium dinitrobisacetylacetonatocobalt (III)[4] (8.0 g, 0.014 mol) was dissolved in 200 m*l* of water, and then methanol (40 m*l*), glycine (2.0 g, 0.027 mol) neutralized with potassium hydroxide (0.86 g) in 30 m*l* of water, and activated charcoal (2.0 g) were added to the solution in this order. The mixture was heated at about 70°C for ten minutes, the activated charcoal was filtered off, and the filtrate was concentrated to about 40 m*l*; the trisacetylacetonatocobalt(III) thus deposited was then filtered off. When acetone (100 m*l*) was added to the filtrate, reddish-purple crystals were separated out. They were subsequently recrystallized from 33% acetone. Yield, about 1.5 g (32%). Found: C, 35.23; H, 5.65; N, 9.00%. Calcd for $C_9H_{15}CoN_2O_6\cdot H_2O$: C, 35.07; H, 5.57; N, 9.09%.

2) cis(N)trans(O)-*Bisglycinatoacetylacetonatocobalt(III) Monohydrate*, cis(N)trans(O)-[*Co(gly)$_2$(acac)*]·H_2O *(II)*: Trisacetylacetonatocobalt(III) (3.6 g, 0.01 mol) was dissolved in 200 m*l* of methanol. Glycine (1.5 g, 0.02 mol) neutralized with potassium hydroxide (1.2 g) in 50 m*l* of water and

activated charcoal (1.0 g) were added, and the mixture was heated at about 60°C for fifteen minutes. The activated charcoal was then filtered off, and the filtrate was concentrated to about 30 ml by evaporating the solvent under reduced pressure. When acetone (100 ml) was added to the solution, reddish-purple crystals were separated out. (These crystals were a 1: 2 mixture of *cis(N)cis(O)* and *cis(N)trans(O)* isomers.) The crystals were dissolved in 50 ml of water, and the solution was concentrated slowly by evaporating the solvent to about 25 ml. When the solution was allowed to stand for a day, only the *cis(N)trans(O)* isomer was separated out. The crystals were subsequently washed with water and methanol. Yield, about 0.5 g (15%). Found: C, 35.12; H, 5.37; N, 9.25%. Calcd for $C_9H_{15}CoN_2O_6 \cdot H_2O$: C, 35.07; H, 5.57; N, 9.09%.

3) cis(N)trans(O)-*Bis*-L-*alaninatoacetylacetonatocobalt(III) Dihydrate*, cis(N)trans(O)-$[Co(\text{L-}ala)_2(acac)] \cdot 2H_2O$ *(III)*: This complex was prepared by the same method as was the complex I. Yield, about 2.0 g (40%). The reaction between trisacetylacetonatocobalt(III) and L-alanine also gave only the *cis(N)trans(O)* isomer. Yield, about 1.2 g (33%). Found: C, 37.35; H, 6.68; N, 7.89%. Calcd for $C_{11}H_{19}CoN_2O_6 \cdot 2H_2O$: C, 37.29; H, 6.56; N, 7.91%.

4) Potassium Bis(acetylacetoneglyciniminato)cobalt(III) Tetrahydrate, trans(N)-$K[Co(acacgly)_2] \cdot 4H_2O$ *(IV)*: A solution of 19.5 g of cobalt(II) chloride hexahydrate in 20 ml of water was added to a solution of 12 g of acetylacetone neutralized with potassium hydroxide (6.6 g) and 17.8 g of glycine in 100 ml of water. The mixed solution was oxidized with a hydrogen peroxide solution and then warmed at 50—60°C for one hour. The solution was concentrated under reduced pressure to a volume of 30 ml; the trisacetylacetonatocobalt(III) and potassium chloride thus deposited were then filtered off. When the resulting solution was cooled to 0°C, reddish-brown crystals were separated out. They were recrystallized from water. Yield, about 4.0 g (10%). Found: C, 35.23; H, 5.52; N, 5.94%. Calcd for $C_{14}H_{18}CoN_2O_6 \cdot 4H_2O$: C, 35.00; H, 5.47; N, 5.83%.

Measurements. The IR spectra were recorded with a Hitachi EPI-S2 infrared abosrption spectrophotometer by using the potassium bromide disk. The visible and ultraviolet abosorption spectra were measured with a Hitachi EPS-3 spectrophotometer in water. The NMR spectra were recorded with a Hitachi R-20 spectrometer (60 MHz) at 35°C. The spectra were measured with about a 5—10% solution of deutrated water by using NaTMS as the internal reference.

Results and Discussion

Infrared Absorption Spectra. The main bands of the IR spectra are listed in Table 1. All the complexes show an asym. ν_{COO} band between 1630 and 1680 cm^{-1}, and $\nu_{C=C}$ and $\nu_{C=O}$ (and $\nu_{C=N}$ for the complex IV) bands between 1500 and 1570 cm^{-1}. Thus, we can conclude that all the carboxylate groups of the amino acid in Complexes I to IV are coordinated to the cobalt(III) ion,[9] and also that the acetylacetonate anions are chelated to the cobalt(III) ion.[10] Complexes I, II, and III give the bands of ν_{NH_2} and δ_{NH_2}, but Complex IV does not. Therefore, in the case of Complex IV, the formation of the Schiff-base between acetylacetone and glycine is confirmed.

Table 1. Infrared absorption spectra (in cm^{-1})

Complex	NH_2 str.	COO asym. str.	NH_2 bend.	C=C str.	C=O str.
I	3260 3140	1675 1640	1586	1566	1512
II	3280 3150	1670 1640	1586	1565	1515
III	3250	1665 1637	1595	1567	1525
IV		1630		1592	1502 (C=N str.)

Table 2. Visible and ultraviolet absorption spectra (in $c/s \times 10^{-13}$)

Complex	ν_{max} (log ε)	ν_{sh} (log ε)	ν_{max} (log ε)
I	55.6 (2.19)	78.8 (2.37)	92.2 (3.61)
II	56.7 (2.22)	78.8 (2.46)	92.0 (3.59)
III	57.1 (2.02)	78.8 (2.30)	92.0 (3.57)
IV	47.5 (1.77) (sh), 57.4 (2.47)		90.6 (3.97)

Electronic Absorption Spectra. The numerical values of the electronic absorption spectra are listed in Table 2. The first abosrption bands of Complexes I, II, and III appear at about 56×10^{13} c/s, and their positions are nearly equal to those of the bisglycinatooxalatocobalt(III) complexes.[11] Since the first bands of Complexes I, II, and III show no splitting, these complexes can be assigned to the *cis(N)*-form structure.

Complex IV, on the other hand, shows a split first absorption band; therefore, a *trans(N)*-form structure can be assigned to this complex.

NMR Spectra. The NMR spectra of the complexes are shown in Figs. 1 and 2, while their numerical values are listed in Table 3.

From these NMR spectra, it can be concluded that Complexes I and II have *cis(N)cis(O)* and *cis(N)trans(O)* forms respectively. Moreover, it can be concluded that Complex III has the *cis(N)trans(O)* form. In the cases of the bisglycinatocobalt(III) complexes, it is confirmed that the *cis(N)cis(O)* isomer shows a CH_2 signal constructed of two peaks, while the *cis(N)trans(O)* isomer gives one peak.[11] Also it is shown that the difference between the *cis(N)cis(O)* and *cis(N)trans(O)* structures is more clearly distinguished by the methyl signals of the acetylacetonate group.

Complex IV shows one C=CH, one CH_2, and two CH_3 peaks with relative intensities of 1: 2: 3: 3. This

Table 3. PMR spectra (in τ)

Complex	C=CH	CH_2		CH_3(acac)	
I	4.22	6.45 6.65		7.71 7.92	
II	4.30	6.34		7.92	
III	4.25	5.91 6.03 6.15	CH(ala)	7.93 8.43 8.55	CH_3(ala)
IV	5.39	6.50		7.58 8.33	

9) T. Sakaguchi and K. Ueno, "Metal Chelates," Vol. II, Nankodo, Tokyo (1963), p. 43.

10) K. Nakamoto, P. J. MacCarthy, A. Ruby, and A. E. Martell, *J. Amer. Chem. Soc.*, **83**, 1066 (1961).

11) N. Matsuoka, J. Hidaka, and Y. Shimura, This Bulletin, **40**, 1868 (1967).

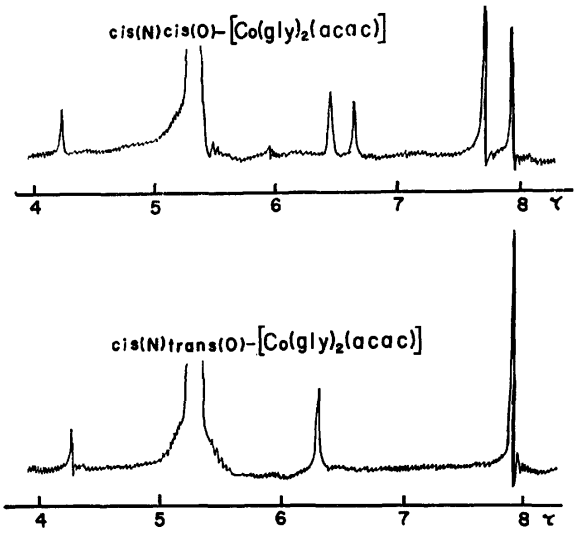

Fig. 1. PMR spectra of the complexes.

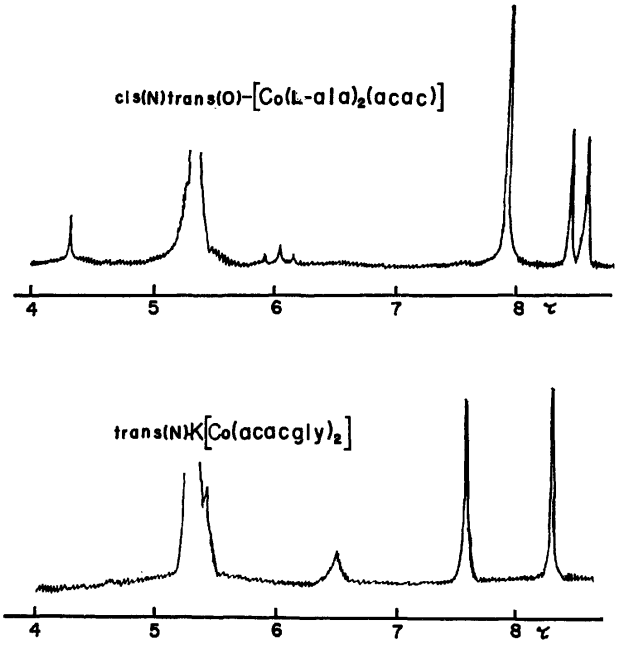

Fig. 2. PMR spectra of the complexes.

spectral pattern clearly implies that Complex IV is a Schiff-base complex in which acetylacetone and glycine are condensed. This fact has also been confirmed by studying the IR spectrum. It is assumed that the formation of the schiff-base complex may be the cause of the difficulty of preparing the *trans(N)cis(O)* isomer.

BULLETIN OF THE CHEMICAL SOCIETY OF JAPAN, VOL. 45, 285—286(1972)

The El Reaction of Menthyl and Neomenthyl Tosylates in Aprotic Solvents

Masatomo NOJIMA, Masakatsu YOSHIMURA, and Niichiro TOKURA
Department of Applied Chemistry, Faculty of Engineering, Osaka University, Suita

(Received May 11, 1971)

The El reaction has been studied, especially in protic solvents, in relation to the S_N1 reaction.[1] In contrast to the insistence of Ingold[2] that the intermediates of the S_N1 and El reactions were the same, and that there was no solvent effect upon the ratio of the afforded olefin and the replaced product, Winstein[3] established that an elimination from the intimate ion pair occurred in the solvent with a low ionizing power:

$$RX \rightleftharpoons R^{\oplus}X^{\ominus} \rightleftharpoons R^{\oplus}//X^{\ominus} \overset{Y^{\oplus}}{\rightleftharpoons} RY + X^{\ominus}$$

$$\downarrow \text{intimate ion pair} \qquad \downarrow \text{solvent separated ion pair}$$

olefin olefin

Chart 1

We examined the El reactions of menthyl and neomenthyl tosylates in dimethylsulfoxide (DMSO), dimethylformamide (DMF), acetonitrile, methylene chloride, and 1,2-dichloroethane respectively in hopes of clarifying the effects of the aprotic solvents upon the rates and to obtain insight into the mechanism of this reaction.

The first-roder rate constants are tabulated in Table 1, along with the derived values of the thermodynamic quantities, the enthalpy and entropy of activation, ΔH^{*} and ΔS^{*}. Although no linearity between the rates and the dielectric constants of the solvents was observed, the rate increased as the dielectric constants of the solvent increased. These results may be explained as follows: the use of solvents with high dielectric constants is advantageous for the ionization and dissociation of the substrate.[4]

The rate ratios between neomenthyl and menthyl tosylates in various solvents are summarized in Table 2. It has been suggested that the hydrogen participation in the ionization step of neomenthyl tosylate contributes to the large acetolysis rate ratio between neomenthy

1) C.K. Ingold, "Structure and Mechanism in Organic Chemistry," Second Edition, Cornell University Press (1969), p. 649.

2) K. A. Cooper, E. D. Hughes, and C. K. Ingold, *J. Chem. Soc.*, **1937**., 1280; E. D. Hughes and B. J. MacNulty, *ibid*,. **1937**; 1283 K. A. Cooper, E. D. Hughes, C. K. Ingold, and B. J. MacNulty, *ibid.*, **1948**, 2038.

3) M. Cocivera and S. Winstein, *J. Amer. Chem. Soc.*, **85**, 1702 (1963).

4) K. B. Wiberg, "Physical Organic Chemistry, " John Wiley & Sons, New York (1966), pp. 267, 381.

Table 1. Summary of rate constants

Compound	Solvent	Temp. °C	k, sec^{-1}	$\Delta H^{\ddagger}$ kcal/mol	$\Delta S^{\ddagger}$ e.u.
Menthyl	DMSO	90	1.09×10^{-4}		
OTs	DMSO	75	2.00×10^{-5}	28.7	2.1
	DMSO	60	2.78×10^{-6}		
	DMF	95	2.62×10^{-5}		
	DMF	85	6.56×10^{-6}		
	DMF	75	2.10×10^{-6}	31.1	4.3
	DMF[a]	60	2.46×10^{-7}		
	CH_3CN	95	2.6×10^{-5}		
	CH_3CN	85	7.63×10^{-6}		
	CH_3CN	75	2.06×10^{-6}	31.6	5.8
	CH_3CN[a]	60	2.38×10^{-7}		
	CH_2Cl_2	95	4.39×10^{-6}		
	CH_2Cl_2	85	1.38×10^{-6}		
	CH_2Cl_2	75	3.48×10^{-7}	31.6	2.4
	CH_2Cl_2[a]	60	4.32×10^{-8}		
	CH_2ClCH_2Cl	95	4.12×10^{-6}		
	CH_2ClCH_2Cl	85	1.13×10^{-6}		
	CH_2ClCH_2Cl	75	3.09×10^{-7}	32.3	4.1
	CH_2ClCH_2Cl[a]	60	3.54×10^{-8}		
Neomenthyl	DMF	60	3.73×10^{-5}		
OTs	DMF	45	6.93×10^{-6}	23.4	−8.8
	DMF	30	1.03×10^{-6}		
	CH_2Cl_2	60	9.71×10^{-7}		

a) Calculated from data at other temperatures.

Table 2. The rate ratios between neomenthyl and menthyl tosylate in the various solvents

Solvent	Rate ratio (II/I)
DMF	150
Methylene chloride	22
EtOH	99
AcOH	59

and menthyl tosylates.[5] The rate ratio in the reaction in DMF was 150, while in methylene chloride it was 22. These results suggest that the hydrogen paticipation does not play an important role, at least in the reaction in methylene chloride.

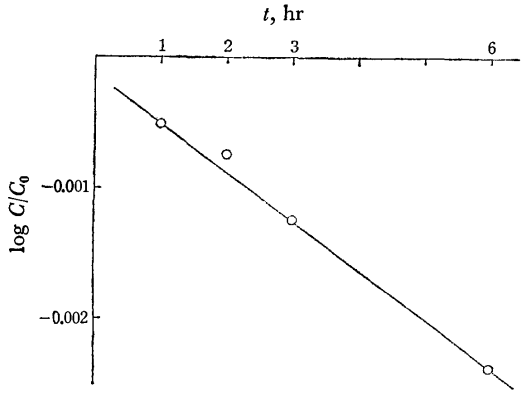

Fig. 1. Isomerization of I to II.
C_0: initial concentration of I. C: concentration of I at time t.

An isomeric change in the configuration of the substrate was found in the reaction in DMF. The E1 reaction of menthyl tosylate in DMF at 75°C, followed by the reduction of the reaction mixture by lithium amide, led to the isolation of neomenthol, olefins, and menthol. From the relationship of log C/C_0 to the reaction time (Fig. 1), the rate of the isomerization of menthyl tosylate to neomenthyl tosylate was estimated to be 2.38×10^{-7} sec^{-1}, which is one order of magnitude smaller than the rate of the olefin formation (2.10×10^{-6} sec^{-1}). The neomenthyl derivative was not detected in the reaction mixtures obtained by reactions in any other solvents except DMF.

Experimental

Materials. DMSO and DMF were purified by drying them over calcium hydride, and they were distilled under diminished pressure. Acetonitrile was purified by the method of Coetzee *et al.*[6] Methylene chloride and 1,2-dichloroethane was dried over calcium chloride and distilled. Menthyl tosylate was obtained by following the method of Winstein;[4] mp 92.2—93.3°C (lit, 93.5—94.0[4]). Neomenthyl tosylate was prepared from neomenthol with tosyl chloride; mp 62.5—63.9°C[7] (lit, 63.0—63.5°C).

Kinetic Procedure. The rates were measured by using glass tubes which could be closed by means of a polyethylene cap. The thermostats were of a conventional design and maintained the temperature within±0.05°C. The reaction mixtures were prepared from the known weight of a solute and from the solvent volumetrically. The reactions were followed by withdrawing ampoules from the thermostat at suitable intervals and by titrating them with a sodium acetate-methanol solution, using bromophenol blue as the indicator.

The Reaction in DMF. The reaction of menthyl tosylate (300 mg) was performed in the presence of two equivalent moles of lutidine in 20 m*l* of the solvent at 75°C. The reaction mixture was poured into ice water, extracted by petroleum ether, and dried over anhydrous sodium sulfate. After the evaporation of the solvent, the reaction mixture was reduced with five equivalent moles of lithium amide in ammonia at 70°C for 4 hr. The reaction mixture was hydrolysed by aq. hydrochloric acid, extracted by ether, and dried over anhydrous sodium sulfate. After the evaporation of the solvent, the products were analyzed by means of a Hitachi K-53 vpc apparatus, equipped with a flame-ionization detector on a PEG 6000 column operated at 180°C.

The Reduction of Menthyl Tosylate.[8] Into a lithium amide-ammonia solution prepared by dissolving 0.8 g (0.05 mol) of lithium in 100 m*l* of ammonia, we added 1.6 g (0.005 mol) of menthyl tosylate dissolved in 10 m*l* of ether. After four hours methanol was added and the mixture was extracted with ether. Then the reaction mixture was treated and analyzed as has been described above; only menthol was present.

5) S. Winstein, B. K. Morse, E. Crunwald, H. W. Jones, J. Corse D. Trifan, and H. Marshall, *J. Amer. Chem. Soc.*, **74**, 1127 (1952).

6) J. F. Coetzee, G. P. Cunningham, D. K. McGuire, and G. R. Padmanabhan, *Anal. Chem.*, **34**, 1139 (1962).

7) W. Hückel, H. Feltkamp, and S. Geiger, *Ann. Chem.*, **637**, 1 (1960).

8) W. G. Dauben and J. Z. Chitwood, *J. Amer. Chem. Soc.*, **92**, 1624 (1970).

BULLETIN OF THE CHEMICAL SOCIETY OF JAPAN, VOL. 45, 287—288(1972)

The Jacobsen Reaction and the Acid-Catalyzed *Ortho-para* Interconversion of Iodoanisoles and Iodophenetoles

Hitomi SUZUKI and Michie YOSHIDA

Department of Chemistry, Faculty of Science, Kyoto University, Sakyo-ku, Kyoto

(Received June 1, 1971)

o-Iodoanisole and *p*-iodoanisole are unstable when brought into contact with sulfuric acid and readily undergo disproportionation to yield 2,4-diiodoanisole.[1] Similarly behave both *o*- and *p*-iodophenetoles, giving 2,4-diiodophenetole in a high yield. Such intermolecular iodo migration is usually referred to as the Jacobsen reaction. When a small amount of *o*- or *p*-iodoanisole is dissolved in sulfuric acid, an intense dark brown color develops, which persists over a period of many days. Dilution of the solution with acetic acid or water, however, causes disappearance of this color and the formation of the iodoanisolesulfonic acid. The deep-colored solution has the iodinating power, but the diluted colorless solution has not. In contrast, *m*-iodoanisole is merely sulfonated to give *m*-iodoanisolesulfonic acid, and the solution neither becomes colored nor possesses the iodinating property.

Several inorganic iodo compounds are known, when dissolved in sulfuric acid, to give deep-colored solutions which contain stable positive iodine (I_3^+ or I_5^+) or multivalent iodine (IO^+ or IO_2^+), and possess the strong iodinating power.[2] In this connection, it seems interesting to examine the intermediate species which is responsible for such an easy intermolecular transfer of the iodine atom in the Jacobsen reaction of iodoanisoles. Being brought into solution, *o*- or *p*-iodoanisole develops at first green, then yellow color, which gradually deepens to yellow brown, and finally to dark brown or black. Within several hours after preparation, both solutions from *o*- and *p*-iodoanisole showed the same ultraviolet absorption (λ_{max}, 205, 227, 238—239 *sh*,[3] 281, 410 *sh*, and 438 nm), and this spectral pattern remained unchanged for days. When a bsaic hydrocarbon such as mesitylene was added to these systems, decoloration soon took place and the formation of iodomesitylene was observed at the time of the disappearance of characteristic color. With a weaker base such as *o*-dichlorobenzene or sterically crowded 1,2,4,5-tetraisopropylbenzene, however, such decoloration was not observed. The solution diluted with acetic acid or water contained neither elementary iodine nor iodic acid, so the possible role of the positive iodine or the multivalent iodine for these coloration was ruled out. The spectral pattern of the above solutions differs from the spectra of the any known inorganic iodo compounds dissolved in sulfuric acid,[2] but resembles the spectrum which is superposition of the spectra of anisolesulfonic acid and the benzenonium complex[4] (Fig. 1). Thus the absorption band in the visible region is thought to be due to the stable σ-complex (for example, I) formed by the addition of sulfur trioxide and stabilized through the conjugative delocalization of positive charge by methoxyl group. Then, the intermolecular transfer of iodine atom would probably proceed through the nucleophilic attack of a more basic substrate upon the iodine atom of this intermediate (Scheme 1).

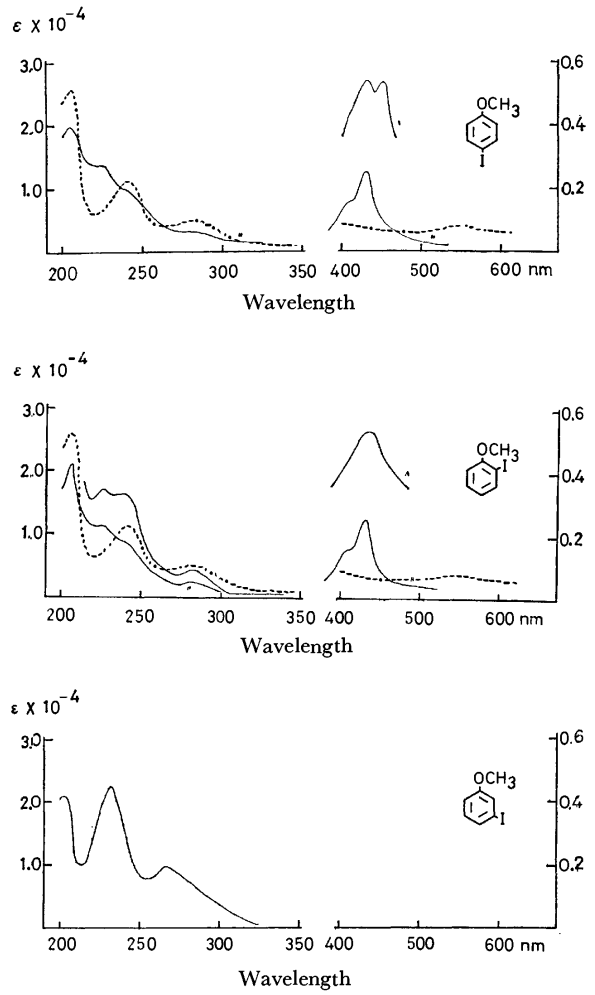

Fig. 1. Absorption curves of iodoanisoles in concentrated sulfuric acid.
Solid line: A. Immediately after dissolution.
B. Several hours later.
Dotted line: After a month's standing.

Intermolecular iodo migration is of some synthetic value. Polyalkylbenzenes can be successfully iodinated by the transfer of iodine atom from *o*-iodoanisole on

1) H. Suzuki and R. Goto, This Bulletin, **36**, 389 (1963); *Nippon Kagaku Zasshi*, **84**, 284 (1963).

2) J. Arotsky and M. C. R. Simons, *Quart. Rev.* (London), **16**, 282 (1962); J. Arotsky, H. C. Mishra, and M. C. R. Simons, *J. Chem. Soc.*, **1962**, 2582.

3) The suffix *sh* denotes shoulder.

4) G. A. Olah and P. R. Schleyer, "Carbonium Ions", Vol. 1, Interscience, London (1968), p. 180.

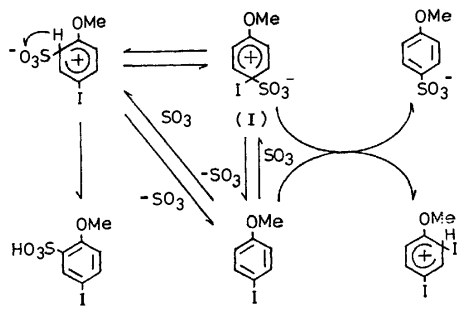

Scheme 1

addition of sulfuric acid.[5] Isomer distribution of the iodination products obtained by the crossed Jacobsen reaction of *o*-iodoanisole with toluene, ethylbenzene, isopropylbenzene, and *t*-butylbenzene is summarized in Table 1. The results clearly indicate the electrophilic nature and the bulkiness of the attacking species.

TABLE 1. ISOMER DISTRIBUTION OF THE PRODUCTS OBTAINED BY THE CROSSED JACOBSEN REACTION OF *o*-IODOANISOLE WITH SOME ALKYLBENZENES

Alkylbenzene	Isomer distribution (%)			
	ortho	*meta*	*para*	1/2 *ortho*-*para* ratio
Toluene	59	a)	41	0.72
Ethylbenzene	41	1	58	0.35
Isopropylbenzene	22	2	76	0.14
t-Butylbenzene	4	0	96	0.02

a) Not determined due to ill resolution from *o*- and *p*-isomers.

Interestingly, *o*- and *p*-iodoanisoles were found to be interconversible in the presence of small amounts of sulfuric acid. This facile isomerization was carried out, agitating the light petroleum solution of each isomer with about 10% weight of sulfuric acid for several hours at room temperature. The relative amount of both isomers in the equilibrium mixture varied to some extent depending on the experimental conditions employed, but the *p*-isomer was always predominant ($o/p=0.32$—0.43). In no case, *m*-isomer was detected, which excludes the intramolecular 1,2-shift process of the isomerization. The present observation is probably the first example of the protogenic acid-catalyzed isomerization of haloanisoles.[6]

The reaction probably involves deiodination and the concurrent rapid reiodination *via* the intermediate I. The interconversion might also be formulated as the intramolecular rearrangement of iodine atom from ortho to para and *vice-versa* through the π-complex. However, the mechanism which involves the iodination of iodoanisoles to 2,4-diiodoanisole, followed by displacement of either one of iodine atoms in the latter seems less probable, since the diiodoanisole was found to be comparatively stable under the same condition.

The reasonable explanation for the lack of iodine migration in *m*-iodoanisole is that the electrophilic attack could hardly occur at the *m*-position where the iodine atom occupies owing to the unfavorable positional condition relative to the methoxyl group, as a result the detachment of the iodine atom as positively-charged species is depressed and *m*-iodoanisole is merely converted to sulfonic acid. The absence of disproportionation with the iodo compounds bearing electron-attracting group[7] or bulky group[8] is probably due to either the difficulty of the formation of the intermediate ion such as I, or the steric hindrance to the S_N2 type intermolecular iodine transfer. Similar disproportionation was observed during the acid hydrolysis of some *o*-iodoacetanilides, which will be described elsewhere.

Experimental

Iodoanisoles (*o*, bp 113—114°C/14 mmHg; *m*, bp 113—114°C/16.5 mmHg; *p*, mp 50—51°C) and iodophenetoles (*o*, bp 126—127°C/16 mmHg; *p*, mp 28—29°C, bp 133—134°C/19 mmHg) were prepared from the corresponding anisidines and phenetidines, respectively. Ultraviolet spectra were measured in 98% sulfuric acid solutions on a Hitachi EPS-300 spectrophotometer and a Shimadzu QV-50 spectrophotometer. The product analysis was performed on a Hitachi Model 063 gas chromatograph using a capillary column coated with Apiezon Grease L.

Jacobsen Reaction of Iodoanisoles and Iodophenetoles. A typical procedure is as follows: A mixture of *o*-iodophenetole (12.4 g) and sulfuric acid (10 g) was stirred at room temperature for 2 hr. The dark thick mixture was diluted with excess of water and the oily precipitate was extracted with ether. The ethereal solution was evaporated and the residue was passed over a column of alumina. Elution with light petroleum, followed by recrystallization from the same solvent gave 2,4-diiodophenetole as white prisms, mp 46—47°C. Yield, 7.7 g (82%). *p*-Iodophenetole gave the same product in somewhat less yield. IR (Nujol): 799, 871, 925, 1042, 1113, 1149, 1242, and 1278 cm^{-1}: PMR (CCl_4): 8.54 (Me, t, $J=7.2$ Hz), 6.00 (CH_2O, q, $J=7.2$ Hz), 3.55 (Aromatic H, d, $J=8.8$ Hz), 2.54 (Aromatic H, q, $J=8.8$ and 1.8 Hz), and 2.03 τ (Aromatic H, d, $J=1.8$ Hz).

Found: C, 25.94; H, 2.19%. Calcd for $C_8H_8I_2O$: C, 25.70; H, 2.16%.

Similarly, *o*- and *p*-iodoanisole gave 2,4-diiodoanisole, mp 68—69°C, in 75—76% yield. IR (Nujol): 800, 872, 1037, 1146, 1187, 1245, 1263, and 1278 cm^{-1}: PMR (CCl_4): 6.14 (MeO, s), 3.48 (Aromatic H, d, $J=8.4$ Hz), 2.48 (Aromatic H, q, $J=8.4$ and 2.4 Hz), and 1.99 τ (Aromatic H, d, $J=2.4$ Hz).

Found: I, 70.73%. Calcd for $C_7H_6I_2O$: I, 70.52%.

5) H. Suzuki, T. Sugiyama, and R. Goto, This Bulletin, **37**, 1858 (1964).

6) Iodophenetoles have been shown to behave similarly. There are several instances known in which the apparent intramolecular bromine shift has been observed during the demethylation of bromoanisoles in the presence of hydrobromic acid. However, these results rather belong to the well-documented isomerization of bromophenols. *Cf.* G. R. Pettit and D. M. Piatak, *J. Org. Chem.*, **25**, 721 (1960), and other papers cited therein.

7) H. Suzuki and R. Goto, *Nippon Kagaku Zasshi*, **84**, 284 (1963).

8) H. Suzuki, K. Nakamura, and R. Goto, This Bulletin, **39** 128 (1966).

BULLETIN OF THE CHEMICAL SOCIETY OF JAPAN, VOL. 45, 289—291(1972)

Reaction of Iodobiphenyls and Iodonaphthalenes with Concentrated Sulfuric Acid. Attempted Extension of the Jacobsen Reaction to Polycyclic Systems

Hitomi SUZUKI and Naotaka YAMAMOTO

Department of Chemistry, Faculty of Science, Kyoto University, Sakyo-ku, Kyoto

(Received June 1, 1971)

In contact with concentrated sulfuric acid, aromatic iodo compounds undergo disproportionation to give higher iodo derivatives. The reaction has been known as the Jacobsen reaction,[1] but its synthetic possibility has received little attension. In some previous papers,[2] we have reported that such disproportionation of aromatic iodo compounds can be used for one-step preparation of certain polyiodobenzene derivatives, which otherwise require lengthy laborious procedure to obtain. Now the reaction has been attempted to extend to the titled polycyclic iodo compounds with the initial aims to define the scope of its synthetic utility as well as to obtain, if possible, previously unknown higher iodo derivatives. Only several triiodo and tetraiodobiphenyls have so far been recorded in literature.[3] No data have been appeared on the preparation of polyiodonaphthalenes containing more than three iodine atoms, with the exception of a recent note that a trace amount of 1,2,3-triiodo and 1,2,3,4-tetraiodonaphthalene was formed in the photolysis of *o*-bis(iodoethynyl)benzene.[4] No product from the sulfonation of the titled compounds seems to have been adequately characterized before.

Treatment of 1-iodonaphthalene with excess of sulfuric acid at room temperature, followed by dilution with water gave a small amount of reddish-brown pasty solid, chromatography of which on alumina using light petroleum as eluant gave a small amount of 1,4-diiodonaphthalene. Yield was usually below 5% and most part of the starting material went into solution as sulfonic acid. The amount of sulfuric acid relative to iodo compound could be varied over a wide range without any significant improvement on the yield of the diiodo product. The change in temperature from room temperature up to 70°C had no effect on the results. Some elementary iodine was liberated at elevated temperature. From the aqueous part, a sulfonic acid was obtained and identified as 4-iodonaphthalene-1-sulfonic acid by comparison with the authentic specimen. On similar treatment, 2-iodonaphthalene was readily sulfonated to give a mixture of sulfonic acids in which 7-iodonaphthalene-1-sulfonic acid and 6-iodonaphthalene-2-sulfonic acid were the main components, the former being predominant. No disproportionation product could be obtained.

4-Iodobiphenyl reacted with sulfuric acid more readily than did 1-iodonaphthalene, giving some 4,4′-diiodobiphenyl as disproportionation product. Yields varied from nearly zero to 8% depending on the conditions employed. Most part of the starting material was converted to sulfonic acid. Similar treatment of 2- and 3-iodobiphenyls merely gave 4′-sulfonic acids. The orientation of sulfo group in these acids was established through the conversion to iodobiphenylsulfonamides, followed by the reductive removal of iodine atom with aqueous ammonia and zinc dust leading to 4-biphenylsulfonamide. Since iodine atom would deactivate the ring in which it is located, the sulfo group has probably entered at the most reactive 4′-position of another ring.

Although the above results delimit the possible use of the Jacobsen reaction for the preparation of the higher iodo compounds, they still seem to provide some information to understand the process of iodine transfer. A sulfur trioxide will add to the substrate to form either the complex I in which the hydrogen atom at the attacking site may migrate to oxygen to give a sulfonic acid III, or the complex II in which the iodine atom may be transferred to the second molecule *via* S_N2 attack on the iodine atom to yield a higher iodo compound. This interpretation is consistent with the findings that only 1-iodonaphthalene and 4-iodobiphenyl which have the iodine atom at the most favorable position for electrophilic attack under go disproportionation. Since the sulfonic acids derived from these compounds are stable in contact with sulfuric acid, a role of the protonated sulfonic acid IV as a possible iodinating species is less probable. 2-Iodonaphthalene will direct the bulky sulfo group to 6 and 8-positions, while 2- and 3-iodobiphenyls are subject to the preferential attack at 4′-position of the unsubstituted ring. Therefore, the inability of these compounds to undergo rearrangement is attributed to the unfavorable structural condition for electrophilic attack at the position where iodine atom occupies.

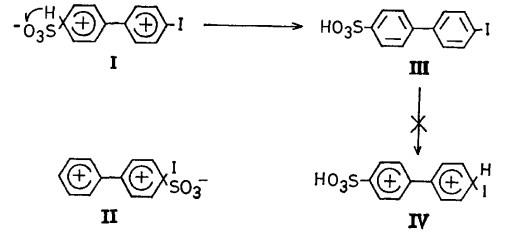

As a parallel study to disproportionation, some effort has been made to iodinate iodobiphenyls and iodo-

1) H. J. Shine, "Aromatic Rearrangement" Elsevier, London (1967), p. 28; H. Cerfontain, "Mechanistic Aspects in Aromatic Sulfonation and Desulfonation," Interscience, London (1968), p. 221.

2) H. Suzuki and R. Goto, This Bulletin, **36**, 389 (1963); *Nippon Kagaku Zasshi*, **84**, 167, 284 (1963).

3) H. Oikawa, *Nippon Kagaku Zasshi*, **84**, 272 (1963); R. B. Sandin, *J. Org. Chem.*, **34**, 456 (1969).

4) I. D. Cambell and G. Egliton, *J. Chem. Soc., C*, **1968**, 2120.

Table 1. Physical properties of some sulfonyl chlorides and sulfonamides derived from iodobiphenyls and iodonaphthalenes

	Mp (°C)	IR spectra[a] (cm^{-1})	Found (%) C	Found (%) H	Calcd (%) C	Calcd (%) H
Sulfonyl Chlorides						
4-Iodonaphthalene-1-sulfonyl chloride	123—124	663, 754, 819, 863, 1131, 1159, 1181, 1199, 1360, 1494, 1550	33.9	1.8	34.0	1.7
6-Iodonaphthalene-2-sulfonyl chloride	138—139	668, 806, 943, 1072, 1165, 1378, 1617	34.2	1.7	34.0	1.7
7-Iodonaphthalene-1-sulfonyl chloride	166—168	680, 744, 813, 832, 1136, 1171, 1176, 1195, 1366, 1492, 1578, 1616	34.1	1.7	34.0	1.7
2-Iodobiphenyl-4-sulfonyl chloride	148—150	686, 769, 808, 1000, 1163, 1373, 1474, 1592	38.1	2.2	38.1	2.1
3-Iodobiphenyl-4-sulfonyl chloride	98—100	687, 786, 835, 1077, 1170, 1367, 1461, 1581	38.2	2.2	38.1	2.1
4-Iodobiphenyl-4-sulfonyl chloride	145—146	770, 809, 1000, 1168, 1373, 1592	38.3	2.2	38.1	2.1
Sulfonamides						
4-Iodonaphthalene-1-sulfonamide	211—213	678, 767, 902, 1138, 1158, 1328, 1501, 1554	36.2	2.6	36.0	2.4
6-Iodonaphthalene-2-sulfonamide	231—232	690—700, 798, 870, 940, 1068, 1124, 1137, 1330, 1562, 1613	35.9	2.4	36.0	2.4
7-Iodonaphthalene-1-sulfonamide	234—237	678, 814, 828, 1080, 1132, 1158, 1327, 1334, 1578, 1621	35.8	2.6	36.0	2.4
2′-Iodobiphenyl-4-sulfonamide	200—204	754, 1096, 1155, 1331, 1460	40.3	2.9	40.1	2.8
3′-Iodobiphenyl-4-sulfonamide	162—163	690, 779, 1096, 1153, 1163, 1330	40.2	3.0	40.1	2.8
4′-Iodobiphenyl-4-sulfonamide	254—256	771, 809, 1000, 1158, 1310, 1337	38.0	2.9	40.1	2.8

a) Principal peaks in 650—2000 cm^{-1} region.

naphthalenes with iodine-periodic acid[5] in order to obtain the reference compounds as well as to know the substitution pattern in these systems. So far, very little information is available on the direct iodination of these compounds except 4-iodobiphenyl, which has been readily converted to 4,4′-diiodobiphenyl in the presence of iodine and suitable oxidizing agent.[6]

1-Iodonaphthalene underwent slow iodination to give mainly 1,4-diiodonaphthalene with a little of 1,5-diiodo isomer. 2-Iodonaphthalene reacts quite slowly to give a mixture of diiodonaphthalenes in a low yield, and infrared spectrum of which proved the major component to be 2,6-diiodonaphthalene. Appreciable amounts of amorphous substances are formed as by-product. None of these diiodonaphthalenes could be iodinated further.

The direct iodination of iodobiphenyls took place more readily than did iodonaphthalenes. 2-Iodobiphenyl gave a mixture of diiodobiphenyls, while 3-iodobiphenyl yielded a diiodobiphenyl and a triiodobiphenyl, relative ratio of these products depending on the amounts of the reagent and length of reaction time. Electrophilic substitution in biphenyl has been known to occur mainly at 4 and 4′-positions, since the transition states are stabilized most effectively when attacking species is attached to these positions. Thus, the major products which would result from the iodination of 2-iodobiphenyl are thought to be 2,4′- and 2,4-diiodobiphenyls, while the products from 3-iodobiphenyl can be formulated as 3,4′-diiodobiphenyl and 3,4,4′-triiodobiphenyl, respectively. 4-Iodobiphenyl gave only 4,4′-diiodobiphenyl in high yield. The iodine atom could not be introduced into 2 or 2′-position even with the use of large excess of the reagent under the conditions employed.

Experimental

Authentic iodonaphthalenesulfonic acids and diiodonaphthalenes were mostly obtained by replacement of amino group in aminonaphthalenesulfonic acid or naphthylamine by iodine, respectively. Infrared spectra were measured in KBr disc, unless otherwise stated, with a JASCO DS-402G spectrophotometer.

General Procedure for the Jacobsen Reaction. A typical procedure is as follows: 1-Iodonaphthalene (5 g) and sulfuric acid (10 g) were placed in a small stoppered flask and then stirred magnetically at 20—30°C for 5 hr. The mixture was diluted with water and the oily solid (*ca.* 0.4 g) was extracted with light petroleum and chromatographed on alumina using the same solvent as eluant. Colorless prisms (0.3 g, mp 85—110°C)[7] were obtained from early eluates and identified as

5) H. Suzuki, K. Nakamura, and R. Goto, This Bulletin, **39**, 128 (1966). Also *cf.* H. Suzuki, "Organic Syntheses," Vol. 51, in press (1971).

6) A. N. Novikov, *Zh. Obshch. Khim.*, **29**, 58 (1959); H. O. Wirth, O. Königstein, and W. Kern, *Ann. Chem.*, **634**, 84 (1960); T. A. Khalimova and A. N. Novikov, *Probl. Poluch. Poluprod. Prom. Org. Sin., Akad. Nauk SSSR, Otd. Obshch. Tekh. Khim.*, **1967**, 82.

7) Some isomeric impurity, possibly 1,5-diiodonaphthalene, might be responsible for the wide melting range of the disproportionation product.

1,4-diiodonaphthalene by infrared spectral comparison with the authentic sample (lit,[8] mp 109—110°C). IR: 743, 775, 808, 942, 1129, 1239, and 1378 cm^{-1}.

Found: I, 67.0%. Calcd for $C_{10}H_6I_2$: I, 66.8%.

The aqueous part was carefully neutrallized with sodium carbonate and the precipitated sodium sulfonate was collected by filtration, dried, and treated with phosphorus pentachloride to give *4-iodonaphthalene-1-sulfonyl chloride*, which was recrystallized from carbon tetrachloride and melted at 123—124°C. On heating with aqueous ammonia, the chloride was converted into *4-iodonaphthalene-1-sulfonamide*, mp 211—213°C.

Physical properties of sulfonyl chlorides and sulfonamides obtained from the reaction of iodonaphthalenes and iodobiphenyls are summarized in Table 1.

Iodination of Iodobiphenyls. Iodine (10.2 g) was added to a mixture of 2-iodobiphenyl (14 g), periodic acid dihydrate (4.56 g), and 80% acetic acid (120 m*l*) containing small amount of sulfuric acid as catalyst, and the mixture was stirred at 70—80°C for 6 hr. Upon cooling, an oily deposit was taken up into light petroleum, washed with aqueous sodium hydrogen sulfate to remove the unchanged iodine, dried, and distilled under reduced pressure to give diiodobiphenyl (19.1 g) as a pale yellow syrup, bp 164—165°C/2 mmHg, which was presumably a mixture of *2,4'- and 2,4-diiodobiphenyls*, the former being predominant. IR: 752, 820, 998, and 1006 cm^{-1}. Found: C, 35.3; H, 2.0%. Calcd for $C_{12}H_8I_2$: C, 35.5; H, 2.0%.

By a similar procedure, 3-iodobiphenyl gave *3,4'-diiodobiphenyl* (mp 75—77°C, IR: 771, 827, and 1003 cm^{-1}. Found: C, 35.4; H, 2.0%. Calcd for $C_{12}H_8I_2$: C, 35.5; H, 2.0%), together with some *3,4,4'-triiodobiphenyl* (mp 114—116°C, IR: 800, and 995 cm^{-1}. Found: C, 27.5; H, 1.6%. Calcd for $C_{12}H_7I_3$: C, 27.1; H, 1.3%). 4-Iodobiphenyl gave *4,4'-diiodobiphenyl* (mp 210—211°C, IR (Nujol), 802, 996, and 1068 cm^{-1}. Found: C, 35.1; H, 1.8%. Calcd for $C_{12}H_8I_2$: C, 35.5; H, 2.0%).

Iodination of Iodonaphthalenes. 2-Iodonaphthalene (5.1 g) mixed with 80% acetic acid (30 m*l*) containing small amount of sulfuric acid as catalyst was treated with iodine (2.6 g) and periodic acid dihydrate (1.14 g) at 70—80°C for 20 hr. The reaction proceeded quite slowly and gave a dark pasty solid, which was taken up into light petroleum-benzene mixture and passed over a column of alumina to yield a low-melting solid substance (*ca.* 3.2 g) from early eluates and fine needles (0.3 g) from later eluates. The former was mainly composed of the unchanged starting material with a little of diiodonaphthalene. The latter product crystallized from ethanol as fine leaflets, mp 210—213°C, had the formula $C_{10}H_6I_2$ and was identified as impure 2,6-diiodonaphthalene on the basis of its high melting point (lit,[9] 203—204°C) and similarity of its infrared spectrum to 2,6-dichloronaphthalene. IR (Nujol): 813, 837, and 888 cm^{-1}. Found: C, 32.9; H, 1.7; I, 66.0%. Calcd for $C_{10}H_6I_2$: C, 31.5; H, 1.6; I, 66.8%.

Similar iodination of 1-iodonaphthalene led mainly to 1,4-diiodonaphthalene with some 1,5-diiodo isomer. The reaction was slow, but polymeric substance was not formed so much.

8) R. Meldola, *J. Chem. Soc.*, **47**, 522 (1885).

9) M. Janczewski and L. Prajer, *Rocz. Chem.*, **28**, 681 (1954).

BULLETIN OF THE CHEMICAL SOCIETY OF JAPAN, VOL. 45, 291—293(1972)

The Synthesis of Methyl 2,4,6-Tri-*O*-benzyl-α-D-glucopyranoside

Shinkiti KOTO, Yuko TAKEBE, and Shonosuke ZEN

School of Pharmaceutical Sciences, Kitasato University, Shirokane, Minato-ku, Tokyo

(Received June 12, 1971)

In synthetic carbohydrate chemistry, the partially benzylated derivative of sugar is, in general, used as an important intermediate.[1] This paper will deal with a facile method of preparing a new, partially-benzylated derivative of D-glucopyranose, methyl 2,4,6-tri-*O*-benzyl-α-D-glucopyranoside (I), directly from methyl α-D-glucopyranoside by means of a controlled benzylation.[2] Methyl α-D-glucopyranoside was very carefully heated below 110°C in benzyl chloride in the presence of sodium hydride (3.3 molar equiv.) to give a mixture of partially- as well as fully-substituted products. After chromatographic separation, the main product, I, was obtained as a distillable oily product with a high reproducible yield; it was fully characterized as crystalline *p*-nitrobenzoate and *p*-phenylazobenzoate. The results of the elemental analysis and the $\varepsilon_{258.5}^{\text{ethanol}}$ value[2] of I indicated the existence of three benzyl groups. The position with a free hydroxyl group was determined by the methylation; *i.e.*, I was converted into the known methyl 4,6-*O*-benzylidene-3-*O*-methyl-α-D-glucopyranoside[3] and 1,2,4,6-tetra-*O*-benzoyl-3-*O*-methyl-β-D-glucopyranose[4] respectively. Thus, the 3-OH of I was unsubstituted.

The high reactivity of the 6-OH and 2-OH of α-D-glucopyranoside compared with that of others is frequently observed[5] and has led to successful preparations of the 2,6-di-*O*-substituted derivative. By the way, the difference between the reactivity of 3-OH and that of 4-OH is usually small, and their order is rather variable according to circumstances. In certain cases, however, a significantly lower reactivity of 3-OH has been reported;[6] the present result may be another example of this.

After the hydrolysis of I, 2,4,6-tri-*O*-benzyl-1,3-di-*O*-

1) C. M. McCloskey, *Advan. Carbohyd. Chem.*, **12**, 137 (1957).
2) M. E. Tate and C. T. Bishop, *Can. J. Chem.*, **41**, 1801 (1963).
3) H. R. Bolliger and D. A. Prins, *Helv. Chim. Acta*, **28**, 465 (1945).
4) J. W. H. Oldham, *J. Amer. Chem. Soc.*, **56**, 1360 (1934).
5) J. M. Sugihara, *Advan. Carbohyd. Chem.*, **8**, 16 (1953).
6) P. Nánási, A. Lipták, and G. Nagy, *Acta Chim. Acad. Sci. Hung.*, **65**, 94 (1970).

Table 1. Physical data of compounds

Cpd. No.	R^1	R^2	Yield %	Mp °C (recryst. solv.)	Bp °C (mmHg)	n_D^{20}	$[\alpha]_D$ (conc.)	$\varepsilon_{258.5}^{EtOH}$	Formula	Elemental analyses Found: % Calcd: % C	H	N
I	CH_3	H	62	——	253—255 (0.002)	1.5582	67.1 (2.9)	598	$C_{28}H_{32}O_6$	72.20 72.39	7.10 6.94	— —
II	CH_3	Ac	88	——	247—249 (0.003)	1.5466	56.8 (1.7)	552	$C_{30}H_{34}O_7$	70.73 71.13	6.81 6.76	— —
III	CH_3	Pnb	>50	133—134 (PE; needles)	——	——	6.1 (2.1)	——	$C_{36}H_{35}NO_9$	68.13 68.50	5.65 5.75	2.22 2.28
IV	CH_3	Az	20	109.5—111 (NH; needles)	——	——	−32.0 (4.5)	——	$C_{41}H_{41}N_2O_7$	72.88 73.20	6.07 5.99	3.88 4.16
V	CH_3	CH_3	78	——	226—229 (0.002)	1.5482	60.4 (1.4)	533	$C_{29}H_{34}O_6$	72.42 72.78	7.16 7.16	— —
VI	Pnb	Pnb	35	247—148.5 (IPA; needles)	——	——	96.0 (1.1)	——	$C_{41}H_{36}N_2O_{12}$	65.61 65.79	4.82 4.85	3.70 3.74

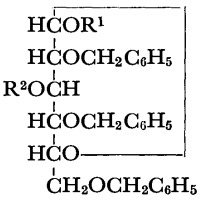

Ac=acetyl PE=petroleum ether
Az=*p*-phenylazobenzoyl NH=*n*-hexane
Pnb=*p*-nitrobenzoyl IPA=isopropyl alcohol

p-nitrobenzoyl-α-D-glucopyranose (VI) was obtained as fine crystals.

Experimental

Tlc was carried out by the use of Silica Gel G (Merck). The silica gel used for the column chromatography was the product of the Kanto Chemical Co. The PMR spectra were measured with Varian S-60T in $CDCl_3$, with TMS as the internal standard. The melting points were determined by means of a Yanagimoto micro-melting-point apparatus; uncorrected values are given. The specific rotation was measured in a 1-dm tube by means of an Atago Polux apparatus in $CHCl_3$ at 25±3°C.

Methyl 2,4,6-Tri-O-benzyl-α-D-glucopyranoside (I). A suspension of methyl α-D-glucopyranoside (5.0 g; 26 mmol) and sodium hydride (*ca.* 50% dispersion; 2.7 g; 2.2 molar equiv.) in freshly-distilled benzyl chloride (26 g; 8 molar equiv.) was cautiously heated at 104—105°C (the oil bath was maintained below 110°C) with very efficient stirring (magnetic) under anhydrous condition. When, after 1.5—2.5 hr, a sharp rising of the reaction temperature and a violent evolution of hydrogen gas began, the oil bath was removed at once and the reaction vessel was immersed in a cold-water bath. After the evolution of the gas had ceased, the vessel was carefully heated at 104—105°C for 2 hr. During the reaction, the mixture became a porous mass, and then it turned into a thin slurry. After cooling to room temperature, another portion of sodium hydride (1.5 g; 1.1 molar equiv.) was added to the mixture; the reaction was then continued at the same temperature overnight. The cooled mixture was filtered through a bed of Hyflo Super-Cel. The filtrate and the washings were combined and evaporated on a boiling-water bath under reduced pressure. A yellow sirup (17 g) was chromatographed on a column of SiO_2 (350 g), eluting it with a mixed solvent of benzene and 2-butanone (20: 1). The order of elution was as follows: a mixture of the dispersion oil, the remaining benzyl chloride and other non-carbohydrate by-products, the tetrasubstituted product, and the main product, I (7.4 g; 62%). I was used directly for the further reactions.

When the original benzylation reaction was continued with additional benzyl chloride (5 g) and sodium hydride (2 g) at 125°C, the perbenzylated glucoside[2] was formed quantitatively.

Methy 2,4,6-Tri-O-benzyl-3-O-methyl-α-D-glucopyranoside (V). I (2.0 g) was heated with methyl iodide (1.1 m*l*) in DMF (3.3 m*l*) in the presence of BaO (1.5 g) at 70—80°C for 3 hr.[7] A brief chromatography gave thin, colorless oil of V.

Methyl 4,6-O-Benzylidene-3-O-methyl-α-D-glucopyranoside. V was hydrogenated quantitatively by the use of palladium on carbon (5%) in methanol and then treated with benzaldehyde in the presence of $ZnCl_2$. Tlc showed the complete exhaustion of the hydrogenated material. Long needles (from diisopropyl ether; 84%). Mp 152—153°C, $[\alpha]_D^{24}$ 118.4° (*c* 2.5, $CHCl_2CHCl_2$). [Lit,[3] mp 150—151°C; $[\alpha]_D^{14}$ 119.5° (*c* 1.6, $C_2H_2Cl_4$)]. The PMR spectrum showed the benzylidene tertiary proton as a singlet at δ 5.56. (Found: C, 61.23; H, 6.91%.)

1,2,4,6-Tetra-O-benzoyl-3-O-methyl-β-D-glucopyranose. The above-mentioned hydrogenolyzed product was hydrolyzed with hot dilute hydrochloric acid and then subjected to neutralization, evaporation, and ordinary benzoylation. Colorless crystals (from methanol; 85%). Mp 203—204°C, $[\alpha]_D^{25}$ 2.5° (*c* 3.9, $CHCl_3$). The authentic sample had a mp of 200—202°C and $[\alpha]_D^{27}$ value of −2.3° (*c* 4.2, $CHCl_3$). [Lit,[4] mp 198—199°C; $[\alpha]_D$ 3.6° (*c* 4.94, $CHCl_3$)]. The mixed mp was 200.5—203.5°C. The IR (KBr) and PMR spectra of the two compound were superimposable. (Found: C, 68.25; H, 4.94%).

2,4,6-Tri-O-benzyl-1,3-di-O-p-nitrobenzoyl-α-D-glucopyranose (VI). I (1.03 g) was heated with aqueous mixed acid prepared from glacial acetic acid (11 m*l*) and sulfuric acid (2N, 2.9 m*l*) for 80 min on a boiling-water bath. After the addition of sulfuric acid (2N, 2.3 m*l*), the mixture was further heated for 9 hr. After neutralization, an oily product (1.27 g) was fractionated on a column of SiO_2 (20 g; benzene: 2-butanone=5: 1). After the recovery of the unchanged mate-

7) R. Kuhn, H. H. Baer, and A. Seeliger, *Ann. Chem.*, **611**, 236 (1958).

rial (0.44 g; 43%), a hydrolyzed product was eluted in a yield of 0.37 g (37%). This was treated with excess *p*-nitrobenzoyl chloride in pyridine. The crude residue thus obtained (95%) was crystallized with diethyl ether.

Spectral Data: I, ν_{max}^{film} (cm^{-1}): 3490, 3460 (OH), 3090, 3070, 3030, 3010, 1955, 1875, 1810, 1720, 1603, 1584, 1145, 739, 699 (benzyl); δ (ppm): 2.40 (1H, broad, exchangeable with D_2O; 3-OH), 3.37 (3H, singlet; *O*-CH_3), 3.43 (1H, quartet; H-2, $J_{1,2}=4.0$ Hz, $J_{2,3}=8.0$ Hz), 4.13 (1H, quartet; H-3, $J_{3,4}=10.0$ Hz). II, ν_{max}^{film} (cm^{-1}): 1746, 1233 (*O*-acetyl); δ (ppm): 1.99 (3H, singlet; *O*-acetyl), 3.43 (3H, singlet; *O*-CH_3), 3.54 (1H, quartet; H-2, $J_{2,3}=10.0$ Hz), 4.77 (1H, doublet; anomeric, $J_{1,2}=3.8$ Hz), 5.63 (1H, quartet; H-3, $J_{3,4}=8.0$ Hz). III, ν_{max}^{KBr} (cm^{-1}): 1729, 1523, 1349 (*p*-nitrobenzoyl). IV, ν_{max}^{KBr} (cm^{-1}): 1714, 1277 (ester). V, δ (ppm): 3.43 (3H, singlet; *O*-CH_3), 3.72 (3H, singlet; *O*-CH_3). VI, ν_{max}^{KBr} (cm^{-1}): 1731, 1529, 1347 (*p*-nitrobenzoyl). δ (ppm): 6.75 (1H, doublet; anomeric, $J_{1,2}=3.4$ Hz).

BULLETIN OF THE CHEMICAL SOCIETY OF JAPAN, VOL. 45, 293—294(1972)

The Synthesis of Silacyclopentane Derivatives

Tsunao ARAKI, Daiyo TERUNUMA, and Toshio FUSE

Department of Applied Chemistry, Faculty of Science and Engineering, Saitama University, Urawa

(Received June 22, 1971)

In the course of our studies of the reaction and polymerization of silacyclopentanes and -pentenes, 6-oxa-3-sila-1,3,3-trimethylbicyclo[3.1.0]hexane(I)[1], 1,3,3-trimethyl-3-silabicyclo[3.1.0]hexane(V), and 1,1,3-trimethyl-1-silacyclopentane(VI) were synthesized. Some of the reactions of I and the hydrogenation reaction of 1,1,3-trimethyl-1-silacyclopentene-3(IV)[2] were investigated.

Results and Discussion

Because of its high strain in the epoxy ring, I was found to be very reactive; the addition of even a small amount of aluminum chloride to I caused a violent reaction, giving a solid polymer. Furthermore, I was found to react with methanol at 50°C giving a mixture of new compounds, 1,1,3-trimethyl-4-methoxy-1-silacyclopentane-3-ol(II) and its isomer, 1,1,3-trimethyl-3-methoxy-1-silacyclopentane-4-ol(III).

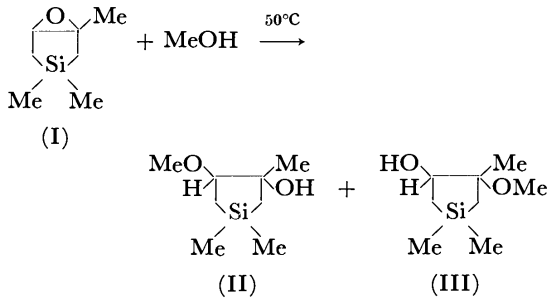

(I) (II) (III)

Under the same reaction conditions, other alcohols, such as ethanol, 1-propanol, and 1-butanol, and alkyl amines, such as methylamine and diethylamine, did not react with I. This lowering of the reactivity toward amines, in contrast with that of ordinary epoxy groups, may be explained in terms of the enhanced basisty of the carbon atomes next to oxygen caused by the electron-releasing effect of the CH_3Si- group. Now, we wish to report another successful synthesis of a new bicyclosilacyclopentane derivative, *i.e.*, 1,3,3-trimethyl-3-silabicyclo[3.1.0]hexane(V). This compound was synthesized by the method of carbene addition using the Simmons-Smith reagent.[3] The structural assignment was accomplished by the analysis of the IR and NMR spectra (IR spectrum; $-CH_2-$ in the cyclopropane ring, 3050 cm^{-1}; its skeletal vibration, 1010 cm^{-1}; NMR spectrum; the two singlets at τ=9.90 and 9.95 for (CH_3^a) (CH_3^b)Si- show that the silacyclopentane ring remains intact).

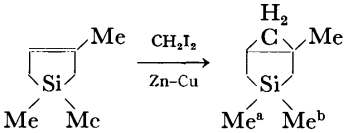

(IV) (V)

Another new compound, 1,1,3-trimethyl-1-silacyclopentane(VI) was also synthesized by hydrogenating IV in the presence of the Pd–C catalyst. In this reaction, when *n*-hexane was used as the solvent hydrogenation proceeded successfully and VI was obtained, but when

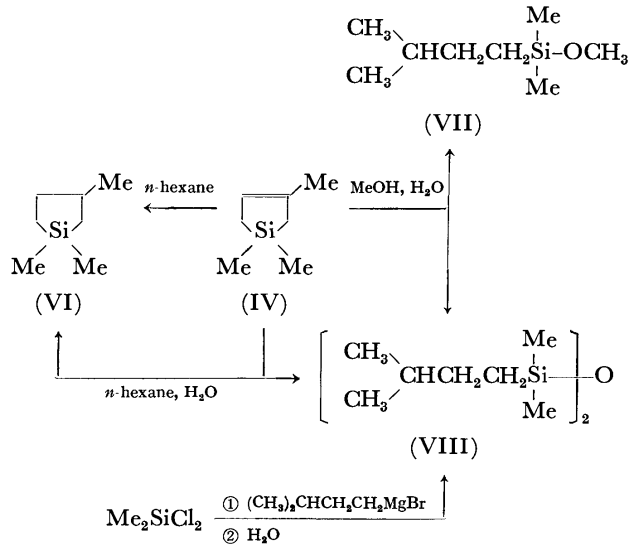

Scheme 1. Hydrogenation of IV using a Pd-C catalyst.

1) G. Manuel, P. Mazerolles, and J. G. Florence, *C. R. Acad. Sci. Paris, Ser. C*, **269**, 1553 (1969).

2) D. R. Weyenberg, L. H. Toporcer, and L. E. Nelson, *J. Org. Chem.*, **33**, 1975 (1968).

3) H. E. Simmons and R. D. Smith, *J. Amer. Chem. Soc.*, **81**, 4256 (1959).

methanol was used in place of *n*-hexane, only a ring-opening product, dimethylisopentylmethoxysilane(VII), was found in the reaction mixture. It was also observed that when a small amount of water was present in the solvent, diisopentyltetramethyldisiloxane(VIII) was formed as a by-product. The structural assignment for VIII was found by comparing its IR and NMR spectra with those of an authentic sample prepared from isopentylmagnesium bromide and dimethyldichlorosilane.

More detailed studies of the reaction of silacyclopentane derivatives are in progress.

Experimental

The NMR spectra were measured by means of a Varian A-60 spectrometer, using tetramethylsilane as the internal standard. The infrared spectra were obtained on a Shimadzu IR-27C spectrophotometer.

Preparation of 1,1,3-trimethyl-1-silacyclopentene-3(IV). A mixture of 34 g (0.5 mol) of isoprene and 64.5 g (0.5 mol) of dimethyldichlorosilane in 80 m*l* of tetrahydrofuran was added to 23 g (1 g atom) of a sodium dispersion in 120 m*l* of tetrahydrofuran over a 3-hr period at 30—35°C (external cooling) under a nitrogen atmosphere. After stirring for 20—25 hr at room temperature, filtration and distillation gave 18.0 g of IV; 28.5% yield; bp 123°C.

Epoxidation of IV. To a solution of 24 g (0.172 mol) of perbenzoic acid in 300 m*l* of chloroform, 20 g (0.157 mol) of IV was added over a 3-hr period at 5—7°C. After maintaining the reaction mixture at 5°C for 48 hr, benzoic acid and the excess perbenzoic acid were extracted with 200 m*l* of N sodium hydroxide. The chloroform solution was washed with two 100-m*l* portions of water and then dried. The removal of the solvent under reduced pressure at room temperature, followed by the frational distillation of the residue, gave 15.6 g of I; 64% yield; bp 60—62°C/34 mmHg, n_D^{25} 1.4442.

Reaction of I with Methanol. Five grams (35.2 mmol) of I and 5.5 g (171.9 mmol) of methanol were placed in a round-bottomed flask. The mixture was maintained for 5 hr at 50°C with stirring. The subsequent fractional distillation of the resulting mixture gave 3.7 g of the product; 60.7% yield; bp 85—90°C/20 mmHg. The H^1 NMR spectrum showed $SiCH_3$ singlets at τ 9.88 and 9.87, a complex multiplet for CH_2 at *ca.* 8.8—9.5, a singlet for C–CH_3 at 8.89, one for O–CH_3 at 6.89, and a quartet for C–H at 6.17. Two hydroxy H^1 peaks, at 7.1 and 8.3, indicate that *tert*-(II) and *sec*-(III) alcohols are present in the product.

Attempts to React I with Other Alcohols. I was reacted with ethanol, 1-propanol, and 1-butanol under the same reaction conditions as were used in the case of methanol. In every case, vapor-phase chromatographic analysis (3m, Thermal-3, 147°C) showed that I and the alcohol remained unchanged in the resulting mixture.

Attempts to React I with Amines. a) Methylamine was introduced into 1 g of I for 5 hr at 50°C. The vpc analysis of the resulting mixture indicated that the reaction did not occur.

b) A mixture of 1 g (7.0 mmol) of I and 2.5 g (34.2 mmol) of diethylamine was maintained for 5 hr at 50°C. The vpc analysis of the resulting mixture indicated that the reaction did not occur.

Preparation of 1,3,3-trimethyl-3-silabicyclo[3.1.0]hexane(V). A mixture of 8 g (0.0635 mol) of IV and 25 g (0.0933 mol) of methylene iodide in 50 m*l* of ethyl ether was refluxed in the presence of 6.5 g of Zinc-Copper couple for 24 hr with stirring. The ether solution was then decanted from the unreacted couple, washed with two 10 m*l* portions of a saturated aqueous ammonium chloride solution, and then dried over anhydrous magnesium sulfate. Fractional distillation gave 2.9 g of V; 33.1% yield; bp 35—36°C/17 mmHg. Found: Si, 20.4%. Calcd for $C_8H_{16}Si$: Si, 20.1%.

Hydrogenation of IV. General Procedure: Ten grams (0.0793 mol) of IV were hydrogenated in a catalytic hydrogenating apparatus in 50 m*l* of the four solvents described below using 0.5 g of palladium charcoal as the catalyst, at room temperature and under atmospheric pressure. The hydrogen uptake was almost theoretical in the case of each solvent. After the removal of the solvent, fractinal distillation gave the following compounds:

1) in the dry *n*-hexane solvent; 9.0 g of VI, bp 120—123°C, n_D^{20} 1.4345. Found: Si, 21.9%. Calcd for $C_7H_{16}Si$: Si, 22.0%.
2) in dry methanol: 10.2 g of VII, bp 60—62°C/80 mmHg, n_D^{20} 1.4120. Found: Si, 17.2%. Calcd for $C_8H_{20}OSi$: Si, 17.6%.
3) in *n*-hexane containing a small amount of water: VI and VIII (bp 120°C/20 mmHg, n_D^{20} 1.4282, Found: Si, 20.1%. Calcd for $C_{14}H_{34}OSi_2$: Si, 20.5%) were obtained. The yields of VI and VIII varied with the amount of water added.
4) in methanol containing a small amount of water: VII and VIII were obtained. The yields of VII and VIII varied with the amount of water added.

Preparation of an Authentic Sample of Diisopentyltetramethyldisiloxane. Isopentylmagnesium bromide prepared from 15.1 g (0.1 mol) of isopentyl bromide and 2.91 g (0.12 g atom) of magnesium in 50 m*l* of ether was stirred into 12.9 g (0.1 mol) of dimethyldichlorosilane in 20 m*l* of ether. The reaction mixture was heated at reflux for 2 hr, and then 30 m*l* of dilute hydrochloric acid were added. The ether layer was dried, subsequent distillation gave 4.8 g of diisopentyltetramethyldisiloxane; 35% yield. Its boiling point and IR and NMR spectra are consistent with those of VIII.

The authors wish to thank Dr. H. Nohira for his many helpful discussions and the Shinetsu Kagaku Co. for providing the dimethyldichlorosilane.

BULLETIN OF THE CHEMICAL SOCIETY OF JAPAN, VOL. 45, 295—296(1972)

Tautomerism in 1-Arylazo-2-naphthols as Studied by Fluorescence

Yoshio MATSUNAGA and Masaaki SHIMANE

Department of Chemistry, Faculty of Science, Hokkaido University, Sapporo

(Received July 10, 1971)

Earlier we examined the diffuse reflection spectra of sixteen 1-arylazo-2-naphthols[1] diluted with sodium chloride and concluded that the azo and hydrazone tautomers coexist in this solid, two-component system.[2] In many cases, the spectra were found to be markedly modified by elevating the temperature. These changes were thermally reversible and were attributed to the movement of the tautomeric equilibrium. A few years ago, Rau studied the fluorescence of hydroxyazo compounds, mostly at 77°K, and concluded that the hydrazone tautomer is the emitting species.[3] Solid 1-phenylazo-2-naphthol was noted by him to be weakly fluorescent at room temperature. Therefore, the examination of the fluorescence in our samples seemed to be a useful means of checking the validity of our earlier conclusions.

The samples of 1-arylazo-2-naphthols diluted with sodium chloride were those used in our previous work.[2] The fluorescence spectra were recorded on a Hitachi Model MPF-2A spectrophotometer. The samples, packed into quartz capillaries, were examined at room temperature and also at the temperature of liquid nitrogen. The wavelength of the exciting light, selected on the basis of experiments on the excitation-dependence of the fluorescence spectra, was 400 or 470 mμ. It is well known that fluorescence spectra are usually mirror-images of the corresponding absorption spectra when plotted on a frequency scale. Unfortunately, the present spectra are located in the region where the sensitivity of the detector decreases drastically; therefore, the attempts at calibration were not successful. In spite of this shortcoming, it is certain that the peak with the longest wavelength in the reflection spectrum arises from the hydrazone tautomer.

Whether or not the samples at a concentration of 1% are fluorescent is summarized in Table 1. Six among the sixteen examined are not fluorescent; however, the following three become fluorescent when diluted more: the *p*-NO_2 derivative at a concentration of 0.1%, and the *p*-Cl and *o*-OH derivatives at 0.01%. In the last column of Table 1, we show which is the major tautomer in the samples diluted with sodium chloride. This information, obtained from the temperature-dependence of the reflection spectra, is cited from one of our earlier works.[2] There is a fairly good parallelism between the detection of fluorescence at 1% and the presence of an appreciable amount of the hydrazone tautomer. The only exceptions are the *o*-OH and *p*-NO_2 derivatives mentioned above. The detection at 0.1 or 0.01% is in accordance with one of our conclusions that the higher the degree of dilution, the more molecules in the hydrazone form. In the case of the *p*-NO_2 derivative, a reexamination of the reflec-

TABLE 1. THE DETECTION OF FLUORESCENCE IN 1-ARYLAZO-2-NAPHTHOLS DILUTED WITH SODIUM CHLORIDE

Substituent	Concentration		Major tautomer[a]
	1%	0.1 or 0.01%	
None	+	+	Comparable
o-Methyl	+		Hydrazone
m-Methyl	+		Comparable
p-Methyl	+		Hydrazone
o-Chloro	+		Comparable
m-Chloro	+		Comparable
p-Chloro	−	+	Azo
o-Hydroxy	−	+	Hydrazone
m-Hydroxy	−	−	Azo
p-Hydroxy	−	−	Azo
o-Methoxy	+		Hydrazone
m-Methoxy	+		Comparable
p-Methoxy	+		Azo
o-Nitro	−	−	Azo
m-Nitro	+		Hydrazone
p-Nitro	−	+	Hydrazone[b]

a) Determined by the temperature-dependence of the reflection spectra with the samples diluted with sodium chloride, see Ref. 2.

b) The azo tautomer may be the major one when the concentration is high.

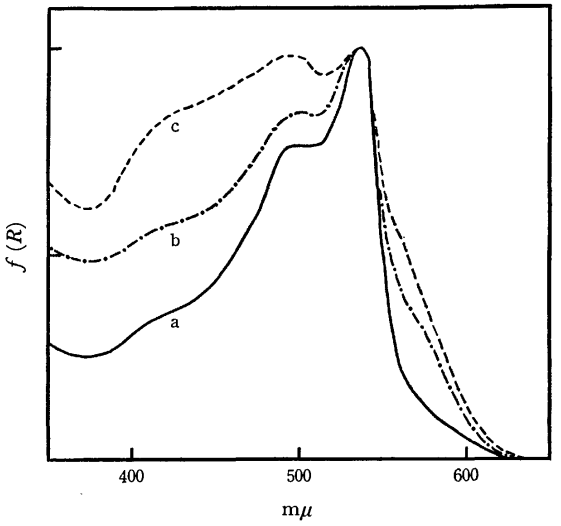

Fig. 1. Diffuse reflection spectra of 1-(*p*-nitrophenylazo)-2-naphthol diluted with sodium chloride at a concentration of 1%; (a) stored for one day after the temperature-dependence measurement, (b) after storage over one year, (c) prepared by grinding at room temperature only. The maximum is arbitrarily taken as 1.00 in each spectrum.

1) This designation is used throughout this paper for convenience; it is not intended to define the structure. The substituents are on the phenyl ring.

2) C. Dehari, Y. Matsunaga, and K. Tani, This Bulletin, **43**, 3404 (1970).

3) H. Rau, *Ber. Bunsenges. Phys. Chem.*, **72**, 637 (1968).

tion spectra revealed that a large change occurred at a concentration of 1% during prolonged storage at room temperature. As is shown in Fig. 1, the sharp peak appearing at 538 mμ is relatively strong when examined one day after the temperature-dependence measurement, but was much weaker after storage for one year. A sample prepared by grinding at room temperature gives the spectrum shown by Curve c. Thus, the hydrazone tautomer of this derivative seems to be less stable than we thought earlier. However, the peak is dominant at concentrations of 0.1 and 0.01% even after storage for nearly two years. It must be noted that the absence of fluorescence cannot be considered as an indication of the absence of the hydrazone tautomer. Nevertheless, fluorescence is not detected at a 1% dilution in most of the cases where the azo tautomer is the major one. All the compounds which are fluorescent at a concentration of 1% are also fluorescent without dilution with sodium chloride. In such cases, it is very likely that the two tautomeric forms exist together, even in crystals.

Cooling brings about a marked increase in the intensity of the fluorescence at the short-wavelength end of the spectrum. In the cases of 1-phenylazo-2-naphthol and the *m*-Cl derivative, the appearance of a fine structure is noted. With the *m*-Me, *p*-Me, *m*-MeO, and *m*-NO_2 derivatives, the change in the relative intensity is so great that the low-temperature fluorescence seems to be shifted to the short-wavelength side by 15—20 mμ.

The authors wish to express their thanks to Professors Hiroaki Baba and Koichi Yagi for permission to use the spectrophotometers.

BULLETIN OF THE CHEMICAL SOCIETY OF JAPAN, VOL. 45, 296—297(1972)

The Reaction of Ethyl Acetoacetate with Benzonitrile in Liquid Ammonia

Noboru SUGIYAMA, Makoto YAMAMOTO, Susumu KOBAYASHI, and Choji KASHIMA

Department of Chemistry, Tokyo Kyoiku University, Otsuka, Tokyo

(Received July 14, 1971)

It is well known that β-diketones[1,2] and β-keto-esters[3,4] condense with an electrophile in the presence of bases in liquid ammonia.

In a previous paper,[5] we reported that acetylacetone condensed with benzonitrile in the presence of alkali amide in liquid ammonia to give 4(1*H*)-pyridone. As one of our series of studies of the syntheses of heterocycles, the present paper will describe the reaction of ethyl acetoacetate (**1**) with benzonitrile (**2**) in liquid ammonia.

If the reaction of **1** with **2** proceeds as the reaction of acetylacetone with **2**, the reaction product may be expected to be 2,4-dioxo-6-phenyl-1,2,3,4-tetrahydropyridine (**4**). However, the reaction of **1** with an equimolar amount of **2** in the presence of twice as many moles of sodium amide in liquid ammonia resulted in the formation of 10% of ethyl 5-amino-3-oxo-5-phenyl-4-pentenoate (**3**), 5.0% of **4**, and 33% of 4-oxo-6-methyl-2-phenyl-1,4-dihydropyrimidine (**5**). The structures of **3**, **4**, and **5** were supported by the spectral data. Compounds **4** and **5** were identified by a direct comparison with authentic samples.[6,7] Since **3** was converted to **4** in liquid ammonia or in ether in the presence of sodium amide, **3** is considered to be an intermediate of the formation of **4** from **1** and **2**. Compound **4** was also formed by heating **3** over 150°C.

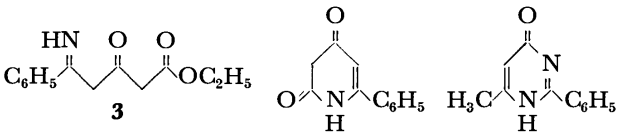

3 **4** **5**

Fig. 1

When the reaction was carried out with a molar ratio of **1**, **2**, and sodium amide of 1 : 1 : 3, the yields of the reaction procduts, based on **1**, were 52.5% of **5** and 20% of **3**, plus a trace of **4**.

It has been reported that **2** is converted into benzamidine[8] in the presence of the amide ion, and that benzamidine and **1** condense to a pyrimidine derivative in the presence of sodium ethoxide in ethanol.[7] This fact suggests that the amide anion attacks the compound **2** to give benzamidine in liquid ammonia, and that benzamidine then condenses with **1** to yield **5**.

The condensation reaction at the terminal methyl group is considered to be initiated by the formation of a dianion by the abstraction of two protons from the methyl and methylene groups of β-diketone. The methyl proton of **1** is less acidic than that of acetylacetone or benzoylacetone.[4] When sodium amide was reacted on **1**, the monoanion of **1** is predominant, this monoanion reacts with **2** to give **5** (Scheme 1). When potassium amide is used instead of sodium amide, the

1) C. R. Hauser and T. M. Harris, *J. Amer. Chem. Soc.*, **80**, 6360 (1958).

2) N. Sugiyama, M. Yamamoto, and C. Kashima, This Bulletin, **42**, 1357 (1969).

3) N. Sugiyama, M. Yamamoto, T. Takano, and C. Kashima, *ibid.*, **40**, 2909 (1967).

4) J. F. Wolfe, T. M. Harris, and C. R. Hauser, *J. Org. Chem.*, **29**, 3249 (1964).

5) C. Kashima, M. Yamamoto, S. Kobayashi, and N. Sugiyama, This Bulletin **42** 2389 (1969).

6) F. Arndt B. Eistert, H. Schloz, and E. Aron, *Ber.*, **69**, 2373 (1936).

7) A. Sitte and H. Paul, *Chem. Ber.*, **102**, 615 (1969).

8) E. F. Cornell, *J. Amer. Chem. Soc.*, **59**, 3311 (1928).

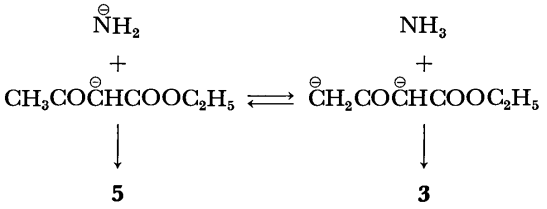

Scheme 1

dianion of **1** is predominant because the ability of dianion formation of potassium amide is a little higher than that of sodium amide in liquid ammonia.[5,9] The dianion reacted with **2** to give **3**. Actually, the yield of **3** increased to 43%, as is listed in Table 1.

Table 1. The products of the reaction of **1** with **2**

Amide	n[a]	Reaction time (hr)	Product (%)		
			3	**4**	**5**
$NaNH_2$	2	2.5	10	5.0	33
$NaNH_2$	3	2.5	20	trace	53
KNH_2	2	2.5	43	trace	3.8
KNH_2	2	5.0	32	15	3.7

a) Molar ratio, **1**:**2**: amide = 1:1:n

The extension of the reaction time leads to an increase in the yield of **4**. This fact suggests that the initially-formed **3** has been converted to **4** by the residual amide ion in liquid ammonia.

This is a simple and convenient method for the synthesis of a compound of the **4** type, because the only method for synthesizing **4** previously reported (F. Arndt *et al.*[6]) is very complicated.

Experimental

Ethyl 5-amino-3-oxo-5-phenyl-4-pentenoate (3). To a solution of 0.1 mol of sodium amide in about 300 m*l* of liquid ammonia in a three-necked flask, we added, drop by drop, 0.05 mol (6.5 g) of **2** in 30 m*l* of anhydrous ether. After this mixture had been stirred for 1 hr, 0.05 mol (5.2 g) of **1** in 30 m*l* of anhydrous ether was added. The dark gray color of the solution soon turned to a brownish green. After being stirred for an additional 2.5 hr, the reaction mixture was neutralized with solid ammonium chloride. The liquid ammonia was evaporated rapidly in a water bath, and 100 m*l* of ether was added. The resulting ethereal suspension was shaken with 2N hydrochloric acid to dissolve the inorganic salts. The acidic aqueous layer was separated and again extracted with fresh ether. The two ether layers were combined and dried over anhydrous sodium sulfate, and the ether was evaporated under reduced pressure. The residue was chromatographed on a silica-gel (Merk 7734, 0.05—0.2 mm) column with a benzene-ethyl acetate (4: 1 v/v) mixture. A fraction which showed a brown color in a ferric chroride test was collected and evaporated to afford **3** (1.17 g, 10%) as an orange oil.

Found: C, 66.50; H, 6.63; N, 5.99%. Calcd for $C_{13}H_{15}NO_3$: C, 66.93; H, 6.48; N, 6.01%. IR(liquid film): 3400 (νNH), 1730 (νC=O, ester carbonyl), 1610 (νC=N) and 695 cm^{-1} (phenyl). UV: λ_{max}^{EtOH} 242 (ε 9390) and 328 nm (ε 17000). NMR(in CCl_4): δ 1.21 (t, 3H, methyl protons), 3.20 (s, 2H, C-2 methylene protons), 4.05 (q, methylene protons of the ester group), 5.32 (s, 1H, C-4 enolic olefin proton), 6.37 (broad, 1H, non-hydrogen bonded NH), 7.40 (m, 5H, aromatic protons), and 9.80 (braod, 1H, hydrogen bonded NH).

The compound **3** was not distilled because of its easy conversion by heat. By heating at 150—170°C for 30 min, about 46% of the **3** was converted into **4**.

After the compound **3** was obtained, **5** was eluted with benzene-ethyl acetate (2: 1 v/v) from the same column. Yield, 0.48 g (5.2%).

2,4-Dioxo-6-phenyl-1,2,3,4-tetrahydropyridine (4). After adjusting the pH to 4—5, the aqueous layer was allowed to stand at room temperature for two hours. The resulting precipitate was collected and then treated with hot acetone. The acetone-insoluble solid was collected and recrystallized from hot pyridine to give **4** as a white solid; 0.47 g (5.0%); mp 312—314°C (lit, 315—318°C[6]). IR(KBr): 3100 (νNH), 1645 (νC=O, conjugated ketone) and 695 cm^{-1} (phenyl). UV: λ_{max}^{EtOH} 308 nm (ε 10300).

4-Oxo-6-methyl-2-phenyl-1,4-dihydropyridine (5). When the hot acetone solution obtained above was cooled, compound **5** was separated as colorless needles. Yield, 2.58 g (28%); mp 215—216°C (lit, 218—221°C[7]).

Found: C, 71.15; H, 5.43; N, 14.92%. Calcd for $C_{11}H_{10}N_2O$: C, 70.95; H, 5.41; N, 15.05%. IR(KBr): 3175 (νNH), 1670 (νC=O, conjugated ketone) and 690 cm^{-1} (phenyl). UV: λ_{max}^{EtOH} 240 (ε 17300) and 293 nm (ε 11200). NMR(in $CDCl_4$): δ 2.38 (s, 3H, methyl protons), 6.28 (s, 1H, olefin proton), 7.52 (m, 3H, aromatic protons), and 8.20 (m, 2H, aromatic protons).

The Condensation Reactions of 1 with 2 under Various Conditions. The condensation reactions of **1** with **2** were carried out by using potassium amide, instead of sodium amide, and were also carried out by changing the molar ratio of amide to **1** and to **2** and/or by changing the reaction time. The results are listed in Table 1.

The Cyclization of 3 to 4. *a*) A solution of 122 mg of **3** in 5 m*l* of anhydrous ether was added to 50 m*l* of liquid ammonia containing 35 mg of sodium amide. The mixture was stirred for two hours and then neutralized with 60 mg of solid ammonium chrolide. After the evaporation of the ammonia, the residue was acidified with 30 m*l* of dilute hydrochloric acid; the resulting white precipitate was collected by filtration. Yield, 74 mg (76%). This compound was identified by comparing its spectral data with those of an authentic sample of 2-phenyl-4,6-dihydroxypyridine.

b) To 80 m*l* of anhydrous ether there were added 30 mg of sodium amide and 100 mg of **3** in 20 m*l* of anyhdrous ether. The solution was then stirred at room temperature for two hours. The **4** was identified by comparison with an authentic sample by means of thin-layer chromatography.

9) Unpublished data by M. Yamamoto *et al.*

BULLETIN OF THE CHEMICAL SOCIETY OF JAPAN, VOL. 45, 298—299(1972)

Rotational Isomerism in Ethylmethylsilane

Michiro HAYASHI, Keiichi OHNO, and Hiromu MURATA
Department of Chemistry, Faculty of Science, Hiroshima University, Hiroshima

(Received July 27, 1971)

Although many experimental data have been accumulated concerning rotational isomerism, a number of molecules have not yet been studied. In this note, we will deal with the vibrational spectra of ethylmethylsilane in relation to the rotational isomerism.

Experimental

The samples of ethylmethylsilane and its deuterated species ($CH_3CH_2SiD_2CH_3$) were prepared as follows. Methyltrichlorosilane was treated by an ethyl Grignard reagent, and the product ($CH_3CH_2SiCl_2CH_3$) was reduced with $LiAlH_4$ or $LiAlD_4$ respectively.[1]

The infrared spectra in the region from 4000 to 200 cm^{-1} were recorded with Perkin-Elmer instruments (model 621 and 521) and Hitachi instruments (EPI-L and FIS-3). For the measurements in the crystalline state, the vapor of the sample was directly condensed on CsI plate in a cell cooled with liquid nitrogen in a vacuum and was then annealed several times in order to keep the sample from being in the supercooled liquid state. The method was also extended to measurements in the liquid state at about 19°C, since the boiling point of the sample is rather low for measurements using the usual technique.

Results and Discussion

According to the reported vibrational assignments for similar molecules, such as dimethylsilane[2] and ethylsilane,[3] CCSi deformation, SiH_2 rocking, twisting, wagging, Si–C symmetric, and asymmetric stretching modes would be expected in the regions around 300, 467(389), 591 (472), 643(558), 659(636), and 728(700) cm^{-1} respectively, where the frequencies in parentheses indicate the expected frequencies for the deuterated species.

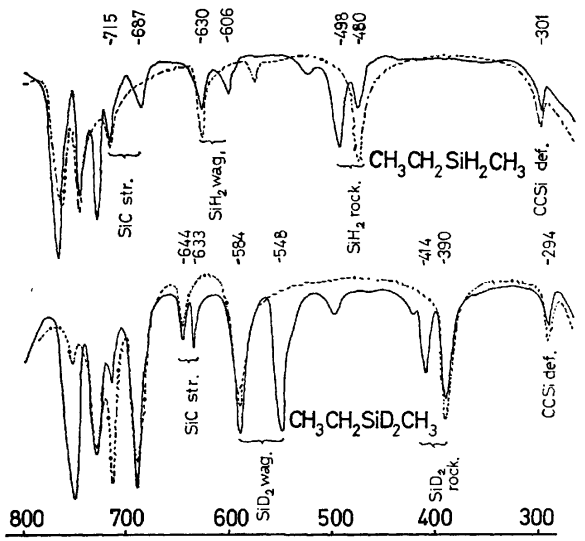

Fig. 1. The infrared spectra of ethylmethylsilane and its deuterated species; —— in the liquid state (19°C), ····· in the crystalline state.

As is shown in Fig. 1, in the region from 700 to 300 cm^{-1}, too many spectra exist there to be an unique molecular form, and some of the spectra vanish in the crystalline state. These facts provide us with evidence of the existence of rotational isomers in the liquid state. The assignments of the observed spectra can easily be found for this region; some are shown in Fig. 1.

The SiH_2 wagging mode and one of the Si–C stretching modes for the parent species are found at frequencies slightly different from those for dimethylsilane. However, this can be understood if these modes originally have nearly equal frequencies and are strongly coupled in ethylmethylsilane, while the corresponding modes in dimethylsilane are separated because of the symmetry of the molecule.

In the gaseous state, the resolution of the spectra becomes worse because of the broad envelopes of the unresolved rotational fine structures.

However, for the deuterated species, the SiD_2 rocking mode is seen as doublets like those in the liquid state; this is considered to be definite evidence of the existence of the rotational isomers in the gaseous state.

As for the parent species, careful measurements with a higher resolution give weak Q branches of the bands at 479 and 498 cm^{-1} over the broad band envelope; these correspond to the bands assigned to the SiH_2 rocking modes in the liquid state. Therefore, the isomers also exist in the parent species. The molecular forms of the isomers would be the *trans* and the *gauche* forms, as in the case of 1,2-dihalogenoethane.

One of the present authors (M.H.) has actually found the *trans* form in the gaseous state by microwave spectroscopy,[4] but he could not find the other form, since the observed microwave spectra were too weak for him to make definite assignments of the transitions for the *gauche* form at the temperature of dry ice.

As usual experimental techniques, such as solvent-effect measurements of the vibrational spectra, seem to be invalid for the determination of the molecular forms of ethylmethylsilane, normal vibration calculations for the skeletal vibrations were attempted regarding ethylmethylsilane as a four-body problem and using a set of force constants which had been obtained from the observed skeletal vibration frequencies of methylsilane,

1) F. S. Kipping, *Proc. Chem. Soc.*, **20**, 15 (1904), W. Dilthey, *Ber.*, **37**, 319 (1904), and A. E. Finholt, A. C. Bond, Jr., and H. I. Schlesinger, *J. Amer. Chem. Soc.*, **69**, 1199 (1947).

2) D. F. Ball, P. L. Goggin, D. C. McKean, and L. W. Woodward, *Spectrochim. Acta*, **16**, 1358 (1960).

3) K. M. Mackay and R. Watt, *ibid.*, **23A**, 2761 (1967).

4) M. Hayashi and C. Matsumura, to be published.

ethylsilane, and dimethylsilane.

However, the observed skeletal frequencies of ethylmethylsilane could not be reasonably reproduced by this over-simplified treatment. Therefore, at present, we cannot conclude whether or not one of the isomers is in the *gauche* form and which isomer persists in the crystalline state.

The authors wish to express their thanks to Professor Tatsuo Miyazawa of Osaka University and to the staff of his research group for allowing us to use their instruments and for their technical assistance.

BULLETIN OF THE CHEMICAL SOCIETY OF JAPAN, VOL. 45, 299—300(1972)

On the Role of the Quadrupole-quadrupole Interaction in the Molecular Arrangements in Crystalline Benzene

Masao HASHIMOTO and Taro ISOBE

The Chemical Research Institute of Non-Aqueous Solutions, Tohoku University, Sendai

(Received August 2, 1971)

It has been said that, in a typical aromatic crystal, quadrupole-quadrupole interaction makes only a negligible contribution to the lattice energy[1-3] and the equilibrium molecular orientation. On the other hand, Kihara[4-6] indicated, after using his molecular models, which simulate magnetically the electric multipoles of actual molecules, that the structure of a molecular crystal corresponds to a minimum of the electrostatic energy between the molecules when the molecules have simple shapes and sufficiently strong electric multipoles. We cannot, therefore, neglect the quadrupole-quadrupole interaction energy against the van der Waals dispersion energy, because only the relative smallness of the former against the latter does not generally justify the discarding of the former.

The crystal packing problem of benzene has been discussed by several authors[1-3,7-8] in terms of the intermolecular potential functions. These authors calculated the dependency of the potential energy of this crystal with respect to the class of the structural variation, in which the molecules are rotated in only small angles from the equilibrium structure, with a preservation of the space-group symmetry. They have obtained a successful explanation in terms of the van der Waals dispersion energy only. However, in principle, we must start to consider the molecular packing problem in two interacting molecules; we must calculate the most stable relative arrangement of the two molecules when the intermolecular distance is known, and then construct the whole crystal from this pair. This is related to the phenomena of condensation and crystallization.

Calculation and Results

One of the two molecules is set on the point of the origin of the cartesian coordinate, while the position of the other is expressed by $P(\theta,\theta',\varphi,\varphi',\gamma,R)$, as is shown in Fig. 1.

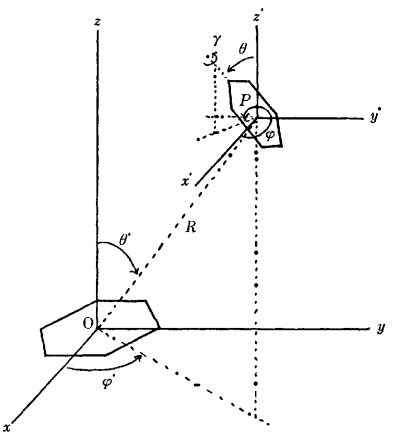

Fig. 1. Geometrical representation of two benzene molecules in interaction.

The intermolecular potential, $v(R)$, is expressed by the sum of the interatomic potentials, $v(r_j)$, as follows:

$$v(R) = \sum_j v(r_j) = \sum_j (b_j \exp(-c_j r_j) - a_j/r_j^6), \qquad (1)$$

where the summation, j, is extended to all pairs of atoms in the two molecules. The three parameters, a_j, b_j, and c_j, were derived from Bartell's function in a way fully described in the text (*cf.* Table 1).[9] A part of the potential energy surface obtained is indicated

TABLE 1. PARAMETER SET

	a_j	b_j	c_j
C···C	298.0	237.0×10^3	4.32
C···H	121.0	31.4×10^3	4.20
H···H	49.2	6.60×10^3	4.08

1) D. P. Craig, R. Mason, P. Pauling, and D. P. Santry, *Proc. Roy. Soc., Ser. A*, **286**, 98 (1965).
2) A. I. Kitaigorodoskii, K. V. Mirskaya, and A. B. Tovbis, *Soviet Phys. -Crystallogr.*, **13**, 176 (1968).
3) D. P. Craig, P. A. Dobosh, R. Mason, and D. P. Santry, *Discuss. Faraday Soc.*, **40**, 110 (1965).
4) T. Kihara, *Acta Crystallogr.*, **16**, 1119 (1963).
5) T. Kihara, *ibid.*, **21**, 877 (1966).
6) T. Kihara, *Bussei*, **10**, 447 (1969).
7) A. I. M. Lae and R. Mason, *Proc. Roy. Soc., Ser. A*, **304**, 487 (1968).
8) D. E. Williams, *Acta Crystallogr.*, **A25**, 464 (1969).
9) A. M. Liquori, *J. Polym. Sci., Part C*, **12**, 209 (1966).

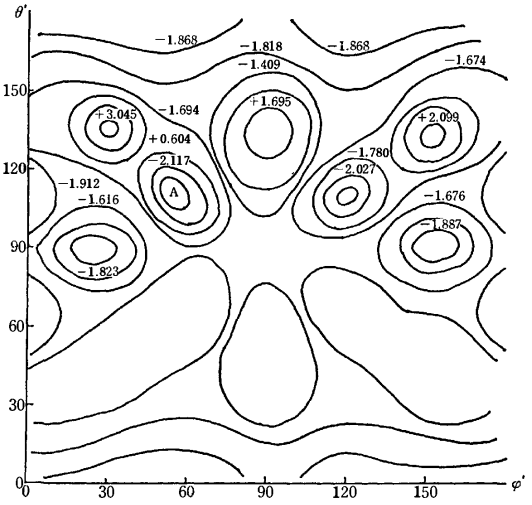

Fig. 2. θ'-φ' energy surface between two benzene molecules. The values in the figure are the minimum with regard to θ, φ, and γ and expressed in kcal/mol unit.

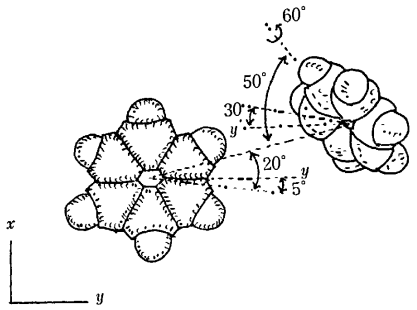

Fig. 3. The most stable orientation of two benzene molecules when R=5.13Å.

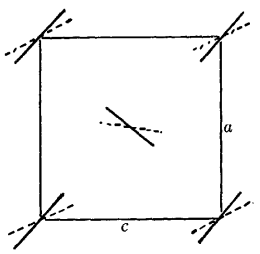

Fig. 4. Diagram of the crystal structure of benzene projected down the b-axis. —— : experimental; ····· our calculation.

in Fig. 2, where R is set at 5.13 Å, the shortest intermolecular distance in the benzene crystal at −3°C. The relative molecular orientation corresponding to the A position in Fig. 2 is indicated in Fig. 3. The corresponding packing in the crystal is indicated by the dashed line in Fig. 4. Thus, it can be observed in Fig. 4 that the molecular packing derived from the two molecules is not consistent with the experimental one, indicating that other types of intermolecular force are acting in addition to the van der Waals interaction.

There are two types of such intermolecular forces. One is the non-additive contribution to Eq. (1), but this is small because of the relatively higher symmetry of the benzene molecules.[10] The other is the quadrupole-quadrupole interaction. The benzene molecules have quadrupole moments[11] perpendicular to the molecular plane:

$$q_{//} = -(5.6\pm2.8)\times10^{-26}\ \text{cm}^2\ \text{e.s.u.}$$

The quadrupole-quadrupole interaction is expressed as follows:

$$\begin{aligned} Q_{ab} = {} & 3qq'[1-5(\cos^2\theta+\cos^2\theta')+17\cos^2\theta\cos^2\theta' \\ & +2\sin^2\theta\sin^2\theta'\cos^2(\varphi-\varphi') \\ & +16\sin\theta\sin\theta'\cos\theta\cos\theta'\cos(\varphi-\varphi')]/4R^5. \end{aligned} \quad (2)$$

Here, the q's are the observed quadrupole moments of the benzene molecule and the θ's and φ's are correlated to the θ's, φ's, and γ in Fig. 1.

The most favourable relative arrangement of two quadrupoles can easily be calculated to be the one in which the molecular planes make a 90° angle. This is almost entirely consistent with the experimental molecular arrangement in the crystal.[12]

Thus, it is necessary, in studying the molecular packing in the benzene crystal, to introduce the quadrupole-quadrupole interaction. The calculated quadrupole-quadrupole interaction energy is −0.95——0.86 kcal/mol at the equilibrium arrangement; this value is attractive.

All the numerical calculations in this paper were done at Computer Center of Tohoku University, using a NEAC 2200 model 700—500 Computer system.

10) M. J. Sparnaay, *Physica*, **25**, 217 (1959).
11) R. L. Shoemaker and W. H. Flygare, *J. Chem. Phys.*, **51**, 2988 (1969).
12) E. G. Cox, D. W. J. Cruickshank, and J. A. S. Smith, *Proc. Roy. Soc., Ser. A*, **247**, 1 (1958).

BULLETIN OF THE CHEMICAL SOCIETY OF JAPAN, VOL. 45, 301(1972)

The Nucleophilic Cyclopropylation of the Condensed Aromatic Ring with Sulfonylcarbanion

Hitosi NOZAKI, Tetuya NISIMURA, and Yasusi YAMAMOTO

Department of Industrial Chemistry, Kyoto University, Yoshida, Sakyo-ku, Kyoto

(Received August 17, 1971)

The nucleophilic methylation of aromatic nuclei has been attained by the action of methylsulfinylcarbanion[1] or dimethyloxosulfonium methylide[2] upon condensed ring hydrocarbons, benzopyridines, or nitrobenzenes. We previously reported that the nucleophilic alkyl-substitution can be effected by the action of sulfonyl-carbanions[3] on anthracene and acridine in hexamethyl-phosphoric triamide (HMPA) as a solvent. We now wish to report a one-step introduction of the cyclopropyl group in anthracene and acridine by means of a sulfonylcarbanion which had been prepared from cyclopropyl phenyl sulfone[4] and sodium hydride in HMPA.

The reaction with anthracene gave 9-cyclopropyl-anthracene (I) (79%). In contrast to the methylation by means of methylsulfinylcarbanion and phenylsulfonylcarbanion, 9,10-dicyclopropylated product was not obtained. The structure of I was supported by its NMR, IR, and mass spectra as well as by the results of elemental analysis.

The treatment of acridine with this carbanion gave 9-cyclopropylacridane (II) (25%) besides a considerable amount of a crystalline, insoluble solid.[5] Phenanthrene, quinoline, or isoquinoline did not react with this carbanion.

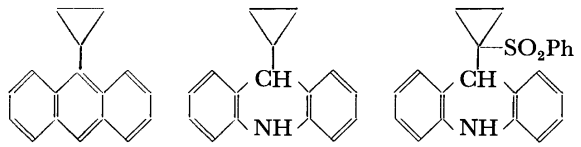

I II III

The cyclopropylated product may be ascribed to the nucleophilic attack of the carbanion on the aromatic ring, followed by a concerted hydride shift and the elimination of the sulfinate anion. This route has previously been proposed in the cases of the methylation by means of methylsulfinylcarbanion[1a] and phenylsulfonyl-carbanion.[3b] On the other hand, 9-cyclopropylacridane seems to be attributable to the decomposition of transient 9-(1-phenylsulfonylcyclopropyl)acridane (III), as 9-(1-phenylsulfonylethyl)acridane is the sole isolable product of the reaction of acridine with the carbanion derived from ethyl phenyl sulfone.[3b]

Experimental

All the mps are uncorrected. The microanalyses were performed by Mrs. Kiyoko Fujimoto of this department. The NMR spectra were taken on a 60 MHz instrument (JEOL C-60 H spectrometer) in deuteriochloroform with tetramethylsilane as the internal standard. The mass spectra were obtained on a Hitachi RMU-6L spectrometer.

Reaction of Anthracene with a Carbanion. A carbanion solution was prepared under N_2 from sodium hydride (0.48 g, 20 mmol) and cyclopropyl phenyl sulfone (3.64 g, 20 mmol) in HMPA (30 m*l*) at 60—70°C for 2 hr. To this, a solution of anthracene (1.78 g, 10 mmol) dissolved in HMPA (20 m*l*) was added, and the reaction mixture was stirred at 90°C for 23 hr. Work-up followed by recrystallization (EtOH) then gave 9-cyclopropylanthracene (I) (1.71 g, 79%); mp 133—134°C. IR (Nujol): 1030 cm^{-1} (cyclopropane ring). MS: 218 (M^+). NMR ($CDCl_3$): δ 0.60—0.95 and 1.25—1.60 (m, 4H, methylenes of cyclopropane), 2.15—2.65 (m, 1H, methine of cyclopropane), and 7.25—8.95 (m, 9H, aromatic protons).

Found: C, 93.3; H, 6.5%. Calcd for $C_{17}H_{14}$: C, 93.5; H, 6.5%.

Reaction of Acridine with a Carbanion. A carbanion solution prepared from sodium hydride (0.48 g, 20 mmol) and cyclopropyl phenyl sulfone (3.64 g, 20 mmol) was allowed to react with acridine (1.79 g, 10 mmol) at 70°C for 15 hr. The reaction mixture was treated with water and extracted with benzene. The evaporation of benzene *in vacuo* and subsequent treatment with ether gave a crystalline solid. The structure of this solid could not be confirmed, as the attempted purification of this solid failed. Meanwhile, the chromatography of the dissolved part in ether on a silica-gel column gave 9-cyclopropylacridane (II) (0.56 g, 25%). The product, II, showed a mp of 122—124°C. IR (Nujol): 3350 cm^{-1} (NH). MS: 221 (M^+). NMR ($CDCl_3$): δ 0.25—0.75 (m, 4H, methylenes of cyclopropane), 0.75—1.00 (m, 1H, methine of cyclopropane), 3.38 (d (J=8 Hz), 1H, benzylic proton), and 6.65—7.75 (m, 9H, aromatic protons and NH).

Found: C, 86.6; H, 6.8%. Calcd for $C_{16}H_{15}N$: C, 86.8; H, 6.8%.

The authors are grateful to Professor Keiiti Sisido for his generous help. The financial support of the Ministry of Education, the Japanese Government, and of the Toray Science Foundation is acknowledged with pleasure.

1) a) H. Nozaki, Y. Yamamoto, and R. Noyori, *Tetrahedron Lett.*, **1966**, 1123. b) P. A. Argabright, J. E. Hofmann, and A. Schriesheim, *J. Org. Chem.*, **30**, 3233 (1965), c) G. A. Russell and S. A. Weiner, *ibid.*, **31**, 248 (1966).

2) a) H. König, H. Metzger, and K. Seelert, *Chem. Ber.*, **98**, 3712 (1965). b) V. J. Traynelis and S. J. V. McSweeney O. P., *J. Org. Chem.*, **31**, 243 (1966).

3) a) H. Nozaki, Y. Yamamoto, and T. Nisimura, *Tetrahedron Lett.*, **1968**, 4625, b) Y. Yamamoto, T. Nisimura, and H. Nozaki, This Bulletin, **44**, 541 (1971).

4) H. E. Zimmerman and B. S. Thyagarajan, *J. Amer. Chem. Soc.*, **82**, 2505 (1960).

5) The structure of this product could not be confirmed, as an attempted purification of this solid failed.

SHORT COMMUNICATIONS

Stereoselective Reactions of Some Anions Derived from 1,3,5-Trithianes

Michio FUKUNAGA, Kazutaka ARAI, Hiizu IWAMURA, and Michinori ŌKI
Department of Chemistry, Faculty of Science, The University of Tokyo, Hongo, Tokyo
(Received August 23, 1971)

While we were studying the base-catalyzed reactions of 1,3,5-trithiane derivatives, Hartmann and Eliel[1] recently reported on the stereoselective protonation and methylation of 2-lithio-1,3-dithiane derivatives. Although the system we have been studying is a little different from the one reported by Hartmann and Eliel, the results are so similar that we feel it is timely to report our independent findings on the 1,3,5-trithianes.

The H-D exchange of the ring-protons of *trans*-2,4,6-trimethyl-1,3,5-trithiane (**1**) was performed in *t*-butyl alcohol-*d* in the presence of alkali *t*-butoxide, and the reaction rate was followed by NMR spectroscopy. The rate of the exchange of the equatorial proton of the compound was found to be 40 times faster[2] than that of the axial, showing the relative ease of the exchange at the equatorial position.

More striking results were obtained with *cis*-2,4,6-trimethyl-1,3,5-trithiane (**2**), which gave a negligible exchange rate under conditions that were convenient for measuring the rate of **1**. Under more severe conditions, the rate of the exchange of the ring-proton of **2** was found to be 550 times lower than that of the axial proton of compound **1**; the rate ratio is now 22000 to 1 when those of the equatorial proton of **1** and the ring-proton of **2** are compared.[3]

The reaction proceeded with retention of configuration. Thus, **1** gave no *cis* isomer containing deuterium as far as NMR spectra showed. Similarly, no *trans* isomer with D was found upon treating compound **2** with *t*-butoxide in *t*-butyl alcohol-*d*.

Quenching the lithio derivatives with H_2O or D_2O provides another stereoselective reaction of the trithianes. Thus, the treatment of either **1** or **2** with butyllithium, followed by quenching with water, gave a 96:4 mixture of **1** and **2**, whereas quenching with deuterium oxide afforded *r*-2-deuterio-2,*cis*-4,*cis*-6-trimethyl-1,3,5-trithiane (**3**).

The preferential reaction at the equatorial position of 1,3,5-trithiane derivatives is not confined to the protonation. We believe that the carbonation is also stereoselective and that only the equatorial isomer is obtained. The treatment of either *cis*- or *trans*-2,4,6-trimethyl-1,3,5-trithiane (**1** or **2**) with equimolar butyllithium in ether-tetrahydrofuran, followed by carbonation with carbon dioxide, produced the identical carboxylic acid (**4**) [mp 137—138.5°C NMR($CDCl_3$) δ: 1.59 (6H, d), 2.07 (3H, s), 4.39 (2H, q), 8—9 (1H, s)]. When this carboxylic acid was treated with an acid catalyst such as BF_3 etherate, a mixture was obtained which contained an isomer (**5**) [mp 135—135.5°C NMR($CDCl_3$) δ: 1.55 (6H, d), 1.78 (3H, s), 4.69 (2H, q), ~10 (1H, s)] as a major component. Since it is well known that, in trithiane derivatives, the proton signals of the equatorial position appear in a higher magnetic field than the axial counterpart,[4] compound **4** may be assigned to the equatorial isomer.

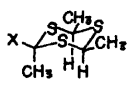

1: X=H
3: X=D
4: X=CO_2H

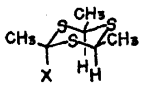

2: X=H
5: X=CO_2H

A possible cause of the stereoselectivity of the above reactions may be mentioned. Since a quantum mechanical study[5] has suggested that the most stable conformation of the $HSCH_2^-$ ion is **6** rather than **7**, the anion lone-pair equatorial conformation which is analogous to conformation **6** will be favored over the anion lone-pair axial. The preferential attack from the equatorial side can be explained on this ground.

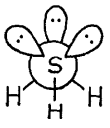

6

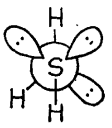

7

It seems difficult to explain why the H-D exchange proceeds with a high retention of configuration on the basis of the above-mentioned results. However, the data on the rates of H-D exchange now available to us conform with the relative population of the H-equatorial isomer. The results suggest that the reaction occurs solely at the H-equatorial conformation. The detail will be published elsewhere.

1) A. A. Hartmann and E. L. Eliel, *J. Amer. Chem. Soc.*, **93**, 2572 (1971).

2) The H-D exchange half-lives for equatorial and axial hydrogens of **1** were 1.5 and 58 hr, respectively, in 0.172 mol/kg *t*-BuOK in *t*-BuOD at 65°C.

3) The H-D exchange half-lives for the axial hydrogens of **1** and **2** were 4.0 min and 37 hr, respectively, in 0.974 mol/kg *t*-BuOK in *t*-BuOD at 100°C.

4) E. Campaigne, N. F. Chamberlein, and B. E. Edwards, *J. Org. Chem.*, **27**, 135 (1962).

5) See a footnote in A. Rauk, S. Wolfe, and I. G. Csizmadia, *Can. J. Chem.*, **47**, 113 (1969).

Gas Chromatography of Rare Earth Pivaloyltrifluoroacetone Adducts with Tri-*n*-butyl Phosphate and Tri-*n*-octylphosphine Oxide

Kei UTSUNOMIYA and Tsunenobu SHIGEMATSU
Institute for Chemical Research, Kyoto University, Uji, Kyoto
(Received September 2, 1971)

Recently the rare earth chelates with 1,1,1,2,2,3,3-heptafluoro-7,7-dimethyl-4,6-octanedione[1] and pivaloyltrifluoroacetone (HPTA)[2,3] have been successfully gas chromatographed. It was shown that gas chromatography following the solvent extraction could be applied for the separation and determination of rare earth elements. The synergic extraction of rare earth ions was thoroughly studied using β-diketones and some organic phosphorus compounds. The high extractability was concluded to be caused by adduct formation. Thus, if the adduct compounds can be eluted, an interesting problem on the gas chromatography of rare earth metal complexes might be presented. In this paper, we wish to describe the gas chromatography of the adduct compounds of europium(III), erbium(III), and lutetium(III) with HPTA and tri-*n*-butyl phosphate (TBP), or with HPTA and tri-*n*-octylphosphine oxide (TOPO).

Five milliliters of an aqueous solution containing rare earth ions (0.01—0.1 mM in the concentration) and sodium acetate (0.2M), having the desired pH (finally pH 5.2—5.3), was shaken with 5 m*l* of benzene solution containing HPTA (0.1M) and TBP (0.1M), or HPTA (0.1M) and TOPO (0.1M), and 10—50 μl of the extract was then employed for gas chromatography. The $pH_{1/2}$ values of the extraction of europium and lutetium are 4.13 and 3.59 with HPTA only, 3.21 and 2.42 with HPTA and TBP, and 2.17 and 1.88 with HPTA and TOPO, respectively. The extracted species in the synergic extraction are $Eu(PTA)_3 \cdot 2TBP$, $Eu(PTA)_3 \cdot 2TOPO$, $Lu(PTA)_3 \cdot TBP$, and $Lu(PTA)_3 \cdot TOPO$. Typical chromatograms of europium complexes extracted are shown in Fig. 1. The retention times (min) obtained under the same conditions as described in Fig. 1 are as follows: europium, 4.4 and 5.5 with the HPTA extract,[4] 4.2 with the HPTA-TBP extract, and 7.2 with the HPTA-TOPO extract; erbium, 3.8, 4.2, and 6.6; lutetium, 2.9, 4.0, and 6.4. The sharp peaks favor the determination of each rare earth element. However, the fact that the separation factors become lower than in the case of the rare earth β-diketonates themselves, makes it unsuitable for the separation. The chromatograms of the synergic extracts which seem favorable for the determination differ a great deal from those of the tris-chelates, and the retention times of the former are generally greater except for europium-HPTA-TBP. This suggests that the adduct compounds can be eluted. For the europium-HPTA-TBP and europium-HPTA-TOPO extracts, the acetone solution of the eluted materials shows fluorescence with the same spectrum as that of the extracted benzene solution. The presence of TBP or TOPO in the eluted complexes is confirmed by comparing the IR spectra of the effluent with those of the tris-chelate, TBP, and TOPO. The results indicate that the rare earth-PTA adducts with TBP and TOPO can be gas-chromatographed without decomposition. Reproducible linear relationships are obtained between the detector response and the original concentration of aqueous europium(III) solution over the range 0.04—0.1 mM in the HPTA-TBP extraction, and 0.01—0.1 mM in the HPTA-TOPO extraction.

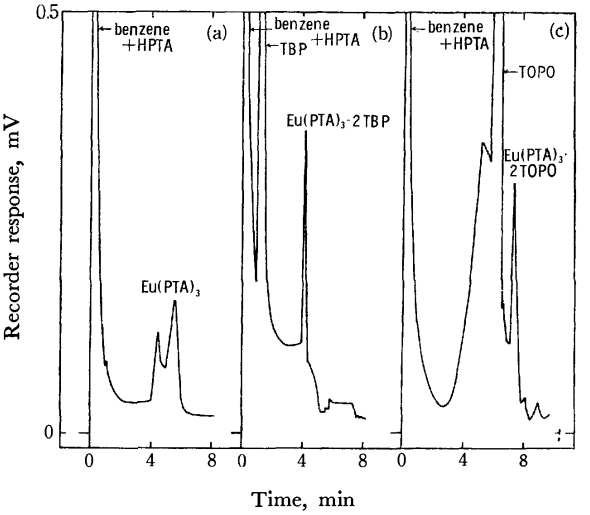

Fig. 1. Gas chromatograms of the extracts of europium(III) with (a) HPTA, (b) HPTA-TBP, and (c) HPTA-TOPO. (a) 152 μg Eu in solvent (50 μl), (b) 91 μg Eu in solvent (50 μl), and (c) 76 μg Eu in solvent (25 μl). Conditions: column, 75 cm × 3 mm i.d. stainless steel; column packing, 5% OV-101 on Chromosorb W AW DMCS (80—100 mesh); column temp., programmed from 150 to 300°C at 20°C/min; helium flow rate, 110 m*l*/min at 150°C. Detector: thermal conductivity detector, 150 mA.

1) C. S. Springer, Jr., D. W. Meek, and R. E. Sievers, *Inorg. Chem.*, **6**, 1105 (1967).
2) T. Shigematsu, M. Matsui, and K. Utsunomiya, This Bulletin, **41**, 763 (1968).
3) M. Tanaka, T. Shono, and K. Shinra, *Anal. Chim. Acta*, **43**, 157 (1968).
4) The chromatogram of the extract shows two peaks (Fig. 1 (a)), whereas tris-chelate, $Eu(PTA)_3$, dissolved in benzene shows single peak having a retention time of 5.5 min.

Catalyst Isotope Effect in *n*-Butene Isomerization Catalyzed by Metal Sulfates

Makoto Misono and Yukio Yoneda

Department of Synthetic Chemistry, Faculty of Engineering, The University of Tokyo, Hongo, Bunkyo-ku, Tokyo

(Received September 13, 1971)

We have reported that rate and selectivity increase monotonously with the acid strength of catalyst in the isomerization of *n*-butene catalyzed by metal sulfates.[1] The results were explained on the basis of the relative rate of proton transfer between catalyst and butene. If the proton transfer is involved in the reaction, it would be expected that (i) over deuterated catalysts, deuterium atoms are incorporated preferentially into the isomerized butenes, and (ii) isomerization proceeds more slowly over deuterated catalysts than normal catalysts (catalyst isotope effect). Preferential deuteration (i) was reported by Ozaki and Kimura for some solid acids.[2] However, catalyst isotope effect (ii) does not seem to have been reported in solid-acid catalysis so far, although it was reported that perdeuterobutene reacted 1.3—1.8 times more slowly than normal butene over silica-alumina.[3]

We observed catalyst isotope effect (ii), in addition to preferential deuterium incorporation (i), in the case of butene isomerization catalyzed by aluminum and magnesium sulfates supported on silica gel (Al-S and Mg-S). The extent of consumption of catalytically active deuteron on the catalyst surface could be examined by the measurement of the deuterium content of butenes.

Reaction apparatus was a closed circulating system (124 cc) connected to a conventional vacuum-line. Catalysts were first evacuated for 1 hr at 100°C in the system and then equilibrated three times with H_2O or D_2O vapor at 70°C. Further equilibration had no effect on the reaction. A catalyst pre-equilibrated with H_2O is denoted by H-catalyst and that with D_2O by D-catalyst. They were evacuated for 1 hr at 70°C, prior to reaction. Reaction temperature was 60±0.5°C. Butene pressure was 10—15 cmHg. Repeated runs on the same catalyst after the same treatment gave sufficiently reproducible results for Mg-S (±3%) and for Al-S (±10%). The rate obviously decreased upon deuteration of Mg-S and the original activity was recovered by re-equilibration with H_2O. The change was much smaller for Al-S. The ratio of the conversion of *cis*-2-butene over H-Mg-S to that over D-Mg-S at the same reaction time is plotted against the latter in Fig. 1. Extrapolation of this ratio to zero conversion gives an isotope effect of 1.7±0.2. A similar effect was also observed for 1-butene isomerization. The rapid decrease in ratio during the course of the reaction may be due to the substitution of deuteron by a more active proton. A slower decrease observed in an experiment with low butene pressure is in accord with this view. The ratio of two isomerized products from *cis*-2-butene (*trans*/1) was 10% lower over D-catalyst (D-Mg-S and D-Al-S), probably reflecting a secondary isotope effect. There was little change in *cis*/*trans* ratio from 1-butene upon deuteration of the catalyst.

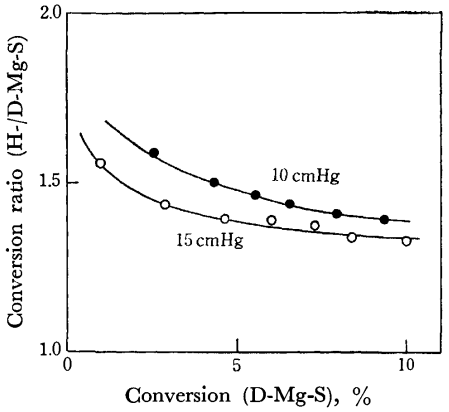

Fig. 1. The ratio of conversion of *cis*-2-butene over normal magnesium sulfate supported on silica gel (H-Mg-S) to that over deuterated magnesium sulfate (D-Mg-S) at 60°C.
Butene pressure: 10 cmHg (●), 15 cmHg (○)

Table 1. Composition of products in the isomerization of *cis*-2-butene over deuterated Mg-S and Al-S at 60°C

		Composition (%)	Isotopic composition (%)[a]	
			d_0	d_1
Mg-S	1-	0.9	38	62
	trans-	0.6	44	56
	cis-	98.5	99.5	0.5
Al-S	1-	3.6	39	61
	trans-	11.9	46	54
	cis-	84.5	91	9

a) Multi-deuterated species observed in small amounts were neglected.

The results of mass spectrometric analysis of the products are given in Table 1. Preferential incorporation of deuterium atoms into isomerized products was obvious. The results show that proton transfer was involved in the reaction and that it was the origin of the observed isotope effect. The fractions of the deuterated products are shown to be only 50—60% and should be compared with the rapid decrease of the conversion ratio in Fig. 1. If the energy profile of the reaction is considered,[4] the observed isotope effect may be regarded as that in the step of proton addition to butene. The reason for the weak effect with a strong acid such as Al-S is now under investigation.

1) M. Misono, Y. Saito, and Y Yoneda, *J. Catal.*, **9**, 135 (1967); **10**, 88 (1968); M. Misono and Y. Yoneda, This Bulletin, **44**, 3236 (1971).

2) A. Ozaki and K. Kimura, *J. Catal.*, **3**, 395 (1964).

3) J. W. Hightower and W. K. Hall, *J. Amer. Chem. Soc.*, **89**, 778 (1967).

4) M. Misono and Y. Yoneda, *Shokubai*, **13**, 22P (1971); *J. Phys. Chem.*, in press.

The Reaction of Disodium Tetracarbonylferrate(−II) with Phthaloyl Dichloride. The Formation of Biphthalidylidene

Take-aki MITSUDO, Yoshihisa WATANABE, Masato TANAKA, Kazuo YAMAMOTO, and Yoshinobu TAKEGAMI

Department of Hydrocarbon Chemistry, Faculty of Engineering, Kyoto University, Sakyo-ku, Kyoto

(Received September 16, 1971)

Previously we reported that acyl halides react with disodium tetracarbonylferrate(−II) (I) to give the acyl tetracarbonylferrates (II), which are then hydrolyzed to the corresponding aldehydes in high yields.[1]

$$\underset{\text{(I)}}{Na_2Fe(CO)_4} + RCOCl \longrightarrow \underset{\text{(II)}}{Na^+[RCOFe(CO)_4]^-} \xrightarrow{H^+} RCHO$$

On the other hand, Sawa and his co-workers[2] reported that lithium acyltetracarbonylferrates (III), which are prepared from $Fe(CO)_5$ and organolithium compounds, react with acyl halides to give ketones and/or α-diketones. It is strongly suggested that the reaction proceeds *via* the aryl- or alkylacyloxycarbene iron complex (IV):

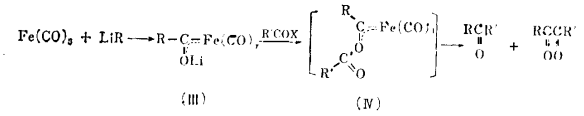

(III) (IV)

In this communication we wish to report that $Fe(CO)_4^{2-}$ reacts with phthaloyl dichloride to give biphthalidylidene possibly *via* the cyclic carbene iron complex.

The reaction was carried out as follows. Into $Na_2Fe(CO)_4$[3] (11 mmol) in tetrahydrofuran, we added 1.6 m*l* (11 mmol) of phthaloyl dichloride with stirring at −40°C under argon. After 1 hr, the mixture was warmed to 40°C and stirred for 2 hr. Then the solvent was distilled off and the residue was washed with water, 6N HCl, water again, and then ethyl ether. The orange-yellow precipitate (0.81 g) thus obtained was recrystallized twice form chloroform to give yellow biphthalidylidene (0.33 g). Yield, 23%. Mp 340—341°C (339—341°C[4]). Found: C, 72.25; H, 3.17%; mol wt (mass) 264. Calcd for $C_{16}H_8O_4$: C, 72.73; H, 3.05%; mol wt 264.22. IR(KBr): 3085 (ν_{C-H}), 1785 ($\nu_{C=O}$), 1605, 1590, 1478 (benzene ring), 1190 (ν_{C-O}), 758 (*o*-disubstituted benzene) cm^{-1}. UV: $\lambda_{max}^{CH_3CN}$ mμ (log ε); 221(4.35), 226(4.38), 257(4.09), 293(4.02), 304(4.07), 356(4.39). These spectra are identical with those of *trans*-formed biphthalidylidene reported previously.[4]

The reaction mechanism is not completely clear at the present time, but a plausible reaction scheme may be presented. First, $Fe(CO)_4^{2-}$ attacks one of the acyl halide groups in phthaloyl chloride to give an acyl carbonylferrate (V). Then the oxygen atom of the acyl group attached to the iron attacks another acyl carbon atom nucleophilically to form a lactonic carbene carbonyliron complex (VI),[5] which then decomposes thermally to biphthalidylidene (VII). Fischer reported that the pyrolysis of a phenylalkoxycarbene-chromium complex gives the dimer of the carbene ligand.[6]

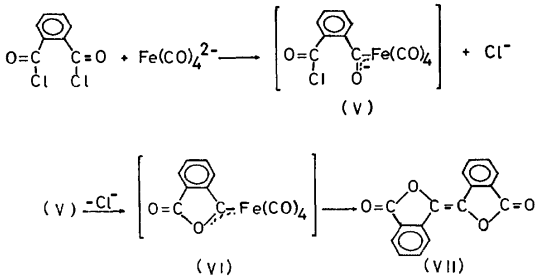

(V) (VI) (VII)

It should be noted that it may be difficult to form the cyclic carbene complex by the reaction of organolithium compounds with metal carbonyls and that two carbene ligands are introduced into this product, biphthalidylidene. In contrast to the present results, only one ligand is introduced into the products in the reaction of lithium tetracarbonylferrate (III) with acyl halide.[2] Further studies of the reaction mechanism are required to explain the difference between these reactions.

The reaction of diacyl halides with metal dianion complexes, $M(L)_n^{2-}$, can possibly be utilized for the preparation of other organic compounds or cyclic carbene metal complexes. We are now investigating these reactions; the results will be published in the near future.

1) Y. Watanabe, T. Mitsudo, M. Tanaka, K. Yamamoto, T. Okajima, and Y. Takegami, This Bulletin, **44**, 2569 (1971).

2) Y. Sawa, M. Ryang, and S. Tsutsumi, *J. Org. Chem.*, **35**, 4183 (1970).

3) M. P. Cooke, Jr., *J. Amer. Chem. Soc.*, **92**, 6080 (1970); V. W. Hieber and G. Braun, *Z. Naturforsch.*, **14b**, 132 (1959).

4) J. C. Sauer, R. D. Cramer, V. A. Engelhardt, T. A. Ford, H. E. Holmqust, and B. W. Howk, *J. Amer. Chem. Soc.*, **81**, 3677 (1959).

5) Lactonic carbene cobalt complex has been prepared by the reaction of $Co_2(CO)_8$ with acetylene and carbon monoxide; H. W. Sternberg, J. G. Shukys, C. D. Donne, R. Markby, R. A. Friedel, and I. Wender, *ibid.*, **81**, 2339 (1959).

6) E. O. Fischer, B. Heckl, K. H. Dötz, J. Müller, and H. Werner, *J. Organometal. Chem.*, **16**, P 29 (1969).

An Unusual Ring Expansion of Lophine to 2,4,6-Triphenyl-s-Triazine

K. SAKAI and J.-P. ANSELME*

Department of Chemistry, University of Massachusetts, Boston, Mass. 02116, U.S.A.

(Received September 6, 1971)

The paucity of *N*-amino imidazoles suitable for our investigation of the fragmentation of *N*-azolylnitrenes[1] prompted us to attempt the generation of these *N*-nitrenes directly *via* the *N*-azides. It has already been shown that in principle all *three* nitrogen atoms of *p*-toluenesulfonyl azide (tosyl azide) can be transferred (*azido transfer* reaction) to anions of secondary amines or imines. Although this reaction has been realized with imines,[2] difficulties arose when side-reactions became the major paths of these experiments.[2,3] These facts notwithstanding, it was anticipated that with the appropriate substrates, *N*-azidation should be possible. The ready availability of 2,4,5-triphenylimidazole (I) prompted us to explore this possibility, particularly since its anion (IIb) is symmetrical with respect to attack of tosyl azide at nitrogen (site 1); since azidation at carbon (site 2) would result in the formation of a non-aromatic ring, it was anticipated that this might favor the formation of the *N*-azide.

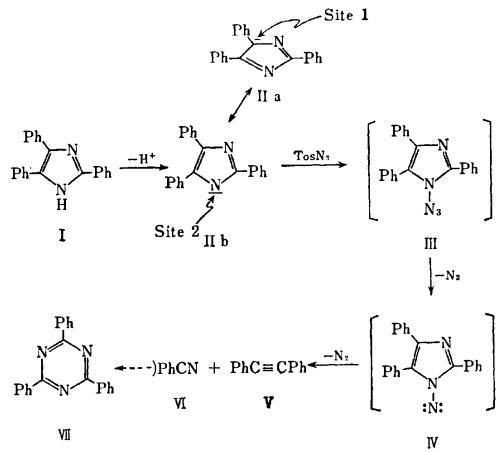

The anion of lophine (II), prepared by the reaction of lophine with one equivalent of methyllithium in tetrahydrofuran, was treated with a two-fold excess of tosyl azide and the reaction mixture was then heated under reflux for 12 hr; vigorous evolution of nitrogen was observed. The reaction mixture was quenched by the addition of water and the organic products were separated by chromatography on alumina. From 20.2 mmol of lophine, there was obtained 4.7 mmol of 2,4,6-triphenyl-*s*-triazine (VII), 2.7 mmol of tolan (as its picrate) and 1.0 mmol of *N*-tosylamino lophine (VIII), in addition to 10.4 mmol of unreacted lophine. Our original assumption was that the triazine arose by trimerization of benzonitrile,[4] one of the primary fragmentation products. On that basis, the yield of benzonitrile (as the triazine) would be over 160% and this coupled with the abnormally low yield of the tolan prompted us to question the fragmentation path as the source of the triazine. If the yield of tolan is taken as the extent to which fragmentation (assuming 100% conversion)[5] was responsible for triazine, then 6.1 mmol of lophine anion was converted to 3.8 mmol of triazine by another route.

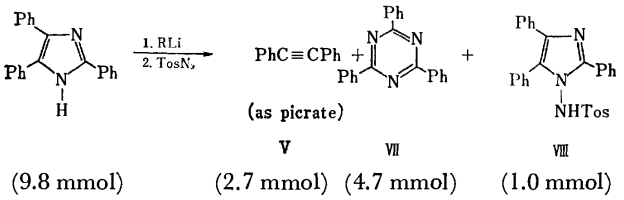

(9.8 mmol) (2.7 mmol) (4.7 mmol) (1.0 mmol)

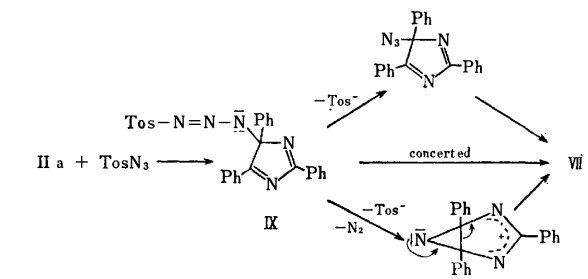

The results obtained can only be rationalized in terms of an attack of tosyl azide at carbon followed by generation of the azide or more likely a concerted ring expansion of the primary addition product (IX) perhaps *via* the highly stabilized bicyclic betaine; bond reorganization would then lead to the observed 2,4,6-triphenyl-*s*-triazine. To our knowledge, this is the first report of a nitrene ring expansion of this type of a five- to a six-membered aromatic heterocycle.[6]

The data obtained show that attack by tosyl azide at carbon is favored by almost 2 to 1 over attack at nitrogen and the ring expansion reaction proceeds in about 64% yield.

* Fellow of the Alfred P. Sloan Foundation.

The generous support of this work by the National Institutes of Health through Grant GM 13689-05 is hereby acknowledged with deep appriciation.

1) K. Sakai and J.-P. Anselme, *Tetrahedron Lett.*, **1970**, 3851.

2) J.-P. Anselme, W. Fischer, and N. Koga, *Tetrahedron*, **25**, 89 (1969).

3) G. Koga and J.-P. Anselme, Unpublished results.

4) We have determined that benzonitrile trimerizes to the triazine under the reaction conditions.

5) The serendipitous formation of VIII allowed us to ascertain that the fragmentation gave the triazine and diphenylacetylene in 48 and 60% yields respectively. *N*-Tosylaminolophine (VIII) was stable under the reaction conditions. The results of the fragmentation will be reported at a later date.

6) For an example of another type, see H. E. Baumgarten, W. F. Wittmann, and G. J. Lehmann, *J. Heterocycl. Chem.*, **6**, 333 (1969).

The Fragmentation of an *N*-Pyrryl Nitrene from the Oxidation of 6-Amino-1,4,5,7-tetramethylpyrrolo[3,4-*d*]pyridazine

K. SAKAI and J.-P. ANSELME*

Department of Chemistry, University of Massachusetts, Boston, Mass. 02116, U.S.A.

(Received September 28, 1971)

While pyrryl *N*-nitrenes do not undergo fragmentation,[1,2] those *N*-nitrenes derived from 1,2,4- and 1,2,3-triazoles,[2,3] tetrazoles,[3] imidazoles,[4] and 1- and 2-benzotriazoles[5] lose elemental nitrogen with formation of the corresponding triply bonded species. We now report evidence which suggests that fragmentation can be a reaction path for some pyrryl *N*-nitrenes.

When a solution of 6-amino-1,4,5,7-tetramethylpyrrolo[3,4-*d*]pyridazine (I)[6] was heated with lead tetraacetate under reflux for 3 hr, nitrogen was generated in about 36% yield. From the very dark brown reaction mixture, a crude semi-solid was obtained which exhibited a medium intensity band at 2035 cm^{-1} (shoulder at 2075 cm^{-1}) and a strong absorption at 1735 cm^{-1}. Treatment of this crude product with 2,4-dinitrophenylhydrazine under acidic conditions gave the bis-(2,4-dinitrophenyl)hydrazone of acetylacetone, mp 209—212°C, identical in all respects with an authentic sample. When the oxidation was carried out overnight at room temperature, the yield of nitrogen was about 22%. Addition of solid sodium carbonate to the dark reaction mixture, followed by removal of the solids and mild acidic hydrolysis of the filtrate, gave a 16% yield of acetylacetone. Its infrared spectrum was superimposable upon that of an authentic sample; its bis-(2,4-dinitrophenylhydrazone) was also identical in all respects to an authentic sample.

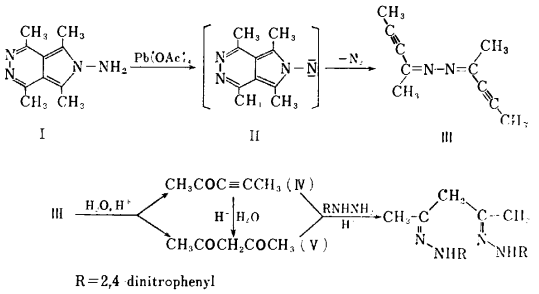

The isolation of acetylacetone coupled with the evolution of nitrogen suggests that, in contrast to the *N*-nitrenes derived from pyrroles and carbazoles,[1,2] the *N*-nitrene (II) generated from I underwent fragmentation to the extent of ~36%. The primary fragment (III) might be expected to be somewhat unstable to the conditions of the reaction and to be hydrolyzed at least partially to 3-pentyne-2-one (IV) which would then presumably be hydrated to acetylacetone; alternatively, IV could give the bis-hydrazone by direct reaction with 2,4-dinitrophenylhydrazine.

The formation of large amounts of dark products suggests that the *N*-nitrene (II) undergoes further reactions *without* expulsion of nitrogen. The occurrence of the fragmentation path in this case may be the result of synergistic effect of two factors, namely the incorporation of the pyrrole ring in a quinoid structure[5] and secondly, the electron withdrawing effect of the two nitrogen atoms of the pyridazine ring which possibly weakens the "backbone" bond[8] sufficiently so that fragmentation can occur.

* Fellow of the Alfred P. Sloan Foundation. To whom inquiries should be addressed.

The support of this work by the National Institutes of Helth (GM 13689-05) is hereby acknowledged with deep appriciation.

1) a) D. M. Lemal, T. W. Rave, and S. D. McGregor, *J. Amer. Chem. Soc.*, **85**, 1944 (1963). b) L. A. Carpino, *J. Org. Chem.*, **30**, 736 (1965).

2) K. Sakai and J.-P. Anselme, *Tetrahedron Lett.*, **1970**, 3851.

3) K. Sakai and J.-P. Anselme, unpublished results.

4) K. Sakai and J.-P. Anselme, This Bulletin, **45**, 306 (1972).

5) C. D. Campbell and C. W. Rees, *J. Chem. Soc., C*, **1969**, 742.

6) W. L. Mosby, *J. Chem. Soc.*, **1957**, 3997; G. Adembri, F. DeSio, R. Nesi, and M. Scotton, *ibid., C*, **1970** 1536.

7) D. S. Noyce and K. E. DeBruin, *J. Amer. Chem. Soc.*, **90**, 372 (1968).

8) K. Sakai, A. Tanaka, G. Koga, and J.-P. Anselme, *Nippon Kagaku Zasshi*, **92**, 1065 (1971).

The CuCl : 1,1-Diphenyl-2-picrylhydrazyl Free Radical Complex

F. LEH and J.K.S. WAN
Department of Chemistry ,Queen's University, Kingston, Ontario, Canada
(Received May 4, 1971)

Although copper ion and hydrazine form a complex readily,[1] none of the disubstituted hydrazines has shown any evidence of complex formation.[2] The reactions of DPPH with copper acetylacetonates[3] and with ferrous ions[4] have been reported. These brief communications are concerned only with the rate of the *apparent* disappearance of free DPPH as monitored by its characteristic visible absorption at 527 mμ, and it was not certain what the nature of the reaction was. The present preliminary report describes the reaction of 2,2-diphenyl-1-picrylhydrazine ($DPPH_2$) and the 1,1-diphenyl-2-picrylhydrazyl radical (DPPH) with Cu(I)Cl and the characterization of the new copper free radical complex formed. Both the $DPPH_2$ and the DPPH reactions lead to the identical solid CuCl:DPPH paramagnetic complex which is remarkably stable. The presence of an unpaired electron in the DPPH ligand may contribute to the donor ability of the molecule to form a metal complex.

The brown solid complex CuCl:DPPH has been prepared *via* different methods involving the reactions of either DPPH with CuCl or $DPPH_2$ with $CuCl_2$ in suitable solvents. The complex can be recrystallized from chloroform and ether and melts with decomposition at 176—178°C. Results of the elementary analysis and molecular weight determinations are consistent with the 1:1 ratio CuCl:DPPH complex. When the complex was dissolved in dilute nitric acid in the presence of Ag^+ ion, gentle heating of the solution regenerated the free DPPH radicals which could be seen readily by the appearance of the characteristic purple color (527 mμ). Prolonged heating resulted in further protonation of DPPH to give the hydrazine. The complex was also found to be unstable in strong acids.

The IR spectrum of the complex in the region 600—4000 cm^{-1} is similar to that of DPPH. The UV-visible absorption spectrum of the complex is, however, distinctly different from that of free DPPH. The characteristic visible absorption band at 527 mμ in the uncomplexed DPPH free radical is probably due to the picryl ring having appreciable delocalized unpaired spin and the second band at ~330 mμ is ascribed to the diphenylamino moiety. The new complexed DPPH absorption spectrum retains the band at ~319 mμ but the visible band at 527 mμ disappears. This suggests that the coordination of Cu^+ ion is probably *via* the picryl ring:

In acid solutions, the complex is not stable; the Cu^+ is oxidized to the Cu^{2+} state and thelig and DPPH is liberated thus regenerating the visible absorption band at 527 mμ.

The oxidation state of copper in the paramagnetic free radical complex was studied by electron spin resonance. The ESR spectrum of the polycrystalline complex shows a single symmetrical line with $g=2.002$. For comparison the Cu(II) complex $Cu^{2+}(N_2H_4)_2(HSO_4^-)_2$ was prepared[1] and its powder ESR spectrum gives the characteristic anisotropic Cu(II)lines. When the CuCl:DPPH complex was dissolved in a degassed benzene solution, a five-line ESR spectrum with additional poorly resolved hyperfine structures resembling a DPPH spectrum, was observed. Since the ESR spectrum of DPPH in a degassed benzene solution is very complicated and has not yet been analysed in detail, it is not practical to speculate on assignments of the CuCl:DPPH spectrum based on some poorly resolved structure. However, ESR spectra of free radical complexes with metal chlorides have been observed with hyperfine couplings assigned to the metal and the chlorine nuclei.[5] γ-Irradiation of the complex CuCl:DPPH in solid state leads to a weak ESR spectrum having the appearance of the paramagnetic Cu^{2+} ion. Detailed investigation of the radiation damage of copper complex is in progress. Based on the ESR results, the copper ion in the solid complex CuCl:DPPH is thought to be in the +1 state. Complementary chemical evidence also showed that the chloride ligand is tightly bound to the copper, characteristic of Cu(I) compounds.

The high resolution PMR spectra of the complex CuCl:DPPH in deuterated acetone or chloroform solvents taken at various temperatures, showed resonance absorptions due to two different groups of protons with intensities in the ratio of 5:1. The large absorption centered at ~538 cps is assigned to the protons on the unsubstituted phenyl rings while the other small absorption at ~435 cps is due to the protons on the picryl ring. In the spectrum of uncomplexed DPPH, the spin delocalization on the picryl ring renders the NMR absorption of the protons on the picryl ring too broad for detection. When the DPPH is complexed to the copper ion *via* the picryl ring, the coordination probably twists the picryl ring more out of the plane of the unpaired electron orbital thus reducing the probability of delocalization and sharpening the picry proton peaks for observation. An X-ray study has shown[6] that in the solid DPPH the picryl ring and the other two phenyl rings are not coplanar with the hydrazine backbone. Thus the observed resonance due to the picryl protons in the complex agrees with the optical absorption evidence suggesting the coordination *via* the picryl ring.

1) A. P. Bhargava, R. Swaroop, and Y. K. Gupta, *J. Chem. Soc., A*, **1970**, 2183.
2) F. Bottomey, *Quart. Rev.*, **24**, 617 (1970).
3) K. Uehara, M. Tanaka, and N. Murata, This Bulletin, **41**, 3034 (1968).
4) V. V. Voevodskii, R. I. Zusman, and Y. N. Molin, *Izv. Sib. Otd. Akad. Nauk SSSR Ser. Khim Nauk*, **3**, 127 (1968).
5) P. Clopath and A.V. Zelewsky, *Chem. Commun.*, **1971** 47.
6) D. E. Williams, *J. Amer. Chem. Soc.*, **88**, 5665 (1966).

Electronic Spectra and Structures of Organic π-Systems. III. Electronic Spectra of Nitrocyclopentadienide Anion and Formylcyclopentadienide Anion[1]

Zen-ichi Yoshida, Tsunetoshi Kobayashi*, and Akihiko Konishi

Department of Synthetic Chemistry, Faculty of Engineering, Kyoto University, Yoshida, Kyoto

(Received February 8, 1971)

The electronic spectra of sodium nitrocyclopentadienide and sodium formylcyclopentadienide have been measured in several solvents. The electronic states of these compounds have been calculated by variable integrals methods I and II (modified Pariser-Parr-Polpe method). The longest wave-length strong absorption band of nitrocyclopentadienide (304 mμ) or formylcyclopentadienide (280 mμ) in isooctane has been assigned to the superimposed band of two intramolecular chage-transfer transitions from the five-membered ring to the nitro or formyl group. Agreement between the calculated and observed transition energies in isooctane is satisfactory.

Among nonbenzenoid aromatic systems the $(CH)_{4n+1}$ ring system having $(4n+2)\pi$ electrons is expected to have interesting electronic characteristics. Cyclopentadienide anion ($n=1$) is the most typical one of this system. However, no detailed investigations have been carried out on the electronic spectra and structures of substituted cyclopentadienide anions. This paper deals with the electronic states of nitro- and formylcyclopentadienide anions.

Experimental

Materials. Sodium nitrocyclopentadienide was prepared by Thiele's[2] method. Sodium formylcylopentadienide was prepared by the method of Hafner and his co-workers.[3] Since the latter compound is quite unstable in atmosphere, treatment was carried out in a nitrogen dry box.

Measurements. Ultraviolet-visible spectra were measured by a Hitachi Model EPS-3T spectrophotometer in isooctane, ether, methanol, water, and acetonitrile.

Results. The ultraviolet-visible spectra of sodium nitrocyclopentadienide and sodium formylcyclopentadienide are shown in Fig. 1. The peak wavelengths are summarized in Table 1.

The ultraviolet and visible spectra of sodium nitrocyclopentadienide in water have been reported also by Kerber and Chick.[4]

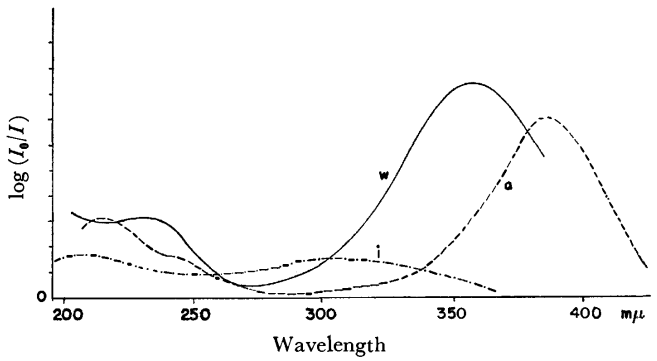

Fig. 1a. Ultra-violet and visible spectra of sodium nitrocyclopentadienide.
Solvents: water (w), acetonitrile (a), and isooctane (i).

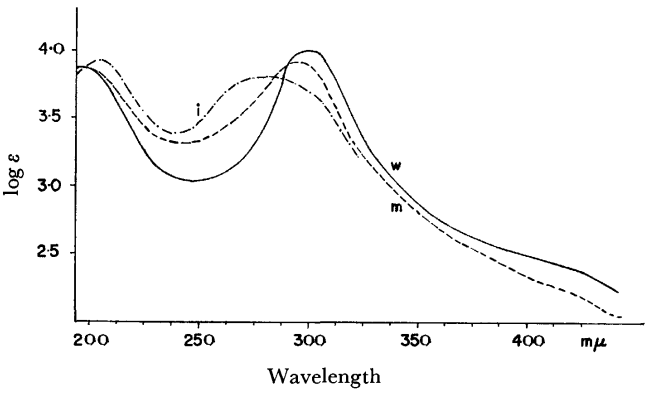

Fig. 1b. Ultra-violet and visible spectra of sodium formylcyclopentadienide.
Solvents: water (w), methanol (m), and isooctane (i).

Theoretical

Methods. The variable integrals methods, VI/1, VI/2/only NNβ, and VI/2/allβ are used.[5] Only the nearest-neighbour β's are taken into consideration in the VI/2/only NNβ, and VI/1 methods while in the VI/2/allβ method all the β's are.

Numberings of the atomic orbitals are shown in Fig. 2. The structures of these molecules are assumed to be as shown in Fig. 2 with reference to the crystallographic data of nitro- and formyl compounds.[6,7] The five-membered rings are assumed to be regular pentagons, and the C–C bond lengths of the pentagons to be 1.40 Å.

The necessary parameters W_p's, α_p's, and $\bar{\alpha}_p$'s are summarized in Table 2.

For the sake of simplicity the variable integrals are reevaluated only in the first five and ten iteration steps of SCF procedures of the VI/1 method and the VI/2 method, respectively.

1) Presented at the 2nd Symposium on Chemistry of Nonbenzenoid Aromatic Compounds, Kyoto, November, 1968.

* Present address: The Institute for Solid State Physics, The University of Tokyo, Roppongi, Minato-ku, Tokyo.

2) J. Thiele, *Ber.*, **33**, 670 (1900).

3) K. Hafner, G. Schulz, and K. Wagner, *Ann.*, **678**, 39 (1964).

4) R. C. Kerber and M. J. Chick, *J. Org. Chem.*, **32**, 1329 (1967).

5) Z. Yoshida and T. Kobayashi, *Theor. Chim. Acta*, **19**, 377 (1970); *J. Chem. Phys.*, **54**, 4538 (1971).

6) "Interatomic Distances," Sp. Pub. No. 11, ed. by L. E. Sutton, The Chem. Soc., London, 1958.

7) "Interatomic Distances," Sp. Pub. No. 18, ed. by L. E. Sutton, The Chem. Soc., London, 1965.

Table 1. The peak wavelengths of sodium nitrocyclopentadienide and sodium formylcyclopentadienide in several solvents in mμ

λ_{max}[a] and ε_{max}[b]

Solvents	Sodium nitrocyclopentadienide	Sodium formylcyclopentadienide
Isooctane	201, 304	205, 280
Ether		283
Methanol		200 (7120), 291 (8590), 430[sh] (200)
Water	232 (4300), 361 (11400)	198 (7280), 297 (12300), 425[sh] (250)
Acetonitrile	213, 244[sh], 386	208, 311, 436[w]

a) in mμ b) in l/(mole·cm), in parentheses

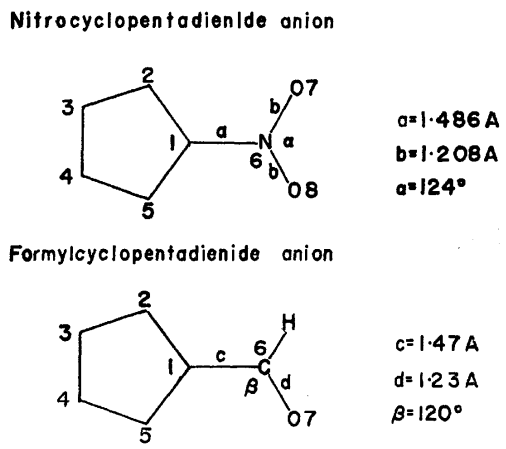

Fig. 2. Assumed structures of molecular species.

Table 2. Parameters

	W_p (eV)	α_p	$\bar{\alpha}_p$
C^+	−11.16	3.8379	3.3697
N^{2+}	−28.71	4.2949	3.7631
O^+	−17.28	3.6357	3.0593

All the singly excited configurations are taken into account in the configuration interactions.

Results. The SCF eigenvalues and eigenvectors given by the VI/2/only NNβ method are shown in Table 3. The π-electron densities and bond orders are given in Table 4, and the calculated $^1\pi^*$–$^1\pi$ transition energies in Table 5 together with the observed values.

Discussion

The β's given by the VI/1 method are on the whole similar to those given by the VI/2 method. The VI/1, VI/2/only NNβ, and VI/2/allβ methods give similar SCF eigenvalues and eigenvectors in the case of nitrocyclopentadienide anion, but slightly different eigenvectors in the case of formylcyclopentadienide anion.

The π-electron densities and bond orders given by these methods resemble each other as shown in Table 4. It is presumed that the contribution of the canonical formula or to the ground state of each anion is large. It may be anticipated that in

Table 3. SCF eigenvalues and eigenvectors given by the VI/2/only NNβ

Nitrocyclopentadienide anion

φ_i	Sym.	C_1	C_2	C_3	C_6	C_7	E_i (eV)
1	b_1	0.1989	0.0646	0.0190	0.6526	0.5126	−12.7434
2	b_1	0.4561	0.4335	0.4292	−0.0072	−0.1545	−8.1958
3	a_2	0	0.0088	0.0027	0	−0.7070	−8.1189
4	b_1	0.6201	0.1001	−0.5004	0.1300	−0.1972	−4.5572
5	a_2	0	0.6020	0.3709	0	0.0090	−4.3972
6	b_1	−0.0008	−0.3090	0.1777	0.6642	−0.3903	4.7152
7	a_2	0	0.3709	−0.6020	0	0.0023	7.8773
8	b_1	0.6066	−0.4499	0.1829	−0.3406	0.1491	8.0330

Formylcyclopentadienide anion

φ_i	C_1	C_2	C_3	C_4	C_5	C_6	C_7	E_i (eV)
1	0.3287	0.2016	0.1324	0.1276	0.1831	0.5212	0.7158	−8.5987
2	0.3241	0.4017	0.4503	0.4387	0.3754	−0.1300	−0.4248	−7.1881
3	0.4602	0.4992	−0.1399	−0.6222	−0.2585	0.1117	−0.2303	−3.6260
4	0.4085	−0.3665	−0.5862	0.0048	0.5506	0.1118	−0.1990	−3.6093
5	0.0474	−0.3364	0.2083	0.1480	−0.3403	0.7205	−0.4295	5.7716
6	0.0628	−0.4047	0.6017	−0.5833	0.3537	−0.0612	0.0319	8.4809
7	−0.6341	0.3708	−0.1051	−0.2048	0.4634	0.4045	−0.1705	9.3373

Table 4. π-Electron densities and bond orders

Atom	Electron densities VI/1	VI/2/ only NNβ	VI/2/ all β	Bond	Bond orders VI/1	VI/2/ only NNβ	VI/2/ all β
Nitrocyclopentadienide anion							
1	1.2700	1.2642	1.2585	1—2	0.5166	0.5452	0.5395
2	1.1093	1·1291	1.1269	1—6	0.4692	0.4142	0.4272
3	1.1396	1.1450	1.1418	2—3	0.7403	0.7210	0.7269
6	0.9044	0.8856	0.8984	3—4	0.5766	0.5948	0.5874
7	1.6639	1.6510	1.6529	6—7	0.6012	0.6200	0.6148
Formylcyclopentadienide anion							
1	1.1805	1.1834	1.1756	1—2	0.5328	0.5530	0.5469
2	1.1596	1.1711	1.1699	1—5	0.5624	0.5755	0.5709
3	1.1638	1.1670	1.1637	1—6	0.4937	0.4524	0.4679
4	1.1966	1.1918	1.1907	2—3	0.7224	0.7052	0.7112
5	1.0641	1.0888	1.0831	3—4	0.5786	0.5974	0.5900
6	0.6198	0.6271	0.6385	4—5	0.7169	0.7031	0.7084
7	1.6156	1.5709	1.5785	6—7	0.7211	0.7607	0.7511

Table 5. Calculated $^1\pi^*$-$^1\pi$ electronic transitions in eV

VI/1 Sym.	E	f	CI Composition[a]	VI/2/only NNβ Sym.	E	f	CI Composition[a]	VI/2/all β Sym.	E	f	CI Composition[a]	Obsd.[b] E
Nitrocyclopentadienide anion												
$^1A_1$	4.267	0.440	4—6 0.935	$^1A_1$	4.028	0.426	4—6 0.947	$^1A_1$	3.992	0.425	4—6 0.947	4.06
$^1B_2$	4.386	0.066	5—6 0.972	$^1B_2$	4.110	0.036	5—6 0.989	$^1B_2$	3.999	0.040	5—6 0.988	
$^1A_1$	6.075	0.439	2—6 −0.353	$^1B_2$	5.848	0.200	3—6 0.897	$^1A_1$	5.801	0.176	5—7 0.705	
			5—7 0.743				5—8 0.352				4—8 −0.656	
			4—8 −0.528									
$^1B_2$	6.279	0.067	3—6 0.729	$^1A_1$	6.064	0.116	5—7 0.695	$^1B_2$	5.865	0.080	3—6 0.627	6.14
			4—7 0.530				4—8 −0.656				4—7 0.336	
			3—8 0.301								5—8 0.666	
$^1B_2$	6.325	0.170	3—6 −0.360	$^1B_2$	6.331	0.013	4—7 0.719	$^1B_2$	6.107	0.061	3—6 0.649	
			4—7 0.654				5—8 0.640				4—7 −0.664	
			5—8 0.606								5—8 −0.322	
Formylcyclopentadienide anion												
	4.159	0.423	3—5 0.387		4.331	0.364	3—5 0.380		4.245	0.258	3—5 0.437	
			4—5 0.866				4—5 0.880				4—5 0.855	
	4.258	0.080	3—5 0.898		4.455	0.129	3—5 0.882		4.308	0.210	3—5 0.832	4.43
			4—5 −0.379				4—5 −0.410				4—5 −0.468	
	5.945	0.342	2—5 0.386		6.230	0.365	2—5 −0.305		5.988	0.463	3—6 −0.479	
			3—6 0.658				3—6 0.645				4—6 0.662	
			4—6 −0.456				4—6 −0.488				3—7 0.395	
			4—7 0.380				3—7 −0.326					
							4—7 −0.330					
	6.082	0.146	3—6 0.422		6.351	0.091	3—6 0.540		6.044	0.102	3—6 0.708	6.05
			4—6 0.757				4—6 0.653				4—6 0.460	
			3—7 −0.373				3—7 0.374				4—7 −0.412	
							4—7 −0.318					
	6.983	0.088			7.385	0.092			7.144	0.299		

a) The transition denoted i-j refers to a one-electron excitation from orbital i to virtual orbital j. The second column gives the CI coefficient of the configuration i-j.

b) In isooctane.

the ground states the five-membered rings are not regular pentagons but slightly bond alternated pentagons in which the C_2–C_3 and C_4–C_5 bonds are slightly shorter than the C_1–C_2, C_1–C_5, and C_3–C_4 bonds.

As is seen in Table 1, the first band ($\sim$300 mμ in isooctane) of nitrocyclopentadienide shows a remarkable red shift by the change of solvent from isooctane to acetonitrile, *viz.*, the energy of this band decreases with the increase in the dielectric constant of the solvent. Thus the band is presumed to be due to the transitions to the excited states with dipolemoments larger than those of the ground state. On the other hand the cyclopentadienide ring is an electron donating group and the nitro group a strong electron accepting group. Thus the first band is also expected to be composed of intramolecular charge-transfer transitions associated with electron transfer from the five-membered ring to the nitro group. As is seen in Table 5 the VI methods explain that this band is composed of two transitions ($^1A_1$, $^1B_2$) associated with electron transfer from the five-membered ring to the nitro group.

From our calculation, the 201 mμ band of nitrocyclopentadienide anion observed in isooctane is expected to be composed of at least two transitions. The fact that this band reveals a shoulder when the solvent is changed from isooctane to acetonitrile may support this interpretation.

The agreement between the calculated and observed transition energies in isooctane is satisfactory in the case of nitrocyclopentadienide (Table 5).

In the case of formylcyclopentadienide the 280 mμ band observed in isooctane is also shifted to 311 mμ by the change of solvent from isooctane to acetonitrile, *viz.*, this band shows a large red shift when the dielectric constant of the solvent increases. Thus the band is expected to be composed of transitions to the excited states with dipole moments larger than those of the ground state. On the other hand, our calculations also explain that this band can be composed of two intramolecular charge-transfer bands caused by electron migration from the five-membered ring to the formyl group (Table 5).

The band around 200 mμ of formylcyclopentadienide shows only a slight solvent shift by the change of solvent from a polar to a nonpolar solvent. This band is predicted to be composed of two transitions localized in the five-membered ring. The prediction is in line with the experimental data.

The longest wavelength weak band around 430 mμ of formylcyclopentadienide can be assigned to a π^*-n transition because it shows a blue shift when the solvent is changed from an aprotic to a protic solvent.

As is seen in Table 5 the argeement between the calculated and observed transition energies in isooctane is satisfactory also in case of formylcyclopentadienide. On the whole the effect of sodium cation on electronic spectra of nitro- and formylcyclopentadienide can be neglected in the calculations.

In conclusion the variable integrals methods[5] give a satisfactory explanation of the electronic spectra of both compounds chosen in this study.

The calculations have been carried out on a HITAC 5020 E computer at the Computer Centre of the University of Tokyo.

Electronic Spectra and Structures of Organic π-Systems. IV. Electronic Spectra of Nitropyrroles

Zen-ichi YOSHIDA, Tsunetoshi KOBAYASHI*, and Hidenori YAMADA

Department of Synthetic Chemistry, Faculty of Engineering, Kyoto University, Yoshida, Kyoto

(Received February 8, 1971)

The electronic spectra of 2-nitropyrrole and 3-nitropyrrole have been measured in various solvents and compared with the values calculated by the variable integrals method II. Agreement between the observed and the calculated transition energies is satisfactory. From eigenvectors of both nitropyrroles, the localization of molecular orbitals to the moiety of molecule has been discussed. The π-electon densities and π-bond orders of both molecules have also been calculated.

We have proposed a new type of modified Pariser-Parr-Pople method, the variable integrals method II, which contains no arbitrary adjusting parameters and needs no guess work in estimating a set of suitable parameters to calculate the electronic spectra of the molecule in question. The method was applied to various kinds of molecules with great success.[1,2]

The electronic spectra of 2-nitropyrrole and 3-nitropyrrole were measured in various solvents and the results were compared with the calculated values.

Experimental

Materials. Nitration of pyrrole was carried out according to Rinkes[3] and needle crystals with mp 60—62°C were obtained. They were dissolved in a benzene-ether (1 : 1) mixture and chromatographed on a silica gel column. Elutions gave substance (I), mp 65°C, as golden yellow coloured needles from carbon tetrachloride (Found: C, 43.03; H, 3.30; N, 24.98; O, 28.42%. Calcd for $C_4H_4N_2O_2$: C, 42.86; H, 3.59; N, 24.99; O, 28.56%, and substance (II), mp 101—102°C, from benzene as yellow crystals (Found: C, 43.02; H, 3.86; N, 25.01; O, 28.60%. Calcd for $C_4H_4N_2O_2$: C, 42.86; H, 3.59; N, 24.99; O, 28.56%). The mass spectrum of each compound showed a parent peak of $m/e=112$. The compounds were identified as monomers of nitropyrroles. There has been some confliction[3-5] concerning the structural identification of nitropyrroles. For instance Safonova and coworkers[4] have reported the mp of 2-nitropyrrole as 55°C and that of 3-isomer to be 64°C. The substance with mp 101°C obtained by the decarboxylation of 4-nitropyrrole-2-carboxylic acid was regarded as a dimer of nitropyrrole.[5] On the other hand, Morgan and Morrey[6] reported that the substances with mp 65—66°C and mp 99—101°C are 2-nitropyrrole and 3-isomer, respectively, and the substance with mp 63—64°C is a mixture of two isomers.

In order to investigate molecular electronic spectra, there should be no ambiguity about the position of the substituent. Thus we confirmed the position of nitro-group by the following infrared method. The infrared spectra of nitropyrroles I and II were measured in carbon tetrachloride on a JASCO DS-402G spectrophotometer. Nitropyrrole I shows three peaks in the NH stretching region at a high concentration. The three peaks at 3470 cm^{-1}, 3390 cm^{-1}, and 3265 cm^{-1} are assigned to the free ν_{N-H}, the intramolecular hydrogen bonded ν_{N-H}, and the intermolecular hydrogen bonded ν_{N-H}, respectively. The peak at 3265 cm^{-1} disappears on dilution. On the other hand, nitropyrrole II shows two peaks in the NH stretching region. The two peaks at 3493 cm^{-1} and 3385 cm^{-1} are regarded as the free and the intermolecular hydrogen bonded N-H stretching vibrations,

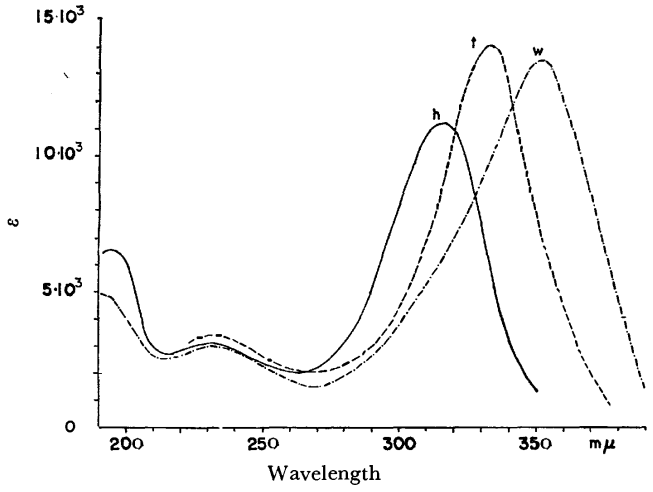

Fig. 1a. Electronic spectra of 2-nitropyrrole.
Solvents: *n*-hexane (h), tetrahydrofuran (t), and water (w).

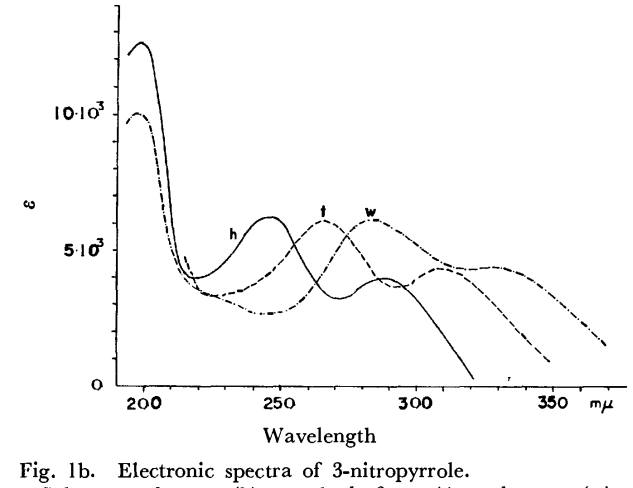

Fig. 1b. Electronic spectra of 3-nitropyrrole.
Solvents: *n*-hexane (h), tetrahydrofuran (t), and water (w).

* Present address: The Institute for Solid State Physics, The University of Tokyo, Roppongi, Minato-ku, Tokyo.

1) Z. Yoshida and T. Kobayashi, *J. Chem. Phys.*, **54**, 4538 (1971).
2) Z. Yoshida, T. Kobayashi, and A. Konishi, *This Bulletin*, **45**, 309 (1972).
3) I. J. Rinkes, *Rec. Trav. Chim.*, **54**, 1167 (1934).
4) E. N. Safonova, V. M. Belikov, and S. S. Novikov, *Izvest. Akad. Nauk* S. S. S. R. Otdel. Khim. Nauk, 1307 (1959).
5) W. J. Hale and W. Hoyt, *J. Amer. Chem. Soc.*, **37**, 2551 (1915).
6) K. J. Morgan and D. P. Morrey, *Tetrahedron*, **22**, 57 (1966).

Table 1. The maximum wavelengths (mμ) and molar extinction coefficients (in parentheses) of nitropyrroles in various solvents

Solvent				
	2-Nitropyrrole			
n-Hexane	193.5 (6590),	230.5 (3090),		315.5 (11190)
Tetrahydrofuran		230 (3400),		332.5 (14020)
Acetonitrile		231 (2930),		335 (12770)
Methanol		230 (3390),		336 (13010)
Water		232.5 (2940),		351.5 (13480)
	3-Nitropyrrole			
n-Hexane	198.5 (12660),		246 (6280),	286.5 (3940)
Tetrahydrofuran		222^{sh} (3380),	265 (6110),	309.5 (4330)
Acetonitrile	202 (10870),	224 (3470),	267.5 (6530),	313.5 (4470)
Methanol		222 (3570),	269 (6330),	313 (4510)
Water	198 (10800),	222.5^{sh} (3400),	281 (6200),	329 (4410)

Table 2. SCF eigenvalues and eigenvectors for 2-nitropyrrole and 3-nitropyrrole

Ψ_i	C_1	C_2	C_3	C_4	C_5	C_6	C_7	C_8	E_i (eV)
2-Nitropyrrole									
1	0.3994	0.4117	0.1808	0.1032	0.1576	0.5937	0.3543	0.3534	−17.9963
2	0.6687	0.1817	0.1321	0.1957	0.3594	−0.3694	−0.3177	−0.3128	−16.3802
3	−0.4282	0.1922	0.5252	0.4608	0.1038	−0.0191	0.2870	−0.4450	−12.7252
4	0.2635	−0.1310	−0.3132	−0.2718	−0.0500	−0.0054	0.6668	−0.5425	−12.6115
5	−0.0309	−0.5716	−0.2300	0.4414	0.5722	−0.0035	0.2054	0.2345	−11.6450
6	−0.2307	0.2068	−0.4358	−0.0164	0.3410	0.5305	−0.3839	−0.4107	−2.0095
7	0.2922	−0.4280	0.0736	0.4242	−0.5442	0.4005	−0.2060	−0.2168	0.5868
8	0.0320	−0.4367	0.5727	−0.5383	0.3048	0.2625	−0.1208	−0.1190	1.6233
3-Nitropyrrole									
1	0.3483	0.2810	0.3675	0.1774	0.1819	0.5822	0.3614	0.3612	−17.5224
2	0.7039	0.2901	0.0286	0.1345	0.3226	−0.3662	−0.2898	−0.2818	−16.5309
3	−0.4750	0.1666	0.5888	0.5142	0.1208	−0.0641	−0.2657	−0.2151	−12.5753
4	−0.0138	−0.0432	−0.0018	0.0612	0.0552	−0.0096	0.7069	−0.7010	−12.3557
5	−0.0320	−0.5478	−0.3013	0.4531	0.6068	0.0020	0.0547	0.1776	−11.5936
6	0.2210	−0.5046	0.2080	−0.1609	−0.0683	0.5484	−0.3992	−0.4033	−1.5166
7	0.3274	−0.3750	0.1956	0.4544	−0.6221	−0.2718	0.1468	0.1586	0.2666
8	−0.0202	0.3346	−0.5875	0.4946	−0.2921	0.3848	−0.1769	−0.1822	1.8670

respectively. The peak at 3385 cm^{-1} disappears on dilution. Thus it was concluded that nitropyrrole I is 2-nitropyrrole and nitropyrrole II 3-isomer.

Measurements. Ultraviolet and visible spectra were obtained with a Hitachi Model EPS-3T spectrophotometer, in *n*-hexane, tetrahydrofuran, acetonitrile, methanol, and water.

Results. The ultraviolet and visible absorption spectra of the compounds in several solvents are shown in Fig. 1. The peak wavelengths of these spectra are summarized in Table 1. Morgan and Morrey[6] have reported the λ_{max} and ε_{max} of these compounds observed in *n*-hexane and methanol. They are consistent with our results, although the spectra around 200 mμ have not been measured.

Theoretical

Method. The variable integrals method II was used.[1,2] The molecular structures of nitropyrroles are assumed as shown in Fig. 2 using the structural data of pyrrole[7] and *p*-nitroaniline.[8] Numberings of the atomic orbitals are also given in Fig. 2.

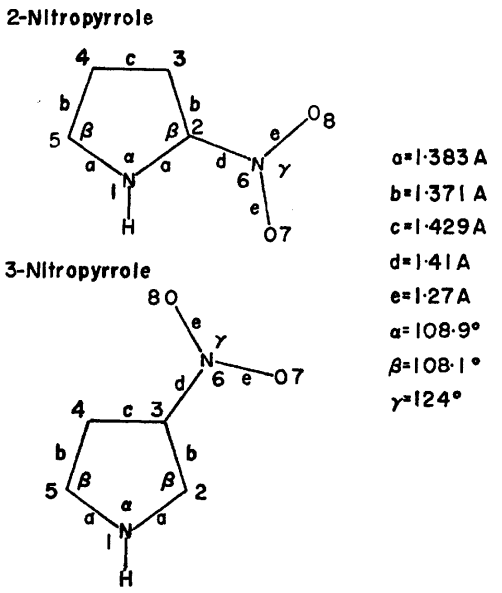

Fig. 2. Assumed structures of nitropyrroles.

7) B. Bak, D. Christensen, L. Hansen, and J. Rastrup-Andersen, *J. Chem. Phys.*, **24**, 720 (1956).

8) J. Donohue and K. N. Trueblood, *Acta Crystallogr.*, **9**, 960 (1956).

Results and Discussion

The SCF eigenvalues and eigenvectors of nitropyrroles are shown in Table 2. The molecular orbitals ψ_5 and ψ_8 of 2-nitropyrrole, and ψ_3, ψ_5, and ψ_7 of 3-nitropyrrole are mainly localized on pyrrole ring, and the molecular orbitals ψ_4's of both nitropyrroles are almost localized in nitro-groups. The other molecular orbitals are delocalized over both pyrrole and nitro-groups.

The π-electron densities and bond orders are summarized in Table 3. In the ground state the charges of about −0.11 *e* and −0.09 *e* are transferred from pyrrole group to nitro-group in 2- and 3-nitropyrroles, respectively.

Table 3. π-Electron densities and bond orders

	2-Nitropyrrole	3-Nitropyrrole
Electron densities		
1	1.7207	1.6871
2	1.1667	0.9857
3	0.9534	1.1467
4	1.0599	1.0461
5	0.9892	1.0461
6	0.9785	0.9546
7	1.5913	1.5757
8	1.5403	1.5581
Bond orders		
1—2	0.3735	0.4821
1—5	0.4560	0.4257
2—3	0.7434	0.7497
3—4	0.5399	0.4704
4—5	0.8010	0.8322
2—6	0.3527	
3—6		0.3304
6—7	0.6357	0.6538
6—8	0.6719	0.6687

The calculated transition energies are summarized in Table 4 with the observed ones in *n*-hexane.

In the case of 2-nitropyrrole the calculated 5.354 eV and 6.457 eV transitions are in good agreement with the observed values. From the CI coefficients we see that the 4.327 eV transition is the so-called intramolecular chage-transfer transition associated with electron migration from pyrrole group to nitro-group. This is consistent with the observed large solvent effect on the longest wavelength band. The 4.729 eV transition is contributed from a charge-transfer configuration, a local excitation configuration in nitro-group and a back charge-transfer configuration associated with electron transfer from nitro-group to pyrrole group. The corresponding band seems to be hidden by the other stronger bands. The 5.354 eV transition is contributed from a charge-transfer configuration, a local excitation configuration in nitro-group and a local excitation configuration in pyrrole group. The 6.457 eV transition is mainly contributed from a localized excitation configuration in pyrrole group.

Table 4. Calculated π-$^1\pi^*$ transition energies in eV

E	*f*	CI Composition[a]		$E_{obsd.}$	$\varepsilon_{obsd.}$
2-Nitropyrrole					
4.327	0.525	5—6	0.941	3.93	11190
4.729	0.162	3—6	0.736		
		4—6	0.551		
		4—7	0.324		
5.354	0.303	3—6	−0.520	5.39	3090
		4—6	0.747		
		5—8	0.344		
6.457	0.032	5—7	0.938	6.41	6590
7.252	0.096				
3-Nitropyrrole					
4.658	0.077	4—6	0.644	4.34	3940
		5—6	0.659		
4.962	0.429	4—6	−0.653	5.04	6280
		5—6	0.511		
		3—6	−0.418		
5.252	0.265	3—6	0.833	5.58[sh]	3380[b]
		5—6	0.423		
6.136	0.397	5—7	0.931	6.25	12660
6.965	0.159				

The observed values are those in *n*-hexane.

a) The transition denoted by *i-j* refers to a one-electron excitation from orbital *i* to virtual orbital *j*. The second column gives the CI coefficient of the configuration *i-j*.

b) Observed values in tetrahydrofuran.

In the case of 3-nitropyrrole the caluclated transition energies are in good agreement with the observed values. The calculated 5.252 eV transition has the character of the so-called intramolecular charge-transfer transition associated with electron migration from pyrrole group to nitro-group. The 4.658 eV and the 4.962 eV transitions are the transitions contributed from charge transfer configurations and back charge-transfer configurations. The 6.136 eV band is the local transition in pyrrole ring. In line with this theoretical interpretation, the corresponding observed band showed no appreciable solvent shift.

In conclusion we found that the variable integrals method II is useful for the systems treated in this paper.

The calculation was carried out on a HITAC 5020 E computer at the Computer Centre of the University of Tokyo.

Electronic Spectra and Structures of Organic π-Systems. V. SCFMO Calculations of Some Fulvenes and Fulvalenes with the Variable Integrals Methods[1)]

Zen-ichi YOSHIDA and Tsunetoshi KOBAYASHI*

Department of Synthetic Chemistry, Faculty of Engineering, Kyoto University

(Received February 8, 1971)

The electronic states of fulvene, 6-vinylfulvene, 6-aminofulvene, 6,6-dialkoxyfulvene, 6-amino-6-alkoxyfulvene, heptafulvene, 8-vinylheptafulvene, sesquifulvalene, and fulvalene have been investigated with the variable integrals methods. The effect of bond alternation is taken into account in the SCF procedure. Agreement between the calculated and observed transition energies is satisfactory.

The variable integrals methods I and II[2)] are applied to fulvene, 6-vinylfulvene, 6-aminofulvene, 6,6-dialkoxyfulvene, 6-amino-6-alkoxyfulvene, heptafulvene, 8-vinylheptafulvene, sesquifulvalene, and fulvalene in order to check the applicability of these methods. The effect of bond alternation is taken into consideration in the SCF procedure. Agreement between the calculated transition energies and the observed ones is satisfactory.

Methods of Calculation

Methods I and II (VI/2/only NNβ) were described in the previous papers.[2)]

In order to introduce the effect of bond alternations, the bond lengths between two adjacent atoms are re-evaluated by the following formulas in each iteration step of the SCF procedures.

$$\text{VI/1} \qquad l_{CC} = 1.515 - 0.177\,P \qquad (1)$$

$$l_{CO} = 1.367 - 0.177\,P \qquad (2)$$

$$l_{CN} = 1.453 - 0.177\,P \qquad (3)$$

$$\text{VI/2} \qquad l_{CC} = 1.515 - 0.177\,P \qquad (4)$$

$$l_{CO} = 1.371 - 0.177\,P \qquad (5)$$

$$l_{CN} = 1.454 - 0.177\,P \qquad (6)$$

Formulas (1)—(6) are obtained on the assumption that bond lengths depend linearly on bond orders. The coefficients of formuals (1) and (4) are obtained using ethylene and benzene as reference standards. Formulas (2) and (5) are obtained with formaldehyde as the standard, and (3) and (6) with pyridine. The difference between double bond length and single bond length of sp^2-hybridized atom is assumed to be equal to that of sp^2-hybridized carbon atom, *viz.*, 0.177 Å.

For the sake of simplicity the variable parameters are reevaluated only in the first five iteration steps of SCF procedures.

In order to check the applicability of formulas (1)—(6), the above methods have been applied also to *trans*-butadiene, *trans*-acrolein, *p*-dimethoxybenzene, benzoic acid, and acetanilide.

For the sake of brevity the numberings of the atomic orbitals in the molecules are given in Fig. 1. The

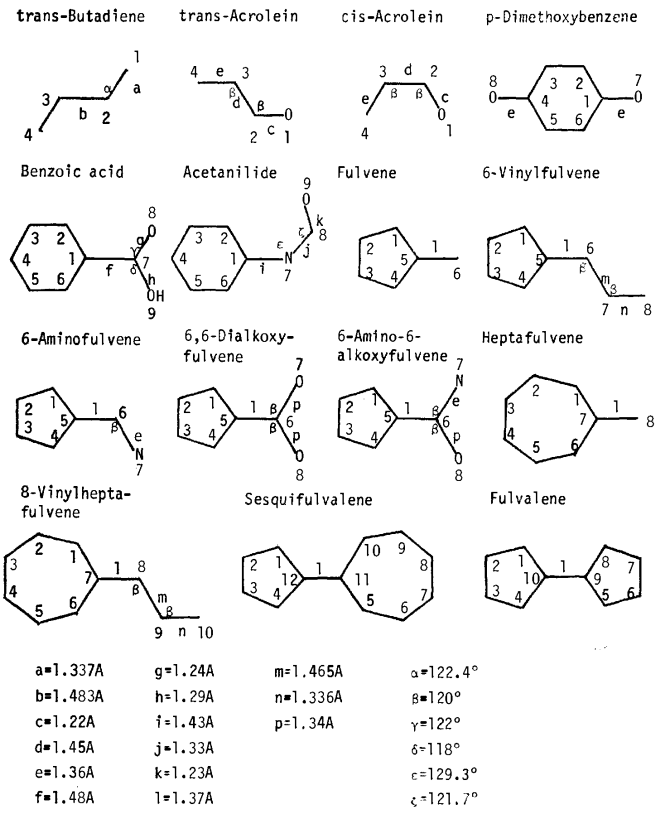

Fig. 1. Assumed structures and numbering systems of molecules.

starting molecular dimensions[3)] are assumed as in Fig. 1, the five-, six-, and seven-membered rings being taken to be regular polygons, the C–C bond lengths of pentagons and heptagons to be 1.40 Å and the C–C bond lengths of benzene rings 1.397 Å.

All the singly excited configurations are taken into account in the configuration interactions.

* Present address: The Institute for Solid State Physics, The University of Tokyo, Roppongi, Minato-ku, Tokyo.

1) Presented at the 3rd Symposium on Chemistry of Non-benzenoid Aromatic Compounds, Osaka, November, 1969.

2) a) Z. Yoshida and T. Kobayashi, *Theor. Chim. Acta*, **19**, 377 (1970). b) Z. Yoshida and T. Kobayashi, *J. Chem. Phys.*, **54**, 4538 (1971). c) Z. Yoshida, T. Kobayashi, and A. Konishi, This Bulletin, **45**, 309 (1972). d) Z. Yoshida, T. Kobayashi, and H. Yamada, *ibid.*, **45**, 313 (1972).

3) "Interatomic Distances," Sp. Pub. No. 11, ed. by L. E. Sutton, The Chem. Soc., London (1958). "Interatomic Distances," Sp. Pub. No. 18, ed. by L. E. Sutton, The Chem. Soc., London (1965).

Table 1. π-Electron densities

	VI/1	VI/2	VI/1	VI/2	VI/1	VI/2
	trans-Acrolein		*cis*-Acrolein		*p*-Dimethoxybenzene	
1	1.4206	1.4087	1.4408	1.4249	0.9906	0.9904
2	0.6444	0.6394	0.6454	0.6410	1.0292	1.0301
3	0.9949	0.9932	1.0350	1.0345		
4	0.9401	0.9587	0.8788	0.8996		
7					1.9510	1.9495
	Bonzoic acid		Acetanilide		Fulvene	
1	1.0365	1.0321	1.0275	1.0208	1.0421	1.0364
2	0.9254	0.9368	0.9855	0.9891	1.0103	1.0094
3	1.0033	1.0018	0.9834	0.9866		
4	0.9707	0.9760	1.0034	1.0051		
5	1.0044	1.0031	0.9891	0.9916	0.9992	0.9998
6	0.9998	1.0053	1.0584	1.0505	0.8960	0.9086
7	0.6448	0.6449	1.7338	1.8009		
8	1.5403	1.5028	0.6618	0.6580		
9	1.8749	1.8974	1.5571	1.4974		
	6-Vinylfulvene		6-Aminofulvene		6-Amino-6-alkoxyfulvene	
1	1.0479	1.0413	1.0475	1.0440	1.0737	1.0664
2	1.0138	1.0123	1.0338	1.0291	1.0329	1.0316
3	1.0138	1.0123	1.0218	1.0198	1.0359	1.0330
4	1.0489	1.0420	1.0742	1·0635	1.0652	1.0621
5	1.0027	1.0029	1.1077	1.0881	1.1622	1.1409
6	0.9016	0.9110	0.8760	0.8848	0.8553	0.8597
7	1.0055	1.0051	1.8390	1.8707	1.8538	1.8815
8	0.9659	0.9732			1.9211	1.9247
	6,6-Dialkoxyfulvene		Heptafulvene		Fulvalene	
1	1.0628	1.0596	0.9731	0.9799	1.0454	1.0382
2	1.0282	1.0278	0.9985	0.9986	0.9965	0.9984
3			0.9920	0.9939		
5	1.1347	1.1271				
6	0.8487	0.8520				
7	1.9173	1.9230	1.0022	1.0017		
8			1.0705	1.0535		
9					0.9163	0.9268
	8-Vinylheptafulvene		Sesquifulvalene			
1	0.9695	0.9768	1.0704	1.0620		
2	0.9972	0.9976	1.0346	1.0305		
3	0.9897	0.9922				
4	0.9896	0.9921				
5	0.9971	0.9976	0.9518	0.9623		
6	0.9688	0.9763	0.9719	0.9749		
7	1.0006	1.0006	0.9761	0.9807		
8	1.0681	1.0534				
9	0.9961	0.9968				
10	1.0231	1.0167				
11			0.9146	0.9145		
12			1.0761	1.0649		

Results and Discussion

The π-electron densities are given in Table 1, and π-bond orders and the calculated final bond lengths in Table 2 together with the observed bond lengths.[3] The bond lengths of 6,6-dimethylfulvene observed by Norman and Post[4] are also shown in the column for fulvene in Table 2. The calculated $^1\pi^*$–$^1\pi$ electronic transition energies are given in Table 3.

trans-*Butadiene*, *Acrolein*, p-*Dimethoxybenzene*, *Benzoic Acid, and Acetanilide.* Agreement between the finally used bond lengths and the observed ones, and that between the finally calculated bond lengths and the observed ones is good, as shown in Table 2. On the whole both methods give similar γ_{pq}-values and β_{pq}-values in these systems, and similar π-electron

4) N. Norman and B. Post, *Acta Crystallogr.*, **14**, 503 (1961).

Table 2. π-Bond orders and calculated bond lengths

	Bond orders		Bond lengths (Å)		
	VI/1	VI/2	VI/1	VI/2	Obsd.[3]
trans-Butadiene					
1—2	0.9584	0.9643	1.345	1.344	1.337
2—3	0.2854	0.2649	1.464	1.468	1.483
trans-Acrolein					
1—2	0.8633	0.8809	1.214	1.215	1.22
2—3	0.3213	0.2741	1.458	1.466	1.45
3—4	0.9462	0.9610	1.348	1.345	1.36
cis-Acrolein					
1—2	0.8438	0.8646	1.218	1.218	
2—3	0.3630	0.3155	1.451	1.459	
3—4	0.9295	0.9469	1.350	1.347	
p-Dimethoxybenzene					
1—2	0.6499	0.6483	1.400	1.400	1.40
1—7	0.2218	0.2252	1.328	1.331	1.36
2—3	0.6676	0.6698	1.397	1.396	1.37
Benzoic acid					
1—2	0.6380	0.6460	1.402	1.401	1.39
1—6	0.6251	0.6352	1.404	1.403	1.39
1—7	0.3059	0.2648	1.461	1.468	1.48
2—3	0.6666	0.6650	1.397	1.397	1.41
3—4	0.6673	0.6693	1.397	1.397	1.37
4—5	0.6571	0.6576	1.399	1.399	1.36
5—6	0.6813	0.6787	1.394	1.395	1.42
7—8	0.7689	0.8058	1.231	1.228	1.24
7—9	0.4079	0.3703	1.295	1.305	1.29
Acetanilide					
1—2	0.6477	0.6503	1.400	1.400	1.38
1—6	0.6398	0.6454	1.402	1.401	1.37
1—7	0.2479	0.2270	1.409	1.414	1.43
2—3	0.6690	0.6686	1.397	1.397	1.39
3—4	0.6640	0.6653	1.397	1.397	1.40
4—5	0.6646	0.6642	1.397	1.397	1.37
5—6	0.6717	0.6709	1.396	1.396	1.41
7—8	0.5285	0.4479	1.359	1.375	1.33
8—9	0.7679	0.8203	1.231	1.226	1.23
Fulvene					
1—2	0.8863	0.8996	1.358	1.356	1.346[4]
1—5	0.2892	0.2760	1.464	1.466	1.439
2—3	0.3848	0.3583	1.447	1.452	1.435
5—6	0.9108	0.9191	1.354	1.352	1.343
6-Vinylfulvene					
1—2	0.8773	0.8918	1.360	1.357	
1—5	0.3090	0.2940	1.460	1.463	
2—3	0.3935	0.3663	1.445	1.450	
3—4	0.8771	0.8916	1.360	1.357	
4—5	0.3089	0.2941	1.460	1.463	
5—6	0.8539	0.8702	1.364	1.361	
6—7	0.3301	0.3028	1.457	1.461	
7—8	0.9425	0.9520	1.348	1.347	

	Bond orders		Bond lengths (Å)	
	VI/1	VI/2	VI/1	VI/2
6-Aminofulvene				
1—2	0.8574	0.8729	1.364	1.361
1—5	0.3385	0.3233	1.455	1.458
2—3	0.4354	0.4054	1.438	1.443
3—4	0.8579	0.8724	1.363	1.361
4—5	0.3290	0.3197	1.457	1.458
5—6	0.8176	0.8388	1.370	1.367
6—7	0.4226	0.3771	1.378	1.387
6,6-Dialkoxyfulvene				
1—2	0.8557	0.8650	1.364	1.362
1—5	0.3361	0.3339	1.456	1.456
2—3	0.4412	0.4199	1.437	1.441
5—6	0.8083	0.8147	1.372	1.371
6—7	0.3073	0.2961	1.313	1.319
Sesquifulvalene				
1—2	0.8444	0.8601	1.366	1.363
1—12	0.3637	0.3491	1.451	1.453
2—3	0.4410	0.4128	1.437	1.442
5—6	0.8400	0.8608	1.366	1.363
5—11	0.3853	0.3565	1.447	1.452
6—7	0.4261	0.3982	1.440	1.445
7—8	0.8334	0.8531	1.368	1.364
11—12	0.7406	0.7680	1.384	1.379
Fulvalene				
1—2	0.8869	0.9016	1.358	1.355
1—10	0.3014	0.2845	1.462	1.465
2—3	0.3616	0.3362	1.451	1.455
9—10	0.8196	0.8393	1.370	1.366
6-Amino-6-alkoxyfulvene				
1—2	0.8460	0.8577	1.365	1.363
1—5	0.3516	0.3457	1.453	1.454
2—3	0.4552	0.4303	1.434	1.439
3—4	0.8463	0.8580	1.365	1.363
4—5	0.3534	0.3463	1.452	1.454
5—6	0.7735	0.7920	1.378	1.375
6—7	0.4067	0.3653	1.381	1.389
6—8	0.2993	0.2918	1.314	1.319
Heptafulvene				
1—2	0.8864	0.9030	1.358	1.355
1—7	0.3075	0.2817	1.461	1.465
2—3	0.3670	0.3406	1.450	1.455
3—4	0.8728	0.8897	1.361	1.358
7—8	0.8981	0.9155	1.356	1.353
8-Vinylheptafulvene				
1—2	0.8778	0.8952	1.360	1.357
1—7	0.3270	0.3004	1.457	1.462
2—3	0.3742	0.3479	1.449	1.453
3—4	0.8677	0.8849	1.361	1.358
4—5	0.3742	0.3480	1.449	1.453
5—6	0.8771	0.8947	1.360	1.357
6—7	0.3285	0.3017	1.457	1.462
7—8	0.8422	0.8654	1.366	1.362
8—9	0.3261	0.3046	1.457	1.461
9—10	0.9439	0.9513	1.348	1.347

Table 3. Calculated $^1\pi^*$-$^1\pi$ electronic transitions in eV

VI/1			VI/2			Obsd.		
Sym.	E	f	Sym.	E	f	E	f	Ref.
trans-Butadiene								
^1B_u	5.965	1.042	^1B_u	6.118	1.016	6.0		5)
^1A_g	7.427	0	^1A_g	7.514	0			
^1A_g	7.762	0	^1A_g	7.845	0			
trans-Acrolein								
	6.158	0.935		6.294	0.806	6.41		6)
	7.591	0.017		7.743	0.038			
	8.384	0.077		8.300	0.159			
cis-Acrolein								
	5.612	0.389		5.736	0.353			
	7.558	0.128		7.651	0.058			
	8.427	0.545		8.366	0.636			
Hydroquinone								
$^1B_{2u}$	4.614	0.026	$^1B_{2u}$	4.596	0.028	4.25	(3.43)[b]	7)
$^1B_{1u}$	5.394	0.023	$^1B_{1u}$	5.368	0.035	5.51	(3.71)[b]	
$^1B_{1u}$	7.056	1.353	$^1B_{2u}$	7.038	1.115			
$^1B_{2u}$	7.066	1.129	$^1B_{1u}$	7.068	1.352			
Benzoic acid								
	4.699	0.020		4.660	0.013	4.5	(3)[b]	8)
	5.207	0.289		5.278	0.174	5.28	(4.3)[b]	
	6.118	0.206		6.302	0.414			
	6.915	0.942		6.872	0.891			
Acetanilide								
	4.705	0.016		4.695	0.009	4.53		9)
	5.156	0.204		5.227	0.152	5.18		
	5.990	0.145		5.983	0.181	6.20		
	6.981	1.054		6.985	1.031			
	7.329	1.150		7.267	0.669			

VI/1					VI/2					Obsd.		
Sym.	E	f	CI Composition[a]		Sym.	E	f	CI Composition[a]		E	f	Ref.
Fulvene												
$^1B_2$	3.425	0.053	3—4	0.998	$^1B_2$	3.663	0.052	3—4	0.999	3.32	0.012	10)
$^1A_1$	5.255	0.507	2—4	0.921	$^1A_1$	5.330	0.524	2—4	0.928	5.13	0.32	
			3—5	0.369				3—5	−0.350			
$^1A_1$	7.083	0.384	1—4	0.825	$^1A_1$	7.117	0.311	1—4	0.831			
			3—5	−0.520				3—5	0.517			
$^1B_2$	7.311	0.163			$^1B_2$	7.357	0.156					
6-Vinylfulvene												
	3.117	0.037	4—5	0.984		3.386	0.038	4—5	0.982	3.12		11)
	4.529	1.108	3—5	0.967		4.636	1.066	3—5	0.968	4.20		
	6.146	0.128	2—5	0.872		6.237	0.092	2—5	0.881			
			4—7	0.443				4—7	0.423			
	6.582	0.365				6.625	0.343					

5) R. S. Mulliken, *Rev. Modern Phys.*, **14**, 265 (1942).
6) A. D. Walsh, *Trans. Faraday Soc.*, **41**, 498 (1945).
7) R. Adams and J. C. Anderson, *J. Amer. Chem. Soc.*, **72**, 5154 (1950).
8) L. Dedel and A. Rosenberg, *Ber.*, **67**, 147 (1934).
9) H. Baba and S. Suzuki, *J. Chem. Phys.*, **32**, 1706 (1960).
10) J. Thiec and J. Wiemann, *Bull. Soc. Chim. Fr.*, **23**, 177 (1956).
11) P. A. Straub, Doris Meuche, and E. Heilbronner, *Helv. Chim. Acta*, **49**, 517 (1966).

Table 3. (Continued)

VI/1					VI/2					Obsd.		
Sym.	E	f	CI Composition[a]		Sym.	E	f	CI Composition[a]		E	f	Ref.
6-Aminofulvene												
	3.483	0.055	4—5	0.998		3.616	0.051	4—5	0.998	3.87	(4.5)[b]	12)
	4.630	0.633	3—5	0.948		4.718	0.654	3—5	0.951			
	6.523	0.222	2—5	0.745		6.577	0.141	2—5	0.764			
			4—6	−0.347				4—6	−0.452			
			4—7	0.458								
	6.860	0.115				7.075	0.095					
6,6-Diethoxyfulvene												
$^1B_2$	3.573	0.061	5—6	0.998	$^1B_2$	3.677	0.055	5—6	0.998	4.28	(4.25)[b]	12)
$^1A_1$	4.724	0.591	4—6	0.941	$^1A_1$	4.785	0.630	4—6	0.946			
$^1A_1$	6.665	0.313	3—6	0.721	$^1A_1$	6.792	0.284	3—6	0.718			
			4—7	0.313				5—7	0.588			
			5—8	0.597				4—8	0.341			
$^1B_2$	6.825	0.098			$^1A_1$	7.015	0.078					
6-Amino-6-ethoxyfulvene												
	3.587	0.059	5—6	0.997		3.657	0.053	5—6	0.998	3.76	(4.4)[b]	12)
	4.510	0.619	4—6	0.948		4.597	0.656	4—6	0.952			
	6.488	0.249	3—6	0.660		6.591	0.177	3—6	0.693			
			4—7	0.418				4—7	0.388			
			5—8	−0.602				5—8	0.567			
	6.691	0.087				6.932	0.067					

VI/1			VI/2			Obsd.		
Sym.	E	f	Sym.	E	f	E	f	Ref.
Heptafulvene								
$^1B_2$	3.056	0.043	$^1B_2$	3.354	0.049	2.91	0.02	13)
$^1A_1$	4.537	0.460	$^1A_1$	4.731	0.424	4.43	0.3	
$^1B_2$	6.205	0.043	$^1B_2$	6.295	0.037			
$^1A_1$	6.406	1.153	$^1A_1$	6.501	1.182			
8-Vinylheptafulvene								
	2.834	0.030		3.131	0.035	2.79		14)
	4.011	1.031		4.210	0.973	3.81		
	5.646	0.677		5.746	0.725			
	5.839	0.070		5.961	0.046			
	5.912	0.045		6.050	0.045			
Sesquifulvalene								
$^1B_2$	2.761	0.001	$^1B_2$	2.956	0.003	3.07	0.47	15)
$^1B_2$	2.954	0.061	$^1B_2$	3.161	0.064			
$^1A_1$	3.513	1.038	$^1A_1$	3.608	1.013			
$^1A_1$	4.593	0.003	$^1A_1$	5.030	0.003			
$^1A_1$	5.336	0.190	$^1A_1$	5.352	0.265			
Fulvalene								
$^1B_{3g}$	2.534	0	$^1B_{3g}$	2.899	0	2.98		16)
$^1B_{2u}$	2.683	0.033	$^1B_{2u}$	3.043	0.035			
$^1B_{1u}$	4.276	1.087	$^1B_{1u}$	4.376	1.050	3.95	0.4	
^1A_g	5·893	0	^1A_g	6.036	0			
^1A_g	6.498	0	^1A_g	6.456	0			

a) The transition denoted by i-j refers to a one-electron excitation from orbital i to virtual orbital j. The second column gives the CI coefficient of the configuration i-j.
b) $\log \varepsilon$

12) K. Hafner, G. Schulz, and K. Wagner, *Ann.*, **678**, 39 (1964).
13) W. von E. Doering and D. W. Wiley, *Tetrahedron*, **11**, 183 (1960).
14) D. J. Bertelli, *J. Amer. Chem. Soc.*, **86**, 3326 (1964).
15) H. Prinzbach, *Angew. Chem.*, **73**, 169 (1961); H. Prinzbach and D. Seip, *ibid.*, **73**, 169 (1961); H. Prinzbach and W. Rosswog, *ibid.*, **73**, 543 (1961).
16) W. von E. Doering, "Theoretical Organic Chemistry, Kekulé Symposium," Butterworths, London (1959), p. 35.

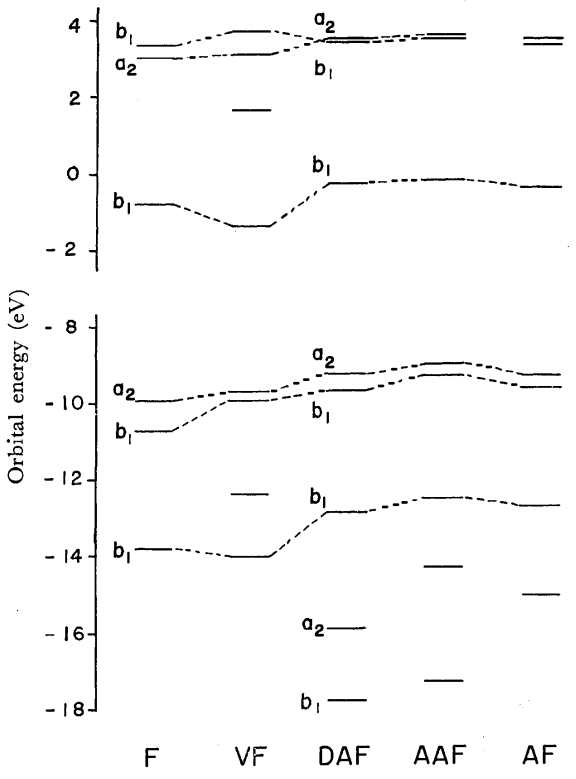

Fig. 2. Correlation diagram for fulvene derivatives with the variable integrals method I.
(F: Fulvene; VF: 6-Vinylfulvene; DAF: 6,6-Dialkoxyfulvene; AAF: 6-Amino-6-alkoxyfulvene; AF: 6-Aminofulvene.)

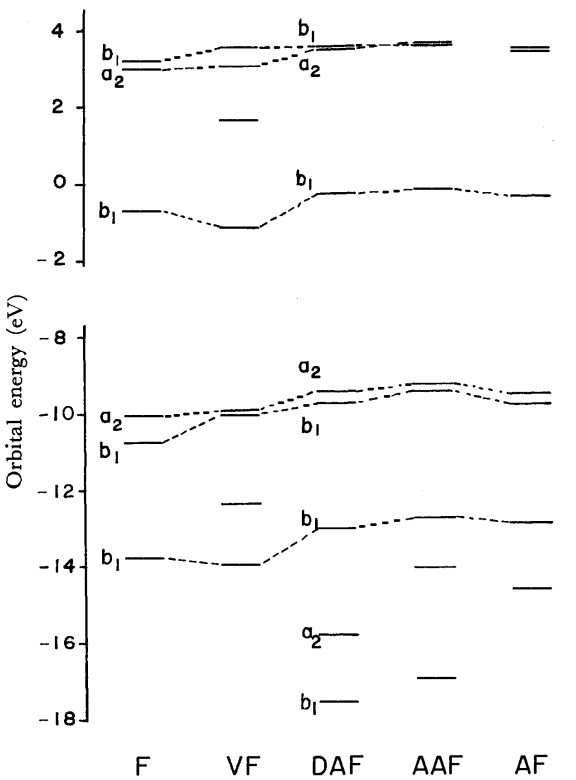

Fig. 3. Correlation diagram for fulvene derivatives with the variable integrals method II.
(F: Fulvene; VF: 6-Vinylfulvene; DAF: 6,6-Dialkoxyfulvene; AAF: 6-Amino-6-alkoxyfulvene; AF: 6-Aminofulvene.)

densities and bond orders (Tables 1 and 2). Agreement between the calculated transition energies by both methods and the observed ones is excellent (Table 3). These results suggest that formulas (1)—(6) can be safely used.

Fulvenes and Fulvalenes. The final parameters or the Coulomb repulsion integrals, γ_{pq}'s, bond lengths, l_{pq}'s, and core resonance integrals, β_{pq}'s, used by both methods are similar to each other except for some cases. In the case of fulvene the finally used bond lengths are in good agreement with the observed bond lengths of 6,6-dimethylfulvene.

The SCF eigenvalues and the eigenvectors given by both methods resemble each other on the whole. The molecular orbitals for fulvene and its derivatives may be approximately correlated as shown in Figs. 2 and 3 for the VI/1 and VI/2 methods, respectively. The correlation diagrams given by the two methods are alike. The lowest occupied orbital of 6-aminofulvene and the two lowest occupied orbitals of 6,6-dialkoxyfulvene or 6-amino-6-alkoxyfulvene are mainly localized on the 6-substituents.

The π-charge densities calculated by both methods are similar to each other (Table 1). The π-bond orders and bond lengths calculated by both methods also resemble each other on the whole (Table 2). The calculated bond lengths of fulvene are in adequate agreement with the bond lengths for 6,6-dimethylfulvene observed by Norman and Post[4] by X-ray crystallographic examination. Both methods reproduce well the bond alternation in the five-membered ring of fulvene. From the table, it is anticipated that slight bond alternations may be present in the five-membered and seven-membered rings of these systems as in fulvene.

The dipolemoment of fulvene calculated by the VI/1 method is 1.231 D and that by the VI/2 method 1.084 D. These values are in good agreement with the observed value (1.1 D) by Thiec and Wiemann[10] in benzene solution. On the other hand the dipolemoment observed by Brown and coworkers[17] by the microwave method is 0.44 D.

The observed transitions are tentatively assigned as in Table 3. Agreement between the calculated transition energies and the observed ones is satisfactory on the whole. The longest wavelength transitions in fulvene, 6-vinylfulvene, 6-aminofulvene, 6,6-diethoxyfulvene and 6-amino-6-ethoxyfulvene are clearly the intramolecular charge-transfer transitions caused by electron transfer from the five-membered rings to the branches.

In conclusion the variable integrals methods I and II are applicable also to these systems.

The calculation was carried out on a HITAC 5020E computer at the Computer Centre of the University of Tokyo.

17) R. D. Brown, F. R. Burden, and J. E. Kent, *J. Chem. Phys.*, **49**, 5542 (1968).

An MO-Theoretical Study of the Decomposition of Hydroperoxides by Sulfonium Compounds and Some Nucleophiles

Katsutoshi OHKUBO and Hirokazu KANAEDA

Department of Synthetic Chemistry, Kumamoto University, Kurokami-machi, Kumamoto

(Received March 3, 1971)

The decomposition reactions of hydroperoxides (ROOH) by sulfonium compounds or some nucleophiles (sulfides, phosphites, and transition metal ions) were treated by the extended Hückel method, augmented by the use of *d*-orbitals. We obtained serveral findings. First, ROOH was more reactive to nucleophiles and was energetically more stable than $(ROOH)_2$. Second, the order of the ability for the ROOH decomposition, sulfonium compounds $\gg$ sulfides $>$ phosphites $\geq$ thiophene, was in good agreement with that of the AO populations of the nonbonding lone pair orbitals of the above compounds. Third, the distinguished ability of the sulfonium compound may be attributed to the contribution of the partially-occupied sulfur *d*-orbitals, in particular, the lowest unoccupied d_{z^2}-orbital; in the ROOH decomposition, these orbitals interact with the lowest unoccupied antibonding $p\sigma$-orbital of the O-O in ROOH at the O_β atom in the direction of the O-O axis. Finally, it was concluded that the sulfur *d*-orbitals contribute to the long-range interaction ($S\text{-}O_\beta > 3.0$ Å) between ROOH and sulfonium compounds.

The thermal[1] and catalytic[2] decompositions of hydroperoxides have been widely investigated by taking notice of the decomposition mechanism. Some chemical properties of hydroperoxides have thus been unveiled such as the kinds of homolytic or heterolytic decomposition products,[1-3] the bond-dissociation energies of the oxygen-oxygen bond[4,5] (including those of alkoxyl radicals[6]), and the association of hydroperoxides.[7,8] On the other hand, some theoretical studies of the electronic structures of hydroperoxides can be found in Refs. 9, 10, and 11, and more recently in Ref. 12. These studies suggest that most hydroperoxides possess the lowest unoccupied antibonding $p\sigma$-type-orbital of the O–O bond and that the bond can easily be cloven by nucleophiles such as low-valent metal ions,[13,14] sulfides[15] and phosphites.[16]

In our previous paper,[17] which referred to the remarkable ability of sulfonium compounds in the catalytic decomposition of hydroperoxides, a presumption was made that the partially occupied d_{z2} and/or d_{xz} (or d_{yz}) orbitals[18,19] play an important role in the scission of the O–O bond as follows:

$$ROOH + R'_3SCl \rightarrow \left[\begin{array}{c} \overset{\alpha}{O}\text{—}\overset{H}{O}\cdots SR'_3\cdots Cl \\ R \qquad \beta \end{array} \right] \rightarrow RO\cdot + \cdot OH + R'_3SCl$$

(R, R' = alkyl or aryl)

The electron transferred from the sulfonium part to the O–O bond through the sulfur *d*-orbitals increases the antibonding character of the O–O bond and promote the scission.

The present study intends to elucidate the role of the *d*-orbitals of sulfonium compounds in the catalytic decomposition of hydroperoxides, comparing their role with those of the nonbonding lone pair orbitals of sulfides and phosphites.

Methods of Calculation

Four systems were investigated in this work: (a) hydroperoxides, ROOH (R=H, CH_3, C_2H_5, *n*-C_3H_7, *n*-C_4H_9, *t*-C_4H_9, and $C_6H_5C(CH_3)_2$), (b) dimeric hydroperoxides $(ROOH)_2$ (R=H, CH_3, and *t*-C_4H_9), (c) trimethylsulfonium chloride ($(CH_3)_3SCl$) and some nucleophiles ($(CH_3)_2S$, $(C_6H_5)_2S$, $(CH_3O)_3P$, and $(C_2H_5O)_3P$, and (d) the interaction of CH_3OOH with $(CH_3)_3SCl$, $(CH_3)_2S$ or $(CH_3O)_3P$. In the case of (d), CH_3OOH was used for the simplicity of computation.

The orbital exponents and the Coulomb integrals ($H_{\mu\mu}$) were supplied by Clementi[20] and Jaffé[21,22] respectively. Especially, the $H_{\mu\mu}$ values of the oxygen

1) For instance, J. W. Forgham and H. L. Williams, *Can. J. Res.*, **B27**, 943 (1949); M, S. Kharasch, A. Fono, and W. Nudenberg, *J. Org. Chem.*, **16**, 113, 1156 (1951); H, C. Bailey and G. W. Godin, *Trans. Faraday Soc.*, **52**, 68 (1956).

2) For instance, M. S. Kharasch, A. Fono, and W. Nudenberg, *J. Org. Chem.*, **15**, 753, 763 (1950); J. W. Forghand and H. L. Williams, *J. Amer. Chem. Soc.*, **72**, 4465 (1950).

3) A. V. Tobolsky and R. B. Mesrobian, "Organic Peroxides," Interscience Publishers, New York (1956), and the references cited therein.

4) A. D. Kirk and J. H. Knox, *Trans. Faraday Soc.*, **56**, 1296 (1960).

5) P. L. Hanst and J. G. Calvert, *J. Phys. Chem.*, **63**, 104 (1959).

6) P. Gray and A. Williams, *Chem. Rev.*, **59**, 239 (1959), and the references cited therein.

7) C. Walling and L. Heaton, *J. Amer. Chem. Soc.*, **87**, 48 (1965).

8) S. Kato, T. Ishihara, and F. Mashio, *Bull. Japan Petrol. Inst.*, **12**, 117 (1970).

9) W. G. Penner and G. B. M. Sutherland, *J. Chem. Phys.*, **2**, 492 (1934).

10) R. S. Mulliken, *ibid.*, **3**, 506 (1935).

11) Y. Amako and P. A. Giguére, *Can. J. Chem.*, **40**, 765 (1962).

12) T. Yonezawa, O. Yamamoto, H. Kato, and K. Fukui, *Nippon Kagaku Zasshi*, **87**, 26 (1966).

13) F. Haber and P. Weiss, *Proc. Roy. Soc., Ser. A*, **147**, 233 (1939).

14) M. H. Dean and G. Skirrow, *Trans. Faraday Soc.*, **54**, 849 (1958).

15) L. Bateman and K. R. Hargauue, *Proc. Roy. Soc., Ser. A*, **244**, 389, 399 (1954); L. Bateman and J. Cunneen, *J. Chem. Soc.*, **1955**, 1596; D. Barnard, *ibid.*, **1956**, 489.

16) D. B. Denney, W. F. Goodyear, and B. Goldstein, *J. Amer. Chem. Soc.*, **82**, 1393 (1960).

17) K. Ohkubo, T. Yamabe, and K. Fukui, This Bulletin, **43**, 1 (1970).

18) K. Fukui, K. Ohkubo, and T. Yamabe, *ibid.*, **42**, 312 (1969).

19) K. Ohkubo and T. Yamabe, *Bull. Japan Petrol. Inst.*, **12**, 130 (1970).

20) E. Clementi and D. L. Raimondi, *J. Chem. Phys.*, **38**, 2686 (1963).

21) J. Hinze and H. H. Jaffé, *J. Amer. Chem. Soc.*, **84**, 540 (1962).

22) J. Hinze and H. H. Jaffé, *J. Phys. Chem.*, **67**, 1501 (1963).

$2p$-orbital and the sulfur $3d$-orbital were taken to be -13.61 eV and -7.00 eV[23] respectively. The resonance integrals ($H_{\mu\nu}$) were evaluated by the Wolfsberg-Helmholtz approximation[24]:

$$H_{\mu\nu} = 0.875(H_{\mu\mu}+H_{\nu\nu})S_{\mu\nu}$$

where $S_{\mu\nu}$ is the overlap integral between AO's.

The orbital contour diagrams were calculated by the use of Slater's AO functions.[26]

Experimental

The decomposition reaction of cumene hydroperoxide was carried out in the following way: cumene hydroperoxide (22.5 mmol) in cumene (50 ml) was vigorously stirred in the presence of sulfonium chloride or a nucleophile (a sulfide, a phosphite, or a transition metal salt), mainly at 80°C for 4.0 hr. Then, the reaction mixture was pipetted out and submitted to analyses of the decomposition products, acetophenone (AP), dicumyl peroxide (DCP), α-cumyl alcohol (CA), and the residual cumene hydroperoxide (CHP). The analytical treatment was carried out in accordance with the method mentioned previously.[17]

Results and Discussion

Electronic Structures of Hydroperoxides. Before discussing the interaction between hydroperoxides (ROOH) and sulfonium compounds (R'_3SCl), the electronic structures of the former should be reviewed. ROOH is characterized by its lowest unoccupied (LU) antibonding $p\sigma$-type O–O bond. Considering that the atom population of the O_β in $RO_\alpha O_\beta H$ is larger than that of the O_α, as is indicated in Fig. 1, such nucleophiles as sulfides and phosphites will interact with ROOH from the O_β side in the direction of the O–O axis.[12] In the case of sulfonium compounds, the interaction will occur between the d-orbitals of the central sulfur and the O–O $p\sigma$-orbital in the same way mentioned above, perhaps because substituents of the sulfonium compound (named R′) sterically hinder the approach of the compound from the O_α side.[17] The characteristic nature of the O–O bond in ROOH is reflected in the orbital contour diagrams for the LU MO of ROOH (R=CH_3) (see Fig. 2).

It is of interest here to discuss which structure of ROOH, monomer or dimer, is energetically more plausible. The total energies listed in Table 1 demonstrated that the ROOH monomer is preferable for the structure of ROOH, especially at low concentrations of the hydroperoxide. In regard to the reactivity of ROOH to nucleophilic reagents, the partial AO bond population of the O–O in the LU MO ($1/2N^{LU}_{p\sigma}$) can be utilized as a reactivity index since the O–O bond is mainly conposed of the $p\sigma$-orbital of the O–O (see Table 1). The value of $1/2N^{LU}_{p\sigma}$ in Table 1 suggests that ROOH is more reactive than $(ROOH)_2$. On the basis of the above discussions, the

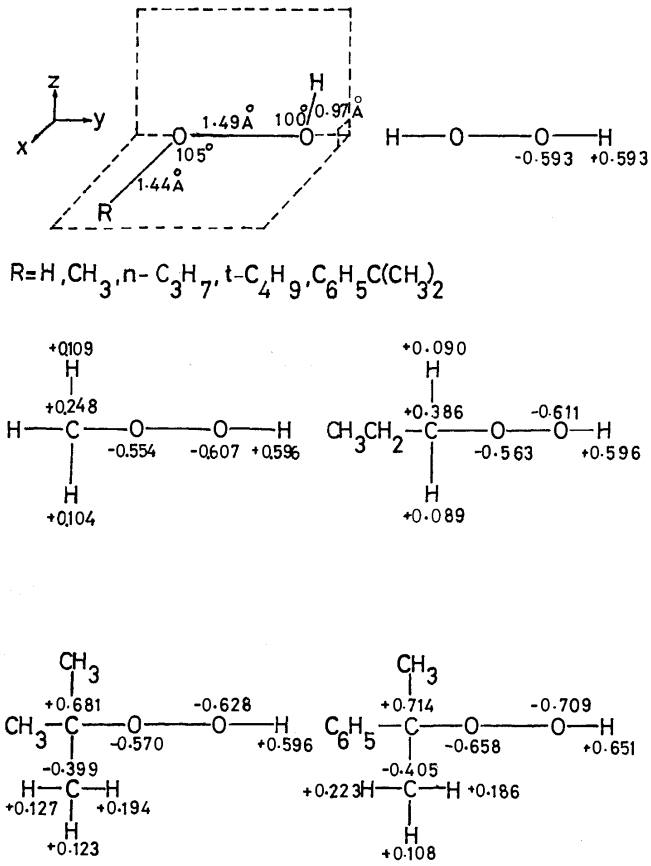

Fig. 1. Atomic charges of some hydroperoxides.

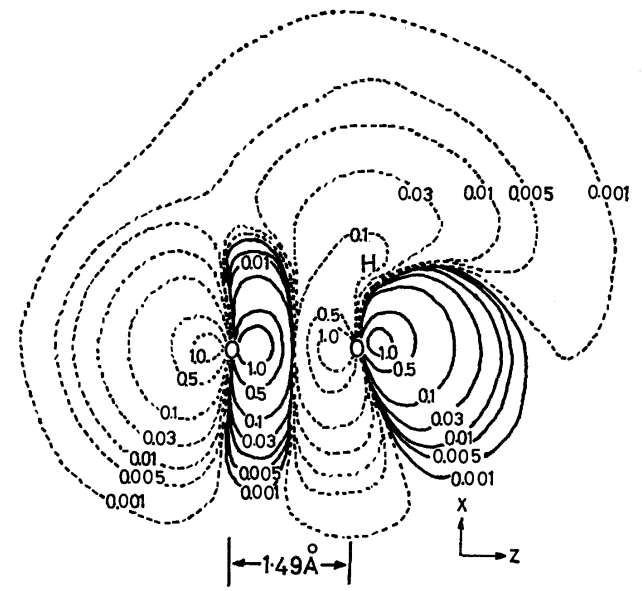

Fig. 2. Orbital contour of CH_3OOH in the LU MO. (the solid and broken lines stand for the positive and negative MO signs, respectively.)

monomer structure of ROOH seems to be the more plausible structure from the standpoints of both the energetic stability and the reactivity to nucleophiles.

Decomposition of Cumene Hydroperoxide by Sulfonium Compounds and Some Nucleophiles. It is of interest also to discuss the abilities of sulfonium compounds and some nucleophiles with regard to the decom-

23) T. Jordan, H. W. Smith, L. L. Lohr, Jr., and W. N. Lipscomb, *J. Amer. Chem. Soc.*, **85**, 846 (1963).
24) M. Wolfsberg and L. Helmholtz, *J. Chem. Phys.*, **20**, 837 (1952).
25) J. C. Slater, *Phys. Rev.*, **36**, 57 (1930).

TABLE 1. SOME ELECTRONIC PROPERTIES OF HYDROPEROXIDES AND THEIR DIMERS

Hydroperoxide	Bond population of O-O bond		$\frac{1}{2}N_{p\sigma}^{LU}$ [a]	Total energy (eV)
	$p\sigma$	total		
H_2O_2	0.349	0.359	−0.309	−309.67
$(H_2O_2)_2$	0.349	0.359	−0.155	−619.30
CH_3OOH	0.346	0.361	−0.309	−413.80
$(CH_3OOH)_2$	0.346	0.361	−0.189	−827.27
C_2H_5OOH	0.345	0.358	−0.308	−517.21
n-C_3H_7OOH	0.345	0.357	−0.308	−620.39
n-C_4H_9OOH	0.345	0.356	−0.308	−723.56
t-C_4H_9OOH	0.343	0.354	−0.306	−722.83
$(t$-$C_4H_9OOH)_2$	0.343	0.356	−0.154	−1442.19
$C_6H_5C(CH_3)_2OOH$	0.342	0.350	−0.143	−1080.21

O···H distance of the dimer was taken to be 1.79 Å.
a) One-electron bond population of the O-O $p\sigma$-orbital in the LU MO.

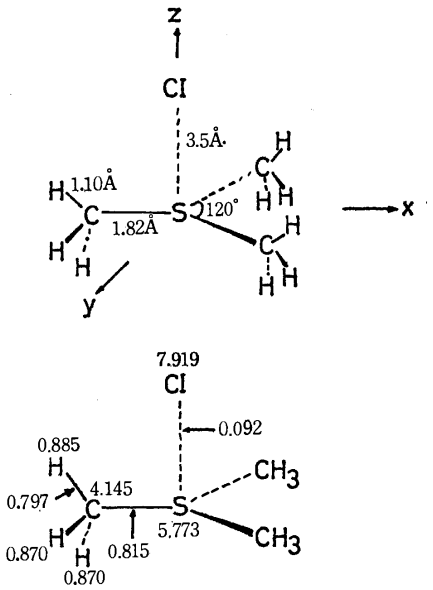

AO population of S d-orbitals
$d_{z^2}=0.068$ $d_{xy}=0.092$
$d_{xz}=0.142$ $d_{x^2-y^2}=0.092$
$d_{yz}=0.142$

Fig. 3. Electronic structure of $(CH_3)_3SCl$.

position of ROOH. Table 2 lists the experimental data obtained from the decomposition reaction of cumene hydroperoxide. Except for transition metal ions, the order of the ability with regard to the ROOH decomposition (estimated from the amount of the hydroperoxide decomposed) was as follows: triphenylsulfonium chloride ≫ diphenylsulfide > triphenylphosphite > trimethylphosphite > triethylphosphite ≃ thiophene. Considering that the ability would be reflected in the AO population of the nonbonding orbital (N_{nbo}) of the central sulfur or phosphorus, in particular, that in the highest occupied (HO) MO ($1/2N_{nbo}^{HO}$), the order of the values of N_{nbo} or $1/2N_{nbo}^{HO}$ listed in Table 3 is in agreement with that of the ability mentioned above. In sulfonium chloride and thiophene, the contribution of the partially-occupied sulfur d-orbitals to the ROOH decomposition should be taken into consideration (this will be discussed, in detail in the later part of this paper).

In regard to the catalytic decomposition of ROOH by the low-valent transition metal ions, the order of the

TABLE 2. ABILITIES OF SULFONIUM COMPOUNDS AND SOME NUCLEOPHILES FOR THE DECOMPOSITION OF CUMENE HYDROPEROXIDE

Compound	Concentration (mol/l)	Temp. (°C)	Time (hr)	CHP decomposed (%)	Products[a] (mmol)		
					AP	DCP	CA
None		80	4	4.44	0.24	trace	0.76
$(C_6H_5)_2S$	0.148	80	4	88.90	1.64	2.2	13.8
$(C_6H_5)_2S$	0.216	25	4	trace			
$(C_6H_5)_2S{=}O$	0.48	80	3	trace			
$\overline{CH(CH)_3S}$	0.12	80	3	20.44	4.0	trace	0.6
$\overline{CH(CH)_3S}$	0.476	80	4	69.33	13.6	—	—
$(C_6H_5)_3SCl$	0.141	80	4	96.89	10.63	4.16	1.91
$(C_6H_5)_3SCl$	0.670	55	4	24.44	2.29	1.12	0.45
$(C_6H_5)_3SCl$	0.424	80	5	99.51	13.28	2.77	3.56
$(CH_3O)_3P$	0.148	80	4	39.11	0.88	trace	7.3
$(C_2H_5O)_3P$	0.148	80	4	28.44	1.04	0.34	4.70
$(C_6H_5O)_3P$	0.148	80	4	42.22	1.10	trace	8.25
Ni(II)[b]	0.006	80	4	27.56	1.38	trace	4.81
Co(II)[b]	0.006	80	4	100.0	4.73	trace	19.1
Fe(II)[c]	0.006	80	4	25.33	1.23	trace	4.42

a) Other products such as methane, phenol, sulfoxide, *etc.* were neglected in this table for the sake of simplicity. See Experimental for the abbreviations.
b) Stearates.
c) A naphthenate.
The initial concentration of cumene hydroperoxide was 22.5 mmol.

Table 3. AO Population of the nonbonding orbitals of a sulfonium compound and some nucleophiles

Compound	N_{nbo}	$\frac{1}{2}N_{nbo}^{HO}$	HO (nonbonding orbital (eV)
$(CH_3)_2S$	1.993	0.729	−11.98
$(C_6H_5)_2S$	1.845	0.312	−11.74
$\overline{CH(CH)_3S}$	1.579 (0.064)		−12.49
$(CH_3)_3SCl$	1.981 (0.068)	0.701	−11.42
$(CH_3O)_3P$	1.298	0.197	−12.28
$(C_2H_5O)_3P$	1.231	0.156	−12.06

Values in parentheses stand for the AO populations of the sulfur d_{z^2} orbtal.

ability with regard to the ROOH decomposition: Co(II)>Ni(II)>Fe(II), can be well explained by its parallelism with the energy required for the electron-releasing from the *d*-orbitals of the transition-metal ion to the O–O $p\sigma$-orbital: Co(II) (7.84 eV)[26]>Ni(II) (9.24 eV)[26]>Re(II) (11.00 eV).[27]

The Interaction between ROOH and the Sulfonium Compound or Some Nucleophiles. First, it is necessary to mention the electronic structure of the sulfonium compound. The ASMO SCF calculations on $(CH_3)_3SCl$[28] supported the planar C_{3v} symmetrical sulfonium cation and suggested a suitable location of the counter chloride (S–Cl=3.5 Å) from the energetic point of view. As has already been mentioned, the sulfonium chloride is characterized by its partially-occupied sulfur *d*-orbitals (see Fig. 3), and the remarkable ability of the compound with regard to the ROOH decomposition as compared with those of sulfides or phosphites

Table 4. Changes in the N_{nbo} of $(CH_3)_3SCl$ and some nucleophiles and the M_{OO} of CH_3OOH due to the interaction

Compound	N_{nbo}	M_{OO}
$(CH_3)_2S$	1.993	
$(CH_3O)P$	1.298	0.361
$(CH_3)_3SCl$	1.981	
	(d_{z^2}=0.068)	
	(d_{xz}=0.142)	
$(CH_3)_2S$[a]	0.622	0.329
$(CH_3O)_3P$[a]	1.129	0.350
$(CH_3)_3SCl$[b]	1.955	
in Type I	(d_{z^2}=0.052)	0.249
$(CH_3)_3SCl$[b]	1.501	
in Type II	(d_{xz}=0.061)	0.266

a) The distance between the O_β in $CH_3O_\alpha O_\beta H$ and the S in $(CH_3)_2S$ (or the P in $(CH_3O)_3P$) was 2.0 Å.
b) The distance between the O_β and the central S was 3.0 Å.

26) F. A. Cotton and T. E. Haas, *Inorg. Chem.*, **3**, 1004 (1964).
27) L. L. Lohr, Jr., and W. N. Lipscomb, *ibid.*, **3**, 22 (1964).
28) K. Ohkubo, *Tetrahedron Lett.*, **1971**, 2897.

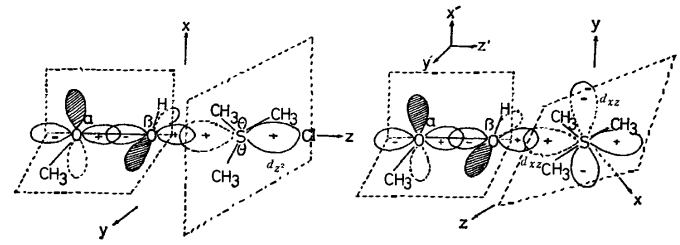

Fig. 4. Two distinct interaction between $(CH_3)_3SCl$ and CH_3OOH.

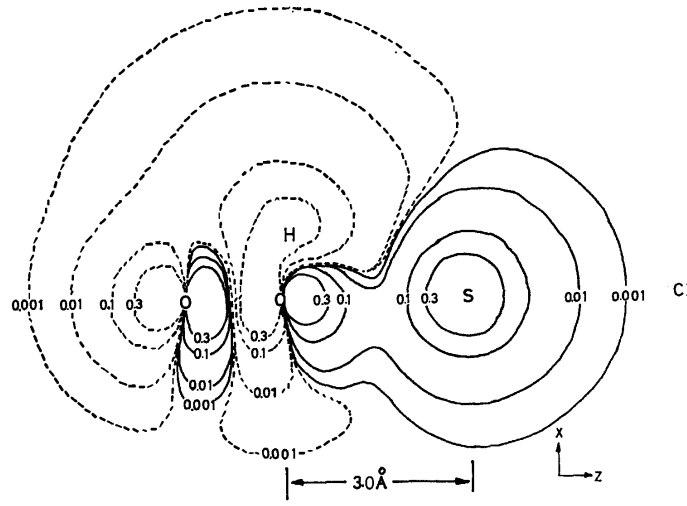

Fig. 5. Orbital contour of LUMO in the long-range interaction between CH_3OOH and $(CH_3)_3SCl$. (the solid and broken lines indicates the positive and negative MO signs, respectively.)

is the result of the contribution of this sulfur *d*-orbitals (especially, the d_{z^2}-orbital) to the interaction with the LU antibonding O–O $p\sigma$-orbital in ROOH. This is consistent with the change in the values of N_{nbo} and the bond population of the O–O (M_{OO}) recorded in Table 4, where two distinct modes of interaction between CH_3OOH and $(CH_3)_3SCl$, *i.e.*, Type I and Type II, are taken into consideration (see Fig. 4); in Type I, the interaction mainly occurs between the sulfur d_{z^2}-orbital of the former and the O–O $p\sigma$-orbital of the latter, while in Type II, the sulfur d_{xz}-orbital interacts predominantly with the $p\sigma$-orbital. In view of the smaller value of M_{OO} in Type I at S–O_β=3.0 Å as compared with that of M_{OO} in Type II, the stronger interaction can be expected by Type I. This long-range interaction between CH_3OOH and $(CH_3)_3SCl$ supports the role of the sulfur *d*-orbital in the catalytic decomposition of hydroperoxides, as can be seen from Fig. 5.

The major portions of the present calculations were carried out on a FACOM 230.60 computer at the Computer Center at Kyushu University while a part of them were done at Kyoto University.

The Adsorption of Polyvinylpyrrolidone at the Mercury/Solution Interface

Tadashi YOSHIDA, Tetsuya OHSAKA, and Shoji TANAKA

Applied Electrochemical Laboratory, Graduate School of Science and Engineering, Waseda University, Nishi-Okubo, Shinjuku-ku, Tokyo

(Received March 13, 1971)

The adsorption of polyvinylpyrrolidone (PVP), known as a water-soluble polymer, at the electrolyte/DME interface was examined by observing the differential capacity *vs.* the time relation, under conditions where the adsorption process was mainly controlled by diffusion. In the case of a relatively low bulk concentration and a short adsorption time, the adsorption rate of PVP at −500 mV(SCE) was controlled almost wholly by the diffusion of the adsorbate to the DME. The relation between the time required to attain the saturated adsorption and the bulk concentration was explained approximately by the Koryta equation, based on the linear diffusion. PVP showed no tendency to form multi-layers within the range of bulk concentrations and adsorption times observed. The maximum surface concentration of PVP decreased almost linearly with the increase in its mean molecular weight. The number of constitutive segments adsorbed per unit of area to form a monolayer at the interface was almost constant, independent of the mean molecular weight. The activation energy for the diffusion was found to be *ca.* 4.7 kcal/mol. On the basis of the results obtained, the configuration of PVP adsorbed at the interface was discussed.

Many water-soluble organic polymers are adsorbed strongly at the interface, and it takes some time to attain an adsorption equilibrium when the adsorption rate is mainly diffusion-controlled in a relatively dilute solution.[1-3]

Polyvinylpyrrolidone (PVP),[4] prepared first by Reppe, has characteristic properties of a good solubility, a strong adsorbability, protective colloid action, *etc.*[5] Some papers[6] on the properties of PVP in an aqueous solution have been published, and Jehring[2] computed the maximum surface concentration (Γ_m) of PVP dissolved in a potassium chloride solution by means of AC polarography. In the present paper, the adsorption of PVP will be investigated by observing the differential capacity in detail for the purposes of examining the diffusion behaviour of PVP in solution and discussing its configuration when adsorbed at the interface.

Experimental

Electrodes and Test Cell. The dropping mercury electrode (DME) was used, and the flow rate (m) and drop time (t_d) of DME were as follows: $m=1.10—1.60\times10^{-4}$ g/sec, $t_d=ca.$ 30 sec/drop. The counter electrode was a cylindrical platinum net with a sufficiently large surface. The electrode potential was referred to the saturated calomel electrode (SCE). The test cell and all parts of the mercury dropping equipment with a capillary, made of Pyrex glass except for the capillary, were connected tightly with ground glass joints without rubber stoppers, and the opening of capillary, prepared from a Molybdenum glass tube, was treated suitably with a tungsten carbide cutter.

Materials. Mercury was distilled twice *in vacuo* after having been treated in the usual way. Four kinds of chemical-grade PVP prepared by BASF were used without further purification; their mean molecular weights ($\bar{M}$) were 10000, 26000, 37000, and 750000 respectively. All the solutions were prepared from guaranteed or purified reagents and triply-distilled water.

Differential-capacity Measurements. A precise impedance bridge of the transformer-connection type, equipped with a cathode-ray oscilloscope detector, was employed. The bridge was fed from the CR-type oscillator, where the sinusoidal wave of 1 kHz was adjusted by an attenuator so as to take an input voltage of *ca.* 10 mV_{p-p}. A cylindrical platinum net, installed around a mercury drop, served as a counter electrode for the DC potentiostatic polarization of the test electrode and for the impedance measurements. On the assumption of a series-equivalent circuit of resistance and capacitance, the differential capacity at the mercury/solution interface was determined synchronously with a certain balance time from the beginning of drop growth. The measurements were conducted in an atmosphere of purified nitrogen.

Theoretical

Adsorption Behavior in the Diffusion-controlled Process. On the assumption of an adsorption process controlled simply by semi-infinite linear diffusion, the surface concentration (Γ_t) of adsorbates on a mercury drop at a certain growth time, t, can be given by the well-known Koryta equation (1),[7] derived from the Ilković formula:

$$\Gamma_t = 0.736 D^{1/2} a t^{1/2} \quad (1)$$

where Γ_t is expressed in mol/cm², and t, in sec, and where D and a are the diffusion coefficient of adsorbates in cm²/sec and its bulk concentration in mol/cm³

1) H. Jehring, *J. Electroanal. Chem.*, **20**, 33 (1969); *ibid.*, **21**, 77 (1969); *Z. Phys. Chem.*, **229**, 39 (1965).

2) H. Jehring and E. Horn, *Monatsber. Deut. Akad. Wiss. Berlin*, **10**, 295 (1968).

3) P. W. Boad, D. Britz, and R. V. Holland, *Electrochim. Acta*, **13**, 1633 (1968).

4) Molecular formula:

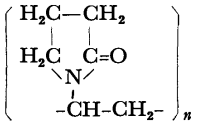

5) R. L. Davidson and M. Sittig, eds., "Water-Soluble Resins," Reinhold Pub. Corp., New York (1962), p. 110.

6) B. Jirgensons, *Makromol. Chem.*, **6**, 30 (1951); W. Scholtan, *ibid.*, **7**, 209 (1951); J. Hengstenberg and E. Schuch, *ibid.*, **7**, 236 (1951); L. E. Miller and F. A. Hamm, *J. Phys. Chem.*, **57**, 110 (1953).

7) J. Koryta, *Collect. Czech. Chem. Commun.*, **18**, 206 (1953).

respectively. According to Frumkin,[8] the relation between the differential capacity and the surface coverage (θ) is written as follows:

$$C = C_{\theta=1}\theta + C_{\theta=0}(1-\theta) \quad (2)$$

where $C_{\theta=1}$ and $C_{\theta=0}$ are the differential capacities per unit of area at $\theta=1$ and $\theta=0$ respectively. Assuming $\theta=\Gamma_t/\Gamma_m$, we obtain from Eqs. (1) and (2):

$$C = C_{\theta=0} - K a t^{1/2} \quad \text{for } t<t_m \quad (3)$$

where $K=0.736(C_{\theta=0}-C_{\theta=1})D^{1/2}\Gamma_m{}^{-1}$

Γ_m and t_m are the maximum surface concentration of the adsorbates and the time required to attain the saturated adsorption respectively. Equation (3) holds only in the case of $t<t_m$ where the adsorption is diffusion-controlled. On the other hand, in the case of $t\gg t_m$, where the adsorption equilibrium is always attainable and where $\theta=1$:

$$C = C_{\theta=1} \quad \text{for } t\gg t_m \quad (4)$$

It is shown by Eq. (3) that, if t is kept constant, C changes linearly with a, while if a is constant, C varies linearly with $t^{1/2}$. Γ_m can be computed from the experimental data by means of Eq. (3) if the value of D is given. At 25°C, the surface area A_t (cm^2) of a mercury drop at its growth time, t, is given by the mercury flow rate, m, as:

$$A_t = 0.85m^{2/3}t^{2/3} \quad (5)$$

Therefore, the observed differential capacity, C_E (μF), is written as follows from Eqs. (3), (4), and (5):

$$C_E = CA_t = 0.85C_{\theta=0}m^{2/3}t^{2/3} - 0.85Km^{2/3}a\,t^{7/6} \quad \text{for } t<t_m \quad (6)$$

$$C_E = C_{\theta=1}A_t = 0.85C_{\theta=1}m^{2/3}t^{2/3} \quad \text{for } t\gg t_m \quad (7)$$

Application of Koutecký-type Equation.[9] The deviation from the Koryta equation can be explained by the Koutecký equation, in which Γ_t is given by Eq. (8), including the supplementary term based on the spherical diffusion:

$$\Gamma_t = 0.736D^{1/2}a\,t^{1/2}(1+3.47D^{1/2}m^{-1/3}t^{1/6}) \quad (8)$$

The (9) and (4)′ relations are obtained from Eq. (8) instead of from the (3) and (4) formulae:

when $t<t_m$, $C = C_{\theta=0} - K a t^{1/2}(1+3.47D^{1/2}m^{-1/3}t^{1/6})$ (9)

if $t\gg t_m$, $C = C_{\theta=1}$ (4)′

Results

Differential-capacity vs. Potential Curves. Figure 1 shows the differential capacity *vs.* potential curves in 1 N sulfuric acid solutions containing PVP ($\bar{M}=10000$) of various concentrations under a fixed balance time, t_B. Relations similar to those in Fig. 1 can be obtained with various t_B values under a fixed value of a instead of t_B. In Fig. 1, the peak due to the ad- or desorption of PVP is found at a noble potential of *ca.* 75 mV(SCE), whereas no peak is given at the less noble side within the potential range observed, and the differential capacity decreases

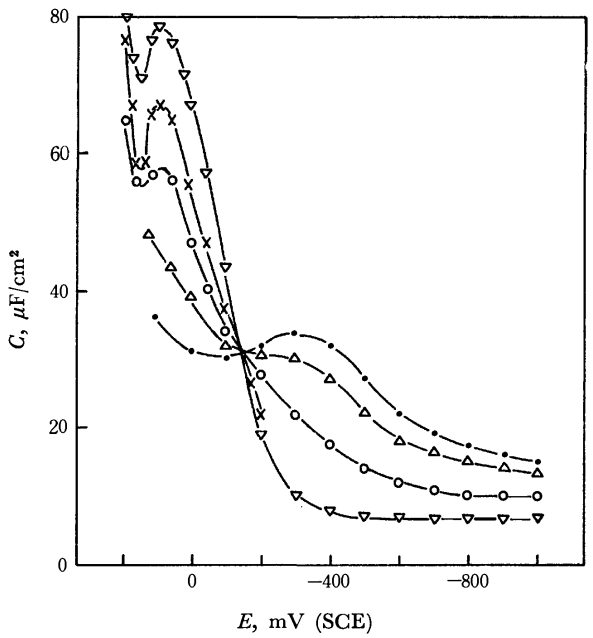

Fig. 1. Differential capacity *vs.* potential curves.
30.0°C, t_B (balance time)=15 sec, 1 N sulfuric acid+PVP ($\bar{M}=10000$); (—·—: PVP 0 mg/*l*, —△—: 5 mg/*l*, —○—: 10 mg/*l*, —×—: 20 mg/*l*, —▽—: 50 mg/*l*)

on the less noble side, while it increases in the peak potential region with an increasing a (or t_B value). The dependence of the capacity on t_B may be understood in terms of the diffusion-controlled adsorption, where the adsorbed PVP increases with the time. Furthermore, it is found that the minimum differential capacity, (C_{min}), due to the adsorption equilibrium or saturation is nearly constant independent of the value of a or t_B within the less noble potential range, while the peak potential is practically independent of the value of a or t_B.

Adsorption attains to its equilibrium or saturation at *ca.* −500 mV(SCE) near the zero-charge potential of mercury upon a reasonable increase in a (or t_B), as may be seen in Fig. 1. Therefore, the interfacial behaviour of PVP will be discussed in most cases at −500 mV(SCE), where the saturated absorption is always attained.

Observed Capacity vs. Time Curves. Figure 2 shows examples of C_E-t curves at −500 mV(SCE) in 1 N sulfuric acid solutions with various values of the concentration of PVP ($\bar{M}=750000$).

In Fig. 2, the C_E for the saturated adsorption with PVP or for the blank solution may be seen to increase with $t^{2/3}$ or A_t [*cf.* Eq. (5) or (7)]. In the diffusion-controlled process [*cf.* Eq. (6)], C_E-t curves are depressed with a, and each curve has a tendency to coincide with the saturated adsorption curve. Diagrams analogous to Fig. 2 were always obtained with PVP's of various $\bar{M}$ values, where for instance, the depression of C_E by the PVP of $\bar{M}=10000$ was about three times that by the PVP of $\bar{M}=750000$ under given a and t_B values.

Oscillograms Observed with a PVP Solution. The oscillograms obtained by the impedance bridge are

8) A. N. Frumkin, *Z. Phys.*, **35**, 792 (1926).
9) A. N. Frumkin and B. B. Damaskin, "Modern Aspects of Electrochemistry," No. 3, Butterworths, London (1964), p. 149.

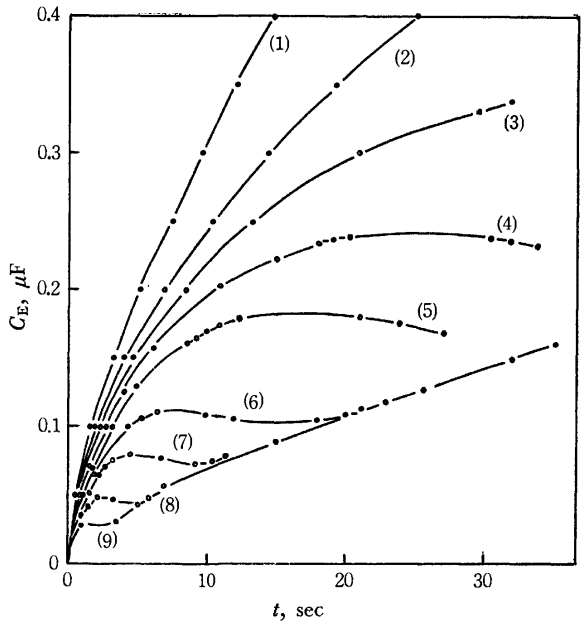

Fig. 2. Observed differential capacity *vs.* time curves.
Observed at −500 mV (SCE), 20.5°C, 1 N sulfuric acid (1) 1 N sulfuric acid+PVP ($\bar{M}$=750000), (2) PVP 15 mg/*l*, (3) 30 mg/*l*, (4) 40 mg/*l*, (5) 50 mg/*l*, (6) 75 mg/*l*, (7) 100 mg/*l*, (8) 150 mg/*l*, (9) 200 mg/*l*

of a simple X type in the case of a blank solution, while they reveal distorted figures in the presence of PVP. Typical cases are shown in Photo. 1 and Fig. 3, where remarkable distortions of figures are revealed in the transient course from the diffusion-controlled process to the saturated adsorption. The oscillograms in Photo. 1 were obtained in a 1 N sodium sulfate solution containing 25 mg/*l* PVP. A figure corresponding to Photo. 1 is shown in Fig. 3, where the three values of the bridge capacitance adjusted

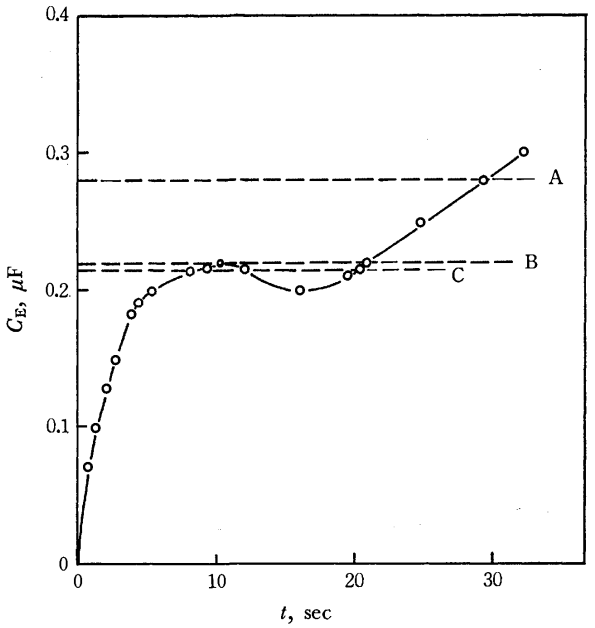

Fig. 3. Observed differential capacity *vs.* time curve connected with Photo. 1.
Observed at −500 mV (SCE), 20.5°C, 1 N sodium sulfate +PVP ($\bar{M}$=10000) 25 mg/*l*, adjusted capacitance; (A: 0.280 μF, B: 0.220 μF, C: 0.215 μF)

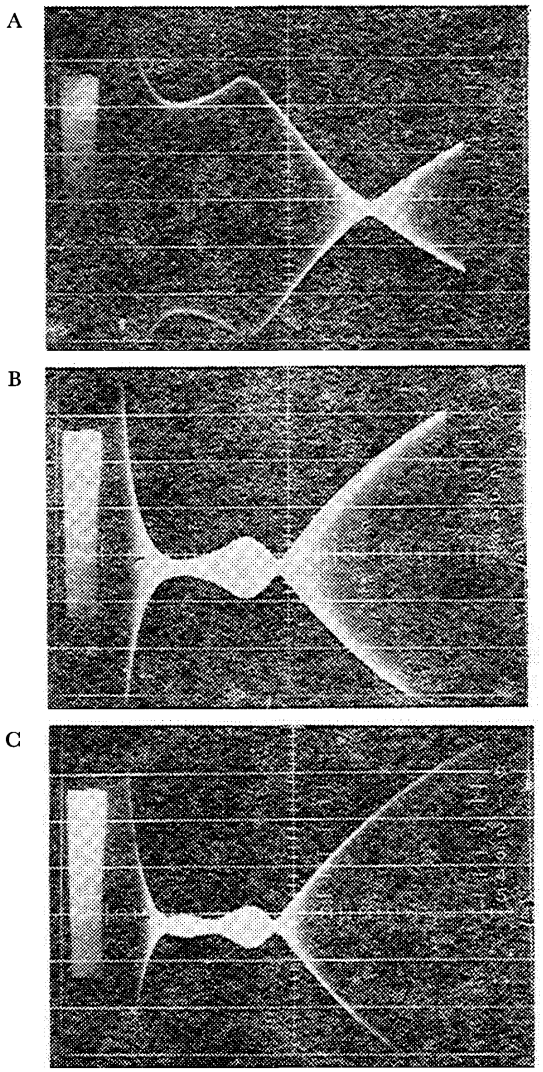

Photo. 1. Oscillograms for the bridge balance.
1 N sodium sulfate+PVP ($\bar{M}$=10000) 25 mg/*l*, X: 5 sec/div., Y: 2 V/div., "A", "B", and "C" correspond to each one in Fig. 3.

are given by dashed lines. Figure 3, showing 1 N sodium sulfate solution, is similar to Fig. 2, showing 1 N sulfuric acid solution. In the case of "C" in Photo. 1, three balance times (t_B) are given, as to be expected from the three points of intersection in the order. It may be considered that the first two balance times are attributable to the diffusion-controlled processes, whereas the last one is due to the saturated adsorption. Similarly, the first and second t_B values for the "B" case in Photo. 1 or Fig. 3 may be due to the diffusion-controlled process and to the saturated adsorption respectively. Next, the balance time related to the "A" case in Photo. 1 or Fig. 3 may be due to the saturated adsorption, while the preceding distortion of the oscillogram is to be expected from the shape of the C_E-t curve in Fig. 3. A figure similar to that in Photo. 1 can be obtained from such data as are shown in Fig. 3 on the assumption that the input admittance due to the unbalanced bridge is approximately proportional to the voltage found on the screen to the detector.

Temperature Dependence of C vs. t Curves. Figure

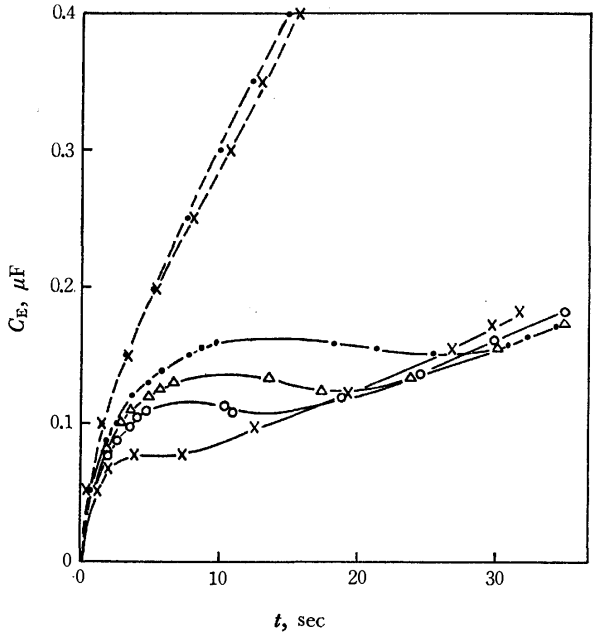

Fig. 4. Observed differential capacity *vs.* time curves obtained at various temperatures.
Obtained at −500 mV (SCE), 20°C, 1 N sulfuric acid; (--.--: 20°C, --×--: 60°C), 1 N sulfuric acid+PVP ($\bar{M}$=10000) 20 mg/*l*; (—·—: 20°C, —△—: 30°C, -○-: 40°C, ·—×—: 60°C)

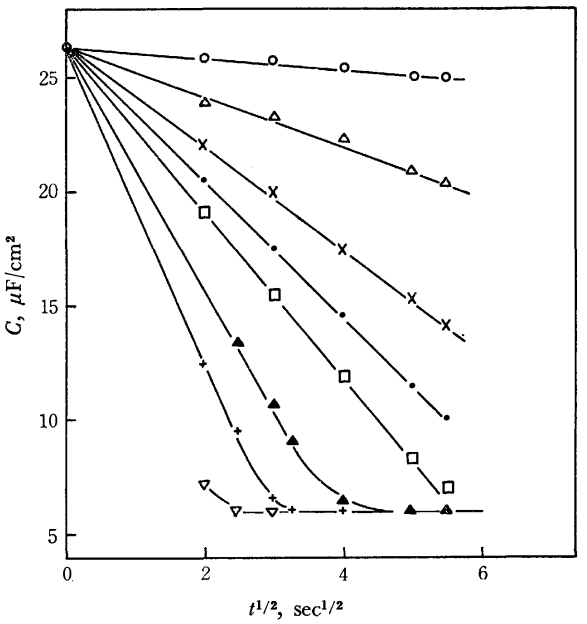

Fig. 5. Differential capacity *vs.* square root of time curves. Observed at −500 mV (SCE), 20.5°C, 1 N sulfuric acid+PVP ($\bar{M}$=750000); (—○—: 5 mg/*l*, —△—: 15 mg/*l*, —×—: 30 mg/*l*, —·—: 40 mg/*l*, —□—: 50 mg/*l*, —▲—: 75 mg/*l*, —+—: 100 mg/*l*, —▽—: 150 mg/*l*)

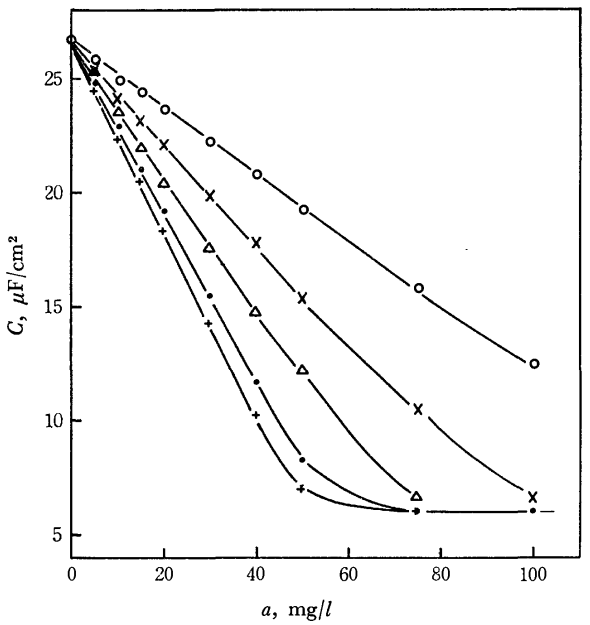

Fig. 6. Differential capacity *vs.* bulk concentration curves. Observed at −500 mV (SCE), 20.5°C, 1 N sulfuric acid+PVP ($\bar{M}$=750000); (—○—: t_B=4 sec, —×—: 9 sec, —△—: 16 sec, —·—: 25 sec, —+—: 30 sec)

4 shows the temperature dependence of the C_E-t curves observed in a 1 N sulfuric acid solution containing PVP ($\bar{M}$=10000) of 20 mg/*l*.

In Fig. 4, the difference between the two curves at 20 and 60°C is nearly negligible in the case of a blank solution. For the solution containing PVP, the time required to attain the saturated adsorption is about 25 sec at 20°C, and it decreases as the temperature rises. The saturated adsorption curves vary somewhat with the temperature, but the differences among them are so small that they are negligible within the temperature range from approximately 20 to 60°C.

Discussion

Application of the Koryta Equation. The variation in the differential capacity, C, with the drop-growth time, t, or with the bulk concentration, a, is expressed by Eq. (3) in the diffusion-controlled process, where $t<t_m$. As may be seen from Figs. 5 and 6 related to the PVP of $\bar{M}$=750000, C decreases linearly with $t^{1/2}$ or a, as to be expected from Eq. (3); it attains a constant value in each case at a certain values of t or a, as to be expected from Eq. (4). The constancy of C shows that the saturated adsorption is achieved. The more a or t_B increases, the steeper the slope of the curve becomes, as may be seen in Figs. 5 and 6. The curves in Figs. 5 and 6 always consist of two linear portions. It is possible to find the time t_m or the bulk concentration, a_m, necessary to attain Γ_m under a certain value of a or t_B from the intersection of these two lines.

It may be concluded that PVP is adsorbed to form the monolayer at the interface, since the minimum differential capacity (C_{min}) observed in the saturated adsorption range is approximately constant independent of a or t (the drop growth or balance time), as may be seen in Fig. 5 or 6.

Saturation Time related to Concentration. The Koryta equation (1) may be modified as follows:

$$\left.\begin{aligned} &\log t_m = -2\log a + K' \\ \text{or:}\quad &\\ &\log t = -2\log a_m + K' \end{aligned}\right\} \qquad (10)$$

where $K'=2\log[\Gamma_m/(0.736D^{1/2})]$

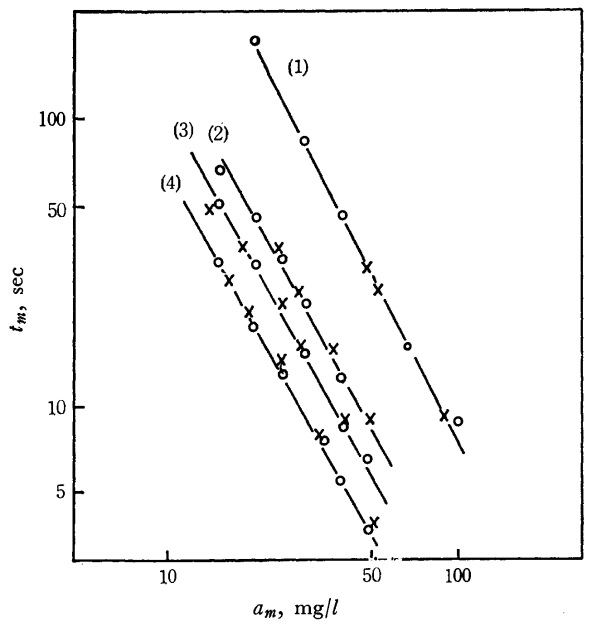

Fig. 7. Time required to attain the saturated adsorption *vs.* bulk concentration curves.
Observed at −500 mV (SCE), 20.5°C, 1 N sulfuric acid+PVP solutions, —o—: derived from C-$t^{1/2}$ curves, - × -: derived from C-a curves, (1): PVP: $\bar{M}$=750000, (2): 37000, (3): 26000, (4): 10000

In Fig. 7, typical plots of $\log t_m$ *vs.* $\log a$ and $\log a_m$ *vs.* $\log t$ are derived from Figs. 5 and 6 with four kinds of PVP. Each plot in Fig. 7 reveals an approximately straight line with a slope deviating by *ca.* −5% from the expected value of −2. Moreover, t_m at a certain definite value of a becomes longer with an increase in the mean molecular weight, as may be seen from Fig. 7; this tendency may result from the lowering of the diffusion coefficient due to the increase in $\bar{M}$.

Reexamination of the Use of the Koryta Equation. Typical C-$t^{1/2}$ and C-a plots based on the Koryta equation are shown in Figs. 5 and 6 with the PVP of $\bar{M}$=750000, the K value in Eq. (3) can be calculated from the slope of each curve. Γ_m can be obtained from the value of K if the diffusion coefficient is known. However, the value of K obtained from the curves in Fig. 5 or 6 shows a slight dependence on a or t_B, *i.e.*, the values of K obtained from the curves in Fig. 5 slightly decreases with an increase in a, while the value derived from the curves in Fig. 6 slightly rises with t_B. Therefore, Γ_m is computed by means of the mean value of K based on the values of the diffusion coefficient[10] as estimated by the Stokes-Einstein equation or experimentally obtained. The dependence of K on a or t_B may be attributable to the variation in the diffusion coefficient with the concentration, or to the effect of the supplementary term of the Koutecký type given in Eq. (9), which was deduced on the basis of the spherical diffusion under a constant Γ_m value, independent of a.

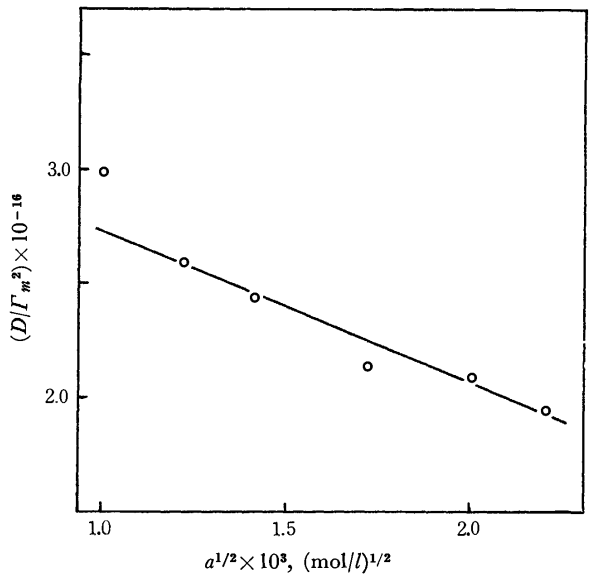

Fig. 8. Concentration dependence of diffusion coefficient for PVP.
Observed at −500 mV (SCE), 20.5°C, 1 N sulfuric acid+PVP ($\bar{M}$=10000) solutions

Friedman *et al.*[12] found a linear relation between the diffusion coefficient and the square root of the bulk concentration for some organic substances (*e.g.*, dextrose, sucrose). An example of the (D/Γ_m^2) *vs.* $a^{1/2}$ plot is shown in Fig. 8, where (D/Γ_m^2) has been calculated from the K derived from the slope of the (C *vs.* $t^{1/2}$) relation at a given a of PVP ($\bar{M}$=10000). As may be seen from Fig. 8, (D/Γ_m^2) shows an approximately linear dependence on the square root of the concentration of PVP. The linear relationship between (D/Γ_m^2) and $a^{1/2}$ in Fig. 8 suggests that the dependence of K on a is attributable to the variation in the diffusion coefficient with a to a certain extent.

A slight deviation of the (D/Γ_m^2)-$a^{1/2}$ relation from linearity may be expected on the basis of the Koutecký equation, in which the effect of the spherical diffusion is taken into consideration. In Eq. (9), the slope of C *vs.* a relation shows $-Kt^{1/2}(1+3.47D^{1/2}m^{-1/3}t^{1/6})$ instead of $-Kt^{1/2}$ in the Koryta Equation (1). The value of K obtained on the basis of the Koryta Equation (1) should be modified to $K(1+3.47D^{1/2}m^{-1/3}t^{1/6})$ in the case of the spherical diffusion, which may be expected to increase with the time. In fact, the value of K obtained from the C-a curve by means of the Koryta equation increases slightly with t_B as has previously been stated.[13]

In short, the variation in the K derived from the Koryta equation may be attributed to the concentration dependence of the diffusion coefficient or to the effect of the spherical diffusion. The deviation of

10) The values of the diffusion coefficient of PVP in the literature[6] as estimated by the Stokes-Einstein equation and as observed with the hanging mercury electrode,[11] are 10.3×10^{-7} cm²/sec for $\bar{M}$=10000, 7.3×10^{-7} for $\bar{M}$=26000, 5.1×10^{-7} for $\bar{M}$=37000, and 1.2×10^{-7} for $\bar{M}$=750000.

11) This Bulletin, to be published.

12) L. Friedman and P. G. Carpenter, *J. Amer. Chem. Soc.*, **61**, 1745 (1939).

13) In the case of $\bar{M}$=10000, for example, the K values derived from the Koryta equation were 1.98×10^9, 2.07×10^9, and 2.19×10^9 for t_B=4, 8, and 16 sec respectively.

the slope by *ca.* −5% from the expected value of −2 in Fig. 7 may be explained by the change in the diffusion coefficient or the effect of the spherical diffusion discussed above. It should be noted that the Koryta equation is approximately applicable to the present system within an error of 10%.

Temperature Dependence of the Diffusion Coefficient. The temperature dependence of the C_E-t relation is shown in Fig. 4 for the case with a 1 N sulfuric acid solution containing 20 mg/l of PVP ($\bar{M}$=10000), and a linear relation is obtained by plotting log [D_T/$D_{(273+20)}$] to T or $1/T$,[14] where the value of (D_T/$D_{(273+20)}$] is derived from the [(t_m at T°K)/(t_m at 273+20°K)] ratio with the Koryta equation at a given a on the assumption that Γ_m is constant independent of T under the present conditions. The temperature coefficient (α) of the diffusion coefficient and the activation energy (Q) of the diffusion are found to be about 0.025 and 4.7 kcal/mol respectively for the present case. The value of Q mentioned above may be reasonable for the diffusion process of PVP ($\bar{M}$=10000).

Configuration of PVP at the Interface. By plotting log Γ_m against log $\bar{M}$ for four kinds of PVP, we obtain an approximately linear relation with a slope of nearly −1, as shown in Fig. 9. From this linear relation, $\bar{M}\Gamma_m$=const. can be obtained; this means that $\bar{P}/S$ is constant, where $\bar{P}$ is the degree of polymerization or the number of segments, and S, the area of the electrode surface occupied by 1 mol of the adsorbed molecule, that is, $S=\Gamma_m^{-1}$. Consequently, it follows that the adsorbed number of the constitutive segment related to PVP at the interface is constant, independent of $\bar{M}$, and that the value of $\bar{P}$ per unit of area can be estimated from Fig. 9 to be *ca.* 4.0×10^{14} seg./cm^2.

The geometrical form of the dissolved PVP molecule in the bulk of the solution was assumed to be a randomly-coiled polymer chain or a revolving ellipsoid.[6] It seems, in the present case, that the geometrical form of PVP in the bulk of the solution may be close to a sphere consisting of a randomly-coiled chain, since the D of PVP, derived from the Stokes-Einstein relation assuming a spherical form, is approximately consistent with the value observed.[11]

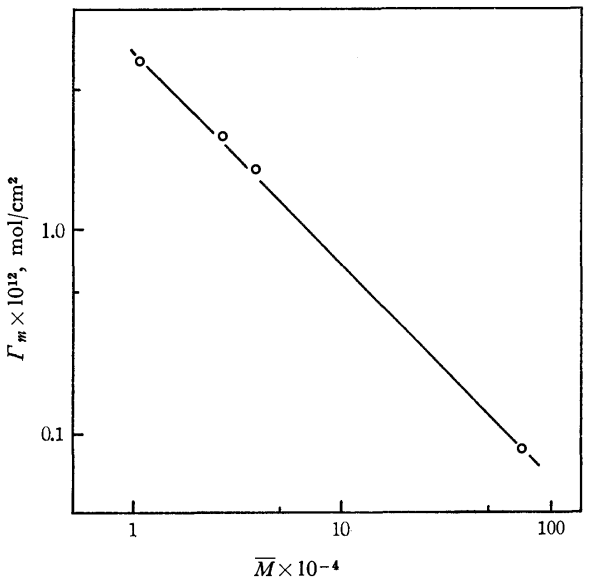

Fig. 9. Maximum surface concentration *vs.* mean molecular weight curve.
Observed at −500 mV (SCE), 20.5°C, 1 N sulfuric acid+PVP solutions

Nevertheless, the spherical form of PVP assumed for the diffusion process cannot explain the fact that the minimum differential capacity observed for PVP differs little from that given by the common organic compound of a non-polymer or from that observed for *N*-vinyl-2-pyrrolidone,[14] which is a component monomer of PVP. Therefore, it may be assumed that the adsorbed PVP at the interface takes a configuration of a spread or flatten form of the chain instead of the spherical form. Moreover, consistent with the above conclusion, the adsorbed number of constitutive segments per unit of area is nearly constant, independent of the $\bar{M}$, as has been mentioned previously.

The authors would like to express their acknowledgements to Dr. Shigemitsu Nomoto for his valuable discussions. The financial aid from the Ministry of Education for this work is gratefully acknowledged.

14) $D=D_0(1+\alpha)^T$ for α and $D=D_0\exp(-Q/\boldsymbol{R}T)$ for Q, where D_0 and Q can be obtained by experimental determinations of the diffusion coefficient at two or more temperatures.

14) This Bulletin, to be published.

Monolayers of Poly(methyl acrylate) Saponified Partially in Homogeneous and Heterogeneous Systems

Seiichiro HIRONAKA* and Kenjiro MEGURO

Department of Chemistry, Faculty of Science, Science University of Tokyo, Kagurazaka, Shinjuku-ku, Tokyo

(Received April 14, 1971)

Poly(methyl acrylate) prepared by radical polymerization of methyl acrylate was saponified partially in acetone-water mixtures (5 : 2 and 100 : 1 by volume), using sodium hydroxide as the catalyst. Saponification in an acetone-water mixture of a 5 : 2 ratio by volume proceeded in a homogeneous state, but the reaction solution of a 100 :1 ratio by volume was in a white-turbid state, in which saponification proceeded in a heterogeneous state. The properties of the monolayers of polymers saponified in different states were studied at the air/water interface by measuring the surface pressure. The limiting areas obtained on distilled water for each polymer saponified in these two systems decreased linearly with an increase in the degree of saponification. However, the monolayers of polymer saponified in a homogeneous system were more stable on sodium chloride solution than those obtained in a heterogeneous system, and gave the limiting areas on solutions above 5% corresponding with the theoretical values calculated from the areas per methyl acrylate and acrylic acid residue and the degree of saponification. This can be explained by the fact that some of the hydrophilic parts of the saponified polymers submerged into the water phase were squeezed out onto the water surface by the salting out effect. On the other hand, those values obtained in a heterogeneous system neither corresponded to the theoretical values nor gave reproducible areas at high concentrations. These facts may be due to the differences in the states of the saponified polymers.

There have been many studies of the hydrolysis of polymers. In particular, a few studies concerned with the hydrolysis of polyacrylate have been reported. Loecker and Smets reported the hydrolysis of copolymers of methacrylic acid and methyl methacrylate in acid-buffered solution.[1] Sakurada *et al.* studied the saponification of poly(methyl acrylate) in binary mixtures of various compositions of water-acetone and reported the effects of solvent on the rate of saponification.[2]

However, studies of the hydrolysis of polymers from the two-dimensional point of view have been scare. Previously, we ourselves investigated the monolayer properties of partially-saponified poly *n*-butyl acrylate at the air/water interface.[3] The relationship between the surface properties and the degree of saponification was discussed.

In the present work, we partially saponified poly(methyl acrylate) with sodium hydroxide in mixtures of different compositions of water-acetone (in homogeneous and heterogeneous systems) and studied the properties of the monolayers of those polymers. The saponification reactions of polymer in homogeneous and heterogeneous systems will be discussed on the basis of the two-dimensional behavior of the polymer when the polymer was spread on water and sodium chloride solutions.

Experimental

Sample Polymers. Methyl acrylate was obtained from Toagosei Co., Ltd. The inhibitor was removed by washing it with 5% sodium hydroxide aqueous solution and distilled water. Methyl acrylate was then purified by distillation under reduced nitrogen atmosphere after having been dehydrated with silicon dioxide. Poly(methyl acrylate) was prepared by radical polymerization in benzene at 50°C under a flow of nitrogen gas, α,α'-azobisisobutyronitrile being used as the inhibitor. After the reaction, this benzene solution was added to a large excess of methanol and the polymer was obtained as precipitate. The polymer thus obtained was purified by repeated precipitation from its acetone solution into a large excess of methanol. The average molecular weight of this polymer was found to be about 659000 by the measurement of the viscosity.

Poly(methyl acrylate) was saponified in a transparent and homogeneous solution of an acetone-water mixture (5 : 2 by volume), with sodium hydroxide as the catalyst, at 50°C until sodium hydroxide was consumed.[3] Saponification in a heterogeneous system was carried out under the same conditions except that the mixture had a different composition of acetone-water (100 : 1 by volume) and except that the reaction solution was a white-turbid suspension of polymer. These saponified polymers for each system were obtained by changing the amount of sodium hydroxide. These polymers were purified by repeated precipitation from their acetone solution into water and methanol. Saponification was confirmed by studying the infrared spectra and by elementary analyses. The degrees of saponification (mol%) of these polymers were calculated by putting the analytical values of carbon as determined by the elementary analyses into Eq. (1), they are listed in Table 1.

$$\frac{c\left(\frac{100-X}{100}\right)+d\frac{X}{100}}{a\left(\frac{100-X}{100}\right)+b\frac{X}{100}}\times 100 = C(\%) \qquad (1)$$

where X is the degree of saponification; a and b are the apparent molecular weights of a methyl acrylate and of an acrylic acid residue respectively; c and d are the weights of carbon in a methyl acrylate and an acrylic acid residue respectively; C (%) is the analytical value of carbon.

Surface-pressure Measurements. The surface pressure-area isotherms were obtained with a modified Wilhelmy-type film balance. The film balance was enclosed in the

* Present address: Faculty of Engineering, Tokyo Institute of Technology, Ookayama, Meguro-ku, Tokyo.

1) W. De Loecker and G. Smets, *J. Polym. Sci.*, **40**, 203 (1959).

2) I. Sakurada, Y. Sakaguchi, and S. Fukui, *Kobunshi Kagaku*, **13**, 355 (1956).

3) S. Hironaka and K. Meguro, *J. Colloid Interfac. Sci.*, **35**, (3), 367 (1971).

Table 1. Elementary analyses of hydrogen and carbon and the degree of saponification of the saponified polymers

Sample	Elementary analysis (%)		Degree of saponification (mol%)
	Hydrogen	Carbon	
Poly(methyl acrylate) theoretical	7.03	55.80	—
Poly(methyl acrylate) experimental	6.86	55.84	—
Homogeneous system			
Saponified polymer	7.20	55.12	13.93
Saponified polymer	6.91	54.59	24.16
Saponified polymer	7.08	53.26	48.34
Heterogeneous system			
Saponified polymer	6.84	55.30	10.38
Saponified polymer	6.88	54.84	18.89
Saponified polymer	6.87	54.24	30.90

chamber adjusted to 20±0.2°C. The distilled water used as the substrate showed a pH of 5.0—6.0. The water in the trough was kept at 20.0±0.2°C by circulating the water from the thermostat bath. Sample polymers were spread on the distilled water and sodium chloride solutions with an "Agla" microsyringe. A mixture of acetone-benzene (1 : 1 by volume) was used as the spreading solvent. Thirty mixutes were allowed for the solvent to evaporate before compression was started. The rate of compression was 7.5 cm²/min.

The surface-pressure measurements were repeated for all polymers at least several times; the results were reproducible within the limits of experimental error.

Results and Discussion

The surface pressure-area isotherms on distilled water for poly(methyl acrylate) and polymers saponified in homogeneous and heterogeneous systems are shown in Figs. 1 and 2. The limiting areas obtained for all the saponified polymers of both systems were smaller than that of poly(methyl acrylate) (Figs. 1 and 2); their theoretical values were calculated as follows.

With the use of the limiting areas of 21.5 Å per methyl acrylate residue and 22.0 Å per acrylic acid residue reported by Crisp,[4,5] the theoretical area (A_t) of the saponified polymer, when all the residues of the polymer were oriented on the water surface, without the hydrophilic parts submerged into the water, was calculated by the following equation:

$$A_t = 21.5\left(1-\frac{X}{100}\right)+22.0\frac{X}{100} \qquad (2)$$

where X is the degree of saponification (mol%).

If the limiting area of the saponified polymer is the sum of the areas of the hydrophilic and hydrophobic parts (acrylic acid and methyl acrylate residues), the measured areas should correspond to the theoretical values calculated by Eq. (2). However, the limiting areas obtained from Figs. 1 and 2 were smaller than the theoretical values and decreased linearly with an increase in the degree of saponification (Fig. 3). The observed decreases in the limiting areas suggest the possibility of some of their hydrophilic parts submerging into the water phase in the compressed state of the films.

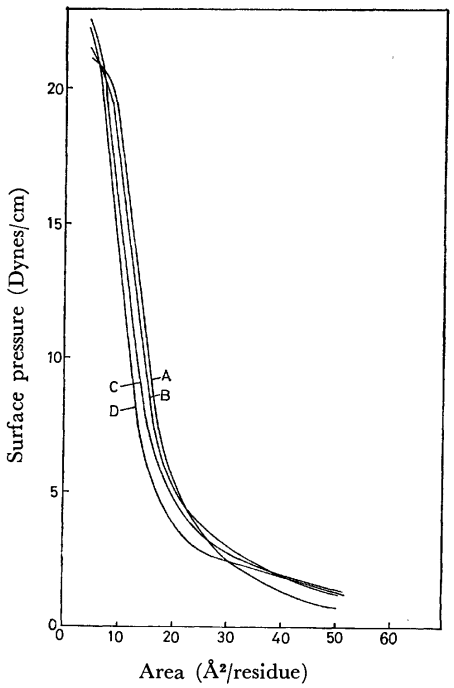

Fig. 1. The surface pressure-area isotherms on distilled water for poly(methyl acrylate) and its saponified polymers in homogeneous system. A-poly(methyl acrylate); B-13.93 mol% saponified polymer; C-24.16 mol% saponified polymer; D-48.34 mol% saponified polymer.

Previously, we investigated the monolayer properties of partially saponified poly *n*-butyl acrylate[3] and discussed them. Saponified polymer monolayers on sodium chloride solution expanded more than those on water. Their limiting areas increased as the salt concentration was increased. The limiting areas obtained on salt solutions above a certain concentration corresponded well to the theoretical values as calculated from the areas per butyl acrylate and per acrylic acid residue. One explanation of this is that the submerged hydrophilic residues of the saponified polymers were forced out of the water phase onto its

4) D. J. Crisp, *J. Colloid Sci.*, **1**, 49 (1946).
5) D. J. Crisp, *ibid.*, **1**, 161 (1946).

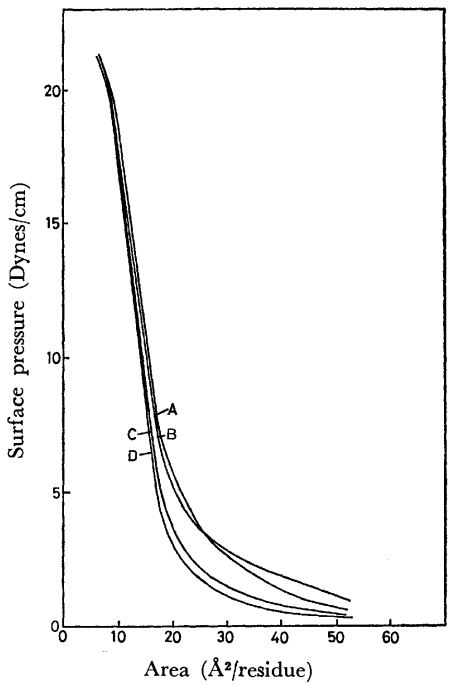

Fig. 2. The surface pressure-area isotherms on distilled water for poly(methyl acrylate) and its saponified polymers in heterogeneous system. A-poly(methyl acrylate); B-10.38 mol% saponified polymer; C-18.89 mol% saponified polymer; D-30.90 mol% saponified polymer.

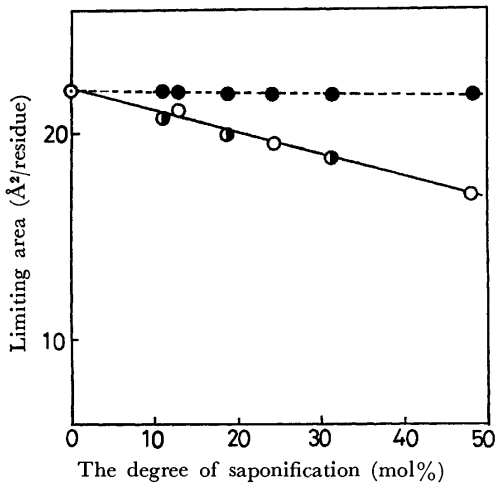

Fig. 3. Plots of the limiting areas of the saponified polymers against the degree of saponification. ○-saponified polymers in homogeneous system; ◑-saponified polymers in heterogeneous system; ⊙-poly(methyl acrylate); ●-theoretical values.

surface *via* the salting out effect.

Figure 4 shows the effect of the salt concentration on the surface pressure-area isotherms for the 48.34 mole% saponified polymer obtained in a homogeneous system. Figure 5 shows the plots of the limiting areas obtained for each saponified polymer *vs.* the concentration of sodium chloride. These curves approached nearly horizontal straight lines on salt solutions above 5%. The extrapolated values of these portions to a zero concentration of sodium chloride were in good agreement with the theoretical values within the limits of experimental error, as Table 2 shows. The agreement suggests that the monolayers of the saponified polymers spread completely on salt solutions above about 5%.

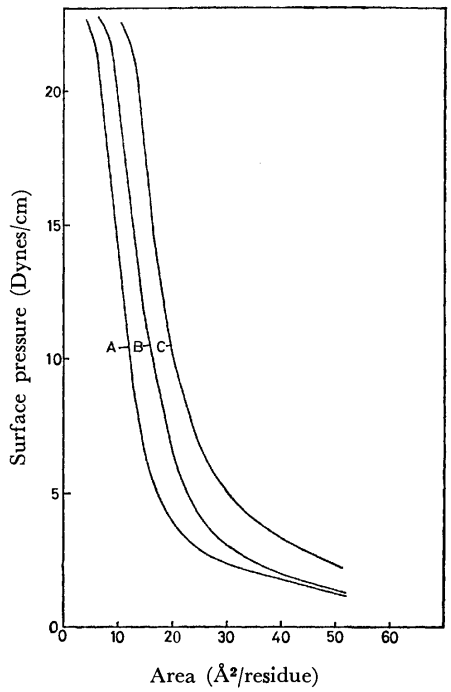

Fig. 4. The surface pressure-area isotherms of 48.34 mol% saponified polymer in homogeneous system on distilled water-(A); 2%-(B); and 5—10% sodium chloride solution-(C).

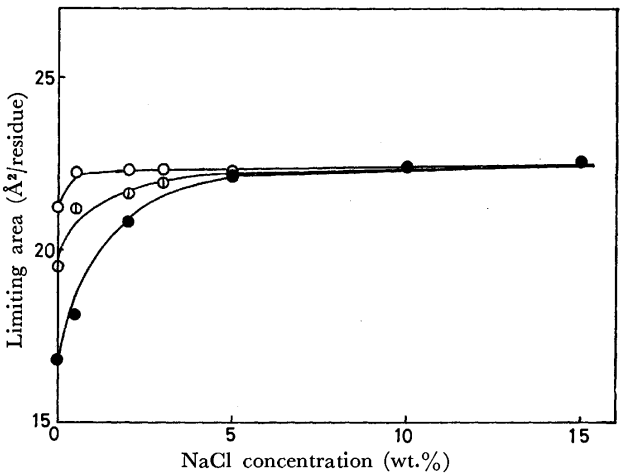

Fig. 5. Plots of the limiting areas of the saponified polymers in homogeneous system against concentration of sodium chloride in the bulk. ○-13.93 mol% saponified polymer; ◑-24.16 mol% saponified polymer; ●-48.34 mol% saponified polymer.

Also, the ratios of the portion submerging into the water phase and the portion remaining on it were estimated from the theoretical and observed values of the limiting areas in Fig. 3.[3] These ratios showed a good linearity against the degree of saponification. In the present work, this linearity was confirmed to hold (in Fig. 6). It can be suggested that the saponification of poly(methyl acrylate) in a homogeneous system proceeds evenly.

On the other hand, the monolayers of polymers

TABLE 2. THE LIMITING AREAS OF POLY(METHYL ACRYLATE) AND ITS SAPONIFIED POLYMERS

Experimental: the values extrapolated to zero concentration of sodium chloride (from Figs. 1 and 2).
Theoretical: the values calculated by Eq. (2).

Sample	Limiting area (Å²/residue)	
	Experimental	Theoretical
Poly(methyl acrylate)	21.6	21.5 (by Crisp)
Homogeneous system		
13.93 mol% saponified polymer	21.8	21.6
24.16 mol% saponified polymer	21.8	21.6
48.34 mol% saponified polymer	21.9	21.7
Heterogeneous system		
10.38 mol% saponified polymer	22.8	21.6
18.89 mol% saponified polymer	21.9	21.7
30.90 mol% saponified polymer	20.3	21.7

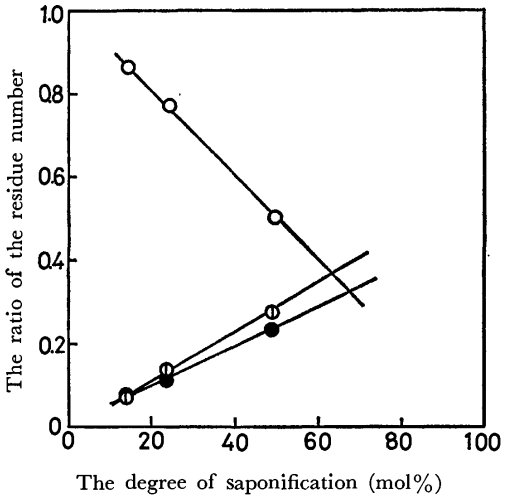

Fig. 6. Plots of the ratio of each residue number against the degree of saponification. The methyl acrylate residue-○, the acrylic acid residue in water-●, the acrylic acid residue on water-◑.

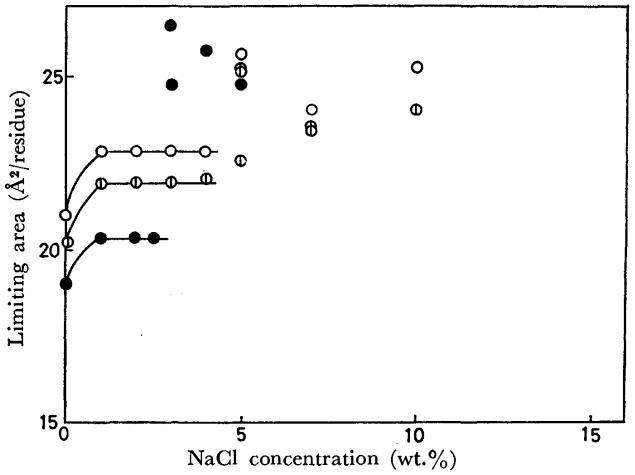

Fig. 7. Plots of the limiting area of the saponified polymers in heterogeneous system against concentration of sodium chloride in the bulk. ○-10.38 mol% saponified polymer; ◑-18.89 mol% saponified polymer; ●-30.90 mol% saponified polymer.

saponified in a heterogeneous system were confirmed to be unstable on salt solution as compared with those in a homogeneous system. Furthermore, the films of these substances had a tendency to show similar linear plots only in the range of low concentrations, as is shown in Fig. 7, and the extraploated values did not agree with the theoretical ones. In the range of higher concentrations above 2.5—4%, the films were less stable than those at low concentrations and were not reproducible, giving much larger limiting areas than the theoretical ones.

The monolayers of polymers saponified under different conditions showed the different two-dimensional behaviors. This may be due to the difference in the saponified states of the polymers. Probably, saponification in a homogeneous solution of the polymer proceeded evenly.

On the other hand, the results obtained for polymers saponified in a heterogeneous system suggest that the states of saponification of the polymers are not steady. Perhaps polymers may be either those saponified in block or mixtures of saponified and unsaponified polymers. If they are mixtures, their monolayers should give the behaviors of the mixed monolayers. Their monolayers, however, did not give the same surface pressure-area isotherms as the mixed monolayers. Therefore, saponification presumably proceeds in block and the saponified polymers consist of both those saponified in block and those not saponified at all.

The unstability and the further expansion of the monolayers of the saponified polymers on salt solutions above 2.5—4% suggest that the parts saponified in block were salted out strongly, exposing many neighboring carboxylates at the water surface. This resulted in an expansion of the monolayer, which was favored by the repulsion between $-COO^-$ ions formed by their dissociation.

The effect of the pH on the monolayers was further examined by adding hydrochloric acid and sodium hydroxide into the water phase, but the films of polymers obtained in both the homogeneous and heterogeneous systems were hardly affected below pH 6, while they expanded a little in the pH range of 8—9.

In conclusion, on distilled water the monolayers of polymers saponified under different conditions showed the same tendency for the limiting areas to decrease

linearly with the increase in the degree of saponification (Fig. 3); the results obtained on salt solutions suggested the difference in the saponified states of polymers detectable by the differences in the stabilities and the reproducibilities of the limiting areas. Further, the submergence theory held good only for polymers saponified in a homogeneous system. A linear relation was obtained by assuming the submergence theory, by assuming, that is, that some of the hydrophilic groups of the saponified polymers submerge into the water phase and are squeezed out of it by the salting out effect. This fact suggests that, while some of the hydrophilic groups are easily submerged into the water phase by compressing the films, one or two hydrophilic groups of both sides of the saponified portions are next to hydrophobic anchors, such as methyl acrylate residues, and remain on the water surface.

On the basis of the above discussion, it may be suggested that studies of the monolayers are of use in connection with the saponification reaction of polymers.

BULLETIN OF THE CHEMICAL SOCIETY OF JAPAN VOL. 45, 336—338 (1972)

The Effect of Pressure on the Sol-Gel Transformations of Macromolecules[1)]

Keizo SUZUKI, Yoshihiro TANIGUCHI, and Toshishige ENOMOTO

Department of Chemistry, Faculty of Science and Engineering, Ritsumeikan University, Kita-ku, Kyoto

(Received April 30, 1971)

The effect of pressure on the gelation of macromolecules, such as gelatin, polyvinyl alcohol, and methyl cellulose, was investigated in order to clarify which binding forces contribute to their gel formations. The values for ΔH and ΔV accompanying the gel formation were calculated from the Eldrige-Ferry's plot and the Clausius-Clapeyron equation respectively. The values for ΔH and ΔV in the gel fromations of gelatin and polyvinyl alcohol are both negative, while those in methyl cellulose are both positive. From the thermodynamical considerations, it has been found that the formation of hydrogen bonds results in negative values of ΔV and ΔH, while that of hydrophobic bonds results in positive values of ΔV and ΔH. Therefore, it may be assumed that the main binding forces in the gelations of gelatin and polyvinyl alcohol may be attributed to hydrogen bonds, and that those in methyl cellulose may be attributed to hydrophobic bonds, at least up to 6000 atm.

Gelations may be classified into three types according to the signs of enthalpy of gelation, ΔH; endothermic ($\Delta H>0$), exothermic ($\Delta H<0$), and athermal ($\Delta H=0$). In each case, there are reversible and irreversible sol-gel transformations. In the present experiment, the non-athermal reversible sol-gel systems are investigated. In reversible gelations, weak binding forces, such as the van der Waals type, hydrophobic bonds, hydrogen bonds, and ionic bonds, are considered to be mainly responsible for the gelation.

In investigating the pressure effect on gelation, it seems worthwhile to classify gelation from the point of view of the volume changes in gel formation, ΔV. The pressure effect can be predicted from the sign of ΔV. That is, the gelation in which ΔV is negative is prompted by hydrostatic compression, while in the gelation in which ΔV is positive, the pressure retards the gel formation.

From the thermodynamical data obtained in the appropriate model systems in which hydrogen bonds or hydrophobic bonds are involved, it has been found that the formation of hydrogen bonds results in negative values of ΔV and ΔH,[2,3)] while that of hydrophobic bonds results in positive values of ΔV and ΔH.[4)] Therefore, we can expect that the pressure will prompt the gel formation in which hydrogen bonds are concerned predominantly, while the pressure will retard the gel formation in which hydrophobic bonds are concerned predominantly.

In the present experiment, gelatin, polyvinyl alcohol, and methyl cellulose were used as samples; the binding forces which are concerned in gel formation will be discussed on the basis of the results of the pressure effect on gel formations.

Experimental

Samples. The gelatin was purchased from the Difco Lab. Co., the polyvinyl alcohol (M. W. 2700) was donated by the Kurashiki Rayon Co. and the methyl cellulose (M.W. 3400, 30.3% methoxyl) was obtained from the Japan Synthetic Chemicals Co., The water used was deionized through an ion-exchange column. These polymer solutions were not buffered.

Sol-Gel Transformation Measurement. The method for the determination of the sol-gel transformation was as follows. The solution was charged into a syringe-type cell, the inner diameter of which was about 10 mm. The cell was set in a high-pressure vessel, and the system was hydrostatically compressed for 10 or 20 min at the desired temperature. As soon as the pressure was released, the state of the system was checked to see if the ball (the diameter of which was 3 mm) inserted in the cell moved or not. In the cases of gelatin and polyvinyl alcohol, the compression was started at the sol state because the gels are formed by compression. The mean value of the lowest pressure at which

1) Presented at the 22nd International Congress of Pure and Applied Chemistry, Sydney, August, 1969, and the 24th Annual Meeting of the Chemical Society of Japan, Osaka, April, 1971.

2) I. M. Klotz, *Fed. Proc.*, **24**, S-24 (1965).

3) E. Fishman and H. D. Drickamer, *J. Chem. Phys.*, **24**, 548 (1956).

4) W. Kauzmann, *Adv. Protein Chem.*, **14**, 1 (1959).

the ball did not move and the highest pressure at which the ball did move was considered to be the sol-gel transition pressure. In the case of methyl cellulose, the gel formed at 1 atm was compressed, because the gel melts by compression. The difference between the highest and the lowest pressure was usually about ±50—100 atm.

Results

Figure 1 shows a sol-gel phase diagram of gelatin at various concentrations. The phase above each curve is a sol phase, while the phase below each curve is a gel phase. It can be seen in this figure that the gelation of gelatin is prompted by raising the pressure. The phase diagram of polyvinyl alcohol in Fig. 2, shows that the pressure favors the gel formation. The curves of the concentrations of 13.35 wt% and 15.24 wt% coincide with each other completely, and above a certain pressure the gel is always formed, whatever the temperature.

Figure 3 shows a sol-gel phase diagram of methyl cellulose at various concentrations. In this figure, the phase above the curve is a gel phase, and the phase below the curve is a sol phase. The methyl cellulose gel is melted by compression; *i.e.*, pressure retards the gel formation of methyl cellulose. This behavior is quite different from that of the two other gels discussed above.

Discussion

Figure 4 shows the relation between the logarithm of the gelatin concentration, c, and the reciprocal of the absolute temperature of sol-gel transformation at each pressure according to the plot of Eldrige and

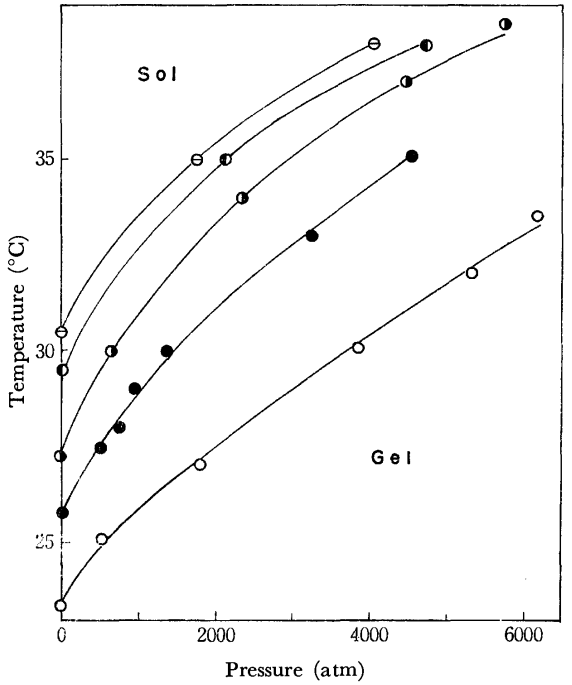

Fig. 1. Sol-gel phase diagram of gelatin-water system at various concentrations.
○: 5 wt%, ●: 10 wt%, ◑: 15 wt%, ◐: 20 wt%, ⊖: 25 wt%

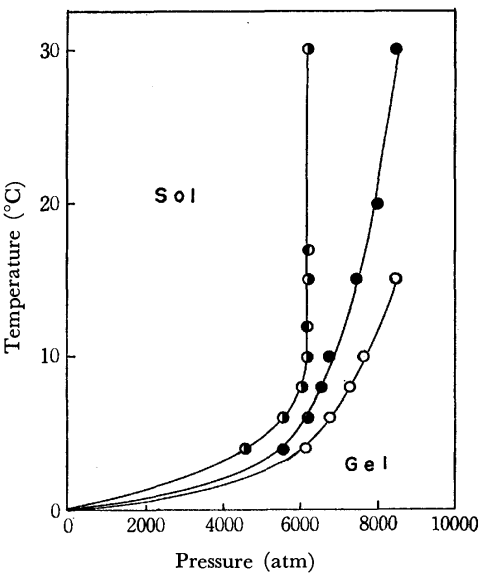

Fig. 2. Sol-gel phase diagram of polyvinyl alcohol-water system at various concentrations.
○: 9.83 wt%, ●: 11.19 wt%, ◑: 13.35 wt%, ◐: 15.24 wt%

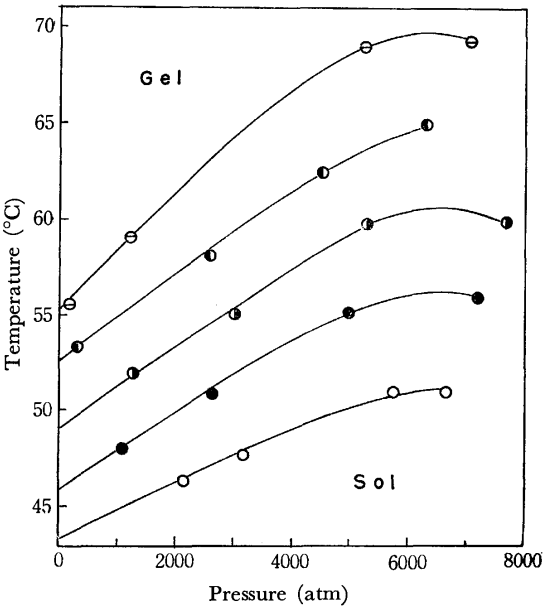

Fig. 3. Sol-gel phase diagram of methyl cellulose-water system at various concentrations.
○: 3.65 wt%, ●: 3.01 wt%, ◑: 2.51 wt%, ◐: 2.07 wt%, ⊖: 1.50 wt%

Ferry.[5] The linear relationship is also applicable to polyvinyl alcohol and methyl cellulose except for the higher concentrations in polyvinyl alcohol. The heat of reaction, ΔH, for the formation of the cross-links in gel is calculated from the slope of Fig. 4 according to the following formula;[5] $\log c = \Delta H/(2.303 RT) + \text{constant}$. The calculated ΔH values are tabulated in Table 1, together with those of polyvinyl alcohol and methyl cellulose.

The volume changes in gel formation were calculated from the relation of Clausius-Clapeyron, $dP/dT = \Delta H/T\Delta V$, assuming that the sol-gel transfor-

5) J. E. Eldrige and J. D. Ferry, *J. Phys. Chem.*, **58**, 992 (1954).

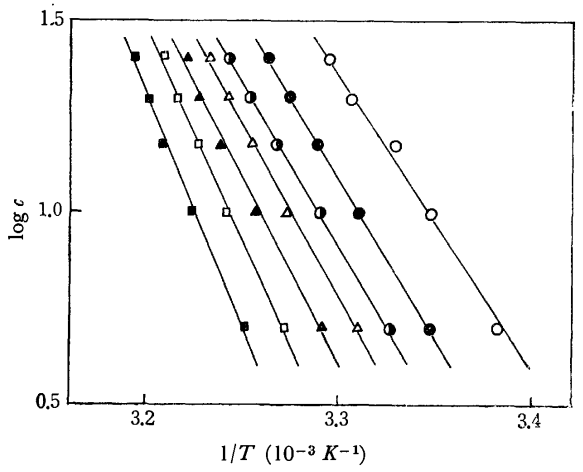

Fig. 4. Relation between the logarithm of the concentration of gelatin and the reciprocal of the absolute temperature of gelation at each pressure.
○: 1 atm, ●: 1000 atm, ◑: 2000 atm, △: 3000 atm, ▲: 4000 atm, □: 5000 atm, ■: 6000 atm

mation of these macromolecules can be treated as a phase transition. In Table 2, these values are listed. It can be found from Tables 1 and 2 that the gel formations in gelatin and polyvinyl alcohol are exothermic (*i.e.*, ΔH is negative) and are accompanied by a volume decrease and that the gelation in methyl cellulose is endothermic (*i.e.*, ΔH is positive) and is accompanied by a volume increase.[6]

As has already been explained in the introduction, when the values of ΔH and ΔV are both negative, hydrogen bonds contribute predominantly to the gel formation, while when the values of ΔH and ΔV are both positive, hydrophobic bonds contribute predominantly to the gel formation. Therefore, it may be assumed that the main binding forces in both gelatin and polyvinyl alcohol gels originate in hydrogen bonds, while in methyl cellulose hydrophobic bonds are mainly responsible for the gel formation.

The changes in ΔH and ΔV for gelatin at each pressure are different from those of polyvinyl alcohol. That is, the absolute values of ΔH and ΔV for gelatin increase with an increase in the pressure, while those of polyvinyl alcohol decrease. Therefore, we may assume that the mechanism for the gelation of gelatin is different in detail from that of polyvinyl alcohol. In methyl cellulose, (Fig. 3), the ΔV values tend to change in sign from positive to negative above 6000 atm. From these facts, it may be assumed that both hydrophobic and hydrogen bonds are concerned with the gel formation in the case of methyl cellulose, and that, with an increase in the pressure, the contribution of hydrogen bonds surpasses the contribution of hydrophobic bonds.

Table 1. ENTHALPY CHANGES, ΔH ACCOMPANYING THE FORMATION OF GEL IN GELATIN-, POLYVINYL ALCOHOL-, AND METHYL CELLULOSE-WATER SYSTEMS

Pressure (atm)	ΔH (kcal/unit)		
	Gelatin	Polyvinyl alcohol	Methyl cellulose
1	−39.4	—	15.0
1000	−42.0	—	13.8
2000	−42.0	—	12.8
3000	−47.6	−28.6	11.6
4000	−50.4	−22.8	10.9
5000	−58.6	−15.8	10.3

Table 2. VOLUME CHANGES, ΔV ACCOMPANYING THE FORMATION OF GEL IN GELATIN-, POLYVINYL ALCOHOL-, AND METHYL CELLULOSE-WATER SYSTEMS

Pressure (atm)	ΔV (cm³/unit)		
	Gelatin Temp. 30°C	Polyvinyl alcohol 5°C	Methyl cellulose 50°C
1	—	—	4.5
1000	—	—	4.2
2000	−8.2	—	3.9
3000	−9.3	−3.5	3.5
4000	−9.8	−3.4	3.3
5000	−11.4	−3.1	—

The finantial support given by the Ministry of Education is gratefully acknowledged.

6) The ΔV values accompanying the gel formation in gelatin (negative) and methyl cellulose (positive) have been obtained at 1 atm by Heymann from dilatometry.[7]

7) E. Heymann, *Trans. Faraday Soc.*, **31**, 846 (1935).

The Temperature Dependence of the Fractionation of Tritiated Water in an Equilibrium between Crystalline Alum and Its Aqueous Solution

Haruhiko TANAKA*

Department of Chemistry, Faculty of Science, Hiroshima University, Higashi-sendamachi, Hiroshima

(Received May 14, 1971)

The temperature dependence of the fractionation of tritiated water (HTO) was examined during the crystal growth of alum from its tritiated aqueous solution. When the ratios of the mole fractions of HTO in the water of crystallization to that of the mother liquid, S, at various temperatures are compared, the following order is established:

$$S_{19.90} \approx S_{29.50} > S_{36.52} > S_{41.95} > S_{47.43} > S_{53.70} \approx S_{69.50},$$

where the suffixes represent the crystallization temperatures, and where $S_{19.90}=0.975$ and $S_{69.50}=0.949$. The concept of the hydration of ions developed recently was applied to the problem of the crystal growth from the solution. Two kinetic parameters, such as the relaxation time of the aluminum ion for entering the surface, τ_c, and that of the hydrated aluminum ion, $Al(OH_2)_6^{3+}$, for the exchange of the water with bulk water, τ_e, were taken into account to explain the fractionation. A surface-diffusion mechanism was suggested as essential in the crystal growth of alum from the solution. The activation free energy for the crystal growth from an unstirred solution was found to be 18.17 kcal/mol, a value which was in good agreement with the value given by Bennema.

Tritium has some advantages over deuterium for examining hydrogen isotope effects. However, the fractionation of tritium in a hydrated crystal in equilibrium with its aqueous solution had scarcely been studied before the results on several hydrated crystals were reported.[1,2] Moreover, the temperature dependence of the fractionation of heavy water has been examined neither by the use of deuterated water nor by that of tritiated water. In this connection, it seemed that it would be quite interesting to study the fractionation of tritium during the crystallization of an inorganic hydrate at various temperatures.

It has been pointed out in a previous report[2] that tritium-fractionation should be useful in the study of phase equilibria between hydrated crystals and their aqueous solutions. Such a study seems to have increasing significance in connection with the recent development of the ionic process in an aqueous solution, particularly with regard to the hydration of various ions. It has become possible to examine the mechanism of the crystal growth of inorganic hydrates from their aqueous solution, as well as the kinetics of the deposition of the hydration water of cations from the solution, in the light of tritium fractionation.

Recently, Fiat and Connick[3] have obtained the kinetic parameters of the hydrated aluminum ion in an aqueous solution by the use of the ^{17}O-NMR technique over a wide range of temperatures. Samoilov[4] has investigated the hydration of alkali metal ions in detail and found that the potassium ion diffuses in an aqueous solution without any hydration water. In addition, the crystal growth of alum from a very slightly supersaturated solution has been studied extensively by Bennema,[5,6] who measured the growth rate as a function of the relative supersaturation of the mother liquid. He concluded from his study that the crystal growth probably occurs by means of a surface-diffusion mechanism originally proposed by Burton *et al.*[7] As he pointed out himself, however, much study remains to be done before a sound theory of crystal growth from an aqueous solution can be worked out.

Potassium aluminum sulfate dodecahydrate, $KAl(SO_4)_2 \cdot 12H_2O$, has been chosen for the present study aiming at the elucidation of the mechanism of crystal growth from an aqueous solution. For this purpose, it seemed that it would be interesting to study the fractionation of tritiated water by slowly growing crystals from a tritiated aqueous solution at various temperatures. Another purpose of the present study is to discuss the behavior of water during the crystal growth from an aqueous solution, behavior which has not been clarified by any other study.

Experimental

Potassium aluminum sulfate dodecahydrate obtained from a commercial source was purified by recrystallization. The solvent was twice-distilled water which contained a trace of tritiated water (*ca.* 1.5×10^{-8} mol/*l*). The single crystals of the hydrated salt were obtained from a very slightly supersaturated solution at constant temperatures of 19.90°, 29.50°, 36.52°, 41.95°, 47.43°, 53.70°, and 69.50°C under unstirred conditions.[8] A seed crystal was obtained from the same solution as that used for the succeeding crystal growth. The form of the small seed crystal was nearly octahedral; the (111) face was well-developed in comparison

* Present address: Shinonome Branch School, Faculty of Education, Hiroshima University, Shinonome, Hiroshima.

1) H. Tanaka and H. Negita, This Bulletin, **43**, 3079 (1970).

2) H. Tanaka and H. Negita, *ibid.*, **44**, 2075 (1971).

3) D. Fiat and R. E. Connick, *J. Amer. Chem. Soc.*, **90**, 608 (1968).

4) O. Ya. Samoilov, "Structure of Aqueous Electrolyte Solutions and the Hydration of Ions," Consultants Bureau Enterprises, Inc., New York (1965), chap. 5.

5) P. Bennema, Thesis, The Technical University of Delft (1965).

6) P. Bennema, *J. Cryst. Growth*, **5**, 29 (1969).

7) W. K. Burton, N. Cabrera, and F. C. Frank, *Phil. Trans. Roy. Soc.*, **A243**, 299 (1951).

8) This condition is necessary to determine the value of the activation free energy needed for the aluminum ion to integrate into the crystal surface, E_{sf}; this value will be discussed later.

with the other faces. The fluctuation of the temperature of the mother liquid was within ±0.02°C in a well-stirred thermostat. The rate of the evaporation of the solvent was so slow that only about 2 g of the well-developed (octahedral) single crystal of the salt was obtained in a week from a large amount of the mother liquid. The relative supersaturation of the mother liquid was kept below *ca.* 1.2×10^{-2} during each crystal growth.

Water from both the mother liquid and the single crystal was recovered by heating them in a stream of nitrogen gas until no further dehydration was observed. The tritium content in the water of crystallization was then compared with that in the corresponding mother liquid by an analysis of the activity of tritium. The activity was measured with a liquid scintillation counter (Packard Tri-Carb), using the scintillant described in a previous paper.[1]

Results and Discussion

The separation factor, S, for the equilibrium between solid and liquid phases can be given as follows in the case of a very low concentration of the relevant isotope (HTO in this case):

$$S = N_s/N_l,$$

where N_s and N_l are the mole fractions of HTO in the solid and liquid phases respectively. Table 1 gives the separation factor, S, together with the net counts per minute (cpm),[9] which are proportional to the amount of HTO, and the value of pH and the maximum relative supersaturation of the mother liquid during the crystal growth.

It may be seen that a considerable dilution of HTO occurs in the solid phase for the whole range of crystallization temperatures. The separation factors apparently decrease with an increase in the temperature in the 29.50°—53.70°C range, implying that more dilution of HTO in the hydrated crystal occurs at higher temperatures. On the other hand, no change in dilution can be seen within the limits of experimental error between 19.90° and 29.50°C or between 53.70° and 69.50°C.

Calculation of the Minimum Separation Factor, S. It has been reported in a previous paper[1] that HTO should be diluted in the crystal of inorganic hydrates during the growth from a solution, if free water behaves according to a surface-diffusion mechanism in which a growth unit essentially diffuses along the crystal surface before integrating into the kink.[7] On the contrary, the value of S has been calculated to be unity when the crystal growth follows a volume-diffusion mechanism; there is a direct integration from the solution into the kink without any surface diffusion.[5] It can thus be assumed here that free water should crystallize from the solution to give the water of crystallization in $KAl(SO_4)_2\cdot12H_2O$ by the surface-diffusion mechanism, since HTO was found to be diluted during the crystal growth of the salt.

Assuming an equilibrium between the free water in the solution and that on the crystal surface, the rate of the integration of the free water into the crystal, R, can be expressed as follows:[1]

$$R = \alpha C_0 \Omega N_0 (kT/2\pi m)^{1/2}(\sigma^2/\sigma_1)\tanh(\sigma_1/\sigma), \quad (2)$$

where

α=correction factor,
C_0=retarding factor,
Ω=volume of a growth unit,
N_0=equilibrium concentration of growth units per ml of the solution,
k=Boltzmann's constant,
T=absolute temperature,
m=mass of a growth unit,
σ=relative supersaturation, and
σ_1=parameter.

The R_{HTO}/R_{H_2O} ratio is thus obtained in the case of the crystal growth by the surface-diffusion mechanism, recognizing that all the factors other than m are independent of the hydrogen isotope:[1]

$$R_{HTO}/R_{H_2O} = (m_{H_2O}/m_{HTO})^{1/2} = 0.949, \quad (3)$$

where R_{HTO}/R_{H_2O} is the ratio of the integration of HTO to that of H_2O molecules into the crystal and where m_{H_2O}/m_{HTO} is the mass ratio of H_2O to HTO molecules. It follows from Eq. (3) that the minimum value of S (or the maximum dilution of HTO in the crystal) is equal to 0.949. This value was derived by assuming

Table 1. Separation factor, S, of tritiated water, HTO, during the crystal growth of alum from its aqueous solution at various temperatures

Temp. (°C)	pH	σ_{max}[d]	Net cpm of HTO[a]		S_{obs}
			Mother liq. (N_l)	Crystal (N_s)	
19.90±0.01	3.31	1.0×10^{-2}	27097±116[b]	26425±115[b]	0.975±0.004
29.50±0.02	3.20	1.2×10^{-2}	45678±210[c]	44477±55[c]	0.974±0.003
36.52±0.01	3.09	1.1×10^{-2}	70925±379[c]	68720±172[c]	0.969±0.004
41.95±0.01	3.05	9.0×10^{-3}	30128±119[b]	29000±143[b]	0.963±0.004
47.43±0.02	2.88	1.0×10^{-2}	67027±266[c]	64284±306[c]	0.959±0.005
53.70±0.01	2.70	1.0×10^{-2}	55500±273[c]	52495±234[c]	0.946±0.004
69.50±0.02	1.85	8.0×10^{-3}	32253±156[b]	30601±116[b]	0.949±0.004

a) cpm in each sample water of 0.1 g with mean square error.
b), c) Measured using counters of 35 and 45% efficiencies respectively.
d) degree of supersaturation.

9) Each cpm listed in Table 1 was obtained by averaging the activities per 0.1 g, which were measured 6—8 times for a given sample of water.

that the fractionation of the isotope results, if at all, only from the free water and, practically speaking, not from the hydration water of the cation.

Free Water in the Aqueous Solution. In the aqueous solution of alum, there are three hydrated ions: $K(OH_2)_p^+$, $Al(OH_2)_6^{3+}$, and $SO_4(H_2O)_q^{2-}$. The hydration number of the aluminum ion has been determined exactly,[10] while those of other ions are ambiguous at this stage. As will be seen, however, the result may be independent of the hydration numbers of K^+ and SO_4^{2-} ions, *i.e.*, p and q. It is improbable that the hydrated aluminum ion, $Al(OH_2)_6^{3+}$, is subject to dehydration in the solution as are the hydrated cations studied in a previous paper,[1] since $Al(OH_2)_6^{3+}$ is rather stable; the order of its lifetime was found to be 7.5 sec at room temperature.[3]

It can be assumed here that the apparent free water molecules may result from the hydration water when the relaxation time needed for $Al(OH_2)_6^{3+}$ to integrate into the crystal surface, τ_c, is longer than that needed for the hydrated ion to exchange its hydration water with bulk water, τ_e. This assumption may be explained by examining a given water molecule rather than the aluminum ion. That is, a given hydration water molecule of Al^{3+} is liberated during the integration into the crystal surface if $\tau_c > \tau_e$. The resulting hydration water of $Al(OH_2)_6^{3+}$ also exchanges with a free water molecule on the surface during the integration into the kink, since the sphere can reside on the surface over the interval of τ_c or a little longer.[6] The water molecules of $Al(OH_2)_6^{3+}$ which integrate into the kink from the surface are thus assumed to result from the originally free water on the surface. On the other hand, half of the hydration water may be taken statistically to come from free water molecules on the surface when τ_c is equal to τ_e.

The hydration of the sulfate ion is supposed to be generally negligible. As for the hydration of the potassium ion, a recent concept by Samoilov[4] may be properly referred to in the present case. According to him, the potassium ion diffuses in a solution without any accompanying hydration water. It follows from the preceding argument that the estimation of the fraction of the free water which plays an important role in the crystal growth can be deduced from the hydration of the aluminum ion.

τ_e of the Aluminum Ion. The relaxation time for the exchange of the hydration water with bulk water has been extensively studied by a number of methods. Although only the order of magnitude of the lifetime of the species, $Al(OH_2)_6^{3+}$, had previously been reported, the exact value has recently been found using a ^{17}O-NMR technique by Fiat and Connick.[3] The measurement was carried out over a wide range of temperatures and the activation free energy for the exchange and the relaxation time were both derived. The lifetime of the $Al(OH_2)_6^{3+}$ species is reproduced in Fig. 1 as a function of the reciprocal of the absolute temperature.

Estimation of the Value of τ_c. The relaxation

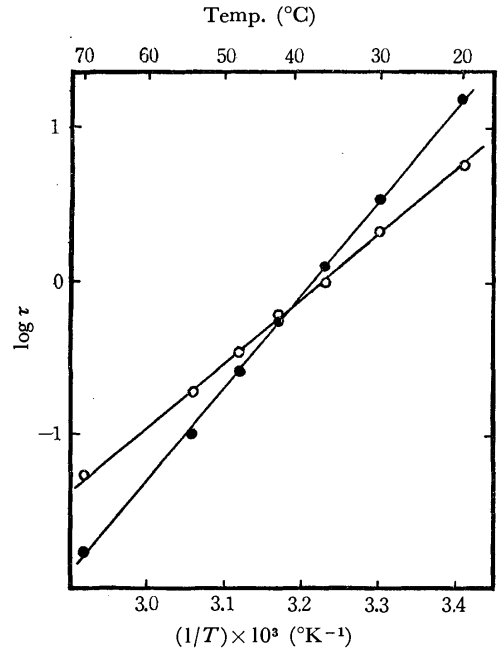

Fig. 1. Plots of τ_c and τ_e *vs.* $1/T$.
● τ_e calculated from Ref. 3.
○ τ_c calculated in terms of Eq. (4) using the value of E_{sf}, 18.2 kcal/mol.

time of the aluminum ion for integrating into the crystal surface, τ_c, can be represented by the equation:[6]

$$\tau_c = (h/kT)\exp(E_{sf}/kT), \quad (4)$$

where E_{sf} is the activation free energy of the ion for integrating into the crystal surface. It seems impossible at this stage to determine the value of E_{sf} accurately, since only the total activation energy for the crystal growth, E_t, can be obtained from the relation between the growth rate, R, and the temperature at a constant relative supersaturation, σ. However, the value of E_{sf} may be nearly equal to that of E_t or a little smaller, if the activation free energy of the aluminum ion for integrating into the kink from the surface, E_k, is relatively small. That is, it is possible to obtain the value of E_{sf} experimentally if the surface-diffusion mechanism is essential in which the integration of the cation into the surface is the rate-determining step. An energy diagram for the

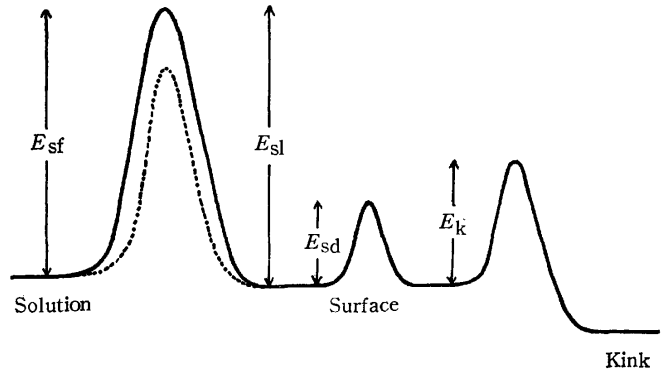

Fig. 2. The free energy diagram of the aluminum ion for integrating into the crystal from an unstirred solution. The dotted line denotes the barrier in the case of a well-stirred solution.

10) H. W. Baldwin and H. Taube, *J. Chem. Phys.*, **33**, 206 (1960); R. E. Connick and D. N. Fiat, *ibid.*, **39**, 1349 (1963).

integration of the cation from the solution into the crystal is shown in Fig. 2.

On the other hand, the value of E_{sf} can also be estimated from a R-σ relation in which the growth rate, R, is expressed as a function of the relative supersaturation, σ, at a constant temperature. According to Bennema, the rate of the crystal growth of $KAl(SO_4)_2 \cdot 12H_2O$ from a well-stirred solution is given in the case of the surface-diffusion mechanism as follows:[6]

$$R = \beta C_0 \Omega (kT/h) \Lambda N_0 \{\exp(-E_{sf}/kT)\} (\sigma^2/\sigma_1) \tanh(\sigma_1/\sigma), \quad (5)$$

where β is a retarding factor and Λ is the thickness of the adsorption layer. He has thus estimated the value of E_{sf} to be 14.0 kcal/mol at 40°C in the case of a stirred solution. The value may, however, have some ambiguity at this stage due to the adjustable parameters, C_0 and Λ.

In the case of an unstirred solution, the following equation may hold:

$$E_{sf} = 14.0 + E_d, \quad (6)$$

where E_d is the activation free energy of the aluminum ion for diffusion in the solution. Equation (6) seems possible, for the activation processes of the cation for the diffusion and the integration into the surface should occur simultaneously. Accordingly, the value of E_{sf} becomes 18.2 kcal/mol in the case of an unstirred solution, assuming the value of E_d to be 4.2 kcal/mol, as was given by Eyring.[11] Neglecting the temperature dependence of the value of E_{sf}, it becomes possible to obtain the value of τ_c using Eq. (4) over the temperature range of 19.90°—69.50°C. Figure 1 shows the values plotted against the reciprocal of the absolute temperature.

Calculation of the Value of S. From the relation between τ_c and τ_e, the separation factor, S, can be calculated at a given temperature, taking account of Eq. (3). Since τ_e is larger than τ_c at 19.90°, 29.50°, and 36.52°C, as may be seen from Fig. 1, the aluminum ion should enter the crystal surface, accompanying the hydration water; that is, the species of the growth units are K^+, $Al(OH_2)_6^{3+}$, SO_4^{2-}, and H_2O for the crystal growth of alum. Assuming for the moment that the hydration water of $Al(OH_2)_6^{3+}$ is not subject to any fractionation of HTO from the bulk water, the value of S at 19.90°, 29.50°, and 36.52°C is calculated to be 0.975 as follows:

$$S = (6 \times 1.000 + 6 \times 0.949)/12 = 0.975. \quad (7)$$

At 41.95°C, τ_c is equal to τ_e. This means that the number of the hydration water of the cation, which integrates into the surface, is reduced to half of the preceding value; *i.e.*, the apparent species of the growth units may become K^+, $Al(OH_2)_3^{3+}$, SO_4^{2-}, and H_2O. The value of S is calculated as follows: $S = (3 \times 1.000 + 9 \times 0.949)/12 = 0.963$. The implication of the assumption that $\tau_c = \tau_e$ at 41.95°C seems quite important in that the value of E_{sf} (or the value of τ_c) can be determined rather exactly in terms of Eq. (4) if the value of τ_e is known, as is the case with the present study. It may be noted here, however, that the evaluated τ_c value may be a little ambiguous, as was pointed out before. As will be shown later, it is more reasonable to assume the reverse, that the $\tau_c = \tau_e$ equation holds when the observed value becomes 0.963.

At a higher temperature, the cation should integrate into the crystal surface apparently, without the hydration water, as was discussed before, because the $\tau_c > \tau_e$ relation holds in this case. It follows that all of the water of crystallization in alum should come from free water molecules, so the value of S becomes 0.949, as may be seen from Eq. (3).

At temperatures around 41.95°C, *i.e.*, at 36.52°C and 47.43°C, however, the separation factors are unlikely to take the extreme values of 0.975 and 0.949 respectively, because both τ_c and τ_e values should have some distribution and so should overlap to some degree. Accordingly, it is necessary to take account of the apparent loss of half of the hydration water of $Al(OH_2)_6^{3+}$ at 36.52°C. As a result, the apparent species of a growth unit for the aluminum ion at 36.52°C becomes $Al(OH_2)_m^{3+}$ with $3 < m < 6$. Similarly, the apparent species at 47.43°C can be given by $Al(OH_2)_n^{3+}$ with $0 < n < 3$. It follows that the separation factors, S, at 36.52° and 47.43°C are, at this stage, calculated to be in the ranges of 0.975—0.963 and 0.963—0.949 respectively. This also means that the apparent species of the growth unit changes continuously into the dehydrated aluminum ion, Al^{3+}, from the $Al(OH_2)_6^{3+}$ species with an increase in the temperature in the range of 29.50°—53.70°C, which thus leads to a continuous decrease in the value of S from 0.975 to 0.949 as the dehydration proceeds.

It should be noted here that the above treatment for the apparent dehydration of the species, $Al(OH_2)_6^{3+}$, is statistically true. The calculated value of S is given in Table 2, together with the values of τ_c and τ_e, and the apparent species of growth units. It seems worthwhile noting that the observed values are in good agreement with the calculated ones.

Factors Which May Influence the Value of S. It is well known that an aqueous solution of alum gives an acidic solution because a hydrolysis of the $Al(OH_2)_6^{3+}$ species occurs in the solution, a hydrolysis which is represented by a reaction such as:

$$Al(OH_2)_6^{3+} + H_2O \rightleftarrows Al(OH_2)_5(OH)^{2+} + H_3O^+.$$

It is thus necessary to obtain the concentration ratio of the tritiated hydronium ion, H_2TO^+, to the tritiated water, HTO. The T_3O^+ and HT_2O^+ species can be neglected as a source of tritium, since the mother liquid used contains a trace amount of HTO.

Salomon[12] has calculated the equilibrium constant of the reaction:

$$H_2O + H_2TO^+ \rightleftarrows HTO + H_3O^+,$$

to be 1.051 at 25°C. Therefore, the concentration

11) S. Glasstone, K. J. Laidler, and H. Eyring, "The Theory of Rate Processes," McGraw-Hill Book Co., Inc., New York (1941), p. 557.

12) M. Salomon, *Can. J. Chem.*, **44**, 689 (1966).

TABLE 2. CALCULATED SEPARATION FACTOR, S_{cal}, THE VALUES τ_c AND τ_e, AND APPARENT SPECIES OF GROWTH UNITS IN THE CRYSTAL GROWTH OF ALUM

Temp. (°C)	τ_c (sec)	τ_e (sec)	Apparent species of growth units	S_{cal}[c]
19.90	5.7	15.7	K^+, $Al(OH_2)_6^{3+}$, SO_4^{2-}, and H_2O	0.975 (0.971)
29.50	2.1	3.4	K^+, $Al(OH_2)_6^{3+}$, SO_4^{2-}, and H_2O	0.975 (0.971)
36.52	1.0_0	1.2_4	K^+, $Al(OH_2)_m^{3+}$ [a], SO_4^{2-}, and H_2O	$\begin{cases}<0.975\ (0.971)\\ >0.963\end{cases}$
41.95	0.6_3	0.6_0	K^+, $Al(OH_2)_3^{3+}$, SO_4^{2-}, and H_2O	0.963
47.43	0.3_6	0.2_7	K^+, $Al(OH_2)_n^{3+}$ [b], SO_4^{2-}, and H_2O	$\begin{cases}<0.963\\ >0.949\end{cases}$
53.70	0.2	0.1	K^+, Al^{3+}, SO_4^{2-}, and H_2O	0.949
69.50	5.4×10^{-2}	1.7×10^{-2}	K^+, Al^{3+}, SO_4^{2-}, and H_2O	0.949

a) $3<m<6$
b) $0<n<3$
c) The value corrected considering the species, $Al(OH_2)_5(HTO)^{3+}$, is given in parentheses.

ratio of H_2TO^+ to HTO in the solution is calculated to be *ca.* $[H_3O^+]/55.6$, where $[H_3O^+]$ refers to the concentration of H_3O^+. It follows that the H_2TO^+ species need not be considered as a source of tritium if $[H_3O^+]<10^{-1}$ gram ion/*l*. In the present study, the pH value of the mother liquid is larger than 1.85, so only HTO molecules have to be considered in calculating the value of *S*.

As for the crystal growth at 19.90° and 29.50°C, the $Al(OH_2)_6^{3+}$ species has been found to integrate into the crystal surface, accompanying the hydration water, as has been discussed before. Therefore, the $Al(OH_2)_5(HTO)^{3+}$ species should be taken into consideration in this case. The more tritiated species, *e.g.*, $Al(OH_2)_4(HTO)_2^{3+}$ are negligible, since the concentration of HTO is extremely low in the present case. Assuming the identical behavior of the species, $Al(OH_2)_5(HTO)^{3+}$, with a free water molecule in fixing into the crystal from the solution, the value of the separation factor for the species is estimated to be *ca.* 0.993 in terms of Eq. (2). The fractionation, if any, of HTO in the hydration water of the cation from bulk water is disregarded at this stage, which may lead to a little ambiguity in the calculation of *S*.

Mechanism of the Crystal Growth and the Fractionation of HTO. Since the $\tau_c=\tau_e$ relation is established when the species of a growth unit for the aluminum ion becomes $Al(OH_2)_3^{3+}$, as has been described above, the value of E_{sf} may be deduced in terms of Eq. (4), using the known value of τ_e.[3] The value of E_{sf} at 41.95°C is thus estimated to be *ca.* 18.17 kcal/mol in the case of an unstirred solution. It is interesting that the activation free energy for the exchange of the water in $Al(OH_2)_6^{3+}$ with bulk water, E_{ex}, becomes equal to the value of E_{sf} at this temperature, as may be seen from the equation:[13]

$$\tau_e = (h/kT)\exp(E_{ex}/kT). \quad (8)$$

The $E_{ex}=E_{sf}$ condition is important in that it is difficult to obtain the value of E_{sf} experimentally as well as theoretically, while the value of E_{ex} can be determined experimentally.

The mean displacement of the growth unit on the surface, x_s, can be estimated approximately, since the value of the activation free energy necessary for leaving the surface, E_{sl}, is nearly equal to the value of E_{sf}. The value of x_s for the aluminum ion is obtained in terms of the expression:[6]

$$x_s = a\exp\{(E_{sl}-E_{sd})/2kT\}, \quad (9)$$

where a is the shortest distance between neighboring growth units in the crystal and where E_{sd} is the activation free energy for the diffusion of the growth unit from one equilibrium position to a neighboring one on the surface. The value of E_{sd} is assumed to be *ca.* 7 kcal/mol according to Bennema,[5] so the value of x_s can be estimated to be *ca.* $7.6\times10^3\,a$. This implies that the cation diffuses over a wide range of the surface before integrating into the kink, because $x_s\gg a$. It follows that the surface-diffusion mechanism should play an essential role in the integration of the cation into the crystal, since the $x_s\gg a$ relation is a necessary condition for integration by means of this mechanism. This also implies that the integration of the cation into the surface should be the rate-determining step; therefore, the value of E_k is relatively small in comparison with the value of E_{sf} (*cf.* Fig. 2).

Accordingly, the crystal of alum should grow by the surface-diffusion mechanism, assuming that the rate of integration of the aluminum ion determines the overall growth mechanism. This assumption is supported by the facts that alum necessarily crystallizes from a slightly supersaturated solution in a stoichiometric way and that the cation has the lowest relaxation time for integrating into the crystal. The preceding discussion may be regarded as another argument for the mechanism of the crystal of alum which has been suggested by Bennema.[5,6] It may be concluded from the present study that isotopic fractionation in phase equilibria is largely influenced by the crystal-growth mechanism and the system of ions and water. The determination of the isotopic fractionation during the crystal growth of hydrated salts from a slightly supersaturated solution should thus contribute to an understanding of the growth mechanism and/or the system of the aqueous solution.

The author wishes to express his gratitude to Professor Hisao Negita of this University for his stimulating discussions and suggestions throughout this work. Thanks are also due to Dr. Osamu Yamamoto for his help in analysing the activity of tritium.

13) H. Eyring, *Chem. Rev.*, **17**, 65 (1935).

Strain Gauge Electromicrobalance for Surface Tension Measurement[1)]

Masakatsu KOSHINUMA, Akio NAKAMURA, Tsutomu SEIMIYA, and Tsunetaka SASAKI

Department of Chemistry, Faculty of Science, Tokyo Metropolitan University, Tokyo

(Received June 3, 1971)

Two types of apparatus using an unbonded strain gauge of a cantilever type for the measurement of surface tension were constructed. One is a sensitive electromicrobalance equipped with an extended arm attached to the cantilever of the strain gauge. The apparatus proved suitable as a surface balance in a completely closed system. By this apparatus, the measurement of surface tension ranging from 0 to 74 dyn/cm is possible with the accuracy of ±0.10 dyn/cm. The other type was constructed by connecting the sensing lever of strain gauge to the arm of a torsion balance with a strip of phosphor bronze. This device together with a counterbalance on the opposite side of the arm also proved to be useful as a tensiometer. Accuracy of this apparatus was a little better than that of the extended arm type balance, although a larger space is required. Both apparatus are inexpensive, easy to construct and simple to operate, and are suitable for the self-recording of time dependence of surface tension or weight change in general with sufficient accuracy. Equations proposed for the time dependence of surface tension of surfactant solution were checked by using the strain gauge tensiometer of the extended arm type.

The Wilhelmy type surface tensiometer is known to give reliable values of surface tension[2)] and is considered to be the best method for the measurement of surface tension, particularly of surfactant solutions where aging is inevitable.[3)]

We previously devised a self-recording tensiometer using torsion balance and differential transformer as a transducer which converts a small vertical displacement of hanging glass plate into an electrical output for recording.[4)] Although the electrical output from the differential transformer was larger than that from a strain gauge of direct loading, skill is required for preparing a good working spiral spring to support the transformer core. In addition, unsteady actions of transformer and oscillator reduced the accuracy of the measurement.

In the present study, the differential transformer was replaced by a strain gauge to improve the performance of the torsion balance. Although surface tension measurements using strain gauge have already been reported,[5-7)] some of them lack detailed descriptions of the apparatus while others turn out to be inapplicable for the self-recording of time dependence of surface tension. Therefore, a self-recording strain gauge tensiometer of a torsion balance type was first constructed. In this apparatus a sensing lever of the strain gauge was connected by a phosphor bronze strip to a fixed point on the arm of the torsion balance and response of the torsion balance due to the action of surface tension was converted into the electrical output which operates a recorder. This apparatus has proved more accurate and sensitive than the former one.[8)]

However, for an accurate measurement of the surface tension of solutions, evaporation of solute or solvent from the solution should be prevented, since slight evaporation frequently produces a profound change in surface concentration[9)] and surface tension. Therefore, the space over the surface of liquid for the measurement should be minimized. The torsion balance is not suitable for this purpose, since a large space is required. A spring balance was constructed but was unfavorable because of its size and sensitiveness towards the temperature change.[10)]

A cantilever strain gauge of extended arm type was finally devised which turned out to be satisfactory for the surface tension measurement of aqueous solution, since it is compact and easy to set in a small chamber together with the solution to be measured. The apparatus proved to be insensitive to temperature and moisture.

By using this apparatus, the time dependence of surface tension of aqueous surfactant solution was measured, uninfluenced by evaporation of the solution and contamination from the surrounding atmosphere, and applicability of various equations proposed for calculating such dependence was checked.

Experimental

Construction of Surface Tensiometer. Strain Gauge: The strain gauge used was of unbonded and cantilever type (UL-120, *Shinko Communication Industry Co., Ltd., Japan*). Its maximum output is ±4 mV for permissible load of ±2 g. A maximum input of 4 volt was supplied from D. C. voltage stabilizer (NA-112, *Nippon Stabilizer Co., Ltd., Japan*). Output voltage from the strain gauge was properly attenuated, biassed with mercury cell, and was recorded by using a 1 mV full scale recorder (*Hitachi* QPD 33, *Hitachi Ltd.*,). A block diagram of the whole electrical setup is shown in Fig. 1 for tensiometer of the extended arm type.

1) Paper presented at the 23rd Annual Meeting of the Chemical Society of Japan, Colloid Section, held in Tokyo, 1970.

2) M. Nakamura and T. Sasaki, *J. Sci. Instr.*, **44**, 855 (1967).

3) G. C. Nutting, F. A. Long, and W. D. Harkins, *J. Amer. Chem. Soc.*, **62**, 1496 (1959); K. L. Sutherland, *Aust. J. Chem.*, **12**, 1 (1959); M. Nakamura and T. Sasaki, This Bulletin, **43**, 3667 (1970); H. Lange, Proc. 3rd. Inter. Congr. Surface Activity, **1**, 279 (1965).

4) K. Obu, T. Seiyama, and T. Sasaki, 18th Colloid Symposium held at Osaka (1965).

5) S. B. Newman and W. M. Lee, *Rev. Sci. Instrum.*, **29**, 785 (1958).

6) V. Jackman, *Anal. Chem.*, **32**, 1055 (1960).

7) R. J. Grabenstetter and J. M. Corkill, *J. Colloid Interfac. Sci.*, **18**, 401 (1965).

8) K. Obu, T. Seiyama, and T. Sasaki, 18th Colloid Symposium held at Osaka (1965).

9) T. Seimiya and T. Sasaki, *J. Colloid Interfac. Sci.*, **21**, 229 (1766).

10) Unpublished.

Strain Gauge Tensiometer of Torsion Balance Type. The apparatus is shown in Fig. 2 in which S is the strain gauge, C, a counterbalance, P, a hanging plate ($20\times20\times0.02$ mm, 300 mg), and D, a magnetic dumper. A tungsten torsion wire of the torsion balance T was 0.22 mm in diameter and 60 mm in length, at the center of which a beam of 230 mm in length was fixed at a point 80 mm from its end. The sensing lever of the strain gauge was connected with the beam at a fixed point on it with a strip of phosphor bronze B ($20\times1\times0.07$ mm). Magnification of the force due to surface tension could be varied by shifting the point of connection of phosphor bronze with respect to the arm. The counterbalance was attached to the opposite side of the arm to offset the weight of the hanging plate and, if necessary, a part of the force due to the surface tension. By this means, together with the electrical attenuation of ouptut and the proper choice of the bias voltage, the range and sensitivity of the balance could be controlled according to the requirement of the experiment. In the present study phosphor bronze was fixed at a point 125 mm from the end of the arm as shown in Fig. 2. This increased the output of strain gauge six times the value of direct loading.

The performance of the apparatus is shown in Table 1. Sensitivity and accuracy are a little better than those of the former apparatus as shown in the table. The apparatus was adjusted so that the surface tension of 73 dyn/cm corresponded to about 1.8 g load of the strain gauge. The apparatus was used under two different conditions. In the first case, the output due to surface tension was so attenuated that 73 dyn/cm corresponded to the full scale of the recorder. In the second case, the output from the strain gauge was applied through the bias voltage to the recorder without electrical attenuation so that the full scale of the recorder covered a range from X_1 to X_1+25 dyn/cm, X_1 being varied between 0 and 55 dyn/cm. Temperature change of several degrees did not affect the surface tension, since the temperature dependence of output (Fig. 3) was found to be 9.05×10^{-6} mV/mg·deg and this corresponded to 0.002 dyn/cm·deg.

Strain Gauge Tensiometer of Extended Arm Type. Figure 4 shows the arrangement of a tensiometer of the extended arm type together with the liquid for measurement and the apparatus for conditioning the chamber containing them. In this apparatus, an extended arm E of thin glass rod, 330 mg in weight was attached to the cantilever of strain gauge S. The effective length of the arm was 93 mm. The tensiometer was fixed to the side column of the chamber. The weight of the Wilhelmy plate P, ($20\times15\times0.02$ mm, 250 mg) was chosen to be the sum of the force due to the surface tension of water (about 73 dyn/cm), and the weights of arm and plate are brought near the limit of a permissible load of the strain gauge. By this arrangement, the weight ranging from 0 to 300 mg could be measured with the accuracy of ±0.4 mg. This corresponds to the surface tension of 0 to 74 ± 0.1 dyn/cm for the plate of 40 mm in horizontal perimeter as shown in Table 1.

For surface tension measurement, a clean glass plate was hung from the arm and the chamber was closed after being flushed with humidified nitrogen (Fig. 4). The liquid then was slowly introduced from the reservoir R into the vessel V until its surface just touched the lower end of the hanging plate P. The vertical force due to the surface tension acting on the plate was converted into an electrical output and recorded through the bias voltage. The recorder was so adjusted that 50 dyn/cm corresponded to a

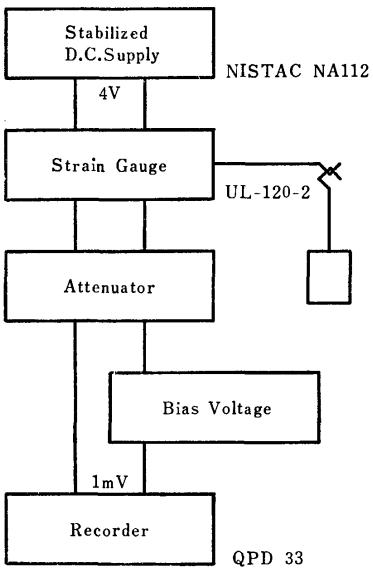

Fig. 1. Electrical setup of the strain gauge tensiometer.

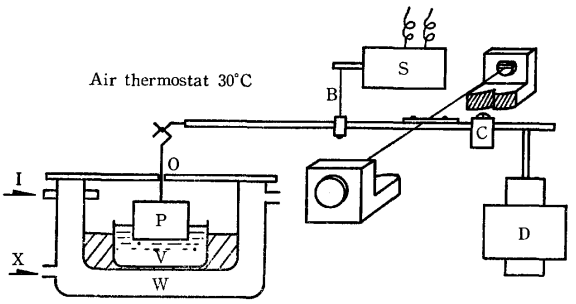

Fig. 2. Strain gauge tensiometer of torsion balance type.
B Phosphor bronze
C Counterbalance
D Magnetic dumper
I Humidified nitrogen gas inlet
O Humidified nitrogen gas outlet
P Hanging glass plate
S Strain gauge
T Torsion balance
V Solution and vessel
W Water jacket
X Thermostated water

TABLE 1. PERFORMANCE OF VARIOUS TYPES OF SURFACE TENSIOMETER

	Strain Gauge			Differential transformer type	
	Torsion balance type	Extended arm type			
Range (dyn/cm)	0—73	X_1—X_1+25	X_2—X_2+50	0—75	X_3—X_3+40
Bias range (dyn/cm)	0	$X_1=0$—55	$X_2=0$—24	0	$X_3=0$—80
Sensitivity (mV/mg)	3.31×10^{-3}	1.00×10^{-2}	4.71×10^{-3}	3.17×10^{-3}	6.45×10^{-3}
Accuracy (dyn/cm)	0.10	0.08	0.10	0.20	0.24

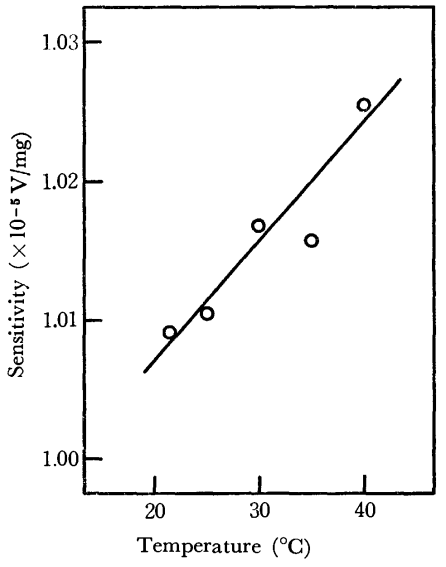

Fig. 3. Temperature dependence of sensitivity of strain gauge tensiometer.

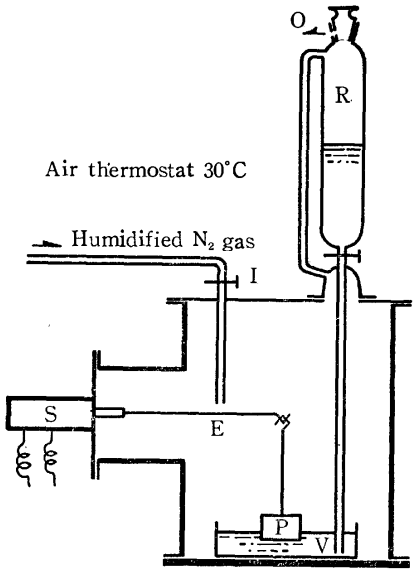

Fig. 4. Strain gauge tensiometer of extended arm type
- E Extended arm
- I Humidified nitrogen gas inlet
- O Humidified nitrogen gas outlet
- P Hanging glass plate
- R Reservoir for a sample solution
- S Strain gauge
- V Vessel and solution

full scale, and the surface tension ranging from X_2 to X_2+50 dyn/cm could be measured, X_2 being varied between 0 and 24 dyn/cm.

Neither the hysteresis due to the load nor the effect of moisture was observed during the course of 24 hr measurement in both types of tensiometers.

Measurement of Time Dependence of Surface Tension and Equilibrium Surface Tension

Surface tension was measured for a 5.4×10^{-6} mol/l aqueous solution of hexaoxyethylene dodecyl ether (homogeneous) by using the extended arm strain gauge tensiometer, at 25°C. The results are shown in Fig. 5. Water used for preparaing the solution was distilled from acid permanganate, then alkaline permanganate solutions and finally distilled without permanganate in borosilicate flasks. Surface tension showed a relatively long aging extending over about 20 hr until it attained an equilibrium. Since measurements were carried out in a closed vessel, evaporation was completely eliminated and the system was free from comtamination from the surrounding atmosphere. Thus the observed changes are considered to be proper to the solution and the data obtained are pertinently for checking the validity of various equations proposed for the time dependence of surface tension of surfactant solution or the equations for obtaining an equilibrium surface tension. Table 2 shows the equilibrium surface tension values calculated from the following empirical equations with various ranges of observed surface tension *vs.* time values.

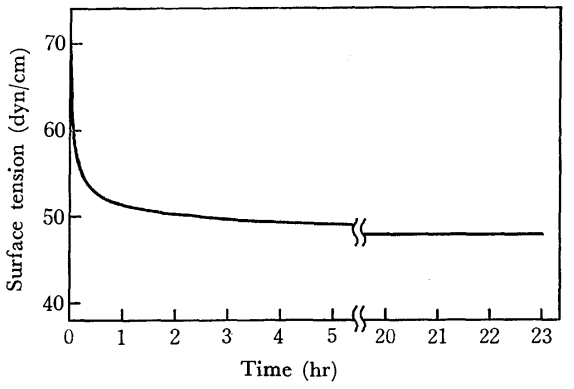

Fig. 5. Surface tension of aqueous hexaoxyethylene dodecyl-ether (at 25°C, 5.4×10^{-6} mol/l).

$$\sigma_t = \sigma_\infty + a/t + b/t^2$$
$$\text{or, } \sigma_t + t(d\sigma_t/dt) = \sigma_\infty - b/t^2 \quad (1)^{11}$$
$$\sigma_t = \sigma_\infty + (\sigma_0-\sigma_\infty)\exp(-\alpha t)$$
$$\text{or, } \sigma_t = (-1/\alpha)(d\sigma_t/dt)+\sigma_\infty \quad (2)^{12}$$
$$\sigma_0 - \sigma_t = (\sigma_0-\sigma_\infty)/(c/\sqrt{t}) + 1 \text{ or,}$$
$$1/(\sigma_0-\sigma_t) = 1/(\sigma_0-\sigma_\infty) + \{c/(\sigma_0-\sigma_\infty)\}(1/\sqrt{t}) \quad (3)^{13}$$

In these equations, σ_t, σ_0, and σ_∞ denote the surface tension of solution at time t, $t=0$ and $t=\infty$ respectively, and α, a, b, and c constants.

It is seen in Table 2 that, as regards the extrapolated equilibrium values of surface tension σ_∞ obtained from the σ-t values of longer time range (0.5—5 hr), Eq. (1) is found to give the best value, being the nearest to the equilibrium value obtained after 20 hr. Since σ_∞ obtained by using σ-t values of shorter and earlier time range is not reliable, the agreement of σ_∞ obtained from Eq. (3) and σ-t values of 5—25 min range is considered to be accidental. Thus, Eq. (1) is recommended here as an empirical formula, but 4 hr measurement is necessary in order to obtain a reliable value of equilibrium surface tension.

11) M. Nakamura and T. Sasaki, This Bulletin, **43**, 3667 (1970).
12) A. Boutaric and T. Berthier, *J. Chim. Phys.*, **36**, 1 (1939).
13) H. Lange, Proc. 3rd. Intern. Congr. Surface Activity, **1**, 279 (1960).

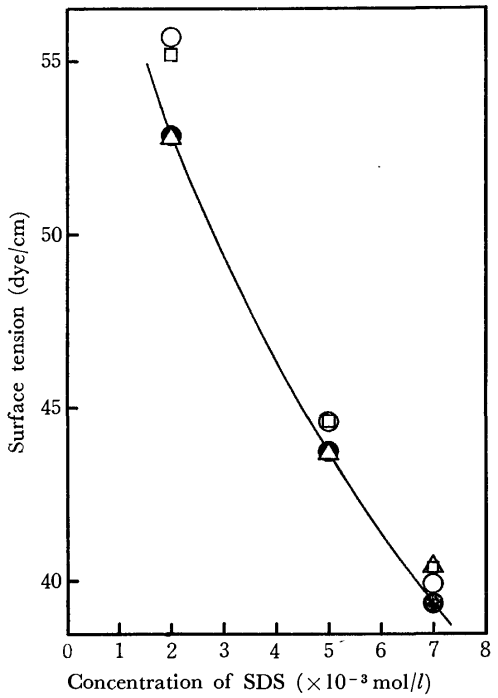

Fig. 6. Calculated and observed equilibrium surface tension.
○: Eq. (1), □: Eq. (2), △: Eq. (3), ● and —: Observed value.

Surface tension was further measured for aqueous solutions of ionic surfactant, sodium dodecyl sulfate, and the validity of the above three equations was checked for three different concentrations. The results are shown in Fig. 6 together with the equilibrium value (solid line) observed after 20 hr. The values of σ_∞ were calculated from σ-t curve of 0.5—4 hr range. We see that the difference between the observed and calculated σ_∞ decreased with increasing concentration and decreasing time dependence of surface tension in the case of Eqs. (1) and (2), while the relation is reverse in the case of Eq. (3). The general tendency is such that the observed equilibrium values of surface tensions to be equal or smaller than the values calculated from these equations.

Table 2. Calculated and observed equilibrium surface tension

	Surface tension (dyn/cm)				
	5—25 min	0.5—2 hr	2—4 hr	0.5—5 hr	After[a] 20 hr
Eq. (1)	50.8	49.3	47.9	47.6	47.8
Eq. (2)	50.8	49.5	48.5	48.8	
Eq. (3)	47.8	46.9	47.3	46.9	

a) Equilibrium surface tension measured for 5.4×10^{-6} mol/l aqueous solution of hexaoxyethylene dodecyl ether at 25°C.

It is concluded from the above observations that the applicability of these equations may differ for different solutions, and a common equation applicable for all systems cannot be obtained. This is quite natural since these equations are empirical, and it is difficult to derive a theoretical equation predicting the change of surface tension with time, because the mechanisms of surface aging may differ for different solutions which are not clear at present, although some explanations have been proposed.[14]

However, from the practical view point Eq. (3) seems convenient since a linear plot is applicable. But also in this case, a 4 hr measurement of surface tension completely free from evaporation and contamination seems desirable for calculation of a reliable value of equilibrium surface tension.

14) K. L. Mysels and A. T. Florence, "Clean Surface," ed. by G. Goldfinger, Marcel Dekker, New York (1970), p. 256.

Adsorption of Sodium and Calcium Dodecyl Sulfates at the Surface of Their Aqueous Solutions

Jun SASAKI, Kazuo TAJIMA, and Tsunetaka SASAKI

Department of Chemistry, Faculty of Science, Tokyo Metropolitan University, Setagaya, Tokyo

(Received June 8, 1971)

Adsorption of sodium dodecyl sulfate (NaDS) and calcium dodecyl sulfate ($Ca(DS)_2$) at the aqueous surface was measured by a radiotracer method using tritium labelled compounds at constant ionic strength of 1×10^{-2} and 7.5×10^{-3} adjusted by the addition of NaCl and $CaCl_2$, respectively. The adsorbed amounts increased with increasing concentration of dodecyl sulfates in both cases, and approached saturation values of 3.65×10^{-10} mol/cm^2 at 25°C for NaDS and 3.8×10^{-10} mol/cm^2 at 55°C for $Ca(DS)_2$. The amounts calculated from surface tension data by applying the Gibbs adsorption isotherm were confirmed to be in good agreement with the values directly measured. The adsorbed amounts of chloride ion, generally assumed to be zero, were confirmed to be negligible in the concentration region from zero up to critical micelle concentration.

Numerous investigations have been reported on the study of surface active substance at air-solution interface with the purpose of examining the applicability of the Gibbs adsorption isotherm under various conditions.[1-5] However, there are only a few discussions based on the direct measurement of surface excess, especially for well defined plane aqueous surface.[5-8]

In the previous studies,[6,8] the Gibbs adsorption isotherm $-d\gamma=nRT\Gamma d\ln a$ was confirmed to hold for the adsorption from aqueous solution of NaDS with $n=2$ for salt free solution, and with $n=1$ for the solution containing excess salt. Several workers have studied the adsorption of ionic surfactant solution at constant ionic strength[2,4,9,10] and eliminated activity coefficients from the Gibbs adsorption isotherm.

In the present study, we have carried out direct measurements of adsorbed amounts of tritiated NaDS and $Ca(DS)_2$ at aqueous interface, and at constant ionic strength by a radiotracer method. Measurements of surface tension were also carried out under the same conditions. From the results the validity of the Gibbs adsorption isotherm at constant ionic strength was checked.

Experimental

Materials. Sodium dodecyl-2,3-t_2 sulfate (TNaDS) was prepared as previously reported.[11] Dodecan-2,3-t_2-1-ol used for the preparation was confirmed to be chemically and radiochemically pure by radiogaschromatography. Calcium dodecyl-2,3-t_2 sulfate ($TCa(DS)_2$) was also synthesized in the same manner as TNaDS from dodecan-2,3-t_2-1-ol, except for the neutralization of dodecyl sulfuric acid by $Ca(OH)_2$. Both surfactants were carefully recrystallized from ethanol and subjected to Soxhlet extraction using ethyl ether for 48 hr to remove unreacted tritiated dodecanol and other surface active impurities. Specific activity of the substances obtained was 16 Ci/mol. Both surfactants were further confirmed to be free from surface active impurities as judged from the absence of minimum in surface tension *vs.* concentration curves. Triply distilled water was used.

Procedure. Ionic strengths of TNaDS and $TCa(DS)_2$ solutions used were kept constant at 1.0×10^{-2} and 7.5×10^{-3} respectively, by diluting 1.0×10^{-2} mol/l TNaDS with NaCl solution of the same concentration and 2.5×10^{-3} mol/l $TCa(DS)_2$ with $CaCl_2$ solution of the same concentration. Radioactivity of tritiated dedecyl sulfate solution was meas-

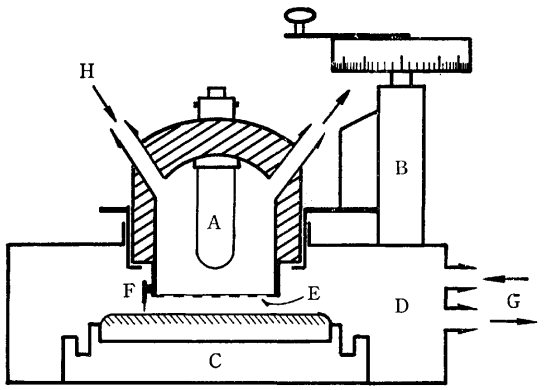

Fig. 1. Thin-window gas-flow GM counter for adsorption measurement.

A:	GM counter	B:	elevator
C:	cell	E:	polycarbonate thin film window
F:	needle point		
G:	N_2 gas	H:	counting gas (Q-gas)

1) A. B. D. Cassie and R. C. Palmer, *Trans. Faraday Soc.*, **37**, 156 (1941).
2) C. P. Roe and P. C. Brass, *J. Amer. Chem. Soc.*, **76**, 4703 (1954).
3) J. T. Davies, *Proc. Roy. Soc.*, **A208**, 224 (1951). E. Matijevic and B. A. Pethica, *Trans. Faraday Soc.*, **54**, 1382 (1958); D. J. Salley, A. J. Weith, A. A. Argyle and J. K. Dixon, *Proc. Roy. Soc.*, **A203**, 42 (1950); G. Nilsson, *J. Phys. Chem.*, **61**, 1135 (1957); E. G. Cockbain, *Trans. Faraday Soc.*, **50**, 874 (1954).
4) K. Shinoda and H. Nakayama, *J. Colloid Sci.*, **18**, 705 (1963).
5) R. Matuura, H. Kimizuka, S. Miyamoto, and R. Shimozawa, This Bulletin, **31**, 532 (1958).
6) K. Tajima, M. Muramatsu, and T. Sasaki, *ibid.*, **43**, 1991 (1970).
7) M. N. Jones and G. Ibbotson, *Trans. Faraday Soc.*, **66**, 2394 (1970).
8) K. Tajima, This Bulletin, **43**, 3063 (1970).
9) M. J. Schwuger, *Kolloid-Z. Z. polym.* **233**, 979 (1968).
10) H. Lange, *Kolloid-Z.*, **153**, 155 (1957).
11) M. Muramatsu and K. Tajima, *J. Labelled Compounds*, **2**, 304 (1966).
12) K. Tajima, This Bulletin, **44**, 1767 (1971).

ured by using a gas-flow GM counter[13] equipped with a thin film (polycarbonate) window as shown in Fig. 1. A counter tube A can be raised or lowered by the rack and pinion device B. Surfactant solution was contained in a polyethylene cell C, 70 mm in diameter. The distance constant to 0.70±0.02 mm by means of electrical contact of the aqueous surface with the point of a needle F fixed to the GM tube. To avoid the effect of carbon dioxide from the surrounding atmosphere, nitrogen gas, well humidified by passing through a glass tube of 6 m in length packed with wet glass wool was slowly introduced and allowed to leak from the chamber D. During the course of measurement, gas flowing was stopped in order not to disturb the solution surface. The whole apparatus was placed in a thermostated glove box filled with humidified nitrogen gas.

After standing both the cell and dodecyl sulfate solution for about 30 min in the glove box, 25 m*l* of the solution was poured into the cell. Radioactivity of the aqueous solutions of TNaDS and $TCa(DS)_2$ was measured at 25±1°C and 55±1°C, respectively. The temperature was chosen several degrees above each Krafft point. Measurements were continued until equilibrium steady counting was obtained. Radioactivity due to the bulk of solution was measured over the surface of tritiated dodecanol dissolved in non-radioactive dodecanol as in the preceeding method[6] and was subtracted from the total radioactivity to give the radioactivity due to adsorption. To convert the radioactivity thus obtained to the amount of adsorbed surfactant, known amount of tritiated stearic acid of 9.0 Ci/mol in specific activity was spread on aqueous solution of 0.1 N H_2SO_4 using the same cell, and the surface count was measured at 25°C and 55°C for TNaDS and $TCa(DS)_2$, respectively. From the inclination of the straight line of count rate *vs.* spread amount multiplied by the ratio of specific activity of tritiated stearic acid to that of tritiated dodecyl sulfate, a conversion factor (mol cm^{-2} cpm^{-1}) was obtained. The surface count rate obtained by subtracting bulk count rate from the count rate over the aqueous solution was converted to surface excess Γ_{D^-} by multiplying it with the conversion factor. Surface tension was measured by the drop volume method applying the Harkins and Brown correction, and by the Wilhelmy plate method, both under the same conditions as in the case of the adsorption measurement.

Results and Discussion

Adsorption. The observed amounts of adsorption Γ_{D^-} were plotted against concentration C for TNaDS and $TCa(DS)_2$ as shown by open circles in Figs. 2 and 3, respectively, The value of Γ_{D^-} for TNaDS rapidly increased with increasing concentration of TNaDS and approched a saturation value of $\Gamma_{D^-}=3.65\times10^{-10}$ mol/cm^2 at the concentration of 2.5×10^{-3} mol/*l*. However, above critical micelle concentration (CMC), it gradually decreased with increasing TNaDS concentration. At the concentration of 1×10^{-2} mol/*l*, where the concentration of NaCl became zero, Γ_{D^-} decreased to 3.09×10^{-10} mol/cm^2, which is in good agreement with the former Γ_{D^-} value of the saturation amount of adsorption for the same system measured by the sheet scintillation counter[6] as shown in Fig. 2. Coincidence of both

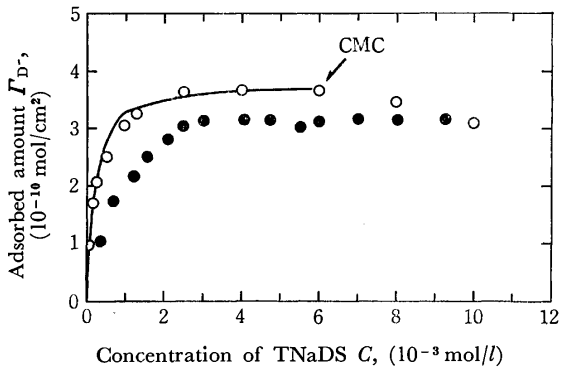

Fig. 2. Adsorption isotherm of TNaDS at constant ionic strength (25°C).
○: present study (TNaDS+NaCl=1×10^{-2} mol/*l*)
●: previous study (without added salt)
—: calculated value

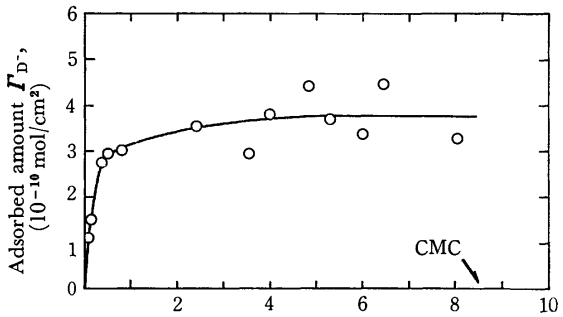

Fig. 3. Adsorption isotherm of $TCa(DS)_2$ at constant ionic strength (55°C).
○: observed value ($TCa(DS)_2+CaCl_2=2.5\times10^{-2}$ mol/*l*)
—: calculated value

results obtained by two different methods of measurement for the same solution shows sufficient reliability of both methods and the absolute value of adsorbed amount obtained. The decrease of Γ_{D^-} above CMC is a direct indication of the effect of decrease of ionic strength or the decrease of NaCl concentration with nearly constant concentration of single dodecyl sulfate ions.[8] Thus, the increase of adsorption of dodecyl sulfate ion due to the addition of NaCl is distinct in a wide range of concentration as shown in Fig. 2. Adsorbed amount from aqueous solution of $TCa(DS)_2$ was also measured for the whole range of concentration up to CMC. It also increased rapidly with increasing concentration and arrived at a saturation value of $\Gamma_{D^-}=3.8\pm0.7\times10^{-10}$ mol/cm^2 at the concentration of 5×10^{-4} mol/*l*, which was roughly equal to the saturation value for TNaDS. Adsorption isotherm for $TCa(DS)_2$ showed fluctuation which might be due to the fluctuations of the count rate. This is inevitable since the absorption coefficient of air space between surface of the solution and window of the GM counter becomes unsteady owing to the incomplete saturation of the space with water vapor at elevated temperature. Gradual contamination of the thin film of the GM counter by radioactive substance, presumably dodecanol produced by hydrolysis of $TCa(DS)_2$ at high temperature, was also observed during the measurement. Radioactivity due to this

13) T. Seimiya, K. Sekine, and T. Sasaki, *J. Sci. Instr.*, **42**, 906 (1956).

contamination was subtracted as background count rate. The water vapor absorbed and permeating through the thin film might have some influence upon the count rate observed. However, it turned out to be negligible in the present experiment.

Surface Tension. Figure 4 shows the surface tension *vs.* concentration curve for the aqueous solution of TNaDS measured by the drop volume and Wilhelmy plate methods. The surface tension obtained by the drop volume method is seen to agree with that obtained by the self-recording Wilhelmy plate method. This differs from the general tendency of the former being somewhat larger. This is due to the rapid attainment of steady surface tension exhibited by the surfactant solution in the presence of added neutral salt. The surface tension of aqueous solution of $TCa(DS)_2$ measured by the Wilhelmy plate method is shown in Fig. 5. In this case, 2 — 3 hr was required to attain equilibrium even in the presence of neutral salt, presumably due to the low concentration of both the surfactant and added salt.

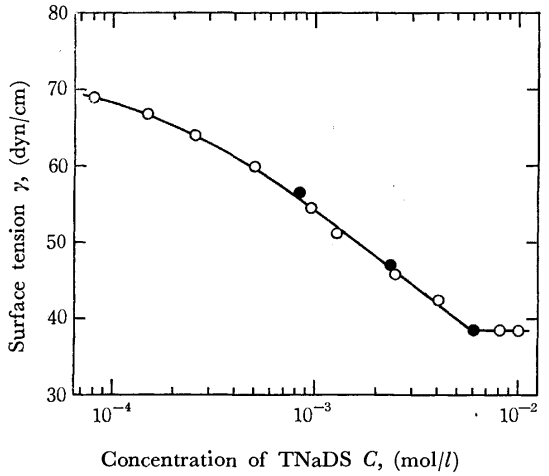

Fig. 4. Surface tension *vs.* concentration of TNaDS solution (25°C).
○: drop volume method
●: Wilhelmy plate method

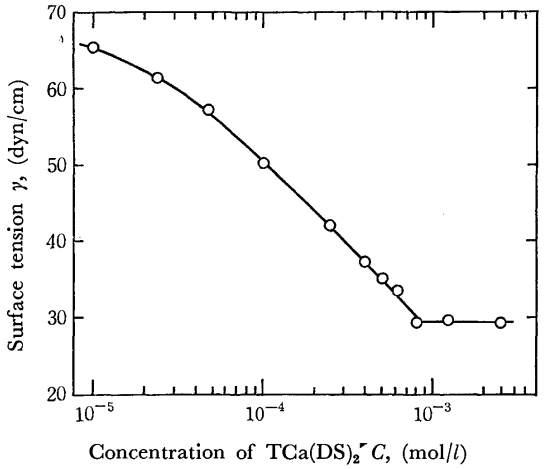

Fig. 5. Surface tension *vs.* concentration of $TCa(DS)_2$ solution (55°C).

Gibbs Adsorption Isotherm. In the present system, where the concentration of hydrogen ion is taken as constant, the Gibbs adsorption isotherm is given by

$$-\frac{d\gamma}{RT} = \Gamma_{D^-}d\ln C_{D^-}f_{D^-} + \Gamma_{M^{n+}}d\ln C_{M^{n+}}f_{M^{n+}} + \Gamma_{Cl^-}d\ln C_{Cl^-}f_{Cl^-}, \quad (1)$$

where f's express activity coefficients, and subscripts D^-, M^{n+}, and Cl^- denote dodecyl sulfate ion, n-valent counter ion and chloride ion, respectively. Activity coefficients of the ions in aqueous solution drop for constant ionic strength and Eq. (1) is reduced to

$$-\frac{1}{RT}\left(\frac{d\gamma}{d\ln C_{D^-}}\right)_I = \Gamma_{D^-} - \Gamma_{Cl^-}\frac{C_{D^-}}{C_{Cl^-}}, \quad (2)$$

where subscript I indicates the constancy of ionic strength. The value of $\Gamma_{D^-}-\Gamma_{Cl^-}(C_{D^-}/C_{Cl^-})$ was calculated with this equation by graphically evaluating $d\gamma/d\ln C_{D^-}$ from γ *vs.* $\ln C_{D^-}$ plot shown in Fig. 4. The results for TNaDS are shown by a solid line in Fig. 2. Satisfactory agreement of calculated value with independently observed Γ_{D^-} might give the experimental evidence that $\Gamma_{D^-}-\Gamma_{Cl^-}(C_{D^-}/C_{Cl^-})$ is essentially equal to Γ_{D^-}, and $\Gamma_{Cl^-}=0$.[12] This confirms the view that the Gibbs adsorption isotherm can be applied in the form

$$-\frac{1}{RT}\left(\frac{d\gamma}{d\ln C_{MD_n}}\right)_I = \Gamma_{D^-} \quad (3)$$

in the concentration region from zero up to CMC for the TNaDS solutions containing a neutral salt with common counter ion at constant ionic strength. Thus it might be concluded that the counter ion of added neutral salt is not adsorbed regardless of the amount added in the solution as is actually indicated, and Eq. (1) is valid without the term $\Gamma_{Cl^-}d\ln C_{Cl^-}f_{Cl^-}$. It is worth noting that although $\Gamma_{Cl^-}=0$ can readily be anticipated from a theoretical viewpoint and this assumption has been adopted by many investigators,[1,4,14] experimental confirmation is not satisfactory. So, the conclusion obtained is significant. Schwuger,[9] in his study of adsorption of divalent metal tetradecyl sulfate at constant ionic strength, neglected the term $\Gamma_{Cl^-}(C_{D^-}/C_{Cl^-})d\ln C_{Cl^-}$ assuming that salt is added in excess. Actually, however, neither was the salt in excess nor the ratio C_{D^-}/C_{Cl^-} small at CMC. It is because of the term Γ_{Cl^-} being zero at any concentration of added salt that the above calculation is justified. Schwuger insisted that at CMC the addition of salt under constant ionic strength has no effect on surfactant adsorption. However, the enhancing effect of salt on the adsorption amount of surfactant is evident as shown in Fig. 2. On close inspection, a small but distinct increase can be observed also in his Γ_{D^-}'s caused by the addition of salt at constant ionic strength, in accordance with our results.

Adsorption of $TCa(DS)_2$ was calculated from Eq.

14) E. J. W. Verwey and T. Th. G. Overbeek, "Theory of the Stability of Lyophobic Colloids," Elsevier, Amsterdam (1948), p. 22.

(3) by applying the data of the surface tension curve shown in Fig. 5. The values of Γ_{D^-} were plotted against the concentration of $TCa(DS)_2$ with a solid line in Fig. 3. Allowing for the experimental error mentioned above, Eq. (3) can also be applied to the adsorption at aqueous surface of $TCa(DS)_2$ solution. The results of the present study also confirmed experimentally the applicability of the Gibbs adsorption isotherm in the form of Eq. (3) for divalent metal dodecyl sulfate from zero concentration up to CMC. It is inferred also in this case that non-adsorption of co-ion in deriving Eq. (3) is not an assumption but the experimental fact, and Eq. (2) without the Γ_{Cl^-} term is safely applicable as is generally believed.

BULLETIN OF THE CHEMICAL SOCIETY OF JAPAN, VOL. 45, 351—355 (1972)

On the Viscosities of Mixtures of Oligotrifluorochloroethylene and *n*-Heptadecane

Naosato YOSHIDA and Shuichi HAMADA

Department of Chemistry, Faculty of Science, Science University of Tokyo, Kagurazaka, Shinjuku-ku, Tokyo

(Received June 18, 1971)

The viscosities, η_m, of mixtures of oligotrifluorochloroethylene and *n*-heptadecane were expressed as follows: $\eta_m=[(1-\Phi_R)-n(1-\Phi_R)]\eta_H+[\Phi_R+n(1-\Phi_R)]^2/[\Phi_R/\eta_R+n(1-\Phi_R)/\eta_H]$, where Φ_R is the volume fraction of the oligotrifluorochloroethylene in the mixture; η_R and η_H, the viscosities of oligotrifluorochloroethylene and *n*-heptadecane respectively, and n, a parameter. The two components were considered to be comparatively well compatible with each other, because the parameter, n, was small (here about 0.1). The free-volume fractions, f_T, of the mixed systems, as calculated from the WLF parameters, were larger than those calculated by assuming a simple additivity between those of the two components. This effect is considered to be caused by the mitigation of physical interactions among oligotrifluorochloroethylene molecules, which are dispersed by *n*-heptadecane as good compatibility is achieved between the two components.

The viscoelastic properties of a mixture of polymers depend on the ratio of the components and on their mixing state.[1] If two components are completely compatible with each other, the mixed system behaves, for example, like a random copolymer with only a glass-transition temperature which is a function of the monomer ratio.[2] Such a compatible system has been obtained, for example, by blending polyvinyl chloride and butadiene-acrylonitrile rubber within a certain volume fraction range of the components.[3] On the contrary, a mixed system of two incompatible or poorly compatible components, such as is observed in ordinary cases, gives properties consistent with those of the original components. If the two components are slightly compatible with each other, they partially dissolve one another according to the natures of the components and the manner of mixing.

In this work, the viscosities of mixtures of oligotrifluorochloroethylene and *n*-heptadecane were studied in connection with their compatibility and free-volume fractions.

Experimental

Materials. Daifloil No. 50, which was obtained from the Daikin Kogyo Company, was used as the sample of oligotrifluorochloroethylene. The oligotrifluorochloroethylene was fractionated by the manner described in our previous paper.[4] Fractionated oligotrifluorochloroethylene samples with the number-average molecular weights of 910, 950, and 1000, which were estimated by the cryoscopic method, were used as polymer components in the mixed systems. A guaranteed-grade *n*-heptadecane, which was obtained from the Kanto Kagaku Company, was used without further purification. The mixed samples of oligotrifluorochloroethylene and *n*-heptadecane were prepared in the following manner: the two components were mixed well together with benzene in various proportions, and then the benzene was removed by vacuum distillation from the mixture at temperatures from 30 to 50°C.

The volume fractions of oligotrifluorochloroethylene in the mixed samples are shown in Table 1.

Procedure. The viscosities and the densities of the liquid samples were measured with an Ubbelohde-type viscometer and a dilatometer respectively in the manner described in the previous paper.[4] The measurements were carried out in the temperature range from 30 to 70°C, with an accuracy of ±0.01°C, in a thermostated water bath.

Results and Discussion

The viscosities of oligotrifluorochloroethylene, *n*-heptadecane, and mixed samples are listed in Table 2-a and 2-b.

Mixing Model for Mixtures of Oligotrifluorochloroethylene and n*-Heptadecane.* The mixing states of oligotrifluorochloroethylene and *n*-heptadecane in the samples have been discussed, on the basis of the dependence of their viscosities on the volume fractions

1) R. Buchdahl and L. E. Nielsen, *J. Polymer Sci.*, **15**, 1 (1955).
2) K. Fujino, K. Senshu, and H. Kawai, *J. Colloid Sci.*, **16**, 262 (1961).
3) M. Kawamata and Y. Inoue, *Kogyo Kagaku Zasshi*, **63**, 1831 (1960).
4) N. Yoshida, S. Hamada, and T. Shirai, This Bulletin, **42**, 3131 (1969).

TABLE 1. VOLUME FRACTIONS Φ_R OF OLIGOTRIFLUOROCHLOROETHYLENE IN SAMPLES AT 50°C

Sample	Φ_R	Sample	Φ_R	Sample	Φ_R
910−0.05[a]	0.0496	910−0.6	0.5992	950−0.8	0.7976
910−0.1	0.0971	910−0.7	0.7015	950−0.9	0.8994
910−0.2	0.1995	910−0.8	0.8000	1000−0.7	0.6985
910−0.25	0.2495	910−0.9	0.8945	1000−0.8	0.7997
910−0.4	0.3995	950−0.7	0.6991	1000−0.9	0.9011

a) The numerical symbol "910" denotes the number-average molecular weight of the oligotrifluorochloroethylene, while the numerical post-script "0.05" denotes the rough volume fraction of the oligotrifluorochloroethylene in the sample.

TABLE 2-a. VISCOSITIES OF LIQUID SAMPLES

Sample	Viscosities η_m, poise					
	30°C	35°C	40°C	45°C	50°C	55°C
n-$C_{17}H_{36}$[a]	0.03183	0.02848	0.02564	0.02320	0.02111	0.01930
910−0.05	0.03728	0.03295	0.02947	0.02665	0.02404	0.02215
910−0.1	0.04237	0.03747	0.03346	0.03016	0.02727	0.02481
910−0.2	0.06073	0.05283	0.04629	0.04083	0.03625	0.03237
910−0.25	0.07369	0.06329	0.05485	0.04815	0.04266	0.03781
910−0.4	0.1574	0.1292	0.1075	0.09057	0.07723	0.06660
910−0.6	0.5849	0.4414	0.3410	0.2692	0.2168	0.1778
910−0.7	1.323	0.9574	0.7109	0.5408	0.4206	0.3340
910−0.8	3.493	2.411	1.711	1.247	0.9305	0.7101
910−0.9	11·20	7.295	4.897	3.381	2.395	1.739
910−1.0[b]	64.97	38.63	23.79	15.13	9.920	6.688

a) n-heptadecane, alone.
b) oligotrifluorochloroethylene with the molecular weight of 910, alone.

TABLE 2-b. VISCOSITIES OF LIQUID SAMPLES

Sample	Viscosities η_m, poise				
	30°C	40°C	50°C	60°C	70°C
910−0.7	1.323	0.7109	0.4206		
910−0.8	3.493	1.711	0.9305		
910−0.9	11.20	4.897	2.395		
910−1.0	64.97	23.79	9.920		
950−0.7		0.8972	0.5174	0.3234	
950−0.8		2.288	1.207	0.6952	
950−0.9		7.880	3.698	1.928	
950−1.0		39.63	15.88	7.124	
1000−0.7		1.225	0.6742	0.4163	0.2835
1000−0.8		3.346	1.715	0.9579	0.5764
1000−0.9		12.32	5.605	2.800	1.518
1000−1.0		63.63	26.74	11.54	5.440

of oligotrifluorochloroethylene, by using the mixing theory proposed by Takayanagi.[5,6] As a consideration of the "R in H" type parallel-model as Fig. 1 shows, the viscosities, η_m, of mixtures of oligotrifluorochloroethylene and n-heptadecane can be expressed as follows:[5]

$$\eta_m = [(1-\Phi_R)-n(1-\Phi_R)]\eta_H+[\Phi_R+n(1-\Phi_R)]^2/[\Phi_R/\eta_R+n(1-\Phi_R)/\eta_H] \quad (1)$$

where the subscripts R and H denote oligotrifluorochloroethylene and n-heptadecane respectively, and where n is a parameter which indicates the degree of contribution of the series element in the parallel-model. The values of the viscosities at 50°C, as calculated by Eq. (1), are shown by solid curves in Fig. 2. The observed values, which are shown by fllled circles in Fig. 2, agree well with those calculated by assuming the "R in H" type parallel-model when is nearly equal to 0.1. These mixed systems were considered to be comparatively well compatible under suitable conditions because of the small value of n, *i.e.*, the smaller contribution of the series element.

5) M. Takayanagi, *Kobunshi*, **10**, 289 (1961).
6) E. Shiraki and G. Okamoto, *Kogyo Kagaku Zasshi*, **65**, 148 (1962).

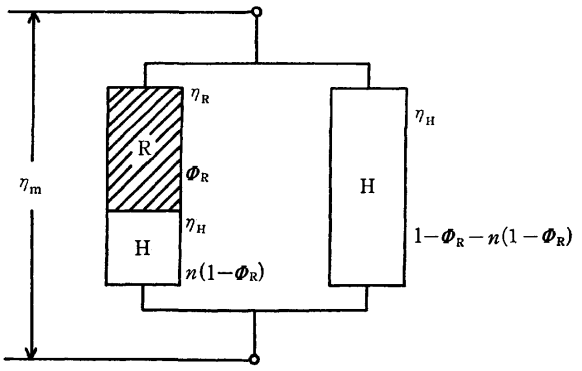

R: Oligotrifluorochloroethylene
H: *n*-Heptadecane

Fig. 1.

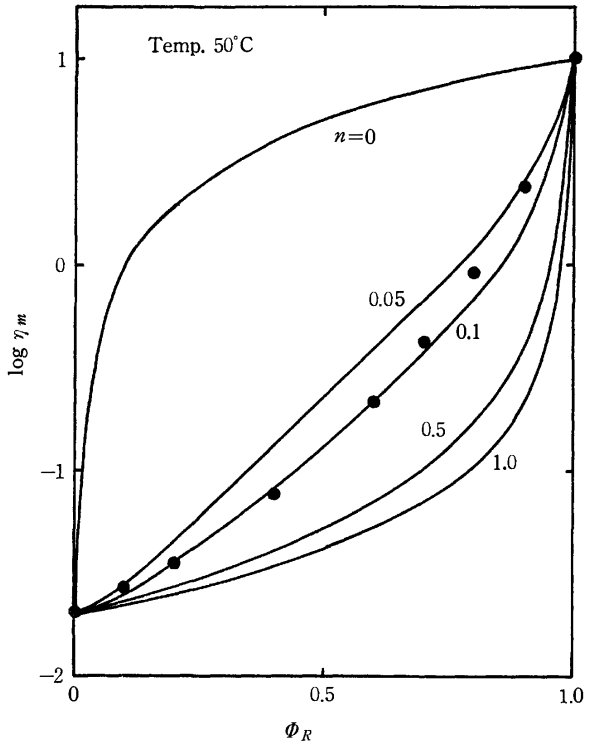

Fig. 2. Relationship between log η_m and Φ_R.

This conclusion was supported by the facts that it was difficult to separate the two components into two phases and that the η_m values did not change even when measured after 2 months, providing the conditions were suitable. A slight deviation of the observed values from the solid line (n is 0.1) in the volume fraction range larger than 0.7 is considered to be caused by the change in the degree of compatibility between the two components.

The η_m/η_H ratio of the viscosities of the mixture and *n*-heptadecane can be expressed by rewriting Eq. (1) as follows:

$$\eta_m/\eta_H = (1-\Phi_R) + [\Phi_R{}^2\eta_R + n\Phi_R(1-\Phi_R)(2\eta_R-\eta_H)]/[\Phi_R\eta_H + n(1-\Phi_R)\eta_R] \quad (2)$$

When the volume fraction, Φ_R, is small and when n is nearly equal to 0.1, η_m/η_H can be approximately expressed as follows:

$$\eta_m/\eta_H = 1+\Phi_R+\Phi_R{}^2/n(1-\Phi_R) \quad (3)$$

because $\eta_R \gg \eta_H$, and $n(1-\Phi_R) \gg \Phi_R\eta_H/\eta_R$. With the assumption of $n=\Phi_R f(\Phi_R)$, the following relationship is obtained:

$$\eta_m/\eta_H = 1 + \Phi_R + \Phi_R/(1-\Phi_R)f(\Phi_R) \simeq 1 + a\Phi_R + b\Phi_R{}^2 \quad (4)$$

where a and b are parameters. Figure 3 shows the relationship between $(\eta_m/\eta_H-1)/\Phi_R$ and Φ_R at 50°C and at volume fractions, Φ_R, smaller than 0.2. The linear relationship was found to be as follows: $(\eta_m/\eta_H-1)/\Phi_R=2.5+5.6\Phi_R$. Similar relations have been found for dilute solutions of polymers.[7-10]

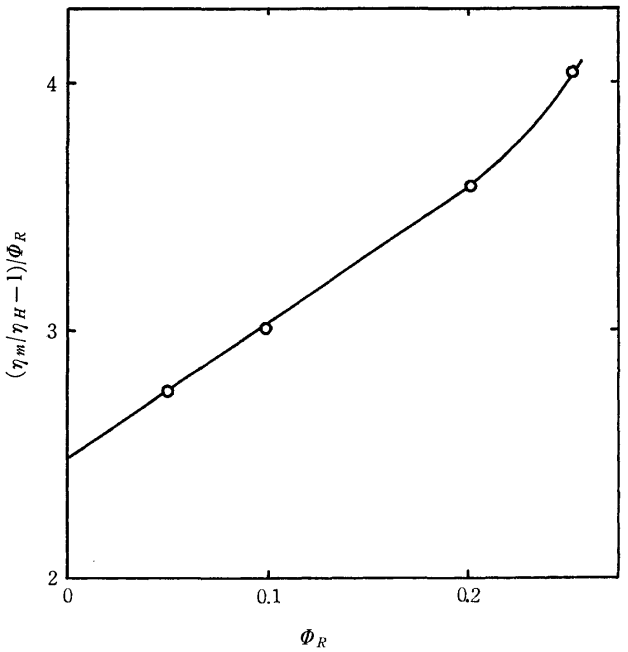

Fig. 3. Relationship between $(\eta_m/\eta_H-1)/\Phi_R$ and Φ_R at 50°C.

Temperature Dependence of Viscosities. Figure 4 shows the relationships between $(T-T_0)$ and $(T-T_0)/\log a_T$. The shift factor, a_T, which was expressed by $\eta\rho_0 T_0/\eta_0\rho T$, was calculated on the basis of an arbitrary fixed temperature, T_0. The linear relationships made it clear that the temperature dependence of the viscosities of the mixed samples could be well explained by the WLF equation.[11] The WLF parameter, $C_1{}^0$ and $C_2{}^0$, were estimated on the basis of T_0 from the linear relationships between $(T-T_0)$ and $(T-T_0)/\log a_T$ in Fig. 4.

The free-volume fraction, f_0, at T_0 and its thermal-expansion coefficient, α_f, were expressed by $1/2.303C_1{}^0$ and $1/2.303C_1{}^0C_2{}^0$ respectively. Table 3 shows the free-volume fractions, f_T, at 30°C and their thermal-expansion coefficients, α_f.

7) E. Guth and R. Simha, *Kolloid-Z.*, **74**, 266 (1936).
8) R. Simha, *J. Appl. Phys.*, **23**, 1020 (1952).
9) N. Saito, *J. Phys. Soc. Jap.*, **7**, 447 (1952).
10) M. Sugita, *ibid.*, **7**, 554 (1952).
11) M. L. Williams, R. F. Landel, and J. D. Ferry, *J. Amer. Chem. Soc.*, **77**, 3701 (1955).

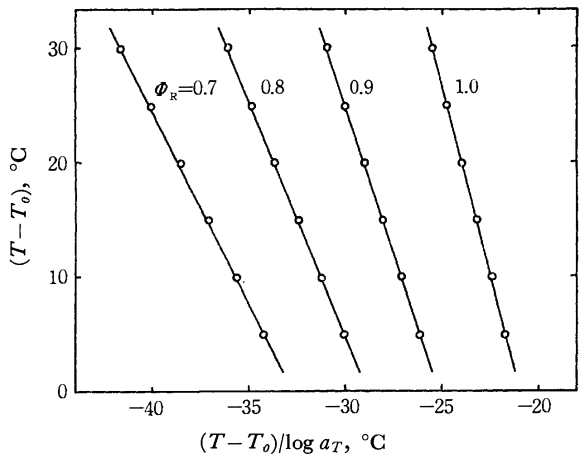

Fig. 4. Relationship between $(T-T_0)$ and $(T-T_0)/\log a_T$.

TABLE 3. VALUES OF f_T AT 30°C AND α_f

Sample	$f_T \times 10^2$	$\alpha_f \times 10^4$
n-$C_{17}H_{36}$	20.52	10.72
910—0.1	18.97	9.83
910—0.2	17.37	9.41
910—0.4	17.09	12.73
910—0.6	15.24	14.37
910—0.7	12.97	11.77
910—0.8	10.54	8.92
910—0.9	8.46	6.59
910—1.0	6.67	4.92
950—0.7	11.99	10.51
950—0.8	9.76	7.92
950—0.9	7.70	5.68
950—1.0	6.32	4.61
1000—0.7	10.93	9.09
1000—0.8	8.98	6.95
1000—0.9	7.14	5.07
1000—1.0	5.79	4.00

If physical interactions between n-heptadecane and oligotrifluorochloroethylene molecules or phases do not exist at all, the volume, V, and the free-volume, v_f, of the mixture may be given by simple additivity as follows:[12]

$$V = V_R + V_H \tag{5}$$

$$v_f = v_{f,R} + v_{f,H} \tag{6}$$

and $$f = v_f/(V_R+V_H) = \Phi_R f_R + (1-\Phi_R) f_H \tag{7}$$

where V_R and V_H are the substantial volumes of oligotrifluorochloroethylene and n-heptadecane in the mixture, and where $v_{f,R}$ and $v_{f,H}$ are the respective free-volumes of the components. Therefore, the temperature dependence of the free-volume fraction, f_T, at T is expressed as follows when the physical interactions do not exist at all:

$$f_T = \Phi_R[f_{0,R}+\alpha_{f,R}(T-T_0)] + (1-\Phi_R) \times [f_{0,H}+\alpha_{f,H}(T-T_0)] \tag{8}$$

12) T. Horino, Y. Ogawa, Y. Soen, and H. Kawai, *J. Appl. Polym. Sci.*, **9**, 2261 (1965).

where $f_{0,R}$ and $f_{0,H}$ are the respective free-volume fractions of oligotrifluorochloroethylene and n-heptadecane at T_0, and $\alpha_{f,R}$ and $\alpha_{f,H}$, their respective thermal-expansion coefficients.

Figure 5 shows the dependence of the free-volume fractions, f_T, of the mixture at 30°C on the volume fractions of oligotrifluorochloroethylene with the molecular weight of 910. The broken line shows

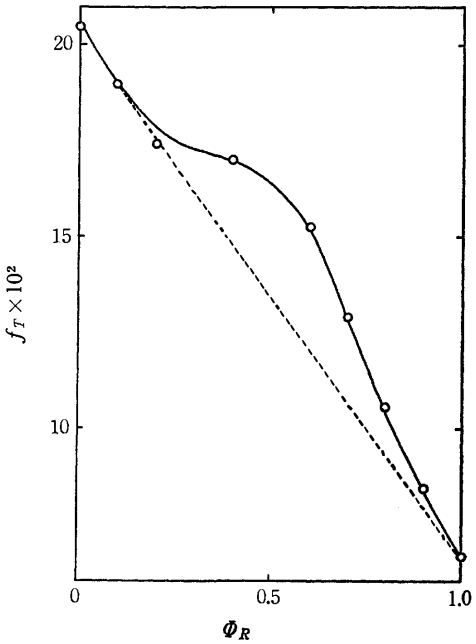

Fig. 5. Relationship between f_T and Φ_R at 30°C.

the relationship calculated by means of Eq. (7). The free-volume fractions, f_T, were larger than those obtained by assuming a simple additivity between the two components. Thus, some physical interactions between the two kinds of molecules or phases are considered to exist. In view of the physical interactions, the free-volume fraction, f_T, of a mixture is generally given by the following equation:

$$f_T = \Phi_R\beta_R(p,T,\Phi_R)f_{T,R} + (1-\Phi_R)\beta_H(p,T,\Phi_R)f_{T,H} \tag{9}$$

where the β's are interaction parameters, and p, the internal pressure induced by one phase on the other due to the difference between the thermal-expansion coefficients of the two phases. The free-volume fractions, f_T, varied abnormally at Φ_R values of about 0.2.

Molecular-weight Dependence of the Viscosities of the Mixture. Figure 6 shows the dependence of the viscosities of the mixtures on the molecular weights of oligotrifluorochloroethylene at 50°C. At molecular weights ranging from 910 to 1000, linear relationships were observed between $\log \eta_m$ and $\log M_n$. The slopes of the linear relationships were much larger than unity, and they decreased with a decrease in the volume fraction, Φ_R.

Figure 7 shows the dependence of the reciporcals of the free-volume fractions, $1/f_T$, on the molecular weights of the oligotrifluorochloroethylene in the mixtures. The reciprocals of the free-volume fractions,

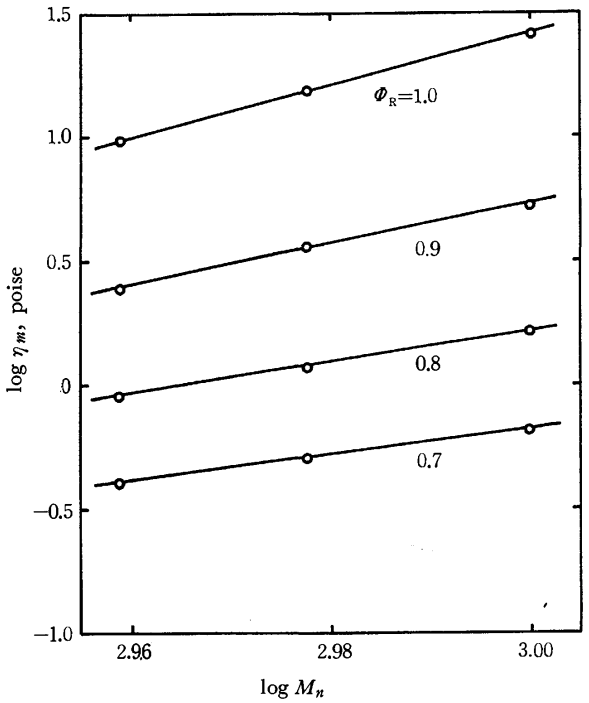

Fig. 6. Dependence of viscosity on molecular weight at 50°C.

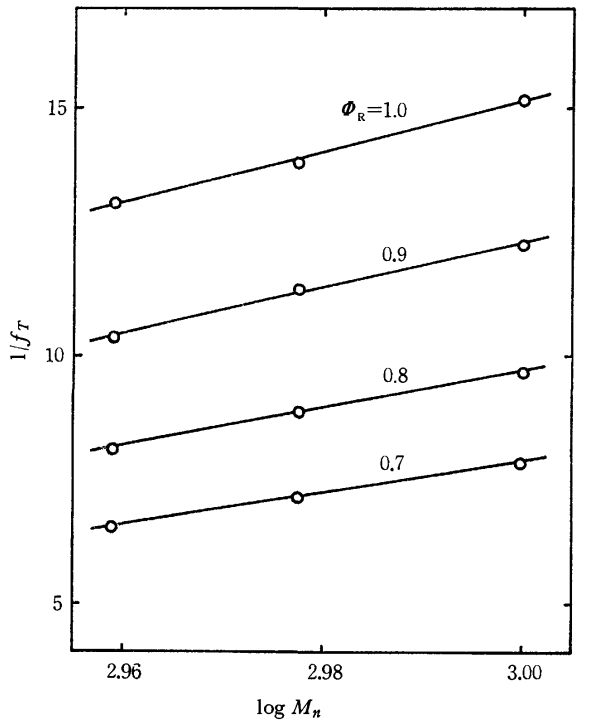

Fig. 7. Relationship between $1/f_T$ and log M_n at 50°C.

$1/f_T$, varied linearly with log M_n. The slopes of the linear relationships were much larger than unity,

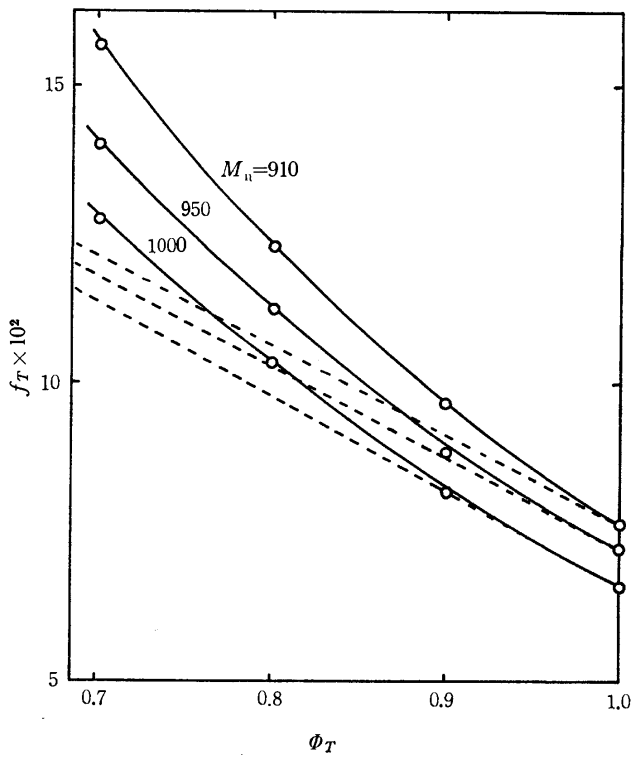

Fig. 8. Dependence of free volume fraction on Φ_T at 50°C.

and they varied with the volume fractions, Φ_R, as did those of log η_m-log M_n relationships.

Figure 8 shows a plot of the free-volume fraction, f_T, against the volume fraction, Φ_R, at 50°C. The broken lines shows the relationships calculated by Eq. (7). The estimated free-volume fractions, f_T, of the mixtures were larger than those calculated by Eq. (7), and the deviation from the calculated values increased with a decrease in the volume fraction, Φ_R, and with a decrease in the molecular weight. A negative effect on the physical interaction among oligotrifluorochloroethylene molecules is implied by the results, because the *n*-heptadecane molecules are considered to disperse among the oligotrifluorochloroethylene molecules and to obstruct the physical interaction among them. The viscosities of liquid oligotrifluorochloroethylene are larger than those of usual chain-polymers with the same chain-lengths.[4,13] Judging from the results shown in Fig. 8, strong interactions may be considered to exist. It has been suggested that these intermolecular actions are a result of the polarization of molecules induced by electronegative atoms or groups bound on the chain-skeletons.[3]

13) N. Yoshida and S. Hamada, This Bulletin, **45**, 88, (1972).

Study of Dielectric Relaxation Mechanism and Mutual Viscosity in Some Aromatic Compounds

N. K. MEHROTRA, T. C. PANT, and M. C. SAXENA
Physics Department, Lucknow University, Lucknow, India
(Received October 23, 1970)

Relaxation time and mutual viscosity of seven substituted benzenes, *p*-toludine, *o*-nitroaniline, 2,4-dichloroanisole, 2,3-dichloroanisole, 2,5-dichloronitrobenzene, 3,4-dichloronitrobenzene, and 4-chloro-1,3-dinitrobenzene have been determined in the 3.13 cm (9585 MHz) microwave region, and at three different temperatures 20, 30, and 40°C. Correlation of mutual viscosity with relaxation time leads to the conclusion that the mutual viscosity is a better representation of the resistance to the rotation of the individual solute molecule.

Investigation of dielectric relaxation in a number of organic compounds shows wide disagreement between the observed values of relaxation time and those calculated using the Debye equation.[1] This discrepancy can be explained if in the Debye equation we use a mutual viscosity parameter η_{12} representing the interaction between both solute and solvent molecules, instead of solvent viscosity η_1. The expression for the coefficient of mutual viscosity η_{12} as proved by Hill[2] is given by:

$$\eta_m\sigma_m = x_1^2\eta_1\sigma_1 + x_2^2\eta_2\sigma_2 + 2x_1x_2\eta_{12}\sigma_{12} \quad (1)$$

where η_m, η_1, and η_2 are the coefficients of viscosity of the solution, solvent and solute, respectively, and the quantities σ represent the average intermolecular distances.

On rearrangement Eq. (1) yields

$$\frac{(\eta_m\sigma_m - x_1^2\eta_1\sigma_1)}{x_2^2\sigma_2^2} = \eta_2 + 2(x_1/x_2)\cdot(\sigma_{12}/\sigma_2)\eta_{12} \quad (2)$$

This equation represents a straight line and its slope gives mutual viscosity η_{12}.

It is interesting to note that an expression involving mutual viscosity η_{12} was also proposed by Vaughan and his co-workers.[3] The results obtained using this expression are in good agreement with those obtained using Hill's equation. Their equation in the present notation is

$$\eta_m = x_1^2\eta_1 + x_2^2\eta_2 + 2x_1x_2\eta_{12} \quad (3)$$

which yields on rearrangement, the relation

$$\frac{(\eta_m - x_1^2\eta_1)}{x_2^2} = \eta_2 + 2x_1/x_2\cdot\eta_{12} \quad (4)$$

The slope of this straight line gives the mutual viscosity.

A good approximation of the relation between the viscosity and relaxation-time was suggested by Kalman and Smyth,[4] who found that the equation

$$\tau = \frac{c'}{T}\eta^{\alpha} \quad \text{where} \quad \alpha = \Delta H\tau/\Delta H\eta$$

gives very satisfactory results over a small temperature range. We have used this equation for a comparative study.

The free energies of activation for the process of dipole orientation and viscous flow have also been calculated using Eyring's equation.[5,6]

Experimental

Chemicals. All the compounds used are of pure quality, obtained from Messrs British Drug House. Purest quality analar benzene obtained from Messrs B.D.H. was distilled before use.

The dielectric constant ε' and the loss factor ε'' were measured using the standing wave technique of Roberts and Von Hippel[7] and its subsequent simplification by Dakin and Works.[8] The estimated accuracies in the measurements of ε' and ε'' were $\pm1\%$ and $\pm5\%$, respectively. The relaxation time was then determined using the concentration variation method of Gopala Krishna.[9]

Viscosities were measured to an accuracy of $\pm2\%$ with a Hoppler precision viscometer. This method requires the determination of time of fall of a glass or metal ball between two marks in a glass tube filled with a liquid with known density. Viscosity η_m of the liquid is calculated using the relation

$$\eta_m = F(S_K - S_F)K \quad (5)$$

where F is the time of fall of the ball in seconds, S_k is the specific gravity of the ball, S_F is the specific gravity of the liquid, and K is the ball constant (=0.009495).

Results and Discussion

Table 1 contains the values of relaxation time τ, mutual viscosity η_{12}, and ratios $T\tau/\eta$, $T\tau/\eta_{12}$ and $T\tau/\eta\alpha$. The values of the relaxation times and molar activation energy parameters at different temperatures are given in Table 2.

The relaxation time of *p*-toluidine is found to be smaller than that of *o*-nitroaniline. This can be explained on the basis that the intramolecular rotation of the $-NH_2$ group is comparatively less hindered by the $-CH_3$ group at the para position than by the $-NO_2$ group at the ortho position in the latter molecule. Further, the variation of relaxation time is in accordance with the

1) P. Debye, "Polar Molecules," Reinhold Publishing Corp., New York, (1929), Chap. 5.
2) N. E. Hill, *Proc. Phys. Soc.*, **67**, 149 (1954).
3) W. E. Vaughan, W. P. Purcell, and C. P. Smyth, *J. Amer. Chem. Soc.*, **83**, 571 (1961).
4) O. F. Kalman and C. P. Smyth, *ibid.*, **82**, 783 (1960).
5) S. Glasstone, K. J. Laider, and H. Eyring, "The Theory of Rate Process," McGraw-Hill Co., Inc., New York (1941), p. 548.
6) N. K. Mehrotra, T. C. Pant, and M. C. Saxena, *Trans. Faraday Soc.*, **65**, 2078 (1969).
7) S. Roberts and A. Von Hippel, *J. Appl. Phys.*, **17**, 610 (1946).
8) T. W. Dakin and C. N. Works, *ibid.*, **18**, 610 (1947).
9) K. V. Gopala Krishna, *Trans. Faraday Soc.*, **53**, 767 (1957).

TABLE 1. VALUES OF THE RELAXATION TIME (τ), AVERAGE MUTUAL VISCOSITY η_{12} AND THE RATIO ($T\tau/\eta_1$), ($T\tau/\eta_{12}$), ($T\tau/\eta_1{}^a$) FOR THE COMPOUNDS INVESTIGATED

Compound	Temp. °K	$\tau\times10^{12}$ sec	η_1 cp	η_{12} cp		$\eta_1{}^a\times10^3$	$T\tau/\eta_1\times10^8$	$T\tau/\eta_{12}\times10^8$	$T\tau/\eta_1{}^a\times10^8$
				Eq. (2)	Eq. (4)				
p-Toluidine	293	7.3	0.65	0.67	0.64	4.42	32.74	31.82	0.48
	303	6.2	0.56	0.61	0.60	3.79	33.59	31.57	0.49
	313	5.4	0.50	0.53	0.52	3.29	34.43	31.74	0.51
o-Nitroaniline	293	7.2	0.65	0.68	0.68	22.77	34.95	32.63	9.29
	303	6.4	0.56	0.64	0.62	20.46	35.88	31.54	9.83
	313	5.7	0.50	0.59	0.55	18.54	35.85	30.07	9.54
2,4-Dichloroanisole	293	10.7	0.65	0.87	0.87	9.02	48.50	36.27	0.34
	303	9.1	0.56	0.75	0.73	7.90	49.33	37.20	0.35
	313	8.0	0.50	0.64	0.67	6.99	50.71	36.40	0.36
2,3-Dichloronitrobenzene	293	11.7	0.65	0.91	0.94	8.12	53.07	37.68	0.42
	303	10.0	0.56	0.79	0.79	7.08	53.78	38.39	0.43
	313	8.7	0.50	0.74	0.73	6.26	55.21	36.86	0.44
2,5-Dichloronitrobenzene	293	13.8	0.65	0.92	0.93	8.97	62.37	43.75	0.45
	303	11.6	0.56	0.89	0.88	7.84	62.81	39.23	0.45
	313	10.4	0.50	0.82	0.80	6.95	67.95	39.05	0.47
3,4-Dichloronitrobenzene	293	17.5	0.65	1.20	1.21	76.14	79.45	42.69	6.74
	303	15.8	0.56	1.19	1.21	70.78	85.17	39.99	6.75
	313	14.5	0.50	1.17	1.18	66.19	92.02	38.58	6.85
4-Chloro-1,3-dinitrobenzene	293	24.1	0.65	1.25	1.25	2.93	108.92	56.52	0.024
	303	19.9	0.56	1.21	1.21	2.48	107.55	49.96	0.024
	313	16.9	0.50	1.19	1.21	2.13	107.38	45.76	0.025

TABLE 2. RELAXATION TIME AND MOLAR ACTIVATION ENERGY PARAMETERS OF POLAR COMPOUNDS IN DILUTE SOLUTION OF BENZENE (at 9585 MHz)

Compound	Temp. °K	$\tau\times10^{12}$ sec	$\Delta F_\tau\times10^{-3}$ J/mol	$\Delta F_\eta\times10^{-3}$ J/mol	$\Delta F_{\eta_{12}}\times10^{-3}$ J/mol	$\Delta H_\tau\times10^{-3}$ J/mol	$\Delta H_\eta\times10^{-3}$ J/mol	$\Delta H_{\eta_{12}}\times10^{-3}$ J/mol	ΔS_τ J/mol	ΔS_η J/mol	$\Delta S_{\eta_{12}}$ J/mol
p-Toluidine	293	7.3	9.34	12.18	12.36	10.26	9.54	8.72	+3.14	−8.99	−12.46
	303	6.2	9.35	12.23	12.56	10.26	9.54	8.72	+3.00	−8.90	−12.69
	313	5.4	9.40	12.30	12.62	10.26	9.54	8.72	+2.64	−8.82	−12.47
o-Nitroaniline	293	7.2	9.39	12.18	12.39	7.16	9.54	5.42	−7.43	−8.29	−22.73
	303	6.4	9.44	12.23	12.67	7.16	9.54	5.42	−7.51	−8.90	−23.91
	313	5.7	9.49	12.30	12.86	7.16	9.54	5.42	−7.43	−8.82	−23.87
2,4-Dichloroanisole	293	10.7	10.28	12.18	13.00	8.91	9.54	8.91	−4.77	−8.99	−13.97
	303	9.1	10.34	12.23	13.07	8.91	9.54	8.91	−4.71	−8.90	−13.75
	313	8.0	10.40	12.30	13.24	8.91	9.54	8.91	−4.78	−8.82	−13.95
2,3-Dichloroanisole	293	11.7	10.53	12.18	13.13	9.11	9.54	8.13	−4.97	−8.99	−17.05
	303	10.0	10.55	12.23	13.19	9.11	9.54	8.13	−4.80	−8.90	−16.71
	313	8.7	10.63	12.30	13.47	9.11	9.54	8.13	−4.86	−8.82	−17.12
2,5-Dichloronitrobenzene	293	13.8	10.92	12.18	13.16	8.92	9.54	4.45	−6.84	−8.99	−29.73
	303	11.6	10.94	12.23	13.53	8.92	9.54	4.45	−6.70	−8.90	−29.97
	313	10.4	11.11	12.20	13.74	8.92	9.54	4.45	−7.05	−8.82	−29.67
3,4-Dichloronitrobenzene	293	17.4	11.52	12.18	13.81	4.86	9.54	1.01	−22.74	−8.99	−43.80
	303	15.8	11.72	12.23	14.27	4.88	9.54	1.01	−22.66	−8.90	−43.76
	313	14.4	12.02	12.30	14.69	4.88	9.54	1.01	−23.22	−8.82	−43.69
4-Chlorc-1,3-dinitrobenzene	293	24.1	12.30	12.18	13.91	11.04	9.54	1.65	−4.29	−8.99	−41.86
	303	19.9	12.31	12.23	14.30	11.04	9.54	1.65	−4.21	−8.90	−41.68
	313	16.9	12.38	12.30	14.73	11.04	9.54	1.65	−4.27	−8.82	−41.78

variation of their molecular volumes. 2,3-Dichloroanisole exhibits a larger relaxation time than 2,4-dichloroanisole, although the size of the two molecules is the same. This can be explained by considering the fact that both molecules contain $-OCH_3$ group at the ortho position, which is capable of intramolecular rotation round its bond with the benzene ring. The rotation of $-OCH_3$ group experiences greater steric hindrances due to the neighbouring chloro groups in 2,3-dichloroanisole than in 2,4-dichloroanisole, resulting in a greater relaxation time in the former molecule.

It is observed from the table that the relaxation time of 2,5-dichloronitrobenzene is smaller than that of 3,4-dichloronitrobenzene, which can be concluded from the consideration that the volume swept out for dipole orientation by the former molecule is also smaller. The largest relaxation time of 4-chloro-1,3-dinitrobenzene among all other compounds investigated can be attributed to its biggest size and the strong polarity of the $-NO_2$ groups.

It is apparent from Table 1 that the ratio increases with the rise of temperature for nearly all the compounds investigated. This is not in conformity with the Debye theory which requires the ratio to be constant for small change of temperature. The anomaly is explained if η_{12} the mutual viscosity of the solute and solvent is used instead of solvent viscosity η_1. The variation in the values of ratios $T\tau/\eta_{12}$ and $T\tau/\eta\alpha$ at different temperatures is negligibly small and this leads us to conclude that either η_{12} or η_1^{α} gives a more convincing account of the resistance confronted by the individual solute molecules during the process of rotation.

The values of the average mutual viscosity η_{12} as determind from Eq. (4) of Vaughan and co-workers are almost equal to those obtained using Hill's equation (2). This is because the form of the two equations is very nearly the same. We have determined the values of η_{12} for chlorobenzene using Eqs. (2) and (4). For chlorobenzene in benzene, Eq. (2) gives 0.74, while Eq. (4) gives 0.73. This indicates a fairly good agreement in the values of η_{12} obtained using the two equations.

The free energies of activation for dipole orientation and viscous flow are found to increase with the rise of temperature while the relaxation time decreases. An explanation is furnished from the consideration that with the rise of temperature, thermal agitation increases, resulting in the increase of the activation energies. Similar results have also been concluded by Shukla and Coworkers[10] for some substituted benzaldehydes. The negative value of the entropy of activation found for most of the compounds investigated indicates that there are fewer configurations possible in the activated state and for these configurations the activated state is more ordered than the normal state. A comparison of the activation energies for the viscous flow using solvent viscosity η_1 and mutual viscosity η_{12} show that $\Delta F_{\eta_{12}}$ is a better representation of the potential barriers offering inner friction to the rotating molecules.

The higher values of ΔF_η as compared to $\Delta F\tau$ indicate that while the process of dipole orientation involves only the rotation of the molecules, the process of viscous flow involves both rotation and translation. Similar results were observed earlier in the case of substituted pyridines.[11]

10) J. P. Shukla, S. I. Ahmad, D. D. Shukla, and M. C. Saxena, *J. Phys. Chem.*, **72**, 1013 (1968).

11) N. K. Mehrotra and M. C. Saxena, This Bulletin, **40**, 19 (1947).

Self-Diffusion of Chloride Ions in Manganese Dichloride Crystallites

Yoshihiro SENSUI

Institute for Atomic Energy, Rikkyo (St. Paul's) University, Yokosuka

(Received June 19, 1971)

The self-diffusion of chloride ions in the powdery crystals of manganese dichloride was studied in the temperature range of 200—420°C by the use of the isotopic-exchange method. The activation energies for self-diffusion were determined to be 0.95 and 1.6 eV in a lower and a higher temperature region respectively. From these, the activation energy for the migration of chloride ions and the formation energy of an anion vacancy or a pair of an anion and a cation vacancy were deduced.

The method of the isotopic-exchange reaction between gaseous molecules and ionic crystals is very useful to the investigation of the self-diffusion of ions in crystals. By this method, the self-diffusion of halide ions in alkali halide crystals has been investigated by several workers[1-5] Laurent and Benard[1] and Barr *et al.*[2-4] have studied mainly the diffusion in the bulk of the crystals, while Takaishi and the present author have studied that of chloride ions in the bulk of sodium chloride and rubidium chloride crystallites, along with the surface exchange reaction[5]. There have, however, been few studies of higher valent metal halide crystals, except for the qualitative studies by Willard and his co-workers.[6-8]

In the present work, the self-diffusion of chloride ions in manganese dichloride crystallites was investigated as a first step in the study of a series of higher valent metal chlorides; we chose this material because it is relatively easy to handle because of its layer structure, its low volatility, and presumed surface homogeneity. Larher studied the adsorption of krypton on several kinds of crystallites with $CdCl_2$-type structures and concluded that their surface were very homotattic.[9] Manganese dichloride, which he did not study has the same structure and may be presumed to have a homotattic surface on the basis of the electron microscopic data (Fig. 1).

Experimental

The apparatus and technique for measuring the self-diffusion of chloride ions by the isotopic-exchange method were described in previous papers.[5] The diffusion measurements were carried out on five specimens of powdery crystals.

Radioactive manganese dichloride was prepared in the form of an aqueous solution from radioactive hydrochloric acid distilled in a vacuum and manganese dichloride (Merks G.R.-reagent, Item No. 5927) by the isotopic-dilution method. In the resultant radioactive chloride, the ratio of ^{36}Cl to Cl was 5.3×10^{-4}.

Anhydrous crystallites of radioactive manganese dichloride were prepared by modifying Marshall's method,[10] *i.e.*, by pouring 100 m*l* of distilled ethyl ether into about 2 m*l* of an anhydrous ethanol solution of manganese dichloride and then baking the precipitate at 420°C for 6 hr in vacuum (3×10^{-7} Torr) prior to the experiment. An electronmicrograph of the anhydrous specimen is shown in Fig. 1. The characteristic layer structure appeared even in the external shape of the crystallites.

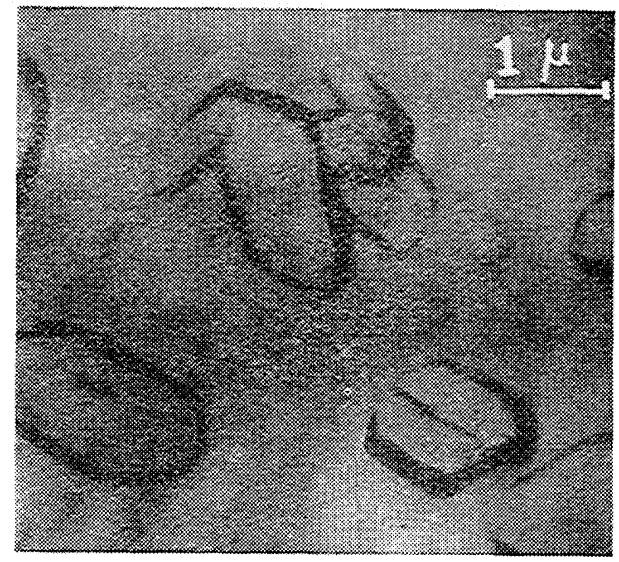

Fig. 1. The external shape of the manganese dichloride crystallites used in the present experiment.

Results and Discussion

Manganese dichloride melts at 650°C and begins to sublime at about 450°C in a vacuum. Therefore, the anion-diffusion measurements were carried out in the temperature range between 200 and 420°C.

At the initial stage of the reaction, only chloride ions near the surface region participate. Accurate data with manganese dichloride were not obtained in this stage, in contrast with the case of alkali chlorides, but it was concluded that the reaction proceed at a high rate. At the later stage, the reaction may be rate-controlled by the bulk-diffusion process. The mean length of the shorter edge of the layer-structural crystallites is estimated from the electronmicroscopic

1) J. F. Laurent and J. Benard, *J. Phys. Chem. Solids*, Pergamon Press **3**, 7 (1957).
2) L. W. Barr, I. M. Hoodless, J. A. Morrison, and R. Rudham, *Trans. Faraday Soc.*, **56**, 697 (1960).
3) L. W. Barr, J. A. Morrison, and P. A. Schroeder, *J. Appl. Phys.*, **36**, 624 (1965).
4) L. W. Barr and D. K. Dawson, *Phys. and Chem. of Ceramic Surfaces, Proceeding* 5 (British Ceramic Soc.), 77 (1965).
5) T. Takaishi and Y. Sensui, *Trans. Faraday Soc.*, **65**, 131 (1969); *Surface Science*, **19**, 339 (1970).
6) M. Blau, W. T. Carnall, and J. E. Willard, *J. Amer. Chem. Soc.*, **74**, 5762 (1952).
7) R. A. Howald and J. E. Willard, *ibid.*, **77**, 2046 (1955).
8) J. R. Wilson and J. E. Willard, *J. Phys. Chem.*, **70**, 1665 (1966).
9) Y. Larher, *ibid.*, **72**, 1847 (1968).
10) F. G. Marshall, *Phys. Rev.*, **58** 642 (1940).

data to be about 0.5 μ (*cf.* Fig. 1). This length corresponds to a few thousand layer in the direction of the *c*-axis of the crystal. In the present experiments, only the ^{36}Cl ions in the bulk of the near-surface gaseous phase; *i.e.*, amounts corresponding to less than 50 layers were counted. Therefore, the diffusion data obtained may be analyzed on the basis of the model of semi-infinite media. For this model, the diffusion equation has the solution;[11]

$$X_g = X_s + 2\alpha(Dt/\pi)^{1/2}$$

where X_g designates the number of ^{36}Cl ions diffused out into the gaseous phases after time t; X_s, that of the ^{36}Cl ions in the surface region which diffused out into the gaseous phase at the initial stage of the reaction; D, the bulk diffusion constant; and α, the product of the surface area and the initial concentration of ^{36}Cl. Denoting the measured counting rate by C, we obtain;

$$C = K \cdot X_g$$

and;

$$C_s = K \cdot X_s$$

where K is the conversion factor. Thus, we obtain;

$$C = C_s + \frac{2\alpha}{K} \cdot \left(\frac{Dt}{\pi}\right)^{1/2}$$

in which the value for C_s cannot be obtained directly from experiments. The exchange process may be expected to be rate-controlled by the bulk-diffusion, and the curve of C against $\sqrt{t}$ may be linear, except at the initial stage. However, there are some ambiguties as to the start of the reaction. The measured time, t, must be corrected; that is, t is replaced by $(t+\delta)$, where the value of δ is determined empirically so as to give a linear curve. The results are given in Fig. 2, in which the intersection of the straight line with the coordinate give the value of C_s.

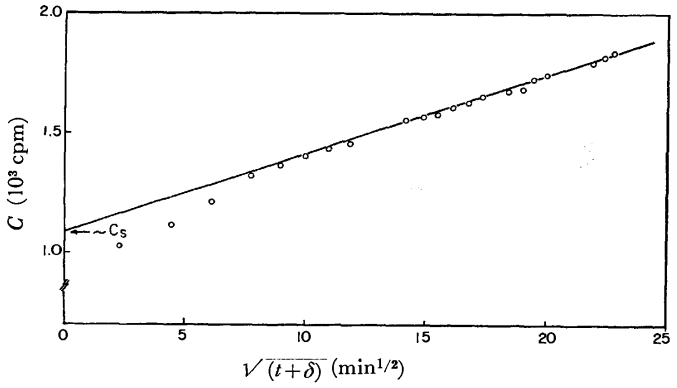

Fig. 2. The plots of C against the square-root of $(t+\delta)$. The data are obtained from the specimen IV at 200°C.

Next, let us suppose that a first diffusion run is made for time t_1 at a temperature T_1 at which the diffusion constant is D_1. If a second run is made for t_2 at a different temperature T_2 (the constant is new D_2), the total counting rate, C, may be shown to be;[11]

$$C = C_s + \frac{2\alpha}{\sqrt{\pi} \cdot K} \cdot (D_1 t_1 + D_2 t_2)^{1/2}.$$

11) A. B. Lidiard and K. Tharmalingam, *Discuss. Faraday Soc.*, **28**, 64 (1959).

This may be extended to further runs and rewritten as follows;

$$(C - C_s)^2 = \frac{4\alpha^2}{\pi K^2} \cdot (D_1 t_1 + D_2 t_2 + \cdots).$$

The values of $(C-C_s)^2$ thus obtained are plotted against the time in Fig. 3. The measured points lie well on the straight lines. If the crystallites contained a lot of dislocations along which diffusion proceeded much faster, complex curve be obtained; that is, the plots of $(C-C_s)^2$ against the time should not fall a straight line when the temperature is changed. This is not the present case, and so it may be concluded that the present model is adequately supported experimentally.

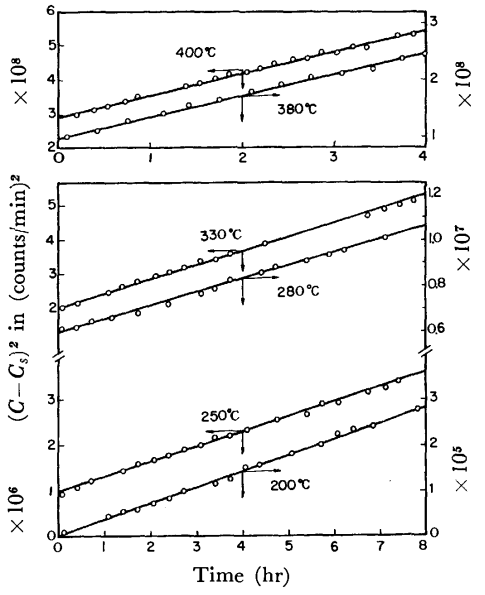

Fig. 3. The plots of $(C-C_s)^2$ against time. All data in this figure are obtained from the specimen IV.

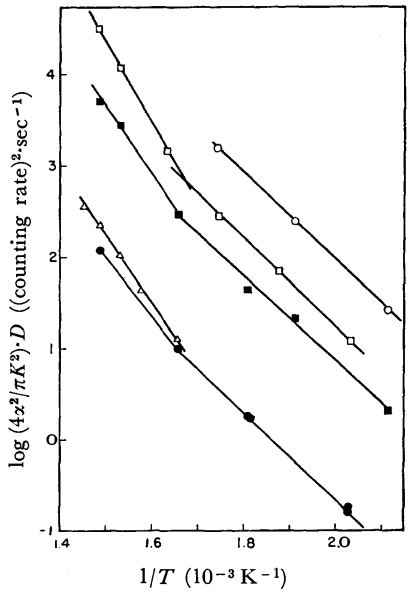

Fig. 4. The Arrhenius plots of apparent self-diffusion rates. ○, ●, □, ■, and △ refer to different specimens, I, II, III, IV, and V respectively.

From the slopes of $(C-C_s)^2$ against the time, the values of $(4\alpha^2/\pi K^2)\cdot D$ can be obtained. The Arrhenius plots of these values are shown in Fig. 4, in which all the curves have break at about 330°C and two kinds of slopes are found. The temperature of the break-point is considerably lower than in the case of alkali chlorides.[1-3] The slope in the lower-temperature region in Fig. 4 gives the activation energy, ΔE, for the migration of ^{36}Cl ions, while that in the higher-temperature region gives $(\Delta E+\Delta W)$, where ΔW denotes the formation energy of an anion vacancy, or a half of that of an anion and a cation vacancy. The values for the activation energies of all the specimens are given in Table 1. The absolute value of D depends on the surface area of the specimen, which was not controlled in the present experiment. Hence, it was possible to determine with confidence only the activation energy in the diffusion process, not the frequency factor. However, if crude estimation from the electronmicroscopic data are used for the surface area of the sample, values, 2×10^{-3} cm^2 sec^{-1} and 1×10^{-8} cm^2 sec^{-1}, are given to the frequency factors corresponding to the formation of a vacancy and the migration of ^{36}Cl respectively. Both of these values are small in comparison with the corresponding values[5] in the crystallites of alkali chlorides, but they are not unreasonable.

Table 1. The value of activation energy for each specimen

Specimen	ΔE (eV)	$\Delta E+\Delta W$ (eV)
I	0.95	
II	0.95	
III	0.96	1.77
IV	0.95	1.50
V		1.58
Average	0.95	1.6

The author's sincere thanks are due to Professor Dr. T. Takaishi of Rikkyo (St. Paul's) University for his valuable discussions.

BULLETIN OF THE CHEMICAL SOCIETY OF JAPAN, VOL. 45, 361—365 (1972)

The Photo-decomposition of 1-Azidopyrene in the Benzene Solution

Tsuguo YAMAOKA,
Department of Printing, Faculty of Engineering, Chiba University, Chiba
Hiroshi KASHIWAGI, and Saburo NAGAKURA
The Institute for Solid State Physics, The University of Tokyo, Roppongi, Minato-ku, Tokyo

(Received June 25, 1971)

1-Nitrenopyrene (Py-N) was produced by the photo-decomposition of 1-azidopyrene (Py-N_3) in the benzene solution at 77°K and at room temperature. At 77°K, Py-N was found to be stable, and its electronic absorption and ESR spectra were measured. The result shows that its ground state is triplet and the fine structure constant, D, is equal to 0.73 cm^{-1}. At room temperature, 1-nitrenopyrene was found to be converted easily into 1,1′-*trans*-azopyrene (*trans*-Py-N=N–Py) in the oxygen-free benzene solution and into 1-nitropyrene (Py-NO_2) in addition to Py-N=N-Py in the oxygen-containing benzene solution. The decay process of Py-N as a reaction intermediate and the formation processes of the reaction products were studied by the flash-photolysis technique, and from an analysis of the results, the rate constants at 23°C were determined to be 2.1×10^9 $l mol^{-1} sec^{-1}$ and 1.4×10^3 sec^{-1} for 2Py–N→*trans*-Py–N=N–Py and for Py–N+O_2→Py-NO_2, respectively.

Nitrenes produced by the photo-decomposition of the corresponding azides are known to be triplet in their ground states.[1-3] Most of the measurements on the nitrenes have hitherto been made in rigid solutions at low temperature;[4-8] studies of them in fluid solutions are few in number.

The flash-photolysis experiment has demonstrated that they exist as transient intermediates in several photochemical reactions of organic azides.[9-11] In particular, Reiser *et al.*[11] studied kinetically three types of reactions of nitrenes, recombination, hydrogen abstraction from a solvent, and reaction with an azido group, taking 1-nitrenonaphthalene, 4,4′-dinitrenobiphenyl, and 1-nitrenoanthracene.

In the present paper, we studied the electronic absorption and ESR spectra of a new nitrene, 1-nitrenopyrene (hereafter to be abbreviated to Py-

1) G. Smolinski, L. C. Snyder, and E. Wasserman, *Rev. Mod. Phys.*, **35**, 576 (1963).
2) G. Smolinski, E. Wasserman, and W. A. Yager, *J. Amer. Chem. Soc.*, **84**, 3220 (1962).
3) J. A. R. Coope, J. B. Farmer, C. L. Gardner, and C. A. McDowell, *J. Chem. Phys.*, **42**, 54 (1965).
4) A. Reiser and V. Froster, *Nature*, **208**, 682 (1965).
5) A. Reiser, H. Wagner, and G. Bowen, *Tetrahedron Lett.*, 2635 (1966).
6) A. Reiser, G. Bowen, and R. J. Horne, *Trans. Faraday Soc.*, **62**, 3162 (1966).
7) A. Reiser, H. M. Wagner, R. Marley, and G. Bowen, *ibid.*, **63**, 2403 (1967).
8) A. Reiser and R. Marley, *ibid.*, **64**, 1806 (1967).
9) R. S. Berry, D. Cornell, and W. Lwowskii, *J. Amer. Chem. Soc.*, **85**, 1199 (1963).
10) A. Reiser, G. C. Terry, and F. W. Wilett, *Nature*, **211**, 410 (1966).
11) A. Reiser, F. W. Wilett, G. C. Terry, V. Williams, and R. Marley, *Trans. Faraday Soc.*, **64**, 3265 (1968).

N), and also its decay process in a benzene solution. We adopted this nitrene as a suitable research subject for the following reasons. Firstly, the photodecomposition quantum yield of the parent azide, 1-azidopyrene(Py-N_3), is very large. Secondly, since the absorption peaks characteristic of Py-N_3, Py-N, and a main final product appear at 360 nm, 415 nm, and 500 nm, respectively, we can easily distinguish the components from one another and can easily follow the reaction process.

Experimental

1-Azidopyrene was prepared by treating the 10% hydrochloric acid solution of 1-aminopyrene with aqueous sodium nitrite and srdium azide solutions below 5°C. The precipitation separated by the filtration of the solution was purified by the aid of a column chromatograph of active alumina.

Commercially-available benzene of a GR grade was purified by shaking it with concentrated sulfuric acid, water, an aqueous sodium hydroxide solution, an aqueous potassium permanganate solution containing sodium hydroxide, and water. The benzene thus treated was dehydrated by calcium chloride and thereafter by sodium metal, and finally it was distilled.

In the present study, the nitrene was prepared in both rigid and fluid benzene solutions. The rigid solution of the parent azide in benzene was illuminated by a 500 W mercury lamp at 77°K. The ESR spectrum of the nitrene thus prepared was measured by a JES ME 3X type spectrometer (X-band, 100 KHz modulation). Since the rigid benzene solution is somewhat opaque for cracking, its electronic absorption spectrum was measured by the aid of the special technique developed by Shibata.[12] Actually, the spectrum was measured by a Shimadzu MPS type spectrophotometer at the Institute of Physical and Chemical Research, an apparatus constructed especially to make possible the application of his method.

The preparation of the nitrene from a fluid benzene solution containing Py-N_3 and the measurement of its electronic absorption spectrum were made by the aid of a flash photolysis apparatus (32 Joule, duration time of 20 μsec) at the Institute of Physical and Chemical Research,[13,14] a cylindrical quartz sample cell 10 cm long and 1 cm in diameter being used. The electronic absorption spectrum was photographed at several stages before and after the flash photolysis.

The decay curve of a transient intermediate and the rise curve of the final product, Py-N=N-Py, in a benzene solution at room temperature were recorded at their peak wavelengths by the aid of an R106 photomultiplier and an oscilloscope.

Final products were separated by the aid of a column chromatography of active alumina, and each component was identified by an elemental analysis, by studying the mass spectrum, and, if possible, by comparing the electronic spectrum, the infrared spectrum, and the gas chromatogram with those of an authentic sample.

The oxygen-free solution, if necessary, was prepared by the freeze-thaw technique.

12) K. Shibata, "Method of Biochemical Analysis," Vol. 7, ed. by D. Glick, Interscience Publishers, New York, N. Y. (1959) p. 77.

13) A. Kira and M. Koizumi, This Bulletin, **42**, 625 (1969).

14) A. Kira and K. Nishi, *Rep. IPCR*, **44**, 56 (1968).

Results and Discussion

Electronic and ESR Spectra of Irradiated Py-N_3 in the Rigid Benzene Solution at 77°K. The electronic absorption and ESR spectra were measured at 77°K with the benzene solution of Py-N_3 (2.7×10^{-4} mol/l) irradiated by a 500W mercury lamp; the results are shown in Figs. 1 and 2, respectively.[15]

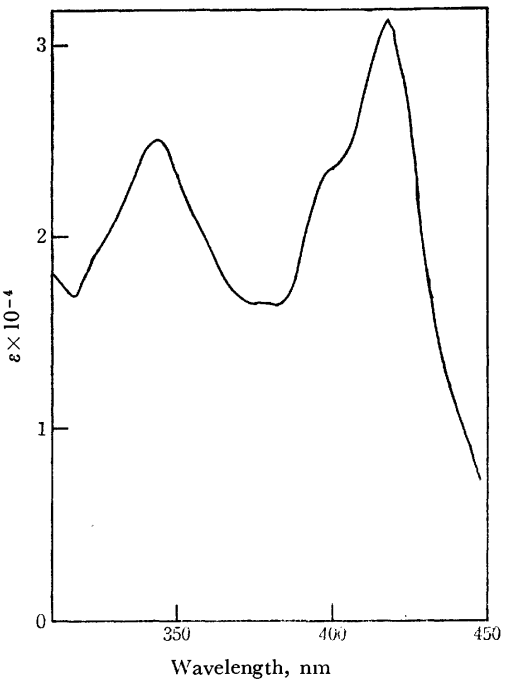

Fig. 1. The electronic absorption spectrum of Py-N in benzene at 77°K.

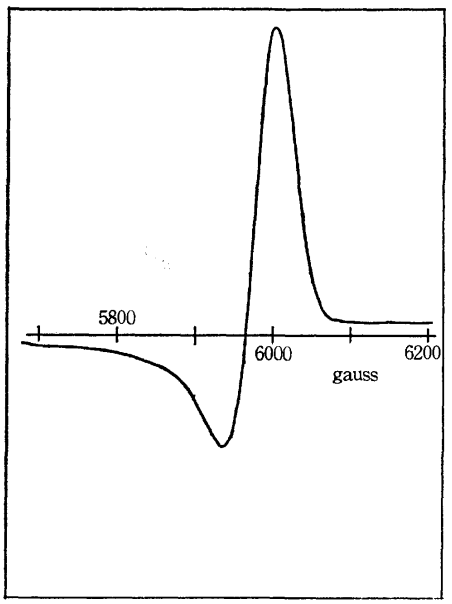

Fig. 2. The ESR spectrum of Py-N in benzene at 77°K.

15) We observed another weak absorption band at 694 nm with a molar extinction coefficient of ~1500 in addition to the strong absorption bands shown in Fig. 1. In the present paper, however, we are concerned with only the strong bands.

The main feature of the ESR spectrum shown in Fig. 2 is that a single, rather broad line appears in a high field (5980 G). This feature is similar to that of the spectra observed for other ground-state triplet nitrenes[1,3] with quite large D and quite small E values. This means that the ESR spectrum shown in Fig. 2 and, therefore, the electronic absorption spectrum shown in Fig. 1 are due to the triplet Py-N. The D value of Py-N was found to be 0.73 cm^{-1} on the reasonable assumptions that $E=0$ and that $g=g_e=2.0023$.[16]

Flash Photolysis of Py-N_3 in Benzene. Figure 3 shows the microphotometer curves of photographs obtained by the flash photolyis of the oxygen-free benzene solution of Py-N_3 ($\sim 1\times10^{-5}$ mol/l). Curves (a), (b), and (c) in this figure are the spectra of the solution taken before, 20 μsec after, and a few minutes after the flash excitation, respectively. Since curve (b) is identical with the spectrum of Py-N shown in Fig. 1, it is evident that Py-N is produced as a transient intermediate in the photoreaction of Py-N_3 in the oxygen-free benzene solution.

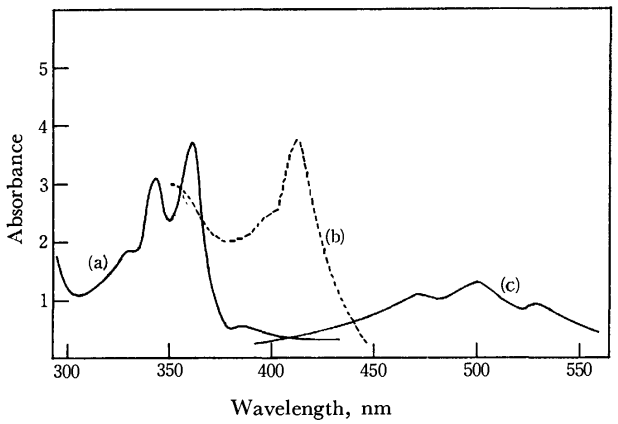

Fig. 3. The microphotometer traces of the absorption spectra measured by the aid of the flash photolysis technique with Py-N_3 in the oxygen-free benzene solution at room temperature.
(a): before a flash irradiation
(b): 20 μsec after a flash
(c): a few minutes after a flash

A final product was isolated from the solution by the aid of the active alumina-column chromatography technique. From the infrared spectrum, and also from a consideration of the electronic absorption spectrum to be described below, the final product was identified with 1,1′-*trans*-azopyrene (abbreviated hereafter to *trans*-Py-N=N-Py).

By stationary irradiation by a mercury lamp of Py-N_3 in an oxygen-free benzene solution at room temperature, we obtained two final products, dark-red and reddish-yellow crystals which were separated from each other by the aid of the active alumina-column chromatography technique in the dark.[17] The elemental analysis of the dark red sample[18] and the mass spectra[19] and infrared spectra[20] of both products show that they have the same chemical composition, Py-N=N-Py. The reddish-yellow crystal is easily converted into the dark red one by warming it from room temperature to ~100°C or by exposing it to sunlight. From these facts, it may be surmised that they are *trans*- and *cis*-Py-N=N-Py. The electronic absorption spectra observed for the dark-red and reddish-yellow samples are shown by curves (a) and (b) in Fig. 4, respectively. In view of the general feature of the electronic absorption spectra that the strongest band of the *trans*-isomer is stronger and appears in a longer-wavelength side than that of the *cis*-isomer, curve (a) in Fig. 4 is due to *trans*-Py-N=N-Py.[21] Since curve (c) in Fig. 3 is identical with this curve, the final product obtained by the flash irradiation of the oxygen-free benzene solution of Py-N_3 is identified with *trans*-Py-N=N-Py.

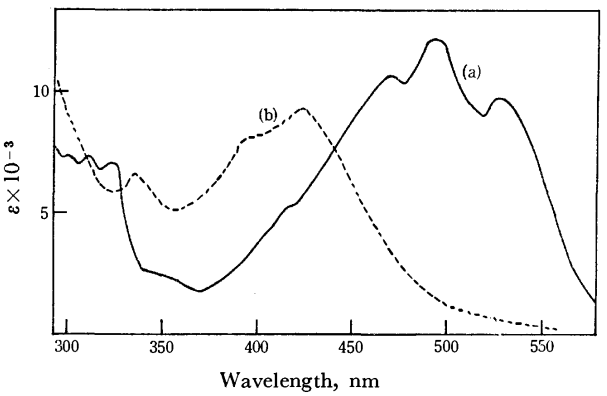

Fig. 4. The electronic absorption spectra of azopyrene.
(a): *trans*-azopyrene
(b): *cis*-azopyrene

The microphotometer curves of photographs obtained by flash photolysis measurements for Py-N_3 ($\sim 1\times10^{-5}$ mol/l) in oxygen-containing benzene solutions are shown in Fig. 5. Curves (a), (b), and (c) in this figure are spectra observed for the solution before, 20 μsec after, and a few minutes after the flash excitation, respectively. Curve (b) in Fig. 5

16) Observed slight broadening in the ESR spectrum of Py-N shows that E is non-zero but is very small. The previously reported E values of nitrenes do not exceed 0.01 cm^{-1}.[3] Therefore, the D value of Py-N may be evaluated by assuming $E=0$ cm^{-1}. Wasserman *et al.* (E. Wasserman, L. C. Snyder, and W. A. Yager, *J. Chem. Phys.*, **41**, 1763 (1964)) could reproduce well by simulation the observed ESR spectrum of methylsulfonylnitrene taking $g=2.0023$. Generally speaking, triplet states of organic molecules have the g value close to 2.0023.

17) Toluene was used as a developing agent. After removing undecomposed Py-N_3, the dark red and reddish yellow parts of the column were cut. The products were extracted by tetrahydrofuran, recrystallized from toluene, washed by toluene and ethyl ether, and finally dried *in vacuo*. All these processes were done in the dark.

18) Found: C, 88.31; H, 4.15; N, 6.59%. Calcd for $C_{32}H_{18}N_2$ (Py-N=N-Py): C, 89.28; H, 4.21; N, 6.51%. A discrepancy between the found and calculated values for carbon may be due to a very small amount of water contained in the sample.

19) Both isomers show a mass spectrum with a signal corresponding to molecular weight of 430.

20) The N=N stretching vibrations were observed for these two isomers in nujol mull.

21) H. Suzuki, "Electronic Absorption Spectra and Geometry of Organic Molecules," Academic Press Inc., New York, N. Y. (1967), p. 504.

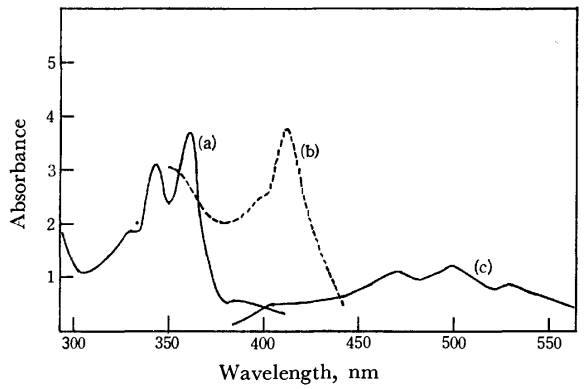

Fig. 5. The microphotometer traces of the absorption spectra measured by the aid of the flash photolysis technique with Py-N_3 in the oxygen-containing benzene solution at room temperature.
(a): before a flash irradiation
(b): 20 μsec after a flash
(c): a few minutes after a flash

is identical with the spectrum of Py-N given in Fig. 1. Therefore, we can conclude that Py-N is a transient intermediate in the photoreaction of Py-N_3 also in the oxygen-containing benzene solution.

In the case of the oxygen-containing benzene solution, we isolated two final products by the aid of column chromatography of active alumina. These procucts were identified with *trans*-Py-N=N-Py and 1-nitropyrene (Py-NO_2); the former was confirmed by comparing its electronic spectrum with that of *trans*-Py-N=N-Py given in Fig. 4(a), and the latter by comparing its electronic and infrared absorption spectra and its gas chromatogram with those of the authentic sample. Curve (c) in Fig. 5 consists of the absorption peaks due to *trans*-Py-N=N-Py given by curve (c) in Fig. 3 and the 400-nm peak of Py-NO_2.

Kinetic Study of the Reaction Process. From the identification of the transient intermediate and the final products, the following reaction mechanisms may applied to for the photoreaction of Py-N_3 in benzene:

for the oxygen-free benzene solution:

$$\text{Py-N}_3 \xrightarrow[\text{fast}]{h\nu} \text{Py-N} + \text{N}_2 \tag{1}$$

$$\text{Py-N} + \text{Py-N} \xrightarrow{k_2} \text{Py-N=N-Py} \tag{2}$$

for the oxygen-containing benzene solution:

$$\text{Py-N}_3 \xrightarrow[\text{fast}]{h\nu} \text{Py-N} + \text{N}_2 \tag{1'}$$

$$\text{Py-N} + \text{Py-N} \xrightarrow{k_2'} \text{Py-N=N-Py} \tag{2'}$$

$$\text{Py-N} + \text{O}_2 \xrightarrow{k_3} \text{Py-NO}_2 \tag{3}$$

From Eq. (2), the following equation can be derived for the oxygen-free benzene solution:

$$k_2 t = \frac{1}{x} - \frac{1}{a} \tag{4}$$

where a and x are the concentrations of Py-N at the start of reaction (2) and at the reaction time, t, respectively, and k_2 is the rate constant for reaction (2). By replacing x and a by A_0 and A, respectively, the latter being the absorbances of Py-N observed at the start of the reaction and at the reaction time t, we can obtain the following equation:

$$k_2 t = \frac{\varepsilon L}{A} - \frac{\varepsilon L}{A_0} \tag{4'}$$

Here, L is the length of the sample cell, and ε is the molar extinction coefficient of Py-N at an appropriate wavelength. In actuality, A, A_0, and ε were measured at 415 nm. The ε value at this wavelength was determined to be 3.0×10^4 from the electronic spectrum of Py-N shown in Fig. 1.

In view of the fact shown by Eq. (2) that one Py-N=N-Py molecule is produced from two Py-N entities, the following equation concerning the concentration of the final product can be obtained:

$$k_2 t = \frac{\varepsilon' L}{2(A'_\infty - A')} - \frac{\varepsilon' L}{2A'_\infty} \tag{4''}$$

where A'_∞ and A' are the absorbances of *trans*-azopyrene at the final stage and at the reaction time t, respectively, and ε' is the molar extinction coefficient of *trans*-azopyrene. These quantities were measured at 470 nm, and ε' at this wavelength was determined to be 1.1×10^4 from the spectrum of the authentic sample shown in Fig. 4(a).

For the oxygen-containing benzene solution, equations similar to Eqs. (4), (4'), and (4'') hold approximately at the initial stage of the reaction. At the stage of the reaction latter than $t\sim400$ μsec, the process shown by Eq. (3) becomes predominant. Since the concentration of oxygen in the solution is $\sim10^{-2}$ mol/l,[22] much larger than that of Py–N ($\sim10^{-5}$ mol/l), the following equations can be derived from Eq. (3):

$$\log x' = \log a' - k_3' t' \tag{5}$$

$$k_3' t' = \log A_0'' - \log A'' \tag{5'}$$

where t' is the reaction time, the origin of which is shifted by ~600 μsec from that of t, a', and x' are the concentrations of Py–N at $t'=0$ and at the reaction time t', respectively, and the corresponding absorbances are shown by A_0'' and A'', respectively. Furthermore, $k_3'=k_3[O_2]$, the concentration of oxygen dissolved in the solution at room temperature being represented by $[O_2]$.

For the purpose of confirming the above mechanism, the kinetic measurements were made for the reaction intermediate, Py–N, and also for the reaction products.

In the case of the photo-decomposition in an oxygen-free benzene solution, the time-dependences of the spectral intensities of Py–N at 415 nm and of Py–N=N–Py at 470 nm were measured by the photometric method until 1 msec after the flash irradiation. The result is shown in Fig. 6.

The plots of $(1/A)$ against t give a straight line, as is shown in Fig. 6(a). This means that Eq. (4') holds well for the oxygen-free benzene solution. From the

22) The Chemical Society of Japan, "Kagaku Benran, Kisohen II," Maruzen, Tokyo (1966) p. 627.

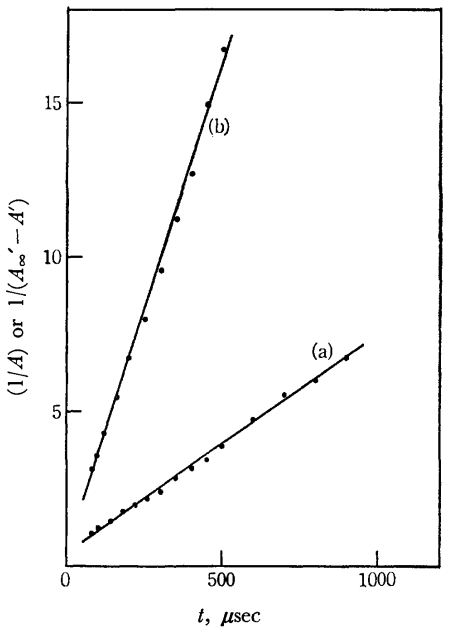

Fig. 6. The time-dependences of the absorption intensities of Py-N and Py-N=N-Py observed for the flash-irradiated Py-N_3 in the oxygen-free benzene solution at 23°C.
(a): $(1/A)$-t plots
(b): $1/(A'_\infty - A')$-t plots

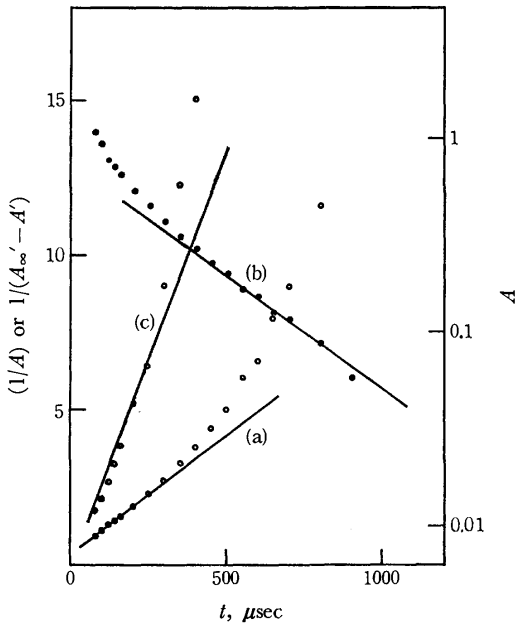

Fig. 7. The time-dependencies of the absorption intensities of Py-N and Py-N=N-Py observed for the flash-irradiated Py-N_3 in the oxygen-containing benzene solution at 23°C.
(a): $(1/A)$-t plots
(b): $\log A$-t plots
(c): $1/(A'_\infty - A')$-t plots

slope of the line, k_2 is determined to be $(2.1\pm0.2)\times 10^9 l\cdot\text{mol}^{-1}\text{sec}^{-1}$ at 23°C. The plots of $1/(A_\infty'-A')$ against t shown in Fig. 6(b) also give a straight line satisfying Eq. (4″), and the rate constant, k_2' is determined from its slope to be $(1.9\pm0.2)\times 10^9 l$ mol^{-1} sec^{-1} at 23°C. This value obtained from the formation velocity of Py–N=N–Py coincides, within the limits of experimental error, with the rate constant obtained from the decay velocity of Py–N. The above-mentioned facts lead to the conclusion that the mechanism given by Eqs. (1) and (2) is satisfied for the photo-decomposition of Py–N_3 in an oxygen-free benzene solution.

Let us turn to the oxygen-containing benzene solution. A decrease in the absorbance, A, with the time was observed at 415 nm for Py–N in this solution; the result is shown in Fig. 7. Curves (a) and (b) in this figure show the $(1/A)$ *vs.* t and $(\log A)$ *vs.* t plots, respectively. These curves indicate that the decrease in A with time is of the second order at the earlier stage of the reaction and of the first order at the stage later than 600 μsec after the flash illumination. The former satisfies Eq. (4) with $k_2'=(2.1\pm0.2)\times 10^9$ l $\text{mol}^{-1}\text{sec}^{-1}$ and the latter Eq. (5) with $k_3'=(1.4\pm 0.2)\times 10^3\ \text{sec}^{-1}$.[23] According to Eq. (2′), the reaction product, *trans*-azopyrene, is formed parallel with the decay of Py–N. This formation process was also followed by measuring A' at 470 nm, and the $1/(A_\infty'-A')$ values were plotted against t; the result is shown by curve (b) in Fig. 7. This curve shows that the formation process follows Eq. (2′) with $k_2=(1.7\pm0.2)\times 10^9\ l\cdot\text{mol}^{-1}\text{sec}^{-1}$. This value agrees, within the limits of experimental error, with the value obtained from the time-dependence of A. The above facts support the reaction mechanism given by Eqs. (1′), (2′), and (3) for the photo-decomposition of Py–N_3 in the oxygen-containing benzene solution.

We should like to express our thanks to Dr. Masashi Imamura and Dr. Akira Kira, The Institute of Physical and Chemical Research, for their kindness in permitting us to use the flash-photolysis apparatus and for many valuable discussions. We are also greatly indebted to Dr. Kazuo Shibata and Dr. Teruo Ogawa, The Institute of Physical and Chemical Research, for their kindness in measuring the absorption spectra of the opaque benzene solutions at the liquid nitrogen temperature.

23) We also tried to obtain the rate constant for the oxygen-containing benzene solution of Py–N_3 according to another analytical method. From Eqs. (2′) and (3), we obtain

$$-\frac{dx}{dt} = k_2'x^2 + k_3'x \qquad \text{(a)}$$

From Eq. (a), the following relations can be derived

$$\frac{k_2'}{k_3'} + \frac{1}{x} = \left(\frac{k_2'}{k_3'} + \frac{1}{a}\right)e^{k_3't} \qquad \text{(b)}$$

or

$$\frac{1}{A} = \frac{1}{\varepsilon L}\left(\frac{k_2'}{k_3'} + \frac{1}{a}\right)e^{k_3't} - \frac{k_2'}{\varepsilon L k_3'} \qquad \text{(b′)}$$

Firstly we evaluated the value of k_3' according to Eq. (5′) and Fig. 7(b). Using this value of k_3', we plotted $1/A$ against $\exp(k_3't)$ and obtained a straight line, the intercept and the slope of which gave k_2'. The value was determined to be $2.15\times 10^9\ l\cdot\text{mol}^{-1}\text{sec}^{-1}$ and $2.08\times 10^9\ l\cdot\text{mol}^{-1}\ \text{sec}^{-1}$, respectively. Both agree with the values obtained from Eqs. (4′) and (4″): But we could not determine precisely a, the initial concentration of Py–N immediately after a flash, from the slope of this straight line. This is because k_2'/k_3' is much greater than $1/a$.

The Exchange Reaction of Deuterium with the Hydroxyl Groups of Zeolite Catalysts

Toshinobu IMANAKA, Yasuaki OKAMOTO, Kazunori TAKAHATA, and Shiichiro TERANISHI

Osaka University, Department of Chemical Engineering, Faculty of Engineering Science, Toyonaka, Osaka

(Received June 28, 1971)

In order to estimate the reactivity of each hydroxyl group, the exchange reaction of deuterium with the hydroxyl groups on the surfaces of the HX, HY, and CaHX zeolites and aerosil was investigated kinetically by an infrared method. The hydroxyl groups appearing at 3660 cm^{-1} on the HX and HY zeolites were more readily exchanged with deuterium than were the other hydroxyl groups on the two zeolites. However, in the case of the CaHX, the order of activities of each hydroxyl group changed with the pressure of deuterium. The rate equation for the reaction is expressed by a Langmuir-type equation. This fact indicates the homogeneity of each hydroxyl group on zeolite. It was found that adsorbed water and carbon dioxide catalyzed the exchange reaction. Furthermore, a compensation effect between the apparent activation energies and the frequency factors occurs in this reaction.

The existence of hydroxyl groups on the surface of zeolite has been shown by infrared spectroscopy.[1-3] The reactivity of a particular hydroxyl group has been estimated from the strength of the interaction with adsorbed olefins,[4,5] bases,[6] and cumene for the HY catalyst.[7] These results show that the hydroxyl group observed at 3650—3640 cm^{-1} is more active than that in the 3550—3540 cm^{-1} region. In this paper, the exchange reaction of deuterium with the hydroxyl groups on the surfaces of zeolites was studied kinetically in order to estimate the reactivity of each hydroxyl group by means of an infrared method. The infrared method has been shown by Carter *et al.*[8] to be useful for investigating the reactivity of a particular hydroxyl group on the surface, as distinct from measuring the overall rate of the exchange of deuterium with a surface hydroxyl group. However, in the kinetic treatment of a reaction, the apparent rate constant, and the adsorption equilibrium constant, and the reactivity of the hydroxyl group must be discussed in terms of the true rate constant.

By the infrared method, Pimentel *et al.*[9] and Eishens and Pliskin[10] have reported the exchange reactions of surface hydroxyl groups on silica gel, and Fry and his co-workers[11] have treated them in some detail. As for alumina, Peri and Hannan[12] have investigated them qualitatively, and Carter *et al.* have studied the reaction kinetically.

The effects of adsorbed water on the reactions catalyzed by zeolites have been reported by many investigators.[13] In the exchange reaction of deuterium with the hydroxyl groups on the zeolite catalyst, similar effects are also found. We found that adsorbed carbon dioxide accelerates its reaction rate. Furthermore, a compensation effect is observed in this reaction; the occurrence of this effect is discussed.

Experimental

Materials. The 13X, 10X, and NaY zeolites were of a commercial grade. The HX, CaHX, and HY zeolites were prepared from their sodium or calcium forms by conventional cation exchange procedures using analytical-grade NH_4Cl. The degree of ion exchange was determined by flame-photometric analysis. In both HX and HY zeolites, 75% of the calcium ions were exchanged. The silica/alumina ratios are 1.4, 1.2, and 2.5 for HX, CaHX, and HY respectively, according to chemical analysis. The aerosil was of a commercial grade. The deuterium used for the exchange reactions had a stated purity of 99.5%.

Procedure. Disks, transparent to infrared radiation, were prepared by pressing the zeolites between polished stainless steel plates to about 10 ton/cm^2. The thickness varied between 7 and 10 mg/cm^2. The platelets were then placed in an IR cell and slid from the salt windows to the center of the IR cell, where they could be heated. The cell can be used in conjunction with a conventional high-vacuum system, and the sample can be treated with gases at any desired temperature. Spectra were taken at room temperature using a Hitachi grating spectrometer. Potassium bromide windows were used on the cell.

The experiments reported in this paper were performed as follows. The disks of HX, HY, CaHX, and aerosil were heated at 300, 400, 350, and 500°C respectively for 14—16 hr under a vacuum of 10^{-5} mmHg in the IR cell. After evacuation, the sample was cooled to room temperature under a vacuum, and the infrared spectrum was recorded. Then, the sample was heated to a reaction temperature and deuterium was introduced. After the desired time had elapsed, sample was cooled to room temperature and the spectrum was again recorded. This procedure was then repeated.

The reaction temperatures were 260—300°C, 280—300°C, 300—330°C, and 400—450°C for HX, HY, CaHX, and

1) J. L. Carter, P. L. Lucchesi, and D. J. C. Yates. *J. Phys. Chem.*, **68**, 1385 (1964).
2) J. B. Uytterhoeven, L. G. Christner, and W. K. Hall *ibid.*, **69**, 2117 (1965).
3) C. L. Angell and P. C. Schaffer *ibid.*, **69**, 3463 (1965).
4) B. V. Liegme and W. K. Hall, *Trans. Faraday Soc.*, **62**, 3229 (1966).
5) P. E. Eberly, Jr., *J. Phys. Chem.*, **71**, 1717 (1967).
6) J. W. Ward *J. Catal.*, **13**, 321 (1961).
7) J. W. Ward *J. Catal.*, **11**, 259 (1968).
8) J. L. Carter, P. L. Lucchesi, P. Corneil, D. J. C. Yates, and J. H. Sinfelt, *J. Phys. Chem.*, **69**, 3070 (1965).
9) G. C. Pimentel, C. W. Garland, and G. Jura, *J. Amer. Chem. Soc.*, **75**, 803 (1953).
10) R. P. Eischens and W. A. Pliskin, *Advan., Catal.*, **10**, 1 (1958).
11) D. L. Fry, P. V. Mohan, and R. W. Lee, *J. Opt. Soc. Amer.*, **50**, 321 (1960)
12) J. B. Peri and R. B. Hannan, *J. Phys. Chem.*, **64**, 1526 (1960).
13) D. W. Basset and H. W. Habgood, *J. Phys. Chem.*, **64**, 769 (1960)

aerosil respectively.

In order to investigate the effect of adsorbed water on the exchange reaction, a small amount of water was added to the system as follows. A trace of adsorbed water was added to the sample by evacuation under a vacuum of 10^{-3} mmHg for 6 hr. Then, the exchange reaction was carried out by adding pure deuterium. In order to add more water to the sample, the reaction was carried out by introducing deuterium containing a small amount of water after the samples had been treated under such conditions.

Mixtures of carbon dioxide and deuterium gas were also placed in contact with the sample in order to study the effects of adsorbed carbon dioxide on the reaction.

Results and Discussion

Typical infrared spectra obtained at room temperature for the sample studied, before and after exposure to deuterium for varying periods of time, are shown in Figs. 1a and 1b. For example, in the original spectrum of the HX zeolite, before exposure to deuterium three different bands due to surface hydroxyl groups were observed. These bands appeared at wave numbers of 3745, 3660, and 3560 cm^{-1}. After exposure to deuterium, additional bands due to OD groups were observed at 2752, 2697, and 2635 cm^{-1}. The wave numbers of the OH groups due to exchange reactions are summarized in Table 1.

Table 1. Wave numbers of OH and OD groups

Sample	Wave number of OH group cm^{-1}	Wave number of additional OD group, cm^{-1}
HX	3745	2752
	3660	2697
	3560	2635
HY	3660	2690
	3548	2622
CaHX	3660	2693
	3595	2659
	3566	2633
aerosil	3755	2760

The reactivity of each hydroxyl group is qualitatively as follows. In the case of the HX zeolite, the OH group occurring at 3660 cm^{-1} is exchanged more readily with deuterium than are the other OH groups under the present experimental conditions. The lowest-frequency OH group (3560 cm^{-1}) has a subsequent activity, while the highest one (3745 cm^{-1}) is most inactive. Although the difference in activities between them is not very great, the OH group observed at 3660 cm^{-1} is 1.5—2 times more active than that at 3745 cm^{-1}. In the case of the HY zeolite, the OH group occurring at 3660 cm^{-1} is a little more active than that at 3548 cm^{-1}. These facts correspond to those estimated from the strength of the interaction with olefins, bases, and aromatics.[12] However, the behavior of the surface hydroxyl groups on the CaHX zeolite is more complecated than in the case with the HX and HY zeolites. When the pressure of deuterium is lower than about 15 cmHg, the OH group observed at 3566 cm^{-1} has the highest activity, that at 3660 cm^{-1} has the next highest one, and that at 3595 cm^{-1} has the lowest one. When the pressure is higher than about 20 cmHg, however, the OH group occurring at 3595 cm^{-1} is more active than those at 3660 and 3566 cm^{-1} which have nearly the same reactivity. The surface OH group on aerosil (3755 cm^{-1}) is much more difficult to exchange than those of the zeolites used. This paper is mainly concerned with the OH groups occurring at 3660 cm^{-1} on HX, HY, and CaHX, and that occurring at 3755 cm^{-1} on aerosil.

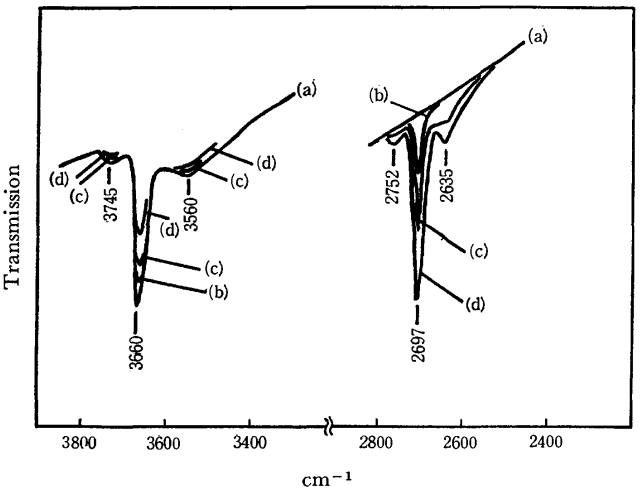

Fig. 1a. Typical infrared spectra of HX as a function of time of treatment with D_2 (13.95 cmHg) at 180°C: (a), 0; (b), 1; (c), 3; (d), 7 hr.

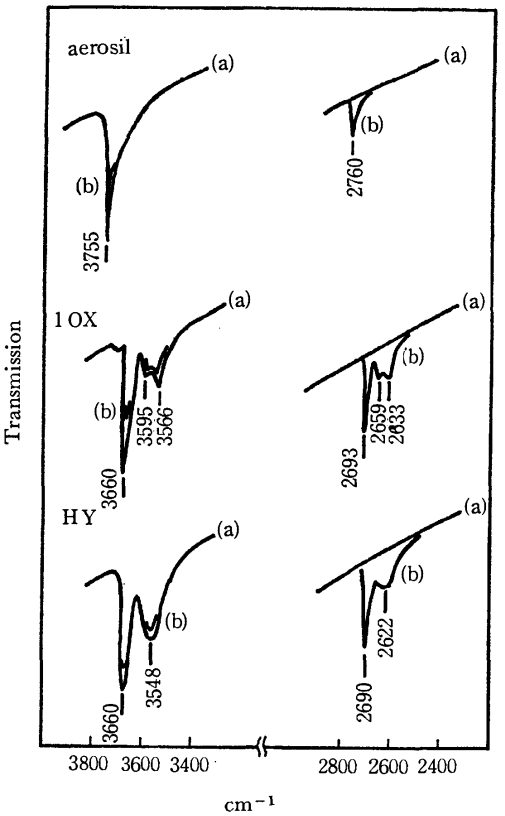

Fig. 1b. Typical infrared spectra of OH and OD groups on HY, CaHX, and aerosil: (a), before exposure to D_2; (b), after exposure to D_2.

If deuterium is adsorbed on the zeolite surface in a Langmuir-type reaction, and the exchange reaction occurs between adsorbed deuterium and hydroxyl groups, the rate equation can be expressed as follows;

$$-\mathrm{d(OH)}/\mathrm{d}t = k\theta\mathrm{(OH)} \quad (1)$$

$$\theta = KP/(1+KP) \quad (2)$$

Therefore,

$$-\mathrm{d(OH)}/\mathrm{d}t = kKP/(1+KP)\mathrm{(OH)} \quad (3)$$

where (OH) is the concentration of surface hydroxyl groups; θ, the coverage of deuterium; k, the rate constant; K, the adsorption equilibrium constant of deuterium; and P, the pressure of deuterium. However, in our experiments, when sliding the samples from the salt windows to the center of the IR cell, the absolute concentration of the hydroxyl group, that is, (OH) in Eq. (3), could not be measured reproducibly. Therefore, Eq. (3) must be transformed into the following equations

$$-\mathrm{d}\ln\mathrm{(OH)}/\mathrm{(OH)_0}/\mathrm{d}t = kKP/(1+KP) \quad (4)$$

$$\mathrm{(OH)_0} = \mathrm{(OH)} + \mathrm{(OD)} \quad (5)$$

where (OD) is the concentration of OD groups and where $(OH)_0$ is the sum of the concentrations of OH and OD groups, that is, the concentration of OH groups before exposure to deuterium. Only $(OH)/(OH)_0$ can be measured in our experiments. Recently it has been reported that the extinction coefficients of OH and OD groups are equal; therefore, the concentrations of OH and OD groups can be represented by their optical densities. Figures 2 and 3 show that the rate equation of the exchange reaction can be expressed by Eq. (4) or (3). That is, each hydroxyl group is considered to be homogeneous. However, for η-alumina, Carter and his co-workers[8] have reported a rate expression which indicates a surface heterogeneity in the alumina. This difference seems to be ascribable to the purity of η-alumina and/or to the crystallinity of zeolite.

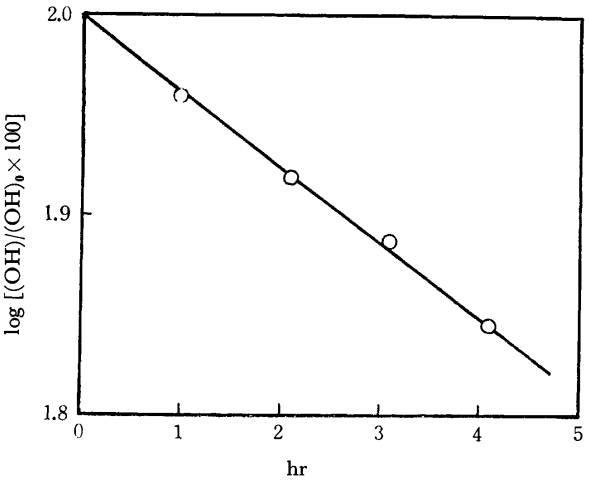

Fig. 2. Exchange of D_2 with the hydroxyl group (HX 3660): reaction pressure; 6.47 cmHg, reaction temperature; 300°C.

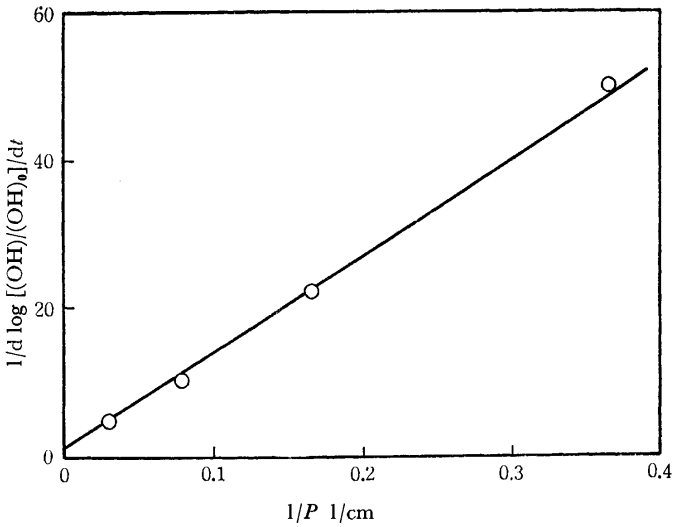

Fig. 3. Langmuir plot of exchange reaction of HX 3660: reaction temperature; 300°C, pressure; cmHg.

From Eq. (4), the rate constant, k, and the adsorption equilibrium constant, K, can be calculated. When the reaction pressure is low, the apparent rate constant, k, can be represented by kK according to Eq. (6):

$$-\mathrm{d(OH)}/\mathrm{d}t = kKP/(1+KP)\mathrm{(OH)}$$
$$= kKP\mathrm{(OH)} \quad (\text{when } KP \ll 1)$$
$$\equiv k'P\mathrm{(OH)} \quad (6)$$

Here, the values of the apparent activation energy, E_a, the frequency factor, A, the activation entropy, ΔS_a, the heat of adsorption, ΔH_a, and the entropy of adsorption, ΔS_a, are calculated from the temperature dependencies of k, k', and K. These values are summarized in Table 2.

The apparent activation energies for the exchange reaction of deuterium with hydroxyl groups have been reported by many investigators. The only value of E_a for a particular OH group, that is, the OH group occurring at 3785 cm^{-1} on η-alumina,[7] is 7—12 kcal/mol. Hall and his co-workers[14,15] have evaluated E_a by measuring the overall rate of exchange for

TABLE 2. KINETICAL CONSTANTS OF EXCHANGE REACTION

OH group	E_a (kcal/mol)	ln A	ΔH_a (kcal/mol)	ΔS_a (e.u.)	$\Delta H^{\neq}$ (kcal/mol)	$\Delta S^{\neq}$ (e.u.)
HK 3660	7.7	2.5	−10	−28	18	−32
HY 3660	41	32	−4.9	−16	46	−5
CaHX 3660	18	9.0	−0.1	−8.2	18	−49
Aerosil 3775	5.3	−2.2	0	−6.7	5.3	−69

14) W. K. Hall, H. P. Leftin, F. J. Cheselshe, and D. E. O'Reilly *J. Catal.*, **2**, 506 (1963).

15) W. K. Hall and F. E. Lutinski, *ibid.*, **2**, 518 (1963).

silica gels (22—23 kcal/mol), γ-alumina (6 kcal/mol) and silica-alumina (8—10 kcal/mol). For the HY zeolite, the value of E_a has been shown to be 20—30 kcal/mol by Imai.[16] The E_a values in Table 2 can not be compared directly with their values, but they seem to be appropriate.

The adsorption heats of the deuterium of the HX and HY zeolites are very large in comparison with those on Na-13(2.06 kcal/mol) and Ca-13(2.49 kcal/mol).[17] They may be explained in terms of the interaction between the electrostatic field of the sodium ion and deuterium. Furthermore, the values of ΔH_a are calculated from the temperature dependence of K in Eq. (4); therefore, they are the values for active deuterium only. Since the values of Na-13Y and Ca-13Y, have, however, been obtained by measuring adsorption isotherms, they are average values of active and non-active deuterium. In the case of the CaHX zeolite, the calcium ions retained in it are considered to exist on the S_1 site only. Therefore, the exchange reaction with the hydroxyl group observed at 3660 cm^{-1} may not be influenced by calcium ions. This is confirmed by the following facts. The OH group occurring at 3660 cm^{-1} on a CaHX zeolite consisting of about 65% of calcium ions is exchanged more readily than that on a CaHX zeolite consisting of 42% calcium ions. Moreover, it has been reported[18] that the activity of the isomerization of *n*-hexane on calcium containing type-Y zeolite catalysts greatly increases when more than 40% of the sodium ions are replaced by calcium ions these facts agree with the effect of calcium ions on the exchange reaction. In the case of aerosil, the heat of adsorption is compatible with that measured on silica.[19]

The adsorption entropies of deuterium on HX and HY are very large. If a deuterium molecule adsorbs on the surface and migrates with two freedoms of translation, the value of the adsorption entropy must be about −9 e.u. Therefore, it is considered that deuterium molecule adsorbed on the HX and HY zeolites migrates in the only defined region, interacting with the cations.

In the case of the CaHX zeolite, however, the adsorption entropy is a degree of free migration. Hence, the deuterium molecule on the CaHX zeolite, which reacts with the surface hydroxyl group of 3660 cm^{-1}, is considered to migrate over a wide region without interacting with the calcium ions in the S_1 sites.

It is found that the small of water adsorbed on the zeolites catalyzes the exchange reaction of deuterium with the surface hydroxyl groups. The rate equation is expressed by Eq. (1) when the amount of adsorbed water is small. The k, k', and K values for the HX zeolite in the presence of adsorbed water are shown in Table 3. In the case of Condition A, the sample was evacuated at 300°C for 6 hr under a vacuum of 10^{-3} mmHg before exposure to pure deuterium. In the case of Condition B, after the sample has been treated under the same conditions as in A, it was placed in contact with the deuterium which contains a small amount of water. The apparent rate constant, k', increases monotonously as the amount of adsorbed water is increased; that is, the exchange rate increases with an increase in the amount of adsorbed water. However, the rate constant, k, has a maximum value. This fact can be explained as follows. The exchange reaction of hydroxyl groups with D_2 is very fast in comparison with that with deuterium. When the amount of adsorbed water is very small, the reaction is accelerated by the exchange reaction between the proton of the water molecule and the deuteron of the deuterium molecule. When the water content is increased, however, water molecules shield the electrostatic field of the cations and, consequently, deactivate the deuterium molecule. The two opposite roles of adsorbed water give the rate constant a maximum value. The increase in K may be explained in terms of the interaction between deuterium and water. The catalytic effect of adsorbed water is more complex than is initially apparent.

Table 3. Effect of adsorbed water on exchange reaction

	No adsorbed water	A	B
k' (1/hr)	1.42×10^{-2}	1.75×10^{-2}	0.113
k (1/hr)	1.50	2.18	0.730
K (1/cmHg)	9.45×10^{-3}	8.03×10^{-3}	0.155

It is found that carbon dioxide also influences the exchange reaction. A typical reaction is shown in

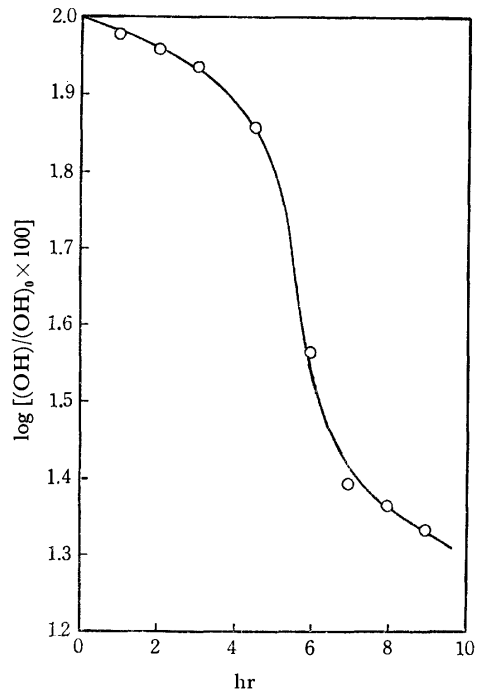

Fig. 4. Effect of carbon dioxide on exchange reaction of HX 3660: reaction temperature; 280°C, pressure of CO_2; 1.34 cmHg, pressure of D_2; 2.08 cmHg.

16) H. Imai, The 21st Annual Meeting of the Chemical Society of Japan (1970).
17) J. E. Bengon and M. Boudart, *J. Catal.*, **8**, 93 (1967).
18) J. A. Rabo, P. E. Pickert, D. N. Stamires, and J. E. Boyle Proc. 2nd Int. Congr. Cat., Paris, 104 (1960)
19) T. King and S. W. Benson, *J. Chem. Phys.*, **44**, 1007 (1966).

Fig. 4. The rate equation cannot be expressed by Eq. (1) or (2) in this case. The reaction rate gradually becomes fast and then slows down with the progress of the exchange reaction. The decrease in the rate is not due to a opposite reaction, because a large excess of deuterium is present during exchange reactions. The effect of carbon dioxide may be interpreted in terms of the interaction between deuterium and carbon dioxide, and in terms of the competitive adsorption of two gases.

A compensation effect is found in this reaction. Figure 5 shows the relation between E_a and $\ln A$. The linear relations between ΔS_a and ΔH_a, and also between $\Delta S^{\ddagger}$ and $\Delta H^{\ddagger}$ hold. Generally, k is considered to be variable in a series of reactions. Therefore, the compensation effect may result from compensatory relations of both k and K. When the apparent rate constant is expressed by kK, a normal compensation effect occurs; when it is expressed by k/K, an anti-compensation effect can occur under specific conditions.

With regard to the detailed mechanism of the exchange, the information presently available is not sufficient to establish it with any certainty. It is conceivable, however, that a proton of the hydroxyl group interacts with an adsorbed deuterium molecule, forms a triatomic intermediate, and removes a HD molecule, with the consequent formation a OD group.

Conclusions

The hydroxyl groups occurring at 3660 cm^{-1} on HX and HY zeolites were more readily exchanged with deuterium than were the other hydroxyl groups on the two zeolites. However, in the case of CaHX, the order of activities of each hydroxy group was changed with the pressure of deuterium; this fact is considered to be ascribable to the effect of calcium ions.

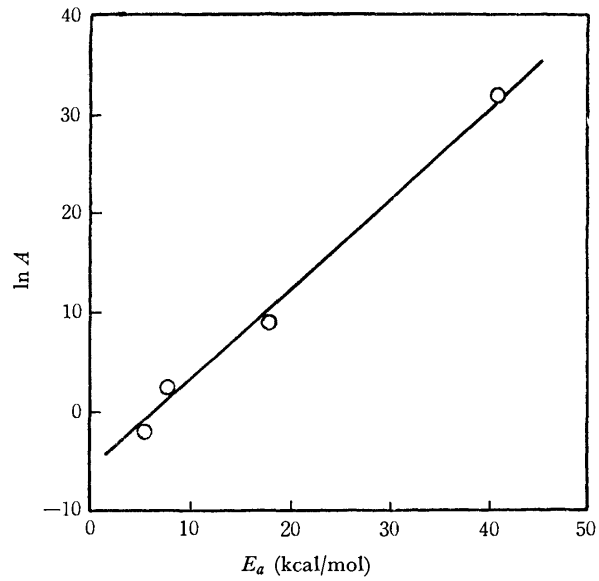

Fig. 5. Compensation effect.

The rate equation for the reaction is expressed by a Langmuir-type equation. This fact indicates the homogeneity of each hydroxyl group on zeolites, contraty to the case with η-alumina. The adsorbed water and carbon dioxide catalyzed the exchange reaction. The adsorbed water accelerates the reaction by the exchange reaction between the proton of the water molecule and the deuteron of the deuterium molecule, but it also shields the electrostatic field, with a consequent deactivation of adsorbed deuterium.

It was found that the compensation effect holds for k, k', and K in this exchange reaction. In general, this effect may result from the existence of the compensatory relation between the entropy and the enthalpy.

Abnormal Hyperfine Splitting in the ESR Spectra of $\alpha,\alpha,\gamma,\gamma$-Tetraphenylallyl-type Organic Stable Free Radicals[1)]

Kohji WATANABE, Jun YAMAUCHI, Hiroaki OHYA-NISHIGUCHI*, Yasuo DEGUCHI**, and Hideo TAKAKI*

Laboratory of Solid State Chemistry, Institute for Chemical Research, Kyoto University, Uji, Kyoto
**Faculty of Science, Kyoto University, Kyoto*
***College of Liberal Arts & Science, Kyoto University, Kyoto*

(Received July 3, 1971)

The ESR spectra of $\alpha,\alpha,\gamma,\gamma$-tetraphenylallyl radical have been first observed. An abnormal ESR hyperfine splitting of this radical has been compared with the ESR hyperfine splitting of other tetraphenylallyl-type radicals; it can be explained very well by introducing the idea of a twisted-allyl model of the molecule.

The history of an organic stable free radical, $\alpha,\alpha,\gamma,\gamma$-tetraphenylallyl(TPA), dates from 1923, when Ziegler published the synthetic method.[2)] Observed in the course of the investigation of the magnetic properties of organic stable free radicals, the electron spin resonance(ESR) spectrum of TPA reveals an unusually large hyperfine splitting of the proton adjacent to the β-position of the allyl group, compared with the results of the familiar theoretical calculation of the spin-density distribution.[3)]

The spectrum of $\alpha,\alpha,\gamma,\gamma$-bisdiphenyleneallyl(BDA) also exhibits an exceptionally large hyperfine splitting of the corresponding proton. ESR studies of the hyperfine structures of $\alpha,\alpha,\gamma,\gamma$-bisdiphenylene-$\beta$-phenylallyl(BDPA),[4,5)] BDA,[4,6)] $\alpha,\alpha,\gamma,\gamma$-bisdiphenylene-$\beta$-methylallyl(BDMA),[3)] and $\alpha,\alpha,\gamma,\gamma$-bisdiphenylene-$\beta$-azoallyl(BDAA)[7)] have already been reported by several authors, but not that of TPA; moreover, no systematic explanation of the relation between the hyperfine coupling constant of the β-position and the framework of the allyl group of these radicals has ever been given.

In the present paper, the ESR spectra of BDA and BDAA were remeasured carefully, and that of TPA was measured for the first time in diluted solutions. A possible explanation was also presented, one based on the model that $2p_z\pi$-*orbitals* of the three carbons in the allyl group of the radicals will twist one another by a certain angle with respect to the two C-C bonds. The validity of this model was examined by comparing the proton hyperfine coupling constant of TPA with those of other tetraphenylallyl-type radicals (Fig. 1).

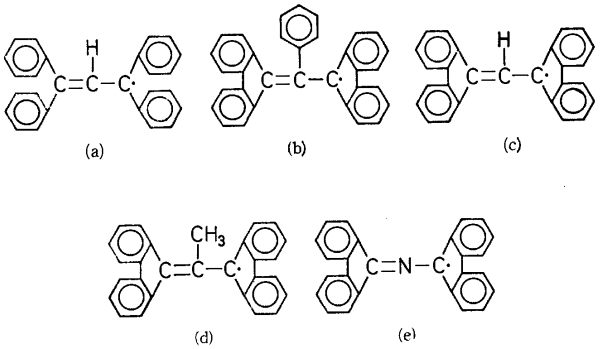

Fig. 1. Tetraphenyl-allyl type radicals.
(a) TPA (b) BDPA (c) BDA (d) BDMA (e) BDAA

Experimental

The samples were prepared following the process described in Refs. 2, 7, and 8. For the observation of the ESR spectra the solvents were well purified, dehydrated, and degassed by the usual methods.[9)] An aqueous solution of peroxylamine disulfonate was used as the standard, and the value of 13.00 gauss was taken for the nitrogen coupling constants.[10)] The hyperfine coupling constants were usually determined by taking the average values of two or three spectra. All the ESR spectra were obtained with a JES-ME3X-type spectrometer of the JEOL Co., equipped with a 100-kHz field modulation. The experimentally-obtained hyperfine coupling constants were then compared with the spectra reconstructed using the ESR spectrum simulator.

Results

Tetraphenylallyl. One of the observed spectra of TPA is shown in Fig. 2.

The spectrum consisted of two groups, which split further into about thirty hyperfine lines. The analysis of the hyperfine structure of the observed spectra revealed that one proton adjacent to the β-position of the allyl group (A_β^H), the eight-phenyl protons at the *ortho*-positions (A_o^H), the eight-phenyl protons at the *meta*-positions (A_m^H), and the four-phenyl protons at the *para*-positions (A_p^H) are attributable to the hyperfine structures. As a result of the reconstruction of the observed spectra by means of the ESR spectrum simulator, the proton hyperfine coupling constants for each solvent were determined to be as is shown in Table 1.

1) Parts of this work were presented at the 8th ESR Symposium of the Chemical Society of Japan, Hiroshima, November, 1969, and at the 9th ESR Symposium, Tokyo, October, 1970.
2) K. Ziegler, *Ann.*, **434**, 34 (1932).
3) H. M. McConnell and D. B. Chesnut, *J. Chem. Phys.*, **28**, 107 (1958).
4) R. Kuhn and F. A. Neugebauer, *Monatsh.*, **95**, 3 (1964).
5) K. H. Hausser, *Z. Naturforsch.*, **14a**, 425 (1959).
6) K. H. Hausser, *ibid.*, **17a**, 158 (1962).
7) R. Kuhn and F. A. Neugebauer, *Monatsh.*, **94**, 16 (1963).
8) R. Kuhn, H. Fischer, F. A. Neugebauer, and H. Fischer, *Ann.*, **654**, 64 (1962).
9) Y. Deguchi, This Bulletin, **35**, 910 (1962).
10) G. E. Pake, J. Townsend, and S. I. Weissman, *Phys. Rev.*, **85**, 683 (1952).

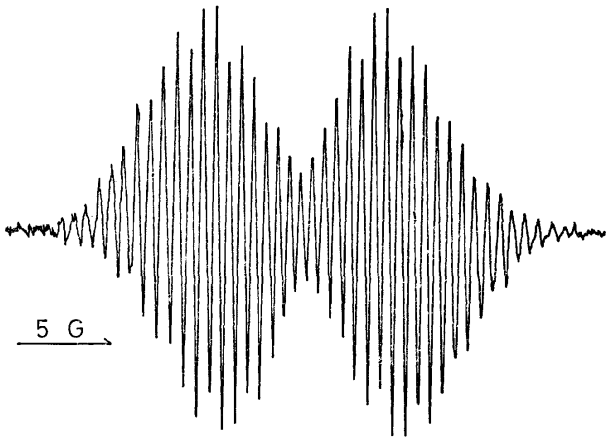

Simulated spectrum

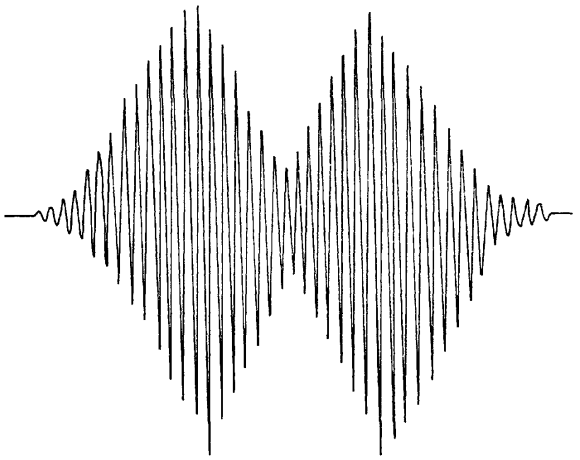

Observed spectrum

Fig. 2. ESR spectrum of TPA in THF and its simulated spectrum.

TABLE 1. HYPERFINE COUPLING CONSTANTS FOR TPA AT 20°C (IN GAUSS)

Solvent	A_β^H	A_o^H	A_m^H	A_p^H
CCl_4	8.65	1.30	0.65	1.95
CS_2	8.50	1.45	0.60	1.80
n-Hexane	8.80	1.25	0.70	2.10
D.E.A.[a]	8.90	1.25	0.75	2.25
T.H.F.[b]	8.95	1.20	0.70	2.10
Ethanol	8.75	1.35	0.65	1.95

a) Diethylamine b) Tetrahydrofuran

The temperature dependence of the coupling constant (A_β^H) in the THF solution is shown in Fig. 3 as a function of the temperature. In these ESR spectra, it can be noticed that the A_β^H changes rather markedly than the others, A_o^H, A_m^H, and A_p^H.

Bisdiphenyleneallyl. The ESR hyperfine structure of BDA in diluted CS_2 solution was observed by Kuhn and Neugebauer[4] and Hausser.[6] The spectrum of BDA in a diluted CS_2 solution measured at 20°C is shown in Fig. 4.

In Table 2, the hyperfine coupling constants of the protons of BDA are also tabulated.

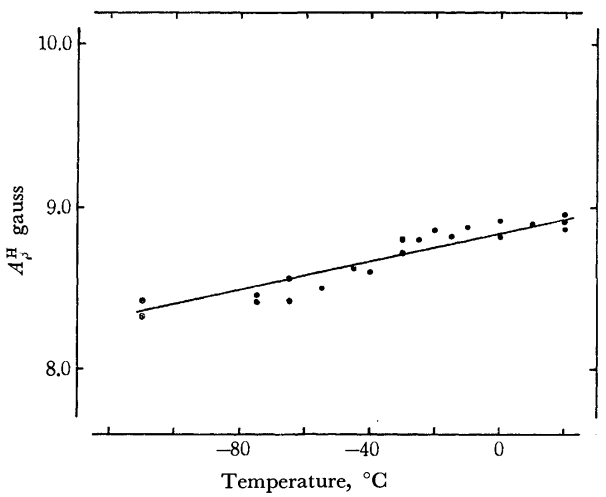

Fig. 3. Temperature dependence of the coupling constant A_β^H of TPA in THF.

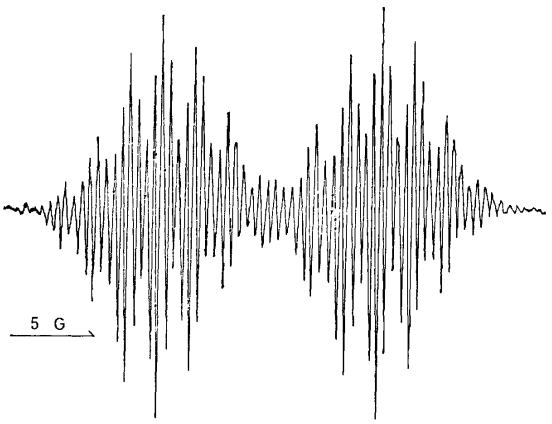

Fig. 4. ESR spectrum of BDA in CS_2.

TABLE 2. HYPERFINE COUPLING CONSTANTS OF BDA IN CS_2 SOLUTION AT ROOM TEMPERATURE (IN GAUSS)

A_β^H	A_1^H	A_2^H	A_3^H	A_4^H	
13.4	1.99	1.99	0.46	—	
13.2	1.92	1.86	0.48	0.36	(Ref. 4)
13.2	1.89	1.89	0.42	0.06	(Ref. 6)

Bisdiphenyleneazoallyl. Although the ESR hyperfine structure of BDAA in a diluted benzene solution has already been observed by Kuhn and Neugebauer[7] they did not analyze the spectrum in detail. In this investigation, the ESR spectra were investigated in several organic solvents at 20°C (Fig. 5) and analyzed in detail.

Reconstructing the observed spectra by the ESR spectrum simulator, the hyperfine coupling constants for nitrogen, and each ring proton were determined, as is shown in Table 3.

From the observed ESR spectra of these tetraphenylallyl-type radicals, it can be concluded that the four phenyl groups or two biphenylene groups are equivalent.

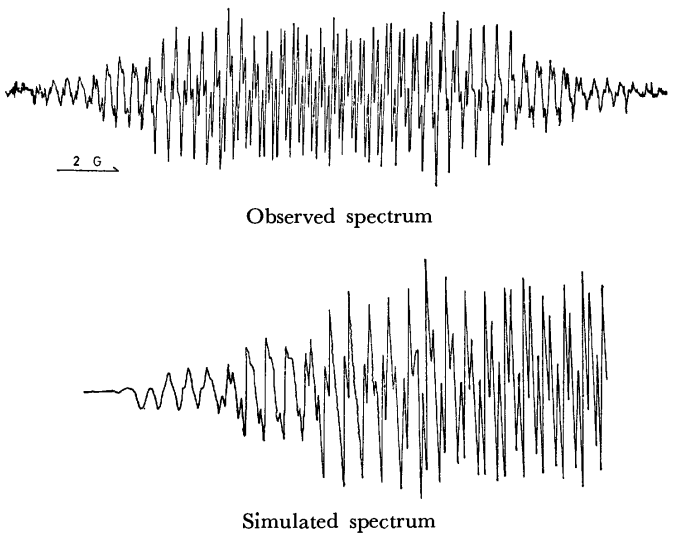

Fig. 5. ESR spectrum of BDAA in benzene and its simulated spectrum.

TABLE 3. HYPERFINE COUPLING CONSTANTS FOR BDAA AT 20°C (IN GAUSS)

Solvent	A_β^H	A_1^H	A_2^H	A_3^H	A_4^H
Benzene	3.38	1.69	1.61	0.44	0.40
T.H.F.[a]	3.26	1.73	1.66	0.45	0.42
D.M.E.[b]	3.39	1.82	1.75	0.44	0.40

a) Tetrahydrofuran b) Dimethoxyethane

Discussion

The theoretical spin densities on each carbon position were enumerated by means of McLachlan's Molecular Orbital method,[11] and also by means of the odd alternant method[12] in the case of TPA. The coupling constants calculated by means of McConnell's relation are also shown in Table 4.

Table 4 indicates that the observed hyperfine coupling constants of the ring protons are in fair agreement with the calculated hyperfine coupling constants. This coincidence indicates the validity of McLachlan's calculation. It should be noted, however, that in TPA and BDA the theoretical hyperfine coupling constants of β-protons are too small to account for the experimentally-determined hyperfine coupling constants; this is in contrast to the close agreement between the observed and the calculated values about the ring protons.

In the ESR spectra of the allyl radical, Fessenden and Schuler[13] have observed three different hyperfine coupling constants due to protons, $A_\beta^H=4.06$ gauss, $A_{\alpha,\gamma}^H=13.93$ gauss, and $A_{\alpha,\gamma}^H=14.83$ gauss. One of them (A_β^H) is a hyperfine coupling constant of the proton adjacent to C_β; it is in satisfactory agreement with the predicted value,[14] on condition that the allyl radical has *sp*² *hybrid orbitals* where the configuration angle of C_α-C_β-C_γ is 120° and that the $2p_z\pi$-*orbitals* of each carbon situated in a C_α-C_β-C_γ plane are parallel. The substitution of phenyl groups for four hydrogen atoms attached to the end carbons, C_α and C_γ, which is the case with TPA, may affect the $2p_z\pi$-*orbital* configuration of the allyl group. The most probable situation is that the allyl group is twisted at an angle of φ, as in Fig. 6, because of the steric effect of the phenyl groups. Assuming this twisted model about the allyl group, the $2p_z\pi$-*orbitals* of C_α and C_γ will result in a nonzero spin density at the proton adjacent to C_β, as is shown in Fig. 7.

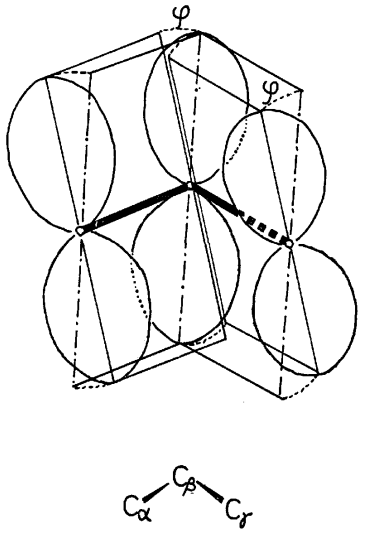

Fig. 6. Twisted allyl model.
$2p_z$ *orbitals* of C_α and C_γ are twisted along the C_α-C_β and C_β-C_γ bonds.

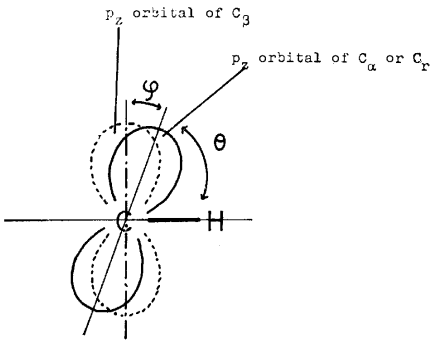

Fig. 7. Relation of the proton adjacent to C_β with $2p_z\pi$-*orbital* of C_α or C_γ.

An interaction between the spin densities of C_α or C_γ and the proton adjacent to C_β can be described by the following relation[15]:

$$A'^H_\beta = (4+50\cos^2\theta)(\rho_{C\alpha}+\rho_{C\gamma}).$$

If the allyl group of TPA or BDA is twisted as in Fig. 6, the experimentally-obtained coupling constant of the proton adjacent to C_β can be estimated by

11) A. D. McLachlan, *Mol. Phys.*, **3**, 233 (1960).
12) R. Lefebore, H. H. Dearman, and H. M. McConnell, *J. Chem. Phys.*, **32** 176 (1960).
13) R. W. Fessenden and R. H. Schuler, *ibid.*, **39**, 2147 (1963).
14) H. M. McConnell, *ibid.*, **30**, 328 (1960).
15) C. Heller and H. M. McConnell, *ibid.*, **32**, 1535 (1960).

Table 4. Observed and calculated coupling constants

Compound		β	γ	1	2	3	4	5	6	7	8
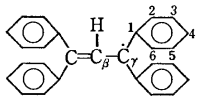	Observed	8.90			1.30	0.65	1.95	0.65	1.30		
	Odd. Alter.	0.74 −0.032	— +0.222	— −0.028	1.77 +0.077	0.64 −0.028	1.77 +0.077	0.64 −0.028	1.77 +0.077		
	McLachlan[a]	1.45 −0.063	— +0.251	— −0.023	1.38 +0.060	0.53 −0.023	1.38 +0.060	0.53 −0.023	1.38 +0.060		
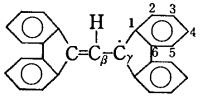	Observed	13.4			1.99	0.46	1.99	—			
	Ref. 4	13.2			1.92	0.48	1.86	0.36			
	Ref. 6	13.2			1.89	0.42	1.89	0.06			
	McLachlan[b]	2.16 −0.094	— +0.256	— −0.023	1.75 +0.076	0.35 −0.015	1.50 +0.065	0.14 −0.006	— +0.050		
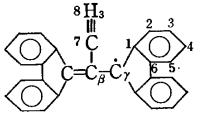	Ref. 4	1.12[c]			1.76	0.44	1.64	0.33			
	McLachlan[b]	2.18[d] −0.087	— +0.260	— −0.025	1.77 +0.077	0.23 −0.010	1.50 +0.065	0.12 −0.005	+0.050	+0.001	−0.007
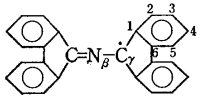	Observed	3.38			1.69	0.30	1.69	0.14			
	McLachlan[b]	4.20[e] −0.103	— +0.254	— −0.025	1.75 +0.076	0.35 −0.015	1.50 +0.065	0.12 −0.005	+0.049		

Calculated coupling constants are obtained using the formula

$A^{H}_{CH}=Q^{H}_{CH}\cdot\rho_{C_1}$ $\qquad Q^{H}_{CH}=-23.0$

a) Each phenyl group is rotated by 10° as that of triphenyl methyl and allyl group is also twisted by 28°.
b) Allyl group is twisted by 37°.
c) Methyl protons.
d) $A^{H}_{C-CH_3}=Q^{H}_{C-CH}\cdot\rho_{C-CH_3}$ $\qquad Q^{H}_{C-CH_3}=+25.0$
e) $A^{N}=Q_1\cdot\rho_N+Q_2\cdot\sum\rho_{C_1}$ ρ_{C_1}s are the spin densities of nuclei attached to the nitrogen. $Q_1=+30.9$, $Q_2=-2.$[19]

the following equation:

$$A^{H}_{\beta} = \frac{Q^{H}_{CH}\cdot\rho_{C\beta} + A'^{H}_{\beta}}{Q^{H}_{CH}\cdot\rho_{C\beta} + (4+50\cos^2\theta)(\rho_{C\alpha}+\rho_{\gamma})}.$$

In the case of TPA, using $\rho_{C\alpha}=\rho_{C\gamma}=+0.251$, $\rho_{C\beta}=-0.063$, $Q^{CH}_{H}=-23.0$ gauss, and $\theta=62°$, A^{H}_{β} becomes 9.05 gauss. In other words, if the twisted angle is assumed to be 28°, A^{H}_{β} will become about 8.90 gauss, which is the most suitable value in this case. Similarly, the twisted angle is estimated to be 37° in the case of BDA. The twisted allyl model mentioned above can easily be applied to the other tetraphenylallyl-type radicals.

For the BDMA, the experimentally-measured hyperfine coupling constants of $A^{H}_{CH_3}$ are close to the theoretically calculated values, as is shown in Table 4. This fact can also be explained by this model, as is shown in Fig. 8, assuming $\rho_{C\alpha}=\rho_{C\gamma}=+0.260$, $\rho_{C\beta}=-0.087$, $Q^{H}_{C\text{-}CH_3}=+25.0$ gauss, and $Q^{H}_{C\text{-}C(CH_3)}=0.85$ gauss;[16] thence, $A^{H}_{CH_3}$ becomes 2.62 gauss or 1.74 gauss.[17] Hence, the protons of the methyl group adjacent to C_β are considerably far apart from C_α or C_γ compared with the proton attached directly to C_β. Consequently, the contribution of $\rho_{C\alpha}$ or $\rho_{C\gamma}$ to the spin density on the methyl proton is negligibly small. On the other hand, the nitrogen nucleus of BDAA is placed at a nodal plane of the $2p_z\pi$-*orbital* of C_α or C_γ. Therefore, the hyperfine coupling constants of nitrogen (A^{N}_{β}) will not be affected directly by the spin density on C_α or C_γ.

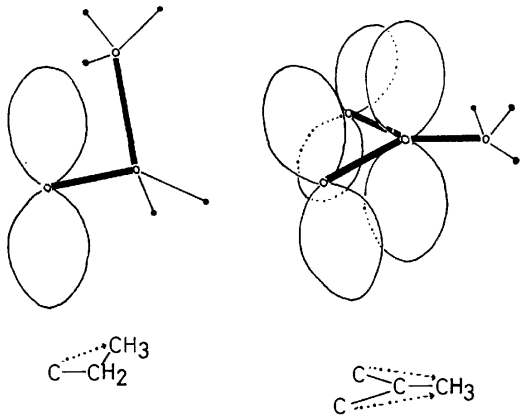

Fig. 8. Twisted allyl model for BDMA.

In addition, the temperature dependence of the coupling constant (A^{H}_{β}) of TPA can also be explained as follows: at high temperatures a vigorous wagging of the allyl group of the TPA molecule will cause the $2p_z\pi$-*orbitals* of C_α and C_γ to come nearer to the proton adjacent to C_β; thence, A^{H}_{β} will become larger, while, at low temperatures, the situation will be reversed.

In order to interpret magnitude of the C_β-proton splitting, a torsion of the phenyl rings from the molecular plane was taken into account at first. However, the spin density of C_β was, at most, the same as that of the allyl radical (the hyperfine coupling constant of the proton adjacent to C_β is only 4.06 gauss[13]). The observation of unusually large splitting of the C_β-proton in TPA or BDA can not be interpreted by means of this mechanism. The other possible explanation is that the configuration angle of C_α–C_β–C_γ is larger than a normal configuration angle of 120° because of the repulsive interaction of phenyl or biphenylene groups. Fraenkel calculated the variation in Q^{H}_{CH} with the bond angle, taking into account the σ-π interaction of the C–H bond.[18] In view of his calculations, the configuration angle of C_α–C_β–C_γ in tetraphenylallyl-type radicals must be smaller than 120°, but this is not plausible in view of the structures of tetraphenylallyl-type radicals.

Conclusion

The abnormal hyperfine coupling constants that have been observed in TPA and BDA could be explained very well, using the method of anisotropic hyperfine interaction. Therefore, in view of the ESR spectra series of these tetraphenylallyl-type radicals, those spectra can be understood by introducing the idea of the twisted allyl model.

The authors wish to thank Professor Kazuhiko Ishizu for his helpful discussion and Mr. Hideo Hasegawa and Mr. Koichi Kubo for the treatment using the ESR spectrum simulator.

16) K. Mukai, H. Nishiguchi, K. Ishizu, Y. Deguchi, and H. Takaki, *This Bulletin*, **40**, 2731 (1967).

17) $A^{H}_{C\text{-}CH_3}=Q^{H}_{C\text{-}CH_3}\cdot\rho_{C\beta}+Q^{H}_{C\text{-}C(CH_3)_3}(\rho_{C\alpha}+\rho_{C\gamma})$ The sign of $Q^{H}_{C\text{-}C(CH_3)_3}$ has not been defined. If the signs of $Q^{H}_{C\text{-}CH_3}$ and $Q^{H}_{C\text{-}C(CH_3)_3}$ are identical, $A^{H}_{C\text{-}CH_3}$ will be 2.62 gauss; if the signs are the opposite, $A^{H}_{C\text{-}CH_3}$ will be 1.74 gauss.

18) K. Fraenkel, *J. Chem. Phys.*, **37**, 1489 (1962).

19) E. W. Stone and A. H. Maki, *J. Chem. Phys.*, **39**, 1635 (1963).

Some Physico-chemical Properties of Vanadium Oxide Supported on Silica or γ-Alumina[1)]

Satohiro YOSHIDA, Toshikatsu IGUCHI, Shingo ISHIDA,* and Kimio TARAMA

Department of Hydrocarbon Chemistry, Faculty of Engineering, Kyoto University, Sakyo-ku, Kyoto

(Received July 6, 1971)

The interactions between vanadium(V) oxide and carriers were investigated in the vanadium oxide catalysts supported on silica and γ-alumina by measuring X-ray diffraction patterns, ESR spectra, solubilities into 0.3 N ammoniacal solutions and reduction rates by benzene. A part of vanadium oxide on the carriers was insoluble in an ammoniacal solution, while unsupported vanadium oxide was easily soluble, and the reduction rates of the catalysts were remarkably affected by the carriers and the vanadium oxide contents. ESR spectra revealed that the vanadium oxide was stabilized by interaction with carriers as a square pyramidal one (VO_5) and a tetrahedral one (VO_4) on the surfaces of γ-alumina and silica, respectively. Massive vanadium(V) oxide crystals grew on these interacted layers with the increase of the oxide contents.

Vanadium oxide has been extensively used as a main catalyst in gas phase oxidation of hydrocarbons and extensive studies have been carried out on its catalytic action.

We also studied the vanadium oxide catalysts especially from the view point of structural chemistry.[2)] Our works mainly dealt with unsupported vanadium catalysts. In the cases of practical catalysts, however, vanadium oxides are generally supported on carriers such as silica and alumina with high surface area. It is known that these carriers have a profound effect on the activities of catalysts.

It is important to elucidate the action of the main component of the supported catalysts. Nevertheless, very few fundamental research works on this problem have been carried out for vanadium oxide catalysts.[2b,3)]

In the present work, some physico-chemical properties of vanadium oxide supported on silica or γ-alumina have been investigated by measuring X-ray diffraction patterns, ESR spectra, solubilities into ammoniacal solutions and reduction rates by benzene vapor in order to clarify the state of vanadium ions in the supported catalysts.

Experimental

Materials. *Silica*: Ethyl silicate purified by distillation three times was hydrolyzed in a water-ethanol mixture at the boiling point. The gel obtained was washed, dried and calcinated at 500°C for 5 hr in dried air stream and was ground to powder of less than 100 mesh.

Alumina: γ-Alumina was obtained by hydrolysis of aluminum isopropoxide, followed by calcination at 650°C for 3 hr, and ground to powder of less than 100 mesh.

Catalysts: Vanadium oxide catalysts supported on silica or γ-alumina were prepared by impregnation of the carrier into an ammoniacal solution of ammonium methavanadate, followed by drying at 110°C and calcination at 500°C for 5 hr in dried air stream. The amount of supported vanadium oxide was analyzed by the usual oxidation-reduction titration method after dissolution of the catalyst into sulfuric acid. Catalysts thus obtained are summarized in Table 1, the vanadium oxide contents being calculated by assuming that vanadium oxide existed as vanadium pentoxide.

TABLE 1. SAMPLES

Samples	V_2O_5 Content (wt%)	Color dry	Color wet	Surface area (m^2/g)
SiO_2	0.0	white	white	633
γ-Al_2O_3	0.0			282
V_2O_5	100.0	orange	orange	5.2
Samples supported on SiO_2				
1 S	1.0	white	l. yel. brown	579
2 S	2.0			564
5 S	4.9	cream	yel. brown	530
10 S	9.9	l. yel. brown	d. yel. brown	491
20 S	19.8			339
30 S	29.3			303
50 S	48.4			203
Samples supported on γ-Al_2O_3				
1 A	1.0	white	white	267
2 A	2.0			251
5 A	4.9	cream	cr. gr. yellow	242
10 A	10.0	l. gr. yellow	l. yel. brown	230
15 A	14.9			206
20 A	19.7			192
30 A	29.5	gr. yel. brown	yel. brown	176
50 A	49.2	yel. brown		126

l; light, d; dark, yel; yellowish, cr; creamy, gr; greenish

Procedures. *X-Ray Diffraction*: A Shimadzu X-ray diffractometer GX-3 with copper target was used. The tube voltage and current were 35 kV and 15 mA, respectively. *ESR*: ESR spectra of catalysts evacuated at 400°C for 2 hr and sealed in glass tubes were recorded with a JEOL JES-3BSX spectrometer at room temperature.

* Present address: Department of Industrial Chemistry Chubu Institute of Technology, Kasugai.

1) S. Yoshida, T. Iguchi, S. Ishida, and K. Tarama, Presented at the 24th Annual Meeting of the Chemical Society of Japan, Osaka, April, 1971.

2a) K. Tarama, S. Teranishi, S. Yoshida, and N. Tamura, "Proceedings 3rd Int. Congress on Catalysis," North-Holland Pub. Co. Amsterdam (1965), p. 282; K. Tarama, S. Teranishi, S. Yoshida, N. Tamura, and S. Ishida, *Kogyo Kagaku Zasshi*, **68**, 1499 (1965); K. Tarama, S. Yoshida, S. Ishida, and H. Kakioka, This Bulletin, **41**, 2840 (1968); K. Tarama, S. Teranishi, and S. Yoshida, *Bull. Inst. Chem. Research, Kyoto Univ.*, **46**, 185 (1968); S. Yoshida, N. Tamura, S. Teranishi, and K. Tarama, *ibid.*, **47**, 246 (1969). b) K. Tarama, S. Teranishi, K. Hattori, and T. Nichibori, *Kogyo Kagaku Zasshi*, **57**, 490 (1954).

3) L. van Reijen and P. Cossee, *Discussion Faraday Soc.*, **41**, 277 (1966); H. Takahashi, M. Shiotani, H. Kobayashi, and J. Sohma, *J. Catalysis*, **14**, 134 (1969).

Dissolution into an Ammoniacal Solution: The catalyst containing *ca.* 1 g of vanadium oxide was impregnated into 300 m*l* of 0.3 N ammoniacal solution for 24 hr at room temperature. Under this treatment the isolated massive vanadium oxide was easily soluble. Thus, the residue vanadium oxide was regarded to be chemically interacting with the carrier.

Reduction by Benzene Vapour: Reduction rates of vanadium oxide on carriers were determined by measuring the weight loss of the catalysts in a flow of benzene-nitrogen gas by a Shimadzu MTB 50 micro-thermanobalance. Nitrogen gas was saturated with benzene at 2, 5, and 10°C with a flow rate of 30 cc/min and reduction temperatures were in the range 380—450°C.

Results

X-Ray Diffraction. Diagrams of the X-ray diffraction of catalysts are shown in Fig. 1. The catalysts containing more than 20% vanadium oxide on both silica and γ-alumina carriers exhibited diffraction lines due to vanadium(V) oxide (abbreviated as V_2O_5), while those containing less than 10% showed no distinct lines. As a whole, the diffraction lines became intense with the increase of the vanadium oxide content. By precise inspection of the diffraction lines due to V_2O_5 in catalysts, the interplaner spacing of (001) planes (the strongest line) of the catalysts supported on silica (group S) was the same as that of unsupported V_2O_5, while the spacing of the catalysts supported on γ-alumina (group A) was slightly shorter than that of group S. The diffraction lines in the range of high diffraction angle were clearer in group S than in group A.

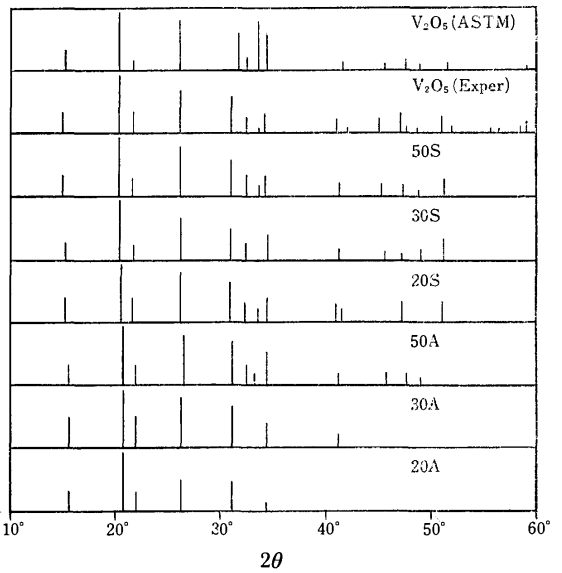

Fig. 1. Diagrams of X-ray diffration of catalysts. Refer to Table 1 for symbols.

Treatment by Ammoniacal Solutions. The residual amount of vanadium oxide in catalysts after treatment with a 0.3 N ammoniacal solution are shown in Table 2 together with the coloration of samples. Generally the amount of the residual vanadium oxide in group A was greater (2—4%) than in group S (1.5—3%). As shown in Table 1, group A had a tinge of green showing existence of a small amount of low-valent vanadium ions and the tone of this color was deepened after treatment with ammoniacal solutions.

Table 2. Samples treated with a 0.3N NH_4OH

Sample	Raw material	V_2O_5 Cont. (wt%)	Colour dry	Colour wet	Surface area (m^2/g)
Samples supported on SiO_2					
10SN	10 S	1.5		cream	595
20SN	20 S	2.2	cream	yellow	554
30SN	30 S	2.6			532
50SN	50 S	2.9		l. yel. brown	472
Samples supported on γ-Al_2O_3					
10AN	10A	2.2			268
15AN	15A	2.9	cream		261
20AN	20A	3.1		l. gr. yellow	254
30AN	30A	3.5	yellow		250
50AN	50A	4.0			240

l; light, yel; yellowish, gr; greenish

Reduction Rates by Benzene Vapour. In the case of the reduction of unsupported V_2O_5 by hydrogen, the change of the weight loss of catalysts caused by reduction consisted of the following three processes as reported by Matsuura.[4] (1) The autocatalytically accelerating process in the initial step of the reduction, (2) the steady reduction process and (3) the retarding process.

In process (2), the weight of the catalysts decreased almost linearly with reduction time and reached the value corresponding to the average composition of

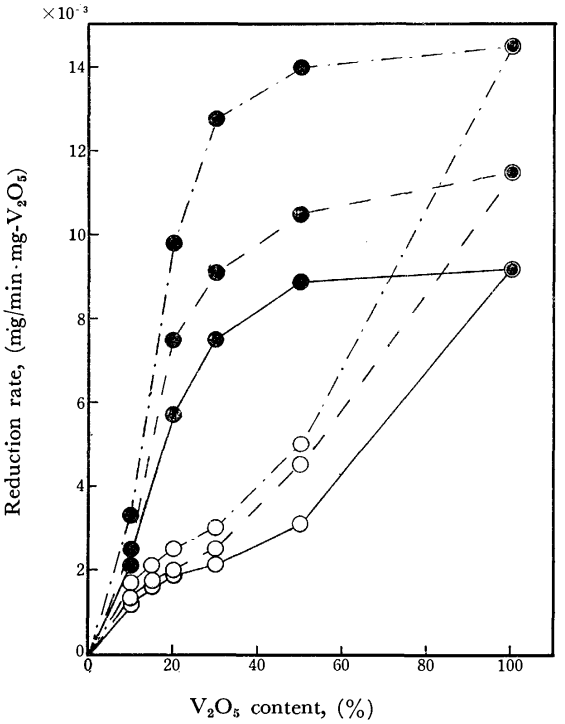

Fig. 2. Reduction rates of catalysts at 420°C.
●; Catalysts supported on silica
○; Catalysts supported on γ-alumina
——; Benzene concentration in feed 6.1%, – –; 4.6%, ——; 3.2%.

4) R. Matsuura, *Nippon Kagaku Zasshi*, **82**, 276, (1961).

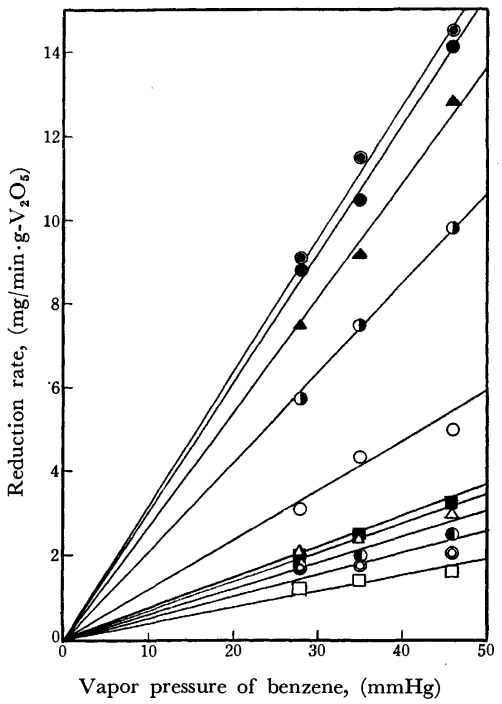

Fig. 3. Reduction rates of catalysts at 420°C.
⊙; V_2O_5, ●; 50S, ▲; 30S, ◑; 20S, ■; 10S, ○; 50A, △; 30A, ◐; 20A, ◎; 15A, □; 10A

vanadium oxide V_2O_4. In process (3), the vanadium oxide on carriers was further reduced from vanadium (IV) oxide to vanadium(III) oxide. The gradient of the linear relation in process (2) was adopted in this paper as the measure of the rate of reduction expressed as weight loss (mg) per unit time (minute) and unit mass of vanadium oxide (mg) contained in the starting samples. Dependence of the reduction rates on the vanadium oxide contents and the vapour pressures of benzene in the feeds are shown in Figs. 2 and 3, respectively. It is clear that the rate of reduction decreased with the decrease of the vanadium oxide content of the catalysts. For the same content of the oxide, the reduction rates were faster for group S than for group A. Figure 3 shows that the reduction rates are proportional to the first order of the vapor pressure of benzene.

The characteristics of the rate of reduction were maintained in the range of reduction temperatures 380—450°C. The apparent activation energies of the reduction ΔE determined from the variation of the rates with reduction temperature are shown in Table 3. The activation energies varied with carriers and vanadium oxide contents.

It was observed that ΔE of group A tended to be larger than that of group S.

The crystalline structures of the reduced samples with the composition V_2O_4 were examined by X-ray diffraction. The sample of unsupported V_2O_5 reduced under the same conditions was composed of two kinds of structures, *i.e.*, the rutile type V_2O_4 and the intermediate "B" named by Sata *et al.*[5,6] In the cases of

5) T. Sata, E. Kodama, and Y. Itoh, *Kogyo Kagaku Zasshi*, **71**, 463 (1968).

Table 3. Apparent activation energy of reduction by benzene vapor

Sample	ΔE (kcal/mol)
V_2O_5	37
Samples supported on SiO_2	
10S	43
20S	37
30S	37
50S	26
Samples supported on γ-Al_2O_3	
10A	43
15A	40
20A	40
30A	37
50A	32

the supported catalysts, only the latter was observed.

ESR Spectra of Catalysts. The evacuated samples of group A exhibited the characteristic ESR spectra with hfs due to $^{51}V(IV)$ in distorted square pyramidal coordination[3,7] and the resolution of hfs became clear with the decrease of vanadium oxide content. In the cases of group S the spectra changed considerably with the vanadium oxide content. While a broad doublet line was observed for 50S and 30S, spectra with not well-resolved hfs over a very broad absorption line were observed for catalysts containing less than 20% vanadium oxide. Typical examples of the spectra are shown in Fig. 4.

When the catalysts were treated with 0.3 N ammoniacal solution, group A exhibited almost the same spectra as 5A in Fig. 4, but group S exhibited only broad absorption lines.

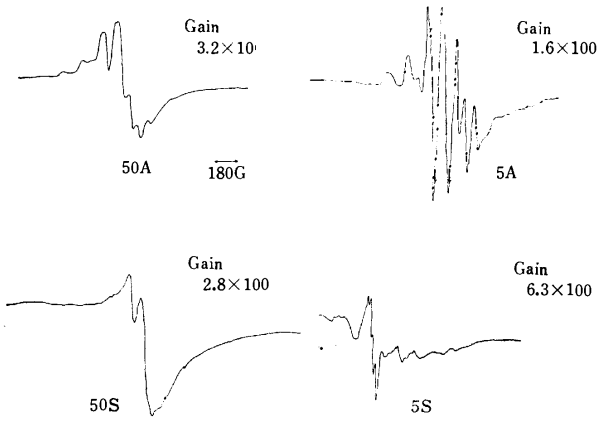

Fig. 4. ESR spectra of catalysts after vacuum treatment at 400°C.

The ESR spectra of group S were affected by moisture and changed to spectra similar to those of group A. As an example, the changes of spectra of 20S by

6) The intermediate B corresponds to VO_x reported by M. Kato, M. Taniguchi, and T. Kubo (*Kogyo Kagaku Zasshi*, **69**, 2102 (1966)) and its composition is believed to be VO_2.

7) K. Tarama, S. Teranishi, S. Yoshida, and H. Yoshida, This Bulletin, **34**, 1195 (1961).

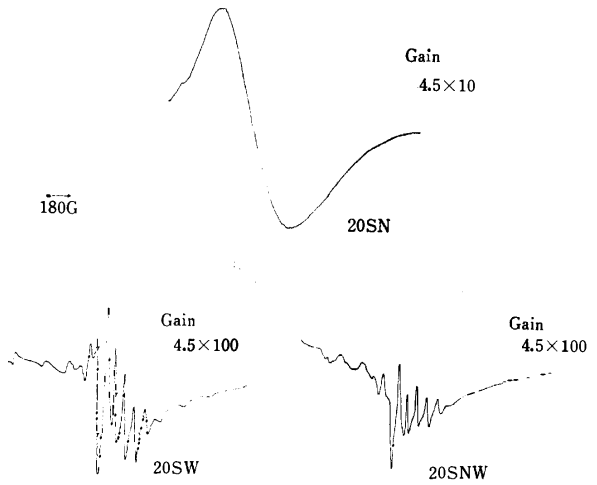

Fig.5 . ESR spectra of 20S after dampening and treatment with a 0.3 N ammoniacal solution.
20SW; Dampened in air after vacuum treatment at 400°C.
20SN; Evacuated at 400°C after treatment with a 0.3 N ammoniacal solution.
20SNW; Dampened sample of 20SN.

treatment with an ammoniacal solution and dampening are shown in Fig. 5.

Discussion

The results obtained indicate that in the supported vanadium oxide catalysts, vanadium oxide is not only dispersed on the carriers with high surface area, but also interacted chemically with the carriers.

Characteristic Behavior of Vanadium Oxide on Carriers. The main features of the results could be summarized as follows. 1) A tinge of green colour and considerable intensity of ESR spectrum of the supported vanadium oxide suggested that tetravalent vanadium ions (V^{4+}) existed in a larger amount in the supported catalysts than in unsupported V_2O_5 (the amount of V^{4+} in V_2O_5 has been estimated to be about 0.6 atom %.[8]).

2) On the carriers, vanadium oxide insoluble in 0.3 N ammoniacal solution existed and the amount was greater in group A than in group S.

3) Both rutile type V_2O_4 and the intermediate "B" were produced in the course of the reduction of unsupported V_2O_5, but rutile type V_2O_4 was not produced in the case of the supported catalysts.

4) The supported samples were more stable against reduction by benzene vapour than unsupported V_2O_5. The tendency was remarkable especially for the samples supported on γ-alumina.

The reduction rates of vanadium oxide catalysts by benzene followed the "parabolic law" which indicates the rate determining step is the diffusion process of oxygen ions within crystals at rather low temtemperature (327°C).[2b,9] In the present research, however, the rate of reduction was proportional to time, that is, of zeroth order with respect to the amount of unreduced vanadium oxide and was proportional to the vapour pressure of benzene. This seems to indicate that the diffusion process of oxygen ions within the crystal is fast enough for the reduction process and the rate determining step of reduction is the uptake of oxygen from vanadium oxide surface by gaseous benzene or adsorbed benzene with low coverage.

If this is the case, the rate would be controlled mainly by the bond strength of oxygen-vanadium ions on the surface. The results obtained reveal that the carriers, especially γ-alumina, affect the bond strength of oxygen-vanadium ions on the surface of vanadium oxide.

Structure of Vanadium Oxide Supported on γ-alumina. Experiments of the reduction and dissolution in 0.3 N ammoniacal solutions of group A showed that considerable interaction between vanadium oxide and γ-alumina took place during the course of preparation, while X-ray diffraction indicated that the vanadium oxide on the γ-alumina was essentially V_2O_5 with a small modification and no special new compounds were formed. The question whether new compounds were formed or not should depend on further investigations since X-ray diffractometry was not useful for samples containing less than 10% V_2O_5. However, such compounds do not seem to be formed because the ESR spectra of 20A and 5A were essentially the same.

The ESR spectra of group A indicated the existence of square pyramidal vanadium oxide (VO_5) which resembled the (VO_5) unit in V_2O_5 crystal.[10] The well-resolved hfs observed for catalysts of low concentration of vanadium showed that unpaired electrons of vanadium(IV) ion were isolated from each other. Thus (VO_5) might be stabilized in an isolated state on the γ-alumina by chemical interaction. For the catalysts of high concentration of vanadium, the ESR spectra were distorted due to interaction of electrons by the possible formation of a small $(VO_5)_n$ network. The massive V_2O_5 crystal observed by X-ray diffraction would be formed by accumulation of vanadium oxide over $(VO_5)_n$ networks.

Structure of Vanadium Oxide Supported on Silica. Although silica has a larger surface area than γ-alumina, X-ray diffraction indicated that the crystal of V_2O_5 developed on silica better than on γ-alumina and the interspacing of the lattice planes was the same as that of pure V_2O_5. The rate of reduction of 50S was almost the same as that of unsupported V_2O_5.

These results show that on silica the same crystal phase exists as pure V_2O_5, when the vanadium oxide content is high. However, the fact that 50S and 30S did not produce rutile type V_2O_5 during the course of reduction by benzene indicated that the crystal phase was slightly perturbed by silica.

In the case of the catalysts of low concentration of vanadium oxide, the ESR spectra were composed of not well-resolved hfs and differ from those of group A.

8) S. Yoshida, *Shokubai*, **10**, 90 (1968).

9) K. Tarama and S. Teranishi, *Kogyo Kagaku Zasshi*, **56**, 302 (1953).

10) A. Bystrom, K. A. Wilhelmi, and O. Brotzen, *Acta Chem. Scand.*, **4**, 1119 (1950).

However, the characteristics of square pyramidally coordinated V(IV) ions was observed when samples were dampened as shown in Fig. 5. It is known that tetrahedrally coordinated V(IV) ions could not be detected by ESR at room temperature.[3] From these facts, the spectra could be assigned to distorted square pyramidally coordinated V(IV) ions $(VO_5)'_n$. The spectrum of 20SN which was obtained by treatment of 20S with a 0.3 N ammoniacal solution was broad singlet and changed to a spectrum characteristic of square pyramidal (VO_5) by dampening (Fig. 5).

From these effects of dampening, the broad absorption line of 20SN does not seem to be produced by dipole-dipole interaction of unpaired electrons, but might be assigned to tetrahedrally coordinated V(IV) ions (VO_4) with short spin-lattice relaxation time.

Thus vanadium oxide would be stabilized on silica surface as (VO_4) at first, followed by the formation of $(VO_5)'_n$ and V_2O_5 with the increase of the vanadium oxide content.

Thus, the structure of vanadium oxide on silica or γ-alumina could be represented schematically as in Fig. 6.

In conclusion, it was found that these carriers interacted chemically with vanadium oxide and affected its structure and that $(VO_5)_n$ which contained square pyramidal VO_5 interacted with γ-Al_2O_3 was more stable against reduction by benzene than $(VO_5)'_n$ which comprised distorted $(VO_5)_n$ and tetrahedral VO_4 on SiO_2.

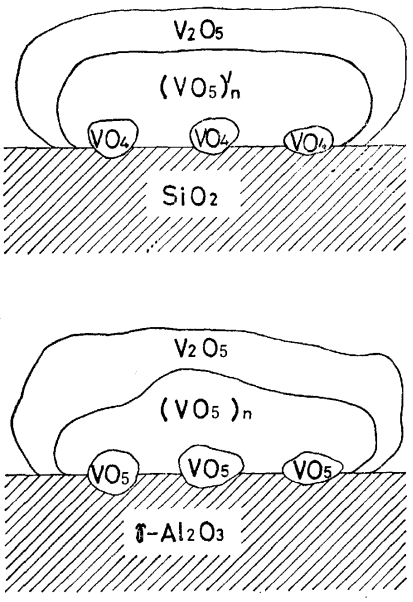

Fig. 6. Schematic representations of vanadium oxides on carriers.

BULLETIN OF THE CHEMICAL SOCIETY OF JAPAN, VOL. 45, 380—383 (1972)

Monolayers of Poly-γ-benzyl-L-glutamate *N*-Alkylamides

Asahi SUZUKI*

Department of Biology, Faculty of Science, Osaka University, Toyonaka, Osaka

(Received July 17, 1971)

To elucidate the effect of long alkyl chains on the surface properties of polypeptides, various poly-γ-benzyl-L-glutamate (PBLG) hexylamides or dodecylamides with different degrees of polymerization were synthesized and their monolayers were examined. PBLG-alkylamides with a low degree of polymerization form expanded-type monolayers on water and their surface pressure-area (π-A) curves have two plateaus. The lower plateau in the π-A curve is not seen in the curves of PBLG-alkylamides with a degree of polymerization of more than 10. The lower plateau in the π-A curve is due to the behavior of the terminal alkyl groups. The effect of temperature on the properties of monolayers was examined. Structures formed in the monolayers were discussed.

From studies on the relation between surface pressure and surface viscosity, it was concluded[1] that the monolayer of poly-γ-benzyl-L-glutamate (PBLG) of low molecular weight is of an expanded type. This was done by comparing polypeptides of rather high molecular weight. The work dealt with the properties of monolayers of low molecular weight PBLG which has a long alkyl chain at its terminal. Ikeda *et al.*[2] discussed to what extent hydrogen bonds between peptides and the van der Waals force between alkyl chains of long chain alkyl amides of poly-α-amino acids contribute to micelle formation in water. It is of interest to see how the van der Waals force between alkyl chains and hydrogen bonds between peptides act in monolayers of polypeptide derivatives, because PBLG-alkylamides are water-insoluble and form monolayers on water.

For this purpose, *n*-hexyl and *n*-dodecyl groups were introduced into polypeptides with different degrees of polymerization. Monolayers of these polymers seemed suitable for studies on the factors making a monolayer stable and on the structures formed in monolayers.

* Present address; Department of Applied Chemistry, Faculty of Engineering, Tokushima University, Tokushima.

1) A. Suzuki and T. Isemura, *Ann. Rep. Biol. Works, Osaka Univ.*, **15**, 75 (1967).

2) S. Ikeda, M. Maekawa, and T. Isemura, This Bulletin., **39**, 105 (1966).

Experimental

A long chain alkylamide of poly-γ-benzyl-L-glutamate was prepared by polymerization of *N*-carboxy-γ-benzyl-L-glutamate anhydride, mp 93°C, in dioxane using hexylamine or dodecylamine as an initiator.[3] The molar ratio of anhydride to initiator, [A]/[I], was varied from 5 to 25 to obtain samples of PBLG-dodecylamide with different degrees of polymerization. The [A]/[I] ratios of the PBLG-hexylamide series were 7, 14, 21, and 28.

The degree of polymerization of polymers was estimated by anhydrous titration of terminal amino groups.[4] Polymers were dissolved in acetic acid and titrated with perchloric acid using methylviolet as an indicator. The activity of perchloric acid was determined by titration with γ-benzyl-L-glutamic acid. The average degrees of polymerization estimated by the titration of amino end groups were approximately equal to the molar ratios of anhydride to initiator: all the ratios of the average degree of polymerization to the [A]/[I] ratio were between 0.9 and 1.2. The polymers were not fractionated into a monodisperse system, so the degrees of polymerization were taken as the [A]/[I] values. In this paper, the [A]/[I] value is given as a suffix *e.g.* PBLG-hexylamide-7 has a value of 7.

Dichloroacetic acid was distilled twice under reduced pressure before use. Benzene was distilled three times. Potassium chloride was heated for about 3 hr at its partial melting temperature.

Polymers were spread at an air/water interface using a conventional Langmuir trough (50.0×14.5×0.9 cm) and their surface properties were measured by means of automatic recording systems.[5] The hanging plate method was employed for measuring surface pressure, the rotatory surface viscometer for surface viscosity and the vibrating electrode method for surface potential.

Polymers were dissolved in a mixture of dichloroacetic acid and benzene (1 : 4, by volume) and spread on water using a micrometer syringe (Alfa, Takara). Potassium chloride was added to the aqueous phase at a concentration of 1 mM to stabilize surface potential. Temperature was controlled by circulating water at constant temperature through a coiled glass tube at the bottom of the trough.

Results and Discussion

The surface pressure (π) and surface viscosity (η) *vs.* surface area (A) curves for the series of PBLG-hexylamide at 20°C are shown in Fig. 1. PBLG-hexylamide-7 has an unusual π-A curve which is of a very expanded type and has two plateaus at surface pressures of 7.8 and 10.0 dyn/cm. The π-A curves of PBLG-hexylamides other than PBLG-hexyl-7 became more condensed as the degree of polymerization increased and their π-A curves had a single plateau at an area of 0.5 m²/mg. Surface viscosity could be detected in monolayers of polymers with a high degree of polymerization when the area was large. Areas where surface viscosities were first detected were distrubuted in the region of the plateaus of the π-A curves.

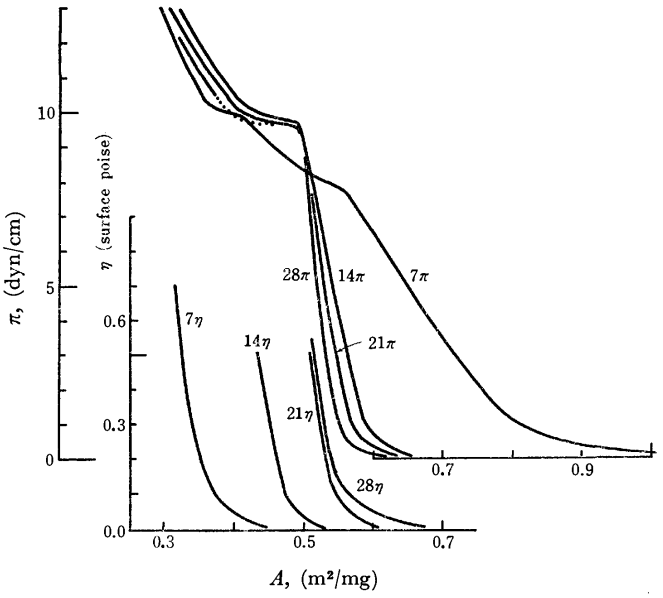

Fig. 1. Variation of the surface properties of PBLG-hexylamide series on water at 20°C.
The degree of polymerization is noted on each curve.

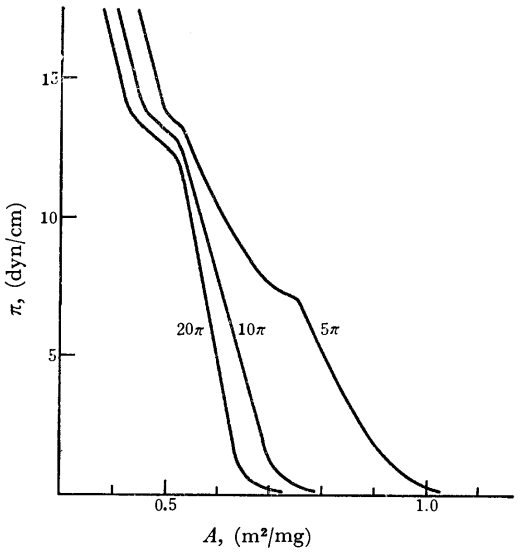

Fig. 2. Variation of π-A curves of PBLG-dodecylamide series on water at 20°C.
The degree of polymerization is noted on each curve.

The π-A and η-A curves of the PBLG-dodecylamide series at 20°C are shown in Fig. 2. There are two plateaus at π=7.2 and 13.0 dyn/cm in the π-A curve of PBLG-dodecylamide-5. The π-A curves of the PBLG-dodecylamide series become a more condensed type with increase in the degree of polymerization. The π-A curves of this series have higher plateaus in the area of 0.55 m²/mg. The surface pressure corresponding to the beginning of the higher plateau varied with the degree of polymerization, but those of the end of the plateau were all at the same pressure of 14.6 dyn/cm.

The temperature dependence of the π-A curve of PBLG-hexylamide-7 is given in Fig. 3. The surface pressure of the lower plateau of the π-A curve does not change appreciably with temperatue but the

3) E. R. Blout and R. H. Karlson, *J. Amer. Chem. Soc.*, **78**, 941 (1956).
4) M. Sela and A. Berger, *ibid.*, **77**, 1893 (1955).
5) A. Suzuki, S. Ikeda, and T. Isemura, *Ann. Rep. Biol. Works, Osaka Univ.*, **15**, 83 (1967).

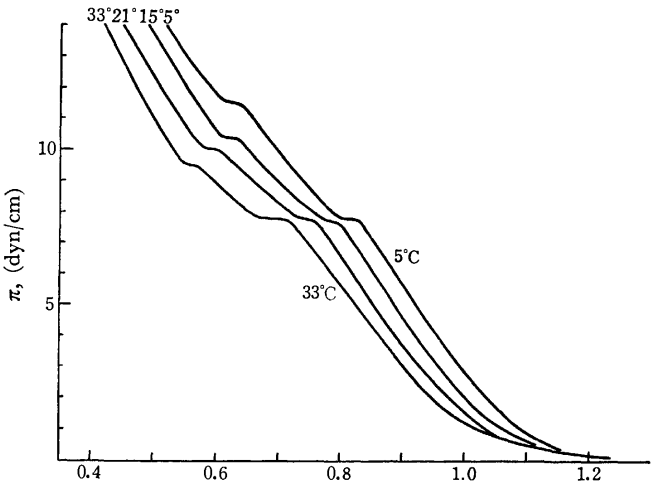

T °C	π_{p1}	π_{p2}
5	7.8	11.5
15	7.8	10.6
21	7.8	10.0
33	7.8	9.5

Fig. 3. Temperature dependence of the π-A curves for PBLG-hexylamide-7 on water.
The critical surface pressure π_p related to the plateaus are shown in the figure.

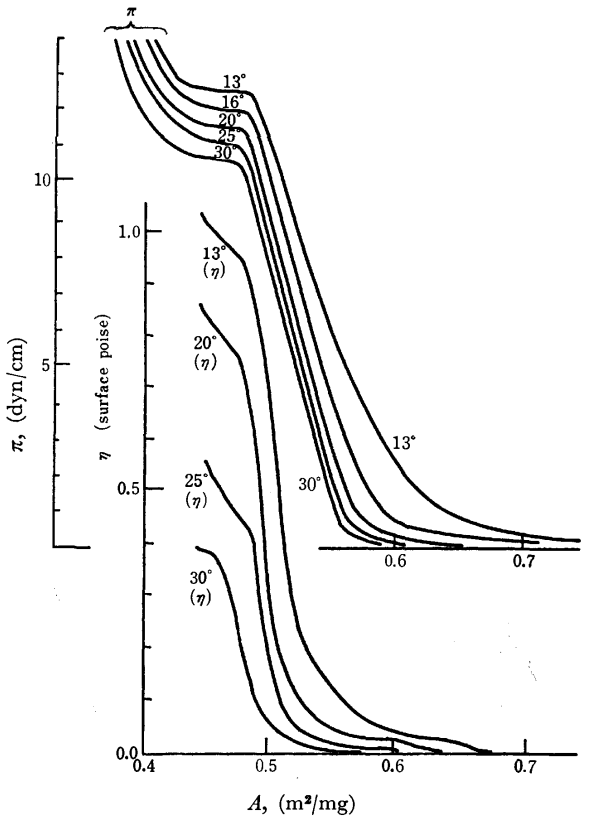

Fig. 4. Temperature dependence of the π-A and η-A curves for PBLG-dodecylamide-10 on water.

surface area corresponding to the beginning of the plateau became smaller with increasing temperature. Both the surface pressure and area of the higher plateau varied with temperature. Temperature had similar effects on the π-A curve of PBLG-dodecylamide-5. Variation of π-A curves of PBLG-dodecylamide-10 with temperature is shown in Fig. 4. The surface pressure corresponding to the higher plateau decreases at high temperature.

The surface moment *vs.* area curves of the PBLG-dodecylamide series are shown in Fig. 5. The surface moment was calculated by the Helmholtz equation $\mu=\Delta VA/4\pi$, assuming that the area occupied by a terminal alkylamine residue is similar to that occupied by an amino acid residue. Since the limiting area of an amino acid residue has been found to be 22 Å^2 in a monolayer of PBLG[1,6] and that of dodecylamine 20.5 Å^2,[7] the above assumption is probably true for a closely packed film.

The smallest area showing the maximum surface moment corresponds to the lower plateau of the π-A curve with PBLG-dodecylamide-5 and also to the area where the surface pressure becomes detectable with PBLG-dodecylamide-10 and PBLG-dodecylamide-20. In an area smaller than that of the plateau, the μ-A curves decrease linearly. In the region from the smallest area showing the maximum surface moment to the area where the surface moment begins to decrease linearly, the plot of μ against A is curved. Assuming that molecules in a monolayer remain in the same conformation when the surface moment is constant, the conformations of the polypeptides seem to remain the same until the surface pressure becomes about 1 dyn/cm, except for PBLG-dodecylamide-5 and PBLG-hexylamide-7 which remain in the same conformations until the lower plateaus are reached. In the region where the plot is curved, the terminal groups contribute considerably to the surface moment since the surface moment varies more for polypeptides of low molecular weight. This suggests that reorientation of terminal groups of polypeptides in associated with decrease in the surface area in this region.

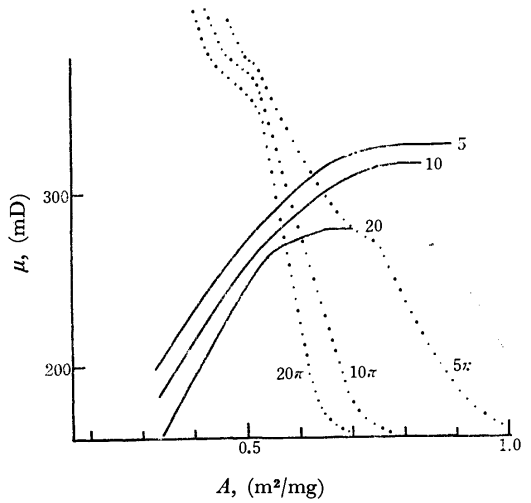

Fig. 5. Surface moment *vs.* area curves for PBLG-dodecylamide series.
The degree of polymerization is noted on each curve.
The π-A curves are shown by dotted lines.

6) S. Ikeda and T. Isemura, This Bulletin,. **34**, 416 (1961).
7) N. K. Adam, *Proc. Roy. Soc.* (London), **A103**, 687 (1923).

Two components of surface moment, due to a peptide and to a terminal group, were estimated from the maximum surface moment, as μ(peptide)$=266\pm29$ and μ(terminal)$=450-1100$ mD. The μ value (peptide) is in accord with that of 265 mD obtained for a monolayer of PBLG.[1,6] The μ value(terminal) varied greatly with polymers. This might be due to complicated factors, such as ionization of these groups.

A hydrocarbon chain should influence the properties of monolayers of polymers of low molecular weight, so the π-A curves of PBLG-hexylamide-7 and PBLG-dodecylamide-5 were compared. The π-A curve of PBLG-hexylamide-7 was found to be more expanded than that of PBLG-dodecylamide-5. The π-A curves of monolayers of PBLG reported previously[1,6] had only one plateau corresponding to the higher plateau observed in this work. This suggests that the lower plateau is due to the terminal alkyl chains. This is supported by the finding that the lower plateau disappeared as the ratio of alkyl groups to peptides became smaller with increase in the degree of polymerization. It seems likely that as the interaction between hexyl groups is smaller than that of dodecyl groups the monolayer of PBLG-hexylamide-7 is more expanded than that of PBLG-dodecylamide-5. The surface pressure related to the lower plateau, which is independent of the temperature, is 7.8 dyn/cm for PBLG-hexylamide-7 and 7.2 dyn/cm for PBLG-dodecylamide-5. Langmuir[8] formulated the interaction between hydrocarbon chains as a function of the number of carbon atoms. Since the polypeptides used in this work have hydrocarbon chains in both their terminals and their side chains, quantitative analyses of their interaction are difficult. The surface pressure at the higher plateau was 10 dyn/cm for PBLG-hexylamide-7 at 20°C and 13 dyn/cm for PBLG-dodecylamide-5 at 20°C, and decreased with increasing temperature.

Surface viscosities become detectable at areas corresponding to the higher plateaus in the π-A curves. It has been reported[9,10] that the surface viscosity of polypeptides is due to the formation of hydrogen bonds between polypeptides. This suggests that hydrogen bonds are formed between peptides in the monolayers when the area corresponds to the higher plateau.

From the shape of the π-A curves obtained with this series of polypeptides, it seems likely that the changes occurring in the monolayers are as follows: (1) molecules in the monolayers become aggregated by the van der Waals force between hydrocarbon chains, (2) reorientation of hydrocarbon chains occurs in the region of the lower plateau, (3) molecules combine by formation of hydrogen bonds between peptide parts of the molecule and (4) reorientation of the side chains of amino acid residues occurs in the region of the higher plateau. The polymers may come in contact with each other by interaction of hydrocarbon chains and the interaction might be too weak to cause any detectable surface viscosity at an area larger than that of the lower plateau. The surface properties of monolayers of PBLG were explained by Yamashita and Yamashita[11] in relation to conformation of the polypeptide. If the conformational change of the oligopeptide studied in this work is considered, it may be related to the higher plateau. Examination of the infrared spectra of the PBLG-dodecylamide series in solid film indicated that low molecular weight PBLG-dodecylamide in the solid film predominantly had β-structure.[12] The conformation of polypeptides in solid films might be related to the π-A curves, as suggested by Yamashita and Yamashita. However, at present information available for further discussion is still insufficient.

8) I. Langmuir, *J. Chem. Phys.*, **1**, 754 (1933).

9) S. Ikeda and T. Isemura, This Bulletin., **32**, 659 (1959).

10) N. L. Gershfeld and C. Y. C. Pak, *J. Colloid Sci.*, **23**, 215 (1967).

11) T. Yamashita and S. Yamashita, This Bulletin, **43**, 3969 (1970).

12) Solid films for the examination of infrared spectra were prepared from solutions in chloroform on silver chloride plates. Infrared spectra were recorded with a Perkin-Elmer Spectrophotometer, model 221, using a sodium chloride prism. The existence of the α-helical or β-structure is deduced from the absorption bands of amide I and II of polypeptides.

Geometrical Structures of Excited States of Conjugated Molecules: Benzene, Naphthalene, Azulene, and Heptalene

Yuichi FUJIMURA, Hiroyuki YAMAGUCHI, and Takeshi NAKAJIMA

Department of Chemistry, Tohoku University, Katahira-cho, Sendai

(Received July 19, 1971)

A semiempirical SCF CI MO method used in combination with the variable bond-length technique, which has proved to be quite successful in predicting the ground-state geometrical structures of conjugated molecules, has been applied with modifications suitable to their excited states. The values of the parameters appearing in the expression of the resonance integral were adjusted so as to reproduce both the absorption and fluorescence spectra of benzene. The lower three singlet states ($^1B_{2u}$, $^1B_{1u}$, and $^1E_{1u}$) and the lowest triplet state ($^3B_{1u}$) of benzene, the lower two singlet states ($^1B_{1u}$ and $^1B_{2u}$) of naphthalene, the lower two singlet states ($^1B_2$ and $^1A_1$) of azulene, and the lowest singlet state of heptalene are examined. It is predicted that the $^1B_{1u}$ and $^3B_{1u}$ states of benzene have the antiquinoidal and quinoidal conformations of the D_{2h} symmetry respectively, and that the symmetry of the lowest singlet state of heptalene is higher than that (C_{2h}) of the ground state.

The prediction of the geometrical structures, that is, of the C–C bond distances of conjugated hydrocarbons, has long been one of the major problems in π-electron theories. For the ground states of benzenoid hydrocarbons, it has been well recognized that the molecular symmetry is always that suggested by superposition with an equal weight of the equivalent Kekulé-type resonance structures, and that the bond orders calculated using molecular orbital methods, assuming the full molecular-symmetry, yield the theoretical C–C bond lengths, which are themselves in good agreement with the experimental values.

On the other hand, it was somewhat amazing to discover that the ground states of certain nonbenzenoid hydrocarbons (*e.g.*, heptalene) and open-shell or charged π-electron systems (*e.g.*, the cyclopentadienyl radical or the benzene positive ion) do not adopt the fully-symmetrical nuclear arrangement to be expected on the basis of the conventional resonance theory, but, rather, a less symmetrical conformation in which the nuclei have been displaced to a certain degree.[1] These nuclear distortions, accompanied by a molecular-symmetry reduction, have now been well interpreted as due to the Jahn-Teller or pseudo-Jahn-Teller effects.[1,2]

Another interesting case of such bond distortion concerns the electronically-excited states. It has been known, for example, that the ESR line shapes of the lowest triplet state ($^3B_{1u}$) of benzene are not those which would be expected from a molecule with at least a trigonal symmetry.[3] The geometrical structures of the excited states of a conjugated molecule are, in general, different from that of the ground state, the difference being reflected primarily in the band shapes of the electronic spectrum. For example, the UV spectrum of heptalene shows a very long absorption tail throughout the visible region,[4] which probably indicates that the geometrical structure of the first excited state is greatly different from that of the ground state. Furthermore, information on the geometrical structures of excited states is quite useful in understanding the inducing and accepting modes of the intramolecular radiationless transitions.[5,6]

It is the purpose of this paper to propose, on the basis of the semiempirical SCF LCAO MO theory, a computational method of determining the molecular symmetries and C–C bond distances for the electronically-excited states of conjugated molecules and to examine the geometrical structures of the lower excited states of benzene, naphthalene, azulene, and heptalene.

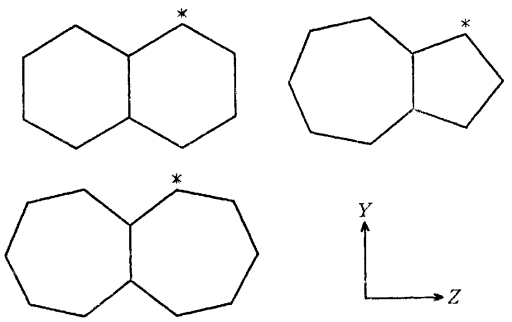

Fig. 1. Numbering of atoms and choice of axes. Carbon atoms are numbered consecutively, starting with the starred atom and proceeding in a clockwise fashion along the periphery.

Method of Calculation

The method used in predicting the energetically most favorable symmetry group and the C nuclear arrangement for an electronically-excited state of a conjugated molecule which is assumed to be planar is a modified version of the semiempirical SCF CI MO method used in combination with the variable bond-length technique, which has proved to be quite successful in predicting the ground-state geometrical

1) L. Salem, "The Molecular Orbital Theory of Conjugated Systems," Benjamin, New York (1966).

2) T. Nakajima, in "The Chemistry of Nonbenzenoid Aromatic Compounds," International Symposium on The Chemistry of Nonbenzenoid Aromatic Compounds, Butterworths, London (1970), in press.

3) M. S. de Groot and J. H. van der Waals, *Mol. Phys.*, **6**, 545 (1963).

4) H. J. Dauben, Jr. and D. J. Bertelli, *J. Amer. Chem. Soc.*, **83**, 4659 (1961).

5) S. H. Lin, *J. Chem. Phys.*, **44**, 3759 (1966).

6) K. F. Freed and J. Jortner, *ibid.*, **52**, 6272 (1970).

structures of a variety of conjugated molecules.[7,8]

Assuming a certain C nuclear arrangement for a conjugated molecule, we carry out the SCF CI MO calculation in the framework of the Pariser-Parr-Polpe approximation.[9,10] Using the wavefunction for an excited state obtained after the inclusion of the configuration mixing all the singly-excited states, we then calculate the C–C bond length for the excited state by the aid of a suitable bond-order—bond-length relationship (*vide infra*). The new C nuclear arrangement is taken as the geometrical structure for the next SCF MO calculation, and the process is repeated until the convergence of the C–C bond lengths for the excited state is reached. As the starting geometrical structures for the iterative calculation, we take all the possible distorted structures in which C–C bond lengths are distorted so that the set of displacement vectors may form a basis for an irreducible representation of the full symmetry group of the molecule.[11,12]

If the self-consistency of the geometrical structure is achieved at two or more different nuclear arrangements, the total energies should be compared with each other in order to determine which one is the energetically most favorable. The total energy of a conjugated molecule is assumed to be the sum of the π-electron energy and the σ-core energy, which may itself be regarded as the sum of the independent contributions from the C–C σ-bonds. Further, for the reduced distance variation, the individual contribution of the σ-bonds may safely be approximated by the quadratic function of the bond-distance variation:

$$E_\sigma = \sum_{\mu<\nu} \frac{k}{2}(\Delta r_{\mu\nu})^2 \tag{1}$$

where k is the force constant for an sp^2 hybridized C–C σ-bond. The value of k used in the present calculations is 714 kcal mol^{-1} Å^{-2}.[13]

It has now been well established[14] that if the total energy of a conjugated hydrocarbon is written as the sum of the π-electron energy, as calculated using a Hückel approximation, and the σ-bond energy, as approximated by Eq. (1), then the minimization of the total energy with respect to the bond-length variations yields a linear relationship between the bond length, r, and the bond order, p:

$$r_{\mu\nu} = r_0 - ap_{\mu\nu} \tag{2}$$

where r_0 is the length for an sp^2–sp^2 C–C single bond and where $a=2\beta'/k$, β' being the first derivative of the resonance integral.

Recently, Julg[15] has shown that the inclusion of electron repulsions in calculating the π-electron energy by the use of the Pariser-Parr-Pople-type semiempirical SCF MO formalism leads to the following relationship between the bond order and the bond length:

$$r_{\mu\nu} = r_0 - ap_{\mu\nu} + bp^2_{\mu\nu} \tag{3}$$

where $b=\gamma'/2k$ and where γ is the Coulomb repulsion integral between neighboring atoms. The b/a ratio being of the order of 0.1 for the bond distance of 1.34 Å, which corresponds to $p=1$, we may safely neglect the p^2 term in Eq. (3) for the longer bond distances with the lower p values. Further, by minimizing the excited-state total energy with respect to the bond-distance variations, Julg[15] has demonstrated that the same linear relationship between p and r that is appropriate for the ground state holds approximately even for both singlet and triplet excited states. In this paper, we adopt, as the bond-order—bond-length relationship for use in excited states, Eq. (2) with $r_0=1.520$ Å and $a=0.186$,[8] the parameter values giving the ground-state bond lengths, which are in good agreement with the experimental values. Miller and Murrell[16] have proposed the following formula for predicting the excited-state bond lengths of conjugated molecules:

$$\Delta r_{\mu\nu} = -0.228\ \Delta p_{\mu\nu} \tag{4}$$

This formula gives $r_0=1.55$ Å, which seems to be somewhat exaggerated as the length for the sp^2–sp^2 C–C single bond.

The one-center repulsion integral for carbon, given as I_c-A_c, is taken to be 11.16—0.03 eV. The two-center repulsion integrals are calculated using the Mataga-Nishimoto formula.[17] The resonance integrals, $\beta_{\mu\nu}$ (in units of eV), are evaluated using the following formula:

$$\beta_{\mu\nu} = -2.38\ \exp[(1.397-r_{\mu\nu})/A] \tag{5}$$

where the pre-exponential factor has been determined so as to reproduce the experimental excitation energies of benzene. On the other hand, the value of A, on which depend sensitively the geometrical structures of conjugated molecules, cannot be determined by reference to the excitation energies of benzene. In this paper, the value of A is adjusted so as to reproduce the emission energy of the fluorescence from the lowest singlet excited state ($^1B_{2u}$) in benzene. Using the experimental emission energy, 4.44 eV[18] we thus obtain $A=0.30$ Å.

Results and Discussion

Benzene. The geometrical structures of the lower three singlet excited states, $^1B_{2u}$, $^1B_{1u}$, and $^1E_{1u}$, and the lowest triplet state, $^3B_{1u}$, are examined. As the starting bond distortions for iterative calculation, we adopt carbon-stretching symmetry coordinates

7) M. J. S. Dewar and G. J. Gleicher, *Tetrahedron*, **21**, 3423 (1965).
8) H. Yamaguchi, T. Nakajima, and T. L. Kunii, *Theor. Chim. Acta*, **12**, 349 (1968).
9) R. Pariser and R. G. Parr, *J. Chem. Phys.*, **21**, 446, 767 (1953).
10) J. A. Pople, *Trans. Faraday Soc.*, **49**, 1375 (1953).
11) T. Nakajima and A. Toyota, *Chem. Phys. Lett.*, **3**, 272 (1969).
12) A. Toyota and T. Nakajima, *ibid.*, **6**, 144 (1970).
13) L. C. Snyder, *J. Phys. Chem.*, **66**, 2299 (1962).
14) G. Binsch and E. Heilbronner, "Structural Chemistry and Molecular Biology," ed. by A. Rich and N. Davidson, Freeman, San Francisco (1968), p. 815.
15) A. Julg, *J. Chim. Phys.*, **65**, 541 (1968).
16) K. Miller and J. N. Murrell, *Theor. Chim. Acta*, **3**, 231 (1965).
17) N. Mataga and K. Nishimoto, *Z. Phys. Chem.* (Leipzig), **13**, 140 (1957).
18) I. B. Berlman, "Handbook of Fluorescence Spectra of Aromatic Molecules, Academic Press, New York (1965), p. 42.

TABLE 1. CARBON-STRETCHING SYMMETRY COORDINATES FOR BENZENE

Mode	Symmetry coordinate[a]
a_{1g}	$S_1=\frac{1}{\sqrt{6}}(\Delta r_{12}+\Delta r_{23}+\Delta r_{34}+\Delta r_{45}+\Delta r_{56}+\Delta r_{61})$
b_{2u}	$S_{14}=\frac{1}{\sqrt{6}}(\Delta r_{12}-\Delta r_{23}+\Delta r_{34}-\Delta r_{45}+\Delta r_{56}-\Delta r_{61})$
e_{2g}	$S_{8a}=\frac{1}{\sqrt{12}}(\Delta r_{12}-2\Delta r_{23}+\Delta r_{34}+\Delta r_{45}-2\Delta r_{56}+\Delta r_{61})$
	$S_{8b}=\frac{1}{\sqrt{2}}(\Delta r_{12}-\Delta r_{34}+\Delta r_{45}-\Delta r_{61})$
e_{1u}	$S_{19a}=\frac{1}{\sqrt{2}}(\Delta r_{12}-\Delta r_{34}-\Delta r_{45}+\Delta r_{61})$
	$S_{19b}=\frac{1}{\sqrt{12}}(\Delta r_{12}+2\Delta r_{23}+\Delta r_{34}-\Delta r_{45}-2\Delta r_{56}-\Delta r_{61})$

a) The plus and minus signs indicate the bond shortening and lengthening, respectively. For the numbering of symmetry coordinates, see E. B. Wilson, *Phys. Rev.*, **45**, 706 (1934).

belonging to a_{1g}, b_{2u}, e_{2g}, and e_{1u} irreducible representations of the D_{6h} point group (Table 1). Further, if a certain carbon-stretching symmetry coordinate and its countertype, in which the bond-length variations are reversed, are not equivalent (*e.g.*, S_{8a}), these two bond distortions should be differentiated as the starting geometry.

As for the lowest singlet excited state ($^1B_{2u}$), it turned out that all the starting bond distortions converge into a unique hexagonal nuclear arrangement with the C–C bond length longer by 0.031 Å than that in the ground state. By applying the Franck-Condon principle to the experimental intensity distribution in the 2600 Å band system of benzene, Craig[19] has found the value of 0.037 Å for the increase in the C–C distance associated with the lowest singlet transition, $^1B_{2u}\leftarrow{}^1A_{1g}$. The predicted increase in bond length is in fairly good agreement with this experimentally-estimated value. The $^1B_{2u}$ state should, in principle, suffer pseudo-Jahn-Teller distortions upon coupling with the closely-spaced $^1B_{1u}$ *via* the a_{2g} vibration and upon coupling with the $^1E_{1u}$ state *via* the skeletal bending modes corresponding to the symmetry coordinate, S_6, of the e_{2g} symmetry.[20] However, the a_{2g} vibration has no influence on the C skeletal arrangement, and the bending displacements, S_6, should cause a change in the small $\beta_{\mu\nu}$ value (zero in the P–P–P approximation) between non-neighboring C atoms.

In case of the lowest triplet state ($^3B_{1u}$), the starting nuclear displacements belonging to a_{1g} and b_{2u} representations converge into a hexagonal conformation with the C–C bond length equal to 1.430 Å, while those belonging to the e_{2g} and e_{1u} representations lead to two D_{2h} conformations; one of these is the quinoidal form (I), and the other, the antiquinoidal form (III) (Fig. 2). As for the symmetry displacements of the e_{2g} symmetry, S_{8a} and its countertype bring about the antiquinoidal and quinoidal forms respectively, while S_{8b} and its countertype lead to the other two equivalent quinoidal forms. In Fig. 2 are shown the bond lengths of these equilibrium conformations, together with their relative total energies. The quinoidal form is more stable than the antiquinoidal form by 0.07 eV, the latter being the metastable quilibrium conformation corresponding to the saddle point of the energy surface. The passage from one of the quinoidal conformations, by way of the antiquinoidal saddle points, to the other two equivalent quinoidal conformations may be caused by the e_{2g} vibration.[1,3,21]

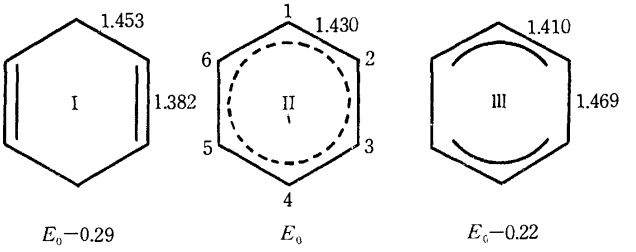

Fig. 2. Predicted equilibrium configurations for the lowest $^3B_{1u}$ excited state of benzene (bond lengths in Å and energies in eV).

In recent years various kinds of experimental studies of the geometry of the $^3B_{1u}$ state of benzene have been attempted. Electron spin resonance experiments by de Groot and van der Waals[3] have indicated that, in solid matrices, the electron-spin distribution in the $^3B_{1u}$ state is far from hexagonal. The study of the phosphorescence spectra of various partly-deuterated benzenes in a C_6D_6 host crystal at 4.2°K by Nieman and Tinti[22] led to the conclusion that the symmetry of the $^3B_{1u}$ state is lower than D_{3h}. The $^3B_{1u}\leftarrow{}^1A_{1g}$ absorption spectrum in benzene vapor mixed with oxygen was studied by King and Pinnington,[23] who concluded that the upper state is of the D_{2h} symmetry. Recently Goncalves and Hutchison[24] studied the electron nuclear double-resonance spectrum of benzene in C_6D_6 single host crystals and suggested that the $^3B_{1u}$ state has an antiquinoidal structure rather than a quinoidal one. It should be noted, however, that, in the experiments in the crystalline or glassy matrix, the degradation of the local D_{6h} symmetry might be due to an environmental effect.

It has been reported that the photochemical reaction of benzene derivatives to Dewar benzene occurs through the $^3B_{1u}$ state.[25–27] To determine the most favorable conformation for the photochemical isomerization, we

19) D. P. Craig, *J. Chem. Soc.*, **1950**, 2146.
20) W. Moffitt, *J. Chem. Phys.*, **22**, 320 (1954).
21) J. H. van der Waals, A. M. D. Berghuis, and M. S. de Groot, *Mol. Phys.*, **13**, 301 (1967).
22) G. C. Nieman and D. S. Tinti, *J. Chem. Phys.*, **46**, 1432 (1967).
23) G. W. King and E. H. Pinnington, *J. Mol. Spectrosc.* **15**, 394 (1965).
24) A. M. Ponte Goncalves and C. A. Hutchison, *J. Chem. Phys.*, **49**, 4235 (1968).
25) E. E. van Tamlem and S. P. Pappas, *J. Amer. Chem. Soc.*, **85**, 3297 (1963).
26) A. W. Burgstahlen and P. L. Chien, *ibid.*, **86**, 2940 (1964).
27) D. Bryce-Smith and H. C. Longuet-Higgins, *Chem. Commum.*, 593 (1966).

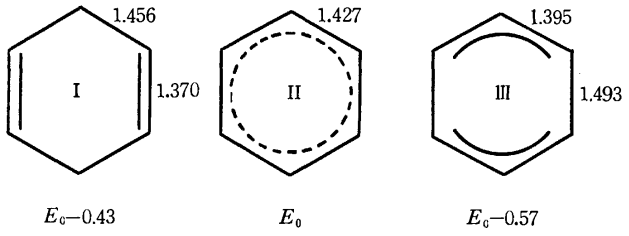

Fig. 3. Predicted equilibrium configurations for the lowest $^1B_{1u}$ excited state of benzene (bond lengths in Å and energies in eV).

examined the nonneighbor 1—4 and 2—5 bond orders of the three conformations, I, II, and III. The predicted 1—4 and 2—5 bond orders of I and III are 0.155 and −0.299, and −0.193 and 0.028, respectively. The predicted 1—4 bond orders of II is −0.057. From the above results, it can be concluded that the most favorable conformation for the reaction in the $^3B_{1u}$ state is I.

For the second singlet state ($^1B_{1u}$), three equilibrium conformations, hexagonal, quinoidal, and antiquinoidal, are obtained. The situation is similar to that predicted for the $^3B_{1u}$ state, except that the relative energies of I and III are interchanged and that the bond length of the unstable hexagonal structure is slightly shorter than that for the $^3B_{1u}$ state (Fig. 3). In the third excited state ($^1E_{1u}$), all the starting distortions lead to the same hexagonal structure, that obtained for the lowest singlet-excited state.

It is well known that the $^1B_{1u}$ state is subjected to the pseudo-Jahn-Teller interaction with the $^1E_{1u}$ state through vibrations of the e_{2g} symmetry[1,21,28] and that the $^1B_{1u}\leftarrow{}^1A_{1g}$ transition is vibronically induced by these vibrations.[29,30] On the other hand, no Jahn-Teller coupling effects are expected to be exhibited at the lowest vibronic level of the $^1E_{1u}\pi^*\leftarrow\pi$ excited state.[31] The results of a recent experimental study by Katz *et al.*[31] of the absorption spectra of benzene and deuterated benzenes in solid rare-gas matrices are in agreement with these predictions. It seems that our results are all consistent with these findings.

Naphthalene. Since the energy difference between the first ($^1B_{1u}$) and second singlets ($^1B_{2u}$) is comparatively small, it may be expected from the symmetry rule[32-34] that the two states will interact strongly with each other through the normal displacement of the b_{3g} symmetry and will suffer a symmetry reduction. Thus, the symmetry groups and the bond lengths for the energetically most favorable nuclear arrangements of the two states were examined. For the two states, the starting bond distortions belonging to the irreducible representations, a_g, b_{3g}, b_{1u}, and b_{2u}, of the full symmetry group, D_{2h}, are taken as the starting bond distortions for iterative calculation. It turns out that, in the two states, all the starting bond distortions converge into a unique self-consistent set of bond lengths corresponding to D_{2h}. The calculated bond lengths of both the states are listed in Table 2 and compared with the experimental values of the ground state.

It is well known that a change in symmetry manifests itself on electronic excitation itself by the appearance of progressions in vibrations which, with respect to the covering symmetry of the ground state, are nontotally symmetrical.

Craig *et al.*[35] have studied the $^1B_{1u}\leftarrow{}^1A_g$ absorption spectrum in naphthalene vapor and shown that such progressions are not found in this absorption band. They have concluded that naphthalene belongs to the D_{2h} symmetry group in the $^1B_{1u}$ electronic state as in the ground state, and that its dimensions are little changed on excitation. The results of Craig *et al.*[35] are in good agreement with the present results.

Table 2. Geometrical structures for various states of aromatic hydrocarbons

Molecule	State	Bond length (Å)					
Napthalene		1—2	1—10	2—3	5—10		
	$^1B_{1u}$	1.399	1.421	1.430	1.457		
	$^1B_{2u}$	1.427	1.417	1.382	1.427		
	^1A_g[a]	1.364	1.421	1.415	1.418		
Azulene		1—2	1—10	4—5	4—10	5—6	6—7
	$^1B_2$ (1)	1.394	1.438	1.439	1.416	1.385	1.416
	$^1A_1$ (2)	1.437	1.381	1.458	1.467	1.376	1.426
	$^1A_1$ (1)[b]	1.398	1.399	1.406	1.469	1.398	1.400
Heptalene		1—2	1—12	2—3	6—12		
	$^1B_{3g}$	1.402	1.412	1.405	1.463		

a) D. W. J. Cruikshank and R. A. Sparks, *Proc. Roy. Soc., Ser. A*, **258**, 270 (1960).
b) A. W. Hanson, *Acta Crystallogr.*, **19**, 19 (1965).

28) A. D. Lieher, *Z. Naturforsch.*, **A16**, 641 (1961).
29) J. N. Murrell and J. A. Pople, *Proc. Phys. Soc.*, **69A**, 245 (1956).
30) A. C. Albrecht, *J. Chem. Phys.*, **33**, 169 (1959).
31) B. Katz, M. Brith, B. Sharf, and J. Jortner, *ibid.*, **52**, 88 (1970).
32) R. G. Pearson, *J. Amer. Chem. Soc.*, **91**, 1252, 4947 (1969).
33) L. S. Bartell, *J. Chem. Educ.*, **45**, 754 (1969).
34) R. G. Pearson, *J. Chem. Phys.*, **52**, 2167 (1970).
35) D. P. Craig, J. M. Hollas, M. F. Redies, and S. C. Wait Jr., *Phil. Trans. Roy. Soc.*, **253**, 543 (1961).

The bond-length changes for excitation to the $^1B_{2u}$ state are calculated by Miller and Murrell,[16] who used Eq. (4) in the framework of the ASMO CI method. The results of these authors are in good agreement with the present ones. By using the predicted bond length changes, they have calculated the intensity of a vibrational progression, which gives a good agreement with the experimental results.

We can draw an important conclusion from the considerations stated above that, on excitation to both the states, there is no change in the symmetry of the molecule.

Azulene. It has been confirmed that azulene does not fluorescence from the lowest singlet ($^1B_2(1)$) state, but instead emits from the second excited singlet ($^1A_1(2)$).[36,37] From this fact, it can be expected that the geometry of the $^1B_2$ (1) state may be considerably deformed compared with that of the ground state ($^1A_1$ (1)). It seemed that it would be interesting to apply the present method to both the excited states.

The starting C-C bond distortions, which are assumed to be inplane, belonging to two irreducible representations, a_1 and b_2, of the full symmetry group, C_{2v}, are taken as the starting ones. Table 2 lists the calculated structures of the $^1B_2$ (1) and $^1A_1$ (2) states, along with the experimental structure of the ground state. For the $^1B_2$ (1) state, the predicted geometrical structure has the C_{2v} symmetry. An analysis of the absorption spectra in the 7000 Å band indicated that azulene retains the C_{2v} symmetry in the $^1B_2$ (1) state.[38] The central bond in the $^1B_2$ (1) state becomes drastically shorter than that in the ground state. In naphthalene, the changes in the bond lengths upon the $^1B_{1u}\leftarrow{}^1A_g$ excitation of naphthalene are comparatively small, so that vibrational frequencies of the upper state can be correlated with those of the ground state. However, a drastic change in the central bond-length of the $^1B_2$ (1) state in azulene would lead to a large variation in the vibrational frequencies of this state. In fact, Hunt and Ross[38] have reported that it is difficult to correlate the vibrational frequencies of the $^1B_2$ (1) state with those of the ground state.

For the $^1A_1$ (2) state, the predicted geometrical structure has the C_{2v} molecular symmetry. McHugh and Ross[39] calculated the structure of the state based on Hückel molecular orbitals with configuration interaction. There are considerable differences between their results and ours in the bond length of the periphery of the molecule. While the C-C bond lengths in the periphery of the molecule are smoothed out in their results, there is a moderate double-bond fixation in the periphery in our results.

From a consideration of the above geometrical structures and the large electronic energy gap[40] between the $^1B_2$ (1) and $^1A_1$ (2) states, it is possible to give a qualitative explanation of the anomalous emission of azulene. The drastic geometrical change in the central bond between the ground and the $^1B_2(1)$ states will lead their two potential surfaces to intersect in the vicinity of the equilibrium point of the $^1B_2$ (1) state. As a result of the intersection, a direct relaxation to the ground state may be the dominant process in the electronic relaxation from the $^1B_2$ (1) state. On the other hand, the bond-length changes in the $^1A_1$ (2) state are moderate, so that the potential surface of the $^1A_1$ (2) state will not intersect with the other potential surfaces ($^1B_2$ (1), $^1A_1$ (1)) in the vicinity of the equilibrium point of the $^1A_1$ (2) state. The large energy gap between the $^1B_2$ (1) and $^1A_1$ (2) states (that is, the small Franck-Condon factors) will cause the nonradiative transition to the lower $^1B_2$ (1) state to be negligibly small. From the above considerations, it can be thought that azulene is emitted from the $^1A_1$ (2) state.

Heptalene. The SCF calculations show that the starting bond distortion, belonging to the b_{3g} representation (that is, alternation), which converges into the geometry of the symmetry group, C_{2h}, in the ground state does not give rise to a symmetry reduction in the lowest excited state; that is, the lowest excited state exhibits no bond alternation. Furthermore, our calculations predict that bond distoritions belonging to b_{1u} and b_{2u} representations do not result in a symmetry reduction, either all the possible starting distortions produce a unique set of bond lengths belonging to the point group D_{2h}. The predicted bond lengths are summarized in Table 2.

The above results may easily be explained on the basis of the symmetry rule[32-34] from the energy-level arrangement in the heptalene molecule with the D_{2h} symmetry. The excitation energies from the ground state to the $^1B_{3g}$, $^1B_{1u}$, and $^1B_{2u}$ states are 0.26, 2.68, and 3.37 eV respectively, and the E_2—E_1 and E_3—E_1 energy gaps are too large to give rise to pseudo-Jahn-Teller distortions in the lowest excited state.

The geometrical structure of the lowest excited state predicted above perhaps gives one of the reasons for the appearance of a long absorption tail in the long-wave length side of the first absorption band in heptalene.[4]

36) H. C. Longuet-Higgins and M. Beer, *J. Chem. Phys.*, **23**, 1390 (1955).

37) G. Viswanath and M. Kasha, *ibid.*, **24**, 574 (1956).

38) G. R. Hunt and I. G. Ross, *J. Mol. Spectrosc.*, **9**, 50 (1962).

39) A. J. McHugh and I. G. Ross, *Aust. J. Chem.*, **21**, 3055 (1968).

40) R. Pariser, *J. Chem. Phys.*, **25**, 1112 (1956).

The Effects of the Crystal-structural Transformation on the Chemical Behavior of ^{64}Cu Recoil Atoms in α-Copper Phthalocyanine

Hiroshi KUDO

Japan Atomic Energy Research Institute, Tokai-mura, Ibaraki-ken.

(Received July 19, 1971)

The Stage-II annealing process of ^{64}Cu recoil atoms in neutron-irradiated α-copper phthalocyanine was carefully examined. The isothermal annealing curve above 270°C showed anomalous inflection point. It was found that the Stage-II annealing process of the α-crystal consisted of a "normal" monotonous annealing process and a "delayed" process caused by the crystal-structural transformation. The results of a kinematic analysis suggested that the fluctuation of the matrix and the change in the crystalographic factors due to the structural transformation play a triggering role in the delayed annealing reaction.

Despite a number of studies of the annealing reaction of ^{64}Cu recoil atoms in neutron-irradiated copper phthalocyanine,[1-12] the details of the mechanism of the reaction do not appear to have been completely elucidated. Yoshihara and Ebihara[9] found striking effects of the crystal structure on the thermal annealing of the ^{64}Cu recoil atoms produced by (n, γ) and (γ,n) reactions. The recoil atoms in the irradiated β-copper phthalocyanine were very easily annealed, while those in the α-crystal were relatively insensitive. The thermal annealing process could be separated into two stages in both the α- and β-crystals; Stage I below 200°C and Stage II above 250°C.

β-Copper phthalocyanine is the most stable crystal modification, and its crystal structure has been reported in detail by Robertson.[13] At least two other crystal forms, designated as the α- and γ-form, have been characterized by a study of their X-ray powder diffraction patterns and by infrared or visible spectroscopy.[14-21] The α-modification (a metastable crystal) is converted into the β-form by treating it in various organic suspension media, by sublimating it *in vacuo*, or simply by heating it above 250°C.[22-27]

It is known that the behavior of the recoil atom in solids depends on such crystallographic factors as the surface activities, the grain size, and the concentration of defects.[12,28] These factors will inevitably be affected by the crystal-structural transformation. An investigation of the effect of the crystal-structural transformation on the thermal annealing process can be expected to give further information on the chemical fate of the ^{64}Cu recoil atoms in neutron-irradiated α-copper phthalocyanine, especially for the Stage-II annealing process. This effect has, however, attracted little attention during the study of the annealing process in α-copper phthalocyanine.[9]

The aim of the present work is to investigate the effect of the crystal-structural transformation on the Stage-II annealing of ^{64}Cu recoil atoms in neutron-irradiated α-copper phthalocyanine. In fact, the isothermal annealing curve above 270°C showed an anomalous inflection point, while no anomaly was observed in the curve below 250°C. The results are discussed in terms of the crystal-structural transformation during the thermal treatment.

Experimental

Target Materials. α-Copper phthalocyanine from Dai-nihon Ink and Chemicals Inc. was carefully purified by recrystallization from sulfuric acid. β-Copper phthalocyanine was obtained by heating the α-crystal for 5 hr at 300°C. The X-ray powder diffraction pattern, the electron micrograph, and the thermogram of the materials were recorded.

1) W. Herr, *Z. Elektrochem.*, **56**, 911 (1952).
2) B. R. Payne, P. Scargill, and G. B. Cook, "Radioisotopes in Scientific Research", Vol. 2, Proc. UNESCO Intern. Conf., Paris 1957 (1958), p. 154.
3) G. B. Cook, *J. Inorg. Nucl. Chem.*, **14**, 301 (1960).
4) D. J. Apers and P. C. Capron, "Chemical Effects of Nuclear Transformations", Vol. 1, Proc. IAEA Symp., Prague 1960 (1961), p. 429.
5) D. J. Apers, F. G. Dejehet, B. S. van Quartyve d'ydewalle, and P. C. Capron, *J. Inorg. Nucl. Chem.*, **24**, 927 (1962).
6) M. Pertessis and R. Henry, *Radiochim. Acta*, **1**, 58 (1963).
7) K. Yoshihara and H. Ebihara, *ibid.*, **2**, 219 (1964).
8) M. Pertessis, *ibid.*, **4**, 44 (1965).
9) K. Yoshihara and H. Ebihara, *J. Chem. Phys.*, **45**, 896 (1966).
10) E. Merz, *Nukleonik*, **8**, 248 (1966).
11) M. H. Yang, H. Kudo, and K. Yoshihara, *Radiochim. Acta*, **14**, 52 (1970).
12) M. H. Yang, K. Yoshihara, and N. Shibata, *ibid.*, **14**, 16 (1970).
13) J. M. Robertson, *J. Chem. Soc.*, **1935**, 615; **1936**, 1195; **1937**, 219.
14) A. A. Ebert, Jr., and H. B. Gottlieb, *J. Amer. Chem. Soc.*, **74**, 2806 (1952).
15) D. N. Kendall, *Anal. Chem.*, **25**, 382 (1953).
16) A. N. Sidorov and I. P. Kotlyar, *Opt. i. Spektroskopiya*, **11**, 175 (1961).
17) J. M. Assur, *J. Phys. Chem.*, **69**, 2295 (1965).
18) B. I. Knudsen, *Acta Chem. Scand.*, **20**, 1344 (1966).
19) B. Honigmann, *J. Paint Tech.*, **38**, 77 (1966).
20) K. Bansho, S. Suzuki, T. Sekiguchi, and I. Saito, *Kogyo Kagaku Zasshi*, **65**, 2005 (1962).
21) T. Sekiguchi, K. Bansho, and O. Kaneko, *ibid.*, **70**, 499 (1967).
22) J. H. Beynon and A. R. Humphries, *Trans. Faraday Soc.*, **51**, 1065 (1955).
23) E. Suito and N. Ueda, *Kolloid Zh.*, **193**, 97 (1963).
24) J. H. Sharp and R. L. Miller, *J. Phys. Chem.*, **72**, 3335 (1968).
25) V. C. Hamann and H. Wagner, *Z. Anorg. Allgem. Chem.*, **373**, 18 (1970).
26) F. H. Moser and A. L. Thomas, "Phthalocyanine Compounds," Reinhold Publishing Corp., New York (1963).
27) A. B. P. Lever, "Advances in Inorganic Chemistry and Radiochemistry," Vol. 7, Academic Press, New York (1965), p. 27.
28) A. G. Maddock and R. Wolfgang, "Nuclear Chemistry," Vol. II, ed. by L. Yaffe, Academic Press, New York (1968), p. 186.

Irradiation. The neutron irradiation of copper Phthalocyanine was performed at the temperature of dry ice (−78°C) for 10 sec by means of a pneumatic tube in the nuclear reactor, JRR-2, of the Japan Atomic Energy Research Institute. The thermal neutron flux at the irradiation position was 5.5×10^{13} n/cm²/sec, and the γ-ray dose rate was about 10^8 R/hr.

Chemical Separation and Radioactivity Measurements. The analytical technique consisted of the dissolution of the target and the separation of the radioactive products by a method described in the literature.[9] After irradiation, the target was dissolved in cold sulfuric acid (<0°C). The solution was slowly poured into a mixture of ice and water to prevent any exchange reaction provoked by a sudden rise of the temperature. The precipitate of copper phthalocyanine was filtered out, and the radioactivity of ^{64}Cu both in the precipitate and in the filtrate was measured by a Baird Atomic single-channel γ-ray spectrometer connected to the NaI(Tl) crystal (well type, 1.75″$\phi\times$2″).

Thermal Annealing. The irradiated sample was heated in a constant-boiling bath with an accuracy of ±0.5°C (<200°C) or in an electric furnace with its temperature controlled within ±1% (>200°C). No thermal decomposition in a gross amount was observed at any temperature.

Results and Discussion

Figure 1 shows the carefully observed isothermal annealing curves of ^{64}Cu recoil atoms in neutron-irradiated α-copper phthalocyanine. As has been described in Ref. 9, the annealable portion in Stage I (below 200°C) is very small, so the State-II process (above 250°C) appears predominant in this system. One can find anomalies in the annealing curves. The isothermal annealing curve of Stage II has an inflection point which moves to the left on the time axis with an increase in its temperature.

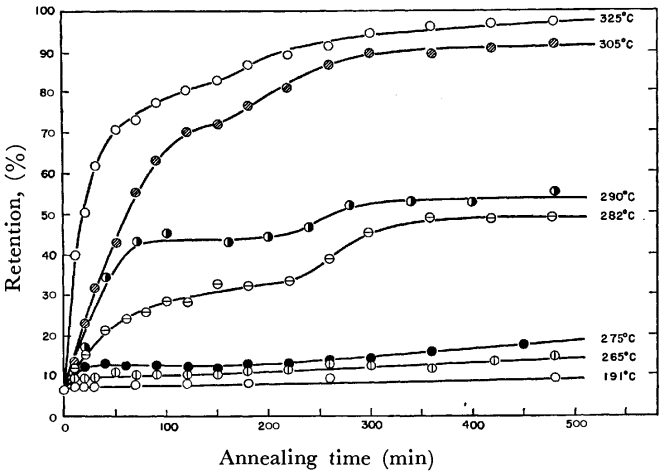

Fig. 1. Isothermal annealing curves of ^{64}Cu recoil atoms in the neutron irradiated α-copper phthalocyanine.

Figure 2 illustrates the isothermal annealing curves of β-copper phthalocyanine. The neutron irradiation and the thermal treatment were carried out under the same condition as those used for the α-crystal. Figure 2 clearly shows the difference between two annealing curves. The annealing process of the β-crystal shows a normal monotonous curve, whereas

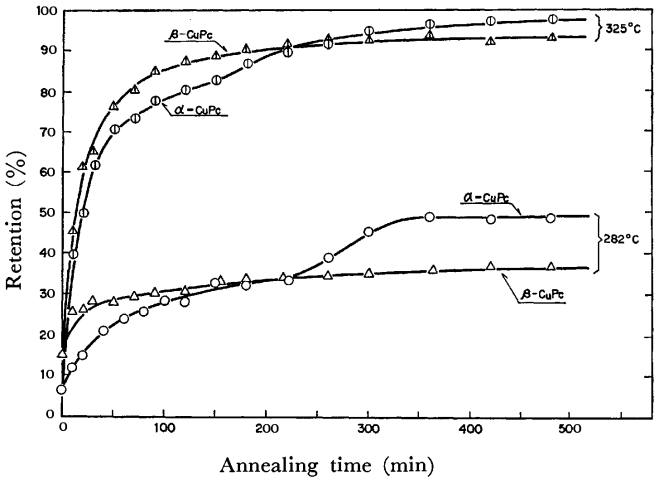

Fig. 2. Comparison of the isothermal annealing curves between α- and β-copper phthalocyanine.

the curve of the α-crystal is not so simple. It can also be pointed out that, although the rate of the annealing reaction of the α-crystal seems somewhat slower than that of the β-crystal at the beginning, the curve for the former reaches a plateau higher than that of the latter, showing a rapid rise around the inflection point. One may attribute these results to the superimposing effect of the crystal-structural transformation in the Stage-II annealing.

The annealing process of the α-crystal appears to consist of the "normal" monotonous annealing process and the "delayed" process which is to be ascribed to the structural transformation. An attempt was made to decompose the curve into two components by assuming that the normal annealing curve can be represented by the first-order rate law. Figure 3 presents two components of the isothermal annealing process of ^{64}Cu recoil atoms in α-copper phthalocyanine. The solid and dotted lines represent the normal annealing process (Component 1) and the other process (Component 2) respectively. Although the magnitude of the annealable portion is not large, the factors determining the features of the curve will hopefully supply

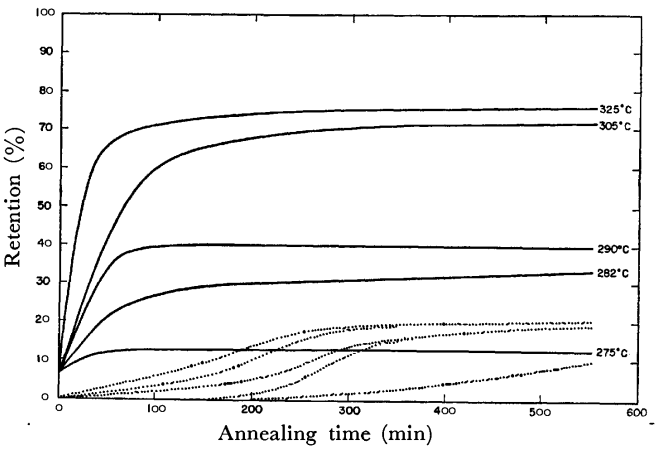

Fig. 3. Two components of the isothermal annealing process in α-copper phthalocyanine; the solid line is the "normal" process (the component 1) and the dotted line is the "delayed" process (the component 2).

information on the mechanism of the delayed annealing process.

A kinematic analysis was undertaken, with special attention being paid to the delayed annealing process. It was found that the following equations could explain all the features of the annealing reaction:

$$[R] = [C_1] + [C_2], \quad (1)$$

where: $$[C_1] = [A_1]\{1 - \exp(-k_0 t)\} \quad (2)$$

and $$[C_2] = [A_2]/\{1 + 1/a \exp(-kt)\}. \quad (3)$$

Here, [R] is the experimentally-observed value of retention; $[C_1]$, $[A_1]$, and k_0 are the retention, the annealable portion, and the rate constant associated with the normal annealing process; $[C_2]$, $[A_2]$, and k are the corresponding quantities of the other process, and a is a parameter. The mechanism proposed above is depicted schematically in Fig. 4, where k' is the rate constant of the structural transformation of α-copper phthalocyanine to the β-form.

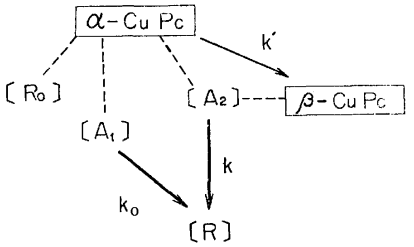

Eig. 4. The possible schematic explanation of annealing process in α-copper phthalocyanine.

As is illustrated in Fig. 5, the curve calculated by the use of Eq. (3) with appropriate values of the a parameter and the k rate constant can satisfactorily explain the delayed annealing reaction. Equation (3) has been derived in the sense of an autocatalytic reaction[29] by assuming that the crystal-structural transformation plays a catalytic role in the course of the delayed process. The parameter a in Eq. (3) determines the induction period, τ, of the delayed process and is closely related to the concentration ratio of the β-modification to the α-crystal in the target under heat treatment. The magnitude of the parameter a becomes smaller with a decrease in the temperature.

The slope of the linear part of the delayed annealing process depends principally on the value of k. The value of k estimated based on the proposed mechanism was found to be of the same order of magnitude as the value of k' associated with the structural transformation of α-copper phthalocyanine. This may indicate that the delayed process is evoked by the crystal-structural transformation.

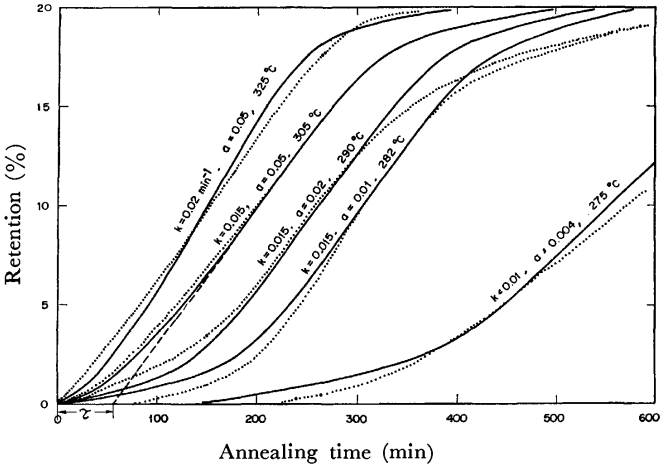

Fig. 5. The calculated curve of the delayed annealing process in α-copper phthalocyanine; the dotted line is the calculated curve and the solid line is the component 2 in Fig. 3.

It is known[30] that the nucleation of a β-particle in a pure α-crystal occurs in the earlier stage of the crystal-structural transformation. After nucleation has begun, the transformation enters the growth stage, the rate of which is controlled by the diffusion process. The electron-micrographic observation revealed that these processes were also involved in the α–β structural transformation of copper phthalocyanine.[31] Consequently, the delayed annealing reaction may be interpreted in terms of the spontaneous fluctuation of the matrix and the change in the crystalographic factors, such as the surface activity and the concentration of defects, due to the structural transformation. These factors probably play a triggering role in the delayed annealing reaction.

The author wishes to express his thanks to Professor T. Shiokawa and Dr. K. Yoshihara of Tohoku University and to Dr. H. Amano and Dr. H. Baba of the Japan Atomic Energy Research Institute for their useful suggestions and discussions throughout this study.

29) A. A. Frost and R. G. Pearson, "Kinetics and Mechanism", 2nd ed., John Wiley & Sons, Inc., New York, London (1961).

30) N. B. Hannay, "Solid-State Chemistry," Prentice-Hall, Inc., New Jersey (1967), p. 136.

31) The detailed observation of the crystal structural transformation of copper phthalocyanine by means of the electron microscope will be published elsewhere.

The Chemical Behavior of ^{64}Cu Recoil Atoms in the Mixed System of Copper Phthalocyanine and Metal-free Phthalocyanine

Hiroshi KUDO

Japan Atomic Energy Research Institute, Tokai-mura, Ibaraki-ken

(Received August 9, 1971)

In order to elucidate the effect of the crystal structure on the chemical behavior of ^{64}Cu recoil atoms in copper phthalocyanine, the author studied the mixed system of copper and metal-free phthalocyanine. It was found that the initial retention increased both in the mixed crystal and in the mixed-disk target. The addition of metal-free phthalocyanine sensitized the target to the thermal annealing reaction, and the rate of the reaction in the mixed crystal was faster than that in the unmixed crystal. The electron acceptor in the target was also found to increase the initial retention. The results were discussed in terms of the electrical properties of the target, which were changed by the change in the spatial arrangement of the molecules.

For the neutron-irradiated copper phthalocyanine, it has already been reported that the chemical consequence of ^{64}Cu recoil atoms depends greatly on the the crystal structure of the target.[1] The initial retention of the β-crystal yielded a higher value than that of the α-crystal. The results have been discussed in terms of the mobility of the recoil atom; *e.g.*, the channeling effect in the crystal depends upon the geometrical configuration of molecules. However, this does not seem the only possible explanation of the difference in the initial retentions in copper phthalocyanine. The intermolecular force and the physical properties of the crystal should inevitably change as the geometrical configuration of the molecules changes. In order to obtain further information leading to a solution of the problem, we studied the mixed system of copper and metal-free phthalocyanine.

Copper phthalocyanine, like other phthalocyanines, shows semiconductivity,[2-6] and the property of its crystal surface necessarily has a significant effect on the fate of the recoil atom. Metal-free phthalocyanine mixed with the target is expected to cause a change in the electrical properties of copper phthalocyanine.[7] It has also been reported[8] that magnesium phthalocyanine disks coated with a film of air-oxidized tetramethyl-*p*-phenylenediamine (TMPD) show a photovoltaic effect, while magnesium phthalocyanine alone exhibits no photovoltaic effect. The addition of chloranil to the surface of films of metal-free phthalocyanine has been found to produce charge carriers in the dark, to increase the quantum yield for the production of charge carriers in the light, and to increase the lifetime of the charge carrier.[9] Interest in the above facts has led to an investigation of the effect of the electron acceptor or the donor in the target.

Experimental

Materials. α-Copper phthalocyanine from Dainihon Ink and Chemicals was carefully purified by recrystallization from sulfuric acid. β-Copper phthalocyanine was obtained by suspending the α-crystal in benzene at 80°C for 2 hr. The α-crystal of metal-free phthalocyanine was prepared from cadmium phthalocyanine by demetallation in a sulfuric acid solution;[10] it was then sublimated *in vacuo* to obtain the β-crystal. The mixed crystal of copper and metal-free phthalocyanine (α-form) was prepared by dissolving appropriate quantities in concentrated sulfuric acid and by then pouring the solution into a large quantity of a mixture of ice and water.[7] The crystal modification of the target material was determined by means of a Philips Norelco X-ray diffractometer, using copper K_α radiation.

For the mixed-disk sample, appropriate quantities of copper and metal-free phthalocyanine were mixed in powder form and then pressed into disk ($\sim$50 mg/cm^2) under a pressure of 100 kg/cm^2. Chloranil from Dai-ichi Pure Chemicals was recrystallized from acetone. *N,N,N',N'*-Tetramethyl-*p*-phenylenediamine dihydrochloride (TMPD), a product of a guaranteed reagent grade from Tokyo Kasei, was used without further purification.

Irradiation. The neutron irradiation of the target was performed at the temperature of dry ice (−78°C) for 10 sec in the nuclear reactor, JRR-2 (thermal neutron flux ϕ_{th}: 5.2×10^{13} n/cm^2/sec) or for 30 sec in the JRR-3 (ϕ_{th}: 2.0×10^{13} n/cm^2/sec). The γ-ray dose rates of the reactors were 1.2×10^8 R/hr and 1×10^8 R/hr respectively.

Chemical Separation and Radioactivity Measurements. The analytical method used here was virtually identical with that described previously.[1] The irradiated target was dissolved in cold sulfuric acid (<0°C), and then the solution was poured into a mixture of ice and water. The precipitate of copper phthalocyanine was then filtered out. The radioactivity of ^{64}Cu in both the precipitate and the filtrate was measured by means of a Baird Atomic single-channel γ-ray spectrometer connected to a NaI(Tl) crystal (well type, 1.75″$\phi\times$2″).

Chloranil and the TMPD did not interfere with the course of the chemical separation.

Thermal Annealing. The irradiated mixed crystal was heated in a constant-boiling bath with an accuracy of ±0.5°C (<200°C) or in an electric furnace with the temperature

1) K. Yoshihara and H. Ebihara, *J. Chem. Phys.*, **45**, 896 (1966).
2) D. D. Eley, *Nature*, **162**, 819 (1948).
3) A. T. Vartanyan, *Zhur. Fiz. Khim.*, **22**, 769 (1948).
4) C. J. Hoffman, *Quart. Rev.*, **18**, 113 (1964).
5) F. H. Moser and A. L. Thomas, "Phthalocyanine Compounds", Reinhold, New York (1963).
6) A. B. P. Lever, "Advances in Inorganic Chemistry and Radiochemistry", Vol. 7, Academic Press, Inc., New York (1965) p. 27.
7) E. A. Lucia and F. D. Verderame, *J. Chem. Phys.*, **48**, 2674 (1968).
8) D. R. Kearns and M. Calvin, *ibid.*, **29**, 950 (1958).
9) D. R. Kearns, G. Tollin, and M. Calvin, *ibid.*, **32**, 1020 (1960).
10) H. Kudo and K. Yoshihara, *J. Inorg. Nucl. Chem.*, **32**, 2845 (1970).

controlled within ±1% (>200°C). No thermal decomposition in a gross amount was observed at any temperature.

Results

Prior to the study of the chemical behavior of the recoil atom in the mixed system of copper and metal-free phthalocyanine, the effect of pressing the crystal in the disk was examined. As is shown in Fig. 1, no discrepancy was observed between the untreated and the pressed targets. The initial retentions of both the pressed target and the untreated one were 5.5% for the α-crystal and 13.5% for the β-crystal.

Figure 2 shows the initial retention of the ^{64}Cu recoil atoms obtained in both the mixed crystal and the mixed disk of α-copper phthalocyanine as a function of the concentration of metal-free phthalocyanine

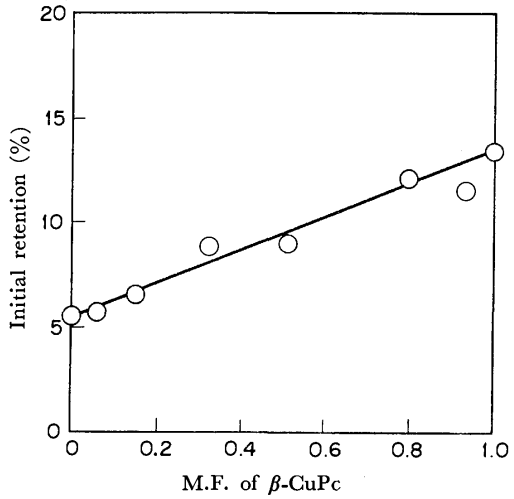

Fig. 1. The initial retention of ^{64}Cu recoil atoms in the mixed disk target of α- and β-copper phthalocyanine. (All samples were pressed under the pressure of 100 kg/cm².)

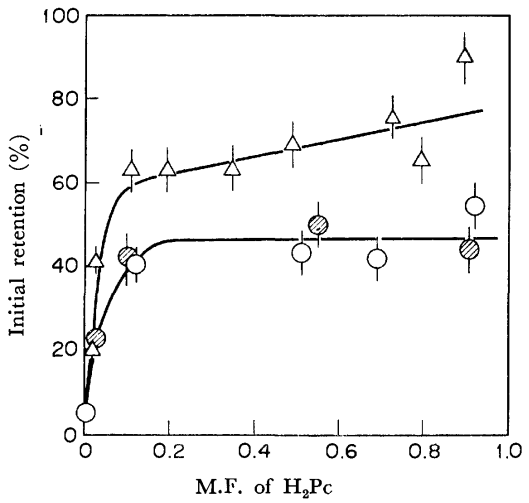

Fig. 2. The initial retention of ^{64}Cu recoil atoms in α-copper phthalocyanine (α-CuPc) mixed with metal-free phthalocyanine (H_2Pc): ○, the mixed crystal (α-form); ◍, the mixed disk with α-H_2Pc; △, the mixed disk with β-H_2Pc.

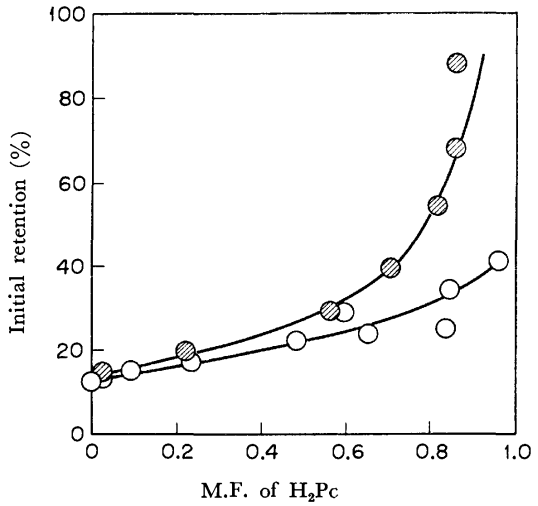

Fig. 3. The initial retention of ^{64}Cu recoil atoms in β-copper phthalocyanine mixed with metal-free phthalocyanine: ○, the mixed disk with α-H_2Pc; ◍, the mixed disk with β-H_2Pc.

in the target. Figure 3 shows the results for β-copper phthalocyanine. Although the shapes of the curves in these figures are not all the same, the initial retention increases in every case in which metal-free phthalocyanine is added. The mixture with the β-form of metal-free phthalocyanine shows a higher value than the mixture with the α-form of metal free phthalocyanine. This tendency is consistent with the finding that the initial retention for β-copper phthalocyanine is larger than that for the α-crystal.

A disk of α-copper phthalocyanine (100 mg/cm²) was irradiated in close contact with a disk of metal-free phthalocyanine in the fashion illustrated in Fig. 4. A disk of α-copper phthalocyanine was attached to a disk (100 mg/cm²) of metal-free phthalocyanine under pressure (Case (a)) or was pressed between two disks (50 mg/cm²) of metal-free phthalocyanine (Case (b)). The initial retentions obtained were 16.8±2.5% and 20.8±3% respectively. These values are clearly higher than those obtained in the unmixed α-crystal.

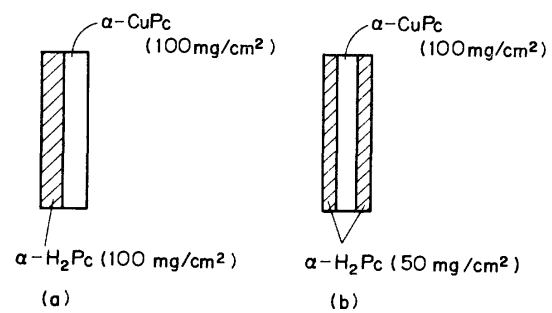

Fig. 4. The cross section of the contact disk target.

The thermal annealing process was studied for the mixed crystal. Figures 5 and 6 show the isothermal annealing curves of ^{64}Cu recoil atoms in the target which contain 0.04 M.F. and 0.53 M.F. of metal-free phthalocyanine respectively. In comparison

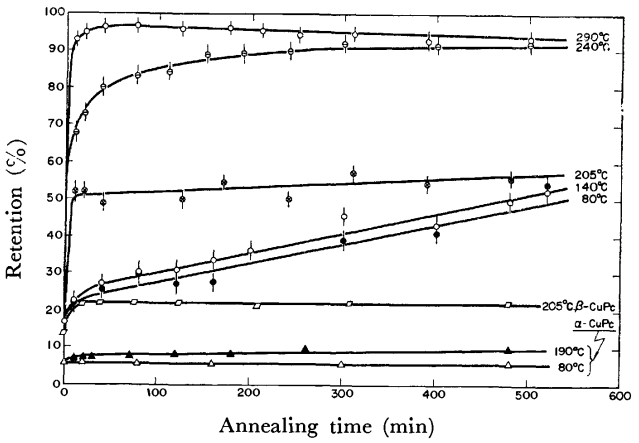

Fig. 5. The isothermal annealing curves for the mixed crystal which contains 0.04 M.F. of metal-free phthalocyanine.

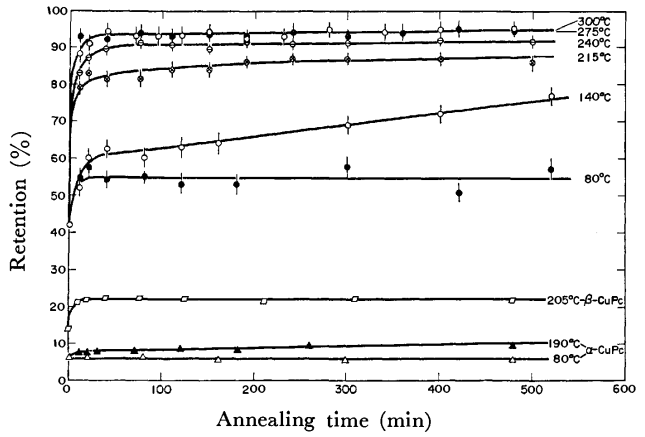

Fig. 6. The isothermal annealing curves for the mixed crystal which contains 0.53 M.F. of metal-free phtha o-cyanine.

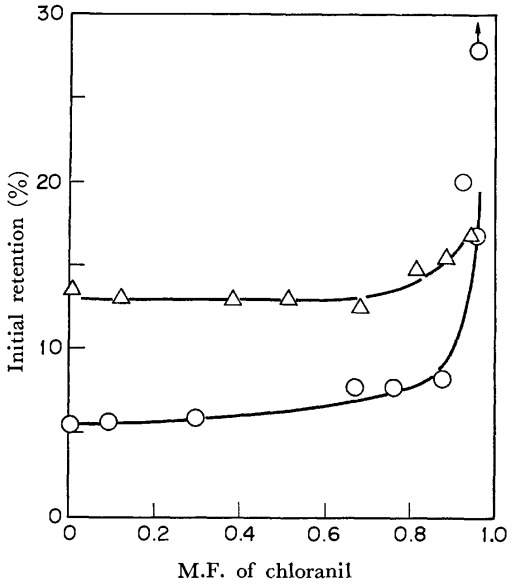

Fig. 7. The effect of chloranil added to copper phthalocyanine on the initial retention of ^{64}Cu recoil atoms. ○, α-crystal; △, β-crystal.

with the curves obtained for the unmixed α-crystal,[1,11] it is clear that, contrary to the case of the unmixed α-crystal, the reaction in the mixed crystal is completed below approximately 250°C. In contrast with the small annealable portion, ΔR, of Stage I (<200°C) in the unmixed crystal, the ΔR in the mixed crystal was very large, even below 200°C. As may be seen in Fig. 5, the retention at 80°C reached a higher value in the mixed crystal, whereas the thermal annealing reaction at the same temperature hardly proceeded at all in the unmixed α-crystal.

The addition of chloranil, as an electron acceptor, to the solid target of copper phthalocyanine was found to increase the initial retention of ^{64}Cu recoil atoms. The results are presented in Fig. 7. When the TMPD was added to the target as an electron donor, no effect on the initial retention was observed.

Discussion

The results presented in Fig. 2 are of great interest. The initial retention increases abruptly in the region of low concentrations of the added metal-free phthalycyanine, the value reaching a plateau in the region above 0.1 M.F. It can also be pointed out that the results obtained with the mixed-disk target of α-copper phthalocyanine with the α-crystal of metal-free phthalocyanine is virtually identical with that obtained in the mixed crystal.

Metal-free phthalocyanine should be distributed homogeneously in the lattice of the mixed crystal, so that it should be possible for the recoil atom to encounter the metal-free molecule in proportion to the concentration of metal-free phthalocyanine. If the recoil atom meets metal-free phthalocyanine in the course of its movement, it may enter the central position of the molecule, thus forming ^{64}Cu-phthalocyanine, since metal-free phthalocyanine has no central metal and two hydrogen atoms in the central space are easily replaced with divalent copper.[5,6] This should lead to an increase in the initial retention.

In the case of the mixed disk target, however, metal-free phthalocyanine may be expected to be mixed rather heterogeneously with copper phthalocyanine. The size of each particle is estimated to be of the order 0.1 μ. Considering the maximum recoil range of ^{64}Cu recoil atoms produced by the ^{63}Cu(n,γ)^{64}Cu reaction in copper phthalocyanine (the order of some tens of Å), it is less probable that the recoil atom interacts directly with metal-free phthalocyanine. Nevertheless, similar results were obtained in the mixed crystal and in the mixed-disk target. From these results, it seems reasonable that metal-free phthalocyanine added to the target indirectly affects the course of the determination of the chemical fate of the recoil atom. The indirect contribution of metal-free phthalocyanine may be supported further by the fact that the initial retention increases when the disk of α-copper phthalocyanine is irradiated in contact with the disk of metal-free phthalocyanine. On the basis of these data, it is possible to say that

11) H. Kudo, This Bulletin, **45**, 389 (1972).

the chemical consequence of the recoil atom strongly depends either on the physical properties of the crystal or on the reaction taking place in the neighborhood of the crystal surface.

As is shown in Figs. 5 and 6, the addition of metal-free phthalocyanine sensitizes the target to the thermal annealing reaction; the annealable portion, ΔR, of Stage I increases remarkably. This may be explained in the same manner as the increase of the initial retention, by assuming that the Stage-I annealing process reflects the initial recoil reaction.[1,12] It is also instructive to note that the rate of the thermal annealing reaction in the mixed crystal, especially at 205°C in the target containing 0.04 M.F. of metal-free phthalocyanine, is faster than that of the unmixed α-crystal. The faster rate of the reaction may be attrubuted to the reaction of the recoil atom at the crystal surface.

Thus, the property of the crystal surface of the phthalocyanine complex may be supposed to play a significant role in determining the chemical behavior of the recoil atom. This is also supported by the results presented in Fig. 7. The addition of chloranil as an electron acceptor to the copper phthalocyanine disk was found to increase the initial retention, although the TMPD, an electron donor, did not appear to affect the initial retention. The results indicate that an electron transfer from copper phthalocyanine to chloranil may have a strong effect on the behavior of the recoil atom.

The conductivity of the α-crystal of metal-free phthalocyanine has been reported[13,14] to be approximately ten times, in special cases more nearly 10^5 times, greater than that of the β-crystal. The values of the energy intervals, based on the band-theory model, of the β-crystals of several metal phthalocyanines lie between 1.5 and 1.7 eV.[15] A much lower value, 0.5 eV, has been reported for the energy interval of the α-crystal.[14] The charge transport in the complex has been explained by an out-of-plane interaction of π-electrons of the conjugated ring structure of the phthalocyanine with the antibonding orbitals of nitrogen atoms in the molecules above and below it.[16] Since the interaction takes place at the distance of the nearest approach of adjacent molecules, the molecular dimensions and the arrangement are important factors in determining the electrical conductivity in the solid. That is, the change in the spatial arrangement of molecules causes a change in the electrical properties of the target and may affect the chemical behavior of the recoil atom in the target.

In the present study of the chemical behavior of ^{64}Cu recoil atoms in the mixed system of copper and metal-free phthalocyanine, the electrical property of the target was suggested to be one of the most significant factors, although it is difficult to conclude at present what parameter of the electrical properties plays a role in determining the chemical fate of the recoil atom. As was mentioned in the last paragraph, the electrical property depends on the spatial arrangement of the molecules. This may lead to an understanding of the crystal-structure dependence of the initial retention in copper phthalocyanine. That is, the channeling effect and also the electrical property of the target might be factors which determine the chemical behavior of the recoil atom.

The author wishes to express his thanks to Professor T. Shiokawa and Dr. K. Yoshihara of Tohoku University for their kind guidance throughout this study. He also wishes to thank Dr. H. Amano and Dr. H. Baba of the Japan Atomic Energy Research Institute for their useful suggestions and discussions.

12) M. H. Yang, *Radiochim. Acta*, **12**, 167 (1969).
13) D. D. Eley and G. D. Parfitt, *Trans. Faraday Soc.*, **51**, 1529 (1955).
14) K, Wihksne and A. E. Newkirk, *J. Chem. Phys.*, **34**, 2184 (1961).
15) D. D. Eley, *Research*, **12**, 293 (1959).
16) G. H. Heilmeir and S. E. Harrison, *Phys. Rev.*, **132**, 2010 (1963).

Calculation of Optical Rotational Strength by Means of Various Types of Molecular Orbitals

Akira IMAMURA, Tsuneo HIRANO,* Chikayoshi NAGATA, and Teiji TSURUTA*

Biophysics Division, National Cancer Center Research Institute, Chuo-ku, Tokyo

**Department of Synthetic Chemistry, Faculty of Engineering, University of Tokyo, Bunkyo-ku, Tokyo*

(Received July 26, 1971)

The optical rotational strengths of the methyl derivatives of cyclohexanone were calculated by means of various types of molecular orbitals, which were converted from those used in the CNDO/2 method. One of them is represented as a Sla ter-basis atomic orbital transformed from molecular orbitals on a CNDO basis by using the overlap matrix. Another was obtained only by modifying the normalization coefficient of the molecular orbitals. From the results, the two-center matrix elements in the calculation of rotational strengths was found to be not negligible, hence, the above-mentioned transformation was indicated to be indispensable. Good agreement with the experimental results was found for the transformed molecular orbitals, especially for those with a modification of the normalization coefficient. The theoretical grounds for these transformations are discussed. The formulae for the matrix elements of the gradient operator which are necessary for the calculation of the rotational strength are given in the appendix.

Recently, several studies of the calculation of the rotational strength by means of molecular orbital theories have been published. Pao and Santry first calculated the rotational strength of methyl-substituted cyclohexanones by the CNDO method,[1] neglecting all the two-center matrix elements.[2] Although only a few experimental data are available, the calculated values agree fairly well with the experimental results. On the other hand, the extended Hückel method[3] was applied to the same molecule, without neglecting the two-center matrix element, by Gould and Hoffmann.[4] Their results seem to be slightly too large.[5] They also calculated the rotational strength of the skewed butadiene chromophore by Pariser-Parr-Pople π-electron-only SCF calculation, with configuration interaction in order to emphasize the importance of the configurational mixing. The rotational strength of the skewed glyoxal at various rotational angles was also calculated[6] by the extended Hückel and CNDO methods, with and without configuration interactions, and with and without the inclusion of two-center matrix elements. This gives the correct sign of the rotational strength for the various α-diketones which were substituted for the skewed glyoxal as a model compound. However, the absolute value of the rotational strength depends remarkably upon the approximations used, that is, whether it is the extended Hückel method or the CNDO method, with or without configuration mixings, and with or without inclusion of two-center integrals. Similar calculations using the Pariser-Parr-Pople method were carried out for skewed butadiene and acrolein by Cheong *et al.*[7] For more complex molecules, the coupled oscillator theory[8] or the method of the composite molecule[9] was employed to find good agreement with the experimental results.

Although the molecular orbital approach to the calculation of the rotational strength is significantly used at present, the quantitative agreement between the calculated and observed values is not always satisfactory. In connection with this, various approximations used in the above calculation should be investigated. For example, the extended Hückel method includes all the overlap integrals; hence, the inclusion of the two-center integrals used for the calculation of the rotational strength is consistent with the approximation of the extended Hückel method However, as is well known, this method is not appropriate for the calculation of polar molecules because of the neglect of the electron-electron repulsion terms. On the other hand, the CNDO method can be expected to give a reasonable wave function for polar molecules, while the inclusion of two-center integrals for the rotational strength is in conflict with the complete neglect of the differential overlap.

In the present investigation, the rotational strength for a few methyl derivatives of cyclohexanone for which experimental data are available were calculated in the CNDO/2 method.[1] The molecular orbital obtained by means of the CNDO/2 method was transformed to that of the Slater-basis set in order to overcome the conflict between the inclusion of two-center integrals in the calculation of the rotational strength and the complete neglect of the differential overlap. The procedure used for the transformation of the molecular orbital from the CNDO basis to the Slater basis will be described in detail in the following section. The rotational strengths thus calculated are in good agreement with the experimental data. The

1) J. A. Pople, D. P. Santry, and G. A. Segal, *J. Chem. Phys.*, **43**, s129 (1965); J. A. Pople and G. A. Segal, *ibid.*, **43**, s136 (1965); J. A. Pople and G. A. Segal, *ibid.*, **44**, 3289 (1966).

2) Yoh-han Pao and D. P. Santry, *J. Amer. Chem. Soc.*, **88**, 4157 (1966).

3) R. Hoffmann, *J. Chem. Phys.*, **39**, 1397 (1963).

4) R. R. Gould and R. Hoffmann, *J. Amer. Chem. Soc.*, **92**, 1813 (1970).

5) In Eq. (6) of Ref. 4, the factor of two is missing on the right side of the equation (private communication). Therefore, the calculated values in Table 1 should be multiplied by two, leading to a slightly large calculated value in comparison with the experimental value.

6) W. Hug and G. Wagniere, *Theor. Chim. Acta*, **18**, 57 (1970).

7) Kam-Khow Cheong, A. Oshita, D. J. Caldwell, and H. Eyring, *Proc. Nat. Acad. Sci. USA*, **67**, 1727 (1970).

8) W. H. Inskeep, D. W. Miles, and H. Eyring, *J. Amer. Chem. Soc.*, **92**, 3866 (1970).

9) S. Hagishita and K. Kuriyama, This Bulletin, **44**, 617 (1971).

difference between the rotational strengths calculated as the CNDO basis and as the Slater basis will be considered in connection with the nature of the atomic basis used in the molecular orbital. Moreover, theoretical grounds for the transformation of the molecular orbitals will be discussed.

Method

Molecular Orbitals. The molecular orbitals employed for the calculation of the rotational strengths were calculated by the CNDO/2 method.[1] The parameters included in the method were the same as those proposed by Pople *et al.*[1] The molecular orbitals thus obtained were transformed to those on the Slater basis in the following way: the molecular orbitals on the CNDO basis were assumed to be represented by the orthogonalized atomic basis defined by Löwdin;[10] hence, the atomic orbitals on the CNDO basis can be represented as an appropriate linear combination of Slater-type atomic orbitals effected by the transformation, so that the atomic orbitals on the CNDO basis are orthogonal with each other. The reverse transformation was already carried out by Pople *et al.* in order to compare the results obtained by the use of the CNDO method with those obtained by the use of the non-empirical method.[1] By making use of Pople's notation, the Slater basis set of atomic orbitals, ϕ', is given as;

$$\phi' = \phi S^{1/2} \tag{1}$$

where ϕ is the CNDO-basis set of atomic orbitals and where S is the overlap matrix calculated by use of the Slater-type atomic orbitals.

Another conversion of molecular orbitals was carried out as the assumption that the ratio of the coefficient in a given molecular orbital remains unaltered, while the corresponding normalizing coefficient of the molecular orbital was calculated including the overlap integrals, which were obtained as if the atomic orbital on the CNDO basis were a Slater-type atomic orbital. Therefore, the new coefficient of the atomic orbital can be obtained by dividing the old one by the normalizing coefficient. For occupied orbitals, the new coefficient is usually less in magnitude than the old one because of the bonding character of the orbitals, but the reverse is true for vacant orbitals because of their antibonding character. The physical meanings of these transformations are given below, along with the results calculated for the rotational strength.

Calculation of the Optical Rotational Strength. The optical rotational strength of the molecule, **R**, can be calculated as follows[11]

$$\mathbf{R} = Im\{\langle\Psi_o|\boldsymbol{\mu}|\Psi_e\rangle\cdot\langle\Psi_e|\mathbf{m}|\Psi_o\rangle\} \tag{2}$$

where Ψ_o and Ψ_e are wave functions of the ground and the excited states respectively, and where $\boldsymbol{\mu}$ and **m** are the electric and magnetic moment vectors respectively. In order to avoid the origin dependence of the rotational strength,[12] the matrix element of the electric dipole moment is converted into the dipole velocity formalism, as has already been done by Hoffmann *et al.*,[4]

$$\langle\psi_i|\mathbf{r}|\psi_j\rangle = \frac{\hbar^2}{m}\langle\psi_i|\nabla|\psi_j\rangle/(E_j - E_i) \tag{3}$$

where ψ_i denotes an i-th molecular orbital, and E_i, its energy. By making use of Eqs. (2) and (3), the reduced rotational strength, $[R_{ij}]$, for the $i\rightarrow j$ transition, in which an electron in the i-th molecular orbital is excited to the j-th molecular orbital, is given by Eq. (4);

$$[R_{ij}] = \frac{-7313}{E_j - E_i}\langle\psi_i|\nabla|\psi_j\rangle\cdot\langle\psi_j|\mathbf{r}\times\nabla|\psi_i\rangle, \tag{4}$$

where energy is represented in eV units, and the gradient operator, in Å units. In the LCAO MO approximation, the matrix element included in Eq. (4) can be expanded into those between atomic orbitals. Therefore,

$$\langle\psi_i|\nabla|\psi_j\rangle = \sum_r\sum_s C_{ir}C_{js}\langle\chi_r|\nabla|\chi_s\rangle, \tag{5}$$

$$\langle\psi_j|\mathbf{r}\times\nabla|\psi_i\rangle = \sum_r\sum_s C_{jr}C_{is}\langle\chi_r|\mathbf{r}\times\nabla|\chi_s\rangle, \tag{6}$$

where the molecular orbital, ψ_i, is represented as in Eq. (7), using the atomic orbital χ_r:

$$\psi_i = \sum_r C_{ir}\chi_r. \tag{7}$$

Calculation of the Matrix Element between Atomic Orbitals. The problem now is to calculate the matrix elements between atomic orbitals. One-center integrals will be considered first. The one-center integrals necessary for the calculation are the gradient and the magnetic moment integrals. These integrals have already been given in a previous paper;[2] hence, only the results will be indicated in this paper, with slight modifications. For a gradient operator, the following equations are obtained by using Slater-type atomic orbitals;

$$\int\chi_{2s}\nabla_x\chi_{2px}d\tau = -\int\chi_{2px}\nabla_x\chi_{2s}d\tau = \frac{1}{\sqrt{3}\,a_0}\frac{(\delta_1\delta_2)^{5/2}}{(\delta_1+\delta_2)}(24\delta_1 - 8\delta_2) \tag{8}$$

where a_0 is the Bohr radius and where:

$$\chi_{2s} = \frac{1}{\sqrt{3\pi}}\left(\frac{\delta_1}{a_0}\right)^{5/2} r\exp\left(-\frac{\delta_1}{a_0}r\right), \tag{9}$$

$$\chi_{2px} = \frac{1}{\sqrt{\pi}}\left(\frac{\delta_2}{a_0}\right)^{5/2} x\exp\left(-\frac{\delta_2}{a_0}r\right). \tag{10}$$

If the $2s$ and $2p$ orbitals have the same Slater exponent, Eq. (8) becomes simpler (Eq. (11)):

$$\int\chi_{2s}\nabla_x\chi_{2px}d\tau = -\int\chi_{2px}\nabla_x\chi_{2s}d\tau = \frac{\delta}{2\sqrt{3}\,a_0}, \quad (\delta=\delta_1=\delta_2). \tag{11}$$

It is apparent that the same formulae are given for the matrix elements between $2s$ and $2py$ or $2pz$ atomic orbitals and that the matrix elements between $2p$ orbitals and those between $1s$ orbitals should vanish because of their symmetrical properties. It should be mentioned that when the matrix element is re-

10) P. O. Löwdin, *J. Chem. Phys.*, **18**, 365 (1950).
11) L. Rosenfeld, *Z. Phys.*, **52**, 161 (1928).
12) A. Moscowitz, "Modern Quantum Chemistry," Vol. 3, ed. by O. Sinanoğlu, Academic Press, New York (1965), p. 31.

presented in atomic units, a_0 (Bohr radius) in the denominator of Eqs. (8) and (11) is unnecessary.

The one-center matrix elements for the magnetic-moment operator can be rewritten as follows:

$$\int \chi_r(\mathbf{r}\times\nabla)\chi_s d\tau = \mathbf{R}_A \times \int \chi_r \nabla \chi_s d\tau + \int \chi_r(\mathbf{r}_A\times\nabla)\chi_s d\tau, \tag{12}$$

where $\mathbf{R}_A$ is the position vector of the atom, A, to which the χ_r and χ_s atomic orbitals belong, and where $\mathbf{r}_A\times\nabla$ is the magnetic moment operator on the A atom. The second term of the right-hand side of Eq. (12) can be calculated by using the following equations:

$$\left.\begin{aligned}
&(\mathbf{r}_A\times\nabla)\chi_{1s}=0\\
&(\mathbf{r}_A\times\nabla)\chi_{2s}=0\\
&(\mathbf{r}_A\times\nabla)\chi_{2px} = \mathbf{j}\chi_{2pz} - \mathbf{k}\chi_{2py}\\
&(\mathbf{r}_A\times\nabla)\chi_{2py} = \mathbf{k}\chi_{2px} - \mathbf{i}\chi_{2pz}\\
&(\mathbf{r}_A\times\nabla)\chi_{2pz} = \mathbf{i}\chi_{2py} - \mathbf{j}\chi_{2px}
\end{aligned}\right\}, \tag{13}$$

where **i**, **j**, and **k** are the unit vectors in the x, y, and z directions. By combining Eq. (12) with Eq. (13) and Eq. (8) or Eq. (11), all kinds of one-center matrix elements for the magnetic-dipole operator can easily be calculated.

The two-center integrals will be considered next. For the calculation of the two-center matrix elements for the gradient operator, two atoms are assumed to be located on the local coordinate Z axis at the distance of R from one another, as is shown in Fig. 1.

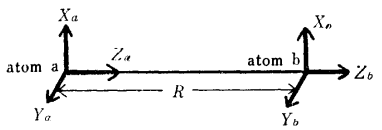

Fig. 1. Local coordinate system.

Then, the matrix elements between the two atomic orbitals on each atom are classified for calculation into several groups according to their symmetrical character, that is, the σ and π characteristics along the Z axis for the atomic orbitals and the gradient operator. The calculation of these matrix elements is followed by the transformation of the coordinate to obtain the matrix element between the atomic orbitals whose coordinates, x, y, and z are defined in the whole molecule. The formulae for the transformation have already been given in the paper by Suzuki *et al.*[13] In Table 1, the equations for the transformation are given; they can be applied by making use of the direction cosines of the local Z-axis with respect to the x, y, z-coordinate system. The two-center gradient matrix elements in the local coordinate can be calculated by using the prolate spheroidal coordinate system, as has already been done by Ehrenson and Phillipson.[14] In this paper, the formulae, which will be given in the appendix, are represented in terms of A and B functions, which are the auxiliary functions frequently used for the calculation of the overlap integrals.[15]

For the calculation of the two-center matrix elements for the magnetic moment operator, the displacement of the origin of the coordinate is necessary, as is shown in the following equation:

$$\int \chi_r(\mathbf{r}\times\nabla)\chi_s d\tau = \mathbf{R}_A \times \int \chi_r \nabla \chi_s d\tau + \int \chi_r(\mathbf{r}_A\times\nabla)\chi_s d\tau \tag{14}$$

where $\mathbf{R}_A$ is the position vector of the atom, A, to which the atomic orbital, χ_s, belongs, and where $\mathbf{r}_A\times\nabla$ is the operator centered on the A atom. The first term of Eq. (14) is easily obtained, since the values of the matrix element for the gradient operator have been calculated in the preceeding step. The second term converts to the calculation of the overlap integrals for p orbitals, but vanishes for s orbitals, according to Eq. (13).

The matrix elements between atomic orbitals thus calculated are substituted into Eqs. (5) and (6) to obtain the rotational strength of the molecules. In order to check the numerical values of these matrix elements, the following equations, which are valid for both the one-center and two-center integrals, should be useful:

$$\int \chi_r \nabla_k \chi_s d\tau = -\int \chi_s \nabla_k \chi_r d\tau \tag{15}$$

TABLE 1. FORMULAE FOR THE TRANSFORMATION OF TWO-CENTER GRADIENT INTEGRALS

$(s|\nabla_i|s) = \gamma_i(S|\nabla_Z|S)$
$(s|\nabla_i|p_i) = \gamma_i^2(S|\nabla_Z|P_Z) + (1-\gamma_i^2)(S|\nabla_X|P_X)$
$(p_i|\nabla_i|s) = \gamma_i^2(P_Z|\nabla_Z|S) + (1-\gamma_i^2)(P_X|\nabla_X|S)$
$(s|\nabla_i|p_j) = \gamma_i\gamma_j\{(S|\nabla_Z|P_Z) - (S|\nabla_X|P_X)\}$
$(p_j|\nabla_i|s) = \gamma_i\gamma_j\{(P_Z|\nabla_Z|S) - (P_X|\nabla_X|S)\}$
$(p_i|\nabla_i|p_i) = \gamma_i[\gamma_i^2(P_Z|\nabla_Z|P_Z) + (1-\gamma_i^2)\{(P_Z|\nabla_X|P_X) + (P_X|\nabla_Z|P_X) + (P_X|\nabla_X|P_Z)\}]$
$(p_i|\nabla_j|p_j) = \gamma_i[(1-\gamma_j^2)(P_Z|\nabla_X|P_X) + \gamma_j^2\{(P_Z|\nabla_Z|P_Z) - (P_X|\nabla_Z|P_X) - (P_X|\nabla_X|P_Z)\}]$
$(p_i|\nabla_j|p_i) = \gamma_j[(1-\gamma_i^2)(P_X|\nabla_Z|P_X) + \gamma_i^2\{(P_Z|\nabla_Z|P_Z) - (P_Z|\nabla_X|P_X) - (P_X|\nabla_X|P_Z)\}]$
$(p_i|\nabla_i|p_j) = \gamma_j[(1-\gamma_i^2)(P_X|\nabla_X|P_Z) + \gamma_i^2\{(P_Z|\nabla_Z|P_Z) - (P_Z|\nabla_X|P_X) - (P_X|\nabla_Z|P_X)\}]$
$(p_i|\nabla_j|p_k) = \gamma_i\gamma_j\gamma_k\{(P_Z|\nabla_Z|P_Z) - (P_Z|\nabla_X|P_X) - (P_X|\nabla_Z|P_X) - (P_X|\nabla_X|P_Z)\}$

i or j or k denotes one of x or y or z. Small letter indicates the atomic orbitals defined in the coordinate of the whole molecule, and large letter the local coordinate in which the Z axis coincides with the line combining two atoms (Fig. 1). γ_i is the direction cosine of the Z axis with respect to the coordinate system x, y and z defined in molecule.

13) M. Suzuki, Y. Nihei, and H. Kamada, This Bulletin, **42**, 323 (1969).
14) S. Ehrenson and P. E. Phillipson, *J. Chem. Phys.*, **34**, 1224 (1961).
15) R. S. Mulliken, C. A. Rieke, D. Orloff, and H. Orloff, *J. Chem. Phys.*, **17**, 1248 (1949).

$$\int \chi_r(\mathbf{r}\times\nabla)_k\chi_s d\tau = -\int \chi_s(\mathbf{r}\times\nabla)_k\chi_r d\tau, \quad (16)$$

where k denotes either the x, y, or z component of the operator. These equations can easily be proved by using integration by parts. Therefore, Eqs. (17) and (18) can also be obtained:

$$\langle\psi_i|\nabla_k|\psi_j\rangle = -\langle\psi_j|\nabla_k|\psi_i\rangle \quad (17)$$

$$\langle\psi_i|(\mathbf{r}\times\nabla)_k|\psi_j\rangle = -\langle\psi_j|(\mathbf{r}\times\nabla)_k|\psi_i\rangle. \quad (18)$$

In our test calculation, the numerical values for the matrix elements were checked against those in Ref. 6, where the numerical values of the z component of the magnetic moment operator of glyoxal are given together with the coordinates of the atoms. It was also confirmed that the rotational strength thus calculated does not vary with the transformation of the coordinate and the displacement of the origin of the coordinate.

Results and Discussion

In Table 2, the calculated rotational strengths of the methyl derivatives are listed for various methods, together with the experimental values. The coordinates of the atoms used for the calculation are the same as those in Ref. 2. By any method, fairly good agreement with the experimental values is found. However, the calculations with only one-center integrals give too large values for 7-, 13-dimethyl cyclohexanone. In other words, the neglect of the two-center integrals results in a large effect on the value of the rotational strength. Therefore, it should be concluded that the rotational strength has to be calculated by the inclusion of two-center integrals, even in the CNDO method.

Theoretically speaking, the molecular orbital employed for the calculation of the rotational strengths including the two-center matrix elements should not be the molecular orbital calculated in the approximation of the complete neglect of the differential overlap, that is, by the CNDO method. In order to overcome this difficulty, the molecular orbitals obtained by the CNDO method were converted to those on the Slater basis or those with a modification of the normalization coefficient described in the previous section. The bonding parameters, β, in the CNDO method were originally determined by corresponding the non-empirically calculated molecular orbitals with those on the Slater basis, which were converted from those on the CNDO basis for diatomic molecules.[1] In this sense, the molecular orbitals on the Slater basis by the CNDO method seem to be appropriate for the calculation of the rotational strength by procedure including two-center matrix elements. However, it should be emphasized that the atomic orbital on the CNDO basis should have a considerable mixing of Slater-type atomic orbitals other than that of the atom considered if the atomic orbital on the CNDO basis is assumed to be the orthogonalized atomic orbital proposed by Löwdin and if the overlap integrals between Slater-type atomic orbitals are relatively large. On the other hand, the bonding parameters are appropriate for diatomic molecules. Therefore, the Slater-type atomic orbitals converted from those on the CNDO basis may not correspond to the Slater-type atomic orbitals used in non-empirical calculations for large molecules. This may be the reason why the rotational strengths calculated by using the molecular orbital on the Slater basis are slightly different from the experimental values.

Table 2. Rotational strengths of methyl derivatives of cyclohexanone for n-π^* transition[a)]

Method \ Molecule		7-, 13- CH_3 cyclohexanone	7-, 8-, 13- CH_3 cyclohexanone
CNDO basis	total	+1.65	+7.26
	one-center[b)]	+4.95	+3.64
Slater basis	total	+4.10	+5.28
	one-center[b)]	+11.44	+5.77
CNDO normalized[c)]	total	+1.95	+8.63
	one-center[b)]	—	—
Experimental[16)]		+1.8	+6.7
Extended Hückel[4)]		+11.06	+12.72

a) The rotational strengths are calculated by using the value of 4 eV for the n-π^* excitation energy.
b) The rotational strength with the one-center matrix element only.
c) CNDO normalized is the method in which the molecular orbital is normalized by using overlap integrals.

Another approach to the calculation of rotational strengths is to use the molecular orbital in which the normalization coefficient is recalculated by including overlap integrals, while the ratio of the coefficients of atomic orbitals in a molecular orbital is assumed to be the same as that in the CNDO method, as has been mentioned in the previous section. Even in this method, there are some faults, one of which is the fact that the molecular orbitals in the CNDO method are calculated in an approximation and with a complete neglect of the differential overlap, contrary to the inclusion of overlap integrals in the recalculation of the normalization coefficient. This discrepancy can be overcome if the ratio of the coefficients of the atomic orbitals in a molecular orbital does not depend upon either the inclusion or neglect of the differential overlap in the CNDO calculation, which cannot be theoretically proved. Another fault included in this method is the non-orthogonality, that is, the molecular orbitals obtained by a modification of the normalization coefficient are usually not orthogonal with each other. However, if the molecular orbitals have different symmetries, even incompletely different ones, such as in the n-π^* transition in methylcyclohexanones, this orthogonality between molecular orbitals is approximately retained. Generally speaking, this non-orthogonal character may not have serious effects on the rotational strength, since the bonding character for occupied orbitals and the antibonding character for vacant orbitals give rise to relatively small overlap integrals between occupied and the vacant orbitals, although the contribution of this overlap term

16) H. Moffitt and A. Moscowitz, *J. Chem. Phys.*, **30**, 648 (1959).

may not be negligible in some cases. At any rate, as may be seen in Table 2, this molecular orbital with a modification of the normalization coefficient seems to give a remarkably good agreement with the experimental results.

In connection with the modification of the molecular orbitals in the CNDO method, we would like to mention that the calculation of the rotational strength with only a one-center matrix element is not always consistent with the approximation in the CNDO method, contrary to the discussion given in a previous paper.[2] The reason for this is that the atomic orbital on the CNDO basis, which can be considered to be the orthogonalized atomic orbital proposed by Löwdin, usually gives non-vanishing two-center matrix elements for the gradient and the magnetic moment operators, even if the corresponding overlap integral vanishes. This is probably supported by the fact that the rotational strengths with only one-center matrix elements calculated by the CNDO molecular orbital (first row of Table 2) are considerably different from those with both one- and two-center matrix elements calculated by the molecular orbitals on the Slater basis (third row of Table 2).

In conclusion, the rotational strengths calculated by the molecular orbitals in the CNDO method with a modification of the normalization coefficients have been found to be in excellent agreement with the experimental result. However, the validity of this treatment must be extensively investigated for various molecules, although the lack of the experimental values of the rotational strength makes it impossible to do so in the present investigation.

Numerical calculations were carried out on the HITAC 5020E Computation Center of the University of Tokyo and on the HITAC 8300 Computer at the National Cancer Center.

Appendix

Formulae of the two-center matrix elements for the gradient operator. As is shown in Fig. 1, the Z axis directs from the a atom to the b atom. R is the distance between a and b atoms in Å units, while P and t are given by the following equation:

$$P = \frac{R}{2a_0}(\delta_a+\delta_b) \tag{A-1}$$

$$t = \frac{\delta_a-\delta_b}{\delta_a+\delta_b} \tag{A-2}$$

where a_0 is the Bohr radius and where δ_a and δ_b are the Slater exponents of the two atomic orbitals, a and b. The auxiliary functions, A_k and B_k, are defined as usual:[15]

$$A_k(P) = \int_1^\infty x^k e^{-Px}dx \tag{A-3}$$

$$B_k(Pt) = \int_{-1}^1 x^k e^{-Ptx}dx. \tag{A-4}$$

The formulae of various types of matrix elements for the gradient operator are given below:

$$(1S_a|\nabla_Z|1S_b) = -\frac{P^4}{4R}(1-t^2)^{3/2}(1-t)$$
$$[A_2B_1+A_1(B_2-B_0)-A_0B_1]$$

$$(2S_a|\nabla_Z|1S_b) = -\frac{P^5}{8\sqrt{3}R}(1-t^2)^{5/2}$$
$$[A_3B_1+A_2(2B_2-B_0)+A_1(B_3-2B_1)-A_0B_2]$$

$$(1S_a|\nabla_Z|2S_b) = \frac{\delta_b}{8\sqrt{3}a_0}P^4(1-t^2)^{3/2}(1-t)$$
$$[-A_3B_1+A_2B_0+A_1B_3-A_0B_2]$$
$$+\frac{P^4}{4\sqrt{3}R}(1-t^2)^{3/2}(1-t)$$
$$[A_2B_1+A_1(B_2-B_0)-A_0B_1]$$

$$(2P_{Za}|\nabla_Z|1S_b) = -\frac{P^5}{8R}(1-t^2)^{5/2}[A_3B_2+A_2B_3$$
$$-A_1B_0-A_0B_1]$$

$$(1S_a|\nabla_Z|2P_{Zb}) = \frac{\delta_b}{4a_0}P^3(1-t^2)^{3/2}(A_2B_0-A_0B_2)$$
$$-\frac{P^5}{8R}(1-t^2)^{3/2}(1-t)^2[A_3B_2+A_2$$
$$\times(B_3-2B_1)+A_1(B_0-2B_2)+A_0B_1]$$

$$(2P_{Xa}|\nabla_X|1S_b) = -\frac{P^5}{16R}(1-t^2)^{5/2}[A_3(B_0-B_2)$$
$$+A_2(B_1-B_3)+A_1(B_2-B_0)+A_0(B_3-B_1)]$$

$$(1S_a|\nabla_X|2P_{Xa}) = \frac{\delta_b}{4a_0}P^3(1-t^2)^{3/2}(A_2B_0-A_0B_2)$$
$$-\frac{P^5}{16R}(1-t^2)^{3/2}(1-t)^2[A_3(B_0-B_2)$$
$$+A_2(B_1-B_3)+A_1(B_2-B_0)+A_0(B_3-B_1)]$$

$$(2S_a|\nabla_Z|2S_b) = \frac{\delta_b}{48a_0}P^5(1-t^2)^{5/2}[A_3(B_0-B_2)$$
$$+A_1(B_4-B_2)+B_1(A_2-A_4)+B_3(A_2-A_0)]$$
$$+\frac{P^5}{24R}(1-t^2)^{5/2}[A_3B_1+A_2(2B_2-B_0)$$
$$+A_1(B_3-2B_1)-A_0B_2]$$

$$(2P_{Za}|\nabla_Z|2S_b) = -\frac{\delta_b}{16\sqrt{3}a_0}P^5(1-t^2)^{5/2}$$
$$[B_2(A_0+A_4)-A_2(B_0+B_4)]$$
$$+\frac{P^5}{8\sqrt{3}R}(1-t^2)^{5/2}$$
$$\times[A_3B_2+A_2B_3-A_1B_0-A_0B_1]$$

$$(2S_a|\nabla_Z|2P_{Zb}) = \frac{\delta_b}{8\sqrt{3}a_0}P^4(1-t^2)^{3/2}(1+t)$$
$$(A_3B_0+A_2B_1-A_1B_2-A_0B_3)$$
$$-\frac{P^6}{16\sqrt{3}R}(1-t^2)^{5/2}(1-t)$$
$$\times[A_4B_2+2A_3(B_3-B_1)+A_2(B_4-4B_2+B_0)$$
$$+2A_1(B_1-B_3)+A_0B_2]$$

$$(2P_{Xa}|\nabla_X|2S_b) = -\frac{\delta_b}{32\sqrt{3}a_0}P^5(1-t^2)^{5/2}$$
$$\times[A_4(B_0-B_2)+A_2(B_4-B_0)+A_0(B_2-B_4)]$$
$$+\frac{P^5}{16\sqrt{3}R}(1-t^2)^{5/2}[A_3(B_0-B_2)$$
$$+A_2(B_1-B_3)+A_1(B_2-B_0)+A_0(B_3-B_1)]$$

$$(2S_a|\nabla_X|2P_{Xb}) = \frac{\delta_b}{8\sqrt{3}a_0}P^4(1-t^2)^{3/2}(1+t)$$
$$\times[A_3B_0+A_2B_1-A_1B_2-A_0B_3]$$
$$-\frac{\sqrt{3}P^6}{96R}(1-t^2)^{5/2}(1-t)$$
$$\times[A_4(B_0-B_2)+2A_3(B_1-B_3)$$
$$+A_2(2B_2-B_4-B_0)+2A_1(B_3-B_1)$$
$$+A_0(B_4-B_2)]$$

$$(2P_{Za}|\nabla_Z|2P_{Zb}) = \frac{\delta_b}{8a_0}P^4(1-t^2)^{3/2}(1+t)$$
$$\times[A_3B_1+A_2B_0-A_1B_3-A_0B_2]$$
$$-\frac{P^6}{16R}(1-t^2)^{5/2}(1-t)$$
$$\times[A_4B_3+A_3(B_4-B_2)-A_2(B_3+B_1)$$
$$+A_1(B_0-B_2)+A_0B_1]$$

$$(2P_{Xa}|\nabla_X|2P_{Zb}) = -\frac{P^6}{32R}(1-t^2)^{5/2}(1-t)$$
$$\times[A_4(B_1-B_3)+A_3(2B_2-B_4-B_0)$$
$$+2A_2(B_3-B_1)+A_1(B_4-2B_2+B_0)$$
$$+A_0(B_1-B_3)]$$

$$(2P_{Za}|\nabla_X|2P_{Xb}) = \frac{\delta_b}{8a_0}P^4(1-t^2)^{3/2}(1+t)$$
$$[A_3B_1+A_2B_0-A_1B_3-A_0B_2]$$
$$-\frac{P^6}{32R}(1-t^2)^{5/2}(1-t)[A_4(B_1-B_3)$$
$$+A_3(B_0-B_4)+A_1(B_4-B_0)+A_0(B_3-B_1)]$$

$$(2P_{Xa}|\nabla_Z|2P_{Xb}) = -\frac{P^6}{32R}(1-t^2)^{5/2}(1-t)$$
$$[A_4(B_1-B_3)+A_3(2B_2-B_4-B_0)$$
$$+2A_2(B_3-B_1)+A_1(B_4-2B_2+B_0)$$
$$+A_0(B_1-B_3)]$$

BULLETIN OF THE CHEMICAL SOCIETY OF JAPAN, VOL. 45, 401—407 (1972)

Spin Relaxation Effects on the ESR Spectrum of Gaseous Oxygen Atoms

Mamoru JINGUJI, Yuji MORI, and Ikuzo TANAKA

Department of Chemistry, Tokyo Institute of Technology, Ohokayama, Meguro-ku, Tokyo

(Received July 7, 1971)

The linewidths of the single-quantum transitions of $O(^3P_1)$ and $O(^3P_2)$ in gaseous diluents, such as oxygen molecules and an inter gas, are measured with an ESR spectrometer of a usual type. The cross sections calculated from the pressure broadening are given. With regard to the multiple-quantum transitions in the Zeeman sublevels of $O(^3P_2)$, the dependence of the linewidths on the pressure is duscussed. The spin-lattice relaxation time, T_1, for the single-quantum transitions of $O(^3P_1)$ or $O(^3P_2)$ is evaluated by employing the standard power saturation technique, and the effectiveness of an inert gas on T_1 is studied. The spin-lattice relaxation between the Zeeman sublevels of the O atom is caused by the coupling between the orbital momentum and the electron-spin state upon collision. With regard to the multiple-quantum, the relaxation mechanism is also studied. Finally, we study the relationship between the spin-lattice relaxation time, T_1, and the corresponding probabilities of $\Delta M_J = \pm 1$, $\Delta M_J = \pm 2$, $\Delta M_J = \pm 3$, and $\Delta M_J = \pm 4$ transition induced by collisions.

Recently studies of spin-relaxation phenomena in the gas phase with two different experimental techniques of ESR spectroscopy have been reported for S-state atoms. One is the measurement of the spin-lattice relaxation time, T_1, for the N atom by Brown and Brennen.[1] They noticed that the N atoms in the N_2 diluent have a long spin-lattice relaxation time and interpreted their data in terms of a lack of equilibration in the portion of the flow tube in the external magnetic field up to the cavity. On the other hand, Westenberg and deHaas[2] have obtained T_1 for the H atom by employing the standard power saturation technique; they have found that O_2 is effective in shortening T_1. We have now investigated the spin relaxation phenomena between Zeeman sublevels of O atoms. It is well known that the ground state of the O atom is ^3P, which is split into three states, $^3P_0$, $^3P_1$, and $^3P_2$, by the spin-orbit interaction. We observed the two absorption lines of the $^3P_1$ state and the four lines of the $^3P_2$ state at a low microwave power level and at a low pressure with the usual ESR technique. At lower pressures, we observed the spectra of the multiple-quantum transitions[3] at the expected position for the $^3P_2$ state with a higher microwave power.

In order to obtain the spin-lattice relaxation time for the single-quantum transition between Zeeman sublevels, we employed the standard power saturation technique formulated theoretically by Westenberg and deHaas.[2] This technique was extended to the measurement of T_1 in the multiple-quantum transitions. From the saturation studies of the four lines of the $^3P_2$ state, it was found that the relative absorption intensity of the two-quantum transition to the single-quantum transition is dependent on the pressure. A decrease in the pressure caused this relative intensity to change from a value of about 1/3 to a value of about 6. Since the spin-lattice relaxation in the gas phase is caused by the collision of the O atom with the oxygen molecule, these data show that the intensity of the multiple-quantum transi-

1) R. L. Brown and W. Brennen, *J. Chem. Phys.*, **47**, 4697 (1967).
2) A. A. Westenberg and N. deHaas, *ibid.*, **51**, 5215 (1969).
3) C. C. McDonald, *ibid.*, **39**, 3159 (1963).

tions is correlated with the spin relaxation phenomena. We measured the spin-lattice relaxation time for the single-, two-, and three-quantum transitions. An interpretation has been given of the dependence of T_1 on the pressure, and for the collisional relaxation mechanism in the gas phase. The analysis indicated that the values of T_1 for the single-, two-, and three-quantum transitions were of the order of 10^{-7}—10^{-6} sec in our system, and that, at any pressure, T_1 increased in this order. Then we investigated the variation in T_1 for the single-quantum transition of $O(^3P_2)$ in inert gas diluents, He, Ne, Ar, Kr, and Xe. The measurement of T_1 yielded the following cross sections for the spin-lattice relaxation: $\sigma_{O-He}=9.9$ Å^2, $\sigma_{O-Ne}=8.5$ Å^2, $\sigma_{O-Ar}=12$ Å^2, $\sigma_{O-Kr}=21$ Å^2, $\sigma_{O-Xe}=25$ Å^2, and $\sigma_{O-O_2}=33$ Å^2. It is concluded that the spin-lattice relaxation in O atoms is caused mainly by collisions between the O atom and inert gases through the strong spin-orbit coupling. Finally, we will discuss the relationship between the transition probabilities and the spin-lattice relaxation, using the experimental values of T_1 for the single-, two-, and three-quantum transitions.

Experimental

A JES-3BSX ESR spectrometer with a cylindrical TE_{011} mode cavity was used; the cavity frequency was about 9170 MHz. The magnetic field was modulated sinusoidally at a rate of 100 kHz, and the modulation amplitude was 28 mG. The loaded Q of the cavity was 2840. In order to obtain the spin-lattice relaxation time, the absolute value of microwave power was measured by a means of a thermister. The power (in gauss squared) of the microwave magnetic field, averaged over time and over the volume of the sample in the cavity, was estimated in the manner outlined by Poole.[4]

The flow of oxygen in the quartz tube, 10 mmϕ, was discharged in a cavity powered by a microwave generator (2450 MHz, 100 W) 50 cm upstream from the center of the ESR cavity. The measurements were carried out at total pressures from 0.02 to 0.3 Torr in order to obtain well-resolved spectra.

Theoretical

(i) The Single-quantum Transitions. Westenberg and deHaas[2] assumed that the homogeneous, unsaturated lineshape was Lorentzian, and they derived a general expression for the complex susceptibility in which the imaginary part represents the absorption of energy. Then, using Wahlquist's treatment,[5] they derived the following relation, which is convenient for saturation studies:

$$\left(\frac{H_1S_s}{H_{1R}S}\right)^{2/3}=\frac{0.53}{(2\mu^2T_1T_2/\hbar^2)^{1/3}H_{1R}{}^{2/3}}+0.53(2\mu^2T_1T_2/\hbar^2)^{2/3}H_{1R}{}^{4/3}\left(\frac{H_1{}^2}{H_{1R}{}^2}\right) \quad (1)$$

where μ^2 is the square of the absolute value of the transition matrix element in the direction of the microwave magnetic field, where $H_1{}^2$ is the average value of the microwave power in the sample, and where $H_{1R}{}^2$ is the absolute reference power of 1.54×10^{-4} G. S is the peak-to-peak amplitude, and S_s is the maximum value of S.

(ii) The Multiple-quantum Transitions. The theory of the multiple-quantum transitions was developed by Hughes and Geiger.[6] From their theory, we can expect that the intensities of the two- and three-quantum transitions will be proportional to the square and cube of the microwave power respectively. This relation is confirmed by the experimental results. There is experimental evidence that the lineshape of the two-quantum transition is adequately approximated by the Lorentzian lineshape, *i.e.*;

$$f(H-H_0)=\frac{\gamma T_2{}^*/\pi}{1+\gamma^2T_2{}^{*2}(H-H_0)^2},$$

where $T_2{}^*$ is a measure of the inverse observed linewidth. It is very closely connected with the area and the peak value of the lineshape. For the two-quantum transitions, we derived theoretically the following equation from the analogy of the single-quantum transitions, considering the dependence of the transition on the microwave power

$$\left(\frac{H_1{}^2S_s}{H_{1R}{}^2S}\right)^{2/3}=\frac{0.53}{(2\mu^2T_1T_2{}^*/\hbar^2)^{1/3}H_{1R}{}^{4/3}}+0.53(2\mu^2T_1T_2{}^*/\hbar^2)^{2/3}H_{1R}{}^{8/3}\left(\frac{H_1{}^2}{H_{1R}{}^2}\right)^2 \quad (2)$$

μ^2 in Eq. (2) is the square of the absolute value of the matrix element for the two-quantum transition, which is different from that of the single-quantum transition as given by Hughes and Geiger.[6] In the case of the three-quantum transitions, the following equation is also derived, where μ^2 is the square of the absolute value of the matrix element for the three-quantum transition, and where $T_2{}^{**}$ is a measure of the inverse observed linewidth:

$$\left(\frac{H_1{}^3S_s}{H_{1R}{}^3S}\right)^{2/3}=\frac{0.53}{(2\mu^2T_1T_2{}^{**}/\hbar^2)^{1/3}H_{1R}{}^{6/3}}+0.53(2\mu^2T_1T_2{}^{**}/\hbar^2)^{2/3}H_{1R}{}^{12/3}\left(\frac{H_1{}^2}{H_{1R}{}^2}\right)^3 \quad (3)$$

In Eqs. (2) and (3), $H_{1R}{}^2$ is an absolute reference power at the sample, the values of which are 9.7×10^{-4} and 7.5×10^{-3} G^2 respectively.

Results and Discussion

(i) Linewidth. Collision with any species perturbs the M_J levels by way of coupling between the orbital momentum and the electron spin state, and causes line broadening. For the O atom, the linewidth, ΔH_{msl}, is governed by the collision frequency; thus, ΔH_{msl} is proportional to the total pressure, by analogy with simple kinetic theory. The plots of ΔH_{msl} *vs.* the total pressure, shown in Fig. 1, all give

4) C. P. Poole, Jr., "Electron Spin Resonance," Interscience Publishers, Inc., New York, pp. 296—302.

5) H. Wahlquist, *J. Chem. Phys.*, **35**, 1708 (1961).

6) V. W. Hughes and J. S. Geiger, *Phys. Rev.*, **99**, 1842 (1955).

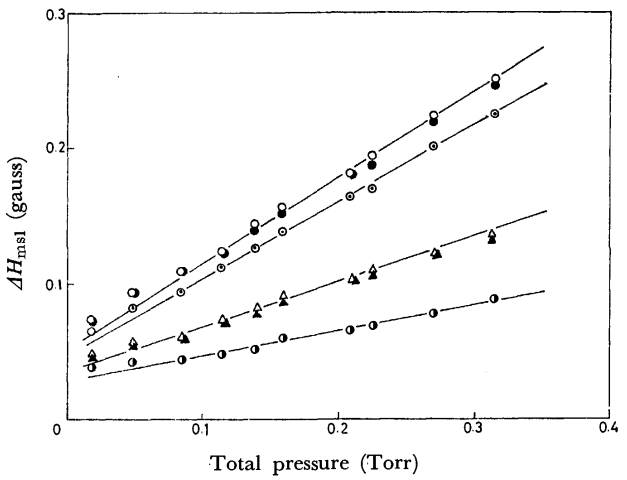

Fig. 1. Linewidths of O atom as a function of total pressure for the single-, two-, and three-quantum transitions.
⊙: $J=1$, $M_J=-1\rightarrow0$, ●: $J=2$, $M_J=-2\rightarrow-1$,
○: $J=2$, $M_J=-1\rightarrow0$, ▲: $J=2$, $M_J=-2\rightarrow0$,
△: $J=2$, $M_J=-1\rightarrow1$, ◑: $J=2$, $M_J=-2\rightarrow1$.

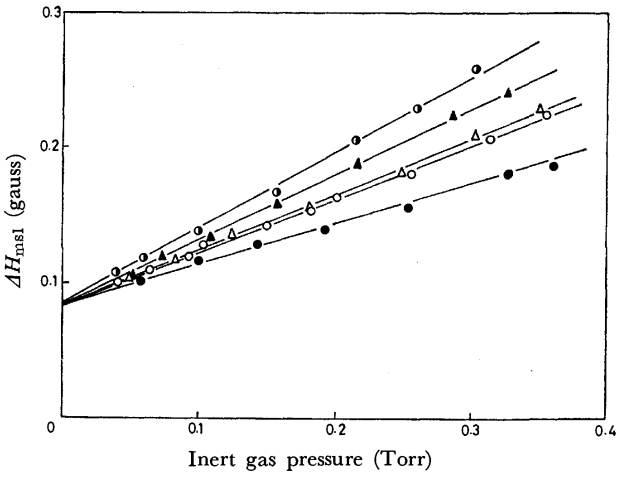

Fig. 2. Linewidths of O ($J=2$, $M_J=-1\rightarrow0$) atom as a function of inert gas pressure.
○: He, ●: Ne, △: Ar, ▲: Kr, ◑: Xe.

straight lines. For the $^3P_1$ state, the linewidths of the $M_J=-1\rightarrow0$ and $M_J=0\rightarrow1$ lines were equal to each other. For the $^3P_2$ state, the linewidths of the $M_J=-2\rightarrow-1$ and $M_J=1\rightarrow2$ lines were equal to each other, and the $M_J=-1\rightarrow0$ and $M_J=0\rightarrow1$ lines were also equal. Thus, the $M_J=-1\rightarrow0$ line of $O(^3P_1)$ and the $M_J=-2\rightarrow-1$ and $M_J=-1\rightarrow0$ lines of $O(^3P_2)$ were used for the width measurement, shown in Fig. 1. The cross sections for the line broadening were calculated for each line of the single-quantum transitions from the data in Fig. 1. The slopes of these linear plots give the values of the cross sections, $\sigma_{O(^3P_2)-O_2}=30.1$ Å^2 and $\sigma_{O(^3P_1)-O_2}=27.7$ Å^2, which are somewhat smaller than the value, $\sigma_{O-O_2}=37$ Å^2, obtained for the $M_J=-1\rightarrow0$ line of $O(^3P_1)$ by Westenberg and deHaas.[2]

The linewidths of the multiple-quantum transitions were noticeably smaller than those of the single-quantum transitions, as is to be expected from the theory of the multiple-quantum transitions.[6] The linewidths of the two- and three-quantum transitions are plotted against the total pressure, together with those of the single-quantum transitions, in Fig. 1. In the case of the two-quantum transition, the plots of the $M_J=-2\rightarrow0$ and $M_J=-1\rightarrow1$ lines are shown in Fig. 1, since the linewidths of the $M_J=-2\rightarrow0$ and $M_J=0\rightarrow2$ lines were equal to each other. In the case of the three-quantum transitions, the linewidths of the $M_J=-2\rightarrow1$ and $M_J=-1\rightarrow2$ lines were also equal; thus, the plots of the $M_J=-2\rightarrow1$ line are shown in Fig. 1. The apparent cross sections for the two- and three-quantum transitions are calculated from the slopes of the linear plots in Fig. 1 to be σ_{O-O_2} 14.6 Å^2 (two-quantum transition) and $\sigma_{O-O_2}=9.4$ Å^2 (three-quantum transition). These cross sections for the two- and three-quantum transitions are nearly 1/2 and 1/3 of those for the single-quantum transitions respectively. These relations coincide with that derived theoretically by Hughes and Geiger.[6]

In order to examine the pressure broadening, we added various inert gases, He, Ne, Ar, Kr, and Xe, as perturbers, keeping the partial pressure of oxygen constant at 0.048 Torr. Then, the variation in the linewidth of the $M_J=-1\rightarrow0$ line of $O(^3P_2)$ was measured; the plots of ΔH_{msl} *vs.* the pressure of inert gases are shown in Fig. 2. The slopes of these linear plots give the cross sections for the line-broadening collision. The values obtained are $\sigma_{O-He}=10.1$ Å^2, $\sigma_{O-Ne}=12.4$ Å^2, $\sigma_{O-Ar}=20.1$ Å^2, $\sigma_{O-Kr}=24.2$ Å^2, and $\sigma_{O-Xe}=28.2$ Å^2. The line-broadening cross sections obtained in this paper are larger than those obtained from the kinetic theory.

(ii) Relaxation Time. S-state atoms, which have no orbital angular momentum in the ground electronic configuration, have a long spin-lattice relaxation time, T_1, in the gaseous state. For N atoms, in the N_2 diluent, or for H atoms in the H_2 diluent, therefore, the saturation of ESR absorption by the atoms can be easily observed at a low microwave power, even at a high diluent pressure.[7] On the other hand, the observation of the saturation phenomena on O atoms in the $^3P_2$ and $^3P_1$ states needs a reduced oxygen diluent pressure and an increased microwave power.

By employing Eq. (1), the T_1 values for six single-quantum transitions of $O(^3P_1)$ and $O(^3P_2)$ are obtained from the saturation data. The plots of $(H_1/H_{1R}\cdot S_S/S)^{2/3}$ against the relative power (H_1^2/H_{1R}^2) at oxygen pressures from 0.02 to 0.3 Torr are shown in Fig. 3 for $O(^3P_2)$. The $(H_1/H_{1R}\cdot S_S/S)^{2/3}$ *vs.* (H_1^2/H_{1R}^2) plots for both $O(^3P_1)$ and $O(^3P_2)$ at a constant pressure of 0.139 Torr are also shown in Fig. 4 for the sake of comparison. These plots give linear lines with slopes of $0.53\ \{(2\mu^2T_1T_2/\hbar^2)^{2/3}H_{1R}^{4/3}\}$ and intercepts of $0.53/\{(2\mu^2T_1T_2/\hbar^2)^{1/3}H_{1R}^{2/3}\}$. It is possible to evaluate $T_1\cdot T_2$ from the value of either slopes or intercept. The values of $T_1\cdot T_2$ obtained in these two different ways almost coincided with each other. Since the lineshapes of the absorption spectra are

7) A. A. Westenberg and N. deHaas, *J. Chem. Phys.*, **40**, 3087 (1964).

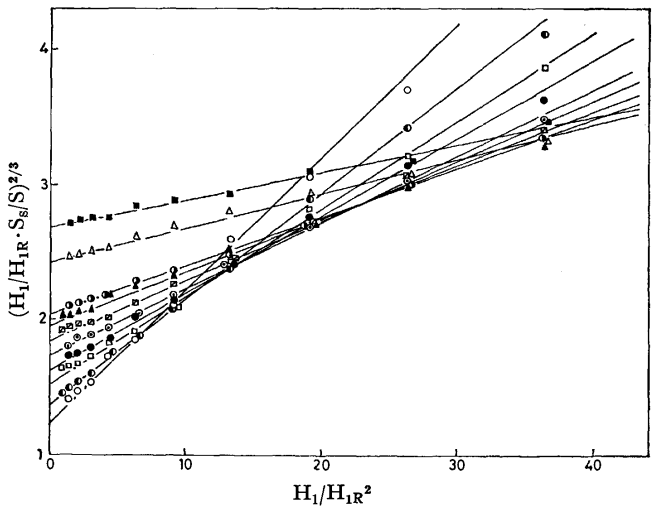

Fig. 3. Saturation data of O ($J=2$, $M_J=-1\rightarrow0$) atom. Data taken at the indicated total pressure in O_2 diluent. ○: 0.018, ◐: 0.048, □: 0.084, ●: 0.114, ⊙: 0.139, ▨: 0.159, ▲: 0.209, ◐: 0.225, △: 0.270, ■: 0.315 Torr.

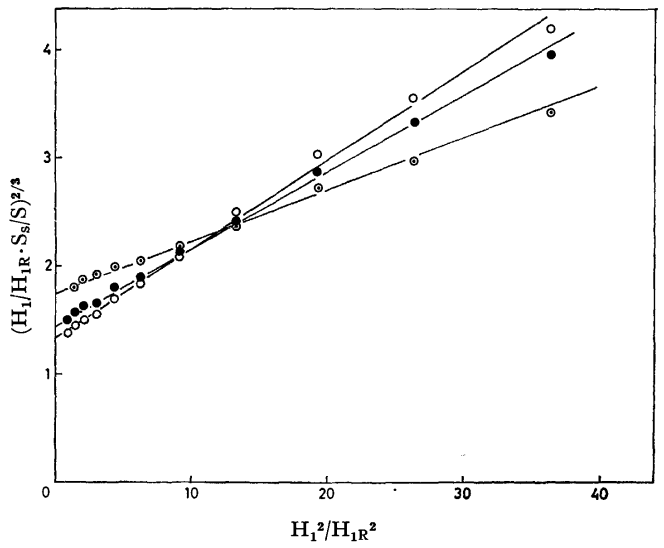

Fig. 4. Saturation data of the single-quantum transitions at total pressure of 0.139 Torr in O_2 diluent. ⊙: $J=1$, $M_J=-1\rightarrow0$, ●: $J=2$, $M_J=-2\rightarrow-1$, ○: $J=2$, $M_J=-1\rightarrow0$.

TABLE 1. EFFECT OF PRESSURE ON T_1 FOR O ATOM IN O_2 DILUENT

Total pressure (Torr)	$O(^3P_2)$ $M_J=-1\rightarrow0$ (μsec)	$O(^3P_2)$ $M_J=-2\rightarrow-1$ (μsec)	$O(^3P_2)$ $M_J=-1\rightarrow0$ (μsec)
0.018	1.15	1.06	1.03
0.048	1.02	0.85	0.81
0.084	0.87	0.81	0.76
0.114	0.84	0.77	0.74
0.139	0.76	0.72	0.65
0.159	0.71	0.66	0.63
0.209	0.60	0.55	0.52
0.225	0.58	0.51	0.48
0.270	0.45	0.42	0.40
0.315	0.37	0.38	0.35

Lorentzian at low modulation amplitudes and at a low microwave power, we can use the well-known relation $T_2=2/(\sqrt{3}\gamma\Delta H_{msl})$, where γ is $g\mu_B/\hbar$. Using this relation, we can calculate T_2, and then determine T_1 from the value of $T_1\cdot T_2$. These values are summarized in Table 1. In the case of inert-gas diluents, we calculated T_1 from the saturation data in the same manner. The values of T_1 thus obtained are summarized in Table 2. In order to obtain information on the relaxation mechanism, the plots of the reciprocal of T_1 *vs.* the total pressure for O_2 and inert-gas diluents are shown in Figs. 5 and 6 respectively. Especially, all of the plots of the inert-gas diluents were obtained from the saturation data on the $M_J=-2\rightarrow-1$ line of $O(^3P_2)$. Using the kinetic theory, the cross sections for the spin-lattice relaxation are calculated from the slopes of the linear portion in Figs. 5 and 6. The resulting cross sections are $\sigma_{O-He}=9.9$ Å^2, $\sigma_{O-Ne}=8.5$ Å^2, $\sigma_{O-Ar}=12.1$ Å^2, $\sigma_{O-Kr}=20.6$ Å^2, $\sigma_{O-Xe}=24.7$ Å^2, and $\sigma_{O-O_2}=33.3$ Å^2. Figure 7 shows plots of the cross sections against the atomic numbers of the inert gases, which serve as convenient indices. The figure also contains similar plots of the elastic scattering cross sections for collisions between electrons and the inert-gas atoms. The cross sections for the spin-lattice relaxation are about 6 times larger, but the sequence of the cross sections appears to be the same in both cases. A similar effect has been observed in the case of M_J mixing induced by potas-

TABLE 2. EFFECT OF INERT GAS ON T_1 FOR O ATOM ($M_J=-2\rightarrow-1$)

He (Torr)	T_1 (μsec)	Ne (Torr)	T_1 (μsec)	Ar (Torr)	T_1 (μsec)	Kr (Torr)	T_1 (μsec)	Xe (Torr)	T_1 (μsec)
0.041	0.88	0.058	0.86	0.048	0.86	0.050	0.84	0.039	0.85
0.064	0.86	0.100	0.83	0.082	0.84	0.073	0.82	0.059	0.81
0.093	0.85	0.143	0.81	0.124	0.81	0.108	0.77	0.099	0.73
0.103	0.81	0.193	0.78	0.181	0.75	0.157	0.68	0.157	0.63
0.150	0.73	0.254	0·70	0.248	0.65	0.216	0.59	0.216	0.53
0.182	0.68	0.327	0.63	0.302	0.61	0.286	0.47	0.260	0.44
0.201	0.66	0.360	0.55	0.350	0.49	0.329	0.45	0·303	0.41
0.256	0.54								
0.314	0.49								
0.355	0.44								

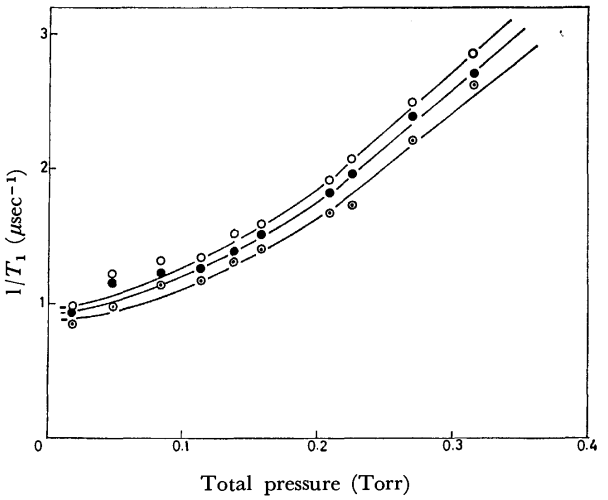

Fig. 5. Reciprocal of T_1 for the single-quantum transitions as a function of total pressure in O_2 diluent.
⊙: $J=1$, $M_J=-1\rightarrow 0$, ●: $J=2$, $M_J=-2\rightarrow -1$,
○: $J=2$, $M_J=-1\rightarrow 0$.

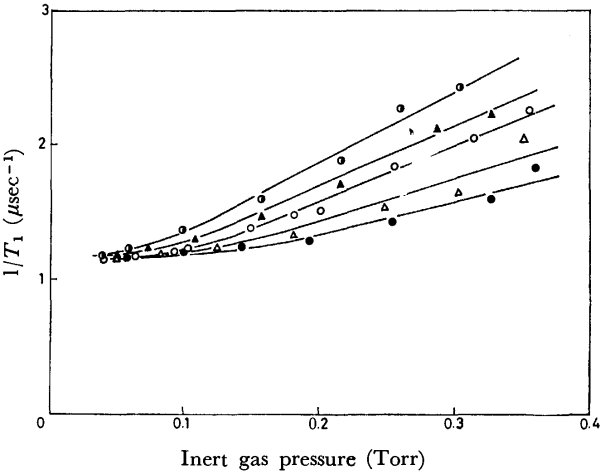

Fig. 6. Effects of added inert gases on T_1 for the single-quantum transitions ($J=2$, $M_J=-2\rightarrow -1$).
○: He, ●: Ne, △: Ar, ▲: Kr, ◑: Xe.

sium-inert gas atomic collisions.[8] It is probable between the orbital momentum and the electron-spin state by collision.

(iii) Multiple-quantum Transition. Observations of the multiple-quantum transitions for O atoms have been reported by Hughes and Geiger[6] and by McDonald.[3] Recently, Atherton and Cook[9] have discussed the lineshapes of the multiple-quantum transitions of $O(^3P_2)$, and Schindler and Tiedemann[10] have studied, both experimentally and theoretically, the change in the line intensities of the multiple-quantum transitions with the microwave power.

At a microwave power level of about 0.2 mW, only single-quantum transitions were detected. As the the power increased, the single-quantum transitions

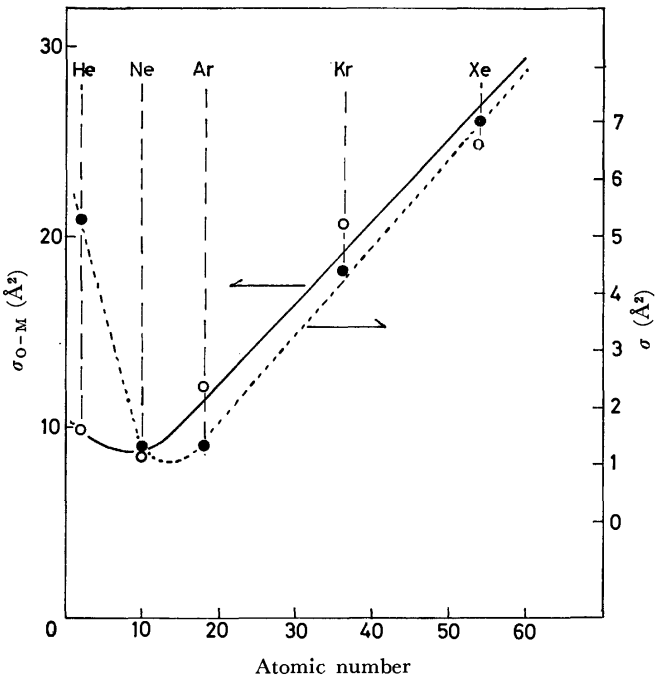

Fig. 7. For comparison of the cross sections (○) for the spin-lattice relaxation with the elastic scattering cross section (●).

showed saturation broadening, and, between each two lines of the four single-quantum transitions of $O(^3P_2)$, the two-quantum transitions appeared and increased in intensity. They became predominant in the spectrum at a microwave power level of about 2.5 mW. A further increase in power produced three-quantum transitions between the two-quantum transition lines, while the single-quantum transitions vanished in the noise level and the two-quantum transitions showed a saturation broadening. At about 20 mW, the three-quantum transitions gave the strongest lines in the spectrum. Finally, between the three-quantum transition lines, the four-quantum transition could be detected at about 100 mW. Thus, by virtue of the different saturation properties of the various transitions, all the possible multiple-quantum transitions for $O(^3P_2)$ can be observed. It is interesting to measure the spin-lattice relaxation time, T_1, of the multiple-quantum transitions, since the saturation property is closely related with the spin-lattice relaxation phenomena.

Extending the treatment employed to measure T_1 for the single-quantum transitions, we tried to obtain for the multiple-quantum transitions from Eqs. (2) and (3), which were derived theoretically. The plots of $(H_1^2/H_{1R}^2 \cdot S_S/S)^{2/3}$ *vs.* $(H_1^2/H_{1R}^2)^2$ for the two-quantum transitions, and those of $(H_1^3/H_{1R}^3 \cdot S_S/S)^{2/3}$ *vs.* (H_1^2/H_{1R}^3) for the three-quantum transitions, are shown in Figs. 8 and 9 respectively. Using Eqs. (2) and (3), we can obtain $T_1 \cdot T_2^*$ and $T_1 \cdot T_2^{**}$ from the slopes of these linear plots in Figs. 8 and 9. We can determine T_2^* and T_2^{**} from the observed linewidths of the two- and three-quantum transition lines, and then calculate T_1 from the values of $T_1 \cdot T_2^*$ and $T_1 \cdot T_2^{**}$. The values of T_1 obtained for the two- and three-

8) W. Berdowski and L. Krause, *Phys. Rev.*, **165**, 158 (1968).
9) N. M. Atherton and Irene P. Cook, *Mol. Phys.*, **19**, 417 (1970).
10) P. Tiedemann and R. N. Schindler, *J. Chem. Phys.*, **54**, 797 (1971).

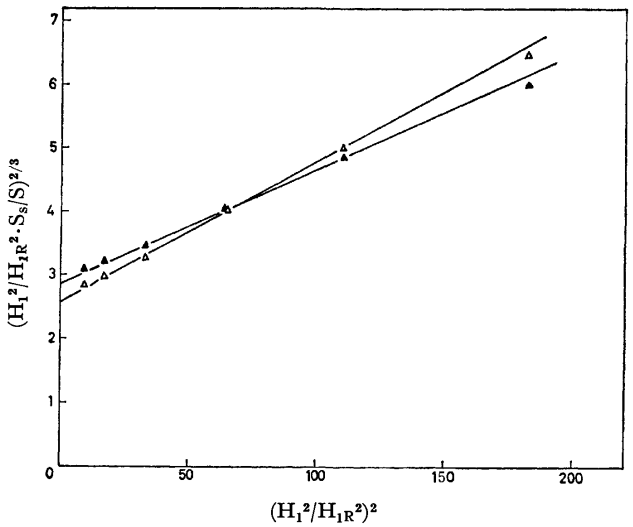

Fig. 8. Saturation data of the two-quantum transitions at total pressure of 0.139 Torr in O_2 diluent.
▲: $J=2$, $M_J=-2\rightarrow0$, △: $J=2$, $M_J=-1\rightarrow1$.

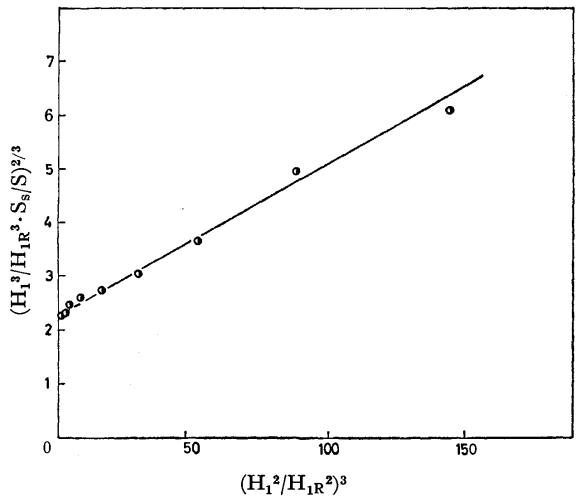

Fig. 9. Saturation data of the three-quantum transitions ($J=2$, $M=-2\rightarrow1$) at total pressure of 0.139 Torr in O_2 diluent.

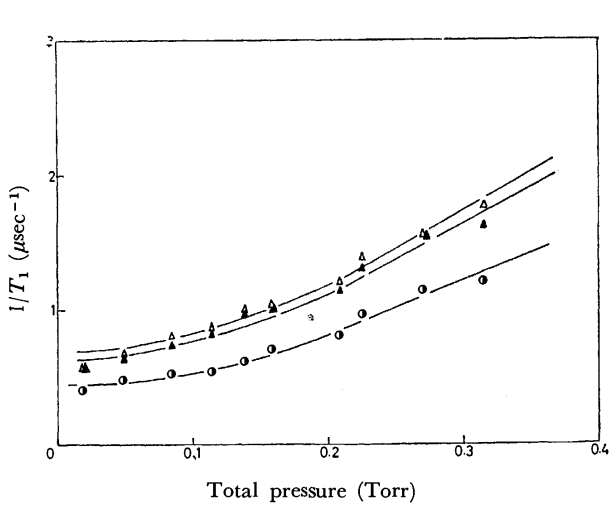

Fig. 10. Reciprocal of T_1 for the two- and three-quantum transitions as a function of total pressure in O_2 diluent.
▲: $J=2$, $M_J=-2\rightarrow0$, △: $J=2$, $M_J=-1\rightarrow1$,
◐: $J=2$, $M_J=-2\rightarrow1$.

TABLE 3. EFFECTS OF PRESSURE OF T_1 FOR THE TWO- AND THREE-QUANTUM TRANSITION IN O_2 DILUENT

Total pressure (Torr)	Two-quantum transition $M_J=-2\rightarrow0$ (μsec)	Two-quantum transition $M_J=-1\rightarrow1$ (μsec)	Three-quantum transition $M_J=-2\rightarrow1$ (μsec)
0.018	1.75	1.74	2.44
0.048	1.62	1.55	2.05
0.084	1.27	1.24	1.89
0.114	1.21	1.16	1.83
0.139	1.02	0.99	1.65
0.159	0.97	0.95	1.40
0.209	0.88	0.84	1.26
0.225	0.77	0.73	1.05
0.270	0.65	0.65	0.89
0.315	0.62	0.57	0.84

quantum transitions are summarized in Table 3. It is found that the values of T_1 for the single-, two-, and three-quantum transitions decrease in that order. In order to examine the relaxation mechanism, we have plotted $1/T_1$ *vs.* the pressure in Fig. 10. The plots are linear except at low pressures, and the dependence of $1/T_1$ on the pressure is in the same sequence for the two- and three-quantum transitions as for the single-quantum transition. From the data in Fig. 10, the values of the apparent cross sections for the spin-lattice relaxation are found to be $\sigma_{O-O_2}=18.0$ Å^2 (two-quantum transition) and $\sigma_{O-O_2}=14.0$ Å^2 (three-quantum transition), which are smaller than $\sigma_{O-O_2}=33.3$ Å^2 of the single-quantum transition for $O(^3P_2)$.

In order to examine the relaxation mechanism in Zeeman sublevels, we derived the relationship between the transition probabilities induced by collisional interaction and the spin-lattice relaxation time (*cf.* the Appendix). From these relationships, the following results can be expected. In the case of the single-quantum transition, the T_1 values of the $M_J=-2\rightarrow-1$ and $M_J=1\rightarrow2$ lines are equal to each other, while those the $M_J=-1\rightarrow0$ and $M_J=0\rightarrow1$ lines are also equal. In addition, the T_1 value of the former pair is smaller than that of the latter. In the case of the two-quantum transition, the T_1 values of the $M_J=-2\rightarrow0$ and $M_J=0\rightarrow2$ lines are equal to each other, and T_1 of this pair has a smaller value than that of the $M_J=-1\rightarrow1$ line. In the case of the three-quantum transition, the T_1 values of the $M_J=-2\rightarrow1$ and $M_J=-1\rightarrow2$ lines are also equal. These results, expected from the Appendix, are in fair qualitative agreement with the experimental results (Tables 1 and 3). As the Appendix shows, the four transition probabilities can be estimated using the values of T_1 for the single-, two-, and three-quantum transitions obtained experimentally. Under these experimental conditions, the $W_1 \gg W_2 > W_3 > W_4$ relation can be expected. Assuming that the values of W_3 and W_4 are negligibly small, the values of W_1 and W_2 can be calculated from the values of T_1 obtained in the pressure range from about 0.2 to 0.3 Torr by the method of least-squares. The average value of W_2/W_1 is 0.0339

in this pressure range, which shows roughtly that the relaxation may be carried out step-by-step; *i.e.* the single-quantum relaxation mainly occurs even in the case of the miltiple-quantum transition.

Appendix

The corresponding probabilities of the $\Delta M_J=\pm1$, ±2, ±3, and ±4 transitions between five Zeeman sublevels ($M_J=-2$, -1, 0, 1, 2) of the $^3P_2$ states induced by the collisions O of atoms with oxygen molecules are $W_{\pm1}$, $W_{\pm2}$, $W_{\pm3}$, and $W_{\pm4}$ respectively, assuming that the sublevels are approximately equally spaced. We suppose that the populations of the substates are N_{-2}, N_{-1}, N_0, N_1, and N_2. In a thermal equilibrium, the steady-state populations obey Boltzmann's law; this requires that the probabilities for transitions up and down be in the ratios of:

$$\begin{aligned}\frac{W_{+1}}{W_{-1}} &= \exp(g\beta H/\boldsymbol{k}T)\\ \frac{W_{+2}}{W_{-2}} &= \exp(2g\beta H/\boldsymbol{k}T)\\ \frac{W_{+3}}{W_{-3}} &= \exp(3g\beta H/\boldsymbol{k}T)\\ \frac{W_{+4}}{W_{-4}} &= \exp(4g\beta H/\boldsymbol{k}T)\end{aligned} \tag{A-1}$$

Since $g\beta H \ll \boldsymbol{k}T$, we can satisfy these conditions by taking:

$$\begin{aligned}W_{\pm1} &= W_1\left(1 \pm \frac{1}{2}\frac{g\beta H}{\boldsymbol{k}T}\right)\\ W_{\pm2} &= W_2\left(1 \pm \frac{g\beta H}{\boldsymbol{k}T}\right)\\ W_{\pm3} &= W_3\left(1 \pm \frac{3}{2}\frac{g\beta H}{\boldsymbol{k}T}\right)\\ W_{\pm4} &= W_4\left(1 \pm \frac{2g\beta H}{\boldsymbol{k}T}\right)\end{aligned} \tag{A-2}$$

By way of example, we will try to obtain the relationship between the transition probabilities and T_1 for the two-quantum transition ($M_J=-1\rightarrow1$). We consider the initial conditions:

$$\begin{aligned}&N_{-2} = N+2n_0,\ N_{-1} = N+n,\ N_0 = N,\\ &N_1 = N-n,\ N_2 = -2n_0\end{aligned} \tag{A-3}$$

with a small n value, where n_0 is the equilibrium value of n. The time evolution of n obeys the following differential equations:

$$\begin{aligned}\frac{dn}{dt} &= -(W_{+1}+W_{-3}+W_{-2}+W_{-1})(N+n)\\ &\quad + W_{+2}(N-n)+W_{+1}N+W_{+3}(N-2n_0)\\ &\quad + W_{-1}(N+2n_0)\\ -\frac{dn}{dt} &= -(W_{+3}+W_{+2}+W_{+1}+W_{-1})(N-n)\\ &\quad + W_{-2}(N+n)+W_{-1}N+W_{+1}(N-2n_0)\\ &\quad + W_{-3}(N+2n_0)\end{aligned} \tag{A-4}$$

Substituting the probabilities from (A-2), we find that:

$$\frac{dn}{dt} = (2W_1+2W_2+W_3)(n_0-n). \tag{A-5}$$

The spin-lattice relaxation time is:

$$\frac{1}{T_1} = (2W_1+2W_2+W_3). \tag{A-6}$$

In the same manner, we can get the following relation between the transition probabilities and T_1 for the single-, two-, three-, and four-quantum transitions.

(i) single-quantum transition

$$\begin{aligned}M_J = -2\rightarrow-1 \quad & \frac{1}{T_1} = \frac{1}{2}(5W_1+2W_2+2W_3+W_4)\\ M_J = -1\rightarrow0 \quad & \frac{1}{T_1} = \frac{1}{2}(6W_1+3W_2+W_3)\\ M_J = 0\rightarrow1 \quad & \frac{1}{T_1} = \frac{1}{2}(6W_1+3W_2+W_3)\\ M_J = 1\rightarrow2 \quad & \frac{1}{T_1} = \frac{1}{2}(5W_1+2W_2+2W_3+W_4)\end{aligned}$$

(ii) two-quantum transition

$$\begin{aligned}M_J = -2\rightarrow0 \quad & \frac{1}{T_1} = \frac{1}{2}(3W_1+5W_2+W_3+W_4)\\ M_J = -1\rightarrow1 \quad & \frac{1}{T_1} = (2W_1+2W_2+W_3)\\ M_J = 0\rightarrow2 \quad & \frac{1}{T_1} = \frac{1}{2}(3W_1+5W_2+W_3+W_4)\end{aligned}$$

(iii) three-quantum transition

$$\begin{aligned}M_J = -2\rightarrow1 \quad & \frac{1}{T_1} = \frac{1}{2}(3W_1+2W_2+4W_3+W_4)\\ M_J = -1\rightarrow2 \quad & \frac{1}{T_1} = \frac{1}{2}(3W_1+2W_2+4W_3+W_4)\end{aligned}$$

(iv) four-quantum transition

$$M_J = -2\rightarrow2 \quad \frac{1}{T_1} = (W_1+W_2+W_3+2W_4)$$

Semiconducting Anion-radical Salts Derived from 3,3′5,5′-Tetrahalo-*p*-diphenoquinones[1)]

Yoshio MATSUNAGA and Yoshihiro NARITA*

Department of Chemistry, Faculty of Science, Hokkaido University, Sapporo

(Received August 2, 1971)

3,3′,5,5′-Tetrachloro- and 3,3′,5,5′-tetrabromo-*p*-diphenoquinones were found to form series of complex anion-radical salts of the $M^+(Q_2)^-$ or $M^+_2(Q_3)^{2-}$ type with various onium cations. These complex salts are dark-colored, almost black in many cases, and show electronic absorptions extending into the rock-salt region. In addition, bluish green-colored simple salts could be isolated with a few cations. The complex salts exhibit electrical resistivities in orders from 10 to 10^4 ohm cm at room temperature. Neither the pattern due to the quinone molecule nor that due to the semiquinone ion is present in their vibrational spectra. A single carbonyl stretching vibration band appears around 1600 cm^{-1}, intermediate between that in the quinone and that in the semiquinone salt.

A new class of electrically-conducting organic compounds formed from various cations and the anion-radical of 7,7,8,8,-tetracyanoquinodimethane (TCNQ) was synthesized by Melby *et al.* about ten years ago.[2-4)] The composition of the anion-radical salts is represented by $M^+(TCNQ)_n^-$, where M^+ is a cation. Naturally, the value of n is 1 in many cases, but for some cations n was found to have multiple values such as 1 and 2, or 1 and 1.5. The complex salts with higher values of n tend to exhibit a lower electrical resistivity than the simple salt, $M^+(TCNQ)^-$.[5)] Since the work of Melby *et al*, the physical properties of the TCNQ anion-radical salts, especially the electrical, magnetic, and optical properties of the complex salts, have been quite extensively studied; however, only relatively few data have been published for new complex ion-radical salts,[6-14)] and far less even for those derived from compounds other than TCNQ.

Goan *et al.* have reported that *p*-chloranil forms molecular complexes with cobaltocene and nickelocene in a mole ratio of donor-to-acceptor of 1 : 2.[15)] The presence of these complexes has been subsequently confirmed by Brandon *et al.* and also by Watanabe *et al.*[16,17)] Their electrical resistivities have been found in the range from 10^4 to 10^6 ohm cm.[17,18)] On the basis of the vibrational spectra, these complexes may be better characterized as complex anion-radical salts containing onium cations. During the course of their work on pentalene derivatives, Le Goff and Lacount obtained a purple-black tetrabutylammonium anion-radical salt of the tetracyanodimethane derivative of dibenzopentalenoquinone. Its composition happened to be $M^+_2(Q_3)^{2-}$. Unfortunately, no resistivity has been reported for this complex salt.[19)] 9-Dicyanomethylene-2,4,7-trinitrofluorene (DTF) was prepared by Mukherjee and Levasseur some years ago. All the anion-radical salts with cations such as methyltriethylammonium, *N*-methyl-quinolinium, methyltriphenylphosphonium, and methyltriphenylarsonium ions have been reported to have the composition of $M^+(DTF)^-$.[20)] Dupuis and Néel have extended the work on the anion-radical salts of DTF and also prepared those of its tetranitro analog. Among the combinations with nineteen cations examined, the only complex (1 : 2) salt was obtained by the reaction between 1,2,3-trimethylbenzimidazolium iodide and DTF.[21)] Here again, the complex salt is much more conducting than the corresponding simple salt. They have observed 50 ohm cm for the 1 : 2 salt and 10^6 ohm cm for the 1 : 1 salt.[22)] A possible complex cation-radical salt has been found in the system of iodine-semiquinoid phenothiazine bromide. The minimum resistivity observed at the composition of $(phenothiazine)_2^+(Br_2I)^-$ is about 4 ohm cm.[23)] Thus, apart from the above-mentioned TCNQ anion-radical salts, our

1) A part of this work was carried out by Y. M. while employed at the Central Research Division of American Cyanamid Co., and was presented at Organic Crystal Symposium, Chicago, 1965.

* Present address, Kurosaki Works, Mitsubishi Chemical Industries, Ltd., Kitakyushu.

2) D. S. Acker, R. J. Harder, W. R. Hertler, W. Mahler, L. R. Melby, R. E. Benson, and W. E. Mochel, *J. Amer. Chem. Soc.*, **82**, 6408 (1960).

3) L. R. Melby, R. J. Harder, W. R. Hertler, W. Mahler, R. E. Benson, and W. E. Mochel, *ibid.*, **84**, 3374 (1962).

4) L. R. Melby, *Can. J. Chem.*, **43**, 1448 (1965).

5) W. J. Siemons, P. E. Bierstedt, and R. G. Kepler, *J. Chem. Phys.*, **39**, 3523 (1963).

6) J. H. Lupinski, K. R. Walter, and L. H. Vogt, Jr., *Mol. Cryst.*, **3**, 241 (1967).

7) P. Dupuis and J. Néel, *Compt. rend. Sér. C*, **265**, 777 (1967).

8) D. Henning, G. Kempter, E. Ahrens, K. D. Benecke, and P. Paul, *Z. Chem.*, **7**, 463 (1967).

9) E. B. Yagubskii, M. L. Khidekel, I. F. Shchegolev, L. I. Buravov, R. B. Lyubovskii, and V. B. Strykov, *Zh. Obshch. Khim.*, **38**, 992 (1968).

10) E. B. Yagubskii, M. L. Khidekel, I. F. Shchegolev, L. I. Buravov, B. G. Gribov, and M. K. Makova, *Izv. Akad. Nauk SSSR, Ser. Khim.*, **1968**, 2124.

11) D. Henning, G. Kempter, and K. D. Worlitzer, *Z. Chem.* **9**, 306 (1969).

12) B. H. Klanderman and D. C. Hoesterey, *J. Chem. Phys.*, **51**, 377 (1969).

13) H. Kusakawa and K. Akashi, This Bulletin, **42**, 263 (1969).

14) D. Henning and G. Kempter, *Z. Chem.* **10**, 343 (1970).

15) J. C. Goan, E. Berg, and H. E. Podall, *J. Org. Chem.* **29**, 975 (1964).

16) R. L. Brandon, J. H. Osiecki, and A. Ottenberg, *ibid.*, **31**, 1214 (1966).

17) H. Watanabe, I. Motoyama, and K. Hata, This Bulletin, **39**, 850 (1966).

18) Y. Okamoto, *J. Phys. Chem.*, **70**, 291 (1966).

19) E. Le Goff and R. B. Lacount, *J. Org. Chem.*, **33**, 2529 (1968).

20) T. Mukherjee and L. A. Levasseur, *ibid.*, **30**, 644 (1965).

21) P. Dupuis and J. Néel, *Compt. rend. Sér. C*, **268**, 557 (1969).

22) P. Dupuis and J. Néel, *ibid.*, **268**, 653 (1969).

23) Y. Matsunaga and K. Shono, This Bulletin, **43**, 2007 (1970).

knowledge of complex ion-radical salts is very fragmentary and scanty. Therefore, it seemed that it would be very interesting to find out whether or not quinones, common electron acceptors which can be as strong as TCNQ and DTF if appropriately selected, can form series of complex anion-radical salts with various onium cations. As the alkali salts of 3,3',5,5'-tetrahalo-*p*-diphenosemiquinones are known to be quite stable,[24,25] the parent quinones were our first choice.

Experimental

Materials. The examples of the anion-radical salts cover only a part of the compounds prepared in this work. However, they illustrate all of the various preparative procedures which we employed.

Tetrahalo-p-*diphenoquinones*: *p*-Biphenol was prepared by the decomposition of tetrazotized benzidine, as has been described by Hirsch, and then halogenated following the procedures reported by Magatti.[26,27] Oxidation to the quinones was carried out in glacial acetic acid by the addition of fuming nitric acid or in carbon tetrachloride with oxides of nitrogen.[28,29] Hereafter, tetrachloro- and tetrabromo-*p*-diphenoquinones will be abbreviated as TCDQ and TBDQ respectively.

Na^+TCDQ^-: Earlier this salt was prepared by the oxidation of tetrachloro-*p*-biphenol dissolved in an aqueous solution of sodium hydroxide with the ferricyanide ion.[25] In the present work, TCDQ was reduced by grinding with an excess of sodium iodide in the presence of acetone. The green crystalline powder was then thoroughly washed with acetone.

(Di-n-propylammonium)$_2$(TCDQ)$_3$: By treating a mixture of 100 mg of powdered TCDQ and 65 mg of di-*n*-propylammonium iodide with acetone, the reddish violet color of the quinone was changed quickly into the black of the anion-radical salt. The yield was 95%. The same product was obtained by the reaction of di-*n*-propylammonium iodide with a mixture of TCDQ and Na^+TCDQ^- suspended in acetonitrile. The complex salt is a purple-black crystalline powder. Found: C, 49.3; H, 4.0; Cl, 36.0%. Calcd for $2C_6H_{16}N\cdot 3C_{12}H_4Cl_4O_2$: C, 49.3, H, 3.8, Cl, 36.4%.

Tetraethylammonium (TCDQ)$_2$: A mixture of 98 mg of TCDQ and 76 mg of tetraethylammonium iodide was added to 20 m*l* of acetone, after which the solution was stirred for a half hour at room temperature. The purple-black solid was collected on a filter and dried in a vacuum desiccator. The yield was 55 mg. Found: C, 49.8; H, 3.6; Cl, 36.5%. Calcd for $C_8H_{20}N\cdot 2C_{12}H_4Cl_4O_2$: C, 49.6; H, 3.7; Cl, 36.6%.

Ferricinium (TCDQ)$_2$: Ferrocene (0.36 g (2 mmol)) was dissolved in 100 m*l* of acetone, and then pulverized TCDQ (1.28 g (4 mmol)) was added. After 5 minutes stirring, the black product was filtered and washed with acetone. The yield was 1.15 g. Found: C, 49.4; H, 2.1; Cl, 34.4%. Calcd for $C_{10}H_{10}Fe\cdot 2C_{12}H_4Cl_4O_2$: C, 49.2; H, 2.2; Cl, 34.4%. The following attempt to prepare the simple salt resulted in the formation of the above-mentioned complex salt. Ferricinium triiodide (2.27 g (4 mmol)) and Na^+TCDQ^- (1.04 g (3 mmol)) were mixed in 50 m*l* of acetonitrile. The suspension was stirred for one hour. Found, C 48.9, H 2.4, Cl, 33.6%. The quinone required for the formation of the complex salt was apparently supplied by the oxidation of the $TCDQ^-$ ion with air during the process of preparation.

Cobalticinium (TCDQ)$_2$: Cobalticinium triiodide, 1.71 g (3 mmol), TCDQ, 0.97 g (3 mmol), and Na^+TCDQ^-, 1.05 g (3 mmol) were mixed in 50 m*l* of acetonitrile. After the mixture had been stirred for a half hour, the black product was filtered and washed with acetone. The yield was 1.8 g. Found: C, 48.1; H, 2.1; Cl, 33.9%. Calcd for $C_{10}H_{10}Co\cdot 2C_{12}H_4Cl_4O_2$: C, 49.0; H, 2.2; Cl, 34.0%.

Tetra-n-*propylammonium TBDQ*: A portion of 150 mg (0.3 mmol) of powdered TBDQ was stirred for one hour with 120 mg tetra-*n*-propylammonium iodide in 20 m*l* of acetone. The bluish-green precipitate was washed with benzene, in which the salt is not soluble. The yield was 130 mg. Found: C, 42.0; H, 4.8; Br, 45.9%. Calcd for $C_{12}H_{28}N\cdot C_{12}H_4Br_4O_2$: C, 42.0; H, 4.7; Br, 46.6%. The corresponding TCDQ salt could be prepared by employing benzene instead of acetone as the reaction medium, but it was found to be too unstable to be examined further.

N-Methyl-acridinium TBDQ: Powdered TBDQ (150 mg (0.3 mmol)) was stirred for 40 min at room temperature with *N*-methyl-acridinium iodide (135 mg (0.5 mmol)) in 30 m*l* of acetone. The green crystalline powder was then filtered. Found: C, 44.7; H, 2.5; Br, 45.9%. Calcd for $C_{14}H_{12}N\cdot C_{12}H_4Br_4O_2$: C, 45.0; H, 2.3; Br, 46.0%.

(N-Methyl-acridinium)$_2$(TBDQ)$_3$: A portion of 100 mg (0.2 mmol) of pulverized TBDQ and one of 50 mg (0.15 mmol) of *N*-methyl-acridinium iodide were ground together and then stirred with 30 m*l* of acetonitrile for a half hour. The violet crystalline solid was filtered and washed with the solvent. The yield was 60 mg. Found: C, 41.0; H, 2.2; Br, 48.9%. Calcd for $2C_{14}H_{12}N\cdot 3C_{12}H_4Br_4O_2$: C, 40.7, H, 1.9; Br, 50.8%.

p-*Phenylenediamine (TBDQ)$_2$*: *p*-Phenylenediamine and TBDQ in a mole ratio of 1 : 2 were added to benzene. After stirring for 15 min, the black product was filtered and washed with benzene. Found: C, 33.0; H, 1.8; N, 3.2; Br, 57.0%. Calcd for $C_6H_8N_2\cdot 2C_{12}H_4Br_4O_2$: C, 32.5; H, 1.5; N, 2.5; Br, 57.7%.

Cobalticinium (p-chloranil)$_2$: Cobalticinium triiodide (1.14 g (2 mmol)), *p*-chloranil (0.49 g (2 mmol)), and K^+-(*p*-chloranil)$^-$ (0.57 g (2 mmol)) were mixed in 50 m*l* of acetone and then stirred for a half hour. The brownish-yellow crystalline product was filtered and washed with acetone. Found: C, 38.9; H, 1.9; Cl, 41.4%. Calcd for $C_{10}H_{10}Co\cdot 2C_6Cl_4O_2$: C, 38.8; H, 1.5; Cl, 41.8%.

Measurements. The electrical resistivities, ρ, at room temperature were examined by a voltage-current method employing a cell similar to that designed by LaFlamme.[30] In some cases, a gradual increase in the resistivity was observed on standing; therefore, the measurements were carried out immediately after drying in a vacuum. The temperature-dependence was measured by a potential-probe method only for some highly-conducting salts. The activation energy for semiconduction, E, was calculated from $\rho=\rho_0\exp(E/kT)$.

The electronic spectra of the solid salts were recorded by means of a Beckman DK-2A spectrophotometer with the aid of a reflectance attachment, and the vibrational spectra, as Nujol mineral oil mulls by means of a Jasco IR-G infrared spectrophotometer. The procedure in the former measurements was described in detail in our previous paper.[23]

24) J. Moir, *S. African J. Sci.*, **9**, 322 (1912).
25) Y. Matsunaga, *Can. J. Chem.*, **38**, 1172 (1960).
26) R. Hirsch, *Ber.*, **22**, 335 (1889).
27) G. Magatti, *ibid.*, **13**, 224 (1880).
28) W. H. Hunter and G. H. Woolett, *J. Amer. Chem. Soc.*, **43**, 135 (1921).
29) A. G. Brook, *J. Chem. Soc.*, **1952**, 5040.
30) P. M. LaFlamme, *Rev. Sci. Instrum.*, **35**, 1193 (1964).

Results and Discussion

Syntheses. The interaction between pyrene and TCDQ (TBDQ) dissolved in chloroform generates a charge-transfer absorption, the maximum of which is located at 13.8 (13.6) kK. This value can well be compared with that of 13.7 kK given by the pyrene complex of tetracyanoethylene (TCNE) and that of 13.1 kK given by the complex of TCNQ dissolved in the same solvent. In other words, the present quinones are electron-acceptors as strong as those famous π-acids. Therefore, it is quite understandable that the quinone molecule oxidizes the iodide ion to free iodine and takes up the electron to form the semiquinone ion.

The major synthetic routes to the present anion-radical salts may be classified into the following three.

Method 1: As has been mentioned above, the iodide serves as the electron source for the formation of the semiquinone ion. This is the most general route for the preparation of both simple and complex salts.

Method 2: The complex salt is prepared by the metathesis of the triiodide and NaTCDQ (NaTBDQ) in the presence of TCDQ (TBDQ). If the quinone is omitted, the amount required for the formation of the complex salt is provided by the oxidation of the semiquinone ion with air in the process of stirring.

Method 3: When the cation source is given as a strong electron-donor, the salt may be prepared by oxidation-reduction, as exemplified by the synthesis of the ferricinium $(TCDQ)_2$. Despite the excess of the electron-donor, the reduction of TCDQ is limited to that which can be stabilized in the form of the complex salt.

With most of the onium cations, M^+, the quinones form only complex anion-radical salts represented by the formulas $M(TCDQ)_2$ or $M_2(TCDQ)_3$ and $M(TBDQ)_2$ or $M_2(TBDQ)_3$. All the complex salts are dark-colored-brown, violet, or black depending upon the kind of cation. When heated, most of the TCDQ salts show color-changes due to decomposition in the temperature-range of 150 to 180°C, while the TBDQ salts show changes in the range from 130 to 170°C. The treatment of TCDQ with tetra-*n*-propylammonium iodide gave a bluish-green product which was too unstable to be analysed. This is the only possible simple TCDQ salt observed in our experiment except those with alkali metal cations. Simple TBDQ salts could be isolated with five cations, namely, tetra-*n*-propylammonium, *N*-methyl-acridinium, *N*-methyl-lepidinium, *N*-methyl-, and *N*-ethyl-isoquinolinium cations. They are green or bluish green, as is the sodium salt. Among the above-mentioned cations, *N*-methyl-acridinium also gives a complex anion-radical salt. So far this is the only combination to be found which forms both simple and complex salts.

Electrical Resistivities. As is summarized in Tables 1 and 2, resistivity values in the range of 10^2—10^3 ohm cm are typical of most of the simple and complex salts examined here. The highest resistivity is exhibited by the simple TBDQ salt of tetra-*n*-propylammonium; however, no appreciable difference is observed in the pair of the simple and complex TBDQ salts of *N*-methyl-acridinium. The TBDQ salts tend to be slightly more conductive than the TCDQ salts. Thus, the TCDQ salts exhibiting resistivities about 100 ohm cm or less include only the following three; the complex salts of cobalticinium, ferricinium, and *p*-phenylenediamine cations. On the other hand, the corresponding complex TBDQ salts and four others, which contain *n*-Pr_2EtNH, *n*-Pr_3NH, Me_3PhN, and Et_3PhN cations, are as conducting as the TCDQ salts mentioned above.

In the study of the tetra-*n*-alkylammonium TCNQ salts, Kusakawa and Akashi have shown that the cation size influences the electrical resistivity as much as by a factor of 10^6.[13] Although the space effects observed in the present work are not large, we can point out some trends. The following orders may be noted in the series of the TCDQ complex salts: quinolinium> *N*-*n*-propylquinolinium, *N*-methyl-isoquinolinium> *N* - ethyl - isoquinolium> *N* - *n* - propyl-isoquinolinium, and *N*-methyl-acridinium< *N*-ethyl-acridinium. When ammonium ions are employed, the effects are more pronounced in the series of the TBDQ salts. The resistivity decreases in this order of the cations: $Pr_2NH_2 > Pr_2MeNH > Pr_2EtNH > Pr_3NH$. Similarly, $Et_3NH > Et_4N$ and $Me_3PhN > Et_3PhN$. The last order is reversed in the TCDQ salts.

TABLE 1. ANION-RADICAL SALTS DERIVED FROM TETRACHLORO-*p*-DIPHENOQUINONE (TCDQ)

Cation	Composition	Resistivity (ohm cm)	Low-energy Band (kK)
Sodium	1 : 1	2×10^3	9.3
Triethylammonium	2 : 3	7×10^3	5.3
Tetraethylammonium	1 : 2	4×10^3	<4
Di-*n*-propylammonium	2 : 3	6×10^2 a)	4.3
Methyldi-*n*-propylammonium	2 : 3	1×10^3 b)	<4
Ethyldi-*n*-propylammonium	1 : 2	1×10^3 c)	4.4
Tri-*n*-propylammonium	1 : 2	3×10^2 d)	4.3
Tetra-*n*-propylammonium	1 : 1 (?)	too unstable to be examined	
Trimethylphenylammonium	2 : 3	6×10^2 e)	4.4
Triethylphenylammonium	1 : 2	4×10^3	<4
p-Phenylenediamine	1 : 2	120	<4
Quinolinium	2 : 3	2×10^5	6.4
N-(*n*-Propyl)-quinolinium	2 : 3	1×10^3	4.3
N-Methyl-isoquinolinium	2 : 3	7×10^3	5.0
N-Ethyl-isoquinolinium	2 : 3	6×10^3	5.0
N-(*n*-Propyl)-isoquinolinium	2 : 3	3×10^3	4.8
Lepidinium	2 : 3	1×10^4	6.2
N-Methyl-lepidinium	2 : 3	1×10^4	4.6
N-Ethyl-lepidinium	2 : 3	7×10^4	5.0
N-Methyl-acridinium	2 : 3	3×10^3	4.7
N-Ethyl-acridinium	2 : 3	5×10^4	6.5
Ferricinium	1 : 2	24 f)	<4
Cobalticinium	1 : 2	50 g)	<4

a) Activation energy 0.21 eV, b) 0.37 eV, c) 0.17 eV, d) 0.18 eV, e) 0.19 eV, f) 0.08 eV, g) 0.07 eV.

Table 2. Anion-radical salts derived from tetrabromo-*p*-diphenoquinone (TBDQ)

Cation	Composition	Resistivity (ohm cm)	Low-energy Band (kK)
Sodium	1 : 1	2×10^3	6.3
Triethylammonium	2 : 3	5×10^3	4.7
Tetraethylammonium	1 : 2	6×10^2	<4
Di-*n*-propylammonium	2 : 3	2×10^3	<4
Methyldi-*n*-propylammonium	2 : 3	1×10^3	<4
Ethyldi-*n*-propylammonium	1 : 2	140	4.3
Tri-*n*-propylammonium	1 : 2	120	4.4
Tetra-*n*-propylammonium	1 : 1	2×10^7	10.5
Trimethylphenylammonium	2 : 3	130	<4
Triethylphenylammonium	2 : 3	84	<4
p-Phenylenediamine	1 : 2	66	<4
N-(*n*-Propyl)-quinolinium	2 : 3	2×10^3	<4
N-Methyl-isoquinolinium	1 : 1	9×10^2	5.8
N-Ethyl-isoquinolinium	1 : 1	2×10^3	4.3
N-(*n*-Propyl)-isoquinolinium	2 : 3	2×10^3	<4
N-Methyl-lepidinium	1 : 1	2×10^3	5.8
N-Ethyl-lepidinium	2 : 3	6×10^4	4.8
N-Methyl-acridinium	1 : 1	3×10^3	5.6
	2 : 3	2×10^3	4.2
N-Ethyl-acridinium	2 : 3	4×10^3	<4
Ferricinium	1 : 2	32 [a]	<4
Cobalticinium	1 : 2	103 [b]	<4

a) Activation energy 0.07 eV, b) 0.10 eV.

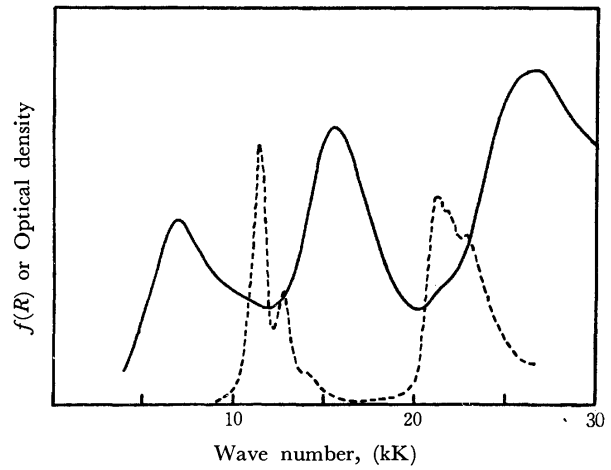

Fig. 1. Electronic spectra of Na^+TCDQ^- in the solid state (——) and in an acetone solution (----).

Electronic Spectra. As is shown in Fig. 1, the solid-state spectrum of NaTCDQ bears no resemblance to that of the salt dissolved in acetone. The solution spectrum comprises bands at 11.3 and 12.7, a shoulder at 14.0, and a strong band with some vibrational structures around 21 kK. It must be noted that this spectrum is very similar to that of the benzidine cation-radical cited in Fig. 2. The latter has bands at 11.6 and 13.1, a shoulder at 14.3, and a strong band around 21.6 kK.[31] Figure 2 presents

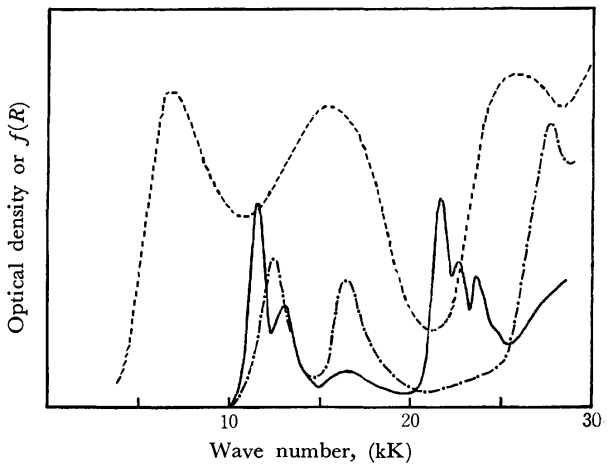

Fig. 2. Electronic spectra of benzidine bromide in an ethanolic solution at room temperature (——) and at low temperature (—·—·—) taken from Ref. 31, and the solid-state spectrum (----) taken from Ref. 32.

the solid-state spectrum of the benzidine bromide, which is very different from the spectra of not only the monomeric but also the dimeric forms of the cation-radical. Considering also the magnetic property, we concluded earlier that the univalent diamine cations in solid benzidine bromide is in a strong, more-than-by-pairs interaction.[32] The solid NaTCDQ shows a solid-state spectrum consisting of three bands located at 6.8, 15.5, and 26.4 kK. Again, this spectrum is very much like that of the benzidine bromide in the solid state. The latter spectrum, shown in Fig. 2, has three bands, at 6.7, 15.5, and 25.8 kK. Therefore, it seems to be quite certain that the anion-radicals in the solid NaTCDQ are also in a strong, more-than-by-pairs interaction. In accordance with this view, a relatively low resistivity, 10^3 ohm cm, is observed for this simple salt.

The spectrum of the solid NaTBDQ presented in Fig. 3 is composed three bands, at 6.2, 15.6, and about 27 kK, and is close to that of the solid NaTCDQ mentioned above. On the other hand, the simple bluish-

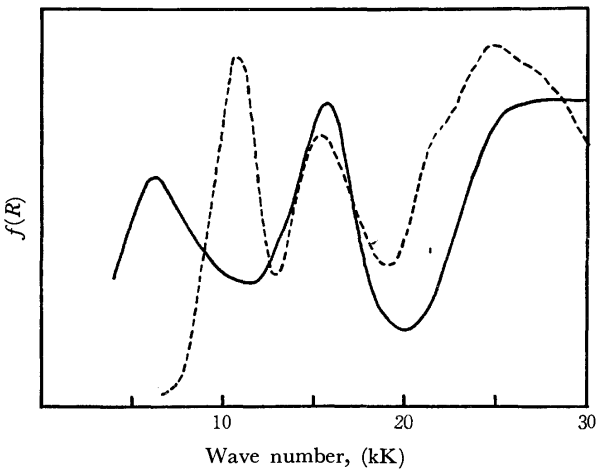

Fig. 3. Diffuse reflection spectra of Na^+TBDQ^- (——) and tetra-*n*-propylammonium-TBDQ (----).

31) K. Takemoto, H. Matsusaka, S. Nakayama, K. Suzuki, and Y. Ooshika, This Bulletin, **41**, 764 (1968).

32) Y. Iida and Y. Matsunaga, *ibid.*, **41**, 2615 (1968).

green TBDQ salt of tetra-*n*-propylammonium exhibits a resistivity as high as 10^7 ohm cm and a solid-state spectrum bearing no resemblance to that of the NaTBDQ. The bands in the spectrum of this ammonium salt are located at 11.5, 15.2, and 24.5 kK. This spectrum seems to correspond well to those of the dimeric form of the benzidine cation-radical: 12.4, 16.4, and 28 kK, as measured in a cold ethanolic solution (see Fig. 2), and 11.5, 15.2, and about 27 kK, as measured with colored acid clays moistened with benzene.[31,33] Thus, the anion-radicals here appear to be essentially in a pair-by-pair interaction. This speculation is consistent with the observed high resistivity.

The spectra of the simple and complex *N*-methyl-acridinium TBDQ salts are presented in Fig. 4. The simple salt exhibits a resistivity of 10^3 ohm cm, which can be well compared with that of NaTBDQ. However, their electronic spectra are different from each other. The *N*-methyl-acridinium salt shows a low-energy band at 5.6 kK, a little lower than that of the corresponding band of the sodium salt. In addition, the presence of an extra band at 10.5 kK must be noted. It is very likely that the interaction of the anion-radicals in this salt is also more-than-by-pairs, but in a mode somewhat different from that in NaTBDQ. The complex *N*-methyl-acridinium salt shows a spectrum consisting of four bands in the infrared and visible regions. The low-energy band appears at 4.2 kK, the limit of our spectrophotometer. The other three are located at 11.0, 18.2, and 24—28 kK. It is rather surprising to see that this spectrum is very much like that of the complex TCNQ salt of *N*-methyl-acridinium. The latter salt, with a composition of 1 : 2, exhibits four bands, located at <4, 11.2, 17.8, and 27.5 kK.[34] The spectra of most of the complex TCDQ (TBDQ) salts are more or less similar to the one shown in Fig. 4.

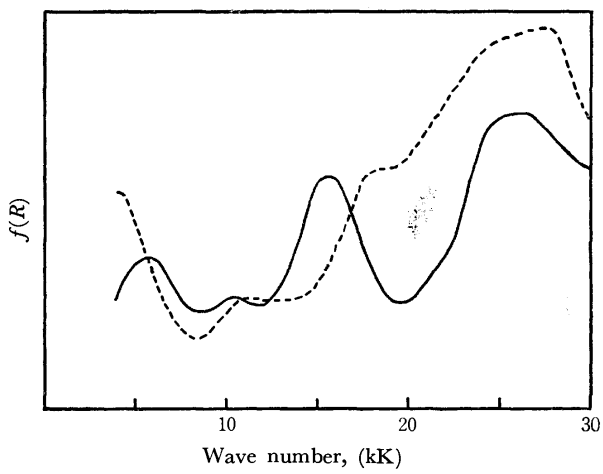

Fig. 4. Diffuse reflection spectra of *N*-methyl-acridinium-TBDQ, the simple salt (——) and the complex salt (----).

Four more examples of the spectra of the complex TCDQ salts are presented in Figs. 5 and 6. In the

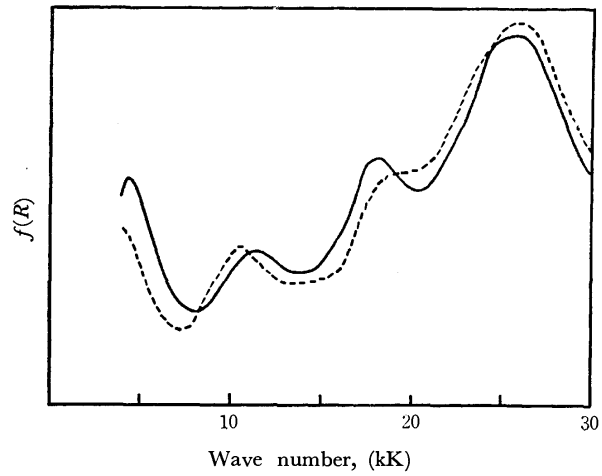

Fig. 5. Diffuse reflection spectra of the complex TCDQ salts containing ethyldi-*n*-propylammonium ion (——) and cobalticinium ion (----).

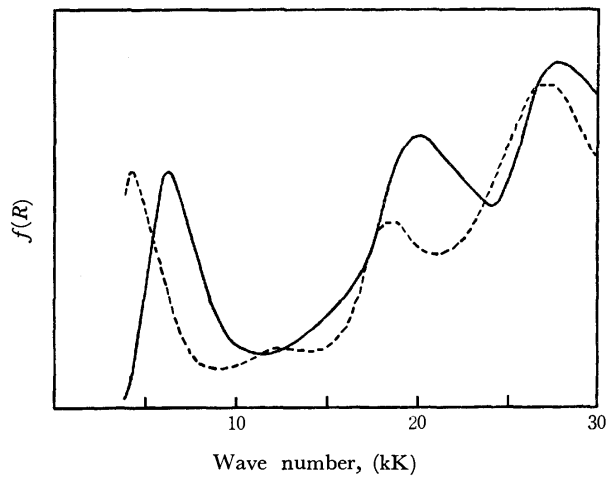

Fig. 6. Diffuse reflection spectra of the complex TCDQ salts containing quinolinium ion (——) and *N*-(*n*-propyl)-quinolinium ion (----).

cases shown in Fig. 5, the cations are quite different in nature and the compositions of the salts are not the same; however, all the patterns are very similar to one another. Absorption bands appear at 4.4, 11.4, 17.8, and 25.6 kK in the ethyldi-*n*-propylammonium salt and at <4, 10.5, 19.0, and 25.8 kK in the cobalticinium salt. On the other hand, the spectra of the TCDQ salts containing cations of the same nature, but exhibiting resistivities different by a factor of two hundred, are compared in Fig. 6. The less-conducting dark-brown-colored quinolinium salt shows bands at 6.4, 20.0 and 27.6 kK. Here, it seems that the weak second band is located around 15 kK, but is hidden by the strong third one. By the introduction of the *N*-*n*-propyl group, the bands are shifted to the low-energy side; that is, they appear at 4.3, 12.8, 18.5, and 27.4 kK. As a result, the salt is violet. In each combination of the salts shown in Figs. 5 and 6, it may be pointed out that the lower the resistivity, the less the energy of the first absorption band. However, such a tendency is only roughly observed in the other cases (see Tables 1 and 2).

33) A. Hakusui, Y. Matsunaga, and K. Umehara, This Bulletin., **43**, 709 (1970).
34) Y. Iida, *ibid.*, **42**, 637 (1969).

For comparison with the complex anion-radical salts derived from TCDQ and TBDQ, the electronic spectra of the solid cobaltocene (*p*-chloranil)$_2$ and nickelocene (*p*-chloranil)$_2$ are shown in Fig. 7. The close agreement between these two suggests that the pattern is essentially determined by the interaction between *p*-chloranil and its anion-radical. Because of the presence of a wide, relatively transparent region, these salts are only lightly colored. However, it must be added that the presence of such a region is not characteristic of the complex salts. The simple sodium salt of *p*-chloranil, where the anion-radicals are supposed to be in a strong interaction, is known to exhibit absorption bands at 11.6 and 26.5 kK.[35] Compared with this, all the spectra of the complex salts are shifted to the low-energy side; the maxima of the strong bands in the cobalticinium salt are found at 5.6 and 22.2 kK.

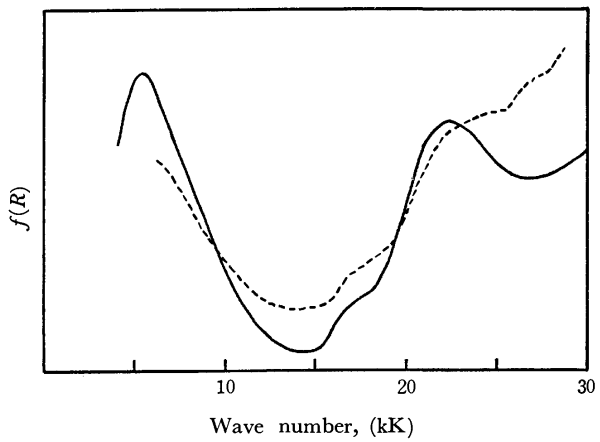

Fig. 7. Diffuse reflection spectra of cobaltocene (*p*-chloranil)$_2$ (——) and nickelocene (*p*-chloranil)$_2$ (----).

Vibrational spectra. It has been established that the vibrational spectrum of the semiquinone ion is markedly different from that of the parent quinone.[34,36] In Fig. 8, the spectrum of TCDQ is compared with that of its simple sodium salt. Instead of the normal carbonyl stretching vibration of TCDQ at 1640 cm^{-1}, a strong absorption band is observed 1530 cm^{-1} in the semiquinone salt. As the wavenumber of the carbonyl mode is known to be mainly determined by the bond order,[37-40] the observed shift can be attributed to the acceptance of one extra electron into the antibonding level of the TCDQ molecule. As a result, the carbonyl bonds more or less lose their double-bond character and the rings lose their quinoid structure. This change over the whole molecule leads to the drastic difference in the vibrational spectrum between the quinone and the

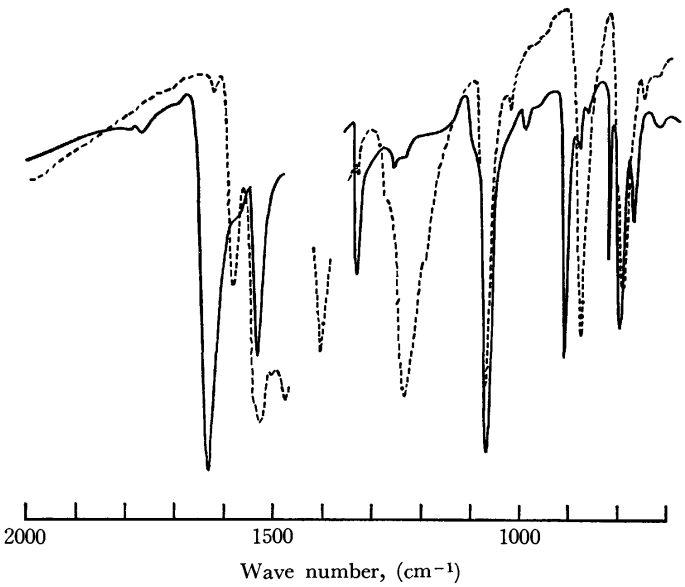

Fig. 8. Vibrational spectra of TCDQ (——) and Na$^+$TCDQ$^-$ (----).

semiquinone ion. Besides a large shift of the carbonyl stretching band, the appearance of a strong broad band at 1240 cm^{-1} must be considered as an indication of the reduction. Moreover, the shift of the band from 910 to 880 cm^{-1} and the replacement of a triplet around 800 cm^{-1} by a strong singlet must be noted.

The spectrum of the complex ethyldi-*n*-propylammonium TCDQ salt bears some resemblance to the spectrum of TCDQ and also that of the semiquinone salt. That is, the presence of bands at 1410, 1250, and 880 cm^{-1} is characteristic of the semiquinone ion. On the other hand, the triplet around 800 cm^{-1} may be ascribed to the original quinone. However, no strong broad band to be assigned to the carbonyl stretching vibration is observed at the wavenumber

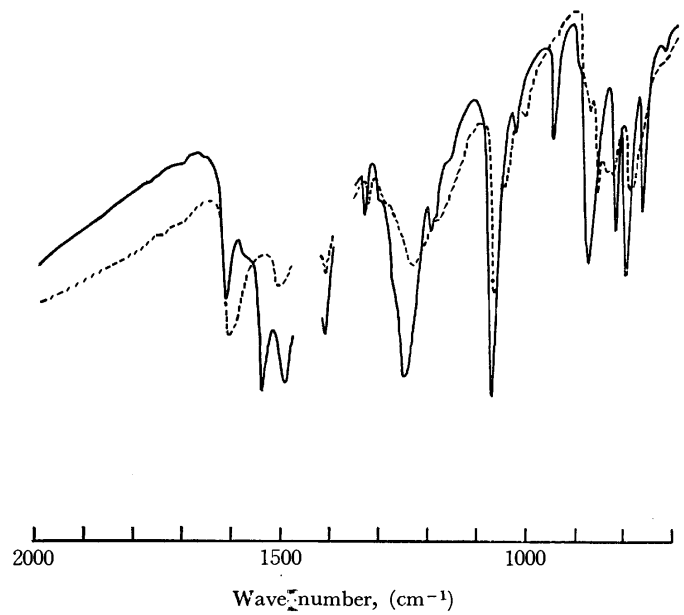

Fig. 9. Vibrational spectra of the complex TCDQ salts containing ethyldi-*n*-propylammonium ion (——) and cobalticinium ion (----).

35) Y. Iida, *ibid.*, **43**, 2772 (1970).
36) Y. Matsunaga, *J. Chem. Phys.*, **41**, 1609 (1964).
37) G. B. Bonino and E. Scrocco, *Atti Accad. Naz. Lincei, Rend. Classe Sci. Fis. Mat. e Nat.*, **6**, 421 (1949).
38) G. Berthier, B. Pullman, and J. Pontis, *J. Chim. Phys.*, **49**, 367 (1952).
39) W. Kemula and M. T. Krygowski, *Bull. Acad. Pol. Sci., Sér. Sci. Chim.*, **15**, 479 (1967).
40) Y. Iida, This Bulletin, **43**, 345 (1970).

corresponding to either that in the quinone or that in the semiquinone ion. A rather narrow band appears at 1610 cm^{-1}. The complex TCDQ salts of di-*n*-propyl-ammonium and methyldi-*n*-propylammonium show spectra similar to this. The spectra of most of the complex TCDQ salts are different from those mentioned above. For example, the spectrum of the cobalticinium salt is shown in Fig. 9. Bands at 860, 1010, and 1410 cm^{-1} form the spectrum of the cation. Here again, we see neither the pattern due to the quinone molecule nor that due to the semiquinone ion. A single broad carbonyl band appears at 1610 cm^{-1}. This wavenumber is intermediate between that in the the quinone, 1640 cm^{-1}, and that in the semiquinone salt, 1530 cm^{-1}. On the basis of this observation, we may conclude that the negative charge is equally shared by the two molecules of the quinone. If so, the quinone molecules in the afore-mentioned three ammonium salts may not be exactly equivalent to each other. The resistivity values seem to have no direct relation with the type of the vibrational spectrum, for the highest value among the complex TCDQ salts is 2×10^5 ohm cm in the quinolinium salt, and the lowest, 24 ohm cm in the ferricinium salt. Their spectra are all of the same type. In all the complexs TCDQ salt, the carbonyl stretching-vibration band is found in the range from 1605 to 1625 cm^{-1} regardless of the composition. This is rather surprising because the formal change per quinone molecule is a half in the 1 : 2 salt and two-thirds in the 2 : 3 salt. Actually, rough estimates derived from a comparison of the red shift of the carbonyl mode in the complex salts with the shift found in the sodium salt are no larger than one-third. The location of the band appearing at 1070 cm^{-1}, in the quinone is hardly affected by the reduction; however, a splitting of as much as 10—25 cm^{-1} is observed in the salts containing some ammonium ions and mostly heterocyclic cations.

The spectrum of TBDQ has a strong carbonyl band at 1630 cm^{-1}. In the simple salts, this band is shifted to the low-energy side by 80—100 cm^{-1}, depending upon the kind of cation. Figure 10 presents the spectra of the simple and complex *N*-methyl-acridinium salts. Here, the carbonyl stretching bands are found at 1545 and 1595 cm^{-1} respectively. The strong broad band located around 1250 cm^{-1} is characteristic of the salts, and it is not observed before the reduction. In the other complex TBDQ salts, the band due to carbonyl stretching appears in the range from 1595 to 1615 cm^{-1}, again regardless of the composition. As in the series of the TCDQ salts, this band is rather weak and narrow in some ammonium salts. Although the band located at 1020 cm^{-1} in the spectra of Fig. 10 apparently corresponds to the 1070 cm^{-1} band in TCDQ, no splitting is observed in any complex TBDQ salts.

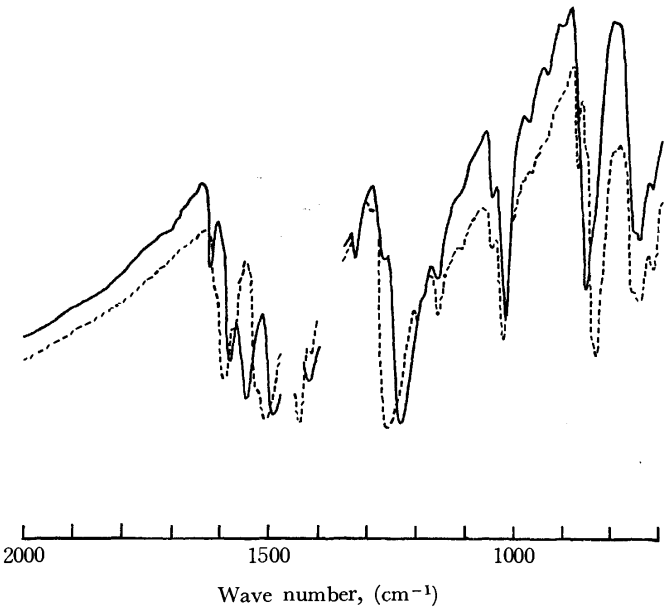

Fig. 10. Vibrational spectra of *N*-methyl-acridinium-TBDQ, the simple salt (——) and the complex salt (----).

Lastly, we wish to emphasize that quinones, if suitably selected, can form series of complex anion-radical salts with various onium cations as well as TCNQ does. Work to prepare a new series of complex anion-radical salts is now in progress using 2,3-dicyano-1,4-naphthoquinone.

The work at Hokkaido University was supported by a grant-in-aid from the Ministry of Education, to which the authors' thanks are due.

Studies of Helical Aggregates of Molecules. III. The Bivalent Metal Soaps of Optically Active 12-Hydroxyoctadecanoic Acid

Taro TACHIBANA, Kazuko KAYAMA, and Hideko TAKENO
Department of Chemistry, Ochanomizu University, Bunkyo-ku, Tokyo

(Received August 20, 1971)

The bivalent metal soaps of optically-active 12-hydroxyoctadecanoic acid were found to crystallize out in the form of twisted fibers from aqueous or anhydrous ethanol solutions. Most soaps of this class produced both right-handed and left-handed fibers from the same specimen, more of the latter in the case of the D-enantiomer. An enantiomorphic relationship of the sense of twist was clearly demonstrated by using both enantiomers of the Ca soap. Under a high-resolution electron microscope, it was observed on the Sr soap that Sr atoms are arranged in lines along the fiber axis with a periodicity of 33—40 Å, showing that the hydroxyoctadecanoate chains of the soap molecules are aligned approximately parallel to the width of the fiber. The twisting of the soap fibers was associated with the layer structure characteristic of soap.

The present work represents an extension of previous studies[1,2] of the sense of twist of helical aggregates of optically active 12-hydroxyoctadecanoic acid and its alkali metal soaps. Some bivalent metal soaps also have been found to form twisted fibers.[3] However, since it had been seen that some soaps of this class, *e.g.*, the Mg soap, produce the right-handed fibers only on some occasions and the left-handed fibers only on other occasions, it was difficult to draw definite conclusions as to the sense of twist of these soap fibers from a small number of experiments. Therefore, experiments have been carried out repeatedly under various conditions.

Generally, the bivalent metal soaps are liable to decompose and release their free acid with a rise in the temperature. For this reason, the crystalline aggregates were allowed to separate out from the C_2—C_8 fatty alcohols into which the soaps are to some extent dissolved without decomposition at temperatures below 100°C. Some soaps thus produced fibrous aggregates, while other soaps, such as the Sr, Ni, and Pb soaps, separated out, in the most part, as amorphous aggregates. Fortunately, we have found that the latter soaps also produced well-developed and twisted fibers when separated out from an alcohol solution containing water. Thus, for the bivalent metal soaps also, it became possible to obtain reliable information about the sense of twist of the soap fibers.

Experimental

The purification of D-12-hydroxyoctadecanoic acid (hereafter abbreviated as "D-acid") from a commercial product has been described previously.[1] The bivalent metal soaps of this acid were prepared by methathesis, at 50°C in aqueous ethanol, between the Na soap and chlorides or sulfates of the corresponding metals. The soaps thus obtained were washed with distilled water, then with ethanol, and finally with acetone, and well dried over P_2O_5 at room temperature. Gravimetric analysis demonstrated that the soaps, which are listed in Table 1, were all the disoaps with the formula of $Me(C_{18}H_{36}O_3)_2$. The water of crystallization was measured by thermogravimetry. The X-ray diffraction patterns, the infrared absorption spectra, and the differential thermographs were also investigated.

To obtain the soap fibers, the soap sample was dispersed into an alcoholic solvent under ultrasonic irradiation and then heated on a water bath. After the excess has been filtered off, the hot solution were allowed to cool to room temperature with stirring. Thus, the Ca and Cd soaps gelled at room temperature, while the other soaps separated out as flocculates or precipitates from the solution. The samples of the Hg and Mn soaps, which are susceptible to thermal decomposition, were carefully treated at a temperature lower than 50°C.

In certain cases, the soap fibers were produced by neutralizing the D-acid in a hydrocarbon solvent, Nujol, with an aqueous solution of the hydroxide of the corresponding metal at a certain high temperature and by then allowing the hot solution to cool to room temperature with stirring. The Nujol solution became grease at room temperature. It was confirmed by infrared analysis that the grease contained no free acid. On the other hand, when the grease was obtained by cooling the Nujol solution in which the soap samples had previously been dissolved at a high temperature (100—160°C), it was demonstrated by infrared analysis that a part of the soap samples was decomposed and free acid was released.

The procedure for observing the aggregates by means of an electron microscope was described in a previous paper.[1]

Results and Discussion

1) Characteristics of the Bivalent Metal Soaps. Since no data on the bivalent metal soaps of 12-hydroxyoctadecanoic acid have yet been described in the literature, some of them are given, together with the data for stearate soaps reported by Matsuura[4] in Table 1. One can see some characteristics of the hydroxyoctadecanoate soaps by comparing them with the stearate soaps.

i) Water of crystallization: With regard to the water of crystallization the hydroxyoctadecanoate soaps are similar to the corresponding stearate soaps.

ii) The infrared absorption spectra: Two infrared absorption bands are found at about 1400 cm^{-1} and 1550 cm^{-1}, they are due to the symmetric and asymmetric stretching vibrations respectively of the carbox-

1) T. Tachibana and H. Kambara, This Bulletin, **42**, 3422 (1969).
2) T. Tachibana, S. Kitazawa, and H. Takeno, *ibid*, **43**, 2418 (1970).
3) T. Tachibana and H. Kambara, *J. Colloid Interfac. Sci.*, **28**, 173 (1968).
4) R. Matsuura, *Nippon Kagaku Zasshi*, **86**, 560 (1965).

TABLE 1. CHARACTERISTICS OF D-12-HYDROXYOCTADECANOATE SOAPS, $Me(C_{18}H_{36}O_3)_2 \cdot xH_2O$
ν=infrared absorption peak for asymmetric vibration of COO^-
d=X-ray long spacing

Me	Mg	Ca	Sr	Ba	Mn	Ni	Cu	Zn	Cd	Hg	Pb
	2	1	0	0	1	1	0	0	0.5	1	0.5
x	(2 & 3	1	0	0	1	2	0	0	0	0	0) [a]
ν (cm^{-1})	1570	1573	1550	1563	1565	1565 sh	1590	1550	1563 sh	1585	1562 sh
	broad	1533	1538	1520	1545	1550		1538	1550	1565	1550
											1525 sh
											1510 sh
										1540 sh	1503
	49.7	50.3	50.2	49.4	49.8	50.5	47.8	46.5	49.6	48.3	50.3
d	49.3	49.8	48.1	47.5	47.7	48.8	47.6	42.6	50.2	50.0	50.8 [b]
(Å)	or										
	52.9										

a), b) Numerical values in parentheses represent those for the corresponding soaps of stearic acid.[4]

ylate ion. Matsuura[4] pointed out that the latter band is broadened or split into two or more bands in the hydrated stearate soaps. However, this splitting of the band was observed for all of the hydroxyoctadecanoate soaps used here, whether hydrated or not.

iii) The X-ray diffraction patterns: The hydroxyoctadecanoate soaps show a long spacing of around 49 Å, this is almost the same value as that of the corresponding stearate soaps, as is shown in Table 1. This value corresponds approximately to double the length of the hydroxyoctadecanoate chain, meaning that the hydroxyoctadecanoate soaps have a layer structure such as that established in the crystal structure of fatty acid and its soaps. It is also common to both the hydroxyoctadecanoate and stearate soaps that the Zn soap gives an abnormally low value of long spacing. It can also be pointed out that the hydrated soaps generally show higher values in the long spacing than do the unhydrated soaps.

The short spacing, which is associated with the interchain distance, is generally broader in the hydroxyoctadecanoate soaps than in the corresponding stearate soaps. The Mn, Ni, and Cu hydroxyoctadecanoates exhibited a diffraction pattern composed of diffuse bands, thus indicating low crystallinity. Here these results will not be taken into consideration further; the present paper will deal mainly with the sense of twist of the soap fibers.

2) The Form of the Aggregates. It was found that the bivalent-metal soaps of the D- (or L-) acid do not always form fibrous aggregates, but produce twisted fibers under appropriate conditions.

Typical electron micrographs are presented in Figs. 1 and 2. These photographs were made to show the same direction as that of the twist of the specimen.

The size and form of the fibrous aggregates and their sense of twist were characteristic of the individual soap under certain conditions. For example, when separated out from ethanol, the Mg soaps produced fibers of a reasonably uniform width of 0.03 μ, while the Sr, Mn, Cu, Cd, Hg, and Pb soaps often produced two types of fibers at the same time: (i) thin fibers of about 0.03 μ wide, with a small pitch of twist, and (ii) ribbons of large dimensions and with a large pitch of twist. The Zn soap precipitated from ethanol in a form of platelets, with a trace of twisted fibers (right-handed and left-handed fibers). This fact may be associated, in some manner, with the abnormally low value of the X-ray long spacing of this soap.

The bivalent metal soaps often produced both right-handed and left-handed fibers at the same time in ethanol. Which type of twisted fibers was more abundant, depended on the solvent used. The Ca soap (D-form) alone exhibited a behavior different from the other soaps in that it produced exclusively the right-handed fibers, not only from alcohols, but also from Nujol. In this connection, the Ca soap showed the same behavior as the Li soap.

3) Enantiomorphic Relationship for the Helical Sense. The relationship between the two enantiomers was previously established for the fibers of the free D- (or L-) acid and of its alkali metal soaps[1] and for the fibers of synthetic polypeptides.[5] As the same relationship can also be expected for the bivalent metal soaps, it was examined by the use of the Ca soap. The fibers from the Ca soap of the D-acid showed a right-handed twist, while those from that of the L-acid showed a left-handed twist, regardless of the solvent used. The Ca soap of the DL-acid (racemic form) gave amorphous precipitates. These micrographs are shown in Figs. 1a, b, and c. Thus it was also demonstrated, for the Ca soap, that the sense of twist in the helical aggregates is primarily associated with the optical isomerism. However, other bivalent metal soaps of the one enantiomer often produced both right-handed and left-handed fibers from the same solution. The same phenomenon was previously observed with the Na and K soaps.[1] This shows that some factors obscure the effect due to the asymmetry of molecule.

4) Solvent Effect on the Sense of Twist. Solvent effects have already been reported for the fibers of the free D- (or L-) acid and of its Li soap, the twist of which showed a one-handed sense in the C_2—C_4 alcohols

5) T. Tachibana and H. Kambara, *Kolloid-Z. Z. Polym.*, **219**, 40 (1967); this paper reports that enantiomorphism is found between helical aggregates of the D-isomer and the L-isomer of poly-γ-benzyl glutamate. Thereafter, we have found the same result with poly-γ-methyl (ethyl, *n*-propyl, or *i*-propyl) glutamate. These polypeptides also gave right-handed fibers for the D-enantiomer and left-handed fibers for the L-enantiomer.

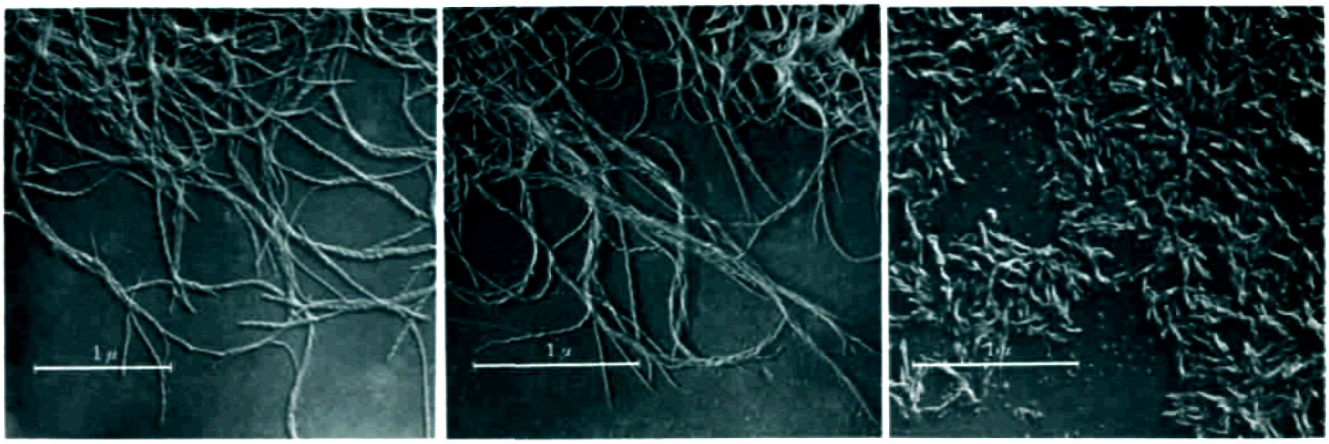
1 μ
1 μ
1 μ

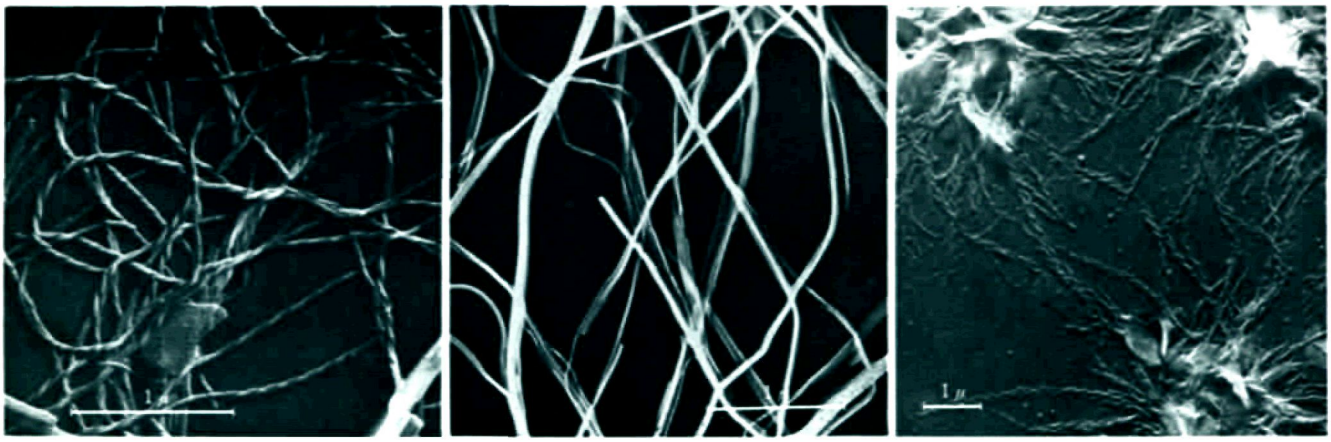
1 μ
1 μ

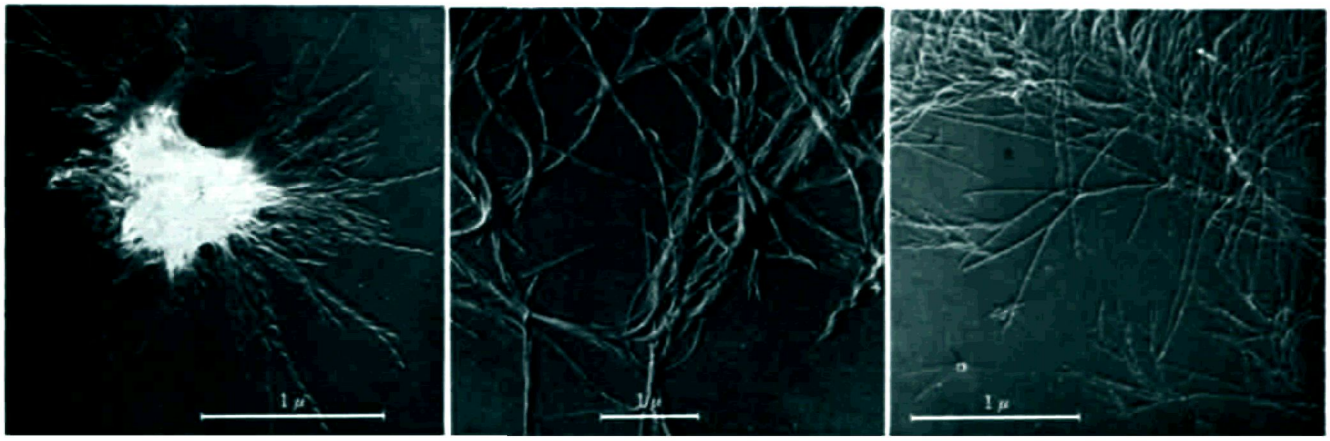
1 μ
1 μ
1 μ

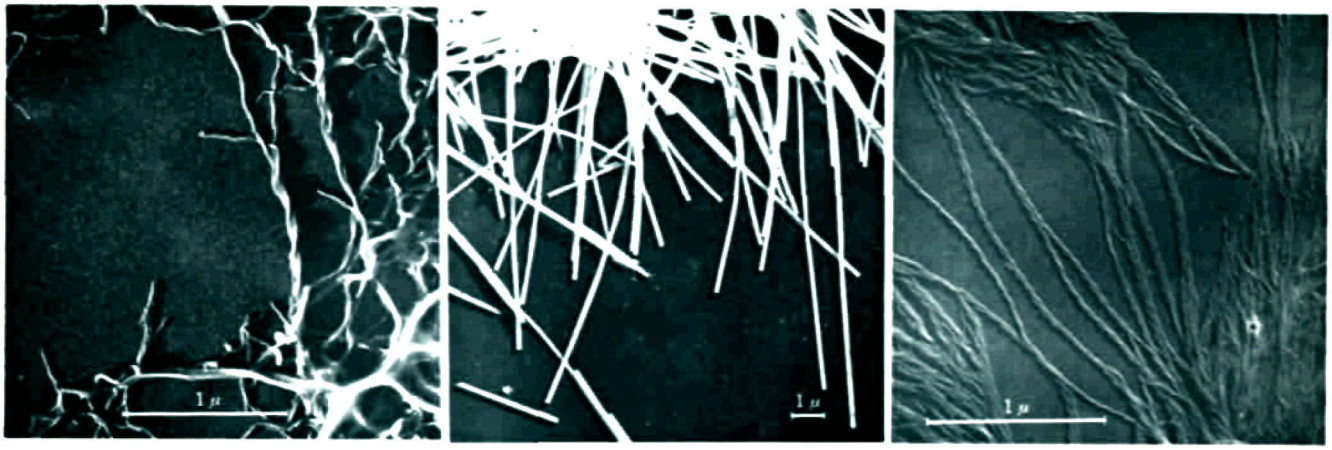
1 μ
1 μ
1 μ

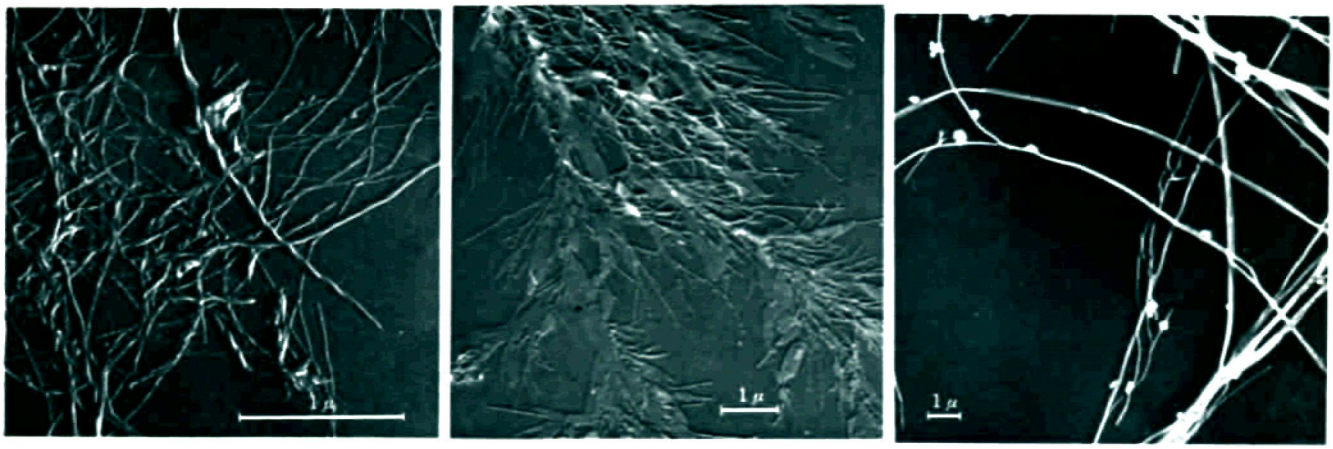
1 μ
1 μ
1 μ

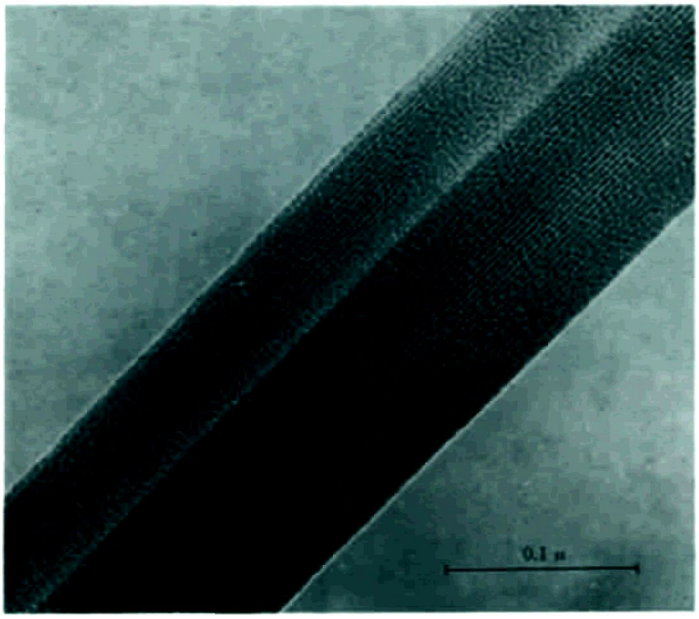
0.1 μ

and both senses in longer alkyl chain alcohols. For the Mg and Cd soaps also, an effect was found similar to that observed with the Li soap. The Mg soap of the D-acid produced predominantly the left-handed fibers from alcohols, while produced predominantly the right-handed fibers from Nujol. On the other hand, the Cd soap produced both right-handed and left-handed fibers from alcohols at the same time, though the fraction of the right-handed fibers increased with the length of the alkyl chain in a series of normal fatty alcohols, and right-handed fibers were exclusively produced from Nujol. It is interesting to note that, with regard to the sense of twist, polar or hydroxy solvents such as alcohols have effects contrary to those of such non-polar solvent as Nujol. This is not due to a difference in the crystalline phase between the soap crystal from alcohols and that from Nujol, since the samples from both solvents gave the same X-ray diffraction patterns. Accordingly, the solvent effect observed here can be regarded as a result of a crystal habit. Probably the polar-nonpolar structure of the soap crystal is associated with the observed effect. The possibility of a solvent effect due to an optically active solvent such as optically active amyl alcohol, was examined in the Ca soap, but no effect was observed.

5) The effect of Water. It was found that the presence of water in alcohols greatly influences the form of the soap aggregates. The Ca soap produced the twisted fibers from anhydrous ethanol, as is shown in Fig. 1a, but it produced only platelets from aqueous ethanol. However, the Sr, Ni, and Pb soaps, which were precipitated mostly as amorphous aggregates from anhydrous alcohols, produced a large number of twisted fibers from aqueous ethanol containing 5%(v/v) water (Figs. 2a, f, and 1). These fibers developed greatly with an increase in the water content, so that the sense of twist was more clearly observed with such fibers. However, the Pb soap from aqueous ethanol gave wider and larger ribbons, in which the twist was little observed. On the other hand, the Zn, Ba, and Cd soaps showed little effect of water on the form of the soap aggregates. An infrared spectral examination showed that the Ca, Sr, and Ba soaps recovered from aqueous ethanol were hydrated salts.

The water effect was observed also when the soaps were crystallized out from Nujol. For example, the Mg, Sr, and Ba soaps yielded fibers twisted a little from Nujol containing no water, but well-developed fibers were obtained when the metal soaps were prepared by neutralizing the D-acid in Nujol with an aqueous solution of the corresponding bivalent metal salts or when soaps previously prepared were dissolved into Nujol containing a certain amount of water at a high temperature. In these experiments, it was necessary to choose the most appropriate temperature.

Previously, Birdsall *et al.*[6] observed in a commercial Ca tallowate-minral oil grease, that the soap fibers were present only when a sufficient amount of water had been incorporated into the grease from which the fibers are formed. In this case, the soap crystallized out was of a hydrated form. These results evidently indicate that water in alcohols or Nujol plays some role in developing the soap crystal as a fibrous form. However, in the case of the hydroxyoctadecanoate soaps, the anhydrous soaps also produced the twisted fibers, as has already been described. Therefore, the twisting is not specific to the hydrated soap. Probably water aids in the development of soap fibers during the crystal growth.

6) Aging Effect. It was observed that the soap fibers changed their form when allowed to stand in the solution from which the fibers had been produced; the Cu soap gave left-handed thin fibers and right-handed wide ribbons immediately after it was separated out from ethanol, but the right-handed ribbons were found predominantly in the aged precipitate; the Ni soap produced a globular aggregates as the initial precipitate, and left-handed fibers from the aged precipitate.

The presence of water in ethanol was found to promote the change of the form of the aggregate; the Sr soap produced left-handed thin fibers and non-twisted ribbons as the initial precipitate, and non-twisted wider ribbons alone after sufficient aging (see Figs. 2a and b); the Pb soap initially produced left-handed fibers, and ribbons after aging. These changes were accelerated by increasing the water content in ethanol.

The Ca and Cd soaps often yielded such large twisted fibers that they were visible under an optical microscope. Such fibers were prepared by crystallizing these soaps out from aqueous ethanol and by then evaporating the solvent very slowly. The sense of twist for the large fibers was the same as that in the thin fibers previously observed by means of an electron microscope.

TABLE 2. THE SENSE OF TWIST IN THE FIBERS FROM BIVALENT METAL SOAPS OF D-12-HYDROXY-OCTADECANOIC ACID

Soap	The sense of twist solvent		
	ethanol	aqueous ethanol	Nujol
Mg	l	l	r & (l)
Ca	r	platelet	r
Sr	(l)	l	(r) & (l)
Ba	(l)	platelet	(r) & l
Mn	r & l		
Ni	(l)	(r) & l	
Cu	r & l	(r) & l	
Zn	(r) & (l)	(r) & l	
Cd	r & l	(r) & l	r
Hg	r & l	l	
Pb	(r) & (l)	l	

r: right-handed twist; l: left-handed twist.
(r) or (l) means the presence of a trace of the corresponding twist.

6) D. H. Birdsall and B. B. Farrington, *J. Phys. & Colloid Chem.*, **52**, 1415 (1948).

7) General Remarks on the Sense of Twist. The sense of twist of the soap fibers is summarized in Table 2. From this table, one can see a tendency for the bivalent metal soaps of the D-hydroxyoctadecanoate to favor, more or less, the formation of the left-handed fibers. The same tendency has also been found for all the alkali metal soaps except for the Li soap. This is considered to be a reflection of molecular asymmetry in the sense of twist of the soap fibers. However, it is characteristic of the bivalent metal soaps that both types of twisted fibers are, except in the case of the Ca soap, produced from the same specimen, although which type is predominant depends on the solvent used.

8) Fine Structure of Fibers. The observation of the structure of soap fibers by high-resolution electron microscopy was made using the Sr soap, which is comparably heat-resistant. The specimens were prepared by allowing a drop of the aqueous ethanol solution to dry on a micro-plastic grid for electron microscopy. The micrographs were photographed at an instrumental magnification of 100,000 X in a JEM-100B electron microscope without further treatment. Twisted thin fibers (width, 0.01 μ) and comparably large ribbons (width, about 0.1 μ) were found; the fine structure could be observed in the latter. Figure 3 shows a typical micrograph, in which striations are seen running parallel to the lengths of the fibers. The spacing of these striations is 33—40 Å, which approximates to the long spacing value of 47.5 Å derived from the X-ray diffraction patterns of the soap. Taking into account the uncertainty of the instrumental magnification, this indicates that Sr atoms all arranged in lines along the fiber axis with a periodicity of about 40 Å, and that the hydroxyoctadecanoate chains of the soap molecules all aligned approximately parallel to the width of the fibers. This is in accord with the observations on Na laurate fibers made by Camp and Shuttleworth[7] and on Ca soap fibers made by Bird and Rooney.[8]

The thickness of the ribbon was too thin to be estimated, probably being less than 50 Å. We observed a considerable disordered part where the striations were not seen on the surfaces of the ribbon; the ribbon consisted of a crystalline region and an amorphous region. From such a fine structure, it is presumed that each surface of a ribbon involves polar groups and non-polar alkyl chains of the hydroxyoctadecanoate molecules, and that the thin sides of it consist of polar groups alone or of non-polar groups alone, depending upon the polarity of the solvent from which the ribbons have been separated. One might expect that such thin ribbons would tend to twist themselves or to associate with one another as the result of the free energy requirement. In fact, the electron micrographs demonstrate that the structure is made up of two or more individual fibers twisted about one another. A similar structure is also encountered in twisted fibers of optically non-active soaps such as Na myristate and Ca tallowate. In these cases, both right-handed and left-handed fibers were observed. On the other hand, it has been established by the X-ray diffraction study that the crystal structure of long chain fatty acid and its salt is composed of alternately ionic layers and hydrocarbon layers, stacked on one another. These facts suggest that the twisting of the soap fibers results from the layer structure characteristic of soap. The one-handed twist of thin fibers composed of optically-active molecules is due to the asymmetry of the fiber structure itself.

In this series of studies, an enantiomorphic relationship in helical aggregates has been clearly demonstrated for 12-hydroxyoctadecanoic acid and its Li and Ca soaps. Other soaps of this acid produced both right-handed and left-handed fibers from the one enantiomer and, then, one of them was more or less predominant: the fibers from the univalent and bivalent metal soaps of the D-acid are inclined to twist to the left. This result is evidence that the sense of twist in the macrohelix is determined by the molecular asymmetry. Since biological fibers often exhibit a one-handed twist, it may be suggested that, in this case also, molecular asymmetry may play a role in determining the sense of twist at any stage of the fiber formation.

These studies were supported by a Scientific Research Grant from the Ministry of Education.

7) M. Camp and T. H. Shuttleworth, *Nature*, **183**, 535 (1959).
8) R. J. Bird and G. Rooney, *ibid.*, **190**, 337 (1961).

The Polymorphism and Physical Properties of the 1,6-Diaminopyrene-*p*-chloranil and Related Molecular Complexes[1)]

Shigeo KOIZUMI and Yoshio MATSUNAGA

Department of Chemistry, Faculty of Science, Hokkaido University, Sapporo

(Received September 2, 1971)

The 1,6-diaminopyrene-*p*-chloranil complex is dark blue when crystallized from chloroform and brown when crystallized from benzene. These two substances are distinctly different in X-ray diffraction, electronic spectrum, vibrational spectrum, and also electrical resistivity. The brown form, the resistivity of which is about 10^5 ohm cm, can be transformed into a third form, exhibiting only a few ohm cm, by compression in the presence of benzene or some other aromatic solvents. Dimorphic forms are also found with the complexes of trichloromonobromo- and dichlorodibromo-*p*-benzoquinones. One of these forms is of a similar nature to the dark blue-colored *p*-chloranil complex. The other form is brown. Only the brown form is obtainable for the complexes of monochlorotribromo-*p*-benzoquinone and *p*-bromanil. All the brown complexes except that of *p*-chloranil are similar and exhibit resistivities of the order of 10^3 ohm cm. In addition, black products exhibiting resistivities of several ohm cm can be prepared by using acetone as the solvent with 1,6-diaminopyrene and tetrahalo-*p*-benzoquinones. Contrary to the afore-mentioned complexes, no definite composition can be assigned to these low-resistivity products.

A large number of molecular complexes formed by interaction between organic electron-donors and acceptors have been examined for semiconductivity and related electronic properties in the past two decades. Among them, the 1,6-diaminopyrene-*p*-chloranil complex seemed to be particularly interesting because of the following reasons: 1) It has been well established that crystal complexes are rather sharply divided into two groups, namely, non-ionic and ionic complexes.[2-4)] Furthermore, the complexes with electrical resistivities of 10^6 ohm cm or less have been shown to be ionic.[5)] The 1,6-diaminopyrene-*p*-chloranil and related molecular complexes were the only exceptions to this rule known before our recent work on benzidine complexes.[6)]

2) The resistivity values recorded for the *p*-chloranil complex are scattered over a wide range, 10^3—10^4 ohm cm for the pressed polycrystalline samples and 10^5—10^9 ohm cm in the three directions of the single crystal.[7-9)] In a preliminary report, one of the present authors suggested that these scattered values can be correlated with the polymorphic forms.[10)]

3) The brown form of the *p*-chloranil complex can be transformed into a new form with a resistivity of only a few ohm cm if compressed with a small amount of benzene.[10)]

Previously we presented a way of demonstrating the effects of the size and shape of the component molecules on the electronic structure of crystal complexes.[11)] The diagram proposed there revealed that the 1,6-diaminopyrene-*p*-chloranil is located near the border line between non-ionic and ionic complexes of this donor. Moreover, the tetramethylbenzidine-*p*-chloranil complex, which exhibits a resistivity of 10^6 ohm cm, is near the above-mentioned location in the diagram. Thus, non-ionic complexes seem to exhibit relatively low electrical resistivities only when their charge-transfer absorptions are in an exceptionally low energy region. Guided by this working hypothesis, we have prepared several non-ionic complexes of benzidine and its derivatives with resistivities of 10^3—10^5 ohm cm.[6)] An examination of the electronic properties of the 1,6-diaminopyrene-*p*-chloranil and related complexes in more detail was highly desirable in order to verify the above-mentioned hypothesis. As the existence of some polymorphic forms has been noted, such a study would provide an excellent chance of demonstrating the importance of the stacking of the component molecules as one of the factors determining the electronic properties of molecular complexes. Furthermore, we were very much interested in the possibility of obtaining low-resistivity complexes without the process of compression.

Experimental

Materials. The *p*-chloranil, 2,5-dichloro-, and 2,6-dichloro-*p*-benzoquinones, and the *o*-chloranil were commercially obtained. The other component compounds were prepared following the procedures described in the references cited: 1,6-diaminopyrene,[12)] trichloromonobromo-*p*-benzoquinone,[13)] 2,5-dichloro-3,6-dibromo-*p*-benzoquinone,[14)] 2,6-dichloro-3,5-dibromo-*p*-benzoquinone.[14)] monochlorotribromo-*p*-benzoquinone,[15)] *p*-bromanil,[16)] 2,3-dichloro-

1) A part of the present work was performed by Y. M. while employed at the Central Research Division of American Cyanamid Company, and was presented at the Symposium on Molecular Structures, Nagoya, 1965.

2) R. Foster and T. J. Thomson, *Trans. Faraday Soc.*, **59**, 296 (1963).

3) Y. Matsunaga, *J. Chem. Phys.*, **41**, 1609 (1964).

4) K. M. C. Davis and M. C. R. Symons, *J. Chem. Soc.*, **1965**, 2079.

5) Y. Matsunaga, *Nature*, **205**, 72 (1965).

6) Y. Matsunaga and G. Saito, This Bulletin, **44**, 958 (1971).

7) M. M. Labes, R. Sehr, and M. Bose, *J. Chem. Phys.*, **33**, 868 (1960).

8) M. Schwarz, H. W. Davies, and B. J. Dobriansky, *ibid.*, **40**, 3257 (1964).

9) P. L. Kronick and M. M. Labes, *ibid.*, **35**, 2016 (1961).

10) Y. Matsunaga, *Nature*, **211**, 183 (1966).

11) Y. Matsunaga, This Bulletin, **42**, 2490 (1969).

12) H. Vollmann, H. Becker, M. Corell, and H. Streeck, *Ann.*, **531**, 121 (1937).

13) S. Levy and G. Schultz, *ibid.*, **210**, 133 (1881).

14) A. R. Ling, *J. Chem. Soc.*, **61**, 558 (1892).

15) A. R. Ling and J. L. Baker, *ibid.*, **61**, 589 (1892).

p-benzoquinone,[17] and *o*-bromanil.[18]

The complexes were crystallized when hot solutions of the components were mixed. For example, a solution of 1,6-diaminopyrene (0.70 g) in 350 m*l* of hot chloroform was added to a solution of *p*-chloranil (0.73 g) in 150 m*l* of hot chloroform. Dark blue crystals were filtered out and washed with the solvent. The yield was 0.85 g. Calcd for $C_{16}H_{12}N_2 \cdot C_6Cl_4O_2$: C, 55.3; H, 2.5; N, 5.9; Cl, 29.7%. Found: C, 55.2; H, 2.4; N, 6.1; Cl, 29.4%. When a solution of the quinone (1.48 g) in 150 m*l* of hot benzene was added to a solution of 1,6-diaminopyrene (1.40 g) in 700 m*l* of the same solvent, brown needles appeared on cooling. The yield was 1.70 g. Found: C, 55.9; H, 2.9; Cl, 28.7%. The *p*-bromanil complex was brown when similarly prepared from both chloroform and benzene. Calcd for $C_{16}H_{12}N_2 \cdot C_6Br_4O_2$: C, 40.3; H, 1.8; N, 4.3; Br, 48.8%. Found: C, 40.6; H, 2.0; N, 4.7; Br, 49.5% for a preparation from chloroform. C, 40.3; H, 1.9; N, 4.4; Br, 48.1% for a preparation from benzene.

When acetone was used as the solvent, the product showed various compositions depending upon the conditions of preparation, *e.g.*, the ratio of the donor to the acceptor employed and their concentrations. The following examples show two extremes in the combination of 1,6-diaminopyrene and *p*-chloranil. The diamine (0.46 g) dissolved in 20 m*l* of acetone was added to 1.48 g of *p*-chloranil in 80 m*l* of hot acetone. The mixture was kept overnight in a stoppered flask, and then the black crystalline deposits were filtered. The yield was 0.43 g. Found: Cl, 16.2% (No. 1 in Table 3). An acetone solution containing 1,6-diaminopyrene and *p*-chloranil in a mole ratio of 1 : 3 was evaporated to dryness at room temperature. The free *p*-chloranil in the deposits was removed by extraction with benzene using a Soxhlet apparatus. The remaining sample was analysed. Found: C, 46.8; H, 2.1; N, 4.6; Cl, 36.3; O, 8.6% (No. 2 in Table 3). One preparation of the 1,6-diaminopyrene-*p*-bromanil crystallized from acetone had the following composition: C, 36.8; H, 1.8; N, 2.9; Br, 53.4% (No. 9 in Table 3).

Measurements. The X-ray measurements were made with a Toshiba recording X-ray diffractometer, Model ADG-301, using filtered copper radiation. The electronic spectra of the crystal complexes were recorded on a Beckman DK-2A spectrophotometer, and the vibrational spectra, on a Jasco IR-G infrared spectrophotometer, both as Nujol mineral oil mulls. The resistivities were measured with a Yokogawa Wheatstone bridge, Type 2768, employing a cell similar to that designed by LaFlamme.[19] During the measurements, the samples were compressed by applying a pressure of about 0.8 kilobars. The temperature was adjusted in the range from room temperature to 100°C using a heating tape wrapped around the cell and with the aid of a Chino temperature-indicating controller.

Results and Discussion

The 1 : 1 Complexes. *p*-Chloranil and trichloromonobromo- and dichlorodibromo-*p*-benzoquinones form dark blue-colored complexes with 1,6-diaminopyrene in chloroform. As they are green when pulverized, hereafter "green form" will be used to designate them. All the quinones give brown-colored

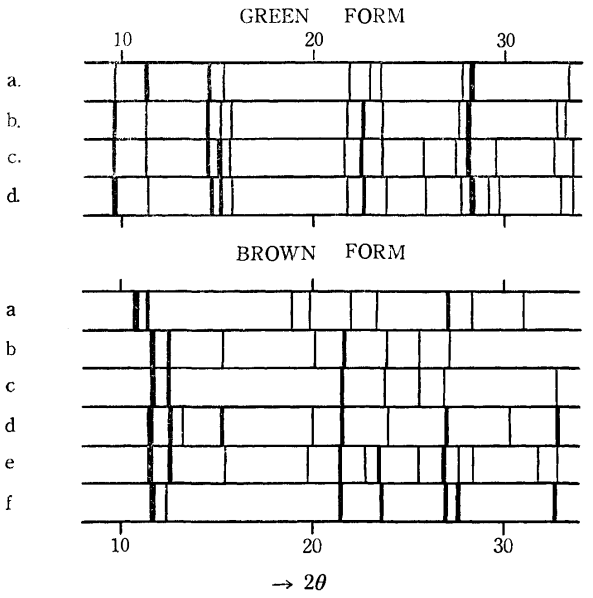

Fig. 1. X-Ray diffraction patterns of the 1,6-diaminopyrene complexes with (a) *p*-chloranil, (b) trichloromonobromo-*p*-benzoquinone, (c) 2,5-dichloro-3,6-dibromo-*p*-benzoquinone, (d) 2,6-dichloro-3,5-dibromo-*p*-benzoquinone, (e) monochlorotribromo-*p*-benzoquinone, and (f) *p*-bromanil.

complexes if mixed with 1,6-diaminopyrene in benzene. The same brown-colored *p*-chloranil complex can be crystallized from the following solvents; toluene, xylene, mono- and *o*-di-chlorobenzenes. The green form is transformed into the brown form when recrystallized from benzene. With monochlorotribromo-*p*-benzoquinone and *p*-bromanil, the brown forms are crystallized even from chloroform. The X-ray diffraction patterns are schematically presented in Fig. 1. The patterns given by all the green forms are similar to each other. However, the brown form of the *p*-chloranil complex is apparently different from the others; hereafter, the latter will be called "the brown form of the second type." Thus, the existence of polymorphic forms in the present complexes is evident. As will be described in the following paragraphs, the difference between the green and brown forms and also that within the brown forms are markedly reflected in their physical and chemical properties. Although only the complexes with *p*-chloranil and *p*-bromanil were analysed, the other complexes mentioned above are doubtlessly of a 1 : 1 composition, also.

The measurements of the electronic spectra of the complexes of *p*-chloranil and *p*-bromanil have been attempted by Kronick *et al.*[20] In their measurements the specimens were ground with potassium bromide and pressed into disks. The absorption spectra obtained by them in the range from about 14 to 40 kK showed the complexes to be mostly radical-ion salts. For instance, the mole fractions of the ionic component of the *p*-chloranil complex was estimated to be as high as 0.90. As was pointed out in our previous paper, the vibrational spectrum is in contradic-

16) H. A. Torrey and W. H. Hunter, *J. Amer. Chem. Soc.*, **34**, 702 (1912).
17) J. B. Conant and L. F. Fieser, *ibid.*, **45**, 2194 (1923).
18) T. Zincke, *Ber.*, **20**, 1776 (1887).
19) P. M. LaFlamme, *Rev. Sci. Instrum.*, **35**, 1193 (1964).
20) P. L. Kronick, H. Scott, and M. M. Labes, *J. Chem. Phys.*, **40**, 890 (1964).

tion with their characterization.[5] Therefore, we examined the electronic spectra of the present complexes by measuring the diffuse reflectance in the range from 6 to 30 kK of the specimens diluted with sodium chloride or naphthalene.[10] Contrary to the spectra presented by Kronick *et al.*, ours showed strong absorptions extended into the near-infrared region. As the charge-transfer absorption of the *p*-chloranil complex is located at 9.9 kK in chloroform and at 8.8 kK in toluene, our observation seemed to be consistent with the view that the complexes are non-ionic. Nevertheless, all the spectra, especially those of the brown forms, contained an extra band appearing at 14 kK. This location can well be compared with a band in the spectrum of 1,6-diaminopyrene monobromide reported in our previous work.[21] The intensity was increased by prolonged grinding, and also by storage; therefore, the cation-radical may be supposed to be formed in these processes. Apparently the discrepancy between the spectra presented by Kronick *et al.* and ours arises from the instability of the complexes ground with potassium bromide. In the present work, we attempted various methods to prevent the appearance of the band at 14 kK. The measurements as Nujol mineral oil mulls was found to be the best from this standpoint. However, with this technique it is not possible to estimate how large the light scattering is or how it depends on the wavenumber, because then the specimens absorb light over the entire measurable range. The apparent spectra newly-obtained for the *p*-bromanil complex and the green and brown forms of the *p*-chloranil complex are shown in Fig. 2. The green form withstands grinding better than the brown form. Consequently, we see that the spectrum of the green form of the *p*-chloranil complex is in essential agreement with that previously measured by the diffuse-reflection method. The spectrum of the brown form is very much improved by the present technique. The absorption maximum of the low-energy band is located around 7 kK. This value is lower by about 2 kK than the energy of the charge-transfer band of this complex dissolved in toluene, from which this form can be crystallized. On the other hand, the low-energy band in the green form appears at exactly the same place as the charge-transfer band of the complex dissolved in chloroform. The overall patterns of these two are similar, and both are certainly of charge-transfer complexes. However, a shoulder on the low-energy side of the absorption band in the visible region is observed only in the spectrum of the brown form, not in that of the green form. Very recently Amano *et al.* presented the crystal spectra of diaminopyrene complexes.[22] In their spectrum of the brown-colored *p*-chloranil complex, there is no charge-transfer band in the near-infrared region. This serious disagreement has yet to be explained. The *p*-bromanil complex, the representative of the brown forms of the second type, shows a spectrum similar to that of the brown-colored *p*-chloranil complex.

As has been reported previously, the vibrational spectrum of the brown form of the *p*-chloranil complex is well approximated by the superposed spectra of the compounds.[5] The green forms and the brown forms of the second type give similar spectra, indicating that they are also non-ionic. However, the patterns in

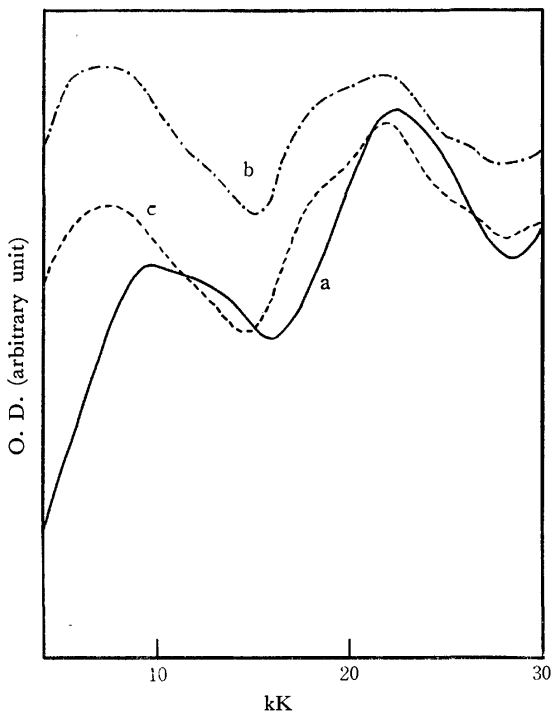

Fig. 2. Electronic spectra of (a) the green form and (b) the brown form of the *p*-chloranil complex and (c) the *p*-bromanil complex.

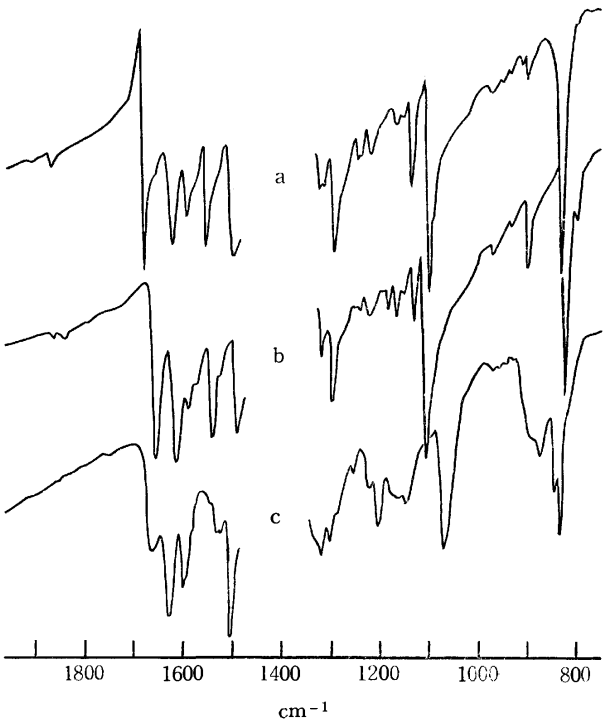

Fig. 3. Vibrational spectra of (a) the brown form and (b) the green form of the *p*-chloranil complex and (c) the *p*-bromanil complex.

21) A. Hakusui, Y. Matsunaga, and K. Umehara, This Bulletin, **43**, 709 (1970).

22) T. Amano, H. Kuroda, and H. Akamatu, *ibid.*, **44**, 1758 (1971).

the region between 1500 and 1700 cm^{-1} are very characteristic of each form. For example, Fig. 3 presents the spectra of the complexes of *p*-chloranil and *p*-bromanil. In the spectrum of the brown-colored *p*-chloranil complex, the bands at 1500, 1595, and 1625 cm^{-1} may be assigned to the donor, and those at 1560 and 1680 cm^{-1}, to the acceptor. The carbonyl stretching band is shifted to 1655 cm^{-1} in the spectrum of the green form. The *p*-bromanil complex gives the highest energy band in this region at 1655 cm^{-1}, but its intensity is markedly weaker than that of the band at 1625 cm^{-1}. Thus, the deviation from the superposed spectrum in the above-mentioned region is appreciable in both the green forms and brown forms of the second type. This observation indicates that the mode of intermolecular interaction is somewhat different in these forms.

The electrical resistivities of compressed polycrystalline samples of the complexes obey the usual exponential law;

$$\rho = \rho_0 \exp(E_a/kT),$$

where ρ is the resistivity, ρ_0 is a constant, and E_a is the activation energy for semiconduction. As has been found in many semiconductors, the value in the high-temperature range is often larger than that in the low-temperature range. For example, the results of the measurements of the complexes of *p*-chloranil, trichloromonobromo-*p*-benzoquinone, and *p*-bromanil are plotted in Fig. 4. The data on all the complexes are listed in Table 1. Kronick and Labes grew their single crystal of the *p*-chloranil complex from chloroform and obtained the following resistivities at 25°C in three directions: 10^5, 10^6, and 10^9 ohm cm.[9] Considering the solvent employed by them, these values may be compared with our value for the green form. The present result agrees reasonably well with the geometric mean of the values observed by Kronick and Labes. In addition, the activation energy in one of the three directions reported by them, 0.19 eV, is in good agreement with our value for the high-temperature range. As may be noted in Table 1, the values of the resistivity and the activation energy in the green forms of the other three complexes are similar to those of the *p*-chloranil complex.

After careful drying, the brown-colored *p*-chloranil complex exhibits a resistivity of the order of 10^5 ohm cm, as is listed in Table 1. This value can be quickly decreased by compression in the presence of benzene. Even a trace of the solvent remaining in the sample can result in a lowering of the resistivity to 10^3—10^4 ohm cm, the values reported by earlier workers.[7,8] If the amount of the solvent is enough, *e.g.*, a few drops per gram, a resistivity as low as a few ohm cm can be achieved. Not only benzene but also the following aromatic liquids were found to be more or less effective in effecting the transformation; toluene, xylene, chlorobenzene, *o*-dichlorobenzene, dimethylaniline, nitro-

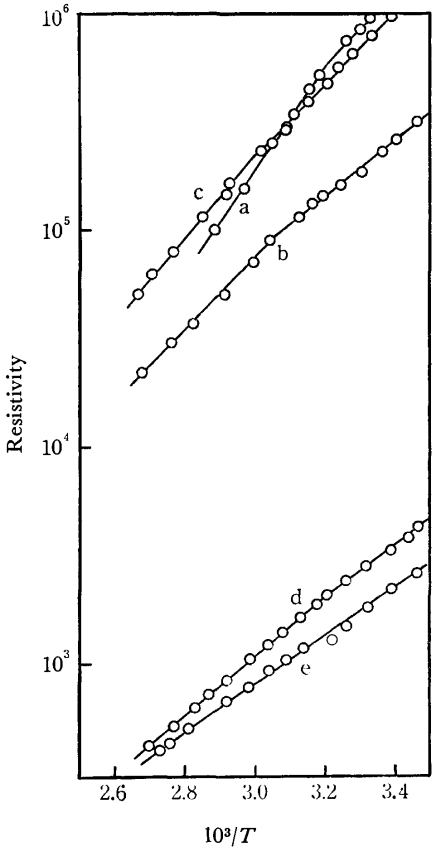

Fig. 4. Electrical resistivities of (a) the green form and (b) the brown form of the *p*-chloranil complex, (c) the green form and (d) the brown form of the trichloromonobromo-*p*-benzoquinone complex, and (e) the *p*-bromanil complex.

TABLE 1. ELECTRICAL PROPERTIES OF THE 1,6-DIAMINOPYRENE COMPLEXES

Acceptor	Form	Resistivity at 20°C (ohm cm)	E_a (eV)[a]
p-Chloranil	Green	1.3×10^6	0.14, 0.20
	Brown	2.7×10^5	0.11, 0.14
Trichloromonobromo-*p*-benzoquinone	Green	9.7×10^5	0.14, 0.17
	Brown (II)	3.3×10^3	0.10, 0.12
2,5-Dichloro-3,6-dibromo-*p*-benzoquinone	Green	3.3×10^6	0.15, 0.19
	Brown (II)	4.0×10^3	0.12, 0.13
2,6-Dichloro-3,5-dibromo-*p*-benzoquinone	Green	2.3×10^6	0.14, 0.16
	Brown (II)	1.3×10^4	0.11
Monochlorotribromo-*p*-benzoquinone	Brown (II)	2.4×10^3	0.10
p-Bromanil	Brown (II)	2.3×10^3	0.10

a) The first value is for the low-temperature range, and the second for the high-temperature range.

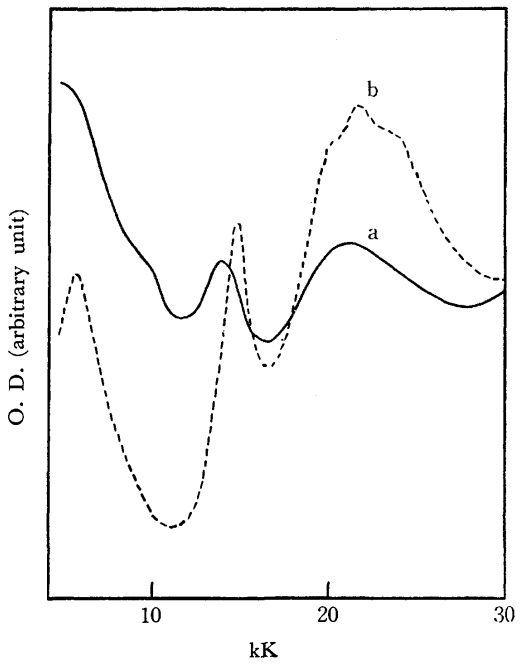

Fig. 5. Electronic spectra of (a) the low-resistivity form of the *p*-chloranil complex and (b) 1,6-diaminopyrene monobromide.

benzene, and pyridine. Contrary to the green and brown forms, which are stable up to about 160°C, the low-resistivity form is not very stable, even at room temperature. After storage for several years, a resistivity of about 100 ohm cm was recorded. The electronic spectrum is shown in Fig. 5, along with that of 1,6-diaminopyrene monobromide measured by the same technique. The absorption in the near-infrared region is appreciably stronger than that in the visible region, and it is shifted to the low-energy side compared with those in the green and brown forms. This behavior seems to be consistent with its low-electrical resistivity, as was noted at the beginning of this paper.

The presence of some diaminopyrene cation-radicals indicated by the peak at 14.0 kK must be mentioned. In the process of the transformation, the complex is compressed; therefore, the pellet produced must be crushed for further examination. As was mentioned earlier, this final step is possibly accompanied by the formation of the cation-radical. The presence of a fair amount of the cation-radical may correlate with the low resistivity, as has been suggested by Kronick *et al*;[20] however, it must be pointed out that the low resistivity can be observed before the crushing. As may be expected from the electronic spectrum shown in Fig. 5, this form shows a strong absorption in the rock-salt region. The vibrational pattern in the above-mentioned characteristic region consists of bands at 1500, 1530, 1580, and 1635 cm^{-1}. If the last one arises from the carbonyl-stretching vibration, it is shifted to the low-energy side as much as 50 cm^{-1}. This unusually large shift may indicate that the crystal structure allows an appreciable contribution of the dative structure to the ground state. It may be suggested that the low-resistivity form has an electronic structure which is intermediate between non-ionic and ionic.

All the brown-colored complexes of the second type exhibit resistivities of the order of 10^3 ohm cm. This value is in accordance with that reported for the *p*-bromanil complex by Labes *et al.*[7] They are stable under compression in the presence of benzene as well as the green forms of the complexes of *p*-chloranil and

Table 2. Classification of the 1 : 1 complexes

Solvent	Halogen atoms on quinonone molecule				
	Cl_4	Cl_3Br	Cl_2Br_2[a]	$ClBr_3$	Br_4
Chloroform	Green form Resistivity 10^6 ohm cm				Brown from (II) 10^3 ohm cm
Benzene	Brown form 10^5 ohm cm		Brown form of (II) Resistivity 10^3 ohm cm		

a) 2,5-dichloro-3,6-dibromo- and 2,6-dichloro-3,5-bromo-*p*-benzoquinones.

Table 3. Resistivities ofn the on-stoichiometric complexes

No.	Quinone	Preparation method	Composition	Resistivity (ohm cm)
1	*p*-Chloranil	Crystallization	See Exptl.	200
2	*p*-Chloranil	Evaporation	See Exptl.	7
3	*p*-Chloranil	Evaporation	1 : 1	870
4	*p*-Chloranil	Evaporation	1 : 1.2	13
5	*p*-Chloranil	Evaporation	1 : 1.4	6
6	*p*-Chloranil	Evaporation	1 : 1.6	4
7	2,5-Dichloro-3,6-dibromo-*p*-benzoquinone	Evaporation	2 : 3	5
8	2,6-Dichloro-3,5-dibromo-*p*-benzoquinone	Evaporation	2 : 3	9
9	*p*-Bromanil	Crystallization	See Exptl.	3
10	*p*-Bromanil	Evaporation	2 : 3	10^7
11	2,3-Dichloro-*p*-benzoquinone	Evaporation	2 : 3	10^6
12	2,5-Dichloro-*p*-benzoquinone	Evaporation	2 : 3	10^4
13	2,6-Dichloro-*p*-benzoquinone	Evaporation	2 : 3	10^5
14	*o*-Chloranil	Evaporation	2 : 3	10^4
15	*o*-Bromanil	Evaporation	2 : 3	10^4

trichloromonobromo- and dichlorodibromo-*p*-benzoquinones. The classification of these 1 : 1 complexes, based on X-ray diffraction and physical properties, is summarized in Table 2. It is interesting to note that the kind of polymorphic form is entirely governed by the number of chlorine (or bromine) atoms on the quinone molecule. The large difference in the optical and electrical properties found in these polymorphic forms shows the importance of the stacking of the component molecules as one of the factors determining the electronic properties of these complexes.

The Non-stoichiometric Complexes.[23] 1,6-Diaminopyrene dissolves well in acetone; therefore, we attempted the preparation of the complexes in acetone in order to avoid the use of a large amount of the solvent. Surprisingly, the complexes prepared in acetone are of an entirely different nature from the 1 : 1 complexes described above. They show no definite composition. The complexes were prepared by crystallization from acetone or by the evaporation of the acetone solution to dryness. The second process was performed by lefting the solution stand in a good hood without heating. As may be seen in Table 3, a low resistivity can be achieved over a fairly wide range of composition (*e.g.*, see Nos. 1 and 2). Although the compositions of Nos. 2 and 9 do not exactly correspond to any simple ratio of the donor to the acceptor, both of them are not far from the calculated values for a mole ratio of 2:3: C, 49.9; H, 2.0; N, 4.7; Cl, 35.5; O, 8.0%, and C, 34.6; H, 1.4; N, 3.2; Br, 55.3%, respectively. Therefore, for the quinones other than *p*-chloranil, the evaporation was carried out only at this mole ratio. It must be added that the complex prepared by the evaporation of an acetone solution to dryness cannot be homogeneous. The composition of No. 1 is markedly different from the ratio of the diaminopyrene to the *p*-chloranil initially dissolved into the solvent. When the solvent is evaporated, the composition of the deposit is expected to vary according to the changes in the mole ratio and also in the concentration. Moreover, we can expect the presence of some decomposition products in the samples made by this method. These two factors may explain the observed difference in resistivity between the samples made by crystallization and those made by evaporation (compare Nos. 9 and 10). In Table 3 we can see that only tetrahalo-*p*-benzoquinones give low-resistivity complexes with 1,6-diaminopyrene in this solvent.

23) The resistivities in this section were measured on compressed pellets by a four-probe method using an A. & M. Fell Model B resistivity test rig and a Keithley Model 502 milliohmmeter.

The authors wish to express their thanks to Dr. Toshio Yokokawa for the use of the X-ray diffractometer.

BULLETIN OF THE CHEMICAL SOCIETY OF JAPAN, VOL. 45, 428—431 (1972)

The Second CMC of the Aqueous Solution of Sodium Dodecyl Sulfate. I. Conductivity

Masaji MIURA and Michiko KODAMA

Department of Chemistry, Faculty of Science, Hiroshima University, Higashisenda-machi, Hiroshima

(Received September 3, 1971)

The conductivity studies of the aqueous solution of sodium dodecyl sulfate (SDS) over the concentration range of 0—0.12 M revealed that there exists a so-called 2nd critical micelle concentration (CMC) at about 65 mM in addition to the 1st CMC at 8.3 mM. The 2nd CMC was greatly influenced by additives; sodium chloride lowered the 2nd CMC, whereas organic substances, such as dodecyl alcohol and *n*-hexane, raised it. Moreover, the specific conductivity-concentration curve of the pure SDS solution broke upward at the 2nd CMC, and its slope increased in the presence of sodium chloride, while it bent toward the concentration axis in the presence of a certain amount of dodecyl alcohol or *n*-hexane. These facts may afford a clue for explaining the micelle structure above the 2nd CMC.

It has been known that, in surfactant solutions, in addition to an initial critical micelle concentration (1st CMC), there occurs a change in the properties of surfactant solutions at a concentration above the 1st CMC, which is usually called the 2nd CMC.

Several works have been done on the 2nd CMC. Tyuzyo *et al.*[1-3] have found a method of estimating the 2nd CMC from the viscosity data. Ekwall and his co-workers[4-9] measured the density, viscosity, and vapor pressure of an aqueous sodium caprylate solution over a wide concentration range above the 1st CMC and discussed the change in the micelle structure. Rovins *et al.*[10] have investigated the 2nd CMC by measuring the viscosity and light-scattering of aqueous solutions of 2-dodecylaminoethanol salts. In our

1) N. Sata and K. Tyuzyo, This Bulletin, **26**, 177 (1953).
2) H. Okuyama and K. Tyuzyo, *ibid.*, **27**, 259 (1954).
3) K. Tyuzyo, *ibid.*, **31**, 117 (1958).
4) P. Ekwall, H. Eikrem, and L. Mandell, *Acta Chem. Scand.*, **17**, 111 (1963).
5) P. Ekwall and P. Holmberg, *ibid.*, **19**, 455, 573, (1965).
6) P. Ekwall, K. Lemstrom, H. Eikrem, and P. Holmberg, *ibid.*, **21**, 1401 (1967).
7) P. Ekwall, H. Eikrem, and P. Stenius, *ibid.*, **21**, 1639 (1967).
8) P. Stenius and P. Ekwall, *ibid.*, **21**, 1643 (1967).
9) P. Ekwall and P. Stenius, *ibid.*, **27**, 1767 (1967).
10) D. C. Robins and I. L. Thomas, *J. Colloid Interface Sci.*, **26**, 415 (1968).

laboratory we measured the conductivity and viscosity of the Aerosol-OT solution,[11] the conductivity, sound velocity, and viscosity of sodium dodecyl sulfate (SDS) solution,[12] and the fluorescence spectrum of acridine orange which was added to an SDS solution;[13] the presence of the 2nd CMC was ascertained in these systems. Thus, it has been revealed by various methods that the 2nd CMC exists in surfactant solutions. However, how the shape and size of the micelle vary at the 2nd CMC is still little known.

It is well known that the impurity of an electrolyte or non-electrolyte which is present in a surfactant solution lowers the 1st CMC and increases the micelle size. It can be expected, therefore, that the 2nd CMC may also be greatly influenced by such impurities.

In our studies, SDS was chosen as the surfactant because it is the most typical anionic surfactant and because the properties of its aqueous solution have been extensively studied by many workers and by various methods. In order to obtain some information about the micelle structure, the effect of additives on the properties of the aqueous solution of SDS was investigated. On the other hand, since there is no direct means to determine simultaneously both the size and shape of the micelle, it is difficult to discuss the micelle structure by only one method. In this studies, therefore, the micelle structure of the aqueous solution of SDS was investigated mainly in the concentration region above the 1st CMC, through systematic studies including measurements of the conductivity, light-scattering, density, viscosity, and depolarization of fluorescence. In the present paper, which is the first of a series of our studies, the results of the conductivity measurements will be reported.

Experimental

Materials. SDS was synthesized according to the method of Dreger.[14] Dodecyl alcohol (DA) was obtained from the Wako Pure Chemical Co., and its purity was determined by means of gas chromatography as 99.7%. The sulfonation of the DA was carried out by adding the DA, drop by drop, to an acetic acid solution of chlorosulfonic acid. The SDS thus obtained was recrystallized several times from the conductivity water and butyl alcohol respectively, and was then purified by a liquid/liquid extraction technique in which a 10% solution of SDS in 50% aqueous alcohol was extracted with 60/80 petroleum ether for 48 hr.[15] Reagent-grade benzene and hexane were purified by fractional distillation. Ultra-pure sodium chloride was obtained from the E. Merck Co. and was used without further purification.

Procedures. The conductivity measurements were carried out by using the apparatus previously described.[16,17] Unplatinized electrodes were employed in order to minimize the adsorption.[18] The concentration of the solution was changed successively by diluting it with conductivity water. The conductivity was measured in a water-thermostat of 25.000±0.005°C after the temperature equilibrium had been established.

In the case of the presence of organic additives, the solutions for conductivity measurements were prepared as follows. Thirty milliliters of a 0.15 M SDS solution were taken in a glass ampoule, and a known amount of DA was added to it. The amount of DA added was below the saturation point.[19] The ampoule was sealed after having been cooled by liquid nitrogen and shaken in a thermostat of 25°C for 48 hr in order to attain an equilibrium of solubilization. A series of ampoules was prepared, each of which contained DA; the molar ratios of DA to SDS were 1/200, 1/100, 1/50, 1/10, and 1/5. The same procedure was also used in the preparation of SDS solutions containing various amounts of solubilized benzene or hexane.[20,21]

Results

No Additives. In general, the 1st CMC of a surfactant solution is determined graphically as the break point in the plot of the specific conductivity *vs.* the concentration. The results of the conductivity measurement of an aqueous solution of SDS in the absence of additives are shown in Fig. 1, where the specific conductivity (κ) is plotted against the concentration of the SDS solution. It may be seen from this figure that a break point appears at about 65 mM in addition to that at 8.3 mM, the latter corresponds to the 1st CMC, while the former, the so-called 2nd CMC, agrees fairly well with the results obtained by other methods.[11-13] It may also be noted that the specific conductivity-concentration curve breaks upward at the 2nd CMC.

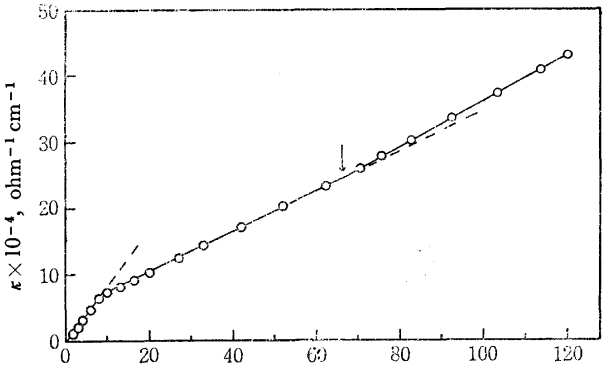

Fig. 1. Specific conductivity of SDS solution. The arrows in Figs. 1 and 2 indicates the 2nd CMC.

11) M. Miura and C. Maeda, Abstract of the 9th Annal Meeting the Chemical Society of Japan, p. 323 (1956).
12) T. Yasunaga, G. Oguri, and M. Miura, *J. Colloid Interface Sci.*, **23**, 352 (1967).
13) M. Miura, Y. Kubota, J. Miyahara, and I. Takeuchi, Abstract of the 20th Annual Meeting of the Chemical Society of Japan, Vol. 1, p. 200 (1967).
14) E. E. Dreger, G. I. Keim, and G. D. Miles, *Ind. Eng. Chem.*, **36**, 610 (1944).
15) S. P. Harrold, *J. Colloid Sci.*, **15**, 280 (1960).
16) G. Jones and R. C. Josephs, *J. Amer. Chem. Soc.*, **50**, 1049 (1928).
17) M. Miura and S. Otani, *Nippon Kagaku Zasshi*, **77**, 517 (1956).
18) A. W. Ralston and C. W. Hoerr, *J. Amer. Chem. Soc.*, **64**, 97 (1942).
19) M. Miura and S. Arichi, *J. Sci. Hiroshima Univ., Ser. A*, **22**, 57 (1958).
20) E. Hutchinson, A. Inaba, and L. G. Bailey, *Z. Physik. Chem.*, **5**, 344 (1955).
21) W. C. Lin, This Bulletin, **28**, 227 (1955).

Effect of Sodium Chloride. In general, crude SDS is apt to contain sodium chloride as an impurity, for the latter is formed as a by-product in the process of the synthesis of SDS. Therefore, the effect of sodium chloride on the 2nd CMC of the aqueous solution of SDS was investigated. The specific conductivities of SDS solutions containing various amounts of sodium chloride are plotted against the concentration of SDS in Fig. 2. The 1st CMC of the SDS solution lowers with an increase in the concentration of sodium chloride; this is in agreement with the results obtained by other workers. It is interesting to note that the 2nd CMC lowers and the slope of straight line above the 2nd CMC rises with an increase in the sodium chloride concentration.

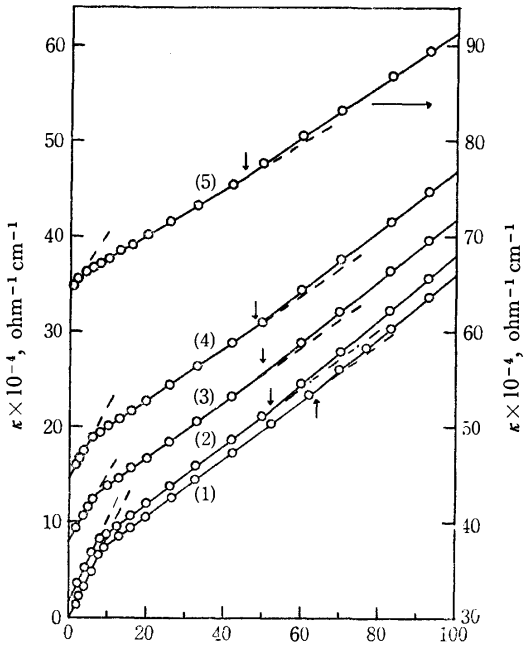

Fig. 2. Specific conductivities of SDS solutions in the presence of NaCl; concentration of NaCl: (1) 0 M, (2) 0.001 M, (3) 0.005 M, (4) 0.01 M, (5) 0.05 M. The plot in the presence of 0.0005 M NaCl was omitted in this figure.

Figure 3 shows the deviation of the specific conductivity ($\Delta\kappa$) from the extrapolation of the linear plot of the specific conductivity *vs.* the concentration below the 2nd CMC in Fig. 2 to a higher concentration. It may be seen from the figure that $\Delta\kappa$ is positive regardless of the sodium chloride concentration and that the angle (α) formed by the two straight lines increases with the sodium chloride concentration.

Effect of Dodecyl Alcohol. It is well known that DA, which is the main starting material in the syntheses of SDS, is apt to remain unreacted as a contaminant in crude SDS and has a profound influence upon the properties of the SDS solution. Therefore, the effect of DA on the 2nd CMC of the aqueous solution of SDS was investigated. DA was added to a SDS solution in a molar ratio of DA to SDS, 1/200, 1/100, 1/50, 1/10, or 1/5. The results of the conductivity measurements are presented in Fig. 4, where $\Delta\kappa$ is plotted against the concentration of SDS. The

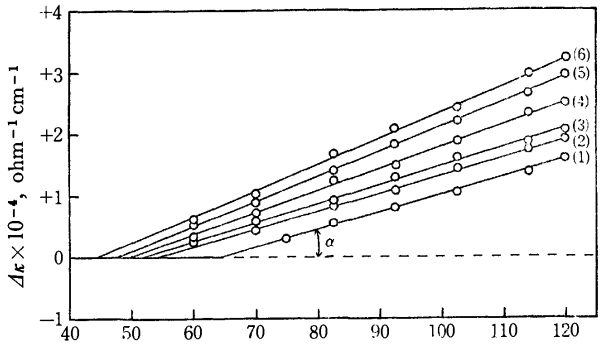

Fig. 3. $\Delta\kappa$ of SDS solutions in the presence of NaCl; concentration of NaCl: (1) 0 M, (2) 0.0005 M, (3) 0.001 M, (4) 0.005 M, (5) 0.01 M, (6) 0.05 M.

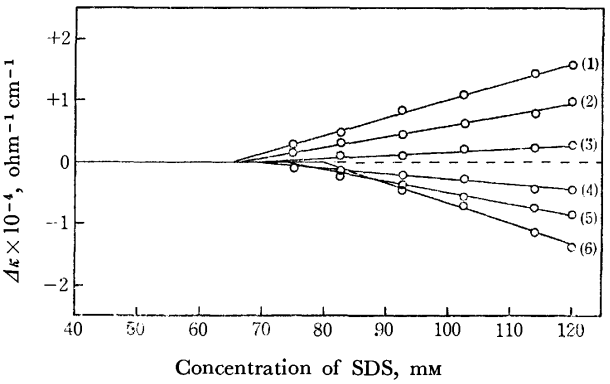

Fig. 4. $\Delta\kappa$ of SDS solutions in the presence of DA; molar ratio of DA to SDS: (1) 0, (2) 1/200, (3) 1/100, (4) 1/50, (5) 1/10, (6) 1/5.

slope of the straight line above the 2nd CMC becomes lower with an increase in the concentration of DA, that is, $\Delta\kappa$ decreases and at last becomes negative when the DA is added in a molar ratio of 1/50 or more to the SDS solution. Moreover, the 2nd CMC increases with the DA concentration. It is of great interest that the results in the presence of DA are quite the opposite of those in the presence of sodium chloride.

Effects of n-*Hexane and Benzene.* Next the effect of non-polar compounds on the properties of the SDS solution were studied. Here, *n*-hexane with a

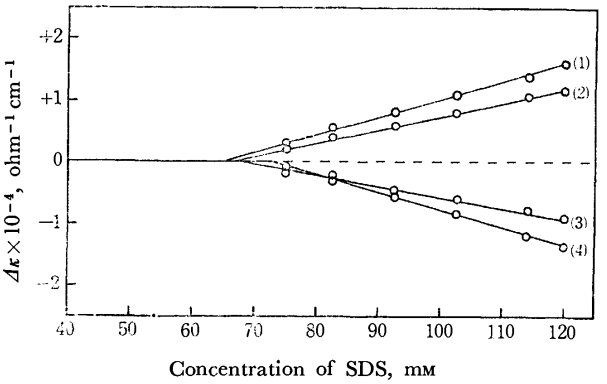

Fig. 5. $\Delta\kappa$ of SDS solutions in the presence of *n*-hexane; molar ratio of *n*-hexane to SDS: (1) 0, (2) 1/100, (3) 1/15 (4) 1/4.

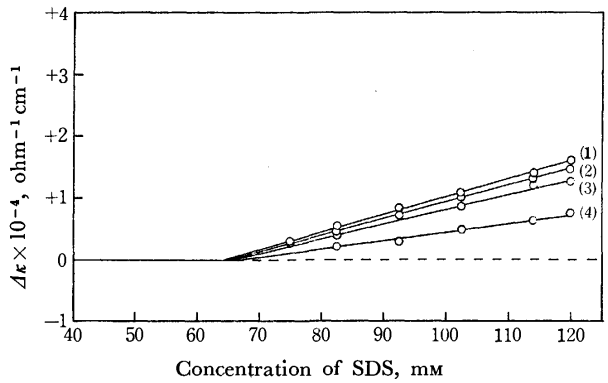

Fig. 6. $\Delta\kappa$ of SDS solutions in the presence of benzene; molar ratio of benzene to SDS: (1) 0, (2) 1/100, (3) 1/10, (4) 1/2.

chain structure and benzene with a ring structure were selected as representatives of nonpolar compounds. The results obtained in the presence of *n*-hexane and those obtained in the presence of benzene are shown in Figs. 5 and 6 respectively. The effect of *n*-hexane is quite similar to that of DA, while benzene does not have such a marked effect.

Effect of Sodium Chloride and DA. Since sodium chloride and DA generally coexist in crude SDS, the effect of these two compounds on the conductivity behavior of the SDS solution was studied; the results are shown in Fig. 7. As may be in Figs. 3 and 4, the results in the presence of sodium chloride are opposed to those in the presence of DA with respect to the 2nd CMC and the slope of the specific conductivity *vs.* the concentration curve above the 2nd CMC. However, when the two compounds coexist, their effects on these two properties compensate each other, as can be seen in Fig. 7.

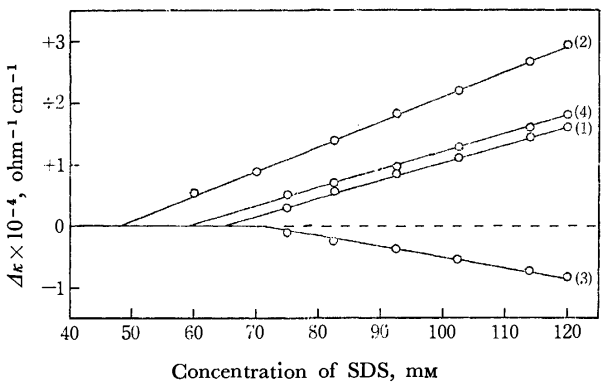

Fig. 7. $\Delta\kappa$ of SDS solutions; (1) no additive, (2) 0.01 M NaCl, (3) DA to SDS 1/10, (4) 0.01 M NaCl and DA in molar ratio of DA to SDS 1/10.

Discussion

As is obvious from Fig. 1, the specific conductivity *vs.* concentration curve of the pure SDS solution breaks upward at the 2nd CMC. When a certain amount of DA is added to the SDS solution, the curve breaks downward, as is seen in Fig. 4. Similar results were obtained for the system of sodium decyl sulfate and decyl alcohol, as is shown in Fig. 8, where the sodium

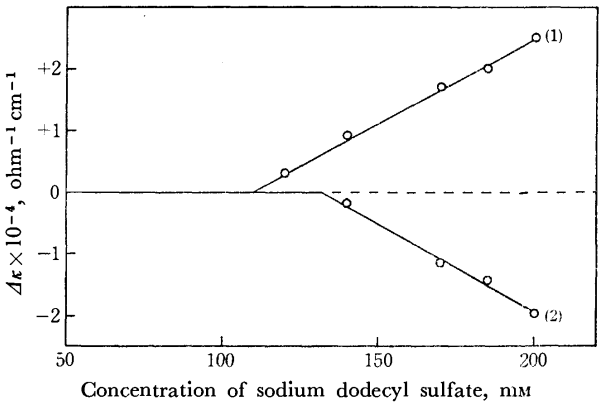

Fig. 8. $\Delta\kappa$ of sodium decyl sulfate solutions; (1) no additive, (2) decyl alcohol in its molar ratio to sodium decyl sulfate 1/10.

decyl sulfate used was carefully purified. In our previous study,[12] the curve bent toward the concentration axis. This may result from the presence of organic impurities such as DA.

In general, the purity of the surfactant can be checked by means of the value of the 1st CMC or by the presence or absence of the minimum in the surface tension *vs.* concentration curve. By the present study, another criterion for the purity of the surfactant was found: the presence of organic contaminants in the surfactant solution can be checked by means of the value of the 2nd CMC and the slope of the specific conductivity *vs.* concentration curve.

In the presence of sodium chloride, the 2nd CMC as well as the 1st CMC lowers, and at the same time $\Delta\kappa$ increases, with an increase in its concentration. On the other hand, in the presence of DA or *n*-hexane, though the 1st CMC loweres, as is well known, the 2nd CMC increases and $\Delta\kappa$ decreases and finally becomes negative with an increase in the concentration of DA or *n*-hexane. It is clear from these results that nonelectrolytes have the same influence on the 1st CMC, but have quite the opposite influence on the 2nd CMC, as compared with electrolytes. These facts may afford a clue for elucidating the micelle structure above the 2nd CMC.

As can be expected from the results shown in Figs. 4 and 5, the specific conductivity *vs.* concentration curve may show no change at the concentration corresponding to 2nd CMC when an appropriate amount of non-electrolyte is present, *e.g.*, an intermediate quantity between 1/100 and 1/50 in molar ratio in the case of DA. The same situation can be deduced when an electrolyte coexists with a non-electrolyte in a certain molar ratio, as can be seen in Fig. 7. In such cases, there may be no 2nd CMC; the presence of a proper amount of the impurities of non-electroytes may stabilize the micelle formed in the region of low concentrations.

Though both *n*-hexane and benzene are nonpolar compounds, the former has a much larger influence upon the 2nd CMC than the latter, as may be seen in Figs. 5 and 6. This may arise from the difference in the mode of solubilization between these two compounds.

Distribution Studies of Alkali Metal Picrates

Tadashi IWACHIDO

College of Liberal Arts, Okayama University, Tsushima, Okayama

(Received March 26, 1971)

Alkali metal picrates are extractable from an aqueous solution into nitrobenzene. The picrates exist mainly as the dissociated form in both the aqueous and the nitrobenzene phases, whereas picric acid exists mainly as the undissociated form in the organic phase. The distribution ratio of the picrates and picric acid at any pH can well be explained in terms of these equilibrium constants. The distribution coefficient of picric acid is evaluated to be $10^{2.63}$.

Polynitroderivatives of phenol and diphenylamine are known as extracting agents of alkali metal cations. However, little is known about the extraction mechanism. Only for alkali metal picrates[1] and hexanitrodiphenylaminates,[2] the distribution coefficient between aqueous and nitrobenzene phases and the association constants in the aqueous phase have been determined by means of the extraction method. As the association constants of the picrates in nitrobenzene phase, the values obtained by means of conductivity measurements have been cited. Such equilibrium constants show that these salts strongly dissociate in nitrobenzene as well as in the aqueous phase. From these data, it can be concluded that the distribution ratio of alkali metals increases with an increase in the dissociation constant in the organic phase and with a decrease in that in the aqueous phase. The present paper will describe that the introduction of the new constant, that is, the dissociation constant of picric acid in the aqueous phase and the distribution coefficient of the acid made it possible to interpret the dependence of the distribution ratio upon the pH of the aqueous solution.

Experimental

Reagents. All the alkali metal picrates except lithium salt were prepared by dissolving picric acid into an aqueous solution containing alkali metal hydroxide or carbonate. The resultant precipitates were recrystallized thrice from water containing a small amount of the corresponding alkali metal hydroxide or carbonate.

Citric acid-lithium citrate buffers (0.1 M) and 0.1 M phosphoric acid-lithium phosphate buffers were used to adjust the pH of the solution to pH 1.5—5 and pH 6—8 respectively.

Extraction. Into a 50-m*l* separatory funnel, 5 m*l* of a 1.000×10^{-2} M picric acid or alkali metal picrate solution were transferred; then the same volume of the buffer solution of a definite pH was added. The resultant aqueous solution was then shaken with 10 m*l* of nitrobenzene for two hours at 25°C.

Determination of Alkali Metal and Picrate Ions. The concentration of alkali metals extracted into the nitrobenzene was determined using an atomic absorption spectrophotometer (Nippon Jarrell Ash, Type AA-1); the concentration of picrate in the aqueous solution was estimated spectrophotometrically at 353 mμ after diluting the solution 250 times with water, and the pH of the solution was adjusted at pH 12. The nitrobenzene existing as a contaminant in the aqueous solution also shows an appreciable absorbance at the same wavelength, but in such a high dilution as 250 times the interference can be almost extinguished.

After equilibration, the pH of the aqueous solution was measured in order to analyse the distribution equilibrium.

Theoretical

Writing the formulae for picric acid and alkali metal picrates as HR and MR respectively, the reactions involved can be represented schematically as in Fig. 1.

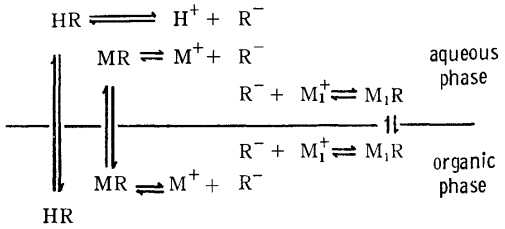

Fig. 1. Schematic representation of the equilibria involved in the extraction.

1) Dissociation of Picric Acid.

$$HR \rightleftarrows H^+ + R^- \qquad K_a^{HR} = \frac{[H^+]_a[R^-]_a}{[HR]_a} \tag{1}$$

2) Association of Alkali Metal Picrates.

$$M^+ + R^- \rightleftarrows MR \qquad K_a^{MR} = \frac{[MR]_a}{[M^+]_a[R^-]_a} \tag{2}$$

$$K_o^{MR} = \frac{[MR]_o}{[M^+]_o[R^-]_o} \tag{3}$$

$$M_I^+ + R^- \rightleftarrows M_IR \qquad K_a^{M_IR} = \frac{[M_IR]_a}{[M_I^+]_a[R^-]_a} \tag{4}$$

$$K_o^{M_IR} = \frac{[M_IR]_o}{[M_I^+]_o[R^-]_o} \tag{5}$$

3) Distribution of the Neutral Molecules.

$$D^{HR} = \frac{[HR]_o}{[HR]_a} \tag{6} \qquad D^{MR} = \frac{[MR]_o}{[MR]_a} \tag{7}$$

$$D^{M_IR} = \frac{[M_IR]_o}{[M_IR]_a} \tag{8}$$

In these equilibrium expressions, the a and o subscripts refer to the aqueous and the organic phases respectively; the brackets, to the molar concentration, and M_I^+, to a competing cation. As the competing cation it is desirable to choose a cation which associ-

1) M. Yamane, T. Iwachido, and K. Tôei, This Bulletin **44**, 745 (1971).

2) S. Motomizu, K. Tôei, and T. Iwachido, *ibid.*, **42**, 1006 (1969).

ates with the picrate ion most weakly in the aqueous solution and most strongly in nitrobenzene. In the present case, the lithium ion suits this purpose.

i) Distribution of Picric Acid. The distribution ratio or the concentration ratio of the reagent species at equilibrium between the two phases can be written as:

$$q^{R}=\frac{[HR]_o+[MR]_o+[M_IR]_o+[R^-]_o}{[HR]_a+[MR]_a+[M_IR]_a+[R^-]_a} \tag{9}$$

Each of the last three terms in the numerator can be expressed in terms of the corresponding constants as follows:

$$[MR]_o=\frac{D^{MR}K_a^{MR}K_a^{HR}[M^+]_a}{D^{HR}\quad[H^+]_a}[HR]_o \tag{10}$$

$$[M_IR]_o=\frac{D^{M_IR}K_a^{M_IR}K_a^{HR}[M_I^+]_a}{D^{HR}\quad[H^+]_a}[HR]_o \tag{11}$$

$$[R^-]_o=\frac{D^{MR}K_a^{MR}K_a^{HR}[M^+]_a}{D^{HR}K_o^{MR}[M^+]_o[H^+]_a}[HR]_o \tag{12}$$

Thus, substituting Eqs. (10), (11), and (12) into Eq. (9) gives the equation:

$$q^{R}=D^{HR}\frac{1+\left\{\left(1+\frac{1}{K_o^{MR}[M^+]_o}\right)D^{MR}K_a^{MR}[M^+]_a+D^{M_IR}K_a^{M_IR}[M_I^+]_a\right\}\frac{K_a^{HR}}{D^{HR}[H^+]_a}}{1+(1+K_a^{MR}[M^+]_a+K_a^{M_IR}[M_I^+]_a)\frac{K_a^{HR}}{[H^+]_a}} \tag{13}$$

A useful approximation for q^R may be obtained from Eq. (13) by making the appropriate assumptions.

(a) If the fourth term in the numerator is assumed to be small enough compared to the second and the third, Eq. (13) can be simplified to:

$$q^{R}=D^{HR}\frac{1+\left\{\left(1+\frac{1}{K_o^{MR}[M^+]_o}\right)\frac{D^{MR}K_a^{MR}K_a^{HR}[M^+]_a}{D^{HR}[H^+]_a}\right\}}{1+(1+K_a^{MR}[M^+]_a+K_a^{M_IR}[M_I^+]_a)\frac{K_a^{HR}}{[H^+]_a}} \tag{14}$$

(b) If the alkali metals are absent in this system, Eq. (13) can be further simplified to the well-known equation:

$$q^{R}=\frac{D^{HR}}{1+\frac{K_a^{HR}}{[H^+]_a}} \tag{15}$$

Equation (13) is the most general expression, but practically Eq. (14) may be the most convenient.

When the aqueous solution is sufficiently acidic, the second and the succeeding terms in the numerator of Eq. (14) may be neglected compared to the first, and in the denominator the first term may be negligible. Thus, Eq. (14) can be simplified to:

$$q^{R}=\frac{D^{HR}}{(1+K_a^{MR}[M^+]_a+K_a^{M_IR}[M_I^+]_a)K_a^{HR}}[H^+]_a \tag{16}$$

The concentration of alkali metals in the aqueous solution can be regarded as constant, because the amounts of these salts extracted into nitrobenzene are very small. Hence, q^R becomes a function of pH alone. A plot of log q^R *vs.* pH will give a straight line with a slope of -1, and from the intercept we can calculate the ratio of the distribution coefficient to the dissociation constant of picric acid, D^{HR}/K_a^{HR}. If the constant, K_a^{HR}, is known, D^{HR} can be calculated.

On the other hand, when the aqueous solution is sufficiently alkaline, the second and the succeeding terms in both the numerator and the denominator of Eq. (14) will become much larger than the first, giving:

$$q^{R}=\frac{\left(1+\frac{1}{K_o^{MR}[M^+]_o}\right)D^{MR}K_a^{MR}[M^+]_a}{1+K_a^{MR}[M^+]_a+K_a^{M_IR}[M_I^+]_a} \tag{17}$$

If $[M^+]_0$ is assumed to reach a certain constant value under sufficiently alkaline conditions, q^R may become a constant value in such a pH region.

The pH value at the intersection of the two constant-slope portions represented by Eqs. (16) and (17) may be calculated using the following equation:

$$[H^+]_a=\left(1+\frac{1}{K_o^{MR}[M^+]_o}\right)\frac{D^{MR}K_a^{MR}K_a^{HR}[M^+]_a}{D^{HR}} \tag{18}$$

ii) Distribution of Alkali Metals. At equilibrium, the distribution of alkali metals between the two phases can be written as:

$$q^{M}=\frac{[MR]_o+[M^+]_o}{[MR]_a+[M^+]_a} \tag{19}$$

The total concentrations of the reagent, C^R, and of alkali metals, C^M, are represented as:

$$C^{R}=[HR]_a+[HR]_o+[MR]_a+[MR]_o+[M_IR]_a+[M_IR]_o+[R^-]_a+[R^-]_o \tag{20}$$

$$C^{M}=[MR]_a+[MR]_o+[M^+]_a+[M^+]_o \tag{21}$$

The electroneutrality in the organic phase is expressed as:

$$[R^-]_o=[M^+]_o+[M_I^+]_o \tag{22}$$

Combining Eqs. (20), (21), and (22) and solving for $[R^-]_a$ gives the following relationships:

$$C^{R}-C^{M}=[HR]_a+[HR]_o+[M_IR]_a+[M_IR]_o+[R^-]_a-[M^+]_a+[M_I^+]_o \tag{23}$$

$$\frac{1}{[R^-]_a}=\frac{1+\frac{(1+D^{HR})}{K_a^{HR}}[H^+]_a+(1+D^{M_IR})K_a^{M_IR}[M_I^+]_a}{C^{R}-C^{M}+[M^+]_a-[M_I^+]_o} \tag{24}$$

On the other hand, the rearrangement of Eq. (19) gives:

$$q^{M}=\frac{[MR]_o\left(1+\frac{1}{K_o^{MR}[R^-]_o}\right)}{[MR]_a\left(1+\frac{1}{K_a^{MR}[R^-]_a}\right)} \tag{25}$$

The substitution of Eq. (24) into Eq. (25) gives this useful expression:

$$q^{M} = D^{MR}\frac{\left\{1+\frac{1}{K_0^{MR}[R^-]_0}\right\}}{\left\{1+\frac{1+(1+D^{HR})[H^+]_a/K_a^{HR}+(1+D^{M_IR})K_a^{M_IR}[M_I^+]_a}{K_a^{MR}(C^R-C^M+[M^+]_a-[M_I^+]_0)}\right\}} \tag{26}$$

If the extraction is carried out when $C^R-C^M=0$, Eq. (26) reduces to:

$$q^{M} = D^{MR}\frac{\left\{1+\frac{1}{K_0^{MR}([M^+]_0+[M_I^+]_0)}\right\}}{\left\{1+\frac{1+(1+D^{HR})[H^+]_a/K_a^{HR}+(1+D^{M_IR})K_a^{M_IR}[M_I^+]_a}{K_a^{MR}([M^+]_a-[M_I^+]_0)}\right\}} \tag{27}$$

Equation (27) is so complex that the dependence of the q^M value upon the pH can not be understood easily from the equation. However, a useful approximation for q^M may be obtained from Eq. (27) by making the following assumptions:

a) that the concentration of alkali metals in the aqueous solution is much greater than that of the competing ion in the organic phase: $[M^+]_a \gg [M_I^+]_0$;

b) that the distribution coefficient of lithium picrate is negligible compared to 1, whereas that of picric acid is much larger than 1: $1 \gg D^{M_IR}$ and $D^{HR} \gg 1$;

c) that the dissociated species are dominant in both phases: $q^M \approx [M^+]_0/[M^+]_a$ and

d) that the concentration of metal ions to be tested in the organic phase is much larger than that of the lithium ion: $[M^+]_0 \gg [M_I^+]_0$. In this manner, Eq. (27) can be simplified to the following expression:

$$(q^M)^2 = D^{MR}\frac{\left([M^+]_0+\frac{1}{K_0^{MR}}\right)}{\left\{[M^+]_a+\frac{1}{K_a^{MR}}\left(1+\frac{D^{HR}}{K_a^{HR}}[H^+]_a+K_a^{M_IR}[M_I^+]_a\right)\right\}} \tag{28}$$

When the aqueous solution is sufficiently acidic, the third term in the denominator will become by far larger than the residual terms, and the first term in the numerator, much smaller than the second, thus yielding:

$$(q^M)^2 = \frac{D^{MR}K_a^{MR}K_a^{HR}}{K_0^{MR}D^{HR}}\frac{1}{[H^+]_a} \tag{29}$$

A plot of log q^M *vs.* pH gives a straight line with a slope of 1/2, and the intercept is given by 1/2 log-$D^{MR}K_a^{MR}K_a^{HR}/K_0^{MR}D^{HR}$.

Alternatively, when the aqueous solution is kept sufficiently alkaline, the term involving $[H^+]_a$ can be neglected; hence, Eq. (28) reduces to:

$$(q^M)^2 = D^{MR}\frac{\left([M^+]_0+\frac{1}{K_0^{MR}}\right)}{\left([M^+]_a+\frac{1}{K_a^{MR}}+\frac{K_a^{M_IR}}{K_a^{MR}}[M_I^+]_a\right)} \tag{30}$$

Since $[M^+]_a$ and $[M^+]_0$ remain almost constant, as has been mentioned, a plot of log q^M *vs.* pH gives a horizontal line.

The logarithm of the q^M-pH curve appears as two constant-slope portions joined by a short curve; the point of intersection can be calculated from Eq. (28) by assuming $[M^+]_0 \ll 1/K_0^{MR}$:

$$\frac{1}{[H^+]_a} = \frac{D^{HR}}{(K_a^{MR}[M^+]_a+1+K_a^{M_IR})K_a^{HR}} \tag{31}$$

Equation (31) shows that the value of D^{HR}/K_a^{HR} can be obtained not only from the log q^R-pH curve, but also from the log q^M-pH curve.

Results and Discussion

i) Equilibria Involved in the Extraction System. The equilibria shown in Fig. 1 are fundamental ones. Of course, these simple expressions are used for convenience to represent the possible complex equilibria in which the solvent molecules participate. Some other equilibria, such as:

$$2HR \rightleftarrows (HR)_2$$

$$RHR^- \rightleftarrows HR + R^- \qquad K_0^{RHR^-} = \frac{[HR]_0[R^-]_0}{[RHR^-]_0}$$

$$HR \rightleftarrows H^+ + R^- \qquad K_0^{HR} = \frac{[H^+]_0[R^-]_0}{[HR]_0}$$

may exist. As has been pointed out by Moore[3] and Brønsted,[4] the dimerization of picric acid need not be considered in the aqueous phase or even in the organic phase. Kolthoff[5] and his collaborators have mentioned that a homoconjugation reaction of picrate anions may be expected to exist in a nitrobenzene solution, and that the dissociation constant evaluated from the solubility measurements is above 10^{-2}. In the same paper, he has also estimated spectrophotometrically the dissociation constant for picric acid in nitrobenzene to be 3.5×10^{-8} at 25°C. Judging from the magnitude of the constants, these reactions were assumed not to be taken into account under the present experimental conditions.

The association constants and the distribution coefficients of the alkali metal picrates are listed in Table 1. It must be noted that K_0^{MR} in this table is used to designate the association constant of the picrates in water-saturated nitrobenzene in place of the $K_0^{MR}{}_{(H_2O)}$ in the original paper.[1]

ii) Distribution of Picric Acid. Plots of log-q^R *vs.* pH are shown in Figs. 2 to 6. Each curve gives a straight line with a slope of exactly −1 in a suf-

3) T. S. Moore, E. Shepard, and E. Goodall, *J. Chem. Soc.*, **1931**, 1447.

4) J. N. Brønsted and R. P. Bell, *J. Amer. Chem. Soc.*, **53**, 2478 (1931).

5) I. M. Kolthoff, D. Stŏcesocà, and T. S. Lee, *ibid.*, **75**, 1834 (1953).

TABLE 1. ASSOCIATION AND DISTRIBUTION CONSTANTS FOR ALKALI METAL PICRATES

Constants	Picric acid	Li-Pic	Na-Pic[1)]	K-Pic[1)]	Rb-Pic[1)]	Cs-Pic[1)]
K_a^{MR}	$10^{-0.42}$ [6)] a)	$10^{1.13}$ b)	$10^{1.38}$	$10^{1.64}$	$10^{1.94}$	$10^{2.07}$
K_0^{MR}	$10^{-7.46}$ a)	$10^{5.80}$ [5)]	$10^{3.67}$	$10^{2.92}$	$10^{2.65}$	$10^{2.43}$
D^{MR}	$10^{2.63}$	$10^{-3.05}$ b)	$10^{-2.55}$	$10^{-1.85}$	$10^{-1.68}$	$10^{-1.17}$

a) Dissociation constants. b) Estimated values.

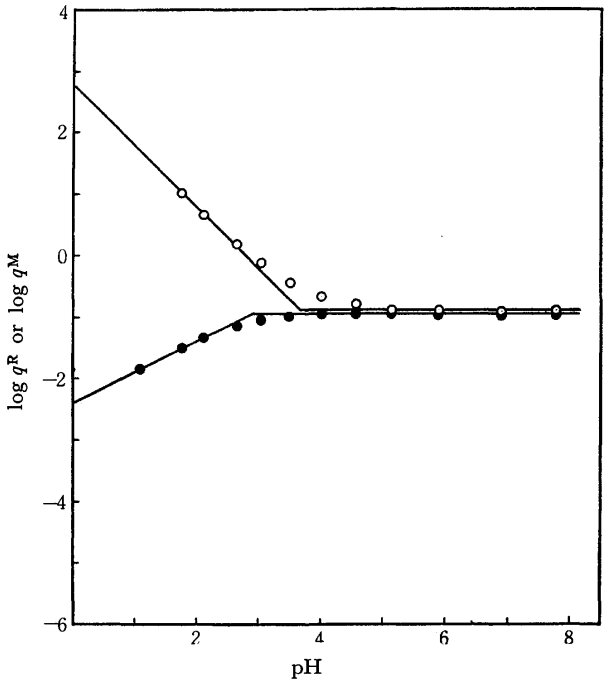

Fig. 2. The distribution of cesium picrate.
log q^R - pH, open circles; log q^M - pH, solid circles.
q^R: open circles, q^M: solid circles

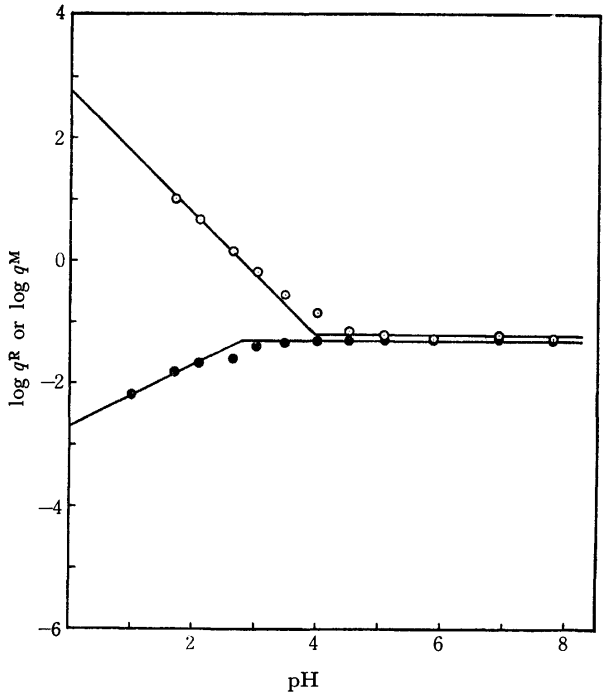

Fig. 3. The distribution of rubidium picrate.
log q^R - pH, open circles; log q^M - pH, solid circles.

6) H. v. Halban and M. Seiler, *Helv. Chim. Acta*, **21**, 385 (1938).

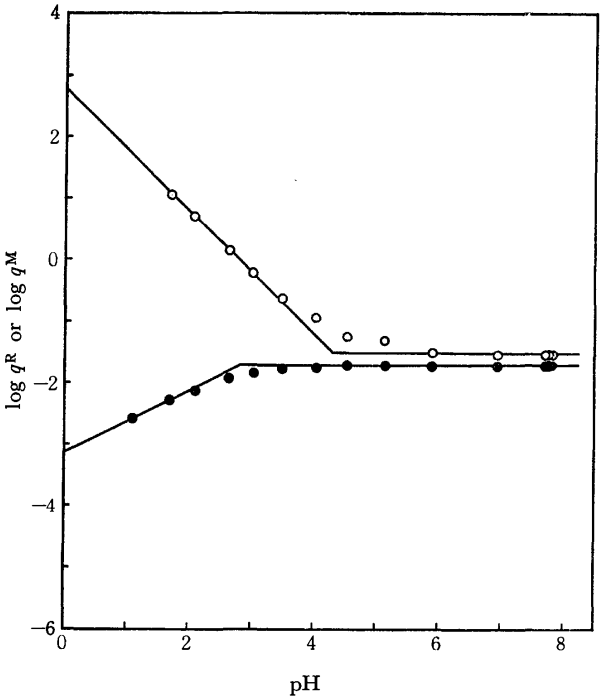

Fig. 4. The distribution of potassium picrate.
log q^R - pH, open circles; log q^M - pH, solid circles.

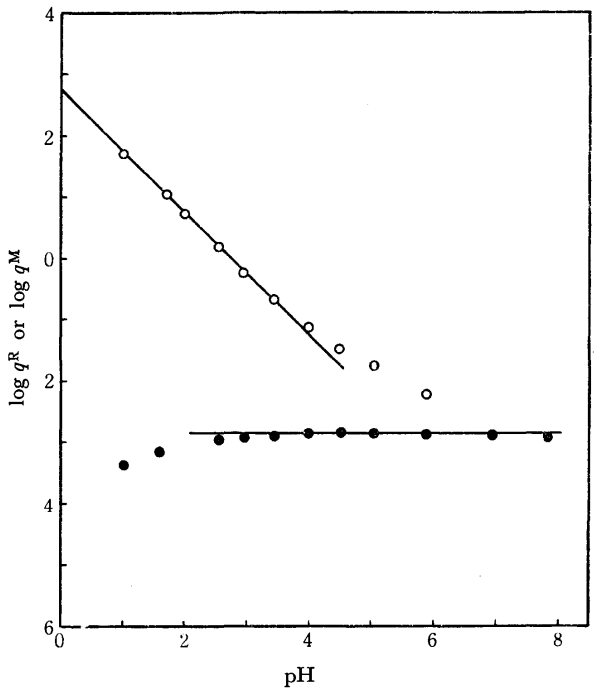

Fig. 5. The distribution of sodium picrate.
log q^R - pH, open circles; log q^M - pH, solid circles.

Table 2. Constants characteristic of log q^R-pH curves

Salts	Intercept at pH=0	D^{HR}/K_a^{HR}	D^{HR}	pH-independent q^R values (Meas.)	pH-independent q^R values (Calcd.)	$[H^+]_a$ values at the intersection (Meas.)	$[H^+]_a$ values at the intersection (Calcd.)
Li-Pic	$10^{2.78}$	$10^{3.00}$	$10^{2.58}$				
Na-Pic	$10^{2.77}$	$10^{3.02}$	$10^{2.60}$		$10^{-2.20}$		
K-Pic	$10^{2.74}$	$10^{3.02}$	$10^{2.60}$	$10^{-1.43}$	$10^{-1.64}$	$10^{-4.19}$	$10^{-4.48}$
Rb-Pic	$10^{2.77}$	$10^{3.09}$	$10^{2.67}$	$10^{-1.19}$	$10^{-1.33}$	$10^{-3.93}$	$10^{-4.13}$
Cs-Pic	$10^{2.77}$	$10^{3.12}$	$10^{2.70}$	$10^{-0.88}$	$10^{-0.83}$	$10^{-3.68}$	$10^{-3.60}$

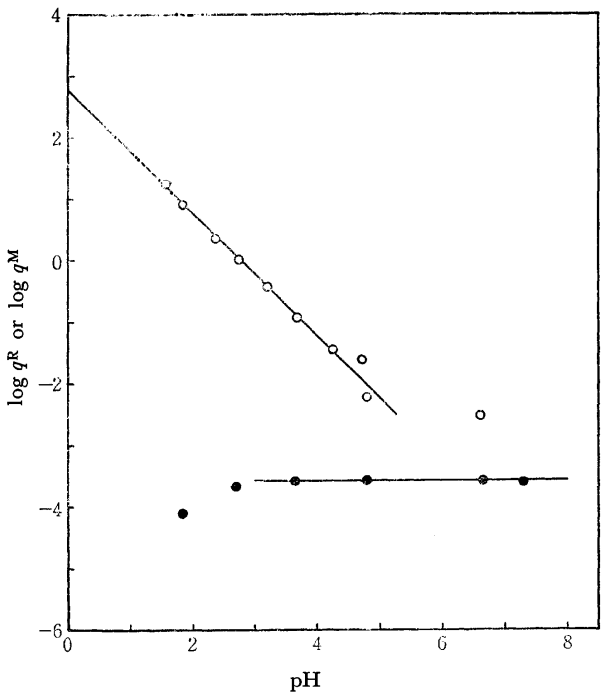

Fig. 6. The distribution of lithium picrate.
log q^R - pH, open circles; log q^M - pH, solid circles.

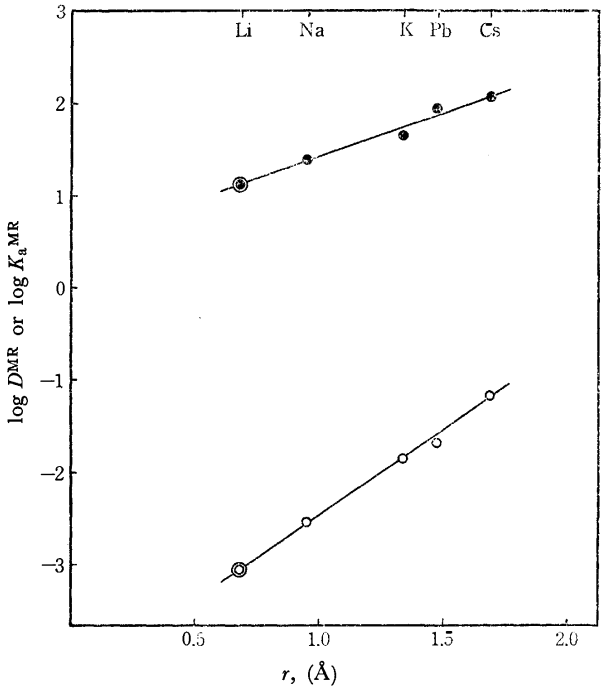

Fig. 7. The evaluation of the distribution constant and the association constant of lithium picrate in aqueous solution.
Distribution constant: open circle
Association constant: solid circle

ficiently acidic solution. A horizontal line was observed only in the extraction of potassium, rubidium, and cesium picrates, which is in accord with the expectation based on Eq. (17). As the errors inherent in the spectrophotometric method are of the order of 1 per cent, small distribution ratios below 10^{-2} can not be determined accurately. Therefore, the values of q^R below $10^{-2.5}$ are not shown in these figures. This is the case for lithium and sodium picrates.

The values of D^{HR}/K_a^{HR} are estimated to be approximately $10^{3.05}$. The evaluation of D^{HR} requires the dissociation constant for picric acid in water saturated with nitrobenzene. For the lack of available data on K_a^{HR}, the constant was replaced by the one obtained in an aqueous solution. The D^{HR} values thus obtained are listed in the fourth column of Table 2. These five values are close to each other within the limits of experimental error, and the mean value, $10^{2.63}$, is in fairly good agreement with $10^{2.41}$.[7] The totals concentration of the picrate ions existing in both phases at a sufficiently high pH were 4.96×10^{-3}, 4.98×10^{-3}, 4.95×10^{-3}, 4.97×10^{-3}, and 4.94×10^{-3} M for lithium, sodium, potassium, rubidium, and cesium picrates respectively. This shows that the accuracy of the experiments is satisfactory.

iii) Estimation of $K_a^{M_1R}$, D^{M_1R}, and $K_0^{M_1R}$.

Due to the very low extractability of lithium picrate, $K_a^{M_1R}$ and D^{M_1R} can not be determined by the extraction method.[1] For the other alkali metal picrates, a plot of log K_a^{MR} or log D^{MR} *vs.* the ionic radii of these cations helps in the evaluation of these values for lithium picrate. The linear extrapolation of each line to r=0.68 Å gives the approximate values of $K_a^{M_1R}$ and D^{M_1R} (Fig. 7). However, the validity of such an approximation is difficult to justify.

Witschonke and Kraus[8] have reported that the dissociation constant of lithium picrate in nitrobenzene containing 0.03 M water is $10^{5.80}$. The dissociation constant tends to increase with the water content in nitrobenzene. Therefore, a somewhat greater value than $10^{5.80}$ might be expected with water-saturated (0.1 M)

7) M. Koyama, O. Tochiyama, and T. Fujinaga, This Bulletin, **44**, 1591 (1971).

8) C. R. Witschonke and C. A. Kraus, *J. Amer. Chem. Soc.*, **69**, 2472 (1947).

TABLE 3. CONSTANTS CHARACTERISTIC OF log q^M-pH CURVES

Salts	Intercept at pH=0		pH-independent q^M values				$[H^+]_a$ values at the intersection	
	(Meas)	(Calcd)	(Meas)	(Calcd by Eq. (32))	(Calcd by Eq. (30))	(Calcd by Eq. (27))	(Meas)	(Calcd)
Na-Pic	10^{-4}	$10^{-3.91}$	$10^{-2.85}$	$10^{-2.42}$	$10^{-2.54}$	$10^{-2.71}$	10^{-2}	$10^{-2.77}$
K-Pic	$10^{-3.11}$	$10^{-3.08}$	$10^{-1.73}$	$10^{-1.57}$	$10^{-1.69}$	$10^{-1.69}$	$10^{-2.80}$	$10^{-2.74}$
Rb-Pic	$10^{-2.68}$	$10^{-2.74}$	$10^{-1.30}$	$10^{-1.18}$	$10^{-1.33}$	$10^{-1.37}$	$10^{-2.76}$	$10^{-2.77}$
Cs-Pic	$10^{-2.39}$	$10^{-2.33}$	$10^{-0.94}$	$10^{-0.77}$	$10^{-0.91}$	$10^{-0.85}$	$10^{-2.92}$	$10^{-2.77}$

nitrobenzene; however, because of the lack of a way to estimate the extent of the effect, $K_o^{M_IR}$ is approximated by $10^{5.80}$ in the present paper.

iv) Distribution of Alkali Metal Picrate. Figures 2 to 6 show a plot of log q^M *vs.* pH by means of solid circles. Each curve consists of two constant-slope portions; that is, one is a line with a constant slope of 1/2, and the other, a horizontal line independent of the pH. These results are in good accord with the expectations based on the formulation.

The q^M values at the intercepts of the log q^M-pH curves agree well with those to be expected from Eq. (29), as is shown in Table 3. For sodium and lithium picrates, the q^M values below pH 2 were so erroneous that the values measured in this pH region are shown without drawing a line.

The pH-independent q^M values obtained and calculated by means of Eq. (30) are listed in the fourth and the sixth columns of Table 3 respectively. The values increased in proceeding from sodium to cesium, and the agreement between the observed and the calculated values was satisfacotry. It must be noted that the such q^M values can also be approximated by the following equation:

$$(q^M)^2 = \frac{D^{MR}K_a^{MR}}{K_o^{MR}} \tag{32}$$

The fifth column of Table 3 shows that such a simple relationship is still valid for potassium, rubidium, and cesium picrates.

Figures 2 to 4 show that, in both the log q^M-pH and the log q^R-pH curves, the q^M and q^R values tend to approach each other in the high pH region. The situation can be well understood by rewriting Eq. (17) as follows:

$$q^R = \frac{\left(1+\frac{1}{K_o^{MR}[M^+]_o}\right)D^{MR}K_a^{MR}[M^+]_a}{1+K_a^{MR}[M^+]_a+K_a^{M_IR}[M_I^+]_a} \tag{17}$$

$$= D^{MR}\frac{\left(\frac{1}{K_o^{MR}}+[M^+]_o\right)}{\left(\frac{1}{K_a^{MR}}+[M^+]_a+\frac{K_a^{M_IR}}{K_a^{MR}}[M_I^+]_a\right)}\frac{[M^+]_a}{[M^+]_o} \tag{17a}$$

The approximation of $[M^+]_a/[M^+]_o$ by $1/q^M$ gives:

$$q^Rq^M \approx D^{MR}\frac{\left(\frac{1}{K_o^{MR}}+[M^+]_o\right)}{\left(\frac{1}{K_a^{MR}}+[M^+]_a+\frac{K_a^{M_IR}}{K_a^{MR}}[M_I^+]_a\right)} \tag{33}$$

The term on the right-hand side of the above equation is identical with $(q^M)^2$ (cf. Eq. (30)), so Eq. (33) reduces to:

$$q^R \approx q^M \tag{34}$$

Such a relationship can also be directly derived from Eq. (9) in a somewhat different manner. If the aqueous solution is kept sufficiently alkaline, the hydrolysis of the picrate ions can be neglected. Thus, Eq. (9) reduces to:

$$q^R = \frac{[M_IR]_o+[MR]_o+[R^-]_o}{[M_IR]_a+[MR]_a+[R^-]_a} \tag{35}$$

If $[M_IR]_a$ and $[M_IR]_o$ are assumed to be negligibly small, $[R^-]_a$ and $[R^-]_o$ in Eq. (35) can be replaced by $[M^+]_a$ and $[M^+]_o$ respectively, because C^R and C^M are kept equal in the present case. This leads to the same relationship:

$$q^R \approx q^M$$

The eighth column in Table 3 shows that the pH value at the intersection of these two constant-slope portions is characteristic of all the picrates, as is to be expected from Eq. (31). The agreement between the observed and the calculated values is very good. This means that, from the intersect, the D^{HR}/K_a^{HR} value can be calculated correctly in the opposite sense.

v) Corrections for the Competing Ions. In the above treatments, the lithium ions in the organic phase have been neglected. Since appreciable amounts of lithium picrate are also extractable by nitrobenzene, as is shown in Fig. 6, the effect of the lithium ions must be taken into account when a stricter treatment is required. Equation (27) is useful for this purpose. The pH-independent q^M values as corrected by the equation are shown in the seventh column of Table 3. As might be expected, the corrections are larger for sodium picrate; this results in a marked improvement of the agreement between the observed and the calculated values. These facts may indicate the validity of the values ($K_a^{M_IR}$ and D^{M_IR}) estimated by the graphical method.

The author wishes to express his gratitude to Professor Kyoji Tôei for his guidance throughout the course of this work.

Kinetics and Mechanisms of the Reaction of Fe(III) with Variamine Blue, [*N*-(*p*-Methoxyphenyl)phenylenediamine] in Aqueous Perchlorate Media

Taira IMAMURA and Masatoshi FUJIMOTO

Department of Chemistry, Faculty of Science, Hokkaido University, Sapporo

(Received May 21, 1971)

The kinetics of the non-complementary reaction of Fe(III) with Variamine Blue was studied under nitrogen atmosphere in perchlorate media of ionic strength $\mu=1.0$ M. The iminoquinone form of Variamine Blue was followed spectrophotometrically by a stopped-flow technique. The rate constants of the stepwise reaction, $Fe(III)+(V.B.)\underset{k_r}{\overset{k_\alpha}{\rightleftarrows}}Fe(II)+(V.B.)_{sox}$, $Fe(III)+(V.B.)_{sox}\xrightarrow{k_\beta}Fe(II)+(V.B.)_{ox}+2\,H^+$, were evaluated to be $k_\alpha=3.28\times10^2$ and $k_\beta=4.29\times10^2$ M^{-1} sec^{-1} at pH$\simeq$2.2 and 25°C. The apparent activation energy was 10 ± 1 kcal·mol^{-1} for both k_α and k_β. The formation rate was not seriously affected by hydrogen ion concentration (pH 2.2—0.77).

Variamine Blue (abbr. V.B.) is used as a redox indicator with many applications.[1] It has been reported that the colorless solution of V.B. undergoes two-electron oxidation to a violet-red iminoquinone (abbr. $(V.B.)_{ox}$) by oxidizing agents such as Ce(IV), Fe(III) and I_2, as follows.[2,3]

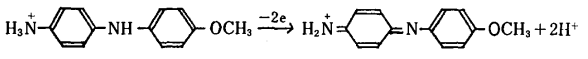

(V. B.) (V. B.)$_{ox}$

Erdey *et al.*[4-6] suggest the following reaction scheme of V.B. with oxidizing agents.

$$(V.B.)\rightleftharpoons(V.B.)_s\rightleftharpoons 1/2(V.B.)_D\rightleftharpoons(V.B.)_{ox},$$

where $(V.B.)_s$ is a semiquinone form, and $(V.B.)_D$ a dimeric one.

We are interested in the possibility of the existence of such intermediates during the course of the reaction, and the mechanisms of the reactions of V.B. with various oxidizing agents such as Co(III), Ce(IV), Tl(III), Fe(III), and I_2.

The present paper reports the reaction of V.B. with Fe(III) in 1.0 M perchlorate media. The reaction was spectrophotometrically followed by a stopped-flow technique at 550 nm corresponding to the λ_{max} of $(V.B.)_{ox}$ under the condition $[Fe(III)]\gg[V.B.]$.

Experimental

Measurements. A Hitachi recording spectrophotometer model EPS-3T was used for spectral measurements. Variations of spectra with time were measured at wavelengths 350—700 nm with a Hitachi RPS-1 rapid scan apparatus. The rates of rapid reactions were measured using a Yanagimoto stopped-flow apparatus SPS-1. Purified nitrogen gas was passed through the reservoirs of the solutions during the course of measurements.

Materials. Deionized and distilled water was used. Iron(III) perchlorate was prepared by heating iron(III) chloride with a small excess of 60% perchloric acid under reduced pressure at about 60—65°C until no trace of chloride ion was detected. Sexihydrate thus obtained was dissolved in water. The concentration of Fe(III) was determined with EDTA titrimetrically.

Iron(II) perchlorate solution was prepared by electrolytic reduction of 1.07×10^{-2} M iron(III) perchlorate in 0.2 M perchloric acid under nitrogen atmosphere until negative tests were attained with thiocyanate. The solution was titrated with Ce(IV) using ferroin as an indicator and stored in a Pyrex bottle under nitrogen atmosphere.

Reagent grade sodium perchlorate and perchloric acid were used to maintain ionic strength at $\mu=1.0$. Sodium perchlorate solution was standardized by titrating with sodium hydroxide the hydrogen ions eluted from a column of Dowex 50W-X8 in the hydrogen form.

Variamine Blue hydrochloride (Dojindo, Kumamoto) was dissolved in water free from oxygen by bubbling with nitrogen purified through an alkaline pyrogallol solution. Variamine Blue solution was freshly prepared before use.

Results

Spectra. The violet solution formed by mixing a large excess of Fe(III) and V.B. has a single absorption peak at 550 nm. With oxidizing agents such as Co(III), Ce(IV), Tl(III), and I_2 the solution also gave similar spectra with a single peak at 550 nm. We have thus ascribed the absorption peak at 550 nm to the iminoquinone form of the Variamine Blue, $(V.B.)_{ox}$.

The absorbance in acidic media was gradually reduced over the visible range, while the absorption peak at 550 nm showed no shift.

Figure 1 shows the fast spectral change in the visible region just after the mixing of Variamine Blue with Fe(III) at pH$\simeq$2.2. Each scan requires 300 millisec. Fourteen scans were manually triggered for about 12 seconds just after mixing the Variamine Blue with Fe(III) in the optical cell from the sample syringes. In the course of the reaction, the peak at 550 nm showed no shift. Thus, under the experimental conditions, any species other than $(V.B.)_{ox}$ do not interfere with the kinetic measurements of the $(V.B.)_{ox}$ using the absorbance at 550 nm.

Reaction Stoichiometry. Erdey reported on the polarographic data suggesting the two-electron transfer reaction between Fe(III) and V.B.[1] We have

1) L. Erdey, *Chemist-Analyst*, **48**, 106 (1959).
2) L. Erdey and A. Bodor, *Z. Analyt. Chem.*, **137**, 410 (1953); L. Erdey and F. Szabadvery, *ibid.*, **155**, 90 (1957); *Acta Chem. Acad. Sci. Hung.*, **13**, 335 (1958).
3) E. Banyai and P. Zuman, *Collection Czech. Chem. Commun.*, **24**, 522, (1959).
4) L. Erdey, I. Buzas, and K. Vigh, *Talanta*, **1**, 377 (1958).
5) L. Erdey and R. C. Pink, *ibid.*, **9**, 329 (1962).
6) L. Erdey, T. Meisel, B. Mohos, and F. Tudos, *ibid.*, **14**, 1477 (1967).

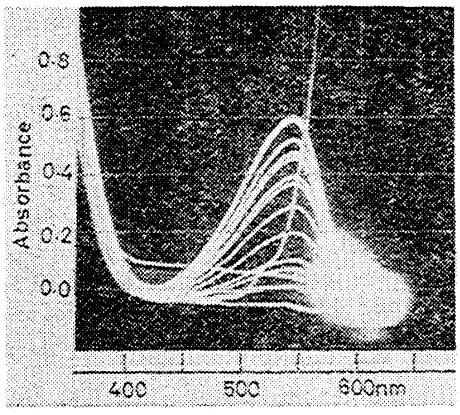

Fig. 1. Fast spectral change in the visible region.
$[Fe(III)]_0=1.07\times10^{-3}$ M, $[V.B.]_0=5.00\times10^{-5}$ M, pH≃2.2, room temperature (≃20°C).

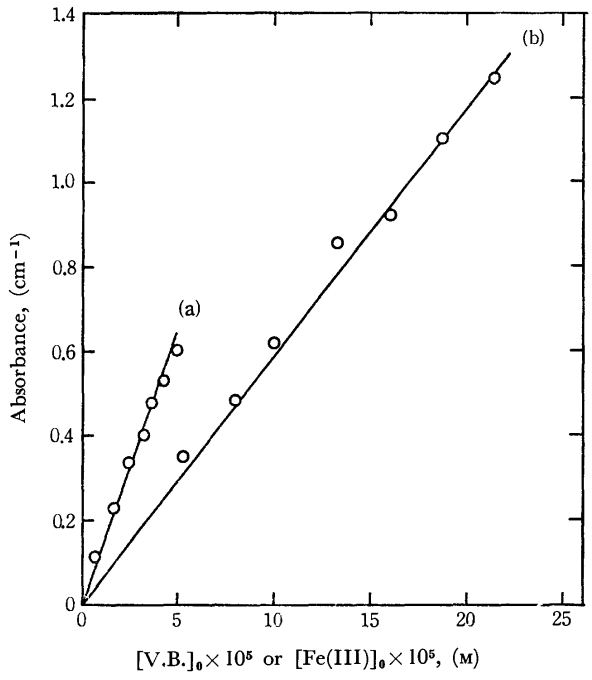

Fig. 2. Absorbance at 550 nm with varying concentration of Variamine Blue or Fe(III) at 25.0°C and $\mu=1.0$ M.
(a) $[Fe(III)]_0=1.07\times10^{-3}$ M, $[V.B.]_0$=abscissa, pH=2.20,
(b) $[Fe(III)]_0$=abscissa, $[V.B.]_0=2.50\times10^{-4}$ M, pH=1.76.

determined the reaction stoichiometry spectrophotometrically at 550 nm by the stopped-flow technique assuming $(V.B.)_{ox}$ as the main product of the reaction even under the condition $[Fe(III)]_0<[V.B.]_0$. Figure 2 suggests that the reaction of Variamine Blue with Fe(III) requires 2 moles of Fe(III) for 1 mole of Variamine Blue, *viz.*, a two-electron transfer reaction.

The molar absorption coefficient of $(V.B.)_{ox}$ in the protonated form at 550 nm was found to be 1.3×10^4 M^{-1} cm^{-1} in the acidic media at 25°C and ionic strength $\mu=1.0$.

Kinetics. In the following two-electron transfer reaction

$$V.B. \xrightarrow{-2e} (V.B.)_{ox} + 2H^+$$

the rate of formation of $(V.B.)_{ox}$ in the presence of large excess of Fe(III) does not obey the first-order rate law. It is assumed that there are some intermediate oxidation states of Variamine Blue in the course of the reaction due to a non-complementary reaction between one mole of reductant, Variamine Blue, and two moles of oxidant, Fe(III).

With Tl(III) as an oxidizing agent under the same conditions, however, the formation rate of $(V.B.)_{ox}$ was expressed by a pseudo-first-order rate law.[7]

Hydrogen Ion Concentration Dependence. The formation rate of $(V.B.)_{ox}$ was not seriously influenced by the hydrogen ion concentration between pH 2.20 and 0.77. The final concentration of $(V.B.)_{ox}$ of this reaction was also not affected by the hydrogen ion concentration (Fig. 3).

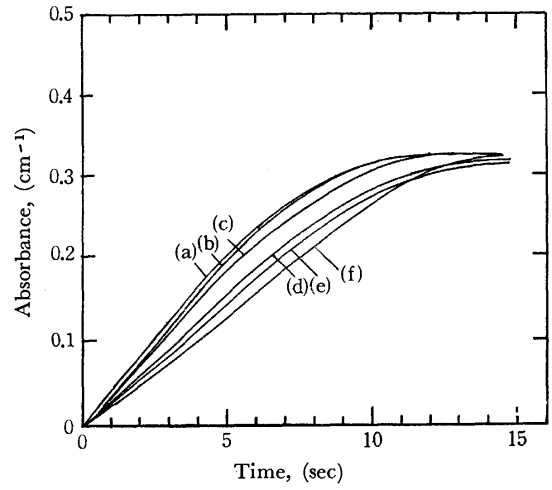

Fig. 3. Hydrogen ion concentration dependence.
$[Fe(III)]_0=1.07\times10^{-3}$ M, $[V.B.]_0=2.50\times10^{-5}$ M, 25°C, $\mu=1.0$: (a) pH=2.195, (b) pH=1.90, (c) pH=1.74, (d) pH=1.20, (e) pH=0.935, (f) pH=0.77.

The initial rate of the formation of $(V.B.)_{ox}$ at pH 2.2 was proportional to the initial concentration of Variamine Blue, the half-life being independent of the initial concentration (Fig. 4).

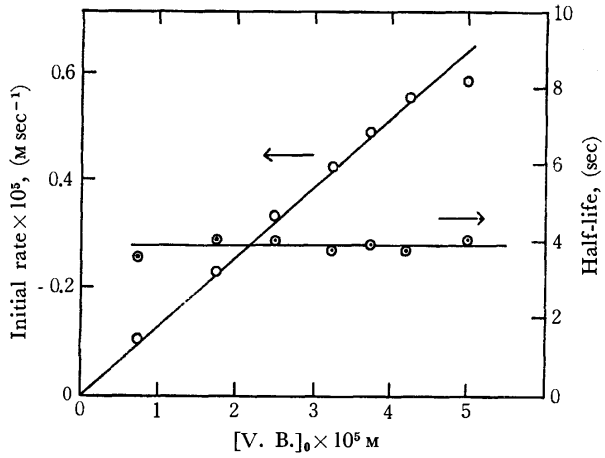

Fig. 4. Initial rate and half-life of the formation of $(V.B.)_{ox}$.
$[Fe(III)]_0=1.07\times10^{-3}$ M, pH=2.20, $\mu=1.0$, 25°C.

Effects of Fe(II). Figure 5 shows the effects of Fe(II) on the rate of formation of $(V.B.)_{ox}$. It is

7) T. Imamura and M. Fujimoto, This Bulletin, **45**, 442 (1972).

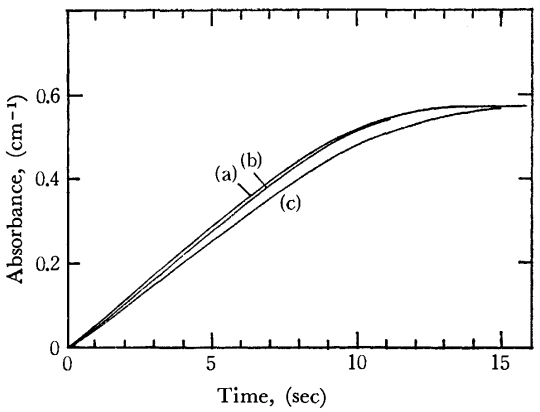

Fig. 5. Effects of Fe(II) on the formation of $(V.B.)_{ox}$ at 25°C and $\mu=1.0$ M.
$[Fe(III)]_0=1.07\times10^{-3}$ M, $[V.B.]_0=5.00\times10^{-5}$ M: (a) $[Fe(II)]_0=0$ M, (b) $[Fe(II)]_0=1.01\times10^{-3}$ M, (c) $[Fe(II)]_0=2.02\times10^{-3}$ M.

suggested that the formation rate of $(V.B.)_{ox}$ was not affected even for $[Fe(II)]_0 \geq [Fe(III)]_0 \gg [V.B.]_0$.

Discussion

Kinetics. The formation of $(V.B.)_{ox}$ in the reaction of Variamine Blue and Fe(III) does not obey the pseudo first-order rate law even with a large excess of Fe(III). It was ascribed to the fact that the intermediate of V.B. was to be considered and the reaction was a non-complementary one.

The overall reaction scheme would be as follows.

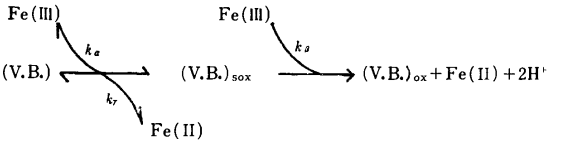

or

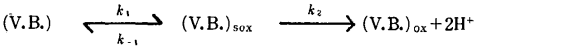

where $(V.B.)_{sox}$ shows a semi-oxidized form of Variamine Blue as semiquinone.

With large excess of $[Fe(III)]_0$ and $[Fe(II)]_0$, the formation of $(V.B.)_{ox}$ is expressed as follows.

$$[(V.B.)_{ox}] = \frac{[(V.B.)]_0}{2q}e^{-pt}[-(p+q)e^{qt}+(p-q)e^{-qt}] + [(V.B.)]_0 \quad (1)$$

where $p=\dfrac{k_1+k_{-1}+k_2}{2}$, $q=\dfrac{\sqrt{(k_1+k_{-1}+k_2)^2-4k_1k_2}}{2}$

and $k_1=k_\alpha[Fe(III)]_0$, $k_2=k_\beta[Fe(III)]_0$, $k_{-1}=k_\gamma[Fe(II)]_0$.

The effect of Fe(II) and hydrogen ion on the formation rate of $(V.B.)_{ox}$ was so small that k_{-1} in the equation was negligible.

Equation (1) is rewritten as follows:

$$[(V.B.)_{ox}] = [(V.B.)]_0\left[1+\frac{1}{k_1-k_2}(k_2e^{-k_1t}-k_1e^{-k_2t})\right]. \quad (2)$$

Let $\tau=k_1t$ and $\kappa=k_2/k_1$, then the equation becomes

$$r=\frac{[(V.B.)_{ox}]}{[(V.B.)]_0}=1+\frac{1}{1-\kappa}(\kappa e^{-\tau}-e^{-\kappa\tau}) \quad (3)$$

where r is the ratio of $[(V.B.)_{ox}]$ to $[(V.B.)]_0$, that is, $r=0$ in the initial state of the reaction, and $r=1$ in the final state, when the reaction is complete. The value of the relative rate constant, $\kappa=k_2/k_1$, obtained by the time ratio method[8,9] was 1.5 at 25°C. The value of k_1 was calculated to be 0.525 sec^{-1} with the observed reaction at $\mu=1.0$, $[Fe(III)]_0=1.067\times10^{-3}$, $[V.B.]_0=5.00\times10^{-5}$ M, 25°C, and pH=2.2.

The specific rates k_α and k_β for the first step and the second step of the reaction were calculated to be 3.28×10^2 M^{-1} sec^{-1} and 4.92×10^2 M^{-1} sec^{-1}, at ionic strength 1.0, pH≃2.2 and 25°C from $k_1/[Fe(III)]_0$ and $k_2/[Fe(III)]_0$, respectively.

In Fig. 6 the concentrations of $(V.B.)_{ox}$ calculated from these values are plotted as a function of time. It is shown that the calculated concentrations of $(V.B.)_{ox}$ agree with the observed ones in the course of the reaction.

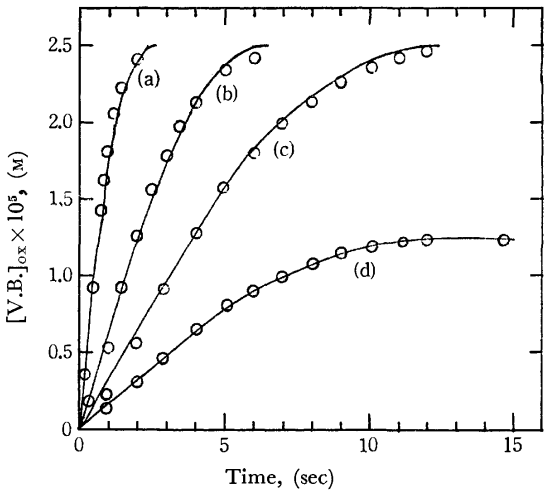

Fig. 6. Calculated concentration of $(V.B.)_{ox}$. Solid lines show the observed concentrations of $(V.B.)_{ox}$.
○ indicate the concentrations of $(V.B.)_{ox}$ calculated with the values, $k_\alpha=3.28\times10^2$ and $k_\beta=4.29\times10^2$ M^{-1} sec^{-1} at 25°C and $\mu=1.0$: (a) $[Fe(III)]_0=6.40\times10^{-3}$ M, $[V.B.]_0=2.50\times10^{-5}$ M, (b) $[Fe(III)]_0=2.13\times10^{-3}$ M, $[V.B.]_0=2.50\times10^{-5}$ M, (c) $[Fe(III)]_0=1.07\times10^{-3}$ M, $[V.B.]_0=2.50\times10^{-5}$ M, (d) $[Fe(III)]_0=1.07\times10^{-3}$ M, $[V.B.]_0=1.25\times10^{-5}$ M.

Temperature Dependence. Values calculated for (k_α, k_β) at 15, 20, 25, 30, and 35°C were found to be (197, 295), (272, 407), (328, 492), (487, 731), and (675, 1010 M^{-1} sec^{-1}) at ionic strength $\mu=1.0$ and pH≃2.2 (see Fig. 7). Apparent energies of activation calculated from these values are 10±1 kcal·mol^{-1} for both k_α and k_β.

Influence of Chloride Ion. Chloride ion was added to the solutions of the reactants in order to investigate the dependence of the reaction rate on the formation of iron(III) chloride complexes.

The formation rate of $(V.B.)_{ox}$ in the presence of large excess of chloride ion was higher than that with

8) A. Frost, R. G. Pearson, "Kinetics and Mechanism," John Wiley & Sons, Inc., New York, London (1961), p. 170.
9) A. A. Frost and W. C. Schwement, *J. Amer. Chem. Soc.*, **74**, 1268 (1952); W. C. Schwemer and A. A. Frost, *ibid.*, **73**, 4541 (1951).

no chloride ion added (Fig. 8). However, the chloride ion affects the reaction rate only slightly.

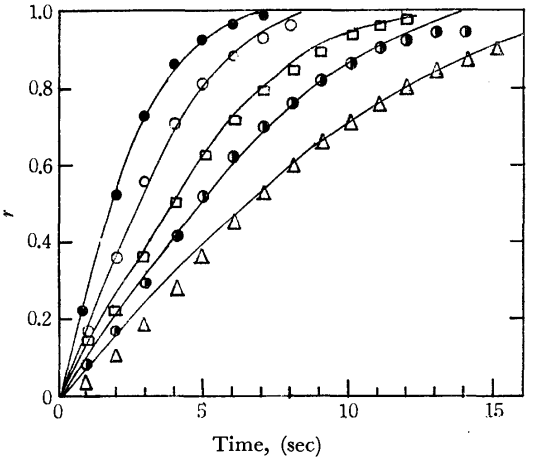

Fig. 7. Temperature dependence.
Solid lines show the observed concentrations of $(V.B.)_{ox}$. ●, ○, □, ◑, and △ indicate the calculated concentrations of $(V.B.)_{ox}$ at 35, 30, 25, 20, and 15°C, respectively: $[Fe(III)]_0=1.07\times10^{-3}$ M, $[V.B.]_0=2.5\times10^{-5}$ M, pH≃2.2, $\mu=1.0$ M.

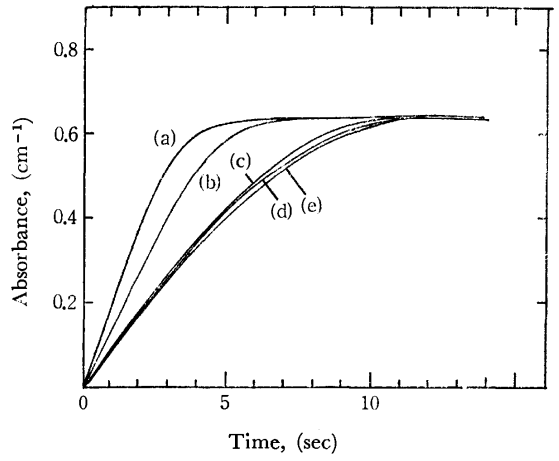

Fig. 8. Influence of chloride ion.
$[Fe(III)]_0=1.07\times10^{-3}$ M, $[V.B.]_0=5.00\times10^{-5}$ M, pH=2.2, 25°C, $\mu=1.0$ M, (a) $[NaCl]=1.0\times10^{-1}$ M, (b) 5.0×10^{-2} M, (c) 1.0×10^{-2} M, (d) 5.0×10^{-3} M, (e) 0 M.

In the reaction of hydroquinone and Fe(III),[10] it was reported that the reaction was either inner- or outer-sphere mechanism. In the reaction of V.B. and Fe(III), it is not clear whether the reaction proceeds by an inner-sphere mechanism or outer-sphere mechanism, as the kinetics was followed by Variamine Blue oxidized form.

That the formation rate of $(V.B.)_{ox}$ is not affected by acid concentration suggests the possibility of the inner-sphere mechanism for the reaction, since $FeOH^{2+}$ would influence the reaction rate for the outer-sphere mechanism. The rate constants as reported in the reaction of $[Fe(CN)_6]^{3-}$ with dichloroindophenol[11] that proceeds by outer-sphere mechanism or by hydrogen-atom transfer are much higher than those in the reaction of Fe(III) with V.B., *viz.*,

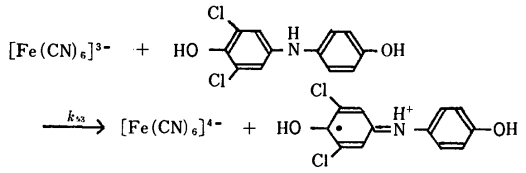

$k_{53} = 1.2\ (\pm0.3) \times 10^4\ M^{-1}sec^{-1}$

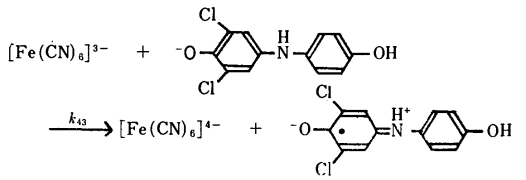

$k_{43} = 3.3\ (\pm0.8) \times 10^7\ M^{-1}sec^{-1}$

The authors wish to thank Prof. H. Baba, Research Institute of Applied Electricity of our University, for use of the rapid scan spectrometer.

The present work has been supported in part by a Grant-in-aid for Scientific Research from the Ministry of Education.

10) J. H. Baxendale, H. R. Hardy, and L. H. Sutcliffe, *Trans. Faraday Soc.*, **47**, 963 (1951).
11) H. Diebler. *Ber. Bunsenges. physik. Chem.*, **4**, 395 (1963).

Kinetics and Mechanisms of the Reaction of Tl(III) with Variamine Blue, [*N*-(*p*-Methoxyphenyl)phenylenediamine] in Aqueous Perchlorate Media

Taira IMAMURA and Masatoshi FUJIMOTO

Department of Chemistry, Faculty of Science, Hokkaido University, Sapporo

(Received May 21, 1971)

A stopped-flow apparatus was used to study the kinetics of the redox reaction of Tl(III) with Variamine Blue under nitrogen atmosphere in acid (0.2—0.6 M) perchlorate media of ionic strength $\mu=1.0$ M. The observed second-order rate constant increases inversely with hydrogen ion concentration. The proposed mechanism involves the overall rate-determining steps

$$Tl^{3+} + (V.B.) \overset{k_1}{\rightleftharpoons} Tl^{+} + (V.B.)_{ox} + 2H^{+}$$

$$TlOH^{2+} + (V.B.) \overset{k_2}{\rightleftharpoons} Tl^{+} + (V.B.)_{ox} + H_2O + H^{+}$$

where (V.B.) and $(V.B.)_{ox}$ are a reduced form and an oxidized form of Variamine Blue respectively. The rate constants are evaluated to be $k_1 \leq 10^2$ M^{-1} sec^{-1}, and $k_2=3.6\times10^4$ M^{-1} sec^{-1} at 25°C. The activation energy E_2 for k_2 is 11 ± 0.8 kcal·mol^{-1}.

It has been reported[1-3] that the aqueous solution of Variamine Blue (abbr. V.B.) undergoes two electron oxidation to yield a violet-red iminoquinone (abbr. $(V.B.)_{ox}$) by oxidizing agents such as Ce(IV), Fe(III), and I_2, as follows.

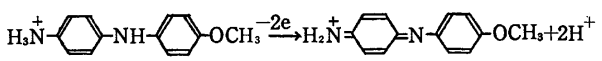

(V.B.) $(V.B.)_{ox}$

In the reaction of V.B. with Fe(III)[4] and Ce(IV),[5] the formation of $(V.B.)_{ox}$ does not obey the pseudo-first-order rate law in the presence of a large excess of metal ions. It was ascribed to the non-complementary reaction, where 2 mol of the oxidizing agent react with 1 mol of the reducing agent.

In the present paper we report the reaction of Tl(III) with V.B. in aqueous perchlorate media. Formation of $(V.B.)_{ox}$ obeys the first order rate law under the condition $[Tl(III)]_0 \gg [(V.B.)_{ox}]$. It seems that the complementary reaction of Tl(III) with V.B. does not proceed through the semioxidized form of Variamine Blue as semiquinone.

Experimental

Materials. Deionized and distilled water was used. The solution of Tl(III) perchlorate was prepared by electrolytic oxidation of Tl(I) perchlorate in 2 M perchloric acid.[6] Thallium(I) perchlorate was precipitated from solutions of Tl(OAc) and $HClO_4$ and purified by repeated recrystallization. The concentration of Tl(III) was standardized with EDTA titrimetrically. Variamine Blue (hydrochloride, Dojindo, Kumamoto) was dissolved in boiled water before use.

Sodium perchlorate and perchloric acid (reagent grade, Koso, Tokyo) were used to maintain the ionic strength at $\mu=1.0$ throughout the work. The concentration of sodium perchlorate was standardized by titrating the eluent from a column of ion-exchange resin, Dowex 50W-X8, in the acid form.

Kinetics. The reaction of V.B. with Tl(III) was followed spectrophotometrically using a stopped-flow apparatus (SPS-1, Yanagimoto, Kyoto) at 550 nm, the λ_{max} of $(V.B.)_{ox}$.

Nitrogen gas purified through an alkaline pyrogallol solution was passed through the solutions in the reservoirs during the course of measurements in order to avoid undesirable air oxidation.

Since in perchloric acid media the absorbance of Variamine Blue at 280 nm decreases gradually on exposure to the air, the solution of Tl(III) in perchloric acid media was mixed with a solution of V.B. of pH about 5. No decrease in absorbance was observed when solid Variamine Blue was directly dissolved *in vacuo* in the 2 M perchloric acid solution freed from oxygen by freezing a few times.

Measurements of the reaction of V.B. with Tl(III) were performed under the conditions $5.0\times10^{-3} > [Tl(III)] > 1.0\times10^{-3}$, $5.0\times10^{-5} \geqq [V.B.]_0 \geqq 5.0\times10^{-6}$, and $0.6 > [H^+]_0 \geqq 0.2$ M.

Results

Stoichiometry. The stoichiometry of the reaction of Tl(III) with V.B. was determined spectrophotometrically at 550 nm using a stopped-flow apparatus.

A definite excess of Tl(III) was mixed with V.B. to determine the molar extinction coefficient of $(V.B.)_{ox}$ as 1.3×10^4 M^{-1} cm^{-1} at 550 nm. The value agreed with that observed in the reaction of Fe(III) with V.B.[4]

Table 1 shows the concentration of $(V.B.)_{ox}$ formed

Table 1. Stoichiometry of the reaction of Tl(III) with V.B.[a]

$[Tl(III)]_0$ (10^{-5} M)	$[V.B.]_0$ (10^{-5} M)	$[(V.B.)_{ox}]$ (10^{-5} M)	$\frac{[(V.B.)_{ox}]}{[V.B.]_0}$	$\frac{[(V.B.)_{ox}]}{[Tl(III)]_0}$
168.0	0.5	0.5	1.0	
2.8	40.0	2.3		0.82
5.6	40.0	5.0		0.91

a) at $[H^+]=0.5$ M, $\mu=1.0$, and 25°C.

1) L. Erdey, I. Buzas, and K. Vigh, *Talanta*, **1**, 377 (1958).
2) L. Erdey and R. C. Pink, *ibid.*, **9**, 329 (1962).
3) L. Erdey, T. Meisel, B. Mohos, and F. Tudos, *ibid.*, **14**, 1477 (1965).
4) T. Imamura and M. Fujimoto, This Bulletin, **45**, 438 (1972).
5) T. Imamura and M. Fujimoto, *ibid.*, submitted for publication.
6) G. Biedermann, *Arkiv Kemi*, **5**, 44 (1953).

from various concentrations of Tl(III) and V.B. The derived stoichiometry is $\Delta[(V.B.)_{ox}]/\Delta[Tl(III)]_0 = -1.0$.

Kinetics. With a large excess of Tl(III) the appropriate pseudo-first-order absorbance plots gave a straight line, as shown in Fig. 1, according to the following equation.

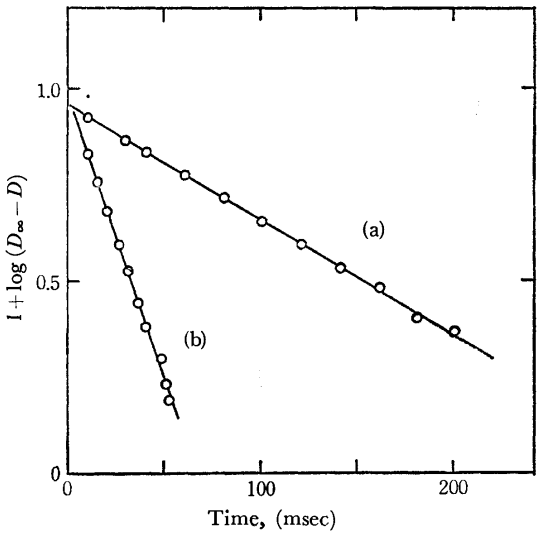

Fig. 1. Typical first-order rate plots at 25°C and $\mu=1.0$. (a) $[Tl(III)]_0=1.68\times10^{-3}$ M, $[V.B.]_0=5.00\times10^{-5}$ M, $[H^+]=0.45$ M, (b) $[Tl(III)]_0=3.36\times10^{-3}$ M, $[V.B.]_0=5.00\times10^{-5}$ M, $[H^+]=0.20$ M.

$$\log(D_\infty - D) = \log(D_\infty - D_0) - \frac{k'}{2.303}t$$

where D_∞, D, and D_0 are the optical densities at 550 nm at equilibrium and $t=t$ and $t=0$, respectively. The observed rate constant k' was plotted against the concentration of Tl(III). Figure 2 shows that the

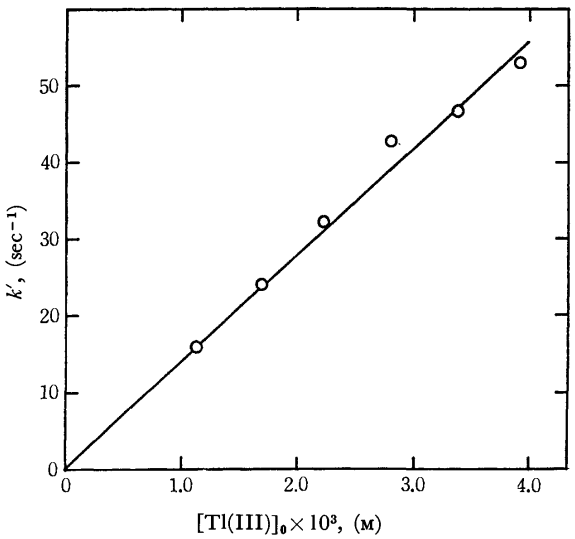

Fig. 2. Plot of pseudo-first-order rate constants against $[Tl(III)]_0$.
$[V.B.]_0=5.00\times10^{-5}$ M, $[H^+]=0.2$ M, 25°C, $\mu=1.0$.

value of k' is proportional to the initial concentration of Tl(III) under the conditions, $\mu=1.0$, $[H^+]=0.2$ M, and 25°C, suggesting the rate equation to be

$$d[(V.B.)_{ox}]/dt = k_a[Tl(III)][(V.B.)]$$

The dependence of the second-order rate constant k_a on $[H^+]$ and temperature was measured in a range $0.6>[H]\geqq0.2$. The plots of k_a *versus* $1/[H]$ at 15, 20, 25, 30, and 35°C fall on a series of straight lines with the intercepts near the origin as shown in Fig. 3.

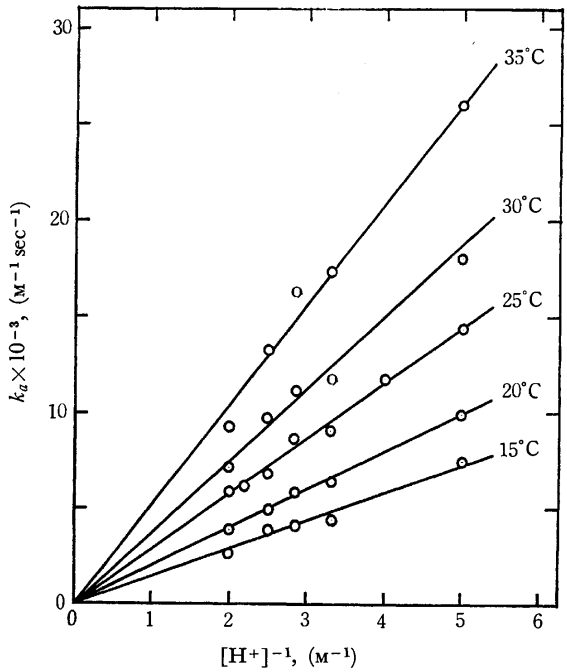

Fig. 3. Plot of second-order rate constants against $1/[H^+]$.

Mechanism and Discussion

In the non-complementary reactions of Tl(III) with Fe(II), the existence of Tl(II) as an intermediate of the reaction is suggested.[7] The reactions of Tl-(III) with V(III) and V(IV) also seem to proceed through the formation of Tl(II).[8] Oxidation of V.B. with Fe(III) and Ce(IV) proceeds through a semi-oxidized form of Variamine Blue as semiquinone to form $(V.B.)_{ox}$.[4,5]

In the complementary reaction of Tl(III) with V.B., however, one mole of Tl(III) reacts with one mole of V.B., and the intermediates as Tl(II) and semiquinone of V.B. seem to be very unstable during the course of the reaction.

Assuming that all protolytic equilibria are rapidly established with respect to Tl(III) and V.B., the mechanism of the reaction is suggested to be as follows.

$$Tl^{3+} \overset{k_1}{\rightleftharpoons} TlOH^{2+} + H^+ \quad (1)$$

$$Tl^{3+} + V.B. \overset{k_1}{\longrightarrow} Tl^+ + (V.B.)_{ox} + 2H^+ \quad (2)$$

$$H^+ + TlOH^{2+} + V.B. \overset{k_2}{\longrightarrow} Tl^+ + (V.B.)_{ox} + 2H^+ + H_2O \quad (3)$$

7) K. G. Ashurst and W. C. E. Higginson, *J. Chem. Soc.*, **1953**, 3044.

8) W. C. E. Higginson, D. R. Rosseinsky. J. B. Stead, and A. G. Sykes, *Discuss. Faraday Soc.*, **29**, 39 (1960).

The second-order rate constant k_a is thus rewritten as $k_a = (k_1[H^+]+k_2K)/([H^+]+K)$, where K is an acid dissociation constant of aqueous Tl(III), $K=7.94\times 10^{-2}$.[7]

When K is neglected against $[H^+]$, we have $k_a = k_1+k_2K/[H^+]$. Values of $k_1 \leq 10^2$ M^{-1} sec^{-1} and $k_2 = 3.63\times 10^4$ M^{-1} sec^{-1} at $\mu=1.0$ and 25°C are evaluated from the intercept and the slope of the straight line shown in Fig. 3.

In Fig. 4 the function $k_a([H^+]+K)$ is plotted against $[H^+]$, from which the value $k_2=3.56\times 10^4$ M^{-1} sec^{-1} is obtained. The value k_2 agreed with the value obtained from the slope of the straight line in Fig. 3 within relative error of about 15%.

Activation energy for k_2, E_a, is also evaluated as 11 ± 0.8 kcal·mol^{-1} from the plot of k_2 against the reciprocal absolute temperature (Fig. 5). The activation energy of the reaction of Tl(III) with V.B. is about the same as that of Fe(III).[4] The apparent activation energy of the reaction of Ce(IV)[5] with V.B. is about zero, the same as observed in the reaction of Ce(IV) with hydroquinone.[9]

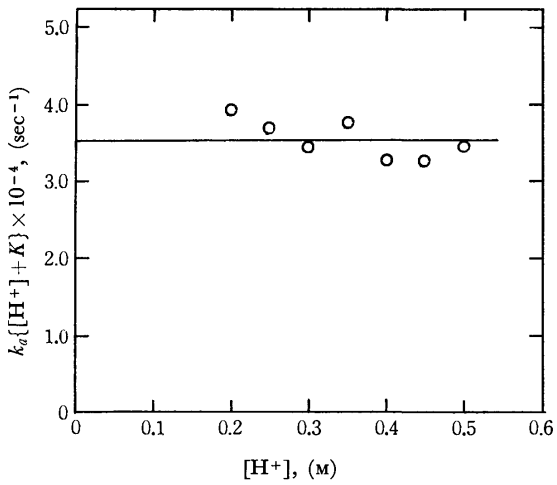

Fig. 4. Plot of $k_a\{[H^+]+K\}$ against $[H^+]$ at 25°C and $\mu=1.0$.

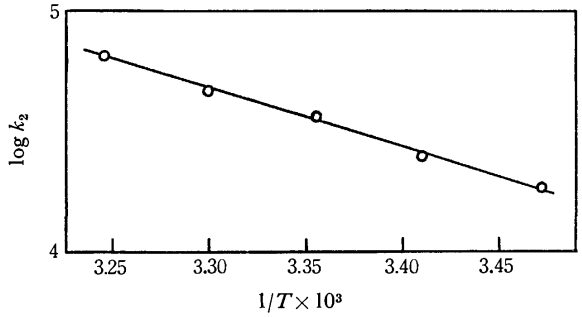

Fig. 5. Plot of second-order rate constant, k_2 against $1/T$.

The apparent rate constant of the reaction of Tl(III) with V.B. is about 10^2 times higher than that of Fe(III) with V.B. It may be ascribed to the difference in the redox potentials of metal ions, $E^0=1.28$ V for Tl(III)[6] and $E^0=0.71$ V for Fe(III).[10]

The values of the apparent second-order rate constants $(1—6)\times 10^4$ M^{-1}sec^{-1} as obtained for the complex formation of Tl(III) with Semi-xylenol Orange at $[H^+]=0.2—0.5$ M and at 25°C[11] suggest the possibility of the complex formation between Tl(III) and V.B. as a rate-determining step for the redox reaction.

The present work was supported in part by a grant-in-aid for Scientific Research from the Ministry of Education.

9) C. F. Wells and L. V. Kuritsyn, *J. Chem. Soc., A*, **1969**, 2575.
10) W. C. Schumb, M. S. Scherrill, and S. B. Sweetser, *J. Amer. Chem. Soc.*, **59**, 2360 (1937).
11) Y. Kawai, T. Takahashi, K. Hayashi, T. Imamura, H. Nakayama, and M. Fujimoto, This Bulletin, in press.

Polarographic Investigation of Alkali Metal Ions in Hexamethylphosphoramide

Kosuke IZUTSU, Sachiko SAKURA, and Taitiro FUJINAGA
Department of Chemistry, Faculty of Science, Kyoto University, Sakyo-ku, Kyoto
(Received May 27, 1971)

The polarographic behavior of alkali metal ions in hexamethylphosphoramide (HMPA) has been found to be greatly influenced by the cations of the supporting electrolytes. With 0.05 M Et_4NClO_4 as the supporting electrolyte, cesium and rubidium ions give diffusion-controlled, reversible waves at −2.32 and −2.35 V, respectively, *vs.* the Ag/0.1 M $AgClO_4$ electrode, but sodium and lithium ions are not reduced until the reduction of the supporting electrolyte (−3.1 V). The potassium ion gives a wave at −2.37 V with a limiting current controlled by the rate of the preceding process. In 0.05 M Bu_4NClO_4 solutions, the reduction wave of the potassium ion is diffusion-controlled, but that of the sodium ion is kinetic and is very small. The lithium ion is not reduced until −3.1 V. In 0.05 M $LiClO_4$, even the sodium ion is reduced reversibly with $E_{1/2}$ at −2.47 V, while the reduction of the lithium ion starts from -2.6_5 V. In mixed supporting electrolytes, the presence of the tetraethylammonium ion is the determining factor of the electrode processes. From the measurements of the electrocapillary curves and of the conductivities, the effect has been attributed to the change in the double-layer properties with the cations of the supporting electrolytes.

Hexamethylphosphoramide(HMPA) is a dipolar aprotic solvent which is often used for organic reactions.[1] It has a highly basic character and solvates strongly to various metal ions.[2] Moreover, it can dissolve alkali metals to yield a blue solution; this solution has been attributed to the formation of solvated electrons.[3]

Voltammetric study at a rotated platinum electrode has been carried out by Dubois *et al.*[4] in HMPA and its mixtures with water. They used lithium and sodium perchlorates as the supporting electrolytes and observed that the behavior of the residual current-potential curves obtained in these two supporting electrolytes differ considerably from each other.

In the present study, the polarographic behavior of alkali metal ions has been investigated in order to elucidate some of the solvation phenomena of these ions in HMPA. The reductions of alkali metal ions in this solvent, being different from those in other aprotic solvents,[5] are greatly influenced by the supporting electrolyte. This effect was found to be due to the change in the double-layer properties with the cation of the supporting electrolyte.

Apparatus and Reagents

Apparatus. The DC polarograms were recorded with a Yanagimoto three-electrode polarograph, Type P8-DP, and the AC polarograms, with a Yanagimoto polarograph, Type 102. An H-type polarographic cell with a fine-porosity sintered glass disc between the two compartments was used. All the potentials were referred to a freshly-prepared Ag/0.1 M $AgClO_4$ (HMPA) electrode, which had a potential of +0.36 V *vs.* aq. SCE when both electodes were immersed in HMPA-0.05 M Et_4NClO_4. A platinum wire served as an auxiliary electrode. The dropping mercury electrodes had the following characteristics in HMPA-0.05 M Et_4NClO_4 and at the mercury head of 62 cm: the A electrode, m=1.72 mg/sec with the circuit open and t=1.40 sec at −2.6 V *vs.* the Ag/Ag^+ electrode, and the B electrode, m=1.88 mg/sec and t=1.39 sec. Except otherwise described, the A electrode was used. Most measurements were carried out at 25°±0.1°C.

Reagents. The cesium and rubidium perchlorates were prepared by adding silver perchlorate to the respective chloride solutions. The sodium perchlorate was prepared by recrystallizing it from its aqueous solution at 70—80°C. The potassium and lithium perchlorates were obtained commercially. All of these alkali perchlorates were vacuum dried at 200°C. The tetraethylammonium perchlorate (Et_4NClO_4), tetrapropylammonium perchlorate (Pr_4NClO_4), and tetrabutylammonium perchlorate (Bu_4NClO_4) were prepared following the procedures in the previous reports[6] and were dried at 80°C under a vacuum. Tetramethylammonium perchlorate (Me_4NClO_4) was prepared from $AgClO_4$ and Me_4NBr and was recrystallized from water.

The HMPA was a product of the Nippon Oil Seal Co., Ltd. It was refluxed over barium oxide under reduced pressure for several hours and then vacuum-distilled. The middle fraction, about 70%, was collected (bp *ca.* 90°C). It was refluxed again over metallic sodium and vacuum-distilled from it. The distillations were carried out with an adiabatic vacuum fractional-distillation column (Shibata Chemical Apparatus Mfg. Co., Ltd.). The HMPA thus obtained gave a specific conductivity of $3—4\times10^{-8}$ ohm^{-1} cm^{-1}, and the water content, as determined by Karl Fischer titration, was approximately 0.01%. It was also confirmed to be pure enough both polarographically and UV-spectrophotometrically. The potential range applicable with a DME was from −0.1 V to −3.1 V *vs.* the Ag/Ag^+ electrode in HMPA-0.05 M Et_4NClO_4. Because the contact of HMPA with air produces an impurity which interferes with the polarographic investigation, the fresh distillate was usually used within a few hours after distillation. Storing at the temperature of dry ice and under a nitrogen atmosphere or under a vacuum was effective in keeping the distillate fresh for more than 24 hr.

* Electrochemical Studies in Hexamethylphosphoramide. I.

1) For review, see H. Normant, *Angew. Chem.*, **79**, 1029 (1967); *ibid., Int. Ed. Engl.*, **6**, 1046 (1967).

2) V. Gutmann, "Coordination Chemistry in Non-Aqueous Solutions," Springer Verlag, Wien (1968).

3) J. M. Brooks and R. R. Dewald, *J. Phys. Chem.*, **72**, 2655 (1968) and the references cited therein.

4) J. E. Dubois, P. C. Lacaze, and A. M. de Fiquelmont, *Compt. Rend.*, **262C**, 181, 249 (1966).

5) J. Broadhead and P. J. Elving, *J. Electrochem. Soc.*, **118**, 63 (1971) and the references cited therein.

6) T. Fujinaga, K. Izutsu, K. Umemoto, T. Arai, and K. Takaoka, *Nippon Kagaku Zasshi*, **89**, 105 (1968).

Results and Discussion

Reductions of Alkali Metal Ions in Tetraalkylammonium Perchlorates as the Supporting Electrolytes. Cesium and Rubidium Ions: With 0.05 M tetraalkylammonium perchlorates as the supporting electrolytes, cesium and rubidium ions give diffusion-controlled, reversible reduction waves at −2.32 and −2.35 V respectively *vs.* the Ag/Ag^+ electrode. The reversibility of the waves was also confirmed AC polarographically. The results are summarized in Table 1 and Fig. 1.

Potassium Ion: When Bu_4NClO_4 or Pr_4NClO_4 is used as the supporting electrolyte, the potassium ion gives a diffusion-controlled wave with a diffusion current constant comparable to those of cesium and rubidium ions in 0.05 M Et_4NClO_4 (see Table 1). In both DC and AC polarographic methods, the wave is reversible and the temperature coefficient of the DC wave height is approximately 1.3%/°C.

If Et_4NClO_4 is used as the supporting electrolyte, however, the reduction of the potassium ion becomes rather complicated. Though the reduction seems to be fairly reversible, judging from both the analysis of the DC wave and the measurement of the AC polarogram, the DC wave height is considerably smaller than in the cases with Bu_4NClO_4 or Pr_4NClO_4 as the supporting electrolyte (Tabe 1) and its temperature coefficient is much larger (ca. 4%/°C in 0.05 M Et_4NClO_4). The test of the dependence of the DC wave height on the height of the mercury column shows that the limiting current is controlled partly by diffusion and partly by chemical reactions.

In Fig. 2, the values of $i_1C^{-1}h^{-1/2}$ are plotted against $h^{-1/2}$ for the reduction waves of 1, 2 and 3 mM potassium ions both in 0.05 M Bu_4NClO_4 and in 0.05 M Et_4NClO_4. Here, i_1 is the limiting current in μA; C, the concentration of the potassium ion in mM, and h, the height of the mercury column corrected

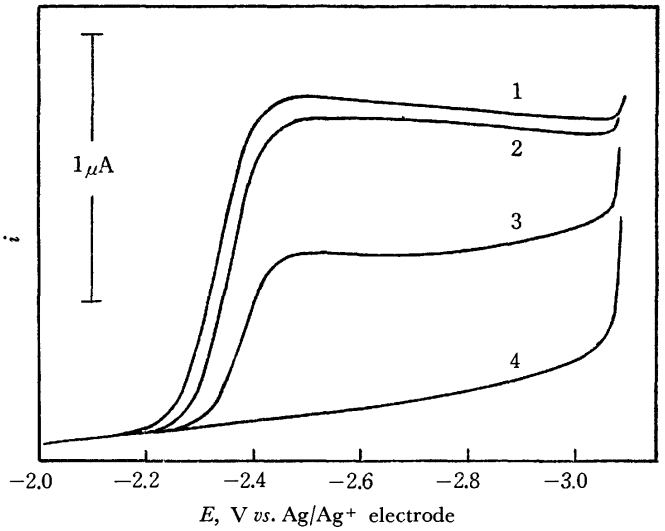

Fig. 1. Polarograms of alkali metal ions in 0.05 M Et_4NClO_4-HMPA. Curve 1, Cs^+; 2, Rb^+; 3, K^+; and 4, Na^+, Li^+ and the residual current. Concn. of each alkali metal ion is 1mM.

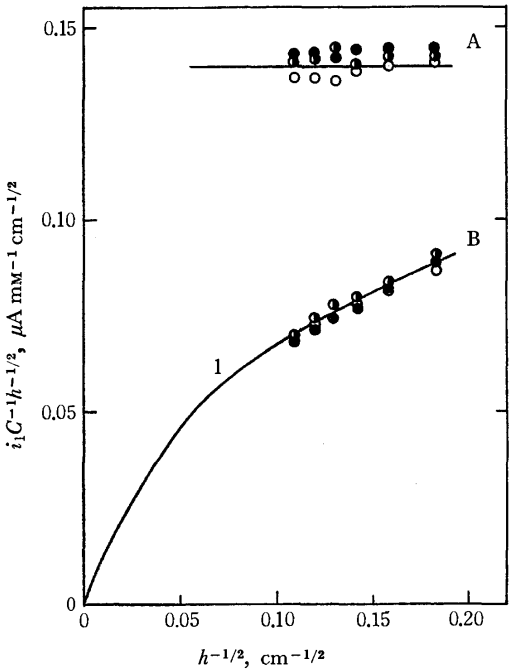

Fig. 2. Relations between $i_1C^{-1}h^{-1/2}$ and $h^{-1/2}$ for potassium waves in 0.05 M Bu_4NClO_4 (A) and in 0.05 M Et_4NClO_4 (B). Concn. of potassium ion: ○, 1 mM; ◑, 2 mM; ● 3 mM. Curve 1 is a theoretical i_1/i_d relation for $i_dC^{-1}h^{-1/2}=0.140$ and $(Kk)^{1/2}=1.23$.

Table 1. Polarographic data of alkali metal ions in 0.05 M tetraalkylammonium perchlorate-HMPA (25°C)[a]

Alkali metal ions	$i_1/Cm^{2/3}t^{1/6}$ μA/mMmg$^{2/3}$ sec$^{-1/2}$	$E_{1/2}$ V *vs.* Ag/Ag^+	$E_{1/4}-E_{3/4}$ mV	$i_p/i_1n\tau^{1/2}$ [b]	Remarks
Cs^+	0.74±0.03	−2.32	59	50	diffusion control
Rb^+	0.69±0.03	−2.35	60	46	diffusion control
	(0.71±0.03)	(−2.35)	(60)	(47)	diffusion control
K^+	0.40±0.03	−2.37	56	38	kinetic+diffusion
	(0.70±0.03)	(−2.38)	(59)	(48)	diffusion control
Na^+	—	—	—	—	not reduced
	(0.024)	(−2.42)[c]	—	—	kinetic control
Li^+	—	—	—	—	not reduced

a) Values in parentheses are in 0.05 M Bu_4NClO_4 and others in 0.05 M Et_4NClO_4.

b) i_p: AC peak height in μmho; τ: drop time at the peak potential, in sec; i_1: limiting current in μA; n: number of electrons. The value of $i_p/i_1n\tau^{1/2}$ for Pb^{2+} in aq. 0.1 M KNO_3 (pH 2) was 101. Measured with the DME B.

c) This value is less negative than the reversible half-wave potential (Ref. 11, p. 376).

for the back pressure. In 0.05 M Bu_4NClO_4 the values of $i_1C^{-1}h^{-1/2}$ are almost independent of $h^{-1/2}$, as is to be expected for the diffusion-controlled current. In 0.05 M Et_4NClO_4, however, the values of $i_1C^{-1}h^{-1/2}$ are smaller than those in 0.05 M Bu_4NClO_4, and they increase with an increase in $h^{-1/2}$, showing that a kinetic factor is involved.

The simplest mechanism considered is that the solvated potassium ion, which is the predominant species in HMPA, is converted into the electroactive state preceding its reduction:

$$K^+_{solvated} \underset{k'}{\overset{k}{\rightleftharpoons}} K^+_{electroactive} \overset{e}{\rightleftharpoons} K(Hg) \qquad (1)$$

$$K=k/k'$$

where the electroactive ion, $K^+_{electroactive}$, seems to be either a (partially) desolvated ion or a solvated ion which has approached to the electrode surface by penetrating through the layer of tetraethylammonium ions, as will be discussed later. According to the theoretical treatment by Koutecky,[7] the average limiting current, i_1, obtained for the above mechanism is shown by Eq. (2):

$$i_1 = i_d\frac{0.886(Kkt)^{1/2}}{1+0.886(Kkt)^{1/2}} \qquad (2)$$

where i_d is the currnt which will be observed if the solvated potassium ion is reduced by diffusion control. ($t^{1/2}$ is equal to $9.1_6h^{-1/2}$ with the A electrode at -2.6 V in 0.05 M Et_4NClO_4.) It seems reasonable to use the limiting current in 0.05 M Bu_4NClO_4, corrected for the change in drop time (see Fig. 8), as the approximate value of i_d in 0.05 M Et_4NClO_4. Curve 1 in Fig. 2 was theoretically obtained by using Eq. (2) for i_d $C^{-1}h^{-1/2}=0.140$ and $(Kk)^{1/2}=1.23$. The good agreement of the curve with the experimental results seems to show that the mechanism expressed by Eq. (1) is valid.

The kinetic current is considerably affected by the experimental conditions. With 0.05 M Et_4NClO_4 as the supporting electrolyte, the values of $(Kk)^{1/2}$ are 0.4_8 at 12.4°C, 1.2_3 at 25°C, and $3._4$ at 41°C. The value of $(Kk)^{1/2}$ also increases with a decrease in the concentration of Et_4NClO_4; thus, $(Kk)^{1/2}$ at 25°C is 0.6_0 in 0.1 M Et_4NClO_4, 1.2 in 0.05 M Et_4NClO_4, and 2.1 in 0.02 M Et_4NClO_4.

Figure 3 shows the effect of water on the limiting current of the potassium ion. In 0.05 M Bu_4NClO_4, the limiting current decreases slightly upon the addition of water (probably due to the increase in viscosity), while, in 0.05 M and 0.1 M Et_4NClO_4, it increases and approaches the value of the purely-diffusion-controlled wave.

In Me_4NClO_4 as the supporting electrolyte, the potassium wave becomes diffusion-controlled again. (See below for a further discussion of the role of the supporting electrolyte.)

Sodium Ion: The polarograms of the sodium ion in HMPA and HMPA-H_2O mixtures containing 0.05 M Et_4NClO_4 as a supporting electrolyte are shown in Fig. 4. The sodium ion in water-free HMPA does not give a reduction wave up to the potential of the reduction of the supporting electrolyte. A fairly large amount of water should be added in order to obtain a well-defined sodium wave. In Bu_4NClO_4 (or Pr_4NClO_4) as the supporting electrolyte, the sodium ion gives a very small wave (probably kinetic in nature) at about -2.4_2 V *vs.* the Ag/Ag^+ electrode (Fig. 5); the wave height is increased more easily by the addition of water than when Et_4NClO_4 is the supporting electrolyte.

Lithium Ion: The reduction of the lithium ion in HMPA-tetraalkylammonium perchlorate solutions is more difficult than that of other alkali metal ions (Fig. 1), and no further experiments were carried out.

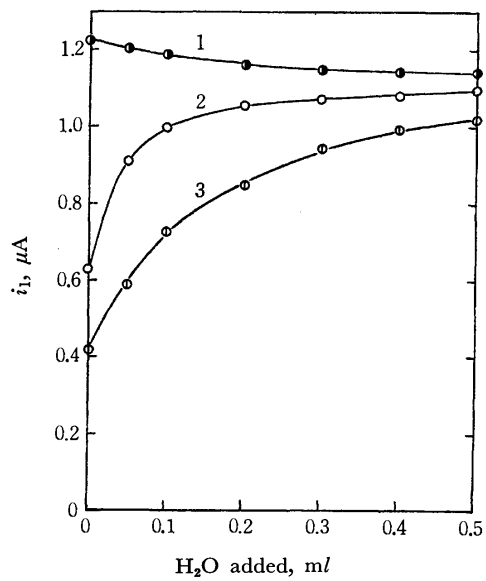

Fig. 3. Effect of water on the limiting current of potassium ions in HMPA. Original volume of the soln.: 10 ml. Concn. of potassium ion: 1 mM. Curve 1, in 0.05 M Bu_4NClO_4; 2, in 0.05 M Et_4NClO_4; and 3, in 0.1 M Et_4NClO_4. (Corrected for the volume change)

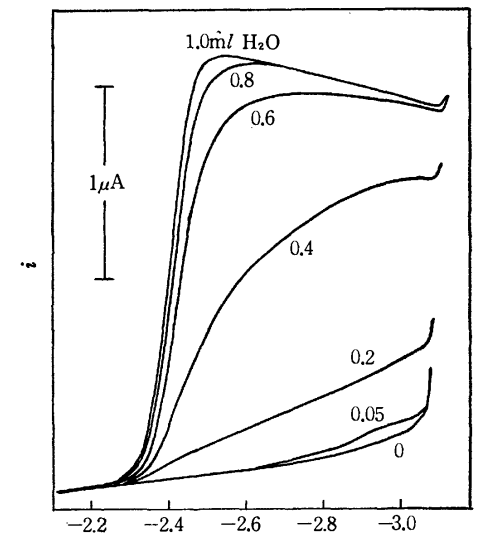

Fig. 4. Effect of water on the sodium wave in HMPA-0.05 M Et_4NClO_4. Water was added to 10 ml of 2.24 mM Na^+ solution. Corrected for the volume change.

7) J. Koutecky, *Collect. Czech. Chem. Commun.*, **18**, 597 (1953).

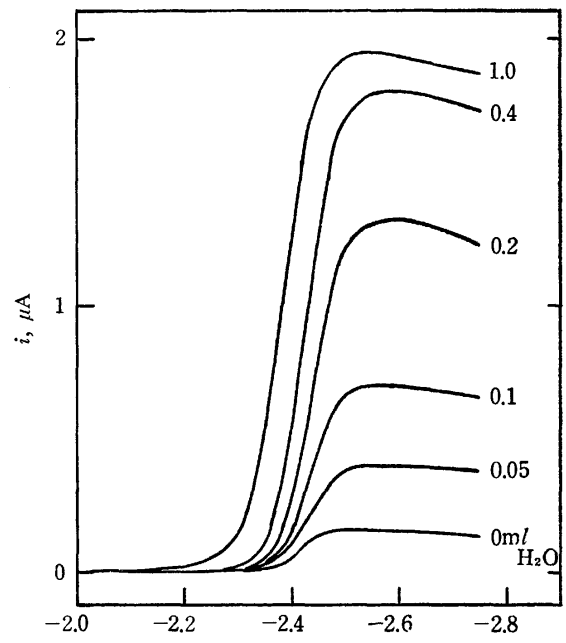

Fig. 5. Effect of water on the sodium wave in 0.05 M Bu_4NClO_4-HMPA. Water was added to 10 m*l* of 2.21 mM Na^+ solution. Corrected for the residual current and the volume change.

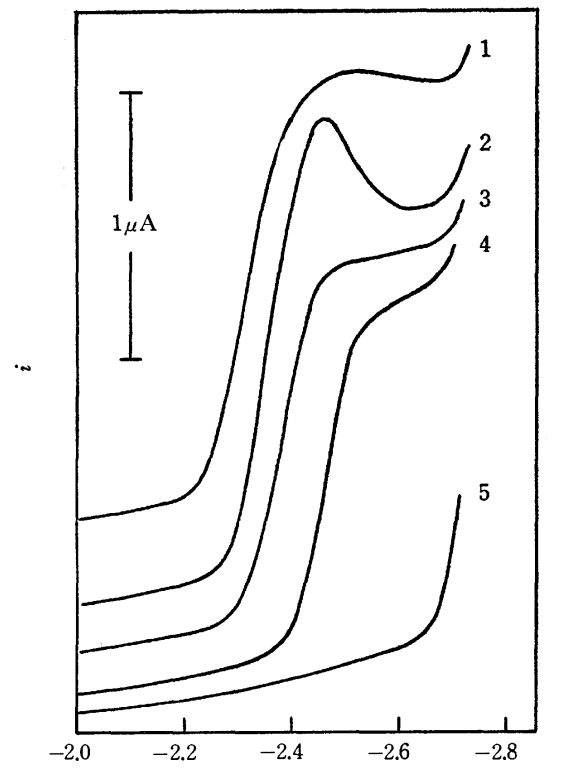

Fig. 6. Polarograms of alkali metal ions in 0.05 M $LiClO_4$-HMPA. Curve 1, Cs^+; 2, Rb^+; 3, K^+; 4, Na^+; and 5, the residual current. Concn. of each alkali metal ion is 1 mM. With the DME B.

Reductions of Alkali Metal Ions in Lithium Perchlorate as the Supporting Electrolyte. As is shown in Fig. 6, the behavior of alkali metal ions in 0.05 M $LiClO_4$-HMPA solutions is quite different from that in tetraalkylammonium perchlorate solutions. The reductions of cesium and rubidium ions in these solutions occur at approximately the same potentials as with the Et_4NClO_4 supporting electrolyte (−2.32 and −2.35 V respectively), though maxima are observed in these waves. The potassium ion also gives a diffusion-controlled wave at −2.37 V, and even the sodium ion, which can not be reduced in the Et_4NClO_4 solution, gives a reversible wave at −2.47 V. The reduction of the lithium ion starts from -2.6_5 V.

Reductions of Sodium and Potassium Ions in Mixed Supporting Electrolytes. The effect of Et_4NClO_4 on the reduction of the sodium ion in 0.05 M $LiClO_4$ was examined. The results are shown in Fig. 7. The sodium wave, which is controlled by diffusion in the absence of the tetraethylammonium ion, is markedly interfered with by the presence of very small amounts of Et_4NClO_4. The presence of Et_4NClO_4 also decreases the drop-time significantly, as is shown in Fig. 7a, indicating that the tetraethylammonium ion is preferentially attracted onto the electrode surface. The reduction of the lithium ion, which starts from about −2.65 V in the absence of the tetraethylammonium ion, is also inhibited by the presence of small amounts of Et_4NClO_4 (Figs. 6 and 7).

In mixed supporting electrolytes, such as $LiClO_4$+Et_4NClO_4, Bu_4NClO_4+Et_4NClO_4, and Pr_4NClO_4+Et_4NClO_4, the reduction of the potassium ion is again

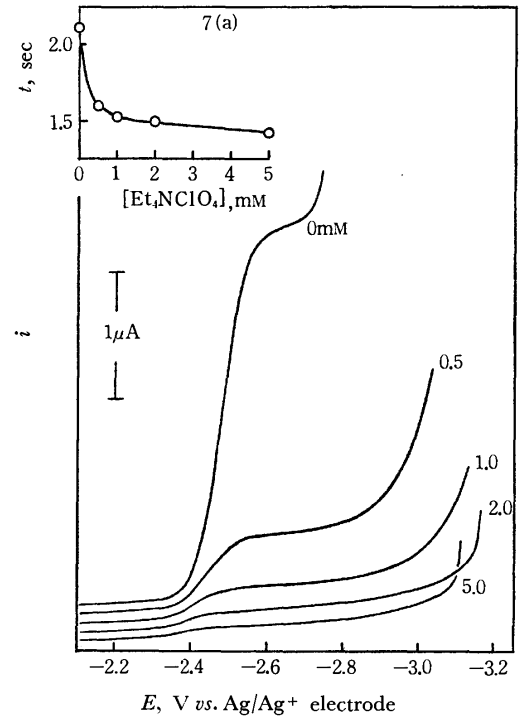

Fig. 7. Effect of Et_4NClO_4 on the sodium wave in 0.05 M $LiClO_4$-HMPA. Concn. of sodium ion: 2.27 mM. Concn. of Et_4NClO_4 is shown on the curves. With the DME B.
Fig. 7(a). Effect of Et_4NClO_4 on the drop time in 0.05 M $LiClO_4$-HMPA.

controlled by the tetraethylammonium ion and a kinetic current is observed, just as when the supporting electrolyte is Et_4NClO_4 only.

Effect of the Supporting Electrolytes on the Electrical Double Layer. The electrocapillary curves obtained by measuring the drop time are shown in Fig. 8. The drop time at extremely negative potentials changes considerably with the supporting electrolytes used; it is largest in 0.05 M $LiClO_4$, smallest in 0.05 M Et_4NClO_4, and between these two in 0.05 M Bu_4NClO_4. The charge densities on the electrode, calculated from the slopes of these electrocapillary curves, are plotted in Fig. 9. The negative charge on the electrode is much larger in 0.05 M Et_4NClO_4 than in 0.05 M Bu_4NClO_4 and $LiClO_4$, showing that the tetraethylammonium ion is more easily attracted to the electrode surface. This difference is probably due to the difference in the sizes of the solvated ions. Figure 10 shows the Stokes law radii of mono-valent cations in HMPA, calculated from the results of conductivity measurements.[8] Though it is questionable to consider that the Stokes law radii are a direct measure of the sizes of solvated ions, it is reasonable to assume that, among the ions in Fig. 10, the tetraethylammonium ion is smallest and the lithium ion is largest. It is natural that the tetraethylammonium ion, which is the smallest cation, is the most easily (or preferentially in the mixed electrolytes) attracted onto the negatively-charged electrode surface.

The big influence of the supporting electrolyte on the reductions of alkali metal ions can be explained by the effect of a competitive approach to the electrode surface of the cation of the supporting electrolyte and of the depolarizing cation. With $LiClO_4$ as the supporting electrolyte, for example, all the alkali metal ions can easily approach the electrode surface and can be reduced. With the Et_4NClO_4 supporting electrolyte, on the other hand, the tetraethylammonium cation is attracted preferentially and its layer inhibits the approach of the bigger solvated cations to the electrode surface. In this case, either the penetration of the solvated cations through the layer or some chemical reactions, such as the (partial) desolvation of the solvated cation, should precede the reduction. If the preceding process is rapid, the reduction is diffusion-controlled (the cases of cesium and rubidium ions), but if it is very slow, the reduction does not occur at all (the cases of sodium and lithium ions). When the rate of the preceding process is in between these two extremes, a kinetic current is observed, as in the case of the potassium ion. With 0.05 M Bu_4NClO_4 as the supporting electrolyte, the inhibition by the tetrabutylammonium ion is less than that by the tetraethylammonium ion, and the potassium ion can be reduced by diffusion control. The reduction of the sodium ion, however, is still controlled by the rate of the preceding process.

The influence of the supporting electrolyte can

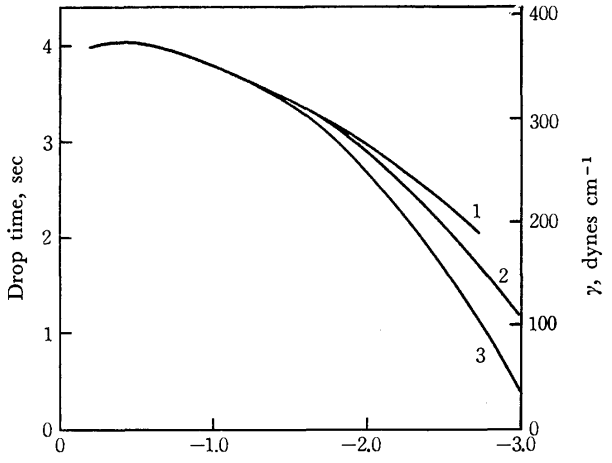

Fig. 8. Drop time-potential curves. Curve 1, in 0.05 M $LiClO_4$; 2, in 0.05 M Bu_4NClO_4; and 3, in 0.05 M Et_4NClO_4. For conversion of drop time t to surface tension γ, the values of t and γ at the ecm in aq. 0.1 M KCl were used as reference. The values of γ at very negative potentials are approximate because correction was not made for the variation of back pressure. With the DME B.

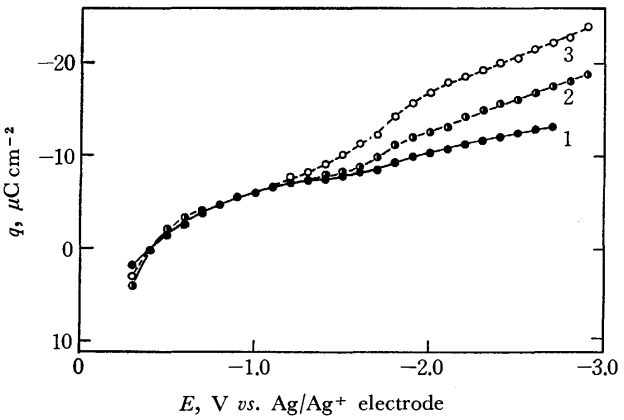

Fig. 9. Charges on the electrode surface obtained from the electrocapillary curves in Fig. 8. Curve 1, in 0.05 M $LiClO_4$; 2, in 0.05 M Bu_4NClO_4; and 3, in 0.05 M Et_4NClO_4.

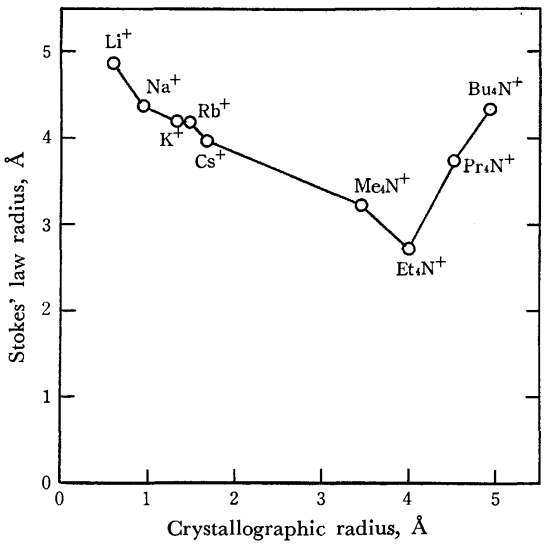

Fig. 10. Stokes' law radii of various mono-valent cations in HMPA.

8) K. Izutsu, S. Sakura, and T. Fujinaga, unpublished results; C. Atlani, J. C. Justice, M. Quintin, and J. E. Dubois, *J. Chim. Phys.*, **66**, 180 (1969).

also be explained qualitatively by means of the double-layer effect. Recently, the kinetics of electrode reactions have been treated by taking into account separately the distance of the outer Helmholtz plane from the geometrical electrode surface (x_2) and that of the plane at the charge center of the reacting species in the transtion state (x_r).[9,10] In HMPA, x_2 is expected to increase with the size of the cation of the supporting electrolyte in the order $Et_4N^+ < Bu_4N^+ < Li^+$, and the x_r values for potassium and sodium ions seem to be between x_2 in $LiClO_4$ and that in Et_4NClO_4. Thus, the potential, ϕ_r, at the plane of the closest approach of these ions will be more negative in $LiClO_4$ than in Et_4NClO_4. The preceding reactions of the depolarizing cations, as shown by Eq. (1), are accelerated significantly when the ϕ_r-potential becomes more negative.[11]

The above explanations are still only tentative. Further studies are now in progress in this laboratory on the electrode double layer at extremely negative potentials and its effects on electrode processes in HMPA and other organic solvents.[12,13]

9) W. R. Fawcett, *J. Electroanal. Chem.*, **22**, 19 (1969); W. R. Fawcett and M. D. Mackey, *ibid.*, **27**, 219 (1970); W. R. Fawcett, D. J. Bieman, and M. D. Mackey, *Collect. Czech. Chem. Commun.*, **36**, 503 (1971).

10) N. Tanaka, Y. Aoki, and A. Yamada, 16th Symposium on Polarography, Kyoto (1970).

11) J. Heyrovsky and J. Kuta, "Principles of Polarography," Academic Press, New York (1966), p. 351.

12) K. Izutsu, S. Sakura, K. Kuroki, and T. Fujinaga, *J. Electroanal. Chem.*, **32**, App. 11 (1971).

13) Quite recently similar inhibiting effect of Et_4N^+ on the reductions of sodium and lithium ions was observed by Gal and Yvernault. J. Y. Gal and T. Yvernault, *Bull. Soc. Chim. France*, **1971**, 2770.

BULLETIN OF THE CHEMICAL SOCIETY OF JAPAN, VOL. 45, 450—456 (1972)

Electronic Spectra and Electronic Structure of Iron(II) Tetraphenylporphins

Hiroshi KOBAYASHI and Yasuo YANAGAWA

Department of Chemistry, Tokyo Institute of Technology Ookayama, Meguro-ku, Tokyo

(Received June 11, 1971)

Tetraphenylporphiniron(II) was synthesized and isolated in a pure state. The iron(II) porphin was in the state of $S=2$. The spin state of iron(II) porphin varies with the axial ligand field. Oxygeneous axial ligands such as tetrahydrofuran and dioxane gave an intermediate spin state ($S=1$), while nitrogeneous ligands such as pyridine gave a diamagnetic state ($S=0$). The electronic spectra of tetraphenylporphin complexes of iron(II) were measured for the three types of the spin state.

Iron of the prosthetic groups in hemoglobin and myoglobin participates as a ferrous ion in oxygen carrying. Iron(II) is stable against oxidation in the hemoproteins even though it is directly bound with an oxygen molecule, whereas iron(II) in the synthetic complexes is hardly stable in the presence of oxygen. Iron(II) in the synthetic porphyrins is not so stable in the presence of oxygen and moisture in the air. However, iron(II) is fairly stabilized in the diamagnetic state obtained for a strong ligand field such as in tris(2,2′-bipyridine)-, tris(1,10-phenanthroline)- or hexacyano complex. The iron(II) porphyrin with a strong axial field is in a diamagnetic state and is relatively stabilized against oxidation.

A systematic study of the effect of axial ligands to the electronic structure of the iron(II) porphyrins was found necessary for the synthetic porphyrins. Recently we succeeded in the preparation of a new series of iron(II) complexes of tetraphenylporphin. In this paper, we present their electronic absorption spectra with special attention to the spin state of the central iron(II).

Experimental

Synthesis of Tetraphenylporphinbis(pyridine)iron(II). Tetraphenylporphinbis(pyridine)iron(II), TPPFe(II)·2Py (TPP is an abbreviation of tetraphenylporphin and Py, pyridine) was prepared by two different methods in a vacuum system.

(A) *Reduction of TPPFe(III)X Complex.* Tetraphenylporphiniron(III) acetate, TPPFe(III)$OCOCH_3$, (500 mg) was dissolved in a mixed solvent of 20 m*l* of pyridine, 150 m*l* of chloroform and 80 m*l* of methanol. After bubbling with dried nitrogen, 300 mg of sodium borohydride was added to the solution. The mixture was stirred for 3 hr at 50—60°C. Chloroform and methanol were distilled off until the volume of the solution became 20—30 m*l*. About 100 m*l* of methanol saturated with dried nitrogen, was added to the concentrated solution. After the solution had been allowed to stand for several hours, blue violet crystals were collected, washed several times with methanol saturated with dried nitrogen and dried in a vacuum. Since TPPFe(II)·2Py was sensitive to the air, it was kept in a glass capsule with inert gas.

(*B*) *Reaction of Iron(II) Acetate with the Metal-Free Base of TPP.* The metal-free base (500 mg) was dissolved in a mixed solvent of 20 m*l* of pyridine and 50 m*l* of chloroform. The solution was sufficiently saturated with dried nitrogen and to it was quickly added about 130 m*l* of a saturated solution of iron(II) acetate in acetic acid prepared by refluxing iron powder in acetic acid saturated with dried nitrogen. Care was taken not to contaminate the porphin solution by unreacted iron powder. The mixture was stirred for 3 hr at 50—60°C. Blue violet crystals were collected and kept in the same way as in (A).

The products prepared by both methods were identified by their characteristic absorption spectra. The product prepared by the method (A) was also identified by elemental analysis.

Found: C, 77.57; H, 4.81; N, 9.99; Fe, 6.80%. Calcd for $C_{54}H_{38}N_6Fe$: C, 78.47; H, 4.88; N. 10.17; Fe, 6.76%.

Synthesis of Tetraphenylporphiniron(II). A capsule of TPPFe(II)·2Py was joined to a vacuum line of 10^{-2} mmHg and was heated for 5 hr in an oil bath at 200°C. TPPFe-(II) was obtained in reddish purple crystalline state. It was much more sensitive to the air than TPPFe(II)·2Py, and was kept in a glass capsule in a vacuum.

Found: C, 80.89; H, 4.35; N, 8.53; Fe, 8.30%. Calcd for $C_{44}H_{28}N_4Fe$: C, 79.00; H, 4.52; N, 8.41; Fe, 8.34%.

Synthesis of Tetraphenylporphinbis(tetrahydrofuran)iron(II). TPPFe(II)·2THF (THF is an abbreviation of tetrahydrofuran) could not be synthesized by the same method as for TPPFe(II)·2Py. This was because of unstable binding of iron(II) and tetrahydrofuran. TPPFe(II)·2THF was prepared from TPPFe(II) with the apparatus shown in Fig. 1. The apparatus was joined to a vacuum line. From

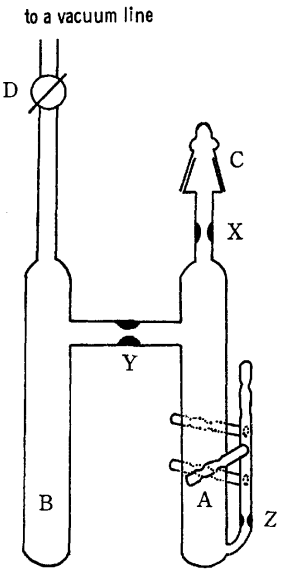

Fig. 1. Apparatus for preparation of TPPFe(II).

C, TPPFe(II)·2Py was carefully placed at the bottom of A under dried nitrogen atmosphere. TPPFe(II)·2py was heated for 5 hr in an oil bath at 200°C, while the apparatus was being evacuated by a vacuum line. After the reaction product had been allowed to stand at room temperature, a sufficient amount of THF saturated with dried nitrogen was added to the reaction product at A. While the THF solution in branch A was cooled in liquid nitrogen, the apparatus was sealed at X and evacuated by a vacuum line. After the cock D had been closed, the frozen solution was allowed to stand at room temperature. The solution was shaken for a while. The solvent THF was then completely transferred to branch B by cooling the branch in liquid nitrogen. Cooling of the frozen THF in the branch B was continued in liquid nitrogen. The apparatus was evacuated down to 10^{-2} mmHg, while the reaction product at A was allowed to stand at room temperature to dry. When the product was dried, the apparatus was sealed off at Y and the product was transferred into a branch of capsules. The branch of capsules was then sealed off at Z.

Found: C, 74.95; H, 4.79; N, 7.06; Fe, 6.91%. Calcd for $C_{52}H_{44}N_4O_2Fe$: C, 76.82; H, 5.45;N, 6.92; Fe, 6.87%.

Synthesis of Tetraphenylporphinbis(pyridine)manganese(II). Tetraphenylporphinmanganese(III) chloride, TPPMn-(III)Cl, (500 mg) was dissolved in a mixed solvent of 20 m*l* of pyridine, 40 m*l* of chloroform and 140 m*l* of methanol. After bubbling with dried nitrogen, 300 mg of sodium borohydride was added to the solution. The mixture was vigorously stirred for 3 hr at 50—60°C. After the reaction mixture was concentrated to 10—30 m*l* by distillation, the crystal of tetraphenylporphinbis(pyridine)manganese(II), TPPMn(II)·2Py, was precipitated by addition of methanol saturated with dried nitrogen. Blue violet lustrous crystals were collected, washed several times with dried oxygen-free methanol, and kept in a glass capsule with dried nitrogen. Since TPPMn(II)·2Py was sensitive to oxygen and moisture in the air, the whole process should be carried out under nitrogen atmosphere.

Found: C, 78.74; H, 4.36; Mn, 6.63%. Calcd for $C_{54}H_{38}N_6Mn$: C, 78.53; H, 4.46; Mn, 6.65%. Manganese was oxidized to permanganate and was determined by colorimetry.

Measurements of Absorption Spectra. Electronic absorption spectra were measured by a Shimadzu automatic recording spectrophotometer Model MPS-50 and a Beckman DU spectrophotometer using quartz cells of 0.1 cm or 1 cm light path. The solvents for absorption measurement were benzene, pyridine, piperidine, tetrahydrofuran, and dioxane purified by the usual methods.[1] They were distilled just before the use and degassed by successive freeze-thaw pumping cycles. Solutions for measurements were prepared in a vacuum system.

Measurements of Magnetic Susceptibilities. Magnetic moments were determined by means of the Gouy method.[2] Measurements were carried out at room temperature with the sample sealed in a capsule with dried nitrogen. After calibrating for the diamagnetic term, the magnetic moment of complex was calculated from the data obtained.

Results and Discussion

Tetraphenylporphiniron(II) has a planar structure as shown in Fig. 2. The central iron might be slightly out of the porphin plane. Such a structure has been found in various metal porphyrins including metal tetraphenylporphins.[3,4] Iron(II) in tetraphenylporphiniron(II), a planar complex, is in the spin state of $S=2$. In the case of TPPFe(II)·2Py, however, σ donation of the nitrogeneous donor of two coordinating pyridines gives rise to a strong axial field and all spins in the central iron are quenched ($S=0$). This was shown by magnetic susceptibility measure-

1) J. A. Riddick and E. E. Troops, "Organic Solvents, Techniques of Organic Chemistry," Vol. 7, ed. by A. Weissberger, Interscience Publishers, New York (1955).

2) B. N. Figgis and J. Lewis, "Modern Coordination Chemistry," ed. by J. Lewis and R. G. Wilkins, Interscience Publishers, New York (1960), p. 415.

3) J. L. Hoard, M. J. Hamor, and T. A. Hamor, *J. Amer. Chem. Soc.*, **85**, 2334 (1963); E. B. Fleischer, C. K. Miller, and L. E. Webb, *J. Amer. Chem. Soc.*, **86**, 2342 (1964).

4) J. L. Hoard, M. J. Hamor, T. A. Hamor and W. S. Caughey, *J. Amer. Chem. Soc.*, **87**, 2312 (1965); D. F. Koenig, *Acta Crystallogr.*, **18**, 663 (1965); J. L. Hoard, "Hemes and Hemoproteins," ed. by B. Chance, R. W. Estabrook, and T. Yonetani, Academic Press, New York (1966); p. 9; M. F. Perutz, *Scientific American*, **211**, 5 (1964); J. C. Kendrew, *Science*, **139**, 1259 (1963).

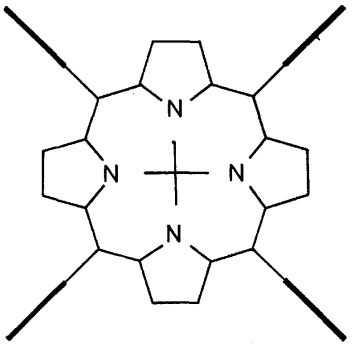

Fig. 2. Molecular geometry of metal tetraphenylporphin. Phenyl groups are actually perpendicular to the molecular plane of porphin.

ments. When the axial ligand field is of moderate strength, the central iron might be in the intermediate spin state, $S=1$. The ligand field of intermediate strength is furnished by such a relatively weak ligand as oxygeneous donor of tetrahydrofuran or dioxane. TPPFe(II)·2THF showed an intermediate value of the magnetic moments for $S=0$ and $S=2$. If a thermal equilibrium exists between the states $S=0$ and $S=2$ of a complex, an intermediate value is expected to be the average of the magnetic moments of two components. In the case of Fe(III) porphyrins, a thermal equilibrium actually exists between two spin states of a complex, giving a mixture absorption spectrum of the species with different spin states.[5] TPPFe(II)·2THF, however, shows no mixture spectrum of the species $S=0$ and $S=2$, but a spectrum characteristic of a species in a spin state other than $S=0$ or $S=2$. Mössbauer spectrum also shows a spectrum characteristic of the intermediate spin state, which differs from a spectrum expected for a mixture of the high spin state and the diamagnetic one.[6] The observed magnetic moments are summarized in Table 1.

The absorption spectra of TPPFe(II) and TPPFe(II)·2Py were measured in benzene and in pyridine

TABLE 1. MAGNETIC MOMENTS OF IRON(II)- AND MANGANESE(II) TETRAPHENYLPORPHINS

Complex	Magnetic moment (Bohr magneton)	Number of unpaired electrons	Spin state
TPPFe(II)·2Py	0	0	$S=0$
TPPFe(II)·2THF	2.75	2	$S=1$
TPPFe(II)	4.75	4	$S=2$
TPPMn(II)·2Py	6.02	5	$S=5/2$

TPP: Tetraphenylporphin, Py: Pyridine, and THF: Tetrahydrofuran.

5) P. George, J. Beetlestone, and J. S. Griffith, "Hematin Enzymes," ed. by J. E. Falk, R. Lemberg, and R. K. Morton, Pergamon Press, Oxford (1961), p. 105.

6) H. Kobayashi, Y. Maeda, and Y. Yanagawa, This Bulletin, **43**, 2342 (1970).

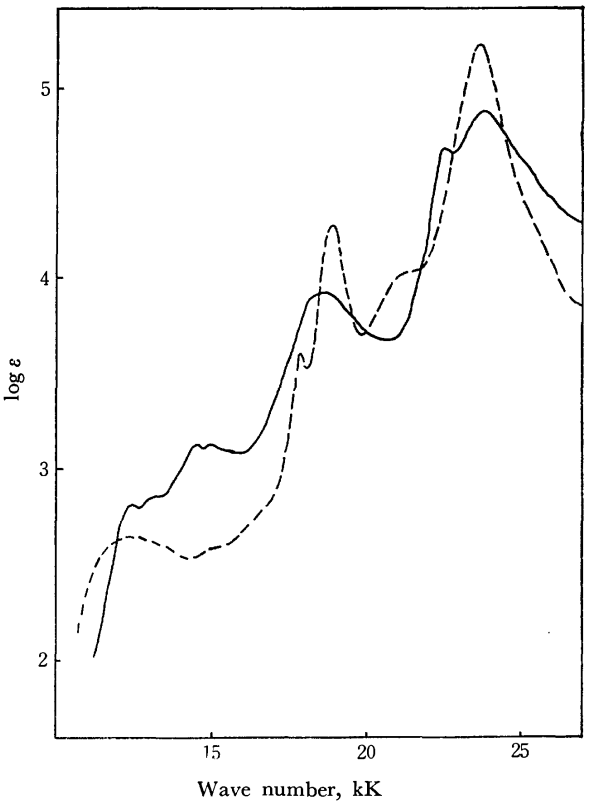

Fig. 3. Absorption spectrum of TPPFe(II).
——: benzene solution
----: pyridine solution

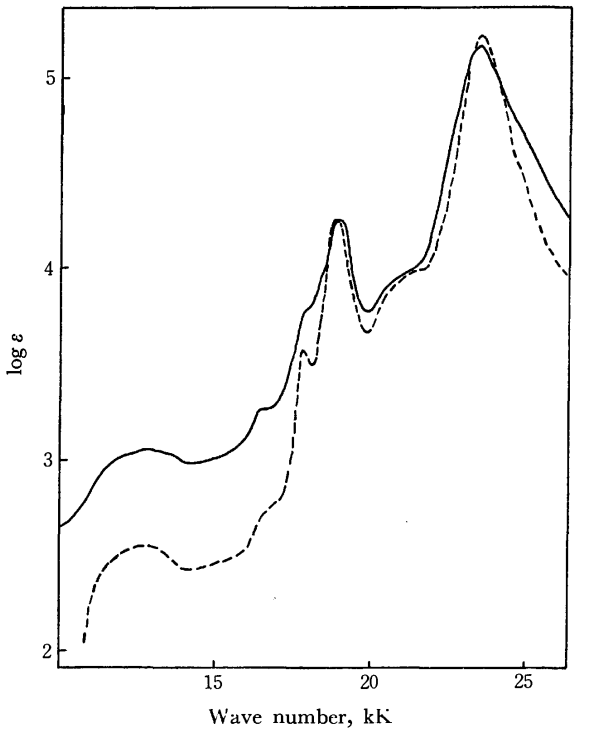

Fig. 4. Absorption spectrum of TPPFe(II)·2Py.
——: benzene solution
----: pyridine solution

(Figs. 3 and 4). Since the absorption spectrum of TPPFe(II) in pyridine solution was in good agreement with that of TPPFe(II)·2Py in pyridine solution, two

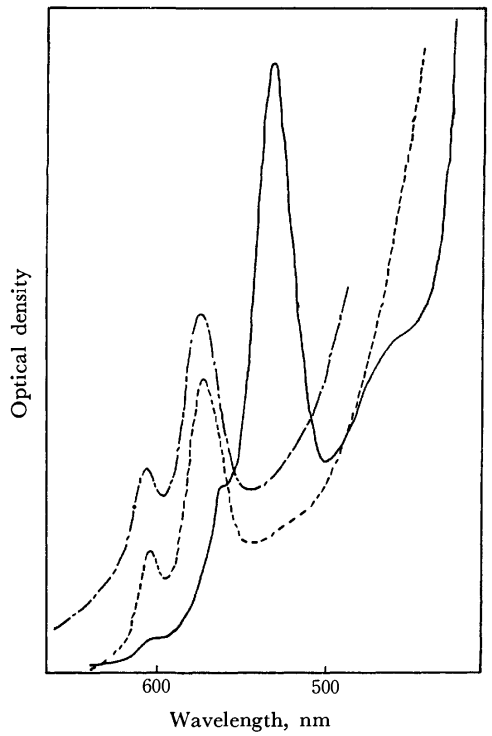

Fig. 5. Spectral change of TPPFe(II)·2Py in benzene when exposed to the air.
——: TPPFe(II)·2Py in dried oxygen-free benzene
----: after the benzene solution was exposed to the air
-·-·: $(TPPFe(III))_2O\cdot 2H_2O$ in benzene

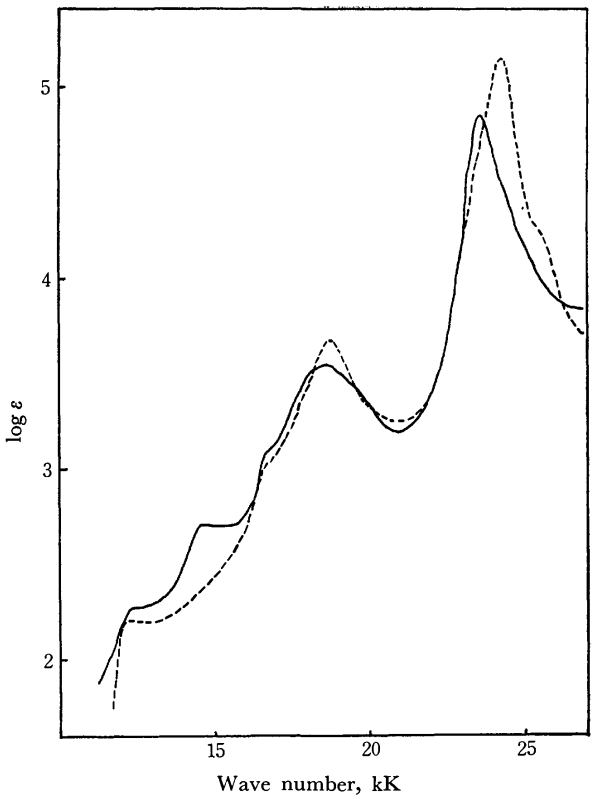

Fig. 6. Absorption spectra of TPPFe(II) in tetrahydrofuran and dioxane.
——: THF solution
----: dioxane solution

molecules of pyridine coordinate to the iron(II) in TPPFe(II) upon dissolution in pyridine. The spectra in the visible region of TPPFe(II)·2Py both in benzene and in pyridine actually coincide. The absorption spectrum of the powder sample of TPPFe(II)·2Py measured by means of the opal glass technique[7] was in good agreement with the solution spectrum. This indicates that the coordination of pyridine in the molecular crystal does not differ much from that in solution. Among the iron(II) complexes of tetraphenylporphin, bis(pyridine) complex in the solid state seems to be the most inert to oxygen and moisture in the air. However, it is readily converted into a ferric complex such as $(TPPFe(III))_2O\cdot 2H_2O$,[8] when the benzene solution of TPPFe(II)·2Py is exposed to the air (Fig. 5).

The absorption spectrum of TPPFe(II) in THF differs from those observed in benzene ($S=2$) and in pyridine ($S=0$). The visible bands observed in THF are close to those observed in benzene, while the Soret band in THF is in fairly good agreement with that in pyridine. The spectrum of TPPFe(II) in THF can not be reproduced by a superposition of the spectra of high spin component and diamagnetic one. Since the intensity of the characteristic bands is almost in the same order in these two components, the mixture spectrum should be a simple superposed spectrum. The observed spectrum of TPPFe(II) in THF is not a simple superposed mixture spectrum. Thus it should be assigned to a spectrum characteristic of a single species other than high spin species or diamagnetic species. As a matter of fact, we could isolate solid TPPFe(II)·2THF from the THF solution of TPPFe(II). It shows an intermediate spin value. TPPFe(II) in dioxane shows a very similar spectrum to that in THF (Fig. 6).

In the case of Fe(III) complexes of tetraphenylporphin, high spin species ($S=5/2$) and low spin species ($S=1/2$) have been synthesized, but not the intermediate spin species ($S=3/2$).[6] In the case of Fe(II) complexes, however, three spin states could be obtained. The most probable d electron configurations of these three spin states are given in Fig. 7. The ordering of the ligand-fielded d orbitals is schematically shown in Fig. 8. The actual values obtained

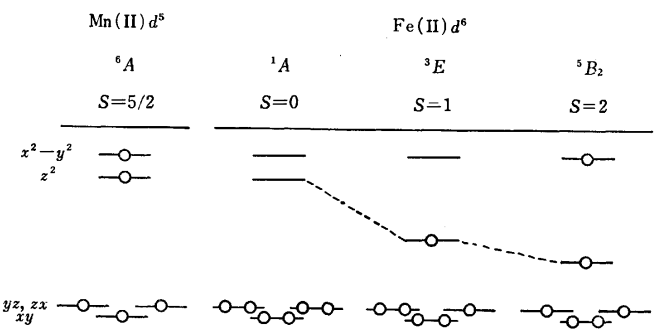

Fig. 7. Configuration of d electrons in iron(II)- and manganese(II) tetraphenylporphins.

7) K. Shibata, "Methods of Biochemical Analysis," Vol. 7, ed. by D. Glick, Interscience Publishers, New York (1959), p. 77.
8) I. A. Cohen, *J. Amer. Chem. Soc.*, **91**, 1980 (1969); E. B. Fleischer and T. S. Srivastava, *J. Amer. Chem. Soc.*, **91**, 2403 (1969).

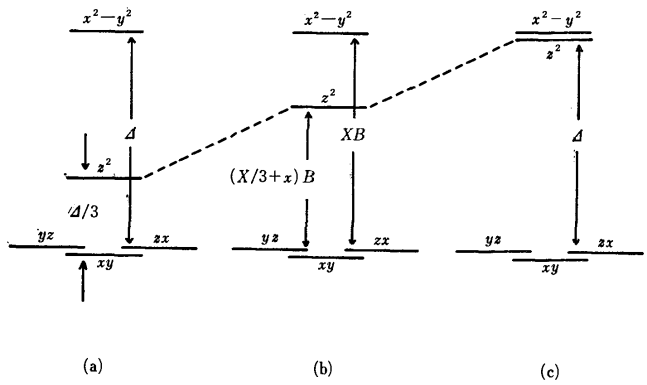

Fig. 8. Energy levels of the ligand-fielded d orbitals.
(a) planar configuration
(b) planar configuration+axial ligand field
(c) octahedral configuration

depend on the model employed. However, a simple argument in terms of molecular orbital theory can readily give the ordering of split d orbitals.[9] The ordering in a planar ligand field:

$$\varepsilon(x^2-y^2)=\Delta,\ \varepsilon(z^2)=\Delta/3,\ \varepsilon(xy)=\varepsilon(yz)=\varepsilon(zx)=0.$$

Δ is the ligand-field splitting parameter. For the sake of simplicity, the small energy difference between yz, zx, and xy orbitals is ignored. Energy difference between x^2-y^2 and z^2 orbitals is crucial. It varies with the axial ligand field. $\varepsilon(x^2-y^2)-\varepsilon(z^2)$ is $2\Delta/3$ for a planar configuration, while it vanishes for an octahedral configuration. $\varepsilon(z^2)$ is parametrized as $\Delta/3+xB$, where xB is an index of the axial ligand field strength in terms of Racah's parameter B. The energy values of d orbitals in iron porphin, in general, are given in B units as follows: $\varepsilon(x^2-y^2)=\Delta=XB$, $\varepsilon(z^2)=\Delta/3+xB=(X/3+x)B$, $\varepsilon(xy)=\varepsilon(yz)=\varepsilon(zx)=0$. The energy of the ground state of iron(II) porphin can be approximately given as a function of the ligand field strength XB, the axial ligand field strength xB and Racah's electrostatic interaction parameters B and C.

$$^1A_1 \quad E_0 - 30B + 15C$$

$$^3E \quad E_0 - 26B + 12C + \frac{2}{3}XB + \frac{1}{2}xB - \frac{B}{2}\sqrt{\frac{4}{9}X^2 + \frac{16}{3}X - \frac{4}{3}xX + x^2 - 8x + 64}$$

$$^5B_2 \quad E_0 - 35B + 7C + \frac{4}{3}XB + xB$$

where E_0 denotes a common term of spherical symmetry. Assuming an empirical relationship $C=4B$,[10] we have

$$^1A_1 - {}^5B_2 \quad \left(37 - \frac{4}{3}X - x\right)B$$

$$^3E - {}^5B_2 \quad \left(29 - \frac{2}{3}X - \frac{1}{2}x - \frac{1}{2}\sqrt{\frac{4}{9}X^2 + \frac{16}{3}X - \frac{4}{3}xX + x^2 - 8x + 64}\right)B$$

9) H. Yamatera, This Bulletin, **31**, 95 (1958).
10) Y. Tanabe and S. Sugano, *J. Phys. Soc. Jap.*, **9**, 766 (1954).

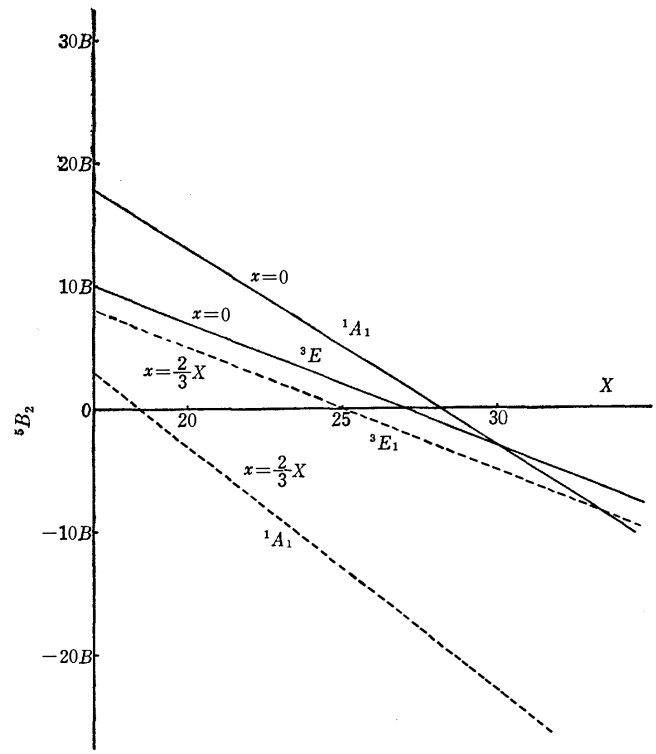

Fig. 9. Energy diagram as a function of the ligand field strength, X, and the axial ligand field strength, x.
----: $x=\frac{2}{3}X$ (octahedral configuration)
——: $x=0$ (planar configuration)

The energy diagram is readily drawn as a function of X and x and is shown in Fig. 9. $^1A_1$ and ^3E are stabilized to a greater extent than $^5B_2$ when X increases. With a fixed value of X, $^1A_1$ is more stabilized than ^3E when the axial ligand field x increases. Unless the axial field is fairly weak, the ground state could not be ^3E. B in iron(II) porphin is estimated to be about 800 cm^{-1} from spectroscopic data.[11] The value of Δ in porphin has been estimated to be 20,000—25,000 cm^{-1} by an extended Hückel molecular orbital calculation.[12] Thus X is in the region 25—31. The value of X predicts $^1A_1$ ground state for an octahedral environment, where $x=2/3X$ which is attained by strongly coordinating axial ligands. For an octahedral ligand field the intermediate spin state ^3E can not be the ground state. For a planar ligand field, where $x=0$, the ground state is $^5B_2$ if $X<27$ and ^1A if $X>30$. When $27<X<30$, the intermediate spin state ^3E is expected to be the ground state. As a matter of fact, the ground state of iron(II) phthalocyanine with no axial ligand is in the state of $S=1$.[13] The ground state of TPPFe(II), however, is in the state of $S=2$. The value of X in TPPFe(II) is smaller than that of iron(II) phthalocyanine. However, in the

11) J. S. Griffith, "The Theory of Transition-Metal Ions," Cambridge University Press (1961), p. 437.
12) M. Zerner, M. Gouterman, and H. Kobayashi, *Theoret. Chem. Acta*, **6**, 363 (1966).
13) B. W. Dale, R. J. P. Williams, C. E. Johnson, and T. L. Thorp, *J. Chem. Phys.*, **49**, 3441 (1968); B. W. Dale, R. J. P. Williams, P. R. Edwards, and C. E. Johnson, *J. ibid.*, **49**, 3445 (1968); C. G. Barraclough, R. L. Martin, S. Mitra, and R. C. Sherwood, *ibid.*, **53**, 1643 (1970).

presence of relatively weak axial ligands such as THF and dioxane, the ground state becomes ^3E. The ^3E ground state, in principle, is reached with a similar X value as in TPPFe(II) as long as the axial ligand field is low. However, a mechanism to enhance the value of X is expected to get the ^3E ground state of TPPFe(II) in THF or dioxane. An effective radius of the central iron in the $^5B_2$ state is rather large and the iron can not be in the central hole and is slightly out of the porphin plane. Once ^3E state or ^1A state is attained, however, the effective radius of the iron is reduced and the iron can be seated in the central hole of porphin. Thus the overlap integral of iron and nitrogen orbitals and the X value increase. The effective radius depends on the occupation number in $d_{x^2-y^2}$ orbital which partially accepts σ electron donated by four nitrogens of porphin. The geometrical change has been pointed out by means of X-ray studies.[4]

TPPMn(II)·2Py in the solid state shows the highest spin state (Table 1). The powder spectrum of TPPMn(II) obtained by the opal glass method was very close to that in benzene. This indicates no change of spin state involved in dissolution. The solution spectrum of TPPMn(II)·2Py in benzene is shown in Fig. 10. The absorption bands are assigned to pure (π, π^*) transitions as that of TPPZn(II).[14] The lowest (π, π^*) transitions are described as a 50–50

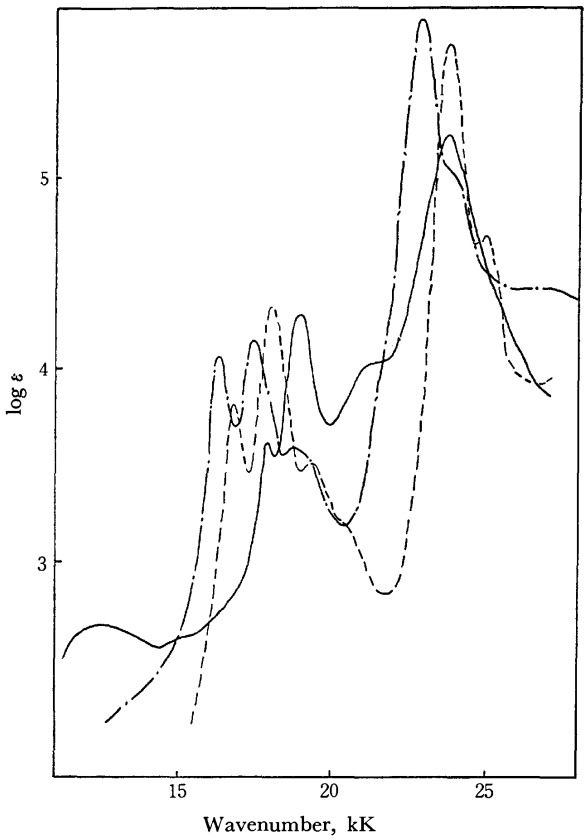

Fig. 10. Absorption spectrum of TPPMn(II)·2Py.
-·-·-: TPPMn(II)·2Py in benzene
——: TPPFe(II)·2Py in pyridine
----: TPPZn(II) in THF

admixture of transitions $2a_1 \rightarrow 4e$ and $3a_2 \rightarrow 4e$.[14-16] When the central metal ion has no appreciable π interaction with the conjugated system of porphin, the lowest excited states can be described by the four-orbital model.[14] When the four-orbital model is applicable, a gap between Q and B bands is fairly constant for a series of central metal ions. This can be seen in the spectra of TPPMn(II)·2Py and TPPZn(II) as shown in Fig. 10. If the central metal ion is replaced by a highly π-donating metal ion, the conjugated system of porphin in the ground and excited states should suffer π electron migration from the central metal ion. Although the absorption spectrum of diamagnetic TPPFe(II)·2Py apparently preserves a character of Q and B bands of a metal porphin less contributed by $d\pi$ electron, a gap between Q and B bands is remarkably smaller than those of TPPMn(II)·2Py and TPPZn(II). Since $d\pi$ ionization potential of the diamagnetic iron(II) in porphin is fairly low, the energy of the charge-transfer from metal $d\pi$ orbitals to the lowest antibonding ligand π orbitals is not so high. Both metal $d\pi$ orbitals zx and yz and the lowest antibonding porphin orbitals $4e$ are of E symmetry. Thus the "metal to ligand" charge-transfer states can mix with the ground state and the lowest exciting states of the π electron system of porphin. In the case of TPPFe(II)·2Py, weak absorption bands are observed in the near-infrared region. These weak bands might be assigned to "metal to porphin" and/or "metal to pyridine" charge-transfer transitions. However, the charge-transfer excited states and the Q and B excited states can not be very pure when their symmetries are the same and their energies are close. The lowest excited states representing the observed spectrum should be described in terms of a configuration interaction admixture of "metal to ligand" charge-transfer excited states and (π, π^*) excited state of porphin ring. As a result, lower charge-transfer states raise the Q state, and thus the gap of Q and B states are reduced. Another charge-transfer is possible from metal to axial ligand. When piperidine which lacks acceptable antibonding π molecular orbitals is used as the axial ligand, the possibility of the "metal to axial ligand" π charge-transfer can be eliminated. The spectrum of TPPFe(II) in piperidine still shows a contribution of charge-transfer states. The charge-transfer is ascribed to "iron to porphin." On the contrary, the spectrum of TPPFe(II) in pyridine gives an evidence of "iron to pyridine" charge-transfer transition at about 21 kK, whereas TPPFe(II) in piperidine lacks the absorption peak (Fig. 11).

Absorption spectrum of a coordination complex, in general, depends upon both the central metal and the ligands. In the case of metalloporphins, especially of iron porphins, the spectrum is predominantly influenced by the spin state of the central metal rather than particular axial ligands. The spin state of the central metal, however, depends upon the axial ligand

14) M. Gouterman, *J. Chem. Phys.*, **30**, 1139 (1959).
15) H. Kobayashi, *J. Chem. Phys.*, **30**, 1362 (1959).
16) C. Weiss, H. Kobayashi, and M. Gouterman, *J. Mol. Spectrosc.*, **16**, 415 (1965).

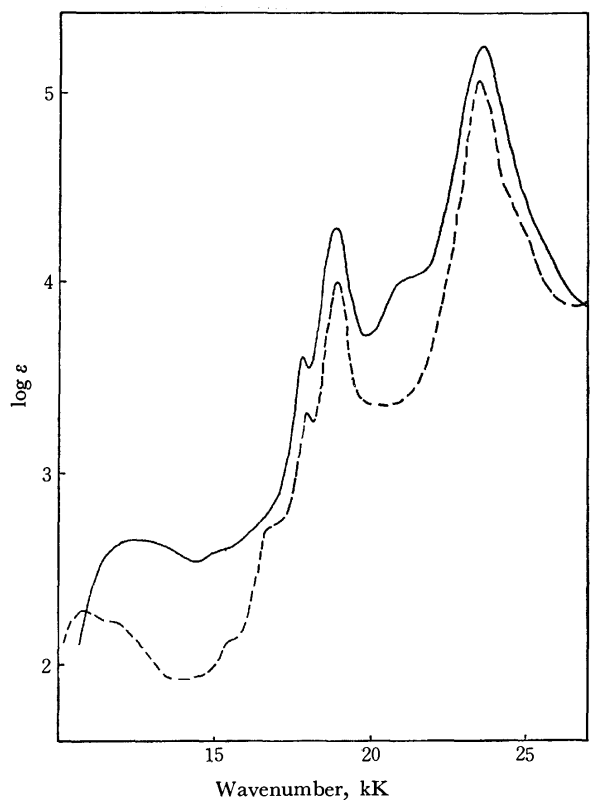

Fig. 11. Absorption spectra of TPPFe(II) in pyridine and piperidine.
——: pyridine solution
----: piperidine solution

field and the spectrum varies with the axial ligands only when the axial ligands can change the spin state of the central metal. It should depend on the properties of the low energy absorption bands of metalloporphin.

When an open shell exists in the central metal ion as in TPPFe(II), "metal to ligand" or "ligand to metal" charge-transfer excited states can mix not only with singlet (π, π^*) excited states but also with triplet (π, π^*) excited states. When a delocalization interaction between iron $d\pi$ orbitals and $4e$ orbitals of porphin is sufficient, such a configuration mixing becomes significant. The usual metalloporphins have two pairs of the spin forbidden singlet-triplet transitions in the near-infrared region.[15,16] The lowest triplet emits phosphorescence. The charge-transfer interaction between the open shell iron and the excited states of porphin will carry an appreciable amount of transition probability to these spin forbidden transitions from the allowed transitions. As a matter of fact, TPPFe(II) shows a rather complicated spectrum in the lower energy region. The near-infrared bands of high spin porphin TPPFe(II), and also intermediate spin porphin TPPFe(II)·2THF should be assigned mainly to weak "metal to porphin" charge-transfer transitions. However, a contribution of the porphin triplets in the near-infrared absorption bands of the open shell iron(II) porphins should be pointed out. Generally speaking, the spin selection rule of molecular electronic transitions is released when the molecule is connected with an open shell system by a charge-transfer process.[17] If the interaction is not so strong as in TPPMn(II)·2Py, it shows just a weak absorption shoulder at the position of the lowest singlet-triplet transition. In the case of the open shell iron(II) porphins, however, the charge-delocalization effect increases mainly due to higher $d\pi$-donating power of iron(II) and thus a configuration mixing of various excitations gives rise to a shift in transition energy and also a redistribution of spectral intensity.

The authors are grateful to Dr. Y. Kaizu for his technical advice in chemical preparations using the vacuum system. One of the authors (H. K.) wishes to express his thanks to Profs. M. Kotani and M. Gouterman for encouragement and helpful discussions.

17) J. N. Murrell, *Mol. Phys.*, **3**, 319 (1960).

The Reaction of Tris(acetylacetonato)cobalt(III) with Bromine in Dichloromethane

Yukio NAKAMURA, Mitsuru GOTANI, and Shinichi KAWAGUCHI
Department of Chemistry, Faculty of Science, Osaka City University, Sumiyoshi-ku, Osaka
(Received June 28, 1971)

Dibromo(acetylacetone)cobalt(II), a new complex containing an acetylacetone molecule as the bidentate ligand, was formed by the reaction of tris(acetylacetonato)cobalt(III) with bromine in dichloromethane, and characterized by elemental and thermogravimetric analyses and electronic and infrared spectra. The same compound was also prepared by direct addition of acetylacetone to anhydrous cobalt(II) bromide. The radical nature of the redox step involved in the reaction pathway from the starting cobalt(III) chelate to the product cobalt(II) complex of acetylacetone was demonstrated by polymerization of methyl methacrylate and styrene remarkably enhanced by the reaction system.

In previous papers we have reported reactions of bromine with several metal acetylacetonates. All metal chelates of this ligand examined so far reacted with bromine quickly in dichloromethane, but products differed depending on the nature of the central metal. In the case of bis(acetylacetonato)copper(II), for instance, the chelate ring was broken, giving γ-bromoacetylacetone and copper(I) bromide or copper(II) bromide according to the reactant mole ratio.[1] In contrast, beryllium and aluminum chelates were so stable as to be subjected to electrophilic ring substitution by bromine at the γ-position of the chelated acetylacetone.[2] Such a direct bromination by elemental bromine without the aid of any buffering mixture was known only for tris(acetylacetonato)-chromium,[3] and the quasiaromatic halogenation[4] of various metal acetylacetonates was effected by making use of *N*-halosuccinimides.[5]

When tris(acetylacetonato)cobalt(III) is allowed to react with excess bromine in dichloromethane, the chelate ring is broken producing cobalt(II) bromide and brominated acetylacetone ultimately. This paper reports the isolation and characterization of a novel cobalt(II) complex of molecular acetylacetone as an intermediary product, and presents some evidence for the radical nature of a redox step involved in the reaction.

Experimental

Materials. Tris(acetylacetonato)cobalt(III) was synthesized according to the standard method.[6] Found: Co, 16.47; C, 50.96; H, 6.22%. Calcd for $Co(C_5H_7O_2)_3$: Co, 16.54; C, 50.57; H, 5.94%. Commercial bromine and dichloromethane were purified by the usual methods.[1] Acetylacetone from Daicel, Ltd. was distilled under reduced pressure and dried with molecular sieves Type 4A8—12, Linde Co. Anhydrous cobalt(II) bromide was prepared by the dehydration of hexahydrate at 135—140°C and purified by sublimation *in vacuo*. Purified methyl methacrylate and styrene were obtained from Prof. Otsu's laboratory and used without further treatment.

Reaction of Tris(acetylacetonato)cobalt(III) with Bromine. The reaction of tris(acetylacetonato)cobalt(III) with bromine in dichloromethane was carried out in a three-necked flask equipped with a burette, a glass tube containing phosphorus pentaoxide, and another tube connected to a filtration equipment by means of a polyethylene tubing. To a chelate solution in the flask of the desired concentration in the range from 0.05 to 0.15 M, was added a bromine solution of the same concentration from the burette with vigorous stirring. The precipitate produced by the reaction was transferred *via* a polyethylene tubing to a vacuum filtration apparatus set up in a desiccator containing phosphorus pentaoxide to remove moisture.

Polymerization Experiments of Vinyl Monomers. When tris(acetylacetonato)cobalt(III) was allowed to react with equimolar bromine in dichloromethane at 0°C, no precipitate was formed. About 10 m*l* of the green solution was quickly transferred to an ampoule, which was then attached to a vacuum line and deaerated by repeated freezing and thawing cycles. Care was taken to keep the sample at temperatures below 0°C. A weighed quantity (about 5 m*l*) of a vinyl monomer was distilled into the ampoule *in vacuo*, which was then sealed off and kept in a thermostat at 35°C for 41 hr. An intermediary compound produced by the reaction between the cobalt(III) chelate and bromine at 0°C underwent further reactions upon heating, concurrently giving rise to the polymerization of a monomer. When the ampoule was opened and the reaction mixture poured into methanol, the cobalt(II) compound was dissolved and a white precipitate of polymer was obtained. This was filtered, washed with methanol and dried *in vacuo*. The polymer specimen for the infrared assay was purified by reprecipitation with benzene-methanol. As a reference the vinyl polymerization was pursued in a similar system including tris(acetylacetonato)cobalt(III) but excluding bromine.

Direct Synthesis of Dibromo(acetylacetone)cobalt(II). About 1 g of anhydrous cobalt(II) bromide was put into an ampoule quickly, evacuated for a while at about 135°C and kept in an ice bath. Into this ampoule about 40 m*l* of purified acetylacetone was distilled *in vacuo*. During the procedure the ice bath was removed occasionally and the reacting mixture was agitated magnetically by means of a small stirrer equipped in the ampoule to prevent aggregation and stimulate dissolution of cobalt(II) bromide. The mixture was then kept at room temperature with continuous stirring. A purple fuzzy product increased as green cobalt(II) bro-

1) Y. Nakamura and S. Kawaguchi, This Bulletin, **38**, 955 (1965); T. Ogura, Y. Kojima, Y. Nakamura, and S. Kawaguchi, *ibid.*, **38**, 1469 (1965).
2) Y. Nakamura and S. Kawaguchi, *ibid.*, **40**, 1179 (1967); Y. Nakamura, M. Hirata, and S. Kawaguchi, *ibid.*, **40**, 2572 (1967).
3) H. Reihlen, R. Illig, and R. Wittig, *Ber.*, **58B**, 12 (1925).
4) J. P. Collman, Advan. Chem. Ser., No. 37, p. 78 (1963).
5) R. W. Kluiber, *J. Amer. Chem. Soc.*, **82**, 4839 (1960); J. P. Collman, R. A. Moss, H. Maltz, and C. C. Heindel, *ibid.*, **83**, 531 (1961).
6) W. C. Fernelius (Ed.), "Inorganic Syntheses," Vol. 5, McGraw-Hill, New York (1957), p. 188.

mide diminished. One or two days were required before the complete disappearance of the latter. The precipitate was increased further by vacuum distillation of some quantity of acetylacetone, filtered and washed with petroleum ether in dry conditions. The product was first evacuated at room temperature. A specimen gave the analytical data: Found: Co, 13,77; Br, 37.84%, which are close to those Calcd for $CoBr_2(C_5H_8O_2)_2$: Co, 14.07; Br, 38.14%. However, the weight decreased gradually with prolonged evacuation. Thus it was finally evacuated at 60°C for about 5 hr to attain constant weight. The color turned from purple to light blue. The compound is very hygroscopic. Found; Co, 18.27; Br, 49.98; C, 19.32; H, 2.83%. Calcd for $CoBr_2$-$(C_5H_8O_2)$: Co, 18.48; Br, 50.12; C, 18.83; H, 2.53%. The purple substance might have contained another molecule of acetylacetone as a solvent of crystallization.

Analysis and Measurements. Solid products were dried *in vacuo* at room temperature and subjected to elemental analysis. Cobalt was determined gravimetrically as sulfate and bromine as silver bromide.

The infrared spectra of solid specimens were measured in Nujol by means of a Hitachi EPI-2 infrared spectrophotometer (4000—700 cm^{-1}) and a Hitachi EPI-L grating infrared spectrophotometer (700—200 cm^{-1}). The infrared spectra of polymers were taken as thin films. Absorption spectra of solutions were obtained using a Hitachi EPS-2 recording spectrophotometer. When the observation was performed at 0°C, ice water was circulated around the cell and dry air was forced to blow against the cell windows to prevent clouding. A solid specimen was ground with Nujol, placed between two plates of opal glass and its transmission spectrum was measured with a Hitachi EPU-2A photoelectric spectrophotometer.[7]

A thermo-spring balance C-282 of Hamada Denki Seisakusho, Ltd. was used for thermogravimetric analysis. The temperature of the sample was raised at a rate of 30°/hr *in vacuo*. The volatile decomposition product was collected in a trap cooled with dry ice and subjected to gas chromatographic analysis. A column of Apiezon Grease L carried on Neosorb NC (Nishio Industries Co., Ltd.) was employed at 59°C, on which hydrogen gas was passed at a flow rate of 72 cm/min. On the other hand the solid decomposition residue was fused together with potassium carbonate. Cobalt and bromine contents were determined gravimetrically.

Magnetic susceptibility was determined at room temperature by the Gouy method with an automatically recording magnetic balance (Naruse Kagakukikai Co., Ltd.). The sample was put into a tube (2 mm in diameter and 70 mm in length) quickly in a dry box. An aqueous solution of nickel(II) chloride was used as a reference.

Results

If tris(acetylacetonato)cobalt(III) is allowed to react with an equimolar quantity of bromine in dichloromethane at 0°C, no precipitate is formed and the dark green solution is quite stable as long as it is kept at 0°C. As shown in Fig. 1 the visible absorption spectrum of this solution is similar to that of the starting complex, suggesting that the intermediary species involved is a cobalt(III) compound. The solution was concentrated by vacuum evaporation at 0°C to isolate a light blue precipitate. The same precipitate

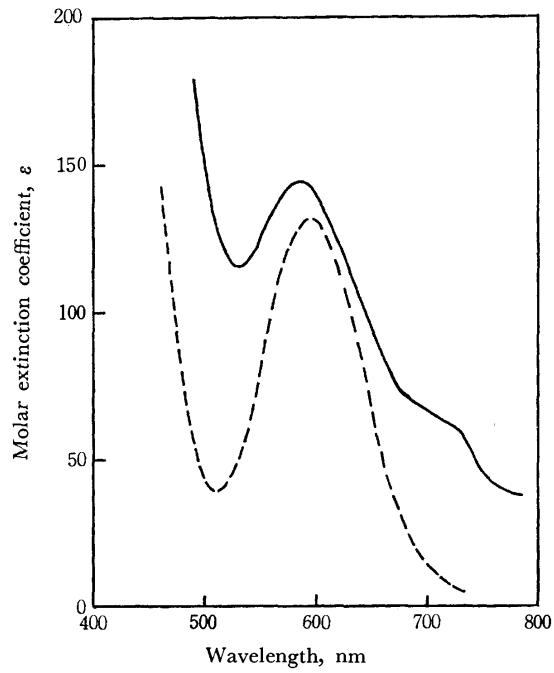

Fig. 1. Absorption spectra in dichloromethane of tris(acetylacetonato)cobalt(III) (----) and a reaction mixture of the chelate and bromine in the mole ratio of 1:1 at 0°C (——).

was also formed by the addition of petroleum ether. However, the solid thus obtained was no longer soluble in dichloromethane, indicating that this is a different compound from the desired soluble intermediate. Elemental analysis disclosed that the secondary product is a cobalt(II) complex of molecular acetylacetone.[8] Found: Co, 18.96; Br, 50.03; C, 18.24; H, 2.60%.

The infrared spectrum of the new complex $CoBr_2$-(acacH) in Fig. 2 shows a characteristic carbonyl band at 1705 cm^{-1} together with a shoulder at 1720 cm^{-1}, coinciding with those observed at 1707 and 1727 cm^{-1} for ketonic molecules of acetylacetone (Table 1).[9] No absorption bands assignable to enolic molecules or chelated enolate anions are observed. The Co–O stretching absorption at 375 cm^{-1} is lower than 422 cm^{-1} of that in $Co(acac)_2$,[10] reflecting weakness of the Co–O bond in the present complex compared to that in the usual enolate chelate. The spectral data reveal unequivocally that a ketonic molecule of acetylacetone is coordinated to the cobalt atom.

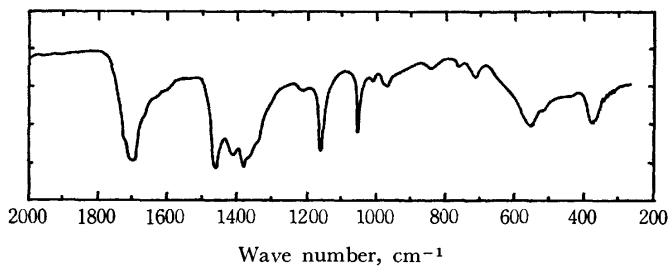

Fig. 2. An infrared spectrum of $CoBr_2$(acacH) in Nujol mull.

7) K. Shibata, "Methods of Biochemical Analysis," Vol. 7, ed. by D. Glick, Interscience, New York (1959), p. 77.

8) A preliminary account of this compound appeared in Y. Nakamura and S. Kawaguchi, *Chem. Commun.*, **1968**, 716.

9) R, Mecke and E. Funck, *Z. Elektrochem.*, **60**, 1124 (1956).

Table 1. IR data in the carbonyl stretching region (cm^{-1})

$CoBr_2(acacH)$	$Co(acac)_2$	$CH_3\,CH_2\,CH_3$ (C=O, C=O)	$CH_3\,CH\,CH_3$ (C=O, C=O, H)
1720 (sh)	—	1727[a]	—
1705	—	1707	—
—	1601	—	1619[a]

a) From ref. 9

The magnetic measurement gave a value of 4.25 B.M. as the effective magnetic moment, indicating the tetrahedral structure[11a] of this cobalt(II) compound.

Since the compound is not soluble in the usual non-coordinating solvents, the absorption spectrum was observed in acetylacetone. The transmission spectrum of a solid specimen was also measured by the Nujol mull method and confirmed to be similar to that in an acetylacetone solution. As depicted in Fig. 3 the absorption curve resembles that observed for $CoBr_2(acetone)_2$ which is considered to assume a tetrahedral structure.[11]

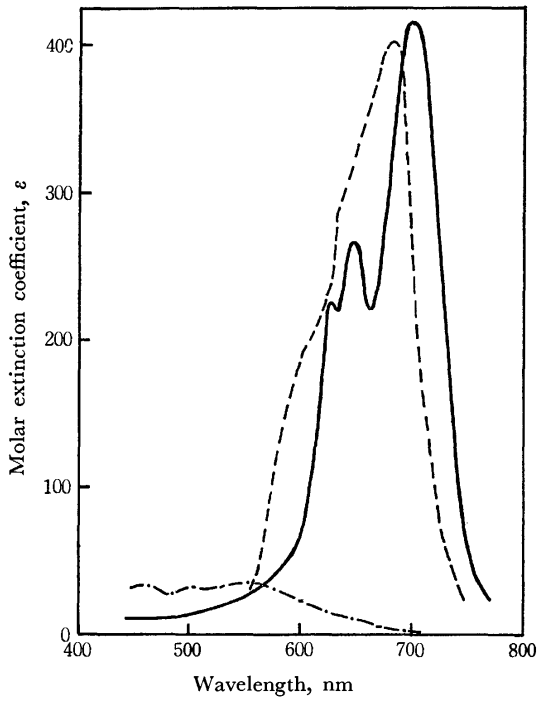

Fig. 3. Absorption spectra of $CoBr_2(acacH)$ in acetylacetone (——), $CoBr_2$ in acetone (----), and $Co(acac)_2$ in dichloromethane (—·—).

In accordance with the supposition that the linkage of acetylacetone to cobalt is weak, the compound begins to decompose at around 70°C. This should be compared with the behavior of bis(acetylacetonato)-cobalt(II), which is quite stable and easily sublimes *in vacuo*. As illustrated in Fig. 4 the weight decrease

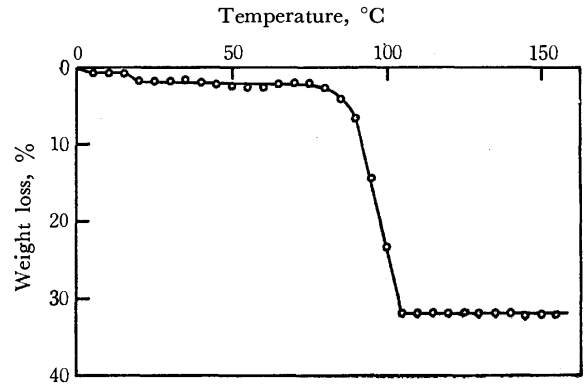

Fig. 4. Thermogravimetric analysis of $CoBr_2(acacH)$. Heating rate: 30°C/hr.

amounts to 30% which coincides with the value 31% calculated for the loss of acetylacetone. The evaporated substance was collected in a trap cooled with dry ice and identified to be acetylacetone by gas chromatography, while the decomposition residue was characterized to be cobalt(II) bromide by elemental analysis (Found: Co, 27.43; Br, 70.54%).

The new complex $CoBr_2(acacH)$ was also prepared by the direct addition reaction of acetylacetone to anhydrous cobalt(II) bromide (see Experimental). Data of the elemental analysis and infrared spectra showed a good coincidence.

When more than 1 mol of bromine was added to 1 mol of tris(acetylacetonato)cobalt(III) in dichloromethane at 0°C, a light blue precipitate appeared. The precipitate produced by the reaction in the reactant mole ratio of 2 : 1 showed an infrared spectrum closely resembling that of $CoBr_2(acacH)$, but gave analytical data showing contamination with cobalt(II) bromide and water. Found: Co, 19.06; Br, 50.64; C, 15.88; H, 2.65; H_2O (Karl Fischer method), 2.82%. Calcd for a mixture $[CoBr_2(acacH)+0.22CoBr_2+0.59H_2O]$: Co, 19.04; Br, 51.63; C, 15.90; H, 2.45; H_2O, 2.82%. Part of the bromine molecules seem to have attacked $CoBr_2(acacH)$, brominating coordinated acetylacetone and liberating cobalt(II) bromide, although the reaction between bromine and a soluble cobalt(III) intermediate occurred predominantly. When a dichloromethane solution of bromine was added dropwise to a dichloromethane solution of tris(acetylacetonato)cobalt(III) at room temperature, a light blue precipitate appeared from the beginning, the amount of which increased with bromine addition. The precipitate was also a mixture of $CoBr_2(acacH)$ and $CoBr_2$. The reaction pattern at room temperature does not differ essentially from that at 0°C, but the reactivity of the cobalt(III) intermediate observed at 0°C (Fig. 1) is much increased at higher temperatures.

A redox process is involved in the conversion of the soluble cobalt(III) intermediate into $CoBr_2(acacH)$. To ascertain the possible radical nature of this redox process, polymerization reactions of methyl methacrylate and styrene were examined in the system. Tris(acetylacetonato)cobalt(III) is known to initiate

10) K. Nakamoto, P. J. McCarthy, and A. E. Martell, *J. Amer. Chem. Soc.*, **83**, 1272 (1961).

11) a) R. L. Carlin, "Transition Metal Chemistry," Vol. 1, Marcel Dekker, New York (1965), p. 1; b) D. A. Fine, *J. Amer. Chem. Soc.*, **84**, 1139 (1962).

TABLE 2. RESULTS OF POLYMERIZATION OF METHYL METHACRYLATE AND STYRENE INITIATED BY $Co(acac)_3$ AND THE $Co(acac)_3$-Br_2 SYSTEM (35°C, 41 hr IN DICHLOROMETHANE)

Monomer	$[Co(acac)_3]$, M	Polymer yield, %	
		$Co(acac)_3$ only	$Co(acac)_3$ + Br_2
MMA	3.41×10^{-2}	2.22	27.6
Styrene	4.11×10^{-2}	0.28	7.7

the radical polymerization of the vinyl monomers,[12,13] but the efficiency is rather low under the present reaction conditions, as shown in Table 2. In contrast the $Co(acac)_3$–Br_2 system exhibits a remarkable initiating ability for vinyl polymerization, revealing that some initiating radicals are formed when the cobalt(III) intermediate is warmed.

The difference in the polymer yield (Table 2) observed for the two monomers reflects the difference in the nature of the monomer. Methyl methacrylate is known to be much more reactive than styrene towards free radicals. The infrared spectrum of a polystyrene film showed a weak but definite absorption peak of the carbonyl group at around 1700 cm^{-1}. This is considered to be due to the acetylacetone radical or its fragment attached to the polymer end. A similar observation was also reported by Otsu, Minamii, and Nishikawa[13] on polystyrene which was prepared employing tris(acetylacetonato)manganese(III) as an initiator. The infrared spectrum of poly(methyl-methacrylate) obtained closely resembles those of polymers prepared by virtue of typical radical initiators such as benzoyl peroxide and azobisisobutyronitrile, but the carbonyl bands due to the acetylacetone group can not be discriminated because of a strong absorption by the ester group.

Discussion

Although the starting material was a cobalt(III) complex, the isolated stable products were cobalt(II) compounds. The reaction step in which cobalt(III) was reduced is not clear enough, but the solution resulting from the addition of equimolar bromine to tris(acetylacetonato)cobalt(III) in dichloromethane at 0°C gave an absorption curve similar to that of the original chelate as shown in Fig. 1, indicating that the first soluble intermediate is an octahedral cobalt(III) complex. Attempts to isolate this compound as a pure solid were unsuccessful, but it could be supposed that a binuclear cobalt(III) complex (A) was formed by the reaction represented by Eq. (1). Either bromine atoms or acetylacetone groups are able to function as bridging ligands.

$$Co(acac)_3 + Br_2 \rightarrow 1/2\,[CoBr(acac)_2]_2 + acacBr \quad (1)$$
(A)

12) E. G. Kastning, H. Naarmann, H. Reis, and C. Berding, *Angew. Chem.*, **77**, 313 (1965).

13) T. Otsu, N. Minamii, and Y. Nishikawa, *J. Macromol. Sci.-Chem.*, **A2**, 905 (1968).

TABLE 3. VISIBLE ABSORPTION MAXIMUM OF THE REACTION MIXTURE OF TRIS(ACETYLACETONATO)COBALT(III) AND BROMINE (1:1) TOGETHER WITH THOSE OF RELATED COMPLEXES[a]

	λ_{max}	log ε
Reaction mixture in CH_2Cl_2 at 0°C	585	2.16
cis-$[Co(acac)_2(NH_3)_2]Cl$ in H_2O	546	2.12
$[Co(acac)_2en]ClO_4$ in H_2O	538	2.20
cis-$[Co(acac)_2py_2]ClO_4$ in CH_3OH	534	1.94
$[Co(acac)_2bipy]ClO_4$ in CH_3OH	553	2.19

a) R. D. Archer and B. P. Cotsoradis, *Inorg. Chem.*, **4**, 1584 (1965).

Visible absorption bands of several related compounds are shown in Table 3. The absorption maximum of the present solution lies on the longer wavelength side corresponding to the weak field of bromine in comparison with other ligands in Table 3. The value of molar absorptivity, however, is similar to values of the related compounds.

The binuclear intermediate (A) changed to the cobalt(II) compound, $CoBr_2(acacH)$ by addition of petroleum ether, concentration at 0°C, or warming to room temperature. We imagine that disproportionation of the intermediate (A) as expressed by Eq. (2) occurred spontaneously, followed by the redox process (3).

$$[CoBr(acac)_2]_2 \rightarrow [CoBr_2(acac)] + Co(acac)_3 \quad (2)$$
(B)

$$[CoBr_2(acac)] + RH \rightarrow CoBr_2(acacH) + R\cdot \quad (3)$$

Here the intermediate (B) is an imaginary compound. Either a solvent molecule or γ-bromoacetylacetone might play the role of the hydrogen donor RH. Similarly the reaction of the intermediate (A) with bromine to produce the ketonic complex will be represented by the following equation followed by (3).

$$1/2\,[CoBr(acac)_2]_2 + Br_2 \rightarrow [CoBr_2(acac)] + acacBr \quad (4)$$

In one experiment 7.14 mmol of tris(acetylacetonato)cobalt(III) was allowed to react with an equimolar quantity of bromine in dichloromethane at room temperature. After 20 hr 2.97 mmol of $CoBr_2(acacH)$ was isolated. If the overall reaction be reproduced by Eqs. (1), (2) and (3) 2.97 mmol of $Co(acac)_3$ and $7.14-2\times2.97=1.2$ mmol (in the monomer basis) of the dimeric intermediate (A) must be contained in the filtrate. The absorption curve of the solution was calculated on this basis by making use of the spectral data as presented in Fig. 1, and found to nearly coincide with the observed one. This supports the proposed scheme (1) through (3).

If a vinyl monomer is mixed with the intermediate (A) in dichloromethane and warmed to higher temperatures, a monomer molecule (M) may take an acetylacetone radical away from (B) liberating cobalt(II) bromide.

$$CoBr_2(acac) + M \rightarrow CoBr_2 + (CH_3CO)_2CHM\cdot \quad (5)$$

Alternatively the intermediate (B) might abstract a hydrogen atom predominantly from γ-bromoacetylacetone, the radical produced initiating polymeri-

zation in turn.

Molecular adducts of acetylacetone with antimony(V) and titanium(IV) chlorides were prepared by Rosenheim, *et al.*[14] in 1903, but the bonding nature was not confirmed. The mercury(II) chloride complex $HgCl_2(acacH)$ was studied by Paoloni[15] in detail, and it was concluded on the basis of the carbonyl stretching band at 1698 cm^{-1} that a ketonic molecule of acetylacetone was coordinated to the mercury atom with two carbonyl oxygen atoms. The present complex $CoBr_2(acacH)$ as well as similar nickel(II) complexes reported by van Leeuwen,[16] $[Ni(acacH)_3](ClO_4)_2$, $[Ni(acacH)_2(AcOH)_2](ClO_4)_2$, and $[Ni(acacH)_2(H_2O)_2](ClO_4)_2$, also contain ketonic molecules of acetylacetone.

In contrast, the acetylacetone adduct of dioxobis(acetylacetonato)uranium(VI) was concluded to involve an enolic molecule of acetylacetone as a unidentate ligand on the basis of IR and NMR data.[17] More recently the same bonding nature was established by X-ray analysis of dibromobis(acetylacetone)manganese(II).[18] It is very interesting that two tautomeric forms of acetylacetone can exist in metal complexes, but factors for preference of one form over the other are not clear. More examples are wanted.

The authors thank Dr. S. Kawai of Osaka University for the magnetic measurement, and Mr. J. Gohda for the elemental analyses. They are also grateful to Professor T. Otsu and Dr. S. Aoki for the supply of purified vinyl monomers, and to Daicel Co., Ltd. for the gift of acetylacetone. Aknowledgement is made to the Ministry of Education for financial support.

14) A. Rosenheim, W. Loewenstamm, and L. Singer, *Ber.*, **36**, 1833 (1903).
15) L. Paoloni, *Gazz. Chim. Ital.*, **89**, 2171 (1959).
16) P. W. N. M. van Leeuwen, *Rec. Trav. Chim. Pay-Bas*, **87**, 396 (1968).
17) J. M. Haigh and D. A. Thornton, *Inorg. Nucl. Chem. Letters*, **6**, 231 (1970).
18) S. Koda, S. Ooi, H. Kuroya, Y. Nakamura, and S. Kawaguchi, *Chem. Commun.*, **1971**, 280.

BULLETIN OF THE CHEMICAL SOCIETY OF JAPAN, VOL. 45, 461—465 (1972)

Magnetic Moments and Electronic Spectra of Low-spin Cobalt(II) Complexes

Yuzo NISHIDA and Sigeo KIDA
Department of Chemistry, Faculty of Science, Kyushu University, Hakozaki, Fukuoka, Japan

(Received June 30, 1971)

Comprehensive elucidation of optical and magnetic properties of low-spin cobalt(II) complexes of various types has been attempted. The g-values and magnetic susceptibilities of the complexes have been calculated, the necessary numerical data being obtained from the spectral data and reasonable assumptions. Fairly good agreement has been obtained between the calculated and experimental values.

As is known, values of magnetic moments of low-spin cobalt(II) complexes fluctuate in a wide range (1.9~2.8 BM., see Table I)[1] higher than the spin-only value (1.73 BM.) for one unpaired electron. High magnetic moments compared to the spin-only value have been attributed to the orbital contribution to the ground state.[2] Theoretical approach to the elucidation of the magnetic properties of phthallocyanine cobalt(II) was reported by Griffith.[3] Recently Martin and Mitra[4] carried out cryomagnetic measurements of the single crystal of the same compound, and were successful in explaining the magnetic anisotropy of the crystal in terms of the ligand field theory. However, such studies were restricted to a few specific compounds, and no comprehensive elucidation of the large variation of the orbital contribution in low-spin cobalt(II) complexes has been given. In order to achieve this, it is necessary to discuss optical spectra and magnetic properties simultaneously, since the orbital contribution is mainly due to mixing of higher ligand-field terms into the ground term through spin-orbit coupling. The theoretical interpretation of electronic spectra of low-spin cobalt(II) complexes does not seem to be satisfactory. In the present study, therefore, we have attempted to elucidate the magnetic and optical properties of various types of low-spin cobalt(II) complexes in terms of ligand field theory.

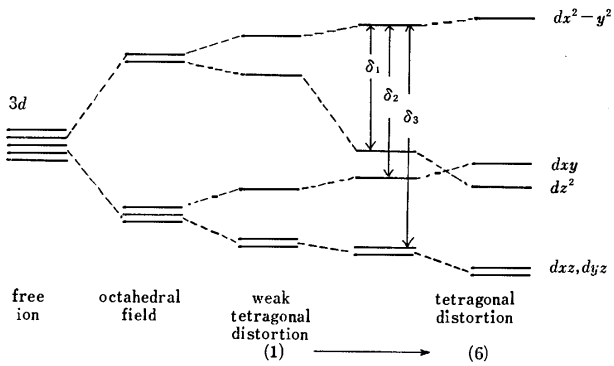

Fig. 1. Assumed *d*-orbital splitting for tetragonal distortion.

1) B. N. Figgis and R. S. Nyholm, *J. Chem. Soc.*, **1954**, 12.
2) B. N. Figgis, "Introduction to the Ligand Field" John Wiley & Sons, New York, (1964), p. 318.
3) J. S. Griffith, *Disc. Faraday Soc.*, **26**, 81 (1958).
4) R. L. Martin and S. Mitra, *Chem. Phys. Letters*, **3**, 183 (1969).

Table 1. The magnetic moment of the low-spin cobalt(II) complexes

	Complex	Coordination number	$\mu_{eff.}$(r. t.)
(1)	$[Co(NO_2)_6]^{4-}$	6	1.88[20]
(2)	$[Co\ diars_3](ClO_4)_2$[a]	6	1.92[21]
(3)	$[Co\ BrAP_2]ClO_4$[b]	5	2.18[19]
(4)	$[Co\ en_2](AgI_2)_2$[d]	4	2.46[5]
(5)	[Co pc][e]	4	2.72[14]
(6)	[Co sals][c]	4	2.30

a) diars=diarsine
b) AP=Diphenyl(*o*-diphenylarsinophenyl)phosphine
c) sals=Bis(salicylaldehyde)-meso-stilbenediimine
d) en=ethylenediamine
e) pc=phthallocyanine

Some spectral and magnetic measurements were carried out to obtain numerical data necessary for the calculations.

Experimental

$[Co\ en_2](AgI_2)_2$ and [Co sals] were prepared by the methods of Lever, Lewis and Nyholm[5], and Nishikawa and Yamada,[6] respectively, where sals represents bis(Salicylaldehyde)stilbenediimine.

The ESR spectra of polycrystalline sample of $[Co\ en_2](AgI_2)_2$ were measured with a JEOL ESR-apparatus model JES-ME-3X at room temperature using an X-band. Manganese(II) doped in MgO powder was used as a standard marker.

The reflection spectra of $[Co\ en_2](AgI_2)_2$ and [Co sals] were measured with a Shimadzu Multipurpose Spectrophotometer model MPS-50L at room temperature.

The magnetic moment of [Co sals] was determined by the Gouy method at room temperature.

The Theoretical Basis for Calculation

Generally, low-spin cobalt(II) complexes are under the effect of the Jahn-Teller distortion to form complexes of axial symmetry changing from a slightly distorted octahedron to a square-planar configuration. The axial symmetry being assumed, the qualitative one-electron energy diagram as shown in Fig. 1 may be drawn from the energy level splitting of copper(II) complexes of similar geometry.[7,8] The qualitative energy-level splitting for the $3d^7$ system of D_{4h} symmetry can be described as the functions of energy differences between *d*-orbitals, δ_1, δ_2 and δ_3 (Fig. 1) and of Slater-Condon parameters, F_2 and F_4, according to the strong field approximation scheme for the d^3 configuration[9] (see Table 11 and Fig. 4). When F_2 and F_4 are estimated as usual at 1000~1200 cm^{-1} and 90~100 cm^{-1}, respectively.[10,11] The relative energy levels of the states might be as given in Fig. 4.

As a result of the above consideration, the case in which an unpaired electron lies in d_{z^2} orbital appears to be most probable for the ground state.[12] Thus, the ground state ($S=1/2$) can be represented by

$$\Psi_{z^2}{}^{+} = |(x^2-y^2)^{+}(x^2-y^2)^{-}(z^2)^{+}|$$
$$\Psi_{z^2}{}^{-} = |(x^2-y^2)^{+}(x^2-y^2)^{-}(z^2)^{-}|.$$

The spin-orbit interaction gives rise to the mixing of some Russell Saunders states. Following the perturbation theory, the ground state is written as

$$\Psi_0{}^{+} = N\left(\Psi_{z^2}{}^{+} + \sum_i \frac{\langle\Psi_i|\zeta\kappa\boldsymbol{L}\boldsymbol{S}|\Psi_{z^2}{}^{+}\rangle}{\Delta E}\Psi_i\right), \quad (1)$$

where N, ζ, and κ represent normalization constant, one-electron spin-orbit coupling constant for 3d orbitals and the orbital reduction factor, respectively, and $\Psi_0{}^{+}$, $\Psi_{z^2}{}^{+}$, Ψ_i are the wave functions of the perturbed ground state, unperturbed ground state, and the excited states respectively. The *g*-values can be calculated according to the equations,

$$g_{\parallel} = 2\langle\Psi_0{}^{+}|\kappa\boldsymbol{L}_z+2\boldsymbol{S}_z|\Psi_0{}^{+}\rangle$$
$$g_{\perp} = 2\langle\Psi_0{}^{+}|\kappa\boldsymbol{L}_x+2\boldsymbol{S}_x|\Psi_0{}^{-}\rangle. \quad (2)$$

Neglecting the second order terms we finally obtain the results.

$$g_{\parallel} = 2N,$$
$$g_{\perp} = N\left(2-\frac{6\kappa^2}{\Delta_1}\right), \quad (3)$$

where Δ_1 is the energy difference between the states $|(x^2-y^2)^{+}(x^2-y^2)^{-}(z^2)^{+}|$ and $|(x^2-y^2)^{+}(x^2-y^2)^{-}(xy)^{+}|$.

According to Van Vleck's theory,[13,14] and assuming a metal complex where the separation between the levels of the ground term is small compared to kT, and the next excited level has an energy large compared to kT (we believe that this is true for the low spin cobalt(II) complexes), the magnetic susceptibility is found to be given by

$$\chi_i = \frac{N\beta^2 g_i^2}{3kT}S(S+1) + N\alpha_i \quad (i=x, y, z), \quad (4)$$

where N and k denote the Avogadro number and the Boltzmann constant, respectively, and Na_i is the temperature-independent term of the susceptibility which is often called the high-frequency term of the susceptibility. α_i can be calculated by the equation

5) A. B. P. Lever, J. Lewis, and R. S. Nyholm, *J. Chem. Soc.*, **1963**, 2552.
6) H. Nishikawa and S. Yamada, This Bulletin, **37**, 8 (1964).
7) Y. Nishida and S. Kida, This Bulletin, **43**, 3814 (1970).
8) B. J. Hathaway and D. E. Billing, *Coord. Chem. Rev.*, **5**, 143 (1970).
9) C. J. Ballhausen, "Introduction to Ligand Field Theory," McGraw-Hill, New York, (1962), pp. 57—97.
10) C. J. Ballhausen and A. D. Lieher, *J. Am. Chem. Soc.*, **81**, 538 (1958).
11) H. Kamimura, S. Sugano, and Y. Tanabe, "Ligand Field Theory and its Application" (in Japanese) Shokabo, Tokyo, (1970), p. 222.
12) Other possibilities for the ground state are where an unpaired electron is (1) in d_{xy} orbital and (2) in d_{xz} (or d_{yz}) orbital. these cases, we could give equations corresponding to equations (2) and (3) on the basis of the same principle. However, it has been found in many compounds that the calculation according to these equation gives results considerably deviating from experimental values, as long as we have assumed reasonable values for the energies of excited states, in contrast to the nice agreement when an unpaired electron is assumed to lie in d_{z^2} orbital.
13) C. J. Ballhausen "Introduction to Ligand Field Theory," MaGraw-Hill, New York, (1962), pp. 139—141.
14) J. H. Van Vleck, "The Theory of Electric and Magnetic Susceptibilities," Oxford University Press, Oxford (1932).

$$\alpha_i = 2\sum_{n,m}\frac{\{\langle\Psi_{0,m}|\beta(\boldsymbol{L}_i+2\boldsymbol{S}_i)|\Psi_{n,m}\rangle\}^2}{j_m(E_0-E_n)}$$

where n and m specify the electronic excited states and the magnetic sub-levels, respectively, and j_m and E_0 are the multiplicity and the energy of the ground state.

In the case of low-spin cobalt(II) complexes, the integrals in equation (5) can be evaluated on the assumption of the energy-level splitting similar to that shown in Fig. 4. Thus we obtain

$$\alpha_z = \alpha_\parallel = \frac{16}{\Delta_3}\beta^2, \tag{6}$$

$$\alpha_x = \alpha_y = \alpha_\perp = \frac{4}{\Delta_2}\beta^2 + \frac{6}{\Delta_1}\beta^2. \tag{7}$$

By combining (4), (6), and (7), we find that χ is expressed by

$$\chi = \frac{N\beta^2}{12kT}(g_\parallel{}^2+2g_\perp{}^2) + \frac{N\beta^2}{3}\left(\frac{12}{\Delta_1}+\frac{8}{\Delta_2}+\frac{16}{\Delta_3}\right), \tag{8}$$

where Δ_1, Δ_2, and Δ_3 are the energy differences between the states $^2A_{1g}$ and ^2E_g, $^2A_{1g}$ and $^2E_g'$, and $^2A_{1g}$ and $^2A_{2g}$, respectively (see Fig. 4 and Table II).

Results and Discussion

Phthalocyanine cobalt(II): The magnetic moment of this complex was reported to be 2.72 BM. at room temperature and 2.22 BM. at 90°K.[15] It is known that this compound has a square-planar structure,[16] and $g_\parallel$ and $g_\perp$ were determined by ESR study[17] to be 1.92 and 2.92, respectively. Substituting the experimental g- and ζ-values ($\zeta=-515\ \mathrm{cm}^{-1}$) into equations (2) and (3), and assuming $k^2=0.8$ as usual,[18] we obtain $\Delta_1 = 2373\ \mathrm{cm}^{-1}\approx 2.4$ kK, which seems to be a reasonable value for the separation of the states $^2A_{1g}$ and ^2E_g.

We can now calculate the low frequency term of equation (8),

$$\chi_l = \frac{N\beta^2}{12kT}(g_\parallel{}^2+2g_\perp{}^2) \approx \frac{N\beta^2}{12kT}\times 20.74. \tag{9}$$

If we neglect the high frequency term of equation (8), the magnetic moment μ would be given by

$$\mu = \sqrt{\frac{3kT}{N\beta^2}\chi_l} = 2.28\ BM.$$

The result is not satisfactory when compared with the experimental value 2.72 BM. Thus, it is evident that we can not neglect the high-frequency term of equation (8). Since it is difficult in this case to estimate the energy differences experimentally, we estimate[19] the probable values of Δ_2 and Δ_3 both at 15 kK on the basis of the estimated energy diagram for a planar Co(II) complex in Fig. 4 (Δ_1 was already estimated at 2.4 kK). Then, we obtain

$$\chi = \frac{20.74N\beta^2}{4kT} + 2.20N\beta^2\times 10^{-3}.$$

This leads to the results

$$\mu_{300°K} = 2.56\ BM$$

$$\mu_{90°K} = 2.37\ \mathrm{BM},$$

which show a fairly good agreement with experimental values.

From this result we may conclude that the remarkably high magnetic moment of the phthalocyaninecobalt(II) relative to the spin-only value is attributable to the orbital contribution through spin-orbit coupling and also to the so called Van Vleck's high frequency term. This conclusion agrees with the result of the recent cryomagnetic measurements by Martin and Mitra.[4] It should be noted that our final formulation for χ_i with the assumption of the above numerical values is essentially the same as that of Martin and Mitra[4], their formulation giving a successful explanation for their results which show that the relation $\mu_\perp > \mu_\parallel$ and $\mu_\parallel$ is nearly independent of temperature whereas $\mu_\perp$ decreases considerably with the lowering of temperature.

Bis(ethylenediamine)cobalt(II)diiodo argentate(I) $[\mathrm{Co\ en_2}](\mathrm{AgI_2})_2$: This compound is known to have the magnetic moment of 2.46 BM[5] and the structure of its cation is thus expected to be square planar. We have measured the optical and the ESR spectra. The results are shown in Figs. 2 and 3. From the latter g-values were obtained to be as follows according to the usual method for the case of $S=1/2$.

$$g_\parallel = 2.00 \text{ and } g_\perp = 2.58. \tag{11}$$

Assuming the energy level splitting similar to that of Fig. 4, we may tentatively assign the bands observed at 7.2 kK and at about 21 kK to the transitions $^2A_{1g}\rightarrow{}^2B_{2g}$ and $^2A_{1g}\rightarrow{}^2E_g'$ (Δ_2) respectively. The transition $^2A_{1g}\rightarrow{}^2E_g$ (Δ_1) can then be estimated at 4~5 kK. The same g-values as the experimental ones (11) were obtained by the calculation according to equation (3) with $\Delta_1 = 4.8$.

Thus we can calculate the susceptibility by use of equation (8), substituting 4.8, 20, and 20 kK into Δ_1, Δ_2, and Δ_3, we get

$$\chi = \frac{0.54}{T} + 320\times 10^{-6}.$$

Hence

$$\mu_{300°K} = 2.26\ \mathrm{BM}\ (\text{exp. } 2.46\ \mathrm{BM}).$$

This is a fairly satisfactory results, considering the degree of the present approximation.

Bis(salicylaldehyde)stilbenediiminatocobalt(II) [Co sals]: Among the derivatives of so-called "Salcomine type" complexes, this compound seems to be the most suitable for the purpose of the present study, since it is known to be unreactive with atmospheric oxygen,[6] and accessible with the usual techniques of optical and magnetic measurements.

15) R. L. Carlin, "Transition Metal Chemistry," ed. by R. L. Carlin, Vol. I, Marcell Decker, New York, (1965), pp. 1—32.

16) A. B. P. Lever, "Advances in Inorganic Chemistry and Radiochemistry," ed. by H. J. Emeleus and A. G. Sharpe, Vol. 7, pp. 27—114.

17) J. F. Gibson, D. J. E. Ingram, and D. Shonland, *Discuss. Faraday Soc.*, **26**, 72 (1958).

18) B. N. Figgis, "Introduction to the Ligand Field", John Wiley & Sons, New York, (1964), pp. 278—291.

19) Since Δ_2 and Δ_3 are much larger than Δ_1, the high-frequency term of (8) will be only sensitive to Δ_1 as readily seen from Eq. (8). Thus, a rough estimation of the values of Δ_2 and Δ_3 is enough for the present purpose.

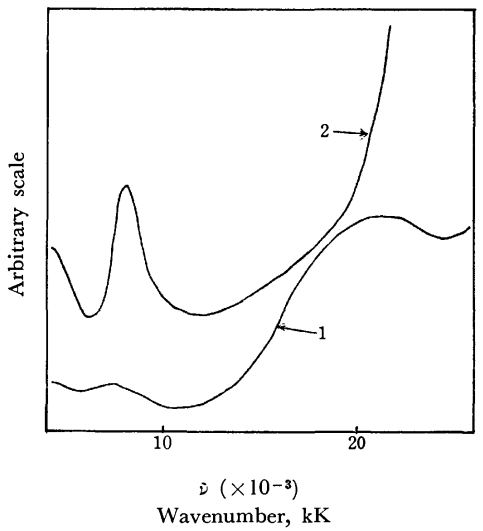

Fig. 2. Reflection spectra of
1—[Co en$_2$](AgI$_2$)$_2$
2 - [Co sals]

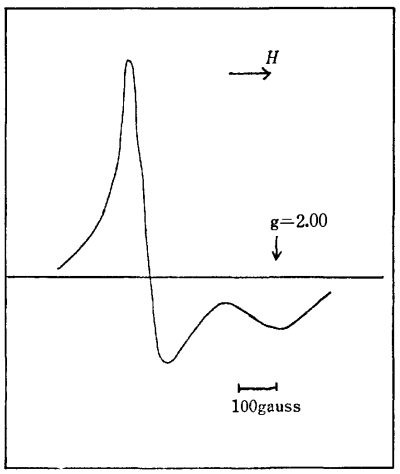

Fig. 3. ESR spectra of [Co en$_2$](AgI$_2$)$_2$ polycrystalline sample at room temperature.

TABLE 2. ELECTRONIC REPULSION ENERGY OF THE LOW-SPIN COBALT(II) COMPLEX

$^2A_{1g}$	$\lvert(x^2-y^2)+(x^2-y^2)-(z^2)+\rvert$	$3F_0-8F_2+33F_4$
$^2B_{2g}$	$\lvert(x^2-y^2)+(x^2-y^2)-(xy)+\rvert$	$3F_0+12F_2-67F_4$
^2E_g	$\lvert(x^2-y^2)+(x^2-y^2)-(xz)+\rvert$	$3F_0-3F_2+8F_4$
$^2B_{1g}$	$\lvert(x^2-y^2)+(z^2)-(z^2)+\rvert$	$3F_0-8F_2+33F_4$
$^2A_{2g}$	$\lvert(x^2-y^2)+(xy)-(z^2)+\rvert$	$3F_0-8F_2-37F_4$
$^2E_g'$	$\lvert(x^2-y^2)+(xz)-(z^2)+\rvert$	$3F_0-8F_2-37F_4$
$^4A_{2g}$	$\lvert(x^2-y^2)+(xy)+(z^2)+\rvert$	$3F_0-4F_2-120F_4$
^4E_g	$\lvert(x^2-y^2)+(xz)+(z^2)+\rvert$	$3F_0-4F_2-120F_4$

In this case, we again assume an energy level splitting similar to that given in Fig. 4-b. Then, the band observed at ~8 kK pointed out by Nishikawa *et al.*[6] as characteristic of the square planar low-spin cobalt(II) complexes and tentatively assigned to the spin-forbidden transition ($^2B_{2g}\rightarrow{}^4A_{2g}$ or ^4E_g), should be assigned to the $^2A_{1g}\rightarrow{}^2B_{1g}$ transition. Accordingly, the transition $^2A_{1g}\rightarrow{}^2A_{2g}$ can be assigned to the shoulder at ~20 kK, and the transition $^2A_{1g}\rightarrow{}^2E_g$ will appear at 5 kK or the lower wave number. Thus, the g-values and magnetic susceptibility can be calculated with the use of equations (2), (3) and (8) with the numerical values $\Delta_1=5$, $\Delta_2=20$, and $\Delta_3=20$ kK as follows.

$$g_{\parallel}=2.0,\ g_{\perp}=2.5$$

$$\chi=\frac{0.52}{T}+310\times10^{-6},$$

and this leads to

$$\mu_{300^\circ K}=2.21\ \text{BM}$$

which is in good agreement with the experimental value 2.30 BM.

Dipotassium barium hexanitrocobaltate(II). $K_2Ba[Co(NO_2)_6]$: This complex has been known to show the lowest magnetic moment (1.88 BM) among the low-spin cobalt(II) complexes. Since the nearly isotropic g-value was observed in the ESR measurements,[21] it is almost evident that this compound has a nearly octahedral structure. Thus, the energy level splitting will be similar to that given Fig. 4-a. We can assign the band observed at 15.5 kK to the $^2A_{1g}\rightarrow{}^2E_g$ transition. The transitions $^2A_{1g}\rightarrow{}^2E_g'$ and $^2A_{1g}\rightarrow{}^2A_{2g}$ would then, correspond to the absorption around 18 kK. Accordingly, we can evaluate the susceptibility using equation (8) with $\Delta_1=15.5$ kK, $\Delta_2=18$ kK and $\Delta_3=18$ kK.

$$\chi=\frac{0.41}{T}+180\times10^{-6}.$$

This leads to

$$\mu_{300^\circ K}=1.92\ \text{BM}.$$

This is in fairly good agreement with the experimental value 1.88 BM.

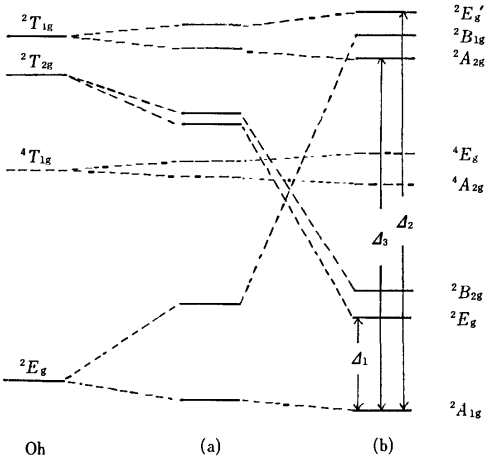

Fig. 4. Energy levels of low-spin cobalt(II) complexes with ground state, $^2A_{1g}$ in D_{4h}-symmetry.

Bromo-bis-diphenyl(o-diphenylarsinophenyl)phosphine cobalt(II) perchlorate $[CoBr(Ap)_2]ClO_4$: Dyer and Meek[20] proposed a five-coordinated square pyramidal structure for this compound from the results of spectral and magnetic measurements. In the optical spectrum they found three peaks at 7 kK, 13 kK, and 22 kK, and have assigned them to the transitions $d_{xy}\rightarrow d_{z^2}$, d_{xz},

20) G. Dyer and D. W. Meek, *J. Am. Chem. Soc.*, **89**, 3983 (1967).

$d_{yz} \rightarrow d_{z^2}$ and $d_{z^2} \rightarrow d_{x^2-y^2}$, assuming that an unpaired electron lies in d_{z^2} orbital in the ground state. Granted this assignment, we might deduce that $\Delta_1 = 13$ kK, $\Delta_2 = 22$ kK, and $\Delta_3 = 22$ kK. Using these numerical values and following equation (8), we obtain

$$\chi = \frac{0.42}{T} + 180 \times 10^{-6}$$

$$\mu_{300^\circ K} = 1.95 \text{ BM}$$

whereas the experimental value is 2.18 BM.

The alternative assignment for the electronic transitions is possible on the assumption of the energy level splitting similar to that given in Fig. 4-b, and this leads to a better agreement between the calculated and experimental values, *viz.*, the bands at 7 kK and 13 kK are assigned to the transitions d_{xz}, $d_{zy} \rightarrow d_{z^2}$ ($^2A_{1g} \rightarrow {}^2E_g$) and $d_{xy} \rightarrow d_{z^2}$ ($^2A_{1g} \rightarrow {}^2B_{2g}$) respectively, and Δ_1, Δ_2, and Δ_3 are evaluated to be 7 kK, 22 kK, and 22 kK. By use of equation (8) and the above numerical values, we obtain a better accordance with the experimental value.

$$\chi = \frac{0.47}{T} + 240 \times 10^{-6}$$

$$\mu_{300^\circ K} = 2.08 \text{ BM}.$$

Conclusion

A quantitative knowledge of the energy-level splittings of the complexes was necessary for the calculation of the magnetic quantities such as *g*-values and susceptibilities. Although we tried to avoid arbitrary methods for obtaining the numerical values necessary for the calculations, some assumptions had to be made. However, it should be noted that (1) all the assumptions are reasonable and probable ones, drawn from other experimental data as well as theoretical considerations, (2) consistency between the calculated results, experimental data and starting assumption is satisfactory throughout this work, and (3) any alternative choice for the energy level splitting of the complexes would not lead to reasonable and consistent results. This implies that our energy level diagrams and assignments of the electronic spectra are correct.

21) H. Elliott, B. J. Hathaway, and R. C. Slade, *Inorg. Chem.*, **5**, 669 (1966).

22) F. Burstall and R. S. Nyholm, *J. Chem. Soc.*, **1952**, 3570.

BULLETIN OF THE CHEMICAL SOCIETY OF JAPAN, VOL. 45, 465—469 (1972)

Studies on Mixed Chelates. I. Mixed Copper(II) Chelates with *N,N,N′,N′*-Tetramethylethylenediamine and a Bidentate Ligand

Yutaka FUKUDA and Kozo SONE

Department of Chemistry, Faculty of Science, Ochanomizu University, Ohtsuka, Bunkyo-ku, Tokyo

(Received July 5, 1971)

Six new mixed copper(II) chelates with *N,N,N′,N′*-tetramethylethylenediamine and a bidentate ligand, *i.e.*, [Cu tmen en] $(ClO_4)_2$, [Cu tmen en] $(NO_3)_2 \cdot H_2O$, [Cu tmen en]$(SO_4) \cdot 4H_2O$, [Cu tmen gly](ClO_4), [Cu-tmen ox]$\cdot 4H_2O$ and [Cu tmen aca](ClO_4) were prepared, and their visible absorption spectra were compared with those of the bis-chelate ions and molecules, $[Cu\ en_2]^{2+}$, $[Cu\ gly_2]$, $[Cu\ ox_2]^{2-}$, and $[Cu\ aca_2]$. The results obtained indicate that steric factors play an important role in the formation and structure of these mixed chelates. The effects of various organic solvents on the electronic spectra of these chelates were also studied. (tmen=*N,N,N′,N′*-tetramethylethylenediamine, en=ethylenediamine, gly=glycinate ion, ox=oxalate ion, aca=acetylacetonate ion.)

Copper(II) chelates with *N,N,N′,N′*-tetramethylethylenediamine (tmen) were investigated by several workers. Meek and Ehrhardt[1] showed that copper(II) ion readily combines with tmen to form a dimeric chelate cation, [tmen $Cu(OH)_2$ Cu tmen]$^{2+}$, while the monomeric bis-chelate cation, $[Cu\ tmen_2]^{2+}$ could not be prepared in spite of all their efforts. These results indicate that, when two molecules of tmen approach the central copper(II) ion, the bulky methyl groups on their donor *N* atoms collide strongly with each other, and the interligand steric hindrance is so large that the formation of bis-chelate becomes practically impossible.[2] On the other hand, Bertini and Mani[3] studied the metal complexes of tmen and related ligands, and showed that various monomeric copper(II) chelates containing one molecule of tmen and simple anionic ligands (Cu tmen X_2) can be prepared.

Recently we studied the formation of mixed copper(II) chelates with tmen and another chelating ligand. The ligands used are common ones (en, gly, ox, and aca) with no bulky groups around the donor atoms, and little steric hindrance is expected when one of them combines with copper(II) together with a tmen molecule. In agreement with this expectation, it was found that all these ligands form quite stable mixed chelates with tmen, the preparation and properties of which will be reported in this paper.

1) D. W. Meek and S. A. Ehrhardt, *Inorg. Chem.*, **4**, 584 (1965).

2) D. W. Meek (*Inorg. Chem.*, **4**, 250 (1965)) pointed out, however, that the larger palladium(II) ion can form the bis-type chelate [Pd $tmen_2$]$(NO_3)_2$.

3) I. Bertini and F. Mani, *Inorg. Chem.*, **6**, 2032 (1967).

4) Elementary analyses were performed at the Organic Microanalytical Section of the Institute of Physical and Chemical Research.

Experimental

Materials. The ligands used were obtained from Wako Pure Chemical Industries Ltd., and Tokyo Kasei Kogyo Co., Ltd. They were reagent grade samples and were used without further purification. Solvents used for spectral measurements were of "extra pure" or "spectro" grade.

Preparation of Mixed Chelates. a) [Cu tmen en]-$(ClO_4)_2$: 10 mmol of copper(II) perchlorate hexahydrate was dissolved in a small amount of water, and equimolar amounts of tmen and en were added with stirring. The resulting solution was concentrated on a water bath. The crude product which separated out was recrystallized from water. Reddish violet crystals (μ=1.84 B.M.).

Found: C, 21.70; H, 5.22; N, 12.69%. Calcd for Cu tmen en $(ClO_4)_2$: C, 21.90; H, 5.51; N, 12.79%.[4]

b) [Cu tmen en]$(NO_3)_2\cdot H_2O$: The method for preparation was the same as in the case of (a) except that copper(II) nitrate trihydrate was used instead of perchlorate. Violet crystals (μ=1.86 B.M).

Found: C, 25.97; H, 6.90; N, 21.37%. Calcd for Cu tmen en $(NO_3)_2\cdot H_2O$: C, 25.16; H, 6.86; N, 22.20%.

c) [Cu tmen en]$(SO_4)\cdot 4H_2O$: 10 mmol of copper(II) sulfate pentahydrate was mixed with equimolar amounts of tmen and en in a small amount of water. A violet paste deposited from the solution. This crude gummy product was purified by suspending it in acetone, and the violet crystalline powder obtained was washed with acetone and ether (μ=2.11 B.M.).

Found: C, 23.24; H, 7.23; N, 13.97%. Calcd for Cu tmen en $SO_4\cdot 4H_2O$: C, 23.55; H, 7.90; N, 13.73%.

d) [Cu tmen gly](ClO_4): 5 mmol of the dimeric chelate, [tmen Cu $(OH)_2$ Cu tmen] $(ClO_4)_2$, prepared according to literature[1] with some modifications and identified by elementary analyses, and 10 mmol of glyH were mixed in a mortar, and about 50 m*l* of methanol was added with stirring. The mixture was filtered and concentrated on a water bath. The crude product which separated out was recrystallized from methanol. Blue-violet crystals (μ= 1.94 B.M.).

Found: C, 27.25; H, 5.79; N, 11.70%. Calcd for Cu tmen gly (ClO_4): C, 27.20; H, 5.70; N, 11.89%.

e) [Cu tmen ox]$\cdot 4H_2O$: The method of preparation was the same as in the case of (a), except that aqueous solutions of copper(II) sulfate pentahydrate, tmen, and potassium oxalate were used as starting materials. Pale blue crystals (μ=2.19 B.M.).

Found: C, 28.54; H, 7.12; N, 8.32%. Calcd for Cu tmen ox$\cdot 4H_2O$: C, 28.26; H, 7.12; N, 8.25%.

f) [Cu tmen aca](ClO_4): 10 mmol of copper(II) perchlorate hexahydrate dissolved in aqueous ethanol (1 : 1) and solutions of tmen and acaH (10 mmol each) in the same solvent were mixed together, and 5 mmol of anhydrous sodium carbonate was added to neutralize acaH. The mixed solution was concentrated on a water bath, and the crude product separated out was recrystallized from ethanol. Reddish violet crystals (μ=1.92 B.M.).

Found: C, 34.81; H, 6.00; N, 7.12%. Calcd for Cu tmenaca(ClO_4): C, 34.92; H, 6.13; N, 7.40%.

Physical Measurements. The electronic absorption spectra of the solutions between 1000 nm (10.0 kK) and 340 nm (29.4 kK) were recorded with a Shimadzu multi-convertible D-40R spectrophotometer and 10 mm silica cells. The reflection spectra of solid samples were obtained with the same spectrophotometer with the reflection attachment and a MgO disks for reference. The magnetic susceptibility measurements were performed by the Gouy method with conventional technique. The IR spectra between 4000 cm^{-1} and 400 cm^{-1} were recorded with a JASCO IR-G spectrophotometer by means of Nujol-mull method.

Results and Discussion

All the mixed chelates obtained are fine crystals or apparently crystalline powders, with compositions shown in the experimental section. All of them have normal magnetic moments (1.84—2.19 B.M.), showing that there is no Cu–Cu interaction in them.

The reflection spectra of these crystals and the absorption spectra of their solutions in various solvents were studied in some detail. Figure 1 illustrates the reflection spectra of four mixed chelates which contain tmen and en, gly, ox, and aca. Figure 2 shows those of three $[Cu\ tmen\ en]^{2+}$ chelates, *i.e.*, perchlorate, nitrate, and sulfate.

We see from Fig. 1 that among the mixed chelates the value of ν_{max} increases in the order en>aca>gly> ox. While the order en>gly>ox is that of the ordinary spectrochemical series, it is noteworthy that the value of the mixed acetylacetonate is remarkably larger than that of the mixed glycinate[5] (in aqueous solution, however, these values are nearly the same; *cf.* Fig. 6).

From Fig. 2, it can be seen that the band maximum

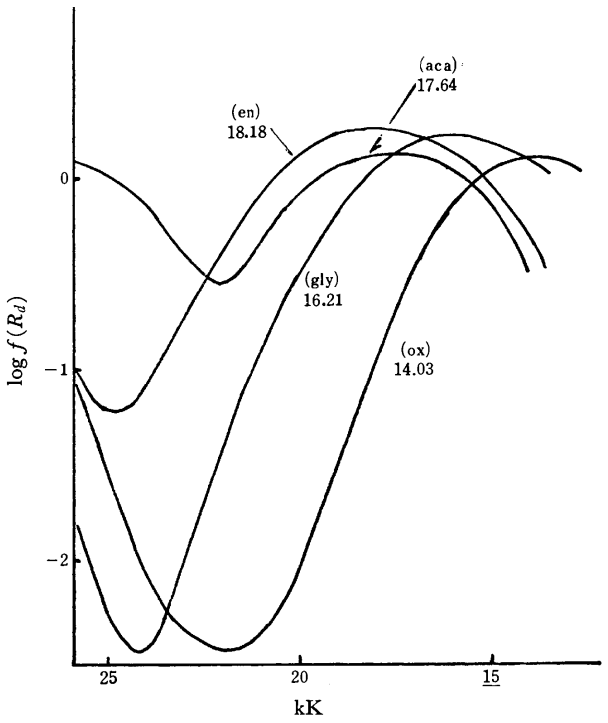

Fig. 1. Reflection spectra of the mixed chelates. Curves denoted by (en), (gly), (aca), and (ox) are those for [Cu tmen en]$(ClO_4)_2$, [Cu tmen gly](ClO_4), [Cu tmen aca](ClO_4) and [Cu tmen ox]$\cdot 4H_2O$, respectively. ν_{max} values are also given.

5) A somewhat similar situation was already pointed out in the spectra of [Cu aca_2] and [Cu gly_2]. Y. Fukuda and K. Sone, This Bulletin, **43**, 556 (1970).

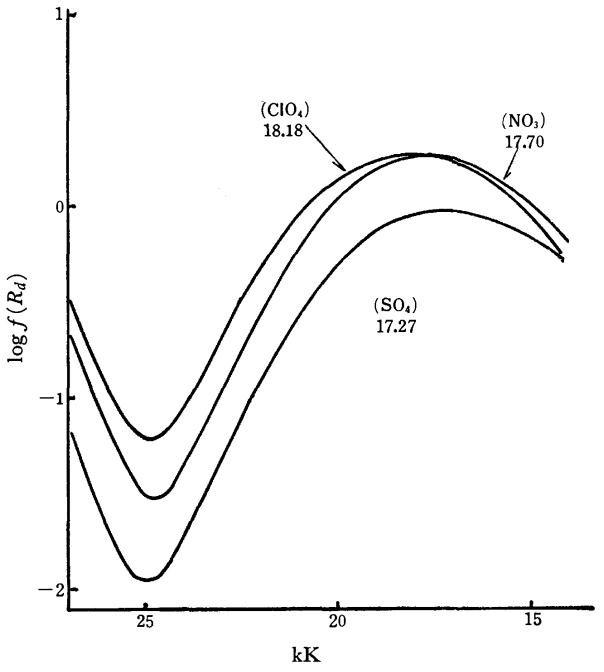

Fig. 2. Reflection spectra of the mixed chelates. Curves denoted by (ClO_4), (NO_3), and (SO_4) are those for [Cu tmen en]$(ClO_4)_2$, [Cu tmen en]$(NO_3)_2 \cdot H_2O$ and [Cu tmen en]$(SO_4) \cdot 4H_2O$, respectively. ν_{max} values are also given.

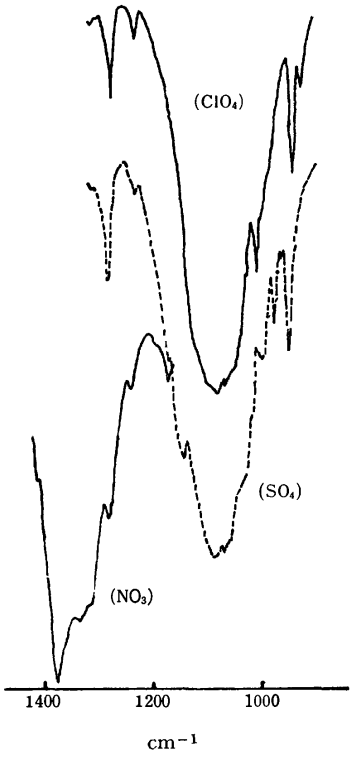

Fig. 3. Anion absorption bands in the infrared spectra of the three chelates shown in Fig. 2. The sharp band at 1375 cm^{-1}, which appears near the top of the NO_3^- band, is due to Nujol.

of [Cu tmen en]X_2 gradually moves to the red in the following order of X: $ClO_4^- \rightarrow NO_3^- \rightarrow SO_4^{2-}$. At first sight this seems to indicate that these anions interact to some extent with the complex cation in the crystals, and that the stronger the interaction (or, in other words, the anion's coordination ability), the lower the ν_{max} value of the mixed chelate. However, the IR spectra of these chelates illustrated in Fig. 3 clearly indicate that the bands of the anions are not remarkably split, *i.e.*, the interaction between the anion and the metal ion in these chelates is quite weak; this result seems reasonable because the mixed chelates contain a very bulky ligand (tmen), which will make the attachment of the oxo-acid anions above and below the planar chelate cation difficult. Therefore, it is more probable that the lowering of the ν_{max} value described above is due to the effect of the water of crystallization in the nitrate and sulfate, the molecules of which probably can coordinate more readily to the chelate cation than the oxo-acid anions.

Figure 4 illustrates the absorption spectra of [Cu tmen aca](ClO_4) in various solvents. This mixed chelate is especially soluble in many organic solvents, and the color of the solution obtained strongly depends on the solvent, varying from reddish violet (in 1,2-dichloroethane) to blue (in dimethylformamide). Figure 5 shows the relation between the ν_{max} value of this chelate in a solution and the donor number (DN) of the solvent; the latter, which was originally proposed by Gutmann,[6] is a measure of the donor strength (coordination or solvation ability) of the sol-

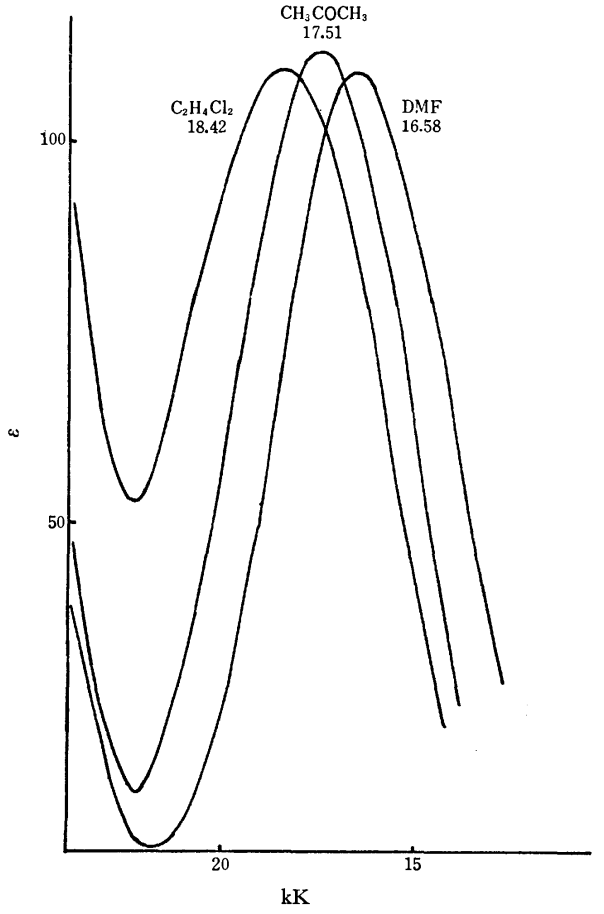

Fig. 4. Absorption spectra of [Cu tmen aca](ClO_4) in 1,2-dichloroethane, acetone, and *N*,*N*-dimethylformamide (DMF). ν_{max} values are also given.

6) V. Gutmann, "Coordination Chemistry in Non-Aqueous Solutions," Springer-Verlag, Wien & New York (1967).

vent. It can be seen that there is an approximately linear relation between ν_{max} and DN, and, the larger the coordinating ability of the solvent, the smaller the corresponding ν_{max} value, the order of change being $CH_3NO_2 > C_2H_4Cl_2 > CH_3COCH_3 \gtrsim C_6H_5CN > CH_3CN > THF > MeOH \gtrsim H_2O > DMF > DMSO$. This solvent effect can be explained in the same manner as in the case of the data in Fig. 2, *i.e.*, by assuming the coordination of the solvent molecules above and below the chelate cation which is in solution. The strength of this coordination will increase with the increase of DN, making the ligand field more and more octahedral, and shifting the absorption band to the lower frequencies.[7]

The spectra of other mixed chelates obtained also show a similar solvent effect; but they are not soluble in many organic solvents, and in certain cases, apparent decomposition takes place. In Table 1 are shown the band maxima of these chelates in some solvents. The reason why the ν_{max} values in DMF of the en, gly, and ox chelates are generally higher than those in H_2O is not clear as yet.

TABLE 1. ν_{max}(kK) AND ε_{max} VALUE (THE LATTER IN PARENTHESES) OF THE MIXED CHELATES IN VARIOUS SOLVENTS

Mixed chelate	CH_3OH	H_2O	DMF
[Cu tmen en]$(ClO_4)_2$	18.25(95)	17.64(85)	17.70(97)
[Cu tmen gly](ClO_4)	17.33(97)	16.95(98)	17.12(102)
[Cn tmen ox]$\cdot 4H_2O$	16.53(127)	16.21(126)	16.72(119)

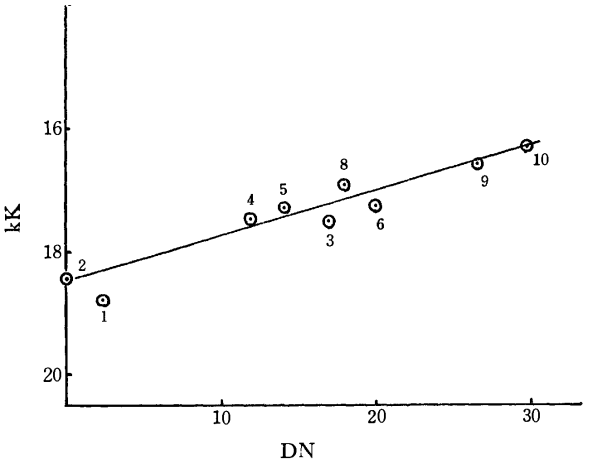

Fig. 5. The relation between ν_{max} and DN in the solutions of [Cu tmen aca](ClO_4) in various solvents. The circles 1 to 10 refer to: 1, CH_3NO_2 (18.80, 2.7); 2, CH_2ClCH_2Cl (18.42, —); 3, CH_3COCH_3(17.51, 17.0); 4, C_6H_5CN(17.48, 11.9); 5, CH_3CN(17.30, 14.1); 6, THF (17.27, 20.0); 7, (not shown) CH_3OH(16.98, —); 8, H_2O(16.92, 18.0); 9, DMF(16.58, 26.6); 10, DMSO(16.31, 29.8). (The numbers in parentheses are those of ν_{max} and DN in each solvent).

Spectral Comparison of the Mixed and Parent Chelates. Recently the nature of the mixed chelates has attracted the interest of many workers[8] and a large number of studies have been published. Among them, Sone and co-workers[9] studied mixed copper(II) chelates containing 2,2′-bipyridine (or 1,10-phenanthroline) and another bidentate ligand(A-A)(=en, gly, ox, or aca), and concluded that the strong interligand steric hindrance in $[Cu\ bip_2]^{2+}$ plays an important role in the following equilibrium:

$$[Cu\ bip_2]^{2+} + [Cu(A\text{-}A)_2]^{m+} \rightleftarrows 2[Cu\ bip(A\text{-}A)]^{n+} \quad (1)$$

In other words, an equilibrium of this type is forced strongly to the right hand side by the fact that the repulsion between two bulky ligands in $[Cu\ bip_2]^{2+}$ disappears in the course of mixed chelate formation.

From the results of the present study, it is easy to see that, in an equimolar mixture of Cu^{2+}, tmen and (A-A), an extreme case of type (1) equilibrium takes place, where one of the components on the left hand side of the equation (*i.e.* $[Cu\ tmen_2]^{2+}$) is so unstable sterically that it cannot exist at all.[1] On the other hand, in the mixed chelate formed, model studies show that the ligand(A-A) does not exhibit any remarkable steric hindrance with tmen; therefore, its formation by way of type (1) equilibrium will be very strongly favored. The facts that the mixed tmen chelates can be obtained easily from such solutions, and they seem to be quite stable in aqueous solutions,[10] are in conformity with this view.

The importance of steric factors in the formation and structure of these mixed chelates is also reflected in Fig. 6, where the positions of the maxima of the mixed and parent chelates in aqueous solutions are illustrated. It is known that, in many types of mixed copper chelates, Kida's rule[11] holds well, which states that the following relation

$$\nu_{AB} = 1/2(\nu_{A_2} + \nu_{B_2}) \quad (2)$$

exists between ν_{AB} (the ν_{max} value expected for a mixed chelate [Cu AB]) and ν_{A_2} and ν_{B_2} (the ν_{max} values of its parent chelates, $[Cu\ A_2]$ and $[Cu\ B_2]$). To test the applicability of this rule to the present data, however, it is necessary to know the value of ν_{tmen_2}. Although this can not be obtained experimentally, an estimate of its magnitude can be made in the following way.

Table 2 shows the data of Meek, Ehrhardt, Yokoi, and Isobe on the ν_{max} values of the bis-chelates $[Cu\text{-}A_2]^{2+}$ of some *N*-alkylated ethylenediamines.[1,12] It can be seen, in general, that the value decreases with

7) a) Other examples of similar spectral effects caused by solvent molecules are found in C. K. Jørgensen, "Inorganic Complexes," Academic Press, London & New York (1963), p. 106, and also in K. Sone and S. Utsuno, This Bulletin, **39**, 1813 (1966). b) Increase of ion-pairs in relatively nonpolar solvents might also influence the spectra to some extent. However, the effect of solvation would be of primary importance since in most cases solvent molecules will be more easily bound by the metal ion than ClO_4^-, which is a very poor donor and also very bulky (*cf.* the preceding text).

8) *Cf. e.g.*, a) R. DeWitt and J. I. Watters, *J. Amer. Chem. Soc.*, **76**, 3810 (1954); S. Kida, This Bulletin, **29**, 805 (1956) (earlier studies); b) "Proceeding of the 3rd Symposium on Coordination Chemistry," ed. by M. T. Beck, Akademiai Kiado, Budapest (1970) (recent results).

9) K. Sone, S. Utsuno, and T. Ogura, *J. Inorg. Nucl. Chem.*, **31**, 117 (1969); *cf.* also Ref. 5.

10) S. Utsuno, unpublished results; G. F. Condike and A. E. Martell, Ref. 13.

11) S. Kida, (see Ref. 8).

12) H. Yokoi and T. Isobe, This Bulletin, **42**, 2187 (1969).

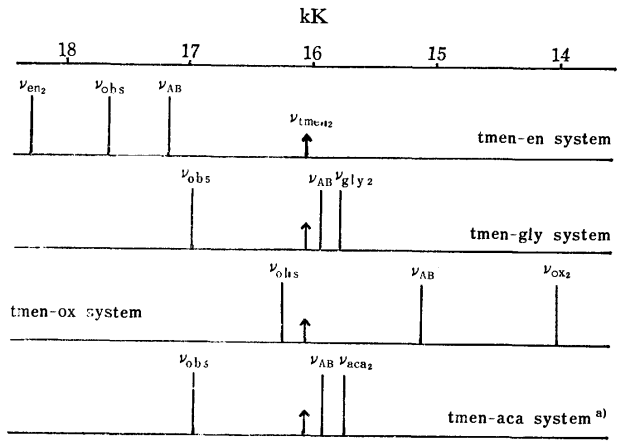

Fig. 6. ν_{max} values of the mixed chelates and the parent bis-chelates in aqueous solutions. The observed values for the mixed chelates and those calculated from Kida's rule are denoted by ν_{obs} and ν_{AB}, respectively, and the imaginary ν_{tmen_2} value (see text) is shown by a short arrow in each system.

(a) Since [Cu aca_2] is insoluble in H_2O, its ν_{max} given in this figure is that of DMF solution, so that only approximate comparison can be made. However, the shift of ν_{obs} from ν_{AB} described in the text is still very evident.

TABLE 2. ν_{max} VALUES (kK) OF THE COPPER(II) CHELATES OF EN AND ITS *N*-ALKYLATED DERIVATIVES (DIFFERENCES NEIGHBORING VALUES ARE SHOWN IN ITALIC; IMAGINARY BETWEEN VALUES ARE SHOWN IN PARENTHESES)

Complex	Solid[1]			Aqueous solution[12] a)
I. [Cu en_2]$(ClO_4)_2$	19.05	→	*0.77*	→ 18.28
	↓ *0.53*			
II. [Cu (*N*,*N'*-Me_2en)$_2$]-$(ClO_4)_2$	18.52	→	*0.85*	→ 17.67
	↓ *0.82*			
III. [Cu (*N*,*N*,*N'*-Me_3en)$_2$]-$(ClO_4)_2$	17.70			
	↓ *(0.82)*			
IV. [Cu $tmen_2$]$(ClO_4)_2$	(16.88)[b]	→	*(0.85)*	→ (16.03)[b]

a) The original data of Yokoi and Isobe refer to solutions in CH_3OH-H_2O (1:1), but it was found that the values in H_2O are nearly the same.

b) Extrapolations leading to these values are based on the assumption that (i) there is a decrease of *ca.* 0.82 kK in going from III to IV, just as in going from II to III, and (ii) there is a shift of *ca.* 0.85 kK in going from solid to solution spectrum of IV. Naturally these assumptions are not entirely reliable, and it is possible that the true values are considerably lower, since the introduction of a fourth CH_3 group in the ligand (*N*,*N*,*N'*-Me_3en) to form tmen will increase the interligand repulsion much more than that of the third in *N*,*N'*-Me_2en. However, even a considerable variation of these values (and those of ν_{AB} derived from them) will not alter the general picture described in the text.

TABLE 3. ν_{max} (kK) VALUES OF EN AND TMEN MIXED CHELATES IN AQUEOUS SOLUTIONS

[Cu en gly]$^+$ [8]	16.95	[Cu tmen gly]$^+$	16.95
[Cu en ox][10]	16.18	[Cu tmen ox]	16.21
[Cu en aca]$^+$ [10]	17.01[a]	[Cu tmen aca]$^+$	16.92

a) 75% dioxane solution.

increasing *N*-methyl groups, indicating the loosening of the coordinate bonds caused by interligand steric repulsion, and there is also a shift of *ca.* 0.8 kK in going from solid to aqueous solution. Extrapolation of these values to the case of aqueous solution of the imaginary bis-chelate [Cu $tmen_2$]$^{2+}$ gives an approximate value of 16.0 kK for its ν_{max}. Substituting this value and the values of ν_{en_2}, ν_{gly_2}, and ν_{ox_2} taken from literature into Eq. (2), the values of ν_{AB} shown in Fig. 6 can be obtained. It can be seen readily that, in all the cases studied, Kida's rule does not hold and ν_{obs} of a mixed chelate is remarkably larger than its ν_{AB}. It is only in the case of [Cu tmen en]$^{2+}$ that ν_{obs} lies between ν_{tmen_2} and ν_{en_2}; in all other cases, ν_{obs} is much larger than both ν_{tmen_2} and $\nu_{(AA)_2}$, and the difference between ν_{obs} and ν_{AB} increases in the order:

$$\text{en} < \text{gly} \simeq \text{aca} < \text{ox} \qquad (3)$$

The reason for these results can be explained in terms of the following two factors. (1) The steric effect is very plausible. Although there will be no remarkable interligand repulsion in any of the mixed chelates studied, it is quite possible that a slight repulsion exists in the case of [Cu tmen en]$^{2+}$, since the four protruding H atoms of the amino groups of en will contact the four methyl groups of tmen to some extent. This repulsion will weaken the coordinate bonds; therefore, the ν_{max} of this chelate will be shifted to the red in comparison with ν_{en_2}, and will be approximately the same as that of [Cu(*N*,*N'*-Me_2en)$_2$]$^{2+}$ in which a repulsion of similar magnitude is expected. On the other hand, this kind of repulsion is probably much smaller in [Cu tmen gly]$^+$, since gly has only one amino group, and is practically absent in [Cu tmen ox] and [Cu tmen aca]$^+$, so that their spectra will generally resemble those of the corresponding en chelates. All these expectations agree quite well with the observed results, as can be seen from the data in Table 2 and Table 3.

(2) The charge of the mixed chela temust also be taken into account. As already pointed out by other investigators,[13] the coordination of a doubly negative ox anion to [Cu tmen]$^{2+}$ will be energetically more favorable than that of a neutral en. Furthermore, the entropy change due to the reduced solvation will also favor the formation of neutral [Cu tmen ox] from the components, in preference to the singly charged gly or aca mixed species and still higher charged [Cu tmen en]$^{2+}$. It is therefore possible that these electrostatic effects also contribute to some extent to the spectral changes described above.

The authors wish to thank Mr. Naoe Tani and Miss Akiko Sakai for their help in carrying out the experiments, Dr. Shunji Utsuno and Mr. Toshio Suzuki whose pioneering work led them to the present study, and also Professor Sigeo Kida of Kyushu University for his stimulating interest in this problem. The work was performed in part by a grant for fundamental research from the Ministry of Education.

13) *Cf.*, *e.g.*, G. A. L'Heureux and A. E. Martell, *J. Inorg. Nucl. Chem.*, **28**, 481 (1966); G. F. Condike and A. E. Martell, *ibid.*, **31**, 2455 (1969); H. Sigel, Ref. 8b, p. 191. The paper of Condike and Martell also contains stability data on [Cu tmen ox].

Complexes Coordinated by 2,2′-Bipyridine Negative Ion. II. Sodium 2,2′-Bipyridinetetracarbonylchromium, -molybdenum, and -wolfram

Youkoh KAIZU and Hiroshi KOBAYASHI

Department of Chemistry, Tokyo Institute of Technology, Ookayama, Meguro-ku, Tokyo

(Received July 8, 1971)

Bipyridinetetracarbonylchromium, -molybdenum and -wolfram and their related complexes were reduced with sodium metal in tetrahydrofuran. Some products in the first stage of reduction were isolated. On the basis of the electronic absorption spectrum and the electron spin resonance, the complex formed in the reduction was concluded to be a complex coordinated by mononegative ion of bipyridine. Metal $d\sigma$ orbital in the complex is still higher than bipyridine π^* orbital, even if it is fairly lowered by a positive charge arising from the "metal to carbonyl" back-donation. Trapped electrons in the bipyridine π^* orbital are, however, readily transferred into $d\sigma$ orbital depending upon molecular environment. This gives rise to the formation of a pentacoordinate complex or complex dimer evolving carbon monoxide.

Coordinating bipyridine captures electrons when a bipyridine complex of less electron-acceptable metal is reduced by strong reducing reagents such as sodium metal. Bipyridine, with its strong σ-donating and π-accepting powers, gives a strong ligand-field to the central metal and a sufficient energy gap between $d\sigma$ and $d\pi$ orbitals. When a tris-bipyridine complex of metal with vacancies in $d\pi$ shell is reduced, electrons furnished by the reducing reagent are captured by the central metal ion. However, a tris-bipyridine complex of metal with no vacancy in $d\pi$ shell should capture electrons either in metal $d\sigma$ orbitals or in the vacant antibonding π molecular orbitals of the coordinating bipyridine. In the higher oxidation states, transition metal ions with $d\sigma$ electrons can exist in various stable coordination complexes.[1] In the lower oxidation states, however, electrons trapped in $d\sigma$ orbitals give rise to a dissociation of the coordinating ligand. Unless some electrostatic attraction between metal and ligand is present as in the higher oxidation states, $d\sigma$ electrons in the antibonding orbital of coordination binding destabilize the coordination binding. Although it shows a trend to form $[Co(bipy)_2]^+$, $[Co(bipy)_3]^+$ can trap two electrons in the metal $d\sigma$ orbitals (bipyridine is abbreviated to bipy).[2] On the contrary, however, $[Mn(bipy)_3]$ and $[Fe(bipy)_3]$ showed an evidence of coordinating bipyridine negative ion.[3] When a vacant antibonding π molecular orbital of the coordinating bipyridine is sufficiently lower than $d\sigma$ orbital of the central metal, electrons furnished upon reduction should be trapped by the coordinating bipyridines.

Porphyrin and phthalocyanine are as highly σ-donating and π-accepting as bipyridine and trap electrons in the conjugated system when the metal complexes are reduced.[4] Such coordinating negative ions have been obtained only for the conjugated nitrogen bases.

In the case of metal carbonyls, sufficient migration of $d\pi$ electron into the antibonding π molecular orbital of coordinating carbon monoxides makes the central metal more positive and therefore more σ-acceptable. Even so, reduction of the metal carbonyls with closed $d\pi$ shell gives rise to a reduction of coordination number or a formation of dimer with metal-metal bond or with carbonyl bridgings. As a matter of fact, a metal carbonyl with d^8 exists in a pentacoordinate structure as in $[Mn(CO)_5]^-$ or $[Cr(CO)_5]^{2-}$,[5] while the one with d^7, in a dimer structure as in $[Mn_2(CO)_{10}]$ or $[Cr_2(CO)_{10}]^{2-}$.[6] Central metal atom in a stable compound has an electronic configuration of the rare gases. It is required by Sidgwick's rule that no open shell exists in a stable structure. However, some monomeric metal carbonyls with open shell have in recent years been successfully prepared. An open shell metal carbonyl $[V(CO)_6]$ was prepared by oxidation of a closed shell metal carbonyl $[V(CO)_6]^-$.[7] In this case, however, a hole exists in a $d\pi$ orbital. Recently we succeeded in the isolation of the first stage reduction product of $[Cr(CO)_4(bipy)]$.[8] If an electron was trapped by the central metal, evolution of carbon monoxide should be expected. In fact, the evolution of carbon monoxide was observed during the second or further stage. As is seen in the formation of $[Cr_2(CO)_{10}]^{2-}$, an electron-capture at the central metal results in a dimer formation. However, in the first stage of reduction, a monomeric open shell species $[Cr(CO)_4(bipy)]^-$ was formed. Thus an electron given by sodium metal was predominantly localized on the coordinating bipyridine. In this paper, we will present a unified study on chromium-, molybdenum-, and wolfram carbonyls with coordinating negative ion of 2,2′-bipyridine.

1) F. H. Burstall and R. S. Nyholm, *J. Chem. Soc.*, **1952**, 3570.
2) Y. Kaizu, Y. Torii, and H. Kobayashi, This Bulletin, **43**, 3296 (1970).
3) Y. Kaizu, T. Yazaki, Y. Torii, and H. Kobayashi, *ibid.*, **43**, 2068 (1970).
4) G. L. Closs and L. E. Closs, *J. Amer. Chem. Soc.*, **85**, 818 (1963). N. Hush and J. Dodd, *J. Chem. Soc.*, **1964**, 4607. D. Clack and H. Hush, *J. Amer. Chem. Soc.*, **87**, 4238 (1965). R. H. Felton and H. Linshitz, *ibid.*, **88**, 1113 (1966). R. Taube, *Z. Chem.*, **6**, 8 (1966).
5) W. E. Wilson, *Z. Naturforsch.*, **13b**, 349 (1958). W. F. Edgell, J. Huff, J. Thomas, H. Lehman, C. Angell, and G. Asato, *J. Amer. Chem. Soc.*, **82**, 1254 (1960).
6) L. F. Dahl, E. Ishishi, and R. E. Rundle, *J. Chem. Phys.*, **26**, 1750 (1957). W. Hieber, W. Beck, and G. Broun, *Angew. Chem.*, **72**, 795 (1960). L. F. Dahl and R. E. Rundle, *Acta Crystallogr.*, **16**, 419 (1963).
7) R. L. Pruett and J. E. Wyman, *Chem. Ind.* (London), **1960**, 119. F. Calderazzo, R. Cini, and R. Ercoli *ibid.*, **1960**, 500, 934.
8) Y. Kaizu and H. Kobayashi, This Bulletin, **43**, 2492 (1970).

Experimental

Materials. 2,2'-bipyridine (bipy) and its 4,4'-dimethyl- (4dmbip) and 5,5'-dimethyl- (5dmbip) derivatives were prepared by the method of Sasse and Whittle.[9] Hexacarbonylmolybdenum [$Mo(CO)_6$] and hexacarbonylwolfram [$W(CO)_6$] were of reagent grade (Pressure Chem. Co., Penn., U. S. A.) and were used without further purification. All other reagents and solvents were commercially available. Tetrahydrofuran (THF) used for solvent was dehydrated by KOH, refluxed on CuCl, carefully distilled under nitrogen atmosphere and a trace of water was removed by $LiAlH_4$.

Preparation of Compounds. [$Mo(CO)_4$bipy] was prepared by the method of Stiddard.[10] Dimethyl substituted bipyridine complexes also were prepared by the same method. [$Mo(CO)_4$bipy]: Hexacarbonylmolybdenum (1.4 g) and bipyridine (0.8 g) were refluxed in toluene (50 m*l*) for 1.5 hr under oxygen-free, dry nitrogen atmosphere. After cooling, reddish orange needle crystals were collected, washed with petroleum ether (60 m*l*) and dried *in vacuo*.

[$Mo(CO)_4$bipy] (reddish orange) Found: Mo, 26.8%. Calcd for [$Mo(CO)_4$bipy]: Mo, 26.3%.

[$Mo(CO)_4$4dmbip] (reddish orange) Found: Mo, 24.9%. Calcd for [$Mo(CO)_4$4dmbip]: Mo, 24.5%.

[$Mo(CO)_4$5dmbip] (yellow) Found: Mo, 24.5%. Calcd for [$Mo(CO)_4$5dmbip]: Mo, 24.5%.

Preparation of [$Mo(CO)_3P(C_6H_5)_3$bipy]. [$Mo(CO)_4$bipy] (0.182 g) and [$P(C_6H_5)_3$] ([$P(C_6H_5)_3$] is abbreviated to $P\phi_3$) (0.184 g) were refluxed in benzene for 5 hr. After cooling, violet needle crystals precipitated were collected by filtration, washed with petroleum ether and dried *in vacuo*.

[$Mo(CO)_3P\phi_3$bipy] (violet needle) Found: Mo, 16.0%. Calcd for [$Mo(CO)_3P\phi_3$bipy]: Mo, 16.0%.

[$Mo(CO)_3P\phi_3$4dmbip] (red purple) Found: Mo, 15.7%. Calcd for [$Mo(CO)_3P\phi_3$4dmbip]: Mo, 15.3%.

[$Mo(CO_3)P\phi_3$5dmbip] (red purple) Found: Mo, 15.0%. Calcd for [$Mo(CO)_3P\phi_3$5dmbip]: Mo, 15.3%.

[$W(CO)_4$bipy] was prepared in xylene instead of toluene by the same method as for molybdenum complexes.[10]

[$W(CO)_4$bipy] (red purple) Found: W, 40.7%. Calcd for [$W(CO)_4$bipy]: W, 40.7%.

Preparation of [$Cr(CO)_4$bipy], [$Cr(CO)_4$4dmbip] and [$Cr(CO)_4$5dmbip] were given elsewhere.[8]

Reduction of [$M(CO)_4L$]. Na[$Mo(CO)_4$L], where L denotes bipy, 4dmbip, or 5dmbip, were prepared by reduction with sodium metal in an apparatus (Fig. 1) in a high vacuum by a similar method as for the preparation of Na[$Cr(CO)_4$L].[8,11]

Na[$Mo(CO)_4$bipy] Found: Mo, 25.5%. Calcd for Na[$Mo(CO)_4$bipy]: Mo, 24.8%.

Na[$Mo(CO)_4$4dmbip] Found: Mo, 22.9%. Calcd for Na[$Mo(CO)_4$4dmbip]: Mo, 23.1%.

Na[$Mo(CO)_4$5dmbip] Found: Mo, 22.5%. Calcd for Na[$Mo(CO)_4$5dmbip]: Mo, 23.1%.

Electronic Absorption Spectra. Absorption spectra were taken on a Shimadzu automatic recording spectrophotometer Model MPS-50. Measurements of the spectra of air-sensitive compounds were described in a previous paper.[11]

Electron Spin Resonance. ESR spectra in THF solution were measured at room temperature using a Japan Electron Optics Laboratory spectrometer Model JES-3BSX. The g-value was determined with the aid of the standard sample of Mn^{2+} ion.

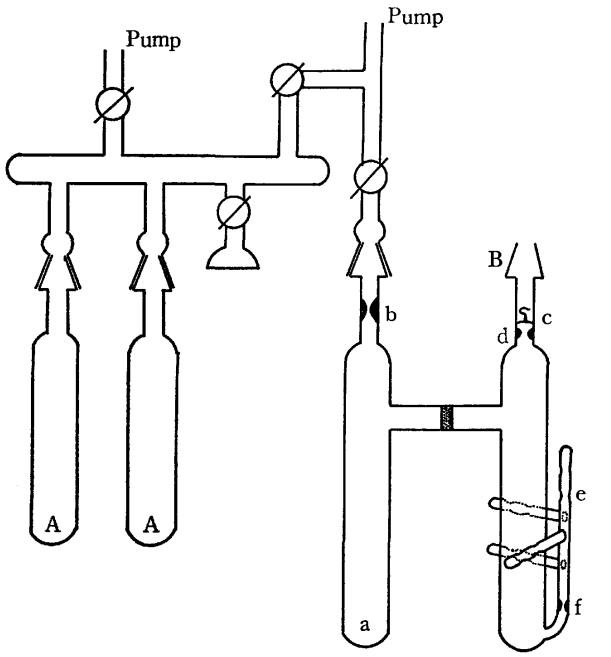

Fig. 1. Apparatus for reduction.
After [$M(CO)_4L$] was placed at a with a slight excess of sodium metal, the apparatus was evacauted up to 10^{-3} mmHg. Dried THF at A, after being thoroughly degassed, was transferred to a by distillation, a being cooled with liquid nitrogen. After being sealed off at b, the THF solution was shaken for about 10 hr and then filtrated. The apparatus was joined with a vacuum line at B. The solvent of the filtrate was then removed by distillation into the vacuum system and the residue was dried *in vacuo*. After being sealed off at d, the product was collected in e and then a branch of sample tubes was sealed off at f. The sample should be stored *in vacuo* and in a dark place.

Results and Discussion

The spectral change of the reduction process of [$Cr(CO)_4$bipy] with sodium metal is shown in Fig. 2. During the first stage of reduction, the spectrum gently changed with the isosbestic points from that of the starting material [$Cr(CO)_4$bipy] to the one shown as (a) in Fig. 2. After that, the curve changed to the spectrum (b), the isosbestic points being shifted. This indicates that the reduction proceeds stepwise. Two steps, at least, are involved in the process. In a previous paper we reported on the isolation of the first stage reduction product of [$Cr(CO)_4$bipy].[8] The spectrum of the isolated Na[$Cr(CO)_4$bipy] is shown in Fig. 3. It coincides with the spectrum (a).

A similar stepwise spectral change was observed in the reduction processes of [$Mo(CO)_4$L], [$W(CO)_4$L], and [$Mo(CO)_3P\phi_3$L] (L: bipy, 4dmbip, 5dmbip) with sodium metal. As a matter of fact, the first reduction product Na[$Mo(CO)_4$L] (L: bipy, 4dmbip, 5dmbip) could be isolated. Absorption spectra of Na[$Mo(CO)_4$L] are shown in Fig. 4. Absorption spectra of the first stage reduction product were obtained for Na[$Mo(CO)_3P\phi_3$L] and Na[$W(CO)_4$L]

9) W. H. F. Sasse, *J. Chem. Soc.*, **1956**, 618. W. H. F. Sasse and C. P. Whittle, *ibid.*, **1961**, 1347.
10) M. H. B. Stiddard, *ibid.*, **1962**, 4712.
11) Y. Torii, T. Yazaki, Y. Kaizu, M. Murasato, and H. Kobayashi, This Bulletin, **42**, 2290 (1969).

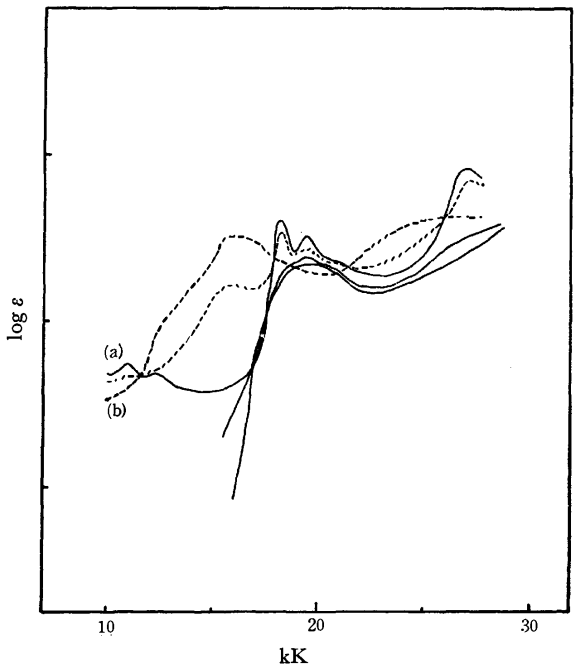

Fig. 2. Spectral changes in the reduction process of [Cr(CO)$_4$bipy] with sodium metal in THF.
——: first stage reduction which forms complex (a)
----: second stage reduction which forms complex (b)

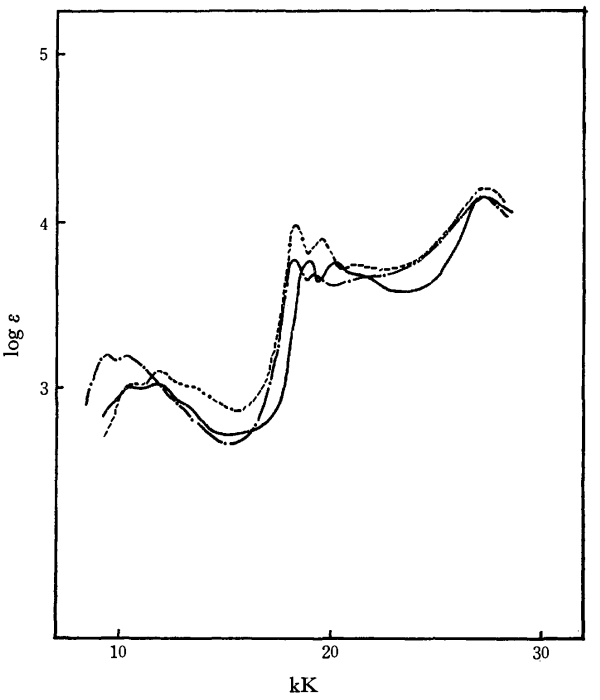

Fig. 4. Electronic absorption spectra of Na[Mo(CO)$_4$L] in THF.
——: L: bipy, ----: L: 4dmbip, —·—·: L: 5dmbip

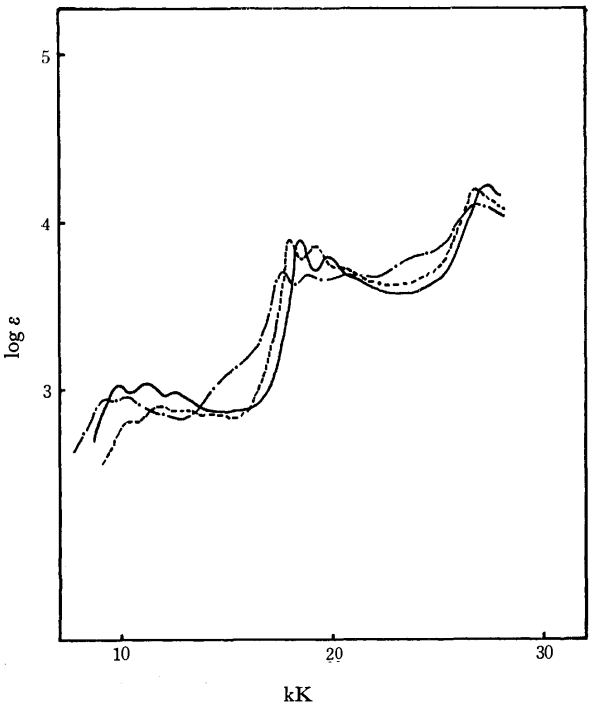

Fig. 3. Electronic absorption spectra of Na[Cr(CO)$_4$L] in THF.
——: L: bipy, ----: L: 4dmbip, —·—·: L: 5dmbip

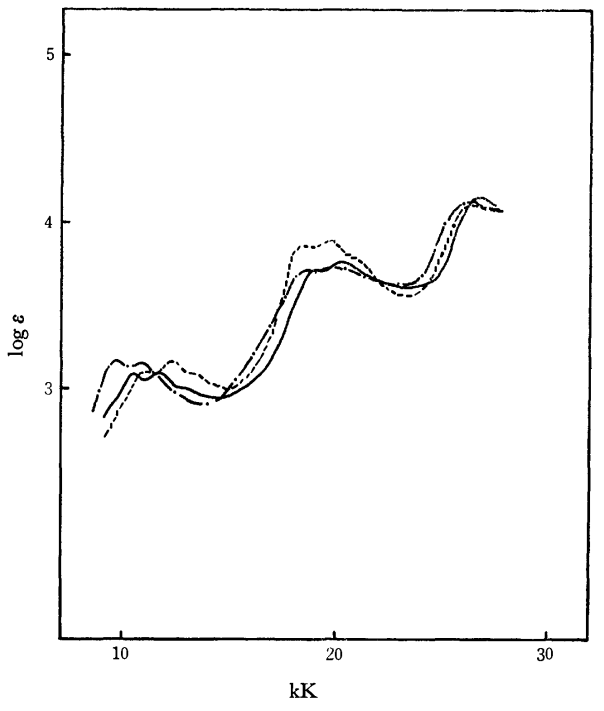

Fig. 5. Electronic absorption spectra of Na[Mo(CO)$_3$Pϕ_3L] in THF.
——: L: bipy, ----: L: 4dmbip, —·—·: L: 5dmbip

(Figs. 5 and 6), although they were not intended to isolate.

Three intense characteristic absorption bands were observed from near-infrared to ultraviolet region. These bands are slightly shifted with a variety of central metals. The second band at about 20,000 cm^{-1} is blue-shifted in the order Cr<Mo≦W. Dimethyl substitutions in the coordinating bipyridine give rise to a blue-shift in the first band in the order 5dmbip< bipy≦4dmbip and a blue-shift in the second band in the order 5dmbip≦4dmbip<bipy, regardless of the central metal species.

ESR spectra of the first stage reduction product of [Cr(CO)$_4$L] (L: bipy, 4dmbip, 5dmbip) and [Mo-

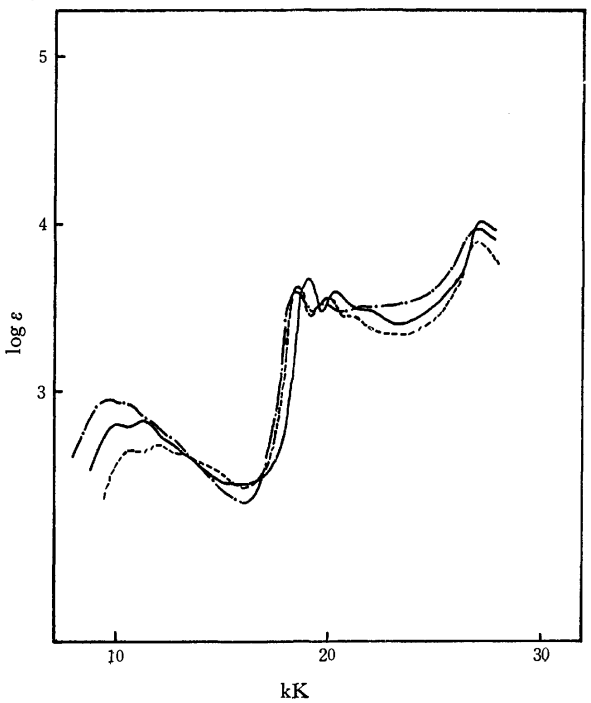

Fig. 6. Electronic absorption spectra of Na[W(CO)$_4$L] in THF.
——: L: bipy, ----: L: 4dmbip, —·—·: L: 5dmbip

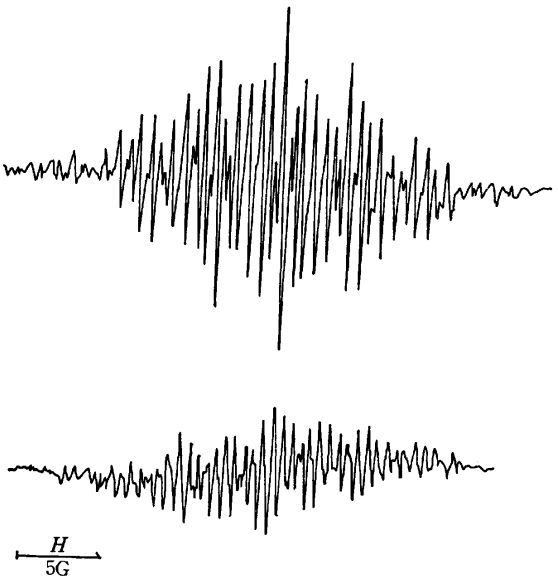

Fig. 7. ESR spectra of Na[Cr(CO)$_4$bipy] and K bipy in THF at room temperature.
upper: Na[Cr(CO)$_4$bipy], lower: K bipy

(CO)$_4$bipy] are shown in Figs. 7—10. ESR spectra of bipyridine negative ions, K bipy, K 4dmbip, K 5dmbip and also Na 4dmbip are shown in Fig. 7 and Figs. 11—13. Observed g-value and line widths are summarized in Table 1. ESR spectrum of Na[Cr(CO)$_4$bipy] is similar to that of K bipy. In the case of K bipy, the binding between K^+ and $bipy^-$ is essentially ionic and the trapped electron in $bipy^-$ has a very poor population on K^+. The ESR spectrum of K bipy does not show a hyperfine structure due to

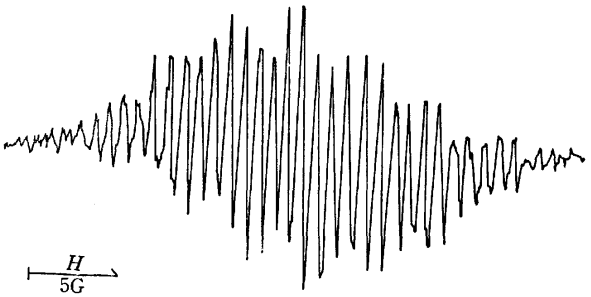

Fig. 8. ESR spectrum of Na[Cr(CO)$_4$4dmbip] in THF at room tempertaure.

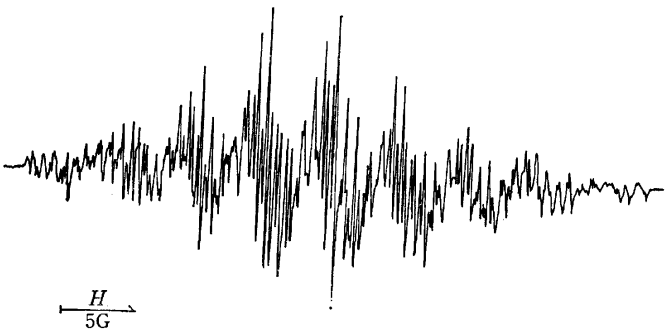

Fig. 9. ESR spectrum of Na[Cr(CO)$_4$5dmbip] in THF at room temperature.

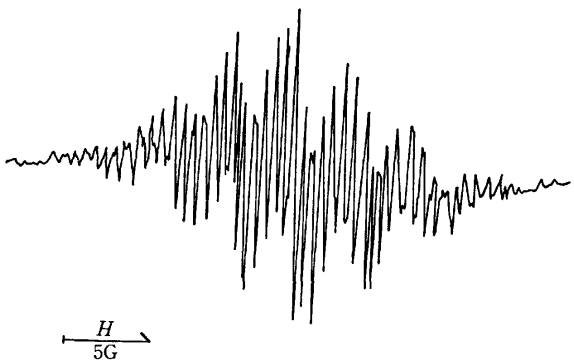

Fig. 10. ESR spectrum of Na[Mo(CO)$_4$bipy] in THF at room temperature.

Table 1. g-value and line width

	g-value	line width
Na[Cr(CO)$_4$bipy]	2.0023	14.5G
Na[Cr(CO)$_4$4dmbip]	2.0019	17.1G
Na[Cr(CO)$_4$5dmbip]	2.0004	15.6G
Na[Mo(CO)$_4$bipy]	2.0021	12.7G
Na[W(CO)$_4$bipy]	2.0031	12.6G
K bipy	2.0026	12.0G
K 4dmbip	2.0024	11.6G
K 5dmbip	2.0025	14.0G

the nuclear spin of potassium ion. The ESR spectrum of Na bipy, however, clearly shows a hyperfine structure due to the nuclear spin of sodium ion (Fig. 13). This phenomenon has been generally observed in

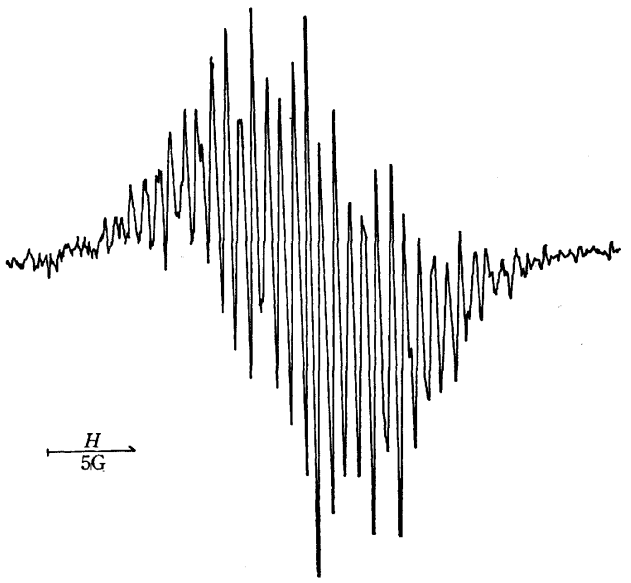

Fig. 11. ESR spectrum of K 4dmbip in THF at room temperature.

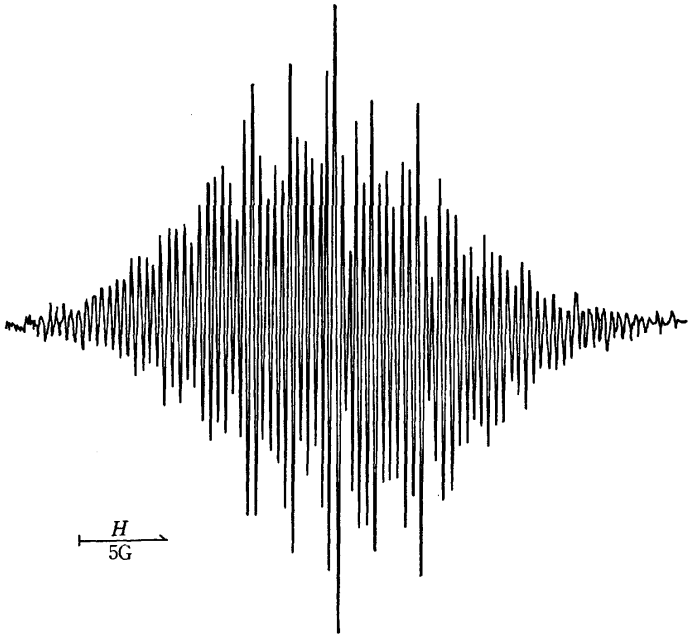

Fig. 12. ESR spectum of K 5dmbip in THF at room temperature.

various aromatic negative ions.[12] Thus ESR spectra of the negative ions obtained by reduction with potassium metal are regarded as those of the respective free negative ions. Na[Cr(CO)$_4$bipy] does not show any hyperfine structure due to either sodium or chromium. An unpaired electron in an antibonding π orbital of bipyridine can not strongly interact with the closed $d\pi$ shell of chromium and also does not migrate over the outer sodium ion.

Apparently the ESR of K bipy, K 4dmbips, and K 5dmbip differs a great deal each other (Figs. 7, 11—

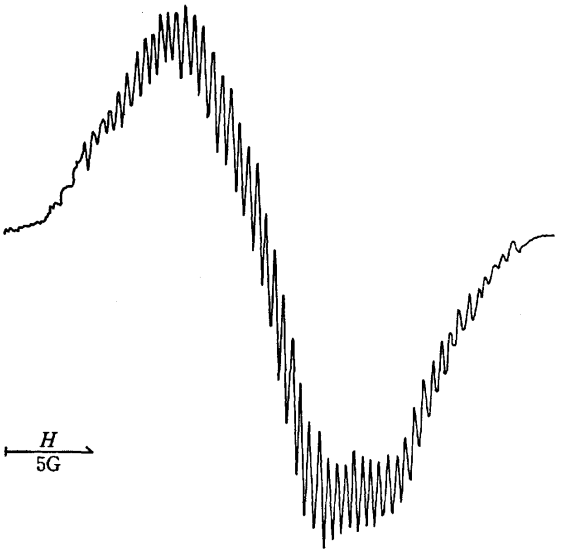

Fig. 13. ESR spectrum of Na 4dmbip in THF at room temperature.

12). Thus many hyperfine structure lines are observed for K 5dmbip, but not so many for K 4dmbip. The hyperfine structure of the ESR of K bipy has been analysed.[13] A similation analysis predicted the highest spin density at 5 and 5′.[14] The highest spin density at the positions 5 and 5′ and lower spin density at 4 and 4′ can give an interpretation of the hyperfine structure due to the dimethyl substitutions. We have never succeeded in similations of the ESR of K 5dmbip and K 4dmbip, however, we can point out that a higher hyperfine constant of six protons of two methyl groups introduced at the positions 5 and 5′ gives a well-resolved hyperfine structure, while the hyperfine constant of 4,4′-dimethyl protons is so small that it just gives an apparent broad line. Actually K 4dmbip gives the simplest ESR spectrum. Another possible interpretation is that the hyperfine structure of K 5dmbip arises from potassium nuclear spin (I=3/2). As shown in Fig. 12, odd number peaks of hyperfine splitting are observed, while even number peaks are expected for I=3/2.

The reduced bipyridine complexes show ESR spectra which actually coincide with those of the corresponding bipyridine negative ions prepared by reduction with potassium metal. Although the magnitude of the hyperfine splitting is, in fact, slightly changed, g-values in the reduced bipyridine complexes actually coincide with that of K bipy (Table 1). In the case of 5,5′-dimethyl bipyridine, however, hyperfine splitting in the reduced bipyridine complex is appreciably changed from that of the negative ion, and g-value of the complex (2.0004) is significantly smaller than the free-spin value, g=2.0023. This indicates that a small interaction between the closed $d\pi$ shell of chromium and the antibonding π orbital of bipyridine changes slightly the electron-trapping molecular orbital and thus spin density at the posi-

12) N. M. Atherton and S. I. Weissman, *J. Amer. Chem. Soc.*, **83**, 1330 (1961). K. Nakamura and Y. Deguchi, This Bulletin, **36**, 359 (1963).

13) E. König and H. Fischer, *Z. Naturforsch.*, **17a**, 1063 (1962).

14) J. S. Veiga, W. L. Reynolds, and J. R. Bolton, *J. Chem. Phys.*, **44**, 2214 (1966).

tions 5 and 5'. Although the spectra have never been reproduced by similation, the electronic structure of bipyridine in the reduced complex is concluded to be very close to that of bipyridine negative ion.

Three characteristic absorption bands of the reduced complexes correspond to respective three bands of bipyridine negative ions. Although these bands are slightly shifted for a variety of the central metal, spectral behavior of the complexes upon a weak perturbation such as dimethyl substitution corresponds to that of bipyridine negative ions regardless of the central metal. As previously reported, the second band at about 20,000 cm^{-1} of bipyridine negative ion is blue-shifted with increasing electrostatic potential due to the coordinating counter cation.[11] The second band of the complexes reported in this paper is blue-shifted in the order $Cr<Mo\leq W$. However, the fact that three characteristic bands of the complexes are changed in spectral intensity and position for the central metal and do not exactly coincide with the corresponding bands of bipyridine negative ion, indicates a binding effect of bipyridine negative ion and metal species. Although an evidence of the existence of bipyridine negative ion is also obtained from the observed *g*-value which is close to the free-spin value, ESR measurements in this particular case do not give a decisive direct evidence of the binding of bipyridine negative ion and metal species. If the coordinating bipyridine is set free upon reduction, the ESR spectrum should show a signal observed for Na bipy in THF. ESR spectrum does not show any hyperfine structure of sodium when $[Mo(CO)_4bipy]$ is reduced with sodium metal in THF. This might be an evidence of the binding.

When $[Cr(CO)_4bipy]$ is reduced by Na bipy instead of sodium metal, absorption spectrum of the first stage reduction product ((a) in Fig. 2) is obtained. The absorption spectrum is observed with no contamination of that of Na bipy unless excess of Na bipy is added. This indicates that Na bipy is wasted to reduce

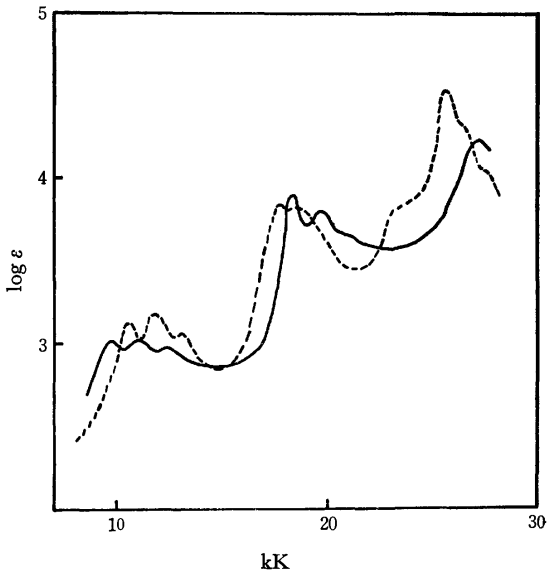

Fig. 14. Electronic absorption spectra of $Na[Cr(CO)_4bipy]$ and Na bipy in THF.

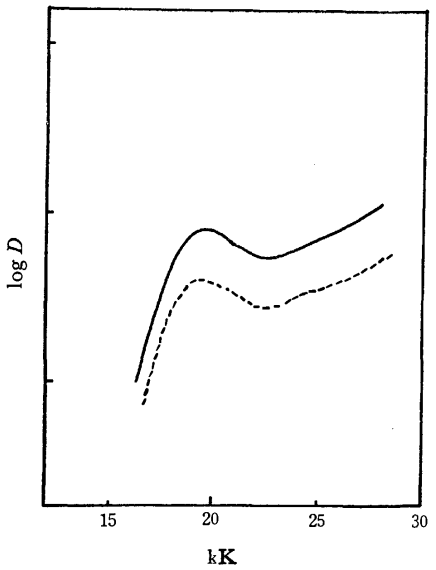

Fig. 15. "Metal to bipyridine" charge-transfer band of a complex formed by oxygen-oxidation of $Na[Cr(CO)_4bipy]$ in THF. ----: $[Cr(CO)_4bipy]$

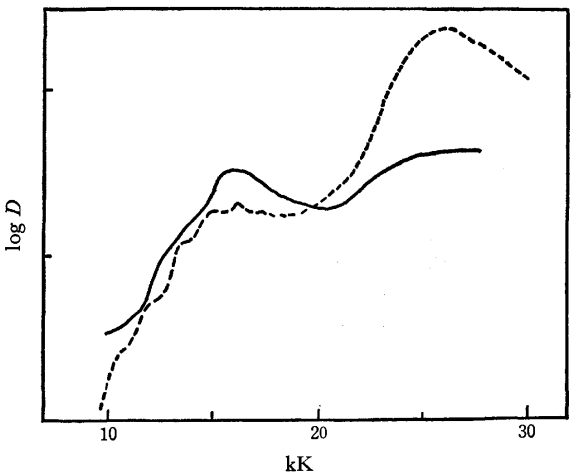

Fig. 16. Electronic absorption spectra of a complex formed in the second stage of reduction (——) and bipyridine dinegative ion, Li_2bipy (----).

the coordinating bipyridine in $[Cr(CO)_4bipy]$. The spectra of the reduced complex and bipyridine negative ion are similar but the difference can be detected (Fig. 14). When the reduced complex is oxidized by oxygen, it gives rise to a characteristic "metal to bipyridine" charge-transfer band in the visible region. From this, a complex formed upon the oxygen-oxidation should be a complex with certain coordinating bipyridine (Fig. 15). Since free bipyridine produced by oxygen-oxidation of free negative ion could not react with a metal carbonyl at room temperature, bipyridine negative ion should be binding to the central metal in the reduced complexes. The second stage complex (b) in Fig. 2 is obtained by reduction with sodium metal but not with Na bipy, a one-electron reducing reagent. Howɔver, the spectrum of complex (b) is different from that of bipyridine dinegative

ion, Li_2bipy, and therefore a complex formed in the second stage could not be assigned to a complex coordinated by dinegative ion (Fig. 16). The first stage reduction product, complex (a), can be obtained even by one-electron donating Na bipy. Thus it is assigned to a one-electron trapping state.

A complex coordinated by bipyridine negative ion, $Na[M(CO)_4L^-]$, could not be obtained by a direct reaction of $[M(CO)_6]$ and Na bipy. When $[M(CO)_6]$ was added with Na bipy in THF, evolution of carbon monoxide was followed by formation of a pale green complex (A). Complex (A) in the solid state was labile at room temperature even in a vacuum. It did not show any similar spectrum of $Na[M(CO)_4L]$. When the isolated solid sample of (A) was oxidized by washing with oxygen-containing toluene or ethanol under nitrogen atmosphere, it gives a very similar spectrum of $[M(CO)_4bipy]$. However, this may indicate the formation of a metal carbonyl complex with bipyridine other than $[M(CO)_4bipy]$. Since free bipyridine could not react with a metal carbonyl at room temperature, bipyridine is expected to enter into the coordination sphere during the reducing process but not the oxidizing process. During the first stage of reaction of $[M(CO)_6]$ and Na bipy, reduction of $[M(CO)_6]$ by Na bipy forms a reactive intermediate $[M(CO)_5]$ evolving carbon monoxide and then, taking a bipyridine molecule, complex (A), probably a metal carbonyl dimer which includes bipyridine. When electrons are trapped in $d\sigma$ orbital, hexacoordinate metal carbonyl gives rise to a pentacoordinate complex or a dimer complex with metal-metal bond or

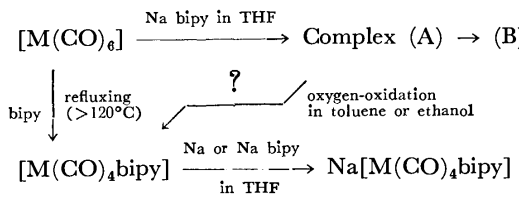

carbonyl bridgings. On the other hand, the first stage of reaction of $[M(CO)_4bipy]$ and Na bipy is just electron-transfer reaction from bipyridine negative ion in Na bipy to the coordinating bipyridine in $[M(CO)_4bipy]$. Since the antibonding vacant π molecular orbital of bipyridine is lower than that of the coordinating carbon monoxide and also is lower than $d\sigma$ orbital which is predominantly localized on the central metal atom, an electron given by Na bipy is trapped in the vacant π orbital of the coordinating bipyridine. The lowest charge-transfer transition in $[M(CO)_4bipy]$ is of "metal to bipyridine" type but not of "metal to carbonyl." Recently we succeeded in the observation of luminescence of $[M(CO)_4bipy]$. The luminescence arises from not a $d\sigma$-$d\pi$ transition but a "bipyridine to metal" charge-transfer transition. As far as a sufficient difference of interelectronic terms does not reverse the order, these observations may indicate that the lowest vacant π molecular orbital of the coordinating bipyridine is the lowest vacant.

An electronic configuration of the rare gas is required for the central metal atom in a stable compound of transition metal in the lower oxidation state. No open shell exists in a stable compound. In various systems including organic and organometallic species, this rule is satisfied. Since $d\sigma$ orbital is occupied in the case of d^7 and d^8 systems, the rule requires d^7 system to form a metal-metal bond with or without carbonyl bridgings ($[Mn_2(CO)_{10}]$ and $[Cr_2(CO)_{10}]^{2-}$) and for d^8 system to decrease the coordination number ($[Mn(CO)_5]^-$ and $[Cr(CO)_5]^{2-}$). In the higher oxidation state, however, transition metal ions with open d shell exist in various stable coordination complexes. Tris-bipyridine complexes, even if in the lower oxidation states, can exist in monomeric state with open shell electronic configurations. In the case of $[Co(bipy)_3]^+$, two electrons with parallel spins are trapped in $d\sigma$ orbitals, though migration of $d\pi$ electron into the antibonding π molecular orbital is appreciable.[2] In the case of isoelectronic $[Fe(bipy)_3]$, however, electrons are trapped in the coordinating bipyridine rather than in the $d\sigma$ orbitals.[3] Electrostatic potential due to a positive charge on the central metal should play an important role to cause the difference. The observed maximum of the lowest (π, π^*) transition of coordinating bipyridine is a function of formal charge on the central metal. The bipyridine (π, π^*) transition of $[Cr(CO)_4bipy]$ is observed at 33,400 cm^{-1} which is close to those observed in $[Cr(bipy)_3]^+$ and $[Co(bipy)_3]^+$. Since back-donation of metal $d\pi$ electrons towards the coordinating carbon monoxides is appreciable and thus the central metal becomes more positive, the coordinating bipyridine in $[Cr(CO)_4bipy]$ is polarized as in $[Cr(bipy)_3]^+$ and $[Co(bipy)_3]^+$ (Fig. 17). Although +1 charge of the complex $[Cr(bipy)_3]^+$ or $[Co(bipy)_3]^+$ is delocalized over the whole

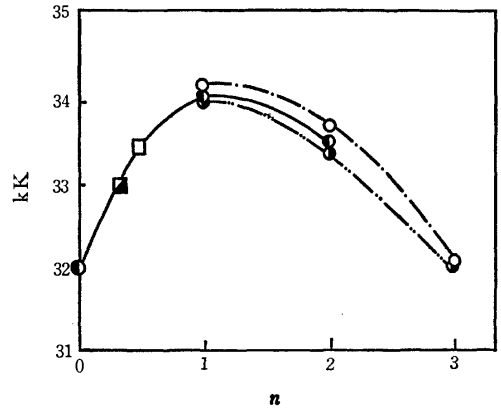

Fig. 17. Energy of the lowest (π, π^*) transition of the coordinating bipyridine *vs.* formal charge of tris-bipyridine complexes, n of $[M(bipy)_3]^{n+}$. The lowest (π, π^*) transition of the coordinating bipyridine in $[M(CO)_4bipy]$ is numerically rather close to those of $[M(bipy)_3]^{2+}$. $P\phi_3$ is a stronger σ donor than CO and therefore a positive charge on Mo of $[Mo(CO)_3P\phi_3bipy]$, for example, should be lower than that of $[Mo(CO)_4bipy]$. The lowest (π, π^*) transition of the coordinating bipyridine is red-shifted for the substitution of CO by $P\phi_3$. This indicates the transition energy of $[M(CO)_4bipy]$ should be plotted in the region from $n=0$ to $n=1$ but not near $n=2$.
-◐-: vanadium compounds, -◑-: chromium compounds
-○-: cobalt compounds, □ : $[M(CO)_4bipy]$
◪ : $[M(CO)_3P\phi_3bipy]$

complex, electron affinity of the metal atom in such an environment is still higher than that of such a neutral complex as $[Cr(CO)_4bipy]$. In the former, metal $d\sigma$ orbital is appreciably lower than bipyridine π^* orbital, while in the latter, metal $d\sigma$ orbital is still higher than bipyridine π^* orbital, even though it is fairly lowered by a positive charge arising from the "metal to carbonyl" back-donation. Actually $[Cr(CO)_4bipy]$ traps an electron in the bipyridine π^* orbital in the first stage of reduction, however, the trapped electron can be readily transfered into the $d\sigma$ orbital. Another electron furnished in the second stage of reduction may occupy $d\sigma$ orbital. When metal $d\sigma$ orbital is occupied, a hexacoordinate complex turns out to be a pentacoordinate complex or a complex dimer evolving carbon monoxide.

BULLETIN OF THE CHEMICAL SOCIETY OF JAPAN, VOL. 45, 477—481 (1972)

Studies on New Derivatives of 8-Quinolinol as Chelating Agents. I. Syntheses, Coloration Reaction with Metal Ions and Acid Dissociation Constants of Some Azomethine and Aminomethyl Derivatives

Takehisa HATA and Toyozo UNO

Faculty of Pharmaceutical Sciences, Kyoto University, Yoshida, Sakyo-ku, Kyoto

(Received July 28, 1971)

Azomethine derivatives of 8-hydroxyquinoline-2-carbaldehyde with aromatic and aliphatic amines and their aminomethyl derivatives were synthesized for the purpose of investigating their applications as analytical reagents. Spot tests with metal ions revealed that azomethine derivatives form intensely colored chelates, whereas aminomethyl derivatives form less intensely colored chelates. The acid dissociation constants were determined by means of potentiometric titration in 50 v/v% aqueous dioxane solution at 25±0.1°C. The values of pK_{NH^+} and pK_{OH} of 8-hydroxyquinoline-2-carbaldehyde, 2-(*o*-hydroxyphenylaminomethyl)-, 2-(*p*-chlorophenylaminomethyl)-, 2-(*p*-tolylaminomethyl)- and 2-(naphthylaminomethyl)-8-quinolinol are lower than those of 8-quinolinol. The phenyl substituent in 2 position of oxine moiety exerts an acid strengthening effect on these ligands. The basicity of the ligand *N*,*N'*-bis-(8-hydroxy-2-quinolylmethyl) ethylenediamine is higher than that of other oxine derivatives.

A number of derivatives of oxine have been prepared for the purpose of finding analytical reagents. However, the search has been confined to derivatives containing only the same coordinative groups as oxine, and little effort has been made to find multidentate ligands. As the ligands having additional coordinative groups, the azo derivatives,[1] 2-aminomethyl-,[2] and 2-hydroxymethyl-8-quinolinol[2] havebeen studied. In fact, 2-aminomethyl-8-quinolinol was confirmed to act as terdentate ligand with Cu^{2+}, Ni^{2+}, Co^{2+}, and Zn^{2+} ions to produce more stable chelates than oxine.

Expecting the multidentate ligands derived from oxine to have excellent properties as analytical reagents, we attempted to synthesize 8-hydroxyquinoline-2-carbaldehyde, azomethine, and aminomethyl derivatives.

Azomethine derivatives were prepared from 8-hydroxyquinoline-2-carbaldehyde and primary amines. Condensation of the aldehyde with ethylenediamine, *o*-aminophenol, *p*-chloroaniline, *p*-toluidine, and naphthylamine in ethanol proceeded easily with gentle warming to give azomethine derivatives. Aminomethyl derivatives were prepared by the reduction of the azomethine derivatives with sodium borohydride in dioxane or ethanol at room temperature. The reaction scheme is given in Chart 1a and 1b.

We investigated the coloration reaction with metal ions and the acid dissociation constants of these derivatives in comparison with those of oxine in order to obtain information on their applicability as analytical reagents.

Experimental

Preparation. 8-Acetoxyquinoline-2-carbaldehyde: To a suspension of 5.8 g of freshly sublimed selenium dioxide in 400 m*l* of dioxane warmed with stirring on a water bath at 50—55°C, was added a solution of 11.4 g of 2-methyl-8-

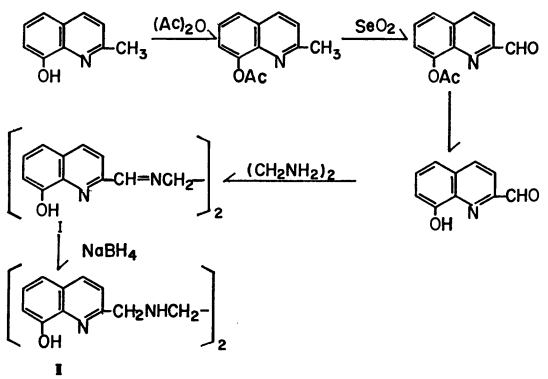

Chart 1a.

* Present address: Yoshida, Shimoadachi-cho, Sakyo-ku, Kyoto.

1) T. Boyd, E. F. Degering, and R. N. Shreve., *Ind. Eng. Chem., Anal.* **Ed.**, 10, 606 (1938).

2) R. L. Stevenson and H. Preiser, *Anal. Chem.*, **39**, 1354 (1967).

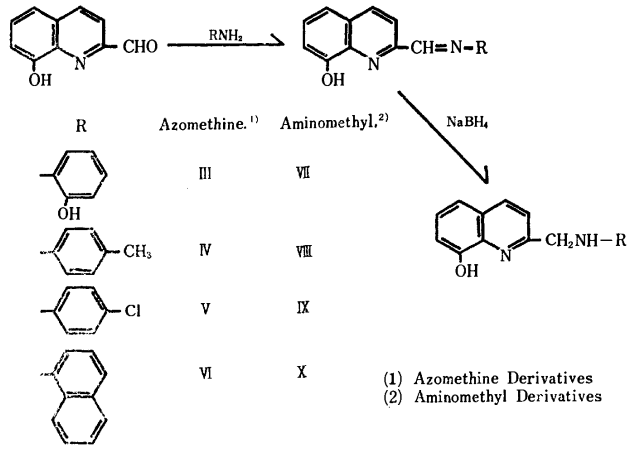

Chart 1b.

acetoxyquinoline in 50 m*l* of dioxane during the course of 3 hours. The mixture was heated to 75—80°C, allowed to stand for 2 hr, filtered, and dioxane was distilled off under reduced pressure. The residue was recrystallized from dioxane to give 9.0 g of light yellow crystals, mp 94—95°C. Found: C, 67.23; H, 4.37; N, 6.71%. Calcd for $C_{12}H_9NO_3$: C, 66.98; H, 4.21; N, 6.51%.

8-Hydroxyquinoline-2-carbaldehyde. A solution of 20 g of 8-acetoxyquinoline-2-carbaldehyde in toluene was cooled to −3°C, and stirred vigorously while 1440 m*l* of aqueous potassium hydroxide was added over 40—50 minutes. The mixture was allowed to stand at room temperature for 30 minutes, and neutralized with 20% aqueous acetic acid. The yellow powder precipitated was recrystallized from cyclohexane to give 13.5 g of yellow crystals, mp 98°C. Found: C, 69.25; H, 3.97; N, 8.26%. Calcd for $C_{10}H_7NO_2$: C, 69.36; H, 4.07; N, 8.08%.

N,N-*Bis(8-hydroxy-2-quinolylmethylene)ethylenediamine (I):* To a solution of 2 g of 8-hydroxyquinoline-2-carbaldehyde in ethanol, was added a solution of 0.35 g of ethylenediamine in ethanol. The mixture was warmed on a water bath for 30 min., cooled in an icebath, and the crystals were filterd. Recrystallization from ethanol gave 1.9 g of white crystals.

N,N′-*Bis(8-hydroxy-2-quinolylmethyl)ethylenediamine (II):* To a suspension of 2.0 g of I in 25 m*l* of ethanol, was added dropwise a solution of 0.8 g of sodium borohydride in ethanol at room temperature. The mixture was kept standing for 1 hr., filtered, and ethanol was removed under reduced pressure. Yellow powder obtained was dissolved in 30% aqueous acetic acid, neutralized with aqueous sodium carbonate. An oily substance appeared on the surface crystallized gradually on standing. Recrystallization from dioxane gave 1.2 g of light yellow crystals.

N-*(8-Hydroxy-2-quinolylmethylene)*-o-*aminophenol (III):* To a solution of 2 g of 8-hydroxyquinoline-2-carbaldehyde in boiling ethanol was added a solution of 1.26 g of *o*-aminophenol in ethanol. The mixture was cooled in an ice bath, and the crystals were filtered and recrystallized from ethanol to give 2.8 g of yellow crystals.

2-(o-Hydroxyphenylaminomethyl)-8-quinolinol (VII): To a suspension of 0.4 g of sodium borohydride in 25 m*l* of dioxane was added dropwise a solution of 1 g of III in 10 m*l* of dioxane at room temperature. The mixture was kept standing for 1.5 hr and was added to the 2—4 equivalent volume of water. This solution was concentrated and the oil separated was crystallized with chilling in an ice bath. Recrystallization from aqueous ethanol gave 0.6 g of white crystals.

The other azomethine and aminomethyl derivatives were prepared by the same method as described above. The melting points and analytical data of the synthesized derivatives are given in Table 1.

Potentiometric titration. Since all the aminomethyl derivatives synthesized are insoluble in water, the potentiometric titration was carried out in 50 v/v% aqueous dioxane solution. A solution containing the ligands (10^{-3} mol/*l*) and perchloric acid ($1.0-2.0\times10^{-3}$ mol/*l*) in 50 v/v% aqueous dioxane solution was titrated with carbonate free 0.1 N KOH solution prepared according to Armstrong's method[3] and standardized against potassium hydrogen phthalate. During the course of titration, the temperature was maintained at 25±0.1°C and a stream of CO_2 free nitrogen was passed through the titration vessel. All the potentiometric measurements of pH were carried out with a Radiometer Titrator TTT 1 and Titrigraph equipped with a Radiometer G 203 B glass electrode and K 401 saturated calomel electrode. The instrument was standardized at pH 4.01 and 6.86 using a Toa Electronics buffer solution. The pH meter correction and ion products of water for solution of 50 v/v% aqueous dioxane were determined to be −0.12 and 15.38, respectively. These values are in agreement with those reported recently by Irving,[4] and Taka-

Table 1. Azomethine and aminomethyl derivatives

Derivative No.	Mp (°C)	Formula	Analysis (%) Calcd C	Calcd H	Calcd N	Found C	Found H	Found N
I	165—166	$C_{22}H_{18}N_4O_2$	71.34	4.89	15.12	71.15	5.19	15.06
II	167—168	$C_{22}H_{22}N_4O_2$	70.57	5.92	14.96	70.58	5.76	14.75
III	168—169	$C_{16}H_{12}N_2O_2$	72.71	4.58	10.60	72.71	4.79	10.44
IV	104—105	$C_{17}H_{14}N_2O$	77.84	5.38	10.68	77.93	5.52	10.56
V	135—136	$C_{16}H_{11}N_2OCl$	67.98	3.92	9.91	67.89	4.08	9.73
VI	123—124	$C_{20}H_{14}N_2O$	80.51	4.73	9.39	80.80	4.97	9.22
VII	134—135	$C_{16}H_{14}N_2O$	72.16	5.30	10.52	72.28	5.25	10.36
VIII	114—115	$C_{17}H_{16}N_2O$	77.25	6.10	10.60	76.99	6.24	10.54
IX	153—154	$C_{16}H_{13}N_2OCl$	67.48	4.60	9.84	67.52	4.34	9.72
X	164—165	$C_{20}H_{16}N_2O$	79.98	5.37	9.33	80.04	5.54	9.26

3) D. M. G. Armstrong, *Chem. Ind.*, (London) **1955**, 1405.
4) H. M. N. H. Irving and H. S. Rossoti, *J. Inorg. Nucl. Chem.*, **30**, 1215 (1968)

Table 2. Spot tests[a)]

Metal Ion	Derivative					
	oxine	I	III	IV	II	VII
Fe^{3+}	dark green(p)[b)]	brownish red(p)	black(p)	black(p)	green	brownish red(p)
Fe^{2+}	dark green(p)	black red((p)	black(p)	black(p)	green	brownish red(p)
Cu^{2+}	green(p)	brownish orange	orange(p)	orange(p)	light yellow	green
Co^{2+}	light yellow	orange(p)	orange(p)	orange(p)	light yellow	light yellow
Ni^{2+}	light yellow	red(p)	red(p)	brown(p)	light yellow	light yellow
Zn^{2+}	yellow	orange	reddish orange(p)	orange(p)	yellow	light yellow
Cd^{2+}	yellow(p)	orange	red(p)	orange(p)	yellow	light yellow
Mn^{2+}	yellow(p)	orange	red(p)	orange(p)	light yellow	light yellow

a) Metal ion solutions were added to 5% dioxane solution of oxine derivatives and the color changes of the solutions were observed at pH 6.8.
b) Precipitation occurred.

moto.[5)]

Results and Discussion

The results of the spot tests are shown in Table 2. The color reaction of the ligands obtained differs considerably from that of oxine as seen in Table 2. The results imply that the ligands may be useful as a metallochromic indicator and the reagents for colorimetric or gravimetric analysis.

The chelates of Fe^{3+}, Fe^{2+}, Cu^{2+}, Ni^{2+}, and Co^{2+} with azomethine derivatives can be extracted into the organic solvents such as isoamyl alcohol and chloroform. Among the ligands whose structures are given in Chart 1, ligands I and III form the most intensely colored chelates.

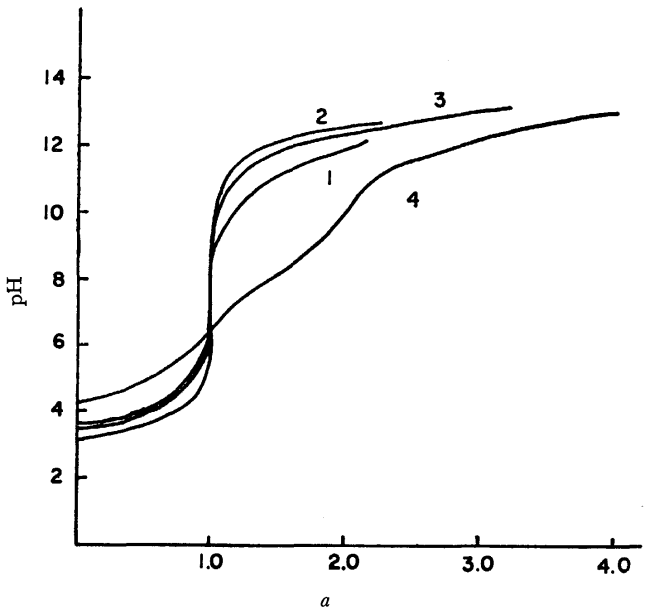

Fig. 1. Potentiometric titration curves of 8-quinolinol derivatives in 50 v/v% aqueous dioxane solution, $\mu=0.1$, 25°C; abscissa a represents moles of base added per mole of ligand.
Curve 1. 8-hydroxyquinoline-2-carbaldehyde
2. 2-(*p*-tolylaminomethyl)-8-quinolinol
3. 2-(*o*-hydroxyphenylaminomethyl)-8-quinolinol
4. *N*,*N*-bis(8-hydroxyquinolyl)ethylenediamine

Azomethine derivatives studied in this work were found to hydrolyze readily in aqueous solution and their acid dissociattion constants could not be determined. The acid dissociation constants of aminomethyl derivatives were determined in 50 v/v% aqueous dioxane solution. The potentiometric titration curves of these ligand are shown in Fig. 1.

As regards the curves of ligands VIII, IX, and X, the separation of two dissociation steps is shown clearly by the pH jump at $a=1$. The first and second steps correspond to the dissociation of proton from the quinoline nitrogen and hydroxyl groups, respectively. The titration curve of ligand VII indicates that the dissociation of proton from quinoline nitrogen occurs in acidic region and the dissociation of two hydroxyl groups overlaps in alkaline region. The titration curve of ligand II exhibits two pH jumps at $a=1$ and $a=2$. This shows that the dissociation of proton from the imino groups occurs in the neutral region and the dissociation from the hydroxyl groups overlaps in the alkaline region.

The acid dissociation constants were calculated by Schwarzenbach's[6)] method with the use of the following equations.

$$K_1 = \frac{[HL]}{[L]\cdot[H^+]},\ K_2 = \frac{[H_2L]}{[HL]\cdot[H^+]},\ \cdots,$$
$$K_j = \frac{[H_jL]}{[H_{j-1}L]\cdot[H^+]} \quad (1)$$

$$[L]_t = \sum_{j=0}^{m}[H_jL] \quad (2)$$

$$[H]_t = [H^+] - [OH^-] + \sum_{j=0}^{m} j\cdot[H_jL] \quad (3)$$

$$\sum_{j=0}^{m}(g-j)\cdot[H^+]^j\cdot\overline{K}_j = 0 \quad (4)$$

$$(\overline{K} = K_1\cdot K_2\cdot K_3\cdots K_j)$$

where

$K_1, K_2, K_3, \cdots, K_j$: the successive acid stability constants

$[L]_t$: total acid concentration

5) S. Takamoto, Q. Fernand, and H. Freiser, *Anal. Chem.*, **37**, 1249 (1965)

6) G. Schwarzenbach, *Helv. Chim. Acta*, **33**, 947 (1950)

$[H]_t$: total acid concentration

g: average number of moles of proton bound per mole of ligand

m: maximum number of moles of proton per mole of ligand

Applying Schwarzenbach's method to ligand [II] (H_4L^{2+}), Eq. (4) is modified to be

$$g + (g-1)\cdot K_1\cdot[H^+] + (g-2)\cdot \bar{K}_2\cdot[H^+]^2 + (g-3)\cdot \bar{K}_3\cdot[H^+]^3 + (g-4)\cdot \bar{K}_4\cdot[H^+]^4 = 0 \quad (5)$$

As is apparent from the titration curve 4 in Fig. 1, there exist two species H_4L^{2+} and H_3L^+ between $a=0$ and $a=1$, two species H_3L^+ and H_2L between $a=1$ and $a=2$, and three spcies H_2L, HL^-, and L^{2-} between $a=2$ and $a=4$. Thus, Eq. (5) can be approximated by the following equations in the first, second, and third buffer regions, respectively.

$$(g-3) + (g-4)\cdot K_4\cdot[H^+] = 0 \quad (6)$$

$$(g-2) + (g-3)\cdot K_3\cdot[H^+] = 0 \quad (7)$$

$$g + (g-1)\cdot K_1\cdot[H^+] + (g-2)\cdot \bar{K}_2\cdot[H^+]^2 = 0 \quad (8)$$

Since g and $[H^+]$ are determined experimentally, the acid stability constants K_3 and K_4 can be calculated from Eqs. (6) and (7), and the overlapping acid stability constants K_1 and K_2 are calculated by the least squares method from Eq. (8). The results are summarized in Tables 3 and 4, and are compared with the dissociation constant of oxine.

As shown in Table 3, the pK_{NH^+} (the dissociation constant of quinoline nitrogen) and pK_{OH} values of these ligands are lower than the corresponding values of oxine. In 8-hydroxyquinoline-2-carbaldehyde, the dissociation constants are in agreement with the values reported in literature (pK_{NH^+} <3, pK_{OH}=10.24).[2]

The pK_{OH} values of 2-(tolylaminomethyl)-, 2-(*p*-chloroaminomethyl)-, and 2-(α-naphthylaminomethyl)-8-quinolinol are almost the same and pK_{NH^+} values increase in the order IX<X<VII<oxine. Thus it is supposed that the electron-withdrawing effect of phenyl group affects the quinoline ring through the $=CH_2NH-$ group and the substituent in the phenyl ring influences 1 position to some extent, but not 8 position of quinoline. Since the methyl group in 4 position of benzene ring behaves as an electron-donating group and the chloro group as an electron-withdrawing group, the pK_{NH^+} value of ligand VIII is higher than that of ligand IX.

In the *o*-hydroxy derivative 2-(*o*-hydroxyphenylaminomethyl)-8-quinolinol (VII), assingnment of the two values of pK_{OH} is very difficult. In 5-(*o*-hydroxyphenylazo)-8-quinolinol,[5] the dissociation constant of the quinoline hydroxyl group and that of the phenyl hydroxyl group have been reported to be 8.51 and 12.0, respectively. As shown in Table 3, the pK_{OH} values of ligands VIII, IX, and

TABLE 3. ACID DISSOCIATION CONSTANTS OF AMINOMETHYL DERIVATIVES IN 50 v/v% AQUEOUS DIOXANE SOLUTION AT 25°C, μ=0.1 (KCL)

Substituent in 8-quinolinol	pK_{NH^+}	pK_{OH}	pK_{OH}
None	3.97	11.54	
2-formyl	<3	9.92±0.02	
2-(*p*-tolylaminomethyl)	3.62±0.02	11.11±0.03	
2-(*p*-chlorophenyl-aminomethyl)	3.19±0.02	11.10±0.02	
2-(naphthyl-aminomethyl)	3.39±0.02	11.11±0.03	
2-(*o*-hydroxyphenyl-aminomethyl)	3.71±0.03	10.86	11.35

TABLE 4. COMPARISON OF ACID DISSOCIATION CONSTANTS

	$pK_{NH_2^+}$	$pK_{NH_2^+}$	pK_{OH}	pK_{OH}
ligand[a]	5.12	8.15	10.81	11.35
EDDA[b]	6.42	9.46		
EDAMP[c]	5.45	8.23		

a) 50 v/v% aqueous dioxane solution, μ=0.1 (KCl), at 25°C.
b) Aqueous solution, μ=0.1 (KCl), at 30°C.
c) Aqueous solution, μ=0.1 (KNO_3), at 25°C.

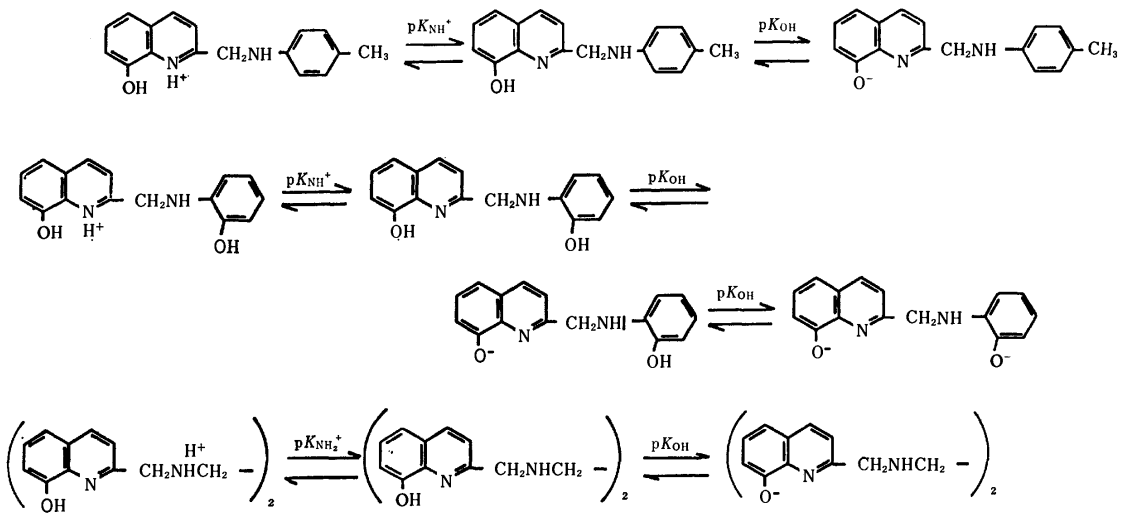

Chart 2

X are lower than those of oxine by about 0.4 log unit. Thus, we assigned the lower value (10.86) of pK_{OH} to the dissociation constant of the hydroxyl group in the quinoline ring and the higher value (11.35) to that of the hydroxyl group in the benzene ring.

In Table 4, the two $pK_{NH_2^+}$ values of ligand II corresponding to the dissociation of the imino groups are compared with those of the aliphatic analog, ethylenediaminediacetic acid (EDDA)[7] and the aromatic analog, ethylene-bis(2-aminomethyl)pyridine (EDAMP).[8] The $pK_{NH_2^+}$ values are similar to those of EDAMP and lower than those of EDDA. This suggests that the dissociation steps between $a=0$ and $a=2$ in the titration curve 4 in Fig. 1 do not correspond to the dissociation of proton from quinoline nitrogen, but to that from the imino group.

Since the basicity of ligand II is higher than that of other oxine derivatives and the ligand is expected to behave as the multidentate ligand, it is presumed that it forms more stable chelates with various metal ions than other oxine derivatives.

The equilibria involving quinoline nitrogen, hydroxyl groups and imino groups in 50 v/v% aqueous dioxane solution may be represented as shown in Chart 2. The dissociation steps of the hydroxyl groups of ligand VII are not completely clarified.

7) S. Chaberek and A. E. Martell, *J. Amer. Chem. Soc.*, **74**, 6228 (1952)

8) R. G. Lacoste and A. E. Martell, *Inorg. Chem.*, **3**, 881 (1964)

BULLETIN OF THE CHEMICAL SOCIETY OF JAPAN, VOL. 45, 481—484 (1972)

Syntheses of Some Medium Sized Cyclic Triamines and Their Cobalt(III) Complexes[1)]

Hiroyuki KOYAMA* and Tamotsu YOSHINO

Department of Chemisty, Faculty of Science, Kyushu University, Hakozaki, Fukuoka

(Received July 30, 1971)

Four cyclic triamines of a medium ring size (9—12-membered ring) which form three mutually-adjacent five- and/or six-membered chelate rings on complexation, such as 1,4,7-triazacyclononane (abbreviated TACN), 1,4,7-triazacyclodecane (TACD), 1,4,8-triazacycloundecane (TACUD), and 1,5,9-triazacyclododecane (TACDD) were synthesized and isolated as their trihydrobromides. The complexation of TACN and TACD with a cobalt(III) salt yielded metal complexes of a sandwich-type structure, such as $[Co(TACN)_2]Br_3$ and $[Co(TACD)_2]Br_3 \cdot H_2O$, which were then isolated. In the case of TACUD, a complex $[Co(TACUD)BrCl_2]$ containing only one molecule of the triamine was isolated. However, although the formation of a cobalt(III) complex with TACDD in solution was inferred spectroscopically, no expected complex was isolable. On the basis of the spectrophotometric data, the ligand-field strength was found to increase in the following order:

$$[Co(NH_3)_6]^{3+} < [Co(TACD)_2]^{3+} < [Co\ en_3]^{3+} < [Co(TACN)_2]^{3+}.$$

In this decade a large number of metal chelates with a quadridentate macrocyclic compound have been synthesized, and most of them have been investigated in considerable detail.[2)] In contrast with this, only a few metal complexes with cyclic tridentate ligands of a medium ring size have been studied.[3,4)] It is well known that an appreciable strain exists in a cyclic hydrocarbon of a medium ring size.

A similar strain appears to exist also in a comparable cyclic triamine,[5)] whose coordination to a metal ion may result in the formation of three mutually-adjacent five- and/or six-membered chelate rings.

The stability of the complex formed by the coordination of such a cyclic triamine to metal ions is expected to depend on the sizes of the three chelate rings in addition to the above-mentioned strain. It seems to be of interest to synthesize such cyclic triamines and to examine the relative stability of their metal complexes.

With this in mind, we synthesized four cyclic triamines of a medium ring size (9—12-membered ring), such as 1,4,7-triazacyclononane (abbreviated TACN, formula I, expected to form three 5-membered chelate rings), 1,4,7-triazacyclodecane (TACD, II, one 6-membered and two 5-membered rings), 1,4,8-triazacycloundecane (TACUD, III, two 6-membered and

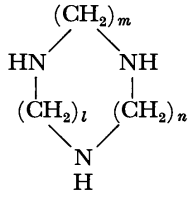

I	$l=2$, $m=2$, $n=2$	TACN
II	$l=3$, $m=2$, $n=2$	TACD
III	$l=3$, $m=3$, $n=2$	TACUD
IV	$l=3$, $m=3$, $n=3$	TACDD

Fig. 1. Structures of the ligands.

1) Presented at the 20th Symposium on Coordination Chemistry, Tokyo, November, 1970.

* Present address: Laboratory of Chemistry, College of General Education, Kyushu University, Ropponmatsu, Fukuoka.

2) B. Bosnich, C. K. Poon, and M. L. Tobe, *Inorg. Chem.*, **4**, 1102 (1965); J. P. Collman and P. W. Schneider, *ibid.*, **5**, 1380 (1966); N. F. Curtis, *J. Chem. Soc.*, **1964**, 2644; E. Ochiai and D. H. Busch, *Inorg. Chem.*, **8**, 1474 (1969).

3) L. T. Taylor and D. H. Busch, *ibid.*, **8**, 1366 (1969).

4) W. Rosen and D. H. Busch, *ibid.*, **9**, 262 (1970).

5) J. Dale, *J. Chem. Soc.*, **1963**, 93.

TABLE 1. PROPERTIES OF THE PRODUCTS

Compound[a]	Formula	Analysis % Found (Calcd) C	H	N	Mp °C	Yield %	Molecular weight Found (Calcd)
I	$C_6H_{18}Br_3N_3$	19.39 (19.38	4.85 4.88	11.25 11.30)	274—275	88	—
II	$C_7H_{20}Br_3N_3$	21.61 (21.78	5.27 5.22	10.65 10.88)	242—243	82	—
III	$C_8H_{22}Br_3N_3$	23.83 (24.02	5.53 5.54	10.51 10.51)	239.5—240	79	—
IV	$C_9H_{24}Br_3N_3$	25.89 (26.11	5.87 5.84	10.08 10.15)	267.5—268.5	62	—
V	$C_{25}H_{31}N_3O_6S_3$	53.28 (53.07	5.35 5.52	7.04 7.43)	173[b]	97	—
VI	$C_{26}H_{33}N_3O_6S_3$	54.02 (53.86	5.82 5.74	7.12 7.25)	119.5—121.5	66	—
VII	$C_{27}H_{35}N_3O_6S_3$	—	—	—	—	57	—
VIII	$C_{28}H_{35}N_3O_6S_3$	55.48 (55.51	5.89 5.82	6.90 6.94)	230—232	24	610 (605.8)
IX	$C_{29}H_{37}N_3O_6S_3$	56.08 (56.17	6.11 6.01	6.80 6.82)	213	25	618 (620.1)
X	$C_{30}H_{39}N_3O_6S_3$	56.67 (56.85	6.32 6.20	6.58 6.63)	172	8	638 (633.9)

a) I, II, III, and IV: As trihydrobromides.
b) Lit, mp 173°C: D. H. Peacock and U. C. Dutta, *J. Chem. Soc.*, **1934**, 1303.

one 5-membered rings), and 1,5,9-triazacyclododecane (TACDD, IV, three 6-membered rings), and isolated them as their trihydrobromides; we also characterized the intermediates obtained in the course of the syntheses as well as the products.

As the central metal ion to which the ligand coordinates, we chose the cobalt(III) ion, which is noted for its typical octahedral coordination, and studied the electronic spectra of the metal complexes formed. We wish now to report the results.

Experimental

All the melting and decomposition points are uncorrected. The infrared spectra were determined in potassium bromide disks on a Hitachi EPI-S2 spectrophotometer.

The NMR spectra were recorded at 60 MHz with a Hitachi R-20 spectrometer with $CDCl_3$ as the solvent, and the chemical shifts were reported in τ values relative to tetramethylsilane as the internal standard except for those attributable to *p*-toluenesulfonyl groups in VIII, IX, and X. The NMR data are given in the order of increasing multiplicity (*s*=singlet, *t*=triplet, *q*=quintet, and *m*=unresolved multiplet), integration, and coupling constant. The molecular weights were determined on a Hitachi Osmometer, type 115, using benzene as the solvent in the case of the tritosyl derivative of cyclic triamines and methanol in the case of the TACUD complex.

N,N',N''-*Tri*(p-*toluenesulfonyl*)*derivative of Open-chain Triamines V, VI, and VII.* To a solution of a triamine $H_2N(CH_2)_{2-3}NH(CH_2)_{2-3}NH_2$ (0.1 mol) and sodium hydroxide (0.3 mol) in water (80 m*l*), there was added, drop by drop, a solution of *p*-toluenesulfonyl chloride (0.3 mol) in ether (150 m*l*); the mixture was then stirred for 1 hr at room temperature. A white precipitate thus formed was collected by filtration, washed with water, and recrystallized from a large amount of methanol to give colorless needles. VII was left as a pale yellow oil and used in the next step without further purification. The data are summarized in Table 1.

N,N',N''-*Tri*(p-*toluenesulfonyl*)*derivative of Cyclic Triamines VIII, IX, and X.* To a vigorously-stirred mixture of anhydrous potassium carbonate (40 g) in dimethylformamide (2 *l*) maintained at 120°C, there was added, drop by drop, a solution of tritosyl triamine (V,VI of VII) (0.03 mol) and 1,3-dibromopropane (0.03 mol) in dimethylformamide (350 m*l*) through a Hershberg's dropping funnel for 30—40 hr at the rate of one drop per 10 sec; the mixture was further stirred for 7 hr at 115—120°C, and then it was cooled to room temperature and filtered to remove any inorganic substances. The filtrate was concentrated to one tenth of the original volume and water (3 *l*) was added to deposit a precipitate, which was then extracted with hot benzene (2 *l*).

The benzene extract was dried over anhydrous sodium sulfate. The solvent benzene was removed to leave a viscous brown-yellow oil of crude tritosyl derivative of the cyclic amine, which was dissolved in ethanol (200 m*l*) and then left to stand to separate colorless needles, which were subsequently recrystallized from ethanolic benzene. The data are summarized in Table 1.

NMR for VIII: τ 7.80 (*m*, 2H), 6.79 (*t*, 4H, J=6 Hz), 6.62 (*s*, 8H).

NMR for IX: τ 8.10 (*m*, 4H), 6.98 (*t*, 4H, J=6 Hz), 6.71 (*s*, 4H), 6.56 (*t*, 4H, J=7 Hz).

NMR for X: τ 8.80 (*q*, 6H, J=6.5 Hz), 6.76 (*t*, 12H, J=6.5 Hz).

Trihydrobromide of 1,4,7-Triazacyclononane (I). This compound (TACN·3HBr) was obtained by hydrolyzing *N,N'*-ditosyl TACN[6] with 30% hydrobromic acid and acetic acid.[7]

Trihydrobromides of Cyclic Triamines II, III, and IV. A tosyl derivative of the cyclic triamine (VIII, IX, or X)

6) D. H. Peacock and Y. S. Gwan, *J. Chem. Soc.*, **1937**, 1468.
7) A mixture prepared by adding glacial acetic acid (9 volume) to 47% hydrobromic acid (16 volume).

(0.004 mol) was dissolved by heating it in 30% hydrobromic acid and acetic acid[7] (300 ml) and then refluxed with stirring for 2 days. The solution was concentrated to one tenth of the original volume; after cooling, ether (200 ml) was added to separate crystals, which were collected, washed repeatedly with ether and then with ethanol, and recyrstallized from 95% acetic acid. The data are summarized in Table 1.

Syntheses of Co(III) Complexes. The amounts of cobalt(II) salt, the cyclic triamine trihydrobromide, and alkali were chosen so as have a molar ratio of 1 : 2 : 5.

Bis(1,4,7-triazacyclononane)cobalt(III) Tribromide (TACN Complex). A solution of $CoCl_2 \cdot 6H_2O$ (94 mg) in water (2 ml) was mixed with a solution of TACN·3HBr(I) (294 mg) and sodium hydroxide (79 mg) in water (3 ml). Air bubbles were passed through the mixture until yellow plates separated fully on the wall of the vessel. After the orange-yellow color of the solution had turned deep red, the precipitate was collected by filtration and washed with ethanol. The concentration of the filtrate gave an additional product (127 mg, 58%); dp>280°C, Λ_M 376 ohm^{-1} cm^2mol^{-1}.

Found: C, 25.95; H, 5.63; N, 14.98%. Calcd for $CoC_{12}H_{30}Br_3N_6$: C, 25.87; H, 5.43; N, 15.08%.

IR: 3080, 3020 (νNH), 990, 905 cm^{-1} (δ_{rock} CH_2).

Bis(1,4,7-triazacyclodecane)cobalt(III) Tribromide Monohydrate (TACD Complex). Air was bubbled for 7 hr into a solution of $CoCl_2 \cdot 6H_2O$ (94 mg), TACD·3HBr(II) (334 mg), and sodium hydroxide (87 mg) in water (10 ml). After the reddish-orange color of the solution had turned dark purple, the solution was concentrated to a half of its original volume; ethanol of twice the volume of the concentrated solution was then added to separate orange needles (135 mg, 56.9%); dp 230—270°C, Λ_M 350 ohm^{-1} cm^2 mol^{-1}.

Found: C, 28.34; H, 6.20; N, 13.50%. Calcd for $CoC_{14}H_{34}Br_3N_6 \cdot H_2O$: C, 27.88; H, 6.02; N, 13.93%.

IR: 3095, 3030 (νNH), 980, 910 cm^{-1} (δ_{rock} CH_2).

Bromodichloro(1,4,8-triazacycloundecane)cobalt(III) (TACUD Complex). Air was bubbled for 6 hr into a solution of $CoCl_2 \cdot 6H_2O$ (85 mg), TACUD·3HBr(III) (286 mg), and potassium hydroxide (100 mg) in 60% aqueous ethanol (10 ml). The mixture was evaporated to dryness. The residue was dissolved in a small amount of hot ethanol. Undissolved inorganic materials were removed by filtration. The filtrate was concentrated on a steam-bath, and the wall of the vessel was rubbed with a glass rod to separate dull red prisms. After the repetition of the treatment to remove the undissolved materials, the crystals were collected, washed with a small amount of ethanol, and dried at 65°C *in vacuo* (51 mg, 38.9%); dp 195—210°C, Λ_M 176 ohm^{-1} cm^2 mol^{-1}.

Found: C, 26.01; H, 5.60; N, 11.21%; mol wt 371. Calcd for $CoC_8H_{19}BrCl_2N_3$: C, 26.18; H, 5.22; N, 11.45%; mol wt 367.0.

IR: 3255, 3095 (νNH), 985, 900 cm^{-1} (δ_{rock} CH_2).

An Attempt to Isolate the TACDD Complex. Although the initial yellow-orange color of a solution of cobalt(II) salt, the ligand (TACDD·3HBr), and alkali in 60% ethanol turned dull red upon an air oxidation similar to that described above, an attempt to isolate the complex was unsuccessful.

Results and Discussion

The trihydrobromide of TACN (I) was obtained by hydrolyzing *N,N'*-ditosyl TACN,[6] whose IR spectrum showed, as expected, a band of medium intensity at 3360 cm^{-1} due to the NH stretching vibration, indicating the existence of a hydrogen atom attached to a nitrogen atom.

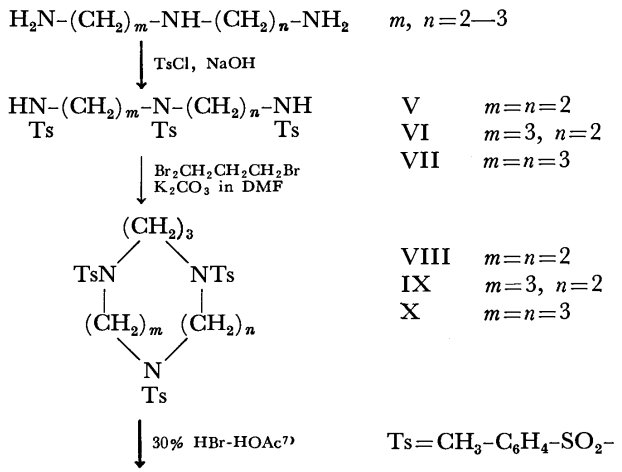

Fig. 2. The synthetic schemes of cyclic triamines (10 - 12-membered ring).

The synthetic schemes of cyclic triamines (10—12-membered ring) are shown in Fig. 2. The tritosylates of TACD (VIII), TACUD (IX), and TACDD (X) were each synthesized by the cyclization of an appropriate tritosylated open-chain triamine with 1,3-dibromopropane in the presence of anhydrous potassium carbonate in dimethylformamide under the conditions of a high dilution. These tritosylated triamines showed no NH stretching band. This means that the tritosylates have no end $-NH-SO_2C_6H_4CH_3$ group. The NMR spectra also supported the lack of the end group. The absence of the end group, coupled with the results of the elementary analyses and of the molecular-weight determination, indicates that these tritosylated triamines are monomers with a cyclic structure.

These tritosylated triamines were hydrolyzed with 30% hydrobromic acid and acetic acid[7] to yield the corresponding trihydrobromides of the triamines.

The IR spectra of the trihydrobromides exhibited complicated absorption bands with a strong intensity between 2900 and 2200 cm^{-1} characteristic of secondary amine salt, and also exhibited two resolved peaks or a peak with a shoulder between 1595 and 1545 cm^{-1} due to the bending vibration of NH_2^+. These facts are also consistent with the cyclic structure of the triamines. In order to study the metal complex, a mixture containing cobalt(II) salt, the cyclic triamine trihydrobromide, and alkali in a molar ratio of 1 : 2 : 5 was oxidized by passing air bubbles through; the separated metal complex was thus isolated. The composition of cobalt(III) complexes of TACN, TACD, and TACUD was confirmed by elementary analyses. The cobalt(III) complexes of TACN and TACD were formulated as, respectively, $[Co(TACN)_2]Br_3$ and $[Co(TACD)_2]Br_3 \cdot H_2O$. Their molar conductance data showed that the complexes of TACN and TACD were 3 : 1 electrolytes.

These facts, as well as their electronic spectra, indicated that all six nitrogen atoms of the cyclic ligands were coordinated to a central metal atom. This means that the complexes of TACN and TACD probably

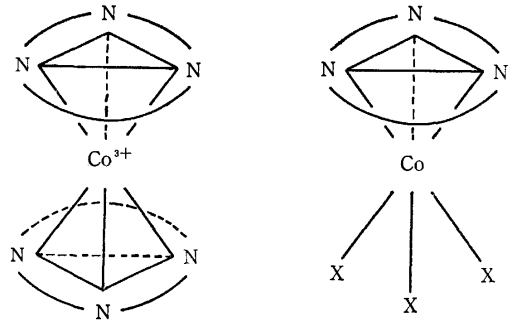

Fig. 3. A sandwich-type complex and a complex molecule (X=halogen).

have the sandwich-type structure shown in Fig. 3. The cobalt(III) complex of TACUD was formulated as $[Co(TACUD)BrCl_2]$. Its electronic spectrum is distinctly different from that of the complex of TACN and TACD described above. These facts suggest that three nitrogen atoms of the cyclic ligand occupy the corners of one octahedral face of the central metal atom, as is shown in Fig. 3. The TACUD complex showed molar conductance data nearly corresponding to those of a 2 : 1 electrolyte.

This suggests that the TACUD complex may be subject to hydrolysis in an aqueous solution much like a diethylenetriamine complex $[Co(dien)Cl_3]$.[8]

The formation of a complex with TACDD in an aqueous solution was inferred from its visible spectral similarity with the TACUD complex. The complexes of TACN, TACD, and TACUD exhibited two NH stretching bands of a strong intensity in the range of 3095 to 3020 cm^{-1}, and also exhibited two bands of medium intensity between 990 and 900 cm^{-1}; they were assigned to the CH_2 rocking vibration. On the basis of X-ray analysis[9] and infrared studies[10] of ethylenediamine complexes, it was confirmed that the conformation of the ethylene portions in the chelate ring of cyclic triamine complexes was nearly *gauche*. The electronic absorption maxima of the complexes in aqueous solutions are summarized in Table 2, along with those of the other $Co-N_6$ complexes. The ligand-field strength increased in the following order:

$$[Co(NH_3)_6]^{3+} < [Co(TACD)_2]^{3+} < [Co\,en_3]^{3+} < [Co(TACN)_2]^{3+}$$

From an examination of the Dreiding model, in the cases of TACN and TACD complexes the interatomic distances for the three inner-oriented hydrogens in a cyclic ligand were estimated to be 2.0—2.2 Å and 1.7—1.9 Å; the distances between hydrogens projecting from the two separate cyclic ligands were measured as 1.9—2.1 Å and 1.8—2.0 Å respectively. From the above investigation, the TACN complex can be said to be almost strain-free with respect to bond lengths and bond angles; therefore, the non-bonded H–H interaction must be negligible. It is interesting to note that TACN has stronger ligand-field strength than ethylenediamine. On the contrary, it appears that the TACD complex is more unstable than the TACN complex because of the increasing repulsion between non-bonded atoms and the expansion of the bond angles of nitrogen-metal-nitrogen.

On the other hand, the sandwich-type complexes of TACUD and TACDD were no longer formed because of cumulative ring strain and repulsion; in return, only one cyclic tridentate ligand and three halogens were coordinated to a metal ion.

TABLE 2. ELECTRONIC ABSORPTION MAXIMA OF THE COBALT(III) COMPLEXES IN AQUEOUS SOLUTIONS

$\tilde{\nu}_{max}$[a] (log ε_{max})

Complex	First band	Second band
$[Co(NH_3)_6]^{3+}$	20.92 (1.75)	29.15 (1.66)
$[Co(en)_3]^{3+}$	21.47 (1.94)	29.60 (1.90)
$[Co(TACN)_2]^{3+}$	21.64 (2.00)	30.03 (1.95)
$[Co(TACD)_2]^{3+}$	21.19 (1.87)	29.24 (1.95)
$Co(TACUD)BrCl_2$[b]	18.69	*ca.* 26.38
TACUD complex[c]	18.94	*ca.* 26.45
TACDD complex[c]	18.52	*ca.* 26.32

a) In the unit of kK.
b) Reflectance data.
c) Aquated complex.

8) P. H. Crayton and J. A. Mattern, *J. Inorg. Nucl. Chem.*, **13**, 248 (1960).
9) A. Nakahara, Y. Saito, and H. Kuroya, This Bulletin, **25**, 331 (1952); K. Nakatsu, Y. Saito, and H. Kuroya, *ibid.*, **29**, 428 (1956).
10) S. Mizushima, I. Ichijima, I. Nakagawa, and J. V. Quagliano, *J. Phys. Chem.*, **59**, 293 (1955).

The Reaction of Bis(acetylacetonato)cobalt(II) with Bromine in Dichloromethane

Yukio NAKAMURA, Nobuko KANEHISA, and Shinichi KAWAGUCHI

Department of Chemistry, Faculty of Science, Osaka City University, Sumiyoshi-ku, Osaka

(Received July 30, 1971)

When bis(acetylacetonato)cobalt(II) is allowed to react with twice molar quantity of bromine in dichloromethane, cobalt(II) bromide and γ-bromoacetylacetone are produced ultimately. From a deep blue solution of an equimolar reaction mixture at 0°C an intermediary product was isolated and characterized to be dimeric bromo(acetylacetonato)cobalt(II) by means of elemental analysis and molecular weight determination. The structure of this compound was inferred to be tetrahedral from absorption spectra and magnetic data. Acetylacetonate groups were supposed to act as bridging ligands on the basis of IR data in the lower frequency region. Dibromobis(acetylacetonato)dicobalt(II) was also derived from dibromo(acetylacetone)cobalt(II) by the reaction with sodium acetylacetonate in acetylacetone at 0°C.

It is very interesting that products of reactions between bromine and various metal acetylacetonates in dichloromethane differ depending on the nature of the central metal. Quasiaromatic γ-substitution was observed in cases of beryllium[1] and aluminum[2] acetylacetonates, but copper(II)[3] and cobalt(III)[4] chelates underwent a rupture of chelate rings. In the latter cases copper(II) and cobalt(III) were reduced to lower oxidation states. In the case of the nickel(II) chelate which is known to be trimeric,[5] stepwise displacement of the acetylacetonate ligand by the bromide anion was observed prior to the final breakdown of the trimeric structure, resulting in nickel(II) bromide and γ-bromoacetylacetone.[6]

Bis(acetylacetonato)cobalt(II) is known to exist as a tetrameric molecule in crystals[7] and is trimeric in non-coordinating solvents.[8] Although the oligomeric structure seems to be much less stable in comparison with the trimeric structure of the nickel(II) chelate, some intermediate might be obtained in the reaction with bromine. In order to confirm this view the present study on the reaction between bis(acetylacetonato)cobalt(II) and bromine in dichloromethane has been undertaken, and a dimeric intermediary product dibromobis(acetylacetonato)dicobalt(II) was isolated and characterized.

Results and Discussion

Final Reaction Products. When a dichloromethane solution of bromine was added dropwise to a dichloromethane solution of bis(acetylacetonato)cobalt(II) at room temperature, the original purple color gradually turned violet, blue, and then greenish blue. The solution became turbid when an equimolar bromine was added, and then a yellow green precipitate separated and increased with further addition of bromine. Finally the solution became colorless after twice molar bromine was added to the chelate. The precipitate was filtered, washed, dried *in vacuo* at 130°C, and identified to be cobalt(II) bromide. Found: Co, 26.62; Br, 72.29%. The yield was 0.969 mol/mol of the starting chelate. The organic bromide in the filtrate was determined by iodimetry to be 1.92 g equiv/mol of the starting chelate. Thus the mass balance in the 1 : 2 reaction is given by

$$Co(acac)_2 + 2Br_2 = CoBr_2 + 2acacBr. \quad (1)$$

Here acac stands for an acetylacetonate anion and acacBr for γ-bromoacetylacetone.

Isolation and Characterization of the Intermediary Product. In order to get some clue to the intermediary product the reaction was studied at 0°C. Even at 0°C when twice molar bromine is allowed to react with bis(acetylacetonato)cobalt(II) in dichloromethane, the same stoichiometry as that at room temperature (1) is observed. On the contrary, when equimolar bromine was added at 0°C, no precipitation took place and the greenish blue solution did not become turbid.

The solution was concentrated by evaporation *in vacuo* at 0°C, to which petroleum ether was added to form a greenish blue precipitate. The precipitate was filtered in a desiccator containing phosphorus pentoxide, washed repeatedly with petroleum ether, and dried *in vacuo* at 100°C. Results of elemental analysis conformed to the formula CoBr(acac). Found: Co, 24.23; Br, 33.32; C, 24.47; H, 3.02%. Calcd for $CoBrC_5H_7O_2$: Co, 24.77; Br, 33.58; C, 25.24; H, 2.97%. When the 1 : 1 reaction was performed in a mixed solvent of dichloromethane and petroleum ether (1 : 5 in volume) at 0°C, the same compound precipitated without evaporation. This compound is stable in dry state even at room temperature. It is readily soluble in dichloromethane and chloroform, but less soluble in dioxane. When a dichloromethane solution is kept standing at room temperature, decomposition proceeds gradually and the solution becomes turbid after about 10 min. However, a dioxane solution is stable enough to allow determination of molecular weight. Special care was

1) Y. Nakamura and S. Kawaguchi, This Bulletin, **40**, 1179 (1967).
2) Y. Nakamura, M. Hirata, and S. Kawaguchi, *ibid.*, **40**, 2572 (1967).
3) Y. Nakamura and S. Kawaguchi, *ibid.*, **38**, 954 (1965); T. Ogura, Y. Kojima, Y. Nakamura, and S. Kawaguchi, *ibid.*, **38**, 1468 (1965).
4) Y. Nakamura, M. Gotani, and S. Kawaguchi, *ibid.*, **45**, 457 (1972).
5) G. J. Bullen, R. Mason, and P. Pauling, *Inorg. Chem.*, **4**, 456 (1965); D. P. Graddon and E. C. Watton, *Nature*, **190**, 906 (1961); F. A. Cotton and J. P. Fackler, Jr., *J. Amer. Chem. Soc.*, **83**, 2818 (1961).
6) K. Isobe, Y. Nakamura, and S. Kawaguchi, *Inorg. Nucl. Chem. Lett.*, **7**, 927 (1971).
7) F. A. Cotton and R. C. Elder, *Inorg. Chem.*, **4**, 1145 (1965).
8) J. P. Fackler, Jr., *ibid.*, **2**, 266 (1963); D. P. Graddon, *Nature*, **195**, 891 (1962).

taken in the isolation and manipulation of this compound to exclude atmospheric moisture.

Molecular weight was determined cryoscopically in dioxane to be 445, close to the value 475 calculated for the dimer $[CoBr(acac)]_2$. However, ebullioscopic determination in a methanol solution gave a value of 252 which is rather near that of monomeric form. It is conceivable that bromo(acetylacetonato)cobalt(II) exists as a dimer in solid state and also in non-donor solvents, but is monomeric in a coordinating solvent such as methanol. Thus the stoichiometry of the 1 : 1 reaction between bis(acetylacetonato)-cobalt(II) and bromine in dichloromethane at 0°C is represented by

$$Co(acac)_2 + Br_2 = \frac{1}{2}[CoBr(acac)]_2 + acacBr. \quad (2)$$

As shown in Fig. 1 the visible absorption spectrum of this compound in dichloromethane at 0°C is quite different from that of bis(acetylacetonato)cobalt(II) in the same solvent, but resembles that of cobalt(II) bromide in acetone,[9a] which is considered to assume a tetrahedral structure.[9] However, the spectrum in methanol is in turn similar to that of bis(acetylacetonato)cobalt(II) in dichloromethane, where the latter complex is oligomeric and seems to maintain the octahedral structure. These spectral data are well reconciled with the results of molecular weight determination, revealing that bromo(acetylacetonato)-cobalt(II) exists as a tetrahedral dimer in dichloromethane and as an octahedral monomer solvate in methanol.

The effective magnetic moment was determined by the Gouy method to be 4.30 B.M. per g-atom cobalt at room temperature. This value is appreciably lower than 5.02 B.M. at 302.6°K of octahedral bis-(acetylacetonato)diaquocobalt(II)[10] and near the usual value of 4.4—4.7 B.M. for tetrahedral cobalt-(II) compounds,[9b] supporting again the tetrahedral structure of the dimeric compound in question.

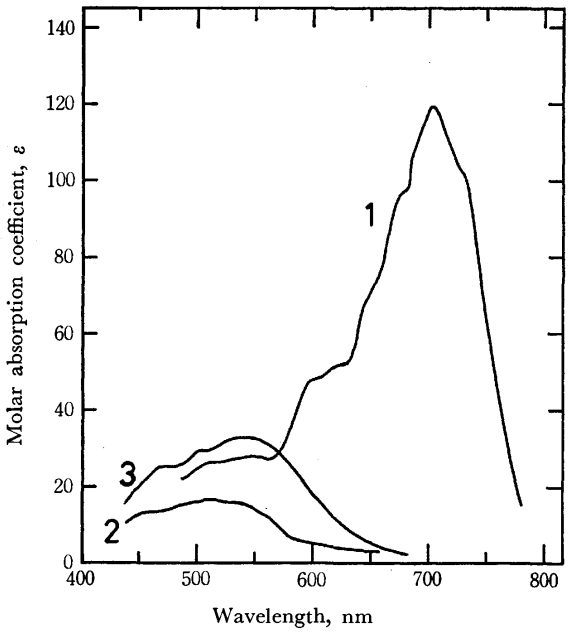

Fig. 1. Absorption spectra of CoBr(acac) in CH_2Cl_2 (curve 1) at 0°C and in methanol (curve 2) at room temperature, and of $Co(acac)_2$ in CH_2Cl_2 (curve 3).

Bromo(acetylacetonato)cobalt(II) is very hygroscopic and it is difficult to get an IR spectrum showing no band due to water. Broadening of the absorption curve in the 1600—1650 cm^{-1} region (Fig. 2) is due to the OH bending absorption of the contaminant water.

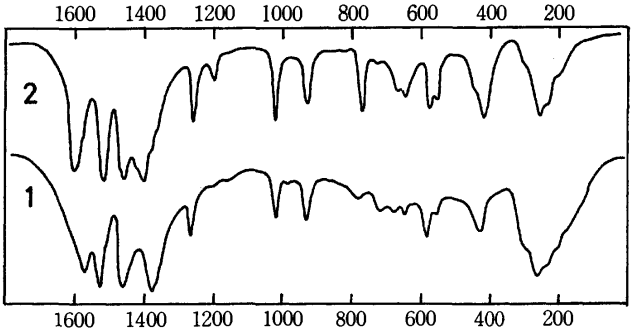

Fig. 2. Infrared spectra of CoBr(acac) (curve 1) and $Co(acac)_2$ (curve 2) in Nujol.

Absorption bands at 435 and around 260 cm^{-1} are assigned to the Co–O stretching vibration.[11] The former frequency is slightly higher than 422 cm^{-1} observed for bis(acetylacetonato)cobalt(II). Recently Nakamoto and his collaborators[12] studied the Co–Br stretching vibrations of $CoBr_2L_2$ type complexes (L=py, 4-chloro-py, or 4-bromo-py), and found that the stretching absorption of the bridging Co–Br bond in the polymeric octahedral form appeared at 118—143 cm^{-1}, while that of the terminal Co–Br bond in the monomeric tetrahedral form was observed at 265 cm^{-1}. Brierley, Geary, and Goldstein[13] also assigned 130 and 168 cm^{-1} bands to the stretching vibration of the bridging Co–Br bond in octahedral $CoBr_2$[1,2-di(4-pyridyl)ethylene], and 247 and 270 cm^{-1} bands to that of the terminal Co–Br bond in tetrahedral $CoBr_2L$ [L=1-(2-pyridyl)-2-(3-pyridyl)-ethylene, or 1-(2-pyridyl)-2-(4-pyridyl)ethylene]. The present compound shows a quite broad absorption in the 200—320 cm^{-1} region exhibiting a maximum at 270 cm^{-1}. This might be due to the terminal Co-Br stretching, but it is not certain since the parent bis(acetylacetonato)-complex also has a broad maximum at 260 cm^{-1} due to the Co–O stretching vibration. However it could be concluded that no band is observed in the 100—150 cm^{-1} region attributable to the bridging Co–Br stretching, and we propose the structure depicted in Fig. 3 for the dimeric bromo(acetylacetonato)cobalt(II) molecule instead of

9) a) D. A. Fine, *J. Amer. Chem. Soc.*, **84**, 1139 (1962); b) R. L. Carlin, "Transition Metal Chemistry," Vol. 1, Marcel Dekker, New York (1965), p. 1.

10) F. A. Cotton and R. H. Holm, *J. Amer. Chem. Soc.*, **82**, 2979 (1960).

11) K. Nakamoto, P. J. McCarthy, and A. E. Martell, *ibid.*, **83**, 1272 (1961).

12) C. Postmus, J. R. Ferraro, A. Quattrochi, K. Shobatake, and K. Nakamoto, *Inorg. Chem.*, **8**, 1851 (1969).

13) M. Brierley, W. J. Geary, and M. Goldstein, *J. Chem. Soc. (A)*, **1969**, 2923.

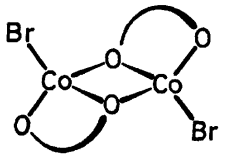

Fig. 3. A proposed structure of dimeric CoBr(acac).

the bromide-bridged structure illustrated previously.[14]

Figure 4 indicates the results of thermogravimetric analysis. The dimeric compound begins to decompose gradually at around 110°C and attains a constant weight at 185°C, but the weight decreases again at around 195°C due to the sublimation of a decomposition product. Heating was discontinued at 300°C and the residue was subjected to elemental analysis. The weight loss by heating up to 185°C was 20.8% corresponding to the release of one acetylacetone group from $[CoBr(acac)]_2$, and acetylacetone collected in a trap cooled by dry ice was identified by gas chromatography.

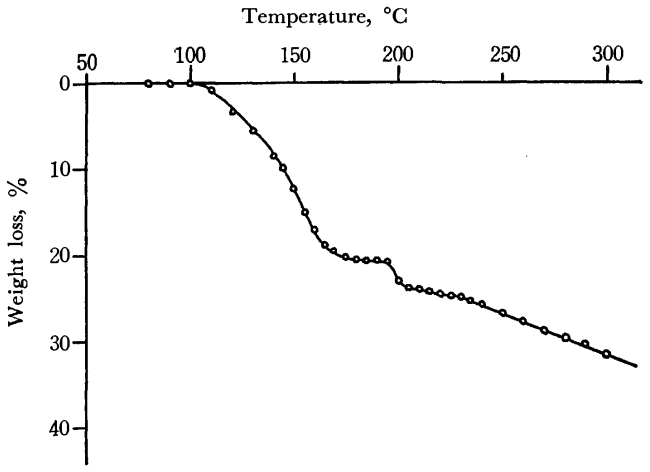

Fig. 4. Thermal decomposition of CoBr(acac) which was dried at 100°C in advance. The rate of temperature elevation was 30°C/hr.

Woodburn and Magee[15] reported that two molecules of dibenzoylmethane (DBMH) were released from an octahedral tetramer, $[Co(DBM)_2]_4$, resulting in a tetrahedral dimer, $(DBM)Co\langle^{OH}_{DBM}\rangle Co(DBM)$. In the present case a corresponding pyrolytic intermediate could not be identified probably because of the succeeding disproportionation, decomposition, or oxidation as represented by

$$[CoBr(acac)]_2 \rightarrow (CoBr)_2acac \rightarrow Co(acac)_2 + CoBr_2 + \text{Co-oxide(s)}. \quad (3)$$

The sublimate deposited on the glass wall was identified by IR assay to be bis(acetylacetonato)cobalt(II). The decomposition residue (0.1089 g) was found to contain 0.0294 g of cobalt and 0.0505 g of bromine. These values should be compared with 0.0369 g of cobalt and 0.0492 g of bromine in the starting specimen [0.1601 g of CoBr(acac)]. It is apparent that a certain quantity of cobalt was lost as a volatile product, but the whole bromine remained in the residue.

The disproportionation reaction of bromo(acetylacetonato)cobalt(II) was also examined in deaerated dichloromethane. Starting with 0.6121 g (2.57 mmol) of CoBr(acac), 0.1935 g of precipitate resulted after being kept standing at room temperature for 160 hr. This was found to contain 0.0441 g (0.84 mg-atom) of cobalt and 0.1267 g (1.59 mg-atom) of bromine indicating that the precipitate was cobalt(II) bromide contaminated with some impurity. Thus the main reaction is represented by

$$[CoBr(acac)]_2 = CoBr_2 + Co(acac)_2. \quad (4)$$

Dimeric bromo(acetylacetonato)cobalt(II) is rather stable in dichloromethane and the extent of the disproportionation reaction (4) was about 65% even after 160 hr.

Derivation of Dimeric Bromo(acetylacetonato)cobalt(II) from Dibromo(acetylacetone)cobalt(II). A new cobalt(II) complex containing a ketonic molecule of acetylacetone as a ligand was prepared by the reaction between tris(acetylacetonato)cobalt(III) and bromine in dichloromethane and also by direct addition of acetylacetone to anhydrous cobalt(II) bromide.[4] As postulated by Pedersen[16] on the mechanism of the metal-ion catalyzed bromination of β-dicarbonyl compounds, a ketonic molecule of acetylacetone coordinated to cobalt(II) is expected to exhibit enhanced acidity by virtue of the polarization effect of the metal ion. In order to verify the postulate the reaction of the ketonic complex with sodium acetylacetonate as a base was forced to occur in deaerated acetylacetone to yield dimeric bromo(acetylacetonato)-cobalt(II) as represented by

$$CoBr_2(acacH) + acacNa \rightarrow \tfrac{1}{2}[CoBr(acac)]_2 + acacH + NaBr. \quad (5)$$

All the procedures of the reaction and separation of products were conducted in a vacuum system to exclude moisture completely. The product obtained after drying at 60°C *in vacuo* was a solvate, $[CoBr(acac)]_2(acacH)$ and was transformed to $[CoBr(acac)]_2$ by prolonged evacuation at 100°C, which showed the same IR and electronic absorption spectra as those of dimeric bromo(acetylacetonato)cobalt(II) obtained by the reaction of bis(acetylacetonato)-cobalt(II) with equimolar bromine in dichloromethane at 0°C.

Experimental

Materials. Bis(acetylacetonato)diaquocobalt(II) was prepared by the method of Charles and Pawlikowski[17] and dehydrated to anhydrous bis(acetylacetonato)cobalt(II) by evacuation at 70°C for 7 hr. Found: Co, 22.98;

14) Y. Nakamura and S. Kawaguchi, *Chem. Commun.*, **1968**, 716.

15) S. I. Woodburn and R. J. Magee, *J. Inorg. Nucl. Chem.*, **30**, 2647 (1968).

16) K. J. Pedersen, *Acta Chem. Scand.*, **2**, 252, 385 (1948).

17) R. G. Charles and M. A. Pawlikowski, *J. Phys. Chem.*, **62**, 440 (1958).

C, 46.28; H, 5.63%. Calcd for $Co(C_5H_7O_2)_2$: Co, 22.91; C, 46.71; H, 5.49%. Bromine and dichloromethane were purified by the usual methods as described previously.[3] Acetylacetone was distilled under reduced pressure and dried with Molecular Sieves Type 4A8—12, Linde Co.

Reaction of Bis(acetylacetonato)cobalt(II) with Bromine. The reaction of bis(acetylacetonato)cobalt(II) with bromine in dichloromethane was conducted in a three-necked flask equipped with a burette, a glass tube containing phosphorus pentoxide, and another glass tube connected to a filtration equipment by means of polyethylene tubing. To a chelate solution in the flask of the desired concentration, usually in the range 0.05—0.20 M, was added a bromine solution of the same concentration from the burette with vigorous stirring. The precipitate formed was transferred *via* polyethylene tubing to a vacuum filtration apparatus set up in a desiccator containing phosphorus pentoxide. The reaction was performed at 0°C or room temperature, the usual precaution being taken against moisture.

Preparation of Dibromobis(acetylacetonato)dicobalt(II) from Dibromo(acetylacetone)cobalt(II). Dibromo(acetylacetone)cobalt[4] (0.957 g, 3 mmol) was dissolved in about 30 m*l* of acetylacetone in an ampoule (A) connected *via* the ground glass joint to a glass tube containing phosphorus pentoxide. To this solution cooled at 0°C, powder of sodium acetylacetonate (0.366 g, 3 mmol) was added and stirred at 0°C for about 2 hr. Ampoule (A) was then attached to the vacuum line as depicted in Fig. 5, and deaerated by cycles of freezing and thawing. Acetylacetone was then distilled *in vacuo* at 0°C into another ampoule (D) leaving deep blue viscous residue, into which dichloromethane was distilled at 0°C. A deep blue solution resulted containing white powder of sodium bromide. The lower ampoule system was detached from the vacuum line at the ground glass joint (C), and the solution was filtered into ampoule (B) through a glass filter (G). After the solvent was vacuum-distilled back into ampoule (A), ampoule (B) was cut and the deep blue viscous residue was dried *in vacuo* at room temperature and finally at 60°C for 5 hr. Results of elemental analyses of the deep blue powder agreed with the formula $[CoBr(acac)]_2(acacH)$. Found: Co, 19.94; Br, 27.16; C, 31.21; H, 4.03%. Calcd for $Co_2Br_2C_{15}H_{22}O_6$: Co, 20.46; Br, 27.74; C, 31.27; H, 3.86%. This adduct lost acetylacetone gradually on evacuation at 100°C and the following analytical results were obtained after 4 hr. Found: Co, 23.14; Br, 31.70; C, 27.54; H, 3.47%. Calcd for $Co_2Br_2C_{10}H_{14}O_4$: Co, 24.77; Br, 33.58; C, 25.24; H, 2.97%. Such poor coincidence suggests the difficulty of complete liberation of excess solvent.

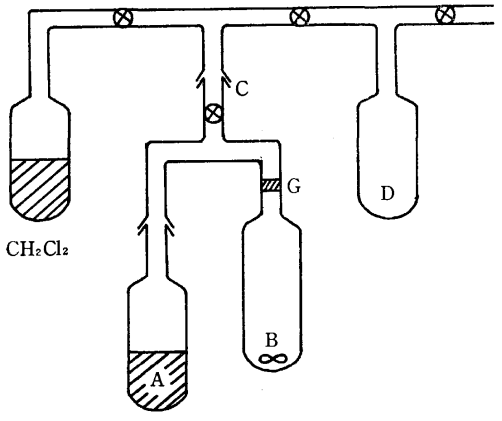

Fig. 5. The ampoule system employed for preparation of CoBr(acac) from $CoBr_2(acacH)$.

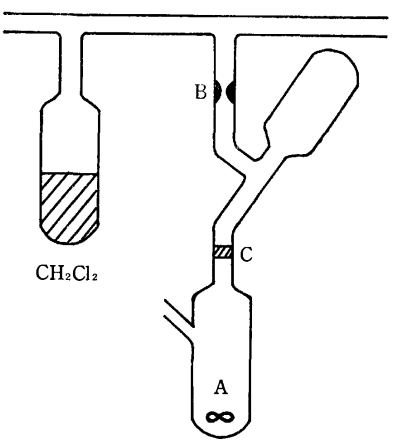

Fig. 6. The ampoule system employed for the disproportionation reaction of CoBr(acac) in dichloromethane.

The Disproportionation Reaction of Dibromobis(acetylacetonato)dicobalt(II) in Dichloromethane. Dibromobis(acetylacetonato)dicobalt(II) (0.6121 g) was put into an ampoule (A) which had been connected to a vacuum system (Fig. 6), and the side tube was sealed off. In the evacuated ampoule (A) about 40 m*l* of dried dichloromethane was distilled, and the ampoule system was sealed off at B from the vacuum line. The solution was kept at around 25°C with stirring for 160 hr. A green precipitate was separated from the solution by virtue of a glass filter (C), dried and subjected to elemental analysis.

Analyses. Solid products were dried at room temperature *in vacuo* unless otherwise stated. Cobalt was determined gravimetrically as sulfate, and bromine as silver salt. For the determination of organic bromide in the filtrate, the solvent was evaporated under reduced pressure. An acetic acid solution of potassium iodide was added to the residue, and the liberated iodine was titrated with a solution of sodium thiosulfate.

Measurements. Infrared spectra were taken in Nujol on Hitachi EPI-2(4000—700 cm^{-1}), EPI-L(700—200 cm^{-1}), and FIS-3(400—30 cm^{-1}) infrared spectrophotometers. Absorption spectra of solutions were measured by means of a Hitachi EPS-2 recording spectrophotometer. For the observation at 0°C, ice-water was circulated through the cell holder and dry air was forced to blow against the cell window to prevent clouding.

A thermo-spring balance C-282 of Hamada Denki Seisakusho, Ltd. was used for the thermogravimetric analysis, and the heating rate was adjusted to 30°C/hr *in vacuo*. The volatile decomposition product was collected in a trap cooled by dry ice and subjected to gas chromatographic analysis. A column (1.5 m) of Apiezon Grease L on Neosorb NC (Nishio Industries Co., Ltd.) was used at 59°C and hydrogen was passed at a flow rate of 72 cm/min. The decomposition residue was fused with potassium carbonate, and cobalt and bromine contents were determined.

The magnetic susceptibility was measured at room temperature by the Gouy method with an automatic recording magnetic balance (Naruse Kagakukikai Co., Ltd.). The sample was kept together with phosphorus pentoxide in a dry box, and then put quickly into a tube (2 mm in diameter and 70 mm in length) and stoppered with silicone grease.

Molecular weight of bromo(acetylacetonato)cobalt(II) was determined by cryoscopy in dioxane and osmometry in methanol with an apparatus manufactured by Knauer,

Germany. Solutions of around 10^{-2} M in the monomer basis were used, and benzil was adopted as a reference.

The authors thank Dr. S. Kawai, Osaka University for the magnetic measurement, and Mr. J. Gohda for the elemental analysis. They are also grateful to the Ministry of Education for financial assistance and to Daicel Co., Ltd. for the supply of acetylacetone.

BULLETIN OF THE CHEMICAL SOCIETY OF JAPAN, VOL. 45, 489—491 (1972)

Reactions of Dibromoalkanes with Dimethyltin Bis(*N*,*N*-dimethylthioseleno- and diselenocarbamates) and Related Compounds

Koji TANAKA and Toshio TANAKA

Department of Applied Chemistry, Faculty of Engineering, Osaka University, Yamada-kami, Suita, Osaka

(Received August 11, 1971)

Dimethyltin-bis(*N*,*N*-dimethylthioselenocarbamate), $(CH_3)_2Sn[SSeCN(CH_3)_2]_2$, dimethyltin-bis(*N*,*N*-dimethyldiselenocarbamate), $(CH_3)_2Sn[Se_2CN(CH_3)_2]_2$, and dimethyltin-bis(*N*-methyl-*N*-phenyldiselenocarbamate), $(CH_3)_2Sn[Se_2CN(CH_3)(C_6H_5)]_2$, react with dibromoalkanes to give bis(1-thia-3-selenacycloalkyl-2-dimethylimminium)dimethyltin tetrabromide, $[(CH_3)_2SnBr_4]^{2-}[(CH_2)_m\langle S, Se\rangle C{=}N(CH_3)_2]_2^{+}$ ($m=2$, 3), 1,3-diselenacycloalkyl-2-dimethylimminium dimethyltin bromides, $[(CH_3)_2SnBr_{n+2}]^{n-}[(CH_2)_m\langle Se, Se\rangle C{=}N(CH_3)_2]_n^{+}$ ($n=1$, $m=2$ and $n=2$, $m=3$), and 1,3-diselenacyclopentyl-2-methylphenylimminium bromide, $[(CH_2)_2\langle Se, Se\rangle C{=}N(CH_3)(C_6H_5)]^{+}Br^{-}$, respectively. The infrared and PMR spectra indicate that the positive charges of 1-thia-3-selena- and 1,3-diselenacycloalkylimminium ions are more delocalized in the higher homologs than in the lower ones.

We have previously reported on the reactions of dihalogenoalkanes with *N*,*N*-dimethyldithiocarbamate and *N*-methyl-*N*-phenyldithiocarbamate complexes of tin(IV), $(CH_3)_2Sn[S_2CN(CH_3)_2]_2$ and $(CH_3)_2Sn[S_2CN(CH_3)(C_6H_5)]_2$.[1,2] The main products of these reactions are 1,3-dithiacycloalkyl-2-dimethylimminium salts (I) and alkylene bis(*N*-methyl-*N*-phenyldithiocarbamate) (II) respectively, depending on the sort of reactant.

$$[(CH_3)_2SnX_{n+2}]^{n-}\left[(CH_2)_m\langle S, S\rangle C{=}N\langle CH_3, CH_3\rangle\right]_n^{+} \quad \text{(I)}$$

($n=1$ or 2; $m=2$, 3, or 4; X=Cl, Br, or I)

$$\begin{matrix} CH_3 \\ C_6H_5 \end{matrix}\rangle N-\overset{\overset{S}{\|}}{C}-S-(CH_2)_m-S-\overset{\overset{S}{\|}}{C}-N\langle \begin{matrix} CH_3 \\ C_6H_5 \end{matrix} \quad \text{(II)}$$

($m=2$, 3, or 4)

1,3-Dithiacycloalkylimminium ions are considered to be intermediates in the formation of ethylene bis(*N*,*N*-disubstituted-dithiocarbamate).[2,3]

Recently, one of the present authors synthesized some *N*,*N*-dialkylthioseleno-[4] and *N*,*N*-dialkyldiselenocarbamate[5] complexes of tin(IV). The purpose of this paper is to study the reaction of dibromoalkanes with dimethyltin-bis(*N*,*N*-dimethylthioselenocarbamate), $(CH_3)_2Sn[SSeCN(CH_3)_2]_2$, -bis(*N*,*N*-dimethyldiselenocarbamate), $(CH_3)_2Sn[Se_2CN(CH_3)_2]_2$, and -bis(*N*-methyl-*N*-phenyldiselenocarbamate), $(CH_3)_2Sn[Se_2CN(CH_3)(C_6H_5)]_2$ (abbreviated as $(CH_3)_2Sn(dmtsc)_2$, $(CH_3)_2Sn(dmdsc)_2$ and $(CH_3)_2Sn(mpdsc)_2$ respectively).

Results and Discussion

The reactions of $Br(CH_2)_nBr$ ($n=2$, 3) with $(CH_3)_2(dmtsc)_2$ give bis(1-thia-3-selenacycloalkyl-2-dimethylimminium)dimethyltin tetrabromide (III) and (IV), and $(CH_3)_2Sn(dmdsc)_2$ reacts with $Br(CH_2)_nBr$ ($n=2$, 3) to yield 1,3-diselenacycloalkyl-2-dimethylimminiumdimethyltin tribromide and tetrabromide, (V) and (VI):

$$[(CH_3)_2SnBr_4]^{2-}\left[(CH_2)_2\langle S, Se\rangle C{=}N\langle CH_3, CH_3\rangle\right]_2^{+} \quad \text{(III)}$$

$$[(CH_3)_2SnBr_4]^{2-}\left[(CH_2)_3\langle S, Se\rangle C{=}N\langle CH_3, CH_3\rangle\right]_2^{+} \quad \text{(IV)}$$

$$[(CH_3)_2SnBr_3]^{-}\left[(CH_2)_2\langle Se, Se\rangle C{=}N\langle CH_3, CH_3\rangle\right]^{+} \quad \text{(V)}$$

$$[(CH_3)_2SnBr_4]^{2-}\left[(CH_2)_3\langle Se, Se\rangle C{=}N\langle CH_3, CH_3\rangle\right]_2^{+} \quad \text{(VI)}$$

On the other hand, $(CH_3)_2Sn(mpdsc)_2$ reacts with $Br(CH_2)_2Br$ to preferentially give 1,3-diselenacyclopentyl-2-methylphenylimminium bromide (VII):

1) T. Tanaka and T. Abe, *Inorg. Nucl. Chem. Lett.*, **4**, 569 (1968).
2) T. Tanaka, K. Tanaka, and T. Yoshimitsu, This Bulletin, **44**, 112 (1971).
3) T. Nakai, Y. Ueno, and M, Okawara, *Tetrahedron Lett.*, **1967**, 3831; This Bulletin, **43**, 156 (1970).
4) T. Kamitani and T. Tanaka, *Inorg. Nucl. Chem. Lett.*, **6**, 91 (1970).
5) T. Kamitani, H. Yamamoto, and T. Tanaka, *J. Inorg. Nucl. Chem.*, **32**, 2671 (1970).

Table 1. Relevant infrared frequencies (cm^{-1}) of 1,3-dichalcogenacycloalkyl-2-dimethylimminium dimethyltin bromides and the related compounds[a,b]

	Compound	ν(C=N)	ν_{as}(Sn-C)	ν_{s}(Sn-C)	ν(Sn-Br)
(Ia)	$[(CH_3)_2SnBr_3]^-$	1587 s	559 s	511 s	215 s
(Ib)[c]	$[(CH_3)_2SnBr_4]^{2-}$	1538 s	568m	505m	210 s
(III)	$[(CH_3)_2SnBr_4]^{2-}$	1588 s	562 s	—	214 s
(IV)	$[(CH_3)_2SnBr_4]^{2-}$	1538 s	561 s	—	215 s
(V)	$[(CH_3)_2SnBr_3]^-$	1574 s	566 s	511 s	216 s
(VI)	$[(CH_3)_2SnBr_4]^{2-}$	1554 s	564 s	—	?
(VII)	Br^-	1520 s	—	—	—

a) Nujol mull. b) The abbreviations used in this table are as follows: s, strong; m, medium. c) This compound is an equimolar mixture of $Br^-[(CH_2)_3(S)_2C{=}N(CH_3)_2]^+$ and $[(CH_3)_2SnBr_3]^-[(CH_2)_3(S)_2C{=}N(CH_3)_2]^+$.

$$Br^-\left[(CH_2)_2(Se)_2C{=}N\begin{matrix}CH_3\\C_6H_5\end{matrix}\right]^+ \quad \text{(VII)}$$

This is in contrast to the reaction of dimethyltin bis(*N*-methyl-*N*-phenyldithiocarbamate) with $Cl(CH_2)_2Cl$, which yields ethylene bis(*N*-methyl-*N*-phenyldithiocarbamate), besides 1,3-dithiacyclopentyl-2-methylphenylimminium salt.[2] The difference between these two reactions seems to result from the different solubilities of 1,3-diselena- and 1,3-dithiacyclopentyl-2-methylphenylimminium salts, which are intermediates in the production of ethylene bis(*N*-methyl-*N*-phenylcarbamate) in the 1,2-dihalogenoethane used as the solvent.

The relevant infrared frequencies of the compounds obtained here are listed in Table 1, together with those of the related 1,3-dithiacycloalkyl-2-dimethylimminium compounds. These 1,3-dichalcogenacycloalkylimminium ions exhibit the ν(C=N) bands at relatively high frequencies, suggesting an appreciable double-bond character of the C=N bond. The ν(C=N) frequencies of IV and VI, with the six-membered rings, are lower than those of III and V, which contain the five-membered ring. This tendency may reflect the fact that the higher homologs are more contributed from the canonical structure (B) than from (A), similar to the case of the 1,3-dithiacycloalkyl-2-dimethylimminium cation described in a previous paper.[2]

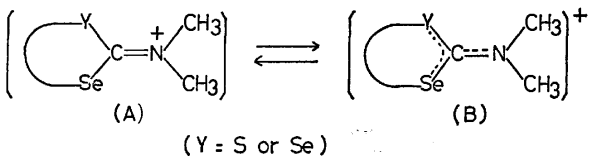

The ν(C=N) band of VII appears at a frequency considerably lower than those of the other 1,3-dichalcogenacyclopentyl-2-dimethylimminium salts, (III and V). This may be interpreted as indicating the decreasing double-bond character of the C=N bond conjugated with the phenyl group.

As is shown in Table 1, the $(CH_3)_2SnBr_3^-$ ion of V exhibits both asymmetric and symmetric ν(Sn–C) bands, while the $(CH_3)_2SnBr_4^{2-}$ ions of III, IV, and VI show only the asymmetric one. This is consistent with the previous report;[2] the former is a trigonal bipyramid with two methyl groups located in equatorial positions, while the latter is an octahedron with an almost linear C–Sn–C moiety.

In the PMR spectra, the N–CH_3 proton signals of the

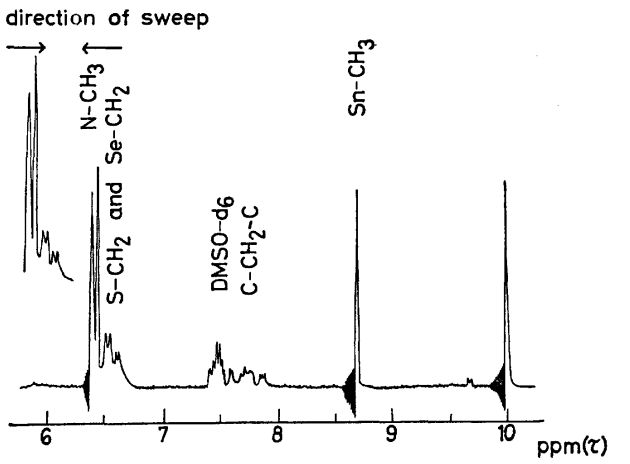

Fig. 1. PMR spectrum $[(CH_3)_2SnBr_4]^{2-}[CH_2(CH_2{-}S)(CH_2{-}Se)C{=}N(CH_3)_2]^+$ in DMSO-d_6, 7 wt%.

TABLE 2. PROTON CHEMICAL SHIFTS (τ, ppm) AND SPIN-SPIN COUPLING CONSTANTS (Hz) OF 1,3-DICHALCOGENACYCLOALKYL-2-DIMETHYLIMMINIUM DIMETHYLTIN BROMIDES AND THE RELATED COMPOUND IN DMSO-d_6[a)]

Compound	τ(Sn-CH_3)	τ(C-CH_2-C)	τ(S-CH_2-) and/or τ(Se-CH_2-)	τ(N-CH_3)	J(^{77}Se-CH_2-)	J(CH_2-CH_2-)	J(^{119}Sn-CH_3)
(Ia)	8.70 s	—	5.92 s	6.44 s	—	—	114
(Ib)	8.70 s	7.78 q	6.56 s	6.46 s	—	7.0	114
(III)	8.71 s	—	5.86 s [b)]	6.45 s 6.40 s	10.5	—	114
(IV)	8.70 s	7.66 s	6.53 t 6.56 t	6.46 s 6.41 s	c)	6.0	114
(V)	8.70 s	—	5.78 s	6.41 s	10.5	—	114
(VI)	8.70 s	7.70 q	6.59 t	6.42 s	c)	7.2	114
(VII)	—	—	5.78m	6.09 s	c)	—	—

a) The abbreviations used in this table are as follow: s, singlet; t, triplet; q, quintet; m, multiplet.
b) The S-CH_2- and Se-CH_2- protons were almost magnetically equivalent, resulting in a slightly broad singlet.
c) Not observed for the main signal being multiplet.

1-thia-3-selenacycloalkyl-2-dimethylimminium ion (III and IV) occur as a doublet at room temperature, because the rotation about the C=N bond is hindered. The lower-field signal is lower and broader than the higher one (Fig. 1). The former may be assigned to the CH_3 protons *trans* to the selenium atom with respect to the C=N bond, since the ^{77}Se (I=1/2, natural abundance 7.58%) could couple more strongly with the *trans*-CH_3 protons than with the *cis*-CH_3 protons, resulting in a decrease in the height and a broadening of the CH_3 proton signal.[4] As is shown in Table 2, the N—CH_3 proton chemical shifts of III are practically in agreement with those of 1,3-dithiacyclopentyl-2-dimethylimminium salt (Ia) and the diselena derivative (V). Quite similarly, the N–CH_3 proton spectrum of IV is observed to be a superposition of those of 1,3-dithiacyclohexyl-2-dimethylimminium salt (Ib) and the diselena derivative (VI). The 4- and 6-CH_2 proton signals of Ib and VI are a simple triplet due to spin-spin coupling with the 5-CH_2 protons, but those of IV shows a doublet of triplets (Fig. 1), although a pair of the lowest signals are concealed by the N–CH_3 proton signals. In addition, the 5-CH_2 proton signals occur as a complicated multiplet. These results may be due to different magnetic environments of the 4- and 6-CH_2 protons attached to the selenium and sulfur atoms respectively.

The J(^{119}Sn–CH_3) value of $(CH_3)_2SnBr_3^-$ and $(CH_3)_2SnBr_4^{2-}$ in DMSO-d_6 is in agreement with that of $(CH_3)_2SnBr_2$ in the same solvent,[6,7] which is known to exist as an octahedral complex ion of $(CH_3)_2Sn(DMSO\text{-}d_6)_4^{2+}$.

Experimental

$(CH_3)_2Sn(dmtsc)_2$,[4] $(CH_3)_2Sn(dmdsc)_2$,[5] and $(CH_3)_2Sn(mpdsc)_2$[5] were prepared elsewhere, while the dihalogenoalkanes are commercially available. The general procedure for the reactions was the same as has been described in the previous paper.[2]

Bis(1-thia-3-selenacyclopentyl-2-dimethylimminium)-dimethyltin Tetrabromide (III). A solution of $(CH_3)_2Sn(dmtsc)_2$ (3.0 g) in 1,2-dibromoethane (20 m*l*) was stirred at 100°C for 10 min to give a yellow precipitate. After the solution had then been cooled to room temperature, the precipitate (III) was filtered off and recrystallized from acetonitrile (4.8 g, 90% yield); mp 146—149°C.

Found: C, 16.71; H, 3.37; N, 3.34%. Calcd for $C_{12}H_{26}N_2S_2Se_2Br_4Sn$: C, 16.78; H, 3.06; N, 3.27%.

Bis(1-thia-3-selenacyclohexyl-2-dimethylimminium)-dimethyltin Tetrabromide (IV). A solution of $(CH_3)_2Sn(dmtsc)_2$ (3.0 g) in 1,3-dibromopropane (20 m*l*) was kept at a temperature of about 100°C for 1 hr in order to liberate a yellow precipitate. Recrystallization from acetonitrile then yielded light yellow crystals of IV (4.6 g, 85% yield); mp 104—106°C.

Found: C, 18.65; H, 3.54; N, 3.12%. Calcd for $C_{14}H_{30}N_2S_2Se_2Br_4Sn$: C, 18.96; H, 3.42; N, 3.16%.

1,3-Diselenacyclopentyl-2-dimethylimminium-dimethyltin Tribromide (V). A solution of $(CH_3)_2Sn(dmdsc)_2$ (5.0 g) in 1,2-dibromoethane (20 m*l*) had been stirred for 1 hr at 100°C and then filtered; the solid product thus obtained was recrystallized from acetonitrile to give light yellow crystals of V (2.2 g, 65% yield); mp 157—159°C.

Found: C, 13.71; H, 2.58; N, 2.64%. Calcd for $C_{17}H_{16}NSe_2Br_3Sn$: C, 13.32; H, 2.54; N, 2.22%.

Bis(1,3-diselenacyclohexyl-2-dimethylimminium)-dimethyltin Tetrabromide (VI). A solution of $(CH_3)_2Sn(dmtsc)_2$ (2.0 g) in 1,3-dibromopropane (20 m*l*) was maintained for 1 hr at 100°C. After it had been cooled to room temperature, yellow solid product (VI) was filtered off and recrystallized from acetonitrile (2.2 g 65% yield); mp 132—133°C.

Found: C, 16.59; H, 2.95; N, 3.06%. Calcd for $C_{14}H_{30}N_2Se_4Br_4Sn$: C, 17.15; H, 3.09; N, 2.86%.

1,3-Diselenacyclopentyl-2-methylphenylimminium Bromide (VII). A solution of $(CH_3)_2Sn(mpdsc)_2$ (2.0 g) in 1,2-dibromoethane (20 m*l*) was stirred for 5 min at 100°C to give a yellow precipitate, which was then recrystallized from an acetonitrile-ether mixture to give pale yellow crystals of VIII (0.76 g 69% yield); mp 190—192°C.

Found: C, 31.38; H, 3.21; N, 3.69%. Calcd for $C_{10}H_{12}NSe_2Br$: C, 31.28; H, 3.15; N, 3.65%.

Infrared and NMR Spectra. The infrared spectra were recorded on Hitachi EPI-2G(5000—400 cm^{-1}) and EPI-L (700—200 cm^{-1}) spectrophotometers. The NMR spectra were measured on a Japan Electron JNM-3H-60 spectrometer operating at 60 MHz at room temperature, using tetramethylsilane as the internal standard.

We are grateful to the Shinko Chemical Co., Ltd., for supplying the elemental selenium.

6) W. Kitching, *Tetrahedron Lett.* **1966**, 3689.
7) T. Tanaka, *Inorg. Chim. Acta*, **1**, 217 (1967).

The Structure of the Pteridine Glycoside from *Aspergillus oryzae*

Sadao MATSUURA, Masaki YAMAMOTO,* and Yasuyuki KANEKO**

Department of General Education, Nagoya University, Chikusa-ku, Nagoya

(Received June 11, 1970)

The structures of two blue-fluorescent substances, asperopterin-A and -B, isolated from *Aspergillus oryzae* were investigated. Asperopterin-B was identified as 2-amino-3,4,7,8-tetrahydro-6-hydroxymethyl-8-methyl-4,7-dioxopteridine (**7**) by studying its chemical degradation, pK_a values, and UV spectra; the structure was confirmed by synthesis. Asperopterin-A was shown to be the β-D-ribofuranoside of **7**, 2-amino-3,4,7,8-tetrahydro-8-methyl-4,7-dioxo-6-pteridinylmethyl β-D-ribofuranoside (**10**).

Two blue-fluorescent substances, asperopterin-A (**1**) and -B (**2**), have been isolated as crystals from *Aspergillus oryzae* T-17.[1,2] In a previous communication,[3] **1** was shown to be a D-riboside of **2**, and a tentative approach to the structure of **2** was made. The present paper will record the complete structures of **1** and **2** as well as the synthesis of the latter.

Results and Discussion

Structure of Asperopterin-B (2). It has previously been established[3] that **2** is a derivative of isoxanthopterin bearing a CH_2OH group at the 6-position and an extra methyl group elsewhere in the molecule. In the present work, this was supported by the NMR spectrum of **2**, which showed two singlets, at 3.22 and 4.52 ppm, representing a methyl and methylene group respectively. Moreover, it is known that isoxanthopterin has the 2-amino-4,7-dioxo-form in an aqueous solution with its two pK_a values (7.34 and 10.06) arising from the hydrogen atoms attached to the N-3 and N-8 positions of the ring.[4] Since **2** has only one acidic pK_a value (8.07), one of these hydrogen atoms must be replaced by a methyl group. In order to find the position of this methyl group, **2** was oxidized with potassium permanganate and the oxidation product (**3**)[3] was compared with the three synthetic *N*-methylisoxanthopterin-6-carboxylic acids (**4a**—**c**); **4c** proved to be identical with **3** (Table 1). Thus, asperopterin-B (**2**) was assumed to be 2-amino-3,4,7,8-tetrahydro-6-hydroxymethyl-8-methyl-4,7-dioxopteridine (**7**); this assumption was eventually confirmed by the following synthesis. 6,8-Dimethylisoxanthopterin (**5**)[4] was brominated using bromine in 48% hydrobromic acid; without isolation, the bromo derivative (**6**) was converted by 0.5 N sodium hydroxide into the 6-hydroxymethyl compound (**7**) which was identical with **2** in R_f and in pK_a value, and also in its UV and IR spectra (Table 1, Fig. 1).

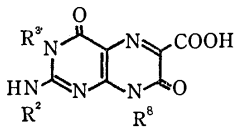

4

	R^2	R^3	R^8
4a	CH_3	H	H
4b[5]	H	CH_3	H
4c[5]	H	H	CH_3
4d[5]	H	CH_3	CH_3
4e	CH_3	CH_3	CH_3

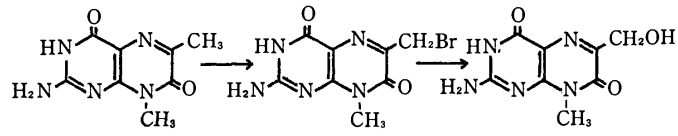

5 **6** **7**

Structure of Asperopterin-A (1). Although it has been shown that **1** was a D-riboside of **2**,[3] the position of the ribosyl group has remained unknown. Because **1** has an acidic pK_a and UV spectra closely

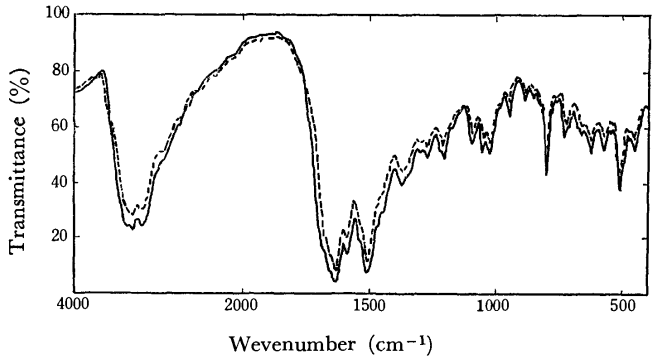

Fig. 1. IR spectra of asperopterin-B (solid line) and **7** (dotted line).

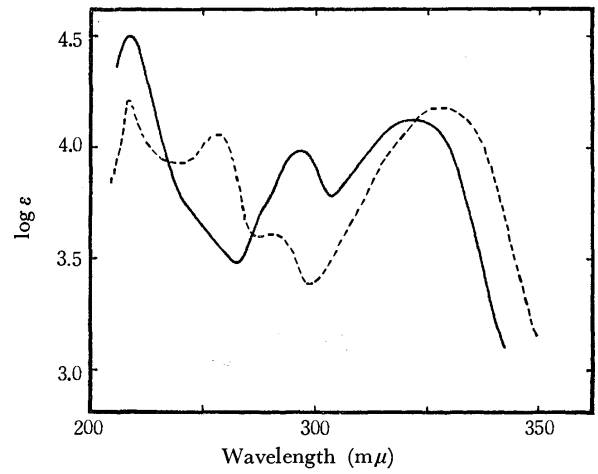

Fig. 2. UV spectra of asperopterin-A.
—— pH 5.5 (neutral molecule)
---- pH 10.5 (anion)

* Present address: Tokyo Research Laboratory, Kyowa Hakkokogyo Co., Ltd., Machida Tokyo.

** Present address: Department of Agricultural Chemistry, College of Agriculture, Nagoya University.

1) Y. Kaneko, *Agr. Biol. Chem.*, **29**, 965 (1965).
2) Y. Kaneko, *Nippon Nogei Kagaku Kaishi*, **40**, 227 (1966).
3) Y. Kaneko and M. Sanada, *J. Ferment. Technol.*, **47**, 8 (1969).
4) W. Pfleiderer and M. Rukwied, *Chem. Ber.*, **94**, 1 (1961).
5) W. Pfleiderer and M. Rukwied, *ibid.*, **95**, 1591 (1962).

TABLE 1. IDENTIFICATION OF PTERIDINES

	R_f[a]			pK_a[b]	UV Spectra				
	a	b	c		pH	Ionic species[c]	λ_{max} (log ε)		
3[d] (Oxidation product of **2**)	0.17	0.69	0.52	3.46 8.17	1.0 5.5 11.0	○ — ——	221 (4.53), 264 (3.79), 290 (3.79), 379 (4.34) 219 (4.51), 293 (3.93), 352 (4.17) 218 (4.25), 260 (4.03), 365 (4.20)		
4c[e]	0.17	0.69	0.52	3.45 8.18	1.0 5.5 11.0	○ — ——	221 (4.53), 264 (3.88), 291 (3.82), 379 (4.37) 219 (4.54), 293 (3.96), 352 (4.20) 218 (4.30), 261 (4.06), 365 (4.24)		
Asperopterin-A (**1**)[f]				8.05	5.5 10.5	○ —	218 (4.57), 292 (4.02), 346 (4.22) 217 (4.27), 259 (4.11), 280 (3.56), 359 (4.26)		
Asperopterin-B (**2**)[d]	0.20	0.46	0.47	8.07	5.5 11.0	○ —	218 (4.57), 292 (4.00), 342 (4.13) 217 (4.22), 257 (4.05), 279 (3.61), 354 (4.17)		
7	0.20	0.46	0.47	8.09	5.5 11.0	○ --	218 (4.53), 292 (4.00), 342 (4.13) 217 (4.21), 257 (4.05), 280 (3.61), 355 (4.16)		
$\mathbf{a}_1$	0.20	0.46	0.47	8.07	5.5 11.0	○ —	217 214	292 256	342 281 354
$\mathbf{b}_2$	0.16	0.75	0.73		1.0 8.5		220 258	253 293	268 355 375
4d[e]	0.16	0.75	0.74	3.74	1.0 8.5	○ —	221 (4.40), 253 (3.90), 269 (3.92), 375 (4.28) 258 (3.75), 292 (3.91), 356 (4.22)		
$\mathbf{c}_2$	0.29	0.75	0.74		1.0 8.5		265 295	292 356	386
4e	0.29	0.75	0.74	3.69	1.0 8.5	○ —	266 (4.02), 293 (3.78), 387 (4.39) 296 (4.00), 358 (4.26)		

a) Descending method was used. Solvent: a: *n*-butanol : 50% acetic acid (2 : 1). b: 4% ammonium chloride. c: 4% sodium citrate. b) Spectroscopic determination. c) ○; neutal molecule. —; monoanion. ——; dianion. d) UV Spectra; *cf.* Kaneko and Sanada.[3] e) UV Spectra and pK_a; *cf.* Pfleiderer and Rukwied.[5] f) UV Spectra; *cf.* Kaneko.[1,2]

resembling those of **2** (Table 1, Figs. 2, 3), either of the two structures (**8** and **9**) seems possible for **1**.

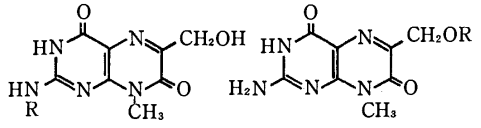

8 **9**

R = D-ribosyl

In order to distinguish between these possibilities, methylation with dimethyl sulfate was carried out. It had previously been reported[6] that isoxanthopterin in an alkaline solution was methylated at N-8, N-3, and the 2-amino group on treatment with dimethyl sulfate; moreover, when **2** was treated similarly, the hydroxyl group of the side chain was methylated together with the ring nitrogen atoms. Therefore, if **1** is **8**, the hydroxyl group of the side chain should be methylated; on the other hand, if **1** is **9**, no methylation could take place at that position, since the hydroxyl group would be protected by the ribosyl group. Using conditions under which no hydrolysis of the glycosidic link occurred, the methylation of **1** in an alkaline solution gave a mixture of products. When this mixture was boiled with 2 N hydrochloric acid, three products, $\mathbf{a}_1$, $\mathbf{b}_1$, and $\mathbf{c}_1$, were obtained. These were then chromatographically separated; $\mathbf{a}_1$ was identified as **2** from its R_f, its pK_a value, and its UV spectrum (Table 1); the permanganate oxidation of $\mathbf{b}_1$ and $\mathbf{c}_1$ gave two acids, $\mathbf{b}_2$ and $\mathbf{c}_2$, which were identical with **4d** and **4e** respectively (Table 1). Since 6-methoxymethylisoxanthopterin[7] was unaffected under the conditions

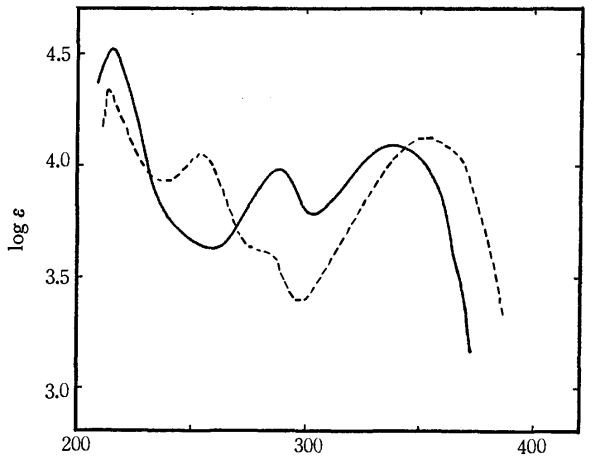

Fig. 3. UV spectra of asperopterin-B.
—— pH 5.5 (neutral molecule)
---- pH 11.0 (anion)

6) T. Sugimoto and S. Matsuura, *Research Bulletin* (Dept. of General Educ., Nagoya Univ.), **11**, 94 (1967).

7) S. Matsuura, S. Nawa, H. Kakizawa, and Y. Hirata, *J. Amer. Chem. Soc.*, **75**, 4446 (1953).

used for the oxidation of **2**, $\mathbf{b}_1$, and $\mathbf{c}_1$, both $\mathbf{b}_1$ and $\mathbf{c}_1$ could be seen to have a hydroxymethyl group at the 6-position, and it could be seen that the glycoside was not methylated at this position, even in the presence of a large excess of dimethyl sulfate. Accordingly, the formula **9**, in which the hydroxymethyl group was protected by a ribosyl group, was confirmed to be that for asperopterin-A.

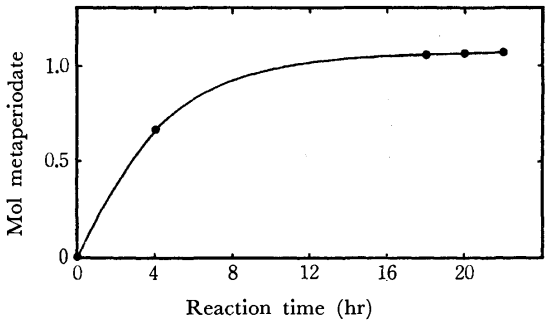

Fig. 4. Periodate oxidation of asperopterin-A.

The structure of the sugar moiety of **1** was determined by periodate oxidation according to the method of Lythgoe[8] and Jackson;[9] **1** consumed one molar equivalent of the reagent and produced no formic acid (Fig. 4). It was clear, therefore, that **1** was a ribofuranoside. The anomeric configuration of **1** was deduced to be β by a comparison of its molecular rotation (−223°) with those of known D-ribofuranosides.[10] Thus, the formula **10** was given to asperopterin-A:

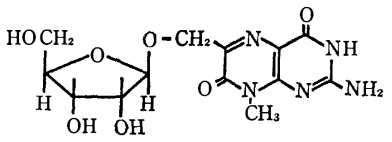

10

Experimental

All the melting points are uncorrected. The NMR spectrum was measured at 60 MHz with a JEOL Model JNM-3 spectrometer, using a 0.5 M KOD solution and TMS as the external reference. The UV spectra were measured on a Shimadzu SV-50 spectrometer and checked on a Shimadzu QR-50 manual instrument. The IR spectra were recorded on a Hitachi Model EPI-G spectrometer. Optical rotations were determined with a Shimadzu Lippich-type polarimeter. The ionization constants were determined spectroscopically.

Permanganate Oxidation of Asperopterin-B (2). 0.1 M Potassium permanganate was added, drop by drop, to **2** (77.6 mg) in 0.01 M sodium hydroxide (100 m*l*) at 60°C until a purple color remained. The solution was then set aside at this temperature for 20 min, and the excess of permanganate was decomposed with 0.05 M potassium sulfite. The manganese dioxide was filtered off and washed with hot water. The combined filtrate and washings were adjusted to pH 2 with hydrochloric acid and passed through a florisil column (1.5×10 cm). The pteridine, adsorbed on the top of the column, was then eluted with water; a small amount of the starting material remained on the column.[13] The eluate was concentrated to a volume of 50 m*l* and adjusted to pH 2. The repeated recrystallization of the precipitate from 1 M potassium hydroxide and finally from an aqueous buffer at pH 2 gave pale yellow needles (45 mg) of the product; mp>300°C.

Found: C, 39.86; H, 3.37; N, 29.02%. Calcd for $C_8H_7N_5O_4 \cdot 1/4H_2O$: C, 39.76; H, 3.13; N, 28.98%.
This product was identical with authentic **4c**.

2,5-Diamino-4-hydroxy-6-methylaminopyrimidine Hydrochloride.[4] 2-Amino-4-hydroxy-6-methylanino-5-nitrosopyrimidine[14] (35 g) and 10% palladized charcoal (5 g) in 400 m*l* water was shaken under hydrogen. After 3 min, 1 M sodium hydroxide (100 m*l*) was added and shaking was continued until the absorption of hydrogen ceased (9700 m*l* within 100 min). After the subsequent acidification of the mixture with 10 M hydrochloric acid (100 m*l*), the catalyst was removed by filtration. The concentration of the filtrate under reduced pressure gave the product in an 85% yield. The catalyst could be used repeatedly without any depression of its activity providing it was washed with ethanolic sodium hydroxide (4 g of sodium hydroxide in 100 m*l* of 20% aqueous ethanol).

In a similar way, 4,5-diamino-6-hydroxy-2-methylaminopyrimidine hydrochloride[4] was prepared from the corresponding 5-nitrosopyrimidine[15] in an 85% yield.

6-Carboxy-3,4,7,8-tetrahydro-2-methylamino-4,7-dioxopteridine (4a). This compound was prepared in an 80% yield from the above 4,5-diamino-6-hydroxy-2-methylaminopyrimidine hydrochloride using the method for its 3-methyl isomer (**4b**);[5] mp>300°C.

Found: C, 38.59; H, 3.67; N, 27.90%. Calcd for $C_8H_7N_5O_4 \cdot 2/3H_2O$: C, 38.56; H, 3.37; N, 28.11%.

2-Amino-3,4,7,8-tetrahydro-6-hydroxymethyl-8-methyl-4,7-dioxopteridine (7). Bromine (1.00 g) was added to **5**[4] (1.20 g) in 48% hydrobromic acid (100 m*l*) at 60°C. The mixture was heated at 80°C until the initially-formed precipitate had dissolved, and then cooled quickly. It was diluted with water (200 m*l*), and its pH was adjusted to 2 with crystalline sodium acetate. The solution was evaporated to dryness under reduced pressure, and the residue was heated at 80°C with 0.5 M sodium hydroxide (200 m*l*) for 15 min. The separated needles (1.01 g) were purified by repeated recrystallization from 1 M potassium hydroxide until only one spot was observed on a paper chromatogram.

8) B. Lythgoe and A. R. Tood, *J. Chem. Soc.*, **1944**, 592.
9) E. L. Jackson and C. S. Hudson, *J. Amer. Chem. Soc.*, **61**, 1530 (1939).
10) It has been reported that methyl β-D-ribofuranoside has a molecular rotation of −102° in contrast to that of the α-isomer (+241°).[11] When the aglycon was replaced by a benzyl alcohol residue, the value for the β-isomer moved to −145°.[12] This displacement (43°) caused by the aglycon exchange is much smaller than the difference (343°) between the rotations of the α- and β-isomers.
11) G. R. Barker and D. C. C. Smith, *J. Chem. Soc.*, **1954**, 2151.
12) R. K. Ness, H. W. Diehl, and G. G. Fletcher, Jr., *J. Amer. Chem. Soc.*, **76**, 763 (1954).
13) The florisil column for chromatography was prepared as before.[2] The behavior of the adsorbed pteridines towards elution depends on their pK_a values. A pteridine with an acidic pK_a below 4 was eluted with water; one with a pK_a between 6 and 9 was eluted with 1% aqueous ammonia or, more effectively, with acetone-ammonia (acetone, 30 m*l*; 1.5% aqueous ammonia, 60 m*l*).
14) W. V. Curran and R. B. Angier, *J. Org. Chem.*, **28**, 2672 (1963).
15) R. Roth, J. M. Smith, Jr., and M. E. Hultquist, *J. Amer. Chem. Soc.*, **73**, 2864 (1951).

Finally, the pH value of the solution of the potassium salt in water (50 m*l*) was adjusted to 5 to give the product as pale yellow needles (270 mg, 22%); mp>300°C.

Found: C, 41.87; H, 4.00; N, 30.24%. Calcd for $C_8H_9N_5O_3 \cdot 1/2H_2O$: C, 41.38; H, 4.34; N, 30.15%.

*Methylation and Subsequent Hydrolysis of Asperopterin-A (**1**).* Dimethyl sulfate was added in portions (0.016 m*l*; 1 equivalent each) to **1** (56 mg, 0.016 mmol) in 0.1 M potassium hydroxide (20 m*l*); the mixture was then maintained at pH 10 by adding 10 M potassium hydroxide. After the addition of every five equivalents of the reagent, the mixture was examined by paper chromatography. Additions were continued until no spot of the starting material was visible. Seventy-five equivalents of dimethyl sulfate were added in all. The reaction mixture, after the inorganic salts had been removed using a florisil column, was heated with 2 M hydrochloric acid (5 m*l*) at 100°C for 10 min. This produced three compounds, $\mathbf{a}_1$, $\mathbf{b}_1$, and $\mathbf{c}_1$ (R_f: 0.20, 0.30 and 0.47 using *n*-butanol–acetic acid), which were separated by a paper-chromatographic method (*n*-butanol–acetic acid as a solvent) and purified using the florisil column.[13]

Permanganate Oxidation of b_1 and c_1. The above $\mathbf{b}_1$ fraction was oxidized with permanganate as has been described before. After the removal of the manganese dioxide, the product was adsorbed on a florisil column (0.3× 3 cm) and eluted with 1% aqueous ammonia. The product ($\mathbf{b}_2$), obtained by the evaporation of the eluate to dryness, was identified as **4d**.

Similarly, the $\mathbf{c}_1$ fraction was oxidized; the product, $\mathbf{c}_2$, was identified as **4e**.

5-Formamido-4-hydroxy-2,6-bismethylaminopyrimidine. Formic acid (98—100%; 60 m*l*) was added, drop by drop, to a vigorously-stirred solution of 4-hydroxy-2,6-bismethylaminopyrimidine[14] (27 g) and sodium nitrite (15 g) in formamide (200 m*l*). The mixture was heated to 90°C, and sodium dithionite (1.2 g) was added. An exothermic reaction occurred, and the nitroso compound dissolved. After 3 min, the formamido compound separated as needles (30.5 g, 90%); mp 282—283.5°C (recrystallized from water).

Found: C, 40.70; H, 6.32; N, 33.94%. Calcd for $C_7H_{11}N_5O_2 \cdot 1/2H_2O$: C, 40.77; H, 5.84; N, 33.97%.

5-Formamido-1,6-dihydro-1-methyl-2,4-bismethylamino-6-oxopyrimidine. Dimethyl sulfate (16.5 g) was added in portions to the above formamidopyrimidine (16 g) in 1 M sodium hydroxide (200 m*l*). The mixture was stirred for 1 hr at 25°C, during which time the pH value of the solution was maintained at 13 by the addition of 10 M sodium hydroxide throughout the reaction. After chilling overnight, the precipitate was collected and recrystallized from water to give colorless needles (9.0 g, 53%) of the product; mp 291—292°C (dec.).

Found: C, 45.23; H, 6.39; N, 33.20%. Calcd for $C_8H_{13}N_5O_2$: C, 45.49; H, 6.39; N, 33.16%.

*6-Carboxy-3,4,7,8-tetrahydro-3,8-dimethyl-2-methylamino-4,7-dioxopteridine (**4e**).* The above 5-formamido-1-methylpyrimidine (2.2 g) was dissolved in 12 M hydrochloric acid (10 m*l*) and set aside at room temperature overnight. Ethanol (20 m*l*) was then added to the mixture, and the precipitated 5-aminopyrimidine was used for condensation without further purification. The 5-aminopyrimidine was added to diethyl oxomalonate (3.2 g), sodium acetate (3 g), and potassium metabisulfite (100 mg) in water (50 m*l*), and the mixture was boiled for 10 min. The yellow needles (2.7 g) were collected and boiled in 1 M sodium bicarbonate (150 m*l*) for 55 min. The precipitate, dissolved in a 0.5 M potassium hydroxide solution (300 m*l*), was added, drop by drop, to boiling 20% acetic acid (300 m*l*) to give yellow needles (2.4 g, 87%); mp>300°C.

Found: C, 44.82; H, 4.19; N, 26.13%. Calcd for $C_{10}H_{11}N_5O_4 \cdot 0.1H_2O$: C, 44.98; H, 4.23; N, 26.23%.

*Periodate Oxidation of Asperopterin-A (**1**).* Sodium metaperiodate (0.113 M, 7.50 m*l*) was added to **1** (57.0 mg) in water (100 m*l*) and diluted to exactly 120.0 m*l*. The solution was incubated at 25°C. Samples (2.0 m*l*) were taken out at intervals, and the excess of metaperiodate in each was estimated iodometrically.[8,9] 0.68, 1.06, 1.07, and 1.07 molar equivalents of periodate were consumed after 4, 18, 20, and 22 hr respectively. After 22 hr, 10 m*l* of the solution was diluted with water and titrated with 0.02 M sodium hydroxide;[8] the diluted solution consumed no sodium hydroxide.

The authors wish to express their appreciation to Professor A. Albert and Dr. D. J. Brown of the Australian National University for their helpful discussions. They also wish to thank the staff of Fujisawa Seiyaku Co., Ltd., for performing the elementary analyses.

Synthetic Reactions by Complex Catalysts. XXIV. A New Catalyst of Copper-Isocyanide Complex for the Michael Addition

Takeo SAEGUSA, Yoshihiko ITO, Shimpei TOMITA, and Hideo KINOSHITA

Department of Synthetic Chemistry, Faculty of Engineering, Kyoto University, Sakyo-ku, Kyoto

(Received December, 23, 1970)

It has been found that some binary systems of a copper compound (or metallic compounds) and an isocyanide catalyze the Michael addition reaction. As the copper component, Cu_2O, metallic copper and copper acetylacetonate are effectual, whereas CuCl, $CuCl_2$, and CuO are ineffectual. The catalyst of copper isocyanide complex is characterized by the selective activation of cyano olefin compounds such as acrylonitrile. This was demonstrated by the competitive addition of an active hydrogen compound to acrylonitrile and methyl acrylate. Some results of kinetics and spectroscopic studies have been explained by assuming a scheme involving coordination of olefin onto copper-isocyanide complex.

This paper deals with the catalyst behavior of some binary systems of a copper compound and an isocyanide for the Michael addition reaction. We have concentrated on new catalyst activity of the copper-isocyanide complexes in the field of synthetic organic reactions, and found several new reactions with the catalytic aid of these complexes. Copper catalyzed formimidation of amine,[1a] phosphine,[1b] alcohol,[1c,d] thiol,[1e] and silane[1f] constitutes a series of new reactions of isocyanide. Dimerization of α,β-unsaturated nitriles and carbonyl compounds (Eq. (1)) is the second series of reactions catalyzed by the copper-isocyanide complexes, where the isocyanide ligand is not incorporated in the products.[2-4]

$$\mathrm{RCH{=}CHX} \longrightarrow \mathrm{RCH{=}\underset{\displaystyle \mathrm{RCHCH_2X}}{\underset{|}{C}}{-}X} \qquad (1)$$

(R=H, primary and secondary alkyl groups; X=CN, CO_2R', COR'')

From the mechanistic consideration on the dimerization reaction, a nucleophilic addition of allyl and vinyl-copper complexes to α,β-unsaturated bond has been reasonably assumed as the key step.[3,4] This assumption prompted us to examine the catalysis of the copper-isocyanide complex in the Michael addition reaction. The expectation has been realized. In addition, the copper-isocyanide complex in the Michael addition is distinguished from the usual base catalysts by the selective activation of cyano olefins such as acrylonitrile.

Experimental

Materials. Commercial reagents diethyl malonate, acetylacetone, benzyl cyanide, malononitrile, *t*-butyl mercaptan, 2-nitropropane, indene, methyl crotonate, methyl acrylate, acrylonitrile, and triethylamine were purified by distillation. Methylacetylacetone (3-methylpentane-2,4-dione) was prepared from acetylacetone and methyl iodide using potassium carbonate catalyst.[5] Diethyl ethylmalonate was synthesized from diethyl malonate and ethyl bromide using sodium ethoxide catalyst.[6] Ethyl propiolate was prepared by the dehydrobromination of dibromosuccinic acid followed by decarboxylation and esterification.[7] Cyclohexyl isocyanide and *t*-butyl isocyanide were prepared according to Ugi's procedure.[8] Metal oxide and salts were all commercial reagents. Metallic copper powder was prepared by the reduction of cupric sulfate with zinc powder in acidic aqueous solution under nitrogen.[9]

Reaction of Diethyl Malonate with Methyl Crotonate. A mixture of diethyl malonate (1.6 g, 10 mmol), methyl crotonate (1.0 g, 10 mmol), cyclohexyl isocyanide (1.09 g, 10 mmol), and cuprous oxide (20 mg, 0.14 mmol) was heated under nitrogen at 90°C for 9 hr. The reaction mixture was subjected to fractional distillation. The fraction boiling at 152—153°C/4 mmHg was collected. The yield of the product was 2.46 g (95%). By IR and NMR spectra as well as elemental analysis, the structure of the product was shown to be $(EtO_2C)_2CHCH(CH_3)CH_2CO_2CH_3$ (I), an adduct of the Michael addition. Principal IR bands (neat): 1730 (s), 1300—1150 (s) cm^{-1}. NMR of I in CCl_4: τ 8.87 (d, CH_3–), 8.64 (t, $-CO_2CH_2CH_3$), 7.52 (d, $-\underset{|}{CH}-$), 7.30 (m, $CH_3\underset{|}{CH}$), 6.64 (d, $-CH_2CO_2CH_3$), 6.30 (s, $-CO_2CH_3$), and 5.79 (q, $-CO_2CH_2CH_3$).

Found: C, 55.43; H, 7.84%. Calcd for $C_{12}H_{20}O_6$: C, 55.37; H, 7.75%.

The reactions of other active hydrogen compounds and acceptor olefins were carried out similarly. The products were identified by IR and NMR spectra. The results are summarized in Table 1.

Effect of Metal Component of Catalyst System. A mixture of 1.60 g (10 mmol) of diethyl malonate, 1.00 g (10 mmol) of methyl crotonate, 1.09 g (10 mmol) of cyclohexyl isocyanide and metal compound (0.14—0.31 mmol) was heated at 90°C for 9 hr under nitrogen. The reaction mixture was subjected to glpc analysis to determine the yield of the Michael adduct, $(EtO_2C)_2CH(CH_3)CH_2CO_2Me$.

Relative Reactivities of Acrylonitrile (AN) and Methyl Acrylate

1) a) T. Saegusa, Y. Ito, S. Kobayashi, K. Hirota, and H. Yoshioka, *Tetrahedron Lett.*, **1966**, 6121; This Bulletin, **42**, 3310 (1969). b) T. Saegusa, Y. Ito, and S. Kobayashi, *Tetrahedron Letters*, **1968**, 935. c) T. Saegusa, Y. Ito, S. Kobayashi, N. Takeda, and K. Hirota, *ibid.*, **1967**, 1273: *Can. J. Chem.*, **47**, 1217 (1969). e) T. Saegusa, S. Kobayashi, Y. Ito, K. Hirota, and Y. Okumura, This Bulletin, **41**, 1638 (1968). f) T. Saegusa, Y. Ito, S. Kobayashi, and K. Hirota, *J. Amer. Chem. Soc.*, **89**, 2240 (1967).

2) T. Saegusa, Y. Ito, S. Kobayashi, and S. Tomita, *Chem. Commun.*, **1968**, 273.

3) T. Saegusa, Y. Ito, S. Tomita, and H. Kinoshita, *J. Org. Chem.*, **35**, 670 (1970).

4) T. Saegusa, Y. Ito, H. Kinoshita, and S. Tomita, This Bulletin, **43**, 877 (1970).

5) A. W. Johnson, E. Markham, and R. Price, "Organic Syntheses", Vol. 42, p. 75.

6) N. Weiner, *ibid.*, Coll. Vol. II, p. 279.

7) T. W. Abbot, R. T. Arnold, and R. B. Thompson, *ibid.*, Coll. Vol. II, p. 10.

8) I. Ugi and R. Meyer, *Chem. Ber.*, **93**, 239 (1960).

9) R. Q. Brewster and T. Groening, "Organic Syntheses", Coll. Vol. II, p. 446.

(MA) in the Michael Addition. The ratio of the reaction rates of AN and MA in the Michael addition reactions by copper-isocyanide catalyst and by the conventional base catalysts were determined by a method of competitive reaction. An equimolar mixture of AN and MA, if necessary with a reaction solvent (toluene), was subjected to the Michael addition with an active hydrogen compound in the presence of a catalyst, and the reaction was short-stopped at a lower conversion. The amounts of the two Michael adducts from AN and MA were determined by glpc. The molar ratio of the two adducts was taken to indicate the ratio of the rate constants of AN (k_{AN}) and MA (k_{MA}) on the basis of the assumption that the Michael addition reactions of AN and MA proceed *via* the same reaction mechanism. The extent of reaction was controlled by the feed concentrations of active hydrogen compound and catalyst and the time of reaction. The rate ratios with various catalysts were determined at the same reaction temperature. The feed compositions, reaction temperatures, reaction times and conversion percentage as well as the rate ratio values are shown in Table 3.

Kinetic Study. An introductory kinetic study was carried out on the Michael addition of methylacetylacetone to MA in the presence of the copper acetylacetonate–cyclohexyl isocyanide system. A homogeneous catalyst solution was prepared by dissolving copper acetylacetonate in cyclohexyl isocyanide at room temperature.

1) *Rate Plot for Methylacetylacetone Concentration.* Under nitrogen, a mixture of MA (30.0 mmol) and methylacetylacetone (variable) was diluted with toluene to 10.0 m*l*, to which 10.0 m*l* of a toluene solution of catalyst containing 0.06 mmol of copper acetylacetonate and 6 mmol of cyclohexyl isocyanide was added. The reaction was carried out at room temperature. A small portion of the reaction mixture was taken out and analyzed by glpc. The initial tangent at time=0 of the time-conversion curve was taken as the rate. Several runs of reactions were performed with various amounts of methylacetylacetone. Fig. 1 shows the relationship between the rate and the concentration of methylacetylacetone.

2) *Rate Plot for MA Concentration.* The reaction was carried out in a similar way. The MA concentration was changed in a region from 1.03×10^{-1} mol l^{-1} to 5.00×10^{-1} mol l^{-1}. A linear relationship between the rate and the MA concentration was obtained as shown in Fig. 2.

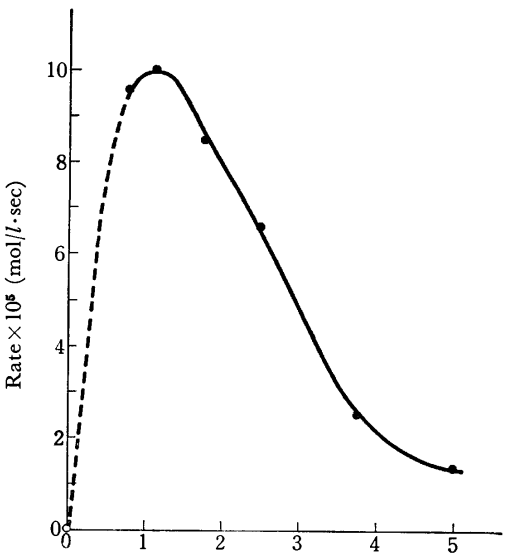

Fig. 1. Relation between the reaction rate and the concentration of methylacetylacetone.

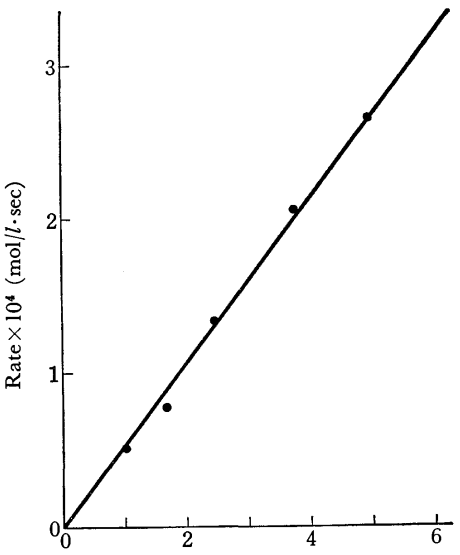

Fig. 2. Relation between the reaction rate and the concentration of methyl acrylate.

UV Examination on the Interaction of AN and MA with Cu_2O-Isocyanide System. 1) *AN - Cu_2O - Cyclohexyl Isocyanide System.* A mixture of 0.7 g (5 mmol) of Cu_2O, 2.18 g (20 mmol) of AN was diluted with acetonitrile to 10.0 m*l*. The mixture was stirred at room temperature for 1 hr. The insoluble Cu_2O was removed by decantation, and the clear homogeneous reddish-yellow solution was separated. This was diluted to AN and isocyanide concentrations of 6.6×10^{-4} mol l^{-1} with acetonitrile, and the diluted solution was subjected to UV spectroscopy examination (Shimadzu SV-50 spectrometer, Shimadzu Seisakusho, Japan). Two absorption bands were observed at $\lambda_{max}=300$ mμ and 360 mμ. The band at 300 mμ was assigned to the AN soluble oligomer formed during the course of preparation of the solution. The band at 360 mμ was observed only in the combination of the three components of AN, Cu_2O, and isocyanide. No single component and combination of two components showed absorption in this region.

2) *MA - Cu_2O - Cyclohexyl Isocyanide System.* A mixture of 0.7 g (5 mmol) of Cu_2O, 2.18 g (20 mmol) of cyclohexyl isocyanide and 1.72 g (20 mmol) of MA was diluted with acetonitrile to 10.0 m*l*, and the mixture was stirred at room temperature for 4 hr. The insoluble Cu_2O was removed by decantation, and the clear yellowish solution was diluted to MA and isocyanide concentration of 2×10^{-2} mol l^{-1} with acetonitrile, and analyzed by UV. A weak absorption band was observed at $\lambda_{max}=325$ mμ. This band was observed only in the combination of these three components.

Results and Discussion

The catalyst activity of the Cu_2O-isocyanide system for the Michael addition reaction is demonstrated in Table 1. As active hydrogen compounds, acetylacetone, malonate, benzyl cyanide, malononitrile, 2-nitropropane, alcohol, thiol, and indene were employed. No single component of Cu_2O and isocyanide alone caused the reaction. Semi-quantitative com-

Table 1. Michael addition reaction by Cu_2O-isocyanide system[a)]

Active hydrogen Compound	mmol	Olefin[b)]	mmol	Catalysts (mmol)	Conditions °C	hr	Adduct yield %
$CH_2(CO_2Et)_2$	10	MC	10	H-NC (10)—Cu_2O (0.2)	90	9	95
$CH_2(COMe)_2$	10	MC	10	H-NC (10)—Cu_2O (0.2)	90	9	72
$PhCH_2CN$	10	MC	10	H-NC (10)—Cu_2O (0.2)	90	9	53
$CH_2(CN)_2$	10	MC	10	H-NC (10)—Cu_2O (0.2)	90	9	22
$MeCH(COMe)_2$	20	MA	20	H-NC (10)—Cu_2O (0.2)	90	1	90
$MeCH(COMe)_2$	20	AN	20	H-NC (10)—Cu_2O (0.2)	90	1	95
$EtCH(CO_2Et)_2$	20	MA	20	H-NC (10)—Cu_2O (0.2)	90	2	50
$EtCH(CO_2Et)_2$	20	AN	20	H-NC (10)—Cu_2O (0.2)	90	2	67
$PhCH_2OH$	30	MA	30	H-NC (10)—Cu_2O (0.5)	90	5	50
$PhCH_2OH$	30	AN	30	H-NC (10)—Cu_2O (0.5)	90	5	80
t-BuSH	30	AN	30	H-NC (10)—Cu_2O (0.2)	70	1[e)]	73
Me_2CHNO_2	30	MA	30	H-NC (10)—Cu_2O (0.2)	80	1[f)]	70
Indene	50	MA	50	*t*-BuNC (30)—Cu_2O (1)	90	4	50[c)]
$MeCH(COCH_3)_2$	10	$CH{\equiv}CCO_2Et$	15	*t*-BuNC (5)—Cu_2O (0.2)	r.t.	24[g)]	78[d)]
$MeCH(COCH_3)_2$	20	AN	15	**1**[i)] (1)	r.t.	6[h)]	86

a) A mixture of an active hydrogen compound, α,β-unsaturated compound, isocyanide, and cuprous oxide was heated at 90°C otherwise e, f, g, h.
b) MC: Methyl crotonate, MA: Methyl acrylate, AN: Acrylonitrile.
c) The adduct was 3-(carbomethoxyethyl)indene.
d) The adduct was $(CH_3OC)_2C(CH_3)CH{=}CHCO_2Et$ (*cis*/*trans* = 1/1).
i) **1** : $C_5H_5Cu(CN\text{-}Bu^t)$

parison of the product yields between the reaction of acrylonitrile (AN) and methyl acrylate (MA) suggests that the olefin component having cyano group at the olefin carbon atom is more reactive than the one bearing carbomethoxyl group. Selective activation of cyano-olefin will be discussed later. As a reaction intermediate, an organic complex of copper derived from the active hydrogen compound might be postulated. Requisiteness of isocyanide for the catalyst activity suggests an organic complex of copper having an essential ligand of isocyanide. In the reaction of indene, a cyclopentadiene homologue, an indenyl copper complex can be assumed to be the intermediate. In fact, we have isolated a cyclopentadienyl copper isocyanide complex (**1**) from Cu_2O, cyclopentadiene and *t*-butyl isocyanide.[10)]

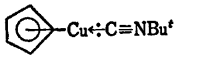

1

An organocopper complex **1** has been found to cause the Michael addition reaction (See Table 1).

Table 2 shows that Cu_2O, $Cu(acac)_2$ and metallic copper are effective as the metallic component in combination with isocyanide. CuO, CuCl, and $CuCl_2$ are much less effective. Besides copper compounds, $Co(acac)_2$ is shown to be fairly effective. The results of the competitive reaction between AN and MA well characterize the Cu_2O - isocyanide system. The rate ratio k_{AN}/k_{MA} changes according to the nature of the catalyst. In the reaction by the Cu_2O-isocyanide system, the rate of AN is much higher than that of MA. The high values of the rate ratio k_{AN}/k_{MA} may be explained by the preferential coordination of AN onto copper in a copper isocyanide complex of a key intermediate. It is reasonable to assume that the coordination of AN by means of the cyano group is stronger than the coordination of MA. The effect of coordination might be explained by the following scheme 1.

$$\underset{\mathbf{2}}{Cu^I(R^1NC)_aL_b} \xrightarrow{R^2H(-LH)} \underset{\mathbf{3}}{R^2Cu(R^1NC)_c} \xrightarrow{Olefin}$$

$$\underset{\mathbf{4}}{R^2Cu(Olefin)(R^1NC)_e} \xrightarrow{R^2H} \text{Michael adduct} + \mathbf{3} \qquad (1)$$

$$(a+b \leqq 4,\ 1 \leqq c \leqq 3,\ 1 \leqq e \leqq 2)$$

The complex of copper compound and isocyanide (**2**) reacts with an active hydrogen (R^2H) to form an

10) T. Saegusa, Y. Ito, and S. Tomita, *J. Amer. Chem. Soc.*, **93**, 5656 (1971).

Table 2. Effect of metal component of catalyst system[a)]

Copper component	(mmol)	Adduct yield (%)
Cu_2O	0.14	95
$Cu(acac)_2$	0.14	77
Cu	0.31	43
CuO	0.25	10
CuCl	0.22	trace
$CuCl_2$	0.14	trace
Other metal components	**(mmol)**	**Adduct yield (%)**
$Co(acac)_2$	0.20	27
Ag_2O	0.20	4
HgO	0.20	0
NiO	0.20	0

a) A mixture of diethyl malonate (10 mmol), methyl crotonate (10 mmol), cyclohexyl isocyanide (10 mmol), and the metal component was heated at 90°C for 9 hr.

organic complex of copper **3**. Replacement of a ligand of **3** by olefin gives rise to the formation of key intermediate **4**, in which the nucleophilic attack of R^2 ligand onto the coordinated olefin occurs in the sphere of ligands. In **4**, the coordination of olefin by means of cyano group will decrease the electron density of olefin bond and increase the electrophilic nature of olefin. In the competitive reaction, the higher rate of AN is due to the fact that the concentration of the complex species **4** of AN is higher than that of the corresponding species of MA. The coordination of olefin to copper/isocyanide complex has not been well established. However, UV absorption bands at 360 mμ of AN - Cu_2O - isocyanide system and at 325 mμ of MA - Cu_2O - isocyanide system might be due to the corresponding complexation. These absorptions were not observed in any single component system or in any combination of two components. Exact assignment of these bands requires further studies. Scheme-1 has been partly supported by some kinetics characters. Preliminary kinetic study was carried out on the reaction of MA with methylacetylacetone (MeAc) in the presence of the $Cu(acac)_2$ - cyclohexyl isocyanide system. As a copper component, copper acetylacetonate was employed in order to insure the homogeneousness of the reaction system. Kinetics has not been fully analyzed, and some fragmentary results which fit Scheme-1 are mentioned. Fig. 1 illustrates a strange dependence of the reaction rate upon the concentration of active hydrogen compound of MeAc. As the concentration of MeAc is increased, the rate first increases and then decreases after reaching a maximum. This exhibits a striking contrast to the corresponding relation in the base catalyzed Michael addition.[11] Anomalous change of the rate in Fig. 1 may be explained by the scheme involving coordination complexes. According to Scheme-1, the concentration of methylacetylacetonyl ligand will increase with the increase of the concentration of MeAc. However, the increase of MeAc concentration will be unfavorable to the coordination of olefin onto copper, and hence it decreases the concentration of the key intermediate of **4**. The decrease of concentration of **4** gives rise to the decrease of rate. The first order dependence of the rate upon the MA concentration is shown in Fig. 2, which is explained by an assumption that the equilibrium constant of the MA coordination onto copper is small and the concentration of **4** is regarded as being nearly proportional to the initial feed concentration of MA.

3 + Olefin ⇄ **4** + isocyanide

Table 3. Relative reaction rates of acrylonitrile (AN) and methyl acrylate (MA) in the Michael reaction with various catalysts

Active hydrogen compd. (mmol)	Catalyst (mmol)	AN, MA[c)] (mmol)	Toluene (ml)	Reaction condition: Temp. (°C)	Reaction condition: Time (min)	Conv.[d)] (%)	k_{AN}/k_{MA}[e)]
	15 Cu_2O (0.3)— 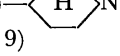 NC (4.5)	15	20		5	0.91	5.47
$MeCH(COMe)_2$	15 EtONa (0.9)	15	20	80	7	1.65	0.198
	3 Et_3N (10)	30	0		15×60	2.10	0.855
	2 Cu_2O (0.5)— 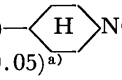 NC (20)	40	0		60	<2.5	15.8
$EtCH(CO_2Et)_2$	2 *t*-BuOK (0.05)[a)]	40	0	room temp.	2	<2.5	1.70
	2 *t*-BuONa (0.1)[b)]	40	0		2	<2.5	0.536
	2 Cu_2O (0.5)— 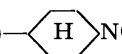 NC (20)	40	0		10	<2.5	7.80
$PhCH_2OH$	2 $PhCH_2OK$ (0.05)	40	0	room temp.	7	<2.5	2.51
	2 $PhCH_2ONa$ (0.1)	40	0		2	<2.5	0.95

a) 0.05 mmol of *t*-BuOK in 0.3 ml of *t*-BuOH.
b) 0.1 mmol of *t*-BuONa in 0.23 ml of *t*-BuOH.
c) An equimolar amount of AN and MA was used.
d) Conversion percent was based on the consumption of combined amount of AN and MA.
e) The ratio of AN and MA.

11) K. T. Finley, D. R. Call, G. W. Solovocool, and W. J. Hayles, *Can. J. Chem.*, **45**, 571 (1967).

Kinetics of the γ-Ray Induced Polymerization of Ethylene in 1,2-Dichlorotetrafluoroethane

Fujio SUGANUMA, Miyuki HAGIWARA, Hiroshi MITSUI, and Tsutomu KAGIYA

Japan Atomic Energy Research Institute, Takasaki Radiation Chemistry Research Establishment, Takasaki, Gunma

(Received February 15, 1971)

The γ-ray induced polymerization of ethylene in bulk or in solution in the presence of 26.9—67.3 g of 1,2-dichlorotetrafluoroethane (R-114) was carried out in a 100-m*l* reactor under a pressure of 210—400 kg/cm² and at 30°C, with a dose rate of 1×10^4—9×10^4 rad/hr. The rate of the polymerization and the molecular weight of the polymer formed increased with the reaction time and the pressure. The rate also increased upon the addition of an appropriate amount of R-114. On the other hand, the molecular weight decreased with an increase in the amount of R-114. The dose-rate exponents of the rate and the molecular weight were found to be 0.8 and −0.2 respectively. These results were analyzed kinetically, and the rates and the rate constants of the initiation, propagation, transfer, and termination reactions were evaluated. Further, the roles of R-114 in the polymerization were discussed.

Polychloromethanes are known as effective radical sources for the initiation reaction of the radiation-induced polymerization of some vinyl monomers, such as styrene and methyl methacrylate.[1] The polymerizations of these monomers are promoted by the presence of such compounds. In the case of ethylene, on the contrary, both the rate of the polymerization and the molecular weight of the polymer formed are markedly depressed. In ethylene polymerization it has been found to be effective to add some fluorinated or chlorofluorinated ethanes, such as hexafluoroethane, chloropentafluoroethane, or 1,2-dichlorotetrafluoroethane.[2] Promotion by chlorofluorinated hydrocarbons is also found in the copolymerization of ethylene with tetrafluoroethylene.[3]

The purposes of this paper are to elucidate the effects of the reaction conditions on the polymerization of ethylene in the presence of 1,2-dichlorotetrafluoroethane (R-114), and to discuss the roles of R-114 in the initiation, propagation, transfer, and termination reactions from the viewpoint of kinetics.

Experimental

The reaction vessel used was a stainless-steel autoclave with a capacity of 100 m*l*. The ethylene monomer was 99.9% pure (free from CO and H_2S), containing less than 3 ppm of O_2. Reagent-grade R-114 was purified by distillation before use. After the reaction vessel had been evacuated, a definite amount of R-114 was charged in. Ethylene was then fed in at 30°C. By using a specially-designed autoclave with a quartz window, the mixture of the monomer and the solvent was observed to be existing in a homogeneous liquid phase, with no separation in the reaction vessel.[3] Polymerization runs were carried out in bulk or in solution in the presence of 26.9—67.3 g of R-114 under a pressure of 210—400 kg/cm² and at a temperature of 30°C, with dose rate of 1×10^4—9×10^4 rad/hr. During the reaction, the temperature was maintained constant within ±1°C by using an automatic controller; the pressure remained essentially constant since the monomer conversion to the polymer was kept less than 10% in all runs (in most cases, less than 5%).

The polymer yield was determined by the direct weighing of the polymer formed after it had been dried to a constant weight in a vacuum oven at room temperature. The number-average molecular weight of the polymer was obtained from osmotic pressure measurements of solutions of the polymer in tetralin at 110°C using a Hewlett-Packard osmometer, Model 502.

Results and Discussion

Effects of Reaction Conditions

Effects of R-114 and Reaction Pressure. The experimental results are summarized in Table 1.

TABLE 1. EXPERIMENTAL RESULTS OF THE POLYMERIZATION IN BULK AND IN THE PRESENCE OF R-114[a]

Reaction pressure kg/cm²	Amount of R-114 g	Reaction time hr	Polymer yield mol/*l*[b]	Molecular weight $\times10^{-4}$
400	0	0.33	0.091	10.7
		0.50	0.201	15.1
		0.75	0.387	21.3
		1.00	0.770	31.6
400	26.9	0.25	0.094	4.12
		0.33	0.166	5.39
		0.50	0.320	6.18
		0.67	0.509	7.10
400	67.3	0.33	0.119	2.73
		0.50	0.232	3.22
		0.67	0.325	3.45
		1.00	0.609	3.93
		1.33	0.830	3.98
310	29.6	0.50	0.166	3.30
		0.67	0.289	3.72
		1.00	0.523	4.51
310	57.4	0.50	0.152	2.14
		0.67	0.210	2.08
		1.00	0.364	2.45
		1.50	0.674	2.79
210	29.6	0.50	0.121	2.57
		0.67	0.173	2.61
		1.00	0.319	2.93
		1.42	0.471	3.18

a) Reaction conditions: temperature, 30°C; dose rate, 9.2×10^4 rad/hr; reactor volume, 100 m*l*.
b) Polymerized monomer.

1) A. Chapiro, "Radiation Chemistry of Polymeric Systems," Interscience Publishers, New York, (1962).
2) M. Hagiwara, H. Okamoto, and T. Kagiya, This Bulletin, **43**, 172 (1970).
3) M. Hagiwara, T. Miura, and T. Kagiya, *ibid.*, **42**, 3380 (1969).

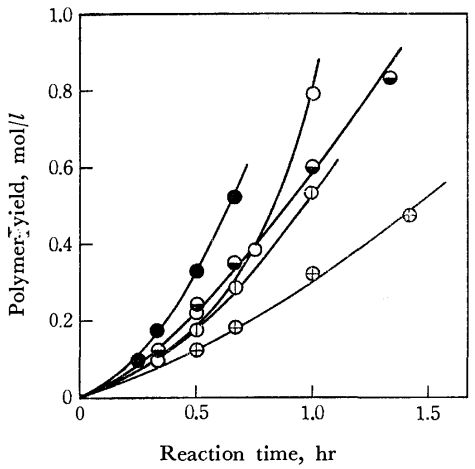

Fig. 1. Polymer yield *vs.* reaction time.
Reaction conditions: Temperature, 30°C; dose rate, 9.2×10^4 rad/hr; reactor volume, 100 m*l*; pressure (kg/cm²) and amount of R-114 (g), (○) 400, 0; (●) 400, 26.9; (◒) 400, 67.3; (◫) 310, 29.6; (⊕) 210, 29.6.

Figure 1 shows the relation between the polymer yield and the reaction time. It is clear that the rate of the polymerization increases with the time, since the time-yield relation gives an upward concave curve in all the polymerizations. A maximum rate was obtained when the amount of R-114 was varied in the range from zero to 67.3 g. The rate increased markedly with the reaction pressure, and was found to be proportional to 1.6 power of the pressure.

As can be seen in Fig. 2, the molecular weight also increases with the time, while it decreases with increase in the amount of R-114 and with the decrease in the pressure.

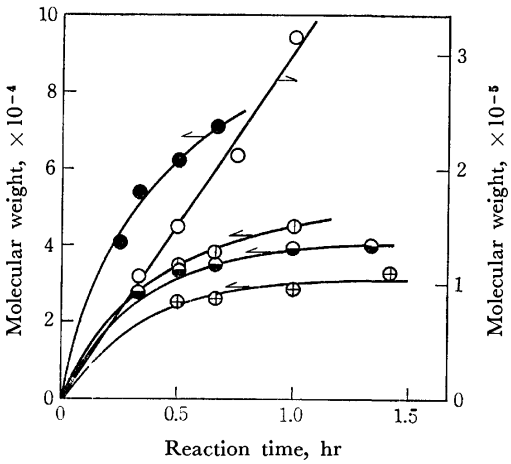

Fig. 2. Molecular weight *vs.* reaction time.
Reaction conditions are the same as in Fig. 1.

The observed increase in the rate and the molecular weight with the reaction time suggests that a stationary state with respect to the concentration of growing radicals is not realized in the polymerization. The time exponents of the polymer yield were found to be 1.9, 1.5, and 1.3 when the amounts of R-114 were 0, 26.9, and 67.3 g respectively at the pressure of 400 kg/cm². The fact that the time exponent of the polymer yield is close to 2.0 without a solvent suggests that the rate of termination is negligibly small in the bulk polymerization.[4] On the other hand, since the time exponent decreases towards unity as the amount of R-114 increases, the termination rate becomes large in the solution polymerization, which approaches a stationary state with an increase in the amount of R-114.[5]

The number of moles of the polymer chain, N_p (defined as the ratio of the polymer yield to the number-average molecular weight) given in Fig. 3 increases with the amount of R-114, and it is almost independent of the reaction pressure. The plots of N_p *vs.* the reaction time give an upward concave curve, while a straight line is obtained in the bulk polymerization. These facts suggest that the rate of transfer is small in the bulk polymerization, and that it increases with the amount of R-114.

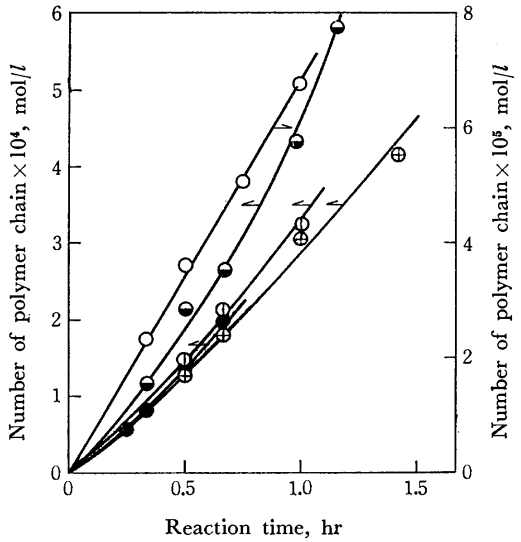

Fig. 3. Number of polymer chain *vs.* reaction time.
Reaction conditions are the same as in Fig. 1.

Effect of Dose Rate. The results are given in Table 2. Dose-rate exponents are determined from Fig. 4 to be 0.8 for the rate of the polymerization and

Table 2. Effect of dose rate on polymer yield and molecular weight[a]

Dose rate $\times10^4$ rad/hr	Polymer yield mol/l[b]	Molecular weight $\times10^{-4}$
0.9	0.089	5.15
2.5	0.171	5.00
5.1	0.307	4.50
9.2	0.609	3.93

a) Reaction conditions; temperature, 30°C; pressure, 400 kg/cm²; amount of R-114, 67.3 g; time, 1 hr; reactor volume, 100 m*l*.
b) Polymerized monomer.

4) S. Machi, M. Hagiwara, M. Gotoda, and T. Kagiya, This Bulletin, **39**, 2696 (1966).
5) M. Hagiwara, H. Mitsui, S. Machi, and T. Kagiya, *J. Polym. Sci., A-1*, **6**, 609 (1968).

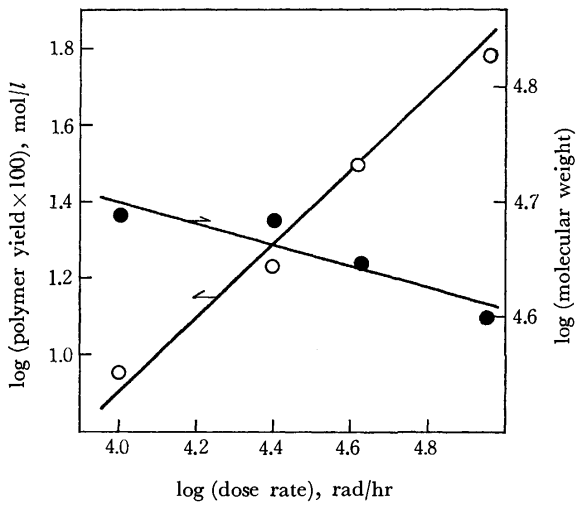

Fig. 4. Effect of dose rase on polymer yield and molecular weight.
Reaction conditions: pressure, 400 kg/cm²; temperature, 30°C, amount of R-114, 67.3 g; time, 1.0 hr; reactor volume 100 m*l*.

—0.2 for the molecular weight respectively. From this and the fact that R-114 is a precipitant of the polyethylene produced, it can be said that the termination by a mutual combination of growing radicals is not important in this polymerization.

Kinetical Consideration

Proposed Scheme of the Polymerization. On the basis of the experimental results presented above, the reaction scheme shown in Eqs. (1)—(6) can be proposed for this polymerization.

Initiation:

$$\text{M, or S} \rightsquigarrow \text{R}_1\cdot \qquad R_i=k_i f([\text{M}],[\text{S}])I \quad (1)$$

Propagation:

$$\text{M} \rightleftarrows \text{M}^*$$

$$\text{M}^* + \text{M} \overset{K_e}{\rightleftarrows} \text{M}_2^* \qquad f_{\text{M}_2^*}=K_e f_{\text{M}}^2 \quad (2)$$

.....

$$\text{R}_n\cdot + \text{M}_2^* \rightarrow \text{R}_{n+1}\cdot + \text{M}^* \qquad R_p=k_p[\text{R}_n\cdot]f_{\text{M}_2^*} = k_pK_e[\text{R}_n\cdot]f_{\text{M}}^2 \quad (3)$$

Transfer:

$$\text{R}_n\cdot + \text{XY} \rightarrow \text{R}_n\text{X} + \text{Y}\cdot \qquad R_{tr}=k_{tr}[\text{XY}][\text{R}_n\cdot] \quad (4)$$

Termination:

$$\text{S} \rightsquigarrow \text{S}\cdot \qquad R_S=k_S[\text{S}]I \quad (5)$$

$$\text{R}_n\cdot + \text{S}\cdot \rightarrow \text{R}_n\text{S} \qquad R_t=k_t[\text{S}\cdot]][\text{R}_n\cdot] \quad (6)$$

where M and S represent the ethylene monomer and R-114 respectively; M* is an excited ethylene monomer, and M_2^*, an excited ethylene dimer; f_{M} and $f_{\text{M}_2^*}$ are the fugacities of the substances indicated; $\text{R}_1\cdot$ is an initiating radical, and $\text{R}_n\cdot$, an active polymer chain composed of n monomers; XY is the substance to which the activity of $\text{R}_n\cdot$ is transferred, and S·, the primary radical formed by the radiolysis of R-114 which causes the termination; R_i, R_p, R_{tr}, R_t, and R_S are the rates of initiation, propagation, transfer, termination, and formation of S· respectively, and k's, the rate constants of these reactions; K_e is an equilibrium constant; [M], [S], [S·], and [XY], are the concentrations of M, S, S·, and XY respectively, and $f([\text{M}],[\text{S}])$, a function of [M] and [S]; where $[\text{R}_n\cdot]$ is the concentration of active polymer chains ($=\sum_{n=1}^{\infty}\text{R}_n\cdot$), and I is the dose rate.

In the above scheme, the initiating radicals are produced from both ethylene and R-114 under γ-ray irradiation. Although we can not entirely exclude the possibility that the initial stage of their formation is influenced by the presence of the hologenated solvent, which may act as a powerful electron scavenger, here it is assumed to be negligibly small. The formation of the excited ethylene dimer and its addition to a growing radical (reactions (2) and (3) are introduced with due consideration of the results of the bulk polymerization.[6,7] Further, the termination is assumed to be a combination of a growing radical with a primary radical from R-114 (reaction (6)).

Rate of Polymerization. For the reasons described above, the kinetics of the non-stationary state should be applied to this polymerization.[8] The overall rate of the polymerization, R, is expressed as:

$$R \fallingdotseq R_p = k_pK_ef_{\text{M}}^2[\text{R}_n\cdot] \quad (7)$$

where $[\text{R}_n\cdot]$ is given by:

$$[\text{R}_n\cdot] = \int_0^t R_i\text{d}t - \int_0^t R_t\text{d}t \quad (8)$$

Since the polymerization was stopped at a low conversion, [M], [S] and f_{M} are considered to be essentially constant during the reaction. Further, if a steady state is assumed with respect to the concentration of the primary radical, [S·], Eq. (9) is obtained from Eqs. (1), (6), and (8):

$$[\text{R}_n\cdot] = R_it - (k_t[\text{S}\cdot]/k_pK_ef_{\text{M}}^2)M_p \quad (9)$$

M_p is the amount of polymer formed, being approximately equal to $\int_0^t R_p\text{d}t$. Hence, the combination of Eqs. (3) and (9) leads to:

$$R_p = k_pK_ef_{\text{M}}^2R_it - k_t[\text{S}\cdot]M_p \quad (10)$$

$$M_p\Big/\int_0^t M_p\text{d}t = (1/2)k_pK_ef_{\text{M}}^2R_i\left(t^2\Big/\int_0^t M_p\text{d}t\right) - k_t[\text{S}\cdot] \quad (11)$$

According to Eq. (11), the plots of $M_p\Big/\int_0^t M_p\text{d}t$ *vs.* $t^2\Big/\int_0^t M_p\text{d}t$ should make a straight line if the proposed scheme is valid. The numerical values of these two terms are obtained from the data in Table 1, while the plots are given in Fig. 5. The intercept of the straight lines obtained gives $k_t[\text{S}\cdot]$, and the slope, $(1/2)k_pK_ef_{\text{M}}^2R_i$.

6) S. Machi, M. Hagiwara, M. Gotoda, and T. Kagiya, *J. Polym. Sci., A-1*, **4**, 1517 (1966).
7) M. Hagiwara, H. Okamoto, and T. Kagiya, *ibid., A-1*, **8**, 3303 (1970).
8) T. Kagiya, M. Izu, S. Machi, and K. Fukui, This Bulletin, **40**, 1049 (1967).

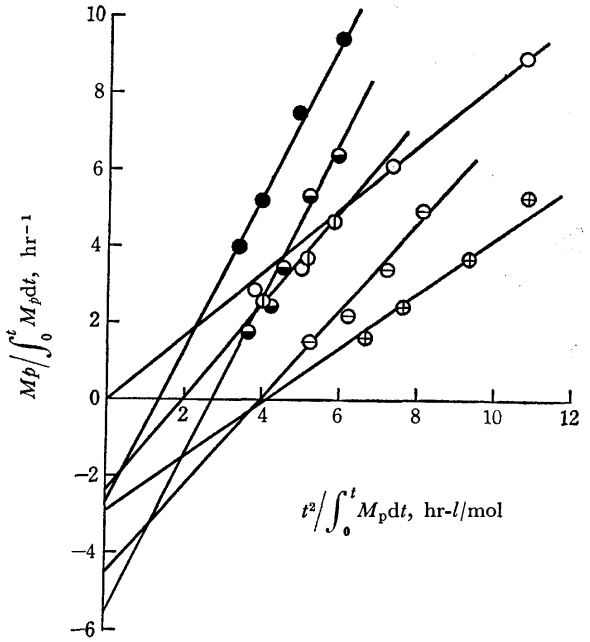

Fig. 5. $M_p/\int_0^t M_p dt$ *vs.* $t^2/\int_0^t M_p dt$.
Reaction conditions: pressure and amount of R-114, (⊖) 310 kg/cm², 57.4 g. Others are the same as in Fig. 1.

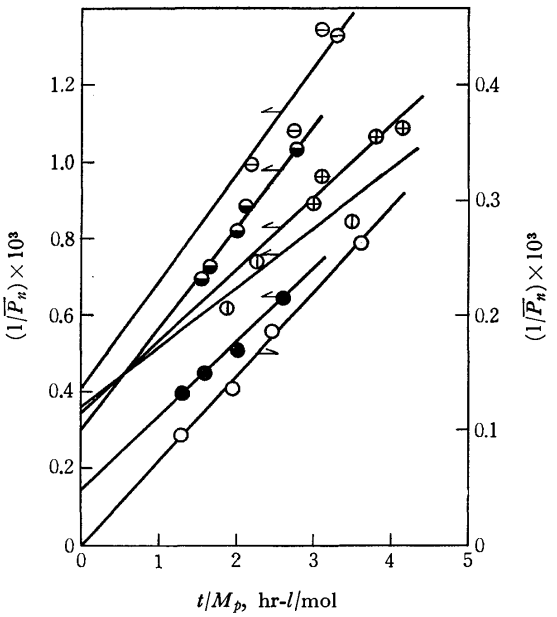

Fig. 6. $1/\overline{P}_n$ *vs.* t/M_p.
Reaction conditions are the same as in Fig. 5.

Degree of Polymerization. For the polymerization with no termination caused by the combination of growing radicals, the number-average degree of polymerization, $\overline{P}_n$, is given by Eq. (12):

$$\overline{P}_n = \int_0^t R_p dt \Big/ \left(\int_0^t R_i dt + \int_0^t R_{tr} dt \right) \qquad (12)$$

Hence, the reciprocal degree of polymerization, $1/\overline{P}_n$, is given as:

$$1/\overline{P}_n = R_i(t/M_p) + k_{tr}[XY]/k_p K_e f_M^2 \qquad (13)$$

In Eq. (13), [XY] can be assumed to be constant throughout the reaction. Figure 6 shows that the plots of $1/\overline{P}_n$ *vs.* t/M_p give a linear relation for every one of the polymerization runs. The slope of the lines is the overall rate of initiation, R_i, and the intercept on the ordinate is $k_{tr}[XY]/k_p K_e f_M^2$. After all, the numerical values of R_i, $k_p K_e$, $k_{tr}[XY]$, and $k_t[S\cdot]$ can be determined by the use of Eqs. (11) and (13). The results are summarized in Table 3.

Initiation Reaction. Since, as is shown in Table 3, the overall rate of initiation, R_i, increases markedly with the addition of R-114, it is clear that R-114 acts as an effective promotor for the initiation reaction. If the energy transfer between ethylene and R-114 does not occur, the overall rate of initiation can be represented as follows:

$$R_i = R_{iM} + R_{iS} = k_{iM}[M]I + k_{iS}[S]I = (k_{iM}[M] + k_{iS}[S])I \qquad (14)$$

where R_{iM} and R_{iS} are the rates of initiation from ethylene and R-114 respectively. Hence, R_{iS} can be evaluated with the use of R_{iM}, which is itself determined by the bulk polymerization. Although Fig. 7 shows some scatter, it can be seen that a linear relation exists between R_{iS} and the concentration of R-114. This indicates the validity of Eq. (14), and also the absence of energy transfer between ethylene and and R-114.

Table 3. Calculated rates and rate constants[a)]

Reaction pressure kg/cm²	Amount of R-114 g	Concentration mol/l		Fugacity[b)] kg/cm²		Rate and rate constant			
		C_2H_4	R-114	C_2H_4	R-114	$R_i\times10^4$ mol/l-hr	k_pK_e hr^{-1} × (kg/cm²)$^{-2}$	k_{tr}[XY] hr^{-1}	k_t[S·] hr^{-1}
400	0	16.7	0	123.6	0	0.72	1.45	0	0
400	26.9	13.8	1.58	108.6	2.77	1.95	1.72	2.63	2.60
400	67.3	9.46	3.95	89.0	6.50	2.80	2.07	4.93	5.55
310	29.6	12.2	1.73	89.1	1.83	2.10	1.45	2.76	2.50
310	57.4	10.3	3.35	69.5	3.65	2.53	1.70	3.84	4.60
210	29.6	11.5	1.73	65.1	1.19	1.83	1.55	2.37	2.90

a) Reaction conditions: temperature, 30°C; dose rate, 9.2×10^4 rad/hr; reactor volume, 100 ml.
b) Calculated by using the equation of state proposed by O. Redlich and J. N. S. Kwong, (Ref. 9).

9) W. C. Edmister, "Applied Hydrocarbon Thermodynamics," Gulf Publishing Co., Houston (1961).

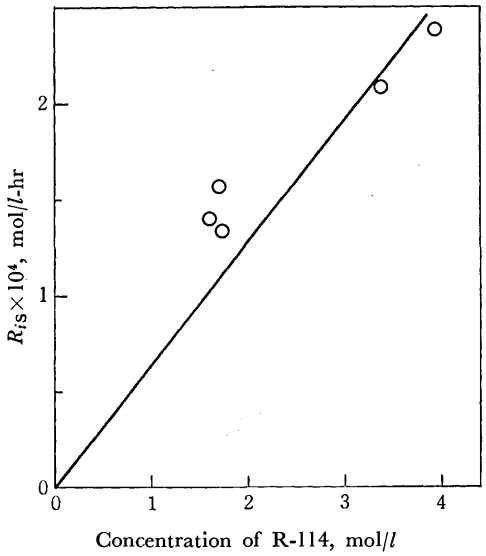

Fig. 7. Rate of initiation from R-114, R_{iS}, *vs.* concentration of R-114.
Reaction conditions: pressure, 210—400 kg/cm²; temperature, 30°C; dose rate, 9.2×10^4 rad/hr; reactor volume, 100 m*l*.

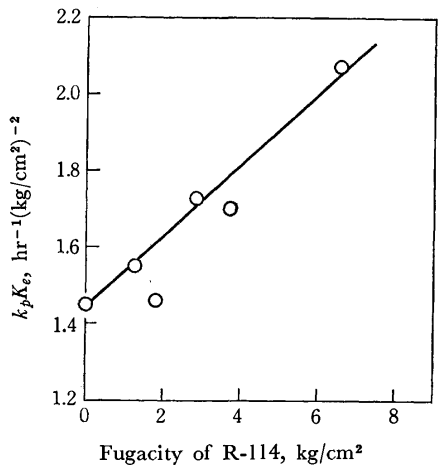

Fig. 8. Apparent rate constant of propagation, k_pK_e, *vs.* fugacity of R-114.
Reaction conditions are the same as in Fig. 7.

Propagation Reaction. The apparent rate constant of propagation, k_pK_e, is shown in Table 3 to increase with the amount of R-114. In Fig. 8 a linear relation is obtained between k_pK_e and the fugacity of R-114, f_{R-114}. This indicates that R-114 acts as promotor of the propagation reaction. The promotive effect of R-114 on the propagation reaction is also suggested by the studies of the copolymerization of ethylene with tetrafluoroethylene.[3] The mechanism of the promotion is not yet clear in detail, however, probably, strongly electronegative fluorine atoms in R-114 molecule have some effect on the reactivity of the growing radical in a solvated state. If that is the case, the linear relation between k_pK_e and f_{R-114} in Fig. 8 can be interpreted as follows.

Equation (15) shows that some of the growing radicals exist in a solvated state:

$$R_n\cdot + S \overset{K_S}{\rightleftarrows} R_n\cdots S \tag{15}$$

$$[R_n\cdots S] = K_S[R_n\cdot]f_{R-114} \tag{16}$$

If the propagation reaction in R-114 consists of the addition of M_2* to the growing radicals in a free state:

$$R_n\cdot + M_2^* \xrightarrow{k_{pf}} R_{n+1}\cdot + M^* \tag{17}$$

and to those in a solvated state:

$$R_n\cdots S + M_2^* \xrightarrow{k_{pS}} R_{n+1}\cdot + M^* + S \tag{18}$$

the rate of the propagation, R_p, can be written as Eq. (19):

$$R_p = \frac{(k_{pf}K_e + k_{pS}K_eK_Sf_{R-114})[R_n\cdot]f_M^2}{1+K_Sf_{R-114}} \tag{19}$$

Therefore, k_pK_e can be derived from a comparison with Eqs. (3) and (19) as follows:

$$k_pK_e = \frac{(k_{pf}K_e + k_{pS}K_eK_Sf_{R-114})}{1+K_Sf_{R-114}}$$

Further, if $f_{R-114}K_S$ is very small compared with unity, the above equation can be rewritten approximately as:

$$k_pK_e \fallingdotseq k_{pf}K_e + k_{pS}K_eK_Sf_{R-114} \tag{20}$$

which satisfies the linear relation in Fig. 8.

Transfer Reaction. As has been stated before, the transfer reaction is absent in the bulk polymerization, but it increases with the addition of R-114. Figure 9 shows that a straight line is obtained when k_{tr}-

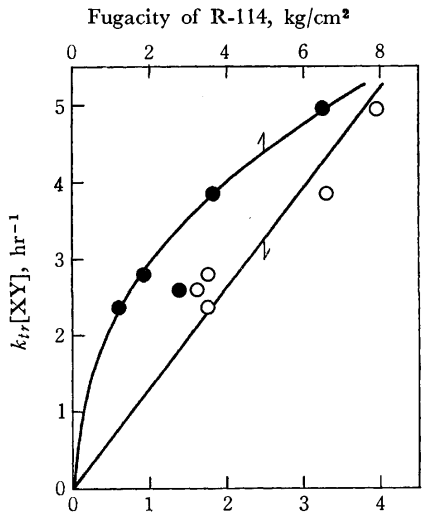

Fig. 9. Apparent rate constant of transfer, k_{tr}[XY], *vs.* concentration of R-114, and fugacity of R-114.
Reaction conditions are the same as in Fig. 7.

[XY] is plotted against the concentration of R-114, [S], rather than against its fugacity, f_{R-114}. This may indicate that radiation energy takes part in the transfer reaction. Since the transfer has been found in a previous work to increase with an increase in the number of the chlorine atoms of a halogenated hydrocarbon solvent,[2] the reaction may be the abstraction of Cl from an excited R-114 molecule by the growing radical:

$$R_n\cdot + ClCF_2CF_2Cl^* \rightarrow R_nCl + CF_2CF_2Cl \tag{21}$$

The existence of a linear relation between $k_{tr}[XY]$ and the concentration of R-114 supports the above conclusion that there is no energy transfer between ethylene and R-114.

Termination Reaction. As can be seen in Table 3, the apparent rate constant of termination, $k_t[S\cdot]$, increases with the addition of R-114. Figure 10 shows that $k_t[S\cdot]$ is nearly proportional to the concentration of R-114.

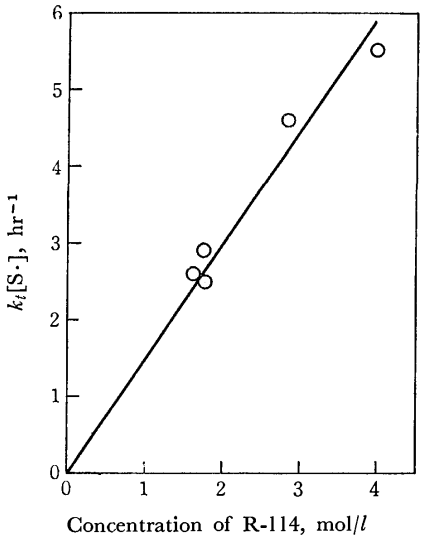

Fig. 10. Apparent rate constant of termination, $k_t[S\cdot]$, *vs.* concentration of R-114.
Reaction conditions are the same as in Fig. 7.

In this polymerization, as has been described above, the radicals formed from R-114 act both as initiators and as terminators. The mass spectrum of R-114 suggests that the radicals from R-114 are mainly CF_2Cl, plus smaller amounts of C_2F_4Cl and Cl.[2] Highly reactive radicals may contribute to the initiation more than those with less reactivity.

Recently, a semi-empirical Eq. (22) was proposed for use in estimating the activation energy of a radical-addition reaction to vinyl monomers (Eq. (23)):[10]

$$E_{a,R} = D_\pi - \phi D_\pi D_f \qquad (22)$$

$$R\cdot + \diagdown C{=}C \diagup \rightarrow R\text{-}\overset{|}{C}\text{-}\overset{|}{C}\cdot \qquad (23)$$

In Eq. (22), D_π is a π-bond dissociation energy of the monomer, D_f is that of the δ-bond formed in the reaction, and ϕ is a constant. Since D_π is constant in this polymerization, it is clear that the activation energy needed to form an initiating radical depends solely on D_f, and that it decreases with an increase in D_f. This means that the radical, R·, will make a greater contribution to the initiation reaction if it can form a strong R-C bond in the reaction with ethylene.

10) T. Kagiya and Y. Sumida, *Polymer J.*, **1**, 137 (1970).

Table 4. Dissociation energy of the bond, R-CH_3

R	D_{R-CH_3} kcal/mol	$\Delta H_{f,R}$ kcal/mol
F	108[12]	
CF_3	90,[13] 117[14]	
CH_2Cl	84.3[a]	27.7[b]
CH_3	83.2[a]	31.5
C_2H_5	81.4[a]	25.1
$CHCl_2$	80.1[a]	20.9[b]
Cl	78.7[a]	28.5
CCl_3	77.7[2], 78.4[a]	16.2[b]

a) Calculated from, $D_{R-CH_3}=\Delta H_{f,R}+\Delta H_{f,CH_3}-\Delta H_{f,R-CH_3}$ where, ΔH_f=standard heat of formation.
b) Estimated from the values of bond dissociation energy listed in Table 9 (p 24) of Ref. 11.

Table 4 gives the dissociation energy of the bonds between several R·'s and the CH_3 radical. If R· is the fluorine atom or a fluorine-containing radical, the bond with CH_3 is stronger than that of such hydrocarbon radicals as CH_3 or C_2H_5. Substitution by the chlorine atom, on the contrary, generally weakens the bond, although one mono-substituted radical, CH_2Cl, exceptionally forms a strong bond. From these facts, it seems reasonable to speculate that the strength of the R-C bond may be in the order of:

$$CF_2Cl,\ C_2F_4Cl,\ CF_3 > CH_2Cl,\ CH_3 > CHCl_2 > Cl,\ CCl_3$$

Hence, the order of the activation energy may be given as:

$$E_{a,CF_2Cl},\ E_{a,C_2F_4Cl} \ll E_{a,Cl}$$

Thus, R-114 can probably contribute to the initiation through reactions (24) and (25):

$$CF_2Cl + CH_2{=}CH_2 \rightarrow CF_2Cl\text{-}CH_2\text{-}CH_2 \qquad (24)$$

$$C_2F_4Cl + CH_2{=}CH_2 \rightarrow C_2F_4Cl\text{-}CH_2\text{-}CH_2 \qquad (25)$$

and to the termination through reaction (26):

$$R_n\cdot + Cl \rightarrow R_nCl \qquad (26)$$

11) N. N. Semenov, "Some Problems in Chemical Kinetics and Reactivity (English translation)," Princeton Univ. Press, Princeton, (1958).
12) J. A. Kerr, *Chem. Rev.*, **66**, 465 (1966).
13) J. B. Farmer, I. H. S. Henderson, F. P. Lossing and D. G. H. Marsden, *J. Chem. Phys.*, **24**, 348 (1956).
14) V. H. Dibeler, R. M. Reese, and F. L. Mohler, *ibid.*, **20**, 761 (1952).

Reactions of Alkylidenetriphenylphosphoranes with Sulfur

Hirokazu TOKUNAGA, Kin-ya AKIBA, and Naoki INAMOTO

Department of Chemistry, Faculty of Science, The University of Tokyo, Hongo, Bunkyo-ku, Tokyo

(Received February 25, 1971)

Reaction of diarylmethylenetriphenylphosphoranes with sulfur gave thiobenzophenones and triphenylphosphine sulfide in good yields. Reaction of benzylidenetriphenylphosphoranes with sulfur gave triphenylphosphine sulfide and 5,7-diphenyl-1,2,3,4,6-pentathiepane. More active alkylidenetriphenylphosphoranes such as isopropylidene- or *sec*-butylidenetriphenylphosphorane gave the corresponding phosphonium betaine containing sulfur atoms or phosphonium salt produced through air oxidation and hydrolysis of the betaine. α-Benzoylbenzylidenetriphenylphosphorane did not react with sulfur. Reactivity of alkylidenephosphoranes toward sulfur was briefly discussed.

Many examples are known on the formation of carbonyl or olefinic compounds by the reaction of alkylidenephosphoranes (I) with oxygen.[1-4] However, only a few examples have been reported on the reactions of I with sulfur,[5,6] although thiocarbonyl compounds could not be isolated.

We investigated the reaction of I with sulfur in more detail, in order to clarify this reaction.

Results and Discussion

Reaction of Diarylmethylenetriphenylphosphoranes (II). Phosphoranes (II) were prepared by adding the corresponding phosphonium bromide to sodium ethoxide in benzene or chlorobenzene, and were allowed to react with sulfur under reflux to give thiobenzophenones (III) and triphenylphosphine sulfide (IV) in good yields. Thiobenzophenones were identified by conversion into their phenylhydrazones. The results are summarized in Table 1.

Table 1. Reactions of II with sulfur

II	Solvent	III	(%)	Mp (Bp) (°C)	IV (%)
IIa	C_6H_6	IIIa	85	49—51	96
	C_6H_5Cl		80	(lit,[7] 53—54)	89
IIb	C_6H_6	IIIb	70[a]	71—76	69[a]
	C_6H_5Cl		52[a]	(lit,[8] 75—76)	62[a]
IIc	C_6H_6	IIIc	50[a]	85—87	67[a]
				(lit,[9] 90.5—91.5)	
IId	C_6H_6	IIId	70[a]	105—110	95[a]
				(lit,[9] 108.5—109.5)	
IIe	C_6H_6	IIIe	57[a]	(136—138/0.3 mmHg)	63[a]
	C_6H_5Cl		63[a]		67[a]
IIf	C_6H_6	IIIf	66[a]	(145—146/0.22 mmHg)	67[a]
	C_6H_5Cl		51[a]		66[a]

a) The yields were calculated on the basis of phosphonium salts used.

$$Ph_3P{=}CArAr' + S_8 \rightarrow ArAr'C{=}S + Ph_3P{=}S$$
II III IV

a: Ar=Ar'=Ph; b: Ar=Ar'=*p*-MeC_6H_4;
c: Ar=Ar'=*p*-ClC_6H_4; d: Ar=Ar'=*p*-BrC_6H_4;
e: Ar=Ph, Ar'=*p*-MeC_6H_4; f: Ar=Ph, Ar'=*p*-ClC_6H_4

Under the present conditions, thiobenzophenones did not react further with II to give olefinic compounds.

Reactions of Benzoylmethylenetriphenylphosphorane (V), α-Benzoylbenzylidenetriphenylphosphorane (VII) and Phenyliminotriphenylphosphorane. Benzoylmethylenetriphenylphosphorane (V) reacted easily with sulfur in refluxing benzene to give IV (88%) and an oily substance (VI), the structure of which corresponds to the trimer or tetramer of benzoylthioformaldehyde.

$$Ph_3P{=}CH{-}COPh + S_8 \rightarrow Ph_3P{=}S + (PhCOCHS)_n$$
V IV VI (n=3—4)

Desulfurization of VI with Raney Ni gave ethylbenzene and acetophenone which were identified by vapor phase chromatography (vpc). Distillation of VI gave only acetophenone.

The reaction of VII with sulfur was attempted in order to obtain monothiobenzil,[10] VII was recovered quantitatively.

$$Ph_3P{=}CPh(COPh) + S_8 \rightarrow \text{no reaction}$$
VII

Phenyliminotriphenylphosphorane did not react with sulfur in refluxing benzene even in the presence of basic catalysts.

Reaction of Benzylidenetriphenylphosphorane (VIII). The reaction of VIII with sulfur gave IV and a new compound (IX), $C_{14}H_{12}S_5$, in 83 and 14% yields in a short time, respectively. The prominent peaks in the MS spectrum of IX were *m/e* 340 (M^+, 4), 276 ($(PhCH)_2S_3^+$, 20), 220 ($PhCHS_4H_2^+$, 10), 219 ($PhCHS_4H^+$, 6), 218 ($PhCHS_4^+$, 48), 156 ($PhCHS_2H_2^+$, 12), 155 ($PhCHS_2H^+$, 35), 154 ($PhCHS_2^+$, 73), 153 ($PhCS_2^+$, 98), 124 ($PhCHSH_2^+$, 14), 123 ($PhCHSH^+$, 49), 122 ($PhCHS^+$, 93), 121 ($PhCS^+$, 100), 78 (PhH^+, 78) and 77 (Ph^+, 78).

$$Ph_3P{=}CHPh + S_8 \rightarrow Ph_3P{=}S + (PhCH)_2S_5$$
VIII IV IX

1) H. J. Bestmann, *Angew. Chem.*, **72**, 34 (1960).
2) H. J. Bestmann and O. Kratzer, *ibid.*, **74**, 494 (1962).
3) H. J. Bestmann and O. Kratzer, *Chem. Ber.*, **96**, 1899 (1963).
4) H. J. Bestmann, H. Häberlein, H. Wagner, and O. Kratzer, *ibid.*, **99**, 2848 (1966).
5) H. Staudinger and J. Meyer, *Helv. Chem. Acta*, **2**, 635 (1919).
6) A. Schönberg, K. H. Brosowski, and E. Singer, *Chem. Ber.*, **95**, 2144 (1962).
7) B. F. Gofton and E. A. Braude, "Organic Syntheses," Coll. Vol. IV, p. 927 (1963).
8) O. Korver, J. U. Veenland, and Th. J. de Boer, *Rec. Trav. Chim.*, **81**, 1031 (1962).
9) A. Lüttringhaus and J. Grohmann, *Z. Naturforsh.*, **10b**, 365 (1955).
10) D. C. Dittmer, G. C. Levy, and G. E. Kuhlmann, *J. Amer. Chem. Soc.*, **89**, 2793 (1967).

With regard to the structure of IX, three isomers, X, XI, and XII, are considered to be possible.

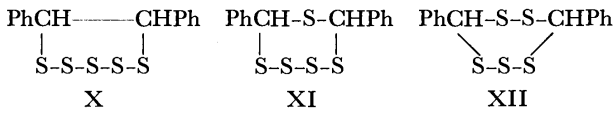

X XI XII

The structure X is excluded, because desulfurization of IX with Raney Ni gave no bibenzyl but toluene (58%). It is difficult to distinguish XI from XII with MS data, but the presence of the weak peak at *m/e* 212, which is attributable to stilbene episulfide, might favor XI to XII.

From the analogy of formation mechanism of ozonide,[11] the structure XI is also more favorable.

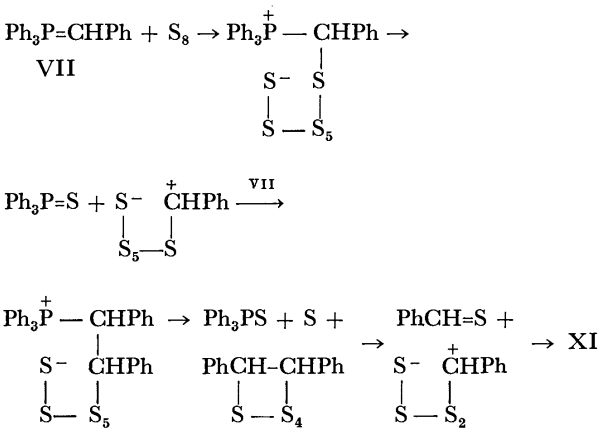

From the above facts, IX is tentatively assigned as 5,7-diphenyl-1,2,3,4,6-pentathiepane (XI).

Very recently, Mägerlein and Meyer have reported that arylmethylenetriphenylphosphoranes gave 1,2-diarylethylenes by reactions with sulfur at 100—120°C, and that triphenylphosphine sulfide and resinous material were obtained at 50—60°C.[12] In our case, a small amount of *cis*- and *trans*-stilbenes was also detected.

Reactions of Active Alkylidenephosphoranes. In the reaction of methylenetriphenylphosphorane (XIII) with sulfur at 70°C, brown precipitates appeared and unidentified gas evolved during the reaction. The gas reacted with metallic mercury but its structure could not be determined by means of IR spectrum. The brown precipitates gradually disappeared during the reaction and only IV was isolated in 74% yield after 6 hr.

More active isopropylidenetriphenylphosphorane (XIV) gave large amounts of brown precipitates, which produced IV on heating at 200°C. During the usual treatment, the brown precipitates changed to phosphonium salt (XV), which possesses sulfonate group and gives isopropyltriphenylphosphonium iodide (XVI) with potassium iodide quantitatively. Absorptions at 1230, 1020, and 605 cm^{-1} in the IR spectrum of XV are consistent with those of sulfonate group.

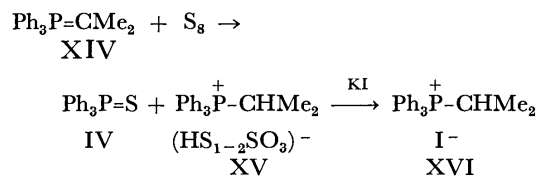

XIV IV XV XVI

In the case of *sec*-butylidenetriphenylphosphorane (XVII), large amounts of brown precipitates appeared in a similar way. The brown precipitates did not show absorptions attributable to sulfonate group in the IR spectrum, when the IR spectrum was measured immediately, but underwent oxidation and hydrolysis in air to give phosphonium salt (XIX), which possesses sulfonate group and also gives the corresponding iodide with potassium iodide.

Therefore, in the cases of the most active phosphoranes the reaction stopped at a stage of addition of sulfur to the P=C bond to give betaine (*e.g.*, XVIII), which is oxidized in air and hydrolyzed to form phosphonium salt possessing sulfonate group during the course of treatment.

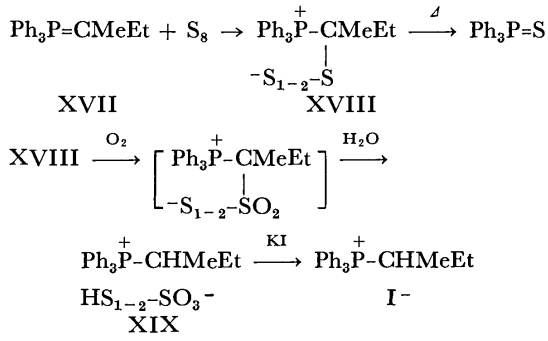

XVII XVIII XIX

Reactivities of Phosphoranes toward Sulfur. The activity of phosphoranes used is considered to decrease in the following order:

$Ph_3P{=}CMeEt \approx Ph_3P{=}CMe_2 > Ph_3P{=}CH_2 > Ph_3P{=}CHPh >$
XVII XIV XIII VIII

$Ph_3P{=}CArAr' > Ph_3P{=}CHCOPh \gg Ph_3P{=}CPh(COPh)$
II V VII

The most active phosphoranes (XIV and XVII) gave betaine with sulfur. The cleavage of the P=C bond scarcely occurred at 70—80°C. Phosphorane XIII also gave brown precipitates, which are considered to be betaine, but the precipitates disappeared after heating for a long period to produce triphenylphosphine sulfide, indicating that the cleavage of the P=C bond occurred very slowly.

The most stable phosphorane (VII) did not react with sulfur, and moderately active phosphoranes (VIII, II and V) underwent a cleavage of the P=C bond with sulfur easily.

Experimental

Materials. Diphenylmethylenetriphenylphosphorane (IIa) was prepared from diphenylmethyltriphenylphosphonium bromide and sodium ethoxide, mp 169—170°C (lit,[13] 174°C). Phosphonium salts were prepared from triphenylphosphine and the corresponding halides without solvent. They are summarized in Table 2.

11) a) P. Bailey, *Chem. Rev.* **58**, 925 (1958); b) A. P. Schaap and P. D. Bartlett, *J. Amer. Chem. Soc.*, **92**, 6055 (1970).

12) H. Mägerlein and G. Meyer, *Chem. Ber.*, **103**, 2995 (1970).

13) L. Horner and E. Lingnaw, *Ann. Chem.*, **591**, 135 (1955)

Table 2. Phosphonium salts ($RPh_3P^+X^-$) used

R	X	Mp (°C) (lit.)	Found (%) C	H
Ph_2CH	Br	231—232 (230)[13]		
$(p\text{-}MeC_6H_4)_2CH$	Br	200—203	73.59	5.70
$(p\text{-}BrC_6H_4)_2CH$	Br	226—230	55.72	3.65
$(p\text{-}MeC_6H_4)PhCH$	Br	230—235	73.38	5.41
$(p\text{-}ClC_6H_4)PhCH$	Br	227—228	68.24	5.10
$(p\text{-}MeOC_6H_4)_2CH$	Br	195—198	68.28	4.32
$(p\text{-}ClC_6H_4)_2CH$	Br	218.5—219	64.50	4.45
sec-Bu	I	204—205.5	59.00	5.44
i-Pr	I	192.7—194.7 (195—196)[14]		
Me	Br	223—234 (232—233)[15]		
$PhCH_2$	Br	231—232 (230)[16]		

Benzoylmethylenetriphenylphosphorane (V) was prepared by the method of Ramirez,[17] mp 180—181°C (lit, 178—180°C). α-Benzoylbenzylidenetriphenylphosphorane (VII) was prepared by the method of Trippett,[18] mp 190.5—191.8°C (lit, 191—192°C). Phenyliminotriphenylphosphorane was prepared by the method of Staudinger,[5] mp 129—131°C (lit, 131—132°C).

Reaction of Diphenylmethylenetriphenylphosphorane (IIa) with Sulfur. *a) In benzene*: A mixture of 23.4 g (0.055 mol) of IIa, 3.5 g (0.11 g atom) of sulfur, and 200 m*l* of dry benzene was heated at 80°C for one hour with stirring under nitrogen. The solvent was distilled off, and the residual blue oil was distilled at 104—107°C under a pressure of 0.5 mmHg. The deep violet distillate (IIIa) solidified, mp 49—51°C (mixt mp 49—51°C, lit,[7] 53—54°C), yield 9.3 g (85%). Recrystallization of the residue of the distillation twice from ethanol gave triphenylphosphine sulfide (IV) (15.5 g, 96%), mp 156—158°C (lit,[19] 157.5°C).

b) In Chlorobenzene: A mixture of 16.7 g (0.039 mol) of IIa, 2.54 g (0.078 g atom) of sulfur, and 150 m*l* of dry chlorobenzene was refluxed, and the reaction mixture was treated in a similar manner to that described in a) to give IIIa (6.2 g, 80%) and IV (10.2 g, 89%).

Reaction of Diarylmethylenetriphenylphosphoranes with Sulfur. A typical procedure is described for the reaction of di-*p*-tolylmethylenetriphenylphosphorane (IIb).

Sodium ethoxide was prepared from 1.17 g (0.051 g atom) of sodium metal and 100 m*l* of absolute ethanol. Ethanol was distilled off, and 400 m*l* of dry benzene was then added and about 100 m*l* of benzene was distilled off to remove ethanol as an azeotropic mixture. After the mixture was cooled to room temperature, 29.7 g (0.055 mol) of di-*p*-tolylmethyltriphenylphosphonium bromide was added. The color of the mixture slowly turned red. After one hour, the red solution was transferred through a G-4 glass-filter to a 500 m*l* three-necked flask, fitted with a reflux condenser, a gas-inlet tube and a stirrer under nitrogen. The filtrated red solution, 3.2 g (0.1 g atom) of sulfur was added. The mixture was then refluxed with stirring for one hour, during which the color of the reaction mixture turned blue rapidly. After the solvent was distilled off, the residual blue oil was distilled at 145—150°C under a pressure of 0.3 mmHg. The deep violet distillate (IIIb) (8.5 g, 70%) solidified, mp 71—76°C (lit,[8] 75—76°C). From the residue of the distillation, 11.0 g (69%) of IV was obtained.

When chlorobenzene was used as a solvent instead of benzene, the yields of IIIb and IV were 52 and 62%, respectively, on the basis of di-*p*-tolylmethyltriphenylphosphonium bromide.

Reaction of Benzylmethylenetriphenylphosphorane (V) with Sulfur. a) A mixture of 9.5 g (0.025 mol) of V and 1.6 g (0.05 g atom) of sulfur and 40 m*l* of dry benzene was refluxed with stirring for one hour under nitrogen and the solvent was distilled off. The residual oil was chromatographed on silica gel. Elution with benzene-petroleum ether (3 : 7) gave white crystals after evaporation of the solvent. White crystals (IV) were recrystallized twice from ethanol, mp 155—158°C, yield 6.5 g (88%). Elution with benzene gave an orange oil (VI) after the evaporation of the solvent. Purification of the oil was unsuccessful. The yield was 3.0 g (80%). IR (neat): 1650 cm^{-1} (C=O); NMR ($CDCl_3$): τ 2.3—3.0 (5H, multiplet) and 5.82 (1H, singlet).

Found: C, 64.49; H, 3.89; S, 17.09%; mol. wt., 450—600 (by freezing point depression of benzene). Calcd for C_8H_6OS: C, 63.97; H, 4.03; S, 21.35%; mol. wt., 150.

A mixture of Raney Ni (W-7) prepared from 4 g of commercial Raney alloy and 0.5 g of the orange oil in 30 m*l* of ethanol was refluxed with stirring for 3 hr. From the filtrate, ethylbenzene and acetophenone were detected by vpc.

b) From the reaction mixture of 19 g (0.05 mol) of V and 3.2 g (0.1 g atom) of sulfur in 200 m*l* of dry benzene, the solvent was distilled off. The residual oil was distilled at 105°C under a pressure of 33 mmHg. The distillate (1.0 g, 17%) was identified as acetophenone by IR and vpc, but acetophenone was not detected from the reaction mixture by vpc.

Reaction of Methylenetriphenylphosphorane (XIII) with Sulfur. XIII was prepared from 19.1 g (0.054 mol) of methyltriphenylphosphonium bromide and sodium amide in liquid ammonia. Ammonia was then removed. After addition of 200 m*l* of dry benzene, the mixture was refluxed for one hour to remove ammonia completely, cooled and transferred to a separating funnel through a glass-filter. The solution was added dropwise to a mixture of 3.2 g (0.1 g atom) of sulfur and 300 m*l* of dry benzene at 70°C with stirring over 2 hr. During the reaction, brown precipitates appeared and a gaseous product which reacted with mercury metal was formed. When refluxing was continued for 6 hr the brown precipitates disappeared. After removal of the solvent the residual oil was chromatographed on silica gel. Elution with benzene - petroleum ether (1 : 1) gave IV (11.7 g, 74%).

Reaction of Benzylidenetriphenylphosphorane (VIII) with Sulfur. VIII prepared from 22.1 g (0.051 mol) of benzyltriphenylphosphonium bromide in liquid ammonia and sodium amide, was added dropwise to a solution of 3.2 g (0.1 g atom) of sulfur in 300 m*l* of dry benzene over a period of two hours at 70°C. The reaction mixture was cooled and the solvent was distilled off. The residual oil was chromatographed on silica gel. Elution with benzene - petroleum ether (1 : 10) gave white crystals after evaporation of the solvent. The white crystals (IX) were recrystallized twice from benzene - petroleum ether (1 : 1) and chloroform, mp 179—181.5°C. The crude yield was 1.23 g (14%).

Found: C, 49.23; H, 3.56; S, 46.67%; mol. wt., 351 (Rast), 340 (MS). Calcd for $C_{14}H_{12}S_5$: C, 49.37; H,

14) G. Wittig and D. Wittenberg, *ibid.*, **606**, 1 (1957).
15) G. Wittig and U. Schöllkopf, "Organic Syntheses" Vol. 40, p. 66 (1960).
16) M. Grayson and P. T. Keough, *J. Amer. Chem. Soc.*, **82**, 3919 (1960).
17) F. Ramirez and S. Derschowitz, *J. Org. Chem.*, **22**, 41 (1957).
18) S. Trippett and D. M. Walker, *J. Chem. Soc.*, **1961**, 1266.
19) A. Michaelis and L. Gleichmann, *Ber.*, **15**, 801 (1882).

3.55; S, 47.07%; mol wt, 340.

A mixture of Raney Ni (W-7), prepared from 2 g of commercial Raney alloy, 57 mg (0.168 mmol) of IX and 30 m*l* of ethanol was refluxed with stirring for 4 hr, and filtered. From the filtrate, toluene (58%) was detected by v.p.c.

Elution with benzene-petroleum ether (1 : 10) gave also a small amount of *trans*-stilbene, mp 122—124°C, and the presence of *cis*-stilbene was indicated by IR spectroscopy. Elution with benzene-petroleum ether (1 : 1) gave 12.5 g (83%) of IV.

Reaction of Isopropylidenetriphenylphosphorane (XIV) with Sulfur. XIV prepared from 25.9 g (0.06 mol) of isopropyltriphenylphosphonium iodide with sodium amide in liquid ammonia, was added dropwise to a solution of 4.0 g (0.12 g atom) of sulfur in 300 m*l* of dry benzene over a period of 3 hr at 70°C. Brown precipitates appeared and a gaseous product which reacted with mercury metal, evolved during the reaction. The reaction mixture was cooled and filtered. The brown precipitates which gave IV on heating to 200°C for 2 hr, were treated with active charcoal in ethanol several times to obtain white crystals (XV) (12.0 g, 46%), which were recrystallized three times from ethanol,mp181—182.0°C.

Found: C, 57.32; H, 5.20; S, 19.30%. Calcd for $C_{21}H_{23}PO_3S_{2.65}$: C, 57.40, H, 5.28; S, 19.34%.

After removal of the solvent from the filtrate, IV (6.8 g, 38.5%) was obtained by silica gel chromatography. Compound (XV) (0.125 g, 0.28 mmol) in 20 m*l* of chloroform was stirred with 1.68 g of potassium iodide in 20 m*l* of water for 10 hr. Yellow crystals obtained from the organic layer were recrystallized twice from ethanol, and identified as isopropyltriphenylphosphonium iodide by comparison of its IR spectrum with that of an authentic sample and by mixed melting point (mp 195.5—196.5°C) with an authentic sample (lit,[14] 195—196°C). The yield was 0.102 g (81%). A mixture of XV (0.457 g, 1.04 mmol) and 6 m*l* of aqueous hydrogen iodide (57%) quickly turned red and black precipitates appeared and hydrogen sulfide evolved. The black precipitates consisted of iodine and isopropyltriphenylphosphonium iodide.

Reaction of sec*-Butylidenetriphenylphosphorane (XVII) with Sulfur.* XVII, prepared from 22.7 g (0.05 mol) of *sec*-butyltriphenylphosphonium iodide with sodium amide in liquid ammonia, was added dropwise to a solution of 3.2 g (0.1 g atom) of sulfur in 300 m*l* of dry benzene over a period of two hours at 70°C. Brown precipitates appeared and a gaseous product which reacted with mercury metal evolved during the reaction. The reaction mixture was cooled and filtered. The yield of brown precipitates was 8.0 g, mp 125—130°C (dec) and the IR spectrum exhibited the absence of sulfonate group. The brown precipitates which also gave IV on heating up to 200°C were treated with active charcoal in ethanol several times. White crystals (XIX) thus obtained were recrystallized three times from ethanol, mp 183.0—185.0°C, yield 7.7 g (33%).

Found: C, 58.38; H, 5.67; S, 18.64%. Calcd for $C_{22}H_{25}PO_3S_{2.65}$: C, 58.28; H, 5.56; S, 18.74%.

After removal of the solvent from the filtrate and chromatography on silica gel, elution with benzene-petroleum ether (1 : 1) gave IV (7.9 g, 54%). Compound (XIX) (0.117 g, 0.25 mmol) in 20 m*l* of chloroform was stirred with 1.17 g of potsssium iodide in 20 m*l* of water for 2 hr. Yellow crystals from the organic layer were recrystallized twice from ethanol-ether, and identified as *sec*-butyltriphenylphosphonium iodide. The yield was 83.4 mg (75%).

BULLETIN OF THE CHEMICAL SOCIETY OF JAPAN, VOL. 45, 509—515 (1972)

Reaction of Enol Ethers with Carbenes. X.[1] Ring Opening of 2,2-Dichlorocyclopropyl Phenyl Sulfides[2]

William E. PARHAM, Shoji KAJIGAESHI,[3] and Siemen H. GROEN[4]

School of Chemistry, University of Minnesota, Minneapolis, Minnesota 55455, *U.S.A.*

(Received March 13, 1971)

The ring opening reactions of six known or new 2,2-dichlorocyclopropyl phenyl sulfides have been carried out with potassium *t*-butoxide in *t*-butyl alcohol and with pyridine. The products were enynes, butadienes, allenes and, as minor products, α,β-unsaturated aldehydes containing the phenylmercapto group. Reaction of a mixture of *cis*- and *trans*-1,1-dichloro-2-methyl-3-phenylmercaptocyclopropane (**2**) with pyridine gave unchanged *trans*-isomer. This apparent selectivity is explained on the basis of the steric effects for ring opening.

In recent years the ring opening of *gem*-dichlorocyclopropanes, derived from enol ethers with dichlorocarbene, have been investigated by Parham *et al.*[5] and by Skattebøl,[6] and the subject has been reviewed by Parham and Schweizer.[7] In order to gain additional information on such ring opening reactions, we have prepared the following six *gem*-dichlorocyclopropanes (**1**—**6**) by the reaction of the corresponding α,β-unsaturated sulfides with dichlorocarbene, and have studied their reactions with potassium *t*-butoxide in *t*-butyl alcohol and with pyridine.

The ring opening reactions probably occur by an El elimination process of the type illustrated in Eq. (1) in a manner analogous to that established for the alkoxy analogues.[5-7]

1) Supported in Part by the U. S. Research Office (Durham) (DA-ARO-D-31-124-G-848). Part IX: W. E. Parham, F. M. Parham, J. F. Dooley and M. K. Meilahn, *J. Org. Chem.*, **33**, 3651 (1968).

2) Presented at the 23rd Annual Meeting of the Chemical Society of Japan, Tokyo, April, 1970.

3) Present address: Department of Industrial Chemistry, Faculty of Engineering, Yamaguchi University, Japan.

4) Present address: The University of Groningen, The Netherlands.

5) W. E. Parham, R. W. Soeder and R. M. Dodson, *J. Amer. Chem. Soc.*, **84**, 1755 (1962).

6) L. Skattebøl, *J. Org. Chem.*, **31**, 1554 (1966).

7) For a review, see W. E. Parham and E. E. Schweizer, "Organic Reactions," Vol. 13, p. 55, (1963).

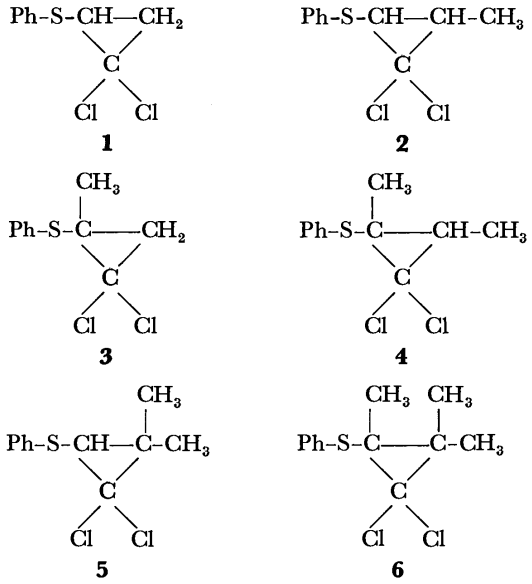

Scheme

In the case of the reaction of **2** with potassium *t*-butoxide in *t*-butyl alcohol, we isolated an α,β-unsaturated aldehyde. Such elimination reaction has been reported.[8] The results of these studies constitute the subject of this report.

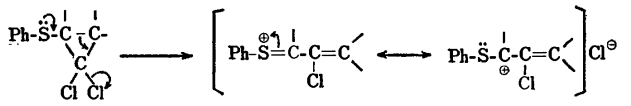

(1)

Results

Preparation of α,β-Unsaturated Sulfides (Carbene Acceptors). 1-Methyl-1-phenylmercaptoethylene (**7**),[9] 2-phenylmercapto-2-butene, (**8**), and 3-methyl-2-phenylmercapto-2-butene (**10**) were prepared by distillation of acetone diphenylmercaptol,[10] ethyl methyl ketone diphenylmercaptol, and isopropyl methyl ketone diphenylmercaptol with potassium bisulfate, respectively. 2-Methyl-1-phenylmercapto-1-propene (**9**)[11] was obtained by isomerization of 2-

Table 1. Syntheses of α,β-unsaturated sulfides $Ph\text{-}S\text{-}C(R_1)=C(R_2)\text{-}R_3$

Compd.	R_1	R_2	R_3	Bp, °C/mmHg (lit)	n_D^t (lit.)	Yield, %	Found (Calcd) % C	H	S	
7[a]	CH_3	H	H	81—86/9 (68—69/6)[9a] (50/2)[9b]	n_D^{25} 1.5656	76	71.69 (71.95	6.85 6.71	21.36 21.34	for $C_9H_{10}S$)
8[b]	CH_3	H	CH_3	81—84/3	n_D^{27} 1.5679	94	72.96 (73.12	7.32 7.36		for $C_{10}H_{12}S$)
9	H	CH_3	CH_3	84—86/4 (111—112/9)[11a] (61—64/0.75)[11b]	n_D^{25} 1.5761 (n_D^{25} 1.5782)[11a] (n_D^{20} 1.5792)[11b]	90	72.99 (73.12	7.37 7.36		for $C_{10}H_{12}S$)
10	CH_3	CH_3	CH_3	114—116/7	n_D^{25} 1.5721	68	74.16 (74.10	7.82 7.91		for $C_{11}H_{14}S$)

a) The distillate from acetone diphylmercaptol should be trapped in an alkali solution because product **7** is easily polymerized by acid (thiophenol) which co-distills.
b) Compound **8** is a mixture of *cis* and *trans* isomers.

Table 2. IR, UV, and NMR spectra of the α,β-unsaturated sulfides

Compd.	IR (neat), cm^{-1} νC=C	δ=C-H	UV, $\lambda_{max}^{95\%\ EtOH}$ mμ (ε)	NMR (in CCl_4) τ
7	1620	870	244(6660), 264(4900)	2.38—2.97 (c,[a] 5, C_6H_5), 4.93, 5.13 (two s, 2, $=CH_2$), 8.06 (s, 3, CH_3)
8	1645	830	247(7320), 263(5750)	2.63—3.04 (c, 5, C_6H_5), 3.90—4.43) (m, 1, =CH-), 8.00—8.47 (m, 6, $2CH_3$)
9		810	250(8150), 266(7960)	2.66—3.12 (c, 5, C_6H_5), 4.08—4.27 (m, 1, =CH), 8.17 (s, 6, $2CH_3$)
10	1635		249(10870), 262.5 (sh., 8240)	2.70—3.06 (c, 5, C_6H_5), 8.00, 8.07 8.14 (three s, 9, $3CH_3$)

a) c: complex

8) W. E. Parham and D. G. Weetman, *J. Org. Chem.*, **34**, 56 (1969). *cf.* a) W. E. Parham and J. F. Dooley, *J. Amer. Chem. Soc.*, **89**, 985 (1967); b) W. E. Parham and J. F. Dooley, *J. Org. Chem.*, **33**, 1476 (1968).
9) *cf.* a) N. K. Kulbovskaya, E. P. Grachova and M. F. Shostakovskii, *Zh. Obshch. Khim.*, **30**, 81 (1960); b) R. Kh. Freidlina, A. B. Terentev, and R. G. Petrova, *Dokl. Akad. Nauk SSSR*, **149**, 860 (1963).
10) A. Schönberg and K. Praefcke, *Chem. Ber.*, **100**, 778 (1967).
11) *cf.* a) R. Adams and A. Ferretti, *J. Amer. Chem. Soc.*, **81**, 4927; (1959); b) E. Benzing, US, 3118002 (c 1260—609), Jan. 14, (1964).

Table 3. Syntheses of 2,2-dichlorocyclopropyl phenyl sulfides

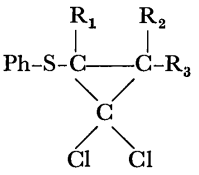

Compd.	R_1	R_2	R_3	Bp, °C/mmHg (Mp, °C)	n_D^t	Yield, %	Found (Calcd) % C	H
3	CH_3	H	H	70—73/0.001 (31—33)	n_D^{25} 1.5809	90	51.69 (51.55	4.25 4.32 for $C_{10}H_{10}Cl_2S$)
4[a]	CH_3	H	CH_3	90—92/0.01	n_D^{25} 1.5771	73	53.70 (53.45	4.87 4.89 for $C_{11}H_{12}Cl_2S$)
5	H	CH_3	CH_3	94—95/0.01	n_D^{25} 1.5764	72	53.51 (53.45	4.89 4.89 for $C_{11}H_{12}Cl_2S$)
6	CH_3	CH_3	CH_3	85—87/0.005 (57—58)		74	55.06 (55.18	5.49 5.40 for $C_{12}H_{14}Cl_2S$)

a) Compound **4** is a mixture of *cis* and *trans* isomers.

Table 4. IR, UV, and NMR spectra of the 2,2-dichlorocyclopropyl phenyl sulfides

Compd.	UV, $\lambda_{max}^{95\%\ EtOH}$ mμ (ε)	NMR (in CCl_4) τ
3	216(sh., 8200), 238(4880), 254(4590)	2.45—2.98 (c, 5, C_6H_5), 8.20—8.60 (m, 5, CH_3 and CH_2, —s peak at 8.36 due to CH_3, two peaks at 8.42 and 8.46 due to CH_2)
4	216(sh., 7880), 241(sh., 5250), 254(5720)	2.40—2.90 (c, 5, C_6H_5), 8.05—9.00 (m, 7, $2CH_3$ and -CH-, —s at 8.37 due to S-C-CH_3, d(J=2.4Hz) at 8.58 due to CH-CH_3)
5	242(sh,, 7720), 251(8460)	2.40—2.80 (c, 5, C_6H_5), 7.40 (s, 1, CH), 8.48 (s, 3, CH_3), 8.63 (s, 3, CH_3)
6	244(sh., 5940), 254.5 (6700)	2.58—2.82 (c, 5, C_6H_5), 8.46, 8.48 (two s, 6, $C(CH_3)_2$), 8.61 (s, 3, C-CH_3)

methyl-1-phenylmercapto-2-propene[12] with sodium ethoxide using a procedure described by Tarbell *et al.*[13] for phenyl propenyl sulfide from allyl phenyl sulfide. The yields, analytical results and some spectral data of the olefins are summarized in Tables 1 and 2.

Preparation of 2,2-Dichlorocyclopropyl Phenyl Sulfides. The reactions of **7**, **8**, **9**, and **10** with ethyl trichloroacetate and sodium methoxide in olefin-free petroleum ether gave **3**, **4**, **5**, and **6**, respectively. The yields, analytical results and some spectral data of the 2,2-dichlorocyclopropyl phenyl sulfides are summarized in Tables 3 and 4.

Ring Opening of 1,1-Dichloro-2-phenylmercaptocyclopropane (1). The product of reaction of **1**[14] with potassium *t*-butoxide in *t*-butyl alcohol was an unidentified black tar. The parent cyclopropane **1** was quite stable in hot pyridine (50 hr) and the starting material was recovered in 80% yield.

Ring Opening of 1,1-Dichloro-2-methyl-3-phenylmercaptocyclopropane (2). The reaction of **2**[14] with potassium *t*-butoxide in *t*-butyl alcohol gave a compound assumed to be 1-formyl-1-phenylmercaptopropene (mixture of two geometrical isomers) (**13**), and a mixture[15] of 1-phenylmercaptobut-3-en-1-yne (**11**)[16] and 1-phenylmercaptobut-1-en-3-yne (*cis*- and *trans*-isomers) (**12**) (Eqs. (2) and (3)). Further evidence for the structure of **11** and **12** was obtained by an independent synthesis (50% yield) of the mixture of **11** and **12** by the reactions of 1-chloro-1-

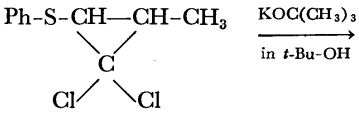

2 (*cis*-, *trans*-)

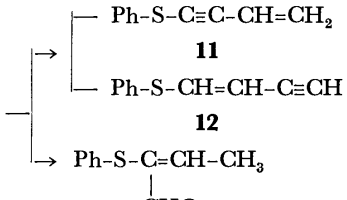

(2)

(3)

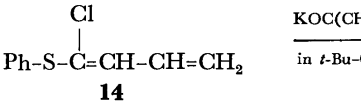

(4)

14

12) W. E. Parham and S. H. Groen, *J. Org. Chem.*, **30**, 728 1965).

13) D. S. Tarbell and M. A. McCall, *J. Amer. Chem. Soc.*, **74**, 55 (1952).

14) W. E. Parham, L. Christensen, S. H. Groen, and R. M. Dodson, *J. Org. Chem.*, **29**, 2211 (1964).

15) The mixture was not separated by fractional distillation.

16) A. A. Petrov, S. I. Radchenko, K. S. Mingaleva, I. G. Savich, and V. B. Lebedev, *J. Gen. Chem., (USSR)*, **34**, 1911 (1964).

phenylmercaptobuta-1,3-diene (**14**)[17] with potassium *t*-butoxide in *t*-butyl alcohol (Eq. (4)).

The reaction of **2** with a large excess of pyridine under conditions of reflux for 40 hr was studied, and a mixture[15] of 2-chloro-1-phenylmercaptobuta-1,3-diene (**15**) and *trans*-**2** was obtained (Eq. (5)). Butadiene **15** and *trans*-**2** were detected by means of their NMR spectra. Compound **2** (mixture of *cis*- and *trans*-isomers) shows two doublets for S–CH, at τ 7.18 with J=10.0 Hz due to *cis*-isomer and at τ 7.68 with J=7.0 Hz due to *trans*-isomer.[14] The above reaction products showed only a doublet for S-CH due to the *trans*-isomer.

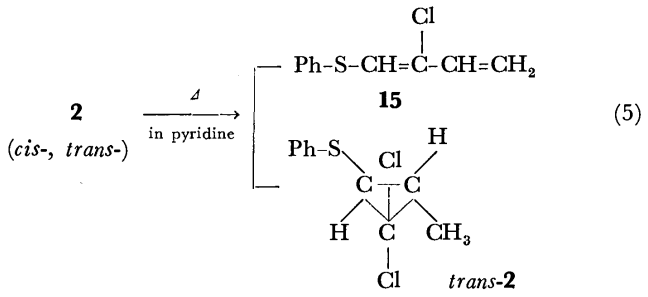

(5)

*Ring Opening of 1,1-Dichloro-2-methyl-2-phenylmercaptocyclopropane (**3**).* The products from the ring opening reaction of **3** with potassium *t*-butoxide in *t*-butyl alcohol were 2-phenylmercaptobut-1-en-3-yne (**16**) (20% yield) and 4-*t*-butoxy-3-phenylmercaptobuta-1,2-diene (**17**) (20% yield) contaminated with a trace amount of a compound containing aldehyde group (the aldehyde group was only detected by IR and NMR spectra: ν_{max} 1670 cm^{-1}; two doublets at τ −0.13, −0.03 (J=6 Hz), and at τ 0.23, 0.33 (J=6 Hz)). Compound **17** was a secondary product derived from **16**. These results are shown in Eq. (6).

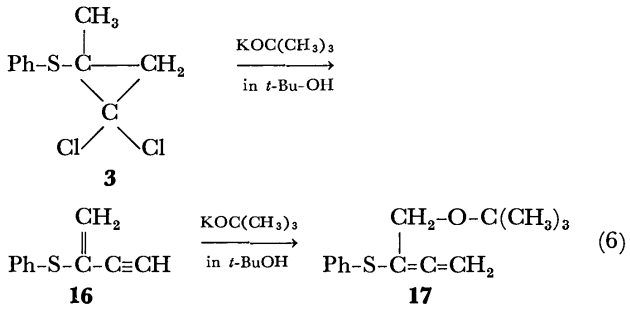

(6)

In order to prove the structure of **17**, the reaction of **17** with Raney nickel (W-2) in ethyl alcohol was performed. Benzene and *n*-butyl *t*-butyl ether (**18**)[18] were identified as reduction products. On the other hand, the products from the reduction of **17** with hydrogen in the presence of Raney nickel (W-2) at room temperature were *sec*-butyl phenyl sulfide (**19**)[19] and *t*-butyl 2-phenylmercaptobutyl ether (**20**).

The isolated **16**[20] was converted into **17** (34% yield) by reaction with potassium *t*-butoxide in *t*-butyl alcohol.

When a solution of **3** in pyridine was refluxed for 70 hr, only black tar was obtained.

*Ring Opening of 1,1-Dichloro-2,3-dimethyl-2-phenylmercaptocyclopropane (**4**).* The products of reaction of **4** (mixture of *cis*- and *trans*-isomers) with potassium *t*-butoxide in *t*-butyl alcohol consisted of a considerable amount of black tar and very unstable enyne derivatives (IR, 3290, 2230, 2110, 920, and 800 cm^{-1}). The derivatives turned dark brown in contact with air, and polymerized. The reaction of **4** with hot pyridine was also studied. A large amount of black tar and a small amount of an unidentified liquid were obtained.

*Ring Opening of 1,1-Dichloro-2,2-dimethyl-3-phenylmercaptocyclopropane (**5**).* The product from the ring opening reaction of **5** using potassium *t*-butoxide was 3-methyl-1-phenylmercaptobut-3-en-1-yne (**21**) (60% yield) (Eq. (7)). The structure of **21** was confirmed by its independent synthesis by dehydrohalogenation of 1-chloro-3-methyl-1-phenylmercaptobuta-1,3-diene (**22**)[12] (Eq. (8)).

The ring opening reaction of **5** with pyridine was carried out, and 2-chloro-3-methyl-1-phenylmercaptobuta-1,3-diene (**23**)[21] (48% yield) was isolated. Compound **23** was easily converted into **21** by refluxing with a solution of potassium *t*-butoxide in *t*-butyl alcohol (50% yield) (Eq. (9)).

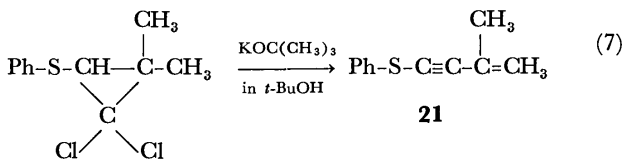

(7)

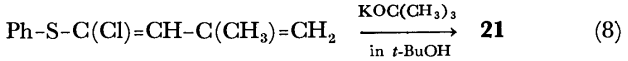

(8)

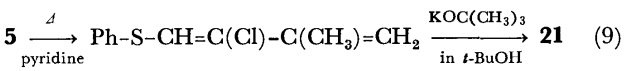

(9)

*Ring Opening of 1,1-Dichloro-2,3,3-trimethyl-2-phenylmercaptocyclopropane (**6**).* Attempts to effect ring opening of **6** with alkoxides (potassium *t*-butoxide in *t*-butyl alcohol, sodium ethoxide in ethyl alcohol and sodium methoxide in methyl alcohol) failed, and starting material **6** was recovered in high yield in every case. When hot pyridine was used as a base and a solvent, a product[21] assumed to be 3-chloro-2-methyl-4-phenylmercaptopenta-1,3-diene (**24**) or 3-chloro-4-methyl-2-phenylmercaptopenta-1,3-diene (**25**) was obtained in 70% yield (Eq. (10)).

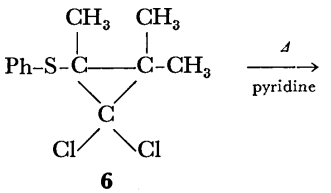

17) W. E. Parham and S. H. Groen, *J. Org. Chem.*, **29**, 2214 (1964).
18) L. Henry, *Rec. Trav. Chim.*, **23**, 329 (1904).
19) W. H. Taylor, *J. Amer. Chem. Soc.*, **58**, 2649 (1936).
20) Compound **16** was unstable, and rapidly turned brown in air.
21) The product appeared to be one compound by its GLPC and NMR spectrum.
22) H. Fischer, "The Chemistry of Alkenes," ed. by Saul Patai, Interscience Publishers, A division of John Wiley and Sons. Inc., New York, N. Y. (1964); p. 1106.

$$\left\{\begin{array}{ll} & \text{Ph-S-C(CH}_3\text{)=C(Cl)-C(CH}_3\text{)=CH}_2 \quad \mathbf{24} \\ \text{or} & \text{CH}_2\text{=C(SPh)-C(Cl)=C(CH}_3\text{)-CH}_3 \quad \mathbf{25} \end{array}\right. \tag{10}$$

Discussion

The accelerating effect of the phenylmercapto group is considered to be a driving force for ring opening

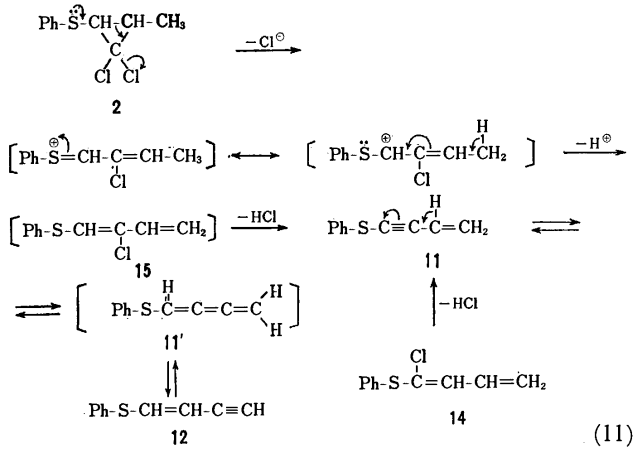

(11)

reaction of these 2,2-dichlorocyclopropyl phenyl sulfides, since the sulfur lone-pair electrons can stabilize the positive charge developed in the transition state or intermediate (Eq. (1)). The formation of **11** and **12** from **2** or **14** by use of potassium *t*-butoxide is explained as shown in Eq. (11). In particular, compound **12** is obtained from an intermediate butatriene (**11'**) by means of retro-propargylic rearrangement[22] in the presence of base. The presumed intermediate **11'** will be derived from **11** by means of prototropic rearrangement.

The ring opening of **2** (mixture of *cis*- and *trans*-isomers) with weak base pyridine led to the mixture of **15** and *trans*-**2** (Eq. (5)). That is, it turned out that *cis*-**2** underwent ring opening more rapidly than *trans*-**2**. As in our previous discussion on the rates of solvolysis of *cis*- and *trans*-1,1-dichloro-2,3-di-*n*-propylcyclopropane,[23] and *cis*- and *trans*-1,1-dichloro-2-ethoxy-3-*n*-propylcyclopropane[24] in the presence of ethanolic silver nitrate, the above experimental results are explained on the basis of steric effects of intermediates (or transition states) derived from the concerted ring opening reactions. Some pertinent arguments for the related preferential formation of only a *trans*-olefin from both *cis*- and *trans*-1,1-dichloro-2-ethoxy-3-methylcyclopropane have been discussed by Skattebøl[6]. Similar steric arguments can account for the stability of **6** in hot *t*-butyl alcohol - potassium *t*-butoxide.

The allene derivative **17** is obtained from **16** by addition of *t*-butoxide ion to **16** as illustrated in Eq. (12).

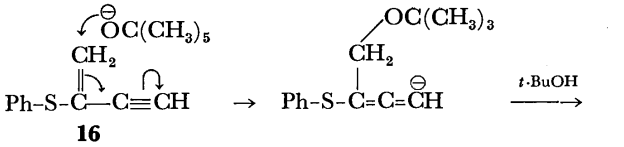

16

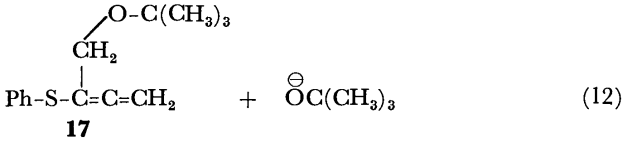

17 (12)

Experimental

Infrared spectra were obtained on a Perkin-Elmer 257 or an Unicam SP 200 spectrometer. Ultraviolet spectra were obtained in spectral grade solvents on a Cary spectrophotometer. Nuclear magnetic resonance spectra were mainly obtained on a Varian Associates Model A-60 or T-60 spectrometer using 20% solutions in carbon tetrachloride and tetramethylsilane as an internal standard. Mass spectra were obtained on a Hitachi Perkin-Elmer RMU-6D mass spectrometer. Gas-liquid partition chromatography analyses were determined on a Beckman GC-4 apparatus.

Materials. Most of the α,β-unsaturated sulfides were prepared by distillation of the corresponding ketone diphenylmercaptol with potassium bisulfate (see Tables 1 and 2). 2,2-Dichlorocyclopropyl phenyl sulfides were prepared from the α,β-unsaturated sulfides, sodium methoxide (from a fresh bottle) and ethyl trichloroacetate by a procedure essentially the same as that for the reaction with phenyl propenyl sulfide[14] (see Tables 3 and 4).

Reaction of **2** *with Potassium* t-*Butoxide in* t-*Butyl Alcohol.* Potassium metal (5.9 g, 0.15 g-atom) was dissolved in *t*-butyl alcohol (150 m*l*) heated at the refluxed temperature in a dry nitrogen atmosphere. To the hot solution was added **2**[14] (9.1 g, 0.039 mol) slowly. The reaction mixture was refluxed for 5 hr, poured into water (300 m*l*) and then extracted with ether (200 m*l*). The organic layer was washed with water (200 m*l*) and dried ($MgSO_4$). Evaporation of the dry ether solution afforded a dark oil which gave two fractions on distillation.

A.—Mixture of 1-phenylmercaptobut-3-en-1-yne (**11**)[16] and 1-phenylmercaptobut-1-en-3-yne (*cis*- and *trans*-isomers) (**12**) : 2.9 g (46%); bp 54—65°C/0.005 mmHg; n_D^{25} 1.6205. A sample of the mixture was redistilled through a 10 cm Vigreux column for analysis: bp 50—53°C/0.002 mmHg; n_D^{25} 1.6208; IR (neat), 3280 cm^{-1} (≡C–H), 2160, 2100 (C≡C), 970, 925, (CH=CH_2); UV ($\lambda_{max}^{95\%EtOH}$), 219 mμ (sh., 12700), 228 (sh., 9500), 241 (9700), 250.5 (10100), 261 (10200); NMR (CCl_4), τ 2.52—2.98 (c, 5, C_6H_5), 2.92—3.43 (m, CH=CH), 3.70—4.83 (m, CH=CH_2), 6.66, 7.11 (two d, J=3 and 3 Hz, ≡C–H of *cis*- and *trans*-isomers), total wt of CH=CH, CH=CH_2 and ≡C–H was 3H; MS m/e, 160 (M^+). The ratio of **11** to **12** was about 7 to 4 (NMR spectrum).

Found: C, 74.51; H, 5.47; S, 20.17%. Calcd for $C_{10}H_8S$: C, 74.95; H, 5.03; S, 20.01%.

B.—A compound presumed to be 1-formyl-1-phenylmercaptopropene (two geometrical isomers) (**13**): 0.7 g (10%); bp 79—84°C/0.001 mmHg; n_D^{25} 1.5798; IR (neat), 1675 cm^{-1} (C=O), 820 (trisubstituted olefin); UV ($\lambda_{max}^{95\%EtOH}$), 252 mμ (ε 6520), 295 (15000); NMR (CCl_4), τ 2.26—3.05 (c, 6, C_6H_6 and C=CH–), 0.78 (s, 1, CHO), 8.66, 8.88 (two d, J=6.0 and 7.2 Hz, 3, CH_3).

Found: C, 67.94; H, 6.19%. Calcd for $C_{10}H_{10}OS$: C, 67.38; H, 5.66%.

2,4-Dinitrophenylhydrazone of **13**: Violet crystal, mp 221—222°C (corr) (from acetone).

Found: C, 53.54; H, 3.73; N, 15.43%. Calcd for $C_{16}H_{14}N_4SO_4$: C, 53.62; H, 3.94; N, 15.63%.

Reaction of **14** *with Potassium* t-*Butoxide in* t-*Butyl Alcohol.* To a hot (85—90°C) stirred solution prepared from potassium

23) W. E. Parham and K. S. Yong, *J. Org. Chem.*, **33**, 3947 (1968).
24) W. E. Parham and K. S. Yong, *ibid.*, **35**, 683 (1970).

metal (0.8 g, 0.02 g-atom) and *t*-butyl alcohol (90 m*l*) was added dropwise **14**[17] (8.9 g, 0.045 mole) in a nitrogen atmosphere. The reaction mixture was refluxed for 5 hr, and the solution was processed essentially as described for the reaction of **2** with potassium *t*-butoxide in *t*-butyl alcohol. A mixture of **11** and **12** was obtained: 3.7 g (51%); bp 62—64°C/0.007 mmHg; n_D^{27} 1.6208. The spectra (IR, UV and NMR) were essentially the same as those of the product derived from **2**.

(Found: C, 74.41; H, 5.31%. Calcd for $C_{10}H_8S$: C, 74.95; H, 5.03%).

*Reaction of **2** with Pyridine.* A mixture of **2** (7.0 g, 0.03 mol. The ratio of *cis*-**2** to *trans*-**2** was approximately 8 to 5—NMR spectrum) and pyridine (50 m*l*) was refluxed for 40 hr under a nitrogen atmosphere. By distilling the solution a considerable amount of residual black red tar and a mixture[15] of 2-chloro-1-phenylmercaptobuta-1,3-diene (**15**) and *trans*-**2** were obtained: 3.0 g; bp 81—82°C/0.06 mmHg; n_D^{25} 1.6235; IR (neat), 900, 980, 1620 cm^{-1} ($CH=CH_2$), 1380, 2920 (CH_3); NMR[25] (CCl_4), τ 2.60—3.10 (c, C_6H_5), 3.56 (s, –S–CH=), 3.60, 3.70, 3.76, 3.86 (J_{AX}=16.0 Hz, J_{BX}=10 Hz, $\underline{H}_X$–C=CH_AH_B), 4.56 (d, J_{AX}=16 Hz, H_X–C=$C\underline{H}_AH_B$), 4.94 (d, J_{BX}=10 Hz, H_X–C=$CH_A\underline{H}_B$), 7.68 (d, J(*trans*)=7.0 Hz, S–CH), 8.28—8.52 (m, $\underline{H}C$–CH_3), 8.60 (d, J=3.6 Hz, CH_3). The ratio of **15** to *trans*-**2** was about 1 to 2 (NMR spectrum).

*Reaction of **3** with Potassium* t*-Butoxide in* t*-Butyl Alcohol.* Potassium *t*-butoxide was prepared from potassium (3.90 g, 0.1 g-atom) and *t*-butyl alcohol (100 m*l*). Compound **3** (7.0 g, 0.03 mol) was added and the solution was heated under reflux and with stirring for 3 hr. Water (300 m*l*) was added and the products were extracted with 200 m*l* of petroleum ether (bp 72°C) and dried ($MgSO_4$). Fractionation gave two products (*A* and *B*) and a considerable amount of residual black tar.

A.—2-Phenylmercaptobut-1-en-3-yne (**16**): 0.9 g (19%); bp 48—51°C/0.02 mmHg; n_D^{25} 1.5712; IR (neat), 3290 cm^{-1} (≡C–H), 2120 (C≡C), 1645, 880 ($C=CH_2$); UV ($\lambda_{max}^{95\%EtOH}$), 253 mμ (ε 9470), 272 (sh., 5420); NMR (CCl_4), τ 2.42—2.88 (c, 5, C_6H_5), 4.33, 4.56 (two s, 2, CH_2=), 7.16 (s, 1, ≡C–H).

Found: C, 74.97; H, 5.35%. Calcd for $C_{10}H_8S$: C, 74.96; H, 5.03%.

B.—4-*t*-Butoxy-3-phenylmercaptobuta-1,2-diene (**17**): 1.3 g (19%); bp 87—90°C/0.02 mmHg. A sample of this product was redistilled for analysis: bp 78°C/0.002 mmHg; n_D^{25} 1.5581; IR (neat), 1950 cm^{-1} (C=C=C); UV ($\lambda_{max}^{95\%EtOH}$), 246 mμ (ε 10800), 270 (sh., 5120); NMR (CCl_4), τ 2.55—3.04 (c, 5, C_6H_5), 5.20 (t, J=2.4 Hz, 2, $=CH_2$), 6.11 (t, J=2.4 Hz, 2, CH_2), 8.88 (s, 9, *t*-Bu); MS m/e, 234 (M^+).

Found: C, 71.46; H, 7.32%. Calcd for $C_{14}H_{18}SO$: C, 71.75; H, 7.74%.

*Reduction of **17** with Raney Nikel (W-2).* A mixture of **17** (2.1 g, 0.009 mol), Raney nickel (W-2) (15 g) and 95% ethyl alcohol (100 m*l*) was refluxed for 5 hr. The alcoholic solution was analyzed by glpc (silicone oil, DC-710, 20% on Chromosorb W), and the spectrum showed the presence of two components (other than ethyl alcohol). The compounds were identified (by injection of authentic samples) as benzene and *n*-butyl *t*-butyl ether.[18]

*Reduction of **17** with Hydrogen Gas on Raney Nickel (W-2).* A mixture of **17** (1.1 g, 0.0047 mol), Raney nickel (W-2) (6 g) and methyl alcohol (150 m*l*) was shaken with hydrogen gas (50 lb) in a hydrogenation apparatus[26] for 28 hr at room temperature. The Raney nickel was filtered and washed with methyl alcohol (100 m*l*). The combined filtrate was distilled through a 10 cm Vigreux column, and a large portion of methyl alcohol was distilled. Further distillation of the brown residue (0.6 g) gave two products.

A.—*sec*-Butyl phenyl sulfide (**19**); 0.1 g (13%); bp 77—80°C/3 mmHg; n_D^{25} 1.5390; NMR (CCl_4), τ 2.57—3.12 (c, 5, C_6H_5), 6.95 (sextet, J=6.6 Hz, 1, –CH–), 8.11—9.22 (m, 8, CH_2—CH_3 and CH_3).

Found: C, 72.02; H, 8.37%. Calcd for $C_{10}H_{14}S$: C, 72.23; H, 8.49%.

This product was identical with an authentic sample of **19**.[19]

B.—*t*-Butyl 2-phenylmercaptobutyl ether (**20**): 0.4 g (36%); bp 72°C/0.001 mmHg; n_D^{25} 1.5191; IR (neat), 1070 cm^{-1} (C–O–C); UV ($\lambda_{max}^{95\%EtOH}$), 255 mμ (ε 5730); NMR (CCl_4), τ 2.56—3.04 (c, 5, C_6H_5), 6.49—7.18 (m, 3, C–CH_2–CH), 8.07—9.18 (m, 14, C_2H_5 and *t*-Bu, —a sharp peak at 8.88 due to *t*-Bu).

Found: C, 69.89; H, 8.93%. Calcd for $C_{14}H_{22}SO$: C, 70.54; H, 9.30%.

*Preparation of **17** from **16** and Potassium t-Butoxide.* Freshly prepared **16** (12 g, 0.0075 mol) was added to a stirred solution prepared from potassium (0.60 g, 0.015 g-atom) and *t*-butyl alcohol (20 m*l*) which was maintained in a nitrogen atmosphere. The reaction mixture was refluxed for 2 hr and then poured into water (100 m*l*), and the resulting mixture was extracted twice with 100 m*l* portions of ether. The ether solution was dried ($MgSO_4$) and concentrated in a rotatory evaporator. Distillation of the residue gave **17**: 0.6 g (34%); bp 80°C/0.005 mmHg; n_D^{26} 1.5678; IR and NMR spectra were identical with those of **17** obtained by the reaction of **3** with potassium *t*-butoxide in *t*-butyl alcohol.

*Reaction of **5** with Potassium* t*-Butoxide in* t*-Butyl Alcohol.* The reaction of **5** (4.94 g, 0.02 mole) with potassium *t*-butoxide (potassium 2.35 g, 0.06 g-atom; *t*-butyl alcohol 60 m*l*) was carried out for 3 hr as described for **2**. 3-Methyl-1-phenylmercaptobut-3-en-1-yne (**21**) was obtained: 2.1 g (60%); bp 60—62°C/0.004 mmHg; n_D^{25} 1.6075; IR (neat), 2140, 2170 cm^{-1} (C=C), 900 ($C=CH_2$), 2970, 2910, 1375 (CH_3); UV ($\lambda_{max}^{95\%EtOH}$) 218 mμ (sh., ε 14600), 228 (sh., 11500), 241 (11200), 249 (11800), 258 (11600): NMR[25] (CCl_4), τ 2.50—3.08 (c, 5, C_6H_5), 4.72, 4.82 (two s, 2, $=CH_2$), 8.06 (s, 3, CH_3).

Found: C, 75.71; H, 5.94%. Calcd for $C_{11}H_{10}S$: C, 75.82; H, 5.78%.

*Dehydrohalogenation of 1-Chloro-3-methyl-1-phenylmercaptobuta-1,3-diene (**22**).* The reaction of **22**[12] (3.7 g, 0.018 mole) with potassium *t*-butoxide (potassium 1.6 g, 0.04 g-atom; *t*-butyl alcohol 40 m*l*) was carried out as described for **14** and gave **21**: 2.3 g (73%); bp 62—65°C/0.005 mmHg; n_D^{27} 1.6041. This product was shown to be identical (IR spectrum) with **21** prepared from **5**.

Found: C, 75.55; H, 5.95%. Calcd for $C_{11}H_{10}S$: C, 75.82; H, 5.78%.

*Reaction of **5** with Pyridine.* The reaction of **5** (4.9 g, 0.02 mol) with pyridine (20 m*l*), carried out for 18 hr as described for **2**, gave 2-chloro-3-methyl-1-phenylmercaptobuta-1,3-diene (**23**): 2.0 g (48%): bp 88—90°C/0.01 mmHg; n_D^{30} 1.6210; IR (neat), 1615, 895 cm^{-1} ($C=CH_2$), 2960, 1370 (CH_3); UV ($\lambda_{max}^{95\%EtOH}$) 252 mμ (ε 5380), 268 (4970), 296 (5560), NMR (CCl_4), τ 2.42—2.97 (c, 5, C_6H_5), 3.42 (s, 1, –CH=), 4.56, 4.99 (two s, 2, $=CH_2$), 8.01 (s, 3, CH_3). The glpc (silicone oil, DC-710, 20% on Chromosorb W) of the product **23** showed only a single peak,

25) The NMR spectrum was obtained on a JEOL MH-100 spectrometer.

26) Made by Parr Instrument Co. Inc. (Moline, III., U. S. A.).

Found: C, 62.35; H, 4.99%. Calcd for $C_{11}H_{11}SCl$: C, 62.72; H, 5.26%.

Dehydrogenation of ***23***. The reaction of **23** (1.6 g, 0.008 mol) with potassium *t*-butoxide (potassium 0.6 g, 0.0016 g-atom; *t*-butyl alcohol 20 m*l*), carried out as described for **14**, gave **21**: 0.7 g (50%); bp 60—61°C/0.001 mmHg; n_D^{27} 1.6002. The IR and NMR spectra of this product were identical with those of authentic **21** prepared from **5** or **22**.

Reaction of ***6*** *with Pyridine*. The reaction of **6** (1.3 g, 0.005 mol) with pyridine (10 m*l*) was carried out for 70 hr as described for **2**, and a compound assumed to be 3-chloro-2-methyl-4-phenylmercaptopenta-1,3-diene (**24**) or 3-chloro-4-methyl-2-phenylmercaptopenta-1,3-diene (**25**) was obtained: 0.8 g (71.4%); bp 66—68°C/0.005 mmHg; n_D^{26} 1.5815; IR (neat), 1635, 890 cm^{-1} ($C{=}CH_2$), 2920, 1370 (CH_3); UV ($\lambda_{max}^{95\%EtOH}$), 218 mμ (sh., ε 10900), 251 (5470), 270 (sh., 3910); NMR (CCl_4), τ 2.38—2.96 (c, 5, C_6H_5), 4.81 4.91 (two s, 2, $CH_2{=}$), 8.00, 8.22 (two s, 6, $2CH_3$). The GLPC (silicone oil, DC-710, 20% on Chromosorb W) of the product showed only a single peak.

Found: C, 63.96; H, 5.74%. Calcd for $C_{12}H_{13}SCl$: C, 64.13; H, 5.84%.

BULLETIN OF THE CHEMICAL SOCIETY OF JAPAN, VOL. 45, 515—519 (1972)

The Photochemical Decomposition of Benzotriazoles

Kazuo Tsujimoto, Mamoru Ohashi, and Teijiro Yonezawa

Department of Hydrocarbon Chemistry, Faculty of Engineering Kyoto University, Kyoto

(Received March 24, 1971)

The photochemical decomposition of several 1-substituted benzotriazoles was investigated. It was observed that in contrast to the thermolytic decompositions of 1-benzyl and 1-benzoylbenzotriazole, the intermediates produced by the loss of nitrogen from these compounds upon irradiation react with hydrogen-donating solvents to yield either reduced or substituted products. The possibility of the presence of an antiaromatic benzoazacyclopropene as an intermediate can be excluded on the basis of the fact that the photolysis of 4′,5-dichloro-1-phenylbenzotriazole gave 3,6-dichlorocarbazole as the sole product. The acetone-sensitized photolysis of 1-benzoylbenzotriazole causes a Wolff rearrangement giving a cyclopentadiene derivative. On the basis of extended Hückel molecular orbital calculations on the intermediates, it is concluded that the photochemical loss of nitrogen from benzotriazoles gives excited-state 1,3-diradicals, while the thermolytic decompositions afford ground-state ones.

Recently Burgess and his co-workers[1] found that the photolysis of 1-phenylbenzotriazole gave carbazole quantitatively. In a previous paper,[2] we reported that the photolysis of various benzotriazoles gave products different from those of thermal decompositions. This fact implies that the spin-correlation effects[3] may be observed in these decomposition process, just as in the case of azides.[4]

To shed some light on the nature of the intermediates produced upon the irradiation of some benzotriazoles, we have examined the difference of benzotriazoles; we based our examination on a molecular-orbital consideration of the electronic structure of the diradical intermediates.

Results and Discussion

The photolysis of 1-benzylbenzotriazole (**I**) in benzene gave *N*-(2-biphenylyl)benzylamine (**II**) in a 29% yield; this amine was the only product which was isolated by column chromatography on silica gel. However, when **I** was photolyzed in acetonitrile, **IV** was obtained together with benzylaniline (**III**), which must be produced by hydrogen abstraction from the solvent (**III** : **IV**=1 : 5).

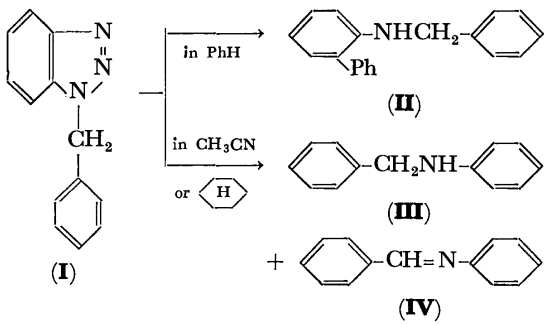

In the photochemical reaction of **I**, two manners must be considered for the addition of benzene to the diradical (**V**), as shown in Scheme 1.

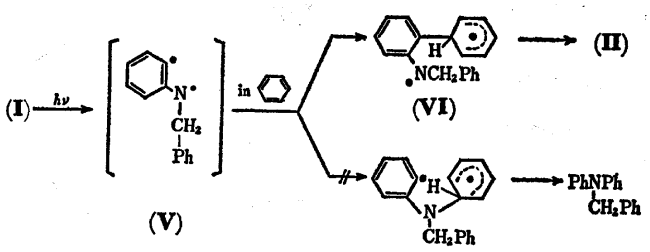

Scheme 1

It is more reasonable to assume that the more reactive center in the diradical (**V**), which presumably has the character of a reactive σ-radical, adds to benzene,[5] and that intramolecular hydrogen transfer in the

1) E. M. Burgess, R. Carithers, and L. McCullagh, *J. Amer. Chem. Soc.*, **90**, 1923 (1968).

2) M. Ohashi, K. Tsujimoto, and T. Yonezawa, *Chem. Commun.*, **1970**, 1089.

3) P. D. Bartlett and P. S. Engel, *J. Amer. Chem. Soc.*, **90**, 2960 (1968).

4) J. S. Swenton, T. J. Ikeler, and B. H. Williams, *ibid.*, **92**, 3103 (1970).

5) D. H. Hey, *Adv. Free Radical Chem.*, **2**, 47 (1967).

resulting adduct (**VI**) then leads to the observed product. When the photolysis of **I** was carried out in cyclohexane, which is thought to be more hydrogen-donating to the produced diradical than is acetonitrile,[6] benzylaniline (**III**) was obtained together with benzylideneaniline (**IV**) (**III**:**IV**=6 : 1).

The formation of **IV** in cyclohexane implies that the diradical resulting from the benzotriazole can abstract intramolecularly a hydrogen atom, even in a hydrogen-donating solvent.

Gibson has reported,[7] that the thermolysis of **I** gave phenanthridine, a cyclized product, in a small yield. However, in the photolysis of **I** we could obtain neither phenanthridine nor 9,10-dihydrophenanthridine, not even in acetonitrile (checked by glpc).

This difference in behavior between the thermolysis and photolysis of **I** suggests that the ground-state diradical of **V** is liable to cyclize and that the diradical produced upon irradiation is either an excited singlet or triplet state and that it abstracts a hydrogen atom intramolecularly or from a solvent cage.

The same sort of difference in behavior between the thermolysis and photolysis is also observed in the case of 1-benzoylbenzotriazole. Drulliner reported[8] that 1-benzoylbenzotriazole (**VII**) decomposed in diphenyl ether at a reflux temperature to give 2-phenylbenzoxazole of **VIII** in an 11% yield. However, in our experiments, only a trace of **VIII** could be obtained in its photolysis in acetonitrile (probably less than 1%). The major product was the amide (**IX**) which had been produced *via* a 1,3- or 1,5-diradical intermediate through hydrogen abstraction from the solvent. The fact that **VIII** could not be obtained in the photolysis of **VII** is analogous to the case of the photolysis of 1-benzylbenzotriazole (**I**), where neither phenanthridine nor 9,10-dihydrophenanthridine was obtained.

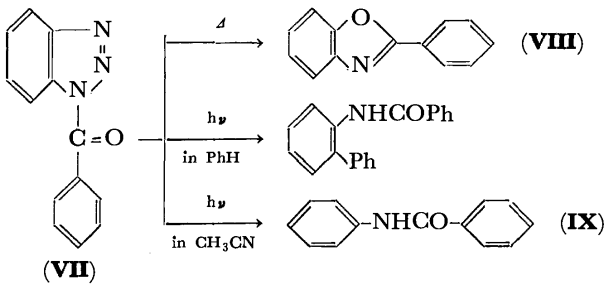

(**VII**) (**VIII**) (**IX**)

The difference in behavior between the thermolytic and photolytic decomposition of **VII** can be interpreted by means of an extended Hückel MO investigation of the electronic structure of the intermediate (**XI**). The atomic-bond populations of C_2-O cited in Table 1 (see Experimental section) show that it is bonding in the ground state but antibonding in the excited state. These results are consistent with the experimental results; that is the thermolytic[8] or mass spectrometric[9] decomposition of **VII** gives the cyclized product, while the photolytic one gives **VIII** in only a small amount.

Table 1. Total energy and atomic bond populations of **XI**.

	Ground state	Excited state
Total Energy	−1313.6 eV	−1311.8 eV
Atomic Bond Population of C_2-N	−0.180	−0.178
Atomic Bond Population of C_2-O	0.050	−0.006

These arguments point to the facts that the thermolytic decomposition of **VII** gives the ground state of **XI** and that the photolysis produces the excited state.

When the photolysis of **VII** was acetone-sensitized, benzanilide (**IX**) and a new type of compound (**X**) were obtained. The assignment of the structure of **X** rests on analytical and spectroscopic data as follows. The results of elemental analysis and the molecular peak (*m/e* 253) of the mass spectrum indicate that its molecular formula is $C_{16}H_{15}NO_2$, suggesting the addition of a molecule of acetone to the diradical intermediate (**XI**). The presence of a strong conjugated carbonyl absorption at 1650 cm^{-1} in the IR spectrum and a strong benzoyl peak at *m/e* 105 in the mass spectrum suggest the benzoyl group. Further information about the structure is obtained from the 220 MHz NMR spectrum. A singlet peak at

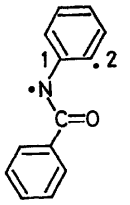

(**XI**)

δ 1.93 (6H) indicates two methyl groups. The complex ABCX signals were demonstrated in the region between δ 5.5 and δ 7.0 in Chart 1; the spectrum given at the bottom was obtained by computer simulation with LAOCOON III.[10]

From these spectral data, two structures, (**X**) and (**X'**), are conceivable. Considering the chemical

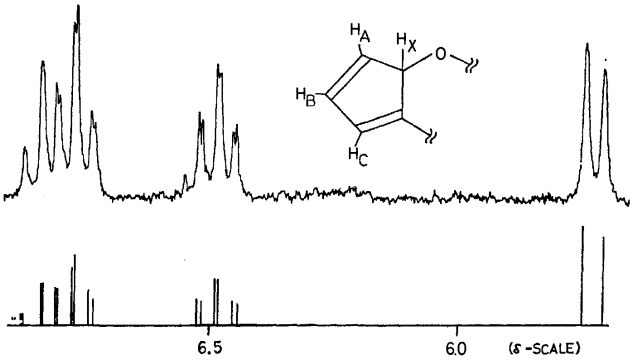

Chart 1. A part of 220 MHz NMR spectrum of **X**.

6) P. Flowerday and M. J. Perkins, *J. Chem. Soc.*, **1970**, 298.
7) M. S. Gibson, *ibid.*, **1956**, 1076.
8) J. D. Drulliner, *J. Amer. Chem. Soc.*, **90**, 6879 (1968).
9) M. Ohashi, K. Tsujimota, A. Yoshino, and T. Yonezawa, *Org. Mass Spectrometry*, **4**, 203 (1971).
10) The resulting parameters were $J_{XA}=J_{AB}=J_{BC}=7.5$ Hz, $J_{AC}=1.5$ Hz, and $J_{XB}=0.6$ Hz; the others were zero. A. A. Bother-By and S. M. Castellano, *J. Chem. Phys.*, **43**, 3863 (1964).

shift of the H_x proton (δ, 5.73 ppm), we concluded that the structure (**X**) must be favored over **X'**.

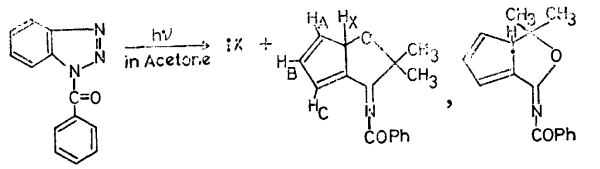

(**VII**) (**X**) (**X'**)

The formation of **X** implies that the reaction proceeds *via* the intermediate (**XI**) formed by triplet acetone-sensitization, which is presumably transformed into the more stable iminofulvene (**XII'**) through an iminocarbene (**XII**), followed by Wolff rearrangement.

No product corresponding to **X** was obtained in the acetophenone- and benzophenone-sensitized photolyses.

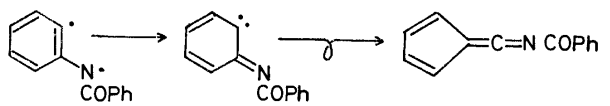

(**XI**) (**XII**) (**XII'**)

These results suggest that the reactions of these intermediates are intimately related to their electronic structures. Therefore, it becomes important to clarify the electronic structure of the intermediates. Boyer and Selvanjan investigated the photolysis of several benzotriazoles and concluded that the 1,3-diradical intermediates have carbene-like structures.[11]

We carried out MO calculations on **XIII'**, which has a fundamental, simple skelton, by means of the extended Hückel method.

Table 2. Atomic and atomic bond polulations of **XIII'**.

	N	C_2
N	6.618	−0.186
C_2	−0.186	3.689

Extended Hückel calculation indicates that the atomic-bond population between C_2 and N is negative (antibonding), and that the atomic-bond populations[12] on the N and C_2 atoms have negative and positive charges respectively. These calculations suggest that the possibility of making a bond between N and C_2 to produce benzoazacyclopropene (**XIIIc'**) is quite small and that the dipolar character predominant over the diradical structure (**XIIIa'**).

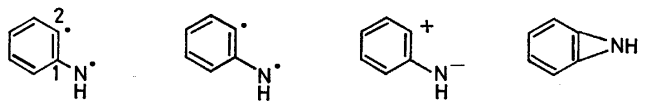

(**XIII'**) (**XIIIa'**) (**XIIIb'**) (**XIIIc'**)

The same calculations also show that the benzoazacyclopropene (**XIIIc'**) is less stable than the associated dipolar intermediate, the difference in their total energies being 3.4 eV (=78 kcal).

In accordance with these calculations, the photolysis of 1H-benzotriazole (**XIII**) in methanol gave *o*-anisidine as a major product (70% yield), along with aniline (30% yield). On the other hand, the photolysis of **XIII** in benzene gave *o*-biphenylamine in a 32% yield, and the similar irradiation of **XIII** in acetonitrile and in cyclohexane gave aniline in 6% and 20% yields respectively.

These results suggest that the character of the intermediate (**XIIIa'** or **XIIIb'**) depends on the polarity of the solvent.

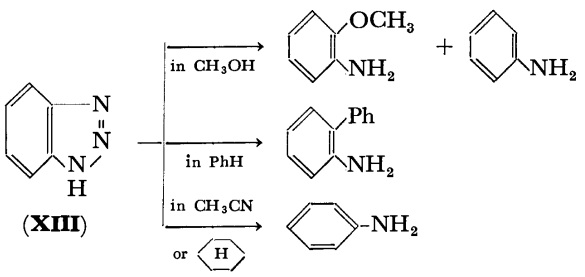

(**XIII**)

Although these molecular orbital calculations indicate that the intermediate (**XIII'**) has no tendency to form benzoazacyclopropene (**XIIIc'**), an antiaromatic compound,[13] we attempted to prove this prediction experimentally. Thus, we examined the behavior of 4',5-dichloro-1-phenylbenzotriazole upon irradiation. The structures of the resulting carbazole were identified by means of the NMR spectra. 3,6-Dichlorocarbazole was isolated as the sole aromatic product in an 89% yield. No 2,6-dichlorocarbazole (**XIX**) was detected, even in the NMR specta of the unpurified product mixture.

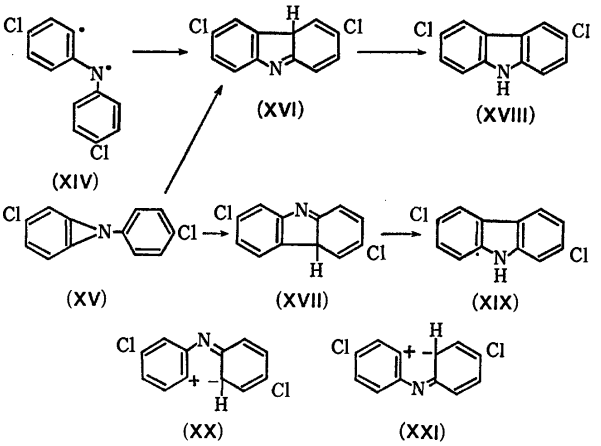

(**XIV**) (**XV**) (**XVI**) (**XVII**) (**XVIII**) (**XIX**) (**XX**) (**XXI**)

If the intermediate was not **XIV** but **XV**, a comparable amount of **XVII** with **XVI** would be obtained in the case of the homolytic cleavage of the azirine ring in **XV**, while the antisymmetric carbazole (**XIX**)

11) J. H. Boyer and R. Selvanjan, *J. Heterocycl. Chem.*, **6**, 503 (1969).

12) R. Hoffman, *J. Chem. Phys.*, **39**, 1397 (1963); R. S. Mulliken, *ibid.*, **23**, 1833, 1841, 2338, 2343 (1955).

13) R. Breslow, J. Brown, and J. J. Gajewski, *J. Amer. Chem. Soc.*, **89**, 4383 (1967).

would be produced when the heterolytic cleavage took place, because the positive charge of **XX** should be more stabilized than that of **XXI** in terms of the electronegativity of the chlorine atom at the *para* position.[14]

In conclusion, we have examined the photochemical decompositions of several 1-substituted benzotriazoles and have found that the photochemical decompositions of 1-benzyl and 1-benzoylbenzotriazoles give products different in their thermolytic and mass spectrometric decompositions.[9] This difference in behavior is accounted for in terms of the electronic structures of the diradical intermediates.

The photochemical loss of nitrogen from the benzotriazoles gives the excited-state intermediates, while the thermolytic decomposition must afford the electronic ground-state intermediates. One exception is the case of 1-phenylbenzotriazole, where both thermolytic and photolytic decompositions[1] gives carbazole almost quantitatively.

In this case, we have no evidence to confirm whether or not the same electronic structute of the intermediates must be considered in both reactions. A detailed investigation of the electronic multiplicities of the intermediates based on SCF-ASMO-CI calculations are now in progress.

Experimental

The IR spectra were recorded on a Hitachi Model 215 grating spectrometer.

The NMR spectra were recorded for solutions in deuteriochloroform (unless otherwise stated) with a Varian HR-220 apparatus, using TMS as the internal standard. The mass spectra were obtained on a double-focussing mass spectrometer, Model JMS-01SG. All the mps were measured on a micro hot stage and are not corrected.

Photolysis of ***I****.* *(A) In Benzene*: The triazole (1.0 g) was dissolved in benzene (500 m*l*), which had previously dried over phosphorus pentoxide and purified by distillation; the solution was than irradiated for 4 hr under a nitrogen atmosphere with a 200-W high-pressure mercury arc lamp surrounded by a quartz filter. The solvent and low-boiling-point materials were removed under reduced pressure. The reaction mixture thus obtained indicated two spots on tlc (silica gel) and was chromatographed on silica gel. Elution with methylene dichloride gave the unreacted triazole and **II** (40 mg); mp 87—88°C (lit, 84—86°C), mass spectrum M$^+$, 259 (93), 180 (32), 167 (28), 91 (100), IR-(KBr), ν_{NH} 3500 cm^{-1}.

(B) In Acetonitrile: The triazole (1.39 g) was irradiated in acetonitrile (330 m*l*) for 13 hr with a 200-W high-pressure mercury lamp. After the removal of the solvent under reduced pressure, the residue was chromatographed on basic alumina. Elution with benzene gave an orange-yellow oil (120 mg), which was discovered by means of vpc analysis using a column of 5% PEG 20 M on chromosorb G to be a mixture of two products. These products had the same retention times as had benzylaniline and benzylideneaniline respectively. The product ratio was determined by vpc using diphenylamine as the internal standard. The oil was rechromatographed on basic alumina, and subsequent elution with cyclohexane - benzene (3 : 1) gave **III** and **IV**, whose structures were identified by the comparison of their IR spectra with the standard IRDC cards.

Photolysis of 1-Benzoylbenzotriazole. *(A) In Benzene*: A solution of the triazole (1.0 g) in benzene (500 m*l*) was irradiated with a 200-W high-pressure mercury arc lamp for 4 hr under a nitrogen atmosphere. The solvent was then removed *in vacuo*, and the residue was chromatographed on silica gel (200 mesh 30$\phi \times$ 190 mm). Elution with methylene chloride (200 m*l*) recovered the unreacted triazole (600 mg). Further elution (400 m*l*) gave a solid (60 mg), which was then crystallized from ligroin to give *N*-(2-biphenylyl)benzamide (mp 88°C). Its IR spectrum was identical with that of an authentic sample. Elution with ethyl acetate and methanol gave polymeric materials which were not identified.

(B) In Acetonitrile: The triazole (120 mg) in acetonitrile (20 m*l*) was irradiated with a 5-W low-pressure mercury lamp for 2 hr under a nitrogen atmosphere. The solvent was then removed *in vacuo*. The residue was chromatographed on silica gel (200 mesh 10 g) with methylene chloride, thus giving three cuts. From the first fraction we obtained 21 mg of the unreacted triazole. The second one gave 9 mg of colorless needles which had a mp of 160—161°C; its IR spectrum agreed with that of the IRDC card of benzaniline. The third fraction gave an identified polymeric material.

(C) In Acetone: A solution of the triazole (1.02 g) in acetone (240 m*l*) was irradiated with a 10-W low-pressure mercury lamp for 15.5 hr under a nitrogen atmosphere. The solvent was then removed. The residue was chromatographed on silica gel. Subsequent elution with methylene dichloride gave three products, whose R_f values on tlc were 0.90, 0.70, and 0.40. The R_f 0.90 fraction (310 mg) turned out to be the unreacted triazole, while the R_f 0.40 fraction (93 mg) was identified as benzanilide by a comparison of its IR spectrum with that of the authentic sample. The recrystallization of the R_f 0.70 fraction (78 mg) from ethanol-water gave colorless needles which melted at 122.0—122.5°C; *m/e* 253 (M$^+$), λ_{max} 311 nm (EtOH), ν_{max} (KBr) 1650 cm^{-1}, δ1.93(s. 6H), 5.73 (d.d. 1H J=7.5 Hz and 0.6 Hz), 6.84(t.d. 1H, J=7.5 and 1.5 Hz), 6.75(d.d. 1H, J=7.5 and 1.5 Hz), 6.84 (t.d. 1H J=7.5 Hz, and 0.6 Hz), and 7.5(m. 5 H) ppm.

Found: C, 75.59; H, 5.86; N, 5.53%. Calcd for $C_{16}H_{15}NO_2$: C, 75.59; H, 5.97; N, 5.53%.

(D) In Acetophenone: The triazole (1.0 g) was dissolved in freshly-distilled acetophenone (240 m*l*). The solution was then irradiated with a low-pressure mercury lamp (10 W) for 13 hr under a nitrogen atmosphere. The solvent was then removed *in vacuo* (max. bath temp. at 63°C). The tlc of the residue on silica gel indicated that almost all of the material was the unreacted triazole. The residue was chromatographed on silica gel. Subsequent elution with benzene gave the starting material and polymeric materials whose structures were not identified.

(E) In Benzophenone: The triazole (500 mg) and benzophenone (508 mg) were dissolved in chloroform (80 m*l*). The solution was irradiated with a high-pressure mercury arc lamp (100 W), using a 2-mm pyrex filter, for 10 hr under a nitrogen atmosphere. The reaction mixture was chromatographed after the removal of the solvent in order to establish the recovery of the starting material.

Photolysis of 1H-Benzotriazole. *(A) In Methanol*: The triazole (1.0 g) in methanol (500 m*l*) was irradiated with a 200-W high-pressure mercury arc lamp for 18.5 hr. The solvent was then removed *in vacuo*, and the residue was chromatographed on silica gel. Elution with methylene

14) M. S. Ao. E. M. Burgess, A. Schauer, and E. A. Taylor, *Chem. Commun.* **1969**, 220.

dichloride gave a red-brown oil (136 mg). A part of the oil was distilled *in vacuo* to give *o*-anisidine, whose IR spectrum was identical with that of an authentic sample. The vpc of the oil on a column of 15% PEG 20 M on Chromosorb W showed the same retention time as that of *o*-anisidine. However, the vpc analysis of the total product showed the presence of an additional product which had the same retention time as that of aniline. A careful vacuum distillation of the oily product gave a colorless oil whose structure was identified by a comparison of its IR spectrum with the IRDC card of aniline.

(B) In Benzene. A benzene solution (500 m*l*) of 1*H*-benzotriazole (1.0 g) was irradiated with a high-pressure mercury arc lamp under bubbling nitrogen gas for 6 hr. The solvent was removed *in vacuo*, and then the residue was chromatographed on silica gel to give biphenylamine (164 mg), whose structure was identified by a comparison of its IR spectrum with the standard IRDC card.

Photolysis of 4',5-dichloro-1-phenylbenzotriazole. The triazole (104 mg) was irradiated in acetonitrile (20 m*l*) for 14 hr. The solvent was then removed, and the residue was chromatographed on silica gel. Subsequent elution with benzene gave colorless needles (81 mg); mp 200.5—201.2°C (lit: 202°C)[15]: IR spectrum (KBr) ν_{NH} 3530 cm^{-1}; *m/e* 237(64), 253(100), and 200(64).

The NMR spectrum showed resonances at δ7.03 (2H, A part of ABX pattern), 7.21 (2H, B part), 7.83 (2H, X part), and 10.0 (br. s. 1H) ppm acetone.

The calculation by means of the extended Hückel method has been described in detail by Hoffmann.[12] The resonance integrals were evaluated by the following equation:

$$KS_{rs}(H_{rr}+H_{ss})/2,\ K=1.75.$$

The Coulomb integrals were estimated by the use of $H_{rr}=-I_p$, where I_p is the ionization potential of the appropriate valence state.

The following values were used in the text:

H	−13.6 eV	
C	−21.43	−11.42
N	−27.5	−14.47
O	−35.3	−15.45

The total energy calculated on the basis of various conformations of **XI** is summarized in Table 3.

Table 3. Dihedral angles θ and total energy

θ	Total Energy (eV)
0	−1313.580
10	−1313.576
90	−1313.559
180	−1312.361

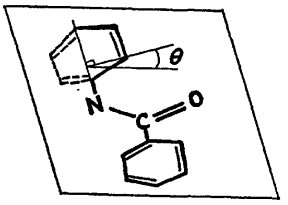

The numerical calculations were carried out at the Kyoto University Computation Center. (FACOM 230—60)

The authors wish to express their hearty thanks to Professor Hiroshi Kato of Nagoya University for his kind advice.

BULLETIN OF THE CHEMICAL SOCIETY OF JAPAN, VOL. 45, 519—525 (1972)

Syntheses of All Isomers of Naphthalenetricarboxylic Acids

Yasuhiko DOZEN

Government Industrial Research Institute, Osaka, Ikeda-shi, Osaka

(Received May 8, 1971)

All the fourteen isomers of naphthalenetricarboxylic acids have been synthesized by the oxidation of trimethylnaphthalenes, dimethylacetonaphthones, dimethylnaphthoic acids, methylnaphthalenedicarboxylic acids, β-(dimethylnaphthoyl)propionic acid, or β-(acenaphthoyl)propionic acids with aqueous sodium bichromate or potassium ferricyanide. Most of these naphthalenetricarboxylic acids, acid anhydrides, and trimethyl esters are new compounds.

During the course of studies on the thermal transformation of alkali salts of naphthalenecarboxylic acids,[1] we realized the necessity of naphthalenetricarboxylic acids for comparison with possible intermediates in the reaction. However, only a limited number of these acids have been reported. Naphthalene-1,4,5-,[2,3] 1,3,8-,[3] and 1,2,8-[3,4] tricarboxylic acids have been prepared by the oxidation of acetylacenaphthenes or cyclohexylacenaphthenes. 1,2,5-[5–7] and 1,2,7-Isomers[8,9] have been synthesized from the corresponding trimethylnaphthalenes. 1,2,4-Tricarboxylic acid is obtained by the oxidation of 1-methylnaphthalene-3,4-dicarboxylic acid.[10] It has been reported that 1-acetyl-2,6-dimethylnaphthalene

1) a) Raecke, *Angew. Chem.*, **70**, 1 (1958). b) E. McNelis, *J. Org. Chem.*, **30**, 1209 (1965). c) J. W. Patton and M. O. Son, *ibid.*, **30**, 2869 (1965). d) Y. Dozen, This Bulletin, **41**, 664 (1968). e) J. Ratusky, *Chem. Ind.* (London), **1970**, 1347. f) M. Matsuoka, T. Kitao, and K. Konishi, *Kogyo Kagaku Zasshi*, **74**, 77 (1971).

2) C. Graebe and P. Haas, *Ann. Chem.*, **327**, 95 (1903).

3) N. G. Sidorova and F. M. Saidova, *Zhur. Obshch. Khim.*, **33**, 2213 (1963); *Chem. Abstr.*, **59**, 13899 g (1963).

4) L. F. Fieser and J. Cason, *J. Amer. Chem. Soc.*, **61**, 1740 (1939).

5) I. M. Heibron and D. G. Wilkinson, *J. Chem. Soc.*, **1930**, 2551.

6) L. Ruzicka and J. R. Hosking, *Helv. Chim. Acta*, **13**, 1402 (1934).

7) C. W. Brandt and L. G. Neubauer, *J. Chem. Soc.*, **1939**, 1037.

8) L. Ruzicka, H. W. Huyser, M. Pfeifer, and C. F. Seidel, *Ann. Chem.*, **471**, 37 (1929).

9) L. Ruzicka and A. G. VanVeen, *Rec. Trav. Chim. Pays-Bas*, **48**, 1023 (1929).

10) K. Alder and R. Schmitz-Josten, *Ann. Chem.*, **595**, 29 (1955).

gives 1,2,6-tricarboxylic acid,[11] but the position of the acetyl group in this acetyldimethylnaphthalene is doubtful.[12,13]

The suitable oxidation procedure of methyl and acetyl groups in naphthalene derivatives with aqueous sodium bichromate has been developed for methylnaphthoic acid,[14] dimethylnaphthalenes,[14] and methylacetonaphthone.[15] Methods for synthesizing the fourteen isomers of trimethylnaphthalene to be oxidized to naphthalenetricarboxylic acids have been reported by some workers,[16-18] but it is not easy to synthesize them all.

In this paper, we wish to report appropriate synthetic methods and the properties of all the fourteen isomers of naphthalenetricarboxylic acid.

Results and Discussion

The preparative methods of naphthalenetricarboxylic acids given so far can be classified into three groups: (1) carboxylation of bromodimethylnaphthalenes by the Grignard reaction, (2) acylation of dimethylnaphthalenes or acenaphthene and (3) cyclization of the methyl- or dimethylphenylbutyric acid derivatives to the naphthalene ring.

1-Bromo-2,4-, 2,3-, 2,6-, and 4,6-dimethylnaphthalenes were prepared by the method of Arnold and Liggett[19] from 1,3-, 2,3-, 2,6-, and 1,7-dimethylnaphthalenes. The orientation for the bromination of these dimethylnaphthalenes has been reported by Kim *et al.*[20] Bromodimethylnaphthalenes were carboxylated to the corresponding dimethylnaphthoic acids by the Grignard reaction with carbon dioxide and then were oxidized with aqueous sodium bichromate to 1,2,4-, 1,2,3-, 1,2,6-, and 1,4,6-naphthalenetricarboxylic acids (Table 3, **2**, **1**, **4**, and **14**).

It has been reported that 2,6-dimethylnaphthalene gives 1-acetyl-2,6-dimethylnaphthalene (mp 70—71°C) by the Friedel-Crafts acetylation reaction in carbon disulfide,[12,13] and the acetyl compound is oxidized with aqueous hypochlorite solution to 2,6-dimethyl-1-naphthoic acid (mp 203—204°C)[13] which is further oxidized with dilute nitric acid to naphthalene-1,2,6-tricarboxylic acid (mp of trimethyl ester: 139—140°C).[11] We prepared 2,6-dimethyl-1-naphthoic acid with mp 173—174°C by the Grignard reaction on 1-bromo-2,6-dimethylnaphthalene. The trimethyl naphthalenetricarboxylate obtained from this compound had mp 141—142°C. On the other hand, trimethyl naphthalenetricarboxylate(**13a**) obtained by the aqueous bichromate oxidation of acetyl-2,6-dimethylnaphthalene(**15**) had mp 172.5—173.5°C. The results indicate that the acetyl group in acetyl-2,6-dimethylnaphthalene(**15**) is not located in the position given in literature. The structure of this acetyl compound was confirmed to be 1-acetyl-3,7-dimethylnaphthalene(**15**) from the fact that both trimethyl naphthalenetricarboxylates(**13a**) obtained by the aqueous bichromate oxidation of acetyl-2,6-dimethylnaphthalene(**15**) (mp 70—71°C) and of acetyl-1,3-dimethylnaphthalene(**16**) (mp 96.5—97.5°C), in which the acetyl group should be located in 7-position as shown in Scheme 1, were the same compound.

β-(5-Acenaphthoyl)propionic acid which had been prepared by the Friedel-Crafts reaction of acenaphthene and succinic anhydride[21] was oxidized to naphthalene-1,4,5-tricarboxylic acid (Table 3, **8**) with aqueous sodium bichromate, but β-(3-acenaphthoyl)propionic acid[21] gave benzene-1,2,3-tricarboxylic acid (Table 3, **6**). On the other hand, β-(3-acenaphthoyl)propionic acid could be oxidized with aqueous potassium ferricyanide to naphthalene-1,2,8-tricarboxylic acid. Naphthalene-2,3,6-tricarboxylic acid(Table 3, **10**) was obtained by the aqueous sodium bichromate oxidation of β-[2-(6,7-dimethylnaphthoyl)]propionic acid prepared by the Friedel-Crafts reaction of 2,3-dimethylnaphthalene and succinic anhydride.[22]

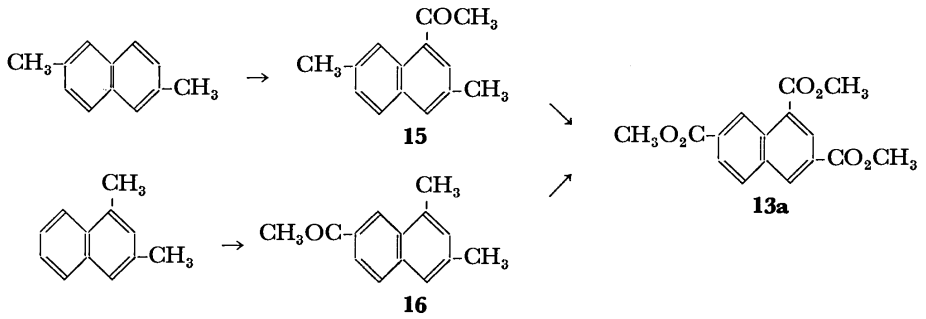

Scheme 1.

11) S. M. Maker, H. F. Bassilios, and A. Y. Salem, *J. Chem. Soc.*, **1958**, 2437.
12) E. Clar, H. Wallenstein, and R. Avenarius, *Ber.*, **62**, 950 (1929).
13) K. Dziewonski, K. Stec, and P. Zagata, *Bull. intern. acad. polon. sci., Classe sci. math. nat.*, **1938A**, 324; *Chem. Abstr.*, **33**, 1713[3] (1939).
14) L. Friedman, D. L. Fishel, and H. Shechter, *J. Org. Chem.*, **30**, 1453 (1965).
15) H. Frischkorn and E. Schinzel, German P. 1291329 (1969); Brit. P. 1173704 (1969).
16) L. Ruzicka, J. R. Hosking, L. Ehman, J. Jensen, and T. Lien, *Helv. Chim. Acta*, **13**, 1411 (1930).
17) L. Ruzicka and L. Ehman, *ibid.*, **15**, 140 (1932).
18) W. Ried and H. Boden, *Chem. Ber.*, **91**, 1354 (1958).
19) R. T. Arnold and R. W. Liggett, *J. Amer. Chem. Soc.*, **64**, 2875 (1942).
20) J. B. Kim, C. Chen, J. K. Krieger, K. R. Judd, C. C. Simpson, and E. Berliner, *ibid.*, **92**, 910 (1970).
21) L. F. Fieser and M. A. Peters, *ibid.*, **54**, 4347 (1932).
22) R. D. Hawarth and F. M. Bolam, *J. Chem. Soc.*, **1932**, 2248.

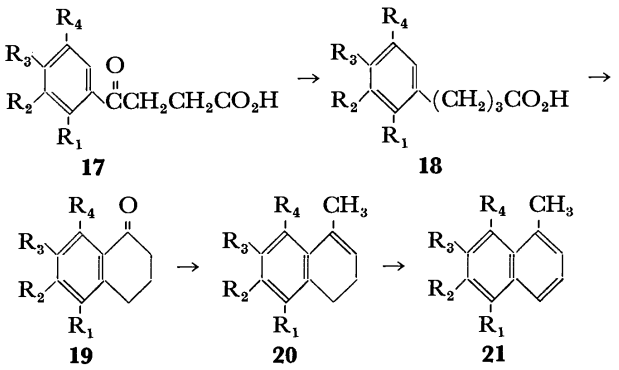

a. 2,3,5-Trimethylnaphthalene: $R_2=R_3=CH_3$ and $R_1=R_4=H$
b. 1,3,5-Trimethylnaphthalene: $R_1=R_3=CH_3$ and $R_2=R_4=H$
c. 1,2,5-Trimethylnaphthalene: $R_1=R_2=CH_3$ and $R_3=R_4=H$
d. 1,3,8-Trimethylnaphthalene: $R_2=R_4=CH_3$ and $R_1=R_3=H$

Scheme 2.

γ-(3,4- or 2,4-Dimethylphenyl)butyric acid(**18a** or **b**) was prepared by the Clemmensen reduction of β-(3,4- or 2,4-dimethylbenzoyl)propionic acid(**17a** or **b**) synthesized from *o*- or *m*-xylene with succinic anhydride.[23] After ring closure of these γ-dimethylphenylbutyric acids(**18a**, **b**) to dimethyltetralones(**19a**, **b**) with polyphosphoric acid,[24,25] the dimethyltetralones were converted into 1,6,7- and 1,5,7-trimethyl-3,4-dihydronaphthalenes(**20a** and **b**) by the Grignard reaction with methylmagnesium iodide and then dehydrogenated to 2,3,5- and 1,3,5-trimethylnaphthalenes(**21a** and **b**) with sulfur as shown in Scheme 2. These trimethylnaphthalenes gave the corresponding naphthalenetricarboxylic acids (Table 3, **9** and **11**). Methyl β-(2,3- or 3,5-dimethylbenzoyl)propionate was obtained by the reaction of 3-bromo-*o*-xylene or 5-bromo-*m*-xylene and β-carbomethoxypropionyl chloride by the method of Dauben and Tilles,[26] who reported on the synthesis of methyl benzoyl- and toluylpropionates. The methyl β-(dimethylbenzoyl)propionates were hydrolyzed to the corresponding free acids(**17c** and **d**) and then converted into 1,2,5- and 1,3,8-trimethylnaphthalenes (**21c** and **d**) by a similar reaction route. These trimethylnaphthalenes gave naphthalene-1,2,5- and 1,3,8-tricarboxylic acids (Table 3, **3** and **7**).

Ethyl 5,7-dimethyl-3,4-dihydronaphthalene-2-carboxylate(**24**) was prepared by the reaction of ethyl γ-(2,4-dimethyl)butyrate (**22**) and ethyl formate in the presence of sodium ethoxide followed by the ring closure with phosphoric acid - sulfuric acid mixture as shown in Scheme 3. This reaction route has been reported on the synthesis of ethyl 6,7-dimethoxy-3,4-dihydronaphthalene-2-carboxylate[27] and ethyl 7-methyl-2-naphthoate.[28] Dihydro compound(**24**)

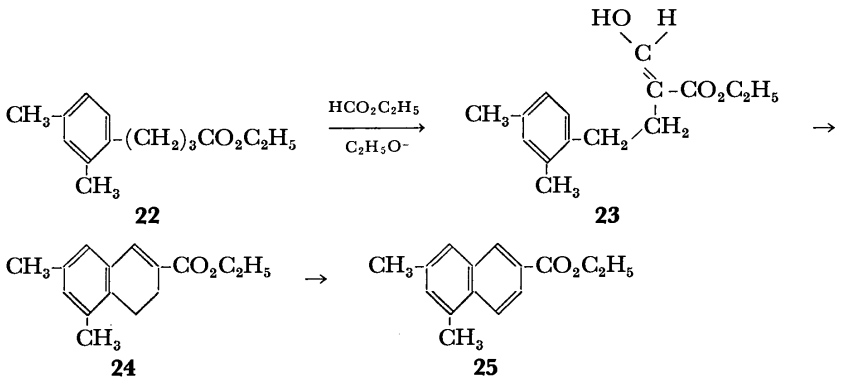

Scheme 3.

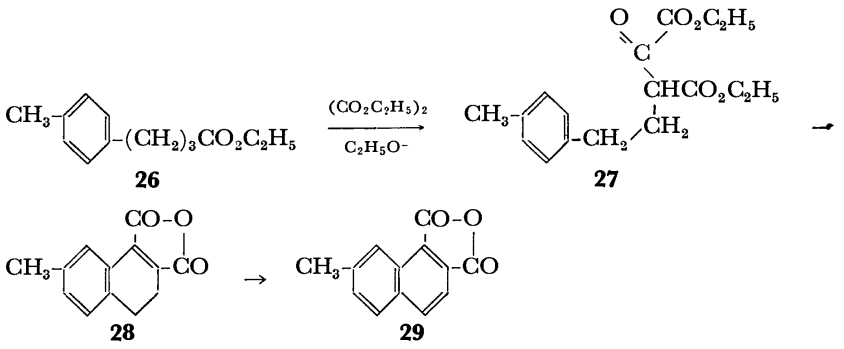

Scheme 4.

23) E. de B. Barnett and F. G. Sanders, *ibid.*, **1933**, 434.
24) H. R. Snyder and F. X. Weber, "Organic Syntheses" Coll. Vol. III, 798 (1955).
25) R. P. Evans and J. C. Smith, *J. Chem. Soc.*, **1954**, 798.
26) W. G. Dauben and H. Tilles, *J. Org. Chem.*, **15**, 785 (1950).
27) H. L. Holmes and L. W. Trevoy, "Organic Syntheses" Coll. Vol. III, 300 (1955).
28) W. Adcock and P. R. Wells, *Aust. J. Chem.*, **18**, 1357 (1965),

was dehydrogenated with sulfur to ethyl 5,7-dimethylnaphthalene-2-carboxylate(**25**), hydrolyzed to free acid and then oxidized to naphthalene-1,3,6-tricarboxylic acid (Table 3, **12**).

Ethyl α-carbethoxy-γ-(*p*-methylphenyl)butyrate(**27**) was synthesized by the reaction of γ-(*p*-methylphenyl)butyrate(**26**) and diethyl oxalate in the presence of sodium ethoxide. This compound was cyclized with sulfuric acid to 7-methyl-3,4-dihydronaphthalene-1,2-dicarboxylic anhydride(**28**) and then dehydrogenated with sulfur to 7-methylnaphthalene-1,2-dicarboxylic anhydride(**29**) as shown in Scheme 4. The preparative method has been reported on the naphthalene-1,2-dicarboxylic anhydride.[29,30]

An attempt to prepare 5-methylnaphthalene-3,4-dihydro-1,2-dicarboxylic anhydride from γ-(*o*-methylphenyl)butyrate by a similar method failed. 7-Methylnaphthalene-1,2-dicarboxylic anhydride gave naphthalene-1,2,7-tricarboxylic acid (Table 3, **5**).

The melting points and analytical data of trimethyl naphthalenetricarboxylates are summarized in Table 1. The esters were hydrolyzed with potassium hydroxide in aqueous ethanol to give free acids, and some of them were dehydrated with acetic anhydride to the corresponding acid anhydrides. Melting points, analytical data, and infrared absorption bands of carbonyl group of naphthalenetricarboxylic acid monoanhydrides are shown in Table 2. In the cases of naphthalene-1,2,8-, 1,3,8-, and 1,4,8-tricarboxylic acids, 1,8-anhydrides were directly obtained by acidification of hot alkaline solution of the corresponding acids.[31]

Table 1. Melting points and analytical data of trimethyl naphthalenetricarboxylates

	Position	Mp (°C) Obsd.	Mp (°C) Ref.	Analytical data[a] Found (%) C	H
1a	1,2,3-	88.5— 89.5	—	63.41	4.77
2a	1,2,4-	119.5—120.5	120[b]	63.40	4.68
3a	1,2,5-	89.0— 89.5	90—91[c] 89[d]	63.46	4.66
4a	1,2,6-	141.0—142.0	139—140[e]	63.58	4.70
5a	1,2,7-	153.0—154.0	153—154[f] 152—153[g]	63.99	4.70
6a	1,2,8-	92.5— 93.5	—	64.04	4.68
7a	1,3,8-	110.5—111.5	—	63.47	4.29
8a	1,4,5-	126.0—127.0	—	63.52	4.77
9a	2,3,5-	128.0—128.5	—	63.43	4.66
10a	2,3,6-	124.5—125.5	—	63.68	4.88
11a	1,3,5-	128.0—129.0	—	63.45	4.70
12a	1,3,6-	194.5—195.5	—	63.62	4.70
13a	1,3,7-	172.5—173.5	—	63.55	4.67
14a	1,4,6-	135.0—136.0	—	63.48	4.70

a) Calcd for $C_{16}H_{14}O_6$: C, 63.58; H, 4.67%. b) Ref. 10. c) Ref. 6, p. 1411. d) Ref. 5. e) Ref. 11. f) Ref. 13. g) Ref. 9.

Experimental[32]

2,3-, 2,4-, 2,6-, and 4,6-Dimethyl-1-naphthoic Acids. 2,3-, 1,3-, 2,6-, and 1,7-Dimethylnaphthalenes were brominated by the method of Arnold and Liggett[19] to give 1-bromo-

Table 2. Physical properties and analytical data of naphthalenetricarboxylic acid monoanhydrides

	Position	Mp (°C) Obsd.	Mp (°C) Ref.	Analytical data[a] Found (%) C	H	Infrared spectrum ν_{CO} (cm^{-1})
2b	1,2,4-	292—293	—	64.79	2.06	1851, 1794, 1701
3b	1,2,5-	277—278	270[b] 270—272[c]	64.46	2.13	1848, 1770, 1759, 1683
4b	1,2,6-	>300	298—300[d]	64.21	2.09	1840, 1792, 1775, 1691
5b	1,2,7-	>300	—	64.86	2.07	1861, 1794, 1695
6b	1,2,8-	298.5—299.5	297.5—298.5[e] 295—297[f]	64.81	1.87	1775, 1742, 1734, 1689
7b	1,3,8-	289—290	287—288[f]	64.28	2.06	1774, 1737, 1693
8b	1,4,5-	273.5—274.5	273—274[f] 273—275[g] 274—275[h]	64.72	2.09	1770, 1737, 1703
9b	2,3,5-	>300	—	64.10	2.06	1843, 1831, 1780, 1676
10b	2,3,6-	288.5—289.5	—	64.22	2.10	1852, 1788, 1695

a) Calcd for $C_{13}H_6O_5$: C, 64.47; H, 2.50%. b) Mp of free acid: Ref. 7. c) Mp of free acid: Ref. 5. d) Mp of free acid: Ref. 11. e) Ref. 4. f) Ref. 3. g) A. A. Morton, J. B. Davidson, T. R. P. Gibb, Jr., E. L. Little, E. E. Clarke, and A. G. Green, *J. Amer. Chem. Soc.*, **64**, 2250 (1942). h) H. E. Nürsten and A. T. Peters, *J. Chem. Soc.*, **1950**, 2389.

29) L. F. Fieser and E. B. Hershberg, *J. Amer. Chem. Soc.*, **57**, 1851 (1935); E. B. Hershberg and L. F. Fieser, "Organic Syntheses" Coll. Vol. II, 194 (1948).

30) E. B. Hershberg and L. F. Fieser, *ibid.*, Coll. Vol. II, p. 423 (1948).

31) Naphthalene-1,8-dicarboxylic acid gives anhydride by recrystallization from nitric acid(S. G., 1,4): C. Graebe and E. Gfeller, *Ber.*, **25**, 653 (1892).

32) Infrared spectroscopy and micro analysis were performed with a Hitachi Infrared Spectrophotometer EPI-S2 (in Nujol) and a Yanagimoto C. H. N. Corder MT-1 apparatus, respectively. The methyl ester of the carboxylic acid was synthesized by the reaction of the silver salt of carboxylic acid and methyl iodide.

2,3-dimethyl-, 1-bromo-2,4-dimethyl-, 1-bromo-2,6-dimethyl-, and 1-bromo-4,6-dimethylnaphthalenes.

2,3-Dimethyl-1-naphthoic acid was prepared by the Grignard reaction of 1-bromo-2,3-dimethylnaphthalene[19]: 52% yield, mp 170—171°C (lit, mp 167—168°C[19]).

1-Bromo-2,4-dimethylnaphthalene gave 2,4-dimethyl-1-naphthoic acid by a similar method; 55% yield, mp 165.5—167.0°C (aqueous EtOH). Found: C, 78.02; H, 6.01%. Calcd for $C_{13}H_{12}O_2$: C, 77.96; H, 6.04%.

1-Bromo-2,6-dimethylnaphthalene gave 2,6-dimethyl-1-naphthoic acid (46.3%) and 2,6-dimethylnaphthalene (24.3%). The acid had mp 173—174°C(aqueous EtOH). Found: C, 77.64; H, 6.02% (the acid reported to have mp 203—204°C[11,13,33] should be assigned to 3,7-dimethyl-1-naphthoic acid). Methyl 2,6-dimethyl-1-naphthoate: mp 89.5—90.5°C (MeOH). Found: C, 78.23; H, 6.73%. Calcd for $C_{14}H_{14}O_2$: C, 78.49; H, 6.58%.

1-Bromo-4,6-dimethylnaphthalene gave 4,6-dimethyl-1-naphthoic acid; 59% yield, mp 196.5—197.0°C (benzene). Found: C, 78.02; H, 6.23%.

Acetylation of 2,6- and 1,3-Dimethylnaphthalenes. 2,6-Dimethylnaphthalene was acetylated with acetic anhydride and anhydrous aluminum chloride in carbon disulfide by the method of Clar, Wallenstein, and Avenarius[12] giving a fraction of bp 151—157°C/4 mmHg in 64.5% yield. This fraction which solidified partly was filtered and recrystallized from ethanol to give 3,7-dimethyl-1-acetonaphthone(**15**); mp 70—71°C(lit, mp 70—71°C).[11-13] This was reported to be 2,6-dimethyl-1-acetonaphthone. 3,7-Dimethyl-1-acetonaphthone (10 g) was oxidized with aqueous sodium hypobromite solution at room temperature for 20 hr to give 1.6 g of 3,7-dimethyl-1-naphthoic acid; mp 202—203°C (aqueous EtOH) (lit, mp 204—205°C[34]) or with aqueous sodium bichromate to naphthalene-1,3,7-tricarboxylic acid (Table 3, **13**). The tricarboxylic acid (2.0 g) was recrystallized from 50 m*l* of acetic anhydride, washed with benzene and dried. The infrared spectrum of this compound has no acid anhydride band.

1,3-Dimethylnaphthalene (37.7 g, 0.242 mol) in 50 m*l* of nitrobenzene was added to a solution of 19.4 g (0.248 mol) of acetyl chloride and 34 g (0.248 mol) of anhydrous aluminum chloride in 80 m*l* of nitrobenzene under chilling with ice-water. Stirring was continued for 2 hr at room temperature and then 2 hr at 60°C. After treatment in the usual manner, 1,3-dimethyl-7-acetonaphthone(**16**) which boiled at 152—159°C/3 mmHg was collected; mp 96.5—97.5°C (EtOH), 56.5% yield(37 g). Found: C, 84.74; H, 7.27%. Calcd for $C_{14}H_{14}O$: C, 84.81; H, 7.11%. The ketone gave naphthalene-1,3,7-tricarboxylic acid (Table 3, **13'**). The trimethyl ester(mp 172.5—173.5°C) was identified to be the same compound by means of mixed melting point and comparison of the infrared spectra with the sample obtained from 3,7-dimethyl-1-acetonaphthone (**15**).

Succinoylation of Acenaphthene and 2,3-Dimethylnaphthalene. β-(3- and 5-Acenaphthoyl)propionic acids were synthesized by the method of Fieser and Peters[21] from acenaphthene and succinic anhydride.

β-[2-(6,7-Dimethylnaphthoyl)]propionic acid was prepared by a modified method of Hawarth and Bolam.[22] 2,3-Dimethylnaphthalene (40.0 g, 0.256 mol) was added to a solution of 78 g (0.58 mol) of anhydrous aluminum chloride and 26.0 g (0.26 mol) of succinic anhydride in 250 m*l* of nitrobenzene under chilling with ice-water. Stirring was carried out overnight at room temperature. The reaction product was treated and purified by a similar method to that in the synthesis of β-(5-acenaphthoyl)propionic acid[21] to give 17.0 g (37%) of β-[2-(6,7-dimethylnaphthoyl)] propionic acid; mp 183.5—184.5°C. Recrystallization from methanol gave mp 184.0—185.0°C (lit, mp 179—180°C[22]).

2,3,5- and 1,3,5-Trimethylnaphthalenes. γ-(3,4- and 2,4-Dimethylphenyl)butyric acid[23] (**18a** and **b**) were cyclized with polyphosphoric acid (200 m*l* of 85% phosphoric acid and 240 g of phosphorus pentoxide)[24,25] to give 6,7- and 5,7-dimethyltetralones (**19a** and **b**); 89% yield, bp 128—130°C/4 mmHg and 90% yield, bp 137°C/5.5 mmHg, respectively. The dimethyltetralones were converted into 1,6,7- and 1,5,7-trimethyl-3,4-dihydronaphthalenes (**20a** and **b**) by the Grignard reaction with methylmagnesium iodide and then dehydrogenated with sulfur at 210°C for 8 hr to give 2,3,5- and 1,3,5-trimethylnaphthalenes (**21a** and **b**); bp 131—131.5°C/11 mmHg (lit, bp 138°C/12 mmHg[17]) and bp 115—116°C/5.5 mmHg, mp 42.5—44.5°C (lit, mp 43°C[16]), respectively.

1,3,8- and 1,2,5-Trimethylnaphthalenes. 4-Acetamido-*m*-xylene[35] was nitrated by a modified method of Haller, Adams, and Wherry.[36] 4-Acetamido-*m*-xylene (100 g, mp 129.5—130.5°C) in 100 m*l* of glacial acetic acid was dropped into 200 m*l* of fuming nitric acid (S. G., 1.52) under stirring at 10°C for 3 hr and further stirred for 20 min. The reaction mixture was poured into 1 *l* of water, filtered, washed with water and finally recrystallized from 500 m*l* of ethanol to give 5-nitro-4-acetamido-*m*-xylene; 70—79% yield, mp 175—176°C (lit, mp 172°C[35]). The compound was deaminated to 5-nitro-*m*-xylene,[36] reduced to 5-amino-*m*-xylene by the Béschamp reduction, brominated to 5-bromo-*m*-xylene by the method of Zanten and Nauta,[37] and then made to react with β-carbomethoxypropionyl chloride to give methyl β-(3,5-dimethylbenzoyl)propionate by the method of Dauben and Tilles[26]; 25.6% yield, bp 153—160°C/2 mmHg. The ester was hydrolyzed to β-(3,5-dimethylbenzoyl)propionic acid(**17d**); 70.3% yield, mp 117—118°C(aqueous EtOH). Found: C, 69.42; H, 7.28%. Calcd for $C_{12}H_{12}O_3$: C, 69.21; H, 7.74%. The Clemmensen reduction of the above keto-acid gave γ-(3,5-dimethylphenyl)butyric acid(**18d**) (95% yield, mp 60—61°C). 1,3,8-Trimethylnaphthalene(**21d**) was then prepared in a similar way *via* 6,8-dimethyltetralone(**19d**) and 1,6,8-trimethyl-3,4-dihydronaphthalene(**20d**); mp 45.5—46.5°C (MeOH) (lit, mp 48°C[5]).

Methyl β-(2,3-dimethylbenzoyl)propionate was prepared from 3-bromo-*o*-xylene[37] in a similar way to that described above; 21—24% yield; bp 145—148°C/2 mmHg. The free acid (**17c**) had mp 100.5—101.5°C (EtOH); 69—72% yield. Found: C, 69.63; H, 7.38%. 1,2,5-Trimethylnaphthalene(**21c**) was then synthesized by a similar way as described above *via* γ-(2,3-dimethylphenyl)butyric acid (**18c**) (mp 109.5—110.5°C from benzene), 5,6-dimethyltetralone(**19c**) (mp 58—59°C) and 1,5,6-trimethyl-3,4-dihydronaphthalene(**20c**); bp 132—134°C/4 mmHg (lit, bp 147—148°C/11 mmHg[16]).

5,7-Dimethyl-2-naphthoic Acid. Into a solution of sodium ethylate prepared from 7.0 g of sodium sand and 17 m*l* of absolute ethanol in 150 m*l* of dry ether, a mixture of 42.0 g (0.191 mol) of ethyl γ-(2,4-dimethylphenyl)butyrate (**22**)[23] and 21.0 g (0.284 mol) of ethyl formate in 100 m*l* of dry ether was added under stirring and chilling with ice-

33) R. Lesser and G. Gad, *Ber.*, **60**, 244 (1927).
34) F. G. Baddar, I. M. Dwidar, and M. Gindy, *J. Chem. Soc.*, **1959**, 1005.
35) W. Willgerodt and F. Schmierer, *Ber.*, **38**, 1473 (1905).
36) H. L. Haller, E. Q. Adams, and E. T. Wherry, *J. Amer. Chem. Soc.*, **42**, 1840 (1920).
37) B. van Zanten and W. T. Nauta, *Rec. Trav. Chim. Pays-Bas*, **97**, 1216 (1960).

salt bath for 20 min and stirred at room temperature for 50 hr. The reaction mixture was worked up as described by Holmes and Trevoy[27] to give 3,4-dihydro-5,7-dimethyl-2-naphthoate (**24**) in 36—40% yield (15.7—17.5 g), bp 163—165°C/2.5 mmHg, mp 75.5—76.5°C. The dihydro compound (52 g, 0.226 mol) was dehydrogenated with 7.5 g (0.234 atom) of sulfur at 240°C for 3 hr to give 44.1 g of ethyl 5,7-dimethyl-2-naphthoate (**25**); bp 165—175°C/3 mmHg. Crystallization three times from 50 m*l* portions of ethanol gave 18.7 g of pure ethyl ester; mp 57.5—58.5°C. Found: C, 79.09; H, 7.27%. Calcd for $C_{15}H_{16}O_2$: C, 78.92; H, 7.06%. The ester(20 g) was hydrolyzed with potassium hydroxide in aqueous ethanol for 30 hr to give 17.4 g of 5,7-dimethyl-2-naphthoic acid in 99% yield, mp 206.5—207.5°C (EtOH). Found: C, 78.09; H, 6.12%. Calcd for $C_{13}H_{12}O_2$: C, 77.97; H, 6.04%. Methyl 5,7-dimethyl-2-naphthoate had mp 70.0—71.0°C (MeOH). Found: C, 78.54; H, 6.66%. Calcd for $C_{14}H_{14}O_2$: C, 78.49; H, 6.58%.

7-Methylnaphthalene-1,2-dicarboxylic Anhydride. Diethyl oxalate (57.5 g, 0.393 mol) in 100 m*l* of dry ether was added to a solution of sodium ethylate prepared from 6.3 g (0.274 atom) of sodium sand and 13 g of absolute ethanol in 100 m*l* of dry ether, during the course of 30 min at room temperature and 53.5 g (0.260 mol) of ethyl γ-(*p*-methylphenyl)butyrate (**26**) in 50 m*l* of dry ether was then added for 5 min. After stirring for 30 hr at room temperature, the product was worked up as described by Fieser and Hershberg[29] to give 27.9 g (50.2%) of 3,4-dihydro-7-methylnaphthalene-1,2-carboxylic anhydride (**28**); mp 138—140°C (from petroleum benzine-benzene). Found: C, 73.00; H, 4.64%. Calcd for $C_{13}H_{10}O_3$: C, 72.88; H, 4.67%. The dihydro compound (21 g, 0.10 mol) was dehydrogenated with 3.2 g (0.10 atom) of sulfur at 200—250°C for 3 hr to give 13.7 g of 7-methylnaphthalene-1,2-dicarboxylic anhydride (**29**). Crystallization three times from benzene(active carbon) gave mp 161.5—163.5°C. The anhydride (26 g) was dissolved in aqueous sodium hydroxide solution by heating to remove trace of hydrogen sulfide, treated with active carbon and reprecipitated with hydrochloric acid. The acid (20.7 g) was treated with 80 m*l* of acetic anhydride at 150°C for 1 hr to give pure 7-methylnaphthalene-1,2-dicarboxylic anhydride (16.7 g); mp 164.5—165.5°C, ν_{CO}: 1842 and 1768 cm^{-1}. Found: C, 73.64; H, 3.45%. Calcd for $C_{13}H_8O_3$: C, 73.56; H, 3.82%. Dimethyl ester: mp 88—89°C (MeOH). Found: C, 69.42; H, 5.52%. Calcd for $C_{15}H_{14}O_4$: C, 69.76; H, 5.46%.

Sodium Bichromate Oxidation. Dimethylnaphthalenecarboxylic acids, methylnaphthalenedicarboxylic acid, dimethylacetonaphthones, β-(acenaphthoyl)propionic acid, β-(dimethylnaphthoyl)propionic acid and trimethylnaphthalenes were oxidized with aqueous sodium bichromate at

Table 3. Conditions and products of sodium bichromate oxidation

	Material: Naphthalene	g (mol)	$Na_2Cr_2O_7 \cdot 2H_2O$ g (mol)	Conditions[a]: Water m*l*	Temp. °C	Time hr	Product: Naphthalene tricarboxylic acid: Position	g (%)
1	1-Carboxy-2,3-dimethyl-[b]	13.0 (0.065)	60 (0.22)	180	260± 5	5	1,2,3-	5.0[c] (25)
2	1-Carboxy-2,4-dimethyl-	12.5 (0.063)	57 (0.19)	150	270±10	5	1,2,4-	12.5 (77)
3	1,2,5-Trimethyl-	9.4 (0.055)	75 (0.25)	150	270±10	21	1,2,5-	0.5 (3)
4	1-Carboxy-2,6-dimethyl-	11.0 (0.055)	55 (0.18)	100	270±10	5	1,2,6-	11.3 (79)
5	1,2-Dicarboxy-7-methyl-	12.5 (0.059)	24 (0.08)	100	265±10	6	1,2,7-	6.8 (44)
6	β-(3-Acenaphthoyl)propionic acid	12.0 (0.047)	75 (0.25)	150	265± 5	6	—[e]	
7	1,3,8-Trimethyl-	3.4 (0.02)	25 (0.083)	75	255± 5	19	1,3,8-	2.2[d] (46)
8	β-(5-Acenaphthoyl)propionic acid	11.2 (0.044)	75 (0.25)	150	280± 5	5	1,4,5-	5.9[d] (55)
9	2,3,5-Trimethyl-	9.0 (0.053)	72 (0.24)	150	270± 5	18	2,3,5-	8.7 (63)
10	β-[2-(6,7-dimethylnaphthoyl)]propionic acid	10.0 (0.039)	70 (0.23)	150	270± 5	6	2,3,6-	7.9 (78)
11	1,3,5-Trimethyl-	8.5 (0.05)	70 (0.23)	150	275± 5	18	1,3,5-	9.6 (74)
12	2-Carboxy-5,7-dimetyl-	8.0 (0.04)	36 (0.12)	100	260± 2	6	1,3,6-	9.9 (95)
13	1-Acetyl-3,7-dimethyl-	9.0 (0.046)	60 (0.22)	150	275± 5	18	1,3,7-	10.9 (92)
13'	7-Acetyl-1,3-dimethyl-	8.0 (0.044)	60 (0.22)	150	275± 5	19	1,3,7-	10.2 (89)
14	1-Carboxy-4,6-dimethyl-	5.0 (0.025)	22.5 (0.075)	100	265± 5	5	1,4,6-	6.0 (92)

a) 300 m*l* Autoclave used as reaction vessel. b) 400 m*l* Autoclave used. c) Separated as methyl ester.
d) Separated as acid anhydride. e) Trimethyl hemimellitate.

250—280°C under autogeneous pressure (*ca.* 30—40 kg/cm²). Sodium bichromate was used 1.3—1.5 times excess per methyl or methylene group. Methylnaphthalenecarboxylic acids, dimethylnaphthoylpropionic acid and acenaphthoylpropionic acids were dissolved in equimolar amount of aqueous sodium hydroxide and oxidized. The reaction mixture was filtered at 70—80°C, and the filtrate was neutralized with hydrochloric acid to pH≃6, treated with active carbon and then acidified with hydrochloric acid to give naphthalenetricarboxylic acids. The reaction conditions and products are summarized in Table 3.

In the cases of naphthalene-1,2,3- and 1,2,5-tricarboxylic acids (Table 3, **1** and **3**), the reaction product was filtered, acidified with nitric acid, neutralized with sodium hydroxide to pH≃9 and treated with active carbon. Excess silver nitrate was then added in order to isolate the carboxylic acid as silver salt owing to the high solubility of these acids in water. The silver salts were converted into trimethyl naphthalenetricarboxylates with methyl iodide. The ester obtained from the 1,2,5-trimethylnaphthalene was dissolved in methanol, chromatographed through the alumina column and eluted with methanol. The eluted solution was evaporated and the residue was recrystallized from methanol to give 0.6 g of trimethyl hemimellitate; mp 100.5—101.5°C. It was identified by means of the mixed melting point and comparison of the infrared spectra with the authentic sample. The mother liquors were evaporated to dryness and the residue (4.5 g) was extracted with 15 m*l* of hot ligroin. After cooling of the ligroin solution, trimethyl naphthalene-1,2,5-tricarboxylate was isolated; 0.4 g, mp 89.0—89.5°C (MeOH).

From the oxidation product of β-(3-acenaphthoyl)propionic acid(Table 3, **6**), trimethyl hemimellitate (mp 101—102°C; 0.2 g) was isolated by a similar treatment to that in the case of 1,2,5-trimethylnaphthalene. The mother liquors gave 1.3 g of impure product; mp 83—93°C.

Potassium Ferricyanide Oxidation of β-(3-Acenaphthoyl)-propionic Acid. β-(3-Acenaphthoyl)propionic acid (5.4 g), 82 g of potassium hydroxide, 470 g of potassium ferricyanide, and 1200 m*l* of water were allowed to react at 60°C for 74 hr. A solution of 24 g of potassium hydroxide, 90 g of potassium ferricyanide, and 200 m*l* of water was added at 24 hr intervals. The product was cooled, acidified with hydrochloric acid and filtered. The filtrate was extracted fifteen times with 300 m*l* portions of ether. The ether was evaporated to give 3.5 g of naphthalene-1,2,8-tricarboxylic acid; mp 288—290°C.

The author wishes to thank Mrs. Shizu Fujishima for the micro analyses.

BULLETIN OF THE CHEMICAL SOCIETY OF JAPAN, VOL. 45, 525—528 (1972)

The Synthesis of the New 1,4,2-Dithiazine Ring[1)]

Kiyoshi HASEGAWA and Syuzi HIROOKA

Department of Industrial Chemistry, Faculty of Engineering, Toyama University, Takaoka-shi

(Received May 21, 1971)

Some derivatives of *N*-(2-phenylethene-1-sulfonyl)-*N'*-alkylthioureas of the $R^1C_6H_4CH{=}CHSO_2NHCSNHR^2$ **2** type were synthesized by a reaction between 2-phenylethene-1-sulfonamides **1** and isothiocyanates in acetone in the presence of K_2CO_3. A new heterocyclic system, 3-alkylamino-5-phenyl-1,1-dioxo-5,6-dihydro-1,4,2-dithiazine **3**, was obtained by the intramolecular Michael cycloaddition of **2** in weakly basic media, and also by the thermal cyclization of **2**. The carbon-sulfur bond in **3** could be cleaved to give **2** again in strongly basic media.

A previous study[2)] in this laboratory has dealt with *N*-benzenesulfonyl-*N'*-alkylthioureas obtained from benzenesulfonamides and alkyl isothiocyanates. When 2-phenylethene-1-sulfonamide[3)] **1**, in which the α, β double bond is activated by a neighboring sulfonyl group,[4)] was used, either the corresponding sulfonylthioureas **2** or the intramolecular cycloadducts, 3-alkylamino-5-phenyl-1,1-dioxo-5,6-dihydro-1,4,2-dithiazines **3**, were formed, depending upon the work-up procedure. Recently, the synthesis of **2** (R^1=H, R^2=allyl and phenyl) was briefly reported,[5)] but **3** has never yet been prepared. This paper will describe the synthesis, cleavage, and structural elucidation of a new heterocycle **3**. The process is outlined below.

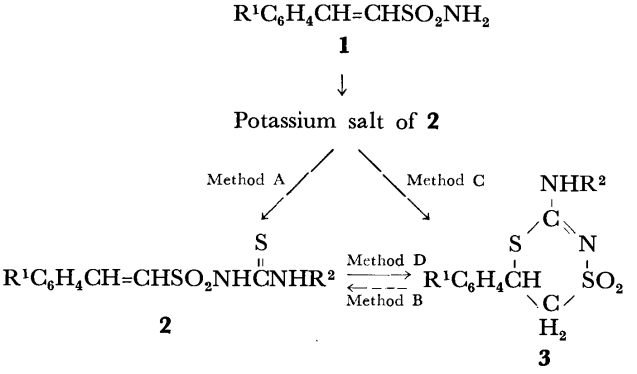

Results

N-(2-Phenylethene-1-sulfonyl)-N'-alkylthioureas **2**. A mixture of **1**, potassium carbonate, and alkyl isothiocyanate in acetone was refluxed for 15—25 hr with stirring to yield the potassium salt of **2** as a normal product. This was filtered, dissolved in water, and acidified to give **2** (Table 1, Method A). The structure of **2** was confirmed by a study of its IR, NMR,

1) Presented in part at the 24th Annual Meeting of the Chemical Society of Japan, Osaka, April, 1971.

2) S. Hirooka, *Nippon Kagaku Zasshi*, **83**, 156 (1962).

3) B. M. Culbertson and S. Dietz, *J. Chem. Soc., C*, **1968**, 90, 992.

4) E. D. Bergmann, D. Ginsburg, and R. Pappo, "Organic Reactions," Vol. 10, New York (1959), p. 241.

5) S. Hartig, *J. Prak. Chem.*, **33**, 216 (1966).

Table 1. $R^1C_6H_4CH_B=CH_ASO_2NHCSNHR^2$ **2**

Compd.	R^2	R^2	Yield (%)		Mp (°C)	UV $\lambda_{max}^{C_2H_5OH}$	Calcd (%)				Found (%)			
			A[a]	B[b]		(ε_{max})	C	H	N	S	C	H	N	S
2a	H	CH_3	95	94	137—138	267 (23700)	46.88	4.72	10.93		46.85	4.89	10.95	
2b	H	C_2H_5	67	87	96— 98	267 (22700)	48.89	5.22	10.37		48.84	5.29	10.26	
2c	H	n-C_4H_9	72	76	110—111	267 (22200)	52.34	6.08	9.39		52.51	6.06	9.30	
2d	H		57	79	130—131		55.55	6.22	8.64		55.80	6.34	8.78	
2e	p-Cl	CH_3	85	90	240—242	274 (11300)	41.30	3.81	9.63	22.05	41.54	4.05	9.75	22.13
2f	p-Cl	C_2H_5	44	87	110—111		43.34	4.29	9.19	21.03	43.41	4.16	9.30	20.99
2g	m-Cl	CH_3	94	92	233—235		41.30	3.81	9.63	22.05	41.37	3.85	9.72	22.05
2h	o-Cl	CH_3	90	93	216—218		41.30	3.81	9.63	22.05	41.05	3.92	9.72	22.16
2i	p-Br	CH_3	80	96	245—247	276 (27500)	35.82	3.31	8.36	19.13	35.90	3.19	8.21	19.28
2j	p-CH_3	CH_3	94	100	149—151	277 (25600)	48.89	5.22	10.37		48.71	5.22	10.30	
2k	p-CH_3	C_2H_5	23	76	108—110	273 (23200)	50.70	5.67	9.86	22.51	50.72	5.57	9.66	21.92

a) Method A, b) Method B.

Table 2. 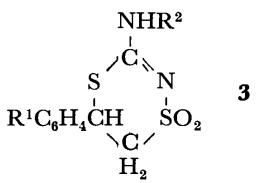 **3**

Compd.	R^1	R^2	Yield (%)		Mp (°C)	UV $\lambda_{max}^{C_2H_5OH}$	Calcd (%)				Found (%)			
			C[a]	D[b]		(ε_{max})	C	H	N	S	C	H	N	S
3a	H	CH_3	87	82	210—211	218 (23500)	46.88	4.72	10.93	24.98	46.75	4.67	10.80	24.70
3b	H	C_2H_5	61	94	174—175	218 (21600)	48.89	5.22	10.37		48.97	5.14	10.29	
3c	H	n-C_4H_9	77	96	150—151	218 (19900)	52.34	6.08	9.39		52.36	5.95	9.26	
3d	H		63	86	201—202	218 (19800)	55.55	6.22	8.64		56.29	6.03	8.35	
3e	p-Cl	CH_3	81	92	250—252	225 (21200)	41.30	3.81	9.63	22.05	41.35	4.05	9.75	22.13
3f	p-Cl	C_2H_5	67	92	201—202		43.34	4.29	9.19	21.03	43.43	4.09	9.19	21.10
3g	m-Cl	CH_3	94	89	234—236	220 (25100)	41.30	3.81	9.63	22.05	41.34	3.96	9.68	22.18
3h	o-Cl	CH_3	84	93	222—224	219 (21800)	41.30	3.81	9.63	22.05	41.48	3.84	9.65	22.12
3i	o-Cl	C_2H_5	71	90	150—151	219 (24800)	43.34	4.29	9.19	21.03	43.53	4.32	9.27	21.17
3j	p-Br	CH_3	68	88	249—251	228 (20400)	35.82	3.31	8.36	19.13	36.01	3.32	8.35	19.20
3k	p-Br	C_2H_5	55	90	230—232	228 (19700)	37.82	3.75	8.02	18.36	37.89	3.61	8.35	18.36
3l	p-CH_3	CH_3	94	86	215—217	223 (27700)	48.89	5.22	10.37	23.68	47.60	5.06	10.00	23.68
3m	p-CH_3	C_2H_5	49	85	204—206	223 (28200)	50.70	5.67	9.86		50.85	5.75	9.82	

a) Method C, b) Method D.

and mass spectra and by the results of elemental analyses. The IR spectrum of **2a** displayed bands at 3320 (ν_{NH}) and 1610 ($\nu_{C=C}$) cm^{-1}. The NMR spectrum of **2a** exhibited an AB pattern centered at δ 7.28 and δ7.77 (J_{AB} = 15.2 Hz) due to the vicinal olefinic protons, H_A and H_B. The large magnitude of this coupling proves that **2** has the *trans* rather than the *cis* configuration.

3-Alkylamino-5-phenyl-1,1-dioxo-5,6-dihydro-1,4,2-dithiazines ***3****. The Base-Catalyzed Intramolecular Cyclization of* ***2****.* When the potassium salt of **2** described above was dissolved in warm water (Table 2, Method C), or when **2** was dissolved in a dilute alkali (Table 2, Method D), a new heterocycle, **3**, began to separate out after a few minutes. This Michael-type reaction carried out at pH values below 12.55 gave **3** in a good yield, and the rate of cycloaddition increased with an increase in the base concentration. Only a one-fourth equivalent of the base was sufficient to effect the cycloaddition of the sulfonylthiourea. In the pH range from 12.55 to 13.40, a mixture of **2** and **3** was obtained. Under strongly basic conditions (pH>13.40), no cycloaddition occurred. The IR spectrum of **3a** displayed a strong band at 1560—1535 cm^{-1} due to the N=C bond, but no absorption due to the C=C group was observed in the region of 1610 $cm.^{-1}$ In NMR pattern of **3a**, ring protons, $H_AH_CH_B$ appeared as an ABX pattern consisting of three quartets of H_A centered at δ3.53, H_C δ 3.67 and H_B δ 5.00 (J_{AC}=14.0 Hz, J_{AB}=11.7 Hz, and J_{BC}=4.4 Hz) respectively (Fig. 1). The observed coupling constants, J_{AB} and J_{BC}, may be compared with those for the axial-axial and axial-equatorial protons respectively. The peak at *m/e* 121.011 in the mass spectrum was in entire agreement with the fragment ion $C_6H_5CS^+$, derived from only the six-membered heterocycle, **3**. The structures of **3b—3m** were inferred because they were analogous with **3a** in their preparations and spectral data. The Michael mechanism is assumed to be like Scheme 1.

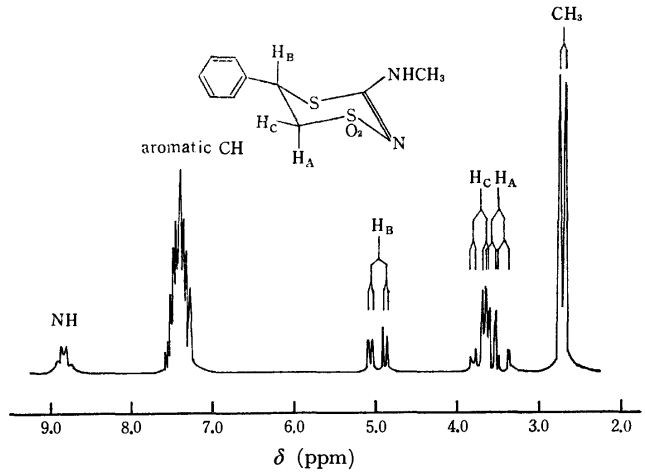

Fig. 1. NMR spectrum of **3a** in DMSO-d_6.

Thermal Cyclization of ***2****.* Thioureas, **2**, were cyclized to **3** by heating; they were then divided into two groups. The changes in their IR spectra showed that the first group, **2a—2d**, **2f**, **2j**, and **2k**, underwent a cyclization upon melting, while the second group, **2e** and **2g—2i**, underwent such a cyclization before melting. The cyclization temperatures of the latter, observed in their DTA curves, were as follows: **2e**, 141—146°C; **2g**, 131—135°C; **2h**, 140—145°C; **2i**, 157—160°C. These cycloadducts, when recrystallized, gave melting points identical with those of the products obtained by Methods C and D.

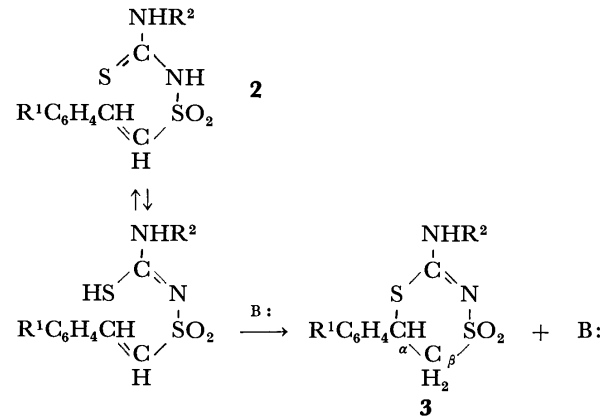

Scheme 1.

Base-Catalyzed Ring-Cleavage of ***3****.* The **3** cycloadduct could be split into **2** when the reaction media were more basic than those used in effecting the cycloaddition (Table 1, Method B). Cleavage proceeded very fast in a solvent such as alkaline aqueous acetone, even at 0°C. Only cleaved **2** was obtained when the pH of the solution was above 13.30. A mixture of **2** and **3** was obtained in the pH range from 12.70 to 13.30. This ring-cleavage is the reverse of the Michael cycloaddition, and a mechanism in the direction the reverse of that in Scheme 1 is assumed.

Discussion

We have been interested in **2** because the SO_2 group can conjugate with and activate a neighboring ethylenic double bond and stabilize the thiolate anion in basic media. As **2** has both donor and acceptor in one molecule, it should be possible to effect intramolecular Michael cycloaddition. It has indeed been found that **2** gives the intramolecular cycloadduct **3** in weakly basic media. Compounds with the general formulation $-CH=CHSO_2NHC(=S)-$ would give intramolecular Michael cycloadducts.

A Michael reversible system can be influenced by the basicity of the solution. Cleavage seems to require a base B:, strong enough to remove active β-hydrogen. A β sulfonyl group is known to accelerate the rate of the base-catalyzed elimination.[6] Cleavage proceeded too rapidly to determine certain details of this reaction, but the higher rate of cleavage was clearly associated with the higher concentration of the base.

Experimental

The melting points were determined on a Yanagimoto micro-melting-point measuring apparatus MP-S2 and are

6) E. S. Gould, "Mechanism and Structure in Organic Chemistry," Holt, Rinehart, and Winston, New York (1959), p. 499.

uncorrected. The IR and UV spectra were recorded on JASCO IRA-1 and Hitachi EPS-3T spectrometers respectively. The NMR spectra were determined with a Varian HA-100 spectrometer, with TMS as the internal standard and the mass spectra, with a JMS-01SG spectrometer.

N-*(2-Phenylethene-1-sulfonyl)*-N'-*methylthiourea* ***2a***.

Method A: To 2-phenylethene-1-sulfonamide (3.00 g, 0.0164 mol) in acetone (30 m*l*), we added methyl isothiocyanate (1.32 g, 0.0180 mol) and anhydrous potassium carbonate (1.32 g, 0.0220 mol), after which the reaction mixture was refluxed for 20 hr with stirring. The resulting potassium salt of **2a** was collected on a filter and washed with acetone to remove the unchanged sulfonamide. This salt was dissolved in water (200 m*l*), and the solution was acidified with concentrated hydrochloric acid to give 4.0 g (95%) of **2a**. Recrystallization from methanol then gave colorless crystals. IR (KBr): 3320 (ν_{NH}), 1610 ($\nu_{C=C}$), 1570 (δ_{NH}), 1495, 1435, 1380 (ν_{SO_2}), 1150, and 1130 (ν_{SO_2}), 1050, 960, 885, 740, and 690 cm^{-1}. NMR (acetone-d_6): δ 3.08 (d, J_{NHCH}=5.0 Hz, 3H, CH_3), 7.28 (d, J_{AB}=15.2 Hz, 1H, H_A), 7.77 (d, J_{AB}=15.2 Hz, 1H, H_B), 7.47±0.05 (m, 5H, phenyl), 8.40 (broad, 1H, SO_2NH), 8.90 (broad, 1H, NH). Mass spectrum (75 eV) *m/e* (rel. intensity): 77 (56), 91 (24), 103 (41), 135 (41), 136 (100), 192 (29), 256 (M^+, 1.8).

Method B: To 3-methylamino-5-phenyl-1,1-dioxo-5,6-dihydro-1,4,2-dithiazine (0.51 g, 0.0020 mol) in acetone (30 m*l*), we added a 1.0 N NaOH solution (4.0 m*l*, 0.0040 mol) and then stirred the mixture for 1 hr at room temperature. The acetone was then evaporated under reduced pressure, and the residual solution was acidified with concentrated hydrochloric acid to give 0.48 g (94%) of ***2a***.

3-Methylamino-5-phenyl-1,1-dioxo-5,6-dihydro-1,4,2-dithiazine ***3a***. *Method C*: When potassium salt of **2a** obtained from 2-phenylethene-1-sulfonamide (2.20 g, 0.0120 mol) by Method A was dissolved in warm water (150 m*l*), **3a** began to separate out after a few minutes. After the mixture had stood overnight, it was filtered to give 1.91 g (87%) of **3a**. Recrystallization from methanol gave colorless crystals. IR (KBr): 3280 (ν_{NH}), 1560—1535 ($\nu_{N=C}$), 1405, 1300 (ν_{SO_2}), 1125 (ν_{SO_2}), 960, 750, and 690 cm^{-1}. NMR (DMSO-d_6): δ 2.74 (d, J_{NHCH_3}=4.5 Hz, 3H, CH_3), 3.53 (q, J_{AC}=14.0 Hz, J_{AB}=11.7 Hz, 1H, H_A), 3.67 (q, J_{AC}=14.0 Hz, J_{BC}=4.4 Hz, 1H, H_C), 5.00 (q, J_{AB}=11.7 Hz, J_{BC}=4.4 Hz, 1H, H_B), 7.41±0.1 (m, 5H, phenyl), 8.70 (broad, 1H, NH). Mass spectrum (75 eV) *m/e* (rel. intensity): 77 (26), 78 (25), 91 (38), 104 (100), 119 (34), 121.011 (13), 135 (38), 136 (25), 177 (6), 191 (20), 256.032 (calculated molecular weight, 256.034, 21).

Method D: When **2a** (0.77 g, 0.0030 mol) was dissolved in a warm 0.1 M K_2CO_3 solution (30 m*l*, 0.0030 mol), **3a** began to separate out in a few minutes. After the mixture had stood overnight, it was filtered to give 0.63 g (82%) of **3a**.

The authors wish to thank Dr. M. Kondo, Mr. H. Kuwano, and Mr. T. Kinoshita of Sankyo Co., Limited, Tokyo, for their help in NMR and mass spectrum study. We are indebted to Mr. Y. Okabe, Mr. H. Yamada, and Mr. K. Hori for assistance in preparing some of the compounds.

BULLETIN OF THE CHEMICAL SOCIETY OF JAPAN, VOL. 45, 528—531 (1972)

The Constituents of *Arthraxon hispidus Makino, Miscanthus tinctorius Hackel, Miscanthus sinensis Anderss,* and *Phragmites communis Trinius*

Makoto KANETA and Noboru SUGIYAMA*

Fukushima Technical College, Iwaki-shi, Fukushima

**Department of Chemistry, Tokyo Kyoiku University, Otsuka, Bunkyo-ku, Tokyo*

(Received May 21, 1971)

From the leaves and stems of *Arthraxon hispidus Makino*, aconitic acid, luteolin, luteolin-7-glucoside, and a new flavone, arthraxin, have been isolated. Luteolin, luteolin-7-glucoside, and arthraxin were also isolated from *Miscanthus tinctorius Hackel*, and tricin was isolated from *Miscanthus sinensis Anderss* and *Phragmites communis Trinius*.

Arthraxon hispidus Makino, called 'Kobunagusa,' in Japanese is widely distributed in Japan. This grass has been used as a source of natural dyestuff for coloring 'Kihachijo,' which is a traditional yellow silk cloth produced on Hachijo Island, Japan. As was stated in our previous paper,[1] a report on a chemical study of the dyestuff has been made by Hayashi *et al.*,[2] but without obtaining a pure material; they presumed that the yellow pigment of the grass was a glucoside of luteolin or quercetin. *Miscanthus tinctorius Hackel*, *Miscanthus sinensis Anderss*, and *Phragmites communis Trinius*, called 'Kariyasu,' 'Susuki,' and 'Yoshi' in Japanese respectively, have also been used as sources of natural yellow dyestuff.

Since no report on chemical studies of the coloring substance have been found in the literature, such a study has been undertaken by the present authors.

Arthraxin hispidus Makino

From the extract of the grass, the following four compounds, **1**—**4**, have been isolated. The methods of isolation for each of these compounds will be described in detail in the Experimental section.

*Arthraxin (**1**).* This substance is a new flavone named arthraxin, the structural formula of which **1** was described in a previous arthraxin paper.[1]

*Aconitic Acid (**2**).* This substance showed an acidic reaction with several reagents. Its analytical, IR and R_f values agreed with those of authentic

1) M. Kaneta and N. Sugiyama, This Bulletin, **42**, 2084 (1969); *J. Chem. Soc., C*, **1971**, 1982.

2) K. Hayashi and T. Inoue, *Acta Phytochimica* **15**, 53 (1949).

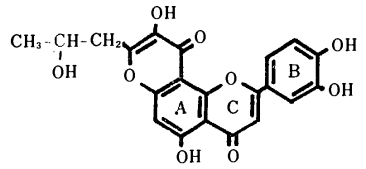

(1)

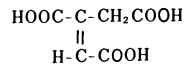

(2)

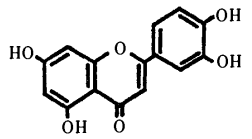

(3)

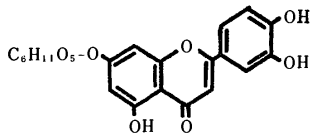

(4)

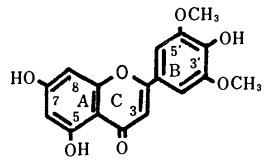

(5)

aconitic acid, and a mixed-melting-point determination with the authentic substance did not show any depression.

Luteolin (3). This substance showed a positive color reaction of flavone, and its analytical values agreed with those of the $C_{15}H_{10}O_6$ formula. On fusion with caustic potash, it yielded protocatechuic acid and phloroglucinol. The agreement of its melting point (325°C), R_f values, and UV spectra with those of luteolin[2-5] further supported its structure.

Luteolin-7-glucoside (4). This substance showed a positive color reaction of flavone, and its analytical values agreed with the $C_{21}H_{20}O_{11}$ formula. The hydrolysis of this compound produced luteolin and glucose. Since the UV λ_{max} of the II band did not shift significantly upon the addition of anhydrous acetate, the sugar was presumed to be attached to the 7-position of the aglycone. Thus, compound (**4**) was considered to be luteolin-7-glucoside. The final identification was based on the agreement of its melting point (255°C), R_f values, and UV spectra with those of luteolin-7-glucoside.[5-7]

3) T. Nakaoki, *J. Pharm. Soc. Japan*, **69**, 70 (1949).
4) T. A. Geissman, "The Chemistry of Flavonoid Compounds," Pergamon Press, Oxford, (1962), p. 111.
5) L. Jurd, *Arch. Biochem. Biophys.*, **63**, 376 (1956).

Miscanthus tinctorius Hackel

A preliminary examination of the ethanol extract of the grass by tlc and ppc showed the presence of almost the same flavonoid compounds as in *Arthraxon hispidus Makino*.

The grass was treated by the procedure to be described in the Experimental section. Consequently, luteolin (**3**) and luteolin-7-glucoside (**4**) were isolated. Moreover, the presence of arthraxin (**1**) was proved by obtaining arthraxin penta methyl ether from the methylated extract of the grass. These compounds were identified by mixed-melting-point determinations, by co-chromatography, and by a comparison of their UV and IR spectra with those of the authentic samples obtained from *Arthraxon hispidus Makino*.

Miscanthus sinensis Anderss

A boiling-water extract of the fresh leaves and stems (approximately 30 kg) of this plant was treated by a method similar to that previously described for the isolation of arthraxin from *Arthraxon hispidus Makino*.[1] The yellow crystalline needles (25 mg) thus obtained were presumed to be tricin (**5**) by studying their behavior.

Tricin (5). This compound had the empirical formula of $C_{17}H_{14}O_7$, and gave a positive color reaction of a hydroxyl flavone with several reagents. Its UV spectrum in ethanol showed peaks at 270 mμ (Band II) and at 350 mμ (Band I). The single well-defined peak of the II band indicates that the compound is a flavone which has one or three substituents in the B ring.[8] The bathochromic shift of 45 mμ of the I band on the addition of aluminum chloride indicates the presence of the 5-hydroxyl group. The fact that the addition of sodium ethylate induced a bathochromic shift of 65 mμ of the I band without decreasing its intensity indicates the presence of the 4′-hydroxyl group and the absence of the 3-hydroxyl group. The fact that the λ_{max} of the I band did not shift significantly on the addition of boric acid and sodium acetate shows the absence of *o*-hydroxyl groups. The NMR spectrum of the compound in deuterated DMSO indicated the presence of hydrogen atoms at the 3-(τ 3.09, s, 1H), 6-(τ3.82, d, 1H, J=2.5), 8-(τ 3.48, d, 1H, J=2.5), 2′-, and 6′-positions (2′- and 6′-equivalent aromatic protons; τ 2.74, s, 2H), the presence of methoxyl groups at the 3′- and 5′-positions (3′- and 5′-equivalent methoxyl groups; τ 6.12, s, 6H), and the presence of hydroxyl groups at the 5-(τ-2.90, 1H), 7-(τ-0.73, 1H) and 4′-(τ0.71, 1H) positions. The mass spectrum of the compound showed *m/e* 330 ($C_{17}H_{14}O_7$), 315 ($C_{16}H_{11}O_7$), 302 ($C_{16}H_{14}O_6$), 287 ($C_{15}H_{11}O_6$), 259 ($C_{14}H_{11}O_5$), 216 ($C_{12}H_8O_4$), 178 ($C_{10}H_{10}O_3$), 163($C_9H_7O_3$), 152($C_7H_4O_4$), 148 ($C_8H_4O_3$), and 124 ($C_6H_4O_3$) ions. The

6) T. Nakaoki and N. Morita, *J. Pharm. Soc. Japan*, **77**, 108 (1957).
7) Ref. 4, p. 324.
8) T. A. Geissman, J. B. Harborne, and M. K. Seikel, *J. Amer. Chem. Soc.*, **78**, 825 (1956).

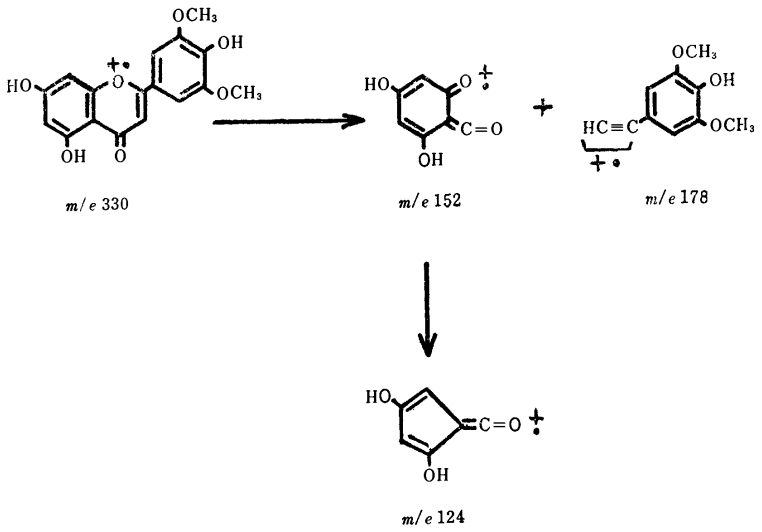

Scheme

parent molecular ion is found at *m/e* 330 as the base peak. The *m/e* 178, 152, and 124 ions are derived from the fission in the heterocyclic ring as is shown in the scheme. These kinds of fragment ions are always observed in the mass spectra of the common flavonoid compound.

Only about 25 mg of this compound were isolated; the lack of a larger sample precluded extensive structural studies. However, Formula (**5**), which is identical with that of tricin, was deduced to be the most probable structure for the compound on the basis of the presented above data.

Phragmites communis Trinius

Fresh leaves and stems of this plant (approximately 20 kg) were treated much as *Miscanthus sinensis Anderss* has been. The isolated substance (*ca.* 10 mg) was identified with tricin by a mixed-melting-point determination, by co-chromatography, and by a comparison of its UV spectra with those of the authentic sample obtained from *Miscanthus sinensis Anderss.*

Experimental

All the melting points were uncorrected. The NMR spectra were measured at 60 MHz with a Hitachi R-20B H. R. NMR spectrometer. The chemical shifts were measured with tetramethylsilane as the internal standard. The high-resolution mass spectrum was determined by direct sample introduction using Hitachi RMS-4 and RMU-7 mass spectrometers.

Arthraxon hispidus Makino. *Extraction and Isolation*: Air-dried leaves and stems (approximately 70 kg) of the grass were treated as has been described in a previous arthraxin paper[1]; 2.85 g of arthraxin (**1**) were thus obtained. The ether solution (see Ref. 1) left after the arthraxin had been removed was concentrated to about one-third the volume and kept in a refrigerator. The deposited solid was recrystallized from acetone-benzene to give 1.95 g of aconitic acid (**2**) as colorless needles. The mother liquor of arthraxin and aconitic acid was concentrated almost to dryness. The residual substance was dissolved in 800 m*l* of boiling water and extracted with ether. The ether solution was then extracted three times with 300-m*l* portions of a saturated aqueous solution of sodium hydrogen carbonate and eight times with 300-m*l* portions of a 1% aqueous sodium carbonate solution. All the extracts were acidified with hydrochloric acid. The product from the hydrogen carbonate extract was recrystallized from alcohol-water to give 120 mg of luteolin-7-glucoside (**4**) as pale yellow micro-needles. The product from the carbonate extract was recrystallized from alcohol-water to give 260 mg of luteolin (**3**) as pale yellow needles.

Aconitic Acid (2): Recrystallization from acetone-benzene gave colorless needles; mp 190°C; λ_{max} (EtOH) 215 mμ; ν_{max} (KBr) 3030, 1730, 1690, 1420, 1285, 1220, 900, 850, and 740 cm^{-1}. The above data agreed with those obtained from authentic aconitic acid. Found: C, 41.37; H, 3.47. Calcd for $C_6H_6O_6$: C, 41.39; H, 3.47%.

Luteolin (3): Recrystallization from alcohol-water gave pale yellow micro-needles; mp 325°C dec., λ_{max} (EtOH) 255, 268 (inflection), 349 mμ, λ_{max} (EtOH+NaOAc) 269, 356 mμ; λ_{max} (EtOH+NaOAc+H_3BO_3) 260, 372 mμ; λ_{max} (EtOH+$AlCl_3$) 263, 277, 362, and 388 mμ; λ_{max} (EtOH+NaOEt) 275, 405 mμ. R_f value on Toyoroshi #51: 0.78 in *n*-butanol - acetic acid - water (4-1-2 by volume). The above results were the same as those reported for luteolin.[2-5] Found: C, 63.15; H, 3.61. Calcd for $C_{15}H_{10}O_6$: C, 62.94; H, 3.52%.

Luteolin-7-glucoside (4): Recrystallization from alcohol-water gave yellow needles; mp 255°C; λ_{max} (EtOH) 257, 268 (inflection), 353 mμ; λ_{max} (EtOH+NaOH) 273, 405 mμ; λ_{max} (EtOH+NaOAc) 261, 362 and 410 mμ; R_f value on Toyoroshi #51: 0.51 in *n*-butanol - acetic acid - water (4-1-5 by volume). The data agreed with the data reported for luteolin-7-glucoside.[5-7] Found: C, 56.43; H, 4.92. Calcd for $C_{21}H_{20}O_{11}$: C, 56.25; H, 4.50%.

Hydrolysis of the Glucoside: Compound (**4**) was hydrolyzed by refluxing with 25% sulfuric acid for 11 hr. The aglycone was collected by filtration and recrystallized from ethanol-water to give luteolin, which was identified by its melting point (325°C), R_f values, and UV spectra, as has been described above. The filtrate was neutrilized with barium carbonate and then concentrated; it was used for the determination of the sugar by paper chromatography, which was carried out on Toyoroshi #51 in four solvent systems: R_f 0.18 in *n*-butanol - acetic acid - water (4-1-5 by volume),

0.27 in *n*- butanol - ethanol - water (4-1-5 by volume), 0.39 in coridine saturated with water, and 0.41 in phenol saturated with water. Identical values were obtained with an authentic sample of glucose.

Misanthus tinctorius Hackel. Extraction and Isolation: The grass was collected in Shiga Prefecture in September, 1970. One kg of air-dried leaves and stems of the grass were treated by the procedure previously described for the isolation of arthraxin from *Arthraxon hispidus Makino*. The resulting product was recrystallized from ethanol-water to give 6 mg of luteolin (**3**). The original mother liquor, which was left after extraction with ether to isolate luteolin, was extracted with 300 m*l* of ethyl acetate. The extract was concentrated under reduced pressure to yield a brownish-orange solid, which was then dissolved in 50 m*l* of boiling water. The solution was then saturated with 50 m*l* of ethyl acetate and kept for a month in a refrigerator. A yellowish crystalline substance which separated at the boundary of water and ethyl acetate was recrystallized from ethanol-water to give 8 mg of luteolin-7-glucoside (**4**) as yellow needles. In this way, approximately 10 kg of the air-dried grasses were processed, yielding *ca.* 50 mg of luteolin and *ca.* 65 mg of luteolin-7-glucoside.

The remaining solution, from which luteolin was obtained, was evaporated to dryness. The residue was dissolved in 200 m*l* of dry acetone and was heated under reflux with 15 m*l* of dimethyl sulfate and 20 mg of anhydrous potassium carbonate for 56 hr, until the ferric chloride reaction became negative. After the inorganic salt has been removed by filtration, the filtrate was evaporated under reduced pressure. The residue was dissolved in a small portion of a mixture of acetone and benzene (1 : 4) and passed through a silica-gel (Kieselgel less than 0.08 mm, Merck) column. Elution was carried out successively with the following solvents: 500 m*l* of benzene, 1000 m*l* of benzene-ethyl acetate (1 : 1), 1000 m*l* of ethyl acetate, and 1000 m*l* of ethyl acetate-acetone (1 : 1). The fraction which was eluted with ethyl acetate-acetone (1 : 1) was evaporated, and the residue was recrystallized from ethanol to give *ca.* 120 mg of arthraxin penta methyl ether as colorless needles.

*Luteolin (**3**) and Luteolin-7-glucoside (**4**)*: The identifications of these compounds were based on the agreement of the melting points, R_f values, and UV spectra with those of the luteolin[2-5] and luteolin-7-glucoside[5-7] isolated from *Arthraxon hispidus Makino*.

Arthraxin Penta Methyl Ether: Recrystallization from ethanol gave colorless needles; mp 204°C; λ_{max} (EtOH) 247, 266, and 338 mμ; ν_{max} (KBr) 2905, 1635, 1590, 1510, 1410, 1395, 1315, 1255, 1200, 1120, 1040, and 835 cm^{-1}. This substance was identified with arthraxin penta methyl ether by a mixed-melting-point determination and by co-chromatography on tlc with authentic sample[1] obtained from *Arthraxon hispidus Makino*.

*Miscanthus sinensis Anderss and Phragmites communis Trinius. Tricin (**5**)*: Recrystallization from ethanol-water gave yellow needles; mp 282°C; Mass (high-resolution mass spectrum): M 330.0730, Calcd for $C_{17}H_{14}O_7$, M 330.0739; λ_{max} (EtOH) 245 (inflection), 270, 350 mμ; λ_{max} (EtOH+NaOAc+H_3BO_3) 272, 355 mμ; λ_{max} (EtOH+$AlCl_3$) 280, 305, 370, and 395 mμ; λ_{max} (EtOH+NaOEt) 262, 325, and 415 mμ. These data are nearly equal to those reported for tricin.[9-11]

The authors wish to express their thanks to Mr. Kyuzaburo Furuhashi, Tokyo Kyoiku University, for the microanalyses and the NMR measurements; to Mr. Hidetora Okuyama for sending a sample of *Arthraxon hispidus Makino* collected on Hachijo Island; to Mr. Tomohiko Takahashi for sending some grass of *Miscanthus tinctorius Hackel* collected in Shiga Prefecture, and to Dr. Tsuguo Tateoka, National Science Museum, for giving an expert opinion on the grass of *Miscanthus tinctorius Hackel*.

9) Ref. 4, p. 114.
10) J. A. Anderson and A. G. Perkin, *J. Chem. Soc.*, **1931**, 2624.
11) W. S. Ferguson, DE B. Ashworth, and R. A. Terry, *Nature* **163**, 606 (1949).
12) J. B. Harborne, *Chem. Ind.*, (London) **1958**, 1950.

The Synthesis of Purine Nucleosides of L-Mycarose and L-Cladinose[1]

Shinkiti Koto, Shonosuke Zen, Satoshi Omura,* and Toju Hata*

School of Pharmaceutical Sciences, Kitasato University

** Kitasato Institute, Shirokane, Minato-ku, Tokyo*

(Received May 26, 1971)

Purine nucleosides of L-mycarose and L-cladinose, neutral branched-chain sugars of macrolide antibiotics, synthesized by a fusion method with the aid of dichloroacetic acid. The structure of these synthesized nucleosides was determined on the basis of the results of elemental analyses and the ultraviolet absorption and proton magnetic resonance spectra, as well as on the basis of the optical rotatory dispersion.

Since the first synthesis of cytotoxic nucleosides of branched-chain sugars by Walton *et al.*,[2] a number of synthetic studies of nucleosides of this class of sugars have been reported; some nucleosides exhibit considerable biological activity.[3] In the course of chemical studies of the macrolide antibiotics, the synthesis of purine nucleosides of the branched-chain sugar was carried out by the use of L-mycarose[4] and L-cladinose;[5] this was of chemical and biological interest. Recently, Howarth *et al.*[6] synthesized a purine nucleoside of arcanose.

As the base components, purine[7] and 6-chloropurine were used. The condensation of the above-mentioned dideoxy branched-chain sugars with these bases was performed by a fusion method,[8] using dichloroacetic acid[9] as the catalyst.

4-*O*-Isovaleryl-L-mycarose, obtained by an acid hydrolysis of leucomycin A_3,[10] was converted into 1-*O*-acetyl, 1-*O*-isovaleryl, and 1-*O*-*p*-nitrobenzoyl derivatives (I, II and III). In the case of the preparation of II, 1-*O*-isovaleryl derivatives of 4-*O*-*n*-butyryl and 4-*O*-acetyl-L-mycarose (II′ and II″), arising from the minor components[11] of the leucomycin complex were also isolated from the reaction mixture.

The fusion procedure was carried out by quickly heating a mixture of the appropriate 1-*O*-acyl derivative of L-mycarose, the base, and dichloroacetic acid at a moderately elevated temperature (95±3°C). 1,4-Di-*O*-Acetyl-L-cladinose was coupled with these bases in an essentially similar fashion. The amount of dichloroacetic acid used was relatively high in comparison with that of the ordinary fusion method.[8] Excess dichloroacetic acid seems to act excellently as a solvent to form a homogeneous melt or to aiding in the smooth mixing of the reaction mixture, even if it is somewhat heterogeneous. In the course of the reaction, the mixture was fused after heating for 1—2 min. A thin-layer chromatogram showed essentially a single spot with the exception of the remaining base, which was detectable under ultraviolet light. The yields of nucleosides were not substantially affected by changing the leaving group. In the coupling of the 1-*O*-nitrobenzoyl derivative of L-mycarose (III) and purine, the yield was slightly improved. In this fusion, *p*-nitrobenzoic acid was quickly deposited from the reaction mixture, thus making evacuation unnecessary, and the duration of the reaction was so diminished that an undesirable decomposition of labile branched chain sugar could

Compds.	R^1	R^2	R^3	R^4
I	Ac	H	Iv	—
II	Iv	H	Iv	—
II′	Iv	H	Bu	—
II″	Iv	H	Ac	—
III	PNB	H	Iv	—
IV	—	H	Iv	H
V	—	H	H	H
VI	—	H	Iv	Cl
VII	—	H	Bu	Cl
VIII	—	H	H	OCH_3
IX	—	CH_3	Ac	H
X	—	CH_3	H	H
XI	—	CH_3	Ac	Cl
XII	—	CH_3	H	OCH_3

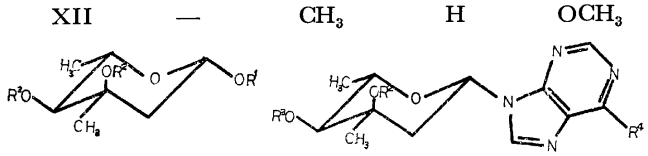

Ac= $-COCH_3$
Bu= $-COCH_2CH_2CH_3$
Iv= $-COCH_2CH(CH_3)_2$
PNB= $-COC_6H_4NO_2(p)$

Chart A

1) Presented at the 24th Annual Meeting of the Chemical Society of Japan, Osaka, April, 1971; Preprint, Vol. III (1971), p. 1838.

2) E. Walton, S. R. Jenkins, R. F. Nutt, M. Zimmerman, and F. W. Holly, *J. Amer. Chem. Soc.*, **88**, 4524 (1966).

3) T. Y. Shen, *Angew. Chem., internat. Edit.*, **9**, 678 (1970).

4) S. Omura, M. Katagiri, H. Ogura, and T. Hata, *Chem. Pharm. Bull.*, **15**, 1529 (1967); R. B. Woodward, *Angew. Chem.*, **69**, 50 (1957); R. Paul and S. Tchelitcheff, *Bull. Soc. Chim. Fr.*, **1957** 443; W. Hofheintz and H. Grisenbach, *Z. Naturforsch.*, **17b**, 852 (1962); R. B. Morin, M. Gorman, R. L. Hamil, and P. V. Vemarco, *Tetrahedron Lett.* **1970** 4737; A. K. Mallams, R. S. Jaret, and H. Reimann, *J. Amer. Chem. Soc.*, **91**, 7506 (1969).

5) P. F. Wiley, K. Gerzon, E. H. Flynn, M. V. Sigal, A. Weaver, V. C. Quark, R. R. Chautvett, and R. J. Monahan, *J. Amer. Chem. Soc.*, **79**, 6062 (1957).

6) G. B. Howarth, W. A. Szarek, and J. K. N. Jones, *J. Org. Chem.*, **34**, 476 (1969).

7) G. Nakamura, *J. Antibiotics*, **14A**, 94 (1961); K. Isono and S. Suzuki, *ibid.*, **13A**, 270 (1960).

8) W. Pigman, D. Horton, and A. Harp, "The Carbohydrates; Chemistry and Biochemistry," 2nd. ed., Academic Press, New York & London (1970), p. 9.

9) M. J. Robins and R. K. Robins, *J. Amer. Chem. Soc.*, **87**, 4934 (1965); F. Perini, F. A. Carey, and L. Long, Jr., *Carbohydrate Res.*, **11**, 159 (1969).

10) S. Omura, M. Katagiri, H. Ogura, and T. Hata, *Chem. Pharm. Bull.*, **16**, 1181 (1968).

11) S. Omura, M. Katagiri, and T. Hata, *J. Antibiotics*, **20**, 234 (1967); *ibid.*, **21**, 272 (1968).

be depressed.

In these fusion reactions, only the β-nucleosides were obtained as fine crystals and no significant formation of their α-anomer was observed. The anomeric configuration of synthetic nucleosides was confirmed by the measurements of their proton magnetic resonance spectra. All the synthesized nucleosides showed a quartet peak of the H-1′ proton, typical of axial anomeric the protons of 2-deoxy sugar, and a doublet of H-4′ with a large splitting constant, indicating the $\mathbf{C}_4^1$ conformation for the sugar moiety. It should be noted that 4′-*O*-isovaleryl derivatives of β-L-mycarosyl nucleoside (IV and VI) show a rather abnormal H-1′ quartet signal, indicating a slight deformation of their pyranosyl ring system. The removal of their isolvaleryl group made them again show the normal quartet pattern.

Table 1. PMR Spectral data (60 MHz)

Compds.	Solv.	(ppm) H-1 (H-1′)	(ppm) H-4 (H-4′)	J (Hz) $1,2_e$	J (Hz) $1,2_a$	J (Hz) 4,5
I	C^d	5.99	4.63	3.1	9.4	9.4
II	C^d	5.82	4.48	3.1	9.4	9.4
II′	C^d	5.83	4.48	2.9	9.1	9.4
II″	C^d	6.00	4.61	3.4	9.8	9.3
III	C^d	6.34	4.75	2.9	9.3	9.5
IV	C^d	6.36	4.88	5.7	8.1	9.8
V	W^d	6.17	3.27	2.7	11.2	9.4
VI	C^d	6.24	4.83	5.7	8.0	9.4
VII	C^d	6.26	4.83	6.9	8.2	9.3
VIII	W^d	6.13	3.33	3.2	10.8	9.6
IX	C^d	6.28	4.95	2.8	10.9	9.9
X	W^d	5.97	3.26	3.1	10.0	9.9
XI	C^d	6.24	4.92	3.1	11.0	10.0
XII	C^d	5.98	3.22	2.9	10.8	9.4

C^d=$CDCl_3$ (TMS, internal)
W^d=D_2O (TMS, external)

The assignment of the β-L-configuration described above was also supported by the optical rotatory dispersion data. All the dispersion patterns of synthetic nucleosides showed features opposite of those of a group of β-D-purine nucleosides.[12,13] In each case, a positive Cotton effect was observed.

The position of the *N*-glycosyl bond was assigned by measuring the ultraviolet absorption spectra.[13] The nucleosides of purine showed spectra similar to those of nebularine.[14] The spectra of the nucleosides of 6-chloropurine also indicated the *N*-9 substitution.[15]

The attempt to de-*O*-acylate the nucleosides of 6-chloropurine (VI and XI) without affecting the chloro group was unsuccessful. Treating them with dilute barium methoxide in methanol afforded corresponding 6-methoxyl derivatives (VIII and XII).

Experimental

Generally, the crude products obtained were purified by column chromatography on silica gel (20 weights of raw product), followed by the examination of each fraction by thin-layer chromatography. The organic layer was dried over sodium sulfate. After the removal of the salt, the solutions were concentrated below 40°C under reduced pressure, unless otherwise stated. Thin-layer chromatography was performed using Silica Gel G (Merck) as the adsorbent. The proton magnetic resonance spectra were measured with a Hitachi H-6013 and, in part, Varian, S-60A apparatuses. The optical rotatory dispersion was measured with a Nihon Bunko spectropolarimeter, Model ORD/UV-5, at 24—25°C.

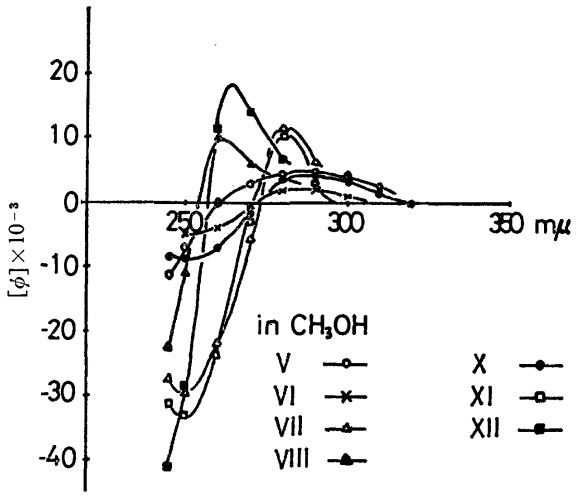

Chart B ORD Curves of Branched-chain Nucleosides

1-O-Acetyl-2,6-dideoxy-4-O-isovaleryl-3-C-methyl-β-L-ribo-hexopyranose (I). Acetic anhydride (3.0 ml) was added to a solution of crude 4-*O*-isovalery-L-mycarose[10] (carimbose) (0.32 g) in pyridine (1 ml). The solution was kept standing for 3 hr. Methanol (4 ml) was then added into the solution and the resulting mixture was kept standing at room temperature for 3 hr. It was concentrated below 55°C to afford a brown syrup (0.54 g), which was then subjected to column chromatography (benzene : 2-butanone=10 : 1). Five-gram fractions were collected. A combination of Fractions #4 and #5 afforded a syrup (0.27 g; 72%) which was then distilled to give an analytically pure acetate; mp 72—74°C, bp 133—135°C/0.01 mmHg, $[\alpha]_D^{25}-15°$ (*c* 1.1, chloroform). ν_{max}^{KBr} (cm^{-1}): 1761 (*O*-acetyl), 1738 (*O*-isovaleryl).

Found: C, 58.10; H, 8.56%. Calcd for $C_{14}H_{24}O_6$ (288.34): C, 58.32; H, 8.39%.

2,6-Dideoxy-1,4-di-O-isovaleryl-3-C-methyl-β-L-ribo-hexopyranose (II). Isovaleryl anhydride (3.3 ml) was added to a solution of crude 4-*O*-isovaleryl-L-mycarose[10] (4.0 g) in pyridine (40 ml), and the resulting mixture was left standing at room temperature for 18 hr. Additional anhydride (2 ml) was then added to the reaction mixture. After

12) T. R. Emerson, R. J. Swan, and T. L. V. Ulbrichit, *Biochem. Biophys. Res. Commun.*, **22**, 505 (1966); W. A. Klee and S. H. Mudd, *Biochemistry*, **6**, 988 (1967); T. Nishimura, B. Shimazu, and I. Iwai, *Biochem. Biophys. Acta*, **157**, 221 (1968); S. Rosenthal and L. (B.) Nguyen, *J. Org. Chem.*, **34**, 1029 (1969).

13) H. Iwamura and T. Hashizume, *J. Org. Chem.*, **33**, 1796 (1968).

14) G. B. Brown and V. S. Weliky, *J. Biol. Chem.*, **204**, 1019 (1953).

15) R. K. Robins, E. F. Godefroi, E. C. Taylor, L. R. Lewis, and A. Jackson, *J. Amer. Chem. Soc.*, **83**, 2574 (1961).

standing for a further 25 hr, methanol (20 ml) was stirred into the mixture under cooling. The solution was allowed to stand overnight and was then concentrated *in vacuo* at 65°C (oil pump), followed by repeated co-evaporation with toluene to give a brown residue with a disagreeable odor. This was fractionated on a silica-gel column (150 g; benzene : 2-butanone=20 : 1; 100 ml fractions). The third and fourth fractions afforded Compound II (2.8 g; 52%). A pure product was obtained by a high-vacuum distillation (79% recovery); bp 155—158°C/0.002 mmHg, n_D^{20} 1.4552, $[\alpha]_D^{23}$ −20° (*c* 4.1, chloroform). ν_{max}^{film} (cm^{-1}): 1735 (*O*-isovaleryl).

Found: C, 61.33; H, 9.02%. Calcd for $C_{17}H_{30}O_6$ (330.43): C, 61.80; H, 9.15%.

The fifth fraction gave crude 4-*O*-*n*-butyryl-2,6-dideoxy-1-*O*-isovaleryl-3-*C*-methyl-β-L-*ribo*-hexopyranose (II′) (1.0 g; 20%), which was purified by high-vacuum distillation; bp 140—145°C/0.06 mmHg, n_D^{20} 1.4543 $[\alpha]_D^{23}$ −29° (*c* 3.9, chloroform). ν_{max}^{film} (cm^{-1}): 1738 (ester).

Found: C, 60.49; H, 8.83%. Calcd for $C_{16}H_{28}O_6$ (316.40): C, 60.74; H, 8.92%.

The seventh fraction gave 0.20 g (4.3%) of 4-*O*-acetyl-2,6-dideoxy-1-*O*-isovaleryl-3-*C*-methyl-β-L-*ribo*-hexopyranose (II″); bp 125—130°C/0.002 mmHg. The proton magnetic resonance spectrum of this compound (in $CDCl_3$ with TMS) had a singlet peak at δ 2.05 attributable to acetoxymethyl.

*2,6-Dideoxy-4-*O*-isovaleryl-*C*-methyl-4-*O*-p-nitrobenzoyl-β-*L*-ribo-hexopyranose (III).* *p*-Nitrobenzoyl chloride (1.28 g) was added stirred into a solution of 4-*O*-isovaleryl-L-mycarose[10] (1.53 g) in pyridine (10 ml), and the resulting mixture was stirred at room temperature for 16 hr. The mixture was moistured with water (0.5 ml), agitated for a while, diluted with a mixture of dioxane (50 ml) and water (5 ml), and then concentrated at 45°C *in vacuo* to give a cake. This was dissolved in benzene (100 ml), and the solution was washed successively with aqueous sodium bicarbonate (1.3%) and water, dried, and evaporated to dryness to afford a syrup (2.42 g), which was then crystallized with isopropanol; yield, 0.58 g (24%); mp 110—112°C. The mother liquor gave a further crop. Recrystallization from isopropanol gave analytical sample. Mp 112.5—114.5°C, $[\alpha]_D^{25}$ −19° (*c* 0.64, chloroform). $\lambda_{max}^{methanol}$ 259 mμ (ε, 13.1×10^3). ν_{max}^{KBr} (cm^{-1}): 1737 (ester), 1607, 1526, 1350, 725 (*p*-nitrophenyl).

Found: C, 57.56; H, 6.38; N, 3.56%. Calcd for $C_{24}H_{25}NO_8$: (395.42); C, 57.71; H, 6.37; N, 3.54%.

*9-(2,6-Dideoxy-3-*C*-methyl-β-*L*-ribo-hexopyranosyl)-purine (V).*
*A. From the 1-*O*-Acetyl Derivative*: A mixture of I (0.27 g), purine (0.11 g), and dichloroacetic acid (0.14 ml) were heated at 99°C for 3 min while being stirred well. A water aspirator vacuum (25 mmHg) was then applied, and the melt was stirred for more 10 min at the same temperature. The resulting greenish melt was quickly cooled with cold water and dissolved in ethyl acetate (20 ml). The solution was washed successively with aqueous sodium bicarbonate (1.3%) and water, dried, and evaporated to dryness to furnish a brown glass (0.27 g), which was then fractionated on a silica-gel column (benzene : acetone= 2 : 1; 5 g fractions). The product (0.14 g, 38%) obtained from Fractions #6 to #9 was dissolved in cold methanol (40 ml), and then chilled methanolic barium methoxide (1N; 5.3 ml) was showly added into the solution. After standing for 48 hr, the solution was carefully bubbled with carbon dioxide, quickly concentrated below 20°C, and purified by means of a silica-gel column (4 g, benzene : acetone= 1 : 1) to give homogeneous glass, 0.090 g (36% from I). Crystallization with diethyl ether (mp 197—199°C (colored)) and subsequent recrystallization from 2-butanone afforded colorless prisms; mp 215—216°C, $[\alpha]_D^{24}$ −25° (*c* 3.3, water). λ_{max}^{water} 265.5 mμ (ε, 6.9×10^3), $\lambda_{max}^{ethanol}$ 262.5 mμ (ε, 7.2×10^3). ν_{max}^{KBr} (cm^{-1}): 1595, 1584, 1497 (purinyl).

Found: C, 54.10; H, 6.12; N, 20.87%. Calcd for $C_{12}H_{16}N_4O_3$ (264.29): C, 54.53; H, 6.10; N, 21.20%.

*B. From the 1-*O*-nitrobenzoyl Derivative*: A mixture of III (0.20 g), purine (0.062 g), and dichloroacetic acid (0.07 ml) was heated in a test tube on a boiling-water bath for 3 min while being efficiently mixed by means of a glass rod. Then, the dark-colored mixture was quickly cooled by cold water and taken up with ethyl acetate (20 ml). The solution was treated as has been described above to give 0.17 g of a crude condensation mixture, which was then subjected to silica-gel column chromatography (5 g, benzene : acetone=2 : 1; 5 g each). The Fractions #3—#5 afforded a homogeneous syrup (0.07 g), which was then de-*O*-isovalerated with methanolic barium methoxide and subsequently treated in the above-described manner to give pure glass (0.049 g; 37% from III). Crystallization and recrystallization were carried out as above. The mixed melting point of this compound with the product from I was not depressed. The IR of the two were superimposable.

Found: C, 54.30; H, 6.16; N, 20.91% Calcd for $C_{12}H_{16}N_4O_3$ (264.29): C, 54.53; H, 6.10; N, 21.20%

*6-Chloro-*O*-(4′-*O*-isovaleryl-2′,6′-dideoxy-3′-*C*-methyl-β-*L*-ribo-hexopyronosyl)-purine(VI).* *A. From the 1-*O*-Acetyl Derivative*: A mixture of I (0.23 g), 6-chloropurine (0.20 g), and dichloroacetic acid (0.12 ml) was heated for 4 min at 95°C while being stirred well; the resulting melt was then stirred for a further 5 min under reduced pressure (25 mmHg, water aspirator) at the same temperature. The reaction was quenced by cooling, and the dark-colored mixture was diluted with 20 ml of ethyl acetate. After the recovery of the unreacted 6-chloro-purine (0.06 g) by filtration, the solution was treated as has been described above and then concentrated to furnish a heavy syrup (0.35 g), which was subsequently fractionated by means of a silica-gel column (benzene: 2-butanone=3 : 1; 5 g each). From Fractions #4 and #5, the product was obtained in a glassy state; yield, 0.11 g (36%). Crystallization and recrystallization were carried out with diisopropyl ether; colorless granular crystals; mp 130—131°C, $[\alpha]_D^{20}$ −28° (*c* 1.0, chloroform). $\lambda_{max}^{ethanol}$ 264 mμ (ε, 9.1×10^3). ν_{max}^{KBr} (cm^{-1}): 1737 (*O*-isovaleryl); 1599, 1567, 1499 (purinyl).

Found: C, 53.13; H, 5.89; N, 14.89%. Calcd for $C_{17}H_{23}O_4N_4Cl$ (382.85): C, 53.33; H, 6.05; N, 14.63%.

*B. From the 1-*O*-Isovaleryl Derivative*: 6-Chloropurine (0.15 g) and dichloroacetic acid (0.10 ml) were heated at 95°C for 2 min while being efficiently stirred, and then the reaction system was connected to a water aspirator while stirring and heating were continued for 2 min at the same temperature. From the resulting mixture, Compound VI was obtained after the above-mentioned treatment; yield, 0.10 g (27%). A mixed melting-point determination with the Compound VI obtained from I was not depressed. The IR of the two samples were superimposable.

Found: C, 52.95; H, 6.01; N, 14.77%. Calcd for $C_{17}H_{23}N_4O_4Cl$ (382.85): C, 53.33; H, 6.05; N, 14.63%.

*C. From the 1-*O*-p-nitrobenzoyl Derivative*: A finely-divided IV (0.20 g) and 6-chloropurine (0.08 g) were mixed well with dichloroacetic acid (0.05 ml) in a test tube with the aid of a glass rod and then heated on a boiling-water bath for 2 min while being efficiently mixed. After the reaction had been quenched, the mixture was subjected to the same treatment as above. The titled compound, 0.06 g (31%), was thus obtained; its melting point was not depressed by ad-

mixture with that from I. The IR of the two were superimposable.

Found: C, 53.14; H, 6.08; N, 15.05%. Calcd for $C_{17}H_{23}N_4O_4Cl$ (382.85): C, 53.33; H, 6.05; N, 14.63%.

6-Chloro-O-(4'-O-n-butyryl-2',6'-dideoxy-3'-C-methyl-β-L-ribo-hexopyranosyl)-purine (VII). A mixture of III (0.295 g), pulverized 6-chloropurine (0.15 g), and dichloroacetic acid (0.10 m*l*) was heated at 95°C at atmospheric pressure for 3 min and then *in vacuo* (23 mmHg). The recovering of the unreacted 6-chloropurine and the extraction of the acidic substances were carried out as has been described in the case of VI. The crude product thus obtained was fractionated on a column of silica-gel (benzene : 2-butanone=10 : 1—3 : 1; gradient elution), having been cut into five-gram portions. The main oily product (0.094 g, 27%) thus obtained was crystallized by trituration with diisopropyl ether. Two recrystallizations from the same solvent gave a pure sample as colorless prisms; mp 144—145°C; $[\alpha]_D^{23}$ −10° (*c* 0.72, chloroform): $\lambda_{max}^{ethanol}$ 264 mμ (ε, 10.1×10^3). ν_{max}^{KBr} (cm^{-1}): 1740 (*O*-*n*-butyryl); 1598, 1561, 1497 (purynyl).

Found: C, 52.21; H, 5.91; N, 15.01%. Calcd for $C_{16}H_{21}N_4O_4Cl$ (368.83): C, 52.12; H, 5.74; N, 15.19%.

6-Methoxy-9-(2',6'-dideoxy-3'-C-methyl-β-L-ribo-hexopyranosyl)-purine (VIII). VI (84 mg) was dissolved in 0.1 N methanolic barium methoxide (10 m*l*), and the resulting mixture was kept standing at room temperature for 4 days. After the careful bubbling in of carbon dioxide, the reaction mixture was quickly concentrated below 20°C under reduced pressure to give a residue which was then passed through a silica-gel column (2 g). By elution with a mixture of benzene and acetone (1 : 1), a product was obtained as a homogeneous glass (42 mg, 65%); it was twice crystallized from a mixed solvent of benzene, acetone, and diisopropyl ether (2 : 1 : 2) to give colorless needles; mp 211—213°C, $[\alpha]_D^{23}$ −18° (*c* 1.0, methanol). $\lambda_{max}^{methanol}$ 249 mμ (ε, 11.5×10^3). ν_{max}^{KBr} (cm^{-1}): 1604, 1581 (purinyl).

Found: C, 53.05; H, 6.16; N, 19.04%. Calcd for $C_{13}H_{18}N_4O_4$ (294.31): C, 52.89; H, 6.22; N, 18.94%.

9-(2',6'-Dideoxy-3'-C-methyl-3'-O-methyl-β-L-ribo-hexopyranosyl)-purine (X). 1,4-Di-*O*-acetyl-β-L-cladinose[16] (0.26 g) was fused and, after quick cooling to room temperature, was well mixed with purine (0.12 g) with the aid of dichloroacetic acid (0.18 m*l*). The mixture was heated with stirring at 98°C for 5 min under atmospheric pressure and then for a further 5 min under reduced pressure (water aspirator). After the quenching of the reaction by cooling with cold water, the greenish-colored mixture was diluted with 30 m*l* of ethyl acetate. The solution was washed and concentrated as in the case of the preparation of VI to afford an oily product (0.297 g), which was fractionated by a silica-gel column (5 g). The column was eluted with a mixed solvent of benzene and acetone (2 : 1). Five-gram fractions were collected. Fractions #3—#6 gave a main product (0.17 g) whose proton magnetic resonance spectrum did not show the presence of the α-anomer. This product was dissolved in methanol (30 m*l*) and treated with 4 m*l* of methanolic 1 N barium methoxide, as has been described in the preparation of V, followed by a similar working-up; it was then passed through a silica-gel column (4 g; benzene : acetone=3 : 2) to afford a glass (0.099 g, 35%). Two crystallizations and recrystallization from diisopropyl ether afforded colorless prisms; mp 155—156°C, $[\alpha]_D^{27}$ −10° (*c* 2.5, water). λ_{max}^{water} 262.5 mμ (ε, 7.2×10^3), $\lambda_{max}^{ethanol}$ 262.5 mμ (ε, 7.1×10^3). ν_{max}^{KBr} (cm^{-1}): 1596, 1581, 1499 (purinyl).

Found: C, 55.90; H, 6.48; N, 19.89%. Calcd for $C_{13}H_{18}N_4O_3$ (278.31): C, 56.10; H, 6.52; N, 20.13%.

6-Chloro-9-(2',6'-dideoxy-3'-C-methyl-3'-O-methyl-4'-O-acetyl-β-L-ribo-hexopyranosyl)-purine (XI). A mixture of 1,4-di-*O*-acetyl-β-L-cladinose[16] (0.26 g), pulverized 6-chloropurine (0.20 g), and dichloroacetic acid (0.13 m*l*) was heated for 4 min at 92—95°C with stirring in an open system and then *in vacuo* (25 mmHg) for 5 min to give a colored mixture; this mixture gave 0.36 g of an oily product after cooling, extraction, and concentration. This was subjected to silica-gel column chromatography (10 g, benzene : 2-butanone=5 : 1; 5 g each). Fraction #3 and #4 gave 0.10 g (28%) of a glass; this glass was subsequently crystallized with diisopropyl ether; mp 126—127°C. Two recrystallizations from the same solvent gave colorless prisms; mp 133—134°C, $[\alpha]_D^{25}$ −26° (*c* 2.5, chloroform). $\lambda_{max}^{ethanol}$ 264 mμ (ε, 9.5×10^3). ν_{max}^{KBr} (cm^{-1}): 1731 (*O*-acetyl); 1590, 1564, 1487 (purinyl).

Found: 50.73; H, 5.57; N, 15.63%. Calcd for $C_{15}H_{19}N_4O_4Cl$ (354.80): C, 54.53; H, 6.54; N, 15.79%.

6-Methoxy-9-(2',6'-dideoxy-3'-C-methyl-3'-O-methyl-β-L-ribo-hexopyranosyl)-purine (XII). XI (61 mg) was treated with 0.1 N methanolic barium methoxide (9 m*l*) for 3 hr, followed by neutralization with carbon dioxide and purification by means of a silica-gel column (5 g; benzene : acetone=2 : 1), to afford a colorless glass (53 mg, quant.). Three crystallizations from diisopropyl ether gave long, colorless needles; mp 179—180°C, $[\alpha]_D^{23}$ −15° (*c* 1.9, methanol), $\lambda_{max}^{methanol}$ 249 mμ (ε, 11.6×10^3), ν_{max}^{KBr} (cm^{-1}): 1608, 1582 (purinyl).

Found: C, 54.54; H, 6.63; N, 18.32%. Calcd for $C_{14}H_{20}N_4O_4$ (308.34): C, 54.53; H, 6.54; N, 18.17%.

This work was supported in part by the Grants-in-aid for cancer research from the Ministry of Education.

The authors wish to thank Dr. Shinichi Kondo and Mr. Seiji Shibahara, Institute of Microbial Chemistry, for the measurements of proton magnetic resonance spectra. We are indebted to Mr. Kazuo Yago for technical assistance.

16) E. H. Flynn, M. V. Sigal, Jr., P. E. Wiley, and K. Gerzon, *J. Amer. Chem. Soc.*, **76**, 3121 (1954).

The Reaction of Diaryl Disulfides with the Cyanide Ion

Kazuhiko TANAKA, Jun-ichi HAYAMI, and Aritsune KAJI

Department of Chemistry, Faculty of Science, Kyoto University, Sakyo-ku, Kyoto

(Received June 8, 1971)

The reaction of symmetrical disulfides with the cyanide ion in various solvents has been investigated. The reaction modes may be summarized as follows: (1) Dialkyl disulfides and diaryl disulfides with electron-withdrawing substituents react with the cyanide ion in DMSO or DMF to give the corresponding monosulfides. (2) Diaryl disulfides with electron-donating substituents react with DMSO to yield aryl methyl sulfides. (3) Diaryl disulfides are cleaved by the cyanide ion into thiolate anions and aryl thiocyanates, which then react with alcohol to afford alkyl aryl sulfides.

The scission of the sulfur-sulfur bond takes place when the attacking nucloeophile has a greater affinity for sulfur than the displaced group. This affinity for sulfur is called "*S*-nucleophilicity" or "thiophilicity".[1] The reaction of unsymmetrical disulfide with various *S*-nucleophiles was studied in detail by Parker and Kharasch.[2] The results indicate that the more stable (less basic) thiolate anion is displaced; the order of thiophilicity is found to be as follows:

$$C_2H_5S^- > C_6H_5S^- > CN^- > SO_3^{2-} > DNPS^- > N_3^- > SCN^-$$

The cyanide ion is a typical anthioanion which has a great affinity for sulfur to form thioanion (the thiocyanate ion).[3] The unsymmetrical disulfides with electron-withdrawing substituents on the aromatic nucleus were cleaved by the cyanide ion to displace thiolate anions at room temperature in aqueous alcohol.[2] Braun *et al.* found that bis(dialkylthiocarbamoyl) disulfides and bis(alkylarylthiocarbamoyl) disulfides react with potassium cyanide to give the corresponding monosulfides.[4] The analogous desulfurization of disulfides has been reported for dixanthyl disulfides,[5] bis(2-benzothiazolyl) disulfide, and dithiodiglycolic acid;[6] however, diphenyl disulfide,[5] bis(*p*-tolyl) disulfide,[6] and dibenzyl disulfide[6] do not react with the cyanide ion. We have previously found that dibenzyl disulfide reacts with the cyanide ion in dipolar aprotic solvents.[7] Therefore, we investigated the reaction of symmetrical disulfides with the cyanide ion in various solvents. We can now classify these reactions into three modes as follows:

$$\text{Mode A:}\quad RS\text{-}SR + CN^- \xrightarrow{\text{DMSO or DMF}} RSR + SCN^- \qquad (1)$$

$$\text{Mode B:}\quad RS\text{-}SR + CN^- + DMSO \rightarrow RSCH_3 \qquad (2)$$

$$\text{Mode C:}\quad RS\text{-}SR + CN^- + R'OH \rightarrow RSR' + RS^- \qquad (3)$$

Results and Discussion

Reaction Mode A. It has been reported that dialkyl disulfide does not react with the cyanide ion in alcohol,[1] since the alkanethiolate anion is a more powerful *S*-nucleophile than is the cyanide ion—*i.e.*, the equilibrium shown in Equation (4) lies to the left:

$$RS\text{-}SR + CN^- \rightleftharpoons RS^- + RSCN \qquad (4)$$

$$RS^- + RSCN \rightarrow RSR + SCN^- \qquad (5)$$

Since the cyanide ion reacts 5×10^5 times faster with methyl iodide in a dipolar aprotic solvent than in a protic solvent,[8] dialkyl disulfide can be expected to be cleaved by the cyanide ion in a dipolar aprotic solvent. Thus, dibenzyl sulfide was isolated in a 58% yield in the reaction of dibenzyl disulfide with the cyanide ion at room temperature in DMSO (Eq. (5)). This result shows that the cyanide ion is a more powerful *S*-nucleophile than is the alkanethiolate anion in the dipolar aprotic solvent. In a similar way, sulfides were obtained from disulfides in fairly good yields. The results are given in Table 1. Bis(*p*-nitrophenyl) and bis(*o*-nitrophenyl) disulfides were easily cleaved by the cyanide ion and gave the corresponding monosulfides in 60% and 76% yields respectively, while bis(*m*-nitrophenyl) and bis(*p*-tolyl) disulfides were not desulfurized to sulfides on treatment with the cyanide ion in DMSO.

Reaction Mode B. Diaryl disulfides, which have electron-donating substituents, were rapidly cleaved by the cyanide ion at room temperature; however, the corresponding monosulfides were not obtained, as has been cited above. When mixtures of diphenyl disulfide and sodium cyanide in DMSO were refluxed for 6 hr, a transparent oil was obtained in a 52% yield. The NMR spectra in CCl_4 exhibited singlet peaks at τ 7.63 (3H, S–CH_3) and at τ 2.66 (5H, aromatic), and the IR spectrum was identical with that of authentic methyl phenyl sulfide. The reaction process can reasonably be explained as follows; diphenyl disulfide was cleaved by the cyanide ion into phenyl thiocyanate and the benzenethiolate anion. Phenyl thiocyanate then reacts with the cyanide ion to afford the benzenethiolate

1) A. J. Parker and N. Kharasch, *Chem. Rev.*, **59**, 583 (1959).
2) A. J. Parker and N. Kharasch, *J. Amer. Chem. Soc.*, **82**, 3071 (1960).
3) R. E. Davis, "Survey of Progress in Chemistry," Vol. 2, ed. by A. Scott, Academic Press, New York (1964), p. 189.
4) J. von Braun and F. Stechele, *Ber.*, **36**, 2275 (1903).
5) G. S. Whitby and H. Greenberg, *Trans. Roy. Soc. Can.*, III, **23**, 21 (1929); *Chem. Abstr.*, **24**, 593 (1930).
6) Y. Minoura, *Nippon Gomu Kyokai Shi*, **23**, 213 (1950).
7) A part of this work was presented at the 21st Annual Meeting of the Chemical Society of Japan, Osaka, April, 1968 (See Abstracts of papers of the Meeting, Vol. 3, p. 1568).
8) A. J. Parker, "Advances in Organic Chemistry *Methods and Results*," Vol. 5, ed. by R. A. Raphael, E. C. Taylor, and H. Wynberg, Interscience Publishers, New York, N. Y. (1965), p. 1.

Table 1. Desulfurization of disulfides with the cyanide ion

$$RS\text{-}SR + CN^- \rightarrow RSR + SCN^-$$

Disulfide R	Cyanide	Solvent	Reaction temp. (°C)	Reaction time (hr)	Monosulfide yield %
n-$CH_3CH_2CH_2$-(Ia)	NaCN	DMSO	80	15	61(Ib)
-$(CH_2)_4$-(IIa)	NaCN	DMF	80	2	43(IIb)
$C_6H_5CH_2$-(IIIa)	NaCN	DMSO	r.t.	72	58(IIIb)
$C_6H_5CH_2$-(IIIa)	NaCN	DMF	60	14	36(IIIb)
p-$CH_3C_6H_4$-(Va)	NaCN	DMSO	65	6	(73)[a](Va)
o-$NO_2C_6H_4$-(VIIa)	NaCN	DMSO	60	3	76(VIIb)
m-$NO_2C_6H_4$-(VIIIa)	NaCN	DMSO	60	3	(36)[a](VIIIa)
p-$NO_2C_6H_4$-(IXa)	NaCN	DMSO	60	3	60(IXb)
3-NO_2-4-ClC_6H_3-(XIa)	NaCN	DMSO	80	9	36(XIb)

a) Recovered disulfide.

Table 2. Formation of alkyl aryl sulfide in the reaction of disulfide with the cyanide ion in DMSO

$$RS\text{-}SR + DMSO \xrightarrow{CN^-} RSCH_3$$

Disulfide R	Cyanide	Reaction temp. (°C)	Reaction time (hr)	Yield of sulfide (%)
C_6H_5-(IVa)	NaCN (1 equiv.)	reflux	6	52(IVc)
C_6H_5-(IVa)	NaCN (2 equiv.)	reflux	6	66(IVc)
p-$CH_3C_6H_4$-(Va)	NaCN (1 equiv.)	reflux	6	63(Vc)

Table 3. Methylation of thiophenols and thiocyanates with DMSO in the presence of the cyanide ion

Starting material	Cyanide	Reaction temp. (°C)	Reaction time (hr)	Product (Yield %)
C_6H_5SH	NaCN (1 equiv.)	reflux	24	$C_6H_5SCH_3$(65)
o-$CH_3C_6H_4SH$	NaCN (1 equiv.)	reflux	19	o-$CH_3C_6H_4SCH_3$(73)
m-$CH_3C_6H_4SH$	NaCN (1 equiv.)	reflux	14	m-$CH_3C_6H_4SCH_3$(73)
p-$CH_3C_6H_4SH$	none	reflux	6	(p-$CH_3C_6H_4S$-)$_2$(86)
p-$CH_3C_6H_4SH$	NaCN (1 equiv.)	reflux	8	p-$CH_3C_6H_4SCH_3$(86)
p-$CH_3C_6H_4SH$	NaCN (1 equiv.)	reflux	24	p-$CH_3C_6H_4SCH_3$(92)
p-$CH_3C_6H_4SH$	NaCN (0.2 equiv.)	reflux	24	p-$CH_3C_6H_4SCH_3$(70)
p-$CH_3C_6H_4SH$	NaOH (1 equiv.)	reflux	7	p-$CH_3C_6H_4SCH_3$(74)
p-$CH_3C_6H_4SNa$	none	reflux	6	p-$CH_3C_6H_4SCH_3$(80)
p-$CH_3C_6H_4SH$	NaCN (1 equiv.)	170	6	p-$CH_3C_6H_4SC_2H_5$(46)[a]
C_6H_5SCN	NaCN (1 equiv.)	reflux	6	$C_6H_5SCH_3$(63)
p-$CH_3C_6H_4SCN$	NaCN (1 equiv.)	reflux	6	p-$CH_3C_6H_4SCH_3$(58)

a) Diethyl sulfoxide was used instead of DMSO.

anion and cyanogen:[9]

$$ArSCN + CN^- \rightarrow ArS^- + (CN)_2 \quad (6)$$

Thus, when mixtures of phenyl thiocyanate and sodium cyanide in DMSO were refluxed for 6 hr, methyl phenyl sulfide was isolated in a 63% yield. The above data show that the thiolate anion, once formed, should react with DMSO to give aryl methyl sulfide. Thus, sodium p-toluenethiolate was treated with DMSO to afford methyl p-tolyl sulfide in an 80% yield. The results are shown in Table 3. The reaction of the thiolate anion with DMSO would form the I adduct, which might then thermally rearrange to aryl methyl sulfide.

$$ArS^- + CH_3\text{-}\underset{\underset{O}{\downarrow}}{S}\text{-}CH_3 \rightarrow \left[Ar\text{-}\overset{\overset{CH_3}{|}}{\underset{\underset{CH_3}{|}}{S}}\text{-}O^- \right] \rightarrow Ar\text{-}S\text{-}CH_3 + [CH_3SO^-] \quad (7)$$

I

[10]

9) Cyanogen was hydrolyzed by introducing into an aqueous solution of sodium hydroxide and the resulting cyanate ion was detected by cobalt ion. See G. J. Jang, "Inorganic Syntheses," Vol. 5, p. 47 (1957); A. Scattergood, *ibid.*, Vol. 2, p. 89 (1946); W. T. Hall, "Analytical Chemistry," Vol. 1, p. 360 (1955).

10) Methanesulfenate anion was not isolated because of its facile disproportionation. See N. Kharasch, S. J. Potempa, and H. L. Wehrmeister, *Chem. Rev.*, **39**, 269 (1946); M. Chaykovsky and E. J. Corey, *J. Org. Chem.*, **28**, 254 (1963); C. Walling and L. Bollyky, *ibid.*, **28**, 256 (1963); D. R. Hogg and P. W. Vipond, *J. Chem. Soc., B*, **1970**, 1242; D. J. Pasto and C. R. Johnson, "Organic Structure Determination," Prentice-Hall, Canada (1969), p. 456.

TABLE 4. FORMATION OF ALKYL ARYL SULFIDE IN THE REACTION OF DISULFIDE WITH THE CYANIDE ION IN ALCOHOL

$$ArS\text{-}SAr + ROH \xrightarrow{CN^-} ArSR + HCN + OCN^-$$

Disulfide Ar	Cyanide	Alcohol	Reaction[a] time (hr)	Yield of sulfide (%)
C_6H_5-(IVa)	NaCN (2.7 equiv.)	CH_3OH	3	66(IVc)
p-$CH_3C_6H_4$-(Va)	NaCN (2.7 equiv.)	CH_3OH	3	67(Vc)
p-ClC_6H_4-(VIa)	NaCN (2.7 equiv.)	CH_3OH	3	60(VIc)
o-$NO_2C_6H_4$-(VIIa)	NaCN (2.7 equiv.)	CH_3OH	3	81(VIIc)
m-$NO_2C_6H_4$-(VIIIa)	NaCN (2.7 equiv.)	CH_3OH	3	81(VIIIc)
p-$NO_2C_6H_4$-(IXa)	NaCN (2.7 equiv.)	CH_3OH	3	79(IXc)
3-NO_2-4-ClC_6H_3-(XIa)	NaCN (1.2 equiv.)	CH_3OH	5	55(XIc)
2-Cl-5-$NO_2C_6H_3$-(XIIa)	KCN (2.5 equiv.)	CH_3OH	4	78(XIIc)
2-Cl-5-$NO_2C_6H_3$-(XIIa)	NaCN (1.7 equiv.)	C_2H_5OH	4	48(XIId)
2-Br-5-$NO_2C_6H_3$-(XIIIa)	NaCN (1.4 equiv.)	CH_3OH	2	55(XIIIc)

a) Refluxing in alcohol.

Although the mechanism of this novel reaction is not yet clear, the *S*-methylation of thiols with DMSO is a useful method for preparing aryl methyl sulfides.

Reaction Mode C. Parker and Kharasch isolated phenyl thiocyanate in the reaction of 2,4-dinitrophenyl phenyl disulfide with sodium cyanide in the presence of 2,4-dinitrochlorobenzene.[2] We found that symmetrical diaryl disulfides were rapidly cleaved by the cyanide ion under refluxing in methanol, and that aryl methyl sulfides were isolated in high yields, as is shown in Table 4. The reaction can be explained by considering the initial formation of *O*-alkyl *S*-aryl thioiminocarbonate (II) from aryl thiocyanate and alcohol.[11] The intermediate (II) is in turn decomposed into the thiolate anion and alkyl cyanate. The nucleophilic attack of the thiolate anion on alkyl cyanate gave alkyl aryl sulfide, with the elimination of the cyanate ion.

The mechanism of the addition of alcohol to thiocyanate in the presence of the cyanide ion and the decomposition of the resulting *O*-alkyl *S*-aryl thioiminocarbonate will be described in detail elsewhere.

Conclusion

The reaction of disulfides with the cyanide ion may be summarized as follows:

i) Dialkyl disulfides and diaryl disulfides with electron-withdrawing substituents in the *ortho*- and *para*-positions give the corresponding monosulfides in dipolar aprotic solvents.

ii) Diaryl disulfides with electron-donating substituents react with DMSO to afford aryl methyl sulfides.

iii) Diaryl disulfides react with alcohol to give alkyl aryl sulfides.

Experimental

The melting points were determined on a hot-stage apparatus and were uncorrected. The NMR spectra were obtained in carbon tetrachloride with a JEOLCO 3H-60 spectrometer against internal TMS. The IR spectra were recorded with JASCO IR-S and DS-402G spectrophotometers, and glc was carried out using a Yanagimoto GCG-5DH gaschromatograph (Silicone DC-550, 3 m).

Material. The disulfides were prepared as has been described in the literature. The physical constants and the results of the elemental analysis of disulfides are listed in Table 5.

TABLE 5. MELTING POINTS AND ANALYTICAL DATA OF DISULFIDES

Disulfide	Mp °C (lit.)	Analysis Found (Calcd) C%	H%	S%
IIIa	69—70 (71[12])	68.31 (68.25)	5.72 (5.73)	25.92 (26.03)
IVa	59.1—60 (62.5—63.5[13])	65.94 (66.01)	4.54 (4.62)	29.30 (29.37)
Va	43.5—44 (48—49[13])	68.49 (68.25)	5.51 (5.73)	25.97 (26.03)
VIIa	198.5—200.5 (195[14])	46.82 (46.72)	2.49 (2.61)	20.88 (20.80)
VIIIa	82—83 (82—83[15])	46.50 (46.74)	2.43 (2.61)	20.93 (20.80)
IXa	186—188 (181[16])	46.89 (46.74)	2.67 (2.61)	20.55 (20.80)
Xa	212—213 (212.8[17])	38.47 (38.21)	1.90 (1.60)	16.99 (17.00)
XIa	115.5—116.5 (116—117[18])	37.96 (38.21)	1.57 (1.60)	17.10 (17.00)
XIIa	145—147 (143—143.5[18])	38.19 (38.21)	1.39 (1.60)	17.09 (17.00)
XIIIa	159—161	30.74 (30.92)	1.49 (1.30)	13.94 (13.76)

Xa: 2-NO_2-4-ClC_6H_3-

11) K. Tanaka, J. Hayami, and A. Kaji, This Bulletin, **44**, 2815 (1971).

12) Y. Minoura, *Nippon Kagaku Zasshi*, **73**, 131 (1952).

13) E. Campaigne, J. Tsurugi, and W. W. Meyer, *J. Org. Chem.*, **26**, 2486 (1961).

14) M. T. Bogert and A. Stull, "Organic Syntheses," Coll. Vol. I, p. 220 (1956).

15) W. A. Sheppard, *ibid.*, Vol. 40, p. 80 (1960).

16) Th. Zincke and S. Lenhardt, *Ann. Chem.*, **400**, 2 (1913).

17) J. N. Elgersma, *Rec. Trav. Chim. Pays-Bas*, **48**, 752 (1929).

18) V. O. Lukashevich, *Dokl. Akad. Nauk SSSR*, **103**, 627 (1955); *Chem. Abstr.*, **50**, 5557a (1956).

Reaction Mode A. General Procedure: Disulfide (0.05 mol) was dissolved in dry DMSO (100 m*l*) or dry DMF (100 m*l*) under stirring, and then powdered sodium cyanide (0.051 mol) was added. After a definite period (see Table 1), the colored solution (red to yellow) was poured into ice-cooled water. The resulting monosulfide was filtered (if solid), dried *in vacuo*, and then recrystallized. If the monosulfide was a liquid, the organic layer was extracted with ether three times, washed with water, and dried with anhydrous sodium sulfate. Distillation gave monosulfide as a transparent liquid. The physical data and the results of the analysis of the monosulfide which was formed by desulfurization are given in Table 6.

Table 6. Melting points and analytical data of monosulfides

Monosulfide	Mp °C (lit.)	Analysis Found (Calcd) C%	H%	S%
IIIb	46.5—47.5 (48.5[12])	78.72 (78.45)	6.60 (6.58)	14.68 (14.96)
VIIb	122—124 (122—123[19])	52.20 (52.17)	3.20 (2.92)	11.35 (11.61)
IXb	162.5—163.5 (160—161[20])	51.87 (52.17)	2.83 (2.92)	11.55 (11.61)
Xb	156.5—158.0 (149—150[21])	41.84 (41.76)	1.96 (1.75)	9.47 (9.29)

Reaction Mode B. General Procedure: A mixture of disulfide and sodium cyanide in DMSO was refluxed for 6 hr. After being cooled to room temperature, the reaction mixture was steam-distilled. The organic layer was extracted with *n*-hexane four times, washed with water, and then dried over anhydrous sodium sulfate. The evaporation of the solvent gave an oil, which was then distilled *in vacuo*. Methyl phenyl sulfide, by 86—87.5°C/20 mmHg (lit,[13] bp 84°C/18 mmHg); methyl *p*-tolyl sulfide, bp 100.8—103°C/19 mmHg (lit,[13] bp 104—105°C/20 mmHg). The NMR and IR spectra and the glc retention time of aryl methyl sulfide were identical with those of authentic samples.

19) R. Nietzki and H. Bothof, *Ber.*, **29**, 2774 (1896).
20) C. C. Price and G. W. Stacy, "Organic Syntheses," Coll. Vol. III, p. 667 (1955).
21) F. Beilstein and A. Kurbatow, *Ann. Chem.*, **197**, 75 (1879).

Table 7. Melting points and NMR data of alkyl aryl sulfides

Alkyl aryl sulfide	Mp °C or bp °C/mmHg (lit.)	τ(*S*-Alkyl)
$C_6H_5SCH_3$ (IVc)	90/22 (84/18[13])	7.63(3H, s)
p-$CH_3C_6H_4SCH_3$ (Vc)	105—106/23 (104—105/20[13])	7.65(3H, s)
p-$CH_3C_6H_4SC_2H_5$ (Vd)	114—117/27 (122—125/20[22])	7.20(2H, q) 8.76(3H, t)
p-$ClC_6H_4SCH_3$ (VIc)	120/23 (170—108/15[23])	7.64(3H, s)
o-$NO_2C_6H_4SCH_3$ (VIIc)	59—60 (60—61[11])	7.53(3H, s)
m-$NO_2C_6H_4SCH_3$ (VIIIc)	125/3 (119—124/1.5[24])	7.44(3H, s)
p-$NO_2C_6H_4SCH_3$ (IXc)	69—70 (69—70[11])	7.45(3H, s)
3-NO_2-4-$ClC_6H_3SCH_3$ (XIc)	70—71.5 (70—72[25])	7.47(3H, s)
2-Cl-5-$NO_2C_6H_3SCH_3$ (XIIc)	98—99[a]	7.47(3H, s)
2-Cl-5-$NO_2C_6H_3SC_2H_5$ (XIId)	68—69.5[b]	6.94(2H, q) 8.54(3H, t)
2-Br-5-$NO_2C_6H_3SCH_3$ (XIIIc)	145—146[c]	7.42(3H, s)

a) Found: C, 41.19; H, 2.90; S, 15.76%. Calcd for $C_7H_6ClNO_2S$: C, 41.28; H, 2.97; S, 15.74%.
b) Found: C, 44.24; H, 3.71; S, 14.62%. Calcd for $C_8H_8ClNO_2S$: C, 44.14; H, 3.70; S, 14.73%.
c) Found: C, 33.83; H, 2.38; S, 13.05%. Calcd. for $C_7H_6BrNO_2S$: C, 33.89; H, 2.44; S, 12.92%.

Reaction Mode C. General Procedure: A mixture of disulfide and sodium cyanide in alcohol was refluxed under stirring. The solvent was evaporated under reduced pressure, and the residue was crystallized or distilled. The physical constants and NMR data of alkyl aryl sulfides are reported in Table 7.

22) H. Gilman and N. J. Beaber, *J. Amer. Chem. Soc.*, **47**, 1449 (1925).
23) J. van der Veen and W. Stevens, *Rec. Trav. Chim. Pays-Bas*, **82**, 287 (1963).
24) A. H. Goldkamp, *J. Org. Chem.*, **34**, 1780 (1969).
25) R. C. Elderfield and F. W. Short, *J. Org. Chem.*, **17**, 758 (1952).

The Reactions of Metal Acetylacetonates and Related Compounds with 2,2-Diphenyl-1-picrylhydrazyl[1)]

Kaku UEHARA, Kiyohiro KAMEI, Makoto TANAKA, and Niro MURATA

Department of Applied Chemistry, College of Engineering, University of Osaka Prefecture: Sakai-shi, Osaka

(Received June 18, 1971)

Some metal acetylacetonates ($M(acac)_n$) were observed to react with the stable free radical 2,2-diphenyl-1-picrylhydrazyl (DPPH) in organic solvents. For the reaction of cupric 3-α-butenylacetylacetonate with DPPH in benzene and cyclohexane, the following rate equation was obtained: $R=k$[cupric chelate][DPPH]. The activation parameters of the reaction were remarkably dependent upon the nature of the substituent and the metal atom in $M(acac)_n$, and upon the solvent. The results of the kinetic studies and the analytical work suggested that $M(acac)_n$ reacted with DPPH to yield 2,2-diphenyl-1-picrylhydrazine (DPPH-H) *via* the reduction of the central metal of the $M(acac)_n$.

In a previous communication,[2)] it was reported that some metal acetylacetonates (M (acac)$_n$) reacted easily with 2,2-diphenyl-1-picrylhydrazyl (DPPH). The reaction will be described in more detail in this paper.

Although DPPH has been known as an efficient radical scavenger, it reacts with species other than radicals. For example, DPPH reacts with compounds having a labile hydrogen atom to produce a radical by the abstraction of the hydrogen atom.[3–13)] Furthermore, DPPH also reacts with some metal salts to form redox systems or complexes.[14–18)]

On the other hand, some $M(acac)_n$ are effective initiators of the radical polymerization of vinyl monomers.[19–22)] To elucidate the reaction mechanism of $M(acac)_n$ with DPPH, we carried out kinetic studies and a determination of the products.

Experimental

Materials. The cupric 3-alkylacetylacetonates were prepared from an aqueous solution of cupric acetate and an ethanol solution of 3-alkylacetylacetone which has been synthesized from sodium salt of acetylacetone and alkyl bromide in the manner reported by Morgan and Martin.[23,24)] The 3-α-butenylacetylacetone and other 3-α-alkenylacetylacetones were synthesized by the condensation of acetylacetone with *n*-butyraldehyde or other aldehydes in the presence of piperidine, according to the method shown in preceding papers.[21,25)] Their cupric chelates were prepared from an aqueous solution of cupric acetate and an ethanol solution of 3-alkenylacetylacetone. The $Cu(acac)_2$, $Fe(acac)_3$, $Mn(acac)_3$, $Co(acac)_3$, $Zn(acac)_2$, $Al(acac)_3$, and $Cr(acac)_3$ were G.R.-grade reagents and were used without further purification. A G.R.-grade sample of DPPH was recrystallized from benzene-ligroin; mp 137—138°C. The solvents were purified by the ordinary method and were distilled before use.

Apparatus and Procedure. The reaction was followed by photometric measurements of the DPPH concentration using a Hitachi recording spectrophotometer, Model EPS-3T. For the reaction in air at atmospheric pressure, aliquots of the reaction mixture were pipetted out at regular intervals from the stock solution in a test tube thermostatted at 25°C. The absorbance of this solution at 525 mμ (in benzene) was measured. For the reaction under a vacuum (10^{-5} mmHg), the following procedure was employed throughout this investigation. The reaction mixture was degassed by the use of the H-shaped tube illustrated in Fig. 1 because the conventional freeze-thaw cycle was unsuitable for this study, as will be described in the next paper.[26)] The solution of $M(acac)_n$ in A and the solution of DPPH in B were simultaneously frozen in liquid nitrogen, and the H-tube was joined to a high-vacuum line after the tube has been sealed at the (a) neck. Each solution was out-gassed by three freeze-thaw cycles under 10^{-5} mmHg, and then the H-tube was sealed at the (b) neck and separated from the vacuum line. The solutions in A and B were mixed thoroughly, and the resulting solution was transferred to the C section. The quartz cell, C, was immediately sealed at the (c) neck

1) paper XIV in a series of "Catalytic Behavior of Metal Chelate Compounds".

2) K. Uehara, M. Tanaka, and N. Murata, This Bulletin, **41**, 3034 (1968).

3) K. E. Russell, *J. Phys. Chem.*, **58**, 437 (1954).

4) E. A. Braude, A. G. Brook, and R. P. Linstead, *J. Chem. Soc.*, **1954**, 3574.

5) J. C. Bevington, *ibid.*, **1956**, 1127.

6) J. E. Hazell and K. E. Russell, *Can. J. Chem.*, **36**, 1729 (1958).

7) J. C. McGowan, T. Powell, and R. Raw, *J. Chem. Soc.*, **1959**, 3103.

8) J. C. Hogg, D. H. Lohman, and K. E. Russell, *Can. J. Chem.*, **39**, 1588 (1961).

9) R. A. Bird, G. A. Harpell, and K. E. Russell, *ibid.*, **40**, 701 (1962).

10) P. J. Proll and L. H. Sutcliff, *Trans. Faraday Soc.*, **59**, 2090 (1962).

11) P. B. Ayscough and K. E. Russell, *Can. J. Chem.*, **43**, 3039 (1965).

12) S. Singh, K. R. Bhaskar, and C. N. R. Rao, *ibid.*, **44**, 2657 (1966).

13) P. B. Ayscough and K. E. Russell, *ibid.*, **45**, 3019 (1967).

14) L. H. Sutcliffe and J. Walkley, *Nature*, **178**, 999 (1956).

15) C. E. H. Bawn and D. Verdin, *Trans. Faraday Soc.*, **56**, 519 (1960).

16) R. I. Zusman, *Kinet. Katal.*, **7**, 414 (1966).

17) V. V. Voevodskii, R. I. Zusman, G. I. Shamovskaya, and Yu. N. Molin, *Izv. Sib. Otd. Akad. Nauk SSSR, Ser. Khim. Nauk*, **1968**, 127. (*Chem. Abstr.*, **70**, 41190 (1969)).

18) H. Imai, Y. Ono, and T. Keii, *J. Phys. Chem.*, **72**, 46 (1968).

19) E. G. Kastning, H. Naarmann, H. Reis, and C. H. Berding, *Angew. Chem.*, **77**, 313 (1965).

20) C. H. Bamford and D. J. Lind, *Chem. Ind.* (London), **1965**, 1627.

21) K. Uehara, T. Matsumura, T. Nishi, F. Tamura, and N. Murata, *Kogyo Kagaku Zasshi*, **69**, 2027 (1966).

22) T. Otsu, N. Minamii, and Y. Nishikawa, *J. Makromol. Sci-Chem.*, **A2**, 905 (1968).

23) G. T. Morgan and A. E. Rawson, *J. Soc. Chem. Ind.*, **44**, 462 (1925). (*Chem. Abstr.*, **20**, 192 (1926)).

24) D. F. Martin, W. C. Fernelius, and M. Shamma, *J. Amer. Chem. Soc.*, **81**, 130 (1959).

25) K. Uehara, T. Matsumura, Y. Murata, M. Tanaka, and N. Murata, *Kogyo Kagaku Zasshi*, **72**, 1825 (1969).

26) K. Uehara, K. Kamei, M. Tanaka, and N. Murata, This Bulletin, *in press*.

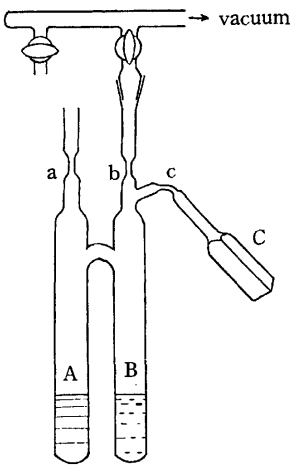

Fig. 1. Schematic drawing of the apparatus.

and separated from the H-tube. It was placed in the cell holder thermostatted at the desired temperature, and the optical density at 525 mμ was measured continuously.

The infrared spectra of the reaction products were measured on KBr disks by means of a Hitachi Model EPI-S2 infrared spectrometer. The mass spectra were recorded on a Hitachi Model RMU-6E mass spectrometer under the following conditions: ionization energy, 15 eV; total emission current, 80 μA; vacuum, 2×10^{-6} mmHg; sample temp., 250°C. The ESR spectra of cupric chelate in the presence of DPPH were measured by means of a Hitachi Model MES-4001 ESR spectrometer.

The isolation of products from the reaction mixture was carried out in the following way. Cupric 3-α-butenylacetylacetonate 1.2 g (0.0033 mol) was allowed to react with DPPH 0.87 g (0.0022 mol) in benzene under a vacuum for 48 hr. After the evaporation of the benzene, the cupric ion and 3-α-butenylacetylacetone were separated by twice extracting the resulting reaction mixture with 200 ml of disodium ethylenediaminetetraacetate (EDTA-2Na) on a hot plate. The residue after the extraction was a viscous brownish-red oil. By the recrystallization of the residue from methanol-water, an orange-brown powder (P) was obtained.

Results and Discussion

Most of the present studies were performed on cupric 3-α-butenylacetylacetonate because it has an appreciable solubility in nonpolar solvents and a high reactivity toward DPPH. Furthermore, this chelate is easily made and has been fairly well studied in our preceding papers.[25,27]

The effects of oxygen on the reaction of cupric 3-α-butenylacetylacetonate with DPPH in benzene are summarized in Table 1. The rate of the reaction

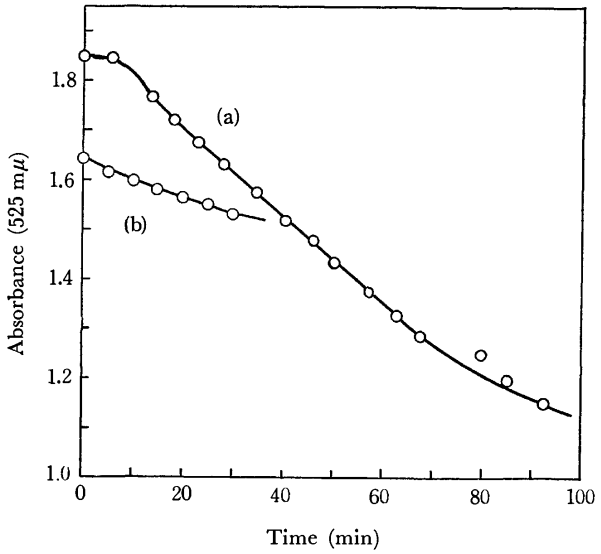

Fig. 2. The change of absorbance in the reaction of cupric 3-α-butenylacetylacetonate with DPPH at 25°C.
(a) in air, [cupric chelate] = 1.40×10^{-4} mol/l
[DPPH] = 1.85×10^{-4} mol/l
(b) *in vacuo*, [cupric chelate] = 4.68×10^{-4} mol/l
[DPPH] = 1.64×10^{-4} mol/l

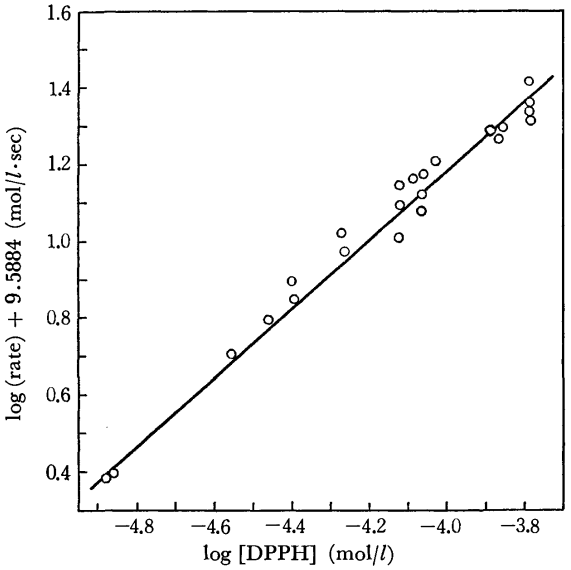

Fig. 3. Plot of log (rate) *versus* log [DPPH].
[Cu(3-α-butenyl-acac)$_2$] = 4.68×10^{-4} mol/l, 25°C.

in atmospheric air was about 10 times that *in vacuo* (10^{-5} mmHg). Fig. 2 shows examples of the time-conversion relation for this reaction. A sigmoid curve was obtained in atmospheric air. The ap-

Table 1. The effects of air on the reaction of cupric 3-α-butenylacetylacetonate with DPPH
(At 25°C, in benzene, [DPPH] = 1.4×10^{-4} mol/l)

Atmosphere	[Cupric chelate] $\times10^4$ mol/l	Rate $\times10^8$ mol/l·sec	Activation energy kcal/mol	Kintic order DPPH	Cu
Vacuo (10^{-5} mmHg)	2.31	0.20	9.2	0.9	1.0
Air	1.40	1.47	11.1	1.6	1.4

27) K. Uehara, Y. Kataoka, K. Kamei, M. Tanaka, and N. Murata, *Kogyo Kagaku Zasshi*, **72**, 1831 (1969).

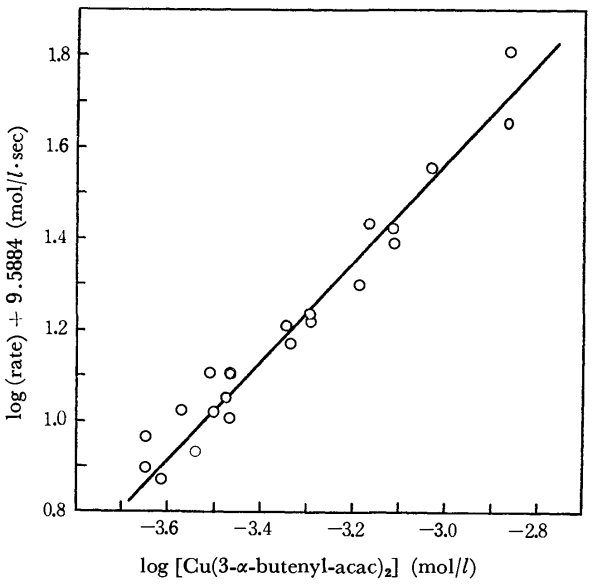

Fig. 4. Plot of log (rate) *versus* log [Cu(3-α-butenyl-acac)$_2$] at 25°C.
[DPPH] $=5.85\times10^{-5}$ mol/*l*

parent activation energy for the reaction was 9.2 kcal/mol *in vacuo* and 11.1 kcal/mol in atmospheric air. The relationships between the reaction rates and the initial concentrations of DPPH for a constant initial cupric chelate concentration *in vacuo* are shown in Fig. 3, from which the rate is found to increase with a 0.9 power[28] of the DPPH concentration. The dependencies of the rate of the reaction *in vacuo* on the concentration of the cupric chelate are shown in Fig. 4, from which the reaction rate is found to be first order with respect to the cupric chelate. In atmospheric air, the rate of the reaction (estimated from the portion of the initial straight line of the sigmoid curve) depended on the 1.4 power of the cupric chelate concentration and the 1.6 power of DPPH. These effects of air suggested that, in atmospheric air, oxygen virtually takes part in the reaction and complicates it. Therefore, to exclude the effect of oxygen, all subsequent experiments were carried out *in vacuo* (10^{-5} mmHg).

The solvent effects on this reaction are summarized in Table 2. In a few solvents the maxima of the absorption spectra of DPPH shifted to shorter wavelengths in the following order: benzene (525 mμ), dioxane (520 mμ), cyclohexane (513 mμ). It was found that the rate of the reaction in these solvents increased with a decrease in the λ_{max} of DPPH. The complex formation of DPPH with several solvents has been confirmed by means of elemental analysis[29] or X-ray diffraction data.[30] Recently, some investigators have reported that the formation of a charge-transfer complex between DPPH and benzene or dioxane was observed from the ESR spectra.[31,32] The solvent effect in the present reaction may be related in some way to the complex formation with these solvents.

Table 2. Solvent effects of the reaction of cupric 3-α-butenylacetylacetonate with DPPH
(*In vacuo*, [cupric chelate] $=4.68\times10^{-4}$ mol/*l*, [DPPH] $=0.545\times10^{-4}$ mol/*l*)

Solvent	Rate at 25°C mol/*l*·sec	Activation energy kcal/mol	Frequency factor *l*/mol·sec	λ_{max} of DPPH mμ	Kinetic order DPPH	Kinetic order Cu
Benzene	3.2×10^{-9}	9.2	7.0×10^{5}	525	0.9	1.0
Dioxane	6.4×10^{-9}	9.8	3.8×10^{6}	520	—	—
Cyclohexane	8.8×10^{-9}	10.6	2.0×10^{7}	513	1.0	1.0

Table 3. Effects of substituents on the reaction of DPPH with Cu(3-R-acac)$_2$ in benzene
([DPPH] $=0.545\times10^{-4}$ mol/*l*, [Cu(3-R-acac)$_2$] $=4.68\times10^{-4}$ mol/*l*)

No	R	Rate at 25°C mol/*l*·sec	Activation energy kcal/mol	Frequency factor *l*/mol·sec	Decomposition rate of the chelate in the polymerization of styrene at 70°C mol/*l*·sec
I	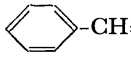	1.4×10^{-8}	9.0	2.2×10^{6}	3.3×10^{-7}
II	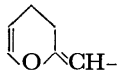	2.7×10^{-9}	—	—	—
III	$CH_3CH=CH-$	3.3×10^{-9}	8.9	4.3×10^{5}	—
IV	$EtCH=CH-$	3.1×10^{-9}	9.2	6.9×10^{5}	2.4×10^{-8}
V	CH_3-	1.0×10^{-11}	21.8	4.9×10^{12}	1.9×10^{-9}
VI	H-	$<10^{-11}$	—	—	—

28) The 0.6 power of the DPPH concentration in the preceding communication[2] is a typographical error and must be corrected to a 0.9 power.
29) J. A. Lyons, W. F. Watson, *J. Polym. Sci.*, **18**, 141 (1955).
30) D. E. Williams, *J. Amer. Chem. Soc.*, **88**, 5665 (1966), *ibid.*, **89**, 4280 (1967).
31) R. Z. Sagdeev, *Zh. Strukt. Khim.*, **7**, 38 (1966). (*Chem. Abstr.*, **64**, 18733 (1966)).
32) Yu. M. Ryzhmanov and A. A. Egorova, *Dokl. Akad. Nauk SSSR*, **191**, 148 (1970). (*Chem. Abstr.*, **73**, 20337 (1970)).

While the activation energies of this reaction increase in the order: benzene<dioxane<cyclohexane, the frequency factors markedly increase in the same order. The net reaction rates observed reflect the fact that the unfavorable activation energies are more than compensated for by the higher frequency factors.

First-order kinetics for each reactant were observed in benzene and cyclohexane. Sutcliffe and Walkly[14] have also pointed out that the redox reaction of metal acetate with DPPH in acetic acid gives first-order kinetics for each reactant and that the rate is reduced by the addition of benzene.

The effects of the replacement of the hydrogen atom in the 3-position of acetylacetone are shown in Table 3. The styryl derivative, I, showing the largest rate among the derivatives studied here had the same activation energy as III or IV, but a much higher frequency factor. It has been reported that the type of substituent markedly affects the frequency factor rather than the activation energy in the radical polymerization of styrene.[25,33]

The effects of metal atoms of metal acetylacetonates on the reaction rate are shown in Table 4. The order of the reactivity of $M(acac)_n$ was as follows:

Mn(III)>Fe(III)>Zn(II)>Co(III)>Cu(II),
Al(III), Cr(III)

The observed reactivity order of $M(acac)_n$ was independent of their stability constants (in water) and of the ionization potentials or electronegativities of their central metals, as was pointed out in connection with the radical polymerization initiated by $M(acac)_n$.[22] The Mn(III) chelate was most reactive toward DPPH, which is in agreement with the activity in the radical polymerization of styrene[19] and methyl methacrylate.[22] On the other hand, the Co(III) chelate, which has a fairly high activity for the radical polymerization, was less reactive to DPPH. The lower reaction rate of $Co(acac)_3$ is attributable to its lower frequency factor.

Table 4. The reaction of DPPH with $M(acac)_n$ in benzene
([DPPH]$=0.545\times10^{-4}$ mol/l, [$M(acac)_n$]$=4.68\times10^{-4}$ mol/l)

$M(acac)_n$	Rete at 25°C mol/l·sec	Activation energy kcal/mol	Frequency factor l/mol·sec
$Mn(acac)_3$	9.8×10^{-10}	8.6	9.8×10^{4}
$Fe(acac)_3$	2.2×10^{-10}	15.3	1.4×10^{9}
$Zn(acac)_2$	1.9×10^{-10}	13.0	2.6×10^{7}
$Co(acac)_3$	0.9×10^{-10}	6.5	2.1×10^{2}
$Cu(acac)_2$	$<10^{-11}$	—	—
$Al(acac)_3$	$<10^{-11}$	—	—
$Cr(acac)_3$	$<10^{-11}$	—	—

The effects of solvents, substituents, and central metals showed that the reactivity of $M(acac)_n$ toward DPPH could not be explained only by the activation energy. The difference between the frequency factors, especially the low frequency factor, is noteworthy.

The ESR spectra of cupric 3-α-butenylacetylacetonate in benzene in the presence of DPPH are shown in Fig. 5. The reduction of the central metal, Cu(II)→Cu(I), is established from the decrease in the intensity of the ESR spectra of Cu(II) with the time.

In order to identify the reaction product (P) isolated

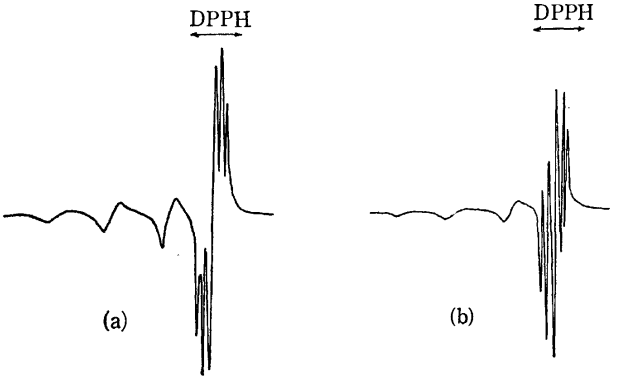

Fig. 5. ESR spectra of $Cu(3\text{-}\alpha\text{-butenyl-acac})_2$ in benzene in the presence of DPPH at room temperature.
(a) $t=0$ min (b) $t=60$ min

by the way described in the Experimental section, the following analyses were carried out. The infrared and ultraviolet absorption spectra of the product (P) agreed with those of an authentic sample of 2,2-diphenyl-1-picrylhydrazine(DPPH-H). The mass spectrum of (P) was closely analogous to that of DPPH-H. It showed the base peak at *m/e* 168 corresponding to that of $(Ar\text{-}NH\text{-}Ar)^+$, *m/e* 212 $(picryl)^+$ and *m/e* 227 $(picryl\text{-}NH)^+$. The value of the elemental analysis of this product also agreed with that of DPPH-H. Found: C, 54.70; H, 3.28; N, 17.28%. Calcd for $C_{18}H_{13}O_6N_5$: C, 54.68; H, 3.28; N, 17.71%.

Cupric 3-α-butenylacetylacetonate has two kinds of labile hydrogen atoms (H^a, H^b). In order to investigate which kind of hydrogen atom takes part in the reaction, the reaction rate of the styryl derivative I, which has no labile H^a was compared with that of the butenyl derivative IV (Table 3). The I derivative showed a higher reactivity than the IV derivative toward DPPH, and the product in this reaction was also DPPH-H. This fact suggests that H^a does not take part in the reaction. Gritter and Ratmore[34] have shown in a study of the site of attack with a *t*-butoxy radical,[34] that a hydrogen atom is abstracted from the 1-position of metal acetylacetonate (H^b). Therefore, it is plausible that labile H^b was abstracted by DPPH in the reaction.

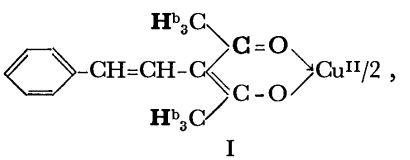

I

33) C. H. Bamford and D. J. Lind, *Proc. Roy. Soc.*, **A302**, 145 (1968).

34) R. J. Gritter and E. L. Ratmore, *Proc. Chem. Soc.*, **1962**, 328.

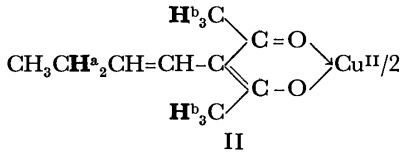

II

Therefore, 3-α-butenylacetylacetone (ligand) was used in place of its cupric chelate in the reaction with DPPH (Table 5). It was found that the reaction rate is one order of magnitude smaller than that for its cupric chelate.

Table 5. The reaction of DPPH with 3-α-butenylacetylacetone (ligand)
([3-α-butenylacetylacetone] = 4.68×10^{-4} mol/l
[Cu(3-α-butenyl-acac)$_2$] = 4.68×10^{-4} mol/l
[DPPH] = 0.545×10^{-4} mol/l)

Reactant	Rate at 25°C mol/l·sec
3-α-butenylacetylacetone	0.35×10^{-9}
Cu(3-α-butenyl-acac)$_2$	3.1×10^{-9}

This lower reactivity of the ligand suggests that the electron transfer from the ligand to the central metal contributes to the reactivity of metal chelates.

As has been described in the Introduction, DPPH forms complexes with several kinds of organic solvents or metal salts. Therefore, it is probable that, in this reaction, the complex formation with M(acac)$_n$ promotes the internal electron transfer from the ligand to the central metal in the same manner as has been described for the system of Cu(acac)$_2$ and tetracyanoethylene.[35] This reaction involves the reduction of the central metal, but does not involve the oxidation of the metallic ion, as has been reported by Bawn and Verdin in the reaction of the ferrous ion and DPPH.[15] Furthermore, the complex formation is considered to lead DPPH to a favorable steric arrangement to abstract a hydrogen atom of the cupric chelate.

A possible mechanism embodying these ideas may be proposed for the reaction of M(acac)$_n$ with DPPH.

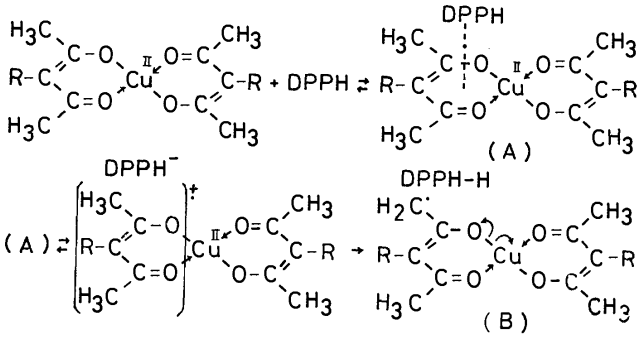

The mechanism is consistent with the observed kinetic results *in vacuo* and the products of the reaction. The internal electron transfer from the ligand to the central metal will facilitate the expulsion of a proton from a methyl group of metal acetylacetonate. The highest reactivity of cupric 3-styrylacetylacetonate (I) seems to result from phenyl group conjugated to the chelate ring, which would be expected to facilitate the internal electron transfer.[25]

35) K. Uehara, Y. Kataoka, M. Tanaka, and N. Murata, *Kogyo Kagaku Zasshi*, **73**, 1053 (1970).

Stereochemical Studies of Monoterpene Compounds. XIV.[1] The Rotational Conformation of the Acetyl and the Formyl Groups of Monoterpene α,β-Unsaturated Carbonyl Compounds

Takayuki SUGA, Kiyoshi IMAMURA, and Tsuyoshi SHISHIBORI

Department of Chemistry, Faculty of Science, Hiroshima University, Higashisenda-machi, Hiroshima

(Received June 21, 1971)

Temperature-dependent circular dichroism measurements in the *n*-π* transition enabled us to predict the preferred rotational conformation of the acetyl and the formyl groups of such monoterpene α,β-unsaturated carbonyl compounds as (+)-1-acetyl-4-methylcyclohexene (**1**), (−)-perillaldehyde (**2**), (+)-1-acetyl-2,4-dimethylcyclohexene (**3**), and (−)-myrtenal (**4**).

The geometry of α,β-unsaturated carbonyl compounds has been determined by means of studying the IR, the UV,[2] and the NMR spectra[3] and by dipole-moment measurements.[4] The temperature-dependent circular dichroism (CD) has recently been found to be useful for studying quantitatively the conformational alteration of optically-active, flexible cyclohexanone derivatives.[5] The conformational analysis of α,β-unsaturated carbonyl compounds, particularly flexible ones, is important, because the conformation of the compounds can be expected to affect their chemical reactivity and physicochemical properties. However, only one attempt[6] to make a conformational study of flexible α,β-unsaturated carbonyl compounds has been made. We now wish to deal with the rotational conformation of the acetyl and the formyl groups of four monoterpene α,β-unsaturated carbonyl compounds, (+)-1-acetyl-4-methylcyclohexene (**1**), (−)-perillaldehyde (**2**), (+)-1-acetyl-2,4-dimethylcyclohexene (**3**), and (−)-myrtenal (**4**). The present study was undertaken on the basis of the temperature-dependent circular dichroism and on the basis of the rule[7] of the correlation between the chirality of an enone system and its sign of a Cotton effect for the *n*-π* transition.

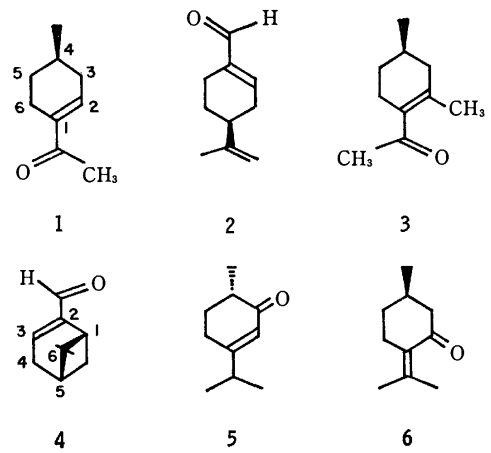

The absolute configuration of the α,β-unsaturated carbonyl compounds used.

Results and Discussion

For the compounds (**1**), (**2**), and (**3**), but not (**4**), both the conformational exchange of the cyclohexene ring and the rotational conformation of the carbonyl group are suspected to be important factors directly affecting the CD curve. However, since the cyclohexene ring substituted with the bulky group would exist in a stable half-chair conformation,[8] the change in the rotational strength depending on the temperature should be considered to indicate truly the equilibrium of the rotational conformation.

The acetyl group of the compound (**1**) can exist in the *s-trans* or the *s-cis* geometry, which may be stabilized by the orbital overlap interaction of the carbonyl and the ethylenic double donds. The geometry of α,β-unsaturated carbonyl compounds can be elucidated by means of the frequency difference and the intensity ratio between the C=O and the C=C stretching bands in the IR spectrum and by means of the molecular extinction coefficient of the π–π* transition in the UV spectrum. The compound (**1**) was identified as taknig preferentially the *s-trans* geometry on the basis of the similarity of its values to those of the representative, *s-trans* α,β-unsaturated ketone, (−)-carvenone (**5**) (Table 1). The CD curve of **1** exhibited a positive Cotton effect with a fine structure in the region of the *n*–π* transition (Fig. 1). The positive rotational strength was increased linearly with a lowering of the temperature. This observation can be explained in terms of the rotational conformations of the acetyl group. This group may be not coplanar with the ethylenic double bond, but may be rotated out of the plane. Accordingly, the compound (**1**) can exist in two possible rotational conformations, **1a** and **1b** (Fig. 2). Since the octant projection diagram predicts a positive Cotton effect for **1a** and a negative one for **1b**, the temperature-dependency of the CD curve indicated the predominancy of **1a** in the conformational equilibrium between **1a** and **1b**.

1) Part XIII of this series: T. Suga and S. Watanabe, This Bulletin, **45**, 240 (1972).
2) R. B. Rurner and D. M. Vaitle, *J. Amer. Chem. Soc.*, **73**, 1403 (1951).
3) D. D. Foulk and A. Fry, *J. Org. Chem.*, **35**, 364 (1970).
4) D. Izsak and R. J. Le Fevre, *J. Chem. Soc., B*, **1966**, 251.
5) K. M. Wellman, W. S. Briggs, and C. Djerassi, *J. Amer. Chem. Soc.*, **87**, 73 (1965).
6) R. E. Ballard, S. F. Mason, and G. W. Vane, *Discuss. Faraday Soc.*, **59**, 43 (1963).
7) G. Snatzke, *Tetrahedron*, **21**, 413, 421, 439 (1965).
8) N. L. Allinger and E. L. Eliel, "Topics in Stereochemistry," Vol. 2, Willey, New York (1967), p. 160.

Table 1. IR and UV spectral data of the α,β-unsaturated carbonyl compounds

Compound	IR[a]				UV[b]	
	$\nu_{c=o}$ (cm^{-1})	$\nu_{c=c}$ (cm^{-1})	$\nu_{c=o}-\nu_{c=c}$ (cm^{-1})	ri(c=o/c=c)[c]	λ_{max} (nm)	ε
1	1674	1652	22	2.4	233.5	14,720
2	1688	1652	36	2.3	232	15,120
3	1685	1619	66	0.9	248	6,340
4	1678	1622	56	3.2	239[d]	8,700
5	1681	1637	44	2.5	235	16,950
6	1691	1614	77	0.7	252.5	8,020

a) In liquid film. b) In ethanol. c) Relative intensity. d) In isooctane.

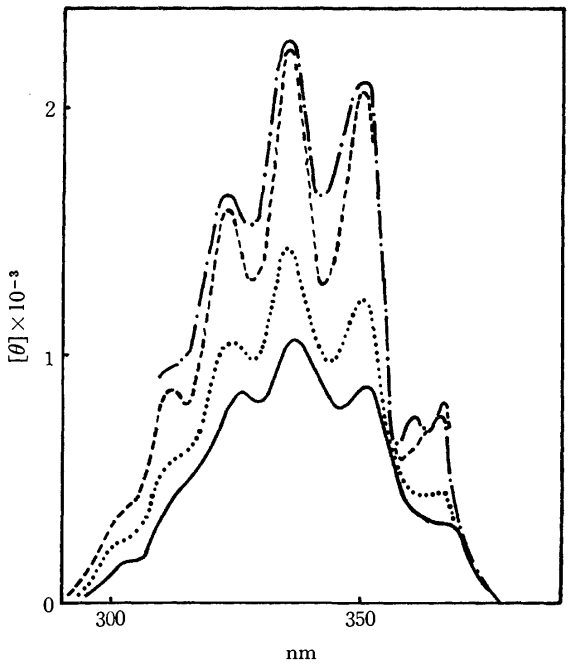

Fig. 1. CD curves of compound **1**: ——, at 25°C, ·····, at −26°C, ----, at −127°C, and —·—, at −186°C in MI solvent.

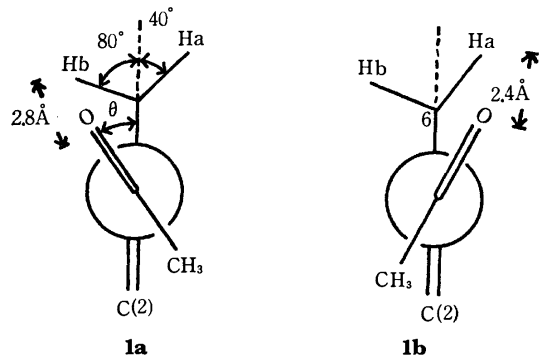

1a **1b**

Fig. 2. The preferred rotational conformation of the acetyl group of compound **1**.

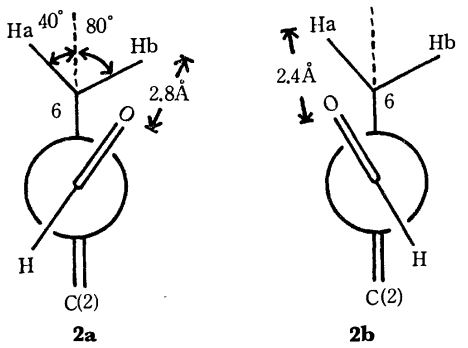

2a **2b**

Fig. 3. The preferred rotational conformation of the formyl group of compound **2**.

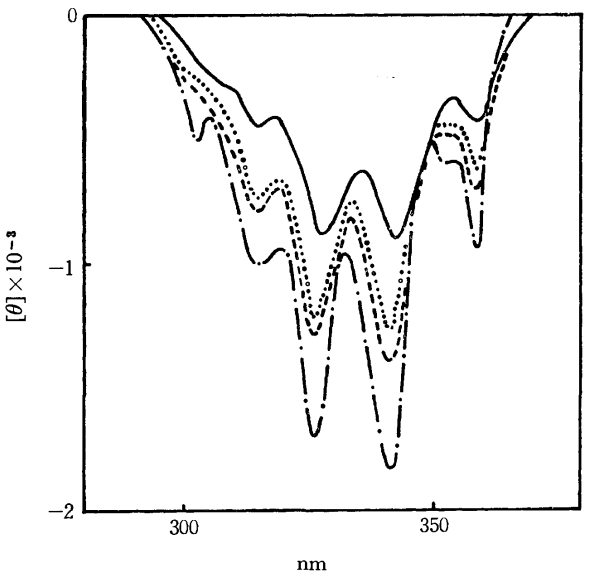

Fig. 4. CD curves of compound **2**: ——, at 25°C, ·····, at −25°C, ----, at −76°C, and —·—, at −115°C in MI solvent.

For the compound (**2**), the **2a** and **2b** conformations (Fig. 3) with the skewed *s-trans* geometry may be favored, as has been discussed above. The temperature-dependency of the CD curve (Fig. 4) showed the presence of the conformational equilibrium between **2a** and **2b**, with a negative and a positive Cotton effect respectively. The increase in the negative rotational strength with the lowering of the temperature indicated the predominance of the **2a** conformer.

According to the Dreiding Model, two allylic hydrogen atoms, (Ha) and (Hb), at the C-6 position are located dissymmetrically in relation to the plane of the ethylenic double bond, keeping the angles of 40 and 80° respectively (Figs. 2 and 3). For the **1b** and **2b** conformers, accordingly, the internuclear distance (2.4 Å) between the Ha and the oxygen atom of the

carbonyl group is shorter than the sum of the van der Waals radius[9] of the hydrogen atom (1.2 Å) and that of the oxygen atom (1.4 Å). On the other hand, the distance between the Hb and the oxygen atom is 2.8 Å for the **1a** and **2a** conformers. These conformers suffer no van der Waals interaction. Thus, the similarity of the temperature-dependent CD curve of the compound (**1**) to that of the compound (**2**) seems to indicate that the bulkiness of the alkyl group (the hydrogen atom or the methyl group) of the carbonyl side chain does not significantly affect the rotational conformation.

The similarity of the IR and the UV spectral data of the compound (**3**) (Table 1) to those of (+)-pulegone (**6**) with a *s-cis*, α,β-unsaturated ketone moiety suggests **3a** and **3b** with a skewed *s-cis* geometry (Fig. 5), as the preferred conformation of **3**. From the

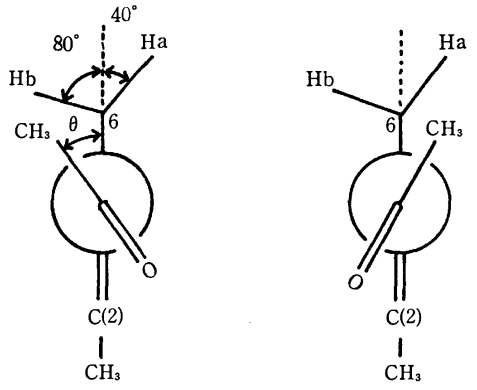

3a **3b**

Fig. 5. The preferred rotational conformation of the acetyl group of compound **3**.

discussion, compared with the compound (**1**), it seems that the steric hindrance of the methyl group at C-2 could enable the compound (**3**) to take the preferred conformation with the *s-cis* moiety. According to the octant projection diagram, a positive Cotton effect can be predicted for **3a**, and a negative one, for **3b**. The CD curve of the compound (**3**) exhibited a weak negative Cotton effect at 25°C. However, with a lowering of the temperature, a strong positive curve appeared in the long-wavelength region at the expense of the negative one (Fig. 6). This result suggests the predominance of the **3a** conformer. This is supported by the fact that the dihedral angle, θ, of the the compound (**3**) between the plane of the ethylenic double bond and that of the carbonyl double bond is larger than that of the compounds (**1**) and (**2**), because the van der Waals radius of the methyl group (2.0 Å) is larger than that of the oxygen atom.

As is shown in Table 1, the IR and the UV spectral data of the compound (**4**), except for the value of the relative intensity, showed an intermediate value between those of the compounds (**5**) and (**6**). This seems to imply that the formyl group may exist in an equilibrium between the *s-trans* and the *s-cis* forms. For the compounds (**1**) and (**2**), however, the conformation with the *s-trans* geometry must be predominant over that with *s-cis*, as has been described above. In addition, it has been pointed out[10,11] that, for butadiene, the *s-trans* form is more stable than the *s-cis* one because of the unfavorable arrangement of the pi orbitals of the latter. Accordingly, the **4a** and **4b** conformations with the skewed *s-trans* geometry are favored for the compound (**4**) (Fig. 7). A positive

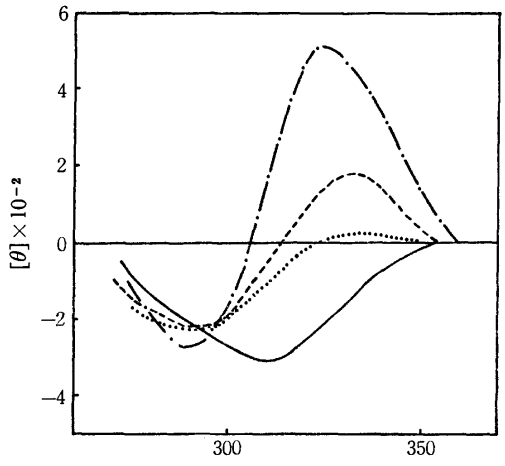

Fig. 6. C.D. curves of compound **3**: ——, at 25°C, ·····, at −57°C, ----, at −136°C, and —·—, at −190°C in MI solvent.

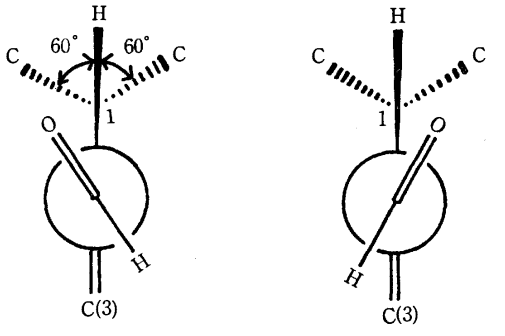

4a **4b**

Fig. 7. The preferred rotational conformation of the formyl group compound **4**.

Cotton effect can be predicted for the **4a** conformer and an opposite one for the **4b** conformer. Actually, the CD curve of **4** exhibited a positive Cotton effect at room temperature. This seems to indicate the preference of the **4a** conformer. However, the compound (**4**) showed unusual variable-temperature CD curves; with a lowering of the temperature, the positive rotational strength in the shorter-wavelength region increased, together with the negative one in the longer-wavelength region (Fig. 8). This indicates the existence of an equilibrium containing more than two rotational conformations, which is considered to show that the conformer population of **4a**, together

9) L. Pauling, "The Nature of The Chemical Bond," Third Eddition, Cornell Univ., New York (1960), p. 260.

10) W. B. Smith and J. L. Massingill, *J. Amer. Chem. Soc.*, **83**, 4301 (1961).

11) R. G. Parr and R. A. Mulliken, *J. Chem. Phys.*, **18**, 1338 (1950).

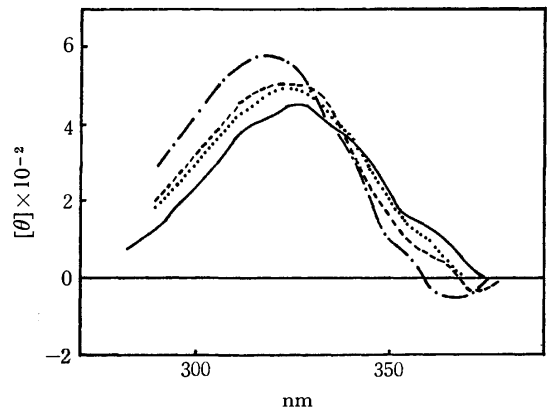

Fig. 8. CD curves of compound **4**: ——, at 25°C, ·····, at −27°C, ----, at −92°C, and —·—, at −184°C in MI solvent.

with that of **4b**, increased at the expense of the *s-cis* form. This can be explained by the symmetry of the spatial arrangement of the allylic carbon-carbon single bonds at the C-1 position to the planes of C-1, C-2, and C-3, a symmetry resulting from the insertion of a cyclobutane ring into the cyclohexene ring, as has been shown in the cases of **4a** and **4b**. Thus, the stabilities of the **4a** and **4b** conformers are nearly equal.

For the cyclohexene derivatives, thus, the predominance of the conformation has been concluded to depend on the dissymmetry on the allylic carbon of the ethylenic double bond.

Experimental

Measurements. The temperature-dependent CD curves were measured by means of a Japan Spectroscopic Co., Ltd., automatically-recording spectropolarimeter, Model ORD/UV-5, equipped with a CD attachment in the MI solvent (methylcyclohexane - isopentane, 1 : 3 by volume) and in the EPA solvent (ether - isopentane - ethanol, 5 : 5 : 2 by volume), using a variable temperature CD cell designed and constructed by the authors.

Materials. (+)-*1-Acetyl-4-methylcyclohexene* (**1**): (−)-10-Nor-8-oxomenthol[12] was treated with a mixture of hydrochloric acid and ethyl alcohol (1 : 4 by volume) overnight to convert it to **1**. The crude oil was then refined by column chromatography over silica gel. The compound (**1**) (100% pure by analytical glc) thus obtained showed the following properties: bp 84.0—85.0°C/5 mmHg, n_D^{25} 1.4786, d_4^{25} 0.9384, $[\alpha]_D^{25}$ +184.4° (neat); NMR $\delta(CDCl_3$, 60 MHz) 0.98 (d, J=6 Hz, −CH−C$\underline{H}_3$), 2.15 (s, −CO−C$\underline{H}_3$), 6.64 ppm (m, −C=C$\underline{H}$−).

(−)-*Perillaldehyde* (**2**): A commercial sample was purified by distillation to give a 99.0% pure compound (**2**), which showed the following properties: bp 89.0—90.0°C/9 mmHg n_D^{25} 1.5036, d_4^{25} 0.9610, $[\alpha]_D^{25}$ −126.5° (neat).

(+)-*1-Acetyl-2,4-dimethylcyclohexene* (**3**): The compound (**3**) was synthesized from (+)-isopulegone (bp 96.0-96.5°C/14 mmHg, n_D^{25} 1.4715, d_4^{25} 0.9745, $[\alpha]_D^{25}$ +9.65° (neat); 90% pure by analytical glc) by the Grignard reaction, followed by ozonization and the dehydration with thionyl chloride. Column chromatography over silica gel impregnated with 15% (v/v) silver nitrate gave a compound (**3**) with the following properties: bp 64.0°C/4 mmHg, $[\alpha]_D^{25}$ +119.0° (*c* 0.185, ethanol); NMR $\delta(CDCl_3$, 60MHz) 0.96 (d, J=6 Hz, −CH−C$\underline{H}_3$), 1.80 (s, −C=C−C$\underline{H}_3$), 2.11 ppm (s, −CO−C$\underline{H}_3$).

(−)-*Myrtenal* (**4**): Following the method in the literature,[13] the oxidation of β-pinene, bp 164.0°C/760 mmHg, n_D^{25} 1.4782, d_4^{25} 0.8692, $[\alpha]_D^{25}$ −19.9° (neat), with selenium dioxide gave a crude compound (**4**), which was then subjected to column chromatography. The pure sample (100% pure by the analytical glc) showed the following properties: bp 58.5°C/4 mmHg, n_D^{25} 1.5002, d_4^{25} 0.9845, $[\alpha]_D^{25}$ −15.8° (neat).

The authors are indebted to the Takasago Perfumery Co., Ltd., and the Nippon Terpene Chemical Co., Ltd., for furnishing us with the samples of perillaldehyde, isopulegol, and β-pinene.

12) T. Shishibori, *J. Sci. Hiroshima Univ., Ser. A-II*, **32**, 125 (1968).

13) W. D. Stallcup and J. E. Hawkins, *J. Amer. Chem. Soc.*, **63**, 3339 (1941).

The Photochemical Reduction of Nitrobenzene and Its Reduction Intermediates. X. The Photochemical Reduction of the Monosubstituted Nitrobenzenes in 2-Propanol

Shizunobu HASHIMOTO and Koji KANO

Department of Applied Chemistry, Doshisha University, Kamikyo-ku, Kyoto

(Received July 9, 1971)

The photochemical reduction of the monosubstituted nitrobenzenes has been investigated in 2-propanol under a nitrogen atmosphere. The nitrobenzenes with electron-withdrawing groups on *meta*- and *para*-positions (*p*-NO_2, *m*- and *p*-CN, *m*- and *p*-$COOC_2H_5$, *p*-$COOCH(CH_3)_2$, and *m*- and *p*-COOH) were photoreduced to the corresponding anilines, and nitrobenzene and the *para*-substituted nitrobenzenes with electron-donating groups (*p*-CH_3 and *p*-OCH_3) were photoreduced to the corresponding phenylhydroxylamines. *p*-Nitroaniline and *p*-nitrophenol were unreactive toward the photoreduction. In the experiments on the determination of the quantum yields for the nitrobenzenes' disappearance upon irradiation with a 313- or 366-nm light, it has been found that there is a linear correlation between the log-values of the relative quantum yields of the substituted nitrobenzenes and nitrobenzene and the Hammett constants, and the ρ value was +1.5. The results obtained suggest that the hydrogen-abstraction reaction of the photoexcited nitrobenzenes may proceed electrophilically.

Hurley and Testa[2] have reported that the reactivity of the hydrogen abstraction of the protonated nitrobenzene triplet is greater than that of the unprotonated nitrobenzene triplet. Similar results have been obtained in the photoreduction of 1-nitronaphthalene in hydrochloric acid (HCl) -2-propanol (IPA) solutions.[3] These results obtained by Testa *et al.* are very interesting in clarifying the mechanism of the hydrogen abstraction of the photoexcited nitro aromatic compounds. On the other hand, we ourselves have previously reported that 4-nitropyridine is not photoreduced in IPA, whereas it is reduced photochemically in a HCl-IPA solution to form 4-hydroxylaminopyridine in a quantitative yield,[4] and that judging from the results of the quantum-yield measurements, the hydrogen abstraction of 4-nitropyridine in the n,π^* excited state may proceed electrophilically.[1] We have also found that, when the photoreduction of the *para*-substituted nitrobenzenes is done in IPA, there is a linear correlation between the log-values of the relative quantum yields for the substituted nitrobenzenes' disappearance and the nitrobenzene and the Hammett constants (ρ : +).[5]

In this paper, we wish to report in detail our findings on the photoreduction of the monosubstituted nitrobenzenes in IPA and to discuss the mechanism of the hydrogen-abstraction reaction of the photoexcited nitrobenzenes. Both the reporting and discussing were begun in a previous communication (Ref. 5).

Experimental

Materials. The *p*-nitrobenzonitrile[6] and phenylhydroxylamine[7] were prepared according to the procedures described in the literature. The monosubstituted anilines were prepared by the reduction of the corresponding substituted nitrobenzenes with zinc dust - HCl, or the reagent-grade anailines were purified prior to use. The monosubstituted phenylhydroxylamines were prepared according to the same procedures as were used in the preparation of phenylhydroxylamine.[7] The other materials, commercially obtained, were purified by recrystalization or distillation.

Identification of the Products. The identification of the photoreduction products was established by comparing the UV spectra with those of authentic samples. A Hitachi 124 spectrophotometer was used to follow the progressive spectral changes in the nitrobenzenes photochemistry.

Determination of Quantum Yields. The determination of the quantum yields for the nitrobenzenes' disappearance was undertaken according to the methods of previous papers.[1,5] The 366-nm light was isolated from a high-pressure 130-W mercury lamp with a Toshiba UV-D1B filter or with a combination filter of Toshiba UV-D1B and UV-35.

Results

Photoproducts of the Monosubstituted Nitrobenzenes. The progressive spectral changes were measured when 1 or 2×10^{-3} mol/*l* solutions of the nitrobenzenes in IPA were irradiated with an immersion-type 130-W high-pressure mercury lamp under a nitrogen atmosphere at room temperature. In most of the reaction, the isosbestic points were observed; therefore, it seems that the photoreaction of the nitrobenzenes in IPA proceeds quantitatively. The isosbestic points in each case were: *p*-NO_2; 233 and 294, *p*-CN; 225 and 242, *m*-CN; 265, *p*-$COOC_2H_5$; 230 and 269, *p*-$COOCH(CH_3)_2$; 231 and 268, *p*-COOH; 232 and 267, H; 244 and 288, *p*-CH_3; 253 and 302, *p*-OCH_3; 228, 266, and 366, *p*-OH; 215 and 264, and *p*-NH_2; 305 and 436 nm, respectively.

Meanwhile, the photoproducts were the corresponding substituted anilines in the photolysis of the *meta*- or *para*-substituted nitrobenzenes with electron-withdrawing groups, and were the corresponding phenylhydroxylamines in the photolysis of nitrobenzene and the *para*-substituted nitrobenzenes with electron-

1) Part IX: S. Hashimoto, K. Kano, and K. Ueda, This Bulletin, **44**, 1102 (1971).

2) R. Hurley and A. C. Testa, *J. Amer. Chem. Soc.*, **89**, 6917 (1967).

3) W. Trotter and A. C. Testa, *J. Phys. Chem.*, **74**, 845 (1970).

4) S. Hashimoto, K. Kano, and K. Ueda, *Tetrahedron Lett.*, **1969**, 2733.

5) S. Hashimoto and K. Kano, *ibid.*, **1970**, 3509.

6) C. S. Miller, "Organic Syntheses," Coll. Vol. III, p. 646 (1955).

7) O. Kamm, *ibid.*, Coll. Vol. I, p. 445 (1934).

donating groups, except for the *p*-NH_2 and *p*-OH derivatives. In the photolysis of *p*-chloronitrobenzene in IPA, no isosbestic points were observed in the UV spectrum; this suggests that the photoreaction of *p*-chloronitrobenzene proceeds in a complicated way. Therefore, we put off the photolysis of the halonitrobenzenes until a latter time.

Quantum Yields for the Disappearance of the Substituted Nitrobenzenes. The quantum yields for the nitrobenzenes' disappearance in IPA at 313 or 366 nm were measured. The photolysis was done under a nitrogen atmosphere at room temperature. The reaction conditions and the results obtained are summarized in Table 1.

TABLE 1. QUANTUM YIELD RESULTS FOR THE DISAPPEARANCE OF THE SUBSTITUTED NITROBENZENES IN 2-PROPANOL

$XC_6H_4NO_2$	Concn. $\times 10^3$ mol/*l*	Light nm	Product	Quantum yield
p-NO_2	1.00	366[a]	*p*-Nitroaniline	0.16
p-CN	1.03	313	*p*-Aminobenzonitrile	0.48[c]
m-CN	1.00	313	*m*-Aminobenzonitrile	0.34
p-$COOC_2H_5$	1.00	313	Ethyl *p*-aminobenzoate	0.15
m-$COOC_2H_5$	1.00	313	Ethyl *m*-aminobenzoate	0.11[c]
p-$COOCH(CH_3)_2$	0.25	313	Isopropyl *p*-aminobenzoate	0.15
p-COOH	1.00	313	*p*-Aminobenzoic acid	0.12
m-COOH	1.17	313	*m*-Aminobenzoic acid	0.18
H	1.10	313	Phenylhydroxylamine	0.03
p-CH_3	1.00	313	*p*-Hydroxylamino-toluene	0.07
p-OCH_3	0.25	313	*p*-Hydroxylamino-anisole	0.02
p-OH	0.50	313	—	0.00
p-NH_2	0.50	366[b]	—	0.004

a) A combination filter of Toshiba UV-D1B and UV-35 was used.
b) A filter of Toshiba UV-D1B was used.
c) In these cases, the quantum yields for the formation of the anilines were measured.

In the UV-spectrum measurements, the n,π^* absorption bands ($\log\varepsilon \leqq 2$) were observed in IPA in the 320—420 nm range for the *m*- and *p*-CN, *m*- and *p*-$COOC_2H_5$, *p*-$COOCH(CH_3)_2$, *m*- and *p*-COOH, H, and *p*-CH_3 derivatives; therefore, the reactivity of the n,π^* excited nitrobenzenes was measured by irradiation with the 313-nm light. On the other hand, since no n,π^* bands were observed in the UV spectrum for the *p*-OCH_3, *p*-OH, and *p*-NH_2 derivatives, the light which excites these compounds at the lowest energy was irradiated.

As Table 1 shows, the quantum yields for the disappearance of the *meta*- and *para*-substituted nitrobenzenes with electron-withdrawing groups ($\Phi_X > 0.1$) were greater than those of nitrobenzene and the *para*-substituted nitrobenzenes with electron-donating groups ($\Phi_X < 0.1$). Particularly, *p*-nitrophenol and *p*-nitroaniline were unreactive toward the photoreduction.

Solvent Effect on the Photoreduction of p-*Nitrobenzonitrile.* A solvent effect on the photoreduction of *p*-nitrobenzonitrile, which was most reactive toward the photoinduced hydrogen-abstraction reaction, was investigated. Table 2 shows the quantum yields for the *p*-nitrobenzonitrile disappearance (Φ_{CN}) upon irradiation with the 313-nm light under a nitrogen atmosphere at room temperature.

TABLE 2. SOLVENT EFFECT FOR THE PHOTOREDUCTION OF *p*-NITROBENZONITRILE

Concn. $\times 10^3$ mol/*l*	Solvent	Quantum yield
1.03	IPA	0.48
1.00	Ethanol	0.11
1.00	Cyclohexane[a]	0.00

a) It contained 10 vol% of IPA to dissolve *p*-nitrobenzonitrile.

The quantum yields were influenced by the hydrogen-donating ability of the solvents. That is, the hydrogen-donating ability of the solvents in this photoreduction may classified, in decreasing order, as: IPA (secondary alcohol), ethanol (primary alcohol), and cyclohexane (parafine).

Oxygen-quenching Effect. The quenching effect by oxygen was studied in oder to clarify the state of the photoreduction.

The 1×10^{-3} mol/*l* solutions of *p*-nitrobenzonitrile and/or *p*-nitrotoluene in air-saturated IPA were irradiated with the 313-nm light at room temperature. In both cases, the photolysis of the nitro aromatic compounds was completely quenched by oxygen. The photoreduction of the nitrobenzenes, therefore, may proceed *via* excited triplet states.

Discussion

The Photoproducts of the Monosubstituted Nitrobenzenes. The photoproducts of the substituted nitrobenzenes were classified by substituent effects as is pictured below:

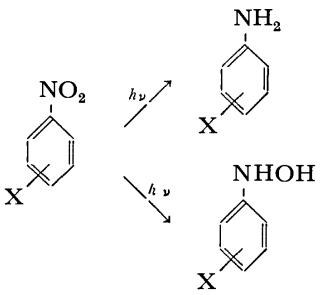

X; *p*-NO_2, *m*- and *p*-CN, *m*- and *p*-$COOC_2H_5$, *p*-$COOCH(CH_3)_2$, *m*- and *p*-COOH

X; H, *p*-CH_3, *p*-OCH_3

It has been established that nitrobenzene, [8,9] 1-

8) R. Hurley and A. C. Testa, *J. Amer. Chem. Soc.*, **88**, 4330 (1966).
9) S. Hashimoto, J. Sunamoto, H. Fujii, and K. Kano, This Bulletin, **41**, 1249 (1968).

nitronaphthalene,[10] 4-nitropyridine 1-oxide,[11,12] and 4-nitropyridine[1,4] in hydrogen-donative alcohols are reduced photochemically to form the corresponding hydroxylamino compounds. However, little attention has been paid until recently to the substituent effect on the photoreduction of nitro aromatic compounds. Finnegan and Knutson[13] have reported that the photoreduction of the *meta*- and *para*-substituted nitrobenzenes in ethanol gives the corresponding anilines, as is summarized as follows:

ethyl *p*-nitrobenzoate →
ethyl *p*-aminobenzoate (32%)
ethyl *m*-nitrobenzoate →
ethyl *m*-aminobenzoate (24%)
t-butyl *p*-nitrobenzoate →
t-butyl *p*-aminobenzoate (52%)
p-nitroacetophenone →
p-aminoacetophenone (16%)
nitrobenzene →
aniline (13%)

Since authentic samples of the *meta*- and *para*-substituted phenylhydroxylamines with electron-withdrawing groups could not be obtained, we could not clarify the process of the aniline formation. However, the *m*- and *p*-$XC_6H_4NO_2H$ radicals may also be generated in the primary steps of the aniline formation, analogous with the nitrobenzene photochemistry.[2]

Correlation between the Quantum Yields and the Hammett Constants. Photoreduction Mechanism. The data on the quantum yields shown in Table 1 indicate a quantitative correlation between the quantum yields and the Hammett constants. A plot of the log-values of the relative quantum yields ($\log \Phi_X/\Phi_H$) of the substituted nitrobenzenes and nitrobenzene *vs.* the Hammett constants[14] is shown in Figure 1. Apparently, the Hammett plots gave a straight line, and the ρ value was + 1.5. The photochemical behavior of nitro compounds in hydrogen-donative solvents may be written as in the following sequence:

$$N + h\nu \rightarrow N^{*1} \quad \text{excitation to a singlet} \quad (1)$$

$$N^{*1} \xrightarrow{k_1} N \quad \text{radiationless decay} \quad (2)$$

$$N^{*1} \xrightarrow{k_2} N^{*3} \quad \text{intersystem crossing} \quad (3)$$

$$N^{*3} \xrightarrow{k_3} N \quad \text{radiationless decay} \quad (4)$$

$$N^{*3} + RH \xrightarrow{k_4} NH + R \quad \text{hydrogen abstraction} \quad (5)$$

A steady-state approximation leads to this expression for the disappearance of nitro compounds:

$$\Phi = \frac{\Phi_T}{1 + [k_3/k_4(RH)]}$$

where Φ is the quantum yield for the disappearance of nitro compounds, Φ_T is the yield of the triplet, and (RH) is the concentration of the hydrogen-donative solvents. As is shown in the equation, Φ should be influenced by Φ_T, k_3, and (RH). However, our findings on the Hammett rule suggest that the only factor which governs the variation in the Φ is k_4(RH), and that the value of Φ_T and k_3 of the substituted nitrobenzenes is scarcely varied by the substituents. By the way, the electronic structure in the photoexcited states may be considerably different from that in the ground states; nevertheless, the Hammett relationship holds for the photoreduction of the nitrobenzenes in IPA. These findings suggest that the hydrogen-abstraction reaction of the photoexcited nitrobenzenes proceeds electrophilically and that the reactivity is governed by the electron density of the nitro groups in the ground states.

The photoreduction of the nitrobenzenes was quenched by oxygen; therefore, the photochemical hydrogen-abstraction reaction might proceed from the n,π^* triplet states (except for the *p*-OCH_3, *p*-NH_2, and *p*-OH derivatives).

The n,π^* transition of the nitro group may be pictured as follows:[15]

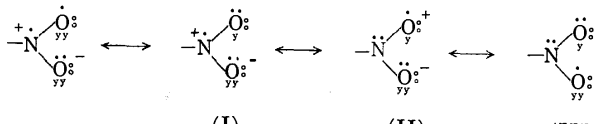

(I) (II) (III)

Ground state n,π^* Excited state
·: π electron; ○: *sp* electron; *y*: p_y electron

Structures (I) and (III) imply that a n,π^* excited state may be found to exhibit biradical properties. On the other hand, as Structure (II) shows, n,π^* excitation removes an electron from the oxygen atom and promotes it to the π^* orbital, which is then shared by the nitrogen and oxygen atoms, formally leaving a 1/2 positive charge on the oxygen. If Structure (I) or (III) participates in the photoreduction, the photoreduction of the nitrobenzenes is similar to the hydro-

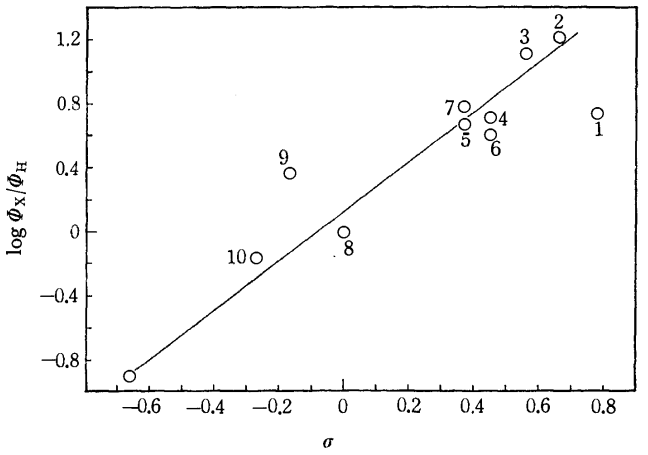

Fig. 1. Plot of $\log \Phi_X/\Phi_H$ *vs.* the Hammett constants.
1: *p*-NO_2; 2: *p*-CN; 3: *m*-CN; 4: *p*-$COOC_2H_5$; 5: *m*-$COOC_2H_5$; 6: *p*-COOH; 7: *m*-COOH; 8: H; 9: *p*-CH_3; 10: *p*-OCH_3; 11: *p*-NH_2

10) S. Hashimoto and K. Kano, *Kogyo Kagaku Zasshi*, **72**, 188 (1969).
11) C. Kaneko, S. Yamada, I. Yokoe, N. Hata, and Y. Ubukata, *Tetrahedron Lett.*, **1966**, 4729.
12) N. Hata, E. Okutsu, ans I. Tanaka, This Bulletin, **41**, 1769 (1968).
13) R. A. Finnegan and D. Knutson, *J. Amer. Chem. Soc.*, **90**, 1670 (1968).
14) D. H. McDaniel and H. C. Brown, *J. Org. Chem.*, **23**, 420 (1958).
15) H. A. Morrison, "The Chemistry of Nitro and Nitroso Compounds," ed. by H. Feuer, Interscience Publications, New York, N. Y. (1969) p. 169.

gen abstraction of the R·radical, which is well-known to proceed electrophilically. Meanwhile, if Structure (II) is an active species, our mechanism can be interpreted on the basis of this structure, because the electron affinity of the nitro groups increases in Structure (II).

The electrophilic hydrogen-abstraction mechanism is supported by the results on the photoreduction of 4-nitropyridine in the HCl-IPA solutions.[1]

It seems that the photoreduction mechanism of the nitrobenzenes is similar to that of the benzophenones. Porter *et al.*[16] have, on the basis of the quantum yields and spectroscopic data, reported that the hydrogen abstraction of the benzophenone triplet, the state of which are classified as n,π^*, π,π^*, and charge-transfer (CT) states, proceeds electrophilically. Meanwhile, Walling and Gibian[17] have found that the Hammett relationship holds for the photoreduction of benzophenone in substituted toluenes ($\rho=-1.15$).

On the other hand, Rosenberg and Servé[18] have reported that, judging from the results of the Stern - Volmer quenching studies, the rate constant for the triplet hydrogen abstraction of 1,1-diphenylethylene (DPE) in IPA is 1.4×10^9 mol^{-1} l sec^{-1}, which is considerably greater than the corresponding value reported for benzophenone, 10^6 mol^{-1} l sec^{-1}.[19] They have suggested that the electron repulsion between the unpaired electrons in the triplet states of DPE and benzophenone strongly induces the delocalization of one electron, so that the ability for the hydrogen abstraction of the two in the triplet states is similar to that of free radicals, such as alkyl and alkoxy radicals.[17,20] In other words, their interpretation means that the localization of one electron on the terminal carbon and/or oxygen atoms is important for the effective photoreduction.

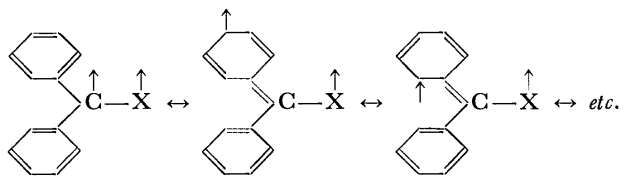

X=O, CH_2

Our results will be interpreted in terms of the mechanism postulated by Rosenberg and Servé. That is, the substituents on the *ortho*- and/or *para*-positions of the nitrobenzenes will facilitate the delocalization of one electron in the triplet states; therefore, the *ortho*- and *para*-substituted nitrobenzenes triplet may act as free radicals. In fact, the quantum yields for the disappearance of the *para*-substituted nitrobenzenes were greater than those of nitrobenzene (except for the *p*-OCH_3, *p*-NH_2, and *p*-OH derivatives). Particularly, the relative quantum yield of *p*-nitrotoluene ($\sigma=-0.170$) was 2.3. However, in the photolysis of the *meta*-derivatives with electron-withdrawing groups, the character of which as free radicals may be weaker than that of the *ortho*- and *para*-derivatives in their excited states, the quantum yields of the photoreduction are markedly greater than those of nitrobenzene. This suggests that the electron distribution of the nitro groups in the photoexcited states or ground states is an important factor in dominating the hydrogen-abstraction reaction of the photoexcited nitrobenzenes.

Hurley and Testa[2] have found that the nitrobenzene triplet is protonated in the higher acidity range, and that the reactivity toward the hydrogen abstraction of the protonated nitrobenzene triplet is greater than that of the unprotonated nitrobenzene triplet. This finding can be interpreted in terms of the electrophilic hydrogen-abstraction mechanism. That is, the positive charge of a proton which adds to the nitro group promotes it to one oxygen atom of the nitro group, so that the electron affinity of the nitro group is enhanced; the photoinduced abstraction of hydrogen may, therefore, effectively proceed. The photochemistry of 1-nitronaphthalene in the HCl - IPA solutions[3] may be understood in terms of the same interpretation.

$$C_6H_5NO_2H^{+*T} + (CH_3)_2CHOH \rightarrow C_6H_5N\dot{O}_2H + H^+ + (CH_3)_2\dot{C}OH$$

Meanwhile, Janzen and Gerlock[21] have reported, in their paper on substituent effects on the photochemistry of the nitro aromatic compounds in tetrahydrofuran, as studied by ESR spin-trapping techniques, that the photolysis of the substituted nitrobenzenes with electron-withdrawing groups gives the correspondingly-substituted nitroxide radicals (IV),

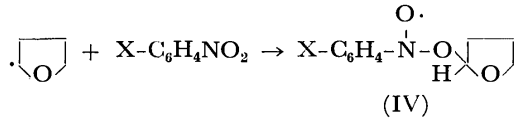

whereas most of the substituted nitrobenzenes with electron-donating groups do not give the (IV) radical except for *p*-phenyl-, *m*- and *p*-methyl-, *p*-ethyl-, *p*-isopropyl-, and *p*-phenoxynitrobenzenes. The results of the studies of the substituent effects by ESR seem to be connected with our findings: the quantum yields for the disappearance of the *meta*- and *para*-substituted nitrobenzenes with electron-withdrawing groups are greater than those of the *para*-substituted nitrobenzenes with electron-donating groups.

Photoreduction of p-*Nitroaniline and* p-*Nitrophenol.* *p*-Nitroaniline and *p*-nitrophenol were unreactive toward the photolysis in IPA; the quantum yields were 0.004 and 0.00 respectively.

The absorption maximum of *p*-nitroaniline at 322 nm ($\varepsilon_{max}=1.4\times10^4$) in *n*-hexane (containing 0.5 vol% of IPA to disolve *p*-nitroaniline) shifted to 377 nm ($\varepsilon_{max}=1.6\times10^4$) in IPA, and the solvent shift

16) G. Porter and P. Suppan *Trans. Faraday Soc.*, **61**, 1664 (1965), and other references cited therein.
17) C. Walling and M. J. Gibian, *J. Amer. Chem. Soc.*, **87**, 3361 (1965).
18) H. M. Rosenberg and P. Servé, *ibid.*, **92**, 4746 (1970).
19) A. Beckett and G. Porter, *Trans. Faraday Soc.*, **59**, 2038 (1963); S. G. Cohen and W. V. Sherman, *J. Amer. Chem. Soc.*, **85**, 1642 (1963).
20) A. Padua, *Tetrahedron Lett.*, **1964**, 3465; S. G. Cohen and R. J. Baumgarten, *J. Amer. Chem. Soc.*, **87**, 2996 (1965).
21) E. G. Janzen and J. L. Gerlock, *J. Amer. Chem. Soc.*, **91**, 3108 (1969).

was +4500 cm^{-1} (the + sign means an increase in the polarity on excitation).[16] This enormous shift shows that the polarity of the molecule is greatly increased in the excited state, and it suggests that the absorption at 377 nm in IPA is an intra-molecular charge transfer (CT) band. In fact, the CT band of *p*-nitroaniline has been observed by Tanaka[22] and Godfrey.[23] The CT configuration of *p*-nitroaniline may pictured as follows:

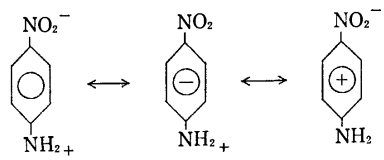

Therefore, if the lowest excited energy level of *p*-nitroaniline is the CT triplet, the electron density of the nitro group may be greatly increased, so that the electrophilic attack will be made very difficult.

Therefore, the photolysis of *p*-nitroaniline in a HCl-IPA solution was carried out in order to clarify the state of the hydrogen abstraction.

A 5×10^{-4} mol/*l* solution of *p*-nitroaniline in a 2.4 mol/*l* HCl solution with 50% IPA-water was irradiated by a 366-nm light under a nitrogen atmosphere at room temperature. The quantum yield for the disappearance of *p*-nitroaniline was 0.004 in IPA, whereas it was 0.03 in the HCl-IPA solution. The increase in the quantum yield in the HCl-IPA solution suggests that the lowest excited state of *p*-nitroaniline hydrochloride is the n,π^* triplet, which is more reactive toward photoreduction than the CT triplet, or that the CT state of *p*-nitroaniline is protonated and has an increased reactivity. This photoreductive behavior of *p*-nitroaniline is similar to that of *p*-dimethylaminobenzophenone in an IPA and/or an IPA-HCl solution.[24] However, *p*-nitroaniline was unreactive in cyclohexane, and in this case, the quantum yield for the disappearance of *p*-nitroaniline was nearly zero.

By the way, *p*-nitrophenol was also completely unreactive toward the photoreduction in IPA. Proter and Suppan[16] have reported that *p*-hydroxybenzophenone in IPA is efficiently deprotonated in the excited singlet and triplet states, and that the lowest excited state of *p*-hydroxybenzophenone is the CT triplet; therefore, the abstraction of hydrogen occurs ineffectively in the photolysis of *p*-hydroxybenzophenone in IPA. The deprotonation of *p*-nitrophenol has not yet been investigated; however, it may be reasonable to conclude that the lowest excited state of *p*-nitrophenol in IPA is the unreactive CT state, because an absorption maximum at 289 nm in *n*-hexane (containing 0.05 vol% of IPA to dissolve *p*-nitrophenol) shifted to 312 nm in IPA, and the solvent shift was enormous (+2500 cm^{-1}).

Photochemical Partial Reduction of p-*Dinitrobenzene.* As has been described above, the *meta-* and *para*-substituted nitrobenzenes with electron-withdrawing groups were relatively reactive toward the photoreduction in IPA, whereas *p*-nitroaniline was unreactive. These findings may be useful for the photochemical partial reduction of *p*-dinitrobenzene to afford *p*-nitroaniline.

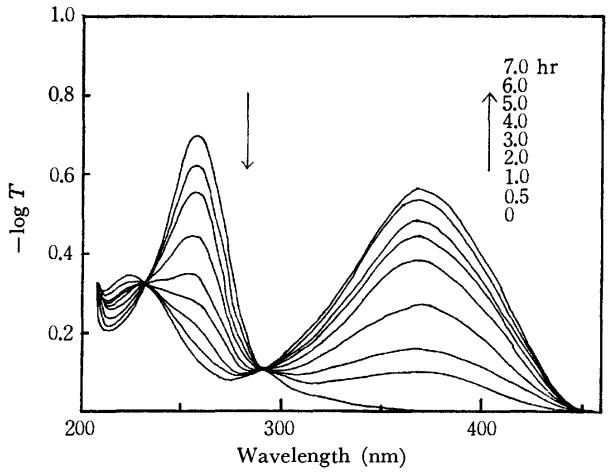

Fig. 2. Progressive spectral change of the photolysis of *p*-dinitrobenzene in IPA.

Figure 2 shows the progressive spectral change when a 2×10^{-3} mol/*l* solution of *p*-dinitrobenzene in IPA was irradiated with a high-pressure 130-W mercury lamp under a nitrogen atmosphere at room temperature. The absorption spectrum of *p*-dinitrobenzene decreased progressively in intensity, and a new absorption band of *p*-nitroaniline with its maximum at *ca.* 370 nm appeared. The isosbestic points were observed at 233 and 293 nm; therefore, the photochemical partial reduction of *p*-dinitrobenzene may proceed quantitatively.

Meanwhile, the n,π^* band of *p*-dinitrobenzene with a maximum at *ca.* 350 nm ($\varepsilon=100$) was observed in IPA. Then a 1×10^{-3} mol/*l* solution of *p*-dinitrobenzene in IPA was irradiated by a 366-nm light under a nitrogen atmosphere at room temperature; the quantum yield for the disappearance of *p*-dinitrobenzene was thus obtained as 0.16. This value (log Φ_X/Φ_H) greatly deviates from the Hammett plot, as is shown in Figure 1. This finding may be interpreted in terms of the inner-filter effect caused by *p*-nitroaniline. That is, the intense CT band with a maximum at 377 nm ($\varepsilon_{max}=1.6\times10^4$) of *p*-nitroaniline produced is absorbed near the 350-nm light, thus promoting the $n\rightarrow\pi^*$ transition of *p*-dinitrobenzene.

22) J. Tanaka, *Nippon Kagaku Zasshi*, **79**, 1373 (1958); J. Tanaka, This Bulletin, **36**, 833 (1963).
23) M. Godfrey and J. N. Murrell, *Proc. Roy. Soc.* **A278**, 71 (1964).
24) S. G. Cohen and M. N. Siddiqui, *J. Amer. Chem. Soc.*, **89**, 5409 (1967).

Synthesis of Chelating Agents. VIII. Synthesis and Acid Dissociation of 3,3-Dimethylbutane-1,2-dinitrilo-*N,N,N',N'*-tetraacetic Acid[1]

Yuzo YANAGIHARA,* Tairoku YANO, Hiroshi KOBAYASHI, and Keihei UENO

Department of Organic Synthesis, Faculty of Engineering, Kyushu University, Hakozaki, Fukuoka

(Received July 12, 1971)

3,3-Dimethylbutane-1,2-dinitrilo-*N,N,N',N'*-tetraacetic acid (BEDTA) has been synthesized by the carboxymethylation of 3,3-dimethylbutane-1,2-diamine (BEDA). The stepwise acid dissociation constants determined by the potentiometric method were found to be $pK_{a1}=6.26$ and $pK_{a2}=9.78$ for BEDA and $pK_{a1}=2.1$, $pK_{a2}=3.62$, $pK_{a3}=5.29$, and $pK_{a4}=11.6$ for BEDTA at 25°C and an ionic strength of 0.1 (KCl). The values were discussed in relation to molecular structures.

In previous papers we have reported on the effect of phenyl-substitution on either 1- or 2-carbons of ethylenedinitrilotetraacetic acid (EDTA) or both,[2] and on the effect of benzene ring fused to 4,5-positions of *trans*-cyclohexane-1,2-dinitrilo-*N,N,N',N'*-tetraacetic acid (CyDTA), on the chelating behavior of these ligands.[3] The major factors governing the chelate stability constant were found to be the ease of taking a *skew* conformation with respect to two nitrilodiacetate groups, as well as the inductive effect which may increase the basicity of nitrogen atoms of the nitrilodiacetate groups.

Introduction of alkyl groups on the ethylene bridge of EDTA would cause a steric effect favorable for chelate formation and also an electron-releasing effect to increase the basicity of nitrogen. Relatively higher chelate stability constants of propane-1,2-dinitrilotetraacetic acid (MEDTA)[4] and butane-2,3-dinitrilotetraacetic acid (BDTA)[5] can thus be understood.

From the results we were interested in the synthesis of EDTA derivatives, in which *t*-butyl groups were introduced on either 1- or 2-carbons of ethylene bridge in EDTA or both. Such bulky groups might cause a highly steric effect in favor of metal chelate formation.

This paper reports on the synthesis and acid dissociation behaviors of 3,3-dimethylbutane-1,2-diamine (BEDA) as well as 3,3-dimethylbutane-1,2-dinitrilotetraacetic acid (BEDTA).

3,3-Dimethylbutane-1,2-diamine (V), which was obtained as dihydrochloride, was synthesized from pinacolone (I) through *t*-butylglyoxal (III) and *t*-butylglyoxal dioxime (IV). 3,3-Dimethylbutane-1,2-dinitrilotetraacetic acid (VI) was synthesized by the carboxymethylation of the diamine (V). The acid dissociation behaviors of diamine (V) and tetraacetic acid (VI) were investigated by the potentiometric method, and the results were discussed in relation to their molecular structures.

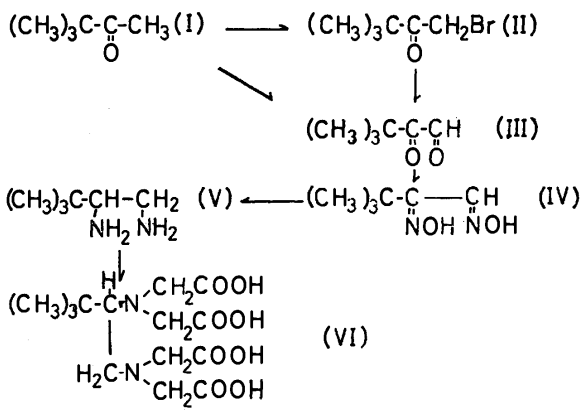

Scheme

Experimental

IR spectra were measured with JASCO DS-301 and DS-403G spectrophotometers. NMR spectra were recorded on a Varian A-60 instrument using acetonitrile as an internal standard, its signal being set at 120 Hz downfield from TMS.

Synthesis of the Ligands. *t-Butylglyoxal (III)* was synthesized by two independent procedures.

(A) Oxidation of pinacolone with selenium dioxide.[6] *t*-Butylglyoxal was obtained in 47% yield according to the procedure in literature, bp 52—71°C/100 mmHg (lit, bp 114—115°C).

(B) Oxidation of bromopinacolone with dimethylsulfoxide. A solution of 78 g of bromopinacolone obtained by the bromination of pinacolone[7] in 400 m*l* of dimethylsulfoxide, was heated at 80—90°C for 3 hr and the reaction mixture was poured into 1 *l* of water. The aqueous solution was extracted with 200 m*l* ether several times. The combined ether extracts were washed with water, then dried over magnesium sulfate. After the solvent evaporated off, the residue was distilled under reduced pressure to give a fraction boiling at 45—50°C/55 mmHg. Yield was 9.3 g (29% from bromopinacolone). The purity of glyoxal (III) was a decisive factor on the yield of glyoxal dioxime (IV). The sample subjected to prolonged standing after the syntheses became inactive for oxime formation because of the hydration of glyoxal by atmospheric moisture. Furthermore, the dioxime from impure glyoxal crystallized with difficulty, resulting in a poor yield. Although procedure (A) gave better yield, procedure (B) was preferred because of a purer

1) Contribution No. 248 from the Department of Organic Synthesis, Kyushu University. Part VII: T. Yano, H. Kobayashi, and K. Ueno, This Bulletin, **43**, 3167 (1970).

* Present Address: Research Laboratories, Kawasaki Plant, Asahi Kasei Co., Ltd., Kawasaki, Kanagawa 210.

2) N. Okaku, Y. Toyota, Y. Moriguchi, and K. Ueno, This Bulletin, **40**, 2326 (1967).

3) T. Yano, H. Kobayashi, and K. Ueno, *ibid.*, **43**, 3167 (1970).

4) J. H. Grimes, A. J. Huggard, and S. P. Wilford, *J. Inorg. Nucl. Chem.*, **25**, 1225 (1963).

5) H. M. N. H. Irving and K. Sharpe, *ibid.*, **33**, 203 (1971).

6) R. C. Fuson, H. Gray, and J. J. Gouza, *J. Amer. Chem. Soc.*, **61**, 1937 (1939).

7) J. H. Boyer and D. Strau, *ibid.*, **74**, 4506 (1952).

product.

t-Butylglyoxal Dioxime (IV). To a solution of 12.6 g (0.18 mol) of hydroxylamine hydrochloride in 30 m*l* of water was added, successively a solution of 2 g (0.0175 mol) of freshly prepared glyoxal (III) in 10 m*l* of ethanol and a solution of 10.1 g of potassium hydroxide in 10 m*l* of water. The mixture was kept standing at room temperature for a few days. An oily layer separated and solidified gradually to afford a pasty mass, from which a solid product was collected by filtration under suction and was recrysrallized from ethanol-water, mp 101—102°C (lit, mp 101—102°C).[5] Yield was 1.3 g (51% of the theoretical). IR: ν_{OH}, 3200—3300 cm^{-1}, ν_{NO}, 950 cm^{-1}.

Found: C, 49.99; H, 8.44; N, 19.23%. Calcd for $C_6H_{12}O_2N_2$: C, 49.99; H, 8.39; N, 19.43%.

3,3-Dimethylbutane-1,2-diamine Dihydrochloride (V). Of the reduction methods including sodium in ethanol, aluminum lithium hydride, hydrogenation with Raney nickel or platinum oxide, tin-hydrochloric acid and zinc-acetic acid, the first one gave the best result in the preparation of diamine-(V) from dioxime(IV).

Metallic sodium (5.8 g) was added portionwise from the top of a condenser to a refluxing solution of 3.3 g of dioxime (IV) in 60 m*l* of ethanol. After the added sodium metal was consumed, 60 m*l* of water was added to the solution, and ethanol was distilled off through a fractionating column. The residue which separated into two layers was extracted with ether, and the ethereal layer was washed with a small amount of water and dried over anhydrous potassium carbonate. To the dried ether solution, dry hydrogen chloride gas was passed to precipitate the diamine dihydrochloride, which was then recrystallized from ethanol. Mp above 270°C. Yield: 1.8 g (42%). IR: $\nu_{NH_3^+}$ 2400—3300 cm^{-1}. NMR (τ in D_2O): 8.99(9H), 6.60—6.80(3H).

Found: C, 37.98; H, 9.49; N, 14.89; Cl, 37.57%. Calcd for $C_6H_{18}N_2Cl_2$: C, 38.10; H, 9.54; N, 14.81; Cl, 37.96%.

3,3-Dimethylbutane-1,2-dinitrilotetraacetic Acid (VI). A solution of 1.0 g (0.048 mol) of diamine dihydrochloride(V) in 3 m*l* of water, was neutralized with a calculated amount of 7 N sodium hydroxide solution. To this solution were added a solution of 3.7 g (0.267 mol) of bromoacetic acid in 5 m*l* of water, which had been neutralized to phenolphthalein with 7 N sodium hydroxide below 10°C, and 30 m*l* (0.21 mol) of 7 N sodium hydroxide solution. The mixture was heated at 100°C for 10 hours under carbon dioxide free atmosphere. The resulting solution was acidified with 6 N hydrochloric acid so that its pH was 1.8—2.0, and was kept in a refrigerator overnight to precipitate the crude tetraacetic acid. The white precipitates were collected by filtration and recrystallized from water. Mp 225°C (decomp.).

Yield: 0.42 g (23%). IR: ν_{COOH} 1763, 1730 cm^{-1}.

Found: C, 47.64; H, 6.60; N, 7.66%. Calcd for $C_{14}H_{24}N_2O_8$: C, 48.27; H, 6.94; N, 8.04%.

Determination of Acid Dissociation Constants. The same apparatus as that described previously was employed.[8] Measurements were carried out at 25.0±0.1°C in an aqueous solution under ionic strength, μ=0.10, with potassium chloride. For the determination of acid dissociation constants, 100 m*l* of 2×10^{-3} M of diamine(V) or of 1×10^{-3} M of tetraacetic acid (VI) was titrated with a solution of 0.1 N potassium hydroxide freed from carbonate ion.

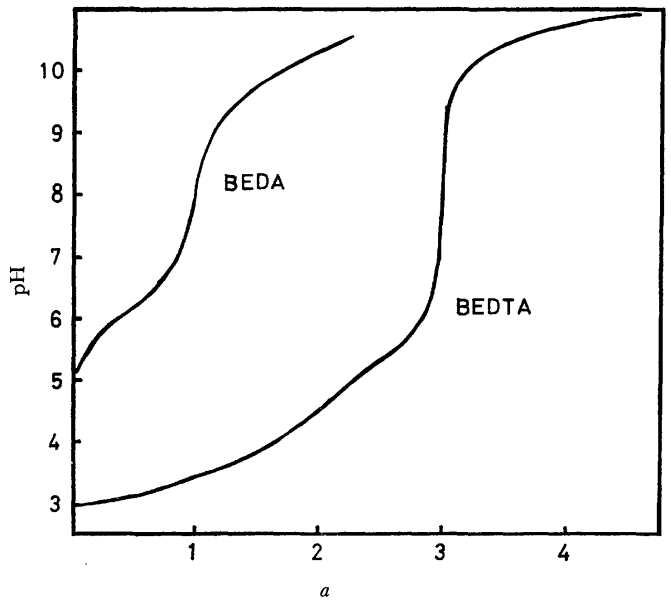

Fig. 1. The pH titration curves of BEDA and BEDTA at 25°C in 0.1 M KCl.

Calculation

The titration curves of BEDA dihydrochloride (V) and BEDTA (VI) are shown in Fig. 1. As the titration curve of BEDA dihydrochloride represents a typical curve of dibasic acid, it can be treated by the standard procedure of Schwarzenbach.[9] The final equations for the procedure are:

$$g + (g-1)[H^+]/K_{a2} + (g-2)[H^+]^2/K_{a1}K_{a2} = 0 \quad (1)$$

$$g = (2-a) + \{[OH^-]-[H^+]\}/C_A \quad (2)$$

where a represents the number of moles of alkali added per mole of the ligand, C_A the total ligand concentration, and K_{a1} and K_{a2} the first and second acid dissociation constants, respectively. In the neighbourhood of a=0.5, equation (1) can be simplified as

$$(g-1) + (g-2)[H^+]/K_{a1} = 0 \quad (3)$$

and in the neighbourhood of a=1.5 as

$$g + (g-1)[H^+]/K_{a2} = 0 \quad (4)$$

Thus, by computing each five sets of experimental values near a=0.5 and a=1.5 into Eqs. (3) and (4), the values of K_{a1} and K_{a2} were obtained, respectively.

As regards BEDTA (VI), the dissociation of the first three steps are clearly separated from the fourth step, as is shown in Fig. 1. Thus, the calculation of the acid dissociation constants can be carried out by the standard procedure of Bjerrum modified by McIntyre. The procedure is essentially the same as described previously.[3] The results of calculations on diamine (V) and tetraacetic acid (VI) are summarized in Tables 1 and 2, respectively, along with the values of related compounds.

Results and Discussion

Acid dissociation constants of diamines. As shown in Table 1, the characteristic of BEDA is its relatively low pK_{a1} value compared with those of other ethylenediamines. We see that the pK_{a1} value of the ethylene-

8) T. Ando, This Bulletin, **36**, 1593 (1963)

9) G. Schwarzenbach, A. Willi, and R. O. Bach, *Helv. Chim. Acta*, **30**, 1303 (1947)

TABLE 1. ACID DISSOCIATION CONSTANTS OF 1,2-DIAMINES

Diamine	pK_{a1}	pK_{a2}	ΔpK_a
BEDA[a]	6.26±0.01	9.78±0.01	3.52
trans-Cyclohexane-1,2-diamine[b, 10]	6.72	9.89	3.17
cis-Cyclohexane-1,2-diamine[b, 10]	6.41	9.99	3.58
Ethylenediamine[b, 10]	7.48	10.18	2.70
Propane-1,2-diamine[c, 11]	7.13	10.00	2.87
dl-Butane-2,3-diamine[c, 11]	6.91	10.00	3.09
meso-Butane-2,3-diamine[c, 11]	6.92	9.97	3.05
2,3-Dimethylbutane-2,3-diamine[c, 11]	6.56	10.13	3.57

a) measured at 25.0±0.1°C and μ=0.10 (KCl)
b) measured at 20°C and μ=0.1 (KCl)
c) measured at 25°C and μ=0.5 (KNO_3)

TABLE 2. ACID DISSOCIATION CONSTANTS OF BEDTA AND RELATED COMPLEXANES MEASURED AT 25.0±0.1°C AND μ=0.10 (KCl)

Complexane	pK_{a1}	pK_{a2}	$\Delta pK_{a(2-1)}$	pK_{a3}	pK_{a4}
EDTA	2.1±0.1	3.62±0.04	1.5	5.29±0.03	11.6±0.3
EDTA[12]	1.99	2.67	0.68	6.16	10.23
MEDTA[a, 4]	2.60	3.03	0.43	6.20	10.84
PEDTA[b, 2]	1.87	3.21	1.34	5.42	9.60

a) Propane-1,2-dinitrilo-*N,N,N',N'*-tetraacetic acid measured at 30°C.
b) 1-Phenylethylenedinitrilo-*N,N,N',N'*-tetraacetic acid measured at 20°C.

diamine homologue decreases with the increasing number of methyl groups introduced on ethylene carbons, and that pK_{a1} values of cyclohexanediamines are also relatively low.

The first dissociation step of 1,2-diammonium ion might be affected by the extent of electrostatic repulsion between the two ammonium groups as well as by the stereochemical ease of hydrogen-bond formation of the amine nitrogen resulting from the first deprotonation of an ammonium group with vicinal ammonium hydrogen. The effects can be evaluated by comparing pK_{a1} values or ΔpK_a ($=pK_{a2}-pK_{a1}$) values, since the pK_{a2} values of these diamines do not differ greatly.

In a bisprotonated stage of 1,2-diamines, in which the rotation of amino groups around the ethylene linkage is not restricted, the stable conformation will be a *trans* form with respect to the amino groups, relieving electrostatic repulsion between the vicinal ammonium groups. Ethylenediamine and *C*-methylated ethylenediamines can take this conformation. Thus, two ammonium groups of such diamines are so remote that less electrostatic repulsion operates between the ammonium groups, and dielectric interaction between the ammonium groups and polar solvent molecules favorably stabilize the highly polarized ammonium groups against the first deprotonation process. Thus the relatively higher pK_{a1} values or relatively smaller ΔpK_a values of ethylenediamine and propane-1,2-diamine can be explained. However, another effect might operate on highly methylated ethylenediamines, where the ammonium groups are embedded in nonpolar hydrocarbon moiety and the polar solvent molecules are restricted to gain access to the ammonium group. This effect would become more significant with the increasing number of methyl groups introduced on ethylene linkage.

In order to explain the significant difference between ΔpK_a values of *cis*- and *trans*-cyclohexane-1,2-diamines, Schwarzenbach[10] proposed the dielectric effect by polar solvent molecules which shielded electrostatic repulsion between the vicinal ammonium groups.

In highly methylated ethylenediamines the dielectric shielding of the ammonium groups by polar solvent molecules is less effective than in ethylenediamine, where the polar solvent molecules are easily accessible to ammonium groups. The effect is responsible for the relatively lower pK_{a1} values of highly methylated ethylenediamines, in spite of the fact that the distance between the two ammonium groups does not differ in both types of ethylenediamines.

In the case of BEDA, two ammonium groups can not take *trans* conformation due to the steric hindrance between *t*-butyl and ammonium groups, but take a stable *skew* conformation with respect to ammonium groups. Thus, the distance between two ammonium groups is comparable to those of cyclohexane-1,2-diamines. At the same time, since one of the ammonium groups is located in the close neighborhood of *t*-butyl group, the polar solvent molecules are less easily accessible. The electrostatic repulsion between two ammonium groups is, therefore, less effectively shielded in BEDA. Simultaneous operation of the conformational and dielectric shielding effects might

10) G. Schwarzenbach and R. Bauer, *Helv. Chim. Acta*, **39**, 722 (1956)
11) F. Basolo, R. K. Murmann, and Y. T. Chen, *J. Amer. Chem. Soc.*, **75**, 1478 (1953)
12) G. Schwarzenbach and G. Anderegg, *Helv. Chim. Acta*, **40**, 1773 (1957)

be responsible for the lower pK_{a1} value and higher ΔpK_a value of BEDA.

It is interesting to note in this connection that pK_{a2} of diamines do not differ greatly. Although the pK_{a2} value is expected to reflect the basicity of nitrogen atom, introduction of alkyl groups on nitrogen or adjacent carbon does not cause any appreciable increase of the value. The result might indicate that the inductive effect of alkyl groups plays a minor role in determining the pK_{a2} values of 1,2-diamines.

Dissociation Constants of BEDTA. In the acid dissociation of EDTA and related tetrabasic complexane-type ligands, deprotonation of the first two and last two steps correspond to the dissociation of carboxylic protons and ammonium protons, respectively. The pK_a values of BEDTA and some related ligands are shown in Table 2.

In previous papers,[2,3] we classified the complexane-type ligands into two groups. The first are those in which the rotation of nitrilodiacetate group is not hindered sterically and two nitrilodiacetates prefer a *trans* conformation due to electrostatic repulsion. This type is characterized by a relatively low $\Delta pK_{a(2-1)}$ value. The second are those in which two nitriloacetate groups sterically favor a *skew* conformation, and this group is characterized by a relatively high $\Delta pK_{a(2-1)}$ value.

The $\Delta pK_{a(2-1)}$ value for BEDTA clearly suggests that this ligand prefers a *skew* conformation with regard to the nitrilodiacetate groups. This can be ascribed to the steric effect by *t*-butyl group, and is in line with the preceeding discussion on BEDA.

The values of pK_{a3} and pK_{a4} are related to the deprotonations of ammonium nitrogens. Thus, a relatively lower value of pK_{a3} can be understood from the low pK_{a1} value of BEDA.

As regards the pK_{a4}, the potentiometric titration of 10^{-3} M solution of the ligand at high pH region might include a considerable error. Thus, the observed pK_{a4} value might not be accurate enough for quantitative discussion, however, pK_{a4} value of BEDTA is obviously higher than the other, the order of magnitude being comparable to that of *trans*-CyDTA ($pK_{a4}=12.35$).[13]

As discussed previously on the pK_{a2} values of methylated ethylenediamines, the introduction of alkyl groups on nitrogen or adjacent carbon does not appreciably contribute to increase of the basicity of nitrogen. The unusually high pK_{a1} value of BEDTA or *trans*-CyDTA might thus be related to some kind of steric and electrostatic effects of deprotonated species.

The authors are grateful to the Ministry of Education for financial support in this work.

13) G. Anderegg, *Helv. Chim. Acta*, **46**, 1833 (1963)

BULLETIN OF THE CHEMICAL SOCIETY OF JAPAN, VOL. 45, 557—561 (1972)

Studies on Stable Free Radicals. VII.[1] The Mechanism for Cyclization Reaction of α-Amino Nitriles with Carbonyl Compounds

Toshimasa TODA, Syoji MORIMURA, and Keisuke MURAYAMA
Central Research Laboratories, Sankyo Co., Ltd., Shinagawa-ku, Tokyo

(Received July 15, 1971)

Substituted 4-oxoimidazolidines were prepared by the condensation of α-amino nitriles with carbonyl compounds, or by the self-condensation of α-amino nitriles. The mechanism of the reaction was studied. The mass spectrum of the condensation product obtained by the reaction of cyclohexanone with 1-amino-1-cyano-^{15}N-cyclohexane (III) or by the self-condensation of III, and the ESR spectrum of corresponding nitroxide radical obtained by the oxidation of the respective condensation products served to elucidate the reaction mechanisms for these condensation reactions. The mechanism for the self-condensation of α-amino nitriles proposed previously was corrected from the spectral data of the reaction product. Possible mechanisms for these condensation reactions are proposed.

In a previous paper,[2] we reported that α-amino nitriles react with aldehydes or ketones to give substituted 4-oxoimidazolidines (I) in an alcoholic solvent and the resulting products yield corresponding stable nitroxide radicals (II) by oxidation.

On the other hand, Noland *et al.*[3] reported that the self-condensation of 1-amino-1-cyanocyclohexane afforded cyclohexane-1-spiro-2′-(4′-oxoimidazolidine)-5′-spiro-1″-cyclohexane (IVa) in the presence of sodium ethoxide in ethanol containing a trace of moisture.

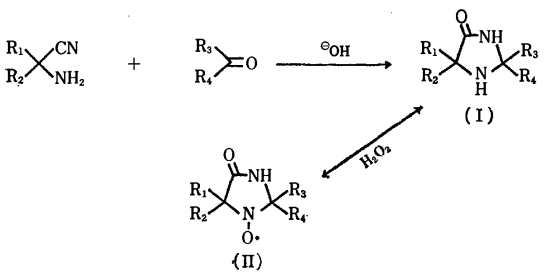

1) Part VI: Ref. 2,

2) T. Toda, S. Morimura, E. Mori, H. Horiuchi, and K. Murayama, This Bulletin, **44**, 3445 (1971).

3) W. E. Noland, R. J. Sundberg, and M. L. Michaelson, *J. Org. Chem.*, **28**, 3576 (1963).

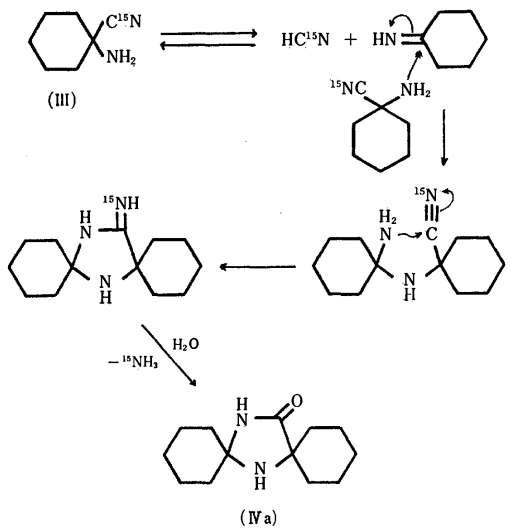

Chart 1.

They proposed for the mechanism of this self-condensation the sequence shown in Chart 1.

This paper deals with the mechanism for the cyclization reaction of α-amino nitriles with carbonyl compounds.

The reaction mechanism was clearly obtained from spectroscopic analysis of the product from the reaction of cyclohexanone with 1-amino-1-cyanocyclohexane (III) in which the nitrogen of cyano-group was replaced by ^{15}N.

We will also discuss the reaction mechanism proposed by Noland *et al.*[3]

Results and Discussion

From our synthetic method for imidazolidinones (I), it was expected that the intermediate would be the Schiff base of an α-amino nitrile with a carbonyl compound.

In order to confirm this, the following reaction was carried out: The condensation of 4-amino-4-cyano-2,2,6,6-tetramethylpiperidine-1-oxyl (V) with benzaldehyde gave 1,3,8-triaza-2-phenyl-4-oxo-7,7,9,9-tetramethyl-spiro[4.5]decane-1-oxyl (VI) in the presence of a catalytic quantity of aqueous sodium hydroxide in ethanol solution, while the reaction of V with benzaldehyde yielded the Schiff base VII under reflux in benzene using ammonium acetate as a catalyst.

The Schiff base VII thus obtained, was treated under similar conditions as in the formation of VI from V, and VI was obtained in good yield.

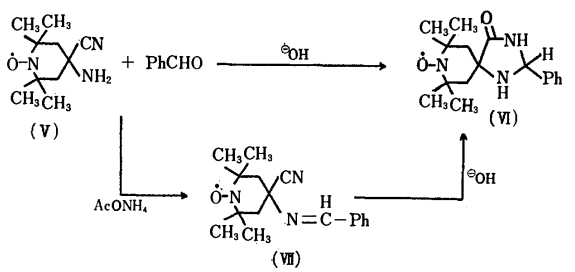

From the results, we assumed the mechanism for cyclization reaction of α-amino nitriles with carbonyl compounds as shown in Chart 2.

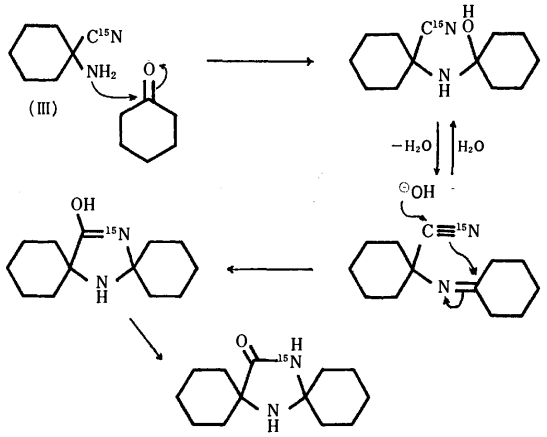

Chart 2.

In order to confirm the assumption and the mechanism proposed by Noland and co-workers,[3] the following experiments were carried out.

The ^{15}N-substituted α-amino nitrile, 1-amino-1-cyano-^{15}N-cyclohexane (III) was prepared by the Strecker reaction of cyclohexanone with ^{15}N-sodium cyanide (95% ^{15}N content) and ammonium chloride. In a similar manner as reported previously,[2] we obtained product A by the reaction of III with cyclohexanone. Likewise, the self-condensation of III in the same way as reported by Noland *et al.*[3] afforded product B. The structures of these products A and B were both designated as cyclohexane-1-spiro-2′-[4′-oxoimidazolidine(3′-^{15}N)]-5′-spiro-1″-cyclohexane(IVb) from their IR spectra. The results are given below.

If the reaction of III with cyclohexanone follows the mechanism as shown in Chart 2, ^{15}N should be incorporated at the 3-position of the imidazolidine ring in product A.

Likewise, if the self-condensation of III proceeded as shown in Chart 1, product B would have no ^{15}N atom in the molecule.

The incorporation of ^{15}N in A or B, can be confirmed by mass spectra measurements; the position of ^{15}N in imidazolidine ring (IVb or IVc) can be determined by ESR measurements of tne corresponding nitroxide radicals (VIIIb or VIIIc) prepared by oxidation[4]

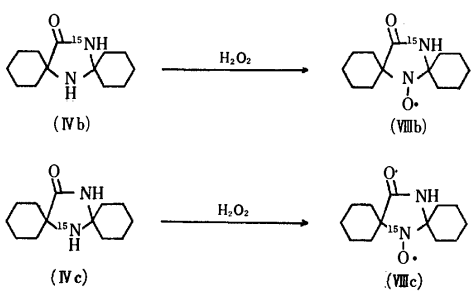

4) K. Murayama, S. Morimura, and T. Yoshioka, This Bulletin, **42**, 1640 (1969).

of A or B with hydrogen peroxide, since in the ESR spectrum triplet lines resulting from a ^{14}N nucleus are expected for VIIIb and doublet lines resulting from a ^{15}N nucleus for VIIIc, respectively.

In the high resolution mass spectrum of product A, the expected molecular ion peak at *m/e* 223.171 assigned to $C_{13}H_{22}ON^{15}N$, and a fragment peak at *m/e* 180.116 to $C_{10}H_{15}ON^{15}N$ were found, while in the case of the imidazolidinone IVa containing no ^{15}N, the corresponding peaks at *m/e* 222.277 ($C_{13}H_{22}ON_2$) and 179.119 ($C_{10}H_{15}ON_2$) were observed.

Oxidation of compound IVa by hydrogen peroxide afforded the corresponding nitroxide radical (VIIIa).[4] Similarly, oxidation of product A gave the nitroxide radical (VIIIb) which was given the following assignment.

Since triplet lines (a_N=14.1 gauss) were observed in the ESR spectrum of this oxidation product, the structure of product A was assigned to IVb. Thus, the mechanism shown in Chart 2 is plausible for the cyclization reaction of α-amino nitriles with carbonyl compounds.

On the other hand, the structure of product B was also assigned to IVb from the mass spectrum of product B and ESR spectrum of the corresponding nitroxide radical.

This shows that the self-condensation reaction of α-amino nitrile does not follow the mechanism (Chart 1) proposed by Noland *et al.*,[3] but might proceed by a mechanism as shown in Chart 5 for the following reasons.

In the cyclization reaction of α-amino nitriles with carbonyl compounds, we found that imidazolidinone compounds I having different substituents from those expected from the mechanism (Chart 2) were obtained.

Treatment of amino nitrile V with cyclohexanone under the same conditions mentioned above gave the normal reaction product, cyclohexane-1-spiro-2′-(4′-oxoimidazolidine)-5′-spiro-4″-(2″,2″,6″,6″-tetramethylpiperidine-1″-oxyl) (IX) and the abnormal reaction product with exchanged substituents IVa, in 44.5% and 36.0% yield, respectively.

Similarly, the reaction of α-amino-α-phenylpropionitrile (X) with cyclohexanone afforded the normal product 1,4-diaza-2-methyl-2-phenyl-3-oxo-spiro-[4.5]-decane (XI) and the same substituent-exchanged product IVa.

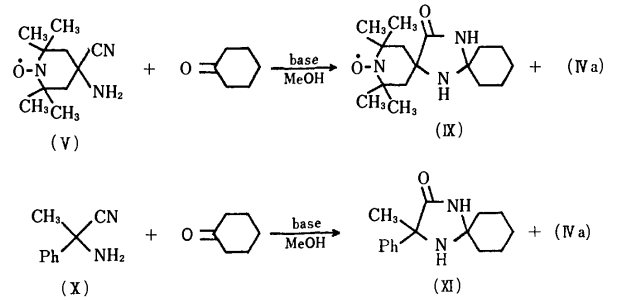

Further experiments showed that in these reactions, the presence of a small amount of water increased the yield of the substituent-exchanged product IVa.

The reaction of α-amino-isobutyronitrile (XII) with cyclohexanone in the presence of basic catalyst was carried out in water free methanol and in methanol containing a small quantity of water. In the former case the normal reaction product 1,4-diaza-2,2-dimethyl-3-oxo-spiro[4.5]decane (XIII) was obtained in 90% yield, while in the latter the substituent-exchanged product IVa in 80% yield.

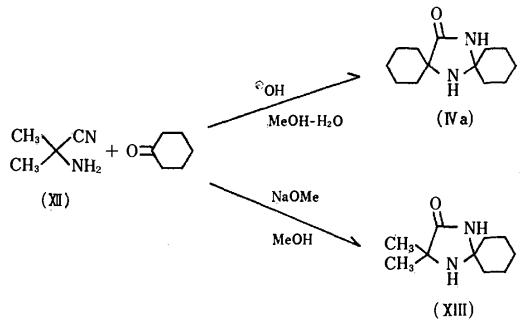

Two possible processes are considered for these exchange reactions: iminopropane reacts with cyclohexanone to give iminocyclohexane (Chart 3); iminopropane is decomposed by water to acetone and ammonia (Chart 4). Cyclohexanone is then converted into 1-amino-1-cyanocyclohexane in the reaction system and the exchange reaction product IVa is formed by the mechanism shown in Chart 2.

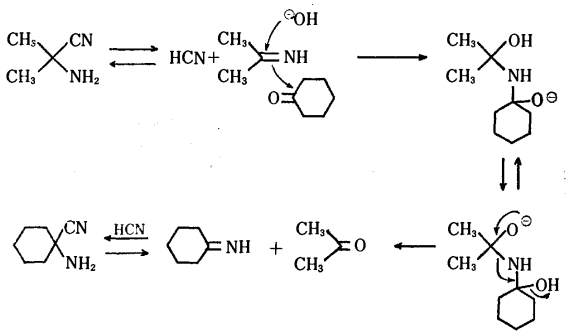

Chart 3.

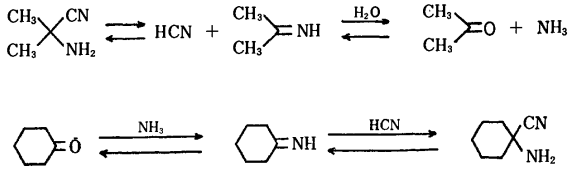

Chart 4.

The second assumption would be more reasonable in explaining the effect of water in promoting the formation of IVa.

In the case of the self-condensation of α-amino nitrile III, iminocyclohexane might also decompose into cyclohexanone and ammonia, and subsequently, the cyclohexanone thus formed would react with the amino nitrile III to give the imidazolidinone IVb by Chart 2 mechanism.

Consequently, the self-condensation reaction[3] of 1-amino-1-cyanocyclohexane might proceed by the mechanism shown in Chart 5.

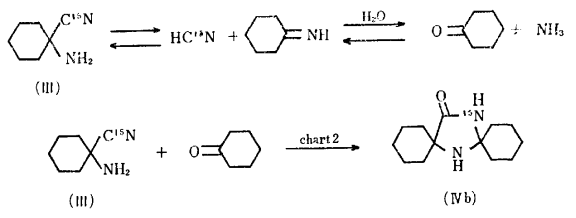

Chart 5.

Presumably the decomposition of iminopropane by water take place faster than that of iminocyclohexane, and cyclohexanone forms an α-amino nitrile more easily than other dialkyl ketones. This hypothesis can be supported by the fact that the reaction of the α-amino nitrile XII with methylisobutyl ketone gave only the normal product 2,2,5-trimethyl-2-isobutyl-4-oxoimidazolidine.[2]

Experimental

Melting points are uncorrected. The IR spectra were determined by means of nujol mulls and liquid films. The mass spectra were obtained using a JEOL-JMS-OIS mass spectrometer. The ESR spectra were recorded on a Hitachi MES 4001 type X-band spectrometer employing 100 kc modulation. Splitting constants were measured relative to the aqueous solution of Fermy's salt.

4-Cyano-4-benzilidenimino-2,2,6,6-tetramethylpiperidine-1-oxyl (VII). A solution of 2.0 g (10 mmol) of 4-amino-4-cyano-2,2,6,6-tetramethylpiperidine-1-oxyl (V)[2] and 1.1 g (10 mmol) of benzaldehyde in 50 m*l* of benzene containing 0.2 g of ammonium acetate was heated under reflux using a Dean-Stark water separator for 8 hr. The solution was cooled to room temperature, washed with water, dried over sodium sulfate and evaporated under reduced pressure to give 2.5 g (86.3%) of crude crystals VII. Recrystallization from benzene gave an analytical sample: mp 84.5°C. Found: C, 71.75; H, 7.82; N, 14.71%. Calcd for $C_{17}H_{22}ON_3$: C, 71.80; H, 7.81; N, 14.77%. IR (cm^{-1}): $\nu_{C\equiv N}$ 2230, $\nu_{C=N}$ 1648.

1,3,8-Triaza-2-phenyl-4-oxo-7,7,9,9-tetramethyl-spiro[4.5]-decane-8-oxyl (VI). (A) To a solution of 19.6 g (0.1 mol) of V[2] and 10.6 g (0.1 mol) of benzaldehyde in 30 m*l* of ethanol was added 1 m*l* of aqueous sodium hydroxide (40%) and the solution were stirred at room temperature for five days. After removal of ethanol under reduced pressure, the resulting crystalline solid was washed with water and dried in a vacuum. VI was obtained analytically pure by recrystallization from methanol: mp 184—185°C, yield 19.2 g (63.5%). Found: C, 67.46; H, 7.92; N, 13.81%. Calcd for $C_{17}H_{24}O_2N_3$: C, 67.52; H, 8.00; N, 13.90%. IR (cm^{-1}): $\nu_{C=O}$ 1703, ν_{NH} 3250 and 3350.

(B) A solution of 2.0 g (7 mmol) of VII and 1 m*l* of aqueous sodium hydroxide (40%) in 20 m*l* of methanol was stirred at room temperature for five days. A yield of 1.8 g (85.0%) of VI was obtained by a similar work-up to that mentioned above. The IR spectrum of the product was consistent with the authentic sample obtained in (A).

1-Amino-1-cyano-^{15}N-cyclohexane (III). A solution of 7.4 g (75 mmol) of cyclohexanone in 30 m*l* of methanol saturated with ammonia was added slowly to a stirred solution of 5.0 g of sodium cyanide-^{15}N (^{15}N content 95%)[5] and 9.3 g of ammonium chloride in 80 m*l* of aqueous ammonia (28%) at 0—5°C. Stirring was continued for 24 hr at room temperature. The resulting precipitate was removed by filtration and the methanol filtrates were evaporated under reduced pressure. The organic layer was extracted with 200 m*l* of diethyl ether, dried over potassium carbonate and evaporated under reduced pressure. The residual oil was distilled to give 5.5 g (64.6%) of III: bp 76—78°C/1 mmHg. IR (cm^{-1}): $\nu_{C\equiv N}$ 2200, ν_{NH} 3350, 3280, and 3200. Mass spectrum: M^+=125.

Cyclization Reaction of III with Cyclohexanone. To a solution of 1.5 g (12 mmol) of III and 1.4 g (12 mmol) of cyclohexanone in 10 m*l* of methanol was added 1 m*l* of a solution of sodium methoxide prepared by adding sodium (2.8 g) to 80 m*l* of methanol, with stirring at room temperature. Stirring was continued for 24 hr. After the solvent had been evaporated under reduced pressure, the resulting crystals were washed with water, dried *in vacuo*. Recrystallization from cyclohexane gave an analytical sample: mp 219—220°C, yield 2.2 g (79.1%). IR (cm^{-1}): $\nu_{C=O}$ 1687, ν_{NH} 3310, 3140, and 3010.

Self-condensation of III. To a solution of 3.8 g (30 mmol) of III in 15 m*l* of 98% (by weight) methanol was added 1 m*l* of a solution of sodium methoxide prepared as above, with stirring at room temperature. Stirring was continued for 24 hr. An analytical sample was obtained by a similar procedure as described above: mp 219—220°C, yield 2.8 g (80.0%). IR (cm^{-1}): $\nu_{C=O}$ 1687, ν_{NH} 3310, 3140, and 3010. Mass spectrum: M^+=223.173, $(M-C_3H_7)^+$=180.115.

Oxidation Reaction. (A) To a stirred solution of 0.6 g (27 mmol) of product A (IVb) in 4 m*l* of acetic acid was added 10 mg of ethylenediaminetetraacetic acid (EDTA) and 15 mg of sodium tungstate and then slowly 4 m*l* of aqueous solution of hydrogen peroxide (30%) at room temperature. The solution was stirred for additional 12 hr at room temperature. The resulting precipitate was separated by filtration, washed with water, and dried *in vacuo* to give 0.5 g (77.6%) of VIIIb: mp 227—228°C. IR (cm^{-1}): $\nu_{C=O}$ 1708, ν_{NH} 3160 and 3050. ESR (in benzene): a_N=14.1 gauss. (B). By a similar method to that described in (A), 0.5 g (77.6%) of VIIIb was obtained from 0.6 g (27 mmol) of the product B (IVb): mp 227—228°C. IR (cm^{-1}): $\nu_{C=O}$ 1708, ν_{NH} 3160 and 3050. ESR (in benzene): a_N=14.1 gauss.

Condensation of 4-Amino-4-cyano-2,2,6,6-tetramethylpiperidine-1-oxyl (V) with Cyclohexanone. A solution of 19.6 g (0.1 mol) of V[2] and 9.8 g (0.1 mol) of cyclohexanone and 1 m*l* of aqueous sodium hydroxide (40%) in 50 m*l* of methanol was stirred at room temperature for three days. After removal of methanol, 50 m*l* of benzene was added and the mixture was stirred at room temperature. After 1 hr, 8.0 g (36.0%) of crude crystals IVa separated; the precipitate was filtrated and washed with water. The crude material was recrystallized from ethanol to give a pure sample IVa which was confirmed by comparison of its IR spectrum with that of an authentic sample. The filtrate was dried over potassium carbonate, evaporated *in vacuo* to give 13.1 g (44.5%) of crude crystals IX. Recrystallization from petroleum ether gave an analytically pure sample: mp 201—202°C. Found: C, 65.22; H, 9.57; N, 14.26%. Calcd for $C_{16}H_{28}O_2N_3$: C, 65.27; H, 9.59; N, 14.27%. IR (cm^{-1}): $\nu_{C=O}$ 1705, ν_{NH} 3280.

Condensation of α-Amino-α-phenylpropionitrile (X) with Cyclohexanone. A mixture of 7.3 g (50 mmol) of α-amino-α-phenylpropionitrile (X) and 4.9 g (50 mmol) of cyclohexanone was heated at 50—60°C in the presence of

5) Available from the Institute of Physical and Chemical Research, Wako-shi, Saitama, Japan.

1 m*l* of sodium methoxide solution mentioned above. After 25 hr, 1.2 g (24.1%) of crude crystals IVa were separated by filtration, washed with water and dried *in vacuo*. By recrystallization from ethanol, IVa was obtained pure as shown by comparison of its IR spectrum and melting point with those of an authentic sample. The filtrate was dissolved in 50 m*l* of benzene, washed with water, dried over potassium carbonate and evaporated under reduced pressure. The residual oil was crystallized on adding petroleum ether to give 3.2 g (40.0%) of crude crystals XI. The crude material was recrystallized from petroleum ether to give an analytical sample: mp 130—131°C. Found: C, 73.69; H, 8.35; N, 11.21%. Calcd for $C_{15}H_{20}ON_2$: C, 73.77; H, 8.25; N, 11.21%. IR (cm^{-1}): $\nu_{C=O}$ 1695, ν_{NH} 3350, 3200 and 3095.

Condensation of α-Aminoisobutyronitrile (XII) with Cyclohexanone. (A). A solution of 8.4 g (0.1 mol) of α-aminoisobutyronitrile (XII) and 9.8 g (0.1 mol) of cyclohexanone and 1 m*l* of aqueous sodium hydroxide (40%) in 50 m*l* of 95% methanol (by weight) were stirred for three days at room temperature. A similar work-up as described above provided 17.8 g (85.0%) of IVa as shwon by comparison of its IR spectrum and melting point with those of an authentic sample. (B). The methanol used was distilled into a receiver containing dried anhydrous sodium sulfate and was used immediately. In a 100 m*l* flask was placed a solution of 8.4 g (0.1 mol) of α-aminoisobutyronirile (XII) and 9.8 g (0.1 mol) of cyclohexanone in 50 m*l* methanol and 1 m*l* of sodium methoxide solution was added. The flask was stoppered to exclude moisture and was heated at 40—50°C with stirring for 6 hr. After removal of methanol under reduced pressure, the resulting crystals were washed with water and dried *in vacuo*. Recrystallization from ethanol gave an analytical sample: mp 193—194°C, yield 16.4 g (90.0%). Found: C, 65.77; H, 9.84; N, 15.14%. Calcd for $C_{10}H_{18}ON_2$: C, 65.89; H, 9.96; N, 15.37%. IR (cm^{-1}): $\nu_{C=O}$ 1693, ν_{NH} 3190 and 3070.

The authors wish to thank Prof. Makoto Okawara, Tokyo Institute of Technology, for his valuable comments and Dr. G. Sunagawa, director of these laboratories, for his encouragement.

BULLETIN OF THE CHEMICAL SOCIETY OF JAPAN, VOL. 45, 561—563 (1972)

Studies on Mannan and Related Compounds. I. The Purification of Konjac Mannan

Noboru SUGIYAMA, Hideo SHIMAHARA,* and Tetsuo ANDOH*

Department of Chemistry, Tokyo Kyoiku University, Otsuka, Tokyo

**Kabushikikaisha Shimizu Manzo Shoten, Laboratory, Onomichi, Hiroshima*

(Received July 22, 1971)

The preparation of pure konjac mannan is described. Its properties and purity are also studied.

A major component of the konjac flour, which is obtained from the tubers of *Amorphophallus Konjac* C. Koch (*Araceae*), is well known to be a glucomannan called konjac mannan. Traditionally, this flour has been used as the stuff of edible *konnyaku*.

We have succeeded in obtaining pure konjac mannan, which retains the most important intrinsic properties of konjac flour; it can make a transparent colloidal solution and can be used in making a *konnyaku* of good quality. The konjac mannan which are obtained by the methods of Ohtsuki[1-4] and Nishida *et al.*[5] do not exhibit these properties. Ohtsuki's method is to prepare the mannan from a colloidal solution of konjac flour by repeated precipitations with alcohol, while Nishida's method is to take the mannan out through the copper complex by treating the super-heated water extract of konjac flour with the Fehling solution. The latter method has been used up to the present as the general procedure for preparing material for chemical studies of konjac mannan.[6-8] The fact, however, that the mannan obtained by these methods lacks important intrinsic properties suggests that the molecular structure of this mannan suffers a kind of denaturing during the processing, as has also been observed in the case of amylose in an alkaline solution.[9] On the other hand, the retention of its intrinsic properties suggests that the mannan has received little or no denaturing effect.

The present method of purification is composed of extraction, dialysis, and lyophylization.

Results and Discussion

Properties. The purified konjac mannan is a light, voluminous, and white cotton-like product.[10] It readily dissolves in water to give a transparent viscous solution and has a *konnyaku*-forming ability. The viscosity of its colloidal solution is almost the samc as that of the mannan before purification. The IR (KBr) of the purified mannan showed bands near

1) M. Mayeda, *Tokyo Igakukai Zasshi*, **18**, 1 (1914).
2) K. Goto, *J. Biochem. Tokyo*, **1**, 201 (1912).
3) T. Ohtsuki, *Acta Phytochim.*, **4**, 1 (1928).
4) S. Miyake, *J. Coll. Agr. Imp. Univ., Hokkaido*, **12**, 164 (1927).
5) K. Nishida and H. Hashima, *Nippon Nogeikagaku Kaishi*, **6**, 991 (1930).
6) F. Smith and H. C. Srivastava, *J. Amer. Chem. Soc.*, **81**, 1715 (1959).
7) K. Kato and K. Matsuda, *Agr. Biol. Chem.*, **33**, 1446 (1969).
8) T. Satoh, A. Moriya, J. Mizuguchi, and S. Suzuki, *Nippon Kagaku Zasshi*, **91**, 1070 (1970).
9) R. E. Reeves, *J. Amer. Chem. Soc.*, **76**, 4595 (1954).
10) S. Kiriyama, H. Morisaki, and A. Yoshida, *Agr. Biol. Chem.*, **34**, 641 (1970).

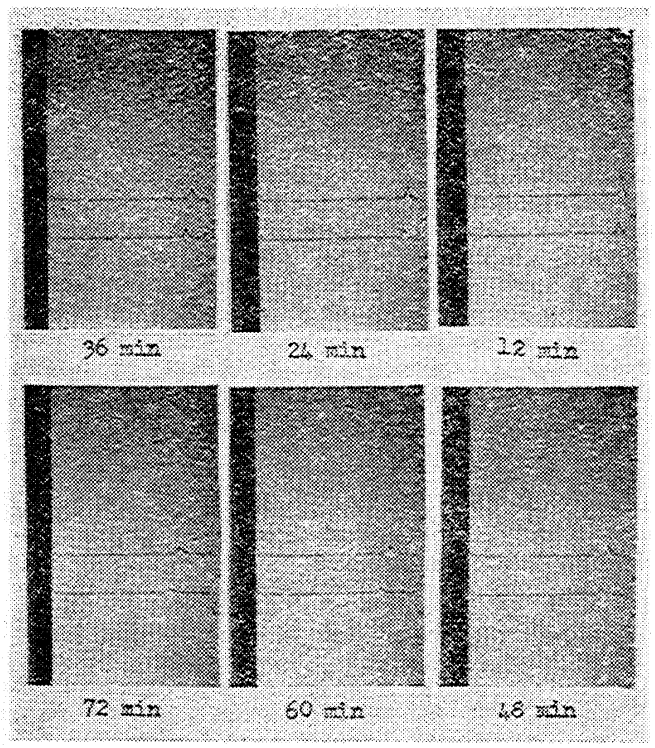

Fig. 1. Sedimentation patterns of purified konjac mannan. Sedimentation analysis was carried out under the following condition: 1.0 mg/m*l* konjac mannan, water, 20°C, 60000 rpm and phase plate angle 70°. Times after reaching the top speed is shown below each diagram. The upper and lower patterns in each diagram are traditional (Zairai-shu) and Chinese species (Shina-shu), respectively. Sedimentation is from light to left.

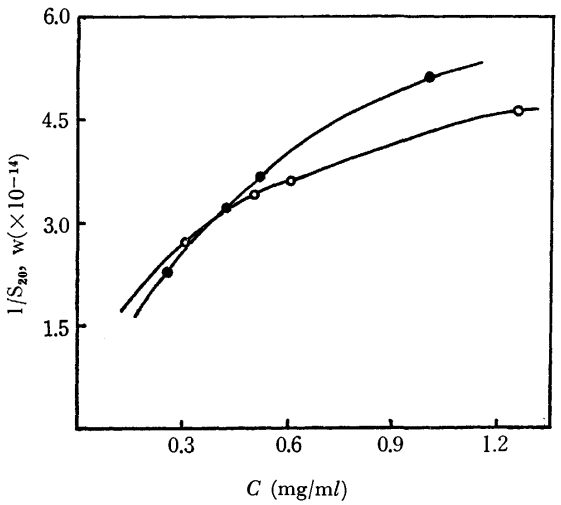

Fig. 2. The sedimentation coefficient as a function of concentration for purified konjac mannan: (○) Traditional species; (●) Chinese species.
Sedimentation analysis was carried out under the follwing condition: water, 20°C and 60000 rpm.

890 (β-glucosidic and β-mannosidic linkages), 1640, and 1720 cm^{-1}. Since the absorptions at 1640 and 1720 cm^{-1} are very weak in the IR chart, they cannot be attributed to uronic acid or the like; rather, it seems that they may be attributed to the trace of absorbed water[11] or to that of protein. However, no entirely reasonable explanation of these absorptions can be given at present. The sedimentation analysis of pure konjac mannan obtained from the traditional species (Zairai-shu) and from the Chinese species (Shina-shu) have been carried out. Each mannan showed only one peak at various intervals of time (Fig. 1). This fact indicates that the konjac mannan purified by the present method consists of ultracentrifugally homogeneous components. Generally, it is known that the linear polymer shows a high concentration dependence of the sedimentation coefficient. Since the purified konjac mannan also shows this phenomenon (Fig. 2), the shape of konjac mannan may be considered to be linear. The difference in the concentration dependence of the mannans suggests that there is some difference in the molecular weight[12] or in the shape of the molecule between the two kinds of mannans.

On complete acid hydrolysis, this purified konjac mannan gave only two spots, corresponding to D-mannose and D-glucose, on paper chromatography. The molar ratio of D-mannose to D-glucose was found to be 1.6 : 1.0 by measuring the spots with a densito-

TABLE 1. PROPERTIES AND RESULTS OF ANALYSES OF THE PURIFIED KONJAC MANNAN

	Konjac flour (intact)	Present method	Nishida and Hashima's method[5,7]	Ohtsuki method[3]
Solubility in water	soluble	soluble	insoluble	insoluble
Solubility in 20% NaOH	insoluble	insoluble	soluble	soluble
Konnyaku forming ability	retained	retained	lost	lost
Reducing power	present	none	none	none
Starch-iodine reaction	positive	negative	negative	negative
C(%)[a]		43.87, 44.01		43.76, 43.47
H(%)[a]		6.16, 6.22		6.47, 6.31
P(%)	0.35	none	trace	
N(%)		trace	0.01—0.02	
Ash(%)	5.23	<0.10	0.10—0.49	0.66—0.81

a) Calculated for $(C_6H_{10}O_5+\frac{1}{8}H_2O)_n$ as indicated by Ohtsuki[3]. C, 43.83%; H, 6.28%.

11) M. Tsuboi, *J. Polymer Sci.*, **25**, 159 (1957).
12) The details of the molecular weight will be described in the following paper.

meter. When the reducing sugar in this acid-hydrolysis mixture was determined by the Bertrand method as modified by Tomoeda, the total content of the reducing sugar was shown to be 96% as D-glucose.

The konjac mannan did not produce any precipitate during the process of the purifying dialysis. This fact and the negligible contents of nitrogen and ashes (Table 1 and Fig. 3) suggest that the inorganic substances and/or the nitrogen-containing substances are not bound with the mannan molecule, as has been mentioned by Kondo and Okimasu.[13]

Purity. This purity was confirmed by elemental analysis, by the ultracentrifuge pattenrs, the ash contentents, and the absence of any reaction of reducing sugars or of starch-iodine. These results are summarized in the above table.

Experimental

Purification Procedure. Ten grams of commercial konjac flour were extracted with three 50 m*l* portions of 50 v/v% ethanol at room temperature for three days. After extraction and filtration, a 50 m*l* portion of 80 v/v% ethanol was added to the residual flour. The flour was then collected and dried at 80—90°C to yield 7.80 g of flour apparently similar to the original flour.

Into 1000 m*l* of water were stirred 4.10 g of the above flour in small portions at room temperature; the stirring was continued for 2—3 hr until the mannan had been completely dissolved. The colloidal solution thus obtained was centrifuged at 15000 rpm for 30 min to remove the insoluble substances. The colorless and transparent supernatant liquid was dialyzed for 72 hr at 9—10°C through a cellulose membrane (VISKING) against running distilled water, and then lyophilyzed. We thus obtained 3.54 g of the purified product.

Preliminary Experiments for the Purification. The above purification procedure was established on the basis of the following experiments.

1) When the commercial konjac flour had been purified without extraction with an ethanol solution, as has been described above, the aqueous solution (0.176%) of the purified product became a slightly yellowish pink after a few days at 9—10°C. Therefore, it seems to have been contaminated with some substance. This substance was removed by extracting the starting flour with 50 v/v% ethanol.

2) The optimum concentration of the dialyzing solution and the necessary time of dialysis have been determined by measuring the ash contents of the lyophilyzed konjac mannan. Figure 3 shows the relationship between the ash content and the dialysis time at various concentrations. These results show that the more concentrated solution is dialyzed more effectively. Thus, the optimum conditions of dialysis were determined to be 0.411 w/w% and 72—96 hr.

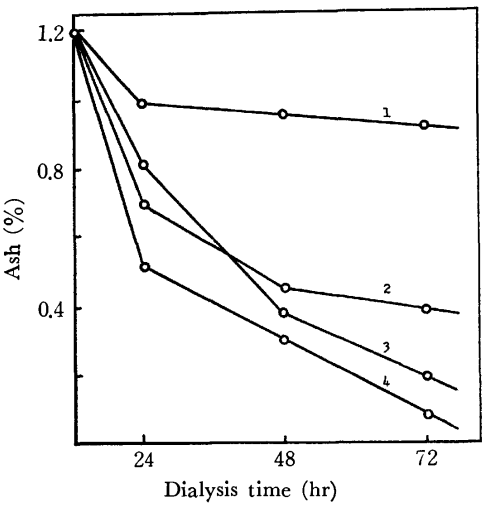

Fig. 3. The Effect of concentration on dialysis.
1: 0.085 2: 0.176 3: 0.252 4: 0.411 w/w%

Hydrolysis and Paper Chromatography. A mixture of 500 mg of the purified konjac mannan and 25 m*l* of N sulfuric acid was heated in a boiling water bath for 24 hr under reflux. According to the usual procedure, the hydrolyzate was paper-chromatographed (Toyo No. 50; *n*-butanol: ethanol : water 40 : 11 : 19; aniline-phthalic acid). The ratio of D-mannose to D-glucose was determined by measuring the area of each intensity integral by means of a densitometer.

The sedimentation patterns were obtained by the use of a Hitachi ultracentrifuge Model UCA-IA.

The authors are grateful to Mr. Koichi Kanna, Tokai Regional Fisheries Research Laboratory, for his measurement of the ultracentrifuge patterns and to Mr. Kyuzaburo Furuhashi, Department of Chemistry, Tokyo Kyoiku University, for the elemental analyses. Thanks are also due to Professor Yutaka Shimizu, Department of Fisheries, Kochi University, his helpful advice and continuous encouragement, and to Mr. Manzo Shimizu, the president of Kabushikikaisha Shimizu Manzo Shoten, for permission to publish this work.

13) Y. Kondo and S. Okimasu, *Journal of Food Science and Technology*, Vol. 14, No. 8, 19 (1967).

Aroyl Arenesulfonyl Peroxides. III. Thermal Decomposition of *p*-Chlorobenzoyl *p*-Toluenesulfonyl Peroxide.[1]

Ryuki HISADA, Michio KOBAYASHI, and Hiroshi MINATO

Department of Chemistry, Tokyo Metropolitan University, Fukazawa, Setagaya-ku, Tokyo

(Received July 21, 1971)

p-Chlorobenzoyl *p*-toluenesulfonyl peroxide was synthesized. Its spontaneous decomposition in benzene or in carbon tetrachloride did not follow a first-order rate equation because of the rate acceleration due to *p*-toluenesulfonic acid produced. When powdery magnesium oxide was suspended in benzene, isomerization to *p*-chlorophenyl *p*-toluenesulfonyl carbonate was completely inhibited, and the rate followed a first-order equation. The products of decomposition (*p*-chlorobiphenyl, *p*-chlorobenzoic acid, *p*-toluenesulfonic acid, phenyl *p*-toluenesulfonate, *etc*) were accounted for in terms of initial formation of *p*-toluenesulfonyloxy and *p*-chlorobenzoyloxy radicals. *p*-Toluenesulfonyloxy radical was found to be a very effective hydrogen-abstractor with little tendency to add to benzene.

The synthesis and decomposition of benzoyl *p*-toluenesulfonyl peroxide was described in a previous paper.[2] Spontaneous decomposition in benzene was mainly an acid-catalyzed isomerization to phenyl *p*-toluenesulfonyl carbonate (42 mol%), but when powdery magnesium oxide was added the extent of isomerization decreased (22 mol%) and products ascribable to phenyl radical[2,3] were found (biphenyl, 44 mol%).

Such facile isomerization is undoubtedly due to the strong electron-withdrawing tendency of the *p*-toluenesulfonyl group. Thus, it is expected that a substituted benzoyl *p*-toluenesulfonyl peroxide with an electron-withdrawing substituent on the benzoyl group may undergo completely homolytic decomposition yielding benzoyloxy radical and *p*-toluenesulfonyloxy radical. As an example of such peroxide, *p*-chlorobenzoyl *p*-toluenesulfonyl peroxide (CTP) was synthesized and its decomposition was investigated.

Results and Discussion

p-Chlorobenzoyl *p*-toluenesulfonyl peroxide (CTP) was prepared by a reaction between *p*-toluenesulfonyl chloride, *p*-chloroperoxybenzoic acid and potassium hydroxide at −22°C.

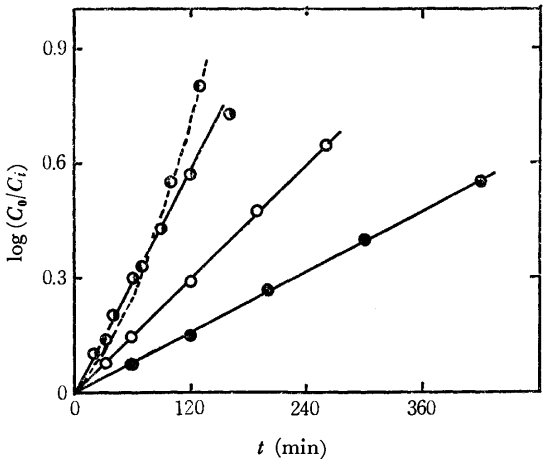

Fig. 1. Plots of $\log(C_0/C_i)$ *vs.* time for the decomposition of CTP in C_6H_6 in the presence of MgO.
● 40.0°C, ○ 45.0°C, ◑ 50.0°C, ◐ 45.0°C, in the absence of MgO

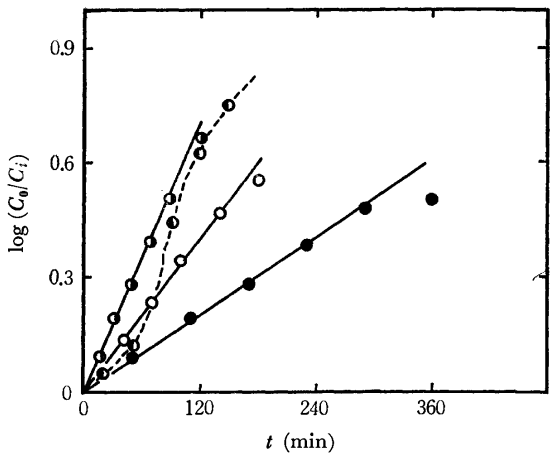

Fig. 2. Plots of $\log(C_0/C_i)$ *vs.* time for the decomposition of CTP in CCl_4 in the presence of MgO.
● 45.0°C, ○ 50.0°C, ◑ 55.0°C, ◑ 50.0°C, in the absence of MgO

Spontaneous decomposition of CTP without any additives in benzene or carbon tetrachloride did not follow a first-order rate equation because of the rate acceleration due to the *p*-toluenesulfonic acid produced. However, when powdery magnesium oxide was suspended in the medium, the decomposition followed an ordinary first-order rate equation. Figures 1 and 2 show the rate of decomposition. The rate constants obtained are listed in Table 1. Arrhenius plots are shown in Fig. 3. In benzene with

Table 1. First-order rate constants for the decomposition of CTP

Temp. (°C)	in C_6H_6 + suspended MgO $k_1\times10^5$ (sec^{-1})	in CCl_4 + suspended MgO $k_1\times10^5$ (sec^{-1})
40.0	5.08	—
45.0	9.56	6.42
50.0	18.0	12.9
55.0	—	20.3
E_a (kcal/mol)	25.4	24.1
$\Delta S^{\neq}$ (e. u.)	+1.0	−3.9

1) Organic Sulfur Compounds. Part XXVII.
2) R. Hisada, H. Minato, and M. Kobayashi, This Bulletin, **44**, 2541 (1971).
3) R. Hisada, N. Kamigata, H. Minato, and M. Kobayashi, This Bulletin, **44**, 3475 (1971).

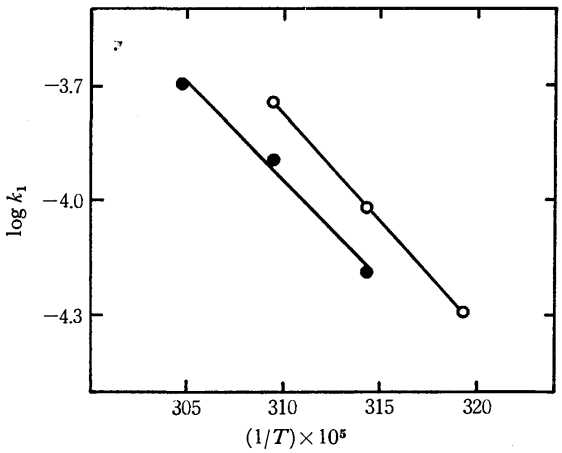

Fig. 3. Arrhenius plot for the decomposition of CTP.
○ in C_6H_6 + MgO, ● in CCl_4 + MgO

TABLE 2. DECOMPOSITION PRODUCTS OF CTP[a)]

CTP (mmol)	5	4.5	2.5	3.5
Solvent (m*l*)	C_6H_6 50	C_6H_6 150	CCl_4 120	CCl_4 170
Additives (mmol)	—	MgO 45	—	MgO 35
Products (mol/mol of CTP)				
Carbon dioxide	—	0.53	0.45	0.60
p-Chlorophenyl *p*-toluenesulfonyl carbonate	0.42	0	0.12	0.07
p-Chlorobiphenyl	0.002	0.56	—	—
Biphenyl	trace	0.01	—	—
p-Dichlorobenzene	—	—	0.42	0.59
Hexachloroethane	—	—	0.19	0.38
p-Chlorobenzoic acid	0.27	0.16	0.26	0.09
p-Toluenesulfonic acid	0.48	0.75	0.71	0.37
Phenyl *p*-chlorobenzoate	0.07	0.10	—	—
p-Tolyl *p*-chlorobenzoate	trace	—	0.005	—
p-Chlorophenyl *p*-chlorobenzoate	0.01	—	trace	—
Phenyl *p*-toluenesulfonate	0.04	0.03	—	—
p-Chlorophenyl *p*-toluenesulfonate	trace	—	0.01	0.08
Chloride ion	—	—	0.06	>0.05
Accounted for				
p-Chlorophenyl- (%)	78	82	81	83
p-Toluenesulfonyloxy- (%)	94	78	84	52

a) Temperature, 45°C; Reaction time, 20 hr. These data are the average of two experiments. Experimental errors are within ±2%.

magnesium oxide, E_a was 25.5 kcal/mol and $\Delta S^{\neq}$ +1.0 e.u., whereas in carbon tetrachloride with magnesium oxide, E_a was 24.1 kcal/mol and $\Delta S^{\neq}$ −3.9 e.u.

Table 2 shows the products of decomposition of CTP in benzene and carbon tetrachloride in the absence and presence of magnesium oxide.

In the absence of magnesium oxide in benzene, isomerization to the mixed anhydride took place to a considerable extent (42 mol%), whereas in the presence of magnesium oxide isomerization was completely inhibited. The yields of various products in benzene can be summarized in the following scheme.

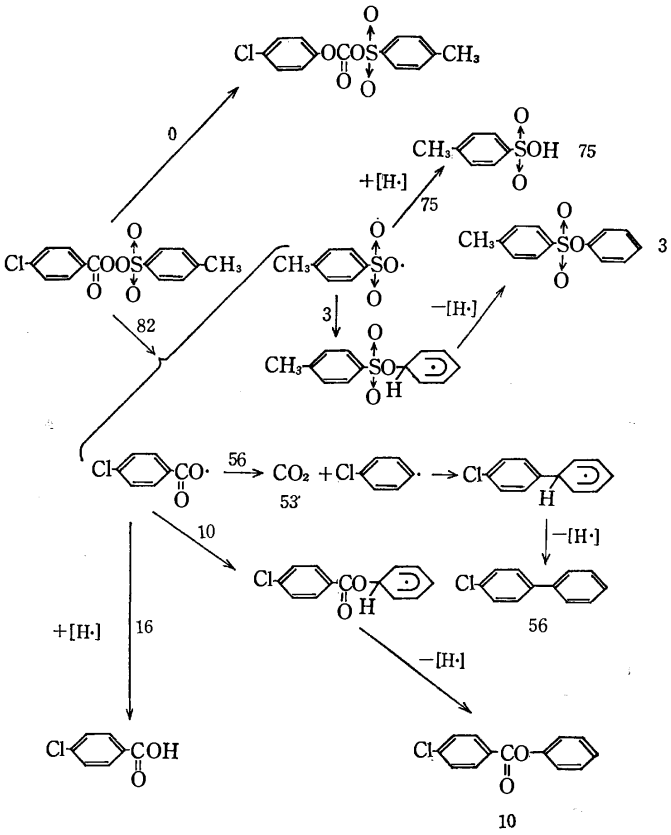

It is interesting to compare the behavior of three different radicals produced, namely, *p*-chlorophenyl, *p*-chlorobenzoyloxy and *p*-toluenesulfonyloxy radicals. Very reactive *p*-chlorophenyl radical almost exclusively adds to benzene molecules surrounding the radical (chlorobenzene was not detected), whereas the fate of *p*-chlorobenzoyloxy radical is 10 addition to benzene *versus* 16 hydrogen-abstraction from cyclohexadienyl radicals. *p*-Toluenesulfonyloxy radical must be a very effective hydrogen-abstractor, since its fate was 3 addition to benzene *versus* 75 hydrogen-abstraction from cyclohexadienyl radicals. The sulfonyloxy radical is stable enough to stay unreacted in the medium until it collides with cyclohexadienyl radicals (*p*-chlorophenyl-, *p*-chlorobenzoyloxy-, or *p*-toluenesulfonyloxycyclohexadienyl radicals.)

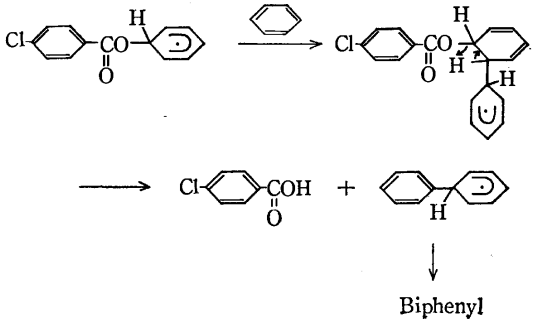

Decomposition of CTP in benzene with magnesium oxide produced unsubstituted biphenyl in 1.1 mol% yield. It was identified by gas chromatography, elution chromatography and infrared spectroscopy. A plausible mechanism of its formation is the above.

When CTP was decomposed in carbon tetrachloride, addition of magnesium oxide did not result in complete inhibition of rearrangement, and the mixed anhydride was produced in 7.4 mol% yield. However, formation of *p*-dichlorobenzene (58.7 mol%) and hexachloroethane (38 mol%) indicates that homolysis is a major reaction. A comparison of the yields of *p*-dichlorobenzene and hexachloroethane ($38\times2-58.7=17.3$) indicates that a part of trichloromethyl radicals arose from the Cl-abstraction of carbon tetrachloride by radicals other than *p*-chlorophenyl radical. *p*-Chlorobenzoyloxy radical may be responsible for this, but it was not possible to isolate *p*-$ClC_6H_4CO_2Cl$, the product of such Cl-abstraction.

Of the four different cases of decomposition of CTP, that in benzene with suspended magnesium oxide is the most interesting, the decomposition being completely homolytic. This paper seems to be the first to describe the formation of a sulfonyloxy radical without competing side reactions.

Experimental

Materials. Benzene, carbon tetrachloride and *p*-toluenesulfonyl chloride were purified according to procedures described previously.[2] *p*-Chloroperoxybenzoic acid was prepared by the method used for the synthesis of *p*-nitroperoxybenzoic acid;[4] yield, 84.1%; mp 110—112°C (lit,[5] 111—113°C). Powdery magnesium oxide was heated in a crucible, cooled and then used.

Preparation of p-*Chlorobenzoyl* p-*Toluenesulfonyl Peroxide (CTP).* This new peroxide could not be prepared by the method used for the synthesis of benzoyl *p*-toluenesulfonyl peroxide. It was synthesized as follows. A solution of *p*-tosyl chloride (9.6 g, 0.05 mol) in dichloromethane (200 m*l*) was cooled to −22°C in a four-necked round-bottomed flask equipped with a mechanical stirrer, a dropping funnel, a thermometer and a calcium chloride tube. Then, an aqueous 50% KOH solution (12 g) was added drop by drop with stirring. The temperature rose to some extent. After the solution was again cooled to −22°C, a solution of *p*-chloroperoxybenzoic acid (11.2 g, 0.06 mol) in dichloromethane (1 *l*) was added slowly while the temperature was kept below −20°C, it was washed with 10 *l* of ice water and dried over anhydrous magnesium sulfate. Evaporation of the dichloromethane under reduced pressure yielded a brownish residue, which gave colorless needles (9.3 g, 57%) upon recrystallization from ether. Recrystallization was repeated twice more and the crystals obtained were used for the experiments. They were stable for a long period at −20°C. Mp, 73—74°C (decomp). The main IR absorptions were observed at 1785, 1395, 1220, 1195, and 1180 cm^{-1}.

Found: C, 51.49; H, 3.17; Cl, 11.01; S, 9.68%. Calcd for $C_{14}H_{11}O_5ClS$: C, 51.46; H, 3.39; Cl, 10.85; S, 9.81%.

Kinetic Measurements. Rates of decomposition were measured by the procedure used for benzoyl *p*-toluenesulfonyl peroxide.[2] A 0.02 N $Na_2S_2O_3$ solution was used instead of a 0.05 N solution.

Analyses of Products of Decomposition. Products of decomposition of CTP were analyzed by a procedure essentially similar to that used in the case of benzoyl *p*-toluenesulfonyl peroxide. Since *p*-chlorophenyl *p*-toluenesulfonyl carbonate was found to decompose in a chromatographic column containing silica gel (Wako Gel Q22; 200 mesh), the reaction mixture was treated with aniline. When the mixture thus treated was subjected to elution chromatography, *p*-chlorophenyl *N*-phenylcarbamate produced was eluted with a hexane-benzene (1 : 2) mixed solvent.

Other products were determined by vapor phase chromatography. For determination of products from the decomposition in benzene, an Apiezon L column was used for *p*-chlorobiphenyl (internal standard, bibenzyl) and various esters (internal standard, *p*-tolyl benzoate). For determination of products in carbon tetrachloride, a silicone oil SE 30 column was used for *p*-dichlorobenzene and hexachloroethane (internal standard, *p*-dibromobenzene) and an Apiezon L column was used for various esters (internal standard, phenyl *p*-chlorobenzoate).

Preparation of p-*Chlorophenyl* p-*Toluenesulfonyl Carbonate.* *p*-Chlorophenyl chloroformate was prepared from *p*-chlorophenol and a 30% toluene solution of phosgene according to the method of Oesper *et al.*[6]; yield, 70.0%; bp 112.5—114°C/20 mmHg (lit,[6] 114°C/20 mmHg).

A solution of *p*-chlorophenyl chloroformate (2.8 g, 0.015 mol) and silver *p*-tosylate (4.2 g, 0.015 mol) in acetonitrile (50 m*l*) was refluxed for 10 hr. The silver chloride precipitated was filtered off, the acetonitrile was evaporated under reduced pressure, and recrystallization of the residue from ether-hexane yielded white crystals (3.1 g, 63.3%). Mp. 123—124°C. This mixed anhydride has not been reported in the literature. Its main IR absorptions were observed at 1785, 1395, 1245, and 1180 cm^{-1}.

Found: C, 51.37; H, 3.44; Cl, 10.58; S, 10.03%. Calcd for $C_{14}H_{11}O_5ClS$: C, 51.46; H, 3.39; Cl, 10.85; S, 9.81%.

Grateful acknowledgement is made to the donors of the Petroleum Research Fund, administered by the American Chemical Society, for support of this research.

4) M. Vilkas, *Bull. Soc. Chim. Fr.*, **1959**, 1401.

5) C. G. Overberger and R. W. Cummins, *J. Amer. Chem. Soc.*, **75**, 4250 (1953).

6) R. E. Oesper, W. Broker, and W. A. Cook, *ibid.*, **47**, 2609 (1925).

The Reduction of Chlorodeoxy Sugars by Tributyltin Hydride

Hitoshi ARITA, Nobuhiko UEDA, and Yoshio MATSUSHIMA

Department of Chemistry, Osaka University College of Science, Toyonaka

(Received July 23, 1971)

Acetylated chlorodeoxy sugars were prepared by the use of sulfuryl chloride. These chlorodeoxy sugars were then successfully reduced to deoxy sugars by the use of tri-*n*-butyltin hydride. α,α'-Azobis-isobutyronitrile, which has been known to be an effective radical initiator, was found to be indispensable for the reaction.

The deoxy sugars, long known as the components of many natural products, form an important class of carbohydrates. There have been many reports on the synthesis of deoxy sugars.[1] The reduction of deoxyhalo-sugars is one of the most important methods, and various effective reducing agents have been employed for this purpose. Lithium aluminum hydride or Raney nickel are excellent reagents, but they are not suitable for the reduction of sugar derivatives labile to alkali. To find milder reduction conditions, the present authors have investigated organotin hydride as a reducing agent of deoxyhalo sugars. Trialkyltin hydride[2] has recently been used for the selective reduction of organic halides. As reported in the previous paper,[3] we were successful in obtaining the 4'-deoxymaltose derivative in a fairly good yield by using organotin hydride and it was found that scarcely any by-product was produced during the course of the reaction. Therefore, this reagent will be useful for the synthesis of deoxy sugars. Jennings and Jones established that sulfuryl chloride could be used for the preparation of chlorodeoxy sugars.[4] We prepared *O*-acetylated chlorodeoxy sugars using this reagent. These *O*-acetyl-chlorodeoxy sugars were successfully converted to deoxy sugars by the use of organotin hydride under mild conditions. The structure of the deoxy sugars synthesized were confirmed by the NMR method and by gas-liquid chromatography. The reaction courses of the preparation of the deoxy sugars are represented in Scheme 1, while the retention times of the deoxy sugars thus obtained are summarized in Table 1.

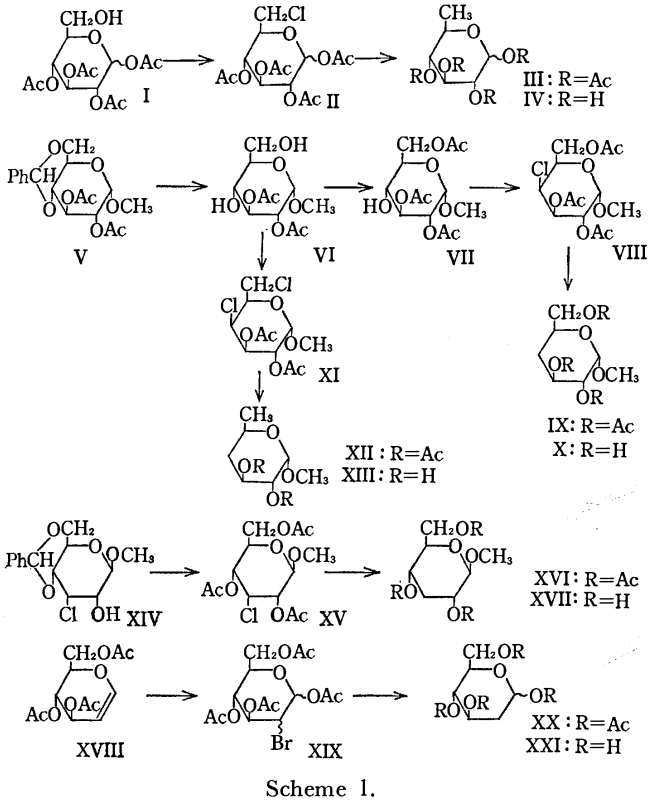

Scheme 1.

TABLE 1. RETENTION TIMES (min) OF DEOXY SUGARS

Methyl 2-deoxy-arabinohexopyranoside	6.8
Methyl 3-deoxy-ribohexopyranoside	6.1
Methyl 4-deoxy-xylohexopyranoside	7.8 8.6
Methyl 6-deoxy-glucopyranoside	8.5 9.0

Gas chromatography was carried out at 185°C. Other conditions are described in the text.

Results and Discussion

Among the various tri-alkyltin hydrides, we chose tri-*n*-butyltin hydride because of its high reactivity and ease of preparation. The compound was stable at room temperature under a nitrogen atmosphere. During the course of this study, we found two important facts. The reduction of chlorodeoxy sugars by organotin hydride was unsuccessful if α,α'-azobis-isobutyronitrile was not present, also. By the addition of a small amount of the latter compound, though reduction proceeded smoothly under mild conditions. Menapace[5] proposed a radical mechanism for the reduction by the use of organotin hydride; in accordance with this proposal, the reduction of chlorodeoxy sugars also needed a radical initiator. The other point concerned the nature of the blocking groups of hydroxyls. We attempted to reduce methyl 4,6-*O*-benzylidene-3-chloro-3-deoxy-β-D-allopyranoside (XIV)[6] without success, in spite of the co-existence of α,α'-azobis-isobutyronitrile. On the other hand, the reduction of methyl 3-chloro-3-deoxy-

1) S. Henessian, *Advan. Carbohyd. Chem.*, **21**, 143 (1966).
2) G. J. M. Van Der Kerk, J. G. Noltes, and J. G. A. Lujiten, *J. Appl. Chem.*, **7**, 366 (1957).
3) H. Arita, and Y. Matsushima, *J. Biochem.*, (Tokyo), **70**, 795 (1971).
4) H. J. Jennings and J. K. N. Jones, *Can. J. Chem.*, **49**, 1408 (1962).
5) L. W. Menapace and H. G. Kuivila, *J. Amer. Chem. Soc.*, **86**, 3047 (1964).
6) H. J. Jennings and J. K. N. Jones, *Can. J. Chem.*, **43**, 2372 (1965).

2,4,6-tri-*O*-acetyl-β-D-allopyranoside (XV) proceeded smoothly. The reduction of methyl 4,6-dichloro-4,6-dideoxy-2,3-di-*O*-acetyl-α-D-galactopyranoside (XI) at 60°C gave methyl 4-deoxy-6-chloro-6-deoxy-2,3-di-*O*-acetyl-α-D-xylohexopyranoside[7] as the main product. The reactivity of primary and secondary halogenide agreed with the data presented by Menapace.[5] The yield of the reduction of each chlorodeoxy sugars was over 85%, and the separation of the product from the reaction mixture was complete and easy.

Experimental

General Methods. All the melting points are uncorrected. The nuclear magnetic resonance spectra were recorded at 60 MHz in chloroform-*d*, with tetramethylsilane as the internal standard. Thin-layer chromatography (tlc) was performed with silica gel G (Merck). The spots were detected by spraying with 5% sulfuric acid in methanol and by subsequent heating at 150°C. A Shimadzu gas chromatograph model GC-4A equipped with a 0.3×300 cm column of 5% SE-30 on chromosorb W (80—100 mesh) was employed. A sample was methanolyzed in a sealed glass tube with 1 N hydrogen chloride in methanol at 100°C for 2 hr. After the methanolysate had been dried up *in vacuo*, the residue was trimethylsilylated.[8]

Tri-n-butyltin Hydride. This reagent was prepared by the thermal decomposition of tri-*n*-butyltin formate according to the method of Okawara and Ohara.[9]

1,2,3,4-Tetra-O-acetyl-D-glucopyranose (I). Compound I was prepared by the detritylation of 6-*O*-trityl-1,2,3,4-tetra-*O*-acetyl-D-glucopyranose according to the method of Helferich and Klein.[10]

6-Chloro-6-deoxy-1,2,3,4-tetra-O-acetyl-D-glucopyranose (II). Compound I (14.5 g) was dissolved in 100 m*l* of anhydrous pyridine, and the solution was cooled in an ice-water bath. Into this solution was then stirred sulfuryl chloride (4.5 m*l*) and the mixture was kept at 4—5°C overnight. The excess sulfuryl chloride was destroyed by a few drops of water, and the mixture was extracted with chloroform (3×150 m*l*). The chloroform extracts were washed with water, 5% aqueous sulfuric acid, and finally with water. Evaporation *in vacuo* gave a reddish residue, which was decolorized with Norit A. Crystallization occurred in absolute methanol, and recrystallization in the same solvent gave 11.5 g of colorless needles. Mp 113—115°C, $[\alpha]_D = +113°$ (*c* 0.51, chloroform). Found: C, 45.43; H, 5.17; Cl, 9.87%. Calcd for $C_{14}H_{19}O_9Cl$: C, 45.85; H, 5.22; Cl, 9.67%.

6-Deoxy-1,2,3,4-tetra-O-acetyl-D-glucopyranose (III). Compound II (1.5 g) was dissolved in anhydrous toluene (10 m*l*), and to the solution were added tri-*n*-butyltin hydride (2.0 g) and α,α'-azobis-isobutyronitrile (15 mg) under a nitrogen atmosphere. The reaction was continued overnight under stirring in an oil bath kept at 80—90°C. On the evaporation *in vacuo* of the solution, crystals appeared immediately. They were washed with ligroin several times to remove the organotin compounds; subsequent recrystallization in methanol gave 1.3 g of colorless needles. Mp 141.5—142.5°C NMR data: δ1.1 (3-H d, C-CH_3), 2.0—2.1 (12-H $-COCH_3$). Found: C, 50.79; H, 6.15%. Calcd for $C_{14}H_{20}O_9$: C, 50.60; H, 6.07%.

6-Deoxy-D-glucopyranose (IV). 6-Deoxy-1,2,3,4-tetra-*O*-acetyl-D-glucopyranose (III, 800 mg) was deacetylated in 0.1 M sodium methoxide in methanol. The solution was deionized with Dowex 50×8 (H^+) and dried up *in vacuo*. Crystallization cocurred in ethyl acetate, giving 380 mg of a colorless specimen. Mp 144—145°C, $[\alpha]_D^{24} = +78°$ (*c* 0.98, H_2O). A previous report[11] gave a mp of 146°C, $[\alpha]_D^{20} + 70°$. Found: C, 43.42; H, 7.23%. Calcd for $C_6H_{12}O_5$: C, 43.90; H, 7.37%.

Methyl 4,6-O-Benzylidene-2,3-di-O-acetyl-α-D-glucopyranoside (V). Compound V was prepared from methyl 4,6-*O*-benzylidene-α-D-glucopyranoside by acetylation with acetic anhydride and pyridine. Mp 108—109°C, $[\alpha]_D = +170°$ (*c* 0.5, chloroform). Found: C, 58.88; H, 6.04%, Calcd for $C_{18}H_{22}O_8$: C, 59.01; H, 6.05%.

Methyl 2,3,-Di-O-acetyl-α-D-glucopyranoside (VI). Compound V (17 g) was dissolved in 80% aqueous acetic acid (200 m*l*) and the solution was kept at 60°C for 2 hr. On the evaporation *in vacuo* of the solution, a syrupy product remained which showed a single spot on thin-layer chromatography.

Methyl 2,3,6-Tri-O-acetyl-α-D-glucopyranoside (VII). Compound VI (6.0 g) was dissolved in a mixture of pyridine (25 m*l*) and chloroform (15 m*l*), after which the solution was cooled in a dry ice-acetone bath. Acetic anhydride (2.25 m*l*) was then added carefully to the solution, and it was kept at −20°C for 24 hr. Subsequent evaporation *in vacuo* gave a syrupy residue, which was put on a silica-gel column; the column was then eluted with ethylacetate-toluene (1 : 1). Methyl 2,3,6-tri-*O*-acetyl-α-D-glucopyranoside (VII) was separated; it showed a single spot on tlc. Yield, 4.2 g.

Methyl 4-Chloro-4-deoxy-2,3,6-tri-O-acetyl-α-D-galactopyranoside (VIII). Compound VII (1.6 g) was dissolved in anhydrous pyridine (20 m*l*) and to this solution was added, drop by drop, sulfuryl chloride (0.7 m*l*) under cooling in an ice-water bath. The mixture was kept at room temperature overnight. The excess sulfuryl chloride was destroyed by the addition of a few drops of water, the reaction mixture was extratced with chloroform (3×50 m*l*), and the extracts were washed with 5% aqueous sulfuric acid and then with water. Evaporation *in vacuo* gave a reddish syrup, which was decolorized in methanol with Norit A. Crystallization occurred in ethanol-ligroin, and recrystallization in the same solvent gave 1.1 g of colorless needles. Mp 80—81°C, $[\alpha]_D^{24} = +180.7°$ (*c* 0.65, chloroform). Found: C, 46.11; H, 5.66; Cl, 10.67%. Calcd for $C_{13}H_{19}O_8Cl$: C, 46.09; H, 5.65; Cl, 10.47%.

Methyl 4-Deoxy-2,3,6-tri-O-acetyl-α-D-xylohexopyranoside (IX). Compound VIII (580 mg) was mixed with toluene (10 m*l*), tri-*n*-butyltin hydride (600 mg), and α,α'-azobis-isobutyronitrile (10 mg), and the reaction was continued overnight under a nitrogen atmosphere in an oil bath kept at 80°C. The reaction mixture was then dired up *in vacuo*, and a residual syrup was crystallized in ligroin. Recrystallization in the same solvent gave 453 mg of colorless crystals. Mp 74—75°C, $[\alpha]_D^{25} = +133.2°$. One previous report[7] gave a mp of 76—77°C, $[\alpha]_D + 134°$, and another[12] a mp of

7) B. T. Lawton, W. A. Szarek, and J. K. N. Jones, *Carbohyd. Res.*, **15**, 397 (1970).

8) C. C. Sweeley, R. Bentley, M. Makita, and W. W. Wells, *J. Amer. Chem. Soc.*, **85**, 2497 (1963).

9) R. Okawara and M. Ohara, *J. Organometal. Chem.*, **3**, 484 (1965).

10) B. Helferich and W. Klein, *Ann. Chem.*, **450**, 219 (1926).

11) K. Freudenberg, H. Eich, C. Knoevenagel, and W. Westphal, *Ber.*, **73** 441 (1940).

12) E. J. Hedgley, W. G. Overend, and R. A. C. Rennie, *J. Amer. Chem. Soc.*, **85**, 4701 (1963).

74°C $[\alpha]_D$+135° (*c* 0.52, chloroform), Found: C, 50.79; H, 6.41%. Calcd for $C_{13}H_{20}O_8$: C, 51.31; H, 6.62%.

Methyl 4-Deoxy-α-D-xylohexopyranoside (X). Compound IX (300 mg) was deacetylated with 0.1 M sodium methoxide in methanol. Crystallization occurred in ethyl acetate, giving 160 mg of a colorless specimen. Mp 91—93°C, $[\alpha]_D^{25}$=+175.2° (*c* 1.0, water) Found: C, 47.32; H, 7.91%. Calcd for $C_7H_{14}O_5$: C, 47.18; H, 7.92%.

Methyl 4,6-Dichloro-4,6-dideoxy-2,3-di-O-acetyl-α-D-galactopyranoside (XI). Methyl 2,3-di-*O*-acetyl-α-D-glucopyranoside (VI, 5.5 g) was dissolved in anhydrous pyridine (65 m*l*) and the solution was cooled in an ice-water bath. To the solution sulfuryl chloride (5.1 m*l*) was then added and it was kept at 4°C overnight. The reddish-colored reaction solution was extracted with chloroform (7×50 m*l*), and the extracts were washed with water, 5% aqueous sulfuric acid, and finally with water. Evaporation *in vacuo* gave a syrup, which was then decolorized in methanol with Norit A. Crystallization in ethanol-ligroin gave 4.2 g of a colorless specimen. Mp, 103.5—105°C; $[\alpha]_D^{25}$=+162.9° (*c* 0.5, chloroform). Found: C, 42.07; H, 5.09; Cl, 22.55%. Calcd for $C_{11}H_{16}O_6Cl_2$: C, 41.92; H, 5.11; Cl, 22.50%.

Methyl 4,6-Dideoxy-2,3-di-O-acetyl-α-D-xylohexopyranoside (XII). Compound XI (1 g) was mixed with anhydrous toluene (20 m*l*), tri-*n*-butyltin hydride (2.8 g), and α,α′-azobis-isobutyronitrile (10 mg), and the mixture was refluxed overnight. Evaporation *in vacuo* gave 780 mg of a colorless syrup, which was purified by silica-gel column chromatography. The syrup thus obtained showed a single spot on tlc. NMR data: δ 1.1 (3-H, d, C-CH_3) 2.0—2.1 (6-H -$COCH_3$), 3.2 (3-H -OCH_3).

Methyl 4,6-Dideoxy-α-D-xylohexopyranoside (XIII). The deacetylation of Compound XII with sodium methoxide gave a colorless syrup, which crystallized on standing. Yield, 450 mg; mp, 106—108°C, $[\alpha]_D^{28}$=+168° (*c* 0.8, methanol). A previous report[13] gave a mp of 107—109°C, $[\alpha]_D$+171° (*c* 1.0 methanol). Found: C, 51.69 H, 8.61%.

Methyl 4,6-O-Benzylidene-3-chloro-3-deoxy-β-D-allopyranoside (XIV). Compound XIV was prepared from methyl 4,6-*O*-benzylidene-β-D-glucopyranoside according to the method of Jennings and Jones.[6] Crystallization occurred in ligroin-benzene. Mp 125.5—127°C, $[\alpha]_D^{25}$=−47° (*c* 1.02, chloroform). Found: C, 56.06; H, 5.74; Cl, 11.81%. Calcd for $C_{14}H_{17}O_5Cl$: C, 55.91; H, 5.70; Cl, 11.79%.

Methyl 3-Chloro-3-deoxy-2,4,6-tri-O-acetyl-β-D-allopyranoside (XV). Compound XIV (5 g) was dissolved in 60% aqueous acetic acid (60 m*l*), and the solution was refluxed for 10 min. After cooling, the solution was dried *in vacuo*. The residual syrup was consecutively acetylated with acetic anhydride and pyridine, giving 5 g of a syrupy product.

Methyl 3-Deoxy-2,4,6-tri-O-acetyl-β-D-ribohexopyranoside (XVI). Compound XV (2.5 g) was dissolved in anhydrous toluene (30 m*l*) and reduced by placing it in tri-*n*-butyltin hydride (2.5 g) and α,α′-azobis-isobutyronitrile (20 mg) at 80°C overnight. A syrupy product crystallized from ligroin in a refrigerator. The crystals were dissolved in methanol and treated with Norit A, and recrystallization in ligroin gave 1.8 g of colorless needles. Mp 64—66°C, $[\alpha]_D^{25}$=−45.3° (c 1.07, chloroform). NMR data: δ 2.0—2.1 (9-H -$COCH_3$) 3.24 (3-H -OCH_3). Found: C, 51.20; H, 6.66%. Calcd for $C_{13}H_{20}O_8$: C, 51.31; H, 6.62%.

Methyl 3-Deoxy-β-D-ribohexopyranoside (XVII). Compound XVI was deacetylated with sodium methoxide to Compound XVII. We thus obtained, a colorless syrup which crystallized on standing for a long period. A melting-point determination failed because of the high hygroscopicity of the crystals, $[\alpha]_D^{25}$=−49.5° (*c* 1.01, water). An earlier report[14] gave $[\alpha]_D^{20}$ −46°.

3,4,6-Tri-O-acetyl-glycal (XVIII). Compound XVIII was prepared from 2,3,4,6-tetra-*O*-acetyl-glucosyl bromide by the method of Fischer.[15]

2-Bromo-2-deoxy-1,3,4,6-tetra-O-acetyl-gluco(manno)pyranose (XIX). 3,4,6-Tri-*O*-acetyl-glycal (XVIII, 6.5 g) was dissolved in dichloromethane (25 m*l*), and to this solution was added bromine in dichloromethane until a slightly red color remained. The solution was then dried *in vacuo*, the syrupy residue was instantaneously dissolved in glacial acetic acid (120 m*l*), and mercuric acetate (12 g) was added to the solution. The mixture was then kept at room temperature overnight. The excess acetic acid was removed by evaporation *in vacuo*, and the residue was extracted with chloroform (3×100 m*l*). The extracts were washed three times with aqueous potassium bromide and finally with water. The chloroform layer was dried over calcium chloride and was evaporated *in vacuo*, giving 9 g of a syrup. Found: Br, 18.98%. Calcd for $C_{14}H_{19}O_9Br$: Br, 19.43%.

2-Deoxy-1,3,4,6-tetra-O-acetyl-D-arabinohexopyranose (XX). Compound XIX (1.5 g) was dissolved in anhydrous toluene (15 m*l*), together with tri-*n*-butyltin hydride (1.5 g) and α,α′-azobis-isobutyronitrile (10 mg) under a nitrogen atmosphere. The reaction was allowed to continue for 2 hr at 50—60°C. Subsequent evaporation *in vacuo* gave a colorless syrup, which was purified by silica-gel column chromatography. A syrup highly pure on thin-layer and gas-liquid chromatography was obtained; it weighed 1.1 g but failed to crystallize.

2-Deoxy-D-arabinohexopyranose (XXI). Compound XX (500 mg) was dissolved in cold 0.1 M barium methoxide in methanol and kept overnight in a refrigerator. The solution was then neutralized by adding 0.1 M aqueous sulfuric acid, and the barium sulfate which was thus precipitated was removed by centrifugation. The supernatant was treated with Dowex 50×8 (H^+) and dried up *in vacuo*. The residual syrup was extracted with acetone and crystallized in the same solvent. Mp 139—141°C. A previous report[16] gave a mp 142—144°C. The specimen was also identified by thin-layer chromatography (*n*-BuOH : EtOH : H_2O=3 : 1 : 1).

The authors are especially indebted to the Nitto Kasei Co., Ltd., for its gift of tri-*n*-butyltin oxide.

13) B. T. Lawton, W. A. Szarek, and J. K. N. Jones, *Carbohyd. Res.*, **14** 255 (1970).

14) B. Lindberg and O. Theander, *Acta Chem. Scand.*, **13**, 1226 (1959).

15) E. Fischer, *Ber.*, **47**, 194 (1914).

16) H. R. Bolliger, *Helv. Chim. Acta*, **34**, 989 (1951).

Stereochemical Studies of Monoterpene Compounds. XV.[1] A Conformational Study of Carvomenthone Derivatives by Means of Temperature-dependent Circular Dichroism[2]

Takayuki SUGA and Satoru WATANABE

Department of Chemistry, Faculty of Science, Hiroshima University, Higashisenda-machi, Hiroshima

(Received August 5, 1971)

The conformations of (1*R* : 4*R*)-(−)-*p*-menth-8-en-2-one (**1**) and of diastereoisomeric pairs of (+)-1-hydroxy-*p*-menth-8-en-2-one, (**2**) and (**3**), (+)-1-hydroxy-*p*-menthan-2-one, (**6**) and (**7**), and (+)-1-hydroxy-8-bromo-*p*-menthan-2-one, (**10**) and (**11**), were examined by a combination of infrared spectra and temperature-dependent circular-dichroism (CD). Explanations are given mainly with regard to the epimeric pair, (**2**) and (**3**). It is demonstrated that α-hydroxyketone (**2**) exists in a conformational equilibrium among **2a**, **2b**, and **2c**. The **2a** conformer predominantly exists in a polar medium and at low temperatures, whereas the **2b** conformer is more stable than **2a** in a nonpolar medium. On the other hand, the epimer (**3**) exists preferentially in the **3a** conformation in both polar and nonpolar media and at low temperatures. The CD curves of compounds **6** and **7** exhibited the exactly same behavior as those in compounds (**2**) and (**3**) respectively. These results are interpreted in terms of the competition of the steric factor and the intramolecular hydrogen bonding.

Circular dichroism (CD) at different temperatures has been found to be very useful for investigating the conformational equilibrium in a flexible cyclohexanone structure.[3] α-Hydroxycyclohexanones provide interesting examples because, in addition to a possible conformational equilibrium, intramolecular hydrogen bonding between the hydroxyl and the carbonyl groups can be expected. Djerassi *et al.*[4] have recently demonstrated the conformational mobility in only (1*S* : 4*R*)-(+)-1-hydroxy-*p*-menthan-2-one (**6**), one of the C-1 epimers, on the basis of measurements of the variable temperature CD curves. This

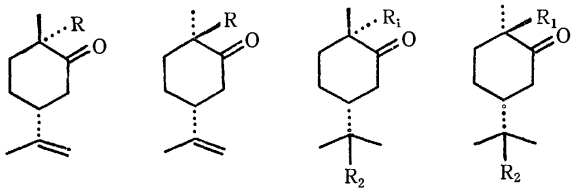

1: R=H **2**: R=OH **4**: R=OAc
3: R=OH **5**: R=OAc
6: R_1=OH R_2=H
7: R_1=OH R_2=H
8: R_1=OAc R_2=H
9: R_1=OAc R_2=H
10: R_1=OH R_2=Br
11: R_1=OH R_2=Br

paper will deal with the conformational analyses of (1*R* : 4*R*)-(−)-*p*-menth-8-en-2-one (**1**) and the epimeric pairs of carvomenthone derivatives, (1*S* : 4*R*)- and (1*R* : 4*R*)-(+)-1-hydroxy-*p*-menth-8-en-2-ones (**2**) and (**3**), their acetates (**4**) and (**5**), (1*S* : 4*R*)- and (1*R* : 4*R*)-(+)-1-hydroxy-*p*-menthan-2-ones (**6**) and (**7**), their acetates (**8**) and (**9**), and (1*S* : 4*R*)- and (1*R* : 4R)-(+)-1-hydroxy-8-bromo-*p*-menthan-2-ones (**10**) and (**11**), all done by means of a combination of infrared spectra and temperature-dependent circular dichroism.

Results and Discussion

The CD curves of (1*R* : 4*R*)-(−)-*p*-menth-8-en-2-one (**1**) in MI and EPA exhibited a positive Cotton effect, and the rotational strength is almost temperature-independent over the range from 25 to −186°C. The menthenone (**1**) may exist in two interconvertible chair conformations, **1a**⇌**1b**. According to the

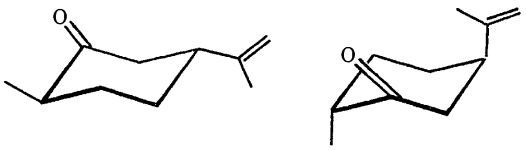

1a **1b**

octant rule,[5] the **1a** conformer should exhibit a positive Cotton effect, and the **1b** conformer, negative one. Therefore, the positive conformer **1a** is more stable than **1b** in respect to the energetic and steric requirements.

The CD curves of α-hydroxyketone (**2**) showed an inversion of the sign of the Cotton effect upon the change in the solvent polarity, as is shown in Fig. 1, in contrast with the corresponding dehydroxyketone (**1**). Such a phenomenon is interpreted in terms of the competition of the steric factor and the intramolecular hydrogen bonding. In the conformational equilibrium, **2a**⇌**2b**, the intramolecularly hydrogen-nonbonded conformer **2a** should exhibit a positive Cotton effect, and the hydrogen-bonded conformer **2b** a negative one. In a nonpolar solvent, the stabili-

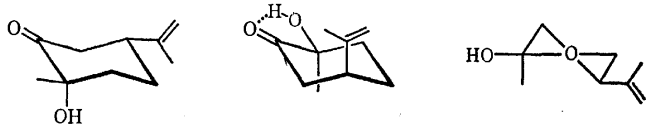

2a **2b** **2c**

1) Paper XIV of this series: T. Suga, K. Imamura, and T. Shishibori, This Bulletin, **45**, 545 (1972).

2) Presented at the 21st Annual Meeting of the Chemical Society of Japan, Osaka, April, 1968.

3) "Optical Rotatory Dispersion and Cicular Dichroism in Organic Chemistry," ed. by G. Snatzke, Heyden & Ltd., London (1967), pp. 16, 335.

4) K. M. Wellman, W. S. Briggs, and C. Djerassi, *J. Amer. Chem. Soc.*, **87**, 73 (1965).

5) W. Moffit, R. B. Woodward, A. Moscowitz, W. Klyne, and C. Djerassi, *ibid.*, **83**, 4013 (1961).

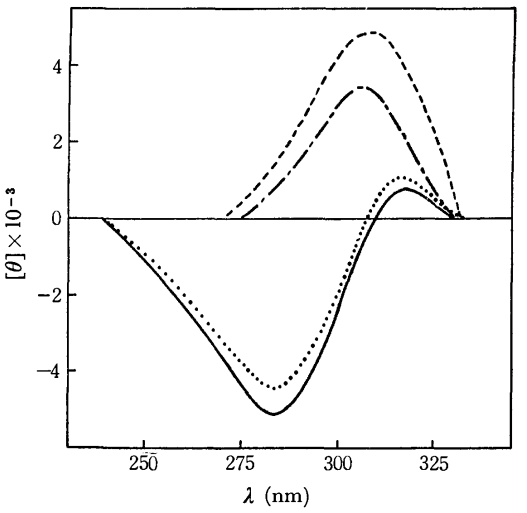

Fig. 1. CD curves of (1*S*: 4*R*)-(+)-1-hydroxy-*p*-menth-8-en-2-one (**2**) in selected solvents at +25°C: ····· in CCl_4, —— in isooctane, ——— in MeOH, and ---- in DMSO.

zation due to intramolecular hydrogen bonding overcomes the steric repulsion.[6] However, the stabilizing intramolecular hydrogen bond will be broken in a polar solvent, so that steric requirements mainly dominate the conformation of **2**. Therefore, the positively-rotating, nonbonded form, **2a**, is preferred in the polar solvents, and the negatively rotating, bonded form, **2b**, in the nonpolar solvents. The conformer populations were calculated[8] on the basis of the CD curves in selected solvents; the results are shown in Table 1.

Table 1. Population of **2b** in selected solvents

Solvent	$R_0^T \times 10^{40}$ (C.G.S.)	Population of **2b** (%)
Isooctane	−3.82	78
CCl_4	−3.67	77
Dioxane	+2.91	13
MeOH	+2.85	13
DMSO	+4.33	0

The predominant existence of the **2b** conformer in a nonpolar solvent, carbon tetrachloride, was further proved by a study of the infrared spectrum, which exhibited two bands, at 3612 (ε 29) and 3512 cm^{-1} (ε 41) (Fig. 2), resulting from a free hydroxyl group and an intramolecularly interacted hydroxyl group[9]

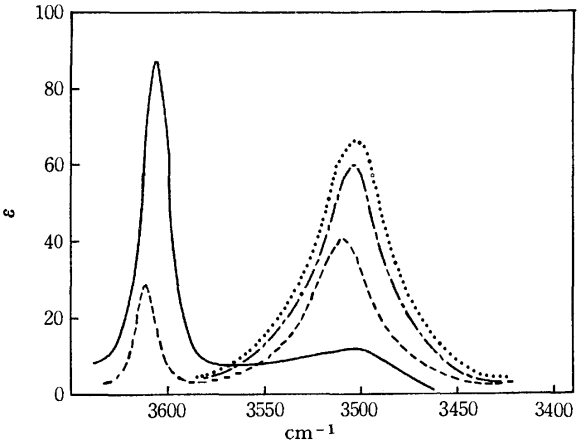

Fig. 2. IR spectra of α-hydroxyketones in carbon tetrachloride at +25°C: ---- for compounds **2**, ——— for **3**, —— for **10**, and ····· for **11**.

between the hydroxyl group and the lone-pair electrons of the carbonyl group. The influence of hydrogen bonding on the conformer population is further supported by the following two facts: (a) The CD curves of its acetate (**4**), in which the intramolecular hydrogen bond is inherently absent, exhibited only a positive Cotton effect, regardless of the solvent polarity, because of the loss of the stabilizing energy by hydrogen bonding. (b) The hydrobrominated compound **10** showed CD curves similar to those of the acetate (**4**) in both the polar and nonpolar solvents, because the positively-rotating, nonbonded conformer is stabilized by the anchoring effect[10] of the bulky 2-bromisopropyl group. This is supported by the infrared spectrum, in which the intensity of the free hydroxyl band of the hydrobrominated compound (**10**) at 3606 (ε 87) cm^{-1} increased greatly at the expense of the bonded peak at 3503 (ε 12) cm^{-1} (Fig.2), in contrast with the case of the parent compound (**2**).

The variable-temperature CD curves of the compound (**2**) in the MI solvent exhibited a double-humped Cotton effect which strikingly implies the temperature dependence of its conformation (Fig. 3). Such a double-humped Cotton effect arising from the n-π^* transition may be explained in terms of the solvational and/or the conformational equilibria. But, the blue-shifted band presumably due to an equilibrium between the solvated and nonsolvated species has been said[11,12] not to show any increase in apparent rotational strength at lower temperatures. Therefore, the double hump observed on the Cotton effect curves has been interpreted as being due to only the conformational equilibria involving the competition of the steric factor and the intramolecular hydrogen bonding. At 25°C, the intramolecularly-hydrogen-bonded form (**2b**) with the negative Cotton effect is preferred. However, the stabilizing intramolecular hydrogen bond will be broken as the tempera-

6) Assuming ΔG of the methyl, hydroxyl, and isopropyl groups to be 1.7, 0.7, and 2.0 kcal/mol,[7] respectively, a free energy difference ($-\Delta G$) for equilibria, **2a**—**2b** and **3a**—**3b**, on the basis of steric factor shows that conformers **2a** and **3b** would be energetically favored by *ca.* 1.0 and 3.0 kcal/mol. However, the **2a** conformer would be less favored and **3a** futher favored by an estimation of the hydrogen bond energy (2—5 kcal/mol). A clear-cut distinction between relative energies of **2a** and **2b** would be diffificult.

7) N.L. Allinger and E. L. Eliel, "Topics in Stereochemistry, Vol. 1," Interscience publishers, New York (1968), p. 199.

8) A. Moscowitz, K. Wellman, and C. Djerassi, *J. Amer. Chem. Soc.*, **85**, 3515 (1963).

9) L. Joris, P. R. Schleyer, and R. Gleiter, *ibid.*, **90**, 327 (1968).

10) S. Winstein and N. J. Holness, *ibid.*, **77**, 5562 (1955); N. L. Allinger and J. Allinger, *ibid.*, **80**, 5476 (1958).

11) K. M. Wellman, P. H. A. Laur, W. S. Briggs, A. Moscowitz, and C. Djerassi, *ibid.*, **87**, 66 (1965).

12) T. Shishibori, T. Suga, S. Watanabe, and T. Matsuura, This Bulletin, **42**, 3284 (1969).

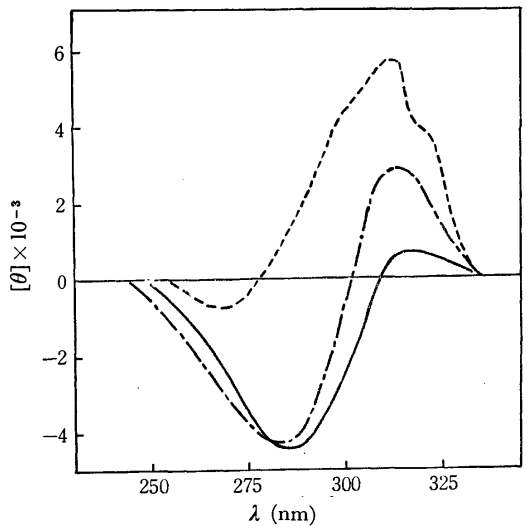

Fig. 3. CD curves of (1*S* : 4*R*)-(+)-1-hydroxy-*p*-menth-8-en-2-one (**2**) in MI: —— at +25°C, ---- at −74°C, and ---- at −186°C.

ture is lowered[4] so the steric requirements mainly dominate the **2a** conformer. The CD curves of **2** in EPA, incontrast with those in MI, showed only a positive Cotton effect with an increase in the apparent rotational strength as the temperature was lowered. This implies that the nonbonded conformer (**2a**) is also energetically preferred in EPA.

On the other hand, the CD curves of **2** in decalin (Fig. 4) exhibited an increase in the rotational strength in the short-wavelength band upon a change in the temperature from −74 to +25°C, and then a decrease from +25 to +150°C. These observations are not consistent with the simple equilibrium, **2a**⇌**2b**. At higher temperatures, the bonded form (**2b**) will diminish with an increase in the amounts of the nonbonded form (**2a**) and/or of the positively-rotating, twist form (**2c**), as has been suggested previously.[4]

Compound **3**, an epimer of **2**, may exist in two such interconvertible chair conformations as the positively-rotating, hydrogen-bonded conformer (**3a**)

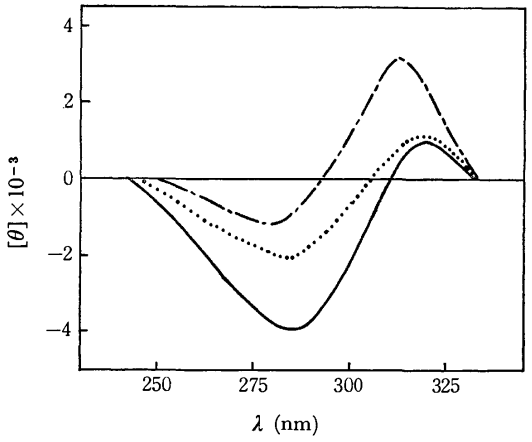

Fig. 4. CD curves of (1*R* : 4*R*)-(+)-1-hydroxy-*p*-menth-8-en-2-one (**2**) in decalin: ---- at −74°C, —— at +25°C, and ····· at +150°C.

and the negatively-rotating, nonbonded one (**3b**).

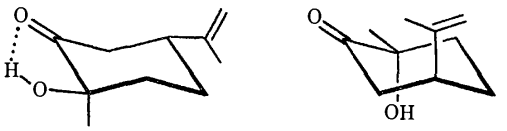

3a **3b**

The compound (**3**) showed only a positive Cotton effect curve with a rotational strength which is almost independent of the solvent polarity. The CD curves of its acetate, **5**, and the hydrobrominated compound, **11**, also showed a solvent-independent, positive Cotton effect at 25°C. Consequently, the **3a** conformer, with an equatorial isopropenyl group, is predominant regardless of the presence of an intramolecular hydrogen bond. The conformer homogeneity of **3** in the nonpolar solvent was ascertained on the basis of infrared spectrum measurements. The spectrum (Fig. 2) in carbon tetrachloride exhibited only a band at 3508 cm^{-1} (ε 61) resulting from an intramolecular hydrogen bond[9] between the hydroxyl group and the lone-pair electrons on the carbonyl oxygen. The two compounds, (**7**) and (**11**), related to the compound (**3**) also exhibited only a similar band assigned to the intramolecular hydrogen bonding (Fig. 2).

The temperature-dependent CD curves of **3** in MI and EPA over the range from 25 to −186°C showed only a positive Cotton effect with a slightly increase in the rotational strength as the temperature was lowered. This implies that the positively-rotating, chair conformer (**3a**) is most stable from the steric and energetic[6] points of view. The compound (**3**) in decalin revealed a decrease in the rotational strength of its positive CD curves at both higher and lower temperatures. This indicates that the hydrogen-bonded conformer (**3a**) would diminish with an increase in the population of the nonbonded conformer when taken out of room temperature.

The saturated compounds **6**, **7**, **8**, exhibited the same phenomena in their CD curves as those in the cases of the corresponding unsaturated compounds, (**2**), (**3**), (**4**), and (**5**) respectively. All the CD data of the saturated compounds are presented in the Experimental section.

Experimental

Measurements. The CD curves were obtained by means of a Japan Spectroscopic Co., Ltd., automatically-recording spectropolarimeter, Model ORD/UV-5, equipped with a circular dichroism attachment, using a variable temperature CD cell designed and constructed by one of the present authors. The EPA solvent is composed of ether-isopentane-ethanol in the ratio of 5 : 5 : 2 by volume. The MI solvent is composed of methylcyclohexane-isopentane in the ratio of 1 : 3 by volume.

The infrared spectra in the hydroxyl-stretching region were measured with a Perkin-Elmer Model 621 Grating Infrared spectrometer at 25°C. A sodium chloride absorption cell (10 mm long) was used; the concentration of the solution was 0.005 mol/*l*.

The NMR, mass, IR, and UV spectra, although not

shown below, supported exactly the structure of the compounds on which the CD curves were measured. Only the methods of preparation of the compounds and the data on the CD curves are given below.

(*1*R : *4*R)-(−)-p-*menth-8-en-2-one* (**1**). The Jones' oxidation of (+)-neodihydrocarveol[13] produced (1*R* : 4*R*)-(−)-*p*-menth-8-en-2-one (**1**): n_D^{25} 1.4650; $[\alpha]_D^{25}$ −200° (MeOH, *c* 0.08); CD (max) in MI (*c* 0.134): $[\theta]_{295}^{+25°}$ +3251, $[\theta]_{300}^{+25°}$ +2955, $[\theta]_{304}^{-186°}$ +3944, $[\theta]_{299}^{-186°}$ +3944, $[\theta]_{309}^{-186°}$ +3199, in EPA (*c* 0.084): $[\theta]_{293}^{+25°}$ +3182, $[\theta]_{290}^{-186°}$ +3206, $[\theta]_{299}^{-186°}$ +2829, $[\theta]_{309}^{-186°}$ +1886.

(*1*S : *4*R)-(+)-*1-hydroxy*-p-*menth-8-en-2-one* (**2**) *and* (*1*R : *4*R)-(+)-*1-hydroxy*-p-*menth-8-en-2-one* (**3**). These compounds were the same as those prepared in the previous paper,[14] to which the physical properties are referred. Their acetates, (**4**) and (**5**) were prepared by the acetylation of **2** and **3** respectively with acetic anhydride in the presence of *p*-toluenesulfonic acid.

The compound (**2**): CD (max) in EPA (*c* 0.0589): $[\theta]_{307}^{+25°}$ +4329, $[\theta]_{307}^{-74°}$ +5101, $[\theta]_{300}^{-186°}$ +6515.

The compound (**3**): CD (max) in MeOH (*c* 0.1684): $[\theta]_{290}^{+25°}$ +10269, in DMSO (*c* 0.1332): $[\theta]_{294}^{+25°}$ +8992, in isooctane (*c* 0.1684): $[\theta]_{286}^{+25°}$ +11195, in decalin (*c* 0.0611): $[\theta]_{285}^{-74°}$ +10307, $[\theta]_{285}^{+25°}$ +9168, $[\theta]_{289}^{+150°}$ +7248, in EPA (*c* 0.0652): $[\theta]_{286}^{+25°}$ +8843, $[\theta]_{290}^{-74°}$ +8898, $[\theta]_{290}^{-182°}$ +10856.

The acetate (**4**): bp 55—56°C/30 mmHg; n_D^{25} 1.4688; $[\alpha]_D^{25}$ +4.81° (MeOH, *c* 0.1454); CD (max) in MeOH (*c* 0.1454); $[\theta]_{288}^{+25°}$ +2931, in DMSO (*c* 0.142): $[\theta]_{294}^{+25°}$ +2945, in isooctane (*c* 0.1644): $[\theta]_{292}^{+25°}$ +3021.

The acetate (**5**): bp 75—80°C/8 mmHg; $[\alpha]_D^{25}$ +61.58° (MeOH, *c* 0.1624); CD (max) in MeOH (*c* 0.1624): $[\theta]_{290}^{+25°}$ +6817, in DMSO (*c* 0.149): $[\theta]_{293}^{+25°}$ +6656, in isooctane (*c* 0.1648): $[\theta]_{294}^{+25°}$ +6534.

(*1*S : *4*R)-(+)-*1-hydroxy*-p-*methan-2-one* (**6**) *and* (*1*R : *4*R)-(+)-*1-hydroxy*-p-*menthan-2-one* (**7**). The reduction of the menthenones (**2**), (**3**), and (**5**) in methanol on 10%-palladium charcoal gave the corresponding saturated compcompounds, (**6**), (**7**), and (**9**).

The compound (**6**): n_D^{25} 1.4621; $[\alpha]_D^{25}$ +23.47° (MeOH, *c* 0.1704); CD (max) in MeOH (*c* 0.1704): $[\theta]_{272}^{+25°}$ −922, $[\theta]_{306}^{+25°}$ 1910, in DMSO (*c* 0.1692): $[\theta]_{308}^{+25°}$ +2255, in dioxane (*c* 0.172): $[\theta]_{276}^{+25°}$ −1566, $[\theta]_{310}^{+25°}$ +1827, in CCl_4 (*c* 0.151): $[\theta]_{282}^{+25°}$ −5201, $[\theta]_{316}^{+25°}$ +594, in isooctane (*c* 0.1686): $[\theta]_{280}^{+25°}$ −4881, $[\theta]_{307}^{+25°}$ +133, in decalin (*c* 0.156): $[\theta]_{282}^{-74°}$ −1827, $[\theta]_{310}^{-74°}$ +2166, $[\theta]_{282}^{+25°}$ −4819, $[\theta]_{318}^{+25°}$ +360, $[\theta]_{282}^{+72°}$ −4161, $[\theta]_{318}^{+72°}$ +371, $[\theta]_{284}^{+150°}$ −2089, $[\theta]_{318}^{+150°}$ +402, in MI (*c* 0.144): $[\theta]_{282}^{+25°}$ −5688, $[\theta]_{316}^{+25°}$ +312, $[\theta]_{274}^{-74°}$ −3072, $[\theta]_{306}^{-74°}$ +2513, $[\theta]_{305}^{-192°}$ +4758, in EPA (*c* 0.143): $[\theta]_{275}^{+25°}$ −1726, $[\theta]_{308}^{+25°}$ +3138, $[\theta]_{307}^{-192°}$ +4696, $[\theta]_{318}^{-192°}$ +3882, (*c* 0.172 at −74°) $[\theta]_{270}^{-74°}$ +683, $[\theta]_{307}^{-74°}$ +2904.

The compound (**7**): n_D^{25} 1.4593; $[\alpha]_D^{25}$ +97.23° (MeOH) *c* 0.1736); CD (max) in MeOH (*c* 0.1736): $[\theta]_{286}^{+25°}$ +2036, in DMSO (*c* 0.064): $[\theta]_{288}^{+25°}$ +7188, in dioxane (*c* 0.076): $[\theta]_{284}^{+25°}$ +9399, in CCl_4 (*c* 0.092): $[\theta]_{282}^{+25°}$ +9634, in isoocatne (*c* 0.0651): $[\theta]_{283}^{+25°}$ +9472, in decalin (*c* 0.06): $[\theta]_{282}^{-74°}$ +8270, $[\theta]_{282}^{+25°}$ +8041, $[\theta]_{282}^{+72°}$ +7341, $[\theta]_{284}^{+150°}$ +5431, in MI (*c* 0.06): $[\theta]_{282}^{+25°}$ +8840, $[\theta]_{284}^{-74°}$ +9596, (*c* 0.056, at −192°) $[\theta]_{286}^{-192°}$ +8828, in EPA (*c* 0.0524): $[\theta]_{284}^{+25°}$ +10706, $[\theta]_{288}^{-74°}$ +11403, $[\theta]_{291}^{-192°}$ +12815, $[\theta]_{298}^{-192°}$ +12132.

The acetate (**9**): n_D^{25} 1.4590; $[\alpha]_D^{25}$ +7.44°; CD (max) in MeOH (*c* 0.121): $[\theta]_{287}^{+25°}$ +7516, in dioxane (*c* 0.12): $[\theta]_{291}^{+25°}$ +7269, in isooctane (*c* 0.1176): $[\theta]_{290}^{+25°}$ +6008.

The acetate (**8**): (1*S* : 2*S* : 4*R*)-1,2-Dihydroxy-*p*-menthane, prepared from the corresponding dihydroxy-*p*-menth-8-ene by hydrogenation, was converted into the hydroxyketone **6** by oxidation with chromic acid-pyridine complex. Then, the hydroxyketone was acetylated in the same manner as above to produce the acetoxyketone, **8**: n_D^{25} 1.4555; $[\alpha]_D^{25}$ +35.47° (MeOH, *c* 0.296); CD (max) in MeOH (*c* 0.296): $[\theta]_{286}^{+25°}$ +1654, in dioxane (*c* 0.353): $[\theta]_{287}^{+25°}$ +753, in isooctane (*c* 0.345): $[\theta]_{290}^{+25°}$ +710.

(*1*S : *4*R)-(+)-*1-Hydroxy-8-bromo*-p-*menthan*-2-*one* (**10**). A benzene solution of the hydroxyketone **2** was treated with a hydrobromic acid-acetic acid solution. After the reaction mixture was then poured into ice water, it was worked up as usual to yield the hydrobrominated compound (**10**) as white crystals: mp 65.5—66.0°C; $[\alpha]_D^{25}$ +63.4° (MeOH, *c* 0.122); CD (max) in MeOH (*c* 0.122): $[\theta]_{304}^{+23°}$ +2825, in CCl_4 (*c* 0.092): $[\theta]_{311}^{+23°}$ +2591.

(*1*R : *4*R)-(+)-*1-Hydroxy-8-bromo*-p-*menthan*-2-*one* (**11**). The treatment of the hydroxyketone **3** in a manner similar to that above gave a hydrobrominated derivative (**11**): mp 61.5°C; $[\alpha]_D^{25}$ +64.4° (MeOH, *c* 0.114); CD (max) in MeOH (*c* 0.114): $[\theta]_{290}^{+23°}$ +5254, in CCl_4 (*c* 0.091): $[\theta]_{286}^{+23°}$ +6227.

The authors wish to thank the Takasago Perfumery Co. for its gift of limonene and Mr. Kiyoshi Imamura of our laboratory for his helpful assistance in the preparation of the hydrobrominated compounds.

13) T. Shishibori, This Bulletin, **41**, 1170 (1968).

14) T. Suga, T. Shishibori, S. Watanabe, and T. Matsuura, *J. Sci. Hiroshima Univ., Ser. A*-11, **32**, p. 331—335 (1968).

A New Steroid with an Unnatural Configuration: 8α,14β-Progesterone

Fumikazu MUKAWA and Wataru NAGATA

Shionogi Research Laboratory, Shionogi & Co., Ltd., Fukushima-ku, Osaka

(Received August 6, 1971)

A modified Wolf-Kishner reduction of certain 5α,8α,14β-11-oxo steroids gave the corresponding 11-deoxy steroids with the same stereochemistry, and the introduction of a double bond at C_4—C_5 leads to 8α,14β-progesterone. The structure and configuration of this compound are discussed on the basis of its physical properties. Its unnatural backbone stereochemistry was established by transformations from the 8α,14β-1,4-diene derivative to the known 8α,14β-estrone.

The demonstration by Westerhof of differences in the biological activity of steroids which feature unnatural backbone stereochemistry has led to the preparation of a variety of such compounds.[1] Although racemic 8α,14β-estrone[2] was prepared by the total synthetic method, no 8α,14β-steroid of the pregnane series has yet been reported on. In view of the current interest in progesterone analogs,[3] we would like to report the synthesis of 8α,14β-progesterone (**7**).

The reduction of 11-oxo-5α,8α,14β-spirostan-3β-ol[4] (**1a**) by a modified Wolf-Kishner procedure, developed in our laboratory[5] for the reduction of highly-hindered ketones, followed by acetylation, led to 8α,14β-spirostan 3β-acetate (**2a**, R_1=Ac). Side-chain degradation then gave the 16-pregnene derivative (**3a**, R=OAc), which, on hydrogenation over a palladium-charcoal catalyst, followed by saponification, yielded the 5α,8α,14β-pregnane derivative (**3b**, R=OH). Compound **3b** (R=OH) was also obtained using the technique described above for spirostan-series compounds, starting from the 11-oxo-8α,14β-pregnane derivative (**1b**, R_2=H).

The partial saponification of the 3β,20β-diacetoxy pregnane derivative, followed by the oxidation of the 3-hydroxyl derivative, provided the 3-ketone (**4a**, X_1,X_2=H). The subsequent introduction of the C_4–C_5 double bond was effected in the following way: the treatment of 2ξ,4ξ-dibromo-3-ketone (**4a**, X_1,X_2=Br) with lithium salts in *N*,*N*-dimethylformamide, and selective hydrogenation with the ruthenium complex[6]

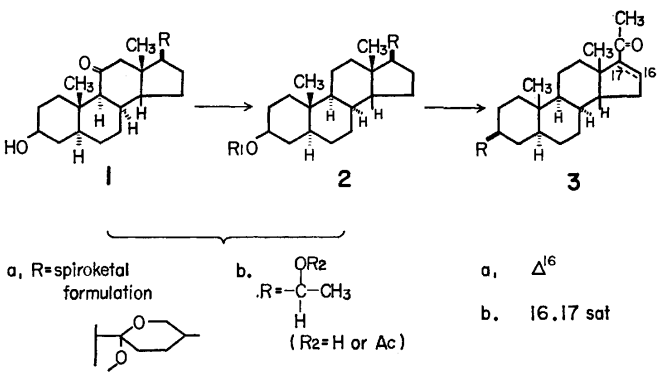

Fig. 1.

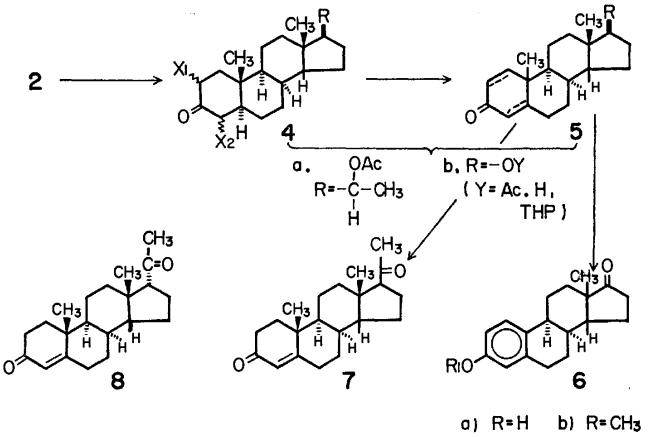

Fig. 2.

of the resulting 1,4-diene-3-ketone (**5a**, $\Delta^{1,4}$), gave the 20β-acetoxy-4-ene-3-ketone derivative (**5a**, Δ^4). This compound, on hydrolysis subsequent to its oxidation, led to the 17β-acetyl derivative (**7**) (predominating) and the 17α-isomer (**8**). These configurations were supported by the circular dichroism data (Table 1). In **7**, a positive Cotton effect appears at 288 nm, in agreement with the 17β-configuration of

TABLE 1. COTTON EFFECT OF UNNATURAL PROGESTERONE AND NATURAL PROGESTERONE

	Circular dichroism (Molecular ellipticity)
7	$[\theta]_{253}$ −12160, $[\theta]_{288}$ +8510, $[\theta]_{325}$ +5600
8	$[\theta]_{253}$ −11200, $[\theta]_{280}$ −3050, $[\theta]_{325}$ +7210
Progesterone	$[\theta]_{240sh}$ +18700, $[\theta]_{286}$ +13320, $[\theta]_{325}$ −4100

The spectra were measured in methanol.

1) a) E. H. Reerink, H. F. L. Schöler, P. Westerhof, A. Querido, A. A. H. Kassnnar, E. Diczfalusy, and K. C. Tillinger, *Nature*, **186**, 168 (1960); b) The nonphotolytic route has been reported: M. Uskokovic, J. Jacobelli, P. Philion, and T. Williams, *J. Amer. Chem. Soc.*, **88**, 4538 (1966); c) E. Farkas, J. M. Owen, and D. J. O'Toole, *J. Org. Chem.*, **34**, 3023 (1969); d) P. Crabbe, A. Cruz, and J. Iriarte, *Can. J. Chem.*, **46**, 349 (1968); e) R. Bucourt, D. Hainait, J. -C. Gase, and G. Nominé, *Tetrahedron Lett.*, **1968**, 5093.

2) C. Rufer, E. Schröder, and H. Gibian, *Ann. Chem.*, **705**, 211 (1967), and the references cited there in.

3) Dr. T. Miyake of our laboratory has discussed (in R. I. Dorfman, ed., "Hormone Research. V," Academic Press, New York, N. Y. (1966), pp. 59—145) the relation between the structure and the physiological activity of progestational steroids.

4) C. Djerassi, W. Frick, G. Rosenkrazz, and F. Sondheimer, *J. Amer. Chem. Soc.*, **75**, 3496 (1953); C. Djerassi, A. J. Manson, and A. Segoloff, *J. Org. Chem.*, **21**, 490 (1956); C. Djerassi, H. Bendas, and A. Segaloff, *ibid.*, **21**, 1056 (1956).

5) W. Nagata and H. Itazaki, *Chem. Ind.* (London), **1964**, 1194.

6) S. Nishimura and K. Tsuneda, This Bulletin, **42**, 852 (1969).

the side chain of progesterone; **8** was shown to have the 17α-configuration by its negative Cotton effect in the same region.[7]

The positive Cotton effect for the n—π^* transition of the α,β-unsaturated ketone, at *ca.* 325 nm, and the negative effect for the π—π^* (253 nm) showed **7** and **8** to have identical 8α and 14β ring junctures. The natural configuration, as in progesterone, is characterized by a negative Cotton effect at 325 nm and a positive one at the π—π^* transition. This evidence indicates the stereochemistry of **7**, though it is not complete.

The Baeyer-Villiger oxidation of **3b** (R=OH) with trifluoroperacetic acid, followed by the oxidation of the C_3-hydroxy group with Jones's reagent, afforded **4b** (X_1,X_2=H, Y=Ac) after alkaline hydrolysis had given 17β-ol (**4b**, X_1,X_2=H, Y=H). This ketone was dibrominated with bromine in acetic acid, giving the dibromide, which, on subsequent treatment with lithium carbonate and lithium bromide, gave the 1,4-dien-3-one (**5b**, Y=H, $\Delta^{1,4}$). The corresponding tetrahydropyranyl ether (**5b**, Y=THP, $\Delta^{1,4}$) was obtained by the standard method. The reductive aromatization of **5b** (Y=THP, $\Delta^{1,4}$) by Dryden's method,[8] followed by the oxidation of 17-hydroxyl, provided 8α,14β-estrone (**6a**), identified with an authentic specimen of 8α,14β-estrone[2] by a comparison of the IR, mass, and NMR spectra. The methyl ether (**6b**) was also identical with an authentic specimen. Thus, we confirmed the assigned stereochemistry of 8α,14β in our synthetic compounds.

Experimental

The melting points are corrected. The UV spectra were obtained using a Hitachi EPS 3-T spectrophotometer, while a Nihon-Bunko DS-201B spectrophotometer was used for the IR spectra. The NMR spectra were obtained on a Varian A-60 spectrometer, with TMS as the internal standard, and the mass spectra were taken with a Hitachi RMU-6 spectrometer. The optical rotations were measured in 1% EtOH-$CHCl_3$ with a Perkin Elmer Polarimeter 141.

*1. (25R)-8α,5α,14β-Spirostan-3β-ol (**2a**, R_1=H).* A mixture of 1.0 g of (25*R*)-5α,8α,14β-spirostan-3β-ol-11-one (**1a**),[4] 9.5 g of 80% hydrazine hydrate, 1.8 g of hydrazine dihydrochloride, and 52 m*l* of triethylene glycol was heated at 130°C for 1.5 hr. After adding 4.5 g of potassium hydroxide pellets, the temperature was raised to 210°C by distilling the low-boiling material out. After 3.5 hr, the reaction mixture was diluted with water and extracted with methylene chloride. The methylene chloride solution was washed with water and dried, and the solvent was evaporated. The crystalline residue was then recrystallized from methanol to give **2a** (R_1=H) (0.73 g); mp 168—172°C. A pure sample melted at 169—173°C, $[\alpha]_D^{23}$ −95.5° (c 0.18); NMR τ: 9.21 (27-C$\underline{H_3}$), 9.05 (21-C$\underline{H_3}$), 8.98 (18-C$\underline{H_3}$), 9.13 (19-C$\underline{H_3}$).

Found: C, 77.7; H, 10.6%. Calcd for $C_{27}H_{44}O_3$: C, 77.8; H, 10.6%.

*2. 5α,8α,14β-Pregn-16-en-20-one 3β-Acetate(**3a**, R=-OAc).*[9] The 5α,8α,14β-tigogenine compound (**2a**, R_1=H) (0.75 g) was refluxed for 12.5 hr with 60 m*l* of acetic anhydride and 0.45 g of pyridine hydrochloride. The mixture was then cooled, diluted with 12 m*l* of acetic acid and 18 m*l* of water, and added to 0.3 g of chromic anhydride in 6 m*l* of 90% acetic acid while being stirred at 15—20°C. After standing at 25°C for 3 hr, the solution was treated first with 0.2 m*l* of 37% formaldehyde and then with 0.65 g of sodium acetate. The stirred suspension was then heated on a water bath for 1 hr, cooled, and diluted with water. After being extracted with ether, the ether solution was dried over anhydrous sodium sulfate and evaporated. The residue was chromatographed[10] on alumina (20 g, Wohlem activity II). Elution with benzene-petroleum ether (4 : 1) and benzene afforded 16-ene (**3a**, R=−OAc) (0.32 g) as plates (from acetone); mp 146—147°C, $[\alpha]_D^{21}$ +56.1° (*c* 0.3).

Found: C, 77.2; H, 9.6%. Calcd for $C_{23}H_{34}O_3$: C, 77.1; H, 9.6%. IR (CCl_4) cm^{-1}: 1745 (3β-acetate), 1670 (20-ketone), 1615 (Δ^{16}). NMR τ: 9.06 (19-C$\underline{H_3}$), 8.81 (18-C$\underline{H_3}$), 8.00 (3β-C$\underline{H_3}$COO), 7.75 (21-C$\underline{H_3}$), 3.40 (Δ^{16}-olefin, t, $J \fallingdotseq 4$ Hz).

*3. 3β-Hydroxy-5α,8α,14β-pregnan-20-one (**3b**, R=-OH).* A solution of 0.22 g of Δ^{16}-ene (**3a**, R=−OAc) in 20 m*l* of ethyl acetate was shaken with a 5% palladium-charcoal catalyst under a hydrogen atmosphere for 15 min. After the removal of the catalyst and the evaporation of the solvent under reduced pressure, a crude acetate was obtained. The saponification of this acetate with 0.2 g of potassium carbonate in ethanol, followed by recrystallization from ether-petroleum ether, gave 0.18 g of **3b** (R=-OH); mp 125—130°C. Analytical samples were recrystallized from methanol; mp 134°C, $[\alpha]_D^{21}$ +82.8° (*c* 0.3).

Found: C, 78.9; H, 10.8%. Calcd for $C_{21}H_{34}O_2$: C, 79.1; H, 10.8%. IR ($CHCl_3$) cm^{-1}: 3600 (3β-OH), 1700 (20-ketone). NMR τ: 9.16 (18-C$\underline{H_3}$), 9.06 (19-C$\underline{H_3}$), 7.91 (21-C$\underline{H_3}$). CD (*c* 0.009, MeOH): $[\theta]_{291}$+7630. Mass: 318 (M·).

*4. 3β,20β-Dioxy-5α,8α,14β-pregnane (**2b**, R_1, R_2=H).* In view of the facile alkaline isomerization at C-14 of 11-oxo-8-ene steroids, the preparation of 11-oxo-14β-pregn-8-en-3β-ol was carried out under Djerassi's conditions:[4] a solution of 12.7 g of 3β,20β-diacetoxy-5α-pregn-8-ene-11-one[11] was refluxed for 40 minutes with 1.2 *l* of 5% methanolic potassium hydroxide. After concentration *in vacuo*, dilution with water, extraction with methylene chloride, evaporation and recrystallization from methanol, we obtained 9.1 g of 11-oxo-5α,14β-pregn-8-en-3β,20β-diol with a mp of 198—202°C; $[\alpha]_D^{26.2}$+152° (*c* 1.0); UV λ_{max}^{MeOH} 248 nm (ε 9200); CD (*c* 0.01, CH_3Cl): $[\theta]_{385}$ 0, $[\theta]_{355}$ −1480, $[\theta]_{330}$ −1230, $[\theta]_{246.5}$ +25600; NMR ($CDCl_3$) τ: 8.88 (18-C$\underline{H_3}$ and 19-C$\underline{H_3}$), 8.81 (d, $J \fallingdotseq 7$ Hz, 21-C$\underline{H_3}$).

Found: C, 75.9; H, 9.6%. Calcd for $C_{21}H_{32}O_3$: C, 75.8; H, 9.7%.

7) G. Snatzke, H. Pieper, and R. Tshesche, *Tetrahedron*, **20**, 107 (1964). Another example favorable to the present discussion is given by P. Crabbe *et al.*, Ref. 1d.

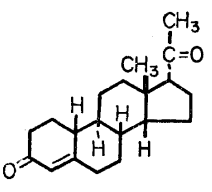

NMR	18-CH_3	21-CH_3
	77	128

CD(in dioxane): $[\theta]_{376}$ 0, $[\theta]_{356}$ −1520, $[\theta]_{342}$ −3630, $[\theta]_{330}$ −4620, $[\theta]_{304}$ −4690, $[\theta]_{286}$ −4690, $[\theta]_{260}$ −610

8) H. L. Dryden, Jr., G. M. Webber, and J. J. Wieczorek, *J. Amer. Chem. Soc.*, **86**, 742 (1964); S. Hayakawa, Y. Kanematsu, and T. Fujiwara, *Biochem. J.*, **115**, 249 (1969).

9) *Cf.* G. P. Mueller, *Nature*, **181**, 771 (1958).

10) T. Reichstein and C. W. Schoppee, *Discuss. Faraday Soc.*, **1949**, 305.

11) E. R. H. Jones and D. A. Wilson, *J. Chem. Soc.*, **1965**, 2933.

The catalytic hydrogenation of this 14β-8-en-11-oxo compound (9.1 g) was carried out in 280 ml of ethanol in an 86-atm autoclave with 4.0 g of 5% palladium-charcoal for 48 hr. Subsequent recrystallization from ether-petroleum ether gave 6.7 g of **1b** (R_2=H); mp 170—173°C; $[\alpha]_D^{23}$+12.0° (*c* 0.35); NMR τ: 9.00 (18-C$\underline{H}_3$), 8.96 (19-C$\underline{H}_3$), 8.85 (d, *J*≒8 Hz, 21-C$\underline{H}_3$); CD (MeOH): $[\theta]_{303}$ −6416.

Found: C, 75.3; H, 10.1%. Calcd for $C_{21}H_{34}O_3$: C, 75.4; H, 10.2%.

1b (R_2=H) (6.8 g) was reduced to the corresponding 11-deoxo derivative (**2b**, R_1,R_2=H) in a 79% yield by a modified Wolf-Kishner reduction, heating with 54 g of 80% hydrazine hydrate and 10.4 g of hydrazine dihydrochloride in 320 ml of triethylene glycol at 130°C for 1.5 hr. After adding 34.5 g of potassium hydroxide, the temperature was raised to 210°C, as in Exp. 1. After cooling, the reaction was worked up as usual. The recrystallization from acetone led to **2b** (R_1=H) (4.8 g) with a mp of 170—173°C. Three recrystallizations from acetone afforded an analytical sample with a mp of 185°C; $[\alpha]_D^{25.8}$ +28.1° (*c* 0.5); NMR τ: 9.10 (19-C$\underline{H}_3$), 9.03 (18-C$\underline{H}_3$), 8.85 (d, *J*≒7 Hz, 21-C$\underline{H}_3$).

Found: C, 78.9; H, 11.3%. Calcd for $C_{21}H_{36}O_2$: C, 78.7; H, 11.3%.

*5. 3,20-Dioxo-5α,8α,14β-pregnane (**3b**, R==O).* The oxidation of 0.70 g of **3b** (R=−OH) with 0.3 ml of Jones's reagent in 0.15 ml of acetone at room temperature produced **3b** (R==O) (0.54 g), with a mp of 133—135°C. Recrystallization from methanol then led to the analytical sample; mp 138°C; $[\alpha]_D^{29}$+115.5° (*c* 0.23); IR (CCl_4) cm^{-1}: 1705; NMR τ: 9.11 (18-C$\underline{H}_3$), 8.86 (19-C$\underline{H}_3$), 7.86 (21-C$\underline{H}_3$); CD (*c* 0.001, MeOH): $[\theta]_{325}$ −3926.

Found: C, 79.7; H, 9.9%. Calcd for $C_{21}H_{32}O_2$: C, 79.7; H, 10.2%.

The same product was obtained when the oxidation of **2b** (R_1,R_2=H) was carried out with stirred chromium trioxide-acetic acid; the mixed melting point and the IR spectra proved to be identical.

The 3,20-dioxo compound (**3b**, R==O) (0.18 g) obtained above was reduced by stirring with 20 mg of sodium borohydride in 20 ml of ethanol for 30 min at room temperature; the mixture was then treated as usual to afford 0.14 g of **2b** (R_1,R_2=H), which was identical with the sample of 3β,20β-diol obtained in Exp. 4.

*6. 3β,20β-Diacetoxy-5α,8α,14β-pregnane (**2b**, R_1,R_2=Ac).* The free 3β,20β-diol **2b** (R_1,R_2=H) (0.5 g) in 2.5 ml of acetic anhydride and 50 ml of pyridine was warmed on a water-bath for 1.5 hr. After dilution with water, filtration, and recrystallization from acetone, we obtained 0.44 g of the diacetate (**2b**, R_1,R_2=Ac) with a mp of 102—104°C; $[\alpha]_D^{26.8}$ +38.2° (*c* 0.9).

Found: C, 74.4; H, 9.8%. Calcd for $C_{25}H_{40}O_4$: C, 74.2; H, 9.9%. IR (CCl_4) cm^{-1}: 1735—1740; NMR τ: 9.16 (19-C$\underline{H}_3$), 9.08 (18-C$\underline{H}_3$), 8.83 (d, *J*≒7 Hz, 21-C$\underline{H}_3$), 8.00 (C$\underline{H}_3$COO).

*7. 20β-Acetoxy-5α,8α,14β-pregnan-3-one (**4a**, X_1,X_2=H).* The partial saponification of the diacetate (**2b**, R_1,R_2=Ac) in 120 ml of 90% methanol with 1.9 g of potassium carbonate gave, after stirring for 2.5 hr at room temperature and dilution with water, 3.5 g of **2b** (R_1=H, R_2=Ac) with a mp of 112—116°C. Further recrystallization from methanol afforded an analytical sample with a mp of 121°C; $[\alpha]_D^{26.8}$ +46.5° (*c* 0.52); IR (Chf) cm^{-1}: 3690, 3600 (3β-OH), 1725 (20β-acetate); NMR τ: 9.18 (19-C$\underline{H}_3$), 9.08 (18-C$\underline{H}_3$), 8.83 (d, *J*=7 Hz, 21-C$\underline{H}_3$), 8.00 (C$\underline{H}_3$COO).

Found: C, 76.1; H, 10.3%. Calcd for $C_{23}H_{38}O_3$: C, 76.2; H, 10.5%.

A mixture of Jones's reagent (1.2 eq.) was added to a solution of 3.2 g of the above 3β-ol **2b** (R_1=H, R_2=Ac) in 15 ml of acetone over a 3-min period, and then the whole mixture was immediately poured into a large volume of ice water. The precipitate was extracted with ether, washed, and dried, and the solvent was removed. Recrystallization from acetone then afforded 3.3 g of **4a** (X_1,X_2=H); mp 140—141°C; $[\alpha]_D^{26.9}$+71.9° (c, 0.12), IR (Chf) cm^{-1}: 1715 (3-ketone), 1735 (acetate); NMR τ: 9.13 (18-C$\underline{H}_3$), 8.88 (19-C$\underline{H}_3$), 8.81 (d, *J*=7 Hz, 21-C$\underline{H}_3$), 8.00 (C$\underline{H}_3$COO); CD (*c* 0.003, dioxane): $[\theta]_{330}$ 0, $[\theta]_{294}$+3635, $[\theta]_{250}$+117, $[\theta]_{218}$+5360.

Found: C, 76.7; H, 9.8%. Calcd for $C_{23}H_{36}O_3$: C, 76.6; H, 10.0%.

*8. 20β-Acetoxy-8α,14β-pregna-1,4-dien-3-one (**5a**, $\Delta^{1,4}$).* One gram of the 3-ketone (**4a**, X_1,X_2=H) was brominated in 70 ml of acetic acid (containing one drop of hydrogen bromide-acetic acid) with 950 mg of bromine in 20 ml of acetic acid. The color disappeared in 10 min, after which the solution was left to stand for 1 hr. The addition of water precipitated the crude 2ξ,4ξ-dibromo-3-ketone (**4a**, X_1,X_2=Br), which was dried and refluxed for 3 hr in 45 ml of *N*,*N*-dimethylformamide with 0.7 g of lithium bromide and 1.2 g of lithium carbonate, avoiding moisture. Most of the solvent was thus evaporated off, and the concentrate was diluted with 2 N-hydrochloric acid. After extraction with methylene chloride, the organic layer was washed with water, dried over anhydrous sodium sulfate, and evaporated. The residue was separated by tlc,[12] using benzene-ethyl acetate (9 : 1) as the developing solvent, to give 0.40 g of **5a** ($\Delta^{1,4}$). An analytical sample was recrystallized three times from ether - *n*-hexane; mp 165°C; $[\alpha]_D^{26.9}$ +220.2° (*c* 0.5); IR (Chf) cm^{-1}: 1730 (acetate), 1655, 1620, 1600 ($\Delta^{1,4}$-3-ketone); UV λ_{max}^{MeOH} 247 mμ (ε 12360); CD: (*c*, 0.001, MeOH) $[\theta]_{345}$+15200, $[\theta]_{320}$+7600, $[\theta]_{299}$+15200, $[\theta]_{273}$ 0, $[\theta]_{255}$−16000; NMR τ: 9.08 (18-C$\underline{H}_3$), 8.83 (d, *J*≒7 Hz, 21-C$\underline{H}_3$), 8.70 (19-C$\underline{H}_3$), 8.00 (C$\underline{H}_3$COO−), 3.96 (d. d., *J*≒2 Hz, C_4–H), 3.80 (d, *J*≒3 Hz, C_2–H), 3.00 (d, *J*≒10 Hz, C_1–H).

Found: C, 77.4; H, 9.1%. Calcd for $C_{23}H_{32}O_3$: C, 77.5; H, 9.0%.

*9. 20β-Acetoxy-8α,14β-pregn-4-en-3-one (**5a**, Δ^4).* 1,4-Diene-3-one (0.13 g) was hydrogenated with 0.1 g of the ruthenium complex in 20 ml of benzene at 40°C under an hydrogen pressure of 88 atm for 1 hr. The residue thus obtained was then separated by tlc, using benzene-ethyl acetate (4 : 1) as the developing solvent, to give 98 mg of **5a** (Δ^4). An analytica sample was recrystallized from ether-petroleum ether; mp 84°C; $[\alpha]_D^{27}$+145.3° (*c* 0.4); IR (Chf) cm^{-1}: 1725 (acetate), 1655, 1600 (4-en-3-one); NMR τ: 8.75 (19-C$\underline{H}_3$), 8.81 (d, *J*≒7 Hz, 21-C$\underline{H}_3$), 8.74 (19-C$\underline{H}_3$), 8.00 (C$\underline{H}_3$COO), 4.25 (t, *J*≒2 Hz, 4H); CD (*c* 0.003, MeOH): $[\theta]_{332}$+12660, $[\theta]_{316}$+8180, $[\theta]_{282}$+8310, $[\theta]_{262.5}$ 0, $[\theta]_{245}$−15510, $[\theta]_{229}$ 0, $[\theta]_{217}$+14800.

Found: C, 77.0; H, 9.5%. Calcd for $C_{23}H_{34}O_3$: C, 77.1; H, 9.5%.

*10. 8α,14β-Pregn-4-en-3-one (**7**) and 8α,14β,17α-pregn-4-en-3-one (**8**).* A solution of 0.90 g of 20β-acetyl-4-en-3-one (**5a**, Δ^4) dissolved in 40 ml of ether was added to a solution of 0.5 g of lithium aluminum hydride in 30 ml of ether, and the mixture was stirred at room temperature for 30 min. The mixture was then cooled, and the excess lithium aluminum hydride was decomposed by the addition of water. On a usual work-up, a syrupy residue was obtained. To a solution of 0.7 g of chromium trioxide in 20

12) For preparative and analytical tlc, silicagel G or GF (E. Merck Co.) was used as the adsorbent.

ml of pyridine, we then added, at 10—15°C, a solution of the syrupy residue in 13 ml of the same solvent. After the reaction mixture had been allowed to stand for 2 hr, the usual work-up gave 0.85 g of a mixture of **7** and **8**, which were separated by tlc. By using a developing solvent (benzene-ethyl acetate, 3 : 1), we obtained 0.71 g of **7** (recrystallization from ether-petroleum ether) with a mp of 78°C; $[\alpha]_D^{24}$+98°C (*c* 0.8). NMR τ: 9.10 (18-C$\underline{H}_3$), 8.75 (19-C$\underline{H}_3$), 7.90 (21-C$\underline{H}_3$), 4.25 (t, $J\doteqdot 2$ Hz, 4H).

Found: C, 80.0; H, 9.6%. Calcd for $C_{21}H_{30}O_2$: C, 80.2; H, 9.6%.

We also obtained **8** (28 mg). It was recrystallized from acetone gave an analytical sample; mp 101°C, $[\alpha]_D^{23.5}$+38° (*c* 0.5). NMR τ: 8.78 (18-C$\underline{H}_3$), 8.68 (19-C$\underline{H}_3$), 7.86 (21-C$\underline{H}_3$), 4.25 (t, $J\doteqdot 2$ Hz, 4H).

Found: C, 80.3; H, 9.3%. Calcd for $C_{21}H_{30}O_2$: C, 80.2; H, 9.6%.

11. Oxidation of ***3b*** *(R=-OH) with Peroxytrifluoroacetic Acid.* Into a mixture of 0.20 ml of 90% hydrogen peroxide and 30 ml of methylene dichloride at 0°C, we stirred 1.5 ml of trifluoroacetic anhydride over a period of 10 min. The mixture was further stirred for five minutes and then transferred to a dropping funnel and stirred drop by drop, into an ice-cold solution of 1.2 g of **3b** (R=OH) in 60 ml of methylene chloride containing 3.8 g of disodium hydrogen phosphate. The mixture was allowed to stand at room temperature under stirring for 1 hr, and then water was added to dissolve the salt. An organic layer was separated and washed with 2 N sodium thiosulfite. After drying, the solvent was removed to give a crystalline residue, **4b** (X_1,X_2=H, Y=Ac); mp 121—123°C. An analytical sample showed a mp of 125°C, $[\alpha]_D$+79° (*c* 0.9).

Found: C, 75.7; H, 9.5%. Calcd for $C_{21}H_{32}O_3$: C, 75.8; H, 9.7%.

The saponification of 0.70 g of **4b** (X_1,X_2=H, Y=Ac) with 700 mg of potassium hydroxide in 16 ml of methanol for 30 min, followed by recrystallization from aq. methanol, produced 0.52 g of **4b** (X_1,X_2=H, Y=H); mp 138—141°C. Analytical sample: mp 142—143.5°C; $[\alpha]_D$+65° (*c* 0.5).

Found: C, 78.6; H, 10.4%. Calcd for $C_{19}H_{30}O_2$: C, 78.6; H, 10.4%.

*12. 8α,14β-Estrone (****6a****) and Its 3-Methyl Ether (****6b****).* The 1,4-dien-3-one (**5b**, $\Delta^{1,4}$) was prepared as has been described above. A solution of 0.20 g of **4b** (X_1,X_2 and Y=H) in 10 ml of acetic acid (containing one drop of hydrogen bromide-acetic acid) was treated with a solution of 0.10 g of bromine in 2.0 ml of acetic acid at room temperature for 20 min. After an additional 30 min's stirring at 45—50°C, the reaction mixture was diluted. The extract was made neutral by washing it with 2 N sodium bicarbonate and water; then it was evaporated to dryness to yield a crude dibromoketone. The dehydrobromination of the crude dibromoketone (0.21 g) with 0.17 g of lithium bromide and 0.21 g of lithium carbonate in 8.5 ml of refluxing *N,N*-dimethylformamide under a N_2 gas stream for 1.5 hr gave the 1,4-dien-3-one compound. The products were separated by tlc. Development with benzene - ethyl acetate (4 : 1) gave crystalline fraction (74 mg); repeated crystallizations from ether - petroleum ether gave **5b** (Y=H, $\Delta^{1,4}$); mp 92—93°C; $[\alpha]_D^{24}$+48° (*c* 0.7), IR (Chf) cm^{-1}: 1655, 1628, 1600 ($\Delta^{1,4}$-3-ketone). UV λ_{max}^{MeOH} 248 nm (ε 12100); CD (*c* 0.0004, MeOH): $[\theta]_{390}$ +13400, $[\theta]_{315}$ +4530, $[\theta]_{299}$+14310, $[\theta]_{268}$ 0, $[\theta]_{250}$−10410, $[\theta]_{225}$ 0; NMR τ: 9.03 (18-C$\underline{H}_3$), 8.70 (19-C$\underline{H}_3$), 3.98 (d, d., $J\doteqdot 2$ Hz, 4-H), 3.75 (d, $J\doteqdot 4$ Hz, 2H), 3.00 (d, $J\doteqdot 10$ Hz, 1H).

Found: C, 79.4; H, 9.4%. Calcd for $C_{19}H_{26}O_2$: C, 79.7; H, 9.2%.

A solution of 0.10 g of **5b** (Y=H, $\Delta^{1,4}$) in 4 ml of dihydropyran was treated with 0.5 ml of a dihydropyran-anhydrous hydrogen chloride solution (10%) by ice-cooling. After 1.5 hr, the mixture was poured into 30 ml of aq. saturated sodium bicarbonate and thoroughly extracted with ether. The organic layer was washed with water and evaporated *in vacuo* to give a residue, which was then purified by tlc. Development with benzene - ethyl acetate (9 : 1) gave 75 mg of the 17ξ-tetrahydropyranyl compound (**5b**, Y=THF, $\Delta^{1,4}$) as an oil. A solution of 60 mg of biphenyl and 0.1 ml of diphenylmethane in 2 ml of freshly-distilled tetrahydrofuran was refluxed under an argon stream with 30 mg of lithium metal with stirring. After this mixture had cooled, into the resulting dark-green solution the above **5b** in 1.5 ml of tetrahydrofuran was slowly stirred under an argon stream, after which the reaction mixture was refluxed for 15 min. The excess of lithium was then decomposed by the addition of methanol and acidified with diluted hydrochloric acid. After the hydrocarbon had been removed by steam distillation, the product was extracted with methylene dichloride. The organic layer was washed with water, dried over anhydrous sodium sulfate, and then evaporated to dryness. The residue was purified ay tlc (elution, benzene - ethyl acetate, 1 : 1) to give a phenolic substance (28.5 mg), which could not be crystallized. This was immediately oxidized with Jones's reagent (0.4 ml) in 4 ml of acetone; subsequent crystallizations from ethanol gave 20.4 mg of **6a** with a mp of 207—213°C. An analytical sample was recrystallized 2 times from ethanol; mp 215—219°C, $[\alpha]_D^{23}$ +11.5° (*c* 0.8). IR (Chf) cm^{-1}: 3600, 3000, 1730, 1605, 1500, 860, 820. (The IR coincided well with the IR of Rufer's sample); NMR τ: 8.85 (18-C$\underline{H}_3$), 3.44 (1H), 3.29 (3H), 2.97 (4H) ($\Delta\tau$ 1,4 ppm, 0.47).[13]

Found: C, 80.0; H, 8.20%. Calcd for $C_{18}H_{22}O_2$: C, 79.9; H, 82.0%.

*3-Methyl Ether (****6b****).* This was prepared by the dimethyl sulfate - 2 N potassium hydroxide treatment of **6a** and was crystallized from methanol; it exhibited a mp of 146—147°C; $[\alpha]_D^{23}$ +14.5° (*c* 0.8, dioxane).

Found: C, 80.1; H, 8.5%. Calcd for $C_{19}H_{21}O_2$: C, 80.2; H, 8.5%. IR (Chf) cm^{-1}: 2995, 2920, 2850, 1730, 1610, 1510, 845. Mass spectrum: 284 ($M^{\cdot}$), 256, 225, 199, 186, 173, 160, 140, 134. The samples of **6a** and **6b** were proven to be identical with authentic samples of *dl*-8α,14β-estrone and its 3-methyl ether (IR spectra, mass spectra, and thin-layer chromatographic behavior).

The authors are very grateful to Dr. C. Rufer (Schering AG) for kindly providing us with the authentic sample of *dl*-8α,14β-estrone.

13) The assignment of the B/C *cis* fusion in **6a** is supported by the small $\Delta\tau$ 1,4-value of 0.47 ppm in NMR (see W. Nagata, T. Terasawa, and K. Tori, *J. Amer. Chem. Soc.*, **86**, 3746 (1964).)

Studies on Geometrical Isomerism by Nulear Magnetic Resonance. V.[1] Stereochemistry of 5-Substituted 4-Alkoxycarbonyl-2-carbamoylimino-1,3-oxathiolanes[2]

Toshio HAYASHI, Makiko AKANO,* Tetsuro YOKONO,** Jun UZAWA, Satoshi KAMBE,*** and Hiroshi MIDORIKAWA

The Institute of Physical and Chemical Research, Wako, Saitama

(Received August 9, 1971)

An equimolar reaction of thiocyanoacetic esters with aldehydes in the presence of potassium fluoride or carbonate leads to a stereoisomeric mixture of *cis* and *trans* isomers of 5-substituted 4-alkoxycarbonyl-2-carbamoylimino-1,3-oxathiolanes. Several of them were separated into two isomeric forms, whose geometrical configurations were determined by means of nuclear magnetic resonance technique. The vicinal coupling constant between the 4- and 5-protons is consistently larger for the *cis* forms than for the *trans*. In the case of the 5-aryl derivatives, the signals of the alkoxycarbonyl group appear at higher field for the *cis* isomers than for the *trans*. The composition ratios of *cis* and *trans* isomers of the oxathiolanes prepared are determined. Infrared data of the *cis* and *trans* oxathiolanes are also reported.

In a previous paper[3] we reported that the reaction of thiocyanoacetic esters (**1**) with aldehydes in the presence of potassium fluoride or carbonate, led to a mixture of 5-substituted 4-alkoxycarbonyl-2-carbamoylimino-1,3-oxathiolanes (**2**) and α,β-unsaturated esters. These oxathiolanes can exist in four isomeric forms, relative to arrangements of the alkoxycarbonyl group and 5-substituent about a single bond in the ring as well as to arrangement of the carbamoyl group about the C–N bond. In the course of study, it has been found that the oxathiolanes prepared in the present work consisted of *cis* and *trans* isomers, some of them being separated into two isomeric forms.[4] The present paper deals with configurational determinations of *cis* and *trans* isomers of the 1,3-oxathiolane derivatives by means of the nuclear magnetic resonance technique.

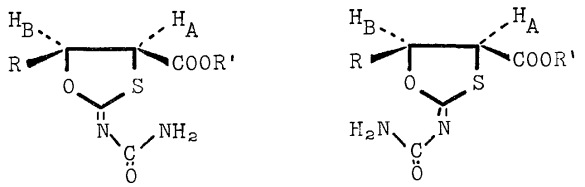

cis forms

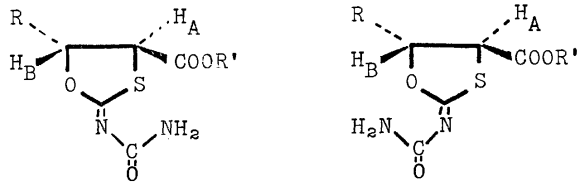

trans forms

Results and Discussion

An equimolar reaction of methyl thiocyanoacetate (**1a**) with benzaldehyde in the presence of potassium carbonate, on standing overnight after removal of the catalyst, gave rise to predominant precipitation of the higher-melting isomer, mp 190—191°C (**6α**).[5] The reaction mixture, on further standing, gradually deposited the lower-melting isomer, mp 138—139°C (**6β**). The *cis* and *trans* isomers of the corresponding ethyl esters (**7α** and **7β**) were isolated similarly. The isomers showed essentially the same mass spectra. With the corresponding *t*-butyl ester only one form, mp 155—156°C (**8β**) was isolated pure.[6] The reaction of **1** with *p*-anisaldehyde, and *p*-chloro- and *p*-bromo-benzaldehydes gave exclusively one isomer. The physical properties of the oxathiolanes are summarized in Table 1. The NMR data for the *cis* and

* Present address: Chiyoda Chemical Engineering and Construction Co., LTD., Tsurumi-ku, Yokohama, Kanagawa.

** Present address: School of Engineering, Hokkaido University, Sapporo, Hokkaido.

*** Oyama Technical College, Oyama, Tochigi.

1) Part IV: T. Hayashi, I. Hori, H. Baba, and H. Midorikawa, This Bulletin, **40**, 2160 (1967).

2) Presented in part at the 23rd Annual Meeting of the Chemical Society of Japan, Tokyo, April, 1970.

3) S. Kambe, T. Hayashi, H. Yasuda, and H. Midorikawa, This Bulletin, **44**, 1357 (1971).

4) Geometrical isomers of several imines were first isolated by Curtin and Hausser.[4a] This was the first unequivocal demonstration of the existence of stereoisomeric compounds in which a carbon atom was bonded to the imino nitrogen. Later, Marullo and Wagner[4b] showed that the isomerization rates of iminocarbonates were so fast that the stereoisomers could not be isolated. However, it was also shown that the isomerization rates are very sensitive to the group on the imino nitrogen. At present we prefer the explanation that the observed separation of the NH_2 signals in the 2-carbamoylimino-1,3-oxathiolanes (Figs. 2 and 3) is due to the existence of *syn* and *anti* isomers, and that the isomerization rates are too fast for isolation. This problem is now under investigation. a) D. Y. Curtin and J. W. Hausser, *J. Amer. Chem. Soc.*, **83**, 3474 (1961); b) N. P. Marullo and E. H. Wagner, *ibid.*, **88**, 5034 (1966).

5) The higher-melting isomers are denoted as α, and the lower-melting isomer, β. In the case where only one isomer was obtained, the isomer having the alkoxycarbonyl signals at higher field than those of the ordinary esters is denoted by C, while the isomer having the alkoxycarbonyl at almost the same field as the ordinary esters is denoted by T. Form C has *cis* configuration, and form T, *trans*.

6) The yield of the α-form was too low for purification. However, the stereoisomeric mixture which contained the α-form predominantly had a melting point higher than the β-form.

Table 1. Physical properties of *N*-carbamoyl-2-imino-4-alkoxycarbonyl-5-substituted 1,3-oxathiolanes

	Compound		Form	Mp (°C)	Formula	Calcd				Found			
						C%	H%	N%	S%	C%	H%	N%	S%
6	C_6H_5	CH_3	α	190—191	$C_{12}H_{12}N_2O_4S$	51.46	4.21	10.63	11.04	51.58	4.35	10.91	11.35
			β	138—139	$C_{12}H_{12}N_2O_4S$	51.46	4.21	10.63	11.04	51.38	4.31	10.14	11.33
7	C_6H_5	C_2H_5	α	190—191	$C_{13}H_{14}N_2O_4S$	53.06	4.80	9.52	10.87	53.42	4.87	9.50	10.88
			β	159—160	$C_{13}H_{14}N_2O_4S$	53.06	4.80	9.52	10.87	53.48	4.62	9.54	10.87
8	C_6H_5	*t*-Bu	β	155—156	$C_{15}H_{18}N_2O_4S$	55.88	5.63	8.69	9.95	55.81	5.67	8.62	9.58
9	*p*-$CH_3OC_6H_4$	CH_3	C	161—162	$C_{13}H_{14}N_2O_5S$	50.35	4.55	9.03	10.31	50.43	4.58	9.07	10.11
10	*p*-$CH_3OC_6H_4$	C_2H_5	C	179—180	$C_{14}H_{16}N_2O_5S$	51.85	4.97	8.64	9.86	51.97	4.95	8.66	9.82
11	*o*-$CH_3OC_6H_4$	C_2H_5	T	197—198	$C_{14}H_{16}N_2O_5S$	51.85	4.97	8.64	9.86	51.83	4.99	8.64	9.89
12	*p*-ClC_6H_4	C_2H_5	T	174—175	$C_{13}H_{13}N_2O_4SCl$	47.50	3.99	8.56	9.74[a]	47.48	3.98	5.56	9.76
13	*o*-ClC_6H_4	CH_3	C	189—191	$C_{12}H_{11}N_2O_4SCl$	45.79	3.52	8.90	10.19[b]	45.68	3.51	8.84	10.27
14	*p*-BrC_6H_4	C_2H_5	T	176	$C_{13}H_{13}N_2O_4SBr$	41.83	3.51	7.51	8.59[c]	41.81	3.51	7.53	8.63
15	*p*-$N{\equiv}CC_6H_4$	C_2H_5	α+β[d]	175—179	$C_{14}H_{13}N_3O_4S$	52.66	4.10	13.16	10.02	52.61	4.10	13.23	9.79
16	CH_3	CH_3	α+β[d]	140—141	$C_7H_{10}N_2O_4S$	38.53	4.62	12.84	14.67	38.74	4.52	12.89	14.69
17	C_2H_5	CH_3	T	145—146	$C_8H_{12}N_2O_4S$	41.38	5.21	12.07	13.78	41.35	5.20	12.11	13.81
18	C_2H_5	C_2H_5	T	150—151	$C_9H_{14}N_2O_4S$	43.90	5.73	11.38	13.00	43.80	5.74	11.33	12.92
19	*i*-C_3H_7	CH_3	α+β[d]	147—150	$C_9H_{14}N_2O_4S$	43.90	5.73	11.38	13.00	43.73	5.71	11.54	12.99

a) Calcd: Cl, 10.79. Found: Cl, 10.69. b) Calcd: Cl, 11.27. Found: Cl, 11.12. c) Calcd: Br, 21.41. Found: Br, 21.49.
d) A stereoisomeric mixture of *cis* and *trans* isomers.

Table 2. NMR data of *N*-carbamoyl-2-imino-4-alkoxycarbonyl-5-substituted 1,3-oxathiolanes (ppm from TMS) in CD_3SOCD_3 solutions

Compound	Configuration		H_A	Δ_c^t [a]	H_B	Δ_c^t [a]	J_{AB}(Hz)	COOR′			Δ_c^t [a]	NH_2	
								CH_3	Δ_c^t [a]	CH_2			
6	C[b]	(α)	4.83	−0.14	5.98	0.11	6.2±0.1	3.25	0.48			7.04	7.32
	T[c]	(β)	4.69		6.09		3.9±0.1	3.73				7.05	7.30
7	C	(α)	4.83	−0.17	5.98	0.07	6.2±0.1	0.72	0.46	3.70	0.46	7.03	7.30
	T	(β)	4.66		6.05		3.9±0.1	1.18		1.18		7.03	7.30
8	C	(α)	4.76	−0.18	5.95	0.01	6.4±0.1	0.99	0.42			7.00	7.30
	T	(β)	4.58		5.96		5.6±0.1	1.41				7.00	7.30
9	C		4.76		5.88		6.2±0.1	3.28				not located	
	T												
10	C		4.76		5.89		6.2±0.1	0.78		3.75		not located	
	T												
11	C	(α)	4.79	−0.10	6.00	0.22	6.1±0.1	0.72	0.53	3.70	0.55	not located	
	T	(β)	4.69		6.22		3.8±0.1	1.25		4.25		not located	
12	C												
	T		4.74		6.13		4.5±0.1	1.23		4.23		7.10	7.35
13	C	(α)	4.79	−0.20	6.00	0.20	6.1±0.1	0.70	0.52	3.65	0.55	not located	
	T	(β)	4.59		6.20		3.8±0.1	1.22		4.20		not located	
14	C												
	T		4.71		6.09		4.4±0.1	1.23		4.21		7.05	7.33
15	C	(α)	4.97	−0.21	6.10	0.14	6.4±0.1	0.76	0.47	3.76	0.46	7.12	7.38
	T	(β)	4.76		6.24		3.8±0.1	1.23		4.22		7.12	7.38
16	C	(α)	4.50	−0.12	4.88	0.23	6.2±0.1	3.72	0.00			6.90	7.14
	T	(β)	4.38		5.11		3.9±0.1	3.72				6.90	7.14
17	C												
	T		4.43		4.94		3.6±0.1	3.74				6.91	7.16
18	C												
	T		4.45		4.95		3.9±0.1	1.22		4.21		6.95	7.20
19	C		4.90	−0.49	4.30	0.47	6.2±0.1	3.71	0.03			6.91	7.15
	T		4.41		4.77		3.9±0.1	3.74				6.91	7.15

a) A differential shift between *trans* and *cis* isomers. b) *Cis* isomer. c) *Trans* isomer.

trans isomers of the oxathiolanes are summarized in Table 2. Assignments of two doublets responsible for the 4- and 5-protons were made by double irradiation technique. Of the doublets of the AB spin system the lines of the doublet at lower field are somewhat broader than those at higher field (Figs. 2 and 3). Irradiation of the benzene protons causes narrowing of the proton α (designated as H_B) to the irradiated group. Such coupling between aromatic and benzylic protons have been observed before in other classes of compounds.[7] The NH_2 signals of the carbamoyl group always appear at two positions, near 7.00 ppm and near 7.30 ppm, which might be due to the presence of *syn* and *anti* isomers.[4]

It can be seen from the Table that there is no clear relation between the electronegativities of the substituent on the benzene ring and the chemical shifts and vicinal coupling constants of the oxathiolane ring

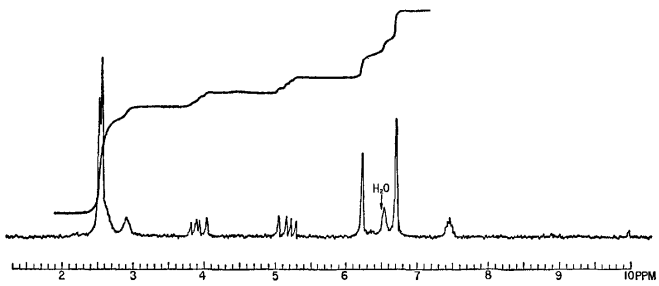

Fig. 1. NMR spectrum of a stereoisomeric mixture of *cis*- and *trans* isomers of *N*-carbamoyl-2-imino-4-methoxycarbonyl-5-phenyl-1,3-oxathiolane (**6**) (60 MHz).

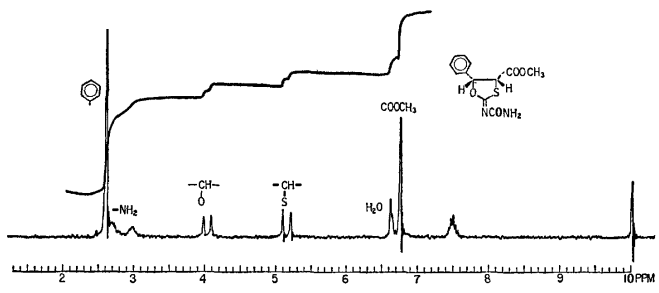

Fig. 2. NMR spectrum of *cis* isomer (**6α**) (60 MHz).

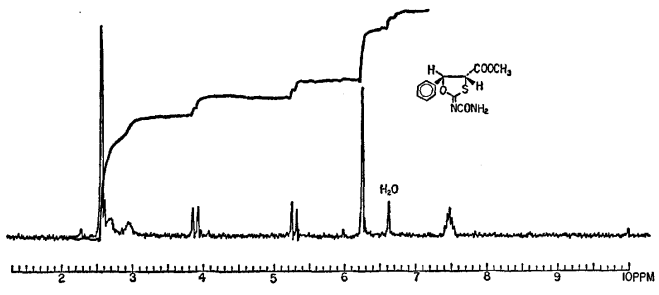

Fig. 3. NMR spectrum of *trans* isomer (**6β**) (60 MHz).

protons. The observed coupling constants (J_{AB}) are in the range 6.0—6.4 Hz for the α-forms and 3.6—4.5 Hz for the β-forms, except for the *t*-butyl ester. It is a common assumption that in five-membered rings which cannot deviate appreciably from planarity, J_{cis} is always larger than J_{trans}[8] as expected from the Karplus rule.[9] However, several reports showed that in the absence of other information such conclusion were doubtful.[10] The Dreiding model indicates that the 1,3-oxathiolane ring should exist predominantly as a very slightly distorted envelope conformation with the oxygen as the "flap" atom. Recently X-ray diffraction studies[11] showed that in the crystal structure of cholest-4-one-3-spiro(2,5-oxathiolane) the oxathiolane ring exists in a slightly distorted envelope conformation with the methylene carbon adjacent to oxygen lying 0.5 Å out of the plane defined by the other four atoms and with a torsional angle of 34.3° between the two carbon atoms. Pasto and coworkers[12] and Bovey and coworkers[13] indicated from analysis of coupling constants for a series of 2-substituted 1,3-oxathiolanes that there is one highly preferred envelope conformation, but the latter concluded that rapid pseudorotation takes place. However, it was shown from an X-ray diffraction study of the structure of ethylene carbonate which is the oxygen analog of 2-imino-1,3-oxathiolane that the molecule has the half-chair C_2 conformation,[14] though 1,3-dioxolane which is the oxygen analog of 1,3-oxathiolane, possesses a slightly distorted envelope conformation.[15] Accordingly, it seems to be difficult to infer from available data the conformation of 2-carbamoylimino-1,3-oxathiolanes. Hence, in the present case the relative values of the coupling constants cannot be considered a reliable indication of the configuration of substituents.

It is interesting to note that with the 5-aryl derivatives the signals of the alkoxycarbonyl groups for the α-forms always appear at a higher field by *ca.* 0.5 ppm than those for the β-forms, while the signals for the β-forms are in almost the same positions as those for the derivatives not having the aryl group (near 3.72 ppm for the methyl and near 1.22 and 4.15 ppm for the ethyl signals). This means that the alkoxycarbonyl protons of the α-forms may experience the long-range shielding of the benzene ring. It should be noted that the H_A proton of the β-form resonates at higher field than that of the α-form, whereas the H_B proton of the former is located at lower field than

7) a) G. P. Newsoroff and S. Sternhell, *Aust. J. Chem.*, **21**, 747 (1968); b) H. Rottendorf and S. Sternhell, *ibid.*, **17**, 1315 (1964); c) G. Ceccarelli, G. Berti, G. Lippi, and B. Macchia, *Organic Magnetic Resonance*, **2**, 379 (1970).

8) L. M. Jackman and S. Sternhell, "Applications of Nuclear Magnetic Resonance Spectroscopy in Organic Chemistry," 2nd Ed., Pergamon Press, New York, N. Y. (1969), p. 288.

9) M. Karplus, *J. Amer. Chem. Soc.*, **85**, 2870 (1963).

10) a) F. A. L. Anet and J. M. Muchowski, *Chem. Ind.* (London), **1963**, 81; b) L. H. Zalkow and M. Ghosal, *Chem. Commun.*, **1967**, 922.

11) A. Cooper and D. A. Norton, *J. Org. Chem.*, **33**, 3535 (1968).

12) D. J. Pasto, F. M. Klein, and T. W. Doyle, *J. Amer. Chem. Soc.*, **89**, 4368 (1967).

13) G. E. Wilson, Jr., M. G. Huang, and F. A. Bovey, *ibid.*, **92**, 5907 (1970).

14) C. J. Brown, *Acta Crystallogr.*, **7**, 92 (1954).

15) S. Furberg and O. Hassel, *Acta Chem. Scand.*, **4**, 1584 (1950).

Table 3. Observed NOE and internuclear distance for H–H interaction

No.	Steucture	Proton irradiated	Proton observed	NOE (%)	Internuclear distance (Å)
6α	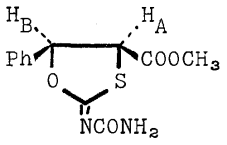	H_B	H_A	28	2.3—2.5
		H_A	H_B	19	
6β	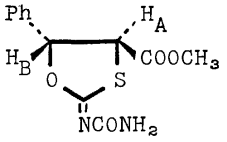	H_B	H_A	7	2.7—3.1
		H_A	H_B	8	
8β	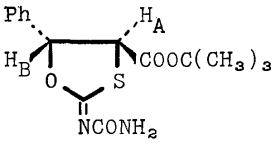	H_B	H_A	14	2.7—3.1
		H_A	H_B	11	

that of the latter. These differential shifts of the ring protons can be attributed to the long-range shielding of the benzene and alkoxycarbonyl groups.[16] The above facts suggest that the higher-melting α-forms possess the *cis* configuration, the lower-melting β-forms the *trans* arrangement.[17,18]

Conclusive evidence supporting these stereochemical assignments can be provided through studies of the nuclear Overhauser effect (NOE). The NOE results obtained when irradiating and observing protons are shown in Table 3, along with the internuclear distance as measured from Dreiding models on the assumptions of the slightly distorted envelope conformation in which rapid pseudorotation occurs. Recetly, Bell and Saunders[19] have shown that there is a linear relationship between the intramolecular nuclear Overhauser effect and the sixth power of the internuclear distance. Table 3 shows that the internuclear distance between the 4- and 5-protons is much shorter for the *cis* form than for the *trans*. Thus, a larger NOE would be expected for the α-form than for the β-form. The results are in good agreement with expectations.

On the assumptions of pseudorotation, one would expect that the molecule would assume the two limiting conformations **2α** and **2α'** for the *cis* isomer and **2β** and **2β'** for the *trans* one, whether in an envelope conformation or in a half-chair C_2 one. In the *cis*

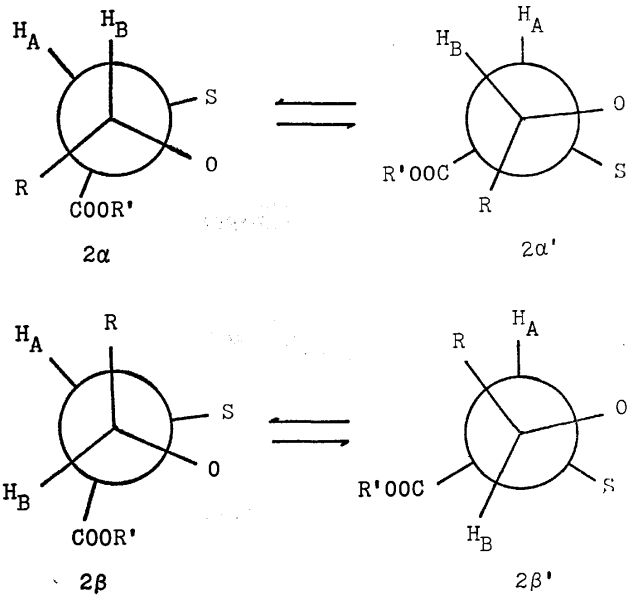

forms, the difference in energy between the two conformations should not be large, because there is no 1 ; 3 diaxial interaction. However, in the *trans* forms, electrostatic repulsion between the two substituents may be larger in **2β'** than in **2β**. Since there is no 1 ; 3 diaxial interaction, conformation **2β** may be preferred to conformation **2β'**. This argument could explain the fact that J_{AB} is larger for the *cis* than for the *trans* isomer. However, since the introduction of the bulkier substituent into the 4- or 5-position should lead to an increase in population of **2β**, the *trans* isomer of *t*-butyl ester (**8β**) might be more heavily populated in **2β** than those of methyl and ethyl esters. This speculation leads to a contradiction to the fact that **8β** has an unusually larger J_{AB}, as compared with **6β** and **7β**. A plausible explanation for this is that the C=NCONH$_2$ group on the 2-position exerts some

16) Similar arguments have been made before in the case of cinnamic ester derivatives,[16a] 4,5-diphenyl-1,3-dioxolan-2-one,[16b] and 4,5-diphenyl-1,3-dithiolane-2-thione.[16b]; a) T. Hayashi, *J. Org. Chem.*, **31**, 3253 (1966); b) C. G. Overberger and A. Drucker, *ibid.*, **29**, 360 (1964).

17) Form C has *cis* configuration, form T, *trans*.

18) In the case of 1,3-dioxolanes[16b),18] and 1,3-dithiolane-2-thiones, the *cis* isomers always have melting points higher than the *trans*; F. A. L. Anet, *J. Amer. Chem. Soc.*, **84**, 747 (1962).

19) R. A. Bell and J. K. Saunders, *Can. J. Chem.*, **48**, 1114 (1970).

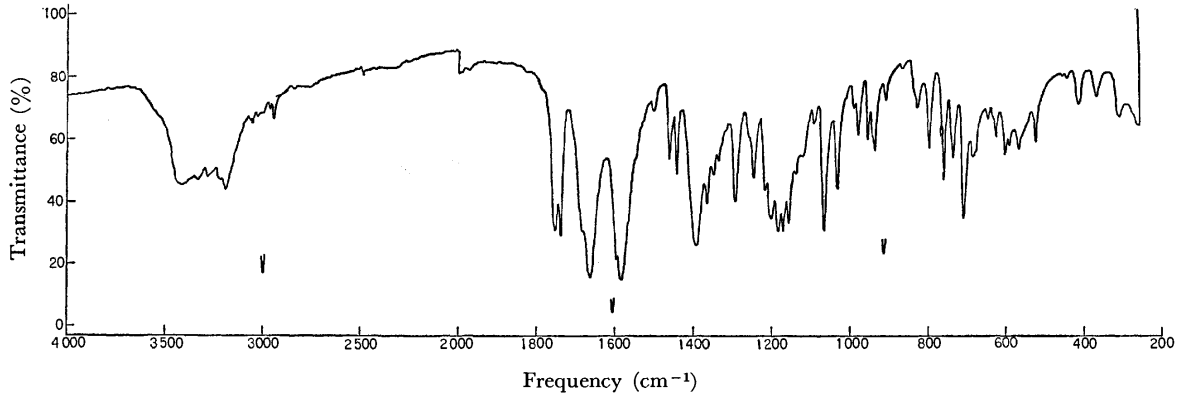

Fig. 4. IR spectrum of *cis*-*N*-carbamoyl-2-imino-4-methoxycarbonyl-5-phenyl-1,3-oxathiolane (**6α**).

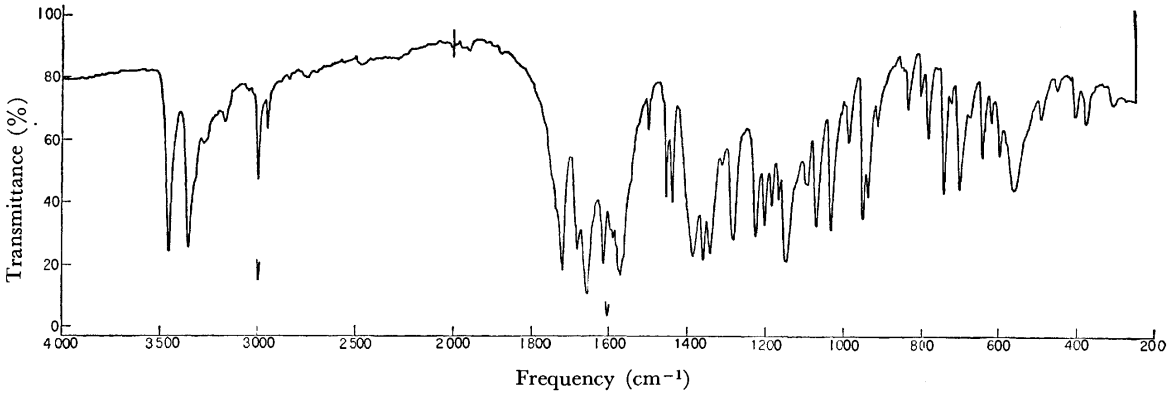

Fig. 5. IR spectrum of *trans*-*N*-carbamoyl-2-imino-4-methoxycarbonyl-5-phenyl-1,3-oxathiolane (**6β**).

Table 4. IR data of *N*-carbamoyl-2-imino-4-alkoxycarbonyl-5-substituted 1,3-oxathiolanes[a)]

Compound	NH_2 stretching		Ester C=O stretching	Carbamoyl C=O stretching	NH_2 deformation	C=N stretching
6α	3300 br	3190 br	1753 s 1740 s	1680 s		1580 s
6β	3454 s	3354 s	1722 s	1658 s	1612 m	1570 s
7α	3300 br	3180 br	1743 s	1680 s		1576 s
7β	3454 s	3354 s	1718 s	1687 s	1610 m	1569 s
8α	3275 s	3212 br	1728 s	1682 s		1560 s
8β	3455 s	3350 m	1714 s	1660 m	1612 m	1575 s
9C	3420 m	3310 br	1744 s	1682 s	1615 m	1580 s
10C	3350 br 3290 m	3240 br 3200 br	1741 s	1687 s	1620 m	1585 s
11α	3360 br	3160 m	1740 s	1695 s		1566 s
11β	3360 br	3160 m	1740 s	1684 s	1605 m	1566 s
12T	3450 s	3352 s	1722 s	1660 s	1615 s	1575 s
13C	3290 br	3180 br	1758 s	1695 s	1625 s	1588 s
14T	3450 s	3350 s	1725 s	1660 s	1618 m	1575 s
15α+β[b)]	3488 br 3335 m	3270 br 3200 m	1735 s 1727 s	1674 s	1610 m	1588 s
16α+β[b)]	3300 br	3180 br	1750 s 1745 s	1685 s	1620 m	1582 s
17T	3360 br 3290 m	3240 br 3200 m	1738 s 1731 s	1678 s		1573 s
18T	3470 s	3200 s	1730 s	1673 s	1620 m	1580 s
19α+β[b)]	3400 br 3330 m	3295 br 3230 m	1740 s	1665 s		1570 s

a) IR spectra were measured in KBr pellets (cm^{-1}). b) A stereoisomeric mixture of *cis* and *trans* isomers.

steric interaction on the 4- or 5-position, which shifts an equilibrium to the **2β′** side to that extent.

Although a stereoisomeric mixture of 5-alkyl substituted derivatives could not be separated, configurational assignments for the measurements of *cis* : *trans* ratios were made on the basis of the relative values of the coupling constants.[20]

The IR spectra are also useful for diagnostic purposes. The ester C=O stretching band for the *cis* isomers always appears at a higher frequency region than that of the *trans* one. The ester C=O band of **6α** exceptionally splits into a doublet (Fig. 4). It was also observed that the NH_2 stretching bands of the carbamoyl group are rather sharp doublet in the *trans* isomers, whereas the *cis* isomers showed broad absorption in the region between 3500 and 3000 cm^{-1} (Figs. 4 and 5).

The isomeric compositions of fourteen oxathiolanes, as evaluated from the integration of the area under the appropriate NMR signals, are given in Table 5. The reaction of **1** with benzaldehyde in the presence of potassium fluoride led to the predominant formation of the *cis* isomer. When potassium carbonate was used as a catalyst, the yield of the *trans* isomer inincreased. The reaction with *p*-anisaldehyde produced exclusively the *cis* isomer, whereas *o*-anisaldehyde afforded predominantly the *trans* isomer. On the contrary, the reaction with *p*-chloro- and *p*-bromobenzaldehydes provided exclusively the *trans* isomer, whereas

Table 5. Stereoisomeric composition of products **2**

Compound	Catalyst	*Cis* %[c]	*Trans* %[c]
6	C[a]	55	45
	F[b]	75	25
7	C	55	45
	F	75	25
8	C	25	75
9	C	100	0
	F	100	0
10	C	100	0
	F	100	0
11	F	21	79
12	C	0	100
	F	0	100
13	F	73	27
14	F	0	100
15	F	24	76
16	C	53	47
	F	53	47
17	C	0	100
	F	0	100
18	C	0	100
	F	0	100
19	F	25	75

a) Potassium carbonate b) Potassium fluoride
c) Figures represent the average of at least three experiments.

20) Since a stereoisomeric mixture of 5-alkyl derivatives could not be separated, the NOE of the 5-methyl derivatives (**16**) was measured in a solution containing the *cis* and *trans* isomers (*ca.* 1 : 1). In this case the 5-methyl protons of the *cis* and *trans* isomers appeared at the same position. When the methyl protons were irradiated, the % area increase in the H_A proton signal was 7% for the *trans* isomer, and 0% for the *cis* isomer.

o-chlorobenzaldehyde resulted predominantly in the *cis* isomer. Furthermore, the reaction of acetaldehyde led to an almost equimolar mixture of the *cis* and *trans* isomers, while propionaldehyde and *n*-butyraldehyde predominantly produced the *trans* isomers. From the results it is difficult to observe any relationship between the electronegativities and steric requirement of the 5-substituent and the stereoisomeric compositions of the products. It was found that the *cis*(α) isomers are always produced more rapidly than the *trans*(β) forms. It was thought at first that the *cis* isomers are the kinetically-favored products and are thermodynamically unstable relative to the more slowly formed *trans* isomers. However, it was shown that under the conditions employed in the reactions the *cis* isomers did not isomerize into the *trans* ones. Under the more drastic conditions the *cis* isomer was converted into a higher-melting product, whose structure still remains undetermined.

Experimental

All melting points were uncorrected. NMR spectra were obtained with Varian HA-100D and JEOL C-60 spectrometers in deuterodimethyl sulfoxide solution using tetramethylsilane as an internal standard. The nuclear Overhauser effects (NOE) were measured as % area increase using the electric integrator of the instrument. The spectra were run as filtered (fine sintered glass) and carefully degassed CD_3SOCD_3 solutions, the concentration varying between 5 and 10%. A small amount of TMS was added as an internal lock.

IR spectra were determined in the KBr pellet using a Perkin-Elmer 521 spectrophotometer. Mass spectra were taken with a JMS-01S instrument operating at 75 eV.

*Reactions of Thiocyanoacetic Esters (**1**) with Aldehydes. General Procedure*: A solution containing thiocyanoacetic ester (**1**) (0.03 mol) and an aldehyde (0.03 mol) in 20 m*l* of moist ether was stirred mechanically in the presence of potassium carbonate or fluoride (5.0 g) at room temperature. The reaction required 3—4 hr, when the benzaldehydes having an electron-attractive substituent were used, and 7—8 hr, when the benzaldehydes having an electron-donating substituent were used. After the catalyst was removed by filtration and washed with 20 m*l* of ether, the filtrate and washings were combined and allowed to stand overnight in an open vessel. The precipitated crystals were collected on a filter and washed with ether, until the crystals became colorless. A small fraction of the crystals was subjected to NMR analysis for the measurement of isomeric ratios. The rest of the crystals were recrystallized from an appropriate alcohol, until the lower-melting isomer was removed (α-form).

The filtrate, from which the crude α-isomer was removed, was allowed to stand for several more days, until the formation of crystals ceased. The precipitate was washed repeatedly with ether and then a small fraction was subjected to NMR analysis. The rest of the precipitate was recrystallized from appropriate alcohol, until a pure lower-melting isomer was obtained.

cis *and* trans *5-Phenyl-4-methoxycarbonyl-2-carbamoylimino-1,3-oxathiolanes (**6α** and **6β**).* A mixture of methyl thiocyanoacetate (3.5 g) and benzaldehyde (3.5 g) in 20 m*l* of moist ether was stirred in the presence of potassium carbonate (5.0 g) for 6 hr. After the catalyst was removed by filtration, the filtrate was allowed to stand overnight at room

temperature. The resulting precipitate was collected on a filter and washed with ether, until the reddish yellow color was removed. After the crystals were weighed, a small fraction was subjected to NMR analysis. The rest of the precipitate was recrystallized from methanol. The crude product contained 80% *cis*-**6**.

The filtrate was allowed to stand for another three days and then the resulting precipitate was washed with ether repeatedly. After the precipitate was weighed, a small fraction was subjected to NMR analysis. The rest of it was recrystallized from ethanol. The crude product contained 40% *trans*-**6**. The *cis* isomer (yield 2.4 g) has mp 190—191°C, molecular ion peak at *m/e* 280. The *trans* isomer has mp 138—139°C, molecular ion peak at *m/e* 280.

cis *and* trans *5-Phenyl-4-ethoxycarbonyl-2-carbamoylimino-1,3-oxathiolanes (***7α** *and* **7β***).* A solution of ethyl thiocyanoacetate (3.5 g) and benzaldehyde (3.5 g) in 20 m*l* of ether was stirred in the presence of potassium carbonate (5.0 g) for 6 hr. The first precipitate was recrystallized from ethanol, giving 2.5 g of **7α**, mp 190—191°C, molecular ion peak at *m/e* 294. The second precipitate was recrystallized from methanol, giving 0.2 g of **7β**, mp 159—160°C, molecular ion peak at *m/e* 294.

Attempted Epimerization of **7α** *with Potassium Carbonate in Ethanol.* To 2.0 m*l* of ethanol were added 0.5 g of **7α** and 0.2 g of potassium carbonate and the mixture was refluxed for an hour and then allowed to stand for two days at room temperature. The solvent was removed in a vacuum. The resulting crystals proved to be the starting material by IR and NMR analyses.

Attempted Epimerization of **6α** *with Sodium Methoxide in Methanol.* In 30 m*l* of methanol was dissolved 0.05 g of sodium and then 0.2 g of **6α**. After the solution was allowed to stand at 50°C for 6 hr, the solvent was removed in a vacuum. The resulting solid product was recrystallized from ethanol. The crystals remained unmelted at 250°C.

The authors wish to express their thanks to Dr. Taro Hayashi of this Institute and Professor Tatsuo Takeshima of Chiba University for their interest and encouragement. Thanks are also due to Mr. Ko-ichi Iyama for his assistance in carrying out the experiments.

BULLETIN OF THE CHEMICAL SOCIETY OF JAPAN, VOL. 45, 584—587 (1972)

Reactions of 5*N*-(1,2,3-Triazol-1-yl)tropolones[1)]

Hiroshi HORINO* and Takashi TODA

Department of Chemistry, Faculty of Science, Tohoku University, Katahira-cho, Sendai

(Received August 16, 1971)

The chemical properties of 5*N*-(1,2,3-triazol-1-yl)tropolones are investigated. The reactions of 5*N*-(4′-ethoxycarbonyl-5′-methyl-1,2,3-triazol-1-yl)tropolone methyl ether (I) with malononitrile and ethyl cyanoacetate gave the corresponding azulene derivatives, but with ethyl acetoacetate the reaction afforded a 1-oxaazulan-2-one derivative. The methoxyl group of I is replaced by aliphatic amines to form 2-aminotropone derivatives. Also, the reaction of I with guanidine and *o*-phenylenediamine gave a 1,3-diazaazulene derivative and a quinoxaline derivative respectively. The brominations of triazolyltropolones afforded the corresponding 3,7-dibromotropolone derivatives, while reactions with thionyl chloride gave 2-chlorotropone derivatives.

Only a few troponoid compounds which possess heterocyclic aromatics on their nuclei have been found, and even their chemical properties have not yet been investigated in detail.[2,3)] Triazole compounds have been known to be interesting, biologically-active substances;[4)] therefore, to synthesize troponoid compounds which possess a triazole ring as a substituent and to investigate their chemical and physiological properties are interesting and important problems. We investigated the reactions of 5-azidotropolones' methyl ethers with several active methylene compounds and obtained 5*N*-(1,2,3-tiazol-1-yl)tropolone methyl ethers.[5)] In this paper, several chemical properties of the triazolyltropolones thus obtained will be presented.

The treatment of 2-methoxy-5*N*-(4′-ethoxycarbonyl-5′-methyl-1,2,3-triazol-1-yl)tropone (I)[5)] with active methylene compounds, such as ethyl cyanoacetate and malononitrile, afforded the corresponding azulene compounds, diethyl 2-amino-6*N*-(4′-ethoxycarbonyl-5′-methyl-1,2,3-triazol-1-yl)azulen-1,3-dicarboxylate (II) and 2-amino-1,3-dicyano-6*N*-(4′-ethoxycarbonyl-5′-methyl-1,2,3-triazol-1-yl)azulene (III) respectively, in fairly good yields. However, the reaction of I with ethyl acetoacetate gave a crystalline substance (IV).

The results of elemental analysis, $C_{17}H_{15}O_5N_3$, and the UV and visible spectra of IV indicated that it is an oxaazulan-2-one type compund.[3)] Ethyl acetoacetate is a weak active methylene compound compared with malononitrile or ethyl cyanoacetate. That is why the second mole of the reagent does not

1) Presented at the 18th Annual Meeting of the Chemical Society of Japan, Osaka, April, 1965.

* Present address: College of General Education, Tohoku University, Kawauchi, Sendai.

2) K. Ogura, This Bulletin, **35**, 808 (1962); S. Seto and Y. Nishiyama, *ibid.*, **35**, 1010 (1962); S. Seto, Y. Nishiyama, and K. Ogura, *ibid.*, **35**, 1958 (1962); T. Nozoe, K. Takase, and Y. Mochizuki, *ibid.*, **37**, 1641 (1964).

3) T. Nozoe and K. Kikuchi, "Dai Yuki Kagaku" (Comprehensive Organic Chemistry), Vol. 13, ed. by M. Kotake, Asakura Shoten, Tokyo (1960), p. 604; and the unpublished results cited therein.

4) F. G. Benson and W. L. Savell, *Chem. Rev.*, **46**, 1 (1950); S. C. Sheehan, *J. Amer. Chem. Soc.*, **73**, 1207 (1951).

5) T. Nozoe, H. Horino, and T. Toda, *Tetrahedron Lett.*, **1967**, 5349, and unpublished results.

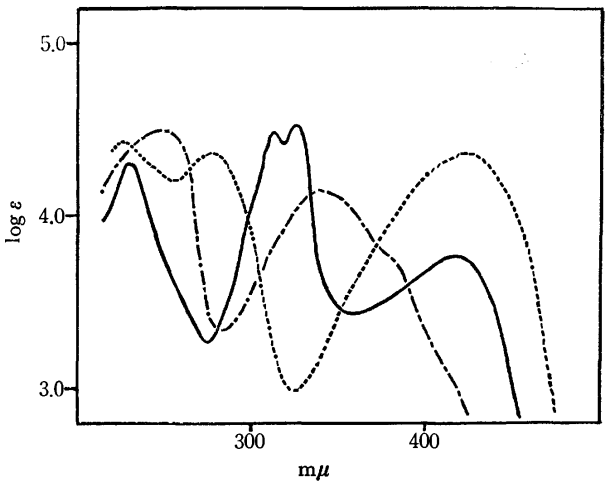

Fig. 1. Ultraviolet absorption spectra of III(——), IV(----) and XVII (------) in methanol.

attack the formed oxaazulanone.

The reactions of I with nucleophilic reagents such as amine were also investigated. When reactions of I were carried out in alcohol with hydrazine, ethylamine, and diethylamine, 2-hydrazino-(V), 2-ethylamino-(VI), and 2-diethylamino-5*N*-(4′-ethoxycarbonyl-5′-methyl-1,2,3-triazol-1-yl)tropone (VII) were obtained respectively. The treatment of 5-azidotropolone methyl ether with aliphatic amines gave the corresponding 2-aminotropone derivatives, but with aromatic amines only the starting substance was recovered under the same reaction conditions.[5] However, I gave a quinoxaline derivative (VIII) in a reaction with *o*-phenylene diamine. This fact suggests that the azido group is a strongly negative one, but that it acts as an electron-donating group by means of its resonance contribution[6] and reduces the reactivity of tropolone nuclei toward nucleophiles.

On the other hand, the triazole ring acts only as an electron-withdrawing group. I afforded 2-amino-6*N*-(4′-ethoxycarbonyl-5′-methyl-1,2,3-triazol-1-yl)-1,3-diazaazulene (IX) in a reaction with guanidine.

The properties are analogous to those of other tropolone methyl ethers.[7] The reactions mentioned above are summarized in the following chart:

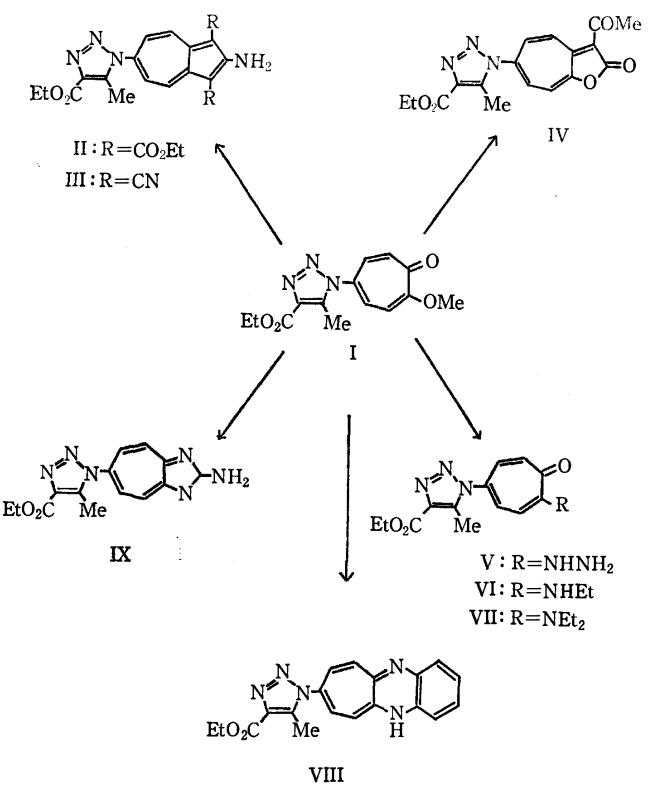

Free triazolytropolones were prepared by the hydrolysis of the corresponding methyl ethers;[5] the tropolones thus obtained are listed in Table 1.

The decarboxylation of XIII and XV in quinoline gave 5′-methyl (XVII) and 5′-phenyl (XVIII) derivatives of 5*N*-(1,2,3-triazol-1-yl)-tropolone. The UV and visible spectra of the triazolyltropolones are analogous to those of other 5-substituted tropolones;[8] being especially similar to that of 5-phenyltropolone.[9]

However, those of XVI and XVIII are shifted to shorter wavelengths compared with those of XVII or 5-phenyltropolone. This phenomenon indicates that the phenyl group at the 5′-position of XVI and XVIII interacts with tropolone nuclei and that the triazole ring can not take a planar position with the tropolone ring. XIV and XVI possess a fairly big shoulder near 400 mμ (log ε, *ca.* 3.5). Signals appear at 2.44 ppm (3H, broad, singlet), 7.44 ppm (4H, tropolone b. s), and 7.60 ppm (1H, triazole b. s) in the NMR spectrum of XVII. Also, those of XVIII appear at 7.32 ppm (1H triazol). These values are in good agreement with the values of the chemical shifts of other known

Table 1.

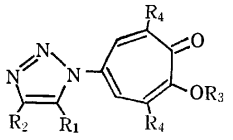

	R_1	R_2	R_3	R_4
I	Me	CO_2Et	Me	H
X	Me	COMe	Me	H
XI	Ph	CO_2Et	Me	H
XII	Ph	COPh	Me	H
XIII	Me	CO_2H	H	H
XIV	Me	COMe	H	H
XV	Ph	CO_2H	H	H
XVI	Ph	COPh	H	H
XVII	Me	H	H	H
XVIII	Ph	H	H	H
XIX	Me	H	H	Br
XX	Me	COMe	H	Br
XXI	Ph	H	H	Br

6) A. S. Smith and J. H. Hall, *J. Amer. Chem. Soc.*, **84**, 480 (1962).
7) *Cf.* pp. 147—148 of Ref. 3.
8) *Cf.* p. 113 of Ref. 3.
9) H. Horino, *Nippon Kagaku Zasshi*, **90**, 85 (1969).

tropolones.[10]

The bromination of 5-methyl-1,2,3-triazol or 1*N*-methyl-1,2,3-triazole takes place at the 4-position.[11] Thus, it is interesting to determine at which moiety (tropolone or triazole) of XVII or XVIII cationoid substitution reactions take place. The treatment of XVII with two moles of bromine gave a dibromide (XIX). The absorption at 861 cm^{-1} of XVII disappeared, and a new band appeared at 887 cm^{-1} in the IR spectrum of XIX. The former corresponds to two adjacent hydrogens, while the latter is an isolated hydrogen of tropolones.[12] The UV spectrum of XIX is analogous with those of 3,7-dibromo- and 3,5,7-tribromotropolones.[13] The NMR spectrum of XIX shows a methyl peak at 2.39 ppm (3H), a triazol hydrogen at 7.63 ppm (1H), and at 8.15 ppm (2H), tropolone hydrogens which shift down field compared with those of XVII under the influence of the substituted bromines. Therefore, the structure of XIX is 3,7-dibromo-5*N*-(5'-methyl-1,2,3-triazol-1-yl) tropolone. Also, the bromination of XIV and XVIII took place at the 3,7-positions of the tropolone moieties, (XX) and (XXI), as shown in Table 1.

These tendencies of the cationoid reactions of 5-triazolyltropolones are analogous to those of 4- and 5-phenyltropolones.[9] The reactions of XVII and XVIII with thionyl chloride afforded the corresponding 2-chlorotropone derivatives; their structures are proved by the results of their elemental analyses and their spectral data.

Experimental[14]

*Diethyl 2-Amino-6*N*-(4'-ethoxycarbonyl-5'-methyl-1,2,3-triazol-1-yl)azulen-1,3-dicarboxylate (II).* Into a mixture of ethyl cyanoacetate (130 mg) and sodium (12 mg) in absolute ethanol (1.5 m*l*), 2-methoxy-5*N*-(4'-ethoxycarbonyl-5'-methyl-1,2,3-triazol-1-yl)tropone (I) (150 mg) was stirred and then the mixture was allowed to stand overnight at room temperature. The solution yielded 260 mg of orange precipitates, which were then extracted with benzene to give 195 mg of II; mp 164—165°C, recrystallized from a benzene-cyclohexane mixture.

Found: C, 59.99; H, 5.41; N, 12.81%. Calcd for $C_{22}H_{24}O_6N_4$: C, 59.99; H, 5.49; N, 12.72%. λ_{max}^{MeOH}, mμ (log ε): 244 (4.60), 320 (4.77 sh), 332 (5.12), 410 (4.05).

*2-Amino-1,3-dicyano-6*N*-(4'-ethoxycarbonyl-5'-methyl-1,2,3-triazol-1-yl)azulene (III).* A suspension of (I) (150 mg) in a solution of malononitrile (76 mg) and triethylamine (115 mg) in absolute ethanol (2.5 m*l*) was stirred overnight. The precipitates thus formed were then separated to afford 222 mg of orange needles of III; mp 285°C, recrystallized from dimethylformamide.

Found: C, 62.45; H, 4.29; N, 24.28%. Calcd for $C_{18}H_{14}O_2N_6$: C, 62.42; H, 4.07; N, 24.27%. λ_{max}^{MeOH}, mμ (log ε): 231 (4.53), 314 (3.64), 327 (4.95), 410 (3.95).

*3-Acetyl-6*N*-(4'-ethoxycarbonyl-5'-methyl-1,2,3-triazol-1-yl)-oxazulan-2-one (IV).* Into a mixture of ethyl acetoacetate (100 mg) and sodium (12 mg) in absolute ethanol (155 m*l*), I (150 mg) was stirred and then the solution was allowed to stand overnight. Then the solvent was removed under reduced pressure, water was added, and the solution was extracted with ethyl acetate to give 47 mg of orange crystals of IV; mp 210°C, recrystallized from ethanol.

Found: C, 59.72; H, 4.72; N, 11.60%. Calcd for $C_{17}H_{15}O_5N_3$: C, 59.82; H, 4.43; N, 12.31%. λ_{max}^{MeOH}, mμ (log ε): 225 (4.41), 278 (4.34), 428 (4.32).

*2-Hydrazino-5*N*-(4'-ethoxycarbonyl-5'-methyl-1,2,3-triazol-1-yl)-tropone (V).* A solution of I (100 mg) and an 80% hydrazine hydrate solution (150 mg) in methanol (2 m*l*) was refluxed on a water bath for 5 min. The yellow precipitates thus formed were collected to give 73 mg of a sand-like crystal, V: mp 202°C, recrystallized from ethanol.

Found: C, 54.02; H, 5.22; N, 24.02%. Calcd for $C_{13}H_{15}O_3N_5$: C, 53.97; H, 5.23; N, 24.21%. λ_{max}^{MeOH}, mμ (log ε): 256 (4.40), 355 (4.27), 414 (4.03).

*2-Ethylamino-5*N*-(4'-ethoxycarbonyl-5'-methyl-1,2,3-triazol-1-yl)-tropone (VI).* A solution of I (200 mg) and an 70% aqueous solution of ethylamine in ethanol (2 m*l*) was stirred and then allowed to stand for 2 hr. The solution produced yellow crystals, which were collected to give 150 mg of VI; mp 142—143°C, recrystallized from ethanol.

Found: C, 59.57; H, 6.03; N, 18.35%. Calcd for $C_{15}H_{18}O_3N_4$: C, 59.59; H, 6.00; N, 18.53%. λ_{max}^{MeOH}, mμ (log ε): 252 (4.57), 350 (4.35), 415 (4.12).

*2-Diethylamino-5*N*-(4'-ethoxycarbonyl-5'-methyl-1,2,3-triazol-1-yl)tropone (VII).* A solution of I (100 mg) and diethylamine (1 g) in 2 m*l* of ethanol was allowed to stand overnight. The solution was then concentrated under reduced pressure without heating and extracted with benzene to afford 84 mg of a paste, which, with a saturated solution of picric acid in alcohol, gave 100 mg of a yellow picrate of VII; mp 163—164°C (dec.), recrystallized from ethanol.

Found: C, 49.49; H, 4.68; N, 17.38%. Calcd for $C_{23}H_{25}O_{10}N_7$: C, 49.73; H, 4.52; N, 17.53%.

*8*N*-(4'-Ethoxycarbonyl-5'-methyl-1,2,3-triazol-1-yl)benz(b)tropazine (VIII).* A solution of I (100 mg) and *o*-phenylenediamine (45 mg) in absolute ethanol (2 m*l*) was refluxed on a water bath for 2 hr. The solution was then concentrated to give 64 mg of crystals of VIII; mp 181°C (dec.), from ethanol.

Found: N, 19.77%. Calcd for $C_{19}H_{17}O_2N_5$: N, 20.16%. λ_{max}^{MeOH}, mμ (log ε): 240 (4.54), 340 (4.13).

*2-Amino-6*N*-(4'-ethoxycarbonyl-5'-methyl-1,2,3-triazol-1-yl)-1,3-diazaazulene (IX).* To a solution of guanidine hydrochloride (60 mg) and sodium (12 mg) in absolute ethanol (2 m*l*), I (150 mg) was added, after which the mixture was refluxed on a water bath for 15 min. The precipitate thus formed was collected and washed with chloroform to afford 135 mg of IX; mp 280°C.

Found: C, 56.33; H, 4.77; N, 28.25%. Calcd for $C_{14}H_{14}O_2N_6$: C, 56.37; H, 4.73; N, 28.18%.

*5*N*-(4'-Carboxy-5'-methyl-1,2,3-triazol-1-yl)tropolone (XIII).* A solution of I (150 mg) in an aqueous 2N sodium hydroxide solution (3 m*l*) was heated on a water bath for 10 min. The solution was then acidified with 2N hydrochloric acid to afford colorless crystals of XIII (127 mg); mp 212—213°C (dec.), recrystallized from ethanol.

Found: C, 53.15; H, 3.86; N, 16.78%. Calcd for $C_{11}H_9O_4N_3$: C, 53.14; H, 3.67; N, 17.00%.

The following substituted triazolyl tropolones were prepared as above.

*5*N*-(4'-Carboxy-5'-phenyl-1,2,3-triazol-1-yl)tropolone (XV).* Mp 177°C (dec.), recrystallized from an ethanol-benzene

10) H. Sugiyama, *Sci. Repts. RITU*, A, 20, 34 (1968).
11) R. Hüttel and G. Welzel, *Ann.*, **593**, 207 (1955).
12) Y. Ikegami, "Infrared Spectra", Kagaku no Ryoiki Special Issue, No. 8, Nanko-Do, Tokyo (1959), p. 33.
13) K. Ogura and Y. Ikegami, *Bull. Chem. Research Institute of Non-Aqueous Solutions, Tohoku Univ.* (in Japanese), **9** (3), 24 (1959).
14) All the melting points are uncorrected.

mixture.

Found: C, 59.26; H, 4.13; N, 12.74%. Calcd for $C_{16}H_{11}O_4N_3 \cdot H_2O$: C, 58.71; H, 4.00; N, 12.88%.

5N-(4'-Benzoyl-5'-phenyl)-1,2,3-triazol-1-yl)tropolone (XVI). Mp 193°C, recrystallized from ethanol.

Found: C, 71.80; H, 4.38; N, 11.47%. Calcd for $C_{22}H_{15}O_3N_3$: C, 71.53; H, 4.09; N, 11.38%.

5N-(5'-Methyl-1,2,3-triazol-1-yl)tropolone (XVII). A solution of XIII (407 mg) in quinoline (2 m*l*) was heated on an oil bath until all the bubbles had evaporated. After it had cooled, the solution was diluted with benzene and extracted with a 2N sodium hydroxide solution, which was then acidified and extracted with chloroform. When the solvent had been removed, XVII was obtained as colorless needles (316 mg); mp 153°C, recrystallized from ethanol.

Found: C, 59.29; H, 4.53; N, 20.57%. Calcd for $C_{10}H_9O_2N_3$: C, 59.14; H, 4.46; N, 20.68%. λ_{max}^{MeOH}, mμ (log ε): 245 (4.10), 334 (4.17), 379 (sh). ν(KBr): 3205, 1672, 863, 849 cm^{-1}.

5N-(5'-Phenyl-1,2,3-triazol-1-yl)tropolone (XVIII). A solution of XV (132 mg) in quinoline (2 m*l*) was treated as above to give XVIII as colorless plates; mp 195°C, from ethanol.

Found: C, 67.80; H, 4.45; N, 15.70%. Calcd for $C_{15}H_{11}O_2N_3$: C, 67.91; H, 4.18; N, 15.84%. λ_{max}^{MeOH}, mμ (log ε): 228 (4.47), 233 (4.49), 334 (4.07), 398 (3.70), 415 (3.31). ν(KBr): 3135, 858, 849, 738 cm^{-1}.

3,7-Dibromo-5N-(5'-methyl-1,2,3-triazol-1-yl)tropolone (XIX). Into a solution of XVII (100 mg) and sodium acetate (82 mg) in acetic acid (1 m*l*), bromine (170 mg) in acetic acid (0.3 m*l*) was stirred at room temperature. The solution was concentrated under reduced pressure, water was added, and then the solution was extracted with chloroform. When all the solvent had been removed, 159 mg of XIX were obtained; they were subsequently recrystallized from ethanol; mp 189°C (dec.).

Found: C, 33.95; H, 2.23; N, 10.90%. Calcd for $C_{10}H_7O_2N_3Br_2$: C, 33.26; H, 1.95; N, 11.64%. λ_{max}^{MeOH}, mμ (log ε): 274 (4.63), 354 (4.17), 436 (4.03). ν(KBr): 2860, 906, 887, 819 cm^{-1}.

The following 3,7-dibromo-5*N*-triazolyltropolones were prepared in the same way as above.

3,7-Dibromo-5N-(4'-acetyl-5'-methyl-1,2,3-triazol-1-yl)tropolone (XX). Mp 170—171°C, recrystallized from ethanol.

Found: N, 10.51%. Calcd for $C_{12}H_9O_3N_3Br_2$: N, 10.42%.

3,7-Dibromo-5N-(5'-phenyl-1,2,3-triazol-1-yl)tropolone (XXI). Mp 230°C (dec.), recrystallized from benzene-ethanol.

Found: N, 9.87%. Calcd for $C_{15}H_9O_3N_3Br_2$: N, 9.93%.

2-Chloro-5N-(5'-methyl-1,2,3-triazol-1-yl)tropone (XXII). A solution of XVII (375 mg) and thionyl chloride (500 mg) in dry benzene (5 m*l*) was refluxed on a water bath until it showed negative ferric chloride test. The subsequent concentration of this solution gave 333 mg of colorless crystals of XXII; mp 169—170°C, recrystallized from benzene.

Found: C, 54.56; H, 3.67; N, 18.20%. Calcd for $C_{10}H_6ON_3Cl$: C, 54.19; H, 3.64; N, 18.96%. λ_{max}^{MeOH}, mμ (log ε): 245 (4.34), 328 (3.98).

The authors are very much indebted to Professor Tetsuo Nozoe for his kind encouragement and guidance during the course of our work.

BULLETIN OF THE CHEMICAL SOCIETY OF JAPAN, VOL. 45, 587—590 (1972)

The Synthesis of 2,3-Dimethyl-3-(5-bromo-2-methoxy-4-methylphenyl)-cyclohexene, a Potentially Useful Intermediate for the Syntheses of Aplysin and Related Sesquiterpenes

Kiyoyuki YAMADA, Hisatoyo YAZAWA, and Yoshimasa HIRATA

Department of Chemistry, Faculty of Science, Nagoya University, Chikusa-ku, Nagoya

(Received August 18, 1971)

As a key intermediate for the syntheses of aplysin, **1**, a bromine-containing sesquiterpene isolated from *Aplysia kurodai*, and related sesquiterpenes, 2,3-dimethyl-3-(5'-bromo-2'-methoxy-4'-methylphenyl)cyclohexene, **2**, was synthesized, starting from an anisole derivative, **6**. The reactivity of the double bond in **2** towards oxidizing reagents was examined: the cyclohexene, **2**, reacted with ozone to give an epoxide, **12**, and a cyclohexanone, **13**, an isomerization product of **12**; **2** could be converted to the diol, **15**, with osmium tetroxide in the presence of pyridine.

The structure of aplysin, a bromine-containing novel sesquiterpene isolated from *Aplysia kurodai*, has been established as **1**.[1] The total synthesis of aplysin, **1**, was previously achieved in our laboratory, employing cyclopentanone as the starting material.[2] A different route for the synthesis of aplysin has since been projected *via* the title compound, **2**, as an important intermediate. A keto aldehyde, **3**, which can be derived from **2**, can possibly be cyclized to a conjugated aldehyde, **4**. The aldehyde, **4**, would then be utilized as an intermediate for the syntheses of aplysin, **1**, and related sesquiterpenes (*e.g.*, laurenisol, **5**[3]). We will describe here the synthesis of the cyclohexene, **2**.

Selective metallation at the C-6 position of the anisole, **6**, was carried out with phenyllithium in ether.[2] The lithium derivative of **6** was reacted with cyclohexanone to afford a cyclohexanol, **7**, the structure of which was confirmed by a study of the NMR

1) S. Yamamura and Y. Hirata, *Tetrahedron*, **19**, 1485 (1963).

2) K. Yamada, H. Yazawa, D. Uemura, M. Toda, and Y. Hirata, *ibid.*, **25**, 3509 (1969).

3) T. Irie, A. Fukuzawa, M. Izawa, and E. Kurosawa, *Tetrahedron Lett.* **1969**, 1343.

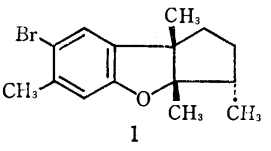
1

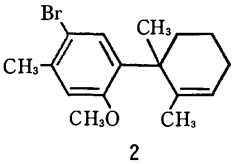
2

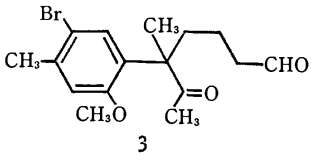
3

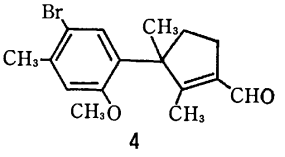
4

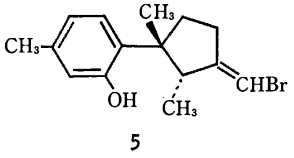
5

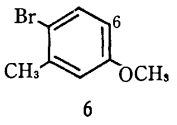
6

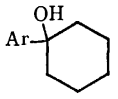
7

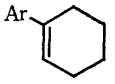
8

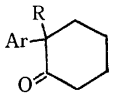
9: R=H
10: R=CH$_3$

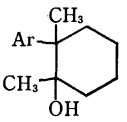
11

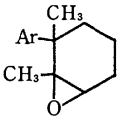
12

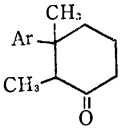
13

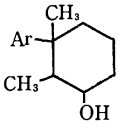
14

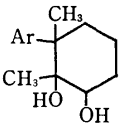
15

Ar=5-bromo-2-methoxy-4-methylphenyl.

spectral evidence: two sharp singlets arising from aromatic protons were observed at δ 6.80 and 7.50, indicating that the condensation took place between the C-6 position of the anisole, **6**, and cyclohexanone. The dehydration of the cyclohexanol, **7**, was smoothly effected by heating it with oxalic acid to give a cyclohexene, **8**. Although the double bond of **8** was inert towards various peracids, the conversion of the cyclohexene, **8**, to a cyclohexanone, **9**, was effected by heating it in performic acid. Methylation at the benzylic carbon atom alpha to the carbonyl group in **9** was performed by treating the cyclohexanone, **9**, with sodium hydride in 1,2-dimethoxyethane and then with methyl iodide. The resulting cyclohexanone, **10**, was submitted to the Grignard reaction under forcing conditions to afford a cyclohexanol, **11**, (~30%) with the recovery of **10** (62%). The rather unreactive nature of the carbonyl group in **10** must be due to steric reasons: the cyclohexanone, **9**, gave the corresponding alcohol in a Grignard reaction in a good yield (~70%). The cyclohexanol, **11**, was dehydrated by heating it in benzene - 50% sulfuric acid to give the desired cyclohexene, **2**.

The double bond of the cyclohexene, **2**, was rather unreactive towards oxidizing reagents. When treated with ozone, the cyclohexene, **2**, afforded an epoxide, **12**, and a cyclohexanone, **13**, and no cleavage of the double bond of **2** occurred. The structures of the two products, **12** and **13**, were established by the spectral data and the following chemical evidence: the epoxide, **12**, was isomerized with 50% sulfuric acid at 80°C to **13**; the reduction of **13** with lithium borohydride yielded a cyclohexanol, **14**, which was then led to the starting cyclohexene, **2**, on treatment with sulfuric acid. The formation of the epoxide, **12**, from **2** suggests that the double bond of **2** is sterically hindered; there are precedents for the formation of an epoxide from a sterically-hindered olefin by ozone.[4] While the *cis*-hydroxylation of **2** with wet silver acetate - iodine[5] did not take place under any conditions, the cyclohexene, **2**, reacted slowly with osmium tetroxide, though only in the presence of pyridine, to afford a diol, **15**. This diol, **15**, was then cleaved by periodic acid to give an oily, rather unstable keto aldehyde, **3**.

Experimental

The melting points are uncorrected. The IR spectra were measured on a JASCO Model IRS spectrophotometer, and the UV spectra (methanol as solvent), on a Perkin-Elmer Model 202 spectrophotometer. The NMR spectra were recorded with a JNMC-60H spectrometer; only the prominent peaks are cited, while the chemical shifts are expressed in ppm downfield from TMS as the internal standard (δ); s, singlet; d, doublet; m, multiplet; the coupling constants are given in Hz. The mass spectra were obtained on a Hitachi RMU-6D mass spectrometer, operating with an ionization energy of 70 eV. Thin-layer chromatography (TLC) was performed on silica gel GF_{254} (E. Merck, A. G., Germany), and column chromatography, on silicic acid (100 mesh, Millinckrodt, U.S.A.). The organic solutions were dried over anhydrous magnesium sulfate and evaporated by means of a rotary evaporator.

1-(5'-Bromo-2'-methoxy-4'-methylphenyl)cyclohexanol (7). A phenyllithium solution was prepared by stirring 16 g (2.28 mol) of metallic lithium into 176 g (1.1 mol) of bromobenzene in 900 m*l* of anhydrous ether under nitrogen. To the solution of phenyllithium, 200 g (1 mol) of the anisole, **6**, was then added, drop by drop, at room temperature. The mixture was stirred for 20 hr at room temperature and then refluxed for 10 hr. After cooling, 97 g (1 mol) of

4) K. W. Bentley, "Technique of Organic Chemistry," Vol. XI, ed. by A. Weissberger, Interscience Publishers, New York, N. Y. (1963), p. 882.

5) R. B. Woodward and F. V. Brutcher, Jr., *J. Amer. Chem. Soc.*, **80**, 209 (1958); *cf.* F. D. Gunstone, "Advances in Organic Chemistry, Methods and Results," Vol. I, ed. by R. A. Raphael, E. C. Taylor, and H. Wynberg, Interscience Publishers, New York, N. Y. (1960), p. 103.

cyclohexanone were added, and the mixture was stirred for 30 min and then refluxed for 5 hr. The mixture was poured into ice water, acidified with 10% hydrochloric acid, and repeatedly extracted with ether. The ethereal extracts were washed with water, dried, and evaporated to give a solid, the recrystallization of which from 95% ethanol afforded pure **7** (94.6 g, 32%); mp 118—119°C; UV 288 (ε 2000), 281 (ε 2000), 233 nm (ε 6700); IR (KBr) 3450, 1600, 1545 cm^{-1}; NMR ($CDCl_3$) 2.36 (3H, s), 3.88 (3H, s), 6.80 (1H, s), 7.50 (1H, s). Found: C, 56.40; H, 6.30; Br, 26.64%. Calcd for $C_{14}H_{19}O_2Br$: C, 56.23; H, 6.41; Br, 26.73%.

*1-(5'-Bromo-2'-methoxy-4'-methylphenyl)cyclohexene (**8**).* A solid mixture of 80 g (0.27 mol) of the cyclohexanol, **7**, and 40 g (0.44 mol) of anhydrous oxalic acid was kept at 210°C for 30 min. After cooling, water was added and the resulting mixture was repeatedly extracted with ether. The ethereal extracts were washed with a 10% sodium hydroxide solution and water, dried, and then evaporated to give a crystalline residue. Recrystallization from 95% ethanol afforded pure **8** (72 g, 96%); mp 51—53°C; UV 291 (ε 2800), 239 nm (ε 9300); IR (KBr) 1600, 1550 cm^{-1}; NMR (CCl_4) 2.35 (3H, s), 3.75 (3H, s), 5.70 (1H, m, vinyl H), 6.62 (1H, s), 7.20 (1H, s); mass, M^+ 282 and 280. Found: C, 59.90; H, 6.05; Br, 28.64%. Calcd for $C_{14}H_{17}OBr$: C, 59.84; H, 6.10; Br, 28.44%.

*2-(5'-Bromo-2'-methoxy-4'-methylphenyl)cyclohexanone (**9**).* To a stirred suspension of 18 g (0.064 mol) of the cyclohexene, **8**, in 60 m*l* of 85% formic acid, we added, drop by drop, 7.5 g of a 30% hydrogen peroxide solution under ice-bath cooling. The mixture was stirred at room temperature for 1 hr and at 90—95°C for 2 hr, and was then allowed to stand at room temperature overnight. The solid thus deposited was filtered and washed with water, a 10% sodium hydroxide solution, and water. The solid was subsequently chromatographed on silicic acid (80 g) with chloroform to give a crystalline material, the recrystallization of which from 95% ethanol afforded pure **9** (11.3 g, 60%); mp 174—175°C; IR (KBr) 1710, 1605, 1550 cm^{-1}; mass, M^+ 298 and 296. Found: C, 56.63; H, 5.55; Br, 27.01%. Calcd for $C_{14}H_{17}O_2Br$: C, 56.61; H, 5.77; Br, 26.91%.

*2-Methyl-2-(5'-bromo-2'-methoxy-4'-methylphenyl)cyclohexanone (**10**).* A mixture of 12 g (0.04 mol) of the cyclohexanone, **9**, and 1.2 g (0.05 mol) of sodium hydride in 160 m*l* of 1,2-dimethoxyethane was kept at 80°C for 2 hr with stirring under nitrogen. After the addition of 8 g (0.056 mol) of methyl iodide, the mixture was stirred at 80°C for 30 min, refluxed for 1 hr, and poured into ice water. The aqueous mixture was repeatedly extracted with benzene. The benzene extracts were washed with water, dried, and evaporated to give a residue, which was then chromatographed on silicic acid (25 g) with chloroform. The crude material thus obtained was recrystallized from 95% ethanol to afford pure **10** (4.9 g, 39%); mp 135—137°C; IR (KBr) 1700, 1602, 1550 cm^{-1}; NMR (CCl_4) 1.18 (3H, s), 2.34 (3H, s), 3.68 (3H, s), 6.64 (1H, s), 7.28 (1H, s); mass, M^+ 312 and 310. Found: C, 57.89; H, 6.08; Br, 25.73%. Calcd for $C_{15}H_{19}O_2Br$: C, 57.93; H, 6.16; Br, 25.70%.

*1,2-Dimethyl-2-(5'-bromo-2'-methoxy-4'-methylphenyl)cyclohexanol (**11**), and 2,3-Dimethyl-3-(5'-bromo-2'-methoxy-4'-methylphenyl)-cyclohexene (**2**).* A solution of methyl magnesium iodide was prepared from 1.7 g (0.07 g-atom) of metallic magnesium and 9.7 g (0.068 mol) of methyl iodide in 120 m*l* of anhydrous ether under nitrogen. The ether was then distilled off, and 120 m*l* of dried benzene were added. To the stirred Grignard solution, 8.5 g (0.027 mol) of **10** in 60 m*l* of benzene were added. The mixture was stirred at room temperature for 30 min, refluxed for 15 hr, and, after cooling, poured into a saturated ammonium chloride solution. The benzene layer was separated, washed with water, and dried. The subsequent evaporation of the benzene afforded an oily residue, which showed two spots on a TLC plate (chloroform as the solvent). The residue was chromatographed on silicic acid (120 g) with chloroform to give the starting ketone, **10** (5.3 g), and a colorless oil, **11** (2.7 g). A solution of 2.7 g of **11** in 27 m*l* of benzene was mixed with 5.5 m*l* of 50% sulfuric acid, after which the mixture was refluxed while being stirred for 3 hr. The benzene layer was separated, washed with a saturated sodium bicarbonate solution and water, and dried. The subsequent evaporation of the solvent afforded an oily product (2.2 g), which was chromatographed on silicic acid (40 g) with chloroform to give a crystalline material. Recrystallization from 95% ethanol afforded pure **2** (1.35 g, 43% from **10**: the yield was calculated from the amount of **10** actually consumed); mp 96—98°C; IR (KBr) 1600, 1550 cm^{-1}; NMR (CCl_4) 1.45 (3H, s), 1.48 (3H, d, J=2), 2.33 (3H, s), 3.76 (3H, s), 5.50 (1H, m, vinyl H), 6.64 (1H, s), 7.17 (1H, s); mass, M^+ 310 and 308. Found: C, 62.06; H, 6.72; Br, 25.89%. Calcd for $C_{16}H_{21}OBr$: C, 62.19; H, 6.85; Br, 25.86%.

*Oxidation of the Cyclohexene (**2**) with Ozone.* Ozone was passed through a solution of 150 mg of **2** in 5 m*l* of dichloromethane at −60°C. The progress of the reaction was examined by TLC. The excess ozone in the solution was flushed out with nitrogen at −60°C. The subsequent evaporation of the solvent afforded a residue, to which water was added. The mixture was allowed to stand at room temperature for 2 hr and was then extracted with benzene repeatedly. The benzene extracts were washed with water, dried, and evaporated to give a yellow oily residue (0.15 g), which showed three spots on a TLC plate. The residue was chromatographed on silicic acid (5 g) with chloroform. The starting material, **2** (35 mg), was thus obtained from the early fractions; the following fractions gave **13**, which was recrystallized from 95% ethanol to give pure **13** (22 mg, 15%); from the later fractions, the epoxide, **12**, was obtained, the recrystallization of which from ethanol afforded pure **12** (75 mg, 50%).

12: mp 116—118°C; IR ($CHCl_3$) 1640, 1600, 1490 cm^{-1}; mass, M^+ 326 and 324.

13: mp 121—122°C; IR (KBr) 1708, 1600, 1545 cm^{-1}; NMR (CCl_4) 0.65 (3H, d, J=7), 1.16 (3H, s), 2.33 (3H, s), 3.82 (3H, s), 6.66 (1H, s), 7.20 (1H, s); mass, M^+ 326 and 324. Found: C, 59.00; H, 6.71%. Calcd for $C_{16}H_{21}O_2Br$: C, 59.13; H, 6.51%.

*Conversion of the Epoxide (**12**) to the Cyclohexanone, (**13**).* A mixture of 19 mg of **12** in 1 m*l* of 50% sulfuric acid was heated at 80°C for 2 hr and then poured into ice water. After the mixture has been repeatedly extracted with benzene, the benzene extracts were washed with water, a saturated sodium bicarbonate solution, and water, dried, and evaporated to give 10 mg of crystalline **13**.

*Conversion of the Cyclohexanone (**13**) to the Cyclohexene (**2**).* A mixture of 15 mg of **13** and 5 mg of lithium borohydride in 2 m*l* of tetrahydrofuran was refluxed for 2 hr. After cooling, the mixture was diluted with water-acetic acid (9 : 1) and extracted with benzene. The benzene extracts were washed with a saturated sodium bicarbonate solution and water, dried, and evaporated to give 15 mg of the alcohol, **14**; IR (neat) 3450 cm^{-1}. A mixture of 15 mg of **14** in 2 m*l* of benzene and 0.1 m*l* of 50% sulfuric acid was refluxed for 2 hr and then poured into a saturated sodium bicarbonate solution. The benzene layer was separated, washed with water, dried, and evaporated, thus affording a crystalline residue. Recrystallization from 95% ethanol afforded 9 mg

of pure **2**.

*Oxidation of the Cyclohexene (**2**) with Osmium Tetroxide.* To a stirred solution of 633 mg (2.05 mmol) of **2** in pyridine (10 m*l*)-tetrahydrofuran (8 m*l*), we added, drop by drop, a solution of 510 mg (2.0 mmol) of osmium tetroxide in tetrahydrofuran (15 m*l*) at room temperature under nitrogen. After two weeks, the dark-red solution was concentrated under reduced pressure to give a residue, which was then taken up in 80 m*l* of 95% ethanol - chloroform (1 : 1). Hydrogen sulfide was passed through the dark-red solution for 10 min, and the resulting black precipitate was filtered. The filtrate was evaporated to afford a dark brown oil, which was chromatographed on silicic acid (60 g); fractions eluted with chloroform gave the starting material, **2** (*ca.* 70 mg), while fractions eluted with chloroform - methanol (v/v, 98 : 2) afforded the crude diol (460 mg), the recrystallization of which from hexane gave the pure diol, **15**; mp 145—146°C. Found: C, 55.88; H, 6.74%. Calcd for $C_{15}H_{23}O_3Br$: C, 56.02; H, 6.76%.

*Periodic Acid Oxidation of the Diol (**15**).* A solution of 106 mg of periodic acid dihydrate in water (1 m*l*) was added to a solution of 140 mg of **15** in tetrahydrofuran (4 m*l*)-water (2 m*l*), after which the mixture was stirred at room temperature for 4 hr. The mixture was then evaporated, neutralized with a sodium bicarbonate solution, and repeatedly extracted with ethyl acetate. The ethyl acetate extracts were washed with a saturated sodium chloride solution, dried, and evaporated to give a colorless oil, **3** (*ca.* 120 mg); IR ($CHCl_3$) 2730, 1725, 1710 cm^{-1}; NMR (CCl_4) 1.35 (3H, s), 1.78 (3H, s), 2.37 (3H, s), 3.73 (3H, s), 6.70 (1H, s), 7.30 (1H, s), 9.60 (1H, t, $J=3$); mass, M^+ 342 and 340.

BULLETIN OF THE CHEMICAL SOCIETY OF JAPAN, VOL. 45, 590—599 (1972)

Solvolysis of Organic Phosphates. V. Participation of the Neighboring Groups and Effects of Metal Ions in the Hydrolysis of 3-Hydroxy-2-pyridylmethyl Phosphate[1]

Yukito MURAKAMI, Junzo SUNAMOTO, and Hideyuki ISHIZU

Department of Organic Synthesis, Faculty of Engineering, Kyushu University, Fukuoka 812

(Received June 15, 1971)

The spontaneous hydrolysis of 3-hydroxy-2-pyridylmethyl phosphate was investigated at 60, 70, and 80°C over the $-\log[H^+]$ range from 1 to 10 in aqueous media with an ionic strength of 0.10. The reactions followed apparent first-order kinetics with respect to the unreacted phosphate species, and the maximum rate was observed at $-\log[H^+]$ 7—8. Reactive species in hydrolysis were neutral zwitterion, monoanion, and dianion species, the reactivity increasing in this order. This trend in reactivity order has not been observed previously. In a moderately acidic region ($-\log[H^+]<2.0$), kinetic data were consistent with the acid catalysis acting on the zwitterion species. Activation parameters provide an evidence for the unimolecular nature of the transition state in spontaneous hydrolysis and suggest the A1 process for the acid catalyzed reaction. The anomalously high reactivity of the dianion species was attributed to participation of the 3-hydroxy group in the reaction process: intramolecular transfer of the hydroxyl proton to the ester oxygen in a pre-equilibrium stage, followed by the P–O bond cleavage in the subsequent transition state to give the products. Hydrolysis was also carried out in the presence of copper(II), nickel(II), zinc(II), aluminum(III), iron(III), and thorium(IV) ions at 60°C and $\mu=0.10$ in a relatively lower pH range. Introduction of the 3-hydroxyl group to 2-pyridylmethyl phosphate resulted in a change of catalytic status of various metal ions. Only iron(III) and thorium(IV) ions accelerated the rate to a significant extent. Validity of the two requirements originally proposed for the bivalent metal catalysis was extended to the polyvalent metal catalysis.

Intramolecular catalysis in the ester hydrolysis is much interesting from a biochemical viewpoint. In the enzymic reaction, the enzyme-substrate complex is formed prior to the rate-determining catalysis reaction as represented by

$$E + S \rightleftarrows ES \rightarrow P \qquad (1)$$

Thus, the enzymic reaction follows first-order kinetics and the loss of entropy in the transition state is rather small. The geometry of the enzyme-substrate complex at the binding site is the major controlling factor for enzyme-specificity rather than the structural environment at the catalysis site. Such mechanistic criteria may also be applied in an analogous sense to the general organic intramolecular catalysis.[2] Recently, investigations of intramolecular catalysis in the ester hydrolyses, particularly in the hydrolyses of phosphates and sulfates, have been extensively carried out. Among them, hydrolyses of salicyl phosphate,[3] *S*-(2-carboxyphenyl)phosphorothioate,[4] and salicyl sulfate[5] are the cases of carboxyl group participation in the intramolecular general acid catalysis. Benkovic and Dunikoski have found the intramolecular acid catalysis by the imidazole-group participation in the hydrolysis of an imidazole substituted phenyl sulfate.[6] Meanwhile, we have actively investigated the

1) Contribution No. 231 from the Department of Organic Synthesis, Faculty of Engineering, Kyushu University. Preliminary communication: Y. Murakami, J. Sunamoto, and H. Ishizu, *Chem. Commun.*, **1970**, 1665.

2) Y. Murakami and J. Sunamoto. *Kagaku no Ryoiki*, **25**, 800, 892, 989, and 1072 (1971).

3) M. L. Bender and J. M. Lawlor, *J. Amer. Chem. Soc.*, **85**, 3010 (1963).

4) T. H. Fife and S. Milstein, *J. Org. Chem.*, **34**, 4007 (1969).

5) S. J. Benkovic, *J. Amer. Chem. Soc.*, **88**, 5511 (1966).

6) S. J. Benkovic and L. K. Dunikoski, Jr., *Biochem.*, **9**, 1390 (1970).

kinetics for the hydrolyses of aryl and alkyl phosphates containing a hetero-aromatic ring in their leaving alcohol groups. In this series of investigations, a unique intramolecular general acid catalysis has been confirmed in the hydrolyses of 2-pyridylmethyl,[7] 6-methyl-2-pyridylmethyl,[8] 2-pyridylethyl,[8] and 8-quinolyl phosphates.[9] We believe that the hydrolyses of the first three phosphates are the first examples of an intramolecular catalysis by the hetero-aromatic moiety in the hydrolyses of the open chain alkyl phosphates. The specific rate enhancement observed in the hydrolysis of these phosphates has been attributed to the participation of hetero-aromatic nitrogen. The intramolecular proton-transfer from pyridyl or quinolyl nitrogen to the ester oxygen seems to be facilitated in the pre-equilibrium step through a five- or six-membered chelate-ring formation, as illustrated by structures **1**, **2**, and **3**. In this work, we designed

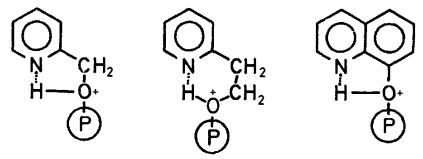

1 **2** **3**

Ⓟ: phosphate moiety

a competing state of affair for the intramolecular general acid catalysis and investigated the hydrolysis of 3-hydroxy-2-pyridylmethyl phosphate which has an additional functional group, 3-hydroxy, to 2-pyridylmethyl phosphate in the proximity of a phosphate moiety. As a result, the present work clarifies which neighboring group, 1-pyridinium or 3-hydroxy group, provides more significant intramolecular catalysis in the hydrolysis.

We also studied the metal-ion catalysis in the hydrolysis of 3-hydroxy-2-pyridylmethyl phosphate. Previously, we investigated the metal-ion catalysis in the hydrolyses of pyridylmethyl phosphates,[7] and 3-pyridyl and 8-quinolyl phosphates.[10] From these studies, we have proposed two requirements for metal ions to yield catalytic efficiency.[7,10] (1) For preliminary chelate formation, the metal ion should form an appropriate chelate of significant stability with an organic phosphate prior to the hydrolysis reaction. (2) For transitional chelate formation, the metal ion should demonstrate an appropriate affinity for the ester oxygen in the transition state, which would give rise to formation of a chelate ring involving the ester oxygen.

3-Hydroxy-2-pyridylmethyl phosphate has three chelating sites. Thus, three kinds of structures for metal-chelate formation can be depicted as shown below by structures **4**, **5**, and **6**. The extent of catalysis due to these metal chelates is subject to the structural nature of the phosphate and the coordination affinity of a metal ion for the donor atoms. We qualitatively investigated the catalytic effects of various metal ions, *i.e.*, copper(II), nickel(II), zinc(II), aluminum(III), iron(III), and thorium(IV). Thus, the present work accumulates the kinetic and mechanistic data for confirmation of the above requirements established for the bivalent metal catalysis, and provides further mechanistic criterion for the polyvalent metal catalysis.[10]

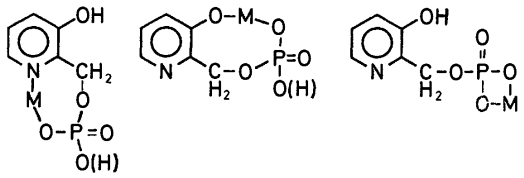

4 **5** **6**

Experimental

Materials. Preparation and purification of 3-hydroxy-2-pyridylmethyl phosphate have been described.[11] Other materials of analytical grade were commercially obtained and used without further purification. The stock solutions of metal ions were prepared from their nitrate salts. The solutions were standardized by means of the usual chelatometric titration.

Kinetic and Potentiometric Measurements. The apparatus and experimental procedures were essentially the same as those described previously.[9,10]

Determination of Acid Dissociation Constants and Specific Rate Constants. The overall rate constant k_0 is given by a summation of each product of a specific rate constant (k) and the corresponding mole fraction (X) over the all ionic species as represented by

$$k_0 = k_{A'}X_{A'} + k_AX_A + k_{HA}X_{HA} + k_{H_2A}X_{H_2A} + k_{H_3A}X_{H_3A} \quad (2)$$

To the present phosphate, the acid dissociation processes shown in Scheme 1 can be reasonably assigned.[11] The symbols suffixed to k's and X's in Eq. (2) (*i,e.*, A', A, HA,

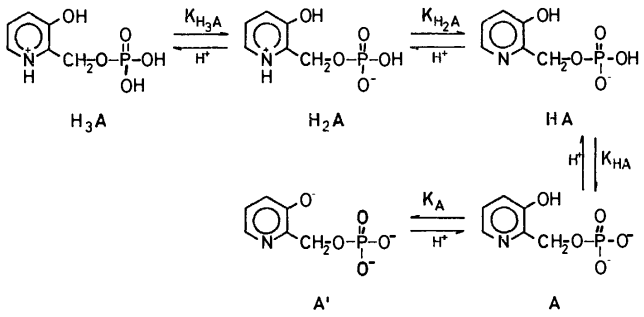

Scheme 1

7) Y. Murakami and M. Takagi, *J. Amer. Chem. Soc.*, **91**, 5130 (1969).

8) Y. Murakami, J. Sunamoto, and N. Kanamoto, presented at the 24th Annual Meeting of the Chemical Society of Japan, Osaka, April, 1971.

9) Y. Murakami and J. Sunamoto, This Bulletin, **44**, 1939 (1971).

10) Y. Murakami and J. Sunamoto, *ibid.* **44**, 1827 (1971).

11) Y. Murakami, J. Sunamoto, H. Sadamori, H. Kondo, and M. Takagi, *ibid.* **43**, 2518 (1970).

H_2A, and H_3A) stand for the ionic species shown in Scheme 1. A mole fraction of each ionic species was calculated by the aid of acid dissociation constants[11] which were determined by the pH-titration at low temperature (25°C) over the whole pH range (1—10.0). The results are illustrated by broken lines in Fig. 1. Thus, if all the acid dissociation constants at a given temperature are known, the specific rate constant for each ionic species can be easily evaluated by means of Eq. (2). However, the acid dissociation constants obtained by potentiometric measurements at higher temperatures (60—80°C) were suspected to involve a little uncertainty. These unavoidable errors might be caused by trace hydrolysis of the phosphate during the course of measurements. Thus, under the circumstances, the dynamic acid dissociation constants and the specific rate constants were simultaneously calculated from the kinetic data by the following procedures.

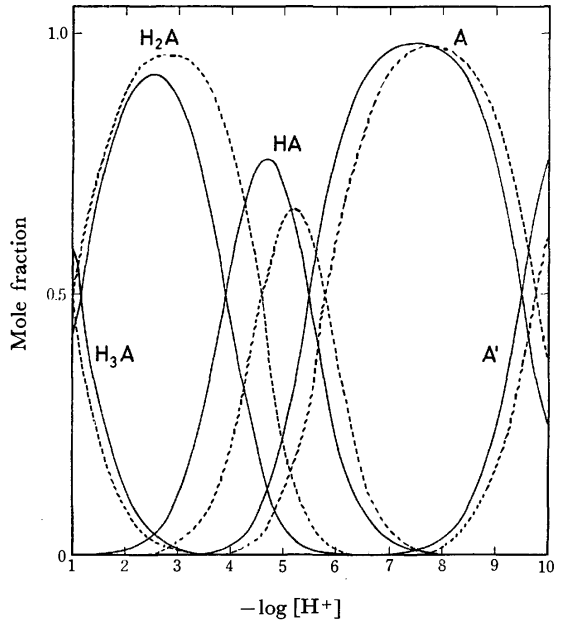

Fig. 1. Distribution of ionic species of 3-hydroxy-2-pyridylmethyl phosphate as a function of $-\log[H^+]$ at $\mu=0.10$, and at 25° (broken lines) and 60°C (solid lines). They were calculated using the pK_a values listed in Table 2.

1) Assumption is made that the trianionic species of the present phosphate (A′) is unreactive in the spontaneous hydrolysis over a pH-range 8.0—10.0 where only two species, trianionic and dianionic, are present. Then, the following relations are valid:

$$T_E = [A] + [A'] \tag{3}$$

$$k_{obs}T_E = k_A[A] \tag{4}$$

where T_E stands for the total concentration of the phosphate species and k_{obs} refers to the observed apparent first-order rate constant. The following equation is derived from Eqs. (3) and (4).

$$[H^+] = k_A\frac{[H^+]}{k_{obs}} - K_A \tag{5}$$

where K_A is the acid dissociation constant of the dianionic species. This equation indicates that a plot of $[H^+]$ *vs.* $[H^+]/k_{obs}$ should give a straight line. The slope of the line is equal to k_A and the intercept at $[H^+]/k_{obs}=0$ corresponds to K_A.

2) In a pH-range 6.0—7.5 where dianionic and monoanionic (HA) species exist exclusively, the following equations are applied to the system:

$$T_E = [HA] + [A] \tag{6}$$

$$k_{obs}T_E = k_{HA}[HA] + k_A[A] \tag{7}$$

where k_A value evaluated in Step 1 can be used. From Eqs. (6) and (7), the following relationship is given:

$$\frac{k_{obs}[H^+]}{k_A-k_{obs}} = k_{HA}\frac{[H^+]}{k_A-k_{obs}} + K_{HA} \tag{8}$$

The relationship between the left hand side and $[H^+]/(k_A-k_{obs})$ in the first term of the right hand side needs to be linear. Thus, k_{HA} and K_{HA} are to be obtained from the slope and the intercept at $[H^+]/(k_A-k_{obs})=0$, respectively.

3) For a pH-range 3.0—5.0, three phosphate species, neutral zwitterion (H_2A), monoanionic and dianionic forms, are to be taken into consideration. Then, the following equations can be given for this state of affair.

$$T_E = [H_2A] + [HA] + [A] \tag{9}$$

$$k_{obs}T_E = k_{H_2A}[H_2A] + k_{HA}[HA] + k_A[A] \tag{10}$$

where k_A and k_{HA} values evaluated in Steps 1 and 2, respectively, can be used. Combination of Eqs. (9) and (10) and the subsequent rearrangement give the following equations.

$$\frac{k_{obs}[H^+]^2}{(k_{HA}-k_{obs})[H^+] + (k_A-k_{obs})K_{HA}} = k_{H_2A}\frac{k[H^+]^2}{(k_{HA}-k_{obs})[H^+] + (k_A-k_{obs})K_{HA}} + K_{H_2A} \tag{11}$$

In a manner similar to those described in the preceding steps, k_{H_2A} and $K_{H\,A}$ are evaluated from the plots.

4) Finally, by using all the values already obtained in the preceding steps and the kinetic data covering a pH-range 1.0—3.0 where cationic, neutral zwitterion, and monoanionic species are considered to be present, we have

$$T_E = [H_3A] + [H_2A] + [HA] \tag{12}$$

$$k_{obs}T_E = k_{H_3A}[H_3A] + k_{H_2A}[H_2A] + k_{HA}[HA] \tag{13}$$

$$\frac{k_{obs}[H^+]^2}{(k_{H\cdot A}-k_{obs})[H^+] + (k_{HA}-k_{obs})K_{H_2A}} = k_{H\cdot A}\frac{[H^+]^2}{(k_{H_2A}-k_{obs})[H^+] + (k_{HA}-k_{obs})K_{H_2A}} + K_{H_3A} \tag{14}$$

k_{H_3A} and K_{H_3A} would be evaluated from the linear plots based on Eq. (14). In general, however, the neutral species of the alkyl phosphates[12] and the monocationic species of pyridylalkyl phosphates[7,8] show much less reactivity in their spontaneous hydrolyses. Therefore, for the present phosphate the kinetic analysis due to Step 4 was discarded. Instead, an acid catalyzed hydrolysis of the neutral zwitterion species was confirmed to proceed in such a moderately acidic region more significantly. The overall rate constant k_0 is, thus, consistent with the equation

$$k_0T_E = k_{H^+}[H^+][H_2A] + k_{H\,A}[H_2A] + k_{HA}[HA] + k_A[A] \tag{15}$$

12) T. C. Bruice and S. J. Benkovic, "Bioorganic Mechanisms," Vol. 2, W. A. Benjamin Inc., New York (1966), Chapt. 5.

Table 1. Specific rate constants for the spontaneous hydrolysis of 3-hydroxy-2-pyridylmethyl phosphate at $\mu=0.10$ ($NaClO_4$ or KNO_3)

Species	Temp. (°C)	$k_{H^+}\times10^4$ $M^{-1}\,sec^{-1}$	$k\times10^5$ sec^{-1}
Zwitterion (H_2A)	60	0.534	
	70	1.60	
	80	4.58	
Zwitterion (H_2A)	60		0.376
	70		1.55
	80		5.16
Monoanion (HA)	60		1.17
	70		4.75
	80		15.7
Dianion (A)	60		2.52
	70		9.23
	80		30.6

Table 2. Acid dissociation constants of 3-hydroxy-2-pyridylmethyl phosphate at $\mu=0.10$ ($NaClO_4$ or KNO_3)

pK_a	25°C[a]	60°C[b]	70°C[b]	80°C[b]
pK_{H_3A}		1.16	1.08[c]	1.00
pK_{H_2A}	4.54	3.88	3.60	3.80
pK_{HA}	5.75	5.48	5.40	5.55
pK_A	9.67	9.48	9.40[d]	9.51

a) Obtained by means of potentiometric titration.
b) Calculated by the kinetic procedures described in the text.
c) Obtained by interpolation using values at 60° and 80°C.
d) Obtained by extrapolation using values at 25° and 60°C.

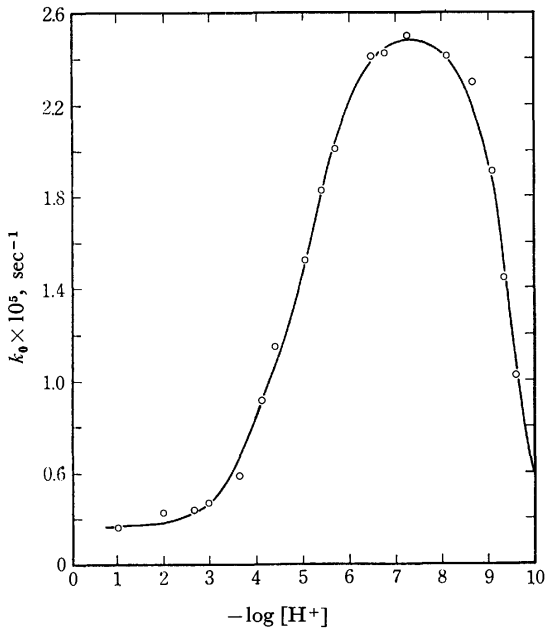

Fig. 2. Rate profile for the spontaneous hydrolysis of 3-hydroxy-2-pyridylmethyl phosphate at 60°C and $\mu=0.10$. Solid line is a theoretical curve calculated from values listed in Tables 1 and 2 by using equation 15.

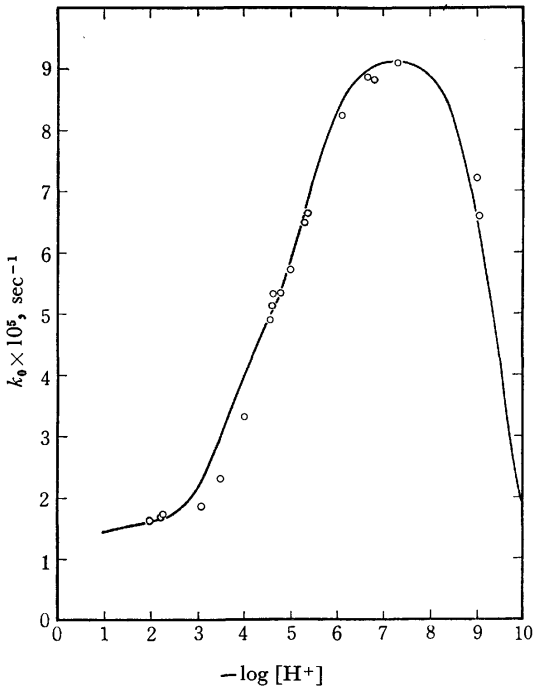

Fig. 3. Rate profile for the spontaneous hydrolysis of 3-hydroxy-2-pyridylmethyl phosphate at 70°C and $\mu=0.10$. Solid line is a theoretical curve calculated from values listed in Tables 1 and 2 by using equation 15.

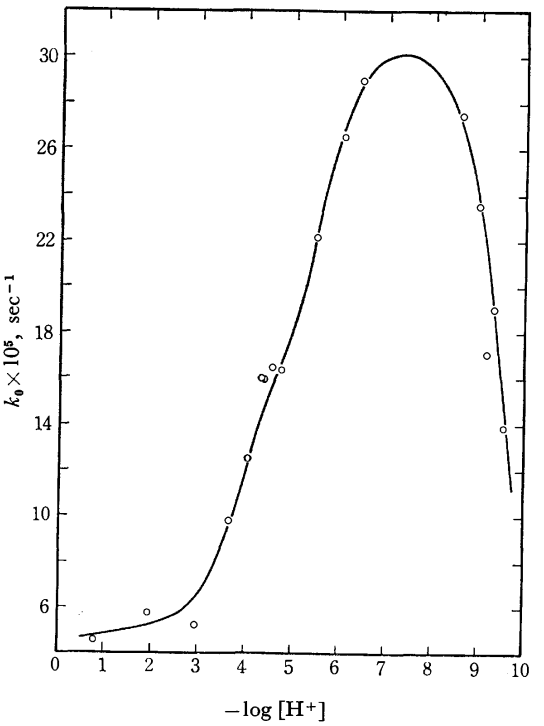

Fig. 4. Rate profile for the spontaneous hydrolysis of 3-hydroxy-2-pyridylmethyl phosphate at 80°C and $\mu=0.10$. Solid line is a theoretical curve calculated from values listed in Tables 1 and 2 by using equation 15.

where

$$T_E = [H_3A] + [H_2A] + [HA] + [A] + [A'] \quad (16)$$

$$\left.\begin{aligned} [H_3A] &= \frac{1}{K_{H_3A}}[H^+][H_2A] \\ [H_2A] &= \frac{1}{K_{H\ A}}[H^+][HA] \\ [HA] &= \frac{1}{K_{HA}}[H^+][A] \\ [A] &= \frac{1}{K_A}[H^+][A'] \end{aligned}\right\} \quad (17)$$

Results

Spontaneous Hydrolysis. The specific rate constants evaluated by the preceding procedure and the acid dissociation constants are listed in Tables 1 and 2, respectively. Moreover, the agreement between the observed and the calculated rate constants at 60, 70, and 80°C is quite satisfactory as illustrated in Figs. 2, 3, and 4, respectively.

In our previous studies on the spotaneous hydrolyses of 2-, 3-, and 4-pyridylmethyl phosphates,[7] 6-methyl-2-pyridylmethyl,[8] 3-pyridyl, and 8-quinolyl phosphates,[9] the reactive species were always the neutral zwitterion and the monoanionic form, and rate-maxima in the pH-rate profiles were observed at —log[H+] 2—3 and 5—6 for all the phosphates. In the present case, however, the maximum rate in the pH-rate profile for the spontaneous hydrolysis appeared at —log[H+] 7—8 with a shoulder at 4.5. Consequently, the most reactive species was the dianionic form followed by the monoanion and then the neutral zwitterion in this order.

Activation Parameters. Each specific rate constant followed the Arrhenius law. The energy, enthalpy, and entropy of activation for each species are listed in Table 3. These values are quite similar in magnitude to those for the monoanions of organic phosphates previously reported,[13] and seem to indicate that all the reactive species of the present phosphate undergo hydrolysis through a unimolecular mechanism in which a pre-equilibrium proton-transfer process followed by P–O fission in the rate-determining step takes place.

Metal Ion Catalysis. In the presence of metal ions, the hydrolysis conditions were set at the upper limit pH and temperature in a range where no noticeable precipitates appeared and no partial hydrolysis of metal ions occurred. Consequently, a good homogeneous phase was maintained during the course of each run. All the reactions were carried out in the presence of equimolar amounts of a metal ion and the substrate at 60°C and μ=0.10 (KNO_3). The hydrolysis reactions in the presence of copper(II), nickel(II), zinc(II), and aluminum(III) ions followed ap-

TABLE 3. ACTIVATION PARAMETERS FOR THE SPONTANEOUS HYDROLYSIS OF 3-HYDROXY-2-PYRIDYLMETHYL PHOSPHATE[a]

Species	E kcal mol^{-1}	$\Delta H^{\neq}$ kcal mol^{-1}	$\Delta S^{\neq}$ e. u.
Acid catalysis zwitterion (H_2A)	25.1[b]	24.4[b]	−5[b]
Zwitterion (H_2A)	30.6	29.9	+6
Monoanion (HA)	30.4	29.7	+8
Dianion (A)	29.1	28.5	+6

a) Errors, standard deviation, in individual rate constants are not greater than ±2%; those in E and $\Delta H^{\neq}$ are approximately ±0.1 kcal mol^{-1}; and those in $\Delta S^{\neq}$ are ±0.1 e.u.
b) Calculated from the second-order rate constants (M^{-1} sec^{-1}), k_{H^+}.

13) J. A. Maynard and J. M. Swan, *Aust. J. Chem.*, **16**, 596 (1963).

TABLE 4. METAL-ION-CATALYZED HYDROLYSIS OF 3-HYDROXY-2-PYRIDYLMETHYL PHOSPHATE AT 60°C AND μ=0.10 (KNO_3)[a]

−Log[H+]	M^{n+}	$k_c\times10^5$ [b] sec^{-1}	$k_0\times10^5$ [c] sec^{-1}	k_c/k_0
2.44	Cu^{2+}	0.388	0.403	0.95
3.53	Ni^{2+}	0.865	0.914	0.95
4.11	Ni^{2+}	0.574	0.616	0.93
3.57	Zn^{2+}	0.634	0.618	1.03
2.74	Al^{3+}	0.360	0.427	0.84
8.57	Al^{3+}	0.224	0.224	1.00
2.86	Fe^{3+}	0.635[d]	0.444	1.43
2.33	Th^{4+}	10.2[d]	0.396	*ca.* 26

a) $T_E=T_M=2.0\times10^{-3}$ M, where T_E and T_M stand for the total molar concentrations of substrate and metal ion, respectively.
b) k_c is the observed overall rate contant for the hydrolysis in the presence of metal ion.
c) k_0 is the overall rate constant for spontaneous hydrolysis.
d) Deviated from the first-order plot; estimated from the initial stage of reaction.

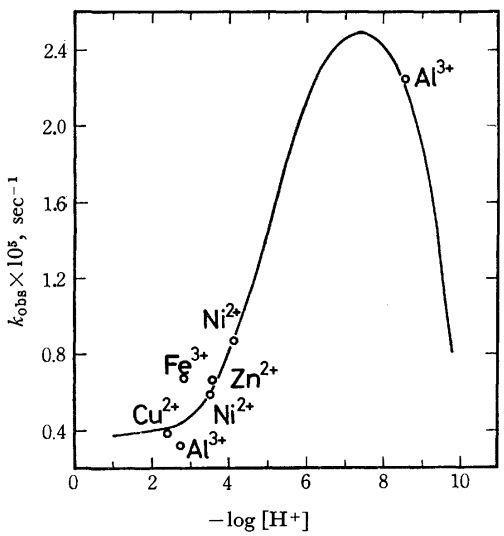

Fig. 5. Effects of metal ions on the hydrolysis of 3-hydroxy-2-pyridylmethyl phosphate at 60°C and μ=0.10 (KNO_3). $T_E=T_M=2.0\times10^{-3}$ M. Solid line represents the rate profile for spontaneous hydrolysis under the same conditions.

parent first-order kinetics with respect to the total concentration of the unreacted phosphate in homogeneous phase at pH's and metal concentrations studied. However, all the metal ions showed no significant catalytic effect. On the other hand, the presence of iron(III) and thorium(IV) ions resulted in a significant acceleration of rate, although the reactions did not follow the simple first-order kinetics and the hydrolysis rates were retarded as reactions proceeded further. During the course of reactions, no formation of insoluble materials was detected and a good homogeneous system was maintained. In particular, the thorium ion showed a profound rate enhancement. The catalytic efficiency of these metal ions is listed in Table 4. The catalytic status of the present metal ions with the exception of thorium(IV) is illustrated in Fig. 5 in reference to the spontaneous reaction.

Discussion

Hydrolysis of Neutral Zwitterion Species. In the hydrolysis of 3-hydroxy-2-pyridylmethyl phosphate, the neutral zwitterion form (H_2A) was the least reactive of the three reactive species, H_2A, HA, and A. This behavior differs noticeably from other heteroaromatic phosphates studied previously.[7-9] Furthermore, for the hydrolyses of the zwitterion species of 2-pyridylalkyl phosphates and 8-quinolyl phosphate, a unique intramolecular general acid catalysis was observed upon participation of 1-pyridinium or 1-quinolinium proton which was transferred to the ester oxygen in the pre-equilibrium stage of reaction. The mechanistic aspect is shown in Scheme 2.

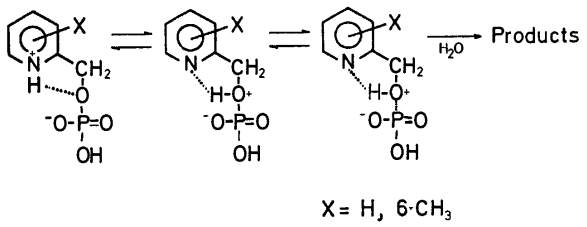

Scheme 2

Thus, for the zwitterion form of the present phosphate, the following two aspects of mechanistic criteria may be considered: (1) An intramolecular general acid catalysis played by the 1-pyridinium proton occurs and the 3-hydroxyl group provides only an electronic effect on the reaction rate as an electron-withdrawing group,[14] in a manner similar to the cases of 2-pyridylalkyl phosphates (Scheme 2). (2) An intramolecular hydrogen bonding of the 3-hydroxyl group to the terminal phosphate oxygen is formed and the phosphate proton is transferred intramolecularly to the ester oxygen, as seen in the usual hydrolyses of alkyl phosphate monoanions. Therefore, if the latter holds, the positive pyridinium group acts only as an electron-withdrawing group as illustrated in Scheme 3. If the driving force for the intramolecular proton

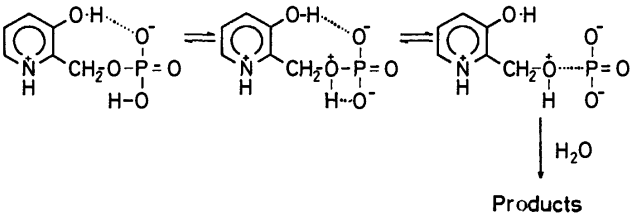

Scheme 3

transfer is due to a preliminary intramolecular hydrogen bonding, Scheme 3 may be more favorable for interpretation of the results than Scheme 2. Since an O–H···O bond is tighter in general than an N–H···O bond in hydrogen bonding strength, the phosphate moiety is to be fixed in space far away from the 1-pyridinium proton due to the intramolecular O–H···O bonding as shown in Scheme 3. Consequently, an intramolecular acid catalysis by the pyridinium group would not be expected, even though the present phosphate is one of 2-pyridylmethyl phosphates. Meanwhile, the absolute hydrolysis rate of the present phosphate is 2.3 times larger than that of 2-pyridylmethyl phosphate in zwitterion form at 70°C. Thus, the 3-hydroxyl group must participate in the reaction process so that the hydrolysis rate is enhanced due to its electronic effect and/or additional intramolecular interaction. As a result, there still remains some uncertainty in elucidating the hydrolysis mechanism. Further confirmation of the present mechanism waits studies of the linear free energy relationship on the hydrolysis of pyridylalkyl phosphates.

Linear free energy relationships (LFER) for the hydrolyses of phosphates and sulfates have been extended by Bunton,[15] Fendler,[16] and Kirby.[17] However, all the esters they studied were aryl esters. So far, the acidity of a leaving group (pK_{OH}) has been usually adopted as the structural parameter for LFER study of ester hydrolyses, where P–O or S–O bond cleavage is the rate-determining step. The pK_{OH} value of an alcohol is, however, generally very large (13—16)[18], even those of the alcohols having an aromatic moiety,[19] compared with those of the phenols (~10).[20] It is, therefore, difficult to determine the correct and reliable acid dissociation constants of alcohols, particularly at higher temperatures, by the usual techniques. Thus, it is quite important to establish some reliable structural parameters other than acid dissociation constants of the leaving alcohols for the LFER study of the hydrolyses of alkyl phosphates.

Activation parameters E, $\Delta H^{\neq}$, and $\Delta S^{\neq}$ for the

14) J. M. Vundennbelt, C. Henrich, and S. G. Vandenberg, *Anal. Chem.*, **26**, 726 (1954).

15) C. A. Bunton, E. J. Fendler, E. Humeres, and K. U. Yang, *J. Org. Chem.*, **32**, 2806 (1967).

16) E. J. Fendler and J. H. Fendler, *ibid.*, **33**, 3852 (1968).

17) A. J. Kirby and A. G. Varvoglis, *J. Amer. Chem. Soc.*, **89**, 415 (1967).

18) P. Ballinger and F. A. Long, *ibid.*, **82**, 795 (1960).

19) M. Tissier and C. Tissier, *Bull. Soc. Chim. Fr.*, **1967**, 3155.

20) G. Kortum, W. Vogel, and K. Andrussow, "Dissociation Constants of Organic Acids in Aqueous Solution," Butterworths and Co., Ltd., London (1961).

hydrolysis of the zwitterion species are quite similar in their magnitude to those for other pyridylalkyl phosphates,[7,8] 3-pyridyl and 8-quinolyl phosphates.[9] Thus, it may be reasonable to assume that the nature of the transition state is essentially the same as that discussed previously, where a unimolecular P–O bond cleavage to give an alcohol and HPO_3^- occurs, irrespective of the source of the transferable proton in the pre-equilibrium stage.

Hydrolysis of Monoanionic Species. Contrary to what would be expected from the previous studies,[7-9] the monoanionic species was more reactive than the neutral zwitterion. The anomalous behavior of the monoanion must be interpreted from two aspects: (1) a simple electron-withdrawing effect of the 3-group (similar to Scheme 3), and (2) an intramolecular general acid catalysis played by the 3-hydroxyl group (Scheme 4).

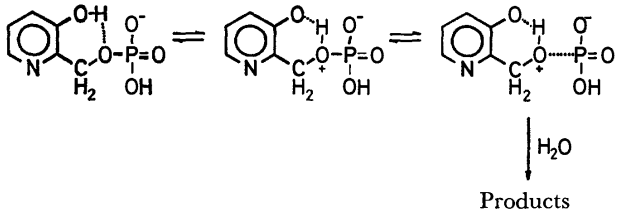

Scheme 4

If Scheme 3 is valid, the electronic effect of the 3-hydroxyl group for this species would be approximately in a similar magnitude to that expected for the zwitterion species. When the substituent effect due to the 3-hydroxyl group on the reaction rate is represented in terms of the ratio of reaction rates against 2-pyridylmethyl phosphate $k_{(3\text{-H-2-PMP})}/k_{(2\text{-PMP})}$, this value is about 2.3 for the hydrolysis of the zwitterion species. On the other hand, the rate ratio is 1.25×10^2 for the hydrolysis of the monoanionic species. This profound rate enhancement should be attributed to the additional proximity effect due to introduction of a hydroxyl group at the 3-position of 2-pyridylmethyl phosphate. Consequently, this neighboring group may be responsible for the intramolecular proton transfer in the transition state as seen in Scheme 4. The driving force for the proton transfer may be due to the preliminary intramolecular hydrogen bonding, primarily to the terminal phosphate oxygen, in which the hydroxyl group is brought about in the neighborhood of the ester oxygen. The hydrogen bonding is then switched to the ester oxygen in the pre-equilibrium stage prior to the transition state, where the stable six-membered ring is formed.

Activation parameters for the hydrolysis of the monoanion are consistent with a unimolecular mechanism accompanied with P–O bond cleavage.

Hydrolysis of Dianionic Species. Generally, the dianionic species of an organic phosphate is unreactive toward spontaneous hydrolysis, except for those of phosphate esters which have a strong electron-withdrawing group in a leaving alcohol moiety, *e.g.*, nitrophenyl and polynitrophenyl phosphates.[15,16] For the present phosphate, the dianionic species was the most reactive and the trianionic species was stable in alkaline media. This presents a unique case in which the dianionic species is more reactive than the zwitterion and monoanionic forms in the hydrolysis of alkyl phosphates. This interesting fact requires some characteristic explanation for the hydrolysis mechanism in reference to hydrolyses of the other ionic species of the present phosphate and of ordinary alkyl phosphates.

The profound rate enhancement must be ascribed to the participation of the 3-hydroxyl group situated in the proximity of the phosphate moiety. No work has been reported on the intramolecular participation of a hydroxyl group in the hydrolysis of alkyl phosphates or sulfates, which consequently gave out to some significant rate enhancement. Bender and Lawlor have shown that 8-hydroxy-1-naphthyl phosphate dianion hydrolyzed about 10-fold faster than the dianion of the 8-methoxyl ester.[3] They considered that this rate enhancement was due to the intramolecular proton transfer from the 8-hydroxyl group to the ester oxygen, although the extent of their investigation was rather limited. Glycerol-1-phosphate **7** was stable in alkaline media and had a rate maximum at around pH 4—5 in its hydrolysis in a manner similar to those observed for usual monoalkyl phosphates. Glycerol-1-methyl phosphate **8** was readily hydrolyzed in alkaline media to give a mixture of glycerol-

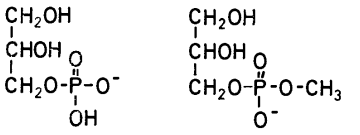

7 **8**

1- and -2-phosphates, no methyl phosphate being produced.[12] Kugel and Halmann have reported the hydrolysis of 1,2-propanediol-1-dihydrogen phosphate,[21] where the phosphate was also hydrolyzed with a maximum rate at pH ~4. In this pH region, the mole fraction of the monoanion reaches its maximum. As a whole, these studies indicate that an alcoholic hydroxyl group at the β-position and/or the γ-position to the phosphate group of alkyl phosphates does not bring about any significant rate enhancement in hydrolysis.

The profound rate enhancement due to the participation of the 3-hydroxyl group may be interpreted from two different aspects: (1) nucleophilic attack of the negatively charged phenoxide group at the phosphorus atom, and (2) intramolecular transfer of the hydroxyl proton to the ester oxygen. Scheme 5 demonostrates the nucleophilic attack of the phenoxide ion at the phosphorus atom forming a cyclic transition state (or a cyclic intermediate), which is followed by the intramolecular transfer of the phosphate group to the phenolic oxygen. A similar state of affair was confirmed in the hydrolysis of glycerol hydrogen

21) L. Kugel and M. Halmann, *J. Amer. Chem. Soc.*, **88**, 3566 (1966).

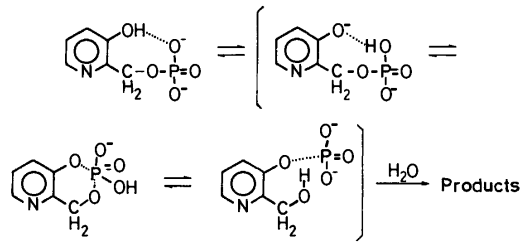

Scheme 5

phosphates,[12] where a cyclic intermediate was formed and subsequently an intramolecular rearrangement of the phosphate group took place. We previously tried to isolate the cyclic phosphate **10** which would be derived from the present phosphate, and 2-hydroxymethyl-3-pyridyl phosphate under various conditions. However, the work failed to give these products, and gave 3-hydroxy-2-pyridylmethyl phosphate exclusively.[22] This suggests that the present phosphate, rather than

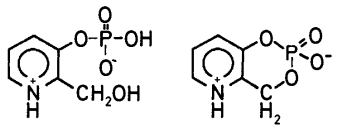

9 **10**

being the precursor of the cyclic phosphate **10** or of the intramolecularly rearranged phosphate **9** should be an intermediate in their hydrolytic decomposition. The dianionic species of 2-hydroxymethyl-3-pyridyl phosphate would not be as reactive as that of 3-hydroxy-2-pyridylmethyl phosphate toward hydrolysis, unless the 2-hydroxymethyl group would participate favorably in the reaction.

Thus, the alternative concept is adopted as the plausible mechanism for elucidation of the enhanced hydrolysis rate. As shown in Scheme 6, the hydroxyl

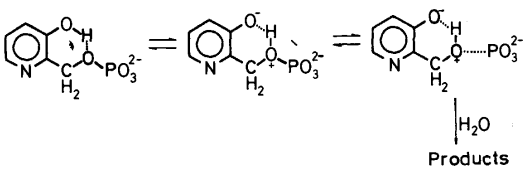

Scheme 6

proton is completely transferred to the ester oxygen in the pre-equilibrium stage, and the P–O bond is then weakened in the subsequent transition state to give the products. This mechanistic aspect is quite analogous to that employed for the hydrolysis of the monoanion as the most plausible mechanism. The six-membered ring formation would stabilize the pre-equilibrium stage in these hydrolytic pathways. For the dianionic species, however, an increase of negative charge on the phosphate moiety will make the proton transfer much more favorable. The small positive entropy of activation again suggests the unimolecular mechanism for the dianion hydrolysis.

Hydrolysis in Moderately Acidic Region. In the moderately acidic region, $-\log[H^+]$ 1.0—2.0, the hydrolysis rates of 8-quinolyl and 3-pyridyl phosphates increased in proportion to the stoichiometric concentration of acid,[9] while pyridylmethyl phosphates underwent no detectable acid catalyzed hydrolysis in a comparable acidic region.[7,8] We attributed the favorable acid catalysis for the former two aryl phosphates to the electron-withdrawing effect caused by the positively charged pyridinium or quinolinium group and also to resonance stabilization given to the generated alcohol of phenolic nature. For the present phosphate, the hydrolysis in a moderately acidic region was not subject to a marked acid catalysis along with the change of hydrogen ion concentration. Under these circumstances, two reaction mechanisms of kinetic equivalence are to be considered: (1) unimolecular spontaneous reaction of the monocationic species, and (2) acid catalyzed reaction of the zwitterion form.

If one assumes that the monocationic species is reactive in the hydrolysis of the present phosphate, the specific rate constants are $k_{H_3A}=0.368\times10^{-5}$, 1.33×10^{-5}, and 4.58×10^{-5} sec^{-1} at 60, 70, and 80°C, where $pK_{H_3A}=1.16$ (60°C), 1.08 (70°C), and 1.00 (80°C), respectively. From these kinetic data, the activation parameters may be estimated: $E=29.5$ kcal mol^{-1}, $\Delta H^{\neq}=28.8$ kcal mol^{-1}, and $\Delta S^{\neq}=+3$ e.u. The specific rate constants and the activation parameters cited here are not necessarily unfavorable to this mechanism. However, we can not show which one of the four protons may be transferred to the ester oxygen at the pre-equilibrium stage in this case.

Under consideration of the results previously obtained on the reactivity of the monocationic species,[7] this species should be much less reactive and the neutral zwitterion is subject to an acid catalysis in this moderately acidic region. The kinetic data and the corresponding activation parameters were evaluated from this aspect as listed in Tables 1 and 3. The entropy of activation in Table 3 suggests that the acid catalysis for the present phosphate proceeds through A1 process as shown in Scheme 7.

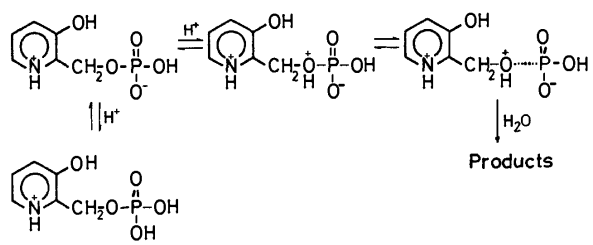

Scheme 7

Effects of Metal Ions. We proposed previously that the two successive interactions were required to yield the metal ion catalysis.[10] Thus, the hydrolysis reaction of 3-hydroxy-2-pyridylmethyl phosphate was investigated in the presence of various metal ions in order to examine the validity and applicability of the proposed mechanisms.

22) Y. Murakami, J. Sunamoto, K. Morooka, and H. Kondo, presented at the Local Meeting of the Chemical Society of Japan, Fukuoka, July, 1968.

3-Hydroxy-2-pyridylmethyl phosphate is related in structure to 2-pyridylmethyl phosphate. Therefore, it may be expected that the copper(II) ion would have a significant catalytic efficiency for the hydrolysis of the present phosphate. Contrary to what would be expected, the copper ion as well as other bivalent metal ions showed no detectable catalysis. When the reaction mixture prepared at pH above 4 in the presence of copper(II) was poured into a reaction vessel, a blue insoluble material appeared about ten minutes after the addition and simultaneously the pH value of the mixture decreased sharply. Apparently, a certain copper complex was produced with liberation of protons. The precipitates were insoluble in almost all of the polar and nonpolar organic solvents as well as in water. In order to examine the nature of the complex, we tried to prepare a complex of 3-hydroxy-2-pyridylmethanol with copper(II): equimolar amounts of the alcohol and copper nitrate were dissolved in water, pH was adjusted to 4—6 using 0.1 N-sodium hydroxide, and the resulting blue precipitates were isolated. The IR spectrum of this copper complex was compared with that of the complex produced during the course of hydrolysis. They differ from each other and the latter is more related to the spectrum of the substrate ester as shown in Fig. 6. As can be seen from Fig. 6-c, absorption bands assigned to the stretching vibration of P–O–C and P=O bonds (900—1200 cm^{-1}) are still observed in the spectrum of the complex formed in the hydrolysis. As a result, the complex is not the one with the hydrolysis product, but that with the unreacted substrate. With the knowledge obtained from the copper catalysis on the hydrolyses of 2-pyridylmethyl[7] and 8-quinolyl[10] phosphates, we can eliminate possibility of the formation of complexes **4** and **6**. If the copper chelate is primarily in structure **4**, the rate enhancement due to the copper ion must be necessarily obtained for the present hydrolysis. Thus, we may assign either **5** or **11** to the blue complex obtained

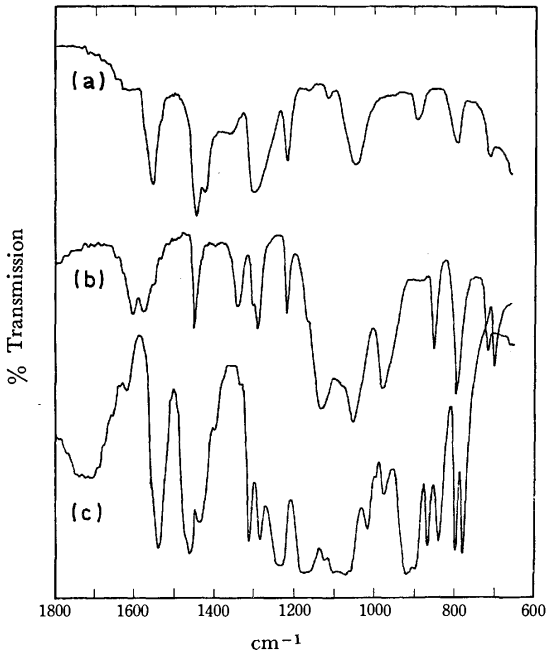

Fig. 6. Infrared spectra (KBr disk method): (a), the copper(II) complex of 3-hydroxy-2-pyridylmethanol; (b), the complex precipitated during the hydrolysis reaction of 3-hydroxy-2-pyridylmethyl phosphate in the presence of copper(II) (see text); (c), 3-hydroxy-2-pyridylmethyl phosphate.

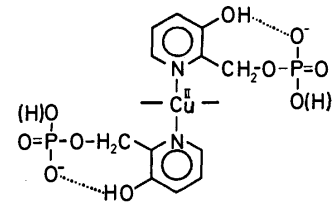

11

during the reaction on the basis of the affinity of the copper ion for nitrogen and/or oxygen donor atoms. There also remains possibility that the complex would be of polymeric nature. Although we are not ready to give a persuasible geometry for the complex, precipitation of the substrate-copper complex may also cause a catalytic inertness of the copper ion. The 3-hydroxy group controlled the geometry of the complex formed in the preliminary equilibrium stage, which resulted in null catalytic efficiency of copper(II) in this work.

For 2-pyridylmethyl[7] and 8-quinolyl[23] phosphoates, the iron(III) ion demonstrated a negative catalytic effect in both hydrolyses. On the other hand, the metal ion showed a large positive catalytic efficiency in the hydrolysis of salicyl phosphate.[24] We ascribed these opposite effects to the difference in affinity of the ferric ion for nitrogen and oxygen donor atoms.[25,26] The iron(III) ion usually demonstrates a larger affinity for an oxygen donor atom rather than for a nitrogen atom. The donor atom existing in the leaving alcohol group of the former two phosphates is nitrogen, while that of the latter phosphate is carboxyl oxygen. 3-Hydroxy-2-pyridylmethyl phosphate has donor atoms of both kinds, the 1-pyridinium nitrogen and the 3-hydroxyl oxygen. Thus, it is of quite interest to examine which donor atom is more effective for catalysis, in reference to the catalytic inertness of the copper ion which demonstrates a larger affinity for a nitrogen donor atom. We see from Fig. 5, that the iron(III) ion shows a positive catalytic effect although the reaction did not follow the strict first-order kinetics. At this stage, validity of the two requirements for the ef-

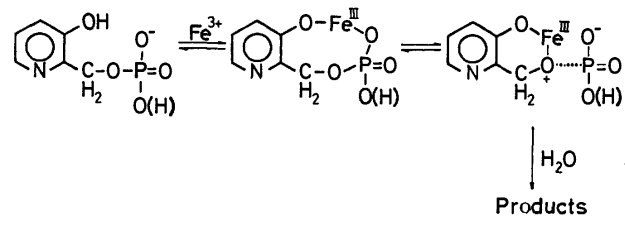

Scheme 8

23) Y. Murakami, J. Sunamoto, and H. Sadamori, *Chem. Commun.*, **1969**, 983.

24) R. Hofstetter, Y. Murakami, G. Mont, and A. E. Martell, *J. Amer. Chem. Soc.*, **84**, 3041 (1962).

fective metal ion catalysis, originally proposed for the bivalent metal ions, is extended to the trivalent metal ion catalysis and a reaction mechanism is put forward in Scheme 8. We take it for granted that this scheme is the most plausible mechanism for the iron catalyzed hydrolysis of 3-hydroxy-2-pyridylmethyl phosphate.

The thorium(IV) ion demonstrated a profound catalytic effect in the hydrolyses of organic phosphates, irrespective of the nature of a leaving alcohol moiety.[10,25] We could, therefore, expect a significant catalysis also for the hydrolysis of the present phosphate. The reaction rate was progressively depressed and consequently deviated from the first-order plot. Nevertheless, a significant effect was observed by all means. For the thorium catalysis observed in the hydrolyses of 3-pyridyl and 8-quinolyl phosphates, the extent of catalytic efficiency in terms of k_c/k_0 was about 10^3 at $-\log[H^+]\sim 2.0$.[10] For the present phosphate, the hydrolysis rate was accelerated only by 30-fold. Although we are not ready to interpret this large difference in catalytic efficiency at present, there is no doubt as to the participation of the 3-hydroxyl group in the present thorium ion catalysis. Judging from the fact that this metal ion does not show a large substrate specificity in hydrolysis relative to other metal ions and possesses the large stability constants with inorganic phosphate,[27] we proposed previously that the catalytic site may be located at the phosphate moiety. The preliminary chelate formation may occur at the terminal phosphate oxygen atoms as illustrated by structure **6**. If this is the case, the relatively strong intramolecular hydrogen bonding between the 3-hydroxyl proton and the phosphate oxygen may interfere with the preliminary chelate formation, shown by structure **12**. Consequently the extent of the catalytic efficiency would be reduced. In addition, the steric hindrance and the inductive effect due to the presence of the 3-hydroxyl group may also affect this chelate formation. In conclusion, through our surveying studies on the polyvalent metal ion catalysis for the hydrolysis of 3-hydroxy-2-pyridylmethyl phosphate, we may advance a concept that the introduction of the 3-hydroxyl group to the 2-pyridylmethyl moiety influences to a great extent the metal ion catalysis and spontaneous hydrolysis due to its electronic and environmental nature.

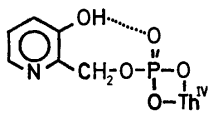

12

25) Y. Murakami and M. Takagi, This Bulletin, **42**, 3478 (1969).

26) Y. Murakami, *Nippon Kagaku Zasshi*, **91**, 185 (1970).

27) L. G. Sillén and A. E. Martell, "Stability Constants of Metal-Ion Complexes," Special Publication No. 17, The Chemical Society, London (1964).

BULLETIN OF THE CHEMICAL SOCIETY OF JAPAN, VOL. 45, 599—603 (1972)

The Rearrangement of 2α-Hydroxy-10β-pinan-3-one with Acetic Anhydride[1]

Toshifumi HIRATA

Department of Chemistry, Faculty of Science, Hiroshima University, Higashisenda-machi, Hiroshima

(Received September, 6, 1971)

The reaction of (+)-2α-hydroxy-10β-pinan-3-one (**1**) with acetic anhydride afforded (+)-2α-acetoxy-10β-pinan-3-one (**2**), (−)-carvone (**3**), (−)-4α-acetoxy-10α-pinan-3-one (**4**), (+)-4β-acetoxy-10β-pinan-3-one (**5**), and (−)-4β-acetoxy-10α-pinan-3-one (**6**). The three products, **4**, **5**, and **6**, were newly identified on the basis of a combination of chemical and physico-chemical methods. By examination using the ^{14}C-labelled acetate (**2**), the formation of **4**, **5**, and **6** was shown to arise from the intramolecular rearrangement of **2**. The mechanistic implications of the reaction are given.

In connection with studies of the stereochemistry and the reaction of pinane derivatives,[3,4] we have now found it necessary to examine the rearrangement of 2α-hydroxy-10β-pinan-3-one (**1**) with acetic anhydride. This paper will deal with the structures of some isomers of an α-acetoxyketone produced newly as well as with the mechanistic implications of the reaction.

Results and Discussion

The reaction of (+)-2α-hydroxy-10β-pinan-3-one (**1**) with acetic anhydride under reflux gave an oily reaction product, which was composed of (+)-2α-acetoxy-10β-pinan-3-one (**2**) (in 14% yield based on the sample taken), (−)-carvone (**3**) (1.3%), and three unknown acetates, **4**, **5**, and **6** (39, 17, and 20% respectively). The structures of the acetates, (**4**), (**5**), and (**6**), were established on the basis of the following evidence. The hydrolysis of the acetate (**4**) gave two unknown ketols, **7** and **8**. By acetylation, the former was returned to the acetate (**4**), whereas the latter was returned to a new acetate **9**. Furthermore, the lithium aluminum hydride reduction of the tosylate (**10**) derived from **7** gave two known compounds,

1) This paper forms Part XVI[2] in the Hiroshima University series of "Stereochemical Studies of Monoterpene Compounds."

2) Part XV: T. Suga and S. Watanabe, This Bulletin, **45**, 570 (1972).

3) T. Suga, T. Shishibori, T. Hirata, and T. Matsuura, *ibid.*, **41**, 1180 (1968).

4) R. G. Carlson, J. K. Pierce, T. Suga, T. Hirata, T. Shishibori, and T. Matsuura, *Tetrahedron Lett.*, **1968**, 5941.

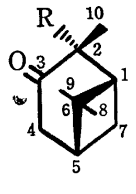

1: R=OH
2: R=OAc

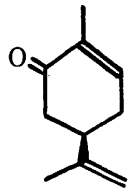

3

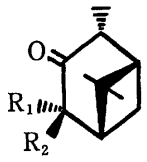

4: R_1=OAc, R_2=H
6: R_1=H, R_2=OAc
7: R_1=OH, R_2=H
10: R_1=OTs, R_2=H

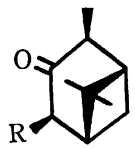

5: R=OAc
18: R=OTs
19: R=OH

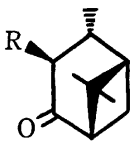

8: R=OH
9: R=OAc
13: R=OTs

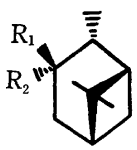

11: R_1=OH, R_2=H
12: R_1=H, R_2=OH

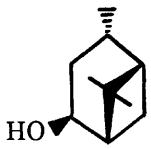

14

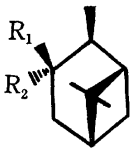

16: R_1=OH, R_2=H
17: R_1=H, R_2=OH

(−)-pinocampheol (**11**) and (+)-neopinocampheol (**12**).[5] These results showed the acetate (**4**) to be 4-acetoxy-10α-pinan-3-one. The ketol (**8**) was similarly confirmed to be 3-hydroxy-10α-pinan-4-one by the fact that its tosylate, **13**, was converted to (+)-neoverbanol (**14**)[5] on reduction with lithium aluminum hydride. It may probably be explained that the ketol (**8**) resulted from the isomerization of the ketol (**7**) through the intermediate (**15**) during the course

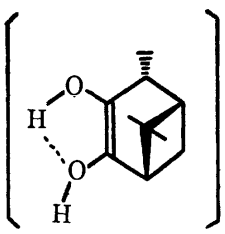

15

of the hydrolysis of the acetate (**4**). The acetate (**5**) was derived to (−)-neoisopinocampheol (**16**) and (+)-isopinocampheol (**17**)[5] on the reduction of the tosylate (**18**) derived from the hydrolyzed product, the ketol (**19**), of the original acetate (**5**) with lithium aluminum hydride. This indicates the structure of **5** to be 4-acetoxy-10β-pinan-3-one. It has been established[3,7–9] that, in the reduction of pinane derivatives with lithium aluminum hydride, the reagent approaches from the opposite side of the *gem*-dimethyl bridge and/or the polar group, because of the steric and/or the polar effects. The reduction of the hydroxyketone (**7**) with lithium aluminum hydride afforded *cis*- and *trans*-glycols, (**20**) and (**21**), in equal amounts. This can be ascribed to the competitive contribution between the *gem*-dimethyl and the hydroxyl groups to the reduction. Accordingly, the hydroxyl group of **7** should be *trans* to the *gem*-dimethyl group. On the other hand, the reduction of the acetate (**5**) with lithium aluminum hydride occurred stereospecifically to result in the formation of glycol, **22**. Therefore, the acetoxy group of **5** is surely *cis* to the *gem*-dimethyl group. This was also the case for the hydroxyketone (**8**), and **8** was converted to glycol, **23**. The acetate (**6**) was also derived to the glycol (**23**) on reduction with lithium aluminum hydride. This shows the structure of **6** to be 4β-acetoxy-10α-pinan-3-one. Consequently, all the structures of acetates, **4**, **5**, and **6**, together with those of ketol, **8**, and the diols, **20**, **21**, **22**, and **23**, were established, as is shown in the Schemes.

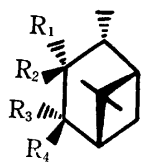

20: R_1, R_3=OH; R_2, R_4=H
21: R_1, R_4=H; R_2, R_3=OH
23: R_1, R_3=H; R_2, R_4=OH

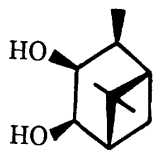

22

Reaction Mechanism. To clarify the mechanism of the formation of the acetates, (**4**), (**5**), and (**6**), from the hydroxyketone (**1**), the ^{14}C-labeled acetate (**2**), being active at the acetoxy carbonyl group, was treated with acetic anhydride in the same manner as above to give the acetates, (**4**), (**5**), and (**6**), in 21, 7, and 10% yields respectively; all of them retained the expected radioactivity. The treatment of the ^{14}C-labeled acetate (**5**) in the same manner as above yielded the radioactive acetates, (**2**), (**4**), and (**6**), in 2, 21, and 14% yields respectively. These findings suggest that the acetate (**2**) produced from the hydroxyketone (**1**)

5) These authentic samples were prepared in our laboratory by the reduction of the appropriate ketones.[3,6,7]
6) G. Zweifel and H. C. Brown, *J. Amer. Chem. Soc.*, **86**, 393 (1964).
7) A. F. Regan, *Tetrahedron*, **25**, 3801 (1969).
8) S. Winstein and N. J. Holness, *J. Amer. Chem. Soc.*, **77**, 3054 (1955).
9) Y. Chretien-Bessiere, *Bull. Soc. Chem. Fr.*, **1964**, 2182.

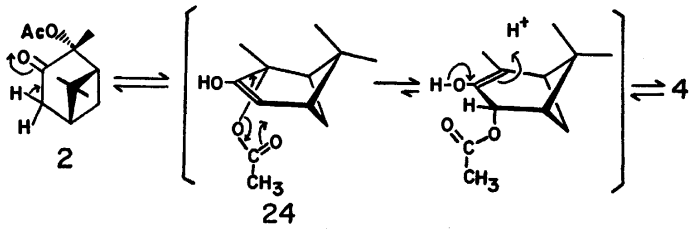

Scheme I

by acetylation suffers intramolecular rearrangements to form **4**, **5**, and **6**. The formation of the acetates is best explained by the initial formation of the acetate (**4**) through the formation of the enolic intermediate (**24**) of the acetate (**2**) by the subsequent intramolecularly-concerted migration of the acetoxy group, and finally by the isomerization of **4** to **5** and **6** through its enolic form, as is shown in Scheme I.

Experimental

The IR spectra were measured on a Perkin-Elmer, 621, Grating Infrared Spectrometer and a Hitachi, EPI-S, Infrared Spectrophotometer. The NMR spectra were recorded on a Varian Associates, HA-100, Spectrometer and a Hitachi Perkin-Elmer, R-20, Spectrometer, using tetramethylsilane as the internal standard. Vapor-phase chromatographic analyses were made on a Perkin-Elmer, F6-D, Gas Chromatograph. Mass spectral analyses were performed on a Hitachi, RMS-4, Mass Spectrometer, ionizing at the order of 80 eV. Radioassays were carried out by converting samples to carbon dioxide by Van Slyke-Folch oxidation,[10] followed by changing the resulting carbon dioxide to barium carbonate, and by counting on planchets at an infinite thickness and with a surface area of 5.0 cm^2 by means of an Aloka, LBC-1, Low-Background 2π-Gas Flow Countmeter. The counts were corrected for the background count, and the counting error was about ±3%.

*Reaction of 2α-Hydroxy-10β-pinan-3-one (**1**) with Acetic Anhydride.* A mixture of 22.0 g of (+)-2α-hydroxy-10β-pinan-3-one [mp 33—34°C, $[\alpha]_D^{25}$ +21.0° (*c* 4.6, EtOH), prepared from (−)-α-pinene following the literature method[11]] and 35.0 g of acetic anhydride was refluxed for 6 hr at 160°C. To the mixture, after cooling, we added 30 m*l* of water, and then it was heated for 30 min at 50°C in order to degrade the remaining acetic anhydride. The reaction mixture was then extracted with ether. The separated ether solution was washed with a dilute sodium bicarbonate solution and water, and then dried over anhydrous sodium sulfate. The removal of the solvent from the ether solution gave 22.9 g of an oily reaction product. The reaction product was chromatographed on a silica-gel column with a mixture of ethyl acetate and *n*-hexane (5 : 95 by volume) in order to separate five eluates.

The first eluate (0.4 g) was composed of complex minor components; it was further subjected to preparative gas chromatography. This resulted in the isolation of (−)-carvone (**3**): $[\alpha]_D^{25}$ −46° (*c* 0.45, MeOH); IR (liq.) 1677 (α,β-unsaturated C=O) and 1651 cm^{-1} (C=C). It was identified by a comparison of the IR spectrum with that of an authentic sample. The second eluate (3.2 g) was proved to be 2α-acetoxy-10β-pinan-3-one (**2**). The third eluate (13.5 g) consisted of two components in the ratio of 2 : 1; it was evaluated from the peak ratio of the C-4 proton signals on the NMR spectrum. A portion (5.0 g) was chromatographed twice on a silica-gel column with a mixture of ethyl acetate and *n*-hexane (1 : 99), but the complete separation was difficult. This procedure resulted in the separation of 4α-acetoxy-10α-pinan-3-one (**4**) (0.66 g) and 4β-acetoxy-10α-pinan-3-one (**6**) (0.11 g), and a mixture of **4** and **6** (4.05 g). The fourth eluate (3.9 g) gave a crystalline mass, which was then recrystallized from *n*-hexane to obtain (+)-4β-acetoxy-10β-pinan-3-one (**5**) (3.5 g). The fifth eluate (1.1 g) consisted of several compounds. One of the compounds was unchanged hydroxyketone (**1**) (0.8 g), but the others failed to separate.

*a) 2α-Acetoxy-10β-pinan-3-one (**2**)*: mp 38—40°C (from *n*-hexane), $[\alpha]_D^{25}$ +23.1° (*c* 0.26, MeOH); UV (MeOH) 300 nm (ε 29.5); IR (KBr) 1745 ($OCOCH_3$) and 1724 cm^{-1} (C=O); NMR (CCl_4) δ 0.86 (s, C_9-3H), 1.37 (s, C_8-3H), 1.49 (s, C_{10}-3H), and 1.92 ppm (s, $OCOCH_3$); mass *m/e* (rel. intensity) 210 (5, M^+), 192 (10), 168 (35) 153 (67), 150 (70), and 43 (100).

*b) 4α-Acetoxy-10α-pipan-3-one (**4**)*: $[\alpha]_D^{25}$ −78.1° (*c* 0.49, MeOH); UV (MeOH) 298 nm (ε 30.2); IR (liq.) 1744 ($OCOCH_3$) and 1728 cm^{-1} (C=O); NMR (CCl_4) δ 1.06 (s, C_9-3H), 1.07 (d, J=7,0 Hz, C_{10}-3H), 1.39 (s, C_8-3H), 2.02 (s, $OCOCH_3$), and 5.28 ppm (b.s, C_4-H); mass *m/e* (rel. intensity) 210 (1, M^+), 168 (2), 150 (7), 127 (16), 85 (56), 83 (25), 55 (30), 43 (82), and 28 (100).

*c) 4β-Acetoxy-10β-pinan-3-one (**5**)*: mp 100.5—101.0°C (from *n*-hexane - ethyl acetate), $[\alpha]_D^{25}$ +66.1° (*c* 6.0, EtOH); UV (MeOH) 292 nm (ε 27.7); IR (KBr) 1747 ($OCOCH_3$) and 1717 cm^{-1} (C=O); NMR (CCl_4) δ 0.93 (s, C_9-3H), 1.21 (d, J=7.0 Hz, C_{10}-3H), 1.33 (s, C_8-3H), 2.06 (s, $OCOCH_3$), and 5.26 ppm (b.s, C_4-H); mass *m/e* (rel. intensity) 210 (1, M^+), 168 (2), 150 (4), 127 (39), 85 (95), 83 (41), 55 (39), and 43 (100).

*d) 4β-Acetoxy-10α-pinan-3-one (**6**)*: $[\alpha]_D^{25}$ −8.5° (*c* 0.37, MeOH); UV (MeOH) 302 nm (ε 27.1); IR (liq.) 1745 ($OCOCH_3$) and 1727 cm^{-1} (C=O); NMR (CCl_4) 0.95 (s, C_9-3H), 1.14 (d, J=7.5 Hz, C_{10}-3H), 1.34 (s, C_8-3H), 2.04 (s, $OCOCH_3$), and 5.09 ppm (b.s, C_4-H); mass *m/e* (rel. intensity) 210 (4, M^+), 168 (2), 150 (7), 127 (20), 85 (25), 83 (20), 55 (11), 43 (25), and 28 (100).

*Hydrolysis of the Acetate (**4**).* To a stirred solution of 10 m*l* of 3 N methanolic potassium hydroxide, we added 2.00 g of **4**; the mixture was kept at room temperature overnight. The mixture was then diluted with 100 m*l* of water and extracted with ether. The removal of the solvent from the ether solution gave 1.40 g of an oily product, which was then chromatographed on a silica-gel column with a mixture of *n*-hexane and an increasing amount of ethyl acetate; we thus separated two components. The first eluate gave 419 mg of **7** and the second eluate, 208 mg of **8**.

*a) 4α-Hydroxy-10α-pinan-3-one (**7**)*: $[\alpha]_D^{25}$ −52.8° (*c* 0.55, MeOH); UV (MeOH) 285 nm (ε 29.7); IR (liq.) 1715 (C=O), and 1371 and 1387 cm^{-1} (*gem*-dimethyl);

10) D. D. Van Slyke and J. Folch, *J. Biol. Chem.*, **136**, 509 (1940).

NMR (CCl_4) δ 1.00 (s, C_9-3H), 1.06 (d, J=7.0 Hz, C_{10}-3H), 1.37 (s, C_8-3H), and 4.07 ppm (b.s. C_4-H). The acetylation of **7** with acetic anhydrade in pyridine gave the acetate (**4**); $[\alpha]_D^{25}$ −75.6° (*c* 0.37, MeOH). The acetate was identified by direct comparisons of its spectral data.

b) 3β-Hydroxy-10α-pinan-4-one (8): mp 44—45°C (from *n*-hexane), $[\alpha]_D^{25}$ −147.7° (*c* 0.27, MeOH); UV (MeOH) 282 nm (ε 36.9); IR (CCl_4) 1716 (C=O), and 1378 and 1391 cm^{-1} (*gem*-dimethyl); NMR (CCl_4) δ 0.74 (s, C_9-3H), 1.23 (d, J=7.0 Hz, C_{10}-3H), 1.37 (s, C_8-3H), and 3.70 ppm (d, J=6.5 Hz, C_3-H). The acetylation of **8** with acetic anhydride in pyridine gave the acetate (**9**); mp 38—39°C (from *n*-hexane), $[\alpha]_D^{25}$ −135.2° (*c* 0.49, MeOH); UV (MeOH) 284 nm (ε 54.9); IR (KBr) 1743 ($OCOCH_3$) and 1723 cm^{-1} (C=O); NMR (CCl_4) δ 0.81 (s, C_9-3H), 1.15 (d, J=7.0 Hz, C_{10}-3H), 1.38 (s, C_8-3H), 2.12 (s, $OCOCH_3$), and 5.12 ppm (d, J=6.5 Hz, C_3-H); mass *m/e* (rel. intensity) 210 (1, M^+), 168 (15), 150 (4), 135 (15) 95 (26), 83 (65), 55 (43), and 43 (100).

4α-Tosyloxy-10α-pinan-3-one (10). The tosylation of 350 mg of **7** with 500 mg of *p*-toluenesulfonyl chloride in 5 m*l* of pyridine at room temperaure for 5 days gave 545 mg of a crude product, which was then subjected to chromatography on a silica-gel column to give 453 mg of the tosylate (**10**); mp 68—69°C (from *n*-hexane - ethyl acetate); IR (KBr) 1722 (C=O) and 1595 cm^{-1} (C=C); NMR (CCl_4) δ 0.98 (s, C_9-3H), 1.05 (d, J=7.0 Hz, C_{10}-3H), 1.39 (s, C_8-3H), 2.44 (phenyl methyl), 4.80 (b.s, C_4-H), and 7.25—7.88 ppm (q, phenyl proton, 4H).

3β-Tosyloxy-10α-pinan-4-one (13). The treatment of 100 mg of **8** with 150 mg of *p*-toluenesulfonyl chloride in 3 m*l* of pyridine gave 137 mg of the tosylate (**13**); mp 118.0—118.5°C (from *n*-hexane - ethyl acetate); IR (KBr) 1740 (C=O) and 1598 cm^{-1} (C=C); NMR (CCl_4) δ 0.78 (s, C_9-3H), 1.26 (d, J=7.0 Hz, C_{10}-3H), 1.34 (s, C_8-3H), 2.44 (s, phenyl methyl), 4.73 (d, J=6.5 Hz, C_3-H), and 7.20—7.90 ppm (q, phenyl proton, 4H).

Reduction of the Hydroxyketone (7), To a stirred solution of 127 mg of **7** in 15 m*l* of ether, we added 100 mg of lithium aluminum hydride under ice-cooling, and then the mixture was refluxed for 2 hr. The mixture, after cooling, was treated with water and then dilute hydrochloric acid. The ether extract gave 120 mg of an oily product, which was separated by preparative thin-layer chromatography on silica-gel with a 3 : 7 mixture of ethyl acetate and *n*-hexane to give 60 mg of the *cis*-glycol, **20**, and 55 mg of *trans*-glycol, **21**.

a) 10α-Pinan-3α,4α-diol (20): mp 52—53°C (from *n*-hexane), $[\alpha]_D^{25}$ −1.0° (*c* 0.59, MeOH); IR (0.002 M CCl_4) 3627 (OH, free) and 3537 cm^{-1} (OH, intramol. bonded); NMR (CCl_4) δ 0.81 (s, C_9-3H), 0.97 (d, J=7.0 Hz, C_{10}-3H), 1.23 (s, C_8-3H), and 4.00 ppm (b.s, C_3- and C_4-H); mass *m/e* (rel. intensity) 170 (0.5, M^+). 152 (2), 137 (3), 85 (100), 43 (73), and 41 (54).

b) 10α-Pinan-3β,4α-diol (21): mp 146.0—146.5°C (from ethyl acetate), $[\alpha]_D^{25}$ −2.9° (*c* 0.14, MeOH); IR (0.002 M CCl_4) 3616 cm^{-1} (OH, free); NMR (pyridine) δ 0.98 (s, C_9-3H), 1.20 (d, J=7.0 Hz, C_{10}-3H), 1.22 (s, C_8-3H), 3.89 (d.d, J=7.0 and 6.0 Hz, C_3-H), and 4.42 ppm (b.d, J=6.0 Hz, C_4-H); mass *m/e* (rel. intensity) 170 (0.5, M^+), 152 (6), 137 (6), 85 (100), 43 (85), 41 (72), and 28 (87).

Reduction of the Hydroxyketone (8). A solution of 113 mg of **8** in 10 m*l* of ether was added to a strired suspension of 100 mg of lithium aluminum hydride in 10 m*l* of ether, and then the mixture was refluxed for 2 hr. After the degradation of the excess reagent, the mixture was extracted with ether to yield 110 mg of a crude product, which was subjected to preparative thin-layer chromatography on silica-gel with a mixture of ethyl acetate and *n*-hexane (3 : 7) to separate 91 mg of 10α-pinan-3β,4β-diol (**23**): mp 95.5—96.0°C (from a mixture of ethyl acetate and *n*-hexane), $[\alpha]_D^{25}$ −24.7° (*c* 0.11, MeOH); IR (0.002 M CCl_4) 3626 (OH, free) and 3547 cm^{-1} (OH, intramol. bonded); NMR (CCl_4) δ 1.00 (s, C_9-3H), 1.02 (d, J=7.0 Hz, C_{10}-3H), 1.19 (s, C_8-3H), 3.48 (m, C_3-H), and 4.10 ppm (b.s, C_4-H); mass *m/e* (rel. intensity) 137 (6), 85 (92), 43 (100), and 41 (77).

Reduction of the Tosylate (10). To a stirred suspension of 300 mg of lithium aluminum hydride in 15 m*l* of ether, we added a solution of 300 mg of **10** in 5 m*l* of ether at room temperature over a 30-min period, after which the mixture was further refluxed for 4 hr. The ether extract gave 139 mg of a reaction product, which was separated into two components by thin-layer chromatography on silica-gel with a mixture of ethyl acetate and *n*-hexane (3 : 7). The more eluted component (89 mg) was confirmed to be (−)-pinocampheol (**11**); mp 66—67°C (from *n*-hexane) (lit,[11] mp 67°C), $[\alpha]_D^{25}$ −57.2° (*c* 0.33, MeOH); IR (KBr) 3350 (OH), and 1370 and 1388 cm^{-1} (*gem*-dimethyl); NMR δ 0.92 (s, C_9-3H), 1.00 (d, J=7.0 Hz, C_{10}-3H), 1.21 (s, C_8-3H), and 3.56 ppm (d.t, J=9.0 and 7.0 Hz, C_3-H); the 3,5-dinitrobenzoate, mp 118—119°C (lit,[12] mp 118—119°C). The other component (21 mg) was found to be (+)-neopinocampheol (**12**); mp 26—27°C (from *n*-hexane) (lit,[11] mp 27°C), $[\alpha]_D^{25}$ +14.0° (*c* 0.15, MeOH); IR (Nujol) 3440 (OH), and 1370 and 1391 cm^{-1} (*gem*-dimethyl); NMR (CCl_4) δ 0.77 (s, C_9-3H), 0.93 (d, J=7.0 Hz, C_{10}-3H), 1.21 (s, C_8-3H), and 3.99 ppm (b.t, J=6.5 Hz, C_3-H). These physical properties and spectral data coincided with those of authentic samples.[5]

Reduction of the Tosylate (13). To a stirred suspension of 140 mg of lithium aluminum hydride in 5 m*l* of ether, we added a solution of 130 mg of **13** in 5 m*l* of ether at room temperature over a 10-min period. After refluxing for 3 hr, the treatment of the mixture in the usual manner gave 61 mg of a reaction product, which was chromarographed on a silica-gel column to separate 13 mg of the pinan-diol (**23**) (mp 95.5—96.0°C) and 42 mg of (+)-neovervanol (**14**); mp 78—79°C (from *n*-hexane), $[\alpha]_D^{25}$ +11.6° (*c* 0.17, MeOH); IR (KBr) 3340 (OH), and 1370 and 1389 cm^{-1} (*gem*-dimethyl); NMR (CCl_4) δ 0.88 (d, J=7.0 Hz, C_{10}-3H), 1.06 (s, C_9-3H), 1.21 (s, C_8-3H), and 4.14 ppm (m, C_4-H). The spectral data coincided with those of an authentic sample.[5]

Hydrolysis of the Acetate (5). To a stirred solution of 420 mg of **5** in 20 m*l* of methanol, we added 10 m*l* of 0.1 N methanolic sodium hydroxide at 15°C over a 10-min period. The mixture was further stirred for 20 min and then extracted with ether to give 292 mg of hydroxyketone, **19**; mp 67—68°C (from *n*-hexane), $[\alpha]_D^{25}$ +33.5° (*c* 0.25, MeOH); UV (MeOH) 288 nm (ε 29.8); IR (KBr) 1710 (C=C), and 1376 and 1390 cm^{-1} (*gem*-dimethyl); NMR (CCl_4) δ 0.86 (s, C_9-3H), 1.20 (d, J=7.0 Hz, C_{10}-3H), 1.32 (s, C_8-3H), and 3.98 ppm (b.s, C_4-H). This hydroxyketone was derived to the acetate (**6**) by acetylation.

4β-Tosyloxy-10β-pinan-3-one (18). The treatment of 200 mg of **19** with 300 mg of *p*-toluenesulfonyl chloride in 4 m*l* of pyridine at room temperature for 5 days gave 370 mg of the tosylate, **19**; mp 97—98°C (from *n*-hexane - ethyl acetate); IR (KBr) 1734 (C=O) and 1597 cm^{-1} (C=C); NMR (CCl_4) δ 0.92 (s, C_9-3H), 1.16 (d, J=7.5 Hz, C_{10}-3H), 1.35 (s, C_8-3H), 2.45 (s, phenyl methyl), 4.78 (b.s,

11) H. Schmidt, *Chem. Ber.*, **77**, 544 (1944).

12) T. Takemoto, G. Kusano, and H. Hikino, *Yakugaku Zasshi*, **86**, 1162 (1966).

C_4-H), and 7.20—7.90 ppm (q, phenyl proton, 4H).

*Reduction of the Acetate (**5**).* A suspension of 110 mg of **5** and 120 mg of lithium aluminum hydride in 50 m*l* of ether was refluxed for 7 hr under agitation, and then it was treated in the usual manner to give 80 mg of glycol, **22**; mp 79—80°C (from *n*-hexane); IR (0.0024 M CCl_4) 3634 (OH, free) and 3533 cm^{-1} (OH, intramol. bonded); NMR ($CDCl_3$) δ 1.10 (d, J=7.5 Hz, C_{10}-3H), 1.16 (s, C_9-3H), 1.20 (s, C_8-3H), and 4.35 ppm (m, C_3- and C_4-H); mass *m/e* (rel. intensity) 170 (1, M^+), 152 (1), 137 (7), 86 (92), 85 (100), 43 (54), and 41 (36).

*Reduction of the Tosylate (**18**).* To a stirred suspension of 300 mg of lithium aluminum hydride in 10 m*l* of ether, we added a solution of 290 mg of **18** in 15 m*l* of ether at room temperature over a 30-min period; this was followed by further refluxing for 3 hr. The mixture, after the usual treatment, gave 185 mg of a reaction product, which was subjected to column-chromatography on silica-gel with a mixture of *n*-hexane and an increasing amount of ethyl acetate to give 90 mg of (−)-neoisopinocampheol (**16**) [mp 50.5—51.0°C (from *n*-hexane) (lit,[11] mp 48°C), $[\alpha]_D^{25}$ −34.5° (*c* 0.75, C_6H_6); IR (KBr) 3340 (OH), and 1369 and 1388 cm^{-1} (*gem*-dimethyl); NMR (CCl_4) δ 1.05 (d, J=7.0 Hz, C_{10}-3H), 1.06 (s, C_9-3H), 1.18 (s, C_8-3H), and 4.35 ppm (d.t, J=5.0 and 10.0 Hz, C_3-H)], 20 mg of (+)-isopinocampheol (**17**) [mp 56—57°C (from *n*-hexane) (lit,[11] mp 57°C), $[\alpha]_D^{25}$ +29.0° (*c* 0.15, C_6H_6); IR (KBr) 3280 (OH), and 1372 and 1388 cm^{-1} (*gem*-dimethyl); NMR (CCl_4) δ 0.91 (s, C_9-3H), 1.08 (d, J=7.0 Hz, C_{10}-3H), 1.20 (s, C_8-3H), and 3.94 ppm (d.t, J=9.0 and 5.0 Hz, C_3-H)], and 18 mg of 10β-pinan-3β,4β-diol (**22**) (mp 79—80°C).

*Reduction of the Acetate (**6**).* A solution of 50 mg of **6** in 15 m*l* of ether was treated with 50 mg of lithium aluminum hydride under reflux for 1 hr to give 39 mg of the pinanediol (**23**); mp and mixed mp 95—96°C, $[\alpha]_D^{25}$ −21.0° (*c* 0.20, MeOH).

Preparation of Radioactive Acetic Anhydride. To a stirred suspension of 1-^{14}C-sodium acetate (3.50 g; 8620±80 dpm/mmol) in ether, we added acetyl chloride (4 m*l*) over a 5-min period at room temperature. The mixture was then further stirred for 3 hr. The distillation of the reaction gave acetic-1-^{14}C anhydride (2.82 g; 4462±40 dpm/mmol).

Rearrangement of Radioactive Acetate. 2α-(1-^{14}C-Acetoxy)-10β-pinan-3-one (**2**) and 4β-(1-^{14}C-acetoxy)-10β-pinan-3-one (**5**) were prepared by treating 2α-hydroxy-10β-pinan-3-one (**1**). The radioactive acetic anhydride in the manner as above. The radioactive acetates, (**2**) and (**5**), were then each treated with acetic anhydride in the manner to be shown below. The reaction product was purified by column-chromatography, followed preparative thin-layer chromatography or recrystallization. The proportion of products was evaluated on the basis of the gas chromatography and the peak ratio of the C-4 proton signals on the NMR spectra.

*a) Rearrangement of the ^{14}C-Acetate (**2**)*: A solution of 840 mg (0.004 mol) of the radioactive acetate (**2**) (187.3±2.0 dpm/mmol) in 1632 mg (0.016 mol) of acetic anhydride was refluxed for 5 hr. The usual treatment of the reaction mixture then gave 830 mg of an oily product, which was composed of 54 mg of the acetate (**4**) (119.2±2.0 dpm/mmol), 58 mg of the acetate (**5**) (97.3±2.0 dpm/mmol), 25 mg of the acetate (**6**) (104.6±2.0 dpm/mmol), and 257 mg of the unchanged acetate (**2**) (136.1±2.0 dpm/mmol).

*b) Rearrangement of the ^{14}C-Acetate (**5**)*: A sample of 1680 mg (0.008 mol) of the radioactive acetate (**5**) (182.4±2.0 dpm/mmol) was refluxed with 3264 mg (0.032 mol) of acetic anhydride for 5 hr. The ether extract of the mixture gave 1632 mg of an oily product, which was composed of 15 mg of **2** (126.5±2.0 dpm/mmol), 91 mg of **4** (138.7±2.0 dpm/mmol), 32 mg of **6** (131.4±2.0 dpm/mmol), and 660 mg of the unchanged **5** (170.2±2.0 dpm/mmol).

The author wishes to express his hearty gratitude to Dr. Takayuki Suga of Hiroshima University for his guidance and encouragement and to Dr. E. von Rudoloff of National Research Council of Canada, Saskatchewan, Canada, for measuring the NMR spectra with a Varian Associates, HA-100, Spectrometer.

Preparation of Cyclamenaldehyde by Selective Hydrogenation in Some Cobalt Carbonyl Complex Catalysts under Oxo Conditions[1]

Kunio KOGAMI,* Osamu TAKAHASHI,* and Ju KUMANOTANI**

*T. Hasegawa Co., Ltd, Nihonbashi, Chuo-ku, Tokyo

**Engineering Research Institute, Faculty of Engineering, The University of Tokyo, Yayoi-cho, Bunkyo-ku, Tokyo

(Received May 18, 1971)

Selective hydrogenation of *p*-isopropyl-α-methylcinnamaldehyde to cyclamenaldehyde in some cobalt carbonyl complex catalyst systems has been investigated under several oxo conditions. The yield of the aimed aldehyde was improved as much as 84 to 86.3% under controlled conditions. Selectivity of the hydrogen increased with the decrease of temperature and the increase of partial pressure of hydrogenation in a water gas. A maximum yield (84%) was obtained with solvents such as isopropyl ether and hexane when used in 2-fold volume for the cinnamaldehyde. A tris(2-bromoethyl) phosphite-substituted cobalt carbonyl complex catalyst gave the best yield (86.3%) as compared with catalysts unsubstituted and substituted with PR_3, $P(OR)_3$, and $PO(OR)_3$ (R=alkyl, aryl).

Cyclamenaldehyde, one of the principal aromatic chemicals, has been prepared industrially by two well known superior processes, *viz.*, dehydrogenation of the corresponding alcohol using a Cu-Zn catalyst[2] and hydrogenation of *p*-isopropyl-α-methylcinnamaldehyde over 5% Pd on a charcoal catalyst.[3-5]

Recently the hydrogenation of α,β-unsaturated carbonyl compounds to give saturated carbonyl compounds was reported on the following catalyst system; tri(triphenylphosphine)chlororhodium by Jardine and Wilkinson,[6] palladium boride by Kawai *et al*,[7] and cobalt hydrocarbonyl by Goetz and Orchin, who found that the saturated carbonyl compounds were produced at 25°C under one atmosphere of carbon monoxide, while the saturated carbonyl compounds formed were reduced very slowly into the corresponding alcohols.[8]

We found that dicobalt octacarbonyl and its complex substituted with tris(2-bromoethyl) phosphite were useful catalysts for selective hydrogenation to the double bond of *p*-isopropyl-α-methylcinnamaldehyde under oxo conditions.

Experimental

Materials. *p*-Isopropyl-α-methylcinnamaldehyde was prepared according to the Knorr method:[9] bp 117—120°C/2 mmHg, d_{20}^{20} 0.9986, n_D^{20} 1.4343.

The dicobalt octacarbonyl (mp 51°C) was prepared in a 51.4% yield according to the method in literature,[11] which involved the reaction between cobalt-hydroxide and a 150 kg/cm² water gas (H_2 : CO, 1 : 1, purchased from the Takachiho Commercial Co., Ltd.).

The complex of dicobalt octacarbonyl substituted with the following ligands in molar ratio of 1 : 2 were prepared in isopropyl ether under a purified nitrogen flow;[10] tiphenylphosphine, triphenyl phsphite, tributylphosphine, tributyl phosphite, tris(2-bromoethyl) phosphite, triphenyl phosphate, and tricresyl phosphate. They were of chemically pure grade and purchased from the Tokyo Kasei Co., Ltd.

Procedure. After *p*-isopropyl-α-methylcinnamaldehyde (18.8 g, 0.1 mol) and a solution of dicobalt octacarbonyl (0.56 g, 0.0016 mol) in 40 m*l* of isopropyl ether had been put into a 300 m*l* stainless steel autoclave equipped with an outlet tube for sampling, the air in the autoclave was flushed with nitrogen several times. The water gas was then charged at pressure from 60 to 80 kg/cm² at room temperature.

The autoclave was then heated up to the desired temperature with stirring. Aliquots of the reaction mixture were withdrawn from the autoclave at the prescribed time interval during the reaction, and submitted to glc.

Hydrogenation was continued until the peak of *p*-isopropyl-α-methylcinnamaldehyde disappeared, and the end point was detected from the gauge pressure-time relation. After the hydrogenation, the autoclave was cooled, purged, and then a solution of triphenylphosphine (1.7 g) in isopropyl ether (300 m*l*) was added. The insoluble precipitates (phosphine complex) were then filtered off. The resulting filtrate was neutralized with 200 m*l* of an aqueous solution of 5% sodium carbonate, and dried over sodium sulfate. After the removal of ether from the solution, an oily product obtained as a residue was distilled *in vacuo* to separate volatile products.

Identification and Analysis of Products. Cyclamenaldehyde and cyclamen alcohol were separated by the distillation of the products of Run 9 in Table 2 with a packed type rectifier, and identified by NMR spectra in carbon deuterium trichloride with tetramethylsilane as an internal standard on a JEOL 4H-100 spectrometer. Cyclamenaldehyde: bp 98—100°C/1 mmHg, d_{20}^{20} 0.9486, n_D^{20} 1.5080. NMR spectrum: 1.05 ppm (d) doublet (J=2.5) methyl 3H; 1.20 ppm (d) doublet (J=2.5) isopropyl methyl 6H; 2.64 ppm (m) multiplet methine H; 2.85 ppm (m) multiplet isopropyl methine H; 7.08 ppm (m) multiplet phenyl 4H; 9.26 ppm (s) singlet aldehyde H.

1) This work was carried out in the Engineering Research Institute, Faculty of Engineering, The University of Tokyo, and presented at the 13th Symposium on the Chemistry of Terpenes, Essential Oils and Aromatics of the Chemical Society of Japan, Kagoshima, 1969.

2) S. Abe and T. Yasukawa, *Yuki Gosei Kagaku Kyokai Shi*, **22**, 144, 209 (1964).

3) J. Levy and A. Friedmann, U. S. 3280192 (1966).

4) P. N. Rylander, U. S. 3372199 (1968).

5) J. Levy and A. Friedmann, Brit. 1086447 (1963).

6) F. H. Jardine and G. Wilkinson, *J. Chem. Soc., C*, **1967**, 270.

7) M. Kawai, T. Imai, and S. Teranishi, *Nippon Kagaku Zasshi*, **90**, 42 (1969).

8) R. W. Goetz and M. Orchin, *J. Amer. Chem. Soc.*, **85**, 2782 (1963).

9) A Knorr, and A. Weissenborn, U. S. 1844013 (1932).

10) E. R. Tucci, *Ind. Eng. Chem., Product Research and Development.*, **7**, 37 (1969).

11) S. Usami, and T. Kondo, The 21st Annual Meeting of the Chemical Society of Japan, Osaka, April, 1969, Preprints, Vol. III, p. 1968.

Cyclamen alcohol: bp 120—122°C/1 mmHg, d_{20}^{20} 0.9492, n_D^{20} 1.5080. NMR spectrum: 0.90 ppm (d) (J=3.0) methyl 3H; 1.21 ppm (d) (J=2.0) isopropyl methyl 6H; 1.80 ppm (bs) broad singlet hydroxy H; 1.91 ppm (m) methine H; 2.87 ppm (m) isopropyl methine H; 3.47 ppm (d) hydroxy methylene 2H; 7.09 ppm (m) phenyl 4H.

The composition of the products was determined by glc using a gas chromatograph (Kotaki GU-21) with a 2 m stainless steel column of KF 54 (5% by weight) on cellite 545 sk (60—80 mesh) at 180°C. Both of the above products were analyzed within a relative experimental error of ±1.5%. The standard materials cyclamenaldehyde and cyclamen alcohol were prepared by the following procedures.[2] Cyclamenaldehyde was prepared by dehydrogenation of cyclamen alcohol with a Cu-Zn catalyst (bp 110—112°C/4 mmHg, d_{20}^{20} 0.9498, n_D^{20} 1.5083), and cyclamen alcohol by the catalytic hydrogenation of *p*-isopropyl-α-methylcinnamaldehyde over a nickel-diatomaceous earth catalyst (bp 130—132°C/4 mmHg, d_{20}^{20} 0.9490, n_D^{20} 1.5076).

Results and Discussion

Hydrogenation of p-*Isopropyl-α-methylcinnamaldehyde Using Dicobalt Octacarbonyl Catalyst.* It is well known that cobalt hydrocarbonyl is formed by the reaction with dicobalt octacarbonyl and a water gas (H_2 : CO, 1 : 1) at 100°C under a pressure greater than 45 kg/cm².

From the results it is suggested that the hydrogenation of *p*-isopropyl-α-methylcinnamaldehyde into cyclamenaldehyde with a minor amount of $Co_2(CO)_8$ under oxo conditions proceeds by the repetition of the process given by the following equations.

$$Co_2(CO)_8 + H_2 \rightleftharpoons 2HCo(CO)_4 \quad (1)$$

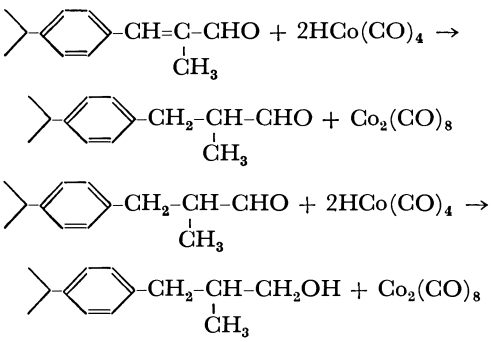

$$\xrightarrow{2HCo(CO)_4}$$

$$\xrightarrow{Co_2(CO)_8}$$

$$\xrightarrow{2HCo(CO)_4}$$

$$\xrightarrow{Co_2(CO)_8} \quad (2)$$

However, it should be noticed that cyclamenalcohol may be formed simultaneously by the reaction of cyclamenaldehyde with $HCo(CO)_4$ at such a high temperature.

Increase in the partial pressure of carbon monoxide in the water gas would decrease the concentration of the cobalt hydrocarbonyl in the system (Eq. (1)), resulting in either a slower or a higher-temperature hydrogenation. The effect of solvents such as isopropyl ether and *n*-hexane upon the product distribution should also be examined under various conditions. The results obtained are summarized in Table 1.

1) Effect of the Amount of Catalyst Complex and Reaction Temperature. Increase in $Co_2(CO)_8$ from 5 to 18% (by weight) for the cinnam aldehyde served to shorten the reaction time, but the undesired cyclamen alcohol and resinous matter tended to increase it (Runs 1—3, Table 1).

A decrease in the catalyst from 5 to 1% (Run 5 and 6) was necessary to raise the reaction temperature, resulting in an increase in the above two compounds.

It was found that the increase of the partial pressure of hydrogen in a water gas at 55 kg/cm² lowered the reaction temperature, resulting in an increase in the yield of cyclamenaldehyde to 80.3% of the theoretical (Run 7, Table 1).

A higher molar ratio of carbon monoxide in a water gas at 45 kg/cm² (H_2 : CO, 1 : 2) raised the reaction temperature from 100—130°C to 140—145°C, giving greater amounts of cyclamen alcohol and resinous matter (Run 3 and 4, Table 1).

2) Solvent Effect. When isopropyl ether or *n*-hexane was used in 5—2-fold volume for the cinnam aldehyde, the reaction temperature was lowered from 100—130°C to 90—125°C, giving rise to an increase in the amount of cyclamenaldehyde as well as a decrease in that of the alcohol and resinous matter (compare Runs 10—12 with Run 8 in Table 1).

The higher molar ratio of hydrogen in the water gas, *e.g.* 65 kg/cm² water gas (H_2 : CO, 12 : 1) used instead of the 100 kg/cm² gas (H_2 : CO, 1 : 1) much lowered the reaction temperature from 90—125°C to 90—96°C and increased the yield of cyclamenaldehyde as much as 84.0% (Runs 11 and 12, Table 1).

By employing an 1.5-fold volume of isopropyl ether, the yield of the cyclamenaldehyde was lowered from 83.2 to 77.8%, accompanied by an increase of distillation residue from 8.9 to 13.6% (Runs 9 and 10, Table 1). From the results, the optimum conditions for yielding cyclamenaldehyde can be given as follows. *p*-Isopropyl-α-methylcinnam aldehyde is reduced at 90—96°C for 6.5 hr under stirring with a 65 kg/cm² water gas (H_2 : CO, 12 : 1) in a 2-fold volume of isopropyl ether with 3% (by weight) $Co_2(CO)_8$ for the cinnamaldehyde.

3) Effect of Ligand Substitution upon Selective Hydrogenation In order to improve the yield of cyclamenaldehyde, hydrogenation was carried out with ligand-substituted cobalt carbonyl complex catalysts. The ligand substitution (Table 2) was performed with the following compounds.

Tributylphosphine, triphenylphosphine, tributyl phosphite, tris(2-bromoethyl) phosphite, triphenyl phosphite, triphenyl phosphate, and tricresyl phosphate.[10] Hydrogenation with these complex catalysts was carried out in a 5-fold volume of isopropyl ether for the cinnamaldehyde at 122—180°C with a 100 kg/cm² water gas (H_2 : CO, 1 : 1). In the case of the tributylphosphine, tributyl phosphite, or triphenylphosphine complex, the reaction proceeded at higher temperature and the yield of cyclamenaldehyde was lowered, while the cyclamenalcohol increased in quantity as compared with the other cases.

The triphenyl phosphite complex catalyst, and triphenyl phosphate- or tricresyl phosphate-$Co_2(CO)_8$ catalyst gave a comparable yield of cyclamenadehyde and a product distribution similar to that given in

Table 1. Selective hydrogenation using dicobalt octacarbonyl catalyst under oxo conditions

Run	*p*-Isopropyl-α-methylcinnamaldehyde (g)	(mol)	Catalyst wt% for cinnamaldehyde $Co_2(CO)_8$	Solvent (ml)	Partial pressure (kg/cm²) H_2	CO	Reaction temperature (°C)	Reaction time (hr)	Composition of reaction product (wt%) Cyclamenaldehyde	Cyclamen alcohol	Distillation residue (%)	Yield of cyclamenaldehyde (%)
1	18.8	0.1	18	*n*-Hexane 100 ml	50	50	110—130	2.5	52.2	29.4	18.4	51.6
2	18.8	0.1	9	*n*-Hexane 100 ml	50	50	110—133	2.5	65.7	20.3	14.0	65.4
3	18.8	0.1	5	*n*-Hexane 100 ml	50	50	100—130	4.5	76.4	10.4	13.2	76.1
4	18.8	0.1	5	*n*-Hexane 100 ml	15	30	140—145	3.0	78.6	10.6	10.8	78.0
5	18.8	0.1	3	*n*-Hexane 100 ml	50	50	120—140	4.0	68.5	17.7	13.8	68.1
6	18.8	0.1	1	*n*-Hexane 100 ml	50	50	120—145	6.5	66.8	17.9	15.3	66.0
7	18.8	0.1	5	*n*-Hexane 100 ml	50	5	90— 96	6.5	81.2	9.6	9.2	80.3
8	18.8	0.1	5	Isopropyl ether (5 folds) 100 ml	50	50	100—130	3.0	79.8	9.7	10.5	78.8
9	18.8	0.1	3	Isopropyl ether (1.5 folds) 30 ml	50	50	90—125	6.5	77.8	8.6	13.6	77.0
10	18.8	0.1	3	Isopropyl ether (2 folds) 40 ml	50	50	90—125	6.5	83.2	7.9	8.9	83.0
11	18.8	0.1	3	Isopropyl ether 40 ml	60	5	90— 96	6.5	83.3	8.2	8.5	82.6
12	18.8	0.1	3	*n*-Hexane 40 ml	60	5	90— 94	6.5	84.0	8.0	8.0	84.0

Table 2. The effect of ligand substitution

Run	*p*-Isopropyl-α-methyl-cinnamaldehyde (g)	(mol)	Catalyst for the cinnamaldehyde (wt%)	Ligand (g)		Solvent (Isopropyl ether) (ml)	Partial pressure (kg/cm²) H_2	CO	Reaction temperature (°C)	Reaction time (hr)	Composition of Product by glc (wt%) Cyclamenaldehyde	Cyclamen alcohol	Distillation residue (%)	Yield (theor.) of aldehyde (%)
1	18.8	0.1	$Co_2(CO)_8$ 1.0	$P(CH_3(CH_2)_3)_3$	1.2	100	50	50	145—160	1.5	65.7	24.3	10.0	65.1
2	18.8	0.1	$Co_2(CO)_8$ 1.0	$P(C_6H_5)_3$	1.7	100	50	50	178—180	1.5	70.6	18.4	11.0	70.0
3	18.8	0.1	$Co_2(CO)_8$ 1.0	$P(CH_3(CH_2)_3O)_3$	1.5	100	50	50	132—145	3.7	68.5	19.5	12.0	68.1
4	18.8	0.1	$Co_2(CO)_8$ 1.0	$P(C_6H_5O)_3$	1.8	100	50	50	126—132	3.2	76.5	11.5	12.0	76.2
5	18.8	0.1	$Co_2(CO)_8$ 1.0	$P(C_6H_5O)_3$	1.8	40	50	50	122—144	6.0	79.2	8.8	12.0	79.0
6	18.8	0.1	$Co_2(CO)_8$ 1.0	$PO(C_6H_5O)_3$	1.9	100	50	50	125—128	4.0	76.5	10.5	13.0	75.9
7	18.8	0.1	$Co_2(CO)_8$ 1.0	$PO(CH_3C_6H_4O)_3$	2.2	100	50	50	126—128	4.0	76.5	10.5	13.0	76.0
8	18.0	0.1	$Co_2(CO)_8$ 1.0	$P(BrCH_2CH_2O)_3$	1.6	100	50	5	120—132	2.0	85.0	6.0	9.0	84.5
9	18.8	0.1	$Co_2(CO)_8$ 1.0	$P(BrCH_2CH_2O)_3$	2.5	100	50	50	130—136	2.0	85.6	5.4	9.0	85.1
10	18.8	0.1	$Co_2(CO)_8$ 1.0	$P(BrCH_2CH_2O)_3$	2.5	40	50	50	128—134	3.0	86.5	4.5	9.0	86.3
11	18.8	0.1	$Co_2(CO)_8$ 1.0	$P(BrCH_2CH_2O)_3$	1.6	50	50	50	128—134	3.0	86.5	4.3	9.2	86.3

the $Co_2(CO)_8$ system unsubstituted (Run 4—7, Table 2).

Use of the tris(2-bromoethyl) phosphite afforded a maximum yield of cyclamenaldehyde (86.3%) (Runs 8—11, Table 2).

The increase in cyclamen alcohol can reasonably be interpreted in terms of the stability of the cobalt carbonyl phosphine and phosphite complexes, in which the scission of cobalt–carbon coordination in the π-oxapropenyl intermediate complex occurred at a relatively higher temperature. Hydridic character of the cobalt hydrocarbonyl complex persisted even at the higher temperature, and resulted in facilitating the hydrogenation of cyclamenaldehyde to cyclamen alcohol.

The increase in cyclamenaldehyde can be interpreted in terms of the fallen electron density of cobalt atom in the complex, which was caused by an electron-attracting effect of the 2-bromoethyl group and which favored the enhancement of the back donation of π-oxapropenyl intermediate as well as the transformation from σ- to π-intermediates of the complex.

The smaller yield in cyclamen alcohol may result from the difficulty in the formation of the cyclic transition state intermediate between the tris(2-bromoethyl) phosphite-substituted cobalt hydrocarbonyl complex and cyclamenaldehyde based on the steric effect of the complex.

The authors wish to express their thanks to Mr. S. Hasegawa, President of T. Hasegawa Co., Ltd, for his permission to publish this paper.

BULLETIN OF THE CHEMICAL SOCIETY OF JAPAN, VOL. 45, 607—612 (1972)

Metal Catalysts Supported on Zeolite. I. A Study on Platinum Particles Distribution

Toshihiko KUBO, Hiromichi ARAI, Hiroo TOMINAGA, and Taiseki KUNUGI

Department of Synthetic Chemistry, Faculty of Engineering, The University of Tokyo, Hongo, Bunkyo-ku, Tokyo

(Received July 14, 1971)

Zeolite 13Y, loaded with platinum cations by ion exchange, was calcined in the air and subsequently reduced in a hydrogen stream. Hydrogen and carbon monoxide adsorption studies, together with an electron microscopic observation of the catalyst, revealed that the size distribution of platinum particles is controlled by the calcination temperature. The hydrogen chemisorption method gave the average particle diameters, which were in fairly good agreement with the observations made by means of an electron microscope on the catalyst with a platinum particle diameter larger than 20 Å, while trace amounts of hydrogen chemisorption were observed for platinum particles less than 20 Å.

In the preparation of metallic catalysts supported on carriers, the relationship between the size distribution of metallic particles and their adsorptive and catalytic activities has constituted one of the most interesting subjects of study. An incentive to the study from a practical point of view is the need for the efficient utilization of metals, especially of such highly priced ones as those in the platinum group. Several physicochemical techniques, such as X-ray diffraction-line-broadening, electron microscope, and gas chemisorption, have been developed for the dispersion state analysis of the metal. These studies involve the following: the influence of the platinum crystallite size on the selectivity of hydrocarbon reforming,[1] the crystallite size and the specific activity for benzene hydrogenation of platinum/silica catalysts,[2] the influence of the crystallite size on the infrared-active nitrogen adsorption on nickel, palladium and platinum,[3] the preparation of a highly dispersed platinum catalyst supported on silica gel,[4] X-ray adsorption edge study of zeolite supported platinum,[5] the adsorptive and catalytic properties of metal crystallites,[6] and some relations between the structural and catalytic properties of alumina-supported platinum.[7] Echigoya *et al.*,[8] and Shirasaki and Furuoya[9] reported that the temperature of calcining $Pd(NH_3)_4^{2+}$ on silica and silica-alumina in the air affected the size distribution of the palladium crystallites formed by subsequent hydrogen reduction. Further, they studied the dispersion state and the structure of palladium crystallites, in particular of the catalysts calcinined at rather high temperatures (>300°C), by X-ray diffraction-line-broadening, electron microscope, and carbon monoxide chemisorption techniques.

In the present study, we were especially interested in the catalysis of fine platinum particles, such as those less than 20 Å in diameter, on zeolite. The platinum

1) H. J. Maat and L. Moscou, The Third International Congress on Catalysis, Section 2, Paper 5 (1964).
2) T. A. Dorling and R. L. Moss, *J. Catal.*, **5**, 111 (1966).
3) R. Van Hardeveld and A. Van Montfoort, *Surface Science*, **4**, 396 (1968).
4) H. A. Benesi, R. M. Curtis, and H. P. Studer, *J. Catal.*, **10**, 328 (1968).
5) P. H. Lewis, *ibid.*, **11**, 162 (1968).
6) G. C. Bond, The Fourth International Congress on Catalysis, Paper 67 (1968).
7) M. Kraft and H. Spindler, *ibid.*, Paper 69 (1968).
8) E. Echigoya, I. Furuoya, and K. Morikawa, *Kogyo Kagaku Zasshi*, **71**, 1768 (1968).
9) T. Shirasaki and I. Furuoya, *ibid.*, **71**, 1774 (1968).

catalysts were prepared by ion exchange and subsequent calcination in the air, followed by reduction in hydrogen. Particularly, we attempted to establish a method of preparation by which to achieve a desired dispersion state of platinum crystallites, which were analyzed by electron microscope and also by hydrogen chemisorption techniques. The temperature of calcining ion exchanged zeolite in the air was found to be the key factor, whereby the particle size distribution after reduction is affected. The hydrogen chemisorption technique was shown to give an average diameter of particles which is in fairly good agreement with that obtained by electron microscopic examination of the catalyst with a platinum particle diameter of over 20 Å on the average.

Experimental

Catalyst Preparation. Platinum catalysts incorporated with a carrier, zeolite 13Y, were prepared by ion exchange, followed by calcination and reduction. The zeolite of Linde molecular sieves Y type SK-40 was employed. Its analysis indicated a chemical composition of SiO_2 63.5%, Al_2O_3 23.5%, Na_2O 13.0%, Cl 0.05%, and Fe 0.05% by weight.

The catalysts of the Pt-NaY type were prepared, in this work, according to the following procedure. The zeolite 13Y was degassed by stirring in deionized water, 20 times by weight, at 98—100°C for 2 hr. Then a given amount of aqueous solution of 0.01 mol/*l* $Pt(NH_3)_4Cl_2$ was added slowly, drop by drop; then the resulting mixture was stirred for another 3 hr at 98—100°C. The ion exchanged zeolite was obtained by filtration and washed thoroughly with deionized water until no chloro anion was detected in the filtrate. The zeolite was dried at 110°C for 3 hr, calcined in the air at a given temperature for 3 hr, and then, prior to use, reduced in a hydrogen stream at 500°C for 3 hr to give a zeolite-supported platinum catalyst.

The catalysts of the Pt-NH_4Y type were prepared in the same way except for the pretreatment of the zeolite 13 Y with aqueous NH_4Cl solution to replace the Na^+ with NH_4^+. This treatment was carried out before the ion exchange with $Pt(NH_3)_4^{2+}$.

The platinum contents in the catalysts were determined the colorimetric method proposed by Ayres and Meyer.[10]

Dispersion State Analysis. Electron microscopic observation and chemisorption experiments were carried out in order to characterize the platinum particle size distribution on zeolite.

The electron microscope employed was of Hitachi-HV·11·DS type. A lightly ground catalyst was dispersed in isopropanol; a drop of the suspension was then evaporated on a carbon film to get a specimen which was subjected to observation at a magnification of 108,000 x. Subsequent photographic enlargement to 324,000 x was practicable.

Conventional BET apparatus was used for the chemisorption experiment. The catalyst sample was allowed to stand in a vacuum system ($<10^{-3}$ mmHg) for 2 hr at 400°C. and then it was cooled to 25°C. A given amount of hydrogen was introduced in order to attain a pressure equilibration in 30—60 min at 25°C. Blank tests were made for the carriers, and a trace amount of hydrogen was found to be adsorbed at pressures ranging from 10^{-3} to 10^{-1} mmHg at 25°C. This might possibly be the result of the presence of iron in the zeolite (0.05%). Due calibration was made for the volume adsorption on carriers in order to obtain the net value of adsorption on platinum particles.

Carbon monoxide adsorption on platinum particles was measured by the same procedure as for hydrogen chemisorption.

Results and Discussion

Electron Micrographs. The electron microscopic observation of the catalyst revealed that the platinum particles supported on zeolite varied in their diameter sizes as a function of the calcination temperature in the air. These experimental results are summarized in Table 1.

Catalyst 1, the zeolite carrier, naturally showed no platinum particle. Catalyst 2 indicated only a few particles, ranging from 10 to 15 Å in diameter. Most of the platinum, therefore, would be dispersed in an atomic state and/or in fine particles less than 10 Å in diameter,[11] which is the limit of resolution of the electron microscope employed. It should be noted that 10 Å is close to the largest pore size of the zeolite 13Y. These findings are similar to the observations

TABLE 1. PLATINUM PARTICLE SIZE DISTRIBUTION AS A FUNCTION OF TREATING PROCEDURE

No.	Catalyst	Treating procedure			Platinum particle diameter range (Å)
		Calcination, 3 hr, at	Calcination in the air, at	H_2 reduction, 3 hr, at	
1	0% Pt-NaY	—	500°C	500°C	—
2		—	100	500	15
4	0.24% Pt-NaY	—	300	500	15— 55
6		—	500	500	30—680
10		—	400	500	30— 65
11		—	500	500	15— 75
12	0.28% Pt-NH_4Y	—	600	500	15— 70
13		N_2, 400°C	500	500	40— 60
14		H_2, 500	500	500	60

10) G. H. Ayres and A. S. Meyer, Jr., *Anal. Chem.*, **23**, 299 (1951).

11) P. H. Lewis[5] found that about 60% of the Pt of his Pt-CaY catalyst was soluble in HF. He attributed this to much smaller crystals, although it may have been due to incompletely reduced or reoxidized platinum.

reported by Benesi *et al.*[4] on silica gel-supported platinum catalyst made by ion exchange. Numerous tiny particles ranging from 15 to 55Å in diameter were found on the catalyst 4 (Fig. 1). These particles must exist on the external surface of the zeolite. In the case of the catalyst 6, bulky particles of platinum were noted; their size distribution was from 30 up to 680 Å (Fig. 2). These results suggest that the growth of platinum was accelerated by the temperature of calcination in the air prior to reduction in a hydrogen stream.

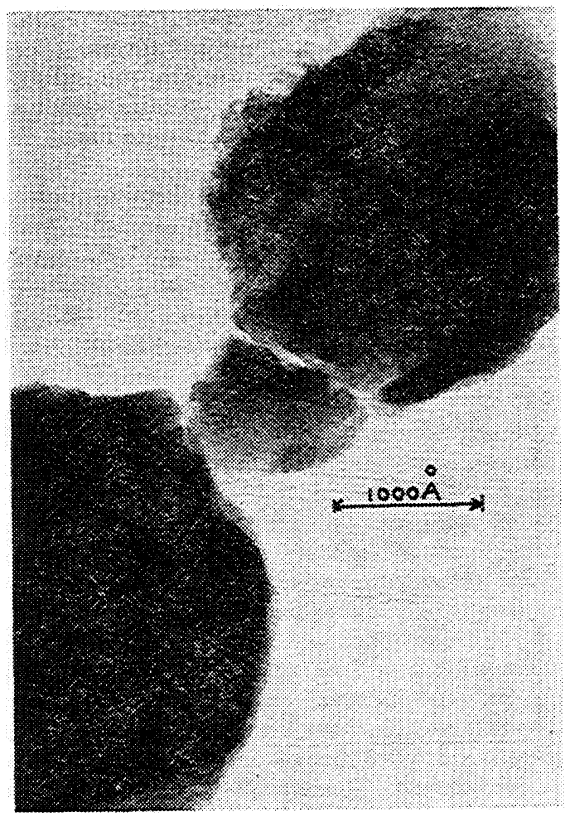

Fig. 1. Electron micrograph of the catalyst 4.

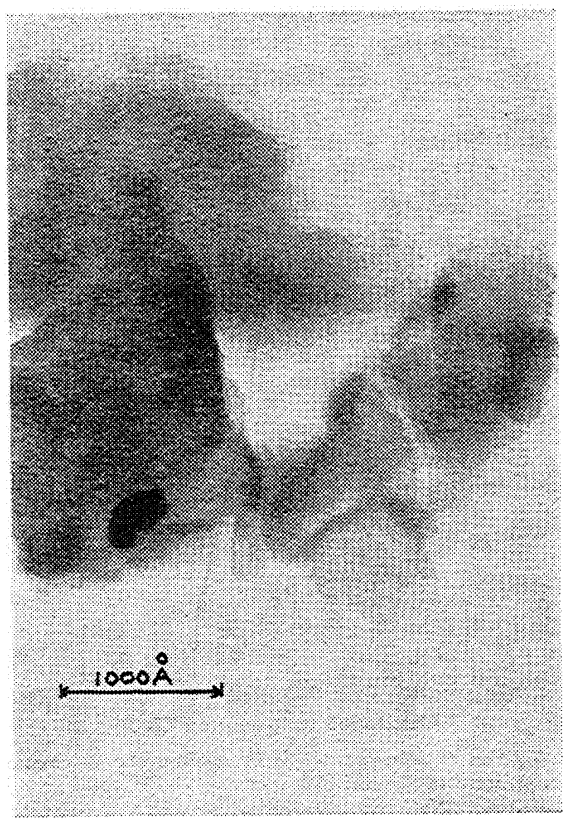

Fig. 2. Electron micrograph of the catalyst 6.

In the cases of the Pt-NH_4Y type catalysts, No. 10 to 12, the platinum particle size distribution seemed less sensitive to the calcination and a fairly good dispersion of platinum on the carrier was still maintained at temperatures ranging from 400 to 600°C. As an example, electron micrograph of the catalyst No. 11

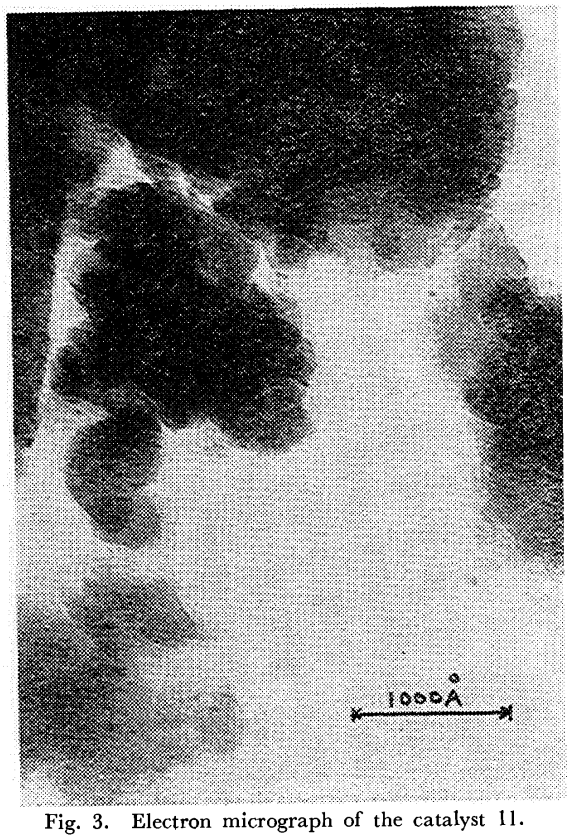

Fig. 3. Electron micrograph of the catalyst 11.

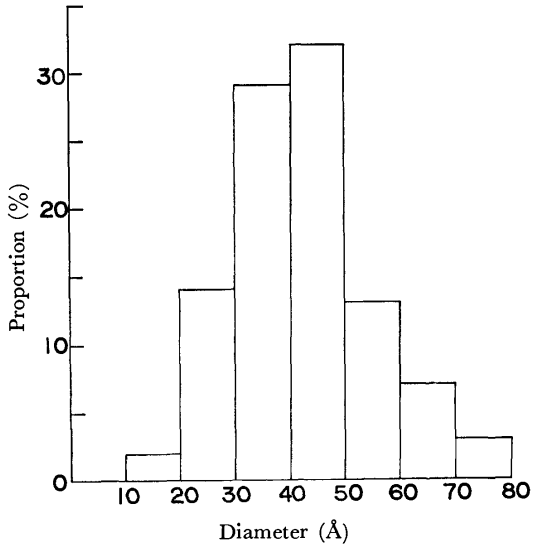

Fig. 4. Size distribution of platinum particles on the catalyst 11.

is shown in Fig. 3, while its particle size distribution is presented in Fig. 4.

The different susceptibilities to the calcining temperature between the Pt-NaY Type and the Pt-NH_4Y type supposedly has some connection with the changes in the crystal structure and electric field of the latter in calcination. That is, at temperatures near 300°C the ammonium ion decomposes into ammonia to leave a proton, while at higher temperatures, near 500°C water is eliminated by the combination of the hydroxyl group with the proton and a defect is formed in the lattice.[12] No definite explanation, however, has yet been developed to account for the above difference.

The pretreatment of ion exchanged zeolites, of both the Pt-NaY and Pt-NH_4Y types, before calcination in the air, by heating in a nitrogen stream (catalyst No. 13) or in a hydrogen stream (catalyst No. 14) respectively, was found to have an adverse effect on the growth of platinum particles in the subsequent calcination in the air. In these two cases, only a small number of tiny particles, 40—60 Å, were found on the carrier (Fig. 5).

Chemisorption. Hydrogen chemisorption on platinum catalysts was measured in the pressure range from 10^{-3} to 10^{-1} mmHg at 25°C. The results, shown in Figs. 6 and 7, indicate that Freundlich-type adsorption isotherms hold for both NaY and NH_4Y type catalysts. These figures also demonstrate that

Fig. 5. Electron micrograph of the catalyst 13.

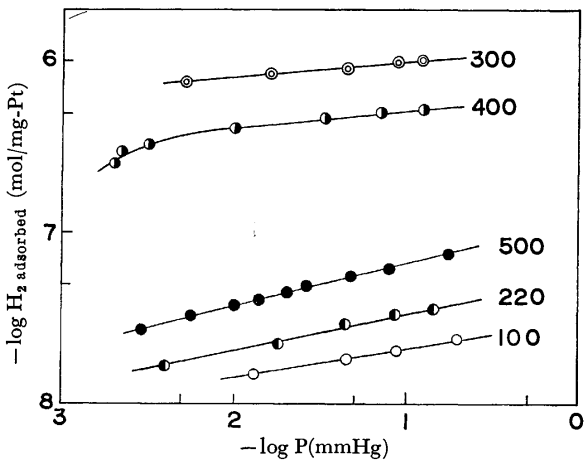

Fig. 6. Freundlich-type hydrogen adsorption isotherms of the Pt-NaY type catalysts. Numerals indicate the calcination temperature in the air.

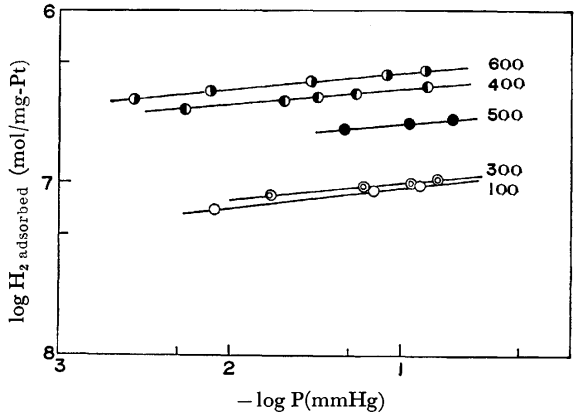

Fig. 7. Freundlich-type hydrogen adsorption isotherms of the Pt-NH_4Y type catalysts. Numerals indicate the calcination temperature in the air.

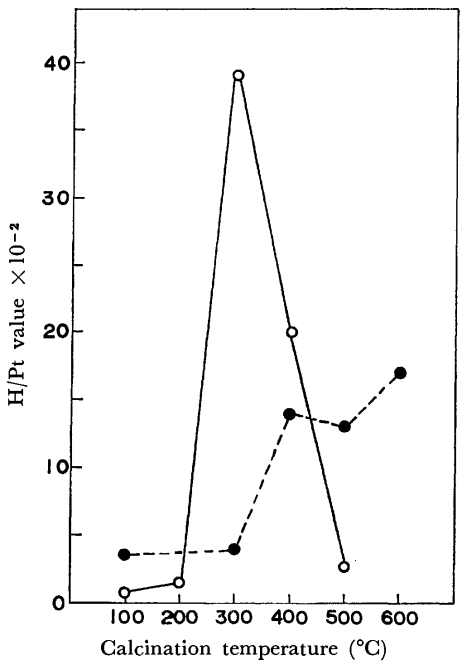

Fig. 8. Plot of atomic ratio H/Pt against the calcination temperature in the air.
—○— Pt-NaY type catalyst.
--●-- Pt-NH_4Y type catalyst.

12) D. N. Stamires and J. Turkevich, *J. Amer. Chem. Soc.*, **86**, 749 (1964).

the volume of hydrogen chemisorption is dependent upon the calcining temperature in the air. The dependency is shown more clearly in Fig. 8, where the number of hydrogen atoms chemisorbed per platinum atom loaded is plotted against the calcination temperature.

Based on the chemisorption data, the average diameter of the platinum particles was calculated. Two assumptions were involved in the calculation, that is, that the platinum particles are in a uniform sphere and that a hydrogen molecule dissociatively chemisorbs covering two platinum atoms. The average diameter is, consequently, given by $6V/S$, where V and S denote the total volume and the total surface area of platinum loaded respectively. S is given by the number of hydrogen atoms adsorbed times the unit area per platinum atom, namely, 8.09Å^2, which is the average the site densities of (100), (110), and (111) of the platinum crystal.[13]

Tables 2 and 3 present the calculated results. The diameters in parentheses, for catalysts 2, 3, 8, and 9, which were calcined at low temperatures, do not seem realistic because no such large particle as those calculated was found by electron microscope inspection. Rather, this could be regarded as meaning that the loaded platinum existed either near atoms or fine particles with diameters less than 10 Å which had little ability to chemisorb hydrogen. In this connection, an interesting fact has been reported by Van Hardeveld and Van Montfoort.[3] They carried out a study of infrared-active nitrogen adsorption on nickel supported on silica. The study consisted of an infrared spectroscopic investigation of the adsorbed nitrogen and of an electron microscopic determination of the metal particle size distribution. They found that the infrared-active adsorption was measurable only if the nickel crystallites were within the range of 15—70 Å. It was also stated that this applies not only to nickel but also to platinum and palladium.

Carbon monoxide adsorption on platinum particles was measured in the same way as hydrogen adsorption. The results are summarized in Figs. 9 and 10. In the case of the Pt-NaY type catalysts, the Freundlich-type adsorption isotherms were found to hold for carbon monoxide, the amount being dependent on the size of the platinum particles.

The gas adsorption behavior of hydrogen or carbon

Table 2. The average diameter of platinum particles calculated from hydrogen chemisorption (Pt-NaY type)

Cat. No.	Calcin. temp. °C	Mol adsorbed at 10^{-1} mmHg mol/g-cat	Atomic ratio, H/Pt	Average diameter, Å
2	100	5.3×10^{-8}	8.6×10^{-3}	(1312)
3	220	8.5×10^{-8}	1.4×10^{-2}	(820)
4	300	2.4×10^{-6}	3.9×10^{-1}	29
5	400	1.3×10^{-6}	2.0×10^{-1}	55
6	500	1.6×10^{-7}	2.7×10^{-2}	425

Table 3. The average diameter of platinum particles calculated from hydrogen chemisorption (Pt-NH_4Y type)

Cat. No.	Calcin. temp. °C	Mol adsorbed at 10^{-1} mmHg mol/g-cat	Atomic ratio, H/Pt	Average diameter, Å
8	100	2.7×10^{-7}	3.7×10^{-2}	(302)
9	300	2.8×10^{-7}	3.9×10^{-2}	(286)
10	400	9.8×10^{-7}	1.4×10^{-1}	82
11	500	9.2×10^{-7}	1.3×10^{-1}	87
12	600	1.2×10^{-6}	1.7×10^{-1}	66

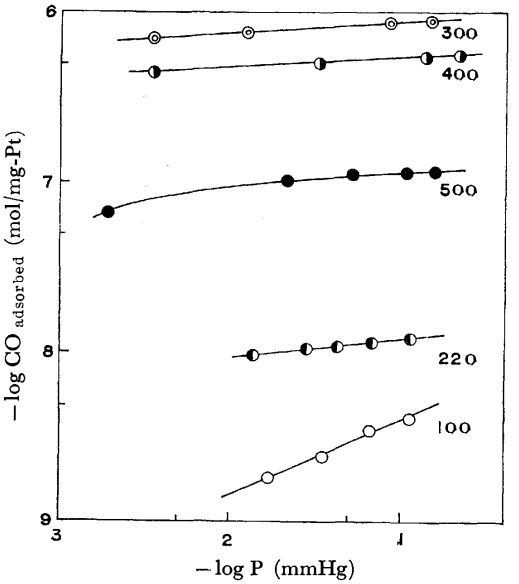

Fig. 9. Freundlich-type carbon monoxide adsorption isotherms of the Pt-NaY type catalysts. Numerals indicate the calcination temperature in the air.

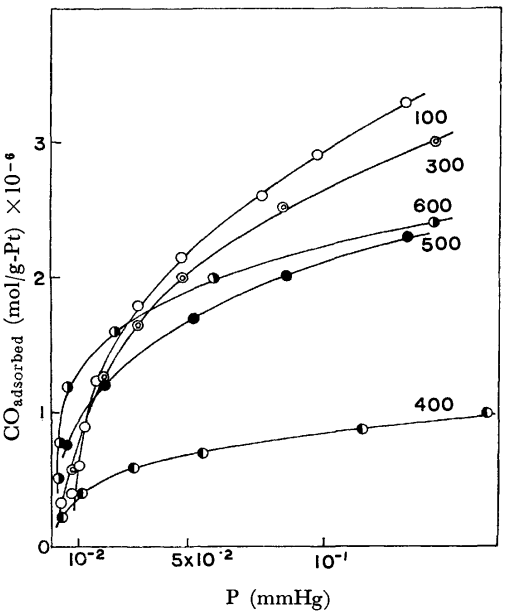

Fig. 10. Carbon monoxide adsorption isotherms of the Pt-NH_4Y type catalysts. Numerals indicate the calcination temperature in the air.

13) H. Chon, R. A. Fisher, E. S. J. Tomezsko, and J. G. Aston, The Second International Congress on Catalysis, Section 1, Paper 3 (1960).

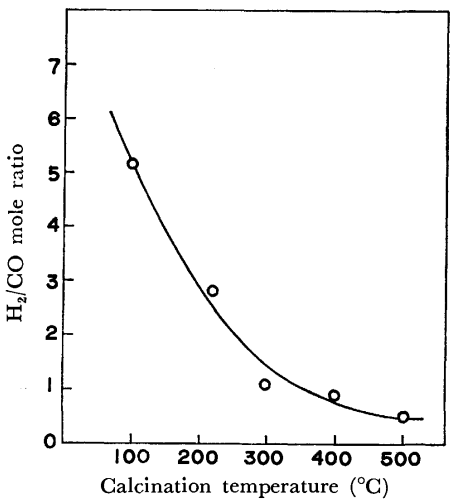

Fig. 11. The ratio of hydrogen and carbon monoxide adsorption on the platinum particles of the P-NaY type catalysts.

monoxide towards platinum particles may change according to their size distribution. This is suggested in Fig. 11, where the amount of hydrogen or carbon monoxide adsorption, at 10^{-1} mmHg and at room temperature, on the platinum supported on NaY zeolite is plotted against the calcining temperature, which has been shown to determine effectively the platinum particle size distribution. Those catalysts which are calcined at low temperatures, and which can consequently be supposed to have fine parparticles, adsorb larger amounts of hydrogen that of carbon monoxide, while those calcined at high temperatures, and having large particles, adsorb less hydrogen than carbon monoxide. The ratio of these two adsorption amounts is given in Table 4. Larger platinum particles, probably more than *ca.* 20 Å in diameter, are shown to have equal number of adsorptive sites for both of the gases by the fact, as is generally recognized, that hydrogen adsorbs in a dissociative fashion, while carbon monoxide does so in a linear form. This is shown by the fact that the ratio, H_2/CO in mole, in Table 4 approaches 0.5 with a rise in the calcining temperature. The reason why the catalyst calcined at a low temperature adsorbs much more hydrogen than carbon monoxide has not yet been made clear;[14] the fact, however, may be accepted that changes in the catalyst preparation procedure and/or conditions generally lead to a catalyst the surface of which is different in gas adsorption susceptibility as a result of some change in its physico-chemical properties, such as lattice defect and work function, in addition to merely physical properties, such as surface area.

TABLE 4. THE RATIO OF HYDROGEN AND CARBON MONOXIDE ADSORPTION ON THE PLATINUM PARTICLES OF THE Pt-NaY TYPE CATALYSTS

Cat. No.	Calcin. temp., °C	H_2/CO
2	100	(5.2)[a]
3	220	2.9
4	300	1.2
5	400	0.9
6	500	0.5

a) The ratio is supposed to be slight reliable, because the amount of carbon monoxide on platinum is little.

14) G. C. A. Schuit and L. L. Van Reijen, "Advances in Catalysis," Vol. 10, ed. by Academic Press, New York and London (1958), p. 250.

On the other hand, the Pt-NH_4Y type catalysts were characteristically distinguished in their adsorptive properties from NaY type catalysts. Carbon monoxide on the carrier was extremely large. Figure 10 shows that the adsorption on the Pt-NH_4Y type carrier was also affected by the calcination temperature in the air.

In conclusion, dispersion state analysis by hydrogen chemisorption gives a result which is in virtual agreement with that obtained by electron microscopic observation with respect to the catalyst with an average particle size over approximately 20 Å in diameter. For the catalyst calcined at low temperatures, however, the hydrogen adsorption method possibly gives rise to a false result. This seems to suggest that the loaded platinum is dispersed in atoms or in fine particles which lose the metallic properties to adsorb hydrogen, supposedly in a more or less cationic state as a result of the pronounced effect of the surrounding oxygen atoms in zeolite. Carbon monoxide adsorption has generally been used to evaluate the metal surface and compared with the catalytic activity. However, the discrepancy between hydrogen and carbon monoxide adsorptions, observed in this study for the platinum fine particles, suggests that the hydrogen chemisorption method is more useful for predicting the catalytic activity, especially for reactions where hydrogen is involved.

These experiments have suggested that, for obtaining a properly dispersed platinum catalyst which has an excellent ability to chemisorb hydrogen, the temperature of calcining the ion exchanged zeolite is one of the most important key factors in the catalyst preparation.

The mechanistic interpretation of the action of oxygen in the calcination of $Pt(NH_3)_4^{2+}$ ion exchanged zeolite to promote the growth of platinum to form crystallites is an interesting subject; it is now under investigation in this laboratory.

For the catalysts calcined at low temperatures, the platinum particles dispersed in atoms or in fine particles, or both, lose their metallic properties to adsorb hydrogen, and supposedly gain a cationic character as a result of the pronounced effect of the surrounding oxygen atoms in zeolite.

A good parallelism that was found to exist between the amount of hydrogen adsorption, which depends on the dispersion states of platinum particles, and their catalytic activities of hydrogenation will be reported in the following paper.

The authors are indebted to Mr. S. Takagi and Mr. S. Takeda for their invaluable assistance in carrying out the electron microscopic study.

Metal Catalysts Supported on Zeolite. II. Dehydrogenation of Cyclohexane and Hydrodemethylation of Toluene over Zeolite-Supported Platinum Catalysts

Toshihiko KUBO, Hiromichi ARAI, Hiroo TOMINAGA, and Taiseki KUNUGI

Department of Synthetic Chemistry, Faculty of Engineering, The University of Tokyo, Hongo, Bunkyo-ku, Tokyo

(Received July 14, 1971)

Correlations between the amount of hydrogen adsorption and the catalytic activities of the zeolite-supported platinum catalysts were interpreted in terms of the dispersion state of platinum particles. The activities for dehydrogenation of cyclohexane and hydrodemethylation of toluene were directly proprotional to the amount of hydrogen adsorption. The tiny platinum particles with diameters of less than 20 Å, which had little ability to chemisorb hydrogen, showed a poor activity in both reactions.

The correlation between the amount of hydrogen adsorption on metal particles and their catalytic activity for hydrogenation or dehydrogenation has been an interesting subject of catalytic study.[1-4] Our previous work[5] demonstrated that zeolite-supported platinum catalysts with a given dispersion state could be obtained by calcining the ion exchanged zeolite in the air and by subsequently reducing in a hydrogen stream. A pronounced effect was observed of the calcination in the air on the growth of the platinum to form particles. Low temperature calcination was found to give a catalyst which had supposedly tiny platinum particles with diameters below 20 Å that chemisorb very little hydrogen. The optimum size of the particles obtained by calcination at 300°C ranged from 20 to 50 Å in diameter and gave the largest hydrogen chemisorption per weight of platinum loaded.

The present paper will report a good parallelism between the amount of hydrogen chemisorption and the catalytic activity of the zeolite-supported platinum catalyst.

Experimental

Catalyst Preparation. The zeolite-supported platinum catalysts were prepared by ion exchange of zeolite 13 Y, followed by calcination in the air and reduction in a hydrogen stream. The catalysts of the Pt-NaY and Pt-NH_4Y types used in this study were prepared in just the same ways as those in the previous work. The catalyst of the Pt-CaY type were prepared in the same way as above except for the pretreatment of the zeolite 13 Y with $CaCl_2$ aqueous solution to replace Na^+ with Ca^{2+}. This treatment was carried out before the ion exchange of the zeolite with Pt-$(NH_3)_4^{2+}$.

Dehydrogenation of Cyclohexane. The experiment was carried out by the use of the pulse-technique. In the reactor (4 mm in diameter), 8 mg of powder of 0.24 wt% Pt-NaY, calcined at a specified temperature in the air, was placed and then reduced in a hydrogen stream at 500°C for 3 hr. After the catalyst temperature has been lowered to 280—320°C, 1 μl of cyclohexane was injected into the large amount of hydrogen stream that continuously flowed down the catalyst bed. The flow rate of hydrogen stream was 60 ml/min, and the pressure was 240 mmHg (gauge). The product stream was analyzed by gas chromatography (column: tricresyl phosphate on cellite, 2.0 m in length). The hydrogen was supplied from a commercial cylinder after purification over Deoxo catalyst and molecular sieve 5A.

For accurately evaluating the relative rate of a reaction by the use of the pulse technique, it is essential to avoid the use of a catalyst in a temperature range where a prolonged adsorption of the reactant or of the product on the carrier takes place. The preferred range of temperature was determined in the following way. Into a reactor with 8 mg of the zeolite 13Y (NaY type, no platinum loaded), 1 μl of cyclohexane or benzene was injected at temperatures ranging from 200 to 340°C; the changes in the height and width of the peak of gas chromatogram were then obtained as is shown in Fig. 1. This figure suggests that a reaction temperature higher than 280°C should be employed.

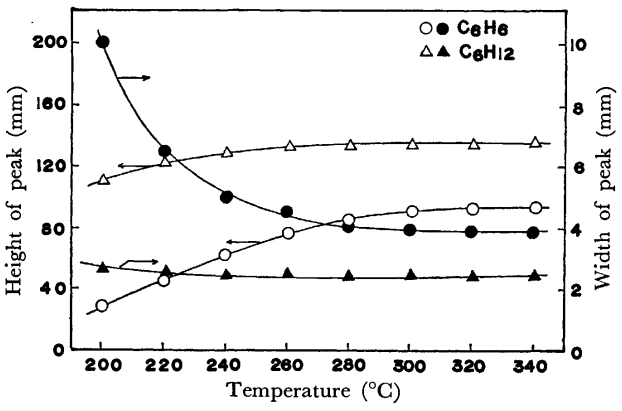

Fig. 1. Adsorption of cyclohexane and benzene on zeolite 13Y.

Hydrodemethylation of Toluene. In a reactor (8 mm in diameter), 0.1 g of a powdered catalyst was placed; 1 μl of toluene was then injected into a large excess amount of hydrogen stream, the flow rate of which was 40 ml/min and the pressure of which was 220 mmHg (gauge). The product stream was analyzed by gas chromatography (column: dinonyl phthalate on cellite, 1.0 m in length). The reaction temperature above 420°C was found to be preferred in the same way as in the cyclohexane experiment.

1) H. J. Maat and L. Moscou, Third International Congress on Catalysis, Section 2, Paper 5 (1964).
2) T. A. Dorling and R. L. Moss, *J. Catal.*, **5**, 111 (1966).
3) H. E. Swift, F. E. Lutinsky, and H. H. Tobin, *ibid.*, **5**, 285 (1966).
4) J. A. Cusmans, G. W. Dembinski, and J. H. Sinfelt, *ibid.*, **5**, 471 (1966).
5) T. Kubo, H. Arai, H. Tominaga, and T. Kunugi, This Bulletin, **45**, 607 (1972).

Results and Discussion

Dehydrogenation of Cyclohexane. The conversions of cyclohexane to benzene remained nearly constant for the first ten injections of cyclohexane at 10 min intervals. Therefore, the average of the conversions in the first ten injections was regared as indicating the catalyst activity. In Fig. 2 the cyclohexane de-

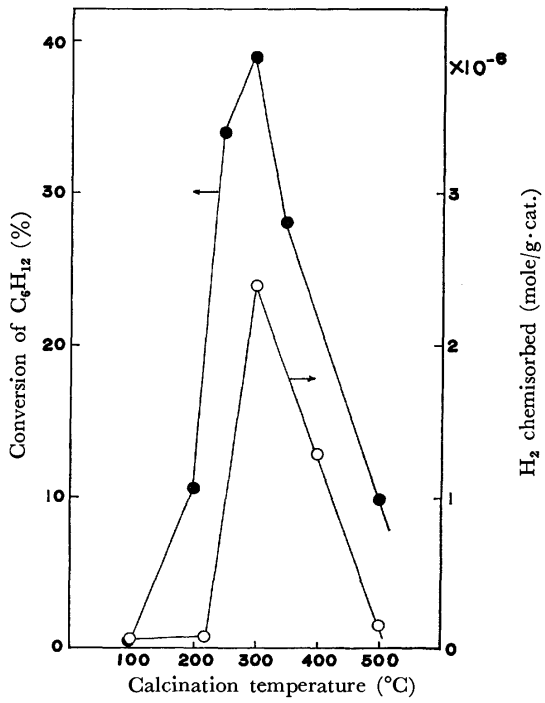

Fig. 2. Dehydrogenation of cyclohexane over 0.24wt% Pt-NaY at 300°C.

hydrogenation activities of the Pt-NaY catalyst at 300°C are plotted against the catalyst calcination temperatures in the air. The change in the amount of hydrogen adsorbed on the catalyst (at 25°C, 0.1 mmHg) is also plotted in the figure. This suggests that the active site for dehydrogenation of cyclohexane is closely connected with the adsorption site of hydrogen.

In our previous report,[5] it has been suggested that the amount of hydrogen adsorption on the zeolite-supported platinum catalyst depends upon the size of the platinum particles, which is a function of the calcination temperature of ion exchanged zeolite. These results show that the catalyst with fine platinum particles, which are less than 20Å in diameter and which have little hydrogen adsorptive capacity, have little activity to convert cyclohexane to benzene. Based on pseudo-first order kinetics with respect to the concentration of cyclohexane, apparent activation energies for the dehydrogenation were obtained for the different catalysts, as is shown in Table 1. All these activation energies were at 31±3 kcal/mol except for that over the catalyst calcined at 200°C in the air. Furuoya and Shirasaki[6] studied sintering mechanism of palladium on silica-alumina and found that the

Table 1. Apparent activation energies in dehydrogenation of cyclohexane over 0.24wt% Pt-NaY catalyst (280—300°C)

(Reduction of the catalysts in a hydrogen stream was carried out at 500°C for 3 hr.)

Run No.	Calcination temp., °C	Activation energy, kcal/mol
1-1	100	—
1-2	200	19
1-3	250	29
1-4	300	31
1-5	350	34
1-6	400	29
1-7	500	32

lattice defect of palladium was mainly determined by the condition of hydrogen reduction and was independent of the condition of previous calcination in air.

In view of these findings, it is considered that the active sites of these catalysts are similar in their quality for dehydrogenation of cyclohexane, and that the difference in the catalytic activities can be attributed to the variation in the effective surface area of the platinum particle.

Hydrodemethylation of Toluene. Hydrodemethylation of toluene over zeolite-supported platinum catalyst of the Pt-NaY type was studied. The activity of the catalyst rapidly decreased with the first ten injections of toluene at 10 min intervals; then it reached a nearly constant level, as is shown in Fig. 3.

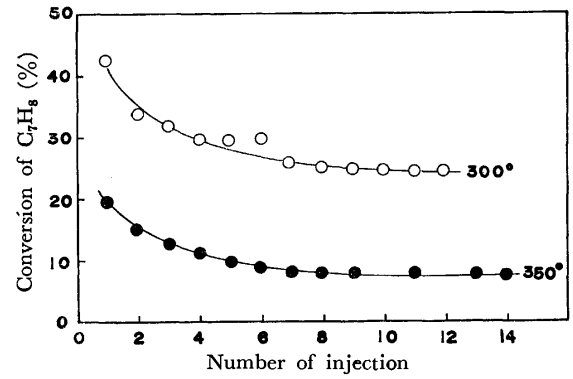

Fig. 3. Hydrodemethylation of toluene over 0.24wt% Pt-NaY at 500°C. Change of activity against the number of injection.
—○— Calcined at 300°C in the air
—●— Calcined at 350°C in the air

All of the catalysts of the Pt-NaY type used in this study showed a similar decline in their catalytic activities. This is considered to come from the deposition of carbonaceous materials on platinum particles because a grey color was found to develop over the catalyst used. After a constant conversion had been attained, the conversion of toluene was taken as a

6) I. Furuoya and T. Shirasaki, *Kogyo Kagaku Zasshi*, **72**, 1223 (1969).

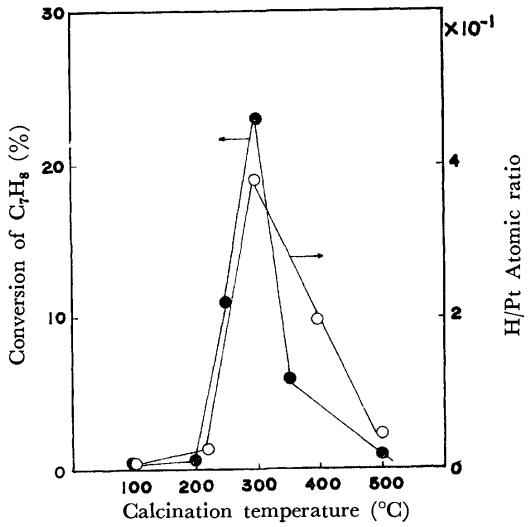

Fig. 4. Hydrodemethylation activity of 0.24wt% Pt-NaY at 500°C against the calcination temperature.

measure of the activity of the respective catalyst. This is plotted against the calcination temperatue in Fig. 4, where the amounts of hydrogen adsorption on the catalyst are also indicated.[5] The figure shows that hydrodemethylation activities of the catalysts are as well correlated with the amounts of hydrogen adsorption as are the cyclohexane dehydrogenation activities. The apparent activation energies for toluene hydrodemethylation were found to lie in the range from 38 to 41 kcal/mol.

Associated with the repeated injection of toluene, a decrease in the activities of the Pt-CaY type catalysts was observed as in the case of the Pt-NaY type catalysts. The hydrodemethylation activity, when a constant level was attained, of the Pt-CaY type catalyst at 500°C is shown as a function of the calcination temperature in the air in Fig. 5. The catalyst calcined at 200°C showed the maximum activity. The characteristic feature of the effect of the calcination temperature was similar to that on the catalysts of the Pt-NaY type.

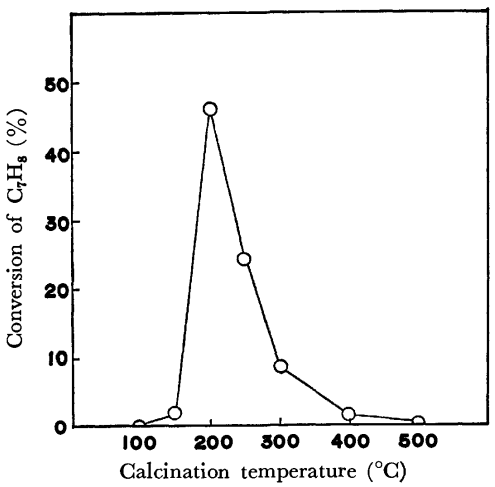

Fig. 5. Hydrodemethylation of toluene over 0.2wt% Pt-CaY at 500°C against the calcination temperature.

In the case of the Pt-NH_4Y type catalysts, no decrease in the initial activity was observed, as is shown in Fig. 6. This makes sharp contrast to the catalysts of the Pt-NaY and Pt-CaY types. The surface proton on the Pt-NH_4Y type catalysts, formed by the decomposition of ammonium ion, might accelerate the cracking of the carbonaceous materials, thus preventing their accumulation. Figure 7 shows the characteristic change in the catalytic activities of the Pt-NH_4Y type catalysts as a function of the calcination temperature. This should be discussed in view of the change in the structure of the zeolite during calcination in the air. That is, the NH_4Y zeolite is transformed by calcination into the decationized type through the HY type, while the structures of the NaY and CaY zeolites are unchanged. At any rate, a good parallelism between the amount of hydrogen

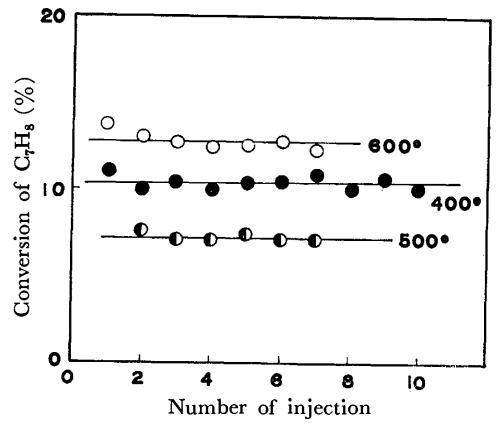

Fig. 6. Hydrodemethylation of toluene over 0.28wt% Pt-NH_4Y at 500°C. Change of the activity against the number of injection.
—●— Calcined at 400°C in the air
—◐— Calcined at 500°C in the air
—○— Calcined at 600°C in the air

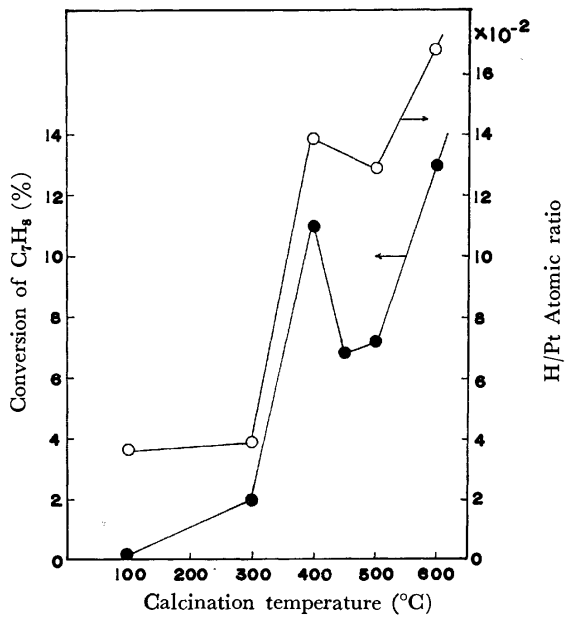

Fig. 7. Hydrodemethylation activity of 0.28wt% Pt-NH_4Y at 500°C against the calcination temperature.

adsorption and the catalytic activity for hydrodemethylation is found to hold. The apparent activation energies for the respective catalysts are shown in Table 2. These experimental facts suggest that the growth of platinum is less favored in the decationized structure of zeolite.

TABLE 2. APPARENT ACTIVATION ENERGIES IN HYDRODEMETHYLATION OF TOLUENE OVER 0.28wt% Pt-NH_4Y CATALYSTS (420—500°C)
(Reduction of the catalysts in a hydrogen stream was carried out at 500°C for 3 hr.)

Run No.	Calcination temp., °C	Activation energy, kcal/mol
2-1	100	—
2-2	300	41
2-3	400	36
2-4	450	37
2-5	500	38
2-6	600	33

Our previous study using electron microscope indicated that the presence of oxygen in the calcination procedure played an important role in the aggregation of platinum, and that the heating of ion exchanged zeolites in a non-oxidizing atmosphere, namely, in a nitrogen or hydrogen stream, had an adverse effect on the growth of platinum particles in the subsequent calcination in the air. The effect of this pretreatment on the Pt-NH_4Y type catalyst is shown in Fig. 8. The hydrodemethylation activity of the catalyst which was pretreated in a nitrogen stream before reduction in the air exhibited a slight activity. The platinum cation or atom may be stabilized on the zeolite by pretreatment in a nitrogen or hydrogen stream at 400—600°C and does not migrate on the surface during the subsequent calcination in the air to form platinum particles. Consequently, the platinum catalyst manufactured by reduction in a hydrogen stream has an ability for neither gas adsorption nor catalytic activity.

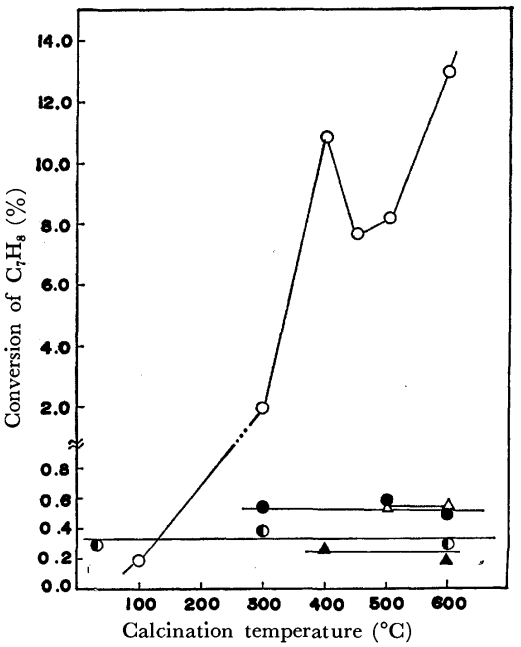

Fig. 8. The effect of pretreatment before calcination in the air and reduction in a hydrogen stream.
—○— Not pretreated.
—◐— Pretreated at 600°C in a nitrogen stream.
—●— Pretreated at 400°C in a nitrogen stream.
—△— Pretreated at 500°C in a nitrogen stream.
—▲— Pretreated at 500°C in a hydrogen stream.

The controlling factors were investigated in preparation of a zeolite-supported platinum catalyst active for hydrogen participating reactions. The most active catalyst, the platinum of which is properly dispersed on the carrier, can be obtained by calcining in the air at a specific temperature prior to reduction in a hydrogen stream. The catalytic activities are in good parallelism with their hydrogen adsorption abilities.

Structural Effects on the Properties of Nonionic Surfactants. I. The Synthesis and Some Surface Activities of Acetal Type Homogeneous Nonionics[1]

Tsunehiko KUWAMURA and Hideo TAKAHASHI

Department of Synthetic Chemistry, Faculty of Engineering, Gunma University, Tenjincho, Kiryu

(Received July 26, 1971)

Higher aliphatic aldehydes (C_8—C_{16}) were treated in the presence of mineral acid with several pure polyoxyethylene glycols (m : 2—6), to give the corresponding acetals (AG types) with a general formula $RCH[O(C_2H_4O)_mH]_2$. These AG types are soluble in water, fairly stable in neutral and weakly basic aqueous solutions, and they exhibited the characteristic properties of nonionics. The hydration of the geminal polyoxyethylene (POE) chains are discussed on the basis of the data of unexpectedly low cloud points. Surface tension measurements on the aqueous solutions of AG types indicated that the critical micelle concentration (CMC) value decreases with an increment of oxyethylene units (m), and that the molecular area does not depend so greatly on m and is significantly smaller than that predicted from the data of conventional nonionics (S types) having one hydrophobic and hydrophilic chain each. For the gross effects of AG types, it has been found that the foam stability is considerably low and the dependence of the wetting power for canvas discs on m is larger than that of S types. The results are discussed on the basis of structural characteristics related to the unfavorable hydration and restricted configuration of the geminal POE chains. The acid-catalyzed hydrolysis of AG types in the micellar solution was significantly slower than that of acetaldehyde diethylacetal in water.

The preparation of pure polyoxyethylene alkanols and alkyl phenols has been described in many reports as thoroughly reviewed by Mulley.[2] In most cases two main methods have been used. (1) The mixture produced by ethylene oxide condensation is separated into individual compounds by distillation and (2) a pure POE glycol is joined to a hydrophobe by the Williamson ether synthesis. However, the yields are insufficient in both procedures. Introduction of two POE chains of definite length to a hydrophobe is, therefore, troublesome and has never been established hitherto.

In previous investigations,[3,4] several new type nonionic surfactants containing one to three hydrocarbon or POE chains have been synthesized from α,α'-glyceryl diethers and mono-, di-, and triethers of pentaerythritol by polyaddition of ethylene oxide, and the structural effects on their properties have been discussed. The role of the multi-chain type hydrophile in the behavior of these nonionics, however, could not be interpreted clearly because of the distribution of the POE chain length and the additional effects of the the joint parts in the surfactant molecules. In this investigation, a series of homogeneous nonionics in which two POE with the same chain length were attached to a hydrophobe by acetal linkage were synthesized and the effect of the multi-chain hydrophile on some surfactant properties was discussed. The reaction scheme and abbreviations are as follows.

$$RCHO + HO(C_2H_4O)_mH \xrightarrow{H^+} RCH\begin{matrix}O(C_2H_4O)_mH\\O(C_2H_4O)_mH\end{matrix}$$

R: C_nH_{2n+1} AG-$(n+1)(2m)$

It is of interest that AG types are easily hydrolyzable in the presence of acid, from the viewpoint of degradation after the utilization in an industrial process. Preliminary information on the hydrolysis of AG types is given in this paper.

Experimental

Materials. Commercially available aliphatic aldehydes were purified by distillation and then checked by gas-liquid chromatography (glc) for satisfactory purity (more than 99%). Pure POE glycols were obtained by fractional distillation of commercial products. The purity and the number of oxyethylene unit were checked and determined by glc, NMR, physical indices and analytical method.

Preparation of AG Acetals. To avoid the formation of diacetals by further condensation of acetal with unreacted aldehyde, a large excess of the glycol was used in each runs. In a 300 m*l* three-necked flask equipped with a reflux condenser, a thermometer, and a mechanical stirrer were placed 0.1 mol of aldehyde, 1 mol of the glycol and a catalytic amount of concentrated hydrochloric acid. The reaction mixture was maintained at room temperature with stirring for 1 hr and then gradually heated up to 60—80°C for 4—6 hr. The contents in the reaction vessel were immiscible and formed a suspension at the initial stage of the reaction. It gradually became homogeneous and produced a foam with the progress of reaction. The mixture was cooled, diluted with benzene and neutralyzed with powdered potassium carbonate. The inorganic salts were filtered off and benzene was then distilled off. Unreacted aldehyde and glycol were removed under reduced pressure. The residue was then dissolved again in benzene, warmed, and washed with a small amount of water several times to remove the remaining glycol and salts. Complete removal of benzene under a high vacuum gave a paste-like product in a high yield. Purity and structure of the products were confirmed by elementary and functional group analyses, paper and thin layer chromatographs and IR and NMR spectra. In paper chromatography, 10 mg of the sample was dissolved in an appropriate amount of benzene, spotted on filter paper (Toyo No. 50), developed by mixed solvents (*e.g.*, upper layer of the mixture of *n*-butanol : pyridine : water=

1) Presented in part at the 23rd Annual Meeting of the Chemical Society of Japan, Tokyo, April, 1970.

2) B. A. Mulley, "Nonionic Surfactant", ed. by M. J. Schick, Marcel Dekker Inc., New York, (1967), p. 421.

3) T. Kuwamura and E. Kameyama, *Kogyo Kagaku Zasshi*, **65**, 1266 (1962).

4) T. Kuwamura and H. Fukutomi, Proc. Intern. Congr. Surface Active Substances, 5th, Barcelona, Vol. I, p. 71 (1968).

5 : 2 : 3) and detected by Dragendorff reagents. In the same way, thin layer chromatography was carried out on silica gel (Wakogel B-5).

Cloud point of the products was measured on a 0.5% aqueous solution.

Surface Activities Measurements. Aqueous surface tension of AG types were continuously measured by the vertical plate method, at 20±1°C using a Shimadzu ST-1 type tensiometer. Wetting power was evaluated by measurement of the sinking time of a canvas disc (diameter : 1 in.) at 40°C, according to the method described by Yano and Kimura.[5] To evaluate foaming properties, volume of the initial foam and foam remaining after 5 min were measured at 25±1°C according to the method by Yano *et al.*[6]

Hydrolysis. No reliable techniques by chemical or chromatographic analysis have yet been establisehd for the kinetic measurement of hydrolysis of AG type acetals in dilute aqueous solution. We have tried to follow the acid-catalyzed reaction through the measurement of cloud point, which might depend upon a concentration of the higher aldehyde produced and solubilized in aqueous solution during the hydrolysis of AG. The following facts are of use for this method. AG acetals are so stable in neutral and weakly basic aqueous solution that the cloud point of the solution was kept practically constant for periods more than 12 hr at 25—35°C as illustrated in Fig. 11. No appreciable depression of the cloud point was observed when a small amount of inorganic salt (less than 0.02 mol/*l*) was added to the solution.

The required calibration curve was obtained in the following way. Aqueous solutions containing three components (AG, the related aldehyde and POE glycol) were prepared at a definite total concentration, in the proportion corresponding to various extents of hydrolysis. Their cloud points were measured and plotted against the calculated % of conversion of AG as in Fig. 12.

Thus, the rate of hydrolysis at 30±0.2°C was measured on the acidic aqueous solutions of 0.5—1.0% initial concentration which are much higher than the CMC. Immediately after sampling, the catalyst in the sample solution was neutralized with a slight excess of alkali.

Results and Discussion

By the procedure mentioned above, a series of AG type homogeneous nonionics containing 8 to 16 carbon atoms in hydrophobe and 4 to 12 oxyethylene units in hydrophile were successfully prepared in one step from the corresponding aldehydes and glycols. Physical properties of the latter are listed in Table 1.

The adsorption band of IR spectra at 1600—1700 cm^{-1} of aldehyde carbonyl was not observed for all products. As an example IR spectrum of AG-12(6) is shown in Fig. 1. In Fig. 2, the strength ratios ($T_{1220/720}$) of IR adsorption bands at 1220 and 720 cm^{-1} and the refractive indices are given as a function of *m*. Deviation from these curves, indicating almost certainly the presence of impurity, was not observed as well as in some cases pointed out by Glassman,[7] Schüring,[8] and Wrigley[9] for S type nonionics. From chromatographic analyses, it was confirmed that the use of a large excess of glycol successfully prevented the formation of diacetal and that the unreacted glycol was almost completely removed by distillation and subsequent washing with water.

NMR spectra provided the proof on the structure of the products. The spectrum (in CCl_4) of AG-12(6) is shown in Fig. 3, where five bands are found at 0.88, 1.27, 3.10, 3.58, and 4.50 ppm in the proton ratio of 3 : 20 : 2 : 24 : 1. They can be ascribed to the protons on methyl, methylene in hydrophobe, hydroxyl, methylene in POE chains and methine groups, respectively. Physical properties, analytical data, and the yields of AG types are listed in Table 2. We see that

Table 1. Properties of the used polyoxyethylene glycols

Glycol	Bp, °C/mmHg (lit[8])	n_D^{20} (lit[8])
Diethylene	140—142/20 (139/18)	1.4475 (1.4477)
Triethylene	120—121/0.5 (121—122/0.3)	1.4567 (1.4567)
Tetraethylene	149—150/0.5 (150—152/0.35)	1.4600 (1.4602)
Pentaethylene	173—175/0.4 (175/0.35)	1.4620 (1.4623)
Hexaethylene	218—221/0.6 (219—222/0.6)	1.4645 (1.4648)

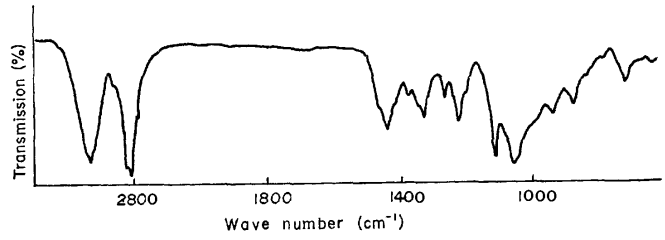

Fig. 1. IR spectrum of AG-12(6).

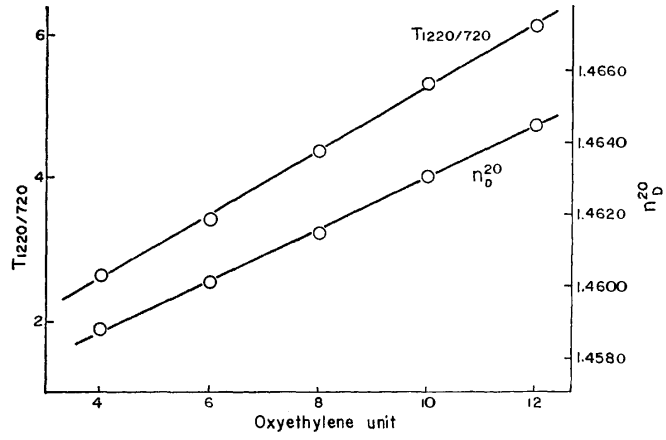

Fig. 2. Plots of the strength ratio ($T_{1220/720}$) of IR absorption *vs.* 2*m* and refractive index *vs.* 2*m* for AG-12 series.

5) W. Yano and W. Kimura, *Yukagaku*, **11**, 138 (1962).
6) W. Yano, T. Isaji, and W. Kimura, *ibid.*, **11**, 183 (1962).
7) V. C. Glassmann and K. Malnnchen, *Fette, Seifen, Anstrichm.* **65**, 741 (1963).
8) S. Schüring and W. Zeigenbein, *Tenside*, **4**, 161 (1967).
9) A. N. Wrigley, A. J. Stirton and E. Howard, *J. Org. Chem.*, **25**, 439 (1960).

Table 2. Properties, analytical data, and yields of AG types

Nonionics	$2m$	Cloud point °C	n_D^{20}	Anal (Calcd) C%	Anal (Calcd) H%	Anal (Calcd) OH%	Yield %
AG-8(6)	6	72.5	1.4591	59.10 (58.51)	10.45 (10.31)	8.0 (8.3)	70
AG-10(6)	6	76.5	1.4618[a)]	59.90 (60.24)	10.24 (10.57)	7.8 (7.9)	85
AG-12(4)	4	<0	1.4588	63.51 (63.45)	11.47 (11.18)	9.3 (9.0)	80
AG-12(6)	6	53.5	1.4601	61.83 (61.77)	11.10 (10.80)	8.0 (7.3)	85
AG-12(8)	8	74.0	1.4615	60.86 (60.67)	10.61 (10.55)	6.9 (6.2)	95
AG-12(10)	10	99.0	1.4631	60.04 (59.79)	10.48 (10.35)	5.3 (5.8)	90
AG-12(12)	12	>100	1.4645	59.74 (59.15)	10.35 (10.20)	4.9 (4.7)	90
AG-14(6)	6	51.0	1.4632	63.88 (63.13)	11.30 (11.00)	6.7 (6.9)	85
AG-14(10)	10	96.5	1.4649	61.76 (60.87)	10.23 (10.52)	5.3 (5.1)	80
AG-16(10)	10	82.0	—	61.92 (61.86)	10.60 (10.67)	4.6 (4.9)	75

a) At 18°C.

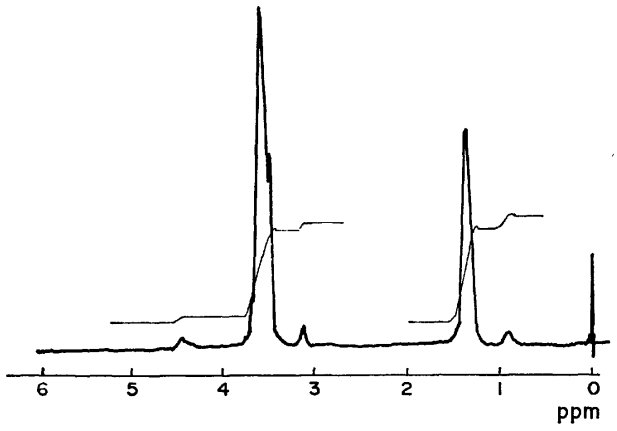

Fig. 3. NMR spectrum of AG-12(6).

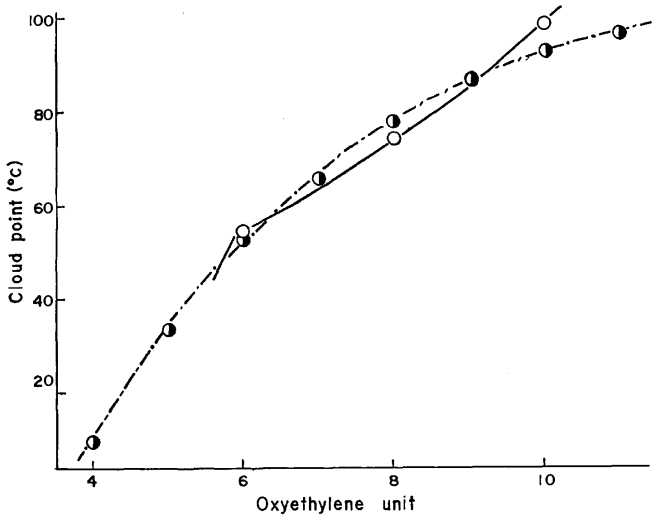

Fig. 4. Plots of cloud point *vs.* number of oxyethylene unit. ○; AG-12 series, ◐; homogeneous polyoxyethylene *n*-dodecanol (S-12 series).[8)]

the method established in this investigation has the advantage of high yield in the preparation of homogeneous nonionics.

The cloud point of nonionics is a measure of the solubility in water and closely related with the hydrophile-lipophile balance (HLB). Smooth and characteristic curves were obtained by the plots of the cloud point *vs.* *m*. A representative example is shown in Fig. 4 for AG-12 series. It can be expected from the structural feature of AG having two terminal hydroxyl groups in a molecule, that the cloud point is higher than that of S types having one hydrophilic chain. On the contrary, the curve for AG lies close to that for S types provided by Schüring[8)] as can be seen in Fig. 4. When the cloud point was plotted against HLB value based on the "group numbers" proposed by Davies,[10)] the curve for AG was apparently shifted to the right side of that for S types as shown in Fig. 5. If the same group numbers are applicable to both type nonionics regardless of the variation in hydrophile structure, the curves for both types would be superimposable. The results suggest that hydration of the geminal POE chains, especially of the oxyethylene unit adjacent to hydrophobe, is significantly hindered and the hydration of two terminal hydroxyl groups in a molecule of AG is incomplete owing to the stronger intramolecular hydrogen-bonding. Such a characteristic hindrance to hydration for AG can be esti-

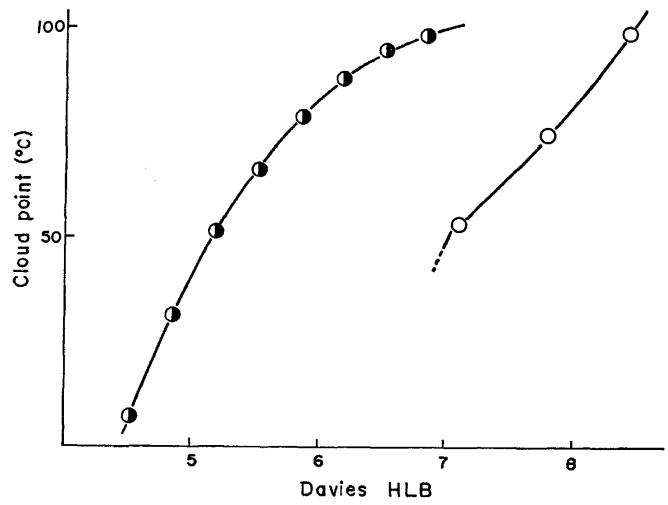

Fig. 5. Plots of cloud point *vs.* Davies HLB value. ○; AG-12 series, ◑; S-12 series.

10) J. T. Davies, Proc. Intern. Congr. Surface Active Substances, 2nd, London, Vol. I, p. 426 (1957).

mated from Fig. 5 to be 1.5—2.0 in Davies's HLB value.

Measurement of surface activities for AG types gave some interesting results. Aqueous surface tension of AG considerably depends upon time as can be seen in Fig. 6. The equilibrium surface tension (γ), was thus taken at the time when the lowering of surface tension is no longer observed. The obtained γ was plotted against logarithm of the concentration and no minima in the γ-log C curves were found for all the AG types studied as shown in Figs. 7 and 8. Surface excess (Γ) and molecular area (A) at CMC were calculated from these γ-log C curves by applying the simple form of Gibbs' adsorption equation, and listed in Table 3. From the fact[12] that A of nonionics of polyglycol ether type is determined by the POE chain, it can be predicted that A of AG types (A_{AG}) is about twice as large as that of S types (A_S) containing the POE chain of the same length as in AG. As can be seen in Table 3, however, A_{AG} are considerably smaller than $2A_S$ and close to A_S.

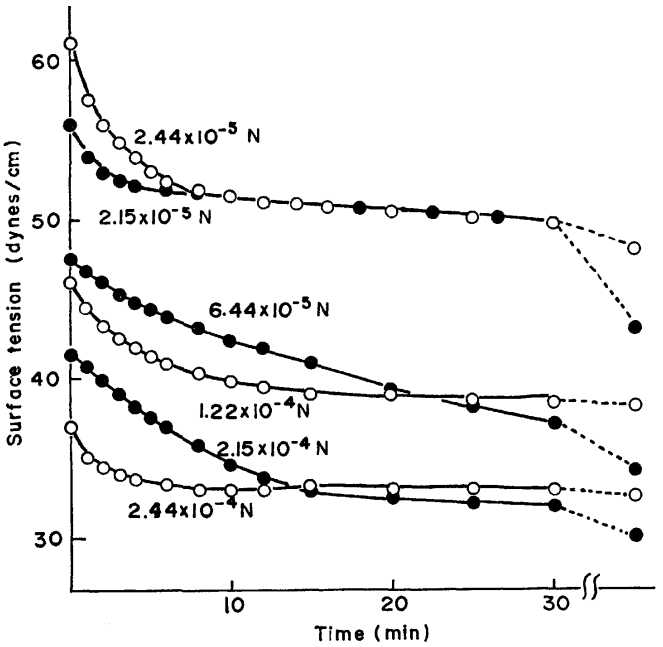

Fig. 6. Time dependence of γ of aqueous solution of AG type at different concentrations (mol/l). ○; AG-8(6), ●; AG-12(6).

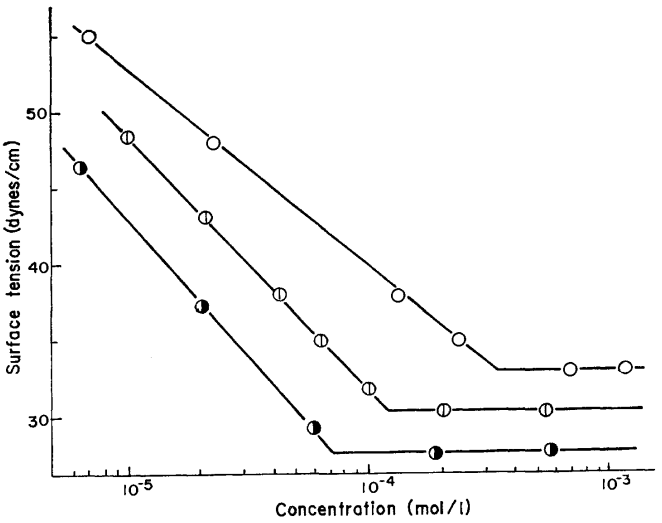

Fig. 7. Plots of γ *vs.* concentration. ○; AG-8(6), ◑; AG-12(6). ◑; AG-14(6).

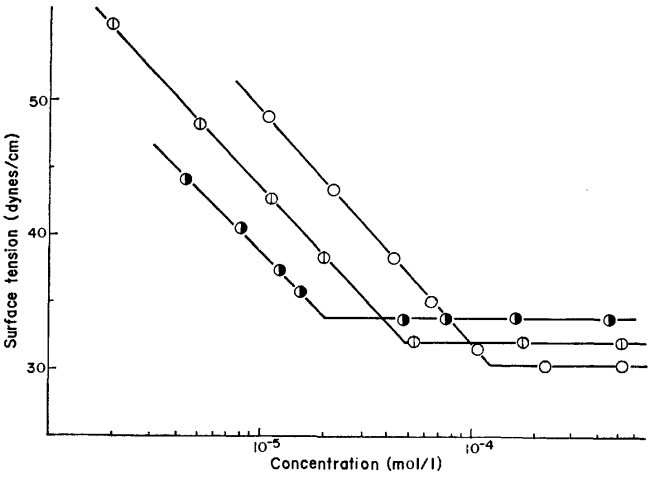

Fig. 8. Plots of γ *vs.* concentration. ○; AG-12(6), ◑; AG-12(8), ◑; AG-12(10).

Table 3. Surface active properties of AG types at 20°C

Nonionics	γ_{CMC} (dyne/cm)	CMC$\times 10^5$ (mol/l)	$\Gamma\times 10^{10}$ (mol/cm^2)	A (Å^2)	$A\times m^{-1/2}$
AG-8(6)	32.9	33.5	2.14	70.0	40.4
AG-12(6)	30.2	12.3	3.05	54.5	31.5
AG-12(8)	31.8	5.00	2.89	57.5	28.8
AG-12(10)	33.8	2.06	2.83	58.6	26.2
AG-14(6)	28.3	6.50	3.19	52.0	30.0
AG-14(10)	36.2	1.70	3.05	54.5	24.4
AG-16(10)	36.0	0.63	3.23	51.5	23.0
S-12(5)[a]	29.7	6.8	3.88	43	19.2
S-12(6)[a]	31.5	7.10	3.52	47	19.2
S-12(5)[b]	—	—	—	56.0	25.0
S-12(7)[b]	—	—	—	64.8	24.5

a) Data in Ref. 11 for the homogeneous polyoxyethylene *n*-dodecanol, the number of oxyethylene unit is shown in parentheses.
b) Data in Ref. 12.

Concerning the surface film of nonionics, van Voorst Vader[13] has given a theoretical explanation for the fact that $A/m^{1/2}$ of S types is constant on the basis of a random coil configuration of POE chain. Fairly good agreement for $A/m^{1/2}$ has been obtained by many investigators as referred to by Lange in his review.[12] For AG-12 and AG-14 series, $A_{AG}/m^{1/2}$ were not constant but decreased with the increment of m, as can be seen in Table 3. Thus, it is suggested for the film state of AG types that two POE chains linked to the same carbon atom in hydrophobic chain never individually hold a random coil configuration but intertwisted with each other and penetrate into the solution.

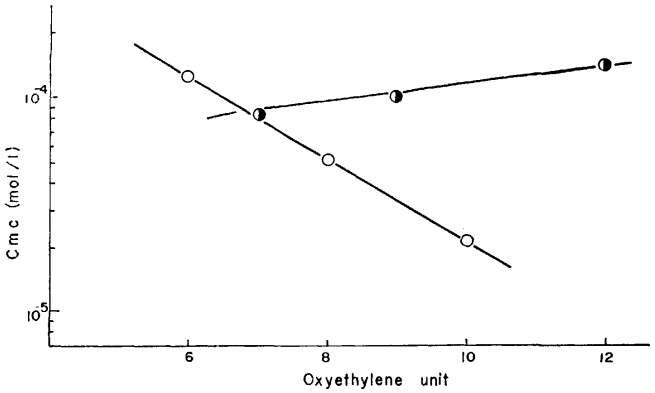

Fig. 9. Plots of log CMC *vs.* number of oxyethylene unit. ○; AG-12 series. ◑; S-12 series, based on the data in the following reference; H. Lange, Proc. Intern. Congr. Surface Active Substances, 3rd, Cologne, Vol. I, p. 279 (1960).

From the sharp inflection point of γ-log C curves in Figs. 7 and 8, CMC was determined and is listed in Table 3. Apparently, in the series of same m, the inflection point shifts to lower concentration region with an increase in the hydrocarbon chain length as shown in Fig. 7, while the CMC of the homologues with same hydrophobe shifts to higher with a decrease in m (Fig. 8) in contrast to S types. It is known that as a surfactant molecule becomes more hydrophilic, *i.e.*, as the POE chain length increases, the CMC increases, although a certain class of nonionics having a shorter hydrocarbon chain exhibits a reverse trend.[14,15] These relations have been quantitatively treated by applying the equation proposed by Hsiao,[16] ln $C_0 = a + bR$, where C_0 is a CMC, a and b are constants for a given hydrophobe and R is length of the POE chain. As shown in Fig. 9, a linear relation between log CMC and m was obtained for AG types. The slope is negative. It is still difficult to explain this anomalous trend from the present data. The phenomenon has been observed for AG series having shorter hydrophilic chains (m : 3—5), which are geminal POE chains unfavorable to hydration and hold a restricted configuration as regards the surface film state of AG. It seems that this configurational feature is closely related to the lowering of CMC with increasing m in a certain region of the smaller m.

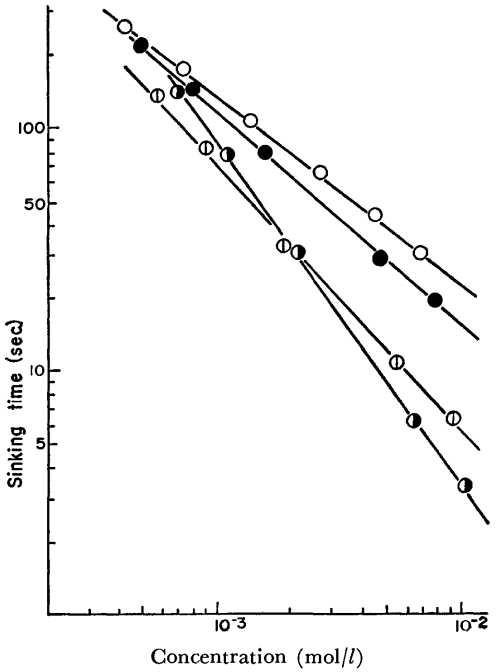

Fig. 10. Plots of log sinking time *vs.* concentration. ○; AG-12(12), ●; AG-12(10), ◐; AG-12(8), ◑; AG-12(6).

Table 4. Foam volume (ml) of AG and S types at 25°C

Nonionics	Concentration of solution (wt%) 0.1			0.5		
	Standing time (min) 0	1	5	0	1	5
AG-12(6)	130	10	0	170	20	0
AG-12(8)	145	15	0	175	20	0
AG-12(10)	185	15	0	200	20	5
AG-12(12)	200	30	15	240	60	15
AG-10(6)	60	0	—	150	0	—
S-12(6.6)[a]	250	240	80	260	260	100

a) Ethylene oxide condensate of *n*-dodecanol prepared by the base-catalyzed method. The average number of ethylene oxide added is shown in parentheses.

On the basis of Draves wetting data obtained for various commercial nonionics of POE monoether type, Komor and Beiswanger[17] reported that textile wetting is primarily dependent upon CMC, and indicated that the concentration dependence of sinking time becomes greater with an increase in CMC of surfactant. Wetting data for a series of AG types are shown in Fig. 10, where sinking time is plotted against concent-

11) N. Ohba and A. Takahashi, Proc. Intern. Congr. Surface Active Substances, 5th, Barcelona, Vol. II, p. 481 (1968).
12) H. Lange, "Nonionic Surfactant", ed. by M. J. Schick, Marcel Dekker Inc., New York, (1967), p. 443.
13) F. van Voorst Vader, *Trans. Faraday Soc.*, **56**, 1078 (1960).
14) D. Becher, *J. Phys. Chem.*, **63**, 1675 (1959).
15) J. E. Carless, R. A. Challis, and B. A. Mulley, *J. Colloid Sci.*, **19**, 201 (1964).
16) L. Hsiao, H. N. Kunning, and P. B. Kolenz, *J. Phys. Chem.*, **60**, 657 (1956).
17) J. Komor and J. Beiswanger, *J. Amer. Oil Chem. Soc.*, **43**, 435 (1966).

ration. The slope, *i.e.*, the concentration dependence of sinking time, increases with decreasing m. This agrees with the result in which CMC becomes greater with decreasing m for a series of AG types studied.

In Table 4, the foaming properties of AG is presented in initial foam volume and after 1 and 5 min. The low foam stability of AG is more characteristic than the foaming ability, like that observed for other multi-chain type nonionics.[3,4,18]

The data of hydrolysis of AG-12(10) were obtained by the cloud point depression method. As can be seen in Fig. 13, they gave good first-order rate plots in the region of conversion below 40%. The plots of the pseudo-first-order rate constant against the concentration of acid also gave a straight line passing the origin with a slope k 5.5×10^{-3} $l$mol^{-1}sec^{-1}. The k value is significantly small in comparison with the specific rate constant 0.39 $l$mol^{-1}sec^{-1}, for acid-catalyzed hydrolysis of acetaldehyde diethylacetal in water.[19] On the acid-catalyzed hydrolysis of monoalkyl sulfates, it was reported that the reaction is strongly accelerated by the aggregation of the reactant anions into micelle.[20-22] However, the result for AG acetal is apparently the reverse. It seems significant that the acetal linkages in the micellar AG are covered by the dome of closely packed POE chains. Probably, the reaction centers compete with many ether linkages in the POE chains for protonation, and the hydrolysis is also subjected to steric hindrance.

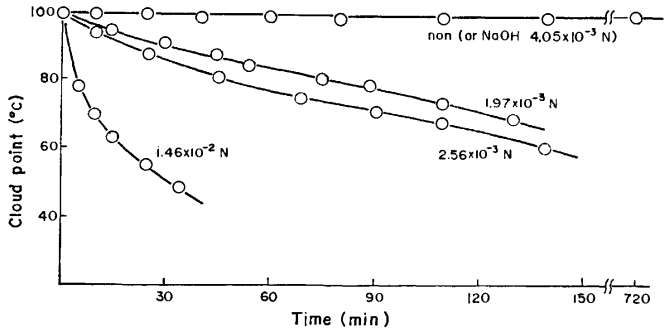

Fig. 11. Depression of cloud point of AG-12(10) in dil. HCl solution at 30°C.

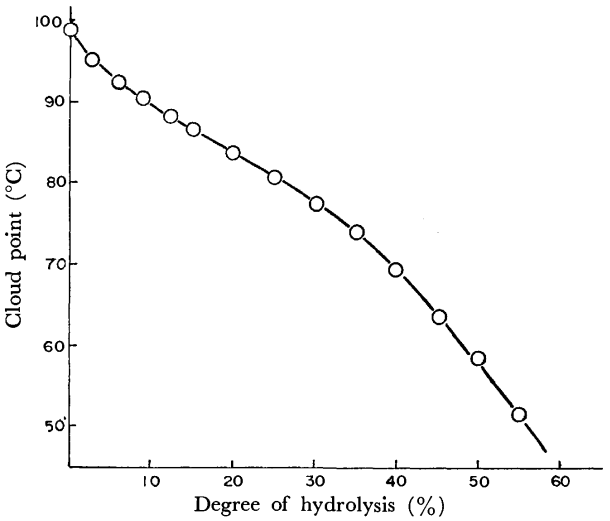

Fig. 12. Calibration curve for the hydrolysis of AG-12(10) at the total concentration of 0.5wt%.

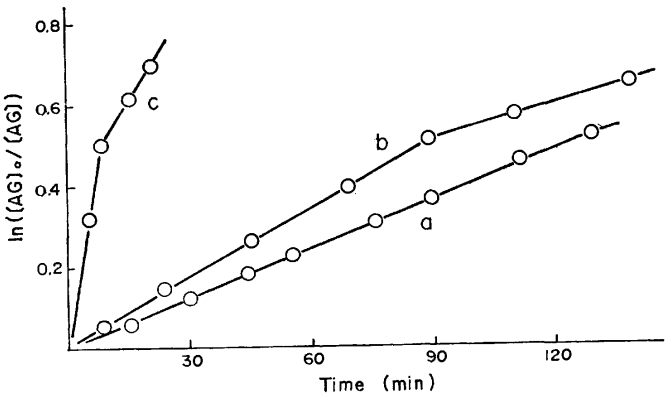

Fig. 13. First-order plots for the hydrolysis of AG-12(10) at 30°C in dil. HCl solutions: a; 1.97×10^{-3} N, b; 2.56×10^{-3} N, c; 1.46×10^{-2} N.

The authors wish to thank Mr. O. Ishikawa and Miss Y. Umezu for their assistance in the experimental work, and Soda Aromatic Co. Ltd., Givaudan Co. Ltd., and Mr. M. Nakajima for the supply of aldehydes. Acknowledgement is made to the Ministry of Education for financial aid.

18) T. Kuwamura and H. Takahashi, Preprints for the 23rd Annual Meeting of the Chem. Soc. Japan, Tokyo, 1970, No. 07333.

19) R. K. Wolford, *J. Phys. Chem.*, **67**, 632 (1963).

20) J. L. Kurz, *ibid.*, **66**, 2239 (1962).

21) V. A. Motsavage and H. B. Kostenbauder, *J. Colloid Sci.*, **18**, 603 (1963).

22) K. Meguro and T. Hikota, *Yukagaku*, **17**, 164 (1968).

NOTES

BULLETIN OF THE CHEMICAL SOCIETY OF JAPAN, VOL. 45, 623—624 (1972)

Effects of $FeCl_3$ on the Graphitizability of Coal Tar Pitch

Sugio OTANI and Asao OYA

Faculty of Technology, Gunma University, Kiryu, Gunma

(Received November 9, 1970)

For the purposes of raising the softening points (S.P.) of pitch materials or increasing the yields of cokes, raw pitch materials are conventionally distilled with some additives or by bubbling in an oxidizing gas, such as Cl_2 or air.[1] This manner, though, generally leads to a lowering of the graphitizability of the resulting carbonaceous materials. In an earlier paper,[2] however, it has been reported that the addition of $AlCl_3$ was remarkably effective in raising the S.P. of the residual pitch materials, but that it did not lower their graphitizability. Consequently, $AlCl_3$ is an interesting additive.

In order to clarify the action of $AlCl_3$ and to determine whether $AlCl_3$ is the only kind of additive having such effects, or whether three are some other additives with the same effects, it was thought advisable to investigate the effects of $FeCl_3$, which has a strong resemblance to $AlCl_3$ in character. The experiments described below deal with the effect of the addition of $FeCl_3$ as compared with that of the addition of Fe powder, and with the case of an entire absence of additives.

Experimental and Results

A mixture of 10 g of coal tar pitch and either 1 g of $FeCl_3$ or 0.5 g of Fe powder (under 100 mesh) was distilled with bubbling N_2 gas at desired temperatures below 550°C for 10 minutes. Coal tar pitch without any additives was also distilled as a reference. From the results shown in Fig. 1, it is clear that the S.P. of the residual pitch materials was more effectively raised by the addition of $FeCl_3$ than in the other two cases.

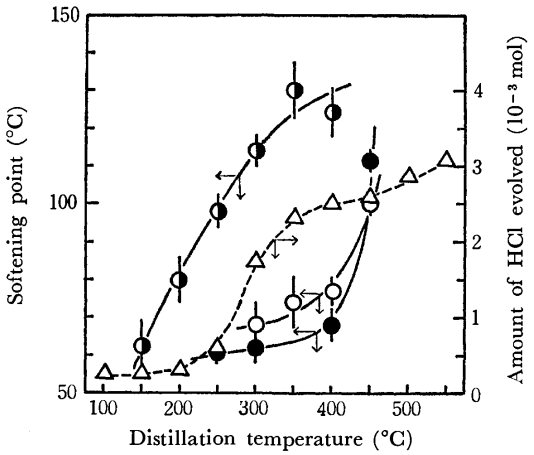

Fig. 1. Changes of softening point and amount of HCl evolved with distillation temperature.
S.P.: —○— no additive, —◑— $FeCl_3$ 10%, —●— Fe 5%, Amount of HCl, —△—

In order to measure the amounts of HCl evolved on heating, the mixture of 10 g of coal tar pitch and 1 g of $FeCl_3$ was heated with bubbling N_2 gas up to 550°C at the rate of 10°C/min, and the HCl thus evolved was absorbed in water and was estimated on the basis of titration with a NaOH solution at 50°C intervals. The evolution of HCl was accelerated at 250—350°C, as is shown in Fig. 1, it corresponded to only 17% of the amount of Cl atoms in $FeCl_3$, even after heating up to 550°C. It is the most characteristic fact that, in spite of the remarkable rise in the S.P. in the distillation temperature range below 250°C, the evolution of HCl in the same range is very small in amount.

In order to estimate the effects of additives on the graphitizability of residues, the following examinations were carried out. First, coal tar pitches were distilled at 550°C for 10 min under the conditions listed in Table 1. The resulting carbonaceous residues were heat-treated at the desired temperatures below 2400°C, and the graphitizability of the resulting carbons was examined by the X-ray diffraction technique.[2] All of the carbonaceous residues which were obtained by bubbling N_2 gas, regardless of the kinds and the amounts of additives, gave graphitizable carbons which show single and symmetrical (002) diffraction patterns upon graphitization. Figure 2 shows the changes in the interlayer spacing d_{002}, and the crystallite thickness, L_c, with

Table 1. Atmospheres of the distillation and the amounts of additives (wt%)

Additive	Atmosphere: N_2	Atmosphere: Cl_2
Fe	3.44	0.69, 1.72, 3.44, 17.21
$FeCl_3$	2, 5, 10, 50	2, 5, 10, 50

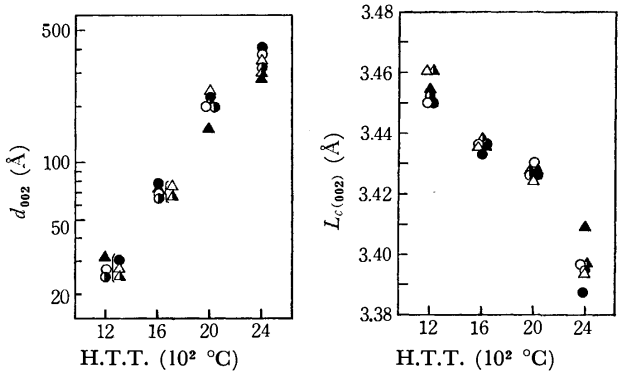

Fig. 2. X-Ray parameters of the residual carbons obtained by the distillation with N_2 gas.
—○—: None, —◑—: $FeCl_3$ 2%, —●—: $FeCl_3$ 5%, —△—: $FeCl_3$ 10%, —▲—: $FeCl_3$ 50%, —▲: Fe 3.44%

1) S. Otani and A. Oya, *Kogyo Kagaku Zasshi*, **73**, 493 (1970).
2) S. Otani and A. Oya, *ibid.*, **73**, 1110 (1970).

the heat-treatment temperature. From the results shown in Fig. 2, it is evident that all the resulting carbons were typically graphitizable. On the other hand, when coal tar pitches were distilled with bubbling Cl_2 gas, all of the resulting carbonaceous residues, regardless of the kinds and the amounts of additives used in this study, gave non-graphitizable carbons which exhibited composite (002) diffraction patterns upon graphitization. It should be pointed out that, when $AlCl_3$ was added in our previous study,[2] the resulting carbonaceous residues gave graphitizable carbons.

Conclusion

The above results show that the addition of $FeCl_3$ is remarkably effective in raising the S.P. of residual pitch without any deterioration of the graphitizability of carbon obtained in the subsequent heating stage. At temperatures below 250°C, the evolution of HCl from the pitch with the addition of $FeCl_3$ is very small in amount in spite of the remarkable rise in the S.P. of the residue. On the other hand, the addition of Fe powder is not effective in raising the S.P. of the residues. Consequently, it seems reasonable to consider that such effects caused by the addition of $FeCl_3$ depend on the action of neither Cl nor Fe, which may be formed by a decomposition of $FeCl_3$ in the distillation stage, but depend on some action of the entire molecule of $FeCl_3$. Such effects of $FeCl_3$ were similar to those of $AlCl_3$ reported previously.[2] Therefore, the effects caused by the addition of $FeCl_3$ or $AlCl_3$ are thought to be due to a certain property, such as the acidic property, which is common to both the reagents.

BULLETIN OF THE CHEMICAL SOCIETY OF JAPAN, VOL. 45, 624—625 (1972)

The Electronic Spectra of the Anion Radical Salts Derived from 2,3-Dicyano-1,4-naphthoquinone

Yôichi IIDA

Department of Chemistry, Faculty of Science, Hokkaido University, Sapporo

(Received July 21, 1971)

Much attention has been paid to solid-ion-radical salts,[1-3] because the ion-radical molecules form, in themselves, a plane-to-plane stacking into columns so as to make a large overlap between their half-filled molecular orbitals.[4] In this case, since any individual radical molecule interacts through charge transfer most strongly with one or two other radicals, the electronic spectrum of the solid salt was found to be different from the monomer spectrum of the radical anion in solution and to show an intermolecular charge-transfer band in the low-energy region.[2,3] In this respect, it was interesting to examine the solid-state spectra of the anion-radical salts of 2,3-dicyano-1,4-benzoquinone and 2,3-dichloro-5,6-dicyano-1,4-benzoquinone.[3]

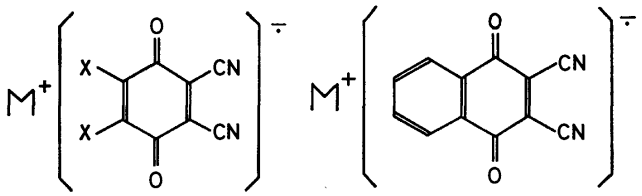

Fig. 1. The anion radical salts of (a) 2,3-dicyano-1,4-benzoquinone, (b) 2,3-dichloro-5,6-dicyano-1,4-benzoquinone and (c) 2,3-dicyano-1,4-naphthoquinone (DCNQ). M^+ represents a diamagnetic counter cation.

The present paper will describe the solid-state spectra, as well as the absorption spectra in solution, of some stable anion-radical salts derived from 2,3-dicyano-1,4-naphthoquinone (DCNQ). The following anion-radical salts were prepared according to the method of Reynolds and VanAllan[5]: Na^+ $DCNQ^-$, K^+ $DCNQ^-$, Rb^+ $DCNQ^-$, and Cs^+ $DCNQ^-$. The purpose of this paper is to show that the charge-transfer interaction between the DCNQ anion radicals also takes place in these solid anion-radical salts. It is interesting that the data indicate that the manner of the charge-transfer interaction is similar to those in the 2,3-dicyano-1,4-benzoquinone anion-radical salts.[3]

The Absorption Spectra in Solution

The absorption spectra of the anion-radical salts in an acetonitrile solution were measured at room temperature. The measurements were made at concentrations of the order of 1×10^{-4} mol/*l*, using a Beckman DK-2A spectrophotometer.

All of the DCNQ anion-radical salts dissolved in an acetonitrile solution appear red, and are quite

1) W. J. Siemons, P. E. Bierstedt, and R. G. Kepler, *J. Chem. Phys.*, **39**, 3523 (1963); R. G. Kepler, *ibid.*, **39**, 3528 (1963).

2) Y. Iida and Y. Matsunaga, This Bulletin, **41**, 2615 (1968); Y. Iida, *ibid.*, **42**, 71, 637 (1969); Y. Iida, *ibid.*, **43**, 2772 (1970); Y. Iida, *ibid.*, **44**, 663 (1971); Y. Iida, *ibid.*, **45**, 105 (1972).

3) Y. Iida, *ibid.*, **44**. 1777 (1971).

4) C. J. Fritchie, Jr., *Acta Crystallogr.*, **20**, 892 (1966); C. J. Fritchie, Jr., and P. Arthur, Jr., *ibid.*, **21**, 139 (1966); P. Goldstein, K. Seff, and K. N. Trueblood, *ibid.*, **B24**, 778 (1968); J. Tanaka and N. Sakabe, *ibid.*, **B24**, 1345 (1968); H. Kobayashi, Y. Ohashi, F. Marumo, and Y. Saito, *ibid.*, **B26**, 459 (1970).

5) G. A. Reynolds and J. A. VanAllan, *J. Org. Chem.*, **29**, 3591 (1964).

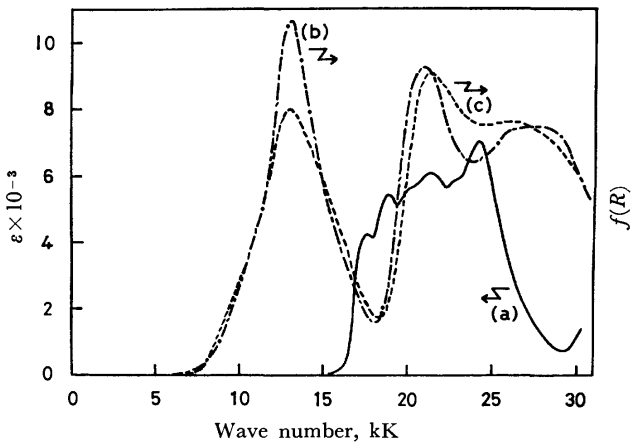

Fig. 2. The electronic spectra of the 2,3-dicyano-1,4-naphthoquinone (DCNQ) anion radical salts; (a) the absorption spectrum of K^+ $DCNQ^-$ in an acetonitrile solution, (b) the solid-state spectrum of Na^+ $DCNQ^-$ and (c) the solid-state spectrum of K^+ $DCNQ^-$.

stable at room temperature. As an example, the absorption spectrum of K^+ $DCNQ^-$ in an acetonitrile solution is reproduced in Fig. 2, Curve (a). It has absorption peaks at 17.6 kK and 18.8 kK, a peak at 21.3 kK with a shoulder around 20.3 kK, and a high-energy band at 24.1 kK with a slight shoulder around 22.7 kK. The spectrum does not change even when the counter cation of the salt is replaced. Since the concentrations are so dilute, the salts seem to be completely dissociated. The obtained spectrum is that of the DCNQ anion radical monomer, because the counter cations of the salts are simple alkali-metal cations.

The Solid-state Spectra

The electronic spectra of the solid DCNQ anion-radical salts were measured by the diffuse-reflection technique. The diffuse-reflection spectra were recorded on a Beckman DK-2A spectroreflectometer in the range from 4.0 kK to 30.8 kK at room temperature. The solid-state spectra were then obtained by plotting the diffuse-reflection spectra using the Kubelka-Munk equation, $f(R)=(1-R)^2/2R$, in which R is the reflectance. The experimental details were the same as those presented in previous papers.[2,3]

All of the DCNQ anion-radical salts were obtained as dark green polycrystals, and all were quite stable at room temperature.

The solid-state spectrum of Na^+ $DCNQ^-$ (Fig. 2, Curve (b)) shows a strong absorption at 13.1 kK, a band at 20.9 kK, and a broad high-energy band around 27.8 kK. This spectrum was found to be quite different from the monomer spectrum of the DCNQ anion radical in solution. The band at 13.1 kK characteristic of the solid salt appears in the low-energy region, where the anion-radical monomer does not absorb. This band has no vibrational structures, and its intensity is remarkably strong. It cannot be assigned to the charge-transfer transition from the anion radical to the counter cation, since its maximum position is scarcely shifted when the counter cation of the salt is replaced (see below). Although, at present, no experimental data on the charge-transfer absorption in the dimer of the DCNQ anion radicals are available for purposes of comparison, the low-energy band at 13.1 kK seems to be attributable to the charge-transfer transition between the DCNQ anion radicals in the solid state. This assignment is analogous to those for the anion-radical salts of the cyano-substituted *p*-benzoquinones,[3] where the charge-transfer band of Na^+ 2,3-Dichloro-5,6-dicyano-1,4-benzoquinone$^-$ has been reported to be located at 12.6 kK, while that of Na^+ 2,3-Dicyano-1,4-benzoquinone$^-$ is located at 10.7 kK with a shoulder around 14.3 kK.

The appearance of the strong charge-transfer band in Na^+ $DCNQ^-$ means that, in the solid state, the DCNQ anion radicals are stacked closely enough together for the half-filled molecular orbitals to make a large overlap. The DCNQ anion radicals seem to form, in themselves, a plane-to-plane stacking into columns; this feature of the crystal structure has also been found in a number of other ion-radical salts.[4] The charge-transfer absorption characteristic of the solid salt should be ascribed to the transition of the $\langle\cdots Q^-Q^-Q^-Q^-\cdots\rangle \rightarrow \langle\cdots Q^-Q^0Q^{2-}Q^-\cdots\rangle$ type, where Q denotes a quinone molecule. In this case, the π–π transitions of the DCNQ anion radical monomer will be perturbed in the field of the other anion radicals. This is shown as appreciable blue-shifts of the high-energy bands at 20.9 kK and 27.8 kK for the solid-state spectrum of Na^+ $DCNQ^-$, compared to the monomer absorptions of the DCNQ anion radical, shown in Fig. 2, Curve (a).

The solid-state spectra of K^+ $DCNQ^-$, Rb^+ $DCNQ^-$, and Cs^+ $DCNQ^-$, although the intensities of the low-energy charge-transfer bands depend slightly on the species of the counter cations, were found to be very similar to that of Na^+ $DCNQ^-$. As an example, the solid-state spectrum of K^+ $DCNQ^-$ is given in Fig. 2, Curve (c). Hence, the electronic structure in the solid DCNQ anion radical salts and the charge-transfer interaction between the DCNQ anion radicals are scarcely affected even though the counter cations of the salts are replaced in the present investigation. It is interesting to note that this situation coincides well with that previously reported for the cyano-substituted *p*-benzoquinone anion-radical salts.[3]

BULLETIN OF THE CHEMICAL SOCIETY OF JAPAN, VOL. 45, 626—627 (1972)

Studies on Salt Solution Aerosols. VI.[1] Droplet Size Determination of Aqueous Sodium Sulfate Solution Aerosols by Chemical Spot Method

Yasuo UENO and Isamu SANO

Department of Chemisty, Faculty of Science, Nagoya University, Chikusa-ku, Nagoya

(Received November 20, 1970)

For the purpose of measuring the size distributions of aqueous sodium chloride solution aerosols, a new method based upon the chemical spot formation was developed.[2] One merit of the method is the easy preparation of a transparent film of polyvinyl alcohol containing the detecting reagent (silver nitrate) which reacts with the solution droplets to give spots of clear outlines. In addition a quantitative relationship holds between the size of the droplets and that of the spots impressed by them.

We have extended this technique to the size measurement of aqueous sodium sulfate solution aerosols. The results were analyzed in combination with those of aqueous sodium chloride solution aerosols.

Experimental

Materials. Ethanol used was of extra pure grade. Polyvinyl alcohol (PVA), obtained from Kurare Co., was 1700 in polymerization degree and 85% in saponification extent. Barium perchlorate was of chemical pure grade.

Preparation of the Reagent Film. To 100 g of an aqueous solution containing 4% by weight of PVA was added 200 m*l* of C_2H_5OH, and then a) 1 m*l*, b) 2 m*l* c) 3 m*l* and d) 4 m*l* of aqueous 40% $Ba(ClO_4)_2 \cdot 3H_2O$ solution was added separately to obtain four solutions of the detecting reagent in different concentrations. On dropping 10 μl of these solutions upon a dry glass slide[3] by means of a micropipette, the solvent (alcohol and water) rapidly evaporated off, leaving a circular transparent film of reagent, about 2.1 cm in diameter.

Generation of Droplets and Measurement of Size Distribution. An aqueous aerosol of 10% Na_2SO_4 solution was introduced into a mist chamber from an atomizer and was subjected to aging for various periods of time under agitation. The droplets were allowed to settle under the action of gravity onto the reagent film and an oil film[2] held on a glass slide. They were put side by side in the chamber. The size of the spots formed on the reagent film was measured with a phase microscope and that of the droplets suspended in the oil film with an ordinary microscope. Microphotographs of the spots and droplets were enlarged and their sizes were recorded with due precaution. The size of the droplets was in the range of about 0.3—12 μ in diameter.

Results and Discussion

Experimental Construction of the Calibration Curve. Both droplets and their spots have their own size distributions. Therefore, taking the volume average diameter D_d for the former and the surface average diameter d_s for the latter, the calibration curve was constructed for four films of varying $Ba(ClO_4)_2$ concentrations (Fig. 1, solid lines). We see that the spot diameter decreases with increasing reagent concentration in film.

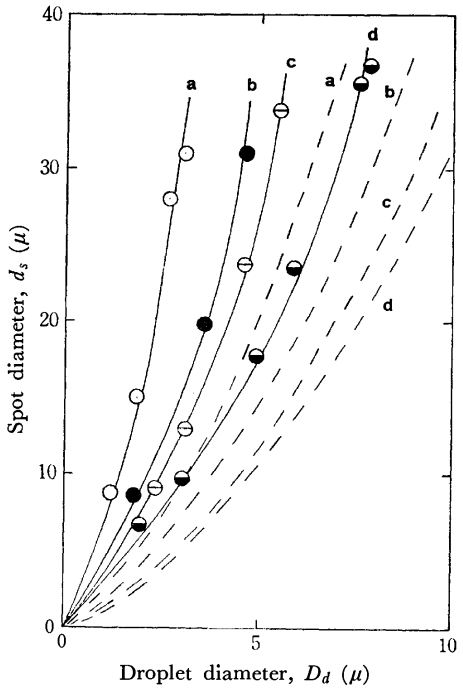

Fig. 1. Relation between the spot and droplet diameters. Solid lines refer to experimental curves and dashed lines calculated ones.
a : 1 m*l* $Ba(ClO_4)_2$ solution, b : 2 m*l* $Ba(ClO_4)_2$ solution
c : 3 m*l* $Ba(ClO_4)_2$ solution, d : 4 m*l* $Ba(ClO_4)_2$ solution

Calculation of the Calibration Curve. Assumptions similar to those of the former report[2] were made, *viz*, the spots of $BaSO_4$ formed are all of a cylindrical form whose height is equal to the film thickness. We thus obtain the relation

$$D_d^3 = 3/2\rho[\text{Film}]C[Ba(ClO_4)_2]M[Na_2SO_4]Hd_s^2/(\rho[Na_2SO_4]C[Na_2SO_4]M[Ba(ClO_4)_2]), \quad (1)$$

where ρ[Film]: density of film,
$\rho[Na_2SO_4]$: density of aqueous Na_2SO_4 solution,
$C[Na_2SO_4]$: concentration of aqueous Na_2SO_4 solution,
$C[Ba(ClO_4)_2]$: concentration of $Ba(ClO_4)_2$ in film,
$M[Na_2SO_4]$: molecular weight of Na_2SO_4,
$M[Ba(ClO_4)_2]$: molecular weight of $Ba(ClO_4)_2$,
H: thickness of film.

Since the concentration of the Na_2SO_4 solution used is known, Eq. (1) takes the form

1) Part V: Y. Ueno and I. Sano, This Bulletin, **44**, 908 (1971).
2) Y. Ueno and I. Sano, *ibid.*, **44**, 637 (1971).
3) cleaned beforehand in the same way as previously reported.[2]

Table 1. Estimated values of ρ[Film], H and $C[Ba(ClO_4)_2]$ and the values of ε.

Film	ρ[Film][a] (g/cm^3)	H[b] (μ)	$C[Ba(ClO_4)_2]$[c] (%)	$\varepsilon_{obs.}$	$\varepsilon_{calc.}$		
(a)	1.40	0.31_2	10.7	0.33	0.32[d]	0.33[e]	0.33[f]
(b)	1.48	0.33_1	19.0	0.42	0.41	0.40	0.40
(c)	1.55	0.34_9	25.7	0.45	0.46	0.46	0.46
(d)	1.61	0.36_8	31.2	0.52	0.51	0.51	0.51

a), b) and c) The values of ρ[Film], H and $C[Ba(ClO_4)_2]$ are calculated by the relations:

$\rho[\text{Film}]=(W[\text{PVA}]+W[Ba(ClO_4)_2\cdot 3H_2O])/(W[\text{PVA}]/\rho[\text{PVA}]+W[Ba(ClO_4)_2\cdot 3H_2O]/\rho[Ba(ClO_4)_2\cdot 3H_2O])$

$H=4(W[\text{PVA}]+W[Ba(ClO_4)_2\cdot 3H_2O]/\rho[Ba(ClO_4)_2\cdot 3H_2O])/\pi D_f^2$

$C[Ba(ClO_4)_2]=100W[Ba(ClO_4)_2\cdot 3H_2O]\cdot M[Ba(ClO_4)_2]/(W[\text{PVA}]+W[Ba(ClO_4)_2\cdot 3H_2O])M[Ba(ClO_4)_2\cdot 3H_2O]$

where W and ρ and the weight and density, respectively, of solid PVA or $Ba(ClO_4)_2\cdot 3H_2O$ in the film having a diameter D_f which is found to be 2.1 cm.

d) $k=1.0$, $\alpha=0.79_1$, $\beta=0.00015_5$. e) $k=2.0$, $\alpha=0.88_6$, $\beta=0.000056_3$. f) $k=5.0$, $\alpha=0.95_3$, $\beta=0.000019_4$.

$$D_d^3 = Kd_s^2 \tag{2}$$

where K is a constant given by

$$K = 5.82\rho[\text{Film}]HC[Ba(ClO_4)_2].^{4)} \tag{3}$$

According to Eq. (2), a plot of log D_d against log d_s should be linear, and this is actually the case, for all concentrations as shown in Fig. 2, the slope being 2/3 for all straight lines. The value of K is found from the intercept on the log D_d axis.

Theoretical curves calculated by Eq. (2) using the values listed in Table 1, are represented by dashed lines in Fig. 1. It is clear that the diameters of the spots found experimentally are larger than those calculated.

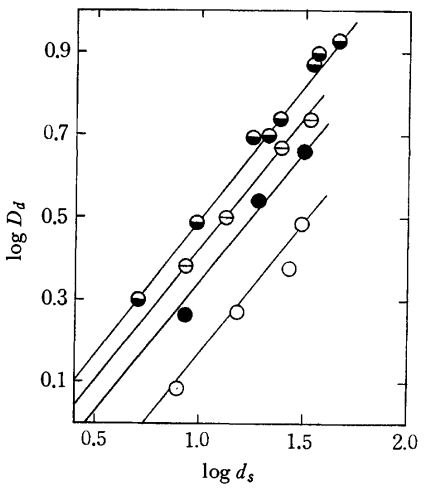

Fig. 2. Plot of log D_d against log d_s.
○: 1 m*l* $Ba(ClO_4)_2$ solution, ●: 2 m*l* $Ba(ClO_4)_2$ solution
⊖: 3 m*l* $Ba(ClO_4)_2$ solution, ◒: 4 m*l* $Ba(ClO_4)_2$ solution

Comparison between Theory and Experiment. It has been shown that for a given D_d[2)]

$$d_{s\ theor.}/d_{s\ exptl.} = (K_{exptl.}/K_{theor.})^{1/2} = \varepsilon \tag{4}$$

The values of ε determined by use of the values of $K_{exptl.}$ and $K_{theor.}$ in accordance with Eq. (4) are listed in Table 1 ($\varepsilon_{obs.}$). All of them are less than unity. For aqueous NaCl solution aerosols it has been shown[2)] that

$$\varepsilon = k(1-\alpha e^{-\beta C}) \tag{5}$$

where C is the concentration (%) of the detecting reagent ($AgNO_3$) in film. The applicability of Eq. (5) for aqueous Na_2SO_4 solution aerosols is shown in Table 1 ($\varepsilon_{calc.}$).

By combining the cases of $AgNO_3$[2)] and $Ba(ClO_4)_2$, we find that

$$\varepsilon = k(1-\alpha e^{-\gamma C/M}) \tag{6}$$

where M is the molecular weight of $AgNO_3$ or $Ba(ClO_4)_2$ and γ a constant.

4) The concentration of the dispersing solution is 10% by weight of Na_2SO_4. The term K, corresponding to $3/2\cdot M[Na_2SO_4]/(\rho[Na_2SO_4]C[Ba(ClO_4)_2]M[Ba(ClO_4)_2]$ in calculated to be 5.82, by replacing the values of 1.09 for $\rho[Na_2SO_4]$, 0.10 for $C[Na_2SO_4]$, 336.2 for $M[Ba(ClO_4)_2]$ and 142.0 for $M[Na_2SO_4]$. For the values of ρ[Film], H and $C[Ba(ClO_4)_2]$, *cf.* Table 1.

BULLETIN OF THE CHEMICAL SOCIETY OF JAPAN, VOL. 45, 628—630 (1972)

Studies on Photo-polarography. V. Theory of Photo-current and Reaction of Aquated Electrons with Scavenger[1]

Kazuo YAMASHITA and Hideo IMAI

Department of Chemistry, Faculty of General Education, Hiroshima University, Hiroshima

(Received December 28, 1970)

The existence of trapped electrons in gamma irradiated glass was directly substantiated by ESR studies[2]. The ESR technique, however, can not be applied to such a transient entity as solvated electrons in solution. On the other hand, the possible existence of free solvated electrons in solution at reasonably close proximity to the parent ion was suggested by spectrophotometric studies[3] using a matrix isolation technique. From kinetics and mass-transport studies[4,5] the reactive but transient entity of an electron in solution is known to be solvated. Accordingly, photo-detached electrons emitted into an aqueous electrolyte solution from an electrode irradiated by ultra-violet light are reasonably assumed to be aquated at a certain distance apart from the electrode surface, where electrons are thermalized. The aquated electrons e^-_{aq} then react with scavenger ions or molecules in solution, producing the photo-current in an electrolytic cell circuit.

The electrolytic photo-current is controlled by the diffusion of e^-_{aq} and its reaction rate with a scavenger. Barker *et al.*[6] gave an equation for the photo-current, but without details. A more generalized solution of this semi-infinite diffusion problem is presented in this paper on the basis of Hatta's theory on the absorption of gases in a reactive solution[7]. The validity of our theory was proved by the dependence of the photo-current on the scavenger concentration and by the Brønsted theory on an ionic reaction with special regard to the solvent effect on the rate process.[8]

Theory

According to Barker's model of the reaction the electrons emitted from the irradiated electrode partly return to the electrode by attraction. Some electrons, however, have sufficient kinetic energy to overcome the attraction,[9] and are thermalized at a distance δ where the attraction is equal to the thermal energy of an electron kT. In this process water molecules are repelled by a thermalized electron, and the liquid is dilated so that a cavity is created in the solution. The electron is then held in the cavity as an aquated electron (Eq. (1)), and enters into the chemical reaction with a scavenger ion or molecule S, as shown in Eq. (2). In this reaction it is assumed that the aquated electrons are wholly depleted through Reaction (2) except the self-decay (Reactions (3) and (4)).

These reactions are schematically shown in the following:

$$e^- + nH_2O \rightleftarrows e^-_{aq} \quad (1)$$

$$e^-_{aq} + S \xrightarrow{k_s} S^- \quad (2)$$

$$e^-_{aq} \rightarrow H_{aq} + OH^-_{aq} \quad (3)^{13}$$

$$2e^-_{aq} \rightarrow H_2 + 2OH^-_{aq} \quad (4)^{13}$$

When the self-decay of e^-_{aq} can be neglected in comparison with the rate of the scavenging reaction, the semi-infinite diffusion equation for the process given by Eqs. (1) and (2) is expressed as follows:

$$\frac{\partial C_e}{\partial t} = D_e \frac{\partial^2 C_e}{\partial x^2} - k_s C_e C_s \quad (5)$$

where C_e and D_e are the concentration and diffusion coefficient of the aquated electron, respectively, k_s the rate constant of Reaction (2), and C_s the scavenger concentration. Under a sufficiently high concentration of scavenger, C_s the scavenger concentration. Under a sufficiently high concentration of scavenger, $C_{s(t=0,x)} = C_{s(t=t,x)}$, we have

$$k_s C_e C_s = kC_e \quad (6)$$

Thus, Reaction (2) can be approximated as a pseudo-first order reaction.

At the stationary state of the diffusion and scavenging process $\partial C_e/\partial t = 0$, and we have from Eq. (5)

$$D_e \frac{\partial^2 C_e}{\partial x^2} = kC_e \quad (7)$$

The boundary conditions for Eq. (7) are

$$\left.\begin{array}{ll} \text{at} & x=0,\ C_e = C_e^s \\ \text{and at} & x=r,\ \dfrac{dC_e}{dx} = 0, \end{array}\right\} \quad (8)$$

1) This paper was presented at the 22nd Annual Meeting of the Chemical Society of Japan, Tokyo, April 1969. For Part IV see, This Bulletin, **42**, 578 (1969).

2) D. C. Walker, *Quart. Rev., London.* **21**, 79 (1967). F. S. Dainton, in Gomberg Centenary Volume, Butterworth, London (1967). J. Zimbrick and L. Kevan, *J. Amer. Chem. Soc.*, **89**, 2483 (1967).

3) M. Anbar and E. J. Hart, *J. Phys. Chem.*, **69**, 1244 (1965).

4) W. C. Gottschall and E. J. Hart, *J. Phys. Chem.*, **71**, 2102 (1967).

5) K. H. Schmidt and W. L. Buck, *Science*, **151**, 70 (1966).

6) G. C. Barker, A. W. Gardner and D. C. Sammon, *J. Electrochem. Soc.*, **113**, 1182 (1966).

7) S. Hatta, *Technol. Reports Tohoku Univ.*, **10**, 916 (1939).

8) For experimental techniques see K. Yamashita and H. Imai, This Bulletin, **41**, 1339 (1968), **42**, 578 (1969).

9) The energy barrier for the emission of electrons in an electrolyte solution has been discussed by Delahay and Srinivasan[10], Brodski and Gurevich[11], and Sharma *et al.*[12]

10) P. Delahay and V. S. Srinivasan, *J. Phys. Chem.*, **70**, 420 (1966).

11) A. M. Brodski and Yu. Ya. Gurevich, *Electrochim. Acta*, **13**, 1254 (1968).

12) V. P. Sharma, P. Delahay, G. G. Susbielles, and G. Tessari, *J. Electroanal. Chem.*, **16**, 285 (1968).

13) Whether the decay is to proceed in the first order reaction (Reaction (3)) or in the bimolecular decay depends upon the concentration of the aquated electrons formed on the deposition plane. For a review see F. S. Dainton, "The Chemistry of the Electron," Nobel Symposium 5, ed. by S. Claeson, Interscience Publishers, New York, N. Y. (1967), pp. 185—209.

where r denotes the distance where e_{aq}^-s are depleted.

The solution of Eq. (7) is given by Hatta[7] as in the following:

$$\frac{C_e}{C_e^\delta} = \frac{\cosh\left\{\sqrt{\frac{k}{D_e}}r\left(1-\frac{x}{r}\right)\right\}}{\cosh\left(\sqrt{\frac{k}{D_e}}r\right)} \quad (9)$$

The rate of electron depletion, v, through the scavenging reaction is expressed by the number of electrons diffusing away from the deposite plane during unit time, *i.e.*,

$$v = -D_e\left(\frac{dC_e}{dx}\right)_{x=0} \quad (10)$$

Thus, the photo-current can be expressed as follows:

$$i_p = -FD_e\left(\frac{dC_e}{dx}\right)_{x=0} = FD_eC_e^\delta\sqrt{\frac{k}{D_e}}\tanh\left\{\sqrt{\frac{k}{D_e}}r\right\} \quad (11)$$

When the reaction rate is sufficiently high, then $\sqrt{k/D_e}\cdot r \to \infty$, and $\tanh(\sqrt{k/D_e}\cdot r)$ can be approximated as unity. Thus, Eq. (11) leads to

$$i_p = FD_eC_e^\delta\sqrt{\frac{k}{D_e}} = FC_e^\delta\sqrt{k_sC_sD_e} \quad (12)$$

On the contrary, when the diffusion is sufficiently high in comparison with the reaction rate, the rate will be expressed simply as

$$v' = kC_e^\delta r \quad \text{and} \quad i_p' = FC_e^\delta k_sC_sr \quad (13)$$

It is noteworthy that Eq. (12) coincides well with the Barker equation[6].

Results and Discussion

In the following the validity of Eq. (12) is proved in relation to the dependence of photo-current on the scavenger concentration, ionic strength of the solution and on the static dielectric constant of the solution.

Field Effect on i_p. The field effect on the photo-current was first pointed out by Barker *et al.*[6] Delahay and Srinivasan applied Fowler's theory of photo-detached electrons *in vacuo* to the solution medium in question, and a quadratic relation of i_p to the electrode potential E was proved in the scavenging of e_{aq}^- by the hydrogen ion. Brodski and Gurevich[10] proposed an improved theory and proved a better linear relationship between i_p and $E^{5/2}$. In our experiment using polychromatic light (250—350 mμ) and nitrate as the e_{aq}^- scavenger[14] a better linear relationship of i_p *versus* $E^{5/2}$ was obtained as shown in Fig. 1.

Dependence of i_p on C_s. Eq. (12) shows a linear relationship between the photo-current and the square root of the scavenger concentration. The photo-current measured at the electrode potential of -1.6 V *vs.* S. C. E. showed a good linearity against the square root of the nitrate concentration as shown in Fig. 2. Even in 44% ethanol-water mixture the linearity was excellent in accordance with Eq. (12).

The Brønsted Theory Applied to the Reaction of e_{aq}^- with Nitrate. We assumed that the photo-current

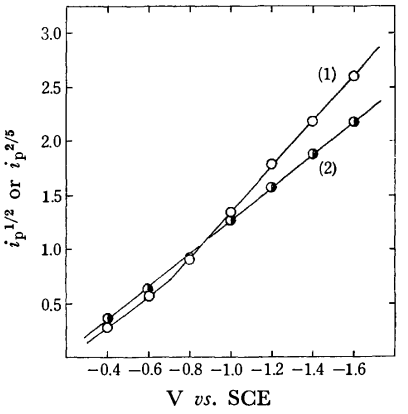

Fig. 1. Dependence of the photo-current on the electrode potential.
0.2 M KCl and 5 mM KNO_3 aq. solution.
(1) $i_p^{1/2}-E$, (2) $i_p^{2/5}-E$.

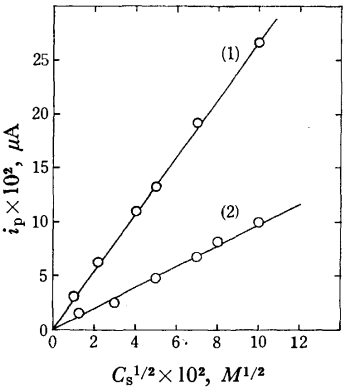

Fig. 2. Dependence of the photo-current on the scavenger concentration.
(1) 1 M KCl aq. solution.
(2) 0.2 M KCl and 44% ethanol aq. solution.
Scavenger, NO_3^-.

flows as a result of Reaction (2) which proceeds in the solution phase at a distance δ apart from the electrode surface (for the reaction model proposed hitherto, *cf.* Ref. 6, 15, 16). The validity of our reaction model, which coincides with the Barker model, can be proved by a solvent effect on the activity coefficient of the reacting species. Thus the Brønsted theory on an ionic reaction was treated, and in the modified expression of the theory a plot of log i_p *vs.* $\sqrt{\mu}/(1+\sqrt{\mu})$ (μ : the ionic strength) should yield a straight line with slope of 0.51 Z_eZ_s, provided C_e and D_e are not significantly varied with changing μ. These data are shown in Fig. 3, which indicates that the values of both Z_e (the charge of the aquated electron) and Z_s (the charge of the scavenger) are univalent and negative.

The effect of the static dielectric constant of a solvent on the rate of an ionic reaction can be discussed in the same way. By combining the Brønsted-Christiansen-Scatchard equation[17,18] and Eq. (12) a plot

14) The scavenging reaction seems to proceed as follows:
$e_{aq}^- + NO_3^- \to NO_3^{2-} + aq \to NO_2 + 2OH^-$
(or $HNO_3^- + OH^-$)

15) H. Berg, *Electrochim. Acta*, **13**, 1249 (1968).
16) M. Heyrovsky, *Nature*, **200**, 880 (1963), *Z. Physik. Chem. (Frankfurt)*, **52**, 1 (1967).
17) G. Scatchard, *Chem. Rev.*, **10**, 229 (1932).
18) B. Krishna and H. S. Singh, This Bulletin, **41**, 325 (1968).

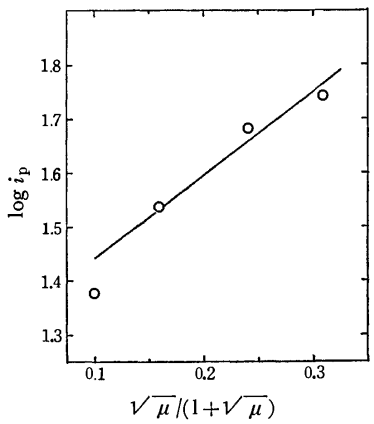

Fig. 3. Effect of the ionic strength on the photo-current.
KCl and 5 mM KNO_3 aq. solution.

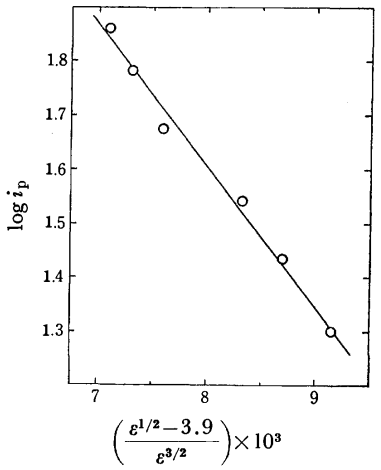

Fig. 4. Effect of the static dielectric constant on the photo-current.
Ethanol-water mixture containing 5 mM KNO_3 and 0.2 M KCl.

of log i_p *versus* $(\sqrt{\varepsilon}-\text{const})/\sqrt{\varepsilon^3}$ (ε : the static dielectric constant) should yield a straight line for solutions constant μ. The data are shown in Fig. 4. The value of D_e was not corrected for the charge of the solution media in this plot. Nevertheless, it gives a fairly good straight line in accordance with the theory. From the plot the charge of an aquated electron is evaluated to be negative, and the rate-determining step of the photo-current is a reaction of an aquated electron with nitrate in the reaction layer.

BULLETIN OF THE CHEMICAL SOCIETY OF JAPAN, VOL. 45, 630—632 (1972)

Formation of the Boron Chelates in the Sodium Borohydride Reduction of the Schiff Bases

Tsuguo TANAKA, Mitsue KOYAMA, Seiji IKEGAMI, and Masako KOGA
Department of Science and Technology, Saga University, Saga

(Received March 25, 1971)

Billman and Diesing[1] reported that the C=N bond of *o*- or *o'*-hydroxy Schiff bases could not be reduced with sodium borohydride in boiling methanolic solutions. Failure of the reduction was ascribed to the resonance stabilization of the Schiff bases (VIIa↔VIIb) in alkaline media. For the purpose of synthesizing the chelating reagents for the spectrophotometric determination of the metal ions,[2] the reduction of a number of Schiff bases with sodium borohydride in the methanolic solutions at 50°C, was attempted and the results are summarized.

When *o*- or *o'*-monohydroxy compounds are reduced, the expected benzylaniline derivatives are precipitated as crystals merely by the acidification of the reaction mixture with dilute acetic acid (procedure A). The Schiff bases having hydroxyl groups on *o*- and *o'*-positions such as Ig and Ih could also be reduced with sodium borohydride, as evidenced by the disappearance of the orange color of the Schiff bases. However, the expected product IIIg or IIIh does not crystallize upon the acidification of the reaction mixture with acetic acid. Therefore, the isolation of the soluble reaction products from the acidified solution was attempted, and the boron chelate *O,O,N*-(*o,o'*-dihydroxybenzylanilino)-borane (Va) was obtained as crystals by the evaporation of the solvents in a vacuum at room temperature (procedure C). The chelate Va was easily dehydrated to give VIa by sublimation in a vacuum at 130—135°C, indicating a weakly coordinated water molecule of Va. The mass spectral data of Va and VIa, and the structures of the ionic species involved are listed in Table 3. The structure of Va and VIa were proved by the *m/e* of 223 and other *m/e* values. Some differences were observed in the mode of fragmentation between Va and VIa.

The normal reduction products *o*-, *o'*-dihydroxybenzylaniline derivatives were also obtained by evaporating methanol from the reaction mixture prior to dilution and acidification (procedure B).

The IR spectra of IIIg, Va and Vb are given in Fig. 2. The 3600 cm^{-1} O-H stretching of Va was ascribed to the coordinated water molecule.[3] Two

1) J. H. Billman and A. C. Diesink, *J. Org. Chem.*, **22**, 1068 (1957).
2) T. Tanaka, This Bulletin, **41**, 1277 (1968).
3) I. Gamo, *ibid.*, **34**, 761 (1961).

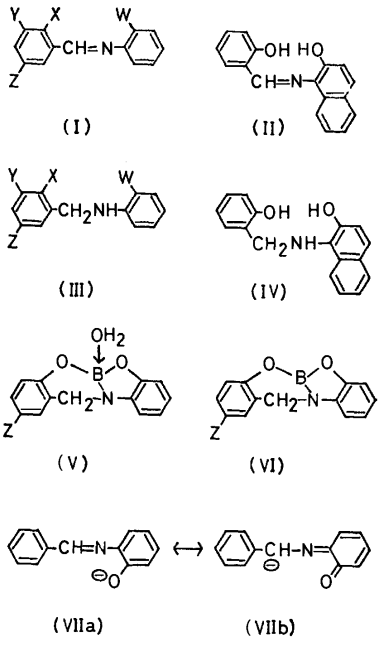

	X	Y	Z	W
Ia	OH	CH_2-CH_2-COOH	CH_3	OH
Ib, IIIb	OH	CH_2-CH_2-COOH	CH_3	H
Ic	OH	CH_2-CH_2-COOH	Cl	OH
Id, IIId	OH	CH_2-CH_2-COOH	Cl	H
Ie	OH	CH_2-COOH	Br	OH
If, IIIf	OH	CH_2-COOH	Br	H
Ig, IIIg	OH	H	H	OH
Ih, IIIh	OH	H	CH_3	OH
Ii, IIIi	H	H	H	OH
IIIj	OH	H	H	H

Va, VIa: Z=H; Vb, VIb: Z=CH_3

Fig. 1.

IR peaks of 3490 and 3060 cm^{-1} seem to be due to the vibration related to the boron chelates. The peaks of 1470, 1280, and 1125 cm^{-1} of the boron chelate were ascribed to the B-N,[4] B-O,[5] and C-N stretching vibrations, respectively, in comparison with the IR spectrum of IIIg.

From the results, it was concluded that the isolation of the normal reduction products of Ig and Ih was prevented by the formation of soluble boron chelates in weakly acidic solutions.

The Schiff base II did not yield the boron chelate but gave the normal reduction product. The yellow color of II is also in contrast with the orange-red color of Ig and Ih. It is deduced that the naphthalene ring is prohibited by the steric hindrance from being in a plane containing the C=N double bond and the phenyl ring of II.

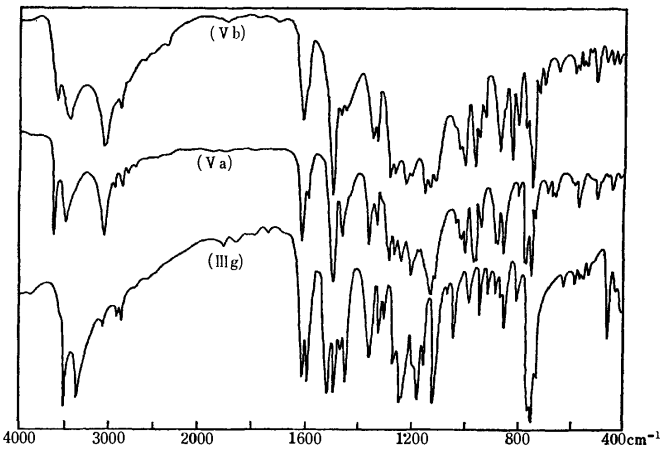

Fig. 2. The IR spectra of (IIIg), (Va), and (Vb).

Table 1. The Schiff bases to be reduced

	Mp °C	Yield %	Anal. Found (%)			Calcd (%)		
			C	H	N	C	H	N
Ia[a]	145—147	80	64.84	6.04	4.44	64.34	6.03	4.41[b]
Ib	110—111	81	71.95	6.11	4.88	72.02	6.05	4.94
Ic[a]	185—186	97	60.05	4.49	4.33	60.10	4.41	4.38
Id	108	99	63.48	4.72	4.62	63.27	4.65	4.61
Ie[a]	217	55.3	51.44	3.43	3.95	51.45	3.45	4.00
If	165	85.5	54.00	3.61	4.00	53.91	3.62	4.19
II	195—198[c]	54	76.65	4.85	5.22	76.38	4.90	5.24

Ig, Ih, Ii: known compounds.

a) The reduction products of these Schiff bases were not identified. They were neither the boron chelate nor the expected reduction product but were a mixture of deoxygenated products.

b) Analytical values of monohydrate.

c) Reported[6] melting point 230°C.

4) H. Steinberg and R. J. Brotherton, "Organoboron Chemistry," John Wiley and sons, New York, 1966, vol. 2. pp. 7—8.

5) J. A. Blau, W. Gerrard, M. F. Lappert, B. A. Mountifield, and H. Pyszora, *J. Chem. Soc.*, **1960**, 380.

6) Z. Holzbecher, *Chem. Abstr.*, **48**, 3198d (1952).

Table 2. Reduction products

	Procedure	Mp °C	Yield %	Anal. Found (%)			Calcd (%)		
				C	H	N	C	H	N
IIIb	A	131—132	90	71.34	6.74	4.85	71.55	6.72	4.91
IIId	A	110	69.5	62.65	5.59	4.57	62.85	5.27	4.59
IIIf	A	142—143	62.5	53.28	4.30	4.03	53.59	4.20	4.17
IIIg	B	88—90	86						
IIIh	B	95—96	72	73.14	6.58	6.13	73.34	6.59	6.11
IIIi[7]	A	79	50						
IIIj	A	45—46	72						
IV	A B	129—131	63.3 75	72.02	5.36	4.60	67.66	5.34	4.65[a]
Va	C	145—146	84.5	64.44 B 4.43[b]	5.08	5.72	64.78 B 4.70	5.02	5.81
VIa		131—133		69.60	4.67	6.12	70.01	4.52	6.28
Vb[c]	C	119—127	67	67.35	5.73	5.45	65.92	5.53	5.49
VIb[c]		108—112		69.81	5.17	6.04	70.93	5.10	5.91

a) Analytical values of hydrochloride mp 162 - 165°C.
b) Atomic absorption analysis of aqueous sodium hydroxide solution using aqueous sodium borohydride solution as a reference.
c) The analytical values were not satisfactory owing to difficulty in purification.

Table 3. The mass spectra of Va and VIa

m/e	Relative intensities (%)[a]		Possible ionic species
	(Va)[b]	(VIa)[c]	
224	7.6	19.9	
223	93	91	$C_{13}H_{10}BNO_2^+$
222	100	100	$C_{13}H_9BNO_2^+$
221	24	71	
111	11.8	24	$C_{13}H_9BNO_2^{++}$
77		27	$C_6H_5^+$
60	29		HBO_3^+
45	37		$H_2BO_2^+$
43	33		BO_2^+
39		11.1	CH_2BN^+
28	20.5		CO^+
18	44		H_2O^+
17	45		HO^+

a) Ions having relative intensities less than 10% are omitted.
b) Ionizing voltage, 75 eV; ionizing current, 200 μA; sample temperature, 105°C; chamber temperature, 140°C.
c) Ionizing voltage, 75 eV; ionizing current, 100 μA; sample temperature, 135°C; chamber temperature, 110°C.

Experimental

Procedure A. To a solution of 100 mg of the Schiff base Id in 15 m*l* of methanol heated to 50°C, crystals of 50 mg of sodium borohydride were gradually added in small portions after frothing had subsided. The reaction mixture was then cooled, filtered, diluted with 12 m*l* of water, and acidified with dilute acetic acid. The solution became turbid and after a while white crystals separated out. Recrystallization from benzene gave 70 mg of IIId with a melting point 110°C (69.5%).

Procedure B. A solution of 1 g of Ig in 20 m*l* of methanol was treated with 114 mg of sodium borohydride as in procedure A. After the reaction was over, methanol was evaporated off in a vacuum at room temperature. The residual purple oil was dissolved in water, and the solution was acidified with dilute acetic acid. White crystals then separated out. Recrystallization from methanol gave 860 mg of IIIg with a melting point 88—90°C (86%).

Procedure C. A solution of 4.5 g of Ig in 150 m*l* of methanol was treated with 3.4 g of sodium borohydride as in procedure A. After the reaction was over, the reaction mixture was cooled and diluted with 120 m*l* of water, when the color of the solution turned green. The solution was then acidified with dilute acetic acid, and the color of the solution turned reddish brown. Evaporation of the solvent at room temperature in a vacuum, yielded 4.3 g of gray precipitate of Va (84.5%). UV, $\lambda m\mu$ (log ε); 203—5 (4.56), 207 (4.59), 244—5 (3.98), 277 (3.67),[8] 282 (3.70), 292 (3.59)[8] in ethanol; 218 (4.27), 230 (4.02), 275 (3.66),[8] 280 (3.70), 285 (3.66)[8] in cyclohexane.

One gram of Va was sublimed at 130—135°C in a vacuum (5 mmHg), to yield 570 mg of yellow crystals of VIa (61.3%). UV, λ mμ (log ε); 218—220 (4.10), 230 (3.92), 275 (3.53),[8] 280 (3.58), 284 (3.54)[8] in cyclohexane.

The authors are grateful to Dr. M. Nakanishi and Mr. T. Kuriyama, Yoshitomi Pharmaceutical Company, for the mass spectra measured on their Nihon-Densi JMS-01S-G mass spectrometer.

7) B. Witkop and J. B. Patrick, *J. Amer. Chem. Soc.*, **74**, 3865 (1952).

8) These bands are obscure owing to overlapping.

BULLETIN OF THE CHEMICAL SOCIETY OF JAPAN, VOL. 45, 633—634 (1972)

Low Frequency Vibrational Spectra of Triarylgermanium Pseudohalides

T. N. SRIVASTAVA and S. K. TANDON*

Department of Chemistry, Lucknow University, Lucknow, India

(Received April 13, 1971)

Infrared spectra of arylgermanium derivatives in the low frequency region have attracted attention of only a few workers[1-3] in recent years. We synthesized some triarylgermanium pseudohalides (Aryl= C_6H_5, p-$CH_3C_6H_4$, pseudohalide=CN, NCO, NCS) and recorded their spectra as KBr discs in the region 650—250 cm^{-1} using a Perkin-Elmer Model 521 Spectrophotometer. The results and fundamental absorption frequencies along with their assignments are given. The characteristic vibrations of pseudohalide groups are identified at the expected positions and have been discussed together with the preparation and purification of the compounds.[4]

Some vibrations of the aromatic rings bonded to germanium atom fall in the recorded range of the spectra. Whiffen's nomenclature[5] has been used throughout to designate various modes of aromatic ring vibrations. A mass sensitive ring stretching vibration t has been observed in all the compounds in the range 370—270 cm^{-1}.[3] It is known[1,3] that when more than one aryl group is present in the molecule, a splitting of this absorption occurs giving rise to a lower component t'. Accordingly we have identified two distinct bands in triphenyl and tri-p-tolylgermanium compounds, the position of the absorption in the former being slightly towards lower frequency side than the latter. The two absorptions have been described by some earlier workers as asymmetric and symmetric phenyl-metal stretching.[2,6-8] The two other mass sensitive aromatic ring stretchings q and r lie above the reported range of the spectra. However, in triphenylgermanium derivatives they have been identified at 1095±1 cm^{-1} vs and 669±1 cm^{-1} w, while in corresponding p-tolyl derivatives they lie at 1088±1 cm^{-1} vs and 702±1 cm^{-1} w respectively.

The strongest absorption in the whole of the spectra is a mass-sensitive out-of-plane ring bending mode which appears as a doublet[6] separated by about 10 cm^{-1} and distinguished by y and y'. Apart from its slight sensitiveness to the mass of the substituent atom,[3] it appears to be dependent on the nature of the substitution of the benzene nucleus. We[9] have identified this absorption in a large number of aryltin compounds and have observed that o-, m- or p- substitution on the benzene ring produces an appreciable change in its position. Some earlier workers[10,11] have mistaken this absorption to be a tin-phenyl stretch. The two other mass sensitive ring deformations u and x are expected to lie below the recorded range of the spectra, although some workers[3,12] have preferred to call the lower component of t by the mode u.

TABLE 1. VIBRATIONAL FREQUENCIES OF TRIARYLGERMANIUM PSEUDOHALIDES

Assignment	$(C_6H_5)_3GeNCS$	$(C_6H_5)_3GeNCO$	$(C_6H_5)_3GeCN$	$(p\text{-}CH_3C_6H_4)_3$-GeNCS	$(p\text{-}CH_3C_6H_4)_3$-GeNCO	$(p\text{-}CH_3C_6H_4)_3$-GeCN
s	617 vw	622 w	614 sh	642 w	643 w	641 w
δ(NCO)		610 sh			606 sh	
CH_3-C_6H_5 rock.				592 s	594 s	595 s
y	471 sh	470 s	468 vs	500 s	500 s	500 s
y'	462 vs	462 vs	456 s	492 vs	492 vs	493 vs
δ(NCS)	478 sh			477 sh		
ν(Ge-NCO)		450 m			—	
Overtone of δ(Ge-CN)			438 m			437 m
w	390 vw	393 vw	390 vw	445 vw(b)	448 vw	447 vw
ν(Ge-NCS)	368 sh			374 sh		
t	340 vs(b)	338 s(b)	365 m	370 m	370 m	376 m
t'	272 w	285 w	276 w	328 m	327 m	327 m

* Present address: Industrial Toxicology Research Center, Chattar Manzil, Lucknow, India.

1) A. L. Smith, *Spectrochim. Acta*, **24 A**, 695 (1968).
2) R. J. Cross and F. Glockling, *J. Organometal. Chem.*, **3**, 146 (1965).
3) K. M. Mackey, D. B. Sowerby, and W. C. Young, *Spectrochim., Acta*, **24 A**, 611 (1968).
4) T. N. Srivastava and S. K. Tandon, *J. Inorg. Nucl. Chem.*, **30**, 1399 (1968).
5) D. H. Whiffen, *J. Chem. Soc.*, **1956**, 1350.
6) R. C. Poller, *Spectrochim. Acta*, **22**, 935 (1966).
7) T. N. Srivastava and S. K. Tandon, *ibid.*, **27 A**, 593 (1971).
8) A. L. Smith, *ibid.*, **19**, 849 (1963).
9) T. N. Srivastava and M. P. Agarwal, *J. Inorg. Nucl. Chem.*, **32**, 3416 (1970).
10) H. Kriegsman and H. Geissler, *Z. Anorg. Allgem. Chem.*, **323** 170 (1963).
11) H. Schumann and M. Schmidt, *J. Organometal. Chem.*, **3** 485 (1965).
12) D. H. Brown, A. Mohammed, and D. W. A. Sharp, *Spectrochim. Acta*, **21**, 659 (1965).

Out of the four mass insensitive ring deformations p, v, s and w only the last two occur in this region. Their position appears to be affected by the nature of the aryl group. An absorption of strong intensity consistently identified in the spectra of *p*-tolyl compounds at 592—595 cm^{-1} has tentatively been assigned to the CH_3-C_6H_5 rocking mode.

BULLETIN OF THE CHEMICAL SOCIETY OF JAPAN, VOL. 45, 634—635 (1972)

Gas Chromatographic Determination of Reversible Adsorption of Hydrogen. XI.[1] Reversible Adsorption of Hydrogen over Some Metal Oxides

Yoshiko SHIGEHARA and Atsumu OZAKI

Research Laboratory of Resources Utilization, Tokyo Institute of Technology, Meguro-ku, Tokyo

(Received July 5, 1971)

It has been shown that the rapid and reversible part of hydrogen adsorption can be measured by means of the gas chromatographic retention volume of deuterium in hydrogen carrier. This method has been applied to metals[2] and metal oxides.[3] It was found that the rapid and reversible adsorption of hydrogen is molecular at low temperature and atomic at higher temperatures. However, not many oxides can remain as oxide at high temperature in a hydrogen stream. The reversible adsorption of hydrogen was determined over some hardly reducible oxides at higher temperatures.

Experimental

The apparatus and procedure for gas chromatographic measurement were essentially the same as before.[2] A deuterium sample was introduced into the hydrogen carrier gas by means of a doser made of glass tubing, and was passed to the catalyst column and detecter.

Vanadium trioxide was obtained from Mitsuwa Chemicals Company, Limited. Chromia was prepared by thermal decomposition of ammonium dichromate. Manganous oxide and zinc oxide were prepared by thermal decomposition of manganous carbonate and zinc oxalate *in vacuo*. The gas chromatographic columns of these oxide samples were made from a glass U tube 10—20 mm in diameter. The amount of samples were as follows. The oxide sample was *in situ* pretreated with hydrogen at rising temperature up to 500°C, during which treatment the following amounts of hydrogen were absorbed as below.

Cr_2O_3	V_2O_3	MnO	ZnO
9.0 g	24.7 g	46.8 g	17.8 g

Results and Discussion

1. Chromia. The deuterium retention volumes are shown in Fig. 1 as a function of temperature. The isobar is independent of the direction of temperature variations. It appears that there is an activated adsorption of hydrogen starting from around 100°C.

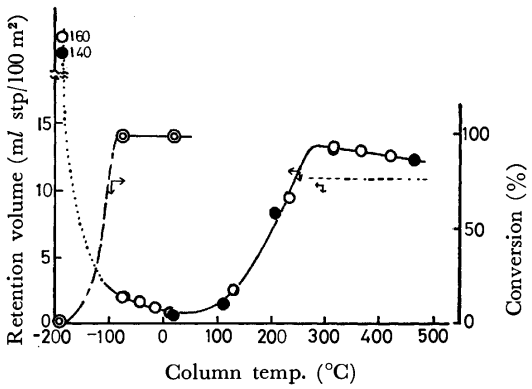

Fig. 1. Deuterium retention volumes and conversion of D_2 into HD by reduced chromia (9.0 g) at different temperatures.
—○— rising temperatures from −195 to 460°C,
—●— lowering temperatures from 460 to −195°C,
—◎— conversion of D_2,
------ difference between retention volume and activated adsorption.

Oxide	Cr_2O_3	V_2O_3	MnO	ZnO
Sorbed hydrogen	18 ml/100 m²	*ca.* 80 ml/g[a]	*ca.* 10 ml/100 m²	14 ml/100 m²
Color of oxide after H_2 treatment	gray	black	pale green	gray

a) This amont of hydrogen corresponds to 0.5 mol per mol of V_2O_3. However, X-ray analysis of hydrogen-treated sample showed only V_2O_3. The large amount of hydrogen consumed might be due to excess oxygen involved.

1) Part IX: Ref 3b, Part X: Ref 3c.

2) A. Ozaki, F. Nozaki, K. Maruya, and S. Ogasawara, *J. Catal.*, **7**, 234 (1967); A. Ozaki, Y. Shigehara, and S. Ogasawara, *ibid.*, **8**, 22 (1967); Y. Shigehara and A. Ozaki, *Nippon Kagaku Zasshi*, **88**, 838, 844 (1967), *J. Catal.*, **10**, 183 (1968), **15**, 224 (1969).

3) Y. Shigehara, and A. Ozaki, a) *ibid.*, **21**, 78 (1971); b) *Nippon Kagaku Zasshi*, **91** 940 (1970); c) *ibid.*, **92**, 297 (1971).

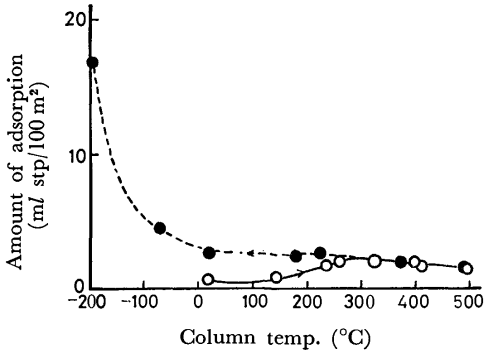

Fig. 2. Hydrogen adsorption isobar on reduced chromia.
—○— 20 → 500°C, —●— 500 → −195°C

In order to examine the contents of the deuterium retention, the static adsorption measurements were carried out on the same sample. The results are shown in Fig. 2. The activated adsorption of hydrogen is clearly demonstrated, but the amount is much less than that of deuterium retention. There must be another type of surface hydrogen which is incorporated into the deuterium retention through an exchange reaction. The amount of exchangeable hydrogen can be estimated by subtracting the activated adsorption from the deuterium retention. It is independent of temperature and is shown in Fig. 1 by the dotted line. Thus the exchangeable hydrogen would be the hydroxyl hydrogen. More than 80% of the deuterium retention accordingly seems to be caused by the surface hydroxyl.

The extent of conversion of D_2 into HD is 100% at above −75°C, while the activatedly adsorbed hydrogen is isotopically equilibrated with the flowing hydrogen above 300°C as shown in Fig. 1. This suggests that the exchange reaction between H_2 and D_2 is catalyzed by an active site other than the adsorption site for high temperature adsorption.

2. Vanadium, Manganese and Zinc Oxides. Three kinds of measurements were made on these oxides, for which activated adsorption of hydrogen is known.[4]

(1) Retention volume of deuterium sample.

(2) Extent of conversion of D_2 into HD in an eluted pulse.

(3) Static measurements of adsorption isobar of hydrogen (summarized in Fig. 3).

The retention volumes over these oxides are commonly null near room temperature, but increase above

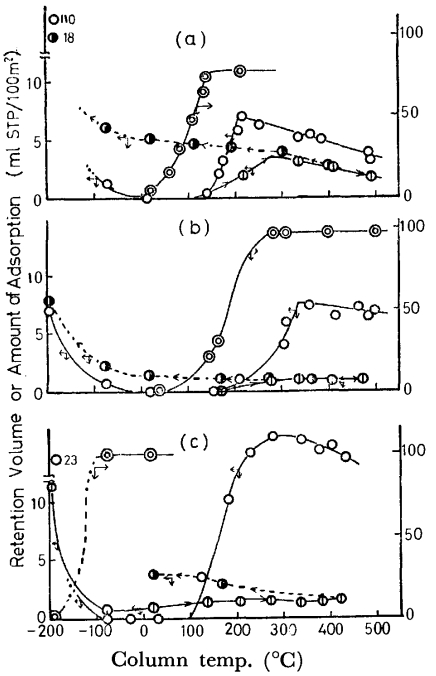

Fig. 3. Deuterium retention volume, amount of adsorption of hydrogen and conversion of D_2 into HD on vanadium (a), manganese (b) and zinc oxides (c).
Retention volume, —○—
Amount adsorbed, —◐— (rising temperature)
—◑— (lowering temperature);
Conversion, —◎—.

about 100°C up to respective maximums. In higher temperature ranges where the retention volumes decrease with rise in temperature, the rate of adsorption and exchange reaction would be fast enough to establish an isotopic equilibrium between gas and solid surfaces.

The extent of conversion of D_2 into HD begins to increase and reaches isotopic equilibrium[5] at a much lower temperature than the retention volume, particularly in the case of zinc oxide, where the conversion is 100% below 0°C. Thus the exchange reaction between H_2 and D_2 seems to be catalyzed by an active site other than the adsorption site for the high temperature adsorption.

The difference between the retention volume and the static adsorption must be due to the isotopic exchange between the adsorbed hydrogen and surface hydroxyl. The exchange is most extensive in the case of zinc oxide.

4) K. Tarama, and S. Teranishi, *Kogyo Kagaku Zasshi*, **55**, 316 (1952); H. S. Taylor, A. T. Williamson, *J. Amer. Chem. Soc.*, **53**, 2168 (1931); H. S. Taylor, S. C. Liang, *ibid.*, **69**, 1306 (1947). V. Kesavulu and H. A. Taylor, *J. Phys. Chem.*, **64**, 1124 (1960).

5) The equilibrium conversion to HD was lower than 100% in the case of V_2O_3 because of the small volume of the sample column of oxide.

BULLETIN OF THE CHEMICAL SOCIETY OF JAPAN, VOL. 45, 636—638 (1972)

Studies on Stable Free Radicals. VIII.[1] The Synthesis and Oxidation of Hindered 4-Oxopiperidine Derivatives

Takao YOSHIOKA, Susumu HIGASHIDA, and Keisuke MURAYAMA

Central Research Laboratories, Sankyo Co., Ltd., Shinagawa-ku, Tokyo

(Received July 22, 1971)

It has been reported that a hindered amine, 2,2,6,6-tetramethyl-4-oxopiperidine (I), was easily oxidized with 30% aqueous hydrogen peroxide in the presence of EDTA and sodium tungstate to give a free radical, 2,2,6,6-tetramethyl-4-oxopiperidine-1-oxyl (II), which was extremely stable in air at room temperature.[2] However, cyclohexane-1-spiro-2′-(4′-oxoimidazolidine)-5′-spiro-1″-cyclohexane (III)[3] did not give the corresponding *N*-oxyl IV (Chart I) and was quantitatively recovered under similar reaction conditions. The difference in the reactivities of I and III can be explained *a priori* by the following factors: a) the effect of the alkyl groups at *C*-2 and *C*-6 (or *C*-5 in imidazolidine ring), b) the character of a heterocyclic ring system. In order to establish the contribution of a), the monocyclohexane derivative V and the dicyclohexane derivative VI (Chart I)

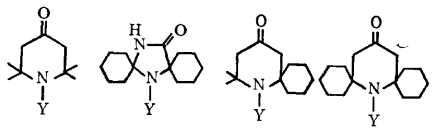

I Y=H III Y=H V Y=H VI Y=H
II Y=O· IV Y=O· VII Y=O· VIII Y=O·

Chart I

were synthesized as is shown in Chart II; the relative ease of the oxidation of V and VI with 30% aqueous hydrogen peroxide into the corresponding *N*-oxyls VII and VIII respectively, was then qualitatively compared with that of I into II.[4] Utilizing a slight modification (in methanol) of the method of Rozantzev,[2] the oxidation of I and V with 30% aqueous hydrogen peroxide into II and VII respectively in good yields was successful, although the ease of the formation of the *N*-oxyl VII was observed to be slightly smaller than that of II. On the other hand, the oxidation of VI into VIII was unsuccessful under the same reaction conditions, and we recovered the starting amine VI. Thus, it was supposed that one of the major factors[4] influencing the rate of the oxidation of such amines is a steric effect. The synthesis of VIII in a good yield was achieved by the oxidation of VI with *m*-chloroperbenzoic acid(CPBA).

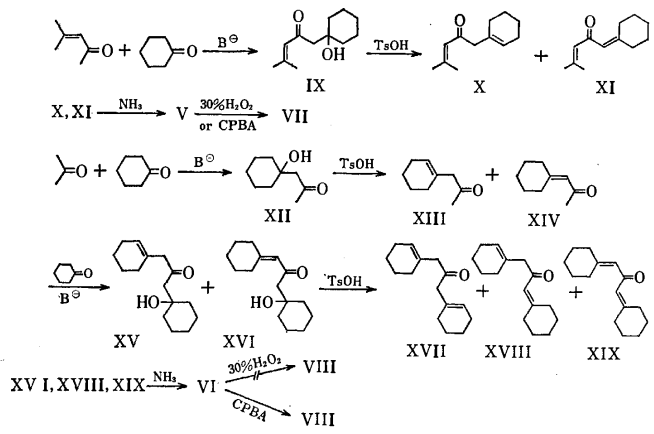

Chart II

Experimental

All the melting points are uncorrected.

Unless otherwise stated, the IR spectra were taken with a Hitachi EPI-S2 spectrometer (Nujol mull or liquid film); the NMR spectra, with a Varian A-60 apparatus, using tetramethylsilane as the internal reference; the mass spectra, with a JEOL-JMS-OIS apparatus, and the ESR spectra, with a Hitachi MES 4001-type X-band apparatus, employing 100-kHz modulation. Table 1 shows the formulae, molecular ion peaks, melting points, boiling points, yields and results of the elemental analysis of all the products, while the spectral data are shown in Table 2.

1-(1-Hydroxycyclohexyl)-4-methylpent-3-en-2-one (*IX*). Into a suspension of 1.00 mol of sodium ethoxide in 500 m*l* of toluene[5] was added slowly and dropwise a mixture of 100 g (1.02 mol) of cyclohexanone and 100.2 g (1.04 mol) of mesityl oxide at −55°C under nitrogen with stirring. After additional stirring for 30 min at −50°C, the reaction mixture was poured into a mixture of 101 g of 35% hydrochloric acid and 700 g of crashed ice. The resulting mixture was allowed to stand at 0°C for 1 hr and then at room temperature overnight. The organic layer was separated, and the aqueous phase was extracted with ether. The combined organic phases were washed three times with water saturated with sodium chloride, and then dried over anhydrous magnesium sulfate. The removal of the solvents and fractional distillation gave 150.3 g of IX.

1-(1-Hydroxycyclohexyl)propan-2-one (*XII*) was similarly prepared from acetone and cyclohexanone.

1-(Cyclohex-1-enyl)-3-(1-hydroxycyclohexyl)propan-2-one (*XV*) *Containing 1-(Cyclohexylidene)-3-(1-hydroxycyclohexyl)propan-2-one* (*XVI*). Similarly, a *ca.* 9 : 1 mixture of XV and XVI was prepared from cyclohexanone and the ketone, XIII, containing XIV.

General Procedure for Dehydration of Ketols IX, XII, XV, and

1) Part VII: T. Toda, S. Morimura, and K. Murayama, This Bulletin, **45**, 557 (1972).

2) a) E. G. Rozantzev, "Free Nitroxyl Radicals," Plenum Press, New York, N. Y. (1970), p. 1. b) K. Murayama, *Yuki Gosei Kagaku Kyokaishi*, **29**, 366 (1971).

3) K. Murayama, S. Morimura, and T. Yoshioka, This Bulletin, **42**, 1640 (1969).

4) Following papers will describe with respect to hindered imidazolidines and piperazines.

5) R. B. Turner and D. M. Voitle, *J. Amer. Chem. Soc.*, **72**, 4166 (1950).

Table 1.

Compound	Formula	M+ (*m/e*)	Mp °C(Solvent for recry.) Bp °C/mmHg	Yield (%)	Elemental analysis (Found/Calcd)		
					C	H	N
V	$C_{12}H_{21}NO \cdot H_2O$	195	50.5—51.5 (acetone: H_2O=2 : 1) 84—87/0.5 (anhydrous oil)	76.8	67.40/67.60	10.82/10.89	6.61/6.57
VI	$C_{15}H_{25}NO$	235	100.5—101.5 (acetone)	89.5	76.53/76.60	10.72/10.72	6.17/5.95
VII	$C_{12}H_{20}NO_2$	210	83.0—84.0 (*n*-hexane)	83.8	68.38/68.53	9.65/ 9.59	6.72/6.66
VIII	$C_{15}H_{24}NO_2$	250	114.0—115.0 (petroleum ether containing benzene)	62.0	71.86/71.96	9.66/ 9.66	5.52/5.59
IX	$C_{12}H_{20}O_2$		105/1.5	75.5	73.24/73.47	10.29/10.20	
X	$C_{12}H_{18}O$[a]		80—81/1	80	80.61/80.85	10.19/10.18	
XII	$C_9H_{16}O_2$	156	67—68/1	32.6	69.31/69.23	10.36/10.38	
XIII	$C_9H_{14}O$[b]	138	82—83/13	75.5	78.03/78.26	10.25/10.22	
XV	$C_{15}H_{24}O_2$[c]	236	128—132/2	30	76.34/76.22	10.10/10.24	
XVII	$C_{15}H_{22}O$[d]	218	124—125/1.5	65	82.85/82.57	10.20/10.18	

a): containing XI, b): containing XIV, c): containing XVI, d): containing XVIII and XIX

Table 2. Spectral data

Compound	IR (cm^{-1})	NMR (τ)
V[a]	3480, 3340(w), 3250, 1715(sh), 1690[b]	7.71(4H, s), 8.76(6H, s), 8.3—8.8(10H, broad)[c]
VI	3280, 1700(sh), 1690[b]	7.67(4H, s), 8.2—9.0(20H, broad)[c]
VII	1710, 1322, 1234[b]	
VIII	1725, 1324, 1212[b]	
IX	3500, 1680, 1620	4.05(1H, m, J=1.2 Hz), 6.55(1H, broad), 7.58[d](2H, s), 7.90(3H, d, J=1.2 Hz), 8—9(10H, broad)
X	1715(sh), 1690, 1670(sh), 1625[e]	3.9(1H, m, J=1.5 Hz), 4.3—4.6(1H, broad m)[d,f], 7.0—7.2(2H, broad m), 7.90(3H, d, J=1.5 Hz), 8.13(3H, d, J=1.5 Hz), 7.8—8.6(broad)
XI[e]		3.9(1H, m, J=1.5 Hz), 4.1(1H, broad m), 7.90[d,f](3H, d, J=1.5 Hz), 8.13(3H, d, J=1.5 Hz), 7.8—8.9(broad)
XII	3490, 1700[b]	6.78(1H, broad), 7.50(2H, s), 7.87(3H, s), 7.87(3H, s), 8—9[d](10H, broad)
XIII	1720, 1690(w), 1670(sh), 1625[g]	4.45(1H, m), 7.06(2H, broad m), 7.93(3H, s)[d,f], 7.8—8.7 (broad)
XIV[g]		4.06(1H, m), 7.90(3H, s), 7.8—8.7(broad)[d,f]
XV	3500, 1700, 1670(sh), 1615[h]	4.3—4.5(1H, m), 6.1—6.5(1H, broad), 6.9—7.1[d,f](2H, broad m), 7.41(2H, s), 7.7—9.0(broad)
XVI[h]		4.0—4.1(1H, m), 6.1—6.5(1H, broad), 7.41(2H[d,f], s), 7.7-9.0(broad)
XVII	1720, 1690, 1670, 1625[i]	4.5(2H, m), 6.9—7.3(4H, broad m), 7.7—8.7[d,f](broad)
XVIII[i]		4.1(1H, m), 4.5(1H, m), 6.9—7.3(2H, broad m)[d,f], 7.7—8.7(broad)
XIX[i]		4.1(2H, m), 7.7—8.7(broad)[d,f]

a) as monohydrate, b) PE-221, c) in $CDCl_3$, d) in CCl_4, e) a mixture of X and XI, f) X/XI=*ca.* 75/25, XIII/XIV=*ca.* 85/15, XV/XVI=*ca.* 90/10, XVII/XVIII/XIX=*ca.* 63/34/3 on the basis of NMR, g) a mixture of XIII and XIV, h) a mixture of XV and XVI, i) a mixture of XVII, XVIII and XIX

XVI, A solution of ketols in benzene was refluxed for 1.5 hr in the presence of *p*-toluenesulfonic acid, using a Dean-Stark separator. After cooling the reaction mixture was washed with water and dried over anhydrous magnesium sulfate. After the removal of the solvent and fractional distillation, IX gave a *ca.* 3 : 1 mixture of *1-(cyclohex-1-enyl)-4-methylpent-3-en-2-one* (*X*) and *1-cyclohexylidene-4-methylpent-3-en-2-one* (*XI*), identified on the basis of the signal intenisty in the NMR spectrum. Similarly, XII gave a *ca.* 85 : 15 mixture of *1-(cyclohex-1-enyl)propan-2-one* (*XIII*) and *1-cyclohexylidenepropan-2-one* (*XIV*) (NMR). Without the separation of XV and XVI, these were dehydrated to give a *ca.* 63 : 34 : 3 mixture of *1,3-(dicyclohex-1-enyl)propan-2-one* (*XVII*), *1-(cyclohex-1-enyl)-3-cyclohexylidenepropan-2-one* (*XVIII*) and *1,3-dicyclohexylidenepropan-2-one* (*XIX*) (NMR).

1-Aza-2,2-dimethyl-4-oxo-spiro[5.5]undecane (*V*). Without the separation of X and XI, these substances(8.7 g, 49.8 mmol) were treated with 12.4 g(730 mmol) of ammonia in 8.7 m*l* of water and 35 m*l* of methanol at 105—110°C for 17 hr in a pressure bottle (glass).[6,7] After the removal of the ammonia and the solvents, the reaction mixture was dissolved into petroleum ether and treated with active char-

6) D. Mackay and W. A. Waters, *J. Chem. Soc., C*, **1966**, 814.

7) It was inferable that the amine V or VI was produced by amination followed by cyclization of XI or XIX *via* isomerization of X or XVII, respectively, under the reaction conditions, although no isomerization was observed on the basis of the NMR and IR spectra under milder reaction conditions (80°C, 7 hr).

coal to give a colorless oil after the removal of the selvents. The oil was dissolved into acetone and diluted with water to give colorless needles of the monohydrate of V.

Cyclohexane-1-spiro-2'-(4'-oxopiperidine)-6'-spiro-1''-cyclohexane (*VI*). Similarly, a ketone mixture of XVII, XVIII, and XIX was treated for 24 hr. Almost pure crystals of VI separated out when the reaction mixture was cooled to room temperature.

Oxidation of Hindered Amine V with 30% Aqueous Hydrogen Peroxide in Methanol. The monohydrate of V(200 mg, 0.94 mmol) was oxidized with 0.5 g (4.41 mmol) of 30% aqueous hydrogen peroxide in 1 m*l* of methanol in the presence of EDTA and sodium tungstate at room temperature for 76 hr. After the removal of the methanol, 10 m*l* of benzene and 0.7 g of potassium carbonate were added to the reaction mixture; the resulting suspension was stirred at room temperature for 1 hr in order to decompose excess hydrogen peroxide. The potassium carbonate was filtered off; the subsequent evaporation of the benzene *in vacuo* gave *1-aza-2,2-dimethyl-4-oxo-spiro[5.5]undecane-1-oxyl* (*VII*) as an oil, which gave reddish needles upon recrystallization from *n*-hexane.
ESR: a triplet (10^{-3} M).

Oxidation of the Hindered Amine VI with 30% Aqueous Hydrogen Peroxide in Methanol. By the same procedures, the amine VI was recovered quantitatively. The oxidation of VI for 9 days gave a trace of the *N*-oxyl VIII, and most of the starting amine VI was recovered.

Cyclohexane-1-spiro-2'-(4'-oxopiperidine-1'-oxyl)-6'-spiro-1''-cyclohexane (*VIII*). A solution of 4.7 g (20 mmol) of the amine VI and 18.0 g (105 mmol) of CPBA in 120 m*l* of chloroform was stirred for 2 days at room temperature and washed with a 10% aqueous solution of potassium carbonate three times and then with water. The chloroform layer was dried over anhydrous magnesium sulfate and concentrated *in vacuo* to give a reddish oil, which solidified on being triturated in a small amount of petroleum ether. The crude product was dissolved into a small amount of benzene, after which petroleum ether was added to give reddish-orange prisms. ESR: a triplet (10^{-3} M).

The *N*-oxyl VII was also synthesized from V by similar procedures(CPBA).

The authors would like to thank Dr. Genshun Sunagawa, the director of these laboratories, for his encouragement and Mrs. Eiko Mori and Mr. Tsutomu Kanai for their technical assistance.

BULLETIN OF THE CHEMICAL SOCIETY OF JAPAN, VOL. 45, 638—639 (1972)

A Novel Synthesis of 3,4-Benzotropolone

Masaru SATO, Josuke TSUNETSUGU, and Seiji EBINE

Department of Chemistry, Faculty of Science and Engineering, Saitama University, Urawa, Saitama

(Received July, 26, 1971)

3,4-Benzotropolone has been synthesized with difficulty from tediously-obtainable 2,3-benzosuberone.[1,2] We now wish to develop a method capable of synthesizing simply 3,4-benzotropolone.

There have appeared several examples of the reaction of diazo compounds with quinones. Diazomethane reacts with β-naphthoquinone (I) to afford a resinous product[3] or a dioxole derivative,[4] although it reacts with *p*-benzoquinone to give tropone derivatives in a few cases.[5-7] On the other hand, diazo compounds can react with quinones in the presence of Lewis acid to induce ring enlargement, thus affording troponoids.[8]

We examined the reaction of I with diazomethane in the presence of boron trifluoride etherate. To a methylene chloride solution of I and boron trifluoride etherate, we added an equal volume of an ethereal diazomethane solution. After working up as usual, followed by chromatographic separation, a bright yellow crystalline product (II) was obtained. II exhibited infrared absorption bands (KBr) at 1424, 1398, 1377, and 1329 cm^{-1} assignable to the chelated carbon-oxygen stretching absorption and at 1100 cm^{-1} due to the oxygen-boron stretching absorption.[9] The NMR spectrum ($CDCl_3$) of II showed only aromatic protons at δ 9.0 (1H) assignable to a benzene ring proton *peri* to the carbonyl group of a tropolone ring and at δ 8.0 (6H) for the other benzene and tropolone ring protons. These spectral data, as well as the complete agreement of the results of elemental analysis, indicated II to be a chelate compound of 3,4-benzotropolonoboron difluoride. The structure of II was established unequivocally by the fact that II was again formed in a high yield on the treatment of 3,4-benzotropolone (III) with boron trifluoride etherate.

The ring enlargement of I was examined under various conditions; the results are shown in Table 1. This reaction gave a very low yield in an ethereal solution but a fairly good yield (25.5%) in a 1 : 1 mixture of ether and methylene chloride. The use of an excess amount of boron trifluoride etherate resulted in no increase in the yield.

II was hydrolyzed with dilute sulfuric acid to afford III in an almost quantitative yield, the overall

1) J. W. Cook, A. R. M. Gibb, R. A. Raphael, and A. R. Sommerville, *Nature*, **163**, 410 (1949); *J. Chem. Soc.*, **1952**, 603. T. Nozoe, Y. Kitahara, and T. Ando, *Proc. Japan Acad.*, **27**, 107 (1952).

2) E. Galantay and W. R. J. Simpson, *Chem. Commun.*, **1970**, 754.

3) L. F. Fieser and J. L. Hartwell, *J. Amer. Chem. Soc.*, **57**, 1479 (1935).

4) W. M. Horspool, *Quart. Rev.* (London), **23**, 204 (1969).

5) G. B. Marini-Bettolo and L. Paoloni, *Gazz. Chim. Ital.*, **84**, 327 (1954).

6) L. I. Smith and W. B. Pings, *J. Org. Chem.*, **2**, 95 (1937).

7) W. Rundel and P. Kastner, *Ann. Chem.*, **737**, 87 (1970); L. Horner and E. Lingnau, *ibid.*, **573**, 30 (1951).

8) B. Eistert and L. Klein, *Chem. Ber.*, **101**, 391 (1968).

9) J. W. Cook, R. A. Raphael, and A. I. Scott, *J. Chem. Soc.*, **1952**, 4416.

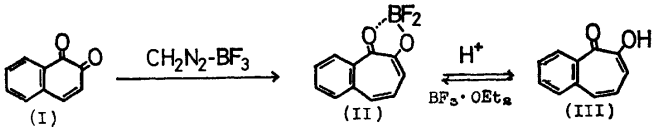

Table 1. The reaction of β-naphthoquinone with diazomethane

Exp. No.	Molar ratio			Solvent	Yied (%)
	Quinone(I)	$BF_3 \cdot OEt_2$	CH_2N_2[b]		
1[a]	1	1	4	Et_2O	2.0
2	1	1	4	CH_2Cl_2	7.1
3	1	1	4	CH_2Cl_2-Et_2O (1:1)	25.5
4	1	1	1.5	CH_2Cl_2-Et_2O (1:1)	18.4
5	1	2	4	CH_2Cl_2-Et_2O (1:1)	22.4

a) The quinone (I) was recovered in 17% yield.
b) Calculated on the basis of *N*-nitrosomethylurea.

yield of III from I amounting to 24%. The present method for the synthesis of III involves a brief sequence starting with the easily-available I; it is markedly superior in its simplicity to another recently-reported method.[2)]

Experimental

Reaction of β-Naphthoquinone (I) with Diazomethane in the Presence of Boron Trifluoride Etherate. A distilled ethereal solution (50 m*l*) of diazomethane prepared from nitrosomethylurea (2.1 g, 0.005 mol) was rapidly added to a solution of freshly-prepared I (0.79 g, 0.005 mol) and 47% boron trifluoride etherate (1.5 m*l*, 0.005 mol) in methylene chloride (50 m*l*) under an atmosphere of nitrogen and with cooling in an ice bath. After having been stirred for 30 min, the mixture was poured into water and extracted with methylene chloride. The organic layer was dried over anhydrous sodium sulfate and evaporated under reduced pressure at room temperature. To the residue we then added a small amount of methylene chloride (*ca.* 10 m*l*), and the insoluble crystals were filtered off. The filtrate and the washings were directly charged on a silica-gel column, which was then eluted with methylene chloride. The evaporation of the solvent from the eluate and the recrystallization of the product from benzene gave 3,4-benzotropolonoboron difluoride (II) as yellow crystals; mp 188—195°C. Yield, 0.281 g (25.5%). Found: C, 59.75; H, 3.21%. Calcd for $C_{11}H_7O_2BF_2$: C, 60.05; H, 3.20%.

This reaction was examined under various conditions; the results are given in Table 1.

Hydrolysis of 3,4-Benzotropolonoboron Difluoride (II). A mixture of II (122 mg), 2 N sulfuric acid (15 m*l*), and ether (10 m*l*) was refluxed for 0.5 hr. After the evaporation of the ethanol, the residue was diluted with water and extracted with cyclohexane. The subsequent removal of the solvent from the extract, after drying over anhydrous magnesium sulfate, gave a product (mp 82—85°C) which was sublimed at 130°C/20 mmHg to give pale yellow crystals of III (mp 85—86°C) in 94.3% yield. Admixture with an authentic sample[1)] showed no depression of the melting point.

Reaction of 3,4-Benzotropolone (III) with Boron Trifluoride Etherate. To a solution of III (30 mg) in absolute ether (3 m*l*) we added 47% boron trifluoride etherate (0.1 m*l*). The product, precipitated after the mixture had stood for 20 min, was collected by filtration and washed with ether to afford II (35 mg, 90% yield); mp 187—193°C (from benzene). The infrared spectrum of this compound was in complete agreement with that of the sample obtained by the ring enlargement of I.

BULLETIN OF THE CHEMICAL SOCIETY OF JAPAN, VOL. 45, 640—641 (1972)

The Formation of Ternary Complexes Involving Mercury(II) and Phenolphthalein Complexone

Toshiaki NOMURA, Kazuo WATANABE, and Sumio KOMATSU

Department of Chemistry, Faculty of Science, Shinshu University, Asahi, Matsumoto

(Received August 6, 1971)

Organic reagents (R) with two iminodiacetate group in a molecule react with mercury(II) to give the corresponding mercury(II) complexes. These complexes then react with anions (X), such as cyanide, thiocyanate, iodide, bromide, and thiosulfate, to form the corresponding mixed-ligand complexes. The molar ratio of Hg(II) : R : X in these mixed-ligand complexes is found to be 1 : 1 : 1.[1,2] In the mixed-ligand complex of thymolphthalein complexone (TPC), the ratio is also 2 : 1 : 1.[2] In this paper phenolphthalein complexone (PPC), which has a structure analogous to TPC, will be discussed with regard to reactions with mercury(II) and anions.

Experimental

Reagents and Apparatus. All the reagents were of an analytical grade and were used without further purification. A PPC solution of 1×10^{-2} M was prepared by disolving Dotite PPC (121.7 mg) with small amounts of water, adding 100 m*l* of methanol, and diluting to 200 m*l* with water. This solution was diluted to a suitable concentration with water when used. Standard mercury(II) ($F=1.041$) and cyanide solutions of 1×10^{-2} M and a buffer solution were prepared as in a preceding experiment.[1]

The absorbances of the solutions were measured by means of a Hitachi Perkin Elmer 139-type spectrophotometer, while the absorption spectra were recorded by means of a Shimadzu Multipurpose Recording Spectrophotometer, MPS-50L type, with quartz cells of an optical length of 10.0 mm. The pH values were measured by means of a Hitachi-Horiba M-5-type pH meter.

Results and Discussion

Reaction of Mercury(II) with PPC. Absorption Spectra: At pH 10.8, a PPC solution showed a weak absorption spectrum with a peak at 565 mμ in the visible region (Fig. 1). When mercury(II) was added to the solution, it gave a strong absorption spectrum in which the peak was shifted to 574 from 565 mμ and in which a new absorption peak appeared at 384 mμ in the visible region. In view of these facts, it can be said that PPC reacted with mercury(II) to form a mercury (II) complex with a strong absorption in the visible region.

Effect of pH: The absorbances of the mercury(II) complex appeared adruptly from a neutral solution, and gave constant values between about pH 10.5 and 11.5.

Composition of the Mercury(II) Complex: The molar ratio of mercury(II) to PPC in the mercury(II) complex was found to be 1 : 2 by the use of the molar-ratio (Fig. 2) and continuous-variation methods. The apparent stability constant (K) of the complex ($Hg(PPC)_2$) was found to be 1.0×10^{11} at an ionic strength of $\mu=0.10$ and at pH 10.8 by the molar-ratio method.

Stability of the $Hg(PPC)_2$ and the PPC Solutions: The absorbance of the PPC solution (reagent blank) at pH 10.8 did not change for 2 hr. The absorbance of the mercury(II)-complex ($Hg(PPC)_2$) solution was constant for about 20 min, but it decreased at a rate of 1.0% an hour beyond this time.

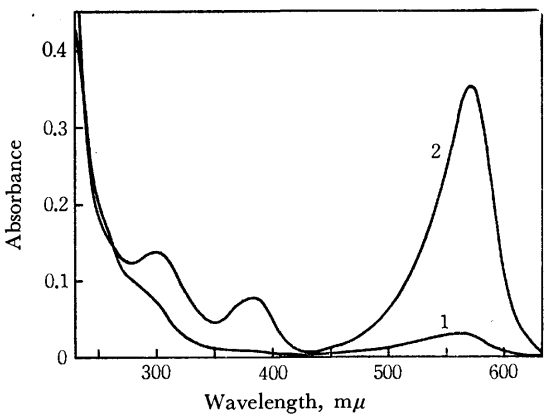

Fig. 1. Absorption spectra of mercury(II) complex and PPC at pH 10.8.
Reference: Water.
1) PPC: 2×10^{-5} M.
2) Hg(II): 1×10^{-5} M, PPC: 2×10^{-5} M.

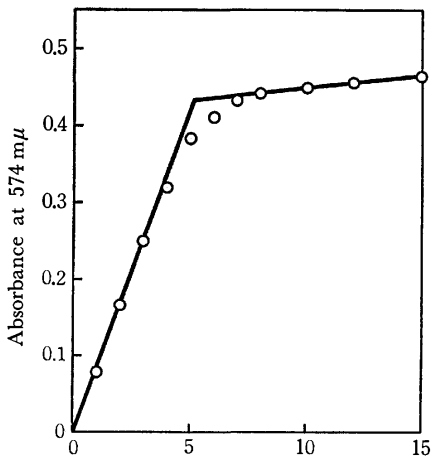

Fig. 2. Composition of mercury(II) complex (Molar ratio method).
Hg(II): 1×10^{-5} M, pH: 10.8, reference: water.

1) T. Nomura, This Bulletin, **43**, 104 (1970).
2) T. Nomura, R. Ikeda, and S. Komatsu, *Nippon Kagaku Zasshi*, **91**, 497 (1970).

Application for the Spectrophotometric Determination of Mercury(II): The above discussion shows that the spectrophotometric determination of mercury(II) with PPC was possible. Mercury(II) up to 60 μg could be determined with a good reproducibility by the following procedure, and the molar extinction coefficient was found to be 3.5×10^4.

Procedure: A mercury(II) sample solution containing up to 60 μg was treated with a buffer solution to adjust the pH to 10.5—11.5, 5 m*l* of a 2×10^{-4} M PPC solution were added, and then the mixture was diluted to 50 m*l* with water. The absorbance of the solution was measured after about 15 min at 574 mμ against the reagent-blank solution.

Reactions of $Hg(PPC)_2$ with Anions. Cyanide, iodide, and thiosulfate reacted with the mercury(II) complex to give the corresponding compounds, colored slightly. The molar ratio of the mercury(II) complex to these anions were determined by means of the molar-ratio (Fig. 3) and continuous-variation methods

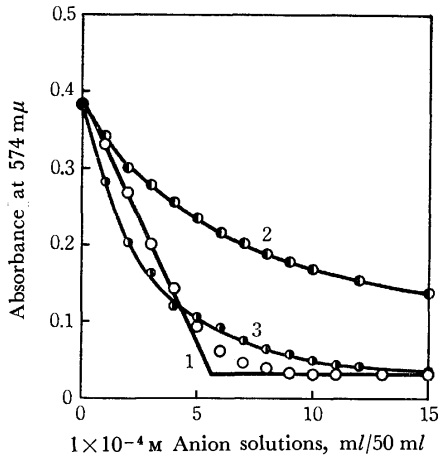

Fig. 3. Reactions of mercury(II) complex with anions. Hg(II): 1×10^{-5} M, PPC: 2×10^{-5} M, pH: 10.8, reference: water.
1) Cyanide ($F=0.928$). 2) Iodide ($F=1.001$).
3) Thiosulfate ($F=1.000$).

and by recording the absorption spectra of mercury(II)-complex solutions containing different amounts of the anions.

The absorption peak, at 574 mμ, of the mercury(II)-complex solution shifted linearly to 570 mμ with cyanide up to $CN^-/Hg(PPC)_2=1$. When an excess of cyanide was added, the absorption spectrum agreed with that of the PPC solution; the maximum absorption at 570 mμ shifted to 565 mμ, and the absorption peak at 384 mμ decreased. When an excess of iodide was added to the mercury(II)-complex solutions, the absorption peak at 574 mμ did not shift to 565 mμ, but to 569 mμ. From the results described above, it was found that cyanide and iodide (X_1) reacted with the mercury(II) complex as follows. When X_1 was added to the mercury(II) complex solution up to $Hg(PPC)_2/X_1=1$, a mixed-ligand complex (Hg-PPC-X_1) was formed and then the PPC was dissociated. When an excess of cyanide was added to the cyano mixed-ligand complex solution, the complex turned into mercury(II) cyanide and PPC. The iodo mixed-ligand complex, however, did not react with an excess of iodide to give mercury(II) iodide and PPC. From Fig. 3(1), it can be seen that the spectrophotometric determination of cyanide could be performed with the mercury(II) complex. This method was especially selective for cyanide because the only interfering anions were sulfide, thiosulfate, and iodide.

The mercury(II) complex reacted with thiosulfate in the molar ratio of 2 : 1. The absorption spectrum of this solution agreed with that of the PPC solution if an amount of thiosulfate about 3 times that in the molar ratio was added.

The absorption spectrum of the mercury(II)-complex solution did not change upon the addition of any other anions, such as fluoride, chloride, bromide, or thiocyanate. Therefore, it can be said that these anions did not react with the mercury(II) complex. The ammonium ion also did not react with this complex.

BULLETIN OF THE CHEMICAL SOCIETY OF JAPAN, VOL. 45, 642—644 (1972)

Some Reactions of Tetrafluorobenzyne with Halogens and Ethers, and with Alcohols

Seiichi HAYASHI and Nobuo ISHIKAWA

Department of Synthetic Chemistry, Faculty of Engineering, Tokyo Institute of Technology, Meguro-ku, Tokyo

(Received August 11, 1971)

As reported previously,[1] tetrafluorobenzyne generated from tetrafluorobenzenediazonium-2-carboxylate behaved as a potential electrophile, and it reacted even with diethyl ether to give 1-ethoxy-2,3,4,5-tetrafluorobenzene(**8**). In our continued studies of this subject, we have found that the tetrafluorobenzyne reacts with halogens and ethers, such as iodine and diethyl ether, or with bromine and dioxane, to give *o*-halogenoalkoxytetrafluorobenzenes.

When tetrafluoroanthranilic acid (**1**) was diazotized with *n*-butyl nitrite in chloroform and the resulting tetrafluorobenzenediazonium-2-carboxylate (**2**) was decomposed in the presence of iodine, two products were obtained : one was the expected 1,2-diiodotetrafluorobenzene (**4**) (15% yield), while the other was 1-butoxy-2,3,4,5-tetrafluorobenzene (**5**) (25% yield).

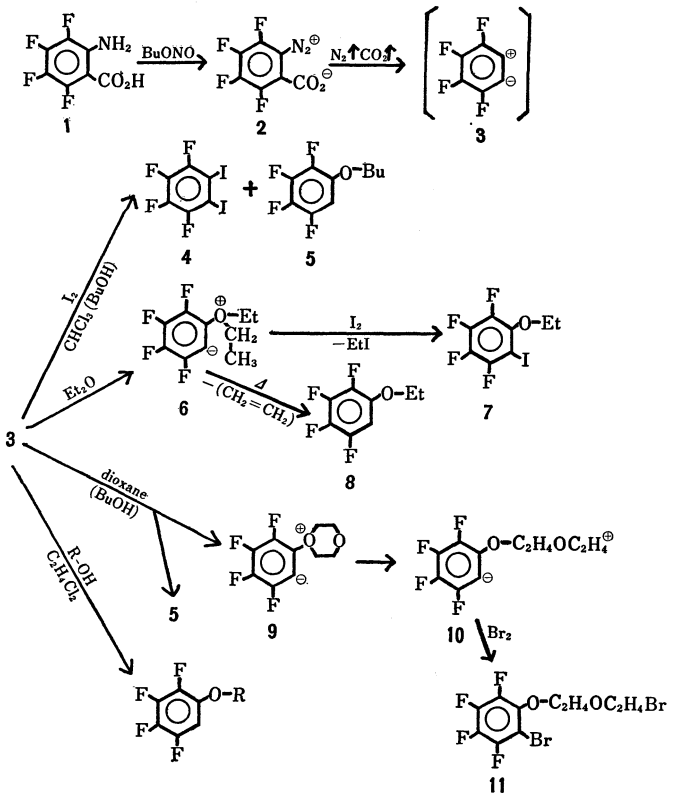

8 (R=Et)
5 (R=Bu)
12a (R=*i*-C_5H_{11})
12b (R=CH_2CH_2Cl)
12c (R=CH_2CH_2OH)
12d (R=CH_2CH_2OEt)

The latter compound was probably formed by the reaction of tetrafluorobenzyne and 1-butanol, which itself resulted from the diazotizing agent, *n*-butyl nitrite.

If the above reaction was carried out in diethyl ether, however, 1-ethoxy-2-iodo-3,4,5,6-tetrafluorobenzene (**7**) was obtained as the main product. In this case, it is evident that iodine reacted with the betaine intermediate **6**, prior to its intramolecular proton-withdrawing to ethoxytetrafluorobenzene (**8**) and ethylene.

Furthermore, if dioxane was used as the solvent and bromine was present in the reaction mixture, tetrafluorobenzyne reacted with both, thus affording 1-(β-(β'-bromoethoxy)ethoxy)-2-bromotetrafluorobenzene (**11**) as the main product. This reaction seemed to have started with the electrophilic attack of tetrafluorobenzyne on dioxane to form **9**, followed by the cleavage of dioxane molecule to **10** and the subsequent reaction of bromine on this betaine intermediate. This is probably the first example of the reaction of any benzyne with dioxane.

In the absence of bromine, however, the only product isolated was 1-butoxy-2,3,4,5-tetrafluorobenzene (**5**), which, as has been mentioned before, had been formed from tetrafluorobenzyne and butanol, which had itself come from *n*-butyl nitrite. In this case, no product which might be formed by the reaction between benzyne and dioxane was confirmed. We assume that this is because the intramolecular proton transfer in the betaine intermediate, **9** or **10**, is sterically more difficult than that in the case of **6**.

Our finding that, in the presence of halogen, dioxane is cleaved by tetrafluorobenzyne seems to be analogous to the facts, which have been reported recently, that tetrahydrofuran is cleaved by benzyne in the presence of water,[2] in the absence of it no product which might result from the cleavage of tetrahydrofuran is observed.[3]

As has been described above, tetrafluorobenzyne reacted with even a small amount of butanol present in the reaction mixture to give a considerable amount of butoxytetrafluorobenzene (**5**). Then, to generalize this reaction we effected the diazotization-decomposition of tetrafluoroanthranilic acid in various alcohols. As we had expected 1-alkoxy-2,3,4,5-tetrafluorobenzene was obtained in a rather good yield in every case. The structures of these compounds were clear from their ^1H and ^{19}F NMR spectra (Table 1).

1) S. Hayashi and N. Ishikawa, *Nippon Kagaku Zasshi*, **91**, 1000 (1970).

2) E. Wolthuis, B. Bouma, J. Modderman, and L. Sytsma, *Tetrahedron Lett.*, **1970**, 407.

3) J. P. N. Brewer, H. Heaney, and J. M. Jablonski, *ibid.*, **1968**, 4455.

TABLE 1 PREPARATION AND SPECTRAL PROPERTIES OF 1-ALKOXY-2, 3, 4, 5-TETRAFLUOROBENZENE (**12**)

No.	Alcohol	Diazotizing agent	Product			
				R	Bp °C/mmHg	Yield %
1	ethanol	*n*-BuONO	[**8**]	Et	71—72/20	67
2	*n*-butanol	*n*-BuONO	[**5**]	*n*-Bu	92—93/20	77
3	isopentanol	*i*-$C_5H_{11}ONO$	[**12a**]	$CH_2CH_2CHMe_2$	110/24	76
4	2-chloroethanol	*n*-BuONO	[**12b**]	CH_2CH_2Cl	108—109/23	66
5	ethyleneglycol	*n*-BuONO	[**12c**]	CH_2CH_2OH	80—81/3	65
6	2-ethoxyethylalcohol	*n*-BuONO	[**12d**]	CH_2CH_2OEt	65—65.5/3	57

No.	Product									
	F Anal		IR		NMR					
					^1H τ (in CCl_4)		^{19}F ppm[a] (in CCl_4, from ext. CF_3CO_2H)			
	Calcd.	Obsvd.	Ar-O-C	C-F	Ar-H	Alkyl-H	2-F	3-F	4-F	5-F
1	—	—	1204	1080	3.50	6.02 (CH_2) 8.56 (CH_3)	82.7	79.2	91.0	63.0
2	34.2	34.5	1198	1082	3.45	6.05 (αCH_2) 8.00—8.75 (βCH_2, γCH_2) 9.00 (CH_3)	82.2	78.2	90.0	62.3
3	32.2	32.0	1200	1076	3.50	6.04 (αCH_2) 8.15—8.60 (CH_2CH) 9.00 (CH_3)	82.1	78.1	90.0	62.3
4	33.2	33.0	1186	1086	3.40	5.78 (αCH_2) 6.25 (CH_2Cl)	81.2	77.4	88.7	61.5
5	36.2	36.6	1200	1080	3.39	6.00 (CH_2CH_2) 5.55 (OH)	82.3	78.3	89.3	61.8
6	31.9	31.5	1200	1080	3.33	5.92 (αCH_2) 6.32 (βCH_2) 6.49 (OCH_2) 8.82 (CH_3)	82.3	78.8	89.8	62.4

a) Values calculated according to Bruce's formula[4] are: 2-F, 80; 3-F, 78; 4-F, 86; 5-F, 63 ppm.

Experimental

All the NMR spectra were run at room temperature, and CCl_4 was used as the solvent unless otherwise noted. The chemical shifts in ^{19}F NMR are shown by δ(ppm) from external CF_3CO_2H.

The Reaction of Tetrafluorobenzyne with Iodine in Chloroform. Into a solution of *n*-butyl nitrite (3.09 g, 0.030 mol) and iodine (7.62 g, 0.030 mol) in chloroform (20 m*l*), a solution of tetrafluoroanthranilic acid (**1**) (4.18 g, 0.020 mol) in chloroform (80 m*l*) was added drop by drop, at 50°C over a 40-min period. After refluxing for 6 hr, the solvent was distilled out in a vacuum and the residue was dissolved in diethyl ether. The ether solution was then treated with an aqueous solution of sodium sulfite to remove the excess iodine, and with a dilute aqueous sodium hydroxide solution to remove any alkaline-soluble matter. After subsequent washing with dilute hydrochloric acid and water, it was dried with magnesium sulfate. The solvent was evaporated, and the oily residue was distilled in a vacuum to give the following two products:

1) 1-*n*-butoxy-2,3,4,5-tetrafluorobenzene (**5**); bp 60—61°C/3 mmHg (1.1 g, 25% yield). Identified with **5** in Table 1 by means of its IR spectrum.

2) 1,2-diiodotetrafluorobenzene (**4**); bp 74°C/3 mmHg, mp 49—51°C (lit. mp 50—51°C[3]). IR: 1110, 1023 cm^{-1} (C-F). ^{19}F NMR (in Me_2CO): +24.7 (3,6-F), +71.7 (4,5-F) ppm.

The Reaction of Tetrafluorobenzyne with Iodine and Diethyl Ether. Into a boiling mixture of *n*-butyl nitrite (2.48 g), iodine (5.08 g), dichloromethane (20 m*l*), and diethyl ether (20 m*l*), a solution of **1** (4.18 g) in diethyl ether (20 m*l*) was added, drop by drop, during the course of 3 hr. The reaction was then run and after-treated in the manner described above; 1-ethoxy-2-iodotetrafluorobenzene (**7**) (bp 65—66°C/3 mmHg, 1.75 g) was thus obtained in a 27% yield.

Found: F, 23.6%; I, 39.5%. Calcd for $C_8H_5F_4IO$: F, 23.7%; I, 39.7%. NMR: ^1H, τ 5.85 q (CH_2), 8.52 t (CH_3); ^{19}F, +38.8 (3-F), +74.9 (6-F), +75.7 (5-F), +82.1 (4-F).

The Reaction of Tetrafluorobenzyne with Bromine and Dioxane. Into a solution of *n*-butyl nitrite (2.60 g) and bromine (3.80 g) in dioxane (30 m*l*), we added a solution of **1** (4.18 g) in dioxane (30 m*l*) at 55—65°C over a 2-hr period. Stirring was continued for 8 more hr at 94°C, and then the reaction mixture was treated as usual, giving 1-(β-(β'-bromoethoxy)-ethoxy)-2-bromo-3,4,5,6-tetrafluorobenzene (**11**) (bp 124—125°C/2 mmHg, 2.2 g) in a 28% yield.

Found: Br, 40.8%; F, 19.3%. Calcd for $C_{10}H_8Br_2F_4O_2$: Br, 40.4%; F, 19.2%. NMR: ^1H, τ 5.78 t (α CH_2) 6.08—6.37 m (β CH_2 and $\alpha'CH_2$), 6.60 t (CH_2Br); ^{19}F,

4) M. I. Bruce, *J. Chem. Soc., A*, **1968**, 1459.

+52.8 (3-F), +75.6 (6-F), +77.6 (5-F), +83.0 (4-F). IR: 1190 (Ar-O-C), 1080 (C-F).

When the above reaction was carried out without bromine, **5** was obtained as the main product (bp 93—94°C/19 mmHg, 1.4 g, 32% yield), as was confirmed by a study of the IR spectrum. The other fraction isolated (bp 120—136°C/3 mmHg, 1.0 g) was a mixture of more than three components, as was shown by gas chromatography; they could not be separated from each other.

*1-Ethoxy-2,3,4,5-tetrafluorobenzene (**8**).* Into a mixture of *n*-butyl nitrite (1.3 g), ethanol (10 m*l*), and 1,2-dichloroethane (10 m*l*), we added a solution of **1** (2.1 g) in ethanol (10 m*l*) at 50—60°C over a 1 hr period. After refluxing for 3 hr with stirring, the solvent was evaporated in a vacuum, and the residue was dissolved in diethyl ether. On treating with an aqueous sodium hydroxide solution to remove the alkaline-soluble matter and washing with dilute hydrochloric acid and then with water, the ether solution was dried on magnesium sulfate. The ether was evaporated, and the residue was distilled to give **8** (1.3 g), which was identified with an authentic sample.[1)]

The reactions with other alcohols were carried out in a similar manner (Table 1).

BULLETIN OF THE CHEMICAL SOCIETY OF JAPAN, VOL. 45, 644—645 (1972)

The Solvent Effect on the Visible Absorption Spectra of the Radical Anion and the Dianion of Anthraquinone[1)]

Masamichi FUJIHIRA and Shigeo HAYANO

Institute of Industrial Science, The University of Tokyo, Roppongi, Minato-ku, Tokyo

(Received August 14, 1971)

In a previous work,[2)] the half-wave potentials of anthraquinone were found to shift to more positive potentials with an increase in the water content in the DMF-alkaline water system. This behavior was interpreted in terms of the hydrogen-bonding of the radical anion or the dianion with water. On the other hand, the change in the hyperfine coupling constants in the ESR spectra of the radical anions[3–6)] has been interpreted also in terms of the hydrogen-bonding of the radial anions with hydroxylic solvents, and a quantitative treatment has been given by Fraenkel *et al.*[5)] The present work will deal with this hydrogen-bonding from the viewpoint of the solvent effect on the visible absorption spectra of the radical anion and the dianion of anthraquinone and with the correlation between the solvent shift of the visible absorption spectra of the anions and the change in the half-wave potentials.

Experimental

The radical anion and the dianion of anthraquinone in the DMF-alkaline water system were generated by controlled-potential electrolysis.[7)] The measurements of the visible absorption spectra of the anions were the same as have been described in a previous paper.[7)]

Results and Discussion

In DMF containing 0.1 N tetraethylammonium perchlorate (TEAP) as the supporting electrolyte, the absorption maxima of AQ^- were 390, 410, and 553 mμ[7)] and those of AQ^{2-} were 420 and 460 mμ. Every visible absorption maximum showed a strong blue shift with an increase in the water content, as is shown in Fig. 1. The results for the radical anion are consistent with the λ_{max} values of 410 and 555 mμ in DMF[8)] and with the λ_{max} values of 400 and 480 mμ in an ethylene glycol-alkaline water system.[9)] As the molar extinction coefficients for these visible absorption bands were of the order of 10^4,[7)] these intense

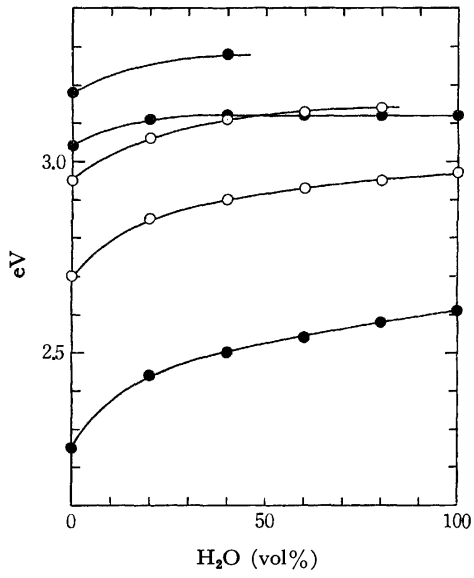

Fig. 1. Variations of λ_{max} of anthraquinone anions with the water content in the DMF-alkaline water system.
● AQ^-, ○ AQ^{2-}.

1) Presented at the 15th symposium of polarography, Sendai, Oct. 7, 1969.
2) S. Hayano and M. Fujihira, This Bulletin, **44**, 2051 (1971).
3) E. W. Stone and A. H. Maki, *J. Chem. Phys.*, **36**, 1944 (1962).
4) Y. Deguchi, This Bulletin, **35**, 260 (1962); K. Umemoto, Y. Deguchi, and H. Takaki, *ibid.*, **36**, 560 (1963).
5) J. Gendell, J. H. Freed, and G. K. Fraenkel, *J. Chem. Phys.*, **37**, 2832 (1962).
6) P. Ludwig, T. Layloff, and R. N. Adams, *J. Amer. Chem. Soc.*, **86**, 4568 (1964).
7) S. Hayano and M. Fujihira, This Bulletin, **44**, 1496 (1971).
8) T. Osa and T. Kuwana, *J. Electroanal. Chem.*, **22**, 389 (1969).
9) Y. Harada and Y. Matsunaga, This Bulletin, **34**, 585 (1961).

absorption bands are presumably due to the $\pi \rightarrow \pi^*$ allowed transition.[10,11]

The blue shifts are similar not only to the change in the hyperfine coupling constants in the ESR spectra,[12] but also to the change in the half-wave potentials.[2] The changes are sharp for small quantities of water, but they gradually level out. The changes in the transition energies of AQ^- and AQ^{2-} were compared with the changes in the half-wave potentials[2] of the first and the second waves respectively. There exists a linear relation between them, as is shown in Fig. 2. Such a relation suggests that both solvent shifts have the same cause, *i.e.*, hydrogen-bonding.

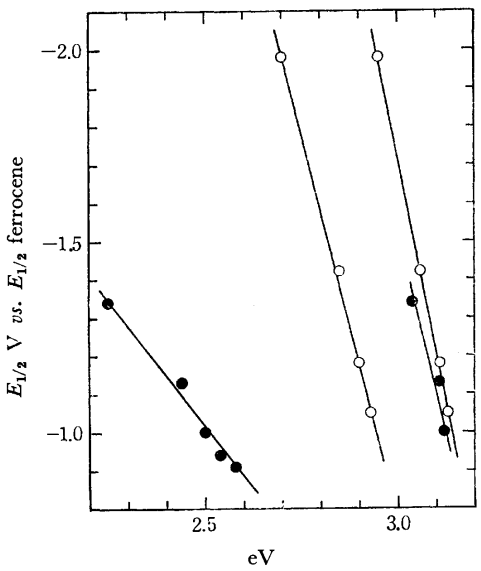

Fig. 2. Correlation between the solvent shifts of λ_{max} and those of $E_{1/2}$.
●, λ_{max} of AQ^- *versus* $E_{1/2}$ of the first wave.
○, λ_{max} of AQ^{2-} *versus* $E_{1/2}$ of the second wave.

The electronic structures of hydrocarbon mono- and dinegative ions have been studied considerably,[13] but no theoretical investigations of those of mono- and dinegative ions of quinones have ever been made except for that of the *p*-benzosemiquinone ion.[11] Thus, we performed the HMO calculations in order to interpret the behavior qualitatively. The oxygen atoms of the anions are expected to be more electronegative in protic solvents, such as water and alcohol, than in aprotic solvents.[5] The Coulomb integral for the oxygen atom was varied in the calculations, since the change in the electronegativity of the oxygen atoms corresponds to the variation in the Coulomb integral for the oxygen atoms.[5] The variations in the energy levels with the change in the values of the parameter, δ, in the $\alpha_o = \alpha + \delta\beta$ relation for the Coulomb integral of the oxygen atom are shown in Fig. 3. The highest occupied energy level of the mono- and dinegative ions of b_{3g}* is found to be lowered remarkably with an increase in the values of δ. Thus, it is clear from such a simple calculation that the blue shift of λ_{max} and the positive shift of $E_{1/2}$ with the increase in the water content can be interpreted in terms of the hydrogen-bonding.

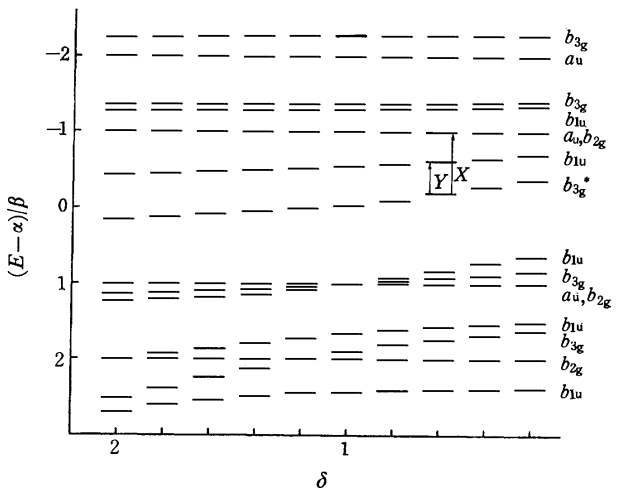

Fig. 3. Variations of the energy levels of anthraquinone with the change in the Coulomb integral for the oxygen atoms. The Coulomb and resonance integrals are assumed as follows:[14,15]

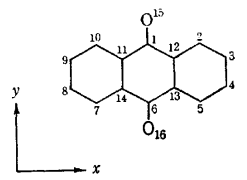

$\alpha_{12}=\alpha_2=\alpha_3=\alpha \quad \alpha_1=\alpha+0.2\beta$
$\alpha_0=\alpha+\delta\beta$

$\beta_{1-15}=\beta_{12-13}=\beta_{12-2}=\beta_{2-3}=\beta_{3-4}=\beta$
$\beta_{1-12}=0.8\beta$

10) Y. Harada and H. Inokuchi, *Mol. Phys.*, **8**, 265 (1964).
11) Y. Harada, *ibid.*, **8**, 273 (1964).
12) J. Q. Chambers and R. N. Adams, *ibid.*, **9**, 413 (1965).
13) P. Balk, S. de Bruin, and G. J. Hoijtink, *Rec. Trav. Chim.*, **76**, 907 (1957); G. J. Hoijtink, *Mol. Phys.*, **2**, 85 (1959); G. J. Hoijtink, N. H. Velthorst, and P. J. Zandstra, *ibid.*, **3**, 533 (1960).
14) A. Kuboyama, This Bulletin, **31**, 752 (1958).
15) Fraenkel *et al.*[5] adjusted α_o and β_{1-15} by varying the parameters δ and γ in the relations $\alpha_o=\alpha+\delta\beta$ and $\beta_{1-15}=\gamma\beta$ in an attempt to fit the proton splittings observed from the radical anions in ethanol - water system. The best values were found to be $\delta=0.9$ and $\gamma=1.4$. The HMO calculations were then performed in an attempt to fit the data for proton splittings in dimethylsulfoxide (DMSO) solution by adjusting the value of δ, while γ used for the ethanol - water system was left unchanged. The best value was found to be $\delta=0.4$ in DMSO. In the present work, other parameters except α_o were quoted from Ref. 9, because the tendency was not affected very much by the choice of parameters.

BULLETIN OF THE CHEMICAL SOCIETY OF JAPAN, VOL. 45, 646—647 (1972)

The Thermal *trans*-to-*cis* Isomerization of $[CrCl_2(en)_2]Cl$ in the Solid Phase

Choei SATO and Suekichi HATAKEYAMA

Department of Chemistry, Faculty of Science, Hirosaki University, Hirosaki

(Received August 30, 1971)

The *cis*↔*trans* isomerization reactions of transition metal complexes have been extensively studied in solution.[1] However, only a few studies have been recently reported on reactions in the solid phase,[2] and little is known about the mechanism of these solid-phase isomerizations. The thermal behavior of *trans*-$[CrCl_2(en)_2]Cl$ in the solid phase was studied by differential thermal analysis (DTA) and compared with that of the *cis*-isomer. *trans*-$[CrCl_2(en)_2]Cl$ showed an endothermic peak at 275°C and then an exothermic peak at 285°C, after which the sample turned reddish violet from gray green, accompanied by an appreciable bulk compression, and above 300°C it decomposed. On the contrary, the *cis*-form showed no peak up to 300°C, and above 300° it decomposed quite like the product obtained by heating *trans*-isomer up to 300°C. The *trans*-to-*cis* isomerization of $[CrCl_2(en)_2]Cl$ at 250—290°C was suggested and confirmed by measurements of the infrared and electronic spectra of the samples.

Experimental

Both *trans*-$[CrCl_2(en)_2]Cl$ and *cis*-$[CrCl_2(en)_2]Cl \cdot H_2O$ were prepared as has been described in the literature.[3] DTA studies were made using the Rigaku-Denki automatic recording DTA apparatus, in which the inert material was alumina, with a helium gas flow through the sample. A powdered sample of 100 mg sandwiched between alumina layers was used, and the heating rate was 5°C min^{-1}. The Rigaku-Denki differential scanning calorimeter (DSC) was also used for a more detailed inspection, with a 20-mg sample and a heating rate of 3°C min^{-1}. The infrared spectra were recorded as Nujol and hexachlorobutadiene mulls on a Model 601-F (4000—200 cm^{-1}) grating spectrophotometer of the Japan Spectro Co., Ltd. The electronic spectra of the samples in aqueous hydrochloric acid solutions were obtained on a Hitachi EPS-2U recording spectrophotometer.

Results and Discussion

The DTA curve obtained for the *trans*-$[CrCl_2(en)_2]Cl$ is given in Fig. 1, together with that of *cis*-$[CrCl_2(en)_2]Cl \cdot H_2O$. In the case of the former, an endothermic peak appears at 275°C and then an exothermic peak at 285°C, but in the case of the latter these peaks do not appear. Above 300°C both complexes decompose in almost the same way. In the heat treatment up to 300°C, the *trans*-complex shows only a slight weight loss (less than one percent), but in the above-peak region it changes in color to a dark-reddish violet from the initial gray green, and there is an accompanying appreciable bulk compression. This product, once obtained from the *trans*-form on being heated up to 300°C, shows no color change upon cooling and no peak in DTA curve when reheated to 300°C. To present the details of the thermal behavior of the *trans*-complex in the 230—300°C region, the DSC curve is shown in Fig. 2. It is noteworthy that small endothermic and exothermic peaks precede the principal peaks.

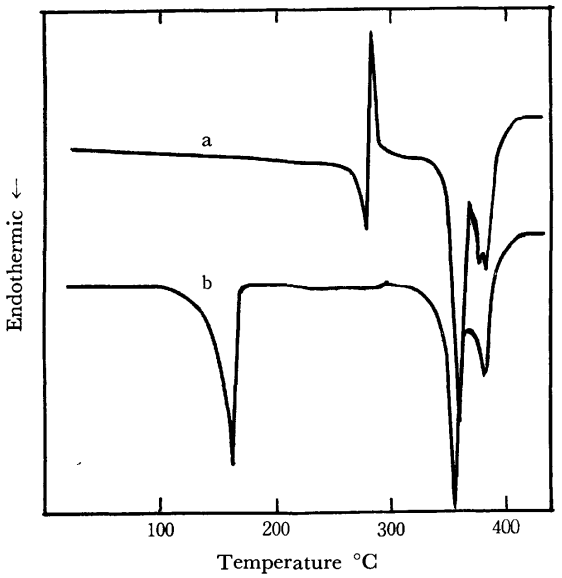

Fig. 1. The DTA curves of *trans*-$[CrCl_2(en)_2]Cl$ (a), and *cis*-$[CrCl_2(en)_2]Cl \cdot H_2O$ (b).

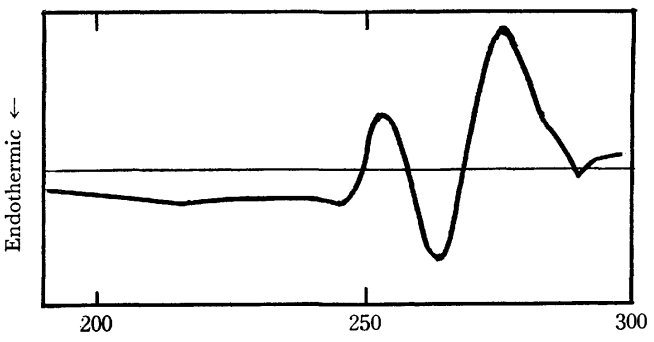

Fig. 2. The DSC curve of *trans*-$[CrCl_2(en)_2]Cl$.

These results suggest that *trans*-$[CrCl_2(en)_2]Cl$ may isomerize to the *cis*-form irreversibly on being heated in the temperature range of 250—290°C. This is confirmed by the results of the measurements

1) F. Basolo and R. G. Pearson, "Mechanisms of Inorganic Reactions," 2nd Ed., John Wiley & Sons, Inc., New York, N. Y. (1967), pp. 274—291.

2) N. Tanaka and K. Nagase, This Bulletin, **42**, 2854 (1969); R. Tsuchiya, K. Murai, A. Uehara, and E. Kyuno, *ibid.*, **43**, 1383 (1970); Y. Kazi, A. Uehara, E. Kyuno, and R. Tsuchiya, *ibid.*, **43**, 1906 (1970); F. C. Chang and W. W. Wendlandt, *J. Inorg. Nucl. Chem.*, **32**, 3535 (1970), *etc.*

3) P. Pfeiffer, P. Koch, G. Lando, and A. Trieschmann, *Ber.*, **37**, 4255, 4269, 4277 (1904).

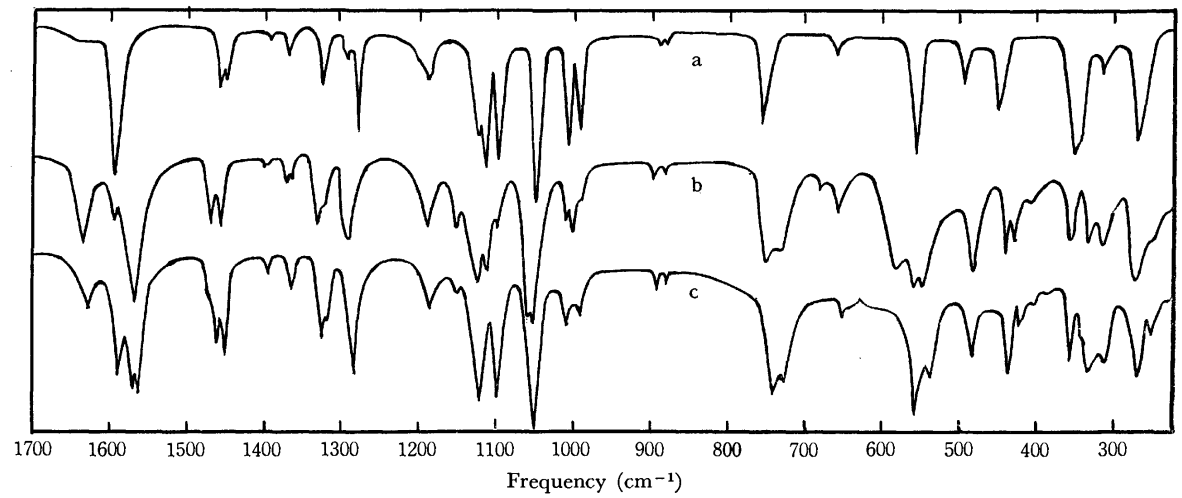

Fig. 3. Infrared spectra of *trans*-$[CrCl_2(en)_2]Cl$ (a), *cis*-$[CrCl_2(en)_2]Cl \cdot H_2O$ (b) and the product obtained from *trans*-form by heating up to 300°C (c).

of the electronic and infrared spectra. The resulting sample, when dissolved in an aqueous hydrochloric acid solution, exhibits absorption maxima at 528 mμ and 402 mμ, these values are in agreement with the values for the *cis*-form.[4] The point group of *trans*-$[CrCl_2(en)_2]^+$ is D_{2h}, on the contrary, that of the *cis*-form is C_2, and the infrared spectra differ appreciably in these two isomers.[5] This is ascertained in our measurements; the results are shown in Fig. 3, together with the results for the sample produced by heating the *trans*-complex up to 300°C. These results clearly indicate the *trans*-to-*cis* isomerization.

The above results suggest that, by the bond-breaking of a Cr-N linkage and the anation of Cl^-, *trans*-$[CrCl_2(en)_2]Cl$ may change first to *cis*,*trans*-$[CrCl_3(en)_2]$, in which one (en) behaves as an unidentate ligand, and may simultaneously melt and subsequently change to *cis*-$[CrCl_2(en)_2]Cl$ and resolidify. A similar type of *cis*↔*trans* isomerization, in which melting, isomerization and resolidification occur successively, has been reported in the case of *cis*-$[PtCl_4\{(C_2H_5)_2S\}_2]$, which isomerizes to the *trans*-form in the temperature range of 120—140°C.[6]

4) M. Esparza and C. S. Garner, *J. Inorg. Nucl. Chem.*, **29**, 2377 (1967).

5) M. N. Hughes and W. R. McWhinnie, *J. Chem. Soc.*, *A*, **1967**, 592.

6) F. G. Angell, H. D. K. Drew, and W. Wardlaw, *J. Chem. Soc.* **1930**, 349; (*cf.* G. B. Kauffman, J. Hwa-san Tsai, and L. T. Takahashi, "Inorganic Syntheses," Vol. VIII, Ed. by H. F. Holtzlaw, Jr., McGraw-Hill, New York (1966) p. 247.

BULLETIN OF THE CHEMICAL SOCIETY OF JAPAN, VOL. 44, 648—649 (1972)

Reactions of Grignard Reagents with Chromium(IV) *t*-Butoxide: Unstable Organochromium(IV) Intermediates

Tetsuo TSUDA* and J. K. KOCHI

Department of Chemistry, Indiana University, Bloomington, Indiana, U.S.A.

(Received February 22, 1971)

Several organochromium(III) compounds have been characterized[1] and others have been postulated as intermediates in reactions.[2] Chromium(IV) is less common and only a few compounds with this oxidation state are known.[3] We have examined the metathesis between chromium(IV) tetra-*t*-butoxide[4] [$Cr(OBu\text{-}t)_4$] and various Grignard reagents with the intention of

$$Cu^{IV}(OBu\text{-}t)_4 + n\text{RMgX} \longrightarrow \underset{\text{I}}{R_nCr^{IV}(OBu\text{-}t)_{4-n}} + n\ t\text{-BuOMgX} \quad (1)$$

probing the properties and stabilities of alkyl and arylchromium(IV) species, I.

Results and Discussion

Aryl Grignard Reagents and Cr(OBu-t)$_4$. Mesityl derivatives of chromium III and II are significantly more stable than their phenyl analogs.[1a,5] The reaction between mesitylmagnesium bromide and $Cr(OBu\text{-}t)_4$ in a 4: 1 molar ratio in tetrahydrofuran (THF) solution at 25°C was observed by following the disappearance of the visible absorption band of $Cr(OBu\text{-}t)_4$ at 630 nm as shown in Fig. 1. After 48 hr the visible absorption spectrum (λ_{max}=518 nm) and the electron paramagnetic resonance (EPR) spectrum ($\langle g\rangle$= 1.983) of the solution were the same as those of trimesitylchromium(III) prepared from mesitylmagnesium bromide and chromium(III) chloride.[5b] Addition of a solution of mercuric chloride in THF quantitatively converted mesitylchromium(III) and unreacted mesitylmagnesium bromide into mesitylmercuric salts,[5] which were separated and the resulting solution was analyzed. Quantitative gas chromatography indicated the presence of 1.11 mol of mesitylene per mol of $Cr(OBu\text{-}t)_4$, but only traces of bimesitylene. The partial stoichiometry of the reaction is:

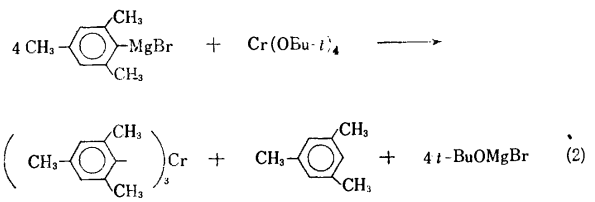

(2)

The analogous reaction between phenylmagnesium bromide and $Cr(OBu\text{-}t)_4$ in a molar ratio of 4: 1 produced after 2 hr a yellow-green solution whose absorption spectrum (λ_{max}=473 nm) was similar to that of a red-brown solution (λ_{max}=445 nm) of triphenylchromium(III) generated from chromium(III) chloride. The presence of other phenylchromium species derived from Ph_2Cr was suspected, but this possibility was discarded by a negative qualitative test. Thus, Ph_2Cr is unstable and is transformed to a π-arene chromium complex which on treatment with sodium tetraphenylboride after aerial oxidation should have afforded a π-arenechromium(I) salt,[6] but none was found. Excess phenylmagnesium bromide also reacted with either $CrCl_3$ or $Cr(OBu\text{-}t)_4$ to afford a solution of phenylchromium(III) species absorbing at 408 nm. On standing both reactions gave rise to dark red-brown solutions showing the same visible absorption spectrum. These differences were attributed to various phenylchromium(III) complexes containing other ligands,[5d] and not to the presence of phenylchromium(II). Analysis of the reaction mixture indicated the presence of biphenyl according to the following stoichiometry:

$$4\text{PhMgBr} + Cr(OBu\text{-}t)_4 \longrightarrow Ph_3Cr + \frac{1}{2}\text{Ph-Ph} + 4\ t\text{-BuOMgBr} \quad (3)$$

Alkyl Grignard Reagents and Cr(OBu-t)$_4$. Ethylmagnesium bromide and $Cr(OBu\text{-}t)_4$ were mixed in a 4: 1 molar ratio in THF solution at −78°C. No reaction occurred until the temperature was raised to −55°C when the color changed abruptly from blue to brown, and a more of less equimolar mixture of ethane and ethylene (no butane) was slowly evolved. The EPR spectrum (g=1.993) of the solution taken at below −20°C was the same as that (g=1.994) of triethylchromium(III) prepared from ethylmagnesium bromide and chromium(III) chloride[1c,d,f] and shown to be relatively stable under these conditions. Approximately 1 mol of hydrocarbons was liberated from each mol of $Cr(OBu\text{-}t)_4$ between −55 and −25°C. We conclude that ethylchromium(IV) species (I, R=CH_3CH_2) are unstable between these temperatures.

$$Cr(OBu\text{-}t)_4 + 4CH_3CH_2MgBr \longrightarrow \underset{\text{I}}{[CH_3CH_2Cr^{IV}]}$$

* Present address: Department of Synthetic Chemistry, Faculty of Engineering, Kyoto University.

1) a) H. H. Zeiss and R. P. A. Sneeden, *Angew. Chem., Intern. Ed.*, **6**, 435 (1967); b) *ibid.*, **7**, 951 (1968); c) *J. Organometal. Chem.*, **22**, 713 (1970); d) *ibid.*, **16**, 449 (1969); e) H. P. Throndsen, W. Metlesics, and H. H. Zeiss, *ibid.*, **5**, 176 (1966); f) Private communication, H. H. Zeiss.

2) a) J. K. Kochi and J. W. Powers, *J. Amer. Chem. Soc.*, **92**, 137 (1970); see also **86**, 5264 (1964); **90**, 1582 (1968); *J. Org. Chem.*, **30**, 1134 (1965); **33**, 1027 (1968).

3) F. A. Cotton and G. Wilkinson, "Advanced Inorganic Chemistry," Interscience Publishers, New York, N. Y. (1966), p. 830—831.

4) N. Hagihara and H. Yamazaki, *J. Amer. Chem. Soc.*, **81**, 3160 (1959).

5) a) G. Stolze and J. Hähle, *J. Organometal. Chem.*, **7**, 301 (1967); b) G. Stolze, *ibid.*, **6**, 383 (1966); c) W. Herwig and H. H. Zeiss, *J. Amer. Chem. Soc.*, **79**, 6561 (1957).

6) M. Tsutsui and H. H. Zeiss, *ibid.*, **81**, 1367 (1959).

$$I \longrightarrow (CH_3CH_2)_3Cr + [CH_3CH_3 + CH_2{=}CH_2] + 4\,t\text{-BuOMgBr} \quad (4)$$

Similarly methylmagnesium bromide and Cr(OBu-t)$_4$ reacted at less than −30°C and only methane (no ethane or ethylene) was liberated as the temperature was raised further to 25°C. The EPR spectrum (g=1.997) of the solution taken at −20°C was the same as that (g=1.995) of trimethylchromium(III) prepared for methylmagnesium bromide and chromium(III) chloride. Hydrolysis of the reaction mixture after completion produced only 65% of methane based on the methylmagnesium bromide used.

$$4CH_3MgBr + Cr(OBu\text{-}t)_4 \longrightarrow (CH_3)_3Cr + CH_4 + 4\,t\text{-BuOMgBr} \quad (5)$$

The latter reflected loss of methyl groups by attack on solvent, incontrast to the good material balance obtained withthe ethyl analog.

Organochromium(IV) Species. We conclude from these studies that alkyl and arylchromium(IV) species are rather unstable intermediates and readily converted to trialkyl and triarylchromium(III) under these conditions. During the slow conversion of Cr(OBu-t)$_4$ by mesitylmagnesium bromide shown in Fig. 1, a metastable species absorbing at approximately 600 nm could be seen after 1.5 hr. Analogous changes in the EPR spectrum of the solution were also observed. Thus, Cr(OBu-t)$_4$ showed only a weak and broad EPR spectrum (g=1.964) in THF solution. On reaction with mesitylmagnesium bromide a new species was found. The multiplet (g=1.983) absorption of this species slowly changed to one characteristic of trimesitylchromium(III). We associate both observations with an intermediate mesitylchromium(IV) species. It is, however, clear that organochromium(IV) species of the kind indicated by I are too unstable for isolation and should be compared with the recently reported trimethylsilylmethyl derivatives.[7a]

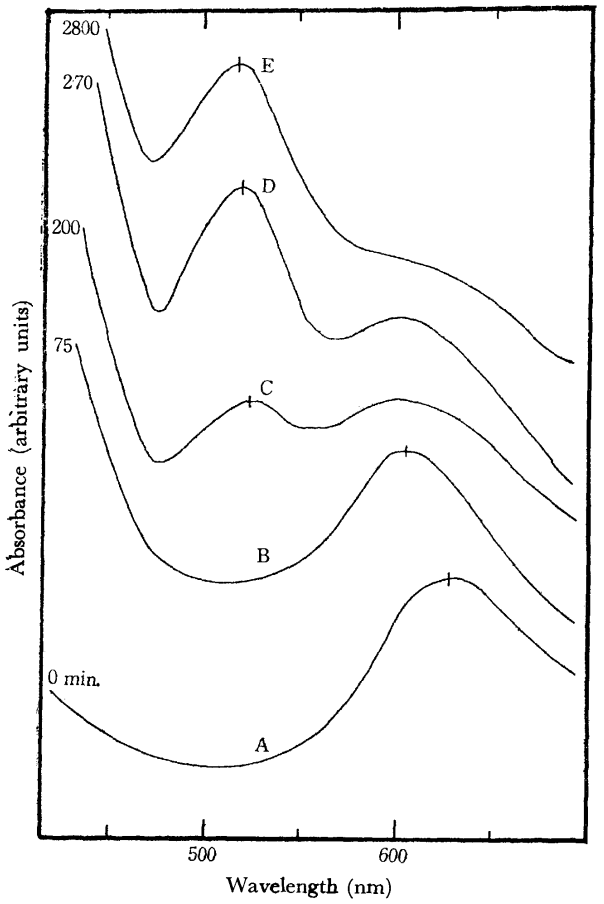

Fig. 1. Reaction of 0.039M Cr(OBu-t)$_4$ and 0.16M mesitylmagnesium bromide in THF at 25°C. A, mix; B, 75 min; C, 200 min; D, 270 min; E, 2800 min. A and E correspond to spectra of Cr(OBu-t)$_4$ and Mes$_3$Cr, respectively.

Experimental

Materials. Cr(OBu-t)$_4$ was prepared according to the reported procedure[8] from bis-benzene chromium[9] and di-t-butyl peroxide in benzene. The purity of Cr(OBu-t)$_4$ checked by iodometry was 95.0%. The Grignard reagents were synthesized under nitrogen by the conventional method. Tetrahydrofuran was refluxed and distilled over LiAlH$_4$ under nitrogen. CrCl$_3$ was used as purchased.

All operations described below were carried out under nitrogen atmosphere except the operation following the addition of HgCl$_2$.

The Reaction of Cr(OBu-t)$_4$ and Mesitylmagnesium Bromide. To the magnetically stirred solution of 4.25 ml THF containing 0.30 mmol Cr(OBu-t)$_4$ in a 100 ml flask, 0.75 ml THF solution containing 0.88 mmol mesitylmagnesium bromide was added at −78°C with a hypodermic syringe. The reaction mixture was gradually warmed to room temperature and kept at ambient temperatures for 50 hr. Of the reaction mixture, 1.80 ml was removed to a 50 ml test tube capped with a rubber septum, and 0.53 ml THF solution of 0.70 mmol HgCl$_2$ was added. After 20 hr the inorganic precipitate was removed by filtration and the resulting solution was analyzed for mesitylene by quantitative gas chromatography (6 ft DEGS on firebrick, durene as a marker).

The Reaction of Cr(OBu-t)$_4$ and Ethylmagnesium Bromide. To a 50 ml test tube capped with a rubber septum, 4.80 ml THF solution of 0.08 mmol Cr(OBu-t)$_4$ was added with a hypodermic syringe chilled to −78°C. Then 0.20 ml THF solution of 0.32 mmol ethylmagnesium bromide was added to this magnetically stirred solution, followed by the injection of 0.50 ml of methane marker gas. The reaction temperature was gradually raised by allowing the ice bath to stand at ambient temperatures. Quantitative gas chromatography analysis using a Porapak column for ethane and ethylene formation was carried out periodically at various temperatures. Standard mixtures of methane, ethane, and ethylene without substrate were calibrated under the same conditions.

EPR Spectra. EPR spectra of THF solutions of the organochromiums were obtained using a Varian E-4 spectrometer. Solutions of the organochromium species were prepared by mixing the degassed THF solutions of Cr(OBu-t)$_4$ and the Grignard reagents at the dry-ice temperature and transferring directly the resulting reaction mixture to an EPR sample tube cooled to dry-ice temperatures. g-Values were determined by calibration with DPPH powder.

We wish to thank the National Science Foundation, U. S. A. for financial support.

7) a) G. Yagupsky, W. Mowat, A. Shortland, and G. Wilkinson, *Chem. Commun.*, **1970**, 1369; b) see also M.R. Collier, M.F. Lappert, and M.G. Truelock, *J. Organometal. Chem.*, **25**, C36 (1970).

8) H. Yamazaki and N. Hagihara, *Nippon Kagaku Zasshi*, **81**, 821 (1960).

9) E. O. Fischer, *Inorganic Synthesis*, **6**, 132 (1960).

BULLETIN OF THE CHEMICAL SOCIETY OF JAPAN, VOL. 45, 650—651 (1972)

The Infrared Spectra of the 1-Propynyl Anion

Isao KANESAKA, Kenji TAKEDA, and Kiyoyasu KAWAI
Faculty of Literature and Science, Toyama University, Gofuku, Toyama

(Received August 31, 1971)

The structure of the 1-propynyl anion, whose electronic structure is anologous to that of acetonitrile $H_3C\text{-}C{\equiv}N:$, is represented by $H_3C\text{-}C{\equiv}C:^-$ (I) as a first approximation. Nest and Gremm[1] have measured the infrared spectra of the alkali acetilides of the R-C CM type, where R is H, CH_3 or C_6H_5 and where M is an alkali metal, in order to investigate the structure of those compounds on the basis of the C≡C stretching frequencies alone; they interpreted the decrease in the C C stretching frequencies from Li to Cs compounds in terms of an increase in the contribution of the $R\text{-}\overset{-}{C}=C:$ structure in the resonance hybride. If so, the contribution of the $H_3C\text{-}\overset{-}{C}=C:$ (II) structure in the 1-propynyl anion(I) would lead to a decrease not only in the C≡C stretching frequencies but also in the C–C stretching frequencies. Radionov *et al.*[2] have studied the infrared spectra of some lithium acetylides and observed the Li-C stretching frequencies in the 440–495 cm^{-1} region, suggesting the presence of a strong covalent character in the Li-C bond. The present paper will deal with the infrared spectra of the 1-propynyl sodium and potassium; except for the lithium compound, which is unsuitable, as has been shown above; we hope to obtain the normal frequencies and the force constants of the 1-propynyl anion and to obtain information concerning their structures.

The 1-propynyl sodium and potassium were prepared by the ordinary method. The infrared spectra were observed for both compounds in the region of 4000—200 cm^{-1} by Nujol or hexachloro-1,3-butadiene mull prepared in a gloved box. The observed frequencies were assigned on the basis of the C_{3v} symmetry; they are shown in Table 1. The C≡C stretching frequencies observed in both compounds differ slightly from that previously reported, *viz.*, 2032 cm^{-1} for the sodium salt and 2023 cm^{-1} for the potassium salt.[1] The normal frequencies of the 1-propynyl anion are listed in Table 2.

The force constants for the 1-propynyl anion were calculated on the assumption of the Urey-Bradley force field, in which F' (linear repulsive force constant) was assumed to be $-0.1\ F$(repulsive force constant), as usual. The atomic distances of the anion were assumed to be C–H=1.11 Å, C–C=1.46 Å, and C≡C=1.21 Å, while the valence angles were assumed to be tetrahedral for the CH_3 group and linear for the C–C C skeleton. For comparison, the force constants were also calculated, on the same assumption of force field, for acetonitrile and propyne, whose normal frequencies have been reported by Pace and Neo[3] and by Crawford[4] respectively, while the atomic

Table 1. The infrared spectra and assignments of $CH_3C{\equiv}CNa$ and $CH_3C{\equiv}CK$ (cm^{-1})

Obs. $CH_3C{\equiv}CNa$	Obs. $CH_3C{\equiv}CK$	Assign.
	3500 w	2852+2×340=3532
3340 w		2040+970+347=3357
2904 s	2905 s	CH_3 asym. str. *E*
2851 w	2852 m	CH_3 sym. str. A_1
2040 vw	2027 w	C≡C str. A_1
1436 s	1442 s	CH_3 asym. bend. A_1
1368 w	1368 w	CH_3 sym. bend. A_1
1316 w		970+347=1317
	1310 w	973+340=1313
970 w	973 w	CH_3 rock. *E*
922 m	915 s	C-C str. A_1
	884 w	
	678 vw	2×340=680
630 w	632 w	
347 m	340 m	C≡C-C bend. *E*

Table 2. The normal frequencies of $CH_3C{\equiv}C^-$ ion (cm^{-1})

Species		Mode	$CH_3C{\equiv}CNa$	$CH_3C{\equiv}CK$
A_1	ν_1	CH_3 str.	2851	2852
	ν_2	C≡C str.	2040	2027
	ν_3	CH_3 bend.	1368	1368
	ν_4	C-C str.	922	915
E	ν_5	CH_3 str.	2904	2905
	ν_6	CH_3 bend.	1436	1442
	ν_7	CH_3 rock.	970	973
	ν_8	C≡C-C bend.	347	340

Table 3. The force constants of $CH_3C{\equiv}CNa$, $CH_3C{\equiv}CK$, $CH_3C{\equiv}N$, and $CH_3C{\equiv}CH$ (md/Å)

	$CH_3C{\equiv}CNa$	$CH_3C{\equiv}CK$	$CH_3C{\equiv}N$	$CH_3C{\equiv}CH$
K(C-H)	4.280	4.284	4.480	4.364
K(C-C)	4.531	4.448	3.945	3.996
K(C≡X)	12.951	12.796	17.488	15.500
H(HCH)	0·407	0.403	0.394	0.397
H(CCH)	0.218	0.223	0.188	0.170
F(H···H)	0.082	0.082	0.071	0.116
F(C···H)	0.385	0.382	0.624	0.659
H(CCX)	0.165	0.160	0.203	0.201

X=C or N.

1) R. Nest and J. Gremm, *Z. Anorg. Allg. Chem.*, **325**, 62 (1963).
2) A. N. Rodionov, G. V. Timofeyuk, T. V. Talalaeva, D. N. Shigorin, and K. A. Kocheshkov, *Izv. Akad. Nauk. SSSR, Sen Khim.* **1965**, 42.
3) E. L. Pace and L. J. Noe, *J. Chem. Phys.*, **49**, 5317 (1968).
4) B. L. Crawford, *ibid.*, **8**, 526 (1940).

distances and valence angles have been reported by Costain.[5] The numerical calculation was carried out by means of computer program reported previously[6] using an electronic computer, HITAC 5020 E, of the Computer Center of Tokyo University. The force constants were fitted by the least-squares method; they are listed in Table 3. The calculated frequencies are in good agreement with the observed ones within the limit of ± 1 cm^{-1} in the two sets of the anion listed in Table 2, and also in the acetonitrile and propyne.

As is shown in Table 3, the C≡C stretching force constant of the 1-propynyl anion is considerably smaller than that of the propyne; it is possible that, because of the increase in the electronic repulsion and the decrease in the *s* character in the bonding, the C C bond in the 1-propynyl anion is less stable than that of the propyne, in which the *sp* hybridisation is postulated for the bonding in the C C bond.

One notices from Table 3 that the C–C stretching force constant of the 1-propynyl anion is larger than that of the acetonitrile or propyne, but that the C–H stretching force constant of the anion is smaller than that of the molecules. In acetonitrile, there is a significant contribution of the $H_3^+C=C=N:^-$ (III)[7] structure. For the 1-propynyl anion, however, we may not expect any important contribution of the $H_3^+C=C=C:^{--}$ (IV) structure in the resonance hybride because the uni-negative-charged carbon in the (I) structure is far less electronegative than the nitrogen atom in the acetonitrile and the distribution of the electronic charge in the (IV) structure is unfavorable. Accordingly, another important structure, $H_3^-C=C=C:$ (V), in which the negative charge is distributed among three hydrogen atoms, may be considered; its contribution may be more significant than that of the (III) structure in the acetonitrile.

The authors wish to express their gratitude to Professor Hiromu Murata for his kind advice.

5) C. C. Costain, *ibid.*, **29**, 864 (1958).

6) T. Shimanouchi, "Computer Programs for Normal Coordinate Treatment of Polyatomic Molecules," Tokyo Univ. (1968).

7) L. Pauling, "The Nature of the Chemical Bond," Cornell Univ. Press, New York (1960), p. 269.

SHORT COMMUNICATIONS

Formation of Ethylenic Compounds by the Decomposition of Cuprated Sulfur Compounds

Teruaki MUKAIYAMA, Koichi NARASAKA, and Masayasu FURUSATO

Laboratory of Organic Chemistry, Tokyo Institute of Technology, Ookayama, Meguro-ku, Tokyo

(Received November 25, 1971)

It was found in our laboratory that bivalent sulfur compounds react easily with some nucleophiles in the presence of $CuCl_2$ to give the corresponding condensation products along with copper mercaptide.[1] A study of the decomposition of α-cuprated sulfides was thus initiated with the expectation that carbenes would be generated by the elimination of copper mercaptide from the α-cuprated sulfides.

α-Cuprated sulfides were prepared according to Gilman's method by the reaction of CuI with α-lithio derivatives of sulfides in tetrahydrofuran at −70°C.[2] Decomposition of the α-cuprated sulfides was then carried out by raising the temperature of the resulting mixtures to room temperature. As an example, a tetrahydrofuran solution of 0.01 mol of benzyl 2-pyridyl sulfide (I) was treated with 0.011 mol of phenyllithium in ether under nitrogen atmosphere at −30°C for 1 hr. After the addition of 0.01 mole of CuI at −70°C, the solution was slowly warmed up to room temperature and allowed to stand for 2 hr with stirring. After hydrolysis, the organic layer was chromatographed on silica gel to afford *trans*-stilbene in 86% yield. The result is explained as shown in Scheme 1; Carbene (III) is initially produced by the elimination of copper mercaptide from the α-cuprated sulfide (II), which changed to stilbene either by dimerization or reaction with the precursor (II).

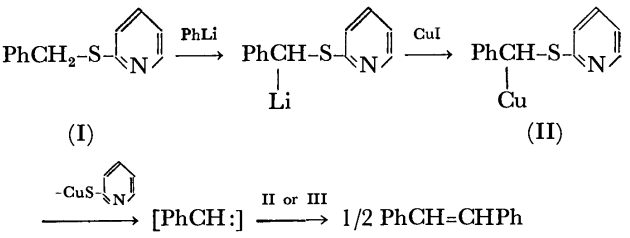

Scheme 1

Similarly, diphenylmethyl and cinnamyl 2-pyridyl sulfides gave tetraphenylethylene and 1,6-diphenylhexatriene in 33% and 10% yields, respectively.

In the cases of sulfide, mercaptals and orthothioformates (IV) with phenylthio or ethylthio group, the reactions also proceeded easily as in the case of 2-pyridyl sulfides. *n*-Butyllithium was used instead of phenyllithium in order to facilitate the formation of lithium salts of IV. The corresponding ethylenic derivatives (V) were obtained in good yields by treatment of the lithium salts with CuI in the same manner as mentioned above (Table 1).

TABLE 1

$R^1R^2CHSR^3$ (IV) $\xrightarrow{BuLi,\ CuI}$ 1/2 $R^1R^2C{=}CR^1R^2$ (V)

IV	R^1	R^2	R^3	V	Yield (%)
a	H	Ph	Ph		45 (*trans*)
b	H	PhS	Ph		82 (*trans*+*cis*)
c	Ph	PhS	Ph		76 (*trans*+*cis*)
d	PhS	PhS	Ph		61[3]
e	EtS	EtS	Et		54

1) T. Mukaiyama, K. Narasaka, and H. Hokonoki, *J. Amer. Chem. Soc.*, **91**, 4315 (1969); T. Mukaiyama, K. Narasaka, K. Maekawa, and H. Hokonoki, This Bulletin, **43**, 2549 (1970); T. Mukaiyama, K. Maekawa, and K. Narasaka, *Tetrahedron Lett.*, **1970**, 4669.

2) H. Gilman, R. G. Jones, and L. A. Woods, *J. Org. Chem.*, **17**, 1630 (1952).

3) Vd was previously formed by carbene route from the lithium salt of IVd; D. Seebach, *Angew. Chem.*, **79**, 468, 469 (1967).

Studies of the Basic Sites of the Silica-Alumina Surface by Means of the Adsorption of Copper(II) Complexes with 2,2'-Bipyridine

Kazuto TAKIMOTO and Masaji MIURA

Department of Chemistry, Faculty of Science, Hiroshima University, Higashisenda-machi, Hiroshima

(Received September 18, 1971)

The basic properties of the silica-alumina surface have been studied by means of the calorimetric titration and phenol-vapor adsorption methods,[1,2] but the nature and structure of its basic sites have not yet been revealed. On the other hand, the basic properties of alumina have been elucidated fairly well in comparison with those of silica-alumina.[3] We have found, from ESR measurements, that one or two OH^- ions coordinate to the copper (II) complex with 2,2'-bipyridine in the aqueous solution of the complex at pH values higher than 8. Such a phenomenon has also been observed in a basic methanol solution. In this paper, the properties of the basic OH groups on the silica-alumina and alumina surfaces will be presented and compared with the ESR spectra in these solutions.

Alumina, 50% silica-alumina, and silica gel were treated *in vacuo* at 300°C for 3 hr. The copper(II) complexes with 2,2'-bipyridine, $[Cu(bip)(OH_2)_4]SO_4$, $[Cu(bip)_2(OH_2)_2]SO_4$, were synthesized in methanol and recrystallized repeatedly from methanol. The water-free methanol solutions of these complexes were evacuated and introduced to the solids through a breakable seal. After the methanol had been eliminated, the ESR spectra were measured at 77°K. The chemical species were determined from the ESR spectra of the 1st and 2nd derivatives.

Figure 1 shows the ESR spectrum for the 1 : 1 complex adsorbed on the surface of 50% silica-alumina. This spectrum suggests the presence of only one chemical species. The $g_{//}$ and $A_{//}$ values of the spectrum were 2.268 and -172×10^{-4} cm^{-1} respectively. This chemical species is identified to that in which two basic OH groups on the surface coordinate to the 1 : 1 complex by means of a comparison with the ESR spectrum of the complex in an aqueous solution at pH>12.5. This is considered to be reasonable, since the axial symmetry of this spectrum is approximately maintained, much as in the solution. On the other hand, when the 1 : 2 complex was adsorbed on the surface, two chemical species were observed; one is the same as that described above, while the other possesses lower values of $g_{//}$ and $A_{//}$, 2.224 and -143×10^{-4} cm^{-1} respectively, than the former. Noack *et al.* have found the species corresponding to these values in 40% ethanol - 60% water and identified it as the *cis* isomer of the 1 : 2 complex.[4]

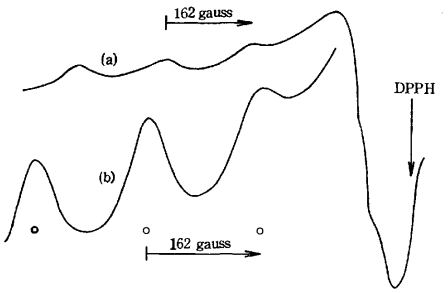

Fig. 1. ESR spectrum of the 1 : 1 complex adsorbed on the surface of 50% silica-alumina; (a) over-all spectrum, (b) parallel components of the spectrum magnified in the lower field region. ○: $g_{//}=2.268$.

The ESR spectrum for the 1 : 1 complex adsorbed on the surface of alumina is represented in Fig. 2. Three chemical species were observed. The species with the lowest value of $g_{//}$ (2.265) is the same as that of the 1 : 1 complex adsorbed on 50% silica-alumina. On the other hand, the species with the middle value of $g_{//}$ (2.306) is identified as that in which one basic OH group coordinates to the 1 : 1 complex by means of a comparison with the ESR spectrum of its aqueous solution in the 8—11 pH range, while the species corresponding to the highest value of $g_{//}$ (2.340) is still uncertain. It is of interest to note that the ESR spectrum of the 1 : 2 complex adsorbed on the surface of alumina was quite the same as in the case of the 1 : 1 complex.

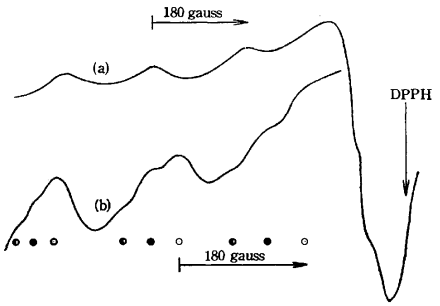

Fig. 2. ESR spectrum of the 1 : 1 complex adsorbed on the surface of alumina; (a) over-all spectrum, (b) parallel components of the spectrum magnified in the lower field region. ○: $g_{//}=2.265$, ●: $g_{//}=2.306$, ◐: $g_{//}=2.340$.

Though the negatively-charged oxygen ion and the OH group are present as basic sites, the effects of these sites on the ESR spectra are quite different; the OH group on $Ca(OH)_2$ and the O^{2-} group on CaO gave rise to different species. It was also found that the O^{2-} on the silica-alumina has a much smaller electron-donating ability than the OH group. The basic sites were thus clarified to exist on the surfaces of 50% silica-alumina and alumina, but they were not observed on the silica gel surface. The basic strength of the sites on the surfaces could also be revealed; the $g_{//}$ value decreases, and that of $A_{//}$ increases, with the electron-donating ability of the ligands. Thus, the adsorption of these complexes on the solid surfaces may be useful means for the elucidation of the basic properties.

1) K. Tanabe and T. Yamaguchi, *J. Res. Inst. Catalysis, Hokkaido Univ.*, **14**, 93 (1966).
2) O. V. Krylov and E. A. Fokina, *Probl. Kinetiki i Kataliza, Acad. Nauk, SSSR*, **8**, 248 (1955).
3) J. B. Peri, *J. Phys. Chem.*, **69**, 220 (1965).
4) M. Noack and G. Gordon, *J. Chem. Phys.*, **48**, 2689 (1968).

p-Nitrophenyl Phosphate as a Phosphorylating Reagent in Nucleotide Synthesis

Tsujiaki HATA and Kyu-Jang CHONG

Department of Chemistry, Tokyo Institute of Technology, Ookayama, Meguro-ku, Tokyo

(Received October 18, 1971)

It is known that tri-substituted esters of phosphoric acid such as triethyl phosphate are transesterified into the corresponding trialkyl phosphate by treatment with alcohol or sodium alkoxide.[1] In the case of mono-substituted phosphates, however, the interchange reaction proceeds very sluggishly and therefore can not be applied to the syntheses of desired monoalkyl phosphates. It was found that pyridine was a remarkably effective solvent for the ester-interchange reaction of *p*-nitrophenyl phosphate (**1**) with alcohols.[2] The reaction is of particular interest since it is an example of ester-interchange reaction, probably proceeding through a reactive *N*-phosphopyridinium intermediate (**2**) towards alcohols.

Phosphorylation of nucleosides by the use of **1** was investigated. When 2',3'-*O*-isopropylidene adenosine (0.3 mmole) was allowed to react with **1** (0.6 mmole) in dry pyridine (0.3 m*l*) at 110°C for two hours, 2',3'-*O*-isopropylidene adenosine 5'-phosphate was isolated by using DEAE cellulose column chromatography. After removal of the protecting group by treating 30% formic acid, adenosine 5'-phosphate was obtained in 85% yield.

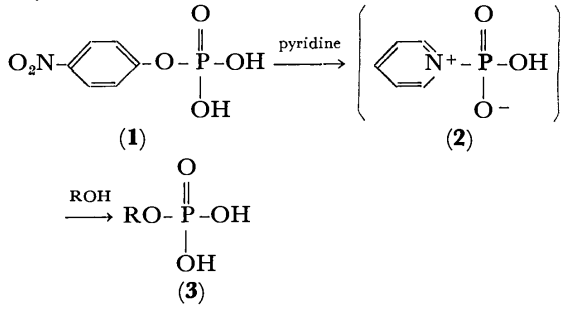

Similarly, other nucleotides were obtained in high yields as shown in Table 1.

It is noted that the yields of nucleotides depend on the concentrations and the molar ratios of **1** to nucleosides. When a large excess of pyridine was employed, nucleoside polyphosphates were formed. 2',3-*O*-Isopropylidene adenosine (0.05 mmol) was treated with **1** (0.25 mmol) in 1.0 m*l* of dry pyridine at 110°C for four hours. After removal of the protecting group, adenosine 5'-diphosphate (ADP) and adenosine 5'-triphosphate (ATP) were obtained in 32% and 33% yields, respectively, along with adenosine 5'-phosphate (35%). These polyphosphates were isolated by means of DEAE cellulose column chromatography.

Phosphorylation of unprotected free nucleoside by the present method was attempted. When adenosine (0.1 mmol) was treated with **1** (0.7 mmol) in dry pyridine (3.0 m*l*) in the presence of tri-*n*-butylamine, adenosine 2',3'-cyclic phosphate (**4**) and adenosine 2'(3'),5'-diphosphate (**5**) were obtained in 43% and 39% yields, respectively. The cyclic phosphate (**4**) was converted with 0.1 N hydrochloric acid into adenosine 2'(3')-phosphate in quantitative yield. When **4** (0.1 mmol) was further treated with **1** (0.7 mmol) in dry pyridine (3.0 m*l*), adenosine 2',3'-cyclic phosphate 5'-phosphate (**6**) was obtained in 57% yield. Data on the chromatographic and spectral properties of these compounds (**4**, **5** and **6**) agree with those of authentic samples.[3,4]

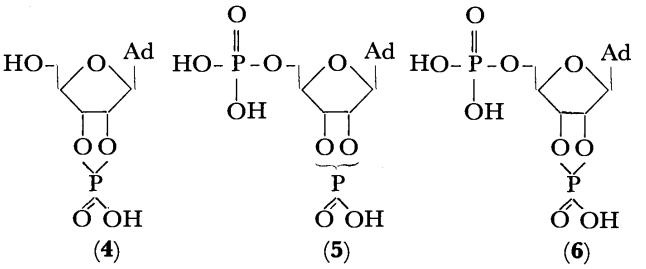

Ad = adenine residue

TABLE 1. PREPARATION OF NUCLEOTIDES

Nucleotide[a]	Yield (%)	R_f value[c]	UV Spectra (pH 2) $\lambda_{max}^{H_2O}$ (mμ)	$\lambda_{min}^{H_2O}$ (mμ)
Adenosine 5'-phosphate	85	0.14	257	231
Guanosine 5'-phosphate	80	0.09	256	228
Uridine 5'-phosphate	82	0.16	262	231
Cytidine 5'-phosphate	70	0.16	279	242
4-*S*-Thiouridine 5'-phosphate	52	0.17	331	285
Thymidine 3'-phosphate[b]	43	0.15	267	235

a) 2',3'-*O*-Isopropylidene nucleoside was used as a starting material except in the case of thymidine derivative.
b) 5'-*O*-Trityl thymidine was used.
c) Paper chromatography was performed by descending technique using Toyo Roshi No. 51 paper. Solvent system used: isopropyl alcohol, concentrated ammonium hydroxide, water (7 : 1 : 2 v/v).

1) W. H. Rueggeberg and J. Chernack, *J. Amer. Chem. Soc.*, **70**, 1802 (1948); A. Morel, *Compt. rend.*, **128**, 508 (1899).
2) K. J. Chong and T. Hata, This Bulletin, **44**, 2741 (1971).
3) M. Smith, J. G. Moffatt, and H. G. Khorana, *J. Amer. Chem. Soc.*, **80**, 6204 (1958).
4) J. G. Moffatt and H. G. Khorana, *ibid.*, 663 (1961).

Butadiene Formation from Ethanol over Silica-Magnesia Catalysts

Hiroo NIIYAMA, Saburo MORII, and Etsuro ECHIGOYA

Department of Chemical Engineering, Tokyo Institute of Technology, Ookayama, Meguro-ku, Tokyo

(Received November 21, 1971)

Butadiene formation reaction from ethanol over various kinds of silica-magnesia having different MgO contents were studied from the standpoint of its acid-base catalysis. Maximum acidity was obtained at 50% MgO, while basicity increased with the MgO content. Silica-magnesia (85% MgO) having adequate acidity and basicity gave the maximum activity. The reaction mechanism and the roles of acidic and basic sites are discussed. The rate controlling step is the acetaldehyde formation catalyzed by basic sites.

Many investigations have been carried out on the reaction of butadiene formation from ethanol.[1,2,3] It was reported that active catalysts should have activities for both dehydration and dehydrogenation reactions. However, the roles of active sites were not clarified. In a previous paper,[4] dehydration and dehydrogenation of alcohols over acid-base bifunctional catalysts were described. It was concluded that the former took place on acidic and the latter on basic sites.

Since butadiene formation reaction includes dehydration and dehydrogenation reactions, acid-base properties of catalysts would be essential. In this paper, the correlations between acidity and/or basicity and the activity of SiO_2-MgO catalysts are given.

Experimental

Catalysts. SiO_2-MgO; A settled amount of magnesium hydroxide (Wako Pure Chem. Co.) and colloidal silica (Nissan Chem. Co.) was kneaded for 3 hr. The gel obtained was dried for 24 hr at 100°C in an oven and then calcined in an electric furnace at 600°C for 3 hr.

SiO_2; Colloidal silica was heated over a water bath. The obtained gel was dried in an oven and then was calcined at 600°C for 3 hr.

MgO; Magnesium hydroxide was calcined at 600°C for 3 hr.

Acidity measurements. Titration (Benesi's method) and gravimetric measurement of pyridine adsorption were used.

Titration was carried out as follows. Samples of the catalysts were calcined at 550°C for 1 hr and then degassed at 300°C under 10^{-5} mmHg. 0.1～0.5 g of the samples were taken in flasks containing water-free benzene. A known amount of *n*-butylamine in benzene solution (0.02N) was added. After four days, Hammett indicators were added and the color of the samples were compared visually with each other.

Adsorption of pyridine was carried out as follows. 0.15～0.3 g of the catalyst was taken in a basket made of quartz and evacuated *in situ* under 10^{-5} mmHg for 3 hr at 350°C. Pyridine was then introduced to the system up to 25 mmHg at 200°C. After adsorption equilibrium had been established (after 1～1.5 hr), desorption was started at the same temperature by trapping the remaining pyridine in the gas phase. The adsorbed amount was determined with a spring balance (sensitivity 10 μg/div.)

Basicity measurements. Titration by benzoic acid using phenolphtalein and nitroaniline[5] as indicators was carried out in order to measure the basicity. Some catalysts, however, showed abnormal color change, making the values obtained unreliable. In this study, the adsorbed amount of boron trifluoride was measured by the gravimetric method and was taken as the index of basicity. Pretreatments and procedures were almost the same as in the acidity measurements.

Infrared spectroscopy. A thin wafer, 1.2×2.0 cm, was prepared by compressing 0.02～0.03 g of the catalyst under 300 kg/cm^2. The infrared cell used was similar to that used by Little.[6] The cell could be attached to the conventional vacuum system and heated *in situ*. The infrared spectra were recorded on a Shimadzu IR spectrometer.

Reaction. Catalytic activities in butadiene formation from ethanol were measured by a conventional flow method. Ethanol and/or other reactants were stored in evaporators maintained at a constant temperature. They were introduced into the reactor with hydrogen, carrier gas. Vaporous products were taken out with a sampling tube and analyzed by gas chromatography.

Results and Discussions

Ethylene, ether, acetaldehyde, butadiene and water were found in the products when SiO_2-MgO catalysts were used. In the case of MgO catalyst, crotonaldehyde and other unknown products were also obtained. SiO_2-MgO catalyst (75 mol% MgO) was used in order to clarify the reaction mechanism.

The effects of contact time on the conversion to all the products were studied. A typical example is given in Fig. 1. Acetaldehyde formation decreased with increase of the contact time, while butadiene formation showed an induction period.[7] This suggests that acetaldehyde is an intermediate product and butadiene a final one in the consecutive reaction.

Several reactants considered[8] to be intermediate products were tested to confirm the reaction mechanism. The results are given in Table 1 and a typical example

1) W. M. Quattlebaum, W. J. Toussaint, and J. T. Dunn, *J. Amer. Chem. Soc.*, **69**, 593 (1947).

2) Yu. A. Gorin, *J. Gen. Chem. USSR*, **16**, 283 (1946), *C.A.*, **41**, 685 (1947), *Zhur. Obshchei Khim.*, **19**, 664 (1949), *C.A.*, **44**, 1006 (1950).

3) M. Ya. Kagan, G. D. Lyubarskii, and O. M. Poduroskaya, *Bull. Acad. Sci. USSR Classe Sci. Chim.*, (1947), *C.A.*, **42**, 4515 (1948).

4) H. Niiyama and E. Echigoya, This Bulletin, **44**, 1739 (1971).

5) J. Take, S. Kikuchi, and Y. Yoneda, *Syokubai (Catalyst)*, **10**, 127 (1968).

6) L. H. Little, "Infrared Spectra of Adsorbed Species", Academic Press, New York and London (1966) p. 31.

7) The induction period is not shown so clearly in this figure, but it was more apparent in the case of SiO_2-MgO catalysts (25 or 50 mol % MgO).

8) M. E. Winfield, "Catalysis Vol. 7" ed. by P. H. Emmett, Reinhold Pub. Co., New York (1960), p. 109.

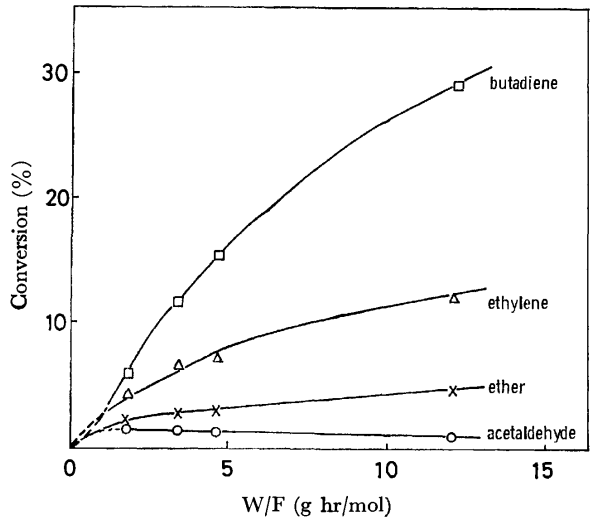

Fig. 1 The effects of contact time on the conversion to all the products. temperature; 380°C, pressure of ethanol; 0.1 atm, catalyst; SiO_2-MgO (75 mol% MgO)

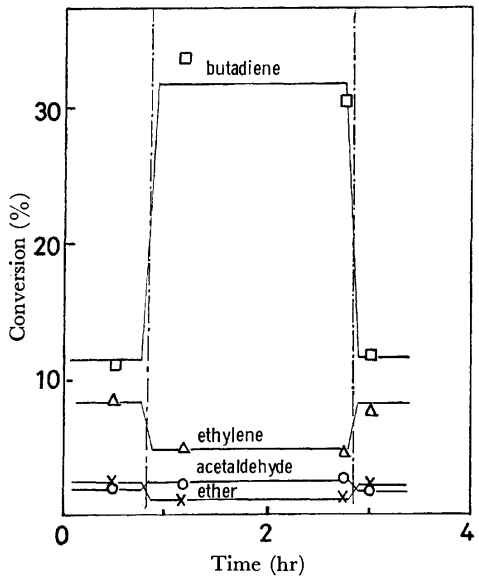

Fig. 2 The effects of acetaldehyde additon. (Reaction conditions were given in table 1)

in Fig. 2. Though neither acetaldehyde nor crotonaldehyde was converted into butadiene, butadiene was readily produced when either of them was fed with ethanol. Moreover, with *n*-propanol or isopropanol instead of ethanol, each produced butadiene with the corresponding dehydrogenated products (propionaldehyde or acetone). Under such reaction conditions, no acetone was found in the products when isopropanol alone was fed. It was also found that any combination of alcohols and ketones or aldehydes brings about hydrogen transfer reaction.[9]

Table 1. Butadiene formation from various kinds of reactants.

Reaction Conditions;
Catalyst; SiO_2-MgO (75 mol% MgO) 1.0 g
Reaction temperature; 380°C
Carrier gas; H_2 100 ml/min stp

run No.	Reactants	Partial Preseure	Conversion to butadiene	By-products
1	ethanol	0.1	0.11	
2	acetaldehyde	0.1	trace	crotonaldehyde
3	crotonaldehyde	0.01	trace	
4	1,3-butanediol	0.01	trace	
5	ethanol acetaldehyde	0.1 0.01	0.31[a]	
6	ethanol crotonaldehyde	0.1 0.01	0.36[a]	
7	1-propanol crotonaldehyde	0.1 0.01	0.18[b]	propionaldehyde
8	2-propanol acetaldehyde	0.1 0.01	0.08[c]	acetone

a) $\frac{\text{butadiene produced} \times 2}{\text{ethanol fed}}$

b) $\frac{\text{butadiene produced} \times 2}{n\text{-propanol fed}}$

c) $\frac{\text{butadiene produced} \times 2}{iso\text{-propanol fed}}$

Various mechanisms have been proposed for butadiene formation reaction. Most investigators considered acetaldehyde as a first intermediate product. Kagan[3] postulated that two acetaldehyde underwent an aldol condensation to form crotonaldehyde. Crotyl alcohol was then produced by the reduction of crotonaldehyde and converted into butadiene. The hydrogen atoms derived from the dehydrogenation of ethanol took part in the reduction. On the other hand, Quattlebaum *et al.* postulated[1] that the hydrogenolysis of crotonaldehyde took place *via* hydrogen transfer from ethanol to crotonaldehyde. 1-hydroxybutene or 1,3-butanediol produced from acetaldehyde and ethanol was also postulated as an intermediate product.[8]

Our results indicate that 1,3-butanediol can not be intermediate product (Table 1, run 4). 1-hydroxybutene is not appropriate, because acetaldehyde and isopropanol gave butadiene instead of isoprene or pentadiene. The mechanisms postulated by Kagan[3] could be rejected because isopropanol gave no dehydrogenated products under the reaction conditions. It was thus concluded that the mechanisms postulated by Quattlebaum *et al.*[1] is valid for this catalyst. This is schematically shown as follows.

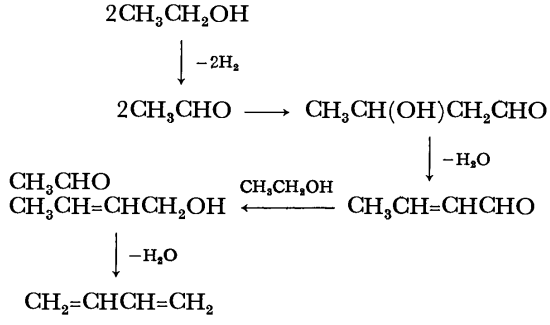

9) H. Niiyama and E. Echigoya, This Bulletin, **45**, 938 (1972).

Table 2. Expected conversion based on the assumption that the first dehydrogenation step is rate determing

reactants	partial pressure	calculated conversion of alcohol	experimental value	run No. in Table 1
ethanol acetaldehyde	0.1 0.01	$0.11+0.10+\sum_{i=1}^{\infty}0.1\times2^{-i}=0.31$	0.31	5
ethanol crotonaldehyde	0.1 0.01	$0.11+0.10\times2+\sum_{i=1}^{\infty}0.1\times2^{-i}=0.41$	0.36	6
1-propanol crotonaldehyde	0.1 0.01	$0.10\times2=0.20$	0.18	7
2-propanol acetaldehyde	0.1 0.01	0.10	0.08	8

Determination of the rate controlling step. On the basis of this scheme and assuming that acetaldehyde formation is the rate controlling step, we can expect the conversion for run 5, taken as an example, in the following way. A mixture of acetaldehyde and ethanol (0.1 : 1) was fed. The relative amount of butadiene derived from ethanol independently of acetaldehyde addition was 0.11 (*cf.* run 1). Since the process after the dehydrogenation of ethanol was assumed to be very fast, all the added acetaldehyde was converted into butadiene. The amount of butadiene from the added acetaldehyde was thus 0.10. Hydrogen transfer between crotonaldehyde and ethanol took place and acetaldehyde was produced again. The secondary acetaldehyde formation was repeated infinitely. Thus the amount of butadiene derived from secondary produced acetaldehyde was $\sum_{i=1}^{\infty}0.1\times2^{-i}$, where i is the cycle number. The expected conversion was calculated as follows.

$$0.11 + 0.10 + \sum_{i=1}^{\infty}0.1 \times 2^{-i} = 0.31$$

The results for runs 5, 6, 7, and 8 are summarized in Table 2. There is a good agreement between the results and the calculated values.

Correlations between catalytic activity and acidity and/or basicity. The acidic properties determined by the Benesi's method and pyridine adsorption method, both of which show a similar tendency, are given in Table 3. The basicity is also given in the table.

The maximum acidity was obtained when MgO content reached 50%, while basicity increased with MgO content. Specific rates of butadiene formation increased with the MgO content up to 85%, but pure MgO showed little activity. This aspect was quite different from that of acidity and also of basicity.

Since the rate controlling step of this reaction was the dehydrogenation of ethanol catalyzed by basic sites,[4] the rate was expected to increase with the MgO content. This, however, was not the case. When MgO catalyst was used, crotonaldehyde was found in the products. This indicates that MgO has a catalytic activity in the aldol condensation reaction.[10] More-

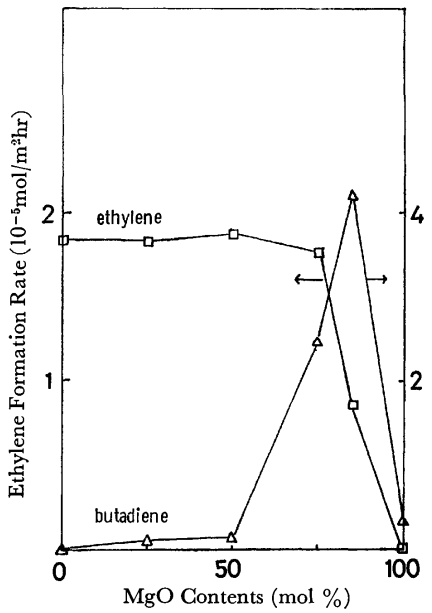

Fig. 3 Rate of production of butadiene or ethylene against MgO contents. temperature; 380°C, pressure of ethanol; 0.1 atm

Table 3. Acidity and basicity of the catalysts

Catalyst	Acidity: Benesi's method: Acidity $H_0>3.3$ 10^{-6} eq/m^2	Acidity: Benesi's method: maximum acid strength H_0	Acidity: Pyridine adsorption at 200°C 10^{-6} eq/m^2	Basicity BF adsorption at 300°C 10^{-6} eq/m^2
SiO_2	—	—	0.09±0.02	0.8±0.2
SiO_2-MgO 25% MgO	1.29±0.1	+1.5	0.68±0.1	4.0±0.5
50% MgO	2.14±0.1	−3.0	0.94±0.1	4.2±0.5
75% MgO	2.14±0.2	+1.5	0.74±0.1	6.2±0.5
85% MgO	1.31±0.2	+1.5	0.28±0.05	7.2±0.5
MgO	—	—	0	15.0±2

10) S. Malinowski and S. Basinski, *J. Catalysis*, **2**, 203 (1963).

over, it showed considerable activity in the hydrogen transfer reaction.[9] Poor activity of MgO catalyst in the reaction could be attributed to the small dehydration activity for the final step catalyzed by acidic sites. It is thus concluded that both acidic and basic sites are necessary to increase the yield of butadiene.

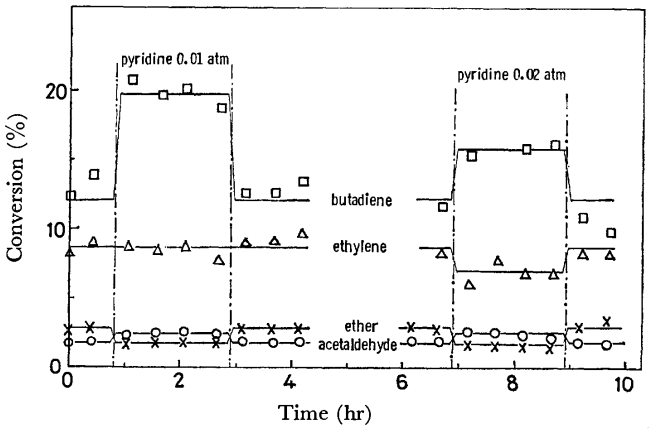

Fig. 4 The effects of pyridine addition. temperature; 380°C, pressure of ethanol; 0.1 atm, W/F=3.4 g hr/mol

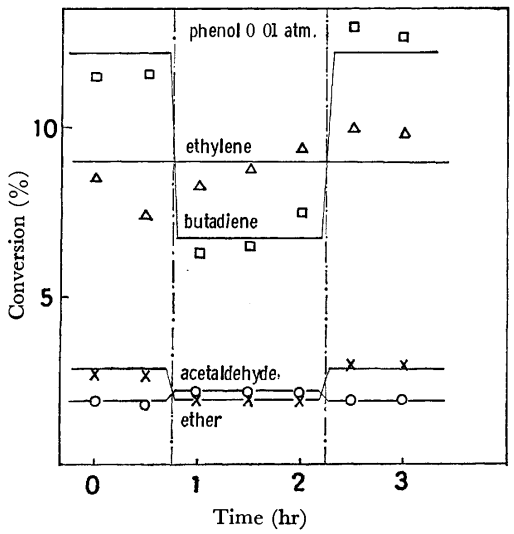

Fig. 5 The effects of phenol addition. temperature; 380°C, pressure of ethanol; 0.1 atm W/F=3.4 g hr/mol

Addition of acidic and basic materials. Pyridine and phenol were introduced into the reaction system in order to poison acidic and basic sites, respectively. The results are shown in Figs. 4 and 5. The addition of phenol brought a marked decrease in butadiene formation, but ethylene formation remained constant. Since the rate controlling step in butadiene formation is the first dehydrogenation catalyzed by basic sites, the effects of phenol are rational.

On the other hand, pyridine had a "promoter action" in butadiene formation. To understand the "promoter action" of pyridine the behavior of surface hydroxyl group was studied by infrared spectroscopy. As is shown in Fig. 6, four absorption bands were observed in 3400—4000 cm^{-1} region. They were assinged to OH stretching vibration bands since they could be exchanged with D_2O. Generally speaking, a hydroxyl group with higher stretching frequency has a basic nature.[11] It was observed that the bands around 3840 cm^{-1} and 3720 cm^{-1} remain while the band around 3650 cm^{-1} readily disappeared in contact with D_2O vapor. Since acidic OH is expected to undergo ex-

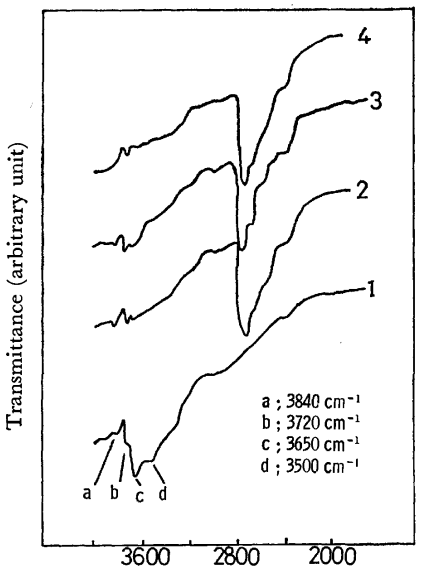

Fig. 6 IR spectra of surface hydroxyl group.
1. evacuated at 350°C for 6 hr.
2. exchanged with D_2O at 350°C for 1 hr and then evacuated at 350°C for 1 hr.
3. exchanged with D_2O again at 350°C for 1 hr and then evacuated at 350°C for 1 hr.
4. exchanged with D_2O again at 350°C for 1 hr and then evacuated at 350°C for 3 hr.

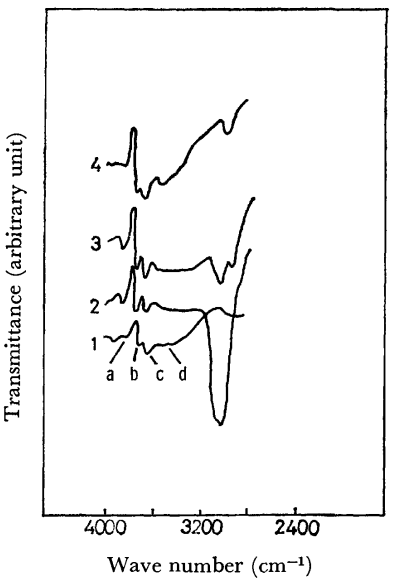

Fig. 7 The effects of pyridine adsorption on surface hydroxyl group.
1. evacuated at 340°C for 3 hr.
2. rehydrated by traces of water under atmosphere of pyridine
3. evacuated again at room temperature for 0.5 hr.
4. evacuated at 100°C for 0.5 hr.

11) J. D. S. Goulden, *Spectrochim. Acta*, **6**, 129 (1954).

change more readily than neutral or basic OH, the band around 3650 cm^{-1} should refer to acidic OH. In other words, bands around 3840 cm^{-1} and 3720 cm^{-1} could be considered to have a basic nature as compared with 3650 cm^{-1} band.

The effects of pyridine on the behavior of these surface hydroxyl group are shown in Fig. 7. Rehydration of the evacuated sample by traces of water (0.03 meq) made little change in the higher frequency bands. In the presence of pyridine, however, rehydration made the intensity of these bands increase. Evacuation at 100°C gave rise to the decrease of the intensity of these bands, with an accompanying decrease of a band around 2900 cm^{-1} assigned to CH stretching of pyridine. This suggests that basic sites are produced by adsorption of pyridine. This would be caused by the inductive effects of adsorbed pyridine.

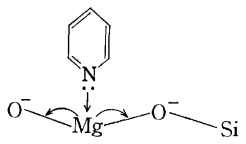

When pyridine is adsorbed on acidic sites, the nearest oxide ions become rich in electron density. This will produce new basic sites available to catalyze the dehydrogenation of ethanol. A small amount of pyridine thus increases basicity accompanied with the increase of dehydrogenation activity. By excess addition, however, pyridine occupies more of the acidic sites than is necessary and makes the "promoter action" retarded.

Conclusion

The reaction mechanism and roles of acidic and basic sites in butadiene formation over silica-magnesia catalysts can be written as follows.

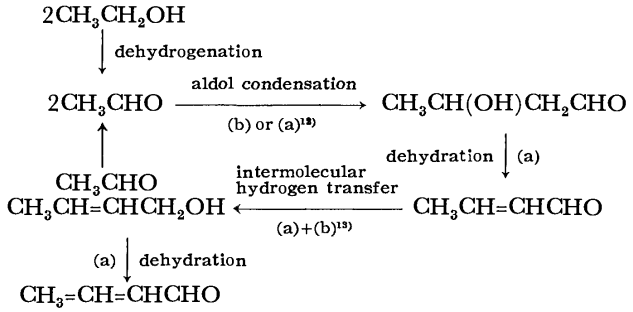

(a) and (b) represent acidic and basic sites, respectively. The rate controlling step over silica-magnesia catalysts is the dehydrogenation of ethanol catalyzed by basic sites. Thus activity increases with basicity. Over magnesia catalyst which has great basicity but no acidity, however, dehydration of crotyl alcohol hardly takes place and the activity is low. It is important to control the acidity and basicity in order to increase the yield of butadiene.

12) Both (a) and (b) are available in this step.[14]

13) This step was considered to take place in an acid-base concerted mechanism.[8]

14) Y. Ogata, "Yuuki Hannoron (Organic Reactions)" Maruzene, Tokyo (1967) p. 279.

BULLETIN OF THE CHEMICAL SOCIETY OF JAPAN, VOL. 45, 659—664(1972)

Photodecomposition of Vinyl Iodide in Gas Phase

Shigeru YAMASHITA, Shigeo NOGUCHI, and Teruo HAYAKAWA

Department of Chemistry, Faculty of Liberal Arts and Sciences, University of Osaka Prefecture, Mozu-Umemachi, Sakai, Osaka

(Received March 20, 1971)

Photodecomposition of vinyl iodide has been studied at 313 and 254 mμ using a high intensity light source. Because of high concentration of the radicals formed primarily due to the high intensity of the light source, only the inter-radical reactions were taken into account in considering the secondary processes.

Both molecular and free radical processes have been observed in the primary process and the ratio of the contribution of molecular process to free radical process was found to be about 1 : 6 in the wavelength range studied. A slight energy dependence of k_d/k_c, the ratio of the rate of disproportionation reaction to that of combination reaction of vinyl radicals, was found in the secondary processes.

The primary process of the photochemical reaction has been studied by many investigators using various instruments for the detection of short-lived intermediates produced in the process.[1)]

In the case of photochemical studies carried out by means of a conventional static reactor and the analysis of the final products, there are ambiguities due to the contributions from so many secondary processes, most of which are the reactions between primary fragment radicals and reactant molecules since the concentration of the primary fragment is usually much lower than that of the reactant molecules.

By use of a high intensity light source in the study of photochemical reactions, the reaction scheme would be simplified even in the conventional static method

1) R. G. W. Norrish and G. Porter, *Nature*, **164**, 658 (1949). G. Porter, *Proc. Roy. Soc.*, **A200**, 284 (1950). G. Herzberg and D. A. Ramsay, *Proc. Roy. Soc.*, **A233**, 34 (1955). F. P. Lossing, D. G. H. Harsden, and J. B. Farmer, *Can. J. Chem.*, **34**, 701 (1956). G. B. Kistiakowsky and P.H. Kydd, *J. Amer. Chem. Soc.*, **79**, 4825 (1957). K. Bergman and W. Demströder, *J. Chem. Phys.*, **48**, 18 (1968).

excluding radical-molecule reactions because of the high concentration of the reactive primary fragment radicals. In the photochemical studies of azoalkanes[2] and alkyl sulfides[3] using high intensity light sources, only the products from the reactions between the free radicals formed in the primary processes were observed. Since the products from the free radical-reactant molecule reactions were not detected in these works, the reaction schemes were rather simplified.

Although a number of data are available for the reactions of alkyl radicals, comparatively few studies have been carried out on the reactions of unsaturated free radicals.[4,5,6]

In the present work, direct photolysis of vinyl iodide in the gas phase at room temperature has been studied under high light intensity conditions. Photolysis of vinyl iodide was reported by Roberge and Herman.[7] However, the study was carried out in carbon tetrachloride solution with a light source of rather low intensity.

The purpose of the present paper was to find the primary process in the photodecomposition of vinyl iodide and to study the energy dependence of the primary and secondary processes by changing the wavelength of the exciting light.

Experimental

Vinyl iodide was prepared by the reaction of 1,2-diiodoethane with sodium ethoxide[8] and purified by vacuum distillation. Before every run, the sample was cautiously degassed at the temperature of liquid nitrogen. The absorption spectrum of vinyl iodide vapor is shown in Fig. 1. The reactor was a conventional drum-type quartz cylinder. The light source was a USH-500D 500W high pressure mercury lamp manufactured by Ushio Electric Co. and the light output was collimated in a housing fitted with condensing lens system and spherical mirror to obtain maximum intensity. The total light flux projected to the surface of the reactor was estimated by ferrioxalate actinometer[9] to be about 3×10^{18} quanta/sec, which is as high as the intensity of the light sources used by previous workers.[2,3]

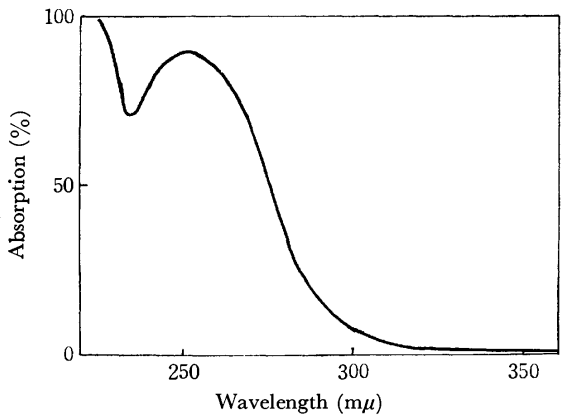

Fig. 1. Absorption spectrum of vinyl iodide vapor. Pressure; 60 torr. Path length; 50 mm.

The reactant gas was irradiated at room temperature in order to exclude thermal reactions. One series of the experiments was carried out using a Toshiba UV-29 filter which transmits a light of wavelength greater than 290 mμ. In the other series, the sample in the reactor was irradiated by a full arc with no filter.

In the UV-29 series experiments, the most abundant quanta absorbed by vinyl iodide are those from the 313 mμ output of the mercury lamp considering the absorption curve of vinyl iodide and other experimental conditions.

In the full arc series experiments, it was not easy to estimate the most effective radiation because of the lack of detailed energy distribution data of the lamp in the wavelength range smaller than 300 mμ. By rough estimation, however, the most effective wavelength in the full arc experiments seems to be 254 mμ line from the mercury lamp. The conversion of the reactant was less than 5% in all runs. Since the dissociation energy of C-I bond in vinyl iodide has been reported to be 66.5 kcal/mol,[10] the light quanta have enough energy for C-I bond rupture both in UV-29 and full arc series. Before the analysis of the reaction products, unreacted vinyl iodide and non-volatile products were condensed by a cold trap cooled at −79°C. The separated volatile products were analyzed by gas chromatograph with a column packed with dimethylsulfolane on alumina and by a Hitachi RMU-5 mass spectrometer.

Results and Discussion

The main products in both UV-29 and full arc series experiments were ethylene, acetylene and 1,3-butadiene. Hydrogen iodide in the reaction products was detected by mass spectrometry. Iodine formation was observed spectrophotometrically by dissolving a small amount of non-volatile products deposited on the reactor wall into *n*-hexane solution. Quantitative de-

Table 1. Photolysis of vinyl iodide

CH_2=CHI (Torr)	Products (micromole)		
	C_2H_4	C_2H_2	C_4H_6
9.26	0.28	0.40	0.07
15.35	0.37	0.53	0.15
22.39	0.51	0.85	0.31
33.70	0.46	0.69	0.36
35.33	0.50	0.75	0.36
40.13	0.49	0.73	0.45
40.47	0.52	0.84	0.45
48.15	0.51	0.68	0.40

Light source; high pressure mercury lamp with a Toshiba UV-29 filter.
Irradiation; 14 min.

2) J. O. Terry and J. H. Futrell, *Can. J. Chem.*, **45**, 2327 (1967).
3) S. Yamashita and F. P. Lossing, *ibid.*, **46**, 2925 (1968). A. Jones, S. Yamashita, and F. P. Lossing, *ibid.*, **46**, 833 (1968).
4) N. A. Weir, *J. Chem. Soc.*, (**1965**) 6870.
5) D. J. LeRoy and A. W. Tickner, *J. Chem. Phys.*, **19**, 1247 (1951).
6) A. G. Sherwood and H. E. Gunning, *J. Phys. Chem.*, **69**, 2323 (1965). M. G. Bellas, J. K. S. Wan, W. F. Allen, P. O. Strausz, and H. E. Gunning, *ibid.*, **68**, 2170 (1964).
7) P. C. Roberge and J. A. Herman, *Can. J. Chem.*, **45**, 1361 (1966).
8) J. Spence, *J. Amer. Chem. Soc.*, **55**, 1290 (1933).
9) C. A. Parker, *Proc. Roy. Soc.*, **A235**, 518 (1956).
10) V. I. Vedeneyev, L. V. Gurvich, V. N. Kondratyev, V. A. Medvedev, and Ye. L. Frankevich, "Bond Energies, Ionization Potentials and Electron Affinities", St Martin's Press, New York, N. Y. (1966), p. 63.

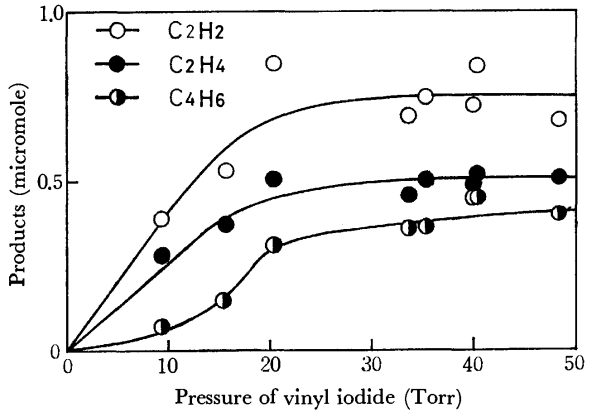

Fig. 2. Pressure dependence of the products formation in vinyl iodide photolysis. Filter; Toshiba UV-29. Irradiation; 14 min.

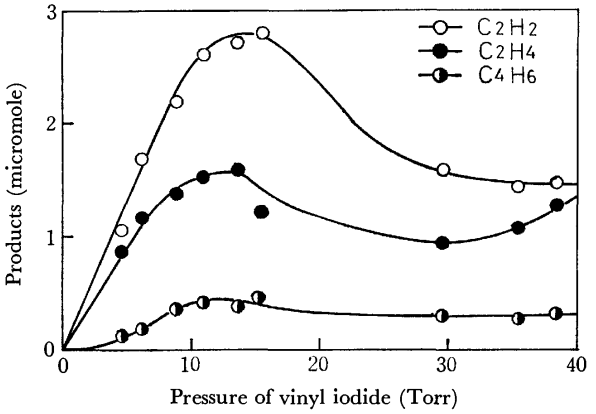

Fig. 3. Pressure dependence of the products formation in vinyl iodide photolysis by full arc without filter. Irradiation; 4 min.

termination of hydrogen iodide and iodine could not be achieved. The rather poor material balance of carbon and hydrogen in the reaction products might be caused by missing hydrogen iodide and a trace of polymeric products in the quantitative determination.

The results of the UV-29 series experiments at various initial pressures of vinyl iodide are shown in Table 1 and Fig. 2. In the pressure range lower than 20 torr, it is seen that the formation of C_2H_2 and C_2H_4 is proportional to the pressure of vinyl iodide and that of 1,3-butadiene to the square of vinyl iodide pressure. Saturation of the product formation takes place in high pressure range. This seems to be due to the fact that the transparency of the reactor wall decreases rapidly in the high pressure runs by the deposition of trace of opaque produsts, probably polymeric, on the reactor wall.

Table 2. Photolysis of vinyl iodide

CH_2=CHI (Torr)	Products (micromole)		
	C_2H_4	C_2H_2	C_4H_6
4.63	0.87	1.06	0.13
6.04	1.17	1.59	0.19
8.67	1.38	2.20	0.37
10.84	1.54	2.63	0.40
13.49	1.61	2.72	0.37
15.20	1.22	2.81	0.46
29.74	0.94	1.59	0.30
35.55	1.07	1.45	0.28
38.59	1.03	1.48	0.31

Light source; full arc of high pressure mercury lamp.
Irradiation; 4 min.

The results of the full arc series are shown in Table 2 and Fig. 3. The results were less reproducible than in the case of the UV-29 series.

These results of high intensity photolyses were expected to differ from those obtained by conventional low intensity light source.

The results obtained with the use of low intensity light source are shown in Table 3 together with those obtained with high intensity source for comparison. The composition of the two reaction products differs.

Table 3. Comparison of the composition of the products in high intensity photolysis of vinyl iodide with the results of low intensity photolysis

	CH_2=CHI (Torr)	Products (micromole)		
		C_2H_4	C_2H_2	C_4H_6
High intensity photolysis	19.40	0.58	1.32	0.52
	24.28	0.73	1.58	0.90
	31.73	0.78	1.66	1.21
Low intensity photolysis	30.71	0.32	0.13	0.03
	30.12	0.32	0.12	0.04
	30.04	0.29	0.15	0.04

Light source for high intensity experiments was a USH-500 high pressure mercury lamp whose incident flux to the reactor was of the order 10^{18} photons/sec.
Light source for low intensity experiments was a SHL-100UV high pressure mercury lamp whose incident flux to the reactor was of the order 10^{16} photons/sec.
Filter; Toshiba UV-29 for both series experiments.
Irradiation time was adjusted for obtaining the products of the same order of amount in the two series.

In contrast to high intensity experiments, the predominant product in low intensity experiments is ethylene as reported by previous workers,[7] indicating that the hydrogen abstraction by vinyl radical-vinyl iodide molecule reaction is more predominant than radical-radical reaction in the low intensity condition because of the low concentration of vinyl radicals.

When nitric oxide was added to the reaction mixture, production of C_2H_4 and C_4H_6 was quenched completely whereas C_2H_2 formation was partly suppressed. The effect of nitric oxide suggests that C_2H_4 and C_4H_6 are formed from free radicals produced in a primary process. On the other hand, C_2H_2 seems to be produced by molecular process as well as by free radical process since its formation was not completely quenched by the addition of the free radical quencher nitric oxide.

It was confirmed that the rate of decomposition was proportional to light intensity as shown in Fig. 4, which means that the reaction rate is proportional to the number of quanta absorbed by the reactant molecules.

Thus, the primary steps of the photodecomposition of vinyl iodide under the conditions of the present work are supposed to be as follows:

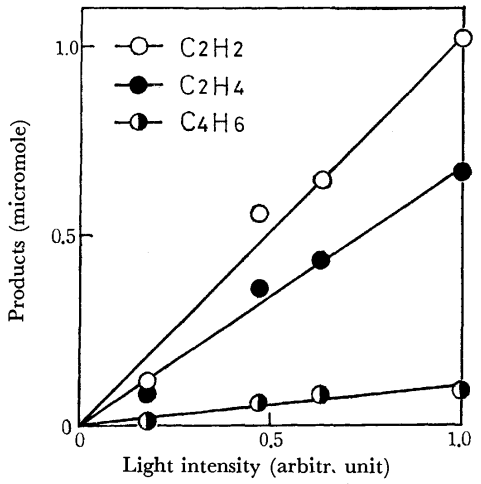

Fig. 4. The effect of light intensity on the products formation.

$$C_2H_3I + h\nu \longrightarrow C_2H_3I^* \quad (1)$$

$$C_2H_3I^* \xrightarrow{k_1} C_2H_3\cdot + I \quad (2)$$

$$C_2H_3I^* \xrightarrow{k_2} C_2H_2 + HI \quad (3)$$

where, the rate of process (1) is approximately expressed by $k_0I_0[C_2H_3I]$, which means that it is proportional to light intensity I_0 and to the pressure of the reactant $[C_2H_3I]$. Process (2) is a free radical process and process (3) a molecular process where the products are molecular species.

Because of the high intensity of the light source, radical-molecule reactions could be neglected in the secondary processes following the primary processes (1), (2), and (3).

The reaction scheme for the secondary processes can be proposed as follows:

$$2C_2H_3\cdot \xrightarrow{k_d} C_2H_2 + C_2H_4 \quad (4)$$

$$2C_2H_3\cdot \xrightarrow{k_r} C_4H_6^* \quad (5)$$

$$C_4H_6^* \xrightarrow{k_{-r}} 2C_2H_3\cdot \quad (6)$$

$$C_4H_6^* + M \xrightarrow{k_s} C_4H_6 + M \quad (7)$$

$$I + I + M \longrightarrow I_2 + M \quad (8)$$

where $C_4H_6^*$ denotes a vibrationally excited complex.

The study of mercury-photosensitized reaction of vinyl chloride in the gas phase by Gunning and his co-workers[6] is instructive for the present work although the reactants and the experimental conditions are different. The process of vinyl radical formation by the reaction of $Hg(6\ ^3P_1)$ atoms with vinyl halide can be ruled out for direct absorption excitation of the reactant molecule. Vinyl radical formation is given by process (2). The hydrogen-abstraction process

$$C_2H_3\cdot + C_2H_3I \longrightarrow C_2H_4 + C_2H_2I$$

can be ruled out because of the high concentration of C_2H_3 radicals since radical-radical reaction is much faster under such conditions. In contrast of the results of Gunning and co-workers the value of the ratio $[C_2H_4]/[C_2H_2]$ was time-independent. The reaction scheme is thus not incompatible with their results,[6] if we consider the difference in experimental conditions.

The contribution of the process

$$C_2H_3\cdot + I \longrightarrow C_2H_3I$$

was assumed to be negligible compared to reactions (4) and (5) by analogy with the fact that the rate constant of the recombination process

$$R\cdot + R\cdot \longrightarrow R\text{-}R$$

is about 10^2 times larger than that of the process

$$R\cdot + X \longrightarrow R\text{-}X$$

where R denotes alkyl radicals and X means NO molecule.[11] Assuming the short life of $C_2H_3I^*$ as in the case of CH_3Cl^*,[6] contribution of the process

$$C_2H_3I^* + M \longrightarrow C_2H_3I + M$$

might be smaller than processes (2) and (3).

The hydrogen-abstraction reaction by iodine atom could be excluded because of its low reaction rate.

Considering the dissociation energy of the C–I bond in vinyl iodide and the energy level of the lowest excited state of iodine atom which is known to be 21.7 kcal/mol,[12] contribution of the electronically excited iodine atom can not be excluded in UV-29 and full arc series while most of the excess energy at the C–I bond rupture would be distributed to the lighter fragment[13] $C_2H_3\cdot$.

Applying the steady state method, the rates of formation of C_2H_2, C_2H_4, and C_4H_6 are expressed as follows:

$$\frac{d[C_2H_2]}{dt} = \frac{I_0k_0k_2}{k_1+k_2}[C_2H_3I] + \frac{I_0k_0k_1k_d(k_s[M]+k_{-r})[C_2H_3I]}{2(k_1+k_2)\{(k_d+k_r)(k_s[M]+k_{-r})-k_rk_{-r}\}} \quad (9)$$

$$\frac{d[C_2H_4]}{dt} = \frac{I_0k_0k_1k_d(k_s[M]+k_{-r})[C_2H_3I]}{2(k_1+k_2)\{(k_d+k_r)(k_s[M]+k_{-r})-k_rk_{-r}\}} \quad (10)$$

$$\frac{d[C_4H_6]}{dt} = \frac{I_0k_0k_1k_rk_s[M][C_2H_3I]}{2(k_1+k_2)\{(k_d+k_r)(k_s[M]+k_{-r})-k_rk_{-r}\}} \quad (11)$$

Assuming the constancy of $d[C_2H_2]/dt$, $d[C_2H_4]/dt$, and $d[C_4H_6]/dt$ in the low conversion period, the following equation is obtained:

$$\frac{[C_2H_2]+[C_4H_6]}{[C_2H_4]+[C_4H_6]} = 1 + \frac{2k_2}{k_1} \quad (12)$$

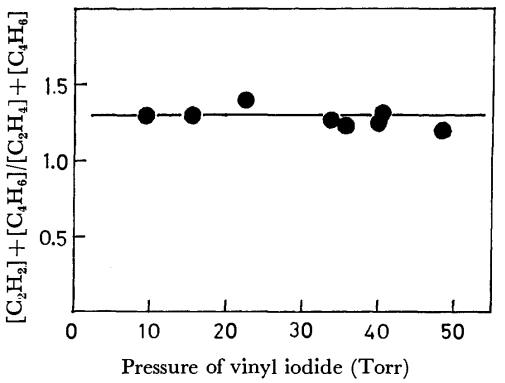

Fig. 5. Reaction product ratio $[[C_2H_2]+[C_4H_6]]/[[C_2H_4]+[C_4H_6]]$ obtained at various pressures of vinyl iodide. Filter; Toshiba UV-29.

11) K. J. Laidler, "Chemical Kinetics", Mc-Graw-Hill Co., New York, N. Y., p. 184 (1965).
12) R. T. Meyer, *J. Phys. Chem.*, **72**, 1583 (1968).
13) J. M. White, R. L. Johnson, Jr. and D. Bacon, *J. Chem. Phys.*, **52**, 5212 (1970).

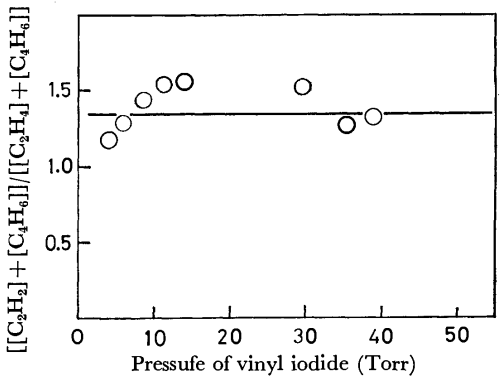

Fig. 6. Reaction product ratio $[[C_2H_2]+[C_4H_6]]/[[C_2H_4]+[C_4H_6]]$ obtained at various pressures of vinyl iodide when full arc was used without filter.

TABLE 4. CONTRIBUTION OF MOLECULAR AND RADICAL PROCESSES IN THE PHOTODECOMPOSITION OF VINYL IODIDE

Experiment	Molecular process	Radical process	k_2/k_1	Most effective wavelength for excitation
UV-29 series	13±2%	87±2%	0.14± 0.02	313 mμ (91 kcal/mol)
Full arc series	17±5%	83±5%	0.20± 0.07	254 mμ (112 kcal/mol)

The equation shows that the reaction product ratio $([C_2H_2]+[C_4H_6])/([C_2H_4]+[C_4H_6])$ is constant and k_2/k_1 value can be obtained.

It is seen in Figs. 5 and 6 that the ratio $[[C_2H_2]+[C_4H_6]]/[[C_2H_4]+[C_4H_6]]$ is constant in both UV-29 and full arc series although the results are rather scattered in the latter. Table 4 shows that the ratio k_2/k_1, ratio of the contribution of molecular process (3) to free radical process (2) in the primary processes, is about 1/6 and almost independent of the exciting energy in the range 91—112 kcal/mol.

The quantum yield for the sum of molecular and radical processes was found to be 0.26±0.2 in the UV-29 series.

In the low pressure range, where $k_s[M] \ll k_{-r}$, Eqs. (9), (10), and (11) are respectively reduced to

$$\frac{d[C_2H_2]}{dt} = \frac{(k_1+2k_2)k_0I_0}{2(k_1+k_2)}[C_2H_3I] \quad (13)$$

$$\frac{d[C_2H_4]}{dt} = \frac{k_0k_1I_0}{2(k_1+k_2)}[C_2H_3I] \quad (14)$$

$$\frac{d[C_4H_6]}{dt} = \frac{k_0k_1k_rk_sI_0}{2(k_1+k_2)k_dk_{-r}}[C_2H_3I]^2 \quad (15)$$

These equations explain the results in which, in the low pressure range, the rates of ethylene and acetylene formation are proportional to the pressure of vinyl iodide, while the rate of 1,3-butadiene formation is proportional to the square of vinyl iodide pressure.

From Eqs. (14) and (15) we obtain

$$\frac{[C_4H_6]}{[C_2H_4]} = \frac{k_rk_s}{k_dk_{-r}}[C_2H_3I] \quad (16)$$

This means that the product ratio $[C_4H_6]/[C_2H_4]$ is proportional to the pressure of vinyl iodide in the low pressure range as shown in Fig. 7.

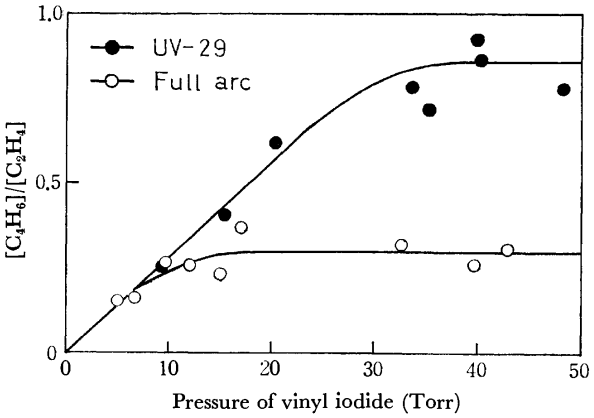

Fig. 7. Linear relation between the ratio $[C_4H_6]/[C_2H_4]$ and vinyl iodide pressure in low pressure range.

From Eqs. (10) and (11), the following equation is obtained:

$$\frac{[C_2H_4]}{[C_4H_6]} = \frac{k_d}{k_r}\left(1+\frac{k_{-r}}{k_s}\cdot\frac{1}{[M]}\right) \quad (17)$$

This shows the linear relation between the ratio $[C_2H_4]/[C_4H_6]$ and $1/[M]$ where [M] denotes the pressure of the reactant. Fig. 8 shows that the linear relation holds both for UV-29 and full arc series. From Fig. 8, the value of the ratio k_d/k_r is found to be 0.43 in UV-29 series and 2.5 for full arc experiments.

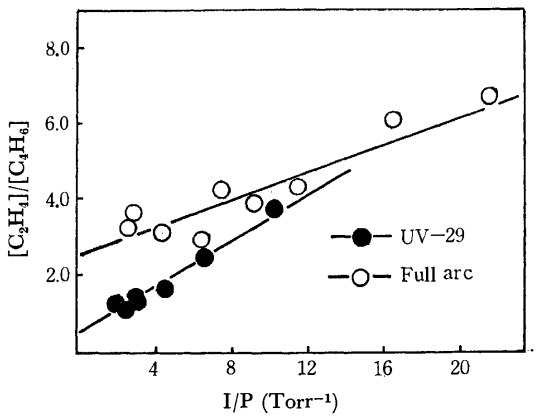

Fig. 8. Linear relation between the ratio $[C_2H_4]/[C_4H_6]$ and the reciprocal of vinyl iodide pressure.

TABLE 5. THE RATIO OF k_d/k_c FOR VINYL RADICAL PRESENTED BY DIFFERENT WORKS

k_d/k_c	Method	Investigators
0.4	Photodecomposition of vinyl iodide mostly at 313 mμ	S. Y. *et al.*
2.5	Photodecomposition of vinyl iodide mostly at 254 mμ	S. Y. *et al.*
1.1	Irradiation of the mixture of vinyl formate and acetaldehyde at a wavelength greater than 300 mμ	N. A. Weir; ref. 4
2	Decomposition of the mixture of vinyl iodide and vinyl bromide by sodium diffusion flame technique	D. J. LeRoy and A. W. Tickner; ref. 5
0.05	Photodecomposition of mercury divinyl by 220—260 mμ	A. G. Sherwood and H. E. Gunning; ref. 6

The value k_d/k_c which is usually used for the rate constant ratio of disproportionation to combination of the radical-radical reaction, is equal to the ratio k_d/k_r in the present paper. The values of k_d/k_c for vinyl radical reactions obtained by the previous and present workers are summarized in Table 5. The results of the present work and those of previous investigators are compatible except for the results of Sherwood and Gunning, although the vinyl radical sources and experimental conditions differ from each other.

Considering the results of photochemical study of Weir[4] and the present work, the value of the ratio k_d/k_c for vinyl radical seems to depend slightly on the exciting energy. When a molecule for free radical source is excited by absorption of quanta of shorter wavelength, the excess energy carried by the photofragment radical should be larger. The results in Table 5 suggest that the excitation by shorter wavelength light causes larger value of k_d/k_c in the case of vinyl radicals. It is difficult, however, to find a regularity from all the data in Table 5 taken from different studies since the conditions for vinyl radical formation differ.

It is generally accepted that recombination and disproportionation reactions of free radicals proceed with almost zero activation energy[14,15] as well as ion-molecule reactions.

It is also known that, in ion-molecule reactions, the "stripping" mechanism is predominant at high energy conditions whereas the "complex" mechanism is effective at low energy conditions.[16,17] In the reaction between CH_4^+ and CH_4, for example, H^+-stripping model was considered while the complex formation was assumed in low energy condition.[18]

$$CH_4^+ + CH_4 \begin{cases} \longrightarrow CH_3 + CH_5^+ & (H^+\text{-stripping}) \\ \longrightarrow C_2H_8^+ \longrightarrow CH_5^+ + CH_3 & (\text{complex}) \end{cases}$$

It might be suggested that the observation of the complex(combination) → disproportionation transition with increasing exciting energy in radical-radical reactions is phenomenologically analogous to the complex→ stripping transition with increasing energy found in ion-molecule reactions.

14) J. C. Walton, *J. Phys. Chem.*, **71**, 2763 (1967).
15) B. H. Mahan, *J. Chem. Phys.*, **32**, 362 (1960).
16) A. Henglein, "Ion-Molecule Reactions in the Gas Phase", American Chemical Society, Washington, D. C., (1966) p. 63.
17) A. Henglein, *J. Chem. Phys.*, **53**, 458 (1970).
18) G.E. Owen and L. Madansky, *Amer. J. Phys.*, **26**, 260(1958).

BULLETIN OF THE CHEMICAL SOCIETY OF JAPAN, VOL. 45, 664—668(1972)

Interaction of Metal Porphyrins with Molecular Oxygen in Solutions

Kenichi YAMAMOTO and Takao KWAN

Faculty of Pharmaceutical Sciences, The University of Tokyo, Bunkyo-ku, Tokyo

(Received May 20, 1971)

The oxidation of divalent metal tetraphenylporphin complexes by molecular oxygen has been investigated in solutions. It was found that the one-electron oxidation of low-spin iron(II) complexes to yield high-spin iron-(III) does not take place, while a low-to-low conversion proceeds with ease. It is suggested that the ready oxidation is due to the delocalization of the d_π electrons of iron(II) to the vacant π-orbital of the porphin ligand. Oxidative mechanisms of manganese(II) and cobalt(II) tetraphenylporphins were also discussed.

It is well known that iron porphyrin complexes take part in oxygen-carrying, electron transfer (redox reaction) and in decomposing hydrogen peroxide in biological processes. These subtle functions may be ascribable to both the iron porphyrin and the axial-ligand environment (protein), and they are quite informative in regard to catalysis.

In the present work, a much simpler reaction system is undertaken; the interaction of synthetic iron tetraphenylporphin (abbreviated to TPP) complexes (Fig. 1) with molecular oxygen is investigated in chloroform solutions, mainly by means of an ESR technique, with special attention paid to the electron-spin configurations of the central metal ion and its ligand environment. Since the spin state of iron in the porphin ring is changeable according to the coordinating capability of the axial ligand, the redox behavior of the iron will be affected more or less by its surroundings. Previous works[1-3]

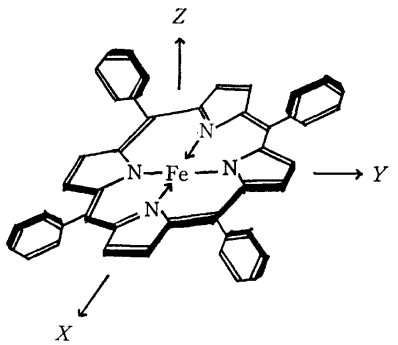

Fig. 1. Iron tetraphenylporphin. Four phenyl groups are bound perpendicular to the porphin plane.

1) K. Yamamoto, K. Marumo, K. M. Sancier and T. Kwan, "Recent Developments of Magnetic Resonance in Biological System," ed. by S. Fujiwara and L. H. Piette, Hirokawa Pub., Tokyo (1968), p. 164.

2) Y. Ogata, K. Marumo, and T. Kwan, *Chem. Pharm. Bull.*, **17**, 1194 (1969).

3) K. Yamamoto and T. Kwan, *J. Catalysis*, **18**, 354 (1970).

on cobalt phthalocyanine and cobalt TPP have, in fact, shown that the oxygenation and oxidation catalysis by these complexes are extensively influenced by the presence of axial ligands.

It is the purpose of the present paper to outline such a redox behavior of iron porphin complexes and to compare it with those of manganese and cobalt TPP complexes.

Experimental

Fe(III)-, Mn(III)-, and Co(II)-TPP complexes were prepared as usual[4] form metal(II) acetate and synthetic TPP. These complexes were dissolved in chloroform with or without a base which was expected to serve as an axial ligand (50—200 times or a saturated concentration). The axial bases used were tetrahydrofuran, quinoline, pyridine, 4-cyanopyridine, 4-methylpyridine, 4-aminopyridine, piperidine, imidazole, and benzimidazole.

Divalent iron and manganese complexes were prepared by reducing the corresponding trivalent metal TPP complexes with sodium dithionite($Na_2S_2O_4$). After the reduction treatment, the reducing reagent was removed from the solution by centrifugation. The concentrations of the metal complex usually ranged from 10^{-3} to 10^{-2}M. Throughout the procedure the complexes were kept in a dried nitrogen atmosphere.

The oxidation of metal(II) complexes was carried out by exposing their chloroform solutions to one atmospheric oxygen at room temperature. The ESR or optical absorption spectra were recorded before and after exposure to oxygen respectively. The ESR spectra were recorded at 77°K by means of a JEOL-P-10 (X-band) spectrometer with a 100-kcps field modulation.

Results and Discussion

Spin State of Iron(III) Complexes. Magnetic susceptibility measurements have served to provide information on the electronic configuration of ferrous or ferric ions. ESR methods have also provided supplementary information. Thus, theoretical analyses[5,6] have shown that high-spin iron(III) porphyrin complexes should exhibit ESR spectra with an axial symmetry at $g_\perp \sim 6$ and $g_{//} \sim 2$, while in low-spin complexes the anisotropic spectra of the three different g components are to be found near $g \sim 2$. The spin state of iron(III) porphin may thus be judged qualitatively from the shape of the obtained spectra.

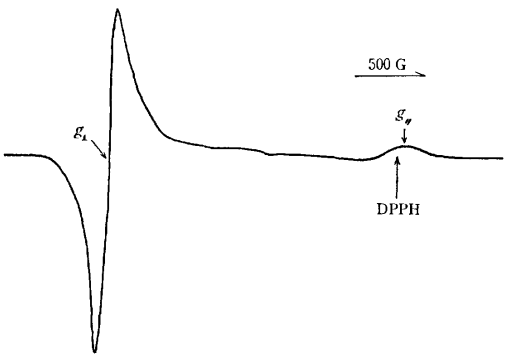

Fig. 2. ESR spectrum of Fe(III)-TPP-Cl in chloroform at 77°K. $g_\perp \sim 6$, $g_{//} \sim 2$.

A typical ESR spectrum of the Fe(III)–TPP complex in chloroform is shown in Fig. 2. It is apparent from the spectral shape of Fig. 2 that the complex is high-spin. The spin configuration is consistent with that determined by the magnetic susceptibility measurements.[7] When excess imidazole was added to this solution, the spectrum of Fig. 2 appeared to change greatly into that shown in Fig. 3 or into that characteristic of low-spin iron. The weak absorption around $g \sim 6$ is probably due to the contamination of high-spin iron.

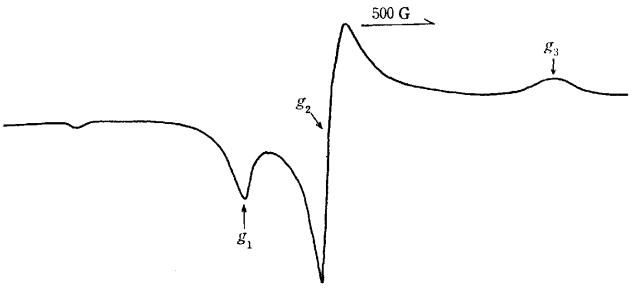

Fig. 3. ESR spectrum of [Fe(III)-TPP-2Im]Cl in chloroform at 77°K.
$g_1=2.98$, $g_2=2.31$, $g_3=1.52$.

A crystalline sample was then found to be isolable when repeated partial evaporation and centrifugation were carefully done. An elementary analysis of the isolated crystal indicated that its composition was consistent with [Fe–TPP–2Im]Cl(imidazole is abbreviated to Im); $C_{50}H_{36}N_8FeCl$, anal. (%), calcd., C: 71.47, H: 4.33, N: 13.34; found, C: 71.29, H: 4.47, N: 14.99. The sample redissolved in chloroform gave almost the same spectrum as that shown in Fig. 3. The diimidazole complexes may, hence, be regarded as stable in chloroform. Their formation may be expressed by:

$$\text{Fe(III)-TPP-Cl} + n\ \text{Im} \longrightarrow [\text{Fe(III)-TPP-2Im}]\text{Cl} + (n-2)\text{Im}$$

The ESR spectra of Fe(III)–TPP complexes coordinated with the other axial bases were further investigated; most complexes were found to be high-spin except that coordinated with 4-aminopyridine, which

Table 1. Electron spin states of Fe(III)-TPP complexes

Complex	ESR Spectra	Spin States
Fe(III)-TPP-Cl	$g_\perp=6.10$, $g_{//}=1.98$	high-spin
[Fe(III)-TPP-2B]Cl		
B: 4-cyanopyridine		
pyridine	$g \sim 6$	high-spin
4-methylpyridine		
4-aminopyridine	anisotropic	low-spin
B: imidazole	$g_1=2.98$, $g_2=2.31$, $g=1.52$	low-spin

4) P. Rothemund and A. R. Menotti, *J. Amer. Chem. Soc.*, **70**, 1808 (1948).

5) J. S. Griffith, "Molecular Biophysics", ed. by B. Pullman and M. Weissbluth, Academic Press, New York (1965), p. 191.

6) J. S. Griffith, Nature, **180**, 30 (1957).

7) H. Kobayashi, M. Shimizu, and I. Fujita, This Bulletin, **43**, 2335, 2342 (1970).

was low-spin. The inspection of these spectra permitted us to confirm that a large basicity of the axial ligand favors a low-spin configuration of iron. The electronic features of the Fe(III) complexes are illustrated in Table 1. It is interesting to note in the Table that the dipyridine iron(III) complex[8] is high-spin, whereas the diimidazole complex is low-spin. This somewhat remarkable difference between pyridine and imidazole ligands can probably be ascribed to the stronger basicity[9] and π-donating capability of imidazole as compared with those of pyridine.[10]

Spin State of Iron(II) Complexes. Low-spin iron(II) complexes have six d electrons in the t_{2g} (d_π) orbital, hence, they are diamagnetic. The ESR absorption for high-spin iron(II) complexes is difficult to measure, probably because of the short spin-lattice relaxation time. Fe(II)-TPP coordinated with various bases has, in fact, shown no ESR spectrum, indicating that this technique is inadequate as far as ferrous iron is concerned.

On the other hand, magnetic susceptibility data were available for Fe(II)-TPP complexes,[7] as is illustrated below:

	μ Bohr magneton
Fe(II)-TPP	4.75
Fe(II)-TPP-2THF	2.75
Fe(II)-TPP-2Py	0

Accordingly, the dipyridine iron(II) complex can be said to be low-spin, while Fe(II)-TPP is high-spin. Unfortunately, no information is available on the diimidazole iron(II) complex. However, it seems very probable, in view of the stronger coordinating capability of imidazole as compared with that of pyridine, that the diimidazole iron(II) complex is also low-spin.

Interaction of Oxygen with Iron(II) Complexes. The oxidative behavior of Fe(II)-TPP complexes has been investigated in the light of both ESR and optical absorption spectra before and after exposure to oxygen at room temperature respectively. Generally speaking, the reactivity of Fe(II)-TPP complexes appeared to vary extensively from one complex to the other. Here, we shall confine ourselves to some extreme cases.

The high-spin Fe(II)-TPP was readily oxidized to yield Fe(III)-TPP upon exposure to oxygen, whereas this was not the case with the low-spin Fe(II)-TPP-2Py. Since the latter complex is hexacoordinated, the fact that oxidation did not occur for Fe(II)-TPP-2Py would, at first sight, indicate that the axial pyridine can not be displaced by oxygen. This interpretation is not correct, however; the hexacoordinated Fe(II)-TPP-2Im complex appeared to be readily and reversibly oxidized under exactly the same reaction conditions as in the case of Fe(II)-TPP-2Py. Such interesting oxidative behavior of Fe(II)-TPP complexes is compared below, together with their electron-spin states (in parentheses).

$$\text{Fe(II)-TPP (high)} \longrightarrow \text{Fe(III)-TPP (high)}$$

$$\text{Fe(II)-TPP-2Py (low)} \;-\!\!\times\!\!\rightarrow\; \text{Fe(III)-TPP-2Py (high)}$$

$$\text{Fe(II)-TPP-2Im (low)} \rightleftharpoons \text{Fe(III)-TPP-2Im (low)}$$

where $\longrightarrow$ indicates "oxidized", and $-\!\!\times\!\!\rightarrow$, "not oxidized". In other words, "oxidized" means the formation of a Fe(III) complex when the corresponding Fe(II) complex is brought into contact with oxygen, while "not oxidized" means no spectral change.

As is shown above, the diimidazole Fe(II) and Fe(III) complexes were both low-spin. On the other hand, the dipyridine Fe(II) was low, with its oxidized form high. The change in the spin state of iron is remarkable for the one-electron oxidation of the dipyridine Fe(II) complex when compared with that for the diimidazole complex. According to X-ray analysis,[11] there exists a substantial difference in structure between the low-spin-iron-porphyrin and high-spin-iron-porphyrin complexes. For high-spin iron porphyrins, the iron atom is known to lie 0.40—0.50 Å out-of-plane from the four porphin-nitrogens, whereas for low-spin iron porphyrins it lies nearly in-plane, hence bringing about rather long bonds between the iron and the porphin-nitrogen, for high-spin iron porphyrins. Thus, a large energy is required for the one-electron oxidation of the Fe(II) complex accompanied by a change in the spin state. The structural difference may arise from the electronic difference that two electrons must be transferred from the nonbonding $t_{2g}(d_\pi)$ to the antibonding $e_g(d_\sigma)$ orbital for the high-spin complex (Fig. 4).

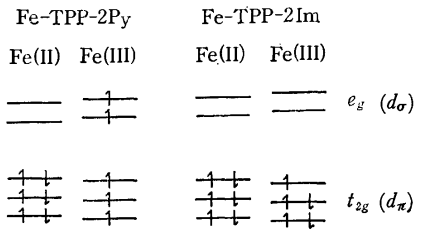

Fig. 4. Electron configuration of Fe-TPP complexes.

The ready oxidation of the diimidazole Fe(II) complex by molecular oxygen to yield Fe(III) is worthy of note, for the mechanism is perhaps associated with that in biological processes, for example, the effective electron transfer by hexacoordinated Cytochrome C. Mössbauer studies[12] of the Fe(II)-porphyrin bond has indicated that the electron of low-spin Fe(II) is extensively delocalized to the porphyrin ligand. Porphyrin itself is known to undergo facile reduction and

8) We were unable to isolate a crystalline dipyridine iron(III) because of some stickiness of the complex, unlike the case of diimidazole iron(III). On the other hand, the dipyridine protoporphyrin iron(III) complex has been isolated by us from a benzene-pyridine solution; $C_{44}H_{42}N_6FeCl$, anal. (%), calcd., C: 65.22, H: 5.24, N: 10.37; found, C: 64.71, H: 5.18, N: 9.69 (unpublished data). The ESR absorption lines of this complex were consistently explained if two pyridine molecules were assumed to be coordinated with the iron atom.[1]

9) pK_a-values: 5.18(pyridine), 1.80(4-cyanopyridine), 6.10(4-methylpyridine), 9.18(4-aminopyridine), 11.12(piperidine), 7.12-(imidazole).

10) L. M. Epstein, D. K. Straub, and C. Maricondi, *Inorg. Chem.*, **6**, 1720 (1967).

11) R. Countryman, D. M. Collins, and J. L. Hoard, *J. Amer. Chem. Soc.*, **91**, 5166 (1969).

12) T. H. Moss, A. J. Bearden, and W. S. Caughey, *J. Chem. Phys.*, **51**, 2624 (1969).

oxidation thus forming a variety of molecular complexes.[13,14]

It may be suggested, therefore, that the oxidation of the diimidazole Fe(II) complex by molecular oxygen takes place by means of a *long-range* interaction mechanism. One electron of the $t_{2g}(d_\pi)$ orbital of Fe(II) is delocalized to the vacant π-orbital of the porphin ligand. Electrons may thus be transferred to molecular oxygen close to the porphin ligand, although the position of the oxygen is still undetermined.

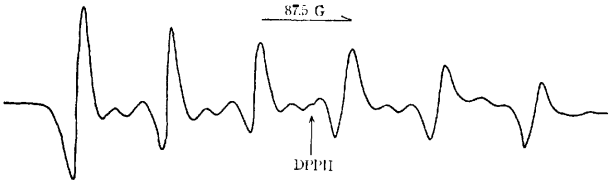

Fig. 5. ESR spectrum of Mn(II)-TPP in chloroform-imidazole solution at 77°K.

Interaction of Oxygen with Manganese(II) Complexes. The Mn(II)-TPP complex dissolved in chloroform gave rise to no ESR spectrum, but when excess amounts of imidazole are added it showed a resonance absorption near $g\sim2$. The spectrum consisted of six hf lines ($I=5/2$) and was characteristic of the high-spin state, provided that the zero field splitting parameters, D and E, are very small.[15,16] The signal is illustrated in Fig. 5. No ESR absorption was observed for most Mn(II)- and Mn(III)-TPP complexes on the addition of axial bases other than imidazole. However, since the magnetic moments have been reported to be in the range of 4.8—5.0 B.M. for a number of Mn(III) porphyrin complexes,[17] it would be highly probable that the Mn-TPP complexes are generally of the high-spin state.

No spectral change was observed when the imidazole Mn(II) complex was exposed to oxygen at room temperature, indicating that the complex was not susceptible to oxidation; we would expect the spectrum of Fig. 5 to disappear if the imidazole Mn(II) complex is oxidized. On the other hand, the Mn(II)-TPP complex was found to be readily oxidized in the absence of a base, because, on adding imidazole to the *oxidized* solution, we found no perceptible ESR spectrum; we should expect that type of spectrum (Fig. 5) to appear if the Mn(II)-TPP complex is not perceptible to oxidation.

Further observations were carried out on the Mn(II)-TPP complexes in the presence of other axial base, mainly by an optical technique. Some representative results are shown below. It is assumed that a dipyridine or diimidazole Mn(II)-TPP complex was formed in chloroform, although the complex was not isolated.

Mn(II)-TPP (high) ⟶ Mn(III)-TPP (high)

Mn(II)-TPP-2Py (high) —x→ Mn(III)-TPP-2Py (high)

Mn(II)-TPP-2Im (high) —x→ Mn(III)-TPP-2Im (high)

Interaction of Oxygen with Cobalt(II) Complexes. All of the Co(II)-TPP complexes coordinated with the axial ligand gave rise to ESR spectra characterized by eight hf lines, as is familiar in the case of cobalt ($I=7/2$). Some of them yielded three shf lines due to ligand nitrogen ($I=1$). The presence of the three shf lines suggests that the cobalt complex is coordinated with a *single* ligand molecule on its z-axis, unlike Fe(II)-TPP or Mn(II)-TPP

$$\text{Co(II)-TPP} + n\text{Py} \longrightarrow \text{Co(II)-TPP-Py} + (n-1)\text{Py}$$

A crystalline sample was isolated from the chloroform-pyridine solution on evaporation, and its composition was consistent with monopyridine complex, or $C_{49}H_{33}N_5Co$; calcd, C: 78.38, H: 4.44, N: 9.32; found, C: 78.38, H: 4.22, N: 9.63. This pentacoordinated form is probably due to the d^7 low-spin electronic configuration of Co(II).[3] The ESR spectrum for Co(II)-TPP coordinated with pyridine is shown in Fig. 6a.

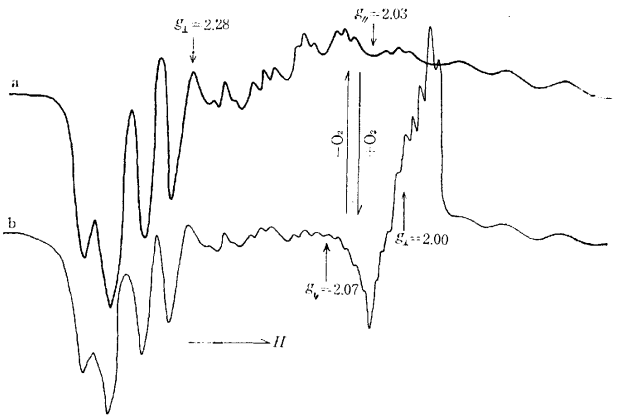

Fig. 6. ESR spectra of Co(II)-TPP-Py in chloroform at 77°K.
(a) evacuated; (b) exposed to O_2 for 10 min at room temperature.

When the Co(II)-TPP-Py complex was exposed to oxygen, the original signal due to Co(II) more or less decayed, while a new signal developed in the vicinity of $g\sim2$ (Fig. 6b). The spectral change was reversible as the oxygen pressures varied. The new signal near $g\sim2$ showed eight shf lines, suggesting that the molecular oxygen ion is formed and combined with cobalt.

An oxygenation took place irreversibly with the Co(II)-TPP coordinated with imidazole. In this case, no ESR signal was detectable after the irreversible oxygenation. The 3 d_{z^2} orbital energy of Co(II) rises especially when a strong base such as imidazole is coordinated. As a consequence, the unpaired electron of Co(II) may readily be transferred to the oxygenated cobalt complex, resulting in a diamagnetic, binuclear cobalt complex.[3] The complexing of oxygen is then no longer reversible.

13) H. A. O. Hill, A. J. Macfarlane, and R. J. P. Williams, *J. Chem. Soc.*, (A) **1969**, p. 1704.
14) J. Fajer, D. C. Borg, A. Forman, D. Dolphin, and R. H. Felton, *J. Amer. Chem. Soc.*, **92**, 3451 (1970).
15) M. Kotani, *Rev. Mod. Phys.*, **35**, 717 (1963).
16) R. D. Dowsing and J. F. Gibson, *J. Chem. Phys.*, **50**, 294 (1969).
17) L. J. Boucher, *J. Amer. Chem. Soc.*, **92**, 2725 (1970).

Summary

So far we have dealt with the oxidation of tetra-, penta-, and hexacooridnated transition metal(II) complexes differing in the spin state. In order to bring about a rapid oxidation, (1) the complexes should provide empty sites for oxygen, and (2) the activation energy should be low. These conditions seem to be fulfilled at least in the oxidation of Mn(II)-TPP, Fe(II)-TPP, and Co(II)-TPP-Py. Conversely, the oxidation will be slow or will be inhibited if empty sites are not available and if significant energy is required for electron transfer. Such a case is the oxidation of Fe(II)-TPP-2Py. These examples are obviously two extreme cases.

We have found an *intermediary* situation in the oxidation of the Fe(II)-TPP-2Im complex, where no more empty sites are available, but where the activation energy must be low enough because of the rapid oxidation that takes place. We have presented a *long-range* interaction mechanism between oxygen and the Fe(II) ion through a conjugated porphin ring. Kinetic data for the oxidation were only qualitative, but the interpretation was consistent with the electronic and structural properties of the complex.

Electron transfer *via* the so-called outer-sphere activated complex has been observed in the electron exchange reaction for $[Fe(CN)_6]^{4-} \rightleftharpoons [Fe(CN)_6]^{3-}$, $[Fe(phenantroline)_3]^{2+} \rightleftharpoons [Fe(phenantroline)_3]^{3+}$, and so on.[18] A net chemical reaction is not involved here. The electron transfer reaction demonstrated above between oxygen and Fe(II)-TPP-2Im thus constitutes a new aspect of the problem of electron transfer.

18) W. L. Reynolds and R. W. Lumry, "Mechanism of Electron Transfer," The Ronald Press, New York (1966), p. 13.

BULLETIN OF THE CHEMICAL SOCIETY OF JAPAN, VOL. 45, 668—677(1972)

The Intermolecular Potential of Hydrocarbon Dimers as Examined by the Perturbation Theory Including Exchange Energy in the PPP Approximation

Hiroko FUJITA and Akira IMAMURA

Biophysics Division, National Cancer Center Research Institute, Tsukiji, Chuo-ku, Tokyo

(Received June 5, 1971)

By using the perturbation method, including the exchange energy, the interaction potential curves for the intermolecular distances from 2.0 Å to 6.0 Å of the ethylene dimer, the butadiene dimer, the hexatriene dimer, and the benzene dimer were obtained. The matrix elements were evaluated in the Pariser-Parr-Pople approximation. Reasonable intermolecular potential curves were obtained for all the dimers studied. The analysis of the perturbation energy leads to the conclusion that the induction and dispersion energies and the exchange repulsion energy of the second order in the overlap integral give the potential minimum for the interaction of small molecules, such as ethylene or butadiene dimers, but for large molecules, such as benzene or hexatriene dimers, the exchange repulsion energy of the fourth order in the overlap integral should also be included in order to obtain the potential minimum. An important role of the charge transfer term was suggested for the chemical reaction; this was in agreement with the indications of previous researchers. The calculated depth of the potential minimum and the equilibrium molecular distance are in fairly good agreement with the experimental data.

The calculation of exact intermolecular potential curves for various large molecules is a very important but still unsolved problem. The relative geometries of charge-transfer complexes and the excimer or exciplex, the orientation of molecules in molecular crystals, and the conformation of such biopolymers as proteins and DNA are intimately related to the intermolecular potential energy between the corresponding molecules. Moreover, for the illustration of reaction mechanisms or the calculation of cross sections for the collisions of molecules, the intermolecular potential curves are indispensable.

The approaches to the evaluation of intermolecular force may mainly be classified into two types, according to whether the system is treated as one molecule or as a composite of two molecules. In the former type, variational methods, including configuration interactions or *ab initio* treatments, have been used. However, especially for large molecules, these methods are not reliable, since the contribution of ionic configurations is apt to be excessively included; hence, plausible intermolecular potential curves have been obtained for only small molecules or atoms.[1,2] In the latter, a difficult problem is the evaluation of the exchange repulsion energy, which heretofore has been treated only semi-empirically, when it has been taken into account at all.[3] One approach to this problem is the perturbation theories including exchange energy recently developed

1) G. Das and A. C. Wahl, *J. Chem. Phys.*, **47**, 2934 (1967).
2) G. H. F. Diercksen, *Chem. Phys. Lett.*, **4**, 373 (1969).
3) M. J. Huron and P. Claverie, *ibid.*, **4**, 429 (1969).

by many authors.[4-9] However, these theories have as yet been applied only to sets of small molecules or atoms.[10,11] On the other hand, for large molecules many phenomena have been studied, for example, the Diels-Alder reactions,[12,13] the excimer formations,[14-16] the spectra of the hydrocarbon dimers,[17] the charge-transfer complexes,[18,19] and the stacking energies of nucleic acid's bases.[20] However, in these calculations various types of approximations are employed, that is, the use of the iterative extended Hückel method, or the neglect of exchanges of electrons or a truncation of the expansion by excited levels.

In this paper, the intermolecular energies of the ethylene dimer, butadiene dimers, the hexatriene dimer, and the benzene dimer were calculated using the Pariser-Parr-Pople (PPP) approximation and by means of the perturbation method, including exchange energy, by Murrell *et al.*[4,5] The potential curves thus obtained are found to be reasonable, giving the potential minimum at an appropriate intermolecular distance. From the analysis of each term of the perturbation energy, it was found that the contribution of exchange energy due to the exchanges of two pairs of electrons, which corresponds to the fourth order term in the overlap integral, is very important for the interaction of large molecules.

Moreover, the contributions of the charge-transfer term is rather small for all the dimers studied except for the *trans*-butadiene-*cis*-butadiene dimer at short distances. The fact that this butadiene dimer has a remarkable contribution of the charge-transfer term is very interesting, since this dimer can be considered to become an activated complex of the Diels-Alder reaction. Those results correspond well with those obtained by Fukui and Fujimoto.[21] The comparison of the calculated intermolecular potential and the equilibrium intermolecular distance with those of the experimental data leads to the conclusion that the theoretical method in the present paper gives relatively reliable results.

Method

The perturbation theories recently developed[4-8] for intermolecular potentials including exchange integrals are multifarious in their formulas. This is because nonperturbed wave functions are not linearly independent of each other; hence, the expansion coefficients of these wave functions for an arbitrary function can not be uniquely determined, as has been pointed out by Lekkerkerker and Laidlaw.[9] However, the various formulas give almost the same results for the interaction energy between two atoms.[10,11] In the present paper, the formulas derived by Murrell and Shaw[4] were adopted for calculating all the intermolecular potential energies except for the charge-transfer term. For the charge-transfer term, the formula of Murrell, Randic, and Williams was employed.[5,22] The outline of the perturbation method will be given below.

The Shrödinger equations of the separated molecules, A and B, are:

$$H_A(i)A_r(i) = E_r^A A_r(i),$$
$$H_B(j)B_s(j) = E_s^B B_s(j). \quad (1)$$

Here, A_r and B_s are wave functions in ground or singly-excited configurations of the A and B molecules respectively.[23] Hereafter, the ground state will be denoted by the suffix '0', *i.e.*, A_0, B_0, *etc.* The Shrödinger equation of the total system is:

$$H\Psi = E\Psi, \quad (2)$$

where:

$$H = H_A(i) + H_B(j) + U,$$

and where U is the interaction potential:

$$U = \sum_s\sum_t e^2/r_{st} - \sum_a\sum_t Z_a^A e^2/r_{at} - \sum_b\sum_s Z_b^B e^2/r_{sb} + \sum_a\sum_b Z_a^A Z_b^B/r_{ab}. \quad (3)$$

Here s and t denote electrons in the A and B molecules respectively, and a and b, nuclei or cores in the A and B molecules. Z is the effective charge, and r represents the distance. The wave function of a configuration constituting the total wave function, Ψ, is constructed from the products of the wave functions of the separated molecules, allowing for exchanges of electrons; that is, for the ground state:

$$\Psi = \Psi_0 + \sum_{t\neq 0} b_t \Psi_t, \quad (4)$$

where:

$$\Psi_0 = \mathcal{A}A_0(i)B_0(j), \quad (5)$$
$$\Psi_t = \mathcal{A}A_r(i)B_s(j), \quad (6)$$

4) J. N. Murrell and G. Shaw, *J. Chem. Phys.*, **46**, 1768 (1967).
5) J. N. Murrell, M. Randic, and D. R. Williams, *Proc. Roy. Soc.*, **A284**, 566 (1965).
6) J. O. Hirschfelder, *Chem. Phys. Lett.*, **1**, 363 (1967).
7) J. O. Hirschfelder and R. Silbey, *J. Chem. Phys.*, **45**, 2188 (1966).
8) J. I. Musher and A. T. Amos, *Phys. Rev.*, **164**, 31 (1967).
9) H. N. W. Lekkerkerker and W. G. Laidlaw, *J. Chem. Phys.*, **52**, 2953 (1970).
10) P. R. Certain, J. O. Hirschfelder, W. Kolos, and L. Wolniewicz, *ibid.*, **49**, 24 (1968).
11) P. R. Certain, *ibid.*, **49**, 35 (1968).
12) L. Salem, *J. Amer. Chem. Soc.*, **90**, 543, 553 (1968).
13) W. C. Herndon and L. H. Hall, *Theoret. Chim. Acta*, **7**, 4 (1967).
14) J. N. Murrell and J. Tanaka, *Mol. Phys.*, **7**, 363 (1964).
15) R. Polak and J. Paldus, *Theoret. Chim. Acta*, **4**, 37 (1966).
16) B. N. Srinivasan, J. V. Russell, and S. P. McGlynn, *J. Chem. Phys.*, **48**, 1931 (1968).
17) A. K. Chandra, *Chem. Phys. Lett.*, **5**, 229 (1970).
18) W. C. Herndon and J. Feuer, *J. Amer. Chem. Soc.*, **90**, 5914 (1968).
19) S. Iwata, J. Tanaka, and S. Nagakura, *ibid.*, **89**, 2813 (1967).
20) R. Rein and M. Pollak, *J. Chem. Phys.*, **47**, 2039 (1967); R. Rein, N. S. Goel, N. Fukuda, M. Pollak, and P. Claverie, *Ann. N. Y. Academy Sci.*, **153**, 805 (1969).
21) K. Fukui and H. Fujimoto, This Bulletin, **41**, 1989 (1968); **42**, 3399 (1969).

22) The charge-transfer term can not be treated together with other locally-excited terms by the perturbation method since the perturbed Hamiltonian for locally-excited terms is different from that for charge-transfer terms. Accordingly, after perturbed wave functions have been obtained for ground and locally-excited configurations, the variational method in which the wave function is represented by a linear combination of charge-transfer and locally-excited configurations (perturbed wave function) should be used. This treatment will give the total wave function for two interacting molecules.

23) Doubly-excited configurations are disregarded since the matrix element between the ground and doubly-excited configurations vanishes.

or:

$$\Psi_t = \mathscr{A}A_k^+(i')B_l^-(j'), \tag{7}$$

where $A_k^+B_l^-$ represents a charge-transfer configuration and where $\mathscr{A}$ is the antisymmetrizing operator, which allows for exchanges of electrons between the i and j sets (or i' and j'); *i.e.*:

$$\mathscr{A} = \{(2n)!(2m)!/(2n+2m)!\}^{1/2}(1+P_{ij}^1+P_{ij}^2+\cdots), \tag{8}$$

where $2n$ and $2m$ are the number of electrons of the i and j sets, respectively. P_{ij}^1 is the operator which exchanges one pair of electrons, accompanied by a change in the sign, while P_{ij}^2 is the one which exchanges two pairs of electrons with no change of the sign, and so on. The total energy for the ground state can be calculated by means of the perturbation method; that is, the substitution of the total energy and the total wave function of Eq. (4) into Eq. (2) yields the following Eqs. (9)—(13):[4,5,9]

$$E^{10} = U_{00}^{10}, \tag{9}$$

$$E^{20} = \sum_{t(\neq 0)} (U_{t0}^{10})^2/(E_0-E_t), \tag{10}$$

$$E^{12} = U_{00}^{12} - S_{00}^{02}U_{00}^{10}, \tag{11}$$

$$E^{22} = \sum_{t(\neq 0)} U_{t0}^{10}(U_{t0}^{12}-S_{t0}^{02}U_{00}^{10})/(E_0-E_t) - S_{00}^{02}E^{20}, \tag{12}$$

$$E^{CT} = \sum_{t(\neq 0)} (U_{t0}^{11}-S_{t0}^{01}U_{00}^{10})^2/(E_0-E_t), \tag{13}$$

where, for convenience, the interaction energies are classified according to the powers of U (the first upper index) and S, *i.e.*, the overlap integral by the electron exchange (the second upper index). E^{10} represents the electrostatic interaction energy between two molecules, A and B; E^{20}, the dispersion and induction energies; E^{12}, the exchange energy of the second order in the overlap integral; E^{22}, the exchange polarization energy, and E^{CT}, the charge-transfer energy. E_0 and E_t are:

$$\begin{aligned} E_0 &= E_0^A + E_0^B \\ E_t &= E_r^A + E_s^B. \end{aligned} \tag{14}$$

The matrix elements are as follows:

$$\begin{aligned} U_{00}^{10} &= \langle A_0(i)B_0(j)\,|\,U\,|\,A_0(i)B_0(j)\rangle, \\ U_{t0}^{10} &= \langle A_r(i)B_s(j)\,|\,U\,|\,A_0(i)B_0(j)\rangle, \\ U_{00}^{12} &= \langle P_{ij}^1A_0(i)B_0(j)\,|\,U\,|\,A_0(i)B_0(j)\rangle, \\ U_{t0}^{12} &= \langle P_{ij}^1A_r(i)B_s(j)\,|\,U\,|\,A_0(i)B_0(j)\rangle, \\ U_{t0}^{11} &= ((2m+1)/2n)^{1/2}\langle A_k^+(i')B_l^-(j')\,|\,U\,|\,A_0(i)B_0(j)\rangle, \\ S_{00}^{02} &= \langle P_{ij}^1A_0(i)B_0(j)\,|\,A_0(i)B_0(j)\rangle, \\ S_{t0}^{02} &= \langle P_{ij}^1A_r(i)B_s(j)\,|\,A_0(i)B_0(j)\rangle, \\ S_{t0}^{01} &= ((2m+1)/2n)^{1/2}\langle A_k^+(i')B_l^-(j')\,|\,A_0(i)B_0(j)\rangle. \end{aligned} \tag{15}$$

As we will show in the latter section, for large molecules the exchange energy up to the second order in the overlap integral, E^{12}, has a negative value at short distances; hence, the potential minimum can not be found. Accordingly we introduce E^{14}, the exchange energy of the 4*th* order in the overlap integral corresponding to the exchanges of two pairs of electrons. According to Murrell and Shaw,[4] the first-order correction for the energy is:

$$E^{(1)} = \langle\psi_0\,|\,U\,|\,\Psi_0\rangle/\langle\psi_0\,|\,\Psi_0\rangle, \tag{16}$$

where Ψ_0 is as given in Eq. (5) and where ψ_0 is:

$$\psi_0 = A_0B_0.$$

The expansion of Eq. (16) up to the 4*th* order in the overlap integral leads to the following formula:

$$\begin{aligned} E^{(1)} &= (U_{00}^{10}+U_{00}^{12}+U_{00}^{14})/(1+S_{00}^{02}+S_{00}^{04}) \\ &= U_{00}^{10} + (U_{00}^{12}-U_{00}^{10}S_{00}^{02}) \\ &\quad + (U_{00}^{14}-U_{00}^{12}S_{00}^{02}-U_{00}^{10}S_{00}^{04}+U_{00}^{10}(S_{00}^{02})^2). \end{aligned}$$

The second term as the right side of the above equation corresponds to E^{12} in Eq. (11), while the last term corresponds to E^{14} *i.e.*, the 4*th*-order term in the overlap integral:

$$E^{14} = U_{00}^{14} - U_{00}^{12}S_{00}^{02} - U_{00}^{10}S_{00}^{04} + U_{00}^{10}(S_{00}^{02})^2), \tag{17}$$

which can be rewritten as Eq. (18) for non-polar molecules since the U_{00}^{10} vanishes:

$$E^{14} = U_{00}^{14} - U_{00}^{12}S_{00}^{02}. \tag{18}$$

The applicability of Eq. (18) to polar molecules was confirmed numerically in the range of the equilibrium distances.

The ground-state wave functions of the separated A and B molecules were assumed to be antisymmetrized molecular orbitals (ASMO's). The coefficients of the atomic orbitals were obtained using the Pariser-Parr-Pople (PPP) method[24] for the π electron system. They can also be obtained by means of other molecular orbital methods such as the CNDO/2 method or *ab initio* calculation. The results by the CNDO/2 method is given in this paper only for the ethylene dimer. The E_t values in Eq. (14) were evaluated as follows: for locally excited configurations,

$$\begin{aligned} E_t &= E_0^A + E_0^B + \varepsilon_k^A - \varepsilon_i^A - J_{ik}^A + 2K_{ik}^A \\ &\quad + \varepsilon_l^B - \varepsilon_j^B - J_{jl}^B + 2K_{jl}^B, \end{aligned} \tag{19}$$

where J and K denote the Coulomb and exchange integrals respectively, and ε, the molecular orbital energies. On the other hand, for charge-transfer configurations,

$$E_t = E_0^A + E_0^B + \varepsilon_l^B - \varepsilon_k^A. \tag{20}$$

Mulliken's approximation was used for the atomic integrals between the different molecules. The two-center electron repulsion integrals (γ) were evaluated using Mataga and Nishimoto's approximation and the nuclear-repulsion potential, $Z_a^AZ_b^B\gamma_{ab}$, in the PPP approximation. The other approximations and parameters used are the same as those in Ref. 25 for the PPP method or in Ref. 26 for the CNDO/2 method. The matrix elements in Eq. (15) are given in terms of molecular orbitals in the Appendix.

Results and Discussion

1. Contribution of Each Term to the Total Interaction Energy. The total intermolecular potential curves in the PPP approximation for the ethylene dimer, the *trans*-butadiene dimer, the *trans*-hexatriene dimer, and the benzene dimer are shown, along with the E^{12}, E^{14},

24) R. Pariser and R. G. Parr, *J. Chem. Phys.*, **21**, 466, 767 (1953); J. A. Pople, *Trans. Faraday Soc.*, **49**, 1375 (1953).

25) C. Nagata, A. Imamura, Y. Tagashira, and M. Kodama, This Bulletin, **38**, 1638 (1965).

26) J. A. Pople and G. A. Segal, *J. Chem. Phy* ., **44**, 3289 (1966).

and E^{20} values, in Figs. 1—4. In all these dimers, configurations of the sandwich type are assumed. In Tables 1—3, the values of all the terms are tabulated in more detail. The calculated intermolecular potential curves are reasonable, because the potential curves have a minimum point at an appropriate molecular distance and increase rapidly when two molecules come closer each other. However, the contributions of such terms as E^{10}, E^{20}, E^{12}, and E^{14} to the total energy differ from molecule to molecule. The electrostatic interaction (E^{10}) between two unsaturated hydrocarbons is very small or non-existent. The second-order term, E^{20}, contains the dispersion interaction energy, the dipole-induced dipole interaction energy, and so on. In the case of hydrocarbons, the former is dominant.

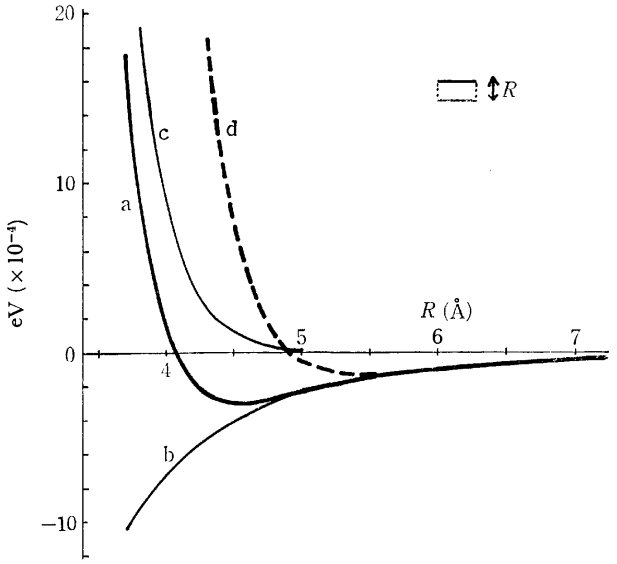

Fig. 1. The interaction energy of the ethylene dimer.
a, total; b, E^{20}; c, E^{12}; d, total in OMAO.

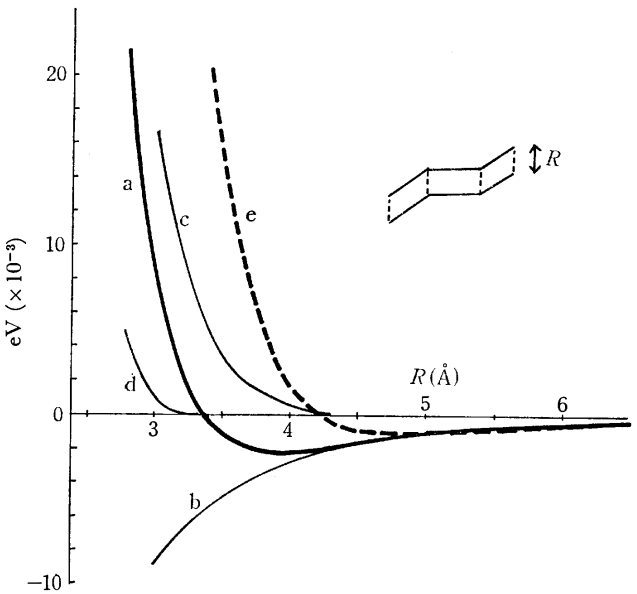

Fig. 2. The interaction energy of the *trans*-butadiene dimer type 1.
a, total; b, E^{20}; c, E^{12}; d, E^{14}; e, total in OMAO.

The magnitude of E^{20} depends upon the sizes of the interacting molecules; that is, this interaction energy is large in magnitude for the benzene dimer, small for the ethylene dimer, and intermediate for the butadiene dimer. The dependence of the magnitude of the dispersion force on the sizes of the molecules may easily be explained by the fact that large molecules have many energy levels. However, this interaction also depends upon the relative orientation between two interacting molecules (see Table 3 and Table 4). At any rate, the dispersion energies stabilize the interacting systems.

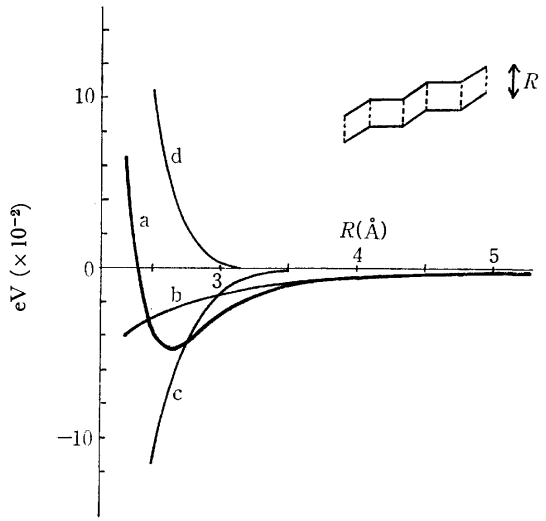

Fig. 3. The interaction energy of the *trans*-hexatriene dimer.
a, total; b, E^{20}; c, E^{12}; d, E^{14}.

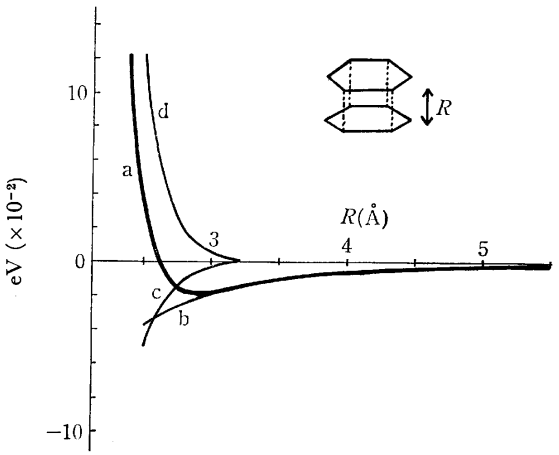

Fig. 4. The interaction energy of the benzene dimer.
a, total; b, E^{20}; c, E^{12}; d, E^{14}.

Table 1. The interaction energies of the ethylene dimer (in eV)

R(Å)	E^{10}	E^{20}	E^{12}	E^{14}	E^{22}	E^{CT}	Total
2.0	0.0	−0.0144	0.4465	0.0478	0.0	0.0	0.4799
3.0	0.0	−0.0027	0.0342	0.0002	0.0	0.0	0.0317
4.0	0.0	−0.0007	0.0009	0.0	0.0	0.0	0.0002
5.0	0.0	−0.0002	0.0	0.0	0.0	0.0	−0.0002
6.0	0.0	−0.0001	0.0	0.0	0.0	0.0	−0.0001

Table 2. The interaction energies of the *trans*-butadiene dimer type 1 (in eV)

R(Å)	E^{10}	E^{20}	E^{12}	E^{14}	E^{22}	E^{CT}	Total
2.0	0.0004	−0.0378	0.0502	0.4356	−0.0012	0.0	0.4472
2.5	0.0003	−0.0174	0.0506	0.0317	0.0	0.0	0.0652
3.0	0.0002	−0.0089	0.0167	0.0011	0.0	0.0	0.0091
4.0	0.0001	−0.0029	0.0006	0.0	0.0	0.0	−0.0022
5.0	0.0	−0.0011	0.0	0.0	0.0	0.0	−0.0011

Table 3. The interaction energies of the benzene dimer (in eV)

R(Å)	E^{10}	E^{20}	E^{12}	E^{14}	E^{22}	E^{CT}	Total
2.0	0.0	−0.0761	−0.3165	1.6435	−0.0092	−0.0	1.2416
2.5	0.0	−0.0377	−0.0503	0.1229	−0.0012	0.0	0.0336
3.0	0.0	−0.0199	−0.0027	0.0043	−0.0002	0.0	−0.0190
4.0	0.0	−0.0064	0.0002	0.0	0.0	0.0	−0.0061
5.0	0.0	−0.0024	0.0	0.0	0.0	0.0	−0.0024

Table 4. The interaction energies of the *trans*-butadiene dimer type 2 (in eV)

R(Å)	E^{10}	E^{20}	E^{12}	E^{14}	E^{22}	E^{CT}	Total
2.0	0.0001	−0.0048	0.0501	0.0619	0.0005	−0.0121	0.0957
3.0	0.0	−0.0014	0.0116	0.0002	0.0	−0.0006	0.0100
4.0	0.0	−0.0005	0.0004	0.0	0.0	−0.0	−0.0
5.0	0.0	−0.0002	0.0	0.0	0.0	0.0	−0.0002
6.0	0.0	−0.0001	0.0	0.0	0.0	0.0	−0.0001

Table 5. The interaction energies of the *trans*-butadiene-*cis*-butadiene dimer (in eV)

R(Å)	E^{10}	E^{20}	E^{12}	E^{14}	E^{22}	E^{CT}	Total
2.0	−0.0	−0.0120	0.0046	0.0097	0.0004	−0.0164	−0.0138
2.5	−0.0	−0.0063	0.0134	0.0013	0.0001	−0.0045	0.0040
3.0	0.0	−0.0035	0.0054	0.0001	0.0	−0.0009	0.0012
4.0	0.0	−0.0012	0.0003	0.0	0.0	−0.0	−0.0010
5.0	0.0	−0.0005	0.0	0.0	0.0	0.0	−0.0005

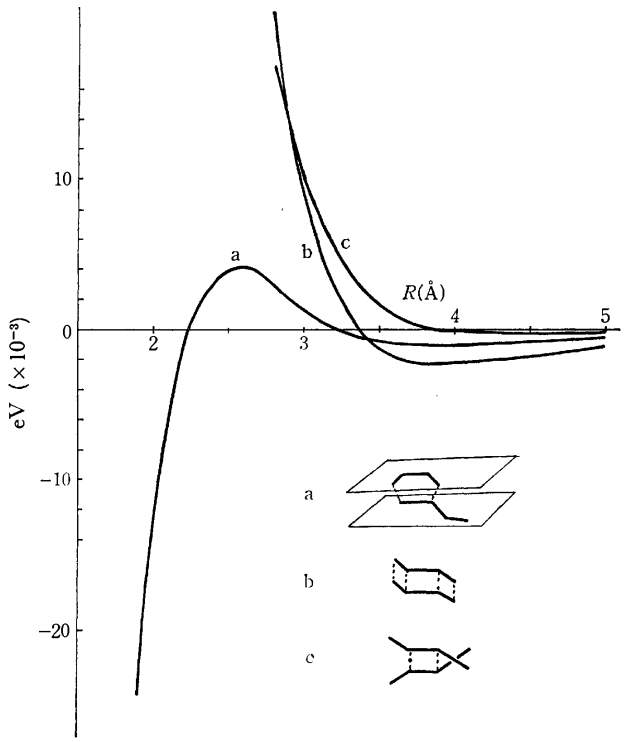

Fig. 5. The interaction energies of the *trans*-butadine-*cis*-butadine dimer (a), the *trans*-butadiene dimer type 1 (b), the *trans*-butadiene dimer type 2 (c).

The contribution of the charge-transfer interaction to the intermolecular potential is negligibly small for hydrocarbon dimers in sandwich-type configuration. On the other hand, the charge-transfer interactions of the *trans*-butadiene dimer in a type-2 configuration (Fig. 5 and Table 4) and of the *trans*-butadiene-*cis*-butadiene dimer (Table 5) are not negligible, especially at short distances. Moreover, among the three butadiene dimers in Fig. 5, only the *trans*-butadiene-*cis*-butadiene dimer has the potential maximum which comes from the remarkable increase in the stabilization energy caused by the charge-transfer interaction, while the other two dimers, the *trans*-butadiene dimer type 1 and type 2, give the increasing potential curves. Although these potential curves at short distances may not be reliable since the contribution of higher-order terms in the perturbation expansion and that of σ-electrons should be taken into account, these features of the potential curves can explain well the fact that the *trans*-butadiene-*cis*-butadiene dimer can bring about a Diels-Alder reaction, while the other two dimers can not. A similar approach to the chemical reaction by making use of the perturbation method has already been made by Fukui *et al.*,[21] emphasizing the importance of the charge-transfer interaction (delocalization interaction in Fukui's nomenclature). Our results are in complete agreement with theirs.

The other terms which depend upon the magnitude

of the overlap integral are the exchange interaction terms, E^{12}, E^{14}, and E^{22}. Among them, the exchange polarization term, E^{22}, is negligibly small for all the molecules studied. The most striking aspect of the results is the relative magnitude of the E^{12} and E^{14} terms at intermediate distances (~2.5 Å). That is, the absolute value of the term of E^{12} is much larger than that of E^{14} for the interaction between small molecules, such as ethylene and butadiene, while the reverse is true for the benzene dimer as well as for the hexatriene dimer. Moreover, E^{12} is negative and E^{14} is positive for large molecules, such as benzene and hexatriene. In other words, if the fourth-order term in the overlap integral is disregarded for the interaction of large molecules, the potential minimum can not be obtained and two molecules come closer to coalescing. Therefore, the inclusion of E^{14} term in the calculation of the intermolecular potential is indispensable for large molecules. However, the situation is different for small molecules; that is, here the potential minimim can be obtained without E^{14}. This characteristic behavior of the exchange interaction term can be ascribed to the fact that the overlap integral between molecular orbitals of the interacting molecules is quite large in magnitude for large molecules, but is relatively small for small

Table 6. The values of σ type overlap integral of two π orbitals of carbons

Distance (Å)			
2.0	2.5	3.0	4.0
−0.2389	−0.1258	−0.0556	−0.0080

Table 7. The values of molecular overlap integral (S^{02}_{00}) for the sandwich type dimers at R=2.5 Å

Dimers			
Ethylene	*trans*-Butadiene	*trans*-Hexatriene	Benzene
−0.0647	−0.1399	−0.2151	−0.2310

molecules, as is indicated in Table 7, although the value of the each atomic overlap integral is the same for all the dimers (Table 6). The signs of the terms of E^{12} and E^{14} are noteworthy since E^{12} is positive for the ethylene and butadiene dimers, except for very short distances, and negative for the hexatriene dimer, while E^{14} is positive for all the dimers. E^{12} is negative at short distances, but positive at the larger distances, for the benzene dimer (Table 3). The sign of E^{12} results from the nine terms with plus or minus signs in U^{12}_{00} given by Eq. (A-5); that is, the No. 1, 2, 3, 4, and 9 terms have negative signs, while the other terms, No. 5, 6, 7, and 8, positive signs. The values of each term for the ethylene and benzene dimers are listed in Tables 8(a) and 9(a) respectively. The dependence of each term on the size of the molecules is shown in Fig. 6. From this figure, it is apparent that the values of the terms, No. 4, 6, 8, and 9, increase rapidly with the increase in the size of the molecules, while the values of the other terms increase only slightly. This tendency can be explained by the number of sums

Table 8. E^{12} and E^{14}, and the values of each term in U^{12}_{00} and in U^{14}_{00} for the ethylene dimer at R=2.5 Å

(a). E^{12} (eV)			(b). E^{14} (eV)		
U^{12}_{00}	No. 1	−0.3864	U^{11}_{00}	No. 1	0.0
	2	−0.3864		2	0.0
	3	−0.3864		3	0.0
	4	−0.2356		4	0.0
	5	0.7727		5	0.0
	6	0.4712		6	0.0
	7	0.7727		7	0.0
	8	0.4712		8	0.0
	9	−0.9424		9	0.0
$-U^{10}_{00}\,S^{12}_{00}$		0.0	$-1/2\,U^{12}_{00}\,S^{02}_{00}$		0.0049
E^{12}		0.1508	E^{14}		0.0049

Table 9. E^{12} and E^{14}, and the values of each term in U^{12}_{00} and in U^{14}_{00} for the benzene dimer at R=2.5 Å

(a). E^{12} (eV)			(b). E^{14} (eV)		
U^{12}_{00}	No. 1	−1.3717	U^{14}_{00}	No. 1	0.0815
	2	−5.0488		2	0.2085
	3	−5.0488		3	0.2085
	4	−18.8695		4	0.4677
	5	6.0876		5	−0.4187
	6	22.6417		6	−0.9344
	7	6.0876		7	−0.4187
	8	22.6417		8	−0.9344
	9	−27.1700		9	1.8689
$-U^{10}_{00}\,S^{02}_{00}$		0.0	$-1/2\,U^{12}_{00}\,S^{02}_{00}$		−0.0058
E^{12}		−0.0503	E^{14}		0.1229

included in each term in U^{12}_{00} (Eq. (A-5)); that is, the former terms are calculated by a fourfold summation, while, on the other hand, the summations for the latter terms are double or triple. From this tendency, the appearance of the negative sign of E^{12} for large molecules can easily be understood. These situations are the same for the terms of U^{14}_{00} except that each term of U^{14}_{00} has a sign opposite to the corresponding one of U^{12}_{00} because of the exchanges of two pairs of electrons. The values of each term in U^{14}_{00} or the ethylene and benzene dimers are listed in Tables 8(b) and 9(b) respectively. As has been mentioned above, all the terms of U^{12}_{00} and U^{14}_{00} have different signs, hence cancel each other out to make the exchange energy positive, as a whole, leading to the appearance of the potential minimum.

The importance of the term of E^{14} for large molecules was pointed out in a previous paragraph. In connection with this, the contribution of the E^{16} term should be investigated since this term probably has a sign different from that of E^{14}. However, the comparison of the magnitude of each term of U^{12}_{00} with that of U^{14}_{00} for the benzene dimer (Tables 9(a) and 9(b)) lead to a finding that each term in the equation of U^{12}_{00} is much larger in absolute magnitude than that of U^{14}_{00}, although the value of E^{14} is, as a whole, larger than that of E^{12}. Accordingly, it can resonably be

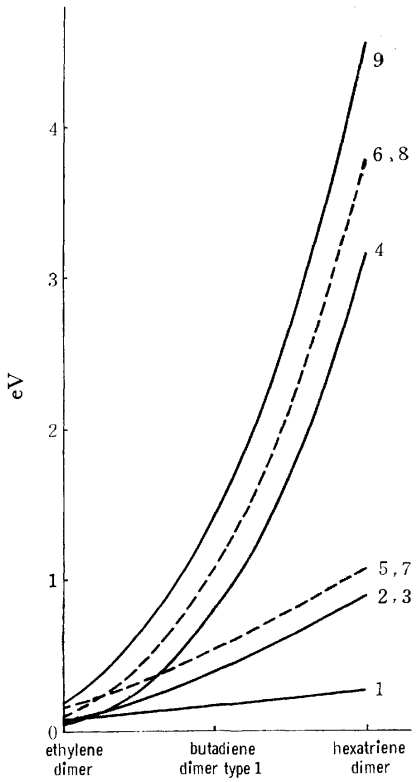

Fig. 6. The absolute value of the each term in U_{00}^{12} at R= 3.0 Å. The numbers represent the each term.———, negative value;--------- positive value.

expected that each term in U_{00}^{16} is too small in magnitude to contribute to the total intermolecular energy, even as a whole. In the present paper, other terms with a fourth order in overlap integrals such as E^{24} are completely neglected. This approximation is reasonable judging from the magnitude of E^{22}.

2. Comparison of the Calculated Values with the Experimental Values. It is very difficult to compare the calculated intermolecular potential and the equilibrium distance with those experimentally obtained, since the value obtained in the gas phase is an average of those of all possible geometries. The relative geometry of molecules in its molecular crystal gives some information, although the interactions between only two molecules are calculated in this paper.

The energy at the calculated potential minimum for both ethylene and butadiene dimers is much less than the thermal energy (0.026 eV at 300°K); hence these molecules have no ability to form stable dimers, a finding which is in accordance with the experimental results. Moreover, the calculated result that the ethylene dimer is more unstable than the butadiene dimer in a type-1 conformation is consistent with the relative stability of these molecules, which can be estimated from the boiling points if the entropic contribution is not serious. For benzene, the potential minimum becomes much deeper than the thermal energy. The experimental value derived from the viscosity (0.015 eV)[27] is very close to that obtained theoretically, although the experimental value corresponds to the average of various relative orientations. On the other hand, the intermolecular energy obtained from the heat of sublimation (0.40 eV) seems to be much larger. However, the difference between the experimental values from the heat of sublimation and the calculated value is not tremendous, since the heat of sublimation includes the interaction energies for all pairs of molecules in the crystal. As a whole, the calculated values of the intermolecular energies agree qualitatively fairly well with the experimental data, although the theoretical values should be calculated in more elaborate approximations in order to compare them with the experimental data quantitatively.

The calculated equilibrium molecular distances are noteworthy in connection with the geometry of the dimer of the molecular crystal. The equilibrium intermolecular distance for the ethylene dimer is located at about 4.5 Å (Fig. 1), which is comparable with the experimental values (4.2—4.8 Å) estimated from the value of viscosity or the second Virial coefficient.[27] On the other hand, the potential minimum for the benzene dimer in Fig. 4 is found at 2.9 Å, which seems to be slightly small in comparison with the value obtained for graphite (3.4 Å). This is because, for the ethylene dimer, the dispersion energy is reasonably balanced with the exchange energy, giving rise to a good agreement with the experimental results for the equilibrium intermolecular distance; on the other hand for the benzene dimer, the dispersion energy overcomes the exchange energy, leading to the slightly short intermolecular distance. From the results described above, we can conclude that the theoretical methods in the present paper are considerably reliable for the prediction of the intermolecular interaction energy and the intermolecular distance, though the quantitative agreement with the experimental data is not entirely satisfactory.

3. Discussion of the Method. In order to improve the present results, the use of a more exact atomic orbital and the explicit inclusion of σ electrons are important. As is well known, the SCF atomic orbitals for various atoms are considerably different form those of the usual Slater atomic orbitals, especially in the region distant from the atomic nucleus. Therefore, the improvement of the atomic orbital may be important for obtaining the exact intermolecular potential.[28] However, the use of the SCF atomic orbital, which is usually represented by the linear combination of several Slater-type atomic orbitals, is cumbersome in the expansion of the matrix elements into atomic orbitals. Instead of the SCF atomic orbital, the overlap matched atomic orbital (OMAO)[29] was employed in order to investigate the dependence of the result on the atomic orbitals used in the present paper. This orbital (OMAO) is a single Slater-type atomic orbital whose exponent was determined so as to reproduce overlap integrals calculated by SCF atomic orbitals. The value of the Slater exponent in OMAO[29] is 1.42, while the

27) J. O. Hirschfelder, C. F. Curtiss, and R. B. Bird, "Molecular Theory of Gases and Liquids", Wiley, New York (1954).

28) J. N. Murrell and G. Shaw, *Mol. Phys.*, **12**, 475 (1967).

29) L.C. Cusachs, B.L. Trus, D.G. Carroll, and P.S. McGlynn, *Int. J. Quant. Chem., Sympo.*, **1**, 423 (1967).

Slater rule gives 1.625 for the carbon atom. Obviously, OMAO has an overlap integral larger in magnitude. The intermolecular potential curves for the ethylene dimer and the butadiene dimer obtained by using OMAO are indicated in Figs. 1 and 2 in comparison with those obtained by the use of the Slater rule. The potential minimum obtained in OMAO is located at a distance longer by about 1 Å for both dimers, because of the increasing contribution of the exchange repulsion energy.

Table 10. The interaction energies in ONDO/2 approximation of the ethylene dimer (in eV)

R(Å)	E^{10}	E^{20}	E^{12}	Total
3.5	0.0051	−0.0150	0.0181	0.0081
4.0	0.0008	−0.0075	0.0030	−0.0037
4.5	0.0004	−0.0040	0.0004	−0.0032

Next, the explicit treatment of σ electrons was carried out in the framework of the CNDO/2 approximation for the ethylene dimer. In this calculation, however, the terms of E^{14}, E^{22}, and E^{CT} are neglected since these terms may not make large contributions to the equilibrium distance and since the calculation of these terms takes much computer time.[30] The results listed in Table 10 indicate that the inclusion of σ electrons increases the contribution of E^{20} because of the increase in the number of energy levels in the summation of Eq. (10). Since E^{20} is negative, the equilibrium distance obtained in the CNDO/2 approximation is shorter than that obtained in the PPP approximation. As a result of the above investigations, it can be concluded that the effects of the improvement of the atomic orbital and the explicit treatment of σ electrons cancel each other out to some extent, resulting in a relatively small correction for the equilibrium distance obtained in the PPP approximation using the usual simple Slater atomic orbitals. On the other hand, the magnitude of the interaction energy in the CNDO/2 approximation is much more than that in the PPP approximation because of the dominant increase in the contribution of E^{20}.

4. Comparison with Other Methods. The finding that the potential curves for the ground state have the minima shown in the present paper may be compared with the results by other authors. The results of the extended Hückel method show that, for example, for the ethylene dimer in Ref. 15 or the benzene dimer in Ref. 16, the potential minimum for the ground state does not appear, contrary to our calculations, while it does exist in the excited states, hence, they concluded that the excimer formations may be expected for these dimers. On the other hand, Chandra investigated the origin of the stability of aromatic hydrocarbon dimers using the Hückel-type π perturbation theory and showed that, in the ground state, the tilted configuration was stable, while the sandwich configuration was not.[17] However, our calculation for the benzene dimer in the sandwich configuration gives the potential minimum, although the magnitude is small because of the use of the π approximation. As was mentioned in the previous paragraph, the inclusion of σ electrons results in an increase in the interaction energy for the ethylene dimer; hence, it can probably be expected that, for the benzene dimer, the interaction energy involving the contribution of σ electrons is also larger by one order than that in the PPP approximation. Therefore, the intermolecular interaction energy obtained by the Hückel or the extended Hückel method, in which the electron-electron repulsion energies are not explicitly included, is substantially different from the results of the present paper with regard to the appearance of the potential minimum.

5. Summary. The method and the approximation used in the present paper give a satisfactory qualitative agreement with the experimental results for the intermolecular potential. In order to obtain a quantitative agreement, more elaborate and cumbersome approximations are required; that is, these must be an improvement in the atomic orbital and in the explicit treatment of σ electrons.

Appendix

The Matrix Elements. The matrix elements in PPP approximation are as followes.

(1)

$$U_{00}^{10} = \sum_a\sum_b Z_a{}^A Z_b{}^B \gamma_{ab}^{AB} - 2\sum_b Z_b{}^B \sum_i^{occ.} \langle \varphi_i{}^A(1) | e^2/r_{1b} | \varphi_i{}^A(1) \rangle$$
$$- 2\sum_a Z_a{}^A \sum_j^{occ.} \langle \varphi_j{}^B(1) | e^2/r_{1a} | \varphi_j{}^B(1) \rangle$$
$$+ 4\sum_i^{occ.}\sum_j^{occ.} \langle \varphi_i{}^A(1)\varphi_j{}^B(2) | e^2/r_{12} | \varphi_i{}^A(1)\varphi_j{}^B(2) \rangle$$
$$= \sum_a (Z_a{}^A - P_a{}^A) \sum_b (Z_b{}^B - P_b{}^B) \gamma_{ab}^{AB}, \qquad \text{(A-1)}$$

where $P_a = 2\sum_i^{occ.} (C_{ai})^2$.

(2) In evaluating the matrix element U_{t0}^{10}, the following cases are separately treated according to the configuration of $A_r(i)B_s(j)$.

(i) When the configuration is A_rB_0, where r denotes the $i \rightarrow k$ singly excitation,

$$U_{t0}^{10} = 2\sqrt{2}\sum_j \langle \varphi_k{}^A(1)\varphi_j{}^B(2) | e^2/r_{12} | \varphi_i{}^A(1)\varphi_j{}^B(2) \rangle$$
$$- \sqrt{2}\sum_b Z_b{}^B \langle \varphi_k{}^A(1) | e^2/r_{1b} | \varphi_i{}^A(1) \rangle$$
$$= -\sqrt{2}\sum_a C_{ak}^A C_{ai}^A \sum_b (Z_b{}^B - P_b{}^B) \gamma_{ab}^{AB}. \qquad \text{(A-2)}$$

(ii) When the configuration is A_0B_s, where s denotes the $j \rightarrow l$ singly excitation,

$$U_{t0}^{10} = -\sqrt{2}\sum_b C_{bj}^B C_{bl}^B \sum_a (Z_a{}^A - P_a{}^A) \gamma_{ab}^{AB}. \qquad \text{(A-3)}$$

(iii) When the configuration is A_rB_s, *i.e.*, both molecules are in excited states, where r denotes the $i \rightarrow k$, singly excitation and s does the $j \rightarrow l$,

$$U_{t0}^{10} = 2\langle \varphi_k{}^A(1)\varphi_l{}^B(2) | e^2/r_{12} | \varphi_i{}^A(1)\varphi_j{}^B(2) \rangle$$
$$= 2\sum_a C_{ak}^A C_{ai}^A \sum_b C_{bl}^B C_{bj}^B \gamma_{ab}^{AB}. \qquad \text{(A-4)}$$

(3)

$$U_{00}^{12} = -2\sum_i\sum_j \langle \varphi_i{}^A(2)\varphi_j{}^B(1) | e^2/r_{12} | \varphi_i{}^A(1)\varphi_j{}^B(2) \rangle \qquad 1)$$
$$-4\sum_l\sum_i\sum_j \langle \varphi_j{}^B(1)\varphi_l{}^B(2) | e^2/r_{12} | \varphi_i{}^A(1)\varphi_l{}^B(2) \rangle$$
$$\times \langle \varphi_i{}^A(3) | \varphi_j{}^B(3) \rangle \qquad 2)$$

30) The calculation of the intermolecular potential including these terms by using the CNDO/2 method is in progress; the results will be published in the future.

(when $l=j$, multiplied by 1/2)

$$-4\sum_{l}\sum_{i}\sum_{j}\langle\varphi_i^A(2)\varphi_l^A(1)\,|\,e^2/r_{12}\,|\,\varphi_l^A(1)\varphi_j^B(2)\rangle \times\langle\varphi_j^B(3)\,|\,\varphi_i^A(3)\rangle \quad 3)$$

(when $l=i$, multiplied by 1/2)

$$-8\sum_{m}\sum_{l}\sum_{i}\sum_{j}\langle\varphi_i^A(1)\varphi_j^B(2)\,|\,e^2/r_{12}\,|\,\varphi_i^A(1)\varphi_j^B(2)\rangle \times\{\langle\varphi_i^A(3)\,|\,\varphi_m^B(3)\rangle\}^2 \quad 4)$$

(when $j=m$ or $i=l$, multiplied by 1/2)

$$+2\sum_{a}\sum_{i}\sum_{j}\langle\varphi_i^A(1)\,|\,Z_a^A e^2/r_{a1}\,|\,\varphi_j^B(1)\rangle \times\langle\varphi_j^B(2)\,|\,\varphi_i^A(2)\rangle \quad 5)$$

$$+4\sum_{a}\sum_{i}\sum_{j}\sum_{l}\langle\varphi_j^B(1)\,|\,Z_a^A e^2/r_{a1}\,|\,\varphi_j^B(1)\rangle \times\{\langle\varphi_i^A(2)\,|\,\varphi_l^B(2)\rangle\}^2 \quad 6)$$

(when $j=l$, multiplied by 1/2)

$$+2\sum_{b}\sum_{i}\sum_{j}\langle\varphi_j^B(1)\,|\,Z_b^B e^2/r_{1b}\,|\,\varphi_i^A(1)\rangle \times\langle\varphi_i^A(2)\,|\,\varphi_j^B(2)\rangle \quad 7)$$

$$+4\sum_{b}\sum_{i}\sum_{j}\sum_{l}\langle\varphi_i^A(1)\,|\,Z_b^B e^2/r_{1b}\,|\,\varphi_i^A(1)\rangle \times\{\langle\varphi_j^B(2)\,|\,\varphi_l^A(2)\rangle\}^2 \quad 8)$$

(when $i=l$, multiplied by 1/2)

$$-2\sum_{a}\sum_{b}Z_a^A Z_b^B\gamma_{ab}^{AB}\sum_{i}\sum_{j}\{\langle\varphi_j^B(1)\,|\,\varphi_i^A(1)\rangle\}^2. \quad 9)$$

(A-5)

U_{00}^{12} is written down here only in terms of the molecular orbitals. In the calculation, if the value of overlap integral between a pair of atomic orbiatls is less than 10^{-4} in magnitude, the contributions of this term could be neglected. This cut off procedure was taken through the computation of any matrix elements including overlap integrals, *i.e.*, U_{00}^{14}, U_{t0}^{12} *etc.*

(4)

$$S_{00}^{02} = -2\sum_{i}\sum_{j}\{\langle\varphi_i^A(1)\,|\,\varphi_j^B(1)\rangle\}^2 = -2\sum_{i}\sum_{j}(\sum_{a}\sum_{b}C_{ai}^{A}C_{bj}^{B}S_{ab}^{AB})^2. \quad \text{(A-6)}$$

(5) The each term of U_{00}^{14} can be obtained by allowing the exchange of one pair of electrons in the electronic configuration of each term in U_{00}^{12}.

If $D_{fg}=\{\langle\varphi_f^A|\varphi_g^B\rangle\}^2$,

$$U_{00}^{14} = 1/2U_{00}^{12}S_{00}^{02}$$

$$+2\sum_{i}\sum_{j}\langle\varphi_i^A(2)\varphi_j^B(1)\,|\,e^2/r_{12}\,|\,\varphi_i^A(1)\varphi_j^B(2)\rangle \times\sum_{\substack{f\\(\neq i)}}\sum_{\substack{g\\(\neq j)}}D_{fg} \quad 1)$$

$$+4\sum_{l}\sum_{i}\sum_{j}\langle\varphi_j^B(1)\varphi_l^B(2)\,|\,e^2/r_{12}\,|\,\varphi_i^A(1)\varphi_l^B(2)\rangle \times\langle\varphi_i^A(3)\,|\,\varphi_j^B(3)\rangle\sum_{\substack{f\\(\neq i)(\neq l,j)}}\sum_{g}D_{fg} \quad 2)$$

(when $l=j$, multiplied by 1/2)

$$+4\sum_{l}\sum_{i}\sum_{j}\langle\varphi_i^A(2)\varphi_l^A(1)\,|\,e^2/r_{12}\,|\,\varphi_l^A(1)\varphi_j^B(2)\rangle \times\langle\varphi_j^B(3)\,|\,\varphi_i^A(3)\rangle\sum_{\substack{f\\(\neq i,l)(\neq j)}}\sum_{g}D_{fg} \quad 3)$$

(when $l=i$, multiplied by 1/2)

$$+8\sum_{m}\sum_{l}\sum_{i}\sum_{j}\langle\varphi_i^A(1)\varphi_j^B(2)\,|\,e^2/r_{12}\,|\,\varphi_i^A(1)\varphi_j^B(2)\rangle \times\{\langle\varphi_i^A(3)\,|\,\varphi_m^B(3)\rangle\}^2\sum_{\substack{f\\(\neq i,l)(\neq j,m)}}\sum_{g}D_{fg} \quad 4)$$

(when $j=m$ or $i=l$, multiplied by 1/2)

$$-2\sum_{a}\sum_{i}\sum_{j}\langle\varphi_i^A(1)\,|\,Z_a^A e^2/r_{a1}\,|\,\varphi_j^B(1)\rangle \times\langle\varphi_j^B(2)\,|\,\varphi_i^A(2)\rangle\sum_{\substack{f\\(\neq i)}}\sum_{\substack{g\\(\neq j)}}D_{fg} \quad 5)$$

$$-4\sum_{a}\sum_{i}\sum_{j}\sum_{l}\langle\varphi_j^B(1)\,|\,Z_a^A e^2/r_{a1}\,|\,\varphi_j^B(1)\rangle \times\{\langle\varphi_i^A(2)\,|\,\varphi_l^B(2)\rangle\}^2\sum_{\substack{f\\(\neq i,l)(\neq j)}}\sum_{g}D_{fg} \quad 6)$$

(when $j=l$, multiplied by 1/2)

$$-2\sum_{b}\sum_{i}\sum_{j}\langle\varphi_j^B(1)\,|\,Z_b^B e^2/r_{1b}\,|\,\varphi_i^A(1)\rangle \times\langle\varphi_i^A(2)\,|\,\varphi_j^B(2)\rangle\sum_{\substack{f\\(\neq i)}}\sum_{\substack{g\\(\neq j)}}D_{fg} \quad 7)$$

$$-4\sum_{b}\sum_{i}\sum_{j}\sum_{l}\langle\varphi_i^A(1)\,|\,Z_b^B e^2/r_{1b}\,|\,\varphi_i^A(1)\rangle \times\{\langle\varphi_j^B(2)\,|\,\varphi_l^A(2)\rangle\}^2\sum_{\substack{f\\(\neq i,l)(\neq j)}}\sum_{g}D_{fg} \quad 8)$$

(when $i=l$, multiplied by 1/2)

$$+2\sum_{a}\sum_{b}Z_a^A Z_b^B\gamma_{ab}^{AB}\sum_{i}\sum_{j}\{\langle\varphi_j^B(1)\,|\,\varphi_i^A(1)\rangle\}^2 \times\sum_{\substack{f\\(\neq i)}}\sum_{\substack{g\\(\neq j)}}D_{fg}. \quad 9)$$

(A-7)

(6) U_{t0}^{12} and S_{t0}^{02} can be classified as follows.

(i) When the configuration is A_rB_0, where r represents the $i\rightarrow k$ singly excitation,

$$U_{t0}^{12} = -\sqrt{2}\sum_{n}\langle\varphi_k^A(2)\varphi_n^B(1)\,|\,e^2/r_{12}\,|\,\varphi_i^A(1)\varphi_n^B(2)\rangle -4\sqrt{2}\sum_{n}\sum_{m}\sum_{f}\langle\varphi_k^A(1)\varphi_n^B(2)\,|\,e^2/r_{12}\,|\,\varphi_i^A(1)\varphi_n^B(2)\rangle \times\{\langle\varphi_f^A(3)\,|\,\varphi_m^B(3)\rangle\}^2$$

(when $m=n$ or $f=i$, multiplied by 1/2)

$$-4\sqrt{2}\sum_{f}\sum_{n}\sum_{m}\langle\varphi_f^A(1)\varphi_n^B(2)\,|\,e^2/r_{12}\,|\,\varphi_f^A(1)\varphi_n^B(2)\rangle \times\langle\varphi_k^A(4)\varphi_m^B(3)\,|\,\varphi_i^A(3)\varphi_m^B(4)\rangle$$

(when $m=n$ or $f=i$, multiplied by 1/2)

$$-2\sqrt{2}\sum_{m}\sum_{n}\langle\varphi_k^A(1)\varphi_n^A(2)\,|\,e^2/r_{12}\,|\,\varphi_i^A(1)\varphi_m^B(2)\rangle \times\langle\varphi_m^B(3)\,|\,\varphi_n^A(3)\rangle$$

(when $n=i$, multiplied by 1/2)

$$-2\sqrt{2}\sum_{m}\sum_{n}\langle\varphi_n^B(2)\varphi_m^B(1)\,|\,e^2/r_{12}\,|\,\varphi_n^B(2)\varphi_i^A(1)\rangle \times\langle\varphi_k^A(3)\,|\,\varphi_m^B(3)\rangle$$

(when $n=m$, multiplied by 1/2)

$$-2\sqrt{2}\sum_{m}\sum_{n}\langle\varphi_n^A(1)\varphi_k^A(2)\,|\,e^2/r_{12}\,|\,\varphi_n^A(1)\varphi_m^B(2)\rangle \times\langle\varphi_m^B(3)\,|\,\varphi_i^A(3)\rangle$$

(when $n=i$, multiplied by 1/2)

$$+\sqrt{2}\sum_{a}\sum_{n}\langle\varphi_k^A(1)\,|\,Z_a^A e^2/r_{a1}\,|\,\varphi_n^B(1)\rangle \times\langle\varphi_n^B(2)\,|\,\varphi_i^A(2)\rangle$$

$$+2\sqrt{2}\sum_{m}\sum_{a}\sum_{n}\langle\varphi_m^B(1)\,|\,Z_a^A e^2/a_1\,|\,\varphi_m^B(1)\rangle \times\langle\varphi_k^A(2)\varphi_n^B(3)\,|\,\varphi_i^A(3)\varphi_n^B(2)\rangle$$

$$+\sqrt{2}\sum_{b}\sum_{n}\langle\varphi_n^B(1)\,|\,Z_b^B e^2/r_{1b}\,|\,\varphi_i^A(1)\rangle \times\langle\varphi_k^A(2)\,|\,\varphi_n^B(2)\rangle$$

$$+2\sqrt{2}\sum_{b}\sum_{n}\sum_{m}\langle\varphi_m^A(1)\,|\,Z_b^B e^2/r_{1b}\,|\,\varphi_m^A(1)\rangle \times\langle\varphi_n^B(2)\varphi_k^A(3)\,|\,\varphi_n^B(3)\varphi_i^A(2)\rangle$$

(when $m=i$, multiplied by 1/2)

$$+2\sqrt{2}\sum_{n}\sum_{m}\sum_{b}\langle\varphi_k^A(1)\,|\,Z_b^B e^2/r_{1b}\,|\,\varphi_i^A(1)\rangle \times\langle\varphi_m^A(3)\varphi_n^B(2)\,|\,\varphi_n^B(3)\varphi_m^A(2)\rangle$$

(when $m=i$, multiplied by 1/2)

$$-\sqrt{2}\sum_{n}\langle\varphi_k^A(2)\varphi_n^B(1)\,|\,\varphi_i^A(1)\varphi_n^B(2)\rangle \times\sum_{a}\sum_{b}Z_a^A Z_b^B\gamma_{ab}^{AB} \quad \text{(A-8)}$$

$$S_{t0}^{02} = -2\sqrt{2}\sum_{j}\langle\varphi_k^A(2)\varphi_j^B(1)\,|\,\varphi_i^A(1)\varphi_j^B(2)\rangle. \quad \text{(A-9)}$$

(ii) When the configuration is A_0B_s, where s represents the $j\rightarrow l$ singly excitation, the matrix elements U_{t0}^{12} and S_{t0}^{02} in this case are obtained from (i) by exchanging upper indices A and B and substituting j and l for i and k, respectively.

(iii) When the configurations A_rB_s, *i.e.*, both molecules are in excited states, where r represents the $i\rightarrow k$ singly excitation and s represents the $j\rightarrow l$,

$$\begin{aligned}U_{t0}^{12} = & -\langle\varphi_k^A(2)\varphi_l^B(1)\,|\,e^2/r_{12}\,|\,\varphi_i^A(1)\varphi_j^B(2)\rangle\\ & -4\sum_n\sum_m\langle\varphi_n^A(1)\varphi_m^B(2)\,|\,e^2/r_{12}\,|\,\varphi_n^A(1)\varphi_m^B(2)\rangle\\ & \times\langle\varphi_k^A(3)\varphi_l^B(4)\,|\,\varphi_i^A(4)\varphi_j^B(3)\rangle\end{aligned}$$

(when $n=i$ or $m=j$, multiplied by 1/2)

$$\begin{aligned}& -2\sum_n\langle\varphi_n^A(1)\varphi_k^A(2)\,|\,e^2/r_{12}\,|\,\varphi_n^A(1)\varphi_j^B(2)\rangle\\ & \times\langle\varphi_l^B(3)\,|\,\varphi_i^A(3)\rangle\end{aligned}$$

(when $n=i$, multiplied by 1/2)

$$\begin{aligned}& -2\sum_n\langle\varphi_k^A(1)\varphi_n^A(2)\,|\,e^2/r_{12}\,|\,\varphi_i^A(1)\varphi_j^B(2)\rangle\\ & \times\langle\varphi_l^B(3)\,|\,\varphi_n^A(3)\rangle\end{aligned}$$

(when $n=i$, multiplied by 1/2)

$$\begin{aligned}& -2\sum_n\langle\varphi_n^B(2)\varphi_l^B(1)\,|\,e^2/r_{12}\,|\,\varphi_n^B(2)\varphi_i^A(1)\rangle\\ & \times\langle\varphi_k^A(3)\,|\,\varphi_j^B(3)\rangle\end{aligned}$$

(when $n=j$, multiplied by 1/2)

$$\begin{aligned}& -2\sum_n\langle\varphi_l^B(2)\varphi_n^B(1)\,|\,e^2/r_{12}\,|\,\varphi_j^B(2)\varphi_i^A(1)\rangle\\ & \times\langle\varphi_k^A(3)\,|\,\varphi_n^B(3)\rangle\end{aligned}$$

(when $n=j$, multiplied by 1/2)

$$\begin{aligned}& -4\sum_m\sum_n\langle\varphi_n^A(1)\varphi_l^B(2)\,|\,e^2/r_{12}\,|\,\varphi_n^A(1)\varphi_j^B(2)\rangle\\ & \times\langle\varphi_k^A(4)\varphi_m^B(3)\,|\,\varphi_i^A(3)\varphi_m^B(4)\rangle\end{aligned}$$

(when $m=j$ or $n=i$, multiplied by 1/2)

$$\begin{aligned}& -4\sum_m\sum_n\langle\varphi_k^A(1)\varphi_m^B(2)\,|\,e^2/r_{12}\,|\,\varphi_i^A(1)\varphi_m^B(2)\rangle\\ & \times\langle\varphi_n^A(4)\varphi_l^B(3)\,|\,\varphi_j^B(4)\varphi_n^A(3)\rangle\end{aligned}$$

(when $m=j$ or $n=i$, multiplied by 1/2)

$$\begin{aligned}& -4\sum_m\sum_n\langle\varphi_k^A(1)\varphi_l^B(2)\,|\,e^2/r_{12}\,|\,\varphi_i^A(1)\varphi_j^B(2)\rangle\\ & \times\langle\varphi_n^A(4)\varphi_m^B(3)\,|\,\varphi_m^B(4)\varphi_n^A(3)\rangle\end{aligned}$$

(when $m=j$ or $n=i$, multiplied by 1/2)

$$\begin{aligned}& +\sum_a\langle\varphi_k^A(1)\,|\,Z_a^Ae^2/r_{a1}\,|\,\varphi_j^B(1)\rangle\langle\varphi_l^B(2)\,|\,\varphi_i^A(2)\rangle\\ & +2\sum_a\sum_n\langle\varphi_n^B(1)\,|\,Z_a^Ae^2/r_{a1}\,|\,\varphi_n^B(1)\rangle\\ & \times\langle\varphi_l^B(2)\varphi_k^A(3)\,|\,\varphi_i^A(2)\varphi_j^B(3)\rangle\end{aligned}$$

(when $n=j$, multiplied by 1/2)

$$\begin{aligned}& +2\sum_a\sum_n\langle\varphi_l^B(1)\,|\,Z_a^Ae^2/r_{a1}\,|\,\varphi_j^B(1)\rangle\\ & \times\langle\varphi_n^B(3)\varphi_k^A(2)\,|\,\varphi_i^A(3)\varphi_n^B(2)\rangle\end{aligned}$$

(when $n=j$, multiplied by 1/2)

$$\begin{aligned}& +\sum_b\langle\varphi_l^B(1)\,|\,Z_b^Be^2/r_{1b}\,|\,\varphi_i^A(1)\rangle\langle\varphi_k^A(2)\,|\,\varphi_j^B(2)\rangle\\ & +2\sum_b\sum_n\langle\varphi_n^A(1)\,|\,Z_b^Be^2/r_{1b}\,|\,\varphi_n^A(1)\rangle\\ & \times\langle\varphi_k^A(2)\varphi_l^B(3)\,|\,\varphi_j^B(2)\varphi_i^A(3)\rangle\end{aligned}$$

(when $n=i$, multiplied by 1/2)

$$\begin{aligned}& +2\sum_b\sum_n\langle\varphi_k^A(1)\,|\,Z_b^Be^2/r_{1b}\,|\,\varphi_i^A(1)\rangle\\ & \times\langle\varphi_n^A(3)\varphi_l^B(2)\,|\,\varphi_j^B(3)\varphi_n^A(2)\rangle\end{aligned}$$

(when $n=i$, multiplied by 1/2)

$$-\langle\varphi_k^A(2)\varphi_l^B(1)\,|\,\varphi_i^A(1)\varphi_j^B(2)\rangle\sum_a\sum_bZ_a^AZ_b^Be^2/r_{ab} \tag{A-10}$$

$$S_{t0}^{02} = -2\langle\varphi_k^A(2)\varphi_l^B(1)\,|\,\varphi_i^A(1)\varphi_j^B(2)\rangle. \tag{A-11}$$

When $(U_{t0}^{10})^2/(E_0-E_t)$ is less than a critical value, the term including U_{t0}^{12} in E^{22}, *i.e.*, $U_{t0}^{10}U_{t0}^{12}/(E_0-E_t)$, can also be expected to be small in magnitude and hence the contribution of this term to E^{22} was neglected in order to save computation time. We found the critical value of 10^{-4} is sufficient for the result within the accuracy of 10^{-4} eV in total intermolecular potential.

(7)

$$\begin{aligned}U_{t0}^{11} = & \sqrt{2}\sum_j\langle\varphi_j^B(2)\varphi_l^B(1)\,|\,e^2/r_{12}\,|\,\varphi_k^A(1)\varphi_j^B(2)\rangle\\ & +4\sqrt{2}\sum_i\sum_j\langle\varphi_i^A(1)\varphi_j^B(2)\,|\,e^2/r_{12}\,|\,\varphi_i^A(1)\varphi_j^B(2)\rangle\\ & \times\langle\varphi_l^B(3)\,|\,\varphi_k^A(3)\rangle\end{aligned}$$

(when $i=k$, multiplied by 1/2)

$$\begin{aligned}& -2\sqrt{2}\sum_i\sum_j\langle\varphi_i^A(1)\varphi_l^B(2)\,|\,e^2/r_{12}\,|\,\varphi_i^A(1)\varphi_j^B(2)\rangle\\ & \times\langle\varphi_j^B(3)\,|\,\varphi_k^A(3)\rangle\end{aligned}$$

(when $i=k$, multiplied by 1/2)

$$\begin{aligned}& -\sqrt{2}\sum_j\langle\varphi_j^B(1)\varphi_l^B(2)\,|\,e^2/r_{12}\,|\,\varphi_k^A(1)\varphi_j^B(2)\rangle\\ & -2\sqrt{2}\sum_a\sum_j\langle\varphi_j^B(1)\,|\,Z_a^Ae^2/r_{a1}\,|\,\varphi_j^B(1)\rangle\\ & \times\langle\varphi_l^B(2)\,|\,\varphi_k^A(2)\rangle\\ & +\sqrt{2}\sum_a\sum_j\langle\varphi_l^B(1)\,|\,Z_a^Ae^2/r_{a1}\,|\,\varphi_j^B(1)\rangle\\ & \times\langle\varphi_j^B(2)\,|\,\varphi_k^A(2)\rangle\\ & -\sqrt{2}\sum_b\langle\varphi_l^B(1)\,|\,Z_b^Be^2/r_{1b}\,|\,\varphi_k^A(1)\rangle\\ & -2\sqrt{2}\sum_b\sum_i\langle\varphi_i^A(1)\,|\,Z_b^Be^2/r_{1b}\,|\,\varphi_i^A(1)\rangle\\ & \times\langle\varphi_l^B(2)\,|\,\varphi_k^A(2)\rangle\end{aligned}$$

(when $i=k$, multiplied by 1/2)

$$+\sqrt{2}\sum_a\sum_bZ_a^AZ_b^Be^2/r_{ab}\langle\varphi_l^B(1)\,|\,\varphi_k^A(1)\rangle \tag{A-12}$$

$$S_{t0}^{01} = \sqrt{2}\langle\varphi_l^B(1)\,|\,\varphi_k^A(1)\rangle. \tag{A-13}$$

The matrix element of the charge transfer from B to A,

$$U_{t0}^{11} = (2n+1/2m)^{1/2}\langle A_l^-(i')B_k^+(j')\,|\,U\,|\,A_0(i)B_0(j)\rangle,$$

is obtained by exchanging upper indices A and B in Eq. (A-12).

The Abnormal Absorption Intensity of the C-H Stretching Vibration Band in Chloroform Vapor. I. The CNDO Calculation Involving the 3*d* Orbitals

Tomoo MIYAZAKI, Tsunehisa SHIGETANI, and Hiroshi YAMAMOTO

Department of Applied Chemistry, Faculty of Science and Engineering, Waseda University, Nishi-Ohkubo, Shinjuku-ku, Tokyo

(Received June 16, 1971)

By the CNDO calculation involving the 3*d* orbitals, the infrared absorption intensity of the C–H stretching vibration band in chloroform vapor has been discussed in comparison with those of methyl chloride and methylene chloride. The value of the 3*d* orbital exponent of the chlorine atom was estimated on the basis of calculations using different values of the 3*d* orbital exponent on methyl chloride. The absolute intensities of the fundamental and the first overtone bands were calculated from the values of the first and the second derivatives of dipole moments with respect to the normal coordinates. From the results of these calculations, it follows that the electrical properties of the vibrating bond are the most effective factors in bringing about the abnormal absorption intensity of the C–H stretching vibration band in chloroform vapor.

The CNDO method was applied by Segal and Klein[1] to the calculation of dipole-moment derivatives $\mu' = \partial\mu/\partial S_j$, where μ is the molecular dipole moment, and S_j, an appropriate symmetry coordinate. They concluded that the theory was reasonably successful in calculating both the magnitude and the sign of μ' for molecules composed of the first-row elements of the periodic table and/or hydrogen.

The CNDO method was extended to the treatment of molecules containing second-row elements by Santry and Segal.[2,3] In their papers, the importance of the 3*d* orbitals to the bonding in the molecule containing the second-row element was discussed and the CNDO parameters of the 3*d* orbitals necessary for calculation on molecules containing these elements were estimated.

The abnormal absorption intensity of the C–H stretching vibration band in chloroform vapor is particularly interesting, since the fundamental band intensity is very weak and the first overtone band intensity is much stronger than that of the former.[4-6] Robinson *et al.* interpreted this experimental result in terms of the electrical properties of the vibrating bond.[4]

In view of the above situation, it appeared of interest to investigate the abnormal intensity of the C–H stretching vibration band in chloroform vapor by the CNDO calculation involving the 3*d* orbitals of the chlorine atom. However, the values of the parameter for the 3*d* orbitals of the second-row elements are not the most desirable.[2] Therefore, in the first step of the treatment in this work, we attempted to estimate the exponent, as a parameter, for the 3*d* orbitals of the chlorine atom by fitting the calculated molecular dipole moment of methyl chloride to the experimental one. By use of the appropriate value of the 3*d* orbital exponent of the chlorine atom, the dipole-moment derivatives referring to the C–H stretching vibration of chloroform have been calculated and the abnormal intensity of this vibration band has been discussed.

1) G. A. Segal and M. L. Klein, *J. Chem. Phys.*, **47**, 4236 (1967).
2) D. P. Santry and G. A. Segal, *ibid.*, **47**, 158 (1967).
3) D. P. Santry, *J. Amer. Chem. Soc.*, **90**, 3309 (1968).
4) C. C. Robinson, S. T. Tare, and H. W. Thompson, *Proc. Roy. Soc.*, **A269**, 492 (1962).
5) M. M. Chalaye and G. Levi, *C.R. Acad. Sci. Paris*, **t.267**, B-45 (1968).
6) I. Rossi, M. Nguyen-Van-Thanh, and C. Haeusler, *Can. J. Chem.*, **47**, 3319 (1969).

Methods of Calculation

The CNDO Calculation Involving the 3d Orbitals. The molecular orbital calculation used in this work followed the CNDO method proposed by Santry and Segal[2] except for the value of the 3*d* orbital exponent. To determine the appropriate value of the 3*d* orbital exponent of the chlorine atom, we adopted the approach of examining the comparative ability of molecular orbitals, as calculated by the various values of the 3*d* orbital exponent, to predict correctly the observed dipole moment of methyl chloride.

The CNDO approximation describes the molecular orbitals, φ_i, as linear combinations of valence atomic orbitals, χ_μ:

$$\varphi_i = \sum_\mu c_{i\mu}\chi_\mu, \tag{1}$$

where the coefficient, $c_{i\mu}$, are the eigenvectors of the Hartree-Fock matrix, $F_{\mu\nu}$. An important characteristic of the calculation in this work is that the 3*d* orbitals are considered to be members of the valence atomic orbital when the atom is a second-row element in the periodic table.

The coefficient of the molecular orbital and the energy can be obtained by solving the appropriate set of secular equations and corresponding secular matrix. The elements of the SCF energy matrix are given in this method by:

$$\begin{aligned} F_{\mu\mu}(\mathrm{S,S}) = &-\frac{1}{2}(I_\mu + A_\mu) + \left\{\left[P_{\mathrm{AA}}(S) - Z_{\mathrm{A}}\right] - \frac{1}{2}(P_{\mu\mu} - 1)\right\}\gamma_{\mathrm{AA}}(\mathrm{S,S}) + P_{\mathrm{AA}}(\mathrm{D})\gamma_{\mathrm{AA}}(\mathrm{S,D}) \\ &+ \sum_{\mathrm{B}\neq\mathrm{A}}\{[P_{\mathrm{BB}}(\mathrm{S}) - Z_{\mathrm{B}}]\gamma_{\mathrm{AB}}(\mathrm{S,S}), \\ &+ P_{\mathrm{BB}}(\mathrm{D})\gamma_{\mathrm{AB}}(\mathrm{S,D})\}, \end{aligned} \tag{2}$$

$$\begin{aligned} F_{\mu\mu}(\mathrm{D,D}) = &-\frac{1}{2}(I_\mu + A_\mu) + \left\{\left[P_{\mathrm{AA}}(\mathrm{S}) - \left(Z_{\mathrm{A}} - \frac{1}{2}\right)\right] \times \gamma_{\mathrm{AA}}(\mathrm{D,S})\right\} + \left[P_{\mathrm{AA}}(\mathrm{D}) - \frac{1}{2}P_{\mu\mu}\right]\gamma_{\mathrm{AA}}(\mathrm{D,D}) \\ &+ \sum_{\mathrm{B}\neq\mathrm{A}}\{[P_{\mathrm{BB}}(\mathrm{S}) - Z_{\mathrm{B}}]\gamma_{\mathrm{AB}}(\mathrm{D,S}) \\ &+ P_{\mathrm{BB}}(\mathrm{D})\gamma_{\mathrm{AB}}(\mathrm{D,D})\}, \end{aligned} \tag{3}$$

$$F_{\mu\nu}(\mathrm{S,S}) = \beta^0_{\mathrm{AB}}\mathrm{S}_{\mu\nu} - \frac{1}{2}P_{\mu\nu}\gamma_{\mathrm{AB}}(\mathrm{S,S}), \quad (4)$$

$$F_{\mu\nu}(\mathrm{S,D}) = \beta^0_{\mathrm{AB}}\mathrm{S}_{\mu\nu} - \frac{1}{2}P_{\mu\nu}\gamma_{\mathrm{AB}}(\mathrm{S,D}) \qquad (\mu \neq \nu), \quad (5)$$

$$F_{\mu\nu}(\mathrm{D,D}) = \beta^0_{\mathrm{AB}}\mathrm{S}_{\mu\nu} - \frac{1}{2}P_{\mu\nu}\gamma_{\mathrm{AB}}(\mathrm{D,D}), \quad (6)$$

where the suffix S refers to s and p orbitals, where D refers to the d orbital, and where γ_{AB} is the electron-repulsion integral calculated as a Coulomb integral involving valence s functions, which are divided into two sets, such as S (involving s and p orbitals) for those with exponents defined by Slater's rules and D (involving d orbital) for those with smaller exponents. In this calculation, the values of the orbital exponent were taken to be 6.1 and 5.5 for the S and D of the chlorine atom respectively. The $-\frac{1}{2}(\mathrm{I}_\mu+\mathrm{A}_\mu)$ term is the core integral, where I_μ and A_μ are the ionization potential and the affinity of the χ_μ orbital. The P_{AA} (S) term is the total charge density of the A atom in s- or p-type orbitals:

$$P_{\mathrm{AA}}(\mathrm{S}) = \sum_{\mu\in\mathrm{A}}^{\mu\neq\mathrm{D}} P_{\mu\mu}, \quad (7)$$

and P_{AA} (D) is the analogous charge density in $3d$ orbitals. The β^0_{AB} term is the resonance integral proportionality constant and is approximated as:

$$\beta^0_{\mathrm{AB}} = \frac{1}{2}K(\beta_{\mathrm{A}}{}^0+\beta_{\mathrm{B}}{}^0), \quad (8)$$

where $\beta_{\mathrm{A}}{}^0$ depends only on the A atom and where K is 0.75 if the A atom and/or the B atom is a second-row element, and 1 otherwise. The Z_{A} term is the core charge on the A atom. The $\mathrm{S}_{\mu\nu}$ term is the overlap integral between the χ_μ and χ_ν orbitals. The numerical values used in this calculation are listed in Table 1. The necessary overlap integrals were evaluated from the master formulas of Lofthus.[7] The electron–repulsion integrals involving s functions were theoretically evaluated from the master formulas, which were provided in the same way as in the derivation of Roothaan.[8]

Table 1. Parameter values (eV)

Atom	H	C		Cl		
Orbital	1s	2s	2p	3s	3p	3d
$1/2(I+A)$	7.176	14.051	5.572	21.591	8.708	0.977
$-\beta_{\mathrm{A}}{}^0$	9	21		22.33		

The Dipole Moments and their Derivatives. The molecular dipole moments were calculated as a sum of three terms, μ_{Q}, μ_{sp}, and μ_{pd}, whree μ_{Q} is the contribution from net charge densities and where μ_{sp} and μ_{pd} are terms which arise from atomic polarization due to the mixing of s and p orbitals and that of p and d orbitals respectively. They can be calculated by means of the following equations:[9]

$$\mu_{\mathrm{Q}}(\mathrm{z}) = 2.5416\sum_{\mathrm{A}}^{\mathrm{atoms}} Q_{\mathrm{A}}z_{\mathrm{A}} \quad \text{(debyes)}, \quad (9)$$

$$Q_{\mathrm{A}} = Z_{\mathrm{A}} - P_{\mathrm{AA}},$$

where z_{A} is the appropriate Cartesian coordinate of the A atom.

$$\mu_{sp}(\mathrm{z}) = -2.5416\sum_{\mathrm{A}}^{\mathrm{atoms}}\left[\frac{10}{\sqrt{3}Z_s'(\mathrm{A})}P_{2s(\mathrm{A}),2p_z(\mathrm{A})} + \frac{21}{\sqrt{3}Z_s'(\mathrm{A})}P_{3s(\mathrm{A}),3p_z(\mathrm{A})}\right] \text{(debyes)}, \quad (10)$$

where Z'_s is the appropriate orbital exponent as defined by Slater's rules.

$$\mu_{pd}(\mathrm{x}) = -2.5416\sum_{\mathrm{A}}^{\mathrm{atoms}} M(\mathrm{A})\left[P_{3d_{xz}(\mathrm{A}),3p_z(\mathrm{A})} + P_{3d_{x^2-y^2}(\mathrm{A}),3p_x(\mathrm{A})} + P_{3d_{xy}(\mathrm{A}),3p_y(\mathrm{A})} - \frac{1^*}{\sqrt{3}}P_{3d_{z^2}(\mathrm{A}),3p_x(\mathrm{A})}\right] \text{(debyes)}, \quad (11)$$

$$\mu_{pd}(\mathrm{y}) = -2.5416\sum_{\mathrm{A}}^{\mathrm{atoms}} M(\mathrm{A})\left[P_{3d_{yz}(\mathrm{A}),3p_z(\mathrm{A})} + P_{3d_{xy}(\mathrm{A}),3p_x(\mathrm{A})} - {}^*P_{3d_{x^2-y^2}(\mathrm{A}),3p_y(\mathrm{A})} - \frac{1^*}{\sqrt{3}}P_{3d_{z^2}(\mathrm{A}),3p_y(\mathrm{A})}\right] \text{(debyes)}, \quad (12)$$

$$\mu_{pd}(\mathrm{z}) = -2.5416\sum_{\mathrm{A}}^{\mathrm{atoms}} M(\mathrm{A})\left[\frac{2^*}{\sqrt{3}}P_{3d_{z^2}(\mathrm{A}),3p_z(\mathrm{A})} + P_{3d_{xz}(\mathrm{A}),3p_x(\mathrm{A})} + P_{3d_{yz}(\mathrm{A}),3p_y(\mathrm{A})}\right] \text{(debyes)}, \quad (13)$$

$$M(\mathrm{A}) = \frac{5376[Z_s'(\mathrm{A})Z_{\mathrm{D}}'(\mathrm{A})]^{7/2}}{5^{1/2}[Z_s'(\mathrm{A})+Z_{\mathrm{D}}'(\mathrm{A})]^8}. \quad (14)$$

The numerical values required to discuss the intensities of the fundamental and the first overtone bands related to the C–H stretching vibration bands were obtained by fitting the calculated dipole moments to a cubic function with respect to the C–H distance and by taking the first and the second derivatives at the equilibrium distance. The dipole moments were calculated for the molecule distorted in the manner dictated by the symmetry coordinate including the C–H stretching modes. All the C–H bond stretching motions were calculated at intervals of ± 0.02 Å.

The Absolute Absorption Intensities of the Vibration Bands. The absolute infrared absorption intensity of the fundamental band, $(A^{*(k)}_{1\leftarrow 0})$, related to the normal coordinate, Q_k, was calculated from the following equation (15), which was derived, by Wilson *et al.*,[10] from a consideration of the 0→1, 1→2, *etc.* transitions, in the harmonic oscillator approximation:

$$A^*_{1\leftarrow 0} = A_{1\leftarrow 0} + A_{2\leftarrow 1} + A_{3\leftarrow 2} + \cdots$$

$$A^{*(k)}_{1\leftarrow 0} = \frac{\pi}{3C}\sum_{i=x,y,z}\left(\frac{\partial\mu_i}{\partial Q_k}\right)^2 [\mathrm{cm^2\cdot sec^{-1}\cdot molecule^{-1}}], \quad (15)$$

where C is the velocity of light and where μ_i is the i-component of the dipole moment of a system.

About the absolute intensity of the overtone band, $(A^{*(k)}_{2\leftarrow 0})$, in relating to the normal coordinate, Q_k, the

7) A. Lofthus, *Mol. Phys.*, **5**, 105 (1962).

8) C. C. Roothaan, *J. Chem. Phys.*, **19**, 1445 (1951).

9) In this calculation, we made a few corrections in Equations (2-32) of the original paper[2]; the revised coefficients are marked by small stars.

10) E. B. Wilson, J. C. Decious, and P. C. Cross, "Molecular Vibrations," McGraw-Hill Book Company, New York (1955).

equation to be used in the calculation was obtained according to the approximation employed for the calculation of the fundamental band intensity by Wilson *et al*:

$$A_{2\leftarrow 0}^{*(k)} = \frac{\Theta^2(1-e^{-2U_k})}{\nu_k}\frac{h}{24\pi C}\sum_{i=x,y,z}\left(\frac{\partial^2\mu_i}{\partial Q_k^2}\right)^2$$

[cm²·sec⁻¹·molecule⁻¹], (16)

where Θ is the partition function for the Q_k vibration: $\Theta=(1-e^{-h\nu_k/kT})^{-1}$, $U_k=h\nu_k/kT$, ν_k is the normal frequency associated with the normal coordinate Q_k, k is Boltzmann's constant, h is Planck's constant, and T is the absolute temperature.

Generally, the dipole-moment derivatives related to the normal coordinates can be written as follows:

$$\frac{\partial\mu_z}{\partial Q_k} = \sum_i Ls_i^{(k)}\frac{\partial\mu_z}{\partial S_i},$$

$$\frac{\partial^2\mu_z}{\partial Q_k^2} = \sum_{i,j} Ls_i^{(k)}Ls_j^{(k)}\frac{\partial^2\mu_z}{\partial S_i\partial S_j}, \quad (17)$$

where Q_k is the kth normal coordinate and where the Ls's are the elements of the $\boldsymbol{L}$ matrix which relate the symmetry cooridnates to the normal coordinates.

As for the normal coordinates considered in this work, all the Ls values are negligibly small except for the Ls(CH) related to the C–H symmetric stretching coordinate, S_{CH}. In other words, it can be assumed that the normal modes considered in this work are approximately equal to the pure C–H symmetric stretching modes. Therefore, $(Ls(CH))^2$ is equal to $Gs(CH)$, where $Gs(CH)$ is the diagonal element of the $\boldsymbol{G}$ matrix related to the C–H symmetric stretching coordinate. Since the molecules lie along the z–axis, as is indicated in Fig. 2, the components of the dipole moments are all equal to zero except for the z–component; also, the derivatives of the x– and y–components of the dipole moments related to the C–H symmetric vibration are equal to zero.

For this reason, the absolute intensities of the fundamental and the first overtone bands of the C–H symmetric stretching vibrations in CH_3Cl, CH_2Cl_2, and $CHCl_3$ can be calculated approximately by the following equations:

$$A_{1\leftarrow 0}^{*(k)} = 3.49307\times 10^{-31}(Ls(CH))^2\left(\frac{\partial\mu_z}{\partial S_{CH}}\right)^2$$

[cm²·sec⁻¹·molecule⁻¹], (18)

$$A_{2\leftarrow 0}^{*(k)} = 2.93118\times 10^{-43}\frac{\Theta^2(1-e^{-2U_k})}{\nu_k}(Ls(CH))^4\left(\frac{\partial^2\mu_z}{\partial S_{CH}^2}\right)^2$$

[cm²·sec⁻¹·molecule⁻¹], (19)

where $\partial\mu_z/\partial S_{CH}$ and $\partial^2\mu_z/\partial S^2{}_{CH}$ are the numerical values calculated in [Debye/Å] and [Debye/Å²] respectively. In this calculation, the Ls(CH)'s were taken to be $1.00797\times\sqrt{N_A}$, $1.02183\times\sqrt{N_A}$, and $1.03698\times\sqrt{N_A}$ in $[gr^{-1/2}]$ units for CH_3Cl, CH_2Cl_2, and $CHCl_3$ respectively, where N_A is Avogadro's number. The value of $\Theta^2(1-e^{-2U_k})$ is practically equal to unity. The observed frequencies of the fundamental bands were used for the values of ν_k's: CH_3Cl[11] $2967.8\times C\,sec^{-1}$, CH_2Cl_2[4] $2989\times C\,sec^{-1}$, and $CHCl_3$[4] $3033\times C\,sec^{-1}$, where C is the velocity of light.

11) G. Herzberg, "Electronic Spectra of Polyatomic Molecules," D. Van Nostrand Company, New York (1966).

Results and Discussion

Figure 1 indicates the variation in the dipole moment of CH_3Cl in the observed geometry when the 3*d* orbital exponent of the chlorine atom is continuously changed from 0 to 6.1; here, the calculation with the zero 3*d* orbital exponent is equivalent to that without 3*d* orbitals, as has been referred to by Santry and Segal.[2] In this figure, it is obvious that the 3*d* orbitals of the chlorine atom play an important role in the molecular properties.

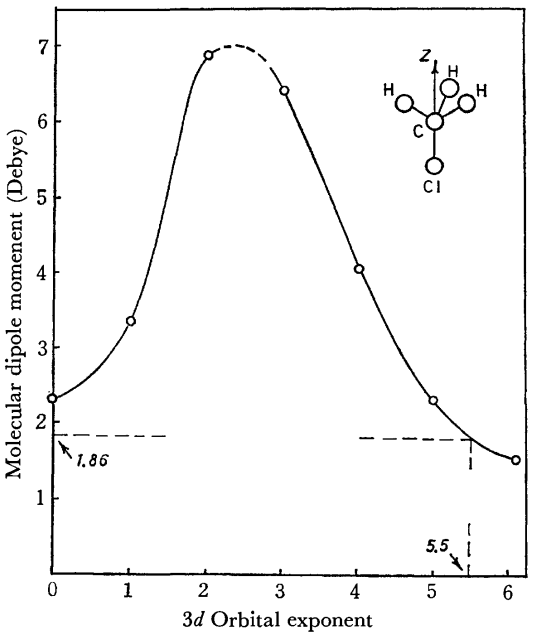

Fig. 1. The variation of dipole moment of CH_3Cl as a function of the 3*d* orbital exponent of chlorine atom.

The study of the results obtained from these calculations suggests that an optimum value of the 3*d* orbital exponent of the chlorine atom is 5.5. Table 2 records the calculated dipole moments of CH_2Cl_2 and $CHCl_3$ obtained by the use of this value. The theoretical dipole moments are in reasonable agreement with the experimental values.

From the results of the preliminary calculations, it is considered that the intensity of the vibration band in chloroform vapor can be discussed in comparison

Table 2. The dipole moments and their derivatives

Molecule	μ_z[Debye] Calcd	Obsd[a]	μ_z'[b] [Debye/Å]	μ_z''[c] [Debye/Å²]
CH_3Cl	1.857	1.86	−0.324	−0.325
CH_2Cl_2	2.004	1.57	−0.157	−0.473
$CHCl_3$	1.710	1.01	0.037_6	−0.650

a) G. A. Barclay and R. J. W. Le Févre, *J. Chem. Soc.*, **1950**, 556.

b) $\mu'_z=\left(\frac{\partial\mu_z}{\partial S_{CH}}\right)_0$

c) $\mu_z''=\left(\frac{\partial^2\mu_z}{\partial S_{CH}^2}\right)_0$

Table 3. The intensities of the C–H vibration bands in CH_3Cl, CH_2Cl_2, and $CHCl_3$

Molecule	Absolute intensity [cm^2 sec^{-1} molecule^{-1}]			
	Fundamental band[a]		Overtone band	
	Calcd ($\times 10^{10}$)	Obsd ($\times 10^{10}$)	Calcd ($\times 10^{10}$)	Obsd ($\times 10^{10}$)
CH_3Cl	225 (70.5)	1006[b] (88), 1010[c]	1.30	
CH_2Cl_2	54.1 (17.0)	334[b] (29), 178,[c] 176[d]	2.89	
$CHCl_3$	3.19 (1)	11.4[b] (1), 22,[c] 8,[d] 15[e]	5.71	50[d], 80[e]

a) Values in parentheses are relative intensities.
b) From Ref. 5.
c) L. A. Gribov and V. N. Smirnov, *Soviet Physics Uspekhi*, **4**, 919 (1962).
d) From Ref. 6.
e) From Ref. 4.

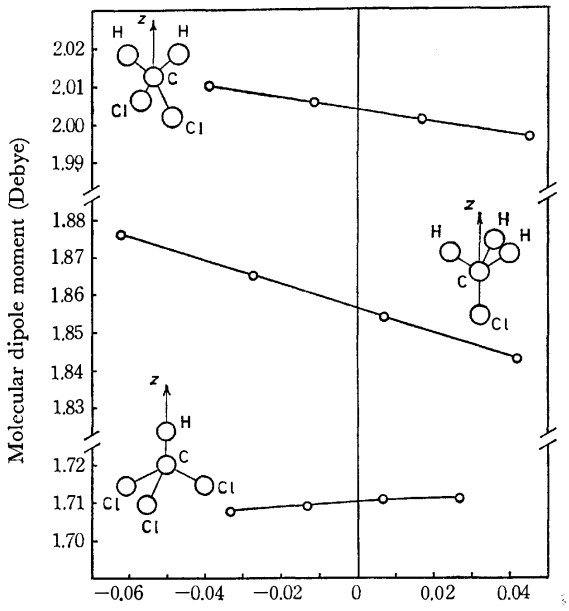

Fig. 2. Calculated variations of the dipole moments as a function of the C–H symmetric stretching coordinate S_{CH}[a].
a) $S_{CH}(CH_3Cl)=(1/\sqrt{3})(\Delta r_1+\Delta r_2+\Delta r_3)$
$S_{CH}(CH_2Cl_2)=(1/\sqrt{2})(\Delta r_1+\Delta r_2)$
$S_{CH}(CHCl_3)=\Delta r$
where Δr's are displacements from the C–H equilibrium distance.

with those of methyl chloride and methylene chloride. Figure 2 indicates the variations in the dipole moments of these compounds as a function of the C–H symmetric stretching coordinate. A cursory glance at this figure will show that the fundamental band intensity of the C–H stretching vibration in chloroform is weaker than those of other compounds. The numerical values of the $\partial\mu_z/\partial S_{CH}$ are indicated in Table 2. As for the molecules considered in this work, the absolute intensities of the fundamental bands can be calculated approximately from these numerical values, $\partial\mu_z/\partial S_{CH}$, as has been stated above. The calculated absolute intensities of the fundamental bands are summarized in Table 3. The calculated values indicate that the intensity of the fundamental band of the C–H vibration in chloroform vapor is much lower than those of methyl chloride and methylene chloride. As for these vibration bands, the intensity ratio of other compounds to chloroform are in fair agreement with those obtained experimentally, although there are some questions about the experimental absolute intensities because the absorption band of the symmetric C–H vibration is difficult to distinguish from that of the antisymmetric C–H vibration, *etc.*

The second derivatives, $\partial^2\mu_z/\partial S^2_{CH}$, necessary for the estimation of the first overtone band intensities are indicated in Table 2. The intensities of the fundamental and the overtone bands cannot be discussed in terms of a direct comparison of $\partial\mu_z/\partial S_{CH}$ and $\partial^2\mu_z/\partial S^2_{CH}$. In order to compare the intensity of the first overtone band with that of the fundamental band, the absolute intensity of the first overtone band should be calculated. The absolute intensities of the first overtone bands, as calculated from Eq. 5, are summarized in Table 3. The values show that the intensity of the first overtone band is stronger than that of the fundamental band in chloroform vapor, although the calculated first overtone band intensity is much weaker than the observed one. The

Table 4. The relative intensity between fundamental and overtone bands

Molecule	Relative Intensity ($A_{1\leftarrow0}^*/A_{2\leftarrow0}^*$)	
	Calcd	Obsd
CH_3Cl	173	
CH_2Cl_2	18.7	
$CHCl_3$	0.558	0.16,[d] 0.2[e]

d) and e) References to footnotes are the same as those in Table 3.

$A^*_{1\leftarrow0}/A^*_{2\leftarrow0}$ ratio in chloroform is indicated in Table 4, in which the ratios for other compounds are also predicted. From the results of these calculations, it was recognized that the electrical properties of the vibrating bond are the most effective factors in bringing about the abnormal absorption intensity of the C–H stretching vibration band in chloroform vapor. Since the calculated absolute intensity of the first overtone band in this work was much weaker than the observed one, the contribution of the mechanical anharmonicity to this abnormal absorption intensity should be examined, for it is a factor which cannot be overlooked.

Tables 5—7 indicated the constituent terms of the dipole moments and their derivatives. From these table, it is obvious that the relative intensity between these compounds and the abnormal intensity of the C–H stretching vibration band in chloroform cannot be ex-

TABLE 5. CONSTITUENT TERMS OF DIPOLE MOMENT
(Unit in Debye)

Molecule	μ_Q	μ_{SP}^{C}	μ_{SP}^{Cl}	μ_{Pd}^{Cl}	$\mu^{a)}$
CH_3Cl	1.498	−0.091	1.398	−0.949	1.857
CH_2Cl_2	1.451	−0.063	1.537	−0.921	2.004
$CHCl_3$	1.108	−0.025	1.235	−0.608	1.710

a) $\mu=\mu_Q+\mu_{SP}^{C}+\mu_{SP}^{Cl}+\mu_{Pd}^{Cl}$

TABLE 6. CONSTITUENT TERMS OF DIPOLE-MOMENT DERIVATIVE $(\partial\mu_z/\partial S_{CH})_0$ (UNIT IN Debye/Å)

Molecule	μ_Q'	$(\mu_{SP}^{C})'$	$(\mu_{SP}^{Cl})'$	$(\mu_{Pd}^{Cl})'$	$\mu'^{a)}$
CH_3Cl	-0.027_5	-0.024_7	-0.009_7	−0.262	−0.324
CH_2Cl_2	0.225	−0.105	0.032_6	−0.309	−0.157
$CHCl_3$	0.449	−0.212	0.109	−0.309	0.037_6

a) $\mu'=\mu_Q'+(\mu_{SP}^{C})'+(\mu_{SP}^{Cl})'+(\mu_{Pd}^{Cl})'$

TABLE 7. CONSTITUENT TERMS OF DIPOLE-MOMENT DERIVATIVE $(\partial^2\mu_z/\partial S_{CH}^2)_0$ (UNIT IN Debye/Å^2)

Molecule	μ_Q''	$(\mu_{SP}^{C})''$	$(\mu_{SP}^{Cl})''$	$(\mu_{Pd}^{Cl})''$	$\mu''^{a)}$
CH_3Cl	-0.038_2	−0.140	-0.021_6	−0.125	−0.325
CH_2Cl_2	−0.005	−0.353	-0.017_5	-0.097_5	−0.473
$CHCl_3$	0.091_3	−0.725	−0.109	0.092_5	−0.650

a) $\mu''=\mu_Q''+(\mu_{SP}^{C})''+(\mu_{SP}^{Cl})''+(\mu_{Pd}^{Cl})''$

plained by the values, such as $\partial\mu_Q/\partial S_{CH}$ and $\partial^2\mu_Q/\partial S^2{}_{CH}$, which are contributed by net charge densities alone. Atomic polarizations and their variations with the vibrating bonds are appreciably effective in determining the molecular dipole moment and the intensity of the vibration band. This is especially the case with the mixing terms of p and d orbitals.

Conclusion

The CNDO calculation involving the 3d orbitals of the chlorine atom was used in discussing the abnormal absorption intensity of the C–H stretching vibration band in chloroform vapor. The results of the calculations have suggested that the 3d orbitals play an important role in determining the molecular properties. The appropriate value of the 3d orbital exponent of the chlorine atom was 5.5. The absolute absorption intensities of the fundamental and the first overtone bands of the C–H symmetric stretching vibration in methyl chloride, methylene chloride, and chloroform were calculated from the dipole-moment derivatives. From the results of the calculations, it was recognized that the electrical properties of the vibrating bond are the effective factors in bringing about the abnormal absorption intensity of the C–H stretching vibration band in chloroform vapor. The contribution of the mechanical anharmonicity to this abnormal intensity will be the subject of future study.

The authors would like to acknowledge the continuing encouragement of Professor K. Higasi. They would like to thank Dr. H. Takahashi for this helpful advice and a critical reading of the manuscript. Thanks are due to Mr. H. Shinoda with whom they have discussed this problem. They are grateful to I.B.M., Japan, Ltd., for lending the computer to Waseda University.

BULLETIN OF THE CHEMICAL SOCIETY OF JAPAN, VOL. 45, 682—684(1972)

The Magnetic Properties of $Cu_3Cl_6(C_6H_7NO)_2 \cdot 2H_2O$

Hirokazu MIYOSHI, Hiroaki OHYA-NISHIGUCHI, and Yasuo DEGUCHI*

Department of Chemistry, Faculty of Science, Kyoto University, Kyoto
**College of Liberal Arts and Science, Kyoto University, Kyoto*

(Received June 17, 1971)

From magnetic susceptibility and ESR measurements, it has been confirmed that polybis(μ-(2-picoline *N*-oxide)-chlorocopper(II)di-μ-chloro)diaquocopper, $Cu_3Cl_6(C_6H_7NO)_2 \cdot 2H_2O$, consists of alternating linear chains with diamagnetic $Cu_2Cl_4(C_6H_7NO)_2$ units and paramagnetic $CuCl_2 \cdot 2H_2O$ units joined by long Cu–Cl bonds. The two copper ions in the $Cu_2Cl_4(C_6H_7NO)_2$ unit are coupled together very strongly by antiferromagnetic exchange interaction and occupy almost entirely the diamagnetic singlet state below room temperature. This interpretation is appropriately supported by the observation of a half-field resonance near 1600 Oe in the ESR spectrum of the powdered sample. On the other hand, the copper ion in the $CuCl_2 \cdot 2H_2O$ unit isolated magnetically can account for the ESR spectrum due to $\Delta M = \pm 1$ transition and magnetic susceptibility, following the Curie law. The magnetic susceptibility of the dehydrate compound, $Cu_3Cl_6(C_6H_7NO)_2$, has also been measured.

There have been many reports on the physical properties of complexes formed between aromatic *N*-oxide and copper(II) halide compounds. They may be divided into general categories which reflect their chemical compositions and magnetic properties. One of them consists of magnetically subnormal substances which are composed of one aromatic *N*-oxide molecule and one $CuCl_2$ group (hereafter termed "1: 1 complexes"). Other well-known complexes with a normal magnetic moment belong to another category consisting of complexes which are formed between two aromatic *N*-oxide molecules and one $CuCl_2$ group ("2: 1 complexes").

Polybis(μ-(2-picoline *N*-oxide)-chlorocopper(II)di-μ-chloro)-diaquocopper, $Cu_3Cl_6(C_6H_7NO)_2 \cdot 2H_2O$, the

complex formed between 2-picoline *N*-oxide and copper(II) halide, is an exceptional compound ("2: 3 complex"). From the magnetic properties and the crystallographical analysis of this complex, it was confirmed by Watson and his co-workers[1,2] that the structure of this complex consists of infinite linear chains containing both five- and six-coordinated copper(II) ions bridged by either chlorine of oxygen atoms. The structure can be regarded as an alternating linear chain consisting of $Cu_2Cl_4(C_6H_7NO)_2$ units and $CuCl_2 \cdot 2H_2O$ units joined by long Cu–Cl bonds. Watson and his co-workers also proposed that the copper ions in the $Cu_2Cl_4(C_6H_7NO)_2$ unit interact antiferromagnetically through the bridging oxygens, while the copper ion in the $CuCl_2 \cdot 2H_2O$ unit does not interact with those of the $Cu_2Cl_4(C_6H_7NO)_2$ units through the bridging chlorine atoms. However, a central problem in this interpretation is whether or not the magnetic ions in the $CuCl_2 \cdot 2H_2O$ units really interact through the chlorine bridges.

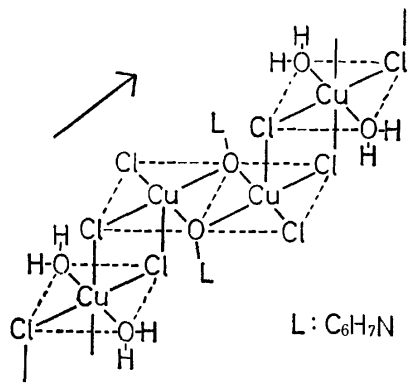

Fig. 1. Schematic crystal structure of $Cu_3Cl_6(C_6H_7NO)_2 \cdot 2H_2O$. The arrow shows the *c*-axis direction.

In the present study, the magnetic susceptibilities of this complex have been measured down to 1.6°K in order to obtain experimental data on the existence of the metal-metal magnetic interaction in this complex. The ESR spectrum of a single crystalline sample has also been observed at room temperature, and that of a powdered sample, at room temperature, 77°K and 4.2°K.

Experimental

$Cu_3Cl_6(C_6H_7NO)_2 \cdot 2H_2O$ (I) was prepared following the procedure of Watson and his co-workers. From the results of a chemical analysis, thermal analysis, infrared and far-infrared spectra measurements,[3] we confirmed the identity of the compound with reference to the preceding data. Found: C, 22.22; H, 2.74; N, 4.38%. Calcd: C, 22.0; H, 2.73; N, 4.27%. The single crystals were grown by the spontaneous evaporation of the solvent from the unsaturated solution. When dried for 50 hr at 100°C, this complex lost two water molecules to its dehydrate, $Cu_3Cl_6(C_6H_7NO)_2$ (II). Found: C, 23.19; H, 2.26; N, 4.56%. Calcd: C, 23.19; H, 2.27; N, 4.51%. The dehydrate (II) has not been reported in the literature, but the identity of this compound was confirmed by a chemical analysis of II and a thermal analysis of I. This complex was a little hygroscopic and reverted to the hydrate after several months. We found some differences in the X-ray powder patterns between I and II.

Results and Discussion

Magnetic susceptibilities were measured in the temperature range from 1.6°K to room temperature by means of a magnetic torsion balance described elsewhere.[4] Mn-Tutton salt was used to calibrate the carbon resistor and the thermocouple. The usual Pascal diamagnetic correction was within the range of experimental error at low temperatures. The X_m-T curves for the two complexes are compared in Fig. 2.

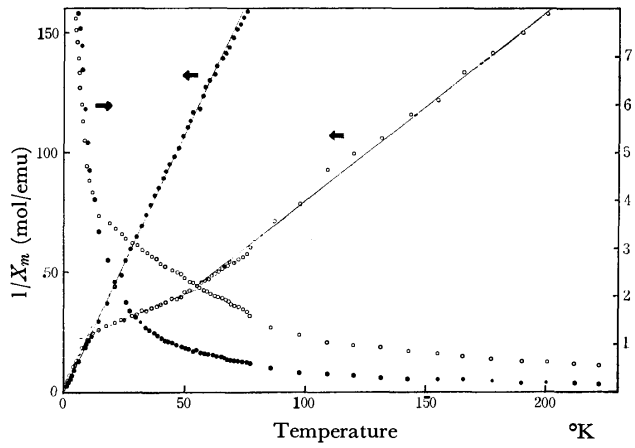

Fig. 2. Molar susceptibilities and their reciprocals as a function of temperature; ●: $Cu_3Cl_6(C_6H_7NO)_2 \cdot 2H_2O$, ○: $Cu_3Cl_6(C_6H_7NO)_2$.

Assuming that $X_m = xNg^2\beta^2 s(s+1)/3k(T-\theta)$, with $s=1/2$ and $g=2.15$, a parameter, x, obtained from the slope of the $1/X_m - T$ plots can offer information about the magnetic state of these complexes. Here the assumption about the *g*-value is consistent with the ESR data to be described later. The most remarkable features of the magnetic data of the compound (I) are that the data obey the Curie law, with $x=1.06$ from room temperature to 1.6°K, and that the molar magnetic susceptibilities can almost all be attributed to only one copper ion per molecule. On the other hand, the dehydrate (II) behaves very differently, as is shown in Fig. 2; this complex seems to be a magnetic trimer with mutual antiferromagnetic interaction.[5] It should be noted, in comparison with I, that the susceptibilities of the II have the values of three copper ions per molecule in the high-temperature range ($x=2.8_3$).

ESR measurements of the hydrate were carried out by using an X-band spectrometer. The hyperfine separation (429.4 Oe) and the *g*-value (2.000) of Mn(II) in MgO were used to calibrate the magnetic field, and DPPH was also used as the magnetic-field indicator. The ESR spectrum of the powdered sample at room

1) R. S. Sager and W. H. Watson, *Inorg. Chem.*, **7**, 2035 (1968).
2) M. R. Kidd, R. S. Sager, and M. H. Watson, *ibid.*, **6**, 946 (1967).
3) R. Whymann and W. E. Harfield, *ibid.*, **6**, 1859 (1967).
4) M. Mekata, *J. Phys. Soc. Japan*, **17**, 796 (1962).
5) K. Kambe, *ibid.*, **5**, 48 (1949); J. H. Van Vleck, "The Theory of Electric and Magnetic Susceptibilities," Oxford (1932).

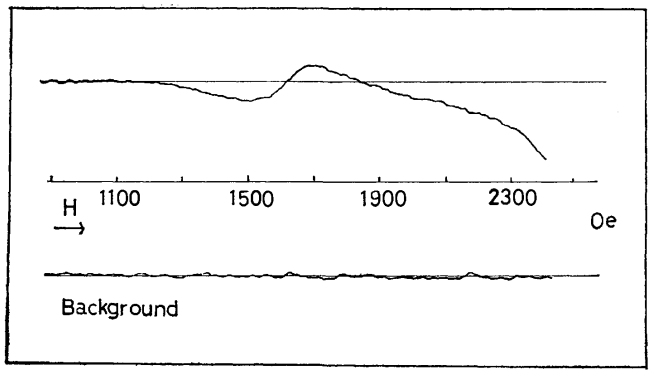

Fig. 3. Low field portion of the polycrystalline ESR spectrum of $Cu_3Cl_6(C_6H_7NO)_2 \cdot 2H_2O$ at room temperature.

temperature exhibited one broad, asymmetric line caused by the anisotropy of the g-value centered at about 3250 Oe, with one additional weak line at about 1600 Oe, as is shown in Fig. 3. The line-shape of the main absorption at 3250 Oe did not show any appreciable change, even at temperatures of liquid nitrogen and helium, implying that the magnetic environment of this complex changes little with the temperature.

Single-crystal studies were undertaken in this complex's three mutually perpendicular planes. The principal values of the g-tensor obtained from the single-crystal measurements are: $g_1=2.302\pm0.005$, $g_2=2.084$, and $g_3=2.032$. The experimental errors are mainly due to the uncertainty of the crystal mounting on the sample holder. The principal values of the g-tensor can be attributed to those of the copper ions, the site symmetry of which is rhombic or approximately orthorhombic and the orbital ground state of which is

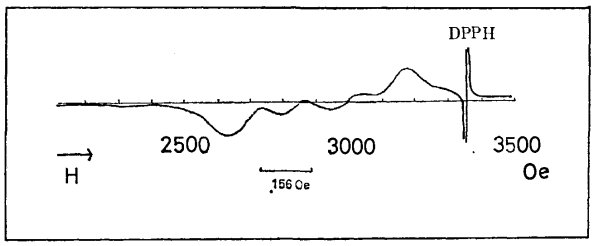

Fig. 4. ESR spectrum at a certain angle of $Cu_3Cl_6(C_6H_7NO)_2 2H_2O$ single crystal at room temperature.

$d_{x^2-y^2}$. This interpretation is supported by a crystallographic consideration of this complex.

The angular variation of the single crystalline ESR spectrum provides much interesting information about the electronic state of the paramagnetic copper(II) ion in this complex. At certain angles, for example, the sample gives an ESR spectrum with four hyperfine lines and a maximum separation between them are about 156 Oe, as is shown in Fig. 4. This splitting arises from copper ions with an electron spin of $s=1/2$ and a nuclear spin of $I=3/2$. The observation of the hyperfine splittings in the ESR spectrum of the single-crystal sample leads to the conclusion that this complex is similar to the magnetically diluted systems. This conclusion can be confirmed further from the results of the temperature variation of X_m with the values attributed to only one copper ion per molecule and with a Weiss constant nearly equal to zero. Other evidence of this consideration is that the dehydrate (II) shows the X_m values due to three copper ions per molecule in the high-temperature range. The absorption near 1600 Oe in the powder ESR spectrum is due to the $\Delta M=\pm2$ forbidden transition, which clearly indicates the existence of the dimer species in this complex, although its signal intensity is very weak. Therefore, it can be concluded that the copper ions of the $Cu_2Cl_4(C_6H_7NO)_2$ units are coupled together very strongly by antiferromagnetic exchange interaction and that they occupy almost entirely the diamagnetic singlet state below room temperature, while the copper ions of the $CuCl_2 \cdot 2H_2O$ units are isolated magnetically. Alternatively speaking, only the copper ions of the $CuCl_2 \cdot 2H_2O$ units diluted magnetically can account for the four hyperfine lines of the ESR spectrum and the molar susceptibilities due to one copper ion per molecule, while a few $Cu_2Cl_4(C_6H_7NO)_2$ units occupying the higher triplet state can give a half-field resonance. This conclusion is consistent with the invariability of the powder ESR line shapes in spite of the temperature variation.

The authors are much obliged to Professor H. Takaki for his continuous encouragement throughout this work and to Dr. M. Mekata for the susceptibility measurement and his helpful discussions.

Polarographic Studies on Substituted 2,2′-Bipyridyl *N*-Oxides[1]

S. S. KATIYAR,* M. LALITHAMBIKA, and R. P. SHUKLA
Department of Chemistry, Indian Institute of Technology, Kanpur-16, India
(Received February 19, 1971)

The polarographic behavior of 4-methoxy-2,2′-bipyridyl 1-oxide has been investigated in 20% dioxane-water solution. Two well defined reduction waves appear in the pH range 0.76—8.8, a third wave in pH 9.3—10.4, but only one wave in more alkaline solutions. The variation of $E_{1/2}$ with pH followed the relations $(E_{1/2})_1 = -0.37—0.10$ pH and $(E_{1/2})_2 = 0.84—0.065$ pH for waves 1 and 2, respectively. The diffusion current constant for the second wave decrease with increasing pH whereas for the first wave it remains constant upto pH 7.0 and decreases afterwards. Variation of diffusion current with temperature and reservoir height indicates the diffusion controlled nature. Wave 1 is produced by the 2 electron reduction of protonated *N*-oxide to 4-methoxy-2,2′-bipyridyl. This intermediate is further reduced, at more negative potentials, to 1,4′-dihydro-4-methoxy-2,2′-bipyridyl by consuming two more electrons and two hydrogen ions simultaneously. The third wave is presumably due to catalytic hydrogen evolution.

The polarographic behavior of pyridine *N*-oxides and purine *N*-oxides has been studied by several workers.[2-8] It has been found that these *N*-oxides give one or more reduction waves in buffered media. Pyridine *N*-oxide in various buffer solutions gives one wave[3,4,6] whose wave height decreases rapidly above pH 6, whereas adenine 1-*N*-oxide[2,7,9] gives a fundamental pattern of three polarographic waves over the pH range 1.4 to 5.6, the third wave being due to catalytic hydrogen evolution. It is also known that *N*-oxides such as nitrogen mustard *N*-oxide[10] and 2-azaadenine 1-*N*-oxide[7] are reduced polarographically to the corresponding amines. Alkaloid *N*-oxides such as narcotine *N*-oxide[3] have been reported to give three waves. It has been observed that the two-electron reduction waves of narcotine *N*-oxide are complicated by the adsorption at the electrode, the kinetic current of protonation and the reversible cleavage of lactone.

A detailed knowledge of the electrochemical behavior of *N*-oxides is of great interest in view of their biological importance, and the possible use of the electrolytic process of reduction for such *N*-oxides which give undesirable reduction products[11] when treated with conventional reductants like hydrogen and Raney nickel. Attempts have been made to correlate the herbicidal activity[12] of 2,2′- and 4,4′-bipyridyl salts to their redox potentials[13] as the herbicidal activity has been found to be dependent on the reversible reduction of the compound. Polarographic investigations on 2,2′-bipyridyl,[14,15] contain certain anomalies in that one report[14] states that it gives one wave while the other indicates that it gives three waves.[15] In view of the absence of polarographic data on substituted 2,2′-bipyridyl *N*-oxides and the existing anomalies in the data on 2,2′-bipyridyl it was considered desirable to investigate systematically the effect of concentration, pH, temperature and other factors on the polarographic reduction of substituted 2,2′-bipyridyl *N*-oxide.

Experimental

Apparatus. A sargent model XXI pen recording polarograph was used to record the current voltage curves. All the potentials were measured against saturated calomel reference electrode. An H-cell, one limb of which contained the calomel electrode and the other the test solution, served as the electrolytic cell. The capillary used had the following characteristics in 0.1M KCl in open circuit:
$m = 1.507$ mg sec^{-1}, $t = 3.38$ sec, $h = 75$ cm of mercury.
The cell was water jacketed and all measurements were made at 25±0.1°C with the help of an external thermostat.

pH measurements were carried out with an Elico pH meter. Ultraviolet spectra were recorded with a Beckman model DU spectrophotometer using 1 cm quartz cells.

Chemicals. The substituted 2,2′-bipyridyl 1-oxides were prepared by the methods given in literature.[16] They were recrystallized several times and checked for their purity by clemental analysis and melting point data. Dioxane used was always freshly distilled before use. All the chemicals used for preparation of buffers were of analytical grade. Buffer systems used in the present study were as follows: NaOAc+HCl (pH 0.65−1.24), KOOC–C_6H_4–COOK+HCl (pH 2.2−2.6), HOAc+NaOAc (pH 3.42−5.89), KH_2PO_4+NaOH (pH 6—8), KCl+H_3BO_3+NaOH (pH 8.5—10.0), Na_2HPO_4+NaOH (pH 11—13).
Nitrogen used for removal of oxygen from solutions was purified by passing through gas washing bottles containing

1) Presented at the Indian Science Congress held at Bangalore, India, Jan. 3—9, 1971.
* To whom all correspondence should be addressed.
2) CH. R. Warner and P. J. Elving, *Collect. Czech. Chem. Commun.*, **30**, 4210 (1965).
3) Y. Asahi, This Bulletin, **34**, 1185 (1961).
4) T. Kubota and H. Miyazaki, *ibid.*, **35**, 1549 (1962); **39**, 2057 (1966).
5) E. Ochiai, *Nippon Yakugaku Zasshi*, **69**, 1 (1949).
6) A. Foffani and F. Fornasari, *Gazz. Chim. Ital.*, **83**, 1051 (1953); **83**, 1059 (1953).
7) F. A. McGinn and G. B. Brown, *J. Amer. Chem. Soc.*, **82**, 3193 (1960).
8) G. Horn, *Monatsber. Deut. Akad. Wiss. Berlin*, **3**, 380 (1961).
9) D. L. Smith and P. J. Elving, *J. Amer. Chem. Soc.*, **84**, 1412 (1962).
10) I. Aiko, *Pharm. Bull.*, **1**, 335 (1953).
11) M. A. Stevens, H. W. Smith, and G. B. Brown, *J. Amer. Chem. Soc.*, **82**, 3189 (1960).
12) R. C. Brain, R. F. Homer, J. Stubbs, and R. L. Jones, *Nature*, **181**, 446 (1958).
13) R. F. Honer, G. C. Mees, and T. E. Tomlinson, *J. Sci. Food Agr.*, **11**, 309 (1960).
14) P. Silvestroni, *Ricerca Sci.*, **24**, 1695 (1954).
15) A. B. Zahlam and R. H. Linnell, *J. Amer. Chem. Soc.*, **77**, 6207 (1955).
16) R. A. Jones, B. D. Roney, W. H. F. Sasse, and K. O. Wade, *J. Chem. Soc., B*, **1967**, 106.

solutions of sodium salt of anthraquinone-2-sulphonic acid and $NaHSO_3$, alkaline pyrogallol, chromous sulphate in about 1N sulfuric acid, NaOH and distilled water in series.

Procedure. Stock solutions of *N*-oxides were prepared in pure dioxane. They were diluted with necessary amounts of water and buffer solutions so that the final volume of 10 m*l* of the test solution contained the desired concentration of *N*-oxide, 20% dioxane and 50% buffer. The final solution was thermostated till it attained a temperature of 25°C and during this time purified nitrogen was bubbled to remove the oxygen. The dropping mercury electrode was then introduced and the polarogram was recorded.

Results and Discussion

4-Methoxy-2,2'-bipyridyl 1-Oxide. 8.11×10^{-5}M solution of 4-methoxy-2,2'-bipyridyl 1-oxide was polarographed in 20% dioxane in various buffers over the pH range 0.85—13.0. A few typical polarograms in different buffers are shown in Fig. 1 and the other data are summarized in Table 1. From pH 0.76—8.8 two well defined and well separated waves were observed. At pH 9.3, 9.5, and 10.4 a third wave appeared which was clearly distinguishable from the second wave. However, in highly alkaline solutions (0.1N NaOH) only one wave was observed. The behavior of diffusion currents and half wave potentials with pH is shown in Figs. 2 and 3. It is of interest to note from Fig. 2 that $E_{1/2}$ becomes more and more negative with increase in pH of the solution. This indicates the participation of hydrogen ions in the electrode reaction. A similar variation of half wave potentials with

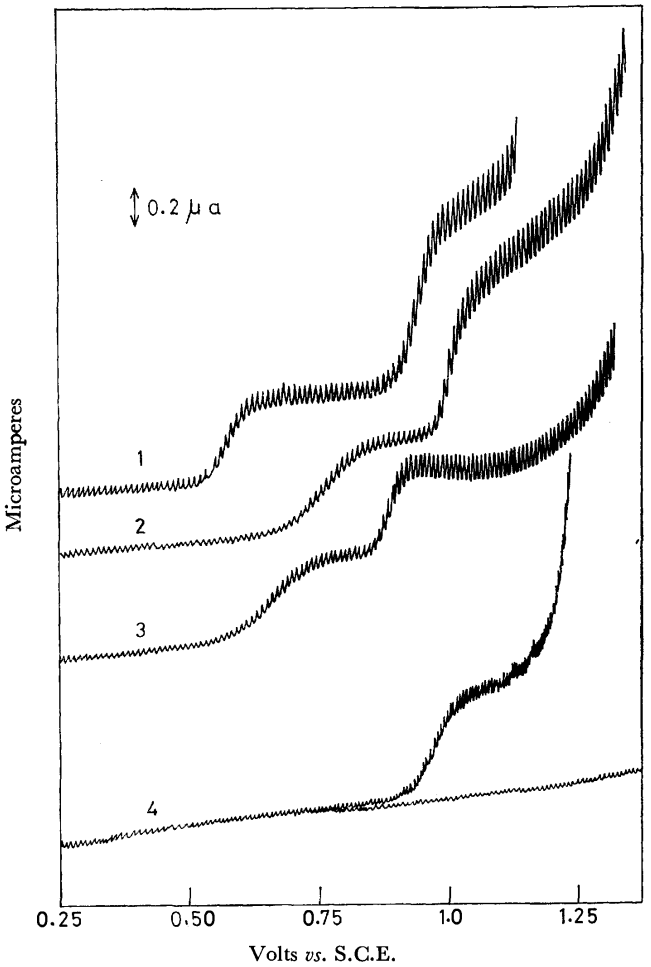

Fig. 1. Polarograms of 4-methoxy-2,2-bipyridyl-1-oxide in various buffers. Curves 1, 2, 3, and 4 are at pH 2.45, 7.55, 8.80, and 0.1N NaOH, respectively. The scale for curves 3 and 4 has been shifted by 0.5 and 0.65 V, respectively, on the abscissa.

TABLE 1. POLAROGRAPHIC CHARACTERISTIC OF 4-METHOXY-2,2'-BIPYRIDYL 1-OXIDE IN VARIOUS BUFFERS AT 25°C
Concentration of *N*-oxide $= 8.11 \times 10^{-5}$ M

pH	Wave 1			Wave 2		
	$(-E_{1/2})_1$ V *vs.* SCE	i_{d_1} μA	I_1	$(-E_{1/2})_2$ V *vs.* SCE	i_{d_2} μA	I_2
0.76	0.58	0.50	3.79	0.95	0.92	7.18
1.14	0.62	0.52	3.90	0.96	0.88	7.14
2.21	0.64	0.50	3.61	1.00	0.70	5.06
3.46	0.72	0.50	3.69	1.06	0.82	6.07
5.65	0.94	0.48	3.73	1.17	0.80	6.07
7.00	1.07	0.50	3.68	1.24	0.72	5.30
9.50	1.18	0.22	1.60	1.42	0.18	1.31
9.70	1.23	0.04	0.29	1.42	0.20	1.47

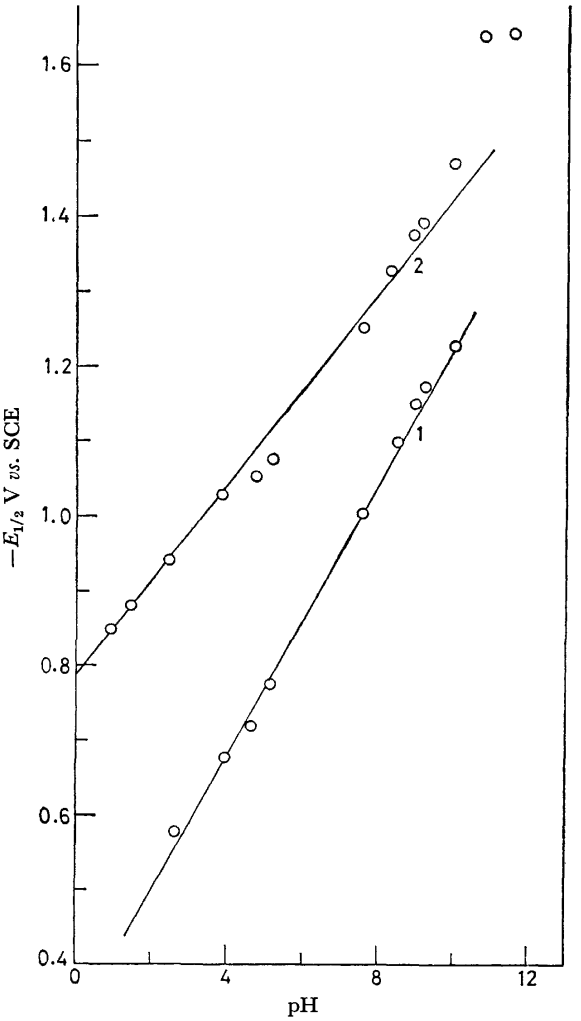

Fig. 2. Variation of half wave potentials of *N*-oxide with pH. 1. First wave; 2. Second wave.

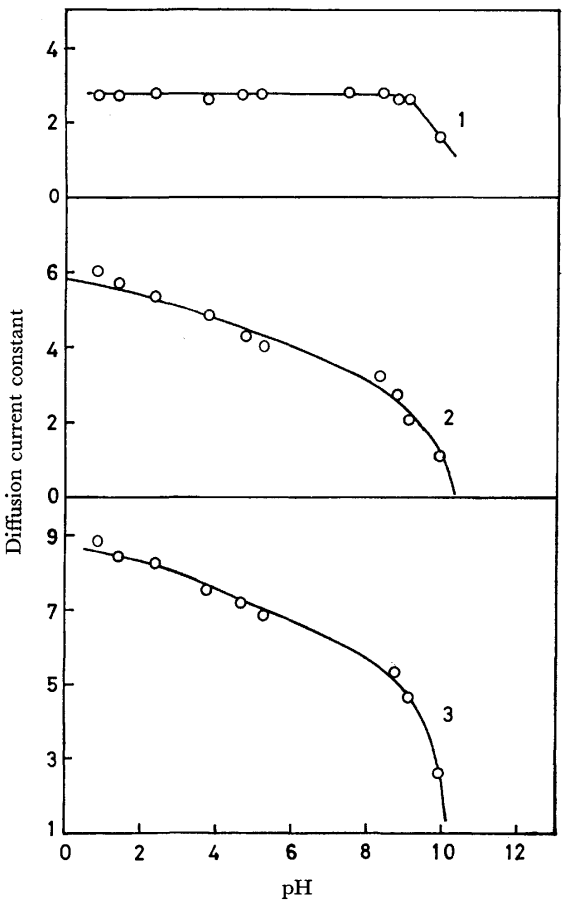

Fig. 3. Variation of diffusion current constant of *N*-oxide with pH. 1. First wave; 2. Second wave; 3. First and second waves.

pH has been reported[15] in the case of other heterocycles, *viz.* 4,4'-, 2,4'-, and 2,2'-bipyridyls, 4-cyanopyridine,[17] alloxan, alloxantin and dialuric acid.[18] The variation of $E_{1/2}$ of both the waves of 4-methoxy-2,2'-bipyridyl-1-oxide with pH is linear almost over the whole pH range investigated. The data for both the waves could be fitted to the following relationships:

$$E_{1/2} = -0.37 - 0.10\,\mathrm{pH}\ \text{(for wave 1)}$$

$$E_{1/2} = -0.84 - 0.065\,\mathrm{pH}\ \text{(for wave 2).}$$

However, for the second wave the half wave potentials appear to become more negative than required by the above relationship beyond pH 9.3. This is presumably due to the third wave which appears at pH 9.3 and almost merges with the second wave at higher pH thus making the accurate calculation of half wave potentials difficult. It can be clearly seen from Fig. 3 that the height of the first wave remains constant up to pH 7 and starts decreasing beyond it. However, the second wave shows a slight decrease in the diffusion current with increasing pH from pH 0.76—5.65 and a larger decrease after pH 7.0. The decrease in wave height with increasing pH has also been reported for pyridine *N*-oxide, 4-methylpyridine *N*-oxide.[4] It is not due to any structural change in 4-methoxy-2,2'-bipyridyl 1-oxide in acid or alkali as indicated by UV spectra of the *N*-oxide in neutral, acid and alkaline media. The spectra of *N*-oxide at various pH are shown in Fig. 4.

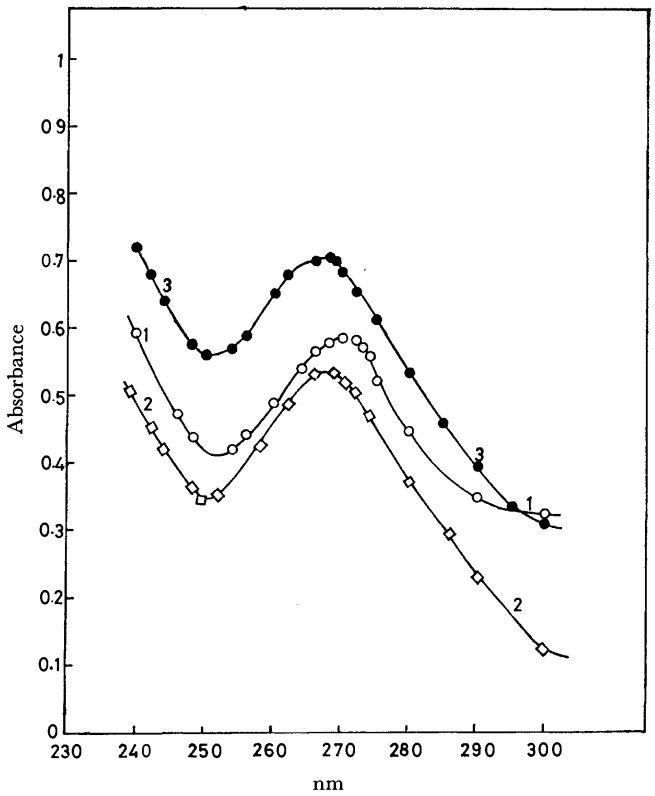

Fig. 4. UV spectra of *N*-oxide at different pH. Conc 3.901×10^{-5}M 1. 0.1N HCl; 2. 0.1N NaOH; 3. pH 7.

Table 2. Polarographic characteristics of 4-methoxy-2,2'-bipyridyl-1-oxide in neutral electrolytes
Temperature 25°±0.1°C

Electrolyte	Concentration $\times10^5$	$(-E_{1/2})_1$	$(-E_{1/2})_2$	$(-E_{1/2})_3$	$(i_d)_1$	$(i_d)_2$	$(i_d)_3$
		V *vs.* SCE			μA		
0.1M KCl	4.38	1.17	1.41	1.62	0.06	0.04	0.20
	6.57	1.17	1.40	1.60	0.14	0.05	0.22
	8.76	1.20	1.43	1.60	0.24	0.06	0.30
0.1M LiCl	4.38	1.18	1.43	1.62	0.22	0.10	0.08
	6.57	1.17	1.42	1.63	0.28	0.16	0.10
	8.76	1.17	1.43	1.61	0.38	0.10	0.12

17) J. Volke and J. Holubek, *Coll. Czech. Chem. Commun.*, **28**, 1597 (1963).

18) W. A. Struck and P. J. Elving, *J. Amer. Chem. Soc.*, **86**, 1229 (1964).

It is clear from this figure that absorption maximum is at 266 nm in 0.1N NaOH and pH 7.0. Wave 1, for reasons subsequently discussed could be assigned to the reduction of protonated *N*-oxide functional group. It is, therefore, expected that in a medium deficient in protons, wave height should decrease and this is what we observed in buffers of increasing pH. This is further substantiated by the polarographic behavior of *N*-oxide in unbuffered media *viz.* neutral supporting electrolytes. The data is presented in Table 2. It can be seen that *N*-oxide gives three waves in KCl, LiCl, and $N(CH_3)_4Cl$. The first two waves appear at a more negative potential than those found in buffered medium of pH 7.0, while the third wave appears at almost the same potential at which the third wave is found in buffered media of pH greater than 9.3. Thus for example $(E_{1/2})_1$, $(E_{1/2})_2$, and $(E_{1/2})_3$ in 0.1M KCl corresponded to −1.17, −1.41, and −1.62 V *vs.* SCE whereas in buffer of pH 7.0 $(E_{1/2})_1$ and $(E_{1/2})_2$ corresponded to −1.07 and −1.24 V *vs.* SCE respectively. More negative half wave potentials in unbuffered solution further substantiate the observation that hydrogen ions are involved in the electrode process. It is instructive to find that the limiting currents for all the three waves in unbuffered media are very small compared to the values for the respective waves in buffer of pH 7.0. Even the total limiting current due to all the three waves in unbuffered media is substantially smaller than the total diffusion current of the two waves observed in buffer of pH 7.0. This observation strongly suggests that it is the protonated *N*-oxide which gets electroreduced, and in unbuffered media due to the paucity of hydrogen ions only a small fraction of *N*-oxide is electroreduced giving very low limiting currents.

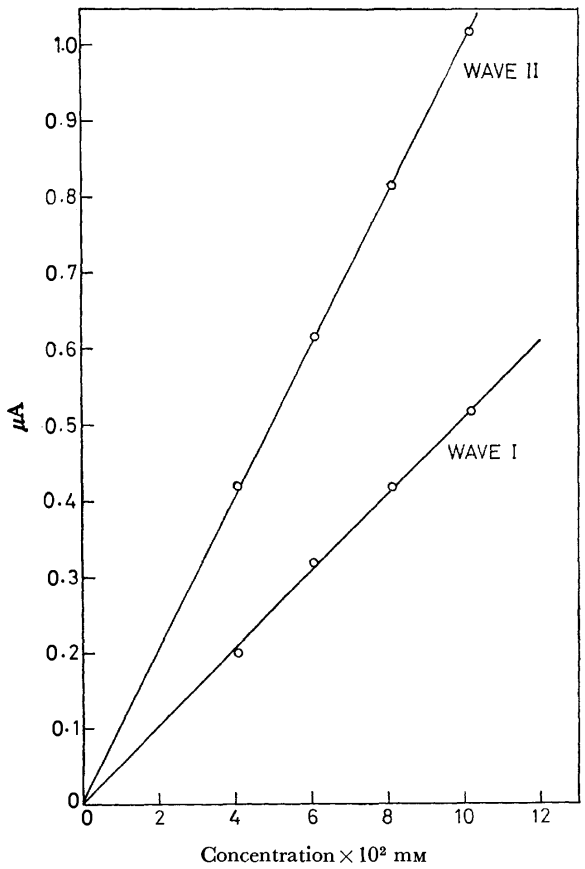

Fig. 5. Linear dependence of diffusion current of *N*-oxide on concentration at pH 0.85.

The characterization of the nature of the electrode process has been done by studying the effect of concentration of *N*-oxide, height of mercury reservior and temperature on the limiting current. The polarograms obtained at varying concentrations of 4-methoxy-2,2'-bipyridyl 1-oxide in the range $4.05-10.13\times10^{-5}$M at pH 0.85 were well difined and well separated. Plot of i_d against concentration gave a straight line as shown in Fig. 5. This indicates the absence of adsorption or catalytic character in both the waves and suggests that both waves are diffusion controlled. Heterocyclic compounds, especially those containing nitrogen, are known to exhibit pronounced adsorption effects at the mercury drop. Even adenine 1-*N*-oxide[2] and Narcotine *N*-oxide are reported to give adsorption waves. In our data we found no evidence for any adsorption wave in the reduction of 4-methoxy 2,2'-bipyridyl-1-oxide at the dme. However, the third wave which appears beyond pH 9.3 does not follow Ilkovic equation and is probably a catalytic wave.

A study of the effect of varying heights of the mercury

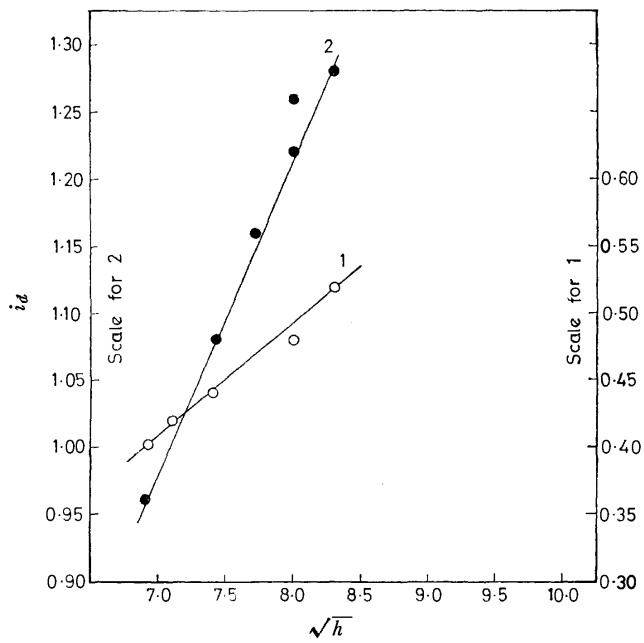

Fig. 6. Effect of mercury height on the diffusion current on *N*-oxide.

TABLE 3. EFFECT OF TEMPERATURE ON THE WAVE HEIGHTS pH=3.3

T °K	i_{d_1}	i_{d_2}	Temperature coefficient	
			Wave 1	Wave 2
303.5	0.40	0.78	—	—
308.5	0.50	0.98	4.6	4.7
312.5	0.58	1.12	3.0	3.6
316.5	0.64	1.20	2.3	1.7
322.5	0.76	1.32	2.9	1.6

column on the diffusion currents as well as the determination of the temperature coefficient of both the waves indicates their diffusion controlled nature. The limiting currents are proportional to the square root of the mercury height as shown in Fig. 6, whereas the temperature coefficients are in the range 1.6—4.6% as summarized in Table 3. The diffusion controlled nature of the waves due to *N*-oxide function has also been reported for adenine 1-*N*-oxide by Elving.[2]

Mechanism of the Electrode Process. The observed polarographic behavior of 4-methoxy-2,2′-bipyridyl 1-oxide can be explained by the following reduction sequence:

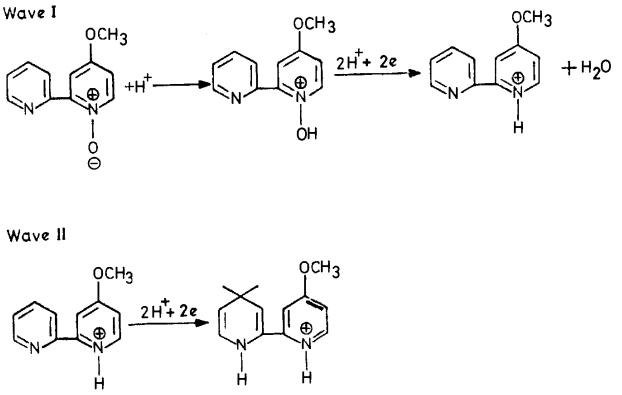

Wave I is produced by the 2 electron reduction of protonated *N*-oxide to 4-methoxy-2,2′-bipyridyl. The *N*-oxide after reaching the electrode picks up two electrons and two protons simultaneously to form 4-methoxy-2,2′-bipyridyl, giving rise to the first two electron wave. 4-Methoxy-2,2′-bipyridyl thus formed as the intermediate is further reduced at more negative potentials to 1′,4′-dihydro-4-methoxy-2,2′-bipyridyl by consuming two more electrons and two hydrogen ions simultaneously, giving rise to the second two electron wave. The latter wave in addition to 4-methoxy-2,2′-bipyridyl reduction may have some contribution from a catalytic hydrogen reduction process. The evidence supporting the above mechanism is discussed below.

The value of diffusion current constant (I) is 3.7 for the first wave and is constant up to pH 7.0; its value is comparable with I value of 3.3 obtained for other *N*-oxide function by Warner and Elving.[2] The I value is also compatible with a two electron reduction process. In a macroscale electrolysis at the potential of the plateau of the first wave, 4-methoxy-2,2′-bipyridyl was detected in the solution.

The second wave is identical in behavior with that of the first wave of 2,2′-bipyridyl. The polarographic data for 2,2′-bipyridyl are summarized in Table 4. It is found that 2,2′-bipyridyl gives a single wave upto pH 3.4 and two waves in the pH range 3.6—10.5, the second wave becoming more and more drawn out in solutions of higher pH. The half wave potentials for the wave 1 of 2,2′-bipyridyl vary linearly with pH as shown in Fig. 7 and fit the relation

$$E_{1/2} = -0.81 - 0.066\,\mathrm{pH}$$

which is similar to that obtained for the second wave of *N*-oxide *viz.* $E_{1/2} = -0.84 - 0.065$ pH. Slightly more negative values obtained for $E_{1/2}$ of wave II of 4-methoxy-2,2′-bipyridyl-1-oxide are due to the presence of *p*-methoxy group in 2,2′-bipyridyl which has a σ value of -0.27.[19] The diffusion current constant for the second wave of *N*-oxide is ~7 (Table 1) which is comparable to the I value (~7) for the first wave of 2,2′-bipyridyl (Table 4). The value of diffusion current constant obtained by Pfeifer[20] for the 2-electron reduction first wave of 2,2′-bipyridyl in the pH range 3.46—7.0 has been reported to be 5.6. This is also in excellent agreement with the I values we obtained in a similar pH range as shown in Table 4. It is thus proved that the electrode reaction producing the second wave is due to the reduction of 4-methoxy-2,2′-bipyridyl.

Table 4. Influence of pH of the medium on the reduction of 2,2′-bipyridyl

Concentration of 2,2′-bipyridyl = 5.7×10^{-5} M

pH	Wave 1			Wave 2	
	$(-E_{1/2})_1$ V *vs.* SCE	i_{d_1} μA	I_1	$(-E_{1/2})_2$ [a] V *vs.* SCE	i_{d_2} [a] μA
0.76	0.88	0.68	7.33	no wave	no wave
1.14	0.91	0.70	7.49	no wave	no wave
2.21	0.95	0.68	6.98	no wave	no wave
3.46	1.01	0.54	5.68	1.20	0.7
5.65	1.17	0.52	5.61	1.34	0.7
7.00	1.25	0.59	5.40	1.41	0.7
10.30	1.45	0.20	2.09	1.79	0.7

a) The half wave potentials and diffusion currents are not accurate since the waves are drawn out.

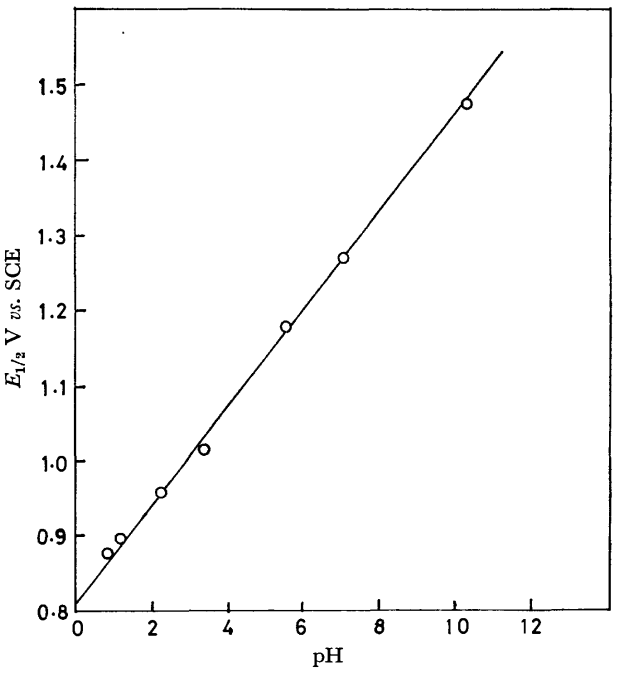

Fig. 7. Variation of $E_{1/2}$ of 2,2′-bipyridyl with pH.

The authors are grateful to Prof. S. Ranganathan and Dr. B. B. Singh of Chemistry Department, Indian Institute of Technology, Kanpur, for help during the course of this work.

19) H. H. Jaffé, *Chem. Rev.*, **53**, 191 (1953).
20) G. Pfeifer, *Veszpremi Vegyipari Egyetim Kozlemenyi*, **3**, 179 (1959).

Structure of the Vanadium-Potassium Catalyst during the Oxidation of Sulfur Dioxide and the Oxidation Mechanism

Akio KATO, Katsuhiko TOMODA, Isao MOCHIDA, and Tetsuro SEIYAMA
Department of Applied Chemistry, Faculty of Engineering, Kyushu University, Fukuoka

(Received July 3, 1971)

The structure of vanadium-potassium catalyst in gas mixtures of various compositions of SO_2, SO_3, and O_2 was investigated at 500, 550, and 600°C to elucidate the mechanism of SO_2 oxidation on the catalyst. It was found that in the catalyst 50—70% of V(IV) is in VO^{2+}-form, 10—15% of V(V) in VO_2^+-form and the rest of the vanadium forms large vanadium-oxygen networks. It was also found that both the reduction of V(V) with SO_2 and oxidation of V(IV) with oxygen are in equilibrium and the desorption of SO_3 from the molten catalyst into gas phase seems to be the rate-determining step in SO_2 oxidation. On the basis of this mechanism, the reaction rate of SO_2 oxidation can be formulated as follows,

$$dSO_3/dt = k'(SO_3) = kP_{SO_2} \cdot P_{O_2}^{1/2}.$$

For the sake of confirmation, the kinetics of SO_2 oxidation (below 10% conversion) over vanadium-potassium catalyst was measured by a flow method at 500, 550, and 600°C over gas compositions of SO_2=5~24% and O_2=10~36%. It was found that the rate expression was correct.

It is generally accepted for sulfur dioxide oxidation by vanadium-potassium catalyst that the active component of the catalyst forms a liquid phase under the reaction conditions[1-8], and that the reaction proceeds according to the reduction-oxidation mechanism.[8,9] However, the composition of the active component is not well established and various contradictory rate-determining steps are proposed for the oxidation. Tandy has suggested the reduction of pentavalent vanadium by sulfur dioxide to be the rate-determining step.[4] On the other hand, Mars *et al.* have proposed the following reduction-oxidation mechanism in which (1) is in equilibirum and (2) is rate-determining.[8]

$$2V^{5+} + SO_2 + O^{2-} = 2V^{4+} + SO_3 \quad (1)$$

$$2V^{4+} + 1/2O_2 = 2V^{5+} + O^{2-} \quad (2)$$

Simecek *et al.* have recently reported a similar mechanism.[9]

We noted that the reduction and oxidation of vanadium in molten salts are closely related to the basicity (activity of oxide ions) of the melts[7,10]. A quantitative estimation of the basicity of the catalyst is, therefore, necessary to elucidate the reaction mechanism of sulfur dioxide oxidation, although Mars and Simecek treated the reduction and oxidation of vanadium assuming a constant activity of oxide ions. The basicity can be estimated by means of the equilibrium relations for pyrosulfate formation:

$$O^{2-} + S_2O_7^{2-} = 2SO_4^{2-} \quad (3)$$

$$\text{or} \quad 2SO_3 + O^{2-} = S_2O_7^{2-} \quad (4)$$

We investigated the structure of potassium-vanadium catalyst under a SO_2-SO_3-O_2 mixture of various compositions, with the emphasis on the determination of the amount of pyrosulfate whose quantitative analyses have never been done. The reaction mechanism of sulfur dioxide oxidation was discussed from the viewpoint based on structural and kinetic investigations.

Experimental

Composition of Catalyst under SO_2-SO_3-O_2 Mixtures. About 0.5 g of V_2O_5–K_2SO_4 mixture was heated in a platinum boat (10×10×30 mm) in the fiowing atmosphere of SO_2(2—16%)–SO_3(3—14%)–O_2(5—40%)–N_2. The boat was placed in a 20-mm diameter quartz glass tube heated with an electric furnace. The temperature was controlled to within ±1°C. The gas mixtures were prepared from SO_2–O_2–N_2 mixture by oxidizing SO_2 partially with an industrial catalyst placed immediately before the catalyst sample. The composition of gas phase was determined by measuring SO_2 contents of the entering and outgoing gas mixtures by an iodimetric method with 0.2N iodine and 0.1N sodium thiosulfate solutions. Heating of catalyst sample in a given gas mixture was continued for 15 hr at 500, 550, and 600°C. The composition of catalyst samples was confirmed to be of steady state value after 8 hr. After the treatment of catalyst sample followed by rapid cooling, the weight change and chemical composition of the sample were determined and measurements of IR spectrum and X-ray powder pattern were carried out.

The concentrations of V(IV) and V(V) in the catalyst sample were determined by titration with ferrous sulfate solution using diphenylamine as an indicator. After dissolving the sample into 0.5N sulfuric acid, V(V) was titrated with 0.1N ferrous sulfate solution with one portion and total vanadium was titrated after oxidizing all vanadium to V(V) with potassium permanganate solution with the other portion. The amount of V(IV) was computed from the two values.

The concentration of pyrosulfate was determined as follows. About 200 mg of the catalyst sample ground was allowed to suspend in 60 ml of water on a water bath for an hour. By this procedure all the sulfate and pyrosulfate dissolved into water, together with some fractions of V(IV) and V(V). Since pyrosulfate hydrolyses to give HSO_4^- ions on dissolu-

1) R. Kiyoura, *Nippon Kagaku Zasshi*, **61**, 72 (1940), *Ryusan*, **2**, 223 (1949).
2) J. H. Frazer and W. J. Kirkpatrick, *J. Amer. Chem. Soc.*, **62**, 1659 (1940).
3) H. F. Topsoe and A. Nielsen, *Trans. Danish Acad. Tech. Sci.*, No. 1, 3 (1948).
4) G. H. Tandy, *J. Appl. Chem.*, (London), **6**, 68 (1956).
5) G. Okamoto, H. Kobayashi, and Y. Kayahara, *Kogyo Kagaku Zasshi*, **63**, 924 (1963).
6) T. Seiyama, A. Kato, T. Harada, and T. Ishida, *Shokubai*, **5**, 221 (1963).
7) T. Sakamoto, T. Ishida, A. Kato, and T. Seiyama, *ibid.*, **7**, 338 (1965).
8) P. Mars and J. G. H. Maessen, *J. Catal.*, **10**, 1 (1968).
9) A. Simecek, B. Kadlec, and J. Michalek, *ibid.*, **14**, 287 (1969).
10) M. Nagano, I. Mochida, A. Kato, and T. Seiyama, *Yogyo Kyokai Shi*, **78**, 401 (1970).

tion, the amount of the former contained in the sample can be determined from that of acid formed. After filtration of the solution, a portion of the filtrate was titrated with 0.05N sodium hydroxide solution using phenolphthalein as an indicator. During the course of titration, V(IV) and V(V) ions undergo the following acid-base reactions or oxidation.[11]

$$VO_2^+ + 2H_2O = H_2VO_4^- + 2H^+ \quad (5)$$

$$2VO^{2+} + 3H_2O = HV_2O_5^- + 5H^+ \quad (6)$$

$$HV_2O_5^- + 1/2O_2 + 2H_2O = 2H_2VO_4^- + H^+ \quad (7)$$

In the indicator range of phenolphthalein, $H_2VO_4^-$ and $HV_2O_5^-$ ions are predominant species for V(V) and V(IV), respectively.[11] The amount of acid produced by reactions (5)—(7) during the neutralization can, therefore, be computed from the concentrations of V(IV) and V(V) before and after the titration with the sodium hydroxide solution. The amount of acid was corrected in the calculation of the amount of pyrosulfate from the consumption of the alkali. Most of V(IV) was oxidized to V(V) during titration.

The amount of SO_3 absorbed was calculated from the weight increase of catalyst sample after making a minor correction for the weight decrease due to the reduction of V(V) to V(IV). Sulfate is given as the difference between the total sulfur, the sum of initial potassium sulfate and SO_3 absorbed, and sulfur in pyrosulfate form.

IR spectra were measured by KBr method. Cu-K_α radiation was used for X-ray examination.

Oxidation Rate of Sulfur Dioxide. Catalysts used in the kinetic study were prepared by mixing the hydrochloric solution of V_2O_5 and K_2SO_4 with carborundum powder of 0.3—0.4 mm diameter and drying the mixture under stirring. The mole ratio K_2SO_4/V_2O_5 was 1(catalyst A) and 2(catalyst B). 42 mg of V_2O_5–K_2SO_4 mixture was supported on 1 g of the carborundum in both catalysts. The oxidation rate was measured by a flow method. Catalyst (0.2—0.3 g) was packed in 12 mm diameter quartz glass tube with quartz glass wool. Temperature was measured by a thermocouple inserted in the catalyst bed and controlled to within ±1°C. Analysis of gas phase was carried out by the iodimetric method.

Table 1. Composition of catalyst sample

K_2O/V_2O_5 and Temperature	Run	Composition of gas phase (%) (balance: N_2)			Composition of catalyst (reference: 1 mol of V_2O_5)				
		SO_2	SO_3	O_2	$\frac{V(IV)\times 100}{V(IV)+V(V)}$	$S_2O_7^{2-}$	SO_4^{2-}	$V(V)_{aq}$ g. ion	$V(IV)_{aq}$
$K_2O/V_2O_5=1$ 500°C	1	3.5	4.7	30.2	32.8	1.08	0.38	0.22	0.43
	2	3.3	5.0	9.9	45.0	1.04	0.48	0.11	0.67
	3	3.4	8.1	30.0	34.6	1.12	0.37	0.30	0.43
	4	4.6	6.8	10.6	47.1	0.94	0.76	0.09	0.69
	5	12.6	4.8	29.8	54.3	0.99	0.61	0.06	0.82
	6	12.1	5.1	9.9	59.9	0.78	1.14	0.08	0.75
	7	12.1	8.0	30.0	55.5	0.94	0.72	0.08	0.73
$K_2O/V_2O_5=1$ 550°C	8	5.0	5.4	7.7	32.3	0.99	0.39	0.24	0.36
	9	11.9	8.9	6.0	40.8	1.13	0.33	0.12	0.53
	10	1.9	3.1	8.7	16.0	0.76	0.63	0.32	0.20
	11	4.4	5.9	5.2	33.4	1.09	0.17	0.13	0.32
	12	1.7	3.5	8.4	19.3	0.99	0.16	0.18	0.16
	13	8.2	13.9	39.8	31.9	1.11	0.31	0.20	0.36
	14	8.4	13.1	25.5	34.3	0.98	0.48	0.19	0.48
	15	10.7	10.4	15.9	38.6	0.85	0.74	0.17	0.61
	16	11.5	10.0	5.4	47.0	0.89	0.71	0.14	0.65
	17	2.2	3.3	9.9	21.8	0.93	0.26	0.17	0.25
	18	6.9	3.2	10.0	30.0	0.86	0.46	0.10	0.40
	19	15.4	5.6	7.9	44.2	0.92	0.57	0.12	0.52
$K_2O/V_2O_5=2$ 550°C	20	3.6	6.4	10.1	33.1	1.27	1.33	0.54	0.45
	21	3.5	6.5	29.2	25.8	1.62	0.55	0.26	0.30
	22	12.2	7.6	30.2	38.2	0.92	1.91	0.57	0.71
	23	12.6	7.4	10.2	44.6	1.44	1.08	0.09	0.62
	24	3.5	8.0	9.8	31.1	1.52	0.91	0.32	0.35
	25	3.2	7.9	29.7	22.5	1.42	0.95	0.49	0.26
	26	12.2	6.3	9.8	43.4	1.41	1.05	0.11	0.56
	27	12.2	6.3	30.0	41.2	1.50	0.85	0.11	0.51
$K_2O/V_2O_5=1$ 600°C	28	2.9	5.4	9.8	15.9	0.93	0.14	0.35	0.13
	29	2.7	5.6	29.9	13.7	0.99	0.02	0.29	0.09
	30	2.9	7.4	30.3	14.7	0.98	0.10	0.32	0.09
	31	12.1	5.9	29.0	22.6	1.02	0.01	0.14	0.19
	32	11.9	5.7	10.0	26.9	0.89	0.35	0.30	0.31
	33	12.1	8.0	10.0	26.3	1.01	0.18	0.12	0.29
	34	12.2	7.7	30.1	22.9	0.93	0.23	0.27	0.22

11) M. Pourbaix, "Atlas of Electrochemical Equilibrium in Aqueous Solution", Pergamon Press. (1966) p. 234.

Table 2. Melting of catalyst sample under SO_2–SO_3–O_2 atmosphere

Run	Temperature (°C)	K_2O/V_2O_5	Composition of gas phase (%) (balance: N_2) SO_2	SO_3	O_2	Melting[a)]
35	450	1	8.2	1.2	41.5	incomplete
36	450	1	2.2	3.6	43.2	incomplete
37	470	2	1.8	4.1	42.3	complete
38	470	2	2.4	3.3	19.8	complete
39	470	2	12.2	1.6	33.0	incomplete
40	470	2	5.9	8.4	33.9	incomplete
41	470	2	2.1	3.6	10.8	incomplete

a) complete: glassy and homogeneous appearance. incomplete: uneven surface, particles differing in colour from surroundings.

Results and Discussion

Composition and Structure of Catalys tunder SO_2-SO_3-O_2 Mixture. The compositions of gas phase and catalyst are shown in Table 1. $V(V)_{aq}$ and $V(IV)_{aq}$ are water-soluble pentavalent and quadrivalent vanadiums, respectively, extracted into water phase. The amount of SO_3 absorbed can be obtained from the relation, $(SO_3) = 2(S_2O_7^{2-}) + (SO_4^{2-}) - (K_2O/V_2O_5)$ (in mol).

Some remarks are given on the melting of catalyst. Experiments were carried out at 450 and 470°C under the conditions given in Table 2. In runs 35 and 36, only a part of the sample appeared to melt.

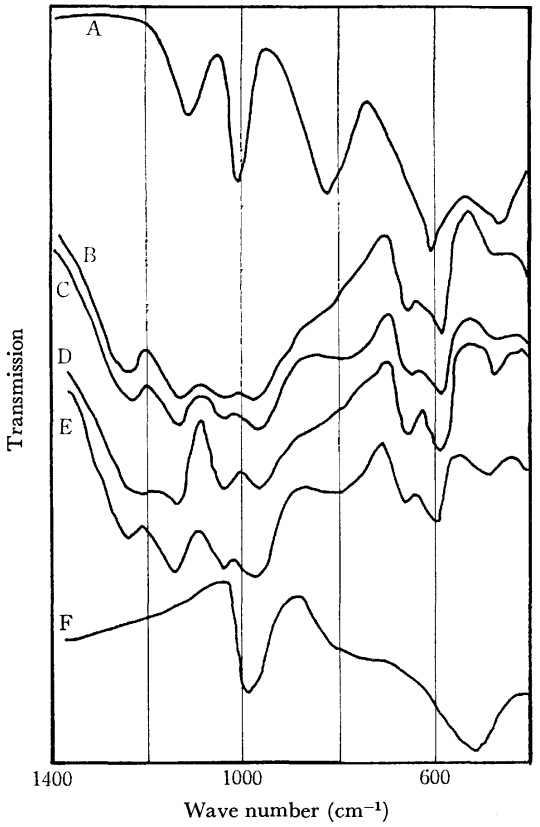

Fig. 1. IR spectra of catalyst samples.
A: Initial $2K_2SO_4$-V_2O_5 mixture, B: Run 7, C: Run 18, D: Run 24, E: Run 34, F: Water-insoluble residue in Run 32.

Even at 470°C, indication of incomplete melting was observed on samples treated under gas mixture of high SO_2/O_2 ratio as in runs 39—41. This casts a doubt on the homogeneity of the molten catalyst over 380—500°C at which the previous kinetic studies were carried out.[8,9] Above 500°C, all the samples had a glassy appearance and showed only a broad diffraction effect around $2\theta = 28°$ in X-ray examinations, indicating the complete melting of catalyst sample. The following discussions are restricted to the results on completely molten catalysts.

IR spectra of catalyst samples are shown in Fig. 1. As compared with the initial mixture of V_2O_5 and K_2SO_4 the sample treated under gas mixture showed complex spectra. IR spectra of the catalyst samples in other runs were very similar to the illustrated spectra of respective temperatures. Absorptions at 1050, 1150, and 1250 cm^{-1} in the spectra B to E can be assigned to ν_3 of SO_4^{2-} and SO_4-groups in $S_2O_7^{2-}$. There is a weak band near 800 cm^{-1}. The frequency coincides with that of asymmetric SOS stretching in $S_2O_7^{2-}$ [12], indicating the presence of pyrosulfate ions. Bands at 600—700 cm^{-1} are considered to be ν_4 vibration of SO_4-groups. Spectrum F of the insoluble residue of water-extraction has a band at 990 cm^{-1} which is assigned to the stretching vibration of double V–O bond.[13] The residue has a compsoition of $K_2O \cdot 1.2V_2O_4 \cdot 7.7 V_2O_5$ which is close to that of a vanadium bronze $K_2O \cdot V_2O_4 \cdot 8V_2O_5$ found in $V_2O_5 \cdot K_2SO_4$ system[6]. Spectrum F is also similar to that of the bronze. Water-insoluble residue in other runs showed very close spectra to F. Thus it seems that the insoluble vanadiums in the catalyst formed a network structure similar to those in vanadium bronzes.[14]

The oxygen atoms in the catalyst should be bound to either a vanadium or a sulfur atom. The compositions of the catalyst sample shown in Table 1 enable us to evaluate the limiting number of oxygen atoms bound to a vanadium atom. The lower limit is given when all sulfur atoms are assumed to be in the form of SO_4^{2-}. The calculated values for the limiting O/V ratio fall in the range 1.3—1.9. This means that each vanadium atom in the catalyst was bound with oxygen atoms on an average of more than 1.3—1.9 atoms. Although Mars *et al.* assumed V^{5+} or V^{4+} ions for vanadiums in vanadium-potassium catalysts under SO_2 oxidation, the present finding appears to be more reasonable considering high ratio of charge to radius of both ions.

The number of oxygen atoms bound a water-soluble vanadium atom is also of interest and can be estimated in a similar way. It was assumed that the ratio of oxygen atom to water-insoluble vanadium atom was 2.5 since the insoluble materials had a composition close to $K_2O \cdot V_2O_4 \cdot 8V_2O_5$, and that all sulfur atoms were in the form $S_2O_7^{2-}$. The second condition gives the upper limit of the ratio O/V_{aq} for water-soluble vanadiums. Caluculations revealed that the limiting O/V_{aq} ratio was in the range 1.3—1.7 for most catalyst samples with $K_2SO_4/V_2O_5 = 1$. Based on this value

12) A. Simon and H. Wagner, *Z. Anorg. Chem.*, **311**, 102 (1961).
13) J. Selbin, *Chem. Rev.*, **65**, 153 (1965).
14) H. G. Bachman and W. H. Barnes, *Z. Krist.*, **115**, 215 (1961).

for O/V_{aq} ratio and the analogy in the forms of vanadium atoms in acidic solution,[11] the water-soluble vanadiums in the catalyst are most likely to be present as VO^{2+} and VO_2^+ ions which will be coordinated with SO_3^{2-} or $S_2O_7^{2-}$ ions. Compounds consisting of K^+, SO_4^{2-}, and VO^{2+} or VO_2^+ ions such as $K_2SO_4 \cdot 2VOSO_4$, $K_2SO_4 \cdot VOSO_4$, and $K(VO_2)(SO_4)$ are highly water-soluble.[15] In the above pyrosulfate determination, the water-soluble vanadiums were thus assumed to be in VO^{2+} or VO_2^+-forms in the catalysts.[16]

From the above findings and compositions in Table 1, it might be concluded on the structure of vanadiums in vanadium-potassium catalysts under reaction conditions that 50 to 70% of V (IV) is in VO^{2+}-form, 10—15% of V(V) in VO_2^+-form and the rest of the vanadium forms large vanadium-oxygen networks.

Rate-determining Step in Sulfur Dioxide Oxidation. Sulfur dioxide oxidation proceeds by the reptition of the reduction of V(V) with sulfur dioxide and oxidation of V(IV) with oxygen. From the conclusions on the structures of vanadiums, the reduction and oxidation can be expressed as follows:

$$2(VO_2^+) + SO_2 = 2(VO^{2+}) + (SO_3) + (O^{2-}) \quad (8a)$$

$$(V(V)_nO_m) + SO_2 = (V(V)_{n-2}V(IV)_2O_{m-2}) + (SO_3) + (O^{2-}) \quad (8b)$$

$$2(VO^{2+}) + 1/2O_2 + (O^{2-}) = 2(VO_2^+) \quad (9a)$$

$$(V(V)_{n-2}V(IV)_2O_{m-2}) + 1/2O_2 + (O^{2-}) = (V(V)_nO_m) \quad (9b)$$

where, $V(V)_nO_m$ and $V(V)_{n-2}V(IV)_2O_{m-2}$ represent the V-O networks, and (8b) and (9b) show their reduction and oxidation, respectively. The desorption of sulfur trioxide formed in molten catalyst according to (8a) or (8b) completes sulfur dioxide oxidation.

$$(SO_3) = SO_3 \quad (10)$$

From the compositions of catalyst and gas phase given in Table 1, the rate-determining step in sulfur dioxide oxidation was examined as follows, where the reaction in molten phase

$$(SO_3) + (SO_4^{2-}) = (S_2O_7^{2-}) \quad (11)$$

$$[SO_3] = \frac{[S_2O_7^{2-}]}{K_{11}[SO_4^{2-}]} \quad (12)$$

was assumed to be in equilibrium and the equilibrium relation was used for the estimation of the concentration of (SO_3). We first examine whether reaction (10) is in equilibrium. If this is so, the ratio $[S_2O_7]/[SO_4^{2-}]$ should be proportional to P_{SO_3}. The observed value, however, was not in agreement with this expectation so that reaction (10) is considered to be not in equilibrium. When reaction (10) is rate-determining, reactions (8a) to (9b) are supposed to be in equilibrium. In this case, the following reaction should necessarily be in equilibrium.

$$SO_2 + 1/2O_2 = (SO_3) \quad (13)$$

The equilibrium conditions of reactions (12) and (13) lead to

$$\frac{[SO_4^{2-}]}{[S_2O_7^{2-}]} \cdot P_{SO_2}P_{O_2}^{1/2} = \frac{1}{K_{11} \cdot K_{13}} \quad (14)$$

When this relation is compared with the observed quantities, $1/K_{11} \cdot K_{13}$ shows no constant value. Flood *et al.*, however, have reported that the polarizing power of cations affects the stability of $S_2O_7^{2-}$ ions in molten state.[17] The inconstancy of $K_{11} \cdot K_{13}$ may be due to a similar effect of cations present. In the present study, correlations among observed quantities are found to be as shown in Fig.2 when $1/K_{11} \cdot K_{13}$ was assumed

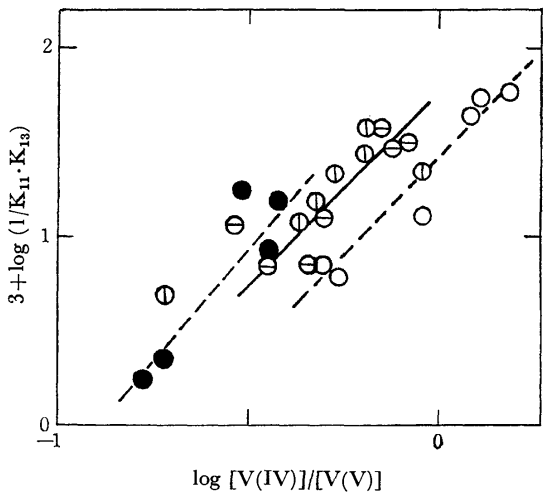

Fig. 2. Dependence of equilibrium constant $1/K_{11}K_{13}$ on the ratio V(IV)/V(V).
○: 500°C, $K_2O/V_2O_5=1$, ◑: 550°C, $K_2O/V_2O_5=1$,
⊖: 550°C, $K_2O/V_2O_5=2$, ●: 600°C, $K_2O/V_2O_5=1$.

to vary in proportion to the square of V(IV)/V(V). It should be noted that quantities observed on both catalyst samples with ratios $K_2SO_4/V_2O_5=1$ and 2 could be correlated by a common line. The dependence of $1/K_{11} \cdot K_{13}$ values on the ratio [V(IV)]/[V(V)] means the decrease in the stability of $S_2O_7^{2-}$ ions with increasing the ratio. This is presumably due to the polarizing effect of VO^{2+} ions on $S_2O_7^{2-}$ ions. The linear relations in Fig. 2 may be considered to support the view that reaction (13) is in equilibrium, although the ratio [V(IV)]/[V(V)] is introduced as a parameter. The effect of the ratio [V(IV)]/[V(V)] was also taken into account in the examination of equilibrium of reaction (10), but no reasonable correlation could be found between the ratio $[S_2O_7^{2-}]/[SO_4^{2-}]$ and P_{SO_3}.

When (SO_3) in the molten catalyst is formed by reactions (8a) to (9b), establishment of equilibrium of reaction (13) means that both reduction and oxidation of vanadiums are in equilibrium as described above. Accordingly, reaction (10) might be considered to be the rate-determining step for sulfur dioxide oxidation with respect to the catalyst at 500—600°C. In this

15) J. W. Mellor, "A Comprehensive treatise on Inorganic and Theoretical Chemistry". Vol. IX, Longmans, London. (1960) p. 818.

16) Although the upper-limit value of V/O_{aq} for catalyst samples with $K_2SO_4/V_2O_5=2$ was in the range 1.9—2.3, VO^{2+} or VO_2^+-forms were assumed in the pyrosulfate determination. A somewhat higher value for the ratio will be due to the relatively higher concentration of sulfate, all of which was assumed to be $S_2O_7^{2-}$ in the calculation.

17) H. Flood and T. Forland, *Acta Chem. Scand.*, **1**, 781 (1947).

this case, the following expression may be expected for the oxidation.

$$dSO_3/dt = k'[SO_3] = kP_{SO_2} \cdot P_{O_2}^{1/2} \quad (15)$$

Oxidation Rate of Sulfur Dioxide as a Function of P_{SO_2} and P_{O_2}. In order to examine the proceeding conclusion on the reaction mechanism, the rate of SO_2 oxidation was measured at 500, 550, and 600°C on vanadium-potassium catalysts. Conversion of SO_2 is shown as a function of contact time in Fig. 3, where

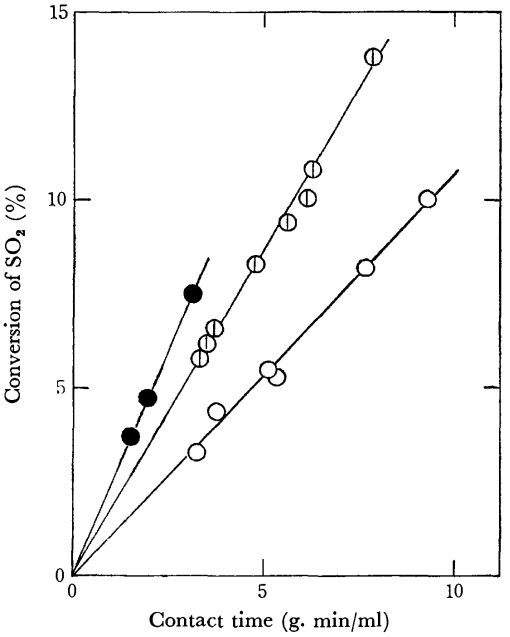

Fig. 3. Conversion of SO_2 as a function of contact time. Catalyst A. Initial gas composition: 10% SO_2, 10% O_2, 80% N_2. ○: 500°C, ◐: 550°C, ●: 600°C.

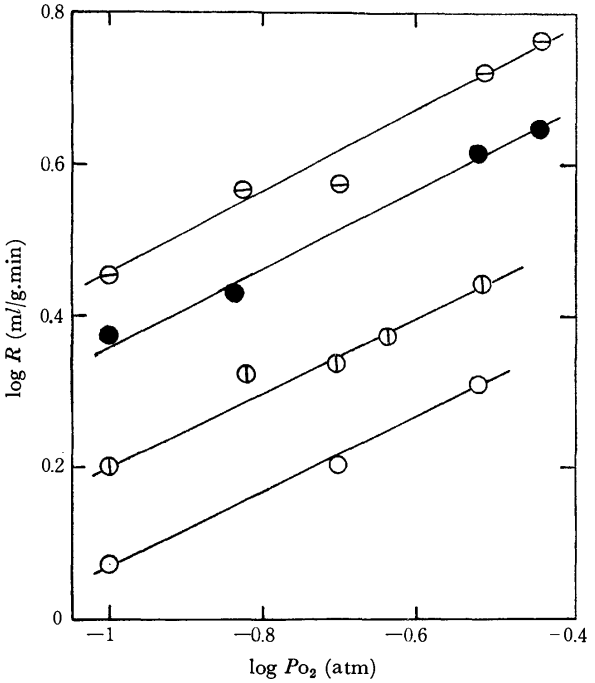

Fig. 4. Influence of the partial pressure of oxygen on the oxidation rate (P_{SO_2}=0.1 atm).
○: 500°C, catalyst A, ◐: 550°C, catalyst A, ●: 600°C, catalyst A, ⊖: 600°C, catalyst B.

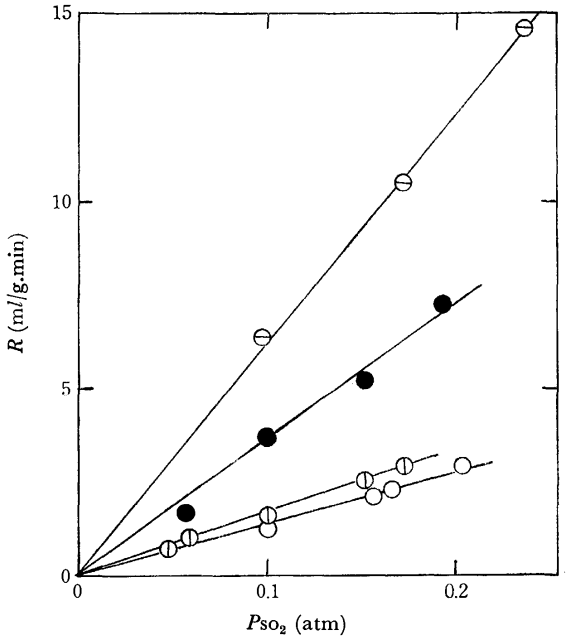

Fig. 5. Influence of the partial pressure of sulfur dioxide on the oxidation rate (P_{O_2}=0.1 atm).
○: 500°C, catalyst A, ◐: 550°C, catalyst A, ●: 600°C, catalyst A, ⊖: 600°C, catalyst B.

the contact time is expressed in terms of the ratio of weight of catalyst to the flow rate of reaction mixture (g·min/m*l*). The oxidation rates are constant up to almost 10% conversion of SO_2. We determined the oxidation rates as a function of P_{SO_2} and P_{O_2} below 10% conversion of SO_2.

The influence of P_{O_2} on the rate is shown in Fig. 4, where the rate R is expressed in m*l*. SO_3(stp)(*g*-catalyst)$^{-1}$ min^{-1}. All the correlations, at three different temperatures on catalyst A and at only one temperature on catalyst B, gives straight lines with a common slope. From the slope, the values 0.50 ± 0.05 can be obtained for the order of the reaction with respect to oxygen. The influence of P_{SO_2} on the rate is shown is Fig. 5, where the oxidation rate is first order with respect to sulfur dioxide.

In summary, the oxidation rate of sulfur dioxide on vanadium-potassium catalyst at 500, 550, and 600°C fits the rate expression (15), showing that the preceeding reaction mechanism concluded from the compositional consideration of catalysts under SO_2–SO_3–O_2 mixture may be valid.

It should be noted that catalyst B showed higher catalytic activity than catalyst A as seen in Figs. 4 and 5. The concentration of vanadium in catalyst A is 1.5 times larger than that in catalyst B. Since the ratio [V(IV)]/[V(V)] for both catalysts is supported to be close to each other from Table 1 and Fig. 2, concentrations of both V(IV) and V(V) will also be about 1.5 times larger in catalyst A than in catalyst B. If the rate-determining step is either the oxidation of V(IV) or reduction of V(V), the catalytic activity should be higher on catalyst A than on catalyst B. This is not the case in the present study. When the desorption of sulfur trioxide from the molten catalysts is rate-determining, a higher activity may be expected

for catalyst B, because the lower concentration of vanadium will give less viscous molten phase and make the desorption of sulfur trioxide from catalyst melt easier. Thus, the higher activity of catalyst B could be taken as another support of the conclusion on the rate-determining step.

Comparison of the Present Kinetics with the Literatures. The present rate expression $R=k\,P_{SO_2}\cdot P_{O_2}$ for the initial stage of SO_2 oxidation differs from the kinetics found in literature,[8] most of which were measured below 500°C. The difference may perhaps be due to that in the reaction temperatures. The lowering of reaction temperature may give two effects.

One is the variation of reaction mechanism. The temperature dependences of oxidation rate in Figs. 3, 4, and 5 give 6—10 kcal as the activation energy. This value is smaller than those obtained at lower temperatures.[8,9] The difference in activation energy suggests the change of the oxidation mechanism with temperature.

The second is the change in the solubility of vanadium component in the molten catalyst. $V_2O_5\cdot K_2SO_4$ mixture is not always a homogeneous melt below 500°C. The appearance of precipitates will influence the observed reaction kinetics and activation energy. This is true especially when the rate-determining step consists of the oxidation or reduction of vanadium. The phase diagram of $V_2O_5\cdot K_2SO_4$ system[6] and the present finding in Table 2 show that the limiting temperature at which the active component of catalyst changes from a homogeneous to a heterogeneous molten phase will depend upon the ratio V_2O_5/K_2O of catalyst and the composition of reacting gas phase. It should be noted that the temperature of the discontinuity in the Arrhenius plot depends on the composition of reaction mixture.[18]

The two effects may be partially responsible for the discrepancies between the present and other works and also for the discontinuity in the Arrhenius plot. To elucidate the reaction mechanism at lower temperatures, it is desirable to investigate the structure of catalyst and oxidation kinetics on catalysts with low V_2O_5/K_2O ratio. A low ratio is necessary to obtain a homogeneous molten catalyst.

The authors are grateful to Mr. T. Hayata for his help in kinetic measurement. A grant from the Matsunaga Science Foundation to A. K. is acknowledged.

18) E. V. Gerburt-Geibovich and G. K. Boreskov, *Zh. Fiz. Khim.*, **30**, 1801 (1956).

BULLETIN OF THE CHEMICAL SOCIETY OF JAPAN, VOL. 45, 695—700(1972)

The Calculation of the Rates of Intramolecular Nonradiative Transitions in Benzene

Noriyuki SHIMAKURA, Yuichi FUJIMURA, and Takeshi NAKAJIMA

Department of Chemistry, Tohoku University, Katahira-cho, Sendai

(Received August 16, 1971)

Intramolecular nonradiative transition rates for various interstates of benzene were calculated from the standpoint of the breakdown of the Born-Oppenheimer approximation. The electronic parts of the coupling matrix elements were explicitly evaluated. These parts vary in the range of $10^{-1}-10^{-3}$ Å^{-1}. The nonradiative transition rates for the $^1E_{1u}\rightarrow{}^1B_{1u}$, $^1B_{2u}$ transitions were predicted to be appreciable. The rate for the $^1B_{1u}\rightarrow{}^1B_{2u}$ transition vanishes as long as the geometrical structure of the $^1B_{1u}$ state is assumed to be of the D_{6h} symmetry. These results are compared with the experimental nonradiative transition widths recently reported by Jortner *et al.*

The ocurrence of intramolecular radiationless transitions in polyatomic molecules in the gas phase is now a well-established experimental fact.[1-10] Previous theoretical investigations concerning radiationless transitions have been based on the implicit assumption that the coupling between the molecule and the medium is essential for the occurrence of the nonradiative process. The theory for intramolecular radiationless transitions in an isolated molecule was set forward by Lin[11] and by Bixon and Jortner,[12] who derived the necessary restricting conditions for the occurrence of a radiationless transition in an isolated molecule in the gas phase from the standpoint of the breakdown of the Born-Oppenheimer approximation.

Information on the rates of the radiationless transi-

1) M. Kasha, *Discuss. Faraday Soc.*, **9**, 14 (1950).
2) N. Stevens and E. Hutton, *Mol. Phys.*, **3**, 71 (1960).
3) M. Kasha, *Radiat. Res. Suppl.*, **2**, 243 (1960).
4) K. F. Greenough and A. B. F. Duncan, *J. Amer. Chem. Soc.*, **83**, 555 (1961).
5) R. Williams and G. T. Goldsmith, *J. Chem. Phys.*, **39**, 2008 (1963).
6) P. Seybold and M. Gouterman, *Chem. Rev.*, **65**, 413 (1963).
7) G. W. Kistiakowsky and C. S. Parmenter, *J. Chem. Phys.*, **42**, 2942 (1963).
8) R. J. Watts and S. J. Strickler, *ibid.*, **44**, 2423 (1966).
9) R. E. Kollogg, *ibid.*, **44**, 411 (1966).
10) P. Pringsheim, "Fluorescence and Phosphorescence," Interscience Publishers, New York (1949), p. 271.
11) S. H. Lin, *J. Chem. Phys.*, **44**, 3759 (1966).
12) M. Bixon and J. Jortner, *ibid.*, **48**, 715 (1968); *ibid.*, **50**, 3284 (1969); *ibid.*, **50**, 4061 (1969).

tions may be inferred from the linewidths in the absorption spectrum. In gas-phase spectra, it is difficult to determine the rates experimentally because of the trivial diffuseness of the linewidths as a result of the molecular rotation, the molecular vibration, and the sequence spectral congestion, but these difficulties are eliminated at low temperature in solid matrices. Recently Jortner *et al.*[13] have observed the linewidths in the absorption spectra of benzene at low temperatures in the rare-gas matrices and have estimated the line broadenings arising from the intramolecular radiationless decay in the lower three excited states ($^1B_{2u}$, $^1B_{1u}$, and $^1E_{1u}$) of benzene.

Our main purpose in this paper is to calculate the radiationless transition rates in the lower three $\pi\rightarrow\pi^*$ excited states of benzene on the basis of the theory for intramolecular radiationless transitions in an isolated molecule and to compare the results with the above experimental information reported by Jortner *et al.*

Robinson and Burland[14] have calculated the radiationless transition probabilities for the internal conversion between the $^1B_{2u}$ and $^1A_{1g}$ states and the intersystem crossing between the $^3B_{1u}$ and $^1A_{1g}$ states in benzene. In their treatment, however, the explicit forms of the perturbation terms which cause the zero-order states to be nonstationary were not given, and the physical meaning of the perturbation terms is somewhat obscure.

Our calculation of the radiationless transition rates in benzene is made on the basis of the following assumptions:

(1) The radiationless transition is regarded as the transition from the lowest zero-order Born-Oppenheimer vibronic level, Ψ_i, in the higher electronic state to a dense manifold of the (zero-order) vibronic levels, Ψ_f, corresponding to a lower electronic state, and the breakdown of the adiabatic approximation is taken as the perturbation which brings about the radiationless decay.

(2) The coupling matrix elements, v, between the Ψ_i and Ψ_f states are assumed to be constant, independent of the channels which connect the initial state with a manifold of the vibronic levels, Ψ_f.

(3) The density, ρ, of the zero-order vibronic states, Ψ_f, is sufficiently high to exceed the reciprocal of the vibronic coupling term, v. This is nothing but a condition for the statistical limit of the intramolecular vibronic coupling and is expressed as:

$$\rho v \gg 1. \tag{1}$$

(4) The vibrational wave functions are approximated by a product of the harmonic oscillator wave functions.

Method of Calculation

In the excited electronic states of a large molecule, the Born-Oppenheimer separability condition for electronic and nuclear motion breaks down, and the intramolecular coupling between the zero-order vibronic level, Ψ_i, and a dense manifold of vibronic levels, Ψ_f, corresponding to a lower electronic state, both of which are eigenstates of the Born-Oppenheimer Hamiltonian, H_o, is induced by the nonadiabatic interaction term (the nuclear kinetic-energy operator), V:

$$V = H - H_o \tag{2}$$

By considering the time evolution of a coherently-excited molecular state, which can be displayed as a time-dependent superposition of molecular eigenstates, each of which is a time-independent superposition of zero-order vibronic states, Bixon and Jortner showed that, with the statistical limits, the rate constant, k, for the nonradiative transition is given by:

$$k = (2\pi/\hbar)\rho v^2 \tag{3}$$

where v is the coupling matrix element and is expressed by:

$$v = \langle\Psi_f|V|\Psi_i\rangle. \tag{4}$$

The adiabatic (zero-order) molecular wave functions, Ψ, are represented in the simple product form:

$$\Psi_i = \Phi_b\theta_{b\beta} \tag{5}$$

and:

$$\Psi_f = \Phi_a\theta_{a\alpha} \tag{5'}$$

where Φ is the electronic wave function and where θ is the vibrational wave function. The non-adiabatic interaction term, V, is given explicitly by the following equation:

$$V\Psi_i = T\Phi_b\theta_{b\beta} - \Phi_b T\theta_{b\beta} \tag{6}$$

where T denotes the kinetic-energy operator for nuclear motion. The coupling matrix element, v, can now be displayed in terms of normal coordinates, Q_i:

$$v = -\hbar^2\langle\Phi_a|(\partial/\partial Q_i)|\Phi_b\rangle\langle\theta_{a\alpha}|(\partial/\partial Q_i)|\theta_{b\beta}\rangle \tag{7}$$

where the Condon approximation[15] has been employed.

We are now in a position to treat the electronic and vibrational parts of Eq. (7) separately. First, the reduction of the electronic part will be considered. Expanding the Hamiltonian in normal coordinates to the first order, we obtain:

$$H = H_o^o + H_{so}^o + \sum_i\{(\partial H_o/\partial Q_i)_o + (\partial H_{so}/\partial Q_i)_o\}Q_i \tag{8}$$

where H_{so} is the spin-orbit coupling Hamiltonian and where the two superscripts of H_o and H_{so} and the two subscripts of $(\partial H_o/\partial Q_i)$ and $(\partial H_{so}/\partial Q_i)$ indicate that the corresponding quantities should be evaluated at the ground-state equilibrium nuclear arrangement. Further, the Φ_a and Φ_b wave functions are expanded into the series of Φ_c^o, and the expansion coefficients, correct to the second order, can be determined using the second-order perturbation theory. We thus obtain for the internal conversion.

$$\langle\Phi_a|(\partial/\partial Q_i)|\Phi_b\rangle = \frac{\langle\Phi_a^o|(\partial H_o/\partial Q_i)_o|\Phi_b^o\rangle}{(E_b^o - E_a^o)}, \tag{9}$$

and for the intersystem crossing:

$$\langle\Phi_a|(\partial/\partial Q_i)|\Phi_b\rangle = \frac{\langle\Phi_a^o|(\partial H_{so}/\partial Q_i)_o|\Phi_b^o\rangle}{(E_b^o - E_a^o)} + \sum_{c\neq b}\sum_{c\neq a}\left\{\frac{\langle\Phi_a^o|H_{so}^o|\Phi_c^o\rangle\langle\Phi_c^o|(\partial H_o/\partial Q_i)_o|\Phi_b^o\rangle}{(E_a^o - E_c^o)(E_b^o - E_a^o)} + \frac{\langle\Phi_a^o|(\partial H_o/\partial Q_i)_o|\Phi_c^o\rangle\langle\Phi_c^o|H_{so}^o|\Phi_b^o\rangle}{(E_b^o - E_a^o)(E_b^o - E_c^o)}\right\}. \tag{9'}$$

13) B. Katz, M. Brith, B. Sharf, and J. Jortner, *J. Chem. Phys.*, **52**, 88 (1970).

14) D. M. Burland and G. W. Robinson, *ibid.*, **51**, 4548 (1969).

15) M. Lax, *ibid.*, **20**, 1752 (1952).

The problem is thus reduced to the calculation of the matrix element:

$$\langle \Phi_a^o | (\partial H_o/\partial Q_i)_o | \Phi_b^o \rangle.$$

According to Albrecht[16] and Liehr,[17] this matrix element is to be written as follows:

$$\langle \Phi_a^o | (\partial H_o/\partial Q_i)_o | \Phi_b^o \rangle = \sum_{f=1}^{3} \sum_{\sigma=1}^{N} (\partial \xi_\sigma^f/\partial Q_i)_o \times \int \rho_{ab}(p) (\partial H_{o,p\sigma}/\partial r_{p\sigma})_o (\partial r_{p\sigma}/\partial \xi_\sigma^f)_o dx_p \quad (10)$$

where σ runs over the N nuclei, where p denotes the pth electron, where ξ_σ^f is the coordinate of the nuclei in the Wilsonian type (Fig. 1), and where the integration of right-hand side of Eq. (10) is over the pth electron. $(\partial \xi_\sigma^f/\partial Q_i)_o$ is a matrix element which transforms the normal coordinates into the local cartesian coordinates, and $(\partial r_{p\sigma}/\partial \xi_\sigma^f)_o$ is the appropriate direction cosine of the vector, $r_{p\sigma}$, connecting the p electron and the σ nucleus with respect to the local cartesian coordinate, f. ρ_{ab} is the one-electron transition density given by:

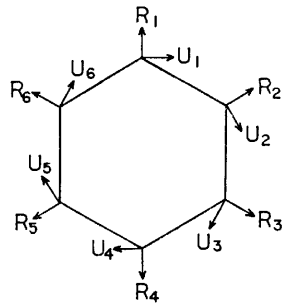

Fig. 1. Wilsonian type coordinate.
R: radial displacement of Wilsonian type coordinate
U: tangential displacement of Wilsonian type coordinate

$$\rho_{ab}(p) = n \int \Phi_a^o \Phi_b^o dx' \quad (11)$$

where n is the number of electrons and the integration is over all but the pth electron. It should be noted that $H_{o,p\sigma}$ is just $(-Z_\sigma e^2/r_{p\sigma})$, because the only nuclear dependent part of the Hamiltonian is the Coulomb potential between the electron and the nucleus. As an example, the electronic part $({}^1B_{2u} \rightarrow {}^1A_{1g})$ will be calculated in the Appendix.

Next, the vibrational part in Eq. (7) will be considered. The vibrational wave functions are approximated in terms of the products of the harmonic-oscillator wave functions, $\chi_{ami}(Q_i)$ and $\chi_{bni}(Q_i')$, where mi and ni correspond to the vibrational quantum numbers:

$$\theta_{bn} = \prod_i \chi_{bni}(Q_i') \quad (12)$$

and

$$\theta_{am} = \prod_i \chi_{ami}(Q_i) \quad (13)$$

where $Q_i' = Q_i + R_i$, R_i being the displacement of the equilibrium points of the its harmonic oscillator between the initial and final states. Using Eqs. (12) and (13), we get the following expression for the vibrational part of the coupling matrix element:

$$\langle \theta_{am} | \partial/\partial Q_i | \theta_{bn} \rangle = \langle \chi_{ami}(Q_i) | (\partial/\partial Q_i) | \chi_{bni}(Q_i') \rangle \times \prod_{j \neq i} \langle \chi_{amj}(Q_j) | \chi_{bnj}(Q_j') \rangle. \quad (14)$$

$\langle \chi_{ami}(Q_i) | (\partial/\partial Q_i) | \chi_{bni}(Q_i') \rangle$ is the non-adiabatic overlap integral; this term can also be expressed in terms of the usual overlap integrals as follows:[11,18]

$$\langle \chi_{ami}(Q_i) | (\partial/\partial Q_i) | \chi_{bni}(Q_i') \rangle = ni^{1/2} \langle \chi_{ami}(Q_i) | \chi_{b,ni-1}(Q_i') \rangle - (ni+1)^{1/2} \langle \chi_{ami}(Q_i) | \chi_{b,ni+1}(Q_i') \rangle \quad (15)$$

All the vibrational wave functions in the initial electronic state are assumed to correspond to the zero-quantum vibrational level.

In Eq. (14), we must take into consideration all the possible combinations of the vibrational overlap integrals under the constraint of the conservation of the excess electronic energy of the final state. Because of the difficulties of the above procedure, the first term on the right-hand side of Eq. (14), which corresponds to a non-adiabatic Franck-Condon overlap, is taken as the average value of the vibrational coupling matrix elements.

The evaluation of the vibrational part of the coupling-matrix element is thus reduced to the calculation of the overlap integral, $S_{mi,ni} (= \langle \chi_{ami}(Q_i) | \chi_{bni}(Q_i') \rangle)$. The analytical expression of $S_{mi,ni}$ as a function of the K_{mi} and K_{ni} constants and the displacement of the equilibrium point, R_i, is given as follows:

$$S_{mi,ni} = c \sum_{j=0}^{[mi/2]} \frac{(\alpha^2-1)^j}{j!} \sum_{k=0}^{ni} \frac{(2\alpha\beta)^{ni-k}(2\gamma)^{mi-2j-ni+k}}{(ni-k)!(mi-2j-ni+k)!} \times \sum_{L=0}^{[k/2]} \frac{(\beta^2-1)^L (2\delta)^{k-2L}}{L!(k-2L)!} \quad (16)$$

where:

$$c = (2^{mi+ni})^{-1/2} (mi!)(ni!) \sqrt{\frac{2K_{mi}K_{ni}}{(K_{mi}^2+K_{ni}^2)}} \times \exp\left\{ -\frac{K_{mi}^2 K_{ni}^2 r^2}{2(K_{mi}^2+K_{ni}^2)} \right\}$$

$$\alpha = \frac{2^{1/2}\rho}{(1+\rho^2)^{1/2}}, \quad \beta = \frac{\alpha}{\rho}, \quad \gamma = \frac{K_{mi} r}{1+\rho^2}, \quad \delta = -\rho r$$

$$\rho = \left(\frac{\nu_{mi}}{\nu_{ni}}\right)^{1/2}, \quad K_{mi} = \left(\frac{\mu \nu_{mi}}{\hbar}\right)^{1/2}, \quad K_{ni} = \left(\frac{\mu \nu_{ni}}{\hbar}\right)^{1/2}$$

where ν_{mi} and ν_{ni} are the vibrational frequencies for the initial and final states and where μ is the effective mass. This formula for $S_{mi,ni}$ applies only to a one-dimensional harmonic oscillator. For a two-dimensional case, we use the formula derived by Bell and Warsop.[19]

For the vibrational frequencies in both the ${}^1A_{1g}$ and ${}^1B_{2u}$ states of benzene, we employ the values proposed by Bernstein *et al.*[20] and by Garforth *et al.*[21] For the other states, the vibrational frequencies are unknown. Recently the differences in the zero-point vibrational energy between the ground state and excited states in benzene have been obtained by observing the deuteration effects on the transition energies.[13] We assume

16) A. C. Albrecht, *J. Chem. Phys.*, **33**, 156 (1960); *ibid.*, **50**, 169 (1960).
17) A. D. Liehr, *Z. Naturforsch.*, *A*, **13**, 596 (1960).
18) T. Matsushita, Doctoral Dissertation, Univ. of Tokyo (1967).
19) S. Bell and P.A. Warsop, *J. Mol. Spectrosc.*, **20**, 425 (1966).
20) E. R. Bernstein, S. D. Colson, D. S. Tinti, and G. W. Robinson, *J. Chem. Phys.*, **48**, 4632 (1968).
21) F. M. Garforth, C. K. Ingold, and H. G. Poole, *J. Chem. Soc.*, **1948**, 491.

that the vibrational frequencies for the $^1B_{1u}$ and $^1E_{1u}$ states can be estimated from these data.

Apart from the coupling matrix element, the remaining parameter determining the radiationless transition rate is the density, ρ, of the vibrational energy levels. The classical approximation[22-24] for the density of vibrational states is not sufficiently accurate, the main reason for the inaccuracy being the neglect of the zero-point energy. We adopt in this paper the semiclassical approximation proposed by Haarhoff,[25] where the density is expressed as follows:

$$\rho = [(E+E_z^o)^{n-1}/(n-1)!](\prod_i^n h\nu_i)^{-1} \quad (17)$$

and where ν_i is the frequency of the ith oscillator, n is the number of the vibrational freedom, E is the energy difference between the initial and final electronic states, and E_z^o is defined by the equation:

$$E_z^o = \sum_i^n (h\nu_i/2). \quad (18)$$

Results and Discussion

The nonradiative transition rates between the various states shown in Fig. 2 have been calculated by the method described in the preceeding section. The vibrational level densities calculated for the various electronic states are shown in Table 1. The calculated

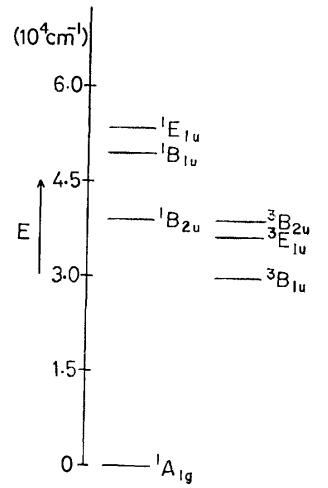

Fig. 2. Energy-level diagram showing the low-lying states of benzene.

matrix elements are summarized in Tables 2, 3, and 4. As can be seen from Table 3, the electronic parts of the vibronic matrix elements for the nonradiative transitions vary over a wide range, from about 10^{-1} to 10^{-3} (Å^{-1}). The electronic part for the $^1B_{1u}\rightarrow{}^1B_{2u}$ nonradiative transition vanishes, because all types of the transition density give zero. These results indicate that the electronic parts cannot be taken as constants in calculating the nonradiative transition rates. The calculated nonradiative transition rates are summarized in Table 4.

Table 1. Calculated level densities

Electronic state		Level density[a] $\frac{1}{\text{cm}^{-1}}$
Initial	Final	
$^1B_{2u}$	$^1A_{1g}$	9.26×10^{15}
$^1B_{1u}$	$^1A_{1g}$	1.13×10^{17}
$^1B_{1u}$	$^1B_{2u}$	6.50×10^{8}
$^1E_{1u}$	$^1A_{1g}$	4.25×10^{17}
$^1E_{1u}$	$^1B_{2u}$	9.60×10^{9}
$^1E_{1u}$	$^1B_{1u}$	1.17×10^{5}
$^1B_{2u}$	$^3E_{1u}$	2.25×10^{4}
$^1B_{2u}$	$^3B_{1u}$	1.90×10^{6}

a) The level densities are given by Eq. (17).

Table 2. Calculated electronic parts

Electronic state		$\langle\Phi_a\lvert\frac{\partial}{\partial Q_i}\rvert\Phi_b\rangle$	Inducing mode (cm^{-1})
Initial	Final		
$^1B_{2u}$	$^1A_{1g}$	1.3×10^{-1} (Å^{-1})	b_{2u} (1313)
		2.8×10^{-2}	b_{2u} (1147)
$^1B_{1u}$	$^1A_{1g}$	2.0×10^{-3}	b_{1u} (3069)
		1.9×10^{-2}	b_{1u} (1011)
$^1B_{1u}$	$^1B_{2u}$	0	a_{2g} (1340)
$^1E_{1u}$	$^1A_{1g}$	7.0×10^{-6}	e_{1u} (3063)
		7.5×10^{-2}	e_{1u} (1478)
		2.6×10^{-2}	e_{1u} (1035)
$^1E_{1u}$	$^1B_{2u}$	8.0×10^{-3}	e_{2g} (3042)
		1.9×10^{-2}	e_{2g} (1584)
		8.6×10^{-3}	e_{2g} (1174)
		5.6×10^{-2}	e_{2g} (606)
$^1E_{1u}$	$^1B_{1u}$	7.5×10^{-2}	e_{2g} (3042)
		2.1×10^{-1}	e_{2g} (1584)
		8.4×10^{-2}	e_{2g} (1174)
		3.7×10^{-1}	e_{2g} (606)

Table 3. Calculated non-adiabatic Franck-Condon factors

Electronic state		Non-adiabatic Franck-Condon factor[a]	Inducing mode (cm^{-1})
Initial	Final		
$^1B_{2u}$	$^1A_{1g}$	9.5×10^{-52}	b_{2u} (1313)
		$<10^{-60}$[b]	b_{2u} (1147)
$^1B_{1u}$	$^1A_{1g}$	9.1×10^{-34}	b_{1u} (3069)
		$<10^{-60}$[b]	b_{1u} (1011)
$^1B_{1u}$	$^1B_{2u}$	1.3×10^{-11}	a_{2g} (1340)
$^1E_{1u}$	$^1A_{1g}$	3.2×10^{-31}	e_{1u} (3063)
		$<10^{-60}$[b]	e_{1u} (1478)
		$<10^{-60}$[b]	e_{1u} (1035)
$^1E_{1u}$	$^1B_{2u}$	1.1×10^{-7}	e_{2g} (3042)
		9.3×10^{-12}	e_{2g} (1584)
		1.8×10^{-19}	e_{2g} (1174)
		1.5×10^{-37}	e_{2g} (606)
$^1E_{1u}$	$^1B_{1u}$	9.9×10^{-1}	e_{2g} (3042)
		4.6×10^{-2}	e_{2g} (1584)
		3.6×10^{-3}	e_{2g} (1174)
		6.0×10^{-5}	e_{2g} (606)

a) The non-adiabatic Franck-Condon factors are given by Eq. (15).
b) These values are less than 10^{-60}.

22) R. A. Marcus, *J. Chem. Phys.*, **20**, 359 (1952), *ibid.*, **43**, 2658 (1965).
23) R. A. Marcus and O. K. Rice, *J. Phys. Colloid. Chem.*, **55**, 894 (1951).
24) M. Vestal, A. L. Wahrhaftig, and W. H. Johnston, *J. Chem. Phys.*, **37**, 1276 (1962).
25) P. C. Haarhoff, *Mol. Phys.*, **7**, 101 (1963).

Table 4. Calculated nonradiative rate constants

Electronic state		Nonradiative rate constant
Initial	Final	k (sec^{-1})
$^1B_{2u}$	$^1A_{1g}$	1.1×10^{-27}
$^1B_{1u}$	$^1A_{1g}$	1.2×10^{-6}
$^1B_{1u}$	$^1B_{2u}$	0
$^1E_{1u}$	$^1A_{1g}$	5.5×10^{-6}
$^1E_{1u}$	$^1B_{2u}$	1.1×10^{-11}
$^1E_{1u}$	$^1B_{1u}$	1.7×10^{-15}

It is interesting to compare the calculated widths with the experimental ones. As the present results have been obtained on the basis of many assumptions which can be thought to be justified within the statistical limits, we cannot expect to reproduce the experimental widths exactly. Katz *et al.*[13] have experimentally determined the absorption widths of the $^1E_{1u}$, $^1B_{1u}$, and $^1B_{2u}$ excited states in solid rare-gas matrices and reported that they are about 300, 300, and 0 cm^{-1} respectively. The calculated width of the $^1E_{1u}$ state is about twenty times as large as the experimental one. This discrepancy between the calculated width and the experimental one may be ascribed in part to the evaluation of the level density by means of the semiclassical method. Frost *et al.*[26] have concluded, from a comparison of the semiclassical method with other methods, that the value of the level density based on the semiclassical method is about ten to twenty times as large as the true value in the case of a relatively low energy.

The calculated width of the $^1B_{1u}$ state is zero, in contrast to the experimental one. The width can be expected, from a consideration of the Franck-Condon factor, to have an appreciable order. The zero width stems from the basic assumption that the zero-order wave function, $\Psi(B_{1u})$, is constructed from the adiabatic wave function. In the present calculations, the vibronic coupling between the $^1B_{1u}$ and $^1E_{1u}$ states is not considered. It is well known [13,17,27,28] that the $^1B_{1u}$ state is subjected to the pseudo-Jahn-Teller interaction with the $^1E_{1u}$ state through vibrations of the e_{2g} symmetry. It can be expected, therefore, that, if $\Psi(B_{1u})$ is constructed by means of the configurational mixing, the calculated width will have a non-zero value. In a subsequent paper, the vibronic-coupling matrix element between the $^1E_{1u}$ and $^1B_{1u}$ states *via* e_{2g} vibrations will be evaluated on the basis of the crude adiabatic approximation.[29-31]

Table 5. Relative magnitudes of local cartesian coefficients $\xi_\sigma^R(b_{2u})$ and $\xi_\sigma^U(b_{2u})$ and relative magnitudes of electronic integrals $I_\sigma^R(B_{2u}, A_{1g}, b_{2u})$ and $I_\sigma^U(B_{2u}, A_{1g}, b_{2u})$

Wilsonian coordinate	Center number					
	1	2	3	4	5	6
R	O	O	O	O	O	O
U	x	$-x$	x	$-x$	x	$-x$

The width of the $^1B_{2u}$ state remains to be confirmed. It is shown in Table 4 that the calculated width of the nonradiative transition is negligibly small. We have calculated the width of the intersystem crossing from the $^1B_{2u}$ state to the $^3E_{1u}$ and $^3B_{1u}$ states. The results of the calculation are as follows:

$$\Gamma(^1B_{2u}\rightarrow{}^3E_{1u}) = 1.2\times10^{-6}\ cm^{-1},$$
$$\Gamma(^1B_{2u}\rightarrow{}^3B_{1u}) = 5.0\times10^{-13}\ cm^{-1}.$$

It may be concluded that the most favorable energy dissipation of the $^1B_{2u}$ state is the intersystem crossing to the $^3E_{1u}$ state. The width from other works gives 2.0×10^{-6} cm^{-1}.[7,32]

Appendix

The evaluation of the matrix element, Eq. (10), for the radiationless transition ($^1B_{2u}\rightarrow{}^1A_{1u}$) will be outlined as an example. Q_t should belong to the b_{2u} mode, judging from the selection rule for the nonradiative transition.

It is often convenient to symbolize the normal coordinate coefficient by $\xi_\sigma^f(b_{2u})$, and the electronic integral, by $I_\sigma^f(B_{2u}, A_{1g}, b_{2u})$, and to rewrite Eq. (10) as follows:

$$\langle\Phi(B_{2u})^o|\{\partial H_o/\partial Q(b_{2u})\}_o|\Phi(A_{1g})^o\rangle = \sum_f^3\sum_\sigma^N \xi_\sigma^f(b_{2u}) I_\sigma^f(B_{2u}, A_{1g}, b_{2u}), \quad \text{(A1)}$$

where:

$$\xi_\sigma^f(b_{2u}) = \{\partial\xi_\sigma^f/\partial Q(b_{2u})\}_o, \quad \text{(A2)}$$

$$I_\sigma^f(B_{2u}, A_{1g}, b_{2u}) = \int\rho(B_{2u}, A_{1g})(\partial H_{o,p\sigma}/\partial r_{p\sigma}) \times (\partial r_{p\sigma}/\partial\xi_\sigma^f)dx_p. \quad \text{(A3)}$$

All the types of the transition density, $\rho(B_{2u}, A_{1g})$, are shown in Fig. 3. Applying a group theoretical reduction[16] (Table 5) shows how Eq. (A1) may be greatly simplified. It is proven that the identical relationships holding among the $\xi_\sigma^f(b_{2u})$ values hold among the $I_\sigma^f(B_{2u}, A_{1g}, b_{2u})$ values, thus

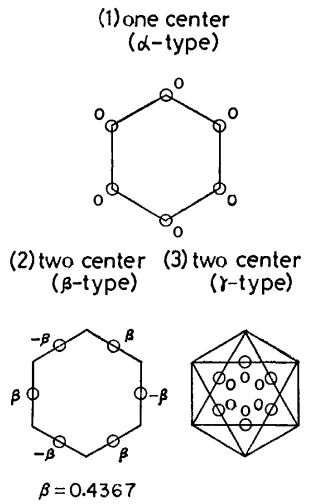

Fig. 3. Calculated transition density.

26) W. Frost and Z. Pasil, *J. Chem. Phys.*, **51**, 3006 (1969).
27) L. Salem, "The Molecular Orbital Theory of Conjugated Systems," Benjamin, New York (1966).
28) A. D. Liehr, *J. Phys. Chem.*, **67**, 389 (1963).
29) B. Sharf and R. Silbey, *Chem. Phys. Lett.*, **4**, 423 (1969).
30) B. Sharf and R. Silbey, *ibid.*, **4**, 561 (1970).
31) B. Sharf and B. Honig, *ibid.*, **7**, 132 (1970).
32) J. W. Donovan and A. B. F. Duncan, *J. Chem. Phys.*, **35**, 1389 (1961).

permitting one to write:

$$\langle\Phi(B_{2u})^o|\{\partial H_o/\partial Q(b_{2u})\}_o|\Phi(A_{1g})^o\rangle = \sum_{f^*}\sum_{\sigma^*}\xi^{f^*}_{\sigma^*}(b_{2u})I^{f^*}_{\sigma^*}(B_{2u}, A_{1g}, b_{2u})\sum_{f}^{3}\sum_{\sigma}^{N}\gamma^2_{\sigma f}(b_{2u}, \sigma^*, f^*) \quad \text{(A4)}$$

where the sum over f^* and σ^* goes over a minimum number of atomic centers and the corresponding cartesian coordinates. The expression in brackets is group-theoretically determined, where:

$$\eta_{\sigma f}(b_{2u}, \sigma^*, f^*) = I_\sigma{}^f(B_{2u}, A_{1g}, b_{2u})/I^{f^*}_{\sigma^*}(B_{2u}, A_{1g}, b_{2u}) = \xi_\sigma{}^f(b_{2u})/\xi^{f^*}_{\sigma^*}(b_{2u}). \quad \text{(A5)}$$

Thus, we may write:

$$\langle\Phi(B_{2u})^o|\{\partial H_o/\partial Q(b_{2u})\}_o|\Phi(A_{1g})^o\rangle = 6\xi_1{}^U(b_{2u})I_1{}^U(B_{2u}, A_{1g}, b_{2u}). \quad \text{(A6)}$$

$I_1{}^U$ can be expanded as follows:

$$I_1{}^U = \beta[I_o(d_1)\cos(d_1, U_1) - I_o(d_2)\cos(d_2, U_1) + I_o(d_3)\cos(d_3, U_1) - I_o(d_4)\cos(d_4, U_1) + I_o(d_5)\cos(d_5, U_1) - I_o(d_6)\cos(d_6, U_1)] \quad \text{(A7)}$$

where d_1, d_2,$\cdots$and d_6 represent the distance between the atomic center, 1, and the six centers of the transition density. We assume that the geometry of benzene is a hexagon whose bond distance is 1.397 Å. The following values, which have been calculated by Liehr, are then substituted on the right-hand side in Eq. (A7):

$$\beta = 0.4367$$

$$\cos(d_1, U_1) = \frac{7}{2}, \qquad \cos(d_2, U_1) = \frac{21}{7},$$

$$\cos(d_3, U_1) = \frac{39}{26}, \qquad \cos(d_4, U_1) = -\frac{39}{26},$$

$$\cos(d_5, U_1) = -\frac{21}{7}, \qquad \cos(d_6, U_1) = -\frac{7}{2},$$

$$I_o(d_1) = I_o(d_6) = 0.8239, \quad I_o(d_2) = I_o(d_5) = 0.1834,$$

$$I_o(d_3) = I_o(d_4) = 0.0950.$$

Thus, we obtain:

$$I_1{}^U(\beta) = 0.5378/5.201 \text{ (eV/Å)}. \quad \text{(A8)}$$

There are two normal modes in b_{2u} species, whose vibrational frequencies are 1147.7 and 1306.7 (cm^{-1}) respectively. The $\xi_1{}^U$ value corresponding to each normal mode is obtained as follows:

$$\xi_1{}^U(b_{2u}-1306.8) = -0.10716$$
$$\xi_1{}^U(b_{2u}-1147.7) = 0.04894. \quad \text{(A9)}$$

By inserting Eq. (A8) and Eq. (A9) into Eq. (A1), we obtain $\langle\Phi(A_{1g})^o|(\partial/\partial Q_i)|\Phi(B_{2u})^o\rangle = 0.136$ and 0.0281 ($Å^{-1}$) for the modes of 1306.8 and 1147.7 (cm^{-1}) respectively.

BULLETIN OF THE CHEMICAL SOCIETY OF JAPAN, VOL. 45, 700—705(1972)

The Heat of Adsorption from Solution. I. The Heat of Adsorption of Benzene on Silica Gel from the Benzene-Cyclohexane Solution

Tetsuo MORIMOTO and Hiromitu NAONO
Department of Chemistry, Faculty of Science, Okayama University, Tsushima, Okayama

(Received August 23, 1971)

The sensitivity and reliability of the improved-flow micro-calorimeter have been examined by supplying given amounts of electric energy to the calibration heater inserted in the calorimeter. The detection limit of the heat amount was found to be 0.01 mcal, and its probable error to be ± 0.5 and $\pm 0.3\%$ at the heat evolutions of 10 and 40 mcal respectively. The heat of the adsorption of benzene on silica gel from a cyclohexane solution has been measured at 30°C by the calorimeter thus constructed. The adsorption calorimetry indicates that benzene is adsorbed reversibly on silica gel, and that the differential heat of the adsorption of benzene is independent of the amount of adsorbed benzene, but that it depends strongly on the pretreatment temperature of the silica gel. The heats of adsorption were found to be 1.2, 1.6, 2.0, and 3.8 kcal/mol on silica gel samples treated at 100, 300, 500, and 800°C respectively. The findings on the heats of adsorption have been elucidated in terms of the interaction between benzene molecules and silanol groups on silica gel.

The heat of adsorption from a solution is of great significance, since it is considered to be a measure of the interaction energy between the adsorbed molecules dissolved in the solution and the solid surface concerned.[1] Many reports have been published on the heat of adsorption from a solution, as calculated from the temperature dependence of the adsorption isotherm. The data obtained, however, seem to be lacking in reliability, because of such difficulties as the temperature effect on solubility and the uncertainties both in regard to the activity coefficient of the adsorbed molecules and in regard to the thickness of the adsorbed layer.[2,3]

So far, two direct calorimetric methods have been developed to measure the heat of adsorption from solu-

1) J. J. Kipling, "Adsorption from Solution of Nonelectrolytes," Academic Press, London-New York (1965), Chapter 10.

2) *ibid.*, Chapter 14.

3) F. E. Bartell, T. L. Thomas, and Y. Fu, *J. Phys. Chem.*, **55**, 1456 (1951).

tion. Young *et al.*[4] have developed a method of measuring the heat of adsorption from solution by means of the technique of the heat of immersion. On the other hand, Groszek[5] has constructed a flow micro-calorimeter, in which the heat of adsorption was measured by injecting a solution of a known concentration into a solvent flowing through an adsorbent bed placed in the column.

In the present investigation, a flow micro-calorimeter has been constructed which is suitable for the exact measurement of a small heat evolution. By using this calorimeter, the heat of adsorption has been measured on a system of silica gel and the benzene-cyclohexane solution. Several investigators have reported the preferential adsorption of an aromatic hydrocarbon dissolved in an aliphatic hydrocarbon on the surface of silica gel.[6-11] However, the direct calorimetric measurement of the heat of adsorption has not yet been made in this system. Here, it will be reported that the direct calorimetric measurement by our improved flow micro-calorimeter can give a highly precise value of the interaction energy of adsorption in the same system.

Experimental

Materials. Silica gel was prepared by the hydrolysis of ethyl orthosilicate. The latter was purified by fractional distillation, and the fraction between the boiling points of 167.1 and 167.8°C was used. Two hundred grams of ethyl orthosilicate and 1015 g of redistilled water were mixed violently at 97—99°C for 4 hr in a 2-*l* flask. In this process, silica gel was produced by the hydrolysis reaction. After that, the excess water was evaporated out at *ca.* 80°C. The silica gel thus obtained was dried at 100°C in an air-bath for 24 hr, calcined at 500°C in the atmosphere for 15 hr, and treated in an agate ball-mill. The benzene and cyclohexane were purified by the usual method.[12] Glass beads of 65—100 mesh, used as a column bed of the flow micro-calorimeter, were treated with hot concentrated hydrochloric acid, washed thoroughly with distilled water, and then dried at 100°C in an air-bath.

Surface Area of Silica Gel. The specific surface area of the silica gel was determined by the BET method from the nitrogen adsorption at the temperature of liquid nitrogen. The surface areas of the samples pretreated *in vacuo* for 4 hr at 100, 300, 500, and 800°C were found to be 423, 422, 431, and 396 m^2/g respectively.

Flow Micro-calorimeter. The calorimeter was constructed by setting a heater circuit in the detection column of the liquid-column chromatograph manufactured by the Japan Electron Optics Laboratory Co., Ltd. The calorimeter, shown diagrammatically in Fig. 1, consisted of a constant flow pump, solvent and solution reservoirs, purification, reference and detection columns, exchange valves, and a metal thermostat. The flow rate was regulated by means of the constant flow pump. The thermistor was used as the temperature-sensitive element. A heater made of platinum wire with a diameter of 0.01 mm and a resistance of 12Ω was placed 1 cm above the thermistor in the detection column. The change in resistivity of the thermistor was amplified and recorded; it was caused by the temperature change due to the heat evolved by the adsorption on silica gel or by the electric current flowing through the heater. Furthermore, it should be noticed that this calorimeter performed excellently in several more points, *i.e.*, the method of injecting the solution, the temperature control of the metal thermostat, and the construction of the double-column system.

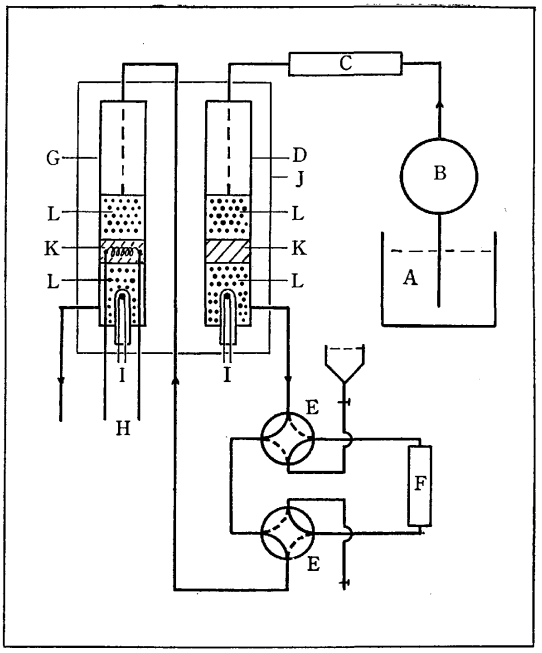

Fig. 1. Block diagram of flow micro-calorimeter.
A, solvent reservoir; B, constant flow pump; C, purification column; D, reference column; E, exchange valves; F, solution reservoir; G, detection column; H, calibration heater; I, thermistor; J, metal thermostat; K, silica gel (adsorbent); L, glass beads.

Adsorption Calorimetry. The primary purpose of the present adsorption calorimetry is to test the performance of the improved flow micro-calorimeter by applying it to the investigation of the interaction between the surface of silica gel and benzene molecules dissolved in cyclohexane. Silica gel (60—140 mg) was pretreated at a reduced pressure of 10^{-3} Torr for 4 hr at an elevated temperature and then placed in a bed at the same position as the calibration heater. In this case, care was taken so that the silica gel sample did not directly come in contact with the atmosphere. The silica gel bed, several millimeters thick, was sandwiched by glass beads (65—100 mesh) in the detection column. Both of them were similarly packed in the reference column. In the purification column, a large quantity of silica gel was used for the filteration of any impurities. At first, the cyclohexane used as a solvent was forced to flow through at the rate of 0.21 ml/min. The flow direction of cyclohexane is shown by arrows in Fig. 1. In order to reduce the fluctuation of the temperature in the detection column, the reference column

4) G. J. Young, J. J. Chessick, and F. H. Healey, *J. Phys. Chem.*, **60**, 391 (1956).
5) A. Groszek, *J. Chromatogr.*, **3**, 454 (1960); *Chem. Ind.*, 482 (1965).
6) C. L. Lloyd and B. L. Hariss, *J. Phys. Chem.*, **58**, 899 (1954).
7) L. R. Snyder, *ibid.*, **67**, 2622 (1963).
8) C. N. Rowe and R. W. Schiessler, *ibid.*, **70**, 787 (1966).
9) B. C.-Y. Lu and R. F. Lama, *Trans. Faraday Soc.*, **63**, 727 (1967).
10) S. K. Suri and R. W. Ramakriskna, *J. Phys. Chem.*, **72**, 1555 (1968).
11) T. Kagiya, Y. Sumida, and T. Tachi, This Bulletin, **44**, 1291 (1971).
12) A. Weissberger, E. S. Proskauer, J. A. Riddick, and E. E. Toops, Jr., "Organic Solvent," 2nd ed., Interscience Publishers, Inc., New York (1955), p. 306, 315.

was connected with the flow circuit and was positioned close to the detection column in the metal thermostat. After the thermal equilibrium had been established in the measuring system, a stable base line with no slope was recorded; then the flowing liquid was replaced with a benzene solution of a given concentration by using the exchange valves. Thus, the temperature rise caused by the adsorption of benzene was recorded. During the flow of the benzene solution, the temperature rose initially, passed through maximum, and then went down to the same level as the original base line. This means that the adsorption equilibrium of benzene has been attained. The A curve in Fig. 6 is an example of such an adsorption peak. The desorption peak was obtained after exchanging the flow of the solution with that of the solvent by means of the exchange valves, as is shown in the B curve in Fig. 6. The calibration of the calorimeter was made with the aid of the calibration heater; the peak area recorded was plotted against the electric energy supplied by the heater.

Adsorption Measurement of Benzene on Silica-gel from the Benzene-Cyclohexane Solution. The amount of benzene adsorbed on silica-gel from the cyclohexane solution was obtained from the difference in the concentrations before and after the adsorption. In a 2-m*l* ampoule, silica gel (0.5—1.0 g) was pretreated under the same conditions as those described in the adsorption calorimetry. A known amount (*e.g.*, 2 g) of the solution of a given concentration was poured into the ampoule, and then it was sealed. In this case, precaution was taken so that the solid powder did not come into direct contact with the atmosphere by cutting off the top of the ampoule in the solution. The sealed ampoule was shaken for 15 hr at 30°C; this resulted in the attainment of the adsorption equilibrium. The concentration of benzene in the supernatant solution was determined by means of absorption spectroscopy at the wave length of 254.5 mμ by using a spectrophotometer of the Hitachi 139 type.

Results and Discussion

Reliability and Sensitivity of the Flow Micro-calorimeter. In Fig. 2, several calibration peaks are illustrated. These peaks are recordings of the resistivity change in the thermistor set in the detection column when different amounts of electric energy were supplied to the calibration heater at the heat-evolution rate of 4.60 mcal/min and at the flow rate of the solvent of 0.21 m*l*/min. Figure 3 presents the relation between the peak area and the electric energy supplied, which was obtained by varying the rate of the solvent flow and that of the heat evolution. It may be seen from Fig. 3 that the peak area is exactly proportional to the heat evolved and that the slope of the straight lines varies

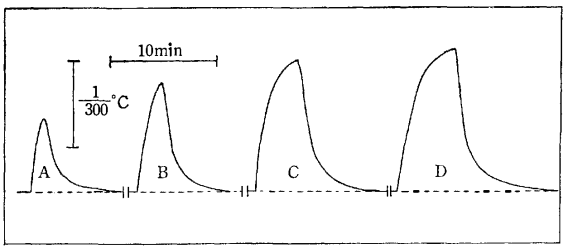

Fig. 2. Calibration peaks at 30°C.
Solvent, cylcohexane; flow rate, 0.21 m*l*/min; heat-evolution rate, 4.60 mcal/min. Peak A, 4.62 mcal; B, 9.28 mcal; C, 18.5 mcal; D, 23.2 mcal.

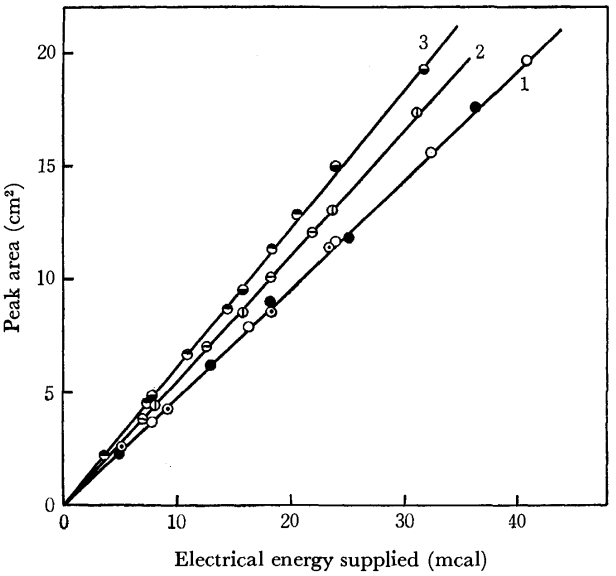

Fig. 3. Relation between peak area and heat.
1: flow rate, 0.21 m*l*/min; heat-evolution rate, ⊙: 4.60 mcal/min, ●: 12.7 mcal/min, ○ 16.3 mcal/min.
2: flow rate, 0.31 m*l*/min; heat-evolution rate, ⊖: 3.67 mcal/min, ⏀: 15.9 mcal/min.
3: flow rate, 0.46 m*l*/min; heat-evolution rate, ◓: 3.72 mcal/min, ◒: 15.9 mcal/min.

with the flow rate of the solvent, independently of the heat-evolution rate. The slope for the straight lines in Fig. 3 increases with the flow rate of the liquid. This fact may be interpreted as follows: the heat generated in the detection column escapes in all directions of the column, but the enhanced flow rate of the liquid causes an increase in the heat sensitivity of the thermistor. Thus, it can be understood that, in flow calorimetry, it is necessary to operate the calorimeter at a constant flow rate.

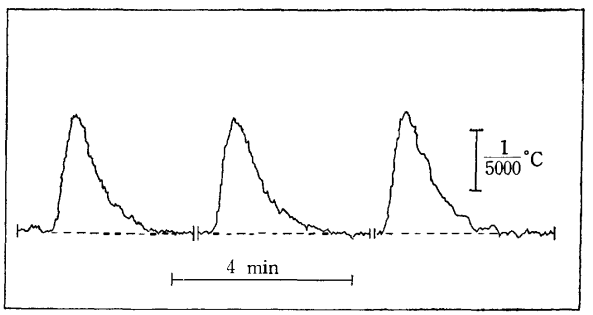

Fig. 4. Response of flow micro-calorimeter for 0.1 mcal at 30°C.
Solvent, cyclohexane; flow rate, 0.21 m*l*/min.

Next, the accuracy of the calorimeter was examined for the heat amounts of 10 and 40 mcal. Five measurements were repeated in each case. The peak area obtained gives probable errors of ± 0.5 and $\pm 0.3\%$ for 10 and 40 mcal respectively. The sensitivity of the calorimeter was also tested. Figure 4 shows the three peaks obtained for 0.1 mcal. Although there is appreciable noise, the peak area can be measured within an error of $\pm 5\%$, which corresponds to the detection limit

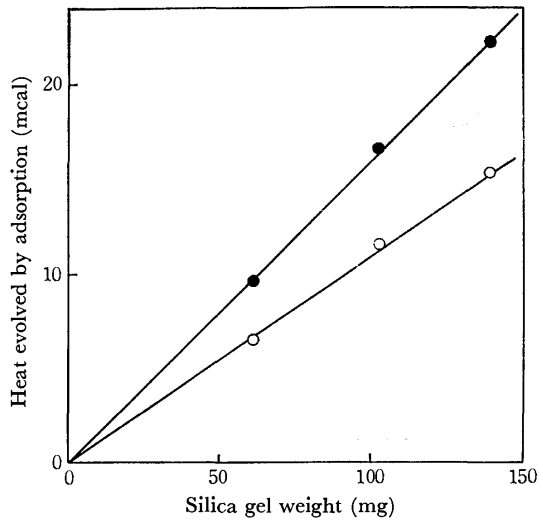

Fig. 5. Relation between heat evolved by adsorption of benzene and silica gel weight in flow micro-calorimeter. Pretreatment temperatrue of silica gel, 100°C; benzene concentration,
○: 0.050 molality, ●: 0.085 molality.

of the heat of 0.01 mcal.

Finally, the relation between the amount of the heat evolved by adsorption and the weight of the adsorbent used for the calorimetry was examined at a constant concentration of benzene. The results obtained are shown in Fig. 5, which indicates that the heat evolved by the adsorption of benzene is proportional to the weight of the silica gel used within the range of the present experiments. The above examinations prove that the present flow micro-calorimeter is useful for the measurement of the heat of adsorption from solution, especially for the investigation of a system with a weak interaction energy.

In comparison with the micro-calorimeter employed by Groszek,[5] the following points are improved in the present calorimeter: (1) the temperature of the metal thermostat is regulated within an error of $\pm 10^{-3}$°C, (2) the noise arizing from the fluctuation in the flow rate of the liquid and in the temperature of the metal thermostat is eliminated by adopting the double-column system, and (3) the solution in the reservoir is smoothly injected into the detection column by using the exchange valves. The sensitivity of his calorimeter was approximately the same as that of the present one. He reported that the slope was recorded by the base line, and that the peak areas are nearly linearly related to the heat produced by the heater up to 20 mcal. On the contrary, the present results give a straight base line, one with no slope over a prolonged period, and a good linearity between the peak area and the amount of heat supplied.

Heat of Adsorption of Benzene on Silica Gel from the Benzene-Cyclohexane Solution. Figure 6 shows the response of the flow micro-calorimeter, including both the exothermic peak due to the adsorption of benzene on silica gel and the endothermic one due to the desorption from silica gel. The silica gel samples used in the experiments in Fig. 6 were pretreated at 100°C *in vacuo*. In each sample of silica gel, no matter what the pretreatment temperature, the area of the adsorption peak is in good agreement with that of the desorption peak within the limits of experimental error. This agreement establishes that benzene molecules are adsorbed reversibly on the silica gel surface.

Taking into account the specific surface area of silica gel, the heat evolved by the adsorption of benzene, H, can expressed in calories per 100 Å^2 of silica gel. This is plotted in Fig. 7 as a function of the concentration. The silica-gel samples used were pretreated at 100, 300, 500, and 800°C *in vacuo*. It can be seen from Fig. 7 that the value of H increases with an increase in the concentration of benzene. Moreover, the H value

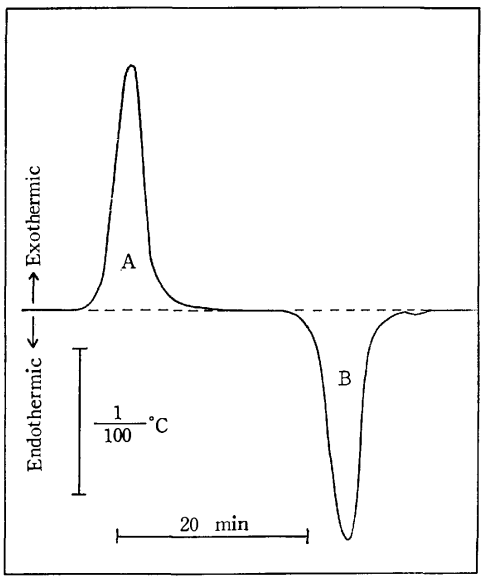

Fig. 6. Adsorption and desorption peaks of benzene at 30°C. A, adsorption peak; B, desorption peak. Solvent, cyclohexane; flow rate, 0.21 ml/min; benzene concentration, 0.095 molality; silica gel weight, 120 mg.

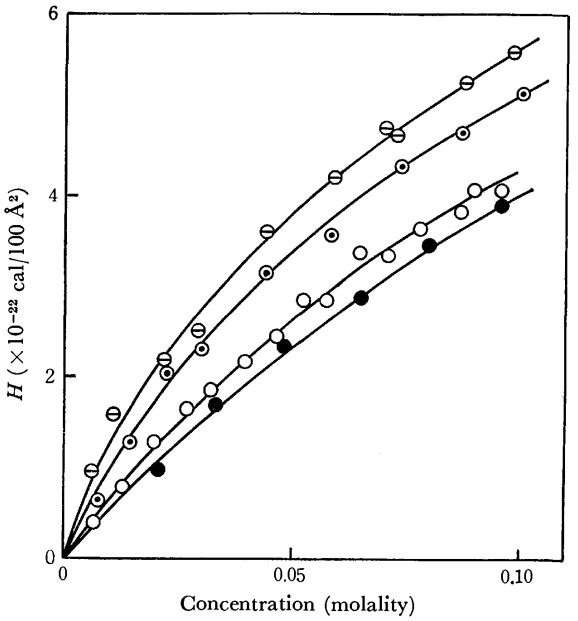

Fig. 7. Heat evolved by adsorption of benzene, H, on silica gel from cyclohexane solution at 30°C.
Pretreatment temperature of silica gel,
○: 100°C, ⊙: 300°C, ⊖: 500°C, ●: 800°C.

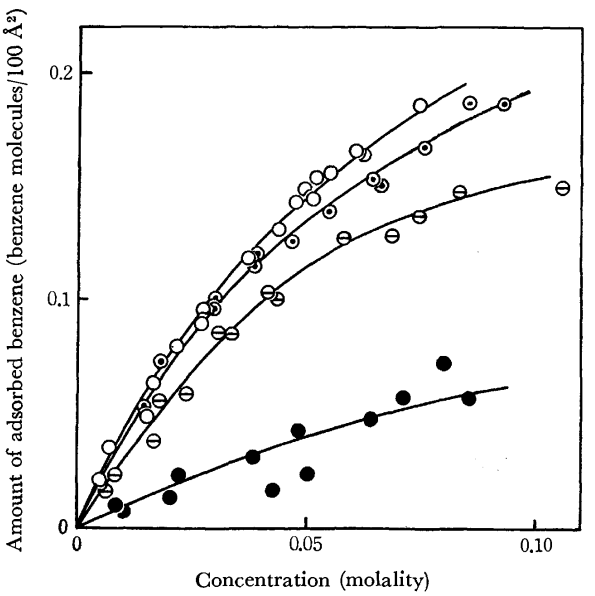

Fig. 8. Adsorption isotherm of benzene on silica gel at 30°C.
Pretreatment temperature of silica gel,
○: 100°C, ⊙: 300°C, ⊖: 500°C, ●: 800°C.

depends on the pretreatment temperature, *i.e.*, it increases in the order of 800, 100, 300, and 500°C treatment.

On the other hand, the adsorption isotherm of benzene on silica gel from the benzene-cyclohexane solution is as is shown in Fig. 8, where the amount of adsorbed benzene is expressed in benzene molecules per 100 Å² of silica gel. An appreciable fluctuation is observed in the experimental data on the amount of benzene adsorbed on the silica gel samples pretreated at 800°C, probably because of the remarkably reduced amount of adsorption. Taking the molecular area of benzene adsorbed in the close-packed state on graphitized carbon black to be 40 Å²,[13] it may be seen from Fig. 8 that only a small part of the silica gel surface is covered by benzene molecules within the concentration range examined here. Furthermore, it can be seen from Fig. 8 that the higher the pretreatment temperature of silica gel, the smaller the amount of benzene adsorbed.

From the smooth curves shown in Figs. 7 and 8, the relation between H and the amount of adsorbed benzene is obtained (*cf.* Fig. 9). A good linear relationship holds between them, and the slope increases with the pretreatment temperature of silica gel. Since the slope directly indicates the differential heat of adsorption, it can be seen from Fig. 9 that the differential heat of adsorption of benzene on silica gel from the cyclohexane solution is independent of the amount of adsorbed benzene within the concentration range examined. Therefore, we can conclude that the surface of silica gel is energetically homogeneous for the adsorption of benzene from the cyclohexane solution at a low coverage of benzene. Furthermore, it should be noticed that the heat of the adsorption of benzene depends greatly on the pretreatment temperature; the values are 1.2, 1.6, 2.0, and 3.8 kcal/mol on the samples pretreated at 100, 300, 500, and 800°C respectively. These values show that the interaction between the silica gel surface and benzene molecules is relatively weak compared to that between the same surface and polar molecules.[14]

In the present calorimetric measurements, the heat of dilution should be a factor in addition to the heat evolved by adsorption. In the benzene-cyclohexane system, the heat of dilution can be calculated from the heat of the mixing of benzene with cyclohexane. Ac-

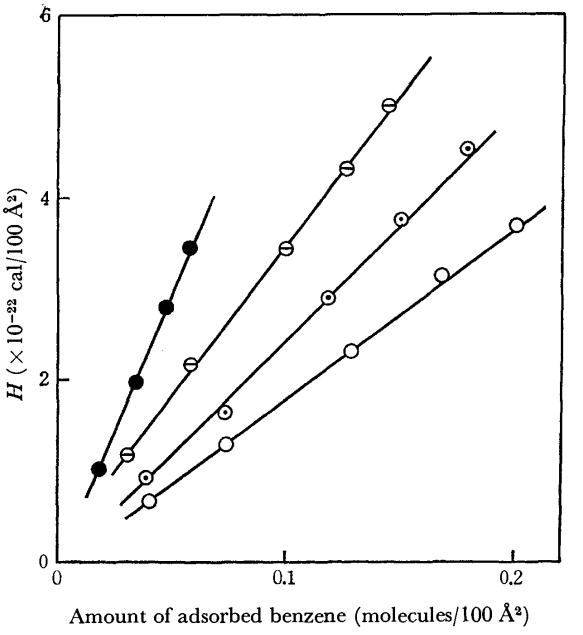

Fig. 9. Relation between H and amount of adsorbed benzene pretreatment temperature of silica-gel,
○: 100°C, ⊙: 300°C, ⊖: 500°C, ●: 800°C.

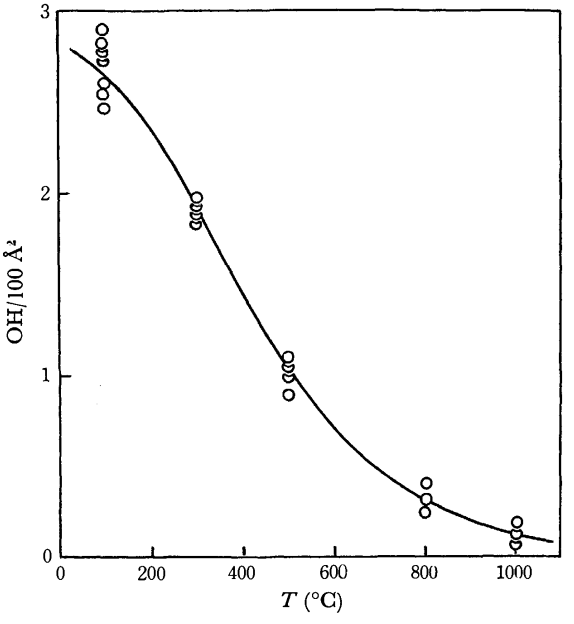

Fig. 10. Relation between silanol content and pretreatment temperature of silica gel, T.

13) A. A. Isirikyan and A. V. Kiselev, *J. Phys. Chem.*, **65**, 601 (1961).
14) T. Morimoto and H. Naono, Unpublished data.

cording to the data reported by Maagek *et al.*,[15] the heat of dilution is less than 5 cal/mol in the concentration range of benzene examined here; this is negligibly small compared with the heat of the adsorption of benzene.

So far, it has been clarified that the silanol groups play an important role in the interaction between the silica gel surface and aromatic hydrocarbon molecules, whether in the gaseous or in the liquid phase.[7,11,16,17] In the present investigation, the surface silanol groups were determined by an analysis of the active hydrogen atoms;[18] the results are presented in Fig. 10 as a function of the pretreatment temperature of silica gel. Figure 10 shows that the silanol content decreases remarkably with an increase in the pretreatment temperature. On the other hand, as is shown in Fig. 8, the amount of benzene adsorbed on the silica gel surface also decreases with an increase in the pretreatment temperature. These results suggest that benzene molecules are selectively adsorbed on silanol groups on the silica gel surface. Moreover, a benzene molecule may be considered to interact with a single silanol group on the basis of the following facts. Assuming that the surface silanol groups are distributed uniformly, the area of silica gel per silanol group can be calculated from the data in Fig. 10: the area are 38, 53, 100, and 320 Å^2 for the surfaces treated at 100, 300, 500, and 800°C respectively. Thus, the area per silanol group is almost equal to, or is larger than, the molecular area of benzene (40 Å^2) mentioned above.[13]

In order to examine the quantitative relationship between the amount of benzene adsorbed and the silanol content, the ratio of the former to the latter was replotted against the concentration of benzene (*cf.* Fig. 11). First, it may be seen from Fig. 11 that the ratio is always far less than unity over the concentration range of benzene examined; this indicates that the surface silanol groups are only partly covered by benzene molecules over the range of the amount of adsorbed benzene examined, in spite of a quite small population of silanol groups. Figure 11 also shows that the higher the pretreatment temperature, the larger the ratio. This latter fact implies that the silanol groups on the surfaces treated at higher temperatures can attract benzene molecules more strongly than those on the surfaces treated at lower temperature; this corresponds with the results in Fig. 9. The heat treatment of silica gel at higher temperatures may change the structure of the surface and make it feasible to adsorb benzene molecules.

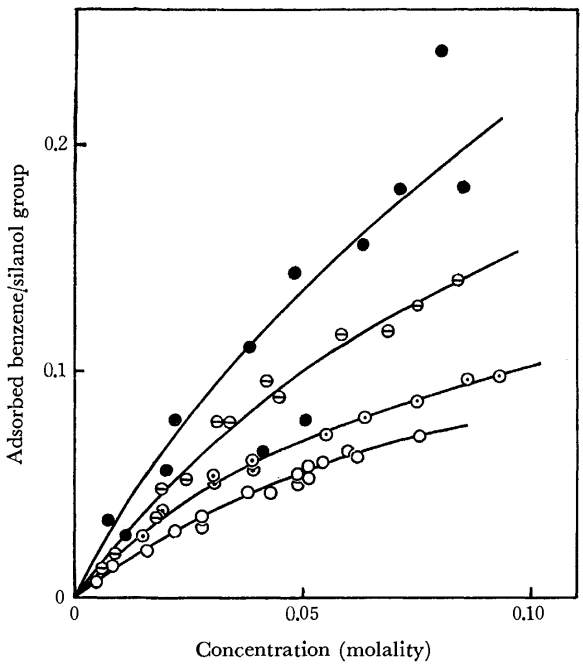

Fig. 11. Effect of pretreatment temperature of silica gel on the ratio of adsorbed benzene to silanol group.
○: 100°C, ⊙: 300°C, ⊖: 500°C, ●: 800°C.

The authors wish to thank Dr. M. Nagao for the measurements of the specific surface area of silica gel and Mrs. K. Moori for her assistance in a part of experiments.

15) R. V. Maagek and H. C. Van Ness, *A. I. Ch. E. Journal*, **7**, 190 (1966).
16) N. Okuda, *Nippon Kagaku Zasshi*, **82**, 1118 (1961).
17) G. A. Galkin, A. V. Kiselev, and V. I. Lygin, *Trans. Faraday Soc.*, **60**, 431 (1964).
18) The experimental details will be published in the next report; *cf.* J. J. Fripiat and J. Uytterhoeven, *J. Phys. Chem.*, **66**, 800 (1962).

A Chlorine NQR Study of Some Perchloro-compounds

Masao HASHIMOTO and Koichi MANO*

Department of Chemistry, Faculty of Science, Kobe University, Nada-ku, Kobe
**Research Institute for Atomic Energy, Osaka City University, Sumiyoshi-ku, Osaka*

(Received September 3, 1971)

The NQR frequencies of chlorines in seven perchloro-compounds were measured at 77°K and above. The assignments of the frequencies were made for each compound. It was found that the resonance frequency is considerably influenced by the electrostatic repulsion between chlorine atoms due to the close Cl···Cl distances. For several compounds, the resonance was found to fade out at rather low temperatures.

Several investigations of the nuclear quadrupole resonance, NQR, of the chlorine nucleus in perchloro-compound, C_mCl_n, have been reported.[1-4] Recently, West and his co-workers applied the NQR method to the determination of the molecular structure of some perchloro-compounds.[5-8] Their study constituets an important chemical application of the NQR technique. In order for this application to be reliable, however, it is necessary to establish the correlations between the molecular structure and the NQR frequencies. In the present work, we measured and assigned the NQR frequencies of chlorines in seven perchloro-compounds (Fig. 1) for which the crystal or molecular structures have been well established.

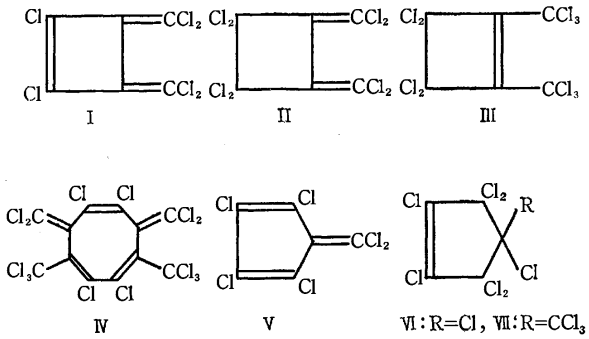

Fig. 1.

In perchloro-compounds, some of the chlorine atoms are expected to approach one another closely, because half or more than half of the atoms in the molecule are chlorine atoms. In fact, intramolecular and/or intermolecular Cl···Cl distances shorter than twice the van der Waals radius have been found in the crystals of some perchloro-compounds.[9-12] In this paper, we will report on the effect of the close Cl···Cl distance on the chlorine NQR frequency of perchloro-compounds. Agranat *et al.* have reported the effect of intramolecular interactions due to overcrowding on the NQR frequencies of chlorines in octachloropentafulvalene.[3]

Experimental

NQR Measurements. The NQR spectra were observed with an externally-quenched super-regenerative spectrometer; the absorption lines were displayed either on an oscilloscope or, when greater sensitivity was required, on a recorder after amplification by means of a lock-in amplifier. The frequencies were measured with a National VP-415 digital frequency counter. The accuracy of the frequency measurements was within ±2 KHz. The frequency measurements were carried out at 77°K (liquid nitrogen bath), at 198°K (dry ice-petroleum ether bath), and at room temperature. In some cases, the frequencies were measured at other temperatures by using a petroleum ether bath cooled by liquid nitrogen or dry ice. The temperature was determined by means of a copper-constantan thermocouple.

Materials. Perchloro-(3,4-dimethylenecyclobutene), I, was prepared by the dechlorination of perchloropropene with aluminum amalgam in ether.[13] This sample was purified by sublimation in a vaccum and by subsequent recrystallization from *n*-hexane under an atmosphere of nitrogen; mp 154—155°C.

Perchloro-(1,2-dimethylenecyclobutane), II, was prepared from I by means of chlorination with antimony pentachloride.[13] The sample of II was purified by chromatography on aluminum oxide. Recrystallization from acetone; mp 93°C.

Perchloro-(1,2-dimethylcyclobutene), III, was prepared from II by the same method as II. The product was purified by chromatography on aluminum oxide and by subsequent recrystallization from acetone; mp 153—154°C. The IR spectrum of this sample was identical with that of an authentic sample.[14]

Perchloro-(1,4-dimethyl-5,8-dimethylenecycloocta-1,3,6-triene), IV, was prepared from perchloro-(3,4,7,8-tetramethylenecyclooctadiene) by chlorination with liquid chlorine in a sealed tube.[13,15] It was then recrystallized from chloroform; mp 275°C.

Perchloro-(5-methylenecyclopentadiene), perchlorofulvene,[16] V, was obtained from perchloropropene by dechlorination with cuprous chloride in hydrous tetrahydro-

1) I. P. Biryukov, M. G. Voronkov, and I. A. Safin, "Tables of Nuclear Quadrupole Resonance Frequencies," Israel Program for Scientific Translations, Jerusalem (1969).
2) M. Hayek, D. Gill, I. Agranat, and M. Rabinovitz, *J. Chem. Phys.*, **47**, 3680 (1967).
3) I. Agranat, D. Gill, M. Hayek, and R. M. J. Loewenstein, *ibid.*, **51**, 2756 (1969).
4) E.A.C. Lucken and C. Mazeline, *J. Chem. Soc.*, (*A*), **1968**, 153.
5) R. West and K. Kusuda, *J. Amer. Chem. Soc.*, **90**, 7354 (1968).
6) A. Roedig, R. Helm, R. West, and R. M. Smith, *Tetrahedron Lett.*, **1969**, 2137.
7) R. M. Smith and R. West, *ibid.*, **1969**, 2141.
8) R. M. Smith and R. West, *J. Org. Chem.*, **35**, 2681 (1970).
9) P. J. Wheatley, *J. Chem. Soc.*, **1961**, 4936.
10) A. Furusaki, This Bulletin, **40**, 758 (1967).
11) A. Furusaki, *ibid.*, **40**, 2518 (1967).
12) A. Furusaki, *ibid.*, **41**, 2886 (1968).
13) K. Mano, D. Sc. Thesis, Osaka City University, **1969**.
14) A. Fujino, Y. Nagata, and T. Sakan, This Bulletin, **38**, 295 (1965).
15) K. Mano, K. Kusuda, and A. Fujino, *Tetrahedron Lett.*, **1968**, 1375.
16) A. Roedig, *Ann.*, **569**, 161 (1950).

Table 1. Measured frequencies for ^{35}Cl in some perchloro-compounds at various temperatures

Compound	No.	77°	198°K	Room temperature	Extrapolated value
		(Frequency in MHz)			
I	ν_1	38.066 (30.005)[a]	37.787		38.15
	ν_2	37.972 (29.936)	37.671		38.07
	ν_3	37.831 (29.822)	37.582		37.90
	ν_4	37.750 (29.758)	37.537		37.80
	ν_5	36.520 (28.783)	36.279		36.59
	ν_6	36.371 (28.663)	36.068		36.46
II	ν_1	38.839 (30.607)	38.527	38.144 (304°K)	38.94
	ν_2	38.639 (30.450)	38.292	37.881	38.75
	ν_3	38.072 (30.007)	37.701	37.292	38.18
	ν_4	37.901 (29.870)	37.634	37.252	38.00
III	ν_1	40.540 (31.953)	40.189	(298°K)	40.66
	ν_2	40.398 (31.953)	40.189		40.56
	ν_3	40.280 (31.753)	39.796		40.44
	ν_4	39.007 (30.742)	38.768	38.473	39.08
	ν_5	38.826 (30.600)	38.583	38.298	38.90
IV	ν_1	40.303 (31.769)	39.873	(294°K)	40.47
	ν_2	39.764 (31.344)	39.298		39.92
	ν_3	39.581 (31.199)	39.168		39.74
	ν_4	37.898 (29.871)	37.650	37.389	37.98
	ν_5	37.804 (29.794)	37.480	37.161	37.94
	ν_6	37.695 (29.710)	37.351	37.011	37.84
	ν_7	37.308 (29.406)	37.042	36.770	37.41
V	ν_1	38.314 (30.200)	38.002		38.41
	ν_2	38.190 (30.101)	37.852		38.31
	ν_3	38.094 (30.026)	37.755		38.21
	ν_4	37.806 (29.801)	37.514		37.94
	ν_5	37.169 (29.297)	36.928		37.27
	ν_6	36.792 (28.998)	36.570		36.89
VI[b]	ν_1	41.187	40.753	40.317 (293°K)	41.35
	ν_2	40.254	39.865	39.452	40.39
	ν_3	39.998	39.696	39.338	40.09
	ν_4	39.771	39.420	39.024	39.88
	ν_5	39.607	39.335	39.002	39.70
	ν_6	39.365	39.072	38.709	39.48
	ν_7	37.900	37.522	37.119	38.02
	ν_8	37.431	37.025	36.600	37.58
VII	ν_1	41.143 (32.432)	40.900	40.629 (300°K)	41.24
	ν_2	41.047 (32.355)	40.720	40.380	41.18
	ν_3	40.923 (32.254)	40.617	40.305	41.03
	ν_4	40.709 (32.086)	40.405	40.122	40.83
	ν_5	40.638 (32.031)	40.332	40.052	40.77
	ν_6	40.182 (31.670)	39.925	39.673	40.28
	ν_7	40.046 (31.562)	39.785		40.15
	ν_8	39.951 (31.484)	39.742	39.533	40.02
	ν_9	38.194 (30.105)	37.958	37.687	38.28
	ν_{10}	37.673 (29.697)	37.410	37.135	37.78

a) The value in ( ) is the measured frequency for ^{37}Cl.
b) Our results obtained for this compound at 77°K are in good agreement with the results of Semin *et al.* (Ref. 1).

furan.[17] The sample was identified by a comparison of the λ_{max} of its UV spectrum and its mp with the values reported for perchlorofulvene.[18] It was then purified by recrystallization from *n*-hexane at about 0°C. Deep-red needles; mp 155—156°C.

Perchlorocyclopentene, VI, was prepared by the chlorination of perchlorocyclopentadiene with antimony pentachloride.[13] Recrystallization from ethanol; mp 38—39°C.

Perchloro-(4-methylcyclopentene),[19] VII, was prepared from perchlorohexadiene-1,5 by treatment with anhydrous aluminum chloride in dichloromethane. Recrystallization from acetone; mp 133°C.

17) Details of this new convenient method will be described in a later publication.

18) E. T. McBee, C. W. Roberts, and J. D. Idol, Jr., *J. Amer. Chem. Soc.*, **77**, 4375 (1955).

19) H. J. Prins, *Chem. Abstr.*, **44**, 1022c (1950).

Results and Discussion

The NQR frequencies of ^{35}Cl in these perchloro-compounds are summarized in Table 1, together with the frequencies of ^{37}Cl at 77°K.

The intensities of the resonance lines of II, III, IV, VI, and VII were found to be much stronger than those of I and V.

The number of resonance lines found for II and III was equal to half the number of chlorines in the corresponding molecule. This indicates that these molecules must possess one or more symmetry elements in their crystals.

In order to minimize the effect of lattice vibrations on the resonance frequency, the observed frequencies were extrapolated to 0°K. The extrapolated values are listed in the last column of Table 1.

The assignments of the frequencies are shown in Fig. 2.

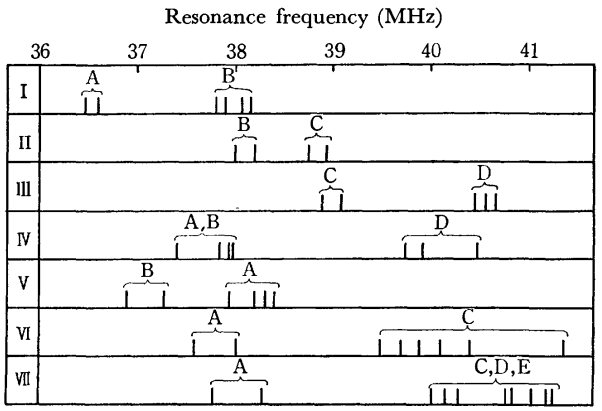

Fig. 2. Resonance frequencies extrapolated to 0°K. Vertical lines show the locations of the frequencies. The notations, A, B, C, D, and E, indicate the functional groups: A, =C–Cl: B, $=CCl_2$; C, $>CCl_2$, D, $-CCl_3$; E, $>\underset{|}{C}-Cl$.

The NQR spectrum of I consists of six resonance lines. Obviously these lines fall into two groups, one of two lines and one of four, centred at about 36.5 and 38.0 MHz respectively. From a structural point of view, the lower two lines may be attributed to the two vinyl chlorines attached to the cyclobutene ring, and the higher four lines, to the four chlorines in the two dichloromethylene groups. The frequencies of chlorines attached to the double bond in the cyclobutene ring are rather lower than those in the five- and eight-membered rings (see the spectra of IV, V, VI, and VII). Roedig *et al.* have reported unusually low resonance frequencies of vinyl chlorines on a cyclobutene ring, 35.53 and 35.95 MHz.[6] This supports our assignment above.

The NQR spectrum of II consists of two groups of lines. From a comparison of the spectrum of II with the spectra of III and I, it is evident that the two lines at about 38 MHz are assignable to the $=CCl_2$, and the other two lines at about 38.7 MHz, to the $>CCl_2$. Because of the conjugative effect, the frequency of an olefinic chlorine is somewhat lower than the frequency of a paraffinic chlorine.

The III molecule has two functional groups, $-CCl_3$ and $>CCl_2$. The three resonance lines at about 40.5 MHz were found to disappear gradually at about 210°K (the so-called "fade-out" phenomenon). This phenomenon has also occasionally been observed for compounds containing trichloromethyl groups, $-CCl_3$.[20,21] Therefore, the three lines at about 40.5 MHz are assignable to the $-CCl_3$, and the other two lines at about 39 MHz, to the $>CCl_2$.

At room temperature, Furusaki has investigated the crystal structure of IV and found that the symmetry of this molecule is C_2.[12] He also found that there were seven crystallographically-nonequivalent chlorine atoms in the unit cell, while, in our NQR study of IV, only four resonance lines were observed at room temperature. Since the frequencies of these four lines decrease monotonously with an increase in the temperature, this crystal seems to undergo no phase transition between 77°K and room temperature. Therefore, the experimental fact that seven resonance lines were observed at 77°K is consistent with this crystal structure. The NQR spectrum of IV consists of two groups: three lines appeared in the frequency region from 39.7 to 40.5 MHz, and four lines, in the region from 37.4 to 38.0 MHz. The higher three lines, ν_1, ν_2, and ν_3, were found to fade out at about 260°K; they are assigned to the $-CCl_3$.

The six resonance lines found for the V compound may be divided into two groups, four lines centered at about 38.2 MHz and two lines centered at about 36.9 and 37.3 MHz. Since this molecule has four olefinic chlorines adjacent to the double bonds in the cyclopentadiene ring and two chlorines in the $=CCl_2$ group, the four higher-frequency lines may be attributed to the olefinic chlorines adjacent to the five-membered ring, and the two lower-frequency lines, to the chlorines in the $=CCl_2$ group. This assignment requires some explanation. If the assignemnt mentioned above for V is correct, the resonance frequencies of the chlorines in the $=CCl_2$ of V are lowered by about 1 MHz below the frequencies of the chlorines in the $=CCl_2$ of I, II, and IV. The decrease in the resonance frequency may be due to the contribution of the following structure to the ground state of V.

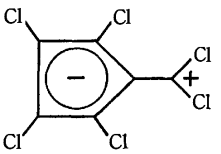

Fig. 3.

In this structure, the electrons of the p_π orbitals of chlorines in the $=CCl_2$ may be in part transferred to the adjacent carbon atoms. According to the theory of Townes and Dailey,[22,23] this decrease in the electron density of the p_π orbitals of chlorine atoms accounts for the decrease in the resonance frequency. Recently, Agranat *et al.* have suggested, in their study of dipole moments, a certain contribution of a dipolar structure to the ground state of V.[24] This supports the above

20) H. C. Allen, Jr., *J. Amer. Chem. Soc.*, **74**, 6074 (1952).
21) H. S. Gutowsky and D. W. McCall, *J. Chem. Phys.*, **32**, 548 (1960).
22) C. H. Townes and B. P. Dailey, *ibid.*, **17**, 782 (1949).
23) B. P. Dailey and C. H. Townes, *ibid.*, **23**, 118 (1955).
24) I. Agranat, H. Weiler-Feilchenfeld, and R. M. J. Loewenstein, *Chem. Commun.*, **1970**, 1153.

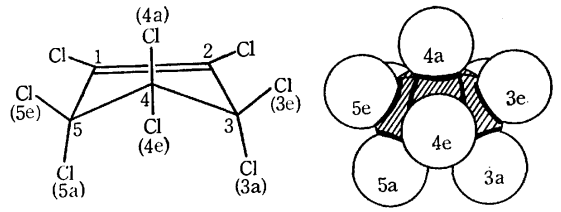

Fig. 4. Molecular model of perchlorocylcopentene, VI.

considerations.

In the NQR spectrum of VI, it is seen that one of the six frequencies of the geminal chlorines is considerably higher than the frequencies of the other geminal chlorines. This can be explained in terms of a strong electrostatic repulsion between the chlorine atoms. An examination of the molecular model of VI (Fig. 4) leads to the following results.

It can be seen in Fig. 4 that the distance between Cl (4e) and Cl(3a), and that between Cl(4e) and Cl(5a), are the shortest among those between the geminal chlorines. Thus, the equatorial chlorine, Cl(4e), is subject to a stronger electrostatic repulsion than any other geminal chlorine. The repulsive electrostatic interaction between chlorine atoms causes the migration of the electronic charge from the chlorine atoms to carbon atoms, and thus causes a diminution in the ionic character of the C–Cl bond. The decrease in the ionic character results in the shift of the resonance frequency to the higher-frequency side.[22,23] The highest frequency line, ν_1, of VI thus assignable to the equatorial chlorine, Cl (4e).

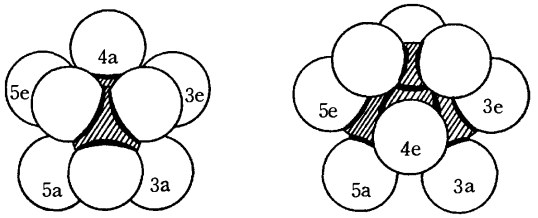

equatorial conformer axial conformer

Fig. 5. Two conformations of perchloro-(4-methylcyclopentene), VII.

The VII molecule has two possible conformations (Fig. 5). In either conformation, the degree of all the intramolecular Cl···Cl repulsive interactions may be larger than that in VI because of the extreme bulkiness of the $-CCl_3$ group. The ionic character of C–Cl bond in the $>CCl_2$ of VII is expected to be smaller than that of VI. This diminution of the ionic character accounts for the experimental fact that the average value of the resonance frequencies of VII shifts to a higher-frequency side compared to that of VI.

It should be noted that the average value of the resonance frequencies of the chlorines in carbon tetrachloride, CCl_4, is comparable to those of the chlorines in the $>CCl_2$ of VI and VII. According to the theory of Townes and Dailey,[22,23] the observed NQR frequency is related to the ionic and double-bond characters of the C–Cl bond and to the *s* character of the chlorine-bonding orbital. They also proposed that the amount of the *s* character was about 15% for the chlorine-bonding orbital in a C–Cl bond.[23] The double-bond character of the C–Cl bond in the $>CCl_2$ and CCl_4 may be neglected. Therefore, the ionic character of the C–Cl bond in the $>CCl_2$ of VI and VII is comparable to that of CCl_4.

Table 2. Resonance lines found to fade out and the temperatures, T_f, at which the resonance lines disappeared

No. of resonance lines	T_f (°K)
All lines of I	255
ν_1, ν_2, and ν_3 of III	210
ν_1, ν_2, and ν_3 of IV	260
All lines of V	255
ν_7 of VII	280

For several compounds, the fade-out phenomena were found at rather low temperatures. The temperatures, T_f, at which the resonance lines disappeared are summarized in Table 2. The fade-out of chlorine resonances has been reported for a number of compounds.[20,21,25,26] From the fact that the fade-out apparently occurs only in a solid where internal or molecular rotation is either definitely known to ocuur or is very likely to occur, it has been considered that such motions are responsible for the fade-out.[21] In the cases of III and IV, a similar mechanism may operate and the disappearance of the $-CCl_3$ chlorine resonances could results from the internal rotaion or rotational oscillation of the $-CCl_3$ group. This view is supported by the large X-ray temperature factors found for the chlorine and the carbon atoms in the $-CCl_3$ groups of IV.[12]

Furusaki, in his X-ray study of IV, has found close intermolecular Cl···Cl distances, 3.43, 3.56, and 3.58 Å for the $-CCl_3$ group.[12] Although the crystal structure of III has not yet been determined, the intramolecular Cl···Cl distances between the two $-CCl_3$ groups in this molecule are expected to be extremely short, for two bulky $-CCl_3$ groups are attached to either end of the C=C bond. However, the fade-out phenomena found for III and IV seem to suggest that the steric hindrance is not severe enough to prevent the internal rotation or rotational oscillation of the $-CCl_3$ group. Detailed studies of the mechanism of the fade-out phenomena found for I and V are now being undertaken by means of investigations of the crystal structures (at room temperature and at low temperatures), by thermal analysis (DTA and DSC), and by studying the temperature dependence of the dielectric constant and the electrical conductivity.

The authors wish to thank Professor Akira Fujino, Research Institute for Atomic Energy, Osaka City University, for his kind gift of the sample for identification. We also wish to thank Dr. Yoshio Kamishina, Faculty of Science, Kobe University, for his valuable suggestions.

25) M. T. Rogers and J. A. Ryan, *J. Phys. Chem.*, **72**, 1340 (1968).

26) M. Hashimoto, T. Morie, and Y. Kato, This Bulletin, **44**, 1455 (1971).

Photoemission of Ion Radical Salts. Benzonitrile- and Triphenylene-Alkali Metal Complexes

Haruki KAWAMURA and Hiroo INOKUCHI

The Institute for Solid State Physics, The University of Tokyo, Roppongi, Minato-ku, Tokyo

(Received September 8, 1971)

The photoelectric emission of the benzonitrile-alkali metal salts were measured and compared with those of the hydrogen-chemisorbed samples. The adsorption of hydrogen onto the salt caused a decrease in the quantum yield of the photoemission at a higher energy region and also a decrease in the threshold energy. The threshold energies were 5.05±0.02 eV for the benzonitrile-rubidium ion radical salt and 4.95±0.02 eV for its hydrogen-chemisorbed sample. Further, the spectral response of the quantum yield of the photoemission for the triphenylene-cesium complex was measured. The threshold energies of the mono- and dinegative ions were 2.40 eV and 2.43 eV respectively, and the quantum yield of the mononegative salt was ten times than that of the dinegative one.

The photoemission from inorganic solids—metals and semiconductors —— has been studied by many workers. However, few studies have been reported on the photoemission from organic materials, especially for organic complexes. Suhrmann first showed that the efficiency of the photoelectric emission of alkali metals is enhanced by the evaporation of hydrocarbon, naphthalene, or anthracene onto sodium (or potassium) metal film;[1] this enhancement may arise from the formation of a complex between alkali metal and aromatic hydrocarbon.

Since this pioneer work, several studies of the photoemission from the aromatic-alkali metal salts have been made in order to clarify the mechanism of the charge-transfer process of the complexes.[2,3]

In this paper, we will present out results on the photoemission from the ion radical salts, benzonitrile-alkali metals and triphenylene-alkali metal. The effect of hydrogen adsorption onto the surface of the benzonitrile-alkali metal complex on the photoemission will be discussed. Further, the change in the photoemission efficiency from the triphenylene-alkali metal salt as a function of the valencies of the aromatic anion is reporsed.

Experimental

Preparation of the Thin Film of the Ion-radical Salt. Benzonitrile-alkali metal salts[4]: Commercial benzonitrile was refluxed with diphosphorous pentoxide in a sealed glass vessel to eliminate all traces of water, subsequently degassed by alternate boiling under a vacuum, and distilled repeatedly. Cesium and rubidium metals, the electron donors, were prepared from their chlorides by reduction with calcium metal in an evacuated glass vessel.[5] The sodium metal was purified by distillation *in vacuo*.

Both the preparation of the ion-radical salt and the measurement of the photoemission from the salt were carried out *in vacuo* (10^{-5}—10^{-6} Torr) because of the instability of the ion-radical salt in air; the purified alkali metal was first evaporated on the surface of a glass vessel, and then purified benzonitrile liquid was introduced into the vessel. By these operations, a dark red solution (excess benzonitrile acts as a solvent) was made. The coloured solution was then dropped onto a copper-disc cathode (emitter) 10 mm in diameter, and the excess benzonitrile was evaporated completely for about 20 hr to make the radical-salt thin film. Then, the copper disc with the deposited salt film was moved towards the centre of the glass photocell, the inside of which had been coated with evaporated gold thin film and which was used as collector. Figure 1 shows the delicate glass photocell.

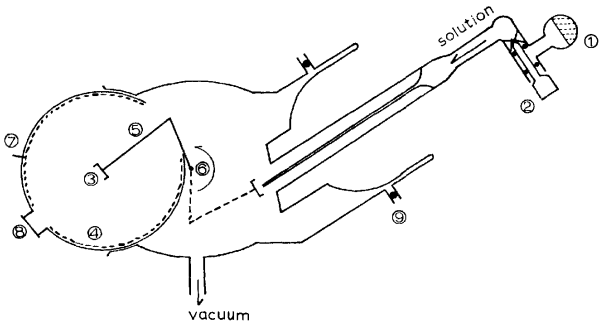

Fig. 1. The schematic diagram of the apparatus for photoemission measurement *in vacuo*. (1); The ion salt solution, (2); greaseless tap, (3); copper disc with the film, (4); Au evaporated film, (5); copper rod, (6); tungsten rod and moving apparatus, (7); collector lead (tungsten rod), (8); quartz window, (9); O-ring.

Triphenylene-cesium ion-radical salt: Commercial triphenylene was recrystallized several times from its alcohol solution and then sublimed in a vacuum. The triphenylene-cesium complexes, both mono- and dinegative ion salts, were prepared as precipitates from their tetrahydrofuran (THF) solution when the triphenylene in THF was brought in contact with Cs metal.[6] The THF solution, in which the radical salt had been suspended, was dropped onto the copper disc through a glass capillary, and then the THF was completely evaporated from the solution, during about a 4 hr period, to make a thin film.

Measurement of the Photoemission. An incident light from a hydrogen-discharge lamp was monochromatized with a Hilger-type monochromator with a quartz prism (for the benzonitrile salt) and also with a Shimadzu Baush-Lomb monochromator (for the triphenylene salt). The absolute measurement of the light intensity was made by means of an

1) R. Suhrmann, *Z. Phys.*, **94**, 742 (1935), **111**, 18 (1937).

2) H. Inokuchi and Y. Harada, *Nature*, **198**, 477 (1963); T. Hirooka, M. Kochi, J. Aihara, H. Inokuchi, and Y. Harada, This Bulletin, **42**, 1481 (1969).

3) M. Batley and L. E. Lyons, *Mol. Cryst.*, **3**, 357 (1968).

4) M. Tsuda and H. Inokuchi, This Bulletin, **43**, 3410 (1970).

5) $2MCl+Ca=2M+CaCl_2$ (M=Cs and Rb).

6) The triphenylene-Cs ion radical salt was precipitated as deep-coloured crystallites; in the salt, triphenylene forms mono- and dinegative ions, depending on the amount of alkali metal. The details will be reported elsewhere.[7]

7) K. Kimura and H. Inokuchi, to be published.

Epply circular thermopile, the sensitivity of which was 0.3 μV/μW *in vacuo*. The output potential was applied from a Keithley 241 voltage supply; 10 V for the benzonitrile salt[8] and 50 V for the triphenylene salt. The photoemissive current was amplified and measured by means of a Cary 32 vibrating-reed electrometer, as a function of the wavelength of the incident light.

Results and Discussion

Benzonitrile-Alkali Metal Salts. The photoemissions from the benzonitrile-sodium, rubidium, and cesium ion-radical salts were measured as functions of the wavelength of the incident light; at first, the measurement of the photocurrent of the freshly prepared film was carried out, and then the salt film was placed in contact with purified hydrogen gas of 10 Torr for 100 min and then pumped up to 10^{-5} Torr. The photocurrent from the hydrogen-exposed film was measured and compared with that of the fresh one.[9] Figures 2, 3, and 4 show the photoelectric yield curves as functions of the photon energy.

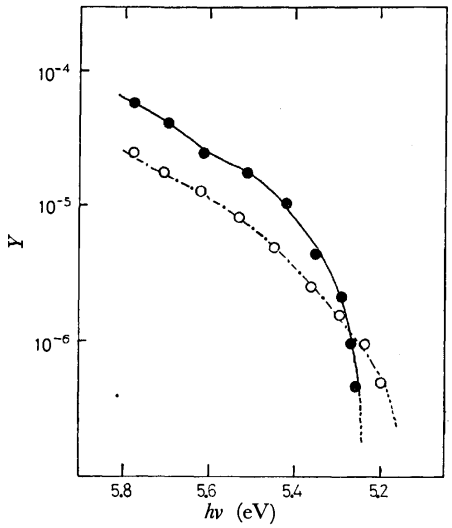

Fif. 2. The spectral distribution of the quantum yield for the Na-Benzonitrile film -●- and for its hydrogen-exposed film -○- -.

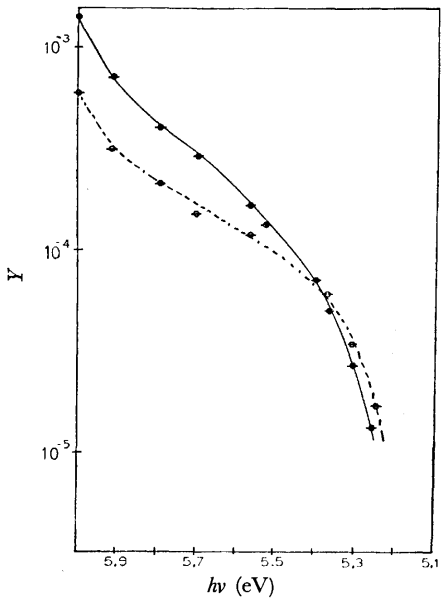

Fig. 3. The spectral distribution of the quantum yield for the Rb-Benzonitrile film -●- and for its hydrogen-exposed film -○- -.

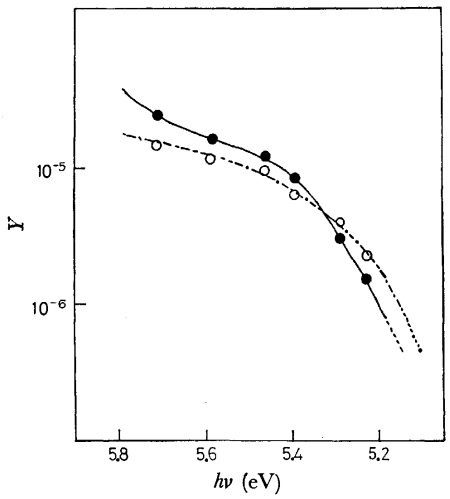

Fig. 4. The spectral distribution of the quantum yield for the Cs-Benzonitrile film -●- and for its hydrogen-exposed film -○- -.

In the present work, the quantum yield (in electrons/quantum unit) was measured only down to 10^{-6}; thereafter, the threshold energy, E_{th}, could not be determined by an extrapolation method.[10] Therefore, the value of the threshold energy had to be obtained another method. By analogy with the Fowler plots for the photoemission of metals, the quantum yield of the ion radical salts near the threshold energy may be subjected to the conventional power law:

$$Y \propto (E-E_{th})^n \qquad (1)$$

where Y is the quantum yield and E is the incident

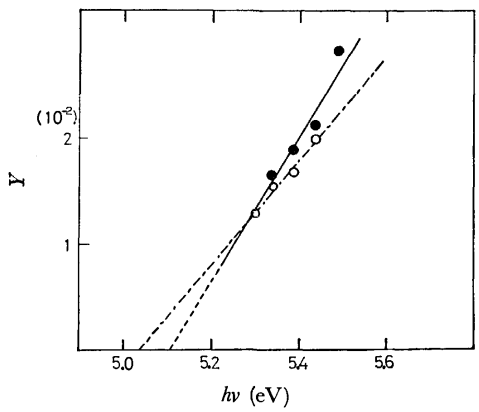

Fig. 5. The power-law fit for the photoelectric quantum yield near the threshold region (Cs-benzonitrile salt).
for the fresh film -●- and
for the hydrogen-exposed film -○- -.

8) The applied voltage was enough for a saturated photoemissive current to be found.

9) H. Kawamura, M. Tsuda, and H. Inokuchi, *Chem. Phys. Lett.*, **5**, 80 (1970).

10) The values of E_{th} are determined by extrapolation from a quantum yield of 10^{-7}—10^{-9} electrons per incident quantum.

photon energy. For the organic complexes, it has been shown empirically that a cube-root plot of the quantum yield ($n=3$) becomes almost linear as a funciton of the incident photon energy, as is illustrated in Fig. 5.[2,11] Table 1 summarizes the values of E_{th}. In Table 1, the accuracy of the work function of the salts is kept within the range of the resolving power of the monochromator for an incident light; the resolving power is 0.02 eV. The values of E_{th} thus obtained are, for example, 5.05 ± 0.02 eV for the benzonitrile-Rb ion radical salt and 4.95 ± 0.02 eV for the H_2-exposed sample. The energy differences, ΔE, between the fresh sample and the H_2-exposed one are 0.07—0.1 eV.

TABLE 1. THE THRESHOLD ENERGY in eV OF PHOTOEMISSION OF BENZONITRILE-ALKALI METAL ION RADICAL SALTS

Donor	Fresh	H_2-exposed	ΔE
Na	5.01	4.92	0.09
Rb	5.05	4.95	0.10
Cs	5.11	5.04	0.07

Generally, in the formation of the salt there is a sharp increase in the electronic conductivity and in the quantum yield photoemission in comparison with its components. The mobile electrons in the salt may originate from the excess charge which transfers from the donor, the alkali metal, to the acceptor, aromatics. The adsorption of hydrogen causes a decrease in the quantum yield in the higher energy region and also a decrease in the threshold energy, as is illustrated in Figs. 2—4. A similar phenomenon appeared in the behavior of the electronic conductivity; that is, there was a marked decrease in the conductivity with the chemisorpition of hydrogen onto the ion-radical salt.[12] The above findings suggest that the excess charge of the radical salt participates in forming a chemisorption-bond with hydrogen.

The quantum yield near the threshold energy of the H_2-exposed sample was larger than that of the fresh one, and the work function of the salt was decreased by the adsorption of hydrogen gas. It seems that the dcrease in the work function derives from the appearance of the surface state, located 0.07—0.1 eV[13] above the highest occupied level of the salt. When the hydrogen-exposed sample was pumped out for a week, the value of the quantum yield of the H_2-exposed sample recovered the value of the fresh sample. Figure 6 shows the time dependence of the photoemission for the benzonitrile-cesium complex under pumping.[14] This result shows that the hydrogen is chemisorbed onto the salt, but does not react.

Triphenylene-Cesium Complex. Figure 7 shows the quantum yield curve of photoemission for the triphenylene-cesium complex. The threshold energies of

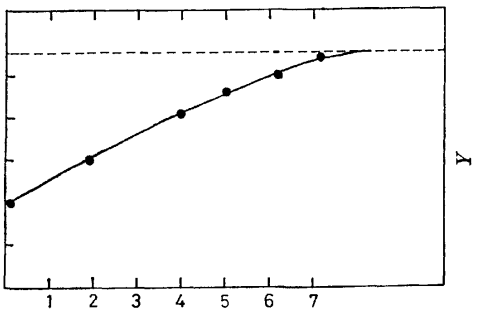

Fig. 6. The time dependence of the photoemission for the H_2-exposed benzonitrile-cesium complex under pumping. I_0 is the value of quantum yield for the fresh film.

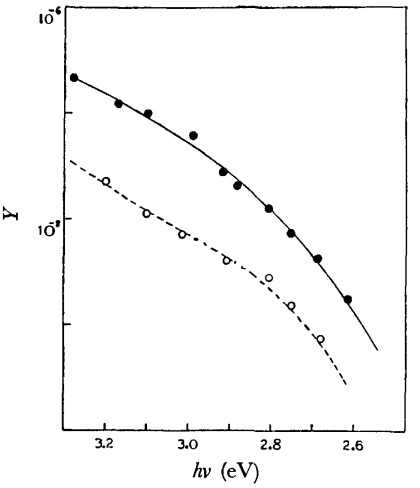

Fig. 7. The quantum yield curve of photoemission for triphenylene-cesium complex.
for Tp^- film -●- and
for Tp^{2-} film --○--

the mono- and dinegative ion salts are 2.40 and 2.43 eV respectively. The quantum yield of the mononegative salt is ten times that of the dinegative one. In the case of the dinegative solid, there are many cesium ions surrounding the aromatic anion; therefore, it is more difficult for the electrons to jump out than in the case of the mononegative sample.

Some aromatic-alkali metal ion radical salts have been found to have a good catalytic activity for hydrogen-deuterium equilibration, $H_2+D_2=2HD$; this catalytic activity may arise from the excess charge, which participates in forming the chemisorotion bond with H_2 on the ion-radical salt in the solid phase.[15] This proposal is supported by these photoemission results.

On the other hand, we have already reported that the distinction of the valencies on the anion produces a large difference in their catalytic acitvity; the reaction rate for the dinegative ion salt was found to be ten times that of the mononegative ion salt at room temperature.[5,15,16] Although no quantitative correlation between the catalytic acitvity and the photoemissive character as functions of the valencies of the anion can be found, we

11) M. Kochi, Y. Harada, T. Hirooka, and H. Inokuchi, This Bulletin, **43**, 2690 (1970).

12) H. Inokuchi, N. Wakayama, and T. Hirooka, *J. Catal.*, **8**, 383 (1967).

13) The value corresponds to ΔE, the energy difference between the E_{th} values of the fresh sample and the H_2-exposed one.

14) During this experiment, the photoemission was measured with a 220-mμ incident light.

15) T. Kondow, H. Inokuchi, and N. Wakayama, *J. Chem. Phys.*, **43**, 3766 (1965); H. Inokuchi, *Discuss. Faraday Soc.*, **51**, 183 (1971).

16) N. Wakayama, Y. Mori, and H. Inokuchi, *J. Catal.*, **12**, 15 (1968).

now intend to make further studies of the behaviour of the excess charge in ion-radical salts.

The authors wish to express their thanks to Drs. Motoyuki Tsuda and K. Kimura for the preparation of the samples and for their useful suggestions.

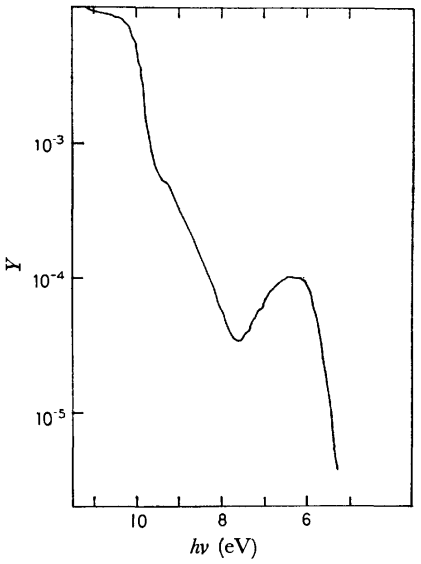

Fig. 8. The spectral response curve of the photoemissive quantum yield for triphenylene-cesium salt in the vacuum ultraviolet region.

Appendix

The photoemission from the benzonitrile-Cs complex was measured in the vacuum-ultraviolet region. Figure 8 shows the spectral response curve of the photoemissive quantum yield. In the curve, a sharp minimum at the photon energy of 7.65 eV was found. The minimum may be the emission from the second-highest occupied level of the benzonitrile anion. This assumption is supported by the fact that the difference (7.65−5.11=2.54 eV) between the minimum (7.65 eV) and the threshold value (5.11 eV) agrees with the absorption peak of the anion, 490 mμ (2.54 eV), and corresponds to the transition between the highest occupied level and the second highest occupied level, as is shown in the following diagram.

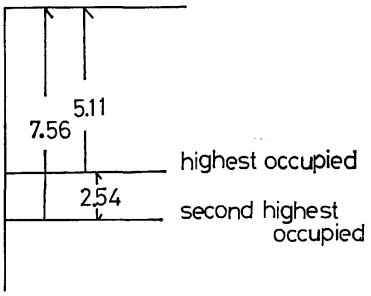

BULLETIN OF THE CHEMICAL SOCIETY OF JAPAN, VOL. 45, 713—716(1972)

Magnetic Properties of Some Iminoxyl Polyradicals. III. Exchange Interaction in Iminoxyl Biradicals

Akira NAKAJIMA, Hiroaki OHYA-NISHIGUCHI, and Yasuo DEGUCHI*

Department of Chemistry, Faculty of Science, Kyoto University, Kyoto

**College of Liberal Arts and Science, Kyoto University, Kyoto*

(Received September 11, 1971)

The EPR spectra of TEMPAD and Sulfite biradicals in a dilute solution have been reasonably interpreted in terms of the variation in the ratio of the intra-molecular exchange interaction to the ^{14}N hyperfine interaction. Comparing these spectra with the theoretical ones, the authors have estimated the intra-molecular exchange interactions as $10.0 \cdot A = 2 \times 10^{-2} k$ and $3.0 \cdot A = 5 \times 10^{-3} k$ respectively. The magnetic susceptibility of the TEMPAD biradical exhibits a broad maximum at a temperature of 16.5°K, while 50 and 75% TEMPAD diluted in corresponding diamine have no maximum in the temperature range measured. The magnetic susceptibility of the sulfite biradical also shows a broad maximum at 15.0°K, in spite of the weak intra-molecular exchange interaction. These results indicate that the origin of the short-range ordering is the inter-molecular exchange interaction between unpaired electrons in different molecules.

There have been a number of investigations with regard to the magnetic properties of organic, stable free radical solids; these investigations will be adequately introduced elsewhere.[1] In these works, some short-range ordering effects caused by the exchange interaction between unpaired electrons are of special interest. The mechanism of the exchange interaction, namely, intra- or inter-molecular exchange interaction, is also an interesting subject to us.[1]

Previously, the present authors reported the magnetic susceptibility of bis(2,2,6,6-tetramethylpiperidine-4) azine-1,1′-dioxyl (the TEMPAD biradical), which indicates a broad maximum at 16.5°K. In order to explain this result, we assumed a thermal equilibrium between the singlet ground state and the excited triplet

1) A. Nakajima, H. Ohya-Nishiguchi, and Y. Deguchi, This Bulletin, to be published.

state caused by the strong exchange interaction between the two unpaired spins in a molecule. On the basis of this model, one could estimate the exchange parameter as $J=-1.14\times10^{-3}$ eV;[2] however, we could find no evidence supporting the model.

On the other hand, recent EPR studies of other iminoxyl biradicals indicate fairly weak exchange interaction in a molecule which is of the same order as the hyperfine interaction.[3-5] These results are inconsistent with our estimation.

In order to clarify this discrepancy, one should take into account the existence of an inter-molecular exchange interaction in addition to an intra-molecular one. As for the experimental study of these two exchagne mechanisms, one must apply some techniques for the elimination of either intra- or inter-molecular exchange interaction. The present authors have made a couple of experiments along those lines: one of them was the dilution of TEMPAD in a diamagnetic matrix in order to decrease the inter-molecular exchange interaction, and the other was the study of other biradicals with a weak intra-molecular exchange interaction aimed at enhancing the inter-molecular exchange interaction.

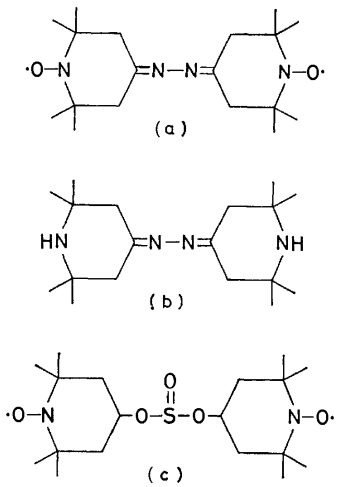

Fig. 1. Molecular structures of the TEMPAD biradical (a), the corresponding diamine (b), and the Sulfite biradical (c).

In this paper, the authors shall report the EPR spectra and the magnetic susceptibilities of the TEPMAD biradical (Fig. 1a) diluted in the corresponding diamine (Fig. 1b) and bis(2,2,6,6-tetramethylpiperidine-4)sulfite-1,1'-dioxyl (the sulfite biradical, Fig. 1c), which has a weak intra-molecular exchange interaction.[4]

Experimental

The TEMPAD biradical and the corresponding diamine were prepared from 2,2,6,6-tetramethyl-4-piperidone (triacetoneamine supplied by the Aldrich Chemicals Co.) following the method described by Rassat *et al.*[6] After purification by chromatography and recrystallization, pure diamine and TEMPAD (mp 139±0.5°C and 182±1.0°C) respectively were obtained. The sulfite biradical was prepared from the TANOL radical (2,2,6,6-tetramethyl-4-hydroxypiperidine-1-oxyl) obtained by the oxidation of the corresponding amine with hydrogen peroxide, following the process of Rozantsev *et al.*[4]

The EPR measurements were carried out using X-band spectrometers, JEOLCO's JES-3BX and JES-P-10, equipped with a 100-kHz field modulation. As a standard sample, peroxylamine disulfonate $[\cdot ON(SO_3)_2]^=$ ($A_N=13.0$ gauss, $g=2.00537$) was used. In all the EPR measurements, the samples were degassed and sealed in glass tubes *in vacuo*.

The static magnetic susceptibility measurements were performed with powder samples of about 50—100 mg over the temperature range of 1.8—273 °K and in magnetic fields of 8—9 kOe, using a torsion balance which has been described elsewhere.[7] The temperature of the samples was determined by means of a Au·Co-Cu thermocouple and a carbon resister set on samples which had been calibrated by means of a standard sample, Mn-Tutton's salt. All the data were corrected for the diamagnetic contributions calculated by the Pascal method, *i.e.* $\chi_{dia}=-2.37\times10^{-4}$ emu/mol for TEMPAD and $\chi_{dia}=-2.62\times10^{-4}$ emu/mol for the sulfite biradical.

Results and Discussion

EPR Spectra. The spin Hamiltonian applied by Lemaire and his co-workers to nitroxide biradicals is:[5,6]

$$\mathcal{H}=g\beta H\cdot S_z+A(S_{1z}I_{1z}+S_{2z}I_{2z})+2|J|(\boldsymbol{S}_1\cdot\boldsymbol{S}_2). \quad (1)$$

The Hamiltonian is expressed in units of h, and the three righthand terms correspond to the Zeeman, hyperfine, and exchange energies. The electron spin operators, $\boldsymbol{S}_i$ and $\boldsymbol{S}_{iz}$, refer to an electron spin wavefunction at the i-th side of the biradical; I_{iz} is the corresponding ^{14}N nuclaer spin operator, and $\boldsymbol{S}$ is the total electron spin operator. One can then show the eigen values of Eq. (1) as:

$$\begin{aligned}
E_{+1}(m_1m_2) &= g\beta H+|J|/2+(A/2)(m_1+m_2)\\
E_{\pm0}(m_1m_2) &= -|J|/2\pm(1/2)D\\
E_{-1}(m_1m_2) &= -g\beta H+|J|/2-(A/2)(m_1+m_2)\\
D^2 &= 4|J|^2+A^2(m_1-m_2)^2 \qquad (D>0)
\end{aligned} \quad (2)$$

and the theoretical EPR absorption energies and the relative intensities as:

i) $m_1\neq m_2$

$$\begin{aligned}
W_{1\pm}(m_1m_2) &= g\beta H+|J|+(A/2)(m_1+m_2)\mp(1/2)D\\
W_{2\pm}(m_1m_2) &= g\beta H-|J|+(A/2)(m_1+m_2)\pm(1/2)D\\
I_{t\pm} &= A^2(m_1-m_2)^2/(D^2+4|J|\cdot D)
\end{aligned} \quad (3)$$

ii) $m_1=m_2$

$$\begin{aligned}
W_3(m_1m_2) &= g\beta H+(A/2)(m_1+m_2)\\
I &= 1
\end{aligned} \quad (4)$$

The theoretical EPR absorption lines for different values $|J|/A$ are of shown in Fig. 2.

The experimental EPR spectrum of the TEMPAD

2) A. Nakajima, H. Nisniguchi, and Y. Deguchi, *J. Phys. Soc. Jap.*, **24**, 1175 (1968).
3) H. Lemaire, B. Levy, and A. Rassat, *Colloque du Centre National de la Recherche Scientifique, Paris*, 1966.
4) E. G. Rozantsev, G. F. Davelko, A. L. Buchachenko, and M. B. Neiman, *Izv. Akad. Nauk SSSR Ser. Khim.*, **1967**, 2306.
5) S. H. Glarum and J. H. Marshall, *J. Chem. Phys.*, **47**, 1374 (1967).
6) R. Briere, R. M. Duperyre, H. Lemaire, C. Morat, A. Rassat, and P. Rey, *Bull. Soc. Chim. Fr.*, **1965**, 3290.
7) M. Mekata, *J. Phys. Soc. Jap.*, **17**, 796 (1962).

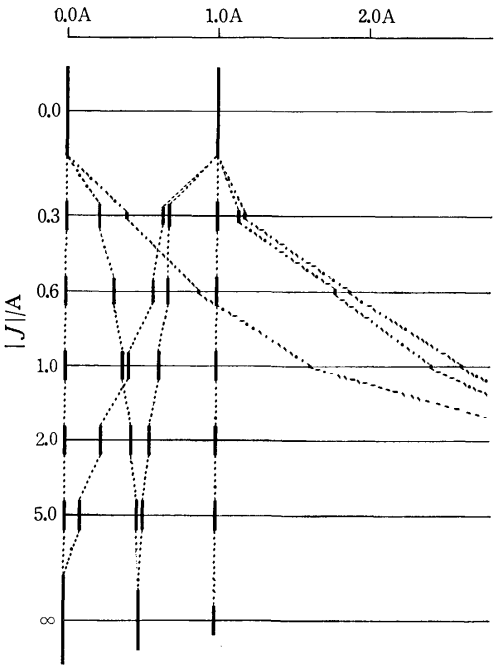

Fig. 2. The theroretical EPR absorption lines for the different values of $|J|/A$.

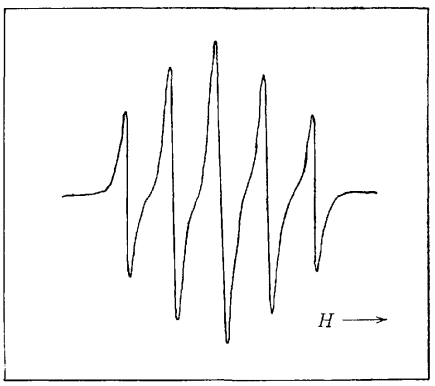

Fig. 3. The EPR spectrum of the TEMPAD biradical in THF solution.

biradical in a tetrahydrofurane (THF) solution at room temperature, as shown in Fig. 3, consists of five lines, with an intensity ratio of 1:2:3:2:1. This result implies that the spectrum corresponds to the case of $|J| \gg A$. The line-width of the center line, however, is considerably broader than that of the four side lines. This is caused by the incomplete superposition of the $W_{1\pm}(\pm 1, \mp 1)$, $W_{2\pm}(\pm 1, \mp 1)$, and W_3 (0, 0) lines. From the line-width of the center line, one can estimate the exchange parameter as $|J| \simeq 10.0 \cdot A = 2 \times 10^{-2} k$ (A= 15.0 gauss).

In the case of the sulfite biradical (see Fig. 4), the EPR spectrum consists seven lines, with an integrated intensity ratio of 1:2:1:1:2:1. This spectrum corresponds to the case of $|J| \sim A$; thus, the exchange energy can be estimated as $|J| \simeq 3.0 \cdot A = 5 \times 10^{-3} k$ (A= 15.6 gauss).

The magnitudes of the intra-molecular exchange interaction estimated from the EPR spectra are listed in Table 1 in units of the hyperfine energy, A. From

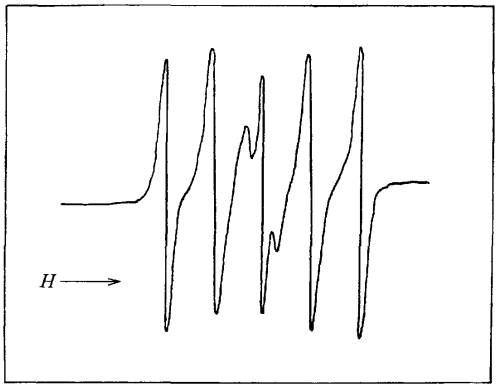

Fig. 4. The EPR spectrum of the Sulfite biradical in THF solution.

Table 1. Magnitude of the intra-molecular exchange interaction of some iminoxyl biradicals in the unit of the hyperfine energy, A.

Biradical	Solvent	Temperature	Magnitude	Reference
TEMPAD	THF	room temp.	10.0	our result
Sulfite	THF	room temp.	3.0	our result
	THF	20°C	2.8	4
Dimethyl-silicate	THF	20°C	1.7	4
Diphenyl-silicate	THF	20°C	6.0	4
Diallyl-silicate	THF	20°C	6.2	4
Carbonate	DMF	0°C	0.92	3
	DMF	−60°C	1.0	3
	n-Hexane	0°C	0.8	5
	CS_2	−100°C	1.1	5
Oxalate	CS_2	−60°C	0.15	5

this table, one can understand that the $|J|$ magnitudes of these biradicals range from 10^{-4} to $10^{-2}k$, that is, that their intra-molecular exchange interactions are fairly weak compared with those estimated from the susceptibility measurements.

Magnetic Susceptibility. The magnetic susceptibility of the 100% TEMPAD biradical *versus* the temperature[1] is shown in Fig. 5. From 273 to 77°K,

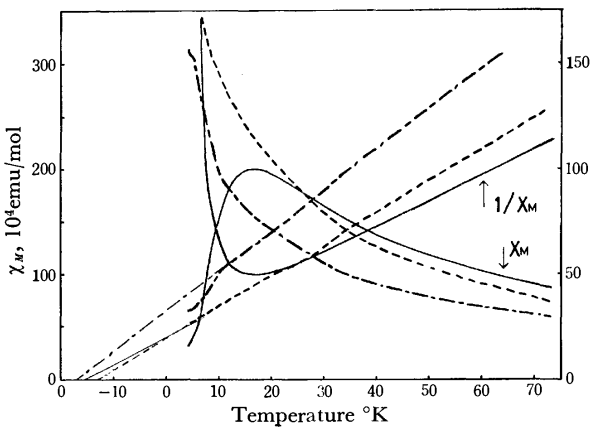

Fig. 5. Temperature dependence of the magnetic susceptibilities (χ_M) and their inverse ($1/\chi_M$) of the diluted TEMPAD biradical;
——: 100%, ----: 75%, and -·--: 50% TEMPAD.

χ_M increases paramagnetically with a decrease in the temperature and obeys the Curie-Weiss law: the Weiss constant is found to be about -15 ± 2°K. When the temperature is lowered further, the χ_M-T curve gradually deviates from the Curie-Weiss law and shows a broad maximum at the temperature of 16.5 ± 0.5°K. χ_M drops rapidly below that temperature. This behavior apparently suggests that a short-range ordering occurs as a result of the negative exchange interaction between unpaired electrons.

If one may apply some practical models, one can calculate the exchange interaction from three experimental values, *i.e.*, the temperature at the broad maximum, the value of χ_M at the broad maximum, and the Weiss constant. These values and the corresponding exchange parameters for the pair and the Ising linear-chain models are listed in Table 2.

The magnetic susceptibilities of 50 and 75% TEMPAD solid solutions diluted with the corresponding diamine, which are shown in Fig. 6, have been corrected for the diamagnetic contributions of the same value as that of the TEMPAD biradical. It should be noted that they show no maximum in the presently adopted temperature range and that their Weiss constants are nearly the same as that of 100% TEMPAD (-13°K for 75% and -16°K for 50%).

The diluted TEMPAD system, we can assume, will consist of two parts; inter-molecular dimers and isolated molecules. On this assumption, the paramagnetic susceptibility can be described as the superposition of these two parts; then, the Weiss constant obtained from the high-temperature region of the $1/\chi_M$-T curve may be to be contributed mainly by the intermolecular dimers. In the low-temperature region, these dimers almost entirely fall into the singlet ground state and the Curie constant is contributed to by only the isolated part. Our experimental results indicate these inclinations. The full details will be given in the following work.

TABLE 2. SOME MAGNETIC CONSTANTS OF 100% TEMPAD BIRADICAL AND CORRESPONDING EXCHANGE PARAMETERS FOR THE PAIR AND THE ISING LINEAR-CHAIN MODELS

	Experimental results	Exchange parameter J (°K)	
		Pair	Ising L-C
T (χ_{max})	16.5 ± 0.5°K	-13.4	-16.8
χ_{max}	$200\pm10\times10^{-4}$ emu	-15	-14
θ	-15 ± 2°K	-30	-15

θ: the Weiss constant

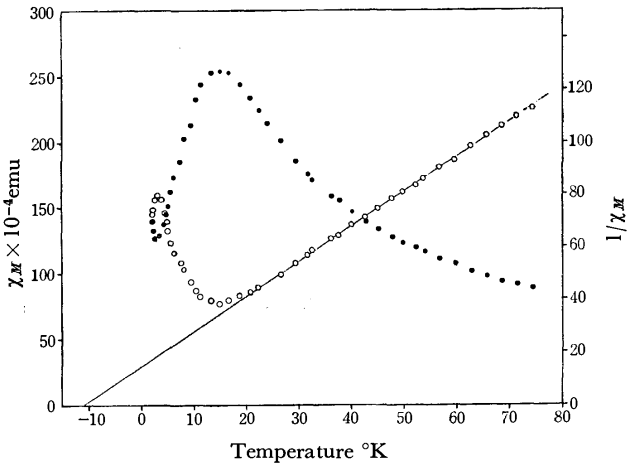

Fig. 6. Temperature dependence of the magnetic susceptibility of the Sulfite biradical;
●: χ_M, ○: $1/\chi_M$.

TABLE 3. SOME MAGNETIC CONSTANTS OF SULFITE BIRADICAL AND CORRESPONDING EXCHANGE PARAMETERS FOR THE PAIR AND THE ISING LINEAR-CHAIN MODELS

	Experimental results	Exchange parameter J (°K)	
		Pair	Ising L-C
T (χ_{max})	15 ± 1°K	-13	-15
χ_{max}	$254\pm10\times10^{-4}$ emu	-19	-18
θ	-11 ± 2°K	-22	-11

θ: the Weiss constant

The magnetic susceptibility of the sulfite biradical shows nearly the same behavior as that of 100% TEMPAD except for the rapid increase below 3°K. In order to explain this behavior, the pair model and the Ising linear-chain model can be applied. The exchange parameters of the models estimated from a comparison with the experimental results are listed in Table 3. Scince the intra-molecular exchange interaction of the sulfite biradical is fairly weak ($5\times10^{-3}k$), the large exchange interaction appearing in the magnetic susceptibility must be attributed to the inter-molecular exchange interaction.

The authors are very much indebted to Professor Hideo Takaki for his continuing guidance and encouragement through this work. They also wish to thank Professor Mamoru Mekata, Dr. Jun Yamauchi, and their collaborators for their helpful advice and discussions.

The Laser Photolysis of Methylene Blue in the Presence of *p*-Chlorophenylglycine

Kinichi Obi and Hiroshi Makino

Department of Chemistry, Tokyo Institute of Technology, Ohokayama, Meguro-ku, Tokyo

(Received September 20, 1971)

The photoreduction of methylene blue by a ruby laser light has been studied. The kinetic treatment and the measurement of the apparent activation energy show that, under the high-intensity irradiation, the excited triplet state of methylene blue plays a main role in the photoreduction by *p*-chloro phenylglycine. The apparent activation energy of the reduction of methylene blue is reduced from 7.4 to 2.8 kcal as the laser light energy increases from 23 to 530 mJ.

The photoreduction of methylene blue (MB) has been extensively studied by continuous irradiation[1-5] and by flash photolysis.[6-9] From these studies, it has become apparent that the photoreduction of MB by a reducing agent such as *N*-phenylglycines proceeds through the interaction between the lowest triplet state of MB and the reducing agent.

In a previous paper,[10] the saturation of the light absorption was observed using a giant-pulse ruby laser. Under such circumstances, the photoreduction of MB in the presence of dimethyl-phenylglycine (DMPG) has been proposed to take place through the excited triplet state of MB, which itself results from the subsequent photon absorption by the lowest triplet state.

The present paper is concerned with the reinvestigation of the excited triplet-state mechanism of MB using *p*-chloro-phenylglycine (*p*-CPG) as the reducing agent, for it is a mild reductant; the quantum yield of the photoreduction[2] of MB by *p*-CPG of an infinite concentration is 0.185, while that by DMPG is 0.388 at pH 7.0. Furthermore, new experimental proof of the excited-triplet-state mechanism was obtained from the apparent activation energies of the reduction of MB corresponding to two kinds of triplet states.

Experimental

The ruby laser head used in this work was the NEC model O-N583, which accommodates a ruby rod 8 mm in diameter and 150 mm long. The Q-switch accomplished by using an ethanol solution of cryptocyanine. The laser pulse 6943 Å was *ca.* 20 nsec in duration and had an energy of *ca.* 530 mJ, which corresponds to 1.85×10^{18} photons. The cross-sectional area of the laser beam was *ca.* 0.25 cm^2. Several neutral density filters, whose transmittance percentages were calibrated for the laser light, were used to reduce the light intensity. The quartz reaction cell used was cylindrical, 13 mm in diameter and 18 mm in path length.

Commercially available MB was obtained from the Koso Chem. Co. and was recrystallized from ethanol and water. The *p*-CPG was kindly offered by Professor Shiro Matsumoto. Dye solutions were prepared in borate buffer solutions in order to keep the pH at 8.0, at which the quantum yield of the photoreduction was at its maximum.[2,3] Degassing was carried out by freeze-pump-thaw cycles. The concentrations of MB were determined from the reported extinction coefficient[11] at the absorption peak ($\varepsilon=9.5\times10^4$ at 665 mμ). The energy of the laser pulse was measured by means of a TRG-100 thermopile. The temperature of the reaction cell was regulated by means of an electric furnace.

Results and Discussion

The transmitted light intensity (I_T) was measured as a function of the incident light intensity (I_0) for the MB solution without the reducing agent; the results are shown in Table 1. No reaction was observed under the laser-pulse irradiation. Using the value of 1.3×10^4 as the extinction coefficient of MB[11] at 6943 Å, the I_T/I_0 ratio was estimated to be 0.70 for the 6.6×10^{-6} M solution. However, the experimental results show a much higher transparency than the value estimated above. This indicates that the saturation of the laser light absorption is realized in the MB solution without the reducing agent. Since the radiative lifetime of the MB singlet-excited state is estimated to be 9.8 nsec from the spectral data[11], and since the fluorescence quantum yield is quite low,[12] the actual lifetime of this state is at least an order of magnitude smaller

Table 1. The transmittance of MB solution and the number of absorbed photons as a function of the dose light intensity

I_0 (mJ)	I_T (mJ)	I_T/I_0	$N_{abs.}$ (photons/molecule)
530	477	0.88	87
440	392	0.86	79
244	215	0.83	48
66	59	0.78	16
23	19	0.75	7

[MB]$=6.6\times10^{-6}$M

1) G. Oster and N. Wotherspoon, *J. Amer. Chem. Soc.*, **79**, 4836 (1957).
2) S. Matsumoto, This Bulletin, **35**, 1860 (1962).
3) S. Matsumoto, *ibid.*, **35**, 1866 (1962).
4) M. Koizumi, H. Obata, and S. Hayashi, *ibid.*, **37**, 108 (1964).
5) N. Kosui, K. Uchida, and M. Koizumi, *ibid.*, **38**, 1958 (1965).
6) C. A. Parker, *J. Phys. Chem.*, **63**, 26 (1959).
7) S. Kato, M. Morita, and M. Koizumi, This Bulletin, **37**, 117 (1964).
8) S. Matsumoto, *ibid.*, **37**, 491 (1964).
9) S. Matsumoto, *ibid.*, **37**, 499 (1964).
10) I. Tanaka, Y. Mori, Y. Minagawa, and E. Okutsu, *J. Phys. Chem.*, **72**, 2684 (1968).
11) K. Bergmann and C. T. O'koshi, *J. Amer. Chem. Soc.*, **67**, 2169 (1963).
12) N. Wotherspoon and G. Oster, *ibid.*, **79**, 3992 (1957).

than the radiative lifetime. Actually, the fluorescence lifetime of MB has been directly measured to be 0.4 nsec using a mode-locked He-Ne laser.[13] This short lifetime indicates that the intersystem crossing rate is quite fast. Thus, in an early stage of the laser-pulse duration, almost all the MB molecules are probably stored in the lowest triplet state. As the absorption coefficient of the lowest triplet state is lower than that of the ground state[14] at 6943 Å, the saturation of the laser-light absorption results from the absence of the ground-state molecules in the pulse duration.

The last column in Table 1 shows the number of photons absorbed (N_{abs}) by each MB molecule. The number of photons absorbed increases with the light intensity; at 530 mJ, one MB molecule absorbs nearly 90 photons. This may be interpreted by the following repetitive process. An MB molecule in the lowest triplet state is excited to the higher triplet state by photon absorption, followed by relaxation to the lowest triplet state in its lifetime, that is, the order of 10^{-11} -10^{-12} sec; it may then absorb another photon. According to the repetitive process, the apparent lifetime of the excited triplet state is extended to 10^{-9} -10^{-10} sec at a high intensity of laser light.

When *p*-CPG was added to the MB solution as a reducing agent, the photoreduction of MB was observed by means of laser-light irradiation. Flash photolysis studies[7-9] have shown that the photoreduction of MB is accomplished through the lowest triplet state of MB. Therefore, the reaction scheme may be shown as follows:

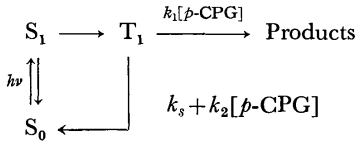

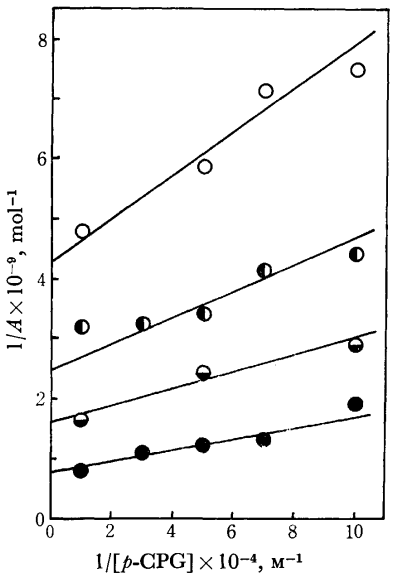

Fig. 1. The reciprocal of the reduced MB *vs.* the reciprocal of the concentration of *p*-CPG at 25°C.
● 530 mJ, ◒ 66 mJ, ◐ 23 mJ, ○ 8 mJ.

13) H. Merkelo, S. R. Hartman, T. Mar, and G. S. S. Govindjee, *Science*, **164**, 301 (1969).
14) R. M. Danziger, K. H. Bar-Eli, and K. Weiss, *J. Phys. Chem.*, **71**, 2633 (1967).

where S_0, S_1, and T_1 are the ground state, the excited singlet state, and the lowest triplet state of MB respectively. According to this mechanism, the following equation is obtained:

$$\frac{1}{A} = \frac{1}{T}\left\{\frac{k_s}{k_1}\cdot\frac{1}{[p\text{-CPG}]} + \left(1+\frac{k_2}{k_1}\right)\right\} \quad (1)$$

where A is the quantity of MB reduced and T is total amount of MB converted to the triplet state. The plots of $1/A$ against $1/[p\text{-CPG}]$ fall on straight lines at various laser-light intensities, as is shown in Figs. 1 and 2 at 25 and 50°C respectively.

Equation (1) also indicates that the ratio of the intercept to the slope $(k_1+k_2)/k_s$ should be independent of the light intensity. Table 2 shows the values of $(k_1+k_2)/k_s$ for *p*-CPG, together with those for DMPG.[10] The values obtained with ordinary light[2] are also included. At a low intensity, this ratio is $1.1\times10^5\text{M}^{-1}$ for 8 mJ at 25°C and $4.7\times10^4\text{M}^{-1}$ for 23 mJ at 50°C.

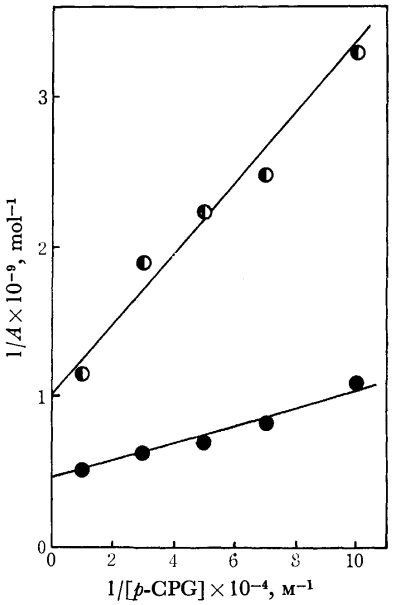

Fig. 2. The reciprocal of the reduced MB *vs.* the reciprocal of the concentration of *p*-CPG at 50°C.
● 530 mJ, ◐ 23 mJ.

Table 2. The ratio of $(k_1+k_2)/k_s$ for *p*-CPG and DMPG

p-CPG		
Laser intensity	25°	50°
530 mJ	$1.4\times10^5\text{M}^{-1}$	$8.1\times10^4\text{M}^{-1}$
66	1.3	
23	1.2	4.7
8	1.1	
Ordinary light[a]		40°
		$3.99\times10^4\text{M}^{-1}$
DMPG		
Laser intensity		25°
101 mJ		$14\times10^4\text{M}^{-1}$
45		5.7
4.4		2.8
Ordinary light[a]		40°
		$3.37\times10^4\text{M}^{-1}$

a) See Ref. 2

These values are compared with the value for the ordinary light given by Matsumoto.[2] However, this ratio increases with the dose intensity; in case of *p*-CPG, increases of 30 and 70% are observed with an increase in the dose energy from the lowest values to 530 mJ at 25 and 50°C respectively. These values are much smaller than that for DNPG, for which a five-fold increase was observed with the increase in the energy from 4.4 to 101 mJ.

In case of DMPG, the increase in the $(k_1+k_2)/k_s$ ratio with the laser-light intensity is interpreted as the result of the contribution of MB in the excited triplet state.[10] If this is the case for *p*-CPG, the reaction scheme can tentatively be written as follows:

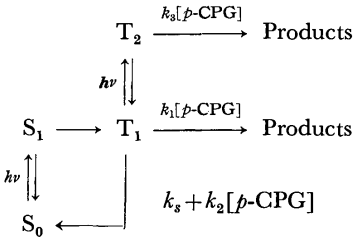

According to the above mechanism, the following equation is obtained:

$$\frac{1}{A}=\frac{1}{T(1+a)}\left\{\frac{k_s}{k_1+bk_3}\frac{1}{[p\text{-CPG}]}+\left(1+\frac{k_2}{k_1+bk_3}\right)\right\} \quad (2)$$

where $a=[T_2]/[T_1]$ and $b=\int[T_2]\,dt/\int[T_1]\,dt$. At a low intensity, $a\to 0$, $b\to 0$, and Eq. (2) is identical with Eq. (1). From Eq. (2), it can be understood why the ratio of the intercept to the slope increases with the dose intensity.

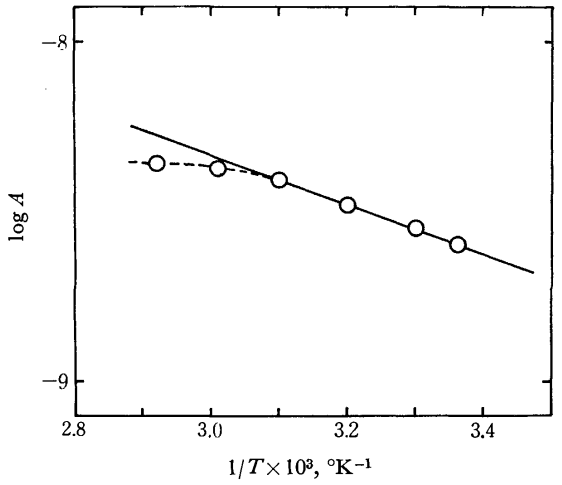

Fig. 3. The typical Arrhenius plot of the reduced MB at 530 mJ. The concentration of *p*-CPG is 10^{-4} M.

The photoreduction of MB was carried out at a rising temperature. Figure 3 shows a typical Arrhenius plot of the quantity of the reduced MB at the dose intensity of 530 mJ. At temperatures lower than 50°C, the plots give a straight line. The apparent activation energy is obtained from the straight part of the Arrhenius plots. It is not clear why the curve deviates from straight line in the temperature region higher than 50°C. The apparent activation energy of the reduction of MB was obtained by varying the laser-light intensity. The results are shown in Fig. 4. The curve shows a decline with an increase in the dose energy up to 270 mJ, while it becomes flat at energy higher than 270 mJ.

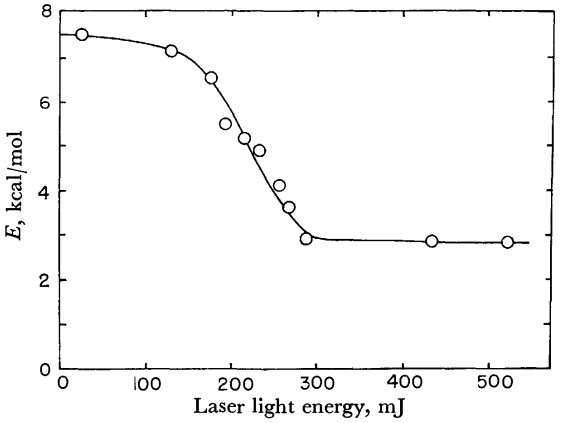

Fig. 4. The apparent activation energy *vs.* the laser light intensity. The concentration of *p*-CPG is 10^{-4}M.

It is supposed that the photoreductions through both the lowest triplet state and the excited triplet state contribute to the apparent activation energy. The activation energy extrapolated to zero light intensity should correspond to the activation energy for the lowest triplet state; it is estimated to be 7.4 kcal mol^{-1}. Since the apparent activation energy of the reaction through the excited triplet state is expected to be lower than that for the lowest triplet state, the decline in the activation energy with the laser intensity is thought to result from the contribution of the reduction of MB through the excited triplet state.

At energy higher than 270 mJ, the apparent activation energy is constant. This can be interpreted by the mechanism in which the reduction mainly occurs through the excited triplet state. Thus, the activation energy in this region would correspond to that of the reduction through the excited triplet state; it can be estimated from Fig. 4 to be 2.8 kcal mol^{-1}.

It is interesting to ascertain the nature of T_2, which was tentatively called the excited triplet state in the previous discussion. As has been mentioned above, the effective lifetime of T_2 is estimated to be 10^{-9}—10^{-10} sec in the absence of the reducing agent at the high-laser intensity, while it is estimated from the diffusion theory that a MB molecule collides with *p*-CPG molecules every 1.4×10^{-6} sec when the concentration of *p*-CPG is 10^{-4} M. This interval between collisions is much longer than the effective lifetime of the excited triplet state. Provided the photoreduction occurs as a result of direct interaction between the excited triplet states of MB and *p*-CPG, the reactionary radii must be about 100 times larger than the diffusional radii. However, if a molecular complex is formed between MB in the lowest triplet state and *p*-CPG, the MB in the excited triplet state may have a better chance to encounter *p*-CPG than would be expected from the simple diffusion theory. This may be the reason why the photo-

reduction occurs during the short effective lifetime of the excited triplet state.

An alternative interpretation of the nature of T_2 is as follows. When the MB molecule in the excited triplet state relaxes to the lowest triplet state, the electronic excitation energy is consumed in heating the solvent around the MB molecule. If the rate of the heat dissipation is slower than the rate of the heat formation by relaxation, the solvent around the MB molecule is locally heated by the repetitive photo-absorption: thus, the activation energy apparently decreases with a rise in the temperature. Since the apparent activation energy decreases from 7.4 to 2.8 kcal with an increase in the dose intensity, the average temperature of the reaction site is estimated to be 520°C.

At the present stage, it is not possible to determine which mechanism is operative in the photoreduction of MB. However, the long-range interaction proposed in the former case seems to be unreasonable in this case. Thus, we may suppose that the complex mechanism or the temperature effect is responsible for the reduction of MB.

The authors wish to express their thanks to Professors Ikuzo Tanaka and Yuji Mori for their helpful advice and support during the course of this work. They are also grateful to Professor Shiro Matsumoto for help in obtaining the compound used in this study.

BULLETIN OF THE CHEMICAL SOCIETY OF JAPAN, VOL. 45, 720—725(1972)

Excimer and Monomer Defect Emissions of Perylene and Pyrene Crystals as Studied by the Nanosecond Time-resolved Spectroscopy Technique

Akinori INOUE, Keitaro YOSHIHARA,* Takahiro KASUYA,* and Saburo NAGAKURA

The Institute for Solid State Physics, The University of Tokyo, Roppongi, Minato, Tokyo
**The Institute of Physical and Chemical Research, Wako, Saitama*

(Received September 21, 1971)

Nanosecond time-resolved fluorescence spectra were measured at 77°K for pyrene and perylene crystals, and anomalous emissions which have lifetimes of ~8 nsec and are difficult to be found by the usual steady excitation, were observed at the higher-wave number sides of the usual excimer emissions. From the band position and the vibrational structure, the anomalous emission was interpreted as being due to monomer defects in each crystal. The analysis of the observed rise and decay curves of the monomer defect and excimer emissions shows that the excited states of both emissions are populated independently from the band level of each crystal excited by light irradiation. The temperature dependence of the emission indicates that a thermal activation of 0.035 eV is required for the excimer formation in a perylene single crystal, while no activation energy is required for the excitation of the monomer defect.

Excimer fluorescences from crystals of aromatic compounds were studied by various investigators[1-5] and were found to be observed for only dimeric crystals, such as pyrene and perylene, in which the molecules exist in pairs.[3] Birks, Kazzaz, and King[5] observed the time dependence of the excimer fluorescence of the pyrene crystal. According to their findings, the excimer is formed at 293°K within one nanosecond after the excitation. Beside the excimer band, a partially-structured anomalous emission band was observed with the microcrystalline layer of pyrene.[2,5] The band was assigned by Birks *et al.* to an emission from surface monomer defects excited by the encounter with excimer excitions.[5]

An anomalous fluorescence band with a vibrational structure was also observed by Tanaka for a single crystal of perylene at low temperatures below 50°K.[4] This band is very similar in position and shape to the monomeric perylene band and was assigned to a monomer emission. Tanaka assumed that the excimer state was populated *via* an excited monomer state and estimated the potential barrier of the process to be 285 cm^{-1} from an analysis of the observed temperature dependence of the excimer emission.[4] According to this mechanism, the excimer emission may be expected to have a rise time which corresponds to the decay time of the monomer emission.

Under these circumstances, we have undertaken to study, by the nanosecond time-resolved spectroscopy technique, the rise and decay processes of fluorescent states of pyrene and perylene, in order to clarify the nature of the anomalous fluorescence and the energy-transfer mechanism in both dimeric crystals.

Experimental

Materials. Pyrene was purified by zone refining after vacuum sublimation. Perylene was purified by the vaccum

1) J. Ferguson, *J. Chem. Phys.*, **28**, 765 (1958).
2) J. B. Birks and A. J. W. Cameron, *Proc. Roy. Soc.*, **249A**, 297 (1959).
3) B. Stevens, *Spectrochim. Acta*, **18**, 439 (1962).
4) J. Tanaka, This Bulletin, **36**, 1237 (1963).
5) J. B. Birks, A. A. Kazzaz, and T. A. King, *Proc. Roy. Soc.*, **291A**, 556 (1966).

sublimation of a synthetic material.[6] A single crystal of perylene was obtained by recrystallization from the toluene solution.

Nitrogen Gas Laser. A pulsed, coaxial-type nitrogen gas laser[7,8] was built as an exciting source. The discharge voltage of the laser is about 30 kV, and the pressure of nitrogen is approximately 4 Torr. Coaxial transmission lines are used as a condenser for the discharge. The wavelength of the laser emission is 3371 Å, and the laser pulse has a duration of approximately 3 nanoseconds, with a peak power of about 20 kW. The repetition rate is 20 Hz, and the oscillatory behavior is quite regular.

Fluorescence Measurements. Fluorescence spectra were measured by means of a Bausch and Lomb monochromator, being detected by an RCA 1P28 photomultiplier. By means of the repetitive operation of the laser, the sampling technique was used to measure the time-resolved spectra, a Tektronix 3S1 sampling oscilloscope being used. By setting the delay of a Tektronix 3T77A sampling sweep unit at a fixed time, a time-resolved spectrum was obtained by scanning the wavelength and recording the average photocurrent. The spectral response of the photomultiplier was not calibrated.

The laser light was attenuated by filters in order to prevent the excition-exciton interaction which causes a remarkable change in the decay characteristics of the fluorescences.[9-11]. A Toshiba UV-39 filter was set in front of the monochromator entrance slit in order to eliminate scattered laser light. For the purpose of analyzing the initial rise of emission, the exact pulse shape of the laser was measured by a Hamamatsu TV R317 biplanar photodiode and the sampling oscilloscope. The time resolution of the system was estimated to be about 0.5 nsec. A 3650 Å line from a high-pressure mercury lamp was used for the measurement of the fluorescence spectra by means of steady excitation.

Results and Discussion

Time-resolved Fluorescence Spectra and Lifetimes. Nanosecond time-resolved fluorescence spectra were measured at 77°K for perylene and pyrene single crystals; the results are shown in Figs. 1 and 2, respectively. Fluorescence spectra observed by the steady-excitation technique for both crystals are also shown in these figures for purposes of comparison. Furthermore, the fluorescence lifetimes measured for both crystals at 293°K and 77°K are listed in Table 1. This table also includes the wave numbers of the observed fluorescence maxima. Two fluorescence spectra with different lifetimes were observed at 77°K for each crystal: one is at shorter wavelengths and is short-lived, while the other is at longer wavelengths and is long-lived.

By the steady-excitation technique, the short-lived emission is difficult to be observed distinctly for the single crystals in the temperature range from 77°K to 293°K. This is because it has a relatively low fluorescence quantum yield in this temperature range. By the nanosecond time-resolved spectroscopy technique, however, we can observe separately each of the short-lived and long-lived components of the emission spectrum. For example, the fluorescence spectrum of the perylene single crystal, observed 4 nsec after the trig-

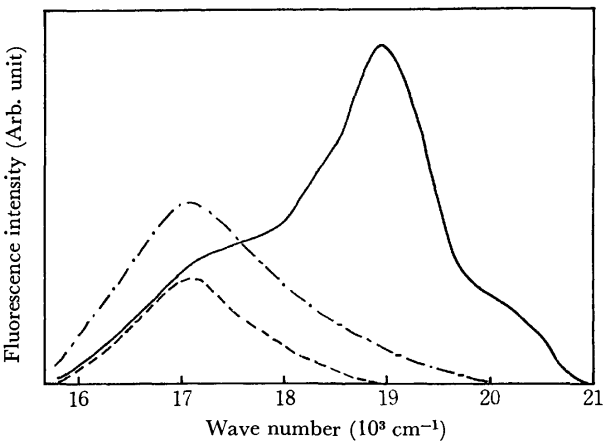

Fig. 1. Time-resolved fluorescence spectra of a perylene crystal at 77°K:———, 4 nsec after trigger; ------, 20 nsec after trigger; ·-·-·-, fluorescence by steady excitation.

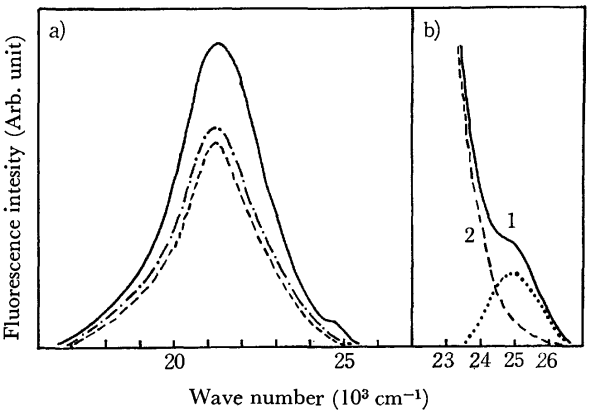

Fig. 2. a) Time-resolved fluorescence spectra of a pyrene crystal at 77°K:——, 4 nsec after trigger;·-·-·-, 10 nsec after trigger; ----, fluorescence by steady excitation.
b) Time-resolved fluorescence spectra in the 25000 cm^{-1} region observed with a pyrene crystal at 77°K, the emission higher than ~26000 cm^{-1} being cut off by the used of a Toshiba UV-39 filter. The ordinate in b) is magnified compared with that in a):——, 4 nsec delay;----, 10 nsec delay;····, spectrum of the monomer defect fluorescence obtained by subtracting curve 2 from curve 1.

Table 1. Fluorescence lifetimes (τ) and maximum wave numbers (ν_{max}) of pyrene and perylene single crystals at 293°K and at 77°K

	293°K		77°K	
	τ (ns)	ν_{max}(cm^{-1})	τ (ns)	ν_{max}(cm^{-1})
Pyrene	—	—	8	25300
	70	21500	180	21500
Perylene	—	—	8	19000
	44	17800	91	17000

6) The synthetic perylene was provided by Professor S. Iwashima, Meisei University and Professor H. Inokuchi, The University of Tokyo.

7) M. Geller, D. E. Altman, and T. A. DeTemple, *J. Appl. Phys.*, **37**, 3639 (1966).

8) A. Inoue, K. Yoshihara, S. Nagakura, T. Kasuya, A. Minoh, S. Kobayashi, and K. Shimoda, *Reports I.P.C.R.*, **47**, 40 (1971).

9) A. Bergman, M. Levine, and J. Jortner, *Phys. Rev. Lett.*, **18**, 593 (1967).

10) C. R. Goldschmidt, Y. Tomkiewicz, and I. B. Berlman, *Chem. Phys. Lett.*, **2**, 520 (1968).

11) A. Inoue, K. Yoshihara, and S. Nagakura, to be published.

ger pulse, has an intense structured band at ~19000 cm^{-1} besides the band at ~17000 cm^{-1} which still remains in the fluorescence spectrum observed 20 nsec after the trigger pulse. The long-lived components are identified with the excimer fluorescences for the following reasons: (1) the lifetime of the emission at longer wavelengths of the pyrene crystal at 77°K, 180 nsec, is very close to that of the excimer emission obtained by Birks, Kazzaz, and King[5] (185 nsec); and (2) in both crystals, the time-resolved spectra of the long-lived emission coincide in their positions and shapes with the corresponding excimer fluorescence spectra obtained by the steady excitation.[1-5] The short-lived fluorescence at ~19000 cm^{-1} is very similar to that observed with the monomeric (β-type) perylene crystal and can safely be assigned to the excited monomer.[4]

Concerning the pyrene single crystal, in addition to the excimer fluorescence at 21500 cm^{-1}, the short-lived emission was observed at 25300 cm^{-1} in the spectrum 10 nsec after the trigger pulse. The latter is similar to the spectrum due to the monomer defect observed by Birks *et al.*[2,5] with a very thin film of pyrene.

The emissions at shorter wavelengths observed for both single crystals are anomalous in the sense that they are distinctly observed only by the nanosecond time-resolved spectroscopy technique at 77°K. On the other hand, when thin evaporated films are used instead of the single crystal, the anomalous emission can be observed by the steady-excitation technique for both aromatic hydrocarbons, even at room temperatures.

Examination of the Previous Mechanisms of the Anomalous Emissions. The two mechanisms were presented previously by Birks *et al.* and by Tanaka for the anomalous emissions observed for the pyrene and perylene crystals, respectively.

First, let us consider the mechanism presented by Birks *et al.*[5] If the anomalous emission of the pyrene crystal is assumed to originate from excited surface monomer defects which are populated by the encounter with excimer excitons,[5] the anomalous fluorescence should have a rise time comparable to the decay time of the excimer exciton. The time dependence of the anomalous emission observed with pyrene crystals at 25000 cm^{-1} at 77°K is shown in Fig. 3. The rise time of the anomalous fluorescence is very short compared with the decay time of the excimer fluorescence. This clearly contradicts the mechanism presented by Birks *et al.*

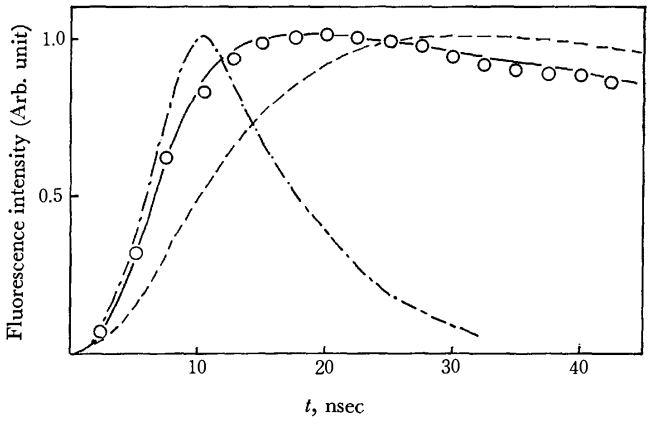

Fig. 3. Time dependence of the fluorescence of a pyrene crystal:——, calculated for the excimer fluorescence based on the present mechanism;----, calculated for the excimer fluorescence based on the mechanism presented by Tanaka; ·–·–, observed curve for the monomer defect fluorescence; –○– observed points for the excimer fluorescence at 77°K.

We will check, from the kinetic point of view, the mechanism presented by Tanaka, which is schematically shown as follows:

$$\mathrm{M} \xrightarrow[①]{h\nu} \mathrm{M}^* \xrightarrow[④]{\mathrm{M}} \mathrm{E}$$
$$②\swarrow \quad ③\searrow \quad ⑤\swarrow \quad ⑥\searrow$$

Here, processes ①, ②, ③, ④, ⑤, and ⑥ are respectively concerned with the excitation of the monomer M, the radiative and radiationless decay processes of the excited monomer, M*, the excimer formation process, and the radiative and radiationless decay processes of the excimer, E. According to this mechanism, the exciton concentrations of the monomer and excimer under pulse excitation may be represented as follows:

$$\mathrm{d[M^*]}/\mathrm{d}t = I(t) - (k_2+k_3+k_4[\mathrm{M}])[\mathrm{M^*}] \quad (1)$$

$$\mathrm{d[E]}/\mathrm{d}t = k_4[\mathrm{M^*}][\mathrm{M}] - (k_5+k_6)[\mathrm{E}] \quad (2)$$

Here, [M*], [E], and [M] represent the concentrations of the corresponding specimens, k_n is the rate constant for the above-mentioned process n, and $I(t)$ is the rate of the generation of singlet monomer excitons, which may be expected to be proportional to the intensity of an incident light pulse. Equations (1) and (2) can be solved as follows:

$$[\mathrm{M^*}] = \exp(-t/\tau_\mathrm{M})\int_0^t \exp(\xi/\tau_\mathrm{M})I(\xi)\mathrm{d}\xi \quad (3)$$

$$[\mathrm{E}] = \exp(-t/\tau_\mathrm{E})\int_0^t \exp((1/\tau_\mathrm{E}-1/\tau_\mathrm{M})\xi)\mathrm{d}\xi \times \int_0^\xi \exp(\eta/\tau_\mathrm{M})I(\eta)\mathrm{d}\eta \quad (4)$$

Here, τ_M and τ_E are the lifetimes of the monomer and excimer defined as $1/\tau_\mathrm{M}=k_2+k_3+k_4[\mathrm{M}]$ and $1/\tau_\mathrm{E}=k_5+k_6$, respectively. The monomer and excimer fluorescences are proportional to the concentrations of the monomer and excimer excitons, respectively. The equations were numerically integrated using the experimentally-determined shape of $I(t)$ and the measured lifetimes shown in Table 1. It is necessary to consider the distortion in the observed fluorescence time-dependence curve due to the inability of the measuring circuit to follow an extremely fast rise. The actual method for correcting the distortion by the aid of a simple theory of the four-terminal network will be described in the Appendix. The time dependence of the excimer fluorescence was evaluated by applying Eq. (4) to the perylene crystal at 77°K; the result is shown by a broken line in Fig. 4. In this figure, the observed result is also shown by open circles for the purpose of comparison. A marked discrepancy exists between the calculated and experimental results. A similar discrepancy was also found for the pyrene crystal, as clearly seen in Fig. 3.

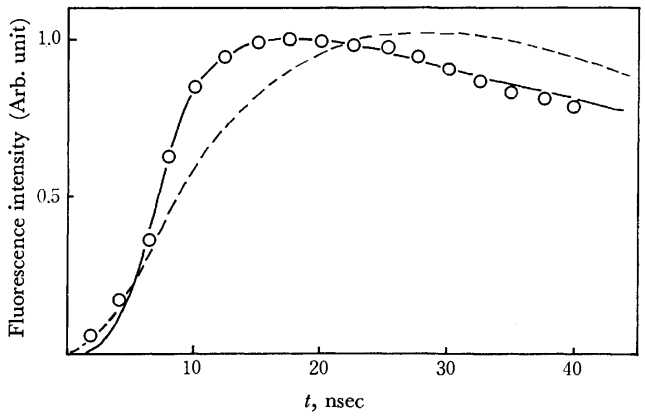

Fig. 4. Time dependence of the excimer fluorescence of a perylene crystal:—, calculated based on the present mechanism;----, calculated based on the mechanism presented by Tanaka; —○—, observed points at 77°K.

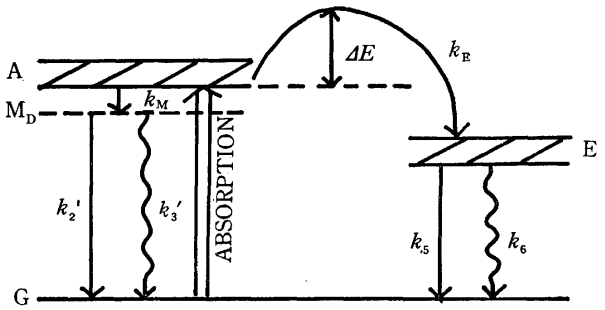

Fig. 5. Schematic diagram representing the mechanism of the excimer and the defect fluorescence of perylene and pyrene crystals.

It is obvious that neither of the two mechanisms presented previously can explain the rise and decay processes of the emissions of pyrene and perylene crystals.

A New Mechanism for the Excimer and Anomalous Emissions. Here, we propose a new mechanism for the appearance of the monomer defect and excimer fluorescences. (see Fig. 5). Crystals are excited to a band whose excitation energy corresponds to the photon energy of 29700 cm^{-1} of the nitrogen gas laser. After the excitation, a slight change in the orientation of paired molecules may take place in the formation of the excimer fluorescent state. The rate constant, k_E, for this process can be represented by $k_E=k_{EO}\exp(-\Delta E/kT)$, where ΔE is a potential barrier for this process and where k_{EO} is a temperature-independent constant. A relaxation to the monomer-defect states also takes place from the excited band level with the rate constant k_M, which has been experimentally determined to be temperature-independent. Actual dimeric crystals contains a number of defect sites occupied by "unpaired" molecules, particularly at the crystal surface. In the perylene crystal, the most intense component around 19000 cm^{-1} of the defect emission corresponds to the 0—1 band of the perylene-monomer emission, while the 0—0 band appears near 20000 cm^{-1} [12] and its intensity is considerably reduced by reabsorption.

12) K. Kawaoka and D. R. Kearns, *J. Chem. Phys.*, **45**, 147 (1966).

The following rate equations are obtained according to the new mechanism:

$$d\rho/dt = I(t) - (k_M+k_E)\rho \quad (5)$$

$$d[M_D]/dt = k_M\rho - (k_2'+k_3')[M_D] \quad (6)$$

$$d[E]/dt = k_E\rho - (k_5+k_6)[E] \quad (7)$$

Here, ρ is the exciton population in the excited band level, and the population of the monomer defect is represented by $[M_D]$. The rate constants k'_2 and k'_3 stand for those of the radiative and radiationless deactivations of the defect state, respectively, while k_5 and k_6 stand for those of the excimer state. Since k_M and k_E are much larger than k'_2, k'_3, k_5, and k_6, the stationary state condition may safely be applied to Eq. (5). Thus, the two concentrations $[M_D]$ and [E] can be expressed as:

$$[M_D] = k_M/(k_M+k_E)\exp(-t/\tau_M)\int_0^t \exp(\xi/\tau_M)I(\xi)d\xi \quad (8)$$

and

$$[E] = k_E/(k_M+k_E)\exp(-t/\tau_E)\int_0^t \exp(\xi/\tau_E)I(\xi)d\xi \quad (9)$$

Here, τ_M and τ_E are the lifetimes of the defect and excimer emissions, defined as $1/\tau_M=k'_2+k'_3$ and $1/\tau_E=k_5+k_6$. The rise curve of the excimer fluorescence was obtained by the numerical integration of Eq. (9) using the measured lifetime and the shape of the laser pulse. The curve obtained for the perylene crystal at 77°K is shown by a solid line in Fig. 4; it is in good agreement with the experimental results. The same mechanism was also applied to the pyrene crystal, with a good agreement between the calculated and observed rise curves, as is shown in Fig. 3. These results show that, in both crystals, the excimer excitons are not produced *via* the excited monomer; rather, both excited states are populated independently from the band levels of the crystals excited by the light irradiation.

Temperature Dependence of Emissions. According to our new mechanism, the intensity ratio of the excimer fluorescence to the anomalous fluorescence obtained by the steady excitation, I_E/I_M, can be written as:

$$I_E/I_M = k_Ek_5(k_2'+k_3')/k_Mk_2'(k_5+k_6) \quad (10)$$

The experimental value, τ_E^{-1}, can be expressed[5] by the sum of the temperature-dependent and temperature-independent rate constants:

$$\tau_E^{-1} = k_5 + k_6 = k_5 + k_6' + k_6^0\exp(-\Delta W/kT) \quad (11)$$

where k_6^0, k'_6, and ΔW are the frequency factor, the temperature-independent rate constant, and the activation energy. The plots of $\ln(\tau_E^{-1}-k_5-k'_6)$ *versus* $1/T$ give a linear relation, as shown in Fig. 6, with $k_5+k'_6=1.2\times10^7$ sec^{-1} and $\Delta W=680$ cm^{-1} for the perylene crystal. This may be compared with the value of $\Delta W=530$ cm^{-1} for the pyrene crystal given by Birks, Kazzaz, and King.[5] The results show that the exponential term may be disregarded in the temperature range below 100°K and that, therefore, k_5+k_6 may be regarded as temperature independent in this temperature range. Furthermore, the present experiment shows that the lifetime of the monomer-defect emission is temperature independent between 77—135°K within the limits of experimental error. Since the radiative

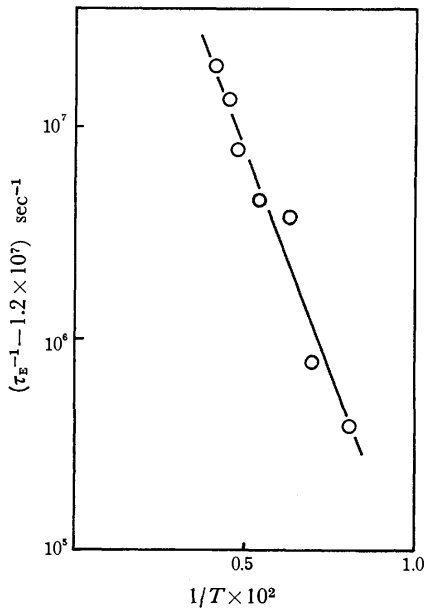

Fig. 6. Temperature dependence of the excimer fluorescence lifetime of a perylene crystal. Semilogarithmic plots of $(\tau_E^{-1}-1.2\times10^7)$ *versus* $1/T$.

rate constants may reasonably be assumed to be temperature independent, the temperature dependence of I_E/I_M given by Eq. (10) actually shows that of k_E/k_M.

To elucidate the natures of k_M and k_E, the temperature dependences of $k_E/(k_M+k_E)$ and $k_M/(k_M+k_E)$ were measured for the perylene crystal between 92—220°K and between 83—135°K, respectively. These values can be obtained by measuring the fluorescence intensity divided by the lifetime, *i.e.*,

$$I_E/\tau_E = C_1(k_E/(k_M+k_E))(k_5/(k_5+k_6))(k_5+k_6) = C_1k_Ek_5/(k_M+k_E) \quad (12)$$

In a similar way,

$$I_M/\tau_M = C_2k_Mk_2'/(k_M+k_E) \quad (13)$$

Here, C_1 and C_2 are temperature-independent constants. The fluorescence intensities, I_E and I_M, can be written as follows:

$$I_E = \int d\nu\int_0^\infty F_{E\nu}(t)dt \qquad I_M = \int d\nu\int_0^\infty F_{M\nu}(t)dt \quad (14)$$

where $F_{E\nu}(t)$ and $F_{M\nu}(t)$ are the time dependences of the excimer and monomer-defect fluorescences at a wave number, ν. The integrals for I_E and I_M with respect to the wave number are performed over the excimer- and defect-emission bands, respectively. Setting $F_{E\nu}(t)=F_{E\nu}^{t_0}\exp((t_0-t)/\tau_E)$ and $F_{M\nu}(t)=F_{M\nu}^{t_0}\exp((t_0-t)/\tau_M)$, where $F_{E\nu}^{t_0}$ and $F_{M\nu}^{t_0}$ are the fluorescence intensities at $t=t_0$, we can obtain:

$$I_E/\tau_E = \exp(t_0/\tau_E)\int F_{E\nu}^{t_0}d\nu \qquad I_M/\tau_M = \exp(t_0/\tau_M)\int F_{M\nu}^{t_0}d\nu \quad (15)$$

Therefore, the temperature dependence of $k_E/(k_M+k_E)$ was obtained by integrating each of the time-resolved spectra (at a fixed time, t_0) of the excimer observed at several different temperatures and by being multiplied by $\exp(t_0/\tau_E)$. Since, according to our experiment, the monomer-defect emission exhibits no change in its position and shape in the temperature range of 77—

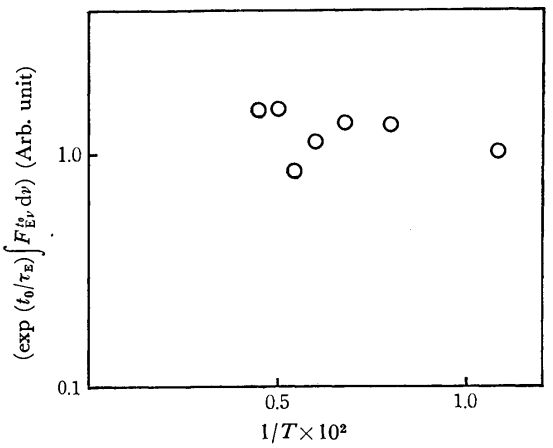

Fig. 7. Temperature dependence of the excimer fluorescence intensity of a perylene crystal obtained by the integration of time-resolved spectra at 20 nsec delay. Semilogarithmic plots of $(\exp(t_0/\tau_E)\int F_{E\nu}^{t_0}d\nu)$, $t_0=20$ nsec *versus* $1/T$.

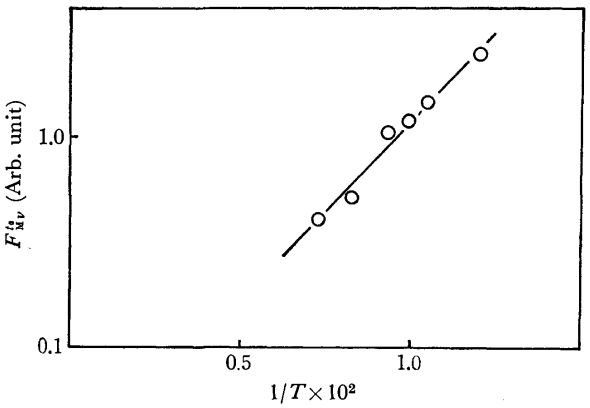

Fig. 8. Temperature dependence of the peak intensity of the defect fluorescence of a perylene crystal. Semilogarithmic plots of $F_{M\nu}^{t_0}$, $t_0=4$ nsec *versus* $1/T$.

135°K, the temperature dependence of $k_M/(k_M+k_E)$ was measured by observing the emission intensity 4 nsec after a trigger pulse at 19000 cm^{-1}. The results are shown in Figs. 7 and 8. The plots of $\ln(k_M/(k_M+k_E))$ *versus* $1/T$ in the temperature range of 96—135°K give a straight line, with an activation energy of $\Delta E=280$ cm^{-1}. On the other hand, $k_E/(k_M+k_E)$ is almost independent of the temperature within the range of 92—220°K. This directly indicates the inequality relation $k_E \gg k_M$ in this temperature range. The temperature dependences of $k_M/(k_M+k_E)$ and $k_E/(k_M+k_E)$ show that the monomer defect emission is intense at lower temperatures, while the excimer emission is almost constant at the temperatures above 90°K. This is in good agreement with the results obtained by the steady-excitation experiment. The results are also consistent with the fact that the quantum yield of the monomer defect emission is relatively small.

The activation energy thus obtained is in agreement with that obtained previously by the steady-excitation experiment,[4] but the mechanism of energy transfer should be reinterpreted according to the present mechanism.

Emissions from the Thin Films of Perylene and Pyrene. In a thin evaporated film which has a much higher concentration of the monomer defect relative to the regular site than a single crystal, the defect emission may be expected to be observed easily by the steady excitation at as high a temperature as 77°K. This is actually the case for a perylene evaporated film (thickness ~0.3 μm), and its peak intensity at 19000 cm^{-1} is comparable with the excimer fluorescence intensity at 77°K. The monomer-defect emission was also observed for a pyrene-evaporated layer.[2,5]

We wish to express our thanks to Dr. M. Geller of the U.S. Naval Electronics Laboratory Center for his kind suggestions about making a coaxial transmission line nitrogen gas laser. We are also greatly indebted to Professor S. Iwashima, Meisei University, and Professor H. Inokuchi, The University of Tokyo, for their kindness in providing us with synthetic materials. Our thanks are also due to Dr. M. Takami, The Institute of Physical and Chemical Research, and Mr. T. Kobayashi for their helpful discussions.

Appendix

The correction for the measured time dependence of the fluorescence was made as follows. An integration circuit assumed for the detector system including the photomultiplier and the oscilloscope, consists of a resistor, R, and a capacitor, C, as shown schematically in Fig. 9. From the theory of the four-terminal network, the ratio of the Fourier-transformed output signal, $G(\omega)$, to the input signal, $F(\omega)$, is given by:

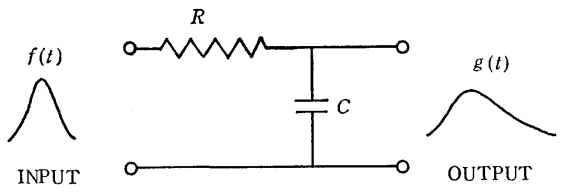

Fig. 9. A model circuit containing a resistor R and a capacitor C of the measuring system.

$$G(\omega)/F(\omega) = 1/(1+i\omega CR) \tag{A1}$$

where

$$F(\omega) = \int_0^\infty dt \exp(-i\omega t) f(t),$$

$$G(\omega) = \int_0^\infty dt \exp(-i\omega t) g(t), \tag{A2}$$

and $f(t)$ and $g(t)$ are the time dependences of the input and output signals, respectively. The output signal, $g(t)$, is obtained by an inverse transformation of $G(\omega)$ and by the aid of the equation (A1):

$$g(t) = (1/CR) \exp(-t/CR) \int_0^t f(\xi) \exp(\xi/CR) d\xi \tag{A3}$$

By the aid of Eq. (A3), the time constant, CR, can be determined in such a way that the integration of the experimentally-determined $f(t)$ fits into $g(t)$ as well as possible. Both $f(t)$ and $g(t)$ were obtained by observing the same laser pulse by a fast photodiode and a 1 GHz sampling oscilloscope, and by a photomultiplier and an 80 MHz oscilloscope, respectively. The actual integration of $f(t)$ fits well into $g(t)$ over a wide range of t with CR=3.5 nsec, suggesting that the original assumption is correct.

The Dye-sensitized Photooxygenation of Hexamethyleneammonium Hexamethylenedithiocarbamate by Xanthene Dyes

Toshihiro YAMASE, Hiroshi KOKADO, and Eiichi INOUE

Imaging Science and Engineering Laboratory, Tokyo Institute of Technology, Ookayama, Meguro-ku, Tokyo

(Received November 5, 1970)

The photoelimination of hexamethyleneammonium hexamethylenedithiocarbamate (HMTC)[1] can be sensitized by xanthene dyes, such as rose bengal and eosine yellowish. In contrast to the direct photolysis results, the presence of HMTC in the dye-sensitized decomposition produces no carbon disulfide and consumes oxygen during the irradiation. The quantum yield of photoelimination in an aerated ethanol solution was measured. The quantum yield was almost unchanged on the variation of the xanthene dye concentration from 10^{-5} to 10^{-6}M. This is different from the former observation[2] that there was an apparent tendency for the quantum yield to decrease monotonously with an increase in the thiazine dye concentration. The singlet oxygen mechanism, in which the photochemical reaction is initiated by the interaction between the triplet dye and the ground-state oxygen molecules, has been inferred for the dye-sensitized photoelimination of HMTC. It has been explained in terms of the effect of 1,4-diazabicyclo [2.2.2] octane, β-carotene, and tetramethylethylene in reducing the quantum yield. The photooxygenation of HMTC by dyes seemed to be caused by attack of the singlet oxygen on the thiocarboxylion group, which has a rate constant of 10^{8}M^{-1}sec^{-1} in ethanol.

In the previous papers of this series,[2,3] the direct and thiazine-dye-sensitized chemistry of hexamethyleneammonium hexamethylenedithiocarbamate (HMTC) has been studied. In contrast to the direct photolysis results, the presence of HMTC in the dye-sensitized decomposition produces no carbon disulfide. It seems that the sensitization by thiazine dye takes place by means of the interaction of the triplet state of the sensitizing dye with dissolved oxygen. In this paper we will try to ascertain the role of oxygen in the dye-sensitized photoelimination of HMTC using xanthene dyes, further, we will describe how the dye-sensitization is not observed for nonionic dithiocarbamates, while it is observed for ionic dithiocarbamates such as HMTC.

Experimental

The HMTC was prepared by a method described previously,[2] Methyl dimethyldithiocarbamate[4] was obtained from Dr. Takeshi Nakai. The compound melted at 45°C and was used without further purification. The butyl ester of hexamethylenedithiocarbamic acid and 2,4-dinitrophenyl hexamethylenedithiocarbamate were prepared using the following general procedure.[5] 8 g of sodium hydroxide were dissolved in 80 m*l* of water, and the mixture was cooled to 5°C. 20 g of hexamethyleneimine and 15 g of carbon disulfide in small portions were stirred in well alternately. The sodium salt hexamethylene dithiocarbamic acid began to crystallize from the solution and was recovered as a white solid by the evaporation of the water and by drying at 110°C. 8.8 g of sodium hexamethylenedithiocarbamate were treated with 3.8 g of *n*-butyl chloride in 60 m*l* of ethanol, and then the mixture was kept at 50°C for 30 min. The sodium chloride thus precipitated was filtered off and the filtrate treated with water. The *n*-butyl ester of hexamethylenedithiocarbamic acid separated as a straw-colored liquid and was used without further purification. 44 g of sodium hexamethylenedithiocarbamate were treated with 40 g of 2,4-dinitrochlorobenzene in 300 m*l* of ethanol, and the solution was heated for 30 minutes at 50°C. The reaction mass was treated with water to dissolve the sodium chloride. The residue was crystallized from ethanol to form bright yellow needles of 2,4-dinitrophenyl hexamethylenedithiocarbamate which melted at 107.5°C.

The acetophenone, benzophenone, Michler's ketone, β-acetonaphthone, and naphthalene were purified by the methods described previously.[6]

The solvents and other reagents were of a GR grade (Tokyo Kasei Corp.), and they were used without further purification. The experimental procedure used in this study was almost the same as that described previously.[2] Degassing was carried out in the usual freeze-pump-thaw cycle at 10^{-5} mmHg. A 1-kW incandescent lamp was used as a source of actinic light for the dye-sensitization. Green light was isolated by means of an interference filter (KL-54) with a maximum in transmission at 546 nm and a transmitting glass filter which cut off light shorter than 520 nm. In most of the experiments, a heat-absorbing filter (HR 1-69) was also employed. The light intensities were measured by means of a Reinecke's salt actinometer. The concentration of oxygen in the ethanol solution was continuously measured using a dissolved-oxygen meter (Kyusuikagaku Kenkyusho D. O. Meter-TP) with a Galvanic electrode, and the output was recorded on a recorder with a 10-mV deflection. Overall, we estimate our absolute error to be within ±10%. For measuring the oxygen concentration, a glass reaction cell was used; it consisted of a cylinder 5 cm in diameter, with a total volume of 80 m*l*, and equipped with a stirrer.

Results

Participation of Oxygen. As was expected, the presence of oxygen was essential to the sensitization by xanthene dyes as well as to that by thiazine dyes,[2] as is shown in Table 1.

Dye Concentration Effects on Quantum Yields. Aerated ethanol solutions containing about 10^{-5}M xanthene

1) $\left(\begin{matrix}CH_2CH_2CH_2\\ |\quad\quad N-C-S\\ CH_2CH_2CH_2\end{matrix}\right)^{-}\left(\begin{matrix}{}^{+}CH_2CH_2CH_2\\ H_2N\quad\quad |\\ CH_2CH_2CH_2\end{matrix}\right)$

2) T. Yamase, H. Kokado, and E. Inoue, This Bulletin, **43**, 669 (1970).

3) T. Yamase, H. Kokado, and E. Inoue, *ibid.*, **43**, 934 (1970).

4) $(CH_3)_2N-\overset{\overset{S}{\|}}{C}-S-CH_3$

5) Ira Williams, U.S. 2187719 (1940).

6) T. Yamase. H. Kokado, and E. Inoue, *Kogyo Kagaku Zasshi*, **72**, 162 (1969).

Table 1. Effect of oxygen

Dye	$[HMTC]_{ini} \times 10^4$, M	$\eta^{a)}$	$\eta^{b)}$
Rose bengal	3.31	0.357	0
Erythrosine	3.30	0.251	0
Phloxine	2.86	0.142	0
Thionine[2)]	5.33	0.251	0
Methylene blue[2)]	5.57	0.227	0

a) Atmospheric condition.
b) Deaerated condition.

dyes and 10^{-4}M HMTC were irradiated at 546 nm. The quantum yield for HMTC elimination was then determined by colorimetric analysis using copper acetate.[7)] The quantum yields obtained for different dye concentrations are tabulated in Table 2. The quantum yield was unchanged within the range of experimental uncertainty as long as all the factors were held constant. This forms a striking contrast with the case of the sensitization by thiazine dyes, where the reciprocal of the quantum yield changed linearly with the dye concentration.[2)]

Table 2. Dye concentration effects on quatum yields

Dye	$[HMTC]_{ini}$, M	[Dye], M	Quantum yield (η)
Erythrosine	3.7×10^{-4}	5.2×10^{-6}	0.222
		2.1×10^{-5}	0.226
		3.6×10^{-5}	0.228
		5.2×10^{-5}	0.263
Rose bengal	3.5×10^{-4}	9.2×10^{-6}	0.378
		3.7×10^{-5}	0.320
		5.5×10^{-5}	0.348
		7.4×10^{-5}	0.352
		9.2×10^{-5}	0.360

Effect of HMTC Concentration. Aerated ethanol solutions containing 10^{-5}—10^{-6}M xanthene dyes and various concentrations of HMTC were irradiated at 546 nm. The results are depicted in Fig. 1. As is represented there, a linear relation between the reciprocal of the quantum yield and that of the HMTC concentration holds for all of the dyes investigated. Apparently the efficiency of sensitization increased in the following order: eosine yellowish<phloxine<erythrosine<rose bengal. This order was the same as that of the dye-sensitized photolysis of 4-methoxy-α-naphthol[8)] or sodium *N,N*-dimethyldithiocarbamate,[7)] which have previously been reported by us.

Effect of the Reducing Agent, Allylthiourea. To examine if the dye-sensitized reaction is initiated by the semiquinone form of dye, allylthiourea was added as a reducing agent and the quantum yield was measured. Aerated ethanol solutions containing 9.2×10^{-6}M of rose bengal, 3.7×10^{-4}M of HMTC, and various concentrations of allylthiourea as a reducing agent were irradiated at 546 nm. Figure 2 shows the Stern-Volmer plots thus obtained. The value of the slope is of the order of 10^3M^{-1}, while it was of the order of 10M^{-1} in the case of thiazine dye. Allylthiourea did not increase, but

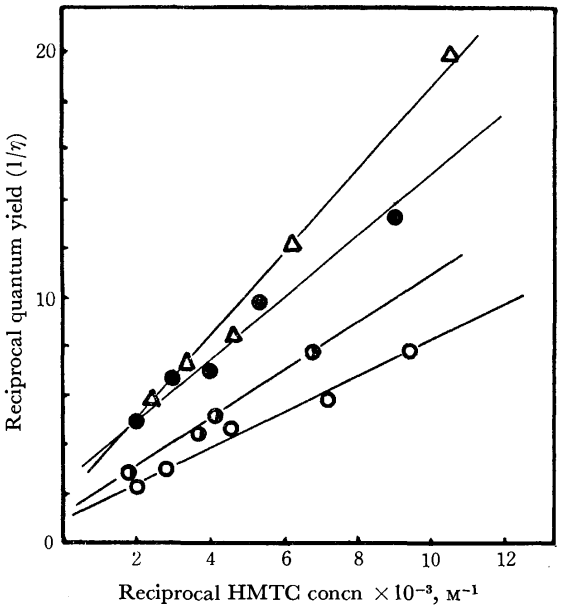

Fig. 1. Dependence of the quantum yield on the HMTC concentration.

	Rose bengal (○),	Erythrosine (◑)	Phloxine (●),	Eosine yellowish (△)
Dye concn	9.2×10^{-6}M	5.2×10^{-6}M	9.2×10^{-6}M	1.8×10^{-5}M
$(Slope)^{-1}$	1.33×10^3	9.8×10^2	8.3×10^2	6.2×10^2

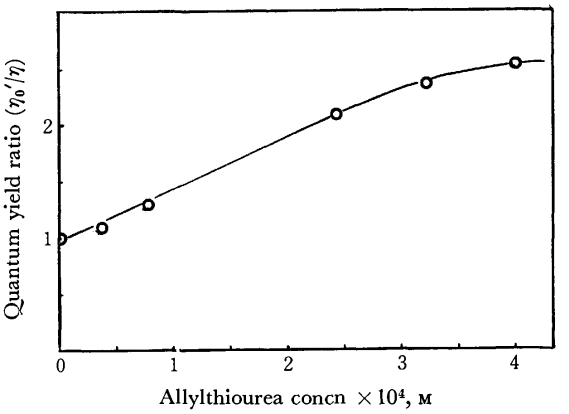

Fig. 2. Effect of allylthiourea on the quantum yield. η and η_0' indicate the quantum yields for the system with and without allylthiourea, respectively.
$[HMTC]_{ini}=3.7\times10^{-4}$M; [Rose bengal]$=9.2\times10^{-6}$M

decreased the efficiency of the sensitization. The present investigation suggests that a reducing agent is not necessary for dye-sensitization. It may be inferred that the sensitization does not take place *via* the semiquinone radical.

Effects of Singlet Oxygen Quencher and Trap. The fact that HMTC did not affect the fluorescence of the xanthene dye ruled out the excited-dye singlet as the sensitizing species under our conditions. From the essentiality of oxygen and the decreasing effect of allylthiourea on the quantum yield, the dye-sensitized photoelimination of HMTC may proceed by means of the singlet oxygen ($^1O_2$) formed by energy transfer from the triplet sensitizer, as was discussed in a previous paper.[2)] It therefore seems interesting to find out if an actual decrease in quantum yield is observed by adding

7) T. Yamase, H. Kokado, and E. Inoue, *ibid.*, **71**, 1587 (1968).
8) E. Inoue, H. Kokado, and T. Yamase, *ibid.*, **70**, 2337 (1967).

a $^1O_2$ quencher, such as 1,4-diazabicyclo[2.2.2.]octane (DABCO),[9] or efficient $^1O_2$ traps, such as tetramethylethylene (TME)[10] and β-carotene.[11] Aerated solutions containing 9.2×10^{-6}M of rose bengal, $2—4\times10^{-4}$M of HMTC, and various concentrations of DABCO, TME, or β-carotene in ethanol solvents were irradiated at 546 nm. The results are shown in Figs. 3, 4, and 5. The resulting quantum yields were reduced; the best fit of the data to the Stern-Volmer equation gave the slope values of 5.8×10, 2.7×10^2, and 7.0×10^4M^{-1} for DABCO, TME, and β-carotene respectively. This decreasing effect on the quantum yields supports the idea of the involvement of the singlet oxygen in the dye-sensitized photoelimination of HMTC.

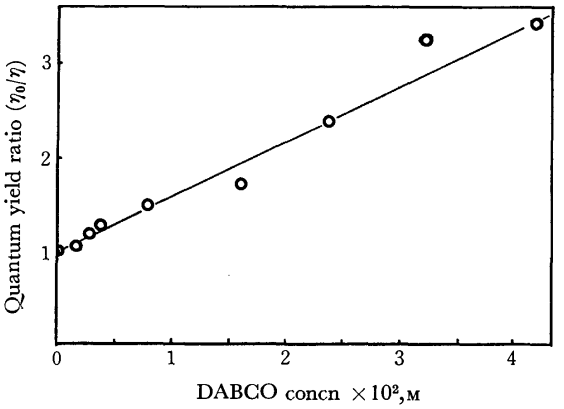

Fig. 3. Effect of DABCO on the quantum yield. η and η_0 indicate the quantum yields for the system with and without DABCO, respectively.
η_0=0.435, Slope=5.8×10 M^{-1}
[HMTC]$_{ini}$=4.48×10^{-4} M; [Rose bengal]=9.2×10^{-6} M

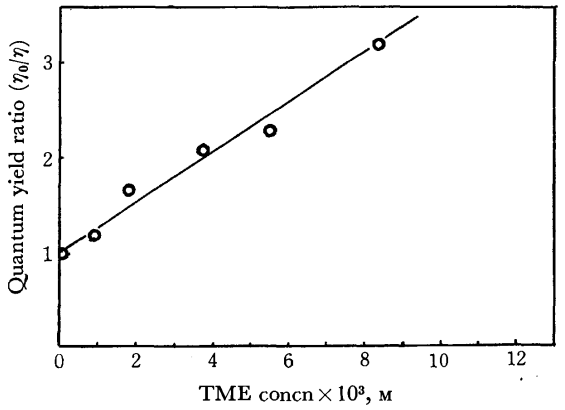

Fig. 4. Effect of TME on the quantum yield. η and η_0 indicate the quantum yields for the system with and without TME, respectively
η_0=0.303, Slope=2.7×10^2 M^{-1}
[HMTC]$_{ini}$=2.80×10^{-4} M; [Rose bengal]=9.2×10^{-6} M

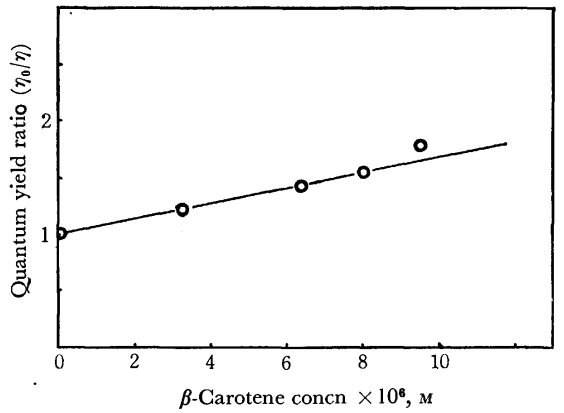

Fig. 5. Effect of β-carotene on the quantum yield. η and η_0 indicate the quantum yields for the system with and without β-carotene, respectively.
η_0=0.357, Slope=7.0×10^4 M^{-1}
[HMTC]$_{ini}$=3.35×10^{-4} M; [Rose bengal]=9.2×10^{-6} M

Consumption of Oxygen. When aerated solutions containing 9.2×10^{-6}M of rose bengal with HMTC in ethanol were irradiated at 546 nm, the dissolved oxygen contained decreased as is shown in Fig. 6. This

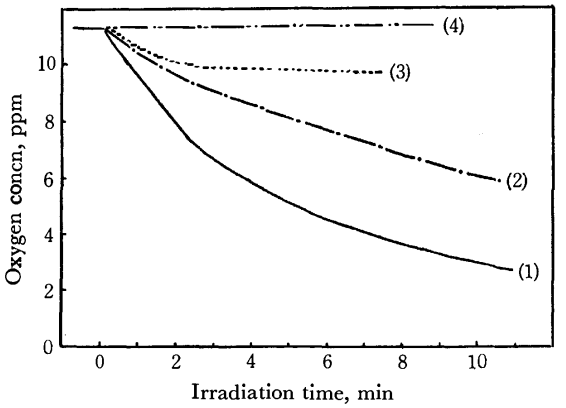

Fig. 6. Intake of oxygen during the irradiation.
(1) [HMTC]$_{ini}$=1.0×10^{-3} M, [DABCO]=0
(2) [HMTC]$_{ini}$=1.0×10^{-3} M, [DABCO]=3.4×10^{-2} M
(3) [HMTC]$_{ini}$=4.0×10^{-4} M, [DABCO]=0
(4) [DABCO]=1.0×10^{-1} M, [HMTC]$_{ini}$=0
[Rose bengal]=9.2×10^{-6} M

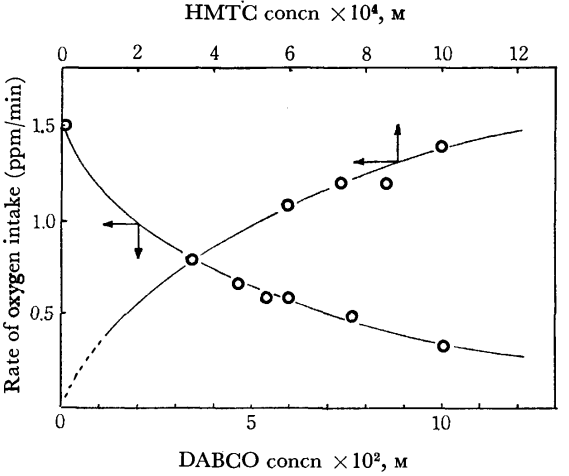

Fig. 7. Effect of DABCO or HMTC on the rate of oxygen intake.
[Rose bengal]=9.2×10^{-6} M
[HMTC]=1.0×10^{-3} M for DABCO effect

9) C. Ouannès and T. Wilson, *J. Amer. Chem. Soc.*, **90**, 6527 (1968).

10) C. S. Foote, S. Wexler, and W. Ando, *Tetrahedron Lett.*, No. **46**, 4111 (1965).

11) C. S. Foote and R. W. Denny, *J. Amer. Chem. Soc.*, **90**, 6233 (1968).

TABLE 3. ATTEMPT AT SENSITIZATION IN OTHER DITHIOCARBAMATES

Substrate	Substrate concn, M	Sensitizer	Sensitizer concn, M	Quantum yield
Methyl dimethyldithiocarbamate	$3.0—12.0\times10^{-5}$	Dye[a]	$\sim10^{-5}$[b]	0[16]
Butyl hexamethylenedithiocarbamate	$1.0—10.0\times10^{-5}$	Dye[a]	$\sim10^{-5}$[b]	0[16]
2,4-dinitrophenyl hexamethylene-dithiocarbamate	$1.0—5.0\times10^{-5}$	Dye[a]	$\sim10^{-5}$[b]	0[16]
Tetramethylthiuram monosulfide[14]	$1.0—5.0\times10^{-5}$	Dye[a]	$\sim10^{-5}$[b]	0[16]
Tetramethylthiuram disulfide (TMTD)[15]	$1.0—10.0\times10^{-5}$	Dye[a]	$\sim10^{-5}$[b]	0[16,17]
	2.1×10^{-4}	Acetophenone	8.0×10^{-2}	0.053[17]
	2.0×10^{-4}	Benzophenone	8.0×10^{-2}	0.043[17]
	3.5×10^{-4}	Michler's ketone	$1—2\times10^{-4}$	0[17]
	2.5×10^{-4}	β-Acetonaphthone	8.0×10^{-3}	0[17]
	3.0×10^{-4}	Naphthalene	6.2×10^{-3}	0[17]

a) Rose bengal or methylene blue.
b) The initial dye concentrations in all of the experiments were 4.0×10^{-5}M and 2.0×10^{-5}M for rose bengal and methylene blue respectively.

shows that the photooxygenation of HMTC took place. Furthermore, DABCO was found to be apparently unreactive toward $^1O_2$, yet to retard the oxidation of HMTC. This is identical with what Wilson had said regarding the effect of DABCO on the rubrene photooxygenation.[9] If the rate of oxygen consumption corresponds to the slope of the linear portion of the curve during the initial stage of the reaction in Fig. 6, the effect of the DABCO or HMTC concentration on the rate of oxygen consumption is also determinable. The results are given in Fig. 7.

Attempts at Dye-sensitization in Other Dithiocarbamates. Unfortunately, we encountered difficulty in identifying the photoproducts. Instead of the direct way of identification, therefore, we attempted to examine the sensitization in the variation of the dithiocarbamates. Esters of dithiocarbamic acid or thiuram sulfide show two strong ultraviolet bands in the 275—290 nm (N conjugation) and 245—260 nm (S conjugation) regions, both with log ε about 4, and another weaker absorption in the 325—360 nm region (log ε about 1.8), as well as HMTC, which represents a true ionic salt.[12] These dithiocarbamates were photolyzed by UV light.[13] In the course of the study we examined whether or not dye-sensitization takes place in these dithiocarbamates. Some representative results of sensitized photolysis in an aerated solution are presented in Table 3. No detectable dye-sensitized reaction occurred, though tetramethylthiuram disulfide (TMTD) was photo-sensitized by a few aromatic ketones possessing a high triplet energy. Furthermore, ethanolic solutions of these dithiocarbamates containing excess hydrogen peroxide were not oxidized by adding dilute aqueous sodium hypochloride.

Discussion

An attempt to check further the singlet-oxygen mechanism for the photooxidations by the action of H_2O_2 mixed with NaOCl, which is known to produce singlet oxygen, failed because HMTC was completely eliminated when NaOCl was injected into a HMTC ethanol solution in the dark. However, all the data presented here on the dye-sensitized photooxidation of HMTC are entirely consistent with a mechanism *via* the singlet oxygen. Because of the spin conservation, only a triplet-triplet transfer (Eq. 1) or a triplet-triplet annihilation (Eq. 2) can be responsible for the excitation of oxygen. Here, $^1D_0$, $^1D_1$, $^3D_1$, and $^3O_2$ represent the singlet ground state, the first excited singlet state, the lowest triplet state of the photosensitizing dye, D, and the ground state of oxygen respectively:

$$^1D_1 + {}^3O_2 \longrightarrow {}^3D_1 + {}^1O_2 \quad (1)$$

$$^3D_1 + {}^3O_2 \longrightarrow {}^1D_0 + {}^1O_2 \quad (2)$$

In dyes, the singlet-triplet splitting is very small.[18] Unfortunately, no literature on the energies of the triplet states of thiazine dyes is available except for thionine.[19] However, if the singlet-triplet splitting (ΔE_{ST}) is smaller than 10 kcal, as is the case with eosine and other xanthene derivatives, then the triplet-triplet transfer can not be responsible for the excitation of oxygen even to the lowest $^1\Delta_g$ state. This can be achieved only by the triplet-triplet annihilation (Reaction 2), in which the whole of the triplet energy of the sensitizer is available. This hypothesis is supported by the conclusion of Stevens and Algar[20] that the singlet oxygen is produced solely by energy transfer from the sensitizer triplet state, even when transfer from excited singlet state is spin-al-

12) M. J. Janssen, *Rec. Trav. Chim. Pays-Bas*, **76**, 827 (1957).
13) For esters of dithiocarbamic acid, see: M. Okawara, T. Nakai, K. Morishita, and E. Imoto, *Kogyo Kagaku Zasshi*, **67**, 130, (1964). For thiuram sulfide, T. Yamase, H. Kokado, and E. Inoue, unpublished results.
14) $(CH_3)_2N-\overset{\overset{S}{\|}}{C}-S-\overset{\overset{S}{\|}}{C}-N(CH_3)_2$
15) $(CH_3)_2N-\overset{\overset{S}{\|}}{C}-S-S-\overset{\overset{S}{\|}}{C}-N(CH_3)_2$
16) The quantities of dithiocarbamate listed in Table 3 were determined by measuring the optical densities of undiluted or diluted samples of irradiated and nonirradiated solutions, if possible, in regions where the dithiocarbamate had a UV absorption which was not interfered with by the dye absorption.
17) An excess of cupric acetate was added to the TMTD solutions and then, after they had stood at room temperature for at least half an hour (in case the reaction was not complete), the quantity of TMTD was determined by almost the same method as that employed for HMTC.
18) L. S. Forster and D. Dudley, *J. Phys. Chem.*, **66**, 838 (1962).
19) H. E. A. Kramer and M. Hafner, *Z. Naturforsch.*, **24b**, 452 (1969).
20) B. Stevens and B. E. Algar, *J. Phys. Chem.*, **73**, 1711 (1969).

lowed and exothermic. The reaction scheme which can explain the experimental data consists of the following steps:

$$^1D_0 + h\nu \xrightarrow{I_{abs}} {}^1D_1 \quad \text{Absorption} \quad (3)$$

$$^1D_1 \xrightarrow{k_1} {}^1D_0 \quad \text{Fluorescence and internal conversion} \quad (4)$$

$$^1D_1 \xrightarrow{k_2} {}^3D_1 \quad \text{Intersystem crossing to the triplet state} \quad (5)$$

$$^3D_1 \xrightarrow{k_3} {}^1D_0 \quad \text{Intersystem crossing to the ground state} \quad (6)$$

$$^3D_1 + {}^3O_2 \xrightarrow{k_4} {}^1D_0 + {}^1O_2 \quad \text{Formation of the singlet oxygen} \quad (7)$$

$$^3D_1 + \text{Red} \xrightarrow{k_5} D\cdot + \text{Red}\cdot \quad \text{Radical formation} \quad (8)$$

$$^1O_2 \xrightarrow{k_6} {}^3O_2 \quad \text{Deactivation of the singlet oxygen} \quad (9)$$

$$^1O_2 + H \xrightarrow{k_H} H\text{–}O_2\ ? \quad \text{Product formation} \quad (10)$$

$$^1O_2 + Q \xrightarrow{k_Q} \begin{matrix} Q + {}^3O_2 \\ Q\text{–}O_2 \end{matrix} \quad \text{Quenching or trapping of the singlet oxygen} \quad (11)$$

where Red, Red·, D·, H, and Q are, respectively, the reducing agent, the radical of Red, the semiquinone radical of D, HMTC, and the singlet-oxygen quenches or trap. If any reducing agent is rigorously excluded, the quantum yield (η) for HMTC photoelimination is given by:

$$\eta = \frac{k_2}{k_1+k_2}\cdot\frac{k_4[O_2]}{k_3+k_4[O_2]}\cdot\frac{k_H[H]}{k_6+k_Q[Q]+k_H[H]} \quad (12)$$

Under [Q]=0, the quantum yield (η_0) is given by:

$$\eta_0 = \alpha\cdot\beta\cdot\frac{k_H[H]}{k_6+k_H[H]} \quad (13)$$

where

$$\alpha = \frac{k_2}{k_1+k_2}, \qquad \beta = \frac{k_4[O_2]}{k_3+k_4[O_2]} \quad (14)$$

By dividing Eq. (13) by Eq. (12), we obtain the Stern-Volmer expression:

$$\frac{\eta_0}{\eta} = 1 + \frac{k_Q[Q]}{k_6+k_H[H]} \quad (15)$$

and a plot of η_0/η *vs.* [Q] should result in a straight line with a slope of $k_Q/(k_6+k_H[H])$. Such a plot is found to be linear for a quencher and two traps, as is shown in Figs. 3, 4, and 5. The value of k_H can be calculated as 1.5×10^8M^{-1}sec^{-1} from the $k_Q/(k_6+k_H[H])$ (7.0×10^4M^{-1}) obtained from Fig. 5, since k_6 and k_Q are 10^4 sec^{-1} and 5.0×10^9M^{-1}sec^{-1} respectively.[11,12] Using $k_H=1.5\times10^8$M^{-1}sec^{-1}, the k_Q values for DABCO and TME were calculated to be 5.3×10^6 and 1.6×10^7M^{-1}sec^{-1} respectively. The data obtained by the indirect kinetic approach are summarized in Table 4.[22]

Table 4. Rate constants for the process

Quencher or trap	$[HMTC]_{ini}\times10^4$, M	$k_Q/k_6+k_H[H]\times$M	$k_Q\times$M sec	$k_H\times$M sec
DABCO	4.48	5.8×10	5.3×10^6	
TME	2.80	2.7×10^2	1.6×10^7	1.5×10^8
β-carotene	3.35	7.0×10^4	5.0×10^9 [11]	

The rate of the oxygen consumption ($-d[^3O_2]/dt$) is given by:

$$-\frac{d[^3O_2]}{dt} = k_4[^3D_1][^3O_2] - k_{QD}[^1O_2][DO] - k_6[^1O_2] \quad (16)$$

where k_{QD} refers to the rate constant for DABCO (DO). Assuming the steady concentrations for $^1O_2$ and $^3D_1$,

$$[^1O_2] = \frac{k_4[^3O_2][^3D_1]}{k_6+k_H[H]+k_{QD}[DO]} \quad (17)$$

$$k_4[^3O_2][^3D_1] \approx \alpha I \quad (18)$$

since $k_4[^3O_2] \gg k_3$.[26] The substitution of Eqs. (17) and (18) into (16) gives the rate of oxygen consumption:

$$-\frac{d[^3O_2]}{dt} = \alpha I\cdot\frac{k_H[H]}{k_6+k_H[H]+k_{QD}[DO]} \quad (19)$$

Eq. (19) can be rewritten as:

$$1/-\frac{d[^3O_2]}{dt} = \frac{1}{\alpha\cdot I}\left(1+\frac{k_6}{k_H[H]}+\frac{k_{QD}}{k_H[H]}[DO]\right) \quad (20)$$

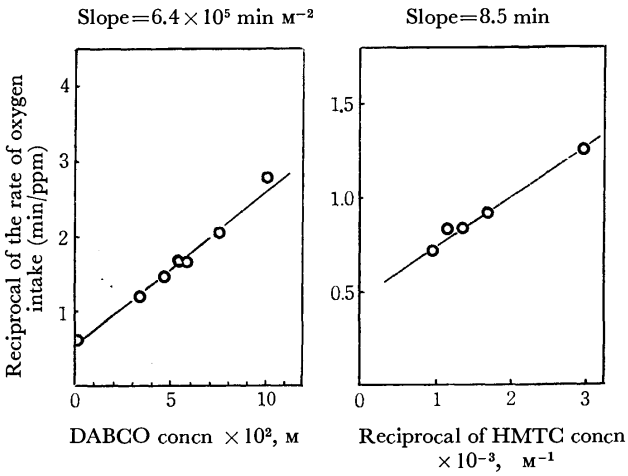

Fig. 8. Relationship between the rate of oxygen intake and DABCO or HMTC concentration.
[Rose bengal]=9.2×10^{-6} M

The best fit of the data in Fig. 7 to this equation gives $k_{QD}/\alpha I\cdot k_H[H]=6.4\times10^5$ min M^{-2} for the plot of $1/(-d[^3O_2]/dt)$ *vs.* [DO], with the [H] and αI constants, as shown in Fig. 8. Experimentally, the values of I and [H] were determined to be $4\text{—}5\times10^{-5}$ Einstein/l min and 1.0×10^{-3}M respectively. If k_{QD} is taken to be

21) P. J. Wagner and I. Kochevar, *J. Amer. Chem. Soc.*, **90**, 2232 (1968).

22) In the gas phase, k_Q for DABCO has recently been found to equal $1.2\pm0.1\times10^7$M^{-1}sec^{-1},[23] so the present value of $k_Q=5.3\times10^6$M^{-1}sec^{-1} seems reasonable. The value of k_Q obtained for TME is less than 10^8M^{-1}sec^{-1},[24] but greater than 10^5M^{-1}sec^{-1},[25] though these values were obtained in the gas phase.

23) E. A. Ogryzlo and C. W. Tang, *J. Amer. Chem. Soc.*, **92**, 5034 (1970).

24) S. J. Arnold, M. Kubo, and E. A. Ogryzlo, "Oxidation of Organic Compounds," Advances in Chemistry Series, No. **77**, American Chemical Society, Washington, D. C., 1968, p. 133.

25) W. S. Gleason, A. D. Broadbent, E. Whittle, and J. N. Pitts, Jr, *J. Amer. Chem. Soc.*, **92**, 2068 (1970).

26) R. M. Danziger, K. H. Bar-Eli, and K. Weiss, *J. Phy. Chem.*, **71**, 2633 (1967).

$5.3\times10^{6}\text{M}^{-1}\,\text{sec}^{-1}$, as is shown in Table 4, then k_H can be calculated to be about $1—2\times10^{8}\text{M}^{-1}\,\text{sec}^{-1}$ from the value of the slope with 6.4×10^{5} min M^{-2}, since α and k_6 are about unity[27] and $10^{4}\,\text{sec}^{-1}$ [11] respectively. The value of k_H calculated here is in good agreement with that obtained by the plot of η_0/η *vs.* [Q]. As a further check, plots of $1/(-\text{d}[^3O_2]/\text{d}t)$ *vs.* 1/[H] were carried out for the data in Fig. 7; they gave a straight line, as is shown in Fig. 8. Then, k_H can be calculated to be about $5\times10^{7}\text{M}^{-1}\,\text{sec}^{-1}$ from the value of the slope with $k_6/\alpha I\cdot k_H=8.5$ min. The values of k_H obtained by different methods are in satisfactory agreement if one allows for the difference in reaction conditions and the errors included in the measurements. The best value of k_H is, therefore, probably around $10^{8}\text{M}^{-1}\,\text{sec}^{-1}$. These results illustrate the sensitivity of HMTC as a photometric detector of oxidation *via* $^1O_2$.

Considering the findings, shown in Table 3, that dye-sensitization did not take place for each dithiocarbamate representing a true nonionic structure, it may be suggested that the thiocarboxyl-ion group ($-C\overset{S}{\underset{S^{\ominus}}{<}}$) plays the important role in the dye-sensitized photooxygenation of HMTC. In connection with the involvement of the singlet oxygen, it was inferred that the singlet oxygen attacked the thiocarboxyl-ion group of HMTC with a rate constant of $10^{8}\text{M}^{-1}\,\text{sec}^{-1}$ in ethanol.[28]

Returning now to the dye reactions, the effects of the dye concentration and of allylthiourea delineated the differences between xanthene dyes and thiazine dyes (Table 2, Fig. 2).[2] As one conceivable mechanism to explain the differences, the D-D mechanism (Eq. 8′) may be mentioned:

$$^3D_1 + {}^1D_0 \xrightarrow{k_5'} D^+\text{–}D^- \qquad (8')$$

The occurrence of a D-D mechanism, in which the photochemical reaction is initiated by the interaction of the triplet-dye and the ground-state-dye molecules, is established for the ethanol solution of xanthene or thiazine dye.[29] When the rate constant of the D-D mechanism is represented by k_5', Eq. (15) can be rewritten to:

$$\eta_0'/\eta = 1 + \frac{k_5}{k_3+k_4[O_2]+k_5'[D]}[\text{Red}] \qquad (21)$$

with a η_0'=quantum yield under [Red]=0. Fig. 2 and a previous paper show that the concentration of allylthiourea, which reduces η to one-half of its original value, is of the order of 10^{-4}M for rose bengal and of 10^{-2}M for methylene blue. In connection with the fact that, on the quantum yield, there is a remarkable effect of the thiazine-dye concentration in comparison with the case of the xanthene dye, for rose bengal, k_5' must be smaller than that for methylene blue provided that k_3, k_4, and k_5 are of similar magnitudes for the two dyes. The above estimation suggests that the D-D mechanism easily occurs for the thiazine dye, resulting in a decrease in the rate of T-T annihilation. Further studies are necessary to examine the above possibility, however.

27) K. Gollnick and G. O. Schenck, *Pure Appl. Chem.*, **9**, 507 (1964).

28) As one conceivable reaction, if the singlet oxygen is to cycloadd to a isolated thiocarboxyl anion group (I), one possible product is an intermediate endoperoxide (II):

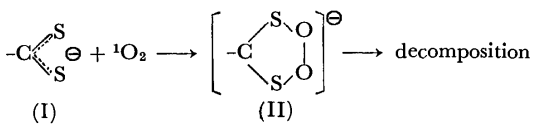

(I) (II)

though we can not construct a state correlation diagram for this reaction because of the lack of thermochemical data.

29) M. Koizumi, *Nippon Kagaku Zasshi*, **90**, 1 (1969).

The Microwave Spectrum of *trans*-Ethylmethylsilane

Michiro HAYASHI and Chi MATSUMURA*

Department of Chemistry, Faculty of Science, Hiroshima University, Higashisenda-machi, Hiroshima
**Government Chemical Industrial Research Institute, Tokyo, Honmachi, Shibuya-ku, Tokyo*

(Received July 14, 1971)

The microwave spectra of $CH_3CH_2SiH_2CH_3$ and $CH_3CH_2SiD_2CH_3$ in the *trans* form were studied. The rotational constants calculated from the spectra can be explained satisfactorily with a model which has structural parameters transferred with only a slight modification, from the values reported for dimethylsilane and ethylsilane. From the observed splittings of the spectra, the barrier to the internal rotation of the $SiCH_3$ group was calculated to be 1520 ± 30 cal/mol, assuming that the coupling effect of the torsional motions of the other groups can be ignored. From the Stark shifts, the dipole moment was determined to be $\mu_a=0.036\pm0.030$, $\mu_b=0.757\pm0.003$, and $\mu_{total}=0.758\pm0.005$ D, making an angle of 2°44′ with the *b* axis for the parent species, while it was determined to be $\mu_a=0.024\pm0.030$, $\mu_b=0.758\pm0.003$, and $\mu_{total}=0.758\pm0.005$ D, making an angle of 1°49′ with the *b* axis for the deuterated species. From these results, the orientation of the dipole moment in the molecule was concluded to be along the direction slightly inclined from the bisector of the CSiC angle toward the ethyl group in the molecule.

Ethylmethylsilane has been investigated by means of microwave spectroscopy as an expression of the current interest in rotational isomerism and in the barriers to internal rotation.

The infrared and Raman spectra of this molecule have also been previously investigated by one of the present authors[1]; they give evidence of the existence of two rotational isomers, which will be published separately. However, the observed microwave spectra were very weak, and assignments are possible for only the *trans* isomer at present.

Therefore, in the present paper, a brief consideration will be given of the structure, the barrier to the internal rotation of the $SiCH_3$ group, and the electric dipole moment of the *trans* isomer.

Experimental

The samples of $CH_3CH_2SiH_2CH_3$ and $CH_3CH_2SiD_2CH_3$ were prepared by the method of reacting CH_3CH_2MgBr with CH_3SiCl_3 in ethyl ether and by subsequently reducing the resultant $CH_3CH_2SiCl_2CH_3$ with $LiAlH_4$ or $LiAlD_4$ in *n*-butyl ether.[2]

The microwave spectra of the samples were measured in the region from 8000 to 36000 MHz with conventional sinu-

TABLE 1. OBSERVED MICROWAVE TRANSITION FREQUENCIES OF *trans*-$CH_3CH_2SiH_2CH_3$ AND $CH_3CH_2SiD_2CH_3$ (MHz)

Transition	$CH_3CH_2SiH_2CH_3$			$CH_3CH_2SiD_2CH_3$		
	ν_A[a]	ν_E[a]	$\Delta\nu$[c]	ν_A[a]	ν_E[a]	$\Delta\nu$[c]
$1_{10}\leftarrow 1_{01}$	12651.59[b]	12650.45	0.00	10230.24[b]	10229.48	−0.01
$2_{11}\leftarrow 2_{02}$	12895.12[b]	12893.67	0.00	10475.60[b]	10474.71	−0.02
$3_{12}\leftarrow 3_{03}$	13266.87[b]	13265.33	0.01	10851.74[b]	10850.77	0.01
$4_{13}\leftarrow 4_{04}$	13774.53	13772.91	0.04	11368.18	11367.11	0.06
$5_{14}\leftarrow 5_{05}$	14428.10	14426.47	0.06	12037.34	12036.25	0.14
$6_{15}\leftarrow 6_{06}$	15239.78	15238.05	0.02	12874.05	12872.87	0.14
$7_{16}\leftarrow 7_{07}$	16223.66	16221.95	−0.01	13895.02	13893.78	0.04
$8_{17}\leftarrow 8_{08}$	17394.92	17393.08	−0.07	15117.86	15116.53	−0.05
$9_{18}\leftarrow 9_{09}$	18769.16	18767.28	−0.23	16559.29	16557.94	−0.33
$10_{19}\leftarrow 10_{010}$	20361.34	20359.28	−0.65	18234.22	18232.72	−0.62
$1_{11}\leftarrow 0_{00}$	17578.12[b]	17576.10	0.02	15061.75[b]	15060.42	0.04
$2_{12}\leftarrow 1_{01}$	22504.58[b]	22502.84	−0.03	19893.14[b]	19892.08	−0.04
$3_{13}\leftarrow 2_{02}$	27312.40[b]	27310.78	0.01	24605.76[b]	24604.80	0.01
$4_{14}\leftarrow 3_{03}$	32005.82	32004.24	0.02	29205.52	29204.58	0.61
$4_{04}\leftarrow 3_{13}$	8805.49	8807.00	−0.01	10841.67	10842.55	−0.03
$5_{05}\leftarrow 4_{14}$	14390.11	14391.55	−0.17	16318.84	16319.72	−0.20
$6_{06}\leftarrow 5_{15}$	20051.50	20052.84	−0.39	21862.78	21863.60	−0.44
$7_{07}\leftarrow 6_{16}$	25773.80	25775.08	−0.80	27454.40	27455.20	−0.71
$8_{08}\leftarrow 7_{17}$	31539.72	31540.92	−1.15	33072.94	33073.60	−0.97

a) ν_A and ν_E designate the observed frequencies belonging to the "A" and "E" components of the doublets, respectively and estimated uncertainty of the frequencies is ±0.05 MHz.
b) The observed frequency used for the determination of the rotational constants by the least-squares technique.
c) $\Delta\nu$=(the observed frequency of the "A" component of the doublet) −(the calculated frequency in the rigid rotor model).

1) M. Hayashi, K. Ohno, and H. Murata, This Bulletin, **45**, 298 (1972).

2) F. S. Fipping, *Proc. Chem. Soc.*, **20**, 15 (1904); W. Dilthey, *Ber.*, **37**, 319 (1904); A. E. Finhalt, A. C. Bond, Jr., and H. I. Schlesinger, *J. Amer. Chem. Soc.*, **69**, 1199 (1947).

TABLE 2. ROTATIONAL CONSTANTS AND MOMENTS OF INERTIA OF *trans*-ETHYLMETHYLSILANE

	$CH_3CH_2SiH_2CH_3$	$CH_3CH_2SiD_2CH_3$
Observed rotational constants for the "A" sublevel (MHz)[a]		
A	15114.85±0.20	12645.98±0.20
B	2703.36±0.10	2656.80±0.10
C	2463.25±0.10	2415.73±0.10
Rotational constants for the unperturbed level (MHz)[b]		
A	15113.80	12645.30
B	2703.34	2656.79
C	2463.25	2415.73

Observed and calculated moments of inertia (amu·Å²)

		Observed[c]	Model I (δ)[d]		Model II (δ)[d]	
$CH_3CH_2SiH_2CH_3$	I_a	33.4381	33.4720	−0.10	33.4198	0.05
	I_b	186.9454	185.8801	0.57	186.7817	0.09
	I_c	205.1668	204.2243	0.46	205.0770	0.04
$CH_3CH_2SiD_2CH_3$	I_a	39.9656	40.0181	−0.13	39.9790	−0.03
	I_b	190.2209	189.1896	0.54	190.1100	0.06
	I_c	209.2026	208.2991	0.43	209.1837	0.01

a) The rotational constants were determined by the least squares technique from the observed frequencies of the following six transitions; $1_{11}\leftarrow 0_{00}$, $1_{10}\leftarrow 1_{01}$, $2_{11}\leftarrow 2_{02}$, $2_{12}\leftarrow 1_{01}$, $3_{12}\leftarrow 3_{03}$, and $3_{13}\leftarrow 2_{02}$. The root mean square deviations on the calculations were 0.016 and 0.024 MHz for the parent and deuterated species, respectively.

b) The unperturbed rotational constants were calculated by the formulas;
A (unperturbed) $=A$(A sublevel)$-F\alpha^2 W_{0A}^{(2)}$, B(unperturbed) $=B$(A sublevel)$-F\beta^2 W_{0A}^{(2)}$, C(unperturbed) $=C$(A sublevel)

c) The moments of inertia were calculated from the unperturbed rotational constants. Conversion factor; 505377 MHz/amu·Å².

d) Observed−calculated in %.

TABLE 3. STRUCTURE OF *trans*-ETHYLMETHYLSILANE[a]

Model I. Structural parameters transferred from those for $(CH_3)_2SiH_2$ and $CH_3CH_2SiH_3$.

CH_3–(C)		–CH_2–		CH_3–(Si)		–SiH_2–		skeleton	
r(CH)	1.093 Å	r(CH)	1.097 Å	r(CH)	1.095 Å	r(SiH)	1.483 Å	r(CC)	1.540 Å
∠(H_sCC)	111°57′	∠(HCH)	105°46′	∠(H_sCSi)	110°56′	∠(HSiH)	107°50′	r(CH_2–Si)	1.867 Å
∠(H_aCC)	111°41′	∠(CCH)	109°28′	∠(H_aCSi)	110°56′	∠($HSiCH_2$)	109°30′	r(CH_3–Si)	1.867 Å
∠(H_sCH_a)	107°15′	∠(SiCH)	109°28′	∠(H_sCH_a)	108°	∠($HSiCH_3$)	109°30′	∠(CCSi)	113°11′
∠(H_aCH_a)	106°59′			∠(H_aCH_a)	108°			∠(CSiC)	110°59′

Model II. Structural parameters adjusted.

∠(CCSi) 114°11′ ∠($HCCH_3$) 109°13′ ∠(SiCH) 109°13′

Other structural parameters remain unchanged.

a) H_s and H_a designate the hydrogen atoms in the molecular plane and out of the plane, respectively.

soidal and square wave Stark modulation spectrometers at the temperature of dry ice.

Results and Discussion

Spectra and Structure of the Molecule. Although *b*- and *a*-type transitions are expected for *trans*-ethylmethylsilane, the observation of the *a*-type spectra was impossible because of the small dipole moment component along the *a* axis.

As is shown in Table 1, the observed *b*-type spectra are doublets resulting from the internal rotation of the $SiCH_3$ group.

The "A" components of the doublets can be explained by an asymmetric rotor model with the rotational constants of A=15114.85, B=2703.34, and C=2463.25 MHz for the parent species and of A=12645.98, B=2656.80, and C=2415.73 MHz for the deuterated species, with reasonable centrifugal distortion contributions.

These rotational constants were determined by the least-squares technique from the observed frequencies of the "A" components of the doublets for the following six transitions; $1_{11}\leftarrow 0_{00}$, $1_{10}\leftarrow 1_{01}$, $2_{12}\leftarrow 1_{01}$, $2_{11}\leftarrow 2_{02}$, $3_{12}\leftarrow 3_{03}$, and $3_{13}\leftarrow 2_{02}$.

From these rotational constants, the unperturbed rotational constants were calculated by subtracting the contributions due to the internal rotation for the "A" sublevel.

As is shown in Tables 2 and 3, the moments of inertia obtained from the unperturbed rotational constants can be explained by a model (Model I in Table 3) which has structural parameters transferred from the reported values for $(CH_3)_2SiH_2$[3] and $CH_3CH_2SiH_3$.[4] Furthermore, a very good agreement is obtained between the calculated and the observed moments of inertia if the CCSi angle is increased by about 1° from the original value and if the CCH and SiCH angles are decreased by about 15′ (Model II in Table 3). Although the models described above should be tested further by

3) L. Pierce, *J. Chem. Phys.*, **34**, 498 (1961).

4) D. H. Petersen, Doctoral thesis, The University of Notre Dame (1961).

means of the observed rotational constants for other isotopic species which have not yet been measured, the agreement is so good and so reasonable that the structure of Model II may be proposed as the best structure for *trans*-ethylmethylsilane.

Internal Rotation of the $SiCH_3$ Group. The analysis of the fine structures of the observed spectra has been carried out by the principal-axis method.[5]

A preliminary analysis indicates that the doublet structures of the observed spectra originate mainly from the coupling of the over-all rotation and the internal rotation of the $SiCH_3$ group if the barriers are taken to be equal to the reported value for the similar molecules.

On the assumption that the coupling terms among the internal rotation of the $SiCH_3$ group, that of the CH_3CH_2 group and the skeletal torsion of the C–SiH_2–CH_2–C part of the molecule, can be neglected, the effective Hamiltonian for the v-th torsional state of the $SiCH_3$ group is given as;

$$H_{v\sigma} = H_r + F\sum_n W_{v\sigma}^{(n)}\mathscr{P}^n$$

$$H_r = AP_a^2 + BP_b^2 + CP_c^2,\ \mathscr{P} = \alpha P_a + \beta P_b$$

$$\alpha = \lambda_a I_\alpha/I_a,\ \beta = \lambda_b I_\alpha/I_b$$

$$F = \hbar^2/2rI_\alpha,\ r = 1 - \lambda_a\alpha - \lambda_b\beta$$

where I_α is the moment of inertia of the $SiCH_3$ group around the top axis and where the λ's are the direction cosines between the internal top axis and the principal axes of the entire molecule. σ stands for either the "A" or "E" sublevel.

I_α was calculated from the structural parameters of Model II, and the λ's were obtained on the assumption that the top axis coincides with the SiC bond.

According to the bootstrap method,[5] the perturbation coefficients, $W_{v\sigma}^{(n)}$, are simply proportional to a quantity, w_1, for a reasonably high barrier if the corrections due to the shape of the barrier are negligible.

By the least-squares technique, the w_1's were determined from the observed frequency splittings of the spectra, neglecting the terms higher than the fourth-order in the effective Hamiltonian for both parent and deuterated species. Then, the reduced barrier s's ($=4V_3/9F$) were obtained by the interpolation of the values of w_1 *vs.* s in the table.[6]

The barrier V_3's calculated from the interpolated s values are found to be 1522 and 1515 cal/mol, respectively, for the two species; the agreement between the two species is good within the limit of experimental error. The results are shown in Table 4.

As the analysis described above was made on the assumption that the coupling can be neglected among the torsional motion of the $SiCH_3$ group and those of the other groups, any comparison with the reported values for the similar molecules would be rather invalid. However, it is noticeable that the barrier of the $SiCH_3$ group in *trans*-ethylmethylsilane is lower than those of methylsilane[7] (1595 cal/mol), dimethylsilane[3] (1640 cal/mol), and trimethylsilane[8] (1830 cal/mol).

Table 4. Observed and calculated splittings ($\nu_A - \nu_E$) of *trans*-ethylmethylsilane (MHz)

Transition	$CH_3CH_2SiH_2CH_3$		$CH_3CH_2SiD_2CH_3$	
	Obsd	Calcd	Obsd	Calcd
$1_{10}\leftarrow 1_{01}$	1.14	1.11	0.76	0.73
$2_{11}\leftarrow 2_{02}$	1.45	1.44	0.89	0.94
$3_{12}\leftarrow 3_{03}$	1.54	1.54	0.97	1.01
$4_{13}\leftarrow 4_{04}$	1.62	1.60	1.07	1.06
$5_{14}\leftarrow 5_{05}$	1.63	1.66	1.09	1.11
$6_{15}\leftarrow 6_{06}$	1.73	1.72	1.18	1.17
$7_{16}\leftarrow 7_{07}$	1.76	1.79	1.24	1.23
$8_{17}\leftarrow 8_{08}$	1.84	1.86	1.33	1.31
$9_{18}\leftarrow 9_{09}$	1.88	1.95	1.35	1.39
$10_{19}\leftarrow 10_{010}$	2.06	2.04	1.50	1.49
$1_{11}\leftarrow 0_{00}$	2.02	2.04	1.33	1.30
$2_{12}\leftarrow 1_{01}$	1.74	1.73	1.06	1.11
$3_{13}\leftarrow 2_{02}$	1.62	1.64	0.94	1.05
$4_{14}\leftarrow 3_{03}$	1.58	1.59	0.94	1.02
$4_{04}\leftarrow 3_{13}$	−1.51	−1.52	−0.88	−0.94
$5_{05}\leftarrow 4_{14}$	−1.44	−1.44	−0.88	−0.88
$6_{06}\leftarrow 5_{15}$	−1.34	−1.36	−0.82	−0.82
$7_{07}\leftarrow 6_{16}$	−1.28	−1.29	−0.80	−0.75
$8_{08}\leftarrow 7_{17}$	−1.20	−1.21	−0.66	−0.69
R.M.S.[a]	0.02_4		0.04_4	
I_α (amu·Å^2)	3.1635		3.1635	
λ_a	0.8645		0.8562	
λ_b	0.5095		0.5166	
s	41.07		41.44	
V_3 (cal/mol)	1522±30		1515±30	

a) Root mean square deviation (MHz)

Dipole Moment. The electric dipole moments were quantitatively determined from Stark-effect measurements of $1_{11}\leftarrow 0_{00}$, $1_{10}\leftarrow 1_{01}$, and $2_{11}\leftarrow 2_{02}$ ($M=2$) transitions. For the deuterated species, very fast Stark shifts were found for $1_{11}\leftarrow 0_{00}$ and the $M=1$ lobe of $2_{11}\leftarrow 2_{02}$ transitions, since the energy levels of 1_{11}, 2_{02}, and 1_{10} are, accidentally in near degeneracy.

The spectrometer was calibrated with OCS[9] on the measurements.

The Stark shifts of the "A" and "E" components of the doublets were found to be essentially the same, and the averaged values were used for the calculations.

However, it was found that some of the observed Stark coefficients, $\Delta\nu/E^2$, show slight but regular variations with the field strength, E, beyond the limit of experimental error. This is probably due to the presence of the higher-order terms, since the second-order perturbation sums for the μ_a component are possibly considerably influenced by the contributions from the μ_b component as the field strength becomes stronger.

Considering the contributions from the higher-order terms as well as from the first-order term, which is especially significant for the $1_{11}\leftarrow 0_{00}$ transition of the deuterated species, the theoretical Stark shifts were calculated by the direct diagonalization of the energy

5) D. R. Herschbach, *J. Chem. Phys.*, **31**, 91 (1959).
6) M. Hayashi and L. Pierce, "Tables for the Internal Rotation Problem," Department of Chemistry, The University of Notre Dame, South Bend, Ind. (1961).
7) R. W. Kilb and L. Pierce, *J. Chem. Phys.*, **27**, 108 (1957).
8) L. Pierce and D. H. Petersen, *ibid.*, **33**, 907 (1960).
9) J. S. Muenter, *ibid.*, **48**, 4544 (1968).

TABLE 5. STARK COEFFICIENTS AND DIPOLE MOMENTS[a)]

Transition	Stark coefficient[b)] ($\Delta\nu/E^2$) $\times 10^5$(MHz/(V/cm)^2)	
	Obsd	Calcd
$CH_3CH_2SiH_2CH_3$		
$1_{11}\leftarrow 0_{00}$ ($M=0$)	3.818	3.831
$1_{10}\leftarrow 1_{01}$ ($M=1$)	2.601	2.605
$2_{11}\leftarrow 2_{02}$ ($M=2$)	2.914	2.894
$\mu_a=0.036\pm0.030$, $\mu_b=0.757\pm0.003$		
$\mu_{total}=0.758\pm0.005$D		
The angle between the b axis and μ, 2°44′		
$CH_3CH_2SiD_2CH_3$		
$1_{11}\leftarrow 0_{00}$ ($M=0$)	−22.578	−22.911
$1_{10}\leftarrow 1_{01}$ ($M=1$)	3.082	3.096
$2_{11}\leftarrow 2_{02}$ ($M=2$)	3.541	3.522
$\mu_a=0.024\pm0.030$, $\mu_b=0.758\pm0.003$		
$\mu_{total}=0.758\pm0.005$D		
The angle between the b axis and μ, 1°49′		

a) The measurements were made on the recorder at five or six different field strengths in the range from 0 to 600 V/cm except the $1_{11}\leftarrow 0_{00}$ transition of the deuterated species for which the range was from 0 to 150 V/cm.

b) In order to simplify the table, the observed and theoretical Stark coefficients are shown, though the frequency shifts were actually used for the determination of the diplole moments. These coefficients are the averaged values of the quantities $\Delta\nu/E^2$ for different field strengths.

matrices instead of by the usual perturbation calculation.[10)]

The energy matrices were truncated at the terms with $J=4$ and higher after the negligible influences of the truncation were confirmed.

Since more elaborate considerations are required for the application of the least-squares technique to this procedure, the dipole moments were determined by changing the magnitudes of the μ_a and μ_b components little by little until the minimum values of the $S=\sum_i(\Delta\nu_{i\text{obsd}}-\Delta\nu_{i\text{calcd}})^2$ quantity were obtained for each of the two species. The details of the procedures will be reported elsewhere.

As is shown in Table 5, the dipole moments were determined to be $\mu_a=0.036\pm0.030$, $\mu_b=0.757\pm0.003$, and $\mu_{total}=0.758\pm0.005$ D for the parent species, which makes an angle of 2°44′ with the b axis, while they were determined to be $\mu_a=0.024\pm0.030$, $\mu_b=0.758\pm0.003$, and $\mu_{total}=0.758\pm0.005$ D for the deuterated species which makes an angle of 1°49′ with the b axis.

The structural calculation indicates that the bisector of the CSiC angle makes angles with the b axis of 3°53′ for the parent species and 3°24′ for the deuterated species.

The values obtained from these observations lead to the conclusion that the orientation of the dipole moment of the molecule is along the direction making an angle of about 1°20′ with the bisector of the CSiC angle toward the ethyl group in the molecule.

As the reported value for dimethylsilane is 0.75 D[3)], the dipole moment of *trans*-ethylmethylsilane can be said to be equal to that for dimethylsilane.

One of the present authors (M.H.) especially wishes to thank Mr. Keiichi Ohno for his assistance in making the samples and Mrs. Hisae Imaishi for her assistance in calculating the theoretical Stark shifts.

10) S. Golden and E. B. Wilson, Jr., *J. Chem. Phys.*, **16**, 669 (1948).

Molecular Structures of Acetyl Chloride and Acetyl Bromide as Determined by Gas Electron Diffraction

Shuzo TSUCHIYA and Masao KIMURA

Department of Chemistry, Faculty of Science, Hokkaido University, Sapporo

(Received July 14, 1971)

The molecular structures of acetyl chloride and acetyl bromide have been investigated by the sector-microphotometer method of gas-phase electron diffraction. The thermal average distances, r_g, and the valence angles, φ_a, have been determined, with estimated limits of error, to be as follows: for acetyl chloride, r_g(C=O)=1.187±0.003 Å, r_g(C–Cl)=1.798±0.003 Å, r_g(C–C)=1.508±0.005 Å, φ_a(OCCl)=120.3°±0.6°, φ_a(CCCl)=112.2°±0.9°, and φ_a(CCO)=127.5°±0.9°; and for acetyl bromide, r_g(C=O)=1.184±0.004 Å, r_g(C–Br)=1.975±0.004 Å, r_g(C–C)=1.518±0.008 Å, φ_a(OCBr)=120.8°±0.9°, φ_a(CCBr)=109.5°±1.2°, and φ_a(CCO)=129.7°±1.1°. The C=O distances in these molecules are shorter than those in acetaldehyde and acetone by about 0.02 Å. This may be attributed to the effect of a highly electronegative halogen atom adjacent to the carbonyl group.

The interatomic distances of acetyl chloride and acetyl bromide were first investigated by the visual method of electron diffraction.[1-3] The purpose of the present study is to determine more accurate structure parameters of these molecules by the sector-microphotometer method.[4] Sinnott observed the microwave spectra of ten isotopic species of acetyl chloride and determined the r_s structure parameters from the rotational constants.[5] He showed further that, at the equilibrium conformation, a methyl hydrogen atom is eclipsed to the oxygen atom. The microwave spectrum of acetyl bromide was investigated by Krisher,[6] but the interatomic distances were not determined. These rotational constants are being used in our laboratory as additional information in a more complete and more accurate analysis of the structure parameters and the barrier to internal rotation. The results will be reported in a forthcoming paper.

Experimental

The samples of acetyl chloride and acetyl bromide were special-grade and extra-pure reagents respectively, obtained from commercial sources. The unit used in the present study has been reported elsewhere.[7] Both short (109.3 mm) and long camera lengths (244.3 mm) were used. Diffraction photographs were taken at room temperature (~16°C) with an r^3-sector. The experimental conditions were as follows: accelerating voltage, about 42 kV; sample pressure, about 60 Torr; exposure times, 25—35 sec; electron-beam current, 0.1—0.3 μA. The developing and photometric process were described in a previous work.[8] In order to calibrate the wavelength of the electron beam, carbon disulfide was used as the reference material.

Analysis

Reduction of the Molecular Intensity. The relation between the optical desity, D, and the scattering intensity, I, was previously estimated to be $I=D(1+0.03D)$ for the plates used in the present study (Fuji Process Hard).[9] The observed intensities were obtained from the optical densities by the use of this relation. The data adopted for analysis covered the range of q=30—130 for the short camera length and that of q=10—60 for the long camera length. After correction for the deviation of the sector shape from an ideal r^3-curve, the leveled total intensities, I_T, were obtained by dividing I by the theoretical background.[10] The experimental background was obtained by Karles' non-negativity criterion for the radial distribution curve.[11] The molecular intensity curves, $qM(q)^{obs}$, derived in this way and the experimental radial distribution curves for the short camera length are shown in Figs. 1 and 2.

Least-squares Analysis. The molecular parameters were determined by applying the least-squares method to the $qM(q)^{obs}$ with a conventional weight function.[9] The molecular model for the least-squares fitting was assumed as follows:

(i) An eclipse conformation for the H and O atoms;

(ii) r_a(C–H)=1.1070 Å (a value observed for ethane)[12] and the nonbonded distances related to the H atoms were fixed at calculated values, and

(iii) ∠CCH=110°21′ (Sinnott's r_s value) and the tilt angle of the methyl group=0°.

In addition to these assumptions, all the mean amplitudes were fixed at the values calculated from the spectroscopic data, since it was impossible to adjust the distances and the mean amplitudes simultaneously. The asymmetry parameters, κ, were estimated according to the equation given by Kuchitsu,[13] while the Morse parameters were assumed to be 2.0 Å^{-1} for the bonded atom pairs and zero for the nonbonded pairs. The elastic and inelastic scattering factors were obtained from the sources cited in a previous work.[9] It is not clear whether or not the H atom is eclipsed to the O atom in acetyl bromide. However, this ambiguity is not relevant to the present work, because the molecular intensity

1) R. W. Dornte, *J. Amer. Chem. Soc.*, **55**, 4126 (1933).
2) P. W. Allen and L. E. Sutton, *Trans. Faraday Soc.*, **47**, 236 (1951).
3) Y. Morino, K. Kuchitsu, M. Iwasaki, K. Arakawa, and A. Takahashi, *Nippon Kagaku Zasshi*, **75**, 647 (1954).
4) The study by this method was once carried out by G. A. Boulet, Dissert. Abstract (Univ. of Michigan), **25**, 3283 (1964), but the accuracy of the results was unsatisfactory.
5) K. M. Sinnott, *J. Chem. Phys.*, **34**, 851 (1961).
6) L. C. Krisher, *ibid.*, **33**, 1237 (1960).
7) Y. Murata, K. Kuchitsu, and M. Kimura, *Oyo Butsuri*, **9**, 591 (1970).
8) H. Fujii and M. Kimura, This Bulletin, **43**, 1933 (1970).
9) S. Konaka and M. Kimura, *ibid.*, **43**, 1693 (1970).
10) The experimental data of the leveled total intensity have been filed with the Chemical Society of Japan. A copy may be secured by citing the document number (Document No. 7201) and by remitting, in advance, ¥300 for photoprints. Payment may be made by check or money order payable to the Society.
11) J. Karle and I. L. Karle, *J. Chem. Phys.*, **18**, 957 (1950).
12) L. S. Bartell and H. K. Higginbotham, *ibid.*, **42**, 851 (1965).
13) K. Kuchitsu, This Bulletin, **40**, 498 (1967).

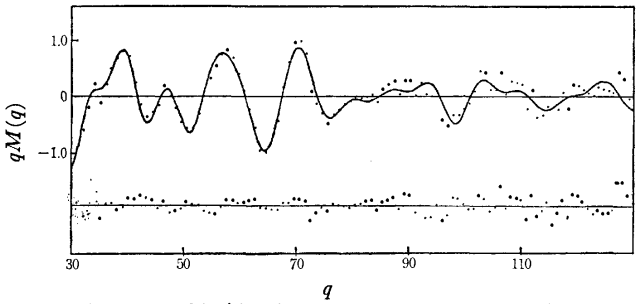

(a) Acetyl chloride (for the short camera length)

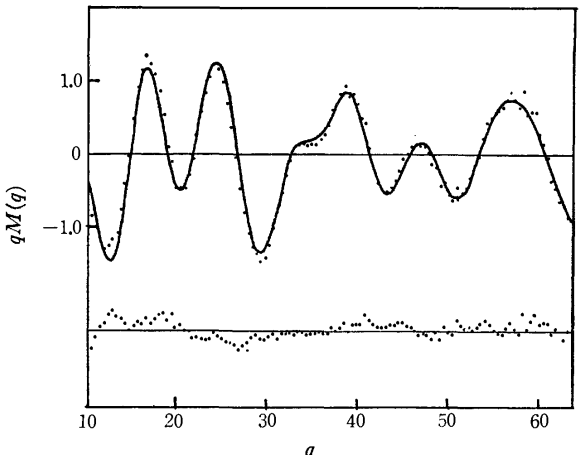

(b) Acetyl chloride (for the long camera length)

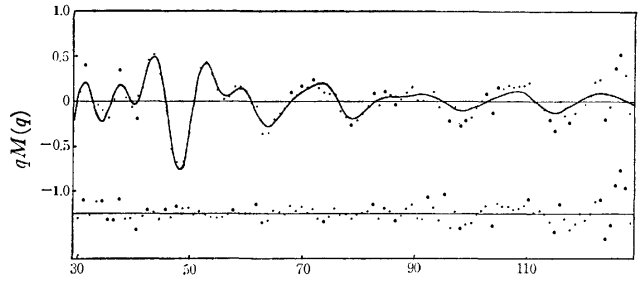

(c) Acetyl bromide (for the short camera length)

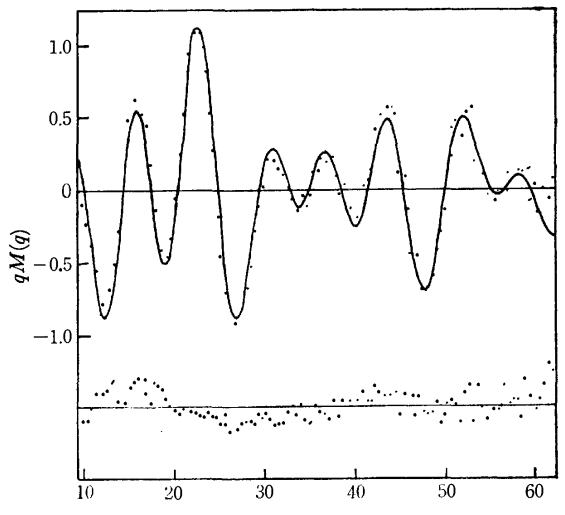

(d) Acetyl bromide (for the long camera length)

Fig. 1. Molecular intensity curves. The dots and the solid curves show the observed and best-fit theoretical values, respectively.

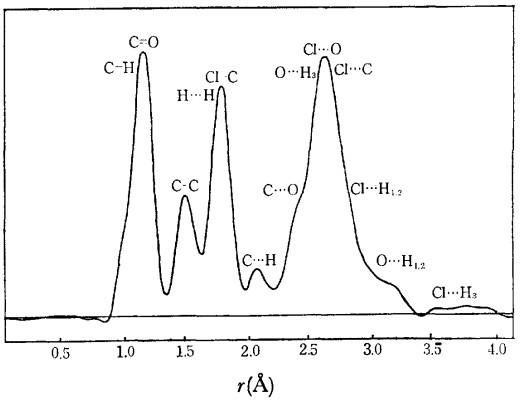

(a) Acetyl chloride

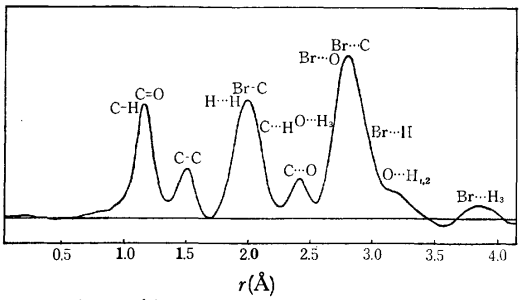

(b) Acetyl bromide

Fig. 2. Experimental radial distribution curves for the short camera length data.

curves for the eclipsed and staggered models are indistinguishable from each other.

Four plates for each of the two camera distances were used for analysis. The averages of the parameters were taken using weights inversely proportional to the squares of the standard deviations obtained by the least-squares fitting. The

Table 1. Results of the least squares adjustment (in Å units)

(a) Acetyl chloride

		σ_1	σ_2
r_a(Cl–C)	1.7968	0.0011	0.0003
r_a(Cl···C)	2.7440	0.0024	0.0006
r_a(Cl···O)	2.6031	0.0016	0.0005
r_a(C–C)	1.5058	0.0021	0.0005
r_a(C=O)	1.1862	0.0010	0.0007
r_a(C···O)	2.4153	0.0033	0.0008
k[b]	0.917	0.009	0.003

(b) Acetyl bromide

		σ_1	σ_2
r_a(Br–C)	1.9736	0.0015	0.0014
r_a(Br···C)	2.8594	0.0043	0.0017
r_a(Br···O)	2.7691	0.0028	0.0023
r_a(C–C)	1.5158	0.0032	0.0011
r_a(C=O)	1.1828	0.0016	0.0009
r_a(C···O)	2.4430	0.0050	0.0029
k[b]	0.849	0.008	0.006

a) Weighted averages of the results for eight plates (four from the long camera length and four from the short camera length). The definitions of σ_1 and σ_2 are given in Ref. 14.

b) Index of resolution (dimensionless).

14) Y. Morino, K. Kuchitsu, and Y. Murata, *Acta Crystallogr.*, **18**, 549 (1965).

Table 2. Error matrices[a] (in 10^{-4} Å units)

(a) Acetyl chloride

	Cl–C	Cl···C	Cl···O	C–C	C=O	C···O	k
Cl–C	28	11	0	0	0	11	20
Cl···C		80	47	−11	0	39	53
Cl···O			45	−11	0	41	11
C–C				52	0	0	0
C=O					23	0	28
C···O						87	70
k[b]							293

(b) Acetyl bromide

	Br–C	Br···C	Br···O	C–C	C=O	C···O	k
Br–C	68	36	26	−30	13	−46	24
Br···C		132	24	−26	18	−63	150
Br···O			74	−9	−9	−37	−98
C–C				97	−13	26	79
C=O					41	−9	60
C···O						158	72
k[b]							516

a) σ_{ij}=sgn $[(B^{-1})_{ij}]\cdot[|(B^{-1})_{ij}|\cdot V^*PV/(n-m)]^{1/2}$, where the notations follows Ref. 14.
b) Index of resolution k is dimensionless.

structure parameters and the standard errors, σ_1 and σ_2,[14] derived are shown in Table 1. Table 2 shows the error matrices which were computed for the best-fit models, corresponding to the theoretical intensity curves for the short camera length depicted in Figs. 1(a) and 1(c).

Mean Amplitudes. The mean amplitudes of vibration used for the analysis were calculated by the normal coordinate treatment.[15] The force constants for the Urey-Bradley force field determined by Overend *et al.* were used for acetyl chloride.[16] The force constants for acetylbromide were transferred from those for acetyl chloride and methyl bromide, and adjusted by a trial-and-error method so as to reproduce the vibrational frequencies obtained from the infrared spectra.[17] The force constants thus determined and the vibrational frequencies of acetyl bromide are shown in Tables 3 and 4 respectively. Evans and Overend estimated[19] the out-of-plane bending force constant for acetyl bromide to be 0.39 mdyn·Å[20] from Taft's inductive and resonance substituent constants. This value is slightly smaller

Table 3. Force constants for acetyl bromide (K, H, and F in mdyn/Å; Y and Θ in mdyn·Å)

K(C–H)	4.62	H(O–C–Br)	0.105
K(C–C)	2.93	F(H···C)	0.445
K(C=O)	12.05	F(H···H)	0.064
K(C–Br)	1.45	F(C···O)	0.360
H(H–C–C)	0.240	F(C···Br)	0.419
H(H–C–H)	0.398	F(O···Br)	0.560
H(C–C–O)	0.270	Y[a]	0.014
H(C–C–Br)	0.247	Θ[a]	0.455

a) Y and Θ are the force constants of the torsional and out-of-plane bending modes respectively.

Table 4. Vibrational frequencies of acetyl bromide (in cm^{-1} units)[a]

		Obs.[b]	Calc.			Obs.	Calc.
A′	ν_1	3017	3017		ν_9	335	344
	ν_2	2945	2946		ν_{10}	305	313
	ν_3	1826	1826				
	ν_4	1426	1419	A″	ν_{11}	3029	3017
	ν_5	1363	1397		ν_{12}	1426	1420
	ν_6	1089	1079		ν_{13}	1005	1045
	ν_7	945	946		ν_{14}	490	490
	ν_8	563	575		ν_{15}	150[c]	151

a) The numbering of the modes follows Ref. 16.
b) Ref. 17.
c) Ref. 18.

Table 5. Mean amplitudes of acetyl chloride and acetyl bromide calculated by the normal coordinate treatment at 289°K (in Å units)

	CH_3COCl	CH_3COBr
C–X	0.0512	0.0547
C···X	0.0666	0.0713
X···O	0.0565	0.0638
X···$H_{1,2}$[a]	0.1322	0.1359
X···H_3[a]	0.1012	0.1012
C–C	0.0506	0.0505
C=O	0.0376	0.0371
C···H	0.1060	0.1054
C···O	0.0584	0.0604
C–H	0.0780	0.0779
O···$H_{1,2}$	0.1092	0.1112
O···H_3	0.1359	0.1367
H···H	0.1274	0.1276

a) The hydrogen atom on the symmetry plane is numbered 3.

than the constant, Θ, listed in Table 3. The calculated mean-square amplitudes, l, are shown in Table 5.

Estimation of Errors. The limits of error were estimated from 2.5 times σ_1 and from the systematic errors. The error due to the uncertainties in the fixed structure parameters was taken into consideration as one of the systematic errors. Yokozeki and Kuchitsu[21] treated this error by a Monte-Carlo technique. However, the present authors have dealt with it by a different and simpler method as follows:

(a) *Procedure*: It was assumed that a variation in one of the fixed parameters, Δ, caused a displacement in each adjusted parameter, δ, linearly proportional to the variation, and that such displacements were simply additive. A least-squares adjustment was carried out by varying only one of the fixed parameters at a time as much as its uncertainty. This procedure was applied to all the fixed parameters.

(b) *Uncertainties in the Fixed Parameters*: The uncertainties in the C–H and C···H distances were assumed to be 0.010 Å, while those for the other nonbonded distances related to the hydrogen atoms were assumed to be; r(O···H): 0.010 Å, and r(Cl···H): 0.010 Å for acetyl chloride, r(O···H): 0.010 Å and r(Br···H): 0.015 Å for acetyl bromide. The uncertainties in the mean amplitudes were assumed to be 10%.

By analogy with the estimation of errors in a previous work,[9] the uncertainties in the asymmetry parameters,

15) S. J. Cyvin, "Molecular Vibration and Mean Square Amplitudes," Elsevier Publishing Co., Amsterdam (1970).
16) J. Overend, R. A. Nyquist, J. C. Evans, and W. J. Potts, *Spectrochim. Acta*, **17**, 1205 (1961).
17) J. A. Ramsey and J. A. Ladd, *J. Chem. Soc., B*, **1968**, 118.
18) L. C. Hall and J. Overend, *Spectrochim. Acta*, **23A**, 2535 (1967).
19) J. C. Evans and J. Overend, *ibid.*, **19**, 701 (1963).
20) The original value 0.39×10^{-5} dyn/rad should read 0.39 mdyn·Å.
21) A. Yokozeki and K. Kuchitsu, This Bulletin, **44**, 2356 **(1971).**

Table 6. Displacements, δr, of the adjusted parameters due to the uncertainties of the fixed parameters (in 10^{-4} Å units)

Fixed parameter	Acetyl chloride			Acetyl bromide	
	δr (C···Cl)	δr (O···Cl)	δr (C···O)	δr (C···Br)	δr (O···Br)
l(C···X)	+15	+11	+1	−2	+40
l(O···X)	−32	−22	−59	−77	−9
l(C···O)	+31	+23	+23	0	0
r(O···H_3)	−1	−1	+1	+4	+1
l(O···H_3)	−6	−2	+2	+2	−3
r(X···$H_{1,2}$)	+7	+3	−2	+4	+6
l(X···$H_{1,2}$)	−5	−5	0	+15	+2
$(\sum\delta_i^2)^{1/2}$	48	34	64	79	41
$\sum\|\delta_i\|$	97	67	88	104	61

Fixed parameter	Acetyl chloride δr(C=O)	Acetyl bromide δr(C=O)
l(C=O)	0	+6
r(C–H)	+5	−10
l(C–H)	−12	−10
$(\sum\delta_i^2)^{1/2}$	13	15
$\sum\|\delta_i\|$	17	26

a) Assumed uncertainties in the fixed parameters are described in text. The plus and minus signs indicate the directions of the displacements δ, when the variations $\Delta>0$.

κ, for the bonded atom pairs were considered to be insignificant. The κ of a nonbonded atom pair was estimated by Kuchitsu to be nearly equal to or less than that of a bonded atom pair.[22] Even if a large value of 100×10^{-7} Å^3 is used for the κ's of the nonbonded atom pairs, the resulting changes in the distances amount to only 0.0004 Å. Therefore, the errors due to the uncertainties in the κ values were ignored.

The results of the calculations are shown in Table 6, where only significant contributors to the error-estimation are presented. In general, the error in an adjusted distance due to the uncertainty in a fixed parameter is significant only if the adjusted distance and the fixed parameter are involved in the same peak in the radial distribution curve. The C=O distance was sensitive to only the uncertainties in the distance and mean amplitude of the C–H bond and in the mean amplitude of the C=O bond. For the C···O distance in acetyl bromide and the C–C and C–X distances, which have no close-by distances except for those which make very small contributions to the molecular intensity, the effect of the uncertainties in the fixed parameters was negligible. It is to be noted that more than about 80% of each error for the nonbonded distances comes from the uncertainties in the mean amplitudes for the C···X, C···O, and O···X pairs.

(c) *Error Estimation*: The last two entries, $(\sum\delta_i^2)^{1/2}$ and $\sum|\delta_i|$, in Table 6 are two possible estimates of the uncertainty in an adjusted parameter due to the uncertainties in the fixed parametes, where δ_i is the displacement due to the variation in the ith fixed parameter. Of the two estimates, $\sum|\delta_i|$ has been adopted as the systematic error to be included in the limits of error. Were the uncertainties in these fixed parameters perfectly random and mutually independent,—in other words, were the law of propagation of error valid in this case, then $(\sum\delta_i^2)^{1/2}$ instead of $\sum|\delta_i|$ might have been taken. However, it seems proper to adopt the latter larger value, unless the nature of the error is clear. The errors due to the uncertainties in the fixed parameters for r(C···X), r(O···X), and r(C···O in chloride) were four times as large as that of the scale factor and were nearly equal to 2.5 σ_1.

The errors in the scale factor were estimated to be 0.05% for acetyl chloride and 0.06% for acetyl bromide. Systematic errors due to the other sources were not included in the limits of error, for they were considered to be insignificant.[9]

Results and Discussion

The parameter, r_a, determined by the least-squares refinement was transformed to the thermal average distance, r_g, by the relation $r_g=r_a+l_a^2/r_a$.[23] The r_a parameter was evaluated by subtracting the harmonic and the centrifugal contributions from r_g, following the equation $r_a=r_g-(<\Delta x^2>+<\Delta y^2>)/2r_e-\delta r$.[24] Here, the third term, δr, was neglected. The angle, φ_a, composed of the thermal-average nuclear position[25] was calculated from the r_a parameters. The final r_g distances and the φ_a angles are listed in Table 7, together with the limits of error. The sums of the φ_a(OCX), φ_a(CCX), and φ_a(CCO) angles for acetyl chloride and acetyl bromide equal 359°56′ and 359°57′ respectively. These values are consistent with the planar structure of the CCOX skeleton. For a comparison of these results for acetyl chloride and acetyl bromide with those reported by Sinnott[5] and Krisher[6] respectively, it is necessary to take into consideration the corrections for the molecular vibrations, including internal rotation. The procedure for dealing with these systems and the results obtained will be reported in forthcoming papers.

Table 7. Thermal average distances r_g and φ_a angles of acetyl chloride and acetyl bromide (distances in Å units)

	CH_3COCl		CH_3COBr	
r_g(C=O)	1.1874	0.0028[a]	1.1840	0.0044[a]
r_g(C–X)	1.7983	0.0029	1.9751	0.0039
r_g(C–C)	1.5075	0.0053	1.5175	0.0080
r_g(C···X)	2.7456	0.0112	2.8612	0.0150
r_g(O···X)	2.6043	0.0077	2.7706	0.0093
r_g(C···O)	2.4167	0.0119	2.4445	0.0126
φ_a(OCX)	120°19′	38′	120°48′	54′
φ_a(CCX)	112°10′	51′	109°29′	1°12′
φ_a(CCO)	127°27′	53′	129°40′	1°6′

a) Limits of error.

The interatomic distances, the stretching vibrational frequencies, and the force constants for carbonyl bonds in various compounds are compared in Table 8. The r_g distances were chosen as the interatomic distances except for the CH_3COF, COF_2, $COCl_2$, and CH_3COCN molecules, for which the r_g distances are not known. The r_g distance may be larger, by as much as about 0.01 Å, than the corresponding r_s (or r_o) value. Even so, it is evident that molecules with at least one halogen

22) K. Kuchitsu, *ibid.*, **40**, 505 (1967).

23) K. Kuchitsu and L.S. Bartell, *J. Chem. Phys.*, **35**, 1945 (1961).

24) Y. Morino, K. Kuchitsu, and T. Oka, *ibid.*, **36**, 1108 (1962).

25) K. Kuchitsu, This Bulletin, **44**, 96 (1971).

Table 8. Interatomic distances, stretching frequencies and force constants of carbonyl groups in the gas state (r in Å, ν in cm^{-1}, and K in mdyn/Å)

No.	Compound	r(C=O)[a]		Ref.	ν(C=O)	Ref.	K(C=O)	Ref.
1	CH_3COF	1.181 (10)	r_s	26	1867	17	12.13	44
2	CH_3COCl	1.187 (3)	r_g	c)	1820	17	11.23	16
3	CH_3COBr	1.184 (4)	r_g	c)	1826	17	12.05	c)
4	CH_3COI				1808	17		
5	COF_2	1.174 (10)	r_0	27	1928	37	12.61	44
6	$COCl_2$	1.166 (2)	r_0	28	1827	38	12.54	44
7	HCHO	1.209 (3)	r_g	29	1744	39	11.07	39
8	CH_3CHO	1.209 (3)	r_g	29	1743	39	10.61	39
9	OCH–CHO	1.212 (2)	r_g	30	1745	40	10.60	45
10	H_2C=CH–CHO	1.217 (3)	r_g	30	1724	40	10.30	46
11	C_6H_5–CHO	1.210 (5)	r_g	31	1725	41		
12	CH_3COCH_3	1.211 (4)	r_g	29	1738	39	10.32	47
13	HCOOH[b]	1.217 (3)	r_g	32	1794	41	11.20	48
14	CH_3COOH[b]	1.214 (3)	r_g	33	1788	42	10.90	48
15	CH_3CH_2COOH[b]	1.211 (3)	r_g	34	1787	41		
16	$(COOH)_2$	1.208 (1)	r_g	35	1756[b]	43		
17	CH_3COCN	1.226 (5)	r_s	36	1740	36	10.90	44

a) Expermimental errors quoted in references are shown in parentheses.
b) Monomer.
c) The present work.
d) α-Oxalic acid.

atom attached to a carbonyl group have shorter r(C=O)'s and higher ν(C=O)'s than do molecules containing no halogen atom, as may be seen in Table 8. Since the carbonyl-stretching frequencies are relatively insensitive to variations in the masses of atoms or groups attached to the carbonyl groups, a relation between the stretching frequency and the distance was frequently discussed in the past by assuming the carbonyl frequency to be one of the characteristics of the carbonyl bond. Margoshes *et al.*,[49] for example, plotted the bond distances *versus* the stretching frequencies for the carbonyl groups and mentioned that the points lie on a smooth curve with average deviations of 0.013 Å from the curve, with the largest error being 0.05 Å. They adopted the distances of not only simple molecules in the gas state, but also complex molecules such as amino acids in the crystalline state. However, now that we have more accurate structures in the gas state, a similar plot may

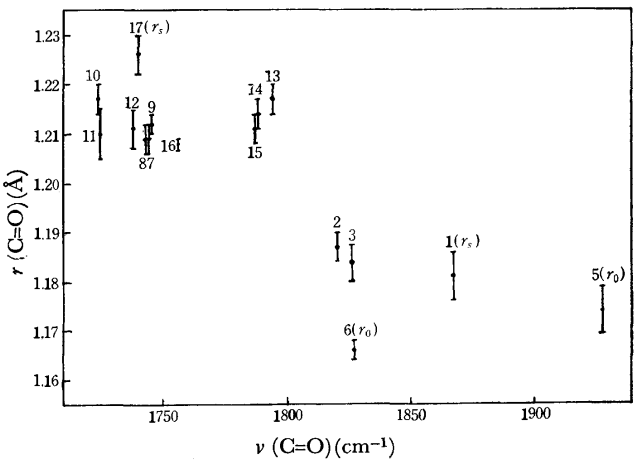

Fig. 3. Relation between bond length and stretching frequency for carbonyl groups. The numbers correspond to the compound numbers listed in Table 8 and the distances are entered in r_g unless remarked as r_s (or r_0). The vertical bars show the errors quoted in references.

26) L. Pierce and L. C. Krisher, *J. Chem. Phys.*, **31**, 875 (1959).
27) V. W. Laurie and D. T. Pence, *ibid.*, **37**, 2995 (1962).
28) G. W. Robinson, *ibid.*, **21**, 1741 (1953).
29) C. Kato, S. Konaka, T. Iijima, and M. Kimura, This Bulletin, **42**, 2148 (1969).
30) K. Kuchitsu, T. Fukuyama, and Y. Morino, *J. Mol. Structure*, **4**, 41 (1969).
31) M. Ogasawara, The 23rd Annual Meeting of the Chemical Society of Japan, Tokyo (1970).
32) A. Almenningen, O. Bastiansen, and T. Motzfeldt, *Acta Chem. Scand.*, **23**, 2848 (1969).
33) J. L. Derissen, *J. Mol. Structure*, **7**, 67 (1971).
34) J. L. Derissen, *ibid.*, **7**, 81 (1971).
35) Z. Náhlovská, B. Náhlovský, and T. G. Strand, *Acta Chem. Scand.*, **24**, 2617 (1970).
36) L. C. Krisher and E. B. Wilson, Jr., *J. Chem., Phys.*, **31**, 882 (1959).
37) A. H. Nielsen, T. G. Burke, P. J. H. Woltz, and E. A. Jones, *ibid.*, **20**, 596 (1952).
38) J. Overend and J. C. Evans, *Trans. Faraday Soc.*, **55**, 1817 (1959).
39) P. Cossee and J. H. Schachtschneider, *J. Chem. Phys.*, **44**, 97 (1966). The force constant with the least errors was selected among those reported by the authors.
40) R. K. Harris, *Spectrochim. Acta*, **20**, 1129 (1964).
41) E. J. Hartwell, R. E. Richards, and H. W. Thompson, *J. Chem. Soc.*, **1948**, 1436.
42) M. Haurie and A. Novak, *J. Chim. Phys.*, **62**, 137 (1965).
43) L. J. Bellamy and R. J. Pace, *Spectrochim. Acta*, **19**, 435 (1963).
44) J. Overend and J. R. Scherer, *ibid.*, **16**, 773 (1960).
45) T. Fukuyama, K. Kuchitsu, and Y. Morino, This Bulletin, **41**, 3019 (1968).
46) T. Fukuyama, K. Kuchitsu, and Y. Morino, *ibid.*, **41**, 3021 (1968).
47) G. Dellepiane and J. Overend, *Spectrochim. Acta*, **22**, 593 (1966).
48) K. Nakamoto and S. Kishida, *J. Chem. Phys.*, **41**, 1554 (1964).
49) M. Margoshes, F. Fillwalk, V. A. Fassel, and R. E. Rundle, *ibid.*, **22**, 381 (1954).

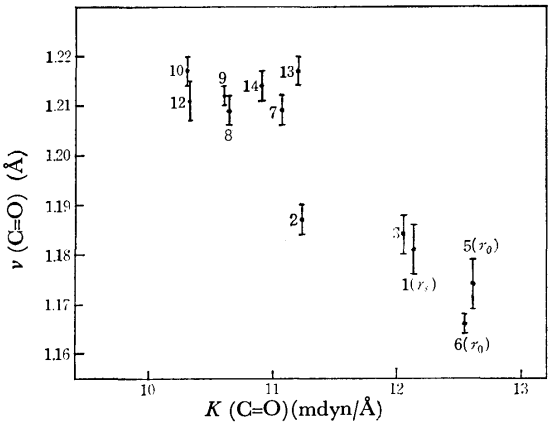

Fig. 4. Relation between bond length and force constant for carbonyl groups.

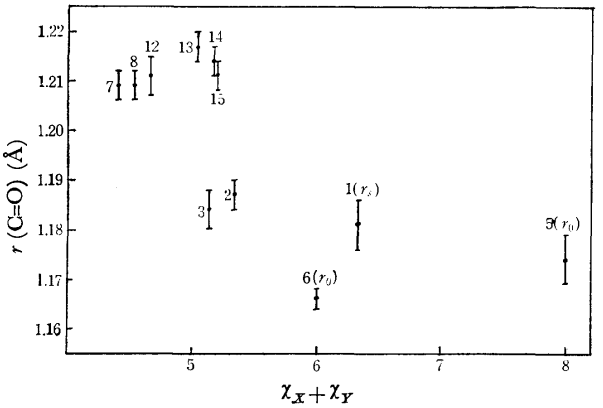

Fig. 5. Relation between the bond length of a carbonyl group and the sum of the electronegativity values of substituents for gaseous carbonyl-containing compounds. The electronegativity values of atoms are on the Gordy-Thomas scale[53] and those of the atomic groups, $-CH_3$, $-CH_2CH_3$, and -OH were evaluated by Kagarise's method.[52]

be made with the latest data (shown in Fig. 3). Roughly speaking, there exists a tendency for a molecule with a shorter r(C=O) to have a higher ν(C=O), as was pointed out by Margoshes *et al.* However, the plotted points can hardly be said to fall on a smooth curve in view of the accuracy of the current distance data.

The frequency-distance curve will serve for diagnostic purposes, but it is inappropriate for use in discussing the nature of the carbonyl bond, because the effect of the coupling between different normal modes of vibration is neglected. This has been particularly stressed by Overend *et al.*[16,44,50] A more physically significant quantity may be the force constant for the C=O bond. In Fig. 4, the r(C=O) values are plotted against the force constants, K(C=O), which, except for acetyl chloride, were calculated on the basis of the simple or a modified Urey-Bradley force field, with certain approximations where necessary. The value for acetyl chloride (Compound 2) is only an estimate made by Overend *et al.* by the use of the corresponding values for acetone and phosgene.[16] Since the calculated C=O stretching frequency for acetyl chloride is about 40 cm^{-1} smaller than the observed value, the best-fit force constant must be larger than this value, probably close to the force constants for acetyl bromide (Compound 3). The force constants for acids fall in the same region as those for the other compounds with no halogen atom. This is encouraging for the purpose of finding a relation between the force constant and bond length. However, the force constants listed in Table 8 have fairly large uncertainties, presumably ± 0.5 mdyn/Å on the average, and the r(C=O) values for the carbonyl halides cannot be compared directly with those for the other compounds. Nevertheless, it is clear, in surveying Table 8 and Fig. 4, that the halogen-containing compounds have the larger C=O force constants and the shorter bond lengths.

The shortening in the C=O bond length mentioned above may be considered to be partly due to the "*inductive effect*" and, perhaps, partly to the "*dipolar field effect.*"[51] Kagarise pointed out a linear relation between the sum of the electro-negativity values, χ_X and χ_Y, of the substituents, X and Y, and the carbonyl stretching frequencies for molecules of the X.CO.Y type, not including acids; *i.e.*, the higher the sum of the electronegativity values, the higher the frequency.[52] A plot of the sum of the electronegativity values against the r(C=O) bond length is shown in Fig. 5. The χ's for the $-CH_2CH_3$ and -OH groups were estimated to be 2.36 and 2.83 respectively, according to Kagarise's idea. The data for glyoxal, acrolein, benzaldehyde, oxalic acid, and acetyl cyanide were not plotted, since estimations of the χ's of the substituents, $-CH{=}CH_2$, $-C_6H_5$, and $-C{\equiv}N$, were difficult. However, since the χ's of the vinyl and phenyl groups are supposed to be similar to that of the H atom,[54] the data for acrolein and benzaldehyde would be in the region representing aldehydes, ketones, and acids on the electronegativity-distance map. It should be noticed that the sums of the electronegativity values for acids are nearly equal to those for acetyl chloride and bromide, while the r(C=O) distances for acids are much longer than those for the halides. This suggests that the C=O bonds in the halogen-containing compounds have partly a triple-bond character.[55]

Empirical relations between the bond lengths and the force constants for very simple molecules have been proposed by several workers.[56-58] Among them, Ladd *et al.*[58] have applied the relation for the carbonyl bond to amide molecules as well as to some of the molecules listed in Table 8, and have predicted the C=O stretching force constants. Their predicted values are generally reasonable. However, since the data of the bond

50) J. Overend and J. R. Scherer, *ibid.*, **32**, 1296 (1960).
51) L. J. Bellamy and R. L. Williams, *J. Chem. Soc.*, **1957**, 4294.
52) R. E. Kagarise, *J. Amer. Chem. Soc.*, **77**, 1377 (1955).
53) W. Gordy and W. J. Orville-Thomas, *J. Chem. Phys.*, **24**, 439 (1956).
54) L. N. Ferguson, "The Modern Structural Theory of Organic Chemistry," Prentice-Hall Inc., U. S. A. (1963).
55) See, *e.g.*, S. Bratož and S. Besnainou, *J. Chem. Phys.*, **34**, 1142 (1961).
56) R. M. Badger, *ibid.*, **2**, 128 (1934); **3**, 710 (1935).
57) C. H. Douglas Clark, *Phil. Mag.*, **18**, 459 (1934).
58) J. A. Ladd, W. J. Orville-Thomas, and B. C. Cox, *Spectrochim. Acta*, **20**, 1771 (1964).

lengths and the force constants are as yet incomplete, it is not possible for the time being to proceed to an unequivocal discussion of the relation between the bond length, the force constant, and the nature of the carbonyl bond.

The authors wish to thank Professor Takao Iijima and Dr. Shigehiro Konaka for their helpful discussions. Most computations were carried out on the FACOM 230-60 in the Computing Center of Hokkaido University.

BULLETIN OF THE CHEMICAL SOCIETY OF JAPAN, VOL. 45, 742—749(1972)

Electronic Spectra and Structures of Organic π-Systems. VI. Electronic States of Diazomethane, Ketene, Diazocyclopentadiene and Benzenediazonium Ion[1]

Zen-ichi YOSHIDA and Tsunetoshi KOBAYASHI*

Department of Synthetic Chemistry, Faculty of Engineering, Kyoto University, Yoshida, Kyoto

(Received February 8, 1971)

The electronic states of diazomethane, ketene, diazocyclopentadiene and benzenediazonium ion were studied by the semi-empirical ASMO LCAO SCF CI method. Both π- and $\bar{\pi}$-systems were taken into consideration. Two types of approximations, Mulliken's formula and a new semitheoretical formula, were used in the evaluation of the core resonance integrals. The latter gives satisfactory results though it contains no arbitrary adjustable parameters. The longest wavelength singlet-singlet transition of diazomethane, ketene or diazocyclopentadiene is $^1\pi^*-{}^1\bar{\pi}$, and that of benzenediazonium ion $^1\pi^*-{}^1\pi$.

Cumulated systems such as diazomethane, ketene, diazocyclopentadiene and benzenediazonium ion are interesting from both physicochemical and organochemical view points. Orville-Thomas and Jones[2] treated diazomethane and ketene by the Hückel method. Hoffmann[3] treated diazomethane by his extended Hückel method. Evleth and Cox[4] treated benzenediazonium ion by the Hückel method and the free electron theory. Sukigara and Kikuchi[5] treated benzenediazonium ion by Pariser-Parr's ASMO LCAO CI method. Dixon and Kirby[6] treated ketene by the open shell SCFMO method. However, so far we have not come across the Pariser-Parr-Pople type SCFMO treatments of diazocyclopentadiene and benzenediazonium ion.

We wish to report on the study on the electronic states of diazomethane, ketene, diazocyclopentadiene, and benzenediazonium ion by the semiempirical ASMO LCAO SCF CI method. The $\bar{\pi}$-systems (in-plane π-systems) of these compounds are explicitly taken into consideration. In the evaluation of the core resonance integrals two types of approximations, Mulliken's formula and a new semi-theoretical formula containing no arbitrary adjusting parameters,[7] are used.

Method of Calculation

The self-consistent field molecular orbital theory[8] has been used to calculate the π-electronic charge distributions and the spectra of diazomethane, ketene, diazocyclopentadiene and benzenediazonium ion. Both

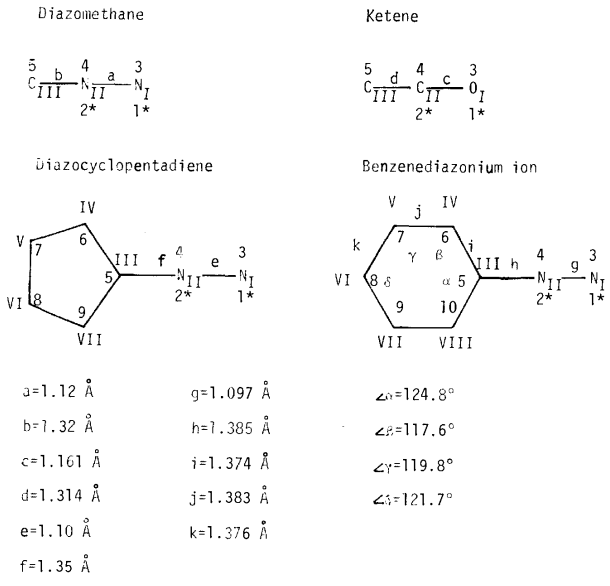

Fig. 1. Assumed structures and numberings of atoms (in Roman numerals) and numberings of atomic orbitals (in Arabic numerals) of diazomethane, ketene, diazocyclopentadiene and benzenediazonium ion. ('*' denotes an in-plane $2p_{\bar{\pi}}$-atomic orbital.)

1) Partly presented at the 20th Annual Meeting of the Chemical Society of Japan, Tokyo, March, 1967 and at the Symposium on Molecular Structure, Sapporo, October, 1967.

* Present Address: The Institute for Solid State Physics, The University of Tokyo, Roppongi, Minato-ku, Tokyo.

2) W. J. Orville-Thomas and W. J. Jones, *Zeit. Elektrochem.*, **64**, 714 (1960).

3) R. Hoffmann, *Tetrahedron*, **22**, 539 (1966).

4) E. M. Evleth and R. J. Cox, *J. Phys. Chem.*, **71**, 4082 (1967).

5) M. Sukigara and S. Kikuchi, This Bulletin, **40**, 461 (1967).

6) R. N. Dixon and G. H. Kirby, *Trans. Faraday Soc.*, **62**, 1406 (1966).

7) Z. Yoshida and T. Kobayashi, *J. Chem. Phys.*, **54**. 4538 (1971).

8) C. C. J. Roothaan, *Rev. Mod. Phys.*, **23**, 69 (1951).

the π- and the $\bar{\pi}$-systems are considered explicitly.

The molecular structural data of diazomethane and ketene obtained by Cox, Thomas, and Sheridan[9,10] on the basis of the microwave spectral study were used. The molecular structure of benzenediazonium ion is assumed as that in benzenediazonium chloride determined by X-ray crystal analysis.[11] The molecular dimension of diazocyclopentadiene is assumed to be as shown in Fig. 1 using the structural data of benzenediazonium chloride and diazomethane. The five-membered ring of diazocyclopentadiene is assumed to be a regular pentagon. The carbon-carbon bond lengths of diazocyclopentadiene are assumed to be 1.40 Å.

The numberings of the atomic orbitals (in Arabic numerals) and the atoms (in Roman numerals) in the molecules are also given in Fig. 1.

The molecular orbitals (MO's), ϕ_i's, are taken as linear combinations of $2p_\pi$- and $2p_{\bar{\pi}}$-atomic orbitals (AO's), χ_r's.

$$\phi_i = \sum_r C_{ir}\chi_r \tag{1}$$

The total Hamiltonian, H, is given by

$$H = \sum_\mu H_\mu^{\text{core}} + \sum_{\mu<\nu}\frac{e^2}{r_{\mu\nu}} \tag{2}$$

$$H_\mu^{\text{core}} = -\frac{1}{2}A(\mu) - \sum_A \frac{e^2 Z_A}{r_{\mu A}} \tag{3}$$

where the Greek subscripts denote electrons, and Z_A the core charge of atom A left by removal of π-(and $\bar{\pi}$-) electrons.

For the closed-shell molecular species, the Roothaan SCF equation[8] is written as follows.

$$\sum_r C_{ir}(F_{rs} - S_{rs}\varepsilon) = 0 \quad (s = 1, 2, \cdots) \tag{4}$$

where

$$F_{rs} = H_{rs} + \sum_{t,u} P_{tu}\left[\langle rs\,|\,tu\rangle - \frac{1}{2}\langle rt\,|\,su\rangle\right]$$

$$S_{rs} = \int \chi_r\chi_s d\tau$$

$$H_{rs} = \int \chi_r(\mu) H_\mu^{\text{core}} \chi_s(\mu) d\tau_\mu$$

$$\langle rs\,|\,tu\rangle = \int \chi_r(\mu)\chi_s(\mu)\frac{e^2}{r_{\mu\nu}}\chi_t(\nu)\chi_u(\nu) d\tau_\mu d\tau_\nu$$

$$P_{tu} = 2\sum_i^{\text{occ}} C_{it}C_{iu}$$

For the sake of simplicity we used the Goeppert-Mayer and Sklar potential[12] and the so-called zero-differential overlap approximation.[13] We neglected non-neighbour core resonance integrals and penetration integrals of neutral atoms but not one-centre exchange integrals.

One-centre Coulomb repulsion integrals, $\langle rr|rr\rangle$'s, are evaluated using appropriate electron-transfer repulsions as proposed by Pariser.[14]

$$\langle rr\,|\,rr\rangle = I_r - A_r$$

where I_r and A_r denote the valence state ionization potential and the valence state electron affinity of the atomic orbital r, respectively. All the necessary values of I_r's and A_r's are taken from Hinze and Jaffé's tables.[15]

One-centre Coulomb repulsion integrals of the type $\langle rr|rr\rangle$'s are evaluated according to the formula

$$\langle rr\,|\,\bar{r}\bar{r}\rangle = \langle rr\,|\,rr\rangle - 6F_2^{\text{pp}}$$

where $\bar{r}$ and r are the $2p_\pi$-atomic orbitals of the same atom and orthogonal to each other. F_2^{pp} is the Slater-Condon parameter and the values of F_2^{pp}'s are taken from Pilcher and Skinner's table.[16]

One-centre exchange integrals are also evaluated using the Slater-Condon parameters as follows.

$$\langle r\bar{r}\,|\,r\bar{r}\rangle = 3F_2^{\text{pp}}$$

Two-centre Coulomb repulsion integrals $\langle tt|uu\rangle$'s and $\langle tt|\bar{u}\bar{u}\rangle$'s are evaluated using the parabolic formula when the distance R is shorter than 4 Å.

$$\langle tt\,|\,uu\rangle = \frac{\langle tt\,|\,tt\rangle + \langle uu\,|\,uu\rangle}{2} + aR + bR^2$$

$$\langle tt\,|\,\bar{u}\bar{u}\rangle = \frac{\langle tt\,|\,\bar{t}\bar{t}\rangle + \langle uu\,|\,\bar{u}\bar{u}\rangle}{2} + a'R + b'R^2$$

where the coefficients a, b, a', and b', are evaluated using the $\langle tt|uu\rangle$ values or the $\langle tt|\bar{u}\bar{u}\rangle$ values calculated at distances R=4 Å and 5 Å by the point charge approximation. When R is greater than 4 Å, $\langle tt|uu\rangle$'s and $\langle tt|\bar{u}\bar{u}\rangle$'s are evaluated by the point charge approximation.

The overlap integrals, S_{rs}'s, are evaluated according to Mulliken and coworkers' table.[17]

The H_{rr} term in Eq. (4) is given by

$$H_{rr} = \int \chi_r(\mu)\left(-\frac{1}{2}A(\mu) - \frac{e^2 Z_A}{r_{\mu A}}\right)\chi_r(\mu) d\tau_\mu - \sum_{B\neq A}\chi_r(\mu)\frac{e^2 Z_B}{r_{\mu B}}\chi_r(\mu) d\tau_\mu = \alpha_r + \sum_{B\neq A}\langle B\,|\,rr\rangle$$

where

$$\alpha_r = \int \chi_r(\mu)\left(-\frac{1}{2}A(\mu) - \frac{e^2 Z_A}{r_{\mu A}}\right)\chi_r(\mu) d\tau_\mu$$

$$\langle B\,|\,rr\rangle = -\int \chi_r(\mu)\frac{e^2 Z_B}{r_{\mu B}}\chi_r(\mu) d\tau_\mu$$

The core attraction integrals of the $\langle B|rr\rangle$ type are given as follows.

$$\langle B\,|\,rr\rangle_{B=1} = -\frac{Z_1}{2}\{\langle 11\,|\,rr\rangle + \langle 33\,|\,rr\rangle\}$$

$$\langle B\,|\,rr\rangle_{B=11} = -\frac{Z_{11}}{2}\{\langle 22\,|\,rr\rangle + \langle 44\,|\,rr\rangle\}$$

$$\langle B\,|\,rr\rangle_{B\neq 1,11} = -\langle rr\,|\,2P_{\pi_B}, 2P_{\pi_B}\rangle$$

9) A. P. Cox, L. F. Thomas, and J. Sheridan, *Nature*, **181**, 1000 (1958).
10) A. P. Cox, L. F. Thomas, and J. Sheridan, *Spectrochim. Acta*, **15**, 542 (1959).
11) Chr. Römming, *Acta Chem. Scand.*, **17**, 1444 (1963).
12) M. Goeppert-Mayer and A. L. Sklar, *J. Chem. Phys.*, **6**, 645 (1963).
13) R. Pariser and R. G. Parr, *ibid.*, **21**, 466, 767 (1953).
14) R. Pariser, *ibid.*, **21**, 568 (1953).
15) J. Hinze and H. H. Jaffé, *J. Amer. Chem. Soc.*, **84**, 540 (1962); J. Hinze and H. H. Jaffé, *J. Phys. Chem.*, **67**, 1501 (1963).
16) G. Pilcher and H. A. Skinner, *J. Inorg. Nucl. Chem.*, **1962**, 952.
17) R. S. Mulliken, C. A. Rieke, D. Orloff, and H. Orloff, *J. Chem. Phys.*, **17**, 1248 (1949).

TABLE 1. ATOMIC PARAMETERS

	$C_{trtrtr\pi}$	$C_{didi\pi\pi}$	$C^{+}_{didi\pi}$	$N_{didi\pi^2\pi}$	$N^{+}_{didi\pi\pi}$	$N_{di^2di\pi\pi}$	$O_{di^2di\pi^2\pi}$
ζ[a]	1.625	1.625	1.8	1.95	2.125	1.95	2.275
W'(eV)[b]	−11.16	−11.19	−23.86	−14.11	−28.70	−14.18	−17.91
α(eV)[c]	−11.16	−20.922	−23.86	−34.181	−43.266	−24.766	−43.418
$<rr\|rr>$(eV)	11.13	11.09	14.03	11.97	16.64	12.52	15.20
$<rr\|\bar{r}\bar{r}>$(eV)	10.044	10.004	12.747	10.423	14.981	10.973	13.243
$<r\bar{r}\|r\bar{r}>$(eV)	0.543	0.543	0.642	0.774	0.830	0.774	0.978
Z[d]	1.0	2.0	2.0	3.0	3.0	2.0	3.0
Z'[e]	4.0	4.0	4.0	5.0	5.0	5.0	6.0
n_{2s}[e]	1.0	1.0	1.0	1.0	1.0	2.0	2.0
n_{2p_σ}[e]	1.0	1.0	1.0	1.0	1.0	1.0	1.0
N[f]	1.0	1.0	1.0	1.0	1.0	1.0	1.0
$\bar{N}$[f]	1.0	1.0	0.0	2.0	1.0	1.0	2.0

a) Slater's orbital exponent.
b) See formulas (5), (6), and (7) in the text.
c) See formula (5) in the text.
d) See formula (3) in the text.
e) See formula (9) in the text.
f) See formulas (5) and (7) in the text.

α_r's are approximated as follows.

$$\alpha_{r_A}(r=1\sim4) = W'_{r_A} - (N_A-1)\langle rr|rr\rangle - (\bar{N}_A)\left\{\langle rr|\bar{r}\bar{r}\rangle - \frac{1}{2}\langle r\bar{r}|r\bar{r}\rangle\right\} \quad (5)$$

$$\alpha_r(r=5\sim10) = -11.16\,\text{eV}$$

where N_A and $\bar{N}_A$ in Eq. (5) are the numbers of electrons in the $2p_\pi$-atomic orbitals r and $\bar{r}$ of the atom A, respectively. Here the atomic orbital $\bar{r}$ is orthogonal to the atomic orbital r. $-W'_{t_A}$ is approximately equal to the first or second valence state ionization potential of the atomic orbital r. The values of α_r, W_r', N, $\bar{N}$, $<rr|rr>$, $<rr|\bar{r}\bar{r}>$ and $<r\bar{r}|r\bar{r}>$ are given in Table 1.

Two methods of approximations were employed in the evaluation of core resonance integrals, β_{tu}'s.

a) Mulliken's formula

$$\beta_{tu} = \frac{0.8676^7}{2} S_{tu}(W_t' + W_u') \quad (6)$$

The coefficient 0.86767 was evaluated using the empirical β_{CC}-value of benzene. This might be referred to as Eβ-approximation.

b) Theoretical formula

$$\beta_{t_Au_B} = \frac{S_{tu}}{2}\{W'_{t_A} + W'_{u_B} - \langle u|U_A|u\rangle - \langle t|U_B|t\rangle - \langle tt|uu\rangle(N_A+N_B-2) - \langle uu|\bar{t}\bar{t}\rangle(\bar{N}_A+\bar{N}_B)\} - \frac{1}{2}\{\langle t|T|u\rangle + \langle u|T|t\rangle\} \quad (7)$$

This might be referred to as Tβ-approximation. Formula (7) is derived as follows. We can easily obtain the following formula for the β_{tu} in the $\pi+\bar{\pi}$-systems as in the VI/2 method,[7] if the electron density change is taken into consideration.

$$\beta_{t_Au_B} = \frac{S_{tu}}{2}\{W'_{t_A} + W'_{u_B} - \langle u|U_A|u\rangle - \langle t|U_B|t\rangle - \langle tt|uu\rangle(P_{tt}+P_{uu}-2) - \langle uu|\bar{t}\bar{t}\rangle(P_{\bar{t}\bar{t}}+P_{\bar{u}\bar{u}})\} - \frac{1}{2}\{\langle t|T|u\rangle + \langle u|T|t\rangle\} \quad (8)$$

where W'_{t_A} is the orbital energy of the atomic orbital t_A and depends on the electron density of the atom in the molecule.

$$\langle u_B|U_A|u_B\rangle \fallingdotseq -\langle u_B|e^2Z_A'/r|u_B\rangle + n_{2s_A}\langle 2s_A 2s_A|u_Bu_B\rangle + n_{2p_{\sigma_A}}\langle 2p_{\sigma_A}2p_{\sigma_A}|u_Bu_B\rangle \quad (9)$$

$\langle u|e^2Z'_A/r|u\rangle$, $\langle 2s_A2s_A|u_Bu_B\rangle$, $\langle 2p_{\sigma A}2p_{\sigma A}|u_Bu_B\rangle$ and $\langle t|T|u\rangle$ are evaluated theoretically using the Slater atomic orbitals according to Roothaan.[18] Z_A' is the core-charge left by removal of electrons of principal quantum number 2 of the atom A. n_{2s_A} and $n_{2\sigma p_A}$ are the numbers of electrons in the atomic orbitals $2s_A$ and $2p\sigma_A$, respectively. If we put $P_{tt}=N_A$, $P_{uu}=N_B$, $P_{\bar{t}\bar{t}}=\bar{N}_A$ and $P_{\bar{u}\bar{u}}=\bar{N}_B$ in (8) we get (7).

For the sake of simplicity we used the fixed β_{tu}-values evaluated by (7) at certain limiting cases, where $P_{tt}=N_A$, $P_{uu}=N_B$, $P_{\bar{t}\bar{t}}=\bar{N}_A$ and $P_{\bar{u}\bar{u}}=\bar{N}_B$.

Two kinds of approximations were used in the evaluation of the atomic parameters of atom II: a) atom II is regarded as neutral (abbreviated as N-approximation) and b) atom II is regarded as positive (abbreviated as P-approximation). Thus all together four possible sets of approximations, NEβ, NTβ, PEβ, and PTβ, are used for each molecule.

The atomic parameters necessary in the calculation are given in Table 1.

The β_{tu}-values calculated by formulas (6) and (7) are given in Table 2.

The starting set of coefficients of MO's is obtained by the Hückel method. The eigenvalues and the eigenvectors are made self-consistent, and the electronic transition energies are then calculated by the configuration interaction (CI) method, all the singly excited configurations being taken into account.

The calculation has been carried out on a HITAC 5020 computer at the computation centre, the University of Tokyo, and on a FACOM 230-60 computer at the computation centre of Kyoto University.

18) C. C. J. Roothaan, *ibid.*, **19**, 1445 (1951).

TABLE 2. CORE-RESONANCE INTEGRAL, β_{ij}, IN eV

Bond	NEβ	NTβ	PEβ	PTβ
Diazomethane				
1—2	−3.292	−3.404	−4.512	−4.128
4—5	−2.437	−2.225	−3.384	−2.811
Ketene				
1—2	−3.043	−3.309	−3.988	−3.559
4—5	−2.731	−2.863	−3.797	−3.270
Diazocyclopentadiene				
1—2	−3.424	−3.588	−4.706	−4.361
4—5	−2.304	−2.059	−3.189	−2.602
5—6	−2.364	−2.359	−2.364	−2.359
6—7	−2.367	−2.363	−2.367	−2.363
7—8	−2.366	−2.361	−2.366	−2.361
Benzenediazonium ion				
1—2	−3.444	−3.616	−4.736	−4.397
4—5	−2.156	−1.877	−2.973	−2.373
5—6	−2.471	−2.506	−2.471	−2.506
6—7	−2.434	−2.455	−2.434	−2.455
7—8	−2.463	−2.495	−2.463	−2.495

Results

The molecular diagrams of these compounds are given in Fig. 2.

The calculated and the observed transition energies are summarized in Table 3. CI coefficients are also given.

Discussion

As is shown in Table 2, with diazomethane β_{12}- and β_{45}-values calculated by formula (6) are slightly larger than those given by formula (7) in P-approximation. The same tendency is also observed with ketene, diazocyclopentadiene and benzenediazonium ion. In the cases of diazocyclopentadiene and benzenediazonium

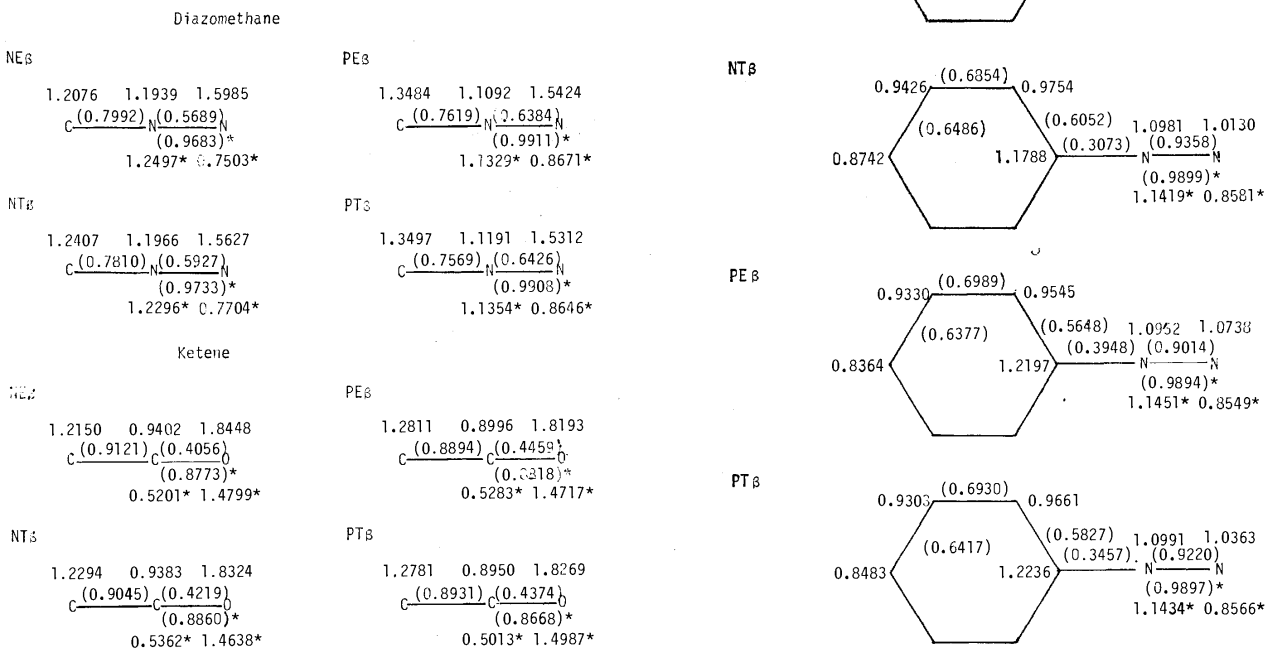

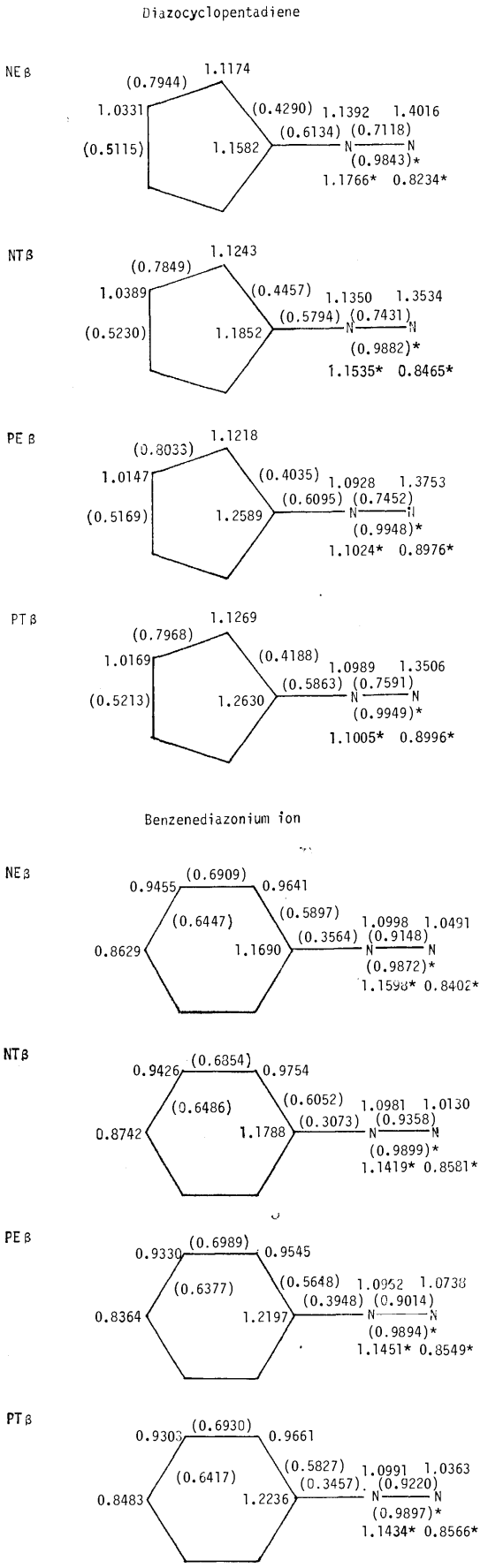

Fig. 2. Electron densities and bond orders (in parentheses).
('*' denotes a P_{ij} of an in-plane π-system.)

Table 3. Calculated transition energies in eV

Sym.	E	f	CI Composition[a)]		Sym.	E	f	CI Composition[a)]		Obsd E	Obsd $\log\varepsilon$
Diazomethane											
	NEβ approximation					NTβ approximation					
$^1A_2$	1.642	0.0	3—4	0.993	$^1A_2$	1.621	0.0	3—4	0.994	3.14[21)]	
$^1A_1$	4.666	0.379	3—5	0.936	$^1A_1$	4.512	0.407	3—5	0.949	5.77[22)]	
			2—4	−0.342							
$^1A_2$	7.567	0.0	1—4	0.973	$^1A_2$	7.593	0.0	1—4	0.973		
$^3A_2$	1.097		3—4	0.986	$^3A_2$	1.125		3—4	0.987		
$^3A_1$	1.550		3—5	0.998	$^3A_1$	1.295		3—5	0.999		
$^3A_1$	5.197		2—4	0.994	$^3A_1$	5.373		2—4	0.992		
	PEβ approximation					PTβ approximation					
$^1A_2$	2.849	0.0	3—4	0.998	$^1A_2$	2.417	0.0	3—4	0.998	3.14[21)]	
$^1A_1$	6.335	0.619	3—5	0.967	$^1A_1$	5.635	0.566	3—5	0.969	5.77[22)]	
$^1A_2$	9.675	0.0	1—4	0.978	$^1A_2$	8.641	0.0	1—4	0.977		
$^3A_2$	2.424		3—4	0.995	$^3A_2$	2.009		3—4	0.995		
$^3A_1$	3.099		3—5	0.998	$^3A_1$	2.321		3—5	0.998		
$^3A_1$	6.924		2—4	0.995	$^3A_1$	6.146		2—4	0.993		
Ketene											
	NEβ approximation					NTβ approximation					
$^1A_2$	2.668	0.0	3—4	0.994	$^1A_2$	2.834	0.0	3—4	0.995	3.87	1.1[6,19)]
$^1A_1$	6.133	0.302	3—5	0.923	$^1A_1$	6.378	0.352	3—5	0.937	6.36∼	
			2—4	0.372				2—4	0.338	7.29[23)]	
$^1A_2$	7.345	0.0	1—4	0.992	$^1A_2$	7.893	0.0	1—4	0.993		
$^3A_2$	2.373		3—4	0.993	$^3A_2$	2.541		3—4	0.994	2.61∼	
$^3A_1$	3.285		3—5	0.998	$^3A_1$	3.500		3—5	0.998	3.22[6)]	
$^3A_1$	5.439		2—4	0.999	$^3A_1$	5.943		2—4	0.999		
	PEβ approximation					PTβ approximation					
$^1A_2$	3.949	0.0	3—4	0.999	$^1A_2$	3.454	0.0	3—4	0.999	3.87	1.1[6,19)]
$^1A_1$	8.178	0.512	3—5	0.951	$^1A_1$	7.382	0.481	3—5	0.956	6.36∼	
$^1A_2$	9.549	0.0	1—4	0.996	$^1A_2$	8.569	0.0	1—4	0.996	7.29[23)]	
$^3A_2$	3.655		3—4	0.998	$^3A_2$	3.165		3—4	0.999	2.61∼	
										3.22[6)]	
$^3A_1$	5.020		3—5	0.996	$^3A_1$	4.149		3—5	0.995		
$^3A_1$	7.271		2—4	0.999	$^3A_1$	6.497		2—4	0.998		
Diazocyclopentadiene											
	NEβ approximation					NTβ approximation					
$^1A_2$	1.857	0.0	4—7	0.950	$^1A_2$	1.828	0.0	4—7	0.954	2.70[sh 24)]	
$^1B_2$	2.483	0.024	5—6	0.999	$^1B_2$	2.376	0.019	5—6	0.999	3.35[sh]	∼2.7
$^1B_1$	3.533	0.0	5—7	1.0	$^1B_1$	3.315	0.0	5—7	1.0		
$^1A_1$	3.737	0.746	4—6	0.951	$^1A_1$	3.576	0.709	4—6	0.957	4.13	4.1
$^1A_1$	6.008	0.0	3—6	0.708	$^1A_1$	6.011	0.003	3—6	0.685		
			5—9	0.471				5—9	0.500		
			4—8	−0.373				4—8	−0.440		
			2—7	−0.317							
$^1B_2$	6.365	0.095	5—8	0.874	$^1B_2$	6.246	0.100	5—8	0.878	6.05	3.5
			4—9	0.472				4—9	0.467		
$^1A_1$	6.595	0.124	4—8	−0.667	$^1A_1$	6.459	0.049	4—8	0.661		
			3—6	−0.556				3—6	0.614		
			5—9	0.434				5—9	−0.360		
$^1A_2$	6.709	0.0	3—7	0.782	$^1A_2$	6.727	0.0	3—7	0.839		
			1—7	−0.530				1—7	−0.446		
$^1A_1$	7.392	1.107	5—9	0.661	$^1A_1$	7.413	1.113	5—9	0.739		
			4—8	0.478				4—8	0.535		
			2—7	0.448				2—7	0.330		
$^3A_1$	0.995		4—6	0.968	$^3A_1$	0.914		4—6	0.967		

Table 3. Calculated transition energies in eV (continued)

Sym.	E	f	CI Composition[a]		Sym.	E	f	CI Composition[a]		Obsd E	Obsd log ε
Diazocyclopentadiene											
	PEβ approximation					PTβ approximation					
$^1A_2$	2.991	0.0	4—7	0.933	$^1A_2$	2.530	0.0	4—7	0.938	2.70[sh 24]	
			3—7	0.357				3—7	0.344		
$^1B_2$	3.413	0.066	5—6	0.997	$^1B_2$	3.017	0.041	5—6	0.998	3.35[sh]	~2.7
$^1B_1$	4.402	0.0	5—7	1.0	$^1B_1$	3.894	0.0	5—7	1.0		
$^1A_1$	4.697	0.873	4—6	0.948	$^1A_1$	4.346	0.875	4—6	0.956	4.13	4.1
$^1A_1$	6.692	0.434	5—9	0.656	$^1A_1$	6.388	0.135	4—8	0.607	6.05	3.5
			3—6	0.512				5—9	−0.568		
			4—8	−0.504				3—6	−0.521		
$^1B_2$	6.702	0.069	5—8	0.872	$^1B_2$	6.404	0.111	5—8	0.900		
			4—9	0.476				4—9	0.425		
$^1A_1$	7.347	0.367	3—6	0.780	$^1A_1$	7.035	0.102	3—6	0.791		
			5—9	−0.528				4—8	0.425		
$^3B_2$	2.125		5—6	0.933	$^3A_1$	1.675		4—6	0.956		
Benzenediazonium ion											
	NEβ approximation					NTβ approximation					
$^1A_2$	3.492	0.0	4—7	0.912	$^1B_2$	3.582	0.035	5—6	0.979	4.13	3.25[25]
			3—7	0.387							
$^1B_2$	3.513	0.043	5—6	0.977	$^1A_2$	3.639	0.0	3—7	0.373		
$^1A_1$	3.869	0.398	4—6	0.919	$^1A_1$	3.891	0.329	4—6	0.925	4.77	4.05
$^1B_1$	4.179	0.0	5—7	1.0	$^1B_1$	4.092	0.0	5—7	1.0		
$^1B_2$	5.512	0.001	5—8	0.752	$^1B_2$	5.446	0.004	5—8	0.764		
			4—9	−0.627				4—9	−0.616		
$^1A_1$	5.615	0.066	5—9	0.662	$^1A_1$	5.628	0.054	5—9	0.680		
			4—8	0.626				4—8	0.660		
$^1A_1$	6.507	0.199	2—7	0.432	$^1A_1$	6.678	0.114	1—6	−0.343		
			3—6	0.651				3—6	0.696		
			4—6	−0.367				4—6	−0.346		
			1—6	−0.328				2—7	0.439		
			5—9	−0.317							
$^3A_1$	2.426		4—6	0.901	$^3A_1$	2.695		4—6	0.894		
			3—6	0.348				3—6	0.343		
	PEβ approximation					PTβ approximation					
$^1B_2$	4.043	0.091	5—6	0.942	$^1B_2$	3.927	0.068	5—6	0.958	4.13	3.25[25]
$^1A_1$	4.550	0.450	4—6	0.894	$^1A_2$	4.245	0.0	4—7	0.901		
			5—8	0.343				3—7	−0.422		
$^1A_2$	4.628	0.0	4—7	0.894	$^1A_1$	4.395	0.441	4—6	0.906	4.77	4.05
			3—7	0.435							
$^1B_1$	5.364	0.0	5—7	1.0	$^1B_1$	4.764	0.0	5—7	1.0		
$^1B_2$	6.150	0.040	4—8	0.675	$^1B_2$	5.784	0.0	5—9	0.751		
			5—9	−0.663				4—8	0.603		
			5—6	0.321							
					$^1A_1$	5.906	0.280	5—8	0.679		
								4—9	−0.605		
$^3B_2$	3.007		5—6	0.933	$^3A_1$	3.006		4—6	0.899		

a) The transition, indicated by i—j, refers to a one-electron excitation from orbital i to virtual orbital j. The second column gives the CI coefficient of the configuration i—j.

ion the β_{CC}-values calculated by formulas (6) and (7) are similar to each other.

In the case of diazomethane the four sets of approximations, NEβ, NTβ, PEβ, and PTβ, give similar eigenvector to one another. However, E_t-values obtained by P-approximation slightly differ from those given by N-approximation. Similar tendencies are also observed with ketene and diazocyclopentadiene. Estimated ionization potentials of diazomethane and ketene from SCF eigenvalues are 10.974—9.923 eV and 10.881—11.582 eV, respectively. The values are slightly larger than the observed ones, 8.99 eV (diazomethane[22]) and 9.607 eV (ketene[22]), respectively. Hoffmann[3] treated

19) K. Knox, R. G. W. Norrish, and G. Porter, *J. Chem. Soc.*, **1952**, 1477.
20) Z. Yoshida and T. Kobayashi, *J. Chem. Phys.*, in press.
21) F.W. Kirkbride and R.G. W. Norrish, *J. Chem. Soc.*, **1933**, 119.
22) G. Herzberg, "Molecular Spectra and Molecular Structure III. Electronic Spectra and Electronic Structure of Polyatomic Molecules," D. van Nostrand Co., Toronto, Inc. (1967).
23) W. C. Price, J. P. Teegan, and A. D. Walsh, *J. Chem. Soc.*, **1951**, 920.
24) W. von E. Doering and C. H. De Puy, *J. Amer. Chem. Soc.*, **75**, 5955 (1953).
25) C. H. Harberts, P. M. Heertjes, L. J. N. van der Hulst, and H. I. Waterman, *Bull. Soc. Chim. Fr.*, **3**, 643 (1936).

diazomethane by his extended Hückel method. He obtained the value of −11.964 eV as the orbital energy of the highest occupied π-orbital. This is by about 1—2 eV smaller than ours. Dixon and Kirby[6] treated ketene by the PPP method. They made the π- and the $\bar{\pi}$-systems self-consistent independently. The eigenvectors they obtained are qualitatively similar to ours, but their eigenvalues differ from ours. Their orbital energy might lead to a large value of the ionization potential.

In the case of benzenediazonium ion the E_i- and the C_{ij}-values calculated by N-approximation differ slightly from those calculated by P-approximation.

The molecular diagrams of these compounds are shown in Fig. 2. In the case of diazomethane all the four sets of parameters give similar molecular diagrams. Every set of parameters suggests that nitrogen atom II bears a large positive charge and that the terminal carbon atom III and nitrogen atom I bear negative charges. The π-bond order of the nitrogen-nitrogen bond is 1.5—1.6. The molecular diagrams suggest that the carbon-nitrogen bond has a large double bond character.

In the case of ketene all the four sets of parameters give similar molecular diagrams and suggest that the central carbon atom II bears a charge of about +0.6 and the terminal oxygen atom a charge of about −0.3. The bond order of the carbon-oxygen bond is about 1.3. The bond order of the carbon-carbon bond is 0.9, suggesting that this bond has a large double bond character. Orville-Thomas and Jones[2] treated diazomethane and ketene by the simple Hückel method with and without π-hyperconjugation. The bond orders they obtained without hyperconjugation are similar to those shown in Fig. 2. The molecular diagram obtained from Dixon and Kirby's[6] SCF eigenvectors shows that the terminal oxygen atom is slightly positive and that carbon atom II is slightly negative in the ground state.

In the case of diazocyclopentadiene also the four sets of parameters give similar molecular diagrams. Nitrogen atom II bears a charge of about +0.7—0.8. This is larger than that of diazomethane. The terminal nitrogen atom I bears a charge of about −0.20——0.27. This is slightly smaller than that in diazomethane. The bond order of the nitrogen-nitrogen bond is about 1.7 and is larger than that in diazomethane. This suggests that the triple bond character of the nitrogen-nitrogen bond in diazocyclopentadiene is larger than that in diazomethane. The bond order of the carbon-nitrogen bond in diazocyclopentadiene is smaller than that of the corresponding bond in diazomethane. This suggests that the double bond character of the carbon-nitrogen bond in diazomethane is larger than that of the corresponding bond in diazocyclopentadiene. In the ground state a charge of about −0.5 is distributed over the five-membered ring. Thus it is anticipated that the contribution of the canonical formula $R^-–N_2^+$ to the ground state is not small. From the bond orders it can be anticipated that in the ground state the five-membered ring is not a regular pentagon but a slightly bond alternated pentagon in which the carbon(IV)-carbon(V) and the carbon(VI)-carbon(VII) bonds are slightly shorter than the carbon(III)-carbon(IV), the carbon(V)-carbon(VI), and the carbon(III)-carbon(VII) bonds.

In the case of benzenediazonium ion nitrogen atom II and terminal nitrogen atom bear charges of about +0.75 and +0.1 respectively. The carbon-nitrogen bond order is about 0.3—0.4 and smaller than that of diazomethane and diazocyclopentadiene. Thus the double bond character of the carbon-nitrogen bond in benzenediazonium ion might be smaller than that of diazomethane or diazocyclopentadiene. The nitrogen-nitrogen bond order is about 1.9 and is greater than that of diazomethane or diazocyclopentadiene, suggesting that the nitrogen-nitrogen bond has a greater triple bond character than that of diazomethane or diazocyclopentadiene. The greater part of the +1 charge of the cation exists on nitrogen atom II in the case of benzenediazonium ion.

From the above discussions the extent of contribution of the canonical formula $R^-–N_2^+$ or $R–N_2^+$ to the ground state might be in the order: diazomethane < diazocyclopentadiene < benzenediazonium ion. The triple bond character of the nitrogen-nitrogen bond might be in the order: diazomethane < diazocyclopentadiene < benzenediazonium ion. The double bond character of the carbon-nitrogen bond might be in the order: benzenediazonium ion < diazocyclopentadine < diazomethane. This is consistent with the observed nitrogen-nitrogen bond lengths and carbon-nitrogen bond lengths of diazomethane and benzenediazonium ion.

Evleth and Cox[4] treated benzenediazonium ion by the simple Hückel method. The π-electron densities ($P_{N_I}=0.706$, $P_{N_{II}}=1.340$) of nitrogen atoms I and II they gave differ from ours.

The calculated transition energies and the observed ones are summarized in Table 3. In the case of diazomethane, agreement between the calculated and the observed transition energies is best with PTβ-approximation. This is consistent with the molecular diagram. The observed 5.77 eV band can be assigned to $\pi—{}^1\pi^*$ transition. The observed 3.14 eV band is tentatively assigned to $\pi—{}^1\bar{\pi}^*$ transition. The calculated 2.417 eV $\pi—{}^1\bar{\pi}^*$ transition has the character of charge-transfer transition caused by electron migration from carbon III to the diazo-group. Hoffmann[3] assigned the longest wavelength transition to $\pi—\bar{\pi}^*$ by his extended Hückel method. This is consistent with our result.

In the case of ketene the observed bands can be assigned as in Table 3. Also in this case the long wavelength weak bands are π-${}^{1,3}\bar{\pi}^*$ transitions. From the MO coefficients it is anticipated that these two transitions have a large character of the intramolecular charge-transfer bands caused by the electron migration from carbon III to the CO-group. The strong band observed between 6.36—7.29 eV can be assigned to $\pi—{}^1\pi^*$. The transition energies calculated by Dixon and Kirby[6] are similar to ours. Knox, Norrish, and Porter[19] observed a weak band between 5.77—6.36 eV (max: 5.77 eV; log ε: 1.8). This band has been tentatively assigned to $\pi—{}^1\sigma^*$ by us[20] using the

ASMO-LCAO-SCF-CI method for the valence electron systems.

In the case of diazocyclopentadiene PTβ-approximation gives the best result as anticipated from the molecular diagrams. PEβ-approximation also gives a result similar to that given by PTβ-approximation. The 2.530 eV, 3.017 eV, 3.894 eV, and 4.346 eV transitions calculated by PTβ-approximation have the character of intramolecular charge-transfer bands caused by electron transfer from the five-membered ring to the diazo-group. The longest wavelength weak shoulder observed at about 2.70 eV is $\pi-{}^1\bar{\pi}^*$ transition.

In the case of benzenediazonium ion PEβ-approximation gives the best result. PTβ-approximation also gives a result similar to that given by PEβ-approximation. NEβ- and NTβ-approximations give unsatisfactory results. This is also anticipated from the molecular diagrams in Fig. 2. The 3.927, 4.245, and 4.395 eV transitions by PTβ-approximation have the character of intramolecular charge-transfer bands caused by electron migration from the benzene-ring to the diazo-group. In the case of benzenediazonium ion the longest wavelength singlet-singlet transition is $\pi-\pi^*$. On the other hand, as we have seen, the longest wavelength singlet-singlet transition is $\pi-\bar{\pi}^*$ in the case of diazomethane, ketene, and diazocyclopentadiene within $\pi+\bar{\pi}$-approximation. Sukigara and Kikuchi[5] have treated benzenediazonium ion by the PP type ASMO LCAO CI method taking the π-system only into consideration. They adjusted two parameters β_{NN} and ω (ω is the $\bar{\pi}$-electron density on nitrogen atom II) so as to reproduce the observed transition energies. They obtained -3.10 eV as β_{NN} and 1.05 as ω. The ω-value is close to the $\bar{\pi}$-electron density we obtained. This β_{NN}-value is slightly smaller than ours. They used $\beta_{CN}=-2.42$ eV and $\beta_{CC}=-2.39$ eV, which are similar to our values. The transitions they calculated by adjusting parameters β_{NN} and ω are similar to our results.

Conclusion

The molecular diagrams suggest that the triple bond character of the nitrogen-nitrogen bonds of these compounds is in the order, diazomethane < diazocyclopentadiene < benzenediazonium ion; and the double bond character of the carbon-nitrogen bonds in the order, benzenediazonium ion < diazocyclopentadiene < diazomethane. This is consistent with the observed carbon-nitrogen and nitrogen-nitrogen bond lengths of diazomethane and benzenediazonium ion. The extent of the contribution of the canonical formula $R^-\text{–}N_2^+$ or $R\text{–}N_2^+$ to the ground state may be in the order, diazomethane<diazocyclopentadiene<benzenediazonium ion.

The longest wavelength singlet-singlet transition is $\pi-\bar{\pi}^*$ in diazomethane, ketene, and diazocyclopentadiene and $\pi-\pi^*$ in benzenediazonium ion.

The semitheoretical formula (7) for the core resonance integral proposed in this paper gives satisfactory results though it contains no arbitrary adjustable parameters.

BULLETIN OF THE CHEMICAL SOCIETY OF JAPAN, VOL. 45, 749—753(1972)

Electronic Spectra and Structures of Organic π-Systems. VII. Electronic States of Benzoylium, Acryloylium, and Cinnamoylium Ions[1)]

Zen-ichi Yoshida and Tsunetoshi Kobayashi*

Department of Synthetic Chemistry, Faculty of Engineering, Kyoto University, Yoshida, Kyoto

(Received February 8, 1971)

The electronic states of benzoylium, acryloylium and cinnamoylium ions have been studied by a semiempirical ASMO LCAO SCF CI method including both π- and $\bar{\pi}$-systems.

The results suggest that the contribution of the canonical formula $R^{-}-\overset{+}{C}O$ or $R-\overset{+}{C}O$ to the ground state in ketene should be smaller than that in benzoylium, acryloylium or cinnamoylium ion. The longest wavelength singlet-singlet transition of benzoylium or cinnamoylium ion is $\pi-{}^1\pi^*$ as in benzenediazonium ion, and that of acryloylium ion is $\pi-{}^1\bar{\pi}^*$ as in ketene, diazomethane and diazocyclopentadiene.

As a part of our investigations on the electronic states of cumulated systems, we reported on the electronic states of diazomethane, ketene, diazocyclopentadiene, and benzenediazonium ion.[2)] This paper deals with the electronic states of benzoylium (isoelectronic with benzenediazonium), cinnamoylium, and acryloylium ions. These systems called oxocarbonium ions are of

1) Presented at the Symposium on Molecular Structure, Fukuoka, October 1969.

* Present Address: The Institute for Solid State Physics, The University of Tokyo, Roppongi, Minato-ku, Tokyo.

2) Paper VI: Z. Yoshida and T. Kobayashi, This Bulletin, **45**, 742 (1972).

importance as the reaction intermediates in Friedel-Crafts type acylation.

The method used in this study is a semiempirical ASMO-LCAO-SCF-CI method in which π-systems are duly taken into consideration.

Method of Calculation

The method used in this study being the same as that used in the calculation of diazomethane, ketene, diazocyclopentadiene, and benzenediazonium ion,[2] its details are not given. Four types of approximations NEβ, NTβ, PEβ, and PTβ are used for each molecule.

For the sake of brevity the numberings of the atomic orbitals and the atoms in the molecules are given in Fig. 1.

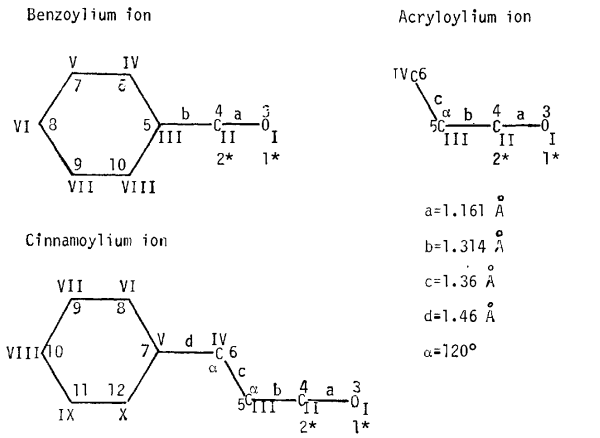

Fig. 1. Assumed structures and numberings of atoms (in Roman numerals) and numberings of atomic orbitals (in Arabic numerals) of benzoylium ion, acryloylium ion, and cinnamoylium ion. ('*' denotes an in-plane $2p_{\pi}$-atomic orbital.)

The molecular dimensions of these compounds are assumed to be as shown in Fig. 1. The carbon-oxygen bond length of methyloxocarbonium hexafluoroantimonate is 1.116 Å according to Boer.[3] This is slightly shorter than the carbon-oxygen bond length of ketene (1.161 Å) given by Kox, Thomas, and Sheridan.[4] We assumed the carbon-oxygen bond lengths and the carbon(II)-carbon(III) bond lengths of benzoylium ion, acryloylium ion, and cinnamoylium ion to be equal to those of ketene given by Kox and co-workers as shown in Fig. 1. This is because the CO-groups are in conjugation with other π-systems. The carbon(III)-carbon(IV) bond length of acryloylium ion or cinnamoylium ion is assumed to be 1.36 Å from the structural data of *trans*-acrolein.[5] The carbon(IV)-carbon(V) bond length of cinnamoylium ion is assumed to be 1.46 Å from the data of *syn-p*-chlorobenzaldoxime.[6] The benzene rings of benzoylium ion and cinnamoylium ion are assumed to be regular hexagons with the carbon-carbon bond lengths of 1.397 Å. Carbon (III), carbon(II), and the oxygen atom of each compound are assumed to lie on a straight line according to the structural data of methyloxocarbonium hexafluoroantimonate.[3,7]

The calculated core resonance integrals β_{tu}'s are summarized in Table 1.

Table 1. Core-resonance integrals, β_{ij}'s, in eV

bond	NEβ	NTβ	PEβ	PTβ
Benzoylium ion				
1—2	−3.043	−3.309	−3.988	−3.559
4—5	−2.731	−2.863	−3.797	−3.270
5—6	−2.378	−2.378	−2.378	−2.378
6—7	−2.378	−2.378	−2.378	−2.378
7—8	−2.378	−2.378	−2.378	−2.378
Acryloylium ion				
1—2	−3.043	−3.309	−3.988	−3.559
4—5	−2.731	−2.863	−3.797	−3.270
5—6	−2.529	−2.586	−2.529	−2.586
Cinnamoylium ion				
1—2	−3.043	−3.309	−3.988	−3.559
4—5	−2.731	−2.863	−3.797	−3.270
5—6	−2.529	−2.586	−2.529	−2.586
6—7	−2.137	−2.049	−2.137	−2.049
7—8	−2.378	−2.378	−2.378	−2.378
8—9	−2.378	−2.378	−2.378	−2.378
9—10	−2.378	−2.378	−2.378	−2.378

The calculation has been carried out on a FACOM 230-60 computer at the computation centre of Kyoto University.

Results

The molecular diagrams of these compounds are shown in Fig. 2. The reported molecular diagrams of ketene are also given. The calculated and the observed transition energies are given in Table 2 together with CI coefficients.

Discussion

In the case of benzoylium ion, the β_{12}- and β_{45}-values calculated by PEβ-approximation are slightly larger than those calculated by PTβ-approximation as shown in Table 1. In N-approximation the β-values given by both methods NTβ and NEβ are similar to each other. The other β_{CC}-values calculated by formulas (6) and (7) in Ref. 2 are in good agreement with each other.

On the whole the four sets of parameters give similar SCF eigenvalues and eigenvectors. The eigenvectors of benzoylium ion are similar to those of benzenediazonium ion.

As is seen in Fig. 2, in the case of benzoylium ion carbon atom II carries a charge of about +0.7—+0.8 and the terminal oxygen I is nearly neutral. The bond

3) F. P. Boer, *J. Amer. Chem. Soc.*, **88**, 1572 (1966).
4) A. P. Cox, L. F. Thomas, and J. Sheridan, *Spectrochim. Acta*, **15**, 542 (1959).
5) R. Wagner, J. Fine, J. W. Simmons, and J. H. Goldstein, *J. Chem. Phys.*, **26**, 634 (1957).
6) B. Jerslev, *Nature*, **180**, 1410 (1957).
7) G. A. Olah, C. U. Pittman, Jr., and M. C. R. Symons, "Carbonium Ions," Vol. 1, p. 153, ed. by G. A. Olah, and P. von R. Schleyer, Interscience, New York (1968).

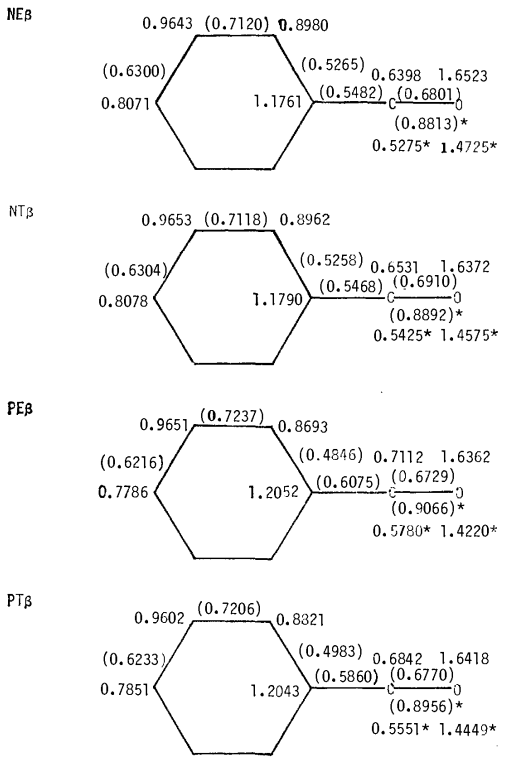

Fig. 2a. Electron densities and bond orders (in parentheses) of benzoylium ion.

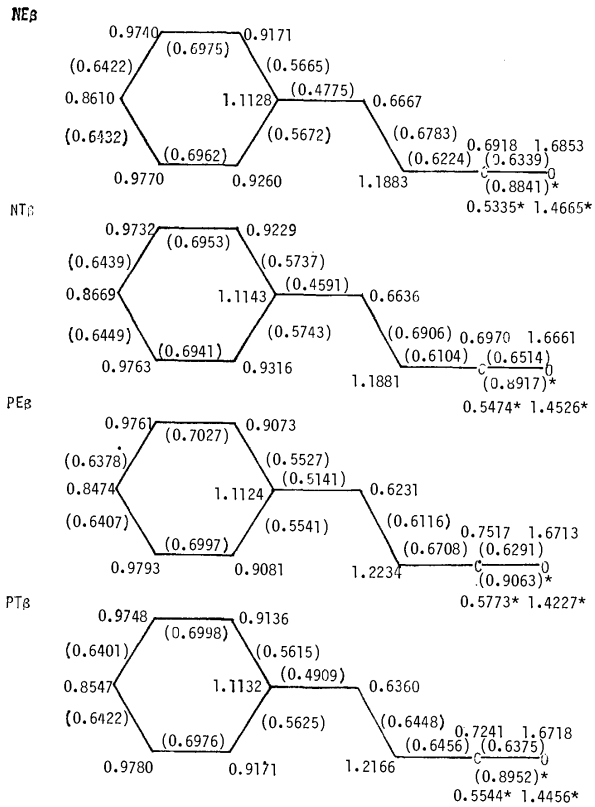

Fig. 2b. Electron densities and bond orders (in parentheses) of cinnamoylium ion.

order of the carbon(II)-oxygen bond is about 1.6. The bond order of the carbon(II)-carbon(III) bond is about 0.54—0.60. A charge of about +0.7 exists on the CO-group. If we compare the molecular diagrams of

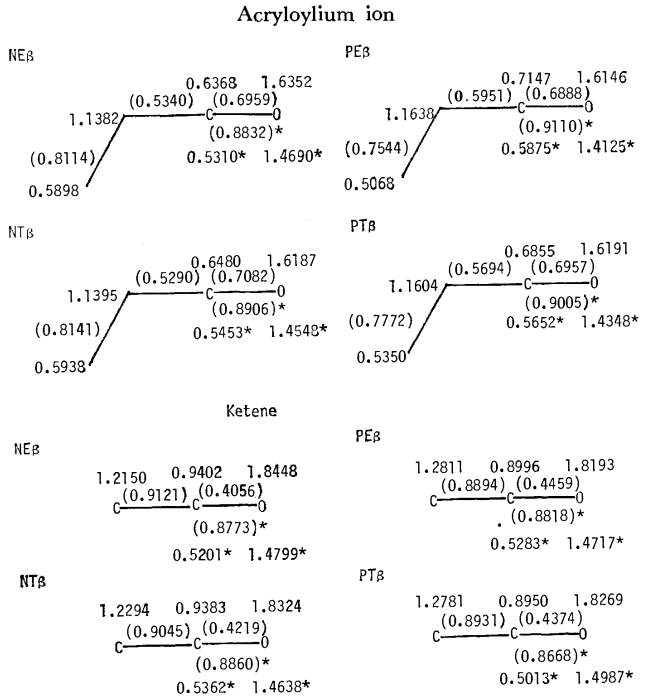

Fig. 2c. Electron densities and bond orders (in parentheses) of acryloylium ion and ketene.

ketene with those of benzoylium ion, the CO bond of benzoylium ion can be anticipated to have a larger triple bond character than the CO bond of ketene, and the C_{II}–C_{III} bond of ketene, a larger double bond character than the C_{II}–C_{III} bond of benzoylium ion. The electron density on the oxygen or carbon atom (I) in ketene is greater than that of the corresponding atom of benzoylium ion. On the whole the extent of contribution of the canonical formula $R–C^{+}\equiv O$ or $R^{-}–C^{+}\equiv O$ to the ground state may be greater in the case of benzoylium ion than in ketene.

In the case of acryloylium ion carbon atom II carries a charge of about +0.7—0.8 as in benzoylium ion. The terminal oxygen is nearly neutral as in benzoylium ion. The bond orders of the carbon(II)-oxygen bond and the carbon(II)-carbon(III) bond are about 1.6 and 0.53—0.60, respectively. These values are similar to those of benzoylium ion. The CO-group in acryloylium ion bears a charge of about +0.73—0.67. The extent of contribution of the canonical formula $R–C^{+}\equiv O$ to the ground state of acryloylium ion might be nearly equal to that in benzoylium ion.

In the case of cinnamoylium ion carbon atom II bears a charge of about +0.7—0.8 as in benzoylium ion and acryloylium ion. The terminal oxygen is nearly neutral also in this system. The bond order of the carbon(II)-oxygen bond is about 1.53 which is slightly smaller than those in benzoylium ion and acryloylium ion. The bond order of the carbon(II)-carbon(III) bond is about 0.61—0.67 which is slightly larger than those of acryloylium ion and benzoylium ion. The results suggest that the triple bond character of the carbon(II)-oxygen bond is slightly smaller than those of benzoylium ion and acryloylium ion, and the double bond character of the carbon(II)-carbon(III) bond is slightly larger than those of the other two com-

Table 2. Calculated transition energies in eV

Sym.	E	f	CI Composition[a)]		Sym.	E	f	CI Composition[a)]		Obsd E	Obsd log ε
Benzoylium ion											
	NEβ approximation					NTβ approximation					
$^1B_2$	3.706	0.099	5—6	0.961	$^1B_2$	3.769	0.105	5—6	0.957	4.03	3.57[7)]
$^1A_2$	4.216	0.0	3—7	0.463	$^1A_2$	4.428	0.0	4—7	0.876	4.75	4.23
			4—7	0.872				3—7	0.459		
$^1A_1$	4.373	0.384	4—6	0.894	$^1A_1$	4.444	0.372	4—6	0.892		
			5—8	0.349				5—8	0.371		
$^1B_1$	5.127	0.0	5—7	1.0	$^1B_1$	5.321	0.0	5—7	1.0		
$^1A_1$	5.997	0.293	3—6	−0.467	$^1A_1$	6.146	0.544	3—6	−0.429		
			2—7	−0.356				5—8	0.685		
			5—8	0.611				4—10	−0.427		
			4—9	−0.441							
$^3B_2$	2.628		5—6	0.958	$^3B_2$	2.663		5—6	0.960		
	PEβ approximation					PTβ approximation					
$^1B_2$	3.876	0.143	5—6	0.957	$^1B_2$	3.811	0.128	5—6	0.959	4.03	3.57[7)]
$^1A_1$	4.694	0.324	4—6	0.874	$^1A_1$	4.607	0.355	4—6	0.880	4.75	4.23
			5—8	−0.445				5—8	−0.422		
$^1A_2$	5.266	0.0	4—7	0.844	$^1A_2$	4.788	0.0	4—7	0.848		
			3—7	−0.522				3—7	−0.514		
$^1B_1$	6.471	0.0	5—7	1.0	$^1B_1$	5.910	0.0	5—7	1.0		
$^3B_2$	2.562		5—6	0.975	$^3B_2$	2.562		5—6	0.970		
Acryloylium ion											
	NEβ approximation					NTβ approximation					
$^1A''$	4.516	0.0	3—5	0.976	$^1A''$	4.766	0.0	3—5	0.980	(5.28∼6.20)[7)]	
$^1A'$	5.009	0.488	3—4	0.953	$^1A'$	5.193	0.540	3—4	0.966		
$^1A'$	6.859	0.209	2—5	0.655	$^1A'$	7.295	0.177	1—4	−0.562		
			1—4	−0.589				2—5	0.649		
			3—6	0.342				3—6	0.427		
$^3A'$	2.701		3—4	0.990	$^3A'$	2.828		3—4	0.990		
	PEβ approximation					PTβ approximation					
$^1A''$	5.492	0.0	3—5	0.987	$^1A''$	5.052	0.0	3—5	0.984	(5.28∼6.20)[7)]	
$^1A'$	5.578	0.682	3—4	0.986	$^1A'$	5.471	0.644	3—4	0.976		
$^1A'$	8.328	0.070	1—4	0.497	$^1A'$	7.607	0.137	1—4	0.542		
			2—5	0.636				2—5	0.664		
			3—6	0.541				3—6	0.427		
$^3A'$	2.974		3—4	0.996	$^3A'$	2.918		3—4	0.996		
Cinnamoylium ion											
	NEβ approximation					NTβ approximation					
$^1A'$	3.356	0.046	5—7	0.417	$^1A'$	3.374	0.044	6—7	0.898	3.80	4.471[7)]
			6—7	0.855				5—7	0.316		
$^1A'$	3.570	0.954	5—7	0.844	$^1A'$	3.585	0.906	5—7	0.886		
			6—7	−0.419				6—7	−0.320		
$^1A''$	3.830	0.0	4—8	−0.621	$^1A''$	4.057	0.0	4—8	−0.621		
			5—8	−0.679				5—8	0.702		
$^1A'$	5.255	0.215	4—7	0.709	$^1A'$	5.333	0.287	4—7	0.685		
			6—10	0.500				6—10	0.557		
$^3A'$	2.099		4—7	−0.375	$^3A'$	2.178		4—7	−0.375		
			5—7	0.830				5—7	0.867		
			6—7	−0.364							
	PEβ approximation					PTβ approximation					
$^1A'$	3.307	0.053	6—7	0.958	$^1A'$	3.279	0.047	6—7	0.955	3.80	4.471[7)]
$^1A'$	3.726	0.923	5—7	0.942	$^1A'$	3.654	0.915	5—7	0.937		
$^1A''$	4.904	0.0	3—8	−0.316	$^1A''$	4.423	0.0	3—8	0.345		
			4—8	0.664				4—8	0.644		
			5—8	0.675				5—8	−0.679		

Table 2. Calculated transition eneregies in eV (continued)

Sym.	E	f	CI Composition[a)]	Sym.	E	f	CI Composition[a)]	Obsd E	Obsd $\log \varepsilon$
$^1A'$	5.530	0.433	4—7 −0.685	$^1A'$	5.485	0.424	4—7 −0.661		
			6—9 0.625				5—9 −0.319		
			5—10 0.316				6—10 0.621		
$^3A'$	2.259		5—7 0.939	$^3A'$	2.183		5—7 0.921		
							4—7 −0.319		

a) The transition, indicated by i—j, refers to a one electron excitation from orbital i to virtual orbital j. The second column gives the CI coefficient of the configuration i—j.

pounds. The bond order of the carbon(III)-carbon (IV) bond in acryloylium ion is 0.75—0.80 which is greater than that of cinnamoylium ion, 0.61—0.69. This suggests that the double bond character of the carbon(III)-carbon(IV) bond of acryloylium ion is larger than that of cinnamoylium ion. The CO-group of cinnamoylium ion bears a charge of about +0.58—0.64. The value is smaller than those in benzoylium and acryloylium ions. On the whole the triple bond character of the carbon(II)-oxygen bond of benzoylium ion, acryloylium ion or cinnamoylium ion is more enhanced than that of ketene. The double bond character of the carbon(II)-carbon(III) bond of ketene may be larger than those of benzoylium, acryloylium, and cinnamoylium ions. Contribution of the canonical formula $R^-–\overset{+}{C}O$ or $R–\overset{+}{C}O$ to the ground state of benzoylium ion, acryloylium ion, or cinnamoylium ion might be larger than in ketene.

Calculated transition energies are summarized in Table 2. In the case of benzoylium ion P-approximation gives better results than the other. This is consistent with the molecular diagram. Calculated 4.788 eV and 5.910 eV transitions (PTβ-approximation) are $\pi—{}^1\bar{\pi}^*$ transitions and are the so-called intramolecular charge-transfer transitions. The character of the transitions of this system is similar to that of benzenediazonium ion.

In the case of acryloylium ion P-approximation gives a better result as in the case of benzoylium ion. This is also consistent with the molecular diagrams. The calculated 5.052 eV transition has the character of the so-called intramolecular charge-transfer transition. This is $\pi—{}^1\bar{\pi}^*$ transition.

In the case of cinnamoylium ion the four methods give similar results but P-approximation gives slightly better results. The calculated 4.423 eV transition by PTβ-approximation has the character of the so-called intramolecular charge-transfer transition, and is $\pi—\bar{\pi}^*$ transition.

Conclusion

The triple bond character of the CO bond of benzoylium ion, acryloylium ion or cinnamoylium ion may be larger than that of ketene. The double bond character of the carbon(II)-carbon(III) bond of ketene may be larger than that of acryloylium ion, cinnamoylium ion or benzoylium ion. The contribution of the canonical formula $R^-–\overset{+}{C}O$ (or $R–\overset{+}{C}O$) to the ground state in ketene may be smaller than in benzoylium ion, acryloylium ion, and cinnamoylium ion.

The longest wavelength singlet-singlet transitions of benzoylium and cinnamoylium ions are $\pi—\pi^*$ as in benzenediazonium ion, and that of acryloylium ion is $\pi—\bar{\pi}^*$ as in diazomethane, ketene, and diazocyclopentadiene.

The Benzene-photosensitized Decomposition of Carbonyl Sulfide in a Cyclohexane Solution

Shin SATO, Hiroshi MIYAMOTO, Shun-ichi HIROKAMI, and Shigeru TSUNASHIMA

Department of Applied Physics, Tokyo Institute of Technology, Ookayama, Meguro-ku, Tokyo

(Received July 27, 1971)

The decomposition of carbonyl sulfide photosensitized by benzene in the solution of cyclohexane has been investigated at room temperature. The quantum yield of CO formation, ϕ_{CO}, at an infinite concentration of COS was estimated to be 1.0. The COS concentration dependence of ϕ_{CO} corresponded well to that of the quenching efficiency of COS on benzene fluorescence. These results suggest that, of the two possible photosensitization processes:

$$C_6H_6(^1B_{2u}) + COS \longrightarrow C_6H_6 + CO + S(^1D)$$

and

$$C_6H_6(^3B_{1u}) + COS \longrightarrow C_6H_6 + CO + S(^3P),$$

the former is responsible for the formation of CO. The very small yield of cyclohexanethiol may be explained by the fact that benzene is an efficient catalyzer for the transition process, $S(^1D) \rightarrow S(^3P)$.

When electronically excited at around 5 eV, carbonyl sulfide has two energetically-possible decomposition channels. The one is through an excited singlet state:

$$COS = CO(^1\Sigma^+) + S(^1D) \qquad \Delta H = 98.8 \text{ kcal/mol}$$

the other is through a triplet:

$$COS = CO(^1\Sigma^+) + S(^3P) \qquad \Delta H = 72.4 \text{ kcal/mol}$$

Therefore, the benzene-photosensitized decomposition of carbonyl sulfide at 2537 Å, if it occurs, has two possible processes. The reaction mechanism may be described as follows:

$$C_6H_6 + h\nu \longrightarrow C_6H_6^*(^1B_{2u}) \quad (1)$$

$$C_6H_6^* \longrightarrow C_6H_6 + h\nu_f \quad (2)$$

$$C_6H_6^* \longrightarrow C_6H_6^{**}(^3B_{1u}) \quad (3)$$

$$C_6H_6^{**} \longrightarrow C_6H_6 \quad (4)$$

$$C_6H_6^* + COS \longrightarrow C_6H_6 + CO + S(^1D) \quad (5)$$

$$C_6H_6^{**} + COS \longrightarrow C_6H_6 + CO + S(^3P) \quad (6)$$

This report will be mainly concerned with which process, Reaction (5) or (6), is more important for the decomposition of carbonyl sulfide.

The gas-phase photolysis of carbonyl sulfide was extensively investigated by Gunning and Strausz.[1] Regarding the liquid-phase, Gollnick and Leppin reported several important observations.[2] When COS is photolyzed at 2537 Å in liquid alkanes such as cyclohexane and cyclopentane, the quantum yield of CO formation is 0.9 and that of mercaptan is in the range of 0.3—0.5. They also showed that methyl, ethyl, and isopropyl alcohols and acetonitrile efficiently catalyze the transition process, $S(^1D) \rightarrow S(^3P)$.

Recently, we showed that COS molecules act as effective electron scavengers in the radiolysis of benzene.[3] Consequently, the benzene-photosensitized decomposition of COS has become an urgent problem to be solved.

Experimental

The COS was a product of the Merck Company. Further purification was not made except for bulb-to-blub distillation, with the rejection of the head and tail fractions. The cyclohexane (Tokyo Kagaku Seiki Co., spectro grade) was passed through a 1 m silica-gel column before use. The benzene (Tokyo Pure Chemical Co., spectro grade) and ethylene (Takachiho Chemical Co.) were used as supplied.

A low-pressure mercury resonance lamp containing 5 Torr Ne was used for irradiating solutions at room temperature in a 30 m*l*, 1 cm thick, cylindrical quartz vessel. The solution was stirred with a magnetic stirrer in order to maintain the homogeneity of the solute concentration. The irradiating light was passed through a Toshiba UV-25 glass filter to cut off the wavelengths shorter than 2000 Å. The reaction vessel was irradiated horizontally to let the gas produced escape from the reaction zone.

In order to estimate the light intensity, the mercury-photosensitized decomposition of ethylene was carried out in a reaction vessel of exactly the same size. The quantum yield of hydrogen at 45 Torr of ethylene was assumed to be 0.203.[4]

The benzene fluorescence spectra were measured using a Hitachi PMF-2A fluorometer. The exciting light was set at 2537 Å. The cell used for the measurement was modified so as to evacuate it and to introduce a quencher gas.

The gas noncondensable at the temperature of liquid nitrogen was collected and measured by means of a Toepler pump. After passing the gas through a cuprous oxide furnace at 390°C, the noncondensables at the temperature of dry ice-methanol were again collected and measured. Cyclohexanethiol and benzenethiol were analyzed, using a Hitachi 023 gas chromatograph equipped with a FID detector and a 1 m tricresylphosphate column at 80°C. Bromobenzene was used as a reference to estimate the absolute yield because its elution time is close to that of cyclohexanethiol.

The solubility of carbonyl sulfide in cyclohexane and in benzene was measured by a technique already reported.[5] Ostwald's coefficients obtained at 20°C are 8.0 in cyclohexane and 13 in benzene.

1) H. E. Gunning and O. P. Strausz, "Advances in Photochemistry," Vol. 4 ed. by W. A. Noyes, Jr., G.S. Hammond, and J. N. Pitts, Jr., Interscience Publishers, New York (1966), p. 143.

2) K. Gollnick and E. Leppin, *J. Amer. Chem. Soc.*, **92**, 2217 (1970).

3) S. Hirokami, S. Shishido, and S. Sato, This Bulletin, **43**, 973 (1970).

4) B. DeB. Darwent, *J. Chem. Phys.*, **19**, 258 (1951).

5) T. Saito, K. Takahashi, and S. Sato, This Bulletin, **41**, 2603 (1968).

Results

Benzene-photosensitized Decomposition of COS. A rather high concentration of benzene (0.43 mol/l) was used to prevent the direct photolysis of COS ($\varepsilon_{2537} \approx 10\ l\,mol^{-1}cm^{-1}$).[6] At this concentration, more than 99% of the impinging light at 2537 Å is absorbed in the solution. The quantum yield of CO is listed in Table 1 as a function of the COS concentration. The values of ϕ_{CO} may be a little overestimated, because the resonance line absorbed by mercury at room temperature is sharper than that emitted by the light source and because benzene molecules can absorb the foot of the resonance line. No gas noncondensable at 77°K other than CO could be obtained.

Table 1. The quantum yield of carbon monoxide in the benzene-photosensitized decomposition of carbonyl sulfide in the solution of cyclohexane

Benzene consentration is 0.43 mol/l

Concentration of COS 10^{-2} mol/l	Quantum yield of CO ϕ_{CO}
0.22	0.17
0.24	0.19
0.26	0.21
0.37	0.25
0.41	0.27
0.42	0.30
0.44	0.35
0.53	0.42
0.65	0.40
0.75	0.40
0.87	0.47
1.09	0.48
1.21	0.64
2.17	0.73
2.84	0.82
3.09	0.76

Gas-chromatographic analysis showed that cyclohexanethiol is the only product in the liquid. The formation of benzenethiol could not be detected. As the yield of cyclohexanethiol was very small, the benzene concentration dependence was checked. The results are shown in Fig. 1. Obviously, the presence of benzene severely prevents the formation of cyclohexanethiol. In the absence of benzene, the light is absorbed by COS and the [cyclohexanethiol]/[CO] ratio obtained is in agreement with that reported by Gollnick and Leppin.[2]

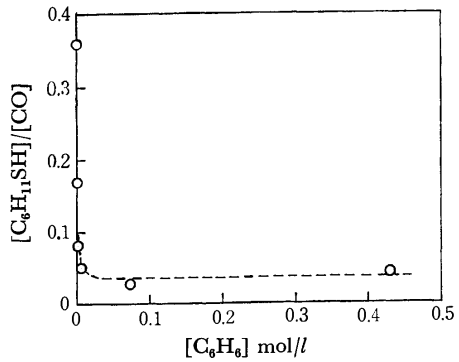

Fig. 1. The relative yield of cyclohexanethiol as a function of the concentration of benzene.

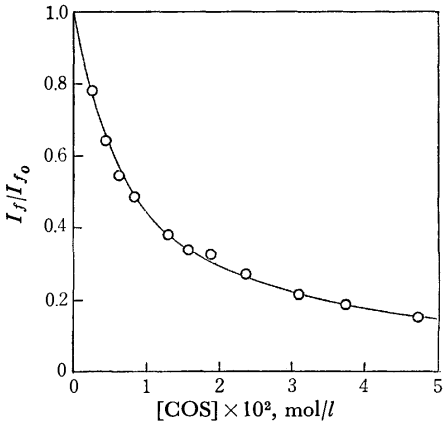

Fig. 2. The relative intensity of the benzene fluorescence as a function of the concentration of carbonyl sulfide.

Quenching of Benzene Fluorescence by COS. The benzene fluorescence was measured at 2800 Å, where the spectrum showed its maximum. In Fig. 2, the relative intensity of the fluorescence is plotted as a function of the concentration of COS. Exactly the same quenching curve was obtained by using the fluorescence intensity at a different wavelength (2950 Å). The benzene concentration used was 0.43 mol/l; the value was the same as that used for the photosensitized decomposition.

Discussion

The steady-state-treatment of the reaction mechanism described in the Introduction gives the following Stern-Volmer equation:

$$I_{f_0}/I_f = 1 + k_5\tau[COS] \qquad (I)$$

Here, I_{f_0} and I_f denote the fluorescence intensity in

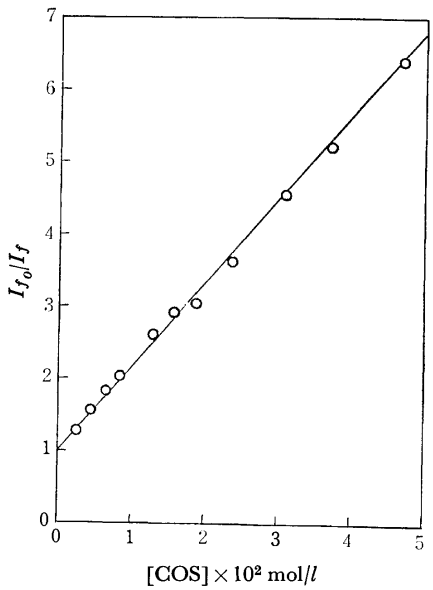

Fig. 3. The Stern-Volmer plot on the benzene fluorescence. The quencher is carbonyl sulfide.

6) K. Gollnick and E. Leppin, *Mol. Photochem.*, **2**, 179 (1970).

the absence and in the presence of the quencher, COS, respectively. k_5 is the rate constant of Reaction (5), and τ is the lifetime of the $^1B_{2u}$ benzene in this solution. From the linear relationship shown in Fig. 3, the $k_5\tau$ value could be calculated to be 110 ± 10 l/mol by the least-squares method. This value may be compared with 300 l/mol, the value which was obtained in the gas phase.[7]

Since the CO formation has two possible channels, the quantum yield of CO has a somewhat complicated dependence on the concentration of COS.

$$\phi_{CO}^{-1} = \left(1+\frac{1}{k_5\tau[COS]}\right)\left(1+\frac{k_3k_6}{k_5k_6[COS]+k_5/\tau'}\right)^{-1} \quad \text{(II)}$$

Here, τ' is the lifetime of the $^3B_{1u}$ benzene in the solution. If only one of the two possible channels is operative for the formation of CO, Eq. (II) can be simplified as follows:

$$\phi_{CO}^{-1} = A^{-1}\left(1+\frac{1}{B[COS]}\right) \quad \text{(III)}$$

In the case of the channel through the singlet-excited state, $A\leq1$ and $B=k_5\tau$, while in the case of the channel through the triplet state, A cannot exceed the quantum yield of the intersystem crossing, ϕ_{SC} and $B=k_6\tau'$. Figure 4 shows the reciprocal of the yield of CO as a function of the reciprocal of the COS concentration. Although the plots are a little scattered, the least-squares method gives $A\approx1.0$ and $B=80\pm30$ l/mol. This value of B roughly agrees with the $k_5\tau$ value obtained by the measurement of the fluorescence quenching.

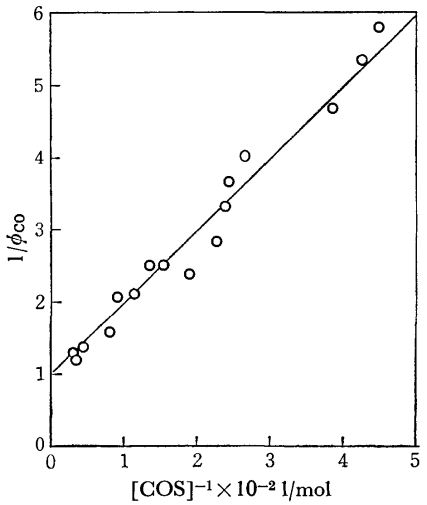

Fig. 4. The reciprocal of the quantum yield of carbon monoxide as a function of the reciprocal of the concentration of carbonyl sulfide.

The lifetime of the $^1B_{2u}$ benzene in cyclohexane at room temperature is reported to be 29 nsec, where the concentration of benzene is 3.4×10^{-2} mol/l.[8] Ludwig and Amata observed that the lifetime in n-nonane is a little dependent upon the concentration of benzene, but its value is not smaller than 26 nsec, even in pure benzene.[9] In the present discussion, therefore, τ may be assumed to be 29 nsec.

The situation is very obscure for the lifetime of the $^3B_{1u}$ benzene. Cundall *et al.* estimated that the lifetime in pure benzene is of the order of 10 nsec.[10] In a previous paper, we investigated the benzene-photosensitized isomerization of butene-2 in a solution of cyclohexane and estimated the lifetime of the $^3B_{1u}$ benzene to be of the order of 0.1 μsec at 5×10^{-4} mol/l of benzene.[11]

Consequently, the agreement between the B value and the $k_5\tau$ value obtained in the fluorescence measurement cannot establish that Reaction (5), the singlet-singlet energy transfer, is responsible for the formation of CO. If the triplet-triplet energy transfer, Reaction (6), is responsible for this process, however, the A value should be equal to or less than ϕ_{SC}. Our previous paper showed that ϕ_{SC} is less than 0.25, while Cundall *et al.* estimated that ϕ_{SC} in pure benzene is 0.6. The present experiment obviously shows that the quantum yield of CO at an infinite concentration of COS is much higher than 0.6. As stated in the Results section, the quantum yields obtained in the present experiment may be a little overestimated. The error is probably within 10%, however, because the quantum yield of cyclohexanethiol in the absence of benzene is in good agreement with that reported by Gollnick and Leppin.[2]

Thus, the discussion of the B factor could not distinguish whether Reaction (5) or Reaction (6) is responsible for the formation of CO, but that of the A factor strongly suggested that Reaction (5) is responsible. It may be concluded, therefore, that the CO formation in the benzene-photosensitized decomposition of COS in cyclohexane results from the singlet-singlet energy transfer. As has been stated above, the $k_5\tau$ value is 80—110 l/mol. The k_5 value, therefore, is $3.3\pm0.6\times10^9$ l/mol sec. This value suggests that Reaction (5) is diffusion-controlled.

As was shown in the Results section, the presence of benzene severely hindered the formation of cyclohexanethiol. This is probably because benzene molecules effectively catalyze the transition process, $S(^1D)\rightarrow S(^3P)$. In the benzene-photosensitization, the following process may be operative:

$$C_6H_6(^1B_{2u}) + COS \longrightarrow C_6H_6\cdots S + CO$$
$$\longrightarrow C_6H_6 + S(^3P) + CO$$

Here, $C_6H_6\cdots S$ represents the intermediate complex.

Since the benzene concentration used in the present experiment is high, the formation of the benzene singlet excimer cannot be ruled out. If the excimer formation is included in the reaction mechanism, the steady-state-treatment becomes a little more complicated. However, the conclusion of the singlet-singlet energy transfer cannot be altered regardless of whether or not the

7) E. K. Lee, M. W. Schmidt, R. G. Shortridge, Jr., and G. A. Haninger, Jr., *J. Phys. Chem.*, **73**, 1805 (1969).

8) I. B. Berlman, "Handbook of Fluorescence Spectra of Aromatic Molecules," Academic Press, New York and London (1965), p. 42.

9) P. K. Ludwig and C. D. Amata, *J. Phys. Chem.*, **72**, 3725 (1968).

10) R. B. Cundall, G. B. Evans, P. A. Griffiths, and J. P. Keene, *ibid.*, **72**, 3871 (1968).

11) S. Sato, H. Kobayashi, and K. Fukano, *Kogyo Kagaku Zasshi*, **72**, 209 (1969).

excimer is quenched by COS.

In this work, the presence of the $^3E_{1u}$ state (4.5 eV) of benzene is completely ignored because its property is unknown. If the property becomes apparent, the inclusion of this state in the reaction mechanism can be easily done.

BULLETIN OF THE CHEMICAL SOCIETY OF JAPAN, VOL. 45, 757—764(1972)

Amino Wagging of the *tert*-Butylamine in $\tilde{A}$ Electronic State

Akiko Y. Hirakawa, Hideyuki Miyazaki, and Masamichi Tsuboi

Faculty of Pharmaceutical Sciences, The University of Tokyo, Bunkyo-ku, Tokyo

(Received August 24, 1971)

Ultraviolet absorption spectra of two isotopic *t*-butylamines, $(CH_3)_3CNH_2$ and $(CH_3)_3CND_2$, have been observed in their gaseous state in the spectral region 2000—2500 Å. There is an electronic band, whose 0—0 band peaks are observed respectively at 2351.2 and 2334.9 Å. The vibrational structure of the band, caused by the amino wagging vibration, was analyzed. On the basis of the observed energy levels, the potential function of the excited molecule along the amino wagging coordinate was determined; it is nearly harmonic with a small positive quartic term. The dependence of intensity on the vibrational quantum number and the intensity ratio of the fundamental and the hot bands indicate that the equilibrium structure of the amino group is the same as that of methylamine; the angle between the C–N axis and the HNH plane has been determined to be $51\pm4°$.

Every aliphatic amine has a strong electronic absorption band in the 2300 Å region. We have examined previously the vibrational structure of the bands of four isotopic methylamines.[1] The result indicated that the amino group has a plane structure in the lowest excited electronic state ($\tilde{A}$), while in the ground state ($\tilde{X}$) it has a pyramidal structure.[2] Along the amino wagging coordinate there are two potential minima separated by a barrier of 1688 cm^{-1} in height in the $\tilde{X}$ state,[3,4] whereas in the $\tilde{A}$ state the potential function is nearly harmonic up to tenth vibrational quantum states. The ammonia molecule is also planar in the lowest excited electronic state according to the result of an analysis[5] of the rovibronic spectrum of ND_3. In the work reported here we have examined the corresponding band of *t*-butylamine and its amino deuterated compound in an attempt to elucidate the effect of an adjacent bulky group on the amino wagging potential. As will be detailed below, the amino group of *t*-butylamine is also found to be planar in the lowest excited electronic state. It has been shown, however, the potential function along the amino wagging coordinate is appreciably different from that in methylamine.

Experimental

t-Butylamine was purchased from Tokyo Kasei Company. *t*-Butylamine-d_2 gas was obtained from deuterated *t*-butylamine hydrochloride by adding concentrated D_2O solution of NaOD. $(CH_3)_3CND_2\cdot DCl$ was obtained by the exchange reaction of $(CH_3)_3CNH_2\cdot HCl$ with D_2O. NaOD used was obtained by the reaction of metallic sodium with D_2O vapor at lower temperature. All the procedures for deuteration were carried out in a vacuum line.

Ultraviolet absorption measurements of these two isotopic *t*-butylamines in the 2000—2500 Å region were made by the use of a Hitachi EPS-3T spectrometer with a quartz prism. The calibration was made by the absorption lines of the γ system of nitric oxide in the region from 1955 to 2270 Å.[6] The relative position of each vibrational peak has been determined with an experimental error of about ±0.5 Å.

A gas cell with quartz windows and with 10 cm path length was used. The pressure of the gas was in the range

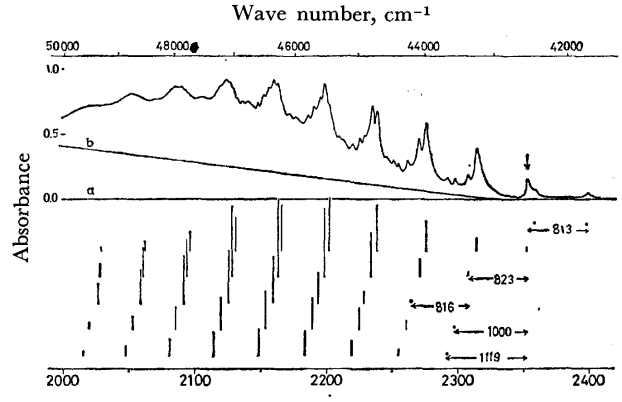

Fig. 1. The structure of the $\tilde{A}$–$\tilde{X}$ band of *t*-butylamine, $(CH_3)_3CNH_2$, in the gaseous state. The continous curve is a reproduction of the observed absorption cruve. Vertical lines indicate the calculated intensities of the bands (See the text). In the calculated spectrum the intensity ratios of the main progression ($v'_1, v'_2=v'_3=v'_4=0$) and other progressions are chosen so that it fits the observed spectrum. The arrow indicates the position of the 0—0 band. Lines a) and b) are the base lines for two possible cases (See the text).

1) M. Tsuboi, A. Y. Hirakawa, and H. Kawashima, *J. Mol. Spectrosc.*, **29**, 216 (1969).

2) T. Itoh, *J. Phys. Soc. Jap.*, **11**, 246 (1956).

3) M. Tsuboi, A. Y. Hirakawa, T. Ino, T. Sasaki, and K. Tamagake, *J. Chem. Phys.*, **41**, 2721 (1964).

4) M. Tsuboi, A. Y. Hirakawa, and K. Tamagake, *J. Mol. Spectrosc.*, **22**, 272 (1967).

5) A. E. Douglas, *Discuss. Faraday Soc.*, **35**, 158 (1963).

6) A. G. Gaydon, *Proc. Phys. Soc.*, **56**, 95 (1944).

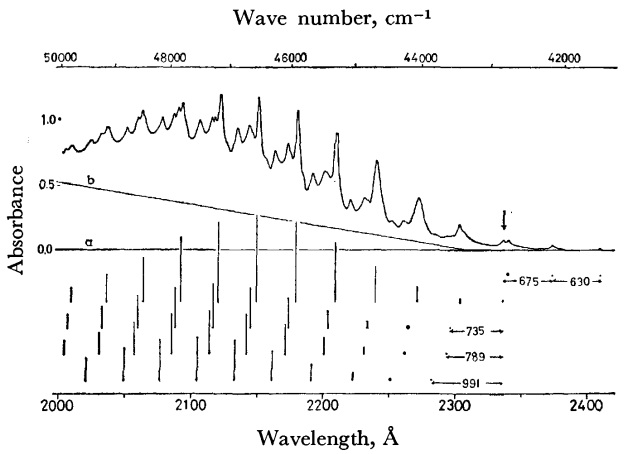

Fig. 2. The structure of the $\tilde{A}$–$\tilde{X}$ band of *t*-butylamine-d_2, $(CH_3)_3CND_2$, in the gaseous state. The continous curve is a reproduction of the observed curve. Vertical lines indicate the calculated intensities of the bands (See the text). In the calculated spectrum, the intensity ratios of the main progression (v'_1, $v'_2=v'_3=v'_4=0$) and other weak progressions are chosen so that it fits the observed spectrum. The arrow indicates the position of the 0—0 band. Lines a) and b) are the base lines for two possible cases (See the text).

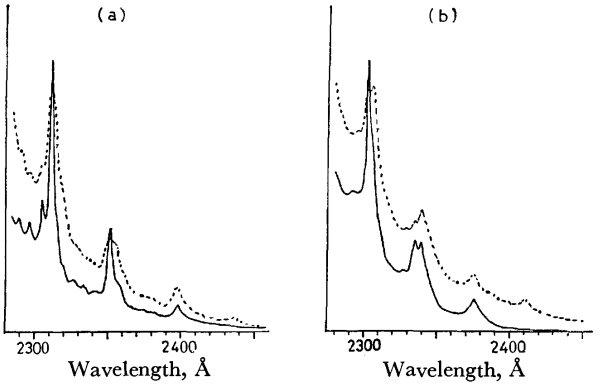

Fig. 3. Temperature dependence of the absorption intensities (a) of $(CH_3)_3CNH_2$ and (b) of $(CH_3)_3CND_2$. The solid line indicates the spectrum at 300°K and the dotted line at 350°K.

of 0.5—1.5 mmHg to obtain spectra of suitable absorption intensity. In Figs. 1 and 2, the absorption curves of two isotopic *t*-butylamine obtained at 300°K are given. To distinguish the hot bands (v'←1) from the fundamental bands (v'←0), the spectra at 350°K were also examined and are given in Fig. 3.

Experimental Results and Analysis of the Spectra

The ultraviolet absorption spectrum of *t*-butylamine in the 40000—50000 cm^{-1} region consists of a few sets of long progressions of bands. First of all, the 0–0 band of each isotopic molecule was determined. The intensities of the peaks at 2397.0 and 2356.8 Å of $(CH_3)_3CNH_2$ increase as the temperature is elevated. Therefore, these peaks are assigned to hot bands and the peak at 2351.2 Å, whose intensity decreases as the temperature is raised, is assigned to the 0–0 band of A–X electronic transition. The frequency difference between the 0–1 band (the peak at 2397.0 Å) and the 0–0 band is 813 cm^{-1}, and this agrees with the frequency of the amino wagging vibration, 811 cm^{-1} observed in the infrared absorption spectrum.[7] Similarly, for $(CH_3)_3CND_2$, the temperature effects on the spectrum show that the peaks at 2408.3, 2372.3, 2338.9, and 2306.1 Å are hot bands and the peak at 2334.9 Å is assignable to the 0–0 band. The frequency difference between the 0–1 band (the peak at 2372.3 Å) and the 0–0 band, 675 cm^{-1}, is equal to the infrared absorption frequency, 673 cm^{-1} [7] within the experimental error.

In the analysis of the bands now in question, every detail of the observed structures should be regarded to be caused by the vibrations of the molecules. The rotational structure should not appear, because even if the rotational lines form a P or R head it should be located within 15 cm^{-1} from each band center, *i.e.* at a smaller distance than the resolution (25 cm^{-1}) of the spectrometer used. For both isotopic *t*-butylamines, all the observed vibronic bands are explained in terms of four vibrational frequencies, ν'_1, ν'_2, ν'_3, and ν'_4, of the excited state and one vibrational frequency ν''_1 of the ground state. The observed frequencies of the bands with their peak heights are given in Tables 1 and 2. Every observed frequency can be assigned to one of the calculated frequencies

$$\nu_{00}+v_1'\nu_1'+v_2'\nu_2'+v_3'\nu_3'+v_4'\nu_4'+f(v_1', v_2', v_3', v_4')-v_1''\nu_1''.$$

The assignment are shown in Tables 1 and 2 in terms of a set of vibrational quantum numbers v_1', v_2', v_3', v_4', and v_1''. The values of ν_{00}, ν'_1, ν'_2, ν'_3, ν'_4, ν''_1 and $f(v_1', v_2', v_3', v_4')$ are derived as shown in the follwing paragraphs and are given in the footnotes of Tables 1 and 2. In the bands of *t*-butylamines, there are a few long progressions of v_1'. The vibrational frequencies of the members of these progressions are given by

$$\nu(v_1') = \nu_{obs}(v_1', v_2', v_3', v_4', v_1'') - \nu_{obs}(v_1'=0, v_2', v_3', v_4', v_1''). \quad (1)$$

These frequencies $\nu(v_1')$ are given in Tables 3 and 4.

The vibrational structure of the band of the undeuterated species $(CH_3)_3CNH_2$ looks slightly complicated, because there is a short progression of v_2' as well as the long progression of v_1'. In other words, there is a progression of progression. The intensities and frequencies of peaks crowded in the 2270 Å region, those in the 2235 Å region, those in the 2200 Å region, and those in the 2160 Å region are all well explained by considering such a progression of progression. The frequencies $\nu(v_1')$ of the members of this progression of progression are given in the second, third, and forth columns of Table 3. In addition, there are two progressions of weaker bands, whose frequencies $\nu(v_1')$ are given in the fifth and sixth column of Table 3. In the seventh column the frequencies $\nu(v_1')$ of the members of a hot band progression are given. The observed $\nu(v_1')$ values presented in the second, third, and fourth columns of Table 3 can be reprodced by an empirical formula.

$$\nu(v_1') = 702.5v_1' + 5.64(v_1')^2 - 1.0(v_1')(v_2'). \quad (2)$$

The $\nu(v_1')$ values calculated from Eq. (2) with $v_2'=0$ are given in the last column of Table 3. The cal-

7) H. Miyazaki, A. Y. Hirakawa, and M. Tsuboi, unpublished work.

Table 1. Observed peaks of the $\tilde{A}$–$\tilde{X}$ band of *t*-butylamine and their vibrational assignments

Å	cm^{-1}	I_h[a]	Assignment[b]					Å	cm^{-1}	I_h	Assingment				
			v_1'	v_2'	v_3'	v_4'	v_1''				v_1'	v_2'	v_3'	v_4'	v_1''
2434.9	41069	<0.001	0	0	0	0	2	2201.2	45430	0.745	4	0	0	0	0
2397.0	41718	0.040	0	0	0	0	1	2197.1	45515	0.880	3	1	0	0	0
2356.8	42430	0.067	1	0	0	0	1	2194.0	45579	0.782	2	2	0	0	0
2351.2	42531	0.145	0	0	0	0	0	2189.6	45670	0.695	3	0	1	0	0
2312.3	43247	0.375	1	0	0	0	0	2185.6	45754	0.641	3	0	0	1	0
2306.6	43354	0.182	0	1	0	0	0	2174.4	45990	0.635					
2297.2	43531	0.147	0	0	1	0	0	2169.0	46104	0.655					
2290.9	43650	0.155	0	0	0	1	0	2165.0	46189	0.750	5	0	0	0	0
2274.2	43971	0.580	2	0	0	0	0	2161.6	46262	0.890	4	1	0	0	0
2269.8	44056	0.445	1	1	0	0	0	2158.6	46326	0.905	3	2	0	0	0
(2264.0	44170	0.360)	0	2	0	0	0	2155.2	46400	0.850	4	0	1	0	0
2261.0	44228	0.295	1	0	1	0	0	2151.2	46486	0.800	4	0	0	1	0
2254.3	44359	0.275	1	0	0	1	0	2146.7	46584	0.745					
2249.6	44452	0.290						2139.3	46745	0.750					
2244.9	44546	0.318						2135.5	46828	0.750					
2237.8	44687	0.680	3	0	0	0	0	2131.2	46922	0.770	6	0	0	0	0
2233.5	44773	0.719	2	1	0	0	0	2127.2	47010	0.850	5	1	0	0	0
2229.0	44863	0.490	1	2	0	0	0	2124.0	47081	0.900	4	2	0	0	0
2224.9	44946	0.472	2	0	1	0	0	2121.3	47141	0.905	5	0	1	0	0
2219.7	45051	0.423	2	0	0	1	0	2117.7	47222	0.875	5	0	0	1	0
2212.7	45193	0.448						2086.6	47925	0.860	6	0	1	0	0
2209.0	45270	0.482						2083.4	47999	0.860	6	0	0	1	0

a) Peak height

b) Every observed frequency is nearly equal to a calculated frequency, $42531+702.5\,v_1'+5.64\,(v_1')^2+823\,v_2'+1000\,v_3'+1119\,v_4'-813\,v_1''$

Table 2. Observed peaks of the $\tilde{A}$–$\tilde{X}$ band of *t*-butylamine-d_2 and their vibrational assignments

Å	cm^{-1}	I_h[a]	Assignment[b]					Å	cm^{-1}	I_h	Assingment				
			v_1'	v_2'	v_3'	v_4'	v_1''				v_1'	v_2'	v_3'	v_4'	v_1''
2408.3	41523	0.007	0	0	0	0	2	2161.8	46258	0.761	4	0	0	1	0
2372.3	42153	0.023	0	0	0	0	1	2153.9	46427	0.720	*t*-bytyl NHD				
2338.9	42755	0.062	1	0	0	0	1	2149.1	46531	1.177	6	0	0	0	0
2334.9	42828	0.065	0	0	0	0	0	2144.9	46622	0.889	5	1	0	0	0
2306.1	43363	0.135	2	0	0	0	1	2143.2	46659	0.929	5	0	1	0	0
2302.6	43429	0.190	1	0	0	0	0	2133.3	46876	0.923	5	0	0	1	0
2295.5	43563	0.100	0	1	0	0	0	2125.9	47039	0.828	*t*-butyl NHD				
2292.7	43617	0.100	0	0	1	0	0	2120.3	47163	1.188	7	0	0	0	0
2282.1	43819	0.114	0	0	0	1	0	2116.8	47241	1.010	6	1	0	0	0
2270.7	44039	0.398	2	0	0	0	0	2114.5	47293	1.010	6	0	1	0	0
(2264.3	44164	0.207)	1	1	0	0	0	2104.7	47513	0.985	6	0	0	1	0
2261.5	44218	0.217	1	0	1	0	0	2091.8	47806	1.130	8	0	0	0	0
2251.1	44423	0.223	1	0	0	1	0	2089.2	47865	1.088	7	1	0	0	0
2239.1	44661	0.683	3	0	0	0	0	2086.7	47923	1.042	7	0	1	0	0
(2233.9	44765	0.370)	2	1	0	0	0	2076.9	48149	1.008	7	0	0	1	0
2231.2	44819	0.400	2	0	1	0	0	2063.6	48459	1.030	9	0	0	0	0
2220.2	45041	0.382	2	0	0	1	0	2062.0	48497	1.045	8	1	0	0	0
2208.5	45280	0.890	4	0	0	0	0	2059.3	48560	1.007	8	0	1	0	0
(2203.7	45378	0.555)	3	1	0	0	0	2050.0	48780	0.935	8	0	0	1	0
2201.1	45432	0.595	3	0	1	0	0	2035.2	49135	0.932	10	0	0	0	0
2190.9	45643	0.580	3	0	0	1	0	2030.9	49239	0.890	9	1	0	0	0
2183.2	45804	0.590	*t*-butyl NHD					2024.2	49402	0.840	9	0	0	1	0
2178.5	45903	1.063	5	0	0	0	0	2008.3	49793	0.790	11	0	0	0	0
(2173.8	46002	0.750)	4	1	0	0	0	2005.6	49860	0.775	10	1	0	0	0
2172.0	46041	0.810	4	0	1	0	0								

a) Peak height

b) Every observed frequency is nearly equal to a calculated frequency, $42828+601.1\,v_1'+2.70\,(v_1')^2+735\,v_2'+789\,v_3'+991\,v_4'-675\,v_1''$

Table 3. Vibrational frequencies in the long progressions of v_1' of *t*-butylamine in $\tilde{A}$ state

			obs[b]				calc[c]
v_1''(813)[a]	0	0	0	0	0	1	0
v_2'(823)	0	1	2	0	0	0	0
v_3'(1000)	0	0	0	1	0	0	0
v_4'(1119)	0	0	0	0	1	0	0
v_1'=0	0	0	0	0	0	0	0
1	716	702	693	697	709	712	708
2	1440	1419	1409	1415	1401		1428
3	2156	2161	2156	2139	2104		2158
4	2899	2908	2911	2869	2836		2903
5	3658	3656		3610	3572		3654
6	4391			4394	4349		4418

a) The values of v_1'', v_2', v_3', and v_4' are given in parentheses (in cm^{-1}).
b) $v(v_1')$ given by Eq. (1).
c) Calculated values by Eq. (2).

Table 4. Vbrational frequencies in the long progressions of v_1' of *t*-butylamine-d_2 in $\tilde{A}$ state (See Text)

			obs[b]			calc[c]
v_1'(675)[a]	0	0	0	0	1	0
v_2'(735)	0	1	0	0	0	0
v_3'(789)	0	0	1	0	0	0
v_4'(991)	0	0	0	1	0	0
v_1'=0	0	0	0	0	0	0
1	601	601	601	604	602	604
2	1211	1202	1202	1222	1211	1213
3	1833	1815	1815	1824		1828
4	2452	2439	2424	2439		2448
5	3075	3059	3042	3057		3073
6	3703	3678	3676	3694		3704
7	4335	4302	4306	4330		4340
8	4978	4934	4943	4961		4982
9	5631	5572	5622	5583		5629

a) The values v_1', v_2', v_3', and v_4' are given in parentheses (in cm^{-1}).
b) $v(v_1')$ given by Eq. (1).
c) Calculated values by Eq. (3).

culated values are in an agreement not only with the observed values of the main progression, but also with those of the two progressions of v_2' progression, because the cross term between v'_1 and v_2', ($x_{12}=-1.0$) is negligibly small. The cross terms (x_{13} and x_{14}) between v_1' and v_3' and between v_1' and v_4' are considered to be a little larger than x_{12}. They are estimated to be -7.5 and -13 respectively.

The vibrational structure of the band of the deuterated species $(CH_3)_3CND_2$ is simpler. There is a main progression whose members are markedly strong and easily picked out. Their frequencies are given in the second column of Table 4. Three other progressions of weak bands, whose frequencies are given in the third, fourth, and fifth columns of Table 4, are also easily found out. In the sixth column of Table 4, the frequencies $v(v_1')$ of the members of a hot progression are given. The observed $v(v_1')$ values of the main progression (second column of Table 4) can be reproduced by an empirical formula

$$v(v_1') = 601.1v_1' + 27.0(v_1')^2. \quad (3)$$

The $v(v_1')$ values calculated from Eq. (3) are given in the last column of Table 4. The cross terms x_{12}, x_{13}, and x_{14} are estimated to be -4.4, -4.5, and -14 respectively.

Amino Wagging Potential for the Upper State

The energy value of the vibronic levels for the upper state of the main progression is now found to be expressed in the form

$$\nu = \nu_e + \omega_1\left(v_1'+\frac{1}{2}\right) + x_{11}\left(v_1'+\frac{1}{2}\right)^2. \quad (4)$$

On the basis of the empirical formula (2) and (3), ν_e= 41771, ω_1=696.9, and x_{11}=5.64 cm^{-1} for the undeuterated species and ν_e=42528, ω_1=598.4, and x_{11}=2.70 cm^{-1} for the deuterated species. The frequency appearing in the main progression (with the suffix 1) is assigned to the amino wagging vibration. This assignment is based upon its frequency (696.9 cm^{-1}), the isotope effect on its frequency (598.4 cm^{-1} for the ND_2 compound), and the character of the electronic band now in question. The band is considered to be caused by a transition in which one of the lone pair electrons on the nitrogen atom is taken up from its original orbital onto the 3*s* orbital of the nitrogen atom.[8] For such a transition, the most pronounced change in the geometrical structure of the molecule is expected

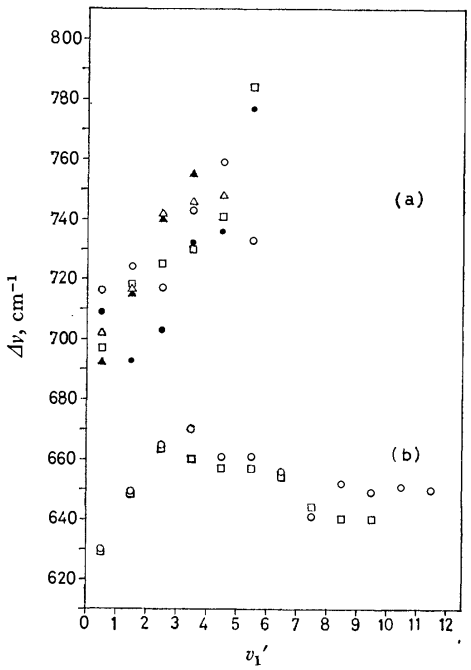

Fig. 4. Spacing of the adjacent vibronic bands in the progression of the amino wagging vibration in the $\tilde{A}$-$\tilde{X}$ band plotted against the vibrational quantum number v_1' for this vibration. (a) For $(CH_3)_3CNH_2$, ○ (for the main progression), △(for the v_2'=1 progression), ▲(for the v_2'=2 progression), □(for the v_3'=1 progression) and ●(for the v_4'=1 progression). (b) For CH_3NH_2, ○(for the main progression) and □(for the v_2'=1 progression).

8) K. S. Mulliken, *J. Chem. Phys.*, **3**, 506 (1935).

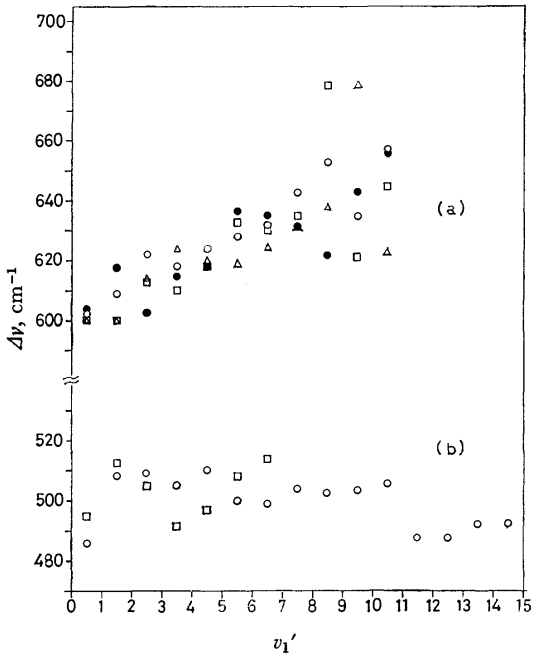

Fig. 5. Similar plotting to that in Fig. 4 for (a) $(CH_3)_3CND_2$ and (b) CH_3ND_2. For (a), ○(for the main progression), △(for the $v_2'=1$ progression), □(for the $v_3'=1$ progression) and ●(for the $v'_4=1$ progression). For (b), ○(for the main progression) and □(for the $v_2'=1$ progression).

to take place along the amino wagging coordinate, as in the case of methylamine.[1] Therefore, the amino wagging vibration is expected to form the main progression in the vibrational structure of the band. Thus, Eq. (4) is regarded to give the energy levels of the amino wagging vibration of the *t*-butylamine molecule in the $\tilde{A}$ electronic state. It is noteworthy that the interval of the adjacent levels increases with increasing v_1'. In this respect, *t*-butylamine is similar to ammonia,[9] but it presents a contrast to methylamine, for which the interval is almost independent of v_1'. This contrast is demonstrated in Figs. 4 and 5. This fact indicates that the potential function along the amino wagging coordinate involves a positive quartic term for *t*-butylamine, whereas the function is nearly harmonic for methylamine.[1]

Let us now assume that the potential function along the amino wagging coordinate, θ (the external angle between the HNH plane and the C–N bond), has the form,

$$hcV = \frac{1}{2}k\theta^2 + j\theta^4. \tag{5}$$

The potential constant k and j are related to the observed ω_1 and x_{11} as

$$\omega_1 = \frac{1}{2\pi c}\sqrt{\frac{k}{\mu}} \tag{6}$$

and

$$x_{11} = \frac{3h^2}{32\pi^4\omega_1{}^2\mu^2c^2}\,\frac{j}{hc} \tag{7}$$

where μ is the reduced moment of inertia (amu·Å^2), h the Planck's constant, and c the light velocity. A transformation, leads to the potential function,

$$Q = \sqrt{\mu}\theta, \quad (\text{in amu}^{1/2}\text{Å}) \tag{8}$$

leads to the potential function,

$$hcV = \frac{1}{2}KQ^2 + JQ^4, \tag{9}$$

where

$$K = k/\mu^2 \tag{10}$$

and

$$J = j/\mu^2. \tag{11}$$

By the use of the observed values of ω_1 and x_{11}, we obtain the potential functions,

$$V(\text{cm}^{-1}) = 7200Q^2 + 1610Q^4 \quad \text{for } (CH_3)_3CNH_2 \tag{12}$$

and

$$V(\text{cm}^{-1}) = 5310Q^2 + 567Q^4 \quad \text{for } (CH_3)_3CND_2. \tag{13}$$

The potential fuction for the excited state of *t*-butylamine -d_2 is shown graphically in Fig. 6 (a).

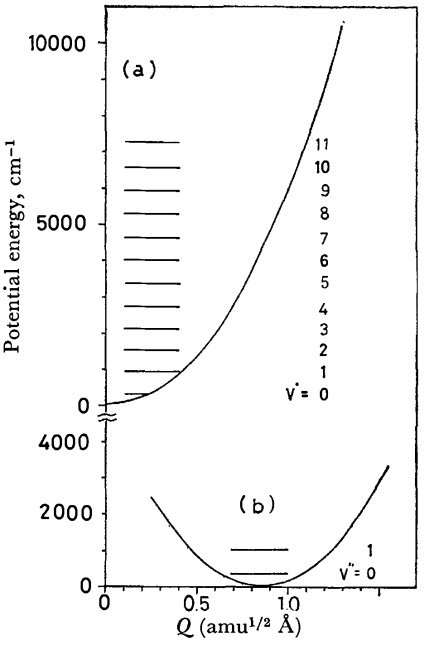

Fig. 6. Potential functions and vibrational energy levels of the amino wagging vibration of *t*-butylamine-d_2. (a) in the first excited electronic state $\tilde{A}$ and (b) in the ground state $\tilde{X}$.

Position of the Potential Minimum in the Lower State

The amino-wagging potential just described indicates that the *t*-butylamine molecule in the upper state has a planar amino group in its equilibrium conformation. It is probable, on the other hand, the amino group of *t*-butylamine is pyramidal in its ground electronic state as it is usually so in any aliphatic primary amine. In other words, the potential minimum in the lower state is considered to be greatly shifted along the amino wagging coordinate from that in the upper state as is shown in Fig. 6. The amount of shift (or the position of the potential minimum in the ground state, Q_{min}) can be estimated from the intensity distribution among the members of each of the progressions mentioned above.

Thus, according to the Franck-Condon principle, the

9) A. D. Walsh and P. A. Wasrop, *Trans. Faraday Soc.*, **57**, 345 (1961).

integrated intensity I of each vibronic band $v'\leftarrow v''$ is given by

$$I = \int \varepsilon(\nu)\mathrm{d}\nu = (8\pi^2 N\nu_{v'\leftarrow v''}/3\boldsymbol{h}c)\,|R_e|^2|S_{v'v''}|^2, \quad (14)$$

where N is the population in the lower state, R_e is the electronic transition moment of the band in question, and $S_{v',v''}$ is the overlap integral,

$$S_{v'v''} = \langle\phi_{v'}(Q)\cdot\phi_{v''}(Q)\rangle, \quad (15)$$

in which $\phi_{v'}$, (Q) and $\phi_{v''}(Q)$ are the vibrational eigenfunctions of the upper and lower states, respectively. In an approximation, both of these vibrational eigenfunctions are assumed to be those of harmonic oscillators, so that

$$\phi_{v'}(Q) = N_{v'}\exp[-(\gamma'/2)Q^2]H_{v'}(\sqrt{\gamma'}Q) \quad (16)$$

and

$$\phi_{v''}(Q) = N_{v''}\exp[-(\gamma''/2)(Q-Q_{\min})^2] \times H_{v''}[\sqrt{\gamma''}(Q-Q_{\min})]. \quad (17)$$

Here, $N_{v'}$ and $N_{v''}$ are the normalization factors, $\gamma' = 4\pi^2\omega'/\boldsymbol{h}$, and $\gamma'' = 4\pi^2\omega''/\boldsymbol{h}$. ω' and ω'' are the harmonic frequencies of the amino wagging vibrations in the upper and lower states respectively. In Eq. (14), all the fraction except $|S_{v'v''}|^2$ in the expression of the integrated intenisty are considered to be practically independent of v'. We therefore calculated $|S_{v'v''}|^2$ as a function of v' by the use of various assumed values of $Q_{\min}$, and compared the results with the observed intensities.

The relative value of absorbance determined at the peak of each vibronic band is given in Tables 1 and 2. In determining the intensities of the bands from these values a possibility of the superposition of the absorptions caused by the second electronic transition $\tilde{B}\leftarrow\tilde{X}$ must be taken into account. In each of Figs. 1 and 2, is shown by a line (b) what is considered to be the upper limit of such background absorption. In other words, the background absorption is considered to be some where between the lines (a) and (b) in Fig. 1 or 2. By subtracting this background absorption from the observed peak height, we can estimate the peak intensity of each band. The integrated intensity is considered to be proportional to the square of the peak intensity because each vibrational band should have the similar rotational structure, therefore, it has a similar contour to another.

The integrated intensities of the members of the v_1'-progressions, thus estimated, are given in Figs. 7 and 8. Each vertical line indicates a range of ambiguity caused by the difficulty of estimating the background absorption, and each range given by the line coresponds to the range (a) to (b) of the background absorption (Figs. 1 and 2).

In Figs. 7 and 8, are also shown the calculated intensities, *i.e.* the calculated values of $|S_{v'v''}|^2$ for a few different assumed values of $Q_{\min}$. The calculations were made by the use of a HITAC 5020E computer in the Computer Centre of the University of Tokyo. A comparison of the observed and calculated intensities indicates that $Q_{\min}=0.65\pm0.05$ amu$^{1/2}$ Å for $(CH_3)_3CNH_2$ and $Q_{\min}=0.85\pm0.05$ amu$^{1/2}$ Å for $(CH_3)_3CND_2$.

An estimation of the $Q_{\min}$ value can also be made

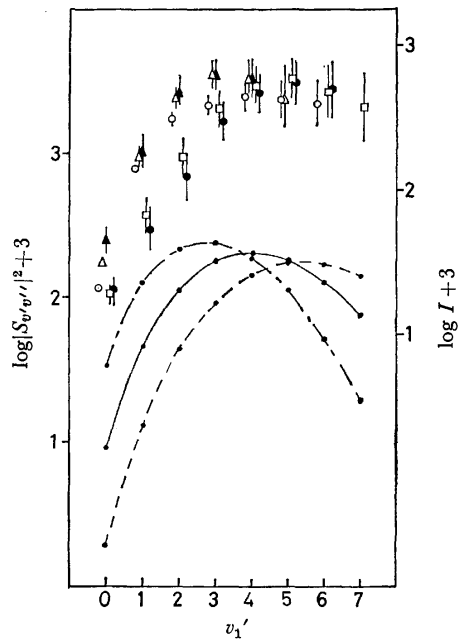

Fig. 7. The relative intensities of the vibronic bands in the progression of the amino wagging vibration of $(CH_3)_3CNH_2$, plotted against the vibrational quantum number v_1'. The points connected with curves represent the calculated values for $Q_{\min}=0.75$ amu$^{1/2}$ Å (---), for $Q_{\min}=0.65$ amu$^{1/2}$ Å (—) and for $Q_{\min}=0.55$ amu$^{1/2}$ Å (—·—·). The observed integrated intensities are shown by ○(for the main progression), △(for the $v_2'=1$ progression), ▲(for the $v_2'=2$ progression), □(for the $v_3'=1$ progression) and ●(for the $v_4'=1$ progression). The vertical line indicates the range of ambiguity of the observed intensity, which corresponds to the range of the background absorption defined by (a) and (b) in Fig. 1.

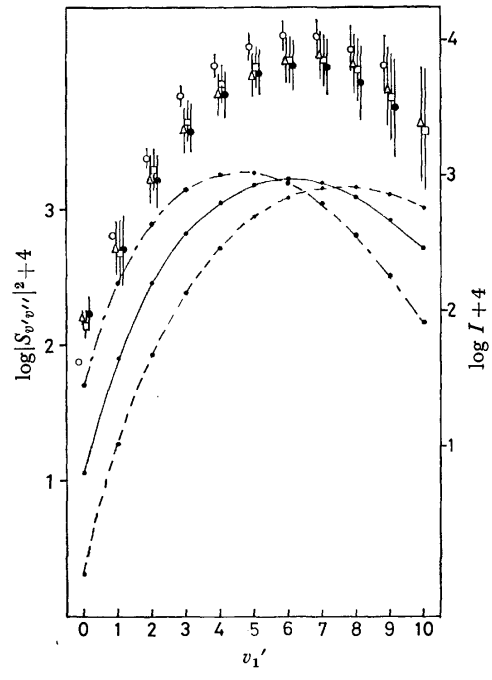

Fig. 8. Similar plotting to that in Fig. 7 for $(CH_3)_3CND_2$. The calculated values for $Q_{\min}=0.95$ amu$^{1/2}$ Å (---), for $Q_{\min}=0.85$ amu$^{1/2}$ Å (—) and for $Q_{\min}=0.75$ amu$^{1/2}$ Å (—·—·) are shown. The observed integrated intensities are shown by ○(for the main progression), △(for the $v_2'=1$ progression), □(for the $v_3'=1$ progression), and ●(for the $v_4'=1$ progression).

from the observed integrated intensity ratio (R) of the $(v'=1)\leftarrow(v''=1)$ band *versus* $(v'=0)\leftarrow(v''=0)$ band or of the $(v'=2)\leftarrow(v''=1)$ band *versus* $(v'=1)\leftarrow(v''=0)$ band. In general, a pair of bands $(v'+1)\leftarrow 1$ and $(v')\leftarrow 0$ come close to each other, and therefore in estimating the intensity ratio (R) of these bands the ambiguity caused by the background absorption is relatively small. On the other hand, the intensity ratio R should be sensitive to the $Q_{\min}$ value. A calculation has been made of the theoretical values of R for a few assumed values of $Q_{\min}$ by the use of Eqs. (15), (16), and (17). In Figs. 9 and 10, the observed and calculated intensity ratios (R) of such pairs of bands are given. In comparison, it is shown again that $Q_{\min}=0.65$ amu$^{1/2}$ Å for $(CH_3)_3CNH_2$ and $Q_{\min}=0.85$ amu$^{1/2}$Å for $(CH_3)_3CND_2$.

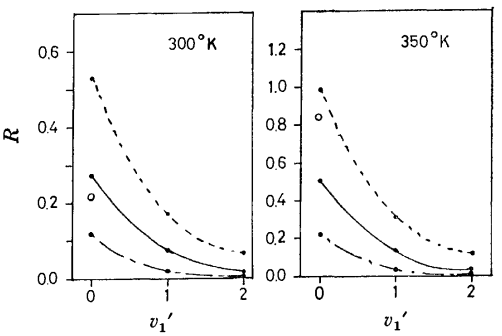

Fig. 9. Intensity ratio of the $v_1'\leftarrow 0$ band *versus* $v_1'+1\leftarrow 1$ band of *t*-butylamine plotted against v_1' at 300 and 350°K. The points connected with curves represent the calculated values for $Q_{\min}=0.75$ amu$^{1/2}$ Å (---), for $Q_{\min}=0.65$ amu$^{1/2}$ Å (—), and for $Q_{\min}=0.55$ amu$^{1/2}$ Å (—·—·). Circles represent the observed values.

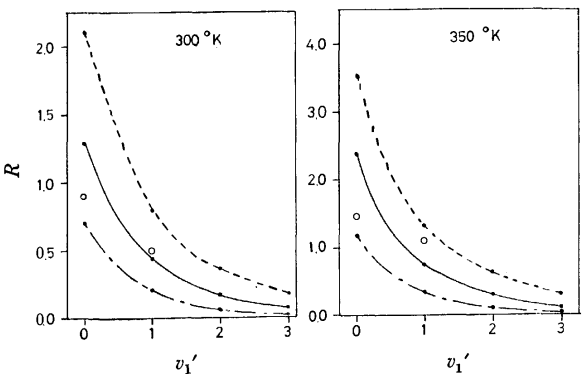

Fig. 10. Intensity ratio of the $v_1'\leftarrow 0$ band *versus* $v_1'+1\leftarrow 1$ band of *t*-butylamine-d_2 plotted against v_1' at 300 and 350°K. The points, connected with curves, represent the calculated values for $Q_{\min}=0.95$ amu$^{1/2}$ Å (---), for $Q_{\min}=0.85$ amu$^{1/2}$ Å (—) and for $Q_{\min}=0.75$ amu$^{1/2}$ Å (—·—·). Circles represent the observed values.

Discussion

From our analysis of the bands, an amount of information has now been obtained on the potential function along the amino wagging coordinates of upper and lower states of *t*-butylamine and *t*-butylamine-d_2. The values of potential constants obtained are given in Table 5.

The position of potential minimum in the ground state has been estimated to be at $Q=0.65\pm0.05$ and 0.85 ± 0.05 amu$^{1/2}$ Å respectively for $(CH_3)_3CNH_2$ and $(CH_3)_3CND_2$. These values are equal to the corresponding values (0.655 and 0.845 amu$^{1/2}$ Å, respectively) of methylamine.[4] If we know the reduced moment of inertia μ we can estimate the equilibrium angle θ by Eq. (8). Let us assume that the value of μ is equal to the inverse of the diagonal element of the G matrix (inverse kinetic energy matrix) corresponding to the wagging coordinate of the planar amino group. Then $\mu=0.540$ amu Å^2 for $(CH_3)_3CNH_2$ and $\mu=0.885$ amu Å^2 for $(CH_3)_3CND_2$. With these values of μ, the equilibrium θ value should be $50.7\pm4°$ for $(CH_3)_3CNH_2$ and $51.7\pm3°$ for $(CH_3)_3CND_2$. Both of these are practically equal to the known value of θ (=51.3°) of methylamine.[2] Thus, the equilibrium conformation of the amino group for *t*-butylamine in the ground state is now found to be quite similar to that for methylamine.

Table 5. Estimated potential constants of amino wagging motion for *t*-butylamine and *t*-butylamine-d_2 in $\tilde{X}$ and $\tilde{A}$ electronic state

$(CH_3)_3CNH_2$		
	ground ($\tilde{X}$)	excited($\tilde{A}$)
ν_1(cm^{-1})	813	702.$_5$
ω_1(cm^{-1})	—	696.$_9$
x_{11}(cm^{-1})	—	5.6$_4$
$Q_{\min}$(amu$^{1/2}$Å)	0.65±0.05	0
θ(degree)	50.$_7$°±4°	0
$(CH_3)_3CND_2$		
	ground ($\tilde{X}$)	excited ($\tilde{A}$)
ν_1(cm^{-1})	675	601.$_1$
ω_1(cm^{-1})	—	598.$_4$
x_{11}(cm^{-1})	—	2.7$_0$
$Q_{\min}$(amu$^{1/2}$Å)	0.85±0.05	0
θ(degree)	51.$_7$°±3°	0

The potential function in the upper state for *t*-butylamine, on the other hand, has been found to be somewhat different from that for methylamine. As has been demonstrated in Figs. 4 and 5, the potential function is nearly harmonic in methylamine, while in *t*-butylamine the potential rises up more steeply as the wagging angle of the amino group increases. As a possible cause of the difference it may be proposed to consider the repulsive force between the bulky *t*-butyl group and the amino group. To test this proposal, a calculation of the repulsive potential has been made for various positions (θ) of the amino group in both of these amines on the basis of a probable set of bond lengths and bond angles and on the basis of potential functions for the non-bonded C···H and H···H atom pairs given by Hendrickson[10] or those given by Bartell.[11] The result indicated that at least a part of the observed difference is explained by the extra repulsive potential caused by the bulkiness of the *t*-butyl group.

Lastly, a brief discussion will be made of the observed vibrational frequencies of the undeuterated and deu-

10) J. B. Hendrickson, *J. Chem. Soc.*, **83**, 4537 (1961).
11) L. S. Bartell, *J. Chem. Phys.*, **32**, 827 (1960).

terated *t*-butylamines in the excited states. The frequency 1000 cm^{-1} of the former is considered to correspond to the frequency 991 cm^{-1} of the latter, and 1119 cm^{-1} to 789 cm^{-1}. The two frequencies 697 and 823 cm^{-1} of the undeuterated species are considered to be caused by a strong vibrational coupling. The intrinsic amino wagging frequency of the undeuterated species should be 765 cm^{-1} if it is 598 cm^{-1} in the deuterated compound. This vibration may couple with the 735 cm^{-1} vibration and may split into the 697 and 823 cm^{-1} vibrations. It is probable that the 735 cm^{-1} vibration which takes place in both deuterated and undeuterated molecules is a skeletal stretching vibration on the basis of a normal vibration calculation of isobutane[12] and of a comparison with the frequencies of *t*-butylfluoride (750 cm^{-1}),[13] *t*-butylalcohol (748 cm^{-1}) and *t*-butylalcohol-d (744 cm^{-1}).[14]

12) H. Takahashi, *Nippon Kagaku Zasshi*, **83**, 799 (1962).
13) D. E. Mann, N. Acquista, and D. R. Lide, Jr., *J. Mol. Spectrosc.*, **2**, 575 (1958).
14) C. Tanaka, *Nippon Kagaku Zasshi*, **81**, 1042 (1960).

BULLETIN OF THE CHEMICAL SOCIETY OF JAPAN, VOL. 45, 764—769(1972)

Laser Photolysis Studies on the Formation of Solvated Ion Radicals in the Pyrene—*N,N*-Dimethylaniline System in Various Solvents

Yoshio TANIGUCHI, Yasuzo NISHINA, and Noboru MATAGA*

Department of Chemistry, Faculty of Engineering Science, Osaka University, Toyonaka, Osaka

(Received August 27, 1971)

Formation of solvated ion radicals in the pyrene-*N,N*-dimethylaniline (DMA) system (which is a typical one showing heteroexcimer (HE) fluorescence) in various solvents has been studied by means of the laser photolysis and transient photoconductivity as well as transient absorption measurements. Ion radical formation due to the encounter collision between an excited pyrene and DMA in moderately as well as in strongly polar solvents has been established. This result is quite important in explaining the experimentally observed relation between the solvent dependent HE fluorescence quantum yield and decay time.

In relation to the electron transfer mechanism of fluorescence quenching in solution, somewhat detailed studies concerning the solvent effects on the HE fluorescence have been carried out.[1,2] According to those investigations, the fluorescence yield as well as fluorescence decay time of HE decrease as the solvent polarity is increased, where the solvent dependence of the fluorescence yield is much stronger than the decay time. One of the present authors (N.M.)[1] has interpreted this result as due to the decrease of the radiative transition probability and the increase of the radiationless transition probability of HE as the solvent polarity is increased. On the other hand, Weller and coworkers[2] have proposed an alternative interpretation for this phenomenon. They assumed the competition of the following two processes for an aromatic hydrocarbon (acceptor) and an aromatic amine (donor) system

$$A^* + D \xrightarrow{k_C} (A^- \cdot D^+)^*$$

$$A^* + D \xrightarrow{k_I} (A_s^- \cdots D_s^+)$$

where $(A^- \cdot D^+)^*$ is the fluorescent HE and $(A_S^- \cdots D_S^+)$ represents solvent-shared ion-pair which is non-fluorescent. It is assumed that the rate of process k_I increases with the increase of the solvent polarity, while process k_C is independent of the solvent polarity.

In order to examine the validity of the assumption of the existence of the non-fluorescent ion-pair state in a solvent which is not very polar, we have undertaken nsec laser photolysis studies on aromatic hydrocarbon-amine system in various solvents. If the dissociation of the ion-pair $(A_S^- \cdots D_S^+)$ into the solvated ion radicals $(A_S^- + D_S^+)$ occurs to some extent in a solvent which is more or less polar, it may be possible to confirm the existence of the dissociated ions by means of the nsec laser photolysis and conductivity measurements. Of course, it may be also possible to observe the non-fluorescent ion-pair and/or the solvated ion radicals by means of the nsec laser photolysis and the measurement of absorption spectra of ions as well as time variations of absorption intensities. However, the sensitivity of the detection by photoconductivity measurements may be higher than that by the absorption spectral measurements. Accordingly, the method of the nsec laser photolysis and conductivity measurement appears to be quite suitable for the detection of ion radicals of rather small concentration in the solvent which is not very polar.

In the following, we show the results of our measurements on the ion radical formation in the pyrene-*N*, *N*-dimethylaniline (DMA) system in various solvents with different polarities.

Experimental

We have used a Q-switched ruby laser (Japan Electron Optics, JLR-O2A) with the out-put power of about 1.5 joule.

* To whom the correspondence should be addressed.

1) N. Mataga, T. Okada, and N. Yamamoto, *Chem. Phys. Lett.*, **1**, 119 (1967).

2) H. Knibbe, K. Röllig, F. P. Schäfer, and A. Weller, *J. Chem. Phys.* **47**, 1184 (1967).

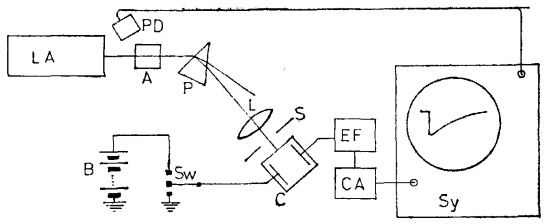

Fig. 1. Schematic diagram of the apparature for the transient photoconductivity measurement. LA: Q-switched ruby laser, PD: photo-diode, A: ADP frequency doubler, P: prism for separating the 694 and 347 nm beams, L: lense, S: slit, C: cuvette, B: battery, SW: switch, EF: emitter follower amplifier, CA: cascade amplifier type CA-2, Sy: Tektronix 585A oscilloscope.

The exciting light pulse of 347 nm was produced through the ADP frequency doubler with conversion efficiency of about 8%. The light pulse has a duration of 15—20 nsec.

The optical arrangement for the photocurrent measurments is shown in Fig. 1. The position of the quartz cuvette for the measurement of photocurrents or transient spectra was settled by using the light beam of a He-Ne gas laser which reproduced the optical path of 347 nm pulse. The optical path of the 347 nm beam was recorded by burned spots on coloured paper produced by irradiating with the 347 nm pulse.

The quartz cuvette for the photocurrent measurments contains two 9 mm × 10 mm Ni plate electrodes spaced each other by 7 mm. The direct irradiation on the electrodes was avoided by putting an optical slit on the front face of the cuvette. The supplied D.C. voltage between electrodes was adjusted in the range from 90 V to 540 V. Current signal obtained was converted to voltage signal through a 50Ω resister or home-made emitter follower amplifiers, the frequency characteristics of which covered the range from about 2 kHz to 150 MHz. The input impedance of our emitter followers was 13.2, 4.12, and 0.887 kΩ, respectively. Some weaker signals of photocurrent were measured by using Iwatsu cascade amplifier type CA-2. The time constant of the electronic circuit was less than 5 nsec when a 50Ω resister was used. In the other cases where the amplifiers were used, the time constant of the electronic circuit increased because of stray capacities of the cuvette and cables. The DC dark current was omitted by using the AC coupling of an emitter follower as well as the AC coupling of an input of Tektronix 585 A oscilloscope. For examining the effect of the exciting light intensity on the photocurrent, the intensity of the laser pulse was varied by using neutral filters composed of wire gauzes.

Transient absorption spectra of ion radicals produced by laser photolysis were measured by means of the methods explained in detail elsewhere.[3] The absorption spectra of ion radicals were photographed by using laser breakdown sparks in O_2 and Xe gases as spectroflashes. On the other hand, the spectra as well as time variations of their intensities were measured by using a Xe flash lamp as a monitoring light source.

Acetonitrile was refluxed repeatedly over phosphorus pentoxide, distilled into potassium carbonate and fractionally distilled. Merck spectrograde *n*-hexane, toluene, ethylether, monochlolobenzene, ethylene dichloride, methylethylketone, and acetone were used without further purification. Pyrene was chromatographed on activated alumina and silica gel, and extensively zone-refined. DMA was refluxed with acetic anhydride, washed with water, dried over potassium hydroxide, and distilled in vacuum several times. All the solutions measured were deaerated completely by repeated freeze-pump-thaw cycles.

Results and Discussion

Generally speaking, the photocurrent density may be given by,

$$i(t) = \sum_j z_j e n_j(t) \mu_j E_{eff} \quad (1)$$

where $z_j e$, μ_j and $n_j(t)$ represent an electric charge, the mobility of j-th carrier and its number in unit volume, respectively. E_{eff} is an effective electric field working on the carriers.

In the case of three compoment system of pyrene-DMA-solvent, the charge carriers may be mainly pyrene anions and DMA cations. We have confirmed the simultaneous production of these anions and cations by means of the laser photolysis and the measurement of the transient absorption spectra. For example, the spectra observed in acetonitrile and pyridine are indicated in Fig. 2 where the absorption bands appearing in the region from 440 to 510 nm can be ascribed to those of pyrene anion and DMA cation and those around 400 nm are due to the T-T absorption of pyrene.[4]

The effective electric field may be given by, $E_{eff} = E_{app}/\varepsilon$, where E_{app} is an applied electric field and ε is

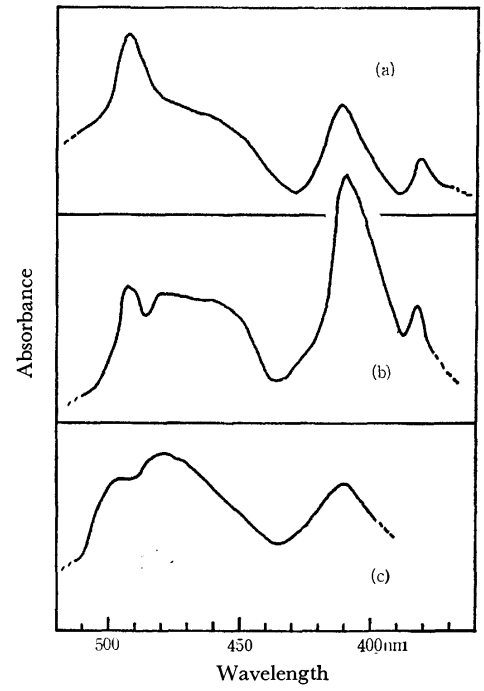

Fig. 2. Transient absorption spectra measured photographically by using laser break down sparks in O_2 and Xe gas.
[Pyrene] = 5×10^{-4} M, [DMA] = 8×10^{-2} M
(a) acetonitrile solution. O_2 spark.
(b) acetonitrile solution. Xe spark.
(c) pyridine solution. O_2 spark.

3) H. Masuhara, M. Shimada, N. Tsujino, and N. Mataga, This Bulletin, to be published.

4) T. Okada, H. Oohari, and N. Mataga, This Bulletin, **43**, 2750 (1970).

the static dielectric constant of solution. Accordingly, Eq. (1) can be reduced to the following.

$$i(t) = en(t)(\mu_{\text{anion}}+\mu_{\text{cation}})E_{\text{app}}/\varepsilon \qquad (2)$$

For the actual evaluation of the concentrations of produced ions in various solvents from the observed photocurrent, the value of the mobility of ion radicals in each solvent is necessary. Because the concentration of ions is rather low, we assume here that the mobility is independent of the ion concentration and is inversely proportional to the viscosity η of the solvent.[5] Then, the concentration of ions may be proportional to the product of (photocurrent) $\times\eta\times\varepsilon$.

In the case of the three component system, the ion radicals may be produced by the encounter collision between A* and D, and the produced ions may decay mainly due to the recombination reaction, *i.e.* electron transfer from anion to cation. Since the concentration of DMA in the present study is approximately 10^{-2}—10^{-1} M, the formation of ion radicals seems to occur very rapidly during nsec time region. Actually, we have confirmed that the formation of ion radicals is quite rapid and the rise curve of the photocurrent is the same as that of a time-integrated function of a 347 nm pulse. As an example, the rise curve of photocurrent and that of the optical absorption at 493 nm (pyrene anion) of the pyrene-DMA-acctonitrile system are indicated in Fig. 3 together with the shape of an exciting light pulse.

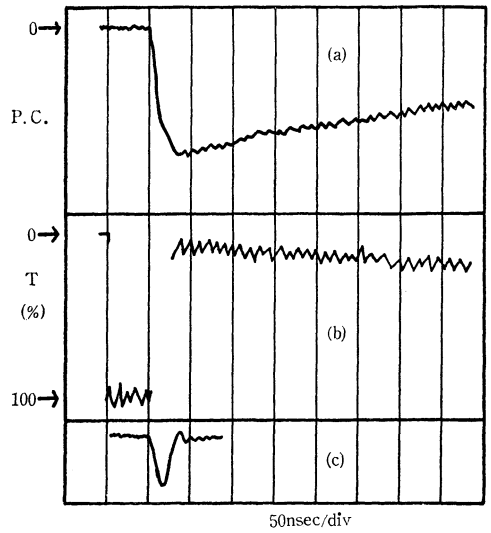

Fig. 3. The rise curve of photocurrent and that of the optical absorption of pyrene anion in the case of pyrene-DMA-acetonitrile system. Concentrations of pyrene and DMA are the same as those in Fig. 2.
(a) photocurrent. (b) transmittance at 493 nm. (c) shape of an exciting light pulse.

Since the concentration of the produced ion radicals may be rather small, the rate of the disappearance of ions due to the recombination reaction will be much slower compared to the rate of their production. We have confirmed that the photocurrent as well as the absorbance due to the ions decay slowly during times

5) J. O'M. Bockris and A. K. N. Reddy, "Modern Electrochemistry," Vol. 1, Plenum Press, New York (1970).

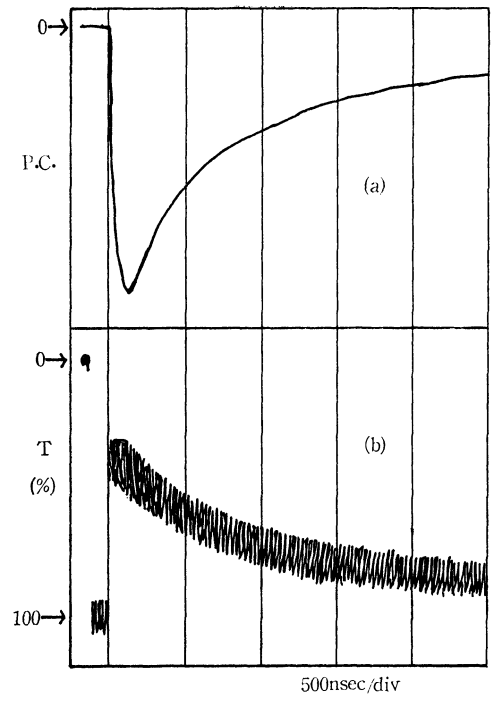

Fig. 4. The decay process of ions in the case of pyrene-DMA-acetone system. Concentrations of pyrene and DMA are the same as those of Fig. 2
(a) photocurrent (b) transmittance at 493 nm.

of μsec. As an example, the observed results for pyrene-DMA-acetone system are shown in Fig. 4.

If the decay of ions is mainly due to the bimolecular reaction between the acceptor anion and the donor cation radicals, both of the reciprocal of the photocurrent and that of the absorbance due to the ions should be proportional to time. This requirement is well satisfied as it is indicated in Fig. 5 for the same system as in Fig. 4. The difference in the slope between (a) and (b) in Fig. 5 can be ascribed to the difference in the initial concentrations of produced ions.

Now, because the formation of ion radicals is quite

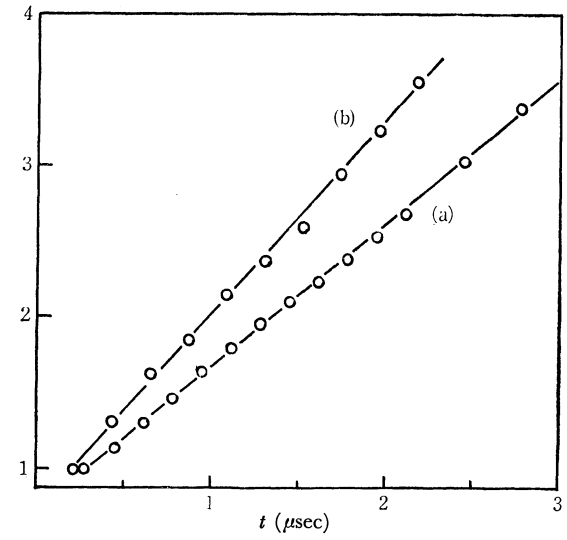

Fig. 5. The reciprocal of the photocurrent *vs.* time relation (a) and the reciprocal of the absorbance *vs.* time relation (b). The same system as indicated in Fig. 4.

rapid while they decay slowly during times of μsec as it is described above, the value of the peak photocurrent obtained immediately after the excitation appears to be proportional to the concentration of dissociated ions. However, there is another problem to be taken into account for the evaluation of ion concentrations in various solvents. Since the light pulse in the present work is fairly strong, it may be possible that the ionization of pyrene due to the double photon absorption occurs and that we are observing the photoconductivity due to pyrene cations and solvated electrons. In order to examine this problem, we have investigated the effect of the exciting light intensity on the peak photocurrent. As an example, the result for pyrene-DMA-acetonitrile system is indicated in Fig. 6, from which one can see that the ionic dissociation in this case is a one photon process. Therefore, in these systems of pyrene-DMA-solvent, the most predominant process leading to the photoionization appears to be the encounter collision between DMA and excited pyrene molecule followed by one electron transfer from DMA to pyrene.

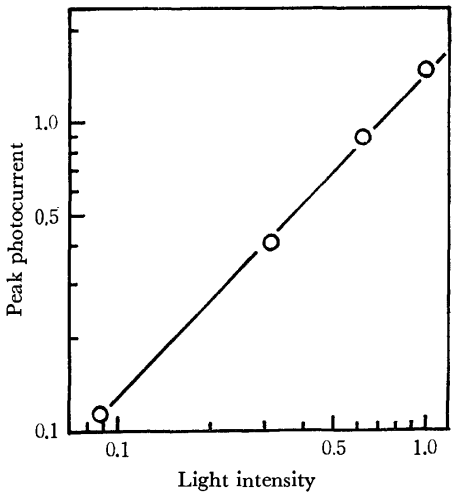

Fig. 6. The effect of exciting light intensity on the peak photocurrent of pyrene-DMA-acetonitrile system. Concentrations of pyrene and DMA are the same as those of Fig. 2, respectively.

In the actual experimental measurements, we have checked not only the photocurrent of the pyrene-DMA system in a solvent but also that of the two component system, pyrene or DMA in the same solvent, as well as that of the pure solvent. We have confirmed that the laser induced photoconductivity of a DMA-solvent system and also that of the pure solvent are negligibly small compared with that of the pyrene-DMA system in the same solvent. However, the photocurrent of pyrene-solvent two component system was not negligible compared with that of the three component system, especially in the case of less polar solvent. For example, the observed value of photocurrent of pyrene-acetonitrile system was *ca.* 5% of that of pyrene-DMA-acetonitrile system. The percentage of the photocurrent of pyrene-solvent system to that of the corresponding three component system becomes larger as the dielectric constant of solvent is decreased. Namely, it is 10% in acetone and pyridine, 30% in methylene dichloride, 50% in monochlorobenzene, and almost 100% in ethylether. These results indicate that the photoionization of pyrene-DMA-solvent system is affected by the solvent polarity more strongly than that of pyrene-solvent two component system.

The laser induced ionization of two component system is not limited to the case of pyrene-solvent systems. Although the details of our studies on the laser induced ionization of various aromatic molecules in organic solvents will be published elsewhere, some fundamental points will be given here.

According to our investigations, this photoionization is mainly caused by a biphotonic process which is a direct two quantum absorption by the ground state to give a high energy state which ionizes. Our studies have indicated further that the photoionization is partially due to mono-photonic absorption process, where the electron transfer from the excited Franck-Condon state of the solute to the solvent molecules seems to occur. At any rate, the laser induced ionization of the pyrene-solvent system is a very rapid process (faster than the encounter collision between A* and D). Therefore, in a rough approximation, the amount of ion radicals produced by the encounter collison between A* and D may be given by subtracting the value of photocurrent of two component system from that of the corresponding three component system. In this way, we have evaluated the relative concentrations of ions given in Table 1.

Although it was not possible to observe the ion radical formation due to the encounter collision between A* and D in *n*-hexane by means of the photocurrent measurements, we have observed transient absorption bands quite similar to those of pyrene anion in the case of pyrene-DMA-*n*-hexane system. The decay curve of the transient absorption at 719 nm is shown in Fig. 7

Table 1. Observed relative concentration of ions, I_C, free energies of HE state, ΔF(HE), the solvated ionpair state, $\Delta F(A_S^- \cdots D_S^+)$, and the dissociated ion radical state, $\Delta F(A_S^- + D_S^+)$, above the gound state, A+D. Free energies are given in units of eV.

Solvent	ε	ΔF (HE)	ΔF $(A_S^- \cdots D_S^+)$	ΔF $(A_S^- + D_S^+)$	I_C[a]
Acetonitrile	37.5	3.02	2.80	2.86	1.0
Acetone	20.7	3.03	2.85	2.95	0.3_0
Methylethyl ketone	18.5	3.03	2.86	2.97	0.2_1
Pyridine	12.3	3.03	2.92	3.08	0.1_1
Ethylene chloride	10.4	3.04	2.95	3.15	0.01_4
Methylene chloride	9.08	3.04	2.98	3.20	0.01_0
Chlorobenzene	5.62	3.06	3.12	3.48	0.004
n-Hexane	1.89	3.28	3.84	4.93	—

a) Strictly speaking, not only the dependence of mobility on the solvent viscosity but also its dependence on the degree of solvation of ions should be taken into consideration in the evaluation of I_C values. The mobility will be smaller in the case of stronger solvation in polar solvents, leading to the stronger dependence of I_C value on the solvent polarity than indicated here.

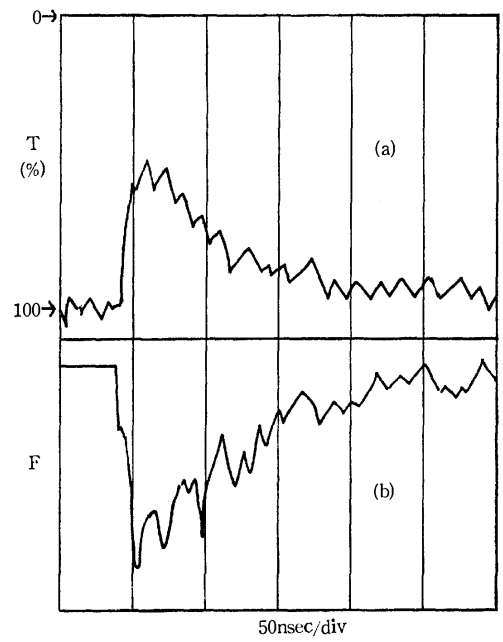

Fig. 7. Rise and decay curves of absorption at 719 nm (a) and those of pyrene-DMA HE fluorescence (b) in the case of *n*-hexane solution. Concentrations of pyrene and DMA are the same as those of Fig. 2, respectively.

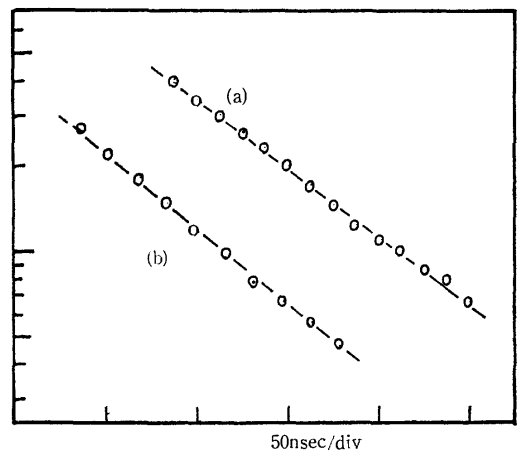

Fig. 8. Semilogarithmic plots of decay curves of Fig. 7. (a) absorption (b) fluorescence

together with the fluorescence decay curve of the pyrene-DMA HE. Semi-logarithmic plots of these decay curves are indicated in Fig. 8. One can see clearly from Fig. 8 that both decay curves are single exponential and they have approximately the same decay constant. Accordingly, the transient absorption bands similar to those of pyrene anion can be assigned to those of pyrene-DMA HE. Thus, the pyrene-DMA HE seems to have a quite polar electronic structure even in the *n*-hexane solution.

Now let us return to the discussion on the results given in Table 1. In Table 1, free energies of the HE state, ΔF(HE), the solvated ion-pair state, $\Delta F(A_S^- \cdots D_S^+)$, and the dissociated ion radical state, $\Delta F(A_S^- + D_S^+)$, respectively above the ground state, A+D, in various solvents are given together with the relative yield of the dissociated ions, I_C. ΔF(HE) has been evaluated by means of the relation,

$$\Delta F(\mathrm{HE}) = \Delta F(\mathrm{A}^* + \mathrm{D}) + \Delta F_c(\varepsilon) \quad (3)$$

where $\Delta F(A^* + D)$ has been estimated to be 3.346 eV, the excitation energy of pyrene to the fluorescent state, and $\Delta F_C(\varepsilon)$ is the free energy change associated with the formation of the HE in a solvent with dielectric constant ε, which can be calculated according to,

$$\Delta F_c(\varepsilon) = \Delta F_c(n\text{-hexane}) - \left(\frac{\varepsilon-1}{2\varepsilon-1} - 0.186\right)(\vec{\mu}_c^2/a^3) \quad (4)$$

The first term denotes the free energy change in *n*-hexane which has been estimated to be about −0.066 eV[6] and the second term the difference in solvation free energy of the complex with dielectric constant ε and *n*-hexane. a and $\vec{\mu}_C$ in the second term represent respectively the cavity radius in Onsager's theory of reaction field and dipole moment of the HE, and the value of $(\vec{\mu}_c^2/a^3)$ has been estimated to be 0.8 eV[7] by applying the equation,

$$h c \bar{\nu}_f \approx -\left(\frac{2(\varepsilon-1)}{2\varepsilon+1} - \frac{n^2-1}{2n^2+1}\right)(\vec{\mu}_c^2/a^3) \quad (5)$$

for the observed values of fluorescence wave numbers. (n is the refractive index of the solvent). $\Delta F(A_S^- \cdots D_S^+)$ can be calculated according to,

$$\Delta F(A_s^- \cdots D_s^+) = (E^+ - E^-) - (e^2/\varepsilon R_0) + \Delta F_s \quad (6)$$

The first term represents the difference between the oxidation potential of the donor and the reduction potential of the acceptor in acetonitrile, the second term the Coulomb attraction energy between the ions A_S^- and D_S^+ separated by the distance R_0 (assumed to be 7 Å), and the third term denotes the difference of the free solvation energies of ions in acetonitrile (ε=37.5) and a solvent with dielectric constant ε. ΔF_S can be calculated with the aid of Born's equation,

$$\Delta F_s = (e^2/2)\left(\frac{1}{R_+} - \frac{1}{R_-}\right)\left(\frac{1}{\varepsilon} - \frac{1}{37.5}\right) \quad (7)$$

where we have assumed $R_+ \approx R_- \approx 3.5$ Å. Finally, ΔF-$(A_S^- + D_S^+)$ is given simply by

$$\Delta F(A_s^- + D_s^+) = \Delta F(A_s^- \cdots D_s^+) + e^2/\varepsilon R_0 \quad (8)$$

The calculated ΔF values and the observed I_C values are plotted against ε values in Fig. 9 for convenience's sake.[8]

One can see clearly from Fig. 9 that the I_C value increases strongly and the $\Delta F(A_S^- + D_S^+)$ as well as $\Delta F(A_S^- \cdots D_S^+)$ values are lowered remarkably as the solvent dielectric constant is increased. The increase of the I_C value is especially notable for the range of $\varepsilon \gtrsim 10$. Thus, in these rather polar solvents with ε values larger than 10, the existence of the dissociated ions has been clearly proved by the present study. In the range of $\varepsilon \approx 5$—10, although the experimental errors for the

6) Unpublished result by T. Okada, H. Matsui, and N. Mataga.
7) Unpublished result by T. Okada and N. Mataga.
8) Quite similar plots of ΔF(HE) and $\Delta F(A_s^- \cdots D_s^+)$ against ε value have been given already by Weller. A. Weller, in Nobel Symposium 5, Fast Reactions and Primary Processes in Chemical Kinetics (S. Claesson, ed.,) Almqvist and Wiksell, Stockholm (1967), p. 413.

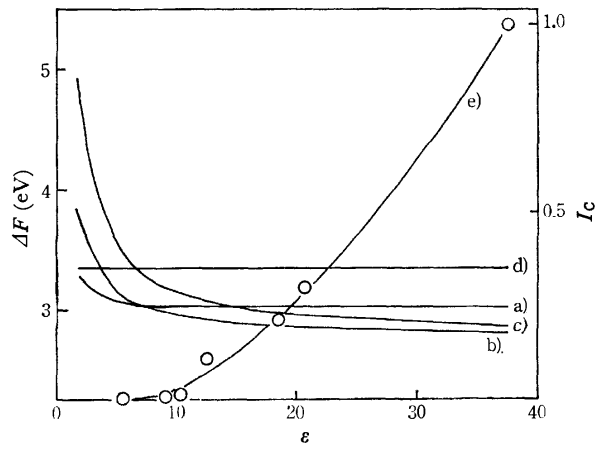

Fig. 9. Plots of ΔF values and I_C values given in Table 1 against ε values of solvents.
(a) ΔF(HE) (b) $\Delta F(A^-_S \cdots D^+_S)$ (c) $\Delta F(A^-_S + D^+_S)$
(d) $\Delta F(A^* + D)$ (e) I_C

determination of I_C values are rather large, the existence of a small quantity of dissociated ions produced by the encounter collision seems to be certain. However, the formation of such ions was not observable in the range of ε smaller than 5.

Of course, the precursor of the dissociated ions is the solvated ion-pair ($A^-_S \cdots D^+_S$) which is formed by the electron transfer process in the encounter complex. Then, the reaction scheme of the dissociated ion radical formation may be written as

$$A^* + D \rightleftarrows A^* \cdots D \rightleftarrows A_s^- \cdots D_s^+ \rightleftarrows A_s^- + D_s^+ \quad (9)$$

However, the difference, $\Delta F(A^-_S + D^+_S) - \Delta F(A^-_S \cdots D^+_S)$, is much larger than the thermal energy at room temperature even at $\varepsilon \approx 10$. Accordingly, it might be possible that the dissociation occurs in the non-relaxed state of the ion-pair immediately after the electron transfer, competing with the relaxation process to the equilibrium solvation state of the ion-pair and/or the relaxation process to the ground state, (A+D). At any rate, since the formation of solvated ion radicals in solvents, which are not very polar and where the HE fluorescence is fairly strong, has been proved in this work, the reaction scheme of the competition of the exciplex formation process with the electron transfer process in the encounter complex seems to be more suitable than the assumption of the continuous structural change of HE with the change of solvent polarity. Of course, there should be more or less structural change of HE induced by the solute-solvent interactions, in principle. However, this effect may play rather small role[9] in explaining the experimentally observed relation between the solvent dependent HE fluorescence quantum yield and decay time, in the case of moderately polar solvents.

As we have described already, the formation of dissociated ion radicals was not observable in *n*-hexane. The circumstance was the same also in toluene. One may see from Fig. 9 that not only the formation of the dissociated ions but also the formation of the solvated ion-pairs, $A^-_S \cdots D^+_S$, seems to be rather difficult in *n*-hexane and toluene (ε=2.38). However, according to the experimental results, the HE fluorescence yield in toluene is only one third of that in *n*-hexane, while the HE fluorescence decay time in toluene is practically the same as that in *n*-hexane.[1] It seems to be rather difficult to explain this result by assuming only the reaction of Eq. (9) which competes with the HE formation process, if the relations between the free energies in Fig. 9 are approximately correct.

Possible explanations for the observed results in toluene solution may be as follows. (a) Toluene molecules will make a specific short range interaction with the ions in the solvated ion-pair ($A^-_S \cdots D^+_S$) in addition to the long range dielectric interactions. This short range interaction (for which the π-electron system of toluene might be playing some role) may lower the $\Delta F(A^-_S \cdots D^+_S)$ value in toluene solution more strongly than indicated in Fig. 9, which makes possible the reaction of Eq. (9) to occur considerably. This is a kind of structural change of the complex involving the surrounding solvent molecules. (b) Owing to a specific interaction of excited molecules with π-electron systems of toluene, there arises some quenching process in the course of HE formation reaction *i.e.* in the encounter complex, as follows.

$$A^* + D \rightleftarrows A^* \cdots D \longrightarrow (A^- \cdot D^+)^* \xrightarrow{\text{solvent}} A + D \text{ or } A^*(T) + D$$

where A*(T) represents the triplet state of pyrene. The quenching process which competes with the HE formation in the encounter complex has been assumed also by Ottolenghi and co-workers[10] in order to interpret quite efficient and very rapid intersystem crossing in some aromatic hydrocarbon-DEA (*N*,*N*-diethylaniline) systems in several solvents. However, it seems to be rather difficult, at the present stage of investigation, to determine the true mechanism of the above described solvent effects on the HE fluorescence in almost non-polar solvents.

9) H. Beens, Thesis, Free University, Amsterdam, 1969.
10) C. R. Goldschmidt, R. Potashnik, and M. Ottolenghi, *J. Phys. Chem.*, **75**, 1025 (1971).

The Diffuse Reflection Spectra of Bentonites Colored with Various Aromatic Compounds and Related Ion-radical Salts

Yoshio MATSUNAGA

Department of Chemistry, Faculty of Science, Hokkaido University, Sapporo

(Received September 9, 1971)

Bentonites colored with each of the following aromatic compounds were examined by the method of diffuse reflection in the range from 4 to 30 kK: benzidine, 4,4'-dihydroxybiphenyl, 4,4'-dimethoxybiphenyl, perylene, tetrathiotetracene, and phenothiazine. By comparison with the spectra of the related ion-radical salts, the oxidation of the aromatic compounds to the mono- and/or di-valent cations could be proven in all of them. Except in the case of phenothiazine, the species in the colored clays was found to be drastically modified by moisture. In addition, the spectra of the copper-arene complexes recently reported by Mortland *et al.* were measured. The oxidation of perylene, tetrathiotetracene, and phenothiazine was found to proceed to a greater extent in the copper-exchanged clays.

Earlier we examined the coloration of acid clay upon the addition of benzidine and related aromatic diamines and showed that the diamines are oxidized to the mono- and di-valent cations.[1] The former cations were found to be in various modes of intermolecular interaction, depending on the kind and amount of the liquid. For instance, acid clay colored with benzidine is blue when moistened with water and yellow when dried. The spectrum of the wet sample consists of bands at 7.5, 12.0, 17.0, and about 27 kK, and closely resembles that of the solid benzidine bromide, where the monovalent diamine cations are supposed to be in a strong, more-than-by-pairs interaction.[2] The spectrum displayed by the dried sample has only one absorption maximum, located at 22.5 kK. Between these two situations, a pattern with maxima at 9.5, 14.5, and 26 kK and a shoulder at 16 kK can be observed by carefully controlling the amount of water. This spectrum can be more easily developed by moistening with methanol instead of water. Finally, when benzene is added to the dried sample, absorption maxima appear at 11.5, at 15.2, and somewhere around 27 kK. The last is similar to that of the dimeric cation in solution and is assigned to the cations in a pair-by-pair interaction.

Bentonite, a clay of the montmorillonite type, has been well known to be colored with aromatic amines;[3-5] therefore, it seemed interesting to study the spectra of bentonites colored with benzidine and to compare them with those of the colored acid clay. In recent years, the formation and stabilization of the monovalent cation from aromatic compounds by contact with silica-alumina and synthetic zeolite has been extensively examined by several workers.[6-10] On the other hand, a limited amount of work has been done on the coloration of natural clays with aromatic compounds other than amine. Takahashi observed that acid clay turns green upon the addition of 4,4'-dihydroxybiphenyl dissolved in aqueous ethanol.[5] Recently Mortland *et al.* reported that the color of well-dried copper(II) bentonite changes from a pale blue to dark red when exposed to benzene vapor.[11,12] Similarly, toluene forms a bright green complex, and xylene, a dark purple complex. In the present work, the following were selected in order to cover various types of aromatic compounds: benzidine, 4,4'-dihydroxybiphenyl, 4,4'-dimethoxybiphenyl, perylene, tetrathiotetracene, and phenothiazine. The ion-radical salts derived from most of these compounds are available, so that the spectra of the colored bentonites can be compared with those of the oxidized forms. The cupric ion has been found necessary to the coloration with benzene; the effect of the cation exchange was examined with perylene, tetrathiotetracene, and phenothiazine.

Experimental

Materials. Natural bentonite supplied by the Koso Chemical Co., Ltd., was refined by repeated elutriations. The colored clays were prepared by grinding an organic compound and the clay together in a ratio of 1 : 99 by weight. If the color was not well developed by this technique, a small amount of chloroform was added to the mixture. The copper exchange was carried out following the procedure given by Yariv *et al.*[13] As this clay was found not to be intensely colored with benzene, the copper-exchanged clay prepared from Wyoming bentonite was mostly employed in the rest of the work.

Van Alphen's 4,4'-dimethoxybiphenyl dinitrate was obtained by the addition of a mixture of fuming nitric acid and carbon tetrachloride to the compound dissolved in carbon tetrachloride.[14] The sodium salt of *p*-diphenosemiquinone was made by the oxidation of 4,4'-dihydroxybiphenyl dissolved in aqueous sodium hydroxide with ferricyanide ions, as has been described by Willstätter and Kalb.[15] The solid

1) A. Hakusui, Y. Matsunaga, and K. Umehara, This Bulletin, **43**, 709 (1970).
2) Y. Iida and Y. Matsunaga, *ibid.*, **41**, 2615 (1968).
3) E. A. Hauser and M. B. Leggett, *J. Amer. Chem. Soc.*, **62**, 1811 (1940).
4) H. Weil-Malherbe and J. Weiss, *J. Chem. Soc.*, **1948**, 2164.
5) H. Takahashi, This Bulletin, **28**, 5 (1955).
6) N. Okuda and T. Tachibana, *ibid.*, **33**, 863 (1960).
7) J. J. Rooney and R. C. Pink, *Trans. Faraday Soc.*, **58**, 1632 (1962).
8) W. K. Hall, *J. Catal.*, **1**, 53 (1962).
9) D. M. Brouwer, *ibid.*, **1**, 372 (1962).
10) D. N. Stamires and J. Turkevich, *J. Amer. Chem. Soc.*, **86**, 749 (1964).
11) H. E. Donor and M. M. Mortland, *Science*, **166**, 1406 (1969).
12) M. M. Mortland and T. J. Pinnavaia, *Nature Phys. Sci.*, **229**, 75 (1971).
13) S. Yariv, L. Heller, Z. Sofer, and W. Bodenheimer, *Israel J. Chem.*, **6**, 741 (1968).
14) J. van Alphen, *Rec. Trav. Chim.*, **49**, 767 (1930).
15) R. Willstätter and L. Kalb, *Ber.*, **38**, 1232 (1905).

salts of the mono- and di-valent tetrathiotetracene cations were prepared according to the methods of Marschalk and Niederhauser.[16]

Measurements. The spectra were recorded on a Beckman DK 2A spectrophotometer with the aid of a reflectance attachment.[1] The colored clays were moistened by leaving them in a desiccator containing water, while they were dried in a desiccator containing silica gel. If stable, the clays were dried in an oven kept near 100°C.

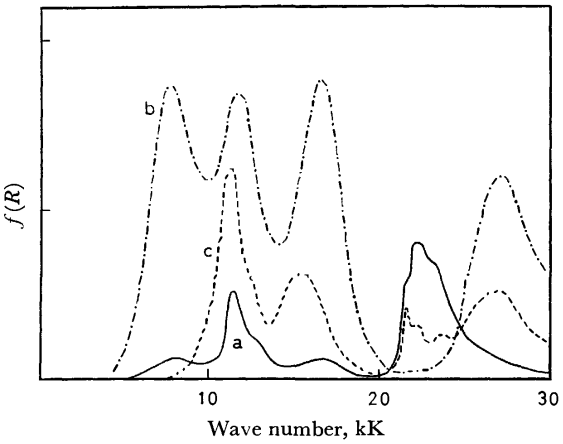

Fig. 1. Diffuse reflection spectra of benzidine-bentonite; (a) prepared by grinding, (b) moistened with water, (c) moistened with benzene.

Results and Discussion

Benzidine-bentonite (Fig. 1). When benzidine and the clay are ground together, absorption bands appear at 11.5, about 13, 21.6, 22.2, and about 23 kK. This spectrum, Curve a in Fig. 1, is in good agreement with that of the monovalent benzidine cation in an ethanolic solution at room temperature. The latter is known to have bands at 11.6 and 13.3, a shoulder at 14.3, and a strong band with a vibrational structure around 22 kK. Therefore, the cation formed at this stage is essentially free from intermolecular interaction. Upon moistening with water, a pattern with bands 7.8, 11.7, 16.6, and 27.3 kK is developed (see Curve b). The locations are close to those in the B-1 pattern which is observed in the wet benzidine-acid clay, as was reported in our earlier paper. The same pattern can be seen as the background of Curve a. However, the band at 7.8 kK becomes relatively less intense when the sample is partially dried. This observation leads to the conclusion that the spectrum given by Curve b is a superposition of the spectra of two species. The sample moistened with benzene exhibits bands at 11.3, 15.5, and 27.0 kK and a shoulder around 12.4 kK. This pattern can well be compared with the B-3 pattern recorded with the colored acid clay moistened with the same solvent. As this spectrum is similar to that of the dimeric form of the benzidine cation observed in a cold ethanolic solution,[17] the monovalent cations here may be supposed to be essentially in a pair-by-pair interaction. The spectrum shown by Curve b may be explained as a superposition of the B-1 and B-3 patterns. As was mentioned in our previous paper, the cations exhibiting the former pattern are likely in a more-than-by-pairs interaction, and this fraction is apparently increased by the presence of water. The band with some structure appearing in the range from 21 to 24 kK of Curve c indicates that the monomeric cations are left in this sample. Because of the presence of isosbestic points at 20.7 and 24.7 kK among the a, b, and c Curves, it may be concluded that the species giving the spectra shown by Curves b and c are in equilibrium with the monomeric cations.

Although a broad background, possibly arising from some decomposition products, appears upon drying, the pattern of the monomeric action reappears. It must be noted that this behavior is quite different from that found in the benzidine-acid clay. In the latter case, the dried sample is yellow and its spectrum has only one absorption maximum, at 22.5 kK which has been assigned to the divalent cation, the quinoidal form in Hasegawa's nomenclature.[1,18] This species is consumed in the development of the blue color in the acid clay upon moistening. From these observations, it can be argued that the mean oxidation state of benzidine in the bentonite complex is lower than that in the acid clay complex.

Dihydroxybiphenyl- and Dimethoxybiphenyl-bentonites (Figs. 2 and 3). 4,4'-Dihydroxybiphenyl, which has an isoelectronic structure with benzidine, gives a green-colored complex with bentonite.[5] A relatively weak band at 14.0 kK and a strong one at 24.2 kK are generated in the moistened sample. Both of them disappear when dried. The behavior of the dimethoxybiphenyl complex is essentially the same as has been described above (compare Curves a and b in Fig. 2). No cation-radical salt derived from dihydroxybiphenyl is known; however, salts of the $OC_6H_5 \cdot C_6H_5O^-$ anion, which is isoelectronic with the $HOC_6H_5 \cdot C_6H_5OH^+$ cation, are available. Figure 3 presents the spectrum of the solid sodium salt as well as the spectrum in an

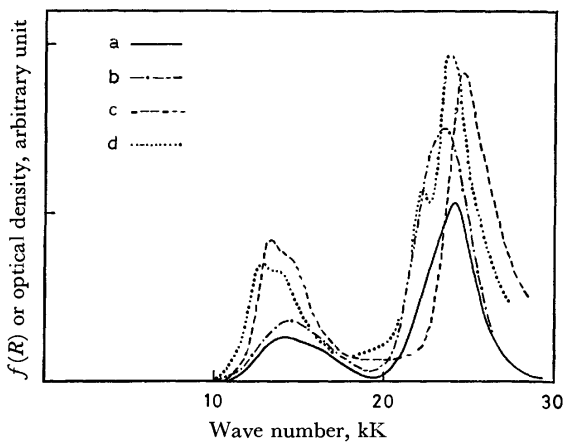

Fig. 2. Diffuse reflection spectra; (a) dihydroxybiphenyl-bentonite, (b) dimethoxybiphenyl-bentonite and absorption spectra of sulfuric acid solutions; (c) dihydroxybiphenyl, (d) dimethoxybiphenyl.

16) C. Marschalk and J. P. Niederhauser, *Bull. Soc. Chem. France*, **1952**, 151.

17) K. Takemoto, H. Matsusaka, S. Nakayama, K. Suzuki, and Y. Ooshika, This Bulletin, **41**, 764 (1968).

18) H. Hasegawa, *J. Phys. Chem.*, **65**, 292 (1961).

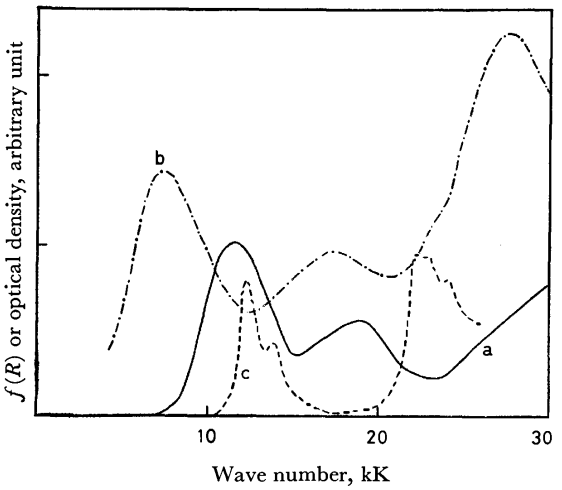

Fig. 3. Diffuse reflection spectra; (a) sodium salt of *p*-diphenosemiquinone, (b) van Alphen's dimethoxybiphenyl dinitrate and absorption spectrum of *p*-diphenosemiquinone ion in ethanol (c).

ethanolic solution. The former exhibits absorption maxima at 11.5 and 19.0 kK, and the latter, at 12.2, at 13.8, and around 22 kK. As to dimethoxybiphenyl, the blue-colored dinitrate prepared by van Alphen has been reported by Buck *et al.* to show an ESR absorption.[19] This observation may be considered as an indication that the salt contains a monovalent cation rather than a divalent one; therefore, we will examine the spectrum of this dinitrate (see Curve c of Fig. 3).

As this compound is not stable, especially when diluted for the spectral measurements, the recorded spectrum is distorted because of the fading during the measurement. A comparison with the spectrum recorded without dilution suggests that the band at 7.4 kK is as intense as that at 27.5 kK. Among the spectra presented in Fig. 3, only the spectrum of *p*-diphenosemiquinone ion dissolved in ethanol bears some resemblance to those of the colored clays. However, the intensity ratio of the low-energy band to the high-energy one in the monovalent anion is far larger than that observed with the colored clay. In addition, the former spectrum is shifted to the low-energy side as much as several kK compared to the latter.

Hydroquinone and 1,4-dimethoxybenzene, closely related to the present compounds, have been known to be converted into monovalent cations upon being dissolved in concentrated sulfuric acid.[20] Therefore, the measurements of the spectra of dihydroxybiphenyl and dimethoxybiphenyl in sulfuric acid were attempted. The spectra recorded immediately after the dissolution are similar to each other, as is shown in Fig. 2. These species are transitory. In the case of dimethoxybiphenyl, the band at 22.2 kK is considerably increased on standing. As we may expect on the basis of their isoelectronic structures, the spectrum of the dihydroxybiphenyl cation is similar to that of the monovalent anion given in Fig. 3. Nevertheless, the general shift to the high-energy side and the enhancement of the high-energy band make the spectrum closer to that of the bentonite complex. Thus, it is very likely that the species in the colored clays are the monovalent cations derived from these compounds.

It should be noted that, although the spectrum of the *p*-diphenosemiquinone ion in ethanol is essentially the same as those of the tetrahalo derivatives reported earlier, the solid-state spectrum is markedly different from those of the derivatives. For example, the sodium salt of 3,3',5,5'-tetrachloro-*p*-diphenosemiquinone shows a solid-state spectrum composed of three bands located at 6.8, 15.5, and 26.4 kK.[21] This feature is rather similar to that of the spectrum of the dimethoxybiphenyl dinitrate, which consists of bands at 7.4, 17.4, and 27.5 kK. In accordance with the results of the ESR measurement made by Buck *et al.*, this spectral similarity and the presence of an absorption maximum as low as 7.4 kK strongly suggest that the cation in the dinitrate is monovalent rather than divalent, and that it is in a more-than-by-pairs interaction. The tetra-*n*-propylammonium salt of tetrabromo-*p*-diphenosemiquinone has been found to show a spectrum consisting of bands located at 11.5, 15.2, and 24.5 kK. Because these locations nearly correspond to those in the dimeric form of the benzidine cation (12.4, 16.4, and 28 kK), the monovalent anions in this ammonium salt have been assumed to be in a pair-by-pair interaction.[21] Although the location of the middle band in the spectrum of the sodium salt of unsubstituted *p*-diphenosemiquinone does not agree with the corresponding band in the above-mentioned ammonium salt, the semiquinone ions here might also be in a pair-by-pair interaction.

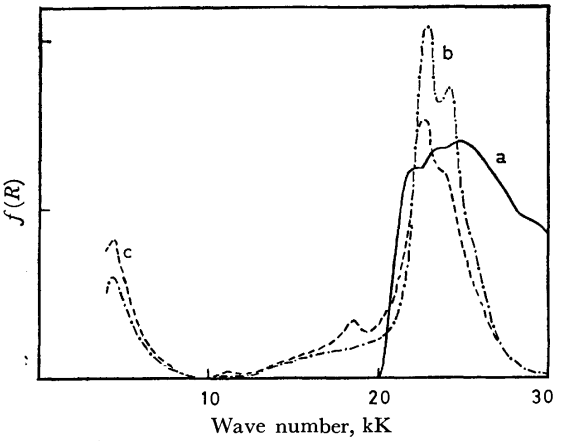

Fig. 4. Diffuse reflection spectra; (a) perylene, (b) perylene-bentontie, dried, (c) the same, moistened.

Perylene-bentonite (Fig. 4). The dried sample is yellow, but it is darker than the hydrocarbon itself because of the presence of a tail extending into the near-infrared region. In addition, the presence of a band at 4.4 kK must be noted. Upon moistening, this low-energy band is intensified and the bands corresponding to those of perylene are weakened (compare Curves b and c in Fig. 4). Furthermore, the appearance of a little peak is observed at 18.5 kK, where the well-known

19) H. M. Buck, J. H. Lupinski, and L. J. Oosterhoff, *Mol. Phys.*, **1**, 196 (1958).

20) K. Kimura and H. Yamada, This Bulletin, **42**, 3032 (1969).

21) Y. Matsunaga and Y. Narita, *ibid.*, **45**, 408 (1972).

monovalent cation exhibits a strong sharp absorption.[22-24] The weak absorptions in the range from 12 to 20 kK may be considered as a part of the spectrum of the perylene cation. In the solid-state spectrum of perylene perchlorate reported by Sato *et al.*, the low-energy band is found at 7.7 kK;[25] it arises from the interaction between the cations. On the other hand, the band appearing at 4.4 kK in the colored clay may be attributed to the interaction between the cation and the neutral molecule. Very recently Chiang *et al.* reported the preparation of (perylene)$_2$ ClO_4,[26] where

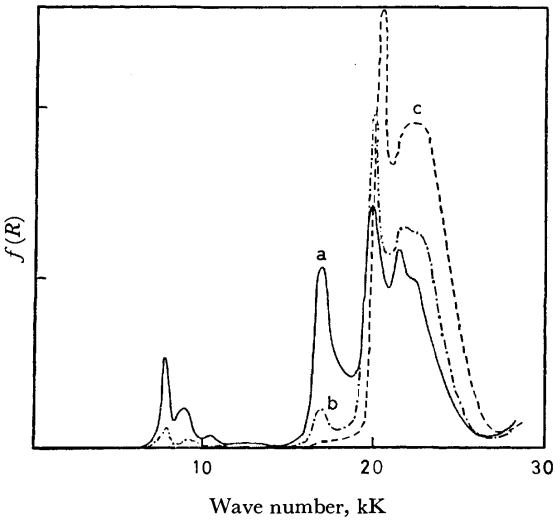

Fig. 5. Diffuse reflection spectra; (a) tetrathiotetracene-bentonite, dried, (b) the same, moistened, (c) tetrathiotetracene-Cu bentonite, dried.

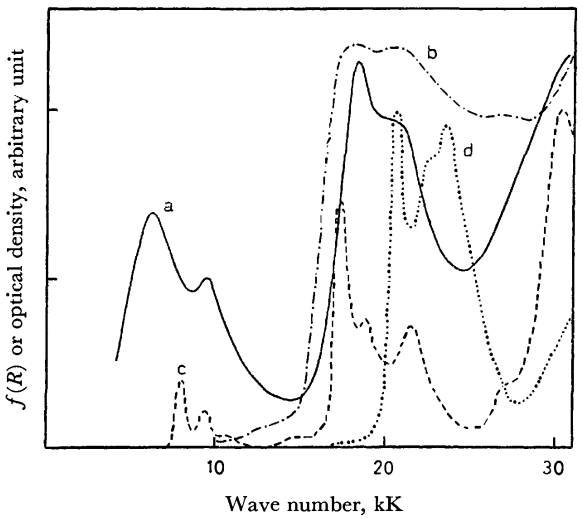

Fig. 6. Diffuse reflection spectra; (a) (tetrathiotetracene$^+$)$_2SO_4$, (b) tetrathiotetracene^{++} $(HSO_4)_2$ and absorption spectra; (c) the monovalent cation in ethanol, (d) the divalent cation in dilute acid.

22) G. J. Hoijtink and W. P. Weijland, *Rec. Trav. Chim.*, **76**, 836 (1957).

23) W. Ij. Aalbersberg, G. J. Hoijtink, E. L. Mackor, and W. P. Weijland, *J. Chem. Soc.*, **1959**, 3049.

24) H. Kuroda, T. Sakurai, and H. Akamatu, This Bulletin, **39**, 1893 (1966).

25) Y. Sato, M. Kinoshita, M. Sano, and H. Akamatu, *ibid.*, **42**, 3051 (1969).

26) T. C. Chiang, A. H. Reddoch, and D. T. Williams, *J. Chem. Phys.*, **54**, 2051 (1971).

such an interaction may be expected to be observed. Unfortunately, though, no spectrum was given for this ion-radical salt.

Tetrathiotetracene-bentonite (Figs. 5 and 6). When a mixture of tetrathiotetracene and clay is moistened with chloroform, it turns dark red and then yellow. The red color reappears easily when it is dried in an oven. This color change is reproducible and can be observed even after storage for over a year. As may be seen by a comparison of Curves a and b in Fig. 5, the spectrum is a superposition of two patterns. One of them consists of three weak bands in the range from 7 to 11 kK and two strong ones located at 17.0 and 21.4 kK. The other has a sharp band at 20 kK and a rather broad one around 22 kK. As will be mentioned in the next paragraph, the former pattern can be ascribed to the monovalent cation, and the latter, to the divalent cation. Both of them seem to be free from intermolecular interactions. The equilibrium between these two species moves to the divalent cation upon the addition of moisture, as is shown in Fig. 5. In addition, the measurements of the spectrum in the range from 100 to 150°C, which is selected to avoid the effect of moisture, revealed the movement of the equilibrium towards the monovalent cation upon an elevation of the temperature.

Since the preparation of dark green-colored tetrathiotetracene, it has been discovered to be easily oxidized to the red-colored monovalent cation and the yellow-colored divalent cation. Several pairs of the salts of these two cations have been isolated by Marschalk and Niederhauser.[16] Moreover, tetrathiotetracene forms ionic molecular complexes with many strong electron-acceptors.[27] The spectra of the solid monobromide and the *o*-chloranil complex have been measured, and their red color has been attributed to bands appearing around 20 kK. To elucidate the species in the colored clays, the spectra of (tetrathiotetracene$^+$)$_2SO_4$ and tetrathiotetracene^{2+}$(HSO_4)_2$ were examined in both the solid and dissolved states. The former salt exhibits absorption maxima at 6.3, 9.5, and 18.4 and a shoulder at 21 kK. On the other hand, the spectrum of the monovalent cation in ethanol is characterized by the presence of three weak maxima, at 8.0, 9.5, and 10.7 kK, and a strong maximum at 17.3 kK. It must be noted that the bands in the near-infrared region are very much more widened and intensified in the solid state than in the dissolved state. The spectrum of the brown-colored bisulfate is rather similar to the above-mentioned in the visible region; that is, the maxima are found at 18.0 and 20.8 kK. However, no absorption is detected in the infrared region. When dissolved in dilute acid, the absorption bands become sharper and are shifted to 20.7 and 23.6 kK respectively. Furthermore, a shoulder at 22.7 kK can be observed (see Curve d in Fig. 6). Apparently the spectra of the colored clays are close to those of the cations in the dissolved state. We also examined the solid-state spectra of tetrathiotetracene$^+$ $Cl\cdot H_2O$, tetrathiotetracene$^+$ Br, and tetrathiotetracene$^+$ NO_3. They are similar to the above-mentioned spectrum; however, the intensity ratio

27) Y. Matsunaga, *ibid.*, **42**, 2248 (1965).

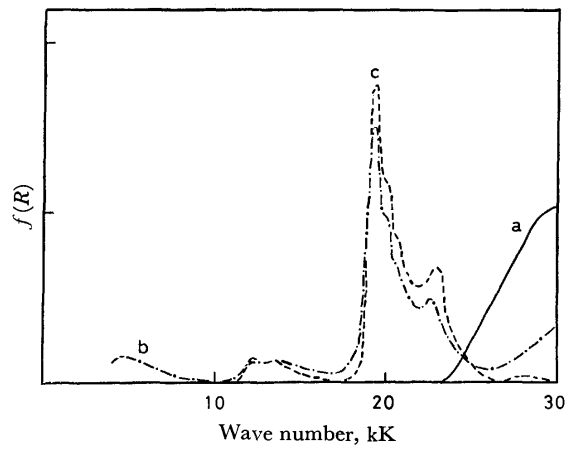

Fig. 7. Diffuse reflection spectra; (a) phenothiazine, (b) phenothiazine-bentonite, (c) phenothiazine-Cu bentonite.

between the band in the infrared region and that in the visible region depends markedly on the kind of anion; that is, it is 0.76: 1 in the chloride, 0.65: 1 in the bromide, 0.60: 1 in the sulfate, and 0.20: 1 in the nitrate.

Phenothiazine-bentonite (Fig. 7). The spectrum of this colored clay in the region between 10 and 25 kK is in good agreement with that of the monovalent cation in solution.[28] However, there are extra absorptions — a weak one in the infrared region and a relatively strong one above 25 kK (see Curve b in Fig. 7). The former may be due to the interaction between the cation and the neutral molecule, for the latter agrees well with that of phenothiazine itself. As was reported earlier, the solid semiquinoid bromide may show an absorption in the infrared region.[29] Nevertheless, the possibility that the weak absorption with a maximum at 4.7 kK in the colored clay is due to the interaction between the cations may be ruled out, because the spectrum of the colored clay between 10 and 25 kK is far from the solid-state spectrum of the bromide. No clear effect of moisture is noted in this case.

Mortland's Copper-arene Complexes (Fig. 8). It has been reported by Donor and Mortland that the benzene complex of copper(II)-exchanged Wyoming bentonite is green or gray when partially hydrated and dark red when well dried.[11] On the basis of the vibrational spectra, Mortland and Pinnavaia have concluded that the green form of coordinated benzene possesses a D_{6h} local symmetry, while the red form does not.[12] It has been suggested that a reduction in the symmetry of the benzene ring occurs if the copper(II) ion is bonded to an edge of the ring, as in the copper(I) complex C_6H_6-$CuAlCl_4$. As no electronic spectrum has been reported by them except for the statement that a very broad intense absorption extends from 1.7 to beyond 4.0 kK, the diffuse reflection spectra of these two forms of the benzene complex as well as those of the toluene and *p*-xylene complexes were measured.

The spectrum of the red form of the benzene complex has a broad maximum located at 19.4 kK and a shoulder around 23 kK in the visible region, and a very intense maximum at 4.4 kK. The electronic absorption mentioned by Mortland and Pinnavaia must be the tail of the last-named one. When this sample is exposed to ambient temperatures and humidity for a while, it turns gray. Contrary to the remarkable change in the vibrational spectrum reported by Mortland, the only change found in the electronic spectrum is the appearance of an additional strong band at 26.7 kK. The low-energy band of the green toluene complex is located at about 10 kK, and that of the purple *p*-xylene complex, at about 9 kK. Compared to the low-energy band of the benzene complex, they are appreciably weaker and at higher energies.

Perylene-Cu Bentonite (Fig. 9). After drying in an oven, the color is a bluish violet. The spectrum between 10 and 20 kK is essentially that of the monovalent cation (see Curve a). Nevertheless, the band in the infrared region and the one at 22.6 kK cannot be assigned to this ion. Upon moistening, the absorptions due to the cation become less intense, while the other two become more intense. The latter pattern is different from both the spectrum of the dimeric perylene cation, which has been shown by Kimura *et al.* to have bands at 10 and 20 kK,[30] and the spectrum of the

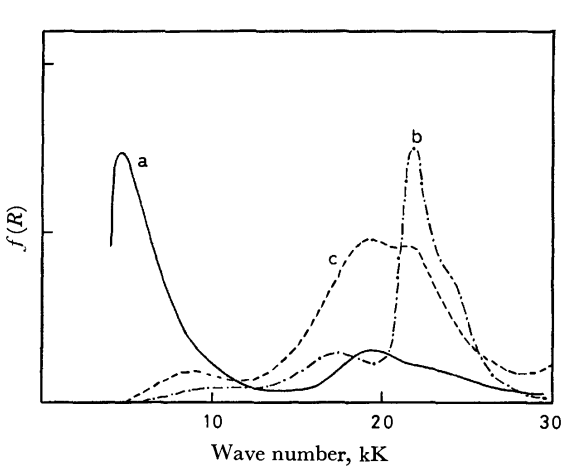

Fig. 8. Diffuse reflection spectra of Mortland's copper-arene complexes; (a) the benzene complex, (b) the toluene complex, (c) the *p*-xylene complex.

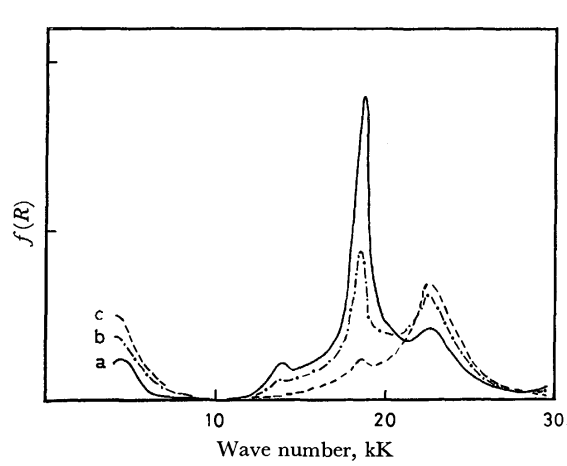

Fig. 9. Diffuse reflection spectra of perylene-Cu bentonite; (a) dried, (b) moistened, (c) moistened further.

28) H. J. Shine and E. E. Mach, *J. Org. Chem.*, **30**, 2130 (1965).
29) Y. Matsunaga and K. Shono, This Bulletin, **43**, 2007 (1970).
30) K. Kimura, T. Yamazaki, and S. Katsumata, *J. Phys. Chem.*, **75**, 1768 (1971).

solid cation-radical salt studied by Sato *et al.*[25] Therefore, the species to which the new pattern is assignable may be the divalent cation or the neutral molecule. The electronic spectra of the alternant hydrocarbon cation and anion of the same valency may theoretically be expected to be practically identical.[31] As the spectrum of the divalent anion of perylene reported by Balk *et al.* bears no resemblance to the above-mentioned pattern,[32] it is not likely that a hitherto-unknown divalent cation is the major species in the moistened sample. The absorption at 22.6 kK may be attributed to the neutral molecule, and that in the infrared region, to the interaction between the monovalent cation and the neutral molecule. If this interpretation is correct, the effect of moisture on the equilibrium is in the direction opposite to that observed with the perylene-unexchanged bentonite. Finally, it must be added that the coexistence of perylene and its monovalent cation has been noted in experiments on the oxidation of this hydrocarbon by silica-alumina.[8,9]

Tetrathiotetracene-Cu Bentonite. The only species found in this sample is the yellow-colored divalent cation (see Curve c in Fig. 5).

Phenothiazine-Cu Bentonite. The spectrum is presented in Fig. 7 (see Curve c). There are no absorptions but those arising from the monovalent cation. Contrary to the case of phenothiazine-bentonite, the oxidation appears to be complete. The same tendency has already been noted in the other two cases discussed above.

As the species in the colored bentonites are mono- and/or di-valent cations, one may expect that the ionization potentials of these aromatic compounds correlate with the degree of the oxidation by bentonite, as has been demonstrated with silica-alumina.[33] The energy of the charge-transfer absorption generated by mixing with *p*-chloranil in chloroform is 1.52 eV for phenothiazine, 1.64 eV for perylene, 1.81 eV for benzidine, and 2.20 eV for dimethoxybiphenyl.[34] The ability to donate an electron should decrease in this order. The solid-state ionization potentials of perylene and tetrathiotetracene have been estimated to be 5.33 and 4.42 eV respectively by the photoemission method.[35] Thus, tetrathiotetracene is the best electron-donor among the compounds examined and, in fact, is the only compound to form the divalent cation when added to bentonite. The presence of the neutral molecule is noted in the cases of phenothiazine and perylene. In accordance with the order of the ionization potential, the latter spectrum is more dominated by the unionized component than is the former. The coloration of bentonite with the poorest donors, dihydroxybiphenyl and dimethoxybiphenyl, is very faint. Possibly only a small part of the added compound is oxidized to the monovalent cation. However, benzidine does not seem to show the tendency observed above. The absorption to be assigned to benzidine, 30.0 kK in the solid state, is absent in Fig. 1. This anomaly may be due to the protonation. If so, the absorption is not in the range covered by the present work. It should be pointed out that all the monovalent cations except the benzidine cation are found to be essentially free from mutual interaction. Apparently this observation cannot be explained by the difference in the concentration of the monovalent cation.

The author wishes to express his thanks to Professor Hiroshi Takahashi of the University of Tokyo for his gift of the sample of Wyoming bentonite.

31) W. P. Weijland, Thesis, Free University, Amsterdam (1958), cited in Ref. 23.
32) P. Balk, G. J. Hoijtink, and J. W. H. Schreurs, *Rec. Trav. Chim.*, **76**, 813 (1957).
33) G. M. Muha, *J. Phys. Chem.*, **74**, 2939 (1970).
34) G. Saito and Y. Matsunaga, This Bulletin, **44**, 1788 (1971).
35) M. Kochi, Y. Harada, T. Hirooka, and H. Inokuchi, *ibid.*, **43**, 2690 (1970).

The Electric Conductivity of the H_2O-B_2O_3 Melt

Hiroshi KODAMA, Toshio YOKOKAWA,* and Kichizo NIWA*

National Institute for Research in Inorganic Materials, 29-3, 2-chome, Honkomagome, Bunkyo-ku, Tokyo

**Faculty of Science, Hokkaido University, Sapporo*

(Received September 20, 1971)

Electric conductivity was measured over the whole composition range of H_2O–B_2O_3 in the liquid state. A peculiar conductivity-temperature relation was observed in a low B_2O_3-to-intermediate composition. The equivalent conductance of H_3BO_3 increases with its content in this range. Both the concentration of proton and its mobility through the proton-jump mechanism seem to change with the composition. The comparison of the results in the B_2O_3-rich range with those of alkali borates indicates a low extent of the dissociation of the –B–O–H group.

Various physico-chemical properties of binary metal borate melts have been investigated by many workers,[1] and it has been made clear that the addition of such metal oxides as Li_2O, Na_2O, K_2O, and PbO to B_2O_3 causes a variation in the coordination state from BO_3 to BO_4, that those binary borates completely dissociate into ionic liquids, and that the metal ion is the sole charge carrier in an electric field. Recently, Ag_2O has been shown to behave similarly, as determined from both the solubility of Ag_2O in Na_2O-B_2O_3 melt[2] and the electric conductivity.[3] H_2O-B_2O_3 provides another interesting system if its behavior is compared with that of the other borates. Considering such experimental evidence as the B–OH absorption band and the dependence of the solubility of water on its partial pressure,[4] the dissolution can be expressed by the following equation:

$$>B\text{–}O\text{–}B< + H_2O = 2>B\text{–}O\text{–}H \qquad (1)$$

Thus, the water molecule modifies the network as do the alkali metal oxides. The solubility of water in the alkali borate melt decreases with the alkali content. Water can be regarded as a basic oxide of the R_2O type, the basicity being quite weak. A recent study related to the density of H_2O-B_2O_3 suggests a change in the coordination number of oxygen around the boron atom in the composition range between $3B_2O_3 \cdot H_2O$ and $B_2O_3 \cdot H_2O$.[5]

The purpose of the present study is to make clear the conduction mechanism and to get structural information about this system through the whole composition range.

Experimental

The procedures used to prepare sample melts with desired compositions and to determine the melts' composition were similar to those used in the density measurements for this system.[5] Four types of cells, shown in Figs. 1, 2, 3, and 4, were used, depending on the compositions of the melts. The type of cell shown in Fig. 1(cell A) was used in the composition range from 0.5 to 2.5 mol% B_2O_3. The B and C cells in Fig. 3 were used in the range from 5.0 to 25.4 and from 33.3 to 80.5 mol% respectively. Each type of cell was sealed and set up as is shown in the b sections of Figs. 1, 2, and 3.

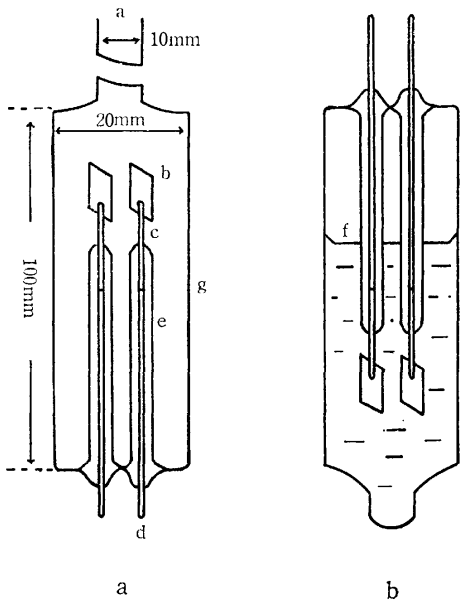

Fig. 1. Cell A used in the composition range of 0.5—2.5 mol % B_2O_3.
a: inlet of sample, b: Pt plate, c: Pt wire, d: W wire, e: thin Pyrex glass tube, f: liquid level of sample, g: Pyrex glass tube.

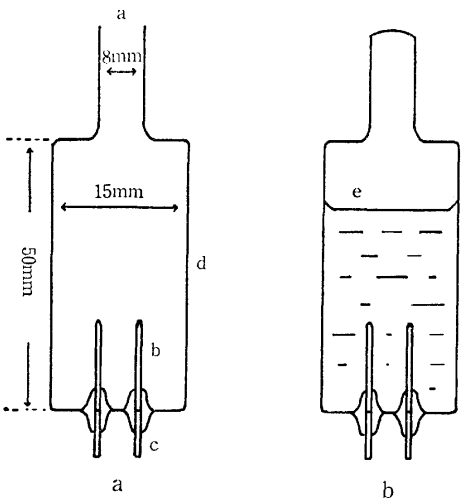

Fig. 2. Cell B used in the composition range of 5.0—25.4 mol% B_2O_3.
a: inlet of sample, b: Pt wire, c: W wire, d: Pyrex glass tube, e: liquid level of sample.

1) J. D. Mackenzie, "Modern Aspect of the Vitreous State," **1**, **2**, **3**, Butterworths, London (1964).
2) T. Maekawa, T. Yokokawa, and K. Niwa, This Bulletin, **42**, 677 (1969).
3) H. Kodama, Y. Kimura, T. Yokokawa, and K. Niwa, *ibid.*, **42**, 681 (1969).
4) H. Franz, *J. Amer. Ceram. Soc.*, **49**, 473 (1966).
5) H. Kodama, T. Yokokawa, and K. Niwa, This Bulletin, **43**, 1036 (1970).

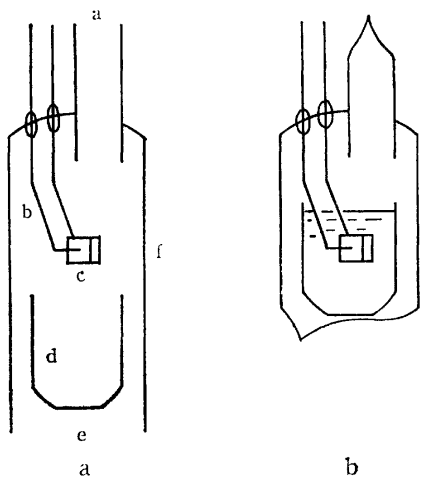

Fig. 3. Cell C used in the compositon range of 33.3—80.5 mol% B_2O_3.
a: inlet of sample, b: Pt wire, c: Pt plate, d: Pt crucible, e: inlet of Pt crucible.

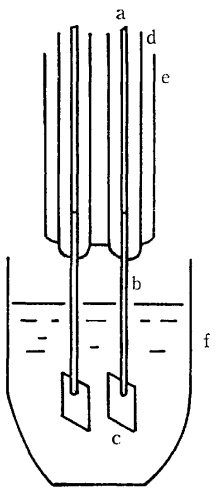

Fig. 4. Cell D used at the concentration of about 99.6 mol % B_2O_3.
a: W wire, b: Pt wire, c: Pt plate, d,e: quartz tube, f: Pt crucible.

For the glass-to-lead wire seal, we used tungsten wire. The last type of cell, the open cell (cell D), was used only in the range of a dilute water content (about 0.1 wt% H_2O). The platinum plate electrodes were platinized by the standard procedure.

Above the liquidus temperature, the vapor pressures of H_2O and HBO_2 become high in the intermediate composition range. The sealed cells, B or C, were so set in a autoclave that the stress due to pressure difference could be moderated. A diagramatic sketch of the apparatus is given in Fig. 5. Nitrogen gas was introduced into the autoclave to compensate the internal pressure of the cell. The data reported by Von Stackelberg[6] and F. Kracek *et al.*[7] were used for doing so.

The cell constant of each cell was calibrated with a 0.1 or 0.01 F KCl aqueous solution prior to the measurement. The cell constant of the A cell was independent of the depth

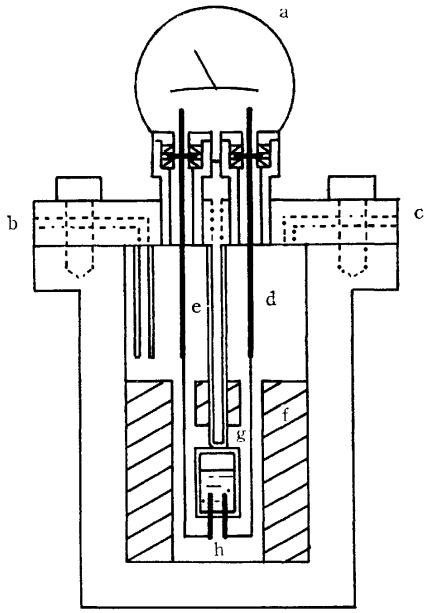

Fig. 5. Autoclave with cell B.
a: pressure gauge, b: gas inlet, c: gas outlet, d: lead wire(Cu), e: thermocouple seath, f: Cu-cylinder, g: cell, h: Pt electrodes.

if the Pt plate electrodes were more than 3 cm below the liquid level. The cell constant of the B cell was also independent of the depth provided that the tips of the electrodes were 5 mm from the liquid level. The corresponding values of the C and D cells depended on the liquid level and had to be calibrated according to its function. The resistance was measured by means of the AC method. A Kohlraush bridge (Y.H.P. type 4255A) was employed. A variable capacitor was coupled when effective. Since the resistance was shown to be independent of the frequency between 1 Hz and 10 kHz, except in the range of intermediate composition, an AC current of 1 kHz was used throughout the experiments.

Since the measured resistance was several hundred Ω and over, any error due to the solution-electrode interfacial capacitance seems to have been small.[8] The measurement with the A cell of a dilute aqueous solution of H_3BO_3 was carried out in an oil bath, its temperature being kept constant within ± 0.05°C. Electric-resistance furnaces were used for the rest of the measurements. The temperature was controlled within ± 0.2°C. The use of the autoclave made the region of homogeneous temperature shorter and the temperature reading somewhat ambiguous. However, the final uncertainty of the conductivity is estimated to be less than 5%, except when the C cell was employed in which case the uncertainty was estimated to be 10%.

Results

The results obtained in the present investigation are shown in Figs. 6, 7, and 8, in which the logarithm of the specific conductivity is plotted against the reciprocals of the absolute temperature.[9] One may note that the Arrhenius linear relation does not hold for most of the compositions. In a solution with an extremely

6) Von Stackelberg, F. Quatram, and J. Dressel, *Z. Elektrochem.*, **43**, 14 (1937).
7) F. C. Kracek, G. W. Morey, and H. E. Merwin, *Amer. J. Sci.*, **35A**, 143 (1938).
8) G. D. Robbins, *J. Electrochem. Soc.*, **116**, 813 (1969).
9) For the numerical data, see the doctors thesis of Hiroshi Kodama, Hokkaido University (1970).

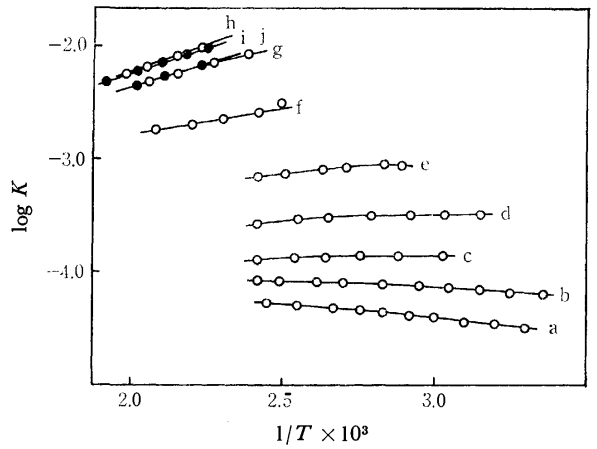

Fig. 6. Relation between specific conductivity and temperature.
a: 0.5, b: 0.7, c: 1.0, d: 1.5, e 2.5, f: 5.0, g(open circle): 10.0, h(open circle): 15.0, i(closed circle): 20.0, j(closed circle): 25.4 (mol% B_2O_3)'

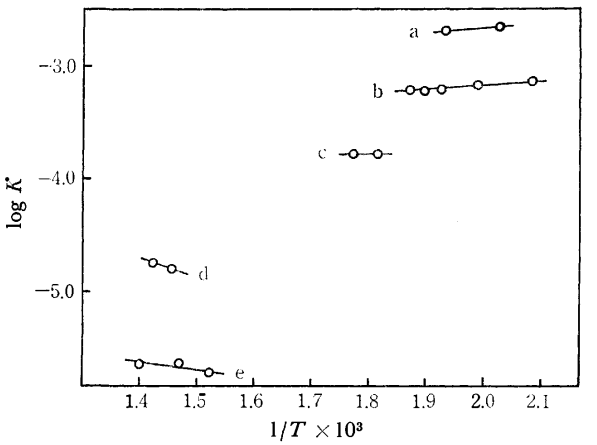

Fig. 7. Relation between specific conductivity and temperature.
a: 33.3, b: 42.2, c: 50.1, d: 74.3, e: 80.5 (mol% B_2O_3).

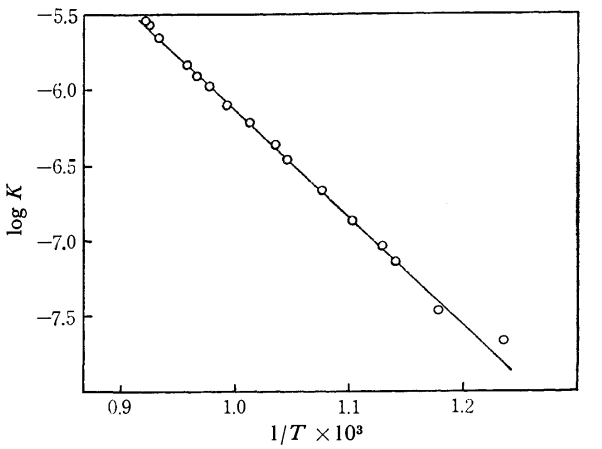

Fig. 8. Relation between specific conductivity and temperature at the concentration of 99.6 mol% B_2O_3.

small B_2O_3 content, the specific conductivity increases with the temperature. With the rise in B_2O_3 content, however, the temperature coefficients of the specific conductivity fall to negative values. The temperature coefficient, strangely enough, returns to positive values beyond a 50 mol % B_2O_3 melt.

Discussion

In ionic conductors, the specific conductivity is given by the following equation:

$$K_{sp} = n_i \times |z_i| \times eu_i \qquad (2)$$

where n_i, z_ie, and u_i are the number of ions per cubic centimeter, the charge, and the mobility of the ion respecitively. Any change in the conductivity can be attributed to a change in either the carrier's concentration or its mobility, or both. The present experimental results indicate that: (1) an Arrhenius-type linear relation does not hold in the H_2O-rich region and (2) the fact that the apparent activation energy is negative in the intermediate range must be interpreted in accordance with the above equation. It is convenient to divide the whole system into ranges from H_2O to H_3BO_3 (25 mol % B_2O_3) and from H_3BO_3 to B_2O_3. The former will be considered as a aqueous solution, and the latter, as a B_2O_3 melt containing H_2O.

H_2O-H_3BO_3 range. H_3BO_3 dissociates into four ionic species, H^+, $H_2BO_3^-$, HBO_3^{2-}, and BO_3^{3-}. Among these species, the numbers of the last two ions are negligible compared with the other two over all the composition ranges in the present measurements. The first dissociation constant (pK) of H_3BO_3 is 9.234 at 25°C. Although there are nearly equal numbers of H^+ and $H_2BO_3^-$ in the solution, the mobility of the hydrogen ion is considerably greater than that of the other. The electric current must be carried mostly by the hydrogen ion.

The mobility of the hydrogen ion in an aqueous solution does not increase steadily with an increase in the temperature. For example, the conductivity of the hydrochloric acid solution has been throughly studied by Owen and Sweeton[10] over a wide range of concentrations and temperatures. They measured the mobilities of the hydrogen and chloride ions separately and found that the absolute temperature coefficient, $(\partial\lambda_-/\partial T)_c$, of the anoin increases from 1.405 at 5°C to 1.753 at 45°C. This increase is about 20%. Under the same conditions, the $(\partial\lambda_+/\partial T)_c$ for H^+ decreases about 18%. This decrease at higher temperatures can be partly explained by the proton-jump mechanism[11,12], since the rate of the proton jump is closely related with the liquid structure, especially the ordering. However, the decreases in the specific conductivity in the present work can not be interpreted only in terms of the decrease in the mobility resulting from the increase in the disorder with the rise in the temperature, for the temperature at which disordering becomes effective may vary from system to system. Further, since the information of the dissociation constant is available at present only for extremely dilute solutions, no firm conclu-

10) B. Owen and F. Sweeton, *J. Amer. Chem. Soc.*, **63**, 2811 (1941).
11) S. Glasstone, K. Laidler, and H. Eyring, "The Theory of Rate Processes," McGraw-Hill, New York and London (1941).
12) R. Gurney, "Ionic Processes in Solution," Dover, New York (1962).

sion can be reached as to the reason for the negative temperature coefficient. However, the present authors feel on the basis of the following data that the variation in the dissociation constant with the temperature must lead to the variation in the hydrogen ion concentration.

In 1934, Harned and Embree,[13] surveying all the data on aqueous solutions, found a remarkable generality in the dissociation of acids. When a parabola of the form

$$\log K = \log K_m - P(T-\theta)^2 \qquad (3)$$

was applied to a set of data for each system, a single value of P, namely $P=5\times10^{-5}$, was found to fit all the data very well. Here θ is the temperature at which the dissociation constant reaches its maximum value, K_m. This phenomenon is related to the temperature dependence of the dielectric constant of water, which plays a decisive role in an acid's dissociation. Only in the case of boric acid do the results appear to be anomalous; there, P is 8×10^{-5} [14]. Although alternative equation,[15] which are thermodynamically more reasonable, have since been proposed, the simpler Eq. (3) is serviceable for the present discussion. For a dilute boric acid solution, the value of θ lies at 77.0°C.[16] In Fig. 9, the logarithmic specific conductivity is plotted against the temperature. These curves may be regarded as parts of a parabola. These results suggest that the concentration of the charge carrier plays an important role in the change of the specific conductivity with the temperature of the present system. As a matter of fact, the relation of the specific conductivity to the concentration was found to be puzzling. In Fig. 10, log K is plotted as a function of log $C_{H_3BO_3}$ at 144°C, where C denotes the number of moles per cubic cm. An almost linear line is obtained up to 25 mol % H_3BO_3. The slope was found to be 1.76, while it should be 0.5 if H_3BO_3 dissociates only at the first step and if the activity coefficients of the species are constant. This extra increase in conductivity with the H_3BO_3 content may be attributable to the change in mobility. In accordance with this the equivalent conductance of H_3BO_3 shown in Fig. 11 reaches a maximum at 25 mol % H_3BO_3. The proton jump mechanism may still be operative in the solution incorporated with the boric acid molecule. One must also note the decrease in the equivalent conductivity with the concentration in an extremely dilute solution, which is not shown in Fig. 11.

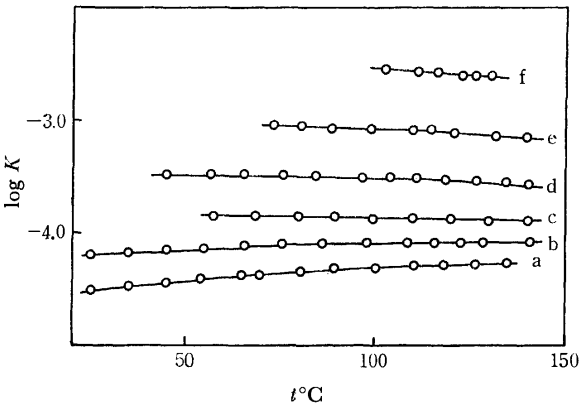

Fig. 9. Relation between specific conductivity and temperature (°C). see Fig. 6 for composition.

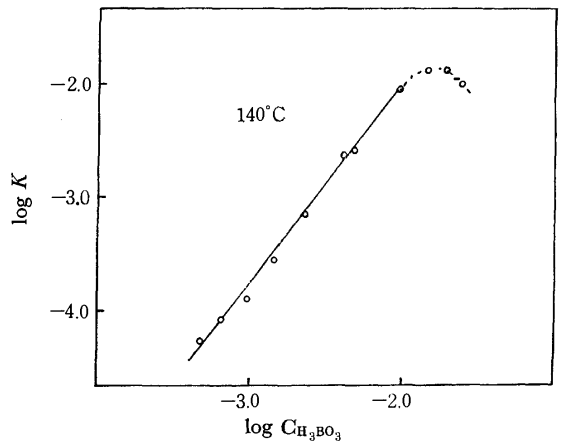

Fig. 10. Relation between the logarithmic specific conductivity and the logarithmic concentration of H_3BO_3 in mole per cm³ at 144°C. Three points beyond −2.0 by $C_{H_3BO_3}$, extrapolated values below the solidus line.

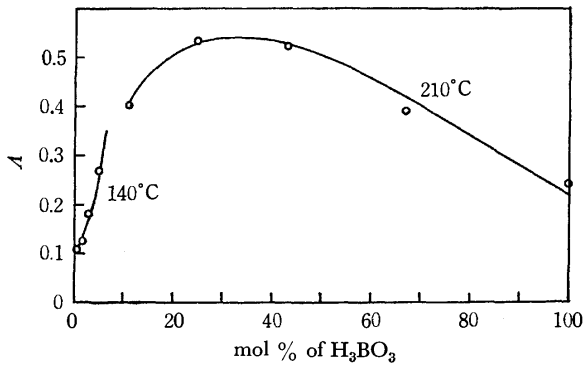

Fig. 11. Equivalent conductance of H_3BO_3 as a function of composition at 140 and 210°C in H_2O-H_3BO_3 range.

H_3BO_3-B_2O_3 Range. In the intermediate range of composition, the experimental data are not enough to allow a quantitative analysis because of the experimental difficulties. However, one may note that the temperature coefficient of the specific conductivity changes in sign near the composition of 50 mol %.

Finally, as is shown in Fig. 8, an Arrhenius-type equation is obtained in the melt of 0.1 wt % (0.4 mol %) water. The apparent activation energy is about 32 kcal/mol. Mackenzie[17] has measured the electric conductivity of B_2O_3 containing a small amount of water (0.1 to 0.2 wt %). He reported a value of about 25 kcal/mol for the activation energy in the region from 850 to 1300°C. The absolute value of the specific consuctivity is $1.9\cdot10^{-6}$ at 850°C, while the extra-

13) H. Harned and N. Embree, *J. Amer. Chem. Soc.*, **56**, 1050 (1934).

14) B. Owen, *J. Amer. Chem. Soc.*, **57**, 1526 (1935).

15) E. King, "Acid-Base Equilibria" "The International Encyclopedia of Physical Chemistry and Chemical Physics: Equilibrium Properties of Electrolyte Solutions," **4**, Pergamon Press, Oxford (1965).

16) H. S. Harned and B. Owen, *Chem. Rev.*, **25**, 50 (1939).

17) J. D. Mackenzie, *J. Phys. Chem.*, **63**, 1875 (1959).

polation of the present results gives $4.5 \cdot 10^{-6}$ at this temperature. Since the specific conductivity and its temperature coefficient are sensitive to the content of water and any impurities, the agreement seems to be satisfactory.

The activation energy for alkali borates, as measured by Shartsis *et al.*,[18] is about 20 kcal at 800°C, which is of an order of magnitude similar to that of the present system. The equivalent conductance of the alkali-metal ions is about unity at a high dilution and increases with the concentration (10 at 20 mol % alkali oxide) at 900°C, while the corresponding H value of the present system varies, being $1.5 \cdot 10^{-4}$ (0.4 mol % water, 560°C), $2.2 \cdot 10^{-4}$ (19.5 mol %, 407°C), and $1.3 \cdot 10^{-3}$ (25.7 mol %, 429°C). Considering the higher mobility of the proton compared with that of any other cation, we may consider that the extent of the dissociation of the –B–O–H group is quite small. The rather perculiar tendency for the equivalent conductance to increase with the concentration is common to both systems, it must be related to the disintegration of the network. No appreciable influence of the coordination change from BO_3 to BO_4 was observed. It is highly desirable to measure the mobility and the concentration of the proton separately.

18) L. Shartsis, W. Capps, and S. Spinner, *J. Amer. Ceram. Soc.*, **36**, 319 (1953).

Conclusion

Electric conductivity was measured over the whole composition range of H_2O–B_2O_3 in the liquid state. The previous data on the dilute aqueous solution of H_3BO_3 and on the B_2O_3 melt with a trace of water are in good agreement with the present results. A perculiar conductivity-temperature relation was observed in the intermediate composition range. As to the conduction mechanism, the proton-jump mechanism and the usual ionic migration seem to be operative in the H_2O-rich and B_2O_3-rich ranges respectively. In the B_2O_3 melt, water behaves in the same manner as do alkali metal oxides except for a partial dissociation of the –B–O–H group.

BULLETIN OF THE CHEMICAL SOCIETY OF JAPAN, VOL. 45, 780—785(1972)

The Characterization of the Electronic Spectra of Heterocyclic Amine *N*-Oxides by Means of the Non-Aqueous Oxidation and Reduction Potentials and the Substituent Effects on Them

Hiroshi MIYAZAKI, Tanekazu KUBOTA, and Masumi YAMAKAWA
Shionogi Research Laboratory, Shionogi and Co., Ltd., Fukushima-ku, Osaka

(Received September 20, 1971)

The half-wave potentials of the voltammetric oxidation and the reduction of various heterocyclic amine *N*-oxides have been measured in CH_3CN by the technique of a rotating platinum electrode. The reversibility of the electrode process was particularly examined for the oxidation reaction by analyzing the oxidation wave and by recording the ESR spectra. Then, the mutual relationship between the electronic spectra of these *N*-oxides and the values of the oxidation-reduction potentials was discussed in detail; we found that this kind of treatment is very useful in assigning the spectra. Finally, a good linear relation between the oxidation potentials of substituted pyridine *N*-oxides and the Hammett σ^+ (Brown-Okamoto) constants was demonstrated and discussed.

It is well known that the polarographic reduction and the oxidation potentials of organic compounds are closely correlated with the molecular orbital energies or with the total energy difference between the starting molecule and the product (free radical) after electrolysis.[1-6] That is, the oxidation ($E_{1/2}^{oxd}$) and the reduction ($E_{1/2}^{red}$) potentials are in a linear relation to the highest occupied molecular orbital (HOMO) and the lowest vacant orbital (LVMO) energies respectively. In other words, the $E_{1/2}^{oxd}$ and the $E_{1/2}^{red}$ seem to be a good measure of the ionization potential and the electron affinity of solvated organic molecules.[7,8] Keeping in mind these facts it can easily be expected that the oxidation and the reduction potentials are correlated quite well with the ultraviolet (UV) absorption spectra of organic compounds if the effect of the configuration interaction is small, and that a singly-excited configuration from HOMO to LVMO contributes mainly to these UV spectra. Typical examples of this kind previously reported are the charge-transfer (CT) ab-

1) J. Koutecky, *Z. Phys. Chem. N. F.*, **52**, 8 (1967) and the other papers cited therein.
2) M. J. S. Dewar, J. A. Hashmall, and N. Trinajstic, *J. Amer. Chem. Soc.*, **92**, 5555 (1970) and the other papers cited therein.
3) K. B. Wiberg and T. P. Lewis, *ibid.*, **92**, 7154 (1970).
4) T. Kubota, K. Nishikida, H. Miyazaki, K. Iwatani, and Y. Ōishi, *ibid.*, **90**, 5080 (1968).
5) E. S. Pysh and N. C. Yang, *ibid.*, **85**, 2124 (1963).
6) W. C. Neickam, G. R. Dimeler, and M. M. Desmond, *J. Electrochem. Soc.*, **111**, 1190 (1964).
7) F. A. Matsen, *J. Chem. Phys.*, **24**, 602 (1956).
8) B. Case, N. S. Hush, R. Parsons, and M. E. Peover, *J. Electroanal. Chem.*, **10**, 360 (1965), *etc.*

sorption bands of CT complexes,[9-11] which are in a good linearity with the half-wave potentials of the polarographic reduction and the voltammetric oxidation of the electron acceptor and the electron donor respectively.

We will in this paper be concerned with an examination of the mutual relation between the half-wave reduction and oxidation potentials and the UV spectra of heterocyclic amine *N*-oxides; it is believed that the results obtained here will be quite useful in characterizing the UV absorption bands of the *N*-oxides, which were extensively studied hitherto in our laboratory. In connection with these dicussions, we will also study what kind of substituent effect on the oxidation and reduction potentials can be expected.

Experimental

Measurements. A Yanagimoto polarograph, Model P8-AP, was used to record the DC and AC polarograms. This instrument uses the three-electrode system, so that the potential due to the so-called *IR* drop term arising from the resistance of the cell circuit is automatically corrected. In the case of polarographic reduction, the details of the experimental technique for obtaining the accurate values of reduction potential have already been reported elsewhere.[4] The capillary used for the dropping mercury electrode was: $m=0.855$ mg/sec and $t=5.17$ sec at $h=70$ cm in distilled water at an open circuit. On the other hand, the half-wave potential of the oxidation voltammogram has been measured using the rotating platinum electrode illustrated in Fig. 1. This electrode has a platinum rod 1 mm in diameter, which was sealed in a soft glass tube with a diameter of ~6.5 mm, as may be seen in Fig. 1. Just before the use of this electrode, we polished the plane head of the rotating platinum electrode with very fine emery paper in order to keep the platinum surface always fresh. This simple technique gave reproducible results.[12] To record the voltammogram, a combination of the above rotating platinum electrode (600 rpm) and a Yanagimoto polarograph, Model P8-AP, was employed, a saturated calomel electrode (SCE) being

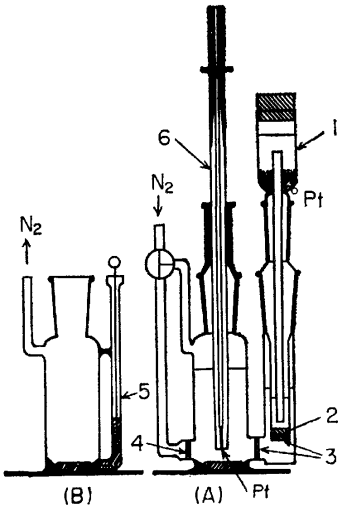

Fig. 1. Electrolysis cell used for recording DC and AC voltammograms. A and B show front and side views, respectively. (1) SCE. (2) salt bridge (see reference 4). (3, 4) fine (3) and coarse (4) glass filters. (5) terminal for ac measurement or three-electrode system. (6) rotating platinum electrode.

Table 1. Various heterocyclic amine *N*-oxides investigated, with their numbering, half-wave reduction and oxidation potentials (V *vs.* SCE), electron number (n) entering in the electrode oxidation reaction, SCF-MO energies (eV) at LVMO and HOMO, and observed band position (eV) at ^1L_a (CT) and ^1L_b bands[a]

No.	Compound	Reduction $E_{1/2}^{red}$	Oxidation $E_{1/2}^{oxd}$	Oxidation n	SCF-MO E_{lv}	SCF-MO E_{ho}	Observed band positions ^1L_a(CT)	Observed band positions ^1L_b
1	Pyridine *N*-oxide	−2.302	1.802	1.0	−2.277	−9.564	4.40	3.81
2	Pyrazine mono-*N*-oxide	−1.836	2.312	1.07	−2.558	−9.923	4.53	
3	Pyrazine di-*N*-oxide	−1.615	1.741	1.32	−3.256	−9.679	3.87	3.4
4	Pyrimidine mono-*N*-oxide	−1.927	2.352	0.81	−2.413	−9.613	—	
5	Quinoline *N*-oxide	−1.840	1.537	0.82	−2.983	−9.223	3.54	3.54
6	Isoquinoline *N*-oxide	−1.948	1.600	0.66	−2.997	−9.372	3.95	3.20
7	Quinoxaline mono-*N*-oxide	−1.456	1.971	0.28[b]	−3.220	−9.588	3.75	
8	Quinoxaline di-*N*-oxide	−1.247	1.598	1.03	−3.639	−9.305	3.02	
9	Phenanthridine *N*-oxide	−1.814	1.482	0.62	−3.061	−9.206	3.62	3.22
10	Acridine *N*-oxide	−1.358	1.280	0.91	−3.500	−8.740	2.73	3.22
11	Phenazine mono-*N*-oxide	−1.021	1.745	0.81	−3.752	−9.110	2.94	3.26
12	Phenazine di-*N*-oxide	−0.851	1.344	0.81	−4.022	−8.825	2.51	
	Tetramethyl-*p*-phenylenediamine	—	0.128	1.0	—	—	—	—

a) See text for detailed explanation.
b) The maximum wave appeared only for this oxidation wave, whose temperature dependence is large (6.34%) and concentration dependence is irregular, although $E_{1/2}^{oxd}$ value almost unchanged with the variation of concentration. Small n value for this case may be due to those irregular phenomena.

9) M. E. Peover, *Trans. Faraday Soc.*, **58**, 1656, 2370 (1962); **60**, 479 (1964).
10) M. E. Peover and J. D. Davies, *ibid.*, **60**, 476 (1964).
11) R. D. Holm, W. R. Carper, and J. A. Blancher, *J. Phys. Chem.*, **71**, 3960 (1967).
12) Here, note that the oxidation voltammogram itself does not change whether or not the dissolved oxygen in solution is removed by bubbling pure nitrogen gas in the solution. Needless to say, however, the reduction voltammogram should be recorded under a pure nitrogen atmosphere.

Table 2. Half-wave oxidation potentials (V *vs.* SCE) of substituted pyridine *N*-oxides recorded with rotating platinum electrode, and the Brown-Okamoto σ^+ values of the substituents

Substituent[a]	$E_{1/2}^{oxd}$	σ^+
H	1.802	0
4-CH_3	1.606	−0.311
4-C_2H_5	1.575	−0.295
4-OCH_3	1.362	−0.778
4-$NHCOCH_3$	1.315	−0.6
4-$N(CH_3)_2$	0.759	−1.7
4-Cl	1.795	0.114
4-$COOC_2H_5$	1.977	0.482
4-CN	2.27	0.659
4-NO_2	2.13	0.790
3-CH_3	1.793	−0.066
3-OCH_3	1.717	0.047
3-Cl	1.900	0.399
3-$COOC_2H_5$	1.918	0.366
3-CN	2.013	0.562

a) The positions 4 and 3 correspond respectively to para- and meta-positions against *N*-oxide group.

used as the reference electrode. Usually all the experiments were made at 25±0.1°C in a CH_3CN solvent containing 0.1 M tetra-*n*-propylammonium perchlorate (TNPAP) as the supporting electrolyte, the sample concentration being ~5×10^{-4} mol/*l*. As typical examples, the oxidation voltammograms of 1,4-dimethoxybenzene and 9,10-diphenylanthracene have been recorded; they are compared with the values in the literature[13,14] where the experimental conditions were the same as ours. The observed values of $E_{1/2}^{oxd}$ (in volts) are 1.310 (1.34) for the former and 1.241 (1.22) for the latter; here, the values in parentheses are those reported in the literature.[13,14] The agreement of the values seems to be good. Finally, the electron-spin-resonance measurements of the anion and the cation radicals of the compounds studied have been carried out by using a technique reported in a foregoing paper.[15]

Samples and Solvents. The samples used are listed in Tables 1 and 2 along with the experimental results. The preparation, the purification, and the physical constants of these samples have been described in our previous papers.[4,16] The supporting electrolyte, TNPAP, was synthesized in the usual manner[17] and was recrystallized several times from a CH_3CN–H_2O mixture. Acetonitrile has been employed as the solvent throughout the present electrode reaction of oxidation and reduction. Spectrograde CH_3CN was rectified carefully after dehydration with CaH_2. Dimethylformamide (DMF) was also used for comparing the data with those in CH_3CN in the case of voltammetric or polarographic reduction, the quality of DMF being the same as has been described elsewhere.[4]

Results and Discussion

Half-wave Potentials, $E_{1/2}$'s, of the Voltammetric Oxidation and Reduction. It is worthy of note that the electrode reactions of the aromatic amine *N*-oxides used are not all the same. An examination of the oxidation voltammograms shows that some compounds exhibit a reversible electrode reaction due to the cation-radical formation of a mother compound, while other compounds give an irreversible reaction. A typical example of the former is phenazine di-*N*-oxide, whose oxidation and reduction voltammograms are shown in Fig. 2. The high value of the first wave peak-height of alternating-current (ac) voltammograms should be noted; it indicates a reversible electrode reaction. In fact, the ESR spectra of the cation and of the anion radicals of phenazine di-*N*-oxide were observed by controlled potential electrolysis at the first wave of the oxidation and the reduction voltammograms respectively.[4,15,18] The following oxidation voltammetric data on phenazine di-*N*-oxide also support the above interpretation: (i) the temperature dependence of the limiting current, i_l (μA), is 0.87%, as computed by the compound-interest method; (ii) the plotting of i_l *vs.* the concentration gave a good straight line through the point of origin, and (iii) the value of 0.063 V of the log-plot (the value of $\Delta E/\Delta\log[i/(i_l-i)]$ indicates a one-electron oxidation process.

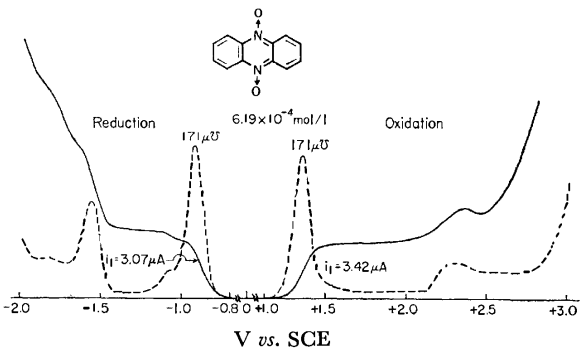

Fig. 2. DC (solid curve) and AC (dotted curve) voltammograms obtained by rotating platinum electrode for oxidation and reduction of phenazine di-*N*-oxide. The absolute value of current is taken at the ordinate for the convenience's sake.

On the other hand, the oxidation voltammograms of quinoxaline mono-*N*-oxide, *etc.*, which have nitrogen lone-pair electrons in a molecule, are typical examples of an irreversible electrode reaction. The participation of the lone-pair electrons in the process of electrode oxidation is the main reason for these irreversible reactions, where the voltammograms change with repeated runs of the measurements unless the platinum electrode is kept on the fresh surface before each recording.

Tables 1 and 2 list the data on the oxidation voltammograms of all the samples used in this report. The *n* value shown in Table 1 stands for the electron number entering in the reaction; it was determined by comparing the wave height with that (standard) of tetramethyl-*p*-phenylenediamine recorded under the same condi-

13) A. Zweig, W. G. Hodgson, and W. H. Jura, *J. Amer. Chem. Soc.*, **86**, 4124 (1964).
14) R. E. Visco and E. A. Chandross, *ibid.*, **86**, 5350 (1964).
15) K. Nishikida, T. Kubota, H. Miyazaki, and S. Sakata, *J. Mag. Resonance* (1972), in press.
16) T. Kubota and H. Miyazaki, This Bulletin, **39**, 2057 (1966).
17) D. H. Geske and A. H. Maki, *J. Amer. Chem. Soc.*, **82**, 2671 (1960).
18) The interpretation and the assignment of the hyperfine coupling constants of these radicals, and also the non-aqueous polarographic data on the electrode reduction, have already been reported in detail.[4,15]

tions. The oxidation voltammogram of tetramethyl-*p*-phenylenediamine is typical of those due to the one-electron oxidation process.[19]

As was mentioned above, the reversibility of the electrode oxidation reaction is more or less different and depends on the compounds. Nevertheless, we have adopted the $E_{1/2}^{oxd}$ values obtained here for the following discussions, since it may be assumed that the effect of the reversibility on the half-wave potential value is not severe. The circumstances as to the $E_{1/2}^{red}$ values are somewhat similar to those presented above in the oxidation voltammogram. However, generally speaking, the reversibility in the electrode reduction process seems to be better than in the case of the oxidation process for many compounds. The polarographic behaviour of various aromatic *N*-oxides has already been reported in detail.[4,15,20] The results of the present reduction voltammetric study are quite similar to, and well reproduce those of the previous polarographic investigation,[4] so in this report we will not discuss these experimental results further. Since the values of $E_{1/2}^{oxd}$ and $E_{1/2}^{red}$ yielded under the same conditions are most reasonable for checking the theoretical treatment (*vide infra*), the $E_{1/2}^{red}$ values observed by using the rotating platinum electrode in CH_3CN solvent are included in Table 1.

The Mutual Relation between UV Spectra and the Half-wave Oxidation and Reduction Potentials. It is well known that the HOMO and the LVMO are in a linear relation to the $E_{1/2}^{oxd}$ and the $E_{1/2}^{red}$ values respectively.[1-8,21,22] Also, the electronic spectra are intimately correlated with the energy difference between the electron-occupied orbitals and the vacant orbitals, so we can except a reciprocal correlation, which would be useful in the assignment of the electronic spectra, of the electronic spectra to the half-wave oxidation and reduction potentials.[23]

If we let ε_{ho} and ε_{lv} be the orbital energies for the highest occupied and the lowest vacant orbitals respectively, Eqs. (1) and (2) are satisfied:

$$E_{1/2}^{red} = k_1\varepsilon_{lv} + k_2 \quad (1)$$

$$E_{1/2}^{oxd} = k_1\varepsilon_{ho} + k_3 \quad (2),$$

where k_1, k_2, and k_3 are all constants. It is assumed here that the electrode reaction is a reversible one-electron process, such as ($R+e \rightleftharpoons R^{\dot{-}}$) or ($R-e \rightleftharpoons R^{\dot{+}}$), and that the difference in diffusion coefficients, activity coefficient, and entropy terms between R and $R^{\dot{-}}$ or $R^{\dot{+}}$ can be disregarded because the values[2] are similar. The left-hand-side terms of Eqs. (1) and (2) can now be expressed by $\Delta F/\mathcal{F}$, where ΔF is the free-energy change for the above electrode process in an non-aqueous solution and is related mainly to the electron affinity[24] for the formation of $R^{\dot{-}}$ or to the ionization potential[24] for the formation of $R^{\dot{+}}$, and also to the solvation-energy change (ΔF_{solv}) between R and $R^{\dot{-}}$ or $R^{\dot{+}}$.[2] Accordingly, the slope, k_1, in Eqs. (1) and (2) becomes $1/\mathcal{F}$. Because $\mathcal{F}$ in a Faraday constant (1 eV/1 V), $|k_1|$ is equal to 1 when an electron volt is taken as the energy unit. The ΔF_{solv} term would be constant under the same experimental conditions in a series of similar compounds (see also later discussions), and would contribute greatly to the k_2 and k_3 terms in Eqs. (1) and (2). We can now write Eq. (3) by taking account of the difference between Eqs. (1) and (2) (here k_4 is a new constant):

$$(E_{1/2}^{red} - E_{1/2}^{oxd}) = k_1(\varepsilon_{lv} - \varepsilon_{ho}) + k_4 \quad (3)$$

In turn, the singlet energy corresponding to a one-electron transition from HOMO to LVMO is given by[25]:

$${}^1E_{ho\to lv} = \varepsilon_{lv} - \varepsilon_{ho} + 2K_{ho\cdot lv} - J_{ho\cdot lv} \quad (4)$$

The excited state pertinent to the transition energy, ${}^1E_{ho\to lv}$, may be mixed with the other excited states having the same symmetry, so that the ${}^1E_{ho\to lv}$ should be changed by the amount of the configuration interaction energy, ${}^1E_{CI}$. The observed energy, $E_{ho\to lv}^{UV}$, attributable mostly to the HOMO→LVMO transition, is thus written as $E_{ho\to lv}^{UV} = \varepsilon_{lv} - \varepsilon_{ho} + 2K_{ho\cdot lv} - J_{ho\cdot lv} + {}^1E_{CI}$. $K_{ho\cdot lv}$ and $J_{ho\cdot lv}$ are, respectively, the well-known two-electron exchange and the Coulomb repulsion integrals[25] pertaining to the two MO's given in the suffixes. The combination of the above equations leads to Eq. (5):

$$(E_{1/2}^{red} - E_{1/2}^{oxd}) = k_1[E_{ho\to lv}^{UV} + J_{ho\cdot lv} - 2K_{ho\cdot lv} - {}^1E_{CI}] + k_4 \quad (5)$$

The linear relation between the experimental values of $(E_{1/2}^{red} - E_{1/2}^{oxd})$ and $E_{ho\to lv}^{UV}$ may be obtained under the binding conditions that in a series of similar compounds, (i) the effect of ${}^1E_{CI}$ on the ${}^1E_{ho\to lv}$ is small or is considered to be constant throughout the compounds, and (ii) the magnitude of the electron repulsion terms ($J_{ho\cdot lv} - 2K_{ho\cdot lv}$) may be put constant in all the samples. In these cases, we can simply write Eq. (6):

$$(E_{1/2}^{red} - E_{1/2}^{oxd}) = k_1 \cdot E_{ho\to lv}^{UV} + k_5 \quad (6)$$

Previously we reported detailed Pariser-Parr-Pople (P.P.P.)-type SCF MO calculations of many aromatic tertiary amine *N*-oxides for use in interpreting the electronic spectra and the electronic structures.[26] These calculation results can be used to check Eqs. (3) and (6). For the compounds whose P.P.P. calculations have not yet been reported, the calculations have been newly carried out here using the same method as in

19) T. A. Gough and M. E. Peover, "Polarography," Vol. 2, ed. by G. J. Hills, Macmillan, London (1964), p. 1017.

20) T. Kubota, H. Miyazaki, and Y. Mori, *Rev. Polarog.*, (Kyoto), **14**, 313 (1967).

21) a) T. Tani and S. Kikuchi, Report of the Institute of Industrial Science, the University of Tokyo, **18**, No. 2 (1968), p. 51. b) T. Tani, K. Honda, and S. Kikuchi, *J. Electrochem. Soc. Japan*, **37**, 17 (1969), and the other papers cited in 21a and 21b.

22) R. Takahashi, "Reaction in Non-aqueous Solvents," Kagakuzōkan 44, ed. by N. Ise, N. Tokura, and T. Fujinaga, (in Japanese) Kagaku-Dōjin (Kyoto) (1970), p. 147.

23) a) A. T. Watson and F. A. Matsen, *J. Chem. Phys.*, **18**, 1305 (1950). b) I. Bergman, *Trans. Faraday Soc.*, **50**, 829 (1954); **52**, 690 (1956).

24) Assuming that there is no change in the molecular geometry upon the $R^{\dot{-}}$ or $R^{\dot{+}}$ formation and no change in the electronic state compared to that of the ground state except for the one-electron addition to LVMO or the one-electron removal from HOMO, these values may be put equal to ε_{lv} or ε_{ho}.

25) N. Mataga and T. Kubota, "Molecular Interactions and Electronic Spectra," Chapter 2, Marcel Dekker, New York (1970).

26) M. Yamakawa, T. Kubota, and H. Akazawa, *Theoret. Chim. Acta* (Berl.), **15**, 244 (1969), and the other papers cited therein. See also C. Leibovici and J. Streith, *Tetrahedron Lett.*, **1971**, 387; J. C. D. Brand and K.-T. Tang, *J. Mol. Spectrosc.*, **39**, 171 (1971).

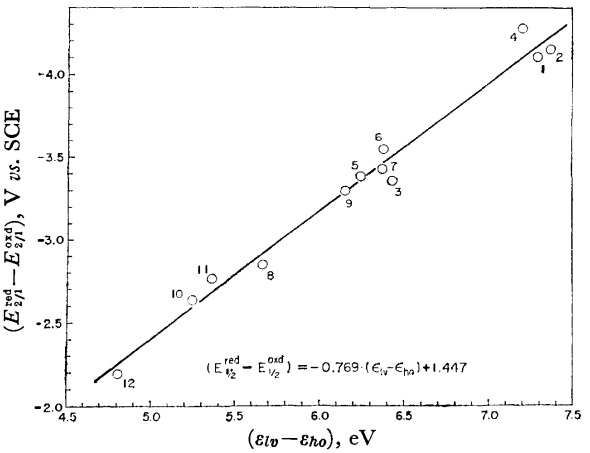

Fig. 3. The relationship between calculated values of $(\varepsilon_{lv}-\varepsilon_{ho})$ and observed values of $(E^{red}_{1/2}-E^{oxd}_{1/2})$ for heterocyclic amine *N*-oxides. See Table 1 for the numbering of each compound.

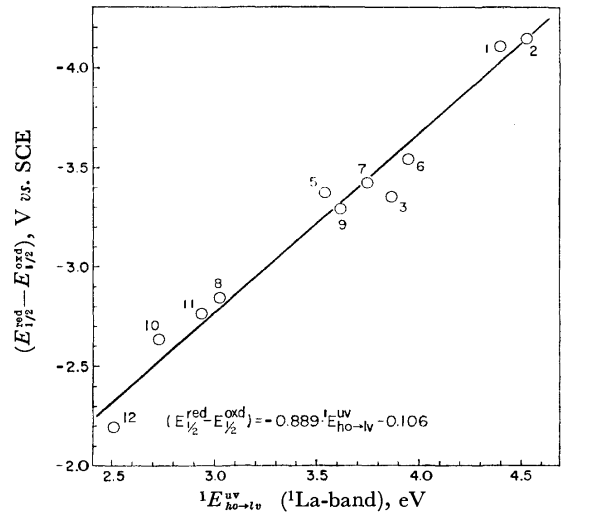

Fig. 4. The relationship between observed values of ^1L_a ($^1E^{uv}_{ho\to lv}$) band and $(E^{red}_{1/2}-E^{oxd}_{1/2})$ for heterocyclic amine *N*-oxides. See Table 1 for the numbering of each compound.

foregoing papers.[26,27] The calculation results are listed in Table 1.

Let us now focus attention on the intramolecular charge-transfer band (^1L_a band) of the amine *N*-oxides,[26] which is mainly due to an electron transition from HOMO to LVMO, where the effect of the configuration interaction is small except for the case of isoquinoline *N*-oxide (0.394 eV). On the basis of the calculation results made hitherto, we may say that the values of $^1E_{CI}$ and $(2K_{ho\cdot lv}-J_{ho\cdot lv})$ are within the maximum variation of 0.11 ± 0.10 eV and -2.21 ± 0.80 eV respectively, and that, except for a few exceptional cases, these values may be seemed to be nearly constant. Therefore, the linear relation of Eqs. (3) and (6) can reasonably be expected to be as is given in Figs. 3 and 4. The mutual correlations are very good. That the slope of the straight line obtained in Figs. 3 and 4 is less than, but near, the |1| should be noted. It can safely be said that the previous conclusion[26] that the ^1L_a (or CT) band of aromatic *N*-oxides arises mainly from a one-electron transition from HOMO to LVMO has been supported by the electrochemical study illustrated in Figs. 3 and 4. From the other standpoint, one can also discuss as follows. It may be remembered that, of the methods employed for analyzing the electronic spectra of a series of similar compounds, the so-called spectroscopic β method is a useful technique[28,29]; here the exchange integral, β, is taken to be a constant applied only to absorption bands which belong to electronic transitions similar in character (*i.e.*, for the ^1L_a and ^1L_b bands the β (^1L_a) and $\beta(^1L_b)$ values are separately assigned). In principle, the β value may be considered as a value including the electron repulsion terms pertinent to the electronic transitions in the same species; it is taken as a constant throughout the series of absorption bands in question, so that the assumptions used in deriving the present equation (6) (except for the discussion of the $^1E_{CI}$ term) and in estimating the spectroscopic β value seem to be similar to each other. Thus, the experimental results shown in Figs. 3 and 4 confirm the usefulness of the above-mentioned spectroscopic β method.

Next, let us discuss the slope of the straight lines shown in Figs. 3 and 4, which is less than the theoretical value of |1|. In previous discussions, we assumed that there was no change in the solvation energy of a variety of cation or anion radicals. The *N*-oxides used, however, can be roughly grouped in three groups by size; *i.e.*, the substances range from monocyclic to tricyclic *N*-oxides, so that the effective ion radii of the cation or anion radicals fall in three groups. As may be understood from Born's equation,[30] these may turn out to be different solvation energies, which would more or less destroy our first assumption. In the present case, we may say, in general, that as the molecular size increases, the values of $|E^{red}_{1/2}-E^{oxd}_{1/2}|$, $(\varepsilon_{lv}-\varepsilon_{ho})$, $^1E^{uv}_{ho\to lv}$, and *the solvation energy* of the anoin or cation radical ions, decrease, which may lead to the slope smaller than |1| that is found for the data obtained *in vacuo*. The following experimental data can also account for the deviation from the ideal linear relationship of Eqs. (3) and (6). That is, the reversibility of the electrode process may be a little different between the reduction and oxidation voltammograms, since, in general, the heterocyclic compound producing the corresponding stable anion radical brings about a lesser stability in the corresponding cation radical, and *vice versa* (see also the first section of "Results and Discussion").

Finally, we would like to discuss the relationship between the ^1L_b bands of the *N*-oxides and the $(E^{red}_{1/2}-E^{oxd}_{1/2})$ values. Generally speaking, the ^1L_b band has a very different character from that of the ^1L_a (or CT) band; not only is the contribution from the HOMO→

27) For the pyridine-type nitrogen atom the values of 14.51 eV and 1.20 eV were employed as the valence-state ionization potential and the electron affinity respectively. *Cf.* G. Pilcher and H.A. Skinner, *J. Inorg. Nucl. Chem.*, **24**, 937 (1962).

28) H. Baba, This Bulletin, **34**, 76 (1961); H. Baba and S. Suzuki, *ibid.*, **34**, 82 (1961); *J. Chem. Phys.*, **32**, 1706 (1960); L. Goodman and H. Shull, *ibid.*, **27**, 1388 (1957).

29) T. Kubota and M. Yamakawa, This Bulletin, **36**, 1564 (1963); M. Yamakawa, T. Kubota, H. Akazawa, and I. Tanaka, *ibid.*, **41**, 1046 (1968).

30) M. Born, *Z. Physik.*, **1**, 45 (1920); see also Ref. 25, p. 225.

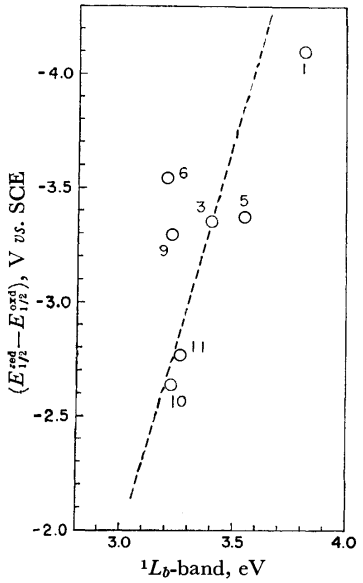

Fig. 5. Plot of the observed values of $(E^{red}_{1/2}-E^{oxd}_{1/2}$ against the observed ^1L_b band energies for heterocyclic amine *N*-oxides. See Table 1 for the numbering of each compound.

LVMO transition very small (if one considers the C_{2v} molecule, the contribution is zero), but also the effect of the configuration interaction on that band is quite large. Accordingly, we can not expect a linear relationship as in Eq. (6). For some *N*-oxides we plot (Fig. 5) the values of $(E^{red}_{1/2}-E^{oxd}_{1/2})$ against the ^1L_b band positions, whose assignment has already been reported.[26] It is now clear that there is no good linear relation and that, roughly speaking, the ^1L_b band position is quite independent of the values of $(E^{red}_{1/2}-E^{oxd}_{1/2})$, so the slope of the dotted line in Fig. 5 is very much larger than |1| and is theoretically unreasonable. Conversely speaking, we can say that the bands employed in Fig. 5 can not be assigned to the ^1L_a (or CT) and that the experimental test of Eqs. (3) and (6) is quite usefull in confirming the band assignment.

Substituent Effect on the Oxidation Potentials of Pyridine N-Oxide Derivatives. In our previous papers, we have already reported a good linear correlation between the $E^{red}_{1/2}$ values and Hammett's σ constants on pyridine *N*-oxide derivatives[4,16] and discussed the physical meaning of this. Here, we have tested whether or not such a correlation holds in the case of the $E^{oxd}_{1/2}$ values, also. Fig. 6 shows the correlation of the $E^{oxd}_{1/2}$ values, which are listed in Table 2, with the Brown-Okamoto σ^+ constants.[31] A good linear relation, written as $E^{oxd}_{1/2}=0.565\ \sigma^+ + 1.745$, with a root mean-square deviation equal to ± 0.066, is found to hold. It should be noted that, in the present case, if one adopts usual Hammett's σ or σ^- values[4,16] we can not find, in particular for the case of larger electron-donating substituents, a good linear relation such as is found in Fig. 6. The free-energy change due to the electrode oxidation reaction is, of course, electrophilic in nature and is just the reverse of that in the case of the electrode reduction process, where the use of σ^- and σ values was suitable[4,16] (the reaction is nucleophilic). Therefore, it is reasonable to say that the better description of the activated state of the oxidation reaction is made using the σ^+ values. Lastly, it is worthwhile to point out that the most important molecular orbital entering into the electrode oxidation is the HOMO, which is destabilized by introducing an electron-donating substituent such as NR_2 in the pyridine ring. This brings about the oxidation reaction more easily and makes the $|E^{oxd}_{1/2}|$ value smaller. These circumstances are just the reverse of those for the process of electrode reduction, where the $|E^{red}_{1/2}|$ value increases when the ring hydrogen atom is replaced with an electron-donating substituent.

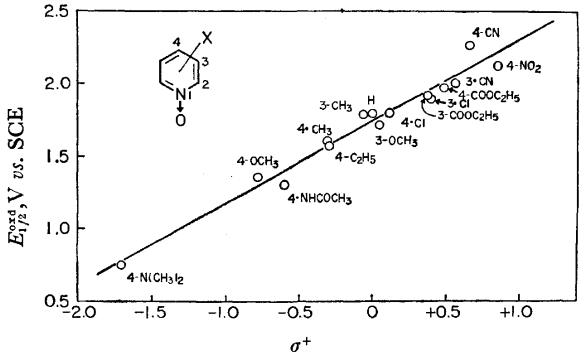

Fig. 6. Linear relation between Brown-Okamoto's σ^+ values and the half-wave oxidation potentials at the first wave of substituted pyridine *N*-oxides.

The authors wish to express their thanks to Professors Soichiro Musha and Makoto Munemori of the College of Engineering, University of Osaka Prefecture, and to Professor Saburo Nagakura of the Institute for Solid State Physics, the University of Tokyo, for their useful discussions.

31) H. C. Brown and Y. Okamoto, *J. Amer. Chem. Soc.*, **80**, 4979 (1958).

Dipole Moment and Force Constants of NSCl from Microwave Spectrum

Setsuko MIZUMOTO, Jun IZUMI, Tatsuro BEPPU,* and Eizi HIROTA
Department of Chemistry, Faculty of Science, Kyushu University, Fukuoka
(Received October 4, 1971)

Dipole moment of $^{15}N^{32}S^{35}Cl$ has been determined to be $\mu_a=0.564_5\pm0.0085$, $\mu_b=1.74_7\pm0.035$, $\mu_{total}=1.83_6\pm0.036$D by analyzing the Stark effect of the $1_{1,1}\leftarrow0_{0,0}$ transition.

Twenty-eight rotational transitions of $^{14}N^{32}S^{35}Cl$ in the ground state have been analyzed to determine four centrifugal distortion constants: $\tau_{aaaa}=-6.9_9\pm0.30$, $\tau_{bbbb}=-0.011_0\pm0.0013$, $\tau_{aabb}=0.17_6\pm0.014$, and $\tau_{abab}=-0.033_4\pm0.0068$ MHz. These constants are combined with the vibrational frequencies and inertia defects to recalculate force constants: $F_{11}=10.032$ md/Å, $F_{22}=1.44_4$ md/Å, $F_{33}=0.74_9$ mdÅ, and $F_{23}=-0.08_6$ md.

The microwave spectrum of NSCl has recently been reported by Beppu *et al*,[1] who determined the molecular structure and the quadrupole coupling constant of the chlorine nucleus, and also estimated force constants using the inertia defects and vibrational frequencies. However, the dipole moment has not been evaluated because the Stark effect of the rotational spectrum of NSCl is complicated by the nuclear quadrupole coupling. In the present work the Stark effect of the $1_{1,1}\leftarrow0_{0,0}$ transition of $^{15}N^{32}S^{35}Cl$ is analyzed in detail to determine the dipole moment and its components along the a- and b-axes.

The general quadratic force field may be determined combining vibrational frequencies with other physical constants such as the inertia defects.[2] The centrifugal distortion constants have also been proved useful in force field determinations.[3-11] It may be worthwhile to improve the force field estimated in Ref. 1 using the centrifugal distortion constants and to compare derived force constants with those of related molecules such as NSF.[10,11]

Experimental

The sample of NSCl was prepared by a method described in Ref. 1. The spectrometer used was of conventional Hughes-Wilson type with a 120 kHz oscillator as a Stark modulator. The spectrum was observed at room temperature.

* Department of Chemistry, Faculty of Science, The University of Tokyo. Present address: Central Research Laboratory, Tokyo Shibaura Electric Co., Ltd., Kawasaki.

1) T. Beppu, E. Hirota, and Y. Morino, *J. Mol. Spectrosc.*, **36**, 386 (1970).
2) Y. Morino, Y. Kikuchi, S. Saito, and E. Hirota, *J. Mol. Spectrosc.*, **13**, 95 (1964).
3) D. Kivelson, *J. Chem. Phys.*, **22**, 904 (1954).
4) L. Pierce, *ibid.*, **24**, 139 (1956).
5) M. G. K. Pillai and R. F. Curl, Jr., *ibid.*, **37**, 2921 (1962).
6) L. Pierce, N. DiCiani, and R. H. Jackson, *ibid.*, **38**, 730 (1963).
7) R. L. Cook, *ibid.*, **42**, 2927 (1965).
8) G. E. Herberich, R. H. Jackson, and D. J. Millen, *J. Chem. Soc.* (A), **1966**, 336.
9) A. M. Mirri and E. Mazzariol, *Spectrochim. Acta*, **22**, 785 (1965).
10) R. L. Cook and W. H. Kirchhoff, *J. Chem. Phys.*, **47**, 4521 (1967). It is to be noted that this reference uses 0.7124D of the OCS moment as a standard. Since the value given by Ref. 12 is 0.7152_1D, dipole moment of NSF (1.902D) is recalculated to be 1.910D.
11) A. M. Mirri and A. Guarnieri, *Spectrochim. Acta*, **23A**, 2159 (1967).

Dipole Moment

The Stark effect of the $1_{1,1}\leftarrow0_{0,0}$ transition of $^{15}N^{32}S^{35}Cl$ is shown in Fig. 1, where the observed frequencies of Stark components are indicated by open circles. Electric field is calibrated using the OCS molecule as a standard.[12] In the limit of the zero field the transition consists of three lines corresponding to $F=3/2\leftarrow3/2$, $5/2\leftarrow3/2$, and $1/2\leftarrow3/2$, whereas two Stark lobes, $M_I=\pm3/2$ and $\pm1/2$, are observed at strong field. In the intermediate region there are five Stark lobes, of which three are $M_F=\pm1/2$ and two $M_F=\pm3/2$. Analysis is carried out according to a procedure described previously,[13] where the rotational constants are fixed to the values reported in Ref. 1: $A=40\,355.96$, $B=4\,019.65$, and $C=3\,649.36$ MHz. A least-squares analysis gives the a and b components of dipole moment and the bb component of the quadrupole coupling constant of the chlorine nucleus as follows: $\mu_a=0.564_5\pm0.0085$D, $\mu_b=1.74_7\pm0.035$D, and $\chi_{bb}=23.8_4\pm0.50$ MHz, where errors are 2.5 times the standard deviations. The frequencies of the Stark lobes calculated using these parameters are drawn by solid lines in Fig. 1 and compared with the observed in Table 1. The χ_{bb} constant may be compared favorably with the value already reported,[1] 23.51 MHz. The total dipole moment is $\mu_{total}=1.83_6\pm0.036$D.

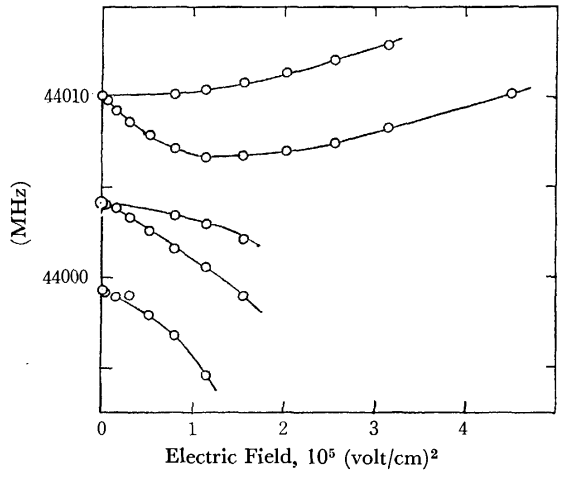

Fig. 1. Stark effect of $1_{1,1}-0_{0,0}$ of $^{15}N^{32}S^{35}Cl$.

12) J. S. Muenter, *J. Chem. Phys.*, **48**, 4544 (1968).
13) E. Hirota and Y. Morino, This Bulletin, **34**, 341 (1961).

TABLE 1. STARK EFFECT OF THE $1_{1,1}\leftarrow 0_{0,0}$ TRANSITION OF $^{15}N^{32}S^{35}Cl$ (MHz)

square of field[a]	obsd	obsd −calcd	obsd	obsd −calcd[b]	obsd	obsd −calcd[b]
$M_F=\pm 1/2$						
0.0	44 010.10	+0.01	44 004.15	+0.02	43 999.36	+0.00
4.70	44 009.77	−0.13			43 999.17	−0.07
14.10	44 009.30	−0.22			43 998.90	−0.08
29.77	44 008.68	−0.22			43 999.00	+0.51
51.70	44 007.90	−0.20			43 997.91	+0.18
79.90	44 007.23	−0.01	44 003.46	−0.24	43 996.75	+0.08
114.37	44 006.73	+0.10	44 003.00	−0.14	43 994.60	−0.68
155.10	44 006.82	+0.28	44 002.20	+0.31		
202.10	44 007.05	+0.16				
255.37	44 007.50	+0.01				
314.90	44 008.29	+0.02				
452.77	44 010.23	+0.00				
$M_F=\pm 3/2$						
0.0	44 010.10	+0.01	44 004.15	+0.02		
4.70			44 004.05	+0.02		
14.10			44 003.83	+0.02		
29.77			44 003.28	−0.11		
51.77			44 002.63	−0.08		
79.90	44 010.19	+0.07	44 001.65	−0.08		
114.37	44 010.40	−0.01	44 000.60	+0.18		
155.10	44 010.82	−0.02	43 999.00	+0.22		
202.10	44 011.34	−0.08				
255.37	44 012.10	−0.03				
314.90	44 012.90	−0.06				

a) In 10^3 (volt/cm)^2.
b) Calculated frequencies are obtained using $\mu_a=0.564_5$D, $\mu_b=1.74_7$D, and $\chi_{bb}=23.8_4$ MHz.

TABLE 2. ROTATIONAL SPECTRUM OF NSCl IN THE GROUND STATE (MHz)

Transition	obsd line center	calcd	distortion correction	obsd −calcd
$1_{1,0}-1_{0,1}$	37 983.1[a]	37 983.05	−1.69	0.05
$2_{1,1}-2_{0,2}$	38 361.72[a]	38 361.61	−1.47	0.11
$3_{1,2}-3_{0,3}$	38 934.40[a]	38 934.68	−1.17	−0.28
$4_{1,3}-4_{0,4}$	39 708.73[a]	39 708.48	−0.80	0.25
$5_{1,4}-5_{0,5}$	40 690.41[a]	40 691.29	−0.41	−0.88
$6_{1,5}-6_{0,6}$	41 893.52[a]	41 893.33	−0.04	0.19
$7_{1,6}-7_{0,7}$	43 327.0[a]	43 326.68	0.24	0.32
$8_{1,7}-8_{0,8}$	45 005.0[a]	45 005.14	0.35	−0.14
$1_{1,1}-0_{0,0}$	45 460.22[a]	45 460.24	−1.70	−0.02
$2_{1,2}-1_{0,1}$	52 937.9[a]	52 937.61	−1.55	0.29
$3_{1,3}-2_{0,2}$	60 228.4[a]	60 228.29	−1.36	0.11
$1_{1,1}-2_{0,2}$	21 904.86	21 904.83	−1.63	0.03
$2_{1,2}-3_{0,3}$	13 687.89	13 688.09	−1.26	−0.20
$6_{0,6}-5_{1,5}$	11 958.30	11 958.17	−1.78	0.13
$7_{0,7}-6_{1,6}$	20 801.36	20 801.51	−3.67	−0.15
$8_{0,8}-7_{1,7}$	29 768.26	29 768.40	−6.10	−0.14
$9_{2,8}-10_{1,9}$	24 744.92	24 745.48	−1.62	−0.56
$10_{2,9}-11_{1,10}$	14 923.31	14 922.54	5.86	0.77
$14_{1,13}-13_{2,12}$	15 490.03	15 489.52	−36.69	0.51
$15_{1,14}-14_{2,13}$	25 920.70	25 920.94	−50.13	−0.24
$12_{2,10}-13_{1,13}$	30 601.97	31 601.92	0.31	0.05
$13_{2,11}-14_{1,14}$	27 486.13	27 486.10	3.00	0.03
$14_{2,12}-15_{1,15}$	23 807.70	23 807.66	4.92	0.04
$15_{2,13}-16_{1,16}$	20 594.13	20 594.33	5.72	−0.20
$16_{2,14}-17_{1,17}$	17 872.57	17 872.24	5.05	0.33
$17_{2,15}-18_{1,18}$	15 665.16	15 665.32	2.50	−0.16
$18_{2,16}-19_{1,19}$	13 994.59	13 994.64	−2.34	−0.05
$19_{2,17}-20_{1,20}$	12 877.96	12 877.95	−9.92	0.01

a) Ref. 1.

Centrifugal Distortion Constants and Force Constants

The line centers of all transitions assigned to the parent species, $^{14}N^{32}S^{35}Cl$, in the ground state are listed in Table 2. The hyperfine structures, where resolved, are corrected for using the quadrupole coupling constants previously reported.[1]

The first-order perturbation theory is applied to determine three rotational constants and four distortion constants. Higher-J transitions may include larger contributions of the distortion effects, but simultaneously the higher-order terms such as the P^6 terms should be taken into consideration to determine the P^4 terms precisely.[6] In the present analysis the transitions of J up to 20 are included. The values of parameters obtained by a least-squares analysis[14] are listed in Table 3, where the errors are 2.5 times the standard deviations. The line frequencies calculated using these

TABLE 3. ROTATIONAL CONSTANTS AND CENTRIFUGAL DISTORTION CONSTANTS OF $^{14}N^{32}S^{35}Cl$ IN THE GROUND STATE (MHz)[a]

A	41 723.3$_4$ ±0.16	τ_{aaaa}	−6.9$_9$ ±0.30
B	4 114.15$_4$±0.026	τ_{bbbb}	−0.011$_0$±0.0013
C	3 738.60$_5$±0.021	τ_{aabb}	0.17$_6$ ±0.014
		τ_{abab}	−0.033$_4$±0.0068

a) Errors are 2.5 times the standard deviations.

14) E. Hirota, T. Tanaka, A. Sakakibara, Y. Ohashi, and Y. Morino, *J. Mol. Spectrosc.* **34**, 222 (1970).

parameters are compared with the observed in Table 2. The average deviation is 0.18 MHz.

In Ref. 1 the four force constants, three diagonal and one off-diagonal, are determined using two vibrational frequencies, ω_1 and ω_2, and two vibrational increments of the inertia defects, Δ_2 and Δ_3. It may thus be interesting to see whether four distortion constants obtained in the present work are useful in determining two remaining force constants, F_{12} and F_{13}. This is unfortunately not the case.

A least-squares analysis is carried out using ω_1, ω_2, Δ_2, Δ_3, τ_{aaaa}, τ_{bbbb}, τ_{aabb}, and τ_{abab} as input data with the following weights: 1.0 for ω_1, 2.0 for ω_2, 1000.0 for Δ_2 and Δ_3, 0.5 for τ_{aaaa}, 130.0 for τ_{bbbb}, 10.0 for τ_{aabb}, and 25.0 for τ_{abab}. The units used here are cm^{-1} for ω, amu Å^2 for Δ, and MHz for τ. The inertia defect should be accurate to about 0.005 amu Å^2, and the weights for the distortion constants might therefore be too small. Calculation with weights of distortion constants increased by a factor of ten gives, however, force constants which agree with the former results within 2.5 times the standard deviations. When F_{12} or F_{13} or both are included as parameters, a least-squares analysis is not convergent. However, a negative F_{12} (about -0.5 md/Å) and a positive F_{13} (about 0.3 md) give much closer fitting to the observed constants, provided that the four force constants are adjusted accordingly. The result shown in Table 4 is obtained assuming both F_{12} and F_{13} equal to zero. Agreement between the observed and the calculated constants is satisfactory except for τ_{bbbb} and τ_{abab}, for which the discrepancies exceed the error limits (see Table 4). A larger discrepancy remains for ω_3, although the "observed" value is estimated, but not measured directly.[15] It is difficult to increase the calculated ω_3 to 273 cm^{-1}, because of the conditions imposed by the inertia defect.

TABLE 4. FORCE CONSTANTS OF NSCl

Force constant	Present[a]	Ref. 1
F_{11}(md/Å)	10.032 ± 0.003	10.03_1
F_{22}(md/Å)	$1.44_4\pm0.013$	1.46_5
F_{33}(mdÅ)	$0.74_9\pm0.036$	0.76_7
F_{23}(md)	$-0.08_6\pm0.022$	-0.067
Constant	**obsd**	**calcd**
$\omega_1(cm^{-1})$	1325	1325
$\omega_2(cm^{-1})$	414	414
$\omega_3(cm^{-1})$	(273)[b]	253.6
Δ_1(amuÅ^2)	(-0.006_8)[c]	-0.0063
Δ_2(amuÅ^2)	0.120_4	0.1240
Δ_3(amuÅ^2)	0.359_9	0.3627
τ_{aaaa}(MHz)	-6.9_9	-6.9_1
τ_{bbbb}(MHz)	-0.011_0	-0.0154
τ_{aabb}(MHz)	0.17_6	0.179
τ_{abab}(MHz)	-0.033_4	-0.0482

a) Errors are 2.5 times the standard deviations.
b) Estimated (Ref. 15). c) Calculated, see Ref. 1.

Discussion

The total dipole moment of NSCl is $1.83_6\pm0.036$D, which is very close to that of NSF, 1.910D.[10]

After the completion of the present work Guarnieri sent us his results on dipole-moment determination.[16] He analyzed the Stark effect of three transitions, $2_{1,1}\leftarrow 2_{0,2}$ ($F=7/2\leftarrow7/2$), $3_{1,2}\leftarrow3_{0,3}$ ($F=9/2\leftarrow9/2$), and $1_{1,1}\leftarrow 0_{0,0}$, of the parent species. For the former two transitions he measures the Stark effect of the component of the largest F value (7/2 and 9/2, respectively) which is independent of the quadrupole effect, and for the last transition only the Stark effect in the strong field is used in the analysis. Dipole moment he obtains is $\mu_a=0.57\pm0.03$D, $\mu_b=1.77\pm0.02$D, and $\mu_{total}=1.87\pm0.02$D. To compare the present results with these values it is necessary to transform the principal axes of the ^{15}N species to those of the parent species, and the angle of transformation is calculated to be $31.4_4'$ using the structural parameters of Ref. 1. When μ_a and μ_b are of the same sign, the a- and b-components of the parent species are calculated to be $\mu_a=0.580_5\pm0.01$ and $\mu_b=1.74_2\pm0.04$D, whereas they are $\mu_a=0.548_5\pm0.01$ and $\mu_b=1.75_2\pm0.04$D in the case of opposite sign (see Ref. 1 for the signs of the coordinate axes). It is seen that both cases are in agreement with Guarnieri's results within experimental errors. On the other hand, the latter case ($\mu_a\mu_b<0$) is shown to be more realistic from consideration of bond moment. As shown in Table 5, the total moment of the ^{15}N species makes an angle of 57°2′ with S–Cl and 60°40′ with S–N, when μ_a and μ_b are of the same sign, whereas the two angles are 92°50′ and 24°52′ for the case of opposite sign. The total moment of 1.83_6D is then accounted for by μ(S–Cl) of 1.80_8D and μ(S–N) of 1.74_0D for the former case and μ(S–Cl) of 0.87_2D and μ(S–N) of 2.07_1D for the latter. A similar analysis is carried out for NSF, and the result is also given in Table 5. Because the

TABLE 5. BOND MOMENTS OF NSCl AND NSF

	NSCl	NSF
I. $\mu_a\mu_b>0$		
θ_1	57°2′	58°18′
θ_2	60°40′	58°37′
μ(S–X)	1.80_8D	1.82_8D
μ(S–N)	1.74_0D	1.82_2D
II. $\mu_a\mu_b<0$		
θ_1	92°50′	72°56′
θ_2	24°52′	43°59′
μ(S–X)	0.87_2D	1.48_7D
μ(S–N)	2.07_1D	2.04_7D

θ_1: angle between μ and S–X.
θ_2: angle between μ and S–X.

bond moment of S–Cl is normally of the order of 0.7D,[17] the second case is more reasonable for NSCl, although a larger moment is expected for S–Cl because of larger fraction (57%) of a resonance form N=S$^+$Cl$^-$, as discussed in Ref. 1. As for NSF, the difference between the bond moments for the two cases is smaller, because the total moment is nearly parallel to the b-axis. Yet the second case is a bit more reasonable: although the bond moment of S–F is not known, the

15) A. Müller, G. Nagarajan, O. Glemser, S. F. Cyvin, and J. Wegener, *Spectrochim. Acta*, **23A**, 2683 (1967).
16) A. Guarnieri, personal communication; to be published.
17) C. P. Smyth, "Dielectic Behavior and Structure," McGraw-Hill, New York, N. Y. (1955).

electronegativity difference for F and S is 1.5, whereas it is 0.5 for Cl and S. Therefore, the S–F moment of 1.48_7D of NSF in the second case seems to be more reasonable. It may be interesting to note that the value of S–N, 2.04_7D for NSF and 2.07_1D for NSCl, is very close to dipole moment of the NS radical, 1.81D.[18]

It is rather disappointing that it has not been possible to determine all three off-diagonal force constants, even if the inertia defects and centrifugal distortion constants are used in addition to vibrational frequencies. The situation is similar to the case of NSF investigated by Cook and Kirchhoff,[10] although they did not take into account the inertia defects in the excited vibrational states. The F_{11} constant of NSF (10.703 md/Å) is nearly the same as that of NSCl (10.032 md/Å), just as the bond length N–S, 1.448 Å for NSF and 1.450 Å for NSCl. The force constants associated with the halogen atom decrease their values from the case of fluoride to the chloride. It may be interesting to note that F_{23} becomes negative for the chloride. In order to improve the force constants of NSCl it is indispensable to observe the ν_3 band in the infrared spectrum.

The calculation in the present work was carried out at the Computation Center at Kyushu University.

18) T. Amano, S. Saito, E. Hirota, and Y. Morino, *J. Mol. Spectrosc.*, **32**, 97 (1969).

BULLETIN OF THE CHEMICAL SOCIETY OF JAPAN, VOL. 45, 789—793(1972)

Mordant Blue 31 as a New Fluorometric Reagent for Aluminum, Gallium, and Scandium

Keizō HIRAKI

Department of Chemistry, Faculty of Science and Technology, Kinki University, Kowakae, Higashi-Osaka

(Received June 2, 1971)

A sensitive fluorometric determination of aluminum, gallium, and scandium with Mordant Blue 31 was worked out. The reagent reacts with aluminum, gallium, scandium, yttrium, lanthanum, lutetium, indium, and magnesium in acidic or basic medium to form complexes with reddish yellow fluorescence. The complexes of aluminum (pH: 5—7), gallium (pH: 4), and scandium (pH: 6) exhibit strong fluorescence with an emission maximum at 590, 600, and 610 nm, respectively. The effects of time, pH and the concentration of the reagent were investigated. In acidic medium, aluminum, gallium, and scandium were found to form 1:1 complex with Mordant Blue 31. Under the optimum conditions, 0.1—3 μg of aluminum, 1—12 μg of gallium, and scandium in 25 m*l* sample solution could be determined. Although the fluorescence intensity of aluminum and gallium complexes was a little lower than that of the lumogallion complexes, Mordant Blue 31 was also applicable as a fluorometric reagent for aluminum and gallium. Since scandium-Mordant Blue 31 complex exhibits the strongest fluorescence of all other scandium-azo dye complexes, the reagent was used as a fluorometric reagent for scandium.

o,o'-Dihydroxyazo compounds are useful as sensitive fluorometric reagents for various metal ions.[1-6] Donald *et al.*[7] described the fluorescent properties of several metal complexes of *o,o'*-dihydroxyazo compounds. In these series chromotropic acid derivatives in particular are very sensitive and form stable fluorescent complexes with aluminum and gallium ions.

The present author describes the preparation of Mordant Blue 31 [2-(2-hydroxy-5-sulfophenylazo)-1,8-dihydroxynaphthalene-3,6-disulfonic acid], and the fluorometric determination of several metal ions.

The reagent reacts with magnesium ion to form a stable fluorescent complex in alkaline solution, determination of magnesium is described.

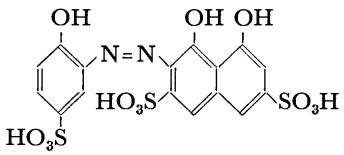

Mordant Blue 31

Apparatus

Spectrofluorometric measurements were carried out with a Hitachi spectrophotometer, Model FPU-2A, equipped with a Hitachi fluorometric attachment, Model G-3. A Hitachi fluorometer, Model EPL-2, was used for fluorometric measurements and a Hitachi-Horiba glass electrode pH meter Model M-5 for pH measurements.

Reagents and Materials

Synthesis of Mordant Blue 31. 2-Amino-1-phenol-

1) A. Weissler and C. E. White, *Ind. Eng. Chem., Anal. Ed.*, **18**, 530 (1946).
2) Y. Nishikawa, K. Hiraki, K. Morishige, and T. Shigematsu, *Japan Analyst*, **16**, 692 (1967).
3) Y. Nishikawa, *ibid.*, **7**, 549 (1958).
4) R. Olsen and H. Diel, *Anal. Chem.*, **35**, 1142 (1963).
5) J. A. Radley, *Analyst*, **68**, 368 (1943).
6) Y. Nishikawa, K. Hiraki, and K. Morishige, *J. Faculty of Science and Technology, Kinki Univ.*, **2**, 15 (1967).
7) C. Donald, J. Freeman, and C. E. White, *J. Amer. Chem. Soc.*, **78**, 2678 (1956).

4-sulfonic acid dissolved in 6N hydrochloric acid was diazotized with an equivalent amount of sodium nitrite under cooling with ice. Chromotropic acid dissolved in about 6N sodium hydroxide was coupled with the diazonium salt solution under cooling below 5°C. The azo compound thus obtained was repeatedly recrystallized from 6N hydrochloric acid, and dried at room temperature in a desiccator on silica gel.

Reagent. 0.1% Mordant Blue 31 solution; 0.25 g of Mordant Blue 31 was dissolved in water and diluted with water to 250 m*l*.

Standard solution of aluminum; 1.6803 g of $Al(NH_4)(SO_4)_2 \cdot 12H_2O$ was dissolved in a small amount of water and 5 m*l* of concentrated hydrochloric acid, and diluted to 100 m*l* with water (1 mg Al/m*l*). The solution was diluted with water to prepare a solution of 1.00 μg Al per m*l*.

Standard solution of gallium; 0.1344 g of Ga_2O_3 (99.99%) was dissolved in concentrated hydrochloric acid, and diluted to 100 m*l* with water (1 mg Ga/m*l*). The stock solution was diluted with 0.1N hydrochloric acid to prepare a solution of 1.00 μg Ga per m*l*.

Standard solution of scandium; 0.1534 g of Sc_2O_3 (99.9%) was dissolved in concentrated hydrochloric acid and diluted to 100 m*l* with water (1 mg Sc/m*l*). The solution was diluted with water to make a standard solution containing 1.00 μg of Sc per m*l*.

Standard Rhodamine B solution; 0.100 g of Rhodamine B was dissolved in water and diluted to 100 m*l*. The solution was diluted with water to prepare a solution of 0.168 μg per m*l*.

Experimental

Fluorescence Spectra of Metal Mordant Blue 31 Complexes. Mordant Blue 31 reacts with aluminum, gallium, scandium, yttrium, lanthanum, lutetium, indium, and magnesium in acidic or basic medium to form complexes with reddish yellow fluorescence. The excitation and emission spectra of aluminum-, gallium-, and scandium-Mordant Blue 31 complexes, which show strong fluorescence, are given in Figs. 1 and 2, respectively.

The reddish yellow fluorescent aluminum complex exhibited excitation maxima at 330 and 540 nm and fluorescence emission maximum at 590 nm. The red fluorescent gallium complex showed excitation maxima at 340 and 580 nm, and fluorescence maximum at 600 nm. The scandium complex showed excitation maxima at 340 and 535 nm, and emission maximum at 610 nm.

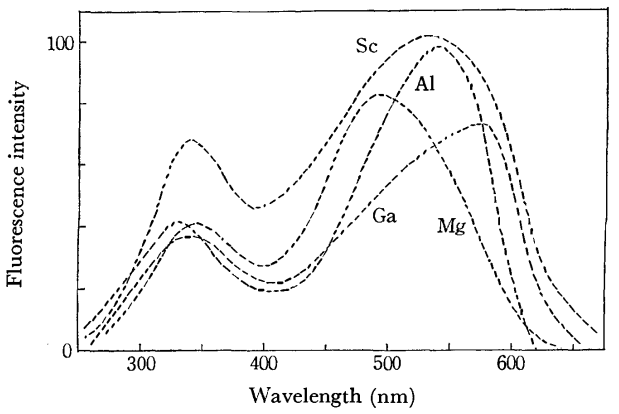

Fig. 1. Excitation spectra of metal Mordant Blue 31 complex
Al: 5×10^{-6}M, emission monochromator set at 590 nm;
Ga: 5×10^{-6}M, emission monochromator set at 600 nm;
Sc: 1×10^{-5}M, emission monochromator set at 610 nm;
Mg: 1×10^{-4}M, emission monochromator set at 585 nm

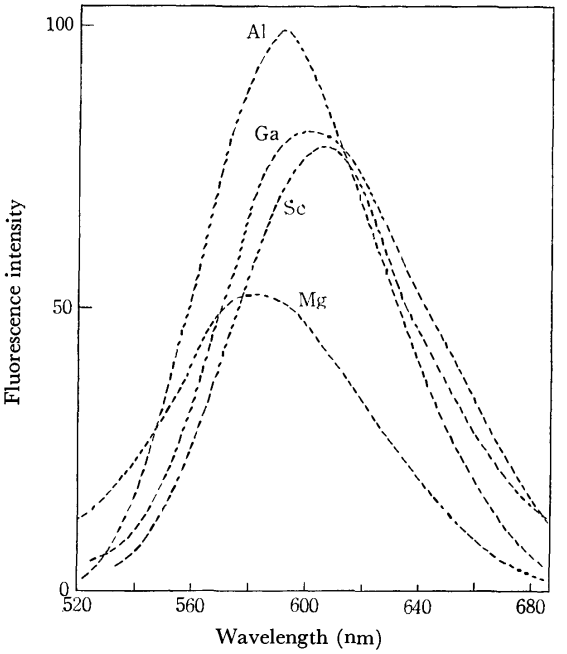

Fig. 2. Emission spectra of metal Mordant Blue 31 complex
Al: 5×10^{-6}M, excitation monochromator set at 330 nm;
Ga: 5×10^{-6}M, excitation monochromator set at 340 nm;
Sc: 1×10^{-5}M, excitation monochromator set at 340 nm;
Mg: 1×10^{-4}M, excitation monochromator set at 340 nm

Fluorometric Determination of metals. *(1) Aluminum*: To about 15 m*l* of the sample solution containing 0.1—3 μg of aluminum, 0.15 m*l* of 0.1% Mordant Blue 31 solution and 2 m*l* of 20% ammonium acetate solution were added. The pH value of the solution was adjusted to 6 with dilute hydrochloric acid or ammonia water and the solution was diluted to 25 m*l* with water. After being stood for 60 min at room temperature, the fluorescence intensity of the solution was measured at 590 nm (excitation: 330 or 540 nm) against the standard Rhodamine B solution.

(2) Gallium: To the sample solution containing 1—12 μg of gallium, 0.25—0.3 m*l* of 0.1% Mordant Blue 31 solution and 2 m*l* of 20% ammonium acetate solution were added. The pH was adjusted to 4, and diluted to 25 m*l*. After being stood 15 min, the fluorescence intensity of the solution was measured at 600 nm (excitation: 340 or 580 nm) against the standard Rhodamine B solution.

(3) Scandium: Scandium was determined by the same procedure as for gallium, adjusting the pH to 6 (excitation: 340 or 535 nm, emission: 610 nm).

Results and Discussion

Effect of Time. The fluorescence of the gallium- and the scandium-complex in aqueous medium was fully developed within a few minutes after mixing the solutions, and was stable for at least 2 hr. On the other hand, the fluorescence of aluminum complex required 120 min to reach the maximum as shown in Fig. 3. The fluorescence of some metal-azo-complex

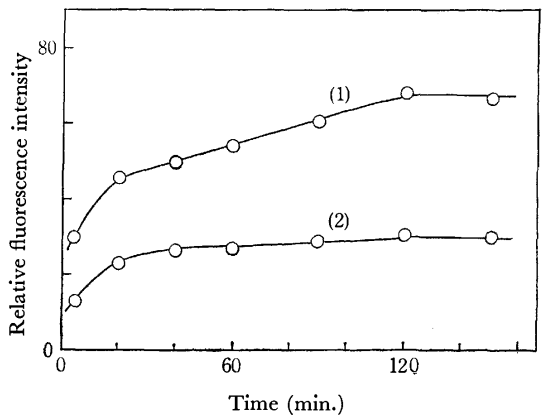

Fig. 3. Stability of fluorescence intensity of aluminum Mordant Blue 31 complex
(1) Al 2 μg, 0.1% reagent solution 0.15 m*l*, pH 6.0, 20 div. (*viz.* 0.168 μg Rhodamine B/m*l* standard solution, FPL-2-primary filter 365, secondary filter 61)
(2) Al 2 μg, 0.1% reagent solution 0.15 m*l*, pH 6.0, 10 div. (*viz.* 0.168 μg Rhodamine B/m*l* standard solution, FPL-2-primary filter 546, secondary filter 61)

readily reached the maximum intensity on warming at 80°C for several minutes. The aluminum complex was unstable on heating and the fluorescence intensity was measured after standing for 1 hr.

Effect of pH. The effect of pH on the fluorescence intensity of the metal-complexes is shown in Fig. 4. The pH values were adjusted with hydrochloric

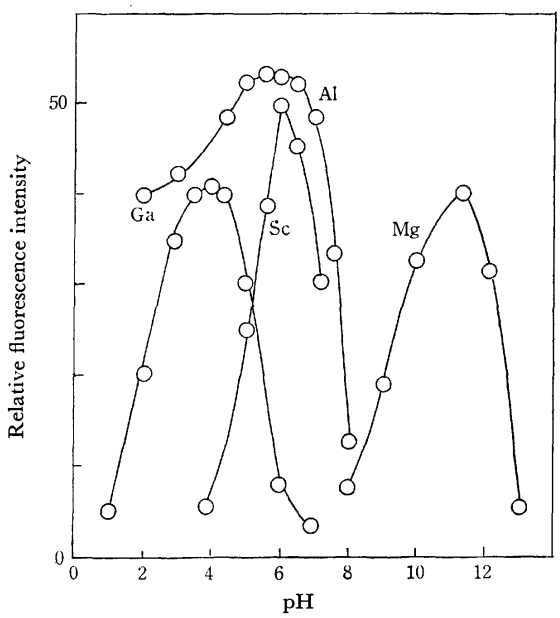

Fig. 4. Effect of pH of solution on fluorescence intensity
Al: 2 μg, 0.1% reagent solution 0.15 m*l*, 40 div. (*viz.* 0.168 μg Rhodamine B/m*l* standard solution, FPL-2-primary filter 365, secondary filter 61)
Ga: 10 μg, 0.1% reagent solution 0.25 m*l*, 40 div. (*viz.* 0.168 μg Rhodamine B/m*l* standard solution, FPL-2-primary filter 365, secondary filter 61)
Sc: 10 μg, 0.1% reagent solution 0.30 m*l*, 60 div. (*viz.* 0.168 μg Rhodamine B/m*l* standard solution, FPL-2-primary filter 365, secondary filter 61)
Mg: 30 μg, 0.1% reagent solution 1.00 m*l*, 100 div. (*viz.* 0.168 μg Rhodamine B/m*l* standard solution, FPL-2-primary filter 365, secondary filter 61)

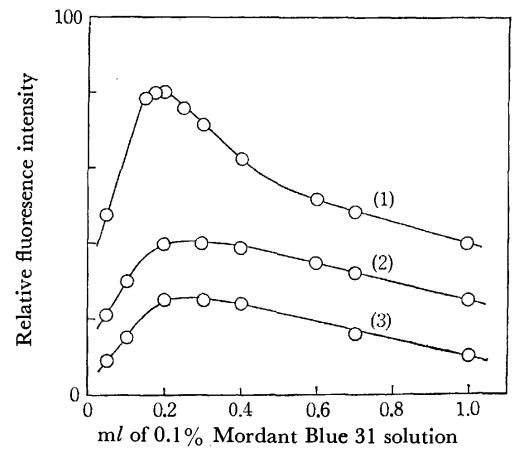

Fig. 5. Effect of reagent concentration
(1) Al 3 μg, pH 6.0, 20 div. (*viz.* 0.168 μg Rhodamine B/m*l* standard solution, FPL-2-primary filter 365, secondary filter 61)
(2) Ga 10 μg, pH 4.0, 40 div. (*viz.* 0.168 μg Rhodamine B/m*l* standard solution, FPL-2-primary filter 365, secondary filter 61)
(3) Sc 10 μg, pH 6.0, 30 div. (*viz.* 0.168 μg Rhodamine B/m*l* standard solution, FPL-2-primary filter 365, secondary filter 61)

acid or ammonia water, except in the case of the magnesium complex where ammonium chloride-ammonia buffer solution and sodium hydroxide solution were used for pH control.

The aluminum and scandium complexes show the maximum fluorescence intensity at pH 6. The pH-intensity curve for the aluminum complex shows maximum value at pH 5—7. The maximum fluorescence intensity of the gallium complex is obtained at pH 4, while the magnesium complex fluoresces in basic medium and gives the maximum intensity at pH 11.

Effect of Concentration of Mordant Blue 31. The effect of concentration of the reagent was examined by adding the different amounts of Mordant Blue 31 to the solution containing 3 μg of aluminum, 10 μg of gallium or 10 μg of scandium, followed by adjusting the pH to the optimum value for the metal complex.

As shown in Fig. 5, the maximum fluorescence intensity was achieved with the use of 0.15 m*l* of 0.1% Mordant Blue 31 solution for the determination of 0.1—3 μg of aluminum. For 1—12 μg of gallium, and 1—12 μg of scandium, respectively 0.25 m*l*, 0.3 m*l* of the reagent solution were required. In all cases, the fluorescence intensity decreases gradually in proportion to the amount of the reagent added. This is due to inner filter effects. Thus a definite amount of reagent was used.

Calibration Curves. Figure 6 shows the calibration curves for aluminum, gallium, and scandium obtained by the above procedures by setting up the fluorometer at 20—40 division using the standard Rhodamine B solution. A linear relationship holds between the fluorescence intensity and the metal ion concentration, showing that aluminum, gallium, and scandium could be determined in the following range: Al; 0.1—3 μg, Ga; 1—12 μg, Sc; 1—12 μg, with an average error of 3 percent.

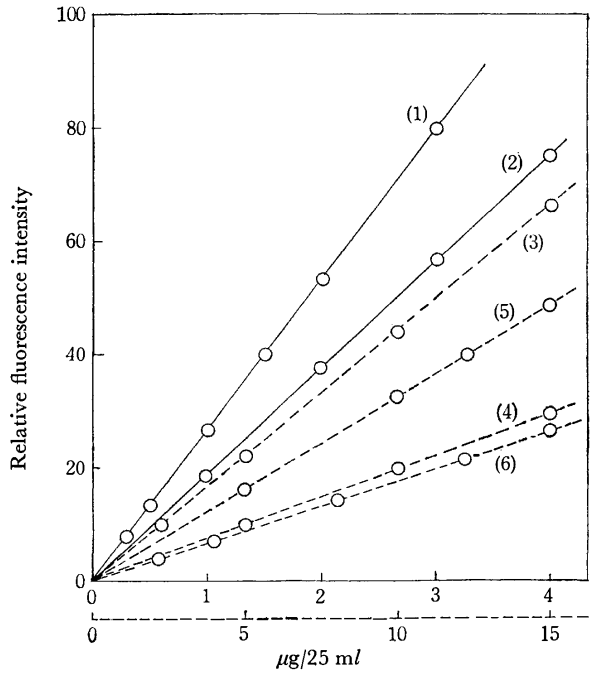

Fig. 6. Calibration curves for aluminum, gallium, and scandium
(1) Al: 20 div. (0.168 μg Rhodamine B/m*l* standard solution), 0.1% reagent solution 0.15 m*l*, FPL-2 (primary filter; 365, secondary filter; 61)
(2) Al: 20 div. (0.168 μg Rhodamine B/m*l* standard solution), 0.1% reagent solution 0.15 m*l*, G-3 (330 nm/590 nm)
(3) Ga: 40 div. (0.168 μg Rhodamine B/m*l* standard solution), 0.1% reagent solution 0.25 m*l*, FPL-2 (primary filter; 365, secondary filter; 61)
(4) Ga: 40 div. (0.168 μg Rhodamine B/m*l* standard solution), 0.1% reagent solution 0.25 m*l*, G-3 (340 nm/600 nm)
(5) Sc: 25 div. (0.168 μg Rhodamine B/m*l* standard solution), 0.1% reagent solution 0.30 m*l*, FPL-2 (primary filter; 365, secondary filter; 61)
(6) Sc: 25 div. (0.168 μg Rhodamine B/m*l* standard solution), 0.1% reagent solution 0.30 m*l*, G-3 (340 nm/610 nm)

Figure 7 shows the calibration curves for some ions forming fluorescent complexes with Mordant Blue 31. The conditions for the fluorometric determinations are summarized in Table 1.

We see that magnesium, yttrium, lanthanum, lutetium, and indium can also be determined with Mordant

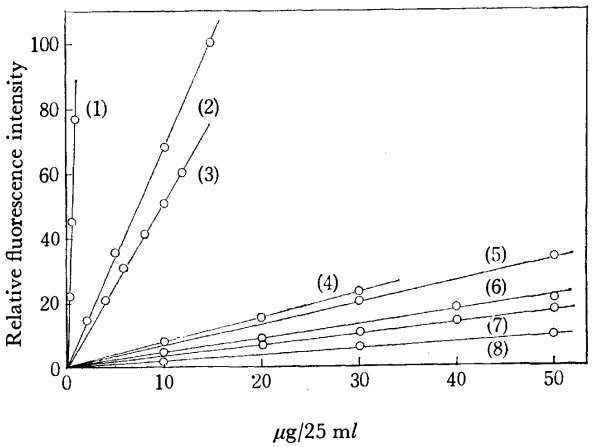

Fig. 7. Calibration curves for some fluorescent complex forming ions at 60 div. (*viz.* 0.168 Rhodamine B/m*l* standard solution, FPL-2-primary filter 365, secondary filter 61).
(1) Al, (2) Ga, (3) Sc, (4) Mg, (5) Y, (6) La, (7) Lu, (8) In

Blue 31 but with low sensitivities. Thus Mordant Blue 31 is excellent as a fluorometric reagent for aluminum, gallium, and scandium.

Effect of Diverse Ions. The effect of 26 cations on the determination of aluminum, gallium, and scandium was studied. The results are summarized in Table 2.

Determination of aluminum. Cobalt(II), iron(III), hafnium(IV), and vanadium(V) reduced the fluorescence intensity. Indium, yttrium, and scandium ions gave a positive error. The following ions did not interfere: magnesium, calcium, nickel(II), copper(II), manganese(II), zinc, cadmium, beryllium, tin(II, IV), thallium(III), arsenic(III), zirconium(IV), selenium(IV), titanium(IV), tungstate(VI), chromate(VI), and molybdate(VI) ions.

Determination of gallium. Fifty micrograms of magnesium, calcium, nickel(II), manganese(II), zinc, cadmium, cobalt(II), beryllium, indium, yttrium, thallium(III), iron(III), arsenic(III), hafnium(IV), zirconium(IV), selenium(IV), titanium(IV), and tungstate(VI) ions did not interfere. Scandium and aluminum ions gave a positive error. Copper(II), tin(II, IV), vanadate(V), chromate(VI), and molybdate(VI) ions reduced the fluorescence of gallium.

Determination of scandium. Cobalt(II), iron(III), hafnium(IV), zirconium(IV), and chromate(VI) ions

Table 1. Conditions for fluorometric determination

		Ion							
		Al	Ga	Sc	Mg	Y	La	Lu	In
Fluorescence excitation band (nm)		330 (540)	340 (580)	340 (535)	340 (500)	335 (540)	340	340 (550)	340 (500)
Fluorescence emission band (nm)		590	600	610	585	590	590	590	620
Optimum pH (pH range)		6.0 (2—8)	4.0 (1—6)	6.0 (4—8)	11.0 (8—13)	7.0 (5—9)	6.0 (5—8)	6.0 (5—8)	6.0 (4—7.5)
Used amounts of 0.1% reagent soln. (m*l*)		0.15	0.25	0.30	1.00	0.25	0.50	0.50	1.00
Standing time (min)		60	15	15	15	15	15	15	15
Fluorescence intensity at 60 div./1 μg	G-3	66.0	3.02	2.7	0.63				
	FPL-2	79.5	6.78	5.05	0.77	0.66	0.37	0.36	0.19
Fluorescence intensity ratio	weight	421	35.9	26.7	4.09	3.49	1.94	1.90	1.00
	molar	114	25.2	12.1	1.00	3.12	2.70	3.35	1.15

TABLE 2. EFFECT OF DIVERSE IONS

Ion	Taken (μg)	Al Found (μg)	Taken (μg)	Ga Found (μg)	Taken (μg)	Sc Found (μg)
Be^{2+}	10	2.1	50	10.0	—	—
Mg^{2+}	10	2.0	50	10.0	50	10.0
Ca^{2+}	10	2.0	50	10.0	50	10.0
Co^{2+}	10	1.0	50	10.0	50	3.3
Ni^{2+}	10	2.1	50	10.5	—	—
Mn^{2+}	10	2.1	50	10.5	50	10.7
Cu^{2+}	10	1.9	50	0.6	—	—
Zn^{2+}	10	2.1	50	10.3	—	—
Cd^{2+}	10	2.0	50	10.6	—	—
Sn^{2+}	10	1.9	50	6.6	—	—
Al^{3+}	—	—	2	13.7	2	##
Sc^{3+}	10	2.5	50	11.5	—	—
Fe^{3+}	10	0.5	50	9.1	50	8.1
Ga^{3+}	10	1.9	—	—	50	12.0
As^{3+}	10	2.0	50	10.0	—	—
Y^{3+}	10	2.4	50	10.0	50	10.0
In^{3+}	10	2.4	50	10.7	50	9.0
Tl^{3+}	10	2.1	50	10.4	50	10.8
Ti^{4+}	10	2.0	50	9.1	—	—
Se^{4+}	10	2.1	50	9.5	50	10.7
Zr^{4+}	10	1.8	50	10.0	50	6.2
Sn^{4+}	10	2.0	50	7.7	—	—
Hf^{4+}	10	1.3	50	10.8	50	8.0
VO_3^-	10	1.7	50	0.9	—	—
CrO_4^{2-}	10	2.1	50	8.0	50	6.5
MoO_4^{2-}	10	2.1	50	6.5	—	—
WO_4^{2-}	10	2.0	50	10.0	—	—

Al taken: 2 μg, Ga, Sc taken: 10 μg respectively.
Serious positive intereference.

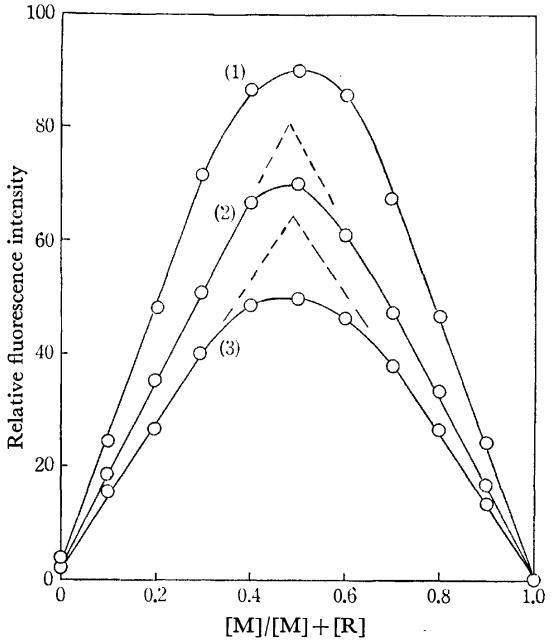

Fig. 8. Continuous variation method
(1) [Ga]=[R]=1.92×10^{-3} mol, 20 div.
(2) [Al]=[R]=5×10^{-4} mol, 10 div.
(3) [Sc]=[R]=1.92×10^{-3} mol, 30 div.

gave negative error. Gallium and aluminum ions gave a positive error.

Determination of the Metal to Ligand Ratio. The mole ratio of metal to the reagent in the metal-Mordant Blue 31 complexes was fluorometrically determined by

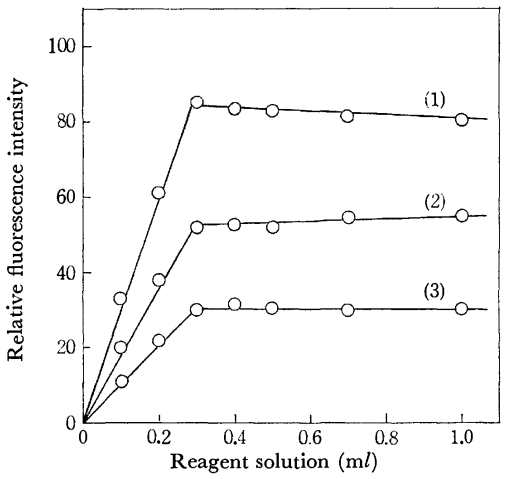

Fig. 9. Mole ratio method
(1) [Al]=[R]=5×10^{-4} mol, Al 0.3 ml, 20 div.
(2) [Ga]=[R]=1.92×10^{-3} mol, Ga 0.3 ml, 20 div.
(3) [Sc]=[R]=1.92×10^{-3} mol, Sc 0.3 ml, 30 div.

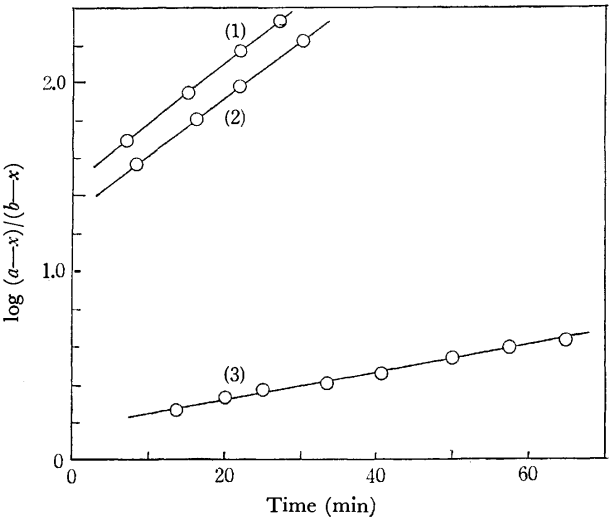

Fig. 10. Kinetics of chelate formation as indicated by fluorescence, a is initial concentration of aluminum, b is initial concentration of Mordant Blue 31, and x is concentration of chelate as indicated by fluorescence.
(1) Al 50 μ mol, reagent 5 μ mol (2) Al 5 μ mol, reagent 50 μ mol (3) Al 50 μ mol, reagent 50 μ mol

continuous variation and mole ratio methods. Figure 8 shows the results of the continuous variation method indicating the formation of a 1 : 1 complex. Mole ratio studies (Fig. 9) also gives the evidence of a 1 : 1 complex. The metal to ligand ratio can be kinetically determined when the complexes are formed with a measurable rate. Figure 10 shows the second order kinetics in the fluorescence development of aluminum-Mordant Blue 31 complex. Kinetic studies also indicate the formation of a 1 : 1 complex. The formation constants of aluminum and gallium complexes were found to be 1×10^6 at 15°C from the curves in Fig. 8.

The author wishes to express his appreciation to Prof. Tsunenobu Shigematsu, Institute for Chemical Research, Kyoto University, and Prof. Yasuharu Nishikawa, Faculty of Science and Technology, Kinki University, for their advice and suggestions.

Copper(II) Chelates of 2,4,6-Heptanetrione and Its Homologues[1]

Fumio SAGARA, Hiroshi KOBAYASHI, and Keihei UENO

Department of Organic Synthesis, Faculty of Engineering, Kyushu University, Fukuoka 812

(Received July 3, 1971)

Copper(II) chelates of heptane-2,4,6-trione as well as its methylated derivatives such as 3-methylheptane-2,-4,6-trione, 3,5-dimethylheptane-2,4,6-trione, and 2-methoxy-2-heptene-4,6-dione have been synthesized. All the ligands gave 1:2 (metal ion:ligand) chelates. The first two ligands gave in addition binuclear 2:2 chelates. The fact that a 1:2 chelate was relatively easily converted into a 2:2 chelate and the conversion occurred more easily with the chelate of the first ligand than with that of the second one was interpreted by the steric effect of the methyl group. The structures of the 1:2 and 2:2 chelates were discussed on the basis of spectroscopic and other data. Reversible addition of heterocyclic bases to the 2:2 copper chelates was observed, and the coordinating structure of pyridine adduct was found to be of a pentacoordinate square pyramid.

Heptane-2,4,6-trione (H_2daa) or diacetylacetone is a higher homologue of acetylacetone. The ligand exists as a monoanionic (Hdaa$^-$) or dianionic form (daa^{2-}), and can behave as a bidentate as well as a terdentate ligand in complex formation.

Although organic chemistry of this compound and its complexing properties have been studied to some extent,[2-8] no systematic investigation of the compound as a multidentate ligand had been reported before the publication of our communication.[9] Recently, the keto-enol tautomerism as well as the copper(II) chelates of heptane-2,4,6-trione and related triketones have been investigated by Dudley *et al.*[10,11] The characteristics of binuclear copper(II) chelates of the related β,δ-triketone ligands have also been reported by Graddon and Townsend,[12] Toy *et al.*,[13] and Murtha and Lintvedt.[14]

Three oxygen atoms in the β,δ-triketone ligands can be seen to be fixed in the same plane unable to coordinate to the same metal ion simultaneously, and it is of interest to investigate the behavior of the β,δ-triketone ligands as a multidentate ligand upon complex formation. We have investigated the fundamental properties, including keto-enol tautomerism of heptane-2,4,6-trione and its methylated derivatives,[15] the synthesis and structure of the chelates of [M(HL)$_2$] and [M$_2$L$_2$] type of divalent transition metal ions and related β,δ-triketones.[16]

In this paper we present the results of syntheses, structures, and the properties of copper(II) chelates of heptane-2,4,6-trione (H_2daa), as well as its methylated derivatives such as 3-methylheptane-2,4,6-trione (H_2-mmd), 3,5-dimethylheptane-2,4,6-trione (H_2dmd), and 2-methoxy-2-heptene-4,6-dione (Hmod).

Experimental

The Ligands. Synthesis and characterization of the ligands have been reported.[15]

Synthesis of the Chelates. 1 : 2 Chelates. Bis(heptane-2,4,6-trionato)copper(II) Dihydrate, Cu(Hdaa)$_2$·2H$_2$O. (a): A methanol solution of heptane-2,4,6-trione (1.0 g, 0.0070 mol) was added to an aqueous solution of cupric acetate monohydrate (0.70 g, 0.0035 mol, in 20 m*l* of water) under cooling in an ice-water bath. Blue precipitates were collected and dried in the air. Yield, 0.85 g (63%). Attempts to recrystallize the sample from various organic solvents were unsuccessful, because the compound was easily converted into Cu$_2$(daa)$_2$ when dissolved in the solvent even at room temperature, mp about 50°C (decompn.). However, it was converted into Cu$_2$(daa)$_2$ upon heating so easily that no reproducible melting point could be observed. Two moles of water, probably coordinated water, could not be removed even at reduced pressure and lower temperature, without causing rearrangement into Cu$_2$(daa)$_2$.

(b): Two grams (0.0049 mol) of bis(heptane-2,4,6-trionato)dicopper(II) and 10.0 g (0.070 mol) of heptane-2,4,6-trione were dissolved into 20 m*l* of pyridine containing a small amount of water at 0°C, and the solution was concentrated to about 5 m*l* by evaporating pyridine at reduced pressure at 0°C, to give blue precipitates which were collected and air-dried. Yield, 2.4 g (64%).

Bis(3-methylheptane-2,4,6-trionato)copper(II), Cu(Hmmd)$_2$. A chloroform solution (20 m*l*) of 3-methylheptane-2,4,6-trione (0.50 g, 0.0032 mol) was stirred together with an aqueous solution of cupric acetate monohydrate (0.32 g, 0.0016 mol) at room temperature. The resulting mixture was kept to stand and the chloroform layer formed was evaporated off at room temperature to give blue precipitates which were purified on a silica gel (WAKOGEL Q-23) column. Yield, 0.45 g (75%), mp about 80°C (decompn.). However, the compound converted into Cu$_2$(mmd)$_2$ by heating so easily

1) Contribution No. 209 from the Department of Organic Synthesis, Kyushu University.

2) F. Feist, *Ann. Chem.*, **257**, 276 (1890).

3) J. N. Collie and A. A. B. Reilly, *J. Chem. Soc.*, **121**, 1984 (1922).

4) F. Feist and H. Belart, *Ber.*, **28**, 1817 (1895).

5) S. S. Deshapande, Y. V. Dingankar, and D. N. Kopil, *J. Indian Chem. Soc.*, **11**, 595 (1934).

6) R. Kaushal, *ibid.*, **23**, 16 (1946).

7) V. B. Billore, R. P. Nigam, R. Kaushal, and S. S. Deshapande, *ibid.*, **23**, 19 (1946).

8) J. R. Bethel and P. Maitland, *J. Chem. Soc.*, **1962**, 3751.

9) F. Sagara, H. Kobayashi, and K. Ueno, This Bulletin **41**, 266 (1968).

10) C. W. Dudley, T. N. Huckerby, and C. Oldham, *J. Chem. Soc., A*, **1970**, 2605.

11) D. Baker, C. W. Dudley, and C. Oldham, *ibid., A*, **1970** 2608.

12) D. P. Graddon and I. T. Townsend, *Aust. J. Chem.*, **22**, 505 (1969).

13) A. D. Toy, T. D. Smith, and J. R. Pilbrow, *J. Chem. Soc., A*, **1970** 2600.

14) D. P. Murtha and R. L. Lintvedt, *Inorg. Chem.*, **9**, 1532 (1970).

15) F. Sagara, H. Kobayashi, and K. Ueno, This Bulletin, **45**, 900 (1972).

16) Y. Taguchi, F. Sagara, H. Kobayashi, and K. Ueno, *ibid.*, **43**, 2470 (1970).

that no reproducible melting point could be observed.

Bis(3,5-dimethylheptane-2,4,6-trionato)copper(II), Cu(Hdmd)$_2$. A similar procedure to the above was carried out using a chloroform solution (50 m*l*) containing 3,5-dimethylheptane-2,4,6-trione (2.00 g, 0.0118 mol) and an aqueous solution (100 m*l*) of cupric acetate monohydrate (1.20 g, 0.0060 mol). The chloroform solution was evaporated to give greenish grey residue, which was purified by elution chromatography on a silica gel column. Yield, 1.42 g (60.1%), mp 162—162.5°C.

Bis(2-methoxy-2-heptene-4,6-dionato)copper(II), Cu(Hmod)$_2$. Heptane-2,4,6-trione (5.0 g, 0.035 mol) was added at 5°C into ether (30 m*l*) containing diazomethane which was prepared from nitrosomethylurea (5.0 g, 0.049 mol) and a 40% potassium hydroxide solution (9.0 m*l*). After being put to stand overnight at room temperature, the ethereal solution was evaporated to give a viscous oil which was dissolved in chloroform (100 m*l*) and treated with an aqueous cupric acetate monohydrate (15.0 g, 0.075 mol). The chloroform layer formed was evaporated to dryness, giving pale blue precipitates, which were recrystallized three times from ethanol. Yield, 2.10 g (32%), mp 160—162°C. The product was assigned to be bis(2-methoxy-2-heptene-4,6-dionato)copper(II).

A chloroform solution of the copper chelate was stirred together with 0.1N hydrochloric acid until the chloroform layer became colorless. The chloroform layer was evaporated to give an oil which was assigned to be heptane-2,4,6-trione by infrared spectral comparison and gas-liquid chromatography. The chloroform solution of the oil was again treated with aqueous cupric acetate. The resulting blue solution was evaporated to give a solid residue which was identified to be $Cu_2(daa)_2$ by infrared spectral comparison.

2:2 Chelates. Bis(heptane-2,4,6-trionato)dicopper(II), $Cu_2(daa)_2$. (a): A methanol solution of heptane-2,4,6-trione (1.0 g, 0.0070 mol) was added portionwise to an aqueous solution of cupric acetate monohydrate (1.4 g, 0.0070 mol) at 30°C with stirring. Resulting green precipitates were insoluble in most organic solvents except for strong coordinating solvents such as pyridine or dimethyl sulfoxide. The precipitates were collected, recrystallized from pyridine and dried under reduced pressure at 65°C for several hours to give green powders, decomposing at about 280°C. Yield, 1.20 g (83%).

(b): A methanol solution (10 m*l*) containing bis(heptane-2,4,6-trionato)copper(II) dihydrate, $Cu(Hdaa)_2\cdot 2H_2O$, (1.00 g, 0.00262 mol) was heated under reflux for 2 hr. The green precipitates were collected and dried under reduced pressure. The complex was identified to be the above mentioned binuclear chelate by elemental analysis and infrared spectroscopy. Yield 1.02 g (95.3%), mp 280°C (decompn.).

Bis(3-methylheptane-2,4,6-trionato)dicopper(II) $Cu_2(mmd)_2$. A similar procedure to the above (procedure (b)) was carried out using a methanol solution of bis(3-methylheptane-2,4,6-trionato)copper(II) (1.0 g, 0.0027 mol). The resulting green precipitates were recrystallized from pyridine and dried under reduced pressure at 65°C. Yield, 0.82 g (70%), mp about 280°C (decompn.).

The properties and the results of elemental analyses as well as the conditions of synthesis of the copper chelates investigated are summarized in Table 1.

Base Adducts of 2:2 Chelates. Pyridine or 4-methylpyridine adducts of $Cu_2(daa)_2$ and $Cu_2(mmd)_2$ were prepared by dissolving 1 g of the copper chelate into 50 m*l* of pyridine or 4-methylpyridine, and putting the resulting solution to stand for 1—2 days at 0—15°C. The crystalline precipitates afforded were collected by filtration and air-dried. Yield 0.3—0.6 g (29—43%). The base adducts were dark brown crystals, fairly stable in nonpolar solvents such as hexane or cyclohexane, but readily decomposed in polar solvents such as methanol or water, precipitating green 2:2 chelates.

The amount of base coordinated to the 2:2 chelates and the temperature at which the base began to dissociate were determined by thermogravimetric analysis. The results are summarized in Table 2.

When bis(heptane-2,4,6-trionato)copper(II) dihydrate ($Cu(Hdaa)_2\cdot 2H_2O$) was treated with concentrated aqueous ammonia, an ammonia adduct was obtained as brown powder. The product was not stable enough to be subjected to thermogravimetric analysis to get reliable results on the number of mole of ammonia added. However, the product was supposed to be the ammonia adduct of $Cu_2(daa)_2$, since the remaining compound after thermal decomposition was found to be $Cu_2(daa)_2$.

Attempts to prepare the solid base adducts of 2:2 chelate with other amine ligands such as ethylamine, diethylamine, triethylamine, aniline, and quinoline were unsuccessful, although adducts were formed in solution as indicated by the color change from green solid to brown solution when the solid 2:2 chelates were dissolved in these amine ligands.

Apparatus and Procedure. All melting points are uncorrected. Visible spectra were measured with a Hitachi

Table 1. Copper chelates of heptane-2,4,6-trione and its methylated derivatives

Chelate	Reaction condition: Temp. °C	Reaction condition: Solvent	Soluble in	Color	Molecular formula	Elemental analysis Found (Calcd): C%	H%	M%
$Cu_2(daa)_2$	30	Methanol or water	Pyridine, THF (ca. 10^{-3}M)	Green	$C_{14}H_{16}O_6Cu_2$	41.41 (41.27)	3.89 (3.93)	31.0 (31.2)
$Cu(Hdaa)_2\cdot 2H_2O$	0	Methanol or water	Methanol, chloroform, acetone, THF	Blue	$C_{14}H_{22}O_8Cu$	43.75 (43.80)	6.09 (5.81)	16.4 (16.6)
$Cu_2(mmd)_2$	Reflux in methanol (from $Cu(Hmmd)_2$)		Pyridine	Green	$C_{16}H_{20}O_6Cu_2$	44.01 (44.01)	4.42 (4.58)	28.7 (29.2)
$Cu(Hmmd)_2$	Room temp., water		Chloroform	Blue-violet	$C_{16}H_{22}O_6Cu$	51.34 (51.40)	6.12 (5.93)	16.56 (16.99)
$Cu_2(dmd)_2$	Not obtainable		—	—	—	—	—	—
$Cu(Hdmd)_2$	Room temp., water		Chloroform	Blue-violet	$C_{18}H_{26}O_6Cu$	53.47 (53.79)	6.61 (6.52)	15.71 (15.81)
$Cu(Hmod)_2$	Room temp., water		Chloroform	Pale blue	$C_{16}H_{22}O_6Cu$	51.37 (51.40)	5.99 (5.93)	17.06 (16.99)

Table 2. Base adducts of 2:2 chelates

Chelate	Base	Mole ratio of base/chelate	Decomposition temp. °C[a)]
$Cu_2(daa)_2$	pyridine	2.0	34
	4-methylpyridine	2.1	38
$Cu_2(mmd)_2$	pyridine	2.0	44
	4-methylpyridine	2.0	49

a) The temperature at which the base begins to dissociate.

124 recording spectrophotometer. Solid reflectance spectra were measured with a Hitachi EPU-2A spectrophotometer. Infrared absorption spectra were recorded with a JASCO DS-301 spectrophotometer. Molecular weights were determined with a Mechrolab vapor pressure osmometer. Thermogravimetric analysis on the base adducts were conducted with a Shimadzu automatic recording thermobalance TB-10B. A weighed amount of a chelate (20—100 mg) was placed on a weighing pan of the thermobalance and the temperature of the furnace was raised at a rate of 5°C per minute under atmospheric pressure. The weight change was recorded automatically up to 150°C.

Infrared spectra and visible spectra of some representative copper chelates are shown in Figs. 1 and 2 respectively.

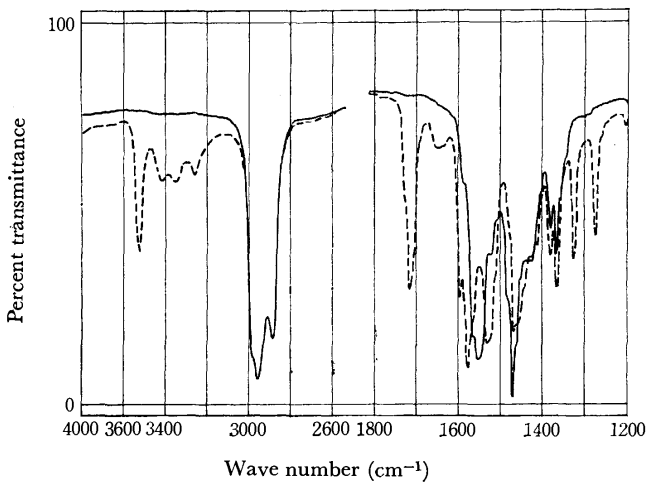

Fig. 1. IR spectra of the copper chelates in Nujol mull. ——: $Cu_2(daa)_2$.------: $Cu(Hdaa)_2 \cdot 2H_2O$

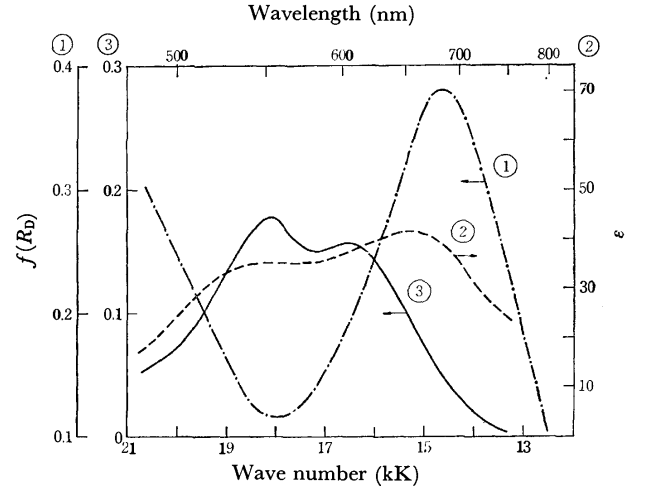

Fig. 2. Visible spectra of the copper chelates and copper acetylacetonate.
1: Powder reflection spectrum of $Cu_2(daa)_2$
2: Absorption spectrum of copper acetylacetonate in chloroform
3: Powder reflection spectrum of $Cu(Hdaa)_2 \cdot 2H_2O$
$f(R_D)$ is calculated according to the Kubelka-Munk equation

Results and discussion

Synthesis of Copper Chelates. Heptane-2,4,6-trione and its homologues can form two types of copper chelates; a mononuclear type, $Cu(HL)_2$, and a binuclear type, Cu_2L_2.[9] As shown in Table 1, heptane-2,4,6-trione and the 3-methyl derivative gave both types of chelates, while the 3,5-dimethyl derivative afforded only the former.

Synthetic procedures of these chelates can be classified as follows; For $Cu(HL)_2$ type chelate: Procedure 1. A cold methanol solution of a ligand was added dropwise into half a mole of aqueous cupric acetate at a lower temperature. Procedure 2. A cold chloroform solution of a ligand was stirred with half a mole of aqueous cupric acetate at a lower temperature. Procedure 3. A cold pyridine solution containing a Cu_2L_2 type complex and a large excess of the corresponding ligand was evaporated under reduced pressure at a lower temperature. For Cu_2L_2 type chelate: Procedure 4. An aqueous cupric acetate was added dropwise into a hot methanol solution of an equimolar amount of the ligand. Procedure 5. A methanol solution of $Cu(HL)_2$ type chelate was heated with or without an equimolar amount of cupric acetate as long as necessary.

Mononuclear $Cu(HL)_2$ type chelates are not so stable, and tend to convert into binuclear Cu_2L_2 chelates at higher temperatures accompanied by the liberation of free ligand (See Experimental). The maximum temperature below which $Cu(HL)_2$ type complex is stable in methanol, is 0°C for $Cu(Hdaa)_2$ and 30°C for $Cu(Hmmd)_2$. Thus, the reaction temperature in the synthetic procedure 1, 2, and 3 has to be kept below −5°C for the first, and at room temperature for the second, otherwise the mixture of $Cu(HL)_2$ and Cu_2L_2 will be obtained as the reaction product. For the third, there was no indication of conversion into binuclear complex even when heated at refluxing temperature in methanol.

The binuclear chelates can be obtained by either procedure 4 or 5, most easily from heptane-2,4,6-trione and less easily from monomethyl derivative. Thus, $Cu_2(daa)_2$ was obtained by the reaction at room temperature, but $Cu_2(mmd)_2$ was obtained at refluxing temperature in methanol. Attempted syntheses of a binuclear chelate with the dimethyl derivative were unsuccessful under various reaction conditions including those for the above ligands. The *O*-methyl derivative gave only the mononuclear chelate as expected from its bidentate structure.

Structure of $Cu(HL)_2$ Chelates. The result of the elemental analysis on 1:2 chelate of heptane-2,4,6-trione suggests the molecular formula of $Cu(Hdaa)_2 \cdot 2H_2O$. The infrared spectra of 1:2 chelates from three

ligands, H_2daa, H_2mmd, and H_2dmd, showed a free carbonyl band at about 1720 cm^{-1} and multiplet bands in the region of 1600—1500 cm^{-1} due to a coordinated carbonyl and an olefinic group involved in the chelate ring which were not observed in the free ligand (Fig. 1). Broad bands in 1700—1600 cm^{-1} observed in the free ligands disappeared in infrared spectra of the copper chelates. The results suggest that the adjacent two of three carbonyl oxygen atoms are involved in the chelate formation with copper, leaving the side carbonyl oxygen uncoordinated.

Powder reflection spectrum of $Cu(Hdaa)_2 \cdot 2H_2O$ shows two broad bands at 16500 and 18100 cm^{-1} which are fairly close to those of bis(acetylacetonato)copper(II) in chloroform (15300, 18200 cm^{-1}). The result indicates that four carbonyl oxygen atoms around copper ion in $Cu(Hdaa)_2 \cdot 2H_2O$ are of square planar configuration as in the case of bis(acetylacetonato)copper(II), and the coordination of two moles of water to the z axis of copper ion is not strong enough to influence the electronic spectra of *d–d* transition.

Thus, the structure of bis(heptane-2,4,6-trionato)-copper(II) dihydrate is proposed as Structure I. In the case of 3-methylheptane-2,4,6-trione, however, there remains a question as to the site of coordination of the ligand, because the ligand is no more symmetric. Although there is no definite data, NMR study on the keto-enol tautomerism of this ligand in $CDCl_3$ revealed that the fractions of monoenol (A), monoenol (B), bisenol and triketo forms were 76, 9, 12, and 3%, respectively, and these fractions did not change appreciably with temperature.[15]

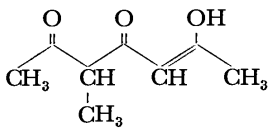
monoenol (A)

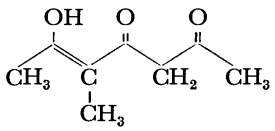
monoenol (B)

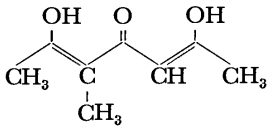
bisenol

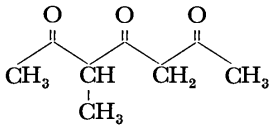
triketo

If one recalls that 1 : 2 copper chelate of 3-methylheptane-2,4,6-trione was synthesized by contacting the chloroform solution of the ligand with an aqueous solution of cupric acetate, the possible structure of 1 : 2 copper chelate might be the one in which the methyl group is located on the middle carbon of uncoordinated side as illustrated in structure I.

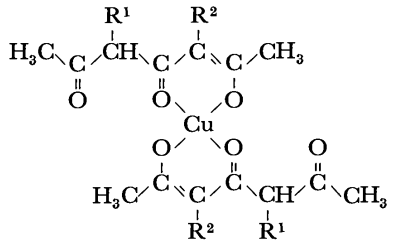

		R^1	R^2
Ia)	$Cu(Hdaa)_2 \cdot 2H_2O$	H	H
Ib)	$Cu(Hmmd)_2$	CH_3	H
Ic)	$Cu(Hdmd)_2$	CH_3	CH_3

Structure I

It is of interest to note that 1 : 2 chelate of heptane-2,4,6-trione differs from those of the *C*-methylated derivatives with respect to the coordinated water. The former contained two moles of water with a multiplet band at 3530—3260 cm^{-1}, could hardly be removed. Attempted dehydration of the two moles of water under reduced pressure at room temperature resulted in conversion into an anhydrous Cu_2L_2 chelate. Thus, bis-(heptane-2,4,6-trionato)copper(II) seems to be stable only in the presence of coordinated water. On the other hand, the 1 : 2 chelates of 3-methyl- and 3,5-dimethyl derivatives can be obtained as anhydrous chelates respectively. Similarly, replacement of one or both terminal methyl groups with the phenyl group also resulted in anhydrous 1 : 2 chelates.[11]

A multiplet band at 3530—3260 cm^{-1} observed on bis(heptane-2,4,6-trionato)copper(II) dihydrate may be responsible for ν_{OH} of coordinated water as well as the enolic hydroxyl group. This suggests the partial enolization of the uncoordinated carbonyl group in the chelate. A similar situation was also observed on bis-(heptane-2,4,6-trionato)palladium(II) by NMR study.[17]

1 : 2 Copper chelates of methylated ligands $Cu(Hmmd)_2$ and $Cu(Hdmd)_2$ were obtained as anhydrous chelates. No meaningful absorption was observed in 3200—3500 cm^{-1} region. This indicates that the uncoordinated carbonyl group in the chelates of methylated ligands do not enolize appreciably. This can be explained by the steric effect of the methyl group on 3-position. In the case of keto form, the uncoordinated terminal acetyl group can rotate freely, so that there operates little steric repulsion between the methyl groups on terminal- and 3-position. On the other hand, the olefinic double bond of the enol form restricts the free rotation of the terminal group, resulting in the stable configuration. Such steric effect does not exist in bis(heptane-2,4,6-trionato)copper(II), allowing a partial enolization of the uncoordinated carbonyl group.

As to the copper chelate of 2-methoxy-2-heptene-4,6-dione, the result of elemental analysis suggests the molecular formula $Cu(Hmod)_2$. The reaction of diazomethane with heptane-2,4,6-trione gave only the *O*-methyl derivative (H_2mod) and no *C*-methyl ones (H_2mmd or H_2dmd). Methylated position of the product should be a side oxygen and not the central one, because the *O*-methyl derivative still showed the ability of chelate formation with beryllium(II) and copper (II) ions to give 1 : 2 chelate. NMR spectrum of the beryllium chelate indicated the presence of an *O*-methyl group in theligand.[17] The compound, however, could be isolated only in the form of a metal complex, and attempts to liberate the free ligand from the copper chelate were unsuccessful, and resulted in decomposition in an acid medium to give the original heptane-2,4,6-trione even at a lower temperature. This is not surprising because the enol-ether bonding usually degradates rather easily. The process of the decomposition of freed ligand could be traced by gas-liquid chromatography; a chloroform extract immediately after libera-

17) Unpublished results.

tion from the copper chelate with an acid gave a single glc peak at $R_T=1.1$ min, and after about 10 min, glc showed four broad peaks in a shorter R_T range in additon to the original peak. Forty min after the glc again showed a single peak but at $R_T=4.1$ min, which was identical with that of heptane-2,4,6-trione. Additional glc peaks which appeared on the process from the *O*-methyl derivative to heptane-2,4,6-trione were not studied in detail, though they were apparently due to tautomers of the *O*-methyl derivative.

Thus, the coordination with metal ion prevented the cleavage of the enol-ether bonding in 2-methoxy-2-heptene-4,6-dione. Since the enol-ether group does not seem to be directly involved in the coordination with metal ion, the stabilization was presumed to be due to steric hindrance in nucleophilic attack of an anion to a protonated intermediate upon the cleavage of the ether bonding.

Infrared bands in the region 1600—1500 cm^{-1} could be assigned in a similar manner to those of heptane-2,4,-6-trione and its *C*-methyl derivatives. The band at 1635 cm^{-1} was due to an olefinic group connected to oxygen. No positive evidence could be obtained to suggest a macrocyclic chelate ring. The result also indicates that diazomethane attacked a side carbonyl group in heptane-2,4,6-trione and not the central one. Volatility of the copper chelate (130°C /5 × 10^{-1} mmHg) and solubility in organic solvents such as chloroform, ethanol, and methanol suggested the 1:2 copper chelate to be of a monomeric form containing a six-membered chelate ring as shown in structure III.

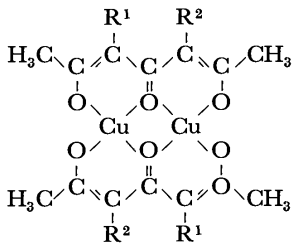

		R^1	R^2
IIa)	$Cu_2(daa)_2$	H	H
IIb)	$Cu_2(mmd)_2$	H	CH_3

Structure II

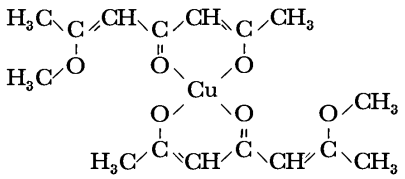

III) $Cu(mod)_3$

Structure III

Structure of Cu_2L_2 Chelates. The results of elemental analysis of the 1:1 heptane-2,4,6-trione chelate suggests the molecular formula Cu(daa). The infrared spectra of 1:1 chelates show multiplet bands in the region 1600—1500 cm^{-1}, which could be assigned to a coordinated carbonyl and an olefinic group involved in the chelate ring as in the case of 1:2 chelates. On the other hand, no characteristic absorption band can be observed in the range 1800—1600 cm^{-1}. This suggests that all the three carbonyl oxygen atoms are involved in coordination. If we consider that the ligand is planar through its conjugated double bond system, and that three carbonyl oxygen atoms eventually can not coordinate to the same metal ion, dimeric structure II becomes the most probable. Although the polymer structure could also be assigned to the chelate, the construction of molecular model gives rise to too great strain to be acceptable. The dimeric structure was also supported by the magnetic moment study down to the liquid helium temperature as well as the ESR study. The strong antiferromagnetism of the copper(II) chelate suggests the dimeric structure. A detailed magnetic study on this system has been recently reported by Baker and others.[11]

The powder reflection spectrum of $Cu_2(daa)_2$ shows one broad band at 14700 cm^{-1}, which suggests a slight distortion from planar structure. The construction of molecular model of $Cu_2(daa)_2$ also needs the displacement of copper ion slightly above or below the plane of ligands.

Interconversion of 1:2 and 2:2 Chelates. The mononuclear and binuclear copper chelates of heptane-2,4,6-trione and its monomethyl derivative are interconvertible, as can be understood from their synthetic procedures. Mononuclear 1:2 chelate can be converted into 2:2 chelate by procedure 5, and 2:2 chelate can be converted into 1:2 chelate by procedure 3. In general, a lower temperature in the presence of excess ligand favors $Cu(HL)_2$ type chelate and a higher temperature Cu_2L_2 type chelate. As no common solvent was found for both types of chelates, equilibrium study on this system was not undertaken. $Cu(Hdaa)_2$ and $Cu(Hmmd)_2$ can be converted into $Cu_2(daa)_2$ and $Cu_2(mmd)_2$ quantitatively by heating methanol solution at 30 and 60°C, respectively.

Facility to form 2:2 chelate of heptane-2,4,6-trione as compared with 3-methyl derivative can be related to the relative enolizability of uncoordinated carbonyl group in 1:2 chelate. Partial enolization of uncoordinated carbonyl group was suggested on bis(heptane-2,4,6-trionato)copper(II), no indication of enolization being observed on bis(3-methylheptane-2,4,6-trionato)-copper(II). Thus, 2:2 chelate of heptane-2,4,6-trione can be obtained at relatively lower temperatures. However, 2:2 chelate of methylated ligand needs a higher temperature to overcome the steric repulsion of methyl groups.

In the case of 3,5-dimethylheptane-2,4,6-trione, NMR study proved that this ligand could not take the *cis*-dienol form, responsible for the 2:2 chelate, because of the steric repulsion of methyl groups.[15] Thus, attempts to synthesize 2:2 chelate of dimethyl derivative have been unsuccessful so far.

Base Adducts of 2:2 Chelates. Chelates of binuclear Cu_2L_2 type are thermally stable. They are not soluble in most organic solvents except for strong coordinating solvents such as pyridine or dimethyl sulfoxide. Green chelates turn brown when they are dissolved in pyridine, from which pyridine adducts can be obtained as brown crystalline precipitates at

higher concentration. The thermogravimetric investigation on the pyridine adducts proved that their composition is $Cu_2L_2Py_2$, in other words, each molecule of pyridine added to each copper ion, and that pyridine can be removed by heating the adduct at a relatively low temperature.

Infrared spectra and X-ray diffraction pattern of powdered sample before the addition and after the dissociation of pyridine were found to be identical. The molecular weight of 2:2 chelates in pyridine determined by a vapor pressure osmometer was found to be 412 (calcd.: 407.4) for $Cu_2(daa)_2$ and 439 (calcd.: 436) for $Cu_2(mmd)_2$.

Visible absorption spectrum of pyridine solution and powder reflection spectrum of pyridine adduct showed a maximum at the same frequency of 13520 cm^{-1}, indicating that the coordinating structure around copper ion in pyridine solution does not differ from that in solid adduct. As regard the infrared spectrum of pyridine adduct, no absorption band due to uncoordinated carbonyl group could be observed, and new bands at 410 cm^{-1} and 386 cm^{-1}, possibly due to the deformation of pyridine ring and the streching mode of N-Cu bond respectively, were observed in addition to the bands observed in the pyridine-free complex.

The results suggest that the dissolution of the 2:2 chelates in pyridine does not destroy the binuclear structure, and that the addition of pyridine is a reversible process. Thus, the structure of pyridine adduct may be of pentacoordinate square pyramid around copper(II) ion, with pyridine molecule coordinating from one side of z-axis of copper ion.

The reversible addition of heterocyclic bases to copper β-diketonates in solution has been investigated extensively.[18] If the adducts were stable, they could be isolated as definite solid adducts. In the case of bis(acetylacetonato)copper(II), mono-4-methylpyridine adduct has been obtained but not with pyridine.[19] In the cases of copper chelates of trifluoro- and hexafluoroacetylacetone, very stable mono- and bis-pyridine adducts were obtained.[20,21] The relative stability in these base adducts can be interpreted by the electron donating property of the heterocyclic nitrogen as well as the electron withdrawing property of β-diketones.

The results of thermogravimetric analysis on pyridine and 4-methylpyridine adducts of the 2:2 copper(II) chelate, as shown in Table 2, indicates a similar tendency as regards the electronic effect of the methyl group introduced on pyridine or heptane-2,4,6-trione, though the effect was not as great.

Financial support from the Ministry of Education is acknowledged.

18) For example; W. R. Mat and M. M. Jones, *J. Inorg. Nucl. Chem.*, **25**, 507 (1963).
19) D. P. Graddon and E. C. Watton, *ibid.*, **21**, 49 (1961).
20) R. D. Gillard and G. Wilkinson, *J. Chem. Soc.*, **1963**, 5885.
21) W. Partenheimer and R. S. Drago, *Inorg. Chem.*, **9**, 47 (1970).

BULLETIN OF THE CHEMICAL SOCIETY OF JAPAN, VOL. 45, 799—802(1972)

Oxovanadium(IV) Complexes of Schiff Bases Obtained from Salicylaldehyde Derivatives and Arylamines

Yoshio KUGE

Environmental Pollution Control Centre, Morimachi, Higashinari-ku, Osaka

and Shoichiro YAMADA

Institute of Chemistry, College of General Education, Osaka University, Toyonaka, Osaka

(Received July 9, 1971)

Oxovanadium(IV) complexes of Schiff bases obtained from salicylaldehyde derivatives and arylamines (abbreviated as $VO(X\text{-}SAL.R)_2$) have been synthesized, where X=H, 5,6-benzo, 5-Cl, and 5-Br, and R=Ph, CH_3-Ph, 2,6-$(CH_3)_2$-Ph and 2,6-$(C_2H_5)_2$-Ph, Ph being phenyl nucleus. Complexes of the type $VO(5\text{-}X\text{-}SAL.Ph)_2$ in the solid state, X being Cl and Br, consist of the species having a different configuration from that of the other complexes. For the latter complexes, distortion from the square-pyramidal configuration is not apparent in the solid state or in non-donor solvents, but in pyridine they combine with one pyridine molecule to form six-coordinate vanadium(IV) complexes. Comparison shows that the tendency toward the distortion in the solid state is lower with R=aryl than with R=α-branched alkyl groups.

In a previous paper[1] we reported the synthesis of

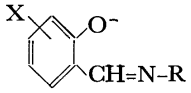

(I)

oxovanadium(IV) complexes with *N*-alkylsalicylideneiminates (abbreviated as X-SAL.R, I). Their structure in the solid state and in solution was examined in connection with the steric effect caused by bulky α-branched alkyl groups.

As regards the corresponding complexes with *N*-

1) S. Yamada and Y. Kuge, This Bulletin, **42**, 152 (1969).

arylsalicylideneiminates, however, only a few of them have been reported,[2] and no systematic examination of the aryl complexes has ever been carried out. In the present work, oxovanadium(IV) complexes with *N*-arylsalicylideneiminates have been studied, and the results have been compared with those of the *N*-alkyl-complexes and the corresponding complexes of some other metal ions.

Experimental

Materials. Complexes of the type $VO(X\text{-}SAL.R)_2$ were synthesized by a method similar to that previously reported.[1,2] Analytical data of new complexes are shown in Tables 1 and 2. A typical method of preparation is given below.

TABLE 1. ANALYTICAL DATA OF OXOVANADIUM(IV) COMPLEXES OF THE TYPE $VO(X\text{-}SAL.R)_2$

R	Calcd, %			Found, %		
	C	H	N	C	H	N
X=H						
2-CH_3-Ph	68.99	4.96	5.75	68.49	4.86	6.23
3-CH_3-Ph	68.99	4.96	5.75	68.30	4.95	6.09
4-CH_3-Ph	68.99	4.96	5.75	68.80	4.92	5.55
2,6-$(CH_3)_2$-Ph	69.90	5.47	5.43	69.26	5.31	5.06
X=5,6-benzo						
Ph	72.99	4.32	5.01	72.76	4.29	4.77
2-CH_3-Ph	73.59	4.80	4.77	73.81	5.03	4.64
3-CH_3-Ph	73.59	4.80	4.77	72.54	4.89	4.46
4-CH_3-Ph	73.59	4.80	4.77	73.53	4.84	4.60
2,6-$(CH_3)_2$-Ph	74.13	5.24	4.55	73.83	5.19	4.67
2,6-$(C_2H_5)_2$-Ph	75.10	6.00	4.17	74.76	5.99	3.99

To a solution of oxovanadium(IV) chloride (0.01 mol) in ethanol were added salicylaldehyde or its derivative (0.02 mol) and an appropriate arylamine (0.02 mol). The solution was stirred at room temperature for about 3 hr and allowed to stand overnight. The precipitate was collected by filtration and recrystallized from ethanol containing a small amount of pyridine.

TABLE 2. ANALYTICAL DATA OF OXOVANADIUM(IV) COMPLEXES OF THE TYPE $VO(X\text{-}SAL.Ph)_2$

X	Calcd, %			Found, %			μ
	C	H	N	C	H	N	
5-Cl	59.11	3.43	5.30	59.00	3.47	5.28	1.49
5-Br	50.59	2.95	4.54	51.23	3.10	4.36	1.57

μ: magnetic moment in B. M. at room temperature

All the complexes were obtained as yellow-brown or olive-green microcrystals. They are soluble in chloroform, dichloromethane and pyridine, but almost insoluble in methanol and ethanol. Some of them undergo decomposition on dissolution.

Measurements. Electronic absorption spectra of the complexes in solution and in the solid state were determined with a Shimadzu MPS-50L spectrophotometer.

Magnetic susceptibilities were determined by the Gouy method at room temperature.

2) L. Sacconi and U. Campigli, *Inorg. Chem.*, **5**, 606 (1966).

Results and Discussion

It is known that the vanadium(IV) ion in most oxovanadium(IV) complexes assumes a square-pyramidal configuration.[1,2] Therefore, when R denotes such a group as phenyl and 3- or 4-substituted phenyl causing very little steric hindrance, the complexes of the type $VO(X\text{-}SAL.R)_2$ are expected to have a square-pyramidal configuration, with the two X-SAL.R groups most

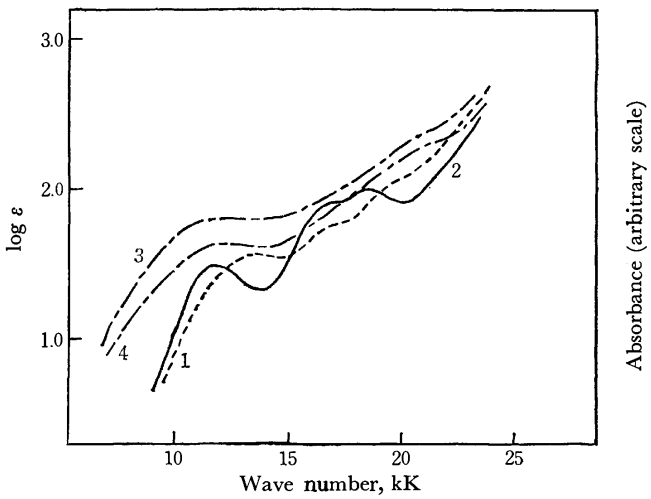

Fig. 1. Electronic absorption spectra of $VO(H\text{-}SAL.R)_2$: 1, R=Ph, solid; 2, R=2,6-$(CH_3)_2$-Ph, in pyridine; 3, R=2-CH_3-Ph, in pyridine; 4, R=2,6-$(CH_3)_2$-Ph, in pyridine.

TABLE 3. ABSORPTION MAXIMA OF OXOVANADIUM(IV) COMPLEXES OF THE TYPE $VO(X\text{-}SAL.R)_2$

R	State	Absorption max, kK (log ε for solution)
X=H		
Ph	solid	12.0 16.6sh, 18.6
	$CHCl_3$	11.9(1.25), 16.5(1.65)sh, 18.5(1.79)
	pyridine	13.6(1.28)
2-CH_3-Ph	solid	11.9, 16.8, 18.6
	$CHCl_3$	11.9(1.40), 16.4(1.72)sh, 18.6(1.86)
	pyridine	12.1(1.81)br
3-CH_3-Ph	solid	11.7, 16.9sh, 18.7
	pyridine	12.9(1.58)
4-CH_3-Ph	solid	11.6, 16.9sh, 18.7
	pyridine	12.9(1.57)
2,6-$(CH_3)_2$-Ph	solid	11.9, 17.0sh, 18.6
	pyridine	12.0(1.60)br
X=5,6-benzo		
Ph	solid	11.9, 16.7sh, 18.5
	pyridine	13.4(1.72)
2-CH_3-Ph	solid	11.9, 16.5sh, 18.5
	$CHCl_3$	12.0(1.51), 16.4(1.91)sh, 18.4(2.04)
	pyridine	13.4(1.76)
3-CH_3-Ph	solid	11.8, 16.7sh, 18.5
	pyridine	13.4(1.76)
4-CH_3-Ph	solid	11.9, 16.9sh, 18.6
	pyridine	13.3(1.74)
2,6-$(CH_3)_2$-Ph	solid	12.2, 16.5sh, 18.2
	pyridine	13.3(1.76)
2,6-$(C_2H_5)_2$-Ph	solid	12.3, 16.5sh, 18.0
	pyridine	13.3(1.70)

br: broad, sh: shoulder

probably having a nearly planar configuration.[1,2] This is borne out by their electronic absorption spectra in non-donor solvents and in the solid state, as shown in Figs. 1 and 2, and Table 3. The spectra are similar to each other and also to those of the N-alkyl-substituted complexes.[1] The absorption maxima at about 12, 16, and 18 kK may be assigned to transitions $d(xy)\rightarrow d(xz)$ $d(yz)$, $d(xy)\rightarrow d(x^2-y^2)$ and $d(xy)\rightarrow d(z^2)$, respectively, as in the previous papers.[1,2] Comparison of their band maxima with those of the *N*-alkyl-substituted complexes[1] shows that the ligand field produced by X-SAL·aryl is slightly weaker than that by X-SAL·alkyl.

It is interesting to note that, even for R=2-CH_3-Ph, 2,6-$(CH_3)_2$-Ph and 2,6-$(C_2H_5)_2$-Ph, a significant distortion from the square-pyramidal configuration does not occur in these complexes, since their absorption maxima in the solid state and in non-donor solvents are nearly the same as those of VO(X-SAL·Ph)$_2$ as shown in Figs. 1 and 2, and Table 3. A similar result was obtained with the corresponding nickel(II) and copper(II) complexes.[3]

The electronic spectra of the complexes of the type VO(5,6-benzo-SAL.R)$_2$ in pyridine clearly differ from those of the same complexes in the solid state or in chloroform as shown in Fig. 2 and Table 3. Since their spectral change on going from the solid state to the pyridine solution is nearly the same, irrespective of whether R denotes 2,6-$(CH_3)_2$-Ph, 2,6-$(C_2H_5)_2$-Ph or Ph, and resembles that of VO(X-SAL·*n*-alkyl)$_2$,[1] their pyridine adducts are considered to have a similar configuration to that of VO(X-SAL·*n*-alkyl)$_2$.

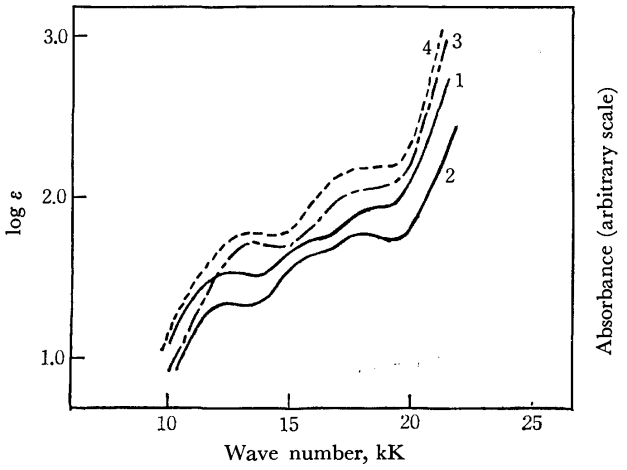

Fig. 2. Electronic absorption aspectr of VO(5,6-benzo-SAL.R)$_2$: 1, R=Ph, solid; 2, R=2,6-$(CH_3)_2$-Ph, solid; 3, R=Ph, in pyridine; 4, R=2,6-$(CH_3)_2$-Ph, in pyridine.

The complexes of the type VO(H-SAL.R)$_2$ in pyridine, R being Ph, 3-CH_3-Ph and 4-CH_3-Ph, exhibit similar spectra to those of the corresponding 5,6-benzo-complexes. On the contrary, for R=2-CH_3-Ph and 2,6-$(CH_3)_2$-Ph and X=H, the spectral change on going to the pyridine solution is different from the other complexes of the type VO(H-SAL.aryl)$_2$, as shown in Fig. 1 and Table 3, the *d-d* bands of the former in pyridine being shifted toward much lower frequencies than in the solution of the latter. This anomalous spectral change indicates that VO(H-SAL.2-CH_3-Ph)$_2$ and VO(H-SAL.2,6-$(CH_3)_2$-Ph)$_2$ in pyridine form six-coordinate pyridine adducts having a more distorted configuration than that of the corresponding adduct of VO(H-SAL.Ph)$_2$. This difference between the complexes with X=H and those with X=5,6-benzo may be ascribed to the effect of the field strength produced by the in-plane ligands. A similar difference in the stereochemistry of the complex, as a result of the introduction of a substituent in the benzene nucleus, was sometimes observed with the corresponding complexes of cobalt(II), nickel(II) and copper(II).[4]

TABLE 4. THE CONFIGURATION OF COMPLEXES OF THE TYPE M(H-SAL.R)$_2$ IN THE SOLID STATE AND IN PYRIDINE

M	R=*iso*-C_3H_7		R=2,6-$(CH_3)_2$-Ph	
	solid	in pyridine	solid	in pyridine
VO(IV)[a]	pl	dist. add.	pl	dist. add.
Co(II)[b]	td	equil.	td	equil.
Ni(II)[c]	td	oct. add.	pl	pl
Cu(II)[d]	td	td	pl	5-co. add.

pl: planar; td: tetrahedral; dist. add.: adduct with a distorted configuration; equil.: equilibrium consisting of two or more different species; 5-co. add.: 5-coordinate adduct; oct.: octahedral

a) Present study and ref. (1). b) Ref. (4).
c) Ref. (3). d) S. Yamada, unpublished.

Comparison of the present results with those of the previous papers[3,4] is summarized in Table 4. We see that the distortion in the solid state occurs more easily with R=α-branched alkyl groups than with R=aryl groups.

Table 4 also shows that the vanadium(IV) ion seems to take up an additional ligand such as pyridine to form a six-coordinate adduct more readily than do the cobalt(II), nickel(II), and copper(II) ions.

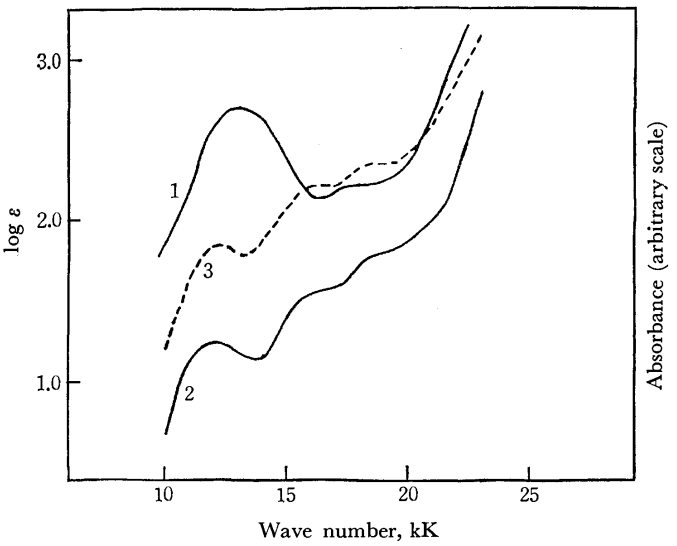

Fig. 3. Electronic absorption spectra of VO(X-SAL.Ph)$_2$: 1, X=5-Br, solid; 2, X=5-Br, in chloroform; 3, X=H, solid.

3) S. Yamada, A. Takeuchi, K. Yamanouchi, and K. Iwasaki, This Bulletin, **42**, 131 (1969).

4) S. Yamada, *Coord. Chem. Rev.*, **1**, 415 (1966).

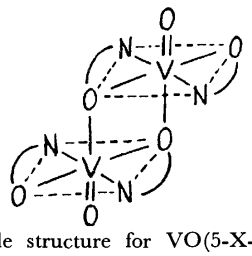

Fig. 4. A possible structure for VO(5-X-SAL.Ph)$_2$ in the solid state, X being Cl and B .

TABLE 5. ABSORPTION MAXIMA OF OXOVANADIUM(IV) COMPLEXES OF THE TYPE VO(5-X-SAL.Ph)$_2$

X	State	Absorption max, kK (log ε for solution)
Cl	solid	13.1, 18.2
	pyridine	13.5(1.62)
Br	solid	13.0, 18.0
	$CHCl_3$	12.0(1.24), 16.5(1.56)sh, 18.7(1.70)sh
	pyridine	13.7(1.58)

sh: shoulder

The spectra of VO(5-Cl-SAL.Ph)$_2$ and VO(5-Br-SAL.Ph)$_2$ in the solid state, shown in Fig. 3 and Table 5, differ remarkably from those of other complexes such as VO(H-SAL.Ph)$_2$ and VO(5,6-benzo-SAL.Ph)$_2$. Moreover, their magnetic moments (Table 2) are lower than the spin-only moment 1.73 B. M. for the d^1 system, showing that some sort of interaction may be present between vanadium(IV) ions. It is therefore likely that their configuration differs from the square pyramidal one. One of the probable configurations for these two complexes in the soid state is a binuclear one, as shown in Fig. 4. For a definite conclusion, however, an X-ray study is necessary. Examination of their infrared spectra yielded no significant conclusion. The low solubility of these compounds did not allow the determination of their molecular weights.

The 5-bromo-substituted complex is moderately soluble in non-coordinating solvents, although the 5-chloro-substituted complex is only slighlty soluble. The spectrum of VO(5-Br-SAL.Ph)$_2$ in chloroform, as shown in Fig. 3, is different from that of the same complex in the solid state but similar to the spectrum typical of the square-pyramidal oxovanadium(IV) complex of this series. It is thus found that the 5-bromo-substituted complex has a uninulcear, square-pyramidal configuration in the non-donor solvent. Inspection of the spectra also indicates that these complexes in pyridine form pyridine adducts having a similar configuration to that of VO(H-SAL.Ph)$_2$ or VO(5,6-benzo-SAL.Ph)$_2$.

Financial support of this work by the Ministry of Education is gratefully acknowledged. Thanks are also due to Mr. Hiro Kuma for his assistance in the experiments.

BULLETIN OF THE CHEMICAL SOCIETY OF JAPAN, VOL. 45, 802—806(1972)

Stereoselective Formation of Isomers of the *Bis*(L-aspartato)-L-(or D-)alaninatocobaltate(III) Complex[1)]

Toshitsugu MATSUDA, Tetsuro OKUMOTO, and Muraji SHIBATA
Department of Chemistry, Faculty of Science, Kanazawa University, Kanazawa

(Received July 22, 1971)

The reaction of racemic α-alanine, in the presence of active charcoal, on a reaction mixture of the $[Co(CO_3)_3]^{3-}$ complex with L-aspartate led to the stereoselective formation of the $[Co(L\text{-}asp)_n(ala)_{3-n}]^{n-}$ (n=0—3) complexes. By means of ion-exchange chromatography and a recrystallization procedure, three stereoisomers of the *bis*(L-aspartato)alaninato complex have been obtained; *mer*$_1$-*Λ*-$[Co(L\text{-}aspH)_2(L\text{-}ala)]\cdot H_2O$, *mer*$_2$-*Λ*-$[Co(L\text{-}aspH)_2(L\text{-}ala)]\cdot 2H_2O$, and *fac*-*Λ*-$[Co(L\text{-}aspH)_2(D\text{-}ala)]\cdot 4H_2O$ (where the *mer*$_1$ and *mer*$_2$ isomers have different geometries). These isomers have been characterized by comparing their CD and PMR spectra with those of the corresponding isomers obtained using L- or D-alanine in place of racemic alanine. The *fac*/*mer* ratio has been estimated to be *ca.* 64/36. The *Δ*/*Λ* ratio in the *fac* isomer has been estimated to be *ca.* 95/5, while the *Δ*/*Λ* ratio in both the *mer*$_1$ and *mer*$_2$ isomers has been estimated as *ca.* 25/75.

Previously, we reported that, when a large excess of racemic α-alanine was reacted with a reaction mixture of the tricarbonatocobaltate(III) complex with L-aspartate, a water-insoluble *fac-tris*(alaninato)cobalt(III) complex was precipitated, and that the precipitates consisted mainly of the *fac*-*Δ*(−)-$[Co(D\text{-}ala)_2(L\text{-}ala)]$ isomer (the (−) sign refers to the sign of the main CD peak in the first absorption band region).[2)] In those experiments, the yield of the insoluble material was usually less than 50%. This fact was an indication of the existence of water-soluble complex species in such a reaction mixture; therefore, we wanted to isolate some of those complexes.

On the other hand, we have recently reported the pra-

1) Presented at the 24th Annual Meeting of the Chemical Society of Japan, Osaka, April, 1971.

2) M. Shibata, H. Nishikawa, and K. Hosaka, This Bulletin, **41**, 130 (1968).

paration of a series of glycinato-L-aspartato complexes, $[Co(gly)_{3-n}(L\text{-asp})_n]^{n-}$ ($n=1,2$), and discussed the stereoselective formations of the complexes.[3] In connection with the earlier work, the present paper will report the isolation and characterization of *bis*(L-aspartato)alaninato complexes, and will discuss the stereoselectivity in the complex formations.

Experimental

Preparation. To a green solution of tricarbonatocobaltate(III) ($CoCl_2 \cdot 6H_2O$ 6.0 g scale; 0.025 mol) prepared by the usual method,[4] 6.7 g (0.050 mol) of L-aspartic acid were added; the mixture was then stirred at 60°C for 2 hr. After adding 4.5 g (0.050 mol) of racemic α-alanine and 1.0 g of active charcoal, the solution was stirred at *ca.* 50°C for 3 hr; the color of the solution then changed from violet to red-violet, and a small amount of a water-insoluble material was precipitated. After the removal of this precipitate and the active charcoal by filtration, the filtrate was adjusted to pH *ca.* 7 with 6N acetic acid. This solution was charged on an anion-exchange column containing 100—200 mesh Dowex 1×8 resin in the chloride form (diameter, 7.0 cm; resin height, 30 cm). When water was passed through the column, a non-charged *tris*(alaninato) complex was eluted out. Then a 0.03M aqueous solution of calcium chloride was poured into the column at the rate of *ca.* 0.5 ml/min. After prolonged elution, seven bands were completely separated; the first band consisted of the univalently-charged *bis*(alaninato)-L-aspartato complex including isomers of both the *mer* and *fac* forms. The second and third bands were of the bivalently-charged *bis*(L-aspartato)alaninato complex belonging to the *mer* form. The fourth and fifth bands were of the same complex belonging to the *fac* form. The last two bands were the *mer* and *fac* isomers of the *tris*(L-aspartato) complex. An attempt at crystallization was actually made for the complex species of the 2—5 bands, because the first band gave a mixture of the stereo isomers of the *bis*(alaninato)-L-aspartato complex, and because the isomers of the complex corresponding to the last two bands, the isomers of the *tris*-(L-aspartato)cobaltate(III), had already been isolated.[5]

Four bands (2—5) were collected in fractions; they were conveniently labelled mer_1, mer_2, fac_1, and fac_2 according to the elution order. Each fraction was then concentrated to a small volume under reduced pressure at temperatures below 40°C. When ethanol was added to the resulting concentrate, the desired complex was obtained as calcium salt. This was then dissolved in a minimum amount of water, and the solution was acidified with 6N hydrochloric acid to precipitate the complex as hydrogen compound. This treatment was also employed for the calcium salts precipitated from the mer_1, mer_2, and fac_1 fractions. The calcium salt precipitated from the fac_2 fraction was dissolved in a minimum amount of water, and the solution was added to a small column containing Dowex 50W×8 resin in the hydrogen form. The effluence was concentrated, and ethanol was added to the concentrate to precipitate the hydrogen compound of the complex. The recrystallization of these hydrogen compounds was performed by dissolving each of them in slightly alkaline water and by then acidifying the solution with diluted hydrochloric acid. This procedure was repeated until the main CD peak of the compound showed a constant intensity. Although the exact yields were not obtained because of the repeated crystallization, the compounds were obtained in yields of roughly 8, 50, and 50 mg for the mer_1, mer_2, and fac_2 fractions respectively. The fac_1 fraction gave a trace of the solid.

A similar experiment was carried out by using L- or D-alanine in place of racemic alanine; the amount of L-(or D-)-alanine used was 2.3 g (0.025 mol). The procedures used in the chromatographic separation and in the isolation of the isomers were those described above.

The results of the elemental analyses of the isolated compounds will be shown below.

Formation Ratios. The formation ratios were compared among the *bis*(L-aspartato)alaninato complex species and actually determined spectrophotometrically using the ε_{max} value of the first absorption band and the $\Delta\varepsilon$ value at the main CD peak in the same absorption band region. However, in the determination we assumed that the Λ and Δ isomers of a complex have the same ε_{max} and $|\Delta\varepsilon|$ values, because only the Λ or Δ isomer could be obtained as a crystal from each of the fractions.

Measurements. The electronic absorption spectra were measured with a Hitachi Perkin-Elmer Model 139 UV-VIS spectrophotometer. The circular dichroism spectra were recorded on a JASCO Model ORD/UV-5 spectropolarimeter. The proton magnetic resonance spectra were recorded on a JEOL Model C-60H spectrometer (60 MHz) at about 25°C, using deuterium oxide containing an equivalent mole of Na_2CO_3 as the solvent. The values of the chemical shifts were measured in relation to sodium 3-(trimethylsilyl)-1-propanesulfonate (Na-TPS) used as an internal reference.

Results and Discussion

Characterization of the Complexes. Since the experiments on the isolation of the isomers of the desired complex were done using racemic (DL-), L-, and D-alanine separately, the isomers obtained from these experiments may conveniently be labelled as (DL), (L), and (D); for example, a compound obtained from the mer_1 fraction in the experiment using DL-alanine will be labelled mer_1 (DL).

The results of the elemental analyses and the numerical data on the absorption and CD spectra are summarized in Table 1. There is a lack of data for the fac_1-Λ because of an extremely poor formation of the species, while the lack of data for the mer_1-Λ(D) arises from a difficulty in crystallization. The geometrical form (*mer* or *fac*) could easily be determined on the basis of the absorption spectral data.[6,7] The absolute configuration (Λ or Δ) was also assigned on the basis of the sign of the main CD peak of each isomer.[8,9] The compounds obtained from the mer_1, mer_2, and fac_1 fractions were identified as the Λ isomers, while the compound obtained from the fac_2 fraction was identified as the Δ isomer. The CD and absorption spectra for the mer_2-Λ and fac_2-Δ are shown in Figs. 1 and 2.

3) K. Kawasaki, J. Yoshii, and M. Shibata, *ibid.*, **43**, 3819 (1970).
4) M. Shibata, *Nippon Kagaku Zasshi*, **87**, 771 (1966).
5) M. Shibata, H. Nishikawa, and K. Hosaka, This Bulletin, **40**, 236 (1967).
6) F. Basalo, J. Bjerrum, and C. J. Ballhausen, *Acta Chem. Scand.*, **9**, 810 (1955).
7) Y. Shimura and R. Tsuchida, This Bulletin, **29**, 311 (1956).
8) M. G. B. Drew, J. H. Dunlop, R. D. Gillard, and D. Rogers, *Chem. Commn.*, **1966**, 42.
9) R. G. Denning and T. S. Piper, *Inorg. Chem.*, **5**, 1056 (1966).

TABLE 1. ANALYSES, ELECTRONIC ABSORPTION AND CD SPECTRA

Complex	Anal. %			Absorption		CD	
	C	H	N	$\nu^{b)}$	ε_{max}	$\nu^{b)}$	$\Delta\varepsilon$
$[Co(L\text{-}aspH)_2(ala)]\cdot H_2O$							
mer_1-Λ(DL)	30.21 (30.77)[a)]	4.94 (4.70)	9.46 (9.79)	56.1	112	56.7	+3.96
				80.4	162	82.4	−0.57
mer_1-Λ(L)	30.95	5.07	9.27	56.1	112	56.7	+3.96
				80.4	162	82.4	−0.56
$[Co(L\text{-}aspH)_2(ala)]\cdot 2H_2O$							
mer_2-Λ(DL)	29.63 (29.53)	5.01 (4.96)	9.46 (9.39)	56.1	123	56.8	+3.98
				80.4	183	82.4	−0.64
mer_2-Λ(L)	29.83	5.14	9.62	56.1	124	56.8	+3.96
				80.4	183	82.4	−0.60
mer_2-Λ(D)	29.39	4.62	9.39	56.1	123	56.8	+4.50
				80.4	183	82.4	−0.89
$[Co(L\text{-}aspH)_2(ala)]\cdot 4H_2O$							
fac_2-Λ(DL)	27.82 (27.33)	5.89 (5.43)	8.52 (8.69)	57.9	183	56.1	−1.69
				80.0	144	74.5	−0.18
						82.0	+0.57
						90.5	−0.06
$[Co(L\text{-}aspH)_2(ala)]\cdot 2H_2O$							
fac_2-Λ(L)	29.70 (29.53)	4.86 (4.96)	9.09 (9.39)	57.9	183	56.2	−1.85
				80.0	144	74.5	−0.19
						82.0	+0.53
						90.5	−0.06
fac_2-Λ(D)	29.63	5.28	9.40	57.9	184	56.1	−1.70
				80.0	144	74.5	−0.18
						82.0	+0.58
						90.5	−0.06

a) Calcd; b) 10^{13} sec^{-1}

The stereochemistry of a *tris*-type complex containing two different aminoacidato ligands provides the existence of three geometrical isomers belonging to the *mer* form and one of the *fac* form (Fig. 3), but in the present work one *fac* isomer and two *mer* isomers labelled as mer_1 and mer_2, were obtained. The PMR spectra for the fac_2-Λ(L), mer_1-Λ(L), and mer_2-Λ(L) are shown in Fig. 4. The two *mer* isomers showed different spectra in the methylene proton resonance of the chelated aspartates.

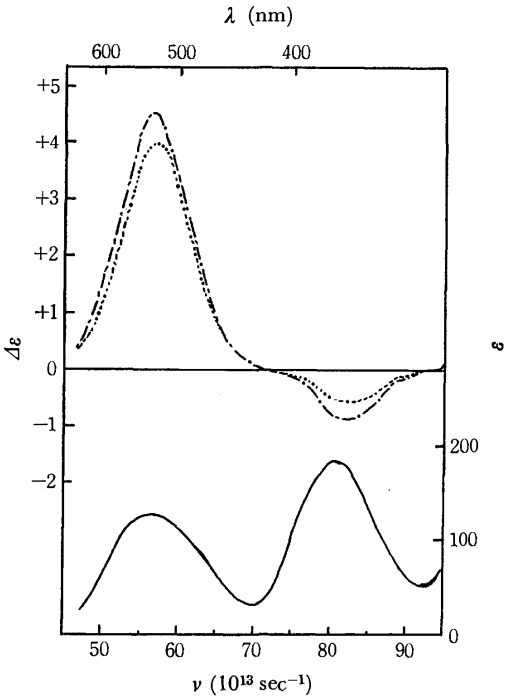

Fig. 1. Absorption and CD spectra for mer_2-Λ isomers in 60% $HClO_4$.
——Absorption spectra
-----CD spectra for mer_2-Λ-(L)
-·-·-CD spectra for mer_2-Λ-(D)

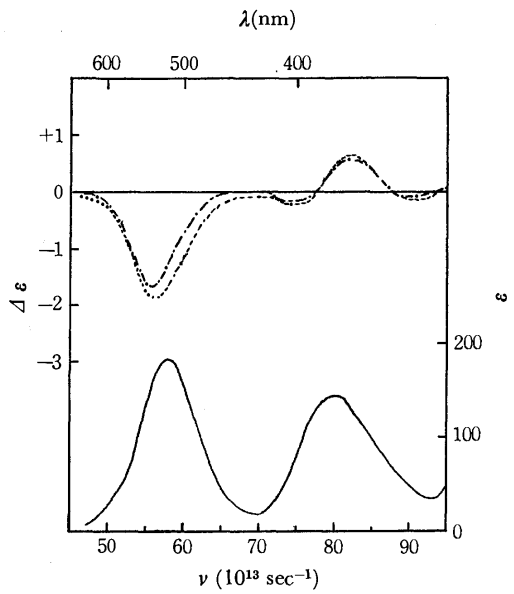

Fig. 2. Absorption and CD spectra for fac_2-Λ isomers in 60% $HClO_4$.
——Absorption spectra
-----CD spectra for fac_2-Λ-(L)
-·-·-CD spectra for fac_2-Λ-(D)

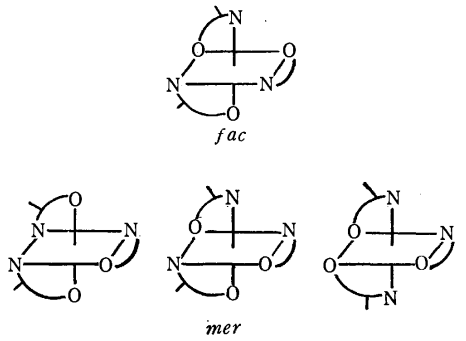

Fig. 3. The possible geometrical isomers of [Co(L-aspH)$_2$-(ala)].

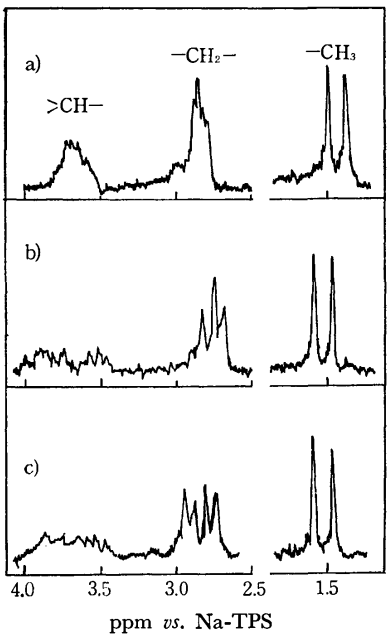

Fig. 4. PMR spectra in D_2O.
a) fac_2-Λ-(L)
b) mer_1-Λ-(L)
c) mer_2-Λ-(L)

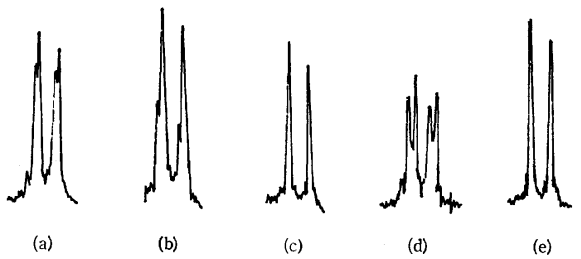

Fig. 5. Methyl proton resonance on;
a) mixed sample of mer_2-Λ-(L) and mer_2-Λ-(D),
b) crude sample of mer_2-Λ-(DL)
c) pure sample of mer_2-Λ-(DL),
d) crude sample of fac_2-Λ-(DL)
e) pure sample of fac_2-Λ-(DL),

This fact suggests that the isomers have different geometries.

The methyl proton resonance spectra of the chelated alanine are shown in Fig. 5. The spectrum for the mer_2-Λ(L) gives a single doublet at 1.55 ppm, while the spectrum for the mer_2-Λ(D) gives a similar doublet at 1.57 ppm. When a mixed sample of the two mer_2 compounds in the same amounts was measured, the spectrum revealed two closed doublets with a slight separation of *ca.* 1.5 Hz. On the other hand, when a compound from the mer_2-Λ(DL) fraction, which had been taken in the course of the recrystallization procedure, was measured, the spectrum showed a pattern similar to that of the mixed sample. The complex on which the recrystallization procedure had been completed showed only one doublet, at 1.54 ppm. Similarly, the fac_2-Λ(L) and fac_2-Λ(D) compounds showed a single doublet due to the methyl protons at 1.43 and 1.48 ppm respectively. The fac_2-Λ(DL) compound gave a doublet at 1.48 ppm, whereas a crude material of the same compound gave two pairs of doublets with a separation of *ca.* 2.5 cps. These results indicate that the crude material of an isomer, in an experiment using racemic alanine, includes both D- and L-alanine as ligands, and that the completely recrystallized material includes either L- or D-alanine as a ligand.

In order to identify the active form (D or L) of the coordinated alanine in the completely recrystallized material obtained by the use of racemic alanine, the $\Lambda\varepsilon$ value of the isomer was compared with that of the corresponding isomer obtained by the use of L- or D-alanine. As may be seen in Table 1, the value of the mer_2-Λ(DL) is almost identical with that of the mer_2-Λ(L) and considerably different from that of the mer_2-Λ(D) isomer. When a similar comparison is made among the fac_2-isomers, a better agreement of the value of the (DL) isomer is found in that of the (D) isomer. These comparisons indicate that the mer_2-Λ(DL) isomer contains L-alanine and that the fac_2-Λ(DL) isomer contains D-alanine. Additional support is obtained from the previously-mentioned PMR data. Since the CD data for the mer_1-Λ(DL) and mer_1-Λ(L) isomers are almost identical, the former perhaps contains L-alanine.

Stereoselectivity. The percent compositions of the *mer* and *fac* isomers, and also the percent compositions of the Λ (or Δ) isomer predominantly formed for each geometrical isomer, are given in Tables 2 and 3. Simi-

Table 2. Percent compositions of the *mer* and *fac* isomers

Amino acids used	Isomers		
	mer (%)	(mer_1/mer_2)	*fac* (%)
DL-ala	36	(1/3)	64
L-ala	34	(1/3)	66
D-ala	39	(2/7)	61
gly[3]	42	—	58

Table 3. Percent compositions of Λ or Λ isomers

Amino acid used	Isomers		
	mer_1-Λ (%)	mer_2-Λ (%)	fac_2-Λ (%)
DL-ala	78	76	95
L-ala	76	78	97
D-ala	73	78	93
gly[3]	73		95

lar data for the glycinato(L-aspartato) complex[3] are also cited in the Tables for the sake of comparison. The figures themselves are not very exact because of the assumed values of ε and $\Delta\varepsilon$ for non-isolated isomers, that is, since the vicinal contribution of the optically active ligands are disregarded, but they do seem to be useful for the estimation of the stereoselectivity. The composition of the *fac*$_2$-Δ (DL, D, or L) isomers was estimated to be *ca.* 95%, and a marked stereoselectivity was found in the Δ configuration. The compositions of all the *mer*-isomers ranged from 70 to 80%, and an appreciable selectivity was found in the Λ configuration. These results are similar to those for the *bis*(L-aspartato)glycinato complex (Table 3). The compositions of the *mer* and *fac* isomers could be estimated to be around 35 and 65%, not very different from those in the corresponding glycinato complex (Table 2). From this fact, we can consider that the orientation of the methyl group of the coordinated alanine scarcely affects the stereoselectivity in the complex concerned, and that the β-carboxylate groups of the coordinated L-aspartates affect the selectivity. In a previous paper,[3] we have assumed an enhanced stability through hydrogen-bonding between the β-carboxylate group in the L-aspartato ligand and the amino group in the adjacent ligand. In the present case, this assumption also gives an explanation of the stereoselectivity.

The fact that the *mer*$_2$-Λ(DL) and *fac*$_2$-Δ(DL) contain L- and D-alanine respectively may be caused by the difference in solubility between the diastereoisomers, rather than by the preferential coordination of one of the active forms of alanine. This is confirmed by the above-mentioned PMR study.

BULLETIN OF THE CHEMICAL SOCIETY OF JAPAN, VOL. 45, 806—811(1972)

Stereochemical Studies of Metal Chelates. VI. The Separation and Stereochemistry of Isomers of Dichloro((3*S*, 8*S*)-dimethyltriethylenetetramine)cobalt(III) Perchlorate

Masahiko SABURI and Sadao YOSHIKAWA

Department of Synthetic Chemistry, Faculty of Engineering, The University of Tokyo, Hongo, Bunkyo-ku, Tokyo 113

(Received September 10, 1971)

The *cis*-α and *cis*-β isomers of dichlorocobalt(III) complexes with (3*S*, 8*S*)-dimethyltriethylenetetramine were isolated. These isomers were stereospecifically formed in the *Λ* and *Δ* absolute configurations respectively. The *cis*-β isomerh as the *Δ*-β(*RS*) geometry, in which the configurations with respect to the coordinated secondary nitrogen centersof tetramine differ from one another. The difference between the *Δ*-β(*RS*) and *Δ*-β(*RR*) (and *Λ*-β(*SS*)) forms was noticed in the circular dichroism curves in the first absorption band region.

In a study of the diacidocobalt(III) complexes of triethylenetetramine (trien),[1] Basolo first pointed out the possibility of three geometrical isomers, *i.e.*, *cis*-α, *cis*-β, and *trans* (*c.f.* Fig. 1). These were isolated and resolved into optically-active antipodes by Sargeson and Searle for the first time.[2,3] The exact geometries of trien in the α and β configurations have recently been shown by X-ray diffraction studies.[4,5] Furthermore, it was suggested that the second *cis*-β form exists as a product of the Hg^{2+}-promoted acid hydrolysis reaction of the optically-active *trans*-$[Co(trien)Cl_2]^+$ ion.[6]

The difference between the two *cis*-β geometries arises from the combination of the configuration of the coordinated secondary nitrogen centers. The asymmetric character of the coordinated secondary nitrogen atom has been well established for some cobalt(III) com-

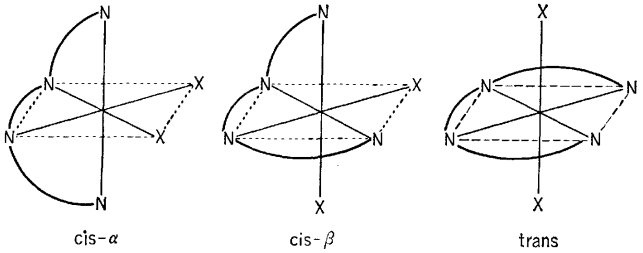

Fig. 1. The geometrical isomers of $[Co(trien)X_2]^{n+}$.

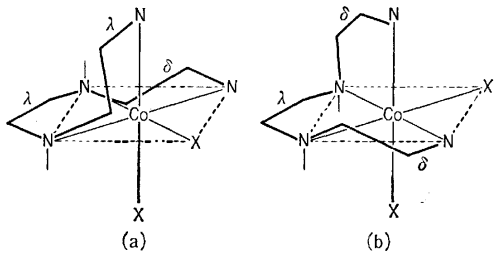

Fig. 2. Diastereoisomeric forms of *cis*-β-$[Co(trien)X_2]^{n+}$ (a) *Λ*-β(*SS*) and (b) *Δ*-β(*RS*)

1) F. Basolo, *J. Am. Chem. Soc.*, **70**, 2634 (1948).
2) A. M. Sargeson and G. H. Searle, *Inorg. Chem.*, **4**, 45 (1965).
3) A. M. Sargeson and G. H. Searle, *ibid.*, **6**, 787 (1967).
4) M. Dwyer and I. E. Maxwell, *ibid.*, **9**, 1450 (1970).
5) H. C. Freeman and I. E. Maxwell, *ibid.*, **8**, 1293 (1969).
6) D. A. Buckingham, P. A. Marzilli, and A. M. Sargeson, *ibid.*, **6**, 1032 (1967).

plexes.[7-12] The structures of the two isomers of *cis-β* geometry are shown in Fig. 2. They are illustrated for the enantiomer, in which the central chelate ring takes the λ[13] conformation. The absolute configurations of the coordinated secondary nitrogen centers are the same for one isomer, designated as Λ[13]-*cis*-β(*SS*)[14] in Fig. 2 and its enantiomorph (Δ-*cis*-β(*RR*)), and different for the other, Δ-*cis*-β(*RS*)[14] in Fig. 2 and its enantiomorph (Λ-*cis*-β(*SR*)[14]). The former geometry was, in fact, observed for some *cis-β* isomers of trien complexes.[5,15-17] On the other hand, the trien cobalt(III) complex with the latter geometry has not yet been isolated except for some β_2-amino acidato complexes.[18]

A detail discussion of the chelate ring conformation of the *β*-configuration was published recently.[19] It is interesting to note that the conformations of the outer-side chelate rings are the same (δ and δ) for the Δ-*cis*-β(*RS*) geometry, while they are different (δ and λ) for the Λ-*cis*-β(*SS*) geometry, as is indicated in Fig. 2. In a recent study of the minimization of the conformational potential energy, it was suggested[20] that the most stable structures for the Δ-β_2-(*RS*) and Λ-β_2(*SR*) isomers of the $[Co(trien)(S\text{-pro})]^{2+}$ ion are those in which the side arms of trien have the same conformation.

It has been well established by X-ray diffraction[21,22] and proton magnetic resonance[23] studies that the methyl group of propylenediamine adopts preferentially the equatorial position with respect to the diamine chelate ring. (2*S*,9*S*)-Dimethyltriethylenetetramine ((2*S*,9*S*)-dimetrien) and (3*S*,8*S*)-dimethyltriethylenetetramine ((3*S*,8*S*)-dimetrien) are optically-active derivatives of trien. The abbreviations and structures of trien derivatives used in the present study are summarized in Table 1. The absolute configuration of the asymmetric carbon atoms is the same *S* configuration for these tetramines, since all the asymmetric centers are derived from the *S*-alanine used as a starting material. If the substituted methyl groups prefer the equatorial orientation, the outer-side chelate rings should have the δ conformation. Accordingly, it was supposed that the *cis-β* isomer containing (2*S*,9*S*)- and (3*S*,8*S*)-dimetrien belongs to the Δ-*cis*-β(*RS*) geometry (shown in Fig. 2), since both the outer-side chelate rings for this structure are expected to have the δ conformation, as has been mentioned previously.

Table 1. Abbreviation and structure of ligands

Abbreviation	Structure
(2*S*,9*S*)-dimetrien	
(3*S*,8*S*)-dimetrien	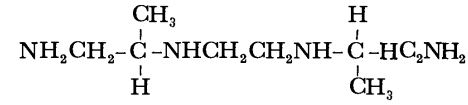
5(*R*)-metrien	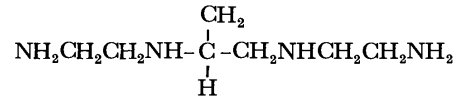
(5*S*,6*S*)-dimetrien	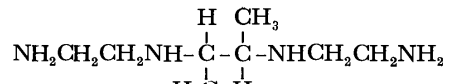
(*R*)-ECE	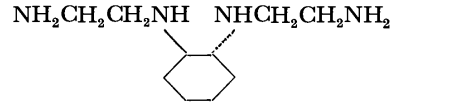

Asperger and Liu[24] isolated three geometrical isomers of dichlorocobalt(III) complexes coordinated with (2*S*,9*S*)-dimetrien, *i.e.*, *cis-α*, *cis-β*, and *trans*. It was noticed by these authors[24] that the *cis-α* and *cis-β* isomers have stereospecifically the Λ- and Δ-absolute configurations respectively. Although the Δ-*cis-β* isomer was isolated, the detailed structure of this complex has not yet been clarified. It was supposed that the *cis-α* and *cis-β* isomers of dichlorocobalt(III) complexes with (3*S*,8*S*)-dimetrien, if obtained, should have the Λ and Δ-configurations respectively, as well as the (2*S*,9*S*)-dimetrien complexes. This is based on the expectation that, for both ligands, the outer-side chelate rings are fixed in the δ conformation due to the substituted methyl groups, though their positions are different in the two ligands. We have succeeded in the isolation of Λ-*cis-α* and Δ-*cis*-β-$[Co((3S,8S)\text{-dimetrien})Cl_2]ClO_4$ and will report our results in the present paper.

Experimental

(2S,9S)-Dimethyltriethylenetetramine Tetrahydrochloride. This was prepared according to the method described by Asperger and Liu.[24]

7) B. Halpern, A. M. Sargeson, and K. R. Turnbull, *J. Am. Chem. Soc.*, **88**, 4630 (1966).
8) D. A. Bucknghan, S. F. Mason, A. M. Sargeson, and K. R. Turnbull, *Inorg. Chem.*, **5**, 1649 (1966).
9) J. F. Blount, H. C. Freeman, A. M. Sargeson, and K. R. Turnnull, *Chem. Commun.*, **1967**, 324.
10) D. A. Buckingham, L. G. Marzilli, and A. M. Sargeson, *J. Am. Chem. Soc.*, **89**, 825 (1967).
11) D. A. Buckingham, L. G. Marzilli, and A. M. Sargeson, *Inorg. Chem.*, **7**, 915 (1968).
12) M. Saburi, Y. Tsujito, and S. Yoshikawa, *ibid.*, **9**, 1476 (1970).
13) *Inorg. Chem.*, **9**, 1 (1970).
14) The nomenclature used is as follows: *R* and *S* designate the asymmetry about the "angular" and "planar" asymmetric N atoms of trien in that order and follow the rules suggested by R. S. Chan, C. K. Ingold, and V. Prelog (*Angew. Chem. Intern. Edn.*, **5**, 385 (1966), *cf.* ref. (6).
15) D. A. Bucknghan, H. C. Freeman, L. G. Marzilli, I. E. Maxwell, and A. M. Sargeson, *Chem. Commun.* **1969** 583.
16) H. C. Freeman, L. G. Marzilli, and I. E. Maxwell, *Inorg. Chem.* **9**, 2408 (1970).
17) H. C. Freeman and I. E. Maxwell, *ibid.*, **9**, 649 (1970).
18) C. Y. Lin and B. E. Douglas, *Inorg. Chim. Acta*, **4**, 1 (1970).
19) D. A. Bucknghan, I. E. Maxwell, A. M. Sargeson, and H. C. Freeman, *Inorg. Chem.*, **9**, 1921 (1970).
20) D. A. Buckingham, I. E. Maxwell, A. M. Sargeson, and M. R. Snow, *J. Am. Chem. Soc.*, **92**, 3617 (1970).
21) Y. Saito and H. Iwasaki, This Bulletin, **35**, 1131 (1962).
22) H. Iwasaki and Y. Saito, *ibid.*, **39**, 92 (1966).
23) S. Yano, H. Ito, Y. Koike, J. Fugita, and K. Saito, *ibid.*, **42**, 3184 (1969).
24) R. G. Asperger and C. F. Liu, *Inorg. Chem.*, **4**, 1395 (1965).

(3S,8S)-Dimethyltriethylenetetramine Tetrahydrochloride. A tetraamide (11.5 g) obtained by the reaction of *S*-alanine amide with oxalyl chloride (described earlier[25]) was stirred into a suspension of lithium aluminum hydride (13.3 g) in anhydrous tetrahydrofuran (300 m*l*), after which the mixture was stirred and heated under reflux for 24 hr. After cooling to room temperature, 25 m*l* of water diluted with 50 m*l* of tetrahydrofuran was vigorously stirred, drop by drop, into the reaction mixture, after which the mixture was stirred for a further 30 min. The resultant slurry was filtered off and washed with tetrahydrofuran (100 m*l*). The residue was extracted with boiling tetrahydrofuran (200 m*l*) under reflux for 2 hr, filtered off, and washed as above. The filtrates and washing were combined, and the tetrahydrofuran was removed under reduced pressure. To the remaining liquid we added 20 m*l* of concentrated hydrochloric acid, and then ethanol was gradually added while hot until the mixture became turbid. After the solution has been cooled to room temperature overnight, the white crystals which separated were collected, washed with ethanol and ether, and dried under vacuum. Yield, 7.0 g.

Trans-*Dichloro((3S,8S)-dimethyltriethylenetetramine)cobalt(III) Perchlorate.* The preparation of this compound was described previously.[26]

Δ-cis-*α*-*Dichloro((3S,8S)-dimethyltriethylenetetramine)cobalt(III) Perchlorate.* The filtrate from which the *trans*-isomer has been removed as above was again cooled to 5°C, and the small amount of green crystals (*trans*-isomer) which precipitated was filtered off. To the filtrate we added 2 more m*l* of 60% perchloric acid, and the solution was stored at 5°C for 2 hr after scratching the side of the vessel with a glass rod. The violet crystals which separated was collected, washed with methanol and acetone, and air-dried. Yield, 0.1 g. *Anal.* Calcd for $[Co(C_8H_{22}N_4)Cl_2]ClO_4$: C, 23.81; H, 5.50; N, 13.88. Found: C, 23.20; H, 5.84; N, 13.51.

Δ-cis-*β*-*Dichloro((3S,8S)-dimethyltriethylenetetramine)cobalt(III) Perchlorate.* The filtrate from the separation of the *Δ*-*cis*-*α*-isomer was left to stand at room temperature for one or two days. The reddish-purple crystals which separated were filtered off, washed with ethanol and acetone, and air-dried. Yield, 0.3 g. A second crop could be obtained by letting the filtrate stand for one or two more days. Yields, 0.2 g. *Anal.* Calcd for $[Co(C_8H_{22}N_4)Cl_2]ClO_4$: C, 23.81; H, 5.50; N, 13.88. Found: C, 23.72; H, 5.63; N, 13.84.

Δ-cis-*α*-*Dinitro((2S,9S)-dimethyltriethylenetetramine)cobalt(III) Chloride.* To a solution containing (2S,9S)-dimetrien·4HCl (3.40 g) and $LiOH \cdot H_2O$ (1.25 g) in 50 m*l* of water, we added $CoCl_2 \cdot 6H_2O$ (2.38 g) and then the solution was cooled in an ice bath. After $NaNO_2$ (1.47 g) had been added, the resultant solution was aerated with carbon dioxide-free air in an ice bath for 1 hr and then for 4 more hr at room temperature. The precipitated impurity was filtered off and washed with a small volume of water. The filtrate and washings were combined and evaporated on a steam bath to a volume of 15 m*l* and then cooled in an ice bath overnight. The yellow-brown crystals which separated were filtered off and washed with a small volume of cold water and ethanol. Yield, 1.5 g. The combined filtrate and washings were further evaporated on a steam bath to about 7 m*l* and then cooled as above. The crystals were filtered off and washed with cold water and ethanol. Yield, 1.0 g. The crude products, which were contaminated with a black impurity, were dissolved in a minimum volume of warm water, filtered, and cooled to room temperature. After the solution had stood overnight, the yellow-brown crystals were filtered off, washed with a small volume of cold water and ethanol, and air-dried. *Anal.* Calcd for $[Co(C_8H_{22}N_4)(NO_2)_2]Cl$: C, 26.64; H, 6.15; N, 23.30. Found: C, 26.52; H, 6.20; N, 23.41.

Δ-cis-α-Dichloro((2S,9S)-dimethyltriethylenetetramine)cobalt(III) Chloride Monohydrate. *Δ-cis-α*-$[Co((2S,9S)$-dimetrien$)(NO_2)_2]Cl$ (1.0 g) was dissolved in 30 m*l* of hydrochloric acid (1:1), and the resultant solution was evaporated on a steam bath almost to dryness. The residue was treated with 10 m*l* of methanol with gentle boiling, and the crystallized product was filtered off, washed with cold methanol and acetone, and air-dried. Yield, 0.7 g. *Anal.* Calcd for $[Co(C_8H_{22}N_4)Cl_2]Cl \cdot H_2O$: C, 26.88; H, 6.76; N, 15.67. Found: C, 26.60; H, 6.60; N, 15.97.

Δ-cis-β-Dichloro((2S,9S)-dimethyltriethylenetetramine)cobalt(III) Perchlorate. A mixture of *Δ-cis-α*-$[Co((2S,9S)$-dimetrien$)]Cl_2 \cdot H_2O$ (0.51 g) and Li_2CO_3 (0.15 g) in 5 m*l* of water was heated on a steam bath for 30 min, cooled to room temperature, and filtered to remove the excess Li_2CO_3. To a solution of *Δ-β*-$[Co((2S,9S)$-dimetrien$)CO_3]^+$ prepared *in situ.* as above, we added 5 N HCl (2 m*l*); the resultant solution was evaporated under a current of air on the surface at room temperarure. When the volume of solution was reduced to 2 m*l*, 60% perchloric acid (1 m*l*) was added. The green crystals of *trans*-$[Co((2S,9S)$-dimetrien$)Cl_2]ClO_4$ which separated were removed whenever necessary, and the filtrate was allowed to stand at room temperature. The reddish-purple crystals which separated were collected, washed with methanol, and air-dried.

Measurements. The visible absorption spectra were measured with a Shimadzu MPS-50L spectrophotometer. The circular dichroism spectra were measured with a JASCO J-20 automatic spectropolarimeter. The spectra of the *cis-α* isomers and of the *cis-β* isomers were measured in 5 N HCl and concentrated HCl solutions to avoid aquation of the complexes.

Results and Discussion

Yoshikawa, Sekihara, and Goto isolated a green *trans* isomer of the dichlorocobalt(III) complex with (3*S*,8*S*)-dimetrien.[25] In spite of the poor agreement between the calculated and found values, especially for

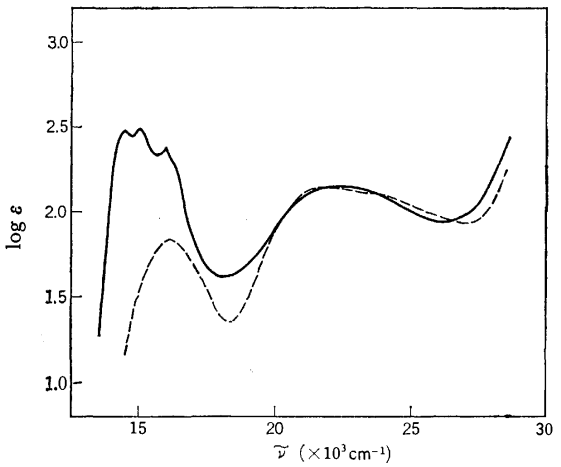

Fig. 3. Absorption Spectra of *trans*-$[Co((3S,8S)$-dimetrien$)Cl_2]_2CoCl_4$ in concentrated hydrochloric acid (———) and *trans*-$[Co((3S,8S)$-dimetrien$)Cl_2]ClO_4$ in methanol (--------).

25) S. Yoshikawa, T. Sekihara, and M. Goto, *Inorg. Chem.*, **6**, 169 (1967).

26) M. Goto, A. Okubo, T. Sawai, and S. Yoshikawa, *ibid.*, **9**, 1488 (1970).

the hydrogen proportion (Found 5.5%; Calcd 6.5%), the constitution of this compound was considered to be $[Co(C_8H_{22}N_4)Cl_2]Cl\cdot HCl\cdot 1.5\ H_2O$. However, it has now been found that the exact constitution of this complex is $[Co(C_8H_{22}N_4)Cl_2]_2(CoCl_4)$. The calculated and found values for this constitution are as follows; Calcd: C, 23.8; H, 5.5; N, 13.9; Cl, 35.1. Found: C, 24.0; H, 5.5; N, 13.9; Cl, 35.2.

The absorption spectrum of the above *trans* complex, measured in concentrated hydrochloric acid, is shown in Fig. 3, where the ε value is evaluated per mole of the Co(III) complex. The complicated strong absorption bands found in the region of 14000—17000 cm^{-1} in a concentrated HCl solution are characteristic of the tetrachlorocobaltate(II) anion.[27] The diffusion reflectance spectrum shows similar peaks in this region, indicating that the $CoCl_4^{2-}$ ion is present in the solid state as the counter ion of this dichlorocobalt(III) complex. This complex anion was also found as the counter ion of *trans*-dichlorocobalt(III) complexes containing *N*-alkyl ethylenediamines.[28] The $CoCl_4^{2-}$ ion appears to be decomposed immediately after the complex is dissolved in methanol, and so it was overlooked in the former study.[25]

We perceived some difficulties in the course of isolating the pure crystalline product of *Λ-cis*-α-[Co((2*S*, 9*S*)-dimetrien)Cl_2]Cl by the method of Asperger and Liu,[24] which can be regarded as an ordinary procedure for preparing the dichlorocobalt(III) complex. This was probably the result of the coexistence of the $CoCl_4^{2-}$ ion, which disturbs the crystallization of the desired products.

It was effective to use anions other than the chloride ion in order to isolate the pure crystalline products of the *cis*-α and *cis*-β isomers of the dichloro complex with (3*S*,8*S*)-dimetrien. We succeeded in isolating the *cis*-α and *cis*-β isomers by the use of perchlorate ion along with the *trans* isomer.

On the addition of 60% perchloric acid to a concentrated solution which seemed to contain three possible isomers of the [Co((3*S*,8*S*)-dimetrien)Cl_2]$^+$ ion, green crystals of the *trans*-[Co((3*S*,8*S*)-dimetrien)Cl_2]ClO_4 immediately crystallized out.[26] The absorption spectrum of this isomer (given in Fig. 3) resembles that of the *trans*-[Co((3*S*,8*S*)-dimetrien)Cl_2]$_2$($CoCl_4$) except for the region of the absorption due to the $CoCl_4^{2-}$ complex anion. The CD spectra of the complexes of such a type have been discussed previously.[25,29]

After the *trans* isomer has been completely removed, a small amount of blue-violet crystals was separated from the filtrate by the addition of more perchloric acid. The visible absorption and CD spectra of this complex are shown in Fig. 4. The spectral data are summarized in Table 2. The absorption spectrum shows a shoulder at a lower wave-number side of the first absorption band. The same feature in the first absorption band was also observed for the *cis*-α-[Co(trien)Cl_2]$^+$ ion, but it was not detected for the *cis*-β isomer of the trien complex. This suggests that the blue-violet isomer has the *cis*-α configuration. Further, the CD spectrum shown in Fig. 4 apparently resembles that of $(+)_D$-*cis*-α [Co(trien)Cl_2]ClO_4 shown by Sargeson and Searle,[2] which was assigned the *Λ* configuration. Therefore, it was determined that the blue-violet isomer of [Co((3*S*,8*S*)-dimetrien)Cl_2]ClO_4 takes, stereospecifically, the *Λ-cis*-α configuration.

The dichlorocobalt(III) complex of (2*S*,9*S*)-dimetrien, which has been shown to adopt preferentially the *Λ-cis*-α configuration, was also prepared. As has been mentioned previously, it was slightly difficult to

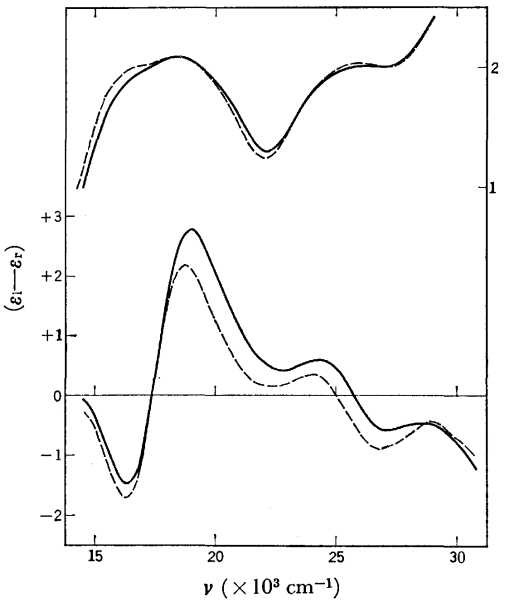

Fig. 4. Absorption and CD spectra of *Λ*-α isomers; (3*S*,8*S*)-dimetrien (——) and (2*S*,9*S*)-dimetrien (------)

Table 2. Spectral data

Complex	Absoption spectra		CD spectra	
	λ_{max} (cm^{-1})	log ε_{max}	λ_{max} (cm^{-1})	$\Delta\varepsilon_{max}$
Λ-cis-α-[Co((3*S*,8*S*)-dimetrien)Cl_2]ClO_4	18450	2.09	16340	−1.49
			18940	+2.78
	26040	2.02	24270	+0.59
			27100	−0.57
Λ-cis-α-[Co((2*S*,9*S*)-dimetrien)Cl_2]Cl·H_2O	18350	2.09	16290	−1.71
			18690	+2.19
	25970	2.04	24100	+0.35
			26810	−0.89
Λ-cis-β-[Co((3*S*,8*S*)-dimetrien)Cl_2]ClO_4	18420	2.11	18690	−1.18
	25190	2.10	24330	−0.60
Λ-cis-β-[Co((2*S*,9*S*)-dimetrien)Cl_2]ClO_4	18800	2.21	19050	−1.55
	25320	2.18	24630	−0.40
Λ-cis-β-[Co((5*R*)-metrien)Cl_2]Cl·0.5H_2O	18690	2.12	(14750	−0.04)
			17090	+0.94
	25640	2.10	24270	+0.34
Λ-cis-β-[Co((5*S*,6*S*)-dimetrien)Cl_2]Cl·H_2O	18800	2.14	17090	−1.05
	25580	2.10	23980	−0.38
Λ-cis-β-[Co((*R*)-ECE)-Cl_2]Cl·H_2O	18590	2.14	(14490	−0.04)
			16860	+1.37
	25640	2.12	24390	+0.33

27) L. I. Katzin, *J. Am. Chem. Soc.*, **76**, 3089 (1954).
28) E. W. Gillow and G. M. Harris, *Inorg. Chem.*, **7**, 394 (1968).
29) D. A. Buckingham, P. A. Marzilli, A. M. Sargeson, S. F. Mason, and P. G. Beddoe, *Chem. Commun.*, **1967**, 433.

obtain the pure crystalline product of this complex by the method of Asperger and Liu.[24] Hence, we prepared it through a reaction of the corresponding dinitro complex with hydrochloric acid. The product thus obtained showed visible and CD spectra identical with those of the complex obtained by the method of Asperger and Liu,[24] shown in Fig. 4. Apparently, the first absorption band has a shoulder on the lower wave number side. This spectral feature may be regarded as a characteristics of the *cis*-α isomer of the dichlorocobalt(III) complex with tetramines. The CD curve is also similar to those of the (+)$_D$-*cis*-α-[Co(trien)Cl_2]ClO_4 and of the blue-violet isomer of the (3*S*,8*S*)-dimetrien complex.

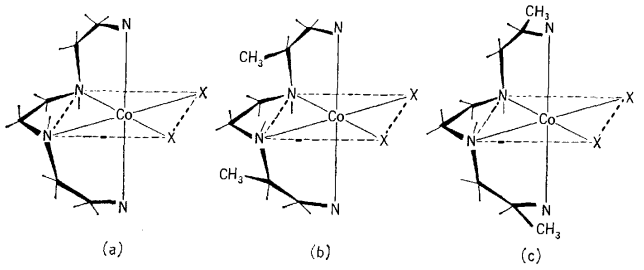

Fig. 5. Structures of *Λ*-α configurations; (a) trien, (b) (3*S*,8*S*)-dimetrien, and (c) (2*S*,9*S*)-dimetrien.

According to a recent X-ray analysis study,[4] the structure of the *Λ*-*cis*-α trien complex has been determined to be as shown in Fig. 5(a), where both the outer-side chelate rings adopt the *δ* conformation. Since the preferred conformation of the outer chelate rings of the (3*S*,8*S*)- and (2*S*,9*S*)-dimetrien is the *δ*-gauche form, as has been mentioned previously, it is reasonable that the *cis*-α isomers of these complexes give rise to the *Λ* configuration. Their probable structures are illustrated in Fig. 5, (b) and (c) respectively. For these configurations, the methyl groups are all situated in the equatorial orientations. The *Λ* isomer, in which the methyl groups should adopt the axial orientations, is energetically unstable as compared with the *Λ* isomer. This is a reason why the former isomer could not be obtained in this study.

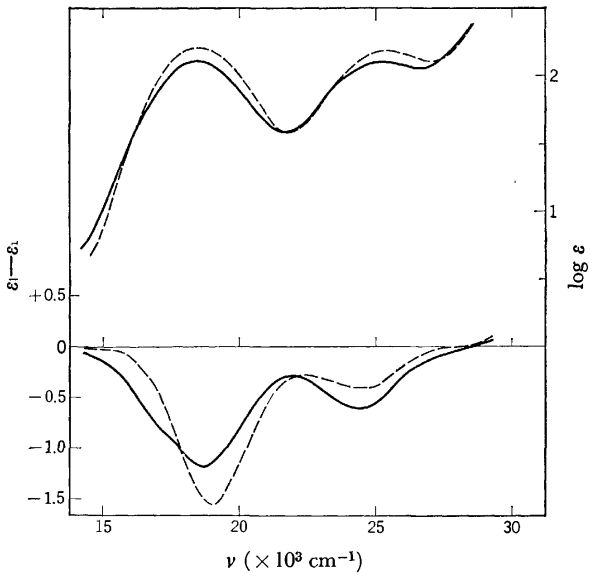

Fig. 6. Absorption and CD spectra of *Λ*-*β* (*RS*) isomers; (3*S*,8*S*)-dimetrien (——) and (2*S*,9*S*)-dimetrien (- - - -).

The third isomer of [Co((3*S*,8*S*)-dimetrien)Cl_2]ClO_4 was obtained as reddish-pink precipitates, which are separated out by letting the filtrate from which the *cis*-α isomer has been removed stand for two or three days. The visible absorption and CD spectra of this compound are shown in Fig. 6. No shoulder of the first absorption band was detected for the present complex, suggesting that it takes the *cis*-*β* configuration. The CD curve of this isomer shows only one negative peak in the first absorption band region. The *Λ*-*cis*-*β*-[Co((2*S*,9*S*)-dimetrien)Cl_2]$^+$ ion, which was first obtained by Asperger and Liu,[24] was prepared by a different method through the *Λ*-*cis*-α isomer in the present study. This complex shows the absorption and CD curves given in Fig. 6. They are apparently similar to the corresponding curves of the reddish-pink isomer of the (3*S*,8*S*)-dimetrien complex. Thus, it was determined that the reddish-pink isomer takes, stereospecifically, the same absolute configuration as the *cis*-*β* isomer of the (2*S*,9*S*)-dimetrien complex, *i.e.*, the *Λ*-*cis*-*β* configuration.

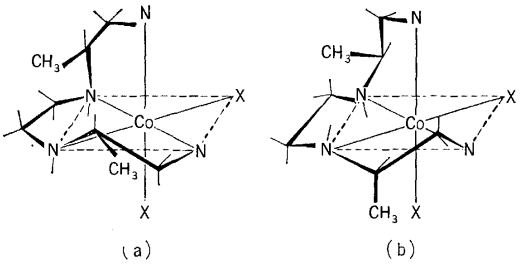

Fig. 7. Structures of *Λ*-*β* isomers of (3*S*,8*S*)-dimetrien; (a) *Λ*-*β*(*RS*) and (b) *Λ*-*β*(*RR*).

The probable structures for the *Λ*-*cis*-*β* isomer of (3*S*,8*S*)-dimetrien are illustrated in Fig. 7(a) and (b). For the *Λ*-*cis*-*β*(*RS*)[30] geometry (a), both the methyl groups are equatorially oriented, and the outer chelate rings take the *δ* conformation. On the other hand, one of the methyl groups, which is present in the "in-plane" chelate ring, having the *λ* conformation, takes the axial orientation for the *Λ*-*cis*-*β*(*RR*) geometry, though the other is in the equatorial position. Because of the difference in methyl orientation, the former geometry is more probable than the latter. The difference in axial and equatorial methyl groups was estimated to be 2.0 kcal/mole for the propylenediamine chelate ring.[31] It is reasonable to consider that the above estimation is applicable to the (2*S*,9*S*)-dimetrien complex. It was demonstrated by the X-ray diffraction method for the dinitro complex that the *Λ*-*cis*-*β*

30) The *RS* representation of the absolute configuration of the coordinated nitrogen centers is complicated in the substituted triens by the presence of methyl groups. For example, (3*S*, 8*S*)-dimetrien and trien complexes have the opposite configurations in the *Λ*-α form; (*SS*) for the former and (*RR*) for the latter. Therefore, the absolute configuration of the coordmated secondary nitrogen centers is represented by *R* and *S*, neglecting, for simplicity, the substituted methyl groups in this paper.

31) A. M. Sargeson, *Transition Metal Chem.*, **3**, 303 (1966).

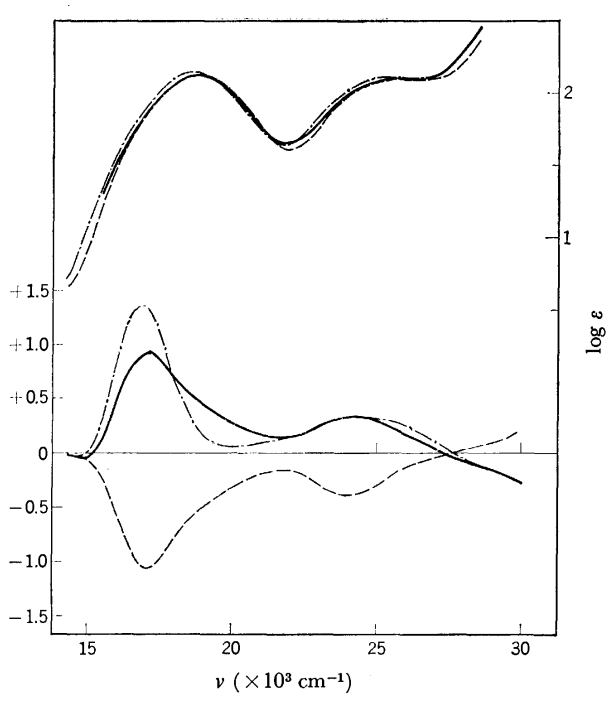

Fig. 8. Absorption and CD spectra for *Λ*-*β*(*SS*) and *Λ*-*β*(*RR*) geometries; (5*R*)-metrien (*Λ*) (——), (5*S*,6*S*)-dimetrien (*Λ*) (– – –), and (*R*)-ECE (*Λ*) (–·–·–·).

isomer of (3*S*,8*S*)-dimetrien possesses the *Λ*-*cis*-*β*(*RS*) geometry, as has been expected.[32]

It seems likely that CD curves are affected by the structural differences, *i.e.*, the absolute configuration of the coordinated secondary nitrogen center and the conformation of each chelate ring. The CD curves of the *Λ*-*cis*-*β*(*SS*) or *Δ*-*cis*-*β*(*RR*)-dichloro complexes of trien derivatives with equatorially-oriented substituents at the central diamine linkage were examined. The structures of these complexes had previously been established as indicated.[33] Their CD and absorption curves are shown in Fig. 8.

There was no definite difference in the absorption spectra of the two types of *cis*-*β* isomer. The *Δ*-*β*(*RS*) isomer exhibited its first absorption maxima at about 18500 cm^{-1}, while the *Λ*-*β*(*SS*) and *Δ*-*β*(*RR*) isomers exhibited theirs at about 18600—18800 cm^{-1}. This suggests that the difference in ligand field due to the structural changes is negligibly small for both the geometries.

On the contrary, an obvious difference in their CD curves could be noted between the *Δ*-*β*(*RS*) and *Δ*-*β*(*RR*) (or *Λ*-*β*(*SS*)) forms in the first absorption band region. The *Δ*-*β*(*RS*) isomers of (3*S*,8*S*)- and (2*S*,9*S*)-dimetrien complexes showed dominant negative CD maxima at about 19000 cm^{-1}. The *Δ*-*β*(*RR*) isomer of (5*S*,6*S*)-dimetrien showed a negative CD peak at 17000 cm^{-1}. The *Λ*-*β*(*SS*) isomers of (5*R*)-metrien and (*R*)-ECE also exhibited the corresponding positive CD peaks at about 17000 cm^{-1}. It was clearly observed that the dominant CD peak for the *Δ*-*β*(*RS*) forms is shifted by 2000 cm^{-1} to the higher wavenumber side than those for the *Δ*-*β*(*RR*) and *Λ*-*β*(*SS*) forms. The observed shift of the CD maxima in the first absorption band region may be useful for distinguishing the geometries of *cis*-*β* dichlorocobalt(III) complexes with any trien derivatives.

32) M. Ito, F. Marumo, and Y. Saito, *Acta Crystallogr.*, **B26**, 1408 (1970).

33) M. Goto, M. Saburi, and S. Yoshikawa, *Inorg. Chem.*, **8**, 358 (1969).

Chemical Studies of Minerals Containing Rarer Elements from the Far East District. LXV.[1] Pollucite from Nagatare, Fukuoka Prefecture, Japan

Kin-ichi SAKURAI, Akira KATO, Noriyuki KUWANO,* and Kozo NAGASHIMA**

Department of Geology, National Science Museum, Ueno Park, Tokyo
**Institute of Metallurgy, Faculty of Technology, Kyushu University, Fukuoka*
***Department of Chemistry, Tokyo Kyoiku University, Otsuka, Tokyo*

(Received September 29, 1971)

The chemical analysis of pollucite found in a granite pegmatite at Nagatare, Fukuoka Prefecture, gave SiO_2 46.03, Al_2O_3 17.76, Fe_2O_3 0.02, MnO 0.01, CaO 0.03, Li_2O 0.16, Na_2O 2.08, K_2O 1.81, Rb_2O 0.61, Cs_2O 28.88, and H_2O 2.74; total 100.13%; recalculated as $(Cs,Rb)_{0.573}(Na,K,Li,Mn,Ca)_{0.316}(Al,Fe)_{0.943}Si_{2.071}O_6 \cdot 0.411\ H_2O$ as O=6, thus satisfying the crystallochemical formula advocated by Beger. X-ray single crystal and powder studies have shown it to be cubic, the space group is Ia3d; $a_0=13.674\pm0.005$ Å. It is optically isotropic or very faintly birefringent, with $n=1.520\pm0.002$.

Granite pegmatites exposed at Nagatare, Fukuoka Prefecture, include some rare alkali-bearing minerals, such as lepidolite,[2] petalite,[3] and amblygonite-montebrasite-series minearals,[4] all except the first one being unique occurrences in Japan.

TABLE 1. X-RAY POWDER DATA FOR POLLUCITE FROM NAGATARE, FUKUOKA PREFECTURE

1		2				
d(Å)	I	d(Å)	I	Q_{obs}	Q_{calc}	hkl
5.55	20	5.56	2	0.032	0.032	211
4.818	20	4.83	2	0.043	0.043	222
3.652	80	3.65	30	0.075	0.075	321
3.421	100	3.416	100	0.0857	0.0856	400
		3.225	2	0.0962	0.0963	330, 411
3.048	10	3.058	3	0.1070	0.1070	420
2.907	100	2.913	45	0.1178	0.1177	332
		2.791	1	0.1284	0.1284	422
2.674	20	2.682	7	0.1390	0.1391	510, 431
2.492	20	2.497	4	0.1604	0.1604	521
2.406	80	2.416	24	0.1713	0.1711	440
2.211	60	2.218	17	0.2033	0.2032	611
		2.162	1	0.2139	0.2139	620
2.007	40	2.015	6	0.2462	0.2460	631
1.970	40	1.973	4	0.2569	0.2567	444
1.886	20	1.897	3	0.2780	0.2781	640
1.855	80	1.860	18	0.2890	0.2888	633
		1.827	1	0.2995	0.2995	642
1.731	80	1.736	22	0.3318	0.3316	651
1.705	60	1.709	10	0.3424	0.3423	800
1.679	20	1.683	3	0.3531	0.3530	811
		1.658	2	0.3640	0.3639	644
1.630	20	1.634	3	0.3744	0.3744	653
		1.589	3	0.3957	0.3958	750
		1.548	4	0.4173	0.4172	752
		1.529	7	0.4280	0.4279	840

1. Pollucite. Buckfield, Maine, U.S.A. A.S.T.M. Card No. 15—317. Cu/Ni radiation. Camera method.
2. Pollucite. Nagatare, Fukuoka Prefecture. Cu/Ni radiation. Diffractometer method.

1) Part LXIV: K. Nagashima, K. Nakao, H. Wakita, and A. Kato, This Bulletin, **44**, 867 (1971).
2) H. Shibata, *J. Geological Soc. Japan.* **41**, 582 (1936).
3) Y. Okamoto, *Kobutsu to Chishitsu*, **3**, 1 (1950).
4) J. Ito, H. Minato, and Y. Okamoto, *J. Mineralogical. Soc. Japan*, **2**, 263 (1955).

A white mass with a rugged, weathered surface collected by the third author from the dump derived from one of the pegmatites turned out to be the first pollucite in Japan, as has previously been reported.[5] The present paper will report the results of its X-ray, chemical, and optical studies.

Description of the Studied Specimen

The analyzed specimen is a part of a white mass more than 10 cm across and 500 g in weight. It is white in color and semitransluscent, with a vitreous luster. It has no cleavage, and the hardness is 5½—6 by Mohs' scale.

The associated minerals found in the mass include pale blue albite, and light and deep purple-colored lepidolites and petalite. Besides them, there are minute soft, white veinlets composed of earthy hydromica (?) with quartz. Under a microscope, pollucite is colorless and isotropic between crossed Nicols, except for a few grains which have a faint birefringence. The refractive index, as measured by the immersion method, is 1.520 ±0.002. The birefringence could not be masured by that method, but it is less than 0.002.

TABLE 2. CHEMICAL ANALYSIS OF POLLUCITE FROM NAGATARE, FUKUOKA PREFECTURE

	wt%	Molecular quotient	Metal number	Oxygen number	Metal number as O=6
SiO_2	46.03	0.7661	0.7661	1.5322	2.0708
Al_2O_3	17.76	0.1742	0.3483	0.5226	0.9417
Fe_2O_3	0.02	0.0001	0.0002	0.0003	0.0008
MnO	0.01	0.0001	0.0001	0.0001	0.0003
CaO	0.03	0.0005	0.0005	0.0005	0.0014
Li_2O	0.16	0.0054	0.0108	0.0054	0.0292
Na_2O	2.08	0.0336	0.0672	0.0336	0.1816
K_2O	1.81	0.0192	0.0384	0.0192	0.1038
Rb_2O	0.61	0.0033	0.0066	0.0033	0.0178
Cs_2O	28.88	0.1025	0.2050	0.1025	0.5541
H_2O	2.74	0.1521			0.4111
Total	100.13				

Analyst: K. NAGASHIMA

5) N. Kuwano, *Chigaku Kenkyu*, **21**, 416 (1970).

X-ray Studies

We used the X-ray single-crystal and powder methods to check the space group and the unit-cell constant. In its precession photographs of zero, first, and second layers, there was no diffraction spectrum violating the extinction rule of Ia3d. The X-ray powder data obtained by the diffractometer method are given in Table 1. The unit-cell constant calculated from them is 13.674± 0.005 Å, well coincident with the known value.[6]

Chemical Analysis

The chemical analysis was carried out adopting the following procedures: Cs_2O, Rb_2O, and Li_2O——atomic absorption analysis; Na_2O, K_2O——flame photometry; SiO_2, Al_2O_3, CaO, H_2O——gravimetry; Fe_2O_3, MnO——spectrophotometry. The results are shown in Table 2. The empirical formula based on O=6 is $(Cs_{0.554}Rb_{0.018})_{0.572}(Na_{0.182}K_{0.104}Li_{0.029}Mn_{0.003}Ca_{0.001})_{0.316}(Al_{0.942}Fe_{0.001})_{0.943}Si_{2.071}O_6 \cdot 0.411\ H_2O$, well satisfying the ideal formula. The adoption of the crystallochemical formula proposed by Beger,[6] $Cs_xNa_yAl_{x+y}Si_{48-x+y}O_{96} \cdot (16-x)H_2O$, where $2y \geq 16-x \geq y$, gives the following results:

empirical formula: $(Cs, Rb)_{9.150}(Na, K, Li, Mn, Ca)_{5.061}Al_{15.080}Si_{33.133}O_{96} \cdot 6.578\ H_2O$

crystallochemical formula: $(Cs, Rb)_{9.150}(Na, K, Li, Mn, Ca)_{5.061}Al_{14.211}Si_{33.789}O_{96} \cdot 6.850\ H_2O$

There is a minor excess of tetrahedrally-co-ordinated ions and a deficiency of water, both being within the limits of analytical error.

6) R. M. Berger, *Z. Krist.*, **192**, 280 (1969).

BULLETIN OF THE CHEMICAL SOCIETY OF JAPAN, VOL. 45, 813—817(1972)

Studies on the Isomerization of 2,4-Dinitrophenylhydrazones of Some Aliphatic α-Keto Acids and the Preparation of Their Geometrical Isomers

Hirohiko KATSUKI, Chizuko TANEGASHIMA,* Masanobu TOKUSHIGE, and Shozo TANAKA**
Department of Chemistry, Faculty of Science, Kyoto University, Sakyo-ku, Kyoto

(Received February 22, 1971)

Cis-trans isomerization of 2,4-dinitrophenylhydrazones of some aliphatic α-keto acids takes place in water and some organic solvents by the catalysis of hydrogen ions. *Trans* isomer is more stable than *cis* isomer for lower keto acids and the reverse is the case for higher keto acids. The fraction of *cis* isomer in isomeric mixture at equilibrium in organic solvents such as ethyl acetate and ethyl ether, saturated with 6N hydrochloric acid, was larger than that in aqueous solution. The two isomers could be separated by means of the difference in their solubility characteristics in 1N sodium carbonate except for some keto acids with tertiary or quaternary β-carbon. Melting points of some pairs of the hydrazone isomers were found to be the same when measured by the usual method. This is due to the isomerization of one isomer to the other which takes place during the course of heating.

For the separation, identification and determination of carbonyl compounds, the 2,4-dinitrophenylhydrazine method is most often used in the fields of organic and biological chemistry. Studies have been carried out on physical and chemical properties of the 2,4-dinitrophenylhydrazones. However, only a limited number of studies has been reported on their geometrical isomers and isomerization.

Separation and assignment of *cis* and *trans* isomers of the hydrazones of the following α-keto acids and the related compounds were reported after the discovery of double spots on paper chromatograms of 2,4-dinitrophenylhydrazones of some α-keto acids:[1,2] pyruvic acid,[3,4] α-oxo-β,β-dimethyl-γ-butyrolactone,[5] and phenylglyoxylic acid.[6]

Although separation of the isomers has been conveniently performed by the use of paper or thin layer chromatography, preparation of a pure sample of the isomer or its identification was difficult due to the isomerization of the hydrazone during its development or elution in chromatography.[4] The first large scale separation of pure isomers has become feasible by the combination of salting-out method[3,6] with the isomerization treatment. Studies on the spectrographic properties and the isomerization with the pure hydrazone isomers thus prepared resulted in the detection[7,8] and

* Present address; Mukogawa Women's University, Nishinomiya, Hyogo.
** Present address; Kyoto Women's University, Higashiyamaku, Kyoto.

1) D. E. Metzler, J. Olevard, and E. E. Snell, *J. Amer. Chem. Soc.*, **76**, 644 (1954).
2) A. Meister and P. A. Abendshein, *Anal. Chem.*, **28**, 171 (1956).
3) T. Moriwaki, H. Katsuki, and S. Tanaka, *Nippon Kagaku Zasshi*, **76**, 1367 (1955).
4) F. A. Isherwood and R. M. Jones, *Nature*, **175**, 419 (1955).
5) A. Matsuyama, *J. Agr. Chem. Japan*, **29**, 736, 977, 982 (1955).
6) I. Hayashi, *Nature*, **178**, 40 (1956).
7) T. Yoshida, S. Egashira, and H. Katsuki, *Nippon Kagaku Zasshi*, **88**, 203 (1967).
8) H. Katsuki, T. Yoshida, C. Tanegashima, and S. Tanaka, *Anal. Biochem.*, **24**, 112 (1968).

determination[9,10] of some aliphatic α-keto acids which are important intermediates in metabolism, irrespective of the presence of geometrical isomers in their hydrazones.

This paper deals with the isomerization of 2,4-dinitrophenylhydrazone isomers of some aliphatic α-keto acids and separation of both isomers.

Keto acids used are classified into two groups, **A**(I-VI) and **B**(VII-IX). The hydrazones of keto acids in group **A** gave *cis* and *trans* isomers. *Cis* and *trans* hydrazones are represented by notations *c* and *t*, respectively, *e.g.* I*c*, I*t*. On the other hand, the presence of the two isomers of the hydrazones in group **B** could not be demonstrated and gave two different forms by recrystallization from different solvents. The hydrazones of VII, for example, are represented by VII*x* and VII*y*, respectively.

R-CO-COOH

Group **A**

	I	II	III	IV
R:	H-,	CH_3-,	CH_3CH_2-,	$CH_3CH_2CH_2$-,

	V	VI
R:	$CH_3(CH_2)_2CH_2$-,	$(CH_3)_2CHCH_2$-

Group **B**

	VII	VIII	IX
R:	$(CH_3)_2CH$-,	$CH_3CH_2(CH_3)CH$-,	$(CH_3)_3C$-

The assignment of the geometrical isomers based on their infrared and visible spectra and other properties was described in the preceeding paper.[11]

Experimental

Preparation of Keto Acids. Most of the keto acids used were synthesized by the condensation of fatty acid esters with diethyl oxalate, followed by hydrolysis with hydrochloric acid.[12] I, II, and IX were prepared by the methods of Radin and Metzler,[13] Haward and Fraser,[14] and Glucksmann,[15] respectively.

Preparation of the Isomers and Forms of the Hydrazones. The crude hydrazone of keto acid in group **A** obtained from aqueous solution by the usual method was first mixed with sufficient 1 N sodium carbonate to dissolve the *trans* isomer. After stirring the mixture for about half an hour, the insoluble hydrazone was filtered off. The filtrate was cooled in an ice bath. Hydrochloric acid (1 N) was then added dropwise until the solution became slightly acidic. After standing it for a few minutes, the precipitate was filtered and washed several times with 0.2 N hydrochloric acid, then with cold water. When necessary, especially in the case of higher keto acid hydrazones, the separation procedure with sodium carbonate was repeated. The hydrazone thus obtained was dried in a vacuum desiccator. It was recrystallized from acetone-benzene (1:3). Paper chromatography was effectively used to confirm complete purification.

The *cis* isomer of the hydrazone of keto acid in group **A** was prepared by utilizing the isomerization treatment as follows: The crude hydrazone was dissolved in ethyl acetate saturated with 6 N hydrochloric acid. After being left to stand at 10°C for 1 hr, 1 N sodium carbonate was added and the mixture was agitated vigorously in a separatory funnel. The resulting insoluble sodium salt of the *cis* isomer was collected by filtration. The treatment of the filtrate with sodium carbonate was repeated until insoluble hydrazone no longer separated out. When necessary, the sodium salt of *cis* hydrazone was dissolved in water and the salting-out separation was repeated. The sodium salt of *cis* hydrazone was washed with 1 N sodium carbonate until the color of the filtrate became yellow and it was then suspended in a small amount of cold water. Hydrochloric acid (1 N) was added until the mixture became slightly acidic. The free *cis* hydrazone produced was immediately collected by filtration,

Table 1. Elementary analyses of the hydrazones

Hydrazones of keto acids	Formulae	C (%)		H (%)		N (%)	
		Calcd	Found	Calcd	Found	Calcd	Found
I*t*	$C_8H_6O_6N_4$	37.81	37.98	2.38	2.47	22.05	22.12
I*c*			38.07		2.51		22.26
II*t*	$C_9H_8O_6N_4$	40.31	40.15	3.01	3.08	20.89	20.61
II*c*			40.12		3.24		20.72
III*t*	$C_{10}H_{10}O_6N_4$	42.56	42.79	3.57	3.83	19.85	19.72
III*c*			42.82		3.69		20.08
IV*t*	$C_{11}H_{12}O_6N_4$	44.59	44.45	4.08	4.32	18.92	18.86
IV*c*			44.30		4.25		19.16
V*t*	$C_{12}H_{14}O_6N_4$	46.46	46.56	4.58	4.75	18.06	18.12
V*c*			46.63		4.65		18.18
VI*t*	$C_{12}H_{14}O_6N_4$	46.46	46.26	4.58	4.82	18.06	18.21
VI*c*			46.22		4.86		17.90
VII*x*	$C_{11}H_{12}O_6N_4$	44.59	44.78	4.08	4.05	18.92	18.62
VII*y*			44.90		4.03		18.95
VIII*x*	$C_{12}H_{14}O_6N_4$	46.46	46.29	4.58	4.83	18.06	18.22
VIII*y*			46.59		4.76		18.21
IX*x*	$C_{12}H_{14}O_6N_4$	46.46	46.75	4.58	4.80	18.06	17.82
IX*y*			46.23		4.61		18.17

9) H. Katsuki, C. Kawano, T. Yoshida, H. Kanayuki, and S. Tanaka, *Anal. Biochem.*, **2**, 433 (1961).
10) H. Katsuki, T. Yoshida, C. Kawano, and S. Tanaka, *ibid.*, **43**, 349 (1971).
11) H. Katsuki, T. Yoshida, J. Nagai, and S. Tanaka, This Bulletin, **44**, 3108 (1971).
12) F. Adickes and G. Andresen, *Ann.*, **555**, 41 (1943).
13) N. S. Radin and D. E. Metzler, "Biochemical Preparations," Vol. 4, 1955, p. 60.
14) J. W. Haward and W. A. Fraser, "Organic Syntheses," Coll. Vol. I, 1941, p. 475.
15) C. Glucksmann, *Monatsh. Chem.*, **10**, 770 (1889).

washed and dried as described for the *trans* isomer in order to prevent isomerization. Recrystallization was carried out in exactly the same way as described for the *trans* isomer.

In the case of the hydrazone of keto acid in group **B**, the two forms were obtained by the following method: crystals of *x* form were obtained by recrystallization of the crude hydrazone from benzene and those of *y* form from 50% aqueous ethanol.

The results of elementary analyses of the hydrazones obtained are summarized in Table 1.

Each isomer as well as each form thus obtained contained no impurities detectable by paper chromatographic analysis.[8] The *cis* isomers gave higher R_f values than the corresponding *trans* isomers in normal phase systems and *vice versa* in reversed phase systems.

Isomerization of the Hydrazones. Determination of the proportions of the two isomers of the hydrazones during their formation was carried out as follows: One m*l* of 2,4-dinitrophenylhydrazine reagent (2.5 μ mol/m*l* in 1.2 N hydrochloric acid) was added to 2 m*l* of keto acid solution containing 0.2 to 0.7 μ mole of keto acid at 30°C. At varying time intervals up to 1 hr, 7 ml of 1.6 N sodium hydroxide solution was added to an aliquot of the mixture to stop the reaction. The red color produced upon addition of alkali was measured at two different wave lengths (W_1 and W_2) after allowing the solution to stand for 10 min at room temperature. W_1 is the wavelength at which two curves representing the absorption spectra of the hydrazone isomers in alkali intersect each other. Thus both isomers show the same absorption coefficient. W_2 is the wavelength at which the difference of the two curves is the largest. If the measured absorbances at W_1 and W_2 are represented as A_1 and A_2, respectively, A_1 or A_2 is equal to the sum of the absorbance due to each isomer of hydrazones formed and the one due to the remaining hydrazine reagent. Thus the following two equations are derived:

$$A_1 = k_1(m+n) + l_1(2.5-m-n)$$

$$A_2 = k_{2c}\cdot m + k_{2t}\cdot n + l_2(2.5-m-n)$$

where m and n represent the amounts of *cis* and *trans* hydrazones (μ moles), respectively, and k_1 and l_1 represent the absorbances of 1 μ mole of *cis* and *trans* hydrazones and of the hydrazine reagent at W_1 under these conditions, respectively. Similarly, k_{2c}, k_{2t}, and l_2 represent the absorbances of 1 μ mole of the *cis* and *trans* hydrazones and of the hydrazine reagent at W_2, respectively. The wavelengths, W_1 and W_2, and the specific absorption coefficients of the hydrazones in group **A** and of the hydrazine, *viz.*, k_1, l_1, k_{2c}, k_{2t}, and l_2, are summarized in Table 2.

Experiments on the isomerization of hydrazones in organic solvent containing hydrochloric acid were carried out as follows: A definite amount of hydrazone (0.3 to 0.6 μ mole) was dissolved in 1 m*l* of organic solvent and to this solution was added 4 m*l* of the same organic solvent saturated with 6 N hydrochloric acid. The solution was kept at 30°C for various periods of time. A few drops of concd. aqueous ammonia were then added to neutralize the solution and stop the isomerization reaction. The organic solvent was evaporated *in vacuo* and the residual hydrazone was dissolved in 5 m*l* of 0.1 N sodium hydrogen carbonate. Five m*l* of 2.0 N sodium hydroxide was added and the absorbances at W_1 and W_2 were determined as described above. In this case, l_1 and l_2 in the equations were negligible because no excess reagent was present. The interference due to the decomposition products from the hydrazone was also negligible under these conditions.

Table 2. Absorption coefficient of the hydrazones and the hydrazine

Hydrazones of keto aicds	W_1	k_1	l_1	W_2	k_{2c}	k_{2t}	l_2
	mμ			mμ			
I	406	1.12	0.088	460	0.40	2.60	0.017
II	417	1.54	0.068	470	1.00	1.68	0.013
III	416	1.59	0.070	470	1.22	1.63	0.013
IV	422	1.68	0.059	470	1.26	1.63	0.013
V	420	1.65	0.060	470	1.25	1.65	0.013
VI	420	1.67	0.060	470	1.25	1.68	0.013

The method for determination of the hydrazone isomers of I and II in ethyl acetate, ethyl ether and isopropyl ether was modified in the following way: After a few drops of aqueous ammonia were added to stop the reaction, 5 m*l* of petroleum ether and 2 m*l* of 0.1 N sodium hydrogen carbonate were added. By shaking the mixture in a separatory funnel, the hydrazones were transferred completely from the upper to the lower layer, and were determined spectrophotometrically by the method described above.

Solubility in Aqueous Sodium Carbonate. An excess amount of the hydrazone was shaken thoroughly with 1 m*l* of 1 N sodium carbonate for 1 hr at 25°C or 0°C, to let the hydrazone remain undissolved in the solution. The concentration of the hydrazone in the saturated solution was determined spectrophotometrically.

Partition between ethyl acetate and 0.1 N sodium carbonate. The hydrazone was dissolved in 2 m*l* of 0.1 N sodium carbonate containing 0.01 N sodium hydrogen carbonate. The hydrazone in the solution was then extracted with 10 m*l* of ethyl acetate and the amount of residual hydrazone in the lower layer was determined spectrophotometrically.

Rusults and Discussion

Isomerization during Hydrazone Formation. The proportion of *cis* to *trans* isomer during the course of hydrazone formation in dilute hydrochloric acid upon addition of the hydrazine reagent was determined. In the case of II, completion of hydrazone formation required 5 min at 30°C. The proportion of *cis* to *trans*

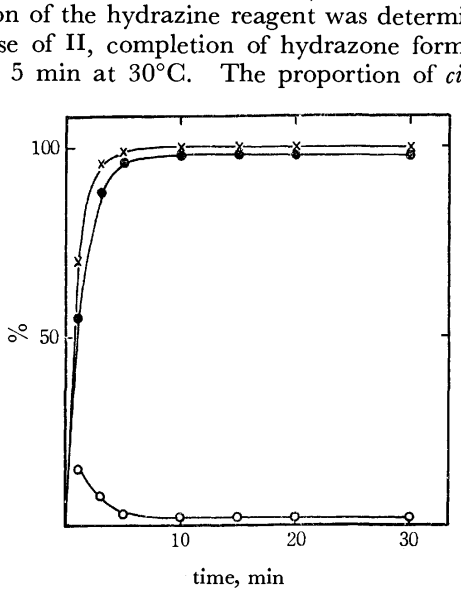

Fig. 1. Proportions of the *cis* and *trans* isomers during the formation of the hydrazone of II.
○, *cis* isomer; ●, *trans* isomer; ×, total hydrazone

isomer was found to vary depending upon experimental conditions. After the reaction for 1 min, about 23% of the hydrazone was present as the *cis* isomer. However, the *cis* isomer once produced was gradually converted into the *trans* isomer during further reaction by the action of hydrogen ions. The fraction of the *cis* isomer at equilibrium was negligible as shown in Fig. 1.

The reaction of I with hydrazine was rapid as in the case of II, but the other keto acids (III–VI) required 10—20 min for the completion of the reaction. The fraction of *cis* isomer in isomeric mixture after attainment of equilibrium in the hydrazone formation was as follows: **I**, negligibly small; III, 62%; IV, 50%; V, 81%; VI, less than 5%. Unlike the case of II, the fraction of *cis* isomer in V after 1-min reaction was 71% and increased to 81% at equilibrium state.

Although isomerization of the hydrazone in dilute hydrochloric acid in the absence of the hydrazine reagent occurred in a similar manner to that in the presence of the hydrazine reagent, hydrolysis of the hydrazone took place to a considerable extent. In the case of II, decomposition by hydrolysis after 30 min was more than 28%. The proportions of the two isomers at equilibrium were similar to those in the presence of the reagent.

The fact that one isomer is separated from the hydrazones of keto acids in group **B**, together with the above results, indicate various differences in the relative stabilities of both isomers of the hydrazones of keto acids. It might be said that, in general, the *trans* isomer is more stable than the *cis* isomer for lower keto acids, and *vice versa* for higher keto acids.

Isomerization in Organic Solvents. The hydrazones are stable in pure organic solvents unless exposed to strong light. However, in organic solvents containing hydrogen ions isomerization took place. Table 3 shows the isomerization of the hydrazones in ethyl acetate containing hydrogen ions. The fractions of *cis* isomers in an equilibrium mixture showed high values except for VI. The values in ethyl acetate were larger than the corresponding values in aqueous solution without exception.

The proportions of the two isomers at equilibrium also varied depending upon the nature of the organic solvent. The isomerization of the hydrazones of II at 10°C in several organic solvents containing hydrogen ions was investigated. The fractions of *cis* isomers in isomeric mixture at equilibrium were as follows: 14% in isopropyl ether, 23% in ethyl ether, 58% in acetone, 44% in ethanol and 56% in 50% aqueous ethanol. The decomposition of the hydrazone of II was much less (less than 7.5%) in isopropyl ether, ethyl ether and ethyl acetate than in acetone, ethanol, and aqueous ethanol. In the latter, it reached 25—55%.

Preparation of the Isomers. For the preparation of *trans* isomer, hydrazones of the keto acids in group **A** were conveniently prepared by the usual method. The hydrazine reagent dissolved in dilute hydrochloric acid was added to the aqueous solution of keto acid and the mixture was left standing for 1 hr to convert the *cis* hydrazone into the *trans* hydrazone as completely as possible. The crude hydrazones thus obtained contained more *trans* isomer than in those obtained from organic solvent as is shown in Table 3. The separation of the *trans* isomer from the *cis* isomer was carried out based on the fact that the *cis* isomer is scarcely soluble in a concentrated sodium carbonate solution.

The difference in solubilities of the two isomers in

Table 3. Isomerization of the hydrazones in ethyl acetate containing hydrogen ions

Hydrazones of keto acids	Time (min)	Hydrazone decomposed (%)	*Cis* isomer in isomeric mixture (%)
I	20	—	71
	60	—	72
II	20	8.2	64
	60	8.6	63
III	20	—	82
	60	—	86
IV	20	2.4	86
	60	2.5	88
VI	20	1.2	<5
	60	1.2	31

Table 4. Solubilities of the hydrazones in 1N sodium carbonate

Hydrazones of keto acids	Solubilities (mmol/ml)	
	0°C	25°C
I*t*[a)]	434	
I*c*[a)]	0.12	
II*t*[a)]	78	
II*c*[a)]	0.03	
III*t*	3.92	6.83
III*c*	0.01	0.07
IV*t*		1.50
IV*c*		0.18
V*t*		5.11
V*c*		0.28
VI*t*[a)]	60.9	
VI*c*[a)]	0.18	
VII*x*,*y*		0.28
VIII*x*,*y*		0.53
IX*x*,*y*		0.27

a) Solubilities of these hydrazones were measured at 0°C instead of 25°C for economical reasons.

Table 5. Partition of the hydrazones between ethyl acetate and 0.1N sodium carbonate

Hydrazones of keto acids	Amounts of hydrazones in 0.1N Na_2CO_3	
	trans isomer (%)	*cis* isomer (%)
I	100	66
II	98	59
III	82	26
IV	69	18
V	49	8
VI	67	68
	x form (%)	*y* form (%)
VII	22	22
VIII	13	13
IX	22	22

1N sodium carbonate varied considerably depending upon the kinds of keto acids as can be seen in Table 4. The difference was the largest in the case of I and gradually decreased as the number of carbon atoms of the keto acid molecule increased, though VI showed an unexpectedly large difference. Separation of the isomers from each other was thus more difficult in the case of the hydrazones of higher keto acids as compared to those of I and II. The hydrazones of keto acids in group **B** were found to be scarcely soluble in sodium carbonate solution in a similar way to the *cis* hydrazones in group **A**.

The difference in behavior of the two isomers in the salting-out is also seen in the partition of each isomer from ethyl acetate and sodium carbonate solution. Table 5 shows the amount of the hydrazone remaining in sodium carbonate solution when the hydrazone was extracted with ethyl acetate from sodium carbonate solution. Thus we see that the *cis* isomer is more easily extracted into ethyl acetate than the *trans* isomer, with the exception of VI, where the two isomers showed nearly the same value. A considerable portion of the hydrazones in group **B** showed the values of the same order of magnitude as those of *cis* isomers in group **A**. Since each hydrazone shows a characteristic value varying greatly in magnitude, measurement of the value is useful for the characterization of the hydrazone.

For the purpose of isolation of the *cis* isomer, isomerization treatment was carried out before the separation procedure by salting-out in order to increase the fraction of the *cis* isomer in the mixture. (For the details of the separation method of both isomers (group **A**), see Experimental).

Although, in general, the existence of *cis* and *trans* isomers is feasible in 2,4-dinitrophenylhydrazones of most unsymmetrical carbonyl compounds, α-keto acids can form highly stable hydrazone derivatives of *cis* form.[3,16] Curious behavior of the *cis* isomers in salting-out, solubility in sodium carbonate solution and in partition between ethyl acetate and 0.1 N sodium carbonate is due to their characteristic structures. Thus, the separation method described above is applicable only to the isomers of α-keto acid hydrazones.

Failure of isolation of the two isomers from keto acid hydrazones in group **B** indicates the instability of one isomer under the usual conditions. So far the behavior of the hydrazones seems to be concerned with keto acids with such structure as $\begin{matrix}R\\R'\end{matrix}\!>\!CHCOCOOH$ or $\begin{matrix}R\\R'\\R''\end{matrix}\!>\!CCOCOOH$.

Isomerization during Melting Point Determination. When a bath with melting point apparatus was heated gradually in the usual manner, some hydrazones did not show sharp melting points. Some pairs of the isomers showed no appreciable difference in their melting points when heated by the usual technique. However, when a capillary containing a sample was steeped into a bath preheated up to a temperature a few degrees below melting point by the usual procedure, sudden melting was often observed in one of the isomers. In such a case, the procedure was repeated in the above mentioned manner, lowering the temperature of the bath by a few degrees each time until the hydrazone did not melt any more. The melting point thus obtained was regarded as the true melting point of the hydrazone. On the other hand, no depression of the melting point was observed on the other isomer even by this method. In Table 6 shown are the melting pontis of the isomers of the hydrazones obtained by this method. The values by the conventional technique are also given when a difference was observed between the two measurements. *Trans* isomers of I and II showed higher melting points than their corresponding *cis* isomers, whereas *cis* isomers higher melting points than their corresponding *trans* isomers. Such a remarkable difference between the melting points of the isomers measured by the two methods suggests the possibility of isomerization of one isomer to the other during heating process. In fact, occurrence of isomerization could be demonstrated by subjecting the hydrazone to paper chromatography after it was kept for some time at certain temperature between the two melting points.

Table 6. Melting points of the hydrazones

Hydrazones of keto acids	Mp (Corrected) *cis* isomer	Mp (Corrected) *trans* isomer	Mp given in literature
I	182.5—183.5	205.5	203[17]
II	210—211	217—218.5	216[18]
III	202—202.5	170—171 (202—202.5)[a]	198[19]
IV	166.5—167.5	129—130 (166—168)[a]	167[19]
V	156—157	120	153[19]
VI	177—178	145.5—146.5	162[19]
	x form	*y* form	
VII	187.5—188	196—196.5	196[19]
VIII	169—170	170—171	169[20]
IX	172.5—173.5	177—178	180[15]

a) The values in parentheses show melting points measured by the usual method.

It is noticeable that the relative stabilities of both isomers, when their crystals are being heated, seem to accord with those in solution.

Although the two forms of hydrazones of keto acids in group **B** showed different melting points, they were not affected by the manner in which measurement was made. No isomerization was observed during the heating process.

The authors with to thank the late Miss Tsuya Yoshida, deceased May 4th, 1970, for her technical assistance.

16) H. Katsuki, K. Sumizu, T. Moriwaki, S. Tanaka, and I. Hayashi, *Nature*, **181**, 639 (1958).

17) S. Weinhouse and S. Friedmann, *J. Biol. Chem.*, **191**, 707 (1951).

18) V. E. Price and L. Levintow, "Biochemical Preparation," Vol. 2, 1952, p. 22.

19) A. Meister, *J. Biol. Chem.*, **197**, 309 (1952).

20) A. Meister *ibid.*, **190**, 269 (1951).

The Dissociation Constants of Weak Acids in a Methanol-Water Mixture

Yasuhiko KONDO and Niichiro TOKURA

Department of Applied Chemistry, Faculty of Engineering, Osaka University, Suita, Osaka

(Received April 24, 1971)

The theoretical expression of the Henry constant has been derived on the basis of the concept of an ideal associated mixture for the system in which a solute, M, exists as such clusters as $M\cdot(H_2O)_j\cdot(MeOH)_{z-j}$, which are related to each other by the equation:

$$M\cdot(H_2O)_{j-1}\cdot(MeOH)_{z-j+1} + H_2O \overset{K_j}{\rightleftarrows} M\cdot(H_2O)_j\cdot(MeOH)_{z-j} + MeOH$$

Making use of the theoretical expression, the transfer-free energies of halogen acids from water to water-methanol mixtures and the dissociation constants of weak acids in water-methanol mixtures have been analyzed and the following equilibrium constants have been obtained for a proton, assuming that a proton is in a higher free energy state in methanol than in pure water, while a counter ion is in the same free-energy state:

$$K_1 = 210, \quad K_2 \doteqdot 16, \quad K_3 \doteqdot 2, \quad K_4 \doteqdot 1$$

The maximum phenomena observed for the dissociation constants of charged acids in the same mixture could be reproduced by the combination of the above Henry constants; emphasis has been placed on the importance of the assumption of a multi-step solvation mechanism.

The solvation of electrolytes and related phenomena in mixed solvents have received very much attention and have been analyzed from various points of view. These may be classified into four categories: *i.e.*, the theoretical treatment developed by Debye[1] and refined recently by Padova,[2] the attempts taking into account the distribution of protons between water and alcohol,[3-8] Marshall's treatment of complete equilibrium constants,[9-12] and several modified forms of the Born equation.[13] A common feature of these attempts is that they all refer to some liquid state as the standard state.

In contrast to these treatments, taking an ideal gas state as the standard state, the present authors have developed a method of analyzing rate constants measured in mixed solvents from the view point of the theory of a nonelectrolyte solution.[14-16] Since the method is based on an equilibrium assumption between reactants and an activated complex, after a few modifications, it is, in principle, reasonable to apply it to the analysis of equilibrium constants measured in mixed solvents.

As will be discussed later, the behavior of dissociation constants in mixed solvents is more complex than that of rate constants. Therefore, several refinements were required for the method to be applicable to the analysis of equilibrium properties in mixed solvents. This paper is an extension of a previous series of works on the solvation of a solute in mixed solvents.[14-16]

Theoretical Expression of an Activity Coefficient in Mixed Solvents.

It is appropriate to define the following activity coefficient, β_{ij}, for the description of the partition of a component, i, between gas and solvent, j:[14]

$$\beta_{ij} = (m_{gi}/m_{li}) \tag{1}$$

where m_{gi} and m_{li} stand for the molar concentration of a component, i in the gas phase over the solution and that of the component, i, in solution.

The Henry constant of a component, i, in a solvent, j, H_{ij}, is defined by the equation:

$$H_{ij} = \lim_{x_i \to 0} (f_i/x_i)_j \tag{2}$$

where f_i and x_i stand for the fugacity and the mole fraction of a component, i, respectively.

At sufficiently low concentrations of a component, i, the following relations hold;

$$f_i = p_i \tag{3}$$

$$p_i = (n_{gi}/V) \times \boldsymbol{RT} = m_{gi} \times \boldsymbol{RT} \tag{4}$$

$$m_{li} = (n_{li}/\textstyle\sum_i n_{li} \times V_i) = x_i \times V_j^{-1} \tag{5}$$

where f_i, P_i, n_{gi}, n_{li}, V_i, x_i, and V_j stand for the fugacity, the pressure, the number of moles in a gas phase, that in a solution, the partial molar volume, and the mole fraction, each of a component, i, and the molar volume of a solvent, respectively.

At sufficiently low concentrations of a component, i, by a combination of Eqs. (1), (2), (3), (4), and (5), we obtain:

$$\beta_{ij} = (H_{ij} \times V_j/\boldsymbol{RT}) \tag{6}$$

where V_j stands for the molar volume of a solvent, j.

An electrolyte, M, can be expected to exist as such

1) P. Debye, *Z. Physik. Chem.*, **130**, 56 (1927).
2) J. Padova, *J. Phys. Chem.*, **72**, 796 (1968).
3) R. W. Gurney, "Ionic Processes in Solution," Dover, New York (1962).
4) C. F. Wells, *Trans. Faraday Soc.*, **61**, 2194 (1965).
5) C. F. Wells, *ibid.*, **62**, 2815 (1966).
6) C. F. Wells, "Hydrogen-Bonded Solvent Systems," ed. by A. K. Covington and P. Jones, Taylor & Francis, London (1968), p. 323.
7) C. E. Newall and A. M. Eastham, *Can. J. Chem.*, **39**, 1752 (1961).
8) H. Ohtaki, This Bulletin, **42**, 1573 (1969).
9) W. L. Marshall and A. S. Quist, *Proc. Natl. Acad. Sci., U.S.*, **58**, 901 (1967).
10) W. L. Marshall, *J. Phys. Chem.*, **74**, 346 (1970).
11) E. M. Woolley, D. G. Hurkot, and L. G. Hepler, *J. Phys. Chem.*, **74**, 3908 (1970).
12) R. A. Matheson, *ibid.*, **73**, 3635 (1969).
13) R. G. Bates, "Hydrogen-Bonded Solvent Systems," ed. by A. K. Covington and P. Jones, Taylor & Francis, London (1968), p. 49.
14) Y. Kondo and N. Tokura, This Bulletin, **40**, 1433 (1967).
15) Y. Kondo and Tokura, *ibid.*, **40**, 1438 (1967).
16) Y. Kondo, Y. Honjo, and N. Tokura, *ibid.*, **41**, 987 (1968).

clusters as $M\cdot(S_1)_m\cdot(S_4)_n$ in mixed solvents, where S_1 and S_4 stand for a solvent, 1 and 4; it has been suggested that the ratio of m to n changes with the composition of the solvent mixture (Refs. 25, 26, and *loc. cit*).

In order to make an explicit formula for an activity coefficient based on the above concept, let us assume the following equilibrium:

$$M + zS_4 \rightleftarrows M\cdot(S_4)_z;\ K_0$$

$$M\cdot(S_4)_{z-j+1}\cdot(S_1)_{j-1} + S_1 \rightleftarrows M\cdot(S_4)_{z-j}\cdot(S_1)_j + S_4;\ K_j$$

$$M\cdot(S_4)\cdot(S_1)_{z-1} + S_1 \rightleftarrows M\cdot(S_1)_z + S_4;\ K_z$$

where M, z, and K_j stand for an unsolvated electrolyte, the solvation number, and the equilibrium constant of a relevant step, respectively.

Hereafter, subscripts 1 and 4 will be used for a solvent, subscript 2 for a solute, and subscript jz for a cluster except for those of equilibrium constants.

One advantage of the discrete model is that it makes it possible to introduce a mathematical formalism expressing the variation in the standard-state free energy with respect to the composition changes in the solvents. Consistent results have been obtained based on the predictions of the model, as will be shown later. However, it would be safe to take the view that this does not necessarily prove the real existence of the clusters.

When the above equilibrium steps exist, for the mixture containing components 1, 2, and 4 the following material balances hold:

$$N_1 = M_1 + M_{1z} + 2\times M_{2z} + \cdots + j\times M_{jz} + \cdots + z\times M_{zz} \quad (7)$$

$$N_2 = M_2 + M_{0z} + M_{1z} + \cdots + M_{jz} + \cdots + M_{zz} \quad (8)$$

$$N_4 = M_4 + z\times M_{0z} + (z-1)\times M_{1z} + \cdots + (z-j)\times M_{jz} + \cdots + M_{z-1,z} \quad (9)$$

where N_i, M_i, and M_{jz} stand for the number of moles of a component, i, before mixing, that of a free component, i, in solutions, and that of such a cluster containing j molecules of a solvent 1, and $(z-j)$ molecules of a solvent 4, such as $M\cdot(S_4)_{z-j}\cdot(S_1)_j$.

Three kinds of mole fraction will be used in the following calculations:

$$x_i = N_i/\sum_i N_i \quad (10)$$

$$y_i = M_i/(\sum_i M_i + \sum_j M_{jz}) \quad (11)$$

$$y_{jz} = M_{jz}/(\sum_i M_i + \sum_j M_{jz}) \quad (12)$$

where x_i, y_i, and y_{jz} stand for the mole fraction defined in terms of the number of moles of a component, i, before mixing and of the number of moles of a component, i, and of a cluster, jz, in solution.

For the above equilibria, the equilibrium constant of each step is defined as follows:

$$K_0 = (y_{0z}/y_2\times y_4^z) \quad (13)$$

$$K_j = (y_{j,z}\times y_4/y_{j-1,z}\times y_1) \quad (14)$$

From Eqs. (7), (8), (9), (10), (11), and (12), we obtain:

$$x_2 = (y_2+\sum_{j=0}^{z} y_{jz})/(1+z\times\sum_{j=0}^{z} y_{jz}) \quad (15)$$

$$(y_2/x_2) = (1+z\times\sum_{j=0}^{z} y_{jz})/(1+\sum_{j=0}^{z}(y_{jz}/y_2)) \quad (16)$$

At sufficiently low concentrations of a solute 2:

$$\lim_{x_2\to 0}(y_2/x_2) = 1/(1+\sum_{j=0}^{z}(y_{jz}/y_2)) \quad (17)$$

From Eqs. (13), (14), and (17), we obtain:

$$\lim_{x_2\to 0}(y_2/x_2) = 1/(1+\sum_{i=0}^{z}(\prod_{j=0}^{i} K_j)\times x_4^{z-i}\times x_1^i) \quad (18)$$

since $x_2\to 0$, $y_1\to x_1$, and $y_4\to x_4$.

For an ideal associated mixture, a fugacity of a component, 2, f_2, is related to the fugacity of that component in the pure state, f_2^0, by the equation:

$$f_2 = f_2^0\times y_2 \quad (19)$$

$$\lim_{x_2\to 0} f_2 = H_{2,\mathrm{mix}}\times x_2 \quad (20)$$

From Eqs. (18), (19), and (20), we obtain:

$$H_{2,\mathrm{mix}} = f_2^0/(1+\sum_{i=0}^{z}(\prod_{j=0}^{i} K_j)\times x_4^{z-i}\times x_1^i) \quad (21)$$

$$H_{2,1} = \lim_{x_1\to 1} H_{2,\mathrm{mix}} = f_2^0/(1+\prod_{j=0}^{z} K_j) \quad (22)$$

$$H_{2,4} = \lim_{x_1\to 1} H_{2,\mathrm{mix}} = f_2^0/(1+K_0) \quad (23)$$

As is clear from Eqs. (13) and (23), the equilibrium constant, K_0, serves as a measure of the stability or of the solvation energy of a solute in a solvent 4.

By combining Eqs. (6) and (21), the activity coefficient of a solute in such a mixture is given by:

$$\lim_{x_2\to 0}\beta_{2,\mathrm{mix}} = \{f_2^0/(1+\sum_{i=0}^{z}(\prod_{j=0}^{i} K_j)\times x_4^{z-i}\times x_1^i)\}\times(V_{\mathrm{mix}}/\boldsymbol{R}T) \quad (24)$$

where V_{mix} means the molar volume of the mixed solvent.

Transfer-free Energy of a Solute from the Solvent 1 to a Mixed Solvent

The transfer-free energy of a solute 2 from the solvent 1 to a solvent mixture, ΔG_t°, can be defined as follows by making use of the above activity coefficient:

$$\Delta G_t^0 = \boldsymbol{R}T\ln\beta_{2,\mathrm{mix}} - \boldsymbol{R}T\ln\beta_{2,1} = \boldsymbol{R}T\{\ln(1+\prod_{j=0}^{z} K_j) - \ln(1+\sum_{i=0}^{z}(\prod_{j=0}^{i} K_j)\times x_4^{z-i}\times x_1^i)\} + \boldsymbol{R}T\ln(V_{\mathrm{mix}}/V_1) \quad (25)$$

where V_1 stands for the molar volume of a pure solvent 1.

Similarly, for the transfer of a solute from the solvent 1 to a solvent 4:

$$\Delta G_t^0 = \boldsymbol{R}T\{\ln(1+\prod_{j=0}^{z} K_j) - \ln(1+K_0)\} + \boldsymbol{R}T\ln(V_4/V_1) \quad (26)$$

For grasping the concept of the above equations, numerical calculations were performed making use of the parameters in Table 1 for the case where $V_4=V_1$, $(1+K_0\times K_1\times\cdots\cdots\times K_z)/(1+K_0)\fallingdotseq K_1\times K_2\times\cdots\cdots\times K_z$[17] $=3{,}000$; then $\Delta G_t^\circ = 2.303\ \boldsymbol{R}T\ \log(\beta_4/\beta_1) = 4.74$ (kcal mol^{-1}) at 25°C.

17) Since the solvation energy of an electrolyte is very large in usual solvents, it is reasonable to assume $K_0 \gg 1.0$. Therefore, K_0 may be dropped out of the final equation.

TABLE 1. EQUILIBRIUM CONSTANTS USED IN THE CALCULATION

Model	z	K_1	K_2	K_3	K_4	K_5	K_6	Relations between ΔG_j° and ΔG_{j-1}°
I	4	3000	1.0	1.0	1.0	—	—	$\Delta G_j^\circ=0, j\geq 2$
II	4	1000	1.88	1.37	1.165	—	—	$\Delta G_j^\circ=(1/2)\Delta G_{j-1}^\circ\ j\geq 3$
III	4	222.0	6.06	1.82	1.225	—	—	$\Delta G_j^\circ=(1/3)\Delta G_{j-1}^\circ$
IV	4	27.8	9.18	4.38	2.683	—	—	$\Delta G_j^\circ=(2/3)\Delta G_{j-1}^\circ$
V	4	7.40	7.40	7.40	7.40	—	—	$\Delta G_j^\circ=\Delta G_{j-1}^\circ$
VI	6	19.0	7.10	3.70	2.39	1.79	1.40	$\Delta G_j^\circ=(2/3)\Delta G_{j-1}^\circ$

$(\Delta G_j^\circ=-RT\ln K_j)$

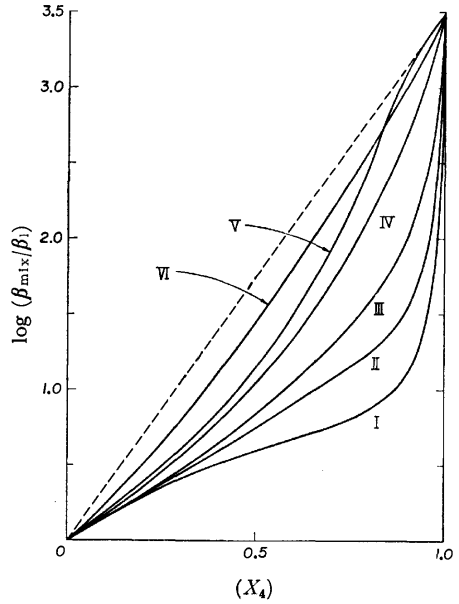

Fig. 1. Calculated values of log (β_{mix}/β_i) as a function of the solvent composition. Numbers in the figure correspond to the model number in Table 1.

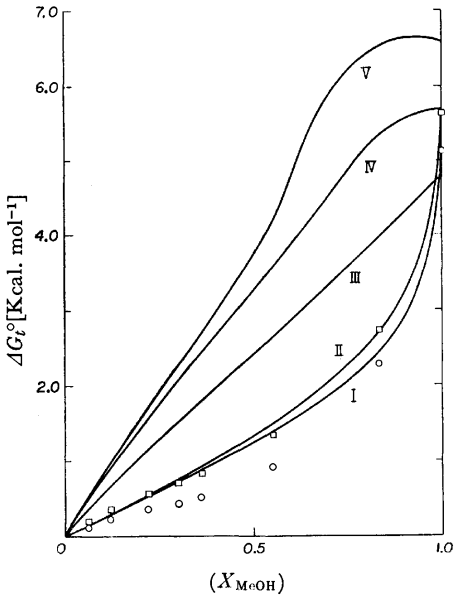

Fig. 2. Transfer-free energies of alkali metal halides and halogen acids from water to methanol-water mixtures.
Experimental results;[17] ○; HBr, □; HCl, III; LiCl, IV; NaCl, V; KCl
Theoretical values, I: HBr, II; HCl

The calculated values are shown in Fig. 1.

As is clear from Fig. 1, the negative deviation from the dotted line increases as the proportion of ΔG_1° to ΔG_t° increases. As $(\Delta G_{j-1}^\circ/\Delta G_j^\circ)\rightarrow 1.0$, and as the solvation number, z, increases, the transfer-energy curve approaches the dotted line. Thus, an important factor in controlling the shape of a transfer-energy curve may be concluded to be the ratio of ΔG_1° to ΔG_t°.

In order to compare the above idea with the experimental results, the transfer-free energies measured by Feakins *et al.*[18,19] are shown in Fig. 2. For most of the electrolytes in Fig. 2, the transfer-free energies from water to methanol are fairly close to each other. However, there is a very sharp distinction between alkali metal halides and halogen acids concerning transfer-free energy curves. The phenomena clearly demonstrate the well-known inadequacies of the Born equation.

Provided that the above model applies to the present system, the difference in transfer-free energy curves reveals that the $(\Delta G_1^\circ/\Delta G_t^\circ)$ ratio of a proton is considerably larger than that of alkali metal ions.

This idea is partly supported by the thermodynamic data for the following step-by-step addition of water to an ion, M^+, as measured by means of a mass spectrometer:

$$M^+\cdot(H_2O)_{n-1}+H_2O=M^+\cdot(H_2O)_n$$

For the reaction in the gas phase, it has been reported that the $(-\Delta H_{0,1})$ value of a proton is considerably larger than that of alkali metal ions and that, in addition, the rate of the decrease in $(-\Delta G^\circ_{n-1,n})$ with an increase in n is smaller for larger ions.[20-23]

Also, the chemical intuition of a preferential solvation of a cation by water has been experimentally proved by Mills and King for the Cr^{3+} ion;[24] it has also been suggested from mass-spectroscopic studies of the competitive solvation of a proton in a water methanol vapor mixture.[21]

18) D. Feakins, B. C. Smith, and L. Thakur, *J. Chem. Soc.* (A), **1966**, 714.

19) A. L. Andrews, H. P. Bennetto, D Feakins, K. G. Lawrence, and R. P. T. Tomkins, *ibid., (A)*, **1968**, 1486.

20) P. Kebarle, S. K. Searles, A. Zolla, J. Scarborough, and M. Arshadi, *J. Amer. Chem. Soc.*, **89**, 6393 (1967).

21) P. Kebarle, R. N. Haynes, and J. G. Collins, *ibid.*, **89**, 5753 (1967).

22) I. Džidic, and P. Kebarle, *J. Phys. Chem.*, **74**, 1466 (1970).

23) M. Arshadi, R. Yamdagni, and P. Kebarle, *ibid.*, **74**, 1475 (1970).

24) C. C. Mills, III, and E. L. King, *J. Amer. Chem. Soc.*, **92**, 3017 (1970).

TABLE 2. EQUILIBRIUM CONSTANTS OBTAINED FROM THE DISSOCIATION CONSTANTS AND TRANSFER-FREE ENERGIES IN MIXED SOLVENTS (25°C)

Acid	z	K_1	K_2	K_3	K_4	K_5	K_6
2,6-Dinitrophenol	4	210.	16.8	1.0	1.0	—	—
Benzoic acid	6	210.	17.0	4.0	2.0	2.0	1.2
Acetic acid	4	210.	17.0	5.0	1.8	—	—
Hydrochloric acid	4	210.	19.0	1.5	1.0	—	—
Hydrobromic acid	4	210.	12.0	1.0	1.0	—	—

Dissociation Constants of Neutral Acids and the Distribution of Clusters in Mixed Solvents

The importance of the entropy terms in determining the magnitude and the sign of the transfer-free energy of solutes from one solvent to another[27,28] has been demonstrated. However, the question of which of the constituents of the electrolyte, *i.e.*, the cation or the anion, is responsible for determining the magnitude of the transfer energy is still a matter of considerable discussion.

In the dissociation of a neutral acid, the perturbation effect brought about on a carbon skelton by the release of a proton may be expected to be small. Especially for the 2,6-dinitrophenolate anion, a negative charge is distributed over the aromatic ring and is partially prohibited from the approach of solvent molecules by two adjacent nitro groups. Also, the non-electrostatic effects by a carbon skelton may be expected to cancel each other out of the total transfer energy since the effect appears on both sides of equations. Thus, it is reasonable to assume that the dissociation constant of a neutral acid is mainly affected by the variation in the standard-state free energy of a proton accompanying the changes in the composition of the solvents.

The dissociation constant as measured in a mixed solvent, $K_{d,\mathrm{mix}}$, is given by;

$$\mathrm{HA} \rightleftarrows \mathrm{H^+} + \mathrm{A^-}$$

$$K_{d,\mathrm{mix}} = K_g(\beta_{\mathrm{HA},\mathrm{mix}}/\beta_{\mathrm{H^+},\mathrm{mix}} \times \beta_{\mathrm{A^-},\mathrm{mix}}) \qquad (27)$$

where K_g is a dissociation constant in a gas phase at an ideal state.

Based on the above assumption, and from Eqs. (21), (22), (23), and (27):

$$\begin{aligned}\ln (K_{d,\mathrm{mix}}/K_{d,4}) &= \ln \Big(1+\sum_{i=0}^{z}\Big(\prod_{j=0}^{i}K_j\Big)x_4^{z-i}x_1^{i}\Big) \\ &\quad - \ln (1+K_0) + \ln (V_4/V_{\mathrm{mix}}) \\ &\fallingdotseq \ln \Big(x_4^{z}+\sum_{i=1}^{z}\Big(\prod_{j=1}^{i}K_j\Big)x_4^{z-i}x_1^{i}\Big) \\ &\quad + \ln (V_4/V_{\mathrm{mix}}) \qquad (28)\end{aligned}$$

$$\begin{aligned}(K_{d,1}/K_{d,4}) &= \{(1+\prod_{j=0}^{z}K_j)/(1+K_0)\}(V_4/V_1) \\ &\fallingdotseq (\prod_{j=1}^{z}K_j)(V_4/V_1) \qquad (29) \\ &(\because \quad K_0 \gg 1)\end{aligned}$$

Comparisons of the calculated values with the experimental results are shown in Fig. 3, where the subscript 1 refers to water and the subscript 4, to methanol, since $(K_{d,\mathrm{water}}/K_{d,\mathrm{MeOH}})>1$. Similar calculations were performed for the transfer energies of hydrochloric acid and of hydrobromic acid on the basis of Eqs. (25) and (26) (the molar volume of the mixture was calculated from the density data of the mixture).[29]

The parameters obtained from the calculations are listed in Table 2.[30]

The most interesting feature of the table is the fact that, for all five cases, the experimental results are fairly well reproduced by similar values of K_j.

The equilibrium constants of the following reaction have been measured by several people:

$$\mathrm{MeOH_2^+} + \mathrm{H_2O} = \mathrm{H_3O^+} + \mathrm{MeOH}$$

The values are *ca.* 110—140 on the pure methanol side[3,7,34-36] and *ca.* 0.20 on the pure water side.[4-6]

At first sight, our equilibrium expression looks a little different from the above equation. However, at each step the net reaction actually taking place is the substitution of water for methanol in the cluster; as a result, the other remaining molecules in the cluster do not appear in the mass-action equation. Therefore, there is no essential difference between the two approaches.

As may partly be inferred from Fig. 3, a proton would exist as $\mathrm{H^+\cdot(MeOH)}_n$ in methanol and as $\mathrm{H^+\cdot(H_2O)}_n$ in water. Thus, our value of K_1 and K_4 should correspond to the equilibrium constant measured on the pure methanol side and on the pure water side rescpectively. They agree with each other generally, but not completely.

25) H. Schneider and H. Strehlow, *Ber. Bunsenges. Physik. Chem.*, **66**, 309 (1962).
26) E. Grunwald, G. Baughman, and G. Kohnstam, *J. Amer. Chem. Soc.*, **82**, 5801 (1960).
27) C. M. Criss and E. Luksha, *J. Phys. Chem.*, **72**, 2966 (1968).
28) C. M. Criss, R. P. Held, and E. Luksha, *ibid.*, **72**, 2970 (1968).
29) International Critical Tables, Vol. III, p. 115.
30) The calculations were performed as follws: the comparison of the theoretical values of Fig. 1 with the log $K_{d,\mathrm{mix}}$ *vs.* $x_{\mathrm{H_2O}}$ plot led to rough estimates of z and of the relation between equilibrium constants, *i.e.*, ΔG°_j and ΔG°_{j-1}, for the relevant system. For an assumed value of z (usually $z=3$), the value of $\prod_{j=1}^{z}(K_j)$ has been obtained on the basis of the boundary condition, *i.e.*, Eq. (29). After that, the values of $\log(K_{d,\mathrm{mix}}/K_{d,4})$ have been calculated on the basis of Eq. (28) for various sets of equilibrium constants. Similar calculations were repeated for several values of z until satisfactory agreements with the experimental results were attained. Similar procedures were adopted for the other systems.
31) G. Kortüm and K. W. Koch, *Ber. Bunsenges. Physik. Chem.*, **69**, 677 (1965).
32) T. Shedlovsky and R. L. Kay, *J. Phys. Chem.*, **60**, 151 (1956).
33) A. L. Bacarella and E. Grunwald, *J. Org. Chem.*, **20**, 747 (1955).
34) L. S. Guss and I. M. Kolthoff, *J. Amer. Chem. Soc.*, **62**, 1494 (1940).
35) J. Koskikallio, *Acta. Chem. Scand.*, **13**, 671 (1959).
36) H. Strehlow, *Z. für Physik. Chem.* (Frankfurt), **24**, 240 (1960).

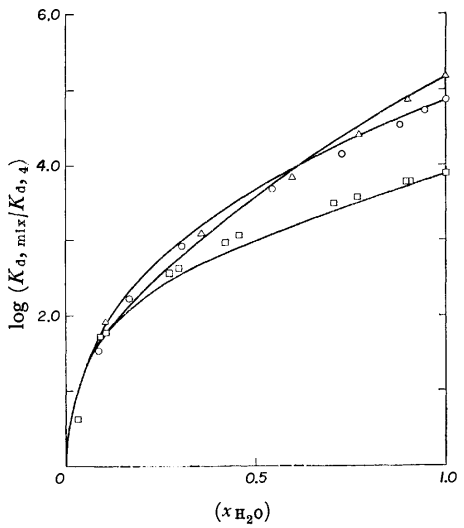

Fig. 3. Dissociation constants in water-methanol mixtures.
Experimental results, □; 2,6-dinitrophenol,[31] ○; acetic acid,[32] △; benzoic acid,[33]
Theoretical values; ——

The results in the table are also of interest in showing the fall in equilibrium constants as the number of water molecules in a cluster increases.

A trend of the equilibrium constants similar to that obtained above, *i.e.*, $K_1 > K_2 > K_3 > K_4$, has been observed for the proton hydration equilibria in acetonitrile.[37-39]

Thus it may be seen that completely different procedures can lead to similar conclusion about the proton hydration equilibria in mixed solvents.

By making use of the equilibrium constants in Table 2, it is possible to calculate the distribution of each cluster, F_{iz}, over the full composition ranges of the solvent by means of Eq. (30):

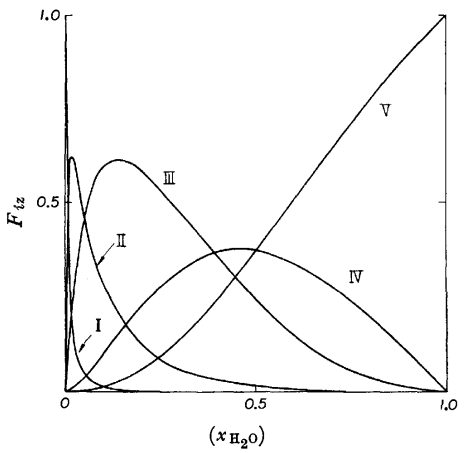

Fig. 4. Distributions of the clusters as a function of the solvent composition.
I: $H^+ \cdot (MeOH)_4$, II: $H^+ \cdot (MeOH)_3 \cdot (H_2O)$, III: $H^+ \cdot (MeOH)_2 \cdot (H_2O)_2$, IV: $H^+ \cdot (MeOH) \cdot (H_2O)_3$, V: $H^+ \cdot (H_2O)_4$.

37) I. M. Kolthoff and M. K. Chantooni, Jr., *Anal. Chem.*, **39**, 1080 (1967).
38) I. M. Kolthoff and M. K. Chantooni, Jr., *J. Amer. Chem. Soc.*, **90**, 3320 (1968).
39) M. K. Chantooni, Jr., and I. M. Kolthoff, *ibid.*, **92**, 2236 (1970).

$$\lim_{x_2 \to 0} F_{iz} = \lim_{x_2 \to 0} M_{iz} / \sum_{j=0}^{z} M_{jz}$$
$$= (\prod_{j=0}^{i} K_j) x_4^{z-i} x_1^{i} / \sum_{i=0}^{z} (\prod_{j=0}^{i} K_j) x_4^{z-i} x_1^{i} \quad (30)$$

The calculated values of F_{iz} for the set of equilibrium constants of hydrochloric acid are plotted against the mole fraction of water in Fig. 4.

As may be inferred from the figure, such clusters as $H^+ \cdot (MeOH)_4$ and $H^+ \cdot (MeOH)_3(H_2O)$ exist only over quite narrow ranges of solvent compositions. In contrast, on the water side, the fraction of the $H^+ \cdot (H_2O)_4$ cluster decreases nearly linearly with the composition of the solvent and the following relation holds over a fairly wide range.

$$F_{44} + F_{34} \doteqdot 1 \quad (31)$$

These factors should be taken into account when attempts are made to correlate the solvation-related properties with the macroscopic properties of the mixed solvents.

Similar distribution curves of a hydrated proton were estimated by Chantooni and Kolthoff in acetonitrile-water mixtures.[39]

Dissociation Constants of Charged Acids in Mixed Solvents

There is a marked difference in the dissociation behavior of charged acids and uncharged acids as measured in mixed solvents. One of the main reasons for such a difference is the charge type of the acids. Since, for the charged acids, electrostatic charging effects appear on both sides of the equilibrium expression, most parts of the effects compensate one another. Thus, the result of such a compensation is a maximum in the plot of log K_d *vs.* the composition of the solvents.

As has been mentioned above, in contrast to the case of hydrogen halogenide acids, the transfer-free energy of alkali metal halides varies monotonously with the change in the composition of the solvents. Also, the

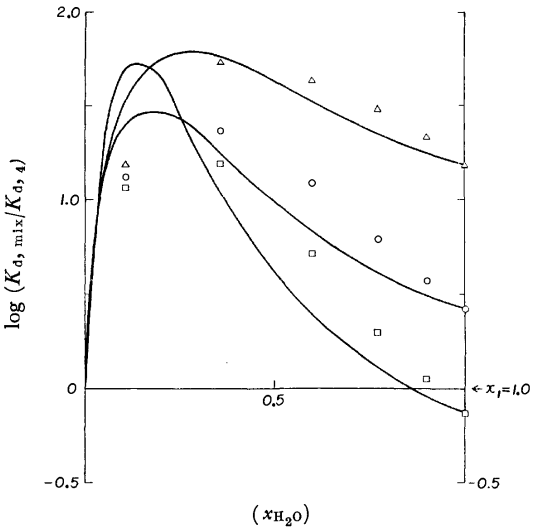

Fig. 5. Dissociation constants of charged acids in water-methanol mixtures.
Experimental results,[33] △; anilinium ion, ○; N-methyl anilinium ion, □: N,N-dimethyl anilinium ion
Theoretical values; ——

Table 3. Equilibrium constants for charged acids (25°C)

Acid	z	K_1	K_2	K_3	K_4	K_5	K_6	Relations between ΔG_j° and ΔG_{j-1}°
Anilinium	6	12.0	5.25	3.0	2.1	1.6	1.4	$\Delta G_j^\circ = (2/3)\Delta G_{j-1}^\circ$
N-Methylanilinium	6	13.53	7.05	4.3	3.0	2.3	1.8	$\Delta G_j^\circ = (3/4)\Delta G_{j-1}^\circ$
N,*N*-dimethylanilinium	6	5.15	5.15	5.1	5.1	5.1	5.1	$\Delta G_j^\circ = \Delta G_{j-1}^\circ$

behavior of the transfer energy of tris(hydroxymethylamine) hydrochloride, *i.e.*, a charged acid, has been reported to resemble that of LiCl.[13]

Thus, the following calculations have been performed from the point of view that the variation in the dissociation constants of charged acids in mixed solvents are mainly controlled by the dissimilarities of the transfer-energy behaviours between charged acid and a proton.

By a procedure similar to that used for uncharged acid, for the equilibria:

$$BH^+ \rightleftarrows B + H^+$$

$$\ln(K_{d,\mathrm{mix}}/K_{d,4}) = [\ln\{1+\sum_{i=0}^{z}(\prod_{j=0}^{i}K_j)x_4^{z-i}x_1^{i}\}-\ln(1+K_0)]_{H^+} - [\ln\{1+\sum_{i=0}^{z}(\prod_{j=0}^{i}K_j)x_4^{z-i}x_1^{i}\}-\ln(1+K_0)]_{EH^+} + \ln(V_4/V_{\mathrm{mix}}) \quad (32)$$

$$(K_{d,1}/K_{d,4}) = [\{(1+\prod_{j=0}^{z}K_j)/(1+K_0)\}_{H^+}/ \{(1+\prod_{j=0}^{z}K_j)/(1+K_0)\}_{BH^+}]\times(V_4/V_1) \quad (33)$$

As is clear from Eqs. (32) and (33), it is necessary to determine two sets of equilibrium constants, *i.e.*, for a proton and for a charged acid. The set of equilibrium constants obtained from the transfer energy of hydrochloric acid has been substituted into Eqs. (32) and (33) for those of a proton; the other parameters used in the calculations are listed in Table 3. A comparison of the experimental results with the calculated values is shown in Fig. 5.

It may be seen from Fig. 5 that the general tendency of the dissociation behaviors of charged acids can be reproduced in mixed solvents by the procedure described above.

In several aqueous-organic mixtures, the acidity function, $-H_0$, goes through a minimum with changing water concentration at fixed concentration of the acid (which corresponds to the maximum in the log K_{BH^+} of the indicator used for the measurements); several attempts have been made to interpret this phenomenon.[40]

A similar maximum phenomenon has been observed for the rate of Wolff-Kishner reaction in mixed solvents.[41]

In previous works, the present authors developed theoretical methods for analyzing the rate constants in solvent mixtures and performed theoretical calculation for the rate constants based on several solvation patterns.[14-16] However, in none of these calculations could a maximum or a minimum phenomenon be simulated. Thus, it is inevitable to assume a multi-step solvation mechanism for reproducing a maximum or a minimum phenomenon in solvent mixtures, although the necessary procedure is much more complicated.

40) C. H. Rochester, "Acidity Functions," Academic Press, London and New York (1970).

41) H. H. Szmant and M. N. Roman, *J. Amer. Chem. Soc.*, **88**, 4034 (1966).

A Consideration of Orbital Interaction in Nitrogen Extrusions of Cyclic Azo Compounds

Satoshi INAGAKI and Kenichi FUKUI

Department of Hydrocarbon Chemistry, Kyoto University, Sakyo-ku, Kyoto

(Received June 9, 1971)

The stereochemical paths of nitrogen extrusions from cyclic azo compounds have been examined from the point of view of particular orbital interaction. The stereoselectivity of the recyclization of 1-pyrazoline derivatives and the homologues on the extrusion can be understood in terms of interaction between the frontier orbitals of the C–N–N–C σ-bond system and of N–N π-bond. Other cyclic azo compounds are found also to behave consistently with the direction of the particular orbital interaction between the relevant parts *e.g.*, strained σ-bonds, π-bonds and lone pairs, and two weakened C–N bonds, and of the interaction between approximate *p* orbitals at the α carbons with respect to the nitrogen and unstrained σ-bond to be cleaved.

Both pyrolytic and photolytic reactions of cyclic azo compounds have been reported in many papers. However, no comprehensive, detailed mechanism and steric course have yet been discussed. Here, we intend to interpret the experimental results from the point of view of orbital interaction. The use of a particular orbital interaction scheme is recommended for the purpose of recognizing steric paths in chemical reactions in general.[1] The fundamental proposition lies in the following statement; "A majority of chemical reactions should take place at the position, and in the direction, of maximum overlapping of the highest occupied (HO) molecular orbital (MO) and the lowest unoccupied (LU) MO of the reacting species; in the reacting species with a singly-occupied (SO) MO, this plays the part of the HOMO or the LUMO, or of both." The consideration of the interaction of these particular MO's is convenient in describing the nature of chemical reactions.[2,3] The procedure for discussing the direction and the position of chemical reactions has been established on the basis of the proposition given in a preceding article.[1] In short, reacting species involved in intramolecular reactions are divided into two parts so that new bonds may form across the surface which borders the parts. The sign relation of the orbital lobes in these parts plays an important role in the reaction. The resultant sketch of the reacting molecules shows the path which they should trace; the reaction should proceed so that the signs are congruent on the atoms where the bonds are newly formed. This formularized procedure will here be applied to the nitrogen extrusion of cyclic azo compounds, of which the stereospecificity has so far been suspended without any comprehensive understanding. The following speculation may assist in understanding the extrusion reactions.

First of all, the decompositions of cyclic azo compounds are classified, in terms of their intrinsic difference as chemical species, into three groups; (1) the nitrogen extrusions of the derivatives of 1-pyrazolines and the homologues, (2) those of the compounds with a conjugative part interacting with weakening C–N bonds, and (3) those of the compounds undergoing a cleavage of the unstrained σ-bond bridging the β and β′ carbons. Now our discussion is compelled to enter upon a treatment of each class, since the way of dividing the reactants and the assignment of the frontier orbitals depend on the nature of the reactants as well as on the reaction environments.

The Derivatives of 1-Pyrazolines and the Homologues

In the case of the pyrolysis, the respective interactions between the HOMO and the LUMO of the N–N π-bond system and the LUMO and the HOMO of the C–N–N–C σ-bond system presumably initiate the extrusion reaction, whereas in the photo-induced reactions the energy incorporated through $n\rightarrow\pi^*$ or $\pi\rightarrow\pi^*$ excitation at the nitrogens is transferred to the σ-bond system by way of the orbital interaction between the LUMO of the σ-bond system and the SOMO at the N=N moiety to weaken the C–N bonds and promote the extrusion. The results of the sensitized photolysis of azo compounds tempt us to expect that cyclic azo compounds decompose through both excited singlet and triplet states, while acyclic azo compounds dissociate and undergo *cis-trans* isomerization by way of singlet and triplet states respectively.[4]

Now it is necessary to know the nodal properties of each bond system in order to further our thinking. In the ground state, two electrons, localized at the N–N π-orbital, occupy the MO which is symmetrical (S) with respect to the mirror plane passing through the middle of the N–N bond. The LUMO or the SOMO has an anti-symmetrical (A) character with respect to the plane. In contrast with π-orbital systems, the symmetry of the σ-bond system has not been established completely. The knowledge obtained from the hybrid-based MO calculations[5] is helpful on the present occa-

1) K. Fukui, *Accounts Chem. Res.*, **4**, 57 (1971) and reference therein.

2) K. Fukui and H. Fujimoto, This Bulletin, **41**, 1989 (1968).

3) K. Fukui and H. Fujimoto, *ibid.*, **42**, 3399 (1969).

4) (a) B. S. Solomon, T. F. Thomas, and C. Steel, *J. Amer. Chem. Soc.*, **90**, 2249 (1968). (b) P. S. Engel, *ibid.*, **91**, 6903 (1969); P. D. Bartlett and P. S. Engel, *ibid.*, **90**, 2960 (1968); P. S. Engel, *ibid.*, **89**, 5731 (1967); I. I. Abram, G. S. Milne, B. S. Solomon, and C. Steel, *ibid.*, **91**, 1220 (1969); P. S. Engel and P. D. Bartlett, *ibid.*, **92**, 5883 (1970).

5) See *e.g.* K. Fukui, in "Sigma Molecular Orbital Theory," ed. by O. Sinanoğlu and K. B. Wiberg, Yale Univ. Press (1970), p. 121.

sion. Among the three MO's essentially occupied by the six bonding electrons in the C–N–N–C system, the lowest has no node; the three bonds being bonding therefore symmetrical (S) with respect to the mirror plane (Fig. 1A). The next has one node between the nitrogens (A), while the last one, which is also the HOMO of this system, has two (S) (Fig. 1B and 1C respectively). Moreover, the LUMO has three nodes, alternating the signs along the bond chain (A) (Fig. 1D).

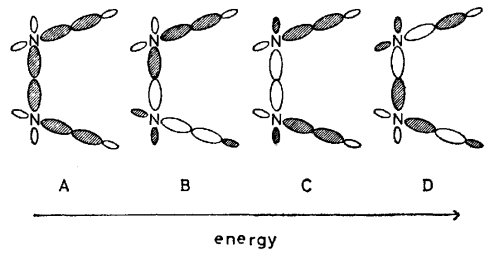

Fig. 1. Relation between orbital symmetry and energy level of three σ-bonds chain.

Assuming that the orbital interaction between the C–N–N–C bond system and the N=N π-bond responsible for the weakening of the C–N bonds governs the stereochemical path both in the pyrolysis and in the photolysis, it is unquestionably necessary to divide 1-pyrazoline and to assign an orbital symmetry for the pyrolysis (A) and the photolysis (B), as is shown in Fig. 2.

In the thermolysis, the particularly important orbital interactions are that between the HOMO of the N–N π-bond system and the LUMO of σ-bond system and that between the LUMO of the former and the HOMO of the latter. One of the interactions, that between π-HOMO and σ-LUMO, is illustrated in Fig. 2A. Fig. 2B represents the mode of the interaction between the LUMO of the σ-bond system and the lowest-excited N–N π-bond, which is caused by an excitation transfer from the neighboring excited N=N π-bond. As a result, 1-pyrazoline decomposes into cyclopropane and nitrogen under both thermal and light-irradiated conditions, with single inversion and with retention at C_α or/and $C_{\alpha'}$ during the recyclization respectively. At first sight, the orbital interaction consideration seems unable to cover all the experimental results listed in Tables 1 and 2. However, it still proves effective in explaining the steric course with the help of the stereochemistry of the reactants. In the pyrolysis, by taking account of the reluctance to rotation of the bulky group at C_α and $C_{\alpha'}$ inward to the breaking five-membered ring, and in the photolysis, by taking account of the multiplicity of the excited state, the particular orbital

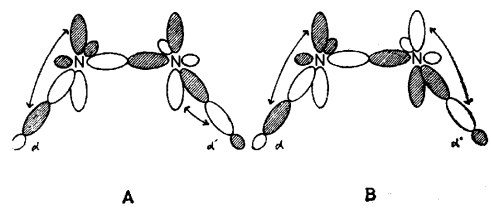

Fig. 2. The modes of orbital interaction in the pyrolysis (A) and in the photolysis (B) of 1-pyrazoline and the homolgue.

Table 1. Product ratios of pyrolyses of 1-pyrazoline derivatives and its homologues

Reactants	Products (%)		Remarks	Ref.
	cis	*trans*		
cis-Ia	33.2	66.1	in vapor	5
trans-Ia	72.6	25.4		
cis-Ib	43.6	57.0	in toluene	6
trans-Ib	6.7	93.3		
cis-IIa	14.7	48.3	in neat liquid	7
trans-IIa	16.6	27.9		
cis-IIb	14.2	31.0	in neat liquid	7
trans-IIb	19.6	38.2		
cis-IIIa	1.00	0.70	under nitrogen	8
trans-IIIa	1.00	1.22	in ratio	
cis-IIIb	31	9	in neat liquid	9
trans-IIIb	11	72		
cis-IIIb	47	19	in vapor	9
trans-IIIb	18	74		
cis-IIIc	1	1	in the gas phase	10
trans-IIIc	1	1	in ratio	
cis-IIId	43.7	35.2	in vapor	5
trans-IIId	46.0	21.8		
meso-IV	43	2.5	in benzene	11
dl-IV	3.5	42		

Table. 2. Product ratios of photolyses of 1-pyrazoline derivatives and its homologues

Reactants	Products (%)		Remarks	Ref.
	cis	*trans*		
cis-Ia	47.5	42.5	in the gas phase	5
trans-Ia	59.5	26.7		
cis-Ia	33.9	61.7	in EtOH	5
trans-Ia	44.5	45.6		
trans-Ia	42.4	43.9	in neat liquid	5
cis-Ia	39.3	60.4	in the presence	5
trans-Ia	38.3	61.2	of benzophenone	
cis-Ib	57.2	42.8	in THF	6
trans-Ib	0.7	99.3		
cis-IIIa	63—76		in neat liquid	8
trans-IIIa		72		
cis-IIId	43.0	37.6	in vapor	5
trans-IIId	24.4	37.2		
cis-IIId	60.4	26.4	in EtOH	5
trans-IIId	13.0	50.7		
cis-IIId	32.1	66.2	in the presence	5
trans-IIId	27.0	72.2	of benzophenone	
meso-IV	35	3.5	in benzene	11
d,l-IV	4	33		
meso-IV	11.5	8	in the presence	11
d,l-IV	8	12	of thioxanthone	

6) R. Moore, A. Mishra, and R. J. Crawford, *Can. J. Chem.*, **46**, 3305 (1968).
7) C. G. Overberger, N. Weinshenker, and J.-P. Anselme, *J. Amer. Chem. Soc.*, **87**, 4119 (1965).
8) C. G. Overberger, J. W. Stoddard, C. Yaroslavsky, H. Katz, and J.-P. Anselme, *ibid.*, **91**, 3226 (1969).
9) T. V. Van Auken and K. L. Rinehart, Jr., *ibid.*, **84**, 3736 (1962).
10) D. E. Mcgreen and W. S. Wu, *Can. J. Chem.*, **45**, 461 (1967).
11) R. J. Crawford and G. L. Erickson, *J. Amer. Chem. Soc.*, **89**, 3907 (1967).

interaction turns out to work clearly in directing the path of these reactions as follows.

The Pyrolysis. The thermolytic reactions of α,α′-disubstituted cyclic azo compounds will be discussed first. They obey the directions of orbital interaction to invert singly at either α or α′ carbons, when the repulsive force is not considerably outstanding between the approaching groups with the progress of the reaction (*cis*- and *trans*-Ia, *cis*-Ib, *cis*-IIa, and *cis*-IIb). *Trans*-species which have bulky groups at both α and α′ carbons suffer such a repellent action during the single inversion that they neglect the orbital interaction, giving the corresponding compounds with a retention of the original configurations (*trans*-Ib and *trans*-IIa and b). In these cases, thermodynamics overcome the orbital interaction.

The second object of our discussion is the group of α, α-disubstituted cyclic azo compounds. When α carbon is occupied by two substituents (except for very small groups, for instance, hydrogen and deuterium), the single inversion undoubtedly occurs more probably at the unsubstituted α′ carbon to produce apparent retention products (IIIa and b).

Thirdly, α,β-disubstituted-1-pyrazolines will be treated. If these compounds dispose the substituent at the β carbon with respect to leaving nitrogens in the *anti*-position in the transition state of the thermolysis, as has been proposed by Crawford and Mishra,[13] *cis*- and *trans*-α, β-disubstituted-1-pyrazolines will have methyl groups at the α carbon at the axial and the equatorial positions respectively. Since the axial group is compelled to rotate inwardly, the *cis*-reactant must rotate a methyl group but *trans*-species rotate hydrogen. From these requirements, it is evident that *trans*-pyrazolines yield more an apparent inversion product than *cis*-pyrazoline. The experiments on *cis*- and *trans*-IIId exhibit this tendency, but it cannot be explained by these discussions why *trans*-IIId apparently gives more of the single inversion product than the retention product. However, in the case of a small substituent at the β carbon (IIIc), the reactants, whether in the *cis*- or *trans*-form, yield *cis*- and *trans*-products in equal amounts, since the small substituent has no influence on the inward rotation at the α carbon.

The Photolysis. Subsequently, let us proceed to a detailed discussion of the photolysis on the assumption that orbital interaction favors the configurational retention path. If these compounds undergo dissociation through the excited singlets, the stereochemical course will be consistent with our predictions based on Fig. 2B. There can, however, exist some factors independent of the orbital interaction. For example, the interventions of triplets would add to a thermodynamically stable product or *trans*-compound, and the deactivation of an excited singlet to the vibrationally-exicted ground state would compete with the path through excited singlets, in some case giving the inversion product. That is why the stereochemical path in thermolysis is complicated.

All the compounds listed in Table 2 except for *cis*-Ia in 95% ethanol and *trans*-Ia in the gas phase more or less exhibit a tendency toward obedience to orbital interaction control. Here, we may find the causes of the two exceptions and some poorly stereoselective reactions mainly in the intervention of triplets, but it is premature to arrive at conclusive interpretations because of the insufficiency of physical information about 1-pyrazolines, the quantum yield of intersystem crossing, the structural geometry of triplets, *etc.* However, it seems that it will be meaningful to make a tentative proposal.

Some experimental results suggest that cyclic azo compounds extrude nitrogen molecules *via* triplets as well as singlets, but that acyclic azo compounds undergo *cis-trans* isomerization *via* triplets, while they dissociate only through singlets.[4] From this generalization, it can be expected that the dissociation through the triplets depends upon the geometrical structure of the reacting molecules. The geometry in the triplet is considered to suffer some twist, which is probably caused by electronic repulsion between two electrons with parallel spins. Assuming that relief from the twisted strain drives the extrusion, the more the triplet species is

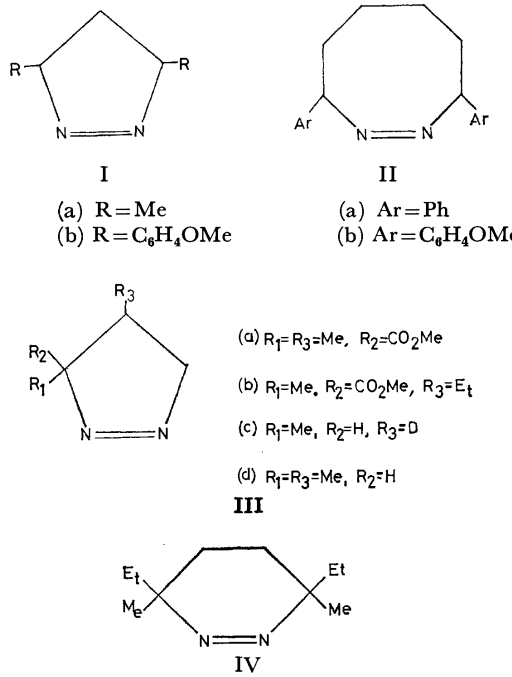

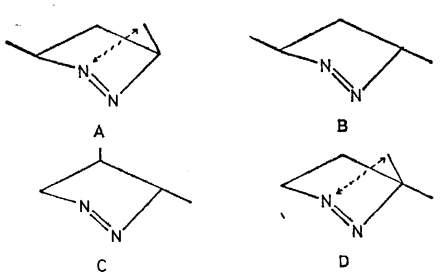

Fig. 3. The repulsion of twisted 1-pyrazoline derivatives in the triplets; (A) *trans*-α,α-dimethyl-1-pyrazoline, (B) *cis*-α,α-dimethyl-1-pyrazoline, (C) α,β-dimethyl-1-pyrazoline, and (D) α,α-substituted 1-pyrazoline.

12) P. D. Bartlett and N. A. Porter, *J. Amer. Chem. Soc.*, **90**, 5317 (1968).
13) R. J. Crawford and A. Mishra, *ibid.*, **88**, 3963 (1966).

strained, the more facile a decomposition it is submitted to.

Now let us proceed to a detailed discussion of this assumption. The distortion of α,α'-disubstituted 1-pyrazolines (I) brings about strains of different extents between *cis*- and *trans*-isomers. With respect to *cis*-I, a suitable repulsion arises from the unavoidable approach of the substituent and the originally remoter nitrogen (Fig. 3A), thus accelerating the extrusion through the triplets so remarkably as to compete with the singlet path. The participation of triplets contributes to the formation of thermodynamically stable products or *trans*-isomers. That probably results in the low stereospecificity of *cis*-I (*cis*-Ia in the gas phase and *cis*-Ib in tetrahydrofuran). Further, in the liquid phase, as the deactivation of an excited singlet to the vibrationally-excited ground state by collision with the surrounding molecules adds to inversion products by way of the ground state, the mode of stereospecificity may be reversed in *cis*-reactants (*cis*-Ia in ethanol). In contrast, *trans*-I can be twisted without bringing the substituents close to the nitrogens (Fig. 3B); therefore, the triplet species might decompose too slowly, as compared with the excited singlets, to exert any remarkable influence on the distribution of products. That implies the predominant control of orbital interaction in determining the stereochemical path in the gas phase (this conclusion contradicts the experimental finding with regard to *trans*-Ia in the gas phase).[14] Since there is little intervention of triplets, the stereospecificity of *trans*-I in the solution is lower by an extent corresponding to the deactivation of the excited singlets to the ground state by solvents (*trans*-Ia in ethanol). However, large substituents at both α and α' carbons keep themselves from approaching at the cost of thermodynamical stability. That is why *trans*-Ib is converted with a high stereospecificity of configurational retention.

Some 1-pyrazolines, α,β-disubstituted compounds (IIId), can avoid the strain, as is illustrated in Fig. 3C. Accordingly, these species obey the direction of orbital interaction in the excited singlets without any disturbance.

The α,α-disubstituted compounds, IIIa and IV, also suffer an appropriate strain (Fig. 3D) enough to take the triplet path of competing explicitly with the singlet path. However, the triplet reactions of these compounds do not affect the product ratios, since the resulting biradical intermediates have nearly equal thermodynamical stabilities whether they assume the *cis*-form or *trans*-form. In fact, the experiments seem to show that IIIa and IV behave as if the triplets were not concerned in distributing the product in spite of the suitable strains. This interpretation is supported by the fact that, while the photo-induced transformation of *meso*- and *d,l*-IV yield the respective products, thus maintaining the configuration, both *cis*- and *trans*-reactants in general give the same product as the major component in the triplet-sensitized reactions under thermodynamical control.

The Compounds with a Conjugative Part Interacting with Weakening C-N Bonds

Before discussing other cyclic azo compounds, we must consider how they diverge from 1-pyrazolines and their homologues. The cyclic azo compounds treated in this section have a "conjugative" part interacting with incipient orbitals appearing at the carbons as the C–N bonds are weakened. This orbital interaction, rather than that which is responsible for the weakening of the C–N bonds, presumably governs the stereochemical path. This assumption is founded on the fact that two C–N bonds can be approximately separated from the N–N σ-bond since weakening σ-bonds tend to have a π character to some extent. In consequence, the whole of the reactant may be divided into the part and two C–N bonds. The respective MO's of the C–N bond system are assigned in Fig. 4.

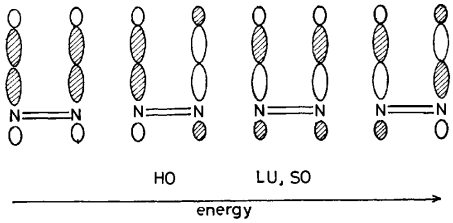

Fig. 4. Relation between orbital symmetry and energy level of two σ-bonds system.

Our discussions will begin with the reaction of 1-pyrazoline and the analogue bearing a conjugative part at the β carbon. When the conjugative part consists of *exo* π-orbitals, *e.g.*, 4-alkylidene-1-pyrazolines, the particularly important orbital interactions are probably that between the HOMO (S) of the π-orbitals and the LUMO (S) of the C–N bonds and that between the LUMO (S) of the former and the HOMO (A) of the latter.[15] Accordingly, the stereospecificity of the compounds depends upon the balance between these two competitive modes of orbital interactions. That is, the configuration may be retained during the reaction when the interaction between symmetrical and symmetrical MO's prevails over the other and may be singly inverted when symmetrical and anti-symmetrical interaction dominates. No information has been obtained so far which shows which mode is predominant. However, when the conjugative part is a lone pair (V), there is no appropriate LUMO localized on this part. This implies the exclusive operation of the orbital interaction between the lone pair as the HOMO (S) and the LUMO (S) the C–N-bond system (Fig. 5). It follows that V goes through thiocarbonyl ylide as an intermediate to produce an adduct with a certain dipolarophile by way of a 4+2 π thermally-allowed-cycloaddition process, with the configuration retained throughout the re-

14) This exceptional distribution of products which slips out of our consistent interpretation does not argue radically against the effectiveness of orbital interaction scheme. The internal conversion of electronic excited state to vibrationally excited state in photolysis take place considerably even in the gas phase. (See Ref. 4a and the references therein.)

15) However there is a communication that the thermolysis of VII yields as a major the recyclization product due to C_α–$C_{\alpha'}$ bond formation against the distribution in the equilibrium. This observation suggests that 4-alkylidene-1-pyrazoline could partially neglect the alkylidene part to behave as 1-pyrazoline. (See Ref. 18c.)

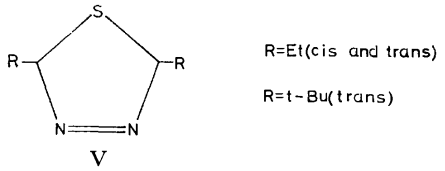

V

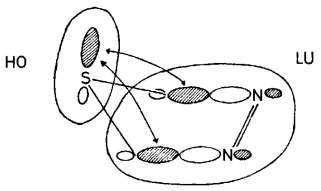

Fig. 5. The mode of orbital interaction in the pyrolysis of thiadiazoline.

action.[16]

The orbital symmetry assigned to 1-pyrazoline under irradiation is still quite important in any discussion of the photochemical transformation of 4-alkylidene-1-pyrazoline on the grounds that an orbital interaction responsible for weakening C–N bonds is desirable for the incipient orbitals at the carbons to move in the same direction.[17] As a result, the extrusion reaction provides, as a major product, the product arising from the direct bond formation by overlapping between the orbitals which result as the C–N bonds weaken. A few related experiments are known.[18]

In the sensitized reaction, the resultant unpaired electrons with parallel spins have an opportunity to redistribute themselves, which would allow the trimethylenemethane intermediate to reach a stable state. That these reactions occur under the thermodynamical control is supported by the experiment which has demonstrated that the distributions of two possible alkylidenecyclopropanes due to recyclization, originating from VIa and from VIb, are nearly identical.[18] The further the two unpaired electrons with parallel spins are separated from each other, and the greater the extent to which these electrons can be delocalized, the more stable the electronic state becomes. According to this principle, all sorts of unsaturated groups or those substituents with lone-pair electrons, attached to the carbon atom at which an unpaired electron appears, will facilitate

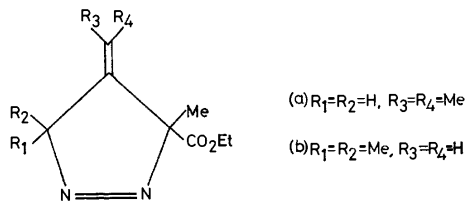

VI

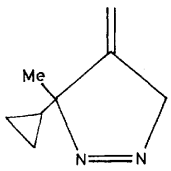

VII

the cyclization. A few experiments are compatible with the results of this discussion, showing that lone pairs at chlorine and at oxygen of the ester group help unpaired electrons to delocalize.[18] With respect to VII, the π character of the cyclopropane ring acts a part corresponding to that of the pure π orbitals.[18c]

The stereochemical behavior of the compounds with one conjugative or strained bond between β and β' carbons will now be discussed. The particularly important orbital interactions in the thermolysis include that between the HOMO (S) of the C_β–$C_{\beta'}$ bond and the LUMO (S) of the C–N bonds and that between the LUMO (A) of the former and the HOMO (A) of the

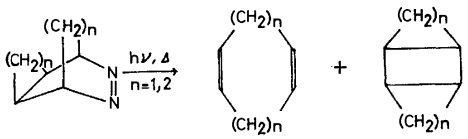

Experiment 1.[19]

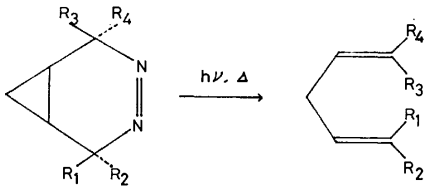

R_1,R_2.R_3,R_4=Me,H

Experiment 2a.[20a]

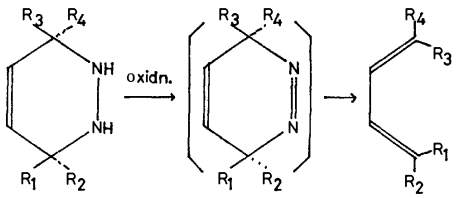

Experiment 2b.[20b]

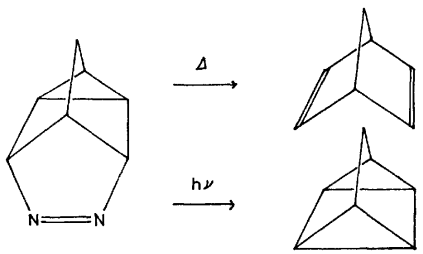

Experiment 3.[21]

16) R. M. Kellog, S. Wassenaar, and J. Bunter, *Tetrahedron Lett.*, **1970**, 4689.

17) The orbital interaction identical with that in pyrolysis might also play an important role in these photolysis, since n-π^* excitation at a nitrogen results only in weakening C–N bonds to give the transition state identical with that in thermolysis.

18) a) S. D. Andrews and A. C. Day, *J. Chem. Soc. (B)*, **1968**, 1271; *Chem. Commun.*, **1966**, 667. b) T. Sanjiki, H. Kota, and M. Ohta, *ibid.*, **1968**, 496. c) T. Sanjiki, M. Ohta, and H. Kato, *ibid.*, **1969**, 638.

19) H. Tanida, S. Teratake, Y. Hata, and M. Watanabe, *Tetrahedron Lett.*, **1969**, 5341, 5345, H. Tanida and S. Teratake, *ibid.*, **1970**, 4991; E. V. Allred, J. C. Hinshaw and A. L. Johnson, *J. Amer. Chem. Soc.*, **91**, 3382 (1969).

20) a) J. A. Berson and S. S. Olin, *ibid.*, **92**, 1086 (1970). b) J. A. Berson, *ibid.*, **91**, 777 (1769).

21) N. J. Turro, "Molecular Photochemistry," W. A. Benjamin, Inc., New York, (1967) p. 230, references cited therein. The analogous reaction are reported in the following paper; L. A. Paquette and L. M. Leichter, *J. Amer. Chem. Soc.*, **92**, 1765 (1970).

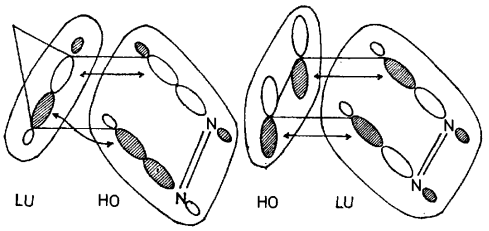

Fig. 6. The mode of orbital interaction in the pyrolysis of bicyclic azo compounds with strained β,β' σ-bond.

Fig. 7. The mode of orbital interaction in the pyrolysis of cyclic azo compounds with a π-bond.

latter. These modes of orbital interaction favor the disrotatory opening of a fused small ring (Fig. 6) or the formation of two π-bonds adjacent to the original π-bond (Fig. 7). These processes accompanying the extrusion are thermally possible (Experiments 1, 2, and 3). The steric paths of the photochemical reactions are complicated by the variable extent to which the photochemically generated SOMO participates directly in the orbital interaction determining the stereochemical course. The initial orbital interaction between the LUMO of the C–N–N–C-bond system and the SOMO of the N–N π-bond may only weaken the C–N bonds, without having any other effects. The HOMO, the level of which must be considerably elevated by this bond weakening, will participate in the interaction with the LUMO of the C_β–$C_{\beta'}$ bond. This orbital interaction is identical with that which operates in the pyrolytic extrusion, leading to the corresponding compounds as well as to thermolysis (Ex. 1 and 2a). The bond formation between the carbons next to the nitrogen (Ex. 1 and 3) may be ascribed to the favorable movement of the atomic orbital lobes in the same direction as was illustrated in connection with the photolysis of 1-pyrazoline (Fig. 2B).

The Compounds Undergoing Cleavage of the Unstrained σ-Bond Bridging between β and β' Carbons

Fig. 8 shows a presumptive energy level relationship between the HOMO and the LUMO of strained and unstrained C_β–$C_{\beta'}$, bonds as well as the C–N-bond system. The reactants with a strained C_β–$C_{\beta'}$ bond could initiate the orbital interaction between the strained bond and the C–N bonds on the weakening of the C–N bonds, for the energy gaps between the frontier orbitals

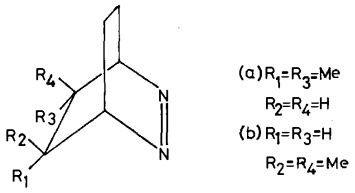

(a) $R_1=R_3=Me$, $R_2=R_4=H$
(b) $R_1=R_3=H$, $R_2=R_4=Me$

VIII

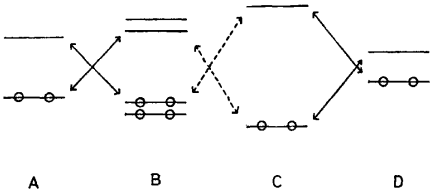

Fig. 8. Estimated energy levels of frontier orbitals of a strained σ-bond (A), two C–N bonds system. (B), an unstrained σ-bond (C) and a quasi-σ-bond (D).

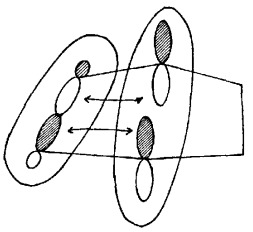

Fig. 9. The mode of orbital interaction in the pyrolysis of cyclic azo compounds with unstrained β,β' σ-bond.

are narrow. In contrast with the strained bond, the level separation between the frontier orbitals of the unstrained bond are so large that the orbital interaction will not be sufficient to break the C_β–$C_{\beta'}$ bond until the C–N bonds become seriously weakened. According to the weakening of the C–N bonds, the appearing orbitals on α carbons come to have an approximate π character. "quasi-π" orbitals can interact with the unstrained C_β–$C_{\beta'}$ bond to cause the fission. The assignment of the orbital lobes and the mode of division of the reactant are analogous to the ring opening of cyclobutene, as is depicted in Fig. 9. This illustration explains the conrotatory bond scission of the unstrained bond in the pyrolysis.[22]

Remarks

The stereospecificity of the extrusion reactions of cyclic azo compounds, which seems to be chaotic, is found to be put into order comprehensively under the government of orbital interaction between the relevant parts in the molecule. During a consideration on the basis of orbital interaction we have found that the parts between which the orbital interaction should be considered to determined the stereochemical course are variable, even in the reaction of similar compounds, and that thermal and photochemical reactions are not always counterparts of each other in the sense of stereospecificity.

22) W. R. Roth and M. Martin, *Tetrahedron Lett.*, **1967**, 3865. It is meaningful to refer to the thermolysis of a bicyclo[2.1.0]pentane derivative. The mechanism is proposed by the reporters that the compound undergoes conrotatory ring opening after the bridge bond cleaves to produce cyclopentane-1,3-diyl biradical; J. A. Berson, W. Bauer, and M. M. Campbell, *J. Amer. Chem. Soc.*, **92**, 7515 (1970).

Synthetic Reactions by Complex Catalysts. XXV.[1] The Copper-catalyzed Reaction of Allyl Isocyanide with Carbonyl Compounds and Olefins. Syntheses of 4-Vinyl-2-oxazoline and 5-Vinyl-1-pyrroline Derivatives

Takeo SAEGUSA, Ichiki MURASE, and Yoshihiko ITO
Department of Synthetic Chemistry, Faculty of Engineering, Kyoto University, Sakyo-ku, Kyoto
(Received June 11, 1971)

This paper describes two reactions of allyl isocyanide (AIC) by means of the Cu_2O catalyst; these reactions produce heterocyclic compounds with vinyl substituents. First, the reactions of AIC with such carbonyl compounds as ketones and aldehydes produce 4-vinyl-2-oxazoline derivatives (**1**) in good yields. Second, AIC also reacts with the C=C double bond of α,β-unsaturated nitriles and esters to produce 5-vinyl-1-pyrroline derivatives (**4**, **5**, and **6**). A mechanistic scheme involving an isocyanoallylcopper complex (**11**) has been assumed.

This paper will describe the Cu_2O-catalyzed reactions of allyl isocyanide (AIC) with carbonyl compounds (Eq. (1)) and with olefins (Eq. (2)). The products are 4-vinyl-2-oxazoline and 5-vinyl-1-pyrroline derivatives respectively. These synthetic reactions have been found

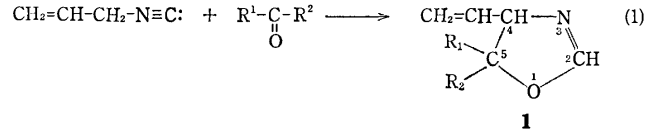

(1)

1

a. $R^1=R^2=CH_3$ **b.** $R^1=Me$, $R^2=Ph$
c. $R^1=R^2=-(CH_2)_4-$ **d.** $R^1=R^2=-(CH_2)_5-$
e. $R^1=H$, $R^2=Ph$ **f.** $R^1=H$, $R^2=i\text{-}Pr$

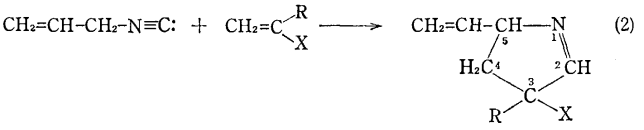

(2)

2

in a series of exploration studies of the catalytic behavior of the copper-isonitrile complexes.[2-4] Especially, they are closely related to our recent finding of oxazoline and pyrroline syntheses[4] in which benzyl isocyanide (**3a**) and carbethoxymethyl isocyanide (**3b**) are reacted with carbonyl compounds and with olefins respectively in the presence of Cu_2O as the catalyst (Eqs. (3) and (4)).

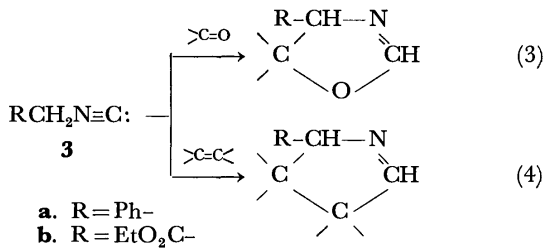

(3)

(4)

3

a. R=Ph-
b. $R=EtO_2C-$

Results and Discussion

Reaction of AIC with Carbonyl Compounds. Synthesis of 4-vinyl-2-oxazoline Derivatives. The results of the reaction of AIC with carbonyl compounds by means of the Cu_2O catalyst are shown in Table 1. 4-Vinyl-2-oxazoline derivatives (**1**) were obtained in high yields with high selectivities. Here, the oxazolines, **1b**, **1e**, and **1f**, are mixtures of the two diastereomers due to the 4-C and 5-C configurations. The ratios are given in Table 1.

In this reaction, the isomerization of AIC to propenyl isocyanide (PPIC) takes place concurrently. After the reaction, the unreacted AIC was found to isomerize to PPIC. The IR spectrum of the lower-boiling fraction (at 5 mmHg, room temperature) from the reaction mixture showed an absorption at 2120 cm^{-1} of $\nu_{N\equiv C}$ of PPIC,[5] which differed from that of AIC ($\nu_{N\equiv C}$ at 2150 cm^{-1}). The isomerization from AIC to PPIC is, however, reversible. With the Cu_2O catalyst, PPIC was reacted with benzaldehyde to produce **1e** in an almost quantitative yield (Table 1). As will be mentioned later, the reversible isomerization of AIC⇄PPIC probably proceeds through the α-isocyano-organocopper complex (**11**), which is also the key intermediate in the reaction of AIC with carbonyl compounds to produce oxazoline derivatives.

Reaction of AIC with Olefins. Synthesis of 5-Vinyl-1-pyrroline Derivatives. The results of the Cu_2O-catalyzed reaction of AIC with α,β-unsaturated esters and nitriles are shown in Table 2. The derivatives of 1-

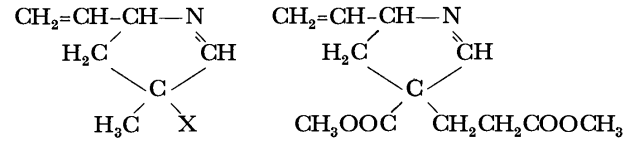

4 **5**

a. $X=COOCH_3$
b. X=CN

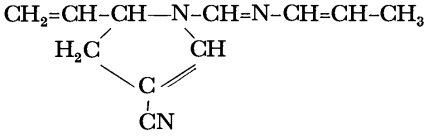

6

1) Part XXIV: T. Saegusa, Y. Ito, S. Tomita, and H. Kinoshita, This Bulletin, **45**, 496 (1972).
2) T. Saegusa, Y. Ito, S. Tomita, and H. Kinoshita, *J. Org. Chem.* **35**, 670 (1970).
3) T. Saegusa, Y. Ito, H. Kinoshita, and S. Tomita, This Bulletien, **43**, 877 (1970).
4) T. Saegusa, Y. Ito, S. Tomita, and H. Kinoshita, *J. Org. Chem.*, **36**, 3316 (1971).
5) T. Saegusa, I. Murase, and Y. Ito, *Tetrahedron*, **27**, 3795 (1971).

Table 1. Reactions of allyl isocyanide with carbonyl compounds[a]

Carbonyl compds (mmol)		Cu_2O (mmol)	Solvent toluene (ml)	Time (hr)	Yield[b] (%) of **1**	Isomers ratio[c]
Ketones						
acetone	(20)	0.7	5[d]	12	**a** ≈69	—
acetophenone	(20)	0.35	5	12[e]	**b** ≈60	66:34
cyclopentanone	(12)	0.7	4	24[e]	**c** ≈23	—
cyclopentanone	(12)	0.35	4	12	**c** ≈65	—
cyclohexanone	(12)	0.35	3	12	**d** ≈60	—
Aldehydes						
benzaldehyde	(20)	0.35	5	6	**e** ≈77	62:38
2-methylpropanal	(20)	0.35	5	12	**f** ≈75	66:40
benzaldehyde	(6)[f]	0.35	3	12	**e** ≈95	—

a) In the presence of Cu_2O, an equimolar mixture of allyl isocyanide and carbonyl compound in toluene was heated at 80°C unless otherwise described.
b) Determined by distillation.
c) Determined by NMR.
d) Benzene was used as solvent.
e) Reaction at room temperature.
f) Propenyl isocyanide instead of allyl isocyanide was used.

Table 2. Reaction of allyl isocyanide with olefins[a]

Olefins (mmol)		Cu_2O (mmol)	Solvent (ml)	Time (hr)	Yield[b] (%)	Isomers ratio[c]
Methyl methacrylate	(20)	0.35	C_6H_6 (3)	12	≈34	54:46
	(6)	0.35	C_6H_6 (3)	96	≈36	
	(6)[d]	0.35	C_6H_6 (3)	12	**4a** ≈ 9.8	
	(6)[d]	0.35	C_6H_6 (3)	96	≈33	
	(6)[d]	0.35	CH_2Cl_2 (3)	12	≈ 1.7	
Methacrylonitrile	(20)	0.7	C_6H_6 (5)	12	**4b** ≈24	55:45
Methyl acrylate	(20)	0.7	DMF (5)	12	**5** ≈73[e]	69:31
Crotononitrile	(20)	0.7	CH_3Ph (5)	12	**8** ≈62[f]	
					6 ≈23[f]	
Acrylonitrile	(10)	0.35	DMF (5)	24	**10** ≈trace	

a) An equimolecular mixture of allyl isocyanide and olefin was heated at 80°C.
b) Determined by glpc.
c) Determined by NMR.
d) Propenyl isocyanide instead of allyl isocyanide was employed.
e) Calculated on the basis of methyl acrylate.
f) Calculated on the basis of crotononitrile.

pyrroline, **4**, **5**, and **6**, were produced. In this reaction, **4a**, **4b**, and **5** were obtained as mixtures of the two isomers due to the 3-C and 5-C configurations (The ratios are given in Table 2).

As is shown in Table 2, the selectivity of the pyrroline synthesis by the AIC-olefin reaction is generally lower than that of the oxazoline synthesis shown in Table 1. The dimerization and polymerization of olefin by the Cu_2O-isonitrile system occur simultaneously, and together they decrease the pyrroline yield.

Similarly to the case of the reaction with carbonyl compounds, the isomerization of AIC to PPIC occurred concurrently. Sometimes PPIC was isolated from the reaction mixture of AIC by vacuum distillation (5 mmHg) at room temperature. Furthermore, the reversibility of AIC⇄PPIC isomerization was also demonstrated in this reaction; *i.e.*, **4a** was produced in the reaction of PPIC with methyl methacrylate. The conversion of PPIC to a dark tarry material disturbed the pyrroline formation. In the PPIC-olefin reaction, only a trace of unreacted PPIC remained, and the PPIC was converted mostly to a dark-brown tar. The strong tendency of PPIC to polymerize to a dark tar was observed also in an experiment isomerizing AIC to PPIC.[5]

As has been mentioned previously, the AIC-olefin reaction is not always clean. In the reaction of AIC with methyl acrylate, **5** was isolated as the main product; it was thought of as being formed by the Michael addition[3,4] of the first pyrroline product, **7**, to another molecule of olefin. Here, the first pyrroline product was not isolated. Probably the rate of the formation of **7** is slower than that of the Michael reaction of **7** with methyl acrylate.

In the case of crotononitrile, the main reaction was its dimerization. The dimerization of crotononitrile by the Cu_2O-isonitrile system has already been found by us.[2] In the AIC-crotononitrile·Cu_2O mixture, the crotononitrile dimerization suppressed the pyrroline formation (Table 2). In addition, the pyrroline product of

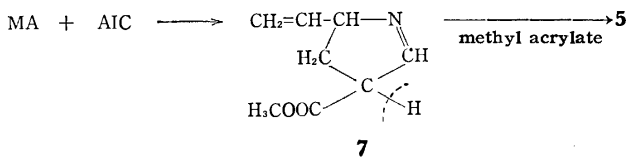

7

$$CH_3\text{-}CH{=}CH\text{-}CN \xrightarrow{Cu_2O/RNC} CH_3\text{-}CH{=}C(CH_3\text{-}CHCH_2CN)\text{-}CN$$

8

this reaction was **6**, which was explained as being derived from the primary product (**9a**) by the copper-catalyzed formimidation[6] of this tautomer (**9b**) with PPIC. The tautomerization of **9a**⇄**9b** has been found in our previous study of the pyrroline synthesis;[4] the copper-catalyzed formimidation of the >NH bond has also been reported.[6]

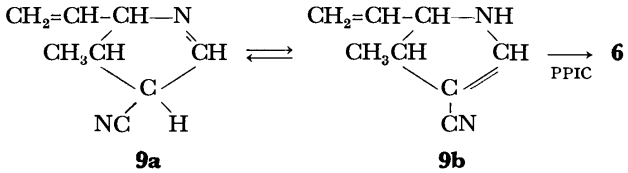

9a **9b**

In the reaction of AIC with acrylonitrile in benzene and DMF, only a trace of the pyrroline product, **10**, was detected by glpc (silicones; column temperature, 200°C). This was due to the polymerization of acrylonitrile by Cu_2O-isonitrile.[7] The polymerization of acrylonitrile by the Cu_2O-isonitrile system as well as the Cu_2O-isonitrile-active hydrogen compound system has been reported by us.[7]

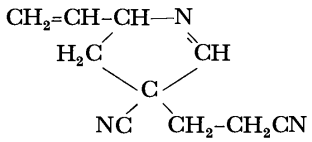

10

Reaction Scheme

On the basis of the scheme for the reactions of benzyl and carbethoxymethyl isocyanide with carbonyl and olefinic compounds, the following scheme may be presented for the reactions of AIC in the present study. First, the isocyanoallylcopper-isonitrile complex (**11**) is formed by the abstraction of α-hydrogen from AIC by Cu_2O. Probably, the coordination of the isocyano group of AIC to another copper complex facilitates the hydrogen abstraction by decreasing the electron density of the α-carbon atom. The α-isocyanoallylcopper complex (**11**) adds to the >C=O or >C=C< group to produce a new-formed copper species (Step 2), and the intramolecular reaction between the copper species and the isocyano group in **12** gives rise to the ring closure, thus producing **13** (Step 3). The abstraction of the α-hydrogen of another AIC molecule by **13** produces **11** and the final product, **14** (Step 4). Thus, the organocopper species is regenerated and the reactions proceed catalytically.

The α-isocyanoallylcopper complex acts as the key intermediate in the AIC⇄PPIC isomerization[5] also as is indicated in the scheme. The formation of **11** is supported by the fact that when the AIC-Cu_2O mixture was treated with allyl bromide, 3-isocyano-1,5-hexadiene (**15**) was isolated.[5]

$$\mathbf{11} + CH_2CH\text{-}CH_2Br \longrightarrow CH_2{=}CHCH(CH_2CH{=}CH_2)\text{-}NC$$

15

Experimental

Reagents. AIC was prepared according to Ugi's procedure,[8] while PPIC was prepared by the isomerization of AIC by the Cu_2O catalyst.[5] The carbonyl compounds were all commercial reagents and were purified by distillation under nitrogen. The α,β-unsaturated esters and nitriles were all commercial reagents which has been purified by distillation under nitrogen. The cuprous oxide was a commercial reagent of an analytical reagent grade and was dried under a nitrogen atmosphere prior to use.

Reactions with Carbonyl Compounds. An equimolecular mixture of isonitrile and carbonyl compounds and catalytic amounts of Cu_2O in benzene was reacted in a sealed test tube under nitrogen under the conditions shown in Table 1. The products were then isolated by vacuum distillation and purified by preparative glpc. The product structures were determined by IR, NMR, and elementary analysis. The identification data of the products are summarized in Table 3.

Reactions with Olefins. The reactions were carried out by a procedure similar to those used with carbonyl com-

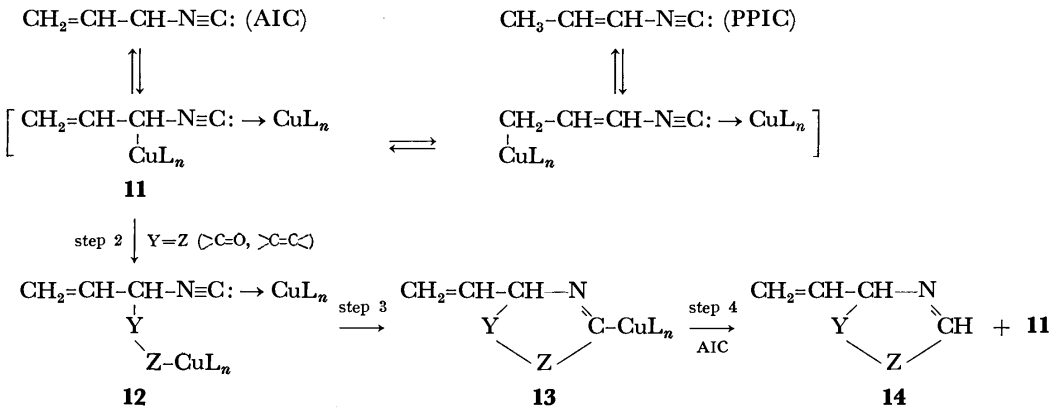

11 **12** **13** **14**

6) a) T. Saegusa, Y. Ito, S. Kobayashi, K. Hirota, and H. Yoshioka, *Tetrahedron Lett.*, **1966**, 6121. b) T. Saegusa, Y. Ito, S. Kobayashi, K. Hirota, and H. Yoshioka, This Bulletin, **42**, 3310 (1969).

7) T. Saegusa, S. Horiguchi, and H. Fujii, Presented at the 19th Symposium of Polymer Science, Oct. 1970, Kyoto.

8) I. Ugi, *Angew. Chem.*, **77**, 492 (1965).

Table 3. Identifications of 2-oxazoline derivatives (**1**)

Compds	Bp (°C/mmHg)	Formula	Anal Calcd C	H	N	Found C	H	N	IR spectrum (neat) cm^{-1}	NMR, τ, ($CDCl_3$)
1a	85— 90/170	$C_7H_{11}NO$	67.17	8.86	11.19	66.91	8.93	11.39	3075, 1640 (C=C) 1625 (N=C) 930 (C=C)	8.56, 8.80(s, 6H, $-CH_3$), 5.86(d, 1H, >CH–N=), *ca.* 4.7(m, 3H), 3.2(broad s, 1H, –N=CH–)
1b	114/8	$C_{12}H_{13}NO$	76.96	7.00	7.48	76.88	7.03	7.35	1645 (C=C) 1628, 1630 (N=C)	8.21, 8.42(s, 3H, $-CH_3$), 5.45(broad d, 1H, >CH–N=), *ca.* 4.7(m, 3H), 2.9(1H, –N=CH–)
1c	65— 69/11	$C_9H_{13}NO$	71.49	8.63	9.26	71.56	8.73	9.34	3075 (C=C) *ca.* 1630 (C=C, N=C)	5.72(broad, d, 1H, >CH–N=), *ca.* 4.7(m, 3H), 3.15(1H, –N=CH–)
1d	75— 80/3	$C_{10}H_{15}NO$	72.69	9.15	8.48	72.24	9.46	8.50	3075, 1645, 935 (C=C), 1625 (N=C)	5.96(d, 1H, >CH–N=), *ca.* 4.6(m, 3H), 3.17(1H, –N=CH–)
1e	115—121/10	$C_{11}H_{11}NO$	76.27	6.40	8.09	75.80	6.61	7.94	1642 (C=C), 1608 (N=C)	5.60(broad, t, 1H) *ca.* 4.8 (m, 2H, $-CH=CH_2$), *ca.* 4.2 (m, 1H, $-CH=CH_2$), 3.05 (1H, –N=CH–)
1f	66— 70/46	$C_8H_{13}NO$	69.03	9.41	10.06	68.51	9.74	10.63	3075, 1645 (C=C) 1630 (NC)	5.75(broad, t, 1H) *ca.* 4.8, 4.2(m, 3H), 3.15(d, 1H, –CH=N–)

Table 4. Identifications of pyrroline derivatives

Compds	Bp (°C/mmHg)	Formula	Anal Calcd C	N	H	Found C	H	N	IR spectrum (neat) cm^{-1}	NMR, τ, ($CDCl_3$)
4a	50— 55/1	$C_9H_{13}NO$	64.65	7.84	8.38	64.67	8.12	8.50	3080, 645 (C=C) 1735 (C=O) 1635 (N=C)	8.57(d, 3H, >CH–CH_3), 6.25 (s, 3H, –O–CH_3), *ca.* 5.21(m, 1H, >CH–N=), *ca.* 4.8(m, 2H, $-CH=CH_2$), *ca.* 4.15(m, 1H, $-CH=CH_2$), 2.55(1H, –N=CH)
4b	55— 63/4	$C_8H_{10}N_2$	71.61	7.51	20.88	71.72	7.78	20.78	3080, 645 (C=C) 2232 (N≡C) 1628 (N=C)	8.57(d, 3H, >CH–CH_3), *ca.* 5.35(m, 1H, >CH–N=), *ca.* 4.85(m, 2H), *ca.* 4.20(m, 1H), 2.65(1H, –N=CH–)
5	135—136/2.5	$C_{12}H_{17}NO_4$	60.28	7.16	5.85	59.84	7.29	6.50	3080, 645 (C=C) 1738 (ester) 1625 (N=C)	7—8(m, 6H, $-CH_2-$), 6.62, 6.72(s, 6H, $-COOCH_3$), *ca.* 5.35(m, 1H, >CH–N=), *ca.* 4.8 (m, 2H, $-CH=CH_2$), *ca.* 4.1(m, 1H, $-CH=CH_2$), 2.52 (d, 1H, >CH=N–)

6 IR (neat) ; 3080 (C=C), 2202 (C≡N), 1650 (C=C), 1600 (N=C)
NMR ($CDCl_3$ τ); 8.69 (d, 3H, >CH–CH_3), 8.15 (d, 3H, CH_3–CH=), 7.06 (q, 1H, CH_3–CH<), 5.70 (t, 1H, >CH–N=), 4—5 (m, 4H, olefin protons), 3.45 (d, 1H, =N–CH=C<^{CH_3}), 2.60 (s, 1H, >N–CH=C(CN)–), 2.41 (s, 1H, N–CH=N)

10 IR (neat) ; 3090, 1662, 985, 908 (C=C), 2200 (C≡N), 1630 (N=C)

pounds under the conditions indicated in Table 2. The structures of **4a**, **4b**, and **5** were determined by IR, NMR, and elementary analyses. The identification of **8** was made by a comparison of its IR and NMR with those of an authentic sample.[2] The identification of **6** was made by means of its IR and NMR, while the structure of **10** was assumed on the basis of its IR spectra. The identification data of the AIC-olefin reaction products are summarized in Table 4.

Studies of Thioiminocarbonates. II. The Cyanide Ion-catalyzed Addition of Alcohols to Thiocyanates

Kazuhiko TANAKA

Department of Chemistry, Faculty of Science, Kyoto University, Sakyo-ku, Kyoto

(Received June 17, 1971)

It was found that thiocyanates reacted with methanol in the presence of a catalytic amount of cyanide ion to give thioiminocarbonates. The effects of other catalysts upon the addition of methanol to thiocyanates were examined: the azide ion and the methoxide ion were effective, while triethylamine, sodium thiocyanate, potassium iodide, triphenylphosphine, sodium acetate, and mercuric cyanide were ineffective. A plausible reaction mechanism involving the addition of the cyanide ion to thiocyanates was proposed.

Although the scission of unsymmetrical diaryl disulfides by various S-nucleophiles has been discussed by Parker and Kharasch,[1] the cleavage products have not been isolated and characterized. Hiskey and Carroll investigated the cyanide-ion cleavage of unsymmetrical disulfides in detail.[2]

They reported that, when methyl phenyldithioacetate was treated with the cyanide ion, 12.5% yields of phenyl thiocyanate were obtained. However, no report has appeared concerning the scission of symmetrical diaryl disulfides by the cyanide ion. In a previous paper, we reported that symmetrical diaryl disulfides were readily cleaved by the cyanide ion in alcohol to afford aryl mercaptides and aryl thiocyanates, which then reacted with the alcohol used as the solvent to afford alkyl aryl sulfides:[3]

$$ArS\text{-}SAr + CN^- \rightleftharpoons ArS^- + ArSCN \quad (1)$$

$$ArSCN + ROH \longrightarrow ArS\text{-}\underset{\displaystyle OR}{\underset{|}{C}}{=}NH \quad (2)$$

$$ArS\text{-}\underset{\displaystyle OR}{\underset{|}{C}}{=}NH + CN^- \longrightarrow ArSR + OCN^- + HCN \quad (3)$$

When *p*-tolyl thiocyanate was treated with an equimolecular amount of the cyanide ion in methanol at a low temperature, a mixture of methyl *p*-tolyl sulfide and *O*-methyl *S*-*p*-tolyl thioiminocarbonate was obtained.[4] In continuing these investigations, we have found that the treatment of thiocyanates with methanol in the presence of a catalytic amount of the cyanide ion gave thioiminocarbonates in good yields.

Results and Discussion

When phenyl thiocyanate (0.1 mol) was treated with methanol in the presence of a catalytic amount of sodium cyanide (0.014 mol) at 0°C for 6 hr, *O*-methyl *S*-phenyl thioiminocarbonate was obtained in a 72% yield. The product showed NMR peaks at τ 5.94 (OCH_3), 2.86 (NH), and 2.27 (C_6H_5), with relative intensities of 3: 1: 5. Its infrared spectrum contained a strong band at 1628 cm^{-1} (C=N) and a weak band at 3300 cm^{-1} (NH). In a similar way, various thioiminocarbonates were prepared from thiocyanates and methanol by using the cyanide ion as the catalyst. The results are summarized in Table 1. Of the various catalysts examined, it was found that sodium azide and sodium methoxide were effective, while triethylamine, sodium thiocyanate, potassium iodide, triphenylphos-

Table 1. Preparations of thioiminocarbonates

$$RSCN + CH_3OH \longrightarrow RS\text{-}\underset{\displaystyle OCH_3}{\underset{|}{C}}{=}NH$$

R–SCN R	Catalyst	R-SCN: Catalyst (mol ratio)	Reaction temp. (°C)	Reaction time (hr)	Yield of thioiminocarbonate (%)
C_6H_5–	NaCN	7:1	0	6	72
C_6H_5–	$NaOCH_3$	9:1	0	6	77
C_6H_5–	NaN_3	7:1	0	7	73
p-$CH_3OC_6H_4$–	NaCN	8:1	0	17	84
p-$CH_3C_6H_4$–	NaN_3	5:1	0	1	70
p-$CH_3C_6H_4$–	$NaOCH_3$	5:1	0	1	64
p-$CH_3C_6H_4$–	NaCN	5:1	0	1	70
p-$CH_3C_6H_4$–	NaCN	8:1	0	8.5	74
m-$CH_3C_6H_4$–	NaCN	11:1	0	17	84
p-ClC_6H_4–	NaCN	7:1	0	6	74
C_2H_5–	NaCN	8:1	0	24	60

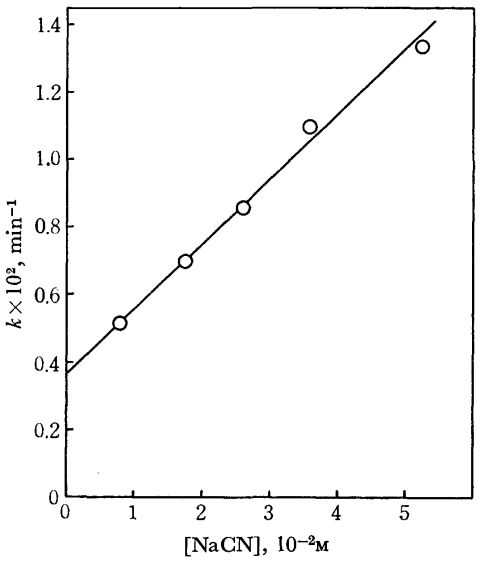

Fig. 1. First-order rate constants for cyanide ion-catalyzed addition of methanol to *p*-tolyl thiocyanate at 0°C.

1) A. J. Parker and N. Kharasch, *J. Amer. Chem. Soc.*, **82**, 3071 (1960).

2) R. G. Hiskey and F. I. Carroll, *ibid.*, **83**, 4647 (1961), and references cited therein.

3) K. Tanaka, J. Hayami, and A. Kaji, This Bulletin, **45**, 536 (1972).

4) K. Tanaka, J. Hayami, and A. Kaji, *ibid.*, **44**, 2815 (1971).

phine, sodium acetate, and mercuric cyanide were ineffective, in the formation of thioiminocarbonates.

Information about the mechanism of the base catalysis can be obtained by measuring the pseudo-first-order rates at varying cyanide-ion concentrations. The plot of [NaCN] against 10^2k gives a straight line, showing that the catalytic effect is directly proportional to the concentration of the cyanide ion. The calculated values of 10^2k in Table 2 are derived from the expression: $k=3.70\times10^{-3}+1.90\times10^{-1}$[NaCN], where the 3.70×10^{-3} value is that for the slow uncatalyzed reaction and 1.90×10^{-1}, that for the catalytic coefficient (k_c) of the cyanide ion.[5]

The pseudo-first-order rates of the reaction of substituted aryl thiocyanates are listed in Table 3. The rates are slightly accelerated when the substituent is electron-withdrawing. On the basis of the observations presented earlier, the reaction scheme of the addition of methanol to thiocyanates in the presence of a cyanide-ion catalyst may be postulated to be as follows:

Table 2. Rates of cyanide ion-catalyzed addition of *p*-tolyl thiocyanate with methanol at 0°C

$CH_3C_6H_4SCN$ [M]	NaCN [M]	$k\times10^2$ (min^{-1})	k_c ($l\cdot mol^{-1}\cdot min^{-1}$)
0.147	0.0084	0.51	0.17
0.147	0.0177	0.70	0.19
0.147	0.0260	0.86	0.19
0.147	0.0357	1.10	0.20
0.147	0.0525	1.33	0.18
		mean	0.19

Table 3. First-order rate constants of the addition of methanol to aryl thiocyanates at 0°C

X–C$_6$H$_4$–SCN (X)	$k\times10^2$ (min^{-1})	Relative rates
p-CH_3O	0.44	0.85
p-CH_3	0.51	0.98
H	0.52	1.00
p-Cl	0.95	1.83
m-Cl	1.04	2.00

[ArSCN]=0.147M, [NaCN]=0.0058M.

$$\mathrm{ArS{-}C{\equiv}N + CN^- \longrightarrow ArS{-}\underset{\displaystyle CN}{\underset{|}{C}}{=}N^-} \quad (4)$$

$$\mathrm{ArS{-}\underset{\displaystyle CN}{\underset{|}{C}}{=}N^- + CH_3OH \longrightarrow ArS{-}\underset{\displaystyle CN}{\underset{|}{C}}{=}NH + CH_3O^-} \quad (5)$$

$$\mathrm{ArS{-}\underset{\displaystyle CN}{\underset{|}{C}}{=}NH + CH_3O^- \longrightarrow ArS{-}\underset{\displaystyle OCH_3}{\underset{|}{C}}{=}NH + CN^-} \quad (6)$$

Experimental

Materials. Phenyl thiocyanate,[6] *p*-methoxyphenyl thiocyanate,[7] *p*-chlorophenyl thiocyanate,[8] *m*-chlorophenyl

Table 4. Physical properties and elemental analyses of thioiminocarbonates

$$\mathrm{R{-}S{-}\underset{\displaystyle OCH_3}{\underset{|}{C}}{=}NH}$$

R	Mp (°C) bp (°C/mmHg)	NMR absorption, τ (Solvent: CCl_4)	Analytical data (%) Found (Calcd) C	H	N	S
C_6H_5–	35—36	2.27 (5H, s, aromatic) 2.86 (1H, s, NH) 5.94 (3H, s, OCH_3)	57.39 (57.46)	5.44 (5.42)	8.35 (8.38)	19.20 (19.17)
p-$CH_3OC_6H_4$–	127.5—129/3.5	2.83 (4H, m, aromatic) 3.30 (1H, s, NH) 6.20 (3H, s, OCH_3) 6.24 (3H, s, CH_3O)	54.83 (54.80)	5.89 (5.62)	7.05 (7.10)	16.46 (16.26)
p-$CH_3C_6H_4$–	106—109/4	3.10 (4H, m, aromatic) 3.45 (1H, s, NH) 6.40 (3H, s, OCH_3) 7.75 (3H, s, CH_3)	59.65 (59.64)	6.21 (6.12)	7.70 (7.73)	17.56 (17.69)
m-$CH_3C_6H_4$–	100—101.5/2	2.68 (4H, m, aromatic) 3.02 (1H, s, NH) 6.20 (3H, s, OCH_3) 7.63 (3H, s, CH_3)	59.74 (59.64)	6.06 (6.12)	7.63 (7.73)	17.94 (17.69)
p-ClC_6H_4–	60—61	2.46 (4H, m, aromatic) 3.00 (1H, s, NH) 6.15 (3H, s, OCH_3)	47.77 (47.64)	4.10 (4.00)	6.84 (6.95)	15.79 (15.90)
C_2H_5–	69—70.5/26	2.66 (1H, s, NH) 6.09 (3H, s, OCH_3) 7.20 (2H, q, $-CH_2-$) 8.65 (3H, t, CH_3)	40.34 (40.31)	7.81 (7.61)	11.78 (11.75)	26.61 (26.90)

5) Triethylamine catalyzed reaction of isocyanates and methanol has been reported. See J. W. Baker and J. B. Holdsworth, *J. Chem. Soc.*, **1947**, 713.

6) L. Gattermann and W. Haussknecht, *Ber.*, **23**, 738 (1890).

7) J. W. Dienske, *Rec. Trav. Chim. Pays-Bas*, **50**, 165 (1931).

8) A. Hantzsch and B. Hirsch, *Ber.*, **29**, 947 (1896).

thiocyanate,[9] and ethyl thiocyanate[10] were prepared as has been described in the literature. *p*-Tolyl thiocyanate and *m*-tolyl thiocyanate were prepared by the same method from the corresponding toluidines. *p*-Tolyl thiocynate, bp 127—129°C/19 mmHg; *m*-tolyl thiocyanate, bp 111—115°C/11 mmHg.

Preparation of Thioiminocarbonates. After a mixture of phenyl thiocyanate (0.1 mol, 13.5 g) and powdered sodium cyanide (0.0143 mol, 0.7 g) in absolute methanol (200 m*l*) has been stirred at 0°C for 6 hr, the methanol was evaporated *in vacuo*. Petroleum ether (200 m*l*) was added, and the mixture was washed with water two times. An organic layer was separated and dried with anhydrous sodium sulfate. The filtrate was evaporated, and the residual oil was distilled *in vacuo*; bp 82—89°C/3 mmHg. The recrystallization of the distillate, which solidified at room temperature, from petroleum ether gave 12 g (72%) of *O*-methyl *S*-phenyl thioiminocarbonate as a transparent rhombic crystal; mp 35—36°C. IR: 3300 (NH), 1628 cm^{-1} (C=N). NMR (in CCl_4) τ 5.94 (3H, s, OCH_3), 2.86 (1H, s, NH), 2.27 (5H, s, C_6H_5). In a similar way, other thioiminocarbonates were prepared. Their physical properties and elemental analyses are listed in Table 4.

Effects of Catalysts. To a solution of *p*-tolyl thiocyanate (0.05 mol) in absolute methanol (50 ml), we added 0.01 mol of a catalyst, after which the mixture was stirred at 0°C for 1 hr. Then the methanol was evaporated under reduced pressure, and ether was added to the residue. A usual work-up and distillation gave a colorless oil. Sodium cyanide, sodium azide, and sodium methoxide were effective, and *O*-methyl *S*-*p*-tolyl thioiminocarbonate was obtained, as is shown in Table 1. Triethylamine, sodium thiocyanate, potassium iodide, triphenylphosphine, sodium acetate, and mercuric cyanide were ineffective, and the *p*-tolyl thiocyanate was recovered unchanged (77—99%).

Determination of the Reaction Rates. Sodium cyanide ($1.17—10.5\times10^{-3}$ mol) was dissolved in a solution of 2.94×10^{-2} mol of aryl thiocyanates in 200 m*l* of absolute methanol placed in a constant-temperature bath at 0 ± 0.05°C. At various intervals, 15-m*l* aliquots were removed and poured into a mixture of *n*-hexane (10 m*l*) and saturated aqueous sodium chloride (50 m*l*). The sample was extracted and again with 10 m*l* of *n*-hexane. From each run thus obtained, the amount of thiocyanate were measured by glc.

The author wishes to thank Professor A. Kaji and Dr. J. Hayami for their discussions.

9) F. Challenger, C. Higgingbottom, and A. Huntington, *J. Chem. Soc.*, **1930**, 26.
10) P. Walden, *Ber.*, **40**, 3214 (1907).

BULLETIN OF THE CHEMICAL SOCIETY OF JAPAN, VOL. 45, 836—840(1972)

Isolation of the Intermediate in the Tricyanovinylation of Indole and *N*-Methylindole

Yasuhiko SHIROTA, Sadayuki EZAKI,* Shigekazu KUSABAYASHI,** and Hiroshi MIKAWA
Department of Applied Chemistry, Faculty of Engineering, Osaka University, Yamadakami, Suita, Osaka
(Received June 28, 1971)

The intermediate has been isolated in the tricyanovinylation of indole and *N*-methylindole. The neutral adduct structure at the 3-position is assigned on the basis of spectroscopic as well as chemical evidence. The mechanism for tricyanovinylation is discussed.

The tricyanovinylation of aromatic amines at either N-position or *para*-position by the reaction with tetracyanoethylene is well known.[1] Indole and its derivatives are also known to undergo tricyanovinylation at the 3-position.[2,3] In these tricyanovinylation reactions tetrahydrofuran, dimethylformamide or pyridine has usually been used as the solvent. Kinetic studies in chloroform or in dichloromethane have shown that the reaction involves three steps:[4,5] (a) rapid formation of a 1: 1 charge-transfer complex (π-complex), (b) formation of a zwitterionic σ-complex, (c) elimination of hydrogen cyanide from the σ-complex to form the final product. In the process of hydrogen cyanide elimination which is the rate-determining step, the

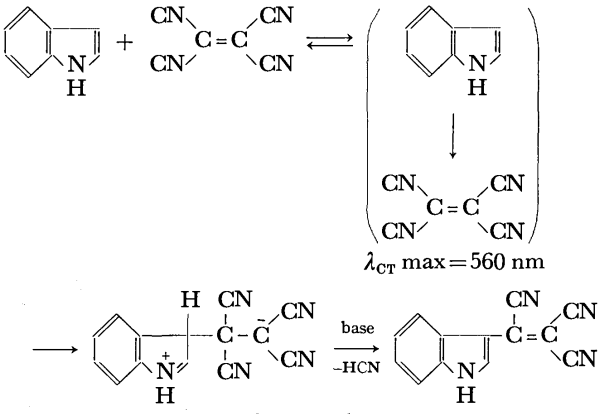

λ_{CT} max = 560 nm

Scheme 1

* Present address: Mitsui Toatsu Chem. Co. Ltd., Omuta, Fukuoka.

** Present address: Department of Chemical Engineering, Faculty of Engineering, Yamaguchi University, Ube, Yamaguchi.

1) B. C. Mckusick, R. E. Heckert, T. L. Cairns, D. D. Coffman, and H. F. Mower, *J. Amer. Chem. Soc.*, **80**, 2806 (1958).
2) G. N. Sausen, V. A. Engelhardt, and W. J. Middleton, *ibid.*, **80**, 2815 (1958).
3) W. E. Noland, W. C. Kuryla, and R. F. Lange, *ibid.*, **81**, 6010 (1959).
4) Z. Rappoport, *J. Chem. Soc.*, **1963**, 4498.
5) R. Foster and P. Hanson, *Tetrahedron*, **21**, 255 (1965).

amine or indole is suggested to act as a proton-abstractor. The proposed mechanism with indole is shown as an example in Scheme 1.

Concerning the above mechanism it should be mentioned that while the formation of the charge-transfer complex is visually observable, the intermediacy of the σ-complex was inferred by indirect evidence.[6] Recently Farrell *et al.* have succeeded in isolating an intermediate from the tetracyanoethylene-*N,N*-dimethylaniline reaction by changing the solvent. The structure of the isolated intermediate had first been assigned to the zwitterionic σ-complex (I),[7] but later the neutral adduct structure (II) was shown to be the correct one.[8] Rappoport and

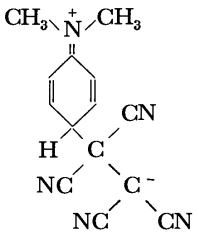

(I)

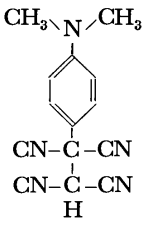

(II)

Shohamy have also achieved the isolation of intermediates in the tricyanovinylation of several primary aromatic amines by introducing the *ortho*-substituents to the amino group.[9] In this case tricyanovinylation occurs at the *para*-position instead of the N-position owing to steric crowding. It has been claimed that the *ortho*-substituted amine is too bulky to be very effective as a proton-abstractor from the intermediate, thus increasing its lifetime and enabling its isolation. Neutral adduct structure like II is assigned from the spectroscopic evidence.

Indole and its derivatives are less basic than aromatic amines, and thus less effective as a proton-abstractor since the unpaired electrons on nitrogen atom participate in the aromatization. It was therefore expected that under favorable conditions isolation of the intermediate would be possible.[10] In the present study we have isolated the intermediate in the tricyanovinylation of indole and *N*-methylindole. Spectroscopic evidences are presented to indicate the neutral adduct structure (III), and the mechanism for tricyanovinylation is discussed.

Results and Discussion

When a half equimolar amount of tetracyanoethylene was mixed with *N*-methylindole in benzene at room temperature, a blackish purple color characteristic of the charge-transfer complex developed immediately. The solution was left at room temperature for 24 hr, during which time the initial blackish purple color slowly faded away to become slighlty reddish yellow. White crystalline solids were precipitated from the solution, collected by filtration and recrystallized from benzene to give white needles. Removal of the solvent *in vacuo* gave additional white solids together with recovered *N*-methylindole. When equimolar amounts of tetracyanoethylene and *N*-methylindole were refluxed in benzene for 7 hr, white needles and the final tricyanovinylated compound, *N*-methyl-3-tricyanovinylindole (VIIa), were obtained simultaneously. The isolated white needles were almost quantitatively converted into VIIa with a loss of hydrogen cyanide when heated in methanol for a few hours. The molecular ion peak of the isolated white needle is observed at *m/e* 259 in the mass spectrum. From these results and from other spectral evidences described below together with the elemental analysis, the isolated white needle was concluded to be the intermediate adduct between *N*-methylindole and tetracyanoethylene, which led to the final substitution product VIIa. The yields of the isolated intermediate were 97% in the reaction at room temperature and 65% in the reaction under reflux. Simultaneous formation of VIIa under reflux appears to result from a thermal decomposition of the isolable intermediate.

The intermediate in the tricyanovinylation of indole was similarly isolated. A benzene solution of indole was added to a solution of a half equimolar amount of tetracyanoethylene in benzene. The initial blackish purple color faded slowly and after 24 hr the solution turned reddish orange. From this solution the intermediate adduct and the final tricyanovinylated compound, 3-tricyanovinylindole (VIIb), were obtained in 83% and 16% yields, respectively. When the reaction solution was refluxed for 7 hr, the main product isolated was VIIb (54%), the intermediate adduct being obtained only in a 14% yield. The isolated intermediate from the reaction of indole was likewise con-

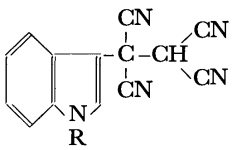

IIIa R=CH_3
IIIb R=H

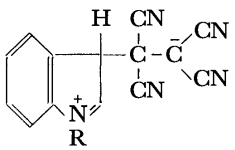

IVa R=CH_3
IVb R=H

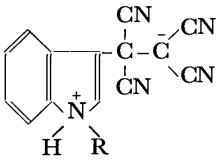

Va R=CH_3
Vb R=H

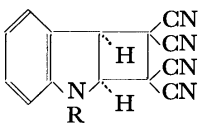

VIa R=CH_3
VIb R=H

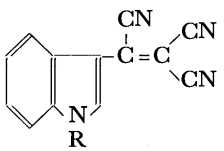

VIIa R=CH_3
VIIb R=H

6) The appearance of the final substitution product is much slower than a decay of the chage-transfer complex.

7) P. G. Farrell, J. Newton, and R. F. M. White, *J. Chem. Soc., B*, **1967**, 637.

8) P. G. Farrell and R. K. Wojtowski, *ibid., B*, **1970**, 1390.

9) Z. Rappoport and E. Shohamy, *ibid., B*, **1969**, 77.

10) Before kinetic studies of the tricyanovinylation reaction were made by Rappoport,[4] and Foster and Hanson,[5] Noland *et al.*[3] had reported in their synthetic studies of tricyanovinylated compounds from indole and its derivatives that in one case, with 2-methylindole, the intermediate was isolated and found to be the adduct tetracyanoethane based on a brief characterization.

verted almost quantitatively into VIIb when heated in methanol. The elementary analysis of the intermediate was in good agreement with the adduct structure between indole and tetracyanoethylene.

Both of the isolated intermediates are relatively stable and can be stored for several days when kept dry below room temperature. The intermediate derived from indole is less stable than that derived from *N*-methylindole, which is also reflected in the results of their preparative reactions described above. They are almost insoluble in carbon tetrachloride but soluble in acetone or tetrahydrofuran. On contact with moisture or basic solvent they slowly turn through pink to red to form the final tricyanovinylated compounds.

The follwing possible structures from IIIa and IIIb to VIa and VIb are conceivable for the isolated intermediates which lead to the final substitution products VIIa and VIIb. Of these structures IIIa and IIIb were assigned from the sepctral evidences.

Infrared Spectra. The infrared spectrum of the isolated intermediate from *N*-methylindole in KBr disk shows a sharp strong absorption at 2900 cm^{-1} which is characteristic of the intermediate and assignable to the aliphatic tertiary C–H stretching vibration. The absorption at 2900 cm^{-1} in the intermediate corresponds to that observed at 2900 cm^{-1} in tetracyanoethane and in *N,N*-dimethyl-4-(1,1,2,2,-tetracyanoethyl)aniline (II).[9] While a sharp absorption characteristic of the conjugated C≡N group appears at 2200 cm^{-1} in VIIa, only a very weak absorption of the unconjugated C≡N group appears at 2260 cm^{-1} in the isolated intermediate. Similarly the spectrum of the intermediate derived from indole in KBr disk shows the characteristic absorption at 2900 cm^{-1}. In this case a very weak absorption at 2260 cm^{-1} and a sharp absorption at 2200 cm^{-1} are observed in the cyano-band region. It is suspected that the intermediate decomposed partly to VIIb during the preparation of the disk as suggested from its reddish orange color. When the spectrum is taken in Nujol mull with a freshly prepared sample, no absorption appears at 2200 cm^{-1}, although in VIIb a sharp strong band appears at 2200 cm^{-1} due to the conjugated C≡N group. The absorption of the unconjugated C≡N group of the intermediate at 2260 cm^{-1} is so weak as to be hardly detectable in Nujol mull. It is generally accepted that cyano-compounds with electron-withdrawing substituents at the α-position frequently show only weak absorption or sometimes no absorption of the C≡N group.[11] It should also be noted that many compounds containing $-C(CN)_2$ moiety are reported to show two medium bands at the unsaturated cyano-band region.[12] In the spectrum of the intermediate derived from indole a single, rather strong band of the secondary N–H stretching vibration appears at 3300 cm^{-1} as observed in indole and in VIIb at 3380 and 3200 cm^{-1}, respectively. No absorption ascribable to the $-\overset{+}{N}H_2$ or $C=\overset{+}{N}H$ group is observed in the regions, 2780—2500 cm^{-1} or 2500—2325 cm^{-1}, respectively[13,14] in both intermediates. The infrared spectra eliminate the σ-complex structures such as IV or V for the isolated intermediates, thus favoring structure III.

NMR Spectra. The NMR spectra of the isolated intermediate were measured in hexadeuterioacetone as soon as possible after the solutions were prepared. The intermediate derived from *N*-methylindole shows a singlet at τ 6.0 due to *N*-methyl protons, a singlet at τ 3.75 and multiplets at τ 1.9—2.8 due to aromatic protons including the proton at the 2-position in the indole ring, the relative ratios being 3 : 1 : 5. The singlet peak at τ 3.75 is reasonably attributed to the methine proton of the dicyanomethyl moiety in structure IIIa from consideration of the chemical shift value of τ 4.19 for tetracyanoethane.[9] The peak due to the *N*-methyl protons appears as a singlet at τ 6.63 (in $CDCl_3$) in *N*-methylindole[15] and at τ 5.84 in VIIa. Similarly the spectrum of the intermediate derived from indole exhibits a singlet at τ 3.74 and multiplets at τ 1.9—2.8 in the relative ratios of 1 : 6. In the latter the indole ring protons and the N-H proton are included. The NMR spectra exclude the cyclo-adduct structure VI with two methine protons which should couple with each other. Structures IV and V are also unlikely from the position and the relative intensity of the signals. In these structures the methine proton at the 3-position should be coupled with the neighboring carbon-bound hydrogen at the 2-position.[14] Thus the isolated intermediates leading to the tricyanovinylated compounds VIIa and VIIb are assigned to structures IIIa and IIIb, respectively, from both the infrared and NMR spectra.

Electronic and Mass Spectra. The electronic spectra of the intermediates IIIa and IIIb in benzene show maxima at 282 nm (log ε 3.62) and 279 nm (log ε 3.76), respectively.

Although the mass spectrum is of no particular use for distinguishing between the adduct structures, it is briefly described. Both intermediates IIIa and IIIb show very low molecular ion peaks at *m/e* 259 and *m/e* 245, respectively. The base peak appears at *m/e* 232 in IIIa and at *m/e* 218 in IIIb, which corresponds to the loss of hydrogen cyanide from the molecular ion. The position and relative intensity of the peaks below *m/e* 232 in IIIa and *m/e* 218 in IIIb are almost the same as those of the tricyanovinylated compounds VIIa and VIIb, respectively, except for the peaks at *m/e* 195 (very low intensity) and *m/e* 194 in IIIa and *m/e* 181 (very low intensity) and *m/e* 180 in IIIb. The characteristic peaks at *m/e* 195 and *m/e* 194 in IIIa and at *m/e* 181 and at *m/e* 180 in IIIb which are absent in the spectra of VIIa and VIIb correspond to the direct loss of $:C(CN)_2$ and $\cdot CH(CN)_2$ from the molecular ion, respectively. Other fragments below *m/e* 232 in IIIa and *m/e* 218 in IIIb are suggested to be formed by the fragmentation of VIIa and VIIb. The main peaks over *m/e* 180 observed in IIIa and IIIb are listed in the Table and the fragmentation course from the molecular ion to the ion of

11) L. J. Bellamy, "The Infra-Red Spectra of Complex Molecules," 2nd ed., Methuen, London, (1958), p. 265.

12) Z. Rappoport and S. Gertler, *J. Chem. Soc.*, **1964**, 1360, and references cited therein.

13) L. J. Bellamy, "The Infra-Red Spectra of Complex Molecules," 2nd ed., Methuen, London, (1958), p. 259.

14) R. L. Hinman and J. Lang, *Tetrahedron Lett.*, **1960**, 12.

15) L. A. Cohen, J. W. Daly, K. Kny, and B. Witkop, *J. Amer. Chem. Soc.*, **82**, 2184 (1960).

Table 1. Fragmentation of IIIa and IIIb in the mass spectra

			IIIa			
m/e	259	233	232	205	194	190
Abundance	1.6	15.6	100	14.4	9.5	8.6
Assignment	P	M–CN	M–HCN	M–2HCN	M–$CH(CN)_2$	M–2HCN–Me
			IIIb			
m/e	245	219	218	191	180	
Abundance	3.6	16.2	100	41.5	7.2	
Assignment	P	M–CN	M–HCN	M–2HCN	M–$CH(CN)_2$	

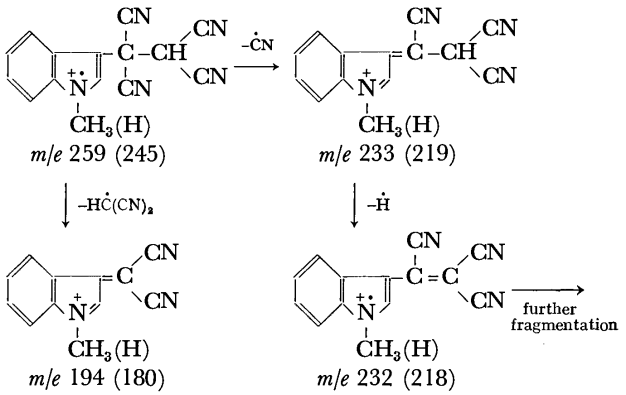

Scheme 2

the tricyanovinylated compound is depicted in Scheme 2.

Mechanism for Tricyanovinylation. It was shown from kinetic studies that the tricyanovinylation of aromatic amines or indole by tetracyanoethylene proceed in three steps as shown with indole in Scheme 1. However, a neutral adduct tetracyanoethane has recently been isolated as an intermediate in the tricyanovinylation of aromatic amines, and a general mechanism as shown in Scheme 3 has been proposed by Rappoport and Shohamy[9] for the tricyanovinylation of aromatic amines. In the present study a similar adduct tetracyanoethane has been isolated as an intermediate in the tricyanovinylation of indole and *N*-methylindole. Consequently, the same general mechanism as has been proposed for the tricyanovinylation of aromatic amines may be written also for the tricyanovinylation of indole and its derivatives.

Reactants $\rightleftarrows$ Charge-transfer Complex (π-Complex)
$\longrightarrow$ Zwitterionic σ-Complex $\rightleftarrows$ Neutral Adduct
Final Substitution Product

Scheme 3

Although the neutral adduct intermediate was isolated under the present reaction conditions, it should be noted that there might be a possibility that the reaction proceeds as described in Scheme 1 under different reaction conditions. Especially, in strongly basic solvents such as pyridine or dimethylformamide it is likely that the tricyanovinylated compound is formed directly from the σ-complex, the basic solvent abstracting a proton from the 3-position in the σ-complex. Whether the final tricyanovinylated compound is formed *via* the neutral adduct intermediate or directly from the σ-complex under the given reaction conditions, where the intermediate can not be isolated, can be seen by examining the hydrogen isotope effect, the presence of which is expected in the elimination of hydrogen cyanide from the σ-complex (IV) owing to the relatively low acidity of the hydrogen at the 3-position.[16]

Experimental

Materials. Indole was obtained commercially and purified by recrystallization from *n*-hexane three times, mp 52°C. *N*-methylindole was prepared from indole as described by Potts and Saxton.[19] Crude distilled product was contaminated with unreacted indole as revealed by the N–H absorption in the infrared spectrum. Chromatograph over alumina and subsequent two distillations *in vacuo* yielded pure *N*-methylindole, bp 128—129°C/25 mmHg (lit.[19] bp. 133°C/26 mmHg). Tetracyanoethylene was obtained commercially, recrystallized from chlorobenzene and sublimed twice *in vacuo*, mp 201°C. Benzene was purified and dried in the usual way, and distilled from sodium wire immediately before use.

Spectra. Infrared spectra were taken with Hitachi EPI-G2 and Jasco IR-G infrared spectrophotometers. Electronic spectra were taken with a Hitachi 124 spectrophotometer. NMR spectra were obtained with a Japan Electron Optics Laboratory JNM 3H-60 spectrometer. Mass spectra were recorded with a Hitachi RMU-6E mass spectrometer by means of a direct inlet with an ionization energy of 70 eV.

Isolation of N-methyl-3-(1,1,2,2-tetracyanoethyl)indole (IIIa). Reaction 1. To a solution of tetracyanoethylene (0.64 g, 0.005 mol) in 40 m*l* benzene was added *N*-methylindole (1.31 g, 0.01 mol) dissolved in 5 m*l* benzene. A blackish purple color appeared immediately and the solution was left at 20°C for 24 hr. During that time the initial characteristic color of the charge-transfer complex slowly faded to a slightly reddish yellow. From the solution were precipitated white crystalline solids (IIIa), which were collected by filtration. Evaporation of the solvent *in vacuo* gave additional IIIa together with recovered *N*-methylindole (0.34 g). The total yield of IIIa was 1.26 g (97%). It was recrystallized from dry benzene to give a white needle. Prolonged heating or repeated recrystallization caused its partial decomposition to *N*-methyl-3-tricyanovinylindole (VIIa). On heating it gradually turned through pink to red above 100°C accompanied by its decomposition to VIIa, and melted at *ca.* 210°C.

Found: C, 70.07; H, 3.48; N, 26.22%. Calcd for $C_{15}H_9N_5$: C, 69.49; H, 3.50; N, 27.02%.

16) A kinetic hydrogen isotope effect was observed with a k_H/k_D value of 3.6 in the tricyanovinylation of *N,N*-dimethylaniline in chloroform owing to the relatively low acidity of *para*-hydrogen in I, while no isotope effect was found in the amine-catalyzed elimination of hydrogen cyanide from II due to the more acidic hydrogen in II[17,18]

17) P. G. Farrell and J. Newton, *Tetrahedron Lett.*, **1964**, 189.

18) P. G. Farrell and J. Newton, *J. Chem. Soc., B*, **1970**, 1630.

19) K. T. Potts and J. E. Saxton, "Organic Synthesis," Vol. 40, (1960), p. 68.

Reaction 2. Solutions of tetracyanoethylene (1.28 g, 0.01 mol) and *N*-methylindole (1.31 g, 0.01 mol) were mixed and refluxed in 45 m*l* benzene for 7 hr. In this case the color of the solution remained black at the end of the reaction. Purple solids were obtained on cooling of the reaction solution. Evaporation of the solvent from the mother liquor also gave additional solids. They were collected and 50 m*l* of benzene was again added and reheated. The hot benzene solution was filtered to separate the insoluble red solids (VIIb, 0.23 g, 10%), which were recrystallized from methanol to give red fine needles. Cooling of the filtrate gave slightly pinkish white needles (IIIb, 1.69 g, 65%).

Isolation of 3-(1,1,2,2-tetracyanoethyl) indole (IIIb). Reaction 1. To a solution of tetracyanoethylene (0.77 g, 0.006 mol) in 40 m*l* benzene was added indole (1.41 g, 0.012 mole) in 5 m*l* benzene and left at 20°C for 24 hr. The initial blackish purple color faded slowly to a deep bluish purple and then to yellow and after 24 hr the solution turned reddish orange. The precipitated reddish pink solids were collected and dissolved rapidly in warm benzene. Insoluble red solids (VIIb) were separated (0.2 g, 16%) and from the filtrate was obtained IIIb as slightly pinkish white needles on cooling. The yield of IIIb was 1.23 g (83%). When heated to determine the mp, it gradually turned pink above 50°C and bove 100°C it turned reddish brown, decomposing to VIIb, mp *ca* 273—278°C. IIIb is less stable than IIId and prolonged heating or repeated recrystallizations from benzene caused considerable decomposition to VIIb.

Found: C, 68.29; H, 2.74; N, 28.50%. Calcd for $C_{14}H_7N_5$: C, 68.56; H, 2.88; N, 28.56%.

Reaction 2. Indole (1.17 g, 0.01 mol) dissolved in 5 m*l* benzene was added to a benzene solution (40 m*l*) of tetracyanoethylene (1.28 g, 0.01 mol) and refluxed for 7 hr. The solution was then cooled to 20°C and the precipitated blackish purple-colored solids were filtered off. Benzene (50m*l*) was again added, reheated to boiling for several minutes and filtered to separate the insoluble red solids (VIIb, 1.18 g, 54%). When the filtrate was cooled, slightly pinkish white needles (IIIb, 0.34 g, 14%) precipitated. In addition, small amounts of brown-colored solids were obtained from the initial mother liquor, which appeared to be *N*-tricyanovinylindole, since N–H absorption disappeared and strong conjuagted C≡N absorption was observed at 2200 cm^{-1} in the infrared spectrum.

Decomposition of IIIa and IIIb to VIIa and VIIb. IIIa or IIIb was heated in methanol for a few hours. The solution gradually turned red, and on cooling red fine needles VIIa or VIIb precipitated. The decomposition of the neutral adduct tetracyanoethane to the final substitution product was almost quantitative in each case.

Identification of VIIa and VIIb. VIIa: mp 226—226.5°C (recryst. from MeOH), (lit.[3] mp 218—219°C). IR: $\nu_{C\equiv N}$ 2200 cm^{-1}. Mass: M^+ *m/e* 232 (calcd 232). NMR: (in acetone) τ 5.84 (3H, singlet, N–CH_3), τ 1.9—2.8 (5H, multiplet, aromatic protons). UV and V: λ_{max} (in MeOH), 252 (log ε 3.91), 286 (log ε 3.99), and 460 nm (log ε 4.39). [lit.[3] in 95% EtOH. 262 (log ε 4.11), 280 (log ε 3.97), and 465 nm (log ε 3.91).]

Found: C, 71.89; H, 3.29: N, 24.06%. Calcd for $C_{14}H_8N_4$: C, 72.40; H, 3.47; N, 24.13%.

VIIb: mp 273—275°C (recryst. from MeOH), (lit.[3] mp 268—270°C). IR: $\nu_{C\equiv N}$ 2200 cm^{-1}, ν_{N-H} 3200 cm^{-1}. Mass: M^+ *m/e* 218 (calcd 218). NMR: (in acetone), τ 1.9—2.8 (multiplets, N–H proton and aromatic protons), UV and V: λ_{max} (in MeOH), 249 (log ε 3.95), 284 (log ε 4.00), and 454 nm (log ε 4.34). [lit.[3] in 95% EtOH, 251 (log ε 3.86), 285 (log ε 3.90), 357 (log ε 4.08), and 464 nm (log ε 4.33).]

Found: C, 71.84; H, 2.36; N, 25.11%. Calcd for $C_{13}H_6N_4$: C, 71.56; H, 2.57; N, 25.69%.

The Cope Rearrangement of Bridged Homotropilidenes Studied by MINDO Methods[1)]

Hiizu IWAMURA, Kazuhiko MORIO, and Tosiyasu L. KUNII*

*Department of Chemistry, Faculty of Science, and *Information Science Laboratory, Faculty of Science, The University of Tokyo, Bunkyo-ku, Tokyo*

(Received July 2, 1971)

The theoretical structures and heats of formation of semibullvalene (**1a**), barbaralane (**1b**), and bullvalene (**1c**) have been investigated by the MINDO methods. The strain energies are estimated to be 19.7, 8.8, and 0.5 kcal/mol, respectively. The activation energies for the Cope rearrangement of these bridged homotropilidenes were obtained by a comparison of the results of a similar study on the biallylic transition states for the rearrangement. They are in good agreement with the experimental values. Extremely facile rearrangement in **1a** is attributed to the partial release of strain energy through the formation of the transition state, and to the proximity (2.16 Å) of the non-bonded termini of the divinylcyclopropane unit in the ground state.

Semibullvalene (**1a**) is unique for its extremely facile Cope rearrangement. The activation energies for the Cope rearrangement of homotropilidenes generally fall into the range 12 ± 1 kcal/mol when they are bridged by a chain of two carbon units as in bullvalene (**1c**) and dihydrobullvalene. One carbon bridged homotropilidenes undergo rearrangement more easily; barbaralane (**1b**) and barbaralone have an activation energy of *ca.* 8 kcal/mol.[2)] The NMR spectrum of **1a** consists of only three multiplets at δ 2.97, 5.08, and 4.17 ppm in the intensity ratio of 2:2:4, indicating that the chemical shift between the protons α and α' is averaged out in the time scale of NMR spectroscopy. The spectral pattern remains unchanged even at $-100°$ at 100 MHz.[3)] The activation energy of the degenerate Cope rearrangement represented by the following equation is thus expected not to exceed 5 kcal/mol.

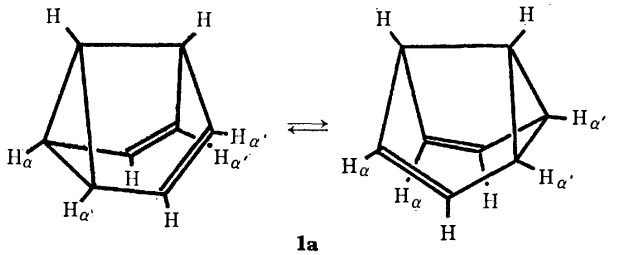

1a

With no experimental technique available for obtaining further kinetic information on **1a**, and in view of recent success in the quantitative evaluation of the heat of formation by the all valence electron SCF MO theory at various levels of sophistication,[4)] we adopted this theoretical tool to clarify the structural uniqueness of semibullvalene which causes the lower barrier to the Cope rearrangement.

Method of Theoretical Calculation

In order to evaluate the activation energy for the Cope rearrangement theoretically, it is necessary to calculate and compare the total energy or heat of formation of the ground state and the corresponding transition state of the bridged homotropilidenes. Since the rearrangement is degenerate, the transition state geometry should be

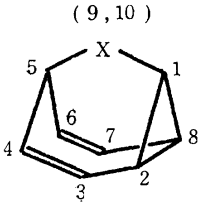

1a, X = zero carbon bridge
1b, X = CH_2
1c, X = CH=CH

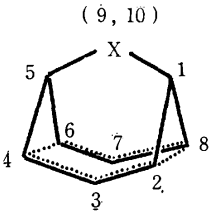

2a, X = zero carbon bridge
2b, X = CH_2
2c, X = CH=CH

symmetric with respect to the plane passing through the center of X and the carbon atoms numbered 3 and 7 as represented by **2a**—**c**, of which there is no *a priori* information as regards the precise geometry. Even the ground state conformation of the bridged homotropilidenes **1a**—**c** has not been reported except for bullvalene.[5)] The equilibrium geometry should be determined by minimizing the molecular energy with respect to all the bond lengths and angles for the ground state as well as the biallylic transition state.

In principle, optimization of geometry has to be made with respect to $3N-6$ internal coordinates. Although the number of the unknown is cut down considerably by the symmetry of the molecule, the computation time required would still be too long. As an example, reasonable assumption of C_s symmetry of **1a** still leaves the number of degree of freedom as 23. Fortunately we are allowed to take many of the bond lengths to be fixed to the standard values. In an extreme case, we may start with the standard bond lengths to effect faster

1) Presented at the 24th Annual Meeting of the Chemical Society of Japan, Osaka, April, 1971. Studies of Reaction Mechanism by All-Valence-Electron Semi-Empirical SCF-MO Theories. III. For paper II of the series note: H, Iwamura, K. Morio, and T. L. Kunii, *Chem. Commun.*, **1971**, 1408; I: H. Iwamura, K. Morio, M. Ōki, and T. L. Kunii, *Tetrahedron Lett.*, **1970**, 4575.

2) G. Schröder, J. F. M. Oth, and R. Merenyi, *Angew. Chem.*, **77**, 774 (1965), and papers cited therein.

3) H. E. Zimmerman and G. L. Grunewald, *J. Amer. Chem. Soc.*, **88**, 183 (1966); H. E. Zimmerman, R. W. Binkley, R. S. Givens, G. L. Grunewald, and M. A. Sherwin, *ibid.*, **91**, 3316 (1969).

4) M. J. S. Dewar, "The Molecular Orbital Theory of Organic Chemistry," McGraw-Hill Book Co., New York, N. Y., (1969); J. A. Pople and D. L. Beveridge, "Approximate Molecular Orbital Theory," McGraw-Hill Book Co., New York, N. Y., (1970).

5) B. Andersen and A. Marstrander, *Acta Chem. Scand.*, **21**, 1676 (1967).

approach to the final geometry. This is necessary, when the MINDO/1 approximation is to be used, becuase the method is parametrized to give the observed heat of formation accurately only with the use of fixed standard bond lengths of Baird and Dewar.[6]

The methods employed here for calculating the geometry of **1** and **2** are based on the MINDO/2 approximation to the full SCF equations of Roothaan. A complete specification of this method together with a discussion of the approximations have been given.[7] The calculations were performed on a HITAC 5020E computer with the use of a modified MINDO program originally written by Baird and distributed by the QCPE organization.[8] The Jacobi method for diagonalization of the F matrices is replaced by the Householder method. The calculations were carried out to a level of self consistency where the change in energies and the maximum change in the bond order matrix were less than 0.0001 eV and 0.0004, respectively.

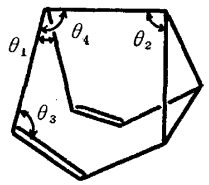

Fig. 1. Definition of angles changed as variables.

The procedure for calculating the geometry is exemplified by **1a**. Essentially the heat of formation was calculated for a systematically chosen set of bond angles shown in Fig. 1, and then minimized graphically. A set of numerical values were assigned to θ_1 to θ_4 and the coordinates of atoms were calculated using the standard bond lengths. The initial set of the angles was measured on molecular framework models of Prentice Hall, Inc.[9] Angle θ_1 was first adjusted by minimizing the molecular energy. Angles θ_2, θ_3, and then θ_4 were similarly calculated with the computed value for θ_1. θ_1 was recalculated with the new values for θ_2 through θ_4. The process was repeated until an absolute minimum in energy was obtained within 1° with respect to all bond angles. The coordinates for H_1 and H_5, the protons attached to C_1 and C_5, respectively, were similarly adjusted on the mirror plane of the molecule. The coordinates for H_3 and H_4 were calculated by assuming that they lie in the $C_2C_3C_4$ and $C_3C_4C_5$ planes, and the C_3–H_3 and C_4–H_4 bonds bisect the $C_2C_3C_4$ and $C_3C_4C_5$ angles, respectively. Finally optimization with respect to the carbon to carbon bond lengths was carried out. Since the optimized bond lengths always differ from the standard values by less than 1%, the change in the bond lengths is considered not to affect the optimized bond angles materially. In the MINDO/1 approximation, a value of 1.09 Å was assumed for all C–H bonds except 1.08 Å for the vinylic C–H bonds. All the C–H bond legths were uniformly shifted by +0.1 Å in the MINDO/2 calculations as suggested by Baird *et al.*[6,7]

As to the conformation of the transition state **2a**—**2c**, the bond lengths of C_1–C_2 and C_2–C_3, the interatomic distance C_1C_5, θ_1, θ_2, and θ_3 were taken as variables. θ_1 is defined as the angle between the planes $C_1C_2C_4C_5$ and $C_5C_6C_8C_1$. Displacement of C_3 and C_7 out of these planes, respectively, is expressed in terms of θ_2.

Results for Ground State Geometry

The theoretical structures for **1a**—**1c** are summarized in Table 1 together with the bond indices of Wiberg.[10] As the method is intended for calculation of the ground state geometry for which no experimental information is so far available, or of the transition state geometry which is not amenable to experimental investigation, it is desir-

TABLE 1. GROUND STATE GEOMETRIES AND BOND INDICES OF THE BRIDGED HOMOTROPILIDENES DETERMINED BY THE MINDO/2 METHOD

		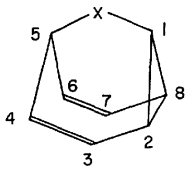	C_1C_2	C_2C_8	C_2C_3	C_3C_4	C_4C_5	C_4C_6[a]
1a	Bond distances (Å)		1.512	1.510	1.481	1.340	1.530	2.158
	Bond indices		0.9277	0.8791	1.0129	1.8448	0.9405	0.0595
			(0.8906	0.8129	0.9130	1.7678	0.8652	0.0466)[b]
1b	Bond distances (Å)		1.512	1.510	1.480	1.339	1.530	2.327
	Bond indices		0.9291	0.8931	1.0049	1.8690	0.9541	0.0280
			(0.8806	0.8468	0.8954	1.7850	0.8595	0.0263)[b]
1c	Bond distances (Å)		1.510	1.510	1.483	1.336	1.529	2.527
	Bond indices		0.9078	0.9078	0.9937	1.8834	0.9488	0.0113
			(0.8558	0.8558	0.8899	1.7855	0.8519	0.0211)[b]

a) Atomic distances b) Bond indices by the MINDO/1 method

6) N. C. Baird and M. J. S. Dewar, *J. Chem. Phys.*, **50**, 1262 (1969); N. C. Baird, M. J. S. Dewar, and R. Sustman, *ibid.*, **50**, 1275 (1969).

7) M. J. S. Dewar and E. Haselbach, *J. Amer. Chem. Soc.*, **92**, 590 (1970); N. Bordor, M. J. S. Dewar, A. Harget, and E. Haselbach, *ibid.*, **92**, 3854 (1970).

8) Quantum Chemistry Program Exchange, Chemistry Department, Indiana University, Bloomington, Indiana 47401.

9) Prentice Hall, Inc., Englewood Cliffs, N. J.

10) K. B. Wiberg, *Tetrahedron*, **24**, 1083 (1968). The bond index is defined as the sum of the squares of the bond orders (P_{jk}).

Table 2. Transition state geometries and bond indices of Wiberg calculated by the MINDO/2 method

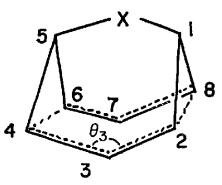

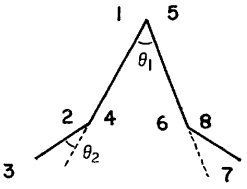

		C_1C_2	C_2C_3	C_2C_8	C_3C_7	Bond angles (°) θ_1	θ_2	θ_3
2a	Bond distances (Å)	1.520	1.400	1.771	2.844	73	5	110.0
	Bond indices	0.9079	1.3853	0.4566	0.0987			
		(0.8588	1.3193	0.4032	0.0700)[a]			
2b	Bond distances (Å)	1.524	1.405	1.798	2.768	72	6	117.5
	Bond indices	0.9214	1.3821	0.4513	0.0936			
		(0.8540	1.3056	0.4023	0.0713)[a]			
2c	Bond distances (Å)	1.520	1.395	1.770	2.587	72	6	124.0
	Bond indices	0.9128	1.3796	0.4503	0.0957			
		(0.8424	1.3006	0.3999	0.0701)[a]			

a) Bond indices by the MINDO/1 method

able to test the computational method with molecules of known geometry. The calculated bond lengths in the cyclopropane rings of **1a—c** are uniformly 1.510 Å and are considerably shorter than 1.544 Å experimentally obtained for bullvalene.[5] They are, however, in good agreement with those usually observed in the cyclopropane derivatives.[11] The adjacent C_2C_3 distance of **1c** is optimized at 1.483 Å; the experimental value is smaller by 0.017 Å. The reason for the discrepancy is as yet not clear. Only for the consistency of comparison, the optimized geometry is adopted in the following discussion.

One of the most significant differences in the ground state geometries of **1a—c** is revealed by the interatomic distances C_4C_6 (=C_2C_8). They are 2.158, 2.327 and 2.527 Å, for **1a**, **1b**, and **1c**, respectively; the order of bond indices is **1a**>**1b**>**1c**. Since the distances should eventually be reduced to *ca.* 1.51 Å to form a carbon-carbon single bond of the cyclopropane ring in the course of the Cope rearrangement, it is interesting that from the present calculation the ground state of **1a** is already forced towards the geometry of the transition state **2a**, while **1b** is less, and **1c** is least perturbed in the direction of the respective transition states.

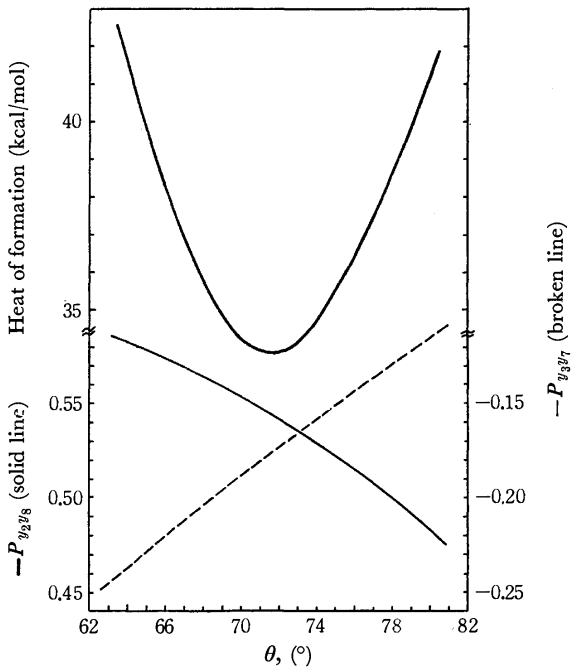

Fig. 2. Heat of formation and bond orders, $P_{y_2y_8}$ (between the $2p_y$ orbitals of C_2 and C_8, the y axis being in the direction $\overrightarrow{C_2C_8}$) and $P_{y_3y_7}$, *vs.* θ_1 for **2b**.

Results for Transition State Geometry

The optimized geometries of **2a—c** are collected in Table 2. It is noted that, contrary to the ground state geometry in which the angle between the wings of the divinylmethane moiety ($C_4C_5C_6$) is in the order **1a**< **1b**<**1c**, θ_1 defined as the dihedral angle between the two allylic planes is almost constant at 72° throughout the transition states **2a—c**. Their C_2C_8 (=C_4C_6) distances differ by not more than 1%. The result suggests that the energy of the transition states **2a—c** basically does not differ. The mode in which the total molecular energy depends on the dihedral angle θ_1 is illustrated in Fig. 2 It is apparent that the potential energy curve is considerably steep on both sides of the equilibrium geometry. A bond population analysis reveals that the energy minimum is reached as a result of an intricate balance between the bonding interaction of both termini of the biallylic systems which stabilizes the transition state to a greater extent as θ_1 decreases and the anti-bonding interaction of the *p*-orbitals on C_3 and C_7 which destabilizes the internal energy. To the latter has to be added the strain energy produced in the angle $C_2C_1C_8$ and $C_4C_5C_6$ as θ_1 decreases. A similar argument based on the simple Hückel approximations has been proposed by Fukui and Fujimoto for preference to the chair-like conforma-

11) E. Goldish, *J. Chem. Educ.*, **36**, 408 (1959).

tion of the transition state for the Cope rearrangement,[12] while Woodward and Hoffmann explained the effect in terms of the orbital symmetry.[13] This orbital repulsion effect first suggested by Doering and Roth[14] also explains why the carbon atoms 3 and 7 tend to be out of the planes defined by $C_1C_2C_4C_5$ and $C_5C_6C_8C_1$, respectively, in the equilibrium geometries of **2**. The average deviation of 6° seems enough to bring the distance between C_3 and C_7 apart without suffering from loss of total conjugative stabilization energy in each allylic group and from strain produced in the ring systems.

Table 3. Heats of formation and strain energies of the homotropilidenes **1a—c** calculated by the MINDO methods

	Heats of formation (kcal/mol)			Strain energies (kcal/mol)
	MINDO/2	MINDO/1	Franklin's group additivity	
1a	27.1	53.0	33.3	19.7
1b	15.5	37.2	28.4	8.8
1c	38.4	52.8	52.3	0.5

Results for Heat of Formation and Charge Distribution of the Ground States 1a—c

Heats of formation corresponding to the equilibrium geometries optimized by the MINDO/2 method and given in Table 1 are listed in Table 3. Border *et al.* reported a value of 42.0 kcal/mol by applying the MINDO/2 method to the observed geometry of bullvalene.[15] The energy minimization along the line outlined in the previous section resulted in heat of formation of 38.4 kcal /mol for bullvalene with the normal 1.51 Å for the C–C bond length of the cyclopropane ring.

In the third column of Table 3 are given heats of formation calculated by the MINDO/1 version on the geometries of the same bond angles determined by the MINDO/2 method. Bond lengths are, however, shifted from the optimized ones to the standard values originally proposed by Baird and Dewar.[6] The MINDO/1 method is considered to give better results as far as heat of formation is concerned.[6,7]

By applying Franklin's group additivity method,[16] heats of formation were estimated for the ideal strain-free molecules corresponding to **1a—d**. The difference between the molecular energies obtained by the MINDO/1 method and those computed by Franklin's method can be regarded to give good estimate for the strain energy of these hydrocarbons.

The charge distributions and resultant dipole moments for the homotropilidenes **1a—c** calculated by the two MINDO methods are summarized in Table 4.

Results for Heat of Formation and Charge Distribution of the Transition States 2a—c

The optimized heats of formation of the biallylic structures **2a—c** representing to the transition states for the Cope rearrangement are listed in Table 5. For the MINDO/1 predictions of the transition state energies, ambiguity remains in the choice of the C_2C_3 bond length. Although it should not be far from 1.40 Å optimized by the MINDO/2 version, we do not know which length will give most accurate heats of formation by the MINDO/1 parametrization.[6] In Fig. 3 is illustrated how heats of formation predicted by the MINDO/1 method depend

Table 4. Electron densities and the resultant dipole moments of **1a—c** determined by the MINDO methods

Atom	**1a**		**1b**		**1c**	
	MINDO/1	MINDO/2	MINDO/1	MINDO/2	MINDO/1	MINDO/2
C_1	3.997	4.018	3.976	3.995	3.917	3.954
C_2	3.905	3.940	3.917	3.951	3.917	3.954
C_3	3.987	4.020	3.972	4.006	3.964	3.993
C_4	3.991	3.995	3.990	4.009	3.993	4.015
C_5	3.864	3.921	3.880	3.924	3.845	3.905
C_9	—	—	3.827	3.924	3.993	4.015
H_1	1.045	1.013	1.047	1.020	1.068	1.029
H_2	1.064	1.029	1.066	1.030	1.068	1.029
H_3	1.038	1.014	1.039	1.011	1.048	1.016
H_4	1.021	1.006	1.043	1.015	1.035	1.011
H_5	1.081	1.039	1.065	1.033	1.080	1.039
H_9	—	—	1.076	1.030	1.035	1.011
	Dipole moments					
Point charge	0.216	0.071	0.131	0.179	0.155	0.172
Hybridization	0.096	0.141	0.105	0.074	0.181	0.146
Sum	0.310	0.137	0.026	0.192	0.026	0.318

12) K. Fukui and H. Fujimoto, *Tetrahedron Lett.*, **1966**, 251.
13) R. B. Woodward and R. Hoffmann, "Conservation of Orbital Symmetry," Academic Press, New York, N. Y., 1970, p. 148.
14) W. von E. Doering and W. R. Roth, *Tetrahedron*, **18**, 67 (1962); *Angew. Chem.*, **75**, 27 (1963).
15) N. Bordor, M. J. S. Dewar and S. D. Worley, *J. Amer. Chem. Soc.*, **92**, 19 (1970).
16) J. L. Franklin, *Ind. Eng. Chem.*, **41**, 1070 (1949).

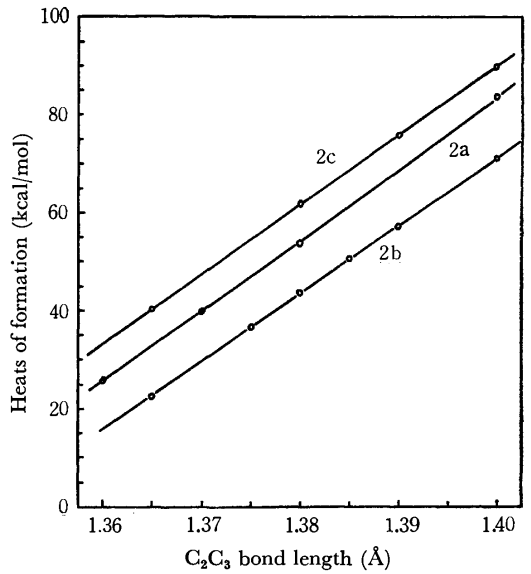

Fig. 3. Dependence of heats of formation by the MINDO/1 method on the C_2C_3 bond length in **2a**—**2c**.

on the C_2C_3 bond length. Although the curves show neither minima nor maxima in the region in question, it is noted that the difference in heats of formation between **2a**—**c** is independent of the choice of the C_2C_3 bond lengths. The numerical values of heat of formation arbitrarily obtained at the intercept of the curves in Fig. 3 at $C_2C_3=1.38$ Å are listed in the third column of Table 5.

Franklin's group additivity method is now employed to calculate the heats of formation of X part of **2a**—**c**,

Table 5. Heats of formation of the transition states **2a**—**c** for the Cope rearrangement

	MINDO/2	Heats of formation (kcal/mol)	
		MINDO/1 ($C_2C_3=1.38$ Å)	Biallyl moiety
2a	45.4	53.6	53.6
2b	33.8	43.9	48.8
2c	64.8	61.9	42.9

they are 0, −4.9, and 19.0 kcal/mol, respectively. By subtracting the latter from the heats of formation predicted by the MINDO/1 method, the partial molecular energies due to the biallylic portion of **2a**—**c** are estimated.

In view of the similar distances between the two allylic moieties in **2a**—**c** as listed in Table 2, we assume that the stability derived from resonance coupling between the two allylic portions does not differ much in **2a**—**c**. A slight difference in stability which is in the order **2a**<**2b**<**2c** in the last column of Table 5 can be attributed to varieties in the strain energy due to the deformation of the "sp^2" hybridized carbon atoms, C_2, C_3, and C_4 in the transition states.

The electron densities and the resultant dipole moments for the transition states **2a**—**c** calculated by the two versions of the MINDO methods are summarized in Table 6.

Discussion on the Origin of Different Activation Energy for Values the Cope Rearrangement

We now arrive at the theoretical activation energy for the Cope rearrangement of the bridged homotropilidenes by comparing the heats of formation of the ground states **1a**—**c** with those of the transition states **2a**—**c**. The results are shown in Table 7. Note that the MINDO/1 method reproduces almost quantitatively the activation energies for the rearrangement. A satisfactory agreement is not unexpected since it is generally accepted that special effort is made during parametrization of the MINDO/1 approximation towards the reproduction of heats of formation.[6] The results of the MINDO/2 approximation are on the contrary less quantitative, and the deviation might be due to underestimation of the strain energy of the cyclopropane ring; the calculated heat of formation of cyclopropane is 3.8 in marked contrast to the observed 12.7 kcal/mol.[6,7] Thus the heats of formation of **1a**—**c** are underestimated relative to **2a**—**c** which have no such strain, with the consequent elevation in the calculated activation energies by the MINDO/2 method.

Satisfactory reproduction of the activation energies

Table 6. Electron densities and the resultant dipole moments of **2a**—**c** determined by the MINDO methods

Atom	**2a**		**2b**		**2c**	
	MINDO/1	MINDO/2	MINDO/1	MINDO/2	MINDO/1	MINDO/2
C_1	3.889	3.953	3.892	3.948	3.866	3.942
C_2	3.985	3.980	3.987	3.978	3.972	3.962
C_3	3.976	4.037	3.964	4.042	3.974	4.050
C_9	—	—	3.832	3.921	3.971	3.996
H_1	1.069	1.021	1.054	1.023	1.083	1.039
H_2	1.029	1.010	1.044	1.018	1.039	1.011
H_3	1.037	1.008	1.039	1.006	1.056	1.021
H_9	—	—	1.072	1.029	1.028	1.006
			Dipole moments			
Point charge	0.378	0.455	0.893	0.699	1.090	0.584
Hybridization	0.731	0.813	0.919	0.753	1.000	0.889
Sum	0.353	0.359	0.026	0.054	0.090	0.305

Table 7. Activation energy for the Cope rearrangement

	Activation energy (kcal/mol)		
	MINDO/1	MINDO/2	obsd
Semibullvalene (**1a**)	0.6	18.3	<5[3]
Barbaralane (**1b**)	6.7	18.3	8.76[2,17]
Bullvalene (**1c**)	9.1	25.4	11.8[18]

by the present SCF MO calculations is surprising in view of the fact that the experimental data are obtained in the condensed phase while the calculation is applied to the isolated molecules in a vacuum. Success can partly be ascribed to special situation where there is no significant deviation of electric charge from even distribution in **1a**—**c** as well as in **2a**—**c** (Tables 4 and 5).

From the NMR spectral behavior of **1a**, it could be postulated that semibullvalene might have the mesovalent structure **2a**.[3] However, this can be easily ruled out by the normal UV spectrum of **1a**.[3] It is supported on theoretical ground that semibullvalene has no such novel bonding but only facile Cope rearrangement. Recently, Anet obtained the value of 6.4 kcal/mol as the activation energy for the Cope rearrangement of the octamethyl derivative of **1a**.[19] The effect of methyl substitution in enhancing or retarding valence isomerization is not uncommon. Complete thermal conversion from cyclooctatetraene to semibullvalene can be achieved only when they are fully methylated,[20] while the interconversion is less efficient in the tetramethyl derivatives.[21] No effort has so far been successful in the parent semibullvalene. In the present case, the effect of the methyl substitution can be rationalized by considering a greater planarity of the five membered ring of C_1 through C_5 in the transition state than in the ground state; the eclipsing methyl groups are sterically more demanding than the more or less staggered orientation.

With respect to the origin of different acitvation energies for the Cope rearrangement of these bridged homotropilidenes,[22] we note from Table 3 and 5 that the strain energies in the ground state are sharply in the order **1a**>**1b**>**1c**, while those of the transition state are moderately in the order **2a**>**2b**>**2c**. Thus it is concluded that one of the possible factors contributing to the different activation energies stems from the strain energies of the ground state of these hydrocarbons. We see from Table 1 and 2 that the bond between carbons 4 and 6 ($=C_2C_8$) in the transition states is conventionally represented by the dotted line, and the bond index is easily expected to be one half; the calculated values by the MINDO/2 methods are 0.46, 0.45, and 0.45 for **2a**, **2b**, and **2c**, respectively. The corresponding values in the ground states, **1a**, **1b**, and **1c**, are 0.06, 0.03, and 0.01, respectively. Although no strict proportionality holds *a priori* between bond indices and bond formation, we can say as a first approximation that the Cope rearrangement has already taken place *ca.* 13% ($=0.06/0.46\times100$) in **1a** to the forward direction of the reaction coordinate. The effect is less pronounced in **1b**, and almost negligible in **1c**.[22]

The authors are indebted to the Ministry of Education for financial support of this work.

17) W. von E. Doering, B. M. Ferrier, E. T. Fossel, J. H. Hartenstein, M. Jones, Jr., G. Klumpp, R. M. Rubin, and M. Saunders, *Tetrahedron*, **23**, 3943 (1967).
18) M. Saunders, *Tetrahedron Lett.*, **1963**, 1699.
19) *Cf.* footnote 2(a) in L. Birladeanu, D. L. Harris, S. Winstein, *J. Amer. Chem. Soc.*, **92**, 6387 (1970).
20) R. Criegee and R. Askani, *Angew. Chem.*, **80**, 531 (1968).
21) H. E. Zimmerman and H. Iwamura, *J. Amer. Chem. Soc.*, **92**, 2015 (1970).
22) During preparation of this manuscript, Dewar and Schoeller (*J. Amer. Chem. Soc.*, **93**, 1483 (1971)) reported in a brief note on a similar theoretical result.

The Photochemical Reaction of α-Diketones

Kazuhiro MARUYAMA,* Keiichi ONO, and Jiro OSUGI

**Department of Chemistry, College of Liberal Arts and Science, Kyoto University, Kyoto*
Department of Chemistry, Faculty of Science, Kyoto University, Kyoto

(Received July 5, 1971)

The relative photochemical reactivity of α-diketones, in particular, 9,10-phenanthraquinone, 1,2-naphthoquinone, acenaphthoquinone, benzil, 4,4′-dimethylbenzil, 2,4,6-trimethylbenzil, 2,5,2′,5′-tetramethylbenzil, 2,3,5,6-tetramethylbenzil, 2,4,6,2′,4′,6′-hexamethylbenzil, phenylglyoxal, 2,5-dimethylphenylglyoxal, and 2,4,6-trimethylphenylglyoxal was investigated in hydrogen donating solvents. Type of the product and relative reactivity differ widely according to the structure of α-diketones. Whereas 9,10-phenanthraquinone gives 1,4-adduct (V) in a hydrogen donating solvent (THF), 2,5,2′,5′-tetramethylbenzil gives 2-hydroxy-2-(2′,5′-dimethylphenyl)indanone (VII) *via* intramolecular hydrogen abstraction in nearly quantitative yield. No photochemical reaction of 2,4,6-trimethylbenzil or 2,3,5,6-tetramethylbenzil could be observed in the same solvent even under a long irradiation.

The photochemical reaction of α-diketones has been studied under various reaction conditions since Klinger.[1] Vapor phase photolysis of biacetyl or hexafluorobiacetyl yields products formed by cleavage of the carbon-carbon bond between two carbonyl groups. However, when *o*-quinones are irradiated in solution in the presence of a hydrogen donor, the resulting products can almost invariably be rationalized taking consideration the mechanistic pathway involving the initial hydrogen abstraction by photo-excited *o*-quinone *via* $n\rightarrow\pi^*$ excitation. As an example, camphorquinone[2] in methanol and 2-propanol gives products derived from initial hydrogen abstraction from the solvent, and 9,10-phenanthraquinone yields 1,2-adduct or 1,4-adduct corresponding to the structure of the sovent when it is irradiated in solution.[3] On the contrary, benzil in cyclohexane gives benzaldehyde formed by cleavage of the carbon-carbon bond between the two carbonyl groups. The present study was undertaken with the aim of elucidating the relationship between reactivity and the structure of α-diketones. 9,10-Phenanthraquinone, 1,2-naphthoquinone, acenaphthoquinone, benzil, methyl substituted benzils and methyl substituted glyoxals have been studied.

Results and Discussion

Reaction Products. Irradiation of 1,2-naphthoquinone in 2-propanol in the absence of oxygen led to an unstable white product identified to be naphthalene-1,2-diol (I). Similarly irradiation of acenaphthoquinone in tetrahydrofuran(THF) in the absence of oxygen give a white product (II) formed by photo-addition. However, in the presence of oxygen, acenaphthoquinone in THF gave naphthalene-1,8-dicarboxylic acid anhydride (III), when it was irradiated. Presumably the first step for the production of this anhydride may be hydrogen abstraction from the solvent resulting in the formation of semiquinone radical, which may react with oxygen to give III according to Scheme 2. Rubin and Zwitkowits reported on the photochemical reaction of phenanthraquinone in some hydrogen donating solvents.[3] They stated that phenanthraquinone reacted with solvents produced 1,2-adduct or 1,4-adduct in the absence of oxygen. Irradiation of phenanthraquinone in mesitylene and in THF gave the corresponding 1,2-adduct (IV) and 1,4-adduct (V), respectively. Relative hydrogen abstraction rate of photo-excited phenanthraquinone in several hydrogen donating solvents have been reported.[4] Recently the reactions have been extensively reinvestigated and their radical nature was confirmed using CIDNP technique.[5] The *o*-quinones unexceptionally abstract hydrogen from the solvent in the first stage of the reaction. The photochemical behavior of benzil, however, differs from that of the *o*-quinones and the principal products in cyclohexane are benzoic acid, benzaldehyde, phenyl cyclohexyl ketone and benzoin.[6]

We have studied in detail the photochemical reaction of benzil and its methyl substituted derivatives, *viz.* 2,5,2′,5′-tetramethylbenzil, 2,4,6-trimethylbenzil, 2,3,5,6-tetramethylbenzil, 2,4,6-trimethylphenylglyoxal, 2,4,6,2′,4′,6′-hexamethylbenzil, and 4,4′-dimethylbenzil. The reaction products are shown in Scheme 1. Irradiation of benzil in THF (in the absence of oxygen) gave a mixture of products containing benzaldehyde, a small amount of benzoin and unidentified products. 2,5,2′,5′-Tetramethylbenzil gave a white product (VII) 2-hydroxy-2-(2′,5′-dimethylphenyl)indanone, *via* intramolecular hydrogen abstraction accompanying 2,5-dimethylbenzaldehyde (VI) when it was irradiated in THF in the absence of oxygen (Scheme 3). In benzene, carbon tetrachloride, or cumene no 2,5-dimethylbenzaldehyde was obtained but product (VII) was exclusively obtained in a nearly quantitative yield. Both 2,4,6,2′,4′,6′-hexamethylbenzil and 2,4,6-trimethylphenylglyoxal dissolved in THF gave 2,4,6-trimethylbenzoic acid as the main product when they were irradiated. Possibly, this acid is formed by the autoxidation of the

1) H. Klinger, *Ber.*, **19**, 1862 (1886).
2) B. M. Monroe and S. A. Weiner, *J. Amer. Chem. Soc.*, **91**, 450 (1969).
3) M. B. Rubin, *J. Org. Chem.*, **28**, 1949 (1963); M. B. Rubin and P. Zwitkowits, *ibid.*, **29**, 2362 (1964).
4) K. Maruyama, K. Ono, and J. Osugi, This Bulletin, **42**, 3357 (1969).
5) K. Maruyama, H. Shindo, and T. Maruyama, *ibid.*, **44**, 585 (1971); K. Maruyama, H. Shindo, T. Otsuki, and T. Maruyama, *ibid.*, **44**, 2756 (1971); H. Shindo, K. Maruyama, T. Otsuki, and T. Maruyama, *ibid.*, **44**, 2789 (1971); K. Maruyama, T. Otsuki, H. Shindo, and T. Maruyama, *ibid.*, **44**, 2000 (1971).
6) D. L. Bunburg and C. T. Wang, *Can. J. Chem.*, **46**, 1473 (1968).

resulting 2,4,6-trimethylbenzaldehyde in the course of separating procedures.[7] However, both 2,4,6-trimethylbenzil and 2,3,5,6-tetramethylbenzil were extremely photo-stable and did not change after being irradiated for over a week.

Determination of Quantum Yields. The quantum yields for the disappearance of α-diketones are shown in Table 1. It has been reported that the quantum yield for the photo-reduction of camphorquinone is very low.[2] On the other hand, the quantum yield of 1,2-naphthoquinone or 9,10-phenanthraquinone was nearly unity. These reactions are characteristic in that the photo-reduction with the solvent acts as a hydrogen donor. The reaction mechanism can be described by the following equations, where Q^s and Q^t are excited singlet and triplet states, respectively and AH the hydrogen donor.

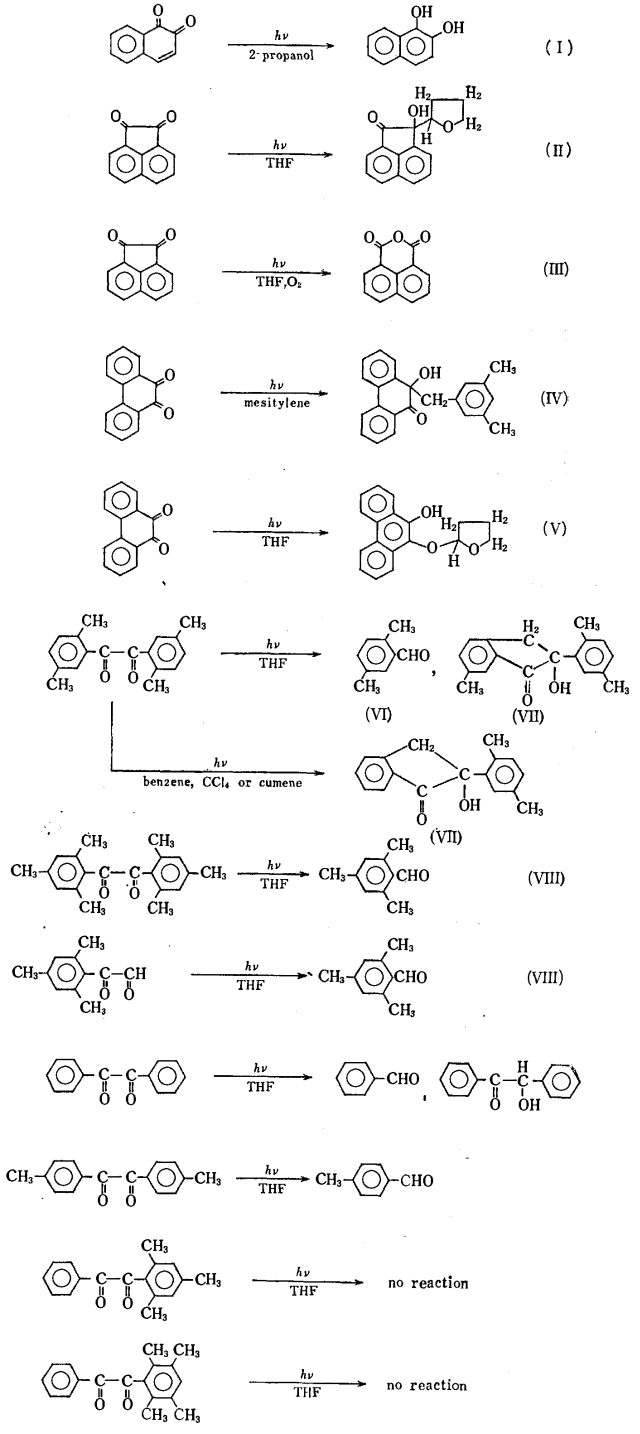

Scheme 1.

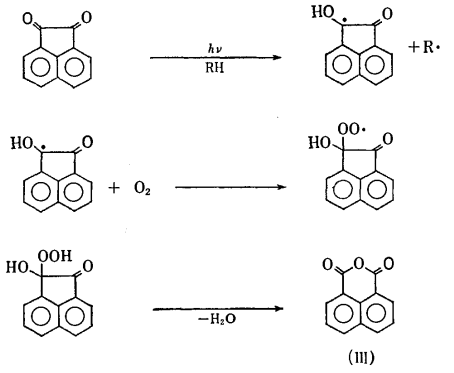

Scheme 2.

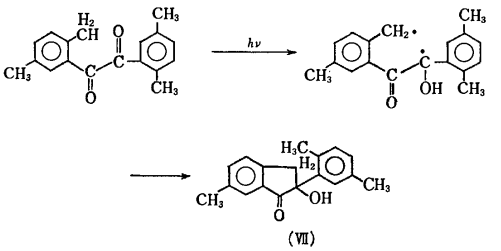

Scheme 3.

TABLE 1. QUANTUM YIELDS OF THE DISAPPEARANCE OF α-DIKETONES IN THF (EXCITING LIGHT: 3640 Å, TEMPERATURE: 25°C)

α-Diketone	Quantum yield	Condition
1,2-Naphthoquinone	1.00	Degassed
9,10-Phenanthraquinone	0.86	Degassed
Acenaphthoquinone	0.75	In the air
Camphorquinone	0.057 (2-propanol)	Degassed
	0.018 (methanol)	Degassed
Benzil	0.85	In the air
2,5,2′,5′-Tetramethylbenzil	1.30	In the air
2,4,6-Trimethylbenzil	<0.02	In the air

Light intensity was determined by a potassium ferrioxalate actinometer.

$$Q^s \longrightarrow Q^t \quad (1)$$

$$Q^t \xrightarrow{k_d} Q \quad (2)$$

$$Q^t + AH \xrightarrow{k_r} QH + A \quad (3)$$

$$QH + A \longrightarrow QHA \quad (4)$$

$$A + A \longrightarrow A_2 \quad (5)$$

If the quantum yield for intersystem crossing is unity, the quantum yield for the disappearance of *o*-quinone is given by

$$\Phi = \frac{k_r[AH]}{k_r[AH]+k_d} \quad (6)$$

7) Methyl substituted benzaldehyde can be oxidised rapidly in the air.

The quantum yield for intersystem crossing of camphorquinone is known to be nearly unity[2] and the life time of its triplet state is similar to those of the other *o*-quinones.[8] Therefore, the difference in the quantum yield of 1,2-naphthoquinone or 9,10-phenanthraquinone and camphorquinone seems to be caused by the difference in the nature of the triplet state. The radical oxygen atom of 1,2-naphthoquinone or 9,10-phenanthraquinone in the photo-excited $n\rightarrow\pi^*$ triplet state should be more electrophilic than that of camphorquinone, for in the former the excited electron to π-orbital may be delocalized entirely on the rest of the molecule.[4] Thus, the $n\rightarrow\pi^*$ triplet state of the 1,2-naphthoquinone or 9,10-phenanthraquinone could be a better hydrogen abstractor.

Table 2. Electronic spectra of α-diketones $n\rightarrow\pi^*$ transition (solvent: THF, room temperature)

α-Diketone	λ_{max} (mμ)
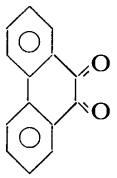	500
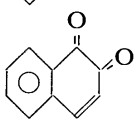	520
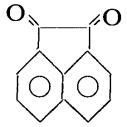	493
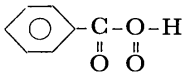	420
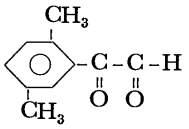	415
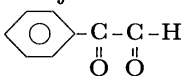	440
OHC·CHO	450
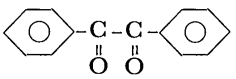	370, 388
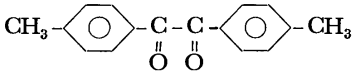	364, 382
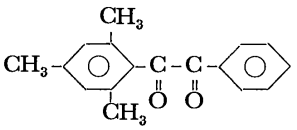	410
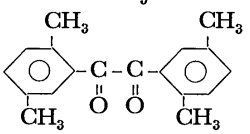	390 (Broad)
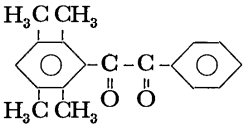	420
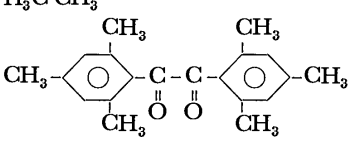	470, 498
$CH_3COCOCH_3$	415—440

8) A. Kuboyama and S. Yabe, This Bulletin, **40**, 2475 (1967).

Thus, we can conclude reasonably that 2,5,2′,5′-tetramethylbenzil or 4,4′-dimethylbenzil has twisted

Photochemical Behavior of Benzil Derivatives. The photochemical behavior of benzil derivatives is more complicated than that of *o*-quinones. Both photo-decomposition and photo-reduction take place at the same time, and in some cases phto-decomposition become the main reaction. Moreover, 2,4,6-trimethylated or 2,3,5,6-tetramethylated benzil derivatives are extremely photo-stable even in THF. We inspected the structural features using UV and PMR techniques and tried to discuss the relationship between the structure and the photochemical behavior of benzil derivatives. The wave lengths of maximum absorption of $n\rightarrow\pi^*$ transition are shown in Table 2 and the chemial shifts of methyl protons of the derivatives in Table 3. Leonard and Blout[9] concluded from the measurement of absorption spectra that non-substituted benzil had a skew structure as shown in Fig. 1 and 2,4,6,2′,4′,6′-hexamethylbenzil had a *trans* planar structure as shown in Fig. 2.

Table 3. PMR chemical shifts of methyl protons of benzil derivatives (room temperature)

Benzil derivative	τ-Values *o*-CH	*m*-CH	*p*-CH
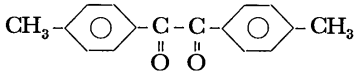			7.59
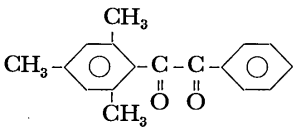	7.68		7.62
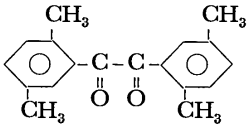	7.24	7.53	
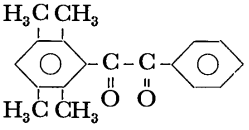	7.85	7.69	
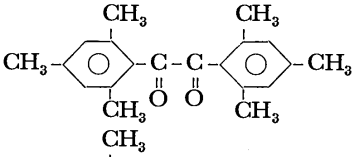	7.87		7.75
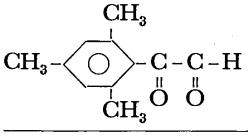	7.86		7.71

60 MHz PMR spectrometer was used.

9) N. J. Leonard and E. R. Blout, *J. Amer. Chem. Soc.*, **72**, 484 (1950).

form around the carbon-carbon bond of the two carbonyl groups like that of non-substituted benzil. As shown in Table 3 τ-values of *meta* or *para* methyl protons (to carbonyl group) remain almost unchanged, but those of *ortho* methyl protons vary in the range $\tau=$ 7.24—7.87. The differences seem to depend on the magnetic anisotropy of carbonyl group. The plane of the two carbonyl double bond and that of the mesityl ring of 2,4,6,2′,4′,6′-hexamethylbenzil would be perpendicular (Fig. 2), but in 2,5,2′,5′-tetramethylbenzil the plane of the dimethylphenyl and the adjacent carbonyl might be nearly co-planar (Fig. 1). Thus, the *ortho* methyl protons of the former might be affected most effectively by the magnetic shielding effect of the carbonyl group. On the other hand, that of the latter is under the influence of the magnetic deshielding effect.

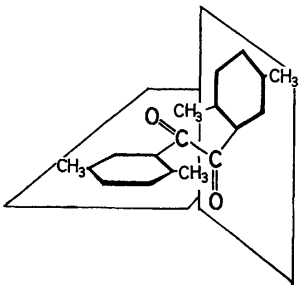

Fig. 1. Skew structure of benzil derivatives.

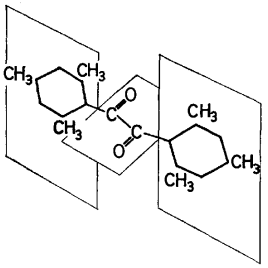

Fig. 2. Trans planar structure of benzil derivatives.

Whereas benzil, 2,5,2′,5′-tetramethylbenzil and 4,4′-dimethylbenzil dissolved in THF react fast in the absence of oxygen, 2,4,6-trimethylbenzil or 2,3,5,6-tetramethylbenzil dissolved in THF remains almost unreacted after a long irradiation over a week. 2,4,6,2′,4′,6′-Hexamethylbenzil reacts slowly. The quantum yields for the photo-reaction of methylated benzils in the presence of oxygen are given in Table 1. We see that 2,4,6-trimethylbenzil or 2,3,5,6-tetramethylbenzil is very unreactive compared with benzil or 2,5,2′,5′-tetramethylbenzil in the presence of oxygen as well as in the absence of oxygen.

Comparing the relative intensity of the phosphorescence of these benzils qualitatively, benzil or 2,5,2′,5′-tetramethylbenzil shows intense phosphorescence in contrast to 2,4,6-trimethylbenzil, 2,3,5,6-tetramethylbenzil, or 2,4,6,2′,4′,6′-hexamethylbenzil, which shows extremely weak phosphorescence. The lifetime of triplet state of benzil and 2,5,2′,5′-tetramethylbenzil in MMA plastic[10] are 0.20 msec and 0.65 msec, respectively, at room temperature, but in the case of 2,4,6-trimethylbenzil, 2,3,5,6-tetramethylbenzil, or 2,4,6,-2′,4′,6′-hexamethylbenzil no T–T, absorption of these benzils could be observed.

Thus, we might consider that the quantum yield for the intersystem crossing of 2,4,6-trimethylbenzil and 2,3,5,6-tetramethylbenzil are strikingly small. These benzil derivatives should be strongly photo-resistive.[11] However, there may be the other possibilities which are remained to be clarified in future. We next examined the solvent effects on the photochemical reactions. The reaction rate of non-substituted benzil showed a remarkable solvent effect. In non-polar solvents such as benzene, toluene, or *n*-hexane, benzil, 4,4′-dimethylbenzil, and 2,4,6,2′,4′,6′-hexamethylbenzil were less reactive than in polar solvents such as THF, *N,N*-dimethylformamide, ether, or methanol, whereas 2,5,-2′,5′-tetramethylbenzil was equally reactive in the polar or non-polar solvents. Qualitative comparison of the relative reactivity of these benzils is given in Table 4.

TABLE 4. RELATIVE REACTIVITY OF α-DIKETONES IN SEVERAL SOLVENTS (LIGHT SOURCE: 400W HIGH PRESSURE Hg LAMP, ROOM TEMPERATURE)

α-Diketones	Qualitative rates in several solvents
Benzil	THF, methanol, DMF, ether $\gg$ benzene, toluene, *n*-hexane
4,4′-Tetramethylbenzil	methanol $\gg$ benzene, *n*-hexane
2,4,6,2′,4′,6′-Tetramethylbenzil	THF $\gg$ benzene
2,5,2′,5′-Tetramethylbenzil	THF, methanol, benzene, toluene, *n*-hexane (reacts fast in all solvents)
2,4,6-Trimethylbenzil	THF, methanol, benzene (does not react in all solvents)

These phenomena seem to be ascribed to the cage effect of solvent for the carbonyl-carbonyl bond scission. However, 2,5,2′,5′-tetramethylbenzil is reactive in non-polar as well as polar solvents. The carbonyl group and the *ortho* methyl proton of this benzil derivative should be positioned very close and nearly overlapping. Consequently VII might be produced *via* intramolecular hydrogen abstraction fairly easily even in the non-polar solvents. On the other hand, 2,4,6-trimethylbenzil and 2,3,5,6-tetramethylbenzil are unreactive in the polar or non-polar solvents. The cause of the low quantum yield for the intersystem crossing of these benzil derivatives remains to be explained. However, it does not seem incidental that these photochemically unreactive benzil derivatives are antisymmetric and the mean value of the dihedral angle between the two carbonyl groups are in the range 90—180°.

Experimental

Materials. 1,2-Naphthoquinone (mp 121—122°C), acenaphthoquinone (decomp. 242°C), and 9,10-phenathraquinone (mp 204°C) were prepared by the oxidation of 2-amino-1-naphthol, of acenaphthene, and of phenanthrene with suitable oxidizing agents. 2,5,2′,5′-Tetramethylbenzil (mp 113—114°C), 2,4,6,2′,4′,6′-hexamethylbenzil (mp 120—121°C), 2,4,6-trimethylbenzil (mp 135°C) and 2,3,5,6-tetramethylbenzil (mp 62—63°C) were prepared by the air-oxidation of the corresponding benzoins[12] produced by the condensation of the corresponding glyoxals with suitable methylated benzenes.[13] Benzil (mp 94—95°C) and 4,4′-dimethylbenzil (mp 104—105°C) were prepared by the oxidation of the corresponding benzoins produced by the benzoin condensation of benzaldehyde and *p*-tolualdehyde.

Irradiation of α-Diketones. A typical photo-reaction was performed as follows. A known amount of α-diketone

10) methyl metacrylate

11) 2,4,6,2′,4′,6′-Hexamethylbenzil reacts very slowly.

12) "Organic Syntheses," Coll. Vol. II, p. 509 (1948); "Organic Reaction," Vol. 4, p. 269.

13) "Organic Syntheses," Coll. Vol. I, p. 87 (1948).

(usually 1/100—1/1000 mol) dissolved (or suspended) in a solvent (20—100 m*l*) was irradiated in an ordinary glass tube through 5 cm thick of water layer from a light source (400W high-pressure Hg-lamp). Change of the substrate was followed spectroscopically. A reaction vessel fitted with a cell for spectroscopic measurement was used for the experiments under degassed conditions.

Analyses of Photochemical Products. 1,2-Dihydroxynaphthalene(I): After the characteristic orange color of 1,2-naphthoquinone dissolved in 2-propanol faded to pale yellow, 2-propanol was evaporated under reduced pressure. The resulting dark orange colored solid was extracted with *n*-hexane. Removal of *n*-hexane left unstable white crystal which changes easily to the corresponding quinhydrone in the air, mp 59—60°C, IR: ν_{OH}=3340—3360 cm^{-1}.

1-Hydroxy-1-α-tetrahydrofuranyl-8-oxoacenaphthene(II): 1,8-Acenaphthoquinone dissolved in THF was irradiated in the absence of oxygen. After two days irradiation the solvent was removed under reduced pressure, and the resulting reddish oil was extracted with petrol ether, and then colorless crystal was obtained, mp 217—223°C (decomp), (yield 80%). Elemental analysis: $C_{16}H_{14}O_3$; Found, C: 75.61%, H: 5.53%; Calculated, C: 75.57%, H: 5.56%.

1,8-Dinaphthoic acid anhydride(III): After the orange yellow color of acenaphthoquinone faded to pale yellow, removal of THF as solvent left a pale yellow solid which was recrystallized from ether. Colorless crystal, mp 273—276°C, $\nu_{C=O}$; 1730, 1770 cm^{-1}. Elemental analysis; Found, C: 72.79%, H: 3.07%, Calculated, $C_{12}H_6O_3$, C: 72.75%, H: 3.13%.

9-Hydroxy-9-(3',5'-dimethylbenzyl)-10-oxo-9,10-dihydrophenanthrene(IV): After 9,10-phenanthraquinone suspended in mesitylene was irradiated for two days, the unreacted mesitylene was removed under reduced pressure. The resulting viscous oil was rinsed with petrol benzene several times, and then yellow crystals were crystallized out, mp 125—126°C, ν_{OH}: 3470 cm^{-1}, $\nu_{C=O}$: 1690 cm^{-1}, $\tau_{m\text{-}CH_3}$: 7.83, $\tau_{\text{-}CH_2\text{-}}$: 7.15, τ_{OH}: 6.20, (yield: 75%). Elemental analysis; Found, C: 82.20%, H: 6.21%, Calculated, $C_{23}H_{17}O_2$, C: 84.93%, H: 5.26%.

9-(10-Hydroxy)phenanthrenyl α-tetrahydrofuranyl ether (V): *i.e.*, 1,4-adduct of 9,10-phenanthraquinone with THF; after 9,10-phenanthraquinone dissolved in THF was irradiated until it became colorless, removal of unreacted THF left crystals which were recrystallized from petrol ether, mp 110—112°C, ν_{OH}: 3250 cm^{-1}, (yield: 80%). Elemental analysis; Found, C: 81.90%, H: 4.48%, Calculated, $C_{18}H_{16}O_3$; C: 81.79%, H: 4.57%.

2-Hydroxy-2-(2',5'-dimethylphenyl)indanone (VII): After 2,5,-2',5'-tetramethylbenzil dissolved in THF (or a suitable solvent) was irradiated for three days under degassed conditions, removal of THF under reduced pressure left heavy viscous oil, which was rinsed with petrol benzene several times. All of the oil then solidified, recrystallized from petrol benzene-benzene, pale yellow crystal, mp 153°C, ν_{OH}: 3390 cm^{-1}, $\nu_{C=O}$: 1705 cm^{-1}, τ_{CH_3}: 7.80, 7.77, 7.55, τ_{OH}: 7.25, $\tau_{\text{-}CH_2\text{-}}$: 6.63, (nearly quantitative yield). Elemental analysis; Found; C: 81.24%, H: 6.75%, Calculated, $C_{18}H_{18}O_2$, C: 81.19%, H: 6.81%. From the mother liquor *2,5-dimethylbenzaldehyde* was isolated after it was treated with aqueous sodium bicarbonate and identified as semicarbazone, mp 217°C. After acidification of the bicarbonate solution a small amount of 2,5-dimethylbenzoic acid was separated, mp 132°C.

2,4,6-Trimethylbenzaldehyde and 2,4,6-trimethylbenzoic acid: After the solution of 2,4,6,2',4',6'-hexamethylbenzil in THF was irradiated for a week, the solution was concentrated and diluted with ether, and then treated with aqueous sodium bicarbonate. From the ethereal solution 2,4,6-trimethylbenzaldehyde was isolated and identified as semicarbazone, mp 184—187°C. After acidification of the sodium bicarbonate extract a fair amount of 2,4,6-trimethylbenzoic acid was isolated, recrystallized from ligroin, mp 153°C, $\nu_{C=O}$: 1690 cm^{-1}, τ_{CH_3}: 7.70, 7.58, τ_{CO_2H}: −2.10.

Benzaldehyde: After benzil dissolved in THF was irradiated under degassed conditions for three days, THF was removed under reduced pressure. The residue dissolved in ether was treated with aqueous sodium bicarbonate and concentrated to a small volume. It was treated with 2,4-dinitrophenylhydrazine hydrochloride solution and then reddish colored crystals were separated, mp 237°C. From a part of the ethereal solution, benzoin was isolated identified by the mp 137°C.

p-*Tolualdehyde*: After the usual treatment of irradiated solution of 4,4'-dimethylbenzil in THF *p*-tolualdehyde was identified to be its 2,4-dinitrophenylhydrazone, mp 232—232°C.

Determination of Quantum Yields and Lifetime of Triplet State. A known amount of an α-diketone was dissolved in THF and irradiated with 400 W high-pressure Hg-lamp through a UV-cut filter (Toshiba VY-42) under the conditions indicated in Table 1. The light intensity was determined with a potassium ferrioxalate actinometer. The lifetime of triplet state of benzil derivatives was determined as follows. Benzil derivatives dissolved in MMA plastic were irradiated by flash method, and the decay of phosphorescence was followed oscillographically. T–T' absorption was also observed spectroscopically through the further activation of triplet state thus attained with a tungsten-lamp.

The Photochemical Reduction of Nitrobenzene and Its Reduction Intermediates. XI. The Photochemical Reduction of Azobenzene in Isopropyl Alcohol[1]

Shizunobu HASHIMOTO and Koji KANO

Department of Applied Chemistry, Doshisha University, Kamikyo-ku, Kyoto

(Received July 9, 1971)

The photochemical reduction of azobenzene in isopropyl alcohol has been investigated. The n-π^* transition of azobenzene caused only the *cis-trans* photoisomerization, while the π-π^* transition caused both photoisomerization and photoreduction. The reduction product was hydrazobenzene. The photoreduction was accelerated by a small amount of oxygen and was quenched by 1,3-pentadiene. The photoreduction was sensitized by fluorene and the aromatic carbonyl compounds (benzophenone, benzaldehyde, and acetophenone). These results suggest that the π,π^* excited triplet state (T_2) of azobenzene abstracts a hydrogen atom.

Previous investigations of azobenzene photochemistry have dealt almost exclusively with the photoisomerization,[2] and so little is known about the photoreduction of the aromatic azo compounds. Irick *et al.*[3] have reported that the photolysis of 4-diethylamino-4′-nitroazobenzen in hydrogen-donative alcohols, such as methanol, ethanol, and isopropyl alcohol (IPA), gives the corresponding hydrazo compound with a low quantum yield (Φ=*ca.* 10^{-4}). On the other hand, we have reported in a previous paper[4] that azobenzene is photoreduced in an IPA or acidic IPA solution to afford hydrazobenzene upon irradiation with a high-pressure mercury lamp. However, the photoreduction mechanisms of azobenzene have been uncertain until recently.

Consequently, this study was undertaken in order to clarify the photoreduction mechansims of azobenzene in IPA.

Experimental

Materials. Azobenzene[5] and *para*-substituted azobenzenes[6] were prepared according to the procedures described in the literature. Reagent-grade IPA was distilled prior to use. 1,3-Pentadiene commercially obtained was further purified by distillation (bp 42—45°C). The other materials, commercially obtained, were recrystallized or distilled as required.

Apparatus and Procedures. In most experiments, an immersion-type Taika 130-W high-pressure mercury lamp was used. We took much a care to remove the oxygen in the reaction system, because the hydrazobenzene produced is photooxidized to give azobenzene.[7] That is, the photolysis was carried out in an atmosphere of nitrogen, freed of oxygen by having been passed through a xylene solution of metal ketyl.

Analytical Procedures. The progressive spectral change in azobenzene photochemistry were measured by means of UV spectroscopy (a Hitachi 124 spectrophotometer was used). The primary amines were determined by means of paper chromatography and/or thin-layer chromatography.[8]

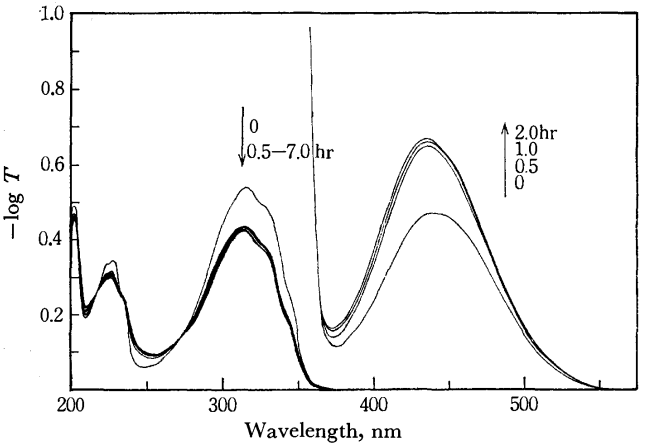

Fig. 1. The progressive spectral change of the photoreaction of azobenzene. For UV spectra measurement, 0.5 m*l* of the photolyzed solution was exactly diluted to 20 m*l* with IPA. The photolyzed solution was directly used as the sample for visible spectra measurement.

Results

Photochemical Reaction of Azobenzene. Figure 1 shows the progressive spectral change during the course of the photolysis of a 1×10^{-2} mol/*l* solution of *trans*-azobenzene in IPA on irradiation with an immersion-type 130-W high-pressure mercury lamp under a nitrogen atomosphere at room temperature. After irradiation, the *trans-cis* photoisomerization proceeded rapidly.[9-11] The formation of *cis*-azobenzene was determined by means of spectroscopy; that is, after the irradiation, the absorption maximum of *trans*-azobenzene at 440 nm in IPA shifted to 435 nm because of the n,π^* excitation of *cis*-azobenzene.[10] *cis*-Azoben-

1) Part X: S. Hashimoto and K. Kano, This Bulletin, **45**, 549 (1972).

2) D. C. Neckers, "Mechanistic Organic Photochemistry," Reinhold Publishing, Co., New York, N. Y. (1967), p. 204.

3) G. Irick, Jr. and J. G. Pacifici, *Tetrahedron Lett.*, **1969**, 1303.

4) S. Hashimoto and K. Kano, *Kogyo Kagaku Zasshi*, **72**, 191 (1969).

5) H. E. Bigelow and D. B. Robinson, "Organic Syntheses," Coll. Vol. III, p. 103 (1955).

6) H. D. Anspon, "Organic Syntheses," Coll. Vol. III, p. 711 (1955).

7) H. Shizuka, H. Kayoiji, and T. Morita, *Mol. Photochem.*, **2**, 165 (1970).

8) S. Hashimoto, K. Kano, and J. Sunamoto, *Kogyo Kagaku Zasshi*, **71**, 864 (1968).

9) G. Zimmerman, L. Chow, and U. Paik, *J. Amer. Chem. Soc.*, **80**, 3528 (1958).

10) S. Yamashita, H. Ono, and O. Toyama, This Bulletin, **35**, 1849 (1962).

11) P. P. Birnbaum and D. W. Style, *Trans. Faraday Soc.*, **50**, 1192 (1954).

zene was also detected by means of thin-layer chromatography. As Fig. 1 shows, the absorption spectra did not change during irradiation after 0.5 hr; this suggests that *cis*- and *trans*-azobenzenes might coexist at equilibrium. Under these conditions, the photoreduction of azobenzene did not proceed; therefore, the initial concentration of *trans*-azobenzene was lowered.

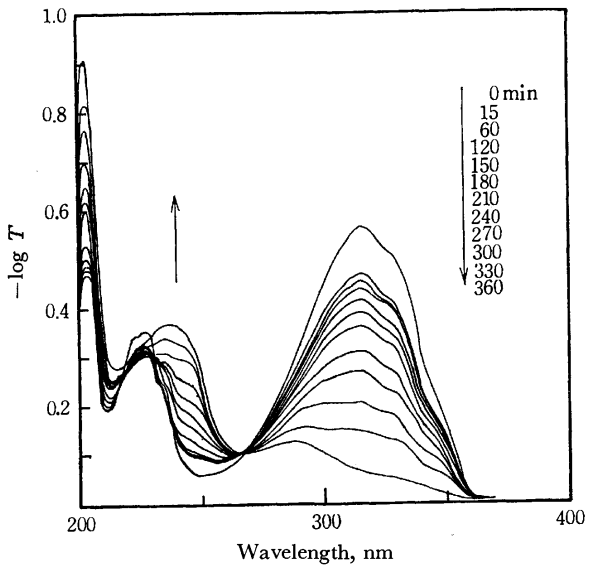

Fig. 2. The progressive spectral change of the photoreduction of azobenzene in IPA.

Figure 2 shows the progressive spectral change during the photolysis of a 5×10^{-4} mol/*l* solution of *trans*-azobenzene in IPA on irradiation under the conditions described above. In this photolysis, the phtoisomerization of azobenzene proceeded in the primary step; then the absorption spectrum of *trans*-azobenzene ($\lambda_{max}=$ 316 nm) decreased progressively in intensity, and a new absorption band with its maximum at *ca.* 242 nm appeared. The new absorption suggested the generation of hydrazobenzene ($\lambda_{max}^{IPA}=242$ nm) as a photoreduction product. When HCl was added to the samples collected after 2 hr, the products of the benzidine rearrangement of hydrazobenzene (benzidine, diphenyline, and aniline)[12] were detected by means of paper chromatography and/or by thin-layer chromatography. This finding supported the idea that a photoproduct of azobenzene was hydrazobenzene.

Effect of Oxygen. The photolysis described above was carried out under an atomosphere of nitrogen which had been freed of oxygen by passage through a xylene solution of metal ketyl; in this case, only the photoisomerization of azobenzene proceeded in an IPA solution when the initial concentration of azobenzene was high (1×10^{-3} mol/*l*). By the way, nitrogen gas commercially obtained contains a small amount of oxygen (*ca.* 1 vol%). Therefore, we studied the effect of oxygen on the photochemistry of azobenzene upon irradiation under an atomosphere of nitrogen containing a small amount of oxygen. The procedures of photolysis were the same to those described above. The initial concentration of *trans*-azobenzene was 1×10^{-3} mol/*l*.

In this reaction, *ca.* 40% of azobenzene was photoreduced to hydrazobenzene after the solution had been irradiated for 8 hr. It was found from this experiment that the rate of the photoreduction of azobenzene was accelerated by a small amount of oxygen.

Meanwhile, when the photolysis was carried out in an air-saturated IPA solution, the photoreduction of azobenzene did not proceed. In this case, it seemed that the photooxidation of hydrazobenzene to azobenzene[7] might proceed or that the triplet state of azobenzene might be quenched by oxygen.

Effect of the Triplet Quencher. The quenching effect on the photoreduction of azobenzene in IPA was investigated by using 1,3-pentadiene as a triplet quencher.

A nitrogen gas was passed into a 5×10^{-4} mol/*l* solution of *trans*-azobenzene in IPA containing 0.4 vol% of 1,3-pentadiene for 1 hr at 0°C. After this procedure, the solution was irradiated with an immersion-type 130W high-pressure mercury lamp at *ca.* 15°C. After 5 hr, the photolyzed solution was analyzed by means of UV spectroscopy. Consequently, it was found that the photoreduction was completly quenched by 1,3-pentadiene and that only the photoisomerization proceeded. In the absence of 1,3-pentadiene, about 13% of the azobenzene was photoreduced to hydrazobenzene upon irradiation under the same conditions. On the basis of the data, it seems reasonable to conclude that the hydrogen abstraction of photoexcited azobenzene proceeds from its triplet state.

The Wavelength Dependence of the Photoreduction of Azobenzene. In the UV spectrum of *trans*-azobenzene in IPA, the n,π^* and π,π^* absorption maxima were observed at 440 ($\varepsilon_{max}=470$) and 316 nm ($\varepsilon_{max}=$

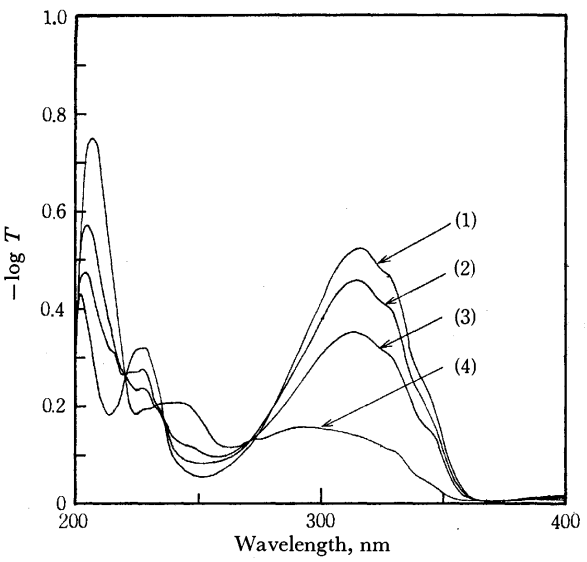

Fig. 3. Wavelength dependence of the photoreduction of azobenzene.
(1): Before irradiation
(2): Irradiation of >420 nm light for 2 hr
(3): Irradiation of a 366 nm light for 1 hr
(4): Irradiation of a 366 nm light for 2 hr

12) H. J. Shine, "Mechanisms of Molecular Migrations," Vol. 1, ed. by B. S. Thyagarajan, Interscience Publishers, New York, N. Y. (1969), p. 191.

2.2×10^4) respectively. Therefore, the reactivity toward the photoreduction of n,π^* and π,π^* excited azobenzene was investigated by using suitable filters.

A 5×10^{-5} mol/l solution of *trans*-azobenzene in a quartz cell (5 cm in diameter and 2 cm in width) was irradiated at wavelengths longer than 420 nm (Toshiba V-Y42 filter) and/or a 366-nm light (Toshiba UV-D2 filter) isolated from a 130W high-pressure mercury lamp under a nitrogen atmosphere at room temperature. The photolyzed solutions were analyzed by means of UV spectroscopy and paper chromatography.

The UV spectra of the photolyzed solutions are shown in Fig. 3. When the solution was irradiated at wavelengths longer than 420 nm, only the *cis-trans* photoisomerization proceeded. However, upon irradiation with a 366-nm light, the azobenzene was photoreduced to hydrazobenzene.

In view of the above facts, it was found that the π,π^* excited triplet of azobenzene abstracted hydrogen atoms.

Photosensitized Reduction of Azobenzene. A 5×10^{-4} mol/l solution of *trans*-azobenzene in IPA containing a photosensitizer (1×10^{-3} mol/l) was irradiated with an immersion-type 130W high-pressure mercury lamp under a nitrogen atmosphere at room temperature. The results obtained are summarized in Table 1.

Table 1. Photosensitized reduction of azobenzene

Sensitizer	E_T[a] kcal/mol	Φ_{ST}[b]	Sensitization	Quenching	Time required for 100% conversion, hr
—	—	—	—	—	6.0
Benzene	85	0.24	—	—	6.0
Benzoic acid	78	—	—	+	—[c]
Benzonitrile	77	—	—	+	—[c]
Acetophenone	74	0.99	+	—	1.5
Benzaldehyde	72	—	+	—	1.25
Diphenylamine	72	0.38	—		—
Thiophene	69	—	—	+	—[c]
Benzophenone	69	1.00	+	—	1.0
Fluorene	68	0.31	+	—	3.5
Biphenyl	65	—	—	—	6.5
Phenanthrene	62	—	—	—	6.0
Michlar's ketone	62	1.01	—		—
Naphthalene	61	0.39	—	—	6.0

a) N. J. Turro, "Molecular Photochemistry," W. A. Benjamin, Inc., New York, N. Y. (1965), p. 132.
b) Ref. a) p. 131.
c) In these cases, the photoreduction is completely quenched.

As is shown in Table 1, the photoreduction of azobenzene was sensitized by fluorene and the aromatic carbonyl compounds (except Michlar's ketone). By the way, thiophene, benzonitrile, and benzoic acid quenched the photoexcited azobenzene.

Substituent Effect on the Photoreduction of Azobenzene. A 5×10^{-4} mol/l solution of 4-methylazobenzene, 4-phenylazobenzonitrile, and 4-phenylazobenzoic acid in IPA was irradiated under the conditions described in the case of azobenzene photochemistry. The results are shown in Table 2.

In the absorption spectra of photolyzed solutions, new absorption bands were observed in the 435—443 nm range; these bands seem to be due to the *cis*-isomers of the azobenzenes in view of the similarity of the visible spectra to that of *cis*-azobenzene. The absorption spectra of photolyzed solutions did not change between 0.5 and 2 hr after irradiation; therefore, the π,π^* absorption at *ca.* 320 nm of the *trans*-azobenzenes consecutively decreased in intensity and new absorption bands which were due to the hydrazobenzenes appeared. The preparation of the hydrazobenzenes was also determined by means of the paper chromatography of the primary amines, which were generated by the acid-catalyzed rearrangement of the hydrazobenzenes[12] as follows:

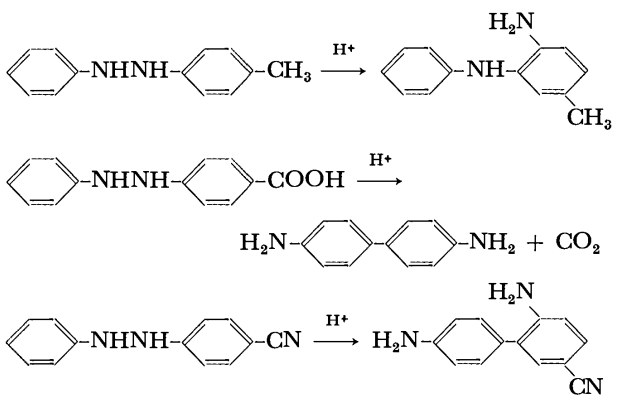

The time required for the complete disappearance of the 4-H, 4-CH_3, 4-COOH, and 4-CN derivatives were 6, 12, 9, and 7 hr respectively. Therefore, it seems that increasing the electronegativity of the substituents tends to increase the apparent rates of photoreduction.

Discussion

Photoreduction Mechanisms of Azobenzene. *trans*-Azobenzene reacted photochemically by way of two

Table 2. Photochemical reduction of 4-substituted azobenzenes

Azobenzenes	n,π^*, nm (ε)	π,π^*, nm (ε, 10^4)	λ_{max} of *cis*-isomers, nm	Time required for 100% conversion, hr	λ_{max} of the products, nm
H	440 (470)	316 (2.2)	435	6	242
CH_3	440 (620)	322 (2.4)	435	12	243
COOH	448 (300)	322 (2.6)	438	9	292
CN	450 (600)	322 (2.5)	443	7	*ca.* 270

In all cases, UV spectra were measured in IPA.

processes, the photoisomerization and the photoreduction.

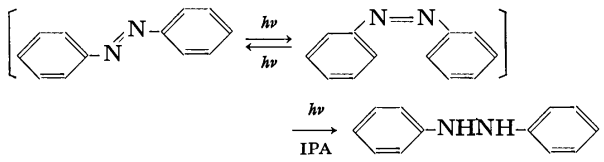

Azobenzene was relatively unreactive toward photoreduction under a nitrogen atmosphere; only the photoisomerization proceeded in a solution with a high concentration (1×10^{-3} mol/l). On the other hand, when a small amount of oxygen existed in the reaction system, the photoreduction was accelerated. It is well-known that oxygen quenches photoexcited species. It might also be mentioned that oxygen also induces the $S^* \rightarrow T$ transition. Before the beginning of the experiments, we inferred that oxygen might quench the triplet state of azobenzene or might oxidize the hydrazobenzene produced to azobenzene; therefore, the photoreduction might be depressed by oxygen. Nevertheless, the fact that the rate of the photoreduction of azobenzene was accelerated by a small amount of oxygen suggests that oxygen induces the $S^* \rightarrow T$ transition. Actually, the excited species of the photoreduction of azobenzene was determined to be the triplet state by the experiment of energy transfer using 1,3-pentadiene.

We also studied the wavelength dependence of the photoreduction of azobenzene. It was found that the $n \rightarrow \pi^*$ transition induced only the photoisomerization, while the $\pi \rightarrow \pi^*$ transition caused the photoreduction. These findings differ from those described for the photoreductions of the benzophenone[13] and/or nitrobenzenes,[1] which are caused by the $n \rightarrow \pi^*$ transition. This wavelength dependence on the azobenzene photochemistry is very interesting; however, we have not obtained sufficient experimental data to interpret the photochemical behavior of azobenzene. We may interpret the mechanisms of azobenzene photochemistry on the basis of the state diagram, as is shown as follows. That is, azobenzene is excited to the S_2 (π,π^*) state by the $\pi \rightarrow \pi^*$ transition. The S_2 state is converted to the $S_1(n,\pi^*)$ state by the internal conversion. The *cis-trans* photoisomerization of azobenzene may mainly be caused by the S_1 state, because the $n \rightarrow \pi^*$ transition causes only photoisomerization in neat IPA or IPA containing 1,3-pentadiene and/or oxygen. By the way, if the S_2 state converts to the $T_2(\pi, \pi^*)$ state by the spin-orbital interaction, this excited species may be able to abstract a hydrogen atom. It seems that the $T_1(n,\pi^*)$ state is not a species of the hydrogen-abstraction reaction, because this state may also be obtained by the intersystem crossing process, $S_1(n,\pi^*) \rightarrow T_1(n,\pi^*)$. The $S_0 \rightarrow T_1$ or $T_1 \rightarrow T_2$ transition has not occurred under our reaction conditions.

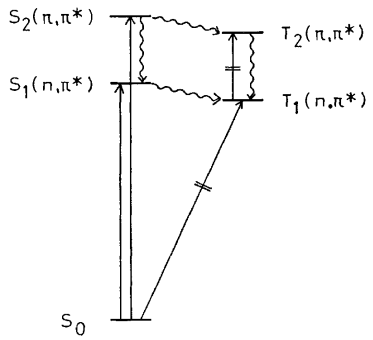

Photosensitized Reduction of Azobenzene. The photoreduction of azobenzene in IPA was sensitized by fluorene (E_T=68 kcal/mol) and by the aromatic carbonyl compounds (benzophenone, benzaldehyde, and acetophenone) except Michler's ketone. If the hydrogen-abstraction reaction of azobenzene proceeds from its π, π^* triplet (T_2), the triplet energy of fluorene may transfer to azobenzene, and then azobenzene may be excited to the T_2 state. Therefore, the energy of the T_2 state of azobenzene may be less than 68 kcal/mol. It seems that the photosensitization by the carbonyl compounds can be interpreted by two mechanisms. One of them is the triplet energy-transfer mechanism, and the other is the hydrogen-transfer mechanism. It is well-known that benzophenone, benzaldehyde, and acetophenone abstract a hydrogen atom from hydrogen donative solvents to generate their ketyl radicals:[14]

$$C_6H_5COR^* + R'H \longrightarrow C_6H_5\dot{C}(OH)R + \dot{R}'$$

Analogously with the IPA ketyl radical,[15] these ketyl radicals may be able to reduce azobenzene in the ground state:

$$C_6H_5\dot{C}(OH)R + C_6H_5N{=}NC_6H_5 \longrightarrow C_6H_5COR + C_6H_5NH\dot{N}C_6H_5$$

13) N. J. Turro, "Molecular Photochemistry," W. A. Benjamin, Inc., New York, N. Y. (1956), p. 137; D. C. Neckers, "Mechanistic Organic Photochemistry," Reinhold Publishing, Co., New York, N. Y. (1967), p. 163.

14) N. C. Yang, D. S. McClure, S. L. Murov, J. J. Houser, and R. Dusenbery, *J. Amer. Chem. Soc.*, **89**, 5466 (1967); J. S. Bradshaw, *J. Org. Chem.*, **31**, 237 (1966).

15) N. J. Turro, "Molecular Photochemistry," W. A. Benjamin, Inc., New York, N. Y. (1965), p. 143.

Reactions Leading to 1,2-Dibenzoylethanes: The Dehalogenation of Phenacyl Bromide and the Photolysis of Methyl Phenacyl Sulfoxide

Hitosi NOZAKI, Tamio SHIRAFUJI, Kiyosi KUNO, and Yasusi YAMAMOTO

Department of Industrial Chemistry, Kyoto University, Yoshida, Kyoto

(Received July 12, 1971)

The dehalogenation of phenacyl bromide by means of lower-oxidation-state metallic ions complexed by DMSO gives 1,2-dibenzoylethane. The by-products are 2,4-diphenylfuran and phenacyl chloride in the presence of Cu(I) chloride, whereas acetophenone and ω-acetoxyacetophenone are produced in the reaction with Cr(II) acetate. Treatment with $K_3Co(CN)_5$/DMSO gives 1,2-dibenzoylethane and acetophenone. The second title reaction consists of the photolysis of methyl phenacyl sulfoxides, the isolated by-products being acetophenones and methyl methanethiolsulfonate. The product distribution is strongly affected by the pH of the reaction mixture and also by the benzene-ring substituents.

Few reactions are known with respect to the formation of 1,2-dibenzoylethane (**1**) *via* the dehalogenation of phenacyl halides (**2**) or the recombination of phenacyl radicals. The treatment of phenacyl bromide (**2a**) with nickel carbonyl gives 1,2-dibenzoylethane (**1a**) in THF, whereas 2,4-diphenylfuran (**3a**) is the sole product in the DMF solvent.[1] The photolysis of dimethylphenacylsulfonium bromide in an aqueous solution gives **1a** besides **2a** and acetophenone (**4a**).[2] We now wish to record two independent reactions producing **1a**: the dehalogenation of phenacyl bromide with lower-oxidation-state metal salts dissolved in DMSO and the photolysis of methyl phenacyl sulfoxide (**5a**).[3]

Dehalogenation of Phenacyl Halide. Complexed metal salts of the lower oxidation state effectively dehalogenate organic halides.[4,5] In continuation of previous studies along this line,[6] we have now examined the reaction of phenacyl bromide with Cu(I) chloride, Cr(II) acetate, and $K_3Co(CN)_5$, all dissolved in DMSO: we thus obtained **1a** in varying yields, along with by-products, as is shown in Scheme 1 and Table 1.

The formation of 2,4-diarylfurans (**3a**, **3b**) in the Cu(I) reaction is parallel to previous observations made

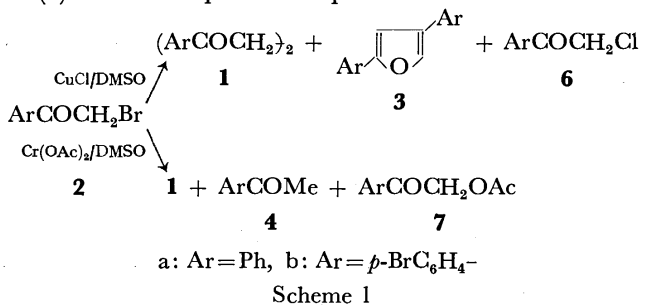

Scheme 1

Table 1. Reaction of $ArCOCH_2Br$ with CuCl, $Cr(OAc)_2$, or $K_3Co(CN)_5$ in DMSO[a]

Components	Reaction time (hr)	Products yield (%)[b] 1	3	4	6	7
2a+CuCl	18.5	13	14		39	
2b+CuCl	38.5	11	13		43	
2a+$Cr(OAc)_2$	12.5	28		—		43
2b+$Cr(OAc)_2$	23	16		32		18
2a+$K_3Co(CN)_5$	24	7		50		
2b+$K_3Co(CN)_5$	17	25		40		

a) Each reaction was carried out at room temperature (CuCl and $Cr(OAc)_2$) and 80—90°C ($K_3Co(CN)_5$) in N_2 atmosphere with 1M DMSO solution or of the salt with Br/metal ratio of 1:2.5.

b) The isolation yields were based on **2**. The recovery was not considered.

of the reactions of α-haloketones with nickel(0) tetracarbonyl,[1] metallic magnesium,[7] or zinc.[8] Analogously with these reactions, we may account for the route to **3a**, and **3b** as in Scheme 2, where the intermediacy of Cu(I) enolate is postulated.[7,8] The Wurtz-type condensation of this enolate with **2** (Route A) or, alternatively, the recombination of phenacyl radicals gives **1**, whereas aldol condensation, followed by dehydro-

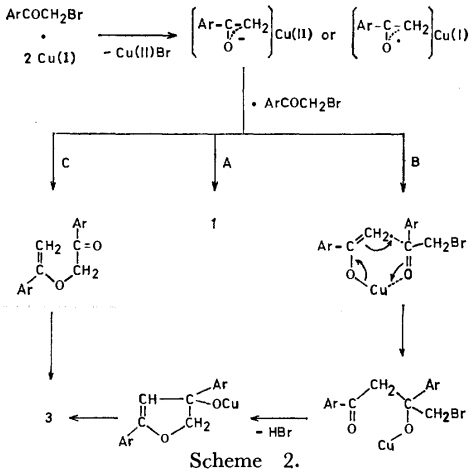

Scheme 2.

1) a) E. Yoshisato and S. Tsutsumi, *Chem. Commun.*, **1968**, 33. b) E. Yoshisato and S. Tsutsumi, *J. Amer. Chem. Soc.*, **90**, 4488 (1968).

2) T. Laird and H. Williams, *Chem. Commun.*, **1969**, 561.

3) Partly communicated in a preliminary form: T. Shirafuji, Y. Yamamoto, and H. Nozaki, *Tetrahedron Lett.*, **1969**, 4097.

4) a) J. K. Kochi and D. Buchanan, *J. Amer. Chem. Soc.*, **87**, 853 (1965), b) C. E. Castro and W. C. Kray, Jr., *ibid.*, **88**, 4447 (1966), c) *ibid.*, **85**, 2768 (1963).

5) K. Onuma, J. Yamashita, and H. Hashimoto, This Bulletin, **43**, 836 (1970).

6) a) H. Nozaki, T. Shirafuji, and Y. Yamamoto, *Tetrahedron*, **25**, 3461 (1969), b) T. Shirafuji, K. Oshima, Y. Yamamoto, and H. Nozaki, This Bulletin, **44**, 1743 (1971).

7) J. E. Dubois and J. Itzkowitch, *Tetrahedron Lett.*, **1965**, 2839.

8) T. A. Spencer, R. W. Britton, and D. S. Watt, *J. Amer. Chem. Soc.*, **89**, 5727 (1967).

Table 2. Photolysis of $ArCOCH_2SOMe$ (5)[a]

	Ar	Solvent	Reaction time (hr)	Products 1	4	8	ArCOOH
5a	Ph	EtOH	5	38	49	8	—
5a	Ph	EtOH[b]	5	20	46	13	—
5a	Ph	*t*-BuOH	4	72	23	52	—
5a	Ph	*i*-PrOH	8	24	20	8	—
5a	Ph	PhH	8	62	trace	61	—
5a	Ph	EtOH(H_2SO_4)[c]	5	12	87	8	—
5a	Ph	EtOH(NaOH)[d]	5	54	27	—	17
5b	*p*-BrC_6H_4	EtOH	5	19	70	10	—
5c	*p*-ClC_6H_4	EtOH	5	33	60	12	4
5c	*p*-ClC_6H_4	EtOH–H_2O[e]	5	30	6	4	—
5c	*p*-ClC_6H_4	EtOH(H_2SO_4)[c]	5	trace	71	trace	—
5c	*p*-ClC_6H_4	EtOH(NaOH)[d]	5	70	15	—	13
5d	*p*-MeC_6H_4	EtOH	6	25	30	—	—
5e	*p*-$MeOC_6H_4$	EtOH	2	trace	88	trace	—
5e	*p*-$MeOC_6H_4$	EtOH(H_2SO_4)[c]	2	—	95	trace	—
5e	*p*-$MeOC_6H_4$	EtOH(NaOH)[d]	2	32	28	—	20
5f	*p*-$Me_2NC_6H_4$	EtOH[f]	46	41	34	—	—
5g	α-$C_{10}H_7$	EtOH	70	—	63	—	—

a) Irradiation was performed on 0.1 M solutions with an external 200W high pressure mercury lamp through a Pyrex filter at room temperature under nitrogen atmosphere.
b) Irradiation under oxygen atmosphere.
c) A trace of concentrated H_2SO_4 was added to adjust the pH of the media at 5—6 on a test paper.
d) A trace of 10% NaOH (EtOH) was added to adjust the pH of the media at 8—9.
e) EtOH:H_2O=2:1 (volume ratio). A by product, *p*-$ClC_6H_4COCH_2SO_2Me$ (18%) was obtained.
f) A by product, *p*-Me_2N-$C_6H_4COCH_2OH$ (20%) was obtained.

bromination (Route B), produces the furans **3**. Schematically, the possibility of Route C cannot be excluded. The anhydrous Cr(II) acetate/DMSO system is apparently less selective than the previously-recorded Cr(II) sulfate/aqueous DMF system,[4c] which produces **4** almost quantitatively. The complete absence of aldol condensation in the Cr(II) reaction may be ascribed to the higher covalency of the chromium-phenacyl bond than that of copper enolate. The ligand-ligand reaction leading to **7** prevails in this case.

Few organic reactions have been recorded to occur under the participation of $K_3Co(CN)_5$.[9-12] The reaction with **2** is mainly reduction to **4** in DMSO. Smaller yields of **1** were obtained.

Photolysis of Phenacyl Sulfoxides (5). The irradiation of β-keto sulfones[13] or β-keto sulfides[14] ($RCOCH_2$-X-CH_2R', X=SO_2 or S) gives $RCOCH_3$ ketones. The reaction of the sulfides is supposed to proceed *via* the Norrish type-II route, whereas that of sulfones has been claimed to involve the homolysis of the C-S bond, followed by hydrogen abstraction by the $RCOCH_2\cdot$ radicals.

The photochemistry of the β-keto sulfoxides[15,16] now readily available has apparently not been described. We will report the formation of **1** and **4** in the photolysis of phenacyl sulfoxides, **5**, mainly in ethanol (Scheme 3), as well as the effects of the pH values of the reacting media and those of aromatic substituents. The results are summarized in Table 2.

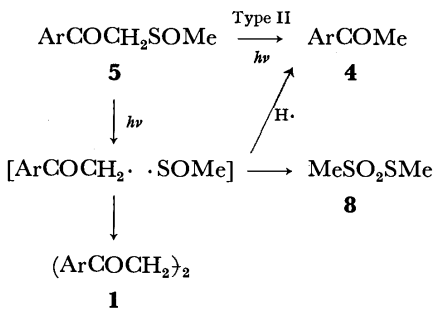

Scheme 3

At the initial stage of this investigation we experienced difficulties in securing reproducible experimental data. Soon it was found that the product distribution is quite sensitive to the pH of the reaction media. Table 2 contains the effect of added acids and bases. Slightly basic conditions favor the yields of dibenzoylethanes, **1**, whereas acetophenones, **4**, are mainly produced under acidic conditions. This effect may be ascribed to the amphoteric character of the phenacyl sulfoxide, that is, to the methylene acidity and the SO

9) T. Suzuki and T. Kwan, *Nippon Kagaku Zasshi*, **88**, 395 (1967).
10) J. Halpern and J. P. Maher, *J. Amer. Chem. Soc.*, **86**, 2311 (1964).
11) J. Kwiatek and J. K. Seyler, *J. Organometal. Chem.*, **3**, 421 (1965).
12) K. Tarama and T. Funabiki, *Nippon Kagaku Zasshi*, **89**, 88 (1968).
13) C. L. McIntosh, P. de Mayo, and R. W. Yip, *Tetrahedron Lett.*, **1967**, 37.
14) (a) H. Hogeveen and P. J. Smit, *Rec. Trav. Chim. Pay-Bas*, **85**, 489 (1966), b) M. C. Caserio, W. Lauer, and T. Novinson, *J. Amer. Chem. Soc.*, **92**, 6082 (1970).
15) E. J. Corey and M. Chaykovsky, *J. Amer. Chem. Soc.*, **87**, 1345 (1965).
16) G. A. Russell and G. J. Mikol, *ibid.*, **88**, 5498 (1966).

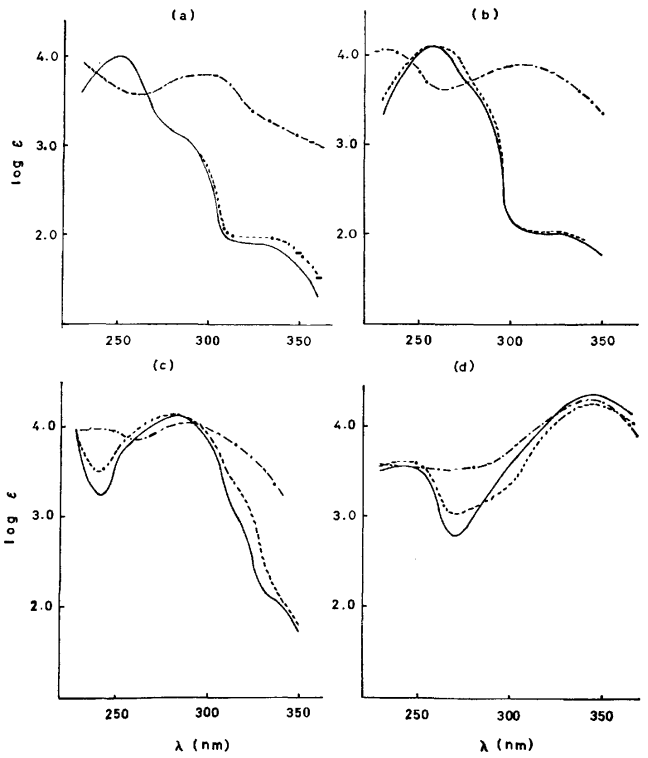

Fig. 1. UV spectra of β-keto sulfoxides in ethanol (——), ethanol-H_2SO_4(------), and ethanol-NaOH (-·-·-).
(a) $PhCOCH_2SOMe$ (**5a**); (b) p-$ClC_6H_4COCH_2SOMe$ (**5c**); (c) p-$MeOC_6H_4COCH_2SOMe$ (**5e**); (d) p-$Me_2NC_6H_4COCH_2SOMe$ (**5f**).

oxygen basicity (*vide infra*). Aromatic substituents also influenced the product distribution; the *p*-dimethylamino group strongly increased the yield of **1**, while *p*-methoxy and *p*-halogen substituents favored **4**. In *t*-butyl alcohol or benzene, **5a** gave **1a** mainly.

The UV absorptions of the reacting mixtures are given in Fig. 1. The bathochromic and hyperchromic shift of longer wavelength (n-π^*) absorptions was observed under basic conditions, the presence of a trace of acid did not change the spectra appreciably. The spectra of the *p*-dimethylamino derivative, **5f**, showed little dependence on the pH and remarkably resembled ot the spectra of **5a**, **5c**, and **5e** under basic conditions. The relationship between the product distribution and the spectral change has not yet been clearly explained. The photolysis appears to involve initial homolysis of the phenacyl-SO bond. The $ArCOCH_2\cdot$ radicals then dimerize to **1** or, alternatively, abstract hydrogen from the solvent to give **4**. Presumably, smaller photoquanta under basic conditions give less energetic $ArCOCH_2\cdot$ radicals, which easily dimerize. The absence of the removable solvent hydrogen also favors the formation of **1**. The counter radicals, ·SOMe, dimerize to give methyl methanethiolsulfonate (**8**), which has been isolated as is shown in Table 2.

Experimental

All the mps are uncorrected. The microanalyses were performed at the Elemental Analyses Center of Kyoto University and by Mrs. K. Fujimoto of this Department. The NMR spectra were taken on a 60 MHz instrument (JEOL C-60H spectrometer) in deuteriochloroform or carbon tetrachloride with tetramethylsilane as the internal standard. The UV spectra were obtained on a Shimadzu MPS-50L spectrometer.

Unless otherwise stated, irradiation was effected externally by means of a 200-W high pressure mercury lamp under a nitrogen atmosphere at room temperature.

Commercial Cu(I) chloride was used without purification. Cr(II) acetate and $K_3Co(CN)_5$ were prepared according to the methods shown in the literature.[12,17] The β-keto sulfoxides were synthesized by the Corey method.[15] The NMR, IR, and microanalyses of novel ones are given below.

Methyl p-*chlorophenacyl sulfoxide (5c)* showed a mp of 128°C. IR (Nujol): 1670 cm^{-1} ($\nu_{C=O}$), 1030 cm^{-1} (ν_{SO}). NMR ($CDCl_3$): δ 2.80 (s, 3H, Me), 4.40 (s, 2H, $-CH_2-$), and 7.35—8.15 (two d, 4H, aromatic protons).

Found: C, 50.2; H, 4.2%. Calcd for $C_9H_9ClO_2S$: C, 49.9; H, 4.2%.

Methyl p-N,N-*dimethylaminophenacyl sulfoxide (5f)* showed a mp of 144—145°C. IR (Nujol): 1600 cm^{-1} ($\nu_{C=O}$), 1020 cm^{-1} (ν_{SO}). NMR ($CDCl_3$): δ 2.74 (s, 3H, -SOMe), 3.10 3.10 (s, 6H, Me_2N), 4.02—4.63 (two d, 2H, $-CH_2-$), and 6.59—7.93 (two d, 4H, aromatic protons).

Found: C, 58.6; H, 6.6%. Calcd for $C_{11}H_{15}NO_2S$: C, 58.6; H, 6.7%.

Reaction of Phenacyl Bromide (2a) with Cu(I) Chloride. In a N_2 atmosphere, Cu(I) chloride (1.5 g, 15 mmol) was dissolved in freshly-distilled DMSO (30 m*l*) (over CaH_2). To this, a solution of **2a** (1.2 g, 6.0 mmol) in DMSO (10 m*l*) was added. The reaction mixture was stirred for 18.5 hr at room temperature, treated with water and extracted with ether. The extract was then washed with water, dried (Na_2SO_4), and concentrated *in vacuo*. Chromatography on a silica-gel column gave 1,2-dibenzoylethane (**1a**) (0.09 g, 13%), 2,4-diphenylfuran (**3a**) (0.09 g, 14%), and phenacyl chloride (**6a**) (0.36 g, 39%). The **1a** product showed a mp of 148—150°C (lit.[1] 145°C) and was identical with an authentic sample. IR (Nujol): 1675 cm^{-1} ($\nu_{C=O}$). NMR ($CDCl_3$): δ 3.47 (s, 4H, $-CH_2-$) and 7.35—8.40 (m, 10H, aromatic protons). The **3a** product showed a mp of 111°C (lit.[18] 111°C). IR (Nujol): 1538 and 910 cm^{-1} (furan ring). NMR (CCl_4): δ 6.82 (s, 1H, proton of the furan ring at the C-3 position) and 7.15—7.65 (m, 11H, protons of the benzene ring and furan ring at the C-5 position). The **6a** product showd a mp of 57—58°C (lit.[19] 58°C), and its structure was supported by NMR and IR.

Reaction of p-*Bromophenacyl Bromide (2b) with Cu(I) Chloride.* A solution of Cu(I) chloride (0.89 g, 9.0 mmol) in DMSO (30 m*l*) was prepared under N_2. To this, a solution of **2b** (0.99 g, 3.6 mmol) in DMSO (10 m*l*) was added and the mixture was stirred at room temperature for 38.5 hr. Chromatography on a silica-gel column gave **1b** (0.08 g, 11%), **3b** (0.09 g, 13%), and **6b** (0.36 g, 43%). The **1b** product showed a mp of 180°C (lit.[1] 180—181°C). IR (Nujol): 1670 cm^{-1} ($\nu_{C=O}$). NMR ($CDCl_3$): δ 3.43 (s, 4H, $-CH_2-$) and 7.54—7.98 (m, 8H, protons of the aromatic ring). The **3b** product showed a mp of 160°C. IR (Nujol): 1539 and 912 cm^{-1} (furan ring). NMR ($CDCl_3$): δ 6.90 (s, 1H, proton of the furan ring at the C-3 position) and

17) J. H. Balthis, Jr., and J. C. Bailar Jr., "Inorg. Synthesis," Coll. Vol. 1, 122 (1939).
18) R. C. Fuson, C. L. Fleming, and R. Johnson, *J. Amer. Chem. Soc.*, **60**, 1994 (1938).
19) S. Goldschmidt, R. Endres, and R. Dirsch, *Ber.*, **58**, 572 (1925).

7.40—7.73 (m, 9H, protons of the aromatic ring and the furan ring at the C-5 position). The **6b** product showed a mp of 116—118°C (from ethanol) (lit.[20] 117—118°C).

Reaction of 2a with Cr(II) Acetate. Under N_2, Cr(II) acetate (1.5 g, 8.8 mmol) was dissolved in DMSO (50 m*l*) so to give *ca.* 0.18 M solution. To this, a solution of **2a** (0.70 g, 3.5 mmol) in DMSO (10 m*l*) was added and the mixture was stirred at room temperature for 12.5 hr. Chromatography on a silica-gel column gave **1a** (0.12 g, 28%), ω-acetoxyacetophenone (**7a**) (0.27 g, 43%). The **7a** product showed a mp of 47—49°C (lit.[21] 49°C); its structure was supported by the IR and NMR.

Reaction of 2b with Cr(II) Acetate. The **2a** halide (2.23 g, 8.0 mmol) in DMSO (10 m*l*) was treated with a solution of Cr(II) acetate (3.40 g, 20 mmol) in DMSO (100 m*l*) at room temperature for 23 hr to afford **1b** (0.25 g 16%), **4b** (0.51 g, 32%), and **7b** (0.37 g, 18%). The **7b** product showed a mp of 84—85°C (lit.[22] 85°C).

Reaction of 2a with $K_3Co(CN)_5$. A solution of the cyanocobalt(II) complex was prepared under N_2 from potassium cyanide (9.75 g, 150 mmol) and Co(II) chloride (3.25 g, 25 mmol) in DMSO (50 m*l*). To this, a solution of **2a** (2.0 g, 10 mmol) in DMSO (5 m*l*) was added, and the mixture was stirred at 80—90°C for 24 hr. A subsequent work-up gave **1a** (0.08 g, 7%) and **4a** (0.60 g, 50%).

Reaction of 2b with $K_3Co(CN)_5$. To a solution of the cobalt complex prepared from potassium cyanide (4.88 g, 75 mmol) and Co(II) chloride (1.63 g, 13 mmol) in DMSO (50 m*l*), a solution of **2b** (1.39 g, 5.0 mmol) in DMSO (10 m*l*) was added, after which the mixture was stirred at 80—90°C for 17 hr. A subsequent work-up gave **1b** (0.25 g, 25%) and **4b** (0.40 g, 40%).

Photolysis of Methyl Phenacyl Sulfoxide (5a). Sulfoxide **5a** (0.182 g, 1 mmol) was dissolved in ethanol (10 m*l*) and degassed under vacuum at −70°C on a dry-ice bath. This was then irradiated by means of high-pressure mercury lamp for 5 hr. After the irradiation, the ethanol was removed *in vacuo* and the residue was chromatographed on a silica-gel column. 1,2-Dibenzoylethane (**1a**) (0.045 g, 38%), acetophenone (**4a**) (0.06 g, 49%), and methyl methanethiolsulfonate (**8**) (0.005 g, 8%) were obtained. The **8** product was identical with an authentic sample.

The photolyses of **5b—5g** were carried out under similar conditions. The results are summarized in Table 2. All the acetophenone derivatives were identical with authentic samples. The **1c**, **1d**, and **1e** products showed mps of 151°C (lit.[23] 151°C), 158—159°C (lit.[24] 159°C) and 154—155°C (lit.[25] 154°C) respectively, their structures were supported by IR and NMR. The **1f** product did not melt below 220°C. IR (Nujol): 1595 cm^{-1} ($\nu_{C=O}$). NMR ($CDCl_3$): δ 3.03 (s, 12H, Me_2N), 3.33 (s, 4H, $-CH_2CH_2-$), and 6.45—8.10 (two d, 8H, aromatic protons). Microanlyses were carried out without purification, as **1f** is difficult to purify in conventional ways.

Found: C, 73.2; H, 7.5; N, 8.4%. Calcd for $C_{20}H_{24}N_2O_2$: C, 74.0; H, 7.5; N, 8.6%.

A by-product, ω-hydroxy-*p*-*N*,*N*-dimethylaminoacetophenone, showed a mp of 155°C. NMR ($CDCl_3$): δ 3.10 (s, 6H, $-NMe_2$), 4.74 (s, 2H, $-CH_2-$), 7.35 (s, 1H, OH) and 6.55—7.97 (two d, 4H, aromatic protons). MS: 179 (M^+).

Found: C, 67.3; H, 7.2; N, 7.6%. Calcd for $C_{10}H_{13}NO_2$: C, 67.0; H, 7.3; N, 7.8%.

Photolysis of 5a in the Presence of Sulfuric Acid. The sulfoxide, **5a** (0.182 g, 1 mmol), was dissolved in ethanol (10 m*l*). A solution of sulfuric acid in ethanol was then added, drop by drop, so to give a solution of pH 5—6 (pH test paper). This solution was degassed and then irradiated under N_2 for 5 hr. The products were isolated and identified as has been described above. The photoreactions of **5c** and **5e** was carried out under similar conditions. The results are summarized in Table 2.

Photolysis of 5a in the Presence of Sodium Hydroxide. The sulfoxide, **5a** (0.182 g, 1 mmol), was dissolved in ethanol (10 m*l*). A solution of sodium hydroxide in ethanol was then added, drop by drop, so to give a solution of pH 8—9. This solution was irradiated under N_2 for 5 hr and the products were confirmed as has been described above. The results are summarized in Table 2.

The authors are grateful to Professor K. Sisido for his generous help. Financial support from the Ministry of Education, Japanese Government, and from the Toray Science Foundation is acknowledged with pleasure.

20) H. H. Pokras and H. I. Bernstein, *J. Amer. Chem. Soc.*, **65**, 2096 (1943).
21) R. G. Linville and R. C. Elderfield, *J. Org. Chem.*, **6**, 270 (1941).
22) W. L. Judefind and E. E. Reid, *J. Amer, Chem. Soc.*, **42**, 1043 (1920).
23) J. B. Conant and R. E. Lutz, *ibid.*, **45**, 1303 (1923).
24) A. Claus, *Ber.*, **20**, 1374 (1887).
25) E. Buchta and G. Schaeffer, *Ann. Chem.*, **597**, 129 (1955).

Thallium(III) Chloride Tetrahydrate as a Lewis Acid Catalyst for Aromatic Alkylation and Acylation[1]

Sakae UEMURA, Kazuhiro SOHMA, and Masaya OKANO
Institute for Chemical Research, Kyoto University, Uji, Kyoto

(Received July 12, 1971)

From a study of aromatic alkylation and acylation using $TlCl_3 \cdot 4H_2O$ catalyst, it was revealed that this metal chloride was a milder Lewis acid catalyst than $AlCl_3$ and $FeCl_3$ and was similar in activity to $ZnCl_2$. Although the yields of the products were generally low, the characteristics of this catalyst were observed in the formation of β,β'-dimethylstyrene and benzoylacetone upon the respective methallylation and acetylation of benzene and in the fact that the hydrated chloride was more effective than the anhydrous one. In a sharp contrast to aromatic bromination, $Tl(OAc)_3$ showed little activity in these reactions.

Although many metal halides have been studied as Lewis acid catalysts for aromatic alkylation and acylation, Tl(III) salts seem to have received little attention so far[2]; only one report on the benzylation, benzoylation, and acetylation of benzene using the anhydrous $TlCl_3$ catalyst has been found in the literature.[3] Recently, Taylor and McKillop showed that the acetylation of anisole could be catalyzed by $Tl(OAc)_3$.[4] On the other hand, the use of Tl(III) salts, such as $Tl(OAc)_3$ and $TlBr_3 \cdot 4H_2O$, has been reported to be very effective in aromatic bromination[5,6], and their role has been considerably clarified.[6]

Our study of the Tl(III) salt-catalyzed aromatic alkylation and acylation has been started in the hope of finding some specific use for the catalyst in these reactions, as in the case of the Tl(III) salt-catalyzed aromatic bromination. Unfortunately, no distinctive feature was found from a synthetic point of view. Considering the yields of the products of butylation, allylation, haloalkylation, and acylation, however, it is clear that the activity of $TlCl_3 \cdot 4H_2O$ is qualitatively comparable to that of $ZnCl_2$ and inferior to that of $FeCl_3$ or $AlCl_3$. Here, it seems to be characteristic that the hydrated Tl(III) salt shows a moderate activity, in contrast to the fact that other active metal halide catalysts are used mostly in the anhydrous state. This report will deal with these observations.

Results and Discussion

The reactions were generally carried out by adding the alkylating or acylating agents to aromatic compounds (in excess as solvents) containing $TlCl_3 \cdot 4H_2O$ at various temperatures and by stirring the resulting mixtures for appropriate periods. Although an $AlCl_3$- or $FeCl_3$-catalyzed Friedel-Crafts alkylation and acylation generally proceeds at a low temperature, it was necessary to heat the reaction mixture in most of these $TlCl_3 \cdot 4H_2O$ catalyzed reactions. Some typical results are summarized in Table 1.

Butylation and Benzylation. It has been reported[7] that, in the presence of $AlCl_3$, *n*- and *t*-butyl chlorides reacted with benzene at 0°C to give *s*- and *t*-butylbenzenes in 50 and 60% yields respectively, and that the reaction of *t*-butyl chloride with benzene gave an 80% yeild of *t*-butylbenzene at 25°C in the presence of the $FeCl_3$ catalyst. In the presence of the $TlCl_3 \cdot 4H_2O$ catalyst, the *s*- and *t*-butyl halides reacted with aromatic compounds to give *s*- and *t*-butylated compounds (I) respectively in 22—39% yields at 60—76°C. The lower the reaction temperature was, the lower the yields of I became. *n*-Butyl chloride or bromide afforded only a small amount of *s*-butylbenzene (*ca.* a 2% yield at 76°C for 10 hr) without any trace of *n*-butylbenzene which was expected to be formed by the attack of the strongly polarized but undissociated alkyl halide molecule. *t*-Butyl alcohol could not be used as an alkylating agent at 70°C because of its rapid oxidation by $TlCl_3 \cdot 4H_2O$; this is in sharp contrast to the reactions with other acidic catalysts (*e.g.*, H_2SO_4, HF, $AlCl_3$, $FeCl_3$, and BF_3), in which *t*-butylbenzene was obtained in high yields from benzene.[7] In the benzylation of toluene with benzyl bromide or acetate, $TlBr_3 \cdot 4H_2O$ showed an activity similar to that of $TlCl_3 \cdot 4H_2O$ as a Lewis acid catalyst. Although $Tl(OAc)_3$ was a very effective catalyst in aromatic bromination, the *s*-butylation of benzene using this catalyst was almost entirely unsuccessful because of the conversion of $Tl(OAc)_3$ to inactive Tl_2O_3.

Allylation and Haloalkylation. It has been reported[8,9] that the reaction of allyl halide and aromatic compounds gives 1-aryl-2-halopropane or 1,2-diarylpropane in the presence of mild Lews acid catalysts, such as $ZnCl_2$, or with strong catalysts, such as $AlCl_3$, respectively, and that both of the products are derived from allylated compounds. Although $TlCl_3 \cdot 4H_2O$ has been shown by the aromatic butylation described above to be a milder Lewis acid catalyst than $AlCl_3$ or $FeCl_3$, it is not known to what kind of metal salts the activity

1) Presented at the 24th Annual Meeting of the Chemical Society of Japan, Osaka, April, 1971.
2) "Friedel-Crafts and Related Reactions," ed. by G. A. Olah, Intersceience, New York (1965), Vol. I, p. 255—256.
3) L. I. Kashtanov, *J. Gen. Chem. (U.S.S.R.)*, **2**, 515 (1932); *Chem. Abstr.*, **27**, 975 (1933).
4) E. C. Taylor and A. McKillop, *Accounts Chem. Res.*, **3**, 338 (1970).
5) A. McKillop, D. Bromley, and E. C. Taylor, *Tetrahedron Lett.*, **1969**, 1623.
6) S. Uemura, K. Sohma, M. Okano, and K. Ichikawa, This Bulletin, **44**, 2490 (1971).
7) C. C. Price, "Organic Reactions," John Wiley and Sons, New York (1946), Vol. III, Chap. 1. p. 30—33.
8) Ref. 2, Vol. II, p. 359—360.
9) C. D. Nenitzescu and D. A. Isacescu, *Chem. Ber.*, **66**, 1100 (1933).

TABLE 1

C_6H_5R R (1mol)	Alkylating or acylating agents (100 mmol)	$TlCl_3 \cdot 4H_2O$ (mmol)	React. temp. (°C)	React. time (hr)	Products (yield, %)[a] I	II	III	IV	V	VI
H	*s*-BuCl[b]	25	76	4	23					
H	*t*-BuBr	10	76	0.3	39[c]					
H	$C_6H_5CH_2OAc$	25	80	5	50[d]					
CH_3	$C_6H_5CH_2Br$	25[e]	70	1	90[f]					
H	CH_2=CH-CH_2Cl	10	57	0.3		4	5	trace		
H	CH_2=CH-CH_2Cl	25	70	4		0	37	trace		
CH_3	CH_2=CH-CH_2Cl	10	57	0.3		7[g]	22[h]	0		
CH_3	CH_2=CH-CH_2Cl	10	65	4		0	52[h]	31[i]		
Cl	CH_2=CH-CH_2Cl	10	65	2		0	18[j]	trace		
H	CH_3COCl	25	56	5					3	6
CH_3	CH_3COCl	25	56	5					19	3
CH_3	CH_3COCl	25	25	0.3					23	0
CH_3	CH_3COCl	25[k]	25	0.3					12	0

a) Based on alkylating of acylating agents.
b) 50 mmol.
c) The 12% yield of di-*p*-*t*-butylbenzene (mp 77—79° C; lit.[17] 76°C) was obtained.
d) Diphenylethane.
e) $TlBr_3 \cdot 4H_2O$.
f) Phenyltolylmethane, $o/p=1.38$.[6]
g) The o/p ratio was not determined.
h) $o/p=0.15$ (determined by NMR).
i) 1,1-Ditolylpropane/1,2-isomer=3 (NMR).
j) $o/p=1.21$ (glc).
k) Anhydrous $TlCl_3$.

of $TlCl_3 \cdot 4H_2O$ is comparable. If $TlCl_3 \cdot 4H_2O$ is a milder catalyst than $ZnCl_2$, we could expect the allylated aromatic compounds to be isolated using this catalyst. In this connection, several aromatic compounds were treated at 55—70°C for 0.3—4 hr with allyl chloride or bromide in the presence of this catalyst. 1-Aryl-2-halopropanes (III) were generally isolated as the main products, along with small or trace amounts of monoallylated compounds (II) and diarylpropanes (IV) (Eq. 1).

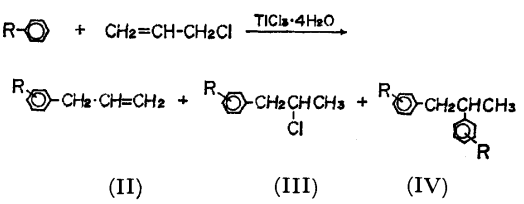

(II) (III) (IV)

This means that the catalytic activity of $TlCl_3 \cdot 4H_2O$ is qualitatively similar to that of $ZnCl_2$ and milder than that of $AlCl_3$ in aromatic allylation. The formation of II was observed only under milder conditions (a short reaction time or a low reaction temperature), though the yields were very poor. The yields of III, which was probably formed by the hydrochlorination of II, decreased in the following order of aromatics, as would be expected; toluene>benzene>halobenzenes. The allylation of halobenzenes with this catalyst at 65—70°C for 1.5—2 hr gave only 9—18% yields of III, while with the $FeCl_3$ catalyst somewhat higher yields (24—53%) were recorded, even at lower reaction temperatures (—21——16°C).[10] Compound IV was probably produced by aromatic alkylation with III. An isomer of IV, 1,1-diarylpropane, was also formed, and the amount of which was larger than that of IV. The presence of such an isomer indicates that the hydrogen transfer has occurred in the intermediary cation ($ArCH_2\overset{+}{C}HCH_3$) derived from III on prolonged heating, as in the case of the *n*-butylation of benzene described above. The use of a solvent led to a significant decrease in the reaction rate; *e.g.*, with benzene and allyl chloride, no reaction occurred at 50°C after 4 hr in carbon disulfide, and only 6% of the III was obtained at 65°C after 4 hr in chloroform. Allyl bromide reacted more easily with benzene than allyl chloride, but a mixture of 2-bromo- and 2-chloro-1-phenylpropanes (in 4: 1 ratio) was obtained in a 43% yield, together with diphenylpropanes (14% yield), when the reaction was at 55°C for 0.3 hr. The allylation with allyl alcohol, which was easily achieved by other Lewis acid catalysts, was unsuccessful when we used $TlCl_3 \cdot 4H_2O$, which has a strong oxidizing property. The reaction with *trans*-crotyl chloride showed a behavior similar to that of the reaction with allyl chloride. With methallyl chloride, however, β,β'-dimethylstyrene was obtained in a 9% yield without any trace of such compounds as III and IV when the reaction was at 75°C for 5 hr. This compound, which is probably formed by the isomerization of the methallylated compound, has not been reported to be formed by a Friedel-Crafts reaction using any Lewis acid catalyst; rather its formation seems to be one of the characteristics of the $TlCl_3 \cdot 4H_2O$ catalyst.

The attacking species in this reaction seem to be rather reactive, because the k_T/k_B ratio in the formation of II and III by the competitive reaction of toluene and

10) T. M. Patrick, Jr., E. T. McBee, and H. B. Hass, *J. Amer. Chem. Soc.*, **68**, 1009 (1946).

benzene with allyl chloride (at 50°C for 0.3 hr) is revealed to be 2.6; this value is comparable with the value (3.2) obtained in the $AlCl_3$-catalyzed benzylation in nitromethane.[11] Further, it is interesting to note that the favorable attack at the *p*-position of toluene by allylic species (the *o*/*p* ratio is 0.15 in III) contrasts strikingly with that at the *o*-position by benzylic species (where the *o*/*p* ratio is 1.38), as is shown in Table 1.

Acylation. Although Kashtanov has obtained a 12% yield of acetophenone from the acetylation of benzene using anhydrous $TlCl_3$,[3] a recent description of Taylor and McKillop of the selective para acetylation of anisole by the $Tl(OAc)_3$ catalyst[4] encouraged us to reinvestigate the acylation using $TlCl_3 \cdot 4H_2O$. In the presence of $TlCl_3 \cdot 4H_2O$, the reactions of acetyl or propionyl chloride with benzene, toluene, and anisole were examined; the *para*-monoacylated compounds (V) were isolated as the main products, although the yields were low. It seems that the low yield is not be accounted for by the hydrolysis of acyl chloride with the water of the hydrated catalyst, because the reaction with anhydrous $TlCl_3$ gave a smaller amount of the product. In a contrast to Kashtanov's report, the acetylation of benzene and toluene at 56°C gave benzoylacetone and *p*-methylbenzoylacetone (VI) respectively, together with V (Eq. 2). When acetophenone

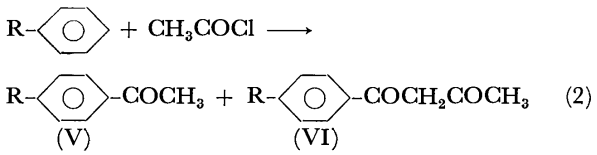

(2)

was heated with $TlCl_3 \cdot 4H_2O$ at 56°C for 5 hr, α-methylchalcone, the Claisen condensation product of acetophenone, was obtained in a 10% yield, as in the $AlCl_3$-catalyzed reaction[12] (in this case, an 11.5% yield was reported); however, the presence of excess (*e.g.*, 5 equiv.) acetyl chloride changed the product to benzoylacetone (9% yield) under the same reaction conditions. Although it has been reported that the methyl group of acetophenone was acetylated with acetic anhydride using the $FeCl_3$ or $ZnCl_2$ catalyst to give benzoylacetone,[12] there have been no reports about acetylation with acetyl chloride. This $TlCl_3 \cdot 4H_2O$-catalyzed acetylation of acetophenone and this formation of VI seem to be characteristic of this catalyst. Acetic anhydride could not be used as the acetylating agent of aromatic compounds with the $TlCl_3 \cdot 4H_2O$ catalyst.

Recently, Taylor and McKillop reported,[4] without any detailed description of the experimental conditions, that, in the CCl_4 solvent, anisole was acetylated by acetyl chloride to give *p*-acetylanisole in an 80% yield when the $Tl(OAc)_3$ catalyst was used. When a similar reaction was carried out with anisole as the solvent and with the $TlCl_3 \cdot 4H_2O$ catalyst, only a 28% yield of the acetylated product was obtained at 25°C after 0.3 hr. For comparison, the reaction of anisole (0.1 mol) and acetyl chloride (0.05 mol) using the $Tl(OAc)_3$ (0.05 mol) catalyst was carried out in CCl_4 (80 ml) at 20°C for 3 hr, but only a 15% yield of *p*-acetylanisole was thus obtained. The reason for the discrepancy with Taylor's result is obscure.

Experimental

Materials. All the organic starting materials were used after distillation. The $TlCl_3 \cdot 4H_2O$ (mp 35—37°C, lit.[13] 37°C; the purity (as determined by iodometry) was more than 96%) and $TlBr_3 \cdot 4H_2O$ (mp 40—42°C, lit.[13] 40°C; purity, 97%) catalysts were of commercial origin. The $Tl(OAc)_3$ was prepared by heating Tl_2O_3 in aceitc acid.[14] Anhydrous $TlCl_3$,[15] which is very hygroscopic, was prepared by dissolving $TlCl_3 \cdot 4H_2O$ into thionyl chloride at room temperature, evaporating the hydrogen chloride, sulfur dioxide, and excess thionyl chloride to dryness on a water bath, and drying under a vacuum for 6 hr (purity, 96.6%). The *n*-, *s*-, and *t*-butylbenzenes, allylbenzene, diphenylmethane, acetophenone, *p*-methylacetophenone, and benzoylacetone were commercial products and were used as the authentic samples for glc analysis. The 1-phenyl-2-chloropropane and 1,2-diphenylpropane were prepared from a benzene-allyl chloride-$FeCl_3$ system at −10—−20°C for 1 hr; the yields were 41% and 14% (1,2-isomer/1,1-isomer= 1.5 by NMR) respectivey. The 1-halophenyl-2-chloropropanes were prepared by the reported method[10] using the corresponding halobenzene, allyl chloride, and $FeCl_3$ catalyst.

Experimental Procedure. The reaction of benzene with allyl chloride in the presence of $TlCl_3 \cdot 4H_2O$ is shown below as a typical example. Allyl chloride (15.2 g, 0.2 mol) was stirred into a suspension of molten $TlCl_3 \cdot 4H_2O$ (9.6 g, 0.025 mol) and benzene (78 g, 1 mol) at 60°C. The color of the reaction mixture changed from pale yellow to orange and finally to deep purple, while the reaction temperature rose to 70°C. After 4 hr, the black precipitates were filtered off, and the filtrate was washed with water and a saturated aqueous $NaHCO_3$ solution and dried over Na_2SO_4. Glc analysis showed that it consisted of almost pure III, 1-phenyl-2-chloropropane (37% yield), and trace amounts of II and IV. III was isolated in a pure state by vacuum distillation; bp 90—93°C/19 mmHg, 9.9 g (64.2 mmol). NMR τ 8.52 (d. J=6.5 Hz, 3H), 6.99 (m. 2H), 5.79 (m. 1H), 2.76 (m. 5H).

Identification of the Products. *Allyltoluene* (II, R=CH_3) was obtained as a mixture with 1-tolyl-2-chloropropane (III, R=CH_3) at bp 50—65°C/7 mmHg (the ratio of II/III=2). The NMR of a mixture of *o*- and *p*-isomers of III τ 7.68 (s. 3H), 6.25—6.05 (m. 2H), 5.30—4.75 (m. 2H), 4.30—3.90 (m. 1H), 3.0—2.75 (m. 5H).

1-Tolyl-2-chloropropane (III, R=CH_3) was obtained as a mixture of *o*- and *p*-isomers at bp 79—82°C/5 mmHg. Found: C, 71.39; H, 7.81%. Calcd for $C_{10}H_{13}Cl$: C, 71.21; H, 7.77%. NMR τ 8.53 (d. J=7.5 Hz, 3H, *o*-isomer), 8.50 (d. J=7.5 Hz, 3H, *p*-isomer).

2-Bromo-1-phenylpropane: Bp 85—89°C/5 mmHg. NMR τ 8.35 (d. J=6.4 Hz, 3H), 6.95—6.78 (m. 2H), 6.0—5.5 (m. 1H), 2.9—2.7 (m. 5H).

Ditolylpropane (IV, R=CH_3) was obtained as a mixture of 1,1- and 1,2-ditolylpropanes at bp 132—135°C/3 mmHg. Found: C, 89.70; H, 8.94%. Calcd for $C_{17}H_{20}$: C, 91.01; H, 8.99%. NMR τ 9.12 (t. J=8 Hz, 3H, 1,1-ditolylpro-

11) G. A. Olah, S. J. Kuhn, and S. H. Flood, *J. Amer. Chem. Soc.* **84**, 1688 (1962).
12) B. M. Perfetti and R. Levine, *ibid.*, **75**, 626 (1953).
13) N. A. Lange, "Handbook of Chemictry," 10th ed., McGraw-Hill, New York (1961), p. 318.
14) L. F. Fieser and M. Fieser, "Reagents for Organic Synthesis," John Wiley and Sons, New York (1967), p. 1150.
15) V. H. Hecht, *Z. Anorg. Allg. Chem.*, **254**, 46 (1947).

pane), 8.78 (d. J=8 Hz, 3H, 1,2-isomer).

β,β'-Dimethylstyrene: Bp 85—86°C/25 mmHg. NMR τ 8.18—8.05 (m, 6H) 3.8—3.65 (m, 1H), 2.8—2.65 (m, 5H).

p-*Anisylacetophenone* (*V*, $R=CH_3O$): Bp 113—122°C/6 mmHg. NMR τ 7.48 (s, 3H), 6.17 (s, 3H), 3.1 (d, J=9.5 Hz, 2H), 2.05 (d, J=9.5 Hz, 2H).

α-Methylchalcone, $C_6H_5C(CH_3)=CHCOC_6H_5$: Bp 160—163° C/2 mmHg (lit.[16] bp 225°C/22 mmHg), IR (liq. film) 1670 (s, $\nu_{C=O}$), 1610 (s, $\nu_{C=C}$) cm^{-1}.

Benzoylacetone: Bp. 115°C/5 mmHg (lit.[12] bp 103—105° C/1.8 mmHg), mp 59°C (lit.[18] 60—61°C). Found: C, 74.03; H, 6.42%. Calcd for $C_{10}H_{10}O_2$: C, 74.05; H, 6.22%.

Spectral Measurements. The IR spectra were measured on Hitachi EPI-2 and EPS-3T spectrometers. The NMR spectra were determined on a Varian A-60 spectrometer, using TMS as the internal standard in $CDCl_3$. Glc analysis was carried out on Shimadzu 5APTF apparatus, using PEG 6000 (25%)-Chromosorb-W 3-m and Apz-L (30%)-Celite 3-m columns, and on a Hitachi F-6 apparatus, using Apz-L 1-m columns.

16) I. Heilbron ed., "Dictionary of Organic Compounds," Maruzen, Tokyo (1965), p. 2153.

17) A. Baur, *Ber.*, **27**, 1608 (1894).

18) Ref. 13, p. 427.

BULLETIN OF THE CHEMICAL SOCIETY OF JAPAN, VOL. 45, 863—866(1972)

Studies of Peptide Antibiotics. XXVII. Synthesis of an Analog of Gramicidin S Containing a Glycine Residue in Place of a Proline[1]

Shuji MATSUURA, Michinori WAKI, and Nobuo IZUMIYA

Laboratory of Biochemistry, Faculty of Science, Kyushu University, Hakozaki, Fukuoka

(Received July 14, 1971)

[Gly^5]-Gramicidin S in which one L-proline residue at 5-position in gramicidin S is replaced with glycine was synthesized and tested for antibacterial properties. The cyclic decapeptide obtained was as active as natural gramicidin S. It was suggested that the mode of antibacterial activity of [Gly^5]-gramicidin S and its conformation are similar to those of GS.

In the studies of synthetic analogs of biologically active peptides, several hybrid analogs which contain two peptide portions suggested from different natural peptides have been synthesized. As such an analog, oxypressin containing the cyclic hexapeptide portion of vasopressin and the linear tripeptide portion of oxytocin was synthesized. The hybrid peptide exhibited unique biological activities compared with the parent hormones.[2] From the results it occurred to us to prepare a gramicidin S analog which contain two peptide portions and to investigate its antibacterial properties.

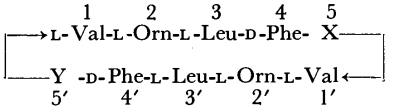

Fig. 1. Structure of GS (X, Y=L-Pro), [Gly^5]-GS (X=Gly, Y=L-Pro) and [Gly$^{5,5'}$]-GS (X, Y=Gly).

In order to understand the relationship between the chemical structure and antibacterial activity of gramicidin S (GS) (Fig. 1), various analogs of GS in which two amino acid residues are substituted with two other amino acids have been synthesized. An analog, [Gly$^{5,5'}$]-GS, was synthesized in this laboratory originally[3] and also in other laboratories,[4] and its strong antibacterial activity has been observed. However, a GS analog in which one amino acid residue is replaced with other amino acid has not yet been synthesized.

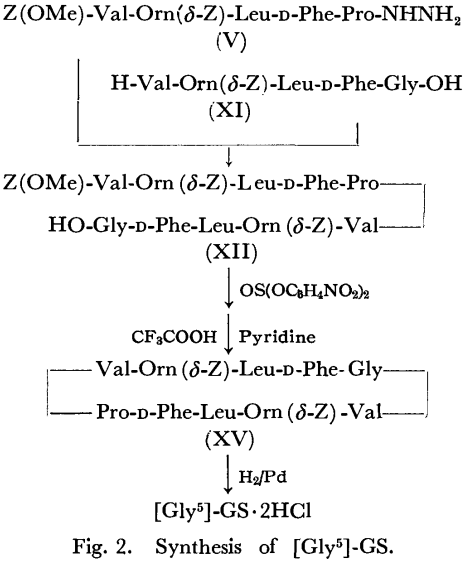

Fig. 2. Synthesis of [Gly^5]-GS.

1) Presented at the 23rd Annual Meeting of the Chemical Society of Japan, Tokyo, April, 1970.

2) R. A. Boissonnas, S. Guttmann, P.-A. Jaquenoud, and J.-P. Waller, *Helv. Chim. Acta*, **39**, 1421 (1957); J. Rudinger, J. Honzl, and M. Zaoral, *Collection Czech. Chem. Commun.*, **21**, 770 (1956); P.G. Katsoyannis, *J. Amer. Chem. Soc.*, **79**, 109 (1957).

3) H. Aoyagi, T. Kato, M. Ohno, M. Kondo, M. Waki, S. Makisumi, and N. Izumiya, This Bulletin, **38**, 2139 (1965).

4) J. Halstrom and H. Klostermeyer, *Ann.* **715**, 208 (1968); A. A. Kiryushkin, Y. A. Ovchinnikov, I. V. Kozhevnikova, and M. M. Shemyakin, "Peptides," North-Holland Pub. Co., Amsterdam (1967), p. 100.

It thus seemd of interest to prepare [Gly^5]-GS (Fig. 1) which is composed of two peptide portions, -Val-Orn-Leu-D-Phe-Pro- from GS and -Val-Orn-Leu-D-Phe-Gly- from [Gly$^{5,5'}$]-GS. This paper describes the synthesis, antibacterial properties and optical rotatory dispersion (ORD) measurement of [Gly^5]-GS.

Figure 2 indicates the route for the synthesis of [Gly^5]-GS.[5] Condensation of the azide derived from Z(OMe)-pentapeptide hydrazide (V) with a neutral pentapeptide (XI) gave an acyldecapeptide acid (XII). Pentapeptide (XI) obtained previously from Z(OMe)-pentapeptide acid[3] was prepared alternately from Boc-pentapeptide acid (X) by the action of formic acid. Z(OMe)-decapeptide acid (XII) was converted into an acyldecapeptide nitrophenyl ester (XIII), and its Z(OMe) group was removed with trifluoroacetic acid. Decapeptide trifluoroacetate (XIV) thus obtained was treated with pyridine for the cyclization reaction. The reaction mixture yielded a pure Z-substituted cyclic decapeptide (XV) which was hydrogenated to afford [Gly^5]-GS as a crystalline dihydrochloride.

TABLE 1. ANTIBACTERIAL ACTIVITY OF THE COMPOUNDS
(Minimum inhibitory concentration, μg/ml)

Compound	*Echerichia coli*	*Staphylococcus aureus*	*Bacillus subtilis*
	(Bouillon agar medium, pH 7.0)		
GS	20	2	2
[Gly^5]-GS	20	5	5
[Gly$^{5,5'}$]-GS	20	5	5
Mixture of GS and [Gly$^{5,5'}$]-GS[a]	20	2—5	2—5
	(Synthetic medium, pH 7.0)		
GS	20	5	5
[Gly^5]-GS	20	5	5
[Gly$^{5,5'}$]-GS	20	5	2—5
Mixture of GS and [Gly$^{5,5'}$]-GS[a]	20	5	5

a) A mixture was prepared with 1:1 weight ratio of GS and [Gly$^{5,5'}$]-GS.

The antibacterial activities of [Gly^5]-GS and several reference compounds toward microorganisms were tested (see Table 1). Three compounds, [Gly^5]-GS, GS and [Gly$^{5,5'}$]-GS, exhibited approximately the same activities for all the microorganisms tested. Erlanger and Goode observed that some linear decapeptides, *e.g.* H-(Val-Lys-Leu-D-Phe-Pro)$_2$-OH, revealed synergistic activity with GS against *E. coli*. They noted that the mode of antibacterial action of such linear peptides might differ from that of GS.[6] As shown in Table 1, a mixture of GS and [Gly$^{5,5'}$]-GS possessed activity in the same degree with each compound GS, [Gly$^{5,5'}$]-GS and [Gly^5]-GS; no synergistic activity of [Gly$^{5,5'}$]-GS on GS was observed. We thus assumed that the mode of action of [Gly$^{5,5'}$]-GS, and then [Gly^5]-GS, is similar to that of GS. This assumption is favored by comparison of ORD curves (Fig. 3) of the compounds referred to above with that of [β-Ala$^{5,5'}$]-GS which possessed no antibacterial activity.[7] The three compounds, [Gly^5]-GS, GS, and [Gly$^{5,5'}$]-GS, afforded a similar shape with a trough at approximately 232 mμ, while [β-Ala$^{5,5'}$]-GS afforded a shape of simple dispersion curve with no trough. The results of ORD measurements suggest that [Gly^5]-GS possesses a conformation similar to that of GS.

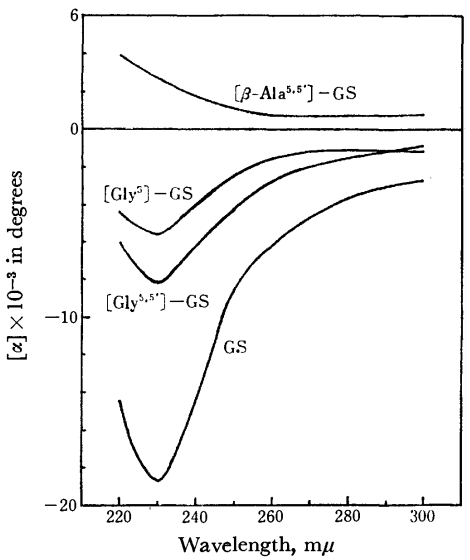

Fig. 3. ORD curves of the four compounds in ethanol. The curve of [β-Ala$^{5,5'}$]-GS is talen from a pre^{v}ious paper.[7]

Experimental

Thin layer chromatography was carried out on Merck silica gel G with the following solvent systems: R_f^1, *n*-butanol-acetic acid-pyridine-water (4:1:1:2, *v/v*); R_f^2, chloroform-methanol (5:1, *v/v*).

H-D-Phe-OEt·TsOH (I). This was prepared according to the procedure for the L isomer.[8] Yield, 88%; mp 153—154°C; $[\alpha]_D^{20}$ −20.0° (*c* 1, ethanol) (Found: C, 59.18; H, 6.48; N, 3.83%). Reported values for the L isomer;[8] mp 153°C, $[\alpha]_D$ +15.5° (DMF).

Z-Leu-D-Phe-OEt (II). This was prepared from Z-Leu-OH·DCHA (21.8 g) and I (17.8 g) with DCC (10 g) in the same way as for Z-Leu-D-Phe-OBzl.[9] Yield, 18.0 g (84%); mp 106—107°C; $[\alpha]_D^{15}$ −7.8° (*c* 1, methanol); R_f^1 0.98, R_f^2 0.76.

Found: C, 67.89; H, 7.34; N, 6.46%. Calcd for $C_{25}H_{32}O_5N_2$: C, 68.16; H, 7.32; N, 6.36%.

Z-Leu-D-Phe-NHNH$_2$ (III). This was prepared from II (17.2 g) and hydrazine hydrate (38 ml) in the same way as for the same product from Z-Leu-D-Phe-OBzl and hydrazine.[9] Yield, 15.8 g (95%); mp 163°C. No depression

5) Abbreviations: Z, benzyloxycarbonyl; Z(OMe), *p*-methoxybenzyloxycarbonyl; Boc, *t*-butyloxycarbonyl; ONp, *p*-nitrophenoxy; DCC, dicyclohexylcarbodiimide; DCHA, dicyclohexylamine; TEA, triethylamine; TsOH, *p*-toluenesulfonic acid; DMF, dimethylformamide. Amino acid symbols except D-Phe and Gly denote the L-configuration.

6) B. F. Erlanger and L. Goode, *Science*, **131**, 669 (1960).

7) S. Matsuura, M. Waki, S. Makisumi, and N. Izumiya, This Bulletin, **43**, 1197 (1970).

8) T. Kato, S. Makisumi, M. Ohno, and N. Izumiya, *Nippon Kagaku Zasshi*, **83**, 1151 (1962).

9) K. Kuromizu and N. Izumiya, This Bulletin, **43**, 2199 (1970).

of melting point was observed on a mixture of III with the product[9] prepared before. III was used for the preparation of Z-Leu-D-Phe-Pro-OEt[9] and Z(OMe)-Val-Orn(δ-Z)-Leu-D-Phe-Pro-OEt (IV)[10] as described in literature.[9,10]

Z(OMe)-Val-Orn(δ-Z)-Leu-D-Phe-Pro-NHNH$_2$ (V). A solution of IV (7.65 g, 8.4 mmol) and hydrazine hydrate (8.3 ml, 167 mmol) in DMF (15 ml) was allowed to stand at room temperature for 7 days. The reaction mixture was poured into water (1000 ml), and the crystals formed were collected by filtration; yield, 7.01 g (93%); mp 131—132°C; $[\alpha]_D^{15}$ −32.8° (*c* 0.5, DMF); R_f^1 0.64.

Found: C, 61.77; H, 7.23; N, 12.13%. Calcd for $C_{47}H_{64}O_{10}N_8 \cdot H_2O$: C, 61.42; H, 7.24; N, 12.19%.

Z(OMe)-D-Phe-Gly-OBzl (VI). This was obtained from Z(OMe)-D-Phe-OH·DCHA[11] (15.32 g) and H-Gly-OBzl·TsOH (10.11 g) with DCC (6.18 g) in the same way as for Z(OMe)-Trp-D-Phe-OBzl.[9] Yield, 11.72 g (82%); mp 115—116°C; $[\alpha]_D^{20}$ +14.2° (*c* 1, ethanol); R_f^1 0.95.

Found: C, 68.12; H, 6.19; N, 5.98%. Calcd for $C_{27}H_{28}O_6N_2$: C, 68.05; H, 5.92; N, 5.88%.

Z-Leu-D-Phe-Gly-OBzl (VII). To a mixture of VI (16.2 g, 34 mmol) and anisole (10 ml) was added 2 N hydrogen chloride in dioxane (240 ml). After 3 hr at room temperature, the solution was evaporated to dryness (yield of a syrup, 11.9 g; R_f^1 0.75). The syrup (H-D-Phe-Gly-OBzl·HCl) was condensed with Z-Leu-OH·DCHA (15.2 g, 34 mmol) and DCC (7.02 g) in chloroform (150 ml) as in the case of Z-Leu-D-Phe-OBzl.[9] Yield, 13.1 g (69%); mp 106—107°C; $[\alpha]_D^{20}$ +13.8° (*c* 1, methanol); R_f^1 0.95.

Found: C, 68.36; H, 6.73; N, 7.62%. Calcd for $C_{32}H_{37}O_6N_3$: C, 68.67; H, 6.66; N, 7.51%.

Z-Leu-D-Phe-Gly-OH (VIII). To a solution of Z-Leu-D-Phe-Gly-OEt[3] (7.0 g, 14.1 mmol) in methanol (70 ml) was added N sodium hydroxide (16.9 ml). The solution was left for 2 hr at room temperature, and N hydrochloric acid (17 ml) was added. The solution was evaporated and the resulting crystals were recrystallized from ethyl acetate-petroleum ether; yield, 5.43 g (82%); mp 116—117°C; $[\alpha]_D^{20}$ +9.3° (*c* 1, methanol); R_f^1 0.75.

Found: C, 62.87; H, 6.96; N, 8.85%. Calcd for $C_{25}H_{31}O_6N_3 \cdot 1/2H_2O$: C, 62.74; H, 6.74; N, 8.78%.

H-Leu-D-Phe-Gly-OH (IX). *(a) From VII*: A solution of VII (13.1 g, 23.4 mmol) in a mixture of acetic acid (70 ml), methanol (35 ml) and water (12 ml) was hydrogenated in the presence of palladium black. The filtrate was evaporated and the resulting crystals were collected with the aid of a mixture of ethanol and acetone; yield, 5.89 g (75%); mp 231—232°C (decomp.); $[\alpha]_D^{20}$ +32.5° (*c* 0.5, acetic acid); R_f^1 0.67.

Found: C, 60.83; H, 7.69; N, 12.30%. Calcd for $C_{17}H_{25}O_4N_3$: C, 60.88; H, 7.51; N, 12.53%.

(b) From VIII. VIII (4.69 g, 10 mmol) was hydrogenated as described above; yield, 2.58 g (77%); mp 230—232°C (decomp.); $[\alpha]_D^{20}$ +32.2° (*c* 0.5, acetic acid).

Boc-Val-Orn(δ-Z)-Leu-D-Phe-Gly-OH (X). Boc-Val-Orn(δ-Z)-NHNH$_2$ (9.69 g, 20.2 mmol)[12] was dissolved in DMF (200 ml) and 2N hydrogen chloride in dioxane (20.2 ml). To the solution at −30°C was added isoamyl nitrite (3.11 ml, 22.2 mmol). After some 10 min, disappearance of the hydrazide was recognized by the detection method of Ertel and Horner.[13] To the reaction mixture was added TEA (3.11 ml, 22.2 mmol). After 5 min at 0°C, a suspension of IX (6.77 g, 20.2 mmol) in DMF (450 ml) and dimethyl sulfoxide (50 ml) containing dicyclohexylamine (4.02 ml, 20.2 mmol) was added to the mixture. After 3 days at 4°C, the reaction mixture was evaporated to approximately 200 ml. To this was added 0.01 M citric acid (5000 ml). The resulting solid was collected and recrystallized from methanol-ether; yield, 12.02 g, (76%); mp 182—183°C; $[\alpha]_D^{25}$ +3.8° (*c* 1, DMF); R_f^1 0.82.

Found: C, 59.52; H, 7.60; N, 10.51%. Calcd for $C_{40}H_{58}O_{10}N_6 \cdot 1/2H_2O$: C, 59.31; H, 7.59; N, 10.38%.

H-Val-Orn(δ-Z)-Leu-D-Phe-Gly-OH (XI). A solution of X (3.9 g, 5 mmol) in 98% formic acid (80 ml)[14] was allowed to stand for 3 hr at room temperature. The solution was evaporated, and a mixture of TEA (20 ml) and methanol (100 ml) was added. The solution was evaporated and the resulting crystals were collected by filtration with the aid of water; yield, 2.59 g (76%); mp 192—193°C; $[\alpha]_D^{25}$ −4.3° (*c* 0.2, acetic acid); R_f^1 0.80, R_f^2 0.55 (Found as monohydrate: C, 59.86; H, 7.44; N, 12.20%). The same compound (XI) was prepared from Z(OMe)-Val-Orn(δ-Z)-Leu-D-Phe-Gly-OH with the action of trifluoroacetic acid;[3] mp 191—192°; $[\alpha]_D^{25}$ −4.2° (acetic acid).

Z(OMe)-Val-Orn(δ-Z)-Leu-D-Phe-Pro-Val-Orn(δ-Z)-Leu-D-Phe-Gly-OH (XII). V (292 mg, 0.32 mmol) was treated with isoamyl nitrite (0.049 ml, 0.352 mmol) as in the case of X. To the azide solution was added a solution of XI (240 mg, 0.352 mmol) in DMF (4 ml) containing TEA (0.049 ml, 0.352 mmol). After being stirred for 5 days at 4°C, the reaction mixture was added to 0.02 M citric acid (250 ml). The resulting solid was collected and recrystallized from methanol-petroleum ether; yield, 343 mg (69%); mp 128—129°C; $[\alpha]_D^{20}$ −21.0° (*c* 0.5, DMF); R_f^1, 0.98, R_f^2 0.62.

Found: C, 61.39; H, 7.16; N, 10.62%. Calcd for $C_{82}H_{110}O_{18}N_{12} \cdot 3H_2O$: C, 61.32; H, 7.28; N, 10.47%.

cyclo-*(Val-Orn(δ-Z)-Leu-D-Phe-Pro-Val-Orn(δ-Z)-Leu-D-Phe-Gly) (XV).* XII (280 mg, 0.18 mmol) was converted into the corresponding *p*-nitrophenyl ester (XIII) (344 mg) with di-*p*-nitrophenyl sulfite (583 mg, 1.8 mmol). After XIII (340 mg) was converted into a decapeptide nitrophenyl ester trifluoroacetate (XIV), XIV was subjected to the cyclization reaction with pyridine.[3] Yield, 76 mg (31% from XII); mp 156—157°C; $[\alpha]_D^{20}$ −93.5° (*c* 0.25, acetic acid).

Found: C, 62.00; H, 7.36; N, 11.43%; mol wt,[15] 1380. Calcd for $C_{73}H_{100}O_{14}N_{12} \cdot 2H_2O$: C, 61.97; H, 7.48; N, 11.67%; mol wt, 1405.

cyclo-*(Val-Orn-Leu-D-Phe-Pro-Val-Orn-Leu-D-Phe-Gly) Dihydrochloride ([Gly^5]-GS·2HCl).* A solution of XV (36mg, 0.026 mmol) in 0.01 N methanolic hydrogen chloride (5.7 ml) was hydrogenated and the filtrate was evaporated. The resulting crystals were recrystallized from methanol-ether-petroleum ether; yield of an air-dried product, 31.8 mg (94%); mp 205—207°C (decomp.); $[\alpha]_D^{20}$ −88.9° (*c* 0.25, ethanol); R_f^1 0.77, R_f^2 0.02. Paper electrophoresis and carboxymethylcellulose column chromatography of this product[7] revealed a single spot or peak, which was at the same position as that by natural GS. Amino acid ratio in acid hydrolysate; Pro 1.08, Gly 0.98, Val 2.11, Leu 2.10, Phe 1.98, Orn 2.05.

Found: C, 52.88; H, 7.91; N, 12.63%. Calcd for $C_{57}H_{88}O_{10}N_{12} \cdot 2HCl \cdot 7H_2O$: C, 52.64; H, 8.06; N, 12.92%.

10) M. Waki and N. Izumiya, This Bulletin, **40**, 1687 (1967).
11) M. Waki and N. Izumiya, *ibid.*, **41**, 1909 (1968).
12) T. Kato, M. Kondo, M. Ohno, and N. Izumiya, *ibid.*, **38**, 1202 (1965).
13) H. Ertel and L. Horner, *J. Chromatog.*, **7**, 268 (1962).
14) B. Halpern and D. E. Nitecki, *Tetrahedron Letters*, **1967**, 3031.
15) Molecular weight was determined by a Hitachi Osmometer, Type 115, using methanol as a solvent.

Microbiological Assays[16] *and ORD Measurements.*[17] The minimum inhibitory concentration was determined by a dilution method. The results are shown in Table 1. ORD measurements were performed as described previously.[7] The curves are shown in Fig. 3.

16) We are indebted to the staff of Takeda Chemical Industries, Ltd. for the assay.

17) We are indebted to the members of Prof. Funatsu's Laboratory, Faculty of Agriculture, for help in ORD measurements.

BULLETIN OF THE CHEMICAL SOCIETY OF JAPAN, VOL. 45, 866—870(1972)

Sulfenylation of Active Methylene Compounds with Sulfenamides

Takanobu KUMAMOTO, Susumu KOBAYASHI, and Teruaki MUKAIYAMA
Laboratory of Organic Chemistry, Tokyo Institute of Technology, Ookayama, Meguro-ku, Tokyo
(Received July 21, 1971)

Equimolar reactions of sulfenamides derived from secondary alkylamines with active methylene compounds afforded mono-sulfenylated compounds in good yields. The reactions of 2 mol of sulfenamides derived from imides with 1 mol of active methylene compounds in the presence of a base gave di-sulfenylated compounds. It was found that α-mono-sulfenylated ketones were prepared by the reactions of enamines with sulfenamides derived from imides. α-*gem*-Di-sulfenylated ketones were prepared by the reactions of α-mono-sulfenylated ketones with sulfenamides derived from imides in the presence of a base. The preparation and reactions of *N*-phenylthiobenzamidine hydrochloride were also examined.

In a previous communication,[1] sulfenylation of active methylene compounds by the use of sulfenamides was reported. The reactions are described more in detail with new results in this paper.

It was found that the equimolar reaction of *N,N*-diethylbenzenesulfenamide with malononitrile in methylene chloride at room temperature for 5 hr resulted in the formation of the dimethylammonium salt of phenylthiomalononitrile in 55% yield. By acid hydrolysis of the salt, phenylthiomalononitrile was obtained in quantitative yield.

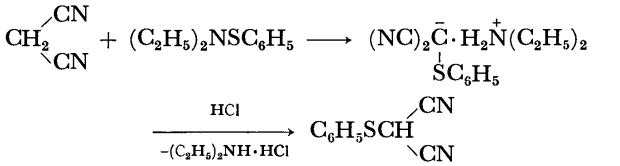

In the case of the reaction of *N,N*-diethylbenzenesulfenamide with dibenzoylmethane, α-phenylthio-β-*N,N*-diethylaminochalcone was obtained in 66% yield instead of the salt. The enamine was converted into phenylthiodibenzoylmethane in quantitative yield by acid hydrolysis.

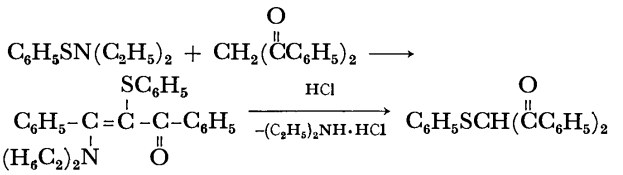

The reactions of *N,N*-diethylbenzenesulfenamide with acetylacetone, ethyl acetoacetate or ethyl malonate under similar conditions without isolation of the intermediates, enamines or salts, afforded corresponding mono-sulfenylated products in good yields (Table 1).

The reactions of *N*-phenylthiopyrrolidine with active methylene compounds were examined. Treatment of *N*-phenylthiopyrrolidine with ethyl acetoacetate at room temperature, followed by acid hydrolysis gave ethyl acetyl(phenylthio)acetate in 60% yield. Similarly, ethyl phenylthiomalonate was obtained in 52% yield by the reaction of *N*-phenylthiopyrrolidine with ethyl malonate. The yields of the mono-sulfenylated products by the above mentioned reactions are higher than those of the reactions of active methylene compounds with *N,N*-diethylbenzenesulfenamide. The results suggest that the reactivity of the sulfenamides depends on the basicity of the amino component of the sulfenamides.

In order to clarify the effects of the amino component of the sulfenamide on this type of sulfenylation, the reactions of ethyl malonate with various sulfenamides such as *N*-phenylthioaniline, *N*-phenylthiopiperidine or *N*-phenylthiobenzamidine[2] were examined (Table 2). The results show that neither *N*-phenylthioaniline, derived from a weak base, nor *N*-phenylthiobenzamidine derived from a strong base, affords a sulfenylated compound. *N,N*-diethylbenzenesulfenamide, *N*-phenylthiopyrrolidine or *N*-phenylthiopiperidine is suitable for mono-sulfenylation of active methylene compounds.

On the other hand, it was found that di-sulfenylated products were obtained by the reactions of *N*-phenylthiosuccinimide with active methylene compounds in the presence of a base. For example, when 2 mol of *N*-phenylthiosuccinimide, 1 mol of dibenzoylmethane and 2 mol of triethylamine were stirred overnight in methylene chloride at room temperature, bis(phenylthio)dibenzoylmethane was obtained in 50% yield.

1) T. Mukaiyama, S. Kobayashi and T. Kumamoto, *Tetrahedron Lett.*, **1970**, 5115.

2) J. Goerdeler, D. Krause-Loevenich and B. Wedekind, *Chem. Ber.*, **90**, 1638 (1957).

Table 1. Reactions of *N,N*-diethylbenzene sulfenamide with active methylene compounds

$CH_2\begin{smallmatrix}X\\Y\end{smallmatrix}$	Yield (%)	Bp (°C/mmHg) or mp [°C]	Elemental analysis (%) Found C	H	S	Calcd C	H	S
$CH_2(COC_6H_5)_2$	66	[93—94]	76.13	4.98	9.86	75.89	4.85	9.63
$CH_2(COCH_3)_2$	77	(152—153/22)	63.62	5.78	15.48	63.45	5.81	15.37
$CH_2(CN)_2$	55	[84—87]	62.37	3.37	18.67	62.07	3.47	18.37
$CH_3COCH_2CO_2C_2H_5$	37	(125—127/4.5)	60.33	6.05	13.30	60.50	5.92	13.43
$CH_2(CO_2C_2H_5)_2$	48	(148 1.7)	58.01	5.99	12.07	58.20	6.01	11.93

Table 2. Reactions of ethyl malonate with sulfenamides

Sulfenamide	Yield of $C_6H_5SCH(CO_2C_2H_5)_2$ (%)
$C_6H_5SNHC_6H_5$	—
$C_6H_5SN(C_2H_5)_2$	48
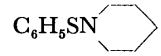	44
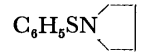	52
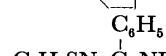	—

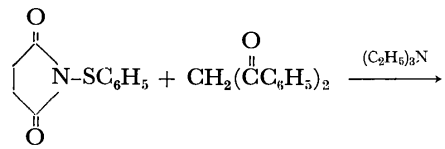

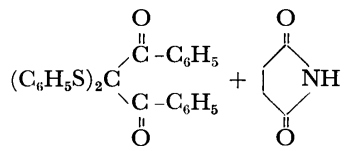

In a similar way, the reactions of *N*-phenylthiosuccinimide with acetylacetone, malononitrile, ethyl acetoacetate or ethyl malonate afforded the corresponding di-sulfenylated products in good yields (Table 3).

The results can be explained as follows. Sulfenylation of active methylene compounds with the sulfenamide derived from the secondary alkylamines would proceed through the activation of sulfur-nitrogen bond by the protonation to the nitrogen atom, followed by the reaction on the sulfur atom with active methylene compounds to give mono-sulfenylated products. These would be converted rapidly to enamines or salts by the subsequent reactions with the secondary alkylamines formed at the same time. Since enamines or salts can not participate in the activation of the sulfenamides, di-sulfenylated products would not be produced in these reactions.

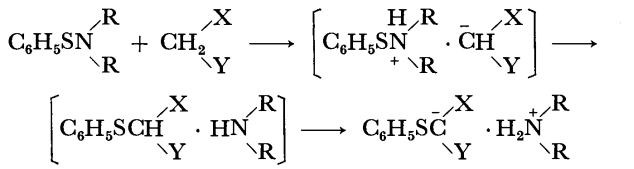

In the case of sulfenylation by the use of sulfenamides derived from imides, the sulfenamide can react with active methylene compounds in basic media to produce sulfenylated products owing to a labile elimination of stable imide anions from the sulfenamides. Thus, the initially formed triethylammonium salts of mono-sulfenylated products further react with sulfenamides to give di-sulfenylated products.

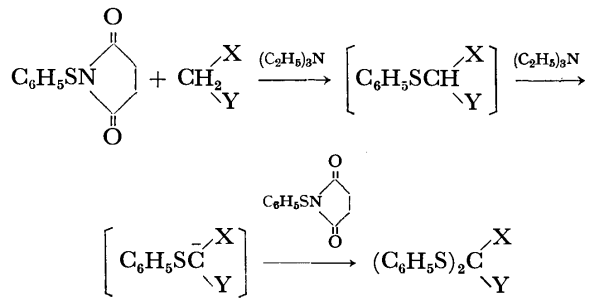

Sulfenylation of the α-carbon of ketones by the use of the above mentioned sulfenamides was next tried in order to establish a convenient method for the preparation of α-mono or α-*gem*-di-sulfenylated ketones considered to be valuable as synthetic intermediates. When *N,N*-diethylbenzenesulfenamide was allowed to react with cyclohexanone in methylene chloride, no sulfenylated product was obtained and only starting materials

Table 3. Reactions of *N*-phenylthiosuccinimide with active methylene compounds

$CH_2\begin{smallmatrix}X\\Y\end{smallmatrix}$	Yield (%)	Mp (°C)	Elemental analysis (%) Found C	H	S	Calcd C	H	S
$CH_2(COC_6H_5)_2$	50	184.5—185.5	73.41	4.87	14.39	73.63	4.58	14.53
$CH_2(COCH_3)_2$	73	117—118	64.72	5.21	19.99	64.55	5.10	20.23
$CH_2(CN)_2$	54	58—59	63.63	3.54	22.62	63.83	3.57	22.67
$CH_2(CO_2C_2H_5)_2$	93	74—75	60.39	5.65	17.14	60.63	5.36	17.01
$CH_3COCH_2CO_2C_2H_5$[a)]	64	122—124[a)]	54.82	4.33	12.22	54.75	4.21	12.16

a) This compound was isolated as its 2,4-dinitrophenyl hydrazone.

were recovered quantitatively. However, the reaction of 2 moles of *N*-phenylthiopyrrolidine and 1 mol of cyclohexanone in methylene chloride at room temperature for 20 hr, followed by acid hydrolysis gave 2,6-bis(phenylthio)cyclohexanone in 67% yield.

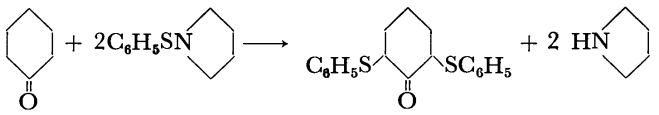

A convenient method for the preparation of α-mono-sulfenylated ketones was established by the reactions of *N*-phenylthiophthalimide with enamines. For example, the reaction of 1-piperidinocyclohexene with *N*-phenylthiophthalimide in tetrahydrofuran at room temperature for 4 hr, followed by acid hydrolysis, afforded 2-phenylthiocyclohexanone and phthalimide in 74% and quantitative yields, respectively.

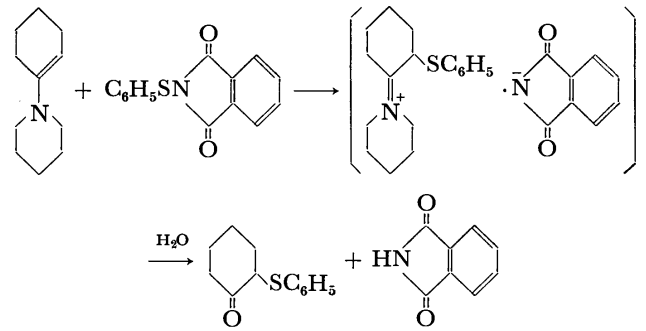

Similarly, α-mono-sulfenylated ketones were obtained in good yields by the reactions of *N*-phenylthiophthalimide with 4-methyl-1-piperidinocyclohexene, β-piperidinostyrene, or 1-piperidino-1-butene (Table 4).

It was found that the α-*gem*-di-sulfenylated ketones were obtained by the reactions of mono-sulfenylated ketones with *N*-phenylthiophthalimide in the presence of a base. When 2-phenylthiocyclohexanone was stirred with *N*-phenylthiophthalimide and triethylamine in methylene chloride, 2,2-bis(phenylthio)cyclohexanone was obtained in 55% yield.

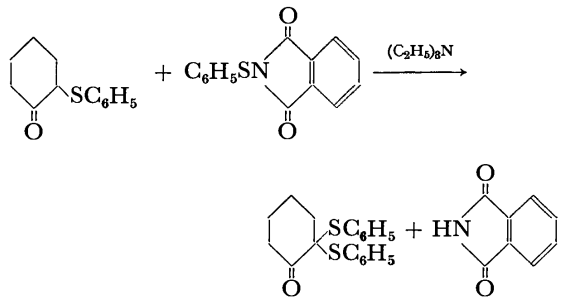

It was found that *N*-phenylthiobenzamidine hydrochloride could be isolated as a white stable solid by the reaction of *N*-phenylthiobenzamidine with hydrochloric acid in benzene. No report has been found on the isolation of hydrochloride of the sulfenamide because of the facile cleavage of the sulfur-nitrogen bond by the action of hydrochloric acid to afford sulfenyl chloride and amine hydrochloride.

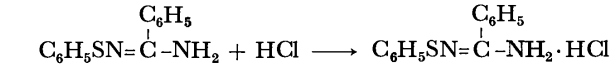

Table 4. Reactions of enamines with *N*-phenylthiophthalimide

Enamine	α-Mono-sulfenylated ketone	
	Yield (%)	Bp °C/mmHg
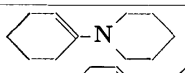	74	122—124/2
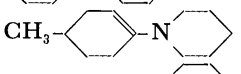	75	127—131/2
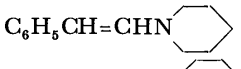	65	135—138/2
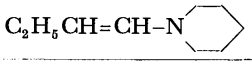	50	98—100/2

It was found that *N*-phenylthiobenzamidine hydrochloride reacted with ketones to afford α-mono-sulfenylated ketones in fairly good yields. For example, the equimolar reaction of *N*-phenylthiobenzamidine hydrochloride with cyclohexanone in dimethyl sulfoxide at room temperature resulted in the formation of 2-phenylthiocyclohexanone and 2,2-bis(phenylthio)cyclohexanone in 40% and 15% yields, respectively.

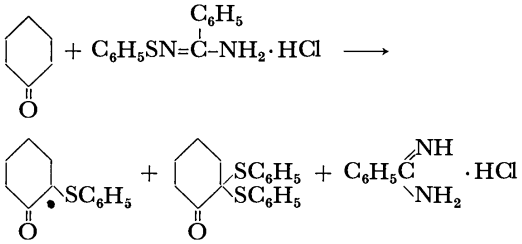

In the case of the reaction of 2 moles of *N*-phenylthiobenzamidine hydrochloride with 1 mol of cyclohexanone in dimethyl sulfoxide at room temperature, 2,2-bis(phenylthio)cyclohexanone was obtained in 70% yield.

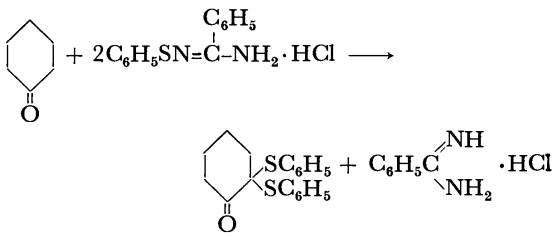

Sulfenylation of unsymmetric ketones by the use of the above mentioned hydrochloride was examined. When 2-methylcyclohexanone was allowed to react with *N*-phenylthiobenzamidine hydrochloride in dimethyl sulfoxide at room temperature, 2-methyl-2-phenylthiocyclohexanone was exclusively obtained in 57% yield.

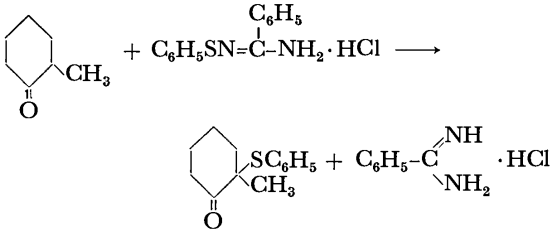

2-Methyl-2-phenylthiocyclopentanone, 2-methyl-2-phenylthio-3-butanone or 3-phenylthio-2-butanone was obtained by the reaction of *N*-phenylthiobenzamidine hydrochloride with 2-methylcyclopentanone, 2-methyl-

Table 5. Reactions of *N*-phenylthiobenzamidine hydrochloride with ketones

Ketone	Structure	Product Yield (%)	Product NMR (τ)	Anal. of 2,4-dinitrophenylhydrazone Found (Calcd) C	H	N	S
	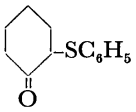	40	—			—	
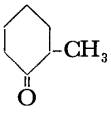	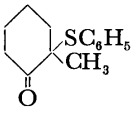	57	8.88(S 3H) 7.6—8.5(M 8H) 2.75(S 5H)	56.98 (56.99	4.85 5.04	13.89 13.99	7.69 7.89)
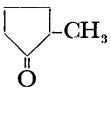	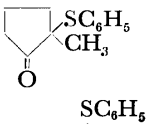	58	8.80(S 3H) 7.3—8.3(M 6H) 2.70(M 5H)	55.32 (55.95	4.69 4.70	14.80 14.50	8.21 8.29)
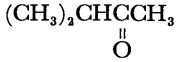	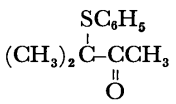	44	8.65(S 6H) 7.70(S 3H) 2.85(S 5H)	54.71 (54.54	4.91 4.86	15.25 14.97	8.39 8.56)
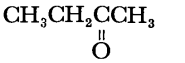	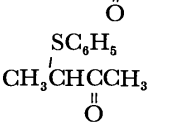	30	8.55(D 3H) 7.75(S 3H) 6.30(Q 1H)2.70(M 5H)	53.60 (53.33	4.46 4.48	16.10 15.55)	

3-butanone or 2-butanone, respectively (Table 5). The results show that sulfenylation of unsymmetric-ketones by the use of *N*-phenylthiobenzamidine hydrochloride occurs on the α-carbon of ketones bearing the larger number of alkyl groups.

The reactions could be interpreted as follows.

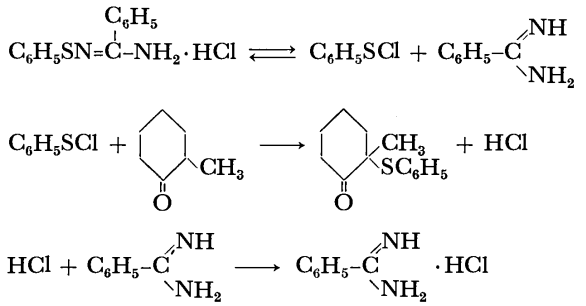

At first, an active intermediate, benzenesulfenyl chloride, is generated from *N*-phenylthiobenzamidine hydrochloride in dimethyl sulfoxide along with benzamidine. The chloride in turn reacts with ketones to afford α-sulfenylated ketones and hydrogen chloride. The benzamidine acts as a hydrogen chloride scavenger. The presence of benzenesulfenyl chloride can be supposed from the following. (1) Sulfenylation of unsymmetric-ketone with the use of *o*-nitrobenzenesulfenyl chloride occurs on the α-carbon of ketone bearing larger number of alkyl groups.[3] (2) The reaction of cyclohexene with *N*-phenylthiobenzamidine hydrochloride in dimethyl sulfoxide affords 2-chlorocyclohexyl phenyl sulfide. The same compound was also obtained by the reaction of cyclohexene with benzenesulfenyl chloride in methylene chloride.[4]

It should be noted that the reactions of active methylene compounds with sulfenamides derived from secondary amines afforded mono-sulfenylated compounds. The reactions of active methylene compounds with sulfenamides derived from imides gave di-sulfenylated compounds.

Mono-sulfenylated ketones are prepared by the reactions of enamines with sulfenamides derived from imide or the reactions of *N*-phenylthiobenzamidine hydrochloride with ketones. *gem*-Di-sulfenylated ketones are prepared by the reactions of α-mono-sulfenylated ketones with sulfenamides derived from imides in the presence of a base.

Experimental

Reaction of N,N-*Diethylbenzenesulfenamide with Malononitrile.* A mixture of *N,N*-diethylbenzenesulfenamide (1.81 g, 0.01 mol) and malononitrile (0.66 g, 0.01 mol) was stirred in methylene chloride (30 m*l*) at room temperature for 5 hr. Removal of the solvent under reduced pressure gave white crystals. Recrystallization from benzene afforded diethylammonium salt of phenylthiomalononitrile 1.36 g 55% mp 85—87°C. Found: C, 62.84; H, 6.87; N, 17.14; S, 12.99%. Calcd for $C_{13}H_{17}N_3S$: C, 63.14; H, 6.93; N, 16.99; S, 12.94%. The salt was stirred in a mixture of 10% hydrochloric acid (30 m*l*) and benzene (30 m*l*) at room temperature. After stirring for 1 hr, the benzene layer was separated. Removal of the solvent gave phenylthiomalononitrile. It was recrystallized from isopropyl alcohol. (0.93 g, guantitative) mp 84—87°C. Found: C, 62.37; H, 3.37; S, 18.67%. Calcd for $C_9H_6N_2S$: C, 62.07; H, 3.47; S, 18.37%.

The reaction of *N,N*-diethylbenzenesulfenamide with dibenzoylmethane was carried out by a similar procedure. In the case of the reaction of *N,N*-diethylbenzenesulfenamide with acetylacetone, ethyl acetoacetate or ethyl malonate, the reaction was carried out without isolation of the intermediates, salts or enamines (Table 1).

3) J. A. Barltrop and K. J. Morgan, *J. Chem. Soc.*, **1960**, 4486.
4) N. Kharasch, "Organic Sulfur Compounds" Pergamon Press, New York, Vol. I, Chapter 32.

Reaction of N-*Phenylthiosuccinimide with Dibenzoylmethane in the Presence of Triethylamine.* A mixture of *N*-Phenylthiosuccinimide (2.09 g, 0.01 mol), dibenzoylmethane (1.14 g, 0.005 mol) and triethylamine (1.11 g, 0.011 mol) was stirred in methylene chloride (40 m*l*) at room temperature. After stirring was continued overnight, the solvent was removed under reduced pressure. Fifty m*l* of water was added to the residue and the resulting oil was extracted with benzene. Removal of the solvent gave a white solid. It was recrystallized from ethanol to give bis(phenylthio)dibenzoylmethane. 1.08 g (50%). Mp 184.5—185.5°C. Found: C, 73.41; H, 4.87; S, 14.39%. Calcd for $C_{27}H_{20}O_2S_2$: C, 73.63; H, 4.58; S, 14.53%.

By a similar procedure, 3,3-bis(phenylthio)-2,3-pentanedione, bis(phenylthio)malononitrile, ethyl α,α'-bis(phenylthio) acetoacetate and ethyl bis(phenylthio)malonate were obtained by the reactions of *N*-phenylthiosuccinimide with acetylacetone, malononitrile, ethyl acetoacetate and ethyl malonate, respectively, in the presence of triethylamine (Table 3).

Reaction of N-*Phenylthiopyrrolidine with Cyclohexanone.* A mixture of *N*-phenylthiopyrrolidine (3.67 g, 0.02 mol) and cyclohexanone (1.00 g, 0.01 mol) was stirred in methylene chloride at room temperature for 20 hr. Removal of the solvent gave an oily residue. Into the residue, a mixture of 10% hydrochloric aicd (30 m*l*) and benzene (30 m*l*) was added under stirring. After stirring for 1 hr, the benzene layer was separated from the mixture and dried with sodium sulfate. The solvent was removed under reduced pressure to give an oily product. It was chromatographed on silica gel. 2,6-Bis(phenylthio)cyclohexanone was obtained from the eluate with a mixture of benzene and petroleum ether (1: 1) 1.96 g, 67%, and was confirmed by conversion into 2,4-dinitrophenylhydrazone. Mp 197—198°C. Found: C, 58.05; H, 4.51; N, 11.50; S, 13.15%. Calcd for $C_{24}H_{22}N_4O_4S_2$: C, 58.30; H, 4.48; N, 11.33; S, 12.95%.

Reaction of 1-Piperidinocyclohexene with N-*Phenylthiophthalimide.* To a suspension of *N*-phenylthiophthalimide (2.55 g, 0.01 mol) in tetrahydrofuran (20 m*l*), a solution of 1-piperidinocyclohexene (1.67 g, 0.01 mol) in tetrahydrofuran (10 m*l*) was added dropwise. With the addition, the precipitate of *N*-phenylthiophthalimide disappeared. After stirring for 4 hr at room temperature, the solvent was removed under reduced pressure. The resulting white solid was added to 10% hydrochloric acid (20 m*l*) under stirring. After stirring for 1 hr, the reaction mixture was extracted with benzene. Removal of the solvent gave an oily residue. Purification of the residue by silica gel column chromatography gave 2-phenylthiocyclohexanone. It was further purified by distillation under reduced pressure. 122—124°C/2 mmHg. 1.52 g (74%). The structure of the compound was confirmed by a direct comparison of its IR spectra with those of the authentic sample.[5]

Similarly, 4-methyl-2-phenylthiocyclohexanone, phenyl(phenylthio)acetaldehyde and 2-phenylthiobutyraldehyde were obtained by the reactions of 4-methyl-1-piperidinocyclohexene, β-piperidinostyrene and 1-piperidinobutene with *N*-phenylthiophthalimide (Table 4).

Reaction of 2-Phenylthiocyclohexanone with N-*Phenylthiophthalimide in the presence of Triethylamine.* A mixture of 2-phenylthiocyclohexanone (41.2 g, 0.2 mol), *N*-phenylthiophthalimide (51 g, 0.2 mol) and triethylamine (22 g, 0.22 mol) was refluxed in methylene chloride (300 m*l*) for 4 hr. The resulting precipitate, phthalimide, was filtered off and filtrate was evaporated under reduced pressure. One hundred m*l* of benzene was added to the residue and the resulting phthalimide was filtered again. Removal of the solvent under reduced pressure gave crystalline solids. Recrystallization from ethanol afforded 2,2-bis(phenylthio)cyclohexanone 36.09 g, 55%, mp 120—122°C. Found: C, 68.77; H, 5.97; S, 20.32%. Calcd for $C_{18}H_{18}OS_2$: C, 68.78; H, 5.77; S, 20.36%.

Preparation of N-*Phenylthiobenzamidine Hydrochloride.* To a solution of *N*-phenylthiobenzamidine (2.28 g, 0.01 mol) in benzene, 6N hydrochloric acid (2 m*l*) was added dropwise. After stirring for 30 min, a white precipitate, *N*-phenylthiobenzamidine hydrochloride, was deposited. The precipitate was filtered under reduced pressure and dried in a desiccator without further purification. 2.30 g, (87%), mp 120—121°C (decomp.). Found: C, 59.28; H, 4.69; N, 10.31; S, 12.12%. Calcd for $C_{13}H_{13}N_2SCl$: C, 58.98; H, 4.91; N, 10.59; S, 12.10%.

Reaction of N-*Phenylthiobenzamidine Hydrochloride with Equimolar Amounts of Cyclohexanone.* A mixture of *N*-phenylthiobenzamidine hydrochloride (1.32 g, 0.005 mol) and cyclohexanone (0.49 g, 0.005 mol) was stirred in dimethyl sulfoxide (20 m*l*) at room temperature for 6 hr. The mixture was added into 300 m*l* of water and the resulting oil was extracted with benzene. The benzene layer was evaporated under reduced pressure to give an oily residue. The residue was chromatographed on silica gel. 2-Phenylthiocyclohexanone (0.41 g, 40%) and 2,2-bis(phenylthio)cyclohexanone (0.12 g, 15%) were obtained from the eluate with a mixture of benzene and petroleum ether (1: 1).

By a similar procedure, 2-methyl-2-phenylthiocyclohexanone, 2-methyl-2-phenylthiocyclopentanone, 2-methyl-2-phenylthio-3-butanone, and 3-phenylthio-2-butanone were obtained from the reaction of *N*-phenylthiobenzamidine hydrochloride with 2-methylcyclohexanone, 2-methylcyclopentanone, 3-methyl-2-butanone and 2-butanone.

Reaction of 2 mol of N-*Phenylthiobenzamidine Hydrochloride with 1 Mol of Cyclohexanone.* A mixture of *N*-phenylthiobenzamidine hydrochloride (1.32 g, 0.005 mol) and cyclohexanone (0.25 g, 0.0025 mol) was stirred in dimethyl sulfoxide (20 m*l*) at room temperature for 6 hr. The mixture was added to 300 m*l* of water and the resulting oil was extracted with benzene. The solvent was removed under reduced pressure and residue was purified by silica gel column chromatography. From the eluate with a mixture of benzene and petroleum ether (1: 1), 2,2-bis(phenylthio)cyclohexanone was obtained, 0.55 g (70%) mp 122—123°C.

5) R. Wilputte and R. H. Martin, *Bull. Soc. Chim. Belg.*, **65**, 874 (1956); *Chem. Abst.*, **51**, 6588i.

The Apparent Molar Volumes of Tetraalkylammonium Halides in Liquid Sulfur Dioxide

Kohei UOSAKI, Yasuhiko KONDO, and Niichiro TOKURA

Department of Applied Chemistry, Faculty of Engineering, Osaka University, Suita, Osaka

(Received July 30, 1971)

The apparent molar volumes, Φv, of tetraalkylammonium halides, R_4NX (R=Me, Et, *n*-Pr, and *n*-Bu; X=Br^- and I^-), have been determined in liquid sulfur dioxide at several concentrations, and from these values the apparent molar volumes at an infinite dilution, Φv°, have been obtained for these salts at 25°C. The results indicate that, for all the salts, the Φv *vs.* $\sqrt{c}$ curves are almost straight over the concentration ranges studied. The slopes of the plots have large positive values for all the salts in this solvent. In order to study the ion-solvent interaction, the apparent molar volumes of the individual ions at an infinite dilution have been determined from those values by Conway's method. While the Φv° values of tetraalkylammonium ions are similar to those in other solvents, the Φv° values of bromide and of iodide ions in this solvent are quite small compared with those in other solvents. The results can be explained in terms of a strong anion-solvent interaction in liquid sulfur dioxide resulting from the formation of a charge-transfer complex of the halide ion with sulfur dioxide.

The study of the ion-solvent interaction is not only very interesting in itself, but also very instructive in making clear the role of a solvent in the process of Finkelstein, **Sn Ar**, and other ionic reactions in solution.[1]

On the other hand, liquid sulfur dioxide has been well known to be a peculiar solvent, for in spite of its low dielectric constant, it dissolves inorganic salts well and has a high ionizing power, and a reaction containing carbonium ion as an intermediate can proceed at an extraordinary fast rate in this solvent.[2] These facts have been explained as being due to a strong anion-solvent interaction in liquid sulfur dioxide,[2] but on the nature of the ion-solvent interaction in the solvent only a few, widely varying studies have been reported, including the studies of electrolytic conductance by Lichtin[3] and a short article on electrostriction volume measurements.[4] Therefore it is very important to investigate the ion-solvent interaction in liquid sulfur dioxide.

Though there are many ways to study ion-solvent interactions, in the present article the authors will discuss it from the view point of the apparent molar volumes of tetraalkylammonium halides, R_4NX (R=Me, Et, *n*-Pr, and *n*-Bu; X=Br^- and I^-) at an infinite dilution, Φ°_V.

The measurements were also performed in acetonitrile and in methanol, and the values obtained were compared with those in the references.

Experimental

Materials. The liquid sulfur dioxide was dried over phosphorus pentoxide for at least one day, distilled twice, and degassed before use. The acetonitrile was refluxed over calcium hydride, distilled, and then repeatedly distilled from phosphorus pentoxide and from calcium hydride.[5] The methanol was treated with magnesium ribbon and distilled.[6] The tetramethylammonium bromide and iodide were obtained from Wako Pure Chemicals and were recrystallized three times each from an ethanol-water mixture and water. The other tetraalkylammonium halides were synthesized from the corresponding trialkylamine and alkyl halide in various solvents at the reflux temperature, and were recrystallized from various solvents. These solvents are summarized in Table 1.

All the salts were dried *in vacuo* at 65°C for one day before use.

Procedure. The densities of an electrolyte solution of liquid sulfur dioxide were measured in a sealed pressure vessel by means of glass float, which was calibrated to a standard state of pure water using mixed solutions of sulfuric acid and water. The values of the density of pure liquid sulfur dioxide (d_0=1.3719 at 25°C) obtained by the present study argeed well with the value (d_0=1.3718) which was obtained by the extrapolation to 25°C of the value quoted

TABLE 1. SOLVENTS FOR THE SYNTHESIS AND RECRYSTALLIZATION OF TETRAALKYLAMMONIUM HALIDES, R_4NX.

R_4NX	R_3N	RX	Solvent for	
			Preparation	Recrystallization
Et_4NBr	Et_3N	EtBr	Acetone	Methanol - acetone mixture
Et_4NI	Et_3N	EtI	Acetone	Methanol - acetone mixture
n-Pr_4NBr	*n*-Pr_3N	*n*-PrBr	Acetone	Methanol - acetone mixture
n-Pr_4NI	*n*-Pr_3N	*n*-PrI	Acetone	Methanol - acetone mixture
n-Bu_4NBr	*n*-Bu_3N	*n*-BuBr	Methyl ethyl ketone	Acetone - ether mixture
n-Bu_4NI	*n*-Bu_3N	*n*-BuI	Methyl ethyl ketone	Acetone - ether mixture

1) A. J. Parker, *Chem. Rev.*, **69**, 1 (1969).
2) N. Tokura, *Bull. Chem. Res. Inst. Non-Aqueous Soln. Tohoku Univ.*, **19**, 47 (1969).
3) N. N. Lichtin, "Progr. Phys. Org. Chem," Vol. 1, S. G. Cohen *et al.*, eds., Interscience Publishers, New York (1963).
4) Y. Kondo, T. Goto, I. Suo, and N. Tokura, This Bulletin, **39**, 1230 (1966).
5) J. F. Coetzee, G. P. Cunningham, D. K. McGuire, and G. R. Padmanabhan, *Anal. Chem.*, **34**, 1139 (1962).
6) A. A. Mayrott, *J. Amer. Chem. Soc.*, **63**, 3079 (1941).

from the International Critical Tables,[7] within the limits of experimental error.

The densities of solutions of acetonitrile and methanol were determined by using a pycnometer with a 50-m*l* capacity.

All the solutions were prepared by weight.

Results and Discussion

The experimental values of the densities of these salt solutions of liquid sulfur dioxide are given in Fig. 1.

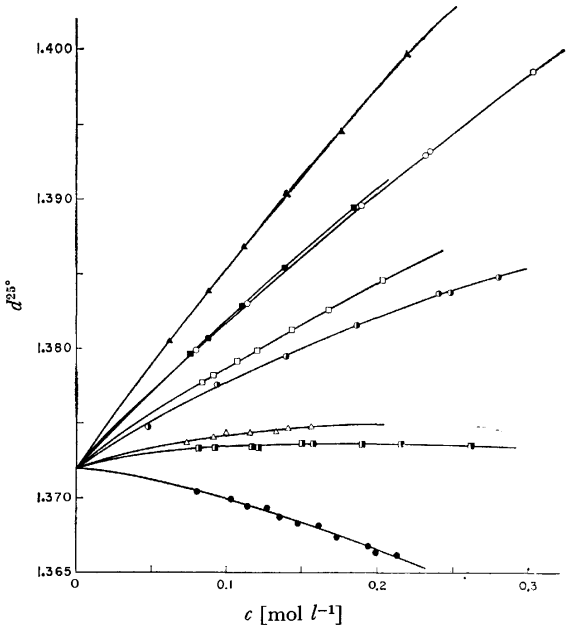

Fig. 1. Densities of liq. SO_2 solutions of tetraalkylammonium halides at 25°C.
○; Me_4NBr, ▲; Me_4NI, □; Et_4NBr, ■; Et_4NI, △; n-Pr_4NBr, ◑; n-Pr_4NI, ●; n-Bu_4NBr, ◨; n-Bu_4NI

The apparent molar volumes, Φv, were calculated from the density data by the equation:[8]

$$\Phi v = (M/d_0) - 1000(d-d_0)/cd_0 \qquad (1)$$

where d_0, M, d, and c are the density of the pure solvent, the molecular weight of the salt, the density of the solution, and the concentration of the solutes respectively.

In Figs. 2, 3, and 4, the apparent molar volumes, Φv, are plotted against the square root of the concentration of the salt, $\sqrt{c}$. In all cases, the plots of Φv *vs.* $\sqrt{c}$ gave nearly straight lines. Then, the apparent molar volumes of the salts at an infinite dilution, Φv°, and the slope, Sv, were obtained on the basis of Eq. (2)[8] by a least-squares method:

$$\Phi v = \Phi v^\circ + Svc^{1/2} \qquad (2)$$

These values are summarized in Tables 2 and 3.

By the Debye-Hückel limitting law, the values of Sv can be calculated from the expression:[10]

$$Sv = Kw^{3/2} \qquad (3)$$

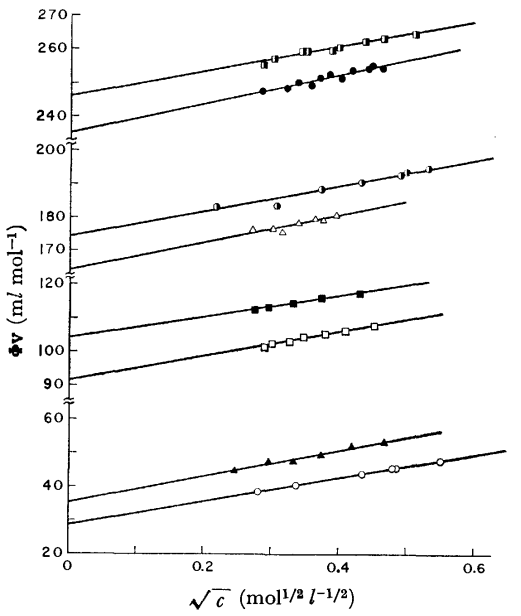

Fig. 2. Plots of Φv *vs.* $\sqrt{c}$ in liq. SO_2 at 25°C.
○; Me_4NBr, ▲; Me_4NI, □; Et_4NBr, ■; Et_4NI, △; n-Pr_4NBr, ◑; n-Pr_4NI, ●; n-Bu_4NBr, ◨; n-Bu_4NI

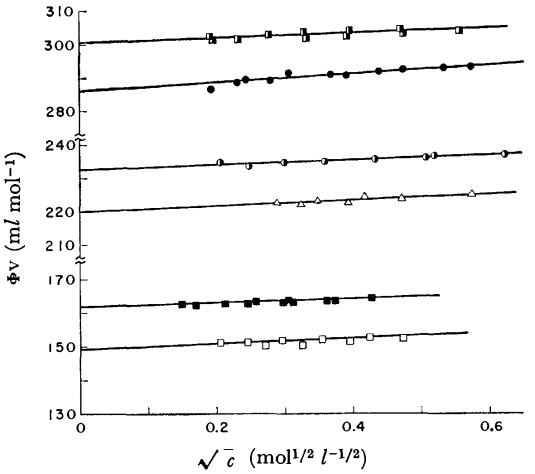

Fig. 3. Plots of Φv *vs.* $\sqrt{c}$ in methanol at 25°C.
□; Et_4NBr, ■; Et_4NI, △; n-Pr_4NBr, ◑; n-Pr_4NI, ●; n-Bu_4NBr, ◨; n-Bu_4NI

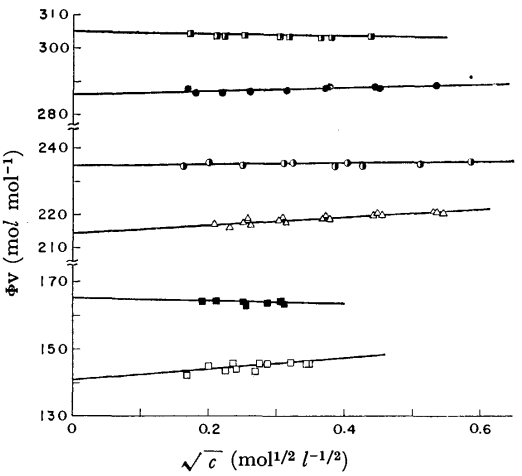

Fig. 4. Plots of Φv *vs.* $\sqrt{c}$ in acetonitrile at 25°C.
□; Et_4NBr, ■; Et_4NI, △; n-Pr_4NBr, ◑; n-Pr_4NI, ●; n-Bu_4NBr, ◨; n-Bu_4NI

7) N. R. C. of U. S. A., "The International Critical Tables," McGrow-Hill, New York (1933), Vol. III, p. 22.
8) O. Redlich and D. M. Meyer, *Chem. Rev.*, **64**, 221 (1964).
9) J. Padova and I. Abrahamer, *J. Phys. Chem.*, **71**, 2112 (1967).
10) O. Redlich, *ibid.*, **67**, 496 (1963).

Table 2. Apparent molar volumes of tetraalkylammonium halides at infinite dilution in various solvents at 25°C

Salt	Liq. SO_2	Acetonitrile	Methanol
Me_4NBr	28.7	—	—
Et_4NBr	91.5	140.8	149.3 149.6[9]
n-Pr_4NBr	164.0	214.7	220.0 222.1[9]
n-Bu_4NBr	235.3	286.1	286.2 285.9[9]
Me_4NI	35.5	—	—
Et_4NI	104.2	165.1	161.9
n-Pr_4NI	173.4	234.9	232.6
n-Bu_4NI	246.3	305.0	300.5

unit: ml mol^{-1}

Table 3. The values of S_V in various solvents

Salt	Liq. SO_2	Acetonitrile	Methanol
Me_4NBr	34.9	—	—
Et_4NBr	36.0	15.1	6.7 7.7[9]
n-Pr_4NBr	41.6	11.4	8.5 6.1[9]
n-Bu_4NBr	43.0	4.6	12.5 11.2[9]
Me_4NI	38.6	—	—
Et_4NI	31.2	−4.3	5.5
n-Pr_4NI	39.4	0.9	6.8
n-Bu_4NI	36.3	−4.8	6.9

unit: ml mol$^{-3/2}$ $l^{1/2}$

where:

$$w = (1/2)\sum_i \nu_i Z_i^2$$

$$K = 2N^2e^3(2\pi/1000RT)^{1/2}D^{-3/2}\,(\mathrm{d}\ln D/\mathrm{d}p - \beta/3)$$

where N, D, β are Avogadro's number, the dielectric constant, and the compressibility of the solvent respectively, and where the other terms have their usual meanings.

Since the concentration ranges used in this investigation are comparatively high, the values of S_V in Table 3 can not reasonably be expected to provide a basis for testing the applicability of the Debye-Hückel limitting law to the solvent system. Also, it is not possible to calculate the theoretical values of S_V from Eq. (3), since the required values of the pressure dependence of the dielectric constant and of the compressibility of the solvent are not available for liquid sulfur dioxide. Though it may be seen that, for all salts studied, the S_V values in this solvent are positive and are quite large compared with those in other solvents, the theoretical implication of the observed difference could not be explored, partly for the reason mentioned above.

In order to make clear the nature of the ion-solvent interaction, it is necessary to assign the absolute ionic partial molal volumes. Conway and his collaborators developed a method by which the Φv values of tetraalkylammonium halides can be divided into the Φv° values of the cation and of the anion in water.[11,12]

Among several methods developed for assigning the absolute ionic partial molar volumes,[13] the most convenient way for the present study seemed to be to follow the one developed by Conway and his collaborators,[11,12] since only a limitted number of the

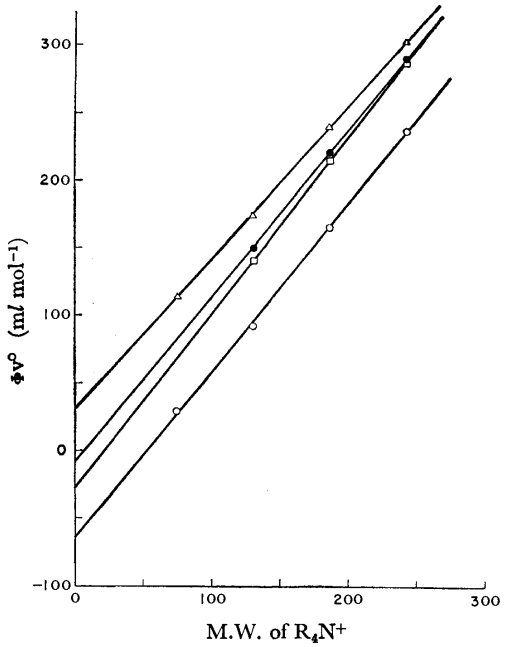

Fig. 5. Plots of Φv° of tetraalkylammonium bromides *vs.* molecular weights of cations.
△; H_2O, ●; MeOH, □; Acetonitrile, ○; liq. SO_2

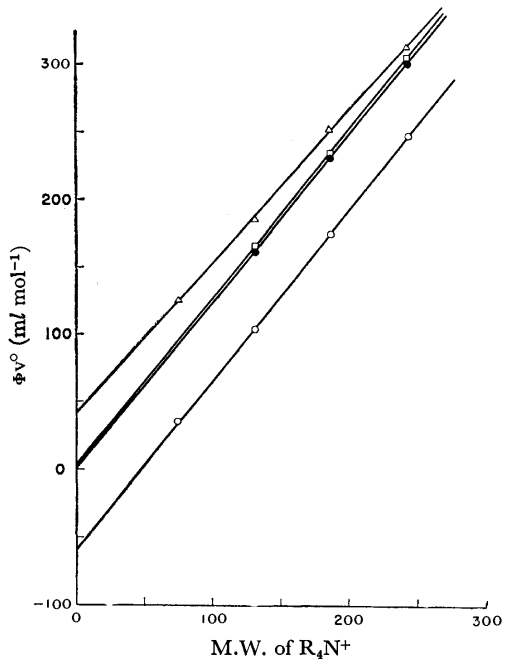

Fig. 6. Plots of Φv° of tetraalkylammonium iodides *vs.* molecular weights of cations.
△; H_2O, ●; MeOH, □; Acetonitrile, ○; liq. SO_2

11) B. E. Conway, R. E. Verrall, and J. E. Desnoyers, *Z. Phy. Chem.*, **230**, 157 (1965).
12) B. E. Conway, R. E. Verrall, and J. E. Desnoyers, *Trans. Faraday Soc.*, **62**, 2738 (1966).
13) F. J. Millero, *Chem. Rev.*, **71**, 147 (1971).

Table 4. Apparent molar volumes of ions at infinite dilution in various solvents at 25°C (ml mol^{-1})

Ions	Liq. SO_2	CH_3CN	MeOH	DMF[a,b) 13]	NMA[a,b) 14]	FA[a) 15]	H_2O[12]
Br^-	−65.5	−27.4	−8.7	—	—	—	30.8
I^-	−58.2	2.8	1.5	5.5	14.2	24.8	42.3
Me_4N^+	93.9	—	—	—	—	—	83.5
Et_4N^+	159.7	165.3	159.2	160.6	161.2	160.7	143.4
n-Pr_4N^+	230.6	237.1	229.9	233.3	233.3	230.7	208.7
n-Bu_4N^+	302.6	307.8	296.9	302.1	308.7	297.6	270.2
b(slope) (ml g^{-1})	1.24	1.27	1.23	1.25	1.26	1.23	1.11

a) $\Phi v^\circ_{R_4N^+}$ have been calculated by $\Phi v^\circ_{R_4NI} = \Phi v^\circ_{R_4N^+} - \Phi v^\circ_{I^-}$.
b) The values at 35°C.

required data are available for the present solvent system.

In the present experiment, the apparent molar volumes of ions in liquid sulfur dioxide, acetonitrile, and methanol were determined on the basis of their method.

According to his procedure, the Φv° values of tetraalkylammonium halides were plotted against the molecular weight of the cation: these plots are shown in Figs. 5 and 6. For the series of tetraalkylammonium bromides and of iodides, straight lines were obtained, as is shown in part in Figs. 5 and 6 for all the solvent systems.

In Fig. 5, the extrapolation of the straight line to a zero-cation molecular weight should directly lead to the apparent molar volumes of the bromide ion at an infinite dilution in the respective solvent,[12] while in Fig. 6, such an extrapolation should correspondingly lead to the Φv° of the iodide ion.[12] Averaging the two series of measurements, the Φv° values of tetraalkylammonium ions, $\Phi v^\circ_{R_4N^+}$, can be calculated by means of Eq. (4):

$$\Phi v^\circ_{R_4N^+} = (1/2)\{(\Phi v^\circ_{R_4NBr} - \Phi v^\circ_{Br^-}) + (\Phi v^\circ_{R_4NI} - \Phi v^\circ_{I^-})\} \quad (4)$$

where $\Phi v^\circ_{R_4NX}$ and $\Phi v^\circ_{X^-}$ are the apparent molar volumes of tetraalkylammonium halide and of halide anion at an infinite dilution.

These apparent molal volumes of ions at an infinite dilution, Φv°_i, and the slopes of the plots of Figs. 5 and 6, b, which were obtained by the least-squares methods on the basis of the equation, are shown in Table 4:

$$\Phi v^\circ_{R_4NX} = \Phi v^\circ_{X^-} + b \text{ (M. W. of cation)} \quad (5)$$

Two or three interesting feature are to be seen in Table 4.

One of these is that the slope of the plot, b, takes a nearly constant value throughout the various solvents with the exception of water. This leads to an insensitive change in the ionic molal volume of the cation, $\Phi v^\circ_{R_4N^+}$, over these solvents. This result is not unexpected provided that the cation-solvent interaction is of an uniform nature throughout these solvents. The smaller values of the slope, b, and of the ionic molal volumes of cations in water may be ascribed to the hydrophobic interaction between the tetraalkylammonium ion and water molecules.

In contrast to the constancy of these slopes, the values of the intercept, which according to Conway's proposal, correspond to the inonic molar volumes of the anions, scatter with a change in the solvent over much wider ranges than would be expected from the experimental uncertainties.

On the basis of the characteristic values of the intercept, the solvents or the nature of the solvent-anion interaction are likely to be classifiable into three or four groups, *i.e.*, large negative (liq. SO_2), small positive (acetonitrile, methanol, *N,N*-dimethyl formamide), moderate positive (*N*-methyl acetoamide, formamide), and large positive (water).

For the case of amides, the observed transition of the $\Phi v^\circ_{I^-}$ from *N,N*-dimethyl formamide to formamide, that is to say, the tendency of the $\Phi v^\circ_{I^-}$ values to approach that of water, with an increase in the number of amino hydrogens, is consistent with the variation in the absolute ionic entropies accompanying the same solvent change.[16] Therefore, some of the solvent characteristics would seem to be specifically reflected in both thermodynamic variables. This might be the "structuredness" of the solvents.[16]

At any rate, water and liquid sulfur dioxide constitute two extreme causes. These results suggest that anion-solvent interaction is markedly strong in this solvent in comparison with that in other solvents. It is well known that sulfur dioxide forms charge-transfer complexes with halide anions in water,[17] methanol,[17] and acetonitrile.[18]

As a result of the formation of a charge-transfer complex of halide anions with sulfur dioxide, the absorption maxima were observed at 341 nm in water at 20°C[17] and at 355 nm in methanol at 22.6°C.[17] The absorption maximum was also observed at 383 nm in liquid sulfur dioxide at 20°C.[19]

Considering these facts, the strong anion-solvent interaction in liquid sulfur dioxide can be explained by the formation of a charge-transfer complex of halide anions with sulfur dioxide.

14) R. Gopal and M. A. Siddigni, *J. Phys. Chem.*, **73**, 3390 (1969).
15) R. Gopal and M. A. Siddigni, *Z. Physik. Chem.* (Frankfurt), **67**, 122 (1969).
16) C. M. Criss, R. P. Held, and E. Luksha, *J. Phys. Chem.*, **72**, 2970 (1968).
17) J. Jander and G. Turk, *Angew. Chem.*, **75**, 792 (1963).
18) E. R. Lippincott and F. W. Welch, *Spectrochim. Acta*, **17**, 123 (1961).
19) K. Uosaki, Y. Kondo, and N. Tokura, unpublished work.

Linear Conjugated Systems Bearing Aromatic Terminal Groups. VII. Syntheses and Electronic Spectra of 1,1′- and 2,2′-Dipyrenylpoly-ynes

Kazuhiro NAKASUJI, Shuzo AKIYAMA, and Masazumi NAKAGAWA
Department of Chemistry, Faculty of Science, Osaka University, Toyonaka, Osaka
(Received August 6, 1971)

1,1′- and 2,2′-Dipyrenylpoly-ynes (I_n and II_n, $n=1$—6) have been synthesized. It was found that the bathochromic shift of the longest-wavelength absorption maxima (λ_L) according to the increase in the number of acetylenic bond (n) can be well expressed by the following formulas:

I_n: $\lambda_L = 3.7n^{1.7} + 430$ (nm in toluene)
II_n: $\lambda_L = 12.6n^{1.4} + 327$ (nm in toluene)

New linear relationships between the longest-wavelength absorption maxima (λ_L) and the xth power of the number of acetylenic bond (n)[$\lambda_L \propto n^x$] observed in various kinds of diarylpoly-ynes have been reported in previous papers.[1-9] Since the value of x is dependent on the nature of terminal groups and the position of linking of polyacetylene chain, we were interested in the behavior of pyrene as the terminal groups of poly-yne system. The present paper deals with the syntheses and electronic spectral properties of 1,1′- and 2,2′-dipyrenylpoly-ynes (I_n and II_n, $n=1$—6).

Syntheses. The syntheses of monoacetylenes (I_1

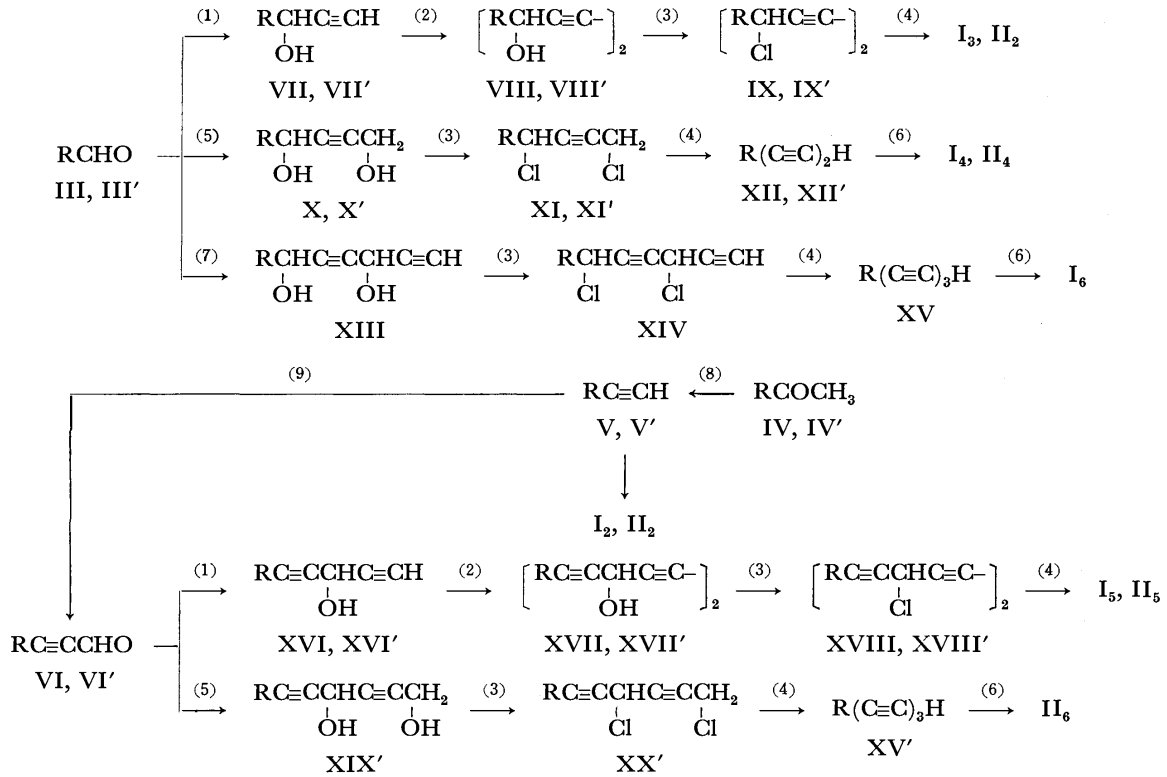

Scheme 1. Syntheses of dipyrenylpoly-ynes (I_n, II_n)

Roman numerals with prime indicate 2-pyrenyl series.
(1) HC≡CMgBr/THF, (2) CuCl-NH_4Cl-O_2/CH_3OH or CH_3OH-acetone, (3) $SOCl_2$-pyridine/THF, (4) $NaNH_2$/liq. NH_3, (5) BrMgC≡CCH_2OMgBr/THF, (6) $Cu(OCOCH_3)_2$/pyridine, (7) BrMgC≡C-CH(OMgBr)C≡CH/THF, (8) i) PCl_5, ii) $NaNH_2$/liq. NH_3, (9) i) i-C_3H_7MgBr, ii) DMF/THF, iii) dil. H_2SO_4.
THF=tetrahydrofuran; DMF=dimethylformamide.

1) S. Akiyama and M. Nakagawa, *Tetrahedron Lett.*, **1964**, 719.
2) K. Nishimoto, R. Fujishiro, S. Akiyama, and M. Nakagawa, This Bulletin, **39**, 2320 (1966).
3) S. Akiyama and M. Nakagawa, *ibid.*, **40**, 340 (1967).
4) S. Akiyama, K. Nakasuji, K. Akashi, and M. Nakagawa, *Tetrahedron Lett.*, **1968**, 1121.
5) S. Akiyama and M. Nakagawa, This Bulletin, **43**, 3561 (1970).
6) K. Nakasuji, S. Akiyama, K. Akashi, and M. Nakagawa, *ibid.*, **43**, 3567 (1970).
7) S. Akiyama, K. Nakasuji, and M. Nakagawa, *ibid.*, **44**, 2231 (1971).
8) S. Akiyama and M. Nakagawa, *ibid.*, **44**, 2237 (1971).
9) S. Akiyama and M. Nakagawa, *ibid.*, **45**, 259 (1972).

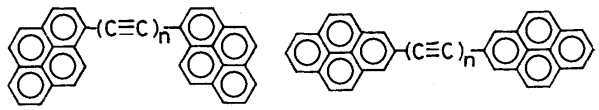

I_n II_n

and II_1) by means of an intramolecular Wittig reaction have been reported.[8] As illustrated in Scheme 1, the reaction sequence used in the syntheses of I_n and II_n is a general method which has been successfully adapted for the preparation of various kinds of diarylpoly-ynes.[6,8,9] 2,2′-Dipyrenylhexaacetylene (II_6) was found to be an unstable, scarcely soluble substance, and gave an unsatisfactory elemental analysis. However, the compound gave a satisfactory electronic spectrum for the present purpose.

Some physical properties of 1,1′- and 2,2′-dipyrenylpoly-ynes (I_n and II_n) are summarized in Tables 1 and 2.

TABLE 1. PHYSICAL PROPERTIES OF 1,1′-DIPYRENYLPOLY-YNES (I_n)

n	Color of crystals	Melting point (°C)	$\nu_{C\equiv C}$(cm^{-1})
1	yellow	266	—
2	yellow	(297—298)	2125
3	yellow	(*ca.* 300)	2185
4	orange yellow	(*ca.* 260)	2190
5	orange	(*ca.* 215)	2175
6	red	(*ca.* 200)	2145

Figures in parentheses indicate decomposition points.

TABLE 2. PHYSICAL PROPERTIES OF 2,2′-DIPYRENYLPOLY-YNES (II_n)

n	Color of crystals	Melting point (°C)	$\nu_{C\equiv C}$(cm^{-1})
1	pale yellow	>330	—
2	light yellow	>330	—
3	yellow	(*ca.* 260—270)	2190
4	yellow	(*ca.* 180)	2195
5	orange yellow	(*ca.* 140)	2185
6	orange		

Figures in parentheses indicate decomposition points.

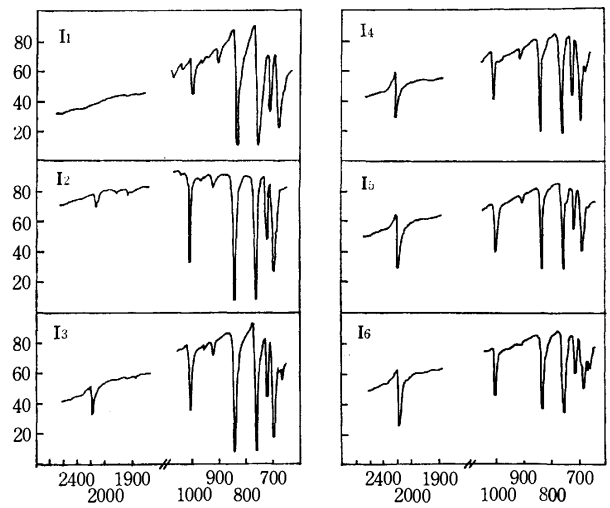

Fig. 1. IR spectra of 1,1′-dipyrenylpoly-ynes (I_n).

The IR spectra of I_n are shown in Fig. 1 as representative of dipyrenylpoly-ynes. The most intense peak in $\nu_{C\equiv C}$ band showed appreciable intensification with increasing number of n. The highest wave number of $\nu_{C\equiv C}$ was observed in the spectra of the tetraacetylenes (I_4 and II_4). The same trend has been observed in the other series of diarylpoly-ynes.[3,4,6,8,9]

Electronic Spectra. The absorption curves and numerical data of the electronic spectra of I_n and II_n are shown in Figs. 2 and 3, and Tables 3 and 4, respectively. In the electronic spectrum of pyrene, there is a low intensity band in the 350—370 nm region (^1L_b) and a strong band in the 290—340 nm region (^1L_a). Both bands exhibit considerable fine structure. The longest-wavelength bands in I_n and II_n seem to arise from the interaction of ^1L_a band of pyrene with polyacetylenic chromophore. The difference in wave-

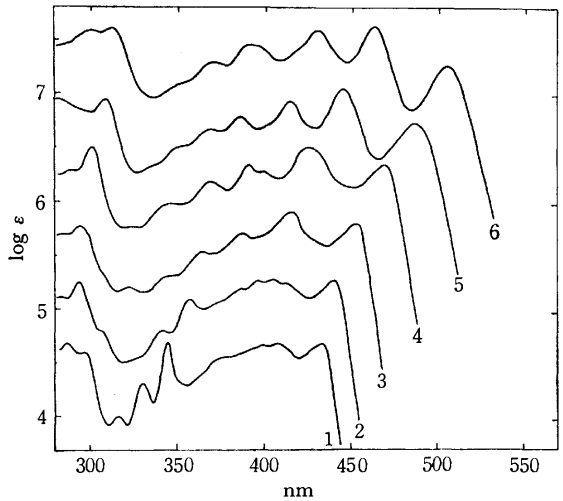

Fig. 2. Absorption curves of 1,1′-dipyrenylpoly-ynes (I_n). With the exception of the monoacetylene at the bottom, the curves are shifted upward along the ordinate by 0.5 log ε unit increments from the curve immediately below (in toluene).

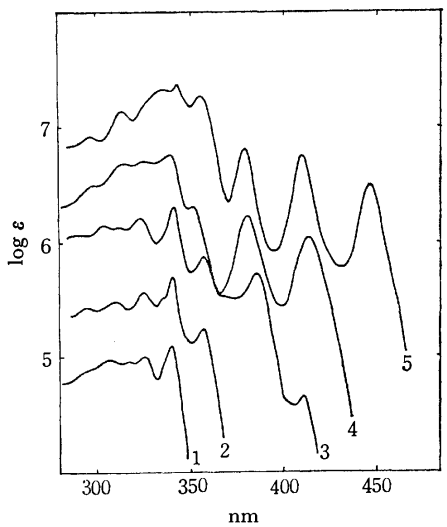

Fig. 3. Absorption curves of 2,2′-dipyrenylpoly-ynes (II_n). With the exception of the monoacetylene at the bottom, the curves are shifted upward along the ordinate by 0.5 log ε unit increments from the curve immediately below (in toluene).

Table 3. Electronic spectral data of I_n

n	λ in nm (log ε) in toluene						
1	287.5 (4.68)	297.5 (4.60)	315.5 (3.99)	330.5 (4.31)	345 (4.68)	401 (4.66)	408 (4.68)
	434 (4.68)						
2	283.5 (4.62)	294 (4.75)	341 (4.29)	367 (4.58)	387 (4.68)	396 (4.74)	405 (4.77)
	413 (4.73)	442 (4.76)					
3	294.5 (4.77)	322.5 (4.20)	345* (4.31)	364 (4.53)	387 (4.70)	417 (4.89)	454 (4.79)
4	289 (4.78)	301.5 (5.00)	325 (4.27)	346 (4.46)	370 (4.67)	392 (4.83)	400 (4.77)
	427 (4.98)	470 (4.83)					
5	282.5 (4.95)	309 (4.94)	352* (4.50)	370 (4.66)	386 (4.78)	415 (4.92)	446 (5.04)
	487 (4.72)						
6	301.5 (5.08)	313 (5.09)	373 (4.78)	393 (4.94)	432 (5.08)	465 (5.10)	507 (4.73)

Asterisks indicate shoulders.

Table 4. Electronic spectral data of II_n

n	in nm (log ε) in toluene							
1	306 (4.99)	317 (4.97)	324 (5.00)	340 (5.10)	373 (a)	380 (a)	394 (a)	403 (a)
2	294 (4.94)	310 (5.00)	325 (5.07)	335 (5.03)	341 (5.21)	358 (4.75)	385 (a)	407 (a)
3	304 (5.05)	313 (5.02)	324 (5.12)	342 (5.21)	359 (4.78)	387 (4.64)	413 (3.52)	
4	297 (5.01)	315 (5.20)	327 (5.21)	340 (5.27)	351 (4.86)	382 (4.78)	415 (4.60)	
5	296 (4.87)	314 (5.12)	336 (5.29)	343 (5.35)	355 (5.28)	379 (4.82)	410 (4.77)	447 (4.51)
6[b]				355	379	404	437	478

a) Accurate ε-values could not be obtained owing to poor solubility.
b) On account of the purity of II_6, only the locations of the long-wavelength bands are shown.

Table 5. Difference of wavelength of λ_L between I_n and II_n

n	1	2	3	4	5	6
I_n	434	442	454	470	487	502
II_n	340	358	387	415	447	478
$\Delta\lambda$	94	84	67	55	40	29

length of the longest-wavelength absorption maxima (λ_L) between I_n and II_n is shown in Table 5. The marked difference ($\Delta\lambda$) between I_n and II_n was found to be the largest ever observed, *i.e.*, the difference between 1,1′- and 2,2′-dinaphthylacetylenes is 23 nm,[6] and that between 2,2′- and 3,3′-, and between 3,3′- and 9,9′-diphenanthrylacetylenes 11.5 and 16.5 nm,[8] respectively. Since the transition associated with ^1L_a band of pyrene is considered to be polarized in the direction of the long axis,[10] the remarkable hypsochromic shift of λ_L of II_n as compared with that of I_n indicates that we do not get what we expect intuitively for dipyrenylpoly-ynes. A similar phenomenon has been observed in phenanthrene derivatives and explained in terms of configuration interaction.[11] Thus, it seems to be pertinent to ascribe the hypsochromism of II_n to configuration interaction.

The absorption band associated with ^1L_b band of pyrene could not be observed in the spectra of I_n. However, II_1, II_2, and II_3 showed low intensity bands at long-wavelength region. The same phenomena were observed in the lower member of 2,2′-dinaphthylpoly-ynes[6] and in that of 2,2′-difluorenylpoly-ynes.[12]

As has been observed in various series of diarylpoly-ynes, increase in the length of poly-yne chain results in a progessive enhancement of the vibrational fine structure. Thus the spectra of higher members of I_n and II_n exhibit a characteristic feature of polyacetylene chromophore. The spacing, *i.e.*, the difference of wavelength between the longest-wavelength sub-band and the next longest-wavelength sub-band, was found to be 1800—2150 cm^{-1} in the case of $n=3$—6 (*cf.* Table 6). The spacing can be considered to correspond to the stretching vibration of acetylenic linkage at excited state. The unusual value of spacing of the diacetylenes (I_2 and II_2) can be attributed to the superposition of vibration of acetylene bond with that inherent to the terminal groups. The same unusual spacing has been observed in the electronic spectra of dianthrylpoly-ynes.[5] The correlation of spacing and $\nu_{C\equiv C}$ with the electronic spectral behavior of diarylpoly-

Table 6. Spacing of electronic spectra of I_n and II_n (cm^{-1})

n	2	3	4	5	6
I_n	(1590)	1950	2140	1890	1790
II_n	(1390)	2030	2080	1990	1960

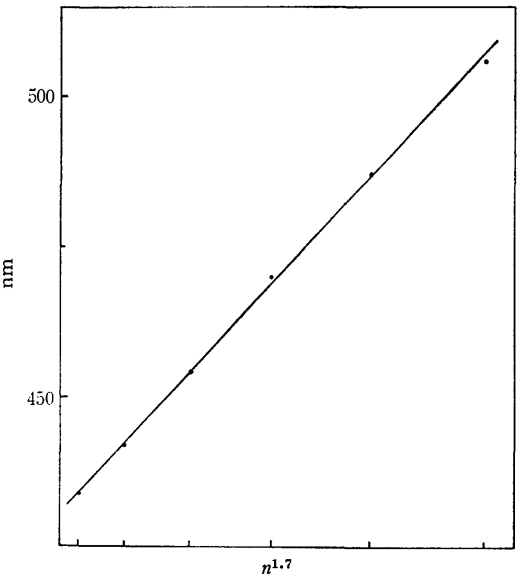

Fig. 4. Plot of λ_L *versus* $n^{1.7}$ for 1,1′-dipyrenylpoly-ynes (I_n).

10) R. S. Becker, I. S. Singh, and E. A. Jackson, *J. Chem. Phys.*, **38**, 2144 (1963) and the references cited therein.
11) S. Akiyama, M. Nakagawa, and K. Nishimoto, This Bulletin, **44**, 1054 (1971).
12) K. Nakasuji, S. Akiyama, and M. Nakagawa, *ibid.*, **45**, 883 (1972).

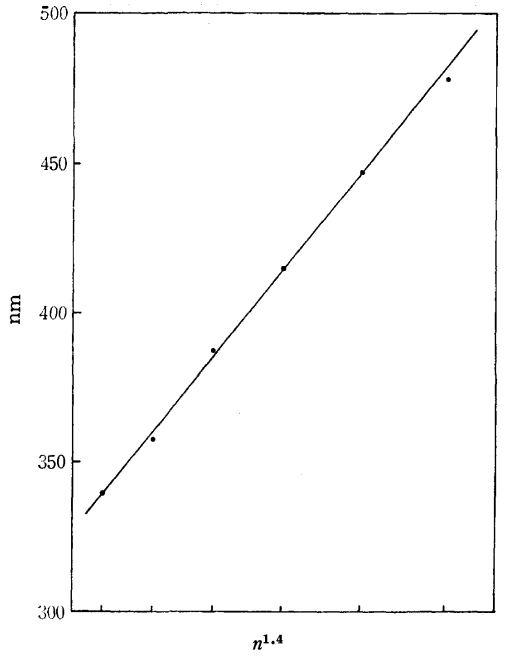

Fig. 5. Plot of λ_L *versus* $n^{1.4}$ for 2,2′-dipyrenylpoly-ynes (II_n).

ynes was discussed elsewhere.[13]

The plots of λ_L of I_n against $n^{1.7}$ and those of II_n *versus* $n^{1.4}$ gave good straight lines as illustrated in Figs. 4 and 5. The linear relationships can be expressed by the following empirical formulas. Agreement of calculated values with observed data was found to be excellent (*cf.* Table 7).

$$I_n: \lambda_L = 3.7n^{1.7} + 430 \quad \text{(nm in toluene)}$$

$$II_n: \lambda_L = 12.6n^{1.4} + 327 \quad \text{(nm in toluene)}$$

TABLE 7. OBSERVED AND CALCULATED λ_L (nm)

	n	1	2	3	4	5	6
I_n	Obs.	434	442	454	470	487	507
	Calcd	434	442	454	469	487	508
	Δ	0	0	0	1	0	−1
II_n	Obs.	340	358	387	415	447	478
	Calcd	340	360	386	415	447	482
	Δ	0	−2	1	0	0	−4

In the above-mentioned dipyrenyl series, the difference in position of linking of polyacetylenic chain exerts a prominent effect on the location of λ_L. This tendency seems to be reflected in the marked difference of the value of x between 1,1′-series (I_n, $x=1.7$) and 2,2′-series (II_n, $x=1.4$).

Experimental

All melting points are uncorrected. The electronic spectra were measured on a Hitachi EPS-3T Spectrophotometer. The IR spectra were obtained on a Hitachi EPI-2 Spectrophotometer by KBr-disk method. Evaporation of solvent or concentration of solution was carried out under reduced pressure.

13) M. Nakagawa, S. Akiyama, K. Nakasuji, and K. Nishimoto, *Tetrahedron*, **27**, 5401 (1971).

1-Ethynylpyrene (V). *Chlorination of 1-Acetylpyrene (IV)*: 1-Acetylpyrene (IV, mp 89°C, 4.88 g, 0.02 mol) prepared by the reported method[14] was mixed with phosphorus pentachloride (4.58 g, 0.022 mol) in benzene (20 m*l*). After the mixture had been refluxed for 1 hr, volatile materials were removed under reduced pressure. The residue was placed in an evacuated desiccator containing potassium hydroxide, thus yielding greenish yellow crystals. This material was used in the subsequent reaction without purification.

Dehydrochlorination. To a stirred suspension of sodium amide [from sodium, 1.80 g (0.08 g-atom)] in liquid ammonia (100 m*l*) was added a solution of the crude chloride in tetrahydrofuran (10 m*l*) over a period of 20 min. After stirring for 3 hr, ammonia was allowed to evaporate. Ether (200 m*l*) was added to the residue and a saturated ammonium chloride solution was added under cooling on an ice-salt bath. The organic layer was washed with water and dried. The residue obtained by evaporation of the solvent was dissolved in benzene (30 m*l*), and the solution was passed through a short column of alumina (15 g). Concentration of the filtrate yielded the ethynyl derivative (V) as pale yellow needles (3.92 g, 87%, mp 112—114°C). Percolation of crude V in petroleum benzine through a column of alumina gave pure V as colorless needles, mp 113—114°C. 1-Ethynylpyrene (V) gave orange cuprous and yellow silver acetylides.

Found: C, 95.45; H, 4.44%. Calcd for $C_{18}H_{10}$: C, 95.54; H, 4.46%. IR: 3310 (≡CH), 2090 (C≡C), 1027 (C–O) cm^{-1}. UV: $\lambda_{max}^{n\text{-hexane}}$ (log ε): 218 (4.10), 236 (4.59), 246.5 (4.78), 261 (4.09), 270.5 (4.47), 281.5 (4.76), 311.5 (3.74), 324 (4.19), 338.5 (4.57), 356.5 (4.80), 373.5 (3.04), 381.5 (3.23) nm.

2-Acetylpyrene (IV′). Acid chloride prepared from 2-carboxypyrene[15] (24.6 g, 0.1 mol) and thionyl chloride (16 m*l*) was dissolved in hot tetrahydrofuran (200 m*l*). The hot solution was added to an ice-cooled solution of diethyl magnesiomalonate [from magnesium, 2.4 g (0.1 g-atom), diethyl malonate, 16.0 g (0.1 mol), anhydrous ethanol, 10.1 g (0.2 mol) and anhydrous toluene (100 m*l*). The excess of ethanol had been removed by an azeotropic distillation with toluene] in toluene. After the addition had been completed, the mixture was stirred for 3 hr at 80°C. 4N Sulfuric acid (40 m*l*) was then added to the reaction mixture. The organic layer was washed with water and dried. The crude ketomalonate obtained by evaporating the solvent was mixed with acetic acid (80 m*l*) and concentrated sulfuric acid (0.5 m*l*). After the mixture had been refluxed for 2.5 hr, 4N sulfuric acid (40 m*l*) was added to the mixture and the reflux was continued for further 2 hr. The reaction mixture was put to stand overnight. The crude crystals deposited were collected by filtration and washed with water and then dissolved in ethyl acetate. After treatment with active charcoal, the solvent was removed to give yellow crystals (16.2 g, 66%). The crude material was recrystallized twice from ethyl acetate to give pure IV′, pale yellow leaflets, mp 145—147°C.

Found: C, 88.27; H, 4.87%. Calcd for $C_{18}H_{12}O$: C, 88.50; H, 4.95%.

2-Hydroxymethylpyrene. Reduction of 2-carbethoxypyrene[15] by means of lithium aluminum hydride afforded 2-hydroxymethylpyrene in a good yield. Recrystallization from ethanol gave pure material as colorless needles, mp 168—169°C.

Found: C, 87.61; H, 5.17%. Calcd for $C_{17}H_{12}O$: C,

14) W. E. Bachmann and M. Carmack, *J. Amer. Chem. Soc.*, **63**, 2494 (1941).

15) H. Vollmann, H. Becker, M. Correll, and H. Streek, *Ann.*, **531**, 1 (1937).

87.90; H, 5.21%.

2-Formylpyrene (III'). A solution of 2-hydroxymethylpyrene (8.68 g, 0.04 mol) in pyridine (60 m*l*) was added to a mixture of chromium trioxide (12.4 g, 0.124 mol) in pyridine (140 m*l*) under ice-cooling. After shaking for 30 min, the cooling bath was removed and the mixture was kept at room temperature for 1 hr. The reaction mixture was then poured into water (1 *l*) and extracted with ether (1.8 *l*). The extract was washed several times successively with 10% hydrochloric acid, a saturated solution of sodium carbonate and water. The residue obtained by evaporating the solvent was recrystallized from ethyl acetate to yield III' (6.2 g, 68%). This material was recrystallized 3 times from the same solvent to give pure III', yellow rods, mp 153—154°C.

Found: C, 88.63; H, 4.36%. Calcd for $C_{17}H_{10}O$: C, 88.67; H, 4.38%.

2-Ethynylpyrene (V'). A mixture of 2-acetylpyrene (IV', 15.9 g, 0.065 mol), phosphorus pentachloride (14.0 g, 0.067 mol) and benzene (200 m*l*) was refluxed for 2 hr, and the volatile materials were removed under reduced pressure. The residue which had been kept in an evacuated desiccator over potassium hydroxide was dissolved in tetrahydrofuran (100 m*l*). The solution was added to a suspension of sodium amide [from sodium, 9.2 g (0.4 g-atom)] in liquid ammonia (500 m*l*) at −70°C. After stirring for 3 hr, the ammonia was allowed to evaporate. A saturated solution of ammonium chloride was added to the residue at −30°C. The aqueous layer was extracted with ether and combined with the organic layer and dried. The residue obtained by evaporating the solvent was dissolved in hot ligroin containing a small amount of benzene. The filtrate obtained by passing the hot solution through a column of alumina (30 g) was concentrated to yield V' as colorless needles, 11.0 g (75%). Recrystallization twice from ethanol gave pure specimen, mp 125—127°C.

Found: C, 95.53; H, 4.41%. Calcd for $C_{18}H_{10}$: C, 95.54; H, 4.46%.

1,1'-Dipyrenyldiacetylene (I_2). Cupric acetate monohydrate (5.0 g) was added to a stirred solution of 1-ethynylpyrene (V, 0.510 g, 2.3 mmol) in pyridine (20 m*l*). The mixture was stirred for 3 hr at 55°C. The insoluble material deposited on cooling the reaction mixture was collected by filtration and washed successively with methanol and water to yield tiny yellow cubes, 0.504 g (98%), mp 297—298°C (dec.). The crude material was dissolved in hot toluene and passed through a short column of alumina. The crystals obtained from the filtrate were recrystallized from toluene, yielding pure I_2, yellow cubes, mp 298°C (dec.).

Found: C, 95.93; H, 4.07%. Calcd for $C_{36}H_{18}$: C, 95.97; H, 4.03%.

2,2'-Dipyrenyldiacetylene (II_2). According to the procedure used in the synthesis of I_2, 2-ethynylpyrene (V') gave II_2, pale yellow needles (from toluene) in a 96% yield. The crystals showed no melting point, but began to decompose at 330°C.

Found: C, 95.91; H, 3.97%. Calcd for $C_{36}H_{18}$: C, 95.97; H, 4.03%.

1-(1-Pyrenyl)-2-propyn-1-ol (VII). A solution of 1-formylpyrene[16] (III, 6.90 g, 0.03 mol) in tetrahydrofuran (60 m*l*) was added to an ice-cooled solution of ethynylmagnesium bromide [from ethyl bromide, 8.20 g (0.075 mol), magnesium, 1.80 g (0.075 g atom) and an excess of acetylene] in the same solvent (85 m*l*). After the mixture had been stirred overnight at room temperature, a saturated solution of ammonium chloride was added to the reaction mixture. The organic layer was dried and the crystals obtained by evaporating the solvent were dissolved in acetone. The insoluble material was removed by filtration. The crystals (6.95 g, 91%, mp 145—150°C) obtained from the filtrate were redissolved in acetone and passed through a short column of alumina. The filtrate was concentrated, and the crystals deposited were recrystallized from ethanol - benzene, yielding pure VII as colorless rods, mp 159—160°C.

Found: C, 88.90; H, 4.67%. Calcd for $C_{19}H_{12}O$: C, 89.04; H, 4.72%. IR: 3600—3100 (OH), 3300 (≡CH), 2100 (C≡C) cm^{-1}.

1-(2-Pyrenyl)-2-propyn-1-ol (VII'). According to the procedure used for VII, 2-formylpyrene (III') gave crude VII' in a 96% yield. The crude material was recrystallized 3 times from carbon tetrachloride - ethanol to give pure VII as colorless needles, mp 132—135°C.

Found: C, 89.06; H, 4.71%. Calcd for $C_{19}H_{12}O$: C, 89.04; H, 4.72%. IR: 3350—3200 (OH), 3250 (≡CH), 1035 (C–O) cm^{-1}.

1,6-Di-(1-pyrenyl)-2,4-hexadiyn-2,6-diol (VIII). A mixture of ethynylcarbinol (VII, 3.98 g, 0.0156 mol), acetone (50 m*l*), methanol (50 m*l*), ammonium chloride (0.30 g), and cuprous chloride (0.40 g) was vigorously stirred at room temperature under a slight excess pressure of oxygen for 48 hr. The crystalline material deposited was collected by filtration and washed with methanol containing hydrochloric acid. The light brown crystals thus obtained (2.02 g, 51%, decomposed at *ca.* 220°C) were dissolved in tetrahydrofuran and passed 4 times through a thin layer of alumina. Concentration of the filtrate gave pure VIII as fine colorless needles. The crystals turned pink at *ca.* 160°C and decomposed at *ca.* 225—260°C.

Found: C, 88.96; H, 4.42%. Calcd for $C_{38}H_{22}O_2$: C, 89.39; H, 4.34%. IR: 3400—3100 (OH), 2250 (C≡C), 1015 (C–O) cm^{-1}.

1,6-Di-(2-pyrenyl)-2,4-hexadiyn-1,6-diol (VIII'). According to the procedure for VIII, the oxidative coupling of ethynylcarbinol (VII') afforded a crude VIII' in a 47% yield which decomposed at *ca.* 245°C. Owing to its poor solubility, the crude material was subjected to the following reaction without purification.

1,1'-Dipyrenyltriacetylene (I_3). Preparation of Dichloride (IX). A mixture of thionyl chloride (0.144 g, 1.2 mmol), pyridine (0.096 g, 1.2 mmol) and tetrahydrofuran (5 m*l*) was added over a period of 30 min to a solution of diacetylenic glycol (VIII, 0.244 g, 0.4 mmol) in tetrahydrofuran (15 m*l*) at −10°C. When the addition had been completed, the mixture was shaken for 10 min at the same temperature and immediately used for the following reaction.

Dehydrochlorination. To a stirred suspension of sodium amide [from sodium, 0.14 g (6 mg-atom)] in liquid ammonia (90 m*l*) maintained at −60°C was added a solution of dichloride (IX). After 30 min, ammonium chloride (1 g) was added and the ammonia was allowed to evaporate. After the organic solvent had been removed, a small amount of water was added to the residue. The insoluble material was collected by filtration, washed with a small amount of methanol and benzene. The solid thus obtained was dissolved in boiling toluene and the hot solution was percolated through a short column of alumina. Concentration of the filtrate afforded fine yellow needles, 0.080 g (42%) which decomposed at *ca.* 295°C. The crystals were redissolved in boiling toluene and passed through a thin layer of alumina, yielding pure I_3 as yellow needles which decomposed at *ca.* 300°C.

Found: C, 96.18; H, 3.85%. Calcd for $C_{38}H_{18}$: C, 96.18; H, 3.82%.

2,2'-Dipyrenyltriacetylene (II_3). The procedure used in the preparation of I_3 was followed. Chlorination of crude

16) A. Rieche, H. Gross, and E. Höft, *Chem. Ber.*, **93**, 88 (1960).

VIII′ followed by dehydrochlorination gave crude II_3 in a 27% yield. Purification of this material gave II_3 as yellow needles (decomp. 260—270°C).

Found: C, 95.93; H, 3.81%. Calcd for $C_{38}H_{18}$: C, 96.18; H, 3.82%.

1-(1-Pyrenyl)-2-butyn-1,4-diol (X). A solution of 1-formylpyrene (II, 6.00 g, 0.026 mol) in tetrahydrofuran (60 m*l*) was added dropwise to an ice-cooled solution of the Grignard derivative of propargyl alcohol [from magnesium, 3.74 g (0.156 g-atom), ethyl bromide, 17 g (0.156 mol), and propargyl alcohol, 4.37 g (0.078 mol)]. The mixture was stirred overnight and then a saturated solution of ammonium chloride was added. The dried organic layer was concentrated. The residue was triturated with benzene and washed with the same solvent, thus yielding pale yellow crystalline powder, 7.20 g (97%), mp 141—145°C. Recrystallization of the crystals from ethanol and from ethanol - benzene afforded pure X as colorless needles, mp 150—151°C.

Found: C, 83.56; H, 4.95%. Calcd for $C_{20}H_{14}O_2$: C, 83.90; H, 4.93%. IR: 3600—3100 (OH), 1055, 1012 (C–O) cm^{-1}.

1-(2-Pyrenyl)-2-butyn-1,4-diol (X′). According to the procedure for X, 2-formylpyrene (III′) gave crude X′ in 82% yield. Recrystallization three times of this material from ethanol yielded pure X′, colorless leaflets, mp 183—185°C.

Found: C, 83.90; H, 4.86%. Calcd for $C_{20}H_{14}O_2$: C, 83.90; H, 4.93%. IR: 3350—3200 (OH), 1000, 1007 (C–O) cm^{-1}.

1-Butadiynylpyrene (XII). Preparation of the Dichloride (XI). A solution of thionyl chloride (4.65 g, 0.039 mol) in tetrahydrofuran (10 m*l*) was added over a period of 1 hr to a mixture of acetylene glycol (X, 4.30 g, 0.015 mol), pyridine (3.08 g, 0.039 mol), and tetrahydrofuran (10 m*l*) kept at −10°C. The temperature of the reaction mixture was gradually raised to room temperature and stirring was continued for 1 hr and then for 1 hr at 30°C. Cracked ice was then added to the reaction mixture. The organic layer was separated and the aqueous layer was extracted with benzene (100 m*l*). The combined organic layer was dried, and concentrated to *ca.* 5 m*l*. The solution of dichloride (XI) thus prepared was used in the subsequent reaction.

Dehydrochlorination. The solution of XI was added over a period of 20 min to a stirred suspension of sodium amide [from sodium, 2.5 g (0.11 g-atom)] in liquid ammonia (100 m*l*) at a temperature of −70°C. After 3 hr ammonium chloride (7 g) was added to the reaction mixture and the ammonia was allowed to evaporate. After the organic solvent had been removed, the residue was extracted with petroleum ether (bp 60—80°C, total 450 m*l*). The extract was passed through a thin layer of alumina (12 g). Concentration of the filtrate afforded extremely unstable XII as fine needles, 1.33 g (36%), mp *ca.* 105°C (dec.). XII gave orange yellow, silver and orange cuprous acetylides.

UV: $\lambda_{max}^{petroleum\ ether}$ 377 nm.

1,1′-Dipyrenyltetraacetylene (I_4). A mixture of 1-butadiynylpyrene (XII, 0.050 g, 0.2 mmol), cupric acetate monohydrate (0.50 g), pyridine (3 m*l*) and methanol (0.5 m*l*) was stirred at room temperature for 12 hr. The insoluble material was collected by filtration and washed successively with water, a small amount of methanol and benzene, yielding fine yellow needles, 0.038 g (76%), which decomposed at *ca.* 255°C. This material was dissolved in hot toluene and percolated through a thin layer of alumina. Concentration of the filtrate gave pure I_4 as fine orange yellow needles, which decomposed at *ca.* 260°C.

Found: C, 96.06; H, 3.64%. Calcd for $C_{40}H_{18}$: C, 96.36; H, 3.64%.

2-Butadiynylpyrene (XII′). Preparation of the Dichloride (XI′). A solution of thionyl chloride (2.33 g, 19.5 mmol) in tetrahydrofuran (10 m*l*) was added to a stirred mixture of the acetylene glycol (X′, 2.15 g, 7.5 mmol), pyridine (1.54 g, 19.5 mmol), and tetrahydrofuran (40 m*l*) under cooling on an ice-salt bath. The temperature of the reaction mixture was allowed to rise gradually to room temperature, and stirring was continued at 30°C for 1 hr. Cracked ice was added to the reaction mixture under external cooling with ice-water. The organic layer was washed successively with water and sodium hydroxide solution, and dried. The concentrated solution of XI′ (*ca.* 10 m*l*) was subjected to the following reaction.

Dehydrochlorination. To a stirred suspension of sodium amide [from sodium, 1.3 g (0.055 g-atom)] in liquid ammonia (50 m*l*) was added the solution of XI′ at −70°C, and stirring was continued for 3 hr. After ammonium chloride (4 g) had been added tothe reaction mixture, ammonia was allowed to evaporate and the organic solvent was removed. The residue was extracted with petroleum benzine (1 *l*). The extract was concentrated to *ca.* 500 m*l* and passed through a short column of alumina, yielding colorless filtrate. It was impossible to isolate diacetylene (XII′) in solid state owing to the unstable nature of the compound. The petroleum benzine solution of XII′ was thus used in the subsequent reaction.

UV: $\lambda_{max}^{benzine}$ 336, 321, 306, 300, 288 nm.

2,2′-Dipyrenyltetraacetylene (II_4). To a stirred solution of cupric acetate monohydrate (4.0 g) in pyridine (20 m*l*) was added a small portion of the solution of diacetylene (XII′), and petroleum benzine was removed under reduced pressure at room temperature. A second portion of the solution was then added, benzine being again removed *in vacuo*. The entire benzine solution was added, portion by portion to the oxidizing reagent, repeating the above procedure. After addition of the solution and removal of the benzine had been completed, additional pyridine (20 m*l*) and methanol (5 m*l*) were added to the solution, and the mixture was stirred overnight at room temperature. After the solvent had been removed, water was added to the residue and the insoluble material was collected by filtration, washed thoroughly with water and then ethanol and benzene. The yellow crystals thus obtained [140 mg, 15% based on the glycol (X′)] were dissolved in hot toluene. The filtrate obtained by percolating the hot solution through a short column of alumina was put to stand to deposit pure II_4 as fine yellow needles. II_4 decomposed at *ca.* 180°C accompanying decoloration.

Found: C, 96.51; H, 3.62%. Calcd for $C_{40}H_{18}$: C, 96.36; H, 3.64%.

3-(1-Pyrenyl)-prop-2-ynal (VI). A solution of 1-ethynylpyrene (V, 10.08 g, 0.045 mol) in tetrahydrofuran (50 m*l*) was added under stirring over a period of 20 min to an ice-cooled solution of isopropylmagnesium bromide [from magnesium, 2.16 g (0.09 g-atom) and isopropyl bromide, 12.18 g (0.099 mol)] in tetrahydrofuran (60 m*l*). The mixture had been refluxed for 1 hr, and then chilled on an ice-salt bath. Dimethylformamide (16 m*l*) was added in one portion to the chilled mixture and stirred for 20 min. Stirring was continued for further 4 hr at room temperature. The reaction mixture was then poured into vigorously stirred 5% sulfuric acid (600 m*l*) and stirred overnight. The mixture was extracted with benzene (1 *l*) and the extract was washed successively with water and a solution of sodium hydrogen carbonate. The organic layer was shaken with a saturated solution of sodium hydrogen sulfite. The adduct deposited was washed with ether, tetrahydrofuran and ether, succes-

sively, and decomposed with a saturated solution of sodium hydrogen carbonate. The crude propynal (VI) thus obtained was extracted with hot benzene (100 m*l*) using a Soxhlet extractor. Orange cubes, 9.19 g (81%), mp 145—147°C, obtained from the extract were recrystallized several times from benzene - cyclohexane. Aldehyde (VI) showed dimorphism, *viz.*, rapid cooling of the benzene - cyclohexane solution gave orange needles, mp 141—142°C. On the other hand, orange cubes, mp 148—149°C were obtained on slow cooling of the solution.

Low mp isomer. Found: C, 89.27; H, 4.01%. High mp isomer. Found: C, 89.63; H, 3.99%. Calcd for $C_{19}H_{10}O$: C, 89.74; H, 3.96%. IR: 2840, 2735 (CHO), 2170 (C≡C), 1645 (C=O) cm^{-1}. Both isomers exhibited almost the same IR spectra, a slight difference being observed in the region 1200—650 cm^{-1}.

3-(2-Pyrenyl)-prop-2-ynal (VI'). To an ice-cooled and stirred solution of isopropylmagnesium bromide [from magnesium, 0.72 g (0.03 g-atom) and isopropyl bromide, 4.06 g (0.033 mol)] in tetrahydrofuran (20 m*l*) was added over a period of 15 min a solution of 2-ethynylpyrene (V', 3.36 g, 0.015 mol) in tetrahydrofuran (20 m*l*). The mixture was stirred for 30 min at room temperature and then refluxed for 30 min. The mixture was then chilled on an ice-salt bath. After dimethylformamide (6 m*l*) had been added in one portion, the temperature of the reaction mixture was gradually raised to room temperature. Stirring was continued for 3 hr and then for 1 hr at 30°C. The reaction mixture was poured into vigorously agitated 5% sulfuric acid (200 m*l*) and stirring was continued overnight. The mixture was extracted with benzene (330 m*l*) and the extract was washed successively, with water, a saturated solution of sodium hydrogen carbonate and water, and dried. The crystalline residue obtained by evaporating the solvent was recrystallized from benzene to afford yellow crystals, 3.1 g (81%). The crystals dissolved in ethanol were treated with active charcoal and recrystallized 3 times from benzene - cyclohexane to yield pure VI' as yellow cubes, mp 160—161°C.

Found: C, 89.60; H, 4.12%. Calcd for $C_{19}H_{10}O$: C, 89.74; H, 3.96%. IR: 2180 (C≡C), 1660 (C=O) cm^{-1}.

1-(1-Pyrenyl)-1,4-pentadiyn-3-ol (XVI). A solution of 1-pyrenylpropynal (VI, 5.09 g, 0.02 mol) in tetrahydrofuran (150 m*l*) was added over a period of 20 min into an ice-cooled and stirred solution of ethynylmagnesium bromide [from magnesium, 1.15 g (0.048 g-atom), ethyl bromide, 5.78 g (0.053 mol) and an excess of acetylene]. The cooling bath was removed after 3 hr, and stirring was continued overnight at room temperature. A saturated ammonium chloride solution was added to the reaction mixture under cooling with ice-salt bath. The organic layer was separated and the aqueous layer was extracted with benzene (100 m*l*). The combined organic layer was dried. A light brown oily material obtained by evaporation of the solvent was mixed with hot benzene (20 m*l*), thus yielding fine light brown needles, 4.07 g (73%), mp 114—119°C. The crystals were recrystallized 4 times from methanol-benzene to yield pure XVI as pale yellow needles, mp 122—123°C. XVI gave yellow cuprous acetylide.

Found: C, 89.69; H, 4.30%. Calcd for $C_{21}H_{12}O$: C, 89.98; H, 4.32%. IR: 3400—3100 (OH), 3295 (≡CH), 2220, 2110 (C≡C), 1010 (C–O) cm^{-1}.

1-(2-Pyrenyl)-1,4-pentadiyn-3-ol (XVI'). Crude crystals of XVI' obtained according to the procedure for the synthesis of XVI were dissolved in benzene - ethanol and treated with active charcoal, yielding light yellow crystals in a 73% yield. The material was recrystallized 3 times from ethanol to give pure XVI' as colorless plates, mp 175—178°C.

Found: C, 89.98; H, 4.35%. Calcd for $C_{21}H_{12}O$: C, 89.98; H, 4.32%. IR: 3500—3400 (OH), 3295 (≡CH), 1180 (C–O) cm^{-1}.

1,1'-Dipyrenylpentaacetylene (I_5). Oxidative Coupling of XVI. A mixture of pentadiynol (XVI, 2.10 g, 7.5 mmol), cuprous chloride (0.20 g), ammonium chloride (0.18 g) and methanol (50 m*l*) was vigorously stirred under a slight excess of oxygen pressure at room temperature for 48 hr. The residue obtained by evaporating the solvent was dissolved in acetone (50 m*l*) and the insoluble material was removed by filtration. The acetone solution was passed through a short column of alumina, and the filtrate was concentrated. The residue solidified on addition of a small amount of benzene. The solid was washed with a small amount of methanol to yield crude XVII as light brown unstable crystalline powder, 1.01 g (58%). The IR spectrum of this material indicates the absence of ethynyl group. The crude material was subjected to the subsequent reaction without purification because of its instability.

Chlorination of XVII. A solution of thionyl chloride (0.18 g, 1.5 mmol) and pyridine (0.12 g, 1.5 mmol) in tetrahydrofuran (5 m*l*) was added over a period of 15 min to a solution of the crude tetraacetylene glycol (XVI, 0.279 g, 0.5 mmol) in the same solvent (15 m*l*) at a temperature of −30°C. After shaking for 10 min, the reaction mixture was used immediately in the following reaction without isolation of XVIII.

Dehydrochlorination of XVIII. The reaction mixture containing XVIII was added to a suspension of sodium amide [from sodium, 0.20 g (8.7 mg-atom)] in liquid ammonia (70 m*l*) at −70°C. After the mixture had been stirred for 30 min, ammonium chloride (1.0 g) was added and the ammonia was allowed to evaporate. The organic solvent in the residue was removed. A small amount of water was added to the residue and the insoluble material was collected and washed successively with water, a small amount of acetone and benzene. A deep brown solid thus obtained was extracted with hot toluene (total 500 m*l*) and the hot extract was passed through a short column of alumina (15 g). I_5 (0.089 g, 34%) was obtained as fine orange needles on putting the orange yellow filtrate to stand. I_5 decomposed at *ca.* 215°C.

Found: C, 96.11; H, 3.55%. Calcd for $C_{42}H_{18}$: C, 96.53; H, 3.47%.

2,2'-Dipyrenylpentaacetylene (II_5). A mixture of diynol (XVI', 1.05 g, 3.75 mmol), cuprous chloride (0.40 g), ammonium chloride (0.36 g), concentrated hydrochloric acid (1 drop) and methanol (80 m*l*) was vigorously stirred in an atmosphere of oxygen under slightly elevated pressure for 48 hr at room temperature. The precipitate collected by filtration was washed with methanol to give brown crystals. The crystals were dissolved in tetrahydrofuran and filtered. Concentration of the filtrate gave crude XVII' as brown crystals, 500 mg (48%). Crude XVII' was converted into dichloride (XVIII') and then dehydrochlorinated to yield II_5 according to the method used in the preparation of I_5. Pentaacetylene (II_5) was obtained as orange yellow needles (13% based on XVII') which decomposed at *ca.* 140°C.

Found: C, 96.43; H, 3.37%. Calcd for $C_{42}H_{18}$: C, 96.53; H, 3.47%.

1-(1-Pyrenyl)-2,5-hexadiyn-1,4-diol (XIII). A solution of 1-formylpyrene (III, 6.68 g, 0.029 mol) in tetrahydrofuran (60 m*l*) was added to a stirred solution of the Grignard derivative of 1,4-pentadiyn-3-ol [from 3.08 g of the alcohol] in tetrahydrofuran (15 m*l*) under cooling on an ice-salt bath. The temperature of the reaction mixture was gradually raised

to room temperature, stirring was continued overnight and a saturated solution of ammonium chloride was then added. The aqueous layer was extracted with benzene (100 m*l*). The combined organic layer was dried and concentrated to give an oily material. The crystals formed by trituration with benzene were washed with a small amount of benzene and dissolved in acetone (50 m*l*). The acetone solution was passed through a short column of alumina (15 g) and the filtrate was concentrated. The oily residue was mixed with hot benzene (25 m*l*) to deposit fine light brown crystals, 6.55 g (73%), mp 115—125°C. Recrystallization of the crystals from ethyl acetate - benzene afforded pure XIII as pale yellow needles which decomposed at *ca.* 145—155°C.

Found: C, 84.88; H, 4.61%. Calcd for $C_{22}H_{14}O_2$: C, 85.14; H, 4.55%. IR: 3600—3100 (OH), 3290 (≡CH), 2110 (C≡C), 1027 (C–O) cm^{-1}.

1-Pyrenyltriacetylene (XV). Chlorination of XIII. To a solution of slightly crude XIII (0.310 g, 1 mmol) in tetrahydrofuran (5 m*l*) maintained at −30°C was added over a period of 15 min a solution of thionyl chloride (0.36 g, 3 mmol) and pyridine (0.24 g, 3 mmol) in the same solvent (5 m*l*). After the addition had been completed, the mixture was stirred for 2 hr at room temperature. Crushed ice was added to the reaction mixture and extraction was carried out with benzene (100 m*l*). The extract was washed successively with water and sodium hydrogen carbonate solution, and dried. The reddish brown oily material obtained by evaporation of the solvent was subjected to the following reaction.

Dehydrochlorination. A solution of crude dichloride (XIV) in tetrahydrofuran (5 m*l*) was added over a period of 10 min to a suspension of sodium amide [from sodium, 0.14 g (6 mg-atom)] in liquid ammonia (50 m*l*) at −70°C. After the mixture had been stirred for 30 min, ammonium chloride (0.7 g) was added and the ammonia was allowed to evaporate. The residue, after the organic solvent had been removed, was extracted with petroleum ether (bp 60—80°C, total 150 m*l*). The extract was passed through a thin layer of alumina (2 g) and the filtrate was used in the subsequent reaction. Extremely unstable yellow crystals (XV) were obtained by concentration of a small portion of the filtrate. The filtrate exhibiting UV maximum at 396 nm gave orange red cuprous acetylide.

1,1'-Dipyrenylhexaacetylene (I_6). The petroleum ether solution of XV was added to a mixture of cupric acetate monohydrate (1.5 g), methanol (5 m*l*), and pyridine (10 m*l*). Petroleum ether was removed under reduced pressure and additional pyridine (5 m*l*) was then added. The mixture was stirred for 2 hr at room temperature. The insoluble material was filtered, washed with water, a small amount of methanol and benzene to yield dark red fine crystals, 0.089 g (33% based on XIII). The crystals were digested with hot toluene (total 400 m*l*) and the extract was passed through a short column of alumina (10 g). On leaving the filtrate to stand, hexaacetylene (I_6) deposited as tiny red crystals which decomposed at *ca.* 200°C.

Found: C, 96.18; H, 3.24%. Calcd for $C_{44}H_{18}$: C, 96.68; H, 3.32%.

1-(2-Pyrenyl)-1,4-hexadiyn-3,6-diol (XIX'). To an ice-cooled and stirred solution of the Grignard derivative of propargyl alcohol [from propargyl alcohol, 1.86 g (0.033 mol)] in tetrahydrofuran (35 m*l*) was added a solution of the propiolaldehyde (VI', 2.80 g, 0.017 mol) in tetrahydrofuran (30 m*l*). After the reaction mixture had been stirred overnight, a saturated solution of ammonium chloride was added. The aqueous layer was extracted with tetrahydrofuran and combined with the organic layer and dried. The combined organic layer was concentrated to yield light brown crystals, 2.9 g (85%). The crystals were recrystallized 3 times from ethanol to give pure XIX' as tiny light brown leaflets, mp 200—203°C (dec.).

Found: C, 85.12; H, 4.58%. Calcd for $C_{22}H_{14}O_2$: C, 85.14; H, 4.55%. IR: 3350—3100 (OH), 2240 (C≡C), 1020, 1040 (C–O) cm^{-1}.

2-Pyrenyltriacetylene (XV'). Chlorination of XIX'. A solution of thionyl chloride (720 mg, 6 mmol) in tetrahydrofuran (10 m*l*) was added to a solution of XIX' (620 mg, 2 mmol) and pyridine (480 mg, 6 mmol) in the same solvent (20 m*l*) at −30°C. The mixture was stirred for 30 min at room temperature and then for 40 min at 30°C. The mixture was chilled again on an ice-salt bath and crushed ice was added. The organic layer was washed with a solution of sodium hydrogen carbonate and dried. The residue obtained by evaporation of the solvent was redissolved in tetrahydrofuran (15 m*l*). The solution of XX' thus prepared was subjected to the following dehydrochlorination.

Dehydrochlorination of XX'. The solution of XX' was added to a suspension of sodium amide [from sodium, 1.3 g (0.055 mg-atom)] in liquid ammonia (100 m*l*) at −70°C. After the mixture had been stirred for 1 hr, ammonium chloride (5 g) was added and ammonia was allowed to evaporate. The residue obtained by evaporation of the organic solvent was extracted with petroleum ether (bp 60—80°C, total 500 m*l*). The extract was percolated through a thin layer of alumina (10 g) and the filtrate was used in the following oxidative coupling without isolation of triacetylene (XV').

2,2'-Dipyrenylhexaacetylene (II_6). The petroleum ether solution of XV' was mixed with a mixture of cupric acetate monohydrate (2 g) and pyridine (20 m*l*) and the petroleum ether was removed under reduced pressure. Pyridine (5 m*l*) and methanol (5 m*l*) were added to the residue and the resulting mixture was stirred for 2 hr at room temperature. The insoluble material was collected by filtration, washed successively with water, methanol and benzene. The yellowish brown solid thus obtained was digested with toluene and the hot extract was passed through a short column of alumina. The filtrate was allowed to cool to room temperature, yielding II_6 as tiny brownish orange yellow crystals. II_6 was found to be rather unstable and gave an unsatisfactory elemental analysis.

Found: C, 94.91; H, 3.90%. Calcd for $C_{44}H_{18}$: C, 96.68; H, 3.32%.

Linear Conjugated Systems Bearing Aromatic Terminal Groups. VIII. Syntheses and Electronic Spectra of Bis(4-biphenylyl)- and 2,2′-Difluorenylpoly-ynes

Kazuhiro NAKASUJI, Shuzo AKIYAMA, and Masazumi NAKAGAWA
Department of Chemistry, Faculty of Science, Osaka University, Toyonaka, Osaka
(Received August 6, 1971)

In order to get further information on the effect of terminal groups on the spectral regularity of diarylpoly-ynes, we carried out the syntheses of bis(4-biphenylyl)poly-ynes (I_n, $n=1$—6) and 2,2′-difluorenylpoly-ynes (II_n, $n=1$—4 and 6). The bathochromic shift of the longest-wavelength absorption maxima (λ_L) along with the increase in n was found to be expressed by the following empirical formulas:

I_n: $\lambda_L = 24.0n^{1.1} + 304$ (nm in tetrahydrofuran)

II_n: $\lambda_L = 9.0n^{1.5} + 350$ (nm in tetrahydrofuran)

The spectral behavior of bis(4-biphenylyl)poly-ynes (I_n) strongly supported the relationship $\lambda_L \propto n$ in diphenylpoly-ynes.

The syntheses and electronic spectral behavior of various diarylpoly-ynes [Ar(C≡C)$_n$Ar] bearing condensed aromatic nuclei as terminal groups have been reported.[1] It was found that the bathochromic shift of the longest-wavelength absorption maxima (λ_L) can

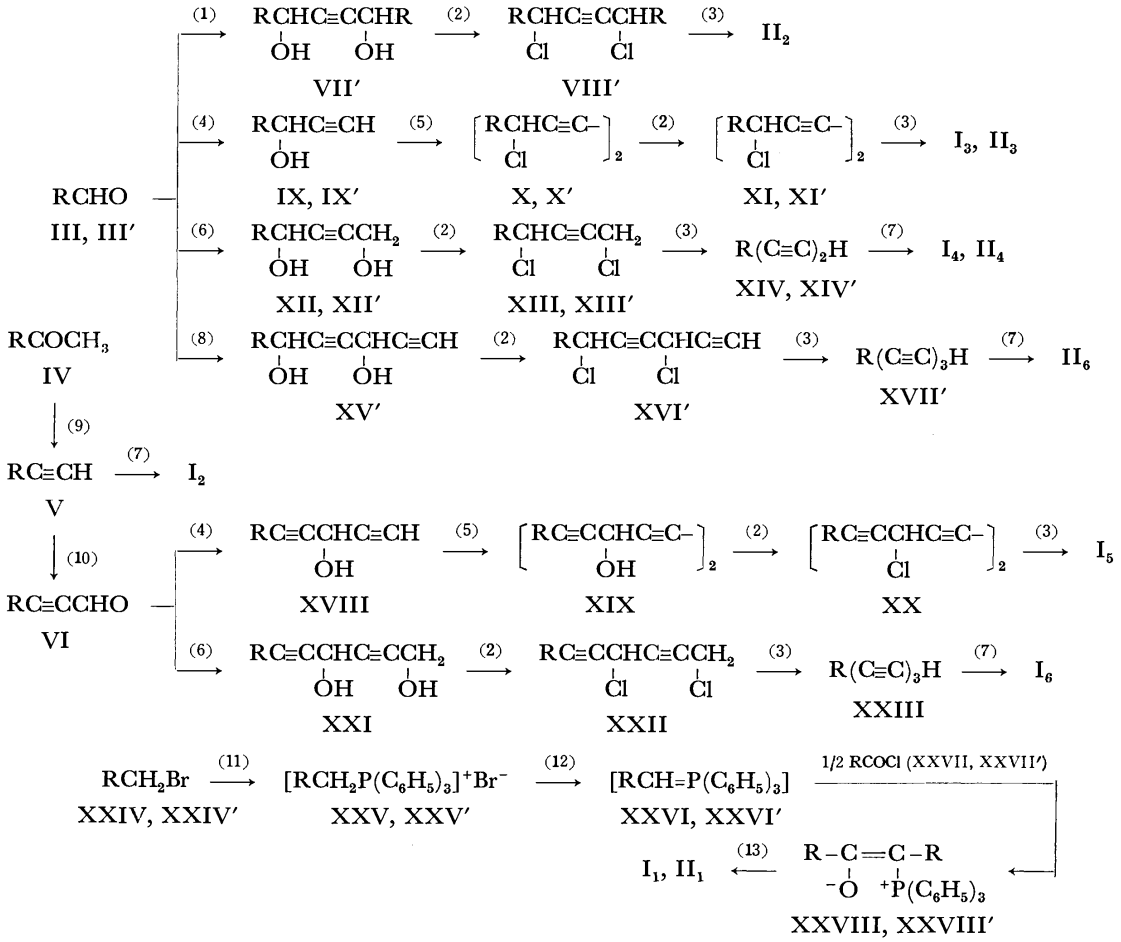

Scheme 1. Syntheses of I_n and II_n

Roman numerals bearing prime indicate the fluorenyl series.
(1) BrMgC≡CMgBr/THF, (2) $SOCl_2$-pyridine/THF, (3) $NaNH_2$/liq. NH_3, (4) HC≡CMgBr/THF or LiC≡CH/liq. NH_3, (5) CuCl-NH_4Cl-O_2/CH_3OH, (6) BrMgC≡CCH$_2$OMgBr/THF, (7) Cu(OCOCH$_3$)$_2$/pyridine, (8) BrMgC≡CCH(OMgBr)C≡CH/THF, (9) i) PCl_5, ii) $NaNH_2$/liq. NH_3, (10) i) C_2H_5MgBr/THF, ii) DMF/THF, iii) dil. H_2SO_4, (11) $P(C_6H_5)_3$/benzene, (12) C_6H_5Li/toluene, (13) thermolysis. THF=tetrahydrofuran, DMF=dimethylformamide.

1) K. Nakasuji, S. Akiyama, and M. Nakagawa, This Bulletin, **45**, 875 (1972) and references cited therein.

be expressed by the empirical formula

$$\lambda_L = An^x + B.$$

The value of x was found to depend on the nature of terminal group as well as on the position of linking of acetylenic chain. In view of the gradual change of the value of x, it was desirable to synthesize diarylpoly-ynes bearing non-condensed aromatic terminal groups to get further information on the effect of terminal groups on the electronic spectra of diarylpoly-ynes. In this paper, we will describe the syntheses and electronic spectral regularity of bis(4-biphenylyl)poly-ynes (I_n, n=1—6) and 2,2'-difluorenylpoly-ynes (II_n, n=1—4 and 6).

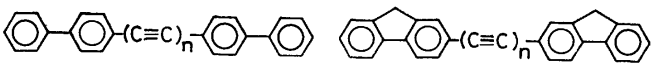

I_n II_n

Syntheses. The reaction sequence used in the syntheses of I_n and II_n are shown in Scheme 1.

The formyl- (III, III') and the propargylaldehyde derivatives (VI) are used as starting materials. In 4-biphenylyl series, the tri- and tetraacetylenes (I_3 and I_4) were obtained from formyl derivative (III), and propargylaldehyde (VI) was used in the preparation of penta- and hexaacetylenes (I_5 and I_6). 2,2'-Difluorenyl-poly-ynes (II_n, n=1—4 and 6) were prepared from 2-formylfluorene (III'). Dehydrochlorination of intermediate chloro-compounds by means of sodium amide in liquid ammonia successfully applied to biphenylyl series resulted in the formation of decomposition products in fluorenyl series, presumably owing to the presence of acidic methylene group. The elimination reactions of fluorenyl series were achieved by means of sodium or potassium ethoxide in ethanol. An attempt to prepare 2,2'-difluorenylpentaacetylene (II_5) according to the following reaction sequence gave fruitless results in the final step: RCHO→RCH(OH)(C≡C)$_2$H→RCH(OH)(C≡C)$_4$(HO)CHR→RCHCl(C≡C)$_4$ClCHR→R(C≡C)$_5$R.

Monoacetylenes (I_1 and II_1) were prepared by the intramolecular Wittig reaction,[2] *i.e.*, by thermolysis of betaines (XXVIII and XXVIII').

The physical properties of I_n and II_n are given in Tables 1 and 2.

The IR spectra of I_n and II_n exhibit the same characteristics observed in the other diarylpoly-ynes, *viz.*, the highest wave number of stretching vibration of acetylenic bond ($\nu_{C\equiv C}$) was observed in the cases of I_4 and II_3 and as illustrated in Fig. 1 the absorption intensity of $\nu_{C\equiv C}$ increased with the increase of n.

Electronic Spectra. The absorption curves and spectral data of I_n and II_n are summarized in Figs. 2 and 3, and Tables 3 and 4.

The marked difference in location of absorption maximum between biphenyl and fluorene has been

Table 1. Physical properties of I_n

n	Color of crystals	Mp (°C)	$\nu_{C\equiv C}$
1	colorless	253—254	—
2	colorless	232—233	2140
3	pale yellow	(*ca.* 250)	2185
4	yellow	(*ca.* 240)	2200
5	yellow	(*ca.* 200)	2180
6	orange yellow	(*ca.* 160)	2145

Numbers in parentheses indicate decomposition points.

Table 2. Physical properties of II_n

n	Color of crystals	Decomposition point (°C)	$\nu_{C\equiv C}$
1	colorless	*ca.* 295	—
2	pale yellow	*ca.* 280	—
3	yellowish brown	*ca.* 250	2190
4	orange yellow	*ca.* 210	2180
6	orange	*ca.* 150	2140

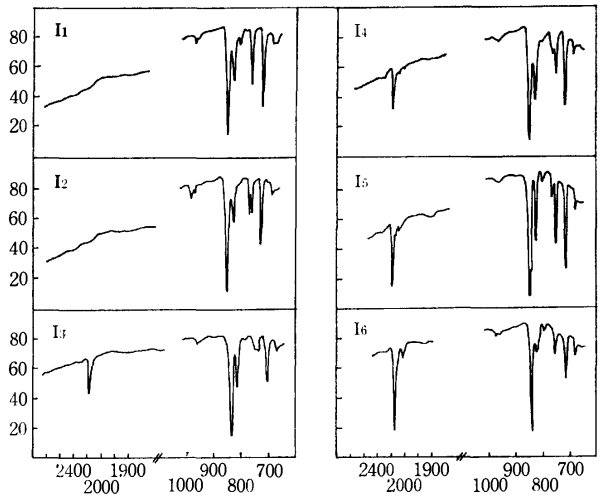

Fig. 1. The IR spectra of bis(4-biphenylyl)poly-ynes (I_n).

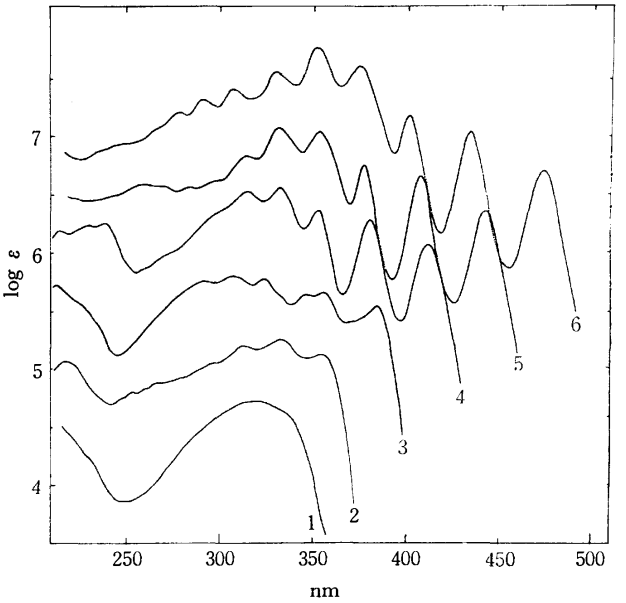

Fig. 2. The absorption curves of bis(4-biphenylyl)poly-ynes (I_n). The curves, with the exception of monoacetylene at the bottom, have been displaced upward on the ordinate axis by 0.5 log ε unit increments from the curve immediately below (in tetrahydrofuran).

2) S. Akiyama, K. Nakasuji, and M. Nakagawa, This Bulletin, **44**, 2231 (1971).

Table 3. Electronic spectral data of I_n

n	λ_{max} (log ε) in nm in tetrahydrofuran										
1	319 (4.62)										
2	217 (4.58)	296* (4.56)	313 (4.71)	332 (4.76)	355 (4.63)						
3	212 (4.75)	292 (4.74)	307 (4.83)	324 (4.81)	345 (4.67)	356 (4.69)	385 (4.57)				
4	214 (4.71)	230 (4.75)	240 (4.77)	314.5 (5.05)	332.5 (5.07)	353 (4.88)	381 (4.79)	413 (4.57)			
5	244 (4.59)	262 (4.68)	270 (4.67)	283 (4.66)	298 (4.72)	314.5 (4.92)	332 (5.16)	353 (5.12)	379 (4.83)	409 (4.72)	445 (4.44)
6	210 (4.61)	278 (4.73)	291.5 (4.84)	306.5 (4.92)	330 (5.06)	353 (5.27)	375 (5.11)	401 (4.69)	434 (4.55)	474 (4.21)	

* indicates shoulder.

Table 4. Electronic spectral data of II_n

n	λ_{max} (log ε) in nm in tetrahydrofuran										
1	229* (4.43)	239* (4.24)	255 (3.89)	335 (4.77)	341 (4.76)	358 (4.83)	383 (4.16)				
2	220 (4.69)	255 (4.24)	331 (4.81)	347 (4.89)	374 (4.84)						
3	220 (4.78)	240 (4.44)	260* (4.23)	273 (4.45)	298.5 (4.67)	312 (4.73)	322 (4.73)	333 (4.96)	352 (4.87)	368 (4.86)	397 (4.79)
4	241 (4.84)	304* (4.71)	324 (4.90)	339 (5.03)	360 (5.08)	389 (4.88)	422 (4.68)				
6	280 (4.83)	295 (4.93)	308 (4.87)	322 (4.84)	340 (5.05)	363 (5.27)	383 (5.11)	407 (5.01)	441 (4.76)	481 (4.42)	

* indicates shoulder

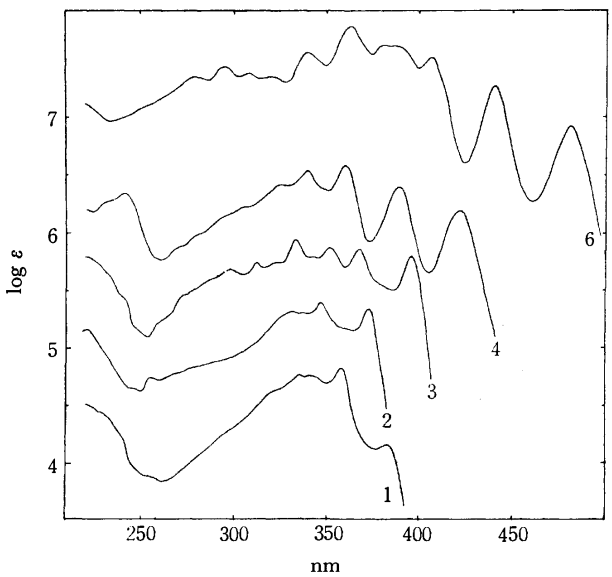

Fig. 3. The absorption cruves of 2,2′-difluorenylpoly-ynes (II_n). The cruves, with the exception of monoacetylene at the bottom, have been displaced upward on the ordinate axis by 0.5 log ε unit increments from the curve immediately below (in tetrahydrofuran.)

attributed to the strained planar structure of the latter.[3] The same characteristic difference was observed between I_n and II_n. Bis(4-biphenylyl)acetylene (I_1) displays a broad and structureless band in the long-wavelength region, while 2,2′-difluorenylacetylene (II_1) exhibits a band with vibrational structure, and an absorption maximum which might be related to ^1L_b band of fluorene can be observed in the longest-wavelength region. However, the members of biphenylyl series higher than diacetylene (I_2—I_6) exhibit vibrational fine structure. As with other diarylpoly-ynes, the fine structure in the spectra of I_n and II_n becomes progressively distinct with the increase of length of the acetylenic chain.

As shown in Table 5, the spacing between the longest-wavelength vibrational sub-band and the next longest-wavelength sub-band was found to be 1900—200 cm^{-1}. Detailed discussion on the spacing and $\nu_{C\equiv C}$ of diarylpoly-ynes is presented elsewhere.[4]

Table 5. Spacing of vibrational fine structure of I_n and II_n

n	2	3	4	5	6
I_n	1950	2120	2030	1980	1940
II_n	2080	1990	2010	—	1890

The plots of the longest-wavelength absorption maxima (λ_L) of I_n and II_n against $n^{1.1}$ and $n^{1.5}$ gave straight lines, as illustrated in Figs. 4 and 5. The linear relationships can be expressed by the following empirical formulas:

I_n: $\lambda_L = 24.0n^{1.1} + 304$ (nm in tetrahydrofuran)

II_n: $\lambda_L = 9.0n^{1.5} + 350$ (nm in tetrahydrofuran)

3) H. Suzuki, "Electronic Absorption Spectra and Geometry of Organic Molecules," Academic Press Inc., New York (1967), p. 261.

4) M. Nakagawa, S. Akiyama, K. Nakasuji, and K. Nishimoto, *Tetrahedron*, **27**, 5401 (1971).

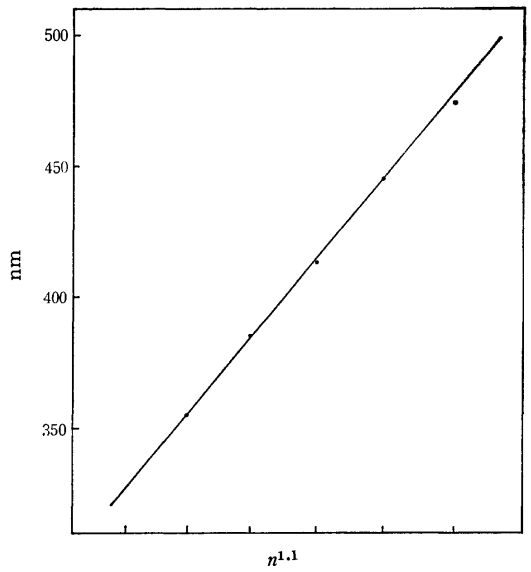

Fig. 4. Plot of λ_L against $n^{1.1}$ for bis(4-biphenylyl)poly-ynes (I_n).

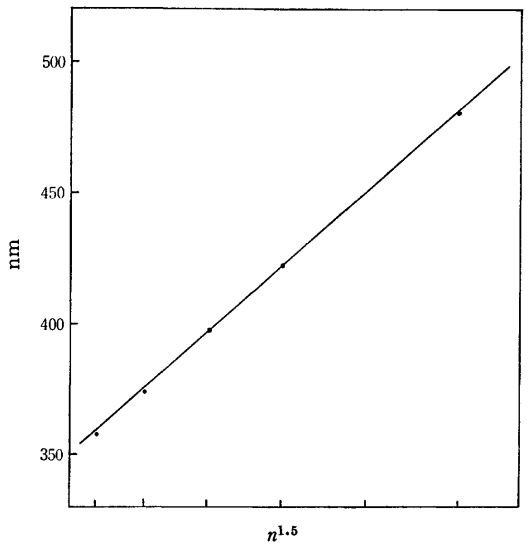

Fig. 5. Plot of λ_L against $n^{1.5}$ for 2,2'-difluorenylpoly-ynes (II_n).

TABLE 6. OBSERVED AND CALCULATED λ_L OF I_n AND II_n

n		1	2	3	4	5	6
I_n	Obsd	—	355	385	413	445	474
	Calcd	328	355	384	414	445	476
	λ		0	1	−1	0	−2
II_n	Obsd	358	374	397	422	—	481
	Calcd	359	375	397	422	451	482
	λ	−1	−1	0	0		−1

As is shown in Table 6, the agreement between observed and calculated values was found to be satisfactory.

It is to be noted that the linear relationship of 1,1'-dinaphthylpoly-ynes[5] could be expressed by the same empirical formula which is valid for 2,2'-difluorenylpoly-ynes (II_n).

We pointed out[6] that the spectral shift of diphenylpoly-ynes should be expressed by the relation $\lambda_L \propto n^{1.0}$ instead of the widely accepted $\lambda_L^2 \propto n$.[7] The spectral behavior of bis(4-biphenylyl)poly-ynes (I_n) seems to afford an additional strong support for the relation $\lambda_L \propto n^{1.0}$ in diphenylpoly-ynes.

A general view of the spectral behavior of various kinds of diarylpoly-ynes and a HMO explanation based on a modified bond-alternation approximation for the novel linear relationship are given elsewhere.[4]

Experimental

All the melting points are uncorrected. The electronic and IR (KBr-disk method) spectra were obtained on Hitachi EPS-3T and EPI-2 spectrophotometers, respectively. Evaporation of solvent or concentration of solution was carried out under reduced pressure throughout this work.

Bis(4-biphenylyl)diacetylene (I_2). Diacetylene (I_2) was prepared by modifying the reported method. Oxidative coupling of 4-ethynylbiphenyl (V)[8,9] by means of the Eglinton method gave I_2 in a 90% yield as colorless needles, mp 232—233°C (lit, mp 232°C,[8] mp 235—236°C[9]).

1-(4-Biphenylyl)-2-propyn-1-ol (IX). A solution of 4-formylbiphenyl[10] (III, 7.3 g, 0.04 mol) in tetrahydrofuran (50 m*l*) was added over a period of 15 min to a stirred solution of lithium acetylide [from lithium, 0.83 g, 0.12 g-atom] in liquid ammonia (200 m*l*) at −60°C. The reaction mixture was stirred for 1 hr at this temperature, then for 17.5 hr at −50——55°C and finally for 3 hr at the boiling point of ammonia. Ammonium chloride (4 g) was added to the reaction mixture at −70°C, and the ammonia was allowed to evaporate. The residue was mixed with a saturated solution of ammonium chloride, and the aqueous layer was extracted with ether. The extract was combined with organic layer and dried. The residue obtained by evaporation of the solvent was crystallized from benzene - cyclohexane to yield brown crystals, 6.7 g (80%). Recrystallization of the crude crystals three times from the same solvent gave pure IX as colorless tiny crystals, mp 114—116°C.

Found: C, 86.31; H, 5.83%. Calcd for $C_{15}H_{12}O$: C, 86.51; H, 5.81%. IR: 3400—3300 (OH), 3290 (≡CH), 2090 (C≡C), 1015 (C–O) cm^{-1}.

1,6-Bis(4-biphenylyl)-2,4-hexadiyn-1,6-diol (X). A mixture of ethynylcarbinol (IX, 3.1 g, 0.015 mol), cuprous chloride (0.3 g, 3 mmol), ammonium chloride (0.23 g, 4.2 mmol) and methanol containing 1 drop of concentrated hydrochloric acid (20 m*l*) was vigorously stirred for 2 hr at room temperature under a slight excess of oxygen pressure. Five drops of concentrated hydrochloric acid was then added to the reaction mixture, and stirring was continued for further 2 hr. Inorganic materials were removed by filtration and washed with methanol. The residue obtained by evaporation of the combined organic layer was dissolved in ether

5) K. Nakasuji, S. Akiyama, K. Akashi, and M. Nakagawa, This Bulletin, **43**, 3567 (1970).

6) S. Akiyama, K. Nakasuji, K. Akashi, and M. Nakagawa, *Tetrahedron Lett.*, **1968**, 1121.

7) H. H. Schlubach and V. Franzen, *Ann.*, **503**, 110 (1951); C. L. Cook, E. R. H. Jones, and M. C. Whiting, *J. Chem. Soc.*, **1952**, 2883; J. B. Armitage, N. Entwistle, E. R. H. Jones, and M. C. Whiting, *ibid.*,, **1954**, 147.

8) H. Tani, F. Toda, and K. Matsumiya, This Bulletin, **36**, 391 (1963).

9) W. Ried and V. Saxena, *Ann.*, **739**, 159 (1970).

10) D. H. Hey, *J. Chem. Soc.*, **1931**, 2476.

containing tetrahydrofuran and washed with 2N hydrochloric acid. The crude material obtained after washing, drying and evaporation was crystallized from benzene - ethanol, giving crude X, 2.1 g (66%). Recrystallization of the crude X three times from the same solvent yielded pure X as light brown plates, mp 215—217°C.

Found: C, 86.73; H, 5.40%. Calcd for $C_{30}H_{22}O_2$: C, 86.93; H, 5.35%. IR: 3450—3350 (OH), 1005 (C–O) cm^{-1}.

Bis(4-biphenylyl)triacetylene (I_3). Preparation of Dichloride (XI). A solution of thionyl chloride (0.72 g, 6 mmol) in tetrahydrofuran (5 m*l*) was added to a stirred solution of the glycol (X, 0.83 g, 2 mmol) and pyridine (0.48 g, 6 mmol) in tetrahydrofuran (10 m*l*) under cooling on an ice-salt bath. Stirring was continued for 1 hr at the same temperature. The reaction mixture was subjected to the subsequent reaction without isolation of XI.

Dehydrochlorination of XI. The solution of XI was added to a stirred suspension of sodium amide [from sodium, 0.4 g, 0.018 g-atom] in liquid ammonia (50 m*l*) at −70°C. After the mixture had been stirred for 2 hr, ammonium chloride (3 g) was added and the ammonia was allowed to evaporate. The residue was mixed with water and the insoluble material was washed with a small amount of ethanol and benzene. The brown crystals thus obtained were dissolved in benzene, and the solution was percolated through a thin layer of alumina (6 g). The filtrate was concentrated to yield yellow crystals, 190 mg (25%). The product was recrystallized twice from benzene to give pure I_3 as pale yellow tiny crystals which decomposed at *ca.* 250°C.

Found: C, 94.74; H, 4.83%. Calcd for $C_{30}H_{18}$: C, 95.21; H, 4.79%.

1-(4-Biphenylyl)-2-butyn-1,4-diol (XII). To an ice-cooled solution of the Grignard derivative of propargyl alcohol [from magnesium, 4.6 g (0.192 g-atom)], ethyl bromide, 25 g (0.23 mol) and propargyl alcohol, 5.4 g (0.096 mol)] in tetrahydrofuran (120 m*l*), was added under stirring a solution of 4-formylbiphenyl[10] (III, 10 g, 0.055 mol) in the same solvent (30 m*l*). The stirred mixture was allowed to warm to room temperature and stirring was continued overnight. 4N Sulfuric acid was then added to the reaction mixture and the organic layer was separated. The aqueous layer was extracted with benzene. The combined organic layer was washed successively with saturated solutions of sodium chloride, sodium hydrogen carbonate and water, and dried. The brown crystals obtained by evaporation of the solvent were dissolved in ethanol and treated with active charcoal and evaporated under reduced pressure. The crude crystals were recrystallized from benzene - ethanol, yielding brown crystals, 9.4 g (72%). The product was recrystallized 3 times from the same solvent to afford pure XII as colorless needles, mp 133—134°C.

Found: C, 80.85; H, 6.04%. Calcd for $C_{16}H_{14}O_2$: C, 80.64; H, 5.92%. IR: 3300—3200 (OH), 1015 (C–O) cm^{-1}.

4-Butadiynylbiphenyl (XIV). Preparation of Dichloride (XIII). A solution of thionyl chloride (14 g, 0.114 mol) in tetrahydrofuran (20 m*l*) was added over a period of 30 min to an ice-cooled mixture of butynediol (XII, 8.8 g, 0.037 mol), pyridine (9.0 g, 0.114 mol) and tetrahydrofuran (80 m*l*) and the reaction mixture was stirred for 1 hr. After the mixture had been stirred for further 40 min at 40°C, crushed ice was added to the mixture under ice-cooling. The aqueous layer was extracted with ether and combined with the organic layer, and washed with water and sodium hydrogen carbonate solution. It was dried and evaporated. Crude XIII thus prepared was used immediately in the following reaction.

Dehydrochlorination of XIII. A solution of the crude XIII in a mixture of tetrahydrofuran (15 m*l*) and ether (5 m*l*) was added in a stirred suspension of sodium amide [from sodium, 6 g (0.26 g-atom)] in liquid ammonia (450 m*l*) at −70°C and the mixture was stirred for a further 2 hr. Ammonium chloride (20 g) was then added and the ammonia was allowed to evaporate. The residue obtained by evaporation of the organic solvent was repeatedly digested with petroleum benzine (total 600 m*l*). The benzine solution was concentrated to *ca.* 200 m*l* and passed through a column of alumina (10 g). Diacetylene (XIV) was obtained as colorless needles, 1.9 g (26%) on concentration of the filtrate. The product was recrystallized from petroleum benzine to give pure XIV, colorless needles, mp 105°C (dec.). XIV was found to be unstable and turned to black insoluble material on standing.

Found: C, 94.57; H, 4.87%. Calcd for $C_{16}H_{10}$: C, 95.02; H, 4.98%. UV: $\lambda_{max}^{n\text{-hexane}}$ (log ε) 302* (4.52), 292 (4.56), 245 (3.99) nm. The asterisk indicates shoulder.

Bis(4-biphenylyl)tetraacetylene (I_4). A solution of 4-butadiynylbiphenyl (XIV, 0.8 g, 4 mmol) in petroleum benzine (20 m*l*) was added to a mixture of cupric acetate monohydrate (4 g) and pyridine (20 m*l*) and the mixture was stirred for 2 hr at room temperature. After benzine had been removed under reduced pressure, stirring was continued for a further 3 hr at 50°C. The reaction mixture was chilled on an ice-salt bath. The solid deposited was filtered and washed with a small amount of methanol and water, successively. The yellowish brown crystals, 620 mg (77%) thus obtained were dissolved in benzene and treated with active charcoal. Recrystallization twice from the same solvent afforded pure I_4 as yellow rods which decomposed at *ca.* 240°C.

Found: C, 95.90; H, 4.48%. Calcd for $C_{32}H_{18}$: C, 95.49; H, 4.51%.

3-(4-Biphenylyl)-prop-2-ynal (VI). To an ice-cooled and stirred solution of ethynylmagnesium bromide [from magnesium, 2.92 g (0.12 g-atom), ethyl bromide, 15.8 g (0.15 mol) and an excess of acetylene] in tetrahydrofuran (70 m*l*) was added over a period of 20 min a solution of 4-ethynylbiphenyl[8,9] (V, 17.8 g, 0.1 mol) in the same solvent (40 m*l*). After 1 hr, the mixture was refluxed for 30 min and then cooled on an ice-salt bath. A solution of dimethylformamide (23 m*l*) in tetrahydrofuran (40 m*l*) was added in one portion to the chilled mixture. The reaction mixture was left to reach room temperature. After stirring for 6 hr, the reaction mixture was poured into cold 5% sulfuric acid (700 m*l*) under vigorous agitation, after which the stirring was continued overnight. The mixture was then extracted with benzene. The extract was washed successively with water and sodium hydrogen carbonate solution and dried. The crude yellow crystals obtained by evaporation of the solvent were recrystallized from benzene - petroleum ether to give colorless needles, 12.3 g (60%), mp 75—78°C. This substance was recrystallized 3 times from benzene - cyclohexane to give pure VI as colorless needles, mp 76—78°C.

Found: C, 87.54; H, 4.89%. Calcd for $C_{15}H_{10}O$: C, 87.35; H, 4.89%. IR: 2180 (C≡C), 1652 (C=O) cm^{-1}.

1-(4-Biphenylyl)-1,4-pentadiyn-3-ol (XVIII). A solution of the aldehyde (VI, 7.22 g, 0.035 mol) in tetrahydrofuran (50 m*l*) was added to an ice-cooled solution of ethynylmagnesium bromide [from magnesium, 2.13 g (0.088 g-atom), ethyl bromide, 11.43 g (0.105 mol) and an excess of acetylene] in tetrahydrofuran (100 m*l*), after which the mixture was stirred for 1 hr at the same temperature. The cooling bath was then removed and stirring continued overnight at room temperature. The reaction mixture was chilled again on an ice-salt bath and a saturated solution of ammonium chloride was added, extracted with benzene. The extract

was dried and evaporated, resulting in crude crystals. The crude material was dissolved in ethanol and treated with charcoal. The crystals obtained from the filtrate were recrystallized from benzene - petroleum benzine to give slightly crude XVIII, 5.6 g (69%), mp 100—103°C. Recrystallization of this substance twice from the same solvent gave pure XVIII, mp 107—109°C.

Found: C, 87.85; H, 5.19%. Calcd for $C_{17}H_{12}O$: C, 87.90; H, 5.21%. IR: 3320—3180 (OH, ≡CH), 2220, 2105 (C≡C) cm^{-1}.

1,10-Bis(4-biphenylyl)-1,4,6,9-decatetrayn-3,8-diol (XIX). A mixture of diacetylene alcohol (XVIII, 4.64 g, 0.02 mol), cuprous chloride (0.40 g, 0.004 mol), ammonium chloride (0.30 g, 0.0056 mol), methanol (30 m*l*) and a drop of concentrated hydrochloric acid was vigorously stirred overnight at room temperature under a slight excess pressure of oxygen. The inorganic materials deposited were removed by filtration. The filtrate was evaporated and the residue was dissolved in ether, washed successively with 2N hydrochloric acid, water, sodium hydrogen carbonate solution and water, and dried. The crystals obtained by evaporation of the solvent were dissolved in ethanol and treated with active charcoal. Slightly impure XIX, 2.8 g (56%), thus prepared, was used in the subsequent reaction without further purification.

Bis(4-biphenylyl)pentaacetylene (I_5). Preparation of the Dichloride (XX). A solution of thionyl chloride (0.54 g, 4.5 mmol) and pyridine (0.36 g, 4.5 mmol) in ether (5 m*l*) was added over a period of 20 min to a stirred solution of the glycol (XIX, 0.69 g, 1.5 mmol) in tetrahydrofuran (10 m*l*) at −58°C and the mixture was stirred for a further 30 min at the same temperature. The reaction mixture was used immediately in the following reaction without isolation of XX.

Dehydrochlorination of XX. The reaction mixture containing XX was added into a stirred suspension of sodium amide [from sodium, 0.6 g (0.26 g atom)] in liquid ammonia (60 m*l*) maintained at −70°C. After stirring for an additional 1 hr at the same temperature, ammonium chloride (3 g) was added and the ammonia was allowed to evaporate. The residue obtained by evaporating the organic solvent was mixed with water. The insoluble material was filtered, washed with ethanol and a small amount of benzene. The deep brown solid thus obtained was dissolved in benzene and the solution was percolated through a short column of alumina (10 g). Yellowish crystals, 345 mg (54%) obtained by evaporation of the filtrate were recrystallized twice from benzene to yield pure I_5 as yellow needles. I_5 decomposed at *ca.* 200°C.

Found: C, 96.03; H, 4.42%. Calcd for $C_{34}H_{18}$: C, 95.75; H, 4.25%.

1-(4-Biphenylyl)-1,4-hexadiyn-3,6-diol (XXI). A solution of biphenylylpropynal (VI, 8.24 g, 0.04 mol) in tetrahydrofuran (20 m*l*) was added to a stirred solution of the Grignard derivative of propargyl alcohol [from magnesium, 2.88 g (0.12 g-atom), ethyl bromide, 15.7 g (0.144 mol) and propargyl alcohol, 3.66 g (0.06 mol)] in tetrahydrofuran (75 m*l*) under cooling on an ice-salt bath, after which the cooling bath was removed and the mixture was stirred overnight at room temperature. To the ice-cooled reaction mixture was added a saturated solution of ammonium chloride and the organic layer was separated. The aqueous layer was extracted with ether. The combined organic layer was washed with sodium chloride solution and dried. The light yellow crystals, 9.0 g (85%) obtained by the evaporation of the solvent were recrystallized twice from benzene to give pure XXI as colorless needles, mp 115—117°C.

Found: C, 82.40; H, 5.51%. Calcd for $C_{18}H_{14}O_2$: C, 82.42; H, 5.38%. IR: 3300—3200 (OH), 2220 (C≡C), 1020 (C–O) cm^{-1}.

1-(4-Biphenylyl)-1,3,5-hexatriyne (XXIII). Preparation of the Dichloride (XXII). To a stirred solution of glycol (XXI) 2.36 g, 9 mmol) in tetrahydrofuran (15 m*l*) maintained at −40°C, was added over a period of 30 min a solution of thionyl chloride (3.12 g, 27 mmol) and pyridine (2.13 g, 27 mmol) in ether (7 m*l*). The mixture was stirred for a further 30 min at the same temperature and then for 1 hr at room temperature. The reaction mixture containing XII was subjected immediately to the following reaction.

4-Biphenylyltriacetylene (XXIII). The solution containing XII was added to a suspension of sodium amide [from sodium, 2.0 g (0.09 g-atom)] in liquid ammonia (150 m*l*) at −70°C. After the mixture had been stirred for 1 hr at the same temperature, ammonium chloride (7 g) was added and ammonia was allowed to evaporate. The residue obtained by removing the organic solvent was digested with petroleum benzine (total 800 m*l*) and the extract was concentrated to *ca.* 200 m*l*. The extract was passed through a short column of alumina (15 g). The filtrate containing extremely unstable XXIII was used in the following reaction.

UV: $\lambda_{max}^{benzine}$ 338, 317, 300 nm.

Bis(4-biphenylyl)hexaacetylene (I_6). The benzine solution of XXIII was evaporated *in vacuo* under continuous addition of ethanol. The ethanol solution of XXIII thus prepared was mixed with a solution of cupric acetate monohydrate (15 g) in pyridine (100 m*l*), and ethanol was removed under reduced pressure. After the reaction mixture had been stirred for 2 hr at 50°C, pyridine was evaporated. The residue was mixed with benzene, and benzene was evaporated to remove the remaining pyridine. The resulting deep brown crystalline mass was dissolved in benzene and percolated through a thin layer of alumina (10 g). Concentration of the filtrate afforded yellowish brown crystals, 180 mg (9%). The procedure of percolation of the benzene solution was rapidly repeated 2 times to give pure I_6, orange yellow needles, which decomposed at *ca.* 160°C.

Found: C, 95.68; H, 4.50%. Calcd for $C_{36}H_{18}$: C, 95.97; H, 4.03%.

1,4-Bis(2-fluorenyl)-2-butyn-1,4-diol (VII'). A solution of 2-formylfluorene[11] (III', 5.4 g, 0.028 mol) in tetrahydrofuran (30 m*l*) was added to an ice-cooled solution of acetylenedimagnesium bromide [from magnesium, 1.9 g (0.08 g-atom), ethyl bromide, 10.7 g (0.096 mol)] in benzene - tetrahydrofuran (1 : 1, 100 m*l*). The reaction mixture was stirred overnight at room temperature, and was then chilled on an ice-salt bath. A saturated solution of ammonium chloride was added to the chilled reaction mixture and the organic layer was separated. The aqueous layer was extracted with ether. The combined organic layer was dried, and evaporated, thus yielding a solid contaminated with a reddish brown oily material. Recrystallization of this material from benzene - ethanol yielded light brown crystalline powder, 3.5 g (60%). The crude material was recrystallized twice from tetrahydrofuran to yield pure VII' as light yellow leaflets, mp 236—238°C.

Found: C, 86.58; H, 5.33%. Calcd for $C_{30}H_{22}O_2$: C, 86.93; H, 5.32%. IR: 3350—3250 (OH), 1005, 980 (C–O) cm^{-1}.

2,2'-Difluorenyldiacetylene (II_2). Preparation of the Dichloride (VIII'). A solution of thionyl chloride (360 mg, 3 mmol) in tetrahydrofuran (5 m*l*) was added to a stirred solution of glycol (VII', 310 mg, 0.75 mmol) and pyridine (240 mg, 3 mmol) in tetrahydrofuran (5 m*l*) under cooling on an ice-salt bath. After the mixture had been stirred for 1 hr at the same temperature and for 2 hr at room temperature,

11) R. Rieche, H. Gross, and E. Hoft, *Chem. Ber.*, **93**, 88 (1960).

crushed ice was added to the reaction mixture under cooling with ice-water. The mixture was extracted with benzene. The extract was washed with water and a solution of sodium hydrogen carbonate and dried. The residue obtained by evaporation of the solvent was used in the following reaction without further purification.

Dehydrochlorination of VIII'. A solution of the crude VIII' in tetrahydrofuran (60 m*l*) and ethanol (20 m*l*) was added dropwise into an ice-cooled solution of potassium ethoxide [from potassium, 0.15 g (3.8 mg-atom)] in ethanol (10 m*l*). After the reaction mixture had been stirred for 2 hr at room temperature, the solvent was evaporated. The residue was extracted with benzene and the extract was passed through a short column of alumina (15 g). The yellow filtrate was evaporated to yield yellowish brown crystals, 180 mg. This material was recrystallized from benzene to yield yellow crystals, 120 mg (42%). The crystals were redissolved in benzene and percolated through a thin layer of alumina (5 g). The crystals obtained from the filtrate were recrystallized twice from benzene to yield pure II_2 as pale yellow needles, mp 280—282°C (dec.). [lit[8] mp 278°C (dec.)].

Found: C, 95.08; H, 4.80%. Calcd for $C_{30}H_{18}$: C, 95.21; H, 4.79%.

1-(2-Fluorenyl)-2-propyn-1-ol (IX'). To an ice-cooled solution of ethynylmagnesium bromide [from magnesium, 1.80 g (0.075 g-atom), ethyl bromide, 8.20 g (0.075 mol) and an excess of acetylene] in tetrahydrofuran (150 m*l*) was added a solution of 2-formylfluorene (III', 5.82 g, 0.03 mol) in tetrahydrofuran (30 m*l*). The reaction mixture was left to reach room temperature and stirring was continued overnight. The mixture was then chilled on an ice-salt bath and a saturated solution of ammonium chloride was added. The organic layer was dried, and evaporated to give crude brown crystals. After recrystallization from benzene, the crystals were dissolved in ethanol and treated with charcoal, giving brown crystals, 5.3 g (80%). A solution of the crystals in ethyl acetate was passed through a thin layer of alumina (10 g). A slightly crude material obtained from the filtrate was recrystallized 3 times from petroleum benzine-benzene to yield pure IX' as pale yellow needles, mp 147—149°C.

Found: C, 87.37; H, 5.50%. Calcd for $C_{16}H_{12}O$: C, 87.24; H, 5.49%. IR: 3450—3300 (OH), 3260 (≡CH), 2120 (C≡C), 1010 (C–O) cm^{-1}.

1,6-Bis(2-fluorenyl)-2,4-hexadiyn-1,6-diol (X'). A mixture of ethynylcarbinol (IX', 2.1 g, 10 mmol), cuprous chloride (200 mg, 3.0 mmol), ammonium chloride (150 mg, 2.8 mmol) and methanol (15 m*l*) containing 1 drop of concentrated hydrochloric acid was vigorously stirred overnight at room temperature under a slight excess of oxygen pressure. The reaction mixture was worked up according to the procedure used in the preparation of X, affording crystals, 1.36 g (63%). The crystals were recrystallized 3 times from benzene - ethanol to give colorless needles, mp 210—212°C (dec.).

Found: C, 87.80; H, 5.11%. Calcd for $C_{32}H_{22}O_2$: C, 87.64; H, 5.06%. IR: 3500—3200 (OH), 1000, 965 (C–O) cm^{-1}.

2,2'-Difluorenyltriacetylene (II_3). Preparation of the Dichloride (XI'). A solution of thionyl chloride (240 mg, 2.0 mmol) in tetrahydrofuran (10 m*l*) was added to a stirred solution of the glycol (X', 220 mg, 0.5 mmol) and pyridine (160 mg, 2.0 mmol) in tetrahydrofuran (10 m*l*) under cooling on an ice-salt bath. The mixture was stirred for 30 min at the same temperature and for 2 hr at room temperature. The reaction mixture was chilled on an ice-salt bath and mixed with crushed ice, then extracted with ether. The extract was washed successively with water and a dilute solution of sodium hydroxide and dried. The brown crystals obtained by evaporating the solvent were dissolved in tetrahydrofuran (30 m*l*) and used in the subsequent reaction.

Dehydrochlorination of XI'. To a stirred and ice-cooled solution of sodium ethoxide [from sodium, 70 mg (3 mmol)] in ethanol (10 m*l*), was added the solution of crude XI' in tetrahydrofuran. After the mixture had been stirred for 2 hr at room temperature, the solvent was removed and the residue was extracted with benzene. The extract was concentrated to *ca.* 80 m*l* and percolated through a short column of alumina (15 g). The brown solid obtained by evaporation of the filtrate was crystallized from benzene, yielding crude crystals, 120 mg (60%). The crude substance was dissolved in benzene and passed through a thin layer of alumina. The crystals obtained by evaporation of the filtrate were redissolved in the same solvent and passed again through a short alumina column. Pure II_3 was obtained from the filtrate as yellowish brown fine crystals, which decomposed at *ca.* 250°C.

Found: C, 95.34; H, 4.47%. Calcd for $C_{32}H_{18}$: C, 95.49; H, 4.51%.

1-(2-Fluorenyl)-2-butyn-1,4-diol (XII'). The crude product obtained by the reaction of 2-formylfluorene[11] (III', 6.4 g, 0.033 mol) in tetrahydrofuran (20 m*l*) with the Grignard derivative of propargyl alcohol [from magnesium, 2.8 g (0.115 g-atom), ethyl bromide, 15 g (0.138 mol) and propargyl alcohol, 3.2 g (0.058 mol)] in the same solvent (75 m*l*) according to the procedure used for XII was recrystallized from benzene - ethanol to give light brown crystals, 6.4 g (82%). Recrystallization of this material 3 times from benzene containing a small amount of ethanol afforded pure XII' as colorless plates, mp 133—135°C.

Found: C, 81.78; H, 5.54%. Calcd for $C_{17}H_{14}O_2$: C, 81.58; H, 5.64%. IR: 3300—3100 (OH), 1105, 1000, 995 (C–O) cm^{-1}.

2-Butadiynylfluorene (XIV'). Preparation of Dichloride (XIII'). A solution of thionyl chloride (3.6 g, 0.03 mol) in tetrahydrofuran (20 m*l*) was added to a solution of butynediol (XII', 2.2 g, 0.01 mol) and pyridine (2.4 g, 0.03 mol) in tetrahydrofuran (50 m*l*) under cooling on an ice-salt bath. The reaction mixture was stirred for 30 min at the same temperature, for 1 hr at room temperature and for 1 hr at 40°C. The reaction mixture was concentrated to *ca.* 30 m*l* and used in the following reaction.

Dehydrochlorination of XIII'. The solution of XII' was added to a stirred solution of sodium ethoxide [from sodium, 2.1 g (0.09 g-atom)] in ethanol (80 m*l*) under cooling on an ice-salt bath. After the mixture had been stirred for 30 min at the same temperature and for 1 hr at room temperature, a saturated solution of ammonium chloride was added to the reaction mixture under ice-cooling. The aqueous layer was extracted with benzene. The combined organic layer was dried and evaporated. The residue was digested with petroleum benzine and the extract was passed through a thin layer of alumina (30 g). The resulting colorless filtrate was concentrated to *ca.* 200 m*l* and subjected to the subsequent reaction without isolation of XIV'.

UV: $\lambda_{max}^{benzine}$ 324, 315, 303 nm.

2,2'-Difluorenyltetraacetylene (II_4). The oxidative coupling used in the synthesis of I_4 was applied to the benzine solution of XIV' yielding crude II_4, 190 mg (9%). The crude material was recrystallized twice from benzene using active charcoal to yield pure II_4 as orange yellow rods which decomposed at *ca.* 210°C.

Found: C, 95.67; H, 4.32%. Calcd for $C_{34}H_{18}$: C, 95.75; H, 4.25%.

1-(2-Fluorenyl)-2,5-hexadiyn-1,4-diol (XV'). A solution of 1,4-pentadiyn-3-ol (3.08 g, 0.039 mol) in tetrahydrofuran (65 ml) was added over a period of 20 min to a solution of ethylmagnesium bromide [from magnesium, 2.05 g (0.086 g-atom) and ethyl bromide, 10.4 g (0.095 mol)] in the same solvent (55 ml) under an atmosphere of nitrogen at 25°C. Stirring was continued for 30 min at the same temperature. A solution of 2-formylfluorene (III', 5.82 g, 0.03 mol) in tetrahydrofuran (60 ml) was then added dropwise to the ice-cooled solution of the Grignard derivative of pentadiyneol. The reaction mixture was left to reach room temperature and stirring was continued overnight. After the reaction mixture had been stirred for 20 min at 40°C, a saturated solution of ammonium chloride was introduced to the mixture under cooling on an ice-salt bath. The organic layer was separated and the aqueous layer was extracted with benzene. The combined orgaic layer was washed, dried and evaporated. The resulting dark reddish brown oily material was mixed with a small amount of hot benzene to give crude crystals, 4.0 g (48%), mp *ca.* 120—140°C. The crude material was recrystallized twice from benzene to yield XV' as light brown crystals, mp 153—173°C.

Found: C, 93.16; H, 5.11%. Calcd for $C_{19}H_{14}O_2$: C, 83.20; H, 5.15%. IR: 3300—3250 (OH), 3260 (≡CH), 2120 (C≡C), 1025, 1010 (C-O) cm^{-1}.

1-(2-Fluorenyl)-1,3,5-hexatriyne (XVII'). Preparation of Dichloride (XVI'). A solution of thionyl chloride (720 mg, 6 mmol) in tetrahydrofuran (8 ml) was added to a stirred solution of glycol (XV', 550 mg, 2 mmol) and pyridine (480 mg, 6 mmol) in tetrahydrofuran (10 ml) under cooling on an ice-salt bath. The reaction mixture was stirred for 1 hr at the same temperature and for 1 hr at 30°C. The reaction mixture was used in the following reaction without isolation of XVI'.

Dehydrochlorination of XVI'. The reaction mixture containing XVI' was added dropwise to a stirred solution of potassium ethoxide [from potassium, 1.2 g (30 mg-atom)] in ethanol (40 ml) under cooling with an ice-salt mixture. After the mixture had been stirred for 30 min at the same temperature and then for 30 min at 30°C, a saturated solution of ammonium chloride (5 ml) was added to the ice-cooled reaction mixture and the volatile material was removed *in vacuo*. The residue was extracted with petroleum benzine, and the extract was concentrated to *ca.* 100 ml. Percolation of the concentrated extract through a short column of alumina (20 g) gave a light yellow filtrate. The filtrate was used in the following reaction without isolation of triacetylene (XVII').

UV: $\lambda_{max}^{benzine}$ 354, 325 nm.

2,2'-Difluorenylhexaacetylene (II_6). To a solution of cupric acetate monohydrate (2 g) in pyridine (10 ml) was added, portion by portion, the benzine solution of the triacetylene (XVII') under reduced pressure. After addition of the solution and removal of benzine had been completed, the pyridine solution was stirred for 30 min at 35°C and then at room temperature overnight. The reaction mixture was concentrated, and benzene was added to the residue. The solvent was again evaporated to remove pyridine completely. The residue was triturated with cold benzene (10 ml) and the insoluble material was collected by filtration and washed thoroughly with water. The brown solid thus obtained was dissolved in hot benzene and the hot solution was passed through a short column of alumina (5 g). The resulting orange yellow filtrate gave orange yellow crystals, 70 mg (7%) on concentration. The crystals obtained by the recrystallization of this substance from benzene were redissolved in benzene and percolated through a short column of alumina. The crystals obtained from the filtrate were recrystallized again from benzene, yielding pure II_6 as orange yellow leaflets which decomposed at *ca.* 250°C.

Found: C, 95.75; H, 3.81%. Calcd for $C_{38}H_{18}$: C, 96.18; H, 3.82%.

4-Biphenylylmethyl-triphenylphosphonium Bromide (XXV). A solution of 4-bromomethylbiphenyl[12] (XXIV, 3.9 g, 0.016 mol) and triphenylphosphine (5.8 g, 0.022 mol) in benzene (40 ml) was refluxed overnight. The solid deposited was collected by filtration and washed with benzene, yielding colorless crystalline powder, 7.4 g (92%). Recrystallization of this material from ethanol gave colorless leaflets, mp 283—287°C.

Found: C, 73.08; H, 5.21; Br, 15.69%. Calcd for $C_{31}H_{26}BrP$: C, 73.10; H, 5.14; Br, 15.69%.

Preparation of the Betaine (XXVIII). To a suspension of the phosphonium bromide (XXV, 1.12 g, 2.2 mmol) in toluene (25 ml) was added an ethereal solution of phenyllithium (0.765N, 3.0 ml) under an atmosphere of nitrogen. Instanteneous deep red coloration took place. After the mixture had been stirred for 30 min at 60°C, a solution of acid chloride (XXVII) [from 4-biphenylcarboxylic acid,[13] 0.20 g (1 mmol) and thionyl chloride, 180 mg (1.5 mmol)] in toluene (20 ml) was added to the solution of phosphorane and stirred overnight. The insoluble material was collected by filtration and digested with boiling toluene (total 200 ml). The extract was concentrated and the residue dissolved in benzene - cyclohexane (1: 1, 5 ml). The crystals deposited, 510 mg (84%), were recrystallized from the same solvent to give pure XXVIII as light yellow rod which decomposed at 215—218°C (foaming was observed at *ca.* 200°C).

Found: C, 87.06; H, 5.53%. Calcd for $C_{44}H_{33}OP$: C, 86.83; H, 5.46%.

Bis(4-biphenylyl)acetylene (I_1). Betaine (XXVIII, 63 mg, 0.103 mmol) was gradually heated to 210°C under reduced pressure (20 mmHg) and kept at this temperature for 15 min. Foaming was observed at *ca.* 190°C. After cooling, the product was extracted with benzene. Evaporation of the solvent gave crude crystals, 32 mg (94%). The crude material was dissolved in benzene and passed through a thin layer of alumina. The crystals obtained by evaporating the filtrate were recrystallized from benzene to yield pure I_1 as colorless leaflets, mp 253—254°C (lit, mp 243—244°C[14]).

Found: C, 94.68; H, 5.44%. Calcd for $C_{26}H_{18}$: C, 94.51; H, 5.49%.

2-Fluorenylmethyltriphenylphosphonium Bromide (XXV'). According to the same procedure as that for XXV, 2-bromomethylfluorene[15] (XXIV', 3.5 g, 0.0134 mol) was converted into phosphonium bromide (XXV', 6.0 g, 87%). The phosphonium bromide (XXV') was recrystallized twice from ethanol - acetone (1:1). The crystals were dried at *ca.* 115°C for 48 hr under reduced pressure to give pure XXV', mp 252—256°C.

Found: C, 73.31; H, 4.99; Br, 15.57%. Calcd for $C_{32}H_{26}BrP$: C, 73.72; H, 5.03; Br, 15.32%.

Preparation of Betaine (XXVIII'). The same procedure as that used for XXVIII was employed. The reaction of phosphonium bromide (XXV', 2.34 g) and acid chloride [from 2-fluorenylcarboxylic acid[16] (0.42 g)] gave the betaine

12) H. Dahn and P. Zoller, *Helv. Chim. Acta*, **35**, 1438 (1952); L. Zervas and I. Dilaris, *J. Amer. Chem. Soc.*, **77**, 5354 (1955).

13) 4-Biphenylcarboxylic acid was prepared by the oxidation of 4-formylbiphenyl (III) by means of Tollens' reagent.

14) G. H. Coleman and R. D. Maxwell, *J. Amer. Chem. Soc.*, **56**, 132 (1934).

15) J. von Braun and H. Engel, *Ber.*, **57**, 191 (1924).

16) M. D. Barnett, G. H. Daub, F. N. Hayes, and D. G. Ott, *J. Amer. Chem. Soc.*, **82**, 2282 (1960).

(XXVIII') in a yield of 87% (1.10 g). The material was recrystallized twice from benzene-cyclohexane to give pure XXVIII' as pale yellow cubes, mp 268—270°C.

Found: C, 87.29; H, 5.45%. Calcd for $C_{46}H_{33}OP$: C, 87.33; H, 5.26%.

2,2'-Difluorenylacetylene (II_1). Pyrolysis of betaine (XXVIII', 192 mg, 0.303 mmol) was performed at 230°C under reduced pressure (*ca.* 20 mmHg). Foaming was observed at *ca.* 220°C. The product was extracted with benzene. The extract was concentrated and passed through a short column of alumina. The crystals, 82 mg (77%) obtained by evaporating the filtrate were recrystallized from benzene affording pure II_1 as colorless rods which decomposed at *ca.* 295°C.

Found: C, 94.50; H, 5.17%. Calcd for $C_{28}H_{18}$: C, 94.88; H, 5.12%.

BULLETIN OF THE CHEMICAL SOCIETY OF JAPAN, VOL. 45, 891—894(1972)

Molecular Orbital Treatment of *Para* Orientation in the Diels-Alder Reactions of 2-Substituted Butadienes with Methyl Acrylate[1]

Takashi INUKAI,[2] Hideo SATO, and Takeshi KOJIMA

The Central Research Laboratories, Chisso Corporation, Kamariya, Kanazawa-ku, Yokohama

(Received August 12, 1971)

The intermolecular orbital method was applied to the orientation phenomena in the Diels-Alder reactions of 2-R-butadienes (R=Me, Ph, Cl, and CN) with methyl acrylate assuming the parallel biplanar transition state geometries. Although qualitatively correct predictions of *para* orientation (major isomer) were obtained with the calculated overlap energies, it is suggested that the non-bonding interactions are overestimated. The simple perturbational molecular orbital method, which takes only the interactions at the terminal positions into account, was also unsatisfactory. However, frontier orbital interactions provided qualitatively correct prediction of the major isomeric product in every case.

The general *ortho/para* orientation in the Diels-Alder reactions between unsymmetrical dienes and dienophiles is questionable with regard to its rationalization in terms of organic electronic theory.[3,4] The experimental vindication of the orientation rule was ill-founded.[3] We recently determined the kinetically controlled isomer ratios of the adducts from 1-Me-, 2-Me-, 2-Ph-, 2-Cl-, 2-CN-, and 2-CF_3-butadienes with methyl acrylate.[5] We are satisfied that the enigmatic orientation rule was qualitatively correct and this led us to seek an explanation.

Since the multicenter mechanism of the Diels-Alder reactions is generally accepted, we have to take into account a number of electronic interactions contributing to the energies of the transition states in order to make a reasonable prediction of the orientation. The relative importance of these contributing factors may not be estimated by the qualitative argument of organic electronic theory. Thus the present problem requires an estimate of various contributing factors by computation.

Feuer *et al.*[4] used a perturbational molecular orbital method (PMO) with considerable success, but their dienes were limited to methyl and phenyl substituted butadienes. For explaining the *ortho/para* orientation by electron-releasing substituents alone, the electronic theory is sufficient.[6] But the real difficulty with this theory lies in rationalizing the same *ortho/para* orientation also by the substituents of opposite polarity. Therefore, in order to know whether the PMO treatment gives a satisfactory solution of the problem or not, the cases with electron-releasing substituents and electron-withdrawing substituents must be studied by application of the PMO method. In this article we describe the results of some attempts of explanation of the orientation phenomena[7] in the Diels-Alder reactions of methyl acrylate with 2-substituted butadienes using the intermolecular orbital (IMO)[8] and the PMO methods.

Method

In the first part of the study the interaction energies $\Delta E_{\text{overlap}}$ of multicenter [4+2] transition states were calculated by the IMO method with the formula,[9]

$$\Delta E_{\text{overlap}} = -\sum_{rr'}(q_r+q_{r'})\gamma_{rr'}S_{rr'} - 2\sum_{j}^{\text{occ}}\sum_{k'}^{\text{vac}}\left(\sum_{rr'}C_{jr}C_{k'r'}\gamma_{rr'}\right)^2/(E_{k'}-E_j) - 2\sum_{k}^{\text{vac}}\sum_{j'}^{\text{occ}}\left(\sum_{rr'}C_{kr}C_{j'r'}\gamma_{rr'}\right)^2/(E_k-E_{j'}) \quad (1)$$

1) Presented in part at the IUPAC Symposium "Cycloaddition Reactions," Munich, Germany, September 9, 1970.

2) To whom inquiries should be addressed.

3) J. Sauer, *Angew. Chem.*, **79**, 76 (1967).

4) J. Feuer, W. C. Herndon, and L. H. Hall, *Tetrahedron*, **24**, 2575 (1968).

5) T. Inukai and T. Kojima, *J. Org. Chem.*, **36**, 924 (1971).

6) For example, J. S. Meek, B. T. Poon, R. T. Merrow, and S. J. Cristol, *J. Amer. Chem. Soc.*, **74**, 2669 (1952).

7) The term *orientation* in this article is used to mean the choice of the major isomeric product.

8) J. Salem, *J. Amer. Chem. Soc.*, **90**, 543 (1968).

9) See Reference 8 for the definition of various symbols.

The first summation denotes the repulsion between π-electron shells of a diene and dienophile. The second summation (hereafter called term 2) denotes the stabilization due to delocalization of π-electrons of a diene to the vacant orbitals of a dienophile, and the third summation (term 3) that due to delocalization of π-electrons of a dienophile to the vacant orbitals of a diene. The unprimed and primed suffixes refer to a diene and dienophile, respectively. The wave functions and energy values for the isolated reactants were calculated by the simple Hückel method. The Hückel parameters used are listed in Table 1. Further parametrization employed is

$$\gamma_{rr'}/S_{rr'} = 3\beta \text{ (for all } r \text{ and } r')^{8)}$$

where β is the standard resonance integral of benzene.

TABLE 1. HÜCKEL PARAMETERS USED[a)]

Coulomb parameter, $h(X)$		Resonance parameter, $k_{x-x'}$	
h(Ċ)	0	C—C	S/S_0
h(Ȯ)	1.5	C—O, carbonyl	0.85
h(Ö)	2.0	C—O, ether	0.6
h(Ṅ)	0.5	O—Me	0.3
h(C̈l)	2.0	C—N, nitrile	1.19
h(M̈e)	2.0[b)]	C—Cl	0.37
		C—Me	0.7[b)]

a) $\alpha_x = \alpha_c + h(X)\beta$; $\beta_{x-x'} = k_{x-x'}\beta$.
b) The heteroatom model of methyl group.

The geometries of the reactant molecules were assumed to be planar and constructed from the probable bond angles and lengths.[10)] The transition state model were constructed by putting the reactants in parallel planes at 3.2 Å distance;[11,12)] there are eight transition state geometries corresponding to possibilities of *para* and *meta* orientation, *endo* and *exo* stereochemistry, and cisoid and transoid conformation of C=C–C=O moiety of methyl acrylate—only two of these are illustrated in Fig. 1.

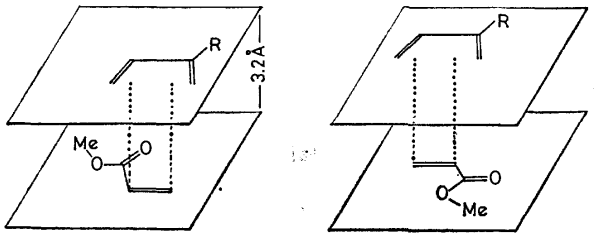

A B

Fig. 1. Transition State Models. A, *para*, *endo*, cisoid; B, *meta*, *exo*, transoid.

The required overlap integrals $S_{rr'}$ were calculated by

$$S_{rr'} = S_{rr'}(\sigma\sigma)\cos^2\theta_{rr'} - S_{rr'}(\pi\pi)\sin^2\theta_{rr'} \quad (2)$$

where $\theta_{rr'}$ is the angle between the interatomic line and the normal on the molecular plane (Fig. 2). $S_{rr'}(\sigma\sigma)$ and $S_{rr'}(\pi\pi)$ are known through the extensive tables by Mulliken *et al.*[13,14)]

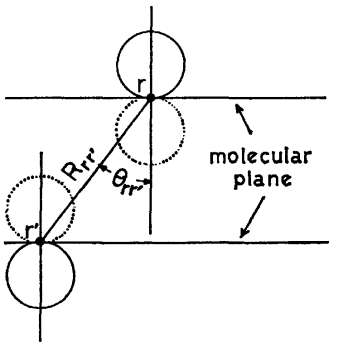

Fig. 2.

Calculation of $\Delta E_{\text{overlap}}$ was performed using a computer program which reads seqular determinants for a pair of isolated reactant molecules and the appropriate overlap matrix ($(S_{rr'})$) for each transition state geometry, and gives the desired energy terms of Eq. 1.

In the second half of the study the same simplest PMO method as that used by previous workers was used.[4)] Thus the perturbational energies, E_p, for the four-center transition states were calculated considering only the terminal interactions, *i.e.*, those between the two pairs of atoms at which σ-bonds will close (Eq. 3).[15)] The Hückel parameters used are those listed in Table 1.

$$E_p = 2[\sum_m^{occ}\sum_n^{vac} - \sum_m^{vac}\sum_n^{occ}](a_{mr}b_{ns} + a_{mu}b_{nv})^2\gamma^2/(E_m - E_n) \quad (3)$$

Results and Discussion

The results by the IMO method for *endo* addition of the cisoid methyl acrylate are shown in Table 2. The main features of interest are:

1) $\Delta E_{\text{overlap}}$ gives correct predictions of *para* orientation by all the substituents.

2) The delocalization energy, namely term 2 plus term 3 of eq 1, indicates *meta* orientation by Ph and CN groups and practically null selectivity in the cases of Me and Cl. It is the repulsion term that makes $\Delta E_{\text{overlap}}$ turn out to be *para* directing.

3) The calculations of the delocalization energy taking only the frontier orbitals into account lead to correct orientation in all cases.

10) Butadiene skeleton [A. Almenningen *et al.*, *Acta Chim. Scand.*, **12**, 1221 (1958)] was assumed to be maintained in all the 2-substituted butadienes. Bond lengths between $C_{(2)}$ (butadiene) and substituent atoms are: $C_{(2)}$—C_{methyl}, 1.50 Å; $C_{(2)}$—C_{phenyl}, 1.46 Å $C_{(2)}$—Cl, 1.70 Å; $C_{(2)}$—C_{cyano}, 1.44 Å, $R_{C\equiv N}$, 1.16 Å. Based on the three-dimensional structure of methyl acrylate [T. Ukaji, This Bulletin, **32**, 1275 (1959)], the following flat structure was assumed: $C_{(1)}=C_{(2)}$, 1.36 Å; $C_{(2)}$—$C_{(3)}$, 1.44 Å; $C_{(3)}$—$O_{(4)}$, 1.36 Å; $O_{(4)}$—$C_{(5)methyl}$, 1.46 Å; $C_{(3)}=O_{(6)}$, 1.22 Å; $\angle C_{(1)}C_{(2)}C_{(3)}$, 120°; $\angle C_{(2)}C_{(3)}O_{(4)}$, 125°; $\angle C_{(2)}C_{(3)}O_{(6)}$, 120°; $\angle C_{(3)}O_{(4)}C_{(5)}$, 115°.

11) W. C. Herndon and L. H. Hall, *Theor. Chim. Acta*, **7**, 4 (1967).

12) P. Markov and P. N. Skancke, *Acta. Chim. Scand.*, **23**, 1295 (1969).

13) R. S. Mulliken, C. A. Rieke, D. Orloff, and H. Orloff, *J. Chem. Phys.*, **17**, 1248 (1949).

14) Those unavailable in the tables were calculated using the appropriate master formula (Reference 13) with the aid of the numerical values of $A_k(p)$, $B_k(pt)$ integrals given by Kotani *et al.* [M. Kotani, A. Amemiya, E. Ishiguro, and T. Kimura, "Tables of Molecular Integrals," Maruzen Co., Ltd, Tokyo (1963)].

15) See Reference 4 for the definition of various symbols.

Table 2. Interaction energies (in units of β) by IMO method for reactions of 2-substituted butadienes with cisoid methyl acrylate by *endo* mechanism

Substituent		Repulsion	Delocalization	$\Delta E_{overlap}$	$\Delta E_{frontier}$ [a]
Me	*para*	−0.0272	0.0178	−0.0094	0.0153 (0.0140)
	meta	−0.0340	0.0175	−0.0165	0.0138 (0.0126)
Ph	*para*	−0.0271	0.0176	−0.0094	0.0123 (0.0108)
	meta	−0.0318	0.0186	−0.0132	0.0099 (0.0083)
Cl	*para*	−0.0270	0.0177	−0.0093	0.0158 (0.0144)
	meta	−0.0292	0.0177	−0.0116	0.0152 (0.0138)
CN	*para*	−0.0268	0.0176	−0.0093	0.0148 (0.0130)
	meta	−0.0301	0.0190	−0.0111	0.0142 (0.0123)

a) The frontier orbital interaction energy, *i.e.* the sum of delocalization energies relative to the highest occupied MO(diene)—lowest vacant MO(dienophile) interaction and the highest occupied MO(dienophile)—lowest vacant MO(diene) interaction. The energy for the former interaction alone is shown in parentheses.

Table 3. Interaction energies (in units of β) by IMO method for reactions of 2-substituted butadienes with cisoid methyl acrylate by *exo* mechanism

Substituent		Repulsion	Delocalization	$\Delta E_{overlap}$	$\Delta E_{frontier}$ [a]
Me	*para*	−0.0216	0.0148	−0.0068	0 0117 (0.0102)
	meta	−0.0218	0.0147	−0.0071	0.0110 (0.0096)
Ph	*para*	−0.0214	0.0146	−0.0068	0.0099 (0.0083)
	meta	−0.0215	0.0150	−0.0065	0.0093 (0.0075)
Cl	*para*	−0.0214	0.0148	−0.0066	0.0117 (0.0102)
	meta	−0.0214	0.0147	−0.0068	0.0114 (0.0099)
CN	*para*	−0.0213	0.0145	−0.0068	0.0110 (0.0092)
	meta	−0.0212	0.0151	−0.0061	0.0110 (0.0090)

a) See Table 2, footnote a.

4) These statements are qualitatively valid also when the transoid conformation of methyl acrylate is assumed.

Similar results for *exo* addition of the cisoid methyl acrylate are listed in Table 3. In this case both the $\Delta E_{overlap}$ and delocalization energy predict preferred formation of *meta* isomer for Ph and CN, in disagreement with experimental facts.[5] The discrepancies are reasonable since the *exo* geometry is evidently improbable in view of the general *endo* rule of the Diels-Alder reactions.[3,16] Similar results are obtained for the transoid methyl acrylate *endo* addition.

16) J. G. Martin and R. K. Hill, *Chem. Rev.*, **61**, 537 (1961).

The above apparent success with $\Delta E_{overlap}$ for *endo* is only superficial, however, as is evident if we compare the results of *endo* (Table 2) and *exo* (Table 3) mechanism. Thus the $\Delta E_{overlap}$ values for the *endo* mechanism are greater (higher $\Delta H^{\neq}$) than the corresponding values for the *exo* mechanism: this erroneous prediction of general predilection for the *exo* addition comes from the excessively large repulsion energy calculated for the *endo* transition state model as shown by exact figures (Tables 2 and 3).

Inclusion of the classical Coulomb potential ΔE_{polar} given by Eq. 4[17] does not give improved results. According to the results (Table 4), 2-Ph- and 2-CN-

$$\Delta E_{polar} = \sum_{r}\sum_{r'} \Delta q_r \Delta q_{r'} / R_{rr'}$$

$$\Delta E = \Delta E_{overlap} + \Delta E_{polar} \quad (4)$$

butadienes should react by the *exo* mechanism in disagreement with Alder's *endo* rule.

Appropriateness of the value of the interplanar distance (3.2 Å) assumed in the present study is questionable. Furthermore, the assumption of a parallel biplanar transition state is debatable although it has usually been made.[11,12,18] Since it is known experimentally that the *endo* mechanism only slightly exceeds the *exo* generally in the Diels-Alder reactions of acyclic dienes,[19] the non-bonding interactions might not be strong enough to pull the reactants close together into

Table 4. Comparison of ΔE^{a} (Eq. 4) for *endo* and *exo* addition of cisoid methyl acrylate

Substituent	Geometry		ΔE_{polar}	$\Delta E_{overlap}$ [b]	ΔE
2-Me	*para*	*endo*	−0.81	+0.65	−0.16
		exo	+0.20	+0.47	+0.67
	meta	*endo*	−0.91	+1.14	+0.23
		exo	+0.22	+0.49	+0.71
2-Ph	*para*	*endo*	0	+0.65	+0.65
		exo	0	+0.47	+0.47
	meta	*endo*	0	+0.91	+0.91
		exo	0	+0.45	+0.45
2-Cl	*para*	*endo*	−0.24	+0.64	+0.40
		exo	+0.05	+0.46	+0.51
	meta	*endo*	−0.29	+0.79	+0.50
		exo	+0.03	+0.47	+0.50
2-CN	*para*	*endo*	+1.08	+0.64	+1.72
		exo	+0.22	+0.47	+0.69
	meta	*endo*	+1.42	+0.77	+2.19
		exo	+0.26	+0.42	+0.68

a) In kcal/mol.
b) Calculated from the values in Tables 2 and 3 with a conversion factor of $\beta = -3$ eV (the spectroscopic value of benzene resonance integral.[8])

17) A. Devaquet and L. Salem, *J. Amer. Chem. Soc.*, **91**, 3793 (1969).

18) N. Tyutyulkov and P. Markov, *Monatsh. Chem.*, **96**, 2030 (1965); *ibid.*, **99**, 861 (1968); P. Markov and N. Tyutyulkov, *ibid.*, **97**, 1229 (1966); K. Somekawa, T. Matsuo, and S. Kumamoto, This Bulletin, **42**, 3499 (1969).

19) T. Inukai and T. Kojima, *J. Org. Chem.*, **32**, 869 (1967); O. Korver, T. L. Kwa, and C. Boelhouwer, *Tetrahedron*, **25**, 4109 (1969); T. L. Kwa, O. Korver, J. W. Hartgerink, and C. Boelhouwer, *ibid.*, **24**, 5711 (1968).

Table 5. Perturbation energies (in units of γ^2/β) by PMO method for reactions of 2-substituted butadienes with methyl acrylate

Substituent		E_p	$E_{frontier}$ [a]
Me	*para*	1.6046	1.1098 (0.5391)
	meta	1.5504	0.9983 (0.4336)
Ph	*para*	1.5731	0.9616 (0.4726)
	meta	1.5466	0.8406 (0.3347)
Cl	*para*	1.5668	1.0710 (0.4819)
	meta	1.5518	1.0397 (0.4523)
CN	*para*	1.5291	0.9115 (0.4431)
	meta	1.5459	0.9072 (0.4115)

a) See Table 2, footnote a.

a near parallel *endo* geometry, making a more open geometry likelier.[20] Our present calculation, therefore, might have overestimated the non-bonding interactions. To make matters worse, the calculated orientation is influenced by the delicate balance of counteracting factors.

An alternative approach is to neglect the non-bonding interactions altogether and see whether qualitatively

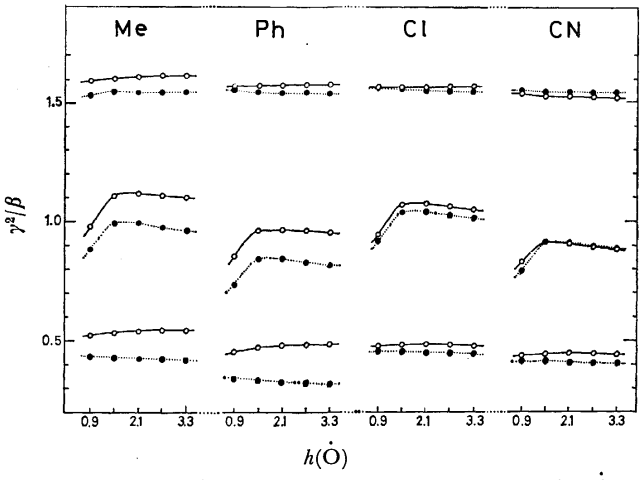

Fig. 3. Perturbation Energy Terms as Functions of $h(\dot{O})$. Upper Curves, Ep; Middle Curves, $E_{frontier}$; Bottom Curves, Highest Occupied MO (Diene)—Lowest Vacant MO (Dienophile). —○— *Para*, ···●··· *Meta*.

20) *Endo* dimerization of cyclopentadiene could be explained by considering only the interactions at the terminal positions when an interplanar angle of 60° was assumed for the *endo* transition state: W. C. Herndon and L. H. Hall, *Tetrahedron Lett.*, **1967**, 3095.

correct predictions can be obtained.[4] The perturbation energies E_p by the PMO method are shown in Table 5. The preferred orientation is predicted correctly in Me, Ph, and Cl cases, but not in the CN case. Thus the claim for successful rationalization of the orientation rule resulted from the hasty conclusion arising from incomplete analysis of the problem.[4]

The frontier orbital interactions, however, agree with the experimental orientation in all the cases, and the delocalization energy corresponding to the highest occupied MO(diene)→lowest vacant MO(dienophile) plays a decisive role in conducing to correct predictions.

Variation of the Coulomb parameter h(Ȯ) of the dienophile from 0.9 to 3.3, far beyond the reasonable range for methyl acrylate itself, did not alter the orientations in terms of both the E_p and $E_{frontier}$ as shown in Fig. 3. This is in line with the fact that the *ortho/para* orientation rule holds over a wide range of dienophile polarity.[3,5,19,21]

It may be appropriate to emphasize the importance of the frontier orbitals in determining reactivity.[22] Their role was undervalued[4] because of the fact that $E_{frontier}$ constitutes only a moderate fraction of total E_p. This reasoning is not convincing, because the most easily perturbed highest occupied MO will play a greater role, in the real transition state, than that allotted to it by the perturbational calculation as Fukui and Fujimoto discussed in general terms.[23] Therefore, unless one treats the transition state more realistically, including the hybridization change *etc.* of the reactants, the full term calculation may turn out to be less accurate, in spite of its formal preciseness, than the frontier orbital method. In fact attention to the frontier orbital interactions alone rather than the full term value was found to be a more judicious choice at least for predictive purposes. Furthermore, the diene→dienophile delocalization part of $E_{frontier}$ plays a decisive role in giving right predictions (Table 5 and Table 2).

21) J. Kazan and F. D. Greene, *J. Org. Chem.*, **28**, 2965 (1963); T. Inukai and T. Kojima, *ibid.*, **31**, 1121 (1966); W. M. Daniewski and C. E. Griffin, *ibid.*, **31**, 3236 (1966); C. M. Wynn and P. S. Klein, *ibid.*, **31**, 4251 (1966); J-C. Soula, D. Lumbroso, M. Hellin, and F. Coussemant, *Bull. Soc. Chim. Fr.*, **1966**, 2059; T. Kojima and T. Inukai, *J. Org. Chem.*, **35**, 1342 (1970).

22) K. Fukui in "Modern Quantum Chemistry," Vol. 1 (Edited by O. Sinanoglu), p. 49, Academic Press, New York (1965).

23) K. Fukui and H. Fujimoto, This Bulletin, **42**, 3399 (1969).

The Palladium-catalyzed Ferrocenylation of Olefins

Akira KASAHARA, Taeko IZUMI, Genji SAITO, Minoru YODONO, Ryu-ichi SAITO, and Yoshiaki GOTO

Department of Applied Chemistry, Faculty of Engineering, Yamagata University, Yonezawa-shi, Yamagata

(Received September 6, 1971)

Ferrocenylpalladium chloride, prepared *in situ* from chloromercuriferrocene and lithium chloropalladite, reacts readily with various olefins to produce alkenylferrocene derivatives. Enol esters and allylic alcohols also react to form (2-oxoalkyl)- and (3-oxoalkyl)-ferrocene derivatives. The synthesis of 1,1′-dialkenylferrocene derivatives from 1,1′-bis(chloromercuri)ferrocene, olefins and palladium salt is also reported. The reaction may proceed by means of a catalytic amount of the metal salt and by the aid of cupric chloride; it provides an extremely convenient method for the synthesis of a wide variety of ferrocene derivatives.

The reactions of olefins in the presence of transition metal compounds have been studied by many workers.[1] Recently, Heck[2] reported that the arylation of unsaturated compounds with Group VIII metal-aryl complexes has proved to be a generally applicable reaction. Several new useful synthetic organic reactions are based upon this arylation: olefinic arylation,[2a,g] aromatic haloethylation,[2c] aromatic allylation,[2e] and the synthesis of aldehydes or ketones with an aryl substituent on the α- or β- position by the arylation of allylic alcohols or enol esters.[2b,d] For example, "phenylpalladium chloride," prepared from phenylmercuric chloride and a palladium salt *in site*, reacts with ethylene to form styrene, hydrogen chloride, and palladium metal:

$$C_6H_5HgCl + PdCl_2 \rightleftarrows [C_6H_5PdCl] + HgCl_2$$

$$[C_6H_5PdCl] + CH_2{=}CH_2 \longrightarrow C_6H_5CH{=}CH_2 + HCl + Pd$$

We have now found that, when Heck's reaction is carried out with ferrocenylpalladium salt prepared *in situ* from chloromercuriferrocene and a palladium salt the ferrocenyl group is introduced into the olefinic system.

Results and Discussion

In the presence of palladium salt, chloromercuriferrocene (**1**) was allowed to react with various olefins in polar solvents, such as methanol, ethanol, acetone, acetic acid, and acetonitrile. As with Heck's olefin arylation, the substitution reaction on the double bond has been observed to lead to the formation of 1-alkenylferrocenes, accompanied by a small amount of biferrocenyl (**2**). Moreover, 1,1′-bis(chloromercuri)ferrocene (**3**) reacts with olefins and palladium catalyst to form 1,1′-di(1-alkenyl)ferrocenes (**4**), accompanied by a small amount of bi-1,1′-ferrocenylene (**5**). The reactions carried out are summarized in Table 1. The properties of the products are given in Table 2.

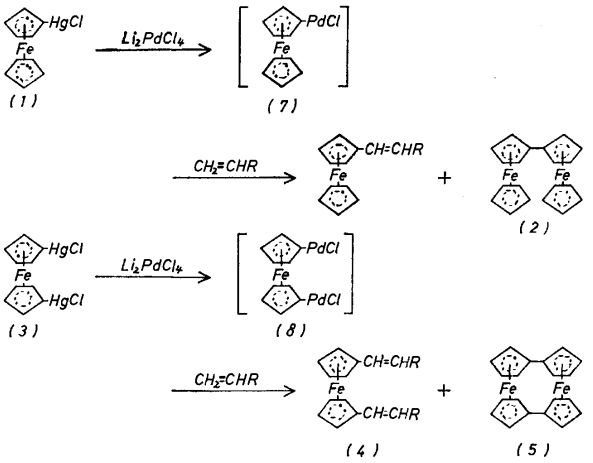

Fig. 1.

Furthermore, it was found that the reactions are generally initiated by a catalytic amount of palladium salt when cupric chloride is added to the reaction system. The latter has been to reoxidize the reduced palladium to the reactive Pd(II) form. Examples of catalytic ferrocenylation are given in Table 3.

The ferrocenylation of simple olefins, such as ethylene, styrene, and ethyl acrylate, resulted in the formation of vinylferrocene, styrylferrocene, and ethyl 3-ferrocenylacrylate respectively in moderate yields, accompanied by a small amount of **2**. In the olefinic palladium salt (**6**) from arylmercuric chloride and palladium salt, followed by the addition of **6** to the olefinic double bond and then the elimination of the hydride ion with palladium.

$$ArHgCl + PdCl_2 \rightleftarrows \underset{(6)}{[ArPdCl]} + HgCl_2$$

$$[ArPdCl] + CH_2{=}CH{-}R \longrightarrow \left[\begin{array}{l} \quad PdCl \\ Ar{-}CH_2{-}\overset{|}{C}H{-}R \end{array}\right] \longrightarrow Ar{-}CH{=}CH{-}R + Pd + HCl$$

1) C. W. Bird, "Transitional Metal Intermediates in Organic Synthesis," Logos Press, London (1966), p. 88; A. Guilo, "Advances in Organometallic Chemistry," Vol. 5, ed. by F. G. A. Stone and R. West, Academic Press, New York (1967), p. 321; E. W. Stern, "Catalysis Review," Vol. 1, ed. by H. Heineman, Marcel Dekker, Inc., New York (1968), p. 74; J. Tsuji, "Advances in Organic Chemistry, Methods and Results," Vol. 6, ed. by E. C. Taylor and H. Wynberg, Interscience Publishers, New York (1969), p. 109.

2) a) R. F. Heck, *J. Amer. Chem. Soc.*, **90**, 5518 (1968); b) *ibid.*, **90**, 5526 (1968); c) *ibid.*, **90**, 5531 (1968); d) *ibid.*, **90**, 5535 (1968); e) *ibid.*, **90**, 5538 (1968); f) *ibid.*, **90**, 5542 (1968); g) *ibid.*, **91**, 6707 (1969).

TABLE 1. FERROCENYLATION OF OLEFINS

Olefin	Solvent	Product	Yield (%)[a]
(a) Reactions with chloromercuriferrocene (**1**).			
Ethylene	C_2H_5OH	Vinylferrocene (**10**)	45
		Biferrocenyl (**2**)	4
Styrene	CH_3OH	Styrylferrocene (**11**)	52
		Biferrocenyl (**2**)	3
Styrene	C_2H_5OH	Styrylferrocene (**11**)	50
		Biferrocenyl (**2**)	4
Styrene	CH_3COCH_3	Styrylferrocene (**11**)	45
		Biferrocenyl (**2**)	4
Styrene	CH_3COOH	Styrylferrocene (**11**)	47
		Biferrocenyl (**2**)	4
Styrene	CH_3CN	Styrylferrocene (**11**)	43
		Biferrocenyl (**2**)	6
Ethyl acrylate	C_2H_5OH	Ethyl 3-ferrocenylacrylate (**12**)	58
		Biferrocenyl (**2**)	3
Ethyl crotonate	C_2H_5OH	Ethyl 3-ferrocenylcrotonate (**13**)	52
		Biferrocenyl (**2**)	3
Methyl methacrylate	CH_3OH	Methyl 3-ferrocenylmethacrylate (**14**)	48
		Biferrocenyl (**2**)	5
Acrylonitrile	C_2H_5OH	3-Ferrocenylacrylonitrile (**15**)	49
		Biferrocenyl (**2**)	5
Acrolein	C_2H_5OH	3-Ferrocenyl-2-propenal (**16**)	45
		Biferrocenyl (**2**)	4
Methyl vinyl ketone	C_2H_5OH	4-Ferrocenyl-3-buten-2-one (**17**)	46
		Biferrocenyl (**2**)	7
Phenyl vinyl ketone	C_2H_5OH	3-Ferrocenyl-1-phenyl-2-propen-1-one (**18**)	45
		Biferrocenyl (**2**)	5
3-Buten-2-ol	C_2H_5OH	4-Ferrocenyl-2-butanone (**19**)	31
		Biferrocenyl (**2**)	9
2-Methyl-2-propenol	C_2H_5OH	2-Methyl-3-ferrocenylpropionaldehyde (**20**)	34
		Biferrocenyl (**2**)	6
5-Phenyl-2-cyclohexenol	CH_3CN	3-Ferrocenyl-5-phenylcyclohexanone (**21**)	14
		Biferrocenyl (**2**)	10
5,5-Dimethyl-2-cyclohexenol	CH_3CN	3-Ferrocenyl-5,5-dimethylcyclohexanone (**22**)	12
		Biferrocenyl (**2**)	12
Isopropenyl acetate	C_2H_5OH	α-Ferrocenylacetone (**23**)	27
		Biferrocenyl (**2**)	6
Acetophenone enol acetate	C_2H_5OH	α-Ferrocenylacetophenone (**24**)	16
		Biferrocenyl (**2**)	11
2-Methylallyl chloride	C_2H_5OH	3-Chloro-1-ferrocenyl-2-methylpropene (**25**)	21
		Biferrocenyl (**2**)	10
(b) Reaction with 1,1′-bis(chloromercuri)ferrocene (**3**)			
Styrene	C_2H_5OH	1,1′-Distyrylferrocene (**26**)	37
		Bi-1,1′-ferrocenylene (**5**)	6
Ethyl acrylate	C_2H_5OH	1,1′-Bis(2-ethoxycarbonylvinyl)ferrocene (**27**)	28
		Bi-1,1′-ferrocenylene(**5**)	8
Ethyl crotonate	C_2H_5OH	1,1′-Bis(2-ethoxycarbonyl-1-methylvinyl)ferrocene (**28**)	25
		Bi-1,1′-ferrocenylene (**5**)	10
Methyl methacrblate	C_2H_5OH	1,1′-Bis(2-methoxycarbonyl-2-methylvinyl)ferrocene (**29**)	31
		Bi-1,1′-ferrocenylene (**5**)	8
Acrylonitrile	C_2H_5OH	1,1′-Bis(2-cyanovinyl)ferrocene (**30**)	28
		Bi-1,1′-ferrocenylene (**5**)	11
Acrolein	C_2H_5OH	1,1′-Bis(2-formylvinyl)ferrocene (**31**)	22
		Bi-1,1′-ferrocenylene (**5**)	10
Methyl vinyl ketone	C_2H_5OH	1,1′-Bis(2-acetylvinyl)ferrocene (**32**)	27
		Bi-1,1′-ferrocenylene (**5**)	12
Phenyl vinyl ketone	C_2H_5OH	1,1′-Bis(2-benzoylvinyl)ferrocene (**33**)	25
		Bi-1,1′-ferrocenylene (**5**)	9

a) Yields are based upon the ferrocenylating agent.

TABLE 2. PROPERTIES AND ANALYSES OF FERROCENYLATION PRODUCTS

Compound	mp °C	Found, % C	Found, % H	Calcd, % C	Calcd, % H	IR Spectrum, (cm^{-1}) and NMR spectrum,[a] ppm (no. of protons)
10[b]	50—51	67.84	5.61	67.96	5.70	IR 1632, 987, 907.
11[c]	120—121	72.78	6.29	72.72	6.10	IR 1634, 960.
12[d]	74—75	63.22	5.48	63.40	5.67	IR 1710, 1620.
13[d]	69—71	64.38	6.01	64.45	6.08	IR 1712, 1618.
14	62—63	63.19	5.52	63.40	5.67	IR 1710, 1620.
						NMR 2.00 d (3) $-C(CH_3)=C-$
						3.73 s (3) $-COOCH_3$
						4.08 s (5), 4.31 q (2), 4.41 q (2) } ferrocene ring protons
						7.40 q (1) $-CH=C-$
15	80—81	65.68 (N, 5.87)	4.55	65.85 (N, 5.90)	4.63	IR 2170, 1612.
						NMR 4.14 s (5), 4.40 s (4) } ferrocene ring protons
						5.36 d (1) $-C=CH-CN$
						7.22 d (1) $-CH=C-CN$
16[e]	94—95	64.88	4.92	65.02	5.03	IR 1688, 1624.
17[f]	84—85	66.05	4.95	66.17	5.07	IR 1670, 1625.
18[g]	136—137	72.07	5.38	72.17	5.55	IR 1660, 1607.
19$_h$[h]	45—46	65.49	6.18	65.66	6.29	IR 1715.
27	53—55	65.55	6.24	65.66	6.29	IR 2850, 1718.
						NMR 1.18 d (3) $-CH_3$
						2.84 d (2) $-CH_2-$
						3.98 m (1) $-CH-$
						4.12 s (9) ferrocene ring protons
						9.74 d (1) $-CHO$
21	71—72	73.66	6.06	73.75	6.18	IR 1710.
						NMR 2.10—3.30 m (8) cyclohexanone ring protons
						4.11 s (9) ferrocene ring protons
						7.28 s (5) phenyl protons
22	89—90	67.08	7.71	67.15	7.74	IR 1710.
						NMR 0.99 s (3) $-CH_3$
						1.08 s (3) $-CH_3$
						1.98—3.24 m (7) cyclohexanone ring protons
						4.13 s (9) ferrocene ring protons
23	46—47	64.81	5.80	64.95	5.86	IR 1713.
						NMR 2.21 s (3) $-CH_3$
						3.92 s (2) $-CH_2-$
						4.12 s (9) ferrocene ring protons
24[e]	80—81	68.43	5.69	68.56	5.75	IR 1687.
25	105—106	59.26	5.61	59.35	5.74	IR 1635, 805.
						NMR 1.48 d (3) $-C(CH_3)=C-$
						2.87 d (2) $-CH_2Cl$
						4.12 s (9) ferrocene ring protons
						7.31 m (1) $-CH=C-$
26[i]	166—168	79.87	5.63	79.99	5.68	IR 1630, 961.
27	83—84	62.88	5.91	62.83	5.80	IR 1710, 1618.
						NMR 1.33 t (6) $-COOCH_2CH_3$
						4.33 d (4) $-COOCH_2CH_3$
						4.55 s (8) ferrocene ring protons
						6.01 d (2) $-C=CH-COOEt$
						7.52 d (2) $-CH=C-COOEt$
28	65—66	64.25	6.31	64.38	6.38	IR 1711, 1620.
						NMR 1.26 t (6) $-COOCH_2CH_3$
						1.98 d (6) $CH_3-CH=C-$
						4.20 q (4) $-COOCH_2CH_3$

Compound	mp °C	Found, % C	Found, % H	Calcd, % C	Calcd, % H	IR Spectrum, (cm^{-1}) and NMR spectrum,[a] ppm (no. of protons)
						4.38 m(4) } ferrocene ring protons 4.53 m(4) } 6.04 q (2) -C=C**H**-COOEt
29	96—97	62.95	5.92	62.83	5.80	IR 1710, 1624. NMR 2.01 d (6) -C=C-C**H**$_3$ 3.77 s (6) -COOC**H**$_3$ 4.37 m(4) } ferrocene ring protons 4.48 m(4) } 7.45 q (2) -C**H**=C-COOCH$_3$
30	101—102	66.78 (N% 9.76)	4.25	66.64 (N% 9.71)	4.19	IR 2170, 1616. NMR 4.42 s (8) ferrocene ring protons 5.39 d (2) -C=C**H**-CN 7.31 d (2) -C**H**=C-CN
31	69—70	65.73	4.21	65.76	4.14	IR 2810, 1687, 1620. NMR 4.39 s (8) ferrocene ring protons 5.43 d (2) -C=C**H**-CHO 7.38 d (2) -C**H**=C-CHO 9.61 d (2) -C**H**O
32	112—113	67.21	5.78	67.08	5.62	IR 1685, 1617. NMR 2.29 s (6) -C**H**$_3$ 4.47 s (8) ferrocene ring protons 6.34 d (2) -C=C**H**-COCH$_3$ 7.46 d (2) -C**H**=C-COCH$_3$
33	145—146	75.44	5.05	75.33	4.96	IR 1680, 1619. NMR 4.49 s (8) ferrocene ring protons 5.57 d (2) -C=C**H**-COPh 7.71 d (2) -C**H**=C-COPh 7.28 s (10) phenyl protons

a) 60 Mc with TMS as internal standard in $CDCl_3$ solution.
b) M. D. Rausch and A. Siegel, *J. Organometal. Chem.* **11**, 317 (1968).
c) P. L. Pauson and E. E. Watts, *J. Chem. Soc.*, **1963**, 2990.
d) P. Da Re and E. Sianesi, *Expirientia*, **21**, 648 (1966).
e) K. Schloegl and H. Egger, *Ann.*, **676**, 76 (1964).
f) J. M. Osgerby and P. L. Pauson, *J. Chem. Soc.*, **1961**, 4604.
g) C. R. Hauser and J. K.Lindsay, *J. Org. Chem.*, **23**, 906 (1957).
h) J. Decombe, J. P. Ravoux, and A. Dormond, *Compt. rend.*, **258**, 2348 (1964).
i) K. Sonogashira and N. Hagihara,*Kogyo Kagaku Zasshi*, **66**, 1090 (1963).

TABLE 3. CATALYTIC FERROCENYLATION OF OLEFINS WITH CHLOROMERCURIFERROCENE (**1**).

Olefin	Solvent	Product	Yield(%)[a]
Styrene	C_2H_5OH	**11**	44
		2	12
Ethyl acrylate	C_2H_5OH	**12**	41
		2	10
Ethyl crotonate	C_2H_5OH	**13**	36
		2	11
Methyl methacrylate	CH_3OH	**14**	38
		2	9
Methyl vinyl ketone	C_2H_5OH	**17**	31
		2	11
Phenyl vinyl ketone	C_2H_5OH	**18**	37
		2	8
Acrylonitrile	C_2H_5OH	**15**	33
		2	10

a) Yields are based upon the ferrocenylating agent used.

In the reactions of olefins with **1** and palladium salt, a δ-bonded ferrocenylpalladium compound (**7**) will function as the ferrocenylation agent, just as arylpalladium salt (**6**) in Heck's arylation reaction. The formation of **2** probably results from a coupling reaction of **7** or from a reaction of **7** with **1**. Similarly, the reactions of olefins with **3** and palladium salt may involve the formation of 1,1'-bis(chloropalladium)ferrocene (**8**) and the mechanism of the formation of **5** as a by-product involves a coupling reaction of **8** or a reaction of **8** with **3**.

$$\underset{(\mathbf{1})}{FcHgCl} + PdCl_2 \rightleftharpoons \underset{(\mathbf{7})}{[FcPdCl]} + HgCl$$

$$2\underset{(\mathbf{7})}{[FcPdCl]} \longrightarrow \underset{(\mathbf{2})}{Fc\text{-}Fc} + PdCl_2 + Pd$$

$$\underset{(\mathbf{7})}{[FcPdCl]} + \underset{(\mathbf{1})}{FcHgCl} \longrightarrow \underset{(\mathbf{2})}{Fc\text{-}Fc} + HgCl_2 + Pd$$

The ferrocenylation of allylic alcohols led to the formation aldehydes or ketones with a ferrocenyl substituent at the β-position. For example, 2-methyl-2-propenol, 5-phenyl-2-cyclohexenol, and 5,5-dimethyl-2-cyclohexenol reacted with **1** in the presence of palladium salt to produce 2-methyl-3-ferrocenylpropionaldehyde, 3-ferrocenyl-5-phenylcyclohexanone, and 3-ferrocenyl-5,

5-dimethylcyclohexanone respectively. These result suggest that the mechanism of the ferrocenylation of allylic alcohol involves the addition of **7** to the allylic double bond, and then hydride elimination from the hydroxylsubstituted carbon:

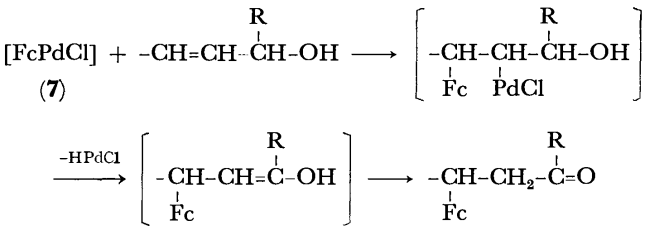

In addition, isopropenyl acetate and acetophenone enol acetate reacted with **1** and palladium salt to yield α-ferrocenylacetone and α-ferrocenylacetophenone respectively. These results suggest that the mechanism of the ferrocenylation of the enol ester involves an addition-elimination sequence; the addition of the ferrocenyl group preferentially occurs on the less substituted carbon atom, followed by the elimination of palladium with an acyl group to produce a carbonyl compound:

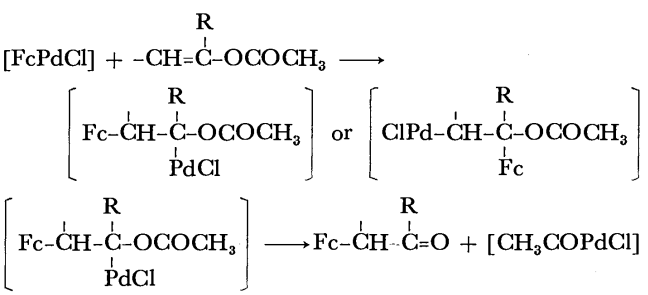

Heck[2c] reported that the reaction of arylpalladium salts with allylic halides produces the allylated aromatic compounds. For example, phenylpalladium salts react with allyl chloride and 2-methylallyl chloride to produce allylbenzene and (2-methylallyl)benzene respectively. He also suggested that this allylation reaction involves the addition of the arylpalladium chloride to the allylic double bond and the elimination of palladium chloride rather than of palladium hydride chloride. However, the reaction of **1** with 2-methylallyl chloride led to the formation of 3-chloro-1-ferrocenyl-2-methylpropene (**9**). This result suggests that the mechanism of the formation of **9** involves the elimination of palladium with a neighboring hydrogen rather than with chlorine.

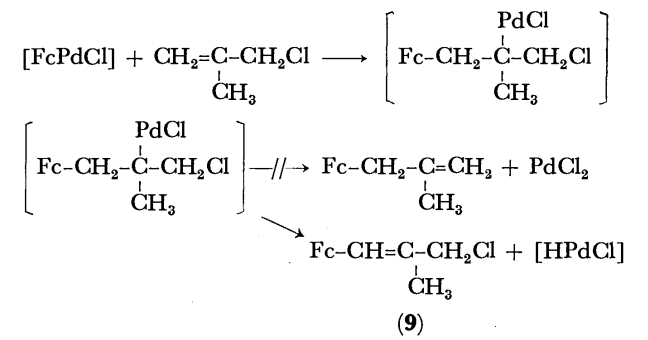

(**9**)

Experimental

Analysis and Materials. All the melting points are uncorrected. The IR spectra were measured on KBr disks with a Hitachi EPI-S2 spectrometer, and the NMR spectra were obtained by means of a Hitachi H-60 spectrometer in $CDCl_3$, using tetramethylsilane as the internal standard.

Chloromercuriferrocene (**1**) and 1,1′-bis(chloromercuri) ferrocene (**3**) were prepared according to the method described by Fish and Rosenblum.[3] 3-Buten-2-ol,[4] phenyl vinyl ketone,[5] and acetophenone enol acetate[6] were synthesized according to known procedures. 5-Phenyl-2-cyclohexenol and 5,5-dimethyl-2-cyclohexenol were synthesized by the lithium-auminum-hydride reduction of 5-phenyl-2-cyclohexenone and 5,5-dimethyl-2-cyclohexenone respectively. The other olefins were of a commercial grade and were purified before use.

General Procedure for the Ferrocenylation of Olefins. Lithium chloropalladite solutions were prepared by stirring 0.84 g (20 mmol) of anhydrous lithium chloride and 1.77 g (10 mmol) of anhydrous palladium chloride overnight at room temperature in 100 m*l* of the respective solvent expect in the case of acetonitrile, where 10 mmol instead of 20 mmol of lithium chloride was used. To this lithium chloropalladite solution, except in the reaction with ethylene, a mixture of 4.20 g (10 mmol) of **1** and four times as much olefin was added, after which the mixture was stirred at room temperature for 12 hr. In the case of the reaction with ethylene, ethylene was bubbled into the reaction mixture under atmospheric pressure. The products were isolated by filtration to remove any precipitated palladium and by distillation under reduced pressure to remove the solvent. The residue was dissolved in benzene; chromatograph on alnmina afforded yellow crystals (mp 228—229°C, 2.12% yields) which were identified as biferrocenyl (**2**)[7] by a comparison of the IR spectra and by a mixed-melting-point determination. Further elution with benzene and recrystallization from methanol, ethanol, or benzene-cyclohexane afforded the respective ferrocenylation product. The structures of the products were confirmed by a mixed-melting-point determinations with an authentic sample and by observation of the IR and NMR spectra. The results are summarized in Table 1, while the analytical results and the properties of the products are listed in Table 2.

In the reactions with **3**, 3.28 g (5 mmol) of **3** and four times olefin as much were added to a lithium chloropalladite solution prepared from 0.84 g of lithium chloride and 1.77 g of palladium chloride; the reactions were then carried out in the manner described above. The crude product was dissolved in benzene and chromatographed on alumina. First, elution with benzene afforded deep yellow crystals (mp 370°C), which were identical as bi-1,1′-ferrocenylene (**5**)[8] by a comparison of the IR and NMR spectra with those of an authentic sample. Further elution with benzene or chloroform afforded 1,1′-divinylferrocene derivatives (**4**). The structures of the products were confirmed by a mixed-melting-point determination with an authentic sample and by observation of the IR and NMR spectra. The results and the

3) R. E. Fish and M. Rosenblum, *J. Org. Chem*, **30**, 1253 (1965).
4) W. G. Young, S. Winstein, and A. N. Prater, *J. Amer. Chem. Soc.*, **58**, 289 (1936).
5) W. G. Young and J. D. Roberts, *ibid.*, **68**, 649 (1946).
6) P. Z. Bedoukian, *ibid.*, **67**, 1430 (1745).
7) H. Shechter and J. H. Helling, *J. Org. Chem.*, **26**, 1034 (1961).
8) F. L. Hedberg and H. Rosenbeg, *J. Amer. Chem. Soc.*, **91**, 1258 (1969): M. D. Rausch, R. F. Kovar, and C. S. Kraihauzel, *ibid.*, **91**, 1259 (1969).

properties of the products are also listed in Tables 1 and 2.

In catalytic reactions, 3.4 g (20 mmol) of cupric chloride dihydrate, 4.2 g (10 mmol) of **1**, and four times olefin as much were added to a lithium chloropalladite solution prepared from 0.17 g (1 mmol) of palladium chloride, 0.08 g (2 mmol) of lithium chloride, and 100 m*l* of ethanol or methanol: the reactions were then carried out in the manner described above. The results are given in Table 3.

The authors would like to express their thanks to Assistant Professor Kaoru Hanaya and Mr. Hideaki Kudo of Yamagata University for the measurements of NMR spectra, and to the Kawaken Fine Chemical Co., Ltd., for a gift of palladium chloride.

BULLETIN OF THE CHEMICAL SOCIETY OF JAPAN, VOL. 45, 900—904(1972)

Spectroscopic Studies on the Tautomers of Heptane-2,4,6-trione and Its Methylated Homologues[1]

Fumio SAGARA, Hiroshi KOBAYASHI, and Keihei UENO

Department of Organic Synthesis, Faculty of Engineering, Kyushu University, Hakozaki, Fukuoka

(Received September 6, 1971)

3,5-Dimethylheptane-2,4,6-trione and 3-methylheptane-2,4,6-trione are synthesized by methylationheptane of-2,4,6-trione *via* alkali metal enolates or an enamine intermediate of the mother compound. In keto-enol tautomerism, the latter two compounds take triketo-, monoenol-, and bisenol forms, while the first one exists in triketo- and monoenol forms, being unable to take a bisenol form. NMR spectra of the tautomers are assigned by combining with IR data. *Keto-enol* ratio in a range of solution phases at various temperatures are estimated by NMR method and effect of the branched methyl groups upon the keto-enol tautomerism is discussed.

A β,δ-tricarbonyl compound is a higher analogue of a β-dicarbonyl compound, and can take triketo-, monoenol- or bisenol forms in its tautomeric equilibrium. Accordingly, the tricarbonyl compound can behave as a bidentate- or terdentate ligand to form a metal chelate complex.

In the course of studies on chelating behavior of some β,δ-tricarbonyl compounds,[2] we were interested in their keto-enol tautomerism in relation to positions of the coordinating sites in the respective ligand molecules, especially in unsymmetric ones.

Tautomerism of compounds of this kind in aqueous media[3] have been studied extensively and recently NMR studies in a range of organic solvents were also reported.[4]

In this paper, we present synthesis and spectroscopic studies on keto-enol tautomerism of three triones; heptane-2,4,6-trione(H_2daa),[5] 3-methylheptane-2,4,6-trione (H_2mmd) and 3,5-dimethylheptane-2,4,6-trione (H_2dmd) in various phases by means of IR and NMR methods.

Results and Discussion

(1) Tautomeric Structures in Crystalline Phases. IR spectrum of H_2daa in a crystalline phase is somewhat different from those of crystalline H_2mmd and H_2dmd despite close similarity in their tricarbonyl skeletons. A band diffused over 3400 to 2200 cm^{-1}, combined together with a broad absorption at 1650 cm^{-1}, indicated the presence of a *cis*-β-ketoenol system with strong intramolecular hydrogen-bonding in crystalline H_2daa, while H_2mmd and H_2dmd exhibit an additional strong peak at 3400 cm^{-1}, which was apparently ascribable to intermolecularly hydrogen-bonded enolic hydroxyl groups in such a condensed phase. Presence of free keto groups is unlikely in the crystalline phases of the three tricarbonyl compounds, since such a keto group, if being present, would display an additional sharp ab-

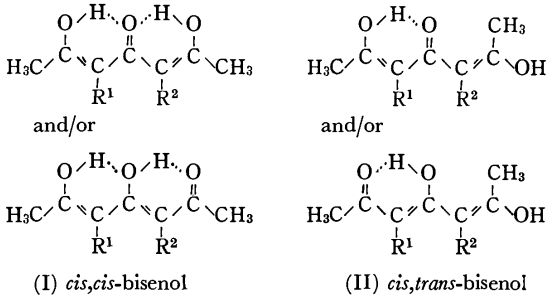

Fig. 1. Possible bisenol structures of the triketones in crystalline phases.

1) Contribution No. 210 from the Department of Organic Synthesis, Kyushu University.

2) a) Preliminary communication: F. Sagara, H. Kobayashi, and K. Ueno, This Bulletin, **41**, 266 (1968). A detailed article in press in this Bulletin. b) Y. Taguchi, F. Sagara, H. Kobayashi, and K. Ueno, *ibid.*, **43**, 2470 (1970).

3) a) G. Schwarzenbach and E. Felder, *Helv. Chim. Acta*, **27**, 576 (1944). b) A. J. Birch, P. Fitton, D. C. C. Smith, D. F. Steere, and A. R. Stelfox, *J. Chem. Soc.*, **1963**, 2209. c) J. Stuehr, *J. Amer. Chem. Soc.*, **89**, 2826 (1967).

4) a) C. W. Dudley, T. N. Huckerby, and C. Oldham, *J. Chem. Soc., A*, **1970**, 2605. b) E. Marcus, J. K. Chan, and C. B. Strow, *J. Org. Chem.*, **31**, 1369 (1966).

5) Abbreviation, H_2daa, comes from *dia*cetyl*a*cetone, and prefixed H_2 shows that the trione contains two dissociable enol protons upon metal-chelate formation, according to usage in coordination chemistry. H_2mmd and H_2dmd correspondingly symbolize the *mono*methyl- and *di*methyl-*d*aa, both prefixed also with H_2 meaning two dissociable protons. Though the prefix, H_2, is no use as far as the present paper is concerned, we feel it more convenient to use consistent symbols with subsequent reports on various metal chelates of the ligands.

sorption near 1710 cm^{-1} as observed in oily H_2mmd or in molten H_2daa.

Above observations in IR absorptions lead reasonably to a presumption that a *cis,cis*-bisenol form with cyclic intramolecular hydrogen-bondings is a major component among the H_2daa tautomers, while a *cis,-trans*-bisenol form is predominant regarding H_2mmd and H_2dmd in their crystalline phases as shown in Fig. 1. The present spectral evidences, however, do not distinguish which two of the three carbonyl groups enolize in the bisenols of crystalline phases, two possible forms in respect to enol positions being equally probable, and neither suggest the detailed stereochemistry of the *cis,trans*-bisenol, which is remained to be elucidated. In any case, the introduction of additional methyl groups at the interposition between carbonyl groups does not favor the formation of *cis, cis*-bisenol tautomer with cyclic intramolecular hydrogen-bondings.

Table 1. NMR spectra of H_2daa (c=1.0M) at 38°C

Assignment	Chemical shifts δ(ppm) in solvent			
	Methanol	$CDCl_3$	CCl_4	Benzene
Bisenol CH_3	1.97	1.97	1.94	1.63
C=C–H	—	5.12	5.02	4.88
Monoenol				
CH_3 (enol side)	2.05	2.07	2.04	1.63
CH_3 (keto side)	2.19	2.23	2.19	1.82
CH_2	—	3.38	3.27	2.97
C=C–H	—	5.53	5.45	5.15
Triketo CH_3	—	2.23	2.19	1.73
CH_2	—	3.67	3.57	3.20
Enol OH		14.10[a]	14.20[a]	14.53
Bisenol fraction (mol %)	18[b]	21	54	57

a) A diffused enol proton signal at room temperature is splitted into two signals at 14.05 and 15.13 ppm at −41°C in $CDCl_3$, and 13.83 amd 15.00 ppm at −21°C in CCl_4, respectively. The sharp peak at a higher field being assigned to that of bisenol and the broad one at a lower field to that of monoenol.

b) Value determined from the respective methyl signal intensities.

(2) Tautomeric Structures in Solution Phases. (2-a) Tautomerism of H_2daa: Table 1 summarizes the NMR spectra of H_2daa in various solvents, including the assignments of signals and bisenol content in solution phases. The assignments are virtually in agreement with those reported by the previous workers[4] except the assignment of the enolic hydroxyl protons. Since the intramolecular hydrogen-bonding in the monoenol would be stronger than those in the bisenol in which two enol protons are chelated to the common central carbonyl oxygen, enol protons in the *cis,cis*-bisenol are conceivably much more shielded than that of the monoenol, and correspondingly the former signal would appear in a higher field than the latter one. Although the conclusion being different from the assignment, by Marcus *et al.*,[4b] this reasoning is confirmed by comparisons of relative intensities of enol protons of the tautomers in H_2daa, and in H_2mmd of variable temperature NMR measurements, which are described below,

Table 2. *Keto-enol* ratio of H_2daa at various temperatures (c=1.0M)

Temp. (°C)	Monoenol (%)	Bisenol (%)	Triketo (%)
	in $CDCl_3$		
48	74	17	9
36	73	21	6
5	68	27	5
−41	68	25	5
	in CCl_4		
56	54	43	3
36	45	54	2
5	36	62	2

especially at lower temperatures. Presence of a monoenol form in the solution phases is consistently indicated in IR spectra which show a sharp intense peak at 1720 cm^{-1}.

Table 2 shows the temperature dependence of keto-enol equilibrium of H_2daa in solution phases, indicating that a higher temperature favors the monoenol form among the tautomeric isomers. This tendency is consistent with the fact that both molten H_2daa and H_2mmd at an elevated temperature reveal a free carbonyl band at 1720 cm^{-1}. Fraction of the triketo form, though being minor, also increases with the elevation of temperature.

On the other hand, as shown in Table 1, bisenol content of H_2daa increases with decrease in polarity of the solvent used. This tendency, being in good agreement with those observed in related pentane-2,4-diones, indicates highly polar character of keto form than an enol form with intramolecular hydrogen-bonding.[6]

Table 3. NMR spectra of H_2mmd at room temperature

Chemical shifts δ(ppm) in CCl_4	Chemical shifts δ(ppm) in $CDCl_3$	Assignment and coupling constants
1.25	1.30	3j; D, J(jm)=7 Hz
	1.32	1g; D, J(gl)=7 Hz
1.73	1.73	4k
1.80	1.80	2h
1.98	2.03	4f
2.03	2.07	3e
2.12	2.14	2d
	2.18	3c
2.17	2.20—2.24	1a; 2b
3.30	3.40	3m; Q, J(mj)=7 Hz
		(1l; Q, J(lg)=7 Hz)
3.40	3.50	2p
3.50	3.62	1n
5.37	5.42	4r
5.48	5.52	3q; multiplet
14.42		4v; broad
14.85		4u; multiplet
15.10	(15.10)[b]	3t; diffused
16.03	16.00	2s

a) Numerals and alphabetical letters indicate the formula number and the positions of protons in Fig. 2 respectively.

b) appeared at −41°C, not observable at room temperature.

D: doublet, Q: quartet

6) a) M. I. Kobachnik, S. T. Ioffe, E. M. Popov, and K. V. Vatsuro, *Tetrahedron*, **12**, 76 (1961). b) S. T. Yoffe, E. M. Popov, K. V. Vatsuro, E. K. Tulikova, and M. I. Kobachnik, *ibid.*, **18**, 923 (1962).

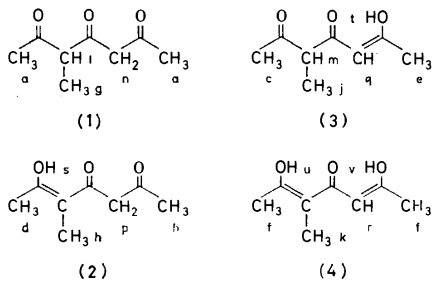

Fig. 2. Tautomeric structures of H_2mmd: (1) triketo, (2) monoenol (B), (3) monoenol (A) and (4) bisenol forms.

TABLE 4. NMR SPECTRA OF H_2dmd AT ROOM TEMPERATURE

Chemical shifts δ(ppm) in CCl_4	Chemical shifts δ(ppm) in $CDCl_3$	Assignment[a] and coupling constants
1.07 1.13	1.13 1.20	2h; D, J(hq)=7 Hz 3j; D, J(jr)=7 Hz
1.25 1.27 1.28	1.32 1.33 1.35	1g(*rac* and *meso*); D, J(gp)=7 Hz 4k, 5k; D, J(kr)=7 Hz
1.40 1.55	1.47 1.62	2l 3m
1.63	1.68	2f, 3f; broad
1.85	1.90	4n
	1.92	5n
1.96	1.98	2b, 3c; broad
2.07	2.17	1a
2.10	2.20	4d
	2.27	5e
2.42 2.48	2.58 2.62	2q; Q, J(qh)=7 Hz 3r; Q, J(rj)=7 Hz
4.64	3.62	all free hydroxyl
3.59 3.70	3.68 3.80	1p(*rac* and *meso*); Q, J(pg)=7 Hz 4r, 5r; Q, J(rk)=7 Hz
16.18	16.25	4s

D: doublet, Q: quartet

a) Numerals and alphabetical letters indicate the formula number and the positions of protons in Fig. 3 respectively.

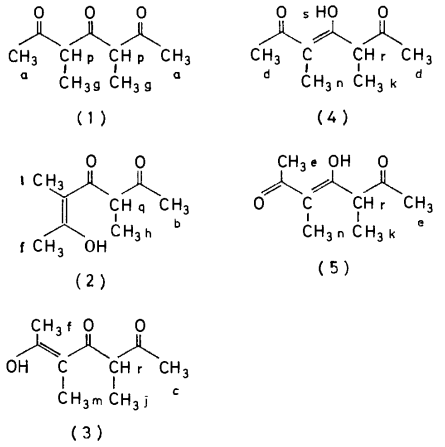

Fig. 3. Tautomeric structurs of H_2dmd: (1) triketo (racemic and meso), (2) *cis*-side-monoenol (A), (3) *trans*-side-monoenol (B), (4) *cis*-central-monoenol and (5) *trans*-central-monoenol forms.

(2-b) Assignments of NMR Signals of H_2mmd and of H_2dmd: Based upon chemical shifts, relative intensities, and spin-spin splitting patterns, NMR signals of H_2mmd and H_2dmd are assigned tentatively as summarized in Tables 3 and 4 accompanied by Figs. 2 and 3. Useful informations are obtained from the results of variable temperature measurements, decoupling measurements, deuterium exchange experiments, and comparisons with IR data in the same solvents.

TABLE 5. *Enol* SIGNALS OF SUBSTITUTED PENTANE-2,4-DIONES (c=1.0M in CCl_4)

1,5-Substituted		3-Substituted	
Substituent	Chemical shifts, δ(ppm)	Substituent	Chemical shifts, δ(ppm)
H- (pentane-2,4-dione)	14.8	methyl-	16.0
1,5-diethyl-	14.9	ethyl-	16.1
1,5-diisopropyl-	15.1	*n*-propyl-	16.1
1,1,1,5,5,5-hexamethyl-	16.7	*n*-butyl-	16.2
(dipivaloylmethane)		benzyl-	16.7[a]

a) Private communication from Prof. Y. Murakami.

The NMR signal of a monoenol proton of H_2dmd appears as a sharp peak at a lower field by 1 ppm as compared with that of H_2daa. Comparisons of chemical shifts of enol protons in some β-dicarbonyl compounds as shown in Table 5, indicate that introduction of an alkyl group to the central carbon causes a deshielding effect upon an enolic hydroxyl signal by about 1 ppm and gives a narrower peak, whereas substitution on side carbons, except with *t*-butyl group does not very much affect the chemical shift, remaining as a broad signal. The deshielding effect observed here is conceivably due to increased hydrogen-bonding of the enol proton which becomes closer to the β-carbonyl oxygen by steric repulsion between methyl groups on the both sides and the alkyl group on the central carbon. Enol proton chemical shift of dipivaloylmethane at an exceptionally lower field may be also explained in a similar manner by steric repulsion between the central hydrogen and bulky *t*-butyl groups on the both sides.

These observations on the enol protons lead that two hydroxyl signals observed at 16.00 and 15.10 ppm in H_2mmd can be assigned to two kinds of enol protons, one carrying an additional methyl group and the other not methylated respectively. Correspondingly the hydroxyl signals at 14.85 and 14.25 ppm of the bisenol form of H_2mmd are also assigned to the two kinds of enol protons in a similar manner.

Measurements on H_2dmd in 100 MHz in deuteriochloroform[7] shows the overlapped doublets centered at 1.33 ppm consisting of three doublets separated by about 0.01 ppm. By deuteration of H_2dmd, the doublet signals of the branched methyl protons coalesce respectively into three broad peaks and signals at a lower field than 2.3 ppm disappear. Combined with the

7) Measured with a JNM-PS-100 by courtesy of Mr. A. Kito in the Government Industrial Research Institute, Osaka, to whom the authors are very grateful.

decoupling data, the above results indicate that the missing signals upon deuteration are undoubtedly due to active protons such as an enolic hydroxyl and methine group interposed between two carbonyls and the coalesced signals are those of the methyl groups on the 3- and 5-carbons of H_2dmd. Also the overlapped doublet signals assigned to three kinds of methyl groups, suggest the presence of two diastereomeric triketo forms, one being a *meso*- and another a racemic form, and a monoenol form at the central oxygen, which is not found among monoenol forms of H_2daa and H_2mmd.

Signals assignable to a bisenol form of H_2dmd can not be found in the NMR spectra either in deuteriochloroform nor in carbon tetrachloride. As reported by Kobachinik *et al.*,[6] the methyl group interposed between two carbonyl groups in a β-diketone does not prevent the formation of a *cis*-enol with cyclic intramolecular hydrogen-bonding. Absence of a *cis,cis*-bisenol form in H_2dmd would be, therefore, conceivably due to steric repulsion between two methyl groups on the 3- and 5-carbons of H_2dmd. A study with molecular model shows that the coplanar *cis,cis*-bisenol form is accompanied by a strong steric hindrance due to the overlapping of the two methyl groups as illustrated in Fig. 4.

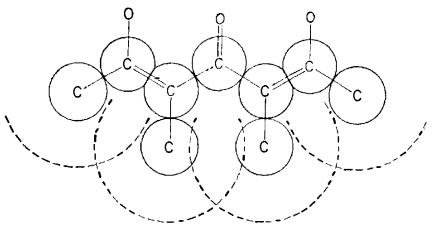

Fig. 4. Coplanar *cis, cis*-bisenol form of H_2dmd, broken semi-circles showing van der Waals radii of the methyl groups.

(2-c) Tautomerism of H_2mmd: H_2mmd in a carbon tetrachloride solution exhibits a widely diffused IR band over the range of 3600 to 2200 cm^{-1}, a sharp absorption at 1720 cm^{-1} and a broad, more intense band from 1650 to 1550 cm^{-1}. In a deuteriochloroform solution the carbonyl band at 1720 cm^{-1} increases in its intensity.

Combined with NMR data, these results indicate that H_2mmd in a solution phase takes in a major portion a *cis*-monoenol as well as a *cis,cis*-bisenol with intramolecular hydrogen-bonding, and that decrease in solvent polarity seemingly favor the *cis,cis*-bisenol form in agreement with a case of H_2daa.

As shown in Table 6, temperature causes substantial effect on the tautomeric composition of H_2mmd in a carbon tetrachloride solution, whereas causing little effect in deuteriochloroform, the keto-enol contents being virtually invariable within the experimental error in so far as a temperature range used (from 55 to 0°C).

Table 6. *Keto-enol* ratio of H_2mmd at various temperatures in mol % (c=0.8M)

Temp. (°C)	Monoenol (A)	Monoenol (B)	Bisenol	Triketo
		in CCl_4		
59	77	8	13	2
36	30	25	46	0
6	13	30	58	0
		in $CDCl_3$		
36	76	9	12	3

(2-d) Tautomerism of H_2dmd: IR spectrum of H_2dmd in deuteriochloroform reveals a prominent hydroxyl band and a free carbonyl band at 3400 and 1720 cm^{-1} respectively, the former absorption indicating evidently the presence of a substantial concentration of a *trans*-enol form. In carbon tetrachloride, the free carbonyl band is splitted into three peaks at 1730, 1715 and 1700 cm^{-1}, which indicate the presence of some configurational isomers in respect to the carbonyl groups.

Consistent with IR data on the hydroxyl group, NMR spectra exhibit a broad signal ascribable to the *trans*-enol proton at 5.90 ppm in deuteriochloroform at −46°C, shifting to a higher field with elevation of temperature as a more sharpened peak, at 3.35 ppm at 46°C. In carbon tetrachloride, the signal appears as a much more diffused band centered at 4.65 and 3.78 ppm at 36 and 55°C respectively.

Table 7. *Keto-enol* ratio of H_2dmd at various temperatures in mol % (c=0.5M)

Temp. (°C)	Side monoenol	Central monoenol	Triketo
		in $CDCl_3$	
50	33	48	19
36	40	45	16
0	51	41	8
		in CCl_4	
56	35	54	11
36	54	30	16

Table 7 shows the temperature dependence of the tautomer content. The presence of a considerable fraction of the triketo form shows a striking contrast to H_2daa and H_2mmd. However, the effect of temperature here seems not so simple as in the other tricarbonyl compounds.

Comparisons of the total enol content of H_2daa, H_2mmd, and H_2dmd suggest that enolizability decreases in the above order and the interposed methyl group seems to hinder enolization. However, the effect of the interposed methyl group seems to be somewhat complicated by combination of both electronic and steric effects. On the other hand, solvents also influence the tautomeric equilibrium in agreement with those observed in β-dicarbonyl compounds, polar solvents favoring the abundance of a keto form and less polar solvents an enol form.

Experimental

Materials. Heptane-2,4,6-trione was prepared according to Bethel and Maitland.[8] Mp 41.0—41.5°C (lit. mp 49°C). Found: C, 58.99; H, 7.27%.

8) J. R. Bethel and P. Maitland, *J. Chem. Soc.*, **1962**, 3751.

3-Methylheptane-2,4,6-trione: (a) Heptane-2,4,6-trione (10.0 g, 0.0703 mol) was dissolved in ethanolic potassium ethoxide which was prepared from absolute ethanol (30 m*l*) and potassium metal (4.10 g, 0.105 mol). After an addition of methyl iodide (80.0 g, 0.563 mol), the solution was kept at 40—50°C for 20 min. The resulting mixture was evaporated under reduced pressure, giving a slurry, which was filtered to remove potassium iodide. A viscous filtrate was dissolved in chloroform (100 m*l*) and treated with an aqueous cupric acetate (14.0 g of the monohydrate in 300 m*l* of water). The resulting blue chloroform solution containing copper complexes was separated by filtration from precipitates, which was mainly the 2:2 (metal ion: ligand) copper complex of H_2daa, being insoluble in chloroform. The filtrate was evaporated to give blue solid, which was dissolved in an aqueous methanol solution of cupric acetate (7.2 g of the monohydrate in 760 m*l* of 10% aq. methanol). The solution, when heated at 50—55°C for 6 hr, gave green precipitates, which, being a 2:2 copper complex of H_2mmd, were collected by filtration and dissolved in 1N hydrochloric acid. Chloroform extract from the above acid solution was evaporated, giving an oil boiling at 45—49°C/5×10^{-3} mmHg. Yield was 3.84 g (35%). Found: C, 61.32; H, 7.92%. Calcd for $C_8H_{12}O_3$: C, 61.52; H, 7.74%. The oil crystallized either spontaneously, but very slowly at room temperature, or from a petroleum ether solution on cooling, to give colorless granular crystals melting at 56.0—56.6°C.

The same compound could be obtained by using sodium or lithium metal in place of potassium in a similar manner as above, but in poorer yields.

In the last methanolic filtrate, there remained the 1:2 complex of H_2dmd, being readily soluble in methanol and not convertible into a form of 2:2 complex.

(b) A mixture of pyrrolidine (10.0 g, 0.141 mol), heptane-2,4,6-trione (20.0 g, 0.141 mol) and ethyl acetate (100 m*l*) was left standing overnight at room temperature. The resulting yellow crystals, which were collected and dried under reduced pressure, were heated with dried methyl iodide (68.4 g, 0.481 mol) under reflux for 24 hr. The resulting solution was evaporated off, giving a semisolid mass which was heated together with water (100 m*l*) at boiling point. The aqueous mixture was extracted with chloroform (50 m*l*). The chloroform extract was shaken with aqueous cupric acetate thoroughly, and a separated chloroform layer was evaporated, giving blue crystalline residue, which was purified by eluting from a silica gel (WAKOGEL Q-23) column with acetonitrile, to give the 1:2 complex of H_2mmd (2.64 g, 20.2%). The free ligand was obtained as described in procedure (a).

The position to which a methyl group was introduced, was confirmed by acid-catalyzed intramolecular condensation of H_2mmd into 2,3,6-trimethyl-γ-pyrone as well as by the following NMR studies on this trione.

3,5-Dimethylheptane-2,4,6-trione: H_2daa (10.0 g, 0.0703 mol) was treated in a similar manner as above, using absolute ethanol (160 m*l*), potassium (8.10 g, 0.210 mol) and methyl iodide (94 g, 0.68 mol). The reaction took 2 hr at 55°C to afford 1.53 g of the 2:2 complex of H_2mmd and 5.8 g of the 1:2 complex of H_2dmd. Decomposition of the H_2dmd complex with 1N hydrochloric acid followed by extraction with chloroform and subsequent evaporation gave colorless oil, which was solidified when treated with petroleum benzine. Recrystallization from a benzene-petroleum benzine (1:1) mixture afforded fibrous needles melting at 81.5—82.5°C. Yield was 2.30 g (19.2%). Bp 105—110°C/4 mmHg. Found: C, 63.23; H, 8.54%. Calcd for $C_9H_{14}O_3$: C, 63.51; H, 8.29%. The methylated positions on the heptanetrione were confirmed by derivation of H_2dmd into 2,3,5,6-tetramethyl-γ-pyrone as well as the NMR studies on this trione.

2,3,6-Trimethyl-γ-pyrone from H_2mmd. A chloroform solution of H_2mmd was heated together with a catalytic amount of 0.1N hydrochloric acid for 5 hr. The resulting solution was evaporated to dryness and solid residue was sublimed. Mp 82.0—84.0°C, yield being 84%. Found: C, 69.58; H, 7.37%. Calcd for $C_8H_{10}O_2$: C, 69.55; H, 7.30%. NMR (1.0M in $CHCl_3$): Four singlets at 1.93 (3H), 2.30 (3H), 2.35 (3H), and 6.64 ppm (1H). IR (Nujol mull): $\nu_{C=O}$ 1675 cm^{-1}.

The structure of the product was characterized by spectral comparisons with 2,6-dimethyl-γ-pyrone[9] (Mp 135.5—137°C. Found: C, 67.47; H, 6.51%. NMR (1.0M in $CHCl_3$): Two singlets at 2.25 (6H) and 6.00 ppm (2H). IR (Nujol mull): $\nu_{C=O}$ 1675 cm^{-1}) and 2,3,5,6-tetramethyl-γ-pyrone[10] (Mp 91.0—92.0°C. Found: C, 70.46; H, 8.06%. NMR (1.0M in $CHCl_3$): Two singlets at 1.92 (6H) and 2.23 ppm (6H). IR (Nujol mull): $\nu_{C=O}$ 1660 cm^{-1}) which were obtained from H_2daa and H_2dmd respectively in a similar manner described above.

Deuteration of H_2dmd. H_2dmd (86 mg) was dissolved in a mixture of methanol-d_4 (328 mg) and heavy water (183 mg). Exchange reaction was traced by NMR measurements immediately after an addition of a drop of pyridine. The reaction was completed in 2 hr at 35°C. The resulting solution was evaporated to dryness under high vacuum (10^{-4} mmHg) at room temperature, to give colorless solid melting at 85—87°C. Treatment with methanol and successive drying afforded the original H_2dmd, which was identified by the infrared spectral comparison.

The β-dicarbonyl compounds quoted in Table 5 were either commercially available or synthesized in our laboratory unless otherwise described.

IR spectra were measured on a JASCO 403-G in both KBr disc and Nujol mull phases for crystalline samples. Of solution phases, the concentrations of samples were prepared so as to be equal to those of NMR samples respectively. NMR spectra were recorded on a Varian A-60 instrument. All chemical shifts from tetramethylsilane were calibrated by use of chloroform proton chemical shift to be 7.27 ppm, both used as internal references. Contents of tautomeric isomers were determined by the least squares calculation from the respective peak areas unless otherwise stated.

The authors are grateful to Messrs. Akira Kito and Isao Yoshida who were engaged in the syntheses of some of the 3-alkyl- and 1,5-dialkylpentane-2,4-diones. The authors also wish to thank the Ministry of Education for a financial support.

9) F. Feist and H. Belart, *Ber.*, **28**, 1817 (1895).
10) J. N. Collie, *J. Chem. Soc.*, **77**, 962 (1900).

The Crystal Structure of 1-Ethyl-5-bromouracil. I. The Crystal Structure of the Form I Crystal of 1-Ethyl-5-bromouracil

Hiroshi MIZUNO, Takaji FUJIWARA, and Ken-ichi TOMITA

Faculty of Pharmaceutical Sciences, Osaka University, Toneyama, Toyonaka, Osaka

(Received September 8, 1971)

1-Ethyl-5-bromouracil, $C_6H_7N_2O_2Br$, is crystallized in two forms. Crystals of the form I are monoclinic with four molecules in a unit cell of dimensions; $a=7.89$, $b=12.01$, $c=9.71$ Å, $\beta=121.0°$, space group $P2_1/c$. Three-dimensional intensity data were collected by diffractometer with Mo-$K\alpha$ radiation. The structure was determined by heavy atom method and refined by the block-diagonal least-squares method. The final R-value was 0.052 for all observed reflections. The molecules are joined together in pairs around a center of symmetry with two N–H···O hydrogen bonds connecting N(3) to carbonyl oxygen O(4), and stacked with the base plane tilted each other.

5-Bromouracil, one of base analogue mutagens, can be incorporated into DNA in place of the normal thymine base. Such an incorporation probably reflects the structural similarity of 5-bromouracil and thymine; the van der Waals radius of bromine atom (1.95 Å) is close to that of methyl group (2.01 Å). In fact, the crystal structure of 1-methyl-5-bromouracil has been found to be isomorphous with that of 1-methylthymine[1] by X-ray study in this laboratory.[2] Once incorporated into DNA, however, the substituted bromine atom may cause to perturb an electron distribution on the pyrimidine ring, since bromine atom has the greater electronegativity than the methyl group. Therefore, this substitution of DNA affects on important biological properties; the increase of the sensitivity to ultraviolet irradiation[3] and the significantly higher melting temperature as compared with that of normal DNA.[4]

The structure analysis of 1-ethyl-5-bromouracil is of great interest in order to examine the influence of bromine atom on the molecular arrangement and the hydrogen bonding. In an earlier report, we described our finding of two forms of 1-ethyl-5-bromouracil, in which the main structural difference between two forms is on the mode of hydrogen bond.[5] In this paper, we describe the precise crystal structure analysis of the form I of 1-ethyl-5-bromouracil.

Experimental

1-Ethyl-5-bromouracil was kindly supplied by Professor A. Rich, M.I.T., U.S.A. and colorless plate-like crystal were obtained by slow evaporation of dimethyl sulfoxide solution. Rotation and Weissenberg photographs around the elongated axis showed the crystals to be monoclinic. The systematic absences for $h0l$ with $l=2n+1$ and for $0k0$ with

TABLE 1. FINAL ATOMIC COORDINATES AND THERMAL PARAMETERS
(Estimated standard deviations are shown in parentheses ($\times 10^4$). Thermal parameters are in the form of exp $[-(h^2\beta_{11}+k^2\beta_{22}+l^2\beta_{33}+hk\beta_{12}+hl\beta_{13}+kl\beta_{23})]$).

Atom	x/a	y/b	z/c	β_{11}	β_{22}	β_{33}	β_{12}	β_{13}	β_{23}
Br	1.2419(1)	0.2499(1)	0.9325(1)	0.0167(1)	0.0073(0)	0.0013(1)	−0.0029(2)	−0.0038(1)	0.0037(0)
C(2)	0.7281(8)	0.2801(8)	0.3950(5)	0.0125(13)	0.0040(5)	0.0062(6)	−0.0004(12)	0.0013(10)	0.0009(3)
C(4)	1.0155(8)	0.3653(6)	0.6369(7)	0.0135(14)	0.0043(5)	0.0051(4)	0.0003(13)	0.0017(10)	−0.0001(3)
C(5)	1.0340(7)	0.2619(6)	0.7172(6)	0.0125(12)	0.0043(5)	0.0054(5)	0.0017(14)	0.0016(9)	0.0017(3)
C(6)	0.9117(9)	0.1766(6)	0.6406(7)	0.0157(15)	0.0053(5)	0.0073(6)	−0.0007(14)	0.0049(10)	0.0021(3)
C(7)	0.6347(10)	0.0866(6)	0.3990(8)	0.0155(16)	0.0055(6)	0.0109(7)	−0.0045(15)	0.0036(13)	−0.0028(4)
C(8)	0.6985(13)	0.0287(8)	0.2949(11)	0.0311(28)	0.0084(8)	0.0238(12)	−0.0131(24)	0.0148(20)	−0.0121(7)
O(2)	0.6003(7)	0.2913(4)	0.2551(6)	0.0155(11)	0.0070(4)	0.0002(5)	−0.0010(11)	−0.0086(10)	0.0018(4)
O(4)	1.1202(6)	0.4480(4)	0.6943(5)	0.0176(11)	0.0042(4)	0.0035(5)	−0.0041(10)	−0.0019(8)	−0.0017(2)
N(1)	0.7610(7)	0.1849(4)	0.4814(6)	0.0136(12)	0.0039(4)	0.0078(5)	−0.0038(11)	0.0025(9)	−0.0013(3)
N(3)	0.8567(7)	0.3678(5)	0.4809(6)	0.0150(13)	0.0050(4)	0.0041(6)	0.0020(12)	0.0010(9)	0.0004(3)
H(1)	0.8715	0.4238	0.4195	3.42					
H(2)	0.9408	0.1006	0.7050	1.56					
H(3)	0.6619	0.0321	0.4984	3.18					
H(4)	0.4886	0.1178	0.3306	2.46	isotropic thermal parameters				
H(5)	0.8430	0.0035	0.3746	4.47					
H(6)	0.6730	0.0839	0.2062	2.82					
H(7)	0.6441	−0.0410	0.2451	3.58					

1) K. Hoogsteen, *Acta Crystallogr.*, **16**, 28 (1963).
2) K. Morita, unpublished result.
3) R. L. Erikson and W. Szybalski, *Biochem. Biophys. Res. Commun.*, **4**, 258 (1961).
4) S. Kit and T. C. Hsu, *ibid.*, **5**, 120 (1961).
5) H. Mizuno, N. Nakanishi, T. Fujiwara, K. Tomita, T. Tsukihara, T. Ashida, and M. Kakudo, *ibid.*, **41**, 1161 (1970).

TABLE 2. THE OBSERVED AND CALCULATED STRUCTURE FACTORS

K	FO	FC	K	FO	FC	K	FO	FC	K	FO	FC	K	FO	FC	K	FO	FC	K	FO	FC	K	FO	FC	K	FO	FC
H,L=	0	0	11	31	32	10	30	-32	9	45	45	3	63	-63	7	40	-40	12	49	50	8	25	28	4	39	40	2	16	15
2	290	321	12	33	32	11	25	21	H,L=	4	5	4	17	19	8	11	-2	13	25	23	9	21	-19	H,L=	-6	0	4	16	-16
4	206	216	13	26	-24	H,L=	2	7	1	16	-18	5	20	-18	10	20	-25	14	39	-32	10	16	-17	0	92	-94	H,L=	-7	6
6	152	-157	14	25	-22	6	17	13	6	15	-19	8	22	21	11	21	22	H,L=	-3	5	H,L=	-4	8	1	33	33	0	48	46
8	97	92	H,L=	1	3	8	18	-13	H,L=	4	6	10	51	-52	12	18	18	1	31	-30	0	96	-108	2	101	100	1	31	29
10	82	-83	1	12	-13	H,L=	2	8	0	60	-60	11	28	-25	H,L=	-2	4	2	17	-17	2	90	103	3	38	-38	2	41	-41
12	37	33	2	68	62	0	60	60	1	23	24	12	37	36	0	40	-42	3	15	-14	4	72	-82	4	86	-86	3	18	-16
14	30	-29	3	28	-27	1	23	23	2	60	56	H,L=	-1	2	1	150	-166	4	13	14	6	51	63	6	44	46	4	44	45
16	28	22	4	27	24	2	59	-62	4	60	-62	0	51	-51	2	44	-47	6	12	11	8	50	-55	7	28	-28	6	55	-55
H,L=	0	1	6	27	25	3	20	-19	5	17	22	1	14	12	3	113	122	7	26	-25	10	32	32	8	26	-24	7	29	-26
2	38	-37	7	12	-10	4	60	60	6	42	47	2	148	162	4	38	38	9	13	11	12	29	-31	9	32	30	8	47	46
4	123	=124	10	11	12	5	31	34	7	17	-9	3	194	-209	5	95	-101	10	13	12	H,L=	-4	9	10	17	17	9	21	23
5	33	-36	11	19	22	6	44	-44	H,L=	5	0	4	127	-134	6	11	-10	12	20	-17	2	35	-37	H,L=	-6	1	10	26	-26
7	16	17	H,L=	1	4	H,L=	3	0	0	22	28	5	123	129	7	127	128	H,L=	-3	6	4	20	22	3	27	-29	H,L=	-7	7
8	31	-31	0	142	139	1	171	172	1	107	-109	6	106	108	8	21	22	0	71	78	6	14	-19	4	10	12	3	22	-21
9	19	20	1	87	81	3	153	-154	2	52	-54	7	95	-99	9	71	-69	1	83	94	7	15	-9	5	11	14	6	15	-16
11	44	-43	2	111	-106	5	93	96	3	83	83	8	76	-76	10	14	12	2	84	-94	8	15	11	6	25	-23	H,L=	-7	8
H,L=	0	2	3	21	-19	7	116	-115	5	74	-79	9	58	57	11	49	49	3	59	-63	H,L=	-4	10	7	18	17	1	72	69
0	91	87	4	160	154	9	58	58	6	18	-24	10	68	69	13	21	-26	4	82	90	0	41	-40	H,L=	-6	2	3	39	-37
1	176	171	5	14	15	11	49	-47	7	91	94	11	31	-29	H,L=	-2	5	5	75	83	1	51	-53	0	78	-76	5	39	39
2	158	-161	6	136	-135	13	34	35	8	23	26	12	53	-51	1	12	11	6	58	-60	2	18	15	1	51	-49	7	31	-28
3	162	-167	8	90	91	H,L=	3	1	9	64	-66	13	34	30	2	37	37	7	34	-30	3	35	36	2	74	72	9	25	22
4	34	39	9	22	29	1	69	-66	11	37	37	14	32	33	4	20	18	8	44	49	5	39	-42	3	64	63	H,L=	-7	9
5	142	145	10	73	=73	2	17	-12	H,L=	5	1	H,L=	-1	3	5	28	26	9	38	38	6	26	24	4	87	-85	1	15	10
6	56	-61	12	42	41	4	15	-16	2	20	-17	1	37	-34	6	26	30	10	42	-43	7	41	44	5	41	-39	H,L=	-7	10
7	108	-112	14	31	-28	5	12	-9	3	13	11	3	20	-19	7	21	-20	11	22	-24	8	21	-20	6	51	53	0	16	-15
8	76	79	H,L=	1	5	6	15	12	4	33	32	4	54	-53	8	13	-16	12	24	22	9	33	-36	7	42	41	1	29	29
9	49	48	1	16	14	7	12	8	6	28	28	5	15	11	9	14	21	14	18	-14	H,L=	-4	11	8	34	-33	2	22	22
10	35	-35	4	23	21	9	13	12	7	20	18	6	38	36	11	17	-19	H,L=	-3	7	4	17	15	9	31	-28	3	31	-30
11	32	-30	6	54	-54	10	15	-9	H,L=	5	2	7	31	32	H,L=	-2	6	1	33	32	5	18	14	10	31	33	5	26	24
12	35	37	9	24	-21	13	14	7	0	80	80	8	23	-25	0	156	150	3	11	15	7	22	-23	11	17	15	6	16	18
13	34	31	H,L=	1	6	H,L=	3	2	1	34	-36	10	23	-22	1	139	-133	5	16	-18	H,L=	-4	12	12	22	-17	7	22	-25
14	20	-18	0	72	75	0	160	-160	2	39	-40	H,L=	-1	4	2	100	-96	7	14	13	1	30	-32	H,L=	-6	3	H,L=	-7	12
H,L=	0	3	1	106	102	1	49	50	3	23	22	0	213	-206	3	102	102	9	21	-26	9	34	31	8	16	18	0	46	-43
1	13	-10	2	71	-70	2	120	118	4	59	57	1	11	11	4	75	75	10	19	-7	H,L=	-5	0	12	18	11	2	30	29
4	19	17	3	81	-79	3	30	-28	5	27	-26	2	160	155	5	74	-73	11	15	12	1	111	109	H,L=	-6	4	4	23	-24
5	30	-30	4	48	47	4	95	-95	6	55	-56	3	21	21	6	86	-89	H,L=	-3	8	2	53	-54	0	15	-14	6	21	21
6	22	17	5	25	26	5	105	105	7	39	39	4	177	-181	7	55	57	1	78	71	3	84	-83	1	104	-100	H,L=	-8	0
7	40	41	6	52	-52	6	98	99	8	26	29	5	32	30	8	50	54	2	24	19	4	13	16	2	46	46	0	59	61
8	15	13	7	59	-59	7	51	-53	9	36	-34	6	96	96	9	36	-33	3	113	-115	5	79	79	3	102	100	2	38	-40
10	16	14	8	38	35	8	87	-88	10	38	-38	8	76	-78	10	50	-52	4	74	78	6	24	-24	5	70	-69	4	27	28
11	22	18	9	49	49	9	46	45	H,L=	5	3	10	71	73	11	29	25	7	66	-70	7	95	-94	6	12	11	6	26	-31
H,L=	0	4	11	29	-29	10	57	58	2	32	-35	12	30	-31	12	25	25	9	41	43	8	24	26	7	34	32	H,L=	-8	1
0	17	15	12	15	11	11	30	-33	6	18	-17	14	27	27	13	25	-27	11	31	-35	9	65	66	8	18	-19	2	14	-14
1	256	249	H,L=	1	7	12	22	-25	H,L=	5	4	H,L=	-1	5	H,L=	-2	7	H,L=	-3	9	11	36	-37	9	31	-31	6	15	4
3	147	-144	10	18	18	13	17	17	0	80	80	1	17	16	1	20	19	2	16	-18	H,L=	-5	1	11	25	22	H,L=	-8	2
5	152	153	H,L=	1	8	H,L=	3	3	1	20	20	4	31	34	2	15	9	3	23	-23	2	17	17	H,L=	-6	5	0	64	67
6	21	17	0	20	-20	2	17	16	2	83	-87	6	12	2	3	19	-21	H,L=	-3	10	3	16	-10	3	21	-17	1	23	22
7	104	-105	1	106	107	3	27	25	4	68	69	8	29	30	4	37	-35	0	62	-60	6	13	11	4	34	-34	2	55	-59
8	15	-17	2	25	22	4	20	-21	6	43	-48	9	16	15	5	13	13	1	46	44	7	13	15	5	26	27	3	22	-21
9	72	75	3	76	-75	5	22	20	7	18	-16	11	21	-26	6	25	25	2	49	49	8	16	17	6	20	-22	4	36	35
11	61	-62	4	25	-25	6	22	21	8	34	38	H,L=	-1	6	11	17	-15	3	48	-49	H,L=	-5	2	7	33	-34	5	16	16
13	23	26	5	76	76	7	45	-43	H,L=	5	5	1	105	-100	H,L=	-2	8	4	38	-39	0	74	-74	9	19	20	6	23	-24
H,L=	0	5	6	16	17	H,L=	3	4	3	15	-9	2	82	78	0	118	111	5	42	43	1	89	85	13	19	12	8	26	29
1	24	23	7	51	-51	0	114	-114	H,L=	5	6	3	119	112	1	16	14	6	24	27	2	76	75	H,L=	-6	6	H,L=	-8	4
2	17	17	8	12	-8	1	22	-24	1	45	52	4	82	-82	2	91	-87	8	20	-19	3	46	-45	0	40	39	1	51	50
3	15	15	9	34	35	2	92	97	H,L=	6	0	5	99	-98	3	43	-42	H,L=	-3	11	4	49	-48	1	65	-63	2	15	-14
4	13	9	H,L=	1	10	3	12	5	0	92	-94	6	77	77	4	68	66	4	19	17	5	75	73	2	80	-80	3	46	-47
5	40	-40	0	54	-54	4	58	-56	1	33	-33	7	58	59	5	35	35	H,L=	-3	12	6	59	59	3	79	77	5	53	55
6	20	-20	1	15	15	5	23	-21	2	100	100	8	60	-62	6	65	-67	0	48	-45	7	50	-50	4	58	59	7	31	-30
9	17	-19	2	47	51	6	67	69	3	37	38	9	57	-56	7	29	-31	2	54	51	8	36	-35	5	60	-61	9	29	23
10	17	14	H,L=	2	0	8	71	-74	4	83	-86	10	21	24	8	65	66	H,L=	-4	0	9	36	37	6	43	-44	H,L=	-8	5
H,L=	0	6	0	232	-237	10	37	38	5	16	-13	11	39	38	10	35	-38	2	179	-174	10	20	19	7	22	24	1	18	13
0	107	-103	1	69	-66	12	29	-30	6	46	46	12	32	-30	H,L=	-2	9	3	15	11	11	39	-36	8	43	43	H,L=	-8	6
1	85	82	2	183	186	H,L=	3	5	7	24	28	13	27	-30	3	14	-11	4	141	134	12	17	-19	9	19	-17	0	25	-24
2	130	124	3	13	11	1	14	-13	8	23	-24	H,L=	-1	7	4	32	-28	5	29	-28	H,L=	-5	3	10	17	-19	1	49	50
3	64	-61	4	193	-199	2	19	16	9	27	-30	1	12	10	5	17	-9	6	83	-82	2	19	-16	11	32	29	2	29	26
4	122	-119	5	117	-113	3	13	8	10	21	17	4	43	-42	6	32	32	8	93	91	3	39	37	12	19	11	3	45	-49
5	14	10	6	116	118	4	23	-23	H,L=	6	1	5	32	-31	7	25	25	10	47	-47	4	20	17	13	23	-25	4	22	-20
6	103	103	8	73	-75	H,L=	3	6	2	31	-30	H,L=	-1	8	8	20	-19	12	39	37	5	20	-20	H,L=	-6	7	5	19	17
7	31	=28	10	55	53	0	69	-71	4	17	15	1	114	-109	H,L=	-2	10	H,L=	-4	1	6	23	-24	2	35	37	6	18	14
8	57	-57	11	13	3	1	90	-91	H,L=	6	2	2	24	-21	0	23	21	1	16	-15	7	16	-17	3	21	-20	7	24	-22
9	39	37	12	44	-43	2	46	46	0	26	-25	3	89	87	1	42	40	2	14	13	8	18	15	6	17	17	9	17	16
10	30	32	14	28	27	3	80	80	1	68	-70	4	12	-13	2	34	-30	4	50	45	H,L=	-5	4	H,L=	-6	8	H,L=	-8	7
11	16	-14	H,L=	2	1	4	40	-39	2	32	31	5	67	-63	3	41	-39	13	18	13	0	97	-95	0	55	54	4	21	19
12	28	-29	1	57	-52	5	62	=65	3	55	57	7	46	45	4	27	28	H,L=	-4	2	1	23	20	1	16	7	5	19	-16
H,L=	0	7	2	19	17	6	35	35	5	45	-49	8	25	25	5	56	56	0	172	166	2	77	72	2	45	-44	6	17	-23
2	13	-11	3	41	-41	7	46	50	6	23	21	9	37	-38	6	36	-33	1	88	83	3	32	-33	4	45	50	7	22	22
4	26	26	4	33	29	8	22	-15	7	39	45	11	27	28	7	30	-31	2	134	-128	4	71	-68	6	41	-42	H,L=	-8	8
5	23	-26	5	37	36	9	29	-27	8	17	-16	H,L=	-1	9	8	35	32	3	74	-75	6	95	93	8	34	40	0	33	-32
6	48	-49	6	18	-15	H,L=	3	7	9	34	-33	3	17	-15	H,L=	-2	11	4	147	141	7	29	-29	10	29	-31	2	38	40
7	19	23	7	11	9	4	17	14	H,L=	6	3	9	17	18	2	16	-6	5	70	69	8	96	-95	12	19	11	4	52	-52
8	14	16	9	15	14	H,L=	3	8	5	17	9	H,L=	-1	10	H,L=	-3	0	6	89	-87	9	29	28	H,L=	-6	9	6	37	37
10	15	-12	11	15	13	0	39	38	H,L=	6	4	0	72	70	1	178	-172	7	18	-16	10	55	53	8	20	-22	H,L=	-8	10
H,L=	0	8	H,L=	2	2	1	50	-51	1	41	-45	1	43	-43	3	158	154	8	32	31	11	15	-4	H,L=	-6	10	2	18	16
0	69	-61	0	170	-165	2	25	-25	2	33	-33	2	62	-63	5	96	-96	9	37	35	12	33	-30	0	44	42	3	14	15
1	21	-21	1	146	-141	3	39	40	3	40	41	3	36	36	7	117	115	10	42	-39	14	17	14	1	32	31	4	18	-21
2	59	56	2	145	141	4	20	21	4	16	22	4	56	54	9	61	-58	11	26	-23	H,L=	-5	5	2	38	-38	5	17	-11
3	20	17	3	151	149	H,L=	4	0	5	39	-42	5	23	-24	10	14	14	12	16	17	1	13	-16	3	40	-40	9	23	-14
4	89	-88	4	100	-99	0	116	112	H,L=	7	0	6	45	-44	11	48	47	13	18	18	2	41	39	4	33	34	H,L=	-8	12
5	18	-18	5	96	-95	1	12	11	1	24	26	7	30	28	13	32	-35	H,L=	-4	3	3	25	25	5	24	26	2	16	2
6	74	73	6	74	73	2	173	-174	2	16	18	H,L=	-2	0	15	19	14	2	15	-19	4	33	-30	6	30	-25	3	20	23
8	49	=46	7	94	94	3	12	-11	3	33	-32	0	234	-237	H,L=	-3	1	3	68	65	7	20	-20	7	24	-26	5	17	-21
10	47	44	8	56	-54	4	135	134	4	14	-17	1	69	66	1	24	27	6	16	14	9	21	21	8	15	14	H,L=	-9	2
H,L=	0	9	9	59	-60	5	26	28	5	51	50	2	187	186	2	16	-14	8	46	-46	H,L=	-5	6	9	25	23	3	24	-27
7	17	-10	10	48	50	6	80	-82	6	17	14	3	70	-11	3	41	-37	9	16	-20	0	104	-98	10	17	-15	5	22	22
H,L=	0	10	11	45	43	7	13	-5	7	30	-31	4	198	-199	4	19	13	10	20	18	1	71	-66	H,L=	-6	11	H,L=	-9	3
0	18	-18	13	34	-34	8	88	91	9	32	33	5	119	113	5	70	68	H,L=	-4	4	2	61	61	1	15	-15	0	15	0
1	50	-50	14	21	15	10	48	-47	H,L=	1	6	6	120	118	6	33	31	0	25	-27	3	64	66	3	20	19	H,L=	-9	4
2	34	33	H,L=	2	3	12	41	37	1	22	21	8	75	-75	7	19	-21	1	205	195	4	59	-58	H,L=	-6	12	0	37	-32
3	50	53	1	15	-14	H,L=	4	1	3	17	-16	10	54	53	8	15	-15	2	13	-13	5	56	-61	0	19	-17	2	15	5
4	23	-18	2	32	30	2	26	-23	H,L=	7	2	12	41	-43	H,L=	-3	2	3	207	-205	6	50	54	1	20	22	4	31	-29
5	44	-44	3	18	17	3	11	14	0	48	-50	14	30	27	0	47	46	5	93	95	7	30	32	5	18	24	5	22	24
H,L=	1	0	5	17	18	4	38	39	1	24	25	H,L=	-2	1	1	120	-114	7	91	-91	8	37	-40	H,L=	-7	0	6	28	24
0	121	114	7	20	-15	7	13	-14	2	44	47	1	129	124	2	39	-36	8	24	-25	9	17	-16	1	29	-26	H,L=	-9	6
1	89	-82	8	13	14	9	16	11	3	36	-38	2	42	-40	3	87	83	9	52	54	10	30	33	2	15	18	4	22	-17
2	28	-26	H,L=	2	4	10	17	-12	4	39	-42	3	23	21	4	88	85	11	43	-41	11	31	28	3	32	32	5	16	-14
3	191	199	0	34	34	H,L=	4	2	5	16	16	4	10	-8	5	99	-94	12	25	26	12	42	-39	4	18	-17	6	18	16
4	25	-25	1	154	-151	0	73	71	H,L=	7	3	5	17	-20	6	115	-111	13	36	32	H,L=	-5	7	5	50	-50	H,L=	-9	8
5	188	-198	2	27	-26	1	117	118	1	16	-7	6	46	42	7	114	113	H,L=	-4	5	2	25	25	7	31	31	1	27	-25
7	141	143	3	158	158	2	70	-70	H,L=	8	0	8	23	24	8	44	43	1	85	-82	4	13	14	9	31	-32	2	16	5
8	22	24	4	71	68	3	131	-131	0	59	61	9	37	-37	9	106	-107	3	58	55	H,L=	-5	8	H,L=	-7	1	3	21	21
9	126	-109	5	114	-114	4	57	58	1	13	14	10	27	-31	10	49	-47	4	18	15	1	73	-70	9	19	13	5	23	-24
10	40	-38	6	68	-68	5	107	109	2	40	-40	12	17	22	11	50	50	5	26	-26	2	22	21	H,L=	-7	2	6	17	21
11	80	80	7	64	62	6	26	-25	3	13	-18	H,L=	-2	2	12	27	27	6	15	-13	3	73	73	0	29	27	H,L=	-9	9
13	33	-34	8	16	13	7	51	-52	4	30	28	0	284	-282	13	17	-19	7	21	25	5	52	-56	1	64	-62	5	18	=10
15	32	28	9	42	-40	9	37	39	5	13	16	1	332	-337	15	24	18	11	17	17	7	46	51	2	40	-38	H,L=	-9	10
H,L=	1	1	11	38	39	10	13	-13	6	27	-31	2	268	271	H,L=	-3	3	13	15	-2	9	36	-32	3	52	55	0	24	23
1	60	58	13	20	-24	11	30	-30	H,L=	8	1	3	136	136	1	33	-30	H,L=	-4	6	11	24	25	4	16	15	1	24	-26
2	53	-50	H,L=	2	5	H,L=	3	5	1	17	-8	4	123	-125	2	114	-107	0	72	=68	H,L=	-5	9	5	48	-49	2	22	-16
3	45	44	1	13	13	1	14	-13	H,L=	-1	0	5	123	-126	3	32	42	1	79	75	5	16	11	6	16	-16	3	16	13
4	14	12	3	28	-25	3	46	46	0	119	114	6	92	94	8	14	-15	2	70	73	8	16	-15	7	54	55	H,L=	-10	4
5	62	-63	4	31	-29	4	12	-13	1	90	82	7	64	66	9	30	-31	3	30	-32	11	19	-14	8	29	31	0	20	-23
6	66	-64	5	52	50	5	20	-16	2	29	-26	8	59	-59	10	24	24	4	53	-54	H,L=	-5	10	9	30	-32	H,L=	-10	5
7	38	37	7	32	-30	6	22	23	3	194	-199	9	81	-80	11	23	20	5	63	65	0	32	37	10	22	-17	2	15	3
H,L=	1	2	10	19	16	8	18	-17	4	23	-25	10	29	30	15	15	-5	6	62	62	1	35	-39	H,L=	-7	3	H,L=	-10	6
0	83	80	H,L=	2	6	H,L=	6	6	5	189	198	11	32	30	H,L=	-3	4	7	43	-44	2	41	-50	4	15	14	3	17	20
1	166	-163	0	63	59	0	36	-37	7	140	-143	12	47	-46	0	109	109	8	50	-54	3

$k=2n+1$, indicate the space group to be $P2_1/c$. From measuring the 2θ setting angles for 14 reflections on the diffractometer with Mo-$K\alpha$ radiation, the unit cell dimensions were determined to be $a=7.89$, $b=12.01$, $c=9.71$ Å, and $\beta=121.0°$. The density measured by the flotation method, with a mixture of benzene and ethylene bromide, was 1.84 gcm^{-3}, whereas the calculated density on the assumption of four molecules in the unit cell is 1.84 gcm^{-3}. Three-dimensional intensity data were collected on a full automatic four-circle diffractometer (Rigaku Denki Co. Ltd.) with Zr-filtered Mo-$K\alpha$ radiation. For the intensity measurement, a plate-like crystal with approximate dimensions of $0.12\times0.20\times0.40$ mm was used and the c-axis was mounted as coincident to the ϕ axis of the goniostat. A total of 2244 independent reflections accessible in $\sin\theta/\lambda$ less than 0.65 were scanned by the ω-2θ technique at a scan speed of 4° per minute through the scan range from $\{2\theta(\alpha_1)-0.65°\}$ to $\{2\theta(\alpha_2)+0.65°\}$ for all reflections, in which a value of 0.65° was determined by measuring the scan range for a sufficiently strong and low order reflection. Background counts of five seconds duration were taken at both sides of each peak. In order to correct the intensities for coincidence loss, the counting rate was kept less than 10000 counts per second with an automatic attenuator mechanism. During the data collection, the intensities for three standard reflections (080), (006), and (800) were measured periodically to check the stability of the electronics and the damage on crystal lattice. After 1187 of all reflections, which have the net intensity exceeded three times of its estimated standard deviations, were recorded and corrected for the usual Lorentz and polarization effects, these data were converted to the absolute scale by means of the usual averaging process.

Structure Determination and Refinement

A three-dimensional Patterson function was calculated, and this easily revealed bromine atom position. Since y paprameter of bromine atom is nearly 1/4, however, the first Fourier synthesis phased on the bromine atom position brought about the pseudo mirror plane at $y=1/4$. To avoid such a trouble, the useful two-dimensional (0 1 0) Fourier synthesis was carried out, and all the non-hydrogen atoms except the terminal ethyl carbon could be assigned. Subsequent Fourier synthesis phased on these positions showed the complete structure including the terminal ethyl carbon.

Three-dimensional refinement was then carried out by block-diagonal least-squares method with unit weight factors for all reflections. The positional parameters of all the non-hydrogen atoms and anisotropic thermal parameters of the bromine atom were initially refined to drop R-index ($\Sigma||F_o|-|F_c||/\Sigma|F_o|$) to 0.08. At this stage, a difference Fourier map clearly revealed the positions of all the hydrogen atoms. Finally, all positional parameters, together with anisotropic temperature factors for the non-hydrogen atoms and isotropic temperature factors for the hydrogen atoms, were refined, and the R-index decreased to 0.052 for all observed reflections.

Final atomic coordinates and thermal parameters together with the corresponding standard deviations are given in Table 1. The observed and calculated structure factors are listed in Table 2.

Results and Discussion

The intramolecular bond lengths and angles are shown in Fig. 1. Within the experimental errors, these values except hydrogen atoms are in good agreement with the values found in other uracil derivatives; 1-methyluracil[6] and 1-methylthymine.[1] The only remarkable deviations were found in the C(2)-N(3) bond length, which is about 0.02 Å longer than those of the above-mentioned derivatives, and in the N(3)-C(4)-C(5) angle which is significantly less here (113.3°) than in 1-methyluracil (116°)[6] and 1-methylthymine (116.1°)[1]. A similar value of this angle is also found in the form II (112.7°) of 1-ethyl-5-bromouracil.[7] Such a smaller angle is commonly found in crystal structures of 5-halogenated uridines; 5-fluoro-2′-deoxy-β-uridine (112.6°)[8], 5-chlorouridine (113.7°),[9] 5-bromo-2′-deoxyuridine (112.4°) and 5-bromouridine (112.8°).[10] Therefore, it seems likely this angle is certainly affected by halogen substitution at C(5).

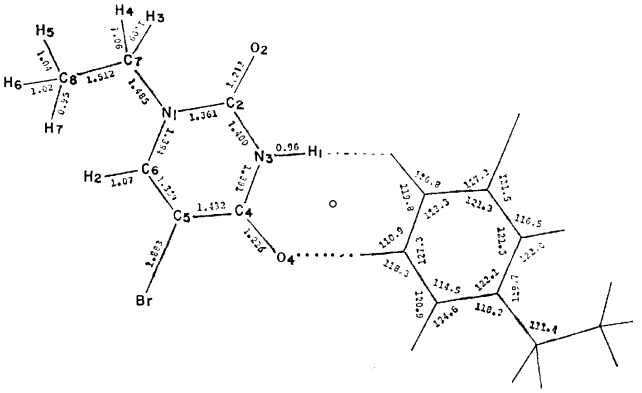

Fig. 1. Bond lengths and bond angles of 1-ethyl-5-bromouracil. The standard deviations are 0.008 Å in bond lengths and 0.6° in bond angles between non-hydrogen atoms.

The best plane through the six ring atoms, as calculated by the least-squares method, is defined by the equation. The distances from the non-hydrogen atoms to

$$-0.89763x + 0.32294y + 0.29995z + 1.30399 = 0.$$

Table 3. Deviations of atoms from the least-squares plane through the six ring atoms

Atom	Deviation (Å)	Atom	Deviation (Å)
Br	−0.008	N(1)	−0.005
C(2)	−0.007	N(3)	0.022
C(4)	−0.022	O(2)	−0.036
C(5)	0.006	O(4)	−0.043
C(6)	0.006	C(7)	−0.068

6) D. W. Green, F. S. Mathews, and A. Rich, *J. Biol. Chem.* **237**, 3573 (1962).
7) T. Tsukihara, T. Ashida, and M. Kakudo, This Bulletin **45**, 909 (1972).
8) D. R. Harris and W. M. MacIntyre, *Biophys. J.* **4**, 203 (1964).
9) S. W. Hawkinson and C. L. Coulter, *Acta Crystallogr*, **B27**, 34 (1971).
10) J. Iball, C. H. Morgan, and H. R. Wilson, *Proc. Roy. Soc., Ser. A*, **295**, 320 (1967).

this plane are listed in Table 3. Both exocyclic oxygen atoms O(2) and O(4) are significantly displaced on the same side of the plane. The substituent carbon atom C(7) is also markedly displaced by 0.068 Å from this plane. Such deviations from the base are frequently observed in crystal structures of purine and pyrimidine derivatives.

The arrangement of the molecules in the crystal is shown in Figs. 2 and 3. The basic molecular unit in this crystal is a dimer formed by two molecules which are joined together in pairs around a center of symmetry, with two N–H···O hydrogen bonds connecting the N(3) atom with the carbonyl oxygen O(4) at a distance of 2.85 Å. It is of particular interest that hydrogen bonded pairing system of the form I is quite different from that of the form II, in which N(3)–H and the carbonyl oxygen O(2) in place of O(4) are used for the hydrogen bond formation.[5,7]

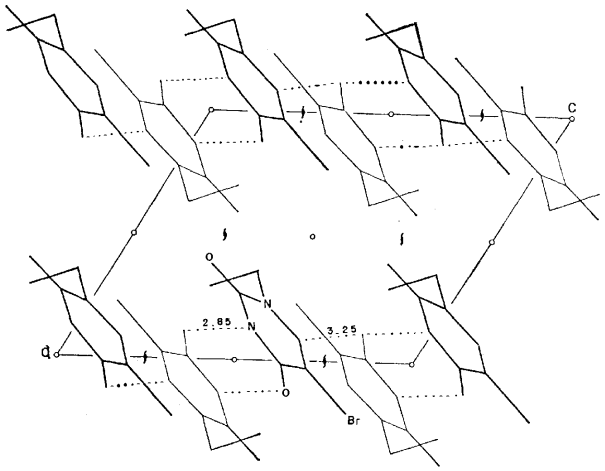

Fig. 2. The crystal structure viewed down the *b* axis.

Figures 2 and 3 show the stacking mode of the adjacent pyrimidine rings related by the *c*-glide plane, forming an infinite stack along the direction of the *c*-axis. This stacking is characterized by the following two points; one is the characteristic arrangement of the adjacent pyrimidine rings tilting to one another with the dihedral angle of 38.° The other is very little overlap of the bases and, therefore, main contact is due to the interactions between the bromine substituent and the adjacent pyrimidine ring as shown in Fig. 3. The distance from the bromine atom to this plane is 3.5 Å. Such a bromine-base contact is frequently found in crystal structures of halogenated purines and pyrimidines.[11]

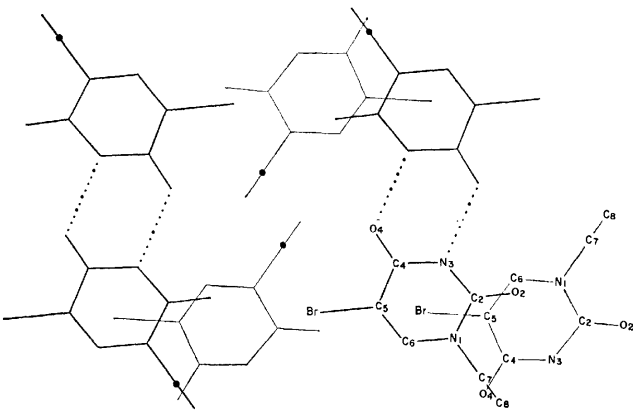

Fig. 3. The stacking of molecules viewed perpendicular to the plane (101).

The closest C···O intermolecular distance in the crystal is found between C(6) and the carbonyl oxygen O(4) of the adjacent molecule, and this distance is 3.25 Å, with the H···O distance 2.24 Å and the C–H–O angle 157.8°, which seems to be a weak hydrogen bond. A similar C–H···O contact has been reported in pyrimidine nucleotides; uridine residue of β-adenosine-2′-β-uridine-5′-phosphoric acid (3.18 Å),[12] calcium thymidine-5′-phosphate (3.42 Å)[13] and barium uridine-5′-phosphate (3.17 Å)[14], and in uracil derivatives; 1-methylthymine (3.11 Å)[1] and uracil (3.19 and 3.28 Å).[15] These values agree quite well with those suggested by Sutor as to the existence of C–H···O hydrogen bond in the solid state.[16]

11) C. E. Bugg, J. M. Thomas, M. Sundaralingam, and S. T. Rao, *Biopolymers*, **10**, 175 (1971).
12) E. Shefter, M. Barlow, R. A. Sparks, and K. N. Trueblood, *Acta Crystallogr.*, **B25**, 895 (1969).
13) K. N. Trueblood, P. Horn, and V. Luzzati, *ibid.*, **14**, 965 (1961).
14) E. Shefter and K. N. Trueblood, *ibid.*, **18**, 1067 (1965).
15) G. S. Parry, *ibid.*, **7**, 313 (1954).
16) D. J. Sutor, *J. Chem. Soc.*, **1963**, 1105.

The Crystal Structure of 1-Ethyl-5-bromouracil. II. The Crystal Structure of the Form II Crystal of 1-Ethyl-5-bromouracil

Tomitake TSUKIHARA,[1] Tamaichi ASHIDA, and Masao KAKUDO
Institute for Protein Research, Osaka University, Osaka

(Received September 8, 1971)

Two crystalline forms of 1-ethyl-5-bromouracil were found. The crystal structure of the form II has been determined. The dimension of the tetragonal unit cell are $a=b=17.13$ Å, $c=5.36$ Å, and $Z=8$. The space group is $P4_2/n$. The final R is 0.064. The hydrogen bond scheme in this crystal, N(3)–H(3)···O(2), is the first finding in alkylated pyrimidine dimers. The carbon atom binding to the nitrogen atom of the pyrimidine ring deviates significantly from the pyrimidine ring plane.

Two crystalline forms of 1-ethyl-5-bromouracil were recently found. The study of these structures showed the presence of different modes of hydrogen bond.[2] The detail of the structure of the form I is presented in the preceeding paper.[3]

The present paper deals with details of the crystal structure of the form II, in which a new hydrogen-bonding type in the alkylated pyrimidine dimers has been found.

TABLE 1. CRYSTAL DATA

$C_6H_7BrN_2O_2$	M.W.=219.05
Tetragonal	$P4_2/n$
$a=b=17.13$ Å	$c=5.36$ Å
$D_{cal}=1.85$ g/cm^3	
$D_{obs}=1.84$ g/cm^3 (by flotation)	

Experimental

Two types of crystals were grown from a dimethyl sulfoxide solution at room temperature. From I crystal is a colorless plate-like crystal and the form II is a transparent needle. Preliminary Weissenberg and Precession photographs established that the form II was tetragonal with the c axis along the needle axis. The systematic extinction of $(00l)$ for l odd and $(hk0)$ for $h+k$ odd restricted the space group to $P4_2/n$. The crystal data are listed in Table 1.

A nickel filtered Cu-$K\alpha$ radiation was used to collect intensity data for all the reflections in the range $0<\sin\theta/\lambda<0.55$ Å^{-1} in octant (hkl) and $(\bar{h}k0)$. All the intensities were measured on a Rigaku Denki computer-controlled four-circle diffractometer (AFC-II). A scintillation counter was used with a pulse-height discriminator. A crystal of approximate dimension, 0.02 mm×0.02 mm×0.10 mm ($0.14<\mu r<0.16$), was mounted with the c axis parallel to the ϕ-axis of the diffractometer. The ω-2θ scan technique was employed with a scan speed of 2°/min by ω, and backgrounds were measured for 6.00 sec at each start and end points of the scan range. A scan range of ω for each reflection was calculated by the formula;[4] scan range$=1.00°+0.15°\times\tan\theta$. Attenuators were automatically inserted when the maximum count rate exceeded 8000 cps. The intensities were corrected only for Lorentz and polarization factors.

Measurements of two reference reflections, (400) and (200), were repeated at every fifty reflections. For 35 time repetition of the measurements, $|F_o(400)|=149.50\pm0.57$ and $|F_o(002)|=93.14\pm0.56$. The standard deviation of $|F_o(hk0)|$ were assigned on the basis of the following equation

$$\sigma^2(|F_o|) = \langle((|F_o(hk0)| - |F_o(\bar{k}h0)|)/2)^2\rangle_{av} \quad (1)$$

where $\langle\ \rangle_{av}$ represents the average of 10 reflections of similar magnitude of F_o. The standard deviations of $|F_o(hkl)|$ were substituted for $\sigma(|F_o(hk0)|)$ of similar $|F_o|$. An index of experimental accuracy

$$\sum_{h,k}(|F_o(hk0)| - |F_o(\bar{k}h0)|)/\sum_{h,k}(|F_o(hk0)| + |F_o(\bar{k}h0)|) \quad (2)$$

is 0.0119, where the summation is over all reflections, of which $|F_o|$ are greater than 10.0. Figure 1 shows the distribution of $\sigma(|F_o(hk0)|)$ *versus* $|F_o|$.

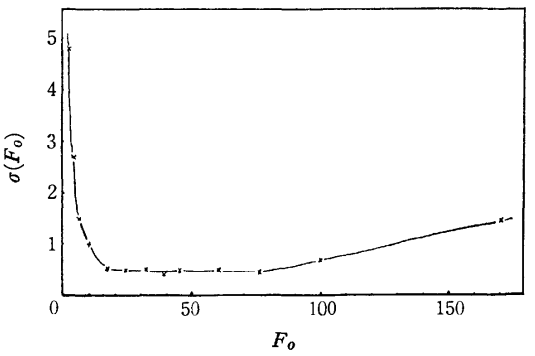

Fig. 1. The standard deviations of $|F_o(hk0)|$. Each symbol (x) represents the average of 10 reflections of similar $|F_o|$.

Structure Determination and Refinement

The position of the bromine atom was found from the three dimentional Patterson function. A Fourier synthesis was computed on the basis of the position of bromine atom. Eight extra atoms except ethyl group showed up on the first map. The definite location of the ethyl group could not be found on the electron density map. The peak which corresponds to the carbon atom C(7) binding to N(1) is too much elongated along the direction perpendicular to the pyrimidine ring plane.

Structure refinements were carried out by the block diagonal least-squares method. The function, $\sum w(|F_o|-|F_c|)^2$, was minimized for the least-squares refinements. The atomic scattering factors were taken from "Inter-

1) Present address: Faculty of Engineering, Tottori University, Tottori.

2) H. Mizuno, N. Nakanishi, T. Fujiwara, K. Tomita, T. Tsukihara, T. Ashida, and M. Kakudo, *Biochem. Biophys., Res. Commun.*, **41**, 1161 (1970).

3) H. Mizuno, T. Fujiwara, and K. Tomita, This Bulletin, **45**, 905 (1972).

4) T. C. Furnas, (1957), Single Crystal Orienter Instruction Manual. Milwaukee: General Electric Co.

Table 2. Final atomic coordinates and thermal parameters with their estimated standard deviations

	x	e.s.d. (x)	y	e.s.d. (y)	z	e.s.d. (z)
Br	0.3591	0.0007	0.6928	0.0006	1.3252	0.0007
C2	0.4139	0.0049	0.4906	0.0046	0.7649	0.0053
C4	0.4448	0.0045	0.6244	0.0047	0.9259	0.0047
C5	0.3841	0.0045	0.6125	0.0046	1.1045	0.0052
C6	0.3451	0.0049	0.5465	0.0052	1.1099	0.0057
N1	0.3587	0.0044	0.4860	0.0043	0.9462	0.0052
N3	0.4556	0.0036	0.5600	0.0036	0.7689	0.0039
O2	0.4279	0.0035	0.4397	0.0033	0.6139	0.0038
O4	0.4860	0.0034	0.6819	0.0031	0.9021	0.0035
H3	0.4962	0.0360	0.5649	0.0346	0.6603	0.0412
H6	0.2979	0.0393	0.5415	0.0388	1.2066	0.0444
C7	0.2884	0.0098	0.4258	0.0097	0.8958	0.0105
C8	0.3069	0.0121	0.3654	0.0120	1.0861	0.0118
C7′	0.3313	0.0109	0.3983	0.0107	1.0249	0.0116
C8′	0.2618	0.0126	0.3926	0.0126	0.8818	0.0134

	$B_{11}\times10^5$	$B_{22}\times10^5$	$B_{33}\times10^4$	$B_{12}\times10^5$	$B_{13}\times10^4$	$B_{23}\times10^4$
Br	663 (3)	459 (3)	485 (2)	174 (6)	6 (2)	−70 (2)
C2	383 (21)	342 (21)	436 (26)	−89 (37)	58 (12)	7 (13)
C4	317 (20)	321 (19)	349 (22)	109 (34)	−44 (12)	40 (12)
C5	308 (19)	323 (20)	358 (23)	−15 (33)	−8 (11)	−11 (12)
C6	338 (22)	532 (26)	470 (29)	20 (40)	92 (14)	−38 (15)
N1	515 (22)	416 (20)	708 (27)	−386 (35)	230 (14)	−79 (13)
N3	304 (15)	348 (16)	366 (19)	−22 (26)	55 (9)	16 (9)
O2	520 (17)	370 (15)	620 (21)	−233 (26)	163 (11)	−68 (10)
O4	481 (16)	320 (14)	501 (19)	−195 (25)	12 (10)	14 (9)

	B
H3	3.500 (0.897)
H6	3.500 (0.903)
C7	4.616 (0.233)
C8	6.747 (0.299)
C7′	5.445 (0.263)
C8′	7.499 (0.331)

Temperature factor
$=\exp(-(B_{11}\times h^2+B_{22}\times k^2+B_{33}\times l^2+B_{12}\times hk+B_{13}\times hl+B_{23}\times kl))$
or
$=\exp(-B(\sin\theta/\lambda)^2)$

national Table for X-ray Crystallography (1962)." To take into account of the anomalous scattering by bromine atom, $\Delta f'(-0.95)$ and $\Delta f''$ (1.40) were included in the calculations. The weighting scheme employed was

$w = 0.0$ ($|F_o|<10.0$ or attenuated reflection)
$w = \sigma^{-1}(|F_o|)$ (others).

Five cycles of least-squares refinement of positional parameters and anisotropic thermal parameters for the nine atoms except ethyl group resulted an a value of R of 0.1394. An (F_o—F_c) synthesis then revealed the two possible site of the ethyl group (Fig. 2).

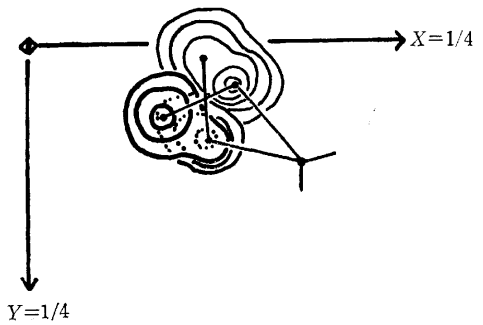

Fig. 2. The composite difference electron density map, for which the contribution of the hydrogen atoms and ethyl group carbon atoms were excluded from the calculated structure factors. Contours are drown at interval of 0.5 e/Å^3, starting at 0.5 e/Å^3.

After three cycles of least-squares refinements of the positional parameters, the anisotropic thermal parameters for the nine atoms except ethyl group and the isotropic thermal parameters for the four atoms of the two sites of the ethyl group, the R value decreased to 0.068. The ethyl group was supposed as equally distributed to the two sites, that is, the occupancies of the both sites are 0.5. In the course of the refinement,

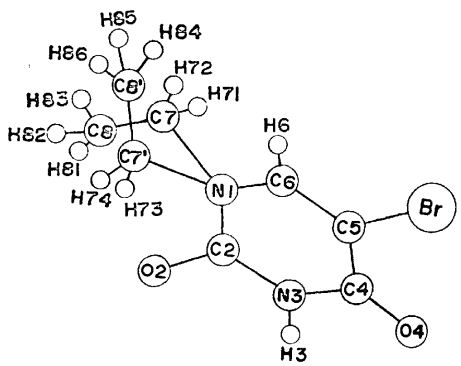

Fig. 3. Structural formula of 1-ethyl-5-bromouracil.

the temperature factor of an atom of the ethyl group compensated for particular choice of the occupancy of the same atom. Accurate occupancies of two ethyl group sites could not be determined, partly because only about 60% of reflections within the limiting sphere of Cu-$K\alpha$ radiation was used in the determination. For several sets of occupancies of two ethyl group sites, similar refinements were tried. These calculations suggested that two ethyl group sites should be multiplied by 0.60—0.45 and 0.45—0.60 respectively. The (F_o—F_c) synthesis at this stage revealed two hydrogen atoms bound to the pyrimidine ring.

The final refinement included all atoms except for the hydrogen atoms of the ethyl group. The final R is 0.064.*

Molecular Structure

Tables 4 and 5 give the bond distances in the pyrimidine ring of this crystal and some other crystals respectively. Comparison with these crystals shows that structure of the pyrimidine ring are in good agreement with each others. The molecule except ethyl group is nearly planar (Table 6), bromine atom being displaced from the plane by 0.04 Å. The carbon atom C(7) and C(7′) deviate significantly from the plane by 0.53 Å and 0.57 Å, respectively. This displacement suggests an increase of p-character in the bond orbitals of C(7)–N(1) and C(7′)–N(1). Triethylpyrazine[5] and bromodihydroacromycine[6] have a similar structure. In form I, the carbon atom C(7) does not displace from the pyrimidine ring plane. In form II, if the carbon atom C(7) is placed on the plane, the distance between the carbon atom C(8) and the oxygen atom O(2) or O(4) of the neighboring molecule is shorter than 3.2 Å.

Table 4. Bond lengths and angles with their estimated standard deviations

Bond	Length	e.s.d.	Angle	θ	e.s.d.
C6–N1	1.376 Å	0.008 Å	C6–N1–C2	121.8°	0.5°
N1–C2	1.360	0.007	C6–N1–C7	117.7	0.6
C2–N3	1.383	0.007	C7–N1–C2	116.1	0.6
N3–C4	1.399	0.006	C6–N1–C7′	118.8	0.6
C4–C5	1.429	0.007	C7′–N1–C2	116.1	0.6
C5–C6	1.313	0.008	N1–C2–N3	113.7	0.5
C2–O2	1.216	0.007	N1–C2–O2	124.7	0.5
C4–O4	1.218	0.006	O2–C2–N3	121.7	0.5
Br–C5	1.864	0.005	C2–N3–C4	128.7	0.4
N1–C7	1.599	0.012	C2–N3–H3	118.8	3.2
C7–C8	1.495	0.016	H3–N3–C4	113.2	3.2
N1–C7′	1.626	0.013	N3–C4–C5	112.7	0.4
C7′–C8′	1.425	0.018	N3–C4–O4	119.9	0.4
N3–H3	0.916	0.041	O4–C4–C5	127.4	0.5
C6–H6	0.963	0.045	C4–C5–C6	120.6	0.5
			C4–C5–Br	119.1	0.5
			Br–C5–C6	120.3	0.4
			C5–C6–N1	123.2	0.5
			C5–C6–H6	123.4	3.3
			H6–C6–N1	112.5	3.3
			N1–C7–C8	100.4	0.8
			N1–C7′–C8′	99.6	0.9

Table 5. Bond lengths and angles of uracil or thymine derivatives

Bond	T[7]	TD[8]	MT[9]	EBU (form I)[3],
C(6)–N(1)	1.382 Å	1.374 Å	1.383 Å	1.384 Å
N(1)–C(2)	1.355	1.385	1.379	1.361
C(2)–N(3)	1.361	1.381	1.379	1.400
N(3)–C(4)	1.391	1.378	1.375	1.381
C(4)–C(5)	1.447	1.453	1.432	1.432
C(5)–C(6)	1.349	1.343	1.346	1.339
C(2)–O(2)	1.234	1.206	1.214	1.212
C(4)–O(4)	1.231	1.230	1.237	1.226
σ	0.005	0.006	0.004	0.008

a) T, TD, MT and EBU represent thymine, thymidine, 1-methylthymine, and 1-ethyl-5-bromouracil respectively.

Table 6. The equation of the least-squares plane through atoms

Equation	Atom	Deviation
$-0.6617X+0.3866Y$ $-0.6425Z+4.0882=0$	Br	0.042 Å
	C2	0.016
	C4	−0.012
	C5	−0.010
	C6	−0.030
	N1	−0.014
	N3	−0.017
	O2	0.034
	O4	−0.010
	*H3	0.041
	*H6	0.092
	*C7	0.545
	*C8	−0.709
	*C7′	−0.563
	*C8′	0.660

where $X=ax$, $Y=by$, $Z=cz$

Atom not included in the least-squares calculation.

Molecular Packing

There are four intermolecular contact regions. Bromine atoms pack closely around a 4_2-axis. Hydrogen bonds, N–H···O, are formed around a center of symmetry. Disordered ethyl groups surround a $\bar{4}$-axis. The hydrogen atom H(6) and the oxygen atom O(4) contact closely with each other. One of the interesting

* Table 3 which gives a complete list of the observed and the calculated structure factors has been submitted to, and is kept as Document No. 7202 by, the office of the Bulletin of the Chemical Society of Japan, 1-5 Kanda-Surugadai, Chiyoda-ku, Tokyo. A copy may be secured by citing the Document number and by remitting, in advance, ¥400 for photo prints. Pay by check or money order payable to: Chemical Society of Japan.

5) J. J. H. McDowell, *Acta Crystallogr.*, **B26**, 954 (1970).
6) J. Z. Gougoutas and B. A. Kaski, *ibid.*, **B26**, 853 (1970).
7) R. Gerdil, *ibid.*, **14**, 333 (1961).
8) D. W. Young, P. Tollin, and H. Wilson, *ibid.*, **B25**, 1423 (1969).
9) K. Hoogsteen, *ibid.*, **16**, 28 (1963).

Table 7. Intermolecular contacts

Atom	Neighbor atom	Distance	Atom	Neighbor atom	Distance
Br	Br g	4.012 Å	C(7)	C(8) e	4.296 Å
Br	Br h	4.012	C(7)	C(8) f	4.360
Br	Br j	4.012	C(7)	C(7′) e	4.328
Br	Br k	4.012	C(7)	C(8′) c	3.999
Br	Br i	4.223	C(8)	C(8) b	4.435
			C(8)	C(8) d	3.553
O(2)	N(3) a	2.866	C(8)	C(7′) d	4.288
O(2)	H(3) a	1.958	C(8)	C(7′) f	4.158
			C(8)	C(8′) b	4.323
O(4)	C(6) k	3.249	C(8)	C(8′) c	3.680
O(4)	H(6) k	2.268	C(8)	C(8′) d	3.857
			C(7′)	C(8′) c	3.711
			C(7′)	C(8′) d	4.357
			C(8′)	C(8′) e	3.781

Key for molecule position

a	$1.0-x$	$1.0-y$	$1.0-z$
b	x	y	$1.0+z$
c	y	$0.5-x$	$1.5-z$
d	y	$0.5-x$	$2.5-z$
e	$0.5-y$	x	$1.5-z$
f	$0.5-y$	x	$2.5-z$
g	$-0.5+y$	$1.0-x$	$0.5+z$
h	$-0.5+y$	$1.0-x$	$-0.5+z$
i	$0.5-x$	$1.5-y$	z
j	$1.0-y$	$0.5+x$	$0.5+z$
k	$1.0-y$	$0.5+x$	$-0.5+z$

aspects of this crystal structure is the packing of bromine atoms. Two non-equivalent distances between bromine atoms are 4.22 Å and 4.01 Å respectively (Table 7). This closest packing region elongates along the needle axis.

The hydrogen bond scheme in this crystal, N(3)–H(3)···O(2), is the first finding in the alkylated pyrimidine dimers. While the hydrogen bond scheme in form I, N(3)–H(3)···O(4), is usually found in the self-dimer of uracil and thymine derivatives, for example, uracil,[10,11] 1-methyluracil,[12] 5-ethyl-6-methyl uracil[13] and 1-methylthymine.[14] It seems that a change of electron distribution in pyrimidine ring by a substitution of a bromine atom or van der Waals interaction between closest packed bromine atoms perturbs the construction of the hydrogen bond scheme. Table 7 gives a list of all the intermolecular contacts between the disordered carbon atoms of the ethyl group. The distances of C(8)–C(8d)[15] and C(8)–C(8'c)[15] are shorter than usual, but a similar intermolecular contact between methyl groups in a crystal of octamethyltetraamidodiphosphono-2,3-butadiene-1,3.[16] The distance between H(6) and O(4), 2.27 Å, is fairly short, and the angle C(6)–H(6)–O(4) is 178.0°. In a thymine or uracil molecule, C(6) has a fairly positive charge.[17] Thus C(6)–H(6)···O(4) may be a hydrogen bond. Similar hydrogen bonds were reported in form I crystal and some other crystals, barium uridine-5′-phosphate,[18] β-adenosine-2′-β-uridine-5′-phosphoric acid[19] and calcium thymine phosphate.[20]

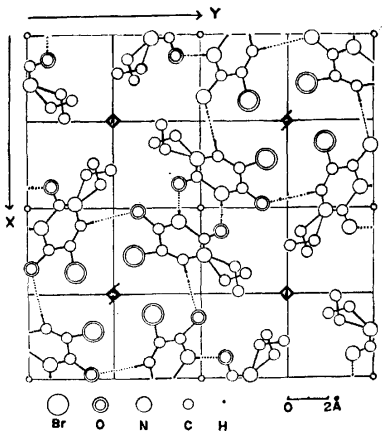

Fig. 4. The crystal structure viewed along the *c* axis. Hydrogen bonds are indicated by broken lines.

10) G. S. Parry, *Acta Crystallogr.*, **7**, 313 (1954).
11) R. F. Stewart and L. J. Jensen, *ibid.*, **23**, 1102 (1967).
12) D. W. Green, F. S. Mathews, and A. J. Rich, *J. Biol. Chem.*, **237**, 3572 (1962).
13) G. N. Reek and R. E. Marsh, *Acta Crystallogr.*, **20**, 703 (1966).
14) T. D. Sakore, H. M. Sobbell, and F. Mazza, *J. Mol. Biol.*, **34**, 385 (1969).
15) The symbols d and c are defined in Table 7.
16) Von L. Born, *Acta Crystallogr.*, **B25**, 1460 (1969).
17) C. Nagata and A. Imamura, *Kagaku*, **24**, 13 (1969).
18) E. Shefter and K. N. Trueblood, *Acta Crystallogr.*, **18**, 1067 (1965).
19) E. Shefter, M. Barlow, R. A. Sparks, and K. N. Trueblood, *ibid.*, **B25**, 895 (1969).
20) K. N. Trueblood, P. Horn, and V. Luzzati, *ibid.*, **14**, 965 (1961).

The Syntheses of 1,3-Oxathiolan-5-one Derivatives

Sadayoshi SATSUMABAYASHI, Shuichi IRIOKA, Hiroshi KUDO,
Kozo TSUJIMOTO, and Shinichi MOTOKI
Department of Chemistry, Science University of Tokyo, Kagurazaka 1-3, Shinjuku-ku, Tokyo
(Received September 17, 1971)

The condensations of aldehydes with thioglycollic acid or α-mercaptopropionic acid were carried out; 2-substituted- or 2,4-disubstituted-1,3-oxathiolan-5-ones were thus obtained. The intermediate of the reaction was isolated only when phenylglyoxal and thioglycollic aicd were used.

We can expect to obtain the 1,3-oxathiolan-5-one derivative by the reaction of α-mercapto acid with aldehyde. However, this heterocyclic system has rarely appeared in the literature except for the 2-trihalomethyl-[1,2] and 2,4,4-triaryl-derivatives.[3-5] In this paper, the syntheses of several 1,3-oxathiolan-5-one derivatives (III) and related compounds will be described.

Acetaldehyde (Ia), propionaldehyde (Ib), and butyraldehyde (Ic) were used as the aliphatic aldehydes and were allowed to react with thioglycollic acid (IIa). The reactions were first carried out in refluxing benzene with an azeotropic removal of the water eliminated in the reaction (Method A). The products thus obtained are presented in Table 1. The results of elementary analyses and the NMR spectra were well in accord with the expected structures. When acetic anhydride was used as the dehydrating agent at 60°C, the product, III, was contaminated with diacetoxyalkane and the separation of the two compounds was almost impossible.

$$\underset{\text{(I)}}{RCHO} + \underset{\text{(IIa)}}{HSCH_2COOH} \longrightarrow \underset{\text{(III)}}{RCH\begin{cases} S-CH_2 \\ | \\ O-CO \end{cases}}$$

The III compounds were also obtained by stirring I and IIa at room temperature without any solvent or dehydrating agent, followed by direct distillation (Method B). As may be seen in Table 1, the yields of the products were here somewhat higher than those given by Method A.

The condensation of IIa with benzaldehyde (Id), *p*-nitrobenzaldehyde (Ie), or *p*-tolualdehyde (If) by Method B was unsuccessful. That is, the bisthioglycollic acid derivative (IV), a condensation product of one mole of I and two of IIa, was thus formed in a nearly quantitative yield. When Method A was adopted, large quantities of the starting materials were recovered, while III was obtained in only about a 15% yield. Therefore, *p*-toluenesulfonic acid was used as the catalyst and the reaction was carried out in refluxing benzene (Method C). Both III and IV were formed in about 30% yields (Table 2).

$$I + IIa \longrightarrow III + \underset{\text{(IV)}}{RCH\begin{cases} SCH_2COOH \\ SCH_2COOH \end{cases}}$$

Since Compound V was considered as an intermediate in the reaction, the isolation of V was attempted.

TABLE 1. $RCHO + HSCH_2COOH \longrightarrow RCH\begin{cases} S-CH_2 \\ | \\ O-CO \end{cases}$ (I) (IIa) (III)

Aldehyde	R	Method	Product (1,3-oxathiolan-5-one)	Yield (%)	Bp (°C/mmHg)
Ia	CH_3	A B	IIIa: 2-methyl-	20.5 36.5	71—73/6
Ib	C_2H_5	A B	IIIb: 2-ethyl-	42.3 43.8	74—75/5
Ic	C_3H_7	A B	IIIc: 2-propyl-	49.3 53.8	90—92/5

	NMR spectral data[a]			Anal (%) Calcd C	H	S	Found C	H	S
IIIa	5.66 (q, 1H)	3.76 (s, 2H)	1.68 (d, 3H)	40.68	5.12	27.10	40.40	5.33	26.88
IIIb	5.48 (t, 1H) 1.03 (t, 3H)	3.68 (s, 2H)	2.23—1.67 (m, 2H)	45.45	6.10	24.22	45.28	6.14	24.30
IIIc	5.55 (t, 1H) 1.00 (t, 3H)	3.68 (s, 2H)	2.13—1.19 (m, 4H)	49.31	6.90	21.90	49.10	7.17	21.72

a) Parts per million downfield from tetramethylsilane; s=singlet, d=doublet, t=triplet, q=quartet, m=multiplet.

1) A. Luttringhaus and H. Prinzbach, *Ann. Chem.*, **624**, 79 (1959).
2) H. E. Simmons and D. W. Wiley, *J. Amer. Chem. Soc.*, **82**, 2288 (1960).
3) A. Bistrzycki and B. Brenken, *Helv. Chim. Acta*, **3**, 447 (1920).
4) A. Romo de Vivar and J. Romo, *J. Org. Chem.*, **24**, 1490 (1959).
5) C. Pedersen, *Acta Chem. Scand.*, **20**, 2314 (1966).

TABLE 2. $RCHO + HSCH_2COOH \longrightarrow RCH(S-CH_2)(O-CO)$ (III) + $RCH(SCH_2COOH)_2$ (IV)

(I) (IIa)

Aldehyde	R	Method	Product	Yield (%)	Mp (°C)
Id	C_6H_5	A	IIId	16.8	57—58
		C	IIId+IVd	31.3+36.5	
Ie	p-NO_2-C_6H_4	A	IIIe	13.8	85
		C	IIIe+IVe	22.5+47.6	
If	p-CH_3-C_6H_4	A	IIIf	19.1	99—100
		C	IIIf+IVf	36.1+32.8	

Product (1,3-oxathiolan-5-one)	NMR spectral data[a]			Anal (%) Calcd C	H	S	Found C	H	S
IIId: 2-phenyl-	7.33 (s, 5H)	6.34 (s, 1H)	3.65 (s, 2H)	60.00	4.48	17.77	59.71	4.70	18.01
IIIe: 2-p-nitrophenyl-	8.30 (d, 2H) 3.86 (s, 2H)	7.62 (d, 2H)	6.55 (s, 1H)	48.01	3.13	14.23	48.00	3.13	14.45
IIIf: 2-p-methylphenyl-	7.37 (d, 2H) 3.78 (s, 2H)	7.16 (d, 2H) 2.36 (s, 3H)	6.44 (s, 1H)	61.85	5.19	16.48	62.01	5.48	16.33

a) Parts per million downfield from tetramethylsilane in $CDCl_3$; s=singlet, d=doublet.

TABLE 3. $RCHO + HSCH(CH_3)-COOH \longrightarrow RCH(S-CH(CH_3)-)(O-CO)$ (VI)

(I) (IIb)

Aldehyde	R	Method	Product (1,3-oxathiolan-5-one)	Yield (%)	Bp (°C/mmHg)
Ia	CH_3	B	VIa: 2,4-dimethyl-	30.9	59—60/3
Ib	C_2H_5	B	VIb: 2-ethyl-4-methyl-	33.9	68—69/3
Ic	C_3H_7	B	VIc: 2-propyl-4-methyl-	55.7	84—86/3

	NMR spectral data			Anal (%) Calcd C	H	S	Found C	H	S
VIa	5.58 (q, 1H) 1.51 (d, 3H)	4.10 (q, 1H)	1.65 (d, 3H)	45.45	6.10	24.22	45.21	6.38	24.46
VIb	5.43 (t, 1H) 1.49 (d, 3H)	4.05 (q, 1H) 1.01 (t, 3H)	2.17—1.67 (m, 2H)	49.31	6.90	21.89	49.23	7.16	21.70
VIc	5.47 (t, 1H) 1.48 (d, 3H)	4.03 (q, 1H) 0.97 (t, 3H)	2.15—1.20 (m, 4H)	52.49	7.55	19.98	52.55	7.81	20.23

In all cases involving the above aldehyde, however, this attempt failed. However, phenylglyoxal (Ig) reacted readily with IIa to give (1-hydroxyphenacyl)-thioacetic acid (V, R=C_6H_5CO), which was then converted to IIIg by means of dehydration with acetic anhydride at room temperature:

$RCH(SCH_2COOH)(OH)$ (V)

The reaction of aliphatic aldehyde with α-mercapto-propionic acid (IIb) was also examined (Method B); the corresponding 4-methyl-1,3-oxathiolan-5-one derivatives (VI) were thus obtained (Table 3).

The above reaction was then applied to the synthesis of the 1,3-oxathian-6-one derivative (VIII) from β-mercaptopropionic acid (IIc) and aldehyde. The hetero-ring VIII has not been reported in the literature. Although VIII was not obtained by the reaction of IIc with Ia—f, it *was* obtained when Ig or chloral (Ih) was used as the aldehyde. In both cases, the intermediates (VII) were isolated in high yields.

$RCHO + HSCH_2CH_2COOH \longrightarrow$

(I) (IIc)

$RCH(OH)-SCH_2CH_2COOH \longrightarrow RCH(S-CH_2)(O-CO)CH_2$

(VII) (VIII)

Experimental

Method A. Into a solution of 0.2 mol of aldehyde (I) and 100 m*l* of benzene, 0.1 mol of thioglycollic acid (IIa)

was added, and then the mixture was stirred for 2 hr at room temperature. The mixture was then refluxed for about 5 hr, the water formed in the reaction being removed continuously by azeotropic distillation. The reaction mixture was washed with a 10% sodium carbonate aqueous solution. Distillation gave the products shown in Table 1.

Method B. Into 0.1 mol of I, 0.1 mol of IIa was added slowly and stirred for 7 hr at room temperature. When the mixture was then distilled, a fraction boiling at 60—110°C/5 mmHg was collected. The distillate was washed with a sodium carbonate solution and then redistilled.

The reaction of α-mercaptopropionic acid (IIb) with aldehyde was carried out in the same manner. The results are shown in Table 3.

Method C. A mixture of 0.2 mol of I, 0.1 mol of IIa, about 0.1 g of *p*-toluenesulfonic acid, and 100 m*l* of benzene was refluxed for about 10 hr, cooled, and washed with a sodium carbonate solution. The benzene was then removed, and the residue was recrystallized from *n*-hexane to give III.

By the acidification of the alkaline solution with hydrochloric acid, IV was precipitated. As IV consists entirely of known compounds,[6] they were confirmed, by studying their melting points and neutralization equivalents to be benzylidenebisthioglycollic acid (IVd) (mp 124°C), *p*-nitrobenzylidenebisthioglycollic acid (IVe) (mp 160—161°C), and *p*-methylbenzylidenebisthioglycollic acid (IVf) (mp 123—125°C). The results are summarized in Table 2.

(1-Hydroxyphenacyl)thioacetic acid (V). To a solution of 0.1 mol of phenylglyoxal (Ig) in 50 m*l* of benzene, 0.1 mol of IIa was added, after with the mixture was stirred for 2 hr at room temperature. The product thus precipitated was collected by filtration and recrystallized from toluene to give V; yield, 81.0%; mp 121°C. Found: C, 52.86; H, 4.31; S, 14.28%; mol wt (neutralization equivalent), 230.4. Calcd for $C_{10}H_{10}O_4S$: C, 53.10; H, 4.46; S, 14.15%; mol wt, 226.2.

2-Benzoyl-1,3-oxathiolan-5-one (IIIg). A solution of 0.05 mol of V, 0.15 mol of acetic anhydride, and 200 m*l* of benzene was stirred at room temperature until the white solid disappeared. When the benzene was then removed under reduced pressure, the residue was poured into a 10% sodium carbonate solution. The product thus precipitated was collected by filtration and recrystallized from ligroin; yield, 58.3%; mp 93—94°C. Found: C, 57.83; H, 3.84; S, 15.33%. Calcd for $C_{10}H_8O_3S$: C, 57.69; H, 3.87; S, 15.37%.

3-(1-Hydroxyphenacyl)thiopropionic Acid (VIIa) and 3-(1-Hydroxy-2,2,2-trichloroethyl)thiopropionic Acid (VIIb). As in the preparation of V, 19.8 g (or 21.4 g) of VIIa (or VIIb) were obtained from 0.1 mol of phenylglyoxal (Ig) (or chloral (Ih)) and 0.1 mol of β-mercaptopropionic acid (IIc). VIIa: yield, 82.5%; mp 107—108°C (recrystallized from toluene). Found: C, 55.23; H, 5.01; S, 13.26%; mol wt (neutralization equivalent), 225.7. Calcd for $C_{11}H_{12}O_4S$: C, 55.00; H, 5.04; S, 13.32%; mol wt, 240.2. VIIb: yield, 84.5%; mp 82—83°C (from ligroin). Found: C, 23.65; H, 2.91; S, 12.88; Cl, 42.08%; mol wt, 245.7. Calcd for $C_5H_7O_3SCl_3$: C, 23.69; H, 2.78; S, 12.65; Cl, 41.95%; mol wt, 253.5.

2-Benzoyl-1,3-oxathian-6-one (VIIIa) and 2-Trichloromethyl-1,3-oxathian-6-one (VIIIb). As in the preparation of IIIg, VIIIa (or VIIIb) was obtained from VIIa (or VIIb). VIIIa: yield, 59.6%; mp 86—87°C (from ligroin). Found: C, 59.27; H, 4.55; S, 14.21%. Calcd for $C_{11}H_{10}O_3S$: 59.46; H, 4.54; S, 14.40%. VIIIb: yield, 48.5%; mp 69—70°C (from hexane). Found: C, 25.58; H, 2.36; S, 13.71; Cl, 44.88%. Calcd for $C_5H_5O_2SCl_3$: C, 25.50; H, 2.14; S, 13.61; Cl, 45.16%.

The authors wish to thank Professor Yojiro Tsuzuki for his helpful advice and encouragement.

6) J. Bongartz, *Ber.*, **21**, 478 (1888).

Asymmetric Reactions. VII. Stereoselectivities in Phenyllithium and Grignard Reactions with Tetrahydrofurfural Derivatives

Juji YOSHIMURA, Yoshiaki OHGO, Katsumi AJISAKA,[1a] and Yaeko KONDA[1b]

Laboratory of Chemistry for Natural Products, Faculty of Science, Tokyo Institute of Technology, Meguro-ku, Tokyo

(Received October 5, 1971)

Stereoselectivities in the phenyllithium and phenylmagnesium bromide reactions with tetrahydrofurfural (**1**), its diacetate (**2**) and 5,5-dimethyl-(*S*)-tetrahydrofurfural (**3**) were examined, in order to clarify the cause of anomalous stereoselectivity of Grignard reactions with *N*-substituted 2,3-*O*-isopropylidene-D-glyceraldimine and the carbonyl analogue(giving *erythro* product predominantly). The presumption that the anomalous stereoselectivity might be caused by coordination ability of magnesium to C_3-oxygen, together with C_1-oxygen or C_1-nitrogen, and C_2-oxygen, was solidified from the present results that no stereoselectivity difference was observed between both reactions with substrates having no C_3-oxygen. Detailed discussion on the stereoselectivity differences between substrates was also made.

The authors have previously reported on the stereoselectivity difference between Grignard and phenyllithium reactions with 2,3-*O*-isopropylidene-D-glyceraldimines, and related compounds, and the difference was explained by assuming that the presence or absence of a coordinative interaction between C_3-oxygen and metal atoms in Grignard or phenyllithium reaction, respectively.[2-4]

In this paper, the presumption was solidified by comparison of the stereoselectivities of tetrahydrofurfural (**1**), its diacetate (**2**), and 5,5-dimethyl-(*S*)-tetrahydrofurfural (**3**) with the previous results.

Results

Synthesis of 5,5-Dimethyl-(S)-tetrahydrofurfural. At first, the synthesis was attempted by process shown in Scheme 1, starting from 2,3-*O*-isopropylidene-5-*O*-benzyl-D-ribonolactone (**6**).[5] Methylation of **6** by methylmagnesium iodide gave the corresponding dimethylated product (**7**) in a good yield. The ring-closure of **7** was attained by heating with anhydrous orthophosphoric acid to give 1,1-dimethyl-1,4-anhydro-2,3-*O*-isopropylidene-D-ribitol (**8**) and its deacetonated derivative (**9**) which was benzoylated for identification to give a monobenzoate with mp 94—96°C. Among two possible structures, it was shown to be 3-*O*-benzoate (**10**) by NMR spectrum (Fig. 1). The doublet at 7.55 τ (J=6.3 Hz) and the triplet at 5.93 τ were assigned to the hydroxyl proton and C_2-proton, respectively, because they changed to a singlet and a doublet (J=6.3 Hz) by addition of a few drop of trifluoroacetic acid. Consequently, other proton signals were easily determined from the coupling constants. Treatment of **9** with thiocarbonylimidazole gave the corresponding

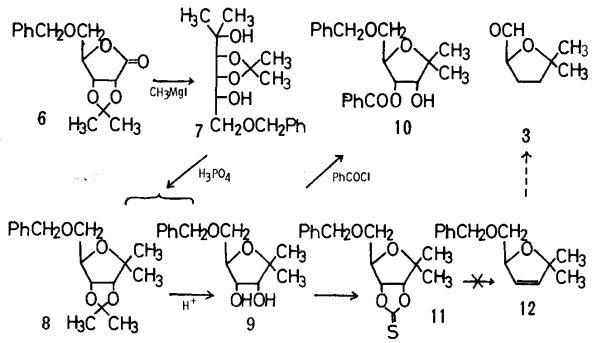

Scheme 1.

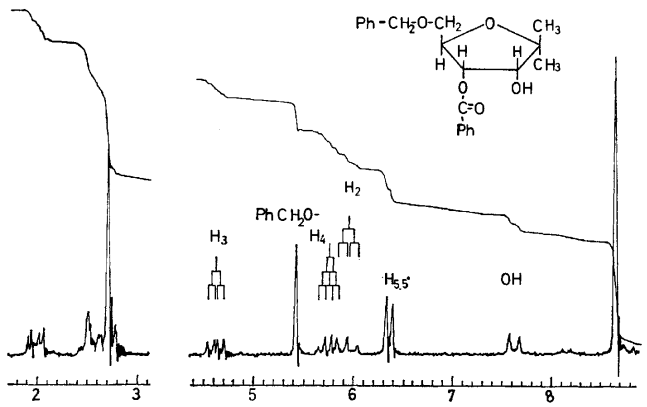

Fig. 1. NMR spectrum of **10** in $CDCl_3$ (τ).

2,3-*O*-thiocarbonate (**11**), however, several trials for elimination of thiocarbonic acid from **11** by refluxing with trimethylphosphite[6] in order to obtain the corresponding unsaturated compound (**12**) gave unsuccessful results.

The successful synthesis of **3** was accomplished by another process shown in Scheme 2, starting from 2,3-*O*-isopropylidene-D-glyceraldehyde. It was converted to ethyl 4,5-*O*-isopropylidene-(4*S*), 5-dihydroxypentenoate-2 (**13**) by Wittig reaction,[7] which was then hydrogenated to the corresponding saturated ester (**14**).

1) a) Present address: Central Reseach Laboratories, Ajinomoto Co., Inc., Kawasaki-shi. b) Present address: School of Pharmacy, Kitasato University, Minato-ku, Tokyo.

2) J. Yoshimura, Y, Ohgo, and T. Sato, *J. Amer. Chem. Soc.*, **86**, 3858 (1964).

3) Y. Ohgo, J. Yoshimura, and T. Sato, This Bullletin **42**, 728 (1969).

4) Y. Ohgo, J. Yoshimura, M. Kono, and T. Sato, *idid.* **42**, 2957 (1969).

5) J. Baddiley, J. G. Buchanan, and F. E. Hardy, *J. Chem. Soc.*, 1961, 2180.

6) E. J. Corey and R. A. E. Winter, *J. Amer. Chem. Soc.*, **85**, 2667 (1965); A. H. Hains, *Carbohydrate Res.*, **1**, 214 (1965); S. D. Horton and W. N. Turner, *ibid.*, **1**, 444 (1966).

7) H. J. Bestmann and O. Kratzer, *Chem. Ber.*, **95**, 1894 (1962).

Treatment of **14** with an excess amount of methylmagnesium iodide gave 1,2-*O*-isopropylidene-5-methyl-1,(2*S*),5-trihydroxy-*n*-hexane (**15**) which was deacetonated with Amberlite IR-120 to **16**. Treatment of **16** with 85% phosphoric acid[8] gave an anhydride with bp 74—75.5°C/15 mmHg. Both five and six-membered ring structures are possible for the anhydride, however, it was confirmed to be 5,5-dimethyl-(*S*)-tetrahydrofurfuryl alcohol (**17**) by the facts that the chemical shifts of CH_2OH and H_2, and splitting patterns of signals in NMR spectra (Fig. 2) are closely similar to those of tetrahydrofurfuryl alcohol,[9] and that the oxidation of it gave an aldehyde. The oxidation product of 5-*O*-chloroformyl derivative of **17** by dimethyl sulfoxide showed an characteristic absorption of aldehyde at 1715 cm^{-1} in IR spectrum, and a signal of it at 0.4 τ (d, J=1.8 Hz) in the NMR spectrum. The elemental analysis of its 2,4-dinitrophenylhydrazone derivative agreed with theoreticals.

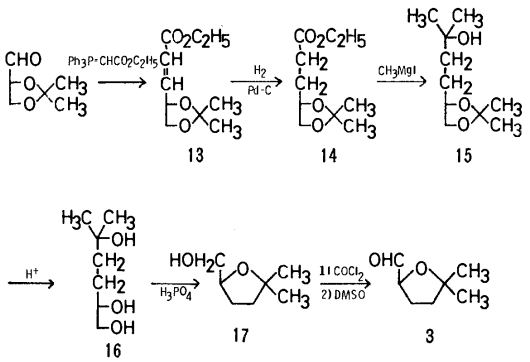

Scheme 2.

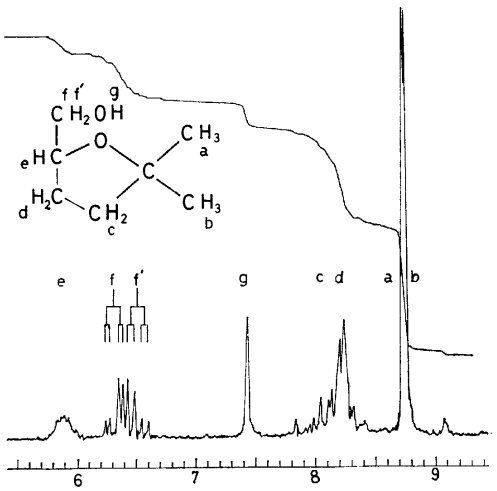

Fig. 2. NMR spectrum of **17** in $CDCl_3$.

Stereoselectivities in the Phenyllithium and Grignard Reactions with Substrates 1, 2, and 3. Substrates **1** and **2** prepared by the method of Scheibler *et al.*,[10] or **3** were treated with an excess amount of phenyllithium or phenylmagnesium bromide by the procedure mentioned in a previous paper.[4] In the case of **1** and **2**, the reaction product was distilled at 80—99°C/0.3 mmHg or purified by column chromatography on silica gel C-100 column, respectively, whose analytical values agreed with those calculated for 2-(hydroxybenyl)tetrahydrofuran (**4**). Although *threo* and *erythro* isomers in **4** could not be isolated, the ratio of them was estimated by glpc and NMR techniques.

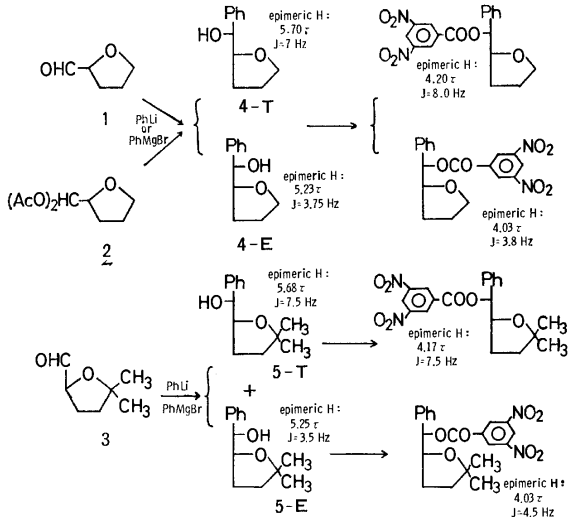

Scheme 3.

Table 1. Diastereomer ratios produced by the reactions of tetrahydrofurfural derivatives with phenyllithium or phenylmagnesium bromide

Substrate	PhLi Product threo : erthro (%)		PhMgBr Product threo : erythro (%)		
1	72.5[a]	27.5[b]	70[a]	30[b]	A
	72.7[a]	27.3[b]	70.5[a]	29.5[b]	B
2	66[a]	34[b]	66[a]	34[b]	C
3	57[c]	43[d]	57.4[c]	42.6[d]	
	(58	42)	(58.7	41.3)	
			58.9[c]	41.1[d]	
			(62	38)	

The diastereomeric ratios except for those in parentheses were estimated by glpc with 20% PEG-6000-Chromosorb AW column, and those in parentheses were estimated from NMR peak areas of epimeric H_1-signals.

A: Fraction 2 of distillates with bp 85—99°C/0.28—0.3 mmHg (PhLi reaction) or with bp 80—99°C/0.28—0.3 mmHg (PhMgBr reaction).

B: Fraction 2′ with bp 99°C/0.3 mmHg which was interceptedly taken. Analytical values of these fractions agreed with those of expected products (see experimental part).

C: The results shwon are of crude products, and the sample purified by silica gel C-100 column chromatography gave analytical values agreed with those of the expected product (see experimental part.)

a) Faster fraction with retention time 633 sec on glpc.

b) Slower fraction with retention time 689 sec on glpc.

c) Faster fraction with retention time 528 sec on glpc.

d) Slower fraction with retention time 556 sec on glpc.

8) J. Colonge and G. Clerc, *Bull. Soc. Chim. Fr.*, **835** (1955).

9) The NMR spectrum of tetrahydrofurfuryl alcohol was taken for comparison with that of 5,5-dimethyl-(S)-tetrahydrofurfuryl alcohol: 5.92 τ (m, H_2); 6.28 τ (q, $J_{HH'}$=12 Hz, J_{HH_2}=4Hz——CH of hydroxymethyl); 6.475 τ (q, $J_{HH'}$=12Hz; $J_{H'H_2}$=6Hz——CH′ of hydroxymethyl).

10) H. Scheibler, F. Sotsckeik, and H. Friese, *Ber.*, **57**, 1443 (1924).

Table 2. Comparison of stereoselectivities in organometallic reactions with several aldehydes and aldimine

	Substrate						
	HC=O	$HC(OAc)_2$	HC=O 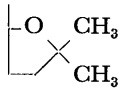	HC=O 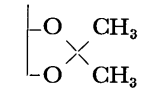		$HC=NCH_2Ph$ 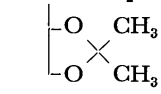	HC=O 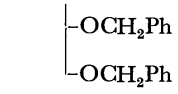
	B	B	B	A[a]	B[b]	A	A
T/E(PhLi)	3.5	1.94	1.33	1.7	1.8	1.7	1.66
T/E(PhMgBr)	2.8	1.94	1.35	0.9	1.1	0.28	1.56
R_{Li}/R_{Mg}	1.25	1.0	0.99	1.8	1.6	6.0	1.06

A: By optical rotation.
B: By gas-liquid partition chromatography using 20% PEG-6000-Chromosorb AW.
a) This Bulletin, **42**, 2957 (1969).
b) Stereoselectivities were reexamined by glpc analysis; NMR analysis gave the same results; signals of the proton attached to carbinol carbon in *erythro* and *threo* isomer appear at 5.2τ (d, J=5 Hz) and 5.5τ (d, J=8 Hz) respectively. The ratio was given by the intergrals of peak areas.
T/E(PhLi): The ratio of *threo* to *erythro* in the PhLi reaction. T/E(PhMgBr): The same ratio in the PhMgBr reaction.
R_{Li}/R_{Mg}: The ratio of T/E(PhLi) to T/E(PhMgBr).

The glpc showed two peaks, of which the amount of faster fraction was larger than that of slower in both the products in organometallic reactions. The NMR spectrum showed two sets of doublet at 5.23 τ (J=3.8 Hz) and 5.70 τ (J=7 Hz), due to epimeric hydrogen attached to carbinol carbon. 3,5-Dinitrobenzoate of **4**, which could not also be isolated, showed the corresponding signals in lower field; at 4.03 τ (J=3.8 Hz) and 4.2 τ (J=8 Hz). It is known that the *erythro* isomers in analogous compounds give a smaller coupling constant than that of *threo* isomers,[4,11-13] and therefore, both the doublets mentioned are assigned to that of *erythro* and *threo* isomers, respectively. These results were presented in Scheme 3 with one presentative structural formula.

In the case of **3**, the product was distilled at 158—160°C/21 mmHg, which showed analytical values consisted with that of 2-(hydroxybenzyl)-5,5-dimethyltetrahydrofuren (**5**). The glpc and NMR analyses of the diastereomeric mixture and the corresponding 3,5-dinitrobenzoate showed the similar results to those in the cases of substrates **1** and **2**, and moreover, two diastereomers of **5** were successfully separated by column chromatography on silica gel C-100 column. Consequently, the relative configurations of the major and the minor products were concluded to be *threo* and *erythro*, respectively.

The diastereomeric ratios in **4** and **5** measured by methods mentioned above were summarized in Tables 1 and 2. These results indicate that there are no substantial differences in stereoselectivities between phenyllithium and phenylmagnesium bromide reactions with **1**, **2**, or **3**. This fact gave a positive support to our previous assumption that Grignard reagents have a coordinative interaction with C_3-oxygen of substrates, but phenyllithium cannot have such an interaction in the transition state of the reaction.

Discussion

For comparison, stereoselectivities of organometallic reactions with *N*-substituted 2,3-*O*-isopropylidene-D-glyceraldimine, its carbonyl analogue and related aldehydes were summarized in Table 2. R_{Li}/R_{Mg} is regarded as an indicator of stereoselectivity difference between phenyllithium and phenylmagnesium bromide reactions. As already pointed out,[4] stereoselectivity difference between phenyllithium and Grignard reactions is brought about when C_3-*O* (or C_β-*O*) of a substrate is sterically fixed at a certain position. The stereoselectivity of phenyllithium reaction should be explained by Cram's model.[14] On the other hand, anomalous stereoselecitvity of the Grignard reactions with aldehydes and aldimines having 2,3-dioxolane ring was explained by assuming that dimeric Grignard species (or two monomeric species) could coordinate to C_3-*O* together with C_2-*O* and imino nitrogen or carbonyl oxygen.[2-4] The validity of the assumption was solidified by the present results that there was no substantial difference in stereoselectivity between phenyllithium and phenylmagnesium bromide reactions with substrate **1**, **2**, and **3** in which C_3-*O* of 2,3-*O*-isopropylidene-D-glyceraldehyde was substituted with methylene group.

However, there still exist questions why there is not so large difference in stereoselectivity between Grignard and phenyllithium reactions with 2,3-*O*-isopropylidene-D-glyceraldehyde[4] as those in the case of *N*-substituted 2,3-*O*-isopropylidene-D-glyceraldimines which are nitrogen analogues of the former and why the reaction with tetrahydrofurfural has higher stereoselectivity than that with 5,5-dimethyltetrahydrofurfural. This can be explained mainly in terms of dual directionality of lone pair orbitals of carbonyl oxygen as follows. As seen from comparison of stereoselectivities with substrate **1** and **3**, stereoselectivity is influenced by existence of methyl on C_5; the methyl group decreases stereoselectivity in either phenyllithium or Grignard reaction. This seems to be concerned with increased difficulty of

11) M. H. Delton and G. U. Yuen, *J. Org. Chem.*, **33**, 2473 (1968).
12) D. Horton and J. M. J. Tronchet, *Carbohyd. Res.*, **2**, 315 (1966).
13) D. Horton, J. B. Hughes, and J. K. Thomson, *J. Org. Chem.*, **33**, 728 (1968).
14) D. J. Cram and K. R. Kopecky, *J. Amer. Chem. Soc.*, **81**, 2737 (1959).

bridged coordination between carbonyl and ring oxygen. Lone pair electron orbitals of carbonyl oxygen extend to two directions (C_2-*O* side and aldehydic *H* side) to which organometallics can coordinate. In the case of 2,3-*O*-isopropylidene-D-glyceraldehyde or 5,5-dimethyltetrahydrofurfural, metal may not necessarily make coordinative bridge between carbonyl oxygen and C_2-*O*, because of steric hindrance of methyl group. Both chelated and non-chelated coordination states, **A**

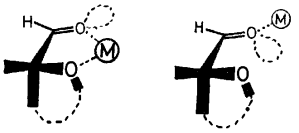

(A) (B)

and **B**, may exist in the transition states. Consequently, reaction may occur from both states and proportion of these two states will depend on the balance of the energy saved by the chelation and repulsion by methyl groups. Increase of non-chelated coordination state in the equillibrium is considered to cause lower stereoselectivity and also smaller difference in stereoselectivity between Grignard and phenyllithium reactions.

It can also be understood that both phenyllithium and Grignard reactions with tetrahydrofurfural have higher stereoselectivity than those with its 5,5-dimethyl derivative, because the substrate has no methyl group and therefore the chelated coordination state would be favored in the equillibrium; rigidity of the bridged coordination and proximity of asymmetry to the reaction center may afford higher stereoselectivity.

On the other hand, imino compounds have alkyl substituent on the nitrogen and the alkyl may be oriented to the sterically less-hindered hydrogen side so that the lone pair electron orbital is oriented to the C_2-*O* side and then dimeric organomagnesium compound may be compelled to form a bridged coordination between C=N, C_2-*O* and C_3-*O*, in spite of the repulsion by isopropylidene group. This allows to explain the unique reversal of stereoselectivity with change from phenyllithium to phenylmagnesium bromide reaction.

Experimental

The NMR spectra were taken with a JNM-4H-100 Spectrometer (Japan Electron Optics Laboratory Co., Ltd.) at 100 MHz in a deuteriochloroform or carbon tetrachloride solution, using tetramethylsilane as an internal standard. The IR spectra were recorded with a Hitachi Model EPI-G2 grating IR spectrophotometer. The optical rotations were measured with a Carl-Zeiss Photoelectric Precision Polarimeter (0.005°). The gas-liquid partition chromatographic analyses were performed with a Hitachi Model K-53 gas chromatograph using a column packed with 20%PEG-6000-Chromosorb AW (1 m column in the case of **4**; 2 m column in the case of **5**).

Reaction of Tetrahydrofurfural with Phenylmagnesium Bromide. To an ice-cooled solution of phenylmagnesium bromide prepared from magnesium (1.2 g) and bromobenzene (4.85 m*l*) in ether (50 m*l*) was added an ethereal solution of tetrahydrofurfural (2.1 g) with stirring. The reaction mixture was refluxed with stirring for 1.5 hr, and then poured into ice-water saturated with ammonium chloride. The ether layer was separated and the water layer was extracted with ether. The combined ether layer was washed, successively with *N*-NaOH, water, *N*-H_2SO_4 and water, and dried over anhydrous sodium sulfate, and concentrated to a syrup (3.2 g). The syrup was fractionally distilled;

Fr. 1 50—60°C/0.3 mmHg 0.8 g.
2 80—99°C/0.3 mmHg 2.2 g.
2′ 99°C/0.3 mmHg 0.2 g.

The fraction 2′ was one which was taken interceptedly only at the boiling point of 99°C/0.3 mmHg. The analytical values agreed with 2-(hydroxybenzyl)tetrahydrofuran.

Found: C, 74.49; H, 8.11%. Calcd for $C_{11}H_{14}O_2$: C, 74.13; H, 7.92%.

These fraction were analysed on glpc using 20% PEG-6000-Chromosorb AW (detector: FID, carrier gas: nitrogen with 0.67 kg/cm², oven temperature: 200°C). The results are shown in Table 1.

NMR: 8.1—8.7 τ (multiplet; H_3 and H_4 in tetrahydrofuryl group (THF group)), 6—6.45 τ (multiplet; H_2 and H_5 in THF group), 5.77 τ (singlet; OH), 5.7 τ (doublet, J=7 Hz; epimeric proton-*threo*), 5.23 τ (doublet, J=3.8 Hz; epimeric proton-*erythro*).

To a solution of Fr. 2 (0.3 g) and 3,5-dinitrobenzoyl chloride (0.5 g) in benzene (20 m*l*) was added 1.5 m*l* of pyridine, and the reaction mixture was poured into water after standing overnight and extracted with chloroform. The organic layer was washed successively with sodium carbonate solution, water, dil-HCl solution and water, and then was concentrated *in vacuo* to dryness. The NMR spectrum of the resulting diastereomeric mixture of 3,5-dinitrobenzoate showed two sets of doublet due to epimeric proton at 4.03 τ (J=3.8 Hz) and 4.2 τ (J=8 Hz).

Reaction of Tetrahydrofurfural (1) with Phenyllithium. The reaction was carried out with the same procedure as in the case of the Grignard reaction. The syrup obtained was fractionally distilled;

Fr. 1 50—85°C/0.28—0.3 mmHg
2 85—99°C/0.28—0.3 mmHg 3 g
2′ 99°C/0.3 mmHg 0.4 g

Yield (2+2′): 3.4 g (91%).

Anal. of fraction 2′. Found: C, 74.41; H, 7.67%. Calcd for $C_{11}H_{14}O_2$: C, 74.13; H, 7.92%.

The products were analysed on glpc under the same condition as in the case of Grignard reaction (Table 1).

Reaction of Tetrahydrofurfural Diacetate (2) with Organometallic Reagents. The reactions were carried out of tetrahydrofurfural diacetate (10 g) with phenyllithium prepared from lithium (4.52 g) and bromobenzene (34.4 m*l*) or phenylmagnesium bromide prepared from magnesium (12 g) and bromobenzene (48.5 m*l*) in ether. Thereafter, the reaction mixture was treated as usual method (described above). The reaction products were tried to purify by distillation, but the aimed products were not separated from diphenyl methyl carbinol. The products were purified by column chromatography using silica gel C-100. The adsorbed products mixtures were successively eluted by *n*-hexane, *n*-hexane-benzene, benzene, and benzene-acetone. Each fraction was analysed by glpc. The acetone-benzene fraction contained the addition products; 2-(hydroxybenzyl)tetrahdrofuran. Found: C, 74.10; H, 8.05%. Calcd for $C_{11}H_{14}O_2$: C, 74.13; H, 7.92%.

Reaction of 5,5-Dimethyl-(S)-tetrahydrofurfural with Phenylmagnesium Bromide or Phenyllithium. A solution of 5,5-dimethyl-(*S*)-tetrahydrofurfural (3.2 g) in 10 m*l* of ether was added with stirring at 0—5°C to an ethereal solution of phenylmagnesium bromide prepared from magnesium (1.8 g) and bromobenzene (11.8 g), and the reaction mixture was

refluxed for 2 hr, and then decomposed with 1N-HCl solution. The products were extracted with ether. The ether layer was concentrated *in vacuo* to a syrup. The syrup was distilled at 158—160°C/21 mmHg. Yield: 2.0 g (39%); $[\alpha]_D$+2.85° (*c* 2, ethanol). Found: C, 75.47; H, 9.06%. Calcd for $C_{13}H_{18}O_2$: C, 75.69; H, 8.80%.

A solution of 5,5-dimethyl-(*S*)-tetrahydrofurfural (3.3 g) was reacted with phenyllithium prepared from 1.1g of lithium and 12.5 g of bromobenzene in ether, and the reaction mixture was treated in the same procedure as in the Grignard reaction; bp 155—160°C/20 mmHg, yield: 2.5 g (48%); $[\alpha]_D$+2.54° (*c* 1.5, ethanol). Found: C, 75.63; H, 9.10%. Calcd for $C_{13}H_{18}O_2$: C, 75.69; H, 8.80%.

NMR spectrum of the diastereomeric mixture: 2.77 τ (Ph), 5.25 τ (doublet, J=3.5 Hz; epimeric proton-*erythro*), 5.68 τ (doublet, J=7.5 Hz; epimeric proton-*threo*), 5.8—6.2 τ (multiplet; H_2 in THF group), 6.85 τ (OH), 8.35—8.5 τ (multiplet; H_3 and H_4 in THF group).

The products were analysed on glpc using 20% PEG-6000-Chromosorb AW (Table 1).

The two diastereomers were separated with column chromatography using silica gel C-100 column and *n*-hexane-benzene (10: 1) as the eluting solvent: faster fraction contained *erythro* isomer and slower fraction contained *threo* isomer. The *erythro* isomer has $[\alpha]_D^{24}$ −3.3° (*c* 0.45, ethanol). NMR spectrum: 2.76 τ (Ph), 5.25 τ (doublet, J=3.5 Hz; epimeric proton), 5.8—6.0 τ (multiplet; H_2 in THF group), 7.58 τ (OH), 8.2—8.5 τ (multiplet; H_3 and H_4 in THF group), 8.73 and 8.78 τ (methyl).

Threo isomer has $[\alpha]_D^{24}$+6.7° (*c* 1.3, ethanol). NMR: 2.76 τ (Ph), 5.68 τ (doublet, J=7.5 Hz; epimeric proton), 5.95—6.2 τ (multiplet, H_2 in THF group), 7.7 τ (OH), 8.2—8.5 τ (multiplet; H_3 and H_4 in THF group), 8.73 and 8.78 τ (methyl).

*1,1-Dimethyl-2,3-O-isopropylidene-D-ribitol (**7**).* 5-*O*-Benzyl-2,3-*O*-isopropylidene-D-ribonolactone (116.4 g) was reacted with 6 molar equivalent of methylmagnesium iodide in ether at 0—5°C. The reaction mixture was left standing overnight and poured into 3 *l* of ice-water. The water layer was extracted twice with 1 litre of ether which was washed with water. The combined ether layer was dried over anhydrous sodium sulfate, concentrated to give a syrup which was distilled at bp 162°C/0.005 mmHg. Yield: 100 g (88%). Found: C, 65.42; H, 8.30%. Calcd for $C_{17}H_{26}O_5$: C, 65.78; H, 8.44%.

*1,4-Anhydro-5-O-benzyl-1,1-dimethyl-D-ribitol (**9**).* 50.4 g (0.16 mol) of 1,1-dimethyl-2,3-*O*-isopropylidene-5-*O*-benzyl-D-ribitol was treated with anhydrous orthophosphoric acid (0.12 mol) with stirring at 100°C for 50 min. The reaction mixture was extracted with 600 m*l* of ether, and the ether layer was washed with water, sodium bicarbonate solution and water, successively. The ether layer was concentrated to give a syrup (36 g). The syrup was fractionally distilled:

Fr. 1 119°C/0.007 mmHg 18.8 g.
2 149°C/0.007 mmHg 10.7 g.

Fr. 1 was dissolved in petroleum ether and extracted with a small amount of water. The evaporation of the petroleum layer gave 1,4-anhydro-1,1-dimethyl-2,3-*O*-isopropylidene-5-*O*-benzyl-D-ribitol (14.8 g) which was hydrolysed with 70% acetic acid (50 m*l*) under reflux for 4 hr, and the reaction mixture was extracted with ether. The ether layer was washed with sodium bicarbonate and water, concentrated to give a syrup (12.8 g) which was distilled at 149°C/0.007 mmHg. Found: C, 66.34; H, 8.16%. Calcd for $C_{14}H_{20}O_4$: C, 66.64; H, 7.99%.

*1,4-Anhydro-1,1-dimethyl-3-O-benzoyl-5-O-benzyl-D-ribitol (**10**).* The above distillate (1.2 g) with bp 149°C/0.007 mmHg was treated with benzoyl chloride (1.4 g) and pyridine (1 m*l*) in chloroform at room temperature. The reaction mixture was poured into ice-water and extracted with chloroform. The organic layer was washed with water and concentrated *in vacuo* to give crystals of mp 94—96°C. The product has absorption bands at 3400 cm^{-1} and 1735 cm^{-1} which correspond to OH and ester carbonyl absorptions, respectively. The structure was confirmed by NMR spectrum (Fig. 1).

*1,4-Anhydro-1,1-dimethyl-2,3-O-thiocarbonyl-5-O-benzyl-D-ribitol (**11**).* To a solution of 15.32 g of **9** in acetone (225 m*l*) was added thiocarbonyldiimidazole (16.3 g) and the solution was refluxed for 1 hr under nitrogen atmosphere. The reaction mixture was concentrated to give a syrup containing crystals which was extracted with ether (300 m*l*). The extract was washed with 400 m*l* of water. The water layer was extracted twice with 200 m*l* of ether. The combined ether solution was dried over anhydrous sodium sulfate. The ether layer was filtered and concentrated under reduced pressure to give a syrup (18 g). The syrup was distilled at bp 145—150°C/0.03 mmHg, yield 11.8 g. Found: C, 61.00; H, 6.68%. Calcd for $C_{15}H_{18}O_4S$: C, 61.22; H, 6.12%.

Elimination of thiocarbonyl group of **11**. 11.1 g of **11** was dissolved in 75 m*l* of trimethyl phosphite and refluxed under nitrogen atmosphere for 3 days. To the reaction mixture was added 6N-NaOH solution under powerful stirring till pH 10, and stirring was continued for 2 hr. The mixture was extracted twice with methylene chloride (200 m*l*), washed with water, and concentrated *in vacuo* to give a syrup. The syrup had no absorption in the region of stretching vibration of olefins.

*Ethyl-4,5-O-isopropylidene-(4S),5-dihydroxypentenoate-2 (**13**).* A solution of carboethoxymethylenetriphenylphosphonium bromide (400 g) in 700 m*l* of abs. ethanol was added with cooling and stirring into sodium alcoholate solution prepared from sodium (23 g) and 500 m*l* of abs. ethanol. To the solution was added 118 g of a freshly distilled 2,3-*O*-isopropylidene-D-glyceraldehyde with cooling and stirring. The reaction mixture was stirred for 48 hr at room temperature, and then concentrated. The resulting sodium bromide and triphenylphosphine oxide were filtered off, and the remainder was distilled at 115—117°C/12 mmHg; $[\alpha]_D^{21}$+83.4° (*c* 0.34, ethanol); yield 112 g (60%). Found: C, 60.59; H, 8.12%. Calcd for $C_{10}H_{16}O_4$: C, 59.98; H, 8.05%.

*Ethyl-4,5-O-isopropylidene-(4S),5-dihydroxypentanoate (**14**).* A solution of **13** (14.4 g) in ethanol (50 m*l*) was shaken with hydrogen in the presence of Pd-C (3 g) for 1 hr during which the substrate absorbed 1.75 *l* of hydrogen at room temperature. The catalyst was removed by filtration and the filtrate was concentrated to a syrup which was distilled at 119—120°C/25 mmHg; yield, 14 g (97%); $[\alpha]_D^{21}$ −5° (*c* 0.42, ethanol). Found: C, 59.85; H, 9.02%. Calcd for $C_{10}H_{18}O_4$: C, 59.41; H, 8.91%.

*1,2-O-isopropylidene-5-methyl-1,(2S),5-trihydroxy-n-hexane (**15**).* To a cooled ethereal solution of methylmagnesium iodide prepared from 400 g of methyl iodide and 70 g of magnesium was added dropwise **14** (70 g) with stirring. The mixture was refluxed for 30 min, poured into ice-water containing ammonium chloride, and the resulting solution was extracted with ether. The ether layer was concentrated to a syrup which was distilled at 108—110°C/9 mmHg; yield, 52 g (82%); $[\alpha]_D^{21}$ −2.2° (*c* 0.50, ethanol). Found: C, 63.86; H, 10.80%. Calcd for $C_{10}H_{20}O_3$; C, 63.79; H, 10.71%.

*5-Methyl-1,(2S),5-trihydroxy-n-hexane (**16**).* A solution of **15** (9.4 g) in water (80 m*l*) and ethanol (20 m*l*) was stirred in the presence of Amberlite IR-120[H] (16 g) at room temperature for 2 hr. The solution filtered was treated with activated carbon and concentrated to give a syrup which was distilled at 110—113°C/0.005 mmHg; yield, 6 g (81%);

$[\alpha]_D^{21}-12.5°$ (*c* 1.0, ethanol). Found: C, 56.16; H, 11.14%. Calcd for $C_7H_{16}O_3$: C, 56.73; H, 10.88%.

5,5-Dimethyl-(S)-tetrahydrofurfuryl Alcohol (17). **16** (25.2 g) was heated with 85% orthophosphoric acid with stirring for 40 min. After cooling the reaction mixture was poured into water, and the resulting solution was extracted with ethyl acetate. The ethyl acetate layer was washed with sodium bicarbonate solution and water, and concentrated to a syrup which was distilled at 74—75.5°C/15 mmHg; yield, 15.7 g (71%); $[\alpha]_D^{18}+13.6°$ (*c* 0.6, ethanol). Found: C, 64.29; H, 11.00%. Calcd for $C_7H_{14}O_2$: C, 64.58; H, 10.84%.

5,5-Dimethyl-(S)-tetrahydrofurfural (3). To a cooled ether solution containing phosgen (3.3 g) was added 4 g of **17** under cooling and the solution was left standing for 2 hr at room temperature. The reaction mixture was concentrated to remove ether and phosgen, and the resulting syrup was distilled at 84—85°C/11 mmHg to give the chloroformate quantitatively. To a solution of 5.6 g of the chloroformate in benzene (10 m*l*) was added 5 g of dimethyl sulfoxide and the reaction mixture was stirred with cooling until carbon dioxide evolution ceased. To this solution 16 m*l* of triethylamine was added and the resulting precipitate of triethylamine hydrochloride was removed by filtration. The mixture was purified through Magnesol-Celite (1:3) column to give 5,5-dimethyl-(*S*)-tetrahydrofurfural. Aldehydic proton signal was observed at 0.4 τ (doublet, $J=1.8$ Hz) in the NMR spectrum.

The reaction of the aldehyde with 2,4-dinitrophenylhydrazin gave an yellow precipitate; mp 119°C. Found: C, 51.26; H, 5.07; N, 18.78%. Calcd for $C_{13}H_{16}N_4O_5$: C, 50.64; H, 5.23; N, 18.18%.

NOTES

BULLETIN OF THE CHEMICAL SOCIETY OF JAPAN, VOL. 45, 922—923(1972)

The Catalytic Decomposition of Nitrous Oxide on Titanium Dioxide; Anatase and Rutile

Yoshito ONISHI

Department of Chemistry, Faculty of Industrial Arts, Kyoto Technical University, Matsugasaki, Sakyo-ku, Kyoto

(Received July 18, 1970)

Many investigations have been published on the catalytic reactions on various metallic oxides,[1] but few deal with the correlation between the catalytic activity and crystal form. From the studies on the catalytic oxidation of carbon monoxide on anatase and rutile, it was confirmed that the catalytic action of titanium dioxide differed with its crystal form.[2,3] In order to examine whether the same result is obtained in other reactions, the catalytic decomposition of nitrous oxide on titanium dioxide was carried out.

The catalytic decomposition of nitrous oxide on various metallic oxides[4] have been studied by many investigators, but there are few on titanium dioxide.

Experimental

The catalysts[2] used were anatase (A) of a guaranteed grade obtained from the East Merck Company, and rutile (R) and an anatase-rutile mixture (AR). The latter two were obtained by heating A at 1150°C for 3 hr and at 1050°C for 1 hr, respectively. Polymorphic forms of the three samples were confirmed by means of the X-ray diffraction method. The specific surface areas of the samples A, R, and AR estimated by the B.E.T. method using nitrogen as the adsorbate were 10.3 m^2/g, 1.0 m^2g, and 3.8 m^2/g, respectively. Nitrous oxide, oxygen, and nitrogen supplied from commercial cylinders were purified by vacuum distillation with liquid nitrogen, or by passing through a liquid nitrogen cooled trap.

The apparatus described in the preceding paper[2] was used. All precautions were taken to keep the samples from contamination. Traps were cooled with dry ice during the run to prevent grease and mercury vapors from the sample. Greaseless stop cocks were used between the traps and the sample tube. Prior to the measurements, the catalyst was pretreated in circulating oxygen of about 70 mmHg for 3 hr at 600°C for the cleaning of its surface.

It was ascertained by the analysis of the decomposition products that there are no side reactions to the main reaction, $N_2O \rightarrow N_2 + 1/2O_2$. The rate of the decomposition was determined by measuring the total pressure. It was confirmed that the gas phase decomposition of nitrous oxide was negligible under the experimental conditions.

Results and Discussion

The decomposition rates of nitrous oxide on three samples were measured under pressures 10^{-3}—80 mmHg at 600—800°C. The rates were proportional to P_{N_2O}. A typical result measured on anatase at 700°C is shown in Fig. 1. The decomposition rates did not change even

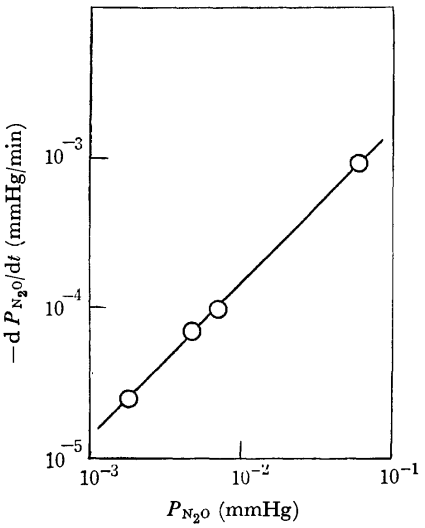

Fig. 1. Effect of N_2O pressure on the decomposition rate.

when oxygen or nitrogen was intentionally introduced into the reaction system. The decomposition rate is thus represented by

$$-d(N_2O)/dt = k_{N_2O} \cdot P_{N_2O} \quad (1)$$

where k_{N_2O} is a constant. The Arrhenius plots of the k_{N_2O} values are given in Fig. 2. The k_{N_2O} value of rutile is much larger than that of anatase at the same temperature, as in the case of oxidation of carbon monoxide. The activation energies of anatase and rutile are 42.3 and 31.0 kcal/mol, respectively. The difference between these values, about 10 kcal/mol, is comparable to the difference in the activation energies of the oxidation of carbon monoxide and that of the thermal desorption of surface oxygen atoms from the catalysts in two crystal forms.[2]

On the catalytic oxidation of carbon monoxide on titanium dioxide,[2] the rate constants k were characteristic for both anatase and rutile, and the k values of the sample AR consisting of particles in both anatase and rutile forms were calculated by assuming that the

1) G. Parravano and M. Boudart, *Advan. Catal.*, **7**, 47 (1955); E. R. S. Winter, *ibid.*, **10**, 196 (1958); F. S. Stone, *ibid.*, **13**, 1 (1962).
2) Y. Onishi and T. Hamamura, This Bulletin, **43**, 996 (1970).
3) Y. Onishi, *ibid.*, **44**, 1460 (1971).
4) G. M. Schwab and H. Schultes, *Z. Physik. Chem.*, **B9**, 265 (1930); C. Wagner, *J. Chem. Phys.*, **18**, 69 (1950); K. Hauffe, *Advan. Catal.*, **7**, 213 (1955); L. Rheaume and G. Parravano, *J. Phys. Chem.*, **63**, 264 (1959); I. Matsuura, Y. Kubokawa, and O. Toyama, *Nippon Kagaku Zasshi*, **81**, 377, 1205 (1960); H. B. Charman, R. M. Dell, and S. S. Teale, *Trans. Faraday Soc.*, **59**, 453 (1963); I. D. Gay and F. C. Tompkins, *Proc. Roy. Soc.*, **293**, 19 (1966); Z. Dzeventski, *Zh. Fiz. Khim.*, **40**, 2309 (1966); *Chem. Abstr.*, **66**, 14303a (1967); K. Tanaka and A. Ozaki, This Bulletin, **40**, 420 (1967); E. R. S. Winter, *J. Catal.*, **15**, 144 (1969).

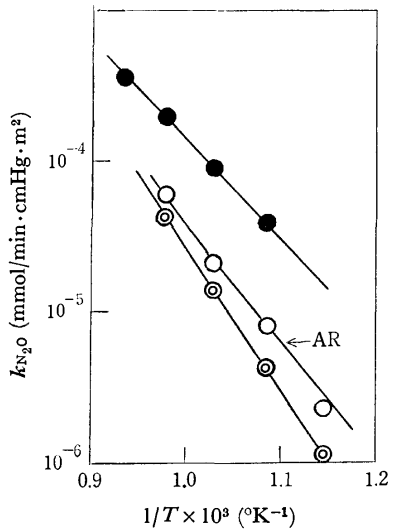

Fig. 2. Effect of temperature on the decomposition rate constant of nitrous oxide.
◎: A, ●: R, ○: AR

catalytic activity of an anatase-type surface and that of a rutile-type surface in AR were equal to those of pure anatase and rutile, respectively. The calculated values agreed well with the experimental values taken at different temperatures. The surface area ratio of the sample AR was estimated to be: anatase/rutile=86.8/13.2. Thus, if we assume that the rate constant k_{N_2O} is characteristic of the crystal form and the surface area ratio of two crystalline surfaces of the sample AR does not change, the rate constants k_{N_2O} of AR can be calculated by using the k_{N_2O} values of samples A and R. The calculated line of k_{N_2O} of the sample AR is shown by curve-AR in Fig. 2 with the experimental values shown by marks ○. The calculated line is in good agreement with the measured values.

It is found from the results that the catalytic action of titanium dioxide for the decomposition of nitrous oxide differs with its crystal form.

The author wishes to thank Prof. Takuya Hamamura, Kyoto Technical University, and Prof. Kumasaburo Kodera, Kyoto University, for their advice and discussions.

BULLETIN OF THE CHEMICAL SOCIETY OF JAPAN, VOL. 45, 923—924(1972)

ESR Spectrum of Bromopyridines Irradiated with Ultraviolet Light. Confirmation of Pyridyl Radical Formation in Irradiated Pyridine and Their Formation Mechanism

Kozo Tsuji and Toshifumi Seiki
Central Research Laboratory, Sumitomo Chemical Co., Ltd. Takatsuki, Osaka

(Received January 21, 1971)

When pyridine was irradiated with electron beams or γ rays, there was observed the three line ESR spectrum with a coupling constant of about 30 gauss at -196°C.[1-5] Although this spectrum was attributed initially to pyridine cation radicals,[1-3] Symons *et al.*[4,5] attributed the spectrum to 2-pyridyl radicals mainly on the basis of observation of a large coupling constant of ^{13}C. The intensity of the ^{13}C signal, however, was not mentioned. The present investigation was carried out in order to confirm this assignment and to discuss about their formation mechanism.

It is well known that carbon-halogen bonds are easily broken homolitically by ultraviolet irradiation. Therefore it is expected that photolysis of halogenated pyridines will produce corresponding pyridyl radicals. Three isomers of bromopyridines were photolized and ESR spectra were recorded.

Experimental

Commercial 2- and 3-bromopyridines were used without further purification. 4-Bromopyridine was received as a hydrochloride and was used as it was. These samples were photolized in an ESR cavity by ultraviolet light from a Xenon short arc lamp (Ushio Electric Inc. UXL-500D) at -196°C. ESR measurements were carried out at -196°C with an X-band ESR spectrometer with 100 Kc field modulation. (Japan Electron Optics Lab. Co., Model JES, 3BS-X)[6]

Results and Discussion

After 2-bromopyridine was photolized at -196°C for 60 min, an ESR spectrum shown in Fig. 1a was observed, which is a three-line spectrum with a coupling constant of about 30 gauss. This spectrum is almost identical with that observed for pyridine irradiated with ionizing radiation.[1-5]

On the other hand 3- and 4-bromopyridines irradiated with ultraviolet light gave apparent singlet spectra with total line widths of about 66 and 60 gauss, respectively, as shown in Figs. 1b and c.

The fact that the triplet spectrum was obtained from only 2-bromopyridine leads to the conclusion that this hyperfine structure is caused by interaction of unpaired

1) K. Tsuji, H. Yoshida, and K. Hayashi, *J. Chem. Phys.*, **45**, 2894 (1966).
2) K. Tsuji, H. Yoshida, and K. Hayashi, *ibid.*, **46**, 2808 (1967).
3) C. David, G. Geuskens, A. Verhasselt, P. Jung, and J. F. M. Oth, *Mol. Phys.*, **11**, 257 (1966).
4) H. J. Bower, J. A. McRae, and M. C. R. Symons, *Chem. Commun.*, **1967**, 542.
5) H. J. Bower, J. A. McRea, and M. C. R. Symons, *J. Chem. Soc., A*, **1968**, 2696.
6) K. Tsuji and T. Seiki, *Polym. Lett.* **7**, 839 (1969).

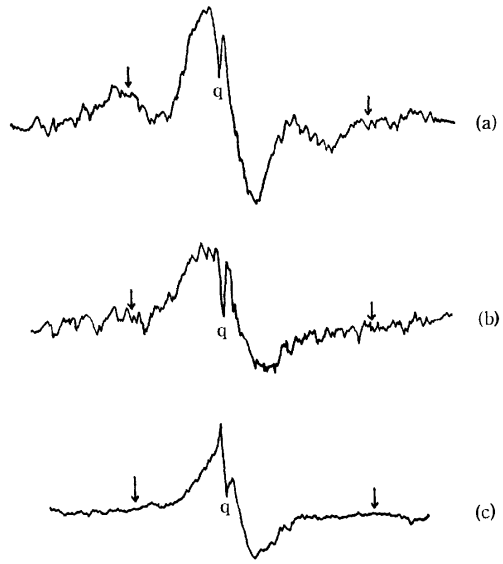

Fig. 1. ESR spectra of bromopyridines irradiated with ultraviolet light at −196°C for an hour.
a) 2-bromopyridine, b) 3-bromopyridine, and c) 4-bromopyridine hydrochloride
Arrow marks represent the positions of Mn^{2+} absorptions. Distance between these two marks is 86.7 gauss.
q represents a quartz signal.

electrons with a nitrogen nucleus, and that the free radicals responsible for the ESR spectrum are 2-pyridyl radicals as expected, although the apparent intensity ratio of the triplet spectrum is not exactly 1 : 1 : 1, probably because of superposition of the spectrum due to the second radicals (II) described in the previous paper.[7] The line widths of the singlet spectra observed for 3- and 4-bromopyridines seem to be reasonable for corresponding pyridyl radicals since a close value is expected for the phenyl radicals[8,9] when the worse resolution of the spectrum is assumed. Therefore it is clear that the 2 pyridyl radical shows the three-line spectrum with a coupling constant of about 30 gauss. Consequently assignment of the ESR spectrum of pyridine irradiated with ionizing radiation at −196°C mainly to the 2-pyridyl radicals is thought to be reasonable.

This pyridyl radical produced in pyridine irradiated with ionizing radiation, however, does not seem to be produced by direct hydrogen atom abstraction from the position-2. The primary process of radiation is ionization of electrons in the nonbonding orbital of the nitrogen nucleus.[1] Cation radicals thus formed could be precursors of the 2-pyridyl radicals, that is consistent with the fact that pyridine hydrochloride[10] and the pyridine complexes with metal salts[7] did not give the pyridyl radicals after γ-irradiation, where lone pair electrons of the nitrogen nucleus are no longer available for ionization. This is also supported by the fact that ultraviolet photolysis of the pyridine-iodine complex with the light corresponding to the charge transfer band of the complex gave the same spectrum even though the intensity is small, since photoexcitation of the complex will produce primarily pyridine cation radicals through the excited state.[2]

Symons *et al.*[5] suggested the 2-pyridyl radicals can be formed by the loss of a proton as follows:

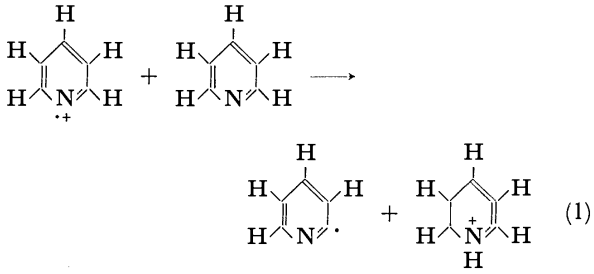

(1)

There is, however, another possibility to produce 2-pyridyl radicals (although they are of protonated form) from pyridine cation radicals, that is, isomerization of pyridine cation radicals.

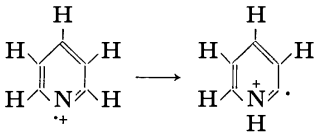

(2)

The protonated pyridyl radical has an extra proton on a nitrogen atom. Although the splitting due to this proton may be expected, the value will be too small to give the splitting in the similar way to the ring proton on position 3.[5] If this is correct, the protonated form can give the similar spectrum to that of unprotonated pyridyl radicals.

These two possible structures of free radicals (protonated- and unprotonated-forms) are quite similar to those of free radicals in irradiated 2-methyltetrahydrofuran.[11]

The protonated form is isoelectric with phenyl radical. Phenyl radicals produced by irradiation seem to be unstable even at −196°C since the ESR spectrum due to phenyl radicals was hardly observed at −196°C in benzene irradiated with ionizing radiation, although their formation is expected as donors of hydrogen atoms to form cyclohexadienyl radicals.[12] The situation is the same for protonated pyridyl radicals in irradiated pyridinium ions.[10] Therefore protonated form might be less stable than unprotonated one. The same conclusion could be drawn by comparison of resonance energies of pyridine (43 kcal/mol) and benzene (40 kcal/mol). Therefore according to this stability consideration, the reaction (1) might be predominant for the mechanism of pyridyl radical formation.

The authors wish to express their gratitude to Drs. S. Kodama, T. Nishikida, A. Segawa, and Y. Kubota for their kind guidance and encouragement. Thanks are also due to Dr. T. Takeshita for his helpful discussion.

7) K. Tsuji, S. Tazuke, K. Hayashi, and S. Okamura, *J. Phys. Chem.*, **73**, 2345 (1969).
8) J. A. Pople, D. L. Beveridge, and P. A. Dobosh, *J. Am. Chem. Soc.*, **90**, 4201 (1968).
9) J. E. Bennett, B. Mile, and A. Thomas, *Proc. Roy. Soc., Ser., A*, 246 (1966).
10) H. J. Bower, J. A. McRae, and M. C. R. Symons, *J. Chem. Soc., A*, **1968**, 1918.
11) D. R. Smith and J. J. Pieroni, *Can. J. Chem.*, **43**, 876 (1965).
12) S. Ohnishi, T. Tanei, and I. Nitta, *J. Chem. Phys.*, **37**, 2402 (1962).

BULLETIN OF THE CHEMICAL SOCIETY OF JAPAN, VOL. 45, 925—926(1972)

1,2,3-Benzotriazole Complexes of Palladium(II)

Yoshihisa WATANABE, Take-aki MITSUDO, Masato TANAKA, Kazuo YAMAMOTO, and Yoshinobu TAKEGAMI

Department of Hydrocarbon Chemistry, Faculty of Engineering, Kyoto University, Sakyo-ku, Kyoto

(Received February 19, 1971)

1,2,3-Benzotriazoles are known to decompose thermally and photochemically to give biradicals, with an accompanying evolution of nitrogen.[1] We attempted to prepare 1,2,3-benzotriazole complexes of transition metals[2] and to compare the complexes with free compounds. This note will describe how the reaction of 1*H*-, 1-benzyl-, and 1-vinyl-1,2,3-benzotriazoles with dichlorobis(benzonitrile)palladium(II) and di-π-allyl-μ,μ'-dichlorodipalladium(II) gives benzotriazole complexes of palladium(II). The pyrolysis and the photolysis of these complexes will bediscussed later.

1*H*-1,2,3-Benzotriazole readily reacts with dichlorobis(benzonitrile)palladium(II) in benzene at room temperature to give a yellow complex of the $PdCl_2$(1*H*-1,2,3-benzotriazole)$_2$ type almost quantitatively. The infrared spectrum of this complex has a very strong band at 3200 cm^{-1}, indicating that the >N–H group remains in the complex and that some of the nitrogen atoms in the benzotriazole act as donors. 1-Benzyl- and 1-vinyl-1,2,3-benzotriazoles react similarly with dichlorobis(benzonitrile)palladium(II) to give complexes of the $PdCl_2$(benzotriazole)$_2$ type. These complexes are also formed from palladium(II) chloride and the benzotriazoles in ethanol, but those reactions proceed very slowly.

The benzotriazoles react with di-π-allyl-μ,μ'-dichlorodipalladium(II) in benzene at room temperature to give white or yellow complexes of the (π-allyl)PdCl(benzotriazole) type. The PMR spectra of these complexes indicate that the allyl group gives a signal of the A_2B_2X type in $CDCl_3$ and of the AX_4 type in dimethyl sulfoxide (DMSO-d_6), and that the chemical shifts and the coupling constants of protons of methylene and the vinyl group are similar to those of the free corresponding benzotriazoles. In DMSO-d_6, the PMR spectra of the allyl groups depend on the temperature (20—70°C). Over 40°C all four terminal protons are equivalent (AX_4, τ 6.2 ppm doublet, 4.2 ppm quintet); this is best described in terms of a rapid dynamic equilibrium between the two possible σ-bonded forms.[3] However, at 20°C, the signal at the higher field appears as a broad singlet, suggesting that the dynamic equilibrium may be affected by the temperature. The fact that the PMR signals of the 1-methylene and 1-vinyl group in the 1-benzyl- and 1-vinyl-benzotriazoles are not affected by the complex formation strongly suggests that the nitrogen atom at the 2 or 3-position of the benzotriazoles acts as the donor in the complexes.

Experimental[4]

All the reactions were carried out in an argon atmosphere. The products, benzotriazole complexes of Pd(II), were stable in air in the solid state.

Dichlorobis(1H-1,2,3-benzotriazole)palladium(II). Into 380 mg of dichloro bis(benzonitrile)palladium(II) in 10 m*l* of benzene, we stirred 240 mg of 1*H*-1,2,3-benzotriazole at room temperature. A yellow substance (340 mg) precipitated out in a few minutes; this was filtered off and washed several times with benzene; mp>290°C; insoluble in benzene, ethanol, water, chloroform, and acetone, but slightly soluble in DMSO and *N,N*-dimethylformamide(DMF).

Found: C, 35.10; H, 2.55; N, 19.95; Cl, 16.80; Pd, 24.80%. Calcd for $C_{12}H_{10}N_6Cl_2Pd$: C, 34.68; H, 2.43; N, 20.23; Cl, 17.06; Pd, 25.60%.

IR (KBr): 3200 (very strong, broad), 1620(m), 1605(m), 1505(m), 1455(m), 1425(w), 1405(m), 1305(m), 1235(s), 1125(m), 1050(s), 915(m), 780(s), 760(m), 740(s) cm^{-1}. (s=strong, m=medium, w=weak intensity)

Dichlorobis(1-benzyl-1,2,3-benzotriazole)palladium(II). 1-Benzyl-1,2,3-benzotriazole[5] (105 mg) in 5 m*l* of benzene was similarly treated with dichlorobis(benzonitrile)palladium(II) (96 mg) for 5 min to give a pale yellow precipitate (120 mg); mp 250°C decomp.; insoluble in benzene, ethanol, chloroform, and acetone, but slightly soluble in DMSO and DMF.

Found: C, 51.58; H, 4.00; N, 13.61%. Calcd for $C_{26}H_{22}N_6Cl_2Pd$: C, 52.41; H, 3.72; N, 14.11%.

IR (KBr): 3080(m), 3050(m), 3000(w), 2940(m), 1615(m), 1595(m), 1495(m), 1480(m), 1455(m), 1330(w), 1310(m), 1300(w), 1245(s), 1165(m), 1140(m), 770(m), 745(s) cm^{-1}.

PMR (60 MHz, in DMSO-d_6); τ 1.8—2.6(multiplet, 4H), 2.65(singlet, 5H), 3.95(singlet, 2H).

Dichlorobis(1-vinyl-1,2,3-benzotriazole)palladium(II). 1-Vinyl-1,2,3-benzotriazole[6] (150 mg) was similarly treated with dichlorobis(benzonitrile)palladium(II) (190 mg) in 5 m*l* of benzene to give a pale yellow precipitate (180 mg); mp 265°C decomp.; insoluble in benzene, ethanol, chloroform, and acetone, but slightly soluble in DMSO and DMF.

Found: C, 41.86; H, 3.11; Pd, 23.31%. Calcd for $C_{16}H_{14}N_6Cl_2Pd$: C, 41.09; H, 3.02; Pd, 22.75%.

1) E. M. Burgess, R. Carithers, and L. MuCullagh, *J. Amer. Chem. Soc.*, **90**, 1923 (1968): A. J. Hubert, *J. Chem. Soc., C*, **1969**, 1334: M. Ohashi, K. Tsujimoto, and T. Yonezawa, *Chem. Commun.*, **1970**, 1089.

2) Benzotriazole complexes of mercury were prepared by the reaction of 1*H*-benzotriazole with mercury salts.

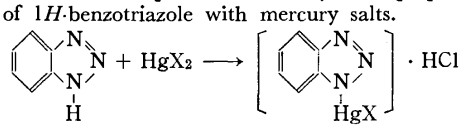

X=O_2CCH_3 and Cl

E. Müller and H. Meier, *Ann. Chem.*, **716**, 11 (1968).

3) J. C. Chien and H. C. Dehm, *Chem. Ind.* (London), **1961**, 745.

4) The PMR and IR spectra were obtained on a JEOL H-60 NMR Spectrometer and a 215 Hitachi Grating Infrared Spectrophotometer, respectively.

5) Prepared by the published method: M. S. Gibson, *J. Chem. Soc.*, **1956**, 1076.

6) Prepared by the published method: J. Hopff, U. Wyss, and H. Lussi, *Helv. Chim. Acta*, **43**, 135 (1960).

IR (KBr): 3100(m), 2940(w), 1645(s), 1600(m), 1500(m), 1460(s), 1360(m), 1320(m), 1310(m), 1210(s), 1170(m), 1140 (m), 1120(m), 960(m), 920(m), 780(m), 760(m), 750(s) cm^{-1}. PMR (in DMSO-d_6); τ 1.5—2.8(multiplet, 5H), 3.8(1H), 4.5(1H).

Chloro(π-allyl)(1H-1,2,3-benzotriazole)palladium(II). Into 183 mg of di-π-allyl-μ,μ′-dichloropalladium(II) in 15 m*l* of benzene, we stirred 300 mg of 1*H*-1,2,3-benzotriazole at room temperature. After 10 min, a pale yellow precipitate (250 mg) was filtered off. Recrystallization from chloroform gave yellow prisms; mp 160°C decomp.; soluble in chloroform and DMSO.

Found: C, 36.50; H, 3.30; N, 14.04; Cl, 11.94; Pd, 36.42%. Calcd for $C_9H_{10}N_3ClPd$: C, 35.79; H, 3.34; N, 13.91; Cl, 11.74; Pd, 35.23%.

IR (KBr): 3080(s), 1620(m), 1600(m), 1455(m), 1390(s), 1280(m), 1220(s), 1150(m), 1105(m), 980(w), 960(m), 935(m), 910(m), 815(m), 780(m), 765(m), 740(s) cm^{-1}. PMR (in DMSO-d_6); at 20°C, τ 2.0—2.5(multiplet, 4H), 4.15(quintet, 1H, J=10.0 Hz), 6.2(singlet, broad, 4H); at 70°C; τ 2.0—2.5(multiplet, J=10.0 Hz), 4.15(quintet, J=10.0 Hz), 6.2 (doublet, J=10.0 Hz).

Chloro(π-allyl)(1-benzyl-1,2,3-benzotriazole)palladium(II). 1-Benzyl-1,2,3-benzotriazole (210 mg) and di-π-allyl-μ,μ′-dichlorodipalladium (270 mg) in 3 m*l* of benzene at room temperature gave a pale yellow precipitate (360 mg). Recrystallization from chloroform gave yellow prisms; mp 125°C (dec.); soluble in chloroform and DMSO.

Found: C, 48.75; H, 3.90; N, 10.71%. Calcd for $C_{16}H_{16}N_3ClPd$: C, 49.00; H, 4.11; N, 10.72%.

IR (KBr): 3100(m), 3050(m), 2960(m), 1595(m), 1500(m), 1455(m), 1385(m), 1310(m), 1240(m), 1230(m), 1160(m), 1140(m), 1120(m), 1005(m), 960(m), 950(m), 770(m), 745(s), 725(s), 700(m) cm^{-1}. PMR (in $CDCl_3$); τ 1.55(multiplet, 1H), 2.6 and 2.7(multiplet and singlet, 8H), 4.15(singlet, 2H), 4.2(multiplet, 1H), 5.85(doublet, 2H, J=7.0 Hz), and 6.85 (doublet, 2H, J=12.0 Hz), (π-allyl: A_2B_2X). PMR (in DMSO-d_6) at 65°C; τ 1.7—2.6(multiplet), 2.65(singlet), 4.0 (singlet), 4.15(quintet, J=10.0 Hz), 6.23(doublet, J=10.0 Hz), (π-allyl: AX_4). At 20°C, the singal at τ 6.23 was a broad singlet.

Chloro(π-allyl)(1-vinyl-1,2,3-benzotriazole)palladium(II). 1-Vinyl-1,2,3-benzotriazole (100 mg) and di-π-allyl-μ,μ′-dichlorodipalladium(II) (126 mg) in 5 m*l* of benzene at room temperature gave a white precipitate (190 mg). Recrystallization from chloroform gave pale yellow prisms; mp 140°C (dec.); soluble in chloroform and DMSO.

Found: C, 40.94; H, 4.04; Pd, 32.43%. Calcd for $C_{11}H_{12}N_3ClPd$: C, 40.27; H, 3.69; Pd, 32.43%.

IR (KBr): 3105(m), 3060(w), 3040(m), 1650(s), 1600(w), 1500(m), 1465(m), 1365(m), 1330(m), 1310(m), 1300(m), 1270(m), 1205(s), 1195(s), 1165(m), 1135(m), 1110(m), 970(m), 910(m), 795(m), 770(m), 760(m) cm^{-1}. PMR (in $CDCl_3$): τ 1.6(multiplet, 1H), 2.2—2.8(multiplet, 4H), 3.97-(doublet of doublets, 1H, J_{ac}[7]=15.0 Hz, J_{ab}=2.0 Hz), 4.2-(multiplet, 1H), 4.63(doublet of doublets, 1H, J_{bc}=12.0 Hz, J_{ab}=2.0 Hz), 5.85(doublet, 2H, J=7.0 Hz), and 6.85(doublet, 2H, J=12.0 Hz), (π-allyl: A_2B_2X). PMR (in DMSO-d_6): at 65°C; τ 4.15(quintet, J=10.0 Hz) and 6.2(singlet, broad).

We wish to thank Dr. M. Ohashi and Mr. K. Tsujimoto for their helpful discussions.

7) 1-Vinyl group:

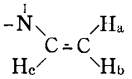

BULLETIN OF THE CHEMICAL SOCIETY OF JAPAN, VOL. 45, 926—928(1972)

The Synthesis of Nucleoside and Nucleotide Analogs

Tooru SEITA, Kiyoshi YAMAUCHI, Masayoshi KINOSHITA, and Minoru IMOTO*

Department of Applied Chemistry, Osaka City University, Sumiyoshi-ku, Osaka

**Department of Applied Chemistry, Kansai University, Suita, Osaka*

(Received April 26, 1971)

During the course of our studies of the preparation of polymers containg nucleic acid bases,[1] we attempted to synthesize nucleoside and nucleotide analogs, replacing the sugar part of the nucleoside or the nucleotide with an aliphatic diol. In the present study, the preparation of nucleoside and nucleotide analogs, such as Ia, IIa, Ia-p, and IIa-p, was investigated. These nucleotide analogs may be useful for the study of the physicochemical properties of nucleic acids when the polymers of these nucleotide analogs are prepared. Moreover, these compounds might be of biological and chemotherapeutical interest because of their structual similarity to Cordycepin, Aristeromycin,[2] etc.

Adenine (I) was chosen as the base part of the nucleoside model. When the sodium salt of I, prepared without isolating from I and sodium hydride, was allowed to react with glycerol α-monochlorohydrin, 3- and 9-(2′,3′-dihydroxypropyl)adenines (Ia and Ib) were obtained. These products were easily separated by fractional crystallization. Both compounds were chromatographically pure. The structures of Ia and Ib were determined by studing their ultraviolet spectra.[3]

1) K. Kondo, H. Iwasaki, N. Ueda, K. Takemoto, and M. Imoto, *Makromol. Chem.*, **120**, 21 (1968); K. Kondo, K. Takemoto, and M. Imoto, *ibid.*, **125**, 42 (1969); K. Kondo, H. Iwasaki, N. Ueda, K. Takemoto, and M. Imoto, *ibid.*. **125**, 298 (1969).

2) E. Waiton, F. N. Nutt, S. R. Jenkins, and F. W. Hally, *J. Amer. Chem. Soc.*, **86**, 2952 (1964); Y. F. Shealey and J. D. Clayton, *ibid.*, **88**, 3885 (1966).

3) It is known that 3-alkyladenines and 9-alkyladenines show λ_{max} at 273±2 mμ (pH:7) and 260±2 mμ (pH:7) respectively. J. A. Montgomery and H. H. Thomas, *J. Org. Chem.*, **28**, 2304 (1963); J. A. Montgomery and H. J. Thomas, *J. Heterocycl. Chem.*, **1**, 115 (1964); N, J. Leonard and T. Fujii, *J. Amer. Chem. Soc.*, **85**, 3719 (1963).

TABLE 1. THE MELTING POINTS, R_f VALUES, UV DATA, AND ELEMENTAL ANALYSES

Compd.	Mp (°C)	R_f[a]	$\lambda_{max}^{H_2O}$ mμ (pH, ε)	Analyses (%) Calcd C	Calcd H	Calcd N	Found C	Found H	Found N
Ia	299—301	0.67	276 (2, 14000) 275 (7, 13500) 274 (12, 14500)	45.93	5.30	33.48	46.09	5.35	33.22
Ib	205—206	0.76	259 (2, 12200) 261 (7, 11600) 262 (12, 12000)	45.93	5.30	33.48	45.86	5.13	32.78
IIa	260 (decomp.)	0.72	265 (7, 11200)	45.71	4.80	26.66	45.50	4.76	26.59
IIb	251—252	0.80	251 (7, 10800)	45.71	4.80	26.66	45.42	5.01	26.38
Ia-p	241—242	0.48	275 (7, 15800)	33.25	4.18	24.22	33.11	4.25	23.89
Ib-p	224—225	0.62	259 (7, 13800)	33.25	4.18	24.22	33.18	4.28	23.97
IIa-p	238—239	0.60	265 (7, 12600)	33.11	3.82	19.31	33.31	3.62	19.21
IIb-p	203—204	0.55	250 (7, 12300)	33.11	3.82	19.31	32.82	3.58	19.01

a) Solvent systems used were: water satulated with *n*-butanol - concd. NH_4OH (15:10) for Ia, Ib, IIa, IIb, and ethanol - conc. NH_4OH - water (15:10:1) for Ia—p, Ib—p, IIa—p, and IIb—p.

In this experiment, 7-(2',3'-Dihydroxypropyl)adenine was not obtained.

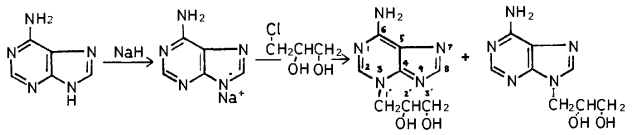

I Ia Ib

When compounds Ia and Ib were treated with concentrated hydrochloric acid and sodium nitrite, the corresponding hypoxanthine derivatives (IIa and IIb) were produced in 70 and 75% yields respectively.

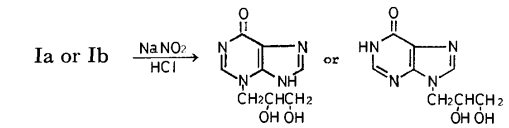

IIa IIb

These compounds were purified by recrystallization. The UV and IR spectra supported the structures.[4]

The phosphorylation of the above compounds was carried out using phosphorus oxychloride in trimethyl phosphate by a modification of the procedure of Yoshikawa, Kato, and Takenishi.[5] By this method, compounds Ia, Ib, IIa, and IIb were phosphorylated to give the corresponding nucleotide analogs, Ia-p, Ib-p, IIa-p, and IIb-p, in 52, 39, 36, and 42% yields respectively. The phosphates were identified by paper chromatography and by elemental analysis. In these experiments, the 2'-phosphates were not obtained since the 2'-position of hydroxyl groups on the nucleoside analogs are sterically hindered.

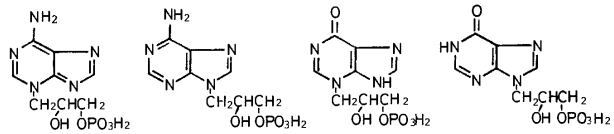

Ia-p Ib-p IIa-p IIb-p

Pharmacological studies and a study of the polymerization reaction of these phosphates are now under way.

Experimental

The melting points are uncorrected. The infrared spectra (IR) were run on a JASCO Model IR-G Spectrometer. The ultraviolet spectra (UV) were measured by a Hitachi Recording Spectrometer Model EPS-3T. Paper chromatography was carried out by the ascending technique using Toyo Roshi No. 50 paper. The results of the elemental analysis, the UV data, the R_f, and the mp of the reported compounds are listed in Table 1.

3-(2',3'-Dihydroxypropyl)adenine (Ia) and 9-(2',3'-Dihydroxypropyl)adenine (Ib). A mixture of adenine (0.67 g, 5 mmol) and sodium hydride (0.25 g, 50%, 5.2 mmol) in anhydrous *N,N*-dimethylformamide (200 m*l*) was stirred at room temperature for 1 hr to give a milky solution of the sodium salt of adenine. To this solution glycerol α-monochlorohydrin (0.55 g, 5.5 mmol) was added, and the mixture was heated at 80—85°C with stirring for 24 hr. The sodium chloride thus precipitated in the cooled reaction mixture was filtered out, and the filtrate was concentrated as much as possible. The resulting solid was filtered and recrystallized from water to afford Ia (0.22 g (21%)) as colorless plates.

The mother liquid was concentrated to dryness. A yellow solid thus obtained was crystallized from ethanol. Recrystallization from water gave 0.47 g (45%) of Ib as colorless needles.

IR of Ia (KBr): 3350(s), 3200(s), 2980(s), 1960(s), 1628(s),

4) J. H. Lister and G. M. Timmis, *J. Chem. Soc.*, **1960**, 327.

5) This method is known to be useful for the selective phosphorylation of the 5'-hydroxyl group of nucleoside (M. Yoshikawa, T. Kato, and T. Tadenishi, *Tetrahedron Lett.*, **1967**, 5065); the selective phosphorylation of nicotinamide nucleoside and riboflavin has also been reported by this method. In the case of riboflavin, as intermediate, 4', 5'-cyclic riboflavin phosphate was isolated; it was exclusively hydrolized to riboflavin 5'-phosphate. Propanediol-1,2-cyclic phosphate and glycerol-1,2-cyclic phosphate produced the corresponding 1-phosphates almost quantitatively under acidic conditions. From these results, it seems that the reaction of diols with phosphorus oxychloride proceed through an intermediate, five-membered cyclic phosphate, which is selectively hydrolyzed into primary phosphates. L. H. Yaynes, N. A. Hughs, G. W. Kener, and A. R. Todd, *J. Chem. Soc.*, **1957**, 3727; H. S. Torrest and A. R. Todd, *ibid.*, **1950**, 3295; T. Ukita, K. Nagasawa, and M. Irie, *Pharm. Bull* (Tokyo), **5**, 127 (1957); E. Baer, ans M. Kates, *J. Biol. Chem.*, **175**, 79 (1948).

1560(w), 1415(m), 1225(w), 1180(w), 1010(m), 890(w), and 710(w) cm^{-1}.

IR of Ib (KBr): 3300(s), 3150(s), 2950(w), 1650(s), 1600(s), 1480(m), 1416(w), 1330(m), 1295(m), 1105(m), 1020(m), 900(m), and 730(s) cm^{-1}.

3-(2',3'-Dihydroxypropyl)hypoxanthine (IIa). Into a solution of Ia (1.0 g, 4.8 mmol) in concentrated hydrochloric acid (20 m*l*), sodium nitrite (1.2 g, 17.1 mmol) in water (40 m*l*) was slowly with vigorously stirring over a 1-hr period. The temperature was maintained at 0°C. After having been stirred at room temperature for an additional 6 hr, the reaction mixture was neutralized with sodium bicarbonate and evaporated to dryness under reduced pressure. The residue was crystallized from water to give IIa (0.7 g (70%)) as colorless plates.

IR (KBr): 3000(s), 2900(s), 2850(m), 1630(s), 1595(m), 1545(s), 1430(s), 1380(w), 1200(m), 1120(m), 1010(m), 940(w), and 790(w) cm^{-1}.

9-(2',3'-Dihydroxypropyl)hypoxanthine (IIb). Compound Ib(1.0 g, 4.8 mmol) was treated with sodium nitrite (1.2 g, 17.1 mmol) in a manner similar to that mentioned above. The reaction mixture was neutrallized with concentrated ammonium hydroxide and concentrated. Crude IIb was crystallized from ethanol. Recrystallization from water afforded IIb (0.75 g (75%)) as colorless needle crystals.

IR (KBr): 3200(s), 2900(s), 1690(s), 1620(w), 1590(m), 1550(m), 1520(m), 1420(m), 1380(w), 1227(s), 1120(s), 1060(m), 1015(m), 870(w), and 770(m) cm^{-1}.

3-(2',3'-Dihydroxypropyl)adenine 3'-Phosphate (Ia-p). Compound Ia (0.5 g, 2.4 mmol) was dissolved in trimethyl phosphate (5 m*l*) and cooled to 0°C. To this solution phosphorus oxychloride (0.4 g, 2.6 mmol) was added slowly over 6-hr period. Water was then added, and the mixture was stirred for 20—30 more min. A white precipitate was then filtered out and crystallized from water. The phosphate, Ia-p (0.36 g (52%)), was obtained as colorless needle crystals.

IR (KBr): 3100(m), 3000(s), 1680(m), 1630(s), 1410(m), 1200(s), 1100(s), 1060(s), 970(s), and 770(w) cm^{-1}.

9-(2',3'-Dihydroxypropyl)adenine 3'-Phosphate (Ib-p). Compound Ib (0.5 g, 2.4 mmol) was treated with phosphorus oxychloride (0.4 g, 2.6 mmol) in trimethyl phosphate (4 m*l*) in a manner similar to that described above. Water added to the reaction mixture and it was stirred for an additional hour. After the reaction mixture had then been concentrated under reduced pressure at below 50°C, the residue was treated with ethanol (20 m*l*). The white precipitate was crystallized from water to give Ib-p (0.26 g (39%)) as colorless needles.

IR (KBr): 3200(s), 3050(s), 1690(s), 1610(m), 1415(m), 1220(m), 1120(s), 990(s), 930(s), and 760(m) cm^{-1}.

3-(2',3'-Dihydroxypropyl)hypoxanthine 3'-Phosphate (IIa-p). Compound IIa (0.5 g, 2.4 mmol) was treated with phosphorus oxychloride (0.4 g, 2.6 mmol) in trimethyl phosphate (5 m*l*) as has been described above. Water the then added to the reaction mixture, and it was stirred for an additional hour. After the evaporation of water below 50°C, a mixture of 20 m*l* of ethanol and 10 m*l* of ether was added. The white precipitate was crystallized from water to give IIa-p (0.25 g (36%)) as colorless crystals.

IR (KBr): 3250(m), 3100(m), 1680(s), 1550(m), 1230(m), 1110(s), 770(w), and 610(w) cm^{-1}.

9-(2',3'-Dihydroxypropyl)hypoxanthine 3'-Phosphate (IIb-p). IIb-p was prepared in the way described in the case of IIa-p; IIb (0.5 g, 2.4 mmol) was treated with phosphorus oxychloride (0.4 g, 2.6 mmol) and trimethyl phosphate (5 m*l*). IIb-p (0.29 g (42%)) was obtained and crystallized from a mixture of ethanol and water (8: 2).

IR (KBr): 3400(m), 3150(s), 1700(s), 1570(m), 1530(w), 1370(s), 1210(s), 1100(s), 990(m), and 910(m) cm^{-1}.

BULLETIN OF THE CHEMICAL SOCIETY OF JAPAN, VOL. 45, 928—930(1972)

The Mass Spectra of 3-Aryl-5-methyl-1,2,3-oxathiazolidine-2-oxides

Tomihiro NISHIYAMA, Yasuyoshi FUJIMOTO, and Fukiko YAMADA
Department of Applied Chemistry, Faculty of Engineering, Kansai University, Senriyama, Suita, Osaka

(Received June 2, 1971)

In continuation of our previous reports concerning the formation of 3-aryl-1,2,3-oxathiazolidine-2-oxides[1] and their mass spectra,[2] this report will deal with the fragmentation schemes of 3-aryl-5-methyl-1,2,3-oxathiazolidine-2-oxides.

We have prepared 3-phenyl-5-methyl-1,2,3-oxathiazolidine-2-oxide (I), 3-tolyl-5-methyl-1,2,3-oxathiazolidine-2-oxides (II), and 3-chlorophenyl-1,2,3-oxathiazolidine-2-oxides (III) by the reported method.[3]

The mass spectral data of the compounds are shown in Table 1, while the major fragmentation paths are shown in Scheme 1. The abundances of the molecular

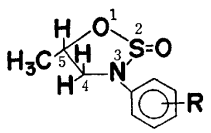

I, R=H
IIa, R=*o*-CH_3
IIb, R=*m*-CH_3
IIc, R=*p*-CH_3
IIIa, R=*o*-Cl
IIIb, R=*m*-Cl
IIIc, R=*p*-Cl

ions of the compounds are quite low. This behavior can be ascribed to the easy cleavage of the oxathiazolidine ring; supporting evidence for this postulate is available from the large peaks (100% abundance) at *m/e* 104, 118, and 138, corresponding to the R-C_6H_4-NCH cation, in the spectra. These peaks occur because of the loss of the SO_2 group from the molecular ion, followed by the loss of both the $CH_2=CH_2$ group and the hydrogen radical (Path 1 in Scheme 1). These fragment ions lose the HCN group to give phenyl cations with *m/e* values of 77, 91, and 111 respectively.

The oxathiazolidines, I, II, and III, exist in the *cis*

1) F. Yamada, T. Nishiyama, M. Nakatani, and M. Kinugasa, This Bulletin, **43**, 3611 (1970).
2) F. Yamada, T. Nishiyama, Y. Fujimoto, and M. Kinugasa, *ibid.*, **44**, 1152 (1971).
3) T. Nishiyama and F. Yamada, *ibid.*, **44**, 3073 (1971).

Table 1. Mass spectral data of compounds I, II, and III (75 eV)

Compound I (*trans*)

m/e	Ion composition[a)]	Rel. Int. (%)
197	$C_9H_{11}NO_2S$	17
133	$C_9H_{11}N$	19
132	$C_9H_{10}N$	25
105	C_7H_7N	22
104	C_7H_6N	100
77	C_6H_5	81

a) The high-resolution mass spectra of these compounds gave the correct composition of all the ions mentioned in the table within an error of ±5 millimass units.

Compound II

m/e	Ion composition	Rel. Int. (%) IIa (*trans*)	IIb (*trans*)	IIc (*cis*)
211	$C_{10}H_{13}NO_2S$	11	32	15
147	$C_{10}H_{13}N$	10	19	19
146	$C_{10}H_{12}N$	6	27	16
132	$C_9H_{10}N$	10	15	14
119	C_8H_9N	15	27	27
118	C_8H_8N	100	100	100
105	C_7H_7N	3	11	14
91	C_7H_7	50	81	56

Compound III

m/e	Ion composition	Rel. Int. (%) IIIa (*cis*)	IIIa (*trans*)	IIIb (*trans*)	IIIc (*trans*)
231	$C_9H_{10}NO_2ClS$	20	18	30	21
167	$C_9H_{10}NCl$	16	14	22	24
166	C_9H_9NCl	14	13	32	23
140	C_7H_5NCl	36	37	36	38
139	C_7H_6NCl	19	19	11	24
138	C_7H_5NCl	100	100	100	100
132	$C_9H_{10}N$	55	53	15	18
113	C_6H_4Cl	13	13	15	16
111	C_6H_4Cl	36	39	53	51

and *trans* configurations between the S=O group and the methyl group in the 5-position, and it is possible to assign the substituent geometry of the isomeric pairs by means of NMR spectroscopy.[3] In the mass spectral data shown in Table 1, the *cis* and *trans* isomers of IIIa show a similar fragmentation pattern. It can be assumed that the fragmentation patterns of the other compounds are the same in the *cis* and *trans* configurations. Thus, the fragmentation pattern for each compound will be discussed by means of the data obtained in the case of either the *cis* or *trans* isomer.

A significant difference in the mass spectral pattern on the position in the ring-substituted group in the III compounds can be observed at *m/e* 132, which is of 55% abundance for the *ortho* isomer, 15% for the *meta*, and 18% for the *para*. On the other hand, in the compounds of II, the abundance of the peak at *m/e* 132 is 10% for the *ortho* isomer, 15% for the *meta*, and 14% for the *para*. This ion at *m/e* 132, corresponding to $C_6H_5NC_3H_5$, can be produced by the loss of the SO_2 group from the molecular ion, followed by the loss of the ring substituent, methyl, or chloro group (Path 2 in Scheme 1). The above findings suggest that the abnudance of IIIa at *m/e* 132 may be caused by the substituent at the *ortho*-position.

In constrast to the present behavior, the above fragment ion was not observed in the spectra of either 3-phenyl-1,2,3-oxathiazolidine-2-oxide or 3-*p*-tolyl-1,2,3-oxathiazolidine-2-oxide bearing no 5-methyl group.

In the compounds of II, peaks at *m/e* 104 and 105, corresponding to the $C_6H_4NCH_2$ and $C_6H_5NCH_2$ cations respectively, were observed. On the contrary to this fact, these peaks were so small as to be negligible in the spectra of III. These differences can be explained by the following fragmentation mechanisms. It is thought that, in the compounds of II, the fragment ion at *m/e* 132 eliminates the $CH_2=CH_2$ group to give the ion at *m/e* 104, and that then a proton adducts to the benzene ring to give the ion at *m/e* 105, as follows:

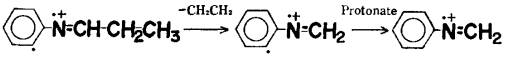

m/e 132 *m/e* 104 *m/e* 105

On the other hand, in the compounds of III, we supposed that the ion at *m/e* 132 can be formed by the elimination of the chloro substituent, followed by the migration of the hydrogen radical from the 5-methyl group to the position on the benzene ring, as follows:

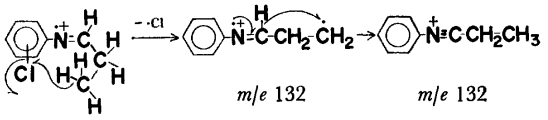

m/e 132 *m/e* 132

m/e 169, 167

As has been described above, there are three principal paths of the fragmentation of the ion corresponding to R-C_6H_4N=$CHCH_2CH_3$ as a result of the loss of the SO_2 group from the molecular ion:

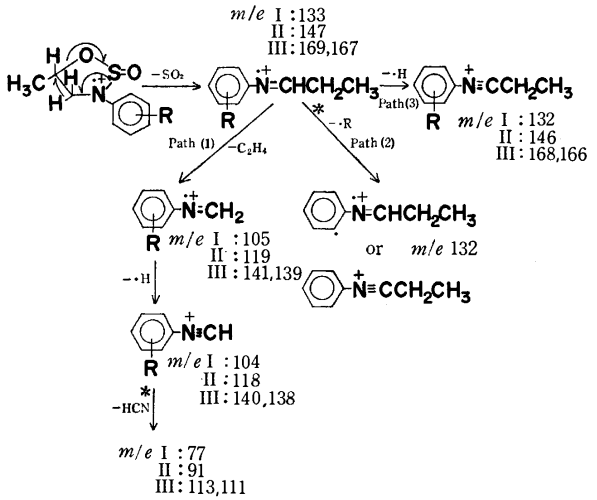

Scheme 1. The major fragmentation pathways of oxathiazolidines, I, II, and III.

* Asterisks denote the processes for which metastable transitions were observed.

(1) the elimination of the $CH_2=CH_2$ group
(2) the loss of the ring substituent (radical)
(3) the loss of the hydrogen radical.

Experimental

The mass spectra were obtained with a Japan Electron Optics Co., Ltd., JMS-O1SG Mattauch-Herzog double-focusing mass spectrometer. In the photographic-plate measurements, a sample was introduced with a marker (PFK), under normal operating conditions (accelerating voltage, 6.4 kV). Accurate masses were determined by the previously-reported method.[2)]

BULLETIN OF THE CHEMICAL SOCIETY OF JAPAN, VOL. 45, 930—931(1972)

The Occurrence of Yangonin, 4-Methoxy-6-(*p*-methoxystyryl)-2-pyrone, in *Ranunculaceae*

Tamotsu SHIBATA,[1] Tsuyoshi SHIBUYA, and Kozo DOI
Department of Chemistry, Faculty of Science, Hirosaki University, Hirosaki

(Received June 21, 1971)

Since the isolation of protoanemonin from the essential oil,[2] little is known about the constituents of *Ranunculus quelpaertensis* Nakai (Kitsunenobotan in Japanese), belonging to *Ranunculaceae*. Recently we have reinvestigated the extractive of stems and leaves of the plant, and have isolated and characterized the following substances as the constituents: fumaric, palmitic, and stearic acids from the acidic fraction, and a long-chain saturated hydrocarbons mixture containing C_{23}—C_{31}, stigmasterol, β-sitosterol, hexacontanol, unidentified C_{27}-alcohol, and yangonin,[3] 4-methoxy-6-(*p*-methoxystyryl)-2-pyrone, from the neutral fraction. As far as we know, yangonin had been isolated only from the root of *Piper methysticum* Forst.[3] (*Piperaceae*), and it is of interest from the stand of chemotaxonomy to occur also in *Ranunculaceae*. The details of the work will be described in the following section.

Experimental

All melting points are uncorrected. The IR spectra were determined as KBr pellets on a Hitachi model EPI-S spectrophotometer. The mass spectra[4] were taken on a Hitachi model RMU-7 mass spectrometer at 70 eV. Gas-liquid chromatographic analyses (glc) were made at 180—220°C, using a Yanagimoto model GCG-5DH apparatus with a hydrogen flame ionization detector (3 mm × 1.5 m column, 10% SE-30/Chromosorb W).

Extraction and Fractionation. Dried stems and leaves (4.2 kg) of the plant were ground and extracted with hot methanol, and the extract were evaporated *in vacuo* to give dark green residue, which was extracted again with ether. The ether solution was then fractionated into the hydrogen carbonate-soluble, carbonate-soluble, and neutral fractions. The former two fractions were extracted respectively with ether after acidifications.

The Hydrogen Carbonate-soluble Fraction. The ether extract was evaporated *in vacuo* to give crystalline residue, from which was isolated fumaric acid, colorless needles (80 mg), mp and mixed mp 284°C (sealed tube), after vacuum sublimation followed by recrystallization from ethanol.

The Carbonate-soluble Fraction. After evaporation of the solvent *in vacuo* followed by crystallization from ethanol, the ether extract afforded a mixture (120 mg) of palmitic and stearic acids, identification of which was made with glc of their methyl esters.

The Neutral Fraction. The *n*-hexane solution of the neutral fraction (22 g) was chromatographed through a column packed with alumina (200 g), an effluent (1200 m*l*) from the same solvent was collected, and the remain was recovered with methanol (1900 m*l*). The former effluent was evaporated *in vacuo* to give colorless crystals (10 g), mp 57—64°C, identified as a mixture of long-chain saturated hydrocarbons containing C_{23}—C_{31}, consisting of mainly C_{27} and C_{29}, from the comparison of glc with standard sample of hydrocarbons.[5] The fraction recovered with methanol, after evaporation *in vacuo*, deposited colorless leaflets (1.6 g), mp 146—148°C, from ethanol. The IR spectrum shows maxima at 970 and 959 cm^{-1}, and the mass spectrum two molecular ion peaks at *m/e* 414 and *m/e* 412. From the comparison of glc, this was proved to be a mixture of stigmasterol and β-sitosterol (2: 1).[6]

The fraction removed from the above sterols was chromatographed through a column packed with alumina (300 g) and developed with a mixed solvent of benzene and ether. An effluent from the system (benzene–ether (99 : 1)) afforded colorless crystals (10 mg) by recrystallization from methanol, mp 68.5—69.5°C, ν_{max}: 3250, 1053, 720, and 710 cm^{-1}. The mass spectrum indicates base peak at *m/e* 31 ($CH_2=O^+H$) and two molecular ion peaks at *m/e* 392.403 (Calcd for $C_{27}H_{52}O$: 392.402) and *m/e* 382.418 (Calcd for $C_{26}H_{54}O$: 382.417), indicative of a mixture of alcohols containing at least hexacontanol.

An effluent from the system (benzene–ether (97: 3)) gave pale yellow prisms by recrystallization from ethanol, mp 152—

1) Present address: Aomori-kenritsu Aomori Nishi High School, Shinjo, Aomori.

2) Y. Asahina and A. Fujita, *Acta Phytochim. Japan*, **1**, 1 (1922).

3) W. Borsche and C. K. Bodenstein, *Ber.*, **62**, 2515 (1929) and previous papers. For the structure, see I. Chmielewska, J. Cieslak, K. Gorczynska, B. Kontnik, and B. Pitakowska, *Tetrahedron*, **4**, 36 (1958). J. D. BuLock and H. G. Smith, *J. Chem. Soc.*, **1960**, 502.

4) We are indebted to Mr. H. Sato, Hitachi Seisakusho, for measurements of the spectra.

5) We are very grateful to Dr. T. Kamano, Taisho Seiyaku Co., for generous gift of the standard sample of hydrocarbons.

6) The authors wish to thank Prof. T. Takemoto, Tohoku University, for carrying out of this analysis.

153°C. Its mass spectrum shows peaks at *m/e* 258 (M^+) and *m/e* 230.092 (M^+–CO) (Calcd for $C_{14}H_{14}O_3$: 230.094), establishing its molecular formula, $C_{15}H_{14}O_4$. The IR spectrum indicates the presence of 2-pyrone ring (1720, 1624, and 1556 cm^{-1}), 1,4-disubstituted phenyl with conjugation (1602, 1575, 1512, 1176, 1110, 1025, 1000, and 827 cm^{-1}), and an extra *trans*-disubstituted ethylene (960 cm^{-1}). The spectral pattern resembles closely that of naturally occurring yangonin. In fact, this constituent showed no depression of mixed melting point with authentic sample.[7] The other mass spectral peaks at *m/e* 215(M^+–CO–CH_3), 202(M^+–2×CO), 187(M^+–2×CO–CH_3), 159(M^+–3×CO–CH_3), 144(M^+–3×CO–2×CH_3), are also compatible to the structure of yangonin.

An effluent from the system (benzene–ether (1:1)) afforded further a mixture of stigmasterol and β-sitosterol.

7) We are very grateful to Dr. R. Hänsel, Freie Universität, Berlin, for generous gift of natural yangonin.

BULLETIN OF THE CHEMICAL SOCIETY OF JAPAN, VOL. 45, 931—932(1972)

The Effect of the Shield Voltage on Appearance Potential Measurements Using a Mass Spectrometer

Susumu TAJIMA, Yukio SHIMIZU,* and Toshikazu TSUCHIYA

Government Chemical Industrial Research Institute, Tokyo, Honmachi, Shibuya-ku, Tokyo

**National Research Institute for Pollution and Resources, Kotobukicho, Kawaguchi-shi, Saitama*

(Received July 7, 1971)

In the usual type of mass spectrometer, a small negative voltage is applied to the filament shield as an aid in confining the largest portion of the filament's emission to the region of the electron slit. In measuring the appearance potential (AP) with the mass spectrometer, the obtained values were found to be affected by the shield voltage. To the authors' knowledge, however the effect of the shield voltage on the AP has not yet been discussed, though it is well known that the measured AP is affected by the repeller voltage[1,2] and/or the source magnetic field.[3] In the present note, the cause of the effect of the shield voltage on the AP will be discussed and a procedure to eliminate the effect will be reported.

Experimental

A CEC 21-103C mass spectrometer was used in measuring the AP. The ionization efficiency (IE) curves were treated by the E.D.D. technique[4] after the data had been smoothed by the least-squares method using a computer. The constant, b, used in the E.D.D. calculation was 0.67. Krypton was used as the calibrating gas for the electron energy scale. The ionization potential (IP) of krypton was taken as 14.00 eV. The sample, benzene, and krypton were introduced into the ion source at the same time. The repeller voltage was kept at a constant value[1,2] for all the measurements. The electron trap current was 10 μA; the temperature of the ion source was 250°C.

The IP value of benzene was measured by using two electric circuits, 1) a standard electric circuit, and 2) a modified electric circuit. In the standard circuit of the CEC 21-103C mass spectrometer, the electron accelerating voltage (V_e) and the shield voltage are supplied from the same circuit by changing the value of the resistor, R, in the circuit, as is shown in Fig. 1. Under usual experimental conditions, the shield voltage changes in proportion to V_e, since the value of the resistor between the filament and the shield electrodes is kept constant ($r \simeq 500$ ohm). In the modified circuit, the voltage, V_e, was supplied from a separate circuit and was set with a 10-turn potentiometer (Sakae Tsushin Kōgyō Co., Ltd.), as is shown in Fig. 2, while the shield voltage was set by the same resistor, R, as in the standard circuit. By this circuit, the shield voltage can be set at any value, independent of the V_e.

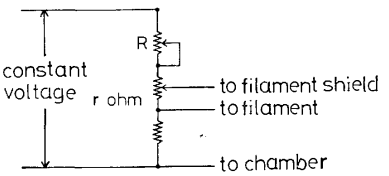

Fig. 1. Diagram of the standard electric circuit for the electron accelerating voltage and the shield voltage of a CEC 21-103C mass spectrometer.

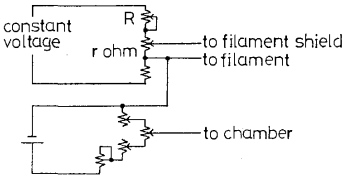

Fig. 2. Diagram of she modified electric circuit for the electron accelerating voltage and the shield voltage.

Results and Discussion

The two IP values of benzene determined in the present study are, in Table 1, compared with those obtained by various other methods.[5-8] As may be seen

1) I. Omura, K. Higashi, and H. Baba, This Bulletin, **29**, 501 (1956).

2) L. Friedman, F. A. Long, and M. Wolfsberg, *J. Chem. Phys.*, **31**, 755 (1959).

3) E. Henderson, P. N. K. Riley, and R. D. Sedgwick, *J. Sci. Instrum.*, **43**, 726 (1966).

4) R. E. Winters, J. H. Collins, and W. L. Courchene, *J. Chem. Phys.*, **45**, 1931 (1966).

5) D. W. Turner, *Tetrahedron Lett.*, **1967**, 3419.

6) M. F. El-Sayed, M. Kasha, and Y. Tanaka, *J. Chem. Phys.*, **34**, 334 (1961).

7) A. J. C. Nicholson, *ibid.*, **43**, 1171 (1965).

8) R. E. Fox and W. M. Hickam, *ibid.*, **22**, 2059 (1954).

Table I. Ionization potential of benzene obtained by using (a) standard electric circuit, and (b) modified electric circuit

	eV
Photoelectron Spectroscopy[5]	9.24
Spectroscopy[6]	9.24_8
Photoionization[7]	9.24_1
Electron Impact (RPD)[8]	9.21
This work[a]	9.52±0.1
This work[b]	9.20±0.1

in the table, the IP value obtained by using the modified circuit agrees reasonably well with the literature values, while that obtained by using the standard circuit is considerably higher. A little higher AP values were obtained for various ions from disubstituted benzenes,[9] too, when the standard circuit was used.

Table 2. Ionization potentials of krypton measured under various shield voltages

Shield voltage (mV)	Ionization potential (eV) (uncorrected)
$1.0\times r$	13.40±0.1
$1.5\times r$	13.30±0.1
$2.0\times r$	13.05±0.1

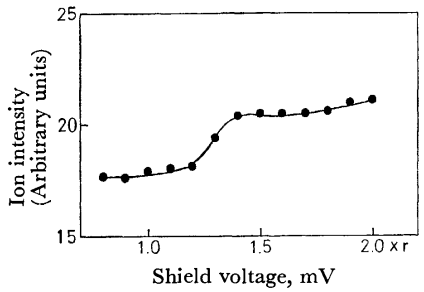

Fig. 3. Variation of the ion intensity of krypton (*m/e* 84) with the shield voltage at the electron accelerating voltage of 15.0 eV (uncorrected), and at ion accelerating voltage of about 1000 V.

To clarify the cause of these results, the IP of krypton was measured at three shield voltages corresponding to current flows of 1.0, 1.5, and 2.0 mA through the resistor ($r\simeq 500$ ohm). The values thus obtained are shown in Table 2. The variation in the krypton-ion (*m/e* 84) intensities with the shield voltage obtained at the electron accelerating voltage of 15.0 eV is shown in Fig. 3. From Figure 3 and Table 2, it may be seen that the ion intensity at a constant electron accelerating voltage increases with an increase in the shield voltage, and that the observed IP for krypton decreases with an increase in the shield voltage. Hence, if the IE curves of the two compounds are measured at different shield voltages, the difference between the two apparent IP's observed will be different from the difference between the true IP's for the two compounds, since different shield voltages exert different influences on the ion intensities of the two compounds. When the IP of benzene is measured by using the standard electric circuit of the CEC 21–103C mass spectrometer and when krypton is used as the calibrating gas for the electron energy scale, different shield voltage are used in each case—*i.e.*, for benzene, about $0.9\times r$ (mV), and for krypton, about $1.4\times r$ (mV). If the factors of the effects due to the shield voltage on the observed IP's of benzene and krypton are taken as $A(C_6H_6)$ and $A(Kr)$ respectively, in this case the following relation can be expected by referring to Table 2, since the shield voltage in the case of benzene is lower than that in the case of krypton:

$$A(C_6H_6) < A(Kr) \quad (1)$$

If the instrumental factors due to the contact potential, *etc.*, are taken as X, then the apparent IP's of benzene, $IP(C_6H_6)$, and of krypton, IP(Kr), are given by the following equations respectively:

$$IP(C_6H_6) = \text{true } IP(C_6H_6) + X - A(C_6H_6) \quad (2)$$

$$IP(Kr) = \text{true } IP(Kr) + X - A(Kr) \quad (3)$$

Since benzene and krypton are introduced into the ion source simultaneously, X is the same for both equations. By subtracting Eq. (2) from Eq. (3), we obtain:

$$IP(Kr) - IP(C_6H_6) = \text{true } IP(Kr) - \text{true } IP(C_6H_6) - A(Kr) + A(C_6H_6) \quad (4)$$

From Eq. (4), it may be seen that the difference detween the apparent IP's is smaller than that between the true IP's, because $A(C_6H_6) < A(Kr)$ in this case. Accordingly, to calibrate the electron energy scale, let the apparent IP of krypton, IP(Kr), be equal to 14.00 eV; then the IP value of benzene obtained will be somewhat higher than the true IP value. This may be the reason why a high IP value, as is shown in Table 1, was obtained when the IP was estimated without taking the effect of the shield voltage into account. On the other hand, the IP value obtained at a constant shield voltage for both benzene and krypton is in good agreement with those of the other workers. At least a part of the reason why a little higher AP values than those accepted were obtained previously[9] for some disubstituted benzenes may be understood in terms of the same explanation. The effect of the shield voltage on the AP may be due mainly to the fact that the electrons from the filament are somewhat accelerated by the shield voltage.

When a CEC 21-103C mass spectrometer is used to measure the AP, a compound which has almost the same ionization potential as that of the sample should be used as the calibration compound for the electron energy scale; otherwise, the shield voltage should be kept at a constant value for measuring the IE curves for both the sample and the calibration compound.

The authous wish to thank Akio Hashizume of this Institute for his valuable discussions.

9) S. Tajima, N. Wasada, and T. Tsuchiya, *Tetrahedron Lett.*, **1970**, 139.

BULLETIN OF THE CHEMICAL SOCIETY OF JAPAN, VOL. 45, 933—935(1972)

Asymmetric Reactions. VI. Asymmetric Hydrogenation of Atropate Catalyzed by Cyanocobalt-Optically Active Diamine Complex[1]

Yoshiaki OHGO, Kazuhiko KOBAYASHI, Seiji TAKEUCHI, and Juji YOSHIMURA
Laboratory of Chemistry for Natural Products, Tokyo Institute of Technology, Meguro-ku, Tokyo

(Received July 20, 1971)

In a previous paper,[2] the authors have reported that the asymmetric hydrogenation of atropate by pentacyanocobaltate - optically active α-amino acid system gives only slightly optically active hydratropic acid.

This paper presents the asymmetric hydrogenation catalyzed by a cyanocobalt complex coordinated with optically active *R*(−)-1,2-propanediamine or *S*(+)-*N*,*N*′-dimethyl-1,2-propanediamine.

Results and Discussion

Piringer *et al.*[3] have reported that μ-ethylenediamine-bis[tetracyanocobaltate(II)] has an ability to activate molecular hydrogen.

At first, the catalytic activity of (1,2-propanediamine)-cyanocobalt(II) complex for the reduction of α,β-unsaturated carboxylic acids, using racemic 1,2-propanediamine, was examined under the atmospheric pressure of hydrogen at room temperature. The results (Table 1) show that reactive α,β-unsaturated carboxylic acids,[2,4] itaconic acid and atropic acid, are catalytically reduced to give the corresponding saturated acids almost quantitatively. Subsequently, catalytic asymmetric hydrogenation of atropate using *R*(−)-1,2-propanediamine as a ligand was attempted and gave *S*(+)-hydratropic acid of $[\alpha]_D$ +0.8—+0.9° which corresponds to about 1% optical yield (Table 2). The optical rotation of the product purified by distillation rose to $[\alpha]_D$ +1.1°. No optical activity was, of course, observed in the hydratropic acid recovered after the treatment of the racemic hydratropic acid under the same conditions. From these facts, it is obvious that the catalytic asymmetric hydrogenation gave a little bit higher stereoselectivity than that in the previously studied system.[2]

It was expected that the coordination of *N*-substituted 1,2-propanediamine to metal would cause more selective asymmetric coordination of the substrate, because the former coordination should induce asymmetry on the nitrogen atom[5] which is placed nearer to the reaction center than asymmetric C_2 carbon. For this purpose, *N*,*N*′-dimethyl-1,2-propanediamine[6] was resolved through L(+)-tartrate salt to give (+)-isomer of $[\alpha]_D$ +53.9° (benzene) in pure state. The configuration was inferred to be *S*(+) from the specific rotation of analogous compound (*R*(−)-*N*[1]-phenyl-*N*[2]-methyl-1,2-propanediamine, $[\alpha]_D$ −29.5°).[7]

The hydrogenation of atropate catalyzed by (*S*(+)-*N*,*N*′-dimethyl-1,2-propanediamine)cyanocobalt(II)

Table 1. Catalytic hydrogenation of activated olefines with (1,2-propanediamine)cyanocobalt(II) complex

Substrate	Time (days)	Product	Yield
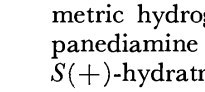	2	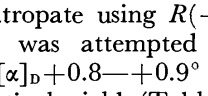	trace
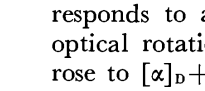	3	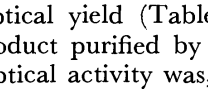	91%
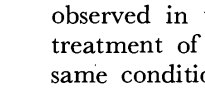	2	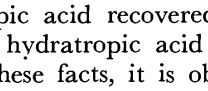	96%

Table 2. Asymmetric hydrogenation of atropate catalyzed by (optically active diamine)cyanocobalt complex

Amine	Catalyst: Mole ratio of Co	CN	Amine	Tb (min)	Tr (days)	Product: Yield	$[\alpha]_D$	Optical yield
Pn	1	4	3	60	3	95.5%	+0.815°	1.0%
Pn	1	2	3	25	2	94.5%	+0.905°	1.1%
Pn	1	2	3	585	2	90.5%	+0.825°	1.0%
diMPn	1	4	2			50%	+5.73°	7.1%

Tb: Time (min) left standing before the reaction. Tr: Reaction time (days).
Pn: *R*(−)-1,2-propanediamine. diMPn: *S*(+)-*N*,*N*′-dimethyl-1,2-propanediamine.

1) This work was presented at the 23rd Annual Meeting of the Chemical Society of Japan, April 1970.
2) Y. Ohgo, S. Takeuchi, and J. Yoshimura, This Bulletin, **43**, 505 (1970).
3) R. Ripan, A. Farcas, and O. Piringer, *Z. Anorg. Allg. Chem.*, **346**, 211 (1966); O. Piringer and A. Farcas, *Z. Phys. Chem.* (Leipzig), **49**, 321 (1966).
4) Y. Ohgo, S. Takeuchi, and J. Yoshimura, This Bulletin, **44**, 283 (1971).
5) D. A. Buckingham, S. F. Mason, A. M. Sargeson, and K. R. Turnbull, *Inorg. Chem.*, **5**, 1649 (1966); S. Saburi and S. Yoshikawa, *ibid.*, **7**, 1890 (1968).
6) W. W. Williams, and A. F. Strobel, U. S. 2619502 (1950).
7) P. S. Portghese and D. L. Larson, *J. Pharm. Sci.*, **53**, 302 (1964).

complex was carried out under the same conditions as above. As expected, it was shown that somewhat greater steric control was affected, *i.e.*, the reduction gave hydratropic acid of $[\alpha]_D+5.73°$ (optical yield, 7%). In consequence, *S*(+)-hydratropic acid was predominantly produced either by use of *R*(−)-1,2-propanediamine or *S*(+)-*N*,*N*′-dimethyl-1,2-propanediamine, despite that these ligands have opposite configurations at C_2 to each other. This discrepancy in appearance may be interpreted as follows, though the asymmetric yields are rather low.

The complex used here showed an absorption spectrum [260 nm (ε, 670); 278 nm (ε, 560); 354 nm (ε, 155); 995 nm (ε, 7.3)] which is closely akin to the spectrum of μ-ethylenediamine-bis(tetracyanocobaltate-(II)) reported by Piringer *et al.*[3] and there is no substantial absorption due to complexes[9,10] produced by disproportionation of the (propanediamine)cyanocobalt complex. These facts indicate that the complex contained in the solution may be such a mixed ligand system as obtained by Piringer *et al.*[3] On the other hand, hydrogenation catalyzed by pentacyanocobaltate-(II) has been reported to proceed with *trans* addition.[8] If this is the case for diamine coordinated cyanocobalt complex described here, coordination models like A and B (Fig. 1) are considered as the transition states of the hydrogenations catalyzed by (*R*(−)-1,2-propanediamine)cyanocobalt(II) and (*S*(+)-*N*,*N*′-dimethyl-1,2-propanediamine)cyanocobalt(II) complexes, respectively. The alkylcobalt complexes are, then formed by hydride addition to the methylene carbon of olefin, and followed by attack of another hydride complex with inversion to give the same *S*(+)-hydratropic acid. However, there are many sites ineffective to asymmetric control. This may be the main cause of resulting in low optical yield.

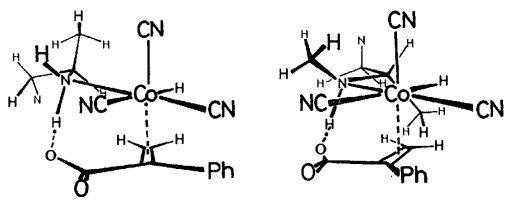

Fig. 1.

It is considered from the results that rigid conformational fixation and proximity of asymmetric groups to the reaction center result in higher optical yield, and that they concurrently prevent, however, coordination of the substrate and therefore the total yield is lowered. This will be an important problem to be overcome in order to design an excellent, homogeneous metal complex catalyst for asymmetric hydrogenation.

8) M. Murakami, S. Suzuki, and J. Kang, *Nippon Kagaku Zasshi*, **83**, 1226 (1962).

9) N. K. King and M. E. Winfield, *J. Amer. Chem. Soc.*, **83**, 3362 (1961).

10) The electronic spectrum of $Co(Ph)_3Cl_2$ (prepared under the same condition as the catalyst did): 354 nm (ε, 11.8); 483 nm (ε, 12.0); 1020 nm (ε, 3.4).

Experimental

Reduction of Some α,β-Unsaturated Acids Catalyzed by (1,2-Propanediamine)cyanocobalt(II). To a solution of $CoCl_2\cdot 6H_2O$ (1 g, 0.0042 mol) in 10 m*l* of water was slowly added a solution of potassium cyanide (1.12 g, 0.017 mol) in water (10 m*l*) with stirring under nitrogen atmosphere to give brown precipitates. The precipitates were dissolved by addition of a solution of 1,2-propanediamine (0.62 g, 0.008 mol) in water (60 m*l*) which had been deoxygenated by bubbling nitrogen gas. To the resulting orange-colored homogeneous solution was added an aqueous solution prepared from 0.6 g (0.004 mol) of atropic acid and sodium hydroxide (0.004 mol). The flask was purged with hydrogen gas and then the reaction mixture was stirred under the atmospheric pressure of hydrogen at room temperature. The solution absorbed the theoretical amount of hydrogen within 2—3 days. The reaction mixture was concentrated and extracted with ether after acidification with conc. hydrochloric acid. The ether layer was washed with water, and concentrated to give a syrup (0.58 g). The product was characterized as hydratropic acid by IR and NMR spectra. Itaconic and tiglic acids were hydrogenated by the same procedure and the results are shown in Table 1.

Asymmetric Reduction by Use of Cyanocobalt Complex Coordinated with Optically Active Diamines (R(−)-1,2-Propanediamine or S(+)-N,N′-Dimethyl-1,2-propanediamine). The asymmetric reduction was carried out by the same procedure as described above, except for using optically active diamines instead of racemic diamine. In the case of the reaction with *R*(−)-1,2-propanediamine the crude product showed only one spot on tlc (silica gel) (R_f, 0.5, ethanol-benzene, 3:1; R_f, 0.65, methanol-water, 3:1). Optical rotation of these crude product was $[\alpha]_D+0.815$—$+0.905$ (see Table 2), and the product was distilled at 90—91°C/0.03 mmHg; $[\alpha]_D+1.1°$ (*c* 10.6, ethanol). The specific rotation corresponds to optical yield of 1.2% [optically pure *S*(+)-hydratropic acid, $[\alpha]_D^{20}$ +81.1° (*c* 3.1, ethanol)]. In the case of the reaction with *S*(+)-*N*,*N*′-dimethyl-1,2-propanediamine, the product was distilled at 83°C/0.0075 mmHg. The NMR spectrum of the distillate showed that the sample was a mixture of 84.1% of hydratropic acid and 15.9% of atropic acid. The optical rotation, $[\alpha]_D+5.73°$ (*c* 6.1, ethanol), corresponds to optical yield of 7%.

S(+)-N,N′-Dimethyl-1,2-propanediamine. Racemic compound was synthesized by reaction of 1,2-dibromopropane and methylamine according to William's method except for using a mixed solvent of benzene and methanol. A mixture of 1,2-dibromopropane (100 g), methylamine (350 m*l*), benzene (200 m*l*) and methanol (200 m*l*) was shaken in an autoclave at 95—105°C for 5 hours, and left standing overnight at room temperature. To the reaction mixture which was transferred to Erlenmeyer flask was added an excess amount of conc. HCl. The solution was concentrated under diminished pressure to give a solid. The solid was dissolved in a small amount of water, covered with benzene (2000 m*l*) and an excess of sodium hydroxide pellets was added to this solution. During this procedure, excess methylamine was evaporated and *N*,*N*′-dimethyl-1,2-propanediamine was transferred to benzene layer which was decanted to another vessel. Water layer was extracted with benzene several times. The combined extracts were distilled through a fractionating column. Bp 127—128°C; yield: 15 g (30%). A part of this sample was benzoylated to give crystals of mp 86—88°C whose analytical values were agreed with those of *N*,*N*′-dimethyl-*N*,*N*′-dibenzoylpropanediamine. Found: C, 73.76; H, 7.06; N, 9.07%. Calcd for $C_{19}H_{22}N_2O_2$: C, 73.52; H,

7.14; N, 9.03%.

Resolution of *N,N'*-dimethyl-1,2-propanediamine was accomplished by fractional crystallization of its L(+)-tartrate. Racemic *N,N'*-dimethyl-1,2-propanediamine (81 g) was dissolved into a solution of L(+)-tartaric acid (226.8 g) in 153 m*l* of water. The mixture was left standing in a refrigerator. The resulting crystals were separated by filtration. The procedures were repeated, and a part of the crystals obtained in some stage of crystallization was used in order to measure specific rotation; an aqueous solution of the crystals was made alkaline and extracted with benzene. The benzene layer was dried by adding sodium hydroxide pellets. The optical rotation of the dried benzene solution was measured, and the concentration was determined by acid titration. Thus obtained specific rotation in each stage of recrystallization was as follows.

Times of recrystallization	1	4	6	8	12
$[\alpha]_{578}$ of benzene solution (°)	+47.3	+51.25	+52.1	+52.6	+53.9
(*c*)	(0.97)		(0.6)	(0.6)	(1.0)

The sample of $[\alpha]_{578}+53.9°$ was used in the experiment of asymmetric hydrogenation.

BULLETIN OF THE CHEMICAL SOCIETY OF JAPAN, VOL. 45, 935—936(1972)

OH Bending Vibrations and Hydrogen Bond in Crystalline *p*-Hydroxybenzaldehyde

Ariyuki AIHARA and Yoshinori SHIROTA*

Department of Materials Science, Denki-Tsushin University, Kojima-cho, Chofu, Tokyo

(Received July 29, 1971)

The energy of hydrogen bond formed in the crystalline state of *p*-hydroxybenzaldehyde was estimated to be 7.3 kcal/mol from the heat of sublimation.[1] However, it has not yet been determined whether the molecules form a hydrogen bond of the type OH···OH or OH···O=C in the crystal.

Recently we carried out IR measurement in relation to our study on dielectric behavior and three-dimensional X-ray crystal structure analysis of this substance. This note reports on the bending vibrations of OH bond and their temperature variation in the crystalline state of *p*-hydroxybezaldehyde with reference to estimating the strength of hydrogen bond spectroscopically.

p-Hydoxybenzaldehyde was purified by vacuum sublimation and used as a KBr disc for the IR measurement. An IR spectrometer of JASCO IR-S type covering a frequency range 650—4000 cm^{-1} was used. Spectra obtained at several temperatures are shown in Fig. 1.

We note a characteristic feature of a broad band at 712 cm^{-1} (15°C) which shifts towards low frequency side with an increasing breadth with the rise of temperature. Similarly a band at 1240 cm^{-1} shifts slightly in the same direction with a tendency of broadening. On the other hand, the temperature variation of a strong and very broad band at 3180 cm^{-1}, which can be identified to be the OH stretching vibration (hydrogen-bonded), is not clear because of the poor resolving power of the instrument in this frequency region. From the characteristic behavior of these bands, it is almost certain that the 712 cm^{-1} band can be ascribed to the out-of-plane bending vibration of the OH bond intermolecularly hydrogen-bonded to neighboring molecules, and that the 1240 cm^{-1} band is due to the in-plane OH bending vibration under the influence of hydrogen bonding.[2-5]

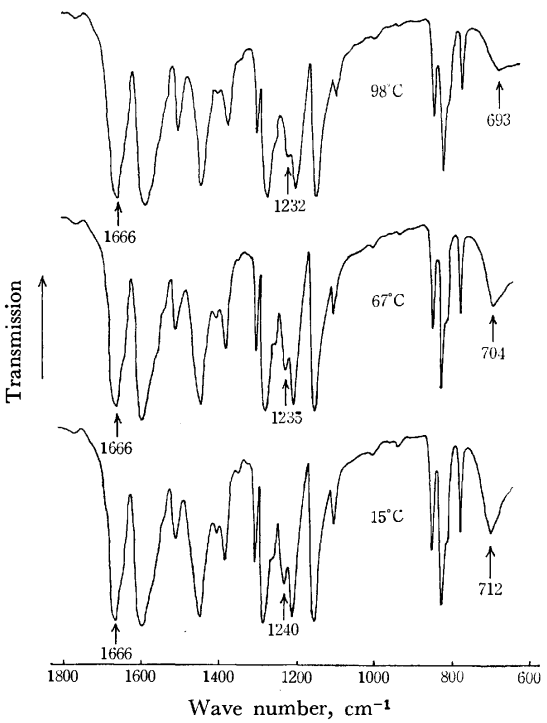

Fig. 1. IR spectra of *p*-hydroxybenzaldehyde (KBr disc) at three temperatures; spectra in the frequeney range, 600—1800 cm^{-1}, are shown.

So far several authors have reported on IR as well

* Present address: Nippon Kōden Kōgyo Co., Shinjuku, Tokyo.

1) A. Aihara, This Bulletin, **33**, 194 (1960).

2) N. Sheppard, "Hydrogen Bonding," ed. by D. Hadzi, Pergamon Press, London (1959), p. 85.

3) G. C. Pimentel and A. L. McClellan, "The Hydrogen Bond," W. H. Freeman and Co., San Francisco (1960), p. 70.

4) W. C. Hamilton and J. A. Ibers, "Hydrogen Bonding in Solids," W. A. Benjamin, Inc., New York (1968), p. 85.

as far-IR absorption of *p*-hydroxybenzaldehyde in solution and solid states,[5-8] but none have mentioned the OH bending vibration except for Bellamy[5a] who identified a band at 1160 cm^{-1} as δ_{OH} (in-plane bending vibration).

It is worthy of mention that the frequency of stretching vibration of C=O group 1666 cm^{-1} remains almost the same all through the temperature variation. This suggests that the carbonyl group is not involved in hydrogen bond formation in the crystalline state and the hydrogen bond in the crystal is very likely of the type, OH···OH···OH···.

A similar suggestion has been made by Fukushima[8] from far-infrared measurement.[9]

In order to estimate the energy of hydrogen bond from the frequency shift of OH vibration on hydrogen bonding, an empirical equation proposed recently by Purcell and Drago[10] has been used: $-\Delta H(\pm 0.5$ kcal/mol$)=0.016\times\Delta\nu_{OH}+0.63$, where ΔH is the energy of the hydrogen bond and $\Delta\nu_{OH}$ the frequency shift in cm^{-1}. Since the equation was derived originally for the anharmonic stretching vibration of a bond involved in hydrogen bonding, estimation of ΔH was made first with the frequency shift of OH stretching vibration observed in this experiment. Taking 3594 cm^{-1} observed in CCl_4 solution[11] as the free OH stretching vibration, $\Delta\nu_{OH}=3594-3180=414$ cm^{-1} leads to ΔH value of 7.25 kcal/mol which is in good agreement with the value 7.3 kcal/mol obtained thermochemically.[1]

A tentative calculation of the energy of the hydrogen bond has been made with the use of the frequency shift of the out-of-plane bending vibration 412 cm^{-1}, the difference between $\gamma_{OH}=712$ cm^{-1} observed in this measurement and $\gamma_{OH}=300$ cm^{-1} assigned to the free OH libration in phenol molecules.[12,13] The result obtained is almost the same as mentioned above, *viz.*, 7.23 kcal/mol. It is reasonable to infer that the anharmonicity of OH libration is reduced to a greater extent due to hydrogen bonding, making the Purcell and Drago equation applicable to the bending vibration in this case.

In the crystalline state of *p*-hydroxybenzaldehyde, the decrease of energy of the hydrogen bond with the rise of temperature can be estimated by following the above procedure as shown in Table 1.

Table 1. Temperature variation of OH bending vibration and the energy of hydrogen bond in crystalline *p*-hydroxybenzaldehyde estimated with the use of the Purcell and Drago equation

Temp. °C	15	50	67	88	98
γ_{OH} cm^{-1}	712	710	704	697	693
ΔH kcal/mol	7.22	7.19	7.10	6.98	6.91
δ_{OH} cm^{-1}	1240	1238	1235	1233	1232
ΔH kcal/mol	1.85	1.62	1.57	1.54	1.53

The decrease in ΔH as seen in the table might be correlated with the increase of O···O distance with the rise of temperature. The OH in-plane bending vibration would be unsuitable to be correlated with the strength of hydrogen bond[5b]: much smaller values of ΔH were obtained from $\Delta\delta_{OH}$ (Table 1) assuming 1176 cm^{-1} observed with phenol vapor[14] to be the free OH bending frequency.

A hindered rotator model with a potential

$$V = (V_0/2)(1-\cos n\theta)$$

can be applied also to calculate the energy of hydrogen bond, if we assume that V_0 is composed of two parts, *i.e.*, an attractive potential due to hydrogen bonding and a repulsive one which is intrinsic to a molecule free from hydrogen bonding. In the above equation, θ is an angle of rotation and n is the number of equilibrium positions the rotator will occupy during the rotation through 360°. Since the frequency of libration in the potential well can be expressed as

$$\nu = (n/2\pi)(V_0/2I)^{1/2}$$

where I is the moment of inertia of the rotator, we get V_0 by substituting the observed value of out-of-plane bending vibration $\gamma_{OH}=712$ cm^{-1} into the equation with appropriate values of I and n. Putting $n=2$, and assuming that the dimension of OH group in *p*-hydroxybenzaldehyde is the same as that of phenol molecule with $I=1.23\times10^{-40}$ gcm^2 (ref. 14), we obtain $V_0=15.96$ kcal/mol. Therefore, subtracting the hindering potential for the OH rotation in a phenol molecule 3.48 kcal/mol[13] from the V_0 value, we get 12.48 kcal/mol as the energy of hydrogen bond in *p*-hydroxybenzaldehyde crystal. The value is somewhat larger than those estimated with the use of the frequency shift on hydrogen bonding 7.22 kcal/mol, probably because the above equation is applicable only in the vicinity of the potential minimum. Or, we might presume that the hindering potential of the OH group in a free molecule of *p*-hydroxybenzaldehyde should be larger than that of a phenol mloecule, due to the reinforced effect of conjugation of the C–O bond with the benzene ring in the presence of an aldehydic substituent at the *para* position.

5) a) L. J. Bellamy, "The Infrared Spectra of Complex Molecules," Methuen and Co., London (1962), p. 91. b) L. J. Bellamy, "Advances in Infrared Group Frequencies," Methuen and Co., London (1968), p. 280.

6) G. M. Barrow, *J. Chem. Phys.*, **21**, 2008 (1953).

7) K. U. Ingold and D. R. Taylor, *Can. J. Chem.*, **39**, 471 (1961).

8) K. Fukushima, This Bulliten, **38**, 164 (1965).

9) Carbonyl stretching frequencies observed in solutions are 1689 cm^{-1} in $CHCl_3$[6], 1701 cm^{-1} in CCl_4.[7] The difference between these values and the one observed in the solid state, 1666 cm^{-1}, must be attributed to dipolar interaction between adjacent carbonyl groups in the crystal.

10) K. F. Purcell and R. S. Drago, *J. Amer. Chem. Soc.*, **89**, 2874 (1967).

11) N. A. Puttnam, *J. Chem. Soc.*, **1960**, 5100.

12) J. C. Evans, *Spectrochim. Acta*, **16**, 1382 (1960).

13) G. Varsányi, "Vibrational Spectra of Benzene Derivatives," Academic Press, New York (1969), p. 368.

14) D. R. Bist, J. C. D. Brand, and D. R. Williams, *J. Mol. Spectrosc.*, **24**, 402 (1967).

BULLETIN OF THE CHEMICAL SOCIETY OF JAPAN, VOL. 45, 937—938(1972)

Lamellar Reactions of Graphite with Aluminum Halides

Tadashi SASA, Yoichi TAKAHASHI, and Takashi MUKAIBO

Department of Nuclear Engineering, The University of Tokyo, Hongo, Bunkyo-ku, Tokyo

(Received July 30, 1971)

Graphite reacts with a large number of substances under suitable conditions to form lamellar compounds. Many kinds of metal chlorides are included. Few studies have been performed on the reaction of graphite with other metal halides such as bromides or iodides. The reactivity of aluminum chloride with graphite has been investigated in detail.[1,2] It was found that aluminum chloride does not react with graphite, by itself, and that the presence of another component such as chlorine, bromine or iodine is necessary for the lamellar reaction to occur. Croft[3] reported the reaction of aluminum bromide and graphite in his early systematic studies. It is doubtful, however, whether excess free bromine was thoroughly eliminated during the course of the reaction. The authors have extended the studies to investigate the reactivity of graphite with aluminum bromide and aluminum iodide.

1. Graphite-$AlBr_3$

High purity artificial graphite (heat-treated at 2400°C or 3000°C) was used for the samples. Aluminum bromide prepared by the reaction between aluminum and bromine of high purity was distilled before the reaction, and excess bromine was carefully removed. The graphite specimen was suspended by a quartz spring balance (sensitivity 20 mm/g) in an evacuated and sealed glass tube, and kept in contact with aluminum bromide vapor of saturation pressure at temperatures 100—250°C for 40 hours. No measurable gain in the weight of the graphite was observed. The electrical conductivity and X-ray diffraction measurement of the sample also showed no measurable change. It is concluded aluminum bromide alone does not react with graphite.

A small amount of gaseous bromine was added in aluminum bromide vapor at 150°C. Graphite is thought to absorb scarcely any bromine at such a high temperature.[4,5] Under these conditions, however, it started to absorb the reactants immediately. When bromine was also added to the graphite in the form of a lamellar compound and residue compound beforehand, absorption of the reactant was also observed. The optimum reaction temperature was 150°C, and the reaction terminated in 24 hours. The observed gain in the weight of the graphite by far exceeded the amounts of existing free bromine, and the existence of aluminum bromide in the graphite was actually confirmed by the decomposition of the reaction products.

It is to be noticed that release of a considerable amount of free bromine was observed at the first stage of the reaction of graphite-bromine residue compound and aluminum bromide. It is known that residue compound of artificial graphite is very stable and scarcely undergoes decomposition by heat treatment below 1000°C.[6,7] However, it was observed that some parts of bromine were released at 70°C and at the same time the reaction with aluminum bromide was initiated. As the reaction proceeded, most of the released bromine was absorbed again by the graphite. For checking the possibility of decomposition of aluminum bromide vapor, the reaction of graphite-bromine residue compound with aluminum chloride was carried out. The release of free bromine was also observed in this case. The released bromine should be attributed to the residual bromine contained in the graphite.

A quantitative investigation of aluminum bromide absorption in relation to the amount of coexisting bromine was carried out. Controlled amount of bromine was doped in graphite in the form of a residue compound or lamellar compound, and the graphite sample was allowed to react with aluminum bromide vapor. The reaction products were weighed for the determina-

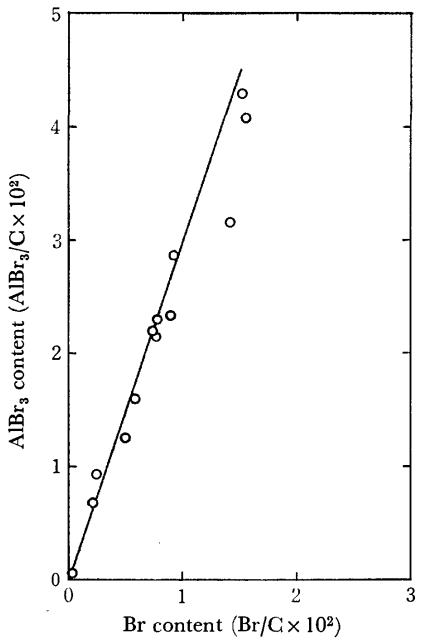

Fig. 1. Ternary lamellar compounds of graphite with aluminum bromide and bromine

1) W. Rüdorff and R. Zeller, *Z. Anorg. Allgem. Chem.*, **279**, 182 (1955).
2) M. L. Dzurus and G. R. Hennig, *J. Amer. Chem. Soc.*, **79**, 1051 (1957).
3) R. C. Croft, *Aust. J. Chem.*, **9**, 184 (1956).
4) J. G. Hooley, *Can. J. Chem.*, **37**, 899 (1959).
5) B. Bach, M. Bagouin, F. Bloc, and A. Herold, *C. R. Acad. Sci. Paris*, **257**, 681 (1963).
6) G. R. Hennig, *J. Chem. Phys.*, **20**, 1433 (1952).
7) Y. Takahashi, K. Miyauchi, and T. Mukaibo, *Tanso (Carbon)*, **1970**, (60), 8.

tion of aluminum bromide uptake. Some samples were decomposed in a vacuum at 500°C, and the released bromine and aluminum bromide were collected separately and analyzed chemically. The relation of aluminum bromide contents and bromine contents of the ternary lamellar compounds is shown in Fig. 1. Aluminum bromide contents depend entirely on the amount of coexisting bromine, and the ratio $AlBr_3$ to Br is found to be nearly three. The result coincides with that of Hennig[2] on $AlCl_3$-Cl, or $AlCl_3$-Br. The atomic composition of the ternary compound was $C_{24}AlBr_3$-$Br_{0.3}$ for the highest reactant contents investigated.

X-ray diffraction study of the reaction products of the highest reactant contents showed the formation of a 'second stage structure' compound, where every other layer spacing of graphite is invaded by the reactants and expands from 3.35 Å to 10.0 Å.

2. Graphite-AlI_3

It was found that aluminum iodide also does not react alone with graphite at temperatures up to 250°C.

When bromine was doped in graphite as the residue compound, the absorption of aluminum iodide took place. However, aluminum iodide reacts easily with bromine to form aluminum bromide and free iodine. No further quantitative studies were carried out.

Free iodine was added to graphite-aluminum iodide system to start the reaction. The intercalation of reactants in graphite was not observed in several careful runs. Thus we conclude that the aluminum iodide and iodine system does not react with graphite.

The authors are grateful to Messrs. N. Arai and K. Matsuoka for their collaboration in a part of the study.

BULLETIN OF THE CHEMICAL SOCIETY OF JAPAN, VOL. 45, 938—939(1972)

Hydrogen Transfer Reaction between Alcohols and Acetone

Hiroo NIIYAMA and Etsuro ECHIGOYA

Department of Chemical Engineering, Tokyo Institute of Technology, O-okayama, Meguro-ku, Tokyo

(Received August 2, 1971)

It was found in the previous paper[1] that hydrogen transfer reaction between alcohol and aldehyde was involved in the butadiene formation from ethanol over SiO_2·MgO. This fact was pointed out by Quattlebaum *et al.*[2] but the mechanism postulated by them was highly improbable. They found purified SiO_2 was most active, while Jones *et al.*[3] reported it was inactive. Basic oxides such as CaO[4] and MgO[5] were also reported as active catalysts.

In this study, various kinds of SiO_2·MgO having different composition and also different acidity and basicity, were used in order to make clear the roles of acidic and basic sites.

Experimental

Catalysts. SiO_2, MgO, and SiO_2·MgO having different MgO contents were prepared by the method described before.[1]

Acidity and Basicity Measurements. Adsorbed amount of pyridine at 200°C and boron trifluoride at 300°C was measured by the gravimetric method described before.[1]

Reaction. A coventional flow type reactor was used. Alcohol and acetone were introduced with hydrogen as a gaseous mixture into a catalyst bed.

Results and Discussion

The reaction took place between any alcohol and ketone or aldehyde. In this study, ethanol, 1-propanol, 2-butanol, and acetone were chosen as reactants. This reaction was confirmed to be an intermolecular hydrogen transfer, because (1) the same activity was observed when helium was used as carrier gas instead of hydrogen, and (2) the hydrogenation of acetone or dehydrogenation of these alcohols did not take place under this reaction condition.

Reactivity of ethanol, 1-propanol, and 2-butanol as hydrogen donors were compared. The sequence of reactivity was, 2-butanol (1.02)$\gg$1-propanol (7.2×10^{-4})$>$ethanol (4.7×10^{-4}) herein, the values in the bracket are the reaction rates in mol/g-cat·hr at 200°C over SiO_2·MgO (85 mol% MgO) catalyst.

It was shown in the previous paper[6] that release of the proton from hydroxy group was the rate determining step in the dehydrogenation of alcohols over basic sites, which gives the sequence of reactivity as follows, 2-butanol$\ll$1-propanol$<$ethanol. The reactivity sequence of alcohols in the hydrogen transfer reaction was quite different from that in the dehydrogenation reaction.

Acid-base properties and the activities of the catalysts were shown in Figs. 1 and 2. The catalytic activity in

1) H. Niiyama, S. Morii, and E. Echigoya, This Bulletin, **45**, 655 (1972).

2) W. M. Quattlebaum, W. J. Toussaint, and J. T. Dunn, *J. Am. Chem. Soc.*, **69**, 593 (1947).

3) H. E. Jones, E. E. Stahly and B. B. Corson, *ibid.*, **71**, 1822 (1949).

4) Y. Schachter and H. Pines, *J. Catal.*, **11**, 147 (1968).

5) S. A. Bullard, H. D. Finch, and D. E. Winkler, "Advances in Catalysis," Vol. 10, Academic Press, New York and London (1959) p. 754.

6) H. Niiyama and E. Echigoya, This Bulletin **44**, 1739 (1971).

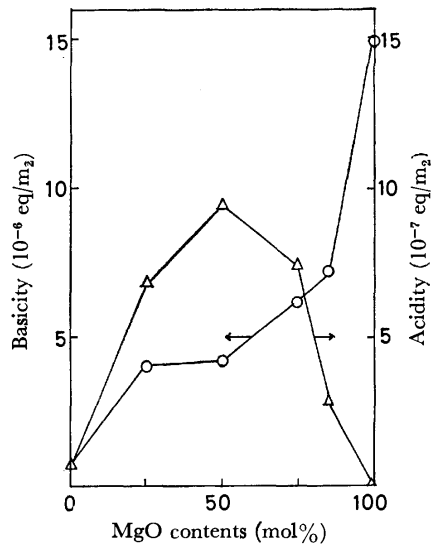

Fig. 1. The correlation between acidity or basicity and MgO contents.
—△— acidity (amount of pyridine adsorbed at 200°C)
—○— basicity (amount of BF_3 adsorbed at 300°C)

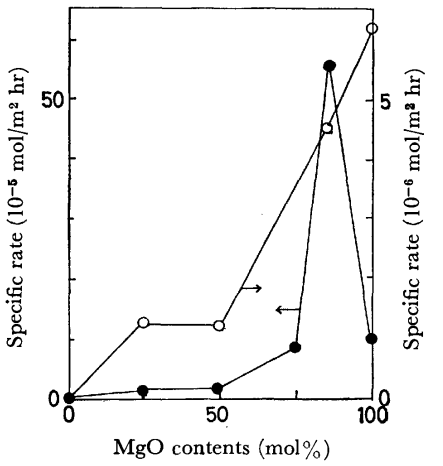

Fig. 2. The correlation between catalytic activity and MgO contents.
—○— ethanol-acetone at 200°C
—●— 2-butanol-acetone at 140°C

the ethanol-acetone system was well correlated with basicity. On the other hand, the profile of the activity against MgO content in the 2-butanol-acetone system was quite different from that of acidity or basicity. It is similar to that of butadiene formation from ethanol.[1] From this profile, it is expected that acidic sites also play important roles in the latter case.[7]

7) Acidic and basic sites are cooperative in the butadiene formation reaction.

Reaction Mechanisms. The reduction of ketone or aldehyde by aluminum isopropoxide is known as Meerwein-Ponndorf reduction. Williams *et al.*[8] and Jackman *et al.*[9] postulated that the reaction proceeded through the following cyclic intermediate. Hydride ion

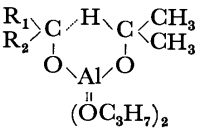

Intermediate postulated by Williams *et al.*[8]

originally attached to the carbinol carbon transferred to ketone to make another alcolate. This mechanisms will be applied in our case.

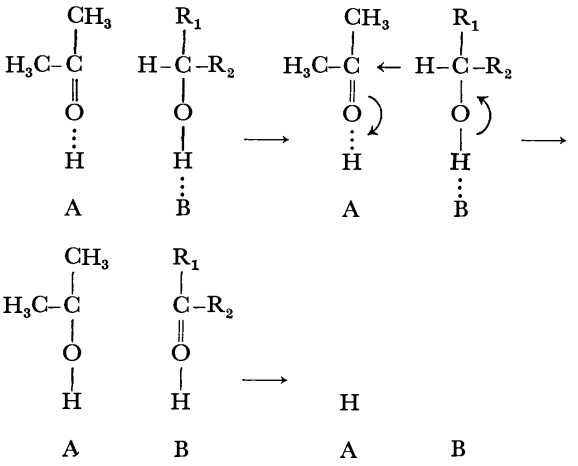

That is, electrophilicity of carbonyl carbon increases by the adsorption on acidic sites (HA) and neucleophilicity of carbinol carbon also increases by the adsorption on basic sites (B). The reactivity of alcohols is expected to depend on the number of aliphatic group attached to the carbinol carbon. Since ethanol has no secondary carbon, it has very small neucleophilicity. Then, the activation of ethanol caused by basic sites is the most important process and so the correlation between activity and basicity is established. On the other hand, 2-butanol is rich in neucleophilicity. Then the difficulty of activation of 2-butanol becomes comparable with that of acetone. Accordingly, no simple correlation with acidity or basicity was obtained, but the catalyst which had adequate acidity and basicity showed high activity.

8) E. D. Williams, K. A. Krieger, and A. R. Day, *J. Am. Chem. Soc.*, **75**, 2404 (1953).
9) L. M. Jackman, A. K. Macketh, and J. A. Mills, *J. Chem. Soc.*, **1947**, 2641.

BULLETIN OF THE CHEMICAL SOCIETY OF JAPAN, VOL. 45, 940—941(1972)

Activation Parameters of the Electrode Reaction of *trans*-1,2-Cyclohexanediaminetetraacetatochromate(III) Complex

Nobuyuki TANAKA, Takeshi TOMITA, and Akifumi YAMADA

Department of Chemistry, Faculty of Science, Tohoku University, Katahira, Sendai

(Received August 6, 1971)

In previous paper,[1] it was reported that in a solution of pH 4.6 the electrode reaction of *trans*-1,2-cyclohexanediaminetetraacetatochromate(II, III) complexes (Cr(II, III)-CyDTA) proceeds as

$$[Cr(III)\text{-}CyDTA]^- + e \rightleftarrows [Cr(II)\text{-}CyDTA]^{2-} \quad (1)$$

A mainly theoretical comparison between the kinetic parameters of the electrode reaction and those of the corresponding homogeneous reaction has been made by Marcus.[2] Although the value of the heat of activation of the electrode reaction is apparent and not absolute, as discussed by Vlček[3] and Tamamushi,[4] the activation parameters corrected for the electrical double layer seem to be useful for a comparison of the electron-transfer reaction at the electrode with those in the solution. The present communication presents the activation parameters of the reaction given by Eq. (1) which were obtained from potentiostatic measurements at various temperatures.

Experimental

Sample solutions of Cr(III)-CyDTA with the supporting electrolyte containing 0.4M sodium chloride, 0.1M sodium acetate buffer and 2×10^{-6}M polyoxyethylene lauryl ether (LEO) were prepared in the same way as previously reported.[1]

For the measurements at 0°C, the temperature was kept constant with an ice-bath, and at 10, 15, 25, and 35°C, controlled by a thermostat. Other apparatus for the measurement were those described previously.[1]

Results and Discussion

The polarograms of Cr(III)-CyDTA complex were measured at several temperatures and the results are given in Table 1. The slopes of log-plots of these polarograms showed that the electrode reaction of the Cr(II, III)-CyDTA system is diffusion-controlled at every temperature. A slope obtained from the Arrhenius plot of diffusion coefficients gave a reasonable value of the activation energy for diffusion. The kinetic parameters determined at various temperatures are given in Table 2.

Table 1. Characteristics of polarographic reduction of 1mM Cr(III)-CyDTA at various temperatures, measured in the supporting electrolyte solutions of pH 4.6 containing 0.4M NaCl, 0.1M acetate buffer and 2×10^{-6}M LEO

Temp. °C	i_d μA	$E_{1/2}$ V *vs.* SCE	Slope of log-plot mV	$D_O\times10^6$ $cm^2\cdot sec^{-1}$
10	−2.42	−1.190	55	3.4
15	−2.60	−1.192	58	4.2
25	−3.00	−1.200	62	5.5
35	−3.47	−1.204	62	7.4

Table 2. Measured kinetic parameters of Cr(III)-CyDTA at various temperatures, obtained in the supporting electrolyte solutions of pH 4.6 containing 0.4M NaCl, 0.1M acetate buffer and 2×10^{-6}M LEO

Temp. °C	$(E_0)_{ms}$ V *vs.* SCE	$(k_s)_{ms}$ $cm\cdot sec^{-1}$	$(\alpha_c)_{ms}$	$(\alpha_a)_{ms}$
0	−1.187	0.0045	0.36	0.78
10	−1.195	0.0011	0.38	0.60
15	−1.189	0.0093	0.39	0.57
20	−1.194	0.018	0.36	0.61
25	−1.198	0.029	0.33	0.67
35	−1.204	0.051	0.33	0.68

The logarithmic values of the standard rate constant, $\log(k_s)_{ms}$, were plotted against $1/T$ in Fig. 1. The measured heat of activation, $(\Delta H_s^*)_{ms}$, and the measured pre-exponential factor, A_{ms}, were obtained from the plot.

In Fig. 2, ϕ_2 potentials, *i.e.*, potentials at the outer Helmholtz plane (OHP), are plotted against the electrode potential E at 15, 25, and 35°C. At more negative potentials than *ca.* −1.18 V *vs.* SCE, ϕ_2 potentials at those temperatures virtually coincide with each other.

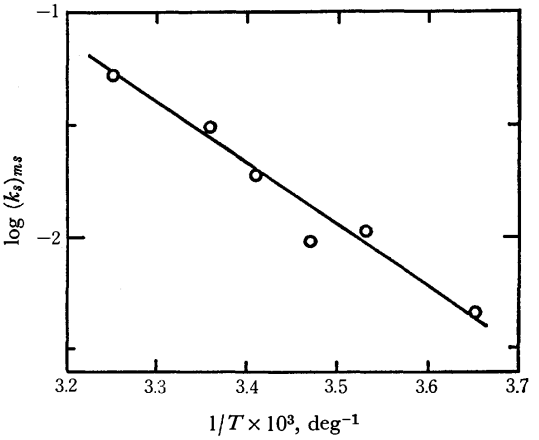

Fig. 1. The Arrhenius plot of $(k_s)_{ms}$ of Cr(III)-CyDTA obtained in the supporing electrolyte solutions of pH 4.6 containing 0.4 M NaCl, 0.1 M acetate buffer and 2×10^{-6} M LEO. The values obtained are: $(\Delta H_s^*)_{ms}=12$ kcal $mole^{-1}$ and $A_{ms}=10^{7.3}$ cm sec^{-1}.

1) N. Tanaka, T. Tomita, and A. Yamada, This Bulletin, **43**, 2042 (1970).
2) R. A. Marcus, *Ann. Rev. Phys. Chem.*, **15**, 155 (1964).
3) A. A. Vlček, *Collect. Czech. Chem. Commun.*, **24**, 3538 (1959).
4) R. Tamamushi, *Rev. Polarog. (Kyoto)*, **10**, 1 (1962).

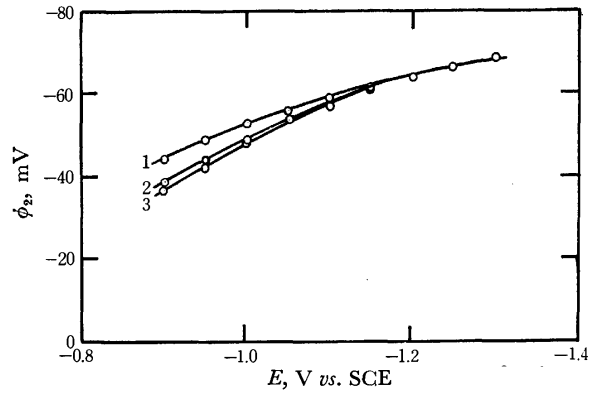

Fig. 2. ϕ_2 potential as a function of the electrode potential E at (1) 15°C, (2) 25°C, and (3) 35°C in a solution of pH 4.6 containing 0.4 M NaCl, 0.1 M acetate buffer and 2×10^{-6} M LEO. ϕ_2 values were estimated from the Gouy-Chapman theory.

TABLE 3. CORRECTED KINETIC PARAMETERS OF Cr(III)-CyDTA AT VARIOUS TEMPERATURES, OBTAINED IN THE SUPPORTING ELECTROLYTE SOLUTIONS OF pH 4.6 CONTAINING 0.4M NaCl, 0.1M ACETATE BUFFER AND 2×10^{-6}M LEO

Temp. °C	$(E_0)_{corr}$ V *vs.* SCE	$(k_s)_{corr}$ cm·sec^{-1}	$(\alpha_c)_{corr}$	$(\alpha_a)_{corr}$
0	−1.186	0.17	0.42	0.72
10	−1.194	0.46	0.49	0.54
15	−1.191	0.37	0.46	0.53
20	−1.195	0.65	0.44	0.55
25	−1.198	0.93	0.40	0.57
35	−1.204	1.5	0.39	0.59

The Frumkin correction can then be applied to the kinetic parameters using these ϕ_2 potentials, assuming that the electron-transfer reaction plane (ERP) is the same as the closest approach of supporting electrolyte (OHP), and none of the chemical species present in the solution is adsorbed on the electrode. The parameters corrected in this way are given in Table 3. The corrected activation parameters are: $(\Delta H_s^*)_{corr}=$ 10 kcal mol^{-1} and $A_{corr}=10^{7.5}$ cm sec^{-1} (Fig.3). There is a great difference between $(k_s)_{ms}$ and $(k_s)_{corr}$, as was reported previously.[1] On the other hand, $(\Delta H_s^*)_{ms}$ is not so much influenced by the correction for the effect of double layer, which was already expected by Joshi *et al.*,[5] when ϕ_2 potential is only slightly dependent on the temperature.

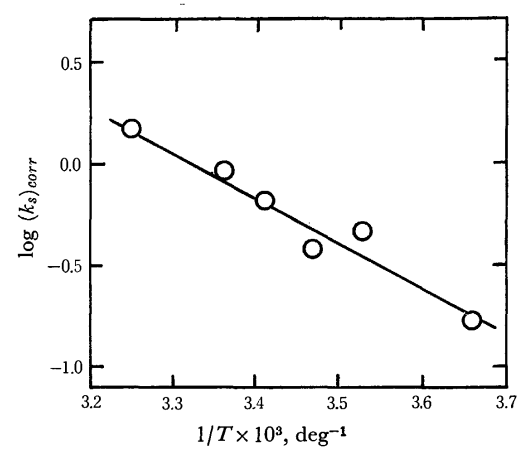

Fig. 3. The Arrhenius plot of $(k_s)_{corr}$ of Cr(III)-CyDTA obtained in the supporting electrolyte solutions of pH 4.6 containing 0.4 M NaCl, 0.1 M acetate buffer and 2×10^{-6} M LEO. The values obtained are: $(\Delta H_s^*)_{corr}=10$ kcal mole^{-1} and $A_{corr}=10^{7.5}$ cm sec^{-1}.

In conclusion, the contribution of the double layer effect to the heat of activation for Cr(II, III)-CyDTA system is relatively small although it can not be neglected.

5) K. M. Joshi, W. Mehl, and R. Parsons, Trans. Symp. Electrode Prosesses, ed. by E. Yeager, (1961), p. 249.

BULLETIN OF THE CHEMICAL SOCIETY OF JAPAN, VOL. 45, 942—943(1972)

The Separation of α- and β-L-Aspartyl-L-phenylalanine Methyl Ester with Aromatic Acids

Yasuo ARIYOSHI and Naotake SATO

Central Research Laboratories, Ajinomoto Co., Inc., Suzuki-cho, Kawasaki, Kanagawa

(Received August 10, 1971)

Although aspartyl peptides can be conveniently prepared by the coupling of *N*-protected aspartic anhydrides with amino acids or amino acid esters, followed by deprotection, this method usually gives a mixture of α- and β-aspartyl peptides.[1-3] Furthermore, the separation of the isomers is generally so difficult and so complicated that only a few methods have been reported; in them techniques of fractional extraction and column chromatography were used.[2,3] Some aromatic acids have been used as specific precipitating reagents for amino acids.[4,5] However, no specific precipitating reagent for the α- and β-aspartyl peptides has been reported in the literature.

α-L-Aspartyl-L-phenylalanine methyl ester (α-APM), which has a sweet taste very similar to that of sucrose, has been found as a new sweetening agent.[6] When α-APM was prepared by the condensation of such *N*-protected L-aspartic anhydrides as benzyloxycarbonyl-L-aspartic anhydride with methyl L-phenylalaninate and by subsequent deprotection, the corresponding β-derivative, β-APM, was also produced as a by-product. α-APM must be sufficiently purified from β-APM, since β-APM has a weakly bitter taste. Purification by recrystallization from water is ineffective because α- and β-APM have almost equal solubilities, and because α-APM is easily changed to the diketopiperazine derivative by heating.

In the course of studies of the sweet peptide, it was

Table 1. Separation of α- and β-APM with various precipitating reagents

Reagent	APM	Grams of α- and β-APM in 100 ml of aqueous solution: Initial solution	Mother liquor
[a] 3,5-Dinitrobenzoic acid	α-APM	1.00	0.10
	β-APM	1.00	0.97
[b] β-Phenylpropionic acid	α-APM	1.00	0.26
	β-APM	1.00	0.91
[a] Cinnamic acid	α-APM	1.00	0.20
	β-APM	1.00	0.92
[b] *p*-Hydroxybenzoic acid	α-APM	1.00	0.30
	β-APM	1.00	1.00
[b] Gentisic acid	α-APM	1.00	0.16
	β-APM	1.00	1.00
[b] β-Resorcylic acid	α-APM	1.00	0.01
	β-APM	1.00	0.96
[b] 5-Chlorosalicylic acid	α-APM	1.00	0.10
	β-APM	1.00	1.00
[a] 2,5-Dichlorophenol	α-APM	1.00	0.06
	β-APM	1.00	1.00
[b] β-Naphthoic acid	α-APM	1.00	0.28
	β-APM	1.00	1.00
[b] β-Naphthoxyacetic acid	α-APM	1.00	0.27
	β-APM	1.00	0.99

To α-APM in the initial solution, 1.2[a] or 2.4[b] molecular equivalents of the reagents were used.

Table 3. Separation of α- and β-APM with various reagents on preparative scale

Mixture: α-APM g	Mixture: β-APM g	Reagent	Water g	Water ml	Recovery: α-APM g (%)	Recovery: β-APM g (%)
5.0	5.0	3,5-Dinitrobenzoic acid	4.2	500	3.1 (62)	2.5 (50)
5.0	5.0	Cinnamic acid	3.0	500	3.2 (64)	3.2 (64)
5.0	5.0	Gentisic acid	6.0	500	3.1 (62)	4.4 (88)
5.0	5.0	β-Resorcylic acid	12.0	500	3.5 (70)	3.9 (78)

Table 2. Characters of precipitated compounds

Compound	Reagent	Component ratio α-APM:Reagent	Mp °C		Elementary analysis (%)
I	3,5-Dinitrobenzoic acid	1:1	141—142	$C_{21}H_{22}O_{11}N_4 \cdot H_2O$	Found: C, 48.09; H, 4.81; N, 10.68 Calcd: C, 48.09; H, 4.61; N, 10.68
II	Cinnamic acid	1:1	140—141	$C_{23}H_{26}O_7N_2 \cdot H_2O$	Found: C, 59.80; H, 6.29; N, 6.35 Calcd: C, 59.99; H, 6.13; N, 6.08
III	Gentisic acid	1:1	133—134	$C_{21}H_{24}O_9N_2 \cdot H_2O$	Found: C, 54.27; H, 5.53; N, 5.75 Calcd: C, 54.07; H, 5.62; N, 6.01
IV	β-Resorcylic acid	1:2	182—186	$C_{28}H_{30}O_{13}N_2$	Found: C, 55.79; H, 5.04; N, 4.83 Calcd: C, 55.81; H, 5.02; N, 4.65

1) W. Grassmann and F. Schneider, *Biochem. Z.*, **273**, 452 (1934).
2) W. J. Le Quesne and G. T. Young, *J. Chem. Soc.*, **1952**, 24; W. D. John and G. T. Young, *ibid.*, **1954**, 2870.
3) D. L. Buchanan, E. E. Haley, and R. T. Markiw, *Biochemistry*, **1**, 612 (1962); D. L. Buchanan, E. E. Haley, F. E. Dorer, and B. J. Corcoran, *ibid.*, **5**, 3240 (1966).
4) D. G. Doherty, W. H. Stein, and M. Bergmann, *J. Biol. Chem.*, **135**, 487 (1940).
5) N. Sato, N. Uchiyama, and T. Akashi, *J. Agr. Chem. Soc. Jap.*, **43**, 504 (1969); Y. Ariyoshi and N. Sato, This Bulletin, **44**, 2787, 3435 (1971).
6) R. H. Mazur, J. M. Schlatter, and A. H. Goldkamp, *J. Amer. Chem. Soc.*, **91**, 2684 (1969).

found that α-APM forms sparingly soluble compounds in water with 3,5-dinitrobenzoic acid, β-phenylpropionic acid, cinnamic acid, *p*-hydroxybenzoic acid, gentisic acid, β-resorcylic acid, 5-chlorosalicylic acid, 2,5-dichlorophenol, β-naphthoic acid, and β-naphthoxyacetic acid. β-APM, on the contrary, did not form such compounds with these reagents. This characteristic was successfully used for the separation of the two isomers of APM. When a mixture of α- and β-APM was placed in contact with these reagents in water, α-APM was selectively precipitated with the reagents, while β-APM remained almost quantitatively in the mother liquor (Table 1).

The separation of the isomers on a preparative scale was achieved with 3,5-dinitrobenzoic acid, cinnamic acid, gentisic acid, and β-resorcylic acid. The elementary analyses showed that the precipitates consist of α-APM and the reagent in a 1:1 molar ratio, except for the precipitate with β-resorcylic acid, which consists of α-APM and β-resorcylic acid in a 1:2 molar ratio (Table 2).

The precipitates and the mother liquors were separately acidified with hydrochloric acid. After removing the liberated reagents by extraction with ether, the acidic solutions were adjusted to the isoelectric point of APM with sodium bicarbonate. The α- and β-APM thus crystallized out were recovered by filtration in fairly high yields (Table 3).

Experimental

The melting points are uncorrected.

α- and β-APM. α- and β-APM were prepared by the method described by Mazur *et al.*[6] α-APM: mp 235—236°C (dec.); $[\alpha]_D^{25}+32.0°$ (*c* 1, acetic acid); $[\alpha]_D^{24}\pm0°$ (*c* 1, water). lit, mp 246—247°C (sintered at 190°C); $[\alpha]_D$ 0° (water).[6] lit, mp 246—247°C; $[\alpha]_D-2.3°$ (*c* 1, N HCl).[7] β-APM: mp 198—199°C (dec.); $[\alpha]_D^{28}+42.5°$ (*c* 1, acetic acid); $[\alpha]_D^{24}+4.0°$ (*c* 1, water). lit, mp 196—197°C; $[\alpha]_D+4°$ (water).[6]

Determination of α- and β-APM. Paper electrophoresis was carried out in aqueous acetic acid of pH 2.77 at 40 V/cm for 1.5 hr; the paper was stained with a cadmium-ninhydrin reagent.[8] The two spots corresponding to α- and β-APM were individually cut off and eluted with methanol, and the absorbances of the eluates were measured at 510 mμ.

Crystalline Compounds of α-APM with the Various Reagents (I, II, III, and IV in Table 2). α-APM Compound with 3,5-Dinitrobenzoic Acid (I): To a stirred solution of 2.0 g of α-APM in 200 m*l* of water, 1.7 g of 3,5-dinitrobenzoic acid was added at room temperature. The solution was kept in a refrigerator overnight. The crystals thus formed as needles were collected by filtration; yield, 3.2 g (89%).

α-APM compound with cinnamic acid (II) was obtained from a mixture of 1.0 g of α-APM and 1.0 g of cinnamic acid in 100 m*l* of 50% aqueous ethanol; yield, 0.9 g (60%).

α-APM compounds with gentisic acid (III) and with β-resorcylic acid (IV) were obtained form a mixture of 1.0 g of α-APM and 0.5 g of gentisic acid or β-resorcylic acid in 100 m*l* of water; yield of III, 0.8 g (50%); yield of IV, 0.5 g (28%). For anal. and mp, see Table 2.

Separation of α- and β-APM with the Various Precipitating Reagents. A typical run was as follows (Table 3): To 500 m*l* of an aqueous solution containing 5.0 g of α-APM and 5.0 g of β-APM, 3.0 g of cinnamic acid was added with stirring at room temperature. The mixture was stirred for 5 hr at room temperature and then kept in a refrigerator overnight. The precipitate was collected by filtration and suspended in 500 m*l* of water. The mixture was adjusted to pH 2.0 with hydrochloric acid. The cinnamic acid thus liberated was removed by extraction with ether. The aqueous solution was adjusted to pH 5.0 with sodium bicarbonate and evaporated *in vacuo* to dryness. The residual crystals were recrystallized from 100 m*l* of water; yield, 3.2 g (64%); mp 235—236°C (dec.); $[\alpha]_D^{26}+32.0°$ (*c* 1, acetic acid). Found: C, 55.50; H, 6.21; N, 9.35%. Cacld for $C_{14}H_{18}O_5N_2\cdot 1/2\ H_2O$: C, 55.44; H, 6.31; N, 9.24%. The compound was confirmed by paper electrophoresis to be free from the β-isomer.

The mother liquor, excluding the α-isomer, was treated as above to give β-APM; yield, 3.2 g (64%); mp 198—199°C (dec.); $[\alpha]_D^{26}+43.0°$ (*c* 1, acetic acid). (Found: N, 9.30%). The compound was confirmed by paper electrophoresis to be pure β-APM.

7) J. M. Davey, A. H. Laird, and J. S. Morley, *J. Chem. Soc.*, *C*, **1966**, 555.

8) J. Heilmann, J. Barrollier, and E. Watzke, *Z. Physiol. Chem.*, **309**, 219 (1957).

BULLETIN OF THE CHEMICAL SOCIETY OF JAPAN, VOL. 45, 944—945(1972)

Reaction of Norbornene with Butadiene Catalyzed by Low-valent Cobalt, Giving *trans*-1-(*exo*-Norbornyl)-1,3-butadiene

Hideo SATO and Takashi INUKAI

The Central Research Laboratories, Chisso Corporation, Kamariya, Kanazawa-ku, Yokohama

(Received August 16, 1971)

Transition metal-catalyzed reactions between olefins and butadiene generally occur through hydrogen transfer from the olefins to butadiene to give substituted 1,4-hexadienes[1] according to

$$CH_2{=}CHR + CH_2{=}CH{-}CH{=}CH_2 \longrightarrow \begin{cases} CH_2{=}CR{-}CH_2{-}CH{=}CH{-}CH_3 \\ RCH{=}CH{-}CH_2{-}CH{=}CH{-}CH_3 \end{cases} \quad (1)$$

(R = H, alkyl, COOEt)

We recently reported,[2] however, that norbornadiene reacts with butadiene in the presence of cobalt catalysts of low valency, involving hydrogen transfer converse to that above, to give 5-butadienylnorborn-2-ene. This seems to be the first example of butadienylation of an internal carbon-carbon double bond. A similar butadienylation of terminal double bonds has been documented but is incomplete[3] and somewhat dubious,[4] except when the olefin is ethylene.[5]

We wish to report here another example of butadienylation, the reaction of norbornene with butadiene by low valent cobalt catalyst giving *trans*-1-(*exo*-norbornyl)-butadiene (I) with high stereochemical selectivity.

Results

Norbornene and butadiene were heated in a stainless steel reactor at 20—40°C for several hours under nitrogen in the presence of the catalysts prepared from $Co(acac)_3$ and Et_3Al. The reaction gave 30—40% yield of a mixture of 1:1 adducts (codimers), which was found by glpc analysis to consist of a main component (80—95%) and four minor ones. Practically no homodimers or oligomers were formed as by-products. The main product was separated by preparative glpc and its structure was determined as (I) from the following observations (Chart 1).

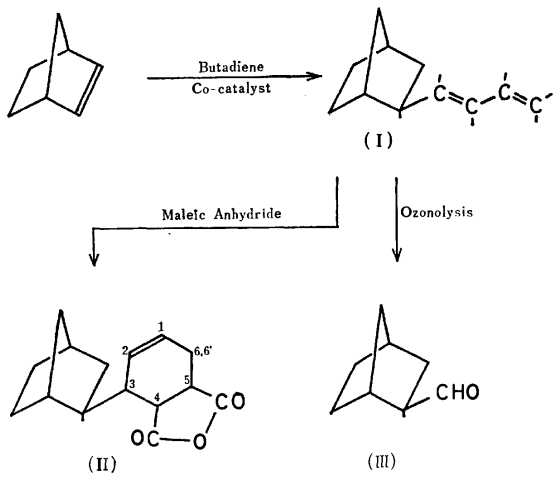

Chart

It has MW 148 (mass spectrum). The UV spectrum shows a typical s-*trans* 1,3-diene absorption, λ_{max} 230 nm, ε_{max} 28100, in cyclohexane, and the IR spectrum (liquid film) shows the $\nu_{C=C}$ at 1603 and 1650 cm^{-1}, δ_{C-H} of vinyl group at 892 and 1000 cm^{-1}, and δ_{C-H} of internal *trans* hydrogens at 949 cm^{-1}. That the butadiene moiety is *trans* substituted at its 1-position is proved by the facile reaction with maleic anhydride to give a Diels-Alder adduct whose NMR and IR spectra are consistent with the assigned structure of 3-norbornylcyclohexene-4,5-dicarboxylic anhydride (II). The butadienyl group is specifically located at the *exo* position of norbornane because *exo*-2-formylnorbornane (III) free from the *endo* isomer is obtained on ozonolysis of the main product. Consequently we conclude that it is *trans*-1-(*exo*-norbornyl)-1,3-butadiene (I).

Temperature around 40°C was found optimum for preparation of (I): at higher temperatures the selectivity for (I) tends to decrease presumably owing to the concomitant Diels-Alder reactions and the conversion decreases sharply. The molar ratio of Et_3Al:

Table 1. Reactions of norbornene with butadiene using several cobalt catalyst systems[a]

Catalyst components (mmol)		Conversion[b] (%)	Selectivity[c] (%)
$Co(acac)_3$ (0.5)	Et_3Al (1.5)	36	84.5
$Co(acac)_3$ (0.5)	Et_3Al[d] (1.5)	36	90
$Co(acac)_3$ (0.5)	Et_3Al[e] (1.5)	34	80
$CoCl_2$ (0.5)	Et_3Al (1.5)	20	80
$Co(acac)_3$ (0.5)	*i*-Bu_3Al (2.0)	32	82
$Co(acac)_3$ (0.5)	$Et_2(OEt)Al$ (2.0)	32	82

a) Reaction at 40°C, 4 hr; norbornene 43 mmol, butadiene 50 mmol, and *ca.* 2 *ml* of benzene.
b) Conversion of norbornene as determined from unreacted norbornene (glpc).
c) Percentage of (I) in the codimer fraction.
d) Plus ethylenediamine (1 mmol).
e) Plus ethanolamine (1 mmol).

1) *Cf.* C. W. Bird, "Transition Metal Intermediates in Organic Synthesis," Academic Press, London (1967), Chapter 2.
2) A. Takahashi and T. Inukai, *Chem. Commun.*, **1970**, 1473. See also A. Carbonaro, F. Cambisi, and G. Dall'Asta, *J. Org. Chem.*, **36**, 1443 (1971).
3) D. Wittenberg, *Angew. Chem.*, **75**, 1124 (1963); H. Müller, D. Wittenberg, H. Seibt, and E. Scharf, *ibid.*, **77**, 318 (1965). Butadienylation of several terminal olefins and acrylates was claimed without evidence to prove the structures of the reaction products.
4) Different structures have been given: A. Misono, Y. Uchida, T. Sato, and K. Uchida, This Bulletin, **40**, 1889 (1967); H. Singer, W. Umbach, and M. Dohr, *Synthesis*, **1971**, 265.
5) T. Saito, Y. Uchida, and A. Misono, This Bulletin, **38**, 1397 (1965).

$Co(acac)_3$ can be varied from 1 to 6 without remarkable effect on selectivity and conversion. The molar ratio of norbornene to butadiene showed only minor effect on yield of (I) within the range 0.5—1.5. Excessive imbalance of the reactant ratio proved undesirable. The results with various catalyst combinations are summarized in Table 1.

Other internal double bond compounds such as cyclopentene, cyclohexene, cyclooctene, *endo*-dicyclopentadiene and *cis*-butene gave little if any codimers with butadiene under similar reaction conditions. Thus butadienylation at an internal double bond seems to be specifically limited to norbornene and norbornadiene.[2]

The reaction provides a convenient route to *exo* norbornane derivatives which are difficult to prepare in stereochemically pure state. As an example, *exo*-2-formylnorbornane prepared by the method given by Alder and Stein[6] was found to be contaminated with the *endo* isomer which could not be completely removed. Pure *exo* (I) and (III) are evidently versatile starting materials for various *exo* substituted norbornanes.

Experimental[7]

Materials. Norbornene (Aldrich Co.) solution in benzene was dehydrated and deaerated by distillation under nitrogen. Butadiene was dried by passing through a $CaCl_2$ column and deaerated by distillation in vacuum. Desiccated $Co(acac)_3$ (EP grade) was used. Alkylaluminums were purified by vacuum distillation of commercial products.

trans-*1-(*exo-*Norbornyl)-butadiene (I).* In a typical example, butadiene (0.2 mol), norbornene (0.2 mol), $Co(acac)_3$ (2 mmol), Et_3Al (6 mmol), and 2 m*l* of benzene were put into a 100 m*l* stainless steel autoclave under nitrogen and heated to 40°C for 4 hr. The catalysts were killed with acetone (2 m*l*) and the mixture was subjected to steam-distillation with a trace of hydroquinone. The oily product was dried with anhydrous sodium sulfate and distilled to give 10.3 g of a codimer fraction, bp 72.5°C at 9 mmHg. The product was 96% pure (I) by glpc (Silicone DC-550). It was purified by glpc using a Silicone DC-550 preparative column.

Found: C, 89.0; H, 11.1%. Calcd for $C_{11}H_{16}$: C, 89.12; H, 10.88%.

Diels-Alder Adduct (II). A solution of 3.01 g of (I) and 1.96 g of maleic anhydride in 25 m*l* of benzene was warmed to 45°C for 5 hr and was let to stand overnight at room temperature. The solvent was removed under reduced pressure, and the residue with mp 95—120°C, was recrystallized repeatedly from benzene-hexane solvent (1:2 by volume) to attain mp 148—149°C.

Found: C, 73.3; H, 7.5%. Calcd for $C_{15}H_{18}O_3$: C, 73.15; H, 7.33%.

NMR (in $CDCl_3$): τ 4.02 (2H; $H_{(1)}$ and $H_{(2)}$, apparent doublet, J *ca.* 4 Hz); τ 6.60 (2H; $H_{(4)}$ and $H_{(5)}$, multiplet); τ 7.28 (1H; $H_{(3)}$, a pair of triplets); τ 7.6—9.2 (13H; $H_{(6)}$, $H_{(6')}$, and norbornyl protons, overlapped multiplets).

*2-*exo-*Formylnorbornane (III).* Ozonized oxygen was bubbled through a solution of 0.034 mol of (I) in methanol (100 m*l*) at −70°C, excess ozone was purged with stream of nitrogen, and triphenylphosphine (0.12 mol) in ether (100 m*l*) was added dropwise to the ozonide solution during a period of 40 min. The dry ice-acetone bath was removed to let the reaction mixture stand overnight at room temperature. (III) was codistilled with the solvent under reduced pressure into a cold trap (−70°C) and redistilled, bp 66—68°C at 12 mmHg; yield 2.5 g (59% of theory). By comparison of its glpc peak (Golay column R-45, polypropylene glycol, Hitachi) with those of the *exo*- and *endo*-2-formylnorbornane mixture obtained by the method of Alder and Stein starting from cyclopentadiene and acrolein,[6] it was found that the product was pure *exo* III free from *endo*.

Semicarbazone, mp 173—174°C (lit,[6] mp 178°C), showed IR and NMR spectra which are superposable with those of the authentic *exo* semicarbazone.

6) K. Alder and G. Stein, *Ann. Chem.*, **525**, 247 (1936).

7) All melting points are uncorrected. IR and UV spectra were determined with Nihon Bunko Model 402G and Hitachi Model EPS-III spectrophotometers, respectively. NMR spectra were taken with a Varian A-60A spectrometer.

BULLETIN OF THE CHEMICAL SOCIETY OF JAPAN, VOL. 45, 946—947(1972)

Cycloaddition of Spiro[2.4]hepta-4,6-diene to Tropone

Hiroshi TANIDA, Toshisada YANO, and Masako UEYAMA*

Shionogi Research Laboratory, Shionogi and Co., Ltd., Fukushima-ku, Osaka

(Received August 16, 1971)

Cycloaddition of cyclopentadiene to tropone leading to *exo*-tricyclo[4.4.1.1^{2,5}]dodeca-3,7,9-trien-11-one was reported by Cookson *et al.*[1] and by Itō *et al.*[2] as the first example of a thermal [6+4] cycloaddition which had been predicted by Hoffmann and Woodward.[3] Whereas in [4+2] cycloaddition dimethylfulvene reacts with dienophile in the same way as cyclopentadiene does,[4] in [6+4] cycloaddition the fulvene was reported to react with tropone as a 6π electron addend due to participation of the exocyclic double bond, the final product being a 2: 1 adduct of tropone and the fulvene.[5] From our interest in the alteration of the reaction pattern we carried out cycloaddition of spiro[2.4]hepta-4,6-diene (**1**) to tropone (**2**). Since cyclopentadiene, dimethylfulvene, and **1** all react in a uniform way in the [4+2] cycloaddition, it would be of interest to know the behavior of **1** in the addition reaction with tropone and, particularly, to determine whether or not the cyclopropane ring in **1** takes part displaying its masked unsaturation character.

When a mixture of an equimolar amount of **1** and **2** was heated at 110°C for 6 days in a tube sealed under nitrogen, two major products in a 79: 16 percent ratio were indicated by vpc, together with two minor products in a total 5%. The vpc peak ratio of the two major products was constant through the reaction period, indicating that they are kinetically-controlled. The 79 and 16% products (**3** and **4**) were isolated by a preparative gas chromatograph (2 m×15 mm) and shown to be both 1: 1 adducts by elementary analyses and molecular weight determinations (osmometry and mass spectroscopy). Catalytic reduction of the adducts over PtO_2 in ethanol resulted in an uptake of 3 mol of hydrogen and in acetic acid that of 4 mol of hydrogen indicating the presence of three double bonds and one

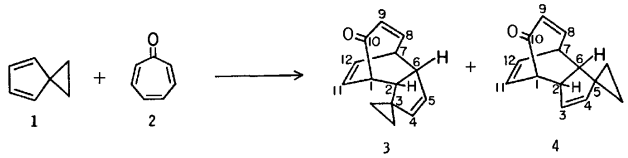

1 2 3 4

cyclopropane ring. The UV and IR properties indicate the presence of an $\alpha\beta$-unsaturated carbonyl group for both the adducts, and consequently, the absence of a [6+4] cycloaddition type product as observed in the reaction of cyclopentadiene.

Conformatory evidence for the indicated structures **3** and **4** was obtained from the 100 MHz PMR spectra, in which the signal assignments were performed by double resonance technique. The NMR parameters (first-order analyses) are summarized in Table 1. It was concluded that the orientation of the cyclopentene moieties in both the adducts was *endo* by the relatively small vicinal $J_{1,2}$ and $J_{6,7}$ and by the presence of long-range $^4J_{2,11}$ and $^4J_{6,12}$ due to the "W" arrangements of

TABLE 1. NMR DATA OF THE ADDUCTS (**3** AND **4**)

1) Chemical shift, τ

	Solvent	H_1	H_2	H_3	H_4	H_5	H_6	H_7	H_8	H_9	H_{11}	H_{12}
3	CCl_4	6.89	7.46	—	4.91	4.72	6.35	6.75	2.99	4.42	4.00	3.76
	C_6D_6	6.73	7.55	—	5.08	4.88	6.64	7.27	3.43	4.26	4.16	3.96
	$\Delta\tau$[a]	−0.16	0.09	—	0.17	0.16	0.29	0.52	0.44	−0.16	0.16	0.20
4	CCl_4	6.68	6.58	4.58	4.95	—	7.16	7.12	3.12	4.39	4.03	3.70
	C_6D_6	6.55	6.69	4.82	4.14	—	7.47	7.66	3.61	4.26	4.19	3.98
	$\Delta\tau$[a]	−0.13	0.11	0.24	0.19	—	0.31	0.54	0.49	−0.13	0.16	0.28

a) $\Delta\tau \equiv \tau$ in $C_6D_6 - \tau$ in CCl_4.

2) Coupling constant, Hz.

3	$J_{1,2}=2.0$	$J_{1,9}=1.9$	$J_{1,5}=\sim0.2$	$J_{1,11}=7.4$	$J_{1,12}=1.2$	$J_{2,6}=8.8$
	$J_{2,11}=\sim0.6$	$J_{4,5}=5.4$	$J_{4,6}=1.9$	$J_{5,6}=2.1$	$J_{6,7}=2.0$	$J_{6,12}=\sim0.5$
	$J_{7,8}=8.8$	$J_{7,9}=0.9$	$J_{7,11}=1.2$	$J_{7,12}=6.9$	$J_{8,9}=11.0$	$J_{11,12}=8.6$
4	$J_{1,2}=2.1$	$J_{1,9}=1.9$	$J_{1,11}=7.3$	$J_{1,12}=1.2$	$J_{2,3}=2.2$	$J_{2,4}=1.8$
	$J_{2,6}=8.8$	$J_{2,11}=0.7$	$J_{3,4}=5.7$	$J_{3,7}=\sim0.4$	$J_{6,7}=2.2$	$J_{6,12}=0.6$
	$J_{7,8}=8.7$	$J_{7,9}=0.7$	$J_{7,11}=1.2$	$J_{7,12}=6.8$	$J_{8,9}=11.1$	$J_{11,12}=8.7$

* Née OHTSURU.

1) R. C. Cookson, B. V. Drake, J. Hudec, and A. Morrison, *Chem. Commun.*, **1966**, 15.

2) S. Itō, Y. Fujise, T. Okuda, and Y. Inoue, This Bulletin, **39**, 1351 (1966).

3) a) R. Hoffmann and R. B. Woodward, *J. Amer. Chem. Soc.*, **87**, 2046, 4388 (1965). b) R. B. Woodward and R. Hoffmann, "The Conservation of Orbital Symmetry," Verlag Chemie GmbH-Academic Press Inc., Weinheim (1970), pp. 83—85.

4) A. S. Onischchenko, "Diene Synthesis," Israel Program for Scientic Translations, Jerusalem (1964).

5) a) K. N. Houk, L. J. Luskus, and N, S. Bhacca, *J. Amer. Chem. Soc.*, **92**, 6392 (1970). b) N. S. Bhacca, L. J. Luskus, and K. N. Houk, *Chem. Commun.*, **1971**, 109.

related protons. The values of $J_{1,2}$ and $J_{6,7}$ are of nearly the same magnitude as the corresponding coupling constants reported for the major [4+2] adduct of cyclopentadiene with 2-chlorotropone, 1-chlorotricyclo-[5.3.2.$0^{2,6(exo)}$]dodeca-3,8,11-trien-10-one.[6] Relative configuration (*anti* or *syn*) of the cyclopropane ring and the carbonyl group in **3** and **4** was determined by the following observations: the presence of spin-couplings between H_6 (or H_2) and the olefinic protons in **3** (or in **4**) (determinable by double resonance experiments); the relatively higher-field positions of H_1 and H_2 signals in **3** and those of H_6 and H_7 in **4** arising from the long-range anisotropy effect of the cyclopropane ring; and the presence of long-range couplings between H_1 and H_5 in **3** ($^5J_{1,5}$) and H_3 and H_7 in **4** ($^5J_{3,7}$) located in the zigzag paths.

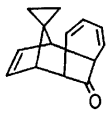

5

Thus it is found that, with tropone, cyclopentadiene reacts as a 4π electron addend, dimethylfulvene as a 6π addend, and the present **1** as a 2π addend. In comparison to the reaction conditions reported for cyclopentadiene and dimethylfulvene,[1,2,5] the occurrence of reaction of **1** seems to require the severest conditions. A molecular model suggests that the [6+4] cycloadduct from **1** and **2** (**5**), if formed, would have severe steric compression around the cyclopropane ring and the butadiene bridge, so that this cycloaddition process would be strongly retarded and the cyclopentadiene moiety in **1** compelled to react as a 2π addend toward the 4π electron system in **2**, despite the higher activation energy required.

Experimental

Melting points were taken in capillary tubes and are corrected. Infrared spectra were determined with a Nippon Bunko IR-S spectrometer, ultraviolet spectra with a Hitachi EPS-3T spectrometer, and NMR spectra with a Varian A-60A and HA-100. VPC analysis was carried out on a Hitachi gas chromatograph K-53 equipped with a hydrogen flame ionization detector, using a 1 m×3 mm glass column packed with 5% XE 60 on Chromosorb W.

Reaction of 1 with 2. Diene **1** was prepared by the reported method.[7] A mixture of 1.5 g of **1** and 1.6 g of **2** was placed in a tube, sealed under nitrogen, and heated at 110°C for 6 days. VPC analysis of the reaction mixture revealed two major products (**3** and **4**) in a 79: 16 percent ratio, with two minor products in a total 5%. Isolation of **3** and **4** was carried out by a Yanagimoto gas chromatograph GCG-3 equipped with 2 m×15 mm glass column packed with 5% XE 60 on Chromosorb W. With a column temperature 180°C and helium carrier gas 300 ml/min, the retention times were 25 min for **3** and 31 min for **4**. Recrystalliaztion of the **3** fraction thus isolated from *n*-pentane gave colorless crystals, mp 66—66.5°; mass spectrum (70 eV) *m/e* 198 (parent peak); molecular weight by osmometry 192; UV λ_{max} (95% EtOH): 225 mμ (shoulder, ε 7000), 265 (1800); IR ($CHCl_3$): 1660 cm^{-1} (CO). Found: C, 84.76; H, 7.17%. Calcd for $C_{14}H_{14}O$: C, 84.81; H, 7.12%. Recrystallization of the **4** fraction from *n*-pentane gave colorless crystals, mp 96.3—97.0°C; mass spectrum (70 eV) *m/e* 198 (parent peak); UV λ_{max} (95% EtOH): 230 mμ (shoulder, ε 5370), 260 (2000); IR ($CHCl_3$): 1656 cm^{-1} (CO). Found: C, 85.10; H, 7.14%. Calcd for $C_{14}H_{14}O$: C, 84.81; H, 7.12%. NMR data for **3** and **4** are summarized in Table 1.

6) S. Itō, K. Sakan, and Y. Fujise, *Tetrahedron Lett.*, **1969**, 775.

7) C. F. Wilcox, Jr., and R. R. Craig, *J. Amer. Chem. Soc.*, **83**, 3866 (1961) and references cited therein.

BULLETIN OF THE CHEMICAL SOCIETY OF JAPAN, VOL. 45, 947—949(1972)

The Kinetics of the Electron-transfer Reactions between Several Chloropentakis(alkylamine)cobalt(III) Complexes and Iron(II)

Kousaburo OHASHI

Department of Chemistry, Ibaraki University, Mito, Ibaraki

(Received August 17, 1971)

In previous papers, the effect of the *cis*-ligand to the bridging chloride ion on the reactivity of *cis*-$Co(en)_2ACl^{2+}$ [1] (A=alkylamine and aminoalcohol) and the effect of amino acid[2] as the nonbridging ligand on the reactivity of *trans*(O,Cl)-Co(dien)(am)Cl^+ (am=amino acid, dien=diethylenetriamine) and *trans*(*N*)-$Co(am)_2(ox)^-$ (ox=oxalic acid) in the iron(II) reductions of these complexes have been reported.

It was demonstrated that the reactivity of *cis*-$Co(en)_2ACl^{2+}$ decreased slightly with an increase in the size of alkylamine and that the specific reduction rate for the β-alanine cobalt(III) complex was considerably larger than that for the other amino acid cobalt(III) complexes investigated.

Buckingham *et al.*[3] found that the base and acid hydrolyses of a series of chloropentakis(alkylamine)-cobalt(III) complexes were very much accelerated by the steric interaction of the alkylamines. The reactivities of these complexes are increased with increases

1) Y. Kurimura and K. Ohashi, This Bulletin, **44**, 1797 (1971).

2) K. Ohashi, K. Yamamoto, I. Hirako, and Y. Kurimura, *ibid.*, in prees.

3) D. A. Buckingham, B. M. Foxman, and A. M. Sargeson, *Inorg. Chem.*, **9**, 1790 (1970).

Table 1. The rate constants, the activation parameters for iron(II) reductions at 25±0.1°C and absorption maximum of cobalt(III) complexes

Complex	Rate constant[a] $M^{-1}\cdot sec^{-1}$	$\Delta H^{\neq}$ kcal/mol	$\Delta S^{\neq}$ eu	nm λ_{max}[b]	nm λ_{max}[c]
$Co(NH_3)_5Cl^{2+}$	7.30×10^{-3}	16.9	−10.4	525	362
trans-$Co(NH_3)_4(CH_3NH_2)Cl^{2+}$	1.26×10^{-2}	16.3	−11.0	535	364
$Co(CH_3NH_2)_5Cl^{2+}$	4.72×10^{-2}	14.8	−13.7	550	380
$Co(n\text{-}C_3H_7NH_2)_5Cl^{2+}$	9.14×10^{-2}	13.4	−16.4	550	383
$Co(i\text{-}C_4H_9NH_2)_5Cl^{2+}$	1.63×10^{-1}	—	—	550	382

a) $[H_2SO_4]=0.050M$, $\sum[SO_4^{2-}]=0.50M$
b) wavelength for the first absorption maximum
c) wavelength for the second absorption maximum

in the size of the alkylamine.

It is interesting to investigate the effect of the coordinated ligands on the reactivity of chloropentakis(alkylamine)cobalt(III) complexes with iron(II). Therefore, the present author wishes to report the results observed in the electron-transfer reactions of several chloropentakis(alkylamine)cobalt(III) complexes.

Experimental

Preparation of Complexes. $[Co(CH_3NH_2)_5Cl]Cl_2$,[4] $[Co(n\text{-}C_3H_7NH_2)_5Cl]Cl_2\cdot HCl$,[3] and $[Co(i\text{-}C_4H_9NH_2)_5Cl]Cl_2\cdot HCl$[3] were prepared by the methods described in the references cited. The *trans*-$[Co(NH_3)_4(CH_3NH_2)Cl]Cl_2$ was prepared by a manner similar to that for the preparation of *trans*-$[Co(^{15}NH_3)(NH_3)_4Cl](ClO_4)_2$.[5]

The wavelengths of the first and second absorption maxima for these complexes are listed in Table 1, along with the rate constants.

Materials. The preparation of a stock solution of iron(II) sulfate and the determination of iron(II), the sulfate ion, and the hydrogen ion were carried out by a method similar to that described in a previous paper.[6] All the other chemicals were of a guaranteed reagent grade. The concentration of sulfuric acid and the total concentration of the sulfate ion of the reaction mixture were adjusted to 0.05M and 0.50M respectively by the addition of sulfuric acid and sodium sulfate solutions.

Measurement of the Reaction Rate. The reactions were followed spectrophotometrically under pseudo-first-order conditions in which the iron(II) concentration was in a large excess to that of the Co(III) complex. The absorbance at the wavelengths corresponding to the first absorption maxima for the complexes were all recorded automatically except for the case of $Co(i\text{-}C_4H_9NH_2)_5Cl^{2+}$. Since the aquation of the $Co(i\text{-}C_4H_9NH_2)_5Cl^{2+}$ proceeded in some extent during the dissolution, the reduction rates were measured at 537 nm, which is the isosbestic point for this complex and $Co(i\text{-}C_4H_9NH_2)_5OH_2^{3+}$. The rate of the aquation of this complex during electron-transfer reaction was negligible small in comparison with that of the reduction during the initial period.

The activation parameters for all the complexes except for $Co(i\text{-}C_4H_9NH_2)_5Cl^{2+}$ were obtained from the log k *vs.* $1/T$ plot, using a linear least-squares method.

Results and Discussion

In the cases of $Co(NH_3)_5Cl^{2+}$, *trans*-$Co(NH_3)_4(CH_3NH_2)Cl^{2+}$, and $Co(CH_3NH_2)_5Cl^{2+}$, the plots of log (A_t-A_∞) *vs.* time were linear for at least two half-lives, but for the $Co(n\text{-}C_3H_7NH_2)_5Cl^{2+}$ and $Co(i\text{-}C_4H_9NH_2)_5Cl^{2+}$, the reaction obeyed a pseudo-first-order sequence for a 60% reaction.

The rates for these reductions are first-order dependences on the Co(III) and Fe(II) concentrations respectively.

In spite of the lability of iron(III) complexes, it has been found, by a direct observation of the transient species $FeCl^{2+}$, that the reactions of cobalt(III) complexes, such as $Co(NH_3)_4OH_2Cl^{2+}$,[7] $Co(HEDTA)Cl^-$,[7] and $Co(OH_2)_5Cl^{2+}$,[8] with iron(II) proceed *via* the chloride-bridged activated states. Therefore, it seems reasonable to assume a similar mechanism for the present reactions. The most important factors in determining the rates of the inner-sphere electron-transfer reactions of cobalt(III) complexes may be: (1) the ligand field strength of the *trans*-ligand which is located at the *trans*-position to the bridging ligand, and (2) the energy for stretching the *trans*-ligand away from the cobalt(III) center. The greater reactivity for *trans*-$Co(NH_3)_4(CH_3NH_2)Cl^{2+}$ than $Co(NH_3)_5Cl^{2+}$ may be ascribed to the weak ligand-field strength for the *trans*-ligand (methylamine) in the former compared with that for the *trans*-ligand (ammonia) in the latter (Table 1).

The rate constants shown in Table 1 indicate that the reactivity of the cobalt(III) complexes of the CoA_5Cl^{2+} type, where A is alkylamine, increases slightly with the size of the alkylamine ligand.

In a previous work,[1] it was suggested that the reactivity of *cis*-$Co(en)_2ACl^{2+}$ in the reduction by iron(II) decreased slightly with an increase in the size of the alkylamine from methylamine to butylamine. The specific rates for CoA_5Cl^{2+} with iron(II) are increased, however, with an increase in the size of alkylamine. The ligand-field strengths of alkylamines are of almost the same degree. Consequently, the small increase in the reactivity of CoA_5Cl^{2+} may be caused by the steric interaction[3] between the coordinated alkylamines. This steric interaction would reduce the reorganization

4) R. Mitzner, P. Blankenburg, and W. Depkat, *Z. Chem.*, **9**, 68 (1960).
5) D. A. Buckingham, I. I. Olsen, and A. M. Sargeson, *J. Amer. Chem. Soc.*, **88**, 5443 (1966).
6) Y. Kurimura, K. Ohashi, T. Ohtsuki, and K. Yamamoto, This Bulletin, **44**, 1293 (1971).
7) A. Haim and N. Sutin, *J. Amer. Chem. Soc.*, **88**, 5343 (1966).
8) T. J. Conochioli, G. Nancollas, and N. Sutin, *ibid.*, **86**, 1453 (1953).

energy for the reduction. No detailed explanation of such a steric effect can be made from the results thus far obtained.

The rates of the base and acid hydrolyses of chloropentakis(alkylamine)cobalt(III) complexes are very much increased with the size of alkylamine. For example, the relative reactivities for the base and acid hydrolyses of $Co(i\text{-}C_4H_9NH_2)_5Cl^{2+}$ are, respectively about 6×10^5 and 10^2 times greater than those of $Co(NH_3)_5Cl^{2+}$.

In the Fe(II) reduction reactions of chloropentakis(alkylamine)cobalt(III) complexes, the effect of the size of alkylamine is very small compared with that in the base and acid hydrolyses reactions. This indicates that the steric effect of the nonbridging ligand in the Fe(II) reduction is not very important.

The authour wishes to express his thanks to Professor K. Yamamoto and Professor Y. Kurimura for their helpful discussions, to Mr. T. Suzuki for his assistance in this work, and to Professor E. Tsuchida for his microanalysis of the Co(III) complexes.

BULLETIN OF THE CHEMICAL SOCIETY OF JAPAN, VOL. 45, 949—950(1972)

Rotational Isomerism in Epihalogenohydrin

Michiro HAYASHI, Kazuki HAMO, Keiichi OHNO, and Hiromu MURATA

Department of Chemistry, Faculty of Science, Hiroshima University, Hiroshima

(Received August 19, 1971)

Thirty years ago, Ballaus and Wagner[1] studied the Raman spectra of epihalogenohydrin in the liquid state and discussed the molecular forms of these substances. Recently, several new investigations have been reported on the molecular forms of these substances.

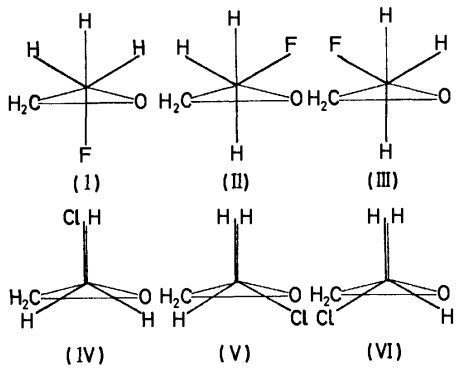

Fig. 1. Molecular forms of epihalogenohydrin.

For epifluorohydrin, the NMR study[2] and the microwave spectroscopy[3] have indicated that the most stable molecular form is the form I in Fig. 1, in which the fluorine atom occupies the *cis* position to the epoxide ring. For epichlorohydrin, however, the electron diffraction[4] has indicated that the preferred form is the form IV, in which the chlorine atom occupies the *trans* position to the epoxide ring.

Not only are the results of these investigations quite different, but the co-existence of the different isomers has never been proved explicitly. We have, therefore, investigated the vibrational spectra of epichlorohydrin, epibromohydrin, and epiiodohydrin in relation to the rotational isomerism, paying special attention to the problem of whether or not the isomers co-exist in the liquid state.

Experimental

Commercial propylene oxide, epichlorohydrin, and epibromohydrin were used without purification since the gas chromatograph showed no remarkable impurities. The epiiodohydrin was prepared from epichlorohydrin by an exchange reaction with KI in acetone.[1]

The infrared spectra were recorded in the region from 4000 to 200 cm^{-1} with a Perkin-Elmer 621 spectrophotometer in both the liquid and crystalline states. The solvent effects of the spectra were also examined using cyclohexane, acetone, and acetonitrile as solvents.

Results and Discussion

As is shown in Fig. 2, some of the spectra vanish in the crystalline state for epihalogenohydrin, while no remarkable change is seen for propylene oxide. The assignments of the observed spectra can be partially made if the spectra of epihalogenohydrin are compared with those of ethylene oxide[5] and propylene oxide.[6,7] Several strong infrared spectra found in the region below 750 cm^{-1} for these substances are regarded as originating from the CH_3 and CH_2X groups.

For propylene oxide, the observed strong bands at 370 and 415 cm^{-1} are assigned to two CCC deformation modes since the CH_3 torsional mode is known to be below 200 cm^{-1}.[7]

For epihalogenohydrin, three skeletal deformation modes may be expected in the region below 500 cm^{-1} for unique molecular form. As Ballaus and Wagner[1] have already pointed out, these skeletal deformations are found at the frequencies close to those of isobutyl

1) O. Ballaus and J. Wagner, *Z. Physik. Chem., B*, **45**, 272 (1939).
2) W. A. Thomas, *J. Chem. Soc., B*, **1968**, 1187.
3) J. Bragin, K. L. Kizer, and J. R. Durig, *J. Mol. Spectrosc.*, **38**, 289 (1971).
4) M. Igarashi, This Bulletin, **28**, 58 (1955).
5) R. C. Lord and B. Nolin, *J. Chem. Phys.*, **24**, 656 (1956).
6) M. C. Tobin, *Spectrochim. Acta*, **16**, 1108 (1960).
7) W. G. Fateley and F. A. Miller, *ibid.*, **19**, 611 (1963).

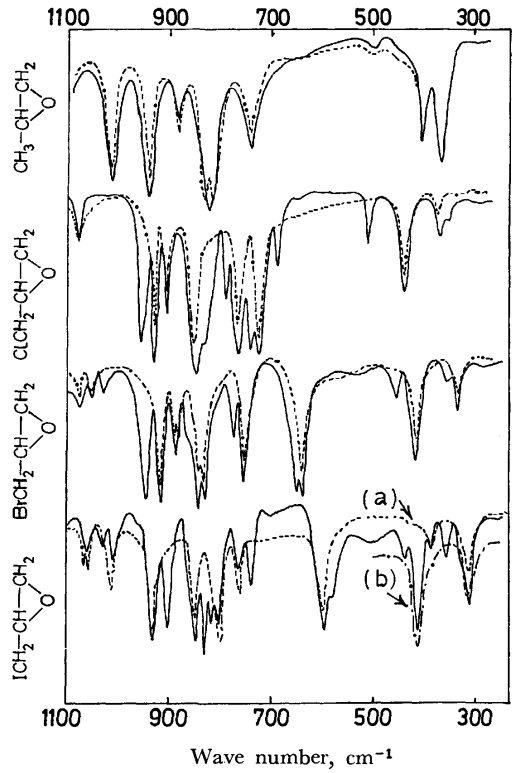

Fig. 2. The infrared spectra of propylene oxide and epihalogenohydrin:—in the liquid state, ----in the crystalline state; (a) in the most stable state, (b) in the metastable state.

halides. From a comparison with the observed spectra of isobutyl halides, the three skeletal deformation modes of epihalogenohydrin can be regarded as falling into two groups, one corresponding to two skeletal deformations of propylene oxide in the region over 300 cm^{-1}, and the other corresponding to the CCX deformation in the region below 300 cm^{-1}.

There are four infrared bands for epichlorohydrin and epibromohydrin and five for epiiodohydrin in this region in the liquid state, while two of them persist in the crystalline state. As is shown in Fig. 2, the frequency *vs.* intensity patterns of the infrared spectra observed around 400, 750, and 900 cm^{-1} show us that the isomers of epichlorohydrin and epibromohydrin in the crystalline state are probably similar to each other, but are different from that of epiiodohydrin. During the repetition of the crystallization procedure, a spectral pattern similar to those for epichlorohydrin and epibromohydrin was also obtained once in the region below 450 cm^{-1} for epiiodohydrin, as is shown in Fig. 2. However, the pattern was changed into an usual one by annealing the sample before recording the spectra around 750 and 900 cm^{-1}.

Although attempts at the reproduction of this special crystalline state have been unsuccessful thus far, these facts suggest that there exist two different crystalline states for epiiodohydrin and that the molecular form is similar to those of epichlorohydrin and epibromohydrin in the metastable crystalline state and is different in the most stable crystalline state.

The solvent effects of the infrared spectra were examined for the skeletal deformations around 400 cm^{-1} and for the C–X stretching modes in the region from 750 to 550 cm^{-1}, which can be easily assigned from the assignments for the similar molecules.[8,9]

For epichlorohydrin and epibromohydrin, the spectra vanishing in the crystalline state become stronger in the cyclohexane solution, while for epiiodohydrin, the spectra persisting in the most stable crystalline state become stronger.

From these results, it can be said that the form in the crystalline state is probably the more polar form for epichlorohydrin and epibromohydrin and the less polar form for epiiodohydrin, in relation to the other forms found only in the liquid state.

As is shown in Fig. 1, there are four other possible molecular forms besides the forms I and IV. Estimation from the bond moments indicates that the magnitudes of the dipole moments for the six different forms decrease in the order of V>I≒II>IV≒VI>III. However, we cannot conclude from these results alone which molecular forms in Fig. 1 correspond to the more polar form and the less polar form described above, though the co-existence of at least two different isomers in the liquid state is proved for these molecules.

8) S. Mizushima, T. Shimanouchi, K. Nakamura, M. Hayashi, and S. Tsuchiya, *J. Chem. Phys.*, **26**, 970 (1957).

9) J. K. Brown and N. Sheppard, *Trans. Faraday Soc.*, **50**, 1164 (1954).

BULLETIN OF THE CHEMICAL SOCIETY OF JAPAN, VOL. 45, 951—952(1972)

The Carbonylation of 1,1′-Bis(chloromercuri)ferrocene with Palladium Salt: A Synthesis of [1.1]Ferrocenophane-1,12-dione

Akira KASAHARA, Taeko IZUMI, and Satoshi OHNISHI

Department of Applied Chemistry, Faculty of Engineering, Yamagata University, Yonezawa-shi, Yamagata

(Received August 23, 1971)

It has recently been found that palladium or palladium chloride can be used as a catalyst for the carbonylation reaction of various compounds:[1] olefins,[2] dienes,[3] acetylene,[4] allyl halides,[5] and amines.[6,7] Furthermore, Henry[7] has reported that arylpalladium salts, prepared *in situ* from arylmercuric salts and palladium compounds, react with carbon monoxide to form arenecarboxylic acids or their derivatives; Heck[8] has also described that diaryl ketones could be formed in moderate yields from arylmercuric salts and carbon monoxide with a palladium-salt catalyst. In this paper, we wish to report that the reaction of 1,1′-bis(chloromercuri)ferrocene (**1**) and carbon monoxide in the presence of a palladium salt results in the formation of [1.1]ferrocenophane-1,12-dione (**2**) and ferrocenedicarboxylic acid derivatives (**3**), plus a small amount of bi-1,1′-ferrocenylene (**4**), while the diferrocenyl ketone (**6**) and methyl ferrocenecarboxylate (**7**) are also produced by the carbonylation reaction of chloromercuriferrocene (**5**) in methanol with a palladium-salt catalyst.

Experimental

Measurements. All the melting points are uncorrected. The NMR spectra were determined in $CDCl_3$ at 60 MHz with a Hitachi H-60 NMR spectrometer, using TMS as the internal reference. A Hitachi EPI-S2 infrared spectrometer was used for the measurements of the infrared absorption spectra. The molecular weight was determined in benzene or in chloroform, using a Hitachi 115 vapor-pressure osmometer.

Materials. 1,1′-Bis(chloromercuri)ferrocene (**1**) and chloromercuriferrocene (**5**) were prepared according to the method described by Fish and Rosenblum.[9]

Carbonylation of 1,1′-Bis(chloromercuri)ferrocene (1). The lithium palladium chloride solution was prepared by stirring 1.68 g (40 mmol) of anhydrous lithium chloride with 3.54 g (20 mmol) of anhydrous palladium chloride overnight at room temperature in 200 m*l* of methanol. Into this lithium chloropalladite solution, **1** (6.56 g, 10 mmol) was then carbonylated at 70°C under a carbon monoxide pressure (50 atm) for 6 hr with shaking; a pressure drop was thus observed. The products were isolated by filtering to remove a precipitated palladium and by distilling under reduced pressure to remove the solvent. The residue was dissolved in benzene and chromatographed on neutral alumina. The first elution with benzene and recrystallization from benzene afforded orange crystals (0.15 g, 8% yields); they were identified as bi-1,1′-ferrocenylene (**4**) by a comparison of the IR spectrum with that of an authentic sample and by a mixed-melting-point determination.[10] Mp 370°C. IR spectrum (KBr): 3090, 1101, 998 cm^{-1}. Found: C, 65.41; H, 4.46%; mol wt (in $CHCl_3$) 363. Calcd for $C_{20}H_{16}Fe_2$: C, 65.54; H, 4.39%; mol wt 368.

The second elution with benzene and recrystallization gave dimethyl 1,1′-ferrocenedicarboxylate[11] (**3**) (1.12 g, 36.8%); this was identified by a comparison of the IR and NMR spectra, and by a mixed-melting-point determination, with an authentic sample. Mp 114—115°C. IR spectrum (KBr): 1704 cm^{-1} (ester). NMR spectrum (ppm): 3.78 ($COOCH_3$, singlet), 4.35 (ring protons, triplet), 4.77 (ring protons, triplet).

Further elution with chloroform and recrystallization from chloroform afforded yellow orange crystals (1.19 g, 29%); they were identified as [1.1]ferrocenophane-1,12-dione[12] (**2**). Mp 350°C. IR spectrum (KBr): 1615, 1104, 998 cm^{-1}. NMR spectrum (ppm): 4.40 (ring protons, triplet); 4.80 (ring protons, triplet). Found: C, 62.17; H, 3.72%; mol wt (in $CHCl_3$) 419. Calcd for $C_{22}H_{16}O_2Fe_2$: C, 62.28; H, 3.80%; mol wt 424.2.

Carbonylation of Chloromercuriferrocene (5). In a lithium chloropalladite solution (prepared from 0.84 g of lithium chloride and 1.77 g of palladium chloride in 100 m*l* of methanol), **5** was carbonylated at 50°C under carbon monoxide (50 atm) for 3 hr with shaking. The isolation of the product in the same manner as was used for **1** gave biferrocenyl[13] (**8**) (mp 236—238°C, 0.21 g, 11.2%), methyl ferrocenecarboxylate[14] (**7**) (mp 70—71°C, 0.78 g, 32.3%), and diferrocenyl ketone[15] (**6**) (mp 205—206°C, 0.54 g, 31.5%). These products were identified by a comparison of the IR and NMR spectra, and by a mixed-melting-point determination, with an authentic sample.

Results and Discussion

The carbonylation of **1** was carried out at 70°C under a carbon monoxide pressure of 50 atm in the presence

1) J. Tsuji, "Advances in Organic Chemistry: Methods and Results," Vol. 6, ed. by E. C. Taylor and H. Wynberg, Interscience Publishers, New York, N. Y. (1969), p. 109.

2) J. Tsuji, M. Morikawa, and J. Kiji, *Tterahedron Lett.*, **1963**, 1063, 1437; *J. Amer. Chem. Soc.*, **86**, 4851 (1964).

3) S. Brewis and P. R. Hughes, *Chem. Commun.*, **1965**, 157, 489; *ibid.*, **1966**, 6; J. Tsuji, S. Hosaka, T. Susuki, and J. Kiji, This Bulletin, **39**, 141 (1966); J. Tsuji and T. Nogi, *ibid.*, **39**, 146 (1966).

4) J. Tsuji, M. Morikawa, and N. Iwamoto, *J. Amer. Chem. Soc.*, **86**, 2095 (1964).

5) J. Tsuji, J. Kiji, S. Imamura, and M. Morikawa, *ibid*,. **86**, 4350 (1964).

6) E. W. Stern and M. L. Spector, *J. Org. Chem.*, **31**, 596 (1966).

7) P. M. Henry, *Tetrahedron Lett.*, **1968**, 2285.

8) R. F. Heck, *J. Amer. Chem. Soc.*, **90**, 5546 (1968).

9) R. W. Fish and M. Rosenblum, *J. Org. Chem.*, **30**, 1253 (1965).

10) F. L. Hedberg and H. Rosenberg, *J. Amer. Chem. Soc.*, **91**, 1258 (1969); M. D. Rausch, R. F. Kovar ,and C. S. Kraihanzel, *ibid.*, **91**, 1259 (1969).

11) K. Yamakawa, H. Ochi, and K. Arakawa, *Chem. Pharm. Bull.*, **11**, 905 (1963).

12) W. E. Watts, *J. Organometal. Chem.*, **10**, 191 (1967).

13) H. Schechlter and J. F. Helling, *J. Org. Chem.*, **26**, 1034 (1961).

14) R. A. Benkser, D. Goggin, and G. Schroll, *J. Amer. Chem. Soc.*, **76**, 4025 (1954).

15) E. O. Fischer and H. Grubert, *ibid.*, **82**, 76 (1960).

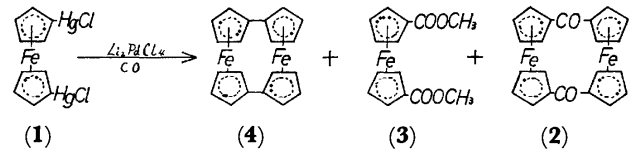

(1) (4) (3) (2)

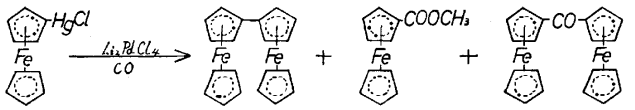

(5) (8) (7) (6)

of lithium chloropalladite in methanol; the main products were **2** and **3**, plus a small amount of **4**. Under the same conditions, the carbonylation of **5** in methanol resulted in the formation of **6**, **7**, and **8**. Heck[8] reported that arylmercuric chlorides react with palladium salts in the absence of carbon monoxide to form biaryls in good yields. We also observed that the reaction of **1** with palladium salts led to the formation of **4** in good yields.[16] The addition of carbon monoxide to the reaction mixture results in the formation of **2** and **3** at the expense of **4**. In the carbonylation of arylmercuric salts, the use of rhodium catalysts for the diaryl ketone has been reported. However, in the carbonylation of **1**, the use of rhodium trichloride as a catalyst did not bring about better results in the formation of **2** compared with the use of the palladium catalyst.

16) T. Izumi, G. Saito, and A. Kasahara, unpublished work.

The mechanism of the formation of **2** from **1**, as Heck pointed out in his carbonylation study,[8] probably involves the reaction of an acyl-palladium compound with a ferrocenylene palladium compound or a ferrocenylene mercuric compound. **3** and **4** are probably formed by side reactions.

$$[C_5H_4(HgCl)]_2Fe + PdCl_2 \rightleftharpoons [C_5H_4(PdCl)]_2Fe + 2HgCl_2$$

$$[C_5H_4(PdCl)]_2Fe + 2CO \rightleftharpoons [C_5H_4(COPdCl)]_2Fe$$

$$[C_5H_4(COPdCl)]_2Fe + [C_5H_4(PdCl)]_2Fe \longrightarrow \mathbf{2} + 2PdCl_2 + 2Pd$$

or

$$[C_5H_4(COPdCl)]_2Fe + [C_5H_4(HgCl)]_2Fe \longrightarrow \mathbf{2} + 2HgCl_2 + 2Pd$$

$$2[C_5H_4(PdCl)]_2Fe \longrightarrow \mathbf{4} + 2PdCl_2 + 2Pd$$

or

$$[C_5H_4(PdCl)]_2Fe + [C_5H_4(HgCl)]_2Fe \longrightarrow \mathbf{4} + 2HgCl_2 + 2Pd$$

$$[C_5H_4(COPdCl)]_2Fe \longrightarrow [C_5H_4(COCl)]_2Fe + 2Pd$$

$$[C_5H_4(COCl)]_2Fe + CH_3OH \longrightarrow \mathbf{3} + 2HCl$$

BULLETIN OF THE CHEMICAL SOCIETY OF JAPAN, VOL. 45, 952—954(1972)

Thiocyanoacetate. III. The Synthesis of 2-Hydrazono-4-thiazolidinone Derivatives[1)]

Satoshi KAMBE and Toshio HAYASHI*

Oyama Technical College, Oyama-shi, Tochigi

**The Institute of Physical and Chemical Research, Wako-shi, Saitama*

(Received August 23, 1971)

Although a number of papers[2-6)] have been published concerning the syntheses of 2-hydrazono-4-thiazolidinone derivatives, no syntheses using ethyl thiocyanoacetate (**1**) as the starting material have been reported. We wish now to report a convenient synthesis of 2-arylidenehydrazono-4-thiazolidinones from **1**, arylideneazines (**2**), and hydrazine hydrate (**3**).

The reaction was performed by refluxing a mixture of **1**, **2**, and **3** (molar ratio 2: 1: 1) in ethanol containing a small amount of acetic acid. For example, the reaction of **1** with **2a** and **3** afforded a pale yellow solid melting at 254—5°C, which was identified as 2-benzylidenehydrazono-4-thiazolidinone (**4a**). The structure of **4a** was inferred from the results of elementary analysis and of spectral studies. The IR spectrum of **4a** revealed the presence of NH (3025 cm^{-1}), C=O (1713 cm^{-1}), and C=N (1645 cm^{-1}) bands. The NMR spectrum showed the NH proton signal at δ 12.1, the CH_2 at 3.9, the =CH at 8.4, and the C_6H_5 at 7.5 ppm. For the structual confirmation of **4a**, an authentic sample was prepared by the treatment of ethyl chloroacetate with benzaldehyde thiosemicarbazone according to the method in the literature.[5)] These products were proved to be identical by a mixed-melting-point determination and by IR and NMR spectral studies. On the other hand, the reaction of **1** with **2a** and **3** (molar ratio 1: 1: 1) in acetic acid gave a product which was identified as 5- benzylidene-2-benzylidenehydrazono-4-thiazolidinone (**5a**). The NMR spectrum of **5a** lacked the CH_2 proton signal and showed the =CH proton as a doublet (δ 8.4 and 8.5 ppm). **5a** was hydrolyzed by hydrochloric acid to

1) Part II of this series: S. Kambe, T. Hayashi, H. Yasuda, and A. Sakurai, *Nippon Kagaku Zasshi*, **92**, 867 (1971).
2) F. J. Wilson and R. Burns, *J. Chem. Soc.*, **121**, 870 (1922).
3) F. J. Wilson and R. Burns, *ibid.*, **123**, 799 (1923).
4) P. Chabrier and E. Cattelain, *Bull. Soc. Chem. Fr.*, **17**, 48 (1950).
5) H. Taniyama, B. Yasui, and T. Imamura, *Yakugaku Zasshi*, **75**, 8 (1955).
6) H. Taniyama and T. Yusa, *ibid.*, **75**, 11 (1955).

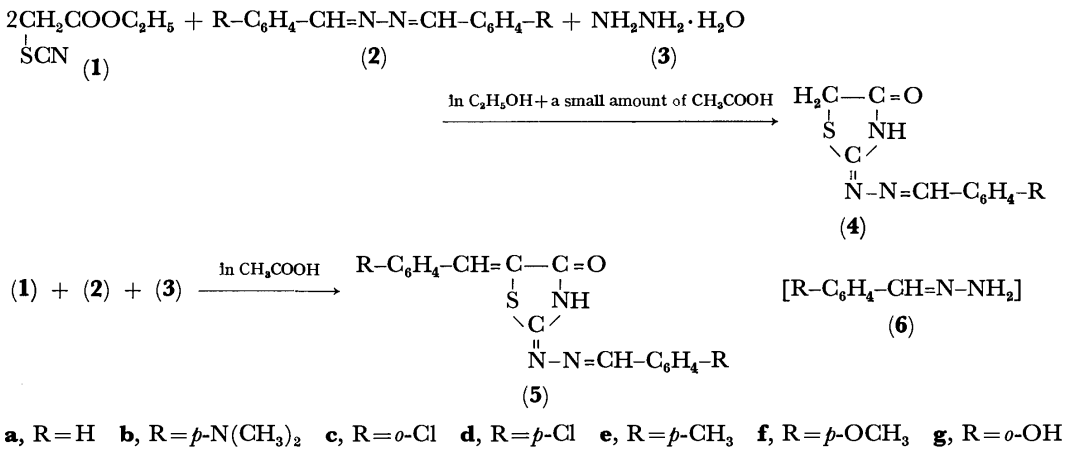

a, R=H **b**, R=*p*-N(CH$_3$)$_2$ **c**, R=*o*-Cl **d**, R=*p*-Cl **e**, R=*p*-CH$_3$ **f**, R=*p*-OCH$_3$ **g**, R=*o*-OH

Scheme 1

give 5-benzylidene-2,4-thiazolinedione, whose IR spectrum showed a carbonyl stretching band as a doublet (1670 and 1740 cm^{-1}). A similar conversion has been reported in the case of 2-isopropylidenehydrazone-4-thiazolidinone.[2] Furthermore, **5a** was also obtained by the reaction of **1** with benzaldehyde acethylhydrazone in acetic acid. However, when **2 g** was employed as the azine reactant, the reaction did not lead to the formation of the corresponding product (**5 g**), but to **4 g**.

A plausible reaction sequence is illustrated in Scheme 1. Presumably, the reaction proceeds through the intermediary of the hydrazone (**6**), which subsequently condenses with **1** to give **4**. The product, **5**, may be formed by the further condensation of **4** with aromatic aldehyde.

Table 1. 2-Arylidenehydrazono-4-thiazolidinones (**4**)

Product	Reac. time (hr)	Yield (%)	Mp °C	Formula	Analysis (%) Found (Calcd) C	H	N	S
4a	2	66	254—255[b]	$C_{10}H_9ON_3S$	55.18 (54.79)	4.03 (4.14)	20.01 (19.17)	14.56 (14.59)
4b	3	52	255—256	$C_{12}H_{14}ON_4S$	55.12 (54.95)	5.28 (5.38)	21.48 (21.37)	12.38 (12.20)
4c	3.5	54	221—222	$C_{10}H_8ON_3SCl$	47.35 (47.33)	3.26 (3.15)	16.72 (16.56)	12.91 (12.62)
4d	4	56	280—282	$C_{10}H_8ON_3SCl$	47.48 (47.33)	3.21 (3.15)	16.62 (16.56)	12.79 (12.62)
4e	3	59	254—255	$C_{11}H_{11}ON_3S$	56.88 (56.65)	4.63 (4.75)	18.03 (18.02)	13.58 (13.72)
4f	2	62	252—253	$C_{11}H_{11}O_2N_3S$	53.04 (53.01)	4.27 (4.45)	16.06 (16.86)	12.32 (12.84)
4g[a]	5	49	307—309[c]	$C_{10}H_9O_2N_3S$	51.19 (51.06)	3.85 (3.86)	17.97 (17.87)	13.86 (13.60)

a) Reac. solv.: CH_3COOH, Crystn. solv.: $(CH_3)_2SO$
b) Lit,[5] 256°C c) Lit,[5] 315°C

Table 2. 5-Arylidene-2-arylidenehydrazono-4-thiazolidinones (**5**)

Product	Reac. time (hr)	Yield (%)	Mp °C	Formula	Analysis (%) Found (Calcd) C	H	N	S
5a	6	32	288—290	$C_{17}H_{13}ON_3S$	66.03 (66.44)	4.17 (4.26)	13.50 (13.68)	10.26 (10.43)
5b	5	25	305—307	$C_{21}H_{23}ON_5S$	64.82 (64.11)	5.90 (5.87)	17.65 (17.80)	8.19 (8.13)
5c	6	28	301—304	$C_{17}H_{11}ON_3SCl$	57.28 (57.08)	2.78 (2.73)	10.49 (10.51)	8.08 (8.01)
5d	8	20	275—277	$C_{17}H_{11}ON_3SCl$	57.10 (57.08)	2.69 (2.73)	10.53 (10.51)	8.04 (8.01)
5e	11	23	269—270	$C_{19}H_{17}ON_3S$	68.09 (68.05)	5.14 (5.11)	12.59 (12.53)	9.56 (9.54)
5f	15	18	254—255	$C_{19}H_{17}O_3N_3S$	62.53 (62.12)	4.79 (4.66)	11.39 (11.44)	8.79 (8.71)

a) Lit,[5] 291—292°C

Experimental[7]

2-Arylidenehydrazono-4-thiazolidinones (4). General Procedure. A mixture of **1** (0.02 mol), **2** (0.01 mol), and **3** (0.01 mol) in ethanol (10 m*l*) containing acetic acid (1 m*l*) was refluxed for a suitable period. Crystalline precipitates were formed during the reaction; these were collected on the filter and washed with ethanol. Recrystallization from acetic acid gave **4**. The results are summarized in Table 1.

5-Arylidene-2-arylidenehydrazone-4-thiazolidinones (5). General Procedure. To a mixture of **2** (0.01 mol) and **3** (0.01 mol) in acetic acid (10 m*l*), we added **1** (0.01 mol), and then the mixture was refluxed for a suitable period. The resulting precipitates were filtered and washed with ethanol. Recrystallization from dimethyl sulfoxide gave **5**. The results are summarized in Table 2.

7) All the melting points are uncorrected. The IR spectra were measured with a Shimadzu IR-27G spectrophotometer in Nujol mulls. The NMR spectra were determined in trifluoroacetic acid with a Nihondenshi JNM-C-60 high-resolution NMR spectrometer (60 MHz), using tetramethylsilane as the internal standard. The chemical shifts of the protons are presented in terms of δ values.

5-Benzylidene-2-benzylidenehydrazono-4-thiazolidinone (5a) from 1 and Benzaldehyde Acetylhydrazone. A mixture of **1** (0.01 mol) and benzaldehyde acetylhydrazone (0.02 mol) in acetic acid (10 m*l*) was refluxed for 14 hr. The resulting precipitate was collected on a filter, washed with ethanol, and recrystallized from dimethyl sulfoxide. Yield, 14%.

The Hydrolysis of 5a. To a solution containing concentrated hydrochloric acid (10 m*l*) and ethanol (10 m*l*), we added **5a** (0.01 mol), and then the mixture was heated for 15 hr. After being cooled, the reaction mixture was poured onto cracked ice. The crystalline matter thus formed was collected, washed with water, and air-dried. Recrystallization from acetic acid gave 5-benzylidene-2,4-thiazolidinones; mp 239—40°C; yield, 26%. IR (cm^{-1}): 3150 (NH), 1740 and 1690 (C=O), 1610 (C=C). NMR (δ): 7.50 (C_6H_5), 8.10 (=CH), 9.55 (NH).

Found: C, 58.65; H, 3.56; N, 6.75; S, 15.54%. Calcd for $C_{10}H_7O_2NS$: C, 58.54; H, 3.44; N, 6.83; S, 15.82%.

The authors wish to express their thanks to Dr. Hiroshi Midorikawa and Dr. Heinosuke Yasuda for their helpful discussions and encouragement throughout the course of this work. Thanks are also due to Dr. Akio Sakurai for his helpful advice in many respects.

BULLETIN OF THE CHEMICAL SOCIETY OF JAPAN, VOL. 45, 954—956(1972)

Molecular Vibrations and Force Fields of Alkyl Sulfides. III. Infrared Spectra of Methyl Ethyl Sulfide

Masaru OHSAKU, Yuji SHIRO,* and Hiromu MURATA

Department of Chemistry, Faculty of Science, Hiroshima University, Higashisenda-machi, Hiroshima

**Shinonome Branch School, Faculty of Education, Hiroshima University, Shinonome-3-chome, Hiroshima*

(Received August 26, 1971)

The vibrational spectra of methyl ethyl sulfide have been extensively examined by several authors.[1-6] The rotational isomerism, C_s (T) and C_1 (G), has also been discussed.[2-5] Lately, Scott *et al.*[6] carried out a normal coordinate treatment using the valence force field. In the previous papers, however, the assignments of the observed bands were not consistent with each other, and in the C–H stretching, CH_3 degenerate deformation, CH_2 bending, and CH_3 rocking regions, the spectra were not well-resolved. In order to obtain the complete infrared data, we have newly recorded the infrared spectra of methyl ethyl sulfide in the gaseous, liquid, and solid states; on the basis of our results, we have then revised a few of the previous assignments. The vibrational data thus obtained will be used in a normal coordinate treatment of methyl ethyl sulfide.

Results and Discussion

The infrared data obtained and the consequent assignments of methyl ethyl sulfide are summarized in Table 1. The C–H stretching, CH_3 degenerate deformation, CH_2 bending, and CH_3 rocking regions are well-resolved in the unannealed or the annealed spectra. In the C–H stretching region, 3000—2800 cm^{-1}, we observed six and ten bands in the liquid and solid states respectively. Among these bands, the overtone bands of the CH_3 degenerate deformation vibrations may be confused. They are hardly distinguishable from each other. In the region around 1300 cm^{-1} two weak bands remain in the annealed spectra (1319 and 1305 cm^{-1}). The band at 1319 cm^{-1} may be assigned to the fundamental with reference to the data of dimethyl sulfide.[7] Scott *et al.*[2] assigned the band at 1305 cm^{-1} to the CH_2 wagging band. We consider this band to be too high to identify as the CH_2 wagging fundamental. The band at 1305 cm^{-1} may be due to the overtone or to the sum-combination. In the CH_2 wagging and twisting regions, some bands disappeared in the solid state. These bands may be

1) D. H. Rank, E. R. Shull, and D. W. E. Axford, *J. Chem. Phys.*, **18**, 392 (1950).
2) D. W. Scott, H. L. Finke, J. P. McCullough, M. E. Gross, K. D. Williamson, G. Waddington, and H. M. Huffman, *J. Amer. Chem. Soc.*, **73**, 261 (1951).
3) M. Hayashi, *Nippon Kagaku Zasshi*, **77**, 1692 (1956).
4) M. Hayashi, T. Shimanouchi, and S. Mizushima, *J. Chem. Phys.*, **26**, 608 (1957).
5) M. Hayashi, *Nippon Kagaku Zasshi*, **78**, 627 (1957).
6) D. W. Scott and M. Z. El-Sabban, *J. Mol. Spectrosc.*, **30**, 317 (1969).
7) M. Ohsaku, Y. Shiro, and H. Murata, This Bulletin, **45**, 113 (1972).

Table 1. Infrared frequencies (cm^{-1}) and assignments of methyl ethyl sulfide[a)]

Gaseous Room temp.	Liquid Room temp.	CS_2 soln	Liquid Low temp.	Solid Annealed	Assignment[b)]
2987 sh, vs 2983 vvs 2977 sh, vs				2985 sh, w	ν_{C-H}
2965 sh, vs			2964 vs	2965 vs	ν_{C-H}
2946 sh, vs				2957 s	ν_{C-H}
2940 vs				2950 sh, s	ν_{C-H}
2925 vs			2926 sh, s	2926 s	ν_{C-H}
2910 sh, s			2915 vs	2915 vs	ν_{C-H}
2896 2888 s 2880				2874 sh, m	ν_{C-H}
2860 s			2868 s	2866 s	
2845 m			2855 sh, s	2855 sh, w	
2830 m			2833 m	2834 m	
1465 m			1465 sh, w	1463 s	$\delta^{d}_{CH_3}$
1454 s			1457 sh, m	1456 s	$\delta^{d}_{CH_3}$
1448 s			1448 vs	1444 s	$\delta^{d}_{CH_3}$
1436 s			1436 vs	1430 s	$\delta^{d}_{CH_3}$
1427 sh, m			1427 vs	1422 m	$\delta^{b}_{CH_3}$
1420 sh, w			1420 sh, s	—	
1405 vvw				1405 vw	
1392 1381 w 1374		1375 s	1374 s	1375 s	$\delta^{s}_{CH_3}$
1335 1327 vw 1320		1319 m	1319 w	1319 w	$\delta^{s}_{CH_3}$
		1305 w	1305 vw	1305 w	
		1278 sh, w	1278 sh, m	—	
1279 1270 vs 1261		1263 vs	1264 vs	1270 s	$\delta^{w}_{CH_3}$
1249 sh, w		1249 sh, m	1249 sh, m	1255 s	$\delta^{t}_{CH_3}$
1246 vw		1246 sh, m	1246 sh, m	—	
~1140 vw				—	
~1130 vw		1116 vvw	1115 vvw	1116 vw	
1072 1066 m 1058		1061 s	1062 s	1061 m	
1046 sh, w		1045 sh, vw	1045 sh, vw	—	
		1010 vw	1008 vw	1009 vw	
993 sh, w 990 w		995 sh, vw	995 sh, vw	996 vvw	
982 sh, w 978 m		982 m	982 m	—	$\delta^{r}_{CH_3}$
970 sh, m 967 m		970 s	968 s	968 vs	$\delta^{r}_{CH_3}$
960 s		961 sh, w	960 sh, w	962 vs	$\delta^{r}_{CH_3}$
953 m 950 m		954 s	955 s	—	$\delta^{r}_{CH_3}$
947 w 941 w		947 sh, s	948 sh, s	947 m	$\delta^{r}_{CH_3}$
				813 vw	
792 vw 786 w 778 sh, w		783 w	783 w	—	$\delta^{r}_{CH_2}$
767 758 w 750		758 m	758 m	764 s	$\delta^{r}_{CH_2}$
730 725 vw 720		727 w	726 m	724 m	ν_{C-S}

TABLE 1. (Continued)

Gaseous Room temp.	Liquid Room temp.	CS_2 soln.	Liquid Low temp.	Solid Annealed	Assignment[b]
671 666 w 660		677 vw	676 vw	—	ν_{C-S}
650 w 647 w 643 sh, vw		654 m	654 m	655 m	ν_{C-S}
	528 vvw, br			—	
	~505 vvw			—	
	363 sh, vw			—	
	354 vw			354 w	δ_{skel}
	272 vvw, br			—	
	238 vvw			235 vvw	δ_{skel}
	~220 vvw			220 vvvw	δ_{skel}
	~215 vvw			—	

s, strong; m, medium; w, weak; v, very; sh, shoulder; br, broad.

a) Above 3000 cm^{-1} and 2800—1500 cm^{-1} regions are omitted.

b) ν, stretching; δ^d, degenerate deformation; δ^b, bending; δ^s, symmetrical deformation; δ^w, wagging; δ^t, twisting; δ^r, rocking; δ_{skel}, skeletal deformation.

due to the less stable conformation. Methyl ethyl sulfide has four CH_3 rocking vibrational freedoms for each conformation. In the 990—940 cm^{-1} region, we observed five and three bands in the liquid and solid states respectively. These bands may be due to the CH_3 rocking fundamentals. Scott *et al.*[2] and Hayashi *et al.*[4] identified one band of this region as the C–C stretching vibration. For the CH_2 rocking vibrations, two bands were obtained in the liquid state and one band remained in the solid state. The C–S stretching vibration has two vibrational freedoms for each conformation. In the liquid state, three bands are observed. Among them, two bands remain in the annealed spectra. If two conformations may coexist in the liquid state, one band may overlap with the other one. In the skeletal deformation region, 400—200 cm^{-1}, three bands for each conformation may be expected. In the liquid state, we observed five bands. Two bands remain in the solid state.

Experimental

The methyl ethyl sulfide was commercially obtained (Tokyo Kasei Co., Tokyo) and distilled; bp 66.5—67°C/760 mmHg. The gaseous spectra (4000—600 cm^{-1}) were recorded at room temperature. The liquid spectra were recorded at room temperature in the 600—200 cm^{-1} region and at low temperatures, slightly above its mp in the 4000—600 cm^{-1} region. The solution spectra (1400—600 cm^{-1}) were obtained in CS_2. The solid state spectra (4000—200 cm^{-1}) were recorded near the temperature of liquid nitrogen. The instrument used for recording was a Perkin-Elmer Model 621 Spectrophotometer.

BULLETIN OF THE CHEMICAL SOCIETY OF JAPAN, VOL. 45, 956—959(1972)

Molecular Vibrations and Force Fields of Alkyl Sulfides. IV. Infrared Spectra of Diethyl Sulfide

Masaru Ohsaku, Yuji Shiro,* and Hiromu Murata

Department of Chemistry, Faculty of Science, Hiroshima University, Higashisenda-machi, Hiroshima

**Shinonome Branch School, Faculty of Education, Hiroshima University, Shinonome-3-chome, Hiroshima*

(Received August 26, 1971)

Many papers on the vibrations of diethyl sulfide have appeared.[1-5] Scott *et al.*[2] postulated three conformations: C_{2v} (TT), C_1 (TG), and C_2 (GG). Hayashi[3] carried out a normal coordinate analysis for skeletal vibrations using a Urey-Bradley type potential and assigned the obtained spectra assuming C_{2v}, C_1, and C_2 conformations. Lately, Scott *et al.*[5] carried out a normal coordinate treatment using a valence force-type potential; they suggested that the C_{2v} and C_1 conformations are stable and that the C_2 conformation must have a high energy. In the previous papers, however, the assignments of the observed bands were not con-

1) N. Sheppard, *Trans. Faraday Soc.*, **46**, 429 (1950).

2) D. W. Scott, H. L. Finke, W. N. Hubbard, J. P. McCullough, G. D. Oliver, M. E. Gross, C. Katz, K. D. Williamson, G. Waddington, and H. M. Huffman, *J. Amer. Chem. Soc.*, **74**, 4656 (1952).

3) M. Hayashi, *Nippon Kagaku Zasshi*, **77**, 1804 (1956).

4) H. J. Boonstra and L. C. Rinzema, *Rec. Trav. Chim. Pays-Bas*, **79**, 962 (1960).

5) D. W. Scott and M. Z. El-Sabban, *J. Mol. Spectrosc.*, **30**, 317 (1969).

TABLE 1. INFRARED FREQUENCIES (cm^{-1}) AND ASSIGNMENTS OF DIETHYL SULFIDE[a)]

Gaseous Room temp.	Liquid Room temp.	CS_2 soln.	Liquid Low temp.	Solid Annealed	Assignment[b)]
2990 sh, vs 2980 vvs 2975 vs				2978 sh, w	ν_{C-H}
2967 sh, vs			2963 vs	2967 vvs	ν_{C-H}
2946 sh, vs				2943 sh, m	ν_{C-H}
2937 vs				2936 sh, m	ν_{C-H}
2929 sh, vs 2926 sh, vs 2923 sh, s			2923 vs	2924 s, br	ν_{C-H}
~2910 sh, s				2904 sh, m	ν_{C-H}
2895 2888 s 2880			2867 s	2873 s	ν_{C-H}
2860 s				2862 sh, vw	ν_{C-H}
2855 s			2855 sh, m	2853 s	ν_{C-H}
~2835 m			2826 sh, w	2823 sh, vvw	
1480 sh, m 1475 s 1471 s			1478 sh, w	1479 m	$\delta^{d}_{CH_3}$
1462 s			1459 sh, s	1463 vs	$\delta^{d}_{CH_3}$
1455 s 1452 sh, s			1453 sh, w	1453 s	$\delta^{d}_{CH_3}$
1449 sh, s			1449 vs	1449 vs	$\delta^{d}_{CH_3}$
1440 m				1442 vs	
1435 m			1438 sh, s	1436 sh, s	
1420 sh, w			1425 m	—	
1393 sh, w 1389 w 1381 w 1375 sh, w		1381 sh, vw	1381 sh, vw	1379 s	$\delta^{s}_{CH_3}$
1373 sh, w 1369 sh, vw 1366 sh, vw		1374 s	1373 s	1375 m	$\delta^{s}_{CH_3}$
1295 sh, vw 1290 sh, w		1294 sh, vw		—	
1285 sh, w 1282 sh, w 1280 sh, w		1282 sh, w	1282 sh, w	1283 vs	$\delta^{w}_{CH_2}$
1271 sh, s		1272 sh, m	1272 sh, m	—	
1265 1261 vs 1255		1257 vs	1258 vs	1254 vs	
1246 sh, m 1243 sh, w		1246 sh, s	1248 sh, s	1242 vw	
~1235 sh, w		1238 sh, m	1236 sh, w	1236 sh, vvw	
1085 w 1081 w		1073 m	1074 m	1081 vw	
1070 w 1067 w		1066 sh, w		—	
1047 vw 1040 vw		1047 w	1047 vw	1042 vw	
1035 vvw		1035 vw		—	
		1028 vvw	1028 sh, vw	1025 vvw	
1005 vvw		1005 vvw	1005 vvw	—	
992 sh, w		992 sh, vw	992 sh, vw	992 s	
984 sh, w		982 sh, w	983 sh, vw	983 m	
980 w		979 sh, m	981 m	—	
972 w		971 s	971 s	—	
969 w 966 w		967 sh, w	967 sh, vw	—	
960 sh, w		958 sh, vw		—	
798 sh, vw		797 sh, w		798 vvs	$\delta^{r}_{CH_2}$
793 sh, vw		792 sh, w	792 sh, vw	—	

TABLE 1. (Continued)

Gaseous Room temp.	Liquid Room temp.	CS_2 soln.	Liquid Low temp.	Solid Annealed	Assignment[b]
787 w		788 sh, m	789 sh, w	—	
783 w 774 w		782 s	782 m	—	$\delta^r_{CH_2}$
765 w		763 m	762 m	—	$\delta^r_{CH_2}$
743 736 vw 730		737 w	738 w	—	ν_{C-S}
705 700 vw 694		695 w	696 w	—	ν_{C-S}
686 vw 680 vw		688 sh, w	688 sh, w	692 w	ν_{C-S}
665 655 vw 647		655 w	656 w	—	ν_{C-S}
635 vw		638 m	638 w	—	ν_{C-S}
	515 vvw			—	
	500 vvw			—	
	475 vvw			—	
	450 vvw			—	
	425 vvw			—	
	390 sh, vw			—	
	384 vw			—	
	376 sh, vw			—	
	345 vw			337 vw	δ_{skel}
	337 sh, vw			330 sh, vw	δ_{skel}
	306 vw			—	
	294 sh, vvw			—	
	~260 vvw			—	
	~255 vvvw			—	
	~245 vvvw			~250 vvw	δ_{skel}

s, strong; m, medium; w, weak; v, very; sh, shoulder; br, broad.
a) Above 3000 cm^{-1} and 2800—1500 cm^{-1} regions are omitted.
b) ν, stretching; δ^d, degenerate deformation; δ^b, bending; δ^s, symmetrical deformaion; δ^w, wagging; δ^t, twisting; δ^r, rocking; δ_{skel}, skeletal deformation.

sistent with each other; moreover, the conformational analyses of this compound have not agreed with each other. In this paper, in order to complete the infrared data, we report anew on the infrared spectra of diethyl sulfide recorded in the gaseous, liquid, and solid states. We will treat the normal coordinates of this molecule and will report its full assignments in the succeeding paper.

Results and Discussion

The infrared data of diethyl sulfide obtained are summarized in Table 1. The existence of the rotational isomers may be confirmed by the spectra in the CH_2 rocking, C–S stretching, and skeletal deformation regions. For the CH_2 rocking region, 800—760 cm^{-1}, we observed five bands in the liquid state and only one band in the annealed film. Diethyl sulfide has two vibrational freedoms of the CH_2 rocking vibrations for each conformation. However, one band of the CH_2 rocking belonging to the A_2 species of the C_{2v} (TT) conformation is infrared-inactive. Therefore, five bands in the liquid spectra would arise from three conformations (TT, TG, and GG); we can not deny the existence of the C_2 conformation at present. The spectra of this region suggest that the stable form in the solid state is the C_{2v} conformation. In the 750—600 cm^{-1} region, C–S stretching vibrations are to be expected. Diethyl sulfide has two vibrational freedoms of the C–S stretching for each conformation. If the three conformations of C_{2v}, C_1, and C_2 coexisted in the liquid state, six bands would arise. In this region we observed five bands in the liquid state and one band in the solid state. Therefore, the stable conformation (TT) represents only one C–S stretching band in the solid state. The other four bands must arise from the other two conformations. Scott *et al.*[2] assigned the band at 688 cm^{-1} (liquid) to the accidentally-degenerate C–S stretching vibration of the C_{2v} conformation. Since this means, however, that the interaction between the two C–S bonds is zero, the assignment is not acceptable. The band at 692 cm^{-1} in the solid state is not overlapped. It is a weak band. Therefore, the dipole change due to the vibration may be small. Another C–S stretching band would be too weak to be observed, since, in the case of dimethyl sulfide,[6] one C–S stretching band is very weak in comparison with the other band. In

6) M. Ohsaku, Y. Shiro, and H. Murata, This Bulletin, **45**, 113 (1972).

the skeletal deformation region, 450—200 cm^{-1}, fifteen bands are to be expected for three conformations, and five bands, including two C–C torsions, for one conformation. Twelve bands are observed in the liquid spectra. Although all of the observed bands are not always considered to be fundamentals, the three bands remaining in the annealed spectra may be due to the skeletal deformation vibrations of the C_{2v} conformation. Therefore, there remain nine bands in this region. Most of these nine bands may correspond to the other two conformations. From the spectra of this region, therefore, we can not deny the existence of the C_2 conformation.

Experimental

The diethyl sulfide was commercially obtained (Tokyo Kasei Co., Tokyo) and distilled; bp 92°C/760 mmHg. The gaseous spectra (4000—600 cm^{-1}) were recorded at room temperature. The liquid spectra were recorded at room temperature in the 600—200 cm^{-1} region and at low temperatures, slightly above its mp in the 4000—600 cm^{-1} region. The solution spectra (1400—600 cm^{-1}) were obtained in CS_2. The solidstate spectra (4000—200 cm^{-1}) were recorded near the temperature of liquid nitrogen. The instrument used for recording was a Perkin-Elmer Model 621 Spectrophotometer.

BULLETIN OF THE CHEMICAL SOCIETY OF JAPAN, VOL. 45, 959—960(1972)

Orientation Patterns in Nematic Liquid Crystal

Mitsunori SUKIGARA, Osamu NAGASAKI,* and Kenichi HONDA
Institute of Industrial Science, The University of Tokyo, Roppongi, Minato-ku, Tokyo

(Received September 4, 1971)

It has been reported by Williams[1] that a periodic optical texture can be observed in certain nematic liquid crystals when an electric field is applied to transparent sandwich cells. There are two different versions of the molecular orientation for the field-induced domain in a sandwich cell. Meyer stressed the piezoelectric effects which cause the alternating regions of splay and bending as seen in Fig. 2-b in his paper.[2] On the other hand, Helfrich predicted a periodic distortion, which was illustrated in Fig. 2 of his report,[3] produced by a space charge electric field on the basis on his theory.[4]

We tried to observe patterns in nematic *N*-*p*'-anisilidene-*p*-*n*-butylaniline in the direction perpendicular to the electric field using a sandwich cell shown in Fig. 1. Observations were made in transmitted light under a polarizing microscope. The walls of the cell were rubbed with a cotton swab before placing the sample.

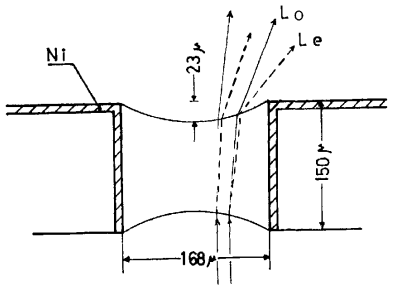

Fig. 1. Schematics of cell configuration and the shape of the sample. The electrodes were made with vacuum sublimated nickel on glass. The shape of the sample was determined with an interference microscope and a contact angle measurement apparatus. L_o and L_e mean the ordinary and extraordinary lights, respectively.

In the fieldless state the projection of the unique axis was aligned perpendicular to the wall near the electrode surface. It was gradually inclined with going away

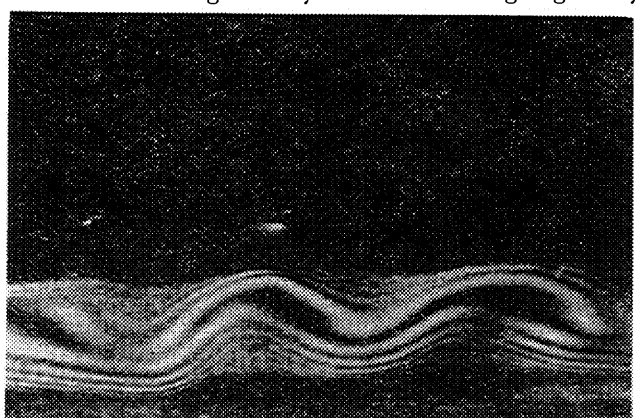

Fig. 2. Wave-like orientation pattern in *N*-p'-anisilidene-*p*-*n*-butylaniline at 25°C observed with crossed Nicols. Applied voltage was 5 V, the upper electrode being anode.

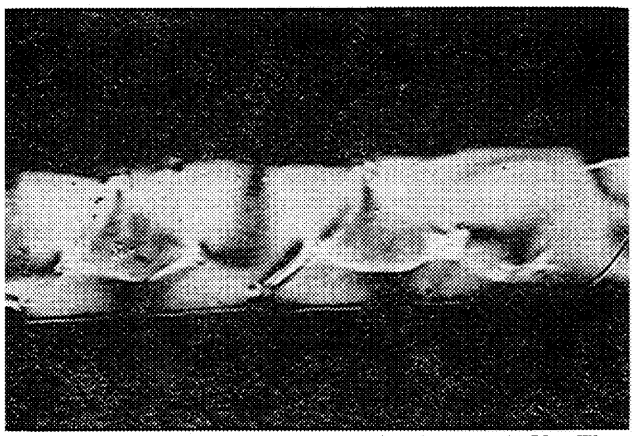

Fig. 3. Novel pattern in the nematic phase at 11 V. The cell was placed between the two parallel Nicols.

* Permanent adress; Seiko-sha Co., Ltd., Sumida-ku, Tokyo.

1) R. Williams, *J. Chem. Phys.*, **39**, 384 (1963).
2) R. B. Meyer, *Phys. Rev. Lett.*,**22**, 918 (1969).
3) W. Helfrich, *J. Chem. Phys.*, **51**, 2755 (1969).
4) W. Helfrich, *ibid.*, **51**, 4092 (1969).

from the wall and finally aligned parallel to the wall. A white turbid part was seen at the center of the cell. The gradual change of the orientation could be seen by observing transmitted light which had been linearly polarized with a polarizer. When the direction of the electric vector of the incident light was rotated from perpendicular to parallel to the wall, a dark band moved from the wall to the center of the cell.

When an electric field ($\geqq$4.5 V) was applied, a wave-like orientation pattern appeared in the white turbid band. A typical pattern observed at 5 V is shown in Fig. 2. The pit in the pattern became deeper and reached the wall with the increase of the applied voltage up to 10 V. When the applied voltage exceeds 12 V, many lines were observed to move to and from the electrodes. This phenomenon corresponds to the dynamic scattering mode.[5] Several novel textures appeared between 10—12 V. An example is given in Fig. 3. The wave-like pattern observed in this experiment is much similar to one predicted by Helfrich.[3] Measurements of electric field distributions in the aligned nematic phase will give much information for the mechanism of the pattern formation.

5) G. H. Heilmeier, L. A. Zanoni, and L. A. Barton, *Proc. IEEE*, **56**, 1162 (1968).

BULLETIN OF THE CHEMICAL SOCIETY OF JAPAN, VOL. 45, 960—961(1972)

Cyclic Disulfides. The Reaction of 1,2-Dithiaacenaphthene with Carbenoids

Seizo TAMAGAKI and Shigeru OAE

Department of Applied Chemistry, Faculty of Engineering, Osaka City University, Sumiyoshi-ku, Osaka

(Received September 4, 1971)

The chemistry of five-membered disulfides has drawn considerable interest mainly because of their characteristic properties in biological reactions and their special role in metabolic sequences.[1] Recently, the electronic features of the five-membered cyclic disulfides have been made clear on the basis of semi-empirical molecular orbital calculations, and the implications on the chemical reactivity have been discussed.[2] At the dihedral angle of 0° around the S–S bond the π-p orbitals of the lone-pairs on the two sulfur atoms are arranged parallel to each other, resulting in a larger splitting of the lone-pair energy levels than in disulfides containing non-parallel-allied lone pairs. Accordingly, electron pairs at the higher level may be expected to display a greater reactivity toward the electrophilic reagents than the less-splitting lone-pairs of the sulfur atom in open-chain disulfides.

The reaction of diaryl disulfide with the methylene formed by the photolysis of diazomethane has been investigated by German chemists and found to proceed in the following manner.[3,4]

$$\mathrm{Ar\text{-}S\text{-}S\text{-}Ar + CH_2N_2} \xrightarrow{h\nu} \mathrm{Ar\text{-}S\text{-}CH_2\text{-}S\text{-}Ar}^{3)}$$

$$\mathrm{Ph\text{-}S\text{-}S\text{-}Ph + Ph_2CN_2} \xrightarrow{h\nu} \mathrm{Ph\text{-}S\text{-}CPh_2\text{-}S\text{-}Ph}^{4)}$$

The similar insertion reaction of five-membered cyclic disulfide is interesting; we carried out the reaction of 1,2-dithiaacenaphthene with bis(arenesulfonyl)diazomethane or with diphenyldiazomethane in the presence of a catalytic amount of copper acetylacetonate.

Experimental

Reaction of 1,2-Dithiaacenaphthene with Bis(toluenesulfonyl)-diazomethane. A mixture of 1,2-dithiaacenaphthene (190 mg) and bis(toluenesulfonyl)diazomethane (350 mg) was refluxed for 15 min in the presence of 15 mg of copper acetylacetonate. After cooling, the solvent was evaporated to afford crystals, which were then recrystallized from benzene (450 mg: 88%) to give, finally, colorless crystals of (A): mp 148—148.5°C. Found: C, 58.36; H, 3.95%. Calcd for $C_{14}H_{14}S_2O_4$: C, 58.60; H, 3.91%.

Decomposition of (A). Compound (A) (140 mg) was decomposed in a test tube at 150°C. Then, the reaction mixture was extracted with hot *n*-hexane. After the evaporation of the solvent, the crystals (60 mg) were sublimated under reduced pressure to afford a carbonyl compound (B): mp 132—133°C. Found: C, 60.64; H, 2.85%. Cacld for $C_{11}H_{16}S_2O$: C, 60.50; H, 2.75%.

Reaction of 1,2-Dithiaacenaphthene with Diphenyldiazomethane. In a similar fashion, the reaction of 350 mg of diphenyldiazomethane with 1,2-dithiaacenaphthene (200 mg) gave 350 mg (91%) of crystals upon recrystallization from benzene-hexane; mp 180—181°C. Found: C, 77.65; H, 4.45%. Calcd for $C_{23}H_{16}S_2$: C, 77.52; H, 4.49%.

Results and Discussion

Diphenyl disulfide was allowed to react with an equimolar amount of bis(toluenesulfonyl)diazomethane in the presence of a catalytic amount of copper acetylacetonate to afford crystals melting at 169—170°C. This structure is at present yet unidentified. However, it is apparent that the reaction mixture did not contain disulfide linkage. Besides, from the reaction mixture no product was isolated which corresponds to the insertion product.

Contrary to the above reaction, the copper salt-

1) L. J. Reed, "Organic Sulfur Compounds," Vol. 1, Pergamon Press, Oxford (1969), p. 443.
2) H. Yamabe, H. Kato, and T. Yonezawa, This Bulletin, **44**, 604 (1971).
3) N. Petragnari and G. Schill, *Chem. Ber.*, **103**, 2271 (1970).
4) A. Schönberg and T. Stalpp, *ibid.*, **63**, 3102 (1930).

catalyzed reaction of 1,2-dithiaacenaphthene with bis-(toluenesulfonyl)diazomethane took place smoothly and was completed within 5 min in refluxing benzene; then the reaction gave crystals (A) with a decomposition temperature of 148—148.5°C. On the basis of the IR and NMR spectra, the compound obtained is considered to be an insertion adduct formed from bis-(toluenesulfonyl)diazomethane and 1,2-dithiaacenaphthene as is shown below.

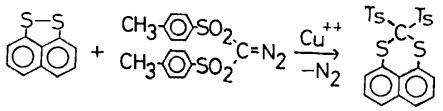

(A)

The IR spectrum showed bands at 1355 and 1175 cm^{-1} corresponding to the stretching frequencies of the sulfonyl group, while the NMR spectrum of the compound fully confirmed the (A) structure. The signals due to two methyl groups appear at δ 2.51 as singlet, and those of 14 aromatic hydrogens as a multiplet centered at δ 7.58.

The pyrolysis of (A) at its decomposition temperature gave carbonyl compound (B). The structure of the resulting compound was confirmed by IR, NMR, MS, and elemental analysis. The IR spectrum showed a strong band at 1610 cm^{-1} corresponding to that of the carbonyl groups. The mass spectrum showed a peak at *m/e* 218 as the molecular peak, followed by an

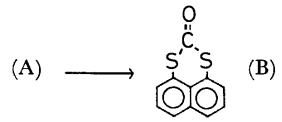

intense peak of *m/e* 190 and with a metastable peak appearing at *m/e* 165.0 due to decarboxylation.

Similarly, upon heating of a benzene solution of an equimolar mixture of 1,2-dithiaacenaphthene and diphenyldiazomethane in the presence of copper salts, a reaction took place promptly and the diphenylmethylene insertion product (C) was obtained as the sole product nearly quantitatively:

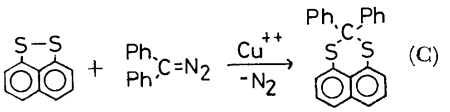

The structure of (C) was confirmed similarly on the basis of IR, MS, and elemental analysis. The mass spectrum showed a peak at *m/e* 356 as calculated from the expected structure (C):

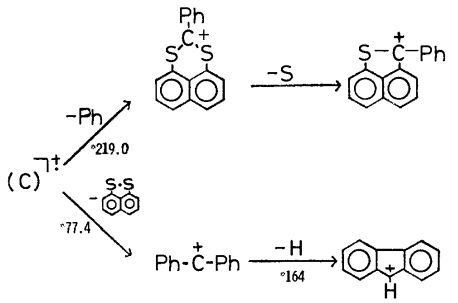

(* indicates the metastable peak)

Unlike 1,2-dithiaacenaphthene, diphenyl disulfide did not give any similar product, as had been anticipated.

All these observations suggest that the reactions of carbenoids are essentially electrophilic. Thus, the effect of lone-pair lone-pair repulsion is evidently demonstrated by the above experiments; that is, the fact that the carbenoids react with 1,2-dithiaacenaphthene readily and not with diphenyl disulfide implies that the five-membered disulfide is much more reactive toward the electrophilic reagents than are the ordinary disulfides.

The formation of the metal carbenoid on the copper salts of acetylacetonate may be followed by the nucleophilic attack of 1,2-dithiaacenaphthene on the carbenoid carbon atom, resulting in the formation of ylide.[5] The mechanism of the carbenoid reaction may be represented as is shown below:

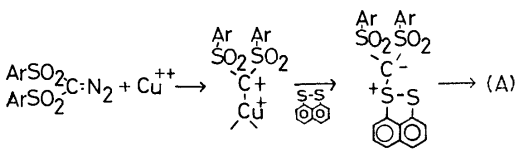

5) S. Searles, Jr., and R. E. Wann, *Tetrahedron Lett.*, **1965**, 2899

BULLETIN OF THE CHEMICAL SOCIETY OF JAPAN, VOL. 45, 962—963(1972)

The MCD Spectrum of the Tropylium Cation

Akio TAJIRI and Masahiro HATANO

The Chemical Research Institute of Non-aqueous Solutions, Tohoku University, Katahira, Sendai

(Received September 7, 1971)

One of the most interesting monocyclic odd-membered non-benzenoid aromatic hydrocarbons, the cycloheptatrienyl (tropylium) cation, $C_7H_7^+$, which has been shown to have a strong aromatic character due to the delocalization of the six π-electrons, was synthesized as early as 1954 by von Doering and Knox.[1]

Because of the intriguing chemical and physical properties of this cation, several authors[2-4] have attempted to calculate its electronic structures, especially its transition energies, on the basis of the π-electron molecular orbital theory. The N→V spectrum was theoretically studied by Murrell and Longuet-Higgins[2] using the SCF-MO theory. They predicted two transitions, an allowed transition at 6.36 eV ($^1A_1'\rightarrow{}^1E_1'$) and a forbidden transition at 4.33 eV ($^1A_1'\rightarrow{}^1E_3'$). The absorption band at 4.51 eV observed by von Doering and Knox was assigned to the latter transition.

The results of PPP-type calculations by Heilbronner and Murrell[4] of various odd-membered non-alternant hydrocarbons, including $C_7H_7^+$, using perimeter models were reported, along with their experimental data. The agreement between the theory and the experiment was quite good, and their results supported the above assignment of the absorption band of the tropylium cation.

TABLE 1. TRANSITION ENERGIES (eV) OF TROPYLIUM CATION

Symmetry	M-LH[2]	J[3]	H-M[4]	This Work[a]	Obsd[b]
$A_1'\rightarrow E_3'$	4.33	3.6	4.52	4.6(forb.)	4.54(ε=4350)
$A_1'\rightarrow E_1'$	6.36	5.7	5.83	6.3(0.32)	5.73(41000)

a) The values in the parentheses are the calculated oscillator strengths.

b) H. J. Dauben, Jr., F. A. Gadecki, K. M. Harmon, and D. L. Pearson, *J. Amer. Chem. Soc.*, **79**, 4557 (1957).

We also calculated the transition energies of $C_7H_7^+$ by use of a modified version of the CNDO/2 method parametrized by Tajiri *et al.*,[5] assuming the carbon skeleton to be heptagonal (D_{7h}) and also assuming each bond length to be 1.40 Å. The calculated transition energies are listed in Table 1, along with the observed values. The values predicted within the framework of the CNDO/2 method are in quite good agreement with the experimental data. The results of the previous authors are also included in the table for the sake of comparison.

On the other hand, recently, with the availability of very sensitive photoelectric spectropolarimeters, interest in optical activity measurements in the magnetic field through absorption bands (Magnetic Circular Dichroism: MCD) has been revived. Many authors[6-9] have used the MCD technique in order to extract information on the ground- and excited-states of ions and molecules. According to the theoretical consideration of Schatz and McCafferry,[10] when either the ground- or excited-state of a compound is degenerate, the Faraday A term is observed. The degeneracy of the ground-state causes the Faraday C term. In addition to these two terms, the B term originates from the mixing of the wavefunctions of the ground- and excited-states with some other states. Therefore, the molar ellipticity $[\theta]_M$(in deg·gauss^{-1}·cm^2·mol^{-1}) may be expressed as:

$$[\theta]_M = -21.348\{f_1A+f_2(B+C/kT)\}$$

where f_1 and f_2 are the functions of the frequency, ν, of the incident light (in general, a damped oscillator model is assumed).

Here let us turn again to the discussion of the electronic state of the tropylium cation. We should observe the A term for each band of the cation in question if we believe the predictions of previous authors, who assigned the $^1A_1'\rightarrow{}^1E_1'$ transition to the shorter wavelength absorption, and $^1A_1'\rightarrow{}^1E_3'$ to the longer. Therefore, we tried to measure the UV and MCD spectra of the tropylium cation in order to confirm the above assignment. The purification of the crude BF_4 salt was achieved by adding ether to its acetonitrile solution

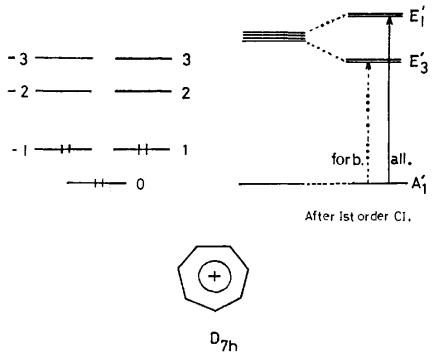

D_{7h}

Fig. 1. π-molecular orbitals labeled by the ring quantum number and the electronic states of tropylium cation.

1) W. von E. Doering and L. H. Knox, *J. Amer. Chem. Soc.*, **76**, 3203 (1954).

2) J. N. Murrell and H. C. Longuet-Higgins, *J. Chem. Phys.*, **23**, 2347 (1955).

3) A. Julg, *J. Chim. Phys.*, **59**, 567 (1962).

4) E. Heilbronner and J. N. Murrell, *Mol. Phys.*, **6**, 1 (1963).

5) A. Tajiri, N, Ohmichi, and T. Nakajima, This Bulletin, **44**, 2347 (1971).

6) B. Briat, D. A. Schooley, R. Records, E. Bunnenberg, and C. Djerassi, *J. Amer. Chem. Soc.*, **89**, 6170 (1967).

7) B. Briat, D. A. Schooley, R. Records, E. Bunnerberg, and C. Djerassi, *ibid.*, **89**, 7062 (1967).

8) B. Briat, D. A. Schooley, R. Records, E. Bunnerberg, C. Djerassi, and E. Vogel, *ibid.*, **90**, 4691 (1968).

9) P. J. Stephens, P. N. Schatz, A. B. Ritchie, and A. J. McCafferry, *J. Chem. Phys.*, **48**, 132 (1968).

10) P. N. Schatz and A. J. McCafferry, *Quart. Rev.*, **23**, 552 (1969).

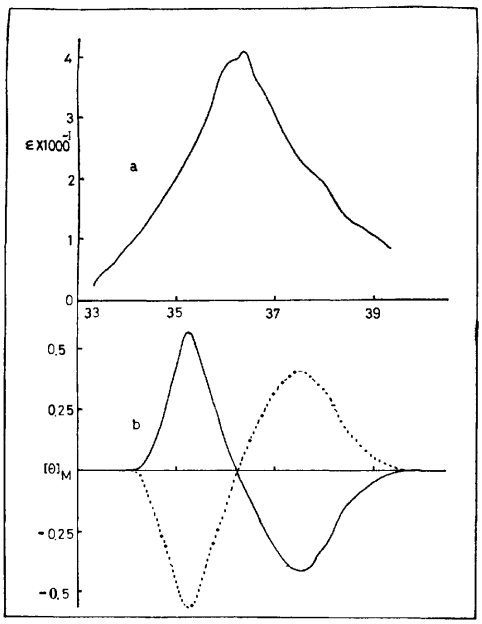

Fig. 2. (a) Molar extinction coefficient of tropylium cation in N/10 HCl solution at room temperature (300°K). (b) Molar ellipticity per unit magnetic field of tropylium cation in N/10 HCl solution at room temperature (300°K). The dotted line is obtained when the current in the magnet is reversed.

until white crystals formed. The concentration of this salt in the N/10 HCl solution was found to be 2.01×10^{-4} mol/*l*. For the measurement of the MCD spectrum, we employed a JASCO ORD/UV-5 recording spectropolarimeter provided with a CD measuring attachment and a 10 KG electric magnet.

Figure 1 shows the π-molecular orbitals and a schematic diagram of the two excited states caused by the lowest electronic transition from the degenerate HOMO to the degenerate LVMO. In Fig. 2 the UV and MCD spectra are shown. Unfortunately, however, because of the difficulties of the MCD measurement in the shorter-wavelength region, we were obliged to limit our measurement to the wavelength region longer than 230 nm.

A clear Faraday A term is shown in Fig. 2; its inflection point coincides with the absorption maximum (4.5 eV) within the limits of experimental error. This, in turn, shows that the lowest excited state of the tropylium cation, corresponding to the longest-wavelength absorption band, which is forbidden by the symmetry but which is partially allowed by the vibrational process, belongs to the $^1E_3'$ irreducible representation of the D_{7h} point group. Furthermore, the ground-state is totally symmetric and non-degenerate because of the lack of the Faraday C term, which should have an extreme in the MCD spectrum near the absorption maximum.

Actually the Faraday A term should be discussed in terms of an A/D which gives the parameters of theoretical interest and, in turn, the magnetic moment of the excited-state, where D is the dipole strength of the particular spectral line. From the observed MCD and UV spectra for this cation, we obtained the A/D value, which was estimated to be $-1.40\ \beta$ by use of the method of Briat *et al.*[6] At the same time, $[B+C/kT]/D$ was found to be negligibly small.

We conclude that the MCD measurements help in the direct assignment of an absorption band and, accordingly, provide us with information on the nature of the ground- and excited-states of ions and molecules.

We awfully acknowledge the generosity of Professor Y. Kitahara and Dr. M. Oda of Tohoku University for providing the sample. We are also grateful to Professor H. Kobayashi of the Tokyo Institute of Technology for giving us an opportunity to measure the MCD spectra.

BULLETIN OF THE CHEMICAL SOCIETY OF JAPAN, VOL. 45, 963—964(1972)

Charge-transfer and Proton-transfer in the Formation of Molecular Complexes. II.[1] Kofler's Ternary Molecular Complex

Yoshio MATSUNAGA and Gunzi SAITO

Department of Chemistry, Faculty of Science, Hokkaido University, Sapporo

(Received September 20, 1971)

The interaction between an aromatic amine and picric acid generally results in the formation of a yellow-colored 1 : 1 salt by means of proton-transfer. By adding pyridine to a mixture of α-naphthylamine and picric acid, Kofler isolated a red-colored complex, the composition of which happened to be α-naphthylamine-pyridine-picric acid (1 : 1 : 1).[2] To explain the deep color of this mixed picrate, he assumed that the pyridine molecule is bound to the hydroxy group of picric acid, while the aromatic amine interacts with the nitro groups of the acid. So far, however, no spectroscopic study of this ternary molecular complex has been reported.

As is shown in Fig. 1, the vibrational spectrum of the 1 : 1 salt derived from α-naphthylamine and picric acid, examined as a Nujol mineral oil mull, has sharp bands at 3075 and 3200 cm^{-1} and broader ones in the

1) Part I: G. Saito and Y. Matsunaga, This Bulletin, **44**, 3328 (1971).

2) A. Kofler, *Z. Elektrochem.*, **50**, 200 (1944).

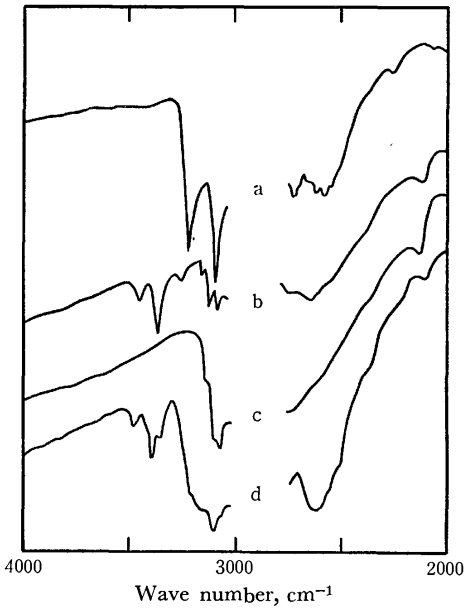

Fig. 1. Vibrational spectra; (a) α-naphthylamine-picric acid (1:1), (b) α-naphthylamine-pyridine-picric acid (1:1:1), (c) pyridine-picric acid (1:1), (d) α-naphthylamine-picric acid (2:1).

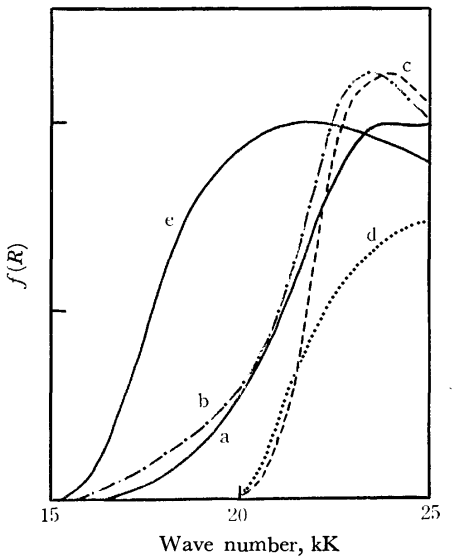

Fig. 2. Diffuse reflection spectra; (a) α-naphthylamine-pyridine-picric acid (1:1:1), (b) α-naphthylamine-picric acid (2:1), (c) α-naphthylamine-picric acid (1:1), (d) pyridine-picric acid (1:1), (e) α-naphthylamine-*s*-trinitrobenzene (1:1).

region from 2500 to 2800 cm^{-1}. This pattern is typical of picrates of primary amines. The first one is assigned to the picrate ion, and the second, to a NH_3^+ stretching frequency.[3] In the spectrum of the ternary complex, bands due to the amine appear at 3250, 3350, and 3450 cm^{-1} instead of at the above-mentioned locations. Although the spectrum in Fig. 1 presents no conclusive evidence for the protonation of pyridine, the pattern in the region below 1700 cm^{-1} includes that of the yellow-colored pyridinium picrate. Thus, the examination of the vibrational spectrum leads to the conclusion that the complex consists of pyridinium picrate and α-naphthylamine. This conclusion is in accordance with the fact that the pK_a value of pyridine is higher than that of the amine, *i.e.*, 5.22 *vs.* 3.92.[4] Kofler also reported the preparation of an orange-colored α-naphthylamine-picric acid (2:1) complex, "semipicrate" in his nomenclature. As may be expected, its vibrational spectrum indicates the presence of both NH_2 and NH_3^+ groups in this complex (see Curve d in Fig. 1).

Both the ternary molecular complex and the 2:1 complex are deeply colored. The diffuse reflection spectra given in Fig 2 clearly show that a broad weak absorption, the maximum of which is located around 20 kK, appears upon the incorporation of pyridine or additional α-naphthylamine into the 1:1 salt. The new absorption must be due to a charge-transfer interaction. The electron donor is undoubtedly α-naphthylamine. As the locations of the absorption maximum are nearly identical, the acceptor component is possibly a common species, namely, the picrate ion. A comparison with the spectrum of the *s*-trinitrobenzene complex suggests that the picrate ion is as strong as trinitrobenzene as an acceptor. The strength of picric acid is comparable with that of *s*-trinitrobenzene; therefore, it may be argued that the acceptor-strength is not much affected by the ionization. Further evidence to support this conclusion will be presented in a subsequent paper.[5] On the basis of this spectroscopic study, one may conclude that, in Kofler's ternary complex, a proton is transferred from picric acid to pyridine and that the interaction between α-naphthylamine and the picrate ion is of the charge-transfer type. It must be added that the explanation suggested by Kofler, of course in the terminology at that time, is in essential agreement with the present conclusion.

3) R. P. Mariella, M. J. Gruber, and J. W. Elder, *J. Org. Chem.*, **26**, 3217 (1961).

4) D. D. Perrin, "Dissociation Constants of Organic Bases in Aqueous Solution," Butterworths, London (1965), pp. 124 and141.

5) G. Saito, and Y. Matsunaga, This Bulletin, submitted.

SHORT COMMUNICATIONS

Small Ring Compounds. I. Anodic Oxidation of 2,3-Dicarbethoxy-cyclopropanecarboxylic Acid

Ichiro MINATO, Tateo TAKASUKA, Koji KIMURA, Tsutomu SAKAKIBARA, and Yoshinobu ODAIRA

Department of Petroleum Chemistry, Faculty of Engineering, Osaka University, Suita-shi, Osaka

(Received November 18, 1971)

Highly strained small ring radicals have recently attracted special interest, and cyclopropyl radicals have been generated by several methods.[1] However, the yields are low and variable, and it would not be feasible to utilize the generated cyclopropyl radicals in various synthetic processes. In the anodic oxidation of cyclopropanecarboxylic acids, a common problem is the facile formation of a cationic intermediate, such as cyclopropyl cation or cyclopropanecarboxonium ion, by the additional one-electron oxidation of a generated cyclopropyl radical.[2] Cyclopropyl cations usually undergo concerted ring opening to afford many rearranged products.

We wish to report on attempts to generate an unrearranged cyclopropyl radical of high efficiency by anodic oxidation. For this purpose, 2,3-dicarbethoxy-cyclopropanecarboxylic acid (I), consisting of *trans,cis*- and *trans,trans*-isomers in the ratio 3: 2, was selected as the starting material. Compound I (0.02 mol) was electrolyzed in methanol (80 m*l*) containing sodium methoxide (0.02 mol) at 20—30°C for 6 hr: Anode, a platinum plate (1.5×20 cm); cathode, mercury-pool (surface area: *ca.* 13 cm^2); distance between the electrodes, *ca.* 1.0 cm; electrolytic cell, beaker-type vessel (150 m*l*) without diaphragm; initial current, 1.5 A (final value, 0.5 A); cell voltage, 60 V (final value 100 V).

2,2',3,3'-Tetracarbethoxy-bicyclopropyl (II) and 1,2-dicarbethoxy-cyclopropane (III) were obtained in 13 and 62.5% yields, along with small quantities of 1,2-dicarbethoxy-3-hydroxymethyl-cyclopropane (IV) and 1,2-dicarbethoxy-3-carbomethoxy-cyclopropane (V). All the products except III were identified by spectroscopic methods and gas chromatographic technique. Compound II can exist in eleven forms, it being confirmed by VPC (DEGSP, 230°C) and their mass spectra that at least nine out of the eleven were formed. Only the major component, mp 155—157°C, was isolated by VPC in *ca.* 30% yield, and determined to be *trans, trans,trans,trans*-isomer. It is significant that no ring opening products were found. Anodic oxidation with platinum anode and cathode (1.5×2.0 cm on each), mounted parallel to each other and 0.3 cm apart, resulted in similar products and their distributions.

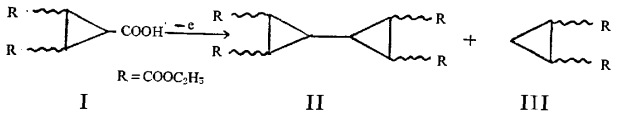

I II III

It should be emphasized that a cyclopropyl radical is consistently generated in *ca.* 70% yield on the electrode. No concerted ring opening occurred through a cationic intermediate. In order to obtain further information on the stability of the radical, the thermal decomposition and photolysis of *t*-butyl-perester of I in benzene have been studied. The radical was also generated almost quantitatively and II and III were obtained in somewhat different yields together with considerable amounts of 3-*t*-butoxyl- and 3-phenyl-1,2-dicarbethoxy-cyclopropanes. Both the present electrolytic conditions employed and the electronic effect of two carbethoxy groups on the increase of the ionization potential of a cyclopropyl radical might be of importance.

1) T. Shono, M. Akashi, and R. Oda, *Tetrahedron Lett.*, **1968**, 1507; H. M. Walborsky, Chen-Tong Chen, and J. L. Webb, *ibid.*, **1964**, 3551; H. M. Walborsky and Chen-Tong Chen, *J. Amer. Chem. Soc.*, **89**, 5499 (1967); D. E. Applequist and A. H. Peterson, *ibid.*, **82**, 2372 (1960); J. K. Kochi and A. Bemis, *ibid.*, **90**, 4038 (1968); D. I. Schuster and J. D. Roberts, *J. Org. Chem.*, **27**, 51 (1962).

2) T. Shono, I. Nishiguchi, S. Yamane, and R. Oda, *Tetrahedron Lett.*, **1969**, 1965; R. Brettle and G. B. Cox, *J. Chem. Soc., C*, **1969**, 1227; T. D. Binnes, R. Brettle, and G. B. Cox, *ibid., C*, **1968**, 584.

The Photochemical Reaction of *p*-Benzoquinone in Water

Shizunobu HASHIMOTO, Koji KANO, and Hiroshi OKAMOTO
Department of Applied Chemistry, Doshisha University, Kamikyo-ku, Kyoto
(Received October 27, 1971)

Although the photochemical oxidation of alcohols by quinones has been extensively studied, few investigations of the photolysis of quinones in aqueous solutions have been done until recently. Broadbent[1] has reported that photoexcited 9,10-anthraquinonesulfonates decompose water to generate the ·OH radical. Hughes and Uaboonkul[2] have reported that photoexcited 9,10-phenanthrenequinone abstracts a hydrogen atom from water to generate a semiquinone radical, which then reacts with triphenylphosphine to produce a dipolar form of 2,2,2-triphenyl-1,3,2-dioxaphospholene. In this communication, we wish to report some preliminary results on the photochemistry of *p*-benzoquinone in water.

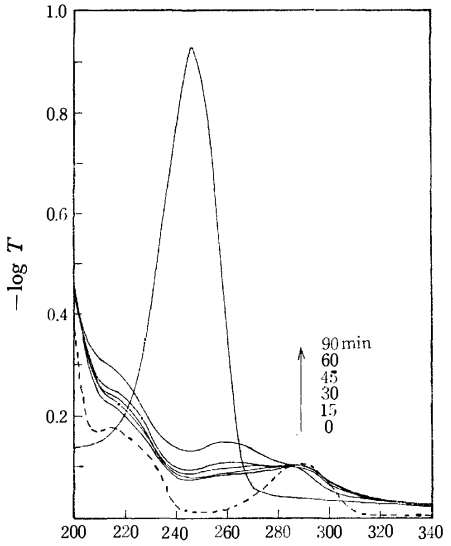

Fig. 1. The UV-spectral change of the photoreaction of *p*-benzoquinone in water. For UV-spectra measurement, 0.8 m*l* of the photolyzed solution was exactly diluted to 20 m*l* with water. The dotted line is the spectrum of the authentic sample of hydroquinone (4×10^{-5}M).

Figure 1 shows the UV-spectral change during the course of the photolysis of a 1×10^{-3}M solution of *p*-benzoquinone in water on irradiation with an immersion-type 130-W high-pressure mercury lamp in a stream of nitrogen. Upon irradiation, the reaction solution became dark orange; this seemed to be due to the formation of quinhydrone. The absorption spectrum of the final photoproduct was the same as that of hydroquinone. Paper chromatography also suggested the formation of hydroquinone (a Toyo filter paper No. 50 was used. Solvent: absolute ethanol; color-producing reagents: ferric chloride and potassium ferricyanide; R_f value of hydroquinone: 0.87).

A solution of *p*-benzoquinone (32.4 mg, 3×10^{-3} mol) in water (300 m*l*) was irradiated with an immersion-type 130-W high-pressure mercury lamp for 30 min at room temperature in a stream of nitrogen. The photolyzed solution was then extracted with ether. The residue obtained upon the removal of the ether was purified by alumina-column chromatography with absolute ethanol and then recrystallized from benzene. Colorless needles of hydroquinone were thus obtained; mp 172—173°C; 12.3 mg (37.2%). In this reaction, we could not detect hydrogen peroxide, which might be produced by the coupling of ·OH radicals.

In the UV spectrum of *p*-benzoquinone in water, the n,π^* and π,π^* absorption maxima were observed at 425 nm ($\varepsilon_{max}=20$) and 246 nm ($\varepsilon_{max}=2.2\times10^4$) respectively. Meanwhile, Kuboyama[3] has reported that the absorption band of *p*-benzoquinone at 539 nm ($\varepsilon_{max}=0.2$) in *n*-heptane can be attributed to the $T_1\leftarrow S_0$ transition (n,π^*). Therefore, we examined the wavelength dependence of the *p*-benzoquinone photochemistry in water. Anaerobic aqueous solutions of *p*-benzoquinone were irradiated with 313 nm (a combination filter of a Toshiba UV-D25 filter, an aqueous nickel sulfate solution, and carbon tetrachloride), 436 nm (a combination filter of a Toshiba V-Y42 filter and a Toshiba V-V42 filter), and >550 nm (a Toshiba V-O56 filter) light respectively. In all cases, *p*-benzoquinone was photolyzed to produce hydroquinone. Since the shoulder of the n,π^* band of *p*-benzoquinone is not observed at wavelengths beyond 550 nm, the n,π^* triplet of *p*-benzoquinone generated by the $T_1\leftarrow S_0$ transition must participate in this photoreaction.

Table 1. Quantum yields for the disappearance of *p*-benzoquinone in water at 313 nm

p-Benzoquinone, M×10³	Quantum yield
9.85	5.2
4.78	6.0
1.00	5.1
0.45	5.8

We determined the quantum yields for the disappearance of *p*-benzoquinone in the anaerobic aqueous solutions at 313 nm. The results are shown in Table 1. The quantum yields were independent of the initial concentrations of *p*-benzoquinone. This finding suggests that a bimolecular deactivation of photoexcited *p*-benzoquinone does not occur, and that photoexcited *p*-benzoquinone does not abstract a hydrogen atom from the quinone ring. Therefore, it seems that water is the hydrogen donor in this reaction. By the way, the quantum yields were greater than unity in all cases. This indicates a chain reaction. The mechanisms of the chain reaction are now under investigation.

1) A. D. Broadbent, *Chem. Commun.*, **1967**, 382.
2) A. N. Hughes and S. Uaboonkul, *Chem. Ind.* (London), **1967**, 1253.
3) A. Kuboyama, *Report of the Government Chemical Industrial Research Institute* (Tokyo), **59**, 347 (1964).

A Convenient Synthesis of Symmetrical and Unsymmetrical Biphenyls by the Oxidation of *N*-Aryl-*N'*-(tri-*n*-butylstannyl)hydrazines

Hiroshi ISHIKAWA and Teruaki MUKAIYAMA[1]
The Noguchi Institute, 1-8, Kaga 1-Chome, Itabashi-ku, Tokyo
(Received November 19, 1971)

Unsymmetrical biaryls are customarily prepared by the Gomberg reaction and its modification,[2] or by arylation with free radicals generated by the decomposition of aroyl peroxides.[2] However, yields of symmetrical biaryls as well as a mixture of isomeric unsymmetrical biaryls are usually below 50%. An alternate procedure is the photolysis of aromatic iodides in benzene solution, giving biaryls in 40—80% yields.[3] Recently, Taylor and his co-workers have reported the photolysis of arylthallium ditrifluoroacetates in benzene giving unsymmetrical biaryls in 80—90% yields.[4]

In this communication we report a new aromatic phenylation reaction which involves an oxidative decomposition of readily accessible *N*-aryl-*N'*-(tri-*n*-butylstannyl)hydrazines, prepared by transamination reaction from diethylaminotri-*n*-butylstannane and arylhydrazine in aromatic solvent. The transamination reaction proceeded usually above 90% as estimated from the amount of diethylamine evolved.

$$Bu_3SnNEt_2 + PhNHNH_2 \longrightarrow Bu_3SnNHNHPh + Et_2NH$$
(I)

When I in benzene was oxidized with mercuric oxide at room temperature, a vigorous evolution of nitrogen took place quantitatively. Biphenyl was obtained in a 35% yield along with a 65% yield of diphenylmercury. Oxidation proceeds quantitatively. Of various metal oxides examined, silver oxide, manganese dioxide, and potassium permanganate proved to be also effective for oxidation. They liberated above 90% of the theoretical volume of nitrogen. Chromium trioxide and cuprous oxide liberated only a small amount of nitrogen under the same conditions. Oxidation of I with diethyl azodicarboxylate or mercury acetamide gave rise to the evolution of nitrogen in a nearly quantitative yield. Although the above reactions proceeded at room temperature, nitrogen was liberated quantitatively. The yield of biphenyl was usually below 30%. When the reaction of I (prepared from 15 mmol of diethylaminotri-*n*-butylstannane and an equimolar amount of phenylhydrazine) with chloranil (20 mmol) was carried out in benzene (300 m*l*) at room temperature, the yield of biphenyl increased to 93%. In an attempt to extend this type of phenylation reaction, similar oxidation of I with chloranil in anisole and pyridine were tried. The results are summarized in the following Table. It is noteworthy that, in pyridine, the oxidative decomposition of I proceeded even at −35°C giving a mixture of phenylpyridines in high yield along with nitrogen. Each mixture of isomeric phenylpyridines and methoxybiphenyls obtained was identical in composition with those observed on other free-radical phenylation of pyridine[5] and anisole.[6] The results suggest that the oxidation of I produced phenyl radicals, which in turn attacked the solvent to form biaryls. The reaction can be represented as follows. Similarly, when *N*-*p*-tolyl-*N'*-(tri-*n*-butylstannyl)hydrazine prepared from diethylaminotri-*n*-butylstannane and *p*-tolyl-hydrazine by transamination reaction was oxidized with chloranil in benzene, *p*-methylbiphenyl was formed in high yield. The yields and isomer distributions are given in the following Table.[4]

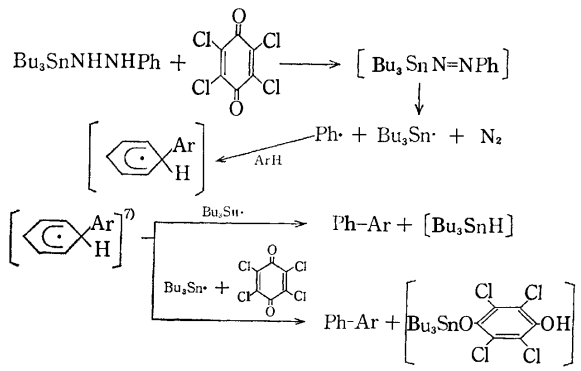

TABLE THE OXIDATION OF *N*-ARYL-*N'*-(TRI-*n*-BUTYLSTANNYL)HYDRAZINES WITH CHLORANIL IN AROMATIC SOLVENTS

Ar	Solvent	Reaction temperature	Yield of biaryls[a] (%)
Phenyl	Benzene	Room temp.	93
	Anisole	−15°——10°	89[c]
	Pyridine	−35°	*ca.* 90[b]
p-Tolyl	Benzene	Room temp.	85[d]

a) Purity of products was determined by glc. The identity of products was established by chromatographic comparison with authentic samples. b) Composition: 64.1% *o*-methoxybiphenyl, 22.5% *m*-methoxybiphenyl, 13.4% *p*-methoxybiphenyls. c) Composition: 59% α-phenylpyridine, 41% β-phenylpyridine. d) Composition: 93.3% *p*-methylbiphenyl, 6.2% *p,p'*-dimethyl-biphenyl, 0.5% biphenyl.

1) Laboratory of Organic Chemistry, Tokyo Institute of Technology, Meguro-ku, Tokyo.

2) See, for example: a) W. E. Bachmann and R. A. Hofman, "Organic Reactions," Vol. II, John Wiley and Sons, Inc., New York (1944), p. 224: b) O. C. Dermer and M. T. Edison, *Chem. Rev.*, **57**, 77 (1957): c) D. R. Augood and G. H. Williams, *ibid.* **57**, 123 (1957).

3) W. Wolf and N. Kharasch, *J. Org. Chem.*, **30**, 2493 (1965).

4) E. C. Taylor, F. Kienzle, and A. McKillop, *J. Amer. Chem. Soc.*, **92**, 6088 (1970).

5) K. Schofield, "Hetero-Aromatic Nitrogen Compounds," Butterworths, Washington, D. C., and London (1967), p. 253.

6) T. Suehiro, *Nippon Kagaku Zasshi*, **72**, 1070 (1951).

7) As shown in the equation, two pathways are conceivable for the hydrogen abstraction form intermediate, arylcyclohexadienyl radical. Since the reaction mixture was treated with aqueous potassium hydroxide in order to remove tetrachlorohydroquinone, tributyltin hydride and tributyltin 4-hydroxyl-2,3-5,6-tetrachlorophenoxide might be hydrolyzed to tributyltin hydroxide which was isolated as major tin-containing component.

The Gas Chromatographic Separation of Germanium Chlorobromides

Yoshihiro MAKIDE and Nobufusa SAITO

Department of Chemistry, Faculty of Science, The University of Tokyo, Hongo, Tokyo
The Institute of Physical and Chemical Research, Wako-shi, Saitama

(Received December 16, 1971)

The formation of mixed halides of germanium in a mixture of germanium tetrachloride and germanium tetrabromide was observed by Delwaulle using Raman spectrometry.[1] However, the attempted mutual separation of these halides by distillation was reported to be unsuccessful.[2] In our recent study of the gas chromatographic behavior of inorganic halides, however, we have found that the mixed halides of germanium can indeed be separated by gas chromatography.

A gas chromatograph equipped with a thermal conductivity detector with platinum filaments was built in our laboratory. The path for the gas flow was made of glass and Teflon to avoid the contact of halides with metal. Kel-F Wax was used as the stationary liquid phase of the partition column. $GeCl_4$ and $GeBr_4$, prepared separately from the elements, were mixed and allowed to stand for a few days so that the halogen interchange equilibrium among the halides could be reached. The mass spectrum of their mixture was then measured by means of a double-focusing mass spectrometer. A mixture of these mixed halides with ^{82}Br-labeled arsenic tribromide was analyzed by means of a radio gas chromatograph. The separated halides were passed through a heated Teflon tube coil, and their activities were measured continuously by means of an NaI scintillation detector placed under the coil.

The formation of mixed halides ($GeCl_3Br$, $GeCl_2Br_2$, and $GeClBr_3$) in the mixture of $GeCl_4$ and $GeBr_4$ was confirmed by mass stectrometry.

The gas chromatogram of the $GeCl_4$–$GeBr_4$ mixture (Fig. 1) shows five peaks. The identification of the three intermediate peaks as mixed halides was confirmed by the following experimental results: (1) as Fig. 2

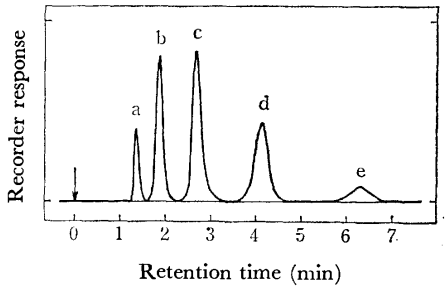

Fig. 1. Gas chromatogram of a mixture of $GeCl_4$ and $GeBr_4$.
Separation column: 200 cm×4 mm i.d., borosilicate glass, filled with 10% Kel-F Wax on silanized Chromosorb W (80—100 mesh). Column temperature: 100°C. Carrier gas: He, 30 ml/min.
a: $GeCl_4$; b: $GeCl_3Br$; c: $GeCl_2Br_2$; d: $GeClBr_3$; e: $GeBr_4$.

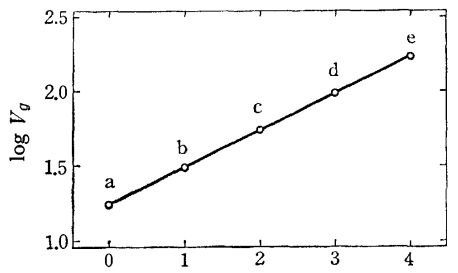

Fig. 2. Log specific retention volume *vs.* number of bromine atoms in a molecule for germanium halides.
a: $GeCl_4$; b: $GeCl_3Br$; c: $GeCl_2Br_2$; d: $GeClBr_3$; e: $GeBr_4$.

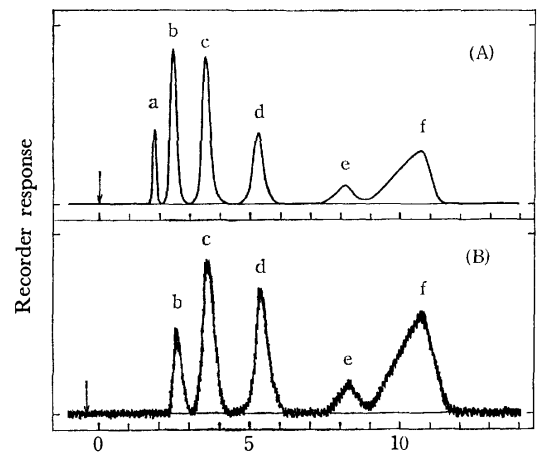

Fig. 3. Gas chromatogram (A) and radio chromatogram (B) of a mixture of $GeCl_4$, $GeBr_4$, and $As^{82}Br_3$.
Column and operating conditions: the same as in Fig. 1, with the exception of the flow rate (He): 20 ml/min. Radiation detector: 3″×3″ NaI(Tl).
a: $GeCl_4$; b: $GeCl_3Br$; c: $GeCl_2Br_2$; d: $GeClBr_3$; e: $GeBr_4$; f: $AsBr_3$.

shows, the logarithm of the specific retention volume has an approximately linear relationship with the number of bromine atoms in a molecule, as in the case of $CCl_{4-n}Br_n$ and $SiCl_{4-n}Br_n$;[3] and (2) the radio gas chromatogram of the mixture with $As^{82}Br_3$ shows that the germanium mixed halides were labeled with ^{82}Br by isotopic exchange (as shown in Fig. 3). Their specific activities were proportional to the number of bromine atoms in the molecule.

Further studies of the gas chromatographic behavior of inorganic halides are in progress and will be published shortly.

1) M. L. Delwaulle, *Compt. Rend.*, **227**, 1229 (1948); **232**, 54 (1951); **234**, 2361 (1952).

2) G. S. Forbes and H. H. Anderson, *J. Amer. Chem. Soc.*, **66**, 931 (1944).

3) Y. Makide and N. Saito, presented at the 24th Annual Meeting of the Chemical Society of Japan (April 1971, Osaka).

Far Infrared Spectra and Internal-Rotation Potential of Ethyl Methyl Ether

Teizo KITAGAWA, Keiichi OHNO,* Hiromu SUGETA, and Tatsuo MIYAZAWA

Institute for Protein Research, Osaka University, Yamada-kami, Suita, Osaka

(Received April 14, 1971)

Far infrared spectra (700～40 cm^{-1}) of ethyl methyl ether and deuterated species ($CH_3CH_2OCD_3$, $CD_3CH_2OCH_3$, $CH_3CD_2OCH_3$, and $CD_3CD_2OCH_3$) were measured in the crystalline, liquid and gaseous states and carbon tetrachloride solution. A low temperature cell was constructed for measuring far infrared absorption of highly volatile samples in the liquid and crystalline states. Far infrared bands due to skeletal bending vibrations of the trans and gauche isomers and lattice vibrations were assigned. From analyses of isotope effects on infrared frequencies, internal-rotation vibrations of the CH_3-CH_2, CH_2-O, and O-CH_3 bonds of the trans isomer of ethyl methyl ether were found at 248, 115, and 202 cm^{-1}, respectively, in the gaseous state. Normal vibrations were treated with the local-symmetry force field and force constants were adjusted by the method of least squares. By the use of Mathieu equation, the threefold potential barriers of the methyl groups of the trans isomer were estimated as $V_3(CH_3\text{-}C)=3.3\pm0.1$ and $V_3(O\text{-}CH_3)=2.5\pm0.1$ kcal/mol.

Studies of the internal-rotation about the CH_2-O bond of the C-CH_2-O-C group are important for treating chain conformations of polyethers including polyethylene glycol[1] $[-CH_2\text{-}CH_2\text{-}O-]_p$. The molecule of ethyl methyl ether CH_3-CH_2-O-CH_3 serves as an appropriate model for studying the internal rotation about CH_2-O bonds.

Analyses of the infrared and Raman spectra[2-5] of ethyl methyl ether suggested that the trans and gauche isomers coexist in the gaseous state and liquid state while the trans isomer remains in the crystalline state. The coexistence of rotational isomers was confirmed by the measurement of the temperature effect on the infrared spectra[6]. Furthermore, from the relative intensity of the infrared bands at ～375 cm^{-1} and ～280 cm^{-1}, the energy difference between the gauche and trans isomers was estimated as 1.5 kcal/mol in the gaseous and liquid states[6]. The electron diffraction of gaseous molecules of ethyl methyl ether was analysed[7] and the predominant isomer was confirmed to be trans and also the weak peaks due to the gauche isomer were recognized in the radial distribution. The molecular structure of the trans isomer was determined precisely by the analyses of the microwave spectra[8]. Recently, the infrared and Raman spectra (3000～500 cm^{-1}) of eight isotopic species of ethyl methyl ether were measured and, from the relative intensity of the infrared bands at 1015 cm^{-1} and 980 cm^{-1}, the energy difference between the gauche and trans isomers was estimated as 1.35 kcal/mol[9].

Vibrational frequencies of internal-rotation modes are important for studying internal-rotation potential. Accordingly, for establishing vibrational assignments of the internal-rotation frequencies of ethyl methyl ether $[CH_3CH_2OCH_3(d_0)]$ and deuterated species $[CH_3CD_2OCH_3(d_2)$, $CD_3CH_2OCH_3(d_3)$, $CH_3CH_2OCD_3$ (d_3') and $CD_3CD_2OCH_3(d_5)]$, the far infrared spectra of the gaseous, liquid and crystalline states were measured in the present study. A low-temperature cell was constructed for measuring far infrared spectra of liquid and crystalline phases of highly volatile samples since the boiling point (6°C) of ethyl methyl ether was lower than room temperature.

Experimental

Ethyl methyl ether and deuterated species were synthesized with Williamson's method. Starting material of ethyl alcohol was prepared, in advance, by the reduction of acetyl chloride with lithium aluminum hydride (or deuteride)[10]. Samples of ethyl methyl ether and deuterated species were purified by repeated distillation from dry ice temperature to liquid nitrogen temperature in vacuum. The samples were dried over phosphorous pentoxide just before spectroscopic measurements and were transferred into absorption cells through vacuum line.

Infrared spectra in the 700～200 cm^{-1} region were recorded on a Hitachi EPI-L Infrared Spectrophotometer. Cesium iodide crystal plates of 3 mm thickness were used as windows of absorption cells. For the 400～50 cm^{-1} region, a Hitachi FIS-3 Far Infrared Spectrophotometer was used with absorption cells of polyethylene windows.

Low Temperature Cell. Figure 1 shows the low-temperature cell constructed in the present study for far infrared measrements. The cryostat consists of Parts A and B. Part A is the outer jacket and is held, with a fringe (1), on the cover of the sample compartment of the spectrophotometer. The fringe is fastened onto the cover (2) with an O-ring and screws, and polyethylene sheets of 1 mm thickness are used as optical windows (3). Part B is the inner jacket and is fastened to Part A with an O-ring and screws. The liquid nitrogen reservoir (4) is as large as 1.8 *l*. The copper block (5) is provided with a channel so that liquid nitrogen is led to the bottom part of the block. However, a small temperature difference is found between the copper block (5) and the sample (6) so that a copper constantan thermo-

* Present address: Department of Chemistry, Faculty of Science, Hiroshima University, Higashi-sendamachi, Hiroshima.

1) T. Miyazawa, K. Fukushima, and Y. Ideguchi, *J. Chem. Phys.*, **37**, 2764 (1962); H. Tadokoro, Y. Chatani, T. Yoshihara. S. Tahara, and S. Murahashi, *Makromol. Chem.*, **73**, 109 (1964); H. Matsuura and T. Miyazawa, *J. Polymer Sci., A-2*, **7**, 1735 (1969).

2) K. W. F. Kohlrausch, *Monatsh. Chem.*, **68**, 349 (1936).

3) Y. Mashiko, *Nippon Kagaku Zasshi*, **80**, 593 (1959).

4) R. G. Snyder and G. Zerbi, *Spectrochim. Acta*, **23A**, 391 (1967).

5) A. D. H. Clague and A. Danti, *ibid.*, **24A**, 439 (1968).

6) T. Kitagawa and T. Miyazawa, This Bulletin, **41**, 1976 (1968).

7) M. Abe, PhD dissertation, the University of Tokyo (1968).

8) M. Hayashi, H. Imaishi, K. Ohno, and H. Murata, This Bulletin, **44**, 299 (1971).

9) J. P. Perchard, *Spectrochim. Acta*, **26A**, 707 (1970).

10) J. D. Cox and H. S. Turner, *J. Chem. Soc.*, **1950**, 3176.

couple is embedded into the window (polyethylene or silicon) of the sample cell. Thermocouple wires are connected outside through hermetic seals (7). The cryostat is evacuated better than 10^{-5} mmHg.

Double-Chopping Operation. In the far infrared region, the emission from the optical wedge in the reference beam of a double-beam spectrophotometer is not negligible as compared with the emission from the far infrared source. When the temperature of the sample in the sample beam is kept low, the emission difference between the wedge and the sample is also compensated by the wedge itself and the transmittance recorded on the chart is appreciably lower than the true transmittance. Accordingly, in the present study, the double-chopping mode (0.9 cps) of FIS-3 was used for absorption measurements of the liquid and crystalline phases at low temperatures and the systematic error due to the wedge emission was eliminated.

Solid Spectra. For absorption measurements of deposited solid, a silicon disk [(6) in Fig. 1] is held on the copper block (5). A glass jet opening is connected to a metal tube (8) so that the sample gas may be introduced from outside onto the silicon disk. Sample gas of ethyl methyl ether was deposited on the silicon disk at 77°K and was then annealed at temperatures as high as 150°K. Far infrared spectra of the solid phase at 77°K are shown in Fig. 2, where transmittance curves of deposited unannealed sample are shown with broken lines and curves of annealed sample are shown with solid lines.

Liquid Spectra. For absorption measurements of condensed liquid, a vacuum tight polyethylene cell (0.2 mm thick) was constructed by welding polyethylene sheets and tubes (entrance and exit). The cell is held on the copper block (5) of the cryostat (Fig. 1) and the entrance and exit are connected to the metal tubes (8). The sample of ethyl methyl ether is introduced through a metal tube and entrance polyethylene tube, and is liquified inside the polyethylene cell kept at low temperature.

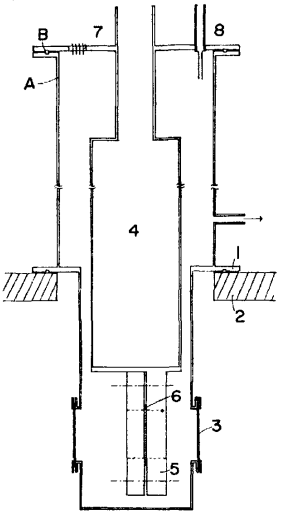

Fig. 1. Cryostat for far infrared absorption measurements.

Far infrared spectra of the liquid phase at ~170°K are shown in Fig. 3. The weak band at 78 cm^{-1} is due to polyethylene sheets of the liquid cell. Since low frequency modes are appreciably influenced by intermolecular interactions, observed peak frequencies of liquid spectra (Fig. 3) are appreciably lower than corresponding peak frequencies of the solid spectra (Fig. 2).

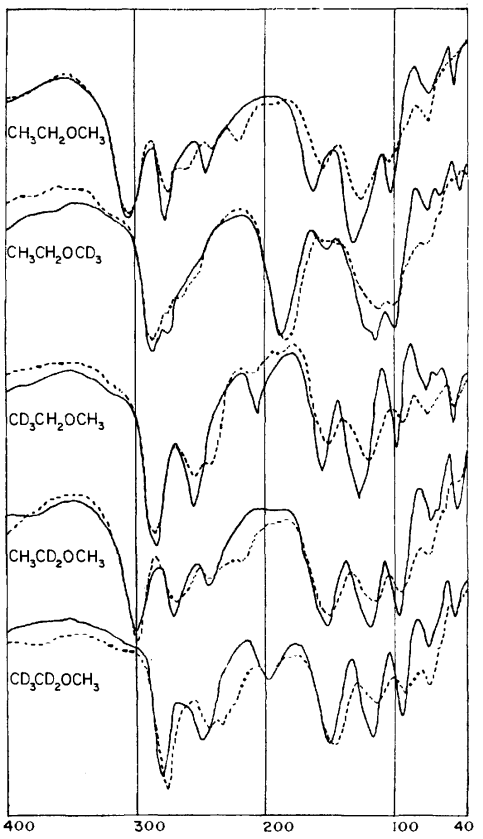

Fig. 2. Far infrared spectra of the solid phase (77°K) of ethyl methyl ether; broken line: deposited unannealed film, and solid line: annealed crystalline film.

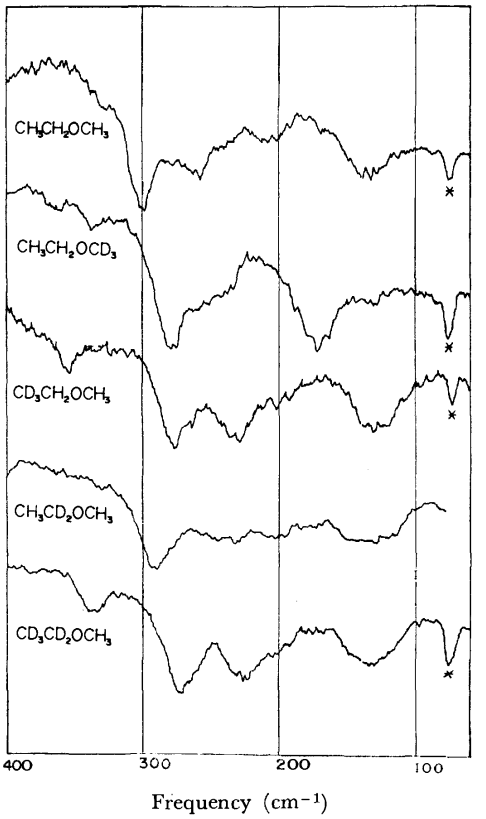

Fig. 3. Far infrared spectra of the liquid phase (~170°K) of ethyl methyl ether. The cell thickness is 0.2 mm. The band marked with * is due to polyethylene sheets.

Gas Spectra. Far infrared spectra of the gas phase (500 mmHg at room temperature) were measured with a 14 cm gas cell. Gas spectra (Fig. 4) are more complex than liquid and solid spectra, because of rotational structures and of overlapping hot bands.

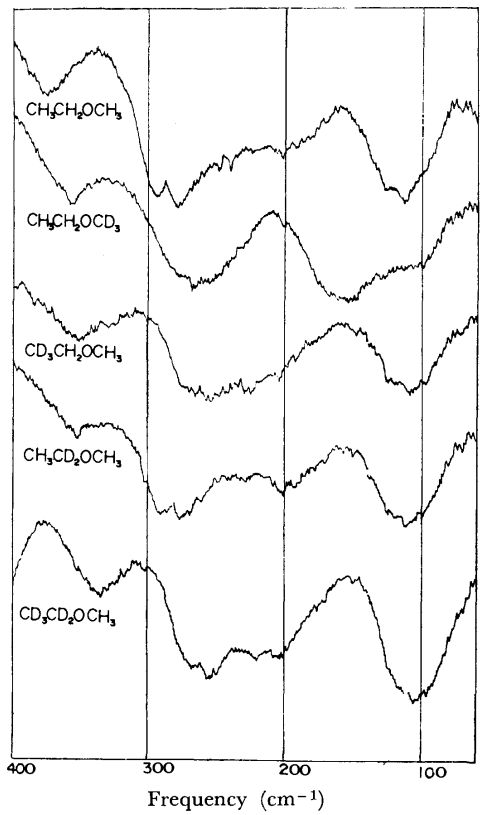

Fig. 4. Far infrared spectra of the gas phase (500 mmHg at room temperatrure) of ethyl methyl ether. The path length is 4 cm.

Solution Spectra. Infrared spectra (500~250 cm^{-1}) of ethyl methyl ether in carbon-tetrachloride solution were measured with a sealed KRS-5 cell (0.2 mm thick). Far infrared spectra of $CH_3CH_2OCH_3$ and $CH_3CH_2OCD_3$ in carbon-tetrachloride solution were measured with a sealed polyethylene cell (0.5 mm thick). Frequencies observed in solution are listed in Table 1, together with the frequencies observed for the solid, liquid, and gas phases.

Normal Vibration Treatments

The normal vibrations of the five isotopic species (d_0, d_3, d_3', d_2, and d_5) of ethyl methyl ether were treated with Wilson's ***GF*** matrix method[11]. In constructing inverse-kinetic energy matrices (***G***), the bond lengths of r(C-C)=1.530 Å, r(C-O)=1.420 Å, and r(C-H)=1.093 Å, tetrahedral bond angles, and the internal-rotation angles of 180°(trans) and 60°(gauche) were used. For the C-H stretching and deformation modes of the CH_3-C, C-CH_2-O, and O-CH_3 groups, local-symmetry coordinates (σ)[12] were used, together with the C-C and O-C stretching, C-O-C bending (ϕ), and internal-rotation coordinates (t).[13]

The potential energy matrices (***F***) were constructed on the basis of a generalized potential function, namely, the local-symmetry force field[12]. The initial set of potential constants of the CH_3-C, C-CH_2-O, and O-CH_3 groups were transferred from ethane[14], polyethylene glycol[15] and dimethyl ether[16], respectively, and were adjusted by the method of least squares[17] with reference to the infrared frequencies observed for the trans and gauche isomers of the five isotopic species (except for internal-rotation frequencies of the gauche isomer)[18]. After six cycles of adjustments, a converged set of potential constants was obtained. However, in the high frequency region (3000~600 cm^{-1}), a unique set of vibrational assignments of the five isotopic species were not yet established. On the other hand, in the low frequency region (<600 cm^{-1}), vibrational assignments were made satisfactorily, and a reliable set of potential constants was obtained for low-frequency modes; $f[\sigma(\text{C-C-O})]=0.925$, $f[\phi(\text{C-O-C})]=1.373$, $f[\sigma(\text{C-C-O})\cdot\phi(\text{C-O-C})]=0.167$, $f[t(CH_3\text{-}CH_2)]=0.0939$, $f[t(CH_2\text{-O})]=0.0769$, $f[t(\text{O-}CH_3)]=0.0682$ mdyn Å/rad², where three force constants were set as $f[r(\text{C-C})\cdot\sigma(\text{C-C-O})]=0.017$, $f[r(\text{C-O})\cdot\delta(\text{C-C-O})]=0.455$ and $f[r(\text{O-C})\cdot\phi(\text{C-O-C})]=0.259$ mdyn/rad.[15] Calculated frequencies lower than 600 cm^{-1} are listed in Table 1.

Lattice Vibrations

Far infrared spectra of the crystal, liquid and vapor phases of $CH_3CH_2OCH_3$ are shown in Fig. 5. In the lowest frequency region, the crystal bands at 52, 67, and 102 cm^{-1} disappear on melting and accordingly are assigned to lattice vibrations. On the other hand, the vapor band at 115 cm^{-1} corresponds to the liquid band at 132 cm^{-1} and to the crystal band at 166 cm^{-1}, since low-frequency internal-rotation vibrations are known to shift appreciably to higher frequency on phase-changes gas→liquid→crystal. Accordingly, the crystal band at 132 cm^{-1} is assigned to a lattice vibration, possibly coupled with internal-rotation modes. Observed frequencies of lattice vibrations of ethyl methyl ether (ν_0) and deuterated species (ν) and their ratios (ν_0/ν) are listed in Table 2.

In the crystal of ethyl methyl ether, the molecule does not have the center of symmetry, and, in principle, translatory and rotatory lattice modes are not separated from each other. However, for 'purely' translatory or rotatory vibrations, frequencies of isotopic molecules would be inversely proportional to the square root of the molecular mass or principal moments of inertia[8],

11) E. B. Wilson, *J. Chem. Phys.*, **7**, 1047 (1939); **9**, 76 (1941).
12) T. Shimanouchi, *Nippon Kagaku Zasshi*, **86**, 261 (1965); "Physical Chemistry", Vol. 4, ed., by H. Eyring, Academic Press, New York, N. Y. (1970), p. 233.
13) T. Miyazawa and K. Fukushima, *J. Mol. Spectry.*, **15**, 308 (1965).
14) J. I. Duncan, *Spectrochim. Acta*, **20**, 1197 (1964).
15) H. Matsuura and T. Miyazawa, This Bulletin, **41**, 1798 (1968).
16) H. Sugeta, Dissertation, Osaka University (1969).
17) D. E. Mann, T. Shimanouchi, J. H. Meal, and L. Fano, *J. Chem. Phys.*, **27**, 43 (1957).
18) K. Ohno, to be published separately.

TABLE 1. INFRARED FREQUENCIES[a] OF ETHYL METHYL ETHER IN THE CRYSTAL, LIQUID, AND GAS PHASES AND CARBON TETRACHLORIDE SOLUTION, CALCULATED FREQUENCIES, AND VIBRATIONAL ASSIGNMENTS

Species	Crystal	Liquid	Solution	Gas	Calc[b]	Assignment[c]
$CH_3CH_2OCH_3$	472 (m)		467 (s)	465 (s)	477 (T)	ϕ_s
					475 (G)	ϕ_a
	—	378 (vw)	376 (m)	374 (w)	375 (G)	ϕ_s
	310 (s)	300 (s)	299 (m)	287 (s)[d]	290 (T)	ϕ_a
	280 (s)	258 (m)	255 (vw)	248 (m)	252 (T)	$t(CH_3\text{-}CH_2)$
	—	240 (vw)	239 (w)	239 (m)	224 (G)	$t(CH_3\text{-}CH_2)$
	249 (m)	208 (w)	~200 (w)	202 (m)	201 (T)	$t(O\text{-}CH_3)$
				192 (w)	197 (G)	$t(O\text{-}CH_3)$
	166 (m)	132 (m)	~127 (w)	115 (s, b)	113 (T)	$t(CH_2\text{-}O)$
					112 (G)	$t(CH_2\text{-}O)$
$CH_3CH_2OCD_3$	449 (m)		448 (s)	451 (s)	452 (T)	ϕ_s
					452 (G)	ϕ_a
	—	360 (vw)	360 (m)	356 (w)	360 (G)	ϕ_s
	290 (s)	276 (s)	279 (m)	265 (s)[d]	273 (T)	ϕ^a
	277 (s)	258 (w)	246 (vw)	241 (w)	247 (T)	$t(CH_3\text{-}CH_2)$
	—	244 (w)		231 (w)	221 (G)	$t(CH_3\text{-}CH_2)$
	191 (s)	172 (m)	~165 (w)	155 (s, b)	156 (T)	$t(O\text{-}CD_3)$
					150 (G)	$t(O\text{-}CD_3)$
	155 (w)	129 (vw)	126 (w)	104 (m, b)	105 (T)	$t(CH_2\text{-}O)$
					100 (G)	$t(CH_2\text{-}O)$
$CD_3CH_2OCH_3$	446 (m)		439 (s)	436 (s)	455 (T)	ϕ_s
					460 (G)	ϕ_a
	—	353 (w)	356 (m)	350 (w)	355 (G)	ϕ_s
	285 (s)	276 (s)	278 (m)	262 (s)[d]	271 (T)	ϕ_a
	254 (m)	236 (m)		230 (m)	224 (T)	$t(O\text{-}CH_3)$
	—	228 (m)		225 (m)	195 (G)	$t(O\text{-}CH_3)$
	205 (w)	202 (w)		~175 (w, sh)	171 (T)	$t(CD_3\text{-}CH_2)$
	—	192 (vw)			167 (G)	$t(CD_3\text{-}CH_2)$
	155 (m)	129 (m, b)		108 (s, b)	109 (T)	$t(CH_2\text{-}O)$
					104 (G)	$t(CH_2\text{-}O)$
$CH_3CD_2OCH_3$	459 (m)		452 (s)	455 (s)	469 (T)	ϕ_s
					455 (G)	ϕ_a
	—	361 (vw)	358 (m)	351 (w)	353 (G)	ϕ_s
	303 (s)	292 (s)	294 (m)	282 (s)[d]	284 (T)	ϕ_a
	275 (m)	245 (w)		240 (vw)	245 (T)	$t(CH_3\text{-}CD_2)$
	—	233 (w)		229 (vw)	224 (G)	$t(CH_3\text{-}CD_2)$
	247 (m)	200 (w)		202 (w)	200 (T)	$t(O\text{-}CH_3)$
				193 (w)	197 (G)	$t(O\text{-}CH_3)$
	156 (s)	130 (m)		111 (b, s)	110 (T)	$t(CD_2\text{-}O)$
					108 (G)	$t(CD_2\text{-}O)$
$CD_3CD_2OCH_3$	437 (m)		419 (s)	416 (s)	448 (T)	ϕ_s
					436 (G)	ϕ_a
	—	336 (w)	342 (m)	336 (m)	338 (G)	ϕ_s
	282 (s)	272 (s)	268 (m)	260 (s)[d]	266 (T)	ϕ_a
	251 (m)	232 (m)		220 (m)	217 (T)	$t(O\text{-}CH_3)$
	—	226 (m)			195 (G)	$t(O\text{-}CH_3)$
	199 (w)	204 (w)		~170 (vw)	169 (T)	$t(CD_3\text{-}CD_2)$
	—	192 (w)			165 (G)	$t(CD_3\text{-}CD_2)$
	152 (m)	129 (m)		104 (s, b)	106 (T)	$t(CD_2\text{-}O)$
					102 (G)	$t(CD_2\text{-}O)$

a) Frequency in the cm^{-1} units; s: strong, m: medium, w: weak, vw: very weak, b: broad, sh: shoulder.
b) T: trans isomer, G: gauche isomer.
c) ϕ_s and ϕ_a are pseudo-symmetric and -antisymmetric skeletal bending modes, respectively, and t is internal-rotation mode.
d) Average frequency of the P and R branch-peaks.

TABLE 2. OBSERVED FREQUENCIES[a] OF LATTICE VIBRATIONS

Species	ν	ν_0/ν	ν	ν_0/ν	ν	ν_0/ν	ν	ν_0/ν
$CH_3CH_2OCH_3$	132	(1)	102	(1)	67	(1)	52	(1)
$CH_3CH_2OCD_3$	119 113	1.11 1.16	98	1.04	63	1.06	47	1.11
$CD_3CH_2OCH_3$	123	1.07	94	1.09	70	0.96	50	1.04
$CH_3CD_2OCH_3$	119	1.11	98	1.04	67	1.00	52	1.00
$CD_3CD_2OCH_3$	116	1.14	93	1.10	66	1.02	52	1.00

a) ν: in cm^{-1} unit, ν_0: frequency of $CH_3CH_2OCH_3$.

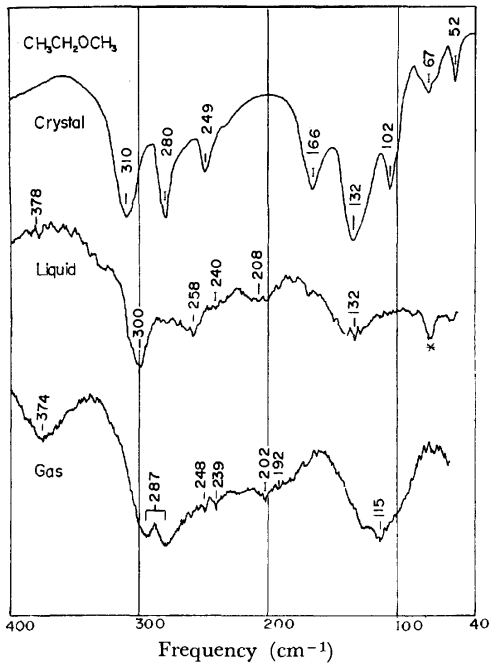

Fig. 5. Comparison of the far infrared spectra of the crystal, liquid, and vapor phases of ethyl methyl ether. The band marked with * is due to polyethylene sheets.

TABLE 3. RATIOS OF THE SQUARE ROOT OF THE MOLECULAR MASS (M) AND PRINCIPAL MOMENTS OF INERTIA (I_a, I_b, and I_c) OF THE TRANS ISOMER[a]

Species	$(M/M^0)^{1/2}$	$(I_a/I_a^0)^{1/2}$	$(I_b/I_b^0)^{1/2}$	$(I_c/I_c^0)^{1/2}$
$CH_3CH_2OCH_3$	(1)	(1)	(1)	(1)
$CH_3CH_2OCD_3$	1.03	1.09	1.06	1.06
$CD_3CH_2OCH_3$	1.03	1.09	1.06	1.06
$CH_3CD_2OCH_3$	1.02	1.12	1.01	1.01
$CD_3CD_2OCH_3$	1.04	1.19	1.07	1.07

a) Ref. 8.

respectively. As shown in Table 3, frequency ratios of the translatory vibrations of ethyl methyl ether and deuterated species are as small as 1.02~1.04, whereas frequency ratios (1.01~1.19) of rotatory vibrations vary with deuterated species and rotation-axes. For the lattice vibration of $CH_3CH_2OCH_3$ (132 cm^{-1}), observed frequency ratios are as high as 1.07~1.14 (Table 2) and accordingly this highest-frequency lattice vibration is primarily due to a rotatory mode, possibly about the axis of the smallest moment of inertia (I_a).

Skeletal Deformation Vibrations

For the trans isomer of ethyl methyl ether CH_3-CH_2-O-CH_3, C-C-O and C-O-C bending vibrations are expected in the region below 600 cm^{-1}. In fact, infrared bands were observed at 472 and 310 cm^{-1} for the crystal phase. Since the mass of the oxygen atom is not much different from the mass of the methylene group, the C–C–O and C–O–C bending modes are hybridized, giving rise to the in-phase (ϕ_s) and out-of-phase (ϕ_a) bending modes. From normal vibration treatments, the bands at 472 and 310 cm^{-1} are assigned to ϕ_s and ϕ_a, respectively (Table 1). Skeletal bending vibrations of the trans isomer (point group C_s) belong to the A′ species and accordingly are expected to give rise to A, B, or AB hybrid bands in vapor spectra. In fact, the band of ethyl methyl ether at 287 cm^{-1} and corresponding bands of deuterated species are observed as B-type (Fig. 4).

The infrared band of liquid ethyl methyl ether at 378 cm^{-1} and corresponding bands of deuterated species disappear on crystallization, and accordingly are assigned to the gauche isomer (ϕ_s mode, Table 1). From normal vibration treatments[4,7], the other skeletal bending vibration (ϕ_a) of the gauche isomer of $CH_3CH_2OCH_3$ is expected at ~510 cm^{-1} but a corresponding band is not observed there. On the other hand, from the temperature dependence of the infrared intensities of the vapor bands at 465, 374, and 287 cm^{-1}, it was suggested[6] that the infrared band due to the ϕ_a vibration of the gauche isomer is overlapped by the band of the trans isomer at 465 cm^{-1}, although the intensity of the composite band is largely due to the gauche isomer. Corresponding bands are also observed for deuterated species (Table 1). It may be remarked that the potential term of $f[\sigma(\text{C-C-O})\cdot\phi(\text{C-O-C})]$ was necessary in least-square adjustments of potential constants with reference to skeletal-bending frequencies of the gauche isomer as well as of the trans isomer.

Internal Rotation Vibrations

For the trans isomer of ethyl methyl ether CH_3-CH_2-O-CH_3, the internal-rotation vibrations (CH_3-CH_2, CH_2-O, and O-CH_3) are all infrared-active. In fact, infrared bands are observed at 280, 249, and 166 cm^{-1} for the crystal phase (Fig. 6). The infrared band at 280 cm^{-1} is shifted appreciably to 205 cm^{-1} on deuteration of the CH_3-C group and is assigned to the internal-rotation vibration about the

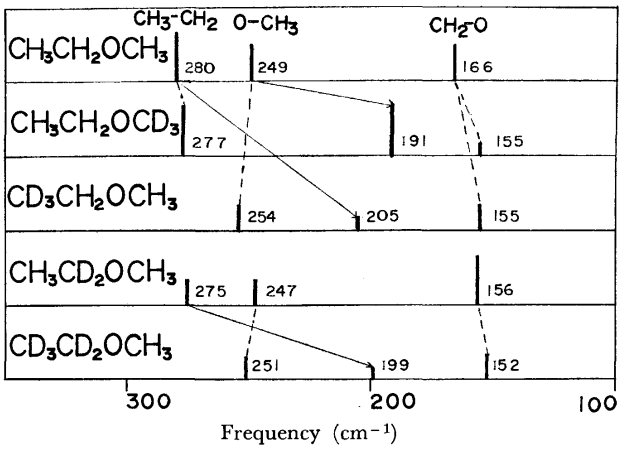

Fig. 6. Isotope shifts of internal-rotation frequencies of the crystal phase.

CH_3-CH_2 bond. On the other hand, the infrared band of $CH_3CH_2OCH_3$ at 249 cm^{-1} is shifted to 191 cm^{-1} on deuteration of the O-CH_3 group and is assigned to the internal-rotation vibration about the O-CH_3 bond. The low-frequency band at 166 cm^{-1} is shifted little on deuteration of the CH_3-C or O-CH_3 group and is assigned to the internal-rotation vibration about the CH_2-O bond. Similar deuteration effects are observed for the infrared bands of CH_3-CD_2OCH_3 at 275, 247, and 156 cm^{-1} (Fig. 6). Thus, the vibrational assignments of the internal-rotation vibrations of the CH_3-CH_2 and O-CH_3 groups are established in the present study. Previous vibrational assignments[4,7] need be revised accordingly.

In the vapor phase, the internal-rotation vibrations of the trans isomer of $CH_3CH_2OCH_3$ give rise to sharp peaks (C-type) at 248, 202, and 115 cm^{-1}, just as expected for the transition moments parallel to the axis of the largest moment of inertia (I_c).

Internal-rotation frequencies of the gauche isomer are calculated to be lower than corresponding frequencies of the trans isomer (Table 1). Frequency differences between the trans and gauche isomers are due to the vibrational coupling between the internal-rotation modes and skeletal bending modes; such coupling is possible for the gauche isomer but not for the trans isomer.

Barrier Height for Internal Rotation of Methyl Group

For the trans isomer of ethyl methyl ether, three internal rotation modes belong to the same species (A″) and hybridization of those modes are expected. Accordingly, potential energy distributions[19] were calculated for internal-rotation vibrations as shown in Table 4. Hybridization of the internal-rotation modes of the CH_3-C and O-CH_3 groups is not negligible although these groups are separated by the central C-O bond. Accordingly, in estimating the barrier height of methyl groups, hybridization. of the two modes need be taken into account.

Table 4. Frequencies and potential energy distributions calculated for internal-rotation vibrations

Species	Freq. (cm^{-1})	Distribution (%)		
		CH_3-CH_2	CH_2-O	O-CH_3
$CH_3CH_2OCH_3$	252	70	0	20
	201	19	1	78
	113	0	95	1
$CH_3CH_2OCD_3$	247	91	0	7
	156	6	3	89
	105	0	93	4
$CD_3CH_2OCH_3$	224	25	1	74
	171	72	1	24
	109	0	95	1
$CH_3CD_2OCH_3$	245	82	0	17
	200	16	1	80
	110	0	96	2
$CD_3CD_2OCH_3$	217	20	1	78
	169	78	0	19
	106	0	95	2

In the present study, threefold potential barriers were estimated first with the harmonic approximation, $V_3(CH_3\text{-}C)=3.00$ and $V_3(O\text{-}CH_3)=2.18$ kcal/mol, from the force constants of $f[t(CH_3\text{-}CH_2)]=0.0939$ and $f[t(O\text{-}CH_3)]=0.0682$ mdyn Å/rad^2. Threefold potential barriers were also estimated as shown in Tables 5 and 6 (third column), with the single-top harmonic approximation, directly from infrared frequencies observed in the vapor phase (Table 1). The structural parameters[20] $F(CH_3\text{-}C)$ and $F(O\text{-}CH_3)$ were calculated (Tables 5 and 6, second column) from the same molecular parameters as used in normal vibration treatments [essentially the same F values were also obtained by the use of the molecular parameters determined by microwave analyses[8]]. Then, with reference to the V_3 values estimated from force constants, the corrections for the single-top approximation were calculated as shown in Tables 5 and 6 (fourth column).

In the second step, the anharmonicity of the three fold potential function was taken into account. Thus, Mathieu equation for the single-top case was used and the V_3 values were calculated (Tables 5 and 6, fifth column) from infrared frequencies of the vapor phase. Finally, the corrections for the single-top approximation were made, yielding corrected V_3 values as shown in the sixth column of Tables 5 and 6. It may be remarked that final V_3 values calculated for the five isotopic molecules agree closely with one another, giving mean values of

$$V_3(CH_3\text{-}C) = 3.3 \pm 0.1 \text{ kcal/mol}$$

$$V_3(O\text{-}CH_3) = 2.5 \pm 0.1 \text{ kcal/mol}$$

19) Y. Morino and K. Kuchitsu, *J. Chem. Phys.*, **20**, 1809 (1952); I. Nakagawa, *Nippon Kagaku Zasshi*, **74**, 243 (1953).

20) D. R. Herschbach, *J. Chem. Phys.*, **31**, 91 (1959).

Table 5. Structure parameters (F) and threefold potential barrier (V_3) of CH_3-C group

Species	F(cm^{-1})	V_3(kcal/mol)			
		Single-top harmonic	Corrected for single-top	Single-top Mathieu	Corrected barrier
$CH_3CH_2OCH_3$	6.18	3.16	−0.16	3.54	3.38
$CH_3CH_2OCD_3$	6.03	3.06	−0.06	3.42	3.36
$CD_3CH_2OCH_3$	3.54	2.75	+0.25	3.01	3.26
$CH_3CD_2OCH_3$	5.99	3.06	−0.06	3.42	3.36
$CD_3CD_2OCH_3$	3.35	2.74	+0.26	2.99	3.25

Table 6. Structure parameters (F) and threefold potential barrier (V_3) of O-CH_3 group

Species	F(cm^{-1})	V_3(kcal/mol)			
		Single-top harmonic	Corrected for single-top	Single-top Mathieu	Corrected barrier
$CH_3CH_2OCH_3$	6.18	2.10	+0.08	2.41	2.49
$CH_3CH_2OCD_3$	3.54	2.15	+0.03	2.38	2.41
$CD_3CH_2OCH_3$	6.03	2.79	−0.61	3.15	2.54
$CH_3CD_2OCH_3$	5.99	2.17	+0.01	2.49	2.50
$CD_3CD_2OCH_3$	5.89	2.61	−0.43	2.96	2.53

It is interesting to note that the threefold potential barrier of the CH_3-C group of ethyl methyl ether agrees closely with the corresponding barrier of propane[21], $V_3(CH_3\text{-}C)=3.325\pm0.020$ kcal/mol. Furthermore, the potential barrier of the O-CH_3 group of ethyl methyl ether agrees closely with the barrier of dimethyl ether recently determined from microwave analyses[22], $V_3(O\text{-}CH_3)=2.56$—2.60 kcal/mol.

21) E. Hirota, C. Matsumura, and Y. Morino, This Bulletin **40**, 1124 (1967).

22) M. Hayashi, private communication.

BULLETIN OF THE CHEMICAL SOCIETY OF JAPAN, VOL. 45, 975—980 (1972)

Studies of Salt Solution Aerosols. VIII.[1] The Effect of Humidity on the Stability of Spray-dried Na_2SO_4 Aerosol and an Estimate of the Particle Density

Yasuo Ueno and Isamu Sano

Department of Chemistry, Faculty of Science, Nagoya University, Chikusa-ku, Nagoya

(Received April 23, 1971)

The aerosols obtained by spraying an aqueous Na_2SO_4 solution of concentrations ranging from 0.1 to 10% by weight were dried by a furnace at 200 to 800°C and were then subjected to stirred aging at room temperature in an atmosphere of 90% relative humidity or less; the variations in both mass concentration and particle size were then measured with the lapse of time.

By employing the results thus obtained and by making some assumptions, the density of the particle in dried aerosols was calculated to be several tenths of one gram per cc, which is smaller by a factor of 3 to 4.5 than the bulk density of solid Na_2SO_4; further, the amount of water which the dried particle might hold if kept in a humidified atmosphere was estimated, with the finding that the density of a particle would decrease with increase in its water content; for example, the density of the particle with composition of $Na_2SO_4 \cdot 10H_2O$ would be 0.32 g/cc, smaller by a factor of 4 to 5 than the bulk density. In addition, the influence of water vapor on the stability of the dried aerosols was studied; it was found that the higher the humidity, the greater the rate of coagulation.

The production of the aerosols of hygroscopic salts and their properties in the presence of water vapor have been investigated by aerosol researchers, especially for the last two decades, from the viewpoint of meterological studies; in recent times, the spray-drying process has come into more frequent use by chemical engineers. The present paper will deal with the dehydration of aqueous Na_2SO_4 solution aerosols, the effect of the water vapor on the coagula-

1) Part VII: I. Sano and Y. Ueno, *J. Res. Assoc. Powder Tech.*, **8**, 94 (1971).

tion rate of the dried aerosols, and, further, the determination of the density of the dried particle.

A number of experiments have been performed in an attempt to determine the influence of such additions as water or some organic vapors upon the stability of aerosols, but the results have shown conflicting trends. For instance, Samokhvalov and Kozhukhova[2] describe that, for anmonium chloride aerosols, water or octyl alcohol vapor acts as a stabilizer, in contrast to the coagulation-promoting effect of water and butyric acid vapor observed by Smirnov and Solnseva.[3]

Concerning the density of an aerosol particle, it is usually assumed to be the same as that in bulk. This is valid for a homogeneous solid particle, but it might lead to erroneous results for an aggregate of solid particles formed by coagulation. It has been shown by Patterson and R. Whytlaw-Gray.[4] that the particles of cadmium, zinc, and magnesium oxides possess a loose or chain-like structure, so that it would be wrong to apply to them the normal bulk density in deducing their size from the rate of settling. After examining dried, microcrystallized particles of several inorganic salts, Duffie[5] has concluded that they are of density far less than normal. For the determination of the density of an aerosol particle, the ultramicroscope method might be used, but it has the disadvantages that reliable value of the settling velocity must be obtained by means of a large number of measurements and that the particles coarser than submicron-sized range can be managed only with difficulty unless a photographic device[6] is utilized; in the present paper, a different method has been adopted to determine the densities.

Experimental

Materials. The Na_2SO_4 used was of extra pure grade, and the H_2SO_4 of chemically pure grade.

Apparatus and Procedure. The mist generated by means of an atomizer of the glass-bead type[7] under a pressure of 2 kg/cm^2 was passed through an electric furnace and charged for 10 minutes into a plastic chamber of a volume of about 0.8 m^3 (1 m in height and 1.02 m in diameter), the inside of which had been kept saturated with water vapor by putting an aqueous H_2SO_4 solution on the bottom and by agitating the atmosphere over it. The aerosol in the chamber was continuously agitated during and after charging by constant-rate stirring (50 rev/min). The time of aging after charging was reckoned from the moment the charging stopped. The concentration of the dispersing solution was varied from 0.1 to 10% by weight, the temperature of the furnace, from 200° to 800°C, and the relative humidity, from 0 to 90%. The temperature in the chamber was held somewhere near 25°C throughout all the experiments. The humidity and the temperature were measured before and after each run by means of an electrical-type hygrometer and a glass set on the walls of the chamber. Table 1 shows the experimental conditions in condensed form.

Analyses of Mass Concentration and Particle Size. The technique of collecting the samples for the analyses has been described previously[9]; the concentration was determined through electrical-conductivity measurements of the solution obtained by dissolving into distilled water the Na_2SO_4 deposit in an electrical precipitator. As for the size, the dried aerosol that came out of the furnace to be aged in the chamber was introduced into a thermal precipitator, where the particles were gathered on electron-microscope collodion-mesh grids; the particles were viewed at a magnification of 2300X, 3000X, or 5000X and were found to be either isolated and rounded ones or chain-like aggregates. As the size of the former, the number-averaged diameter was taken, and while as that of the latter, the number average of the volume-equivalent diameters was taken.

Results and Discussion

Time Variations of Mass Concentration and Particle Size. From the experiment, it was found that the relative mass concentration decreases with the time and, further, that it decreases as the concentra-

TABLE 1. CONDITIONS USED IN THE EXPERIMENT

Run	Concentration of dispersing solution, %	Temperature of furnace, °C	Relative humidity in chamber, %	Temperature in chamber, °C
E_{10}	10.0	200	0	25.0
E_{15}	10.0	800	0	24.9
E_{20}	0.1	800	0	26.0
E_{21}	1.0	800	0	25.5
E_{22}	5.0	800	0	26.0
E_{23}	10.0	500	0	25.3
E_{24}	10.0	500	28.0	25.6
E_{26}	10.0	500	42.3	25.1
E_{28}	10.0	500	65.0	24.8
E_{33}	10.0	500	90.0[8]	25.9

2) K. Samokhvalov and O. K. Kozhukhova, *J. Phys. Chem. (USSR)*, **8**, 420 (1936).
3) L. A. Smirnov and V. H. Solnseva, *Colloid J. (USSR)*, **4**, 401 (1938).
4) H. S. Patterson and R. Whytlaw-Gray, *Proc. Roy. Soc. (London)*, **A113**, 302 (1927).
5) J. A. Duffie and W. R. Marshall, Jr., *Chem. Engr. Progr.*, **49**, 480 (1953).
6) V. D. Hopper and T. H. Laby, *Proc. Roy. Soc. (London)*, **A178**, 243 (1941).
7) I. Sano and Y. Ueno, *Nippon Kagaku Zasshi*, **90**, 47 (1969).
8) It has been enough established experimentally that, in an atmosphere of which humidity is below 93%, there occurs no transition from solid phase to liquid one. *cf.* S. Twomey, *J. Appl. Phys.*, **24**, 1099 (1953).
9) Y. Ueno and I. Sano, This Bulletin, **44**, 908 (1971).

tion of the dispersing solution or the relative humidity of the chamber increases. Here, the relative mass concentration is defined as the ratio of the concentration (m_t) at time (t) to the initial one (m_0), determined by the extrapolation of m_t. It should be added that no influence of the temperature of the furnace upon the concentration change was found in so far an aqueous 10% solution was examined, the points corresponding to Runs E_{10}, E_{15}, and E_{23} overlapping one another.

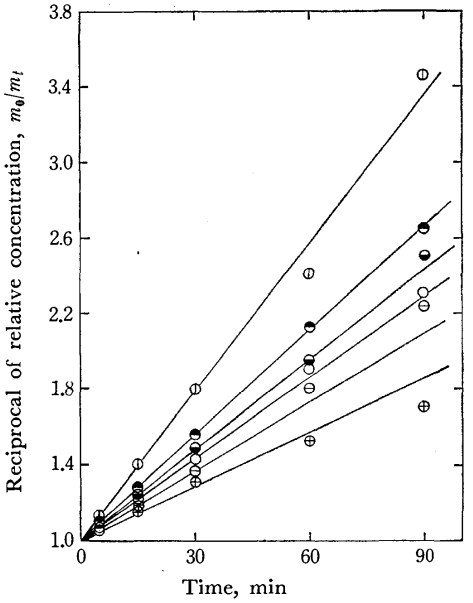

Fig. 1. Plot of the reciprocal of relative mass concentration against time.
◐ E_{33} ◓ E_{28} ◒ E_{26} ○ E_{23} ⊖ E_{22} ⊕ E_{21}

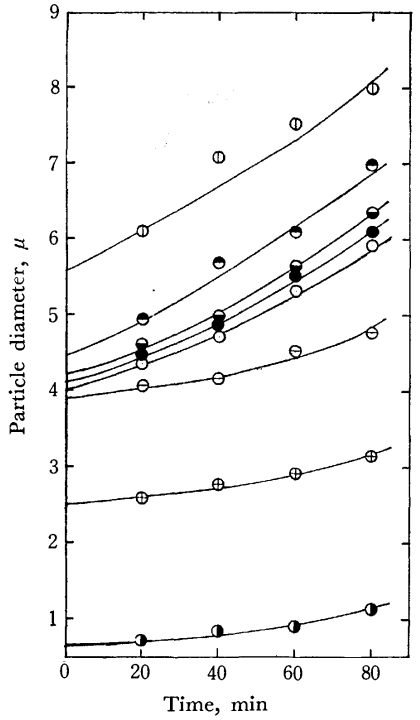

Fig. 2. Time variation of particle size under different conditions.
◐ E_{33} ◓ E_{28} ◒ E_{26} ● E_{24} ○ E_{23} ⊖ E_{22} ⊕ E_{21}
◑ E_{20}

If the reciprocal of the relative mass concentration is plotted against the time, a linear relation is found for the early stage of the run (Fig. 1), suggesting that the time variation in the mass concentration is a second-order reaction.[9]

Figure 2 depicts the change in the particle size with the time under different conditions of the relative humidity in the chamber and of the concentration of the dispersing solution. From the figure, it is obvious that the particle size increases with the time and becomes larger with the increase in both humidity and concentration.

Estimate of the Density of Particle. The settling velocity of a particle of a monodisperse aerosol confined in a chamber under agitation may be expressed as follows[10]:

$$-dn_t/dt = n_t \cdot V_t/H \tag{1}$$

n_t: number concentration at time t
V_t: Stokes' velocity of settling at time t of a particle
H: height of chamber

The integration of Eq. (1) between time t to $t+\Delta t$ yields:

$$-\int_t^{t+\Delta t} dn_t/n_t = 1/H \cdot \int_t^{t+\Delta t} V_t \, dt \tag{2}$$

or

$$\ln n_{t+\Delta t}/n_t = -V_t/H \cdot \Delta t \tag{3}$$

V_t being assumed to be constant for a short interval of time, Δt. On substituting the relations:

$$n_{t+\Delta t} = 6\, m_{t+\Delta t}/\pi D_{t+\Delta t}{}^3 \rho_{t+\Delta t} \tag{4}$$

$$n = 6\, m_t/\pi D_t{}^3 \rho_t \tag{5}$$

m: mass concentration
D: diameter of particle
ρ: density of particle

it follows that:

$$-\ln [m_{t+\Delta t}/m_t \cdot (D_t/D_{t+\Delta t})^3] = V_t \cdot \Delta t/H - \ln [\rho_{t+\Delta t}/\rho_t] \tag{6}$$

Provided that the $\rho_{t+\Delta t}$ term is equal to ρ_t for the short interval Δt, the plot of the left-hand side of Eq. (6) against Δt passes through the point of origin, and the slope at the origin given the settling velocity at time, t, with the height of chamber H=100 cm. In Fig. 3, an example (Run E_{28}) is shown; the slope of the line gets steeper as the time becomes longer. For the other experiment runs, similar results are obtained. The values of the velocities thus found are represented in Fig. 4.

By equating the effective weight of particle at time, t, to the Stokes' drag, we obtain:

$$\pi/6 \cdot D^3(\rho - \rho')g = 3\,\pi\eta VD \tag{7}$$[11]

where D is the diameter of the particle; ρ and V, its density and settling velocity; η and ρ, the viscosity and density of the medium (air), and g, the gravitational acceleration. By neglecting ρ' in comparison with ρ, we obtain:

10) D. Sinclair, "Handbook on Aerosols," Chap. 5, U. S. A. Atomic Energy Commission, Washington D. C. (1950).
11) The subscript t is omitted for simplicity.

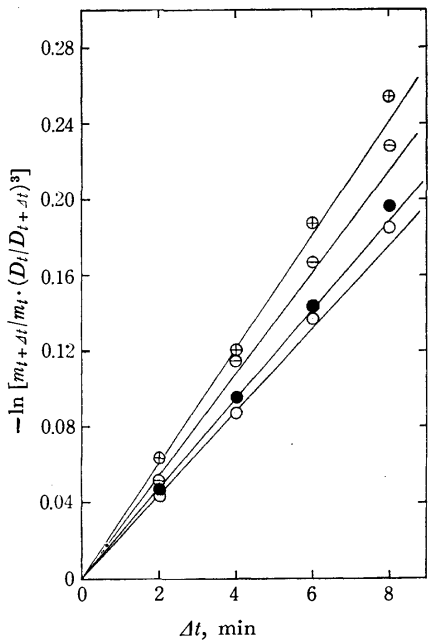

Fig. 3. Plots of Eq. (6) for Run E_{28}.
○ 20 min ● 40 min ⊖ 60 min ⊕ 80 min

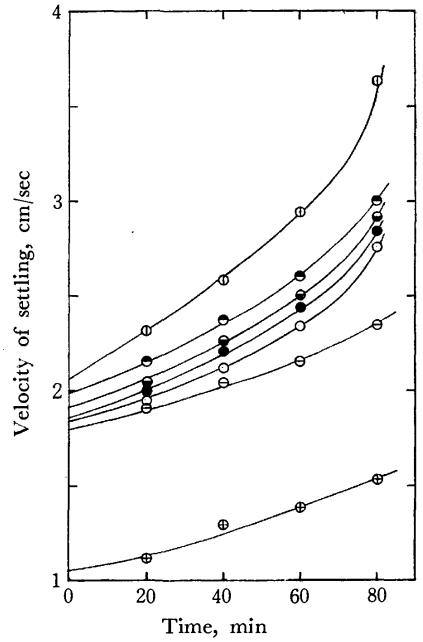

Fig. 4. Variation of the settling velocity of particles with time.
◑ E_{33} ◓ E_{28} ◒ E_{26} ● E_{24} ○ E_{23} ⊖ E_{22} ⊕ E_{21}

$$\rho = 18\,\eta V/gD^2 \qquad (8)$$

From Eq. (8), the value of ρ at time t can be estimated if D and V at time t are known. The values obtained are given in Fig. 5; the points for Runs E_{10} and E_{15} are not shown, since they coincide with those of Run E_{23}. It may be seen in Fig. 5 that the density of the particle decreases with the time of aging and, further, with the increase in the humidity.

Effect of Humidity on the Coagulation Rate. The number concentration (n_t) at the time, t, is obtained by substituting m_t, D_t, and ρ_t (Fig. 5) into Eq. (5);

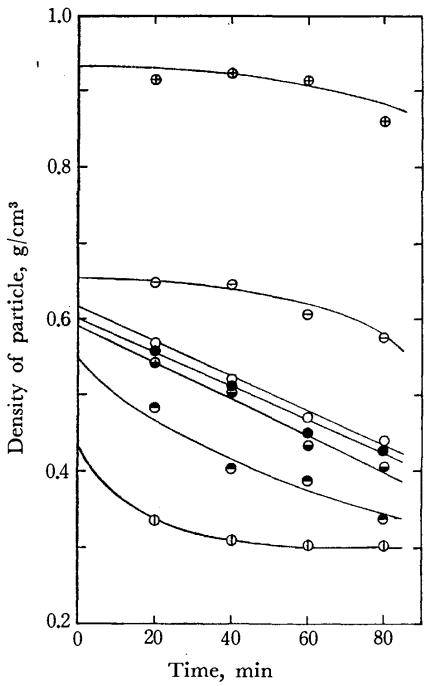

Fig. 5. Time-dependence of the density of air-borne Na_2SO_4 particles.
⊕ E_{21} ⊖ E_{22} ○ E_{23} ● E_{24} ◒ E_{26} ◓ E_{28} ◑ E_{33}

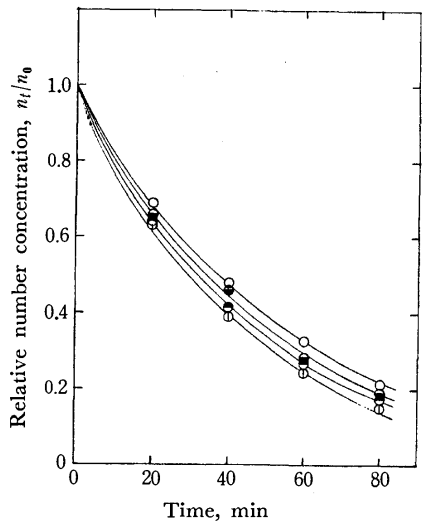

Fig. 6. Plots of n_t/n_0 against time.
○ E_{23} ◒ E_{26} ◓ E_{28} ◑ E_{33}

the concentration at zero time (n_0) is determined by extrapolation to zero time of the plot of n_t against t. Figure 6 represents the plot of the relative number concentration (n_t/n_0) against the time; from the figure, it may be seen that the influence of water vapor is roughly linear with the humidity. The half-decay period in terms of number concentration and the particle size at that time are shown in Table 2; from the table, it may be seen that, as the humidity is increased, the half-decay period gets shorter, the particle size larger, and the particle density smaller. According to Duffie *et al.*[5], spray-dried Na_2SO_4 particles are hollow and crystallized, and they show holes with edges rounded inward and have thin, compact shells with radius/thickness ratios of the order of 10. The

TABLE 2. PARTICLE DIAMETER AND DENSITY AT THE HALF-DECAY PERIOD

Run	Half-decay period, min	Particle diameter, μ	Particle density, g/cm^3
E_{23}	37	4.7(4.0)	0.53(0.62)
E_{26}	34	4.9(4.3)	0.51(0.57)
E_{28}	32	5.3(4.5)	0.43(0.53)
E_{33}	29	6.5(5.6)	0.32(0.43)

The parentheses express the value at zero time (Figs. 2 and 5).

TABLE 3. DRY PARTICLE-LIQUID DROPLET DIAMETER RATIO AND THE DENSITY OF PARTICLE IMMEDIATELY AFTER DRYING

Run	Concentration of dispersing soln, %	Furnace temperature, °C	Diameter of dry particle (d_s), μ	Particle-droplet diameter ratio, d_s/D_l	Density of dry particle (ρ_s), g/cc
E_{21}	1	800	2.5	0.22[15]	0.93[17]
E_{22}	5	800	3.9	0.43[15]	0.65[17]
E_{15}	10	800	4.0	0.56[15]	0.62[17]
E_{23}	10	500	4.0	0.56[15]	0.62[17]
S_{11}[16]	10	274	57.5	0.48	0.78
S_{13}[16]	10	167	64	0.49	0.78
S_8[16]	20	277	69	0.65	0.74
S_9[16]	20	164	74.5	0.67	0.74

formation of hollow particles due to the evaporation rate of water exceeding the diffusion rate of salt back into the inside, thereby creating internal voids after dryness is reached. In view of this fact, it might well be said that the Na_2SO_4 particles now under investigation are also so solidly-built that the particle size does not decrease in the presence of humidity. On the other hand, it was found by Andreasen *et al.*[12] that the particles smaller than 10 μ act as binders between colliding particles; further, Neumann[13] found that moisture leads to an increased stichness of the particles, particularly for hygroscopic ones.

Since the decrease in the relative mass concentration with the time follows the law of the second-order reaction rate (Fig. 1), whose mechanism will be discussed in a later paper, the decrease in the number concentration might be caused mainly by coagulation; some of the aggregates so formed fall to the bottom of chamber, vanishing from the system.

Comparison of the Density Found with Other Published Results. Crosby and Marshall,[14] after carrying out a series of experiment runs on spray-drying, at temperatures between 162° and 285°C, of aqueous Na_2SO_4 solutions with concentrations ranging from 10 to 20 wt%, concluded that, under all the conditions of temperature and concentration studied, the density of the particle increases as the size decreases, the variation being as great as fourfold; this explains, in part, why spraydried commercial products with small particles frequently exhibit higher densities than the corresponding products composed of large particles.

Table 3 presents comparison between the results obtained by the present authors and those obtained by Crosby and Marshall. It is apparent that two sets of figures are different from each other because of the difference in the experimental conditions, but that they are of the same order of magnitude. Concerning the variation in the density gets smaller with the time. This might be due to the formation of loose or chain-like aggregates by coagulation; the situation has been confirmed by the electron-microscope observation referred to above.

Determination of the Water Content of a Dried Particle. Let us suppose that droplets produced by atomization have passed through a furnace to be dried particles, without encountering mutual collision.

Since the solid content of a droplet will remain unaltered, there holds a mass-balance relation between the diameter (D_l) of a droplet produced by atomization and the diameter (d_s) of a particle formed by the dehydration of the droplet:

$$1/6\cdot\pi D_l^3\rho_l[1/(1+W_l)] = 1/6\cdot\pi d_s^3\rho_s[1/(1+W_s)] \quad (9)$$

ρ_l: density of liquid droplet
ρ_s: density of dried particle
W_l: water content of liquid droplet (grams of water per gram of Na_2SO_4)
W_s: water content of dried particle (grams of water per gram of Na_2SO_4)

Solving for the ratio of particle to droplet diameter, we obtain:

$$d_s/D_l = [\rho_l(1+W_s)/\rho_s(1+W_l)]^{1/3} \quad (10)$$

By the use of Eq. (10), the percentage of the water content of a dried particle or the number of H_2O molecules (X) associated with a Na_2SO_4 molecule can be estimated for Runs E_{24}, E_{26}, E_{28}, and E_{33}, all

12) A. H. M. Andreasen, N. Hofman-Bang, and N. H. Rasmussen, *Kolloid Zhur.*, **86**, 70 (1939).
13) B. S. Neumann, "Flow Properties of Disperse System," Chap. X, ed. by J. J. Hermans (Leiden) 1953.
14) E. J. Crosby and W. R. Marshall, Jr., *Chem. Eng. Progr.*, **54**, 56 (1958).
15) Obtained from Eq. (10) by putting $W_s=0$. These runs have been conducted in dry atmosphere (Table 1).
16) The symbol *S* is after Crosby *et al.*'s notation.
17) Obtained from Fig. 5 by extrapolation to zero time.

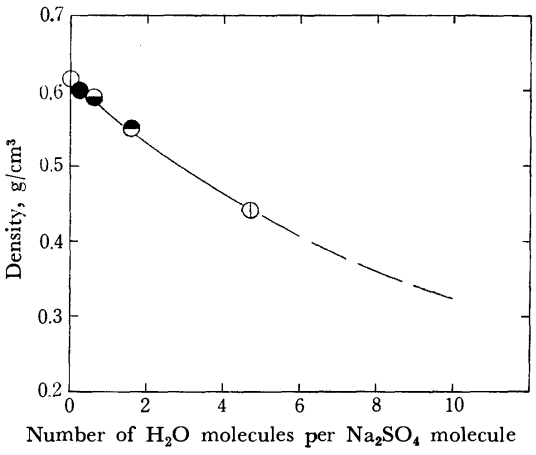

Fig. 7. Relation between density of the solid particle and its water content
○ E_{23} ● E_{24} ◒ E_{26} ◓ E_{28} ◫ E_{33}

of which were carried out in a humidified atmosphere. The results are depicted in Fig. 7. The procedure is as follows. On assuming that the value of D_l ($7.3_2\,\mu$) found with Run E_{23} (Table 3) is the same for these four runs, and, that dried particles leaving the furnace are hydrated in the humidified atmosphere to come to equilibrium with water vapor during charging, the W_s values are, first, calculated from Eq. (10) by substituting 7.3 for D_l, the values of d_s and ρ_s, being determined by extrapolation to zero time (Figs. 2 and 5). We know 1.089 for ρ_l and 9 for W_l: then, the W_s so found is converted into X. It may be seen in the figure that the particle density varies from 0.62 for an anhydrate particle to 0.32 for a decahydrate particles. These values are less than the normal densities, the ratio of normal density to that thus estimated being 4.4 for the former particle and 4.5 for the latter one. Futhermore, on the basis of the fact[5] that hollow particles with a radius/thickness ratio of 10 are formed, the density of the shell can be calculated; the results are 2.3 for an anhydrate particle and 1.2 for a decahydrate one, values close to the normal densities of 2.7 and 1.4.

BULLETIN OF THE CHEMICAL SOCIETY OF JAPAN, VOL. 45, 980—983 (1972)

Hydrogen Exchange Reactions between Olefins or an Olefin and Molecular Hydrogen over Alumina Studied by Microwave Spectroscopy

Yuzo SAKURAI, Takaharu ONISHI, and Kenzi TAMARU

Department of Chemistry, The University of Tokyo, Hongo, Bunkyo-ku, Tokyo

(Received May 29, 1971)

The exchange reaction between propylene and deuterium was studied over alumina. The rate of the reaction was expressed by $V_{ex}=k[P_{D_2}]^{0.5}[P_{Pro}]^{0.0}$. In the initial stages of the reaction the *cis*- and *trans*-1-d_1 species of propylene were the only products of the exchange reaction, but the concentration of the 3-d_1 species increased continuously as the reaction progressed. The activation energy for the exchange reaction was about 8.2 kcal/mol.

Propylene-*cis*-d_1 was reacted over alumina, and the variation in the deuterium distribution of the propylene was followed by microwave spectroscopy. Isotope scrambling and "double-bond migration" occurred to considerable extents, while *cis-trans* equilibration between the two C_1 hydrogen positions proceeded even faster. In the reaction of propylene-3-d_1, the isotope mixing and "double-bond migration" were considerably slower than those of the *cis*-1-d_1 species. *Cis*- and *trans*-1-d_1 species were formed in equal amounts. The possible mechanism of these reactions is discussed on the basis of the results obtained.

n-Butene isomerization, especially double-bond migration, in the presence of perdeuteriopropylene over alumina was studied in a previous paper[1] in order to obtain further information about the reaction mechanism. It was concluded that the isomerization of *n*-butene, or at least the double-bond migration, occurs on some protonic sites formed on the catalyst by the adsorption of olefin molecules, and that extensive deuterium exchange during the isomerization proceeds independently of the isomerization.

In this report the exchange reaction between propylene and molecular deuterium was carried out over alumina to derive more information about the mechanism of the deuterium scrambling among terminal olefins, and to elucidate the nature of the catalytic action of the alumina.

Experimental

γ-Alumina employed in this study was obtained from Degussa Co., and was pretreated in the following manner. Dry oxygen was circulated over the catalyst at 600°C for two hours, and the catalyst was then cooled to 500°C, the oxygen was replaced by dry hydrogen, and the catalyst kept at this temperature for one hour. The system was then evacuated for two hours at 600°C. Usually 9 g of alumina was employed as the catalyst.

Propylene was obtained from Takachiho Shoji Co., and purified by repeated distillation *in vacuo*. The deuterium (Showa Denko Co.) had a quoted purity of 99.5 D%, and was used without further purification.

Methylacetylene from Takachiho Shoji Co. was treated several times with weakly alkaline deuterium oxide to re-

1) Y. Sakurai, T. Onishi, and K. Tamaru, submitted for publication in *Trans. Faraday Soc.*

place its acetylenic hydrogen with deuterium. Methylacetylene-1-d_1 thus obtained was selectively hydrogenated to propylene-*cis*-1-d_1 by a process similar to that developed by Rabinovitch and Looney.[2] Three samples of propylene-*cis*-1-d_1 were obtained and employed for the reaction. The deuterium contents were determined by mass spectrometry, and were found to be around 90% in all three cases. Microwave spectroscopic analysis of the samples revealed that they consisted of only the *cis*-1-d_1 and *trans*-1-d_1 species.

The 3-d_1 species of propylene was synthesized by reacting allyl chloride and deuterium oxide over zinc powder in an acetic anhydride medium. The deuterium content of the propylene-3-d_1 thus obtained was about 83%. According to the microwave spectroscopic analysis, the propylene-3-d_1 consisted solely of the 3-d_1 species without any trace of the other monodeuterated species.

A conventional closed circulating system with a total volume of about 300 cm^3 was employed for the reaction. A mixture of propylene and deuterium was circulated over the alumina catalyst which was kept at a constant temperature (−21—60°C).

Analysis of the isotopic composition of the deuterium was carried out by gas chromatography using a $MnCl_2$-alumina column at liquid nitrogen temperature. The mass spectra of the propylene were recorded with an ionization, and the appropriate corrections were applied.

Microwave spectra of propylene and its mono-deuterated species were observed by Lide and Christensen,[4] and used for the quantitative determination of the deuterium contents at each hydrogen position of propylene-d_1 by Hirota and Morino.[5] Measurements were carried out at dry ice temperature with a conventional Stark modulation spectrometer. The $1_{01}-0_{00}$ transition was employed for the analysis, and the intensities of the neighboring peaks were compared. When the appropriate corrections were applied to the results,[5] the corrected intensity ratio was taken to show the relative abundance of the two species concerned.[6]

Results

Exchange Reaction between Propylene and Deuterium. The initial rate of the hydrogen exchange between propylene and deuterium was studied at propylene pressures between 11 and 44 cmHg, the partial pressure of deuterium being kept constant at 44 cmHg. The results are shown in Fig. 1. The initial rate of the hydrogen exchange was also studied at a constant pressure of propylene (22 cmHg), with a varying partial pressure of deuterium and the results are given in Fig. 2. The results of Figs. 1 and 2 show that proportional to square root of the deuterium pressure. This can be interpreted by postulating that the propylene is strongly adsorbed on the surface of alumina, and the deuterium molecules dissociate on the surface, to take part in the exchange reaction with the adsorbed propylene.

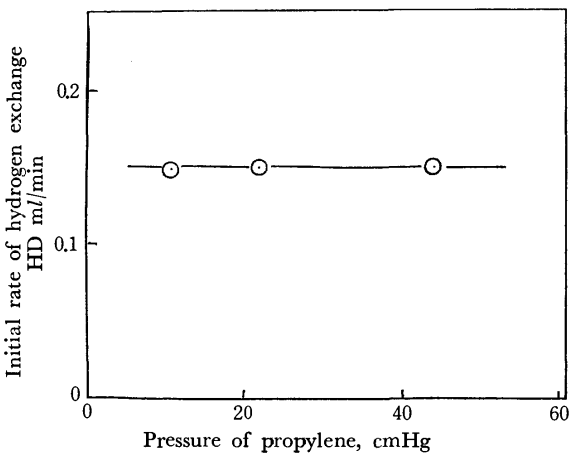

Fig. 1. Hydrogen exchange between propylene and deuterium over alumina. Dependence of the rate on partial pressure of propylene. P_{D_2}=44 cmHg.

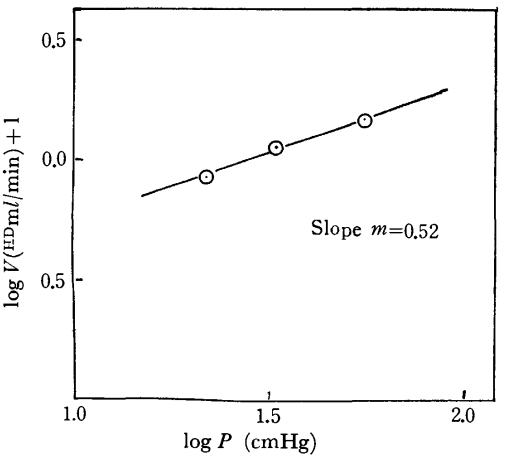

Fig. 2. Hydrogen exchange between propylene and deuterium over alumina. Dependence of the rate on partial pressure of deuterium. $P(C_3H_6)$=22 cmHg.

The hydrogen exchange between and equimolar mixture of propylene and deuterium was studied at temperatures between 0 and 60°C, and the Arrhenius plot of the exchange rate gave an activation energy of 8.2 kcal/mol. Recently deuterium exchange with hydrogen atoms in some olefins such as 1-butene, *cis*-2-butene and isobutene over alumina has been reported by Hightower and Hall.[7] They found an activation energy for the exchange reaction with D_2 of 5∼6 kcal/mol, which is slightly smaller than the value of 8.2 kcal/mol obtained here for the reaction between propylene and deuterium.

As the reaction progressed, hydrogenation of the propylene was found to occur to a small extent, but its rate was always almost one order of magnitude smaller than that of the exchange reaction. Therefore, the hydrogenation of propylene may be neglected under these conditions, and the subsequent discussions will be entirely concerned with the exchange

2) B. S. Rabinovitch and F. S. Looney, *J. Amer. Chem. Soc.*, **75**, 2652 (1953).

3) D. R. Herschbach and L. C. Kirisher, *J. Chem. Phys.*, **28**, 728 (1958).

4) D. R. Lide, Jr. and D. Christensen, *ibid.*, **35**, 1374 (1961).

5) Y. Morino and E. Hirota, *Nippon Kagaku Zasshi*, **85**, 535 (1964).

6) E. Hirota, private communication: the observed intensity ratio should be divided by the following correction coefficient. *cis*-1-d_1/3a-d_1=1.0576, *trans*-1-d_1/3b-d_1=1.0488, and 2-d_1/3a-d_1=1.0990.

7) J. W. Hightower and W. K. Hall, *J. Catal.*, **13**, 161 (1969).

reaction.

A mixture of propylene and deuterium (3 : 5) was reacted over alumina at three different temperatures (0, 24, and 56°C), and the resultant mono-deuterated propylene species were analyzed by microwave spectroscopy. Four mono-deuterated species are distinguishable either by their chemical properties or by microwave spectroscopy;

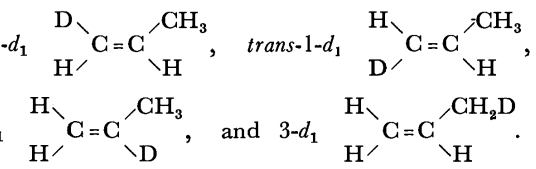

The fractions of the four mono-deuterated species were plotted against the number of deuterium atoms which entered the propylene by the exchange reaction. The results are shown in Fig. 3. The total concentrations of the mono-deuterated species were always normalized to 100%. The notable features of the results in Fig. 3 are: i) The amount of the 2-d species formed in the reaction was negligible. A small amount of 2-d_1 species was observed after prolonged reactions, but its concentration was at most 4—5% of the total mono-deuterated propylene. ii) The *cis*-1-d_1 and *trans*-1-d_1 species were formed in approximately equal amounts throughout the course of the reaction. iii) The fraction of the 3-d_1 species increased continuously as the reaction proceeded, but its contribution was almost zero in the very initial stages of the reaction. In other words, *cis*-1-d_1 and *trans*-1-d_1 propylene were the only mono-deuterated species produced in the early stages of the exchange reaction. iv) At high conversion levels the deuterium in the propylene was equally distributed among the five hydrogen positions at C_1 and C_3. v) Reaction at the three different temperatures gave rise to similar deuterium distributions, which meant that the activation energy for the deuterium shift to form the 3-d_1 species ("double-bond migration") was nearly equal to that of the exchange reaction, 8.2 kcal/mol.

Hydrogen Exchange Reactions between Deuterated Olefins. When propylene-*cis*-1-d_1 was circulated over alumina at 30°C, isotope scrambling resulting in $C_3H_4D_2$ and $C_3H_3D_3$ occurred rapidly as shown in Fig. 4. Microwave spectroscopic analysis of the mono-deuterated propylene revealed that the deuterium which had initially been mainly at the C_1 *cis* position moved rapidly to the other positions on the C_1 and C_3 atoms, and attained an equilibrium distribution within one hour (Fig. 5). As Fig. 4 shows, the relative concentrations of the four isotopic propylene species, *i.e.*, C_3H_6, C_3H_5D, $C_3H_4D_2$, and $C_3H_3D_3$, which were detected in the course of the reaction, became constant after a reaction time of about one hour. These results suggest that the shift of the deuterium to yield the 3-d_1 species ("double-bond migration") is an intermolecular process.

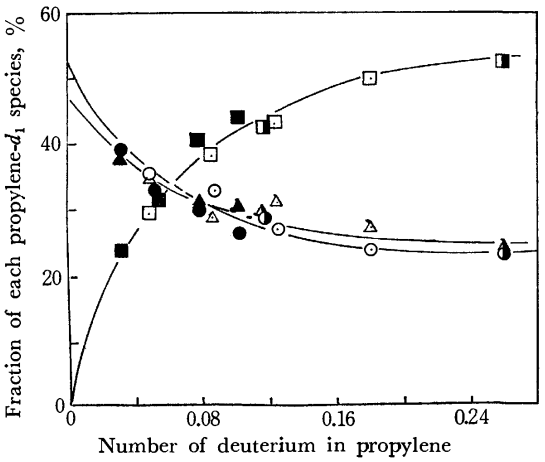

Fig. 3. Temperature dependence of deuterium distribution in propylene.
●▲■: 0°C, ○△□: 24°C, ◑◭◨: 56°C.

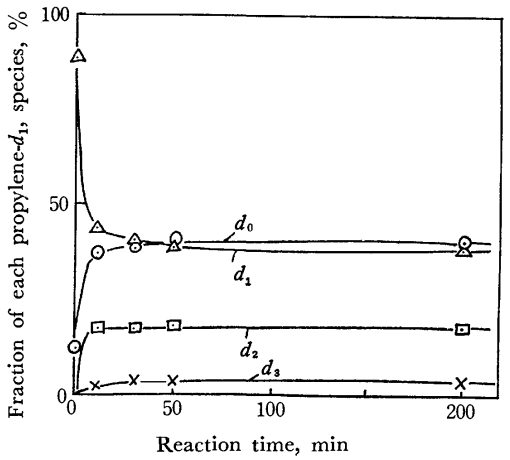

Fig. 4. Isotope mixing among the propylene, the change in deuterium content in propylene over alumina at 30°C.
○: C_3H_6, △: C_3H_5D, □: $C_3H_4D_2$, ×: $C_3H_3D_3$

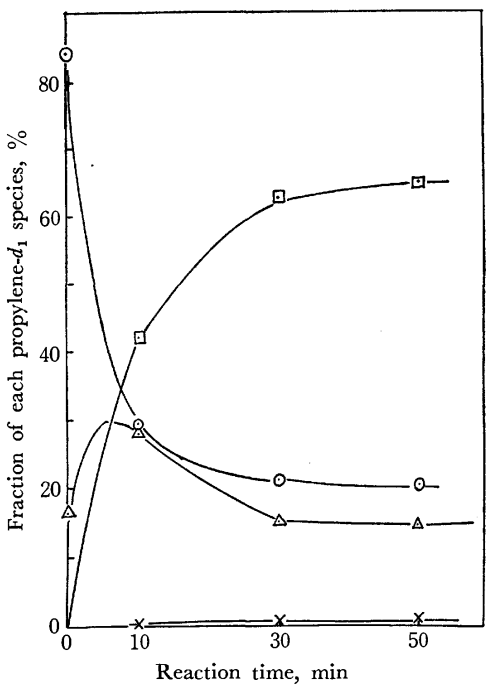

Fig. 5. Position of propylene-d_1 over alumina at 30°C.
□: 3-d_1, ○: *cis*-1-d_1, △: *trans*-1-d_1, ×: 2-d_1

When the reaction temperature was lowered, it was clearly demonstrated that *cis-trans* equilibration between the two hydrogen positions at C_1 atom occurred much more rapidly than "double-bond migration" to yield the 3-d_1 species. The activation energy for the *cis-trans* equilibration is lower than the "double-bond migration." The results are given in Fig. 6. Fig. 6 is for reaction at −21°C using sample B of the propylene-*cis*-1-d_1. The rate of isotope mixing to form $C_3H_4D_2$ and $C_3H_3D_3$ was considerably reduced at these temperatures.

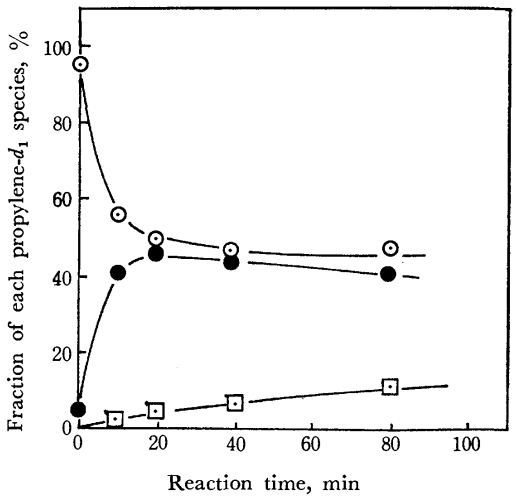

Fig. 6. The change in deuterated position of propylene-d_1 over alumina at −21°C.
○: *cis*-1-d_1, ●: *trans*-1-d_1, □: 3-d_1

When the 3-d_1 species of propylene was circulated over alumina at 0°C. under the similar conditions, *cis*-1-d_1 and *trans*-1-d_1 species formed in exactly equal amounts as shown in Fig. 7. The rate of the formation of the 1-d_1 species, however, was considerably slower than the rate of formation of the 3-d_1 species from *cis*-1-d_1 propylene.

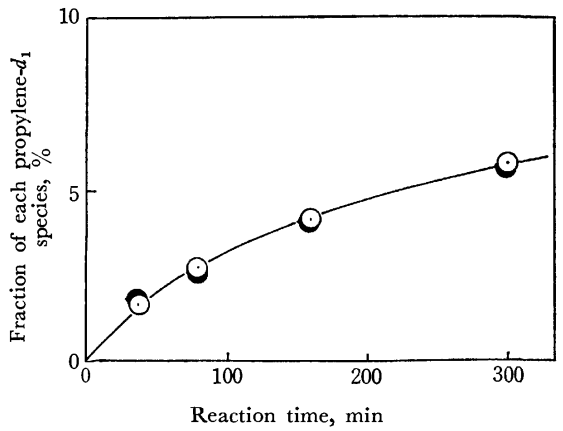

Fig. 7. Reaction of propylene-3-d_1 over alumina at 0°C.
○: *cis*-1-d_1, ●: *trans*-1-d_1

Discussion

Three kinds of the reactions were involved in the experiments described above. The first is the exchange reaction between propylene and deuterium molecule. The second is isotope mixing among the propylene isomers, and the third is *cis-trans* equilibration of the deuterium in the two hydrogen positions on the C_1 atom.

The first reaction can be considered to proceed *via* the interaction of adsorbed propylene and a deuterium atom formed by dissociation of deuterium on the surface. This view is supported by the observed rate equation for the exchange, $V_{ex} = k[P_{D_2}]^{0.5}[P_{Pro}]^{0.0}$. The adsorption of propylene over alumina appears to be dissociative at C_1 position, because the deuterium exchange occurred selectively in the hydrogen positions at C_1 atom. If an associative mechanism is involved, where deuterium adds to the adsorbed propylene to form an isopropyl (or propyl) intermediate, then substantial amounts of the 3-d_1 (or 2-d_1) species should appear even in the initial stages of the reaction. This was not found in the experiments. Thus, propylene can be assumed to adsorb on alumina dissociatively rather than associatively.

The second reaction may correspond to the double-bond migration of *n*-butene over alumina described previously.[1] Isotope mixing among the propylene isomers as shown in Fig. 4 and "double-bond migration" in the mono-deuterated species as shown in Fig. 5 occurred at a comparable rate and both reactions get to final distribution in half an hour at 30°C. At lower temperatures such as −21°C the rates of both reactions were considerably slower. This suggests the hydrogen dissociation at C_3 and its association at C_1 position. Isotope mixing thus accompanies "double-bond migration."

The third reaction, the *cis-trans* equilibration of deuterium in the two hydrogen positions on the C_1 atom occurred very rapidly even at temperatures as low as −21°C. At −21°C the isotope mixing and "double-bond migration" slowed down remarkably. This suggests that the *cis-trans* equilibration reaction which may correspond to the *cis-trans* isomerization of 2-butene proceeds intramolecularly and is probably independent of the above two reaction. Hightower and Hall[8] studied that reaction of a mixture of butene and perdeuterio-butene over alumina, and concluded that *cis-trans* isomerization occurred by an intramolecular rearrangement.

The authors would like to express their gratitude to Professor Y. Morino and Dr. S. Saito of the Sagami Chemical Research Center for the measurement of microwave spectroscopy. The authors are also thankful for the assistance of Dr. A. C. Herd in preparing this manuscript.

8) J. W. Hightower and W. K. Hall, *J. Amer. Chem. Soc.*, **89**, 778 (1967).

The Trapping Efficiency for Electrons in Polar Glasses at 77°K

Takeshi SAWAI, Yoshiharu SHINOZAKI, and Gisuke MESHITSUKA

Tokyo Metropolitan Isotope Research Center, 2—11—1, Fukazawa, Setagaya-ku, Tokyo

(Received August 9, 1971)

The trapped electron yields in alcohols and methanol-water mixtures at 77°K as a function of the electron scavenger concentration have been measured. The reciprocal of the trapped electron yield increased linearly with the concentrations of phenol, acetone, and acrylamide. The relative trapping efficiency for electrons was found to increase with an increase in the dielectric constant of the matrix at room temperature. The relative travelling distance of electrons in these matrices was also estimated.

Extensive studies have been made of the formation of the trapped electrons in irradiated glasses of polar or non-polar substances.[1] The presence of electron scavengers,[1d,2,3] such as acrylamide, nitrate ions, nitrite ions, monochloroacetate, and acetone, decreases the yield of the trapped electrons, and these scavenging experiments showed that the mobile electron was the precursor of the trapped electron. Electrons produced by γ-irradiation or photoionization are trapped efficiently in polar glassy states at 77°K, and the absorption spectra of the trapped electrons are characterized by a very broad band in the visible or near-infrared spectral region.

Ekstrom and Willard[4] measured the optical absorption and ESR spectrum of the trapped electrons in γ-irradiated organic glasses covering a range in polarity, from 3-methylpentane to glycerol. They showed that the absorption maximum was shifted towards shorter wavelengths with an increase in the polarity of the matrix molecules, and the ESR line width increased. These results were explained by using a model in which the electrons are trapped in pre-existing cavities in the matrix.

Recent experiments, such as the pulse radiolysis of polar glasses at 77°K[5] and studies of water-ethylene glycol glass irradiated at 4°K,[6] have suggested that the mobile electrons were trapped in deeper traps at 77°K than at 4°K, indicating an orientational relaxation of the molecules at 77°K, and that the electrons trapped in the deeper traps had an absorption similar to that of the trapped electron irradiated with ^{60}Co γ-rays at 77°K. If the polarity of the solvent correlates with the formation processes of the trapped electrons, one can expect that the travelling distance of electrons prior to trapping in other words, the trapping efficiency of the matrix molecules for the mobile electrons, will depend on the polarity. The present investigation will show that the trapping efficiency depends on the polarity of the matrix molecules. The experiments were performed using glasses of alcohols and methanol-water mixtures containing phenol, acetone, or acrylamide at 77°K.

Experimental

The alcohols (isopropanol, ethanol, and methanol) were purified by distilling them twice after they had been refluxed for 24 hr with 2,4-dinitrophenyl hydrazine-sulfuric acid. The water was triply distilled. The solutions were purged with bubbling nitrogen prior to ^{60}Co γ-ray irradiation at 77°K. Methanol (5 mol% H_2O) and ethanol (5 mol% H_2O) formed clear glasses, and the other solutions were glassy with a few small cracks. Pyrex cells (~2 mm thick) were mainly used for the irradiation and for the optical measurements of trapped electrons. Metal cells (~3 mm thick) with high-purity silica windows were used for the measurement of the optical absorption below 400 nm in phenol solutions. The absorption spectra were measured at 77°K with a Cary Model 14R spectrophotometer. The optical densities of the trapped electrons (OD(e_t^-)) in various matrices were obtained by subtracting the OD after bleaching by light transmitting at $\lambda > 540$ nm (using a Toshiba V-054 glass filter) from the OD after γ-irradiation. Since the Pyrex cell absorbs from the visible to the UV region after γ-irradiation at 77°K, and since the intensity decreases upon optical bleaching, a correction was made for the OD (e_t^-). Irradiation was carried out at 77°K using a 5K Ci ^{60}Co source at a dose rate of 4×10^{19} eV/g hr, as determined by ferrous sulfate dosimetry.

Results and Discussion

The absorption spectra of the trapped electrons were observed in alcohols and methanol-water mixtures.[9] The results are summarized in Table 1. The presence of an electron scavenger decreases the trapped electron yield, but the position of the absorption maximum is not affected. Figure 1 shows the trapped electron yield *vs.* the irradiation dose at

1) For recent reviews of this subject, see: a) W. H. Hamill, "Radical Ions," ed. by E. T. Kaiser and L. Kevan, John Wiley and Sons, Inc., New York, N. Y. (1968) p. 321. b) J. E. Willard, "Fundamental Processes in Radiation Chemistry," ed. by P. Ausloos, John Wiley and Sons, Inc., New York, N. Y. (1968) p. 599. c) L. Kevan, "Progress in Solide-State Chemistry," **2**, ed. by H. Reiss, Pergamon Press, New York, N. Y. (1956) p. 304. d) L. Kevan, "Radiation Chemistry of Aqueous Systems," ed. by G. Stein, John Wiley and Sons, New York (1968) p. 21. e) B. G. Ershov and A. K. Pikaev, "Advance in Chemistry Series, Radiation Chemistry-I," **81**, ed. by R. E. Gould, American Chemical Society Pub., Washington, D. C. (1968) p. 1. f) L. Kevan, *Actions Chim. Biol. Radiations*, **13**, 57 (1969).

2) W. A. Seddon and R. D. Smith, *Can. J. Chem.*, **45**, 3083 (1967).

3) K. Eiben and D. Schulte-Frholinde, *Z. Physik. Chem.*, **45**, 20 (1965).

4) A. Ekstrom and J. E. Willard, *J. Phys. Chem.*, **72**, 4599 (1968).

5) J. T. Richards and J. K. Thomas, *J. Chem. Phys.*, **53**, 218 (1970).

6) T. Higashimura, M. Noda, T. Warashina, and H. Yoshida, *ibid.*, **53**, 1152 (1970).

7) T. Sawai and W. H. Hamill, *J. Phys. Chem.*, **73**, 2570. (1969)

8) P. J. Dyne and O. A. Miller, *Can. J. Chem.*, **43**, 2696 (1965).

9) The composition of the methanol-water mixture is given in a mole percentage.

TABLE 1. ABSORPTION MAXIMUM OF TRAPPED ELECTRONS IN GLASSY ALCOHOLS AND METHANOL-WATER MIXTURES AT 77°K

Matrix	λ_{max} nm
isopropanol	640 (613)
ethanol	530 (530)
methanol	520 (514)
75%methanol-25%water	530 (526)[a]
40%methanol-60%water	555 (550)[b]

( ): λ_{max} measured by G. Ershov and A. K. Pikaev, ref. (1e),
a: 70%methanol-30%water, b: 50%methanol-50%water

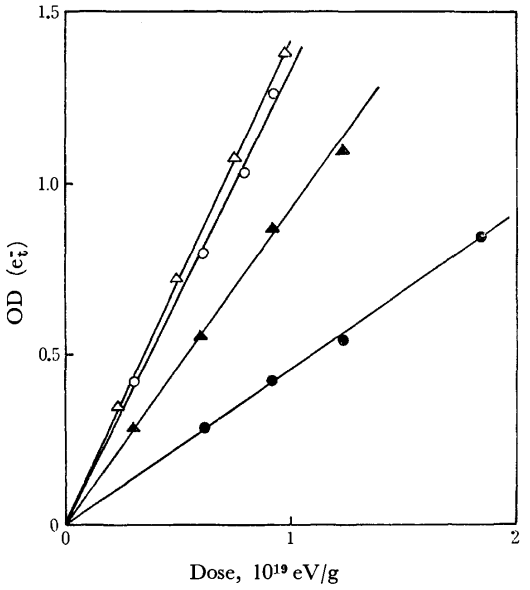

Fig. 1. Trapped electron yield as a function of dose in ethanol and methanol-water at 77°K.
○: ethanol, △: 40% methanol-60% water
●: 1.2 mol% phenol in ethanol
▲: 1.0 mol% phenol in 40% methanol-60% water

77°K obtained from 1.2 mol% phenol in ethanol and 1.0 mol% phenol in a 40% methanol - 60% H_2O mixture, and from the same solutions without any solute. The trapped electron yield is linear in dose in all the systems; the yields from systems without a solute seem to be almost the same, but the effect of phenol on the yield is quite different in different mixtures. This seems to be the effect of the electron-trapping efficiency of the matrices, which is correlated with the polarity. In the presence of phenol, the absorption maximum which is attributed to the C_6H_6OH radical appears at 345 nm in addition to the trapped electron band. It has been shown that phenol scavenges an electron to form the C_6H_6OH radical.[7] The radical yield increases with an increase in the concentration of phenol, and the radiation dose, $OD(C_6H_6OH)$ is larger in methanol than in the 40% methanol - 60% H_2O mixture at the same phenol concentration. The spectra of irradiated phenol in methanol and in 40% methanol - 60% H_2O at 77°K are shown in Fig. 2. Figure 2 suggests that the trapping efficiency by the matrix for the mobile electron is much smaller in methanol than in

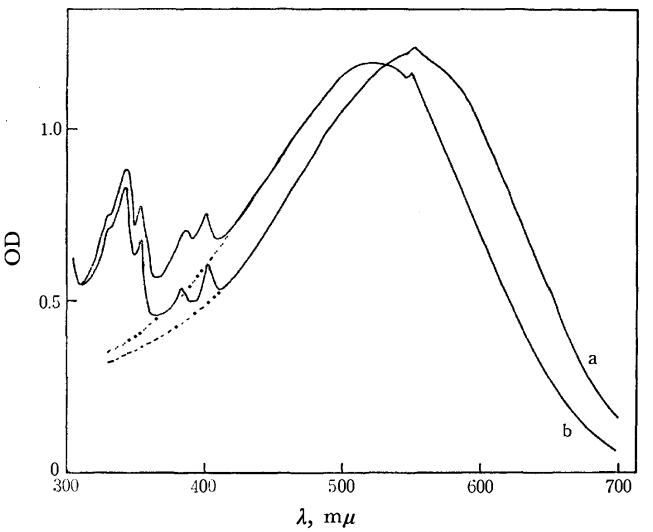

Fig. 2. Spectrum of irradiated phenol in methanol and in 40% methanol-60% water at 77°K.
a : 1.6 mol% phenol in 40% methanol-60% water
b : 0.8 mol% phenol in methanol
Dose: 1×10^{19} eV/g

the methanol-water mixture, since the $OD(C_6H_6OH)$ and $OD(e_t^-)$ in methanol are almost equal to those in the latter matrix, even though the phenol concentration is quite different. The trapping efficiency seems to correlate with the dielectric constant of the matrices; that is, the matrix with higher dielectric constant has the higher trapping efficiency.

It has been considered that the trapped electrons are produced by the reaction of mobile electrons with trapping sites in the solid state, and that the depth of the trapping sites is correlated with the dielectric constant of the matrix. The mechanisms for electron trapping are not very clear, but mobile electrons (e_m^-) may either recombine with positive holes to form excited molecules or react with traps (T) or scavengers (S) as is described in the following scheme:

$$M \rightsquigarrow M^+ + e_m^- \quad (1)$$

$$e_m^- + M^+ \rightarrow M^* \quad (2)$$

$$e_m^- + T \rightarrow e_t^- \quad (3)$$

$$e_m^- + S \rightarrow S^- \quad (4)$$

The linearity of the e_t^- yield with the dose, however, shows that reaction (2) can be neglected. From these simple competition reactions, it follows that:

$$G(e_t^-) = G_0(e_t^-)k_3[T]/(k_3[T]+k_4[S]) \quad (I)$$

where $G(e_t^-)$ and $G_0(e_t^-)$ are the trapped electron yields with and without a solute respectively. Since $G(e_t^-)$ can be replaced by the optical density:

$$1/OD(e_t^-) = 1/OD_0(e_t^-)(1+k_4[S]/k_3[T]) \quad (II)$$

The plot of $1/OD(e_t^-)$ *vs.* [S] at a constant dose should be linear for each matrix. $1/OD(e_t^-)$ plotted as a function of the concentrations of phenol, acetone, and acrylamide in isopropanol, ethanol, methanol, and methanol-water mixtures at 77°K is shown in Figs. 3, 4, and 5. $1/OD(e_t^-)$ is a linear function of

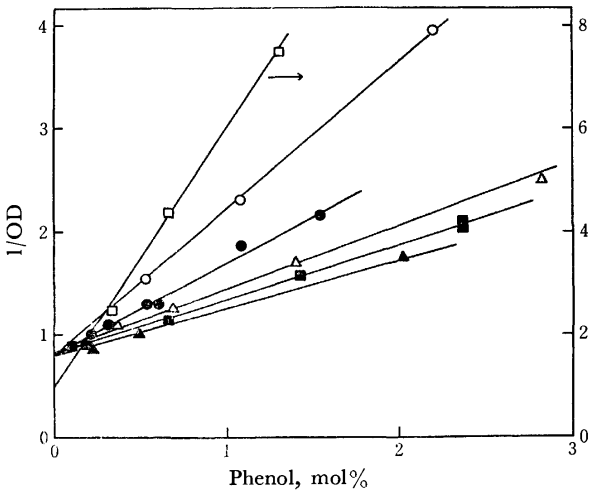

Fig. 3. Trapped electron yield as a function of phenol concentration in various matrices.
□: isopropanol, ○: ethanol, ●: methanol
△: 75% methanol-25% water, ■: 60% methanol-40% water, ▲: 40% methanol-60% water

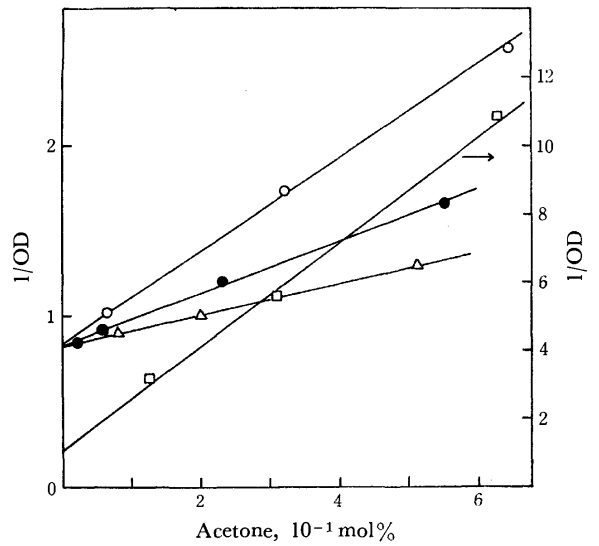

Fig. 4. Trapped electron yield as a function of acetone concentration.
□: isopropanol, ○: ethanol, ●: methanol
△: 75% methanol-25% water

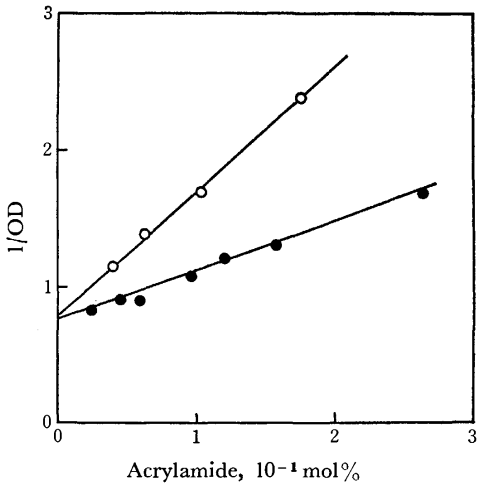

Fig. 5. Trapped electron yield as a function of acrylamide concentration.
○: ethanol, ●: methanol

the solute concentration in all cases. The fact that $1/OD(e_t^-)$ in Fig. 3 is linear with the concentration of phenol to 2 mol% suggests that the trapping sites for e_m^- are unlikely to be destroyed even at a relatively high concentrations of the solute. From the slopes Figs. 3, 4, and 5, the relative trapping efficiencies

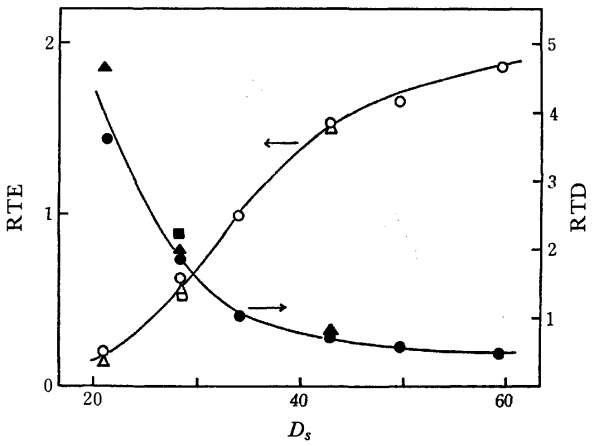

Fig. 6. Relative trapping efficiency (RTE) and relative travelling distance (RTD) for electrons in various matrices at 77°K as a function of dielectric constant of the matrix.
○●: phenol, △▲: acetone, □■: acrylamide

TABLE 2. RELATIVE TRAPPING EFFICINCY FOR MOBILE ELECTRON AND SOLUTE CONCENTRATION REQUIRED TO REDUCE OD TO 1/2 OD_0 IN ALCOHOLS AND METHANOL-WATER MIXTURES

		isopropanol	ethanol	methanol	75%methanol 25%water	60%methanol 40%water	40%methanol 60%water
Phenol	RTE	0.20	0.63	1.0	1.6	1.7	1.9
	[S]	0.22	0.54	0.86	1.26	1.44	1.66
Acetone	RTE	0.12	0.56	1.0	1.6		
	[S]	0.080	0.29	0.53	0.82		
Acryl amide	RTE		0.47	1.0			
	[S]		0.090	0.22			
Dielectric constant*		21	26.8	34.2	43.2	50.0	58.8

*: Dielectric constant at room temperature RTE: Relative trapping efficiency
S: Solute concentration required to reduce OD to 1/2 OD_0, mol%.

$(K_3[T]/k_4)$ in different matrices can be obtained. These results, which are normalized to the methanol matrix, are summarized in Table 2. The relative values of k_3 [T] as a function of the static dielectric constant (D_s) of the matrix at room temperature are plotted in Fig. 6. The trapping efficiency increases with the increase in D_s in the matrices. The intercepts in Figs. 3, 4, and 5 give $1/G_0(e_t^-)\varepsilon$, since OD is related to $G\varepsilon$; these figures show that the $G_0(e_t^-)\varepsilon$ values are almost the same in alcohols and in methanol-water mixtures except for the case of isopropanol.

The relative trapping efficiencies in various matrices should correlate with the travelling distance for mobile electrons prior to trapping. Dyne and Miller[8] and Seddon and Smith[2] have calculated the travelling distance on the bases of experiments with biphenyl in organic glass and acrylamide in alkaline glass respectively. Adopting the mathematical procedure described by Dyne and Miller[8] the root mean-square distance which electrons move prior to trapping, $(\bar{r}^2)^{1/2}$, can be estimated from the concentration of the solutes required to reduce the electron yield to one half its initial value. These concentrations ([S]) in various matrices are listed in Table 2. The relative travelling distances for mobile electrons in alcohols and methanol-water mixtures at 77°K are plotted in Fig. 6. In contrast with the relative trapping efficiency, the distance decreases with the increase in the dielectric constant at room temperature. However, further investigation seems to be necessary, especially concerning the temperature dependence of D_s and various phenomena occuring in the glassy state irradiated at 77°K, in order to correlate these facts with the phenomena in various matrices at 77°K.

The authors are indebted to Professor William H. Hamill for reading and discussing the manuscript.

BULLETIN OF THE CHEMICAL SOCIETY OF JAPAN, VOL. 45, 987—992 (1972)

Energy Transfer Concerning the Lowest Triplet State of Tetracyanobenzene with Methyl-Substituted Benzenes

Takayoshi KOBAYASHI and Saburo NAGAKURA

The Institute for Solid State Physics, The University of Tokyo, Roppongi, Minato, Tokyo

(Received September 3, 1971)

The quantum-yield ratios of phosphorescence to fluorescence and the phosphorescence lifetimes were measured for the charge-transfer complexes of tetracyanobenzene with methyl-substituted benzenes. By combining the observed results with the fluorescence quantum yields and lifetimes reported previously, the upper and lower limits of the rate constants for the intersystem crossing and for the radiative and non-radiative energy-transfer processes from the lowest triplet state to the ground state were obtained with the complexes. The intersystem-crossing rate constant of tetracyanobenzene was found to be decreased by the complex formation. This tendency was explained by the mixing of the charge-transfer configuration with the appropriate singlet and triplet states of the component molecules. The phosphorescence radiative rate constant was found to be determined by the contribution of the higher excited singlet configurations of each complex to the phosphorescent state. The temperature dependence of the phosphorescence-quenching rate constant was determined, and the activation energy of the process was interpreted as being due to intramolecular out-of-plane bending vibrations.

The phosphorescences of charge-transfer (abbreviated hereafter to CT) complexes have been studied by several authors,[1-7] the trinitrobenzene, tetrahalophthalic anhydride, and tetracyanobenzene (abbreviated hereafter to TCNB) complexes with several donors having been taken as examples. The excited triplet states of some CT complexes may be expected to have the characters of a locally-excited (abbreviated hereafter to LE) triplet of acceptor, an LE triplet of donor, and a CT triplet, which can be represented by $^3(DA^*)$, $^3(D^*A)$, and $^3(D^+A^-)$, respectively. In actuality, phosphorescence spectra from these three types of triplet states have been observed.[1,4-7] In this connection, the TCNB complexes are especially remarkable, because the CT phosphorescence was first observed with the complex with hexamethylbenzene (abbreviated hereafter to HMB) and the above-mentioned three types of phosphorescence were all observed by changing donors.[6,7]

The natures of the lowest triplet states of CT complexes have also been studied by the ESR measurement.[8-10] Hayashi *et al.*[8,9] first succeeded in finding

1) C. Reid, *J. Chem. Phys.*, **20**, 1212 (1952).
2) S. P. McGlynn and J. D. Boggus, *J. Amer. Chem. Soc.*, **80**, 5096 (1958).
3) S. P. McGlynn, J. D. Boggus, and E. Elder, *J. Chem. Phys.*, **32**, 357 (1960).
4) J. Czekalla and K. J. Mager, *Z. Elektrochem.*, **66**, 65 (1962).
5) N. Christodouleas and S. P. McGlynn, *J. Chem. Phys.*, **40**, 166 (1964).
6) S. Iwata, J. Tanaka, and S. Nagakura, *J. Amer. Chem. Soc.*, **89**, 2813 (1967).
7) S. Iwata, J. Tanaka, and S. Nagakura, *J. Chem. Phys.*, **47**, 2203 (1967).
8) H. Hayashi, S. Nagakura, and S. Iwata, *Mol. Phys.*, **13**, 489 (1967).
9) H. Hayashi, S. Iwata, and S. Nagakura, *J. Chem. Phys.*, **50**, 993 (1969).
10) P. Krebs, E. Sackmann, and J. Schwarz, *Chem. Phys. Lett.*, **4**, 65 (1969); **8**, 417 (1971).

the ESR signal of the lowest triplet states of CT complexes and in clarifying their nature by analyzing the observed fine structure constants.

From the above-mentioned phosphorescence and ESR studies, the natures of the phosphorescent states of CT complexes have been clarified unambiguously and understood systematically. The dynamical aspects of the phosphorescence of CT complexes, however, are still open to question, although Christdouleas and McGlynn studied the phosphorescence lifetimes and quantum yields for the naphthalene complexes with several acceptors.[5]

Under these circumstances, we have undertaken to study energy-transfer processes concerning the triplet states of several TCNB complexes with methyl-substituted benzenes, by obtaining the rate constants for the intersystem crossing and also for the phosphorescence emitting and quenching processes.

Experimental

The preparation and purification of materials, and also the measurements of the absorption and fluorescence spectra were described in a previous paper.[11] Sample solutions used for the measurements of phosphorescence lifetimes and quantum yields were degassed by the freeze-thaw technique. The phosphorescence lifetimes were determined by analyzing exponential decay curves measured by an oscilloscope. The phosphorescence quantum yields were determined by measuring quantum-yield ratios of phosphorescence to fluorescence, the quantum yields of which were obtained in the previous paper.[11]

During the measurement of the phosphorescence lifetime, the sample was kept in a Dewar vessel into which cold nitrogen gas was allowed to flow, in order to keep it at a temperature between ~100°K and ~280°K.

Results and Discussion

Phosphorescence Quantum Yield. The quantum-yield ratio of phosphorescence to fluorescence was measured by two different methods.

In method I, a fluorescence spectrum was obtained by subtracting the phosphorescence from a total emission spectrum, as is shown in Fig. 1. Thus, we obtained the quantum-yield ratio of the phosphorescence to the fluorescence. For the systems containing TCNB–durene and TCNB–HMB in methyl methacrylate (hereafter abbreviated to MMA), however, the total emission has only one peak: therefore, the separation into the two parts is rather optional and may cause a large error. For these cases, method II was used.

In method II, we measured the intensities of the total emission and phosphorescence by rotating two sectors in-phase and out-of-phase, respectively, as is shown in Fig. 2, keeping the sample in the same position and fixing the voltage of a photomultiplier and the sensitivity of a recorder. The total emission intensity was reduced by a neutral density filter to an intensity appropriate to be measured. The quantum-yield ratio of phosphorescence to fluorescence was evaluated from the observed intensities of total emission, $I_{\mathrm{Tot}}^{\mathrm{in}}$, and phosphorescence, $I_{\mathrm{P}}^{\mathrm{out}}$, with the aid of Eq. (1) derived from Eqs. (A-9)—(A-13) in the Appendix.

$$\frac{\Phi_{\mathrm{P}}}{\Phi_{\mathrm{F}}} \cong \frac{T_1+T_2}{T_1} \frac{I_{\mathrm{P}}^{\mathrm{out}}}{I_{\mathrm{Tot}}^{\mathrm{in}}-I_{\mathrm{P}}^{\mathrm{out}}} \qquad (1)$$

where T_1 and T_2 are the duration times of the "on" and "off" states of the sector.

The quantum-yield ratios obtained by methods I and II are given in Table 1. We adopted the values obtained by method II for the TCNB complexes with durene and HMB and the average values of methods I and II for the other TCNB complexes.

Determination of Rate Constants. The observed phosphorescence lifetimes and the evaluated quantum

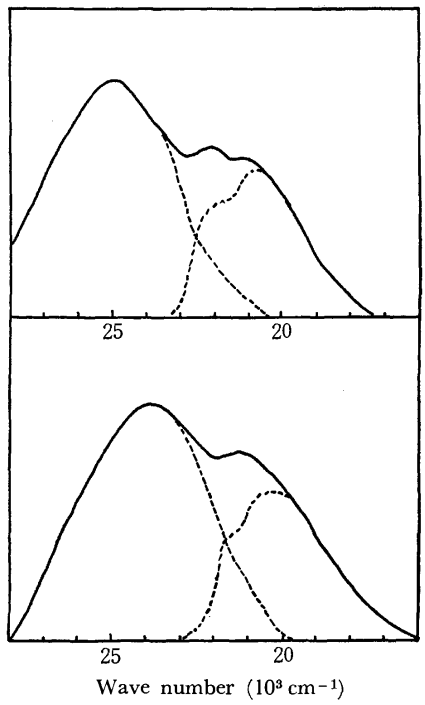

Fig. 1. The total emissions observed for the TCNB complexes with benzene (upper figure) and toluene (lower figure) and separation into fluorescence and phosphorescence.

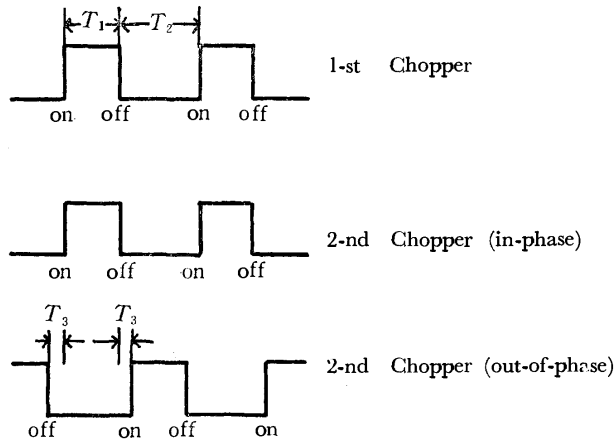

Fig. 2. Phases of the 1-st and 2-nd choppers.

11) T. Kobayashi, K. Yoshihara, and S. Nagakura, This Bulletin, **44**, 2603 (1971).

TABLE 1. PHOSPHORESCENCE LIFETIMES (τ_P), FLUORESCENCE AND PHOSPHORESCENCE QUANTUM YIELDS (Φ_F AND Φ_P), AND SEVERAL RATE CONSTANTS OF TCNB COMPLEXES

Donor[a]	I_P (eV)[b]	Φ_P/Φ_F (I)[c]	Φ_P/Φ_F (II)[c]	$(\Phi_P/\Phi_F)_a$[c]	Φ_F[d]	Φ_P	τ_P (sec)	k_2(max) (10^6	k_3(max) sec^{-1}	k_3(min))	k_4(max) (	k_4(min) sec^{-1}	k_5(max))
Benzene	9.245	0.48	0.44	0.46	0.63	0.29	3.0	2.1	9.7	7.6	0.33	0.26	0.072
Toluene	8.82	0.55	0.53	0.54	0.55	0.30	2.4	2.8	8.8	6.0	0.42	0.29	0.13
m-Xylene	8.56	0.56	0.54	0.55	0.51	0.28	2.3	2.8	6.6	3.8	0.43	0.25	0.19
p-Xylene	8.445	0.69	0.67	0.68	0.46	0.31	2.5	3.2	7.5	4.4	0.40	0.24	0.16
Mesitylene	8.39	0.56	0.52	0.54	0.47	0.25	2.3	3.3	6.2	2.9	0.43	0.20	0.23
Durene	8.03	0.1	0.14		0.25	0.035	1.7	12	13	0.60	0.59	0.027	0.56
HMB	7.85	0.1	0.10		0.16	0.016	0.76	21	22	0.41	1.32	0.025	1.3

a) The measurements were made for the durene and HMB complexes in MMA and for the other complexes in donor.
b) The ionization potential of each donor.
c) Φ_P/Φ_F (I) and Φ_P/Φ_F (II) are the quantum-yield ratio of phosphorescence to fluorescence obtained by methods I and II, respectively, and $(\Phi_P/\Phi_F)_a$ is the average of these two values.
d) Fluorescence quantum yields were obtained in Ref. (11).

yields are given in Table 1. In this table, k_3, k_4, and k_5 are the rate constants for the intersystem crossing, phosphorescence, and phosphorescence-quenching processes, respectively, and k_2 is the rate constant for the fluorescence-quenching process other than the intersystem crossing.

The quantum yields, Φ_F and Φ_P, and also the lifetimes τ_F and τ_P, are obtained with the aid of the rate constants:

$$\Phi_F = \frac{k_1}{k_1+k_2+k_3}, \quad \Phi_P = \frac{k_3}{k_1+k_2+k_3}\frac{k_4}{k_4+k_5} \tag{2}$$

$$\tau_F = \frac{1}{k_1+k_2+k_3}, \quad \tau_P = \frac{1}{k_4+k_5} \tag{3}$$

where k_1 is the fluorescence radiation decay constant. From Eqs. (2) and (3) we obtain the following relationships:

$$k_1 = \frac{\Phi_P}{\tau_F} \tag{4}$$

$$0 \leqq k_2 \leqq \frac{1}{\tau_F}(1-\Phi_F-\Phi_P) \tag{5}$$

$$\frac{\Phi_P}{\tau_F} \leqq k_3 \leqq \frac{1}{\tau_F}(1-\Phi_F) \tag{6}$$

$$\frac{1}{\tau_P}\frac{\Phi_P}{1-\Phi_F} \leqq k_4 \leqq \frac{1}{\tau_P} \tag{7}$$

$$0 \leqq k_5 \leqq \frac{1}{\tau_P}\frac{1-\Phi_F-\Phi_P}{1-\Phi_F}. \tag{8}$$

By the aid of Eqs. (4)—(8), the upper and lower limited values of k_2, k_3, k_4, and k_5 can be represented as follows:

$$k_2(\min) = k_5(\min) = 0 \tag{9}$$

$$k_2(\max) = \frac{1}{\tau_F}(1-\Phi_F-\Phi_P) \tag{10}$$

$$k_3(\min) = \frac{\Phi_P}{\tau_F} \tag{11}$$

$$k_3(\max) = \frac{1}{\tau_F}(1-\Phi_F) \tag{12}$$

$$k_4(\min) = \frac{1}{\tau_P}\frac{\Phi_P}{1-\Phi_F} \tag{13}$$

$$k_4(\max) = \frac{1}{\tau_P} \tag{14}$$

$$k_5(\max) = \frac{1}{\tau_P}\frac{1-\Phi_F-\Phi_P}{1-\Phi_F} \tag{15}$$

The limited values actually evaluated by Eqs. (10)—(15) are tabulated in Table 1.

Intersystem-Crossing Rate Constant, k_3. In discussing the rate constants for intersystem crossing given in Table 1, we divide the systems under consideration into two groups, groups A and B. Group A contains the TCNB–benzene, TCNB–toluene, TCNB–*m*-xylene, TCNB–*p*-xylene, and TCNB–mesitylene systems, and group B, the TCNB–durene–MMA and TCNB–HMB–MMA systems.

First, let us consider the TCNB–benzene and TCNB–toluene systems belonging to group A. In both systems, the sums of the fluorescence and phosphorescence quantum yields are nearly equal to unity as may easily be seen in Table 1; therefore, the fluorescence quenching is mainly due to the intersystem crossing.

The fact that TCNB is nonfluorescent means that, when the internal conversion may be disregarded,[12] its intersystem-crossing rate constant is much larger than its fluorescence radiation decay constant which is evaluated from the intensity of the absorption spectrum to be 2.0×10^7 sec^{-1}. Therefore, the intersystem-crossing rate constants, k_3's, for the systems of group A are smaller than that of the acceptor molecule itself. On the other hand, Christdouleas and McGlynn showed that k_3 of naphthalene was increased by the complex formation with trinitrobenzene and tetrahalophthalic anhydrides.[5] The intersystem-crossing rate constant of naphthalene can be estimated to be smaller than 5.8×10^6 sec^{-1} from the lifetime (103 nsec) and quantum yield (~0.4) in the literature.[13,14]

12) The rate constant of internal conversion from the first singlet state to the ground state was found to be very small for several compounds (T. Medinger and F. Wilkinson. *Trans. Faraday Soc.*, **61**, 620 (1965)).
13) T. V. Ivanova, P. I. Kudrysahov, and B. Ya. Sevshinikov, *Dokl. Akad. Nauk. SSSR*, **138**, 572 (1961).
14) E. H. Gilmore, G. E. Gibson, and D. S. McClure, *J. Chem. Phys.*, **23**, 399 (1965).

The great difference in the intersystem-crossing rate constant between TCNB and naphthalene may be the reason why the TCNB complexes of group A and the naphthalene complexes with trinitrobenzene and tetrahalophthalic anhydrides show reverse tendencies with regard to the effect of complex formation on the intersystem-crossing rate constant. The CT complex formation may bring about the mixing of the CT configuration with the appropriate excited singlet and triplet states of component molecules. This mixing may decrease the great rate constant of TCNB and increase the small rate constant of naphthalene.

For complexes of group B, the $\Phi_F+\Phi_P$ values are considerably smaller than those for the complexes of group A, as is seen in Table 1. This increases the difference between k_3(min) and k_3(max), and makes it difficult to estimate the real values of k_3 for the complexes of group B. In order to remove this difficulty, we discuss the two limiting cases: namely, case 1 where the true k_2, k_3, k_4, and k_5 values are, respectively, close to k_2(min), k_3(max), k_4(min), and k_5(max); case 2, where they are, respectively, close to k_2(max), k_3(min), k_4(max), and k_5(min). As is clearly seen in Table 1, in case 1 k_3 has no correlation with the ionization potentials of the donors, while in case 2 there is a correlation between them. In view of the fact that the ionization potential of the donor may be expected to be related with the contribution of CT configurations to the lowest triplet state[9] and therefore related also with k_3, case 2 is more probable than case 1.

Consideration of k_4. On the assumption that there is only one singlet state $|S_p>$, which makes a major contribution to the perturbation of the lowest triplet state, $|T_i>$, the rate constant, k_4, and the transition moment, $\vec{M}$, for the phosphorescence are written as follows:

$$k_4 \simeq \frac{64\pi^4\nu_P^3}{3hc^3}|\vec{M}|^2 \tag{16}$$

$$\vec{M} = -\frac{<S_p|H_{SO}|T_1>}{E(S_p)-E(T_1)}<S_p|\vec{er}|S_0> \tag{17}$$

where ν_P is the frequency of the phosphorescence maximum, $E(S_p)$ and $E(T_1)$ are the energies of $|S_p>$ and $|T_1>$ states, H_{SO} is the spin orbit interaction hamiltonian, and $\boldsymbol{h}$, $\boldsymbol{c}$, and $\boldsymbol{e}$ are universal constants. Here, $|S_0>$, $|S_p>$, and $|T_1>$ are expanded into the ground, CT, and LE configurations;

$$|S_0> \cong |G> \tag{18a}$$

$$|S_p> \cong c_1^p|{}^1LE^p> + c_2^p|{}^1CT^p> \tag{18b}$$

$$|T_1> \cong c_3|{}^3LE> + c_4|{}^3CT> \tag{18c}$$

where $|G>$ is the ground configuration, $|{}^1LE^p>$ and $|{}^1CT^p>$ are the singlet LE and CT configurations, respectively which make major contributions to the expansion of $|S_p>$, $|{}^3LE>$, and $|{}^3CT>$ are the lowest triplet LE (within the acceptor) and lowest triplet CT configurations, respectively, and c_1^p, c_2^p, c_3, and c_4 are their coefficients in the expansion. By inserting Eqs. (18a—c) into Eq. (17), we can obtain:

$$\vec{M} \cong K\vec{M}(\text{G-LE}) + L\vec{M}(\text{G-CT}). \tag{19}$$

Here, K, L, $\vec{M}$(G–LE), and $\vec{M}$(G–CT) are defined as follows:

$$K = c_1^pN \tag{20a}$$

$$L = c_2^pN \tag{20b}$$

$$N = \{c_1^pc_4<{}^1LE^p|H_{SO}|{}^3CT> + c_2^pc_3<{}^1CT^p|H_{SO}|{}^3LE> + c_1^pc_3<{}^1LE^p|H_{SO}|{}^3LE> + c_2^pc_4<{}^1CT^p|H_{SO}|{}^3CT>\} \times \{E(S_p)-E(T_1)\}^{-1} \tag{20c}$$

$$\vec{M}(\text{G-CT}) = <{}^1CT^p|\vec{er}|G> \tag{20d}$$

$$\vec{M}(\text{G-LE}) = <{}^1LE^p|\vec{er}|G>. \tag{20e}$$

In the case where $|S_p>$ is the lowest excited singlet state, $|S_1>$, which mainly consists of the lowest singlet LE (within the acceptor) configuration, $|{}^1LE>$, and the lowest singlet CT configuration, $|{}^1CT>$,[15] k_4 is given by the following equation from Eqs. (16)—(20):

$$k_4 \propto \frac{\nu_p^3|(c_1^1c_4+c_2^1c_3)|^2\{|c_1^1\vec{M}(\text{G-LE})/\boldsymbol{e}|^2+|c_2^1\vec{M}(\text{G-CT})/\boldsymbol{e}|^2\}}{\{E(S_1)-E(T_1)\}^2} \equiv \frac{A}{\{E(S_1)-E(T_1)\}^2} \tag{21}$$

where c_1^1 and c_2^1 are the coefficients of $|{}^1LE>$ and $|{}^1CT>$ in the expansion of $|S_1>$.

By the use of the values of $|\vec{M}(\text{G-CT})/\boldsymbol{e}|=0.1$ Å and $|\vec{M}(\text{G-LE})/\boldsymbol{e}|=0.3$ Å, and of $|c_1^1|^2$, $|c_2^1|^2$, $|c_3|^2$, and $|c_4|^2$ given in Refs. (9) and (11), we can evaluate the right-hand side of Eq. (21). The relative values of A and $A/\{E(S_1)-E(T_1)\}^2$ are listed in Table 2, the corresponding values of the TCNB–benzene system being taken as the standards. The relative values of $A/\{E(S_1)-E(T_1)\}^2$ are much larger than those of k_4(max) except for the toluene complex.[16] On the other hand, the relative values of A coincide considerably well with those of k_4(max). This means that the discrepancy in the relative values between $A/\{E(S_1)-E(T_1)\}^2$ and k_4(max) is due to the too large change in the $\{E(S_1)-E(T_1)\}^2$ term in Eq. (21) from one complex to another. This difficulty can

15) Amano *et al.* measured the polarization of phosphorescence spectra for several TCNB complexes, and obtained the preliminary results of a ratio $\left|\frac{K\vec{M}(\text{G-LE})}{L\vec{M}(\text{G-CT})}\right| = \left|\frac{c_1^p\vec{M}(\text{G-LE})}{c_2^p\vec{M}(\text{G-CT})}\right|$ to be 2.4, 2.1, 1.4, 1.3, and 1.2 for the complexes with HMB, durene, mesitylene, *p*-xylene, and benzene, respectively. The results shows that the ratio increases with the decrease in the ionization potential of the donor. This means that the $|S_p>$ state has the decreasing $\left|\frac{c_1^p}{c_2^p}\right|$ value with the increasing ionization potential of donor. The lowest excited singlet state satisfied this condition.[11]

16) The relative value of $A/\{E(S_1)-E(T_1)\}^2$ for the TCNB-durene complex is larger than that for the TCNB-HMB complex. This is due to the fact that the energy separation $E(S_1)-E(T_1)$ is smaller for the former complex than for the latter. This tendency is found in solvents other than MMA; namely, the $(E(S_1)-E(T_1))$ are 1000 and 1300 cm^{-1} for the TCNB-durene complex in ethanol and a 1 : 1 mixed solvent of ethyl ether and isopentane, while the corresponding values for the TCNB-HMB complex are 1600 and 1700 cm^{-1}, respectively.

Table 2. The relative values of A, $\frac{A}{\{E(S_1)-E(T_1)\}^2}$, and k_4(max), and the $\{E(S_1)-E(T_1)\}^2$ values

Donor	A	$\frac{A}{\{E(S_1)-E(T_1)\}^2}$	k_4(max)	$\{E(S_1)-E(T_1)\}^2$ (10^6 cm^{-2})
Benzene	≡1.00	≡1.00	≡1.00	16.81
Toluene	1.29	1.99	1.27	10.89
m-Xylene	1.77	6.73	1.30	4.41
p-Xylene	1.85	7.04	1.21	4.41
Mesitylene	1.77	6.13	1.30	4.84
Durene	2.23	46.3	1.79	0.81
HMB	2.30	11.9	4.00	3.24

easily be removed by considering that the $|S_p>$ state is not $|S_1>$ but a higher excited singlet state, the energies of which, $E(S_p)$, is high, and that $\{E(S_p)-E(T_1)\}^2$ changes to a considerably smaller extent than $\{E(S_1)-E(T_1)\}^2$ from the benzene complex to the HMB complex.

Temperature Dependence of k_5. In a preceding paper,[11] we found that k_1 is temperature-independent in a rigid medium (polymethyl methacrylate) in the range from 300°K to 77°K. From the same reason, the phosphorescence radiative rate constant, k_4, can safely be assumed to be temperature-independent in polymethyl methacrylate in a similar temperature range.

Let us express the temperature dependence of k_5 in the following way:[17]

$$k_5 = k_5^0\left[1+B\exp\left(\frac{-\Delta E}{kT}\right)\right]. \tag{22}$$

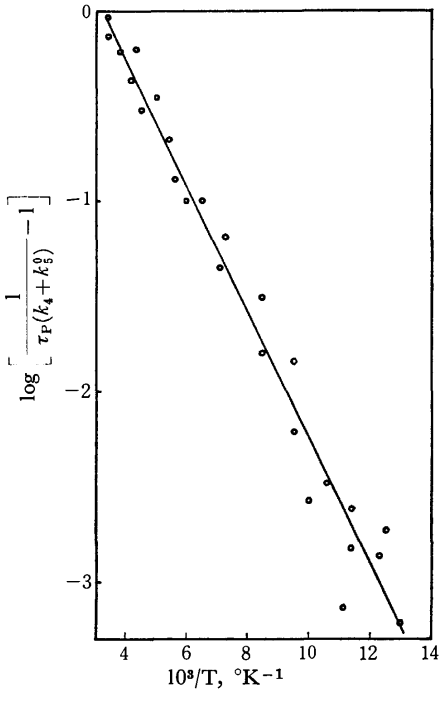

Fig. 3. Plot of $\log\left[\frac{1}{\tau_P(k_4+k_5^0)}-1\right]$ *versus* $1/T$ for the system including TCNB-durene in polymethyl methacrylate.

17) P. F. Jones and S. Siegel, *Chem. Phys. Lett.*, **2**, 486 (1968); *J. Chem. Phys.*, **50**, 1134 (1969).

The temperature dependence of the phosphorescence lifetime is given by the following equations:

$$\tau_P^{-1} = (k_4+k_5^0) + Bk_5^0\exp\left(-\frac{\Delta E}{kT}\right) \tag{23}$$

$$\frac{1}{\tau_P(k_4+k_5^0)} - 1 = \frac{Bk_5^0}{k_4+k_5^0}\exp\left(-\frac{\Delta E}{kT}\right) \tag{24}$$

From the extraporation of the $\tau_P^{-1}-1/T$ plot for the TCNB–durene complex in polymethyl methacrylate to a low-temperature region, we evaluated $1/(k_4+k_5^0)$ to be 1.70 sec. By the use of this value, we plotted $\log\left[\frac{1}{\tau_P(k_4+k_5^0)}-1\right]$ against $1/T$ for the same system. The results shown in Fig. 3 give a straight line as expected from Eq. (24), and ΔE is evaluated to be 535±30 cm^{-1}. From this value, it is revealed that the low-frequency intramolecular vibrations (probably out-of-plane bending modes) are responsible for the temperature dependence of k_5 for the temperature range studied. This is consistent with the conclusion presented by Jones and Siegel[17] after their measurement of the phosphorescence lifetimes of naphthalene-h_8, naphthalene-d_8, phenanthrene-h_{10}, and phenanthrene-d_{10}.

We should like to express our deep gratitude to Dr. Takako Amano, Department of Chemistry, Kyushyu University, for her kindness in offering her experimental results to us before publication.

Appendix

The integrated emission intensity over the observation time region from 0 to T is given by the following equation:

$$I = a\int_0^T D(t)\int_{-\infty}^{t} L(t')E(t-t')\mathrm{d}t'\mathrm{d}t, \tag{A-1}$$

where $L(t')$ is the exciting light intensity at time t', $D(t)$ is the ratio of detected photon number to the one emitted from the sample at time t, $E(t-t')$ is a decay function for the emission, and a is a proportionality coefficient. The integrated emission intensities are given by Eq. (A-2) for the two cases having the excitation and detection sectors "in-phase" and "out-of-phase":

$$I^\alpha = a\int_0^T D^\alpha(t)\int_{-\infty}^{t} L(t')E(t-t')\mathrm{d}t'\mathrm{d}t \tag{A-2}$$

where α indicates "in" or "out" and D, L, and E are as follows:

$$D^{in}(t) = \begin{cases} D_0 & n(T_1+T_2) \leqq t \leqq n(T_1+T_2)+T_1 \\ 0 & n(T_1+T_2)+T_1 \leqq t \leqq (n+1)(T_1+T_2) \end{cases} \tag{A-3}$$

$$D^{out}(t) = \begin{cases} D_0 & T_1+T_3+n(T_1+T_2) \leqq t \leqq 2T_1 \\ & \quad +T_3+n(T_1+T_2) \\ 0 & 2T_1+T_3+n(T_1+T_2) \leqq t \leqq T_1 \\ & \quad +T_3+(n+1)(T_1+T_2) \end{cases} \tag{A-4}$$

$$L(t) = \begin{cases} L_0 & n(T_1+T_2) \leqq t \leqq n(T_1+T_2)+T_1 \\ 0 & n(T_1+T_2)+T_1 \leqq t \leqq (n+1)(T_1+T_2) \end{cases} \tag{A-5}$$

$$E(t) = \frac{\Phi}{\tau}\mathrm{e}^{-t/\tau} \tag{A-6}$$

where n is an integer, L_0 is the number of photons absorbed by a sample when the excitation sector is "on" D_0 is the ratio of the number of photons detected to that emitted by the sample when the observation sector is "on", and τ and Φ are the lifetime and quantum yield, respectively. T_3 is a half of the difference between T_2 and T_1. By putting (A-3), (A-4), (A-5), and (A-6) into (A-2), and by integrating over one period, T_1+T_2, I^{in}, and I^{out} are obtained:

$$I^{\text{in}} = aL_0D_0\Phi\left[\tau(1-e^{-T_1/\tau})(e^{T_1/\tau}-1)\frac{e^{-((T_1+T_2)/\tau)}}{1-e^{-((T_1+T_2)/\tau)}} + T_1 + \tau(e^{-T_1/\tau}-1)\right] \quad \text{(A-7)}$$

$$I^{\text{out}} = aL_0D_0\Phi\left[\tau(e^{-T_3/\tau}-e^{-((T_1+T_3)/\tau)})(e^{T_1/\tau}-1) \times \frac{e^{-((T_1+T_2)/\tau)}}{1-e^{-((T_1+T_2)/\tau)}}\right]. \quad \text{(A-8)}$$

By taking τ and Φ to be τ_F and Φ_F, or τ_P and Φ_P, the integrated intensities of the fluorescence or phosphorescence in-phase and out-of-phase over one period T_1+T_2 can be given as follows:

$$I_F^{\text{in}} \cong aL_0D_0\Phi_F T_1 \quad \text{(A-9)}$$

$$I_F^{\text{out}} \cong 0 \quad \text{(A-10)}$$

$$I_P^{\text{in}} \cong I_P^{\text{out}} \cong aL_0D_0\Phi_P\frac{T_1^2}{T_1+T_2} \quad \text{(A-11)}$$

The intensities of the total emissions, $I_{\text{Tot}}^{\text{in}}$ and $I_{\text{Tot}}^{\text{out}}$, are also given as follows:

$$I_{\text{Tot}}^{\text{in}} \equiv I_F^{\text{in}} + I_P^{\text{in}} \cong I_F^{\text{in}} + I_P^{\text{out}} \quad \text{(A-12)}$$

$$I_{\text{Tot}}^{\text{out}} \equiv I_F^{\text{out}} + I_P^{\text{out}} \cong I_P^{\text{out}}. \quad \text{(A-13)}$$

BULLETIN OF THE CHEMICAL SOCIETY OF JAPAN, VOL. 45, 992—996 (1972)

Polarized Absorption Spectrum of the Second S → T Transition of Phenazine Crystals

Naohiko MIKAMI and Mitsuo ITO

Department of Chemistry, Faculty of Science, Tohoku University, Katahira-cho, Sendai

(Received September 8, 1971)

Polarized absorption spectrum of the second S→T transition of phenazine single crystal was measured at 4.2°K. The transition moments of the individual vibronic bands were determined uniquely from their polarization characteristics. The 0—0 band at 20470 cm^{-1} was found to be polarized along the N-N axis of the molecule and assigned as $^3B_{3u}\leftarrow{}^1A_g$ (n-π^*) transition. The vibronic bands other than the 0—0 band was found to be exclusively polarized along the long axis of the molecule, and they were assigned as the vibronic bands induced by a nontotally symmetric vibration in the $^3B_{3u}$ state. The possible routes of vibronic spin orbit coupling mechanism are discussed on the basis of the observed results.

Recently, high resolution photo-excitation technique becomes popular for detection of extremely weak singlet-triplet absorption spectrum of aromatic molecules. This indirect method[1] has real advantages for the crystals which have delayed fluorescence produced by triplet-triplet annihilation,[2] or in such a case that the excitation energy of triplet state of host crystal transfers well to phosphorescent molecules doped in the crystal.[3,4] In other cases, however, the direct observation of singlet-triplet absorption spectrum always gives unambiguous results. The polarization characteristic of singlet-triplet transition of aromatic molecules is important not only in assignment of the triplet state but also in elucidation of the spin orbit coupling mechanism of the molecules. Especially if the polarization characteristic of individual vibronic bands is determined, it provides reliable information on the mechanism of so called vibronic spin orbit interaction. Many works along this line were performed mainly by measurements of polarization degrees of the phosphorescence spectra.[5] In the absorption studies, however, only a few works have been reported.

The lowest singlet-triplet absorption spectrum of phenazine crystal was first observed by Clarke and Hochstrasser[6] at about 6400 Å and it was assigned by them as $^3B_{1u}\leftarrow{}^1A_g$ (π-π^*) transition on the basis of Zeeman splitting pattern of the factor group components.[7] This assignment for the lowest triplet state is reasonable because of good correspondence to the assignment for anthracene.[8,9] Later, Hochstrasser and Mazzacco[10] reported another weak abosption system in the region of 4800 Å and assigned it to be due to a second singlet–triplet transition. But

1) P. Avakian, E. Abramson, R. G. Kepler, and J. C. Caris, *J. Chem. Phys.*, **39**, 1127 (1963).
2) G. Durocher and D. F. Williams, *ibid.*, **51**, 5405 (1969).
3) G. Castro and G. W. Robinson, *ibid.*, **50**, 1159 (1969).
4) D. M. Burland, G. Castro, and G. W. Robinson, *ibid.*, **52**, 4100 (1970).
5) For example, S. M. Ziegler, and M. A. El-Sayed. *J. Chem. Phys.* **52**, 3257 (1970).
6) R. H. Clarke and R. M. Hochstrasser, *ibid.*, **47**, 1915 (1969).
7) R. M. Hochstrasser and T. S. Lin, *ibid.*, **49**, 4929 (1968).
8) R. Pariser, *ibid.*, **24**, 250 (1956).
9) R. H. Clarke and R. M. Hochstrasser, *ibid.*, **46**, 4532 (1967).
10) R. M. Hochstrasser and C. Marzzacco, *ibid.*, **49**, 971 (1968).

their spectrum was too obscure to ensure detail analysis.

In the present work, the polarized measurements of the 4800 Å absorption were carried out for the single crystal at 4.2°K, and the assignments and the possible routes of vibronic spin orbit coupling mechanism are discussed on the basis of the observed results.

Experimental

The single crystal of phenazine was grown in a high vacuum Pyrex tube by conventional Bridgman method after sample purification by chromatographic extraction followed by extensive zone refinning. The crystal was cleaved along the *bc*-plane, and cut down perpendicular to it. Thickness of the crystal used for spectral measurements was 5 to 30 mm. The polarized absorption spectra were taken on the *bc*-plane with the light polarized along the *b*-axis and with light perpendicular to it. The *b*-axis of the crystal was identified by X-ray diffraction method.

We were also able to obtain another crystal which exposes the *ac*-plane. Polarizing microscopic observation of this crystal through the *b*-axis showed that the angles between the *c*-axis and the directions of the minimum and maximum refractive indices α, γ, were about 50° and 40°, respectively, in agreement with the crystallographic data cited in the literature.[11]

The crystals used were so large that it was difficult to cool them to 4.2°K without cracking. Therefore, we constructed a cryostat having a specially designed thermal exchange tube. With this cryostat, the crystal was cooled very slowly to liquid helium temperature. After many failures, we succeeded in obtaining very clear crystals having no cracking at 4.2°K, and they were subject to the spectral measurements.

The absorption spectra were photographed on Kodak 103a-O plates with a Shimadzu GE-100 grating spectrograph having reciprocal linear dispersion of 8.4 Å/mm in the first order. Continuum from a 500 W xenon arc lamp and/or a tungsten iodine lamp was condensed on the crystal after passing through a water filter of 100 mm path length and a Toshiba UV-39 glass filter. The light passed through the crystal was focussed on a slit of the spectrograph. A Glan-Foucault prism was placed in front of the slit for polarization measurements.

To serve in vibrational analysis of the spectrum, we observed also the Raman spectrum of the crystal. The Raman spectrum was measured with a Narumi double monochromator combining with a He-Ne gas laser. The single crystal cube whose edges are parallel to *a*,*b* axes was used for plarization measurements at room temperature. The depolarization degrees of the Raman lines were also measured for molten phenazine with a high temperature liquid cell.

Results and Discussion

The absorption spectra of the first and the second singlet-triplet transitions are reproduced in Fig. 1. The first singlet-triplet absorption spectrum obtained in this work is the same as that reported by Clarke and Hochstrasser.[6] The half band widths of this absorption region were about 0.5 cm^{-1}. Davydov splittings were observed for the 0—0 band at 15447.5 cm^{-1} and the 0+1328 cm^{-1} vibronic band. The observed frequencies of fundamental vibrations in the first triplet excited state are 415, 452, 599, 740, 1044, and 1384 cm^{-1}.

The second singlet-triplet absorption consists of many bands whose half widths are about 3 cm^{-1}.

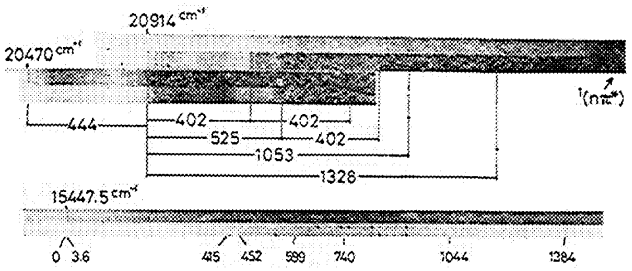

Fig. 1. Absorption spectra of phenazine crystal at 4.2°K. The upper is the second S→T absorption spectrum at about 4885 Å, and the lower is the first S→T transition at 6470 Å.

Table 1. Vibrational analysis of main absorption bands in 2nd S → T transition of phenazine crystal (cm^{-1})

ν	Intensity[a]	Remarks	
20470	w	0	
20498	vw, b	0+28	phonon
20554	vw, b	0+84	phonon
20586	vw, b	0+116	phonon
20815	w	0+345	
20839	w	0+369	
20876	vw, b	0+369+28	phonon
20914	s	0′ (0+444)	
20943	m, b	0′+28	phonon
20974	w	0+504	
21035	w	0+565	
21208	m	0+738	
21315	s	0′+402	
21343	m, b	0′+402+28	phonon
21439	s	0′+525	
21464	m	0′+525+28	phonon
21498	w	0+504+525	
21520	w	0′+606	
21546	w	0′+606+26	phonon
21639	w, b	0′+725	
21719	m	0′+2×402	
21744	w, b	0′+2×402+26	phonon
21843	m	0′+525+402	
21869	w	0′+525+402+26	phonon
21920	m	0′+606+402	
21958	w	0+1488	
21967	m	0′+1053 or 2×525	
21993	m	0′+1053+26	phonon
22023	w, b	0+504+2×525	
22243	w	0′+1329	
22270	vw	0′+1329+26	phonon
22368	w	0′+1053+402 or 2+525+402	
22394	vw	0′+1053+402+26 or 2×525+424+26	
22645	w	0′+1329+402	
22742	m	0′+1628	
22809	m	vibronic band belonging to $^1B_{3u} \leftarrow {}^1A_g(n\pi^*)$ transition	

a) Relative intensity
s: strong, m: medium, w: weak, vw: very weak, b: broad

11) R. G. Wood and G. Williams, *Phil. Mag.*, **31**, 115 (1941).

Davydov splitting was not observed. The longest wavelength band at 20470 cm^{-1}, which was considered as a 0—0 band of this absorption system, was weak compared with the bands at higher frequencies than 20914 cm^{-1}. Frequencies of the main bands and their tentative vibrational analysis are shown in Table 1. Five fundamental frequencies, 402, 525, 606, 1053, and 1328 cm^{-1} were found which start from the band at 20914 cm.$^{-1}$ Of these frequencies, 402 and 525 cm^{-1} belong to totally symmetric vibrations in the excited state, since they form short progressions. The other frequencies 606, 1053, and 1328 cm^{-1} are also probably due to totally symmetric vibrations. On the other hand, no prominent progression starting from the 20470 cm^{-1} band was observed. The frequency difference between this band and the 20914 cm^{-1} band is 444 cm^{-1}. It is probably due to a fundamental frequency in the excited state, but it is not repeated anywhere except the above difference. This fact and the weak intensity of the 20470 cm^{-1} band suggest that the 20914 cm^{-1} band and the higher ferquency bands followed to it are attributed to "*forbidden bands*" induced by a nontotally symmetric vibration.[12] If this interpretation would be correct, 444 cm^{-1} should be a nontotally symmetric vibration in the excited state and the strong intensity of the 20914 cm^{-1} band is explained as the results of intensity borrowing from higher excited states through this perturbing vibration. This situation is very similar to that of the (n-π^*) singlet-singlet absorption spectrum of this crystal at about 4200 Å where a vibronic band perturbed by a b_{1g} vibration occurs[13].

In order to determine the directions of the transition moments of the individual vibronic bands, we observed polarized absorption spectrum. Phenazine forms a monoclinic crystal of space group $P2_{1/a}$ having two molecules in a unit cell, as shown in Fig. 2.[14] It is seen from Fig. 2 that projection of the long axis of the molecules on ac-plane is nearly parallel to the [201] direction shown by **L** in the figure. This direction is easily identified from the direction of the largest refractive index on the ac-plane and the angle made between it and the cleavage plane. It is also seen from the figure that projection of the molecular normal axis on the ac-plane is also almost parallel to **L** because the molecular short axis is nearly parallel to the ac-plane. Thus, polarization measurements were made on the ac-plane with incident light polarized parallel to **L** and with light polarized perpendicular to it. A part of the observed spectrum for a crystal of 28 mm thickness is reproduced in Fig. 3. The weak 0—0 band at 20470 cm^{-1} (which is not shown in the figure) and the band at 21208 cm^{-1} appear dominantly in the $\mathbf{L}_\perp$ component. Then, the transition moments of these bands are parallel to the short axis of the molecule. On the other hand, all the bands above 20914 cm^{-1} except the band at 21208 cm^{-1} is exclusively polarized in the $\mathbf{L}_{//}$ direction. Therefore, we may conclude that their transition moments are parallel to the long or normal axis of the molecule. In order to distinguish between the two possiblities for the latter, we measured the polarized spectrum on the bc crystal plane. The observed intensity ratio $\frac{I(b)}{I(c)}$ was 3 for all the bands exclusively polarized along the **L** direction. The calculated ratios for the long and normal axis transition moments should be 2.7 and 18, respectively, in oriented gas approximation. Therefore, we may conclude that the transition moments of the 20914 cm^{-1} band and its relatives are parallel to the long axis of the molecule.

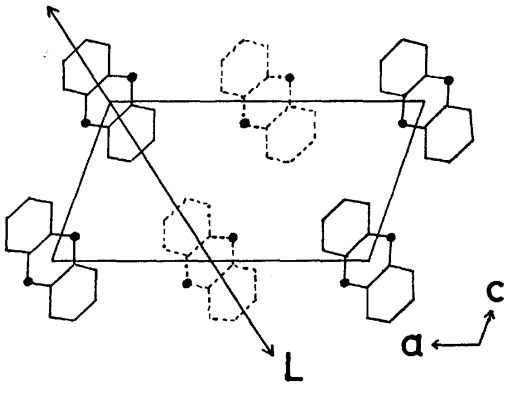

Fig. 2. Projection of the molecules onto the ac plane of the crystal. The molecules which are translationally inequivalent in a unit cell are indicated by the broken line. The direction **L** indicates the [201] in the crystal.

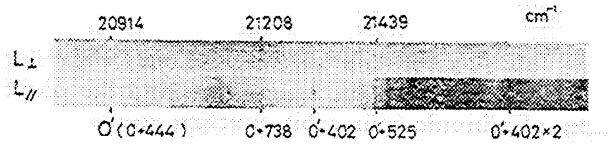

Fig. 3. Polarized absorption spectrum of the second S→T transition of phenazine single crystal at 4.2°K. The 0—0 band at 20470 cm^{-1} is not shown but its polarization characteristices is same as that of the band 0+738 at 21208 cm^{-1}.

Now, we proceed to assignment of the 0—0 band at 20470 cm^{-1} of the second triplet state which is polarized along the short axis (z) of the molecule. $^3B_{1u}$, $^3B_{2u}$, and $^3B_{3u}$ states are considered as candidates. All g-states are excluded because of appearance of the 0—0 band. In Table 2 are listed possible perturbing singlet states coupled with the triplet state by usual spin orbit interaction. It is found from this table that the triplet states which can couple with the $^1B_{1u}$ state of the short axis (z) transition moment must be $^3B_{3u}$ (n-π^*) or B_{2u} (π-π^*). Within the limit of LCAO MO consideration for the one electron spin orbit matrix elements, $^3B_{2u}$ (π-π^*) state can never couple with any short axis polarized singlet state, since operation of the operator l_x on an atomic orbital p_x from which the molecular orbitals are constructed always gives zero eigenvalue[15]. Hence, we have a unique

12) A. C. Albrecht, *J. Chem. Phys.*, **33**, 156 (1960).
13) N. Mikami, *J. Mol. Spectrosc.*, **37**, 147 (1971).
14) F. H. Herbstein and G. M. Schmidt, *Acta, Cryst.* **8**, 406 (1955).
15) For example, S. P. McGlynn, T. Azumi, and M. Kinoshita, "*Molecular spectroscopy of the triplet state*" Prenice-Hall, Inc. 1969 New Jersey.

assignment of $^3B_{3u}$ $(n\,\pi^*)$ for this triplet state. This assignment is supported from the theoretical predictions of the location of the $(n\,\pi^*)$ triplet state[16] and from the smaller energy separation between the singlet and triplet $(n\,\pi^*)$ states of this molecule than that of pyrazine.

TABLE 2. SPIN ORBIT COUPLING SELECTION RULE FOR THE TRIPLET STATE

Γ(T)		$\Gamma(l_\xi)$		Γ(S)
$^3B_{3u}(n\pi^*)$	<	$B_{1g}(l_z)$	—	$^1B_{2u}(y)$
		$B_{2g}(l_y)$	—	$^1B_{1u}(z)$
$^3B_{2u}(\pi\pi^*)$	<	$B_{1g}(l_z)$	—	$^1B_{3u}(x)$
		$B_{3g}(l_x)$	—	$^1B_{1u}(z)$
$^3B_{1u}(\pi\pi^*)$	<	$B_{2g}(l_y)$	—	$^1B_{3u}(x)$
		$B_{3g}(l_x)$	—	$^1B_{2u}(y)$

Γ(T), $\Gamma(l_\xi)$, and Γ(s) indicate irreducible representations of triplet state, angular momentum operator and singlet state of the molecule having D_{2h} symmetry, respectively.

As mentioned before, the band at 20914 cm^{-1} has its transition moment parallel to the long axis (y) of the molecule. If it would be an electronic band origin of another triplet state, it should have the symmetry of $^3B_{3u}$ $(n\,\pi^*)$ or $^3B_{1u}$ $(\pi\,\pi^*)$ as is seen from Table 2. However, $^3B_{1u}$ $(\pi\,\pi^*)$ can not couple with any $^1B_{2u}$ states within the limit of LCAO MO approximation, while $^3B_{3u}$ $(n\,\pi^*)$ can couple only with $^1B_{2u}$ $(n\,\sigma^*)$. Such $(n\,\sigma^*)$ singlet state lies in general in far ultraviolet region and the corresponding absorption is not so intense. Therefore, contribution from the $^1B_{2u}$ $(n\,\sigma^*)$ seems not to be important. From these reasons, we exclude the possibility that the 20914 cm^{-1} band is a band origin of another triplet state. As already suggested before we interprete the band at 20914 cm^{-1} as a vibronic band induced by a nontotally symmetric vibration of the frequency 444 cm^{-1} in the excited state. In the Raman spectral measurement, we observed seven bands in the frequency range from 400 to 750 cm^{-1}. Of them, the Raman bands at 414, 582, 610, and 734 cm^{-1} are readily assigned as due to totally symmetric vibrations from their depolarization degrees observed for the molten sample. Furthermore, the experiment on the polarized Raman spectrum of the single crystal of phenazine indicated that the Raman spectrum of the single crystal of phenazine indicated that the Raman band at 494 cm^{-1} belongs to b_{1g} species and the bands at 449 and 512 cm^{-1} to b_{3g}. It is then very probable that the excited state vibration of 444 cm^{-1} is b_{3g} which corresponds to 449 cm^{-1} in the ground state.[17]

Now, we shall discuss the origin of the 20914 cm^{-1} on the vibronic-spin-orbit interaction scheme.[18] The Hamiltonian containing spin orbit coupling[19] is written to first order in nuclear displacement by

$$\mathbf{H} = \mathbf{H}_o^\circ + \mathbf{H}^\circ_{so} + \sum_a \left\{\left(\frac{\partial \mathbf{H}_o}{\partial \mathbf{Q}_a}\right)^0 + \left(\frac{\partial \mathbf{H}_{so}}{\partial \mathbf{Q}_a}\right)^0\right\}\mathbf{Q}_a$$

where, $\mathbf{H}_o$ is unperturbed term, $\mathbf{H}_{so}$ spin orbit coupling operator and $\mathbf{Q}_a$ indicates normal coordinate, the superscript zero referring to the equilibrium nuclear configurations. The vibronic wave function of the triplet state with which we are concerned is thus written in second order perturbation theory by

$$\begin{aligned}{}^T\theta = {}^T\theta_o &+ \sum_S \frac{\langle S|\mathbf{H}^\circ_{so}|T\rangle}{E_{ST}}{}^S\theta_o + \sum_S \frac{\langle S|\mathbf{H}'_{so}|T\rangle}{E_{ST}}{}^S\theta_o \\ &+ \sum_S \sum_{S'} \frac{\langle S|\mathbf{H}'_o|S'\rangle}{E_{SS'}} \frac{\langle S'|\mathbf{H}^\circ_{so}|T\rangle}{E_{S'T}}{}^S\theta_o \\ &+ \sum_S \sum_{T'} \frac{\langle S|\mathbf{H}^\circ_{so}|T'\rangle}{E_{ST'}} \frac{\langle T'|\mathbf{H}_o'|T\rangle}{E_{TT'}}{}^S\theta_o\end{aligned}$$

where $\mathbf{H}'_o$ and $\mathbf{H}'_{so}$ represent $\left(\frac{\partial \mathbf{H}_o}{\partial \mathbf{Q}_a}\right)^0\mathbf{Q}_a$ and $\left(\frac{\partial \mathbf{H}_{so}}{\partial \mathbf{Q}_a}\right)^0\mathbf{Q}_a$ respectively. S′ and T′ indicate intermediate states. The second term indicates the usual spin orbit coupling for pure electronic state. The third term represents "the direct spin vibronic coupling." The fourth term is called "vibronic coupling in the singlet manifold with spin orbit coupling" and the last term is called "spin orbit coupling with vibronic coupling in the triplet manifold."

As is already described, the vibrationless triplet state is $^3B_{3u}$ $(n\,\pi^*)$ which couple with a $^1B_{1u}$ state through spin-orbit interaction, while the states corresponding to the vibronic band at 20914 cm^{-1} and its relatives must be perturbed by $^1B_{2u}$ state on the same interaction scheme. The selection rule for the spin-orbit coupling with vibronic coupling in the singlet manifold (the fourth term of the above equation) is same as that of the usual spin orbit coupling. Hence, the coupling by this mechanism between the $^3B_{3u}$ $(n\,\pi^*)$ state and the intermediate singlet state $^1B_{2u}$ are almost forbidden from the reason mentioned previously. On the other hand, the last term of the above equation, for which selection rule is shown in Table 3, will be non-zero when the intermediate triplet state is ^3A_u because it interacts vibronically with the $^3B_{3u}$, $^3B_{2u}$, or $^3B_{1u}$ by vibrations of b_{3g}, b_{2g}, or b_{1g} species, respectively and also it interacts with $^1B_{2u}$ by the spin-robit coupling. Since the perturbing vibration to the $^3B_{3u}$ $(n\,\pi^*)$ electronic state is the

TABLE 3. SELECTION RULE FOR VIBRONIC SPIN ORBIT COUPLING WITH THE $^1B_{2u}(y)$ SINGLET STATE

Γ(T)	×	Γ(vib)	=	Γ(vibronic)	$\Gamma(l_i)$		$\Gamma^{obs}_{(S)}$
$^3B_{3u}$	×	b_{3g}					
$^3B_{2u}$	×	b_{2g}	>	^3A_u	——	$B_{2g}(l_y)$	— $^1B_{2u}(y)$
$^3B_{1u}$	×	b_{1g}					
$^3B_{2g}$	×	b_{1u}	—	$^3B_{3u}$	——	$B_{1g}(l_z)$	—
	×	b_{2u}	—	^3A_u	——	$B_{2g}(l_y)$	—

16) L. Goodman and R. W. Harrell, *J. Chem. Phys.*, **30**, 1131 (1959).

17) In the previous paper,[13] we correlated the vibration of 413 cm^{-1} of the excited $(n\,\pi^*)$ singlet state with the ground state vibration of 449 cm^{-1}. However, polarized Raman spectrum reveals that the 449 cm^{-1} must be a b_{3g} vibration and the 494 cm^{-1} belongs to b_{1g} vibration. Then, we revise that the 413 (b_{1g}) vibration of the singlet $(n\,\pi^*)$ state corresponds to the 494 cm^{-1} in the ground state.

18) T. Pavlopoulos and M. A. El-Sayed, *J. Chem. Phys.*, **41**, 1082 (1964).

19) A. C. Albrecht, *ibid.*, **38**, 354 (1963).

b_{3g} vibration of 444 cm^{-1}, the "*forbidden band*" at 20914 cm^{-1} and its relatives borrow their intensities from ^3A_u intermediate state which interacts with $^1B_{2u}$ ($\pi\ \pi^*$) state by spin orbit coupling. Hence, the following scheme is considered as the most possible coupling route,

$$^3B_{3u}(n\pi^*)\frac{Vib}{b_{3g}}{}^3A_u(n\pi^*)\frac{SO}{l_y}{}^1B_{2u}(\pi\pi^*)$$

Group theoretically, the coupling route by the third term of the equation is not excluded, but it gives the same result as that given above.

The MO calculation[20] indicates that the symmetry of the highest occupied π obrital (π_7) of phenazine molecule is b_{2g} and the lowest and the second lowest vacant orbitals (π_8^* and π_9^*) are of b_{3u} and a_u, respectively. The two nonbonding orbitals resulting from the two nitrogen atoms are of $a_g(n_+)$ and $b_{1u}(n_-)$. The first singlet-singlet transition at about 2.9 eV is mainly described as $n_+\rightarrow\pi_8^*$, while the second singlet-singlet transition at 3.2 eV is due predominantly to $\pi_7\rightarrow\pi_8^*$. Roughly speaking, the n_+ orbital is slightly higher in energy than the π_7 orbital. Then, the A_u excited state ($n_+\rightarrow\pi_9^*$), which is forbidden optically, may have almost same excitation energy as that of the $^1B_{2u}$ ($\pi_7\rightarrow\pi_9^*$) state observed at about 5 eV. The singlet–triplet separation of ($n\rightarrow\pi^*$) transition is generally not so large that the ^3A_u ($n_+\rightarrow\pi_9^*$) state state will locate near the $^1B_{2u}$ ($\pi_7\rightarrow\pi_9^*$) state. Therefore, strong spin-orbit coupling between them is expected. The fact that the intensity of the 0—0 band is much weaker than the vibronic bands may be explained from absence of the short axis polarized singlet state in vicinity of this spectral region. This is in accord with the result obtained from the polarized absorption spectrum of ($n\ \pi^*$) singlet state of this crystal.[13]

20) W. R. Carper and J. Stengl, *Mol. Phys.*, **15**, 121 (1968).

Figure Captions

BULLETIN OF THE CHEMICAL SOCIETY OF JAPAN, VOL. 45, 996—1004 (1972)

Vibrational Analysis of Electronic Transition Bands of Coronene

Koichi OHNO, Takashi KAJIWARA, and Hiroo INOKUCHI

The Institute for Solid State Physics, The University of Tokyo, Roppongi, Minato-ku, Tokyo

(Received September 10, 1971)

The fluorescence and absorption spectra of coronene dissolved in organic solvents were measured at room temperature. Their vibrational structures were analyzed by reference to the Raman lines of crystalline coronene measured by means of a He-Ne gas laser, and the observed transition energies were compared with the calculated ones. It was suggested that the p-band of the absorption spectrum of coronene (23000—27000 cm^{-1}) is composed of more than one electronic transition, in contrast with the case of benzene. The fluorescence and phosphorescence spectra of coronene in *n*-octane were also measured at 77°K, and their vibrational structures were successfully analyzed with some perturbing vibrations and a few totally-symmetric ones.

The absorption and emission spectra of the first singlet-singlet transition band of coronene in solution show distinct vibrational structures. Further, a good mirror-image correspondence between the intensities and positions of the vibrational peaks of the fluorescence spectra and those of the α-band of the absorption spectra, both in solution and in vapor, was found. Therefore, it is possible to attempt the vibrational anaysis of the bands; such analysis has been carried out by Sidman,[1] Shpolskii,[2] and Mentzel and Zimmermann.[3] However, their results are somewhat tentative and insufficient because of the lack of Raman spectra and infrared absorption spectra of the hydrocarbon.

In order to analyze the vibronic structure, it is necessary to know the frequencies and symmetries of the intramolecular vibrations, which can be introduced from the observation of the Raman spectra. However, no complete measurement of the Raman spectra of coronene has yet been reported. Only one line has been found by Mentzel and Zimmermann;[3] its frequency is 1363 cm^{-1} in a CS_2 solution and 1346 cm^{-1} in a tetrahydrofuran (THF) solution. No other lines could be detected because of the poor solubility of coronene in the solvents. In this work, however, by means of a He-Ne gas laser as a light source, weak but refined Raman spectra of crystalline coronene could be obtained.

The first singlet-singlet transition band of coronene (23000—27000 cm^{-1}), with $\log \varepsilon = 2.5$[4] in the absorption spectrum, has been interpreted as a weakly-allowed electronic transition one, as was indicated by Brocklehurst and Bowen.[5] This concept is the same as for benzene, for both hydrocarbons, benzene and coronene, have a D_{6h} symmetry. For benzene, the lowest one-electron transition is orbitally fourfold-degenerate in the Hückel MO calculation. The degeneracy is removed by electron-electron interactions; then, one degenerate E_{1u} state and two nonde-

1) J. W. Sidman, *J. Chem. Phys.*, **23**, 1365 (1955).

2) E. V. Shpolskii and L. A. Klimova, *Soviet Physics*, Doklady 1, 782 (1956).

3) N. Mentzel and H. Zimmermann, *Ber. Bunsenges. Physik. Chem.*, **67**, 582 (1963).

4) ε is the extinction coefficient.

generate states, B_{1u} and B_{2u}, are given.

The absorption and fluorescence spectra of benzene vapor have been vibrationally analyzed.[6] The emission spectrum of benzene arises from one quantum addition of an e_{2g} vibration of 606 cm^{-1} to the symmetry-forbidden 0—0 band. The main progression is obtained by several further quanta addition of an a_{1g} vibration of 923 cm^{-1}. In coronene, as was reported by Brocklehurst and Bowen,[5] the vibrational structures of the fluorescence spectrum in heptane at −180°C are largely composed of several series of three bands. There are three remarkable series with interpeak distances of approximately 1360 cm^{-1}. This relation is common in the fluorescence spectrum and also in the α-band of the absorption spectrum, so it is possible to analyze the first singlet-singlet transition bands of coronene with some e_{2g} and a few a_{1g} vibrations, as in the case of benzene.

In this paper, the first singlet-singlet transition bands of coronene will be vibrationally analyzed by reference to the Raman lines of the crystalline sample. The above transition bands and the p- and β-bands of the absorption spectrum will also be analyzed using the transition energies calculated by means of the molecular obtital theory.[7-9] Further, the vibrational structures of the fluorescence and phosphorescence spectra of coronene in glassy *n*-octane (77°K) will be discussed.

Experimental and Results

1.1. Raman Spectra of Crystalline Coronene. In order to analyze the vibronic structures of the electronic spectra of coronene, the Raman lines of crystalline coronene were measured by means of a laser Raman spectrometer with a He-Ne gas laser (Japan Electron Optics Laboratory Co.) attached. The He-Ne gas laser (15803 cm^{-1}) was operated at an output of 40 mW. The applied sample was crystalline powder of high-purity coronene.[10] A single crystal was not employed because the crystal form was of a needle-type, so the polarized Raman spectrum could not be measured.

Although a weak emission spectrum was overlapped on the Raman spectrum, several Raman lines were identified at room temperature and at the temperature of liquid nitrogen (listed in Table 1).

Because a coronene molecule has a D_{6h} symmetry, the e_{2g}, e_{1g}, and a_{1g} vibrations should be Raman-active. Among them, a_{1g} vibrations are generally most intensive; therefore, it can be expected that most of the strong Raman lines obtained in the intramolecular vibration range belong to a_{1g} except for one line of 369 cm^{-1},[12] since, in the lower-frequency region, in general there is no totally symmetric vibration in a large aromatic hydrocarbon such as coronene.

Table 1. Raman lines of the crystalline coronene

	RT		77°K	
Lattice vivration range		40 cm^{-1}		43 cm^{-1}
		57		52
		87		77
				90
Intra-molecular vibration range	S	369 cm^{-1}	M	369 cm^{-1}
	W	435	M	435
	VS	482	VS	487
	W	830	M	571
	VS	1354	W	828
	VS	1371	S	840
	W	1584	VS	1354
	W	1631	VS	1369
			W	1584
			W	1625
			W	1633

Among the observed lines, 1354 and 1371 cm^{-1} are the most intensive lines in the intramolecular vibration range; they may correspond to 1363 cm^{-1} measured in the CS_2 solution by Mentzel and Zimmermann. The complete assignments of the Raman lines have not yet been made because of overlapping with weak emission spectra and because of the difficulty of polarized-Raman-spectra measurements.

In the lattice vibration range, there is a drastic change in the structure of the Raman lines between room temperature and the temperature of liquid nitrogen (Fig. 1). There-

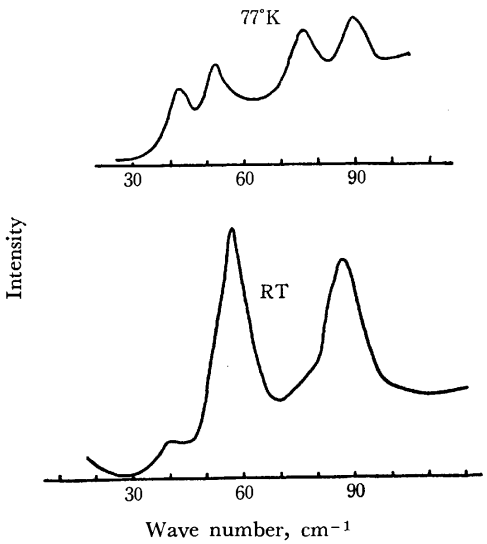

Fig. 1. The lattice vibration range of Raman spectra of coronene crystallites.

5) E. J. Bowen and B. Brocklehurst, *J. Chem. Soc.*, **1954**, 3875; **1955**, 4320.

6) H. Sponer, G. Nordheim, A. L. Sklar, and E. Teller, *J. Chem. Phys.*, **7**, 207 (1939).

7) N. S. Ham and K. Ruedenberg, *ibid.*, **25**, 1 (1956).

8) R. Hummel and K. Ruedenberg, *J. Phys. Chem.*, **66**, 2334 (1962).

9) H. Gutfreund and W. A. Little, *J. Chem. Phys.*, **50**, 4468 (1969); *Phys. Rev.*, **183**, 68 (1969).

10) The purification process has already been reported in another article.[11]

11) S. Iwahima, K. Ohno, T. Kajiwara, and J. Aoki, *Nippon Kagaku Zasshi*, **90**, 884 (1969).

12) See Sec. *2.1.*

fore, it seems that the phase transition takes place within the temperature range; the measurement of the heat capacity will now be undertaken.

1.2. Absorption Spectra of Gaseous Coronene. For understanding the optical properties of the coronene molecule, the absorption spectra of gaseous coronene are useful.[13] This seven-membered aromatic hydrocarbon, coronene, is very stable even at high temperatures of about 500°C, so that it was possible to obtain vapour phase enough to measure the absorption spectra. Purified coronene (46 mg) was enclosed in a cylindrical cell 3 cm in diameter and 30 cm in length *in vacuo*. The cell was placed in an electric furnace and heated to a constant temperature of 400°C in order to observe the α-band and to 250°C to observe the p-band. A tungsten lamp was used as the light source for the optical-absorption measurement. The most appropriate period of exposure was 20 min for the α-band observation and 10 min for the p-band observation, while the slit width of the spectrograph, a Spex Model 1700 III, was 100 μ. The relative intensities of the absorption peaks of the observed α-band are shown in Fig. 2.

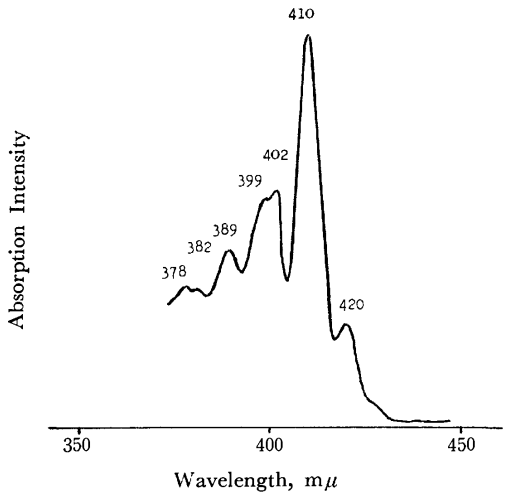

Fig. 2 The absorption spectrum of gaseous coronene.

As is shown in Table 2, the vibrational structure of the α-band of gaseous coronene is very similar to that of the benzene solution of coronene at room temperature reported by Clar,[14] while the p-band of the gaseous state is blue-shifted by a lack of solvent perturbation in comparison with that in solution. The fact that the α-band is hardly affected at all by the solvent supports the assignment of the band to an electronic transition from the $^1A_{1g}$ state to the $^1B_{2u}$ state which is symmetry-forbidden. The absence of the absorption peak at about 4270 Å in the gaseous phase, in contrast with its appearance in the benzene solution, suggests that the peak corresponds to that of the symmetry-forbidden transition.

1.3. Absorption and Emission Spectra of Coronene in Solution. The absorption and fluorescence spectra of coronene in solution were measured at room temperature. Fig. 3 and 4 show the absorption and emission spectra of coronene in THF. The peaks are named, as is shown in the figures,

13) J. Aihara, K. Ohno, and H. Inokuchi, This Bulletin, **43**, 2435 (1970).

14) E. Clar, "Polycyclic Hydrocarbons," Academic Press Inc., N. Y. (1964), p. 83.

Table 2. Absorption spectrum of gaseous coronene in comparison with the absorption spectra in benzene at room temperature

	Vapor	In benzene	In benzene by Clar[14]
α-band	(4264 Å) a)	4275 Å	4280 Å
	4200	4205	4200
	4104	4101	4100
	4022	4028	4020
	3980	3978	3965
	3890	3883	3880
	3820	3817	3815
	3780	3782	3780
		3686	3685
p-band		3560	
		3474	
	3370	3412	3415
	3310	3359	3360
	3260	3311	
		3258	3255
		3193	3195
		3150	3165

a) Very weak absorption was observed in the neighbourhood of 4264 Å, but it is impossible to determine the position exactly.

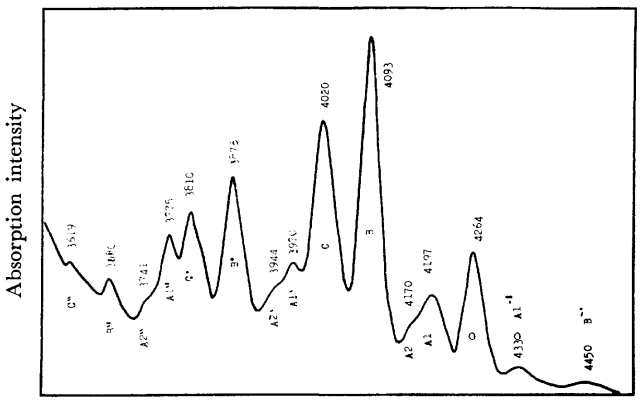

Fig. 3-1. The α-band of the absorption spectrum of coronene in THF at room temperature.

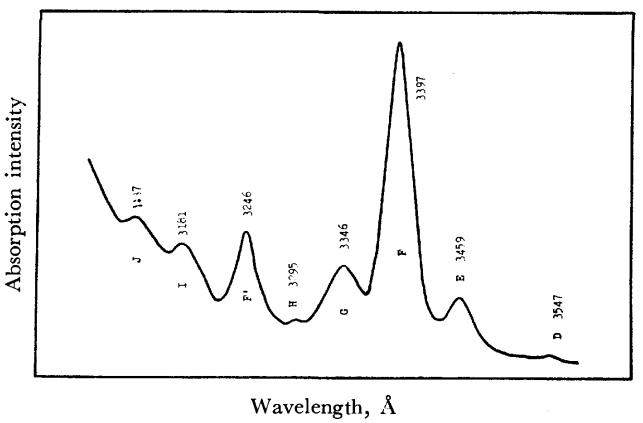

Fig. 3-2. The p-band of the absorption spectrum of coronene in THF at room temperature.

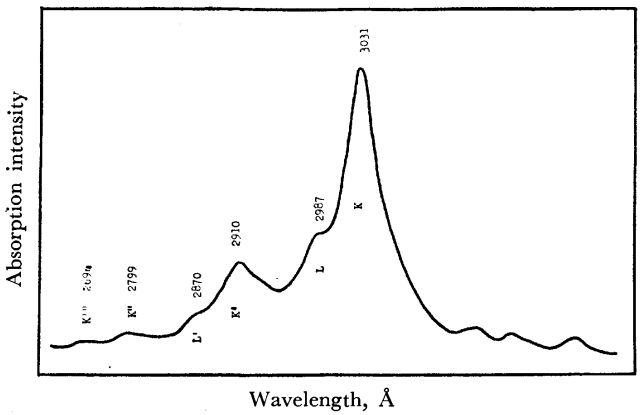

Fig. 3-3. The β-band of the absorption spectrum of coronene in THF at room temperature.

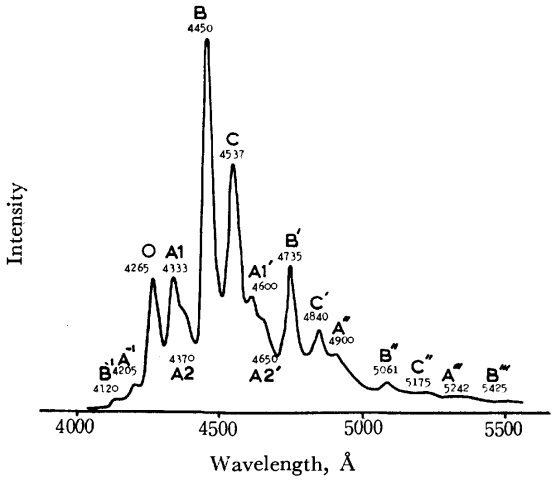

Fig. 4. The fluorescence spectrum of coronene in THF at room temperature.

according to the repeating structures and the mirror-image correspondence.

The vibrational structures of the fluorescence spectra of coronene in solution are composed of three (A_1, B, and C) or four series (A_1, A_2, B, and C), with a common interpeak distance, as in the case of the α-band of the absorption spectra of coronene. Clearly, there is a good mirror-image correspondence between the fluorescence spectra and the α-band of the absorption spectra. The mirror position at about 4270 Å (O-peak) coincides with the O-O position of the first singlet-singlet transition predicted by the absorption spectrum of gaseous coronene.

1.4. Fluorescence and Phosphorescence Spectra of Coronene in n-*Octane at 77°K.* As is well known, the quasi-linear spectra in *n*-paraffin at low temperatures give rather fine vibronic structures.[2,5] Therefore, the fluorescence and the phosphorescence spectra of high-purity coronene in *n*-octane were measured at 77°K in order to analyze the vibronic structures of the $^1A_{1g}$-$^1B_{2u}$ transition band and also the $^1A_{1g}$-$^3B_{1u}$ transition one. The resolving power of the spectra observed by means of a Spex 1700 III spectrograph are satisfactory (Fig. 5); for example, the line-widths at 4320 Å and at 4440 Å are about 4 Å (21 cm^{-1}). It is noted that the envelope of this fluorescence spectrum shows a very similar pattern (A_1, A_2, B, C, and their repetition) to that of the fluorescence bands in THF at room temperature. However, there exist some multiplicities. According to a recent report by Pfister,[15] the splittings are caused by many possible environments of a solute molecule dissolved in *n*-paraffin crystal. Although the number of possible sites depends, in general, upon the method of crystallization, in any of our measurements there were two possible sites for the case of coronene in *n*-octane; there exist two fluorescence origins, 23529 cm^{-1} and 23495 cm^{-1}, but only one phosphorescence origin is observed, at 19399 cm^{-1}. However, if the other phosphorescence origin is assumed to be 19411 cm^{-1}, the vibronic bands can be divided into two series with similar vibronic patterns; one series starts from 19399 cm^{-1}, and the other, from 19411 cm^{-1}.

Vibrational Analysis of the Spectra in THF

2.1. First singlet-singlet Transition Bands. The α-band of the absorption spectrum shows a good mirror-image correspondence to the fluorescence spectrum. The O-peak (4264 Å in Fig. 3 or 4265 Å in Fig. 4) is in the mirror position. As has already been suggested, the O-peak corresponds to the 0—0 position of the transition between the lowest $^1A_{1g}$ state and the lowest $^1B_{2u}$ state, which is a symmetry-forbidden transition and which is allowed with a one-quantum addition of an e_{2g} vibration. The main progressions are obtained by the further addition of several quanta of a_{1g} vibrations.

Therefore, it is possible to analyze the vibronic structure of the first singlet-singlet transition with several e_{2g} vibrations and a few a_{1g} vibrations. The results of the analysis of the α-band and the fluorescence spectrum of coronene in THF are shown in Table 3. The vibrational structure of the α-band (or the fluorescence spectrum) is composed of four series (A_1, A_2, B, and C), with a common interpeak distance of about 1340—1370 cm^{-1}. The adding frequency ν_0 (a_{1g}), reveals the existence of the totally

Table 3. Vibrational analysis of the α-band and the fluorescence spectrum of coronene in THF

	α-band		Fluorescence		Assignment
	ν (cm^{-1})	ν-ν_{00} (cm^{-1})	ν (cm^{-1})	ν_{00}-ν (cm^{-1})	
B^{-1}	22470	−980	24270	−820	$-\nu_3$
A^{-1}	23095	−355	23780	−330	$-\nu_1$
O	23450	0	23450	0	$^1A_{1g}$—$^1B_{2u}$
A_1	23825	375	23080	370	$\nu_1(e_{2g})$
A_2	23980	530	22880	570	$\nu_2(e_{2g})$
B	24430	980	22470	980	$\nu_3(e_{2g})$
C	24875	1425	22040	1410	$\nu_4(e_{2g})$
A_1'	25190	1740	21740	1710	$\nu_1+\nu_0(a_{1g})$
A_2'	25355	1905	21510	1940	$\nu_2+\nu_0$
B'	25800	2350	21120	2330	$\nu_3+\nu_0$
C'	26245	2795	20660	2790	$\nu_4+\nu_0$
A_1''	27490	3040	20410	3040	$\nu_1+2\nu_0$
A_2''	26730	3280	20130	3320	$\nu_2+2\nu_0$
B''	27175	3725	19760	3690	$\nu_3+2\nu_0$
C''	27630	4180	19320	4130	$\nu_4+2\nu_0$
A_1'''			19080	4370	$\nu_1+3\nu_0$
B'''			18430	5020	$\nu_3+3\nu_0$

15) C. Pfister, *J. Chim. Phys.*, **67**, 418 (1970).

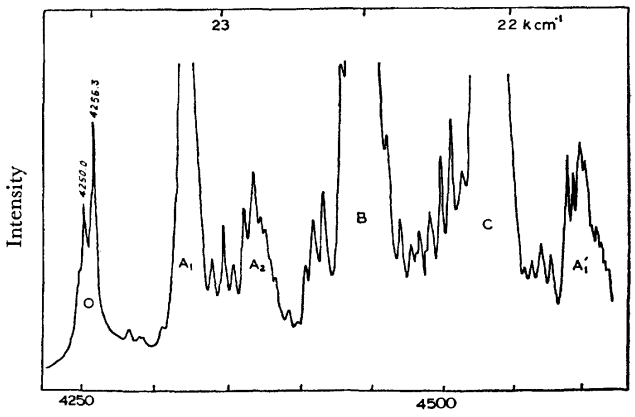

Fig. 5-1.

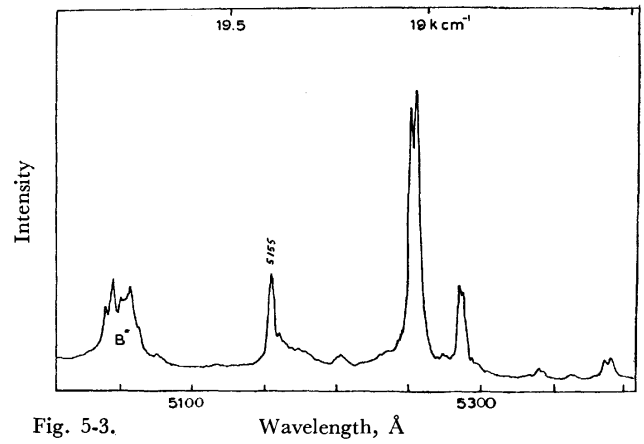

Fig. 5-3.

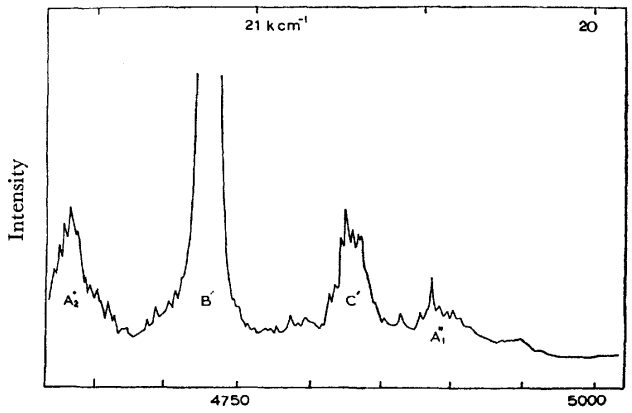

Fig. 5-2.

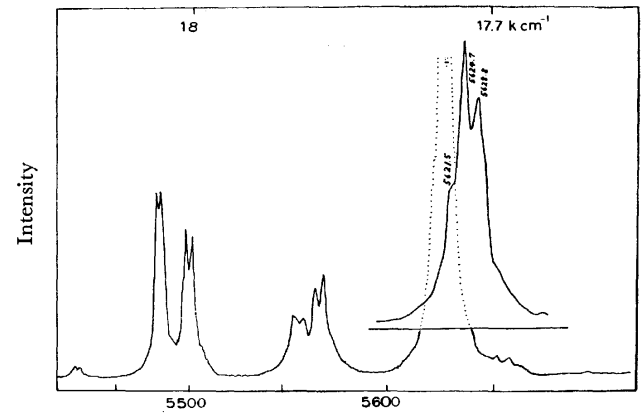

Fig. 5-4.

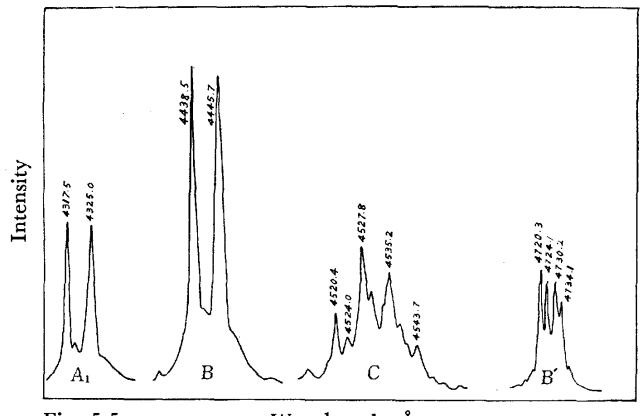

Fig. 5-5.

Fig. 5. The emission spectrum of coronene in *n*-octane at 77°K. Figure 5—5 shows the positions of peaks, A_1, B, C, and B′ illustrated in Fig. 5—1 and —2.

symmetric vibration of 1371 or 1354 cm^{-1} found in the Raman spectrum of crystalline coronene by means of a He-Ne gas laser. This frequency also appears in both the p- and β-bands. ν_1, ν_2, ν_3, and ν_4 in Table 3 are perturbing vibrations belonging to e_{2g}. Among them, ν_1 (375 cm^{-1}) corresponds to the Raman line (369 cm^{-1}), which may be one of the non-totally symmetric Raman active vibrations, e_{2g} or e_{1g}, so that it is possible to predict that the Raman line (369 cm^{-1}) is an e_{2g} vibration.

Two peaks (A_1^{-1} and B^{-1} of Fig. 3—1) apperaing on the longer-wavelength side of the α-band, and also the two peaks, A_1^{-1} and B^{-1} of Fig. 4, on the shorter-wavelength side of the fluorescence spectrum, have almost identical frequency differences form the O-peak which correspond well to the frequencies of the perturbing vibrations, ν_1 and ν_3. As has already been indicated by Brocklehurst and Bowen,[5] these bands seem to be the hot bands of the lowest singlet-singlet transition, for these bands could not be observed at the temperature of liquid nitrogen in either the absorption or in the fluorescence spectra. Although the agreements in the vibrational analysis between the hot-band florescence and the α-band are not adequate, these discrepancies can easily be understood by considering the reabsorption process.

Sidman[1] has assigned 990 cm^{-1} (corresponding to ν_3 in our assignment) to ν_1 (370 cm^{-1}, e_{2g})+ν (620

cm^{-1}, a_{1g}) but the absence of the 620 cm^{-1} line in the Raman spectrum suggests that his assignment is not correct.

2.2. p-Band. In the p-band of the absorption spectrum, the values of log ε range from 3 to 4.8 (Fig. 3—2). The intensity of the *D*-peak at 3547 Å is much weaker than that of any other peak in the p-band, while it is much stronger than the peaks in the α-band. Therefore, this peak seems to belong to another electronic transition.

Taking the *E*-peak (Fig. 3—2) at 3459 Å (28910 cm^{-1}) as the 0—0 position, we can obtain exactly the same frequencies (Table 4) as in the vibrational analysis of the α-band. In the p-band, the vibration of 530 cm^{-1} is the most effective perturbing vibration, and the additional frequency is 1365 cm^{-1}.

The two peaks (I and J of Fig. 3—2) in the shorter-wavelength region of the p-band have an interpeak distance of 445 cm^{-1}, which corresponds to the frequency of 1420—975 cm^{-1}, but the interpeak distance between G and I is 1550 cm^{-1}, which has not yet appeared elsewhere. If I and J are the repeating structure of G and H with a one-quantum addition of a totally symmetric vibration of 1550 cm^{-1}, the repetition of the most intense peak, F, must appear at the 530+1550 cm^{-1} position. Furthermore, although H is much weaker than G, J has an intensity almost comparable to that of I. Therefore, it is unreasonable to assign I and J to the repetition of G and H. It is, then, preferable to assume the existence of another electronic transition.[16] (Table 4)

Table 4. The vibrational analysis of the p-band of coronene in THF

	$\nu(cm^{-1})$	$\Delta\nu(cm^{-1})$	Assignment
D	28195		
E	28910	(0)	$^1A_{1g}-{}^1B_{1u}$
F	29440	(530)	$\nu_5(e_{2g})$
G	29885	(975)	$\nu_3(e_{2g})$
H	30330	(1420)	$\nu_4(e_{2g})$
F'	30805	(1895)	$\nu_5+\nu_0(a_{1g})$
I	31435		
J	31880		

Table 5. The vibrational analysis of the β-band of coronene in THF

	$\nu(cm^{-1})$	$\Delta\nu(cm^{-1})$	Assignment
K	32980	0	
L	33460	480	ν_6
K'	34350	1370	$\nu_0(a_{1g})$
M	34890	1910	ν_7
K''	35710	2730	$2\nu_0$
K'''	37080	4100	$3\nu_0$
K''''	38460	5480	$4\nu_0$
N	39600		
P	42270		
Q	43760		
R	44480		

16) This will be considered in Sec. 3.

2.3. β-Band. The β-band is clearly composed of an allowed transition, with log ε=5.4 at the most intensive absorption peak, which is assigned to the $^1A_{1g}$-$^1E_{1g}$ transition, as in the case of benzene. As is shown in Table 5, the vibrational structure of the β-band also reveals the totally symmetric vibration of 1370 cm^{-1} which appears in the β-band, the p-band, and the Raman spectrum.

3. Comparison of Transition Energies between Calculated and Observed Values

The molecular orbitals of coronene and their energies were first calculated by Moffitt and Coulson[17] by means of the simple LCAO-MO method. According to their calculations, the highest occupied MO belongs to e_{2u} and the lowest vacant MO belongs to e_{1g}, so that the lowest one-electron transition is orbitally fourfold degenerate, as in the case of benzene. The electron-electron interaction removes the fourfold

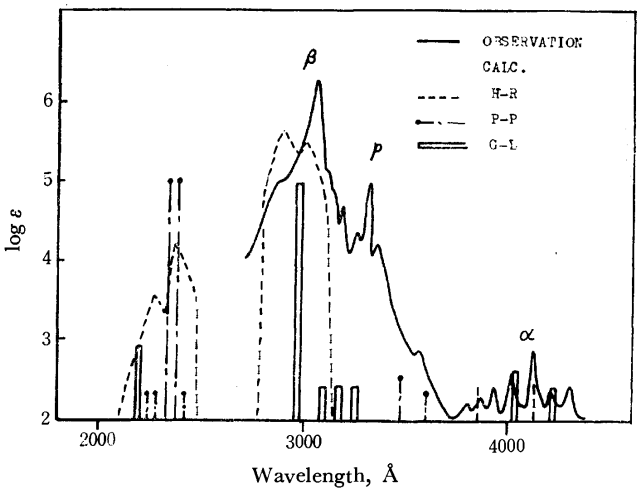

Fig. 6. The calculated and observed spectrum of coronene HR; Calculation by Hummel and Ruedenberg[8] P–P; Conventional Parier-Parr MO calculation[9] and G–L; Calculation by Gutfreund and Little.[9] The calculated spectral lines for forbidden transitions indicate their wavelength postitions only.

Table 6. The transition energy and the oscillator strength of coronene[a]

	$\nu(cm^{-1})$	f
$^1B_{2u}$	24459	0.0000
$^1B_{1u}$	27484	0.0000
$^1A_{1g}$	31751	0.0000
$^1A_{1g}$	32171	0.0000
$^1A_{1g}$	32501	0.0000
$^1E_{1u}$	33893	4.4
$^3B_{1u}$	19762	

a) In this work Nishimoto-Mataga's electron repulsion integrals[18] are used as the bare Coulomb potential in the calculation of the effective interaction potential and 21 configurations are used in the CI calculation.

17) W. Moffitt and C. A. Coulson, *Proc. Phys. Soc.*, **60**, 21 (1948).
18) K. Nishimoto and M. Mataga, *Z. Physik. Chem.* (Frankfurt), **12**, 335; **13**, 140 (1957).

TABLE 7-a. THE VIBRATIONAL ANALYSIS OF THE FLUORESCENCE SPECTRUM OF CORONENE IN *n*-OCTANE AT 77°K

	ν(cm^{-1})	$\Delta\nu$(cm^{-1})	Assignment
M	23529	0	I 0—0 ($^1B_{2u}-{}^1A_{1g}$)
M	23495	34	II 0—0 ($^1B_{2u}-{}^1A_{1g}$)
W	23351	178	I 178
VW	23310	219	II 185
VW	23295	234	
W	23228	301	
VS	23162	367	I 367
W	23145	384	II 384
VS	23121	408	II 374
VW	23100	429	II 395
M	23042	487	I 487
M	23001	528	II 494
M	22959	570	I 570
M	22929	600	II 566
M	22897	632	I 632
M	22862	667	II 633
VW	22847	682	I 682
VW	22815	714	II 680
W	22766	763	I 763
VW	22730	799	II 765
M	22705	824	I 824
M	22680	849	I 849 (II 815)
M	22640	889	II 855
M	22582	947	I 947
VVS	22528	1001	I 1001
VVS	22494	1035	II 1001
M	22424	1105	I 1071
M	22376	1153	I 1153
M	22336	1193	II 1159
W	22321	1208	I 1208
M	22306	1223	I 1223
W	22279	1250	II 1216
M	22274	1255	II 1221
M	22242	1287	I 1287
M	22205	1324	II 1290
M	22163	1366	I 1366
S	22122	1407	I 1407
S	22104	1425	I 1425
VS	22086	1443	I 1443 (II 1409)
S	22072	1457	I 1457 (II 1423)
VW	22056	1473	
VS	22051	1478	II 1444
M	22036	1493	II 1459
M	22024	1505	I 1505
S	22009	1520	I 1520
M	21988	1541	II 1507
M	21973	1556	II 1522
W	21956	1573	I 1573
M	21930	1599	II 1565
M	21901	1628	I 1628
M	21867	1662	II 1628
M	21815	1714	I 367+1347
M	21796	1733	I 367+1366
M	21772	1757	II 374+1349
M	21753	1776	II 374+1368
W	21716	1813	I 1813
W	21701	1828	I 487+1341
VW	21678	1851	II 1817
W	21647	1882	II 494+1354
W	21629	1900	II 494+1372
M	21610	1919	I 570+1349
M	21591	1938	I 570+1368
W	21573	1956	II 566+1356
W	21526	2003	I 632+1371
W	21503	2026	II 633+1359
W	21466	2063	
W	21450	2079	
VW	21419	2110	
VW	21409	2120	
W	21342	2187	I 824+1363
W	21313	2216	I 849+1367
W	21272	2257	II 855+1368
W	21252	2277	
VW	21236	2293	I 947+1346
VW	21211	2318	I 947+1371
S	21184	2345	I 1001+1344
S	21166	2363	I 1001+1362
S	21142	2387	II 1001+1352
S	21124	2405	II 1001+1370
VW	21102	2427	I 1071+1356
VW	21073	2456	II 1071+1351
VW	21053	2476	II 1071+1371
W	21028	2501	I 1153+1348
W	21006	2523	I 1153+1370
W	20958	2571	I 1223+1348
W	20940	2589	I 1223+1366
W	20894	2635	I 1287+1348
W	20853	2676	II 1290+1352
W	20777	2752	I 1407+1345
W	20760	2769	I 1425+1344
M	20741	2788	I 1443+1345 (II 1409+1345)
M	20725	2804	I 1457+1347
M	20708	2821	II 1444+1343
M	20693	2836	II 1459+1343
M	20683	2846	I 1505+1341
VW	20661	2868	I 1520+1348
VW	20642	2887	II 1507+1346
W	20614	2915	II 1522+1359
W	20565	2964	
W	20511	3018	
M	20469	3060	I 367+1347+1346
W	20448	3081	I 367+1347+1367
W	20419	3110	II 374+1349+1353
W	20400	3129	II 374+1349+1372
	20280	3249	
Broad			570+2×1360
	20200	3329	
VW	19908	3611	
W	19841	3688	I 1001+1344+1343
M	19822	3707	I 1001+1362+1344
W	19798	3731	II 1001+1352+1344
M	19771	3758	II 1001+1370+1353
W	19701	3828	
VW	19592	3937	
VW	19535	3994	
W	19376	4153	I 1457+1347+1349
VW	19361	4168	

Table 7-b. The vibrational analysis of the phosphorescence spectrum of coronene in *n*-octane at 77°K

	ν(cm^{-1})	$\Delta\nu$(cm^{-1})	Assignment
	(19411)	(−12)	I Assumed
S	19399	0	II $^3B_{1u}-{}^1A_{1g}$
M	19216	183	II 183
VS	19047	352	I 364
VS	19032	367	II 367
W	18957	442	
S	18924	475	I 487
S	18915	484	II 484
VW	18875	524	I 536
W	18758	541	II 541
W	18727	672	I 684
W	18716	683	II 683
W	18650	749	I 761
M	18570	829	I 841
M	18553	846	II 846
M	18447	952	I 964
M	18435	964	II 964
VS	18254	1145	I 1157
VS	18245	1154	II 1154
VS	18190	1209	I 1221
VS	18175	1224	II 1224
S	18005	1394	I 1406
S	17992	1407	II 1407
S	17972	1427	I 1439
S	17960	1439	II 1439
W	17789	1510	
VVS	17779	1620	I 1632
VVS	17766	1633	II 1633
W	17696	1703	I 364+1351
W	17677	1722	II 367+1355
W	17556	1843	II 484+1359
W	17289	2110	
W	16883	2516	II 1154+1362
M	16846	2553	I 1221+1344
W	16628	2771	I 1439+1344
W	16603	2796	II 1439+1357
W	16412	2987	II 1633+1354

degeneracy to give one degenerate E_{1u} state and two nondegenerate states, B_{1u} and B_{2u}.

The transition energies calculated by Ham and Ruedenberg[7] and those reported by Hummel and Ruedenberg[8] reproduce the experimental absorption spectra somewhat better than the conventional Pariser-Parr SCF-MO calculation, as is shown in Fig. 6.[19] The agreement with the experimental results has been considered plausible. By many authors, it has been assumed that the first weak band at 23400 cm^{-1} might correspond to the 2600 Å band of benzene ($^1B_{2u}$); the band in the 29000 cm^{-1} region, to the 2000 Å band of benzene ($^1B_{1u}$), and the most intensive band, at 33000 cm^{-1}, to the 1800 Å band of benzene ($^1E_{1u}$). However, these correspondences may not always be appropriate, because, in the case of coronene, a much larger number of electronic configurations must be considered in the CI calculation than in the case of benzene.

Recently, a more improved calculation has been presented by Gutfreund and Little.[9] In their calculation, the correlation effects of the π-electrons were considered carefully, and it was shown that the Coulomb interaction between π-electrons in a conjugated molecule is screened by the presence of other π-electrons and that, therefore, the bare Coulomb potential must be replaced by the appropriate effective interaction potential. The obtained transition energies for the low-lying singlet states of polycyclic hydrocarbons, such as coronene, tetracene, and pyrene, agreed plausibly with the absorption spectra experimentally obtained. In the case of coronene, the ambiguous p-band can be explained clearly by their calculation. According to their calculation, it seems that the conventional assignments are not appropriate; thus, it is preferable to conclude that the α-band of coronene corresponds to the two forbidden transitions; the p-band, to the three forbid-

Table 8. The obtained fundamentals and Raman lines

Fluorescence		Phosphorescence		Raman
I	II	I	II	
178 cm^{-1}	185 cm^{-1}		183	
367	374	364	367	369
384	395			
				435
487	494	487	484	487
		536	541	
570	566			571
632	633			
682	680	684	683	
763	765	761		
824				828
849	855	841	846	840
947				
		964	964	
1001	1001			
	1071			
1153	1159	1157	1154	
1208	1216			
1223	1221	1221	1224	
1287	1290			
1347	1349			1354
1366	1368			1369
1407	(1409)	1406	1407	
1425	(1423)			
1443	1444	1439	1439	
1457	1459			
1505	1507			
1520	1522			
1573	1565			1584
1628	1628			1625
		1632	1633	1633
1813	1817			

19) The conventional Pariser-Parr MO calculation gives much larger transition energies.

den transitions, and the β-band, to the one allowed transition.

In the present work, we calculated the transition energies of coronene by the SCF-MO CI method, with effective electron repulsion integrals as in the Gutfreund and Little calculation. The calculated transition energies and oscialltor strengths are listed in Table 6. These results show that there are three states between $^1B_{1u}$ and $^1E_{1u}$, as in the results of Gutfreund and Little.[9] We found that the three states (31751, 32171, and 32501 cm^{-1}) belong to $^1A_{1g}$, so that the transitions between these states and the ground states ($^1A_{1g}$) are forbidden and vibronically allowed by e_{1u} vibrations. Although the e_{1u} vibrations are infrared-active, the infrared spectrum of coronene has not been measured; therefore, we cannot discuss further the vibronic structures of the p-band. In order to analyze the observed p-band, it would be desirable to determine the vibronic states by a calculation including the vibronic interactions among the three A_{1g} states, the lowest $^1B_{1u}$ state, and the $^1E_{1u}$ state. Thus, we should prefer to suggest that the p-band is composed of more than one electronic transition.

4. Vibrational Analysis of Emission Spectra in *n*-Octane

The observed fluorescence and phosphorescence spectra of coronene in *n*-octane at 77°K were analyzed with reference to the results of the preliminary analysis reported in the Experimental and Results sections and with reference to the observed Raman lines. The assignments are shown in Table 7, while the obtained fundamentals are listed in Table 8. The fundamentals obtained from the phosphorescence spectrum agree well with those from the fluorescence one; most of the obtained Raman lines are also found in the fundamentals derived from the fluorescence spectrum. The adding a_{1g} frequencies found in the fluorescence spectra are 1347 cm^{-1} and 1366 cm^{-1} in Series I, and 1349 cm^{-1} and 1368 cm^{-1} in Series II. These frequencies coincide well with the most intensive Raman lines, 1354 cm^{-1} and 1369 cm^{-1}. The most effective perturbing fundamentals are 367, 1001, 1407, and 1443 cm^{-1} in the fluorescence spectrum and 367, 484, 1154, 1224, 1407, 1439, and 1633 cm^{-1} in the phosphorescence one. As was mentiaed in Sec. *2.1*, almost all of these should be e_{2g} vibrations; however, 484 cm^{-1}, corresponding to the intensive Raman line, 487 cm^{-1}, may be an a_{1g} vibration, since the 964 cm^{-1} observed in the phosphorescence spectrum approximately equals $484 \times 2 = 968$ cm^{-1}.

The authors wish to thank Professor Mitsuo Ito, Tohoku University, and Dr. Toru Yokoyama, Japan Optics Laboratory Co., for their kind cooperation in making the Raman-spectrum measurements. The authors are also indebted to Professor Satoshi Iwahima, Meisei University, for preparing the high-purity coronene used for the spectroscopical measurements.

BULLETIN OF THE CHEMICAL SOCIETY OF JAPAN, VOL. 45, 1004—1010 (1972)

Polarized Absorption Spectra of TCNNQ-Aromatic Hydrocarbon Molecular Complexes

Yasumasa J. I'HAYA, Toru YUNOKI,* and Noboru SUZUKI

Department of Materials Science, The University of Electro-Communications, Chofu, Tokyo

(Received September, 11, 1971)

Polarized absorption spectra of TCNNQ and TCNNQ-anthracene, pyrene, phenanthrene (Group 1), 1,2-benzanthracene, chrysene and triphenylene (Group 2) molecular complexes were measured in the frequency range of 13.5—42 kK at room temperature and 80°K. The mole ratio of donor to acceptor was found to be 2 : 1 for Group 1 complexes and 1 : 1 for Group 2 complexes. Two broad bands observed in each spectrum of these complexes were assigned to be the first and the second charge-transfer (CT) bands. The CT bands were enhanced in intensity and displaced to the red at 80°K. The first CT bands were confirmed to be associated with the charge transfer from the highest occupied molecular orbital (HOMO) of donor to the lowest vacant molecular orbital (LVMO) of acceptor. The charge transfer mechanism for the second CT bands may be divided into two classes; for Group 1 complexes it is mainly due to the second LVMO of acceptor, while for Group 2 complexes, in addition to this, there is a possibility of the charge transfer from the second HOMO of donor to the LVMO of acceptor.

TCNNQ (11,11,12,12-tetracyano-1,4-naphthaquinodimethane) is a new cyanocarbon acceptor with the electron affinity 1.49 eV and is known to form sufficiently strong charge-transfer π-complexes with aromatic hydrocarbons.[2] In a previous paper,[2] we have presented a preliminary survey on the polarized absorption spectra of the molecular complexes which involve TCNNQ as an acceptor and anthracene, pyrene, phenanthrene, 1,2-benzanthracene, chrysene

* Present address: ULVAC Corporation, Chigasaki, Kanagawa.

1) S. Chatterjee, *J. Chem. Soc., B*, **1967**, 1170.

2) Y. J. I'Haya, T. Yunoki, and N. Suzuki, This Bulletin, **43**, 3636 (1970).

and triphenylene as donors. We have shown that the second charge-transfer (CT) bands of these complexes are mainly associated with a charge transfer from the highest occupied molecular orbital of donor to the *second* lowest vacant molecular orbital of acceptor.

In the present communication, we shall report the details of the polarized absorption spectra of TCNNQ and these TCNNQ molecular complexes observed at room temperature and liquid nitrogen temperature. To the authors' knowledge, there has been published no spectral datum of CT bands of a molecular complex observed at such a low temperature. We shall show that CT bands enhance their spectral intensities and disclose their vibrational structures at liquid nitrogen temperature. Using the low-temperature data, we re-examine the relationships between charge-transfer transition energies and highest occupied molecular orbital energies of donors.

Experimental

TCNNQ was synthesized by Chatterjee's method,[1] and purified by repetitive recrystallization from methanol and methylene chloride, followed by vacuum sublimation. Anthrancene, pyrene, phenanthrene, 1,2-benzanthracene, chrystene and triphenylene used as electron donors were of reagent grade from commercial sources and they were purified by recrystallization and sublimation. The molecular complex single crystals of microscopic size were prepared from the purified TCNNQ and donors by simultaneous sublimation onto a heated glass plate.

The absorption spectra of TCNNQ and its molecular complexes in solution were measured in methylene chloride by a JASCO ORD/UV-5 spectrophotometer. The mole ratio of donor to acceptor in each molecular complex was determined spectroscopically.

The polarized absorption spectra were measured with a specially designed microspectrophotometer. A 500 W high pressure xenon-arc lamp (Ushio Electric Co.) was used as a light source, which was operated with a 20A stabilized power supply. The light was passed through a grating monochrometer (Hitachi model 139), polarized by a Rochon prism, and focused onto a sample crystal mounted on a sample holder. The sample crystals, selected from among a number of sublimation flakes, were mounted between quartz objective slides which edges were sealed by Araldite cement in order to avoid sublimation of samples. The sample holder and two objectives of reflection type (Olympus Optical Co.) were set in a cryostat which had two cryogen containers. The section of the cryostat is shown in Fig. 1. Sample temperatures were measured with a copper-constantan thermocouple while spectra were being taken. An R-136 photomultiplier tube (Hamamatsu Television Co.) was used as the detector.

The directions of crystal axes were examined by the observation under a polarizing microscope. The crystal thickness was roughly estimated from birefringence and retardation using the polarizing microscope. The crystal spectra were observed from the direction normal to the developed face of a crystal for two polarizations, parallel and perpendicular to the crystal elongated axis which we hereafter call the *l*-axis. To each molecular complex, the spectral measurements were carried out for several crystals of different thicknesses. The position of each absorption maximum was found to be not dependent upon crystal thickness.

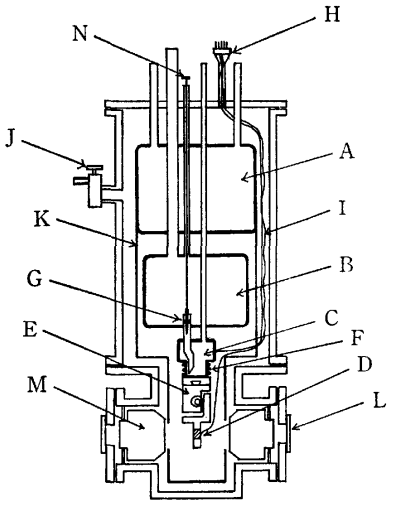

Fig. 1. Cryostat for Microspectrophotometry. A: Liquid nitrogen can; B,C: Liquid nitrogen or helium can; D: Sample holder; E: Vertical adjusting gear; F: Heater; G: Cryogen dropping valve; H: Connector; I: Thermocouple; J: Exhaust valve; K: Radiation shield; L: Fused quartz window; M: Reflection-type objective; N: Pin valve.

Results

1. Crystal and Solution Spectra of TCNNQ. The TCNNQ crystal is orthorhombic, space group *Pbca* with cell dimensions of $a=13.210$ Å, $b=7.209$ Å, and $c=26.629$ Å, eight molecules being contained in the unit cell. Fig. 2, the projection along the *a*-axis, shows that the TCNNQ molecule is non-polar in the crystal.[3] We have observed the *b*-axis and *c*-axis polarized spectra as well as the *a*- and *b*- polarized spectra, since we found the presence of two different crystal habits. They are shown in Figs. 3 and 4 together with the solution spectrum.

The solution spectrum in methylene chloride consists of two main bands, each having a few vibrational structures which maxima are estimated to be located at 25.3 kK ($\varepsilon=33{,}000$) and 34.7 kK ($\varepsilon=6{,}900$). Higher frequency bands have been observed at 45.2 kK and 48.1 kK.[4]

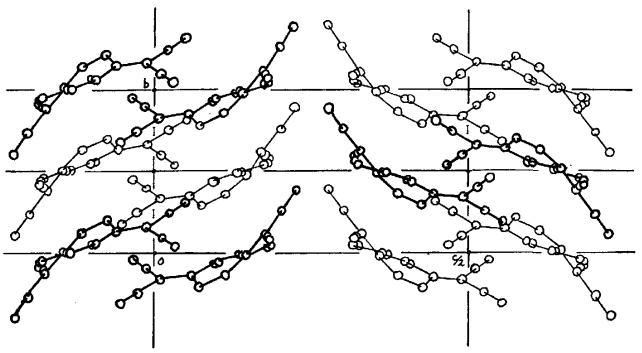

Fig. 2. Projection of the crystal structure of TCNNQ along the *a*-axis on the *bc* plane.

3) F. Iwasaki, private communication.
4) N. Suzuki and Y. J. I'Haya, *Tetrahedron*, **26**, 5379. (1970).

The *a*-axis polarized spectrum in Fig. 3 has two absorption bands; one at 33.8 kK is rather narrow and the other in the 22—27 kK region is quite broad. The *b*-axis polarized spectrum in the same figure has one narrow band at 31.2 kK with an weak shoulder at 25.6 kK.

In the *bc*-face spectra (Fig. 4), the *b*-axis polarized spectrum has a peak at 30.9 kK and a weak shoulder at 26.0 kK, while the *c*-axis polarized spectrum has two peaks at 22.9 kK and 33.6 kK and a shoulder at 25.1 kK.

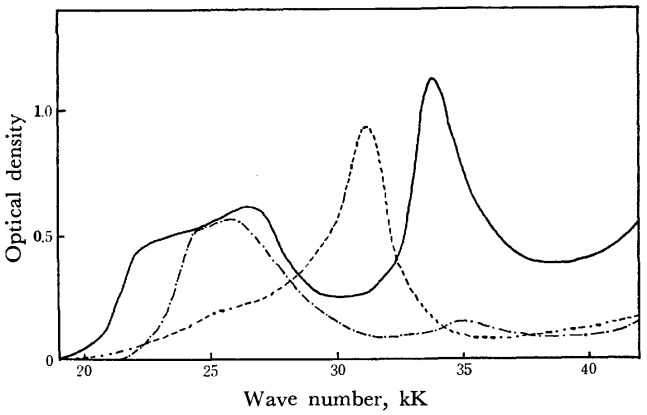

Fig. 3. Polarized absorption spectra of TCNNQ crystal observed from the *c*-axis at room temperature.
(—·—·— solution spectrum in methylene chloride)

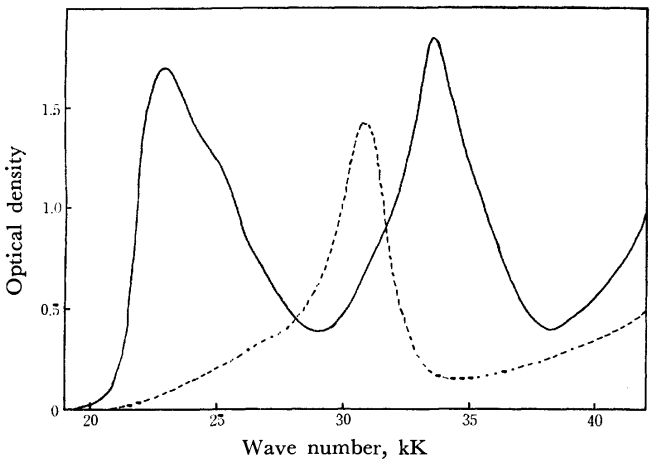

Fig. 4. Polarized absorption spectra of TCNNQ crystal observed from the *a*-axis at room temperature.

At liquid nitrogen temperature, we have not found any significant change in the overall spectrum of each polarization.

2. Composition and Solution Spectra of Molecular Complexes. The mole ratio of donor to acceptor was found to be 2 : 1 for anthracene-, pyrene-, and phenanthrene-TCNNQ complexes, while that for 1,2-benzanthracene-, chrysene-, and triphenylene-TCNNQ complexes was 1 : 1. The former is called Group 1 complexes and the latter Group 2 complexes in the following.

Measurement of the CT bands in a solution spectrum of each molecular complex was very difficult, because TCNNQ itself absorbed strongly in the longer wavelength side. The first CT bands were observed for all the complexes but second CT bands were not clearly observed in solution. The wave numbers of the first CT band maxima observed in solution are listed in the second column of Table 1.

3. Crystal Spectra of Molecular Complexes. Two broad bands were observed in each polarized absorption spectrum of all the molecular complexes studied, as shown in Figs. 5—10. These two bands (14—23 kK) are not local excitation bands but can be assigned to be the first and second CT bands, since the lowest transition of TCNNQ has an absorption maximum at 25 kK and those of electron donors appear at much shorter wavelength region. The wave numbers of these CT band maxima are listed in Table 1.

(a) Anthracene-TCNNQ (2 : 1) Complex: The first CT band appears at 14.3 kK in the room-temperature spectrum and is polarized in the *l*-axis, while the second CT band at 20.8 kK and polarized in a direction perpendicular to *l*. The polarization ratio, $I(//l)/I(\perp l)$, at each band maximum is 2.6 for the first CT band and 0.36 for the second CT band. When the crystal temperature is down to 80°K, the first CT band is displaced to the red by 600 cm^{1} and the second CT band remains unshifted, both bands being remarkably enhanced in intensity. Furthermore, it is seen that the first CT band discloses a vibrational structure at 80°K. The broad band in the 25—30 kK region is a local exci tation band associated mainly with the 25.9 kK transition of TCNNQ and partly with the 26.3 kK transition of anthracene.

Table 1. Wave numbers of absorption peaks in solution and crystal charge-transfer (CT) spectra of aromatic hydrocarbon-TCNNQ complexes (kK)

Donor molecule	Solution[a]	Crystal			
		Room temp.		Liq. N_2 temp.	
	CT	1 st CT	2 nd CT	1 st CT	2 nd CT
Anthracene	14.8	14.3	20.8	13.7	20.8
Pyrene	15.3	14.6	21.9	14.3	20.8
Phenanthrene	20.8	17.6	22.9	16.6	21.2
1,2-Benzanthracene	15.4	15.6	19.2	14.2	19.2
Chrysene	16.7	16.1	19.5	15.5	18.3
Triphenylene	21.7	18.5	21.6	18.1	21.3

a) Solvent: CH_2Cl_2. Only one CT band was observed in solution.

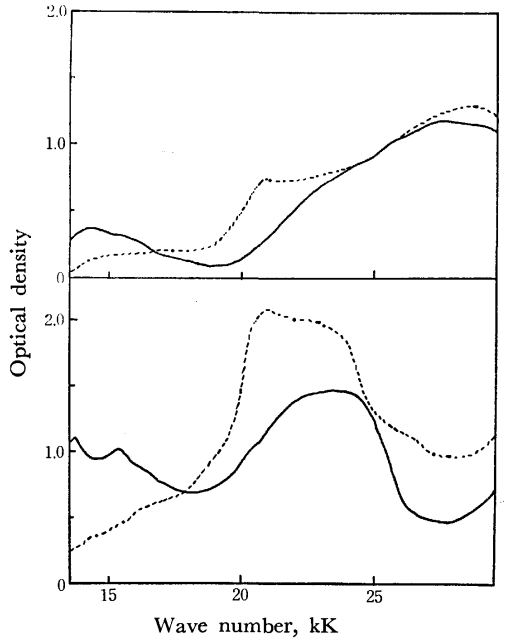

Fig. 5. Polarized absorption spectra of anthracene-TCNNQ complex at room temperature (above) and 80°K (below). Solid line: $//l$ spectrum; Broken line: $\perp l$ spectrum.

(b) Pyrene-TCNNQ (2 : 1) Complex: The 14.6 kK and 21.9 kK absorption bands are assigned to be the first and the second CT bands, respectively, since they are enhanced in intensity at low temperature. The polarization ratio is 3.6 for the first CT band and is 0.46 for the second CT band. The longest wavelength absorption spectrum of TCNNQ and other local excitation bands are to appear around at 25 kK and/or in the frequency region higher than 25 kK. At 80°K, the first and the second CT bands are displaced by 300 cm^{-1} and 1,100 cm^{-1}, respectively, to the red compared with those taken at room temperature. Here again the low temperature spectrum has clear vibrational structure.

(c) Phenanthrene-TCNNQ (2 : 1) Complex: The polarized spectra of this complex resemble those of the anthracene- and pyrene-TCNNQ complexes described above. The first CT band located at 17.6 kK is polarized parallel to the l-axis and the second CT band at 22.9 kK perpendicular to l. The observed polarization ratios are 2.4 for the former and 0.43 for the latter. At 80°K, vibrational structures become clearer in both bands, while their longest wavelength peaks corresponding probably to 0,0 transitions are shifted

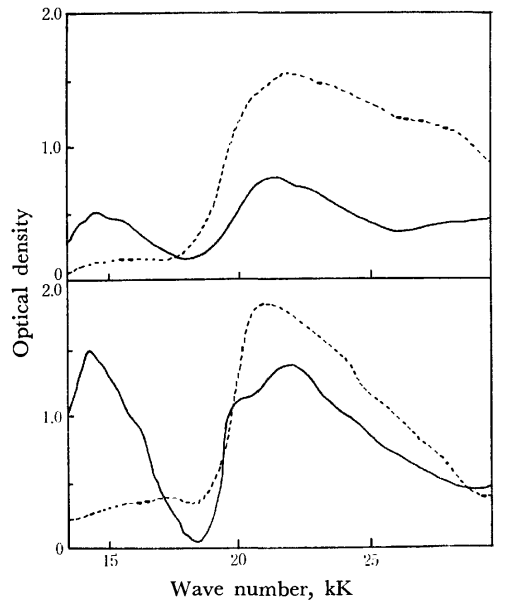

Fig. 6. Polarized absorption spectra of pyrene-TCNNQ complex at room temperature (above) and 80°K (below). Solid line: $//l$ spectrum; Broken line: $\perp l$ spectrum.

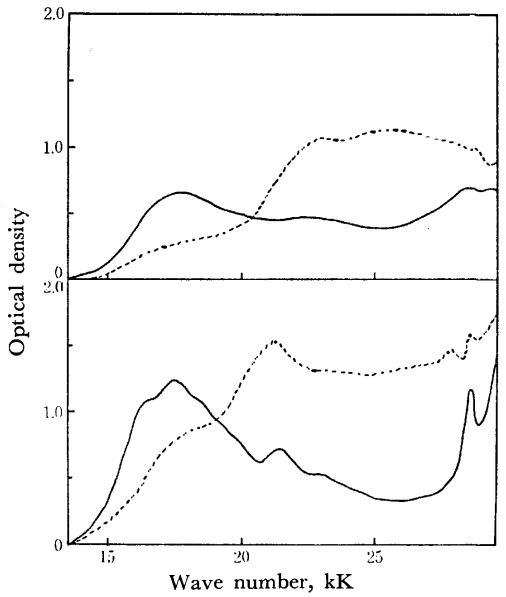

Fig. 7. Polarized absorption spectra of phenanthrene-TCNNQ complex at room temperature (above) and 80°K (below). Solid line: $//l$ spectrum; Broken line: $\perp l$ spectrum.

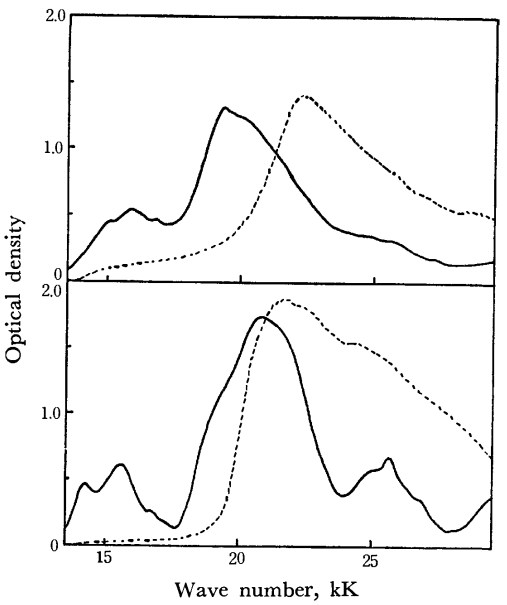

Fig. 8. Polarized absorption spectra of 1,2-benzanthracene-TCNNQ complex at room temperature (above) and 80°K (below). Solid line: $//l$ spectrum: Broken line: $\perp l$ spectrum.

to the red. The sharp absorption bands appearing around at 28.5 kK are due to phenanthrene.

(d) 1,2-Benzanthracene-TCNNQ (1 : 1) Complex: The spectrum of the complex is quite different from those three described above. The first and the second CT bands appear at 15.6 kK and 19.2 kK, respectively, both being polarized along the *l*-axis. At 80°K, the vibrational structure of the first CT band becomes clear-cut and the lowest frequency peak, probably a 0,0 band, is displaced by 1,400 cm^{-1} to the red. There has not frequently been observed an intermolecular CT spectrum that shows such a clear vibrational structure. On the other side, the lowest frequency peak of the second CT band appears as a shoulder of the corresponding band in the low-temperature spectrum, no spectral shift being observed.

Moreover, we have observed another absorption band which is polarized perpendicular to the *l*-axis and the absorption peak of which is located at 22.1 kK. The band is enhanced in intensity and displaced to the red by 500 cm^{-1} at 80°K. The band can not be attributed to any local excitation and is tentatively assigned to be the third CT band. The polarization ratio for this band is 0.61, while those for the first and the second CT bands are 5.2 and 3.9, respectively. Around at 25 kK, there appear the local excitation bands of 1,2-benzanthracene and TCNNQ.

(e) Chrysene-TCNNQ (1 : 1) Complex: The spectrum of the complex is rather broad in both polarization directions, parallel and perpendicular to the *l*-axis. The absorption shoulder at 16.1 kK can be assigned as the first CT band. The *l*-polarized spectrum has a peak at 19.5 kK which may be regarded as the second CT band. The polarization ratios are 2.2 and 1.2, respectively, for the first and the second CT bands. These broad bands become somewhat narrow at low temperature. The 16.1 kK shoulder is still not resolved well and shifted to 15.5 kK, while the 19.5 kK peak

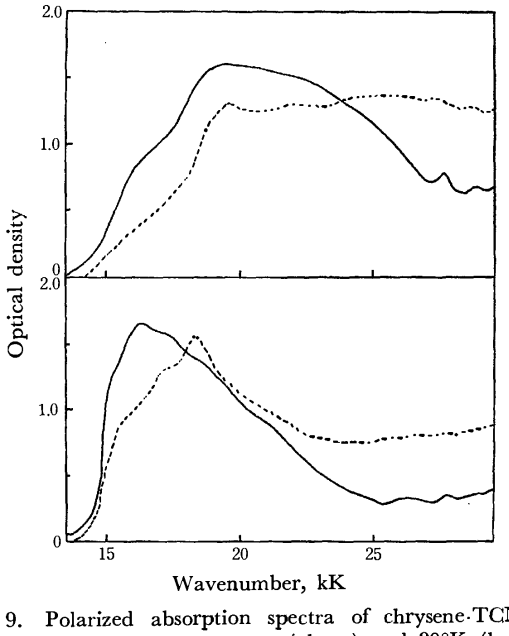

Fig. 9. Polarized absorption spectra of chrysene-TCNNQ complex at room temperature (above) and 80°K (below). Solid line: //*l* spectrum; Brolen line: ⊥*l* spectrum.

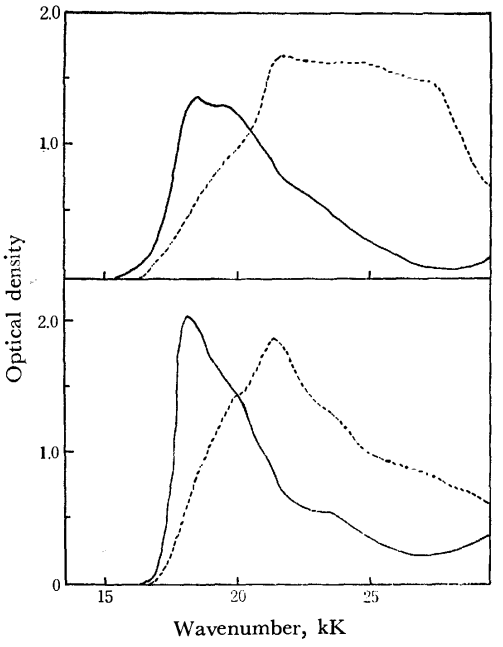

Fig. 10. Polarized absorption spectra of triphenylene-TCNNQ complex at room temperature (above) and 80°K (below). Solid line: //*l* spectrum; Broken line: ⊥*l* spectrum.

appears more clearly at 18.3 kK. The absorption band appearing around at 27 kK is evidently due to the local excitation associated with the *p*-band of chrysene (27.2 kK).

(f) Triphenylene-TCNNQ (1 : 1) Complex: The first CT band is found at 18.5 kK with an *l*-axis polarization and the second CT band at 21.6 kK with a polarization perpendicular to *l*. The broad absorption band in the 23—28 kK region is due to the local excitation associated with the TCNNQ transition and the 28.6 kK transition of triphenylene. At 80°K, both bands become considerably sharp, enhance their intensities, and shift to the red by 900 cm^{-1} and 300 cm^{-1}, respectively. The polarization ratios are 2.2 and 0.46, respectively, for the first and the second CT bands.

Discussion

Our previous calculation of the electronic spectrum of TCNNQ, assuming the molecule to be planar, has shown that in solution the 25.3 kK absorption band corresponds to the lowest B_2 transition polarized along the molecular longer axis and the weak 34.7 kK band to the next to the lowest A_1 transition polarized along the molecular short axis.[4] In the crystalline state, the bands are markedly intensified and broadened compared with the solution spectrum. The fact that the molecular structure of TCNNQ is non-planar in crystal puzzles us how to explain the observed crystal spectra and their polarization. Though a theoretical estimate of optically allowed exciton levels has to be carried out on the basis of the actual molecular structure, we may attribute the 33.8 kK (*a*-polarized) and 31.2 kK (*b*-polarized) bands in Fig. 3 to the two components of the 34.7 kK A_1 transition. The A_1 transition may be split and intensified through an interaction with

the strong B_2 transition. Similarly, the 33.6 kK (*c*-polarized) and 30.9 kK (*b*-polarized) bands appearing in the *bc*-face spectra (Fig. 4) may be attributed to the components of the same 34.7 kK transition. The broad bands in the 22—27 kK region in both the *ab*- and *bc*-face spectra are ascribed to the 25.3 kK B_2 transition of the free molecule.

Unlike the TCNQ- and TCNE-polycyclic aromatic hydrocarbon complexes, there exist two kinds of composition for the TCNNQ complexes as mentioned before, that is those of the mole ratios of donor to acceptor 2 : 1 and 1 : 1. Though the molecular sizes of Group 1 hydrocarbons are certainly smaller than those of Group 2 hydrocarbons, the difference in molecular size is not great enough to explain the existence of the two forms. A similar situation was found in some *p*-benzoquinone complexes.[5] This is probably due to the non-planar structure of the TCNNQ molecule, above and below which conditions for charge transfer interaction may be different.

As shown before, the TCNNQ molecular complexes studied exhibit two broad absorption bands, with the exception of the 1,2-benzanthracene-TCNNQ complex which shows three bands, in the spectral region where no local excitation band is expected to appear. We have assigned them to be the first and the second CT bands. In Group 1 complexes, the first CT bands are clearly polarized along the crystal elongated *l*-axes and the second CT bands are perpendicular to them. The two CT bands of Group 2 complexes, however, have both polarization components, except for the triphenylene-TCNNQ complex which exhibits polarization ratios of the first and the second CT bands quite similar to Group 1 complexes.

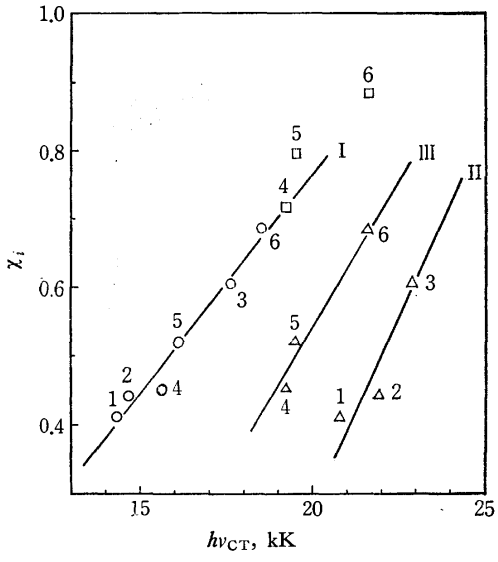

Fig. 11. Charge-transfer transition energies (room temperature) *vs* the Hückel molecular oribtal energy coefficients, χ_i, of the polycyclic aromatic donors. O: lst CT band, Δ: 2nd CT band; 1: anthracene, 2: pyrene, 3: phenanthrene, 4: 1,2-benzanthracene, 5: chrysene, 6: triphenylene-TCNNQ complexes. □ is a plot of 2nd CT band against 2nd HOMO energy of donor.

5) T. Amano, H. Kuroda, and H. Akamatu, This Bulletin, **42**, 671 (1969).

The wave numbers of the absorption maxima of the first and the second CT bands, $h\nu_{CT1}$ and $h\nu_{CT2}$, are plotted in Fig. 11 against the highest occupied molecular orbital (HOMO) energies of the corresponding polycyclic aromatic donors. The values of these HOMO energies are taken from the results of the Hückel molecular orbital calculations (the overlap integrals neglected)[7] and appear as χ_i on the ordinate of Fig. 11. Actual *i*th orbital energy is $\alpha+\chi_i\beta$ where α is the Coulomb integral for carbon and β is the carbon-carbon resonance integral. For the first CT bands, a straight line can be drawn (line I) as usual cases, so that these bands are most probably associated with the charge transfer from the HOMO of donor to the lowest vacant molecular orbital (LVMO) of acceptor. We have found that the energies of the first CT states of these complexes can be well expressed in terms of the ionization potentials, I_p, of the donor molecules as (in eV)

$$h\nu_{CT1} = 0.69\, I_p - 3.29.$$

The 25 kK band of TCNNQ, assigned to be the B_2 transition polarized along the molecular longer axis, appears as a local excitation band polarized perpendicular to the *l*-axis which coincides with the polarization direction of the first CT bands in all Group 1 complexes. The donor molecules and TCNNQ are therefore supposed to be alternately stacked along the *l*-axis in Group 1 complex crystals.

A plot of $h\nu_{CT2}$ *versus* the HOMO energy of donor products two linear relationships, Line II for Group 1 complexes and Line III for Group 2 complexes. The charge transfer mechanism for the second CT bands of these complexes may, therefore, be divided into two classes depending upon the mole ratio of donor to acceptor. A current explanation for the origin of a second CT band is that the band is mainly associated with a charge transfer from the second HOMO of a donor molecule to the LVMO of an acceptor molecule.[7] If we assume such a charge transfer mechanism for Group 1 complexes, the magnitude of $h\nu_{CT2}$ turns out to be in the order anthracene—pyrene—phenanthrene, which is entirely in the reverse order compared with the present observation.

We tentatively conclude, therefore, that the second CT bands of Group 1 complexes may be associated mainly with the charge transfer from the HOMO of donor to the *second* LVMO of acceptor. A similar explanation was given by Iwata, Tanaka, and Nagakura for the 1,2,4,5-tetracyanobenzene-aromatic donor complexes.[8] As they pointed out, Line II should be drawn parallel with Line I in Fig. 11, if a simple relationship is assumed for both first and second CT

$$h\nu_{CT} = I_p - E_A - C$$

bands. Here E_A is the electron affinity for the lowest and/or the second lowest vacant orbital of acceptor and C the sum of several terms including electrostatic

6) C. A. Coulson and A. Streitwieser, Jr., "Dictionary of π-Electron Calculations", W. H. Freeman and Co., San Francisco (1965).

7) H. Kuroda, I. Ikemoto, and H. Akamatu, This Bulletin, **39**, 1842 (1966) and subsequent papers.

interaction energy, which may be supposed to be approximately constant for a given acceptor. The reason why this is not the case is just uncertain.

On the other side, a plot $h\nu_{CT2}$ of Group 2 complexes against the second HOMO energy of donor (the squares drawn in Fig. 11) suggests that there is a roughly linear relationship between them. Thus in this case, we can not exclude the possibility of a charge transfer from the second HOMO of donor. Our tentative conclusion is that the second CT bands of Group 2 complexes may be due to a mixed charge transfer mechanism, one from the HOMO of donor to the second LVMO of acceptor and the other from the second HOMO of donor to the LVMO of acceptor.

As mentioned before, the second CT band in each crystal spectrum is polarized in the direction almost perpendicular to the polarization direction of the corresponding first CT band. This fact suggests that the donor molecule and TCNNQ are alternately and slantly stacked along the *l*-axis so that charge transfer can occur in two directions, almost parallel and perpendicular to the *l*-axis.

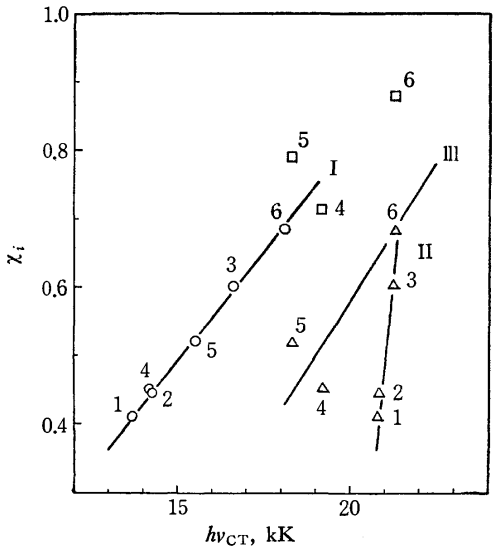

Fig. 12. Charge-transfer transition energies (80°K) *vs.* the Hückel molecular oribtal energy coefficients, χ_i, of the polycyclic aromatic donors. Symbols are the same as in Fig. 11.

The data taken at 80°K are plotted in Fig. 12 in exactly the same manner of Fig. 11. It is seen that the linear relationship for the first CT bands holds more precisely than in the room-temperature data. Line I of Fig. 12 is in parallel with Line I of Fig. 11 and is displaced to the red by 700 cm^{-1} compared with the latter. Line II strongly suggests that the second CT bands of Group 1 complexes are due to the charge transfer from the HOMO of donor to the second LVMO of acceptor, but the situation that its slope is so steep is again puzzling. Plots of $h\nu_{CT2}$ of Group 2 complexes against the HOMO energy of donor (triangles in Fig. 12) and the second HOMO energy of donor (squares in Fig. 12) both deviate considerably from linearity. Rather the datum for the triphenylene-TCNNQ complex seems to join with those for Group 1 complexes, namely Line II. Originally the crystal spectra of the triphenylene-TCNNQ complex taken at room temperature and at 80°K resemble those of Group 1 complexes in regard to their polarizations.

Thus the low-temperature data clearly support our conclusion on the charge transfer mechanism of these complexes obtained from the room-temperature data. On the other side, we can not say anything in detail about the polarization and intensity of these CT bands since the crystal structures of these complexes have not been analysed. Specifically, it is hard to understand that the intensity of each CT spectrum is as large as that of the strong TCNNQ local excitation. A series of studies along such requests is being planned, together with a theoretical estimate of optically allowed exciton levels of the TCNNQ crystal.

This work was supported in part by a grant of Ministry of Education.

8) S. Iwata, J. Tanaka, and S. Nagakura, *J. Amer. Chem. Soc.*, **88**, 894 (1966).

9) G. Briegleb, "Elektronen-Donator-Acceptor-Komplexe", Springer-Verlag, Berlin-Göttingen-Heidelberg (1961), p. 75.

Light-scattering Studies of the Interaction of Sodium Chondroitin Sulfate C with Bovine Serum Albumin[1)]

Masayuki NAKAGAKI and Yoh SANO

Faculty of Pharmaceutical Sciences, Kyoto University, Sakyo-ku, Kyoto

(Received September 29, 1971)

Angular light-scattering investigations were carried out in 0.01 M sodium chloride solutions at 25°C for various mixed solutions of bovine serum albumin (BSA) and chondroitin sulfate (Chs). The experimental values of molecular weight and of the molecular dimensions showed an entirely different tendency from the calculated values, and we may assume that there is no interaction between them. It has, therefore, been concluded that Chs interacts with BSA strongly and that a complex is formed between them. For the soluble complex thus formed, the number of the bound BSA molecules with one Chs molecule was expressed by a Langmuir-type equation as a function of the amount of excess BSA existing free in the solution. When the latter was sufficiently large, the number of bound BSA molecules per Chs molecule approached 20.6.

A Zimm plot of the complex was drawn, and the molecular weight, the radius of gyration, and the second virial coefficient of the complex were determined. It has been concluded from these results that the complex molecule has a long-like shape; the length was about 30% longer, but the diameter was about 6 times thicker, than the Chs molecule at the maximum binding of BSA.

Chondroitin sulfate, one of natural acid mucopolysaccharides composes the primary part of the cartilage, together with collagen-like protein, and is present in the skin or in other connective tissues as mucoproteins, playing important physiological functions. Since the acid mucopolysaccharides are anionic polyelectrolytes, their protein complexes are bound primarily by polar linkages. The interaction between chondroitin sulfate and bovine serum albumin has been studied by quite a few workers.[2-11)] It seems, however, that is studies reported thus far have been little connected with the complexes themselves. Soluble complexes formed between chemically-different macromolecular species have recently come under investigation, but the angular light scattering of solutions containing the soluble complexes[12-14)] has not yet been studied very extensively. In the present paper, the interaction between bovine serum albumin and chondroitin sulfate will be discussed on the basis of the experimental results obtained by the light-scattering technique and the binding coefficient, *i.e.*, the binding ratio of protein to chondroitin sulfate; the molecular shape and size of the soluble complex will also be reported.

Experimental

Materials and Solvents. The sodium chondroitin sulfate (hereafter called Chs) used in this work was of the C type; it was extracted so carefully that it contained no electrolyte except, sometimes, sodium chloride. This sample is the same as that investigated by Nakagaki and Ikeda[15)] by the light-scattering technique in various ionic strengths. For the purpose of the experiments, a stock solution of about 1% was prepared, kept in a refrigerator at 4°C, and used after dilution if necessary. The stock solution was made up a fresh and kept for less than three days because of the denaturation of the sample. Bovine serum albumin (hereafter called BSA) was that made by Armour Co., Ltd., (Fraction V, No. G5717, D. 1029). Much as in the case of Chs, a stock solution of about 1% was prepared and diluted if necessary. The reduced scattering intensity of this sample did not change when it was left as long as 30 hr at 25°C. The water used here was distilled, refined by the use of ion-exchange resin, and distilled again with an all-glass still. Concentrations were corrected for the water content in the sample. The water content necessary for this correction was determined by drying in a vacuum over P_2O_5 at 60°C for two days.

Refractive Index Increment. The refractive index increment (dn/dc) was measured by means of a Shimadzu electrophotometric differential refractometer at 25°C. Measurements were carried out using unpolarized light from a mercury arc (100 V, 85 W), with a spectrum filter whose wavelength was 4360 Å. The instrument constant was obtained by using a standard solution of potassium chloride, whose concentration was 0.01483 g/ml; the value of (dn/dc) of 0.1344 was taken from the literature.[16)] The potassium chloride used was a reagent-grade commercial product dried in a vacuum at about 200°C for more than six hours. The refractive index increments obtained were 0.1535 for Chs and 0.1935 for BSA. The value for Chs agreed with that reported by Nakagaki and Ikeda[15)] for the same sample. The value for BSA agreed well with

1) This paper was presented at the 22nd Colloquy on Colloid and Interface Chemistry, Sendai, November, 1969.

2) E. Gorteg and L. Nanninga, *Proc. Koninkl. Nederl. Acad. Wettenschappen*, Series., **55**, 341 (1952).

3) E. Gorteg and L. Nanninga, *Discuss. Faraday Soc.*, **13**, 205 (1953).

4) J. Badin and M. Schubert, *J. Clin. Invest.*, **34**, 1312 (1955).

5) P. Bernfeld, J. S. Nisselbaum, B. J. Berkeley, and R. W. Hanson, *J. Biol. Chem.*, **235**, 2852 (1960).

6) A. J. Anderson, *Biochem. J.*, **88**, 460 (1963).

7) E. Gramling, W. Niedermeir, H. L. Holly, and W. Pigman, *Biochem. Biophys. Acta*, **69**, 552 (1963).

8) A. J. Anderson and C. H. Slack, *Clin. Sci.*, **26**, 97 (1964).

9) A. Klemer, K. Homberg, and D. Mernpel, *Z. Naturforsch.*, **196(10)**, 961 (1964).

10) S. M. Partrige, *Federation Proc.*, **25(3)**, 994 (1966).

11) S. M. Partrige, "Chem. Physiol. Mucopolysaccharides, Proc. Symp. Milar." (1965) p. 51.

12) E. P. Geiduschek and P. Doty, *Biochem. Biophys. Acta*, **9**, 609 (1952).

13) I. J. Heilweil and Q. V. Winkle, *J. Phys. Chem.*, **59**, 944 (1955).

14) F. Sokol, *J. Polymer Sci.*, **30**, 581 (1958).

15) M. Nakagaki and K. Ikeda, *This Bulletin.*, **43(3)**, 555 (1968).

16) A. Kruis, *Z. Phys. Chem.*, **34B**, 13 (1936).

those of the references.[13,17,18] For mixed solutions of Chs and BSA, the value of the refractive increment obtained by direct determination for each mixture was used for the calculation of the apparent molecular weight.

Light-scattering measurements. The apparatus used in this investigation was a Shimadzu electrophotometric light-scattering photometer, PG-21 type. All the measurements were performed with unpolarized light with a wavelength of 4360 Å in a vacuum and at 25°C, the temperature being kept constant by circulating thermostatted water. The apparatus constant was calibrated on the basis of the value, $R_{90°}=48.5\times10^{-6}$, for the reduced scattering intensity of dust-free benzene at a 90° angle. The benzene was a commercial product of a reagent grade. It was dried with Drynap (an alloy of sodium metal and lead; weight ratio, 1 : 10; specific gravity, 6.4; mp, 368°C),[20-22] distilled twice by means of an all-glass still, and filtered directly into the cylindrical glass cell for light-scattering measurements through a Cella Filter (Mitter, Sartorius Co., Ltd.). The correction of the illuminated volume was done by using a fluorescein solution which had been optically clarified with Membrane Filter No. 15 (Sartorius Co., Ltd.) under pressure. The solutions and the solvent for the light-scattering measurements were optically clarified as well with the same mebrance filter.

All the light-scattering measurements were done over the range of scattering angles between 35°—135° for solutions of BSA, Chs, and their mixtures in various mixing ratios, γ, (gBSA/gChs), in a 0.01 M sodium chloride solutions as a solvent.

$$\gamma = c_{BSA}/c_{Chs} \tag{1}$$

where c_{BSA} and c_{Chs} are concentrations (g/ml) of BSA and Chs respectively. After the solutions had been made up by the dilution of stock solutions, these solutions were kept at 4°C in the refrigerator until the light-scattering experiments were carried out the next day. Dust-free solution were obtained in the way described above. In order to avoid errors due to the temperature difference and due to the existence of tiny bubbles, the scattering intensities were read about an hour after setting.

Density measurements. All the measurements were done with a picnometer of about 35 ml at 25°C. The water was used directly after distillation.

Results

Light Scattering. The results of the light-scattering measurements were analyzed according to the well-known equation:

$$\frac{Kc}{R_\theta} = \frac{K'\phi^2 c}{R_\theta} = \frac{1}{M}\left\{1+\left(\frac{16\pi^2 n_0^2}{3\lambda_0^2}\right)R_g^2\sin^2\left(\frac{\theta}{2}\right)\right\} + 2A_2c \tag{2}$$

where R_θ is the reduced scattering intensity of the solution in an excess over the solvent at the scattering angle, $\theta°$, c is the weight concentration of the polymer, (g/ml), M is the weight-average molecular weight of the polymer, and K' is the optical constant given by the following equation:

$$K = K'\phi^2, \quad K' = 2\pi^2 n_0^2/\lambda_0^4 N_A, \quad \phi = dn/dc \tag{3}$$

where ϕ is the refractive index increment of the solution, λ_0 is the wavelength in a vacuum (the value used in this experiment being 4360 Å), n_0 is the refractive index of the solvent, N_A is Avogadro's number, R_g^2 is the mean square radius of gyration, and A_2 is the second virial coefficient of the system.

In order to obtain the values of the weight-average molecular weight, M, the mean square radius of gyration, R_g^2, and the second virial coefficient, A_2, according to Eq. (2), the experimental data were plotted according to the so-called Zimm plot method, taking Kc/R_θ and $\sin^2(\theta/2)+100c$ on the ordinate and the abscissa respectively.

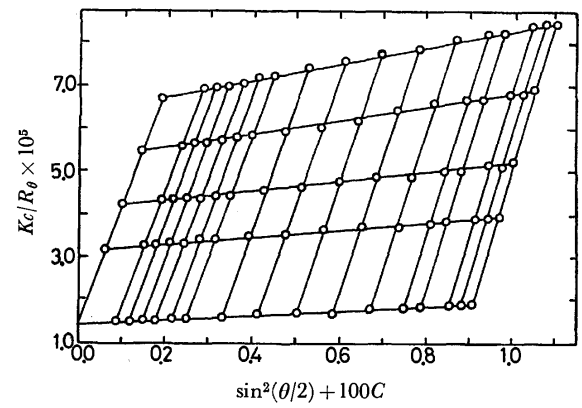

Fig. 1. Zimm plot for sodium chondroitin sulfate C (Chs) in 0.01 M NaCl at 25°C, pH 5.56.

Figure 1 shows the Zimm plot of Chs in 0.01 M sodium chloride (pH=5.56). The apparent weight-average molecular weight thus obtained was 70900. The values of the apparent mean square radius of gyration and the apparent second virial coefficient, as well as the molecular weight, agreed well with those obtained independently by Nakagaki and Ikeda[15] for the same sample. Figure 2 shows the Zimm plot of BSA in 0.01 M sodium chloride (pH=5.00). The molecular weight obtained from this was 71900; this value was in good agreement with the value found in the lite-

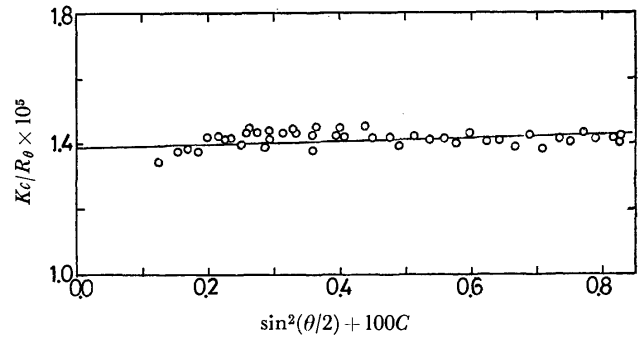

Fig. 2. Zimm plot for bovine serum albumin (BSA) in 0.01 M NaCl at 25°C, pH 5.40

17) G. E. Perlmann and L. G. Longsworth, *J. Amer. Chem. Soc.*, **70**, 2719 (1948).
18) M. Halwer, G. C. Nutting, and B. A. Brice, *ibid.*, **73**, 2786 (1951).
19) C. L. Carr, Jr., and B. H. Zimm, *J. Chem. Phys.*, **18**, 1616 (1950).
20) R. A. Edge and G. W. Fomles, *Anal. Chim. Acta*, **32**, 191 (1965).
21) K. Tabei, H. Hiranuma, and N. Amemiya, This Bulletin., **39**, 1085 (1966).
22) K. Tabei and K. Naton, *ibid.*, **39**, 2300 (1966).

rature.[23] In the case of the mixed solutions of BSA and Chs, the scattering intensity was measured and the data were tentatively analyzed, at first, according to Eq. (2) by assuming them to be solutions of one solute whose weight concentration was equal to the sum of the two components. The apparent values of the molecular weight, the radius of gyration, and the second virial coefficient thus obtained were further examined theoretically as two-solute systems. All the experiments were carried out at concentrations between 3.5×10^{-3} and 5×10^{-4} g/m*l* in the total of the two solutes. Within this concentration range, the light-scattering data could be extrapolated without any difficulty.

Figure 3 (a), (b), and (c) are examples of the Zimm plot for the mixing ratios of $\gamma=12.9$, 24.4, and 101 respectively. As is shown in Fig. 3, the Zimm plot changed its shape and became narrower with an increase in the mixing ratio, γ. The Zimm plot at low γ-values was similar to that of Chs, while the Zimm plot at γ-values higher than 35.2 was similar to that of BSA.

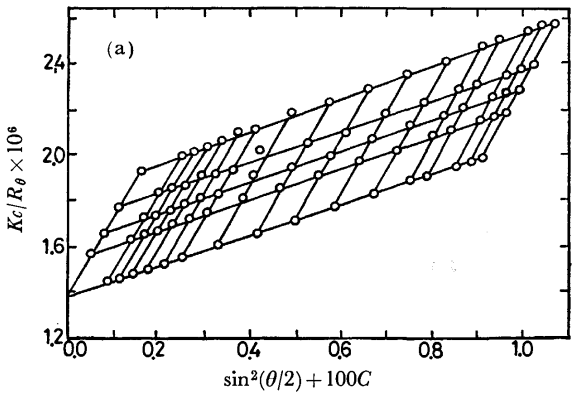

Fig. 3(a)

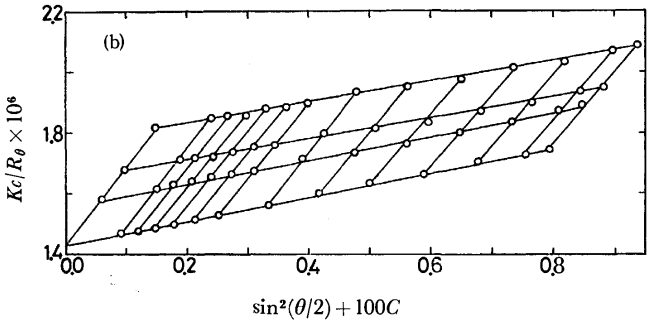

Fig. 3(b)

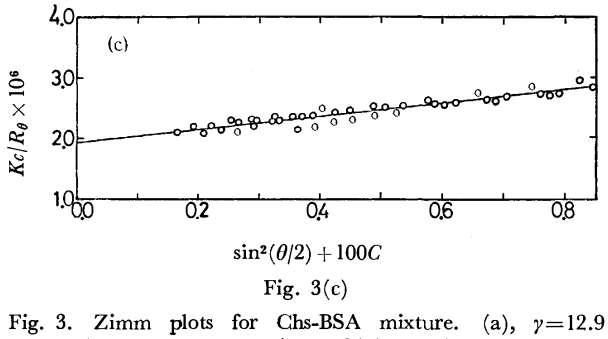

Fig. 3(c)

Fig. 3. Zimm plots for Chs-BSA mixture. (a), $\gamma=12.9$ gBSA/gChs, pH 5.62; (b), $\gamma=24.4$ gBSA/gChs, pH 5.83; (c), $\gamma=101$ gBSA/gChs, pH 5.56. All measurements were carried out at 25°C, in 0.01 M NaCl.

23) J. T. Edsall, H. Edelhoch, R. Lontie, and P. R. Morrison, *J. Amer. Chem. Soc.*, **72**, 464 (1950).

The apparent values of the weight-average molecular weight, the second virial coefficient, and the radius of gyration, M_{app}, R_{gapp}, and A_{2app} respectively, obtained from these Zimm plots according to Eq. (2) are plotted against the mixing ratio, γ, in Fig. 4 for the region of rather low mixing ratios. The dotted curves are the calculated ones, which will be explained later.

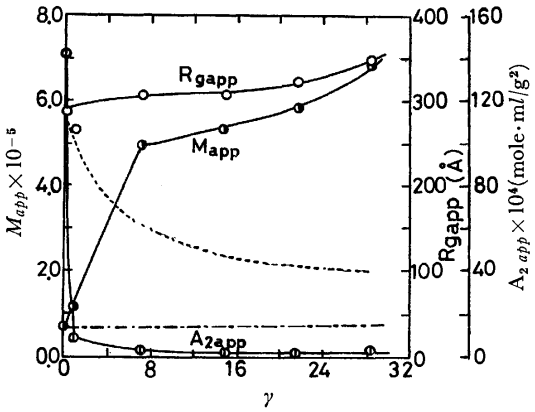

Fig. 4. Apparent molecular weight, M_{app}(◑), apparent radius of gyration, R_{gapp}(○), and apparent second virial coefficient, $A_{2\,app}$(ⓘ), obtained from BSA-Chs mixture of various mixing ratio, γ (gBSA/gChs)
◑,ⓘ,○: experimental values
– – – – theoretical curve of molecular weight for Chs-BSA system caluclated by equation (10)
------- theoretical curve of radius of gyration for Chs-BSA system calculated by equation (11)

It may be seen from this figure that the apparent molecular weight increases appreciably with the mixing ratios. It can further be seen from Fig. 4 that the apparent second virial coefficient decreases remarkably with the increase in the mixing ratio. In the region of the higher mixing ratios, that is, in the region of the higher BSA content, the apparent molecular weight has its maximum, as is shown in Fig. 5, where the mole fraction of BSA, X_{BSA}, is on the abscissa in place of the mixing ratio, γ. The mole fraction of BSA in the total solute, X_{BSA}, is related to by Eq. (4):

$$X_{BSA}=\frac{\gamma M_{Chs}}{M_{BSA}+\gamma M_{Chs}} \tag{4}$$

where M_{BSA} and M_{Chs} are the weight-average molecular weights for BSA and Chs respectively.

Density. The measurements of the density for the mixed solutions were carried out with a picnometer at 25°C. The values of the partial specific volume, V_{app}, of the mixed solute were calculated, they are plotted against the mole fraction of BSA in Fig. 6. It can be seen that the apparent partial specific volume increases linearly with the mole fraction of BSA. The value of the partial specific volume of Chs was 0.4448 m*l*/g. This value agrees well with the value obtained independently by Nakagaki and Ikeda.[15]

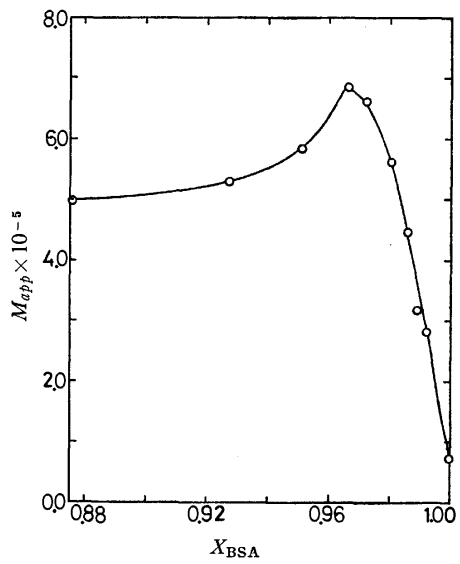

Fig. 5. Apparent molecular weight, M_{app}, plotted against mole fraction of BSA, X_{BSA}.

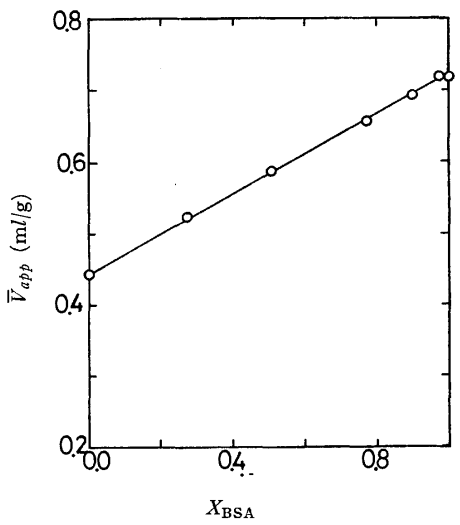

Fig. 6. Apparent partial specific volume, $\bar{V}_{app}$, (ml/g), plotted against mole fraction of BSA, X_{BSA}.

On the other hand, the partial specific volume of the native BSA was 0.7165 ml/g. This value agrees reasonably well with those values listed in the literature.[24-26]

Discussion

Binding of BSA on Chs Molecules. For the light scattering of a solution containing z macromolecular components, the following equation has been derived by Zimm,[27] by Stockmayer,[28,29] and by Blum and Morales[30,31] according to the theory of the fluctuation of the chemical potentials;

$$\frac{R_\theta}{K'c_t} = \sum_{i=1}^{i=z} M_i P_i(\theta) w_i \phi_i^2 - 2c_t \sum_{i=1}^{i=z} \sum_{j=1}^{j=z} A_2^{(ij)} M_i M_j P_i(\theta) P_j(\theta) w_i w_j \phi_i \phi_j \quad (5)$$

where R_θ is the reduced scattering intensity of the solution containing z macromolecular components and where $P_i(\theta)$ is the interference factor of the i-th macromolecular component and is approximately given by the following equation:

$$P_i(\theta) = 1 - \frac{16\pi^2 n_0^2}{3\lambda_0^2} Rg_i^2 \sin^2\left(\frac{\theta}{2}\right) \quad (6)$$

$A_2^{(ij)}$ is the second virial coefficient describing the interaction between the i-th and j-th components, w_i is the weight fraction of the i-th component in the total solute, and c_t is the total weight concentration (g/ml) for the mixed solution. Here,

$$c_t = \sum_{i=1}^{i=z} c_t \quad (7)$$

and

$$w_i = c_i/c_t \quad (8)$$

where c_t is the weight concentration of the ith macromolecular component.

Since the second term of Eq. (5) is smaller than the first term, Eq. (5) can be written as follows by using Eq. (6), in which the second term is again assumed to be smaller than the first:

$$\frac{K'c_t}{R_\theta} = \frac{1}{\sum_{i=1}^{i=z} M_i w_i \phi_i^2} \left\{ 1 + \frac{16\pi^2 n_0^2}{3\lambda_0^2} \left(\frac{\sum_{i=1}^{i=z} M_i w_i \phi_i^2 Rg_i^2}{\sum_{i=1}^{i=z} M_i w_i \phi_i^2} \right) \times \sin^2\left(\frac{\theta}{2}\right) \right\} + 2c_t \frac{\sum_{i=1}^{i=z} \sum_{j=1}^{j=z} A_2^{(ij)} M_i M_j P_i(\theta) P_j(\theta) w_i w_j \phi_i \phi_j}{\left(\sum_{i=1}^{i=z} M_i P_i(\theta) w_i \phi_i^2 \right)} \quad (9)$$

By comparing Eq. (9) with Eq. (2), the following equations can be obtained for a mixed solution of two macromolecular solutes described by the subscripts 1 and 2:

$$M_{app} = (M_1 w_1 \phi_1^2 + M_2 w_2 \phi_2^2)/\phi^2 \quad (10)$$

$$R_{gapp}^2 = (R_{g1}^2 M_1 w_1 \phi_1^2 + R_{g2}^2 M_2 w_2 \phi_2^2)/M_{app}\phi^2 \quad (11)$$

Here, M and R_g in Eq. (2) are replaced by M_{app} and R_{gapp} respectively. The results calculated according to these equations, assuming no interaction between Chs and BSA, that is, by setting 1=Chs and 2=BSA, are shown in Fig. 4 by dotted curves. It may be seen that the experimental values show an entirely different tendency from the calculated curves. This means that the chondroitin sulfate molecules interact with the BSA molecules strongly and that a complex is formed between them.

24) P. G. Squire, P. Moser, and C. T. O' Konski, *Biochemistry*, **7**(**12**), 4261 (1968).
25) C. Tanford, K. Kawahara, and S. Lapanje, *J. Amer. Chem. Soc.*, **89**(**4**), 729 (1967).
26) A. Ullman, M. E. Goldberg, D. Perrin, and J. Monod, *Biochemistry*, **7**(**1**), 261 (1968).
27) B. H. Zimm, *J. Chem. Phys.*, **16**, 1093 (1948).
28) W. H. Stockmayer, *ibid.*, **18**, 58 (1950).
29) J. G. Kirkwood and R. J. Goldberg, *ibid.*, **18**, 54 (1950).
30) J. J. Blum and M. F. Morales, *J. Chem. Phys.*, **20**, 1822 (1952).
31) J. J. Blum and M. F. Morales, *Arch. Biochem. Biophys.*, **43**, 208 (1952).

From Figs. 4 and 5, it can be seen that, with an increase in the mixing ratio, the apparent molecular weight and the apparent radius of gyration increase, while the apparent second virial coefficient decreases remarkably. These results suggest the formation of a complex between BSA and Chs by the following chemical equation:

$$(\text{Chs}) + \delta_m(\text{BSA}) \rightarrow (\text{Chs})\cdot(\text{BSA})_{\delta m}$$

If the affinity between Chs and BSA is strong, the complex is formed to as great an extent as one of these components is mostly used up. In this instance, the concentration of the component is negligibly small, so that the system can be considered to be a solution of two macromolecular solutes for which Eqs. (10) and (11) are applicable. By using these equations, the possibility that either Chs and BSA remains in excess after the complex formation has been examined. To explain the experimental data satisfactorily, it has been concluded that a part of the BSA is left free in the solution and that many BSA molecules are bound on one Chs molecule ($\delta_m > 1$). Equations (10) and (11) can be used, in this case also, by setting 1=complex (to be designated by the subscript m) and 2=free BSA (to be designated by the superscript f). The following equation:

$$M_{app} = [w_{\text{Chs}}M_{\text{Chs}}(\phi_{\text{Chs}} + \phi_{\text{BSA}}\delta)^2 + (w_{\text{BSA}} - w_{\text{Chs}}\delta)M_{\text{BSA}}\phi_{\text{BSA}}{}^2]/\phi^2 \quad (12)$$

can be deriven from Eq. (10) by using the following obvious relations:

$$M_m = M_{\text{Chs}}(1+\delta) = M_{\text{Chs}} + \delta_m M_{\text{BSA}} \quad (13a)$$

$$w_m = w_{\text{Chs}}(1+\delta) \quad (13b)$$

$$w_{\text{BSA}}{}^f = w_{\text{BSA}} - \delta w_{\text{Chs}} \quad (13c)$$

$$\delta = \delta_m M_{\text{BSA}}/M_{\text{Chs}} \quad (13d)$$

together with the Geiduschek-Doty equation:[12]

$$\phi_m = (\phi_{\text{Chs}} + \delta\phi_{\text{BSA}})/(1+\delta) \quad (14)$$

The weight-binding coefficient, δ, can be obtained according to Eq. (12) by using the experimental values of M_{app} and of all other quantities. As a result, it has been concluded that the value of δ increases with the mixing ratio, γ. The molar binding coefficient, δ_m, thus obtained is shown in Fig. 7 as a function of the molar ratio of free BSA, $\gamma_m{}^f$, relative to the molar concentration of Chs.

$$\gamma_m{}^f = (M_{\text{Chs}}/M_{\text{BSA}})\gamma - \delta_m \quad (15)$$

An equation of the same form as Langmuir's adsorption isotherm is often used to describe the amount of binding of a low-molecular-weight substance to macromolecules as a function of the equilibrium concestration of the latter.[32] A similar equation can be expected to be used as well in the case of complex formation between two macromolecular substances. In our case, the number of molecules, δ_m, of BSA bound on one molecule of Chs may be given by the following equation:

$$\delta_m = \delta_m{}^\infty \frac{k\,\gamma_m{}^f}{1 + k\,\gamma_m{}^f} \quad (16)$$

where the constant, k, indicates the strength of adsorption and where $\delta_m{}^\infty$ is the saturated molar binding coefficient.

On the basis of the linear relationship between $\gamma_m{}^f/\delta_m$ *vs.* $\gamma_m{}^f$, which is expected from Eq. (16) and which is shown in Fig. 7 by a dotted line, the parameter values, $\delta_m{}^\infty = 20.6$ and $k = 0.255$, were obtained. The solid curve in Fig. 7 shows the values calculated from Eq. (16) by using these parameter values. From this, it can be seen that the agreement between experimental and calculated values is good and that the maximum number of BSA molecules to be bound to a Chs molecule is about 21.

Since a Chs molecule consists of 145 disaccharide units, according to the observed value of its molecular weight, it may be concluded that, at saturation, one BSA molecule is bound to about seven disaccharide residues.

Zimm Plot of the Complex Molecules. Since it has been concluded in the preceding section that a complex and excess (free) BSA exist in the mixed solution of Chs and BSA, the next step is to obtain the reduced scattering intensity of the complex, $R_{\theta m}$, by subtracting the contribution of free BSA from the total reduced scattering intensity, and to attempt to draw a Zimm plot of the complex. The reduced scattering intensity of the complex may be calculated from the experimental data by the following equation, because the second virial coefficient of BSA is almost zero, as is shown in Fig. 2:

$$R_{\theta m} = R_\theta - K' c_{\text{BSA}}{}^f M_{\text{BSA}} \phi_{\text{BSA}}{}^2 P_{\text{BSA}}(\theta) \quad (17)$$

The Zimm plot may be analyzed according to the following equation, which has the same form as Eq. (2):

$$\frac{K'\phi_m{}^2 c_m}{R_{\theta m}} = \frac{1}{M_m}\left\{1 + \left(\frac{16\pi^2 n_0{}^2}{3\lambda_0{}^2}\right) R_{g_m}{}^2 \sin^2\left(\frac{\theta}{2}\right)\right\} + 2A_{2m}c_m \quad (18)$$

Here, ϕ_m has been given by Eq. (14). Finally, it

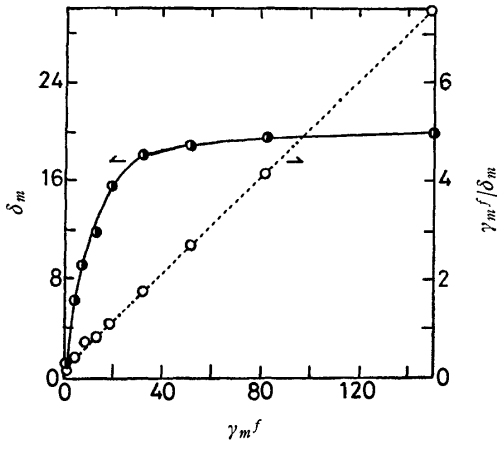

Fig. 7. Molar binding coefficient, δ_m, plotted against molar ratio of free BSA, $\gamma_m{}^f$ (BSA/Chs). The broken line is Langmuir plot of equation 16, where $\gamma_m{}^f/\delta_m$ is plotted against $\gamma_m{}^f$.

32) M. Nakagaki, N. Koga, and H. Terada, *Nippon Yakugaku Zasshi*, **83**(**6**), 586 (1963); *ibid.*, **84**(**6**), 516 (1967); *ibid.*, **86**(**6**), 447 (1966); M. Nakagaki and H. Terada *ibid.*, **87**(**7**), 817 (1967); *ibid.*, **87**(**8**), 980 (1967); *ibid.*, **87**(**9**), 1089 (1967).

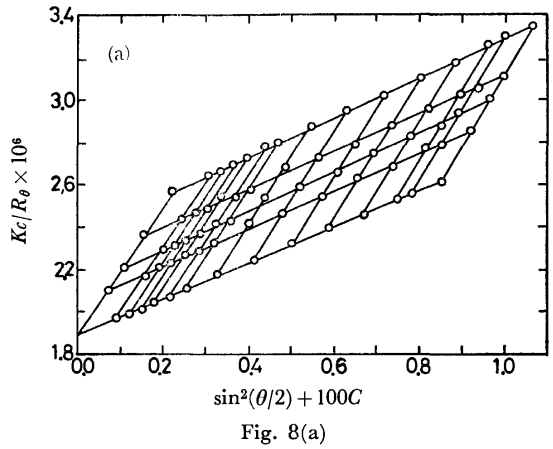

Fig. 8(a)

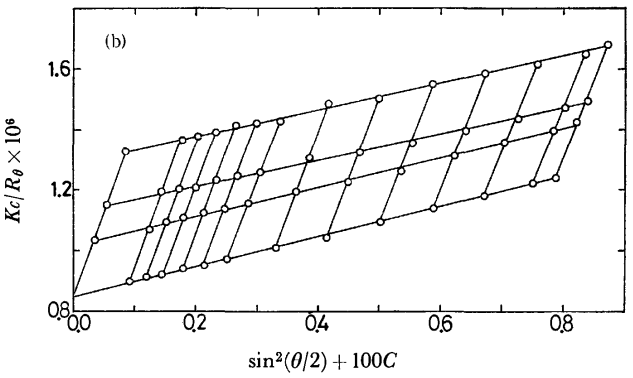

Fig. 8(b)

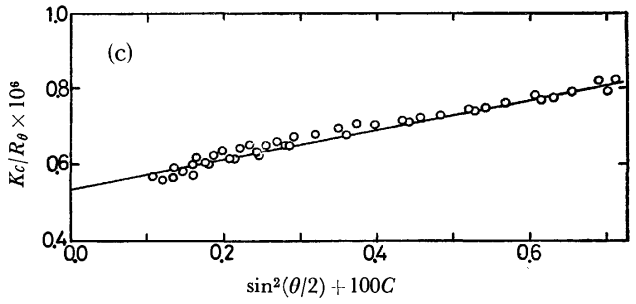

Fig. 8(c)

Fig. 8. Zimm plots for BSA-Chs complex molecule calculated from Fig. 3. Curves (a), (b), and (c) correspond to curves (a), (b) and (c) in Fig. 3.

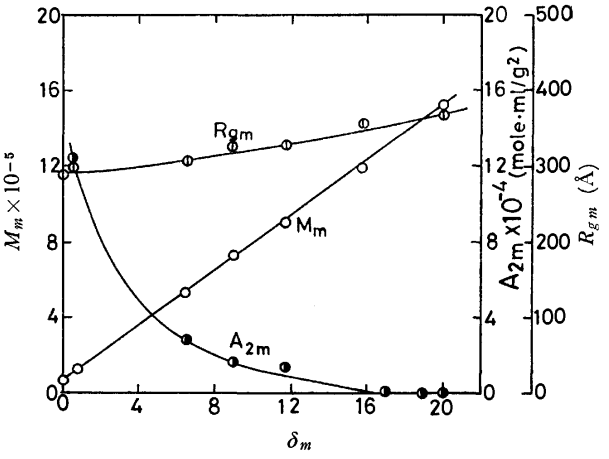

Fig. 9. Molecular weight, M_m(○), radius of gyration, R_{gm} (◫) and second virial coefficient, A_{2m}(◑) for BSA-Chs complex molecule against molar binding coeffient, δ_m, in 0.01 M NaCl at 25°C.

should be mentioned that the A_{2m} term in Eq. (18) is not the second virial coefficient of the complex itself, but contains the contribution due to the interaction between the complex and the free BSA.

Examples of the results are shown in Fig. 8, which corresponds to Fig. 3. The molecular weight, M_m; the radius of gyration, R_{gm}, and the second virial coefficient, A_{2m}, for the complex are plotted against the molar binding coefficient, δ_m, in Fig. 8. It can be seen that M_m increases remarkably and linearly with δ_m but that R_{gm} increases only slightly, while A_{2m} decreases rapidly and approaches the value of BSA alone ($A_{2BSA}=0$).

It is natural that the molecular weight of the complex, M_m, increases linearly with δ_m, as is to be expected from Eq. (13a). The molecular weight of the bound BSA, calculated from the inclination of the straight line of Fig. 9, is 72000, which is in good agreement with the molecular weight of native BSA, M=71900, already cited.

On the other hand, R_{gm} value for the complex is almost equal to R_{gapp} for the mixed solutes, as is clear from a comparison between Figs. 4 and 9, because R_g obtained from the light-scattering measurements is z-average and the radius of gyration of the free BSA is very small. Moreover, the length of the complex molecules seems to be nearly equal to that of Chs itself, because the value of R_g does not increase very much with δ_m. Finally, the second virial coefficient for the complex decreases rapidly with δ_m. This indicates that the electric charges of the Chs are shielded by the binding of BSA molecules. Therefore, it can be concluded that the complex molecule has as its core the chondroitin sulfate molecule, with its surface covered with BSA molecules.

Shape and Size of the Complex Molecule. The shape and size of the complex molecule will be discussed. The chondroitin sulfate is an unbranched linear anionic polyelectrolyte and is stretched extensively by the electrostatic repulsive force if the polyions have a low ionic strength. It is, however, known that the polyions gradually contract with the increase in the ionic strength because of the formation of ionic pairs or because of electrostatic shielding effect of the ionic atmosphere. Nakagaki and Ikeda[15] found, from their viscosity and the light-scattering investigations, that the polyion of chondroitin sulfate is a long rod-like shape which is, at an infinite ionic strength, about 800 Å in long and about 10 Å in diameter. The shape of the complex molecule may be assumed to be almost the same as that of chondroitin sulfate, because the radius of gyration does not change very much. Therefore, the complex molecule is assumed to be a rod-like molecule.

The radius of gyration, R_{gm}, and the volume, V_m, of a rod-like molecule are expressed as follows:

$$R_{gm}^2 = L_m^2/12 + D_m^2/8 \quad (19)$$

$$V_m = \pi(D_m/2)^2 L_m \quad (20)$$

According to these equations, the diameter, D_m, and the length, L_m, of the complex can be calculated, ignoring the solvation, from the value of the radius of gyration and the value of the partial specific volume of the complex.

The partial specific volume of the complex, $\overline{V}_m$, is calculated from Eq. (21), which is based on an additivity rule, as is generally assumed:

$$\overline{V}_{app} = \overline{V}_m w_m + \overline{V}_{BSA} w_{BSA}{}^f \quad (21)$$

Further, the value of the molecular volume of the complex, $M_m\overline{V}_m/N_A$, can be calculated from the data already shown in Fig. 6 according to Eq. (22). The results are plotted against the molar binding coefficient, δ_m, in Fig. 10. This figure shows that the volume of the Chs molecule does not change with the binding of BSA and also that the volume of a bound BSA is 0.862×10^5 (Å^3/molecule), which is 0.7212 m*l*/g in the partial specific volume. The partial specific volume of the native BSA, on the other hand, is 0.7165 m*l*/g. There is a reasonably good agreement between these values and those listed in the literature.[24-26] As has been mentioned above, the length and the diameter of the complex molecule can, therefore, be calculated, according to Eqs. (19) and (20), from the experimental values of $\overline{V}_m$ and

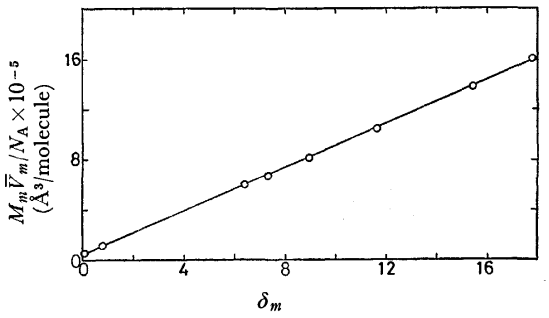

Fig. 10. Partial molar volume per complex molecule, $M_m\overline{V}_m/N_A$, (Å^3/molecule) plotted against molar binding coefficient, δ_m.

R_{gm} if the density in the complex molecule is assumed to be homogeneous. The results obtained are shown in Table 1. It may be seen that the length increases about 20 percent as compared with the Chs molecule, while the diameter increases about five times, upon the binding of BSA.

In contradistinction to the assumption of a homogenous density in complex molecules, if the molecule has a structure in which the core of the Chs molecule with a density of ρ_{Chs} is surrounded by BSA molecules with a density ρ_{BSA}, and if the complex molecule as a whole is assumed to be a rigid prolate spheroid with major axis a and minor axis b, the radius of gyration of the complex will be given by:

$$R_{gm}^2 = \frac{\left(\frac{a^2+2b^2}{5}\right)\rho_{BSA}\left(\frac{4}{3}\pi ab^2\right)+(\rho_{Chs}-\rho_{BSA})\frac{\pi}{4}D_{Chs}^2L_{Chs}\left(\frac{L_{Chs}^2}{12}+\frac{D_{Chs}^2}{8}\right)}{\rho_{BSA}\left(\frac{4}{3}\pi ab^2\right)+(\rho_{Chs}-\rho_{BSA})\frac{\pi}{4}D_{Chs}^2L_{Chs}} \quad (22)$$

$$V_m = \frac{4}{3}\pi ab^2 \quad (23)$$

According to Eqs. (22) and (23), the length of the two axes, $2a$ and $2b$, can be calculated from the experimental values of the radius of gyration and the partial specific volume by assuming that the Chs core has the same length, L_{Chs}, and the same diameter, D_{Chs}, as free Chs molecules. The results thus obtained are shown in Table 1.

If the complex molecule is assumed to be a rigid rod which has a Chs core, much like the structure of the prolate spheroid considered above, the length, L', and the diameter, D', of the complex molecule can be calculated in the same way:

$$R_{gm}^2 = \frac{\left(\frac{L'^2}{12}+\frac{D'^2}{8}\right)\rho_{BSA}\left(\frac{\pi}{4}D'^2L'\right)+(\rho_{Chs}-\rho_{BSA})\frac{\pi}{4}D_{Chs}^2L_{Chs}\left(\frac{L_{Chs}^2}{12}+\frac{D_{Chs}^2}{8}\right)}{\rho_{BSA}\left(\frac{\pi}{4}D'^2L'\right)+(\rho_{Chs}-\rho_{BSA})\frac{\pi}{4}D_{Chs}^2L_{Chs}} \quad (24)$$

Table 1. Molecular dimensions of the complex molecule between chondroitin sulfate C and bovine serum albumin at various molar binding coefficient

δ_m	0	0.707	6.404	8.895	11.628	15.455	20.360
	(rigid rod-like molecule of a uniform density)						
L_m	998	1039	1068	1130	1126	1227	1278
D_m	8.0	12.2	27.1	32.0	36.7	36.7	46.1
	(a prolate ellipsoid of revolution which is considered for a different density between Chs and BSA)						
$2a$		959.2	978.2	1036	1032	1125	1162
$2b$		15.0	18.6	38.6	44.0	48.2	55.2
	(rod-like molecule which is considered for a different density between Chs and BSA)						
L'		1180	1096	1152	1143	1241	1279
D'		11.0	26.3	29.9	34.1	37.5	42.9

These results are also shown in Table 1.

The results shown in Table 1 are in fairly good agreement with each other, irrespective of the model. It seems, at any rate, that the complex molecule has a long, deformed shape. In these models, the prolate spheroid is the most suitable to explain the results of viscosity measurements, as will be published elsewhere.

The authors are indebted to Dr. Kiyoshi Ikeda and Mr. Kenichi Sugimori for their helpful advice on this work.

BULLETIN OF THE CHEMICAL SOCIETY OF JAPAN, VOL. 45, 1018—1021 (1972)

The Polarized Absorption Spectra of Some α-Aminoanthraquinones

Hiroyasu INOUE, Toshihiko HOSHI,* Junko YOSHINO,* and Yoshie TANIZAKI**

Department of Applied Chemistry, Faculty of Technology, Kanagawa University, Kanagawa-ku, Yokohama
**Department of Chemistry, College of Science and Engineering, Aoyama Gakuin University, Chitosedai, Setagaya-ku, Tokyo*
***Department of Chemistry, Faculty of Science, Tokyo Institute of Technology, Meguro-ku, Tokyo*

(Received October 5, 1971)

The π–π^* electronic absorption spectra of 1-amino-, 1,4-diamino-, and 1,4,5,8-tetraaminoanthraquinones were investigated by means of the polarized absorption spectra using stretched PVA sheets and theoretical calculations. Each of these compounds has four absorption bands in the near-ultraviolet region (210—340 nm) and one in the visible region. The bands of the aminoanthraquinones which appear in the visible region can be assigned to the intramolecular charge-transfer transitions associated with the charge migration from the amino group to the carbonyl groups.

In a previous paper,[1] the polarized absorption spectra of sodium anthraquinonesulfonates were measured in stretched PVA sheets, and the polarization directions of the bands of anthraquinone and its sulfonates were discussed. It has been found that anthraquinone has four π–π^* absorption bands above 220 nm. The positions and the polarization directions of the bands are as follows; 324 nm (x-polarization), 272 nm (y-), 252 nm (x-), and about 249 nm (y-), where the y- and x-axes are, respectively, parallel and perpendicular to the C=O bond axis of the molecule.

It has been established that the substituted anthraquinones with electron-donating groups, such as hydroxyl or amino groups, have bands in the visible region.[2,3] For instance, Kuboyama and Wada[2] have measured the absorption spectra of several hydroxyanthraquinones; the visible band of each hydroxyanthraquinone corresponded to the 324 nm band of anthraquinone. Labhart[3] has measured the polarized absorption spectra of several aminoanthraquinones under an external electric field and has determined the polarization direction of each band. According to his results, the visible band at 564 nm of 1,4-diaminoanthraquinone is polarized along the x-axis of the molecule.

In the present paper, the electronic absorption spectra of 1-aminoanthraquinone, 1,4-diaminoanthraquinone, and 1,4,5,8-tetraaminoanthraquinone were studied by means of the polarized absorption spectra using stretched PVA sheets and of theoretical calculations.

Method of Calculation

The method of the calculation was the same as that in our previous works,[4–6] that is, the Pariser-Parr-Pople method[7–9] with a variable β approximation. The resonance integrals, β_{rs}'s, were adjusted at every iteration of the SCF calculations by means of the following equations:

$$\beta_{CC} = -1.84 - 0.51p_{CC}$$
$$\beta_{CN} = -2.02 - 0.53p_{CN}$$
$$\beta_{CO} = -2.20 - 0.56p_{CO}$$

where p_{rs} is a bond order between the r and s atoms. The valence-state ionization potentials, $I_p(r)$'s, and the electron affinities, $E_a(r)$'s, for carbon, nitrogen, and oxygen atoms were taken as:

$$I_p(C) = 11.42\ \text{eV}, \quad E_a(C) = 0.58\ \text{eV}$$
$$I_p(N) = 25.00\ \text{eV}, \quad E_a(N) = 10.0\ \text{eV}$$
$$I_p(O) = 17.32\ \text{eV}, \quad E_a(O) = 2.65\ \text{eV}.$$

The geometries of anthraquinone and its derivatives are shown in Fig. 1, in which the interatomic distances in the anthraquinone skeleton are taken from the results of the X-ray analysis by Sen[10]; all the valence angles are assumed to be 120°.

1) H. Inoue, T. Hoshi, and Y. Tanizaki, *Nippon Kagaku Zasshi*, **92**, 501 (1971).
2) A. Kuboyama and K. Wada, This Bulltin **39**, 1874 (1966).
3) H. Labhart, *Chimia*, **15**, 20 (1961).
4) H. Inoue, T. Hoshi, T. Masamoto, J. Shiraishi, and Y. Tanizaki, *Ber. Bunsenges. Physik. Chem.*, **75**, 441 (1971).
5) T. Hoshi, H. Inoue, J. Shiraishi, and Y. Tanizaki, This Bulltin, **44**, 1743 (1971).
6) H. Inoue, T. Nakamura, and T. Igarashi, *ibid.*, **44**, 1469 (1971).
7) R. Pariser and R. G. Parr, *J. Chem. Phys.*, **21**, 466, 767 (1953).
8) J. A. Pople, *Proc. Phys. Soc.*, **A68**, 81 (1955).
9) K. Nishimoto and L. S. Forster, *Theor. Chim. Acta*, **3**, 407 (1965).
10) S. N. Sen, *Indian J. Phys.*, **22**, 347 (1948).

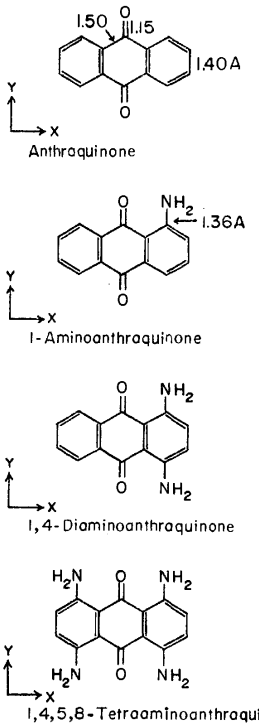

Fig. 1. The geometries of the molecules.

Experimental

Materials. All the anthraquinone derivatives used here were offered by Dr. Kou Naiki of the Tokyo Institute of Technology. The PVA (polyvinyl alcohol) powder used for the preparation of the sheets was obtained commercially (Nippon Gosei Co., Ltd., NM-14) and was used without further purification.

Measurements of the Polarized Absorption Spectra. The polarized absorption spectra using stretched PVA sheets were measured by the method already described.[1]

Notations. $D_{\parallel}$ and $D_{\perp}$: absorbances measured with the incident light polarized, respectively, parallel and perpendicular to the stretched direction of the PVA sheet. *Rd*: ratio between $D_{\parallel}$ and $D_{\perp}$, $D_{\parallel}/D_{\perp}$. R_s: degree of stretching of the sheet. θ: orientation angle, which indicates the angle between a transition moment and the orientation axis of a molecule.

Results and Discussion

The absorption spectra of 1-amino-, 1,4-diamino-, and 1,4,5,8-tetraaminoanthraquinone are shown in Fig. 2, in which the spectrum of anthraquinone is also shown for the sake of comparison. As has been described in a previous paper,[1] anthraquinone has four absorption bands, at 324 nm, 272 nm, 252 nm, and about 230 nm, which are polarized along the *x*-, *y*-, *x*-, and *y*-axes respectively, where the *x*- and *y*-axes are respectively perpendicular and parallel to the C=O bond axis of the molecule. In the case of the aminoanthraquinones studied here, there are four absorption bands in the near-ultraviolet region and one in the visible region. The former four bands may correspond to those of anthraquinone described above.

Figure 3 shows the polarized absorption spectra of 1-aminoanthraquinone in the stretched PVA sheets.

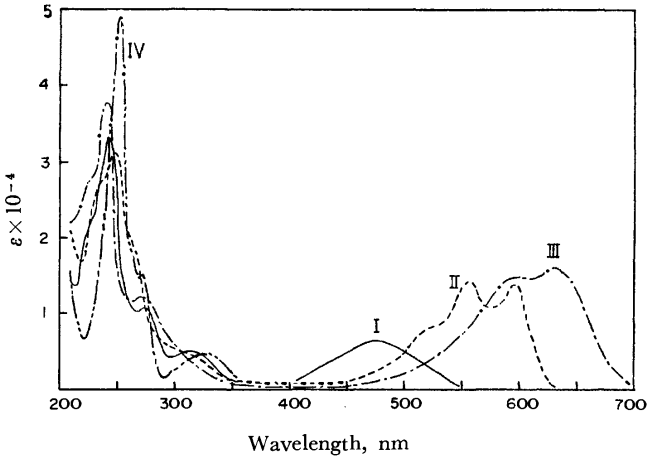

Fig. 2. The absorption spectra of 1-aminoanthraquinone (I), 1,4-diaminoanthraquinone (II), 1,4,5,8-tetraaminoanthraquinone (III), and anthraquinone (IV) in ethanol.

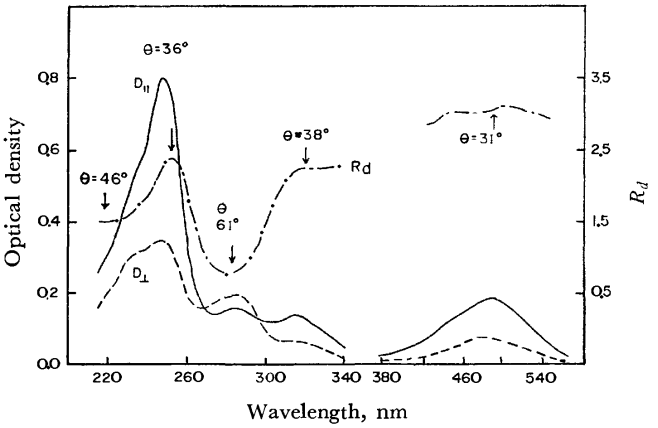

Fig. 3. The polarized absorption spectra of 1-aminoanthraquinone. (R_s=5.8)

From the behavior of the R_d curve, it is clear that the absorption spectrum of this compound consists of five bands in the observed wavelength region. They appear at 490 nm, 315 nm, 282 nm, 248 nm, and 235 nm; the orientation angles of these bands are 31°, 38°, 61°, 36°, and 46° respectively. As has been predicted above, the latter four bands can correspond to those of anthraquinone, because the behavior of the R_d curve in the region of 210—340 nm (Fig. 3) is very similar to that of anthraquinone.[1] A band corresponding to the 490 nm band of 1-aminoanthraquinone is not observed in the case of anthraquinone. The polarization direction of the 490 nm band seems to be almost parallel to those of the 315 nm and 248 nm bands.

These experimental results are compared with the theoretical ones in Table 1. From the comparison of the observed positions of the bands, the relative intensities, and the orientation angles with the theoretical results, the observed bands at 490 nm, 315 nm, 282 nm, 248 nm, and 235 nm can assigned to the calculated transitions, I, II, IV, VII, and VIII respectively. From the polarized absorption spectra obtained using stretched PVA sheets, we can not determine the precise polarization direction of each band unless the orien-

Table 1. The calculated results for 1-aminoanthraquinone

	Transition energy				Oscillator strength	Polarization direction against x-axis
	Calcd		Obsd		Calcd	Calcd
	eV	(nm)	eV	(nm)		
I	3.06	(405)	2.53	(490)	0.2222	3°
II	3.97	(313)	3.90	(315)	0.0528	2°
III	3.99	(311)			0.0028	−41°
IV	4.40	(282)	4.40	(282)	0.1224	−80°
V	4.59	(270)			0.0923	63°
VI	4.73	(262)			0.4501	80°
VII	5.08	(244)	5.00	(248)	0.5546	−5°
VIII	5.35	(232)	5.28	(235)	0.1882	−89°
IX	5.47	(227)			0.2416	16°
X	5.63	(220)			0.1397	87°
XI	5.74	(216)			0.3919	−20°
XII	6.05	(205)			0.0463	70°

Table 2. The relative polarization directions against the polarization direction of the 490 nm band

	Relative polarization	
	Obsd	Calcd
the 314 nm band	7°	1°
the 282 nm band	92°	97°
the 248 nm band	5°	8°
the 235 nm band	77°	88°

tation axis of the molecule is known. However, the relative polarization directions between two bands may be given by the sum or remaider of the two orientation angles.[11] Thus, the relative polarization directions in relation to the polarization direction of the 490 nm band are found to be as is shown in Table 2. These results are in good agreement with those of the theoretical calculations.

Figure 4 shows the polarized absorption spectrum of 1,4-diaminoanthraquinone. It is clear that this molecule has five absorption bands, at 600 nm, 320 nm, 280 nm, 255 nm, and 235 nm, and that their orientation angles are 34°, 52°, 58°, 41°, and 51° respectively. Since this molecule seems to belong to the C_{2v} point group, each π–π^* electronic transition should

11) If the directions of the transition moments of two bands of a molecule are represented by $\overrightarrow{AA'}$ and $\overrightarrow{BB'}$, the relative polarization direction between the two bands is expressed by $\angle AOB'$ or $\angle AOB$. The former angle ($\angle AOB'$) is given by the sum of two orientation angles ($\angle AOC + \angle COB'$), whereas the latter angle ($\angle AOB$) is given by the difference between the two orientation angles ($\angle BOC - \angle AOC$), where $\overrightarrow{CC'}$ represents the orientation axis of the molecule.

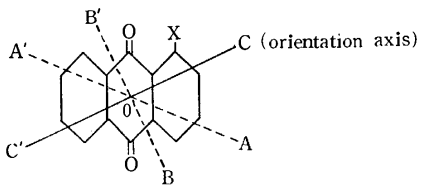

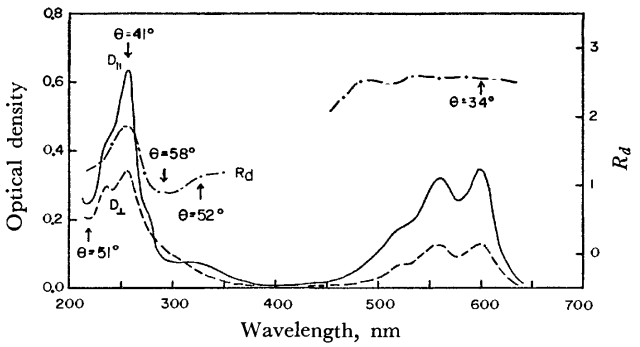

Fig. 4. The polarized absorption spectra of 1,4-diaminoanthraquinone. (R_s=5.1)

be polarized along the x- or y-axis of the molecule. As in the case of the anthraquinonesulfonates described in a previous paper, the x-axis of this molecule is preferentially oriented in the stretched direction of the PVA sheet; this implies that the R_d values of the x-axis polarized bands are larger than those of the y-axis polarized ones. Therefore, it is found that the 600 nm, 320 nm, and 255 nm bands are polarized along the x-axis, and the 280 nm and 235 nm bands, along the y-axis. The 600 nm band may consists of a single electronic band, since this band is isolated from the other bands; the R_d values of this band are almost constant. The sum of the orientation angles of the 600 nm and the 280 nm bands is nearly a right angle (92°), so the 280 nm band may be regarded as being almost pure, whereas the 320 nm and 255 nm bands are overlapped with other ones respectively, because the orientation angles of these bands are smaller than that of the 600 nm band.

These experimental results are compared with the calculated results in Table 3. The observed 600 nm, 320 nm, 280 nm, 255 nm, and 235 nm bands can be assigned to, respectively, the calculated transitions I, III, V, IX, and XI.

The polarized absorption spectrum of 1,4,5,8-tetra-

Table 3. The calculated results for 1,4-diaminoanthraquinone

	Transition energy				Oscillator strength	Polarization direction against x-axis
	Calcd		Obsd		Calcd	Calcd
	eV	(nm)	eV	(nm)		
I	2.59	(479)	2.07	(600)	0.3062	0° (x)
II	3.77	(329)			0.0041	90° (y)
III	4.00	(310)	3.88	(320)	0.0330	0° (x)
IV	4.18	(297)			0.0062	0° (x)
V	4.20	(295)	4.43	(280)	0.0198	90° (y)
VI	4.48	(277)			0.2614	90° (y)
VII	4.67	(266)			0.0120	90° (y)
VIII	4.94	(251)			0.6774	90° (y)
IX	5.11	(243)	4.86	(255)	0.6270	0° (x)
X	5.39	(230)			0.2231	0° (x)
XI	5.66	(219)	5.28	(235)	0.1534	90° (y)
XII	5.94	(209)			0.1895	0° (x)
XIII	5.99	(207)			0.0947	90° (y)

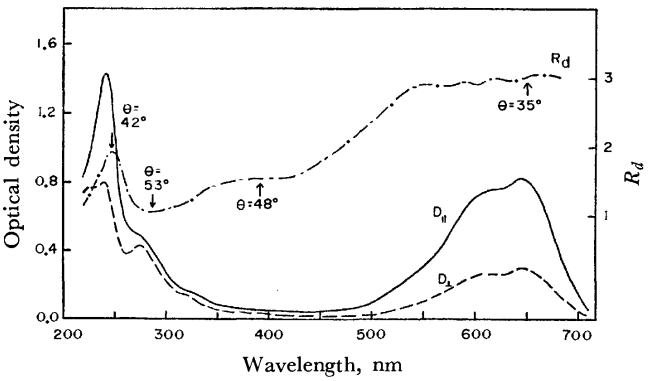

Fig. 5. The polarized absorption spectra of 1,4,5,8-tetraaminoanthraquinone. (R_s=9.6)

Table 4. The calculated results for 1,4,5,8-aminoanthraquinone

	Transition energy				Oscillator strength	Polarization direction against x-axis
	Calcd		Obsd		Calcd	Calcd
	eV	(nm)	eV	(nm)		
I	2.48	(501)	1.92	(645)	0.5058	0° (x)
II	2.88	(430)			0.0000	
III	3.71	(334)			0.0000	
IV	4.12	(301)			0.0000	
V	4.14	(300)			0.0155	90° (y)
VI	4.31	(288)			0.0000	
VII	4.36	(285)	3.82	(325)	0.0005	0° (x)
VIII	4.72	(263)	4.51	(275)	0.7761	90° (y)
IX	4.85	(256)			0.0000	
X	5.18	(239)	5.39	(230)	0.6934	90° (y)
XI	5.27	(235)			0.0000	
XII	5.38	(230)	5.06	(245)	0.9103	0° (x)
XIII	5.64	(220)			0.0000	

aminoanthraquinone is shown in Fig. 5. From the features of the absorption and R_d curves, in this case also, the absorption bands corresponding with those of the above compounds are found at 645 nm (x-axis polarized), 325 nm (x), 275 nm (y), 245 nm (x), and 230 nm (y).

The calculated results are tabulated in Table 4. The observed 645 nm (x), 325 nm (x), 275 nm (y), 245 nm (x), and 230 nm (y) bands are assigned to, resectively, the calculated transitions I, VII, VIII, XII, and X.

As has been described above, the electronic spectra of aminoanthraquinones consist of four bands in the near-ultraviolet region and one in the visible region; the former four bands correspond well to those of anthraquinone.

Table 5 shows the first excited state wave functions,

Table 5. The first excited state wave functions of 1-amino-, 1,4-diamino-, and 1,4,5,8-tetraaminoanthraquinone

1-Aminoanthraquinone

$$\Psi_I=0.0054\phi_{5,10}+0.0407\phi_{5,11}-0.0100\phi_{5,12}-0.0226\phi_{5,13}-0.0149\phi_{5,14}+0.0435\phi_{6,10}-0.0043\phi_{6,11}+0.0344\phi_{6,12}+0.0069\phi_{6,13}-0.0054\phi_{6,14}+0.0189\phi_{7,10}+0.0497\phi_{7,11}+0.0108\phi_{7,12}-0.0762\phi_{7,13}+0.0116\phi_{7,14}-0.0684\phi_{8,10}-0.0795\phi_{8,11}+0.0042\phi_{8,12}+0.1389\phi_{8,13}-0.0074\phi_{8,14}-0.9535\phi_{9,10}+0.0844\phi_{9,11}+0.1667\phi_{9,12}-0.0412\phi_{9,13}-0.0054\phi_{9,14}$$

1,4-Diaminoanthraquinone

$$\Psi_I=0.0643\phi_{6,12}-0.0617\phi_{6,14}-0.0361\phi_{7,11}-0.0334\phi_{7,13}+0.0076\phi_{7,15}+0.0106\phi_{8,12}-0.0446\phi_{8,14}-0.0395\phi_{9,12}+0.1134\phi_{9,14}-0.9777\phi_{10,11}+0.1302\phi_{10,13}-0.0136\phi_{10,15}$$

1,4,5,8-tetraaminoanthraquinone

$$\Psi_I=0.0773\phi_{8,14}-0.0735\phi_{9,14}-0.0907\phi_{10,16}-0.1580\phi_{11,15}+0.9774\phi_{12,13}-0.0111\phi_{12,17}$$

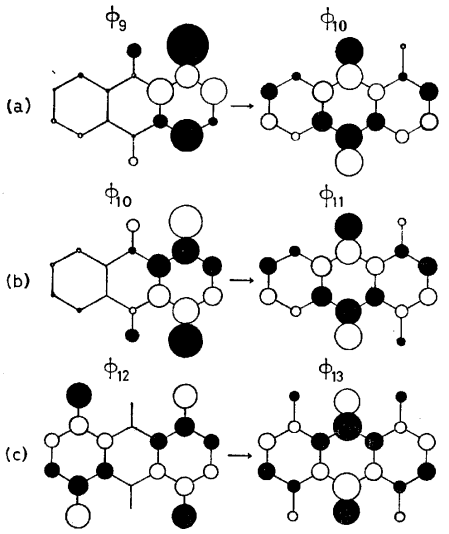

Fig. 6. The coefficients for the MO's.
(a): 1-aminoanthraquinone, (b): 1,4-diaminoanthraquinone, (c): 1,4,5,8-tetraaminoanthraquinone

Ψ's, of 1-amino-, 1,4-diamino-, and 1,4,5,8-tetraaminoanthraquinone. The Ψ_1 of 1-aminoanthraquinone can be approximately represented by $\phi_{9,10}$; that of 1,4-diaminoanthraquinone, by $\phi_{10,11}$, and that of 1,4,5,8-tetraaminoanthraquinone, by $\phi_{12,13}$. The coefficients of the wave functions associated with these configurations are shown pictorially in Fig. 6. From this figure, it may be concluded that the transitions, I, of these compounds are to be assigned to the intramolecular charge-transfer transitions from the amino groups to the carbonyl groups.

Symmetry Rule for Predicting Bond Distortions in Conjugated Hydrocarbons

Takeshi NAKAJIMA, Azumao TOYOTA, and Sadao FUJII

Department of Chemistry, Faculty of Science, Tohoku University, Sendai

(Received October 5, 1971)

A symmetry rule for predicting molecular shapes which is based on the second-order Jahn-Teller effect has been applied to the predictions of bond distortions in a number of nonalternant hydrocarbons in their ground and electronically excited states. In spite of the very crude approximation that only the lowest-lying excited state plays a dominant role in determining the energetically most favorable nuclear displacement, a fairly clear-cut criterion for molecular-symmetry reduction was obtained. The actual types of the most soft bond distortions, determined by examining the two-center components of transition densities, are in good agreement with the results of variable bond-length SCF MO calculations and available experimental results. The problem of symmetry reductions possible in large cyclic polyenes $C_{4n+2}H_{4n+2}$ is briefly discussed.

A symmetry rule for predicting molecular structures has recently been developed by Pearson,[1-3] Salem,[4] and Bartell.[5] The rule is based on the second-order or pseudo Jahn-Teller effect, and follows the earlier work by Bader.[6,7] The symmetries of the ground state and the lowest excited state(s) determine which kind of nuclear motion occurs most easily in the ground state of a molecule. The rule has proved remarkably successful in predicting the stable molecular shapes of inorganic and small organic molecules. Symmetry rules have also been used to predict the course of chemical reactions by Bader,[7] Salem and Wright,[8] and Pearson.[9]

In this paper we consider the application of the symmetry rule to the prediction of the geometrical structures of conjugated π-electron systems. We deal, in particular, with the problem of molecular-symmetry reduction and double-bond fixation in the nonalternant hydrocarbons.[10]

On the basis of the second-order perturbation theory, Binsch *et al.*[11-15] have recently developed a general theory of double-bond fixation in conjugated systems. The symmetry rule is based also on the second-order perturbation theory, but it provides a more intelligible way of predicting the double-bond fixations and of understanding the origin of bond distortions in conjugated systems.

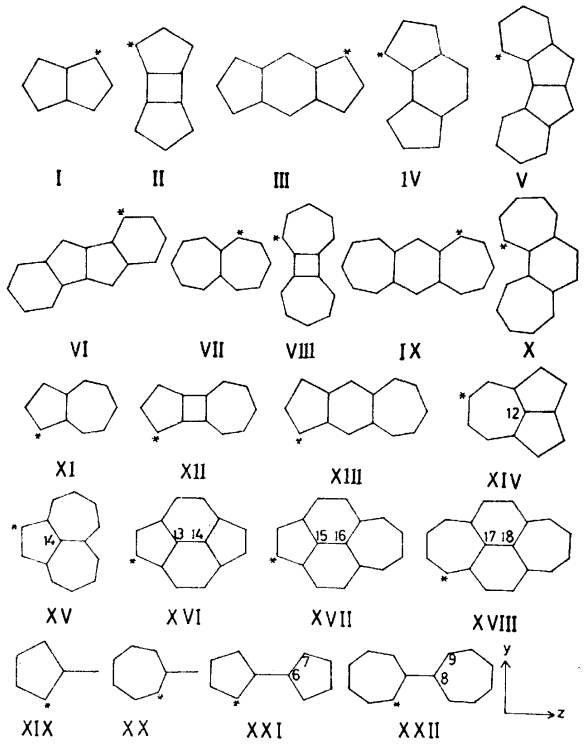

Fig. 1. Numbering of atoms and choice of axes in nonalternant hydrocarbons. Carbon atoms are numbered consecutively, starting with the starred atom and proceeding clockwise along the periphery. For VI the z axis is taken to be perpendicular to the molecular plane.

Theoretical

We start by assuming for a conjugated molecule a fully-symmetrical nuclear arrangement as the unperturbed nuclear configuration. The unperturbed electronic wavefunctions ϕ_0, ϕ_1, $\cdots$, ϕ_n, $\cdots$ and the corresponding eigenvalues E_0, E_1 $\cdots$, E_n, $\cdots$ are assumed to be known. We now distort the nuclei from the initial symmetrical arrangement by means of the ith normal coordinate of nuclear motion Q_i. With the use of the second-order perturbation theory, the energy of the ground state after deformation may be written as

$$E(Q_i) = E_0 + \left\langle \phi_0 \left| \frac{\partial H}{\partial Q_i} \right| \phi_0 \right\rangle Q_i$$

1) R. G. Pearson, *J. Amer. Chem. Soc.*, **91**, 4947 (1969).
2) R. G. Pearson, *ibid.*, **91**, 1252 (1969).
3) R. G. Pearson, *J. Chem. Phys.*, **52**, 2167 (1970).
4) L. Salem, *Chem. Phys. Lett.*, **3**, 99 (1969).
5) L. S. Bartell, *J. Chem. Educ.*, **45**, 754 (1969).
6) R. F. Bader, *Mol. Phys.*, **3**, 137 (1960).
7) R. F. Bader, *Can. J. Chem.*, **40**, 1164 (1962).
8) L. Salem and J. S. Wright, *J. Amer. Chem. Soc.*, **91**, 5947 (1969).
9) R. G. Pearson, *Theoret. Chim. Acta*, **16**, 107 (1970).
10) L. Salem, "The Molecular Orbital Theory of Conjugated Systems," Benjamin, New York (1966).
11) G. Binsch, E. Heilbronner, and J. N. Murrell, *Mol. Phys.*, **11**, 305 (1966).
12) G. Binsch and E. Heilbronner, "Structural Chemistry and Molecular Biology," A. Rich and N. Davidson, Ed., Freeman and Co., San Francisco (1968), p. 851.
13) G. Binsch and E. Heilbronner, *Tetrahedron*, **24**, 1215 (1968).
14) G. Binsch, I. Tamir, and R. D. Hill, *J. Amer. Chem. Soc.*, **91**, 2446 (1969).
15) G. Binsch and I. Tamir, *ibid.*, **91**, 2450 (1969).

$$+\frac{1}{2}\left\{\left\langle\psi_0\left|\frac{\partial^2 H}{\partial Q_i^2}\right|\psi_0\right\rangle - 2\sum_n{}'\frac{\left|\left\langle\psi_n\left|\frac{\partial H}{\partial Q_i}\right|\psi_0\right\rangle\right|^2}{E_n-E_0}\right\}Q_i^2 \quad (1)$$

If the initial ground-state wavefunction ψ_0 is nondegenerate, as is the case with the nonalternant hydrocarbons deal with in this paper (since the fully-symmetrical nuclear arrangements of these molecules belong to point-group D_{2h}, C_{2h}, or C_{2v}), then the second term in Eq. (1) is nonzero only for the totally symmetric nuclear displacements.

Let us assume that the total energy of a conjugated molecule can be written as the sum of the π-electron energy and the σ-core energy, the latter being approximated by a quadratic function of the bond-distance variation

$$E_\sigma = \sum_{\mu<\nu}\frac{k}{2}(\Delta r_{\mu\nu})^2 \quad (2)$$

where k is the force constant for an sp^2 hybridized C–C σ-bond.

It is easily shown[11,12] that by equating the second term in Eq. (1) to zero, the usual linear relationship between bond order and bond length for conjugated hydrocarbons can be derived. It follows that in conjugated hydrocarbons all the symmetrical bond distortions will occur until the first-order energy equilibrium is reached. That is, bond lengths will change to the first-order equilibrium values through the bond-order - bond-length relationship, but still keep the original molecular symmetry.

Assuming that the first-order changes have taken place, we have

$$E(Q_i) = E_0 + \frac{1}{2}\left\{k+\left\langle\psi_0\left|\frac{\partial^2 H_\pi}{\partial Q_i^2}\right|\psi_0\right\rangle - 2\sum_n{}'\frac{\left|\left\langle\psi_n\left|\frac{\partial H_\pi}{\partial Q_i}\right|\psi_0\right\rangle\right|^2}{E_n-E_0}\right\}Q_i^2 \quad (3)$$

If we assume that the change in the π-electron energy on variation of a particular bond length can be considered to arise from a one-electron perturbation which can be incorporated in the core resonance integral $\beta(r)$, the second term in the braces in Eq. (3) can be written as[11,14]

$$\left\langle\psi_0\left|\frac{\partial^2 H_\pi}{\partial Q_i^2}\right|\psi_0\right\rangle = 2\sum_{\mu<\nu}p_{\mu\nu}\beta_{\mu\nu}''\left(\frac{\partial r_{\mu\nu}}{\partial Q_i}\right)^2 \quad (4)$$

where p is the bond order and β'' is the second derivative of $\beta(r)$ with respect to r. We may safely neglect this term since for the reduced bond-distance interval in question the curvature of the $\beta(r)$ curve should be very small.

According to Eq. (3), the force constant for the normal vibration Q_i can be identified with the term in the braces and can be negative if a given matrix element $\langle\psi_0|\partial H_\pi/\partial Q_i|\psi_n\rangle$ is nonvanishing and the associated energy gap E_n-E_0 is sufficiently small. If the force constant is negative, the energy should be lowered by the nuclear deformation Q_i, and a pseudo-Jahn-Teller distortion from the symmetrical nuclear arrangement would occur spontaneously.

In order to estimate the probable value of the force constant, we now make a rather drastic approximation that the infinite sum over excited states in Eq. (3) is replaced by one or two dominant terms corresponding to the lowest one or two excited states. Pearson[2,3] has shown that this approximation is justified in a large variety of small molecules and complex ions. Our approach is then simply to examine whether a given molecule in a symmetrical nuclear configuration has reasonably low lowest excited state(s) and, if so, whether any of the integrals $\langle\psi_0|\partial H_\pi/\partial Q_i|\psi_n\rangle$ are nonvanishing. Since Q_i and $\partial H_\pi/\partial Q_i$ have the same symmetry and the ground state is, in general, totally symmetric, the integral is nonzero only when ψ_n and Q_i have the same symmetry. The symmetry of the lowest excited state(s) now determines which kind of nuclear displacement occurs energetically most easily.

Although the symmetry of the most soft normal nuclear displacement can thus be determined, its actual type cannot always be uniquely determined, because there are, in general, several types of bond distortion belonging to the same symmetry. In order to determine which distortion is energetically most favorable, it is useful to interpret the third term in the braces of Eq. (3) as the "relaxability" of the molecule along the coordinate Q_i, and express the matrix element $\langle\psi_0|\partial H_\pi/\partial Q_i|\psi_n\rangle$ in terms of the transition density ρ_{0n} between the ground and excited states by[4]

$$\left\langle\psi_0\left|\frac{\partial H_\pi}{\partial Q_i}\right|\psi_n\right\rangle = \int\rho_{0n}\frac{\partial v}{\partial Q_i}\,d\tau \quad (5)$$

where v is the one-electron nuclear-electron potential operator. For a one-electron transition between molecular orbitals ϕ_i and ϕ_j, ρ_{0n} is given by $\sqrt{2}\,\phi_i\phi_j$.[10] A given state may contribute much to the molecular relaxability towards mode Q_i, if ρ_{0n} is large near nuclei which contribute much to Q_i, but little to the relaxability if ρ_{0n} is small near such nuclei. We may thus predict the most favorable type of bond distortion by examining the distribution of transition densities over the molecular skeleton.

Eigenvalues and wavefunctions for the fully-symmetrical nuclear arrangements are calculated using the self-consistent configuration-interaction formalism of Pariser-Parr-Pople MO method, in conjunction with the variable bond-length technique in which bond lengths and, consequently, the resonance and Coulomb repulsion integrals are allowed to vary with bond orders at each iteration until self-consistency is reached.[16]

Since it is based on the second-order perturbation theory, the symmetry rule only gives the type of the most favorable bond distortion. In order to obtain information about the actual magnitudes of distortions or the equilibrium bond lengths at which the

16) H. Yamaguchi, T. Nakajima, and T. L. Kunii, *Theoret. Chim. Acta*, **12**, 349 (1968).

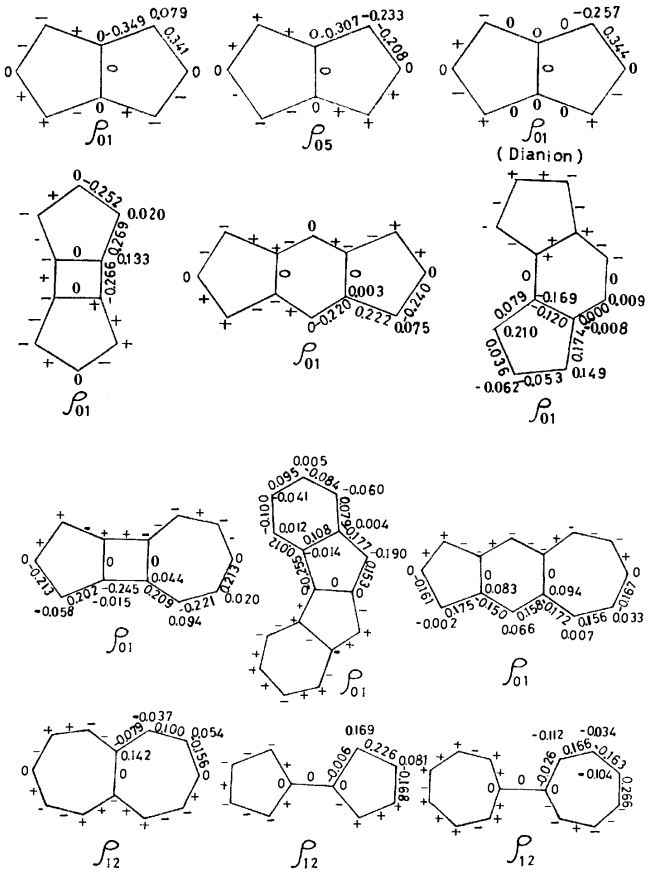

Fig. 2. One-center and two-center components of the transition densities.

nuclei of the real molecule will settle, we use the SCF MO method mentioned above, taking into account, as the starting geometries, all the possible distinct structures in which bond lengths are distorted so that the set of displacement vectors may form a basis for each irreducible representation of the full symmetry group of a molecule.[17,18] In pentalene (I, Fig. 1), for example, there are 3, 2, 2, and 2 distinct bond distortions belonging to respectively a_g, b_{2g}, b_{2u}, and b_{1u} irreducible representations of the point group D_{2h}. When self-consistency is achieved at two different geometries, one having a full symmetry and the other a lower symmetry, the latter should, in principle, be energetically favored as compared with the former. In such a case, we define the stabilization energy as the difference in total energy between the two geometries. The value of the force constant k adopted for use in calculating the σ-core energy is 714 kcal mol^{-1} Å^{-2}.[19]

Results and Discussion

The symmetries and energies (measured from the ground state) of the lowest excited states for the fully-symmetrical nuclear arrangements of the nonalternant hydrocarbons (Fig. 1) and some of their dianions are listed in Table 1. In Fig. 2 are shown the one-center and two-center components of the transition densities for some selected molecules.

TABLE 1. SYMMETRIES AND ENERGIES OF FIRST AND SECOND SINGLET EXCITED STATES OF NONALTERNANT HYDROCARBONS

Molecule (Point group)	First excited state		Second excited state	
	E_1-E_0 (eV)	Symmetry	E_2-E_1 (eV)	Symmetry
I (D_{2h})	0.35	B_{3g}	3.25	B_{1u}
II (D_{2h})	1.22	B_{1u}	2.15	B_{3g}
III (D_{2h})	1.00	B_{3g}	1.54	B_{1u}
IV (C_{2v})	1.47	B_2	1.48	B_2
V (C_{2v})	0.41	B_2	2.27	B_2
VI (C_{2h})	2.54	A_g	0.79	B_u
VII (D_{2h})	0.26	B_{3g}	2.41	B_{1u}
VIII (D_{2h})	0.81	B_{1u}	1.75	B_{2u}
IX (D_{2h})	0.83	B_{3g}	1.20	B_{1u}
X (C_{2v})	1.46	B_2	1.06	B_2
XI (C_{2v})	2.05	B_2	1.48	A_1
XII (C_{2v})	1.07	B_2	1.51	A_1
XIII (C_{2v})	0.81	B_2	1.62	A_1
XIV (C_{2v})	1.73	B_2	1.18	A_1
XV (C_{2v})	1.52	B_2	1.37	A_1
XVI (D_{2h})	2.24	B_{3g}	0.99	B_{2u}
XVII (C_{2v})	2.98	A_1	0.17	B_2
XVIII (D_{2h})	2.15	B_{3g}	0.98	A_1
XIX (C_{2v})	3.32	B_2	1.74	A_1
XX (C_{2v})	2.94	B_2	1.38	A_1
XXI (D_{2h})	2.04	B_{3g}	0.09	B_{2u}
XXII (D_{2h})	1.74	B_{3g}	0.06	B_{2u}
I^{2-} (D_{2h})	4.62	B_{2u}	0.66	B_{1u}
III^{2-} (D_{2h})	3.05	B_{2u}	1.00	B_{1u}
IV^{2-} (C_{2v})	3.93	B_2	0.05	A_1
VII^{2-} (D_{2h})	1.43	B_{2u}	0.44	B_{1u}

The second excited states being, in most cases, well separated from the lowest excited states in these molecules, the symmetries of the most soft nuclear displacements may be given by those of the lowest excited states. In pentalene (I), for example, the most soft nuclear displacement is predicted to be of b_{3g} symmetry. In this molecule there are two distinct types of in-plane vibration both belonging to b_{3g} irreducible representation. In Fig. 2 are shown one-center and two-center components of ρ_{01} for pentalene, together with those of ρ_{05} associated with the fifth excited state which lies at 6.14 eV above the ground state and belongs also to B_{3g} representation. It will be seen from these data that the lowest excited state contributes much to the relaxability of the molecule towards the bond-alternation type of distortion, while the next B_{3g} excited state contributes mainly to that towards the other type of bond distortion. The data in Fig. 2 show that in most of the molecules examined, with the exception of molecules IV and V, the bond alternation in the peripheral carbon skeleton is the energetically soft most bond distortion in the ground state. Such will be the case with the seven-membered analogues of I, II,

17) T. Nakajima and A. Toyota, *Chem. Phys. Lett.*, **3**, 272 (1969).
18) T. Nakajima, in "The Chemistry of Nonbenzenoid Aromatic Compounds," International Symposium on the Chemistry of Aromatic Compounds, Butterworths, London (1970), in press.
19) L. C. Snyder, *J. Phys. Chem.*, **66**, 2299 (1962).

TABLE 2. PREDICTED AND EXPERIMENTAL (IN ITALICS) BOND LENGTHS OF NONALTERNANT HYDROCARBONS

Molecule	Bond	Bond length (Å)	Molecule	Bond	Bond length (Å)	Molecule	Bond	Bond length (Å)
I (C_{2h})	1—2	1.356		5—6	1.457		4—12	1.448
	1—8	1.469		5—16	1.409		5—6	1.381
	2—3	1.450		6—7	1.364		5—11	1.446
	3—4	1.370		7—15	1.455		6—7	1.427
	4—8	1.446		15—16	1.467		7—8	1.376
							8—9	1.429
II (C_{2v})	1—2	1.383	VII (C_{2h})	1—2	1.357		9—10	1.374
	1—10	1.419		1—12	1.460		10—11	1.435
	2—3	1.420		2—3	1.450		11—12	1.404
	3—4	1.381		3—4	1.362			
	4—5	1.431		4—5	1.445	XIII (C_s)	1—2	1.371
	4—10	1.488		5—6	1.371		1—14	1.441
	9—10	1.391		6—12	1.453		2—3	1.428
			VIII (C_{2v})	1—2	1.367		3—4	1.382
III (C_{2h})	1—2	1.372		1—14	1.442		4—5	1.435
	1—12	1.447		2—3	1.440		4—14	1.462
	2—3	1.424		3—4	1.366		5—6	1.376
	3—4	1.392		4—5	1.442		6—7	1.443
	4—5	1.435		5—6	1.366		6—12	1.460
	4—12	1.444		6—7	1.460		7—8	1.369
	11—12	1.381		6—14	1.471		8—9	1.434
				13—14	1.381		9—10	1.373
IV (C_{2v})	1—2	1.449					10—11	1.429
	1—12	1.371	IX (C_{2h})	1—2	1.364		11—12	1.382
	2—3	1.357		1—16	1.452		12—13	1.436
	3—4	1.463		2—3	1.439		13—14	1.376
	4—5	1.368		3—4	1.371	XIV (C_{2v})	1—2	1.404,[c] *1.406*[d]
	4—12	1.454		4—5	1.430		1—11	1.397, *1.394*
	5—6	1.442		5—6	1.385		2—3	1.397, *1.386*
	11—12	1.458		6—7	1.440		3—4	1.435, *1.426*
				6—16	1.449		3—12	1.445, *1.421*
V (C_s)	1—2	1.366		15—16	1.375		4—5	1.371, *1.359*
	1—16	1.440					5—6	1.437, *1.423*
	2—3	1.437	X (C_{2v})	1—2	1.443		6—12	1.395, *1.378*
	3—4	1.364		1—16	1.376			
	4—5	1.446		2—3	1.363	XV (C_{2v})	1—2	1.399,[c] *1.412*,[e] *1.396*[f]
	5—6	1.375		3—4	1.449		1—13	1.400, *1.393*, *1.393*
	5—16	1.449		4—5	1.358		2—3	1.433, *1.437*, *1.436*
	6—7	1.459		5—6	1.457		2—14	1.442, *1.472*, *1.470*
	7—8	1.376		6—7	1.375		3—4	1.374, *1.380*, *1.358*
	7—15	1.439		6—16	1.450		4—5	1.429, *1.434*, *1.418*
	8—9	1.451		7—8	1.432		5—6	1.373, *1.367*, *1.368*
	9—10	1.404		15—16	1.451		6—7	1.435, *1.446*, *1.446*
	9—14	1.413					7—14	1.400, *1.429*, *1.399*
	10—11	1.396	XI (C_{2v})	1—2	1.398,[a] *1.391*[b]			
	11—12	1.398		1—10	1.405, *1.413*	XVI (D_{2h})	1—3	1.353[g]
	12—13	1.397		4—5	1.406, *1.383*		2—3	1.462
	13—14	1.400		4—10	1.469, *1.483*		3—4	1.387
	14—15	1.462		5—6	1.398, *1.401*		3—13	1.426
	15—16	1.390		6—7	1.400, *1.385*		4—5	1.412
							13—14	1.414
VI (C_{2h})	1—2	1.397	XII (C_s)	1—2	1.374			
	1—16	1.399		1—12	1.434	XVII (C_{2v})	1—2	1.362[g]
	2—3	1.397		2—3	1.426		2—3	1.446
	3—4	1.396		3—4	1.380		3—4	1.397
	4—5	1.402		4—5	1.463		3—15	1.428

TABLE 2. continued

Molecule	Bond	Bond length (Å)	Molecule	Bond	Bond length (Å)	Molecule	Bond	Bond length (Å)
	4—5	1.402		6—7	1.410	XXI (D_{2h})	1—2	1.356
	5—6	1.397		17—18	1.413		1—5	1.460
	6—7	1.446					2—3	1.455
	6—16	1.428	XIX (C_{2v})	1—2	1.356		5—6	1.372
	7—8	1.364		1—5	1.462			
	8—9	1.440		2—3	1.449	XXII (D_{2h})	1—2	1.359
	15—16	1.412		5—6	1.353		1—7	1.454
							2—3	1.450
XVIII (D_{2h})	1—2	1.357[g]	XX (C_{2v})	1—2	1.357		3—4	1.360
	2—3	1.452		1—7	1.461		7—8	1.379
	4—5	1.457		2—3	1.449			
	5—6	1.390		3—4	1.360			
	5—17	1.427		7—8	1.355			

a) Ref. 16.
b) X-ray bond lengths; J. M. Robertson, M. M. Shearer, G. A. Sin, and D. G. Watson, *Acta Crystallogr.*, **15**, 1 (1962).
c) H. Yamaguchi, T. Terasaka, and T. Nakajima, *Theoret. Chim. Acta*, **18**, 225 (1970).
d) X-ray bond lengths of a dimethylphenyl derivative; Ref. 35.
e) X-ray bond lengths of a tetramethyl derivative; Ref. 36.
f) X-ray bond lengths of a tetramethyl derivative; Ref. 37.
g) Ref. 38.

TABLE 3. BOND LENGTHS OF DIANIONS OF NONALTERNANT HYDROCARBONS

Dianion	Bond	Bond length (Å)	Dianion	Bond	Bond length (Å)
I^{2-} (D_{2h})	1—2	1.400	IV^{2-} (C_{2v})	1—2	1.401
	1—8	1.423		1—12	1.406
	4—8	1.416		2—3	1.398
				3—4	1.414
III^{2-} (D_{2h})	1—2	1.397		4—5	1.437
	1—12	1.421		4—12	1.416
	4—12	1.432		5—6	1.370
	11—12	1.408		11—12	1.447
			VII^{2-} (D_{2h})	1—2	1.415
				1—12	1.399
				2—3	1.404
				6—12	1.504

and III (molecules VII, VIII and IX, respectively).

The molecular symmetry groups and the bond distances for the energetically most stable nuclear arrangements of the nonalternant hydrocarbons obtained by the variable bond-length SCF MO method are presented in Tables 2, and 3, Inspecting the data in Tables 1, 2 and 3. one may draw a fairly clear-cut criterion for the molecular symmetry reduction in nonalternant hydrocarbons that if the lowest excitation energy is smaller than about 1.2 eV, the force constant for a certain antisymmetric in-plane vibration should be negative and the molecule would be distorted into a less symmetrical nuclear configuration. In Fig. 3 the stabilization energies ΔE_s which favor a lower-symmetry nuclear arrangement are plotted against the lowest excitation energies E_1-E_0 as calculated by assuming the fully-symmetrical nuclear arrangements. It is seen that there exists a good correlation between E_1-E_0 and ΔE_s; the smaller the former, the larger the latter.

The molecular symmetry groups for the most stable nuclear configuration as obtained by using the SCF method are in complete agreement with those brought about by the most soft bond distortions predicted from the symmetry rule. Moreover, in molecules I, II, III, VII, VIII, IX, XII, and XIII which suffer a symmetry reduction, the bond-length distributions obtained by using the SCF method indicate that they exhibit a more or less marked bond-length alternation in the molecular periphery, as is expected from the distributions of transition densities. It is of interest to note in this connection that a fairly strong bond alternation is predicted even in molecules II, VIII, and XIII, the perimeters of which are composed of $4n+2$ carbon atoms.

Of particular notice is dibenzopentalene (V). The transition density ρ_{01} of this molecule (Fig. 2) indicates

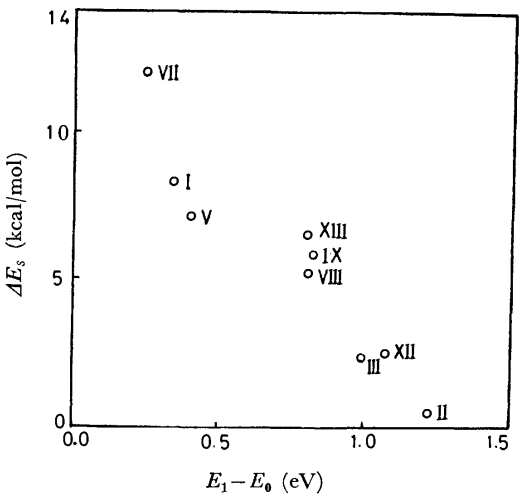

Fig. 3. Correlation of ΔE_s with E_1-E_0.

that strong double-bond fixations are localized in the pentalene segment, but there exists only a slight degree of double-bond fixation in each of the benzene rings. On the other hand, the results of SCF calculations show that in one of the benzene rings of this molecule, bond lengths are smoothed out as in benzene, whereas in the other ring there exists a strong double-bond fixation in the same degree as in the pentalene segment. In the case of V, the symmetry rule is thus insufficient in predicting the actual type of the most favorable bond distortion. In the isomeric dibenzopentalene (VI) which suffers only a first-order bond fixation, the two benzene rings are equivalent and in both the benzene rings bond lengths are almost equalized. Strong double-bond fixations are localized in the butadiene-like skeleton of the pentalene segment. It is therefore expected that the molecule undergoes addition reactions in this region. This is in accordance with experimental facts.[20,21]

Of the cata-condensed nonalternant hydrocarbons examined, pentalene (I) and heptalene (VII) which have been the objects of many theoretical investigations[13,15,19,22-27] are predicted to possess a marked tendency to the second-order double-bond fixation. In both molecules there exists a strong bond-length alternation in the molecular periphery. Available experimental information[28-30] agrees with this in indicating that the π-electrons in these molecules are strongly localized in "double" bonds, rather than uniformly delocalized over the entire molecule.

s-Indacene (III), recently prepared by Hafner *et al.*[31], is predicted to assume a skew structure with a moderate double-bond fixation. The results obtained by using different theoretical methods[13,15,32] agree with this. The theoretical predictions are in good agreement with the available experimental information.

Other molecules worth mentioning are peri-condensed nonalternant hydrocarbons XIV—XVIII; all these molecules are predicted not to suffer second-order bond distortions. As for XIV and XV, it is noted that bond lengths of the peripheral bonds belonging to the 5-membered ring of XV are all predicted to be 1.4 Å. In both molecules there is a pronounced double-bond fixation in the remaining region of the periphery. Derivatives of XIV and XV have been prepared by Hafner and Schneider[33,34] and the predicted distributions of bond lengths are in good agreement with the X-ray data (Table 2).[35-37] In molecules XIV—XVIII, it is predicted that bond lengths of the naphthalene core are almost the same as those in the free naphthalene molecule and there are marked double-bond fixations in the other region of the periphery.[38] The most stable nuclear arrangement in XVI corresponds to the aromatic model proposed by Lo and Whitehead.[39] Molecules XVI and XVIII have been synthesized by Trost and Bright[40] and Boekelheide and Vick,[41] respectively. The present results are in good qualitative agreement with the available experimental facts.

The lowest excitation energies calculated assuming the full molecular-symmetry for dianions of I, III IV, and VII are all larger than the critical value (1.2 eV). This indicates that no symmetry reduction should occur in the ground states of these dianions, the prediction being in agreement with the results of SCF calculations. In I, III, and VII, addition of two more electrons to the neutral molecule to form the dianion results in a complete disappearance of the unsymmetrical bond distortion, and in the dianions the bond lengths of the peripheral C–C bonds are nearly equalized. Dianions of I,[42,43] II,[44] and IV[45,46] have been prepared and are known to be stable species.

In this connection the molecular symmetries of anion and cation radicals of fulvalenes should be mentioned. If the full molecular symmetry (D_{2h}) is assumed, the ground states of the cation radical of pentafulvalene (XXI) and the anion radical of heptafulvalene (XXII) are predicted to be of $^2B_{1g}$ symmetry. The lowest excited states of these radicals are of ^2A_u symmetry and are predicted to be very close to the ground states; in the framework of one-electron approximation the two states are degenerate. In these radicals, therefore, the ground state interacts strongly with the first

20) C. T. Blood and R. P. Linstead, *J. Chem. Soc.*, **1952**, 2255 2263.
21) C. C. Chuen and S. W. Fenton, *J. Org. Chem.*, **23**, 1538 (1958).
22) P. C. den Boer-Veenendaal and D. H. W. den Boer, *Mol. Phys.*, **4**, 33 (1961).
23) P. C. den Boer-Veenendaal, J. A. Vliegenthart, and D. H. W. den Boer, *Tetrahedron*, **18**, 1325 (1962).
24) T. Nakajima and S. Katagiri, *Mol. Phys.*, **7**, 149 (1963).
25) T. Nakajima, H. Yamaguchi, R. Kaeriyama, and Y. Nemoto, This Bulletin, **37**, 272 (1964).
26) P. François and A. Julg, *Theoret. Chim. Acta*, **11**, 128 (1968).
27) N. C. Baird and R. M. West, *J. Amer. Chem. Soc.*, **93**, 3072 (1971).
28) H. J. Dauben and D. J. Bertelli, *ibid.*, **83**, 4659 (1961).
29) E. LeGoff, *ibid.*, **84**, 3975 (1962).
30) R. Bloch, R. A. Marty, and P. de Mayo, *ibid.*, **93**, 3071 (1971).
31) K. Hafner, K. Häfner, C. König, M. Kreuder, G. Ploss, G. Schulz, E. Strum, and K. H. Vöpel, *Angew. Chem.*, **75**, 35 (1963); *Angew. Chem. Int. Ed. Engl.*, **2**, 123 (1963).
32) T. Nakajima, T. Saijo, and H. Yamaguchi, *Tetrahedron*, **20**, 2119 (1964).
33) K. Hafner and J. Schneider, *Angew. Chem.*, **70**, 702 (1958).
34) K. Hafner and J. Schneider, *Ann. Chem.*, **624**, 37 (1957); **672**, 194 (1964).
35) H. J. Lindner, *J. Chem. Soc., B*, **1970**, 907.
36) E. Carstensen-Oeser and G. Habermehl, *Angew. Chem.*, **80**, 564 (1968).
37) R. Quasba, F. Brandle, W. Hoppe, and R. Huber, *Acta Crystallogr.* **B25**, 1198 (1969).
38) H. Yamaguchi and T. Nakajima, This Bulletin, **44**, 682 (1971).
39) D. H. Lo and M. A. Whitehead, *Chem. Comm.* **1968**, 771.
40) B. M. Trost and G. M. Bright, *J. Amer. Chem. Soc.*, **89**, 4244 (1967).
41) V. Boekelheide and G. K. Vick, *ibid.*, **78**, 653 (1956).
42) T. J. Katz and M. Rosenberger, *ibid.*, **84**, 865 (1962).
43) T. J. Katz, M. Rosenberger, R. K. O'Hara, *ibid.*, **86**, 249 (1964).
44) K. Hafner, *Angew. Chem.*, **75**, 1041 (1963); *Angew. Chem. Int. Ed. Engl.*, **3**, 165 (1964).
45) T. J. Katz and J. Schulman, *J. Amer. Chem. Soc.*, **86**, 3169 (1964).
46) T. J. Katz, V. Balogh, and J. Schulman, *ibid.*, **90**, 734 (1968).

TABLE 4. BOND LENGTHS OF CATION AND ANION RADICALS OF FULVALENES

Radical	Bond	Bond length (Å)	Radical	Bond	Bond length (Å)
XXI$^+$(C_{2v})	1—2	1.416	XXII$^+$(D_{2h})	1—2	1.379
	1—5	1.441		1—7	1.427
	2—3	1.396		2—3	1.426
	5—6	1.388		3—4	1.380
	6—10	1.461		7—8	1.422
	8—9	1.477			
	9—10	1.353	XXII$^-$(C_{2v})	1—2	1.400
				1—7	1.437
XXI$^-$(D_{2h})	1—2	1.378		2—3	1.399
	1—5	1.429		3—4	1.422
	2—3	1.428		7—8	1.396
	5—6	1.421		8—14	1.449
				11—12	1.354
				12—13	1.426
				13—14	1.360

excited state through the nuclear displacement of $b_{1u}(z)$ symmetry, with the result that the initial molecular symmetry (D_{2h}) should be reduced to C_{2v} (Table 4).

On the other hand, in the anion radical of XXI and the cation radical of XXII, the energy gaps between the first excited state (which is doubly degenerate in the one-electron approximation) and the ground state are reasonably large (1.4 and 1.7 eV, respectively) and these radicals would not suffer symmetry reduction.

The above predictions are in agreement with the results obtained by using the open-shell SCF method in conjunction with the variable bond-length technique.[47,48]

The cation and anion radicals of XXII have been prepared and their ESR spectra have been investigated by Sevilla *et al.*[49] The analysis of the hyperfine spectra of these radicals has revealed that the cation radical should have D_{2h} symmetry, whereas the molecular symmetry of the anion radical should be lower than D_{2h}.

Finally we consider the application of the symmetry rule to the prediction of the geometrical structures of the excited states of conjugated hydrocarbons. On the basis of the same approximation as used in predicting the ground-state geometrical structures, the force constant for the ith normal nuclear-displacement in the nth excited state may be written as

$$f_n^i = k - 2\sum_m{}' \frac{\left|\left\langle \psi_n \left| \frac{\partial H_\pi}{\partial Q_i} \right| \psi_m \right\rangle\right|^2}{E_m - E_n} \qquad (6)$$

In order to seek the most soft nuclear displacement in the excited state, the approximation is again made of replacing the sum in Eq. (6) by one or two terms correpsonding to the higher one or two excited states. Now, the transition density ρ_{nm} between the nth excited state corresponding to the orbital jump $\phi_i \rightarrow \phi_k$ and the mth one corresponding to $\phi_j \rightarrow \phi_l$ is $\phi_k\phi_l$ if $i=j$, and $-\phi_i\phi_j$ if $k=l$. Therefore, the value of the matrix element $|\langle\psi_n|\partial H_\pi/\partial Q_i|\psi_m\rangle|^2$ in Eq. (6) should be about one half of that of $|\langle\psi_0|\partial H_\pi/\partial Q_i|\psi_n\rangle|^2$ in Eq. (3) in so far as the transition densities are assumed not to vary significantly according to the molecular orbitals concerned. Thus, if the energy gap $E_m - E_n$ is smaller than about one half the critical value obtained above, that is, about 0.6 eV, the force constant in the excited state is expected to be negative.

In Table 1 are presented the energies of the second excited states (measured from the first excited states) as obtained by minimizing the ground-state energy assuming the full molecular symmetry. Use of these eigenvalues and corresponding wavefunctions in Eq. (6) is approximative. The energy values and corresponding wavefunctions to be used in Eq. (6) should, in principle, be those corresponding to the first-order equilibrium nuclear arrangement of the nth excited state, as given by minimizing its energy and keeping the molecular symmetry highest.

Inspection of Table 1 reveals that all those molecules which suffer a molecular-symmetry reduction in the ground state have $E_2 - E_1$ values considerably larger than the critical value and are predicted to possess a fully-symmetrical nuclear arrangement in their first excited state.

TABLE 5. BOND LENGTHS OF FIRST SINGLET EXCITED STATES OF VII, XXI AND XXII

Molecule	Bond	Bond length (Å)	Molecule	Bond	Bond length (Å)
VII (D_{2h})	1—2	1.402	XXII (C_{2v})	1—2	1.399
	1—12	1.412		1—7	1.436
	2—3	1.405		2—3	1.404
	6—12	1.463		3—4	1.421
				7—8	1.406
XXI (C_{2v})	1—2	1.422		8—14	1.442
	1—5	1.435		11—12	1.362
	2—3	1.394		12—13	1.448
	5—6	1.409		13—14	1.365
	6—10	1.442			
	8—9	1.444			
	9—10	1.366			

In the case of heptalene (VII), we have calculated the bond-length distribution in the first excited state using the same SCF procedure as that used for the ground state, except for the use of a different value 3.3 Å^{-1} (1.7 Å^{-1} for the ground state) for the exponent in the exponential expression of the resonance integral.[50] The results are presented in Table 5; all the possible starting bond distortions produce a unique set of bond

47) A. Toyota and T. Nakajima, *Chem. Phys. Lett.*, **6**, 144 (1970).

48) T. Nakajima, A. Toyota, and H. Yamaguchi, "Aromaticity, Pseudoaromaticity and Antiaromaticity." The 3rd Jerusalem Symposium, The Israel Academy of Sciences and Humanities, Jerusalem (1970), p. 227.

49) M. O. Sevilla, S. H. Flajser, G. Vincow, and H. J. Dauben, Jr., *J. Amer. Chem. Soc.*, **91**, 4139 (1969).

50) Y. Fujimura, H. Yamaguchi, and T. Nakajima, This Bulletin, **45**, 384 (1972).

lengths belonging to the point group D_{2h} and the bond lengths of the peripheral bonds are nearly equalized, which supports the prediction given by the symmetry rule. The marked difference in the geometrical structure between the ground state and the lowest excited state in heptalene gives the main reason for the appearance of a long absorption tail throughout the visible region in its absorption spectrum.[28]

On the other hand, there are cases where a molecule has an E_1-E_0 value reasonably higher than the critical value, but the separation between the second and first excited states is relatively small. The E_2-E_1 value for I^{2-} is of the same order of magnitude as the critical value, and those for the peri-condensed hydrocarbon, XVII, the fulvalenes, XXI and XXII, and the dianions, IV^{2-} and VII^{2-}, are significantly smaller than the critical value for the first excited state. For XXI and XXII, the results of SCF calculations presented in Table 5 agree with the predictions given by the symmetry rule in indicating that on exciting to the first excited state, the molecular symmetries are reduced to C_{2v} from D_{2h}. This provides a probable explanation for the fact that the longest wave-length absorption bands of these molecules are relatively broad.[51]

Azulene (XI) has an E_2-E_1 value reasonably larger than the critical value and no symmetry reduction is expected on excitation to the first excited state. A recent analysis of the vibrational structures of the longest wavelength absorption band indicates that azulene retains C_{2v} symmetry in the first excited state.[52]

Conclusion

In predicting the geometrical structures with respect to the C–C bond distances of nonalternant hydrocarbons on the basis of the pseudo Jahn-Teller theorem, we have assumed that only the lowest excited state plays a dominant role in determining the most soft nuclear displacement. In spite of this very crude approximation, the predicted types of the energetically most favorable bond distortions and molecular-symmetry reductions are in good agreement with the results of the variable bond-length SCF MO calculations and available experimental facts.

The criterion for the symmetry reduction obtained above, that if the lowest excitation energy predicted assuming the full molecular-symmetry for a nonalternant hydrocarbon is smaller than *ca.* 1.2 eV, the molecule should be distorted into a less symmetrical nuclear configuration, is applicable to the conjugated hydrocarbons in general. It is interesting to mention, in this connection, the symmetry reductions possible in large cyclic polyenes $C_{4n+2}H_{4n+2}$.[10] The lowest excitation energies calculated assuming the full molecular-symmetry (D_{6h}) for $C_{18}H_{18}$ and $C_{30}H_{30}$, both known to date,[53] have been reported to be about 1.6[54-56] and 0.95 eV,[55] respectively. It is thus expected that $C_{30}H_{30}$ should suffer a symmetry reduction, and that contrary to the previous assumption,[10,55] there exists no symmetry reduction ($D_{6h}\rightarrow D_{3h}$) in the ground state of $C_{18}H_{18}$. Actually, as for $C_{18}H_{18}$, the lowest excitation energy (1.6 eV) predicted assuming D_{6h} symmetry is in good agreement with the position of the longest wave-length absorption band ($^1B_{2u}$) recently discovered by Blattmann *et al.*[54] The symmetry reduction in $C_{4n+2}H_{4n+2}$ is thus predicted to occur at $n\sim5$, which is in agreement with the result obtained by Binsch and Heilbronner using a more sophisticated theoretical procedure.[12]

51) W. von E. Doering, "Theoretical Organic Chemistry, Kekulé Symposium," Butterworths, London (1958), p. 35, and personal communication.

52) G. R. Hunt and I. G. Ross, *J. Mol. Spectrosc.*, **9**, 50 (1962).

53) F. Sondheimer, R. Wolovsky, and Y. Amiel, *J. Amer. Chem. Soc.*, **84**, 274 (1962).

54) H. R. Blattmann, E. Heilbronner, and G. Wagnière, *ibid.*, **90**, 4786 (1968).

55) H. C. Longuet-Higgins and L. Salem, *Proc. Roy. Soc.*, (London), **A257**, 445 (1960).

56) M. Gouterman and G. Wagnière, *J. Chem. Phys.*, **36**, 1188 (1962).

ESR Studies of the Conformational Interconversion of the 9,10-Dihydrophenanthrene Radical Anion and Its Related Compounds

Masamoto IWAIZUMI, Takashi MATSUZAKI, and Taro ISOBE

The Chemical Research Institute of Non-Aqueous Solutions, Tohoku University, Katahira 2—1—1, Sendai

(Received October 6, 1971)

The ESR spectra of the 9,10-dihydrophenanthrene radical anion change drastically with the temperature, and at temperatures around −30°C the spectra show a marked line-width alternation effect. These temperature-dependent ESR spectra and the line-width alternation effect have been interpreted in terms of the conformational interconversion of the 9,10-dihydrophenanthrene radical anion molecule. From an analysis of the spectra, the activation energy of the inversion has been estimated to be 6.3±0.6 kcal/mol. It has also been estimated, from the ratio of the axial and equatorial proton splittings, that the dihedral angle of the axial protons is about 11°. These data are compared with those of the 4,5,9,10-tetrahydropyrene radical anion. The ESR of the 4,5-dihydropyrene radical anion is also presented.

The conformational interconversion of several bridged biphenyls has been investigated by means of NMR[1,2] and ESR,[3] and also by the observation of the racemization of optically-active biphenyls.[4-7] The inversional motion of the neutral molecule of 9,10-dihydrophenanthrene (I) has been studied by the NMR[1] and the optical methods.[6] However, the techniques of NMR or optical measurements were not effective in obtaining information about the inversion process of the 9,10-dihydrophenanthrene molecule, because the inversion process was too fast to be treated by the NMR or optical measurements. In a previous paper,[3] we observed a line-width alternation effect in the ESR of the radical anion of 4,5,9,10-tetrahydropyrene (II) and explained it in terms of the inversional motion of the molecule. The ESR technique is sometimes quite effective in the study of fast rate processes; it makes possible the measurements of much faster rate processes than in the case of the NMR and optical methods.

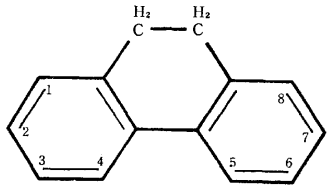

[I]

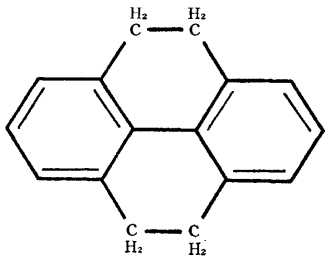

[II]

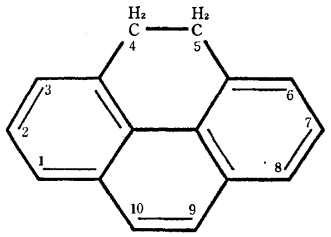

[III]

In this paper, we wish to report on the inversion process of the radical anion of 9,10-dihydrophenanthrene as studied by the ESR method. We observed a line-width alternation effect in the ESR similar to that of the 4,5,9,10-tetrahydropyrene radical anion. This line-width alternation effect can be explained as arising from the rapid modulation of the methylene proton hyperfine splitting constants due to exchange between an axial and equatorial state by means of the inversional motion of the molecule. The data obtained for this inversion process and the structure of the molecule are compared with those of the 4,5,9,10-tetrahydropyrene radical anion. In connection with these compounds, the 9,10-dihydropyrene radical anion has also been studied by the ESR method.

Experimental

The 9,10-dihydrophenanthrene and 4,5-dihydropyrene were obtained commercially. The 9,10-dihydrophenanthrene was purified by recrystallization from ethyl alcohol (mp 34—35°C), and the 4,5-dihydropyrene, by column chromatography (mp 130—131°C). The radical anions were prepared by alkali metal reduction in ethereal solvents by the previously-established technique.[8] ESR measurements were carried out by means of a Hitachi X-band ESR spectrometer. Variable temperature experiments were performed using a gas-flow temperature control method previously described.[3] The temperature of the samples was monitored by means of a copper-constantan thermocouple which was fixed just below the sample tube.

1) M. Ōki, H. Iwamura, and N. Hayakawa, This Bulletin, **36**, 1542 (1963); **37**, 1865 (1964).
2) R. J. Kurland, M. B. Rubin, and W. B. Wise, *J. Chem. Phys.*, **40**, 2426 (1964).
3) M. Iwaizumi and T. Isobe, This Bulletin, **38**, 1547 (1965).
4) K. Mislow and M. A. W. Glass, *J. Amer. Chem. Soc.*, **83**, 2780 (1961).
5) K. Mislow and H. B. Hopps, *ibid.*, **84**, 3018 (1962).
6) K. Mislow, M. A. W. Glass, H. B. Hopps, E. Simon, and G. H. Wahl, Jr., *ibid.*, **86**, 1710 (1964).
7) K. Mislow, R. Graeve, A. J. Gordon, and G. H. Wahl, Jr., *ibid.*, **86**, 1733 (1964).
8) J. R. Bolton and G. K. Fraenkel, *J. Chem. Phys.*, **40**, 3307 (1964).

Results and Discussion

Line-width Alternation Effect in the ESR spectra of the 9,10-Dihydrophenanthrene Radical Anion and the Inversional Motion of the Molecule. As Fig. 1 shows, the hyperfine structure of the ESR spectra of the 9,10-dihydrophenanthrene radical anion changes markedly with the temperature. This change in the hyperfine structure with the temperature comes mainly from the change in the hyperfine components due to the methylene protons. The spectrum at low temperatures (Fig. 1a, 4) can be analyzed in terms of the difference in the splitting constant for the axial and the equatorial methylene protons, and the four sets of triplet splittings due to the four sets of two equivalent ring protons. A typical set of splittings due to the methylene protons are shown with arrows in Fig. 1. As the temperature increases, this methylene proton hyperfine splitting changes extensively; at temperatures around −27°C (Fig. 1a, 1) it becomes a three-line pattern with an intensity ratio of about 1 : 4.2 : 1 and with line separation of $(a_{eq}+a_{ax})$, where the a_{eq} and a_{ax} are the splitting constants of the equatorial and axial protons obtained at low temperatures. This hyperfine pattern is a typical line-width alternation phenomenon, and the intensity ratio coincides well with the one expected, 1 : 4 : 1, from the theory of the line-width-alternation effect[9] for an extremely broadened case.

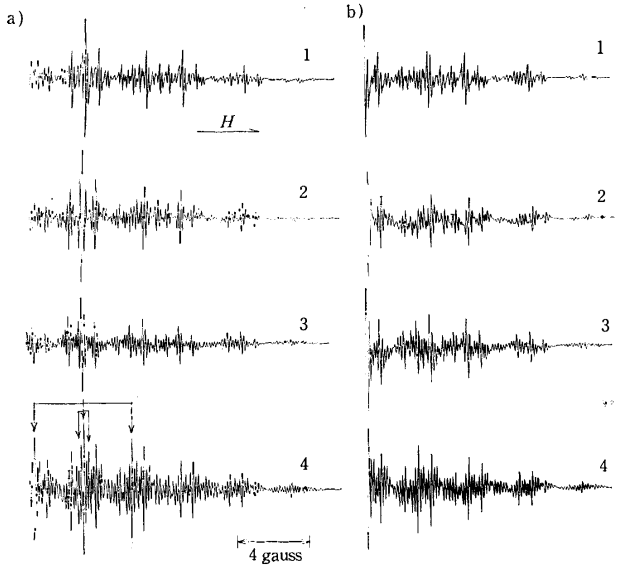

Fig. 1. ESR spectra of the 9,10-dihydrophenanthrene radical anion in tetrahydrofuran with lithium ion as a counter ion.
(a) Spectra observed 1) at −27°C, 2) at −71°C, 3) at −81°C, and 4) at −102°C.
(b) Computer simulation; 1) $\tau=1.4\times10^{-7}$ sec 2) $\tau=2.0\times10^{-6}$ sec, 3) $\tau=5.0\times10^{-6}$ sec 4) $\tau=4.0\times10^{-5}$ sec.

As has been reported in the previous paper,[3] the line-width alternation effect observed here can be attributed to the inversional motion of the 9,10-dihydrophenanthrene anion molecule. At low temperatures, the rate of the inversional motion is slow and the axial and equatorial splitting constants can be separately observed. On the other hand, at high temperatures the inversional motion becomes rapid and it becomes impossible to distinguish the axial and the equatorial protons by rapid exchange between the two states.

This rate process has, therefore, been analyzed by using a modification for the two-jump model of Bloch's equation.[10] The computer-simulated ESR spectra obtained on the basis of this model are compared with the observed spectra in Fig. 1. Although the ring proton hyperfine splitting constants change slightly with the temperature, the neglect of such slight changes in the splitting constants does not result in serious errors in the evaluation of the life-time of the conformation, τ. Therefore, the changes in the hyperfine splitting constants with the temperature were ignored and the hyperfine splitting constants obtained at −102°C were used throughout the ESR

Table 1. Hyperfine splitting constants and spin densities for the 9,10-dihydrophenanthrene radical anion[a] (in gauss)

Position	1,8	2,7	3,6	4,5	CH_2 Axial	CH_2 Equatorial
Hyperfine splitting constants at −102°C[b]	0.161	5.363	0.708	3.359	2.674	0.289
Spin densities[c]	−0.0064	0.2041	−0.0262	0.1154	—	—

a) The radical was prepared with lithium in tetrahydrofuran.
b) Absolute values.
c) The values were obtained by the McLachlan's calculation (*Mol. Phys.*, **3**, 233 (1960)) using the following parameters and $\lambda=1$.

$\delta_{\alpha_1}=-0.1\beta$ $\quad\delta_{\alpha_2}=\delta_{\alpha_3}=-0.1\beta$ $\quad\delta_{\alpha_4}=-0.5\beta$
$\beta_{12}=\beta_{23}=0.7\beta$ $\quad\beta_{24}=2.5\beta$

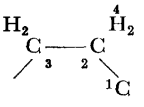

9) J. H. Freed and G. K. Fraenkel, *ibid.*, **39**, 326 (1963); P. D. Sullivan and J. R. Bolton, "Advances in Magnetic Resonance," Vol. 4, ed. by J. S. Waugh, Academic Press, New York, N. Y. (1970), p. 39.
10) H. S. Gutowski and C. H. Holm, *J. Chem. Phys.*, **25**, 1288 (1956).

simulation. In Table 1 the hyperfine splitting constants obtained at −102°C are listed. The assignment of the observed splitting constants to the respective proton positions was made on the basis of the calculated spin distribution.

By applying the estimated τ values to the following relation:

$$k = 1/\tau = k_0 \exp(-E_a/RT) \quad (1),$$

the activation energy, E_a, of the inversional motion can be evaluated. Here, k is the rate constant of the inversion, and k_0 is the frequency factor. Figure 2 shows the plot of $\log_{10} 1/\tau$ against $1/T$. E_a and k_0 were calculated to be 6.3±0.6 kcal/mol and $3.5\pm2.9\times10^{12}$ sec^{-1} respectively from the figure.

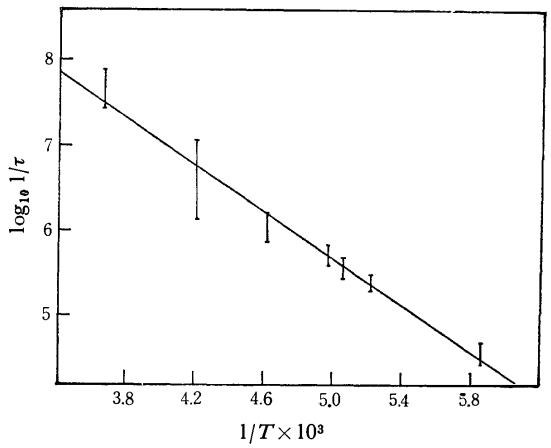

Fig. 2. Plot of $\log_{10} 1/\tau$ against $1/T\times10^3$ for the 9,10-dihydrophenanthrene radical anion.

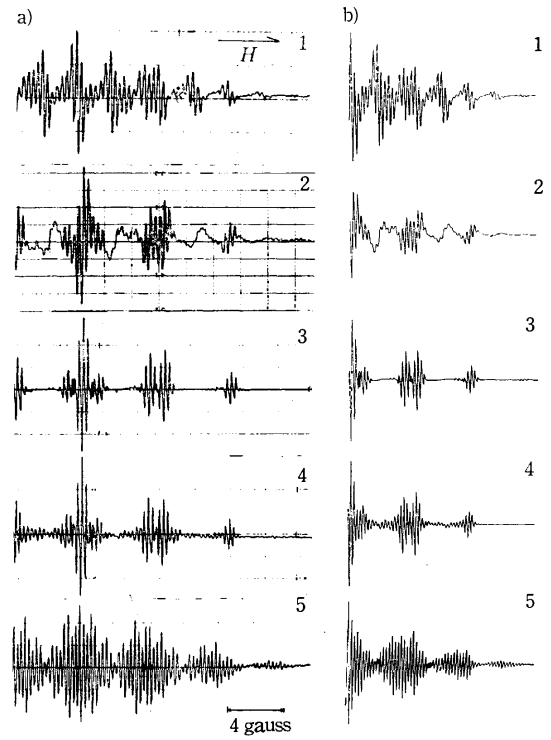

Fig. 3. Comparison of the computer simulated ESR spectra with the observed ones of the 4,5,9,10-tetrahydropyrene radical anion in 1,2-dimethoxyethane with potassium ion as a counter ion.
(a) Spectra observed 1) at +63°C, 2) at +23°C, 3) at −35°C, 4) at −58°C, and 5) at −81°C.
(b) Computer simulation; 1) $\tau=1.2\times10^{-9}$ sec, 2) $\tau=1.2\times10^{-8}$ sec, 3) $\tau=7.0\times10^{-8}$ sec, 4) $\tau=1.6\times10^{-6}$ sec, 5) $\tau=9.0\times10^{-6}$ sec.
The observed spectra are taken from Ref. 3.

For a comparison of the activation energy with that of the inversion of the 4,5,9,10-tetrahydropyrene radical anion, the inversion process of the 4,5,9,10-tetrahydropyrene radical anion previously reported was reexamined through a computer simulation of the spectra. The calculated spectra are compared with the observed ones in Fig. 3. From the plot of $\log_{10} 1/\tau$ against $1/T$ (Fig. 4), the activation energy of the inversion of the molecule was obtained as 8.7± 0.6 kcal/mol, and k_0, as $4.4\pm2.8\times10^{14}$ sec^{-1}.[11] That is, the increase in the activation energy of the inversion from the singly-bridged form to the doubly-bridged form is 2.4 kcal/mol. Milsow estimated, by a simple theoretical consideration, an activation energy of 7—8 kcal/mol for the 4,5,9,10-tetrahydropyrene and one of 4 kcal/mol for the 9,10-dihydrophenanthrene molecules.[6] These predictions are in agreement with our experimental results, although his calculation was made for neutral molecules and gave a larger difference in the activation energies between the two compounds.

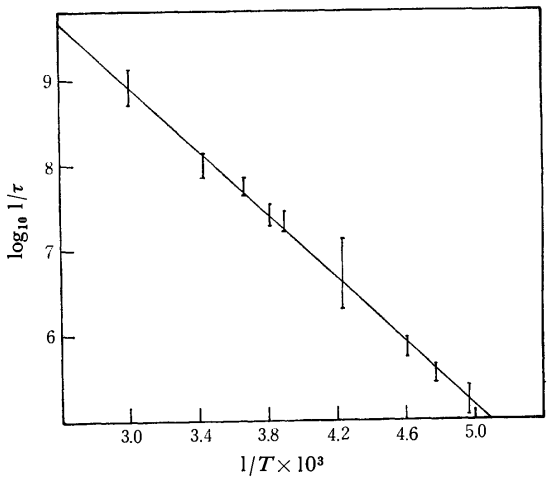

Fig. 4. Plot of $\log_{10} 1/\tau$ against $1/T\times10^3$ for the 4,5,9,10-tetrahydropyrene radical anion.

The Conformation of the 9,10-Dihydrophenanthrene Anion Molecule. β proton hyperfine splitting constants have a pronounced orientation dependence, which is given by the well-known formula:[12]

$$a_\beta = (B_0 + B_2 \cos^2\theta)\rho_t. \quad (2)$$

Here, ρ_t represents the spin density at the trigonal carbon(i), θ is the dihedral angle between the C–H$_\beta$

11) In a previous paper[3] the activation energy was estimated without attempting a computer simulation of the whole hyperfine pattern of the spectra, but by observing the behavior of the pair of lines with spin states (1,0) and (0,1) or (−1,0) and (0,−1). Here, the numbers in the parentheses correspond to the quantum numbers for the total angular momenta of the axial and equatorial protons respectively. In this work adopting the computer simulation of the whole hyperfine pattern of the spectra, it was found that the estimated activation energy in the previous paper contains a large error. The value reported previously must, therefore, be revised.

12) C. Heller and H. M. McConnell, *J. Chem. Phys.*, **32**, 1535 (1960).

bond and the $2p_z$ orbital on the ith carbon, and B_0 and B_2 are constants. In the 9,10-dihydrophenanthrene molecule, if the molecular structure is planar, the two protons in the methylene groups must be equivalent stereochemically and must have the same splitting constants. On the other hand, if the two aromatic rings twist about the bond joining the rings, the hyperfine splittings of the two methylene protons will become different, and the larger the amount of the twist becomes, the larger will the ratio of the axial and the equatorial proton splitting constants be. The observed ratio of the axial and the equatorial proton splittings in the 9,10-dihydrophenanthrene radical anion was 9.25. For the case of the 4,5,9,10-tetrahydropyrene radical anion, this ratio was 4.82. Furthermore, by assuming that $B_0=0$, the dihedral angle for the axial proton of the 9,10-dihydrophenanthrene radical anion is calculated to be 11°. This value is larger than the value, 3°, for the 4,5,9,10-tetrahydropyrene radical anion previously reported. These results indicate that the twist angle between the two benzene rings would be larger in the 9,10-dihydrophenanthrene radical anion than in the case of the 4,5,9,10-tetrahydropyrene radical anion, which is in agreement with the conclusion obtained from the studies by means of the NMR and UV spectra.[6]

ESR of the 4,5-Dihydropyrene Radical Anion. In the case of the 4,5-dihydropyrene radical anion(III), the two methylene protons will probably be in different states stereochemically, *i.e.*, in the axial and equatorial states, as in the cases of the 9,10-dihydrophenanthrene or 4,5,9,10-tetrahydropyrene radical anion, although the distortion of the molecule from a planar structure is small because of the presence of the 9—10 π bond. We examined the ESR spectra of the 4,5-dihydropyrene radical anion in the hope of getting information on the structure of the molecule and the inversional motion.

The observed spectra are shown in Figs. 5 and 6. The spectrum in Fig. 5 is analyzed in terms of four sets of triplet splittings, which can reasonably be assigned to the hyperfine interaction with the ring protons on the basis of a comparison with the spin-density distribution estimated by the MO calculation (Table 2). When the anion is prepared by reduction with potassium in 1,2-dimethoxyethane, the hyperfine splitting due to the methylene protons is not resolved. On the other hand, when the radical is prepared by reduction with potassium in 2-methyltetrahydrofuran, the radical shows a spectrum with further splittings due to the interaction with the methylene protons and a potassium ion associated with the radical anion (Fig. 6). The appearance of the methylene proton

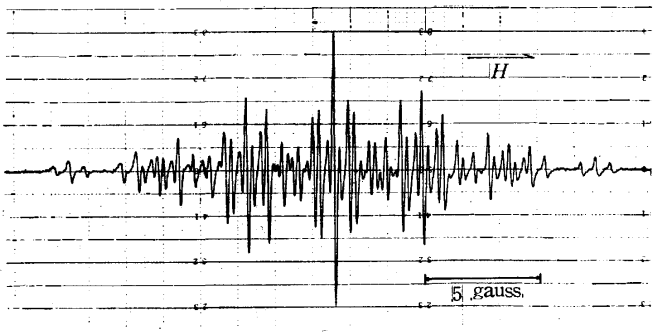

Fig. 5. ESR spectrum of the 4,5-dihydropyrene radical anion in 1,2-dimethoxyethane with potassium ion at 20°C.

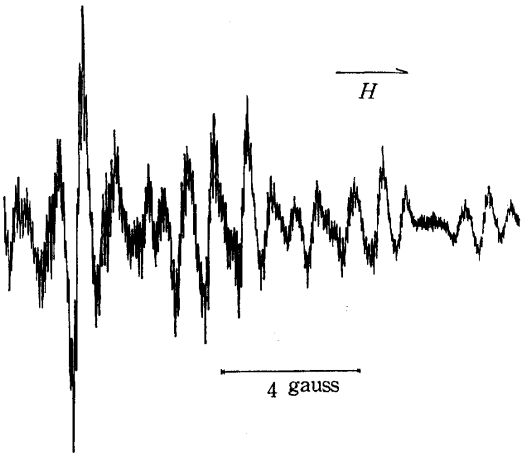

Fig. 6. ESR spectrum of the 4,5-dihydropyrene radical anion in 2-methyltetrahydrofuran with potassium ion at 20°C.

splitting is attributed to the redistribution of the odd electron in the molecule by the cationic field of the associated potassium ion. Unfortunately, the spectra could not be analyzed unequivocally because of the low S/N ratio, the complicated hyperfine pattern, and imperfect resolution. In the spectrum obtained at 20°C, however, the additional hyperfine splittings due to the methylene protons and the associated potassium seem to consist of eight lines. If it is assumed that the four methylene protons show quintet splitting with a binomial intensity ratio, and that potassium show a splitting with a splitting constant of half of the four methylene protons, an eight-line pattern with roughly the same intensity ratio as the observed one can be expected for the methylene proton and the potassium hyperfine splittings. According to this analysis, the two types of methylene protons, axial and equatorial, will be in an averaged state as a result of the fast inversional motion. The inversion rate will

Table 2. Hyperfine splitting constants and spin densities for the 4,5-dihydropyrene radical anion[a]

(in gauss)

Position	1,8	2,7	3,6	9,10	CH_2
Hyperfine splitting constants at 20°C[b]	3.782	0.632	2.887	4.677	<0.06
Spin densities[c]	0.1469	−0.0348	0.1152	0.1969	—

a) The radical was prepared with potassium in 1,2-dimethoxyethane.
b) Absolute values.
c) The values were obtained by the McLachlan's calculation using the parameters shown in the footnote c of Table 1.

then be faster than approximately 10^8 Hz. The NMR spectrum of the neutral molecule of 9,10-dihydropyrene shows a single line for the methylene protons, with a δ value of 3.22. This means that the inversional motion of the neutral molecule is apparently a fast process on the NMR time scale. More reliable information on the methylene protons in ESR is desirable for the analysis of the inversion process of the 9,10-dihydropyrene anion.

The numerical calculations were carried out on the NEAC 2200 Model 700 computer at the Computer Center, Tohoku University.

BULLETIN OF THE CHEMICAL SOCIETY OF JAPAN, VOL. 45, 1034—1038 (1972)

The Reactions between a Rhenium Filament and Nitric Oxide at High Temperatures and Low Pressures

Teijiro TAMURA

Department of Chemistry, Faculty of Industrial Arts, Kyoto Technical University, Matsugasaki, Sakyo-ku, Kyoto

(Received October 22, 1971)

The rates of the reaction of rhenium with nitric oxide under a filament temperature of (1300—1800)°K and a nitric oxide pressure of ($3\times10^{-5}-1\times10^{-3}$)Torr have been measured by a static method. The rate of the reaction increases with an increase in the temperature, and the apparent activation energy is 24 kcal/mol. The rate of the reaction is proportional to the nitric oxide pressure and independent of the nitrogen pressure. The apparent compositions of the rhenium oxide produced in the reaction have been determined from the weight change in the rhenium filament and from the amount of nitric oxide consumed in the temperature range of (1300—2100)°K. The ReO_3 and Re_2O_7 were formed at lower temperatures and at higher temperatures respectively. The Re_2O_7 was presumed to be formed by the oxidation of the ReO_3 deposited on the vessel wall with atomic oxygen evolved in a high-temperature range.

At high temperatures, some metals react with oxidizing gases to form very highly volatile metal oxides. Therefore, the reactions proceed on surfaces practically free from the accumulation of the oxide layers. Adsorption, surface reaction, and desorption are included in these processes, and kinetic studies of such systems are expected to present useful information about the gas-solid interactions. These metals can be heated resistively to a considerably high temperature and can readily provide a clean metal surface when heated at a high temperature in a vacuum. Moreover, if the reactions are carried out at very low pressures, the following advantages may be expected; the diffusion rate of gas coming to and leaving from the surface is so large that it does not limit the overall rate of the process.

Rhenium possesses some advantageous properties;[1,2] that is, many refractory transition metals can form stable carbides and nitrides, while rhenium can not,[3] and it has a high resistance to the "water cycle"[4] at high temperatures. It is of interest to investigate the interaction of nitric oxide with rhenium, since nitric oxide is an odd molecule (possessing an odd number of electrons).

Many studies of the reactions of oxygen with tungsten[5-8] and rhenium[9-11] have been reported. However, although the reaction of tungsten with nitric oxide at very low pressures has been studied by Anderson[12], no reaction of rhenium with nitric oxide has been studied.

In the present investigation, the reaction rates of the rhenium filament with nitric oxide have been measured at pressure from 3×10^{-5} Torr to 1×10^{-3} Torr and in the temperature range from 1300°K to 1800°K by a static method. The apparent compositions of the rhenium oxide have also been determined from the amount of nitric oxide consumed and from the amount of rhenium lost in the temperature range from 1300°K to 2100°K.

Apparatus

The apparatus is shown in Fig. 1. For the measurement of the rate of the reaction, a reaction vessel of 5.2 *l* (including

1) C. T. Sims, C. M. Craighead, R. I. Jaffé, D. N. Gideon, E. N. Wyler, F. C. Todd, D. M. Rosenbaum, E. M. Sherwood, and I. E. Campbell, "Investigations of Rhenium," Battle Memorial Institute, Wright Air Development Center Technical Report, 54—371, June (1954).

2) C. F. Robinson, *Rev. Sci. Inst.*, **29**, 250 (1958).

3) C. T. Sims, "Rhenium," ed. by B. W. Gonser, Elsevier, New York (1962).

4) "Water cycle" is a cyclic process of an oxidation reduction reaction of the hot filament with a residual water vapor in the vacuum tube, which causes the failure of the filament.

5) J. A. Becker, E. J. Becker, and R. G. Brands, *J. Appl. Phys.*, **32**, 411 (1961).

6) J. B. Berkowitz-Mattuch, A. Büchler, J. L. Engelke, and S. N. Goldstein, *J. Chem. Phys.*, **39**, 2722 (1963).

7) P. O. Schissel and O. C. Truson, *ibid.*, **43**, 737 (1965).

8) Yu. G. Ptushinskii and B. A. Chuikov, *Surface Sci.*, **6**, 42 **7**, 90 (1967).

9) T. Hamamura and G. Tomita, This Bulletin, **40**, 1066 (1967).

10) D. E. Rosner and H. D. Allendorf, *J. Chem. Phys.*, **49**, 5553 (1968).

11) R. P. H. Gasser and C. J. Massay, *Surface Sci.*, **20**, 107 (1970).

12) H. U. Anderson, U. S. At. Energy Comm., UCRL-10135 (1962).

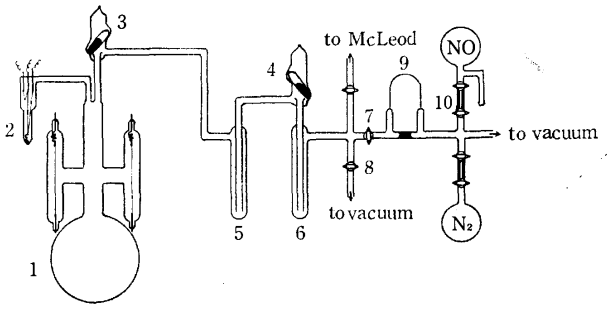

Fig. 1. The apparatus.
1: Reaction vessel, 2: Pirani gauge, 3,4: Greaseless cock, 5,6: Liquid nitrogen trap, 7,8: stop cock, 9: Capillary leak, 10: Gas pipet.

a Pirani gauge) was used. It consisted of a spherical bulb 20 cm in diameter and side tubes 3.5 cm in diameter and 15 cm long. Along the axis of each side tube, a rhenium filament, 0.152 mm in diameter and 130 mm long, was mounted, being stretched by a tungsten spring and connected to lead wires by spot welding. The lead wires were coated with glass in order to exclude any reactions that consume nitric oxide on the lead-wire surface.

For the determination of the oxide composition, the apparatus was similar to that used for the measurement of the reaction rate except that it had a reaction vessel of 98 *l*, and rhenium filaments, each 75 mm long, were mounted in it. They were clamped at both ends with platinum strips which were welded to the glass-coated lead wire so that they could be easily disconnected from the wires for weighing.

Particular care was taken to keep the filaments free from grease and mercury-vapor contamination; liquid nitrogen traps and greaseless stopcocks were used. Nitric oxide in a reservoir was supplied to the reaction vessel by a gas pipet through a capillary tube so placed as to decrease the flow rate of the gas. The pressure in the reaction vessel was measured by a Pirani gauge which was calibrated against a McLeod manometer and which had a sensitivity of 7.2×10^{-5} Torr/mV for nitrogen and nitric oxide.

The rhenium filament was heated electrically by means of a controllable DC power supply, and its temperature was measured with a micro optical pyrometer. The rhenium filament was analyzed spectroscopically (Found: Si : 0.08%, Ti : 0.001%). It was cleaned by dipping it in a boiling 40% caustic potash solution for five minutes and then wiping it off aqua-dag with filter paper; this procedure was repeated several times.

The nitric oxide and nitrogen were prepared by the methods described in the previous paper[13].

Procedure

All the apparatus was evacuated by a mercury-diffusion pump; for degassing the reaction vessel was heated at 360°C for ten hours in an electric furnace, and the filaments were heated to about 2100°K in oxygen of 1×10^{-5} Torr in order to remove any possible carbonaceous surface contamination. This heating was done until the evolution of the inactive gases from the filaments had become negligibly small.

Before each experiment, a filament was flashed at 2200 °K for 2 min in a high vacuum. Then the nitric oxide was introduced into the reaction vessel. When the nitric oxide pressure attained the desired value, the reaction vessel was separated from the evacuating system by means of the greaseless cock. The filament was then heated to the experimental temperature. As the reaction proceeded, the pressure in the vessel decreased; it was measured from time to time after the filament had been switched off and cooled down at room temperature, because the Pirani gauge could not follow the rapid change in pressure.

In the case of the determination of the composition of the rhenium oxide, each filament was weighed with a micro balance before it was mounted in the vessel. The processes of degassing the apparatus and of introducing nitric oxide into the vessel were similar to those described above. Then the filament was heated at the experimental temperature until all the nitric oxide had been consumed. Separate filaments were thus heated at the temperatures between 1300°K and 2100°K. The filaments were then taken out from the reaction vessel, removed from the lead wires, and weighed again with the micro balance in order to determine the loss of the rhenium filament.

Results and Discussion

The Rate of the Reaction. The rate of the reaction between the rhenium filament and nitric oxide was measured at temperatures from 1300°K to 1800°K and at pressures from 3×10^{-5} Torr to 1×10^{-3} Torr.

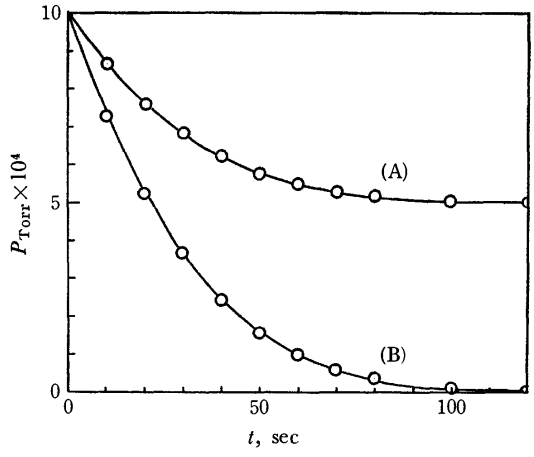

Fig. 2. Pressure *vs.* heating time of the filament.
Filament temperature, 1400°K.
(A) Total pressure of nitric oxide and nitrogen.
(B) Partial pressure of nitric oxide.

A typical plot of the pressure, as measured by the Pirani gauge, against the heating time of the filament is shown by curve A in Fig. 2. Since nitrogen is formed by the reaction, the pressure indicated by curve A is the total of the pressure of nitric oxide still remaining and that of the nitrogen produced. We assume that the overall process is represented by:

$$x\mathrm{NO} + \mathrm{Re} \rightarrow (1/2)x\mathrm{N_2} + \mathrm{ReO}_x,$$

and that nitrogen and a volatile rhenium oxide (it evaporates and sticks to the vessel wall) are produced, the intermediate steps being ignored; for every molecule of nitric oxide consumed, there is a net decrease of half molecules in the gaseous phase. It is thus possible, from measurements of the total pressure, P, at various times, to determine the partial pressure, P_{NO}, of the nitric oxide still remaining, as follows:

13) T. Tamura, This Bulletin, **44**, 590 (1971).

$$P_0 - P = (1/2)(P_0 - P_{NO})$$
$$P_{NO} = 2P - P_0$$

where P_0 is the initial pressure of nitric oxide. The plot of P_{NO} against the heating time is given by curve B in Fig. 2.

From the rate of consumption thus obtained, the amount of nitric oxide which reacts with the rhenium filament, D_{NO} mol/sec, can be calculated. The relation between the rate of reaction and the nitric oxide pressures at various temperatures is shown in Fig. 3.

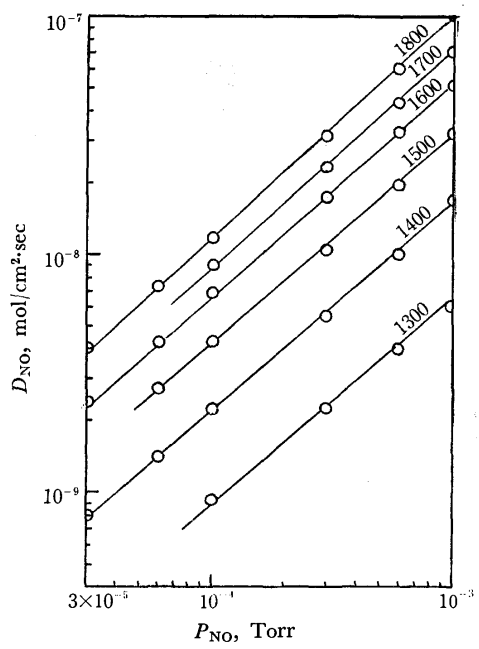

Fig. 3. Effect of nitric oxide pressure on the rate of reaction.

Under these experimental conditions, that is, when the total pressure in the reaction vessel is so low and the surface area of the filament is so small, it is assumed that the temperature of the nitric oxide molecules striking the filament is equal to that of the wall of the reaction vessel and that the pressure is uniform throughout the vessel. Therefore, the number of mols of nitric oxide that strike the filament per second can be calculated from the kinetic theory of gases as follows:

$$P_{NO}S/\sqrt{2\pi MRT}$$

where P_{NO} is the nitric oxide pressure in dyn/cm²; S, the surface area of the filament in cm²; M, the molecular weight of nitric oxide; $\boldsymbol{R}$, the gas constant, and T, the temperature of the reaction vessel. Consequently, the probability, $\boldsymbol{k}$, that a nitric oxide molecule which strikes the filament will disappear from the gaseous phase by some reaction processes can be calculated from the following equation:

$$D_{NO} = \boldsymbol{k}P_{NO}S/\sqrt{2\pi MRT},$$

$\boldsymbol{k}$ is the reaction probability. The reaction probabilities for various temperatures and pressures are given in Table 1. A plot of $\log D_{NO}$ *vs.* $1/T$ is given in Fig. 4. The apparent activation energy is about 24 kcal/mol. The effect of the nitrogen pressure on the rate of the consumption of nitric oxide was also investigated; the filament was heated at a constant temperature with various amounts of nitrogen added to the nitric oxide at first. As a result, the rate of consumption was found to be independent of the nitrogen pressure. This coincides with the fact that the nitrogen desorbs from the surface below 1300°K in the flash-desorption experiments.[13,14] If the filament temperature is kept constant, the rate of consumption is simply given as a function of the nitric oxide pressure alone:

$$D_{NO} = K \cdot P_{NO}^{n}$$
or: $$\log D_{NO} = \log K + n \log P_{NO}$$

Table 1. Reaction probabilities at various temperatures at nitric oxide pressures of 6×10^{-4} torr and 1×10^{-4} torr

Filament temp. °K	$\boldsymbol{k}$ (6×10^{-4} Torr)	$\boldsymbol{k}$ (1×10^{-4} Torr)
1300	0.011	0.015
1350	0.0168	0.024
1400	0.027	0.036
1450	0.039	0.052
1500	0.053	0.069
1550	0.070	0.094
1600	0.0875	0.11
1650	0.101	0.123
1700	0.115	0.141
1770	0.143	0.163
1800	0.161	0.190

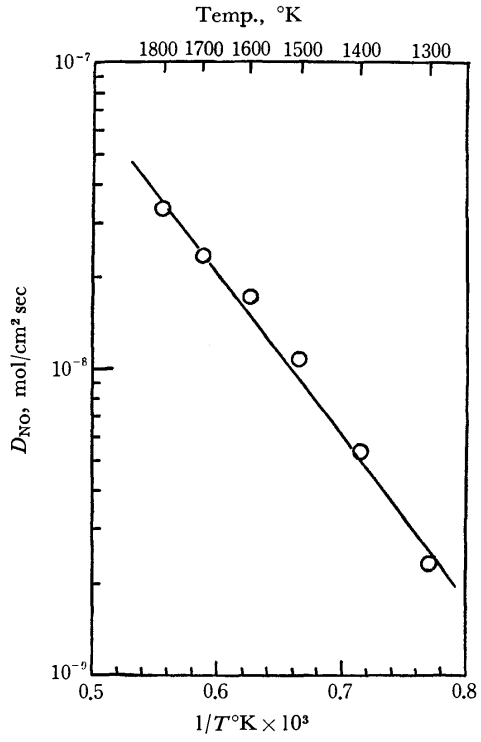

Fig. 4. Effect of filament temperature on the rate of reaction at 3×10^{-4} Torr of nitric oxide pressure.

14) T. Tamura, This Bulletin, **44**, 2116 (1971).

where K and n are constants. As can be seen from Fig. 3, the rate of consumption can be considered to be proportional to the nitric oxide pressure. If this reaction occurs with the direct impact of nitric oxide molecules from the gaseous phase to the rhenium surface, the rate of the reaction should depend on the higher-power of the pressure.

The pressure dependence of the rate of this reaction may be explained as follows. The flash-desorption experiments[13,14] have shown that nitric oxide molecules are dissociated to atomic species at high temperatures under the present experimental conditions, and that nitrogen atoms recombine and evaporate as nitrogen molecules, while oxygen atoms remain on the rhenium surface at a considerably high temperature as an adsorbed oxygen layer. Moreover, in the experiment of thermionic electron emission,[15] it was found that the surface condition for the Re-NO reaction was the same as that for the Re-O_2 reaction, the amounts of species other than oxygen atoms were extremely small on the surface, and that the surface was completely covered with oxygen atoms, whose concentration was independent of the nitric oxide pressure.

Since no rhenium oxides other than ReO_3 evaporate in the temperature range of this experiment,[16] we consider that ReO_3 is formed with oxygen atoms in an oxygen layer and incoming nitric oxide molecules. Therefore, the following steps of the reaction may be described:

$$NO_{(g)} \xrightarrow{k_1} N_{(a)} + O_{(a)} \quad (1)$$

$$N_{(a)} + N_{(a)} \xrightarrow{k_2} N_{2(g)} \quad (2)$$

$$NO_{(g)} + 2O_{(a)} + Re \underset{k_{-3}}{\overset{k_3}{\rightleftharpoons}} ReO_{3(a)} + N_{(a)} \quad (3)$$

$$ReO_{3(a)} \xrightarrow{k_4} ReO_{3(g)} \quad (4)$$

In the step 1, although nitric oxide adsorbs on the rhenium surface as molecules at room temperature, it is decomposed immediately to atomic oxygen and nitrogen at elevated temperatures.[13] No nitric oxide was detected in the desorption from a mixed nitrogen-oxygen layer.[14] Moreover, in another experiment, when the rhenium filament was heated in a mixed gas of nitrogen and oxygen, nitric oxide was not detected by means of an omegatron mass spectrometer. Hence, the backward reaction of step 1 does not occur. In the step 2, hardly any nitrogen exists on the rhenium surface above 1300°K, as has been described above; k_2 in the step 2 is, therefore, very large and the rate of the backward reaction is negligibly small. In the step 3, the recombination and evaporation processes of the adsorbed nitrogen atom are the same as in the step 2; by supposing $k_3 \gg k_{-3}$ and $k_4 \gg k_3$ in such a high temperature range, the step 3 may be regarded as the rate-determining step, and nitric oxide may be regarded as consuming three molecules in one reaction.

15) will be published.

16) B. Weber, J. Fusy, and A. Cassuto, "Recent Developments in Mass Spectroscopy," Proceeding of the International Conference in Mass Spectroscopy, Kyoto, ed. by K. Ogata and T. Hayakawa, University of Tokyo Press (1969) p. 1319.

The rate equation may be written as follows:

$$-d[NO]/dt = D_{NO} = 3k_3P_{NO}.$$

The rate of the reaction between nitric oxide and rhenium is proportional to the nitric oxide pressure.

The Determination of the Composition of Rhenium Oxide. The apparent compositions of rhenium oxides were determined in the temperature range from 1300°K to 2100°K; these results are shown in Table 2, while the O/Re ratios are plotted against the temperature in Fig. 5.

TABLE 2. COMPOSITION OF RHENIUM OXIDE

Filament temp. °K	Consumed NO mol×10⁶	Loss of Re mol×10⁶	Oxide ReO_x value x
1300	7.94	2.62	3.03
1400	14.25	4.89	2.92
1500	7.817	2.56	3.05
1600	7.515	2.57	2.93
1700	15.0	4.76	3.15
1800	16.02	4.98	3.22
1900	11.6	3.23	3.48
2000	7.02	2.00	3.50
2100	9.03	2.51	3.59

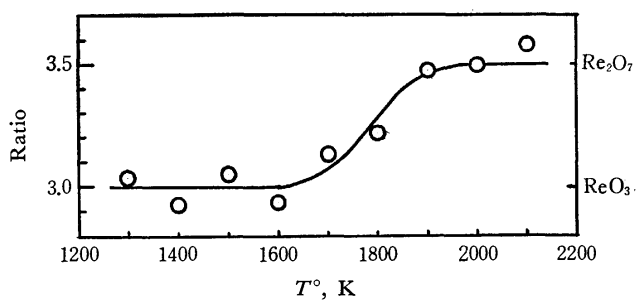

Fig. 5. The ratio, O/Re.

From these results, the ratio is seen to be close to 3.0 below 1700°K and then to increase to a steady value of close to 3.5 above 1900°K. These ratios of 3.0 and 3.5 correspond to the admitted oxides of rhenium trioxide, ReO_3, and rhenium heptoxide, Re_2O_7, respectively. Any ratio that lies between 3.0 and 3.5 may correspond to a mixture of the two oxides. The color of the rhenium oxide deposited on the wall of the reaction vessel depends upon the filament temperature. It is dark blue below 1600°K and colorless above 1900°K, while at intermediate temperatures its color is pale blue. Therefore, from these facts, it is considered that the ReO_3 on the wall is dark blue, that the Re_2O_7 is colorless, and that the pale blue deposit observed in the reactions at intermediate temperatures is composed of these two oxides. Although the apparent composition of Re_2O_7 is obtained at higher temperatures, the formation of Re_2O_7 on the rhenium surface and its evaporation from it at such high temperatures are thermodynamically unfavorable because the heat of the formation of Re_2O_7 is larger than that of ReO_3, and because the ReO_3 is found at lower temperatures. In another

experiment using the omegatron mass spectrometer, when the filament temperature was raised above 1800 °K in nitric oxide, a considerable amount of atomic oxygen was observed. Therefore, we consider that only the ReO_3 evaporates and deposits on the vessel wall, even above 1800°K, and that the ReO_3 on the wall is oxidized succesitively to Re_2O_7 with the atomic oxygen that is evolved in this high-temperature range.

The author wishes to express his deep thanks to Professor Takuya Hamamura of this Institute and to Professor Kumasaburo Kodera and Dr. Masaru Onchi of Kyoto University for their kind discussions and encouragement, and to Dr. Minoru Ozasa of the Matsushita Electronics Corporation, who made the spectroscopic analysis of rhenium.

BULLETIN OF THE CHEMICAL SOCIETY OF JAPAN, VOL. 45, 1038—1044 (1972)

Effects of Chain Molecules on the Temperature of the Maximum Density of Water

Masao SAKURAI, Tsuyoshi KOMATSU, and Tsurutaro NAKAGAWA
Department of Polymer Science, Faculty of Science, Hokkaido University, Sapporo
(Received November 4, 1971)

The shifts in the temperature of the maximum density of water produced by the addition of small amounts of oligomers of polyethylene glycol and polyethylenimine and other related compounds were determined by dilatometry. These effects were interpreted in terms of the change in the structure of water around the various solute molecules in connection with their chain length. It was found that, as the chain length increases, the extent of the modification of the water structure by the chain molecules decreases because of the hydrophobic contact between ethylene groups. The apparent specific expansibility of the solute in the neighbourhood of 4°C was also evaluated as a function of the concentration.

The nature and role of water structure in aqueous polymer solutions have been subjects of great interest and controversy for a long time.[1] For example, recently Klotz[2] has discussed in detail the hydrophobic interactions between water and the alkyl groups of polymers; then, from the results of their near-infrared spectra measurements in H_2O/D_2O mixture, Worley and Klotz concluded that polyvinylpyrrolidone fits into the group of hydrogen-bonded structure makers.[3] On the contrary, Goldfarb and Rodriguez[4] have suggested, from their thermodynamic data, that the hydrated sheath around polyvinylpyrrolidone in water is not "ice-like," but is to be classified as part of the classical scheme of solute hydration.

An alternative approach to the problem of polymer-water interaction may be to examine the effect of chain length on certain properties of aqueous solutions of oligomers. From this point of view, the solubilities of hydrocarbons in oligomeric polyethylenimine solutions have been determined by Okubo and Ise.[5] Their solubility data indicate that the hydrophobicity of the oligomers increases with an increase in the molecular weight. More recently, the volumetric properties of aqueous solutions of the oligomers of polyethylene glycol and polypropylene glycol have been investigated by Sandell and Goring.[6] The apparent specific expansibility, which they have regarded as a measure of the structural effect of a solute,[7] increases with an increase in the chain length; that is, the extent of the hydrophobic hydration is reduced as the chain length increases. This has been interpreted in terms of the increasing hydrophobic contact between ethylene groups.

Since the hydrogen-bonded structure of water is greatly sensitive to the temperature, it seemed that it would be useful to examine the temperature dependence of some thermodynamic properties in order to specify the structural phenomena of aqueous polymer solutions.

In the present paper, we will report some results concerning the effects of the addition of chain molecules on the temperature of the maximum density (TMD) of water. The phenomenon of the TMD of water at 3.98°C has been regarded as coming from the balance of the increase in volume resulting from the thermal expansion and the decrease in volume resulting from the breakdown of the hydrogen-bonded low-density water structure.[1,8,9] Although, in general, the presence of various kinds of solutes depresses the TMD from 3.98°C, it is also well known that some alcohols elevate the TMD in very dilute

1) J. L. Kavanau, "Water and Solute-Water Interactions," Holden-Day, Inc., San Francisco (1964).
2) I. M. Klotz, *Federat. Proc.*, **24**, *Suppl.* 15, s-24 (1965).
3) J. D. Worley and I. M. Klotz, *J. Chem. Phys.*, **45**, 2868 (1966).
4) J. Goldfarb and S. Rodriguez, *Makromol. Chem.*, **116**, 96 (1968).
5) T. Okubo and N. Ise *J. Phys. Chem.*, **73**, 1488 (1969).
6) L. S. Sandell and D. A. I. Goring, *J. Polym. Sci., Part A-2* **9**, 115 (1971).
7) J. L. Neal and D. A. I. Goring, *J. Phys. Chem.*, **74**, 658 (1970).
8) D. Eisenberg and W. Kauzmann, "The Structure and Properties of Water," Oxford Univ. Press, London (1969).
9) "Hydrogen-Bonded Solvent Systems," ed by A. K. Covington and P. Jones, Taylor, and Francis Ltd., London (1968).

solutions.[10-13] This observation implies that these alcohol molecules stabilize the hydrogen-bonded intermolecular structure of water. Wada and Umeda[13] and Franks and Watson[14] have shown that the depression in the TMD produced by the addition of small amounts of many organic compounds is less than that to be expected when ideal mixing takes place, and that, as a rule, this effect is more pronounced when the number of carbon atoms within the solute molecules increases. Thus, the solutes which show a tendency to raise the TMD may be assumed to stabilize the structure of water.

The purpose of this work is to make an attempt to clarify the interactions between polymers and water on the basis of the measurements of the TMD and in connection with the concept of the structural change of water.

Experimental

Procedure. Bicapillary-type dilatometers with a capacity of about 80 m*l* and with capillary tubes 0.7 mm in diameter were used to measure the temperature dependence of the volumes of the aqueous solutions. Measurements were made with a cathetometer at approximately 0.3~0.5°C intervals in the range ±2°C from the TMD. The temperature of the thermostat bath was maintained with a precision of ±0.002°C, and the temperatures corresponding to the measured volumes were read on a Beckmann thermometer. In order to correct the thermal expansion of the dilatometer itself, the shift in the TMD, $\Delta\theta$, produced by the addition of a solute was determined graphically, according to the method of Wada and Umeda,[13] by comparing the meniscus height-temperature curve of the solution with that of pure water. By using this method, the maximum error in estimating $\Delta\theta$ was ±0.02°C. It has been found that the values of $\Delta\theta$ obtained preliminarily with regard to the solutions of both sodium chloride and ethylene glycol are in good agreement with the literature values.[13,15]

The densities of the pure solutes were determined at 5, 15, 25, 35, and 45°C using Ostwald-type pycnometers with a volume of about 20 m*l*.

Materials. The polyethylene glycol (PEG) was furnished by the Sanyo Kasei Co. The PEG-200 and PEG-400 (the average molecular weights are 200 and 400 respectively) were dried under reduced pressure and were used without further purification. The PEG-20000 was recrystallized from methyl ethyl ketone and was dried at room temperature under a vacuum. The polyethylenimine (PEI) was purified by passing its dilute solution through columns containing cation and anion exchange resins in the hydrogen and hydroxide forms respectively. Its molecular weight was estimated viscometrically to be about 2000. The ethylene glycol (EG) was a chromatographically pure reagent, and the ethylenediamine (ED) and triethylamine (TEA) were guaranteed reagents. These materials were dried over molecular sieve and were used without further purification. The diethylene glycol (DEG), triethylene glycol (TEG), ethylene glycol dimethyl ether (EGDME), diethylene glycol dimethyl ether (DEGDME), triethylene glycol dimethyl ether (TEGDME), diethylenetriamine (DT), triethylenetetramine (TT), and tetraethylenepentamine (TP) were fractionally distilled. The water used to prepare the solutions was distilled and then purified by passing it through a column of cation-anion exchange resin mixtures.

Results and Discussion

The specific volumes of the pure solutes at various temperatures are given in Table 1. From these data, the specific expansibilities, $\partial v_2/\partial T$, at 4°C can be

Table 1. Specific volume, v_2, and specific expansibility, $\partial v_2/\partial T$, at 4°C of pure solutes

Solute	v_2 (m*l* g^{-1})					$\partial v_2/\partial T \times 10^3$ (m*l* g^{-1} deg^{-1})
	5°	15°	25°	35°	45°	
EG	0.88967	0.89520	0.90087	0.90660	0.91248	0.547
DEG	0.88713	0.89280	0.89846	0.90433	0.91025	0.557
TEG	0.88071	0.88685	0.89300	0.89926	0.90563	0.606
PEG-200	0.87959	0.88596	0.89230	0.89868	0.90522	0.628
PEG-400[a]	—	—	—	—	—	0.646
PEG-20000	—	—	—	—	—	(0.66)
EGDME[a]	—	—	—	—	—	1.346
DEGDME[a]	—	—	—	—	—	1.064
TEGDME[a]	—	—	—	—	—	0.947
ED	—	1.10796	1.11966	1.13163	1.14388	1.126
DT	1.03803	1.04750	1.05694	1.06647	—	0.943
TT	1.00782	1.01624	1.02445	1.03281	—	0.832
TP	0.99473	1.00273	1.01036	1.01818	—	0.780
PEI	—	—	—	—	—	(0.62)
TEA	1.34836	1.36528	1.38263	1.40080	—	1.647

a) The values of $\partial v_2/\partial T$ of these solutes were calculated from the unpublished density data by T. Nakajima.

10) J. P. McHutchison, *J. Chem. Soc.*, **1926**, 1898.
11) N. Gregg-Wilson and R. Wright, *J. Phys. Chem.*, **35**, 624 (1931).
12) A. G. Mitchell and E. F. K. Wynne-Jones, *Discuss. Faraday Soc.*, **15**, 161 (1953).
13) G. Wada and S. Umeda, This Bulletin **35**, 646, 1797 (1962).
14) F. Franks and B. Watson, *Trans. Faraday Soc.*, **63**, 329 (1967).
15) "International Critical Tables," Vol. III, McGraw-Hill, New York (1933), p. 107.

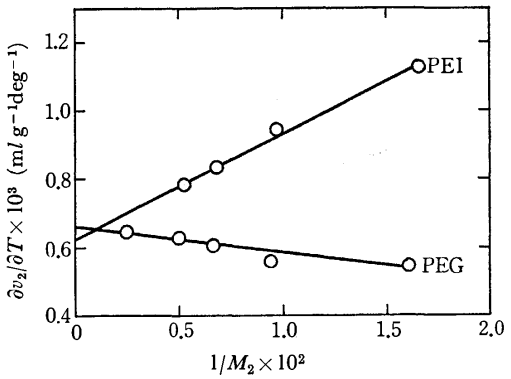

Fig. 1. Plots of specific expansibility at 4°C *vs.* the reciprocal of molecular weight of the oligomers.

evaluated by the least-square method; the values are given in the last column of Table 1. The specific volumes of high polymers in the liquid state are not known, so the $\partial v_2/\partial T$ values of PEG-20000 and PEI were estimated roughly by extrapolating the corresponding values of the respective oligomers to an infinite molecular weight, as is illustrated in Fig. 1.

The shifts, $\Delta\theta$, in the TMD produced by the addition of various solutes are summarized in Table 2. The concentration is expressed in terms of the weight fraction in order to facilitate the comparison of the behavior of polymers with that of low-molecular-weight analogues.

The quantitative analysis of $\Delta\theta$ in terms of the water-structural concept has been proposed by Wada and

TABLE 2. THE SHIFTS IN TMD AND THE APPARENT SPECIFIC EXPANSIBILITIES IN THE NEIGHBOURHOOD OF 4°C AT VARIOUS WEIGHT FRACTIONS

Solute	$w\times10^2$	$\Delta\theta$ (deg)	$\Delta\theta_{str}$ (deg)	$\partial\phi_2/\partial T\times10^3$ (ml g^{-1} deg^{-1})
EG	0.4232	−0.22	−0.07	0.81±0.07
	0.5727	−0.30	−0·10	0.81±0.05
	0.7575	−0.41	−0.14	0.84±0.04
	1.0544	−0.55	−0.18	0.81±0.03
	1.5899	−0.83	−0.26	0.80±0.02
	2.1588	−1.17	−0.40	0.83±0.02
DEG	0.4504	−0.20	−0.04	0.69±0.07
	0.5977	−0.27	−0.06	0.70±0.05
	0.9017	−0.42	−0.10	0.72±0.03
	1.0327	−0.48	−0.11	0.72±0.03
	1.4325	−0.70	−0.18	0.75±0.02
	2.3016	−1.12	−0.28	0.74±0.02
TEG	0.2840	−0.12	−0.01	0.66±0.11
	0.5040	−0.24	−0.04	0.74±0.06
	0.6469	−0.32	−0.07	0.77±0.04
	0.9076	−0.46	−0.10	0.78±0.03
	1.2236	−0.65	−0.17	0.82±0.03
	2.2177	−1.22	−0.34	0.84±0.02
PEG-200	0.1787	−0.11	−0.04	0.96±0.17
	0.3264	−0.20	−0.07	0.95±0.10
	0.5948	−0.33	−0.09	0.86±0.05
	0.8130	−0.45	−0.12	0.86±0.04
PEG-400	0.1319	−0.08	−0.03	0.94±0.23
	0.3379	−0.20	−0.06	0.92±0.09
	0.5463	−0.34	−0.11	0.97±0.06
	0.8555	−0.54	−0.18	0.98±0.03
PEG-20000	0.3357	−0.22	−0.07	1.02±0.09
	0.5752	−0.38	−0.14	1.02±0.06
	1.2382	−0.83	−0.30	1.03±0.03
EGDME	0.1347	−0.04	0.08	0.46±0.23
	0.2726	−0.08	0.16	0.46±0.11
	0.4292	−0.18	0.19	0.65±0.07
	0.4958	−0.20	0.23	0.63±0.06
	0.6276	−0.25	0.29	0.62±0.05
	0.7770	−0.32	0.36	0.64±0.04
	1.0282	−0.42	0.48	0.63±0.03
	1.5267	−0.70	0.64	0.70±0.02
DEGDME	0.5848	−0.33	0.07	0.88±0.06
	0.8516	−0.48	0.11	0.87±0.04
	1.1625	−0.65	0.15	0.86±0.03
	1.6526	−0.95	0.20	0.88±0.02
	2.0689	−1.21	0.23	0.89±0.02
TEGDME	0.5559	−0.30	0.04	0.84±0.06
	0.8191	−0.46	0.04	0.87±0.04
	1.3529	−0.77	0.06	0.88±0.03
ED	0.1263	−0.07	0.02	0.86±0.24
	0.3426	−0.19	0.06	0.86±0.09
	0.5477	−0.33	0.07	0.93±0.06
	0.8811	−0.53	0.11	0.93±0.04
	1.2344	−0.78	0.12	0.97±0.03
DT	0.0983	−0.05	0.01	0.79±0.31
	0.1772	−0.08	0.03	0.70±0.18
	0.5299	−0.25	0.07	0.73±0.06
	1.0397	−0.50	0.13	0.74±0.03
	1.5302	−0.74	0.20	0.74±0.02
	2.4478	−1.25	0.27	0.78±0.02
TT	0.7412	−0.33	0.07	0.69±0.05
	1.0523	−0.47	0.10	0.69±0.03
	1.5883	−0.72	0.14	0.70±0.02
	1.9005	−0.87	0.16	0.70±0.02
	2.7827	−1.32	0.21	0.72±0.01
TP	0.2167	−0.10	0.01	0.72±0.14
	0.4075	−0.18	0.02	0.69±0.09
	0.7812	−0.33	0.06	0.06±0.04
	2.0290	−0.88	0.16	0.66±0.02
	2.5220	−1.13	0.16	0.68±0.01
	3.4949	−1.63	0.18	0.70±0.01
PEI	0.1247	−0.07	−0.02	0.88±0.24
	0.2258	−0.12	−0.03	0.83±0.14
	0.3988	−0.24	−0.08	0.94±0.08
	0.5354	−0.28	−0.07	0.81±0.06
	0.8395	−0.46	−0.12	0.85±0.04
TEA	0.0932	0.02	0.12	−0.33±0.33
	0.1944	0.00	0.21	0.00±0.16
	0.5141	−0.07	0.48	0.21±0.06
	1.2898	−0.39	0.99	0.47±0.03
	1.8690	−0.73	1.28	0.60±0.02

Umeda[13] and has been extended by Franks and Watson.[14] The specific volume, v, of a solution is expressed by:

$$v = (1-w)v_1 + wv_2 + \Delta v_w^M \quad (1)$$

where v_1 and v_2 are the specific volumes of water and a pure solute respectively, and where Δv_w^M is the excess volume of mixing referred to a mixture of the solute weight fraction, w. The temperature dependence of v_1 in the vicinity of the TMD can be given by a parabolic function:[13]

$$v_1 = v_1^*[1+\alpha_1(T-3.98)^2] \quad (2)$$

where v_1^* is the specific volume of water at 3.98°C and where α_1 is the coefficient relating to the thermal expansion. By inserting Eq. (2) into Eq. (1), and differentiating with respect to temperature, and then from the condition: $\partial v/\partial T=0$ at the TMD, one obtains the following relation:

$$\Delta\theta = (T-3.98) = -\frac{w\partial v_2/\partial T}{2(1-w)v_1^*\alpha_1} - \frac{\partial \Delta v_w^M/\partial T}{2(1-w)v_1^*\alpha_1} \quad (3)$$

The first term, denoted by $\Delta\theta_{id}$, on the right-hand side of Eq. (3) indicates that, for ideal solutions, $\Delta\theta$ is always negative and is proportional to the concentration as long as for very dilute solutions. The second term, denoted by $\Delta\theta_{str}$, is referred to the temperature dependence of the excess volume and may be attributed to the change in water structure caused by adding various solutes.

The values of $\Delta\theta_{str}$ have been evaluated for various solutes.[13,14] In general, it appears that the values of $\Delta\theta_{str}$ are large and positive for such solutes as monofunctional alcohols and amines, whereas more hydrophilic solutes such as ethylene glycol and dioxane produce negative $\Delta\theta_{str}$ values. In other words, the sign and magnitude of $\Delta\theta_{str}$ depend mainly on the hydrophilic-hydrophobic balance within the respective solute molecules, or are due to some kinds of water-structure modifications.

There have been various discussions with respect to the structure of water in a pure liquid state and in aqueous solutions. At present, however, no satisfactorily reasonable interpretation and models have been proposed.[1,8,9,16,17] In the present analysis, the so-called two-state model was adopted as a basis for discussion; it is assumed that water is an equilibrium mixture of bulky hydrogen-bonded species and dense unbonded species, and also that the introduction of a small quantity of non-polar molecules or groups into aqueous solutions shifts the equilibrium between the two species from dense species to bulky species.

The effect of a solute on TMD may be interpreted in terms of the difference in the specific expansibility of the pure solute and the apparent specific expansibility of the solute in water. The specific volume of a solution is also expressed using the apparent specific volume, ϕ_2, of a solute as follows:

$$v = (1-w)v_1 + w\phi_2 \quad (4)$$

Then, we obtain the following equation instead of Eq. (3):

$$\Delta\theta = -\frac{w}{2(1-w)v_1^*\alpha_1}\frac{\partial\phi_2}{\partial T} \quad (5)$$

Combining Eqs. (3) and (5) yields;

$$\frac{\partial \Delta v_w^M}{\partial T} = w\left(\frac{\partial\phi_2}{\partial T} - \frac{\partial v_2}{\partial T}\right) \quad (6)$$

Since the hydrogen-bonded structure of water is broken down rapidly with a rise in the temperature, and since, accordingly, the amounts of unbonded water mole-

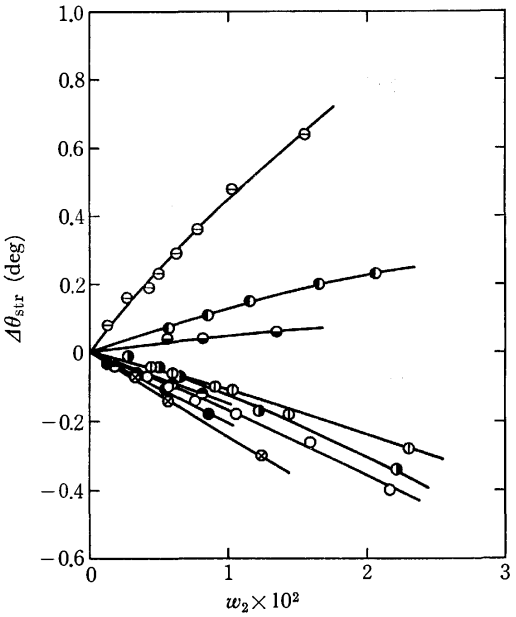

Fig. 2. Variation of $\Delta\theta_{str}$ with the concentration.
○, EG; ⓘ, DEG; ◑, TEG; ◓, PEG-200; ●, PEG-400; ⊗, PEG-20000; ⊖, EGDME; ◐, DEGDME; ◒, TEGDME.

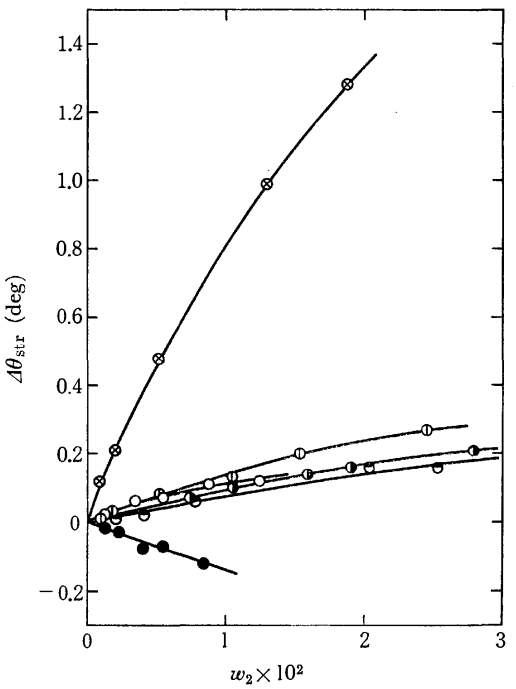

Fig. 3. Variation of $\Delta\theta_{str}$ with the concentration.
○, ED; ⓘ, DT; ◑, TT; ◓, TP; ●, PEI; ⊗, TEA.

16) H. S. Frank, *Federat. Proc.*, **24**, *Suppl.* 15, s-1 (1965).
17) H. S. Frank, *Science*, **169**, 635 (1970).

cules with a higher density are increased, the increase in the apparent specific volume of a hydrophobic solute in aqueous solution caused by the increase in temperature might to some extent be canceled out in comparison with a case where no special hydrophobic interaction, the so-called "hydrophobic hydration," takes place. Therefore, when the solute is a structure-stabilizing one, the value of $\partial\phi_2/\partial T$ is smaller than that of $\partial v_2/\partial T$; namely, a positive $\Delta\theta_{str}$ value can be derived from Eq. (6).

In Table 2 and in Figs. 2 and 3, the values of $\Delta\theta_{str}$ obtained are shown as a function of the weight fraction.[18] From the results shown in Fig. 2, it is clear that, for a series of PEG oligomers, the $\Delta\theta_{str}$ values are all negative over the entire concentration range studied and that they change according to their chain lengths in the following order:

DEG>TEG>PEG-200>EG>PEG-400>PEG-20000

Unfortunately, little is yet known about the influence of such a polar substance on the structure of water, but the fact that negative $\Delta\theta_{str}$ values are obtained may indicate that these solutes disrupt the intermolecular structure of water because of the formation of strong hydrogen bonds between solutes and water. It seems that the increase in temperature produces such larger ϕ_2 values as a result of the disruption of the solute-water hydrogen-bonding, which itself results in the volume contraction around the hydroxyl groups. If this is true, the $\Delta\theta_{str}$ value should become negative according to Eq. (6).

As regards the hydrophilic-hydrophobic balance within a solute molecule, molecules of longer chain length should become more hydrophobic than lower-molecular-weight analogues in this series, because of the relative decrease in the contribution from the hydrophilic terminal hydroxyl groups. The above sequence observed for PEG oligomers is, however, just the opposite of what might be expected from this idea, except for the case of EG. As will be discussed in detail later, we propose another scheme of interpretation, *i.e.*, a concept of hydrophobic contact between ethylene groups.

Figure 3 shows the $\Delta\theta_{str}$ values for the PEI oligomers and TEA. The latter is expected to behave as a typical hydrophobic solute in water. In fact, TEA produces a strikingly large positive $\Delta\theta_{str}$, which is comparable in magnitude to those produced by monohydric alcohols[13] or dialkylamines.[14] It is observed with PEI oligomers that the $\Delta\theta_{str}$ changes according to their chain lengths in the following order:

DT>ED>TT>TP>PEI

which is quite similar to the sequence for the PEG oligomers. However, in contrast to the PEG oligomers, the values of $\Delta\theta_{str}$ are slightly positive except for the case of PEI. This difference suggests that the hydrogen bond between water and the hydroxyl group of the PEG oligomers is stronger than that between water and the amino group of the PEI oligomers. This may be accounted for on the basis that the more electronegative oxygen atom is generally able to form a stronger hydrogen bond than is the less electronegative nitrogen atom.

It could, however, be emphasized that too much significance should not be found in the difference in $\Delta\theta_{str}$ because of the choice of the standard state.[19,20] In the present analysis, the pure liquid state of the solute was used as the standard state in order to calculate $\partial v_2/\partial T$ and $\Delta\theta_{str}$. For the purpose of a more accurate discussion of the solute-water interaction, one should use the hypothetical value of $\partial v_2/\partial T$ in an infinitely dilute aqueous solution (in other words, under the condition that no solute-solute interaction takes place) instead of in the pure liquid state. Especially when liquids exhibits significant intermolecular interactions, the adoption of the pure liquid state as the standard has its disadvantages. We should not ignore this situation in comparing the behavior of the oligomers of the PEG with that of the PEI, since the former possesses a much greater ability of solute-solute hydrogen-bonding than the latter; this is suggested by their high viscosities and the characteristic variation in their specific expansibilities with the increase in the chain length for the PEG oligomers, as is shown in Fig. 1. This may also be closely related to the fact that the $\Delta\theta_{str}$ values of various alcohols and amines do not always increase in a regular manner with the number of carbon atoms within the solute molecules. It may, at any rate, be permissible to consider that the difference in $\Delta\theta_{str}$ indicates at least a relative difference in the solute-water interaction so far as the chain-length dependence of $\Delta\theta_{str}$ for the oligomers of the homologous series is concerned, as we have done in this study.

As is shown in Fig. 2, for the series of glycol dimethyl ethers the $\Delta\theta_{str}$ values are all positive, decreasing more rapidly in magnitude with the increase in chain length than for the series of the PEG and PEI oligomers. The positive $\Delta\theta_{str}$ value suggests a comparatively stronger hydrophobic hydration caused by the terminal methyl groups. This is confirmed by the results of the limiting partial molar volumes of various glycols in aqueous solutions by Nakanishi *et al.*,[21] who stated that such glycol molecules as 1,2-ethanediol and 1,3-propanediol mix "substitutionally" with water, whereas, when one of the hydroxyl groups is not located at the end of the molecule (*e.g.*, 1,2-propanediol or 1,3-butanediol), the "interstitial" contribution due to a possible cavity occupation by a methyl group increases.

As has been described above, ED and EG give rise

18) In order to calculate $\Delta\theta_{str}$ as a first approximation, the value of $\partial v_2/\partial T$ at 4°C is always employed in the present analysis, since it can be considered that there is no effect of the variation of $\partial v_2/\partial T$ in a small range of temperature (the maximum value of $\Delta\theta$ obtained in this experiment is −1.63°C). Also, the use of $\partial v_2/\partial T$ which are estimated roughly by a extrapolation method for the high polymers is believed not to result in a large error in calculating $\Delta\theta_{str}$, or at least this has no influence upon the present discussion relating to the chain length dependence.

19) F. Franks and H. T. Smith, *Trans. Faraday Soc.*, **64**, 2962 (1968).

20) General Discussion in Ref. 9, p. 222.

21) K. Nakanishi, N. Kato, and M. Maruyama, *J. Phys. Chem.*, **71**, 814 (1967).

to unordinary values of $\Delta\theta_{str}$, and EGDME produces a particularly large positive $\Delta\theta_{str}$ value. This observation suggests that, in the case of these small molecules with only one ethylene group, the nature of the terminal group may be one of the decisive factors in the interactions between the solute and the water molecules.

Thus, the results on the $\Delta\theta_{str}$ values of these oligomer solutions prove that the hydrophobic interaction of a chain molecule with water decreases as the chain length increases, provided that the interaction is not affected remarkably by the terminal group. It is plausible to consider that the effect of the chain length on the hydrophobicity is due to the conformational change of a chain molecule. Recently, Neal and Goring[7] measured the temperature dependence of the apparent specific volume, *i.e.*, the apparent specific expansibility, $\partial\phi_2/\partial T$, for various aqueous solutions; they proposed that this quantity might be a useful measure of the effect of a nonelectrolyte on the structure of water. Subsequently, they could show the increase in $\partial\phi_2/\partial T$ with an increase in the chain length for both oligomers of polyethylene glycol and polypropylene glycol.[6] That is to say, the hydrophobic character of a chain molecule decreases with an increase in the chain length. More recently, the partial molar volumes of the series of glycol dimethyl ethers in aqueous solutions have been measured at various temperatures by Nakajima *et al.*[22] According to their analysis, the partial molar volume of the ($-CH_2CH_2O-$) group can be calculated from the differences in the partial molar volumes between DEGDME and EGDME and also between TEGDME and DEGDME. The value obtained from TEGDME is greater than those obtained from DEGDME and EGDME. This fact suggests that the extent of the hydrophobic hydration of these chain molecules in aqueous solutions decreases with an increase in the chain length, if one accepts the hypothesis that such a hydration occurs with an overall economy of space. These results agree very well with the results of our TMD measurements. The most reasonable interpretation of this effect may be that, with an increase in the chain length, the hydrophobic contact between ($-CH_2CH_2-$) groups takes place more easily and that, consequently, the relative decrease in hydrophobic interaction is observed because of the reduction of the ($-CH_2CH_2-$) area which is accessible to water, as was proposed by Sandell and Goring.[6]

By using Eq. (5), the values of $\partial\phi_2/\partial T$ in the neighbourhood of 4°C at various concentrations can be calculated from the TMD data, which are summarized in the last column of Table 2. The maximum error in $\partial\phi_2/\partial T$ was estimated on the basis of the accuracy in determining TMD: ±0.02°C. Some results are shown in Figs. 4 and 5, in which the values for several alcohols calculated from the TMD data by Wada and Umeda[13] are also included. Of course, the values of $\partial\phi_2/\partial T$ at various concentrations cannot be evaluated at a constant temperature by this method; moreover, the accuracy of $\partial\phi_2/\partial T$ is not satisfactory because of the very low concentrations. The data shown in Figs. 4 and 5, however, may be good enough for us to discuss some qualitative tendency of these values in connection with the hydrophobic character of the solutes. The fact that the $\partial\phi_2/\partial T$ values of all the PEG oligomers increase with an increase in the chain length, except for EG, accords qualitatively with the results which were directly measured by Sandell and Goring. For the PEI oligomers, on the other hand, this is not the case. The variation in $\partial v_2/\partial T$ with the chain length is exceedingly larger for the PEI

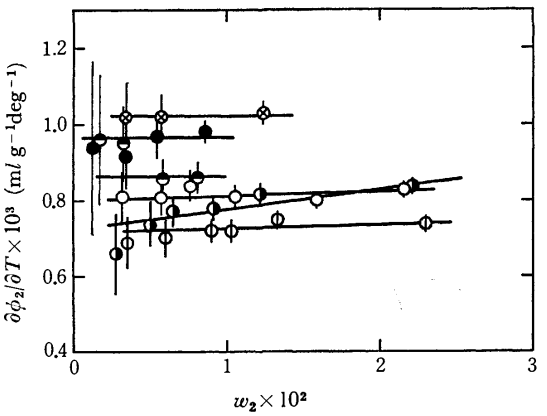

Fig. 4. Concentration dependence of $\partial\phi_2/\partial T$ for PEG oligomers; ○, EG; ◑, DEG; ◑, TEG; ◓, PEG-200; ●, PEG-400; ⊗, PEG-20000.

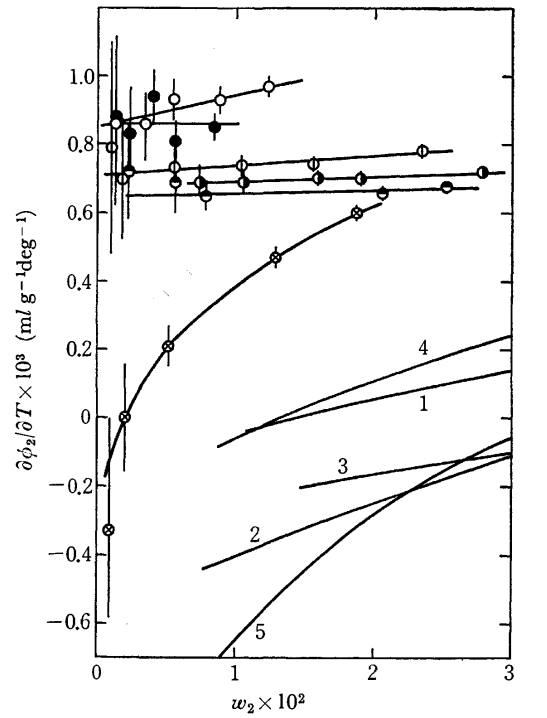

Fig. 5. Concentration dependence of $\partial\phi_2/\partial T$ for PEI oligomers, TEA and some alcohols (the data for alcohols are all calculated from Wada and Umeda, Ref. 13); ○, ED; ◑, DT; ◑, TT; ◓, TP; ●, TEI; ⊗, TEA; 1, MeOH; 2, EtOH; 3, *iso*-PrOH; 4, *sec*-BuOH; 5, *tert*-BuOH.

22) T. Nakajima, T. Komatsu, and T. Nakagawa, *Repts. Progr. Polym. Phys. Japan*, **14**, 1 (1971).

oligomers than for the PEG oligomers, as is shown in Fig. 1; therefore, the variation in the $\partial\phi_2/\partial T$ values with the chain length seems to be largely due to the difference in $\partial v_2/\partial T$ values, though there exists a problem in the choice of the standard state, as has been mentioned above. In such a case it may be inadequate to use the quantity $\partial\phi_2/\partial T$ as a measure of the effect of a solute molecule on the structure of water.[23]

Figures 4 and 5 show the characteristic tendencies of $\partial\phi_2/\partial T$ for various solutes. The solutes which produce small positive or negative $\Delta\theta_{str}$ values, such as the chain molecules used in this experiment, give rise to a slight concentration dependence of $\partial\phi_2/\partial T$, whereas those which produce large positive $\Delta\theta_{str}$ values, such as TEA and many monohydric alcohols, bring about a striking concentration dependence of $\partial\phi_2/\partial T$. The latter have been regarded as hydrogen-bonded-structure makers and will give rise to a larger hydrophobic hydration than the former.

It is well known that the apparent specific volume of a hydrophobic substance in an aqueous solution decreases with its concentration so long as the concentration is low. This behavior has been interpreted in terms of "mutual salting-in"[25] or "mutual co-operative stabilization."[26] According to Franks and Smith,[26] the non-polar solutes form complete or partial clathrate cage systems, resulting in a contraction in the net volume. When two solute molecules approach each other at a suitable distance, such cage systems are stabilized co-operatively and, consequently, ϕ_2 decreases with a rise in the concentration. Therefore, the slope of the ϕ_2-concentration curve becomes more negative as the temperature is lowered or as the sizes of the non-polar groups of the solute molecules become larger. This phenomenon is the same as with the larger concentration dependence of $\partial\phi_2/\partial T$ of the strongly hydrophobic solutes. Thus, the concentration dependence of $\partial\phi_2/\partial T$ may also be regarded as a useful measure of the structural effect of a solute molecule from the viewpoint of solute-solute interaction.

One could find from Eq. (5) that a positive $\Delta\theta$ is equivalent to the negative expansibility. As has been mentioned in the introduction, this anomalous behavior should be considered as an evidence for the stabilization of the water structure surrounding the non-polar groups of a solute molecule. In fact, the negative expansibility has been observed directly with *tert*-butyl alcohol and *sec*-butyl alcohol in very dilute aqueous solutions.[19] As is shown in Fig. 5, it is evident that this phenomenon should also be observed in the very dilute aqueous solutions of many monohydric alcohols and possibly TEA.

Finally, it should be pointed out that our conclusion concerning chain molecule-water interaction is quite similar to that of Sandell and Goring,[6] but it may conflict with the explanation by Okubo and Ise of their solubility results.[5] The solubilities of naphthalene and biphenyl in aqueous solutions of PEI and its oligomers (ED, DT, TT, TP) increase with increases in their chain length. From these results they have concluded that the so-called "iceberg" formation of water molecules may be facilitated by an increasing degree of polymerization. It is difficult to solve the problem of these conflicting results. It can, however, be proposed that the solubility behavior of a non-polar co-solute in aqueous solutions of the chain molecules may be of a rather complicated nature as a result, for instance, of the conformational change of the solute molecules themselves. A more systematic investigation regarding the solubility behavior of nonelectrolytes in aqueous polymer solutions, and especially its temperature dependence, remains a subject for future study.

The authors wish to thank Mr. Toshio Nakajima for his helpful discussion. The present work has been supported in part by a Grant for Scientific Research from the Ministry of Education.

23) According to the data of Sandell and Goring,[6] the values of $\partial v_2/\partial T$ for PEG oligomers are independent of the chain lengths; in such a case $\Delta\theta_{str}$ must be in parallel with $\partial\phi_2/\partial T$. Our own data obtained by pycnometry, however, indicate that $\partial v_2/\partial T$ are clearly dependent on the chain lengths, as shown in Fig. 1. That is to say, it is not always advantageous to discuss any solute-water interaction in terms of $\partial\phi_2/\partial T$ or $\Delta\theta$ (not $\Delta\theta_{str}$). For example, it should be misleading to conclude from the measurements of $\Delta\theta$ alone that the quaternary alkylammonium halides, which are regarded as typical structure stabilizing solutes at room temperature, disrupt the hydrogen-bonded structure of water at low temperatures.[24]

24) A. J. Darnell and J. Greyson, *J. Phys. Chem.*, **72**, 3021 (1968); see also, T. S. Sarma and J. C. Ahluwalia, *ibid.*, **74**, 3547 (1970).

25) J. E. Desnoyers and M. Arel, *Can. J. Chem.*, **45**, 359 (1967).

26) F. Franks and H. T. Smith, *Trans. Faraday Soc.*, **63**, 2586 (1967).

Interaction of 1,2-Dichloroethane with Benzene and other Aromatic Hydrocarbons

Akio MORITA, Hiroaki TAKAHASHI, and Keniti HIGASI

School of Science and Engineering, Waseda University, Shinjuku, Tokyo

(Received August 21, 1971)

Experiments to confirm Kubo's conclusion on the complex formation of 1,2-dichloroethane with benzene were carried out following his procedure. Dielectric measurements were carried out with inert solvents hexane and cyclohexane. The interactions between 1,2-dichloroethane and each of the compounds toluene and *p*-xylene were also studied with inert solvents hexane, cyclohexane, and carbon tetrachloride. The results are discussed in relation to complex formation.

It was found that the dipole moment of 1,2-dichloroethane, when measured in benzene solution, is unaccountably high.[1] It was also found that the Raman lines of the same molecule in the same solvent show abnormal behavior.[2] Later investigation led to the conclusion that the gauche isomers of this molecule gain an extra stability in benzene. However, no satisfactory explanation has been offered since for the nature of the extra energy.[3] From ultrasonic and thermodynamic studies it was concluded that there is some interaction between 1,2-dichloroethane and an aromatic hydrocarbon but no evidenc for complex formation between these molecules was obtained.[4]

The complex formation between 1,2-dichloroethane and benzene has been suggested by many workers.[5] First experimental proof was given by Kubo[6] from the dielectric measurements of mixtures of the two molecules in the medium of carbon tetrachloride. He examined a general case of complex formation:

$$CH_2Cl\text{-}CH_2Cl + nC_6H_6 \rightleftarrows CH_2Cl\text{-}CH_2Cl\cdot nC_6H_6$$

and showed that the number n should be 1 and not 2. He gave the equilibrium constant $K_c=32$ ml/mol and the excess polarization for the solute $\Delta P=97.6$ cm^3 at 20°C. From his ΔP value the dipole moment of the 1 : 1 complex was estimated[7] to be almost equal to the value 2.55 D[8] of the gauche isomer. Thus, we might conclude that the gauche isomer is stabilized in benzene solution through the complex formation, because such formation will certainly result in stronger intensities of the Raman lines of the gauche isomer and give rise to a high dipole moment in benzene solution.

The present paper deals with dielectric measurements on the basis of complex formation; it is in fact an extention of Kubo's work. Three inert solvents were employed, *viz.*, hexane, cyclohexane, and carbon tetrachloride. Benzene, toluene (with polarity), and *p*-xylene (with no polarity) were also chosen as aromatic molecules for the interaction with 1,2-dichloroethane.

Experimental

Dielectric constants of dilute solutions of 1,2-dichloroethane were measured at 25°C with the use of a heterodyne apparatus at 1 MHz. Solvents are mixtures of aromatic and inert solvents. Dielectric constants ε and densities d of dilute solutions can be expressed by linear functions of concentration of the solute (wt. fraction $w<0.05$).

$$\begin{aligned} \varepsilon &= \varepsilon_m + aw \\ d &= d_m + bw \end{aligned} \qquad (1)$$

where ε_m, d_m are the dielectric constant and the density, respectively, of the mixture solvent and a, b are the so-called "slopes". With the use of these "slopes" we can obtain the apparent specific polarization ${}_\infty p^*$ of 1,2-dichloroethane (at zero concentration of the solute) in the mixture of two solvents with a given concentration of aromatic molecules.

$${}_\infty p^* = \frac{\varepsilon_m-1}{\varepsilon_m+2}\cdot\frac{1}{d_m}\left[\frac{3a}{(\varepsilon_m-1)(\varepsilon_m+2)}+\frac{d_m-b}{d_m}\right] \qquad (2)$$

The apparent polarization ${}_\infty p^*$ is a hypothetical polarization calculated on the assumption of no complex formation. It differs from the specific polarization ${}_\infty p$ obtained in the medium of inert solvent alone. The difference ${}_\infty p^*-{}_\infty p = \Delta p$ is, therefore, a measure of the interaction between the solute and the aromatic solvent. Multiplying Δp by the molecular weight M of 1,2-dichloroethane, we obtain the corresponding molecular polarization ΔP_{obs}. This polarization term has been obtained for the system of 1,2-dichloroethane, aromatic and inert solvents.

$$\Delta P_{obs} = M\,\Delta p = M({}_\infty p^* - {}_\infty p) \qquad (3)$$

The relationship between ΔP_{obs} and the concentration of aromatic solvent under the light of Kubo's equation[6] and the Benesi-Hildebrand[9] equation for complex formation were examined.

For the equilibrium of 1 : 1 complex formation

$$CH_2Cl\text{-}CH_2Cl + \text{Arom} \rightleftarrows \text{Complex}$$

we have the relation

$$K_c = \frac{\alpha}{(1-\alpha)c_B} \qquad (4)$$

where α is the fraction of dichloroethane combined with aromatic solvent and c_B the concentration of the aromatic solvent in equilibrium which is taken as equal to its initial concentration.

The following relation is assumed for fraction.

$$\alpha = \frac{\Delta P_{obs}}{\Delta P} \qquad (5)$$

1) L. Meyer, *Z. Physik. Chem.*, **B8**, 357 (1930); K. Higasi, *Bull. Inst. Phys. Chem. Res.*, **13**, 186 (1934).
2) S. Mizushima, Y. Morino, and K. Higasi, *Sci. Pap. Inst. Phys. Chem. Res.*, **25**, 159 (1934).
3) A. Wada and Y. Morino, *J. Chem. Phys.*, **22**, 1276 (1954).
4) O. Kiyohara and K. Arakawa, This Bulletin, **43**, 3037 (1970).
5) H. Müller, *Physik. Z.*, **34**, 689 (1933).
6) M. Kubo, *Bull. Inst. Phys. Chem. Res.*, **13**, 1221 (1934).
7) K. Chitoku and K. Higasi, This Bulletin, **40**, 773 (1967).
8) S. Mizushima, "Structure of Molecules and Internal Rotation," Academic Press, New York (1954), p. 35.
9) H. A. Benesi and J. H. Hildebrand, *J. Amer. Chem. Soc.*, **70**, 2832 (1948); **71**, 2703 (1949).

and

$$\Delta P = P(\mathrm{AB}) - P(\mathrm{A}) - P(\mathrm{B}) \quad (6)$$

where $P(\mathrm{AB})$, $P(\mathrm{A})$, and $P(\mathrm{B})$ are the molecular polarizations of the complex, dichloroethane and aromatic solvent, respectively.

Introducing Eq.(5) into Eq.(4), we get Kubo's formula[6]

$$\frac{\Delta P_{\mathrm{obs}}}{c_{\mathrm{B}}} = K_c(\Delta P - \Delta P_{\mathrm{obs}}) \quad (7)$$

In a similar way Benesi-Hilderband's equation[9] can be derived as

$$\frac{1}{\Delta P_{\mathrm{obs}}} = \frac{1}{K_c \Delta P}\cdot\frac{1}{c_{\mathrm{B}}} + \frac{1}{\Delta P} \quad (8)$$

The following modification of Eq.(8) can be used as well.[10]

$$\frac{c_{\mathrm{B}}}{\Delta P_{\mathrm{obs}}} = \frac{c_{\mathrm{B}}}{\Delta P} + \frac{1}{K_c \Delta P} \quad (9)$$

Plots of $\Delta P_{\mathrm{obs}}/c_{\mathrm{B}}$ against ΔP_{obs} will confirm the validity of Eq. (7); plots of $1/\Delta P_{\mathrm{obs}}$ against $1/c_{\mathrm{B}}$ and those of $c_{\mathrm{B}}/\Delta P_{\mathrm{obs}}$ against c_{B} are related to Eqs.(8) and (9), respectively. If the plots all satisfy the straight-line relationship and provide the consistent values of K and ΔP, we could conclude that 1 : 1 complex is formed between 1,2-dichloroethane and the aromatic solvent. K_c and ΔP are obtained from these plots.

In addition we can estimate the dipole moment μ_{AB} of the complex AB in Debye units from ΔP.

$$P_0(\mathrm{AB}) = \Delta P + P_0(\mathrm{A}) + P_0(\mathrm{B}) \quad (10)$$

$$\mu_{\mathrm{AB}} = 0.0128\sqrt{P_0(\mathrm{AB})T} \quad (11)$$

where $P_0(\mathrm{AB})$, $P_0(\mathrm{A})$, and $P_0(\mathrm{B})$ are the orientation polarizations of the complex, 1,2-dichloroethane, and aromatic solvent, respectively; and $P_0(\mathrm{A}) = P(\mathrm{A}) - P_E(\mathrm{A}) - P_A(\mathrm{A}) = P(\mathrm{A}) - 23.9\ \mathrm{cm}^3$;[8] and $P_0(\mathrm{B}) = 0$ for benzene and p-xylene and $P_0(\mathrm{B}) = 3.8\ \mathrm{cm}^3$ for toluene.[2,11]

Materials. Both 1,2-dichloroethane of special grade (Wako) and carbon tetrachloride were kept over calcium chloride for a week before distillation. Benzene, toluene, p-xylene, hexane, and cyclohexane were stored over sodium wire and distilled.

Results and Discussion

Results of the dielectric measurements are summarized in Tables 1, 2, and 3. The concentration of the aromatic hydrocarbon c_{B} in the system of three components is shown in the first column in the units of mol/m*l*. The dielectric constant ε_m and the densities d_{m} refer to the mixture solvent (with a given c_{B}). Two slopes a and b are obtained from several solutions with the same c_{B} and with the concentration of the solute w=0.01—0.05. With the use of ε_{m}, d_{m}, a, and b, the apparent specific polarization ${}_\infty p^*$ is calculated from which ΔP_{obs} is easily obtained (*cf.* Eqs. (2) and (3)).

The quantity $\Delta P_{\mathrm{obs}}/c_{\mathrm{B}}$ will be a linear function of ΔP_{obs} if Eq. (7) for the complex formation is satisfied in the system under examination. Plots of $\Delta P_{\mathrm{obs}}/c_{\mathrm{B}}$ are made against ΔP_{obs} for nine systems of 1,2-dichloroethane, aromatic, and inert solvents (see Figs. 1, 2, and 3). Deviations from the linear relation are within experimental error. We see that 1,2-dichloroethane forms 1 : 1 complex with an aromatic molecule, benzene, toluene, and p-xylene.

Other plots using the relations given by Benesi-Hildebrand equation (8) and Eq. (9) are repeated for all the systems. No appreciable deviation from the

Table 1. Apparent polarization of 1,2-dichloroethane in mixtures of benzene and inert solvent (25°C)

Benzene $c_{\mathrm{B}}(\times 10^{-3})$	ε_{m}	d_{m}	a	b	${}_\infty p^*$	ΔP_{obs}
a) Inert solvent: hexane						
11.18	2.274	0.8735	3.511	0.2578	89.1	26.6
7.69	2.145	0.8063	2.905	0.2827	84.3	21.8
6.08	2.087	0.7756	2.616	0.2874	81.3	18.8
5.64	2.071	0.7672	2.548	0.2955	80.4	17.9
0.00	1.891	0.6627	1.490	0.3053	(62.5)	0.0
b) Inert solvent: cyclohexane						
11.18	2.274	0.8735	3.511	0.2578	89.1	25.0
8.43	2.200	0.8454	3.187	0.2705	86.2	22.1
5.50	2.126	0.8176	2.815	0.2788	81.8	17.7
4.34	2.099	0.8071	2.663	0.2837	79.6	15.5
0.00	2.014	0.7735	1.819	0.2756	(64.1)	0.0
c) Inert solvent: carbon tetrachloride						
11.18	2.274	0.8735	3.511	0.2578	89.1	22.6
9.86	2.270	0.9573	3.737	0.2248	87.1	20.6
8.06	2.266	1.0708	3.898	0.1365	84.0	17.5
5.68	2.259	1.2243	4.141	−0.0161	79.6	13.1
0.00	2.226	1.5855	4.103	−0.4743	(66.5)	0.0

Values in parentheses correspond to ${}_\infty p$.

10) G. Briegleb, "Electronen-Donator-Acceptor Komplexe", Springer, Berlin (1961).

11) A. L. McClellan, "Tables of Experimental Dipole Moments," Freeman, San Francisco (1963).

TABLE 2. APPARENT POLARIZATION OF 1,2-DICHLOROETHANE IN MIXTURES OF TOLUENE AND INERT SOLVENT (25°C)

a) Inert solvent: hexane

Toluene $c_B(\times 10^{-3})$	ε_m	d_m	a	b	$M_\infty p^*$	ΔP_{obs}
9.35	2.374	0.8618	3.020	0.2669	79.3	16.8
5.74	2.180	0.7852	2.522	0.2956	76.8	14.3
4.38	2.107	0.7562	2.313	0.2962	75.3	12.8
3.32	2.054	0.7333	2.159	0.3061	73.6	11.1
0.00	1.891	0.6627	1.490	0.3053	(62.5)	0.0

b) Inert solvent: cyclohexane

9.35	2.374	0.8618	3.020	0.2669	79.3	15.2
6.73	2.263	0.8314	2.755	0.2739	77.6	13.5
5.92	2.220	0.8258	2.673	0.2772	76.9	12.8
4.40	2.172	0.8109	2.511	0.2761	75.4	11.3
0.00	2.014	0.7735	1.819	0.2756	(64.1)	0.0

c) Inert solvent: carbon tetrachloride

9.35	2.374	0.8618	3.020	0.2669	79.3	12.8
8.03	2.355	0.9642	3.323	0.2121	78.9	12.4
7.39	2.347	1.0135	3.473	0.1771	78.7	12.2
6.62	2.337	1.0733	3.641	0.1345	78.4	11.9
0.00	2.226	1.5855	4.103	−0.4743	(66.5)	0.0

TABLE 3. APPARENT POLARIZATION OF 1,2-DICHLOROETHANE IN MIXTURE OF *p*-XYLENE AND INERT SOLVENT (25°C).

a) Insert solvent: hexane

p-Xylene $c_B(\times 10^{-3})$	ε_m	d_m	a	b	$M_\infty p^*$	ΔP_{obs}
8.065	2.263	0.8562	2.902	0.2674	78.9	16.4
6.05	2.166	0.8096	2.593	0.2882	76.8	14.3
5.37	2.129	0.7940	2.484	0.2739	75.9	13.4
4.55	2.094	0.7750	2.247	0.2448	74.7	12.2
0.00	1.891	0.6627	1.490	0.3053	(62.5)	0.0

b) Inert solvent: cyclohexane

8.065	2.263	0.8562	2.902	0.2674	78.9	14.8
6.65	2.208	0.8399	2.712	0.2525	77.8	13.7
5.94	2.184	0.8319	2.644	0.2588	77.1	13.0
5.10	2.154	0.8222	2.573	0.2723	76.2	12.1
0.00	2.014	0.7735	1.819	0.2756	(64.1)	0.0

c) Inert solvent: carbon tetrachloride

8.065	2.263	0.8562	2.902	0.2674	78.9	12.4
7.16	2.255	0.9366	3.087	0.2197	77.9	11.4
6.68	2.256	0.9808	3.217	0.2020	77.4	10.9
5.86	2.254	1.0552	3.376	0.1460	76.3	9.8
0.00	2.226	1.5855	4.103	−0.4743	(66.5)	0.0

linearity was observed.

Two unknown quantities K_c and ΔP for each system can be determined by the least square method from the data with the use of any of Eqs.(7), (8), and (9). In Table 4 the equilibrium constant and the excess polarization ΔP thus obtained are recorded. Values calculated by Eq. (9) are omitted since they are very similar. All the K_c and ΔP values thus obtained are consistent with each other.

For the system of 1,2-dichloroethane, benzene, and carbon tetrachloride equilibrium constant K_c is found to be 30.0 ml/mol and the excess polarization ΔP= 90.0 cm³ at 25°C from Eq. (7). The values are in agreement with Kubo's K_c=32 ml/mol and ΔP= 97.6 cm³ at 20°C.[6]

We see from Figs. 1—3 that toluene has steeper inclinations. The different behavior of toluene may perhaps be due to the existence of polarity while both benzene and *p*-xylene lack it. The same trend is found in Benesi-Hildebrand's plots.

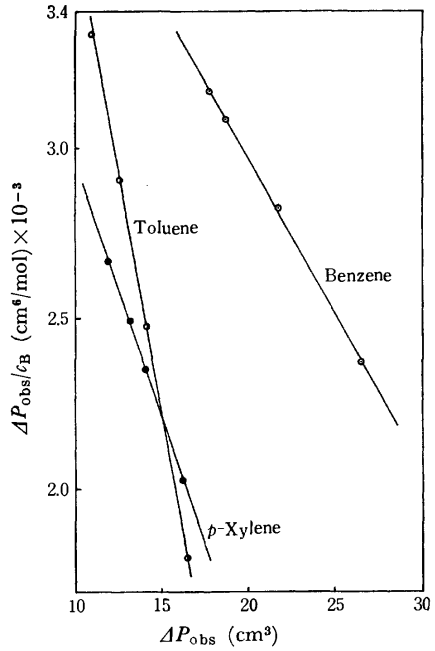

Fig. 1. Interaction of 1,2-dichloroethane with benzene, toluene, and *p*-xylene, in the inert medium of hexane.
⊙: Benzene, ○: Toluene, •: *p*-Xylene

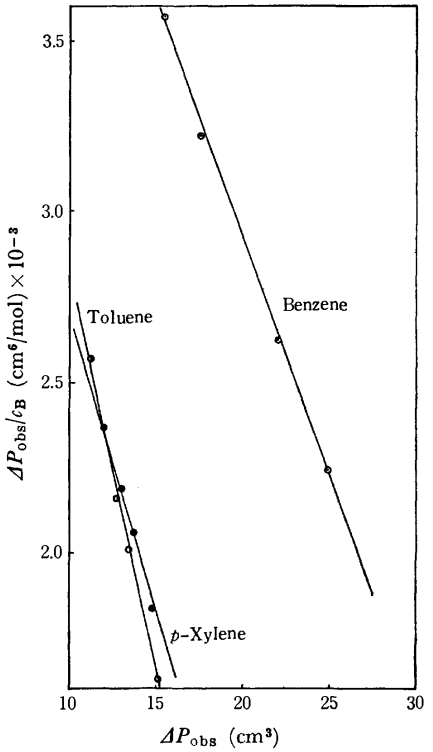

Fig. 2. Interaction as in Fig. 1, in the inert medium of cyclohexane.

From Table 4 we see that K_c in carbon tetrachloride is comparatively high with toluene and low with both benzene and *p*-xylene. Carbon tetrachloride may not be a perfectly inert solvent, some interaction with a solute often being suspected when this solvent is employed.[12,13] However, we have no means to decide the most ideal inert solvent among these non-polar solvents.

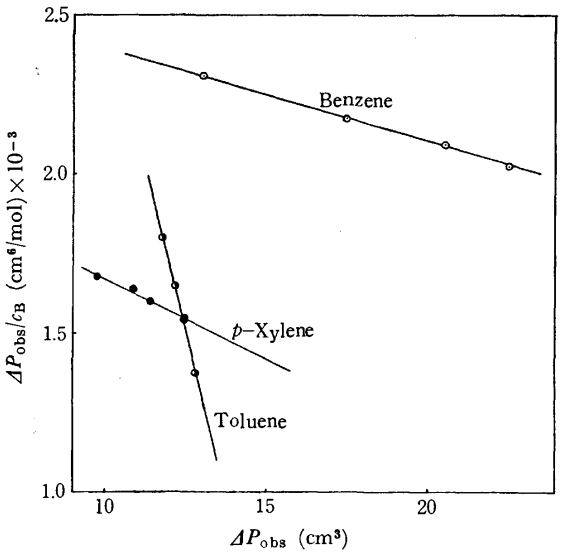

Fig. 3. Interaction as in Fig. 1, in the inert medium of carbon tetrachloride.

Table 4. K_c and ΔP obtained by Eqs. (7) and (8)

Inert solvent	Hexane	Cyclo-hexane	Carbon tetrachloride	
Intraction with Benzene				
K_c	90.7	139	30.0	(7)
(ml/mol)	90.4	140	30.6	(8)
ΔP	52.9	41.0	90.0	(7)
(cm^3)	52.9	40.8	88.5	(8)
Interaction with Toluene				
K_c	272	240	480	(7)
(ml/mol)	271	242	476	(8)
ΔP	23.4	21.9	15.6	(7)
(cm^3)	23.5	21.8	15.8	(8)
Interaction with *p*-Xylene				
K_c	155	196	51.0	(7)
(ml/mol)	154	200	53.1	(8)
ΔP	29.5	24.2	42.5	(7)
(cm^3)	29.6	24.0	41.5	(8)

The equilibrium constant K_c (Table 4) increases in the order

benzene < *p*-xylene < toluene

while the excess polarization varies in the order

toluene < *p*-xylene < benzene.

The trend is of interest since it will explain the apparently contradicting behavior of the relaxation times and the dipole moments obtained in benzene and *p*-xylene.[7]

The average relaxation time τ_0 and the Cole-Cole distribution parameter α of 1,2-dichloroethane increase from 3.69 psec and 0.13 in benzene to 4.53 psec and 0.19 in *p*-xylene. The increase seems parallel to the increase in the equilibrium constant. The ampler the complex, the greater the values of K_c and

12) T. Shibuya and Y. I'Haya, This Bulletin, **37**, 896 (1964).
13) K. Chitoku and K. Higasi, *ibid.*, **39**, 2160 (1966).

also of τ_0, since the average relaxation time becomes greater when the contribution from the complex with larger size is more important. The same contribution will give rise to an increase in α.

The dipole moment of 1,2-dichloroethane is found to be 1.63 D in *p*-xylene which is much less than the value 1.80 D in benzene.[7] This apparent decrease seems to be parallel to the decrease of ΔP from benzene to *p*-xylene. It reveals that the dipole moment of the complex with *p*-xylene becomes smaller compared with the moment of the complex with benzene.

In Table 5 the dipole moments of 1 : 1 complexes between 1,2-dichloroethane and aromatic solvents calculated from ΔP (Kubo's method) are recorded.

Table 5. Dipole moment of 1,2-dichloroethane-aromatic hydrocarbon complexes obtained by Eq. (11)

Aromatic Hydrocarbon	Inert solvent		
	Hexane	Cyclohexane	CCl_4
Benzene	2.11D	1.99D	2.54D
Toluene	1.79	1.79	1.74
p-Xylene	1.82	1.77	2.04

The dipole moment of the complex with benzene obtained in carbon tetrachloride is 2.54D, which is almost the same as the moment 2.55D presumed by Mizushima[8] as the moment of the gauche isomer. The equilibrium constant K_c=30.0 ml/mol (Kubo's method) gives α=0.25 in benzene at 25°C (*viz.*, c_B=$11.18\cdot10^{-3}$ mol/ml).

From the ratio of the intensities of the Raman lines I(gauche)/I trans), we can estimate the number of the gauche isomers in benzene and hexane at room temperature.[2] The mole fraction x_g of the gauche isomers increases from 0.16 (hexane) to 0.39 (benzene). On the other hand we find the increase in x_g is about 0.21 from dipole moment measurements, *viz.*, x_g in hexane 0.276, in carbon tetrachloride 0.289 and in benzene 0.491.[7]

It should be noted that the fraction of the complex 0.25 can be considered equal to the apparent increase 0.21—0.23 in x_g of the gauche isomers when transferred to benzene from a non-aromatic solvent.

This would imply that the extraordinary increase in numbers of the gauche isomers in benzene which is the so-called benzene effect is due to the formation of a complex which has the gauche conformation in the part of 1,2-dichloroethane. In the system of 1,2-dichloroethane - benzene - carbon tetrachloride the above statement appears to be valid since the complex has the same polarity as the gauche isomer. However, the situation is more complicated in other systems. The same problem will be discussed more in detail.[14]

From the dielectric measurements based on Kubo's procedure we get a similar evidence for complex formation between 1,2-dichloroethane and an aromatic hydrocarbon, *viz.*, benzene, toluene, or *p*-xylene, and we find that the so-called "benzene effect" might be related to the complex formation. It should be pointed out that both the equilibrium constant and the polarity of the complex are affected by the choice of inert solvents, hexane, cyclohexane, and carbon tetrachloride.

14) K. Higasi, H. Takahashi, K. Chitoku, and A. Morita, in press. *Memo. Sch. Sci. Eng., Waseda Univ.*, **35** (1971).

Radiolysis of Mixtures of Hydrocarbons and Ammonia. I. Formation of Ethylamine from a Mixture of Ethylene and Ammonia

Okihiro TOKUNAGA, Kumao HAMANOUE, Jiro OKAMOTO, and Akibumi DANNO

Japan Atomic Energy Research Institute, Tokai Research Establishment, Tokai-mura, Naka-gun, Ibaraki-ken

(Received August 18, 1971)

The γ-radiolysis of a gaseous mixture of ethylene and ammonia has been investigated over the whole range of composition. The products of decomposition were primarily hydrogen, ethane, *n*-butane, ethylamine, and acetylene. It was observed that the yields of ethane, *n*-butane, and ethylamine increased with the increasing concentration of ammonia, and that the *G*-values of these products at 98 mol% ammonia were 0.52, 2.12, and 0.89, respectively. Addition of oxygen or nitric oxide as radical scavengers tended to reduce the yields remarkably. The *G*-value of ethyl radical was calculated from the *G*-values of ethane, *n*-butane, and ethylamine, and the limiting value of $G(C_2H_5\cdot)$ was determined by extrapolation to 100 mol% ammonia. The value thus obtained agrees with the initial *G*-value of hydrogen radical, *i.e.*, $G_H=7.0\pm0.6$, which was obtained by Eyre and Smithies in the study of the γ-radiolysis of ammonia gas[1]. From these results, it was concluded that thermal hydrogen radicals produced by the γ-radiolysis react quickly with ethylene, giving ethane, *n*-butane, and ethylamine from ethyl radicals.

The radiolysis of olefins has been studied by many investigators. The primary process of hydrogen formation was investigated in detail by Hatano *et al.* on the simple olefins (ethylene, propylene, butene-1 and butene-2) under the action of γ-ray radiation.[2-7] They concluded that almost all the hydrogens produced were non-scavengeable and that they were produced by the decomposition of the so-called "super-excited state" which had been proposed by Platzman.[8-10]

It is well-known that thermal hydrogen radicals react quickly with olefins to form alkyl radicals *viz.*, the olefins are good radical scavengers.

It is obvious that hydrogen radical formed in the radiolysis of ammonia finally leads to hydrogen molecule or ammonia molecule. Eyre and Smithies reported that the initial *G*-value of hydrogen radical in the radiolysis of ammonia was as large as 7.0 ± 0.6.[1]

It is expected, therefore, that the concentration of ethyl radical may increase in the radiolysis of a mixture of ammonia and ethylene in which ammonia gives a a large *G*-value of hydrogen radical and ethylene is good radical acceptor. Thus the yields of the products produced by the reaction of ethyl radical might increase.

We have studied the γ-radiolysis of a gaseous mixture of ethylene and ammonia and will report on the mechanism of formation of ethane, *n*-butane, and ethylamine.

Experimental

Materials. Ethylene gas of high purity (over 99.8%) from the Takachiho Trading Co. was purified more than five times by bulb-to-bulb distillation, and only the middle fraction of the purified ethylene was used as the reactant. Purity was determined to be over 99.96% by gas chromatography. Ammonia of high purity (over 99.99%) from the Matheson Co. was dehydrated by metallic sodium and distilled by the bulb-to-bulb distillation method as in the case of ethylene, only the middle fraction of the purified ammonia being used as reactant. Purity of the ammonia was determined to be over 99.9% by gas chromatography. Oxygen and nitric oxide from the Takachiho Trading Co. were used without further purification.

Irradiation. A mixture of ethylene and ammonia was led into a 30 m*l* Pyrex glass ampoule fitted with a break-off seal at constant pressure (2 atm, 2.4×10^{-3} mol). Irradiation was carried out at room temperature by Co-60 γ-rays at the exposure-dose rate of 1.9×10^5 r/hr. In the run of hydrogen analysis, the experiment was carried out at 4 atm using a 3.1 m*l* Pyrex glass ampoule (5.0×10^{-4} mol of the mixture).

Analysis. *Ethylamine*: The irradiated sample was frozen at -196°C and dissolved in 1.0 m*l* benzene. 0.1 m*l* of the solution was then injected into a gas chromatograph (Yanagimoto, 3DH) equipped with a flame ionization detector by means of a micro-syringe. A column (2 m$\times$ 3 mm) with 10% KOH and 10% tetraethylene pentamine on 80/100 mesh Porapak Q was connected directly to a column with 10% KOH and 10% Lubrol MO on 80/100 mesh Porapak Q and used at 70°C. The carrier gas was nitrogen. Ethylamine was identified by the following. The retention time of the peak was consistent with that of a standard ethylamine and the peak disappeared when the sample was passed through sulfuric acid.

Hydrocarbons: The analysis was carried out with a gas chromatograph (Yanagimoto, G8) equipped with a flame ionization detector. A column (2 m$\times$4 mm) filled with silica gel was used, with nitrogen as a carrier gas. Measurement was carried out by the temperature promotion method in the range 50—150°C at a rate of 4°C/min.

Hydrogen: Non-condensable gases at -196°C were collected by a Toepler-pump and analyzed by a gas chromatograph (Yanagimoto, GC220) equipped with a thermal conductivity detector. A column (5 m$\times$5 mm) with Molecular Sieve 5A was used at room temperature with argon as a carrier gas.

Hydrazine: The irradiated sample was frozen at -196°C and dissolved in 2 m*l* water. The dissolved sample was analyzed by the method reported by Watt and Chrisp.[11]

1) J. A. Eyre and D. Smithies, *Trans. Faraday Soc.*, **66**, 2199 (1970).
2) Y. Hatano, S. Shida, and S. Sato, This Bulletin **37**, 1854 (1964).
3) Y. Hatano and S. Shida, *ibid.*, **39**, 456 (1966).
4) Y. Hatano and S. Shida, *J. Chem. Phys.*, **46**, 4784 (1967).
5) Y. Hatano, S. Shida, and M. Inokuti, *ibid.*, **48**, 940 (1968).
6) Y. Hatano, S. Shida, and S. Sato, This Bulletin **41**, 1120 (1968).
7) Y. Hatano, *ibid.*, **41**, 1126 (1968).
8) R. L. Platzman, *Radiat. Res.*, **17**, 419 (1962).
9) R. L. Platzman and W. P. Jesse, *Nature*, **195**, 790 (1962).
10) R. L. Platzman, *J. Chem. Phys.*, **38**, 2775 (1963).

Results

The products in the γ-radiolysis of ammonia were hydrogen, nitrogen, and hydrazine. Hydrogen and hydrazine were determined. In the case of ethylene radiolysis, hydrogen, methane, ethane, acetylene, propane, *n*-butane, *n*-pentane, and *n*-hexane were identified. These products were analyzed quantitatively except for *n*-pentane and *n*-hexane. In the γ-radiolysis of a mixture of ammonia and ethylene, formation of ethylamine was confirmed in addition to the above products.

In the radiolysis of pure ammonia, the *G*-value of hydrazine was very small, *i.e.*, $G(N_2H_4)=0.01$. In the case of the mixture of ammonia and ethylene, $G(N_2H_4)$ was not more than 0.01.

Dependence of the *G*-value of hydrogen $G(H_2)$ on the composition of the mixture is shown in Fig. 1. In the case of pure ethylene, $G(H_2)$ is 1.26 ± 0.03 both at 2 atm and 4 atm. This is consistent with the values reported.[6,12] Thus, there is no pressure effect in our experimental condition.

The dependence of the yield of ethylamine on dose at 90 mol% ammonia is shown in Fig. 2. The yield of ethylamine increases linearly with the increasing dose. From the slope of the straight line, the $G(C_2H_5NH_2)$ is calculated to be 0.73.

The depencence of the yield of ethylamine on the composition of the mixture is shown in Fig. 3. The yield of ethylamine increases with the increasing concentration of ammonia and the maximum yield 3.7×10^{-7} mol or $G(C_2H_5NH_2)=0.89$ is obtained at 98 mol% ammonia. In the case of pure ammonia, a small of ethylamine 0.25×10^{-7} mol was also obtained. This seems to be due to the elution of ethylamine by ammonia which was absorbed on the columns of the gas chromatograph.

Oxygen and nitric oxide are often used as radical scavengers in radiation chemistry. Table 1 shows the variations of the yields of ethylamine and *n*-butane by the addition of these scavengers. Both products were reduced completely by the addition of more than 0.15 mol% oxygen or by the addition of more than 0.6 mol% nitric oxide. It can be concluded that ethylamine and *n*-butane are formed through the radical processes.

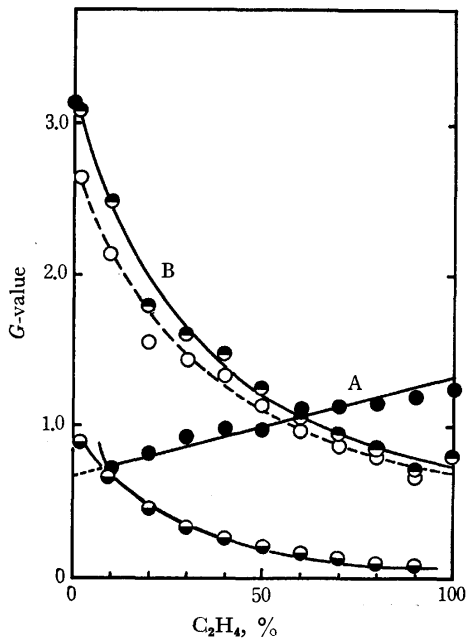

Fig. 1. Composition dependence of *G*-values.
dose; 1×10^{7} rad, $C_2H_4+NH_3=2.4\times10^{-3}$ mol
—●— (A): $G(H_2)$
—◒— : $G(C_2H_5NH_2)$
—○— : $G(C_2H_6)+G(n\text{-}C_4H_{10})$
—◓— (B): $G(C_2H_6)+G(n\text{-}C_4H_{10})+\frac{1}{2}\cdot G(C_2H_5NH_2)$

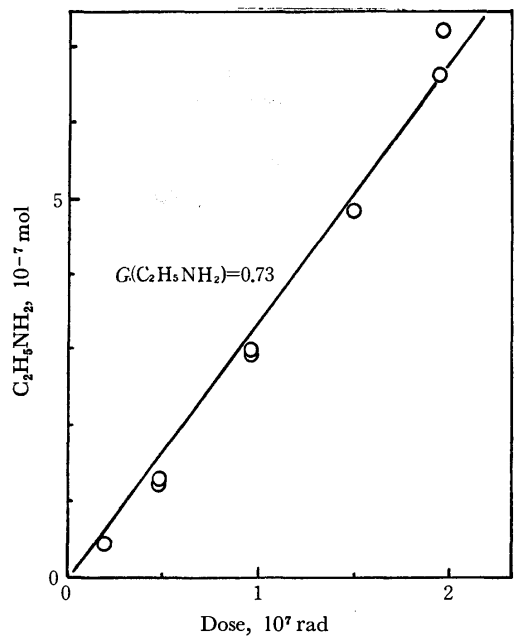

Fig. 2. Dose dependence of the yield of ethylamine.
$C_2H_4+NH_3=2.4\times10^{-3}$ mol, $(C_2H_4/NH_3=1/9)$

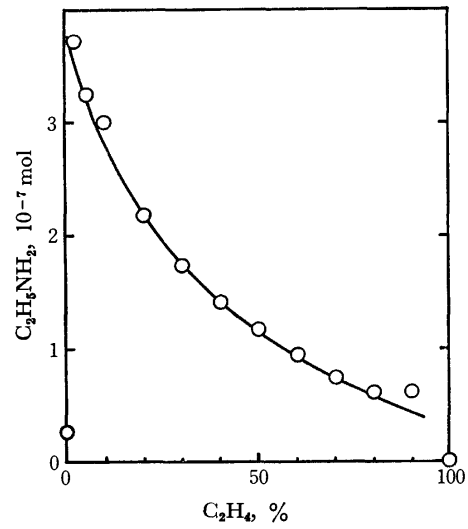

Fig. 3. Composition dependence of the yield of ethylamine.
dose; 1×10^{7} rad, $C_2H_4+NH_3=2.4\times10^{-3}$ mol

11) G. W. Watt and J. D. Chrisp, *Anal. Chem.*, **24**, 2006 (1952).
12) F. W. Lampe, *Radiat. Res.*, **10**, 691 (1959).

Table 1. Effects of additives (NO, O_2)

NO, %	$C_2H_5NH_2$, (10^{-7} mol)	n-C_4H_{10}, (10^{-7} mol)	O_2, %	$C_2H_5NH_2$, (10^{-7} mol)	n-C_4H_{10}, (10^{-7}mol)
0	3.0	7.0	0	3.0	7.0
0.15	1.5	2.5	0.15	0	0
0.3	0.9	1.5	0.6	0	0
0.56	0	0	1.0	0	0
1.0	0	0	1.6	0	0
1.5	0	0			

C_2H_4: NH_3=1 : 9, dose; 1.0×10^7 rad

Figure 4 shows the dependence of the yields of hydrocarbon products (methane, ethane, acetylene, and n-butane) on the composition of the mixture. The yields of n-butane and ethane increased with the increasing concentration of ammonia, and were reduced by addition of nitric oxide. On the other hand, the yield of acetylene, one of the main products, was not only independent of the concentration of ammonia but also was unaffected by the addition of nitric oxide. This fact shows that acetylene was formed through the ionic decomposition or the unimolecular decomposition process of an excited ethylene molecule.

The yield of methane was very small, and the data were not accurate. However, it can be qualitatively concluded that no effect of the addition of ammonia are observed as in the case of acetylene.

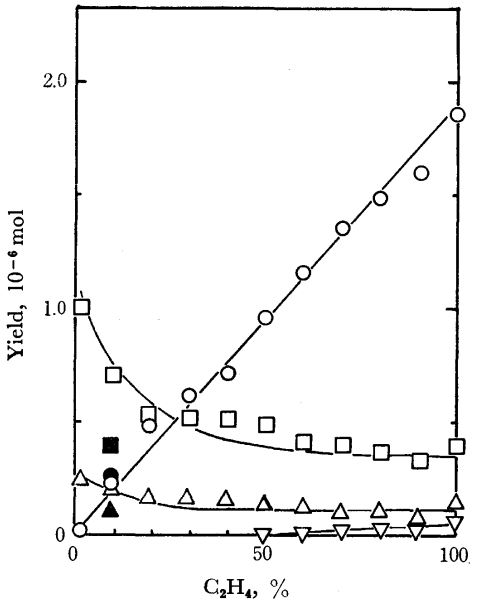

Fig. 4. Composition dependence of the yields of acetylene, n-butane, ethane, and methane.
dose; 1×10^7 rad, $C_2H_4+NH_3=2.4\times10^{-3}$ mol
—○—; C_2H_2 : ●
—□—; n-C_4H_{10}: ■
—△—; C_2H_6 : ▲
—▽—; CH_4
} 0.14 mol% NO

Discussion

The radiolysis of ammonia has been studied in detail by many investigators. Willis *et al.* found by electron beams that $G(H_2)$ was constant, *i.e.*, $G(H_2)=3.58\pm0.08$, in the pressure range 1—2.25 atm.[13] Recently we have obtained $G(H_2)$ to be 3.14 ± 0.11 in the pressure range 2—4 atm in the γ-radiolysis of ammonia.[14]

As shown in Fig. 1, it is obvious that $G(H_2)$ is reduced rapidly by the addition of a small amount of ethylene and then increases linearly with the increasing concentration of ethylene. It is well-known that olefins are effective scavengers of thermal hydrogen radicals, and that almost all the hydrogen formed in the radiolysis of olefins is non-scavengeable. Consequently, the value obtained by extrapolating the straight line (A) in Fig. 1 to 100 mol% ammonia corresponds to the G-value of the so-called non-scavengeable hydrogen or hot hydrogen, which might be produced in the radiolysis of pure ammonia, *i.e.*, $G_{hot}(H_2)$[15]$=0.68$. The value is in good agreement with our results in the radiolysis of a mixture of ammonia and propylene or 1,3-butadiene,[14] and with the result of Eyre and Smithies.[1]

It can be deduced that the difference between $G(H_2)$ which is the value of hydrogen produced in the radiolysis of pure ammonia and $G_{hot}(H_2)$, *viz.*, $G(H_2)-G_{hot}(H_2)=2.46$ corresponds to the G-value of hydrogen formed from the thermal hydrogen radicals.

In Fig. 1 is given the relationship between the G-values of products which seem to be formed from thermal hydrogen radicals, and the composition of the mixture. The value obtained by extrapolating curve B to 100 mol% ammonia is 3.2. The value corresponds to 6.4 which is the G-value (G_H) of hydrogen radicals. This agrees approximately with the initial G-value of hydrogen radical $G_H=7.0\pm0.6$ obtained by Eyre and Smithies[1] and $G_H=7.2\pm0.5$ by Johnson and Simic in the radiolysis of pure ammonia.[16]

As shown in Table 1, the yields of n-butane and ethylamine are reduced by the addition of oxygen or nitric oxide. The yields of products except acetylene are reduced by the addition of nitric oxide (Fig. 4).

It can be deduced that ethane, n-butane, and ethylamine are formed by the following radical processes:

$$H\cdot + C_2H_4 \rightarrow C_2H_5\cdot \quad (1)$$

$$C_2H_5\cdot + C_2H_5\cdot \rightarrow n\text{-}C_4H_{10} \quad (2)$$

$$\rightarrow C_2H_4 + C_2H_6 \quad (3)$$

$$NH_2\cdot + C_2H_5\cdot \rightarrow C_2H_5NH_2 \quad (4)$$

The relation between ethane/n-butane and the composition of the mixture is shown in Table 2. It is obvious that the ratio is independent of the composition, and the constant value is found to be 0.30 ± 0.06. This value is about twice 0.14 which is the ratio of the rate

13) C. Willis, A. W. Boyd, and O. A. Miller, *Can. J. Chem.*, **47**, 3007 (1969).
14) K. Hamanoue, J. Okamoto, O. Tokunaga, and A. Danno, to be published; 24th Annual Meeting of the Chemical Society of Japan, vol. 1, p. 52 (1971).
15) In this paper, $G_{hot}(H_2)$ denotes the yield of non-scavengeable hydrogen.
16) G. R. A. Johnson and M. Simic, "Radiation Chemistry," Vol. 2, p. 197, Am. Chem. Soc., (Washington D. C.) (1968).
17) J. A. Kerr and A. F. Trotman-Dickenson, "Progress in Reaction Kinetics," Vol. 1, p. 105, Pergamon Press (Oxford) (1961).

constant of the disproportionation reaction of ethyl radicals to that of the combination reaction.[17] This suggests that some processes other than reaction (3) might participate in the formation of ethane. Smith *et al.*[18] and Rabinovich *et al.*[19] reported that reaction(5) as well as reaction(3) takes part in the formation of ethane:

$$H\cdot + C_2H_5\cdot \rightarrow C_2H_6 \qquad (5)$$

For the formation of ethylamine, the following reaction as well as reaction(4) might participate.

$$C_2H_5\cdot + NH_3 \rightarrow C_2H_5NH_2 + H\cdot \qquad (6)$$

However, from the bond energies of ammonia and of ethylamine[20], we can calculate the heat of reaction of (6) to be -2.4 kcal/mol, that is, the reaction is endothermic. Consequently, reaction(4) is considered to be more favorable than reaction(6).

Table 2. Relationship between the concentration of ethylene and $C_2H_6/n\text{-}C_4H_{10}$

C_2H_4, %	$\frac{C_2H_6}{n\text{-}C_4H_{10}}$
2	0.24
10	0.27
20	0.29
30	0.31
40	0.31
50	0.30
60	0.34
70	0.25
80	0.31
90	0.30
100	0.35
mean	0.30±0.06

Schurath *et al.* have investigated the photolysis of a mixture of ethylene and ammonia, and reported that the following reaction competes with reaction(4) and that the ratio of k_7 to k_4 is about 0.4:[21]

$$C_2H_5\cdot + NH_2\cdot \rightarrow C_2H_4 + NH_3 \qquad (7)$$

Thus, in our reaction system we have to take the contribution of reaction(7) into consideration.

It is obvious that the higher the yields of ethyl radical, the higher the concentration of ammonia. That is to say, the quantity of hydrogen radicals scavenged by ethylene increases with the increasing concentration of ammonia. On the other hand, it is reasonable to consider that the yield of amino radical increases with increasing concentration of ammonia. Consequently, the composition which gives the maximum yield of ethylamine lies so far to the high concentration of ammonia.

Table 3. *G*-Values of products and ethyl radical

Products	*G*-value	$G(C_2H_5\cdot)$ consumed
CH_4	0.01	
C_2H_6	0.52	(3)[a] 0.60
		(5) 0.22
C_2H_2	1.73	
$n\text{-}C_4H_{10}$	2.12	(2) 4.24
$C_2H_5NH_2$	0.89	(4) 0.89
		(7) 0.27
	Total	6.22

2 mol% C_2H_4, dose; 1.0×10^7 rad
a) Number in parentheses indicates reaction number.

Table 3 shows the *G*-values of products at 2 mol% ethylene. From them we can calculate the *G*-value of each ethyl radical consumed by reactions(2), (3), (4), (5), and (7). The values thus obtained are also given in Table 3. The total *G*-value of ethyl radical consumed is seen to be 6.22 which corresponds to the *G*-value of hydrogen radical consumed by the same processes. On the other hand, the *G*-value of thermal hydrogen radical in the radiolysis of pure ammonia is 6.4 to 7.0. In the radiolysis of pure ammonia, the difference between $G(H_2)=3.14$ and $G_{hot}(H_2)=0.68$ is 2.46. Thus, the apparent *G*-value of thermal hydrogen radical is 4.92. Consequently, the value 6.22 is reasonable and $G(C_2H_5\cdot)$ is considered to be nearly equal to G_H.

In the radiolysis of ethylene, ethyl radicals formed might be consumed not only by reactions(2), (3), and (5), but also by reaction(8).

$$C_2H_5\cdot + C_2H_4 \rightarrow C_4H_9\cdot \qquad (8)$$

Reaction(8) might give hydrocarbons of more than C_4. As shown in Table 3, the $G(C_2H_5\cdot)$ consumed by reactions(2), (3), (4), (5), and (7) is 6.22. k_2, k_3, and k_8 are the order of 10^{11}, 10^{11}, and 10^4 (l/mol sec), respectively.[14] Thus, the concentration of ethyl radical in the steady state can be estimated by the following equation using these values.

$$\frac{G(C_2H_5\cdot)\times I}{100} \simeq (k_2+k_3)[C_2H_5\cdot], \qquad (9)$$

where I is dose-rate in eV/ml sec. The value thus obtained is 0.7×10^{-9} mol/ml. Using these values, the ratio of the reaction rate of reaction(8) to that of reactions (2) plus (3) is as follows.

$$\frac{v_8}{v_2+v_3} = \frac{10^4[C_2H_4][C_2H_5\cdot]}{10^{11}[C_2H_5\cdot]^2} = 2.3\times10^{-4} \qquad (10)$$

Consequently, $v_8 \ll (v_2+v_3)$ and the quantity of ethyl radical consumed by reaction(8) may be negligible. It can be concluded that the thermal hydrogen radicals (scavengeable hydrogen radicals), formed in the radiolysis of a mixture of ethylene and ammonia, react mainly with ethylene and the resulting ethyl radical leads to ethane, *n*-butane, and ethylamine.

The *G*-value of thermal hydrogen radical in the radiolysis of pure ammonia is 6.4 to 7.0. This value must be equal to the *G*-value of amino radical. Con-

18) M. J. Smith, P. M. Beatty, J. A. Pinder, and D. J. Le Roy, *Can. J. Chem.*, **33**, 821 (1955).
19) B. S. Rabinovitch, D. H. Dillis, W. H. McLain, and J. H. Current, *J. Chem. Phys.*, **32**, 493 (1960).
20) N. N. Semenov, "Some Problems of Chemical Kinetics and Reactivity," Vol. 1, p. 16, Pergamon Press, (London) (1958).
21) U. Schurath, P. Tiedemann, and R. N. Schindler, *J. Phys. Chem.*, **73**, 456 (1969).

sidering the *G*-values of hydrazine, ethylamine, and that of reaction(7), amino radical must be also consumed by some other reactions.

The authors wish to express their sincere thanks to Prof. Keiichi Oshima of the University of Tokyo for his valuable guidance.

BULLETIN OF THE CHEMICAL SOCIETY OF JAPAN, VOL. 45, 1054—1057 (1972)

Magnetic Properties of Copper(II) Complexes of 6-Aminopurine and 6-Hydroxypurine

Toshiro ASAKAWA, Motomichi INOUE, Ken-ichi HARA, and Masaji KUBO
Department of Chemistry, Nagoya University, Chikusa, Nagoya
(Received December 6, 1971)

The magnetic susceptibilities of bis(6-aminopurinato)copper(II) trihydrate, dichlorobis(6-aminopurine) copper(II) sesquihydrate, and dichlorobis(6-hydroxypurine)copper(II) monohydrate obey the Bleaney-Bowers equation for binuclear clusters in conformity with the results of X-ray crystal analysis. The exchange integrals within binuclear clusters were evaluated as $J/k = -156$ to -208°K. Superexchange interaction rather than the interaction of direct nature operates predominantly between copper atoms through the $p\pi$ orbitals of the heterocycles. The J/k values of the compounds are nearly equal to the value, -204°K, of copper(II) acetate monohydrate, although the Cu–Cu distance in the former is greater than that in the latter. The magnetic susceptibilities of dibromobis(6-aminopurine)copper(II) dihydrate, dibromobis(6-hydroxypurine)copper(II) dihydrate, dichloro(6-aminopurine)copper(II), dichloro(6-hydroxypurine)copper(II) monohydrate, and dibromo(6-hydroxypurine)copper(II) hemihydrate indicate the presence of paired copper atoms in the crystals.

Copper(II) acetate monohydrate presents a typical example of binuclear structure,[1] its magnetic susceptibility conforming to the simple triplet-singlet formula.[2,3] For the magnetic interaction within a binuclear cluster, two types of mechanism have been proposed, *i.e.*, direct exchange interaction through a δ-bond ($d_{x^2-y^2}-d_{x^2-y^2}$) and superexchange interaction through four Cu–O–C–O–Cu linkages.[3-6] Some experimental results suggest the predominance of the latter mechanism.[4-6] However, no conclusive evidence has been proposed as yet. A recent X-ray crystal analysis has shown that the crystals of bis(6-aminopurinato)copper(II) tetrahydrate, $Cu(ap)_2 \cdot 4H_2O$, contain binuclear clusters closely resembling those of copper(II) acetate monohydrate as shown in Fig. 1.[7] However, the detailed structure of the compounds reveals two significant differences that the Cu–Cu separation, 2.949 Å, in $Cu(ap)_2 \cdot 4H_2O$ is much greater than 2.64 Å in copper(II) acetate monohydrate and that 6-aminopurinato ligands involve a strong π-bond conjugation as compared with acetate groups. The crystals of dichlorobis(6-aminopurine)copper(II) trihydrate, $CuCl_2(apH)_2 \cdot 3H_2O$, and dichlorobis(6-hydroxypurine)copper(II) trihydrate, $CuCl_2(hpH)_2 \cdot 3H_2O$ also have binuclear clusters analogous to those of $Cu(ap)_2 \cdot 4H_2O$.[8,9] The neutral molecules of the heterocycles in the first two compounds have a stronger aromatic character than that of anionic heterocycles in the last compound. The present investigation has been undertaken in order to obtain some information about the mechanism of magnetic interaction between copper atoms in the binuclear clusters of the copper(II) complexes having the nitrogen heterocycles and of copper(II) acetate monohydrate. In addition, we have determined the susceptibilities of some $CuBr_2L_2$ and CuX_2L type complexes (X: halide ions, L: 6-aminopurine or 6-hydroxypurine) to discuss magnetic interaction in relation to crystal structure.

Preparation of Materials

Bis(6-aminopurinato)copper(II) tetrahydrate, $Cu(ap)_2 \cdot 4H_2O$, was prepared by a method described by Weiss and Venner[10] and recrystallized from a 10% ethanol - water mixture.[7] When the crystals were dried over phosphorus pentoxide or silica gel in a desiccator, $Cu(ap)_2 \cdot 3H_2O$ was obtained.[10] The results of chemical analysis are listed in Table 1. Dichlorobis(6-aminopurine)copper(II) sesquihydrate, $CuCl_2(apH)_2 \cdot 1.5H_2O$, dichlorobis(6-hydroxypurine)copper(II) monohydrate, $CuCl_2(hpH)_2 \cdot H_2O$, dichloro(6-aminopurine)copper(II), $CuCl_2(apH)$, and dichloro(6-hydroxypurine)copper(II) monohydrate, $CuCl_2(hpH) \cdot H_2O$, were prepared by methods reported in the literature.[10,11] X-ray crystal analysis has been

1) J. N. van Niekerk and F. R. L. Schoening, *Acta Crystallogr.*, **6**, 227 (1953).
2) B. Bleaney and K. D. Bowers, *Proc. Roy. Soc.* (London), **A214**, 451 (1952).
3) B. N. Figgis and R. L. Martin, *J. Chem. Soc.*, **1956**, 3837.
4) G. F. Kokoszka, H. C. Allen, Jr., and G. Gordon, *J. Chem. Phys.*, **42**, 3693 (1965).
5) L. Dubicki and R. L. Martin, *Inorg. Chem.*, **5**, 2203 (1966).
6) D. B. Yawney and R. J. Doedens, *ibid.*, **9**, 1626 (1970).
7) E. Sletten, *Acta Crystallogr.*, **B25**, 1480 (1969).
8) P. de Meester, D. M. L. Goodgame, P. K. Angela, and A. C. Skapski, *Nature*, **229**, 191 (1971); P. de Meester and A. C. Skapski, *J. Chem. Soc., A*, **1971**, 2167.
9) E. Sletten, *Acta Crystallogr.*, **B26**, 1609 (1970).
10) R. Weiss and H. Venner, *Hoppe-Seylers Z. Physiol. Chem.*, **333**, 169 (1963).
11) R. Weiss and H. Venner, *ibid.*, **340**, 138 (1965).

TABLE 1. ANALYTICAL DATA FOR $CuX_2(apH)_m \cdot nH_2O$ AND $CuX_2(hpH)_m \cdot nH_2O$

Compound	Cu, %		C, %		H, %		N, %	
	Calcd	Found	Calcd	Found	Calcd	Found	Calcd	Found
$Cu(ap)_2 \cdot 3H_2O$	16.5	16.9	31.1	31.5	3.7	3.7	36.3	37.1
$CuCl_2(apH)_2 \cdot 1.5H_2O$	14.7	14.7	27.8	28.5	3.0	2.9	32.5	32.3
$CuCl_2(hpH)_2 \cdot H_2O$	14.9	15.3	28.3	28.1	2.8	2.4	26.4	25.4
$CuBr_2(apH)_2 \cdot 2H_2O$	11.9	12.2	22.7	22.9	2.7	2.6	26.4	25.9
$CuBr_2(hpH)_2 \cdot 2H_2O$	11.9	12.5	22.6	22.8	2.7	2.2	21.1	21.2
$CuCl_2(apH)$	23.6	23.4	22.3	22.2	1.9	2.1	26.0	25.8
$CuCl_2(hpH) \cdot H_2O$	22.1	21.8	20.8	21.0	2.4	2.1	19.4	19.4
$CuBr_2(hpH) \cdot 0.5H_2O$	17.2	17.1	16.3	16.4	1.6	1.6	15.2	15.3

apH: 6-aminopurine, hpH: 6-hydroxypurine.

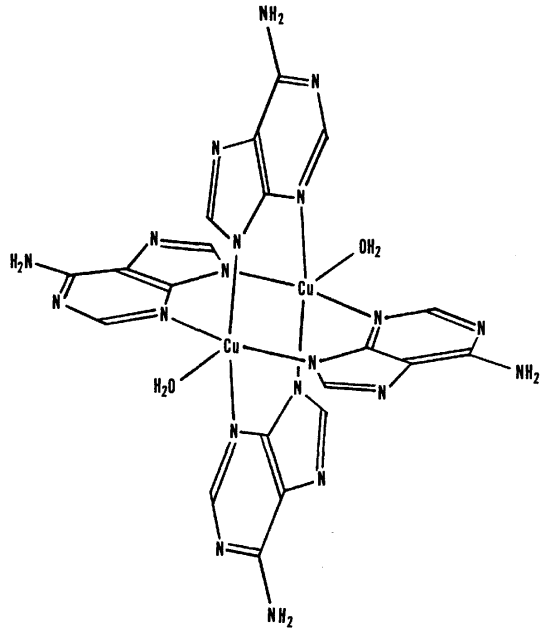

Fig. 1. Binuclear structure of bis(6-aminopurinato)copper-(II) tetrahydrate.

carried out on $Cu(ap)_2 \cdot 4H_2O$, $CuCl_2(apH)_2 \cdot 3H_2O$, and $CuCl_2(hpH)_2 \cdot 3H_2O$. However, the crystals of these complexes gradually lost water of crystallization in air. On standing over silica gel in a desiccator, the crystals yielded $Cu(ap)_2 \cdot 3H_2O$, $CuCl_2(apH)_2 \cdot 1.5H_2O$, and $CuCl_2(hpH)_2 \cdot H_2O$, which were no longer dehydrated in vacuum as well as in air. Therefore, these hydrates were used for magnetic measurements. Dibromobis(6-aminopurine)copper(II) dihydrate, $CuBr_2(apH)_2 \cdot 2H_2O$, and dibromobis(6-hydroxypurine)-copper(II) dihydrate, $CuBr_2(apH)_2 \cdot 2H_2O$, and dibromobis(6-hydroxypurine)copper(II) dihydrate, $CuBr_2(hpH)_2 \cdot 2H_2O$, were prepared by adding a dilute aqueous solution of copper(II) bromide (1 mol) to aqueous solutions of appropriate ligands (2 mol) acidified with a minimum quantity of hydrobromic acid. Dibromo(6-hydroxypurine)copper(II) hemihydrate, $CuBr_2(hpH) \cdot 0.5\ H_2O$, was prepared in the same way as for $CuCl_2(hpH) \cdot H_2O$ using hydrobromic acid in place of hydrochloric acid. We tried to prepare $CuBr_2(apH)$ by a method similar to that for $CuBr_2(hpH) \cdot 0.5H_2O$, but failed to obtain pure samples.

Magnetic Measurements and Results

Magnetic susceptibilities were determined using magnetic balances described in a previous paper.[12] The molar susceptibilities were corrected for diamagnetic contributions (in 10^{-6} emu/mole) from copper(II) ions (−11), chloride ions (−26), bromide ions (−36), water (−13), 6-aminopurine (−62), and 6-hydroxypurine (−59).[13,14] The last value is based

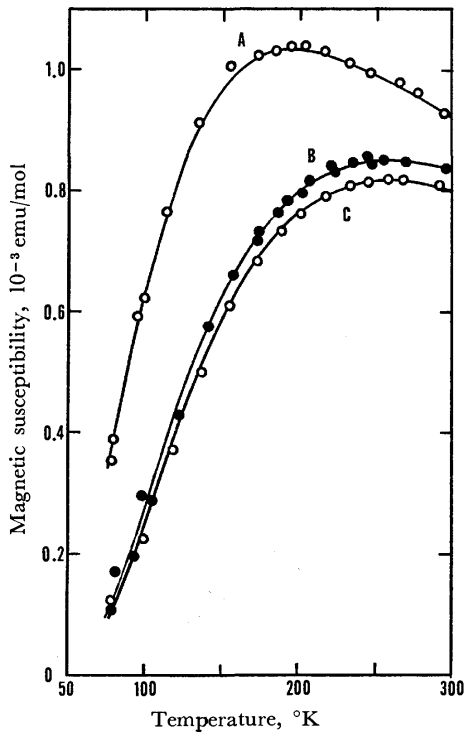

Fig. 2. Magnetic susceptibilities of bis(6-aminopurinato)-copper(II) trihydrate (A), dichlorobis(6-aminopurine)-copper(II) sesquihydrate (B), and dibromobis(6-aminopurine)copper(II) dihydrate (C). The solid curves show theoretical susceptibilities calculated by the triplet-singlet formula.

12) M. Inoue, S. Emori, and M. Kubo, *Inorg. Chem.*, **7**, 1427 (1968).

13) P. W. Selwood, "Magnetochemistry," 2nd Ed., Interscience Publishers Inc., New York, N. Y., 1956.

14) G. Foëx, "Constantes Sélectionées, Diamagnétisme et Paramagnétisme," Masson, Paris, 1957.

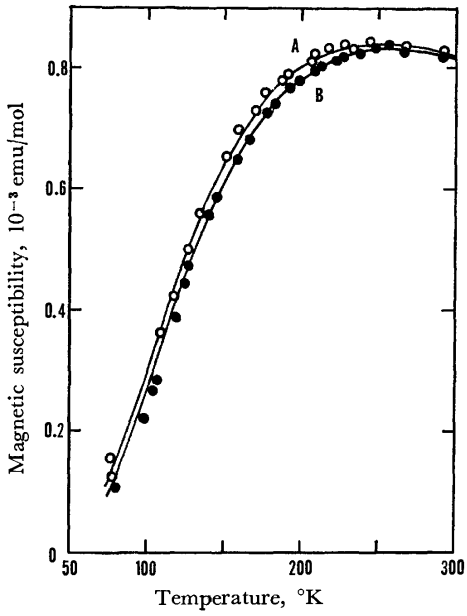

Fig. 3. Magnetic susceptibilities of dichlorobis(6-hydroxypurine)copper(II) monohydrate (A) and dibromobis(6-hydroxypurine)copper(II) dihydrate (B). The solid curves represent the triplet-singlet formula.

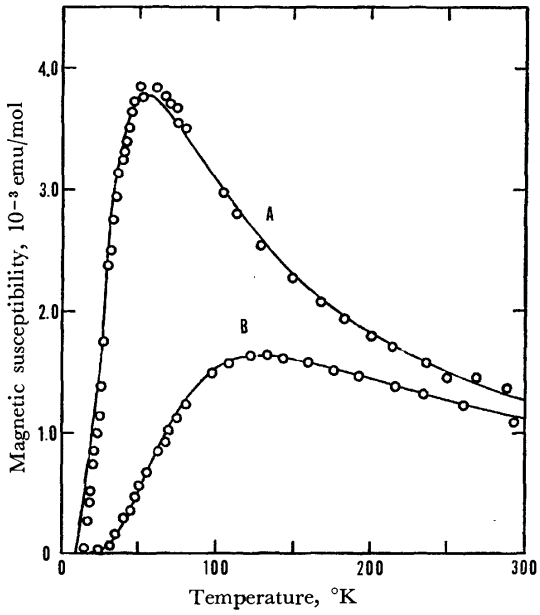

Fig. 4. Magnetic susceptibilities of dichloro(6-aminopurine)copper(II) (A) and dichloro(6-hydroxypurine)copper(II) monohydrate (B). The solid curves represent the triplet-singlet formula.

on the observed values of 6-aminopurine (adenine) and 2-amino-6-hydroxypurine (guanine).[14] The temperature-independent paramagnetism was assumed to be equal to 60×10^{-6} emu/mol.[3] The corrected susceptibilities are plotted against the temperature in Figs. 2—5.

Discussion

The magnetic susceptibility of $Cu(ap)_2\cdot3H_2O$ conforms to the theoretical susceptibility, χ, of binuclear

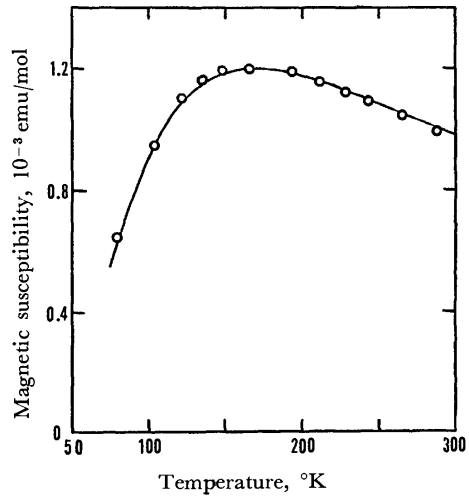

Fig. 5. Magnetic susceptibility of dibromo(6-aminopurine)-copper(II) hemihydrate. The solid curve represents the triplet-singlet formula.

clusters[2] (see Fig. 2).

$$\chi=\frac{Ng^2\beta^2}{3kT}\left[1+\frac{1}{3}\exp\left(-\frac{2J}{kT}\right)\right]^{-1} \quad (1)$$

Here apart from obvious notations, J is the exchange integral between copper atoms within a cluster. The exchange integral and the g-value are evaluated as $J/k=-156$°K and $g=2.07$. The magnetic susceptibility of $Cu(ap)_2\cdot4H_2O$, on which X-ray crystal analysis had been carried out, could not be determined in a reproducible manner because the crystals gradually lost water of crystallization even in air. By use of Eq. 1, the exchange integral, J/k, was roughly estimated to be about -170°K from the susceptibility *versus* temperature curve. Goodgame and Price[15] have measured the susceptibility of $Cu(ap)_2\cdot4H_2O$ and evaluated the parameters as $J/k=-151$°K and $g=2.06$. The exchange integral and the g-value of $Cu(ap)_2\cdot3H_2O$ are almost equal to those of $Cu(ap)_2\cdot4H_2O$, indicating that the binuclear clusters are retained on dehydration without any significant change in bonding arrangement. The disagreement between the J/k values of $Cu(ap)_2\cdot4H_2O$ is due probably to fluctuation in composition. In fact, the magnetic moment of $Cu(ap)_2\cdot4H_2O$ gradually increased with time at room temperature. The J/k value of $Cu(ap)_2\cdot3H_2O$ is more reliable than that of the tetrahydrate because the former crystals were no longer dehydrated in vacuum as well as in air. Therefore, the following discussion is based on the data of $Cu(ap)_2\cdot3H_2O$ and an assumption that the crystals of the trihydrate contain binuclear clusters having the same bonding arrangement as in those of the tetrahydrate.

Dubicki and Martin[5] have pointed out that the δ-bond in the crystals of copper(II) acetate monohydrate is virtually nonbonding and that the configuration of the binuclear clusters is maintained by four bridging acetate groups. This has been supported by the following experimental results. The Cu–Cu

15) D. M. L. Goodgame and K. A. Price, *Nature*, **220**, 783 (1968).

bond length, 2.657 Å, in the crystals of copper(II) formate monourea is nearly equal to 2.64 Å in copper(II) acetate monohydrate,[6] although the former compound shows a magnetic moment, 1.08 B.M. (17°C), much lower than that of the latter, 1.40 B.M. (21.2 °C).[16] Because the Cu–Cu separation, 2.949 Å, in $Cu(ap)_2 \cdot 4H_2O$ is much greater than that in copper(II) acetate monohydrate, δ-bonds are presumed to be very weak in the former compound. Therefore, magnetic interaction is supposed to take place between copper atoms through Cu–ap–Cu linkages.

The crystals of $CuCl_2(apH)_2 \cdot 3H_2O$[8] and $CuCl_2(hpH)_2 \cdot 3H_2O$[9] have binuclear clusters bearing a striking resemblance to those of $Cu(ap)_2 \cdot 4H_2O$: neutral molecules of the heterocycles coordinate to two copper atoms in place of 6-aminopurinato groups and one of the two chloride ions in the chemical formula occupies the same position about a copper atom as does a water molecule coordinating weakly to a copper atom (see Fig. 6). $CuCl_2(apH)_2 \cdot 1.5H_2O$ and $CuCl_2(hpH)_2 \cdot H_2O$ show magnetic properties characteristic of binuclear clusters (see Fig. 3 and Table 2), indicating the retention of the binuclear structure on dehydration. The exchange integrals of $CuCl_2(apH)_2 \cdot 1.5H_2O$ and $CuCl_2(hpH)_2 \cdot H_2O$ are larger than that of $Cu(ap)_2 \cdot 3H_2O$ (see Table 2), although Cu–Cu distance, 3.066 and 3.024 Å, in the former are slightly greater than 2.949 Å in the latter. When paired copper atoms are separated from each other by three diamagnetic atoms (for example, Cu–N–C–N–Cu links), the π-path can give rise to a strong antiferromagnetic interaction between copper atoms,[17] whereas if the contribution from the σ-path is predominant, unpaired electrons of copper atoms are coupled ferromagnetically.[17] In the clusters of $CuCl_2(apH)_2 \cdot 1.5H_2O$ and $CuCl_2(hpH)_2 \cdot H_2O$, nitrogen atoms bonded to copper atoms have $p\pi$ orbitals, because neutral molecules of 6-aminopurine or 6-hydroxypurine coordinate to copper atoms as shown in Fig. 6. Hence, positive holes of copper atoms can migrate through the π-bond system of Cu–N–C–N–Cu links, giving rise to antiferromagnetic interaction in agreement with the sign of the exchange integrals. In the crystals of $Cu(ap)_2 \cdot 3H_2O$, 6-aminopurinato groups coordinate to copper atoms by nitrogen atoms having a negative formal charge (see Fig. 6). This hinders the migration of positive holes through the π-bond system and weakens antiferromagnetic interaction between copper atoms. Owing to this effect, the magnetic interaction is presumed to operate more strongly in $CuCl_2(apH)_2 \cdot 1.5H_2O$ and $CuCl_2(hpH)_2 \cdot H_2O$ than in $Cu(ap)_2 \cdot 3H_2O$ in accordance with the experimental results (see Table 2).

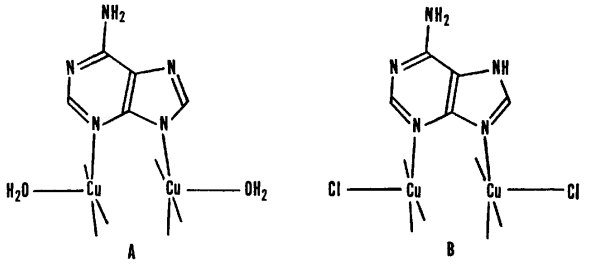

Fig. 6. Bonding arrangements in the binuclear clusters of bis(6-aminopurinato)copper(II) trihydrate (A) and dichlorobis(6-aminopurine)copper(II) sesquihydrate (B).

TABLE 2. EFFECTIVE MAGNETIC MOMENT μ_{eff} AT 17°C, EXCHANGE INTEGRAL J, AND g-VALUE g

Compound	μ_{eff}, B.M.	$-J/k$, °K	g
$Cu(ap)_2 \cdot 3H_2O$	1.46	156	2.07
$CuCl_2(apH)_2 \cdot 1.5H_2O$	1.39	206	2.15
$CuCl_2(hpH)_2 \cdot H_2O$	1.38	200	2.11
$CuBr_2(apH)_2 \cdot 2H_2O$	1.38	208	2.12
$CuBr_2(hpH)_2 \cdot 2H_2O$	1.38	206	2.13
$CuCl_2(apH)$	1.74	44	2.10
$CuCl_2(hpH) \cdot H_2O$	1.62	104	2.12
$CuBr_2(hpH) \cdot 0.5H_2O$	1.52	134	2.07
$Cu(CH_3COO)_2 \cdot H_2O$[a]	1.40[b]	204	2.13

a) Ref. 3, b) at 21.2°C.

The magnetic susceptibility *versus* temperature curves of $CuBr_2(apH)_2 \cdot 2H_2O$ and $CuBr_2(hpH)_2 \cdot H_2O$ conform to Eq. 1 (see Figs. 2 and 3), indicating the presence of binuclear clusters analogous to those in the crystals of the corresponding chlorides. The values of exchange integrals are almost equal to one another as listed in Table 2, indicating that the substitution of chlorine with bromine gives no appreciable effect on magnetic interaction.

The magnitude of superexchange interaction depends to a great extent on the electronic structure of bridging ligands. When superexchange interaction takes place through three diamagnetic atoms, a path through π-orbitals can give rise to a strong antiferromagnetic interaction.[17] Therefore, one would suspect that magnetic interaction operates more strongly in the complexes of 6-aminopurine and 6-hydroxypurine than in copper(II) acetate monohydrate, because the heterocycles are expected to facilitate the migration of positive holes more strongly than do acetate groups. Contrary to this expectation, the exchange integral of copper(II) acetate monohydrate is almost equal to those of $CuX_2(apH)_2 \cdot nH_2O$ and $CuX_2(hpH)_2 \cdot nH_2O$ type complexes and is evidently larger than that of $Cu(ap)_2 \cdot 3H_2O$ (see Table 2). These facts suggest that the effect of direct exchange interaction is not entirely negligible in the binuclear clusters of copper(II) acetate monohydrate despite the predominance of superexchange interaction.

The susceptibilities of $CuCl_2(apH)$, $CuCl_2(hpH) \cdot H_2O$, and $CuBr_2(hpH) \cdot 0.5H_2O$ also can be fitted well to the curves of Eq. 1 (see Figs. 4 and 5). Presumably, paired copper atoms are bridged by the heterocycles in the crystals.

16) M. Kishita, M. Inoue, and M. Kubo, *Inorg. Chem.*, **3**, 237 (1964).

17) M. Inoue and M. Kubo, *ibid.*, **9**, 2310 (1970).

The Chemical Structures of Glasses of the $NaPO_3$-Sb_2O_3 and $NaPO_3$-Sb_2O_5 Systems

Makoto WATANABE and Mineo KATO

Department of Industrial Chemistry, Chubu Institute of Technology, Matsumoto-cho, Kasugai-shi, Aichi

(Received May 12, 1971)

Glassy substances of the $NaPO_3$-Sb_2O_3 and $NaPO_3$-Sb_2O_5 systems with P/Sb ratios in the range from 5.0 to 300 were prepared by heating $NaPO_3$ and Sb_2O_3, or Sb_2O_5 at 1000°C, and by then quenching the melts of the mixtures. The condensed phosphates were separated by paper-chromatographic analysis and determined colorimetrically, and the average degree of polymerization of the phosphates was measured by the pH-titration method. From these results, it has been found that the degree of polymerization of the phosphates increased with the increase in the P/Sb ratio. When the glassy samples of both the systems were treated with water, antimony trioxide was deposited. The results show that, in the glassy samples of both the systems, the valency of antimony is three, assuming that the glasses have the P–O–P, P–O^-, P–O–Sb, and Sb–O^- linkages, a theoretical treatment of the degree of polymerization of condensed phosphates has been made and compared with the experimental data. It has been concluded that the glasses of both the systems with P/Sb ratios larger than 5.0 have P–O–P, P–O^-, and P–O–Sb linkages.

Condensed phosphates containing oxoacid anions of some elements other than phosphorus have been prepared by several investigators.[1-4] In a previous paper,[5] the chemical compositions and structures of glasses of the $NaPO_3$-Sb_2O_3-Na_2O system were reported. It has been revealed in these papers that, in structures of condensed phosphates containing oxoacid anions of an element, X, other than phosphorus, there are P–O–X linkages. In the present work, glassy substances of the $NaPO_3$-Sb_2O_3 and $NaPO_3$-Sb_2O_5 systems were prepared in order to obtain some information on the chemical compositions and the structural framework of the systems. As for the glasses of the $NaPO_3$-Sb_2O_3 system, it has been presupposed that its structural framework is the same as that of the glasses of the $NaPO_3$-Sb_2O_3-Na_2O system, this has been confirmed by the measurement of the degree of polymerization and by a theoretical treatment of that of the condensed phosphates. The theoretical treatment of the degree of polymerization of the condensed phosphates revealed that the glasses of these two systems have P–O–Sb linkages. The compositions of the condensed phosphates have been determined by the paper-chromatographic analysis of their aqueous solutions.

Experimental

Materials. Monosodium dihydrogen orthophosphate dihydrate was heated in a platinum crucible at 1000°C for 3 hr and then converted to a glass of sodium metaphosphate by cooling a melt in a crucible. The average chain length of the glass thus obtained was about 100. The antiomony trioxide and pentoxide were commercial reagents.

Classy substances. A mixture of sodium metaphosphate and antimony trioxide, or pentoxide was melted in a platinum crucible at 1000°C for 2 hr and then quenched by placing the crucible in ice water. By this procedure, glasses of the $NaPO_3$-Sb_2O_3 and $NaPO_3$-Sb_2O_5 systems with P/Sb ratios of 5.0 to 300 were prepared. All the glasses thus obtained were transparent and colorless.

Paper Chromatography. The phosphate species in the solution of the glassy substances were separated by paper chromatography and then determined colorimetrically. Except for the acidic solvent, the procedure was the same as that described in a previous paper.[5] In this experiment, the acidic solvent was made by mixing 26.5 m*l* of water, 0.25 m*l* of concentrated aqueous ammonia, 5 g of trichloroacetic acid, and 73.5 m*l* of isopropyl alcohol. It was used for the separation of ortho-, di-, tri-, tetra-, and long-chain phosphates.

The Measurement of the Average Chain Length of Polyphosphates. The average degree of the polymerization of phosphate species in the glassy samples was also measured by the method described in the previous paper.[5]

X-ray Diffractometry. The samples were ground with an agate mortar until they could pass through a 150-mesh screen. Their X-ray diffraction patterns were taken with nickel-filtered CuKα radiation, by using a Toshiba X-ray diffractometer, ADG-102.

Results and Discussion

The samples with P/Sb ratios larger than 5.0 were completely transparent and opaque. The data of X-ray diffractometry of these samples indicated that they were amorphous. The chemical compositions of the phosphate species contained in the glassy substances were estimated by paper-chromatographic analysis. The data of the paper chromatography for the $NaPO_3$-Sb_2O_3 system with P/Sb ratios of 5.0 to 300 are given in Table 1, while those for the $NaPO_3$-Sb_2O_5 system with P/Sb ratios of 5.0 to 300 are given in Table 2. It is found that the ortho-, pyro-, and tripolyphosphate contents of both the systems decrease with the increase in the P/Sb ratio from 5.0 to 300. The quantities of trimeta- and tetrametaphosphate are less than several percent throughout the range of P/Sb ratios from 5.0 to 300. The quantities of high polyphosphate increase with the increase in the P/Sb ratio.

When the glassy samples of the $NaPO_3$-Sb_2O_3 and $NaPO_3$-Sb_2O_5 systems were treated with a 0.03 N sodium hydroxide solution, a white substance was deposited. A study of the X-ray diffraction patterns

1) K-H. Jost, H. Worzala, and E. Thilo, *Z. Anorg. Allgem. Chem.*, **325**, 98 (1963).
2) S. Ohashi and T. Matsumura, This Bulletin, **35**, 501 (1962).
3) S. Ohashi and F. Oshima, *ibid.*, **36**, 1489 (1963).
4) T. Nakamura and S. Ohashi, *ibid.*, **40**, 110 (1967).
5) M. Watanabe, K. Tanabe, T. Takahara, and T. Yamada, *ibid.*, **44**, 712 (1971).

Table 1. Distribution of phosphates of the $NaPO_3$-Sb_2O_3 system with P/Sb ratios of 5.0-300

P/Sb	Phosphate (P%) Ortho	Pyro	Tri	Tri-meta	Tetra-meta	Higher
5.0	10.2	20.5	17.7	1.6	2.9	47.1
7.0	4.1	16.7	16.1	2.8	5.2	55.1
10	3.9	11.7	11.7	2.9	2.4	67.4
15	1.8	10.3	11.0	2.9	3.6	70.4
20	2.3	8.5	6.9	5.2	4.0	73.1
30	2.4	4.8	9.7	3.5	3.4	76.2
50	2.2	2.2	4.3	3.9	4.6	82.8
80	0.5	1.6	2.9	3.6	4.9	86.5
100		1.5	2.6	4.4	3.1	88.4
150		1.3	1.9	2.7	4.1	90.0
200		1.9	1.7	3.0	3.1	90.3
300		1.7	1.6	3.4	2.9	90.4

Table 2. Distribution of Phosphates of the $NaPO_3$-Sb_2O_5 system with P/Sb ratios of 5.0—300

P/Sb	Phosphate (P%) Ortho	Pyro	Tri	Tri-meta	Tetra-meta	Higher
5.0	16.0	18.1	14.6	6.6	4.0	40.7
8.0	14.1	14.0	6.8	5.1	4.0	56.0
10	5.4	6.6	6.5	3.9	3.7	73.9
15	4.5	4.2	3.0	2.5	3.5	82.3
20	5.1	3.9	2.8	3.2	2.5	82.5
30	3.7	2.9	2.1	2.9	2.2	86.2
50	1.6	2.5	2.8	2.9	2.7	87.5
80	1.0	1.6	2.0	3.5	1.9	90.0
100	0.5	1.5	1.2	3.5	2.4	90.9
150	0.9	1.3	0.5	3.3	2.8	91.2
200				2.5	2.2	95.3
300				1.9	1.4	96.7

of the deposit showed it to be antimony trioxide. This indicates that the antimony pentoxide contained in the samples of the $NaPO_3$-Sb_2O_5 system is reduced to antimony trioxide. The careful treatment of weight change of this system supports the reduction. Therefore, the valency of antimony in the glassy samples of both the systems is three.

The average chain length of the polyphosphates contained in the samples of both the systems was measured. The results of the paper chromatography of these glasses show that the quantities of orthophosphate and of ring phosphates are not very large, therefore, the effect of their presence on the calculation of the average chain length of polyphosphates is disregarded in the following discussion. It is well known that the average chain length, $\bar{n}$, of polyphosphates in a sodium phosphate glass is given by the $Na/P=(\bar{n}+2)/\bar{n}$ equation, where Na/P is the atomic ratio of both the elements. If antimony trioxide or pentoxide does not react with phosphate glass to form P–O–Sb linkages in the melted state, the average chain length of phosphates in the glassy samples does not change when the P/Sb ratio is changed. The straight line,

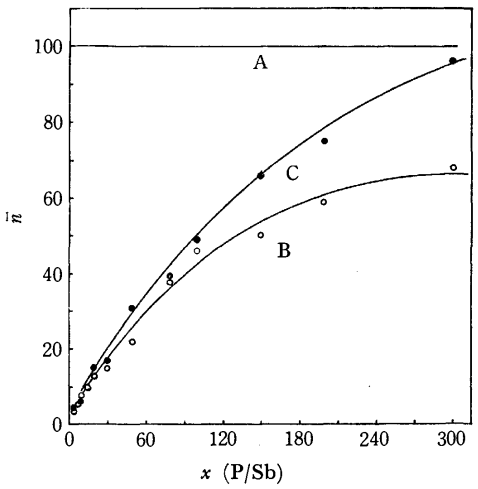

Fig. 1. Variation of average chain length of polyphosphates.
A: Pure sodium metaphosphate
B: Experimental values of the $NaPO_3$-Sb_2O_3 system
C: Experimental values of the $NaPO_3$-Sb_2O_5 system

A, in Fig. 1 exhibits this relation. Curves B and C in Fig. 1 indicate the relation between the measured average chain length of polyphosphates and the P/Sb ratio, x, of the $NaPO_3$-Sb_2O_3 and $NaPO_3$-Sb_2O_5 systems respectively. The great discrepancy between the straight line, A, and the curves B and C, and the results of paper chromatography indicate that the phosphate glass reacts with antimony trioxide or pentoxide at a high temperature to form P–O–Sb linkages.

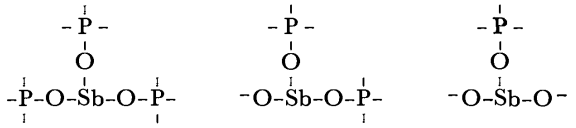

From the finding that, when the glassy samples of both the systems are treated with a 0.03 N sodium hydroxide solution, antimony trioxide is deposited, it may be concluded that there are three possible types of structures containing P–O–Sb and Sb–O^- linkages. The average chain length, $\bar{n}$, of the polyphosphates produced by the hydrolytic scission of P–O–Sb linkages in the glassy samples of both the systems is given by Eq. (1):

$$(\bar{n}+2)/\bar{n} = (x+y-z)/x \qquad (1)$$

where x, y, and z are the numbers of phosphorus atoms, P–O–Sb linkages, and Sb–O^- linkages per atom of antimony respectively. For Structure A, B, or C, y is 3, 2, or 1, and z is 0, 1, or 2, respectively. The average chain length of polyphosphates derived from the $NaPO_3$-Sb_2O_3 and $NaPO_3$-Sb_2O_5 systems with various P/Sb ratios, x, was calculated by inserting these values into Eq. (1). The calculated values of $\bar{n}$ are given in Tables 3 and 4. The underlined values are the average chain length nearest to the measured one. As is shown by Column I of Table 3 or 4, even the calculated values of the average chain length based on Structure A are considerably larger than the measured values when x is larger than 30 or 80 respectively. Other factors that shorten the chain length of the polyphosphates present in the phosphate-antimonate

TABLE 3. AVERAGE CHAIN LENGTH OF POLYPHOSPHATES OF THE $NaPO_3$-Sb_2O_3 SYSTEM

		Column I $\bar{n}$ calcd by Eq. (1)			Column II $\bar{n}$ calcd by Eq. (2) (f=0.02)		
		Structure			Structure		
x	$\bar{n}$	A	B	C	A	B	C
(P/Sb)	Found	$\binom{y=3}{z=0}$	$\binom{y=2}{z=1}$	$\binom{y=1}{z=2}$	$\binom{y=3}{z=0}$	$\binom{y=2}{z=1}$	$\binom{y=1}{z=2}$
5.0	3.5	3.3	10	—	3.2	9.1	—
7.0	5.4	4.7	14	—	4.5	12	—
10	7.4	6.7	20	—	6.3	17	—
15	10	10	30	—	9.1	23	—
20	13	13	40	—	12	29	—
30	15	20	60	—	17	38	—
50	22	33	100	—	25	50	∞
80	38	53	160	—	35	62	267
100	46	67	200	—	40	67	200
150	50	100	300	—	50	75	150
200	59	133	400	—	57	80	133
300	68	200	600	—	67	86	120

TABLE 4. AVERAGE CHAIN LENGTH OF POLYPHOSPHATES OF THE $NaPO_3$-Sb_2O_5 SYSTEM

		Column I $\bar{n}$ calcd by Eq. (1)			Column II $\bar{n}$ calcd by Eq. (2) (f=0.01)		
		Structure			Structure		
x	$\bar{n}$	A	B	C	A	B	C
(P/Sb)	Found	$\binom{y=3}{z=0}$	$\binom{y=2}{z=1}$	$\binom{y=1}{z=2}$	$\binom{y=3}{z=0}$	$\binom{y=2}{z=1}$	$\binom{y=1}{z=2}$
5.0	4.3	3.3	10	—	3.3	9.5	—
8.0	5.9	5.3	16	—	5.2	15	—
10	7.2	6.7	20	—	6.5	18	—
15	10	10	30	—	9.5	26	—
20	15	13	40	—	13	33	—
30	17	20	60	—	18	46	—
50	31	33	100	—	29	67	—
80	39	53	160	—	42	89	—
100	49	67	200	—	50	100	∞
150	66	100	300	—	67	120	600
200	75	133	400	—	80	133	400
300	96	200	600	—	100	150	300

glasses are the existence of a branching point and impurities. If all these factors are represented by the factor, f, Eq. (1) is modified into Eq. (2):

$$(\bar{n}+2)/\bar{n} = (x+y-z+fx)/x \qquad (2)$$

where f is given with respect to an atom of phosphorus. The f factor is arbitrarily set at 0.02 for the $NaPO_3$-Sb_2O_3 system and at 0.01 for the $NaPO_3$-Sb_2O_5 system. The value of f of $NaPO_3$-Sb_2O_3 system is identical with that of the $NaPO_3$-Sb_2O_3-Na_2O system. The average chain lengths shown in Column II of Tables 3 and 4 are obtained by inserting these values into Eq. (2). The average chain length of pure sodium metaphosphate is usually in the range from 80 to 200, depending on the conditions of preparation. The f factor of the pure sodium phosphate glass is given by $(\bar{n}+2)/\bar{n}=(1+f)/1$; it ranges from 0.025 to 0.01. Therefore, the f factor of 0.02 for the $NaPO_3$-Sb_2O_3 system and that of 0.01 for the $NaPO_3$-Sb_2O_5 system seem to be reasonable. As is shown in Column II of Tables 3 and 4, the average chain lengths, as calculated on the basis of Structure A, are very close to the experimental values throughout the range of P/Sb ratios from 5.0 to 300. In view of the above discussion, it may reasonably be concluded that the structural framework of the glasses of the $NaPO_3$-Sb_2O_3 and $NaPO_3$-Sb_2O_5 systems with P/Sb ratios in the range from 5.0 to 300 was composed of Structure A, and that Structures B and C were not involved in the structural framework.

Preparation and Properties of Iron(II) Complexes with Tetraoxime Analogues[1]

Joseph BACKES, Isao MASUDA, and Koichiro SHINRA

Department of Applied Chemistry, Faculty of Engineering, Osaka University, Yamada-kami, Suita, Osaka

(Recdived June 16, 1971)

Three polymeric iron(II)-tetraoxime chelates of the formula $CH_3C(NOH)C(NOH)$-R-$C(NOH)C(NOH)$-CH_3, where R: C_6H_4-O-C_6H_4, C_6H_4-C_6H_4, and 2,6-pyridyl, are characterized and compared with monomeric α-dioxime analogues. Analytical data indicate that in the solid state these Fe-N_4 type chelates do not coordinate an axial base. Axial substitution takes place only upon dissolution into pyridine or similar basic solvents. The resemblance between the substituted polymer chelates and the monomeric dimethylglyoxime compounds, as far as their electronic spectra are concerned, is discussed. While the solid state polymers are all paramagnetic with moments 2.0—2.5 B.M., ESR data show that in solution a conversion into a diamagnetic species takes place. A strong absorption band due to the O–N stretching vibration appears at about 1650 cm^{-1} upon complexing of the nitrogen atoms. The paramagnetism and the reflectance spectra of the solid state samples are related to their structure.

Many works have been presented dealing with the formation and properties of metal chelate polymers.[2] In these works the low solubility of the compounds often rendered a more accurate research impossible. Better understanding of the effect of polymerization on the central metal ion is expected from a further investigation of these chelate compounds.

Tetraoxime coordination polymers with nickel(II) and with cobalt(II), nickel(II), and copper(II) have been reported by Jones *et al.*[3] and Murahashi and Kubota,[4] respectively.

The present work involves an investigation of iron(II) complexes with ligands of the formula $CH_3C(NOH)C(NOH)$-R-$C(NOH)C(NOH)CH_3$, where R stands for C_6H_4-O-C_6H_4, C_6H_4-C_6H_4, and 2,6-pyridyl.

A close look at a molecular model reveals that the two α-dioxime groups within one ligand unit are not parallel to each other, which renders a binuclear structure with a ligand to iron molar ratio of 1 : 1 impossible.

The properties and structure of these chelates are compared with those of the monomeric iron(II)-α-dioximes.

Experimental

Preparation of the tetraoxime ligands. 4,4′-Bis(α,β-dioxopropyl)diphenyl-tetraoxime and 4,4′-bis(α,β-dioxopropyl)diphenylether-(1,1)-tetraoxime were prepared according to the methods described by Jones *et al.*[3] The products obtained showed the following characterstics:

4,4′-Bis(α,β-dioxopropyl)diphenyl-tetraoxime. White crystals; soluble in DMSO, hot DMF and hot pyridine; insoluble in methanol, ethanol, ethyl ether, petroleum ether, *etc.*; mp 358—359°C.

Found: C, 61.41; H, 5.07; N, 15.67%.

4,4′-Bis(α,β-dioxopropyl)diphenylether-(1,1)-tetraoxime. White crystals; soluble in DMSO, hot DMF and hot pyridine; insoluble in methanol, ethanol, ethyl ether, petroleum ether, *etc.*; mp 270—271°C.

Found: C, 58.28; H, 4.98; N, 15.22%.

2,6-Bis(α,β-dioxopropyl)pyridine-tetraoxime. The pyridine ligand was newly prepared according to the following method.

Pyridine-2,6-dicarboxylic acid chloride. This compound was obtained by heating a mixture of 25 g (0.15 mol) pyridine-2,6-dicarboxylic acid and 53.5 g (0.45 mol) of freshly distilled thionylchloride on a water bath for 1 hr. The excess thionylchloride was removed by azeotropic distillation with benzene. The product was not further purified, and immediately dissolved in 50 m*l* dry benzene for the next step.

N,N,N′,N′-*Tetraethylpyridine-(2,6)-diamide.* The compound was synthesized by the Schotten-baumann reaction in dry benzene using 51.2 g (0.7 mol) freshly distilled benzene to yield colorless crystals, soluble in all common solvents, yield 78%, mp 73—75°C.

Found: C, 65.25; H, 8.65; N, 15.30%. Calcd for $C_{15}H_{23}N_3O_2$: C, 65.95; H, 8.35; N, 15.15%.

2,6-Dipropionylpyridine. This compound was obtained by the reaction of *N,N,N′,N′*-tetraethyl-pyridine-(2,6)-diamide with ethylmagnesium bromide in anhydrous ether. Due to the low solubility of the diamide in ether, the Grignard reagent was added slowly to a suspension of the former in the solvent. The compound, after extraction with a benzene-ether mixture (1 : 1), was purified by consecutive column chromatography to yield colorless crystals, soluble in all common organic solvents, yield 33%, mp 64—65°C.

Found: C, 68.94; H, 6.86; N, 7.32%. Calcd for $C_{11}H_{13}O_2N$: C, 69.09; H, 6.85; N, 7.33%.

2,6-Bis(α,β-dioxopropyl)pyridine-2,2′-dioxime. The dioxime compound was obtained from 2.1 g (0.011 mol) of 2,6-dipropionyl-pyridine and 2.2 g (0.022 mol) freshly distilled *n*-butylnitrite in anhydrous benzene, dry hydrogen chloride being bubbled through the reaction mixture. The precipitate was filtered and thoroughly washed with water and benzene. Recrystallization from aqueous alcohol yields colorless crystals, yield 69%, mp 212—213°C.

Found: C, 52.70; H, 4.56; N, 16.80%. Calcd for $C_{11}H_{11}O_4N_3$: C, 52.99; H, 4,45; N, 16.85%.

2,6-Bis(α,β-dioxopropyl)pyridine-tetraoxime. An aqueous-methanolic solution of 1.5 g (0.006 mol) dioxime and 0.84 g (0.012 mol) hydroxylamine-hydrochloride was refluxed for 13 hr, until no more precipitation took place. The precipitate was collected, filtered, washed with cold methanol and dried in a vacuum. Recrystallization from aqueous alcohol yielded colorless crystals, soluble in hot alcohol,

1) Presented at the Annual Meeting of the Chemical Society of Japan, April, 1971.

2) R. J. Cotter and M. Matzner, "Ring-forming Polymerizations," Academic Press, New York and London, (1969), and references therein.

3) M. E. B. Jones, D. A. Thornton, and R. F. Webb, *Makromol. Chem.*, **49**, 62 (1961).

4) Sh. Murahashi and H. Kubota, This Bulletin, **35**, 1465 (1962).

Table 1. Analyses and magnetic moments of the iron(II)-complexes with tetraoximes, CH_3-C(NOH)-C(NOH)-R-C(NOH)-C(NOH)-CH_3[a)]

	Found, %			Calcd, %			μ_{eff}, B.M.[b)]
	C	H	N	C	H	N	
$(C_6H_4$-O-$C_6H_4)TOH_2\cdot$Fe	49.34	4.68	12.84	50.96	3.80	13.20	2.49
$(C_6H_4$-$C_6H_4)TOH_2\cdot$Fe	53.47	5.14	13.84	52.96	3.95	13.72	2.00
(2,6-pyridyl)$TOH_2\cdot$Fe	39.43	3.88	21.80	39.66	3.32	21.02	2.31

a) Tetraoximes with various R are abbreviated as R-TOH_4.
b) Obtained for the powdered sample at room temperature.

DMSO, DMF, and pyridine, yield 56%, mp 241—242°C. Found: C, 47.19; H, 5.15; N, 24.43%. Calcd for $C_{11}H_{13}O_4N_5$: C, 47.31; H, 4.69; N, 25.08%.

Preparation of the complexes. One millimole of an iron(II) salt (Mohr's salt) was dissolved under nitrogen in 5 m*l* of water; to this solution was added at 50°C a solution of 0.5 mmol tetraoxime ligand dissolved in 10 m*l* hot DMF and 3 m*l* pyridine. An intensely red colored precipitate was immediately formed. The reaction mixture was kept at 50°C until the precipitation was completed (about 8 hr). The product was then filtered, washed with hot water, hot DMF and dried. The red powders obtained were insoluble in all common solvents, except pyridine and other organic bases. They were slightly soluble but unstable in DMF and DMSO. The analytical data are shown in Table 1.

Preparation carried out in pyridine yielded products identical to those obtained by the above standard procedure.

Apparatus and Procedures. Infrared spectra were measured by the KBr disk method using a Shimadzu IR-27C spectrophotometer in the 4000—650 cm^{-1} region. The polystyrene spectrum was used for calibration.

Magnetic moments in the solid state were determined by the Gouy method using freshly distilled water and $CuSO_4\cdot 5H_2O$ as reference substances. The molar susceptibilities were corrected using Pascal's constants for the diamagnetism of the component atoms.

Reflectance spectra of the finely ground samples were obtained with a Hitachi Spectrophotometer EPS-3, equipped with a reflectance attachment. Magnesium oxide was used as the standard of light reflectance. Electronic absorption spectra were determined with the same spectrophotometer.

The thermogravimetric analyses (TGA) were carried out using a Rigakudenki automatic recording thermobalance under atmospheric pressure. A sample of about 80 mg was held in a nitrogen stream and heated at a rate of 5°C/min.

ESR spectra were measured in the solid state at room temperature and in pyridine solution at room temperature as well as at the temperature of liquid nitrogen with a Japan Electron Optics Laboratory ESR spectrometer, Model JES-ME-2X, using 100 kHz field modulation. A blank test was run before each measurement using an evacuated sample tube. The magnetic field was calibrated with the EPR marker manganese(II) in magnesium(II) oxide.

Results and Discussion

The analytical data of the complexes, shown in Table 1, are in fair agreement with those calculated for a ligand to iron ratio of 1 : 1, indicating that one mole of ferrous ion coordinates with two α-dioxime groups.

The thermogravimetric curves of the metal chelates (*cf.* Fig. 1) show that a thermal decomposition takes

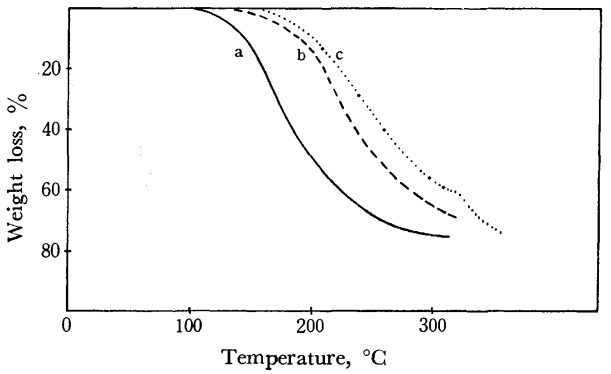

Fig. 1. Thermogravimetric curves of the iron(II)-tetraoximes in nitrogen atmosphere.
a : $(C_6H_4$-O-$C_6H_4)TOH_2\cdot$Fe
b : $(C_6H_4$-$C_6H_4)TOH_2\cdot$Fe
c : (2,6-pyridyl)$TOH_2\cdot$Fe

place according to the same pattern as for the three complexes. They give further evidence that no axial base is actually coordinated.[5)]

The present ferrous tetraoxime complexes are soluble in organic bases such as pyridine, aniline, *etc.* The electronic absorption spectra in pyridine solution show two intense bands at about 18 and 25 kK. This spectral feature is also found in pyridine-substituted iron(II)-dimethylglyoxime complexes, where two absorption maxima appear in the 17.5—19.6 and the 25.0—25.6 kK regions. The one at longer wavelength is attributed to the Fe→oxime charge transfer, the one at shorter wavelength to the Fe→pyridine charge transfer.[6)]

Though the three polymer chelates have all been found to be paramagnetic in the solid state (*cf.* Table 1), the above absorption pattern is consistent with a diamagnetic species.[6)] Spin-pairing is thus thought to take place upon substituting an axial base.

Support for this conversion was found in the ESR spectra of the compounds. For the solid state samples a clear signal without hyperfine structure was detected in the 3000 Gauss region. This signal completely disappeared in a pyridine solution.

Upon dissolving the chelates in organic bases such as piperidine or aniline which do not allow any axial

5) The TGA curve of ferrous tetraoxime compounds with axially coordinated pyridine, $(CH_2)_nTOH_2$-Fe-$(Py)_2$, n=6, 10, shows a weight loss corresponding to the dissociation of two pyridine molecules.

6) M. J. Cowan, J. M. F. Drake, and R. J. P. Williams, *Discuss. Faraday Soc.*, **27**, 217 (1959), and references therein; Y. Yamano, I. Masuda, and K. Shinra, This Bulletin, **44**, 1581 (1971).

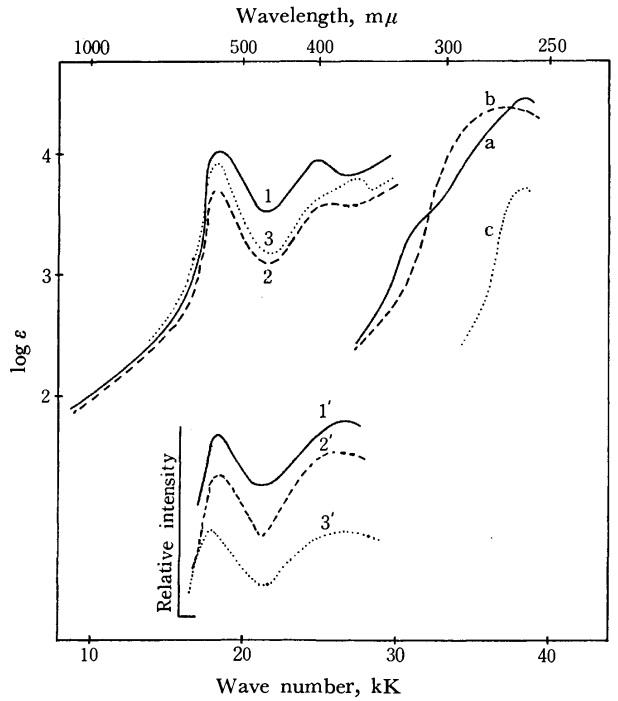

Fig. 2. Absorption spectra: a: $(C_6H_4\text{-}O\text{-}C_6H_4)TOH_4$, b: $(C_6H_4\text{-}C_6H_4)TOH_4$, c: (2,6-pyridyl)$TOH_4$, in dimethylsulfoxide solution; 1: $(C_6H_4\text{-}O\text{-}C_6H_4)TOH_2\cdot Fe$, 2: $(C_6H_4\text{-}C_6H_4)TOH_2\cdot Fe$, 3: (2,6-pyridyl)$TOH_2\cdot Fe$, in pyridine solution.
Reflectance spectra: 1′: $(C_6H_4\text{-}O\text{-}C_6H_4)TOH_2\cdot Fe$, 2′: $(C_6H_4\text{-}C_6H_4)TOH_2\cdot Fe$, 3′: (2,6-pyridyl)$TOH_2\cdot Fe$.

π-delocalization, the absorption band at higher energy, as for the dimethylglyoxime complexes, is no longer found. The band at lower energy, attributed to the Fe→oxime charge transfer, shifts considerably to longer wavelength with the increase of the basicity of the axial substituent (*cf.* Table 2).

In the case of the ferrous dimethylglyoxime complexes, substitution on the axially coordinated pyridine ligand was found to cause strong shifts of the charge transfer bands to longer or to shorter wavelength, depending on whether the donor properties (*cf.* aminopyridine, methylpyridine) or the acceptor properties (*cf.* cyanopyridine) of the pyridine were increased.[6] As can be seen from Table 2, this effect is considerably weaker in the tetraoxime complexes.

A plot of the absorption intensity of the complexes *vs.* the composition of a mixed pyridine-chloroform solvent (Fig. 4) indicates that the axial pyridine forms a very weak bond, which is consistent with the small effect of the pyridine substituents.

It is worth noticing that both the lower and the higher energy bands are shifted to longer wavelength in the pyridine-substituted tetraoxime complexes

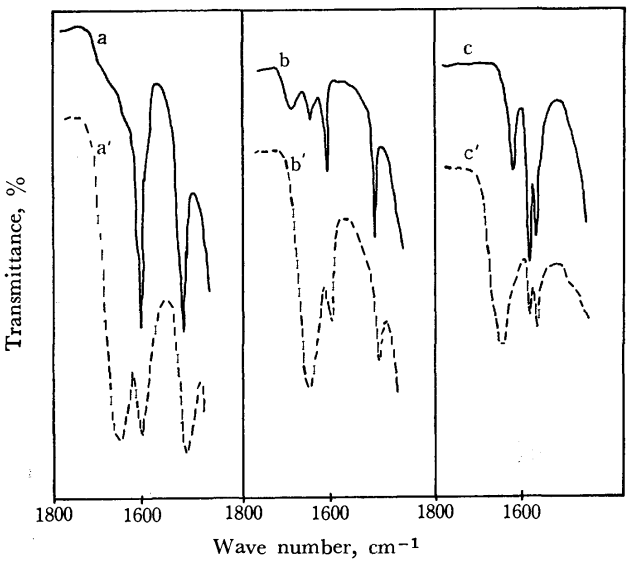

Fig. 3. Infrared spectra of the tetraoxime ligands and their iron(II)-complexes.
a: $(C_6H_4\text{-}O\text{-}C_6H_4)TOH_4$, b: $(C_6H_4\text{-}C_6H_4)TOH_4$, c: (2,6-pyridyl)$TOH_4$, a′: $(C_6H_4\text{-}O\text{-}C_6H_4)TOH_2\cdot Fe$, b′: $(C_6H_4\text{-}C_6H_4)TOH_2\cdot Fe$, c′: (2,6-pyridyl)$TOH_2\cdot Fe$.

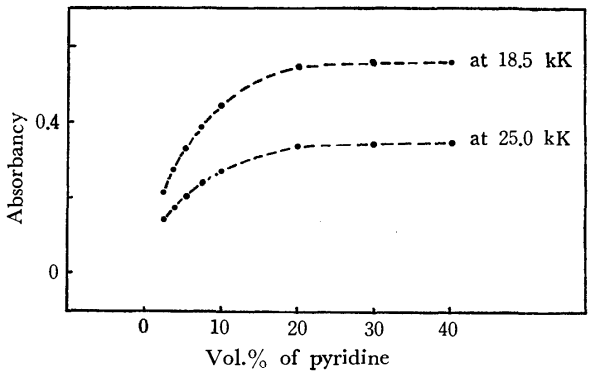

Fig. 4. Absorbancy *vs.* concentration of pyridine.
1.4 mmol $(C_6H_4\text{-}O\text{-}C_6H_4)TOH_2\cdot Fe$ in pyridine/chloroform solution, cell length = 1 cm.

Table 2. Electronic absorption spectra

Complexes	ν_{max}, kK (log ε)		Solvents
$(C_6H_4\text{-}O\text{-}C_6H_4)TOH_2\cdot Fe$	18.4	26.2	20% (4-CN-Py)/$CHCl_3$
	18.5 (4.11)	25.0 (3.87)	Pyridine
	18.5	25.0	20% (3-CH_3-Py)/$CHCl_3$
	18.4	25.8	20% (3-NH_2-Py)/$CHCl_3$
	18.2		Aniline
	17.3		Piperidine
$(C_6H_4\text{-}C_6H_4)TOH_2\cdot Fe$	18.3 (3.70)	25.6 (3.58)	Pyridine
(2,6-pyridyl)$TOH_2\cdot Fe$	18.4 (3.92)	24.8 (shoulder)	Pyridine
		27.5 (3.79)	

(25.0 and 18.5 kK respectively), as compared to the pyridine-substituted dimethylglyoxime complexes (26.0 and 19.6 kK), which can be related to a stronger Fe→oxime bonding in the former.

Comparision of the infrared spectra of the ligands and the iron(II)-complexes reveals a divergent behavior from similar dimethylglyoxime compounds. Figure 3 shows that the complexing of the nitrogen atoms of the oxime compound leads to the appearence of a strong absorption band at about 1650 cm^{-1}.

For the diphenylether- and the diphenyl-tetraoxime ligands, an absorption band attributable to the C=N stretching vibration can hardly be assigned due to the low intensity absorptions in the characteristic 1650 cm^{-1} region. In the pyridine tetraoxime ligand, a sharp but low intensity band appears at 1620 cm^{-1}, which is tentatively assigned to the C=N stretching mode of the free oxime group. For the three complexes, coordination with Fe(II) leads to a strong, broad absorption band at about 1650 cm^{-1}. A similar effect has been found in 1,2-diimine compounds upon chelating with iron(II).[7]

A second noticeable feature of the infrared spectra is that in both the pure ligands and the complexes the OH stretching vibrations at 3250 cm^{-1} can be detected, which in the iron complexes can be assigned to terminal oxime groups within the polymer. The strong intensity of this absorption band within the complexes suggests that the polymer chain is not much extended.

The structure of the ferrous tetraoxime polymer chelates in solvents involving organic bases has so far been found to bear a close resemblance to the axially substituted, octahedral Fe(II)-dimethylglyoxime analogues. While the latter are very unstable in the absence of an axial base,[6] the former could be isolated in the solid state, even from a pyridine solution with no pyridine coordinated.

7) D. H. Busch and J. C. Bailar, Jr., *J. Amer. Chem. Soc.*, **78**, 1137 (1956).

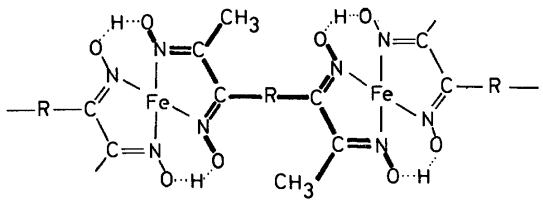

Fig. 5. Schematic representation of the tetraoxime-iron(II) complexes.

However, the reflectance spectra show the presence of a band in the 25 kK region, along with the Fe→ oxime charge transfer band at about 18 kK.

It is clear from a molecular model that, due to the sp^2 bonding between R and the oxime group, the R–C–C angle is equivalent to 120°, which excludes the formation of a monomeric binuclear complex (Fig. 5).

The absorption at shorter wavelength seems to result from an axial interaction of the central ferrous ion with another chelate molecule in the upper and lower-layers of the polymer network forming a pseudo-octahedral structure in the solid state.

Insufficient solubility and infusibility did not allow any accurate molecular weight determination.

Some paramagnetic ferrous chelates with small magnetic moments have been reported.[8] Among the explanations offered were impurities from residual ferrous or ferric ions, a thermal mixture of the low spin and the high spin form[9] or a planar arrangement with a large ligand field splitting.[10]

The present polymer chelates have been found to form a strong bonding in the Fe–N_4 plane, whereas the bonding toward the axial substituents is very weak. This seems to be a major factor determining the small magnetic moment.

8) B. N. Figgis and J. Lewis, *Progr. Inorg. Chem.*, **6**, 37 (1967).
9) W. Klemm and H. Senff, *J. Prakt. Chem.*, **154**, 73 (1939).
10) J. Chatt and B. L. Shaw, *J. Chem. Soc.*, **1961**, 285.

Derivatographic Studies on Transition Metal Complexes. VII.[1] Thermal *cis, trans*-to-*trans, cis* Isomerization of $[CoCl_2(NH_3)_2en]Br \cdot H_2O$ in Solid Phase[2]

Ryokichi TSUCHIYA, Masatatsu SUZUKI, and Eishin KYUNO

Department of Chemistry, Faculty of Science, Kanazawa University, Kanazawa

(Received June 26, 1971)

The *cis, trans*-to-*trans, cis* isomerization as well as dehydration of $[CoCl_2(NH_3)_2en]Br \cdot H_2O$ were investigated by using derivatographic, isothermal, and sealed tube methods. Isomerization in a solid phase proceeded regardless of whether its state was monohydrate or anhydride. Two distinct processes were found for isomerization, one being accompanied by the liberation of water of crystallization and the other taking place after complete liberation of water of crystallization. Both reactions were of the first order. The thermochemical functions were obtained to be $\Delta H = (12 \pm 2)$ kcal/mol, $E^* = (28 \pm 3)$ kcal/mol and $\Delta S^* = (-10 \pm 4)$ e.u. for dehydration. The values $E^* = (28 \pm 3)$ kcal/mol and $S^* (-4 \pm 2)$ e. u. were estimated for isomerization in the first process, and $E^* = (28 \pm 3)$ kcal/mol and $\Delta S^* = (-12 \pm 3)$ e.u. for that in the second process. As a possible reaction mechanism for isomerization, an "aquation-anation mechanism" was introduced for the first process and an "intramolecular mechanism" for the second.

It is known that, owing to the small energy change in isomerization, some cis-complexes turn into the corresponding trans-complexes[3] and other trans-complexes are converted into the cis-complexes[4-7] in a solid phase. A striking feature particularly of isomerization in a solid phase is that the reactions are sensitively affected by the kind of counter ionic species contained, in contrast to the reactions in aqueous solution. As an example, the variation of the counter ion X in *cis, trans*-$[CoCl_2(NH_3)_2en]X$ type gives rise to a different reaction upon heating in a solid phase. In the case of X=Cl, no isomerization could be observed, whereas in the case of $X=ClO_4$, isomerization into the corresponding *trans, cis*-form[3] took place and in the case of X=SCN, the *cis, trans*-complex was converted into *cis, cis*-$[CoCl(NCS)(NH_3)_2en]Cl$.[1]

It is of interest to investigate the cause of isomerization path-ways differing with the kind of counter ionic species. For studying the problem, we attompted to observe the isomerization of *cis, trans*-$[CoCl_2(NH_3)_2en]Br \cdot H_2O$ and its anhydride as one of the series of studies on *cis, trans*-$[CoCl_2(NH_3)_2en]X$ type complexes. Three geometrical isomers of $[CoCl_2(NH_3)_2en]^+$ are schematically drawn in Fig. 1, together with their colors. When the monohydrate and anhydride of the corresponding bromide are heated in a solid phase, a distinct color change from blue to green is observed. This thermal isomerization step is shown by an arrow in Fig. 1. This paper deals with the measurement of rate and the estimation of the kinetics of isomerization as well as dehydration in the complex bromide.

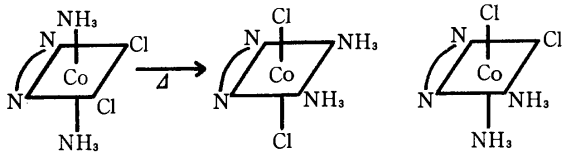

cis, trans-form (blue) — *trans, cis*-form (green) — *cis, cis*-form (violet)

Fig. 1. Geometrical isomers of $[CoCl_2(NH_3)_2en]^+$.

Experimental

Preparation of Complexes. The complex, *cis,trans*-$[CoCl_2(NH_3)_2en]Br \cdot H_2O$ was prepared by the method of Bailar and Pepard.[8] The corresponding bromide was obtained by saturating the solution of the chloride with ammonium bromide at room temperature and by standing it in a refrigerator for a while. Purification was achieved by recrystallization from water. Blue crystals deposited out were filtered, washed with a small amount of cold water, ethanol and ether, and air-dried.

Found: C, 7.46; H, 5.00 N, 17.29%. Calcd for *cis,trans*-$[CoCl_2(NH_3)_2en]Br \cdot H_2O$: C, 7.46; H, 4.95; N, 17.39%.

The complex *trans,cis*-$[CoCl_2(NH_3)_2en]Cl$ was also prepared by the method of Bailar and Pepard for the corresponding *cis,trans*-complex.

Derivatographic Measurement. The apparatus and techniques for derivatography used were the same as described previously.[9]

Isothermal Measurement. A Shimadzu TM-1A Thermano balance and Abderhalden apparatus were used for the isothermal measurment. The measurement and analytical method were also the same as given previously.[9] In order to determine the ratio of the two isomers in the sample in each heating step, the visible and UV absorption spectra of the complexes were measured with a Hitachi R-3 Spectrophotometer. The electronic spectra of the complexes in DMF-water mixture (4 : 1), *cis, trans*-$[CoCl_2(NH_3)_2en]Br \cdot H_2O$, *trans,cis*-$[CoCl_2(NH_3)_2en]Br$ and the reaction product obtained by heating the former are given in Fig. 2. Since *cis,trans*- and *trans,cis*-complexes exhibit the absorption coefficients 110 and 34 at 598 nm ($\nu = 50.17 \times 10^{13}$ sec^{-1}) and 92 and 41 at 625 nm ($\nu = 48.00 \times 10^{13}$ sec^{-1}), respectively,

1) Part VI, R. Tsuchiya, M. Suzuki, and E. Kyuno, This Bulletin, **44**, 709 (1971).
2) Presented at the 24th Annual Meeting of the Chemical Society of Japan, Osaka, April, 1971.
3) R. Tsuchiya, A. Nakata, and E. Kyuno, This Bulletin, **44**, 705 (1971).
4) H. E. LeMay, Jr., and J. C. Bailar, Jr., *J. Amer. Chem. Soc.*, **89**, 5577 (1967).
5) R. Tsuchiya, K. Murai, and E. Kyuno, This Bulletin, **43**, 1383 (1970).
6) R. Tsuchiya, Y. Kaji, and E. Kyuno, *ibid.*, **43**, 1906 (1970).
7) N. I. Lobanov, *Zhur. Neorg. Khim.*, **4**, 151 (1959).
8) J. C. Bailar, Jr., and F. Pepard, *J. Amer. Chem. Soc.*, **62**, 105 (1940).
9) R. Tsuchiya, Y. Kaji, and E. Kyuno, This Bulletin, **42**, 1881 (1969).

the ratios *cis*, *trans*/*trans*, *cis* of two isomers in each product were determined spectrophotometrically by means of the following equations,

$$\left.\begin{aligned} 110X + 34Y &= D_{598} \\ 92X + 41Y &= D_{625} \end{aligned}\right\} \quad (1)$$

where X and Y are the concentrations (mol l^{-1}) of *cis*, *trans*-complex and *trans*, *cis*-complex, respecitvely, and D_{598} and D_{625} are the observed absorbancies at 598 nm and 625 nm, respectively, with 1.0 cm cell.

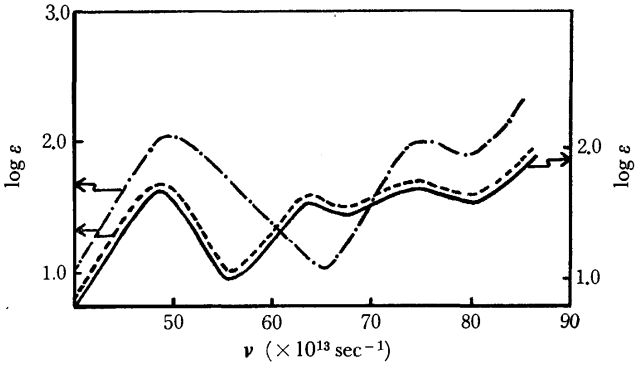

Fig. 2. Electronic spectra of *cis*, *trans*-$[CoCl_2(NH_3)_2en]Br \cdot H_2O$ (———), *trans*, *cis*-$[CoCl_2(NH_3)_2en]Br$ (——), and the product obtained by heating the former (----).

IR Spectral Measurement. The IR and Far IR spectra were measured by a nujol-mull method using JASCO Model IR-E and IR-F Spectrophotometers both in NaCl and in CsBr regions.

Results and Discussion

Structural Assignment. IR spectra of the complexes are shown in Fig. 3. In order to determine the geometric configuration in the thermal reaction product of *cis*, *trans*-$[CoCl_2(NH_3)_2en]Br \cdot H_2O$, δ_{NH_2} bands appearing in 1250—1350 cm^{-1},[1,10] ν_{Co-N} bands in 450—550 cm^{-1},[12] and ν_{Co-Cl} bands in 300—360 cm^{-1},[11] should be carefully studied.

The three wave number regions where the absorption peaks appear differ to some extent in *cis*, *trans*-$[CoCl_2(NH_3)en]Br \cdot H_2O$ and *trans*, *cis*-$[CoCl_2(NH_3)en]Br$ as seen in Fig. 3. On the other hand, the absorption peaks for δ_{NH_2}, ν_{Co-N} and ν_{Co-Cl} in the thermal reaction product were found to be in fair agreement with those in *trans*, *cis*-$[CoCl_2(NH_3)_2en]Br$.

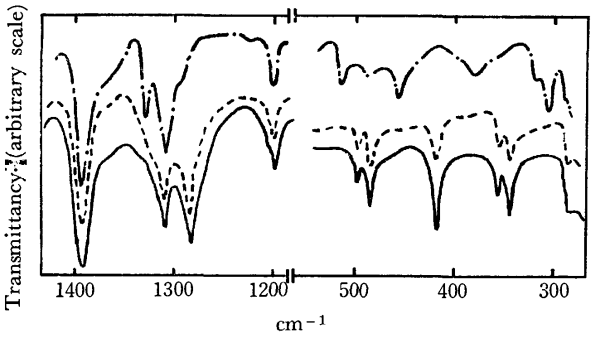

Fig. 3. IR spectra of *cis*, *trans*-$[CoCl_2(NH_3)_2en]Br \cdot H_2O$ (———), *trans*, *cis*-$[CoCl_2(NH_3)_2en]Br$, (——), and the product obtained by heating the former (----).

If the thermal exchange between chloride ion coordinating to the central metal ion and bromide ion in the outer coordination sphere occurs in the isomerization process, the bands in 300—360 cm^{-1} for the reaction rpoduct should differ from those for *trans*, *cis*-$[CoCl_2(NH_3)_2en]Br$. A similar exchange has been found in the isomerization, *cis*, *trans*-$[CoCl_2(NH_3)_2en]SCN \cdot H_2O \longrightarrow$ *cis*, *cis*-$[CoCl(NCS)(NH_3)_2en]Cl$.[1] However, no such exchange could be observed in *cis*, *trans*-$[CoCl_2(NH_3)_2en]Br \cdot H_2O$.

Thus, it is concluded that the thermal reaction product of *cis*, *trans*-$[CoCl_2(NH_3)_2en]Br \cdot H_2O$ is *trans*, *cis*-$[CoCl_2(NH_3)_2en]Br$.

Derivatography. The derivatogram for *cis*, *trans*-$[CoCl_2(NH_3)_2ne]Br \cdot H_2O$, is shown in Fig. 4, where the heating rate applied is 1°/min. The TG curve indicates that dehydration begins at about 90°C and is complete at 125°C and no further loss of weight is detectable until about 150°C. The DTA curve exhibits two overlapped, broad endothermic peaks: the first endothermic peak is centered at 100°C corresponding to genuine dehydration, and is followed by the second, somewhat less intense peak at 120—125°C, corresponding to the dehydration accompanied by the partial isomerization. Other endothermic and exothermic peaks appear at 150—170°C suggesting further decomposition from the TG curve. The DTG curve exhibits similar peaks to those in the DTA curve.

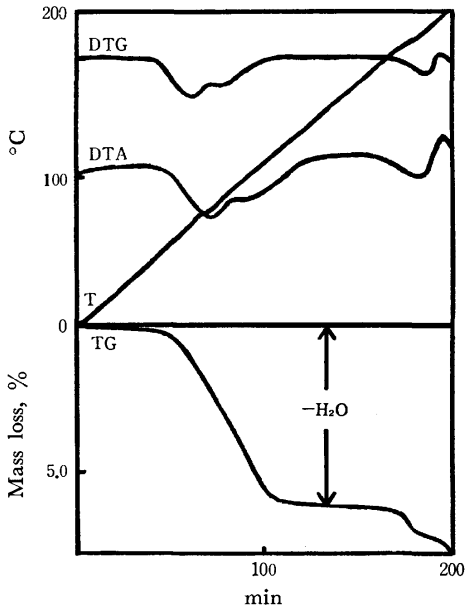

Fig. 4. Derivatogram for *cis*, *trans*-$[CoCl_2(NH_3)_2en]Br \cdot H_2O$.

The enthalpy change ΔH in the genuine dehydration was estimated to be (12±2) kcal/mol by means of analysis of the first endothermic peak.[9] The value is comparable to the enthalpy change in the dehydration from the general hydrate.

10) For *cis*, *trans*- and *trans*, *cis*-$[CoCl_2(NH_3)_2en]Cl$: E. Kyuno, *Nippon Kagaku Zasshi*, **80**, 722 (1959).

11) I. Nakagawa and T. Shimanouchi, *Spectrochim. Acta*, **22**, 759 (1966).

Rate Law for Dehydration and Isomerization. From the measurement of the weight change with a thermobalance at several isothermal temperatures in the region 100—140°C, the relationship between mass loss and time was obtained. By measurement of the absorption of the samples picked up at desired time intervals upon heating and application of equations (1), the conversion ratios of *cis, trans* type complexes to *trans, cis* type complexes were calculated. The results are summarized in Table 1.

Table 1. The rate constant of dehydration k_d, first step isomerization k_1* and second step isomerization k_1**, and thermochemical functions

°C	k_d (sec^{-1})	k_1* (sec^{-1})	k_1** (sec^{-1})
100	$(1.9\pm0.3)\times10^{-4}$	$(1.1\pm0.4)\times10^{-4}$	$(1.1\pm0.3)\times10^{-6}$
110.8	$(4.6\pm0.4)\times10^{-4}$	$(4.1\pm0.4)\times10^{-4}$	$(2.8\pm0.3)\times10^{-4}$
121.8	$(1.2\pm0.3)\times10^{-3}$	$(1.2\pm0.4)\times10^{-3}$	$(9.1\pm0.3)\times10^{-5}$
138.3	$(6.5\pm0.3)\times10^{-3}$	$(7.1\pm0.5)\times10^{-3}$	$(3.3\pm0.3)\times10^{-4}$

$\Delta H = (12\pm2)$kcal/mol
$E^* = (28\pm3)$ kcal/mol $E^* = (28\pm3)$kcal/mol $E^* = (28\pm3)$ kcal/mol
$\Delta S^* = (-10\pm3)$ e.u. $\Delta S^* = (-4\pm2)$ e.u. $\Delta S^* = (-12\pm3)$ e.u.

Let *a* denote the initial amount of *cis, trans*-complex monohydrate (in case of dehydration) or of its anhydride (in case of isomerization), *x* denote the amount of anhydride (dehydration) or *trans, cis*-complex (isomerization) produced, and let the values of log $a/(a-x)$ be plotted against time (Fig. 5.). The results

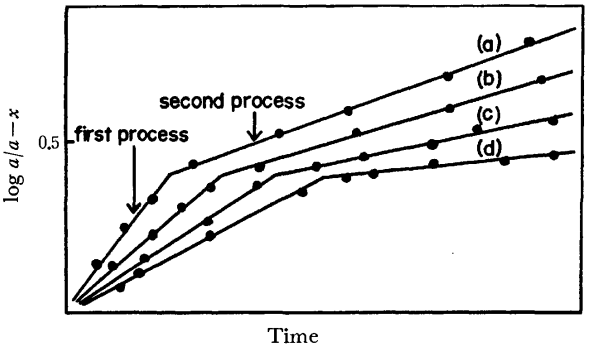

Fig. 5. Plots of log $a/(a-x)$ *vs.* time for isomerization. (a) 138.3°C, (b) 121.8°C, (c) 110.8°C, (d) 100°C Time scales are different in each run.

give two crossed straight lines at each temperature, indicating that the reactions proceed in the first order.

The appearance of a knick point in each plot suggests the presence of the two steps in isomerization. The first step of isomerization was followed by the dehydration from the complex and *cis, trans*/*trans, cis* ratios in the product at all temperatures were found to be 40 : 60 at the end of dehydration. The second step of isomerization proceeded in the absence of water.

Rate constants calculated are listed in Table 1, which includes the thermochemical functions estimated from the temperature-dependence of rate constant: the activation energies were obtained from the inclination of the plottings, and the entropies of activation were calculated by means of absolute rate theory.

The thermal reaction schemes are shown in Fig. 6. It is known that the isomerization accompanying dehydration in solid phase was interpreted in terms of the "aquation-anation mechanism," while the isomerization in anhydrous state was explained with the aid of the intramolecular mechanism[12,13]. In the thermal decomposition of *trans*-$[CoCl_2pn_2](H_5O_2)Cl_2$, the above concepts concerning the reaction mechanism were also applied.[5]

It is known that the activation energies in the dehydration and in the isomerization accompanying dehydration are 25—45 kcal/mol[1,5]. A comparison of the above activation energies with that given in Table 1 suggests that the isomerization of *cis, trans*-$[CoCl_2(NH_3)_2en]Br \cdot H_2O$ in solid phase proceeds through "aquation-anation mechanism" in the same way as in aqueous solution.

In order to confirm the presumption, the same thermal isomerization as above was tried in a sealed tube, since isomerization in a sealed tube is expected to be faster than that in an open system. In the anhydrous complex, no further change in reaction rate was found between the sealed tube and the open system. However, the rate of the first step isomerization accompanying dehydration was found to be considerably affected by the vapor pressure from water contained in the complex. This is probably due to the fact that, in the case of anhydride, a small amount of water coexisting with the sample can act only at the surface of solid, while in the hydrated crystals

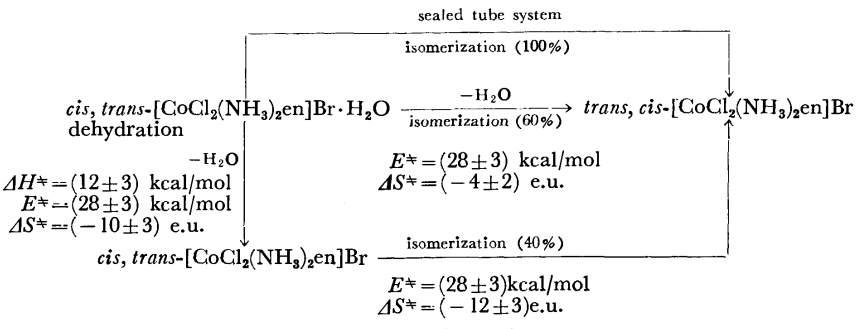

Fig. 6. Thermal reaction schemes.

12) J. C. Bailar, Jr., *J. Inorg. Nucl. Chem.*, **8**, 165 (1958); P. C. Ray and N. K. Dutt, *J. Indian Chem. Soc.*, **18**, 289 (1941); **20**, 81 (1943).

13) See for example, F. Basolo, and R. G. Pearson, "Mechanism of Inorganic Reactions," 2nd ed., John Wiley and Sons, Inc., New York, N. Y. (1967), p. 327.

water molecules can easily react with the complex in a sealed tube.

The "aquation-anation" path-way in the isomerization of the *cis, trans*-complex monohydrate to the *trans,cis*-complex monohydrate,

$$\textit{cis, trans}\text{-}[CoCl_2(NH_3)_2en]Br\cdot H_2O \searrow \rightarrow \textit{trans, cis}\text{-}[CoCl_2(NH_3)_2en]Br + H_2O$$

is presumed to consist of the following two steps:

$$\textit{cis, trans}\text{-}[CoCl_2(NH_3)_2en]Br + H_2O \searrow \rightarrow \textit{trans, cis}\text{-}[CoCl(H_2O)(NH_3)_2en]BrCl \quad \text{(i)}$$
(or *cis, trans*-)

$$\textit{trans, cis}\text{-}[CoCl(H_2O)(NH_3)_2en]BrCl \text{ (or } \textit{cis, trans}\text{-)} \searrow \rightarrow \textit{trans, cis}\text{-}[CoCl_2(NH_3)_2en]Br + H_2O \quad \text{(ii)}$$

Process (ii) may be considered to be the rate determining step since the isomerization was found to proceed according to the first rate law.

On the other hand, it was found that the complex chloride, *cis, trans*-$[CoCl_2(NH_3)_2en]Cl\cdot H_2O$, does not isomerize in the open system but isomerizes in the sealed tube, which gives similar conditions to those in aqueous solution. It may be due to the fact that the water of crystallization has little role in the isomerization of the chloride in the open system.

Since *cis, trans/trans, cis* ratios in the sample obtained immediately after the complete liberation of water of crystallization from *cis, trans*-$[CoCl_2(NH_3)_2en]Br\cdot H_2O$ are independent of the degree of isothermal temperature, a certain amount of water might have no contribution to the isomerization.

The activation energy for the first isomerization, $E^*=(28\pm3)$ kcal/mol, coincides with that for the dehydration. This suggests that the aquation process (i) is very fast, being followed by the slower anation (ii). Thus the consideration that process (ii) may be the rate determining step is supported and the "aquation-anation mechanism" would be accepted in the isomerization of *cis, trans*-$[CoCl_2(NH_3)_2en]Br\cdot H_2O$.

For the isomerization of anhydrous complex, either of the intramolecular mechanisms, "chain-opening-closing" or "twisting" mechanism, may be considered. If the former is predominant in the isomerization of anhydrous complex, the activation energy would be relatively large owing to the requirement of the bond-breaking energies. The activation energy actually obtained in the second isomerization $E^*=(28\pm3)$ kcal/mol was, however, considerably smaller than that expected. Thus, "chain-opening-closing" mechanism can be ruled out. On the other hand, "aquation-anation mechanism" also can not be accepted even if the activation energy is eventually equal to that in the first isomerization, since the second isomerization occurs in the absence of water.

Thus, we might conclude that the second isomerization of anhydrous complex *cis, trans*-$[CoCl_2(NH_3)_2en]Br$ proceeds with the aid of "twisting mechanism," because it does not require much activation energy.

With the values of the activation energy E^* and the entropy of activation ΔS^*, those of free energy of activation ΔG^* were calculated to be 30 kcal/mol and 33 kcal/mol, for the first and second isomerizations respectively. It is obivous from these values that the anhydrous complex is more difficult to isomerize than the hydrate complex.

Formation of Uranium Sesquicarbide by the Partial Decarburization of Uranium Dicarbide Using Magnesium Oxide

Hiroaki TAGAWA

Japan Atomic Energy Research Institute, Tokai-mura, Ibaraki

(Received August 2, 1971)

Formation of U_2C_3 by the reaction of UC_2 with MgO has been studied by means of chemical and X-ray analyses at temperatures 1450—1700°C *in vacuo*. The reaction was found to proceed generating CO and Mg vapor and to produce U_2C_3. The decarburization is represented by

$$2UC_2 + MgO \rightarrow U_2C_3 + CO + Mg.$$

UO_2 and UC were formed as the intermediate compounds. The amount of UO_2 was nearly equal to that formed by the reaction: $UC_2+4MgO=UO_2+2CO+4Mg$. The lattice parameter of U_2C_3 was 8.0890 Å. The lattice parameters of UC_2 and UC varied with the reaction time. The main reaction sequence was suggested to be:

$$1/4UC_2 + MgO = 1/4UO_2 + 1/2CO + Mg$$

$$7/4UC_2 + 1/4UO_2 = U_2C_3 + 1/2CO.$$

The experimental results were in good agreement with those obtained by thermochemical calculation.

In the system uranium-carbon, there are three compounds, monocarbide, sesquicarbide, and dicarbide. Monocarbide UC is NaCl-type face-centered cubic,[1,2] with a lattice parameter of 4.9605 Å. Sesquicarbide U_2C_3 is known to be body-centered cubic (space group I43d) by X-ray[3] as well as neutron diffraction studies[4]. The best parameter seems to be 8.0898 Å[5,6]. Dicarbide UC_2 has two modifications. α-UC_2 is CaC_2-type body-centered tetragonal.[1,2,4,7,8,9] The compound exhibits a non stoichiometric range of composition, $UC_{1.85}$—$UC_{1.96}$. Various lattice parameters are found in literature. They lie in the ranges a_0=3.515—3.526 Å, c_0=5.98—6.00 Å. It was shown that the values of carbon-saturated UC_2 obtained in equilibrium state are a_0=3.5256 Å and c_0=6.000 Å[6,10]. Above 1765°C the tetragonal structure is transformed into the cubic structure[8,11], which is considered to be of the NaCl-type with a C_2 group as in the case of CaC_2 and KCN.

Although uranium sesquicarbide is stable below 1780°C[12], it is not formed easily by the carburization of uranium metal or by the carbothermic reaction of uranium dioxide. In both reactions, the carbide phase of the composition C/U=1.5 is always found to be a mixture of monocarbide and dicarbide. No sesquicarbide is obtained directly. It was reported that sesquicarbide is formed by adding mechanical stress onto a mixture of monocarbide and dicarbide,[13] or by heating and cooling it repeatedly at about the temperature of decomposition of U_2C_3.[14] It was also reported that U_2C_3 is formed by heating a mixture of UC and UC_2 at 1500—1600°C,[15] or by the reaction of pure UC and graphite *in vacuo*.[16,17] The formation of sesquicarbide is apparently inhibited by the presence of dissolved oxygen in the matrix.[17,18] Self-purification is reported when the carbide of composition $UC_{1.5}$ is annealed at 1500°C in a vacuum of 10^{-5} mmHg, producing U_2C_3.[15,17]

However, it was found that uranium sesquicarbide is easily produced by the reaction of dicarbide with uranium dioxide:[19]

$$7UC_2 + UO_2 = 4U_2C_3 + 2CO.$$

In this reaction, U_2C_3 is formed not only by the direct reaction of UC_2 and UO_2, but also by the reaction of UC, which appears as an intermediate with some quantity of oxygen, with UC_2, which dissolves oxygen from UO_2 : $U(C,O)+U(C_2,O)\rightarrow U_2C_3+CO$.
Oxygen has an important role in the formation of sesquicarbide. Thus, if a suitable metal oxide is used instead of uranium dioxide, the oxygen will act to give the product U_2C_3.

The reaction of uranium dicarbide with magnesium oxide as a metal oxide was examined by means of X-ray and chemical analyses. Magnesium oxide was chosen because the vapor pressure of magnesium pro-

1) R. E. Rundle, N. C. Baenzieger, A. S. Wilson, and R. A. Mc-Donald, *J. Amer. Chem. Soc.*, **70**, 99 (1948).
2) L. M. Litz, A. B. Garett, and F. C. Groxton, *ibid.*, **70**, 1718 (1948).
3) M. W. Mallett, A. F. Gerds, and D. A. Vaughan, *Trans. Electrochem. Soc.*, **99**, 197 (1952).
4) A. E. Austin, *Acta Crystallogr.*, **12**, 159 (1959).
5) J. F. A. Hennecke and C. J. Toussaint, *J. Appl. Crystallogr.*, **2**, 301 (1969).
6) H. Tagawa, K. Fujii, and Y. Sasaki, *J. Nucl. Sci. Tech.* (Tokyo), **8**, 244 (1971).
7) M. Atoji and R. C. Medrud, *J. Chem. Phys.*, **31**, 332 (1959).
8) A. L. Bowman, G. P. Arnold, W. G. Witteman, T. C. Wallace, and N. G. Nerson, *Acta Crystallogr.*, **21**, 670 (1966).
9) M. Atoji, *J. Chem. Phys.*, **47**, 1188 (1967).
10) H. Tagawa, *J. Nucl. Mater.*, **34**, 116 (1970).
11) W. B. Wilson, *J. Amer. Ceram. Soc.*, **43**, 77 (1960).
12) E. K. Storms, "The Refractory Carbides," Academic Press, New York, N. Y. (1967) p. 176.
13) M. W. Mallett, A. F. Gerds, and D. A. Vaughan, *Trans. Electrochem. Soc.*, **98**, 505 (1951).
14) W. G. Witteman and M. G. Bowman, USAEC-Report TID-7676, 121 (1964).
15) S. Imoto, T. Sano, and Y. Takada, "Carbides in Nuclear Energy", Vol. 1, ed. by L. E. Russell et al. Macmillan & Co. Ltd., London (1964), p. 7.
16) K. Sato, K. Naito, and T. Mukaibo, *J. Atomic Energy Soc. Japan*, **4**, 754 (1962).
17) J. Henney, UKAEA Report AERE-R 4175 (1962).
18) J. Henney, UKAEA Report AERE-R 4661 (1966).
19) H. Tagawa and K. Fujii, *J. Nucl. Mater.*, **39**, 109 (1971).

duced is very large at high temperatures, and magnesium does not form carbide under the experimental conditions, uranium sesquicarbide thus being expected as the product.

Experimental

Materials. Uranium dicarbide was prepared by the carburization of uranium metal. The procedure was the same as that reported.[6] Uranium hydride and spectroscopically pure graphite powder were mixed at a mole ratio 1 : 2, and cold-pressed to cylindrical pellets. The resulting pellets were heated in a graphite crucible at 400°C to decompose the hydride, and then at 1700°C for 3 hr *in vacuo*. Composition of the dicarbide produced: uranium, 90.767 wt%; total carbon, 8.870 wt% (C/U=1.937), with no free carbon. The lattice parameters were $a_0=3.5252$ Å and $c_0=5.999$ Å. Chemically pure magnesium oxide was ignited at 900°C in the air before use.

Procedure. The UC_2 and MgO powders under 200 mesh were mixed together at the ratio 13 : 1 by weight, and cold-compacted at 3 ton/cm² into cylindrical pellets, 7 mm in diameter and 7 mm in height. The pellets were heated in a graphite crucible *in vacuo* at 1450—1700°C for 0.5 to 7 hr. The reaction was carried out in a tantalum resistance furnace, evacuated to 1×10^{-5} mmHg or below. The temperature of crucible was measured with a two-color eye pyrometer, calibrated by the melting point of platinum.

Chemical and X-ray analyses. Chemical analysis of amounts of total carbon and uranium was carried out by means of combustion technique.[6] The amount of magnesium oxide unreacted was determined by the photometric method with 8-hydroxyquinoline.[20] The method involves TBP extraction to separate uranium, precipitation of magnesium as 8-hydroxyquinolate, and photometric measurement of combined 8-hydroxyquinoline in hydrochloric acid medium.

X-ray measurements were carried out with a diffractometer, the operation conditions being the same as reported.[10] The lattice parameters were calculated from diffraction lines between 165° and 70° of twice the Bragg angle, by the $\cos^2\theta$ extrapolation method. The standard deviations were within 0.0004 Å for UC, U_2C_3, a_0 of UC_2 and UO_2, and within 0.002 Å for c_0 of UC_2. The amounts of three uranium carbides in the product were determined by comparison of relative intensities. The (311) or (222) reflection for UC, the (521) reflection for U_2C_3 and the (211+202) reflection for UC, the (521) reflection for U_2C_3 and the (211+202) reflections for UC_2 were used. No reflection was found for magnesium oxide. The amount of uranium dioxide as an intermediate was determined by comparison of the reflection (111) for UO_2 with the (111) reflection for UC and (101) for UC_2. The results were compared with those of chemical analysis.

Results

Reaction of UC_2 with MgO. The reaction of a pelletized mixture of uranium dicarbide and magnesium oxide at temperatures 1450—1700°C *in vacuo* was found to proceed generating carbon monoxide and magnesium vapor, which condensed at a cold zone in the furnace. At 1500°C the weight change in the pellets before and after the reaction was 8.27, 8.60, 9.21, and 9.30 wt% corresponding to the heating time 0.5, 1, 2, and 7 hr, respectively. It was shown that most of the weight loss took place within 0.5 hr. The reaction at 1700°C terminated after heating about 1 hr. The results of chemical analysis for the products heated at 1500°C are given in Fig. 1. The change in the carbide composition by X-ray analysis obtained by the summation of the composition of the three carbides, is also given. The difference in the data obtained by X-ray and chemical analyses was taken as the amount of uranium dioxide. This was in good agreement with that obtained directly by X-ray analysis. Magnesium oxide unreacted was detected only in the products obtained by 0.5 hr heating and at 1500°C or below; the amount was 0.95 wt% at 1450°C and 0.09 wt% at 1500°C. Figure 2 shows the change in the phases UC_2, U_2C_3, UC, and UO_2 in the products with the reaction time at 1500°C. The amount of UO_2 showed a maximum in 0.5 hr of heating at all the temperatures. We see that UO_2 (10 mol%) was found in the product by heating for 0.5 hr. The amount was nearly the same as that formed by the reaction: $UC_2+4MgO=UO_2+2CO+4Mg$, *i.e.*, 12.5 mol%. On visual inspection of the cross section of the pellets heated for 0.5 hr, uranium dioxide was found to be scattered throughout the area. Uranium monocarbide was also formd as an intermediate; the amount of UC showed a maximum at all the reaction temperatures for 0.5—1 hr of heating time. The quantity of uranium sesquicarbide increased monotonically with the reaction time, UC_2 being rapidly consumed.

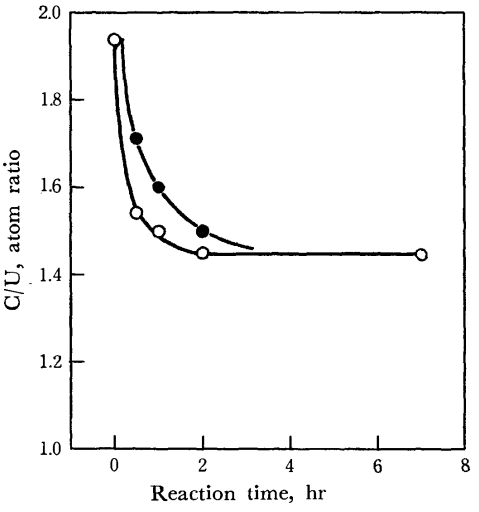

Fig. 1. Variation of the C/U atom ratios of the product at 1500°C by chemical and X-ray analyses with reaction time.
○: chemical analysis
●: X-ray analysis. The difference between X-ray and chemical analysis is taken as UO_2.

Change in the Lattice Parameters. The lattice parameters of the three uranium carbides were found to vary with the reaction time. The results for the products heated at 1500°C are given in Table 1. The lattice parameter of UC at 0.5 hr is slightly smaller

20) H. B. Evans and H. Hashitani, *Anal. Chem.*, **36**, 2032 (1964).

Table 1. The variation of the lattice parameters of uranium carbides and dioxide with the reaction time in the product heated at 1500°C

Time	UC	U_2C_3	UC_2		UO_2
			a_0	c_0	
(hr)	(Å)	(Å)	(Å)	(Å)	(Å)
0.5	4.9598	8.0900	3.5198	5.996	5.4715
1	4.9604	8.0897	3.5238	5.998	—
2	4.9606	8.0895	—	—	—
7	4.9604	8.0888	—	—	—

than that at 1 hr or longer heating times, which is the same as that of stoichiometric UC with a small quantity of oxygen[12]. The value at 0.5 hr at 1450°C was 4.9611 Å, and that for longer heating times was about 4.9605 Å. At 1600° and 1700°C, the UC lattice parameter took the nearly constant value 4.9605 Å. When oxygen is dissolved into UC, the lattice parameter has been shown to deviate from 4.9605 Å[21-24]. The change in the lattice parameter observed indicates that oxygen is dissolved in UC to form a $UC_{1-x}O_x$ phase. It is possible to determine the amount of dissolved oxygen from the change in lattice parameter. In the present work, the amount of oxygen dissolved in the UC phase does not seem to be very large. For example, the parameter 4.9611 Å for UC in the product heated at 1450°C for 0.5 hr corresponds to 2000 ppm of dissolved oxygen, according to Magnier et al.[21] By further heating, UC is converted into U_2C_3 by the reaction with UC_2. The oxygen dissolved would have been removed as CO.

The lattice parameter of U_2C_3 varied between 8.0900 and 8.0885 Å. The values at 7 hr at 1450—1700°C were 8.0890±0.0003 Å.

The lattice parameter of UC_2 varied considerably with the reaction temperature and time. The starting UC_2 phase disappeared within 2 hr in the products heated at temperatures higher than 1500°C. It was found that the lattice parameters varied with the reaction time in the same manner as that reported previously,[19] *viz.*, the parameters, a_0 and c_0, showed minimum values at about 0.5 hr. The change in the UC_2 lattice parameter with time indicates that oxygen is transferred into the carbide phase from MgO and/or UO_2 and then removed gradually.

Discussion

It was reported that the formation of uranium sesquicarbide is inhibited in the presence of dissolved oxygen[17,18]. However, the reaction of UC_2 with UO_2 was found to yield U_2C_3, even when the carbide phase coexisted with unreacted UO_2 and/or dissolved oxygen.[19] We found that partial decarburization of UC_2 with MgO produced U_2C_3 when magnesium oxide was used instead of uranium dioxide. The characteristic in this reaction is the formation of UO_2 as an intermediate. Figure 2 shows that the content of UO_2 in the product heated at 0.5 hr at 1500°C is 10 mol%, and that of UC_2 60 mol%. It is suggested that the reaction of UC_2 with MgO is predominant as compared with the other reactions and the formation of UO_2 by the reaction is complete within 0.5 hr, since the content of UO_2 is 12.5 mol% at a maximum. Uranium monocarbide was also formed as an intermediate dissolving a small amount of oxygen. From the results in Figs. 1 and 2, it is deduced that the reaction of UC_2 with MgO proceeds in three steps:

(1) MgO is consumed by UC_2 to form UO_2 : $UC_2 + 4MgO \rightarrow UO_2 + 2CO + 4Mg$, and UC_2 dissolves oxygen;

(2) U_2C_3 is produced by the reaction of UC_2 with UO_2 formed: $7UC_2 + UO_2 \rightarrow 4U_2C_3 + 2CO$, and at the same time UC is also formed by the paralled reaction: $3UC_2 + UO_2 \rightarrow 4UC + 2CO$; and

(3) UC_2 with dissolved oxygen reacts with UC : $U(C,O) + U(C_2,O) \rightarrow U_2C_3 + CO$.

Figures 1 and 2 show that step (1) terminates within 0.5 hr, step (2) takes place at reaction times between 0.5 and 2 hr or a little longer, and step (3) after 2 hr. The main reaction sequence is given by

$$1/4UC_2 + MgO = 1/4UO_2 + 1/2CO + Mg$$
$$7/4UC_2 + 1/4UO_2 = U_2C_3 + 1/2CO$$

$$2UC_2 + MgO = U_2C_3 + CO + Mg$$

The formation of U_2C_3 should be examined from a thermochemical standpoint. For the various reactions of UC_2-MgO system accompanied by the release of CO and Mg, the following reactions are probable:

$$2UC_2 + MgO = U_2C_3 + CO + Mg \quad (1)$$
$$UC_2 + MgO = UC + CO + Mg \quad (2)$$

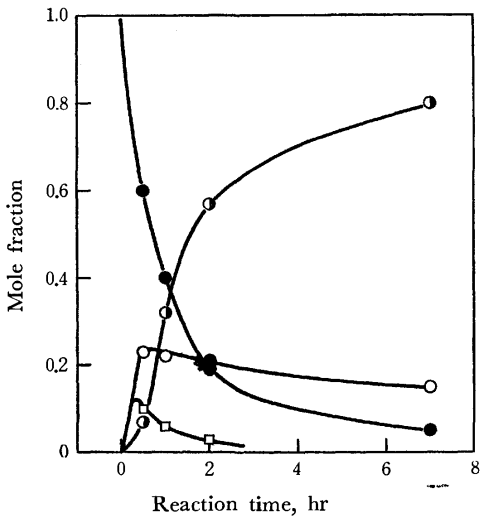

Fig. 2. Variation of mole fractions of UC_2, U_2C_3, UC, and UO_2 in the product at 1500°C with reaction time.
●: UC_2; ◑: U_2C_3; ○: UC; □: UO_2.

21) P. Magnier, J. Trouve, and A. Accary, "Carbides in Nuclear Energy," Vol. 1 ed. by L. E. Russell et al, Macmillan & Co. Ltd., London (1964), p. 95.
22) N. H. Brett, E. A. Harper, H. J. Hedger, and J. S. Pottinger, *ibid.*, p. 162.
23) R. F. Stoops and J. V. Hamme, *J. Amer. Ceram. Soc.*, **47**, 59 (1964).
24) B. C. H. Steele, N. A. Javed, and C. B. Alcock, *J. Nucl. Mater.*, **35**, 1 (1970)

TABLE 2. STANDARD FREE ENERGIES OF FORMATION

Reaction	ΔG°(cal)	Validity Range (°K)	Reference
$U(l)+C(s)=UC(s)$	$-26160+0.4T$	1400—2100	25
$2U(l)+3C(s)=U_2C_3(s)$	$-48500-2.4T$	1400—2000	25
$U(l)+1.93C(s)=UC_{1.93}(s)$	$-21433-2.89T$	1400—2100	25
$U(l)+O_2(g)=UO_2(s)$	$-269700+97.0T-15.4T\log T$	1400—2000	26
$Mg(g)+1/2O_2(g)=MgO(s)$	$-181600+75.7T-7.37T\log T$	1380—2500	27
$C(s)+1/2O_2(g)=CO(g)$	$-26700-20.95T$	298—2500	27

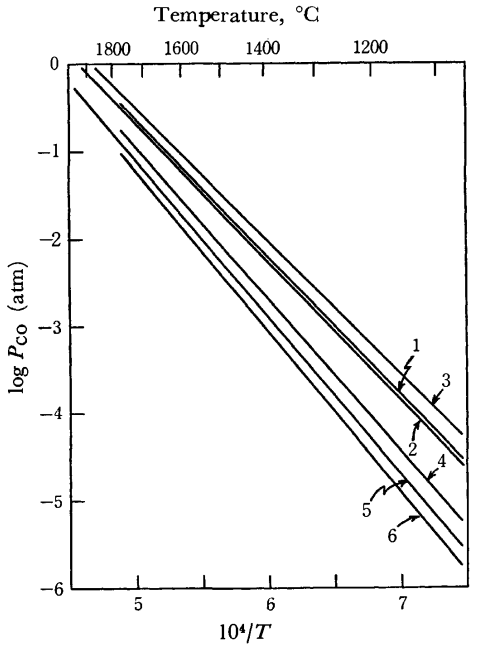

Fig. 3. Calculated equilibrium CO pressures in atm as a function of temperature.
1: $2UC_2+MgO=U_2C_3+CO+Mg$
2: $UC_2+MgO=UC+CO+Mg$
3: $UC_2+4MgO=UO_2+2CO+4Mg$
4: $7UC_2+UO_2=4U_2C_3+2CO$
5: $3UC_2+UO_2=4UC+2CO$
6: $3U_2C_3+UO_2=7UC+2CO$

$$UC_2 + 4MgO = UO_2 + 2CO + 4Mg \quad (3)$$

UO_2 is formed by the reaction of UC_2 and MgO. Consequently, it is necessary to consider the reactions of UC_2-UO_2 system:

$$7UC_2 + UO_2 = 4U_2C_3 + 2CO \quad (4)$$

$$3UC_2 + UO_2 = 4UC + 2CO \quad (5)$$

$$3U_2C_3 + UO_2 = 7UC + 2CO \quad (6)$$

The equilibrium CO pressures for the equations were calculated with use of the standard free energies of formation for UC,[25] U_2C_3,[25] UC_2,[25] UO_2,[26] MgO[27] and CO[27] listed in Table 2. The calculated values are given in Fig. 3. The figure shows that the CO pressure of reaction (3) is the highest at all temperatures. Thus, in the earlier stage of the reaction of UC_2 with MgO, the formation of uranium dioxide quite possibly takes place before that of uranium sesquicarbide. Once UO_2 is produced, U_2C_3 rather than UC is formed preferentially in the reaction of UC_2 with UO_2. The experimental results are in good agreement with those obtained by thermochemical calculation.

The author wishes to express his appreciation to Mr. K. Fujii for his help in the experiment, to Dr. H. Hashitani and Mr. T. Adachi for analyzing magnesium in the carbide samples and to Dr. Y. Sasaki for his continued support in this work.

25) C. E. Holley and E. K. Storms, "Thermodynamics of Nuclear Materials", IAEA, Vienna (1968) p. 397.
26) M. H. Rand and O. Kubaschewski, "The Thermochemical Properties of Uranium Compounds," Oliver & Boyd, London (1963).
27) O. Kubaschewski, E. Ll. Evans and C. B. Alcock, "Metallurgical Thermochemistry," 4th ed., Pergamon Press, London (1967).

Kinetic Studies of the Electron-Transfer Reaction in Iron(II) and Iron(III) Systems. V. The Reaction in Mixed Solvents of Methanol and Water[1)]

Goro WADA and Akiko ENDO

Department of Chemistry, Nara Women's University, Nara

(Received August 9, 1971)

The electron-transfer reaction between Fe(II) and Fe(III) species in mixed solvents of methanol and water was investigated by the use of Fe-59 as the radioactive tracer. The hydrolysis constant of Fe^{3+}, K_H, in the mixed solvent decreases gradually as the mole faction of methanol, x_M, increases. At very high acidities, ionic association between Fe^{3+} and ClO_4^- ions occurs, thus forming an ion-pair in the mixed solvent. The apparent rate constant, k_{app}, of the electron-transfer reaction is a function with respect to x_M; k_{app} does not vary much in the concentration range $x_M \leqq 0.3$, but it decreases as x_M grows higher than 0.3. k_{app} is also dependent upon $[H^+]$ and in a linear relationship with $[H^+]^{-1}$. Thus, the two reaction paths, Fe^{2+}-Fe^{3+} (k_0) and Fe^{2+}-$FeOH^{2+}$ (k_H), are deduced to be prevailing. Both rate constants, k_0 and k_H, decrease with an increase in x_M. The constancy of k_{app} at $0 \leqq x_M \leqq 0.3$ is a result of compensation between the increasing K_H value and the decreasing k_0 and k_H values. By taking into account the values of $\Delta H_H^{\neq} = 7.6$ kcal/mol and $\Delta S_H^{\neq} = -19.1$ e.u. at $x_M = 0.2$, both of which do not differ greatly from those in pure water, the reaction is concluded to proceed through the hydrogen-atom-transfer mechanism in the mixed solvent, the inhibiting effect of methanol being due to the reduction of the hydrogen bondings between water molecules.

The electron-transfer reaction between the hydrated species of iron(II) and iron(III) in aqueous media, $Fe^{2+}{}_{aq} + {}^*Fe^{3+}{}_{aq} \rightarrow Fe^{3+}{}_{aq} + {}^*Fe^{2+}{}_{aq}$, was early deduced by several authors[2-4)] to proceed *via* the hydrogen-atom-transfer mechanism. This mechanism was supported by the finding that the rate of the reaction decreased upon the addition of some substances in the reaction systems, such substances as nitromethane,[5)] 2-propanol,[6)] and other alcohols.[7)] These added substances were supposed to act as breakers of chains of the hydrogen bondings between water molecules, through which the hydrogen-atom-transfer would have occurred. When dimethyl sulfoxide[1)] is added to the reaction system, it is strongly associated with water molecules and, hence, lowers the water activity to a considerable extent, thus, suppressing the reaction rate. On the other hand, both mono- and dimethyl acetamides[8)] rather accelerate the reaction, in which cases their partial coordination to iron(III) ion enables the reaction to proceed faster than in the absence of the acetamides without altering the reaction mechanism.

In the present investigation, a quantitative determination of the reaction rate was performed in the mixed solvents of methanol and water in order to find out how the molecules of methanol participate in the electron-transfer process both as solvent and as ligand, and how they affect the reaction mechanism through hydrogen-atom-transfer.

Experimental

Commercial methanol of a guaranteed reagent grade was distilled and used. The preparation of the other chemical materials used and the procedure of the kinetic measurements have been described previously.[9,10)] The temperature and the ionic strength of the reaction systems were kept at 25°C and $\mu = 0.5$ M respectively, unless otherwise noted.

Determination of the Hydrolysis Constant, K_H, of Fe^{3+} in Methanol-water Mixed Solvents. The hydrolysis constant, $K_H = [FeOH^{2+}][H^+]/[Fe^{3+}]$, in mixed solvents of methanol and water at various mole fractions of methanol, x_M, was determined at a total concentration of iron(III) of 2×10^{-4} M and at a concentration of perchloric acid of 10^{-3}—10^{-2} M by spectrophotometry at wavelengths of 330, 340, and 350 nm. A Hitachi-Perkin-Elmer UV-VIS spectrophotometer, Model 139, with a thermostated cell compartment was used for the optical density determination. In this compartment was used for the optical density determination. In this connection, the optical densities of the solutions of iron(III) at high acidities up to 4 M were determined in order to show the probable occurrence of ionic association between the iron(III) ion and the perchlorate ion with an increase in the mole fraction of methanol, that is, with a decrease in the dielectric constant of the medium.

Since the values of pK for the second-step hydrolysis of the iron(III) ion in aqueous solutions, $FeOH^{2+} \rightleftarrows Fe(OH)_2^+ + H^+$, were found to be as small as 4.70[11)] and 4.59[12)] at 25°C, the contribution of the presence of $Fe(OH)_2^+$ in the reaction system could be ignored, the pK value in the mixed solvents not being determined.

Results and Discussion

Hydrolysis Constant of the Fe^{3+} Ion, K_H, in Mixed Solvents. Considering the balance relations:

1) Part IV: G. Wada and M. Aoki, This Bulletin, **44**, 3056 (1971).
2) R. W. Dodson, *J. Phys. Chem.*, **56**, 852 (1952).
3) R. W. Dodson and N. Davidson, *ibid.*, **56**, 866 (1952).
4) W. L. Reynolds and R. W. Lumry, *J. Chem. Phys.*, **23**, 2460 (1955).
5) A. G. Maddock, *Trans. Faraday Soc.*, **55**, 1268 (1959).
6) N. Sutin, *J. Phys. Chem.*, **64**, 1766 (1960).
7) R. A. Horne, Ph. D. Thesis, Columbia University, New York, N. Y., 1955; R. A. Horne, "Exchange Reactions," International Atomic Energy Agency, Vienna, 1965, p. 67.
8) G. Wada and R. Yoshihara, *Kogyo Kagaku Zasshi*, **73**, 2309 (1970).
9) G. Wada, N. Yoshizawa, and Y. Sakamoto, This Bulletin, **44**, 1018 (1971).
10) J. Menashi, W. L. Reynolds, and G. Van Auken, *Inorg. Chem.*, **4**, 299 (1965).
11) A. B. Lamb and A. G. Jacques, *J. Amer. Chem. Soc.*, **60**, 1215 (1938).
12) T. Ito and N. Yui, *Sci. Rep. Tohoku Univ.*, **37**, 19 (1953).

$$A = \varepsilon_0[Fe^{2+}] + \varepsilon_H[FeOH^{2+}] \quad (1)$$

$$[HClO_4] = [H^+] - [FeOH^{2+}] \quad (2)$$

$$[Fe(III)] = [Fe^{3+}] + [FeOH^{2+}] \quad (3)$$

an equation is established as follows:

$$\frac{1}{A_H} = \frac{1}{\varepsilon_H[Fe(III)]} + \frac{[H^+]}{\varepsilon_H K_H[Fe(III)]} \quad (4)$$

in which [Fe(III)] and [$HClO_4$] are the total concentrations of iron(III) and perchloric acid, and ε_0 and ε_H, the molar extinction coefficients of Fe^{3+}_{aq} and $FeOH^{2+}$, respectively. A stands for the observed optical density of an aqueous solution containing iron(III) perchlorate, perchloric acid, and methanol, and A_H, for the calculated optical density of a solution simply containing $FeOH^{2+}$, which is equal to $\varepsilon_H[FeOH^{2+}]$. Eq. (4) suggests a linear relationship between A_H^{-1} and [H^+]. Since A_H and [H^+] are not known at first, A and [$HClO_4$] are respectively used instead as a first approximation; they give a rough straight line. The intercept and slope of the approximate straight line give a rough value of K_H, which also gives an approximate value of [$FeOH^{2+}$]. By using this value, more precise A_H and [H^+] values are obtained. By repeating the procedure of this successive approximation, the final relation between A_H^{-1} and [H^+] is reached. A typical relation is plotted in Fig. 1. The values of K_H at various mole fractions of methanol, x_M, at μ=0.5 M and 25°C observed at the wavelengths of 330, 340, and 350 nm are listed in Table 1; the table indicates a clear trend for K_H to increase monotonously as x_M increases because of the lowering of the dielectric constant of the mixed solvent.[13] The observed values of K_H are almost reasonably compared with those appearing in the literature, 1.59×10^{-3} M at x_M=0[14] and 1.70×10^{-2} M at x_M=0.52.[15]

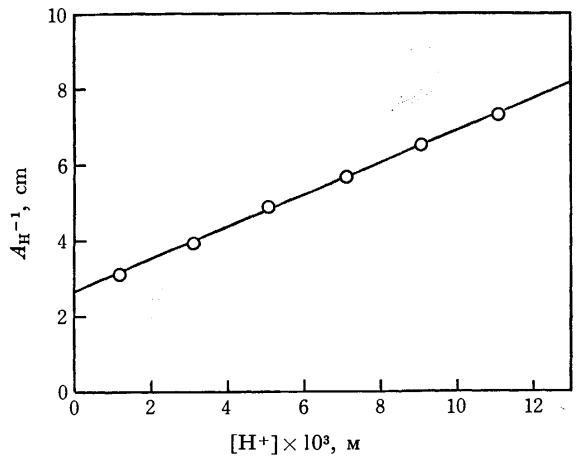

Fig. 1. Linear relation of A_H^{-1} with respect to [H^+] at 330 nm, μ=0.50 M, and 25°C.
[Fe(III)]=2×10^{-4} M, x_M=0.20.

TABLE 1. HYDROLYSIS CONSTANTS K_H AND DIELECTRIC CONSTANTS AT VARIOUS MOLE FRACTIONS OF METHANOL x_M AT μ=0.50 M AND 25°C

x_M	$K_H \times 10^3$ M	Dielectric constant
0	2.2	82.6
0.04	2.4	80.0
0.08	3.0	76.4
0.12	3.3	73.1
0.20	6.2	67.6
0.25	8.7	64.1
0.31	9.4	59.9

The dependence of K_H upon the temperature is shown in Table 2, at x_M=0.20. By plotting log K_H against T^{-1}, the enthalpy of the hydrolysis of Fe^{3+}_{aq} is obtained as ΔH_H=11.6 kcal/mol at x_M=0.20, which, for reference, is compared to a value of 13.7 kcal/mol for the enthalpy associated with the ionization process of the water molecule in the liquid state, $H_2O \rightarrow H^+ + OH^-$.

TABLE 2. TEMPERATURE DEPENDENCE OF K_H AT x_M=0.2 AND μ=0.50 M

Temperature, °C	$K_H \times 10^3$, M
15.5	3.0
20	4.7
25	6.2
30.5	8.3

Ionic Association Between Fe^{3+} and ClO_4^- Ions. The determination of K_H values was carried out at concentrations of perchloric acid of 10^{-3}–10^{-2} M. As the acid concentration is raised within this concentration range, the apparent molar extinction coefficient of the iron(III) solution at 330 nm, ε (which is equal to A/[Fe(III)]), decreases because ε_0 is smaller than ε_H. However, when the acid concentration is raised higher than 10^{-2} M up to as high as 4 M, ε begins rather to increase through a broad minimum in the mixed solvents of methanol and water, although this is not the case in pure water, where the line is horizontal. The observations over the whole concentration range at various x_M's are depicted in Fig. 2. The higher the mole fraction of methanol, the steeper the slope of the curve in the concentrated acid media. The phenomena can reasonably be understood by the possible occurrence of the ionic association between Fe^{3+} and ClO_4^-,[16] as follows.

When an ion-pair between Fe^{3+} and ClO^{4-} is represented by $Fe{\cdot}ClO_4^{2+}$, the total optical density of the solution is expressed in the following form, the ionic association being taken into account:

$$A = \varepsilon[Fe(III)]$$
$$= \varepsilon_0[Fe^{3+}] + \varepsilon_H[FeOH^{2+}] + \varepsilon_a[Fe{\cdot}ClO_4^{2+}] \quad (5)$$

$$[Fe(III)] = [Fe^{3+}] + [FeOH^{2+}] + [Fe{\cdot}ClO_4^{2+}] \quad (6)$$

where ε_a is the molar extinction coefficient of the ion-pair.

13) E. W. Washburn, "International Critical Tables," Vol. 6, (1944), p. 100.
14) A. S. Wilson and H. Taube, *J. Amer. Chem. Soc.*, **74**, 3509 (1952).
15) G. Popa, C. Luca, and E. Iosif, *Z. Phys. Chem.* (Leipzig), **222**, 49 (1963).
16) R. A. Horne, *Nature*, **181**, 410 (1958).

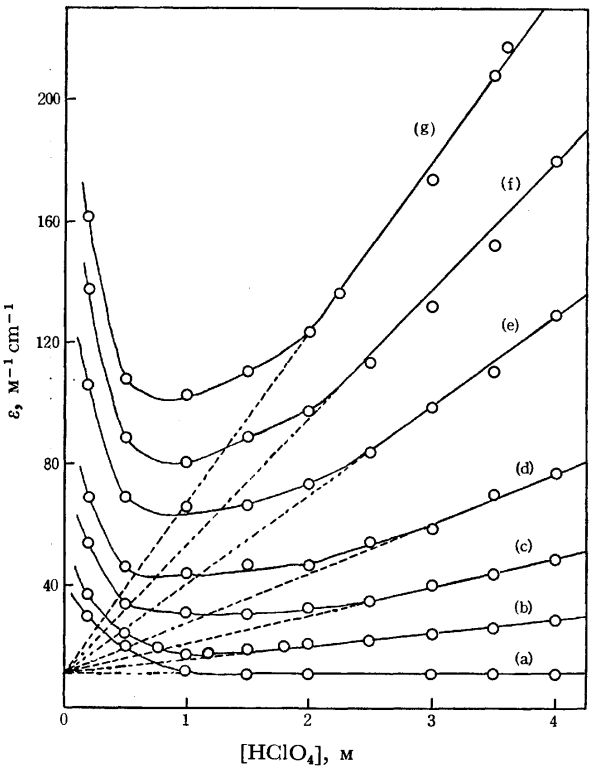

Fig. 2. Apparent molar extinction coefficient of Fe(III) in mixed solvents of methanol and water at 330 nm and 25°C. [Fe(III)]=2×10^{-3} M
a): x_M=0, b): x_M=0.04, c): x_M=0.08, d): x_M=0.12, e): x_M=0.20, f): x_M=0.25, g): x_M=0.31.

Since the formation constant of the ion-pair is defined as $K_a=[Fe\cdot ClO_4^{2+}]/[Fe^{3+}][ClO_4^-]$, ε is given as follows:

$$\varepsilon=\frac{\varepsilon_0+\varepsilon_H K_H/[H^+]+\varepsilon_a K_a[ClO_4^-]}{1+K_H/[H^+]+K_a[ClO_4^-]} \quad (7)$$

Considering that perchloric acid is a strong acid and that, therefore, it dissociates completely in aqueous media, $[H^+]$ is approximately equal to $[ClO_4^-]$ in the present circumstances. Therefore, Eq. (7) may be rewritten in this form:

$$\varepsilon=\frac{\varepsilon_0+\varepsilon_H K_H/[H^+]+\varepsilon_a K_a[H^+]}{1+K_H/[H^+]+K_a[H^+]} \quad (8)$$

When the acidity of the solution is very low as a limiting case, ε will be shown to involve a term in reciprocal proportion to $[H^+]$:

$$\varepsilon\approx\varepsilon_0+\varepsilon_H K_H/[H^+] \quad (9)$$

When the acidity of the solution is very high, as another limiting case, ε will vary under the control of a term proportional to $[H^+]$:

$$\varepsilon\approx\varepsilon_0+\varepsilon_a K_a[H^+] \quad (10)$$

At the intermediate of the two extreme cases, there must occur a minimum nearly at the acid concentration of $[H^+]=(\varepsilon_H K_H/\varepsilon_a K_a)^{1/2}$, actually occurring at $[H^+]\sim1$ M, which indicates that $\varepsilon_H K_H\sim\varepsilon_a K_a$ at each x_M.

Figure 2 also indicates that the slope of the line, $\varepsilon_a K_a$, grows larger as x_M becomes higher, although it is not known whether this is due to the increase in

Table 3. Apparent second-order rate constants at various mole fractions of methanol x_M at μ=0.50 M and 25°C

$[HClO_4]$ M	x_M	[Fe(II)] $\times10^4$, M	[Fe(III)] $\times10^5$, M	$t_{1/2}$ sec	k_{app} $M^{-1}sec^{-1}$
0.035	0.20	0.39	0.60	94	166
0.04	0.20	0.74	1.63	60	128
0.05	0	1.14	1.58	47	114
	0	0.52	1.41	87	121
	0	1.07	8.69	55	109
	0.04	0.69	1.58	73	112
	0.08	0.76	1.74	60	124
	0.08	0.80	1.63	67	108
	0.12	0.71	1.63	75	106
	0.15	1.02	1.63	55	107
	0.20	1.15	1.52	44	121
	0.20	0.93	1.68	62	102
	0.20	0.84	0.43	72	109
	0.25	0.83	1.74	64	108
	0.31	1.02	1.58	54	110
	0.35	0.66	1.90	77	106
	0.38	0.97	1.52	62	99.8
	0.42	0.96	2.39	58	99.5
	0.47	0.78	2.77	85	76.9
	0.51	0.77	1.63	101	73.0
	0.58	0.80	2.44	121	55.1
	0.62	0.98	1.79	140	42.7
	0.68	1.47	2.17	154	26.6
0.07	0.20	1.34	1.79	57	80.0
0.10	0.20	1.01	1.63	108	54.8
0.15	0.20	1.16	1.74	145	35.7
0.20	0	1.50	1.58	135	30.8
	0	1.09	1.58	173	32.0
	0.04	1.34	1.68	138	33.2
	0.04	1.60	1.68	121	32.0
	0.08	1.43	1.68	138	31.4
	0.12	1.23	1.74	157	31.3
	0.15	1.85	1.85	111	30.6
	0.20	1.32	1.68	154	30.4
	0.25	2.13	1.90	98	30.5
	0.31	1.52	1.90	134	30.2
	0.35	1.26	1.85	157	30.6
	0.35	2.11	2.06	103	29.1
	0.35	1.64	2.39	131	28.3
	0.37	1.43	1.74	155	28.0
	0.39	2.27	1.74	102	27.8
	0.39	1.99	2.12	109	28.9
	0.42	1.53	1.96	161	24.9
	0.42	1.79	1.85	130	27.1
	0.48	2.47	1.85	111	23.4
	0.49	1.80	2.28	143	23.9
	0.51	1.83	2.23	174	19.4
	0.56	1.60	1.74	182	21.4
	0.56	1.24	2.39	251	18.6
	0.58	2.31	2.71	159	16.9
	0.58	1.94	2.23	213	15.0
	0.62	2.02	1.74	230	13.8
	0.62	2.46	2.23	174	14.8
	0.68	1.86	2.55	302	10.8
	0.68	3.25	2.34	246	8.1
0.30	0.20	1.38	1.79	246	18.1

ε_a, to that in K_a, or to both. Another interesting indication is that all of the straight lines expressed by Eq. (10) converge on the same point on the axis, giving a common value of $\varepsilon_0=11\ \text{M}^{-1}\text{cm}^{-1}$ regardless of the concentration of methanol. Therefore, the Fe^{3+} ion might not be coordinated at all with methanol below $x_M=0.3$ at least, or might exhibit a constant value for ε_0, regardless of whether or not it is partially coordinated with methanol. At any rate, the value of K_a is not known at this time.

Rate of Electron-Transfer Reaction. Since the electron-transfer reaction between iron(II) and iron(III) has been recognized to be of the first order with respect to both [Fe(II)] and [Fe(III)],[1,7,8] the apparent second-order rate constant, k_{app}, can be calculated by the following equation:

$$k_{app}=\frac{0.693}{([Fe(II)]+[Fe(III)])t_{1/2}} \qquad (11)$$

The experimental results obtained at various mole fractions of methanol, mainly at $[HClO_4]=0.05$ and 0.20 M at $\mu=0.50$ M, and 25°C are shown in Table 3. A survey of k_{app} depending upon x_M is made in Fig. 3. k_{app} seems to be almost constant at $x_M<0.3$, over which point it begins to diminish abruptly. This trend can be noticed more clearly at a lower acid concentration.

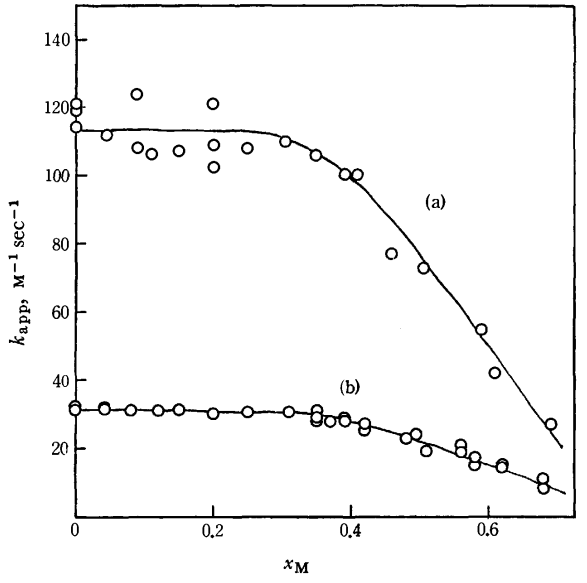

Fig. 3. Plot of k_{app} *vs.* x_M at $\mu=0.50$ M and 25°C.
a) $[H^+]=0.05$ M, b) $[H^+]=0.20$ M

The dependence of k_{app} upon the acidity of the solution at a constant mole fraction of methanol, at $x_M=0.2$ for instance, which belongs to the plateau portion in Fig. 3, was observed; it is shown in Fig.4. The plot of k_{app} *vs.* the reciprocal $[H^+]$ indicates that there may be a linear relationship between them, passing the vicinity of the origin of the coordinates.

Reaction Mechanism. When the facts revealed in Figs. 3 and 4 are taken into account, the following two paths of the electron-transfer reaction can most convincingly be considered to actually occur:

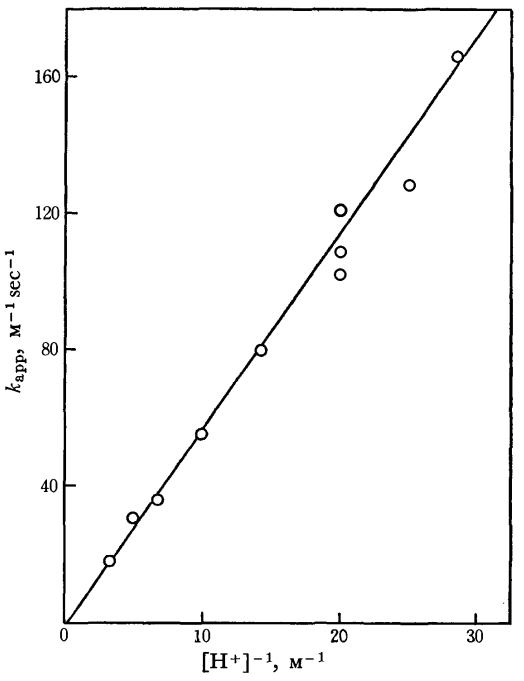

Fig. 4. Plot of k_{app} *vs.* $[H^+]^{-1}$ at $x_M=0.20$, $\mu=0.50$ M and 25°C.

$$Fe^{2+}+{}^*Fe^{3+}\rightarrow Fe^{3+}+{}^*Fe^{2+} \qquad (k_0) \qquad (12)$$

$$Fe^{2+}+{}^*FeOH^{2+}\rightarrow FeOH^{2+}+{}^*Fe^{2+} \qquad (k_H) \qquad (13)$$

By the usual means of calculation, the apparent rate constant, k_{app}, is given as follows, where k_0 and k_H are the rate constants for the (12) and (13) reaction paths respectively:

$$k_{app}=\frac{k_0+k_HK_H/[H^+]}{1+K_H/[H^+]} \qquad (14)$$

If the denominator on the right-hand side of Eq. (14) is regarded approximately as unity, k_{app} must show a linear trend, as has been seen in Fig. 4. When the denominator is precisely computed and multiplied by k_{app}, a more regular straight line than that in Fig. 4 is obtained between $k_{app}(1+K_H/[H^+])$ and $[H^+]^{-1}$, which is again reproduced in Fig. 5. The straight line in the figure passes near the point of origin, pointing out that k_0 is almost zero at $x_M=0.20$. By the use of the K_H values in Table 1, the k_0 and k_H values at different x_M's are similarly obtained from the intercepts and slopes of the respective straight lines; they are collected in Table 4.

The values of k_0 in Table 4 are very approximate, but it can be safely said that k_0 is almost zero at mole fractions of methanol over 0.2. The values of k_H in the table, on the other hand, more regularly decrease with an increase in x_M. The range of x_M values adopted in the table, $x_M=0-0.3$, corresponds to that exhibiting the plateau portion of the curve in Fig. 3.

It can be concluded, therefore, that although both k_0 and k_H decrease as x_M increases, k_{app} holds an approximate constancy, because the increase in K_H cancels the decrease in k_0 and k_H to make k_{app} almost unchanged, by chance. Table 4 also lists the prod-

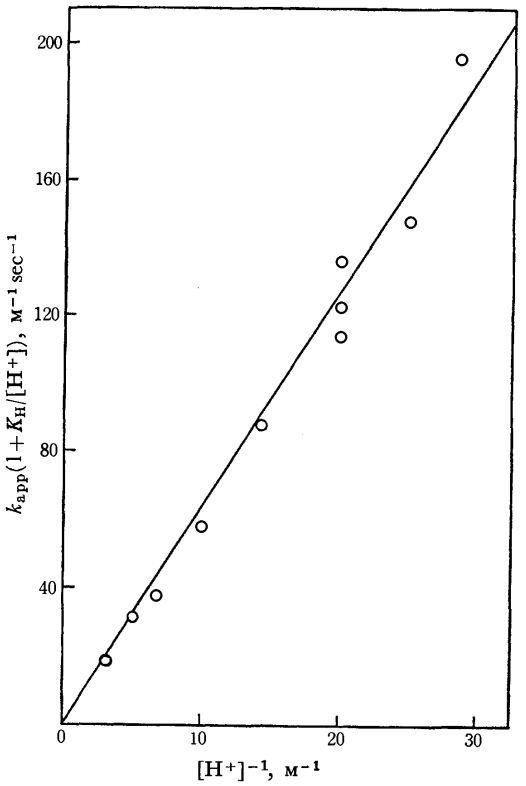

Fig. 5. Plot of $k_{app}(1+K_H/[H^+])$ *vs.* $[H^+]^{-1}$ under the same conditions as in Fig. 4.

TABLE 4. k_0 AND k_H AT DIFFERENT x_M AT μ=0.50 M AND 25°C

x_M	k_0 $M^{-1}sec^{-1}$	k_H $\times 10^{-3}$, $M^{-1}sec^{-1}$	k_HK_H sec^{-1}
0	~2	2.7	6.0
0.04	~4	2.3	5.5
0.08	~2	2.0	6.0
0.12	~5	1.6	5.3
0.20	~0	1.1	6.7
0.25	~0	0.73	6.3
0.31	~0	0.70	6.6

ucts of k_H and K_H; they suggest the apparent constancy of k_{app} within the whole range of x_M values far observed.

Activation Parameters for Reaction. The values of k_H at x_M=0.20 were obtained at different temperatures in the same way as at 25°C; the correlation of log (k_H/T) against T^{-1} is drawn in Fig. 6, from which the activation enthalpy, $\Delta H_H^{\neq}$=7.6 kcal/mol, and the activation entropy, $\Delta S_H^{\neq}$=−19.1 e.u., are calculated. A comparison with the activation parameters in pure water is made in Table 5.

The activation enthalpy and entropy for the electron-transfer reaction between Fe^{2+} and $FeOH^{2+}$ do not greatly differ from each other in pure water and in methanol-water mixtures. This fact indicates that the hydrogen-atom-transfer mechanism[2-4] may still be active even in methanolic media. The effect of methanol on the rate of the reaction is the partial destruction and breaking of the hydrogen bondings in the chains between water molecules by substituting

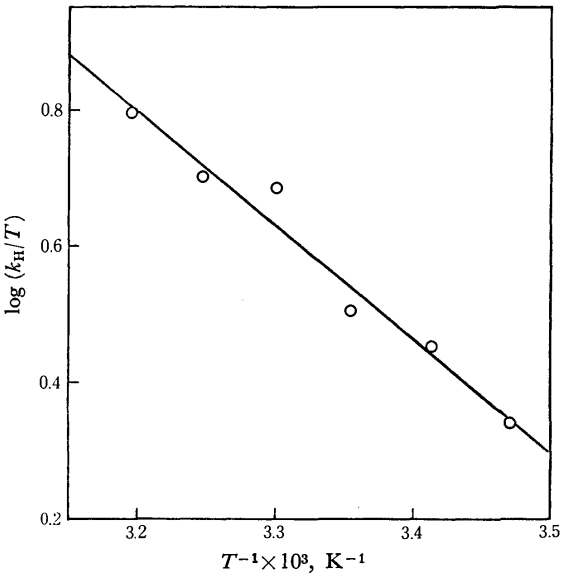

Fig. 6. Plot of log (k_H/T) *vs.* T^{-1} at x_M=0.2 and μ=0.50 M.

TABLE 5. ACTIVATION PARAMETERS FOR THE REACTION Fe^{2+}-$FeOH^{2+}$

x_M	$\Delta H_H^{\neq}$ kcal/mol	$\Delta S_H^{\neq}$ cal/deg·mol	Ref.
0.20	7.6	−19.1	Present work
0	6.9	−18	17)
0	8.4	−14.4	18)

the methanol molecules for water in the bulk solvent.

In the case of a mixed solvent of DMSO and water,[1] the effect of DMSO is so great that it forms a molecular associate with water, thus lowering the activity of water. In the present case of methanol, its effect on the rate constant is not so markedly clear as to influence it explicitly, as a result of compensation for the growth of K_H.

According to the conductivity measurements,[19] Walden's ionic radius and the activation energy for the ionic migration for simple ions are nearly unchanged when the mole fraction of methanol is varied in methanol and water mixtures within the range of its mole fractions of 0—0.3. This suggests no possible occurrence of mixed solvation of methanol around the central ions in this mole fraction range. We have described above the constant molar extinction coefficient of the Fe^{3+} ion, ε_0=11 $M^{-1}cm^{-1}$, in the same mole fraction range of methanol. We attributed this either to the constancy of light absorption by the ions, regardless of the composition of their coordination sphere, or to the constancy of the composition sphere, or to the constancy of the composition of the coordination sphere itself, regardless of the surrounding medium. Now we can obviously decide that the latter is the case. In this concentration range, Fe^{3+}

17) J. Silverman and R. W. Dodson, *J. Phys. Chem.*, **56**, 846 (1952).
18) S. Fukushima and W. L. Reynolds, *Talanta*, **11**, 283 (1964).
19) G. Wada, C. Ito, and K. Horie, *J. Electrochem. Soc. Jap.*, **28**, 58 and E-32 (Overseas Edition) (1960).

may be preferentially solvated only with water molecules. The decrease in the rate of the electron-transfer reaction is, therefore, brought about, not by the reaction species themselves, but by the decrease in the ease of the hydrogen-atom-transfer along the chains of hydrogen bondings between the reacting species, by the insertion of methanol molecules in place of water ones, although the composition of the coordination sphere does not alter upon the addition of methanol.

BULLETIN OF THE CHEMICAL SOCIETY OF JAPAN, VOL. 45, 1078—1080 (1972)

Preparation and Properties of *N,N*-Dialkylethylenediamine *N*-Oxide Complexes of Nickel(II), Copper(II), and Cobalt(III)

Sigeo KIDA and Takayuki ONIKI

*Department of Chemistry, Faculty of Science, Kyushu University, Hakozaki, Fukuoka**

(Received August 23, 1971)

The complexes of Ni(II), Cu(II), and Co(III) with *N,N*-Dialkylethylenediamine (alkyl=CH_3, C_2H_5, and C_3H_7) have been prepared. It was revealed that these ligands coordinate to metal ions as bidentate ligands with amino and tertiary amine oxide groups. Two forms have been obtained for the 1 : 2 nickel(II) complexes, the hydrated green form with $\mu_{eff}=3.3$ and the anhydrous red or reddish brown form with zero or very low magnetic moment. They are easily convertible into each other. Formation of square planar diamagnetic Ni(II) complexes with ionic-type ligand was interpreted in terms of the steric effect of the alkyl groups.

Only a few studies have been made on the metal complexes of tertiary amine oxide[1,2] compared with those of complexes of pyridine *N*-oxide and its derivatives.[3,4] It was reported that trimethylamine oxide forms tetrahedral complexes with cobalt(II), zinc(II), and cadmium(II) in alcoholic solution,[2] but octahedral or square planar complexes were not known.

We have attempted to prepare stable metal chelates involving a tertiary amine oxide as a coordinating group, using *N,N*-dialkylethylenediamine *N*-oxide as a neutral ligand. We succeeded in the preparation of new complexes of Cu(II), Ni(II), and Co(III) of tertiary amine oxide. It is to be noted that diamagnetic square planar nickel(II) complexes were readily obtained by using a ligand of the 2N2O-type which may be expected to form rather ionic bond with a metal ion.

Experimental

Preparation. N,N-*Dimethylethylenediamine* N-*Oxide (abbreviated as dimen-O)*: To 15 g of *N,N*-dimethylethylenediamine diluted with the same amount of water was added dropwise 220 m*l* of 3% hydrogen peroxide. After standing for 24 hours at room temperature, the solution was evaporated at 65°C under reduced pressure and a sirup of *N*-oxide was obtained. This was used for the preparation of complexes without further purification.

N,N-*Diethylethylenediamine* N-*Oxide (abbreviated as dieen-O)* and N,N-*Dipropylethylenediamine* N-*Oxide (abbreviated as dipen-O)*: The above two compounds were prepared by a method similar to that for dimen-O.

Bis-N,N-*(dimethylethylenediamine* N-*oxide)*nickel(II) *Perchlorate 1.5 hydrate (=[Ni(dimen-O)$_2$](ClO$_4$)$_2$·1.5H$_2$O)*: To a solution of 1.2 g of the ligand in 50 m*l* of 95% ethanol was added 2.0 g of nickel(II) perchlorate hexahydrate dissolved in 50 m*l* of 95% ethanol. Green crystals were immediately formed. They were collected on a glass filter and washed with ethanol.

Found: C, 19.61; H, 5.51; N, 11.52%. Calcd for [Ni(dimen-O$_2$)](ClO$_4$)$_2$·1.5H$_2$O: C, 19.49; H, 5.51; N, 11.36%. $\mu_{eff}=3.3$ B.M.

*Bis-(*N,N-*dimethylethylenediamine* N-*oxide)nickel(II) Perchlorate (=[Ni(dimen-O)$_2$](ClO$_4$)$_2$)*: The compound was prepared by recrystallization of the green hydrated form from ethanol as red crystals. It is also obtained by heating the hydrated complex over phosphoric anhydride at 80°C.

Found: C, 20.50; H, 5.24; N, 11.83. Calcd for [Ni(dimen-O)$_2$](ClO$_4$)$_2$: C, 20.62; H, 5.19; N, 12.02%. $\mu_{eff}=0.6$ B.M.

Bis-(N,N-diethylethylenediamine N-*oxide)nickel(II) Perchlorate (=[Ni(dieen-O)$_2$](ClO$_4$)$_2$*: To a solution of 1.5 g of the ligand in 40 m*l* of 99% ethanol was added 2.0 g of nickel(II) perchlorate hexahydrate dissolved in 40 m*l* of 99% ethanol. The resulting deep green solution was cooled in a refrigerator for 24 hr. Reddish brown crystals were formed. Recrystallization was carried out from ethanol.

Found: C, 27.50; H, 6.35; N, 10.51. Calcd for [Ni(dieen-O)$_2$](ClO$_4$)$_2$: C, 27.61; H, 6.18; N, 10.73%. Diamagnetic.

When the reddish brown crystals are kept in the humid atmosphere for one day, they gradually change into pale blue powder containing 2 mol of water for one nickel atom. This is readily reconverted into the reddish brown anhydride by heating at 100°C or keeping it in a desiccator over phosphoric anhydride.

Found: H_2O, 6.51. Calcd for [Ni(dieen-O)$_2$](ClO$_4$)$_2$·2H$_2$O: H_2O, 6.46%. $\mu_{eff}=3.3$ B.M.

*Bis-(*N,N-*di*-n-*propylethylenediamine* N-*oxide)nickel(II) Perchlorate (=[Ni(dipen-O)$_2$](ClO$_4$)$_2$)*: To a solution of 1.9 g of the *N*-oxide in 20 m*l* of 99% ethanol was added 1.5 g

* A part of the work was carried out in the Department of Chemistry, Wakayama University, Wakayama.

1) K. Isslied and A. Kreibich, *Z. Anorg. Allgem. Chem.*, **313**, 338 (1961).

2) S. Kida, This Bulletin, **36**, 712 (1963).

3) J. V. Quagliano, J. Fujita, G. Franz, D. J. Phillips, J. A. Walmsley, and S. Y. Tyree, *J. Amer. Chem. Soc.*, **83**, 3770 (1961).

4) S. Kida, J. V. Quagliano, J. A. Walmsley, and S. Y. Tyree, *Spectrochim. Acta*, **19**, 189 (1963).

of nickel(II) perchlorate hexahydrate dissolved in 20 m*l* of 99% ethanol. Twenty m*l* of dioxane was added to this solution which was then cooled for 48 hr in a refrigerator. Reddish brown crystals were formed. Recrystallization was carried out from a mixed solvent of ethanol and dioxane.

Found: C, 33.20; H, 7.02; N, 9.65. Calcd for $[Ni(dipen\text{-}O)_2](ClO_4)_2$: C, 33.23; H, 6.92; N, 9.60%. diamagnetic.

The hydrated form of this compound was obtained as pale blue powder by the same procedure as for the ethyl homologue. However, the content of water was found to be much higher, *i.e.*, 6 mol of water for one nickel atom.

Found: H_2O, 15.15. Calcd for $[Ni(dipen\text{-}O)_2(ClO_4)_2\cdot 6H_2O$: H_2O, 15.74%. $\mu_{eff}=3.3$ B.M.

*Bis-(*N,N-*dimethylethylenediamine N-oxide)copper(II) Perchlorate (=[Cu(dimen-O)$_2$](ClO$_4$)$_2$*: The complex was prepared by the same method as that for $[Ni(dimen\text{-}O)_2](ClO_4)_2\cdot$ except for using copper(II) perchlorate $1.5H_2O$, instead of nickel(II) perchlorate.

Found: C, 20.58; H, 5.19; N, 11.91. Calcd for $[Cu(dimen\text{-}O)_2](ClO_4)_2$: C, 20.41; H, 5.14; N, 11.90%. $\mu_{eff}=1.74$ B.M.

*Bis-(*N,N-*diethylethylenediamine* N-*oxide)copper(II) Perchlorate (=[Cu(dieen-O)$_2$](ClO$_4$)$_2$*: The complex was prepared by a similar method to that for the above complex.

Found: C, 27.18; H, 5.94; N, 10.68. Calcd for $[Cu(dieen\text{-}O)_2](ClO_4)_2$: C, 27.36; H, 6.12; N, 10.63%. $\mu_{eff}=1.78$ B.M.

*Tris-(*N,N-*dimethylethylenediamine* N-*oxide)nickel(II) Perchlorate (=[Ni(dimen-O$_3$)](ClO$_4$)$_2$*: To a solution of 2.0 g of the ligand in 50 ml of 95% ethanol was added 2.0 g of nickel(II) perchlorate hexahydrate dissolved in 50 m*l* of 95% ethanol. Light blue crystals were formed. They were collected on a glass filter, washed with ethanol and dried *in vacuo* over phosphoric anhydride.

Found: C, 25.00; H, 6.13; N, 14.67. Calcd for $[Ni(dimen\text{-}O)_3](ClO_4)_2$: C, 25.28; H, 6.37; N, 14.74%. $\mu_{eff}=3.2$ B.M.

*Tris-(*N,N-*diethylethylenediamine* N-*oxide)nickel(II) Perchlorate (=[Ni(dieen-O)$_3$](ClO$_4$)$_2$*: Light blue crystals were obtained by a similar method to that for the above complex.

Found: C, 32.38; H, 7.55; N, 12.49. Calcd for $[Ni(dieen\text{-}O)_3](ClO_4)_2$: C, 33.05; H, 7.40; N, 12.84%. $\mu_{eff}=3.0$ B.M.

*Tris-(*N,N-*dimethylethylenediamine N-oxide)cobalt(III) Perchlorate (=[Co(dimen-O)$_3$](ClO$_4$)$_3$*: To an aqueous solution of 3.2 g of the N-oxide in 20 m*l* water were added 2.5 g of $[CoCl(NH_3)_5]Cl_2$ and 1 g of active carbon. The mixture was heated on a water-bath for 3 hr and filtered. To this filtrate were added 50 m*l* of acetone and 60 m*l* of ethanol saturated with sodium perchlorate. Deep blue violet crystals were immediately formed. Recrystallization was carried out from ethanol.

Found: C, 21.24; H, 5.46; N, 12.34. Calcd for $[Co(dimen\text{-}O)_3](ClO_4)_3$: C, 21.52; H, 5.42; N, 12.55%. diamagnetic.

Optical resolution of the complex was undertaken with the use of optically active trioxalato cobaltate(III) ion, but it was unsuccessful.

Reflectance Spectra. The powder reflectance spectra were measured with a Shimadzu Multipurpose Spectrophotometer Model MPS-50L.

Magnetic susceptibility. Magnetic susceptibilities were measured by Guy's method at room temperature.

Results and Discussion

Cobalt(III) Complexes. An aqueous solution of tris (N,N-dimethylethylenediamine N-oxied)cobalt(III) ion (abbreviated as $[Co(dimen\text{-}O)_3]^{3+}$) is fairly stable at room temperature, and gives an absorption spectrum similar in contour to those of *fac*-tris-(alaninato) cobalt(III) and of *fac*-tris-(β-alaninato)cobalt(III),[5] but the absorption peaks show a considerable red-shift (~1.7 kK) relative to those of the amino acid complexes as seen in Table 1. This seems to indicate that tertiary amine oxide is located at a lower position in the spectrochemical series than carboxylic acid.

Table 1. Absorption peaks of some Co(III) complexes of 3N-3O coordination in aqueous solution

	I kK(ε)	II kK(ε)
$Co(dimen\text{-}O)_3^{3+}$	17.62 (120)	24.93 (124)
fac-$Co(\beta\text{-ala})_3$	19.01 (141)	27.03 (61)
fac-$Co(ala)_3$	19.23 (186)	26.74 (160)
mer-$Co(\beta\text{-ala})_3$	17.55 (100) 20.49 (64)	27.03 (84)

Copper(II) Complexes. We see from Table 2 that the *d-d* bands of $[Cu(dimen\text{-}O)_2](ClO_4)_2$ and $[Cu(dieen\text{-}O)_2](ClO_4)_2$ (in solid state) are located in a much shorter wave-length region compared with those of the usual Cu-2N-2O type complexes such as $[Cugly_2]$. This is undoubtedly due to the steric effect of alkyl groups attached to nitrogen atoms, which may hinder the coordination to the axial position of the complex.[6]

Table 2. Peaks of reflectance spectra of some copper(II) complexes

complexes	ν_{max} (kK)
$Cu(CH_3NH_2)_4(ClO_4)_2$	17.24
$Cu(C_2H_5NH_2)_4(ClO_4)_2$	16.64
$Cu(gly)_2$	15.97
$Cu(dimen)_2(ClO_4)_2$	18.02
$Cu(dieen)_2(ClO_4)_2$	20.37
$Cu(dimen\text{-}O)_2(ClO_4)_2$	17.54
$Cu(dieen\text{-}O)_2(ClO_4)_2$	17.54

gly=$NH_2CH_2COO^-$, dimen=$(CH_3)_2NCH_2CH_2NH_2$
dieen=$(C_2H_5)_2NCH_2CH_2NH_2$

Nickel Complexes. The 1 : 3 complexes, $[Ni(dimen\text{-}O)_3](ClO_4)_2$ and $[Ni(dieen\text{-}O)_3](ClO_4)_2$, are undoubtedly hexacoordinated species, judging from their reflectance spectra (Table 3) and the bidentate nature of the ligands. Whereas, in the 1 : 2 complexes, however, there are two types, green hydrate ones and red or brown anhydrous ones. The former are readily converted into the latter when they are heated above 80°C or kept in a desiccator over phosphoric anhydride. The anhydrous complexes are

5) M. B. Celap, *Inorg. Chem.*, **6**, 2064 (1967).
6) B. J. Hathaway and D. E. Billing, *Coord. Chem. Rev.*, **5**, 143 (1970).

TABLE 3. PEAKS OF ELECTRONIC SPECTRA AND MAGNETIC MOMENTS OF SOME NICKEL COMPLEXES

Complexes		ν_{max} (kK)				μ_{eff}
$Ni(gly)_2$	(in water)	16.23			27.10	
$Ni(\beta\text{-ala})_2$	(in water)	16.18			26.67	
$Ni(dimen\text{-}O)_3(ClO_4)_2$	(powder)	16.05			26.74	3.2
$Ni(dieen\text{-}O)_3(ClO_4)_2$		15.92			26.67	3.0
$Ni(dimen\text{-}O)_2(ClO_4)_2 \cdot 1.5H_2O$		15.27		(24.57)	26.18	3.3
$Ni(dimen\text{-}O)_2(ClO_4)_2$			19.34			0.6
$Ni(dieen\text{-}O)_2(ClO_4)_2$			17.64	21.83		diamag.
$Ni(dipen\text{-}O)_2(ClO_4)_2$			16.95	20.83		diamag.
$Ni(dimen)_2(ClO_4)_2$				21.60		diamag.
$Ni(dipen)_2(ClO_4)_2$				20.96		diamag.

β-ala$=NH_2CH_2CH_2COO^-$, dipen$=(C_3H_7)_2NCH_2CH_2NH$

gradually hydrated in the atmosphere to form green complexes. Thus, the conversion of both forms is reversible. The reflectance spectra and the magnetic moments of the former clearly indicate that they are hexa-coordinated ones. Since the latter give the reflectance spectra which show one or two bands in the visible region and no absorption in the near infrared region (800 mμ~1200 mμ), it is evident that they are planar tetra-coordinated complexes. Formation of planar nickel(II) complexes with the ligands expected to form rather ionic bonds with a metal ion should be due to the steric effect of the alkyl groups of the ligand which may hinder coordinating groups from entering the fifth and sixth coordination positions of the tetragonal nickel(II) complex. Measurements of magnetic susceptibility showed that Ni $[dimen\text{-}O)_2](ClO_4)_2$ shows a feeble paramagnetism which could not be eliminated in spite of efforts to purify the complex. Repeated recrystallization and careful dehydration of the sample brought about no magnetic moment smaller than 0.6 B.M. (at room temperature). However, measurements of magnetic susceptibility over the temperature range (300°~77°K) showed that this complex obeys Curie's law.

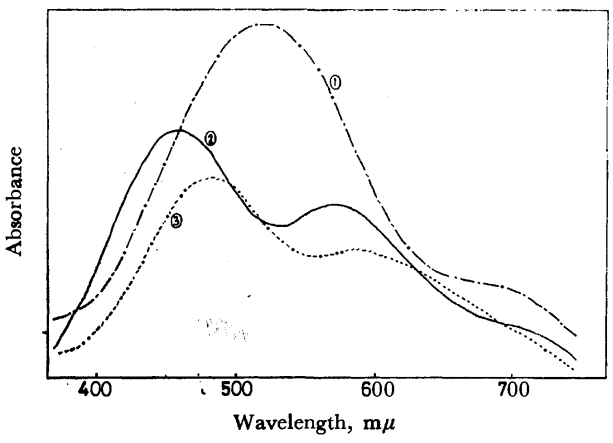

Fig. 1. Refrectance Spectra of ①—— $[Ni(dimen\text{-}O)_2](ClO_4)_2$, ②—— $[Ni(dieen\text{-}O)_2](ClO_4)_2$, and ③---- $[Ni(dipen\text{-}O)_2](ClO_4)_2$.

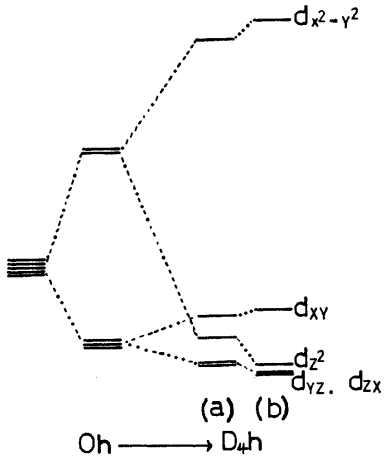

Fig. 2. Assumed energy level splittings of *d*-orbitals for (a) $[Ni(dimen\text{-}O)_2](ClO_4)_2$ and (b) $[Ni(dipen\text{-}O)_2](ClO_4)_2$.

Thus we can conclude that the small paramagnetism is due not to the thermal population of low-lying triplet state as might be anticipated from the energy-level diagram of Maki,[7] but to paramagnetic impurity, probably of the hydrated species. This is consistent with the fact that $[Ni(dimen\text{-}O)_2](ClO_4)_2$ is most easily hydrated among those planar complexes.

It is remarkable that the reflectance spectrum of $[Ni(dimen\text{-}O)_2](ClO_4)_2$ shows one broad band in the visible region, whereas $[Ni(dieen\text{-}O_2](ClO_4)_2$ and $[Ni(dipen\text{-}O)_2](ClO_4)_2$ show two bands in the visible region (Fig. 1). This is explainable in terms of the energy-level diagram[8] given in Fig. 2, granted that the methyl derivatives are less planar than the ethyl and propyl derivatives, i.e., perturbation along the tetragonal axis is somewhat larger in the methyl derivatives.

The authors wish to express their sincere thanks to Prof. Y. Muto, Saga University, for cryomagnetic measurements. They also thank Miss E. Yamagami for her help in the experiment.

7) G. Maki, *J. Chem. Phys.*, **28**, 651 (1958).
8) Y. Nishida and S. Kida, This Bulletin, **43**, 3814 (1970).

Infrared Intensities of Crystalline HCN and DCN

Masakatsu UYEMURA and Shiro MAEDA

Research Laboratory of Resources Utilization, Tokyo Institute of Technology, Meguro-ku, Tokyo

(Received September 3, 1971)

The absolute infrared intensities of crystalline HCN and DCN were measured at the temperature of liquid N_2. In comparison with the gaseous values, both stretching fundamentals (ν_1, ν_3) exhibited a striking increase in the integrated absorption, while the bending (ν_2) was almost unchanged. From the observed intensity change, the change in the dipole-moment derivatives with respect to the molecular internal coordinates was calculated to be $\partial \Delta \boldsymbol{M}/\partial r_{C\equiv N}=1.43$ D/Å and $\partial \Delta \boldsymbol{M}/\partial r_{C-H}=2.01$ D/Å, those values were chosen from two alternative possibilities as the more probable set. The significance of these values, however, is somewhat peculiar to the optically-active crystalline vibrations, so they were then resolved into derivatives with respect to purely intramolecular and intermolecular coordinates: $[\partial \Delta \boldsymbol{M}/\partial r_{C-H}]=0.58$ D/Å and $[\partial \Delta \boldsymbol{M}/\partial r_{H\cdots N}]=-1.43$ D/Å. The general intensity features were reasonably interpreted by considering the contribution of a charge-transfer structure to the H–N hydrogen bonding.

The study of the infrared intensity in condensed phases is supposed to be a potential source of information about the nature of interactions between molecules. It is quite common knowledge that the formation of a hydrogen bond, X–H···Y, gives rise to a striking increase in the integrated absorption of the X–H stretching vibration, as well as to a large frequency shift and a broadening of the band. This intensity behavior has thus far been qualitatively interpreted as being mainly due to the vibronic contribution of the charge-transfer effect.[1-3] In the present investigation, a somewhat detailed study of the intensity was attempted so as to obtain a closer understanding of the electronic features in the hydrogen-bonding interactions. Then, crystalline hydrogen cyanide was chosen as a particularly favorable system for an analytical study of the intensity change, because, besides its simple molecular structure, it forms strictly linear hydrogen-bonded chains, as has been shown by Dulmage and Lipscomb's X-ray data.[4]

Actually, the crystal has two modifications bounded at 170°K, that is, the high-temperature tetragonal phase described by the space group C_{4v}^{9}-*I4mm* and the low-temperature orthorhombic phase described by C_{2v}^{20}-*Imm*. In either phase, HCN (DCN) molecules are linked in a straight chain with a C–H···N distance of 3.18 Å, and such chains are assembled parallel with each other (Fig. 1). So far as the hydrogen bonding is concerned, the difference between these two phases seems to be of little significance; therefore the low-temperature phase crystal, which is experimentally more tractable, has been dealt with exclusively in the present work.

The infrared spectrum of crystalline (low-temperature-phase) HCN has been obtained by Hoffmann and Hornig,[5] and the Raman spectra of HCN and DCN crystals were investigated by Pézolet and Savoie[6]

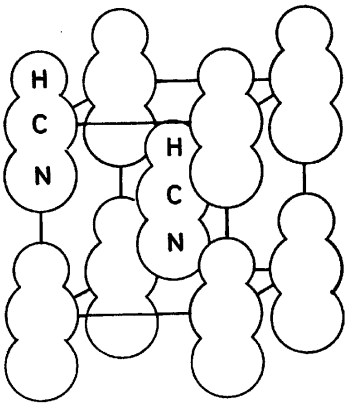

Fig. 1. Crystal structure of hydrogen cyanide (low temperature phase).

recently. In general these observations accord with the above crystal structure and indicate the formation of fairly strong hydrogen bonds. Pézolet and Savoie also observed high-frequency shoulders for each band in their spectra; they ascribed them to longitudinal vibrations, which will be discussed later in relation to the infrared intensities. Now, Hoffmann and Hornig[5] observed a remarkable change in the relative intensities from gaseous to crystalline HCN, and afterwards the absolute intensity was determined exactly for gaseous HCN and DCN by Hyde and Hornig.[7] In comparing the gaseous and crystalline relative intensities described above, it is noticeable that a striking change, certainly an intensification, has occurred not only in the usual C–H stretching vibration, ν_3, but also in the C≡N stretching, ν_1. A possible cause of the latter may be looked for in an increased mixing of the C–H stretching coordinate into the normal coordinate, Q_1, whose effect is further enhanced by the magnified value of the dipole-moment derivative, $\partial \mu/\partial r_{C-H}$. However, a brief consideration suggests that the $\partial \mu/\partial r_{CN}$ may also be influenced by the hydrogen bonding in the crystal. The intensity change in the acceptor-group vibration has been established for some carboxylic acid dimers by Wenograd and Spurr,[8] but

1) G. M. Barrow, *J. Phys. Chem.*, **59**, 1129 (1955).
2) H. Tsubomura, *J. Chem. Phys.*, **24**, 927 (1956).
3) K. Szczepaniak and A. Tramer, *J. Phys. Chem.*, **71**, 3035 (1967).
4) W. J. Dulmage and W. N. Lipscomb, *Acta Crystallogr.*, **4**, 330 (1951).
5) R. E. Hoffmann and D. F. Hornig, *J. Chem. Phys.*, **17**, 1163 (1949).
6) M. Pézolet and R. Savoie, *Can. J. Chem.*, **47**, 3041 (1969).
7) G. E. Hyde and D. F. Hornig, *J. Chem. Phys.*, **20**, 647 (1952).
8) J. Wenograd and R. A. Spurr, *J. Amer. Chem. Soc.*, **79**, 5844 (1957).

the change in hydrogen cyanide is far more conspicuous and may be adequate for the attainment of an unambiguous interpretation.

Experimental

HCN and DCN were obtained by adding aqueous H_2SO_4 or D_2SO_4 to potassium cyanide. The evolved gas was dried over calcium chloride and magnesium perchlorate, and was purified by repeated distillation within a vacuum line. The infrared spectra did not show any indication of impurities except for a minor amount of HCN mixed in the DCN sample, whose deuterium concentration was estimated at 85% from the intensity of the HCN bands.

The infrared spectra of the low-temperature-phase crystals were recorded on a Perkin-Elmer model 125 spectrophotometer. Thin solid films of the samples were obtained by spraying the gas onto a window cooled with liquid nitrogen in a conventional vacuum cell. The thickness of the deposited films was measured by monitoring the interference fringes at a fixed wavelength of one micron during the formation of films on a KRS-5 window.[9] The density at 77°K was calculated based on the X-ray data,[4] and the refractive index for the wavelength of one micron was obtained by extrapolating Anderson *et al.*'s[9a] dispersion data and by adjusting it for 77°K using Lorentz-Lorenz formula. The rate of film growth was about 3 to 4 microns per hour. The slit width was so chosen that it was always less than one-third of the half-width of the measured band.

The experimental quantity,

$$B' = \int_{\text{band}} \ln (T_0/T) \mathrm{d}\nu$$

where T/T_0 is the observed transmittance, was calculated by the use of Lagrange's polynomial of the third order fitted to four successive points among 13 to 20 experimental points. The integrations were carried out over such frequency ranges as cover more than 12 times the half-windth.

Results and Discussion

The Beer's law plots for the fundamental bands are illustrated in Figs. 2 and 3, where n is the concentration in mol/cm^3 and where l is the thickness in cm. The integrated absorption coefficient,

$$A = \int \alpha \mathrm{d}\nu$$

was obtained from the limiting slope of the curves, it is given in Table 1, and compared with the gaseous value by Hyde and Hornig.[7] If the Lorentz curve is assumed for the band shape, the errors caused by the finite slit width and the finite integration range are estimated to be about 3% and 6% at most,[10] but the composite error in the experiment may be roughly estimated at 20% at the maximum, considering other sources of error, such as in drawing the base-line and in the film-thickness determination. It may be seen that both stretching absorptions are intensified very much, whereas the bending intensity is almost unchanged, despite its considerable shift in frequency.

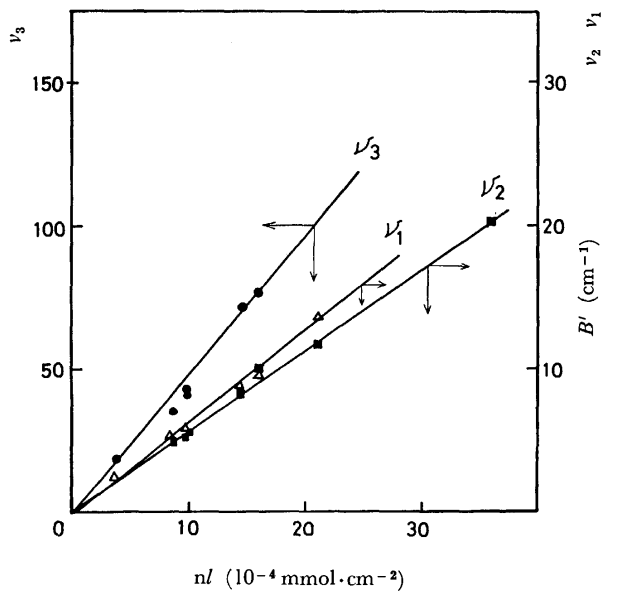

Fig. 2. The Beer's law plots of fundamental bands of crystalline HCN.

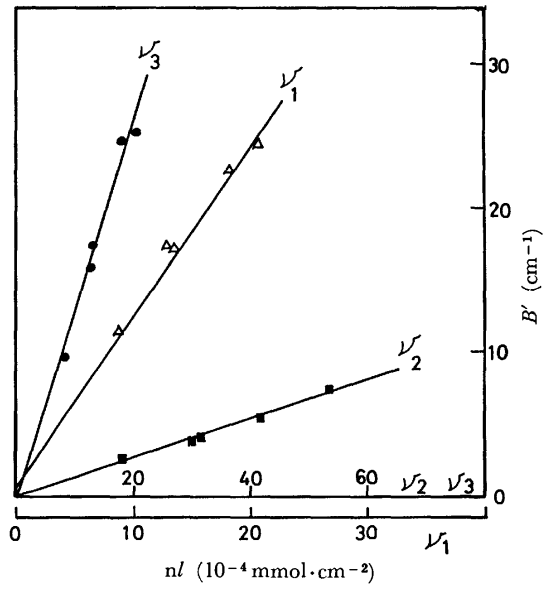

Fig. 3. The Beer's law plots of fundamental bands of crystalline DCN.

In Table 1 are also included the relative intensity values predicted by Pézolet and Savoie[6] based on their Raman observation, as well as those measured by Hoffmann and Horig.[5] The correspondence between the predicted values and the present observations is surprisingly good, supporting the conclusion of Pezolet and Savoie about the longitudinal and transverse frequencies.[11] The observed intensity, A, is related to the dipole-moment derivative by:

$$A_i = (N\pi/3c^2)\,|\partial \boldsymbol{M}/\partial q_i|^2, \qquad (1)$$

where $\boldsymbol{M}$ is the dipole moment of the crystal and where q_i is a molecular vibrational coordinate which partici-

9) J. L. Hollenberg and D. A. Dows, *J. Chem. Phys.*, **34**, 1061 (1961); *ibid.*, **37**, 1300 (1962).

9a) J. L. Lowry and S. T. Anderson, *Proc. Roy. Soc.* (London), **A136**, 474 (1932).

10) D. A. Ramsay, *J. Amer. Chem. Soc.*, **74**, 72 (1952).

11) In that case, however, there remains a question about the interpretation of the splitting of the ν_2 band also observed in the infrared spectra.

TABLE 1.

	Solid					Gas		
	freq. (cm^{-1})	A[a] (10^4 cm/mM)	rel. intensity H.H.[b]	rel. intensity P.S.[c]	$\partial M/\partial q$ (10^2 esu)	freq. (cm^{-1})	A (10^4 cm/mM)	$\partial\mu/\partial q$[e] (10^2 e.s.u.)
HCN								
ν_1	2099	0.518	1.0	1.0	0.81	2096.9	0.00143	0.045
ν_2	828, ~840	0.462	1.4	1.2	0.57	712	0.457	0.57
ν_3	3130	3.94	5.7	7.2	2.36	3311.4	0.540	0.88
DCN								
ν_1	1885	0.99		1	1.18	1925.3	0.0269	0.20
ν_2	649	0.141		1/6	0.32	569	0.137	0.31
ν_3	2545	1.07		1	1.23	2630.3	0.305	0.66

a) Corrected value for the field effect by multiplying 1/1.22 given from Polo-Wilson's equation (Ref. 17).
b) Measured by Hoffmann and Hornig (Ref. 5).
c) Predicted by Pézolet and Savoie (Ref. 6).
d) Measured by Hyde and Hornig (Ref. 7).
e) Calculated based on the Hyde and Hornig's intensity (see text).

pates in an optically-active ($k=0$) normal coordinate, Q_i, of the crystal. In the oriented gas model, q_i is equivalent to the corresponding molecular normal coordinate; this, however, may be unsatisfactory in the present system of strong interactions.

Since the unit cell contains only a single molecules,[4] Q_i is given by the normalized total sum of q_i:

$$Q_i = n\sum_j (q_i)_j, \tag{2}$$

where n is a normalization constants and where $\sum_j$ implies a summation over all the molecules in the crystal. q_i may be expressed in terms of molecular internal coordinates as:

$$q_i = \sum_k L_{ki}^{-1} r_k, \tag{3}$$

so that the dipole-moment derivative with respect to r_k is given by:

$$\frac{\partial M}{\partial r_i} = \sum_j L_{ji}^{-1}\frac{\partial M}{\partial q_j}. \tag{4}$$

Now, let us consider the quantity

$$\Delta M = M - \sum_i \mu_i. \tag{5}$$

which represents the contribution from the intermolecular interaction, where μ_i is the dipole-moment of an isolated molecule, i, and, $\sum_i \mu_i$ is equivalent to the M for the oriented gas model. Eq. (4) is also valid for ΔM; that is,

$$\frac{\partial \Delta M}{\partial r_i} = \sum_j L_{ji}^{-1}\frac{\partial \Delta M}{\partial q_j}, \tag{6}$$

(Bending vibration, ν_2)

As may be seen in Table 1, the gaseous and solid intensities of ν_2 coincide well within the limits of experimental error for both HCN and DCN. This may suggest that the charge distribution in a molecule was changed little as a result of hydrogen bonding. However, this mode of vibration necessarily involves a compensating rotation (or a libration in solids) of the molecule, so that the observed intensity includes the contribution from the accompanying rotation of the molecular dipole moment. It has been shown[12] from the gaseous data that the physically unambiguous

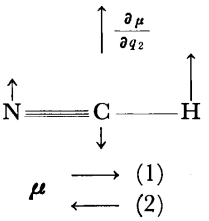

Fig. 4. Relative polarity of μ and $\partial\mu/\partial q_2$ in hydrogen cyanide.

quantity, P_R,[13] which is obtained by subtracting such a rotational contribution from the observed $\partial\mu/\partial q$, is in closer agreement between HCN and DCN, resulting in an average value of 1.08 D/rad, with the polarity shown in Fig. 4. As the molecular dipole moment in solids is not known (although it could be estimated from the intensity of a librational mode), the corresponding quantity in solids can not now be determined. The values tentatively given in Table 2 were calculated assuming that the dipole moment was equal to the gaseous value, 3.00 D.[14] At all events, such a close agreement between gaseous and solid data suggests no remarkable change in the dipole moment due to the hydrogen bonding in this case.

(Stretching vibrations ν_1 and ν_3)

If the stretching coordinates of the C≡N and C–H (C–D) bonds are expressed by r_1 and r_2, Eq. (4) for these parallel modes may be solved to give $\partial M/\partial r_1$ and $\partial M/\partial r_2$ from the observed $\partial M/\partial q$. The L^{-1} matrix was obtained on the basis of the force constants, which were chosen so as to minimize the standard deviation of the frequency for both HCN and DCN. For the sake of consistency, the L^{-1} was also calculated for

12) J. Overend, "Infrared Spectroscopy and Moelcular Structure," ed. by M. Davies, Elsevier Publ. Comp., Amsterdam (1963), p. 374.
13) B. Crawford, Jr., *J. Chem. Phys.*, **20**, 977 (1952); A. D. Dickson, I. M. Mills, and B. Crawford, Jr., *ibid.*, **27**, 445 (1957).
14) C. H. Towns and A. L. Shawlow, "Microwave Spectroscopy," McGraw-Hill, New York (1955).

TABLE 2.

	rel. sign $\partial M/\partial q_2$, μ[a)]	$p_R(\nu_2)$ HCN (D/rad)	$p_R(\nu_2)$ DCN (D/rad)	rel. sign $\partial M/\partial q_1$, $\partial M/\partial q_3$	$\partial M/\partial r_1$ HCN (D/Å)	$\partial M/\partial r_1$ DCN (D/Å)	$\partial M/\partial r_2$ HCN (D/Å)	$\partial M/\partial r_2$ DCN (D/Å)
Gas	(1)	1.06	1.11	++	−0.33	−0.47	1.06	1.08
	(2)	−0.20	0.25	+−	−0.62	−1.67	1.02	0.58
Solid	(1)	1.10	1.14	++	1.19	0.86	3.18	2.98
	(2)	−0.24	0.21	+−	−4.43	−5.72	2.31	−0.28
average								
Gas	(1)	1.08		++	−0.40		1.07	
Solid	(1)	1.12		++	1.03		3.08	

a) (1) and (2) in this column correspond to those in Fig. 4.

TABLE 3.

relative sign $\partial\mu/\partial r_1$ (gas), $\partial M/\partial r_1$ (solid)	$\partial \Delta M/\partial r_1$ (D/Å)	$\partial \Delta M/\partial r_2$ (D/Å)	$[\partial \Delta M/\partial r_2]$ (D/Å)	$[\partial \Delta M/\partial r_3]$ (D/Å)
(i) −+	1.43	2.01	0.58	−1.43
(ii) ++	0.63	4.15	3.52	−0.63

TABLE 4.

	Gas	Crystal
K(CH)	5.799	5.126
K(CN)	17.933	18.542
K(CH, CN)	−0.167	−0.158
H	0.271	0.204
		mdyn/Å

$2V = K(\mathrm{CH})r_2^2 + K(\mathrm{CN})r_1^2 + 2K(\mathrm{CH,\ CN})r_1r_2 + Hr_{\mathrm{CH}}r_{\mathrm{CN}}\Delta\phi^2.$

the gas by the same procedure, Hyde and Hornig[7] adopted a somewhat different criterion in determining their force constants. In Table 4 are given the force constants thus obtained. The dipole moment derivatives $\partial M/\partial r$'s, are summarized in Table 2 and there compared with the corresponding gaseous quantity, $\partial\mu/\partial r$, where the proper choice of a relative sign for $\partial M/\partial q_1$ and $\partial M/\partial q_3$ is definitely (++).

It is remarkable that $\partial M/\partial r_1$ and $\partial M/\partial r_2$ have the same direction of polarity in the solid, while they are opposite in the gas. There may be two possibilities in accounting for the additional contribution, $\partial \Delta M/\partial r$. According to the choice of opposite or equal signs for $\partial M/\partial r_1$ (solid) and $\partial\mu/\partial r_1$ (gas), either (i) or (ii) in Table 3 is obtained.

Now, if an additional coordinate, r_3, is introduced to give the N···H stretching, the condition:

$$r_1 + r_2 + r_3 = 0 \tag{7}$$

is always realized for the optically-active modes in the crystal. Therefore, the dipole-moment derivatives dealt with thus far, which conform with this condition, of course, may be given by the expressions:

$$\frac{\partial \Delta M}{\partial r_1} = \left[\frac{\partial \Delta M}{\partial r_1}\right] - \left[\frac{\partial \Delta M}{\partial r_3}\right]$$
$$\frac{\partial \Delta M}{\partial r_2} = \left[\frac{\partial \Delta M}{\partial r_2}\right] - \left[\frac{\partial \Delta M}{\partial r_3}\right] \tag{8}$$

where the bracketed derivatives imply that they have no connection with Eq. (7). In other words, the dipole-moment derivatives as given from Eq. (6) include inevitably a part which is properly attributable to a wholly intermolecular displacement, $[\partial \Delta M/\partial r_3]$.

As the C–N bonding electrons are supposed to be little involved in the hydrogen bonding, the $[\partial \Delta M/\partial r_1]$ in Eq. (8) may well be neglected in the following. Then, according to (i) or (ii) in Table 3,

$$\text{(i)} \qquad \text{(ii)}$$
$$-[\partial \Delta M/\partial r_3] \approx \partial \Delta M/\partial r_1 = 1.43 \text{ or } 0.63 \text{ D/Å}$$
$$[\partial \Delta M/\partial r_2] = \partial \Delta M/\partial r_2 + [\partial \Delta M/\partial r_3] \approx 0.58 \text{ or } 3.52 \text{ D/Å}$$

where the positive value of the derivatives indicates that the moment is increased in the direction of $\bar{N}\equiv C-\overset{+}{H}$ for the stretching of the bond.

As is commonly recognized, the hydrogen-bond formation may be described properly in terms of electrostatic and charge-transfer interactions. That is, an appropriate wave function for the C–H···N system may be:[15]

$$\Psi = c_1\psi_1 + c_2\psi_2 + c_3\psi_3 \tag{9}$$

where ψ_i represents these structures;

$$\begin{aligned} &\psi_1; \quad \mathrm{C{-}H \quad N} \quad \text{(I)} \\ &\psi_2; \quad \mathrm{C^-\ H^+ \quad N} \quad \text{(II)} \\ &\psi_3; \quad \mathrm{C^-\ H{-\!-\!-}N^+} \quad \text{(III)}. \end{aligned} \tag{10}$$

Although the contribution of ψ_2 may possibly be of greater importance in stabilizing the system, the vibrational change of the dipole moment is mainly ascribable to ψ_3. This is because not only does the structure III have a much greater inherent moment than II, but also the weight of III in the Ψ is expected from theoretical consideration to be more susceptible to the vibrational displacement than that of II. This latter point is supported by the results of Coulson and Danielsson's[15] semi-empirical calculation of the O–H··· O system. Therefore, the (i) set above corresponds to the case in which the approach of the H—N distance is far more effective in causing the charge transfer than the C–H stretching, and the (ii) set, *vice versa*.

Now, in order to obtain an approximate idea, the additional moment due to the contribution from the structure III may be given by:

$$\Delta M = c_3^2 Re, \tag{11}$$

15) C. A. Coulson and U. Danielsson, *Ark. Fys.*, **8**, 239, 245 (1954).

where the intrinsic moment of the structure III is roughly equalized to the C–H···N distance, R, multiplied by the electronic charge, e. Then,

$$[\partial \Delta \boldsymbol{M}/\partial r] = e(c_3^2 + 2c_3 R[\partial c_3/\partial r]), \quad (12)$$

where r may be either r_2 or r_3 and where the brackets imply the same as before. The size of c_3^2 has been estimated at a few per cent even in the O–H···O case, so ec_3^2 may be by far smaller than any possible $[\partial \Delta \boldsymbol{M}/\partial r]$ value given before. Therefore, the relationship:

$$\frac{[\partial \Delta \boldsymbol{M}/\partial r_2]}{[\partial \Delta \boldsymbol{M}/\partial r_3]} \simeq \frac{[\partial c_3/\partial r_2]}{[\partial c_3/\partial r_3]} \quad (13)$$

may be approximately valid in the present case.

The value of this ratio can not be estimated empirically. However, it can be shown that Coulson and Danielsson's findings on the O–H···O system[15] quated above give this ratio a negative value definitely less than unity in size. This fact suggests that the set (i) in Table 3 is preferable.

Finally, let us mention the polarity of the dipole-moment derivatives. Strictly speaking, the sign of those derivatives is significant only in a relative sense, as is obvious from Eq. (1). However, it is fairly conclusive from the above discussions that $[\partial \Delta \boldsymbol{M}/\partial r_3]$ has the polarity of $H^+\cdots N^-$ for $r_3>0$, and that then, $[\partial \Delta \boldsymbol{M}/\partial r_2]$ is the reverse. Therefore, the set (i) adopted above implies the following polarities of individual derivatives for $r_1, r_2>0$:

$$\partial \boldsymbol{M}/\partial r_1 \text{ (solid)} = 1.03 \quad (\cdots \dot{\overset{-}{N}}C\text{-}H\cdots)$$

$$\partial \boldsymbol{M}/\partial r_2 \text{ (solid)} = 3.08 \quad (\cdots N\overset{-}{C}\text{-}\dot{\overset{+}{H}}\cdots)$$

$$\partial \mu/\partial r_1 \text{ (gas)} = 0.40 \quad (N^+ \equiv C^-)$$

$$\partial \mu/\partial r_2 \text{ (gas)} = 1.07 \quad (C^- \text{-} H^+)$$

Critical Considerations

There may be some argument because the above interpretation ignored the possible influences on the intensities other than hydrogen bonding. In fact, there have been found several cases without hydrogen bonding which showed many-fold changes in intensity from a gas to a solid.[16] It may be noticed, however, that the absolute magnitude of such a change was generally much smaller than the present observations, althought it resulted in a remarkable change in ratio for the bands of a small intrinsic intensity. On the other hand, the field effect is of different category and may give some error in the numerical results, because Polo-Wilson's equation[17] employed in Table 1 may not be very satisfactory.[18]

It has been implicitly assumed so far that the sample films were composed of randomly-oriented polycrystals. There may be little doubt about the crystalline nature of the samples, because the observed spectra showed an excellent correspondence to the Raman spectra,[6] for which the samples were crystallized much more carefully. On the other hand, Hoffmann and Hornig observed an apparent change in the relative intensities of the splitted ν_2 components depending on the depositing condition; they attributed this change to the formations of oriented crystals.

In the present work, the features of the ν_2 bands were similar to those of the more scattering films of Hoffmann and Hornig which were looked on as less oriented, and were almost unchanged for various film thicknesses and different window materials. Accordingly, the orientation effect does not seem to be very significant even if it does occur. The close proximity of the gaseous and solid ν_2 intensities may possibly support the above inference.

Supposing the orientation effect to be considerable, the most probable case is one with molecular axes parallel to a window surface, because the parallel bands were observed to have a reasonably great intensity; also Hoffmann and Hornig observed only a single component of ν_2 in their more oriented films. When this is the case, the observed intensity, A, should be multiplied by 1.33 for ν_2 and by 0.67 for ν_1 and ν_3 before applying Eq. (1). Even in this case, however, the essential matter in the discussions so far may be little disturbed, because the stretching and bending vibrations were dealt with quite separately.

16) J. L. Hollenberg and D. A. Downs, *J. Chem. Phys.*, **37**, 1300 (1962); G. M. Wieder and D. A. Dows, *ibid.*, **37**, 2990 (1962).
17) S. R. Polo and M. K. Wilson, *ibid.*, **23**, 2376 (1955).
18) H. Yamada and W. B. Person, *ibid.*, **40**, 309 (1964).

Stereochemical Studies of Metal Chelates. VII.[1] The Preparation, Stereochemistry, and Circular Dichloism of Dinitrocobalt(III) Complexes with (3*S*, 8*S*)-Dimethyltriethylenetetramine and Related Tetramines

Masahiko SABURI, Tsutomu SAWAI, and Sadao YOSHIKAWA

Department of Synthetic Chemistry, Faculty of Engineering, The University of Tokyo, Hongo, Bunkyo-ku, Tokyo

(Received September 10, 1971)

Dinitrocobalt(III) complexes with (3*S*,8*S*)-dimethyltriethylenetetramine((3*S*,8*S*)-dimetrien) and related ligands were prepared and separated into the geometrical isomers. The *cis*-α and *cis*-β isomers of the (3*S*,8*S*)-dimetrien complex gave rise to the Λ and Δ isomers respectively. A similar stereospecificity could be observed for the other dissymmetric ligands employed in this study. The circular dichroism (CD) spectra of the *cis*-β isomers showed three kinds of patterns, which were related to the structural features of the complexes.

There are three topological ways for coordinating triethylenetetramine (trien) to a cobalt(III) ion, *cis*-α, *cis*-β, and *trans*, as is shown in Fig. 1. The actual stereochemistry of the trien complex is, however, more complicated because of the asymmetric feature of the secondary amino groups coordinated. Taking into account this source of asymmetry, the possible isomers of the trien complex are those shown in Fig. 2, where one of the enantiomeric pair is represented for each dissymmetric isomer. Only the *meso trans* isomer is intrinsically optically-inactive. In Fig. 2, the absolute configurations of the coordinated secondary amino groups and those of the central metal ion are denoted by *R* or *S*,[2] and by Λ or Δ,[3] respectively.

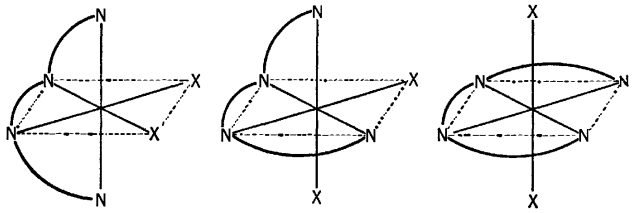

cis-α *cis*-β *trans*

Fig. 1. Topological isomers of trien complex. *cis*-α, *cis*-β, and *trans*.

Although only one enantiomeric pair is probable for the *cis*-α isomer (Λ-α(*RR*) and Δ-α(*SS*)), two kinds of diastereoisomers can be expected for the *cis*-β and *trans* isomers, because of the difference in the combination of the absolute configurations of the coordinated secondary N atoms. These configurations are the same for one of the β isomers (Λ-β(*SS*) and Δ-β(*RR*)) and the dissymmetric *trans* isomer (*trans*(*SS*) and (*RR*)), whereas they are antimeric for the other β isomer (Δ-β(*RS*) and Λ-β(*SR*)) and the *meso trans* form.

The conformations of the three chelate rings are closely related to the stereochemistry of the trien complex. The conformation of each chelate ring is represented by δ or λ,[5] as is shown in Fig. 2. The conformations of both of the outer chelate rings are the same in the *cis*-α form, as has been proved in a recent X-ray diffraction study.[6] On the other hand, they are antimeric in the usual *cis*-β isomers,[7–9] where

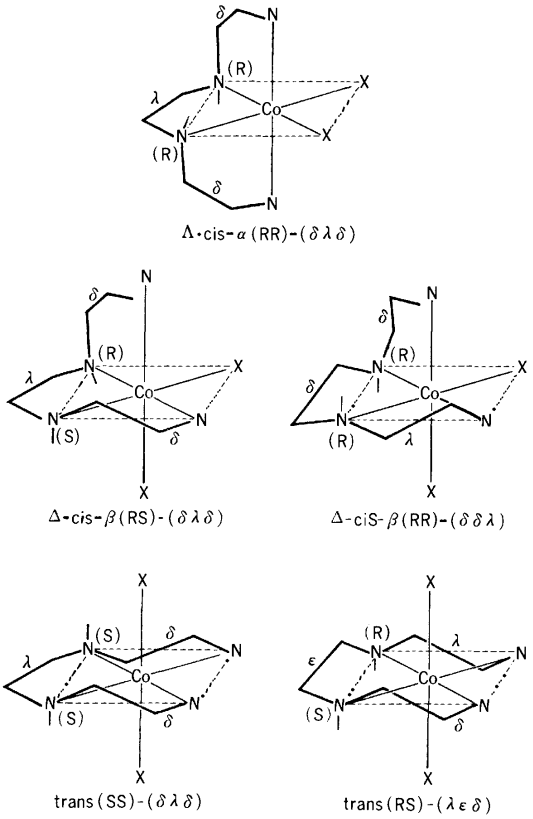

Fig. 2. Probable isomers of octahedral trien complexes. Λ-*cis*-α(*RR*)($\delta\lambda\delta$), Λ-*cis*-β(*RS*)($\delta\lambda\delta$), Δ-*cis*-β(*RS*)($\delta\lambda\delta$), *trans*-(*SS*)($\delta\lambda\delta$), *meso-trans*(*RS*)($\delta\varepsilon\lambda$).

1) Part VI. M. Saburi and S. Yoshikawa, This Bulletin, **45**, 806 (1972).

2) The asymmetric configuration is described as *R* or *S* according to the sequence rule of R. S. Cahn, C. K. Ingold, and V. Prelog, *Angew. Chem. Intern. Ed. Emgl.*, **5**, 385 (1966).

3) The absolute configuration about a central metal ion is described as Λ or Δ according to the tentative rule of *Inorg. Chem.*, **9**, 1 (1970).

4) The order of two kinds of sec-N atoms in the *cis*-β isomers follows the order proposed by D. A. Buckingham, P. A. Marzilli, and A. M. Sargeson, *Inorg. Chem.*, **6**, 1032 (1967).

5) The conformation of diamine chelate ring is represented as δ or λ. See ref. (3).

6) M. Dwyer and I. E. Maxwell, *Inorg. Chem.*, **9**, 1459 (1970).

7) H. C. Freeman and I. E. Maxwell, *ibid.*, **8**, 1293 (1969).

8) H. C. Freeman and I. E. Maxwell, *ibid.*, **9**, 649 (1970).

9) H. C. Freeman, L. G. Marzilli, and I. E. Maxwell, *ibid.*, **9**, 2408 (1970).

the coordinated asymmetric secondary N atoms of trien take the same configurations (see *Λ-cis-β(SS)* in Fig. 2).

However, a detailed examination of the Dreiding stereomodels shows[10] that these chelate rings probably take the same conformations in the *Λ-β(RS)* and its enantiomer. It appears, therefore, that the *cis-β* isomer of such a steric form (*Λ-β(RS)* and/or *Λ-β(SR)*) can be obtained by the use of trien analogues modified in such a way that the outer-side chelate rings are restricted to the same conformation by some steric effect(s) of the substituents.

For (3*S*,8*S*)-dimethyltriethylenetetramine ((3*S*,8*S*)-dimetrien) and (2*S*,9*S*)-dimethyltriethylenetetramine ((2*S*,9*S*)-dimetrien), the absolute configurations of the asymmetric carbon centers of both side arms have the same *S* configuration. The structures and abbreviations for these tetramines, along with the other ligands employed in the present study, are summarized in Table 1. Both the side chelate rings are fixed in the same (*δ*) conformation for these ligands, ((3*S*,8*S*)- and (2*S*,9*S*)-dimetrien); therefore, diacidocobalt(III) complexes with these tetramines give rise to the *Λ-cis-β(RS)* isomer (in which both the outer chelate rings have the *δ* conformation).

Recently, the *Λ-cis-β* isomers of dichlorocobalt(III) complexes with (3*S*,8*S*)-[1] and (2*S*,9*S*)-dimetrien[11] were isolated. The structures of these isomers could be determined to be the *Λ-cis-β(RS)* form on the basis of their circular dichroism (CD) spectra. It was shown that the CD curve of the *Λ-β(RS)* forms are different from those of the *Λ-β(RR)* forms (or *Λ-β(SS)*) in the case of dichloro complexes.

It is interesting to investigate the difference(s) in the CD spectra between the *Λ-β(RR)* and *Λ-β(RS)* forms (or their antipodes) for cobalt(III) complexes other than the dichloro complex. In order to examine this problem, we prepared and separated the isomers of dinitrocobalt(III) complexes coordinated with (3*S*,8*S*)-dimetrien, (2*S*,9*S*)-dimetrien, and related trien derivatives. The CD spectra of these complexes will be measured and discussed in the present paper.

Table 1. Abbreviation and structure of ligands

Structure	Abbreviation
	(3*S*, 8*S*)-dimetrien
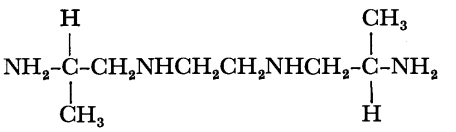	(2*S*, 9*S*)-dimetrien
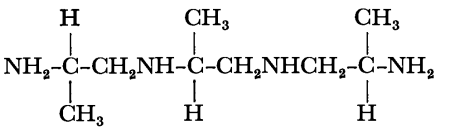	(5*R*)-Me$_3$trien
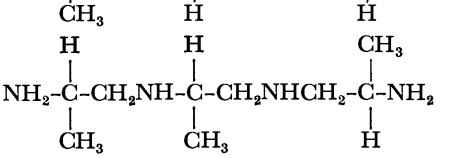	(5*S*)-Me$_3$trien
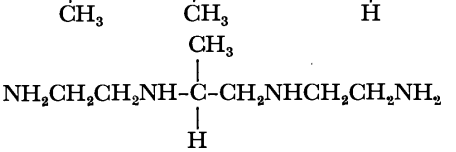	(5*R*)-metrien

Experimental

(3S,8S)-Dimethyltriethylenetetramine Tetrahydrochloride (3S,8S)-dimetrien·4HCl). The method of preparing this ligang has been described previously.[1]

Λ-cis-*α-Dinitro ((3S,8S)-dimethyltriethylenetetramine)cobalt-(III) Perchlorate(Λ*-cis-*α-[Co((3S,8S)-dimetrien)(NO$_2$)$_2$]ClO$_4$).* To a solution of (3*S*,8*S*)-dimetrien·4HCl (2.55 g) and LiOH·H$_2$O (0.94 g) in 30 m*l* of water, CoCl$_2$·6H$_2$O (1.80 g) and NaNO$_2$ (1.10 g) were added successively; then the solution was aerated with carbon dioxide-free air for 10 hr at room temperature. The resultant solution was gradually evaporated on a water bath at 50°C until the volume was reduced to about 10 m*l*; it was then filtered, and 20 m*l* of ethanol were added. The white precipitates were removed quickly, 10 more m*l* of ethanol were added, and the mixture was kept in an ice bath for 1 hr. After the white precipitates has been removed once more, the filtrate was allowed to stand in an ice bath for 3 hr. The yellow precipitates which thus separated were filtered off and washed with a small volume of ethanol. The filtrate and washings were united and cooled in a refrigerator overnight. A further crop of yellow precipitates was then collected and washed with ethanol. The filtrate and washings were stored in order to separate the *cis-β* isomer.

The crude, hygroscopic yellow precipitates were dissolved in a small volume of warm water and then filtered. The pure perchlorate salt could be obtained by adding excess solid LiClO$_4$·3H$_2$O to the filtrate. It was recrystallized from warm water. Found: C, 22.65; H, 5.23; N, 19.62%. Calcd for [Co(C$_8$H$_{22}$N$_4$)(NO$_2$)$_2$]ClO$_4$: C, 22.62; H, 5.22; N, 19.79%.

Λ-cis-*β-Dinitro((3S,8S)-dimethyltriethylenetetramine)cobalt(III) Perchlorate (Λ*-cis-*β-[Co((3S,8S)-dimetrien)(NO$_2$)$_2$]ClO$_4$).* To the combined filtrate and washings from the separation of the *Λ-cis-α* isomer, we added an excess amount of solid LiClO$_4$·3H$_2$O; the yellow-brown crystals which thus separated were collected and washed with ethanol and ether. The product thus obtained was contaminated with the *Λ-cis-α* isomer, and so it was fractionally recrystallized from a warm aqueous solution. After removing the less soluble *Λ-cis-α* isomer, the *Λ-cis-β* isomer could be obtained as yellowish-brown crystals. It was recrystallized from warm water. Found: C, 22.86; H, 5.23; N, 19.31%. Calcd for [Co(C$_8$H$_{22}$N$_4$)(NO$_2$)$_2$]ClO$_4$: C, 22.62, H, 5.22; N, 19.79%.

(2S,9S)-Dimethyltriethylenetetramine Tetrahydrochloride (2S,-9S)-dimetrien·4HCl). This ligand was prepared by the method of Asperger and Liu.[11]

Λ-cis-*α-Dinitro((2S,9S)-dimethyltriethylenetetramine)cobalt(III) Chloride (Λ*-cis-*α-[Co((2S,9S)-dimetrien)(NO$_2$)$_2$]Cl).* The method of preparing this complex has been previosuly described.[1]

Λ-cis-*β-Dinitro((2S,9S)-dimethyltriethylenetetramine)cobalt(III) Perchlorate (Λ*-cis-*β-[Co((2S,9S)-dimetrien)(NO$_2$)$_2$ClO$_4$).* To a solution of *Λ-β*[Co(2*S*,9*S*)-dimetrien)CO$_3$]$^+$ prepared *in situ.* as has been described previously[1] (1.5×10^{-3} mol

10) M. Goto, M. Saburi, and S. Yoshikawa, *ibid.*, **8**, 358 (1969).
11) R. G. Asperger and C. F. Liu, *ibid.*, **4**, 1395 (1965).

scale), we added 5 N $HClO_4$ to pH 1, and then the solution was warmed at 80°C for 2 min. 5 N $HClO_4$ was further added in order to adjust the pH of the solution to 1, after which solid $NaNO_2$ (0.8 g) was added and dissolved. After the mixture had stood at room temperature for 15 min, an excess of solid $LiClO_4 \cdot 3H_2O$ was added to the brown solution. The yellow-brown crystals which separated out immediately were collected after standing 1 hr in an ice bath and washed with a small volume of cold water, ethanol, and ether. The product was slightly contaminated with the *Δ-cis-α*-isomer, and so it was fractionally recrystallized from a warm aqueous solution. The fractions showing a negative Cotton effect in the first absorption band region (~450 mμ) were combined and recrystallized repeatedly from warm water until they showed a constant CD curve. Found: C, 22.55; H, 5.38; N, 19.37%. Calcd for $[Co(C_8H_{22}N_4)(NO_2)_2]ClO_4$: C, 22.62; H, 5.22; N, 19.79%.

(R)-(−)$_D$- and (S)-(+)$_D$-*Propylenediamine.* These substances were obtained by resolving commercially-available racemic propylenediamine according to the method of Dwyer *et al.*[12]

N,N'-*Bis(carbobenzoxy*-(S)-*alanyl)*-(R)-*propylenediamine.* 17.8 g (0.075 mol) of carbobenzoxy-(*S*)-alanine hydrazide, obtained by a usual method,[13] was dissolved in a mixture of acetic acid (90 m*l*), 5 N HCl (38 m*l*), and water (375 m*l*). The solution was cooled to below −5°C in an ice-salt bath, and then a cold aqueous solution of $NaNO_2$ (5.5 g, 0.08 mol) was added in one portion. The carbobenzoxy-(*S*)-alanyl azide thus formed was extracted with 500 m*l* of cold ether. The ether layer was separated, washed with water (100 m*l*) a 3% sodium bicarbonate solution (100 m*l*), and water (100 m*l*) successively, and then dried briefly over anhydrous sodium sulfate. Sodium sulfate was removed and to the ether solution we added 2.22 g (0.03 mol) of (*R*)-(−)$_D$-propylenediamine; the mixture was subsequently stirred for 24 hr in an ice bath and then for 12 hr at room temperature. The resultant white precipitates were filtered off and washed with ether. For elemental analysis, small portion of the product was recrystallized from hot ethanol. mp 199.4—200.0°C (corr.). Found: C, 61.14; H, 6.25; N, 12.19%. Calcd for $C_{25}H_{32}N_4O_6$: C, 61.97; H, 6.66; N, 11.56%.

N,N'-*Bis(*(S)-*alanyl)*-(R)-*propylenediamine Diacetate.* 4.85 g (0.01 mol) of *N,N'*-bis(carbobenzoxy-(*S*)-alanyl)-(*R*)-propylenediamine was hydrogenated for 4 hr in 100 ml of methanol containing 1.5 g of acetic acid and 1 g of paradium black, using a Parr low-pressure apparatus. After the removal of the catalyst, the solution was concentrated to dryness under reduced pressure, giving white prceipitates of *N,N'*-bis((*S*)-alanyl)-(*R*)-propylenediamine diacetate. For the subsequent reaction, the product was used without further purification.

(2S,5R,9S)-*Trimethyltriethylenetetramine Tetrahydrochloride* ((5R)-*Me$_3$trien·4HCl*). 9.48 g (0.282 mol) of *N,N'*-bis((*S*)-alanyl)-(*R*)-propylenediamine diacetate was added to a suspension of 7.6 g of lithium aluminum hydride in 200 m*l* of anhydrous tetrahydrofuran. The mixture was stirred and heated under reflux for 24 hr. After the mixture had then been cooled to room temperature, 14.4 m*l* of water diluted with 50 m*l* of tetrahydrofuran was added, drop by drop; the resultant slurry was filtered off and washed with a small volume of tetrahydrofuran. The residue was extracted with boiling tetrahydrofuran (200 m*l*) under reflux (2 hr) and then filtered again. After repeating the extraction once more, the combined filterates and extracts were concentrated under reduced pressure, leaving an oily residue. This residue was dissolved in ethanol (100 m*l*), and exess dry HCl gas was bubbled through, yielding white precipitates. These were filtered off and recrystallized from 5 N HCl and ethanol. Found: C, 31.98; H, 8.41; N, 16.38%. Calcd for $C_9H_{24}N_4 \cdot 4HCl$: C, 32.35; H, 8.45; N, 16.77%.

Δ-cis-*α*-*Dinitro* ((2S,5R,9S)-*trimethyltriethylenetetramine) cobalt-(III) Chloride* (*Δ*-cis-*α*-[*Co*((5R)-*Me$_3$trien*)(NO_2)$_2$]*Cl*). To a solution of 1.02 g of (5*R*)-Me$_3$ trien·4HCl and 0.36 g of $LiOH \cdot H_2O$ in 25 m*l* of water $CoCl_2 \cdot 6H_2O$ (0.64 g) and $NaNO_2$ (0.42 g) were added and dissolved successively; the resultant solution was aerated for 6 hr at room temperature. The yellow precipitates which were thus separated were collected and washed with cold water and ethanol. A second crop could be obtained by concentrating the filtrate on a water bath (50°). The crude products were recrystallized from water and ethanol. Found: C, 29.03; H, 6.33; N, 22.14%. Calcd for $[Co(C_9H_{24}N_4)(NO_2)_2]Cl$: C, 28.85; H, 6.46; N, 22.43%.

Δ-cis-*β*-*Dinitro* ((2S,5R,9S)-*trimethyltriethylenetetramine)cobalt-(III) Perchlorate* (*Δ*-cis-*β*-[*Co*((5R)-*Me$_3$trien*)(NO_2)$_2$]*ClO$_4$*). To the filtrate from the isolation of the *Δ-cis-α* isomer as above, a large excess of solid $LiClO_4 \cdot 3H_2O$ was added. After the mixture had stood overnight, yellow-brown precipitates were collected, washed with water and ethanol, and dried *in vacuo*. They were then recrystallized from warm water. Found: C, 23.31; H, 5.80; N, 18.01%. Calcd for $[Co(C_9H_{24}N_4)(NO_2)_2]ClO_4 \cdot H_2O$: C, 23.67; H. 5.74; N, 18.40%.

N,N'-*Bis(carbobenzoxy*-(S)-*alanyl)*-(S)-*propylenediamine.* This compound was prepared by a procedure similar to that used for *N,N'*-bis(carbobenzoxy-(*S*)-alanyl)-(*R*)-propylenediamine, but using (*S*)-(+)$_D$-propylenediamine instead of (*R*)-(−)$_D$-propylenediamine. For the elemental analysis, a small portion of the product was recrystallized from ethanol. mp 233.5—234.5°C (corr.). Found: C, 61.92; H, 6.76; N, 12.14%. Calcd for $C_{25}H_{32}N_4O_6$: C, 61.97; H, 6.66; N, 11.56%.

N,N'-*Bis(*(S)-*alanyl)*-(S)-*propylenediamine Diacetate.* *N,N'*-Bis(carbobenzoxy-(*S*)-anlayl)-(*S*)-propylenediamine was hydrogenated in the same way as the corresponding (*R*)-propylenediamine derivative. The product was used in the following reaction without further purification.

(2S,5S,9S)-*Trimethyltriethylenetetramine* ((5S)-*Me$_3$trien*). *N,N'*-Bis((*S*)-alanyl)-(*S*)-propylenediamine diacetate (10.1 g, 0.03 mol) was treated with lithium aluminum hydride (9.1 g) in anhydrous tetrahydrofuran (200 m*l*) in a manner similar to that used in preparing (5*R*)-Me$_3$trien. The oily residue thus obtained was dried over KOH pellets and distilled under reduced pressure. bp 108—109°C (2 mmHg). Since the hydrochloride of this tetramine was hygroscopic, it was converted to the picrate salt for analysis. Found: C, 35.00; H, 3.73; N, 19.45%. Calcd for $C_9H_{24}N_4 \cdot 4C_6H_3N_3O_7 \cdot 2H_2O$: C, 34.75; H, 3.53; N, 19.65%.

Δ-cis-*β*-*Dinitro*((2S,5S,9S)-*trimethyltriethylenetetramine)cobalt-(III) Iodide Monohydrate* (*Δ*-cis-*β*-[*Co*((5S)-*Me$_3$trien*)(NO_2)$_2$]-*I·H$_2$O*). To a solution of (5*S*)-Me$_3$trien (0.565 g) in 20 m*l* of water containing 3 m*l* of 1 N HCl, we added $CoCl_2 \cdot 6H_2O$ (0.714 g) and $NaNO_2$ (0.435 g); the resultant solution was aerated with carbon dioxide-free air for 10 hr at room temperature. The solution was concentrated on a water bath to about 5 m*l*, and then 10 m*l* of ethanol were added. The white precipitates which thus separated (NaCl) were removed by filtration, and more ethanol was added. After removing the white precipitates if necessary, 5.64 g

12) F. P. Dwyer, F. L. Garvan, and A. Shulman, *J. Am. Chem. Soc.*, **81**, 920 (1959).

13) J. P. Greenstein and M. Winitz, "Chemistry of Amino Acid," p. 951. Vol. 2, John Wiley & Sons, Inc., New York, N. Y. (1961).

of $LiI \cdot 3H_2O$ were added. When the mixture was left standing at room temperature, slightly hygroscopic yellow precipitates began to separate; they were collected and recrystallized from methanol and ethanol. A further crop was obtained from the filtrate by adding ethanol and isopropanol. Found: C, 22.41; H, 5.35; N, 16.78%. Calcd for $[Co(C_9H_{24}N_4)(NO_2)_2]I \cdot H_2O$: C, 22.33; H, 5.41; N, 17.36%.

Measurements. The visible absorption spectra were measured with a Shimadzu MPS-50L spectrophotometer. The circular dichroism spectra were measured with a JASCO J-10 automatic spectropolarimeter.

Results and Discussion

The dinitrocobalt(III) complexes coordinated with (3*S*,8*S*)-dimetrien, (2*S*,9*S*)-dimetrien, and other tetramines were prepared by the usual air-oxidation procedures. The isomers were separated by fractional crystallization. In a previous study,[1] the stereospecificity incorporated with the (3*S*,8*S*)- and (2*S*,9*S*)-dimetrien was clarified for the dichlorocobalt(III) complexes; it was revealed that only the *Λ* and *Δ* isomers could be isolated for the *cis*-*α* and *cis*-*β* isomers respectively. Thus, in the case of dinitro complexes, the *cis*-*α* and *cis*-*β* isomers with these tetramines would also take, stereospecifically, the *Λ* and *Δ* absolute configurations respectively. Hence, the structures of the fractionally-separated products were examined by measuring the CD and ORD curves.

The chloride salts of the dinitrocobalt(III) complexes of (3*S*,8*S*)-dimetrien were highly soluble in an aqueous solution. The first and second fractions obtained by adding ethanol showed ORD curves similar to that of the *Λ*-*cis*-*α*-$[Co(trien)(NO_2)_2]^+$ ion[14]

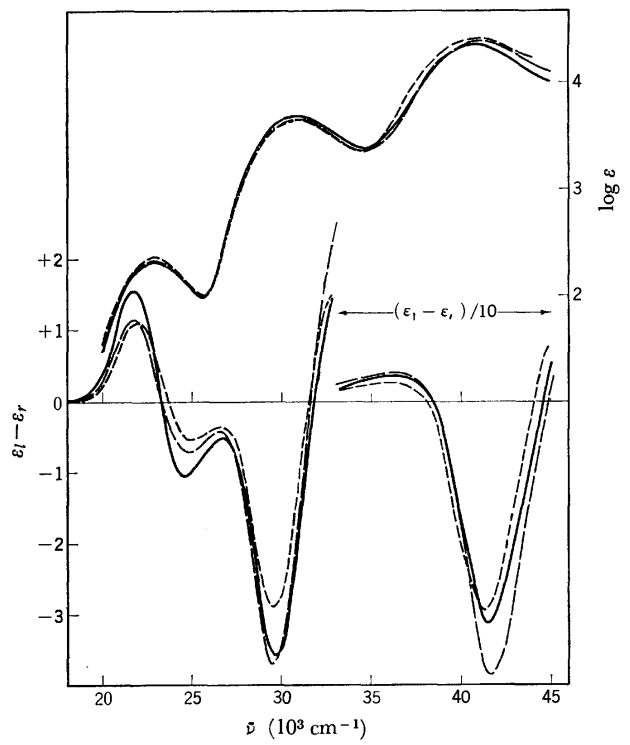

Fig. 3. Electronic absorption and CD spectra of the *Λ*-*cis*-*α* isomers. (3*S*,8*S*)-dimetrien (——), (2*S*,9*S*)-dimetrien (- - -) and 5(*R*)-Me_3trien (— — —).

Table 2. Spectral data

Complex	λ_{max}(cm^{-1})	log ε_{max}	λ(cm^{-1})	$\Delta\varepsilon_{max}$
Λ-*α*-[Co((3*S*, 8*S*)-dimetrien)$(NO_2)_2$]$^+$	22880	2.31	21830	+1.60
			24570	−1.03
	30860	3.68	29670	−3.57
			36500	+4.3
	40650	4.35	41490	−31.3
Λ-*α*-[Co((2*S*, 9*S*)-dimetrien)$(NO_2)_2$]$^+$	22880	2.32	21740	+1.18
			24880	−0.71
	30960	3.65	29500	−3.68
			35970	+4.2
	40980	4.38	41670	−38.6
Λ-*α*-[Co((5*R*)-Me_3trien)$(NO_2)_2$]$^+$	22850	2.33	22080	+1.15
			25000	−0.53
	30960	3.64	29590	−2.94
			35710	+2.8
	40900	4.40	41320	−29.5
Λ-*β*(*RS*)-[Co((3*S*, 8*S*)-dimetrien)$(NO_2)_2$]$^+$	22570	2.40	21880	−2.66
			25000	+0.43
	30860	3.49	31060	+1.72
			36500	+1.1
	40650	4.34	42020	−12.1
Λ-*β*(*RS*)-[Co((2*S*, 9*S*)-dimetrien)$(NO_2)_2$]$^+$	22730	2.36	22120	−2.68
			25380	+0.42
	30960	3.61	31550	+2.01
			37450	+1.5
	40980	4.38	42550	−8.9
Λ-*β*(*RS*)-[Co((5*R*)-Me_3trien)$(NO_2)_2$]$^+$	22570	2.44	22030	−3.40
			25000	+0.85
	31150	3.62	31250	+3.14
			37590	+2.5
	40900	4.45	42190	−14.5
Λ-*β*(*SS*)-[Co(trien)-$(NO_2)_2$]$^+$	22680	2.38	22120	+2.20
			25380	−0.23
	31150	3.63	29850	−1.08
			33110	+0.73
	40980	4.45	42370	−12.3
Λ-*β*(*SS*)-[Co((5*R*)-metrien)$(NO_2)_2$]$^+$	22730	2.40	22170	+2.50
			25320	−0.32
	31250	3.66	29940	−0.82
			32890	+1.08
	40820	4.48	42020	−12.6
Λ-*β*(*RS*)-[Co((5*S*)-Me_3trien)$(NO_2)_2$]$^+$	22450	2.50	22220	−2.56
	30700	3.73	29590	+1.04
			33000	−0.56
			37040	+0.8
	40800	4.54	41320	−5.7

and were regarded as consisting of the *Λ*-*cis*-*α* isomer of $[Co((3S,8S)\text{-dimetrien})(NO_2)_2]Cl$. However, these fractions were slightly hygroscopic and were considered to involve other isomer(s) as well. Thus, the chloride salt was converted into the perchlorate salt, the solubility of which was relatively low in water. The pure perchlorate salt of this isomer shows the absorption and CD spectra given in Fig. 3. The spectral data are summarized in Table 2.

On the basis of the similarity in the CD spectra between the present complex and the *Λ*-*cis*-*α* isomer of the trien complex,[14] the former was identified as

14) A. M. Sargeson and G. H. Searle, *Inorg. Chem.*, **4**, 45 (1965).

Λ-cis-α(RR)[15]-[Co((3*S*,8*S*)-dimetrien)$(NO_2)_2$]ClO_4. An X-ray analysis of this complex[16] revealed that the complex ion takes the *Λ-cis-α* structure illustrated in Fig. 4.

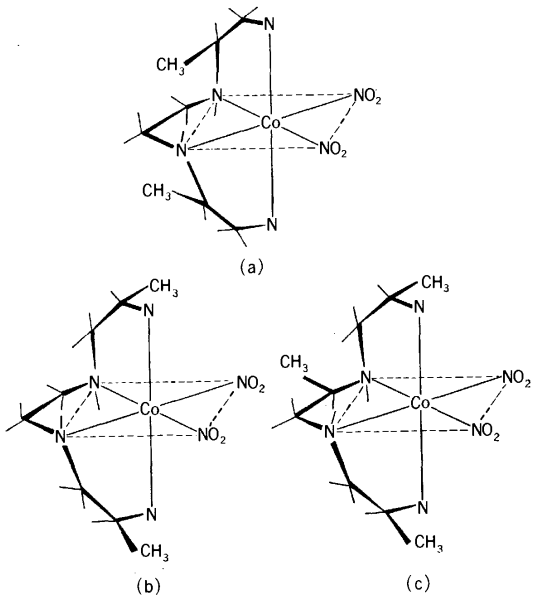

Fig. 4. Probable structures of the *Λ-cis-α* isomers. (a) (3*S*,8*S*)-dimetrien, (b) (2*S*,9*S*)-dimetrien, and (c) (5*R*)-Me_3trien.

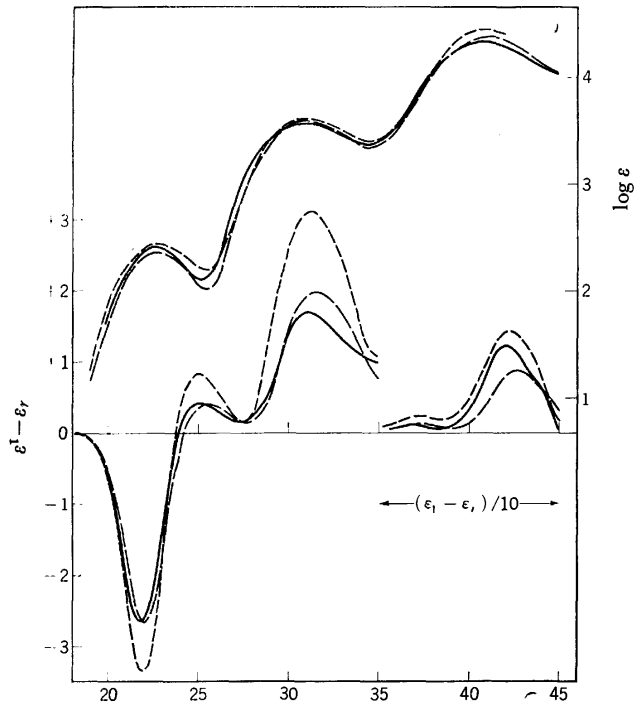

Fig. 5. Electronic absorption and CD spectra of the *Λ-cis-β(RS)* isomers. (3*S*,8*S*)-dimetrien (——), (2*S*,9*S*)-dimetrien (- - -) and (5*R*)-Me_3trien (— — —).

The second isomer of [Co((3*S*,8*S*)-dimetrien)$(NO_2)_2$]-ClO_4 could be obtained from the mother liquor by adding excess $LiClO_4$. The exact structure of the present isomer has been determined by a X-ray crystallographic study,[17] which showed that the complex ion takes the *Λ-cis-β(RS)* geometry, as is illustrated in Fig. 5. The electronic absorption and the CD spectra for this complex are shown in Fig. 6. A detailed comparison of the CD of the *Λ-β(RS)* geometry with that for the diastereoisomeric *β* geometry (*Λ-β-(SS)* and *Λ-β(RR)*) will be presented later.

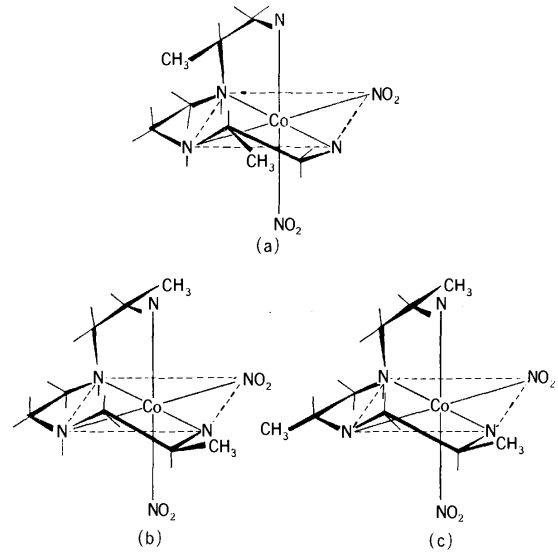

Fig. 6. Probable structures of the *Λ-cis-β(RS)* isomers; (a) (3*S*,8*S*)-dimetrien, (b) (2*S*,9*S*)-dimetrien, and (c) (5*R*)-Me_3trien.

The third isomer of [Co((3*S*,8*S*)-dimetrien)$(NO_2)_2$]-ClO_4, identified as the *trans* form, was eventually isolated from the filtrate of the separation of the *cis-β* isomer. However, the *trans* isomer can be prepared more easily by the reaction of the *trans*-[Co((3*S*,8*S*)-dimetrien)Cl_2]ClO_4 with $NaNO_2$ in hot methanol. The absorption and CD spectra of this isomer have been reported previously.[18]

The *Λ-cis-α* isomer of the dinitrocobalt(III) complex coordinated with (2*S*,9*S*)-dimetrien was readily obtained from an aerated solution as the chloride form because of its low solubility. The absorption and CD spectra of this complex are given in Fig. 3; they are similar to those of the corresponding (3*S*,8*S*)-dimetrien complex. This means that the present complex also has the *Λ-cis-α(RR)* geometry shown in Fig. 4, where the substituted methyl groups are situated in equatorial positions.

On the other hand, it was difficult to obtain the *Λ-cis-β* isomer of the (2*S*,9*S*)-dimetrien complex from the mother liquor of the *Λ-cis-α* isomer. Hence, the

15) The *RS* representation of the absolute configuration of the asymmetric secondary N atoms is complicated in substituted triens by the presence of methyl groups. For example, (3*S*,8*S*)-dimetrien and trien complexes have the opposite configurations in the *Λ-α* form; (*SS*) for the former and (*RR*) for the latter. In this paper the absolute configuration of the coordinated secondary N centers is represented by *R* and *S*, neglecting the substituted methyl groups.

16) M. Ito, F. Marumo, and Y. Saito, to be published.

17) M. Ito, F. Marumo, and Y. Saito, *Acta Crystallogr.*, **B26**, 1408 (1970).

18) M. Goto, A. Okubo, T. Sawai, and S. Yoshikawa, *Inorg. Chem.*, **9**, 1488 (1970).

Δ-β isomer was prepared by the reaction of $NaNO_2$ with *Δ-cis-β*-[Co((2*S*,9*S*)-dimetrien)$(H_2O)_2$]$^{3+}$ ion, which is prepared *in situ* through the carbonato complex. The carbonato complex, prepared *in situ* by the reaction of the *Δ-cis-α*-[Co((2*S*,9*S*)-dimetrien)Cl_2]$^+$ ion with excess Li_2CO_3, was found to show a dominant negative Cotton effect in the first absorption band region, suggesting that the resultant carbonato complex takes the *Δ* configuration predominantly.

The dinitro complex obtained above showed a negative CD band in the first absorption band region. The absorption and CD spectra of this complex are shown in Fig. 5. The CD spectrum markedly resembles that of the *Δ-cis-β*(*RS*) isomer of the (3*S*,8*S*)-dimetrien complex. Therefore, the *cis-β* siomer of the (2*S*,9*S*)-dimetrien complex can be said to adopt preferentially the *Δ-β*(*RS*) geometry, as is shown in Fig 6.

We supposed that a (2*S*,9*S*)-dimetrien analogue with a methyl group introduced into the central ethylenediamine linkage would give rise to the *Δ-cis-β*-(*RS*) isomer more preferentially than the original (2*S*,9*S*)-dimetrien. This was based on the observation[10] that trien derivatives with any equatorially-oriented substituent(s) at the central chelate ring yield, stereoselectively, *cis-β* isomers, though they have the *Δ-β*(*SS*) and/or *Δ-β*(*RR*) geometry. Therefore, it is necessary that the methyl group introduced into the (2*S*,9*S*)-dimetrien skeleton take the equatorial orientation with respect to the central diammine linkage. (2*S*,5*R*,9*S*)-Triemethyltriethylenetetramine ((5*R*)-Me_3trien) satisfies the above requirement. For this tetramine, the central chelate ring would be fixed in the *λ* conformation because of the steric effect of the methyl group, which has the *R* absolute configuration.

By the use of the (5*R*)-Me_3trien, the *Δ-cis-α* and *Δ-cis-β* isomers of dinitrocobalt(III) complex were isolated. The former was obtained as the chloride form by concentrating the aerated solution, while the latter was also obtained as the perchlorate salt by adding $LiClO_4$ to the mother liquor. The absorption and CD spectra of these complexes are shown in Figs. 3 and 5 respectively.

The CD spectra of the *Δ-cis-α* and *Δ-cis-β* isomers are clearly similar to those of the (3*S*,8*S*)- and (2*S*,9*S*)-dimetrien complexes, though the intensity of each CD band of the present cis-*β* isomer is slightly higher than those of the others. This means that the *cis-α* and *cis-β* isomers of the (5*R*)-Me_3trien complex have the *Δ-cis-α*(*RR*) and *Δ-cis-β*(*RS*) geometries respectively. The probable structures of these isomers are also shown in Figs. 4 and 6.

The steric effects incorporated with the equatorial methyl group introduced into the central diamine linkage were clearly observed for the (5*R*)-Me_3trien, since the *cis-β* isomer could be isolated from the mother liquor more readily than in the case of the (2*S*,9*S*)-dimetrien complex; morevoer, it was recognized that the yield of the *cis-β* isomer is larger than that of the *cis-α* isomer. However, the presence of the *cis-α* isomer suggests that the steric effect of the equatorial methyl group in the central chelate ring, which provides preferentially the *cis-β* isomer, is not so sufficient in the case of (5*R*)-Me_3trien as in the previous case.[10]

(2*S*,5*S*,9*S*)-Trimethyltriethylenetetramine ((5*S*)-Me_3-trien) is an epimer of (5*R*)-Me_3trien, and the asymmetric carbon atom at the central chelate ring has the *S* configuration. In this ligand the absolute configurations of all the asymmetric carbon centers are *S*; therefore, all three chelate rings should take the *δ* conformations if the methyl groups tend to take the equatorial orientations. However, it is impossible for complexes of trien derivatives to take a structure in which all three chelate rings have the same configuration at the same time, as is shown in Fig. 2.

It seems likely for the coordination of (5*S*)-Me_3-trien that one of the chelate rings takes the *λ* conformation and that the methyl group comes to lie in the axial orientation in this chelate with the *λ* conformation. Otherwise, a new very strained form may be brought about, in which at least one of the chelate rings no longer has the gauche conformation.

Only one isomer has been isolated for the dinitrocobalt(III) complex coordinated with (5*S*)-Me_3trien. The electronic absorption and CD spectrum of this complex are shown in Fig. 7. The CD curve is obviously different from that of the *Δ-cis-α* (or its enantiomer); it rather resembles those of the *Δ-cis-β*(*RS*) isomers. This suggests that the present complex has a *cis-β* geometry and the *Δ* absolute configuration.

The (5*S*)-Me_3trien complex may belong to either of two diastereoisomeric forms (*Δ-β*(*RR*) and *Δ-β*(*RS*)), though some deformations from the ordinary structures may be involved. The structure of this complex is difficult to identify in detail by only examining the

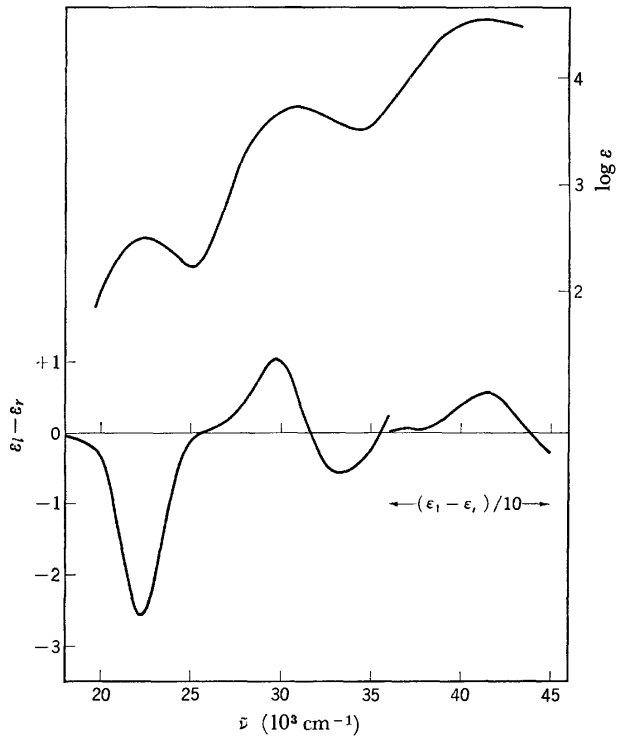

Fig. 7. Electronic absorption and CD spectra of the (5*S*)-Me_3trien complex.

CD spectrum, as will be described later. However, the influence of the difference in the absolute configuration of the methyl group introduced into the central diamine linkage was demonstrated in the different behavior between (5*R*)- and (5*S*)-Me_3trien as (2*S*,9*S*)-dimetrien analogues.

It has been indicated[19,20] that, in a *cis*-bis(diamine) complex, such as the *cis*-$Co(en)_2X_2^{n+}$ ion, with C_2 symmetry, the octahedral $A_{1g}\rightarrow T_{1g}$ transition breaks down into one component with A symmetry and two components with B symmetry. The three transitions have been distinguished, by means of their symmetry and trigonal (D_3) parentages, as $A(E_a)$, $B(E_a)$, and $B(A_2)$ transition.[19] The CD curve of the $(-)_D$-$[Co(en)_2(NO_2)_2]^+$ ion, which has the *Λ*-absolute configuration, shows a dominant positive band and a minor negative band at 21700 and 25000 cm^{-1} respectively. The former band was assigned to the $(A(E_a)+B(E_a))$ transitions, and the latter, to the $B(A_2)$ transition.[19]

The CD spectra of the *Λ-cis-α* isomers shown in Fig. 3 have a dominat positive band and a minor negative band at about 21800 and 25000 cm^{-1} respectively; they are markedly similar to those of $(-)_D$-*cis*-$[Co(en)_2(NO_2)_2]^+$ ion. Therefore, the CD bands at 21800 and 25000 cm^{-1} for the *Λ-cis-α* isomers can be assigned to the $(A(E_a)+B(E_a))$ transitions and the $B(A_2)$ transition respectively. This is reasonable, since both of the bis(en) and the α-trien complexes are related by a common two-fold rotation axis (C_2), as is shown in Fig. 8.

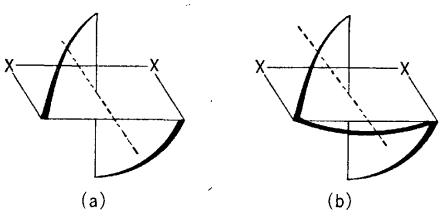

Fig. 8. The common two-fold rotation axis for *cis*-bis(en) and *cis*-α-trien complexes.

The CD spectra of the *Λ-cis-β(RS)* isomers show a dominant negative band and a minor positive band at about 22000 cm^{-1} and 25000 cm^{-1}, respectively. The positions of the band maxima of the major and the minor CD peaks correspond closely between the *Λ-cis-α* and *Λ-cis-β(RS)* isomers. This suggests that the *cis-β* isomer, which no longer has any symmetry elements, can be approximated by the same C_2 symmetry as the *cis-α* isomer. On this supposition, we assign the dominant negative band and the minor positive CD band of the *Λ-β(RS)* isomers to the $(A(E_a)+B(E_a))$ and the $B(A_2)$ transitions respectively.

The CD spectra of the *Λ-cis-β(SS)* isomers are given in Fig. 9. The exact structure of the dinitrocobalt(III) complex with (5*S*)-methyltriethylenetetramine ((5*S*)-metrien), which is enantiomeric to the (5*R*)-

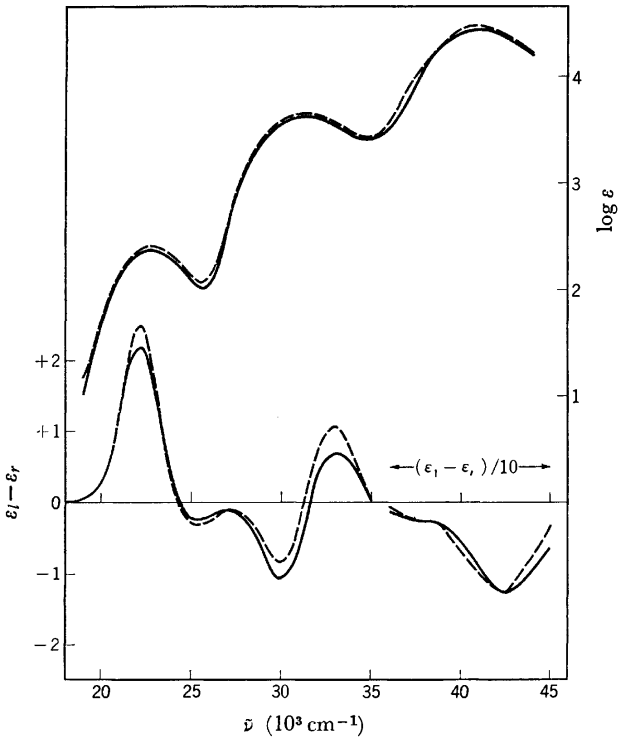

Fig. 9. Electronic absorption and CD spectra of the *Λ-cis-β(SS)* isomers. trien (——) and (5*R*)-metrien (- - -).

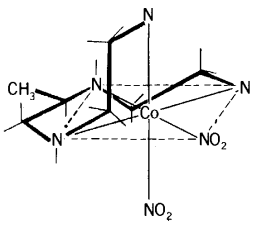

Fig. 10. Probable structure of the *Λ-cis-β(SS)*-[Co(5*R*)-metrien)$(NO_2)_2]^+$ ion.

metrien used in this study, has been determined by a recent X-ray analysis study,[21] which has revealed that the complex ion takes the *Λ-cis-β(RR)* geometry, as expected. Thus, the (5*R*)-metrien complex should have the *Λ-cis-β(SS)* configuration, which is illustrated in Fig. 10. The CD curves in Fig. 9 have a major positive band and a minor negative band at about 22100 cm^{-1} and 25300 cm^{-1} respectively. The patterns of the CD curve of the present isomers are rather similar to those of the *Λ-β(RS)* isomers. Therefore, the two CD bands can be assigned in the same way as for the *Λ-β(RS)* isomers. This is in contrast to the cases of the dichloro complexes, where a notable shift is observed between these geometries in the CD maxima in the first absorption band region.

However, there is a notable difference in the CD curves of the *Λ-β(RS)* and of the *Λ-β(SS)* isomers in the NO_2 specific absorption band region (26000—35000 cm^{-1}). The *Λ-β(SS)* isomers show two CD peaks with opposite signs in this region, a negative

19) A. J. McCaffery, S. F. Mason, and B. J. Norman, *J. Chem. Soc.*, **1965**, 5094.
20) H. Yamatera, This Bulletin, **31**, 95 (1958).
21) K. Tanaka, M. Ito, F. Marumo, and Y. Saito, unpublished result.

band at the lower-wavenumer side (near 30000 cm^{-1}) and a positive band at the higher-wavenumber side (near 33000 cm^{-1}), whereas the *Δ-β(RS)* isomers show only one positive band, near 31000 cm^{-1}, in this region. Since the bands of nitro-cobalt(III) complexes in this region consist not only of the ligand field transition (T_{2g} in the O_h symmetry), but also of the charge transfer transitions (between Co^{3+} and NO_2^-), it was impossible to assign the CD band in this region. However, the observed difference in the CD curves must be attributed to the differences in the structures of the diastereoisomeric complexes, that is, to the configuration of the secondary N centers and the conformations of the three chelate rings.

The CD curve of the (5*S*)-Me_3trien complex shows two CD bands with opposite signs in the specific absorption band region, a positive band at about 30000 cm^{-1} and a negative band at about 33000 cm^{-1}. This appears to indicate that the (5*S*)-Me_3trien has the *Δ-cis-β(RR)* geometry. At present, this complex is considered to have the *Δ-cis-β-(RS)* geometry; this assignment is based on a study of trien derivatives with an axially-oriented methyl group in the central diamine linkage.[22] The new type of *Δ-cis-β(RS)* isomer, which shows two CD bands with opposite signs in the specific absorption band region, has a fairly distorted structure because of the axial methyl group. It is noticiable that the (5*S*)-Me_3trien complex and its homologs show only one CD band in the first absorption band region, as is indicated in Fig. 7.

Thus, it is revealed that the CD curves of *cis-β* dinitrocobalt(III) complexes with trien derivatives can be classified into the following series; (1) the *λ-β(SS)* and *Δ-β(RR)* isomers have two CD bands in the first absorption band region and two CD bands in the specific absorption band region; (2) the *Δ-β(RS)* isomers have two CD bands in the first absorption band region and one CD band in the specific absorption band region, and (3) the distorted *Δ-β(RS)* isomers have one CD band in the first absorption band region and two CD bands in the specific absorption band region. The detailed structure for the distorted *Δ-β(RS)* isomer will be discussed in a subsequent paper.[22]

22) H. Matsushita, M. Goto, M. Saburi, and S. Yoshikawa, unpublished result.

BULLETIN OF THE CHEMICAL SOCIETY OF JAPAN, VOL. 45, 1093—1097 (1972)

Behavior of Alkali Metals in the Hydrogen Flame Ionization Detector for Ultra-Micro Analysis of Alkali and Alkaline Earth Metals

Masaaki YAMADA, Shigetaka SUZUKI, and Shun ARAKI

Department of Industrial Chemistry, Faculty of Engineering, Tokyo Metropolitan University, Setagaya-ku, Tokyo

(Received September 13, 1971)

Behavior of alkali metals in the small hydrogen flame for ultra-micro analysis of alkali and alkaline earth metals were investigated. Distribution of free neutral atoms and formation of alkali hydroxides were studied by the photometric method, distribution of charged particles was determined by the Langmuir probe method, and confirmation of whether negative-charged particles are mostly electrons or negative ions by the sheath method. It was found that only lithium formed hydroxide in the flame, ionization chiefly occurred in the part 0—5 mm above the jet, and that most of negative-charged particles are not electrons but negative ions.

A new method for ultra-micro analysis of alkali and alkaline earth metals was developed by the authors,[1-3] a hydrogen flame ionization detector being used as a sensor. The detector, in which the electric current caused by ionization of the metal in flame is measured, has high sensitivity (*e.g.*, 10^{-14} mol in Rb and Cs).

Since the ionization method is based on the ionization of alkali and alkaline earth metals, it is important to investigate the behavior of the metals in flame. Physical investigations[4-10] have been carried out on ionization mechanisms or kinetics of alkali and alkaline earth metals in flame. Positive ion and electron concentrations were measured by the Langmuir probe method[4] and high-frequency method,[5-10] respectively. The former has been used for determining positive ion concentration in hydrocarbon flames.[11-14]

1) S. Araki, S. Suzuki, and T. Hobo, *Bunseki Kagaku*, **15**, 27 (1966).
2) S. Araki, S. Suzuki, T. Hobo, T. Yoshida, K. Yoshizaki, and M. Yamada, *ibid.*, **17**, 847 (1968).
3) S. Araki, S. Suzuki, T. Hobo, and M. Yamada, *ibid.*, **19**, 493 (1970).
4) H. F. Calcote and I. R. King, Fifth Symposium (International) on Combustion, Reinhold, New York (1955), p. 423.
5) F. M. Page and T. M. Sugden, *Trans. Faraday Soc.*, **53**, 1092 (1957).
6) P. F. Knewstubb and T. M. Sugden, *ibid.*, **54**, 372 (1958).
7) P. J. Padley, F. M. Page, and T. M. Sugden, *ibid.*, **57**, 1552 (1961).
8) P. J. Padley and T. M. Sugden, Eighth Symposium (International) on Combustion, Williams & Wilkins, Baltimore (1962), p. 164.
9) K. Schofield and T. M. Sugden, Tenth Symposium (International) on Combustion, Academic Press, New York (1965), p. 589.
10) A. N. Hayhurst and T. M. Sugden, *Trans. Faraday Soc.*, **63**, 1375 (1967).
11) I. R. King, *J. Chem. Phys.*, **37**, 74 (1962).
12) H. F. Calcote, Eighth Symposium (International) on Combustion, Williams & Wilkins, Baltimore (1962), p. 184.
13) H. F. Calcote, Ninth Symposium (International) on Combustion, Academic Press, New York (1963), p. 622.
14) G. Wortberg, Tenth Symposium (International) on Combustion, Academic Press, New York (1965), p. 651.

Most flames were pre-mixed flames whose temperature distributions were attained only in vertical direction, and were much larger (burner mouth several centimeters in diameter) than the diffusion flame used in this experiment. Metallic elements were added to the inner flame as fine sprays of dilute aqueous solution.

Behavior of alkali metals in a small diffusion flame were studied when alkali chlorides were added to the outer flame as vapor. Distribution of free neutral atoms and charged particles, and mobility of charged particles were determined by the flame photometric method, Langmuir probe method, and sheath method,[15] respectively. The results are discussed.

Experimental

The hydrogen flame ionization detector was the same type as that used previously.[3] The inner diameters of the evaporating and ionizing jets were 0.6 and 1 mm, respectively. The flow rates of hydrogen and oxygen for the ionizing flame (the upper flame) were 240 and 25 ml/min, respectively, and for the vaporating flame 120 and 85 ml/min, respectively. Alkali metals were continuously supplied to the ionizing flame by the evaporation of chlorides of alkali metals. A spiral of platinum wire (0.2 mm in diameter), coated with fused alkali chlorides, was placed near the evaporating flame. A small D.C. voltage was applied to both terminals of the wire and evaporation of these metals could be accurately controlled by regulation of electric current.

The temperature was measured at various points of the ionizing flame with a fine Pt-Pt/Rh 13% thermocouple 0.1 mm in diameter.

The flame photometric method was applied to determine the distribution of free neutral atoms in the flame. A diffraction grating was used as a monochrometer and a photomultiplier tube (Hamamatsu T.V. R213) as a sensor. The spectrum intensities of lithium and sodium resonance lines in emission were measured at several points through a pipe 2 mm in inner diameter.

Distribution of charged particles in the flame was determined by the Langmuir probe method. A fine probe (Pt/Rh 13% wire 0.1 mm in diameter, (1) in Fig. 1) was inserted into the flame and a potential was applied to the probe against the ionizing jet. When the potential was varied, the

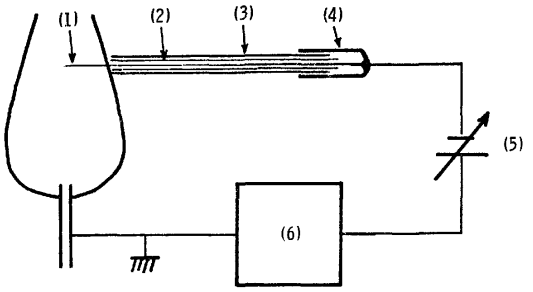

Fig. 1. Circuit for measuring probe characteristic. (1) Fine probe wire (0.1 mm D., Pt/Rh 13%); (2) Thin silica tube; (3) Copper cooling tube (1 mm I.D.); (4) Glass tube for moving the probe in a horizontal direction; (5) Voltage supplier (−3—3 V); (6) D.C. amplifier

15) T. Kinbara and H. Ikegami. *Combustion and Flame*, **1**, 199 (1957).

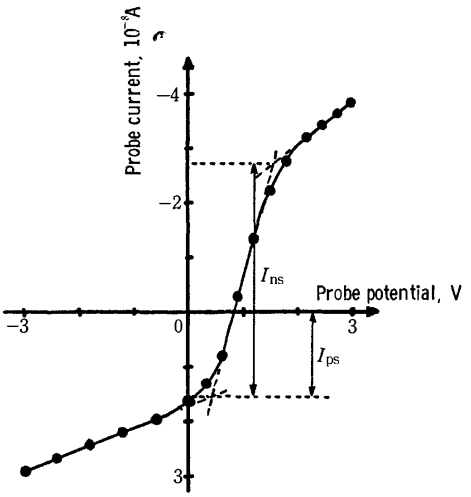

Fig. 2. Current-potential characteristic of Langmuir probe.

current-potential curve as shown in Fig. 2 was obtained. I_{ps} and I_{ns} are saturation currents due to only positive ions and only negative particles, respectively. The probe wire, together with its cooling tube, was mounted on the movable carriage of a cathetometer, the telescope being removed. The saturation current was measured at various points in each half of the flame. Measurements were carried out in a horizontal direction by inserting the probe in every one millimeter, and the saturation current in one position was determined by subtracting the values of two adjacent measurements.

Mobility of ions in the flame was observed by the sheath method to confirm whether the negative particles were chiefly electrons or negative ions. The diagram of the circuit used was the same as that of Kinbara.[15] A platinum wire 0.3 mm in diameter was used as an electrode. A potential difference was applied between the wire electrode and the ionizing jet. In order to observe the potential of the ionized gas, a probe of Pt/Rh 13% wire 0.1 mm in diameter was

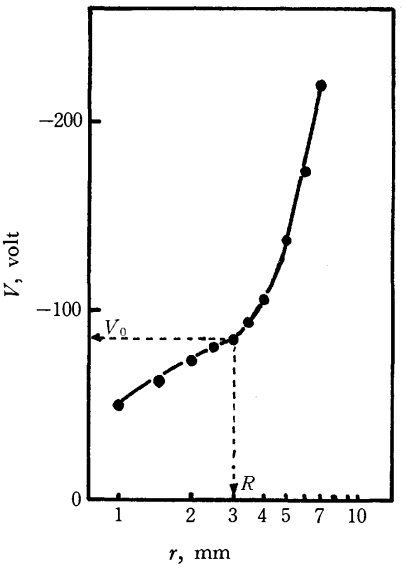

Fig. 3. Potential distribution around positively charged wire electrode.
Height of wire electrode from jet: 8 mm; r_0: 0.3 mm; l: 6 mm; Potential of jet: −600 V; i: 8×10^{-8} A

used. The probe was covered with a thin silica tube (0.4 mm in diameter) except for 6 mm at the end. The probe, together with its silica tube holder, was mounted on the movable carriage of a cathetometer. The uncovered part of the probe was carefully adjusted to be just beneath and parallel to the wire electrode. The potential was observed by the potentiometer. By adjusting the potential V of the probe with respect to the wire electrode under investigation, the probe current could be reduced to zero, at which point the probe would be at the same potential as the adjacent gas. Keeping the probe current at zero, the observed potentials of the probe were plotted as a function of ln r. A curve was obtained as given in Fig. 3. r is the distance between the center of the wire electrode and the probe. The mobility k_- for negative particles around the positive wire electrode is given by the equation.[15]

$$k_- = \frac{i[R^2 \ln(R/r_0) - 1/2(R^2 - r_0^2)]^2}{1.1 \times 10^{-12} l V_0^2 (R^2 - r_0^2)} \quad (\mathrm{cm \cdot sec^{-1}/V \cdot cm^{-1}}), \tag{1}$$

where i is the total current(A) through the flame, V_0 the potential difference (volt) in the sheath, $R - r_0$ the sheath thickness (cm), r_0 the radius (cm) of the wire electrode, and l the length(cm) of the wire electrode in the flame. V_0 and R were determined from Fig. 3 and k_- was calculated by Eq.(1).

It is necessary that the potential distribution is concentric with the wire electrode and uniform along its axis. Thus, measurements were carried out at 8—12 mm above the jet, where the ion distribution was relatively more homogeneous than other parts of the flame.

Results and Discussion

The temperature distribution of the ionizing flame is given in Fig. 4, and the distribution of free sodium atoms in vertical direction in Fig. 5. Determination was carried out as follows. If spectrum intensities in any two points of the flame are I_1 and I_2, the ratio of the numbers of free atoms N_2/N_1 would be as follows.

$$\frac{N_2}{N_1} = \frac{I_2 V_1}{I_1 V_2} e^{E/k(1/T_2 - 1/T_1)}, \tag{2}$$

where k is the Boltzmann constant, E the energy of excitation (2.10 eV for sodium resonance lines), V the volume of observed flame, and T the mean temperature of observed flame. The ordinate of Fig. 5 is given by Eq. (2), where N_1 is the number of free neutral atoms in the region 0—2 mm above the jet and N_2 the number in the region under investigation.

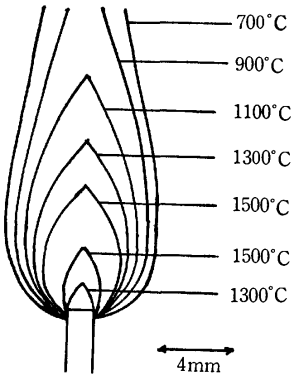

Fig. 4. Temperature distribution of ionizing flame.

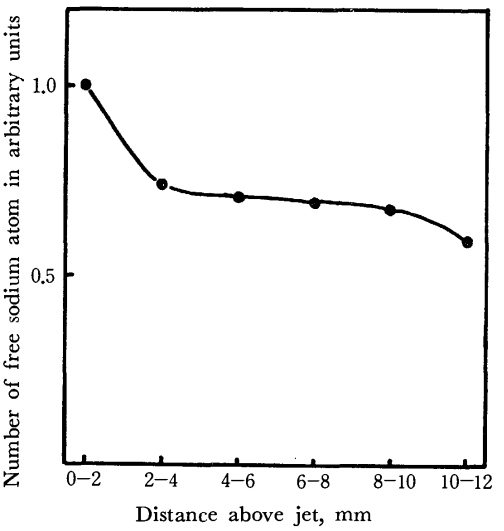

Fig. 5. Vertical distribution of free sodium atom.

The volume of inner flame 0—4 mm above the jet was subtracted from volume V, since it was considered that sodium atoms are not present in this part, or even if they were, the temperature of this part was too low to excite sodium atoms.

We see from Fig. 5 that free sodium atoms are mainly distributed in the lower and outer parts of the flame. In the upper part, the distribution was uniform due to the diffusion of sodium atoms.

Figure 6 shows the observed intensities of the sodium and lithium resonance lines in the emission 3—5 mm above the jet, plotted (logarithmic scale) against the reciprocal temperature. If these metals were present as free atoms, then Fig. 6 should show a straight line with slope $(-E/k)$, where E is 2.10 and 1.85 eV for sodium and lithium resonance lines, respectively.

Any systematic deviation from this line would mean that a significant part of the metals was present other than as free neutral atoms, in an amount depending on

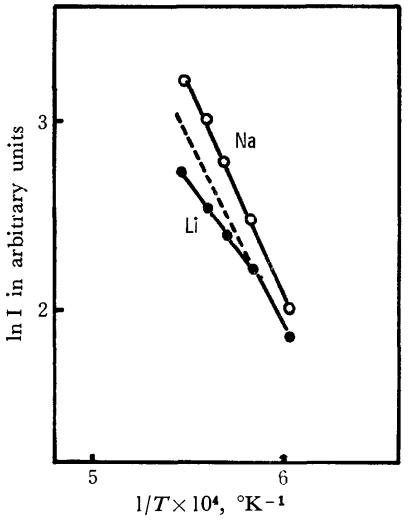

Fig. 6. Plot of ln (intensities of lithium and sodium in resonance lines) against $1/T$.
Emission intensity 3—5 mm above jet was measured. The dotted line corresponds to the theoretical slope, with the assumption that no compounds or ions are formed.

temperature. The plot for sodium showed a straight line, and E agreed with the energy of resonance lines. Hence, most of the sodium is present as free atoms in this region. On the other hand, the plot for lithium deviated from the theoretical straight line with the rise in temperature. Since lithium is more difficult to ionize than sodium, the decrease of free atoms by ionization dose not cause the deviation. A reasonable source of deviation would be formation of a molecular compound. Jensen and Padley[16] considered that gaseous hydroxide was formed as

$$A + H_2O \rightleftarrows AOH + H,$$

where A is alkali metals, and they determined dissociation energies of alkali hydroxides. From their results, LiOH is a most stable compound; the stability decreases in the order CsOH, RbOH, KOH, and NaOH.

If a metal and its position in the flame are given, spectrum intensity I is proportional to the number of free atoms N. If the number of free atoms and spectrum intensity decreased to N' and I' as a result of hydroxide formation:

$$\frac{[LiOH]}{[Li]} = \frac{N-N'}{N'} = \frac{I-I'}{I'}. \quad (3)$$

From the deviation in Fig. 6 and Eq. (3), it was found that [LiOH]/[Li] was 0.1—0.3 at 1500—1550°C. In the case of cesium, spectrum intensity could not be measured owing to lack of sensitivity. However, it was found from Fig. 7 that the hydroxide would be formed at 1700°C or above. Fig. 7 shows a relationship of dissociation energies of alkali hydroxides and formation temperatures of sodium, potassium, and rubidium hydroxides, determined by Jensen and Padley.[16] Only a small amount of lithium hydroxide appeared to formed. This is because the flame temperature was relatively low and alkali elements were not added as fine sprays of dilute aqueous solution.

Distributions of charged particles in the flame by the Langmuir probe method are shown in Figs. 8, 9,

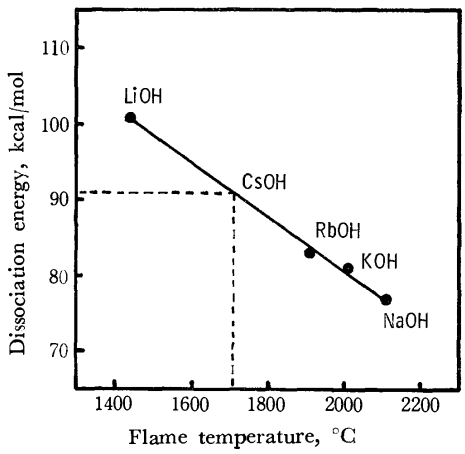

Fig. 7. Plot of dissociation energy against formation temperature of alkali hydroxides.
Temperature for the formation of LiOH was determined.

16) D. E. Jensen and P. J. Padley, *Trans. Faraday Soc.*, **62**, 2132 (1966).

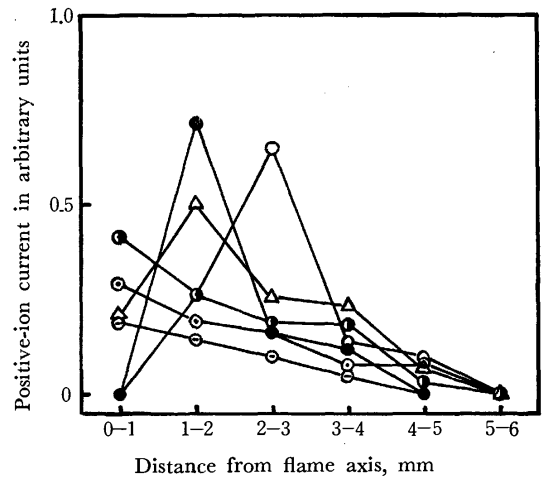

Fig. 8. Horizontal distribution of positive ion in adding sodium chloride in flame.
Distance above jet (mm): ● 1; ○ 3; △ 5; ◑ 7; ⊙ 9; ⊖ 11

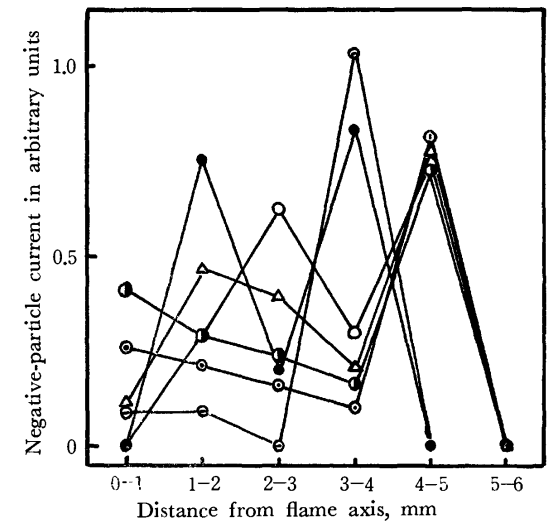

Fig. 9. Horizontal distribution of negative particles in adding sodium chloride in flame.
Distance above jet (mm): as Fig. 8.

and 10. The ordinates of these figures are represented by I_{ps} or I_{ns} in Fig. 2. It seemed reasonable that the positive-ion distributions have maxima in the parts of higher temperature, since alkali metals A are ionized by collisional process with flame gas molecules X, *viz.*,

$$A + X \rightleftarrows A^+ + e + X$$

and the ionization of the alkali metals is near thermal equilibrium. However, the negative-particle distributions also have larger maxima in the outer part of the flame. We see from Fig. 10 that ionization chiefly occurred in the part 0—5 mm above the jet and the negative-particle current was only about twice as large as the positive-ion current.

If negative particles were only free electrons, the negative-particle current should be much larger than the positive-ion current because of the larger mobility of free electrons. In such a small flame, however, it is possible that the higher diffusion rate of electrons allow them to diffuse out of the flame, causing a small

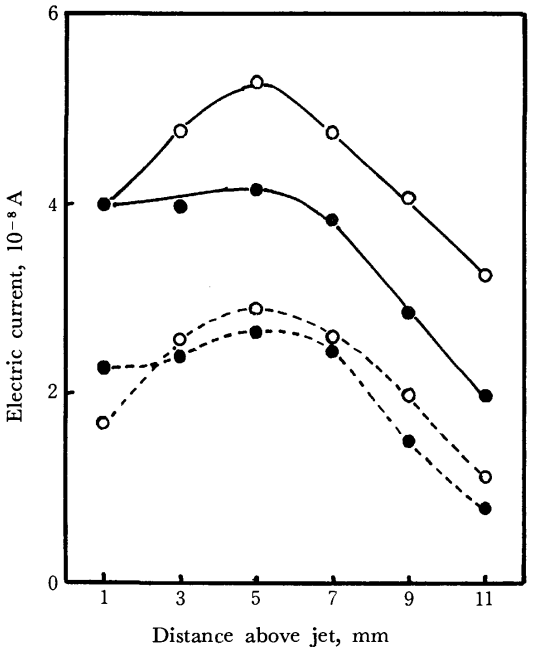

Fig. 10. Vertical distribution of positive ion and negative particles.
●: Sodium; ○: Rubidium
----: Positive ion; ——: Negative particles

negative-particle current. It appears that most negative particles are negative ions of small mobility formed by attachment of free electrons to electronegative gases such as hydroxyl radical, atomic oxygen and chlorine. However, it was not possible to distinguish electrons from negative ions by the probe method. To do this, negative-particle mobility should be measured.

Thus, the positive-ion and negative-particle mobilities were measured by the sheath method when sodium chloride was added to the flame. The plot for negative-particle mobility is shown in Fig. 3. From Eq. (1) and Fig. 3, k_- was calculated to be 9 $cm \cdot sec^{-1}/V \cdot cm^{-1}$, and k_+ to be 0.4 $cm \cdot sec^{-1}/V \cdot cm^{-1}$. If the negative particles were free electrons, the mobility would be of an order of about 10^3. If they were negative ions, it would be the same order as that of the positive-ion mobility. It thus seems reasonable that most of the negative particles were negative ions and a few electrons increased the mean negative-particle mobility. The negative-particle distributions in Figs. 9 and 10 showed maxima in the outer part of ionization zone. It was considered that electrons diffused to the outer surface of the flame, and negative ions were formed by attachment of electrons to the electronegative gases during the course of diffusion.

BULLETIN OF THE CHEMICAL SOCIETY OF JAPAN, VOL. 45, 1097—1100 (1972)

The Synthesis and Properties of *trans*-$[CrCl_2(NH_3)_4]Cl \cdot H_2O$

Kenzo NAGASE and Nobuyuki TANAKA*

Department of Chemistry, Tohoku University, Kawauchi, Sendai

**Department of Chemistry, Faculty of Science, Tohoku University Katahira, Sendai*

(Received October 2, 1971)

A simple method for the synthesis of *trans*-dichlorotetraamminechromium(III) chloride monohydrate was developed, and the configuration of the complex obtained was confirmed by measurements of the infrared and visible absorption spectra. It was found that the *cis-trans* isomerization took place in the solid state upon the thermal treatment of the complex at 200°C. The enthalpy change for the reaction was calculated to be 1.2 kcal·mol^{-1} by an analysis of the DSC curve.

Recently, several reports concerning the syntheses and properties of a *trans* type of tetraamminechromium(III) complex have been presented. Glerup and Schaffer[1] have reported the synthesis of a number of *trans*-diacidotetraamminechromium(III) complexes by the reaction of difluorotetrapyridinechromium(III) iodide with liquid ammonia in an autoclave. Hoppenjans and his co-workers[2] also obtained these complexes by a method based on the acid cleavage of the complex ion, $[(NH_3)_5Cr(OH)Cr(NH_3)_4Cl]^{4+}$. They[3] also investigated the stoichiometry and kinetics of the aquation reaction of *trans*-$[CrCl_2(NH_3)_4]^+$ in an acid solution. Brown *et al.*[4] measured the infrared absorption spectra of *trans*-$[CrCl_2(NH_3)_4]ClO_4$ in the frequency region of 200—600 cm^{-1}.

These syntheses, however, are somewhat complicated, and only a few studies have been made of the properties of these complexes. In the present study, a simple method for the synthesis of *trans*-$[CrCl_2(NH_3)_4]Cl \cdot H_2O$ was developed, and the infrared (400—4000 cm^{-1}) and visible absorption spectra of the complex were measured. Moreover, the thermal reactions of the complex in the solid state were examined.

Experimental

Material. Three complexes, $[Cr(NH_3)_6]Cl_3$,[5] *cis*-$[CrCl(H_2O)(NH_3)_4]Cl_2$[6], and *trans*-$[CoCl_2(NH_3)_4]Cl \cdot H_2O$,[7]

1) J. Glerup and C. E. Schäffer, *Chem. Commun.*, **1968**, 38.
2) D. W. Hoppenjans, J. B. Hunt, and Sr. M. J. Dechant, *ibid.*, **1968**, 514.
3) D. W. Hoppenjans, J. B. Hunt, and C. R. Gregoire, *Inorg. Chem.*, **7**, 2506 (1968).
4) D. H. Brown, D. R. MacSween, and D. W. A. Sharp, *Inorg. Nucl. Chem. Lett.*, **5**, 991 (1969).
5) M. Mori, *Nippon Kagaku Zasshi*, **74**, 253 (1953).
6) M. Mori, *ibid.*, **74**, 255 (1953).
7) S. M. Jφrgensen, *Z. Anorg. Chem.*, **14**, 415 (1897).

were prepared according to the literature, *cis*-$[CrCl_2(NH_3)_4]Cl$ was obtained by heating *cis*-$[CrCl(H_2O)(NH_3)_4]Cl_2$ at 120°C for 3 hr in a vacuum.

Measurements. A Hitachi EPI-2G infrared spectrophotometer was used for the measurement of the infrared absorption spectra. The electronic spectra in solutions were measured by means of a Hitachi EPS-3 spectrophotometer. The diffuse reflectance spectra in the solid state were measured by means of a Hitachi EPS-3 spectrophotometer equipped with a standard integrating sphere attachment. The thermogravimetric(TGA) and differential scanning calorimetric(DCS) curves were obtained with a Rigakudenki 2008 CS thermobalance equipped with a standard differential scanning calorimeter in a dynamic nitrogen atmosphere. A ten-milligram sample in a aluminum crucible was used in each measurement. The furnace-heating rate was about 5°C min^{-1}.

Synthesis of trans-$[CrCl_2(NH_3)_4]Cl \cdot H_2O$. The starting material $[Cr(NH_3)_6]Cl_3$ (5 g) in powder was heated at 230°C in air until the color was converted to green. The product was washed thoroughly with cold water until the washings was colorless. The residue was non-electrolyte, its formula was represented as $[CrCl_3(NH_3)_3]$ on the base of the analytical data.

To the fine powder of $[CrCl_3(NH_3)_3]$ (3 g) in a 100 m*l*-stoppered flask, a 20-m*l* portion of 28% ammonia water was added. The mixture was then maintained at about 25°C for 5 days. *trans*-$[CrCl_2(NH_3)_4]Cl \cdot H_2O$ was formed as green crystals, those crystals were filtered off and washed with a small amount of cold water and then with ethanol, and air dried (yield *ca.* 1.5 g).

The complex thus obtained was purified by recrystallization from water at about 20°C. The crude material was dissolved in a minimum amount of water and filtered off. The green filtrate, in a desiccator with concd. HCl, was kept over night in a refrigerator, the green crystals which thus appeared were filtered off, washed with ethanol, and air dried.

Analysis. Found: Cr, 21.5; H, 5.95; N, 22.81; Cl, 42.9; H_2O, 7.4%. Calcd. for $[CrCl_2(NH_3)_4]Cl \cdot H_2O$: Cr, 21.27; H, 5.77; N, 22.92; Cl, 43.49; H_2O, 7.36%. The water content was determined from the TGA curve.

Results and Discussion

The infrared spectra of the complex and its related complexes are shown in Fig. 1. The M–N stretching band, which provides direct information about the coordination bond, appears in a lower-frequency region. The complex obtained gives the corresponding band at 469 cm^{-1} as a single peak, *trans*-$[CoCl_2(NH_3)_4]Cl \cdot H_2O$ also gives a single peak at 501 cm^{-1}, whereas *cis*-$[CrCl_2(NH)_3]_4Cl$ gives three peaks, at 437, 462, and 475 cm^{-1}.

The electronic spectra of the complex and its analogue are shown in Fig. 2. In the region of the *d-d* transition, the spectrum of the complex has absorption maxima at 17000, 21100, and 25100 cm^{-1}, its pattern very similar to that of *trans*-$[CrCl_2(en)_2]^+$, the spectrum of which has been measured by Carner and Esparza.[8]

The analytical data and the infrared and visible absorption spectra confirm that the complex obtained in this study has a *trans*-configuration and that its

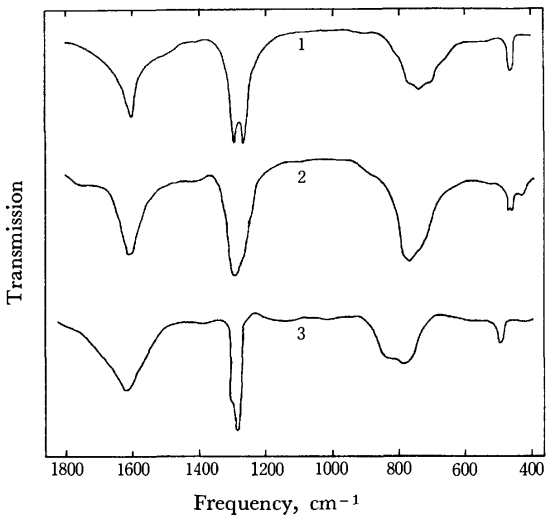

Fig. 1. Infrared spectra of (1) *trans*-$[CrCl_2(NH_3)_4]Cl \cdot H_2O$, (2) *cis*-$[CrCl_2(NH_3)_4]Cl$, and (3) *trans*-$[CoCl_2(NH_3)_4]Cl \cdot H_2O$.

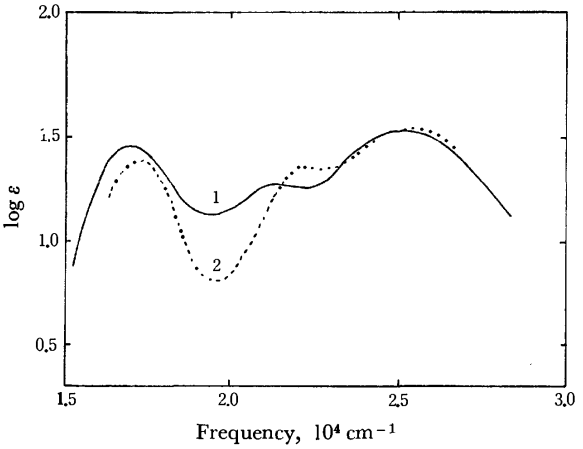

Fig. 2. Visible absorption spectra of (1) *trans*-$[CrCl_2(NH_3)_4]^+$ and (2) *trans*-$[CrCl_2(en)_2]^+$.

formula may be represented as *trans*-$[CrCl_2(NH_3)_4]Cl \cdot H_2O$.

The TGA and DSC curves of *trans*-$[CrCl_2(NH_3)_4]Cl \cdot H_2O$ are shown in Fig. 3. From the TGA curve, it can be seen that the decomposition in the solid state takes place in three steps. The first step, which begins at 65°C and which is completed at 110°C (weight loss, 7.4%), is attributed to the evolution of one mole of hydrated water. The second one, which begins at 210°C and which is completed at 260°C (weight loss, 6.8%), is due to the evolution of one mole of ammonia. The nature of the third step, which begins at 260°C, is not yet clear.

On the DSC curve of *trans*-$[CrCl_2(NH_3)_4]Cl \cdot H_2O$, an endothermic peak for each weight loss was observed, but the peak for the second step splits into two. The shoulder peak may be due to the *cis-trans* isomerization.

In order to confirm the *cis-trans* isomerization, the diffuse reflectance spectra of the samples were measured before and after heating the complex. These spectra are shown in Fig. 4. The spectrum of the dehydrated complex which was obtained by heating

8) C. S. Carner and M. Esparza, *J. Inorg. Nucl. Chem.*, **29**, 2377 (1967).

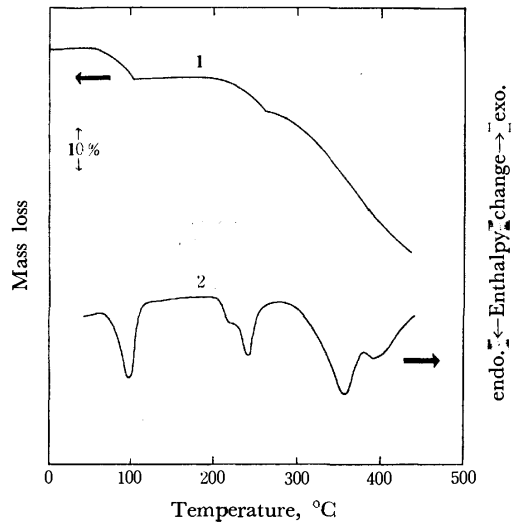

Fig. 3. TGA (1) and DSC (2) curves of *trans*-$[CrCl_2(NH_3)_4]Cl \cdot H_2O$ in a dynamic nitrogen atmosphere.

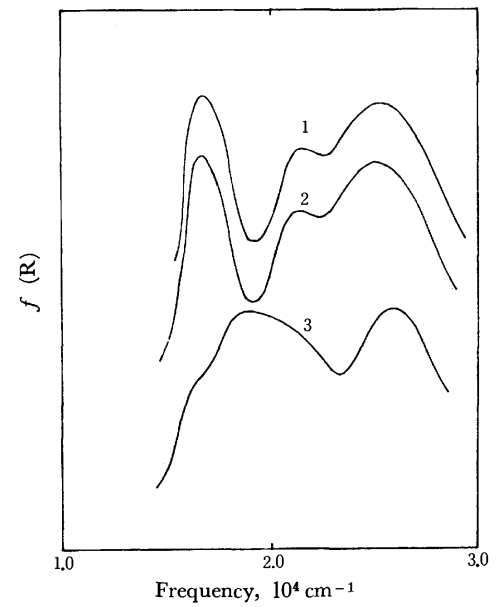

Fig. 4. Reflectance spectra of (1) *trans*-$[CrCl_2(NH_3)_4]Cl \cdot H_2O$, (2) *trans*-$[CrCl_2(NH_3)_4]Cl$, and (3) the sample obtained after heating *trans*-$[CrCl_2(NH_3)_4]Cl$ at 200°C for 24 hr in a sealed capillary tube.

trans-$[CrCl_2(NH_3)_4]Cl \cdot H_2O$ at 110°C for 3 hr in a vacuum is almost identical with that of the hydrated complex, from which it is clear that the *cis-trans* isomerization did not occur in the first step. When the dehydrated complex was heated at 220°C in a sealed capillary tube which was used for the purpose of suppressing the evolution of ammonia, the *cis-trans* isomerization occurred. The spectrum which is given by curve 3 in Fig. 4 suggests that the product was a mixture of the *cis* and *trans* isomers.

The enthalpy change, ΔH, for the isomerization reaction was calculated by means of an analysis of the DSC curve of *trans*-$[CrCl_2(NH_3)_4]Cl$. Since the isomerization was followed by the evolution of ammonia, as may be seen in Fig. 3, the peak area for the isomerization was estimated by drawing a curve which corresponded to the evolution of ammonia. The value of ΔH obtained for the isomerization (*trans*→*cis*) was 1.2 kcal·mol^{-1}. This value seems reasonable in view of the values reported in previous studies[9-11] for other isomerization reactions.

In order to confirm the existence of the reverse reaction, *cis*→*trans*, the *cis* isomer was heated under the same conditions as those employed for the *trans* isomer. The TGA and DSC curves of *cis*-$[CrCl(H_2O)(NH_3)_4]Cl_2$ are given in Fig. 5. From the TGA curves, it can be seen that the decomposition in the temperature

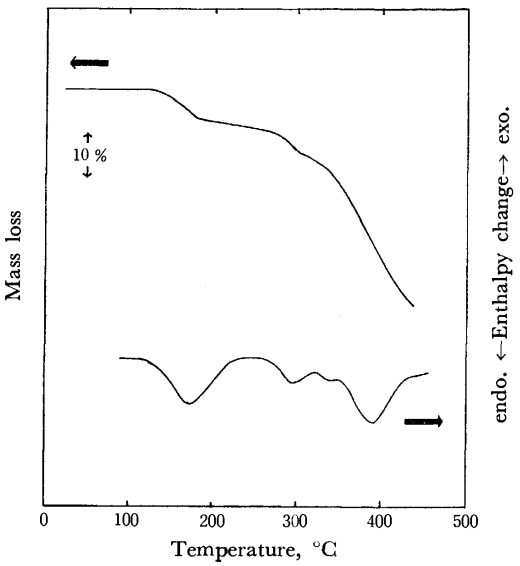

Fig. 5. TGA (1) and DSC (2) curves of *cis*-$[CrCl(H_2O)(NH_3)_4]Cl_2$ in a dynamic nitrogen atmosphere.

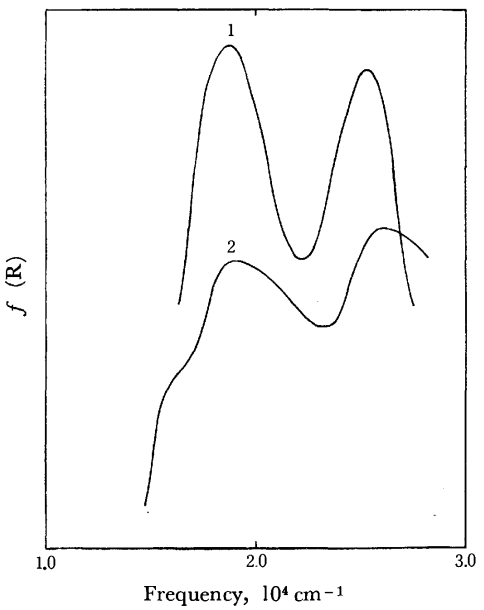

Fig. 6. Reflectance spectra of (1) *cis*-$[CrCl_2(NH_3)_4]Cl$ and (2) the sample obtained after heating *cis*-$[CrCl_2(NH_3)_4]Cl$ at 200°C for 24 hr in a sealed capillary tube.

9) R. Tsuchiya, K. Murai, A. Uehara, and E. Kyuno, This Bulletin, **43**, 1383 (1970).
10) Y. Kaji, A. Uehara, E. Kyuno, and R. Tsuchiya, *ibid.*, **43**, 1906 (1970).
11) R. Tsuchiya, Y. Nakata, and E. Kyuno, *ibid.*, **44**, 705 (1971).

range from 25 to 500°C took place in three steps. In the temperature region from 142 to 200°C, the complex lost coordinated water to form *cis*-$[CrCl_2(NH_3)_4]$-Cl while at temperatures higher than 200°C the evolution of ammonia took place. Since the horizontal mass level was not observed between the evolution of water and the evolution of ammonia, pure *cis*-$[CrCl_2(NH_3)_4]Cl$ could not be obtained by heating *cis*-$[CrCl(H_2O)(NH_3)_4]Cl_2$ under the conditions employed for the measurement of the TGA curve. Therefore, the pure *cis*-$[CrCl_2(NH_3)_4]Cl$ used for the measurement was obtained by heating *cis*-$[CrCl(H_2O)(NH_3)_4]$-Cl at 120°C for 3 hr in a vacuum.

The *cis*-$[CrCl_2(NH_3)_4]Cl$ thus obtained was heated at 200°C for 24 hr in a sealed capillary tube. The reflectance spectrum of the product is given in Fig. 6, along with that of the *cis* isomer. The shoulder peak at 17000 cm^{-1} suggests that the products contained *trans* isomer. In fact, the *trans* isomer was separated from the product by the following procedure.

To the product (1 g) 20 m*l* of water was added, and then the mixture was filtered. The residue on a filter is a mixture of the *cis* isomer and a minute amount of $[CrCl_3(NH_3)_3]$ which was formed by the evolutoin of ammonia. The green filtrate was left over-night in a desiccator with concd. HCl, and then kept standing over night in a refrigerator. The green crystals formed were separated and washed with ethanol. The physical data of the product were identical with those of *trans*-$[CrCl_2(NH_3)_4]Cl \cdot H_2O$.

On the DSC curve, an endothermic peak for each mass loss was observed, but in the case of the *cis* isomer there was no peak corresponding to the *cis-trans* isomerization. From this result, it may be supposed that, when the *cis* isomer is heated in a dynamic nitrogen atmosphere the evolution of ammonia took place at a lower temperature than did the isomerization.

The equilibrium constant for the *cis-trans* isomerization reaction could not be obtained, since the side reaction, *cis*- or *trans*-$[CrCl_2(NH_3)_4]Cl \rightarrow [CrCl_3(NH_3)_3]+NH_3$, took place under the conditions employed in this study.

The authors wish to express their hearty thanks to Masahiro Sakurai for his measurements of the TGA and DSC curves. They also wish to thank the Ministry of Education for the financial support granted this research.

BULLETIN OF THE CHEMICAL SOCIETY OF JAPAN, VOL. 45, 1100—1104 (1972)

Thermochromisms of Some β-Diketone Chelate Copmlexes of Copper(II) in Pure Pyridine[1]

Hiroshi Yokoi, Mitsuru Sai, and Taro Isobe

Chemical Research Institute of Non-aqueous Solutions, Tohoku University, Katahira, Sendai

(Received December 3, 1971)

Two types of thermochromisms have been found for several β-diketone chelate complexes of copper(II) in pure pyridine or γ-picoline. One is observed for such complexes as bis(acetylacetonato)copper(II). In this case, the visible absorption spectra at various temperatures have well-defined isosbestic points; there are two different complex species, L and H, at equilibrium in the solvent, where L and H represent the low-temperature and high-temperature species respectively; they are different in the interaction between the complex and pyridine or γ-picoline molecules. The other is observed for such complexes as bis(salicylaldehydato)copper(II), where the spectral intensity increases remarkably with a rise in the temperature. The equilibrium for bis(acetylacetonato)copper(II) was studied over the temperature range of 0—60°C, and the results were used to derive the approximate thermodynamic parameters, $\Delta H = 4.0 \pm 1.0$ kcal/mol and $\Delta S = 13 \pm 4$ e.u., for the L→H change. The most probable structures for L and H were suggested from a spectrophotometrical point of view.

The thermochromism exhibited by many metal complexes in solution is associated with an equilibrium between the different configurations which the complexes can adopt in the solution at various temperatures.[2-6] It is interesting to us that some kinds of metal complexes change their structural configurations easily according to environmental conditions. Some of the configurations may be chemically labile. Investigations of the thermochromism are, therefore, important in understanding chemical reactions.

The purpose of this paper is to report the new experimental finding that the β-diketone chelate complexes of copper(II) in pure pyridine or γ-picoline exhibit two different types of thermochromisms and

1) Preliminary report: H. Yokoi, M. Sai, and T. Isobe, *Chem. Lett.*, **1972**, 25.

2) D. E. Scaife and K. P. Wood, *Inorg. Chem.*, **6**, 358 (1967); K. Mizutani and K. Sone, *Z. Anorg. Allg. Chem.*, **350**, 216 (1967); R. K. Scarrow and T. R. Griffiths, *Chem. Commun.*, **1967**, 425.

3) K. Sone and M. Kato, *Z. Anorg. Allg. Chem.*, **301**, 277 (1959); C. K. Jφrgensen, *Acta Chem. Scand.*, **11**, 399, 919 (1957); F. Basolo, Y. T. Chen, and R. K. Murmann, *J. Amer. Chem. Soc.*, **76**, 956 (1954).

4) F. A. Cotton and J. P. Fackler, Jr., *ibid.*, **83**, 2820, 3775 (1961).

5) D. M. L. Goodgame and M. A. Hitchiman, *Inorg. Chem.*, **5**, 1303 (1966).

6) M. Nicolini, C. Pecile, and A. Turco, *Coodin. Chem. Rev.*, **1**, 133 (1966); T. Boschi, M. Nicolini, and T. Turco, *ibid.*, **1**, 269 (1966).

to estimate the possible mechanisms for these thermochromisms. This experimental finding indicates that there are different interactions between the complex and pyridine or γ-picoline molecules.

Experimental

Materials. The β-diketone chelate complexes of copper(II) employed here are $Cu(acac)_2$, $Cu(dpm)_2$, $Cu(bzac)_2$, $Cu(sal)_2$, and $Cu(etacest)_2$, where acac, dpm, bzac, sal, and etacest are the anions of acetylacetone, dipivaloylmethane, benzoylacetone, salicylaldehyde, and ethyl acetoacetate respectively. They were prepared and purified by the same general method.[7] All the ligand agents were obtained commercially. G.R.-grade pyridine and γ-picoline were dried over potassium hydroxide and were fractionally distilled.

Spectroscopy. The visible absorption spectra for the complexes in pyridine and γ-picoline were measured over the temperature range of 0—60°C with a Cary model 14 spectrophotometer, using 1-cm quartz cells. Color changes occured reversibly with a change in the temperature for all the sample solutions.

Results and Discussion

The visible absorption spectra at various temperatures for $Cu(acac)_2$ and $Cu(bzac)_2$ in pyridine are shown in Figs. 1 and 2 respectively. The same temperature dependences of the spectra were also observed for $Cu(dpm)_2$ in pyridine and for $Cu(acac)_2$ in γ-picoline. It is characteristic of these three complexes in pyridine and γ-picoline that the visible absorption spectra at various temperatures have well-defined isosbestic points. On the other hand, the spectra of $Cu(sal)_2$ in pyridine at various temperatures are shown in Fig. 3; almost the same temperature dependences of the spectra were observed for $Cu(etacest)_2$ in pyridine and $Cu(sal)_2$ in γ-picoline. It is characteristic of the latter two complexes in pyridine and γ-picoline that the spectral lines observed at various temperatures do not intersect with one another and that only the spectral intensities increase remarkably with a rise in the temperature. The five complexes employed here, accordingly, group themselves in two classes, the former three complexes (Class A) and the latter two complexes (Class B), according to these temperature dependences of the visible absorption. This classification is also consistent with the one based upon the stability of the complexes,[8,9] the composition of the adducts of the complexes with pyridine,[10] and the solvent effect of the positions of the absorption maximum, as are listed in Table 1.

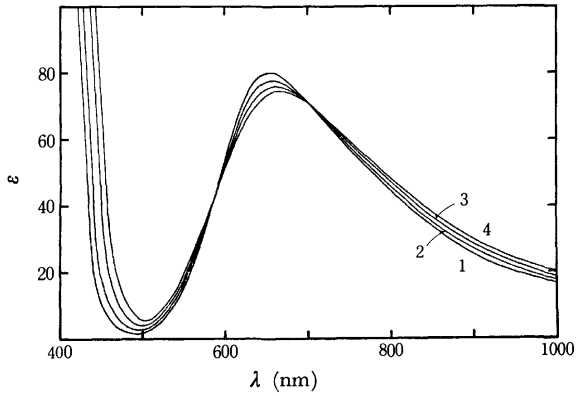

Fig. 1. Visible absorption spectra of $Cu(acac)_2$ in pyridine. (1): 0°C, (2): 20°C, (3): 40°C, (4): 60°C.

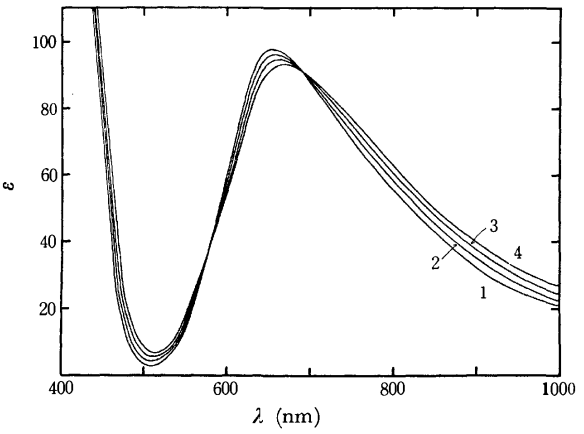

Fig. 2. Visible absorption spectra of $Cu(bzac)_2$ in pyridine. (1): 0°C, (2): 20°C, (3): 40°C, (4): 60°C.

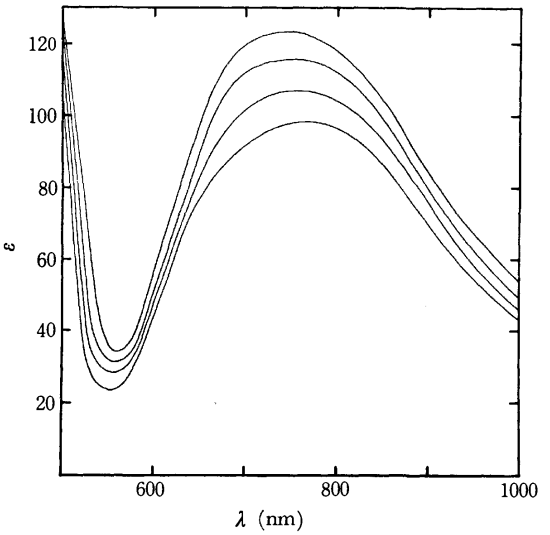

Fig. 3. Visible absorption spectra of $Cu(sal)_2$ in pyridine. (1): 0°C (the lowest line), (2): 20°C, (3): 40°C, (4): 60°C.

Such isosbestic points as are shown in Figs. 1 and 2 indicate that the complexes of Class A are present as two different complex species at equilibrium, even in a pure solvent of pyridine or γ-picoline. The two complex species will hereafter be called the low-temperature species, L, and the high-temperature species,

7) P. Pfeiffer, E. Breith, E. Lubbe, and T. Tsumaki, *Ann.*, **503**, 84 (1933); A. E. Finn, G. G. Hampson, and L. E. Sutton, *J. Chem. Soc.*, **1938**, 1254.

8) L. G. Sillén and A. E. Martell, "Stability Constants of Metal-ion Complexes," (Special Publication No. 7), The Chemical Society, Burlington, London (1964).

9) M. Calvin and K. W. Wilson, *J. Amer. Chem. Soc.*, **67**, 2003 (1945).

10) D. P. Graddon and E. C. Watton, *J. Inorg. Nucl. Chem.*, **21**, 49 (1961); Y. Muto, This Bulletin, **31**, 56 (1958); H. Yokoi, M. Sai, and T. Isobe, *ibid.*, **43**, 1078 (1970).

Table 1. Various properties of the β-diketone chelate complexes of copper(II)

Class	Copper(II) complex	Stability[a]	Adduct with pyridine[c]	Visible absorption spectra: Absorption maximum (at 20°C) Solvent: C-E[d] λ(nm); ε	Visible absorption spectra: Absorption maximum (at 20°C) Solvent: Pyridine λ(nm); ε	Visible absorption spectra: Temperature dependence in pyridine solution λ(nm); ε
A	$Cu(acac)_2$	17.4	$[Cu(acac)_2 \cdot Py]$	654; 44	655; 77	two isosbestic points: 585; 38 / 700; 71
	$Cu(dpm)_2$	ca. 19[b]		658; 44[e]	645; 98	two isosbestic points: 576; 32 / 686; 83
	$Cu(bzac)_2$	18.0	$[Cu(bzac)_2 \cdot Py]$	654; 53	660; 96	two isosbestic points: 562; 33 / 726; 77
B	$Cu(sal)_2$	13.0	$[Cu(sal)_2 \cdot Py_2]$	660; 59	760; 108	Changes in intensity without crossings of spectral lines
	$Cu(etacest)_2$	14.2	$[Cu(etacest)_2 \cdot Py_2]$	650; 40	710; 72	Changes in intensity without crossings of spectral lines

a) Ref. 9. b) an approximately estimated value. c) Ref. 10, Py represents a pyridine molecule. d) an equivolume mixture of chloroform and ethanol. e) A shoulder was observed at about 530 nm.

H.

$$L \rightleftharpoons H \qquad (1)$$

The equilibrium constant, K, for this equilibrium may be obtained from the following equation:

$$K = \frac{[H]}{[L]} = \frac{x}{c^0 - x} = \frac{D - D_L}{D_H - D} \qquad (2)$$

where c^0 represents an initially-given concentration, where D is the measured optical density at any suitable wavelength, and where D_L and D_H are the optical densities at the same wavelength which would be found for the pure L and H species respectively at the concentration of c^0. Unfortunately, neither D_L nor D_H could be determined directly here, but an attempt has been made to estimate them for $Cu(acac)_2$, using the following method.

The measured spectra in the neighborhood of the two isosbestic points are shown in Fig. 4, where the bold line represents the peak position for the measured spectra and the one estimated by extrapolation for the spectra at temperatures besides 0—60°C. Accordingly, if we properly estimate the two temperatures at which the L and H species are present in solution in their pure forms, the spectral peak positions at the temperatures will be determined by the bold line. Since the spectral lines of D_L and D_H pass through the two isosbestic points and the peak positions estimated for them, we can draw smooth curves like the measured spectral lines through the three points; the curves are regarded as assumed spectral lines of D_L and D_H and are shown by dotted lines in Fig. 4. The equilibrium constant at any temperature can then be determined at any suitable wavelength within the range of 585—700 nm by using Eq. (2). The results are listed in Table 2. It is expected, from a consideration of the absorption-line shapes, that the true temperatures at which the L and H species are present in solution in their pure forms do no deviate extremely from the assumed ones listed in Table 2. Although the values of ΔH and and ΔS for the equilibrium were finally determined to be 4.0±1 kcal/mol and 13±4 e.u. respectively, such large errors were introduced for extra safety because of some uncertainty in the values of D_L and D_H.

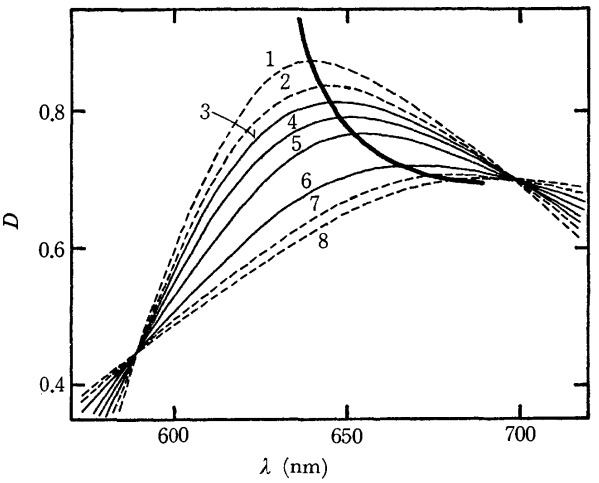

Fig. 4. The measured and estimated spectra in the neighborhood of isosbestic points for $Cu(acac)_2$ in pyridine (——: the measured spectra, ----: the estimated spectra, the bold line shows the spectral peak position).
(1): −60°C, (2): −40°C, (3): 0°C, (4): 20°C, (5): 40°C, (6): 60°C, (7): 110°C, (8): 130°C.

The temperature affects the intensity of an electronic transition induced by a vibrational mode, n, according to $\coth(h\nu_n/2kT)$ in the simplest theory.[11,12] The oscillator strength at t°C will hereafter be expressed as f_t. Assuming that $\nu_n = 150$—$300\ cm^{-1}$, we can calculate the (f_{60}/f_0) ratio to be 1.15—1.19 according to the coth rule mentioned above for the copper(II) complexes in pure forms. The spectral data of the β-diketone chelate complexes of copper(II) in pyridine and γ-picoline are listed in Table 3.

11) A. D. Liehr and C. J. Ballhausen, *Phys. Rev.*, **106**, 1161 (1957); J. H. Van Vleck, *J. Phys. Chem.*, **41**, 67 (1937); R. S. Mulliken and C. A. Rieke, *Repts. Progr. Phys.*, **8**, 231 (1941).
12) J. Ferguson, R. L. Belford, and T. S. Piper, *J. Chem. Phys.*, **37**, 1569 (1962).

Table 2. The equilibrium and thermodynamic constants of L ⇌ H for $Cu(acac)_2$ in pyridine

Assumed temperature[a] (°C)		K				ΔH	ΔS
L	H	0°C	20°C	40°C	60°C	(kcal/mol)	(e.u.)
−40	110	0.71	1.11	2.12	3.12	4.7	16
−60	130	0.98	1.40	2.43	3.33	3.9	12
−60	110	1.05	1.53	2.77	4.00	4.3	13
−40	130	0.66	1.02	1.85	2.63	4.4	13
						av.[b] 4.0±1.0	13±4

a) The assumed temperature at which L or H is present in solution in a pure form.
b) Such large errors were adopted for extra safety.

Table 3. Spectral data of the β-diketone chelate complexes of copper(II) in pyridine and γ-picoline

Copper(II) complex	Solvent[a]	Absorption maximum		Oscillator strength, f[b]		f_{60}/f_0[d]
		0°C λ(nm); ε	60°C λ(nm); ε	0°C (×10³)	60°C (×10³)	
$Cu(acac)_2$	Py	652; 80	667; 75	1.76	1.95	1.10
	γ-Pic	660; 88	675; 81	1.97	2.07	1.05
$Cu(dpm)_2$	Py	660; 98	670; 94	2.20	2.33	1.05
$Cu(bzac)_2$	Py	645; 114	652; 94	2.25	2.44	1.08
$Cu(sal)_2$	Py	*ca.* 750; 98[c]	*ca.* 750; 123[c]	2.72	3.68	1.35
	γ-Pic	*ca.* 740; 107[c]	*ca.* 730; 129[c]	3.01	3.84	1.27
$Cu(etaccst)_2$	Py	730; 67	730; 77	1.63	1.99	1.22

a) Py: pyridine, γ-Pic: γ-picoline. b) Corrected values at 20°C (the observed f value at t°C was multiplied by the ratio of the density of pyridine at 20°C to the density of pyridine at t°C). c) These systems exhibited broad absorption peaks. d) f_t represents the oscillator strength at t°C.

There is a clear difference in the observed ratio (f_{60}/f_0) between the complexes of Class A and Class B, as may be seen in Table 3. The ratios observed for the complexes of Class B are larger than those calculated theoretically according to the coth rule; furthermore, the spectral intensities of the complexes increased remarkably without any crossings of spectral lines with a rise in the temperature, as has been mentioned above. It seems, therefore, probable that a change in structure accompanying a change in spectral intensity takes place continuously according to the temperature for the complexes of Class B in pyridine or γ-picoline.

On the other hand, the observed ratio (f_{60}/f_0) for the complexes of Class A is much smaller than for the complexes of Class B, as may be seen in Table 3. The ratio (f_H/f_L) for $Cu(acac)_2$ in pyridine at any temperature was evaluated to be about 1.1, using the following values: $K_{60°C}=3.3$, $K_{0°C}=1.2$, $f_0=1.76$, $f_{60}=1.95$, and $(f_{60,H}/f_{0,H})=(f_{60,L}/f_{0,L})=1.17$. These results indicate that the spectral intensity of L is almost equal to that of H, and that, therefore, there is almost no difference in the symmetry of the copper-ion environment between L and H.[13] The fact that, for the planar copper(II) complexes, the visible absorption bands shift to longer wavelengths as the axial coordination bondings strengthen, or as the planar coordination bondings weaken, has been confirmed both theoretically and experimentally.[14,15] This gives a basis for the interpretation of the experimental fact that the absorption maximum for H appears at a somewhat longer wavelength than that for L, as is shown in Table 3. It has been reported that the copper atom is penta-coordinated to the four oxygen atoms in the β-diketone and to the nitrogen atom of the pyridine molecule for $Cu(acac)_2$ in pyridine at any temperature.[16,17] Many X-ray diffraction studies have shown that, when the planar metal complexes form some penta-coordinated 1 : 1 adducts,

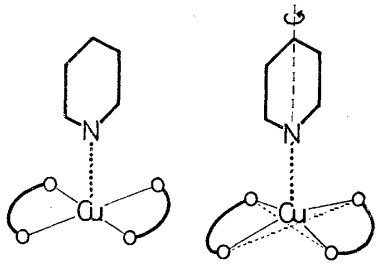

Fig. 5. The estimated structures of L and H for $Cu(acac)_2$ in pyridine.

13) R. L. Belford and W. A. Yeranos, *Mol. Phys.*, **6**, 121 (1963); C. R. Hare, "Spectroscopy and Structure of Metal Chelate Compounds," ed. by K. Nakamoto and P. J. McCarthy, John Wiley & Sons, New York (1968), p. 98.

14) R. L. Belford, M. Calvin, and G. Belford, *J. Chem. Phys.*, **26**, 1165 (1957).

15) D. P. Graddon, *J. Inorg. Nucl. Chem.*, **14**, 161 (1960); H. Yokoi, M. Sai, and T. Isobe, This Bulletin, **42**, 2232 (1969).

16) D. P. Graddon, *Nature*, **183**, 1610 (1959); D. P. Graddon and E. C. Watton, *ibid.*, **187**, 1021 (1960).

17) H. Yokoi, M. Sai, and T. Isobe, to be published.

the metal ion is displaced from the plane in the direction of the fifth coordinating atom.[18] On the basis of all these facts concerning the structures of $Cu(acac)_2$ in pyridine, the most probable structures of L and H were estimated to be those shown in Fig. 5, where both structures are of an approximate C_{2v} symmetry in the copper-ion environment. It may be said that the displacement of the copper atom from the plane of the four oxygen atoms is somewhat larger for H than for L. If we assume that the pyridine molecule in H rotates freely, as is shown by an arrow in Fig. 5, the entropy change can be calculated to be 14.8 e.u. Interestingly, this value is almost equal to the observed entropy change for L→H. The possibility that the pyridine molecule in H may rotate freely can be fully expected, since the difference in structure between L and H seems to be too small to give rise to such a large entropy change because of the environmental difference between them, and since it is considered, from a structural point of view, that the pyridine molecule rotates more easily in H than in L.

18) E. Frasson, R. Zannetti, R. Bardi, S. Bezzi, and G. Giacommetti, *J. Inorg. Nucl. Chem.*, **8**, 452 (1958); P. R. H. Alderman, P. G. Owston, and J. M. Row, *J. Chem. Soc.*, **1962**, 668; S. Ooi and Q. Fernando, *Chem. Commun.*, **1967**, 532.

BULLETIN OF THE CHEMICAL SOCIETY OF JAPAN, VOL. 45, 1104—1110 (1972)

Activation of Iron-Alkyl Bonds in Dialkylbis (dipyridyl) iron(II) by Interaction with Olefins

Takakazu YAMAMOTO, Akio YAMAMOTO, and Sakuji IKEDA

Research Laboratory of Resources Utilization, Tokyo Institute of Technology, Ookayama, Meguro, Tokyo

(Received May 19, 1971)

The reactions of dialkylbis(dipyridyl)iron(II) **1** with various substituted olefins were studied. Tetracyanoethylene, maleic anhydride, and acrylamide gave olefin-coordinated π-complexes on reactions with **1**, whereas other vinyl monomers with relatively large *e*-values were polymerized by the alkyl-iron complex. Kinetic study of the reactions of **1** with olefins by a spectroscopic method revealed that the reaction rate can be expressed by

$$-\frac{d[FeR_2(dipy)_2]}{dt} = \frac{[olefin][FeR_2(dipy)_2]}{A+B[olefin]+C[dipy]}.$$

On the basis of kinetic results and from comparison with the reactions of dialkyl(dipyridyl)nickel with olefins, a mechanism involving partial dissociation of the dipyridyl ligand from **1**, followed by a coordination of the olefin and activation of a Fe-alkyl bond was proposed.

Transition metal-alkyl complexes are generally considered to be the active species in various catalytic reactions involving olefins such as polymerization with Ziegler type catalysts, hydroformylation, hydrogenation, isomerization, and oligomerization[1]. Instability of the transition metal-alkyl bond usually makes isolation of the alkyl complexes difficult, thus hindering a detailed study of the interaction of olefins with the alkyl complexes, a crucial step in catalyses. From Ziegler type catalyst systems we have isolated transition metal-alkyl complexes, the metal alkyl bonds of which are stabilized by the presence of a ligand dipyridyl[2]. These alkyl complexes are very stable and prove to be particularly suitable for studying the mechanism of activation of the metal-carbon bond by coordination of olefins[3),4]. In some cases the reactions of some olefins with the alkyl complexes lead to polymerization[5] while in other cases a scission of the metal-alkyl bonds yielding metal-olefin π-complexes resulted[3]. We previously studied the reactions of dialkyldipyridylnickel with various olefins in detail[3] and found that the essential feature of the reactions of the nickel complex can be expressed by the following scheme.

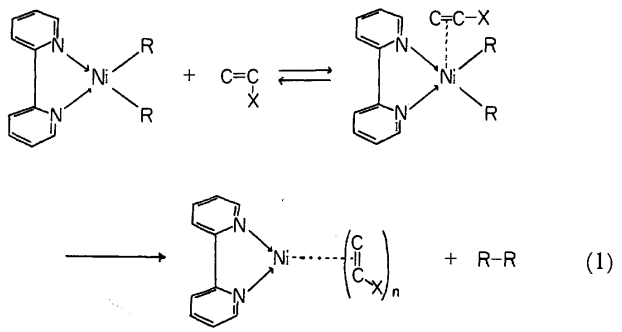

(1)

The rate of the reaction is given by the equation

1) a) M. L. H. Green, "Organometallic Compounds, Vol. 2, The Transition Elements," Methuen and Co. Ltd., London (1968); b) P. Cossee, *J. Catal.*, **3**, 80 (1964).

2) a) A. Yamamoto, K. Morifuji, S. Ikeda, T. Saito, Y. Uchida, and A. Misono, *J. Amer. Chem. Soc.*, **87**, 4652 (1965); b) *ibid.*, **90**, 1878, (1968); c) T. Saito, Y. Uchida, A. Misono, A. Yamamoto, K. Morifuji, and S. Ikeda, *J. Organometal. Chem.*, **6**, 572 (1966); d) *J. Amer. Chem. Soc.*, **88**, 5198 (1966).

3) T. Yamamoto, A. Yamamoto, and S. Ikeda, *J. Amer. Chem. Soc.*, **93**, 3350, 3360 (1971).

4) A general term "olefin" is used throughout this series of papers including a substituted olefin.

5) A. Yamamoto, T. Shimizu, and S. Ikeda, *Makromol. Chem.*, **136**, 297 (1970).

TABLE 1. REACTION OF $FeEt_2(dipy)_2$ WITH OLEFINS

Olefin	*e*-value[7]	Results	Shifts of IR bands
Tetracyanoethlene (TCNE)		Dark brown solid ($Fe(dipy)_2(TCNE)_2$)	$\nu_{C\equiv N}$ 2220 → 2110 cm^{-1}
Maleic anhydride (MAH)	2.25	Red solid ($Fe(dipy)(MAH)_4$)	$\nu_{C=O}$ 1780 → 1780～1730 cm^{-1}
Acrylamide (AcAm)	1.30	Reddish brown solid ($Fe(AcAm)_2$?)	ν_{N-H} 3370 → 3280 cm^{-1} $\nu_{C=O}$ 1670 → 1660 cm^{-1}
Acrylonitrile (AN)	1.20	Polymerization took place.	
Methacrylonitrile (MAN)	0.81	Polymerization took place.	
Acrolein (AC)	0.73	Polymerization took place.	
Methyl vinyl ketone (MVK)	0.69	Polymerization took place.	
Methyl acrylate (MA)	0.60	Polymerization took place.	
Methyl methacrylate (MMA)	0.40	Polymerization took place.	
Vinyl chloride (VCl)	0.20	Dark red solid	
Vinyl acetate (VAc)	−0.22	Reddish purple solid ($Fe(dipy)(Vac)_2$)	$\nu_{C=O}$ 1800～1730 → 1600～1560
2-Vinylpyridine (2-Vi-Py)	−0.50	Polymerization took place.	
Styrene (St)	−0.80	No apparent change was observed.	
Isobutyl vinyl ether (IBVE)	−1.77	No apparent change was observed.	
Ethylene (E)		No apparent change was observed.	

$$r = -\frac{d[NiR_2(dipy)]}{dt} = k_{Ni}[NiR_2(dipy)][olefin] \quad (2)$$

In contrast to the alkyl-nickel complex which does not initiate vinyl polymerization in the absence of oxygen, dialkylbis(dipyridyl)iron(II) (**1**) initiates the polymerization of some vinyl compounds and gives iron-olefin π-complexes. In this paper we report the results of preparative and spectroscopic studies of the reactions of $FeR_2(dipy)_2$ **1** with various olefins. The propagation mechanism in the polymerization of methyl methacrylate was discussed in a previous paper.[6]

Results and Discussion

Alkyl-iron complex **1** is fairly stable in the solid state but decomposes slowly in solution at room temperature. The methyl and ethyl complexes begin to decompose at about 95°C and the propyl complex at about 80°C when heated in the absence of solvent. Pyrolysis of the methyl complex released mainly methane, the ethyl complex ethane (65%) and ethylene (35%) and the propyl complex propane (60%) and propylene (40%). The compositions of the evolved gases differ from those of the pyrolysis products of $NiR_2(dipy)$ which gave ethane from the methyl complex, butane from the ethyl complex and propane and propylene from the propyl complex. The rates of pyrolysis of the solid alkyl-iron complexes[3] are proportional to the amounts of remaining **1**. The activation energy for the pyrolysis of $Fe(CH_3)_2(dipy)_2$ was estimated to be 23 kcal/mol, $Fe(C_2H_5)_2(dipy)_2$ 47—54 kcal/mol and $Fe(n\text{-}C_3H_7)_2(dipy)_2$ 16 kcal/mol. The variation of gaseous decopmosition products and of activation energies of the pyrolysis of the three alkyl-iron complexes suggest that the mechanism of pyrolysis in solid state is not simple.

The results of the reactions of **1** with various olefins are summarized in Table 1. Olefins are arranged in the decreasing order of Alfrey-Price's *e*-value which is considered to reflect the electronegativity of the olefin.[7] Except for the top three olefins, the olefins with large *e*-values were polymerized by **1**. The α,β-disubstituted olefins such as tetracyanoethylene (TCNE) and maleic anhydride (MAH) gave complexes containing a part of the dipyridyl ligands. The ethyl groups were absent in these complexes as proved by IR spectroscopy and methanolysis. Acrylamide has exceptionally high reactivity toward the iron complex and displaces both of the dipyridyl ligands. A similar behavior was observed in other cobalt-dipyridyl[8a] or phosphine complexes[8b]. In the case of vinyl chloride, C–Cl bond was cleaved and a complex of an approximate composition $Fe(dipy)_2Cl_2$ was obtained. With vinyl acetate (VAc) the iron complex gave a reddish purple solid with composition $Fe(dipy)(VAc)_2$ with extraordinarily low $\nu_{C=O}$ bands as compared with those of the free vinyl acetate. The vinyl acetate may be coordinated with iron through both double bond and the carbonyl group as in the case of nickel-vinyl acetate complex[3]. In most cases where olefin-coordinated iron complexes were obtained, purification of the complexes was difficult and the solid complexes appear to be mixtures of $Fe(dipy)_x(olefin)_y$ with different x and y values depending on the relative coordinating abilities of the dipyridyl and the olefin.

With olefins of large negative *e*-values no apparent reaction was observed, although spectral study revealed slow decomposition of **1** in some cases. Among olefins 2-vinylpyridine is exceptional in yielding a high polymer initiated by the alkyl-iron complex. As

6) A. Yamamoto, T. Shimizu, and S. Ikeda, *Polymer Journal* (Japan.), **1**, 171 (1970).

7) J. Brandrup and E. H. Immergut, "Polymer Handbook," II-341, Interscience Publishers, New York, London, Sydney (1966).

8) a) A. Yamamoto, T. Yamamoto, and S. Ikeda, unpublished result; b) A. Yamamoto, Y. Kubo, and S. Ikeda, unpublished result.

in the case of vinyl acetate 2-vinylpyridine may coordinate to iron through both the double dond and the nitrogen of the pyridine ring, thus causing greater enhancement of the reactivity of the alkyl-iron bond.

Kinetics of Decomposition of $FeR_2(dipy)_2$ in Solution. On reactions of $FeR_2(dipy)_2$ with olefins, the deep blue color of the initial solutions turns brown or reddish brown both in polymerization and dealkylation reactions. The color change is considered to reflect the decomposition of the original complex, and the decomposition reaction was followed spectroscopically. As an example of the spectral study, the change of the electronic spectrum of $Fe(C_2H_5)_2(dipy)_2$ in solvents on addition of acrylonitrile is given in Fig. 1. The iron complex **1** decomposes very slowly in tetrahydrofuran even in the absence of olefin (*vide infra*), but the rate of decomposition is strikingly accelerated by the addition of olefins and the decomposition rate in the absence of olefins can be regarded negligible as compared with that in the presence of olefins.

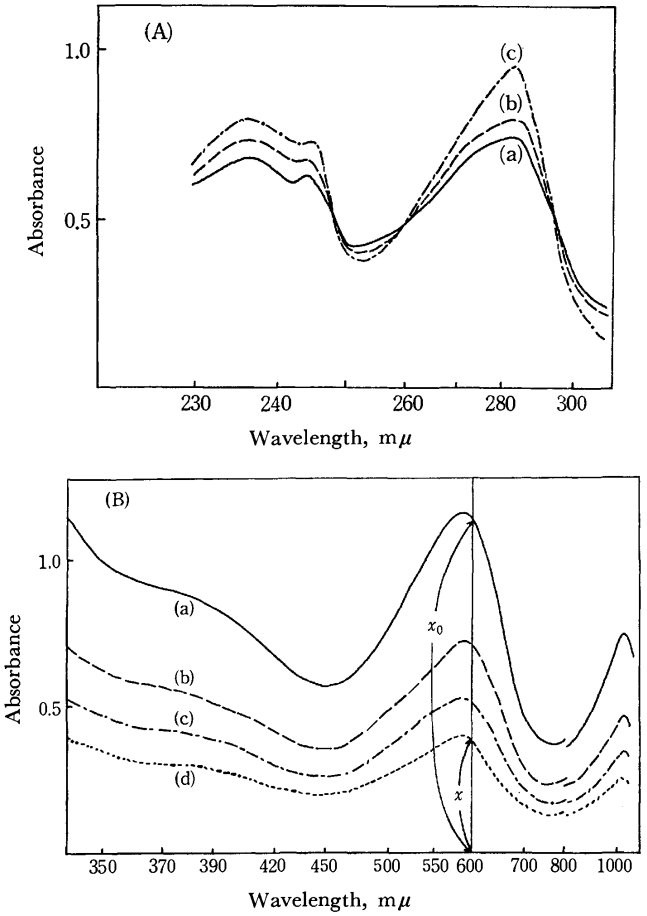

Fig. 1. Change of the ultraviolet (A) and visible spectra (B) of $Fe(C_2H_5)_2(dipy)_2$ by addition of acrylonitrile; (A) in diethyl ether at 24.3°C, [acrylonitrile] $= 1.5 \times 10^{-3}$ M, (a) 0 min, (b) 2.5 min, (c) 18 min,; (B) in tetrahydrofuran at 23.4°C, [acrylonitrile] $= 1.0 \times 10^{-3}$ M, (a) 0 min, (b) 3 min, (c) 6 min, (d) 9 min.

We assigned the two couples of absorption band of $Fe(C_2H_5)_2(dipy)_2$ **1** in UV (237, 282 mμ) and visible rgeions (590, 1010 mμ) to $\pi \rightarrow \pi^*$ excitation bands ($\varepsilon = 2 \times 10^4$) and $d \rightarrow \pi^*$ charge-transfer bands ($\varepsilon = 3 \times 10^3$)[3]. Since the final solution does not absorb

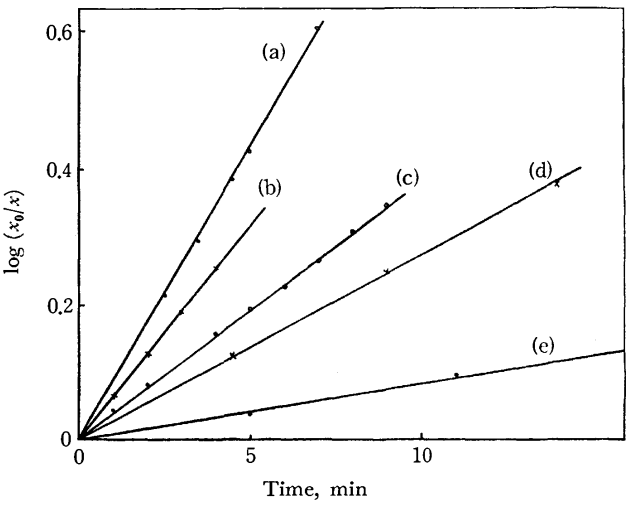

Fig. 2. Plots of log (x_0/x) (*cf.* Fig. 1) against time. (a): methyl acrylate (MA), 0.43 M, 22°C; (b): acrylonitrile (AN), 1.7×10^{-3} M, 22°C; (c): methyl vinyl ketone (MVK), 4.6×10^{-3} M, 23°C; (d): methacrylonitrile (MAN), 5.0×10^{-3} M, 23°C; (e): methyl methacrylate (MMA), 0.21 M. 24°C. solvent = tetrahydrofuran.

at 600 mμ after the reaction, we measured the rate of decomposition of **1** by observing the decrease of the absorbance at 600 mμ. The plots of log (x_0/x) values in Fig. 1 against time give linear relationships for various olefins (Fig. 2). The pseudo-first-order rate constants k were calculated from the slopes of the lines.

Rate of decomposition =

$$-\frac{d[Fe(C_2H_5)_2(dipy)_2]}{dt} = k[Fe(C_2H_5)_2(dipy)_2] \qquad (3)$$

Figure 3 indicates the variation of k with the concentrations of olefins. The k values change with the olefin concentration at low concentrations of olefin but level off at higher concentrations and approach a limiting value independent of the olefins. In the case of isobutyl vinyl ether (IBVE) k does not reach the limiting value even in bulk because of a very weak interaction of isobutyl vinyl ether with the iron com-

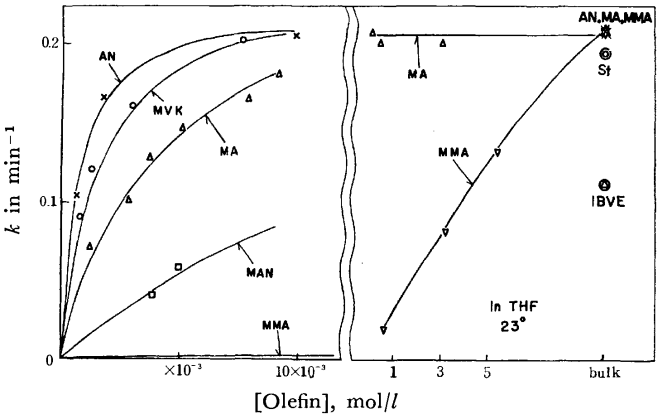

Fig. 3. Pseudo-first-order rate constant k *versus* concentration of olefin at 23°C; solvent = tetrahydrofuran. AN = acrylonitrile, MVK = methyl vinyl ketone, MA = methyl acrylate, MAN = methacrylonitrile, MMA = methyl methacrylate, St = styrene, and IBVE = isobutyl vinyl ether.

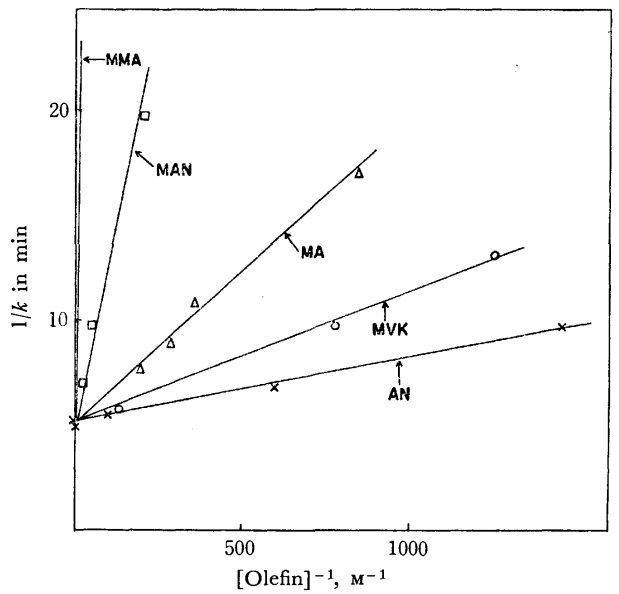

Fig. 4. The reciprocal plot for the data shown in Fig. 3.

plex. The pattern as shown in Fig. 3 suggests an S_N1 mechanism. A similar pattern has been observed in the reaction of methyl manganese pentacarbonyl with nucleophiles.[9] The reciprocal plots of k against olefin concentrations give linear relationships as shown in Fig. 4. The results can be explained by assuming the following three-stage mechanism.

$$\underset{\mathbf{1}}{Fe(C_2H_5)_2(dipy)_2} \underset{k_{-1}}{\overset{k_1}{\rightleftarrows}} \underset{\mathbf{2}}{Fe(C_2H_5)_2(dipy)(dipy)^*} \quad (4)$$

$$\mathbf{2} + \text{olefin} \underset{k_{-2}}{\overset{k_2}{\rightleftarrows}} \underset{\mathbf{3}}{Fe(C_2H_5)_2(olefin)(dipy)(dipy)^*} \quad (5)$$

$$\mathbf{3} \xrightarrow{k_3} \text{decomposition products} \quad (6)$$

Since the initial complex $Fe(C_2H_5)_2(dipy)_2$ is coordinatively saturated and the kinetic results suggest an S_N1 mechanism, it is reasonable to assume a partial dissociation of dipyridyl ligands from **1** to make a coordination site available for the incoming olefin molecule. $Fe(C_2H_5)_2(dipy)(dipy)^*$ represents a partially dissociated species which may have a structure as shown below[10,11].

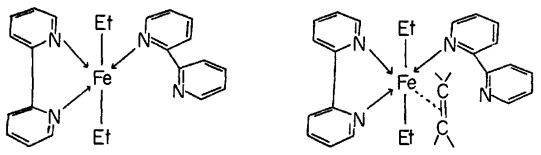

2 **3**

The complex may be either five-coordinated or have a solvent molecule in the sixth coordination position.

For complex **3** we assume an iron complex with an olefin coordinated through the double bond in analogy with that we observed in $Ni(C_2H_5)_2(dipy)(olefin)$.[3] The steady state approximation for the concentrations of **2** and **3** yields the rate equation:

$$\text{Rate} = -\frac{d[Fe(C_2H_5)_2(dipy)_2]}{dt} = k_3[\mathbf{3}]$$

$$= \frac{k_1k_2k_3[\text{olefin}][Fe(C_2H_5)_2(dipy)_2]}{k_{-1}(k_{-2}+k_3)+k_2k_3[\text{olefin}]} \quad (7)$$

The observed pseudo-first-order rate constant k is given by

$$k = \frac{k_1k_2k_3[\text{olefin}]}{k_{-1}(k_{-2}+k_3)+k_2k_3[\text{olefin}]} \quad (8)$$

$$\frac{1}{k} = \frac{1}{k_1} + \frac{k_{-1}(k_{-2}+k_3)}{k_1k_2k_3[\text{olefin}]} \quad (9)$$

The linear relationships between $1/k$ and $1/[\text{olefin}]$ and convergence of plots for different olefins into a single intercept as shown in Fig. 4 are in line with Eq. (9). Intercept $1/k_1$ is a function only of **1** and not of olefin. If we assume the partial dissociation of complex **1** into **2**, the frequency of dissociation can be estimated to be about 0.2/min. If we assume $k_{-2} \gg k_3$, as we observed in the decomposition of the olefin coordinated $Ni(C_2H_5)_2(dipy)$,[3] the reciprocal of the slope becomes $(k_1k_2k_3/k_{-1}k_{-2})$. Since the values k_1 and k_{-1} are functions only of the iron complexes **1** and **2** and not of olefin, the value $k_1k_2k_3/k_{-1}k_{-2}$ is proportional to the relative reactivity of olefin.

Concerning activation of Ni–R bonds by coordination of olefins we observed that electronegative olefins activate the Ni–R bonds more strongly than less electronegative olefins and that the rate constants (k_{Ni}) for decomposition of $NiR_2(dipy)$ are larger in reactions of $NiR_2(dipy)$ with more electronegative olefins. If we assume a similar mechanism of activation for the Fe–Et bond as in Eqs. (5) and (6), we can expect a parallel relation between the k_{Ni} value for the ethyl-nickel complex and the $k_1k_2k_3/k_{-1}k_{-2}$

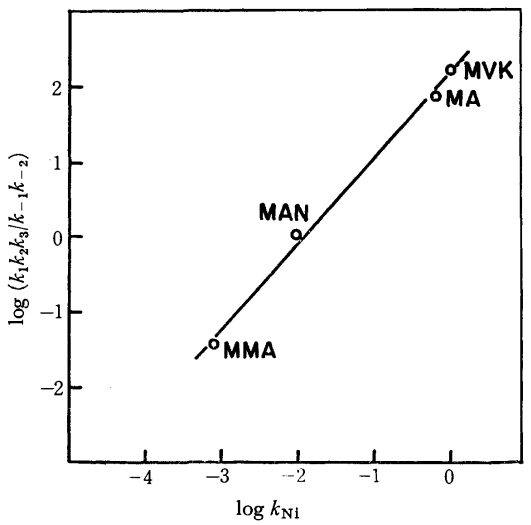

Fig. 5. Plot of log $(k_1k_2k_3/k_{-1}k_{-2})$ obtained from the reciprocal slopes of the lines in Fig. 4 against log k_{Ni} where k_{Ni} is a rate constant for the decomposition of $NiEt_2(dipy)$.[3]

9) B. J. Mawby, F. Basolo, and R. G. Pearson, *J. Amer. Chem. Soc.*, **86**, 3994 (1964).

10) A similar species was assumed in an acid-catalyzed replacement of a dipyridyl ligand from $Fe(dipy)_3^{2+}$, F. Basolo, J. C. Hayes, and H. M. Neuman, *J. Amer. Chem. Soc.*, **75**, 5102 (1953).

11) This is a partial revision of our mechanism[5,6] in which complete dissociation of one dipyridyl ligand was postulated.

value for the ethyl-iron complex. Figure 5 clearly demonstrates that a similar factor operates both in the activation of the nickel–ethyl and iron–ethyl bonds.

1 is stable in the solid state, but slowly decomposes in solution with evolution of ethane and ethylene even in the absence of olefins. The composition of the dark violet decomposition product obtained approximately agreed with the structure $Fe(dipy)_2$.[2b] The ethyl-iron bonds and hydrogen-iron bond, which might be formed through a hydrogen extraction from the ethyl group by iron, were not detected in the decomposition product. The decomposition rate depends on the nature of the solvent as shown in Fig. 6. The decomposition rate was higher in a solvent of greater coordinating ability. Decomposition was not detectable in diethyl ether and *n*-hexane.

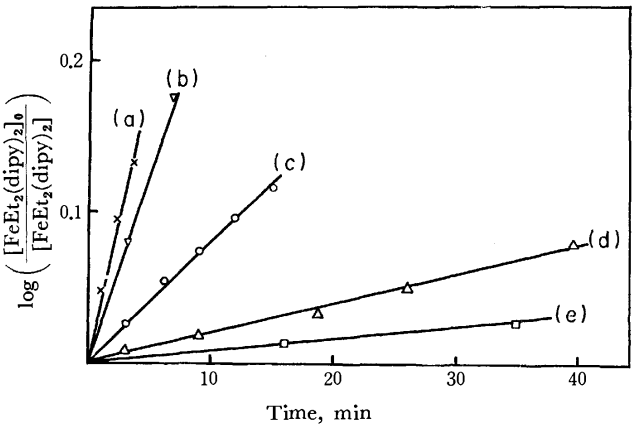

Fig. 6. Decomposition of $Fe(C_2H_5)_2(dipy)_2$ in solvents. (a): acetonitrile, 24.6°C; (b): dimethylformamide (DMF), 24.6°C; (c): Acetone, 23.5°C; (d): DMF, 22.4°C, containing dipyridyl (0.0137 M); (e): tetrahydrofuran, 25.6°C.

We observed a blue shift of the charge-transfer bands of $Ni(C_2H_5)_2(dipy)$ in solvents of strong coordinating ability, and explained this shift as the lowering of the energy of the *d*-orbitals of nickel through the coordination of solvent[3]. We have further postulated that an electron excitation from a σ_{Ni-C} orbital to a vacant *d*-orbital of nickel is a necessary step for the activation of the Ni–C bond. In the case of $Ni(C_2H_5)_2(dipy)$, however, the lowering of the *d*-level by coordination of the solvent was not sufficient to induce scission of the very stable Ni–C bond, whereas olefins with electronegative substituents caused the scission. If we assume that a similar factor operates in determining the activation of the iron-carbon as in nickel-carbon bond and take a smaller activation energy for the pyrolysis of $Fe(C_2H_5)_2(dipy)_2$ (about 50 kcal/mol) compared with the one for the corresponding ethyl-nickel complex (68 kcal/mol) into account, the easier scission of the Fe–Et bond in strongly coordinating solvents can be explained by the lowering of the energy of the vacant *d*-orbital of the iron complex. The decomposition rates of **1** in solvents are proportional to the concentration of **1** (Fig. 6). The decreasing order of the first-order rate constants was in line with that of the magnitude of the blue shifts of

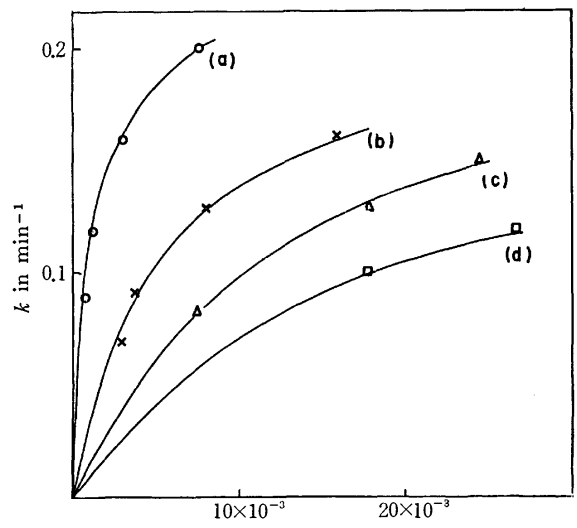

Fig. 7. Effect of the concentration of dipyridyl added on the pseudo-first-order rate constant k for the decomposition of $FeEt_2(dipy)_2$ in tetrahydrofuran at 23°C. (a): [dipy]= 0 mol/*l*, (b): 1.4×10^{-3} mol/*l*, (c): 2.31×10^{-3} mol/*l*, (d): 3.88×10^{-3} mol/*l*.

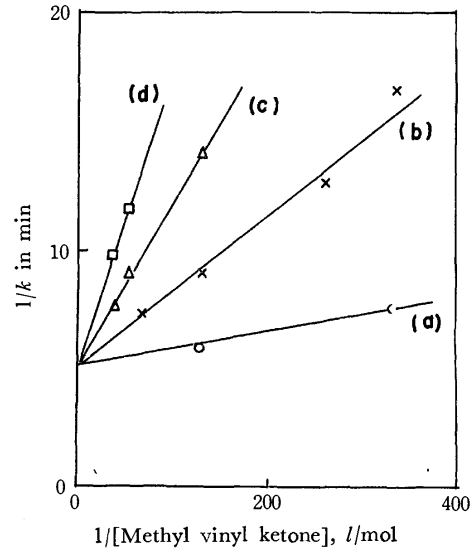

Fig. 8. The reciprocal plot for the data shown in Fig. 7.

$Ni(C_2H_5)_2(dipy)$ caused by coordination of solvents: acetonitrile>dimethylformamide>acetone>tetrahydrofuran>ether, *n*-hexane.

Addition of dipyridyl to the reaction systems hinders the decomposition of $Fe(C_2H_5)_2(dipy)_2$ in the absence of olefin (Fig. 6, curve (d)) as well as in the presence of olefins (Fig. 7). The decomposition rates are still proportional to concentrations of $Fe(C_2H_5)_2(dipy)_2$. Figure 8 shows $1/k$ *versus* 1/[olefin] plots for the data shown in Fig. 7. Since the intercept is common to all lines in Fig. 8, the effect of dipyridyl can be explained in terms of a competitive coordination of dipyridyl with olefin and solvent to **2** to form a complex **4** which may be in equilibrium with **2**. Complex **4** may be converted directly into **1** through the process given below:

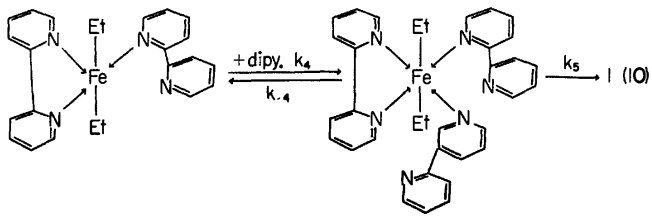

2 4

Using the steady-state approximation for concentrations of the intermediate complexes **2**, **3** and **4**, we get the rate equation:

$$\text{Rate} = -\frac{d[FeEt_2(dipy)_2]}{dt} = k_3[\mathbf{3}]$$

$$= \frac{k_1k_2k_3[\text{olefin}][FeEt_2(dipy)_2]}{k_{-1}(k_{-2}+k_3)+k_2k_3[\text{olefin}]+\dfrac{k_4k_5(k_{-2}+k_3)[\text{dipy}]}{k_{-4}+k_5}} \quad (11)$$

When k_{-2} is much greater than k_3, the observed pseudo-first-order rate constant k is given by:

$$k = \frac{k_1k_2k_3[\text{olefin}]}{k_{-1}k_{-2}+k_2k_3[\text{olefin}]+\bar{k}[\text{dipy}]} \quad (12)$$

where $\bar{k}=k_{-2}k_4k_5/(k_{-4}+k_5)$. The plots of $1/k$ against $1/[\text{olefin}]$ with varying concentrations of dipyridyl added (Fig. 8) substantiate the validity of Eq. (12). The intercept of the lines is $1/k_1$ and the slopes are $(k_{-1}k_2+\bar{k}[\text{dipy}])/k_1k_2k_3$. The effect of variation of the added dipyridyl concentration on the slopes in Fig. 8 is shown in Fig. 9. The linear relationship confirms Eq. (12).

The intercepts of the lines in Fig. 9 represent $k_{-1}k_{-2}/k_1k_2k_3$ values in the absence of added dipyridyl and the slopes $\bar{k}/k_1k_2k_3$. The results are in line with the postulated mechanism expressed by Eqs. (4), (5), (6), and (10), where spontaneous partial dissociation of dipyridyl forming **2** and the succeeding competitive coordination of olefin, solvent, and dipyridyl to **2** are assumed.

When a very polar solvent was employed in place of tetrahydrofuran and extra dipyridyl was not added to the solution, $Fe(C_2H_5)_2(dipy)_2$ decomposed at an appreciable rate even in the absence of olefin. Accordingly we could not obtain the *k versus* [olefin] relationship as shown in Fig. 3 in the polar solvent with no dipyridyl in the solution. When extra dipyridyl was added to the solution, the decomposition of $Fe(C_2H_5)_2(dipy)_2$ caused by the interaction of the polar solvent was hindered and the normal *k versus* [olefin] pattern was obtained.

With $Fe(CH_3)_2(dipy)_2$ and $Fe(n\text{-}C_3H_7)_2(dipy)_2$, similar kinetic patterns as in Fig. 3 have been obtained. The liniting k_1 values with the series of $FeR_2(dipy)_2$ were 0.27 min^{-1} for the propyl, 0.21 for the ethyl, and 0.013 for the methyl complexes. We previously found a linear relation between the inductive effect of the alkyl groups and the highest occupied energy level of $NiR_2(dipy)_2$, and discussed the influence of the alkyl groups on the reactivity of the complexes.[3] We see a similar linear relation between the rate constant k_1 and σ^* value proposed by Taft[12] in Fig. 10. The decrease in the partial dissociation rate of one dipyridyl ligand influenced by the decrease of the inductive effects of the alkyl groups is understandable if the decreasing stability of amine complexes with decreasing electronegativity of a transition metal[13] is taken into account.

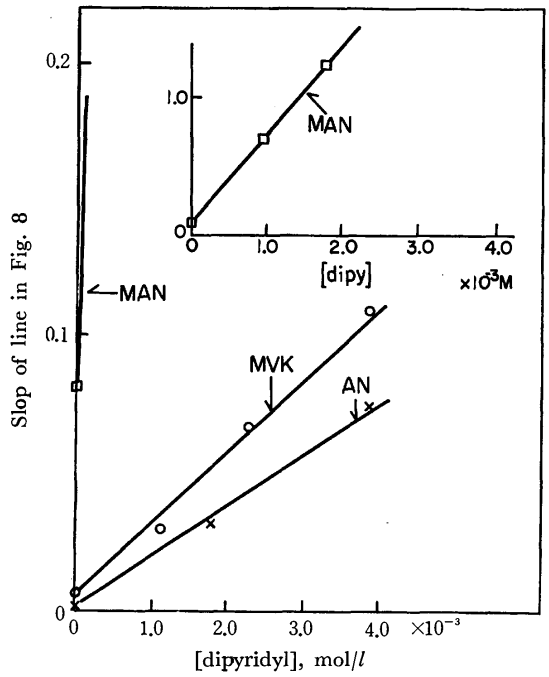

Fig. 9. Plot of the slopes of lines in Fig. 8 against the dipyridyl concentration, (○) for methyl vinyl ketone; analogous plots for methacrylonitrile (□) and acrylonitrile (×).

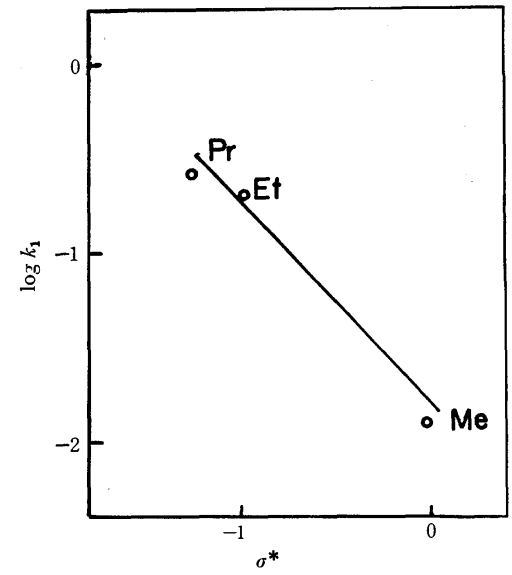

Fig. 10. Relation between the rate constant k_1 and σ^*.

12) R. W. Taft, Jr., *J. Amer. Chem. Soc.*, **75**, 4231 (1953).

13) a) D. P. Graddon, "An Introduction to Co-ordination Chemistry," Pergamon Press Ltd. Oxford, London, (1961); b) F. Basolo and R. G. Pearson, "Mechanism of Inorganic Reaction, Second Edition," John Wiley and Sons, Inc., New York, London, Sydney (1968).

Experimental

I. Materials and General Procedures. $Fe(C_2H_5)_2(dipy)_2$ was prepared by the method reported previously.[2] $Fe(CH_3)_2(dipy)_2$ and $Fe(C_3H_7)_2(dipy)_2$ were prepared in an analogous way. Found: C, 65.8; H, 5.73; N, 13.8%. Calcd for $C_{22}H_{22}N_4Fe$: C, 66.3; H, 5.57; N, 14.1%. Found: C, 67.8; H, 6.65; N, 12.2%. Calcd for $C_{26}H_{30}N_4Fe$: C, 68.8; H, 6.61; N, 12.3%. Olefins and solvents were purified and stored, and general procedures and techniques were almost the same as previously reported.[3] Because of the lack of suitable procedures for purification, some complexes can not be claimed very pure. However, structures which are consistent with the analytical data are given.

II. Reactions of $Fe(C_2H_5)_2(dipy)_2$ with Olefin and Isolations of Olefin-Coordinated Iron Complexes. *1. Tetracyanoethylene (TCNE)*: Ether (10 m*l*) was distilled in a vacuum into a reaction vessel containing 1.58 g of $Fe(C_2H_5)_2(dipy)_2$ (3.7 mmol) and 1.52 g of tetracyanoethylene (12 mmol). The mixture was allowed to react at room temperature for a day. The composition of the gas evolved was ethane, ethylene, and butane in a molar ratio of 1 : 1 : 0.1. The dark brown precipitate was filtered, washed many times with ether, and dired in a vacuum. The dark brown solid was insoluble in almost all organic solvents. The yield of the solid was almost quantitative. Found: C, 59.3; H, 2.16; N, 25.4%. Calcd for $Fe(dipy)_2(TCNE)_2$: C, 61.4; H, 2.56; N, 26.9%.

2. Maleic anhydride (MAH): A mixture of 0.60 g (1.4 mmol) of $Fe(C_2H_5)_2(dipy)_2$ and 4.2 g (43 mmol) of maleic anhydride in 10 m*l* of ether was allowed to react at room temperature for 20 hr. The gas evolved consisted of ethane, ethylene, and butane in a molar ratio of 0.1 : 1 : 1. The red solid was filtered, washed many times with ether and dried in a vacuum. The yield was almost quantitative. Found: C, 51.1; H, 2.52; N, 3.97%. Calcd for $Fe(dipy)(MAH)_4$: C, 51.5; H, 2.64; N, 4.61%.

3. Acrylamide (AcAm): A mixture of 0.38 g (0.89 mmol) of $Fe(C_2H_5)_2(dipy)_2$ and 2.0 g (28 mmol) of acrylamide in 40 m*l* of ether was allowed to react at room temperature for a day. The deep blue color of $Fe(C_2H_5)_2(dipy)_2$ turned reddish brown in 2 or 3 hr. The gas evolved consisted of ethane and ethylene in a molar ratio of 1 : 1. The reddish brown precipitate was filtered, washed, and dried under vacuum. The IR spectrum of the complex gave no peak characteristic of dipyridyl complexes. Found: C, 37.0; H, 4.12; N, 12.8%. Calcd for $Fe(AcAm)_2$: C, 36.4; H, 5.05; N, 14.1%.

4. Polymerization of Acrylonitrile (AN), Methacrylonitrile (MAN), Acrolein (AC), Methyl Vinyl Ketone (MVK), Methyl Acrylate (MA), Methyl Methacrylate (MMA), and 2-Vinylpridine (2-Vi-Py): These olefins were polymerized with $Fe(C_2H_5)_2(dipy)_2$. Temperatures when polymerization started were $-30°C$ for acrylonitrile, $-20°C$ to $-10°C$ for methacrylonitrile, acrolein, 2-vinylpyridine and methyl vinyl ketone, 20°C for methyl acrylate and methyl methacrylate. The compositions of the gases evolved were ethane and ethylene in ratios of 1 : 1~2.5.

5. Vinyl Chloride (VCl): Dry vinyl chloride was introduced into tetrahydrofuran solution (30 m*l*) containing 0.50 g (1.2 mmol) of $Fe(C_2H_5)_2(dipy)_2$. The deep blue color of $Fe(C_2H_5)_2(dipy)_2$ turned dark red in a day at room temperature. The dark red precipitate was filtered, washed with benzene, and dried in a vacuum. Found: C, 50.5; H, 3.63; N, 10.9; Cl, 21.7%. Calcd for $Fe(dipy)_2Cl_2$: C, 55.5; H, 3.66; N, 12.8; Cl, 16.7%. Calcd for $Fe(dipy)Cl_3$: C, 37.4; H, 2.49; N, 8.72; Cl,33.2%. As judged from analytical data, the solid is considered to be a mixture of $Fe(dipy)_2Cl_2$ and $Fe(dipy)Cl_3$ in a molar ratio of about 3 : 1.

6. Vinyl acetate (VAc): Vinyl acetate (5.5 m*l*, 59 mmol) was distilled *in vacuo* into a flask containing 0.91 g (2.1 mmol) of $Fe(C_2H_5)_2(dipy)_2$. The mixture was allowed to react for 3 days at room temperature. The reddish purple solid was filtered and recrystallized from acetone. The gas evolved consisted of ethane and ethylene in a molar ratio of 1 : 3. Found: C, 58.5; H, 5.04; N, 8.23%. Calcd for $Fe(dipy)(VAc)_2$: C, 56.2; H, 5.21; N, 7.31%.

7. Styrene (St), Isobutyl vinyl ether (IBVE), and Ethylene (E): No apparent change took place. Polymer was not obtained when $Fe(C_2H_5)_2(dipy)_2$ was treated with St, IBVE, or E for a few days at room temperature.

III. Spectral Measurements. The infrared spectra were obtained with a Shimadzu model IR 27C or Hitachi Model EPI-G3. Visible and ultraviolet spectra were recorded on a Shimadzu SV-50A spectrometer. When necessary, the temperature was controlled within 0.5°C by circulating water of a constant temperature around the cuvette.

IV. Analysis. The microanalysis of carbon, hydrogen, and nitrogen was performed by Mr. T. Saito of our laboratory with a Yanagimoto CHN Autocorder Type MT-2. Considerable difficulties were encountered in the microanalysis of unstable complexes.

The Mechanism of Vinyl Polymerization by Dialkylbis(dipyridyl)iron(II)

Takakazu YAMAMOTO, Akio YAMAMOTO, and Sakuji IKEDA

Research Laboratory of Resources Utilization, Tokyo Institute of Technology, Ookayama, Meguro, Tokyo

(Received May 19, 1971)

Kinetics of polymerization of vinyl compounds (acrylonitrile, methacrylonitrile, acrolein, methyl vinyl ketone, methyl acrylate, alkyl methacrylates, and 2-vinylpyridine) with dialkylbis(dipyridyl)iron(II), $FeR_2(dipy)_2$ **1** (R= CH_3, C_2H_5, n-C_3H_7), was studied. By comparison with previous kinetic results in which the decomposition of **1** was followed spectroscopically, a polymerization mechanism including a slow initiation process followed by rapid propagation and unimolecular termination processes was proposed. The effects of the concentration of monomer, the addition of dipyridyl and the coordinating ability of solvent on the molecular weight of the polymer were explained by competitive coordination to the iron complex having a growing polymer chain. Results of copolymerization experiments were explained in terms of competitive coordination and insertion reactions between the monomers involved. A linear relationship was found between $\log(1/r_1)$ values and the logarithms of stability constants of nickel–olefin π-complexes with methacrylonitrile as the reference (M_1). From the formation of C_2H_5D in the polymerization of β-*cis*-d_1-methyl methacrylate with $Fe(C_2H_5)_2(dipy)_2$ a unimolecular termination process involving abstraction of β-hydrogens of the growing chain by the alkyl group or the iron complex was proposed.

Although great efforts have been made to unravel the mechanism of coordination polymerization by Ziegler type catalysts, the inherent complexity and instability of the mixed catalyst systems prepared *in situ* have hindered the drawing of a clear-cut conclusion on the kinetic results.[1]. Recently kinetic studies have been carried out successfully on the polymerization mechanisms of vinyl monomers[2] and butadiene[3] using isolated π-allyl-transition metal complexes. We have been studying the properties of isolated alkyl-nickel, cobalt, and iron complexes[4] which are thermally stable and appropriate for studies[5] on catalytic reactions of unsaturated conpounds. Our attention was focused on the activation mechanism of alkyl-iron bonds by interaction of dialkylbis(dipyridyl)-iron(II) with various olefins.[6] In this paper we deal mostly with the propagation and termination mechanisms. Vinyl polymerization by alkyl-iron and cobalt complexes has been communicated briefly.[7] NMR studies on the propagation mechanism have also been reported.[8]

Results and Discussion

Kinetics of Polymerization. The results of polymerization of various monomers with $FeR_2(dipy)_2$ are summarized in Table 1 where R=CH_3, C_2H_5, and n-C_3H_7. The monomers are arranged in decreasing order of Afrey-Price "*e*-value"[9]. The Table indicates a general trend, except for 2-vinylpyridine[6], for monomers with higher *e*-values to polymerize readily, monomers with medium *e*-values to polymerize slowly, and the polymerization of monomers with low or negative *e*-values to proceed either slowly or not take place. These monomers are not polymerized with dipyridyl alone; dipyridyl-iron complexes without R–Fe bonds such as $Fe(dipy)_2$[4], $Fe(dipy)_3$[4] and $Fe(dipy)(vinyl\ acetate)_2$[6] do not initiate polymerization. Methacrylic esters present an interesting intermediate case. Methyl methacrylate (*e*-value= 0.40) can be polymerized by $FeR_2(dipy)_2$ (R=CH_3, C_2H_5, C_3H_7), whereas less electronegative ethyl methacrylate (*e*-value=0.17) can be polymerized by $Fe(n\text{-}C_3H_7)_2(dipy)_2$ but not by the methyl and ethyl homologs (a negligible amount of polymer was obtained with $Fe(CH_3)_2(dipy)_2$). The results clearly indicate the important role of the alkyl-iron bond in the initiation process. In accordance with observation on the activation of alkyl-nickel bonds by interaction with olefins[5], the propyl-iron bond seems to be more easily activated than methyl- and ethyl-iron bonds. Once the polymerization is initiated by activation of the alkyl-iron bond through interaction with a monomer having a more electronegative substituent, a monomer with a less electronegative substituent can be taken into the copolymer; thus, ethyl methacrylate and methacrylonitrile were copolymerized with $Fe(C_2H_5)_2(dipy)_2$, but not ethyl methacrylate.

Figure 1 shows a typical time-conversion curve of the polymerization of acrylonitrile with $Fe(C_2H_5)_2$-$(dipy)_2$ and the dependence of molecular weight of the polymer on conversion. The polymerization was carried out in the presence of extra dipyridyl added in order to control the polymerization rate. Since the polymerization yield is low, the concentration of acrylo-

1) L. Reich and A. Schindler, "Polymerization by Organometallic Compounds," Interscience Publishers, New York (1966).
2) D. G. Ballard, W. H. Jones, and T. Medinger, *J. Chem. Soc., B*, **1968**, 1168, 1176.
3) J. H. Harrod and L. R. Wallace, *Macromolecules*, **2**, 449 (1969).
4) a) A. Yamamoto, K. Morifuji, S. Ikeda, T. Saito, Y. Uchida, and A. Misono, *J. Amer. Chem. Soc.*, **87**, 4652 (1965); b) *ibid.*, **90**, 1878 (1968); c) T. Saito, Y. Uchida, A. Misono, A. Yamamoto, K. Morifuji, and S. Ikeda, *J. Organometal. Chem.*, **6**, 572 (1966); *J. Amer. Chem. Soc.*, **88**, 5198 (1966).
5) T. Yamamoto, A. Yamamoto, and S. Ikeda, *J. Amer. Chem. Soc.*, **93**, 3350, 3360 (1971).
6) T. Yamamoto, A. Yamamoto, and S. Ikeda, This Bulletin, **45**, 1104 (1972).
7) A. Yamamoto, T. Shimizu, and S. Ikeda, *Makromol. Chem.*, **136**, 297 (1970).
8) A. Yamamoto, T. Shimizu, and S. Ikeda, *Polymer J.* (Japan), **1**, 171 (1970).
9) J. Brandrup and E. H. Immergut, "Polymer Handbook," II-341, Interscience Publishers, New York, London, Sydney (1966).

TABLE 1. POLYMERIZATION OF VINYL MONOMERS BY $FeR_2(dipy)_2$

$FeR_2(dipy)_2$ (g)	Monomer (ml)		Temp. (°C)	Time	Yield (%)	Mol. wt. $\times 10^{-4}$
R=C_2H_5, 0.050	Acrylonitrile	5.0	30	9 min	30	1.05
C_2H_5, 0.020	Methacrylonitrile	10.0	room temp.	3 days	53	12.7
C_2H_5, 1.04	Acrolein	6.0	−30	2 days	70	
C_2H_5, 1.37	Methyl vinyl ketone	5.0	−20	10 days	77	
C_2H_5, 0.24	Methyl acrylate	6.0	room temp.	18 hr	64	
CH_3, 0.040	Methyl methacrylate	10.0	25	6 days	16	
C_2H_5, 0.13	Methyl methacrylate	10.0	31	3 days	5.6	12.6
n-C_3H_7, 0.38	Methyl methacrylate	8.0	30	2 days	33	
CH_3, 0.35	Ethyl methacrylate	10.0	room temp.	2 days	trace	
C_2H_5, 0.23	Ethyl methacrylate	10.0	room temp.	7 days	0	
n-C_3H_7, 0.20	Ethyl methacrylate	5.0	room temp.	9 days	3.6	
C_2H_5, 0.91	Vinyl acetate	5.5	room temp.	3 days	0	
n-C_3H_7, 0.50	Vinyl acetate	6.0	room temp.	17 days	0	
C_2H_5, 0.30	2-Vinylpyridine	4.0	20	3 days	45	
C_2H_5, 0.44	Styrene	5.0	room temp.	7 days	0	
n-C_3H_7, 0.43	Styrene	5.0	room temp.	15 days	0	
C_2H_5, 0.62	Isobutyl vinyl ether	5.0	50	20 hr	0	

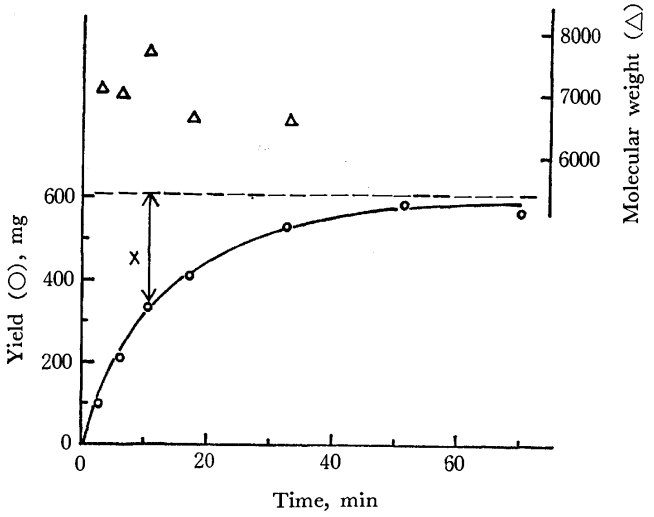

Fig. 1. Polymerization of acrylonitrile with $Fe(C_2H_5)_2(dipy)_2$ at 27.5°C; yield (○) *versus* time and molecular weight (△) of the polymer *versus* time. Acrylonitrile= 12.6 m*l*; dimethylformamide = 51 m*l*; $Fe(C_2H_5)_2(dipy)_2$= 0.19 g; dipyridyl = 1.24 g.

nitrile can be regarded to be constant during the polymerization. Figure 1 indicates that the molecular weight of the polymer is virtually independent of time. As our spectroscopic study revealed[6], the concentration of $Fe(C_2H_5)_2(dipy)_2$ decreases with time in the presence of an olefin. The decrease of the concentration of the ethyl-iron complex should be responsible for the decrease of the polymerization rate. In fact the polymerization stops when the deep blue color of $Fe(C_2H_5)_2(dipy)_2$ disappears. Since the molecular weights of the polymers obtained at different conversions remain virtually constant, the yield of the polymer can be regarded as proportional to the number of polymer chains. The number of polymer chains produced from a single ethyl-iron complex (initiator efficiency) is shown in Table 2. The initiator efficiency increases with the increase of the monomer concentration approaching unity. The polymer yield is thus considered to be proportional to the ethyl-iron complex decomposed at a certain monomer concentration. If we plot the logarithms of the value x (Fig. 1) *versus* time a linear relationship is observed (Fig. 2) indicating the validity of the following equation.

$$-\frac{dx}{dt} = \bar{k}x \qquad (1)$$

The value x can be regarded to correspond to the remaining concentration of the ethyl-iron complex. The change of the slope $\bar{k}$ (Fig. 2) against the acrylonitrile concentration is plotted in Fig. 3. The value $\bar{k}$ increases with the increase of the acrylonitrile concentration approaching a limiting value of 0.2 min^{-1} in the presence of a small amount of dipyridyl added. Addition of a large amount of dipyridyl suppresses

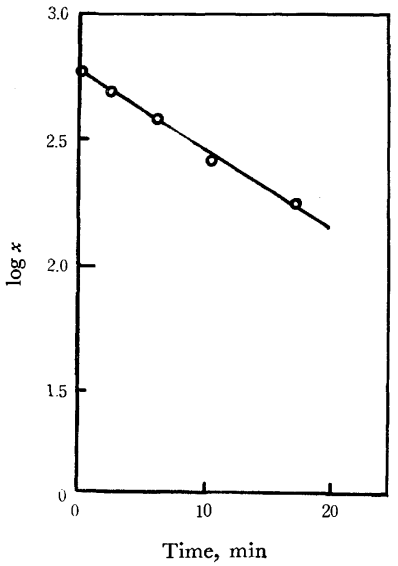

Fig. 2. The plot of logarithm of x (Fig. 1) versus time.

Table 2. Effects of concentration of monomers and dipyridyl on the molecular weights of polymers and the number of polymer chains produced from a single-iron complex

[Monomer][a] (mol/l)		[dipy][b] (mol/l)	$FeEt_2(dipy)_2$ (mmol)	Temp. (°C)	Time	Yield (g)	Mol. wt. $\times 10^{-3}$	n[c]
AN	2.0	0	0.071	10	25 min	1.45	104	0.20
AN	15.1	0	0.047	10	2 days	3.06	205	0.32
AN	1.26	7.0×10^{-3}	0.045	23	1 day	0.17	6.7	0.56
AN	2.42	7.1×10^{-3}	0.049	23	1 day	0.48	12	0.82
AN	4.15	7.4×10^{-3}	0.045	23	1 day	0.81	18.5	0.97
AN	0.69	0.155	0.95	23	1 day	0.60	~1.0[d]	~0.63[d]
AN	1.38	0.147	0.90	23	1 day	0.92	~1.2[d]	~0.85[d]
AN	3.01	0.130	0.77	23	1 day	2.24	~2.1[d]	~1.4[d]
MMA	9.40	0	0.30	30	3 days	0.53	126	1.4×10^{-2}
MMA	8.55	0	0.38	30	3 days	0.58	107	1.4×10^{-2}
MMA	7.80	0	0.33	30	3 days	0.15	94	0.49×10^{-2}

a) [Monomer] = concentration of the monomer; AN = acrylonitrile; MMA = methacrylate. Solvent: dimethylformamide for acrylonitrile and tetrahydrofuran for methyl methacrylate.
b) [dipy] = concentration of added dipyridyl.
c) The number of polymer chains produced from a single ethyl-iron complex (initiator efficiency).
d) Since the molecular weights of the polymers in these cases were very low, only approximate values could be obtained by viscometry.

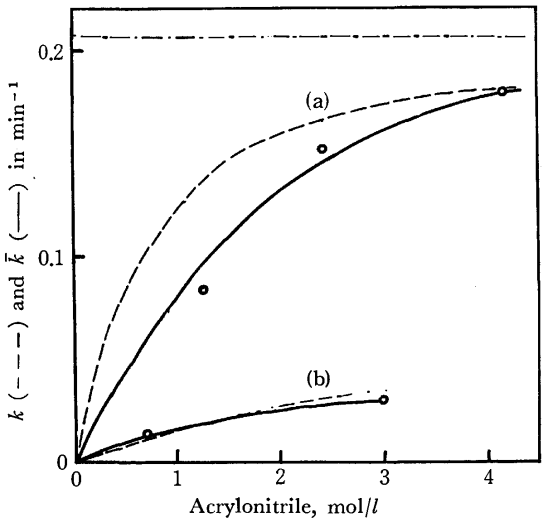

Fig. 3. Pseudo-first-order rate constants, k and $\bar{k}$, against the concentration of acrylonitrile at 23°C. (a), Concentration of dipyridyl was 7.2×10^{-3} mol/l; (b), Concentration of dipyridyl was about 0.14 mol/l. For k and $\bar{k}$ see the text. Solvent: dimethylformamide

the polymerization rate as shown by (b) in Fig. 3. We see a striking resemblance between this and the decomposition pattern of $Fe(C_2H_5)_2(dipy)_2$.[6] In Fig. 3 are also shown the change of pseudo-first-order rate constants k for decomposition of $Fe(C_2H_5)_2(dipy)_2$ with the concentrations of monomers (*cf.* Fig. 3 of the preceding paper[6]). The agreement between the rate constants indicates that the rate of polymerization of acrylonitrile by $Fe(C_2H_5)_2(dipy)_2$ is proportional to the decomposition rate of the ethyl-iron complex. This result implies that the initiation is the rate-determining step followed by rapid propagation and termination processes. The molecular weight of the polymer is independent of the initiator concentration[7] but is affected by the monomer concentration, the

Table 3. Effects of solvent on the molecular weight of poly(methyl methacrylate) at 30°C. Catalyst = $Fe(C_2H_5)_2(dipy)_2$. [dipy] = 0 $[Fe(C_2H_5)_2(dipy)_2] = 23\sim28$ mmol/l

MMA (M)	Solvent	Molecular weight
4.68	Benzene	91000
6.36	Tetrahydrofuran	78000
3.06	Tetrahydrofuran	60000
4.68	Acetonitrile	46000

coordinating ability of the solvent employed and the concentration of dipyridyl added. Table 3 shows the effect of solvent on the molecular weight of poly(methyl methacrylate). Employment of a strongly coordinating solvent decreases the molecular weight of the polymer obtained. Table 2 shows that the molecular weight of the polymer increases with monomer concentration but decreases with the increase of dipyridyl concentration. These results suggest the competitive coordination of the monomer, dipyridyl and solvent toward an iron complex with a growing polymer chain.

Dealing with the kinetics of decomposition of $FeR_2(dipy)_2$ we assumed the following activation mechanism of the metal-alkyl bond:[6]

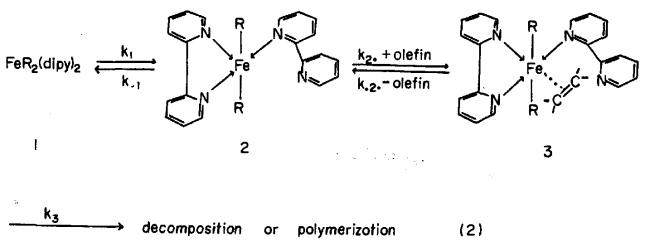

If the above mechanism is valid, an inhibiting effect

TABLE 4. INHIBITION OF POLYMERIZATION BY THE ADDITION OF DIPYRIDYL

Monomer (ml)	Solvent[a] (ml)	Dipyridyl (g)	Temp. (°C)	Time	Yield (%)
MMA 8.0	THF 16	0	30	46 hr	34
MMA 6.5	THF 13	0.30	30	46 hr	21
MMA 5.5	THF 11	0.80	30	46 hr	0
AN 5.0	DMF 20	0	30	30 min	23
AN 5.0	DMF 20	9.0	30	30 min	1.6

a) THF: tetrahydrofuran; DMF: dimethylformamide.

of dipyridyl for polymerization is expected. Table 4 substantiates this expectation showing that the polymerization of methyl methacrylate was completely inhibited and that of acrylonitrile severely retarded by the addition of dipyridyl.

If the polymerization proceeds through an insertion mechanism[7], the coordinated monomer is inserted between one of the two iron-alkyl bonds in complex **3** generating a growing species **4** ($n=1$) as shown below.

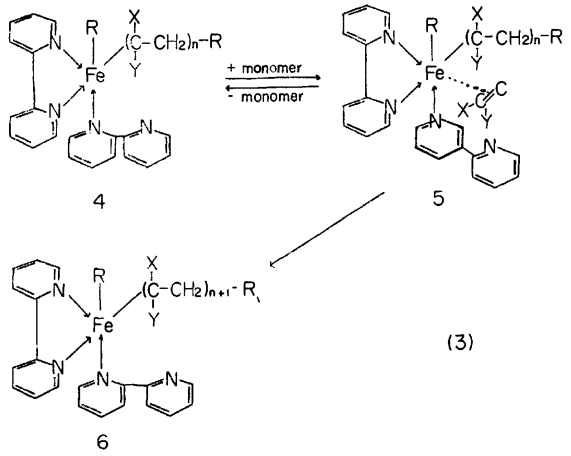

Propagation processes might proceed further by coordination and insertion reactions of monomer molecules as shown in Eq. (3). The partially dissociated dipyridyl ligand may remain attached to iron as in **4**, **5**, and **6**, but the possibility that one dipyridyl is completely displaced as shown below can not be excluded.

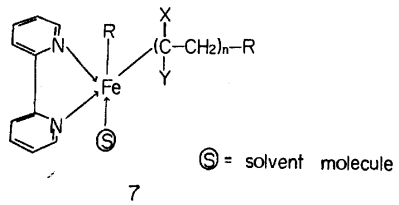

We observed the effects of solvents and alkyl groups on the stereoregularity of methyl methacrylate polymer and the presence of a penultimate effect on the polymer configurations[8]. Penultimate effects in solvents of low coordinating abilities were explained by assuming a species in which a coordination site is occupied by the substituent of the penultimate unit displacing the solvent molecule in **7**. The role of the singly bonded dipyridyl ligand in **4** may be similar at that of a solvent in **7**. If the explanation is reasonable we can anticipate that the proportion of acetone-insoluble stereoblock polymers produced by a propagation process involving a penultimate effect[8] will decrease by the addition of dipyridyl. Table 5 supports this view.

TABLE 5. EFFECT OF DIPYRIDYL ON THE FORMATION OF ACETONE-INSOLUBLE POLY(METHYL METHACRYLATE)

Dipyridyl added (g)	$Fe(C_2H_5)_2(dipy)_2$ (g)	Acetone-insoluble fraction (%)
0	0.50	10.7
0	0.81	7.56
0.30	0.67	2.90
0.30	0.68	5.06
0.50	1.45	2.18

Methyl methacrylate = 10 ml, Benzene = 20 ml, Temperature = 30°C, Time = 2 days.

For an explanation of the difference in stereochemical configuration of poly(methyl methacrylate) obtained with $Fe(CH_3)_2(dipy)_2$ and $Fe(C_2H_5)_2(dipy)_2$, we previously assumed a difference in steric effects between the methyl and ethyl groups bonded to iron. However, an inductive effect of the alkyl group may also be involved. The higher rate constant (k_1) for the breakage of one Fe–N bond of dipyridyl from $Fe(C_2H_5)_2(dipy)_2$ than for the methyl homolog has been explained by the inductive effect of the alkyl group in the preceding paper[6]. If a similar situation holds in the complete dissociation of one dipyridyl ligand from **4** giving **7**, the formation of an acetone-insoluble poly(methyl methacrylate) will be favored for the ethyl-iron complex than for the methyl complex in agreement with the experimental result that the acetone-insoluble stereoblock polymer was obtained with the ethyl complex but not with the methyl homolog.[8]

Copolymerization. We observed previously that acrylonitrile unit is introduced into a polymer chain preferentially to methyl methacrylate which has a less coordinating ability toward the iron complex[7]. We deal herewith with more quantitative aspect of copolymerization. From copolymerization experiments

TABLE 6. MONOMER REACTIVITY RATIOS IN COPOLYMERIZATIONS OF VINYL MONOMERS WITH $Fe(C_2H_5)_2(dipy)_2$.

M_1	M_2	r_1	r_2	$r_1 \times r_2$
Methacrylonitrile	Acrylonitrile	0.17±0.03	17±2	3.0 ±0.9
Methacrylonitrile	Methyl acrylate	0.23±0.06	3.4 ±0.4	0.78±0.23
Methacrylonitrile	Methyl methacrylate	4.2 ±1.2	0.16±0.05	0.73±0.40
Acrylonitrile	Methyl methacrylate	25±5	0.09±0.04	2.6 ±1.6

of vinyl monomers with $Fe(C_2H_5)_2(dipy)_2$, monomer reactivity ratios were obtained by using Fineman-Ross' method[10]. The values are summarized in Table 6.

The results can be explained by assuming the competitive coordination to the iron complex and the ensuing insertion reactions between metal-carbon bonds.

$$\begin{aligned}
&\text{Fe-m}_1\text{-}\sim + \text{M}_1 \underset{k_{11}^{(-1)}}{\overset{k_{11}^{(1)}}{\rightleftharpoons}} \text{Fe-m}_1\text{-}\sim \overset{k_{11}^{(2)}}{\longrightarrow} \text{Fe-m}_1\text{-m}_1\text{-}\sim \\
&\qquad\qquad\qquad\quad \vdots \\
&\qquad\qquad\qquad\quad \text{M}_1 \\
&\text{Fe-m}_1\text{-}\sim + \text{M}_2 \underset{k_{12}^{(-1)}}{\overset{k_{12}^{(1)}}{\rightleftharpoons}} \text{Fe-m}_1\text{-}\sim \overset{k_{12}^{(2)}}{\longrightarrow} \text{Fe-m}_2\text{-m}_1\text{-}\sim \\
&\qquad\qquad\qquad\quad \vdots \\
&\qquad\qquad\qquad\quad \text{M}_2 \\
&\text{Fe-m}_2\text{-}\sim + \text{M}_1 \underset{k_{21}^{(-1)}}{\overset{k_{21}^{(1)}}{\rightleftharpoons}} \text{Fe-m}_2\text{-}\sim \overset{k_{21}^{(2)}}{\longrightarrow} \text{Fe-m}_1\text{-m}_2\text{-}\sim \\
&\qquad\qquad\qquad\quad \vdots \\
&\qquad\qquad\qquad\quad \text{M}_1 \\
&\text{Fe-m}_2\text{-}\sim + \text{M}_2 \underset{k_{22}^{(-1)}}{\overset{k_{22}^{(1)}}{\rightleftharpoons}} \text{Fe-m}_2\text{-}\sim \overset{k_{22}^{(2)}}{\longrightarrow} \text{Fe-m}_2\text{-m}_2\text{-}\sim \\
&\qquad\qquad\qquad\quad \vdots \\
&\qquad\qquad\qquad\quad \text{M}_2
\end{aligned} \tag{4}$$

$$k_{11} = \frac{k_{11}^{(1)}k_{11}^{(2)}}{k_{11}^{(-1)}},\quad k_{12} = \frac{k_{12}^{(1)}k_{12}^{(2)}}{k_{12}^{(-1)}},\quad k_{21} = \frac{k_{21}^{(1)}k_{21}^{(2)}}{k_{21}^{(-1)}},\quad k_{22} = \frac{k_{22}^{(1)}k_{22}^{(2)}}{k_{22}^{(-1)}} \tag{5}$$

$$r_1 = \frac{k_{11}}{k_{12}},\quad r_2 = \frac{k_{22}}{k_{21}} \tag{6}$$

In these equations dipyridyl ligands and the other alkyl group are omitted for the sake of simplification. M_1 and M_2 are coordinating monomers and m_1 and m_2 represent monomer units taken into the polymer chains. We found a linear relationship between log k_{Ni}, the logarithms of rate constants for the scission of Ni–R bonds of $NiR_2(dipy)$, and log K, the logarithms of stability constants of Ni(dipy)(olefin)[5]. We have also found a linear relationship between the log k_{Ni} value for Ni–R scission and log $(k_1k_2k_3/k_{-1}k_{-2})$ which represent the relative reactivities of olefins for the decomposition of $FeR_2(dipy)_2$ (*cf.* Eq. (2),[9] and Fig. 5 of the preceding paper[6]). From these two relationships, a linear relationship between log K and log $(k_1k_2k_3/k_{-1}k_{-2})$ can be derived; $\log(k_1k_2k_3/k_{-1}k_{-2}) = 2.4\log K - 4.3$. Therefore, it is reasonable to assume a linear relationship between log K and the logarithms of rate constants, k_{ij}, for insertion of a monomer (j) into the iron-carbon bond of the preceding monomer unit (i) already introduced into the polymer chain. These assumptions lead to the following relationships.

$$\begin{aligned}
\log k_{11} - \log k_{12} &= a_1(\log K_1 - \log K_2) \\
\log k_{21} - \log k_{22} &= a_2(\log K_1 - \log K_2)
\end{aligned} \tag{7}$$

where a_1 and a_2 are constants depending on the nature of the Fe–m_1 and Fe–m_2 bonds into which the coordinated monomer is to be inserted. From these equations $1/r_1$ and $r_1 \cdot r_2$ can be expressed as follows.

$$\log 1/r_1 = a_1(\log K_2 - \log K_1) \tag{8}$$

$$\log (r_1 \cdot r_2) = (a_1 - a_2)(\log K_1 - \log K_2) \tag{9}$$

10) M. Fineman and S. Ross, *J. Polymer Sci.*, **5**, 259 (1950).

Figure 4 shows the plot of log $1/r_1$ *versus* (log K_2—log K_1), where M_1 is methacrylonitrile chosen as the reference. The roughly linear relationship supports Eq. (8) and demonstrates a unique characteristic of the coordination polymerization. It can be seen from a comparison of r_1 values in Table 6 that the relative reactivity of methacrylonitrile is 0.17 of that of acrylonitrile and 4.2 times of that of methyl methacrylate. If we assume the validity of the proposed coordination mechanism the relative reactivity of acrylonitrile to methyl methacrylate is expected to be 25 in good agreement with the experimental value of 25±5.

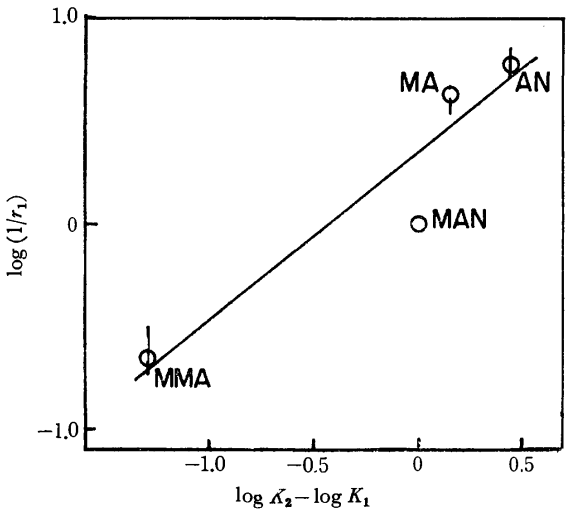

Fig. 4. Copolymerization of methacrylonitrile with olefins. M_1=methacrylonitrile as a reference. K represents the stability constant of the nickel–olefin π complex.[5]

Natta *et al.*[11] observed that $r_1 \cdot r_2$ values are very close to unity in the copolymerization of styrene derivatives with mixed catalysts prepared from aluminum alkyls and titanium halides and that log r_2 values are inversely proportional to the Hammett constants of the substituents. In our system log r_2 or log $1/r_1$ values increase with the increase of the Hammett constants of the substituent and hence with the increase of the log K values, but the $r_1 \cdot r_2$ values show significant deviations from unity. If a_1 should be equal to a_2 (Eq. (9)), $r_1 \cdot r_2$ should be unity. The observed deviations in our system suggest the considerable effects of the ultimate units in the growing polymer chains.

Termination Mechanism. The fact that molecular weights of poly(acrylonitrile) and poly(methyl methacrylate) are independent of the catalyst concentration suggests that the termination reaction is unimolecular as shown by

$$R_t = k_t[\text{Fe*}] \tag{10}$$

where [Fe*] represents the concentration of growing polymer chains attached to the iron complex such as **4** or **7**. In the proposed coordination mechanism the rate of propagation can be expressed by

$$R_p = k_p[\text{Fe*}][\text{M}] \tag{11}$$

11) G. Natta, F. Danusso, and D. Sianesi, *Makromol. Chem.*, **30**, 238 (1959); F. Danusso, *Chem. Ind.* (Milan), **44**, 611 (1962).

Thus from a comparison of Eqs. (10) and (11) the molecular weight of the polymer is expected to be proportional to the monomer concentration. The linear relationship between the molecular weight of poly(acrylonitrile) and the concentration of the monomer in Fig. 5 supports the above assumptions. The fact that the addition of dipyridyl (Fig. 5) and the employment of solvents with greater coordinating abilities caused the decrease of molecular weight suggests that coordination of a solvent and dipyridyl instead of a monomer destabilizes the bond between iron and the growing polymer chain to induce the unimolecular termination process. Further insight into the termination mechsnism was obtained by employing a deuterated monomer and analyzing the gas evolved in the termination process.[12]

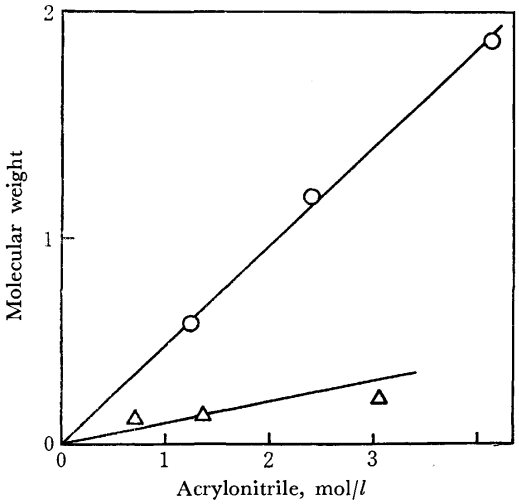

Fig. 5. Effect of the concentration of acrylonitrile and dipyridyl on the molecular weight of poly(acrylonitrile), (○) [dipy]≒7.2×10^{-3}, (△) [dipy]≒0.14 mol/*l*.

In the polymerization of *cis*-β-d_1-methyl methacrylate (78% isotopic purity) with $Fe(C_2H_5)_2(dipy)_2$, the evolution of ethane and ethylene was observed to take place in a molar ratio 1 : 2.5. Analysis of the ethane by mass spectroscopy indicated that it contained 32% of C_2H_5D and 68% of C_2H_6 (average of two experiments). The possibility of direct hydrogen abstraction of the methyl methacrylate monomer by the ethyl groups of $FeEt_2(dipy)_2$ can be excluded since the content of C_2H_5D in ethane evolved in the thermal decomposition of $FeEt_2(dipy)_2$ in benzene-d_6 at room temperature and at 80°C did not exceed the natural abundance of C_2H_5D. The NMR spectrum of the recovered deuterated monomer after the polymerization was identical with that of the deuterated monomer used for the experiment. Thus the source of ethane-d_1 is considered to be the ethyl group of $FeEt_2(dipy)_2$ and the β-hydrogens of the growing poly(methyl methacrylate-d_1) chain.

In a previous paper[8] we concluded that one of the alkyl groups of $FeR_2(dipy)_2$ remains attached to iron during the propagation process. The fact that the initiator efficiency (*n* in Table 2) does not exceed unity (except for one case where the accuracy of the molecular weight determination is not very great) also supports the conclusion. If we assume that ethane-d_1 was formed through an abstraction of β-hydrogens in the ultimate unit of the growing polymer chain attached to iron by the remaining ethyl-group, the theoretical content of C_2H_5D is 39%, which agrees with the experimental value. An experiment carried out with a 1 : 1 mixture of the normal methyl methacrylate and methyl methacrylate-d_1 showed a corresponding decrease in the amount of C_2H_5D in the evolved gas in comparison to C_2H_6.

Thus we believe that the termination involving the formation of ethane and ethylene takes place through one of the following courses:

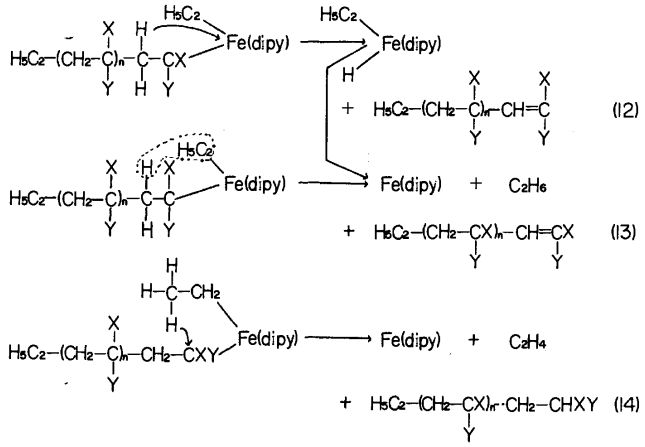

where X=CH_3, Y=$COOCH_3$ for methyl methacrylate.

The coordinated solvent molecule or dipyridyl ligand as in **7** and **4** are omitted for the sake of simplification. From the available data it has not been determined yet whether the elimination (Eq. (12)) leaving the alkyl-iron hydride takes place first followed by an intramolecular elinination of RH, or the alkyl group abstracts the β-hydrogen directly as in Eq. (13). In a similar type of polymerization of methyl methacrylate by tris(allyl)chromium, Ballard *et al.*[2] proposed a termination mechanism in which the addition of an allyl group to the carbonyl group of the ultimate monomer unit was involved. The type of termination seems to be unlikely in our system.

Experimental

Materials. Dialkylbis(dipyridyl)iron(II) was prepared as previously described[4,6]. Methyl *cis*-β-d_1-methacrylate was prepared from methyl acetylene, deuterium chloride, nickel tetracarbonyl and methanol-d_1 by the method of Jones[13] and was purified by distillation 4-times, NMR: τ3.93 *β-cis* proton, (a complex peak with a relative area 0.22); τ4.47 *β-trans* proton (a quartet with a relative area 1); τ6.27 ester methyl proton (a singlet with a relative area 2.9); τ8.07 α-methyl proton (a doublett with a relative area 2.9). The deuterated monomer had 78% isotopic purity based on NMR. Monomers and solvents were purified

12) T. Yamamoto, A. Yamamoto, and S. Ikeda, *J. Polymer Sci.*, part B, **9**, 281 (1971).

13) E. R. Jones, T. T. Shen, and M. C. Whiting, *J. Chem. Soc.*, **1959**, 230.

and stored as previously reported[6].

Polymerization. Polymerization was mostly carried out in a sealed ampoule in which the catalysts, olefin and solvent were transferred in an atmosphere of nitrogen or by trap-to-trap distillation *in vacuo*. After the set time of polymerization, the ampoule was opened and the content poured into acidic methanol. The precipitate was filtered, washed with methanol and dried. The kinetic study on acrylonitrile was carried out in a Schlenk type flask around which thermostatted water was circulated or in a dilatometer immersed in a thermostatted water bath. Acrylonitrile, catalyst, dipyridyl, and dimethylformamide were transferred in an atmosphere of nitrogen. The time-dependent yield was measured by pipetting out each fraction of the solution from the Schlenk type flask at set time or by reading the decrease of the volume of solution in the dilatometer. The density of poly(acrylonitrile) in the solution was measured by comparing the final decrease of volume with the weight of the recovered polymer. The density at 25°C was 1.05 g/m*l*. Poly(methyl methacrylate) was extracted in a Soxhlet extractor with acetone for 1 week and separated into acetone-soluble and acetone-insoluble fractions.

Compositions of the Copolymers. Compositions of the copolymers were calculated from microanalyses of carbon, hydrogen and nitrogen performed by Mr. T. Saito with a Yanagimoto CHN Autocorder Type MT-2.

Molecular Weight. The molecular weights of polymer were measured by viscometry by using the following equations: for poly(methyl methacrylate)[14], $[\eta]=3.80\times10^{-5}M_w^{0.79}$; for poly(acrylonitrile)[15], $[\eta]=1.66\times10^{-4}M_w^{0.81}$; for poly(methacrylonitrile)[16], $[\eta]=9.55\times10^{-4}M_w^{0.56}$.

Mass Analysis. The gas evolved in the polymerization of methyl β-*cis*-d_1-methacrylate was analyzed with a Hitachi type RMU-5B Mass Spectrometer by Mr. H. Sakurai.

14) J. -Y. Chine, L. -H. Shin, and K. -I. Shin, *Acta Chim. Sinica*, **23**, 213 (1957).
15) J. Bisschops, *J. Polymer. Sci.*, **17**, 81 (1955).
16) N. Fuhrman and R. B. Mesrobian, *J. Amer. Chem. Soc.*, **76**, 5281 (1954).

BULLETIN OF THE CHEMICAL SOCIETY OF JAPAN, VOL. 45, 1117—1119 (1972)

The Photochemical Degradation of Diphenyl Sulfone-1-^{14}C

Mamoru NAKAI,* Naomichi FURUKAWA, and Shigeru OAE,

Department of Applied Chemistry, Faculty of Engineering, Osaka City University, Sumiyoshi-ku, Osaka

and Takeshige NAKABAYASHI

Department of Chemistry, Radiation Center of Osaka Prefecture, Sakai, Osaka

(Received May 26, 1971)

The photolysis of diphenyl sulfone-1-^{14}C upon irradiation with 2537 Å light in benzene gave biphenyl-1-^{14}C and benzenesulfinic acid-^{14}C. The yields of both compounds were estimated by means of an isotope dilution method. The ^{14}C activity of the sulfone recovered was equal to that of the sulfone employed, while that of biphenyl formed was found to have nearly one half of the ^{14}C activity. These results reveal that the phenylation reaction by phenyl radical formed by the photolytic cleavage of the C–S bond of the sulfone is an intermolecular reaction in which benzenesulfonyl radical appears to abstract hydrogen from the intermediate cyclohexadienyl radical rather than attacking benzene. The ^{14}C distribution indicates that the ^{14}C activity at 1-position was found to remain at the same position of biphenyl after photolysis of the sulfone. Thus, the photolysis of diaryl sulfones in benzene followed by the oxidation of biphenyl derivatives obtained would be a convenient method for the degradation of diaryl sulfones.

Degradation of ^{14}C-labeled diphenyl sulfone was previously carried out by way of initial alkaline fusion of the sulfone, followed by the subsequent cleavage of the phenol obtained, but the method was tedious. We sought to find a simple and more convenient degradative method of sulfone or sulfide, especially in our studies on the mechanisms of the reactions of diphenyl sulfone and related compounds with either sulfur[1] or diaryl disulfide[2], possible migration of phenyl group in the treatment of diphenyl sulfide with aluminum chloride[3] and also the alkali fusion of these compounds.[4] Recently, Kharasch and Khodair[5] reported that the photolysis of diaryl sulfone, sulfoxide, and sulfide in benzene produces aryl radicals which give the corresponding biphenyl in good yield. They proposed the following intermolecular mechanism since the photolysis of bis-*p*-tolyl sulfone in benzene gave only 4-methylbiphenyl and no 4,4′-dimethylbiphenyl.

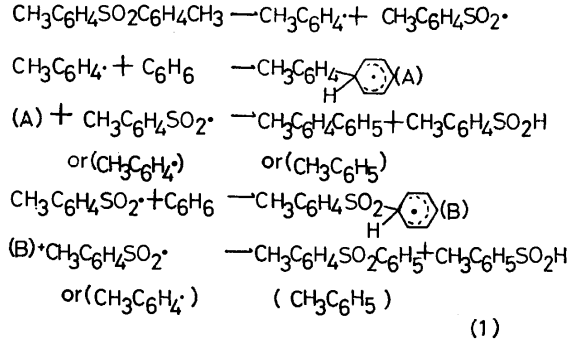

(1)

* Present address: Ube Industries Ltd., Ube, Yamaguchi.

1) S. Oae and S. Kawamura, This Bulletin, **36**, 163 (1963).

2) S. Oae, Y. Tsuchida, and M. Nakai, *ibid.*, **44**, 451 (1971).

3) S. Oae, M. Nakai, and N. Furukawa, *Chem. Ind.* (London), **1970**, 1438.

4) S. Oae and N. Furukawa, This Bulletin, **39**, 2260 (1966).

5) N. Kharasch and A. I. A. Khodair, *Chem. Commun.*, **1967**, 98.

Thus, the photolysis of diphenyl sulfone seems to be a convenient method for the degradation of diphenyl sulfone if there is no skeletal rearrangement. In order to confirm the absence of skeletal rearrangement during the reaction so that the method can be used for the degradation of diphenyl sulfone and sulfide conveniently, the photolysis of diphenyl sulfone-1-^{14}C was carried out, followed by the degradation of the biphenyl-*x*-^{14}C formed.

This paper describes a detailed account and implications of experimental observations.

Results and Discussion

The synthesis of diphenyl sulfone-1-^{14}C has been described.[6] The rather low yield (27%) of biphenyl formation is due to the low efficiency of irradiation and our efforts to minimize any further reaction. Biphenyl formed by photolysis was diluted with an aliquot of inactive biphenyl and then oxidized with CrO_3 in acetic acid at 70—75°C (Eq. (2)). The

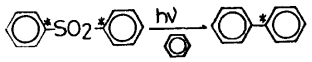

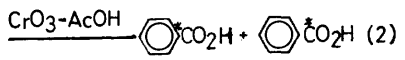

activity of benzoic acid thus obtained was compared with that of biphenyl. The percentage rearrangement of the activity at 1-position of the sulfone was calculated. The result reveals that more than 99% ^{14}C activity remained in the original position. Thus, the photolysis of diphenyl sulfone is shown to be a convenient method for the degradation to determine the ^{14}C activity at 1-position of diphenyl sulfone, sulfoxide and sulfide.

In order to shed further light on the mechanism of the photolysis of diaryl sulfone in benzene a more detailed analysis of products was performed by using the ^{14}C-labeled diphenyl sulfone.

A benzene solution of diphenyl sulfone-1-^{14}C (0.0224 M) was irradiated with 2537 Å light at room temperature for 20 hr. After the reaction, unchanged diphenyl sulfone was recovered while biphenyl formed was isolated and subjected to ^{14}C activity measurement. Determination of the yield of a possible product, benzenesulfinic acid, was carried out by means of isotope dilution. (Eq. (3)). The result of

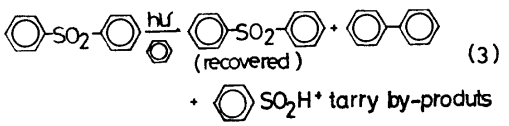

(3)

the photolysis is shown in Table 1.

The following conclusion may be drawn from the data in Table 1. Firstly, the activity of diphenyl sulfone recovered is equal to that of the starting material. Benzenesulfinic acid appears to be formed by the hydrogen atom abstraction from the intermediate cyclohexadienyl radical with benzenesulfonyl radicals produced by the initial C–S bond cleavage of the sulfone, while there is no addition of benzenesulfinyl radical to benzene to reproduce diphenyl sulfone as shown by Eq. (4). If the sulfonyl radical attacks the solvent benzene, the ^{14}C activity of the recovered sulfone would be less than that of the starting sulfone. Secondly, the fact that the activity of biphenyl formed is nearly one half of that of diphenyl sulfone used reveals that phenyl radical produced reacts with benzene to yield biphenyl, *viz.*, the process is an intermolecular free radical arylation reaction of benzene. That the ^{14}C activity of biphenyl (47%) is slightly less than the theoretical value might be due to the isotope effect during the initial C–S bond cleavage of the sulfone-^{14}C.

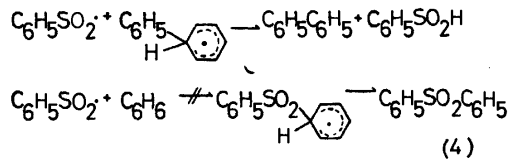

(4)

Thus, the photolysis of diphenyl sulfone in benzene is considered to proceed through the mechanistic route proposed earlier by Kharasch and Khodair as shown by the following equation. Consequently, the photolysis of diphenyl sulfone is found to be a simple

TABLE 1. PHOTOLYSIS OF DIPHENYL SULFONE-1-^{14}C

	Diphenyl sulfone (Starting material)	Diphenyl sulfone (Recovered)	Biphenyl	Benzenesulfinic acid
Activity (dpm/mmol)	8.26×10^5	8.31×10^5 (100.6%)	3.88×10^5 (47.0%)	1.02×10^4 [a]
Yield	Conversion: 58.7%	(41.3%) [d]	71.0% [b]	6.8% [c]

a) Three fifths of the resulting benzene solution diluted with 0.755 g of inactive sulfinic acid.

b), c) Based on the amount which actually underwent photolysis and on the assumption that one mol of diphenyl sulfone yielded one mol of biphenyl.

d) Recovered yield.

6) S. Oae, N. Furukawa, M. Kise, and M. Kawanishi, This Bulletin, **39**, 1212 (1966).

and convenient method of degradation of ^{14}C labeled diphenyl sulfone.

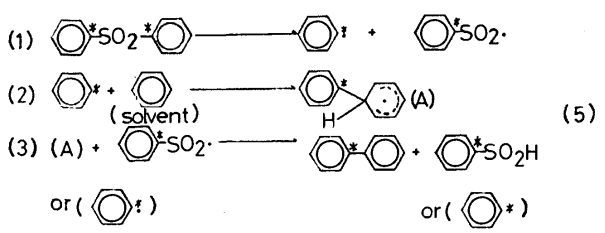

Experimental

Preparation of Diphenyl Sulfone-1-^{14}C. Diphenyl sulfone-1-^{14}C was synthesized through 9 steps starting from barium carbonate-^{14}C. The synthetic method has been given.[6]

The Photolysis of Diphenyl Sulfone-1-^{14}C. The photolysis of sulfone (1.223 g) was carried out in 250 m*l* of benzene at room temperature for 15 hr by the irradiation of 2537 Å light of a low-pressure cold cathode mercury lamp. The reaction mixture turned brown and then become tarry material which coated the lamp reducing the efficiency of prolonged irradiation. The benzene solution was divided into two parts. Three fifths of the contents of the flask was used for the measurement of the activity of diphenyl sulfone recovered and biphenyl formed *in situ* and the rest was subjected to the determination of the yields of the compounds listed in Table 2 by means of an isotope dilution method. The benzene solution was washed with 5% alkali solution to remove the acidic components including benzenesulfinic acid. After evaporation of benzene, both biphenyl and diphenyl sulfone were isolated and separated by means of silica gel column chromatography. Benzenesulfinic acid was extracted with ether from the aqueous layer after acidified with hydrochloric acid. Crude biphenyl thus obtained was purified by recrystallization from water-alcohol and then by sublimation twice. Diphenyl sulfone and benzenesulfinic acid isolated were purified by recrystallization twice from benzene-*n*-hexane and ether-*n*-hexane, respectively. Diphenyl sulfone, biphenyl, and benzenesulfinic acid thus obtained were subjected to the counting of ^{14}C activity.

Oxidation of Biphenyl. An aliquot amount of biphenyl (0.4 g) was dissolved in 5 m*l* of acetic acid, and to this solution was added a solution of 5 g of anhydrous chromic acid in 2 m*l* of water and 5 m*l* of acetic acid dropwise with stirring at 70—75°C. Carbon dioxide evolved during the oxidation. After the oxidation was completed, the content of the flask was stirred for 30 min at 70—75°C. The reactant was then poured into 40 m*l* of water and the whole mixture was extracted with ether. The ether layer was washed with water three times to remove acetic acid and then re-extracted with 5% alkali solution. The alkali solution was reacidified and the benzoic acid precipitated was purified by sublimation. The yield was about 20%. Both benzoic acid and biphenyl were subjected to the counting of ^{14}C activity. The specific activities of both biphenyl-*x*-^{14}C and benzoic acid-^{14}C were found to be the same. Thus no ^{14}C rearrangement occurred during photolysis and oxidation. The benzoic acid obtained was degraded according to the known method[7] and was found to have ^{14}C activity at its 1 position.

Measurement of the ^{14}C Activities. Activities of all the compounds were counted with a liquid scintillation counter (TEN) in toluene solution using POPOP as a scintillator.

We wish to thank Dr. M. Hamada of the Radiation Center of Osaka Prefecture for his advice and for affording facilities for the measurements.

7) J. D. Roberts, H. E. Simmons, Jr., L. A. Carlsmith, and C. W. Vaughan, *J. Amer. Chem. Soc.*, **75**, 3290 (1953); J. D. Roberts, D. A. Semenow, H. E. Simmons, Jr., and L. A. Carlsmith, *ibid.*, **78**, 601 (1956).

Nitrate as an Oxidant in the Reaction of Silver(I) Salts with Grignard Reagents

Masuhiko TAMURA* and Jay K. KOCHI

Department of Chemistry, Indiana University, Bloomington, Indiana 47401, *U.S.A.*

(Received July 19, 1971)

The reaction between various Grignard reagents and silver(I) salts in the presence of nitrogen-containing oxidants such as lithium nitrate, nitrogen dioxide, and methyl nitrate has been examined in tetrahydrofuran solutions. Coupling dimer is formed in high yields almost independently of the structure of the Grignard reagent. From the stoichiometry, it is concluded that these oxidants oxidize two equivalents of metallic silver formed *in situ* to silver(I) species under proper reaction conditions. Other transition metal halides are also oxidized by these oxidants in a similar manner. Soluble forms of reduced silver complexes formed in the reaction of silver(I) nitrate and Grignard reagent are also described.

The reactions of various transition metal salts and Grignard reagents in which alkane, alkene, and coupling dimer are obtained as products have been studied for some time.[1] Silver(I) salts are generally reduced to the metallic state in the presence of excess Grignard reagent, and the stoichiometry[2] of the reaction is generally represented by Eq. (2).

$$2\,RMgY + 2\,AgX \rightarrow [RH, R(-H), R\text{-}R] + 2\,MgXY + 2\,Ag \quad (1)$$

$$Q(R) = \frac{R(-H) + RH + 2\,R\text{-}R}{AgX} = 1.0 \quad (2)$$

The distribution of products is dependent on the Grignard reagent as well as the reaction conditions. The mechanism of the formation of coupling dimer has also been proposed.[3]

$$2\,R\text{-}Ag \rightarrow R\text{-}R + 2\,Ag \quad (3)$$

In most studies for this reaction, diethyl ether has been a medium of choice.[4]

We have examined the mechanism of the Kharasch reaction catalyzed by various transition metal salts and the reactions of transition metal halides with Grignard reagents, especially in tetrahydrofuran (THF) solution.[5] During these studies we found that nitrate is capable of acting as an oxidant in the *catalytic* reaction of silver(I) salt and Grignard reagent in THF.

In this paper we describe the reaction of silver(I) salt and Grignard reagent in the presence of nitrogen-containing oxidants such as lithium nitrate, nitrogen dioxide, and methyl nitrate in THF solutions. We also describe the soluble silver complex formed in the reaction of silver(I) nitrate and Grignard reagent in THF.

Results and Discussion

Reactions of Silver(I) Salts and Grignard Reagents. When a silver(I) salt was mixed with ethylmagnesium bromide in THF, *n*-butane was formed quantitatively together with a metallic silver precipitate as shown in Table 1.

$$2\,EtMgBr + 2\,AgX \rightarrow C_4H_{10} + 2\,Ag + 2\,MgBrX \quad (4)$$

TABLE 1. REACTION OF SILVER(I) SALTS AND ETHYLMAGNESIUM BROMIDE IN TETRAHYDROFURAN[a]

AgX	Q(Et)	Distribution of product (%)			Alkali[c] (mmol)
		C_2H_4	C_2H_6	*n*-C_4H_{10} [b]	
AgBr	1.0	2.1	6.2	91.7	9.6
AgOAc	1.1	2.7	13.3	84.0	n. d.[d]
$AgClO_4$	1.1	2.7	7.2	90.1	9.4
$AgNO_2$	1.5	2.7	21.9	75.4	n. d.[d]
$AgNO_3$	3.6	1.4	11.2	87.4	10.5

a) In 21 m*l* THF solution containing 1.0 mmol AgX and 10.5 mmol EtMgBr at 25°C for 2.0 hr.
b) Percentage of *n*-C_4H_{10} was doubled.
c) Analysis after the reaction was completed.
d) Not determined.

A black precipitate was also formed immediately when silver(I) nitrate reacted with *excess* ethylmagnesium bromide. With this silver(I) salt, however, a part of the black precipitate gradually redissolved, accompanied by the formation of additional *n*-butane as shown in Fig. 1. Moreover, the value of Q(Et) in Eq. (2) was 3.6 in the case of silver(I) nitrate, which suggests that the nitrate acted as an oxidant during the reaction. The reactions of silver(I) nitrate and various organometallic compounds were also carried out in THF in order to see the general tendency of this unique behavior of nitrate. The results are summarized in Table 2 which shows clearly that Q(R) became greater than the usual stoichiometric requirements of 1.0, independently of the Grignard reagent. The coupling dimer was still the main product except

* Present address: Central Research Laboratories, Kuraray Co., Ltd. Sakazu, Kurashiki, Okayama, Japan; To whom correspondence should be addressed.

1) F. A. Cotton, *Chem. Rev.*, **55**, 551 (1955); G. W. Parshall and J. J. Mrowca, *Advan. Organometal. Chem.*, **7**, 157 (1968); G. E. Coates, M. L. H. Green, and K. Wade "Organometallic Compounds" Vol. 2, Third ed., Methuen and Co., Ltd., London, (1968).

2) C. D. M. Beverwijk and G. J. M. Van der Kerk *Organometal. Chem. Rev.*, **A5**, 215 (1970). J. H. Gardner *et al.*, *J. Amer. Chem. Soc.*, **51**, 3375 (1929); **59**, 2583 (1937); **61**, 2551 (1939); *J. Org. Chem.*, **61**, 2551 (1939). H. Gilman and J. M. Straley, *Rec. Trav. Chem. Pays-Bas*, **55**, 821 (1936).

3) G. M. Whitesides and C. P. Casey, *J. Amer. Chem. Soc.*, **88**, 4511 (1966).

4) W. T. Miller *et al.*, *J. Amer. Chem. Soc.*, **90**, 7367 (1968); **91**, 6532 (1969); H. Hashimoto and T. Nakano, *J. Org. Chem.*, **31**, 891 (1966) and references cited therein.

5) M. Tamura and J. K. Kochi, *J. Amer. Chem. Soc.*, **93**, 1483, 1485, 1487 (1971); M. Tamura and J. K. Kochi, *J. Organometal. Chem.*, **29**, 111 (1971); **31**, 289 (1971); M. Tamura and J. K. Kochi, "Synthesis", 303 (1971); K. Wada, M. Tamura, and J. K. Kochi, *J. Amer. Chem. Soc.*, **92**, 6656 (1970); M. Tamura and J. K. Kochi, This Bulletin, **44**, 3063 (1971).

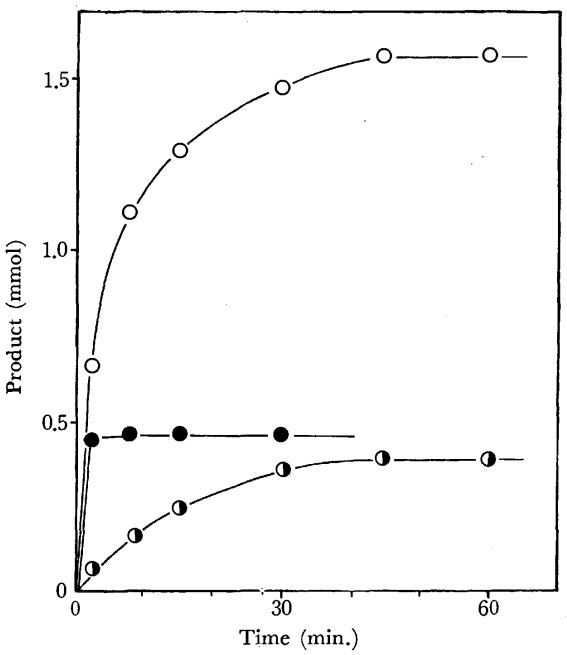

Fig. 1. Rate of formation of products in the reaction of silver(I) salts and ethylmagnesium bromide in tetrahydrofuran at 2°C.
THF: 21 m*l*, AgX: 1.0 mmol, EtMgBr: 7.3 mmol
○: n-C_4H_{10} from $AgNO_3$, ●: n-C_4H_{10} from AgBr
◑: C_2H_6 from $AgNO_3$

for secondary and tertiary alkyl Grignard reagents in which the formation of alkane and alkene predominated. Q(R) remained 1.0 when diethylzinc and triethylaluminum were employed, but no reaction took place between silver(I) nitrate and tetraethyllead or tetraethyltin.

Methyl, ethyl, n-propyl, isopropyl, and t-butylmagsium bromides, ethylmagnesium chloride, diethylmagnesium, and ethyllithium all produced a black-brown solution (*vide infra*) in varying yields after the reactions were complete. On the other hand, phenyl, benzyl, and allylmagnesium bromides, diethylzinc and triethylaluminum did not afford brown solutions. Only a black precipitate and a colorless solution remained after the reaction was complete. These observations suggest that the formation of a black-brown solution is related to the reactivity of organometallic compound since benzyl and allylmagnesium bromides are more reactive, and phenylmagnesium bromide is less reactive than other alkyl Grignard reagents.[6]

The reaction of silver(I) nitrate and ethylmagnesium bromide was also greatly affected by the reaction temperature and the molar ratio of ethylmagnesium bromide to silver(I) nitrate as shown in Table 3. Thus, the value of Q(Et) and the yield of coupling dimer became larger at lower temperatures. The higher yields of soluble silver complex were obtained at lower temperatures and molar ratios of ethylmagnesium bromide to silver(I) nitrate of 5—7. The lower value of Q(Et) and the higher yield of ethane at higher temperature may be ascribed to the reaction of nitrate with ethylmagnesium bromide and the aggregation of metallic silver formed *in situ* (see Experimental, Table 6). Q(Et) also became greater than 1.0 when the reaction of silver(I) nitrate and ethylmagnesium bromide was carried out in diethyl ether, dioxane, and diglyme as indicated in Table 4. However, no soluble silver complex was formed in these solvents.

Reaction of Silver(I) Perchlorate and Ethylmagnesium Bromide in the Presence of an Oxidant. In order

Table 2. Reaction of silver(I) nitrate and various organometallic compounds[a]

Organometallic compound	Temp. (°C)	Period (min)	Q(R)	Distribution of product (%)			Reaction[b] mixture
				R(-H)	RH	R-R	
MeMgBr	2	120	1.0		3.1	96.9	A
MeMgBr	40	180	2.0		8.8	91.2	B
EtMgBr	2	60	3.4	1.2	9.2	89.6	B
EtMgCl	2	60	3.5	0.7	7.4	91.9	B
Et_2Mg	2	60	8.4	1.7	9.3	89.0	B
EtLi	2	60			n. d.		B
Et_2Zn	80	240	1.1	3.5	15.8	80.7	A
Et_3Al	40	60	1.1	7.6	20.0	72.4	A
n-PrMgBr	2	60	1.7	1.3	8.0	90.7	B
iso-PrMgBr	2	60	3.7	26.1	35.3	38.6	B
t-BuMgBr	2	60	3.8	38.7	38.7	22.6	B
CH_2=CHMgBr	2	60	1.6		5.1	94.9	A
CH_2=CHMgBr	25	60	3.5		6.8	93.2	B
PhMgBr	60	60	>1.7		n. d.	>90	A
$PhCH_2MgBr$	2	60	>2.9		n. d.	>90	A
CH_2=$CHCH_2MgBr$	2	60	3.4		8.3	91.7	A

a) In 21 m*l* THF solution containing 1.0 mmol $AgNO_3$ and 6.5—8.0 mmol organometallic compound.
b) Appearance of the reaction mixture after completion
A: Black precipitate and colorless solution
B: Black-brown solution (λ_{max} 415 nm) together with a black precipitate

6) J. H. Wotiz, C. A. Hollings, and R. Dessy, *J. Amer. Chem. Soc.*, **77**, 103 (1955).

TABLE 3. EFFECTS OF TEMPERATURE AND MOLAR RATIO OF ETHYLMAGNESIUM BROMIDE TO SILVER(I) NITRATE[a]

EtMgBr/$AgNO_3$	Temp. (°C)	Q(Et)	Distribution of product (%)			Soluble Ag[b] (%)
			C_2H_4	C_2H_6	n-C_4H_{10}	
7.3	62	2.4	3.8	48.7	47.5	1
7.3	25	3.5	2.6	21.3	76.1	24
7.3	2	3.3	1.8	10.1	88.1	34
7.3	−10	3.3	1.2	9.1	89.7	n. d.[c]
14.6	2	3.3	1.2	9.0	89.8	2
5.1	2	2.8	2.2	13.8	84.0	32
2.9	2	1.9	2.1	14.9	83.0	18

a) In 21 m*l* THF solution containing 1.0 mmol $AgNO_3$ reacted for 60 min.
b) Percentage of soluble Ag in solution, based on $AgNO_3$ charged.
c) Not determined.

TABLE 4. EFFECT OF SOLVENT ON THE REACTION OF SILVER(I) NITRATE AND ETHYLMAGNESIUM BROMIDE[a]

Solvent	Temp. (°C)	Period (min.)	Q(Et)	Distribution of product (%)			Reaction[b] mixture
				C_2H_4	C_2H_6	n-C_4H_{10}	
Et_2O	2	90	1.8	2.7	22.7	74.6	A
Et_2O	25	90	1.6	3.7	34.2	62.1	A
Dioxane	25	60	1.5	6.1	38.5	55.4	A
Diglyme	2	60	3.3	3.0	12.6	84.4	C
Diglyme	20	60	2.4	3.3	18.2	78.5	C

a) In 21 m*l* solution (84 vol% solvent and 16 vol% THF) containing 1.0 mmol $AgNO_3$ and 7.3 mmol EtMgBr.
b) Appearance of the reaction mixture after completion.
A: Black precipitate and colorless solution
C: Brown precipitate and colorless solution

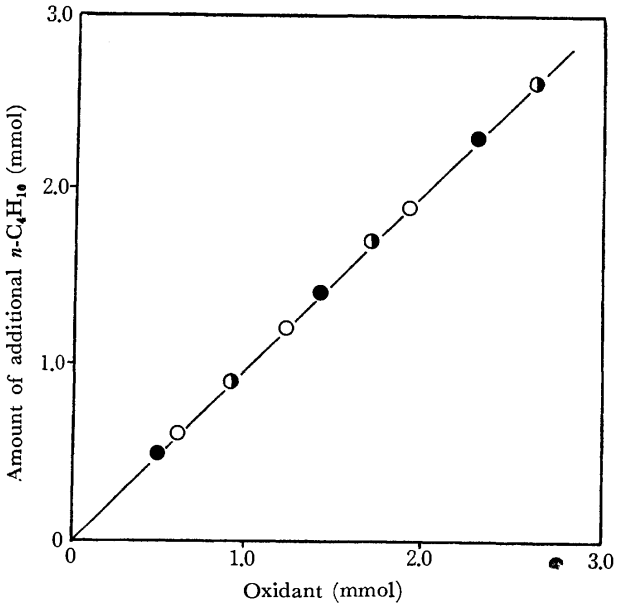

Fig. 2. Increase in the amount of *n*-butane from the reaction of silver(I) perchlorate and ethylmagnesium bromide in the presence of an oxidant in tetrahydrofuran at 2°C for 60 min. THF: 21 m*l*, $AgClO_4$: 1.0 mmol, EtMgBr: 8.7 mmol
●: Methyl nitrate, ○: Nitrogen dioxide, ◑: Lithium nitrate

to determine the role of nitrate as an oxidant, the reaction of silver(I) perchlorate and ethylmagnesium bromide in THF solutions was examined in the presence of other oxidants. When methyl nitrate, lithium nitrate, or nitrogen dioxide was added in the reaction, greater than stoichiometric amounts of coupling dimer was also formed as shown in Fig. 2. Furthermore, additional coupling dimer was formed when lithium nitrate was added to the black suspension resulting from the reaction of silver(I) bromide and excess ethylmagnesium bromide in THF. It is clearly indicated from the slope of the plot in Fig. 2 that these oxidants oxidize two equivalents of metallic silver.[7]

$$AgClO_4 + EtMgBr \rightarrow 1/2\ C_4H_{10} + MgBrClO_4 + Ag \quad (5)$$

$$2\ Ag \xrightarrow{Oxidant} 2\ Ag(I) \xrightarrow{EtMgBr} C_4H_{10} + 2\ Ag \quad (6)$$

Similar results were obtained when silver(I) bromide replaced silver(I) perchlorate. Lithium nitrate and nitrogen dioxide also produced a black-brown solution, but methyl nitrate only afforded a black precipitate and a colorless solution. Sodium nitrite, nitric oxide, isoamyl nitrite, nitroethane and nitrobenzene, on the other hand, showed no evidence of enhancing the value of Q(R) beyond 1.0. The behavior shown by nitrate is, therefore, quite different from the result reported for the reaction of organocuprate with nitrobenzene.[9]

The reaction between nitrate salts and Grignard reagents has not been published. It is known, how-

7) One of nitrogen oxides (nitrogen dioxide *etc.*) formed *in situ* may be the essential oxidant. Oxidation of metallic silver with nitrogen dioxide may involve electron transfer since a small amount of nitric oxide was detected in gas phase during the reaction of silver(I) nitrate with ethylmagnesium bromide.[8]

8) M. Tamura and T. Yasui, *Chem. Commun.*, **1968**, 1209; *Kogyo Kagaku Zasshi*, **72**, 575, 578, 581, 585 (1969).

9) G. M. Whitesides, W. F. Fischer, Jr., J. S. Filippo, Jr., R. W. Bashe, and H. O. House, *J. Amer. Chem. Soc.*, **91**, 4871 (1969).

TABLE 5. REACTIONS OF TRANSITION METAL HALIDES AND ETHYLMAGNESIUM BROMIDE IN THE PRESENCE OF LITHIUM NITRATE[a)]

Transition metal halide	$LiNO_3$ (mmol)	EtMgBr (mmol)	Temp (°C)	Period (min)	Q(Et)	Distribution of product (%)			$\Delta Et^{b)}/LiNO_3$	Reaction[c)] mixture
						C_2H_4	C_2H_6	$n\text{-}C_4H_{10}$		
$MnCl_2$		8.8	30	60	2.2	28.3	71.7	0.0		A
$MnCl_2$	0.95	18.0	30	360	7.0	37.6	61.1	1.3	5.0	B
$FeCl_3$		8.8	2	60	3.7	18.3	67.2	14.5		B
$FeCl_3$	0.50	18.0	2	60	6.8	18.5	37.4	44.1	6.0	B
$FeCl_2$		8.8	2	60	2.1	25.9	67.6	6.5		B
$FeCl_2$	0.95	18.0	2	60	6.3	19.6	37.0	43.4	4.3	B
$CoBr_2$		8.8	2	60	2.6	17.1	78.7	4.2		B
$CoBr_2$	0.95	18.0	2	60	7.2	32.5	55.4	12.1	5.4	B
$NiCl_2$		8.8	2	60	2.5	36.5	61.2	2.3		B
$NiCl_2$	0.95	18.0	2	60	6.1	28.3	50.8	20.9	3.8	B
$PdCl_2$		7.0	2	60	2.2	48.1	51.9	0.0		B
$PdCl_2$	0.95	18.0	2	150	5.0	42.4	56.2	1.4	3.1	B
CuCl		10.5	25	120	1.0	50.8	49.2	0.0		A
CuCl	0.95	18.0	30	60	3.5	19.9	47.7	32.4	2.6	B
$CuCl_2$		10.5	25	60	1.9	26.6	28.7	44.7		A
$CuCl_2$	0.95	18.0	25	60	4.3	18.6	32.5	48.9	2.4	B

a) In 21 ml THF solution containing 1.0 mmol transition metal halide.
b) Differences between the total yield in the presence of $LiNO_3$ and that in the absence of $LiNO_3$.
c) A: Black precipitate and colorless solution, B: Black-brown or brown solution together with varying amounts of precipitate.

ever, that various products are formed in the reactions of nitrogen dioxide, nitroalkanes, and organic nitrates with Grignard reagents.[10] These reactions presumably involve addition of the Grignard reagent to the nitrogen–oxygen bond. Similar reactions are probably involved with nitrates since diethylhydroxylamine was obtained in the reaction of lithium nitrate and ethylmagnesium bromide in THF after hydrolysis (see Table 6).

Reactions of Transition Metal Halides and Ethylmagnesium Bromide in the Presence of Lithium Nitrate. The role of lithium nitrate as an oxidant was also examined in the reactions of other transition metal halides and ethylmagnesium bromide in THF solution. The results summarized in Table 5 show that lithium nitrate can act as an oxidant in varying degrees of efficiency.

$$MX_n \xrightarrow{\text{excess EtMgBr}} \text{Products} + M \quad (7)$$

$$M \xrightarrow{\text{Oxidant}} M^{+m} \xrightarrow{\text{EtMgBr}} \text{Products} + M \quad (8)$$

The higher efficiency was observed with manganous, ferric, ferrous, cobaltous, and nickelous halides since the values of $\Delta Et/LiNO_3$ were larger with these compounds.

Interestingly, the addition of lithium nitrate also afforded soluble metal species from manganous and cuprous(cupric) chlorides.

$$MX_n \xrightarrow{\text{excess EtMgBr}} \text{Products} + M \text{ (Black precipitate)} \quad (9)$$

$$MX_n \xrightarrow{LiNO_3\text{-excess EtMgBr}} \text{Products} + \text{Soluble M species (M; Ag, Cu, and Mn)} \quad (10)$$

10) M. S. Kharasch and O. Reinmuth, "Grignard Reagents of Nonmetallic Substances" Prentice-Hall Co., New York, N. Y. (1954).

The effect of lithium nitrate on the formation of reduced metal species was not clear with other transition metal halides since soluble species were also formed from these transition metals in its absence.

The formation of coupling dimer from other transition metal halides was also facilitated by lithium nitrate. Its effect could not be examined directly since most ethyl transition metal complexes are labile.

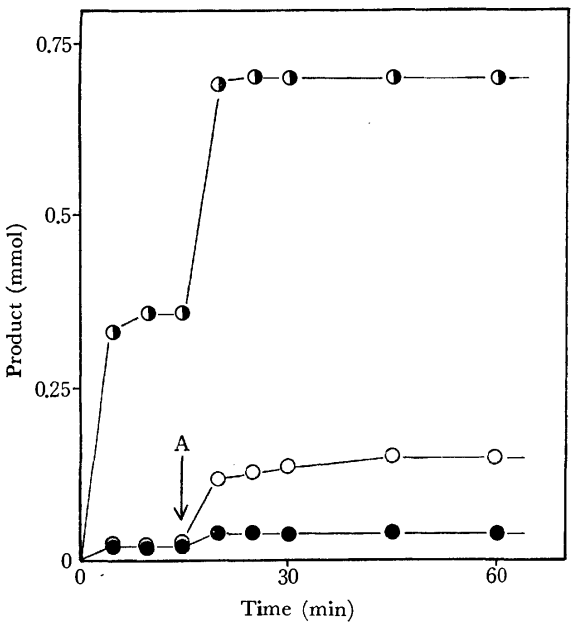

Fig. 3. Rate of formation of products in the reaction of cupric chloride and ethylmagnesium bromide in the presence of nitrogen dioxide.
In 21 ml THF solution containing 1.0 mmol $CuCl_2$ and 1.68 mmol EtMgBr at 2°C
◑: $n\text{-}C_4H_{10}$, ○: C_2H_6, ●: C_2H_4
Nitrogen dioxide (0.80 mmol) was added at point A.

Ethylcopper and ethylmanganese complexes, however, are relatively stable thermally in THF solutions.[5] The rate of the reaction between ethylcopper and nitrogen dioxide is illustrated in Fig. 3 which shows that the coupling dimer was formed immediately in high yield.

$$2\ \mathrm{EtCu} \xrightarrow{\mathrm{NO_2}} \mathrm{Et\text{-}Et} + 2\ \mathrm{Cu\ species} \qquad (11)$$

Ethane and ethylene, on the other hand, were the principal products in the absence of nitrogen dioxide as indicated in Table 5. The oxidation of organocuprates with molecular oxygen to form coupling dimer has been reported in an analogous situation.[9] We also find that the oxidation of ethylcopper species in THF with molecular oxygen affords *n*-butane in excellent yields. Oxidation of a mixture of ethylcopper and *n*-propylmagnesium bromide with nitrogen dioxide in THF yielded a mixture of three coupling dimers (*n*-butane, *n*-pentane, and *n*-hexane) in high yield.

$$\mathrm{EtCu} + n\text{-PrMgBr} \rightleftarrows n\text{-PrCu} + \mathrm{EtMgBr} \qquad (12)$$

$$\mathrm{EtCu} + n\text{-PrCu} \xrightarrow{\mathrm{NO_2}} \mathrm{C_4H_{10}} + \mathrm{C_5H_{12}} + \mathrm{C_6H_{14}} + \mathrm{Cu\ species} \qquad (13)$$

Nitrogen dioxide also oxidized methyl and ethylmanganese species in THF solutions. Coupling dimer was obtained quantitatively from methylmanganese species, and equimolar amounts of ethane and ethylene were formed from ethylmanganese species.[5]

These observations suggest that lithium nitrate increases the yield of coupling dimer by direct oxidation of the alkyl transition metal complex formed *in situ*.

Soluble Form of Reduced Silver Complex. A soluble silver complex was formed, as mentioned above, in the reaction of silver(I) nitrate with Grignard reagent, diethylmagnesium or ethyllithium and in the reaction of silver(I) perchlorate with ethylmagnesium bromide in the presence of lithium nitrate or nitrogen dioxide in THF. It was not formed in the reaction of silver (I) nitrate with phenyl, allyl, benzylmagnesium bromide, diethylzinc, or triethylaluminum or in the reaction of silver(I) perchlorate with ethylmagnesium bromide in the presence of methyl nitrate. The reaction temperature and the molar ratio of ethylmagnesium bromide to silver(I) nitrate also greatly influenced the yield of soluble silver complex (Table 3).

The soluble silver complex designated as (A) showed a sharp λ_{max}, at 415 nm after dilution of the reaction mixture with THF, and the absorption was independent of the organometallic compound (Table 2). When an excess of Grignard reagent was added to the silver complex(A), the λ_{max} was shifted to 400 nm to form a new species(B) as shown in Fig. 4.

The chemical behaviors of the soluble complex(A) obtained from the reaction of silver(I) nitrate with diethylmagnesium are summarized in Fig. 5. The solution did not contain ethyl–metal groups since no ethane was evolved on acidic hydrolysis. Metallic silver was recovered quantitatively as a black precipitate when the solution was hydrolyzed with dilute sulfuric acid. Silver(I) species were absent since no silver(I) chloride was detected after extraction with concentrated ammonium solution followed by neutralization with hydrochloric acid. The soluble silver complex did not appear to react with excess triphenylphosphine and diethylzinc (no change in the visible spectra). The addition of benzyl and allyl bromides to the silver complex(A) afforded dibenzyl and diallyl, respectively, and silver(I) bromide in stoichiometric amounts. Oxidation of the soluble silver complex(A) with oxygen afforded silver(I) species only partially. When an equal amount of diglyme was added to the solution of complex(A), a black-brown precipitate was formed immediately. This precipitate was soluble in fresh THF and the resulting solution showed the same λ_{max} at 415 nm. The black-brown precipitate was washed with a 1 : 1 mixture of diglyme–THF under helium several times until no magnesium compound was detected in the washings. The solid, however, still contained magnesium compound in amounts corresponding to the ratio of silver/magnesium=1.1. The infrared spectra of the purified brown solid, which was dried *in vacuo* at room temperature, showed no characteristic absorptions. Both solutions of the complexes absorbing at 415 and 400 nm also showed no signal when the electron spin resonance spectra were examined.

We infer from these observations that both complexes (A) and (B) are composed of zerovalent silver. No zerovalent silver complexes have been cited.[11]

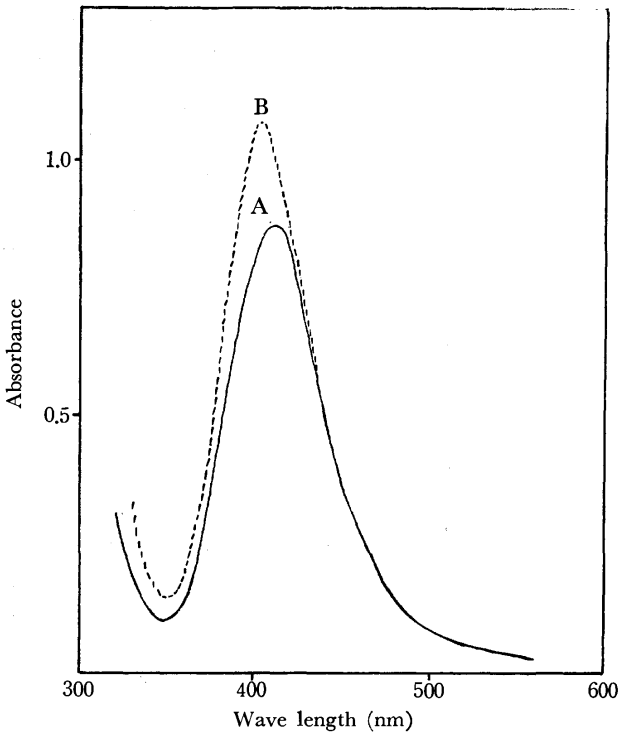

Fig. 4. Visible spectra of soluble silver complexes from the reaction of $AgNO_3$ and EtMgBr in THF.
Ag conc. 0.54×10^{-4} M, at room temperature
A: Reaction solution after dilution with THF
B: In the presence of excess EtMgBr

11) R. R. Dewald, J. M. Brooks, and M. A. Trickey, *Chem. Commun.*, **1970**, 963.

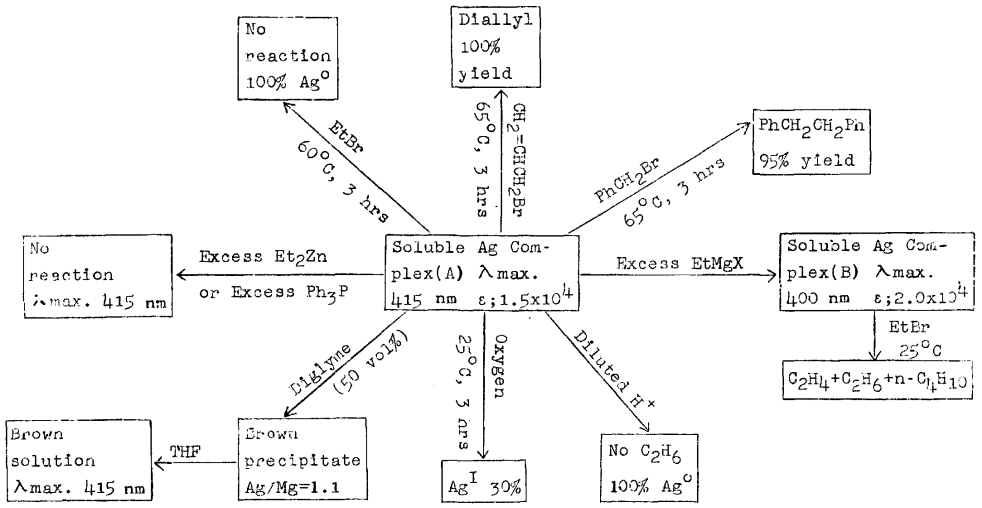

Fig. 5. Properties of the soluble silver complex obtained in the reaction of silver (I) nitrate and diethylmagnesium in tetrahydrofuran.

However, the formation of zerovalent cobalt and iron complexes coordinated with Grignard reagent have been reported under similar conditions.[12] Complex (B) absorbing at 400 nm may be a silver complex coordinated with Grignard reagent and is represented as the complex which shows enhanced catalytic activity in the Kharasch reaction.[5] The structure of complex(A) absorbing at 415 nm is not clear, but we assume that it is a zerovalent silver complex coordinated with one of the nitrogen-containing magnesium compounds formed in the reaction (see Experimental). Complex(B) absorbing at 400 nm was more stable than complex(A) absorbing at 415 nm and could be stored for prolonged periods in a refrigerator.

The lower yields of complex A) obtained at higher temperatures and at higher molar ratios of ethylmagnesium bromide to silver(I) nitrate may be attributed to the aggregation of the silver species presumed to be the catalyst in the Kharasch reaction.[5] The relationship between the organometallic compound and nitrogen-containing oxidant on the yield of complex (A) may also be related to the aggregation of silver.

Experimental

All reactions in this paper were carried out under an inert atmosphere.

Materials. A billet of triply sublimed magnesium was obtained from Dow Chemical Co. Anhydrous nickelous chloride was prepared from the reaction of its hexahydrate and thionyl chloride. Anhydrous ferrous chloride was prepared by disproportionation of iron and anhydrous ferric chloride in THF.[13] Anhydrous manganous chloride was prepared from its tetrahydrate by treating at 150°C for 50 hr *in vacuo*. Anhydrous ferric chloride, palladous chloride, cobaltous bromide, cuprous chloride, cuppric chloride, silver(I) bromide, acetate, nitrate, nitrite and perchlorate, lithium nitrate, nitrogen dioxide, nitric oxide, isoamyl nitrite, and triphenylphosphine were of commercial grade and used without further purification. Nitrobenzene, nitroethane, and all organic bromides were purified by distillation before use. Methyl nitratew as prepared from methyl alcohol and nitric acid.[14]

Organometallic Compounds. All Grignard reagents were prepared as usual except for the use of 1.5 times excess metallic magnesium and low temperature (5~25°C). After filtration under nitrogen, all solutions of the Grignard reagents (0.5~2.0 M) were almost colorless except for vinylmagnesium bromide. The concentration of each Grignard reagent was determined by back titration with base and by the measurement of the amount of hydrocarbon liberated after acidic hydrolysis. Diethylmagnesium was prepared by precipitation of magnesium bromide from the Grignard reagent with dioxane followed by replacement of ether with THF. Ethyllithium (benzene solution, purchased from Lithium Corporation of America, Inc.) and triethylaluminum (supplied from Du Pont Co.) were of commercial grade. Diethylzinc was prepared from the reaction of zinc–copper couple with a mixture of ethyl bromide and ethyl iodide.[15] Tetraethyllead[16] and tetraethyltin[17] were prepared from the Grignard reagent in ether solution.

Solvents. THF was purified by refluxing over lithium aluminum hydride for 2 days, fractionating under nitrogen and stored under helium. Diethyl ether, dioxane, and diglyme were purified in a similar manner.

Analysis of Organic Product. Organic products were analyzed by gas chromatography using the internal standard method as previously reported.[5]

Analyses of Silver and Magnesium. Silver(0) was analyzed by titration[18] with a standard solution of potassium thiocyanate after extraction of silver(I) species with concentrated ammonium solution, filtration and oxidation with

12) M. H. Abraham and M. J. Hogarth, *J. Organometal. Chem.*, **12**, 1 (1968); G. Costa, G. Mestroni, and G. Boscarato, *Ric. Sci.*, **7**, 315 (1964).

13) G. Wilkinson, "Organic Synthesis, Col. Vol. IV, 473 (1963).

14) A. P. Black and F. H. Babers, *ibid.*, Col. Vol. II, p. 412 (1967).

15) C. R. Noller, *ibid.*, Col. Vol. II, p. 184 (1967).

16) R. H. Bullard and W. Robinson, *J. Amer. Chem. Soc.*, **49**, 1368 (1927); R. K. Ingham, S. D. Rosenberg, and H. Gilman *Chem. Revs.*, **60**, 459 (1960).

17) H. Gilman and R. G. Jones, *J. Amer. Chem. Soc.*, **72**, 1760 (1950).

18) A. I. Vogel, "A Text-book of Quantitative Inorganic Analysis" Third ed., Longmans, London (1961),

TABLE 6. REACTION OF NITROGEN-CONTAINING OXIDANT WITH GRIGNARD REAGENTS IN TETRAHYDROFURAN[a]

Oxidant	mmol	Grignard reagent RMgBr	mmol	Temp (°C)	Period (min)	RH (mmol)	R loss[b] (mmol)	Alkali[c] (mmol)
$LiNO_3$	2.5	MeMgBr	15.4	23	120	0.10	~0	15.4
$LiNO_3$	2.0	MeMgBr	7.3	62	120	0.43	2.6	9.2
$LiNO_3$	1.2	EtMgBr	8.1	31	120	1.40[d]	3.2	9.2
$NaNO_2$	2.0	EtMgBr	8.1	31	120	0.07	~0	8.1
$MeONO_2$	1.6	EtMgBr	7.0	2	60	0.47	n. d.[e]	n. d.
NO_2	0.85	EtMgBr	7.0	2	60	0.70	n. d.	n. d.
$EtNO_2$	1.4	EtMgBr	7.3	2	60	0.95	n. d.	7.2

a) In 21 m*l* THF solution.
b) RMgBr charged minus total RH after hydrolysis.
c) Titrated after the reaction was completed.
d) Contained 0.28 mmol C_2H_4 and 0.09 mmol n-C_4H_{10}, A small amount of nitric oxide was detected in gas phase by gc (molecular sieve).
e) Not determined.

nitric acid. Silver(I) species was analyzed gravimetrically after precipitation as silver(I) bromide. Magnesium was determined by EDTA titration.[17]

Reaction of Silver(I) Nitrate and Ethylmagnesium Bromide in Tetrahydrofuran (Typical example). To a 250 m*l* round bottomed flask equipped with a magnetic stirring bar and sealed with a rubber serum cap was added 0.17 g silver(I) nitrate. The nitrogen atmosphere was replaced with helium and 17 m*l* of THF was added with a syringe. After the flask was immersed in a dry ice–acetone bath, 25 ml of methane and 25 m*l* of isobutane (both markers) were added with syringes. The flask was then transferred to an ice–water bath. After 5 min agitation, 4.0 m*l* of ethylmagnesium bromide (7.3 mmol) was added to the solution with stirring. The color of the solution became black (suspension) immediately and then gradually changed to a black-brown solution. A small portion of the gas phase was removed with a hypodermic syringe and analyzed by gas chromatography at intervals of time. After the reaction was complete (60 min), a small portion of the reaction mixture was transferred to a deaerated test tube sealed with a serum cap. The mixture was centrifuged for 5 min and 0.10 m*l* of the black-brown supernatant solution was transferred to UV cell sealed with a rubber septum and containing 20 m*l* of THF. Visible spectrum was measured in the range 300~600 nm (λ_{max} 415 nm, Absorbance; 0.82). λ_{max} shifted to 400 nm (Absorbance; 1.35) when 1.0 m*l* of ethylmagnesium bromide solution (1.8 M) was added to the solution in UV cell. All subsequent reactions were also carried out in a similar manner.

Reaction of Nitrogen-Containing Oxidants with Grignard Reagents in Tetrahydrofuran. The reactions of nitrogen-containing oxidants with Grignard reagents were examined in THF solutions. The results are summarized in Table 6 which shows that the corresponding alkane was formed in varying yield. The reaction of lithium nitrate and methylmagnesium bromide did not proceed smoothly at 23°C but it occurred at 62°C to form predominantly methane. The reaction of sodium nitrite and ethylmagnesium bromide was also negligible. After the reaction was complete, the amount of alkali was greater than that of ethylmagnesium bromide charged.

The rate of formation of ethane in the reaction of lithium nitrate and ethylmagnesium bromide was also examined in THF solution. The amounts of ethane were determined at 5-min intervals and plotted against time. From the slope of the resulting line, the rate of formation of ethane was calculated (initial rate). A systematic variation of the concentration of each component led to the following empirical equation.

$$\frac{dC_2H_6}{dt} = k[LiNO_3]^{1.0}[EtMgBr]^{1.2}$$

The apparent activation energy of this reaction was 17.0 kcal/mol and the apparent second order rate constant was approximately 10^{-3} l mol^{-1}–sec^{-1} at 2.0°C. These results suggest that the following reactions occurred in the reaction between lithium nitrate and ethylmagnesium bromide.[10]

$$LiONO_2 + EtMgBr \xrightarrow{slow} LiOMgBr + EtNO_2$$

$$EtNO_2 + EtMgBr \xrightarrow{fast} C_2H_6 + CH_3CH{=}N\begin{matrix}\nearrow OMgBr\\ \searrow O\end{matrix}$$

$$EtNO_2 + EtMgBr \rightarrow Et_2N\begin{matrix}\nearrow OMgBr\\ \searrow O\end{matrix}$$

$$Et_2N\begin{matrix}\nearrow OMgBr\\ \searrow O\end{matrix} + EtMgBr \rightarrow Et_2NOMgBr + EtOMgBr$$

$$LiOMgBr + H_2O \rightarrow LiOH + MgBrOH \text{ } etc.$$

Diethylhydroxylamine was the main product isolated after acidic hydrolysis from the reaction between lithium nitrate and ethylmagnesium bromide as well as that between silver(I) nitrate and ethylmagnesium bromide. However, these reactions can not be directly related to the oxidant since neither nitroethane or diethylhydroxylamine acted as an oxidant during the reaction of silver(I) perchlorate and ethylmagnesium bromide. It is possible that one of the nitrogen oxides (nitrogen dioxide *etc.*) is the essential oxidant. The formation of nitrogen oxides in the reaction of lithium nitrate and ethylmagnesium bromide may involve electron transfer since nitrogen oxides are formed during the oxidation of metallic palladium with lithium nitrate in acetic acid.[8]

Reaction of Silver(I) Nitrate and n-Butylmagnesium Bromide in the Presence of Lithium Nitrate. Silver(I) nitrate (2.5 mmol), lithium nitrate (20 mmol), and 50 m*l* THF were added to a 500 m*l* round bottomed flask which was previously flushed with nitrogen and sealed with a rubber serum cap. A solution of 1.0 M n-butylmagnesium bromide (100 m*l*) was added and the mixture was stirred for 3 hr

at 10°C. The reaction mixture was worked up in the usual manner after addition of dilute sulfuric acid and extraction with petroleum ether. Distillation afforded 1.85 g (72% based on total nitrate group) of *n*-octane.

We wish to thank the National Science Foundation for generous financial support, the Du Pont Company for the THF and the Dow Chemical Company for the billet of magnesium used in this work.

BULLETIN OF THE CHEMICAL SOCIETY OF JAPAN, VOL. 45, 1127—1132 (1972)

The Reaction Mechanism of 2-Dimethoxymethyl-3-methoxypropionitrile with Acetamidine. I. A Revised Structure of the Intermediate[1]

Takenori NISHINO, Masumi KIYOKAWA, Yoshiyuki MIICHI, and Kanji TOKUYAMA

Shionogi Research Laboratory, Shionogi & Co., Ltd., Fukushima-ku, Osaka

(Received July 29, 1971)

The reaction of 2-dimethoxymethyl-3-methoxypropionitrile (**1**) with acetamidine yields 2,7-dimethyl-5,6-dihydropyrimido[4,5-*d*]pyrimidine (**6**) *via* an intermediate, λ_{max}^{MeOH} 262 mμ. This intermediate has been identified as 2-acetamidinomethylene-3-methoxypropionitrile (**5**) without being isolated. However, this assignment seems to be somewhat inconsistent with the stabilities of an acetal group in basic media and with the UV spectra of compounds with structures similar to **5**. The reaction of **1** with sodium methoxide gave a dimeric compound (**8**). This result suggests the formation of **2**-dimethoxymethylacrylonitrile (**2**) in the initial stage of the reaction of **1** with acetamidine. The reaction of acrylonitrlie with acetamidine yielded 2-methyl-4-amino-5,6-dihydropyrimidine (**23**), whose UV spectrum in methanol showed its absorption maximum at 270 mμ in neutral media and at 258 mμ in basic media. Therefore, the structure of the intermediate may be concluded to be 2-methyl-4-amino-5-dimethoxymethyl-5,6-dihydropyrimidine (**27**) instead of **5**, and the reaction may be concluded to proceed *via* the pathway of **1**→**2**→**27**→**6**.

Interesting and rather complicated results have been reported by Takamizawa and his co-workers dealing with the syntheses of some pyrimidines from derivatives of 2-formyl-3-methoxypropionitrile with acetamidine.[2] Two types of pyrimidines are obtainable by the reactions: 2-methyl-4-amino-5-methoxymethylpyrimidine (**7**) can be obtained directly by the reaction of 2-methoxymethylene-3-methoxypropionitrile (**3**), while 2,7-dimethyl-5,6-dihydropyrimido[4,5-*d*]pyrimidine (**6**) can be obtained from 2-dimethoxymethyl-3-methoxypropionitrile(**1**) or 2-dimethoxymethylacrylonitrile (**2**) *via* a complex pathway, which is proposed to be as shown in Chart 1.[2] An intermediate can be detected spectrophotometrically, λ_{max}^{MeOH} 262 mμ or λ_{max}^{EtOH} 275 mμ, without being successfully isolated. When heated with another mole of acetamidine, this intermediate is converted into **6**. This intermediate has been identified as 2-acetamidinomethylene-3-methoxypropionitrile (**5**).

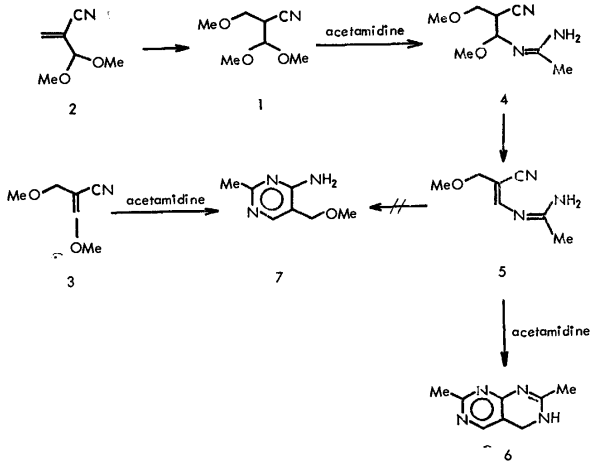

Chart 1

As acetamidine is a strong base (pK_a 12.4),[3] the reactions proceed under basic conditions. The reaction of **3**→**7** is quite natural, judging from the literatures.[4,5] On the other hand, the formation of **6** from **1** or **2** is very unusual and interesting. However, further investigation is thought to be required before we can reach any final conclusion on the reaction mechanism, since the step of **1**→**4**→**5** seems to be inconflict with the stabilities of an acetal group in basic media.[6]

A further question has been raised on the basis of the comparison of the UV spectra of compounds with structures similar to **5**. The absorption maximum of ethyl acetamidinomethylenecyanoacetate[7] appears at 330 mμ in ethanol, and that of 2-aminomethylene-3-ethoxypropionitrile appears at 270 mμ in methanol.[2] From these data the absorption maximum of **5** is expected to appear at a wavelength longer than 270 mμ.

1) Pyrimidines, 8. For Part 7, see F. Takami, S. Wakahara, and T. Maeda, *Chem. Lett.*, **1972**, 159.

2) A. Takamizawa, K. Tokuyama, and K. Tori, This Bulletin, **32**, 188 (1959), and earlier papers in this series.

3) P. A. S. Smith, "The Chemistry of Open Chain Organic Nitrogen Compounds," Vol. 1, W. A. Benjamin, New York (1965), p. 178.

4) H. Andersag and K. Westphal, *Ber.*, **70**, 2035 (1937); R. Grewe, *Z. Phys. Chem.*, **242**, 89 (1936).

5) G. V. Chelinstev and Z. V. Benevalenskaya, *J. Gen. Chem.*, **14**. 1142 (1944); *Chem. Abstr.*, **40**, 4069 (1946),

6) E. Schmitz and E. Eichhorn, "The Chmistry of the Ether Linkage," Interscience, New York (1967), p. 329.

7) T. Matsukawa, *Yakugaku Zasshi.* **62**, 417 (1942),

Consequently, the establishment of unequivocal structure of the intermediate is desired. For this purpose, studies of the behavior of **1** toward bases were attempted.

The treatment of **1** with sodium methoxide at 40°C for 2 hr gave a viscous oil (**8**). The analytical data and the integration of the NMR spectrum showed it to be a dimeric substance, $C_{12}H_{18}N_2O_4$, which was thought to be obtained from the dimerization of **1** by the elimination of one mol of methanol. The UV spectrum in ethanol showed the absorption maximum at 232 mμ suggesting the presence of a partial structure of MeO–C=C–CN.[8] The IR spectrum showed characteristic absorption bands due to non-conjugate and conjugate nitriles, double bond, and acetal and methoxy groups. Therefore, **8** was determined to be 2-dimethoxymethyl-2-methoxymethyl-4-methoxymethyleneglutaronitrile and to be, as will be described below, a mixture of *trans* and *cis* isomers.[9]

Figure 1 shows the NMR spectrum of **8** in carbon tetrachloride. With the 4-methoxymethylene group, the signal due to the methine proton appeared as two singlets at 2.98 τ (⅔H, a) and 3.18 τ (⅓H, b), while the signal due to the methyl group also appeared as two singlets, at 6.10 τ (2H, a) and 6.08 τ (1H, b). The signal due to the methylene proton at the 3-position appeared as an AB-type quartet at 7.43 τ and 7.55 τ (J 14 Hz, ⅔H, a), and as a singlet at 7.57 τ (⅔H, b). These data clearly supported the idea that **8** was a mixture of two isomers whose ratio was about 2 : 1.

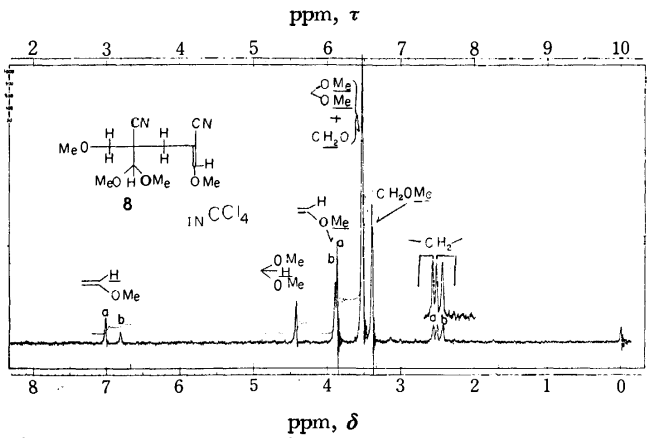

Fig. 1. NMR spectrum of **8** (a mixture of *cis* and *trans* isomers) in carbon tetrachloride at 60 MHz.

The assignment of the other signals was also consistent with the proposed structure. The methyl signal of the 2-methoxymethyl group was observed as a three-proton singlet at 6.60 τ and the two methyls of the acetal group, as a six-proton singlet at 6.45 τ, which overlapped with the two-proton singlet due to the methylene proton of the 2-methoxymethyl group. The methine proton of the acetal group was observed as an one-proton singlet at 5.60 τ.

8) A. Takamizawa, K. Hirai, and S. Sumimoto, *Chem. Pharm. Bull.* (Tokyo), **14**, 238 (1966).

9) "*Cis*" means that the methoxy group of the 4-methoxymethylene moiety is located on the same side of the nitrile group, while "*trans*" means that it is found on the opposite side.

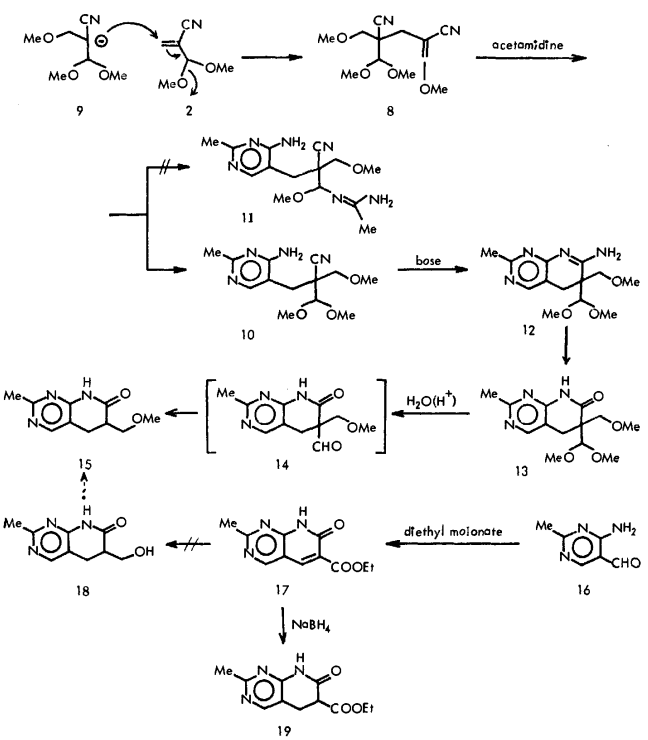

Chart 2

A reasonable pathway for the formation of **8** has been proposed; it is shown in Chart 2. Under basic conditions, an equilibrium of **1**⇌carbanion (**9**)⇌**2** can give **8**. Although the formation of **3** from **9** was also expected, the addition product of **9** to **3** was scarecely detected. Therefore, the initial step of the reaction of **1** under basic conditions must be the predominant formation of **2**. Consequently, in the reaction of **1** with acetamidine, the Michael-type addition of acetamidine to **2** initially formed may be expected as the second step. The disagreement for the initial step of the reaction of **1** with acetamidine between this conclusion (**1**→**2**→Michael-type addition compound→**6**) and the mechanism proposed by Takamizawa *et al.* (**2**→**1**→**5**→**6**)[2] has prompted us to study the reaction of **8** with acetamidine.

If the reaction of **1** with acetamidine proceeded only by the Michael-type addition of acetamidine to a double bond, **8** would be converted into a pyrimidine (**10**), in which the acetal group of **8** remained unchanged. On the other hand, if the reaction of **1** could proceed by the direct substitution of the acetal part, **8** could be converted into another pyrimidine (**11**), which has no acetal group. When **8** was treated with acetamidine in 1,2-dimethoxyethane (DME) at a reflux temperature, a compound, $C_{13}H_{20}N_4O_3$, was obtained which was proved to be 2-methyl-4-amino-5-(2′-cyano-2′-dimethoxymethyl-3′-methoxy)propylpyrimidine (**10**) by physical and chemical methods, as will be reported in detail below.

The UV spectrum showed the characteristic bands due to 4-aminopyrimidines[10,11] and the IR spectrum

10) A. Takamizawa, *Yakugaku Zasshi*, **74**, 748 (1954).

11) D. J. Brown, "The Pyrimidines," Interscience, New York (1962), p. 447.

showed the bands due to non-conjugate nitrile and acetal groups. The NMR spectrum also suggested the presence of pyrimidine ring and an acetal group. Therefore, the structure of **10** was established.

The structure of **10** was further confirmed by the following reactions. The heating of **10** in pyridine containing sodium hydroxide afforded **12**. The IR spectrum showed the absence of a nitrile group and the UV spectrum in ethanol showed the absorption maxima at 221 and 301 mμ, which were shifted to 281 and 322 mμ in acidic media. As these spectral data suggested the presence of a bicyclic structure, **12** was concluded to be 2-methyl-6-dimethoxymethyl-6-methoxymethyl-7-amino-5,6-dihydropyrido[2,3-*d*]pyrimidine.

The hydrolysis of **12** with acetic acid gave **13**, $C_{13}H_{19}N_3O_4$, which was identified as 2-methyl-6-dimethoxymethyl-6-methoxymethyl-7-oxo-8*H*-5,6-dihydropyrido[2,3-*d*]pyrimidine (**13**) from its IR spectrum, which showed the bands due to amidocarbonyl, acetal, and methoxymethyl groups. The UV spectrum in ethanol showing absorption maxima at 242 and 275 mμ which were shifted to 280 mμ in acidic media and to 280 and 301 mμ in alkaline media, also supported the structure. Hydrolysis of **12** under strongly acidic conditions gave **15**, $C_{10}H_{13}N_3O_2$. The IR and NMR spectra showed the absence of an acetal group, and the behavior in the UV spectrum was quite similar to that of **13**. Therefore, the structure of **15** is probably 2-methyl-6-methoxymethyl-7-oxo-8*H*-5,6-dihydropyrido[2,3-*d*]pyrimidine, which can be derived *via* a formyl compound (**14**). To obtain further evidence for the above-described structures, the synthesis of **15** was attempted by means of the scheme outlined in Chart 2 (**16**→**17**→**18**→**15**). 2-Methyl-6-carbethoxy-7-oxo-8*H*-pyrido[2,3-*d*]pyrimidine (**17**) was prepared by the reaction of 2-methyl-4-amino-5-formylpyrimidine (**16**)[12] with diethyl malonate, using piperidine as the catalyst. The IR spectrum, which showed the characteristic band due to the amidocarbonyl group, and the NMR spectrum, which showed signals of the ethoxy group, the methyl group, the pyrimidine-ring proton, and the pyridone-ring proton, confirmed the structure. The behavior in the UV spectrum also supported the structure.

The reduction of **17** with lithium aluminum hydride to **18** was unsuccessful because of the formation of many unexpected products. However, another reduced product (**19**) was obtained by using sodium borohydride as a reducing reagent. The IR spectrum showed two carbonyl bands, and the NMR spectrum exhibited signals due to the ethyl group, the pyrimidine-ring proton, the methyl group on the pyrimidine-ring, and the $-CH_2-CH-$ moiety appearing as an ABX pattern.

These data suggested that **19** was 2-methyl-6-carbethoxy-7-oxo-8*H*-5,6-dihydropyrido[2,3-*d*]pyrimidine. Although the attempt to prepare the expected compound, **18**, for the synthesis of **15** through a different scheme was unsuccessful, the behavior of **19** in the UV spectrum was quite similar to that of **15**. Therefore, the structures of the **13** and **15** and, consequently, the structure of **10** were confirmed. The formation of **10** from only the reaction of **8** with acetamidine suggested that the acetal group of **1** was inert for the substitution with acetamidine under basic conditions and that the Michael-type addition of acetamidine to double bonds was preferable.

As has been described above, under basic conditions, **1** would be predominantly converted into **2** in the initial stage and the Michael-type addition of acetamidine to a double bond would more easily occur as compared with the case of the low reactivity of an acetal group. Therefore, the intermediate, detected spectrophotometrically, is derived from the reaction of **2** with acetamidine, not directly from the reaction of **1**.

Pietra has reported a reaction of acrylonitrile with benzamidine which yields 2-phenyl-4-amino-5,6-dihydropyrimidine (**21**).[13] As no detailed data were presented, however, we reinvestigated this reaction under milder conditions. In the initial stage of the reaction, a new compound (**20**) was isolated; it was then easily converted into **21** on heating. The compound **20** showed the ba nddue to a non-conjugate nitrile group in the IR spectrum and the signal due to an ethylene group appearing as an A_2B_2 pattern in the NMR spectrum (chloroform-*d*). Therefore, **20** was determined to be 3-benzamidinopropionitrile, and this reaction was concluded to proceed through the Michael-type addition of benzamidine to acrylonitrile, followed by cyclization. Consequently, the most likely structure of the intermediate, λ_{max}^{MeOH} 262 mμ, is 2-methyl-4-amino-5-dimethoxymethyl-5,6-dihydropyrimidine (**27**), which is formed by the cyclization of 2-dimethoxymethyl-3-acetamidinopropionitrile (**26**), the addition product of acetamidine to **2**. To obtain further rational evidence of this idea, the synthesis of a model compound, 2-methyl-4-amino-5,6-dihydropyrimidine (**23**), was attempted. The treatment of acetamidine with acrylonitrile afforded a syrup, which was then converted into crystals at room temperature. The crystals, $C_5H_9N_3$, showed no band due to a nitrile group in the IR spectrum. Therefore, it was identified as 2-methyl-4-amino-5,6-dihydropyrimidine (**23**). The purification of the intermediate syrup was unsuccessful, but its IR spectrum, showing the band due to a non-conjugate nitrile group, suggested that it was 3-acetamidinopropionitrile (**22**).

The structure of **23** was also supported by the NMR spectrum in dimethyl sulfoxide-d_6 (Fig. 2), which showed a broad signal due to an amino group at 5.20 τ, a narrow triplet due to the methyl group at the 2-position at 8.18 τ, and signals due to H_5 (7.99 τ) and H_6 (6.78 τ) appearing as an A_2B_2 pattern. The triplet of the methyl group and the broad signal of H_6 must be caused by homoallyl coupling between them (J 1Hz). The value of the coupling constant was consistent with those of the coupling constants of **28** (J

12) S. Mizukami and E. Hirai, *Chem. Pharm. Bull.* (Tokyo), **14**, 1321 (1966).

13) S. Pietra, *Boll. Sci. Fac. Chem. Ind. Bologna*, **11**, 78 (1953).

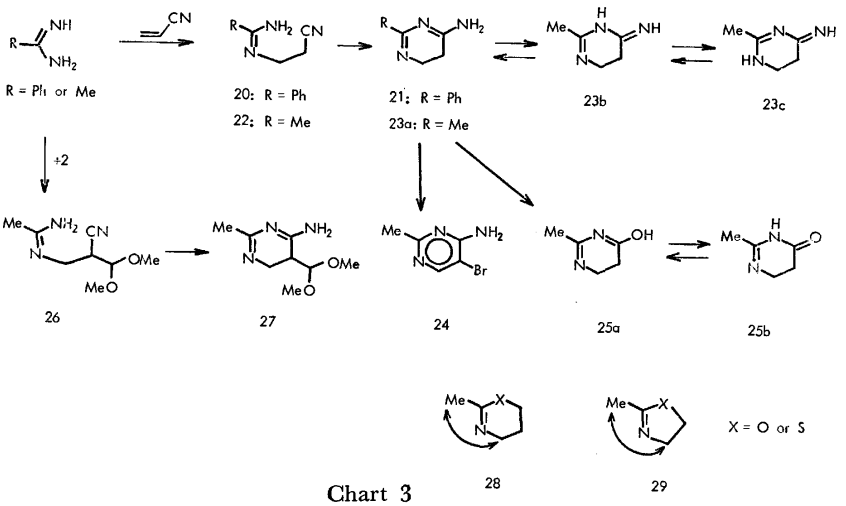

Chart 3

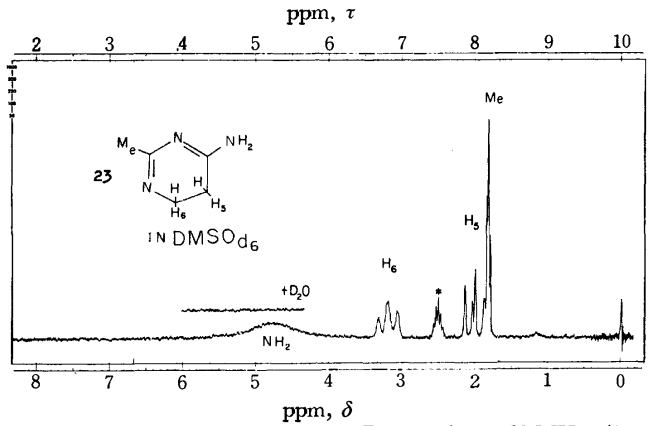

Fig. 2. NMR spectrum of **23** in DMSO-d_6 at 60 MHz (* DMSO-d_5).

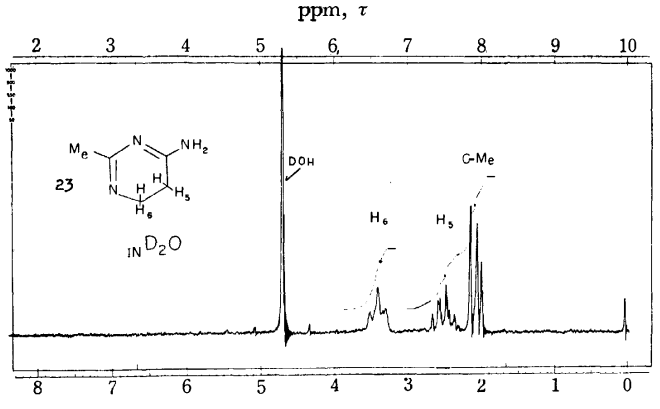

Fig. 3. NMR spectrum of **23** in deuterium oxide at 60 MHz.

1.5 Hz),[14] and **29** (J 1.38—1.65 Hz).[15] The methyl signal of **23** appeared as one triplet in dimethyl sulfoxide-d_6, but as three broad methyl singlets in deuterium oxide (Fig. 3). The spectrum seemed to suggest the existence of three kinds of tautomers, such as **23a**, **23b**, and **23c**.

The structure of **23** was unequivocally established by the following reactions. The bromination of **23** with bromine in acetic acid, followed by dehydrobromination with triethylamine, gave 2-methyl-4-amino-5-bromopyrimidine (**24**).[16] The addition of hydrochloric acid to a methanol solution of **23** immediately gave colorless crystals (**25**), whose molecular formula agreed with that of the hydrolized product of **23**. The NMR spectrum of **25** in methanol-d_4 showed a narrow triplet due to the methyl group, and signals due to H_5 and H_6 appeared as an A_2B_2 pattern. Therefore, **25** was determined to be 2-methyl-4-hydoxy-5,6-dihydropyrimidine (isolated as the HCl salt). As the IR spectrum of **25** showed the band due to an amidocarbonyl group, it seemed to have preferably the **25b** structure in a crystalline state rather than the **25a** structure. Easy hydrolysis of 4-amino group of **23** supported the presence of the partial structure of amidine, and the structure of **23**.[17]

The behavior of **23** in the UV spectrum was very important. The spectrum in methanol showed its absorption maximum at 270 mμ (ε 8,100); it was shifted to 275 mμ in acidic media and to 258 mμ in basic media. The values of the absorption maxima, 270 mμ and 258 mμ, were close to that of 262 mμ of the intermediate previously observed under basic conditions because of the presence of acetamidine. Therefore, the idea that **27** is the intermediate instead of **5** was supported.

In conclusion, for the reaction of **1** with acetamidine we would like to propose the following pathway **1**→**2**→**26**→**27** (the intermediate, λ_{max}^{MeOH} 262 mμ) → **6**, which accounts for the observed results. The mechanism of the step of **27**→**6** is also interesting; studies of it will be presented separately.

Experimental

All the melting points were recorded on a Kofler block and have not been corrected. The NMR spectra were taken with a Varian A-60-A spectrometer, using tetramethylsilane as the internal reference, and the chemical shifts were expressed in τ value (s: singlet, d; doublet, t: triplet, q:

14) E. Cherbuliez, *Helv. Chem. Acta*, **50**, 331 (1967).
15) M. A. Weinberger and R. Greenhalgh, *Can. J. Chem.*, **41**, 1038 (1963).
16) Z. Budĕšisky, *Collect. Czech. Chem. Commun.*, **14**, 223 (1949).
17) L. Doub and U. Krolls, *J. Heterocycl. Chem.*, **7**, 527 (1970).

quartet, m: multiplet). The molecular weights were determined by means of a vapor-pressure osmometer in chloroform unless otherwise stated. The solvents used were removed under reduced pressure.

*Reaction of 2-Dimethoxymethyl-3-methoxypropionitrile (**1**) with Sodium Methoxide.* A mixture of sodium methoxide (2.5 g) and **1** (50 g) was stirred at 40°C, while the methanol produced during the reaction period was eliminated under reduced pressure. After 2 hr, the mixture was dissolved in benzene (600 m*l*); the benzene solution was washed with water, 1 N hydrochloric acid, saturated sodium bicarbonate, and water, dried, and then the solvent was removed. The distillation of the residue (40 g) gave 2-dimethoxymethyl-2-methoxymethyl-4-methoxymethyleneglutaronitrile (**8**) (22.3 g, bp 177—183°C/2 mmHg). $UV_{m\mu}^{EtOH}$ 232 (ε 11100) $IR_{cm^{-1}}^{film}$ 2250, 2240 (CN), 1640 (C=C), 1080, 1150 (C–O–C, acetal). Found: C, 56.74; H, 7.33; N, 10.98%; mol wt, 260 (benzene). Calcd for $C_{12}H_{18}N_2O_4$: C, 56.68; H, 7.14; N, 11.02%; mol wt, 254.28.

*Reaction of 2-Dimethoxymethyl-2-methoxymethyl-4-methoxymethyleneglutaronitrile (**8**) with Acetamidine.* Acetamidine hydrochloride (2.6 g) was neutralized by methanolic sodium methoxide prepared from sodium (554 mg), and then the methanol was removed. To the residue, DME (100 m*l*) and **8** (2.2 g) were added, after which the mixture was refluxed for 2 hr. The solvent was evaporated to dryness and then extracted with ether (50 m*l*). From the ether layer, **8** (748 mg) was recovered. The recrystallization of the ether-insoluble residue from ethyl acetate gave 2-methyl-4-amino-5-(2'-cyano-2'-dimethoxymethyl-3'-methoxy)propylpyrimidine (**10**) (needles; 985 mg). Mp 139—140°C. $UV_{m\mu}^{MeOH}$ 235 (ε 6900), 278 (ε 3400); (+HCl) 252 $IR_{cm^{-1}}^{KBr}$ 2240 (CN), 1100, 1070 (acetal). NMR ($CDCl_3$) 1.93^s (1H, H_6), 5.63^s (1H, C<u>H</u>$(OMe)_2$), 7.53^s (3H, 2-Me), 6.43^s (6H, $CH(O\underline{Me})_2$), 6.59^s (3H, $CH_2O\underline{Me}$), 7.13^q (2H, $\underline{CH_2}OMe$). Found: C, 55.70; H, 7.10; N, 20.21%, mol wt, 279. Calcd for $C_{13}H_{20}N_4O_3$: C, 55.70; H, 7.19; N, 19.99%; mol wt, 280.32.

*2-Methyl-6-dimethoxymethyl-6-methoxymethyl-7-amino-5,6-dihydropyrido[2,3-d]pytimidine (**12**).* To a solution of 2-methyl-4-amino-5-(2'-cyano-2'-dimethoxymethyl-3'-methoxy)propylpyrimidine (**10**; 300 mg) in pyridine (1.5 g), a 48% sodium hydroxide solution (1 g) was added; the solution was then heated at 100°C for 20 min. After the removal of the pyridine, the residue was extracted with chloroform (200 m*l*), and then the chloroform was removed. The recrystallization of the residue from acetonitrile gave **12** (needles; 44 mg). Mp 195—196°C. $UV_{m\mu}^{EtOH}$ 221 (ε 13200), 301 (ε 14200); (+HCl) 281, 322. Found: C, 55.85; H, 7.18; N, 19.86%; mol wt, 285. Calcd for $C_{13}H_{20}N_4O_3$: C, 55.70; H, 7.19; N, 19.99%; mol wt, 280.32.

*2-Methyl-6-dimethoxymethyl-7-oxo-8H-5,6-dihydropyrido[2,3-d]pyrimidine (**13**).* A solution of 2-methyl-6-dimethoxymethyl-6-methoxymethyl-7-amino-5,6-dihydropyrido[2,3-*d*]pyrimidine (**12**; 0.5 g) in 10% acetic acid (10 m*l*) was heated at 100°C for 0.5 hr. The solution was concentrated and neutralized with a saturated sodium carbonate solution, and then the solvent was evaporated to dryness. The residue was extracted with ethyl acetate. From the extract, crude crystals of **13** were obtained (400 mg; mp 118—120°C). Recrystallization from ether gave pure plates of **13** (mp 125–125.3°C). $UV_{m\mu}^{EtOH}$ 242 (ε 5600), 275 (ε 10700); (+HCl) 280; (+NaOH) 280,301. $IR_{cm^{-1}}^{KBr}$ 1700 (CONH), 1065, 1100, 1120 (C–O–C, acetal). NMR ($CDCl_3$) 1.73^s (1H, H_4), 5.25^s (1H, C<u>H</u>$(OMe)_2$), 6.48^s (6H, $CH(O\underline{Me})_2$), 6.28^d, 6.33^d (2H, $\underline{CH_2}OMe$, J 9 Hz), 6.73^s (3H, $CH_2O\underline{Me}$), 6.82^m, 7.03^m (2H, H_5), 7.35^s (3H, 2-Me). Found: C, 55.52; H, 6.77; N, 15.07%, mol wt, 285. Calcd for $C_{13}H_{19}N_3O_4$: C, 55.52; H, 6.76; N, 14.95%, mol wt, 281.31.

*2-Methyl-6-methoxymethyl-7-oxo-8H-5,6-dihydropyrido[2,3-d]pyrimidine (**15**).* A solution of 2-methyl-6-dimethoxymethyl-6-methoxymethyl-7-amino-5,6-dihydropyrido[2,3-*d*]pyrimidine (**12**; 1 g) in 1 N hydrochloric acid (7 g) was heated at 100°C for 50 min. The solution was neutralized with a saturated sodium bicarbonate solution and then concentrated to 2 m*l*. After the extraction of this solution with chloroform (20 m*l*), the chloroform was evaporated to give a powder (723 mg). Recrystallization from methanol gave **15** (175 mg). Mp 185—186°C (columns). NMR ($CDCl_3$) 1.63^s (1H, H_4), 6.25^m (2H, $-CH_2O-$), 6.61^s (3H, OMe), 7.05^m (2H, H_5), 7.05^m (1H, H_6), 7.33^s (3H, 2-Me). Found: C, 58.11; H, 6.43; N, 20.37%. Calcd for $C_{10}H_{13}N_3O_2$: C, 57.96; H, 6.32; N, 20.28%.

*2-Methyl-6-carbethoxy-7-oxo-8H-pyrido[2,3-d]pyrimidine (**17**).* A mixture of 2-methyl-4-amino-5-formylpyrimidine[12] (**16**; 1.35 g), diethyl malonate (1.6 g), benzoic acid (45 mg), piperidine (100 mg) and benzene (18 m*l*) was refluxed for 2 hr, during which time the water produced was removed by azeotropic distillation with benzene. Then, more piperdine (110 mg) was added to the solution, and it was refluxed for an additional 4 hr. After cooling, the crystals which appeared were separated from the solution by filtration. The crystallization of the crystals from ethanol–methanol gave **17** (1.36 g). Mp 230—231.5°C (needles). $UV_{m\mu}^{EtOH}$ 265 (ε 3400), 274 (ε 3100), 324 (ε 9300), (+HCl) 265, 275, 320; (+NaOH) 256, 275, 353. $IR_{cm^{-1}}^{KBr}$ 1690 (CONH). NMR ($CDCl_3$) 5.29^q (2H), 8.58^t (3H)(OC_2H_5), 7.17^s (2-Me), 1.53^s (1H, H_4), 1.05^s (1H, H_5). Found: C, 56.39; H, 4.69; N, 17.79%; mol wt, 249. Calcd for $C_{11}H_{11}N_2O_3$: C, 56.65; H, 4.75; N, 18.02%; mol wt, 233.32.

*Reduction of 2-Methyl-6-carbethoxy-7-oxo-8H-pyrido[2,3-d]pyrimidine (**17**) with Sodium Borohydride.* To a solution of **17** (1.08 g) in ethanol (84 m*l*), sodium borohydride (470 mg) was added at 0°C. After the solution has been stirred for 1 hr at 0°C, the solution was adjusted to pH 4 with hydrochloric acid and then evaporated to dryness under reduced pressure. The residue was extracted with acetone (80 m*l*), and then the solvent was removed. The residue (powder 1.169 g) was purified by silica gel column chromatography [Wakogel Q-23 (30 g) was used]. The desired 2-methyl-6-carbethoxy-7-oxo-8*H*-5,6-dihydro[2,3-*d*]pyrimidine (**19**) was eluted with a mixture of chloroform and ethanol (8 : 1 v/v, 250 m*l*) after initial elution with chloroform (150 m*l*). The recrystallization of the eluted compound from ethanol gave **19** (333 mg). Mp 200—200.5°C. $UV_{m\mu}^{EtOH}$ 240 (ε 8200), 271 (ε 14100); (+HCl) 277; (+NaOH) 298. $IR_{cm^{-1}}^{KBr}$ 1740, 1690 (C=O). NMR ($CDCl_3$) 5.78^q (2H), 8.75^t (3H) (OC_2H_5), 1.63^s (1H, H_4), 7.35^s (3H, 2-Me), 6.78^m (2H, $-\underline{CH_2}-CH$), 6.32^m (1H, $-CH_2-C\underline{H}-$). Found: C, 56.21; H, 5.65; N, 17.71%; mol wt, 249. Calcd for $C_{11}H_{13}N_3O_3$: C, 56.16; H, 5.77; N, 17.86%, mol wt, 235.24.

Reaction of Acrylonitrile with Benzamidine. Benzamidine (4.5 g) was dissolved completely in acrylonitrile (2 g) at −30°C and then left at room temperature. After 1 hr, crystals of 3-benzamidinopropionitrile (**20**) appeared. $IR_{cm^{-1}}^{Film}$ 2280 (CN). NMR ($CDCl_3$) 6.48^m (2H, H_3), 7.27^m (2H, H_2). The crystals were heated for 20 min on a boiling water-bath and then recrystallized from chloroform-benzene. Colorless plates of 2-phenyl-4-amino-5,6-dihydropyrimidine (**21**) (mp 178—180°C)[13] were thus obtained (3.1 g).

Reaction of Acrylonitrile with Acetamidine. A solution of acetamidine hydrochloride (11.8 g) in methanol (30 m*l*) was neutralized with methanolic sodium methoxide pre-

pared from sodium (2.56 g) and methanol (50 ml). The solution was filtered, and then the filtrate was evaporated to dryness. To the residue, acrylonitrile (4 g) was added at 10—20°C, after which the solution was allowed to stand at room temperature for 1 day. The reaction mixture was then solidified. Recrystallization from ethanol–ether (3/8 v/v) gave crude crystals of 2-methyl-4-amino-5,6-dihydropyrimidine (**23**). The further recrystallization of **23** from ethanol gave a pure sample (cubics, 1.45 g). Mp 188—192°C. Found: C, 53.85; H, 8.39; N, 37.82%; mol wt, 125 (ethanol). Calcd for $C_5H_9N_3$: C, 54.03; H, 8.16; N, 37.81%; mol wt, 111.15.

*Dehydrogenation of 2-Methyl-4-amino-5,6-dihydropyrimidine (**23**).* Into a solution of **23** (222 mg) in acetic acid (6 ml) in portions was stirred below 15°C. After the solution had been stirred for 40 min, precipitates were collected by filtration and washed with ethanol. A mixture of precipitates, triethylamine (300 mg), and ethanol (3 g) was refluxed for 3 min, evaporated to dryness, and extracted with benzene, and the benzene was removed. The recrystallization of the residue from water gave 2-methyl-4-maino-5-bromopyrimidine (**24**) (80 mg), mp 138—140°C.[16]

*Hydrolysis of 2-Methyl-4-amino-5,6-dihydropyrimidine (**23**).* To a solution of **23** (111 mg) in methanol, 21% methanolic hydrochloric acid (w/w 0.4 g) was added. Crystals of hydrochloric acid salt of **23** thus appeared. Water (25 mg) was added to the solution, and the solution was stirred at room temperature. After 1 hr, the crystals dissappeared and columnar crystals were newly precipitated. Recrystallization of the columnar crystals from methanol gave 2-methyl-4-hydroxy-5,6-dihydropyrimidine hydrochloride (**25**) (40 mg). Mp>250°C. $UV_{m\mu}^{MeOH}$ 227 (ε 7,570); (+NaOH) 208. $IR_{cm^{-1}}^{KBr}$ 1740 (CONH). NMR (CD_3OD) 7.60^s (3H, 2-Me), 7.15^m (2H, H_5), 6.15^m (2H, H_6). Found: C, 40.41; H, 6.10; N, 18.86%. Calcd for $C_5H_9N_2OCl$: C, 40.36; H, 6.14; N, 19.06%.

The authors wish to express their deep gratitude to Professor Toshihiko Okamoto, University of Tokyo, and to Dr. Ken'ichi Takeda, Director of this Laboratory, for their encouragement.

BULLETIN OF THE CHEMICAL SOCIETY OF JAPAN, VOL. 45, 1132—1136 (1972)

Study on Oxidation of Chalcones with Lead Tetraacetate and Manganic Acetate

Kazu KUROSAWA and Junko HIGUCHI

Department of Chemistry, Faculty of Science, Kumamoto University, Kurokami-machi, Kumamoto

(Received July 31, 1971)

2′-Hydroxychalcones were oxidized with lead tetraacetate and manganic acetate to give *trans*- and *cis*-aurones, together with substituted benzoic acids and cinnamic acid. In the oxidation, 2′-benzyloxy-4,4′-dimethoxychalcone gave 2-acetoxy-1-(2′-benzyloxy-4′-methoxy)phenyl-3-(4′-methoxy)phenylpropane-1,3-dione and *erythro*-2,3-diacetoxy-1-(2′-benzyloxy-4′-methoxy)phenyl-3-(4′-methoxy)phenylpropan-1-one. Structures of the products were elucidated spectrometrically and confirmed by syntheses.

Several papers[1-4] have been published on the oxidation of various organic compounds with manganic acetate. In a previous communication,[5] it was reported that 2′-hydroxychalcones (Ia–i) were oxidized with manganic acetate to give aurones (IIa–i). In some cases,[3,4] however, it was shown that under certain conditions the reagent has a strong similarity to lead tetraacetate.[6] We therefore carried out the oxidation of Ia–i with lead tetraacetate and also examined the oxidation with manganic acetate more in detail. We wish to report both results in this paper.

When 2′-hydroxychalcones (Ia–c) were oxidized with either manganic acetate or lead tetraacetate in acetic acid, several compounds were isolated (Table 1). From mother liquors of the main products aurones (IIb and IIc), compounds IIIb and IIIc, respectively, were separated by successive thin layer chromatography and were found to be isomers of IIb and IIc from the following evidences. IR spectra of IIIb and IIIc showed absorptions at 1676—1679 cm^{-1} which are slightly lower than those of IIa, IIb, and IIc (1700 cm^{-1}) (Table 2). In 60 MHz NMR spectra of IIa, IIb, IIc, IIIb, and IIIc (Table 3), the difference was shown in a signal corresponding to $H_{2'}$ and $H_{6'}$/ or $H_{6'}$. The signals of $H_{2'}$ and $H_{6'}$ of IIIb and $H_{6'}$ of IIIc appeared at δ8.29 and 8.77, respectively, rather lower field shifts as compared with those of IIb (δ 8.06) and IIc (δ 8.12). The cause of the shifts could be ascribed to the anisotropic effect of a carbonyl group. Thus, the NMR spectra indicated that IIa, IIb, and IIc have a *trans*-configuration with respect to the carbonyl and the phenyl groups, and IIIb and IIIc have a *cis*-configuration. Their UV spectra showed a characteristic absorption pattern, *viz.*, the *trans*-isomer (IIa–c) has an absorption maximum at a longer wavelength (376—392 nm) and the *cis*-isomer at a shorter wavelength (350—352 nm) (Table 2).

Three acidic compounds were isolated and they were found to be a 2-hydroxybenzoic acid (IV), a

1) T. Aratani and M. J. S. Dewer, *J. Amer. Chem. Soc.*, **88**, 5479 (1966).
2) E. I. Heiba, R. M. Dessau, and W. J. Koehl, Jr., *ibid.*, **91**, 138 (1969).
3) J. B. Bush, Jr. and H. Finkbeiner, *ibid.*, **90**, 5903 (1968).
4) E. I. Heiba, R. M. Dessau, and W. J. Koehl, Jr., *ibid.*, **90**, 5905 (1968).
5) K. Kurosawa, This Bulletin, **42**, 1456 (1969).
6) E. I. Heiba, R. M. Dessau, and W. J. Koehl, Jr., *J. Amer. Chem. Soc.*, **90**, 2706 (1968).

Table 1. Oxidation of chalcones

Chalcone[6]	Reagent	Reaction conditions: Mole ratio of I and Reagent	Time (min)	Aurone[6]: *trans*-	Aurone[6]: *cis*-	Product (yield, %), mp (°C): Acid		Aldehyde	Ketone	
Ia	$Pb(OAc)_4$	1 : 1.5	30	IIa (20) 137			V (0.52) 184	VIa[8] (1.9) 170		
Ia	$Mn(OAc)_3$	1 : 3	25	IIa (32) 137		IVa (2.8) 149	trace	VIa (0.56) 170		
Ib	$Pb(OAc)_4$	1 : 1.5	30	IIb (33) 133	IIIb (0.52) 163—164		V (1.3) 184	VIa (0.38) 170		
Ib	$Mn(OAc)_3$	1 : 3	20	IIb (30) 133	IIIb (0.55) 163—164	IVb[7] (4.0) 150				
Ic	$Pb(OAc)_4$	1 : 1.5	30	IIc (48) 138[a]		IVb (1.4) 150		VIc[9] (1.2) 168		
Ic	$Mn(OAc)_3$	1 : 3	30	IIc (53) 138[a]	IIIc (0.82) 143—144	IVb (2.2) 150				
Id	$Pb(OAc)_4$	1 : 1.5	30	IId (35) 190						
Ie	$Pb(OAc)_4$	1 : 1.5	30	IIe (25) 182						
If	$Pb(OAc)_4$	1 : 1.5	30	IIf (30) 145						
Ig	$Pb(OAc)_4$	1 : 1.5	30	IIg (20) 178						
Ih	$Pb(OAc)_4$	1 : 1.5	30	IIh (35) 186						
Ii	$Pb(OAc)_4$	1 : 1.5	30	IIi (37) 184						
Ij	$Pb(OAc)_4$	1 : 2	450			IVj (2.3) 101—102	V (4.6) 184	VII (5.0)	VIII (6.0) 155—156	IX (5.5) 164—166
Ij	$Mn(OAc)_3$	1 : 4	480			IVj (7.0) 101—102	V (2.1) 184	VII (9.0)	VIII (8.3) 155—156	IX (3.5) 164—166

a) This was previously reported as 129°C, but has been corrected.

Table 2. IR and UV spectral data for IIa, IIb, IIc, IIIb, and IIIc

Compound	ν_{max} (cm^{-1}): C=O	C=C	λ_{max} (nm) (log ε)		
IIa	1700	1640	255 (4.18)	333 (4.13)	392 (4.45)
IIb	1700	1647	253 (4.11)		376 (4.49)
IIIb	1676	1637	256 (4.15)	350 (4.36)	394 (inf) (4.25)
IIc	1700	1645	261 (4.07)		382 (4.42)
IIIc	1679	1637	263 (4.12)	352 (4.29)	369 (inf) (4.19)

inf; inflection

Table 3. NMR spectral data for IIa, IIb, IIc, IIIb, and IIIc (δ value at 60 MHz)

Compound	H_4[a]	H_5[a]	H_6	H_7[a]	H_8: *trans*	H_8: *cis*	$H_{2',6'}$/or $H_{6'}$[b]: *trans*	$H_{2',6'}$/or $H_{6'}$[b]: *cis*	$H_{3',5'}$/or $H_{5'}$[b]: *trans*	$H_{3',5'}$/or $H_{5'}$[b]: *cis*	OCH_3
IIa		7—8 (4H)			7.06		8.06		7.14		3.95 (3H)
IIb	7.89	6.92	—	6.92	6.97		8.06		7.13		3.95 (3H) 4.02 (3H)
IIIb	7.72	6.74	—	6.67		6.90		8.29		7.00	3.90 (3H) 3.87 (3H)
IIc	7.78	6.80	—	6.80	7.32		8.12		6.86		4.02 (3H) 3.99 (9H)
IIIc	7.79	6.77	—	6.71		7.37		8.77		6.86	4.00 (6H) 3.95 (6H)

a) $J_{4,5}$=8.5 Hz, $J_{5,7}$=2 Hz, $J_{2',3'}=J_{5',6'}$=8.5 Hz, analysed as an AB system.
b) $J_{5',6'}$=8.5 Hz.

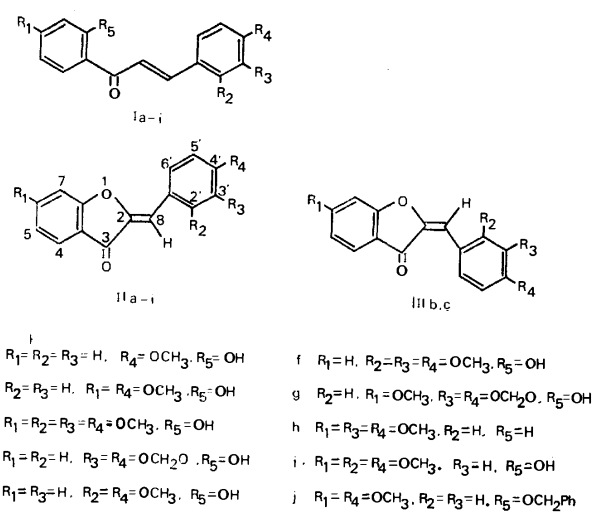

Fig. 1.

benzoic acid (V) and a cinnamic acid (VI). They were identified with authentic samples by their IR spectra.

It was reported recently[10] that the reaction of of chalcones with thallium acetate gave a product in which a skeletal rearrangement took place. This prompted us to investigate the oxidation of 2'-benzyloxy-4,4'-dimethoxychalcone (Ij)[11] with lead tetraacetate and manganic acetate. With both reagents, identical products IVj, V, VII, VIII, and IX were obtained (Table 1).

Product (VIII), $C_{26}H_{24}O_7$ (analysis and mass spectrum), mp 155—156°C, was isolated from chloroform extract of the reaction mixture by preparative tlc and recrystallization. The IR spectrum of VIII (ν_{max} 1750, 1250, and 1675 cm^{-1}) suggested the presence of an acetoxyl group and an aroyl group. The NMR spectrum (100 MHz) of VIII indicated the presence of a *p*-methoxybenzoyl group {δ 6.68(d, 2H), δ 7.61 (d, 2H) (AA'BB' system, $J_{AB}=J_{A'B'}=9$ Hz), and δ 3.64 (s, 3H)}, a 2-benzyloxy-4-methoxybenzoyl group δ 7.09 (broad s, 5H), δ 4.70 (d, 1H) and δ 4.82 (d, 1H) (AB system, $J=12.0$ Hz), δ 6.26 (d, 1H), δ 6.46 (dd, 1H) and δ 7.92(d, 1H)(ABX system, $J_{AB}=2$ Hz, $J_{AX}=0$ and $J_{BX}=9$ Hz), and δ 3.73(s, 3H)}, and an acetoxyl group {δ 2.08(s, 3H)}. This spectroscopic evidence indicated that product (VIII) is 2-acetoxy-1-(2'-benzyloxy-4'-methoxy)phenyl-3-(4'-methoxy)phenylpropane-1,3-dione.

Product (IX), $C_{28}H_{28}O_8$ (analytical and mass spectrum), mp 164—166°C, was isolated also from the chloroform extract. The IR spectrum of IX indicated the presence of an acetoxyl and a benzoyl groups (1745 and 1250, and 1675 cm^{-1}, respectively). The NMR spectrum (100 MHz) of IX indicated the presence of a *p*-methoxyphenyl group {δ 6.80(d, 2H), δ 6.58 (d, 2H) (AA'BB' system, $J_{AB}=J_{A'B'}=9$ Hz) δ 3.68(s, 3H)}, a 2-benzyloxy-4-methoxybenzoyl group {δ 7.3—7.6(m, 5H), δ 5.18(s, 2H), δ 6.52(d, 1H), δ 6.50(dd, 1H) and δ 7.76(d, 1H)(ABX system, $J_{AB}=2.5$, $J_{AX}=0$, and $J_{BX}=9.4$ Hz), δ 3.78(s, 3H)}, two acetoxyl groups {δ 1.92(s, 3H) and δ 2.02(s, 3H)}, and a CH=CH unit{δ 6.28 (d, 1H), and δ 6.36(d, 1H)(AB system, $J=3.0$ Hz)}. All the spectroscopic evidence showed that the product (IX) has a structure of 2,3-diacetoxy-1-(2'-benzoyloxy-4'-methoxy)phenyl-3-(4'-methoxy)phenylpropan-1-one (IX).

The third product isolated from the chloroform extract was found to be anisaldehyde (VII), being identified with an authentic sample by IR spectra.

The fourth product, mp 184°C, was isolated by sodium bicarbonate extraction of the chloroform extract and was proved to be anisic acid (V). This was confirmed on the mixed melting point test with an authentic sample.

The fifth product, mp 100—101°C, was found to be 2-benzyloxy-4-methoxybenzoic acid(IVj) by its NMR spectrum(60 MHz) {δ 7.53(s, 5H), δ 5.32 s, 2H), δ 3.88(s, 3H), δ 6.65(d, 1H), δ 6.70(dd, 1H) and δ 8.22 (d, 1H) (ABX system, $J_{AB}=2$, $J_{AX}=0$, and $J_{BX}=8.5$ Hz), and δ 12.0(s, 1H)}.

The structures of VIII and IX were finally confirmed by syntheses.

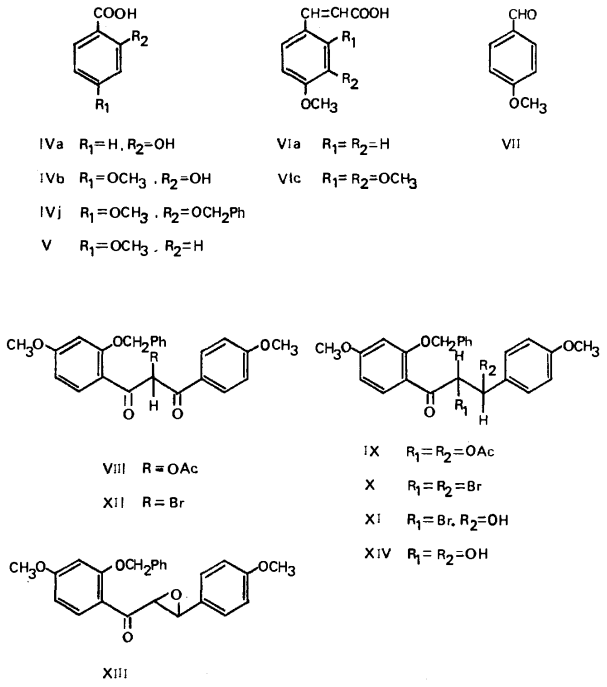

Fig. 2.

A chalcone dibromide (X), mp 163—165°C, obtained from Ij, was treated with wet acetone.[12] This yielded a bromohydrin (XI), mp 129—130°C. XI was oxidized with chromic acid to a diketone (XII), mp 80—82°C. XII was then heated with sodium acetate in acetic acid to give an acetate. The acetate has a melting point and IR spectrum identical with those of VIII.

7) "Beilsteins Handbuch der Organischen Chemie," Vol. 10, p. 379.
8) *ibid.*, Vol. 10, 298.
9) *ibid.*, Vol. 10, 508.
10) W. D. Ollis, K. L. Ormand, *J. Chem. Soc., C*, **1970**, 119.
11) W. D. Ollis, K. L. Ormand, B. T. Redman, R. J. Roberts, and I.O. Sutherland, *ibid.*, **1970**, 125.
12) M. G. Marathey, *J. Org. Chem.*, **20**, 563 (1955).

IX was synthesized as follows. The chalcone epoxide (XIII), mp 93°C, was treated with aqueous acetic acid and the resulting glycol (XIV), mp 134—135°C, was acetylated with acetic anhydride in pyridine. This acetate was found to be identical with product (IX). It is also shown by this synthesis that IX has an *erythro* diacetoxy configuration as a *trans*-chalcone epoxide is hydrolysed to a glycol by S_N2 mechanism and this makes a *trans* addition to a *trans* double bond.

Thus, the reaction of manganic acetate and lead tetraacetate with chalcone proceeded in a similar way to each other, but differed from the reaction of thallium acetate.[10] Rearranged products have not been isolated. It was also shown that the reaction takes place differently from those of a substituted styrene and a compound having an isolated double bond, which gave a lactone[3,4,6] and a 1,2-diacetate,[13] respectively. It can be said that the carbonyl group must have a significant influence in the oxidation of the chalcone. This was illustrated by the formation of the diketone (VIII), which seemed to be the first example. It seems unlikely that product (IX) is an intermediate in the formation of VIII as the former is not reactive with manganic acetate.

Table 4. Analysis of new compounds

Compound	Formula	Found		Calcd	
		C%	H%	C%	H%
IIc	$C_{19}H_{18}O_6$	66.83	5.38	66.66	5.30
IIf	$C_{18}H_{16}O_5$	69.23	5.20	69.22	5.16
IIi	$C_{18}H_{16}O_5$	69.28	5.26	69.22	5.16
IIIb	$C_{17}H_{14}O_4$	72.45	5.03	72.33	5.00
IIIc	$C_{19}H_{18}O_6$	66.42	5.40	66.66	5.30
IVj	$C_{15}H_{14}O_4$	69.62	5.48	69.75	5.46
VIII	$C_{26}H_{24}O_7$	69.65	5.53	69.63	5.39
IX	$C_{28}H_{28}O_8$	68.43	5.85	68.28	5.73
X	$C_{24}H_{22}O_4Br_2$	53.80	4.33	53.96	4.15
XI	$C_{24}H_{23}O_5Br$	60.88	4.96	61.16	4.92
XII	$C_{24}H_{21}O_5Br \cdot 1/3\ C_6H_6$	62.80	4.80	63.04	4.68
XIII	$C_{24}H_{22}O_5$	73.96	5.81	73.83	5.68
XIV	$C_{24}H_{24}O_6$	70.38	6.03	70.57	5.92

Experimental

All NMR spectra were recorded for deuteriochloroform solutions with a JEOL JNM-MH-100 and a JNM-MH-60 spectrometers with tetramethylsilane as an internal standard; IR spectra were recorded for chloroform solution with a JASCO DS 403G grating spectrometer; UV spectra were obtained for methanol solutions with a Hitachi EPS-3T spectrophotometer. Preparative and analytical tlc were carried out with a Wakogel BlO. Melting points were determined with a Yanagimoto micro melting point apparatus and uncorrected.

Lead tetraacetate and manganic acetate were prepared according to references.[14,15]

Reaction of Lead Tetraacetate with Chalcones (Ia—i). Chalcone (1 mmol), dissolved in acetic acid (15 ml) was heated with lead tetraacetate (1.5 mmol) at 100°C for 30 min. After removal of the acetic acid *in vacuo*, the resulting solid was treated with 2 N sulfuric acid (10 ml) and then extracted with chloroform (20 ml). The chloroform layer was separated from the aqueous solution and then evaporated. The residue was dissolved in a small amount of chloroform and separated on tlc (10 g×5) with chloroform as an eluent. The crude aurone was recrystallized from ethanol.

Reactions of Lead Tetraacetate and Manganic Acetate with Chalcones (Ia—c) in a Large Scale. Chalcone (20 mmol) was oxidized as above with lead tetraacetate (30 mmol) or manganic acetate (60 mmol) and the products were separated on alumina (Wako, 100 g) with chloroform as an eluent. *cis*-Aurone was separated from a *trans*-aurone by repeated tlc and recrystallization from ethanol. Sodium bicarbonate extraction of the chloroform solution yielded a mixture of carboxylic acids (IV, V and VI), which were separated by fractional recrystallization from water.

Reaction of Manganic Acetate with 2'-Benzyloxy-4,4'-dimethoxychalcone (Ij).[11] Ij (2 mmol) was dissolved in acetic acid (20 ml) containing acetic anhydride (1 ml) and then heated with manganic acetate (8 mmol) at 100°C for 8 hr. After removal of the acetic acid, the resulting mixture was hydrolyzed with 2 N sulfuric acid and then extracted with chloroform. The chloroform layer was washed with aqueous sodium bicarbonate. The chloroform being removed, the resulting liquid was chromatographed on preparative tlc (35 g×5) effected with chloroform. From a band running just below Ij, product (VIII) was obtained and recrystallized from ethanol to give colorless plates, mp 155—156°C. From a slow running band, product (IX) was separated after recrystallization from ethanol as colorless needles, mp 164—166°C. From a band just above Ij, colorless liquid was isolated and identified as anisaldehyde (VII) on comparison of its IR spectrum with that of an authentic sample. Upon acidification of the sodium bicarbonate extract, two acids, IVj and V were obtained after recrystallization from water.

Reaction of Lead Tetraacetate with Ij. Ij (2 mmol) was oxidized with lead tetraacetate (4 mmol) in acetic acid (20 ml) at 100°C for 7.5 hr. Working up in a manner as described above, products (IVj, V, VII, VIII, and IX) were isolated.

1-(2'-Benzyloxy-4'-methoxy)phenyl-2,3-dibromo-3-(4'-methoxy)-phenylpropan-1-one (X). Ij (3.74 g) in carbon disulfide (50 ml) was treated with bromine (1.6 g) at 0°C for 15 min. The precipitates were collected and recrystallized from benzene to give microcrystals, mp 163—165°C (3.54 g, 67%).

1-(2'-Benzyloxy-4'-methoxy)phenyl-2-bromo-3-hydroxy-3-(4'-methoxy)phenylpropan-1-one (XI). X (3.00 g) was treated with 60% aqueous acetone (30 ml) under reflux for 15 min. After removal of the acetone, the aqueous solution was extracted with benzene. Benzene was removed and the resulting liquid was allowed to crystallize from a small amount of benzene. Recrystallization of the crude product from the same solvent yielded colorless cubes, mp 129—130°C, (1.22 g, 46%).

1-(2'-Benzyloxy-4'-methoxy)phenyl-2-bromo-3-(4'-methoxy)-phenylpropane-1,3-dione (XII). To XI (412 mg) in acetic acid (10 ml), was added chromic acid (246 mg) in acetic acid (25 ml) at room temperature and the mixture was warmed on a steam bath for 2.5 min. The reaction mix-

13) K. B. Wiberg, "Oxidation in Organic Chemistry," Part A, Academic Press, New York and London (1965), p. 335.

14) L. F. Audrieth, "Inorganic Syntheses," Vol. 3, McGraw-Hill Co. Inc. (1950), p. 47.

15) P. J. Andrulis, Jr., M. J. S. Dewer, R. Dietz, and R. L. Hunt, *J. Amer. Chem. Soc.*, **88**, 5473 (1966).

ture was treated with 2 N sulfuric acid (100 ml) and then extracted with chloroform. After removal of the chloroform, the resulting liquid was allowed to crystallize from benzene. Recrystallization of the crude product from benzene gave colorless microcrystals, mp 80—82°C, (199 mg, 54%).

2-Acetoxy-1-(2'-benzyloxy-4'-methoxy)phenyl-3-(4'-methoxy)phenylpropane-1,3-dione (VIII). XII (112 mg) was treated with a mixture of anhydrous sodium acetate (500 mg) and acetic acid (2 ml) under reflux for 7.5 hr. The reaction mixture was treated with 2 N sulfuric acid and then extracted with chloroform. The chloroform layer was concentrated and separated on silica gel (10 g×3) with chloroform as an eluent. From appropriate band, a crude material was separated and recrystallized from ethanol to give colourless plates, mp 154—155°C, (30 mg, 28%).

2'-Benzyloxy-4,4'-dimethoxychalcone Epoxide (XIII). To a mixture of the chalcone(Ij) (1 g), acetone (20 ml) and methanol (10 ml), and 2 N sodium hydroxide (2.0 ml) was added 30% hydrogen peroxide (2.5 ml) at 50°C during a period of 50 min. The reaction mixture was poured into ice water and extracted with chloroform. After removal of the chloroform, the resulting liquid was allowed to crystallize from ethanol. This yielded colorless microcrystals, mp 93°C, (49%).

1-(2'-Benzyloxy-4'-methoxy)phenyl-2,3-dihydroxy-3-(4'-methoxy)-phenylpropan-1-one (XIV). XIII (248 mg) was dissolved into a mixture of acetone (25 ml) and 10% acetic acid (25 ml) and kept at room temperature for 16 hr. The mixture was diluted with water and the precipitates were collected. Recrystallization of the crude product from ethanol gave colorless needles, mp 134—135°C, (117 mg, 45%).

2,3-Diacetoxy-1-(2'-benzyloxy-4'-methoxy)phenyl-3-(4'-methoxy)-phenylpropan-1-one (IX). XIV (117 mg) was treated with a mixture of acetic anhydride (0.5 ml) and pyridine (1 ml) at 0°C for 18 hr. The reaction mixture was poured into ice water and the precipitates were collected. Recrystallization of the precipitates from ethanol gave colorless needles, mp 164—166°C, (52 mg, (37%).

The authors wish to thank Professor Shin-ichi Sasaki and Mr. Hidetsugu Abe, Miyagi University of Education, for measuring NMR spectra. The authors also deeply thank the staff of JEOL Co. Ltd. for recording 100 MHz NMR and mass spectra.

BULLETIN OF THE CHEMICAL SOCIETY OF JAPAN, VOL. 45, 1136—1139 (1972)

Synthesis and Conformation of Cyclopropane Intermediates in the Total Synthesis of Illudin M and S

Takeshi MATSUMOTO, Haruhisa SHIRAHAMA, Akitami ICHIHARA, Hyonsobb SHIN, Shohei KAGAWA, Toshiaki HISAMITSU, Toshihiro KAMADA, and Fujio SAKAN

Department of Chemistry, Faculty of Science, Hokkaido University, Sapporo

(Received August 6, 1971)

Several promising cyclopropane intermediates in the total synthesis of illudin M and S have been prepared. Survey of NMR of these compounds showed the conformation **17** to be unfavourable.

Preliminary reports were given on the total synthesis of illudin M and S[1,2]. Cyclopropyl ketone derivatives of general formula **1**, where X represents hydrogen or any groups activating methylene group, were desirable for the Michael reaction (Scheme 1) which was expected for combined cyclopropane and cyclopentane moieties to give useful intermediates **3** for illudins. This paper describes the synthesis of several cyclopropane derivatives **6**, **9**, **12**, **13**, **14**, and **15** of this type and their preferred conformation.[3] Ethyl 2,2-ethano-3-ketobutyrate (**4**), bp 90—102°C/20 mmHg, was prepared by the alkylation of acetoacetic ester with ethylene bromide in 24% yield and the carbonyl group of compound **4** was masked with ethylene glycol in the usual manner to give ketal **5**, bp 127—137°C/20 mmHg, in 68% yield. Ketal **5** was converted into 1-methanesulfinyl-3,3-ethano-4,4-ethylenedioxy-2-pentanone (**9**), mp 41—43°C in 91% yield by treatment with methylsulfinyl carbanion according to Corey's general procedure.[5] The Pummerer reaction of **9** by heating with acetic anhydride at reflux temperature for 3 hr afforded acetoxysulfide **12**, mp 44—46°C, in 79% yield. On treatment with amalgamated aluminum in aqueous ethanol at room temperature, the methylthio group of **12** and

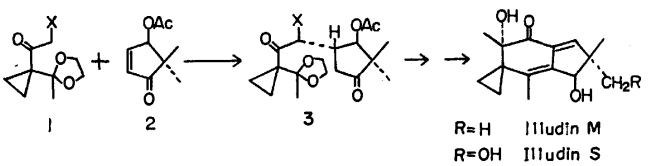

Scheme 1.

1) T. Matsumoto, H. Shirahama, A. Ichihara, H. Shin, S. Kagawa, S. Matsumoto, and S. Nishida, *J. Amer. Chem. Soc.*, **90**, 3280 (1968).

2) T. Matsumoto, H. Shirahama, A. Ichihara, H. Shin, S. Kagawa, F. Sakan, and K. Miyano, *Tetrahedron Lett.*, **1971** 2049.

3) Our purpose was finally achieved[4] by the Michael reaction of β-ketosulfoxide **9** (**1**, X=$SOCH_3$) with cyclopentenone **2**. Attempted Michael reactions of cyclopropyl ketones **6**, **12**, **13**, **14**, and **15** with **2** were unsuccessful.

4) T. Matsumoto, H. Shirahama, A. Ichihara, H. Shin, S, Kagawa, N. Ito, T. Hisamitsu, T. Kamada, F. Sakan, K. Saito, S. Nishida, and S. Matsumoto, *Tetrahedron Lett.*, **1968**, 1925.

5) E. J. Corey and M. Chaykovsky, *J. Amer. Chem. Soc.*, **87**, 1345 (1965).

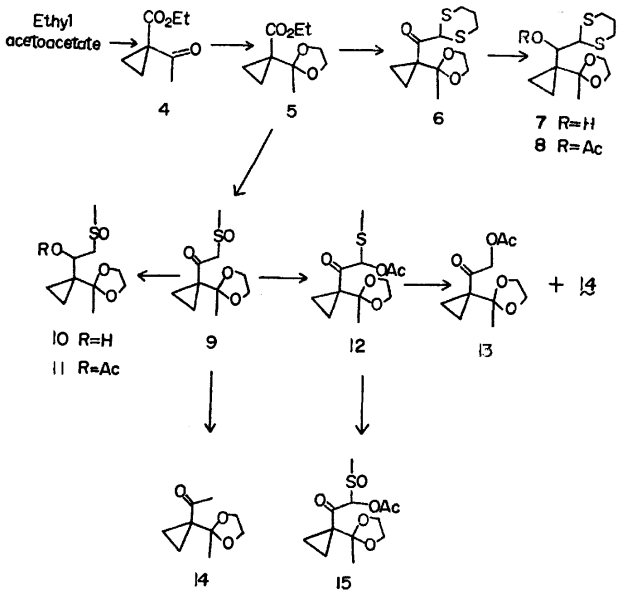

Fig. 1.

part of the acetoxy group were removed to give acetoxymethyl ketone **13**, bp 89—92°C/1 mmHg (30%) and methyl ketone **14**, bp 45—50°C/1 mmHg (25%). The latter was directly obtained by the treatment of **9** with the same reagent in aqueous tetrahydrofuran. Sulfide **12** was converted into sulfoxide **15** by oxidation with hydrogen peroxide in acetic acid (26%).

1,1-Trimethylenedithio-3,3-ethano-4,4-ethylenedioxy-2-pentanone (**6**), mp 59—60°C, was obtained by the action of an anion of 1,3-dithiane on the ester **5** according to Corey's method[6] in 45% yield.

We would like to add a note on the conformation of the cyclopropyl methyl ketone ethylene ketals. The long range shielding effect of the cyclopropane ring is well known[7,8] from which the instability of the conformation **16** of cyclopropyl methyl ketones has been

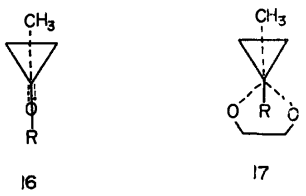

Fig. 2. Unstable conformations of cyclopropyl methyl ketones and their ketals.

deduced[7]. By comparison of chemical shifts of methyl group on the dioxolane rings with those of the compounds with *gem*-dimethyl group in the place of cyclopropane ring, information on the conformation of the above cyclopropyl methyl ketone ethylene ketals might be obtained. Three of such *gem*-dimethyl compounds (**21**, **18**, **22**) were prepared for another purpose[9] and some more pairs of cyclopropyl ketone ketals and the corresponding *gem*-dimethyl compounds were available. Cyclopropyl ketones **6** and **9** were reduced with sodium borohydride to give hydroxydithiane derivative **7** and hydroxysulfoxide **10**, mp 120—122°C, respectively. Both alcohol **7** and **10** were converted into acetates **8** and **11** in the usual manner. The *gem*-dimethyl compounds corresponding to **10** and **11**, 1-methanesulfinyl-3,3-dimethyl-4,4-ethylenedioxy-2-pentanol (**19**) and its acetate **20**, were prepared from dimethylmethanesulfinylpentanone **18** in the same manner as in the preparation of **10** and **11**.

As shown in Table 1, the methyl signals of the cyclopropyl compounds invariably appeared at a lower field than those of the *gem*-dimethyl compounds, showing that conformation **17** of the cyclopropyl compounds is not preferable. The fact that conformation **17** in which the methyl group situated just above the cyclopropane ring is unfavorable can be explained by the repulsion between cyclopropane ring and eclipsed methyl group. Instability of the so called transoid cyclopropyl methyl ketones **16** might be due, at least in part, to the same effect.

Table 1. Chemical shifts (τ) of methyl groups on the dioxolane rings

Compounds							
R=CH_3, CH_3	**21**	**18**	**22**	**19**	**23**	**20**	**24**
	8.69	8.77[a,9]	8.74[9]	8.70[a]	8.71[9]	8.66[a]	8.70[9]
R=CH_2—CH_2	**5**	**9**	**6**	**10**	**7**	**11**	**8**
	8.44	8.53[a]	8.48	8.55	8.68	8.55	8.60
Differences	0.25	0.24	0.26	0.15	0.03	0.11	0.10

a) $CDCl_3$ was used as a solvent. Other data were observed in CCl_4.

6) E. J. Corey and D. Seebach, *Angew. Chem.*, **77**, 1134, 1135 (1965).
7) J. L. Piere and Arnaud, *Bull. Soc. Chim. Fr.*, **1967**, 1690.
8) K. Tori and K. Kitahonoki, *J. Amer. Chem. Soc.*, **87**, 386 (1965) and the literature cited.
9) T. Matsumoto, H. Shirahama, A. Ichihara, H. Shin, and S. Kagawa, This Bulletin, **45**, 1144 (1972).

Experimental

NMR spectra were taken on JEOL Co. Model 3H60 and Hitachi Model H60 spectrometers.

*Ethyl 2,2-Ethano-3-ketobutyrate (**4**).* An ethanolic solution prepared from 46 g of sodium and 900 ml of ethanol was added dropwise over a period of 6 hr with stirring, to a mixture of 130 mg of ethyl acetoacetate and 188 g of ethylene bromide. The temperature was maintained so that the the mixture was just refluxed. After addition was completed, the reaction mixture was further refluxed for 14 hr with stirring and concentrated under reduced pressure at temperatures below 50°C until most of the ethanol was removed. The residue was extracted with benzene several times and the combined extracts were washed with a saturated salt solution and dried. After evaporation of the solvent, the crude product was distilled to yield 39.1 g of an oil boiling at 85—90°C/25 mmHg. The distillate was dissolved in benzene and washed with 10% aqueous potassium hydroxide solution several times and then with a saturated salt solution and dried. Evaporation of the solvent gave 37.4 g (24%) of desired cyclopropane derivative: IR (neat) 3050, 1725, 1685 cm^{-1}.

*Ethyl 2,2-Ethano-3,3-ethylenedioxybutyrate (**5**).* A mixture of 115 g of **4**, 134 g of ethylene glycol, 300 mg of *p*-toluenesulfonic acid and 370 m*l* of benzene was refluxed for 46 hr. The water formed was removed by azeotropic distillation with a Dean-Stark separator. After cooling down to room temperature the reaction mixture was washed with a saturated sodium bicarbonate solution and then with water and dried. Evaporation of the solvent gave crude product which, on distillation, gave 100 g (68%) of the desired ketal; bp 127—137°C/20 mmHg; IR (neat) 1725 cm^{-1}; NMR $\tau(CCl_4)$ 9.00 (4H, m, cyclopropane), 8.73 (3H, t, $J=7$ Hz, CH_3CH_2O), 8.44 (3H, s, CH_3CO), 6.16 (4H, s, OCH_2CH_2O), 5.96 (2H, q, $J=7$ Hz, OCH_2CH_3).

Found: C, 59.98; H, 8.06%. Calcd for $C_{10}H_{16}O_4$: C, 59.98; H, 8.05%.

*1-Methanesulfinyl-3,3-ethano-4-ethylenedioxy-2-pentanone (**9**).* A portion of ether (210 m*l*) and 42.2 g of ester **5** were added dropwise over a period of 1 hr to a dimethyl sulfoxide solution of methanesulfinyl carbanion, prepared from 140 m*l* of dimethyl sulfoxide and 12.9 g of sodium hydride (50% mineral oil dispersion), under ice-water cooling and mechanical stirring in the atmosphere of nitrogen. The ice-water bath was removed and stirring was continued for additional 1.5 hr at room temperature and the reaction mixture was then poured into about 1 *l* of water washed three times with benzene, neutralized with diluted acetic acid to a pH of 5—6 (pH paper), and extracted five times with chloroform. The combined extracts were washed with a saturated salt solution until the washings were no longer acidic, dried over sodium sulfate and evaporated to yield 44.5 g (91%) of keto sulfoxide **10** as a pale yellow crystalline solid. A sample was recrystallized from ethyl acetate for analysis: mp 41—43°C; IR (Nujol) 1680, 1045 cm^{-1}; NMR $\tau(CDCl_3)$ 8.87 (4H, bs, cyclopropane), 8.53 (3H, s, CH_3), 7.32 (3H, s, CH_3SO), 6.07 (4H, s, OCH_2CH_2O), 5.99 and 5.73 (2H, ABq, $J=15$ Hz, CH_2SO).

Found: C, 51,65; H, 6.86%. Calcd for $C_{10}H_{16}O_4S$: C, 51.70; H, 6.94%.

*1-Methanesulfenyl-1-acetoxy-3,3-ethano-4,4-ethylenedioxy-2-pentanone (**12**).* A solution of 4.0 g of sulfoxide **9** in 40 g of acetic anhydride was gently refluxed for 3 hr. Most of the acetic anhydride was evaporated under reduced pressure and the residue was dissolved in chloroform, washed with a saturated sodium bicarbonate solution and a saturated salt solution and dried. Removal of the solvent gave an oil which was chromatographed on silica gel to give 3.8 g (79%) of crystalline product; mp 44—46°C; IR (Nujol) 1740, 1690, 1240, 1040 cm^{-1}; NMR $\tau(CCl_4)$ 8.7—9.4 (4H, m, cyclopropane), 8.45, (3H, s, CH_3), 8.12 (3H, s, CH_3S), 7.92 (3H, s, AcO), 5.9—6.3 (4H, m, OCH_2CH_2O), 3.62 (1H, s, SCHO).

Found: C, 52.74; H, 6.79%. Calcd for $C_{12}H_{18}O_5S$: C, 52.55; H, 6.62%.

*1-Acetoxy-3,3-ethano-4,4-ethylenedioxy-2-pentanone (**13**).* Aluminum amalgam freshly prepared from 2.4 g of aluminum foil was added with stirring to a solution of 2 g of the Pummerer reaction product in 120 m*l* of 10% aqueous ethanol. The mixture was stirred for 2 hr at room temperature, then filtered and the residue was washed with ethanol. The combined filtrate was concentrated under reduced pressure at a temperature below 50°C till the most of ethanol was removed. The residue was dissolved in ether and the solution was washed with water and dried over anhydrous sodium sulfate. Evaporation of the ether gave 1.2 g of the crude products which was subjected to preparative vpc (column: Apiezon Grease (1 m), at 175°C, carrier gas: He 120 m*l*/min) to give *ca.* 300 mg (25%) of methyl ketone **14** and 460 mg (30%) of the desired product: bp 89—92°C/1 mmHg; IR (neat) 1750, 1710, 1230, 1045 cm^{-1}; NMR $\tau(CCl_4)$ 8.9—9.2 (4H, m, cyclopropane), 8.51 (3H, s, CH_3), 7.90 (3H, s, AcO), 6.60 (4H, s, OCH_2CH_2O), 5.12 (2H, s, CH_2OAc).

Found: C, 57.89; H, 7.12%. Calcd for $C_{11}H_{16}O_5$: C, 57.88; H, 7.07%.

*3,3-Ethano-4,4-ethylenedioxy-2-pentanone (**14**.)* Amalgamated aluminum freshly prepared from 2.7 g of aluminum foil was added with stirring to a solution of 2.32 g of the sulfoxide **9** in 150 m*l* of 10% aqueous tetrahydrofuran. The mixture was stirred for 1 hr in an ice-water bath, then filtered and the filtered solid was washed with tetrahydrofuran. The filtrate was concentrated till most of the tetrahydrofuran was removed. The residue was dissolved in ether, washed with water and dried over anhydrous sodium sulfate. Removal of the solvent gave 1.28 g of desired ketone: bp 45—46°C/1 mmHg; IR (neat) 1688, 1045 cm^{-1}; NMR $\tau(CCl_4)$ 8.91 (4H, s, cyclopropane), 8.44 (3H, s, CH_3), 7.79 (3H, s, CH_3CO), 6.08 (4H, s, OCH_2CH_2O).

*1-Methanesulfinyl-1-acetoxy-3,3-ethano-4,4-ethylenedioxy-2-pentanone (**15**).* Hydrogen peroxide (30% solution, 500 mg, 2 equivalent) was added to a solution of 450 mg of the Pummerer reaction product **12** in 5 m*l* of acetic acid. The solution was kept at a temperature below 10°C for 20 hr, neutralized with saturated sodium carbonate solution and extracted with benzene several times. The combined extracts were dried over anhydrous magnesium sulfate and the solvent was removed to give an oil. The oil was purified by silica gel chromatography to yield 122 mg (26%) of the sulfoxide; IR (neat) 1745, 1690 cm^{-1}; NMR $\tau(CDCl_3)$ 9.5—8.0 (4H, m, cyclopropane), 8.36 (3H, s, CH_3), 7.7 (3H, s, AcO), 7.46 (3H, s, CH_3SO), 6.3—5.7 (4H, m, OCH_2CH_2O), 3.05 (1H, s, $OSHC<^{OAc}_{CO}$).

*1,1-Trimethylenedithio-3,3-ethano-4,4-ethylenedioxy-2-pentanone (**6**).* A solution of 7 g of *n*-butyl bromide in 10 m*l* of ether was added dropwise to 0.8 g of lithium metal covered with 20 m*l* of ether at −30——40°C and stirred for 1.5 hr at 0—10°C. To the resulting solution was added dropwise 4.3 g of 1,3-dithiane in 70 m*l* of tetrahydrofuran at −30——40°C and stirred. To the solution thus prepared was added dropwise 7 g of ester **5** in 10 m*l* of tetrahydrofuran

at −60——70°C with stirring. The reaction mixture was allowed to stand at the same temperature range for 3 days and then poured into water. The solution was acidified with dilute hydrochloric acid and extracted with *n*-hexane. The extract was washed with a saturated salt solution and dried over anhydrous sodium sulfate. After evaporation of the solvent, the residue was distilled to give 4.2 g (45%) of **6**: bp 146°C/2 mmHg which was soon crystallized, mp 59—60°C; IR (nujol) 3030, 1675, 1040 cm^{-1}; NMR τ($CDCl_3$) 8.90 (4H, bs, cyclopropane), 8.49 (3H, s, CH_3), 6.3—8.3 (6H, m, $S(CH_2)_3S$), 6.09 (4H, s, OCH_2CH_2O), 5.18 (1H, s, $COCH\langle^{S}_{S}$).

Found: C, 52.43; H, 6.86%. Calcd for $C_{12}H_{18}O_3S_2$: C, 52.52; H, 6.61%.

*1,1-Trimethylenedithio-3,3-ethano-4,4-ethylenedioxy-2-pentanol (**7**).* To a solution of ketone **6**[9] in dry ether was added a solution of excess lithium aluminum hydride in dry ether and stirred overnight at room temperature. The mixture was cooled in an ice bath and excess reagent was decomposed with a small amount of water. The mixture was extracted several times with ether. The extract was dried and concentrated to give a paste: IR (neat) 3400, 1040 cm^{-1}; NMR τ(CCl_4) 9.40 (4H, s, cyclopropane), 8.57 (3H, s, CH_3), 6.38 (1H, d, J=7 Hz, CHOH), 6.19 4H, s, OCH_2CH_2O), 5.66 (1H, d, J=7 Hz, SCHS); *m/e*: 276 (M^+).

*Acetate **8**.* A sample of alcohol **7** was acetylated with acetic anhydride and pyridine in the usual manner to give acetate **8** as a crystalline mass: mp 77—78°C; IR (Nujol) 1730, 1240, 1050 cm^{-1}; NMR τ(CCl_4) 8.4—9.7 (4H, m, cyclopropane), 8.55 (3H, s, CH_3), 7.90 (3H, s, AcO), 6.7—8.2 (6H, m, $S(CH_2)_2S$), 6.10 (4H, bs, OCH_2CH_2O), 5.77 (1H, d, J=10 Hz, SCHS), 5.09 (1H, d, J=10 Hz, AcOCH).

Found: C, 52.67; H, 7.01%. Calcd for $C_{14}H_{22}O_8$: C, 52.82; H, 6.97%.

*1-Methanesulfinyl-3,3-ethano-4,4-ethylenedioxy-2-pentanol (**10**).* To a solution of 1.97 g of **9** in 10 m*l* of ethanol was added a solution of 80 mg of sodium borohydride in 2 m*l* of ethanol. The mixture was allowed to stand overnight at room temperature with stirring. After removal of most of the ethanol under reduced pressure, the residue was dissolved in water and extracted with chloroform. The aqueous phase was concentrated under reduced pressure and extracted with chloroform. The combined extracts were dried over sodium sulfate and the solvent was removed to give 1.7 g (84%) of colorless paste which crystallized gradually. A sample of the product was recrystallized from ethyl acetate: mp 120—122°C; IR (Nujol) 3200, 1045, 1025, 995 cm^{-1}; NMR τ($CDCl_3$) 9.1—9.5 (4H, m, cyclopropane), 8.55 (3H, s, CH_3), 8.03 (1H, s, OH), 7.33 (3H, s, CH_3SO), 7.07 (2H, d, J=6 Hz, $SOCH_2$), 6.06 (4H, s, OCH_2CH_2O), 5.77 (1H, t, J=6 Hz, OCH).

Found: C, 51.33; H, 7.67%. Calcd for $C_{10}H_{18}O_4S$: C, 51.27; H, 7.75%.

*Acetate **11**.* A sample of above alcohol **10** was acetylated with acetic anhydride and pyridine in the usual manner to give acetate **11**: IR (neat) 1745, 1240, 1045 cm^{-1}; NMR τ (CCl_4) 9.1—9.5 (4H, m, cyclopropane), 8.55 (3H, s, CH_3), 7.95 (3H, s, AcO), 7.45 (3H, s, CH_3SO), 6.88 (2H, d, J=6 Hz, CH_2SO), 6.10 (4H, s, OCH_2CH_2O), 4.98 (1H, t, J=6 Hz, CHOAc); *m/e*: 276 (M^+).

*1-Methanesulfinyl-3,3-dimethyl-4,4-ethylenedioxy-2-pentanol (**19**).* To a solution of 249 mg of 1-methanesulfinyl-3,3-dimethyl-4,4-ethylenedioxy-2-pentanone (**18**) in 10 m*l* of water was added a solution of 15 m*l* of sodium borohydride in 1 m*l* of water. The mixture was stirred in an ice bath for 3 hr and left in a refrigerator overnight. The mixture was extracted several times with chloroform and the extract was dried and evaporated to give 202 mg (81%) of a crystalline mass which was recrystallized from ethyl acetate: mp 140—144°C; IR (neat) 3200, 1030, 1005 cm^{-1}; NMR τ ($CDCl_3$) 9.05 (3H, s, CH_3), 8.98 (3H, s, CH_3), 8,70 (3H, s, CH_3), 7.26 (3H, s, CH_3SO), 6.8—7.5 (2H, m, CH_2SO), 6.06 (4H, s, OCH_2CH_2O), 5.80 (1H, d, J=8 Hz, OCH).

*Acetate **20**.* A sample of alcohol **19** was acetylated with acetic anhydride and pyridine in the usual manner to give acetate **20**: IR (neat) 1740, 1235, 1035 cm^{-1}; NMR τ ($CDCl_3$) 9.00 (6H, s, 2×CH_3), 8.66 (3H, s, CH_3), 7.90 (3H, s, AcO), 7.39 (3H, s, CH_3SO), 6.3—7.3 (2H, m, CH_2SO), 6.06 (4H, s, OCH_2CH_2O), 4.40 (1H, d, J=10 Hz, of *d*, J=2.5 Hz, OCH).

Synthesis of 5,5-Dimethyl-4-acetoxy-2-cyclopentenone and 5-Methyl-*t*-5-acetoxymethyl-*r*-4-acetoxy-2-cyclopentenone Intermediates for Illudin M and S

Takeshi MATSUMOTO, Haruhisa SHIRAHAMA, Akitami ICHIHARA, Hyonsobb SHIN, Shohei KAGAWA, Fujio SAKAN, Shuji NISHIDA, Sojiro MATSUMOTO, Kenichi SAITO, and Hisanobu HASHIMOTO

Department of Chemistry, Faculty of Science, Hokkaido University, Sapporo

(Received August 6, 1971)

5,5-Dimethyl-4-acetoxy-2-cyclopentenone and 5-methyl-*t*-5-acetoxymethyl-*r*-4-acetoxy-2-cyclopentenone, intermediates for illudin M and S respectively, have been synthesized from ethyl adipate.

In an earlier communication[1] we reported a total synthesis of *dl*-illudin M[2] (**4**) through the Michael reaction between **1** and the cyclopentenone **2**. A total synthesis of illudin S[2,3] (**5**) has also been presented[4] by an analogous route employing **3a** (Scheme 1). In this paper we should like to describe synthesis of these cyclopentenone intermediates **2**[5] and **3a**.

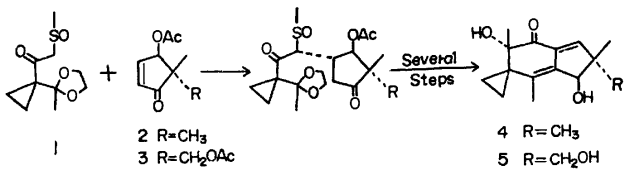

Scheme 1.

At first attempts were made to derive the cyclopentenone **2** from 2,2-dimethylcyclopentanone[6] (**20**). However, **20** had been obtained as a mixture with some other methylated cyclopentanones by methylation of either cyclopentanone or methylcyclopentanone. Thus another route for **20** was desirable.

2-Methyl-2-carbethoxycyclopentanone[7] **6** was reduced by lithium aluminum hydride to give a semicrystalline 2-methyl-2-hydroxymethylcyclopentanol (**18**) in 80% yield, bp 148—153°C/4 mmHg, which was converted into a monotosylate **19** quantitatively. Treatment of one mol of **19** with 1.5 mol of lithium aluminum hydride afforded in 64% yield 2,2-dimethylcyclopentanol[7] (**17**) which furnished on Jones oxidation the desired ketone **20**, bp 139°C, in 70% yield. Alcohol **17** was also prepared by a modified Eschenmoser's method[7] through **8**→**9**→**15**→**16**. Attempted transformation of 2-methyl-2-tosyloxymethylcyclopentanone ethylene ketal (**14**) to **20** with lithium aluminum hydride was unsuccessful, *O*-tosyl bond being cleaved to regenerate **8**. The steric hindrance probably changed the vulnerable point of the tosyloxy group.[8] Bromination of **20** with bromine followed by dehydrobromination with lithium chloride in dimethylformamide gave, in 60% yield (two steps), 5,5-dimethyl-2-cyclopentenone (**22**), bp 150—154°C, which was again brominated with *N*-bromosuccinimide. Subsequent treatment with silver acetate in acetic acid gave 5,5-dimethyl-4-acetoxy-2-cyclopentenone (**2**), bp 92—94°C/10 mmHg, as an oil in 43% yield (from **22**).

The above method for the preparation of acetoxycyclopentenone **2** is advantageous in that diacetoxycyclopentenone **3**, the

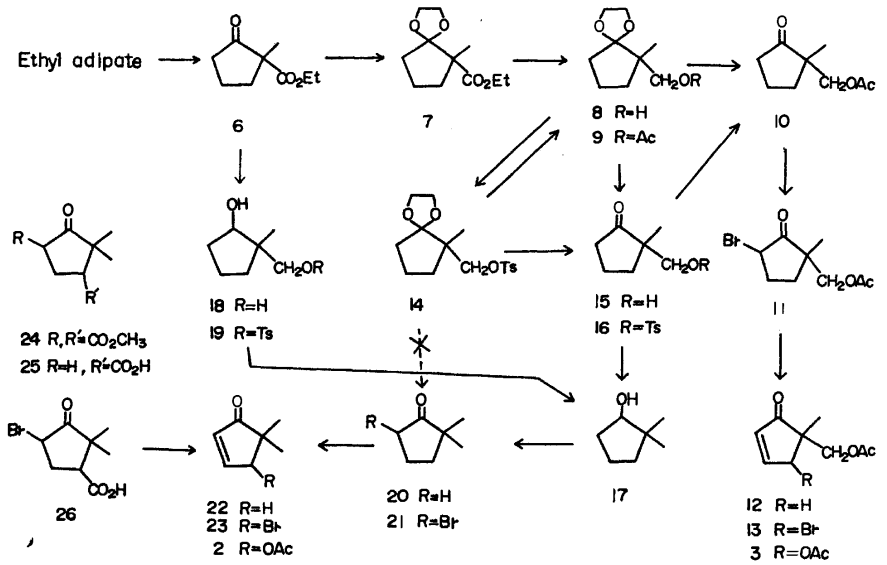

Fig. 1.

1) T. Matsumoto, H. Shirahama, A. Ichihara, H. Shin, S. Kagawa, F. Sakan, S. Matsumoto, and S. Nishida, *J. Amer. Chem. Soc.*, **90**, 3280 (1968).

2) T. C. McMorris and A. Anchel, *ibid.*, **87**, 1594 (1965).

3) T. Matsumoto, H. Shirahama, A. Ichihara, Y. Fukuoka, T. Takahashi, Y. Mori, and M. Watanabe, *Tetrahedron*, **21**, 2671 (1965); T. Matsumoto, Y. Fukuoka, A. Ichihara, Y. Mori, H. Shirahama, Y. Takahashi, and M. Watanabe, This Bulletin, **37**, 1716, (1964); K. Nakanishi, M. Ohashi, M. Tada, and Y. Yamada, *Tetrahedron*, **21**, 1231 (1965).

4) T. Matsumoto, H. Shirahama, A. Ichihara, H. Shin, S. Kagawa, F. Sakan, and K. Miyano, *Tetrahedron Lett.*, **1971**, 2049.

5) The synthesis of **2** was partly presented in a preliminary report. T. Matsumoto, H. Shirahama, A. Ichihara, H. Shin, S. Kagawa, N. Ito, T. Hisamitsu, T. Kamada, F. Sakan, K. Saito, S. Nishida, and S. Matsumoto, *Tetrahedron Lett.*, **1968**, 1925.

6) H. O. House and B. M. Trost, *J. Org. Chem.*, **30**, 2502 (1965); F. G. Gault, J. E. Germain, and Jean-Marie Conia, *Bull. Soc. Chim. Fr.*, **1957**, 1064.

7) A. Eschenmoser and A. Frey, *Helv. Chim. Acta*, **35**, 1660 (1952).

8) H. Schmid and P. Karrer, *ibid.*, **32**, 1371 (1949).

intermediate for illudin S, can be prepared through common compounds. However, for the synthesis of illudin M, a simpler method for **2** was desirable. Readily accessible 5,5-dimethyl-2,4-dicarbethoxycyclopentanone **24**[9] was converted by boiling with dilute perchloride acid into 5,5-dimethyl-4-carboxycyclopentanone (**25**), mp 107°C, in 60% yield. Bromination of **25** with bromine afforded, in quantitative yield, 5,5-dimethyl-4-carboxy-2-bromocyclopentanone (**26**), mp 152—154°C, which was converted into **22** by treatment with lithium chloride in dimethylformamide in 43% yield with simultaneous decarboxylation.

The second five membered intermediate 5-methyl-*t*-5-acetoxymethyl-*r*-4-acetoxy-2-cyclopentenone (**3a**) was prepared in a similar way through bromination-dehydrobromination from 2-methyl-2-hydroxymethylcyclopentanone (**10**), bp 83.5°C/4 mmHg, which was obtained through the steps **6**→**7**→**8**[6]→**9**→**10** or **8**→**15**[6]→**10**. Cyclopentenone **12** was then converted into diacetoxycyclopentenone **3**, bp 134—160°C/20 mmHg, (70%), by the same method as employed in the preparation of acetoxycyclopentenone **2** from **22**. Compound **3** thus obtained was a mixture of two configurational isomers with respect to 4-acetoxy and 5-acetoxymethyl groups. The isomers were separated by preparative gas chromatography (3 m DEGS column) to give **3a** and **3b**. Isomer **3b**, which has a shorter retention time, exhibited in its NMR spectrum AB quartet peaks due to the acetoxymethyl group attached to a chiral center at τ 6.23 and 5.77 (J= 12 Hz). The other isomer **3a** showed a smaller difference of chemical shift between the diastereotopic methylene protons (ABq, τ 5.99 and 5.89, J=11 Hz). The larger magnitude of nonequivalence suggested that **3b** might have *cis* arrangement of the acetoxymethyl group to the acetoxy group on cyclopentanone, since in **12** the corresponding methylene protons showed a singlet at τ 6.07.

For the confirmation of stereochemistry, **3b** was converted into diol **18** to observe intramolecular H-bond between the two hydroxyl groups. Treatment of **3b** with sodium borohydride gave a single saturated alcohol **27**[10] which was oxidized with Jones reagent to give rise to 2-methyl-2-acetoxymethyl-3-acetoxycyclopentanone (**28**). Reduction of **3b** with sodium borohydride proceeded stereospecifically[11] and the the attack of the reagent took place from the less hindered site to give an alcohol **27**. The OAc/CH_2-OAc *cis* structure of alcohol **27** was deduced because the monoacetate of **27** exhibited in the NMR spectrum a sharp singlet due to methylene protons of acetoxylmethyl group suggesting the presence of the plane of symmetry in the triacetate (monoacetate of **27**). Pentanone **28** was converted into thioketal **29** which was desulfurized with Raney nickel to give diacetate **30**. On the other hand, an isomeric mixture of diol **18** obtained from **6** by reduction with lithium aluminum hydride was separated by chromatography to yield two stereoisomeric diols with the weight ratio of *ca.* 1 : 4. On observation on the IR spectrum of each isomer in highly diluted solution, the major diol **18a** exhibited absorption bands due to hydroxyl group at 3648 and 3590 cm^{-1} ($\Delta\nu$OH=58 cm^{-1}) and the minor one **18b** at 3645 and 3570 cm^{-1} ($\Delta\nu$OH=75 cm^{-1}). Thus the latter should have *cis* configuration with respect to hydroxyl and hydroxymethyl groups. Comparison of the diacetylated *trans* and *cis* diols (**18a** and **b**) with the diol diacetate **30** derived from isomer **3b** revealed that **3b** actually had *cis* configuration.

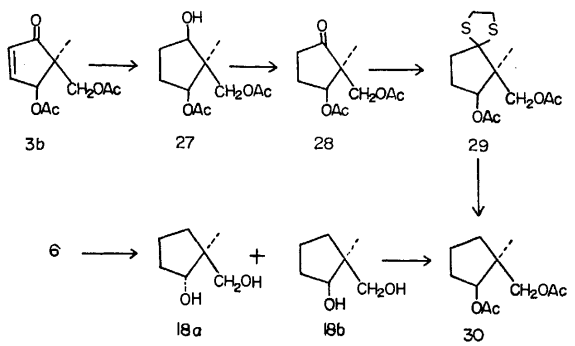

Fig. 2.

Experimental

*2-Methyl-2-hydroxymethylcyclopentanol (**18**).* To an ice cooled solution of 32 g of lithium aluminum hydride in 1.5 *l* of dry ether was added dropwise a solution of 127 g of 2-methyl-2-carbethoxycyclopentanone (**6**) in 100 m*l* of dry ether over a period of 2 hr with mechanical stirring. The resulting mixture was allowed to stand at room temperature and then refluxed for 5 hr. After the reaction was completed water was added dropwise to the ice cooled reaction mixture to decompose the excess of the reagent. The ethereal solution was washed with saturated salt solution, dried over anhydrous sodium sulfate and distilled to give 78 g (80%) of diol **18**: bp 148—153°C/4 mm; IR (neat) 3330, 1030 cm^{-1}.

Found: C, 64.70; H, 10.70%. Calcd for $C_7H_{14}O_2$: C, 64.58; H, 10.84%.

Chromatographic separation of *cis* and *trans* diols was achieved on a column of silica gel employing a mixture of benzene and ethyl acetate (3 : 2) as a solvent. Crude diol (450 mg) gave 121 mg of *trans* isomer **18a** (later eluted): IR (CCl_4, 0.005 M) 3648, 3590 cm^{-1}; NMR τ ($CDCl_3$) 9.00 (3H, s, CH_3), 6.71 (2H, s, OH), 6.52 (2H, s, CH_2O), 6.10 (1H, m, CHO) and 34 mg of *cis* isomer **18b** (earlier eluted): IR (CCl_4, 0.005 M) 3645, 3570 cm^{-1}; NMR τ ($CDCl_3$) 9.00 (3H, s, CH_3), 6.93 (2H, s, OH), 6.40 and 6.27 (2H, ABq, J=11 Hz, CH_2O), 6.04 (1H, m, CHO).

*2-Methyl-2-tosyloxymethylcyclopentanol (**19**).* To a solution of 260 g of diol **18** in 1 *l* of dry benzene were added 208 g of pyridine and 500 g of *p*-toluenesulfonyl chloride. After standing overnight at room temperature pyridine hydrochloride formed was removed by filtration. The benzene solution was washed six times with 6 N hydrochloric acid under ice cooling, three times with aqueous sodium carbonate solution, once with saturated salt solution and then dried over anhydrous sodium sulfate. Removal of the solvent left 567 g (quantitative) of tosylate **19**. An analytical sam-

9) G. Stork and F. H. Clarke, Jr., *J. Amer. Chem. Soc.*, **83**, 3114 (1961).

10) In general, the reduction of 2-cyclopentenone with complex hydrides gives saturated alcohol. See H. C. Brown and H. W. Hess, *J. Org. Chem.*, **34**, 2206 (1969).

ple was prepared by chromatography on silica gel: IR (neat) 3500, 3400, 1600, 1360, 1180 cm^{-1}.

Found: C, 58.85; H, 6.91%. Calcd for $C_{14}H_{20}O_4S$: C, 59.13; H, 7.09%.

*2,2-Dimethylcyclopentanol (**17**).* *A) By Reduction of **19**:* To an ice cooled solution of 57 g of lithium aluminum hydride in 1.8 *l* of dry ether was added dropwise 284 g of of tosylate **19** over a period of 2 hr with mechanical stirring. The resulting solution was allowed to stand at room temperature and then refluxed for 19 hr. After the reaction was completed the excess reagent was decomposed by water under ice cooling. The ethereal solution was washed, dried and distilled to afford 73 g (64%) of dimethylcyclopentanol **17**: bp 59.5—62°C/10 mmHg (lit,[7] 100°C/110 mmHg); IR (neat) 3370, 1380, 1360 cm^{-1}.

*B) By Reduction of **16**:* Tosylate **16** (19.2 g) was reduced by lithium aluminum hydride in dry ether in the same manner as above to yield 5.2 g (71%) of the alcohol **17**.

*2,2-Dimethylcyclopentanone (**20**):* To a solution of 57 g of cyclopentanol **17** in 130 m*l* of acetone was added dropwise the Jones reagent (prepared from 44 g of chromic anhydride in 130 m*l* of water and 38.2 m*l* of concentrated sulfuric acid) over a period of 2 hr with stirring by a mechanical stirrer under ice cooling. The resulting mixture was allowed to be warmed up to room temperature for 1 hr. The reaction mixture was then poured into 1 *l* of water and extracted with ether and the ethereal extract was washed with sodium carbonate solution and saturated salt solution, dried and distilled. 39 g (70%) of fragrant oil **20**, was obtained: bp 139°C; IR (neat) 1740, 1410, 1380, 1360 cm^{-1}.

Found: C, 74.98; H, 10.66%. Calcd for $C_7H_{12}O$: C, 74.95; H, 10.78%.

*5,5-Dimethyl-2-cyclopentenone (**22**).* *A) Preparation from Dimethylcyclopentanone **20**.* To a solution of 11.2 g of **20** in 250 m*l* of chloroform was added dropwise a solution of 16 g of bromine in 100 m*l* of the same solvent with stirring over a period of 5 hr. The reaction mixture was washed with aqueous sodium bicarbonate, then with saturated salt solution and dried. After removal of the solvent the residual bromoketone was dissolved in 130 m*l* of dimethylformamide and 11.4 g of lithium chloride was added. The solution was heated to reflux for 4 hr. The reaction mixture was poured into a large quantity of water and extracted several times with ether. The combined extracts were washed with sodium bicarbonate solution and saturated salt solution, dried and distilled to give 6.6 g (60%) of dimethylcyclopentanone **22**: bp 150—154°C; IR (neat) 3040, 1710, 1590, 1380, 1360, 810 cm^{-1}; NMR τ (CCl_4) 8.97 (6H, s, $2\times CH_3$) 7.53 (2H, t, J=2 Hz, CH_2), 4.02 (1H, d (J=6 Hz) of t (J=2 Hz) =CHCO), 2.53 (1H, d (J=6 Hz) of t (J=3 Hz), =CH–). Dinitrophenylhydrazone: mp 172—173°C.

Found: C, 53.77; H, 5.10; N, 19.49. Calcd for $C_{13}H_{14}N_4O_4$: C, 53.78; H, 4.86; N, 19.30%.

*B) Preparation from Bromoacid **26**:* A solution of 30 g of bromoacid **26** and 32 g of lithium chloride in 300 m*l* of dimethylformamide was refluxed for 1.5 hr. After cooling the reaction mixture was poured on 1 *l* of ice water and extracted three times with ether. The combined extracts were washed with saturated salt solution and dried. The solvent was removed and the residual oil was distilled, 6.1 g (43%).

*5,5-Dimethyl-4-acetoxy-2-cyclopentenone (**2**).* A solution of 2.2 g of cyclopentanone **22**, 5 g of *N*-bromosuccinimide and 80 mg of benzoyl peroxide in 70 m*l* of CCl_4 was heated to reflux for 2 hr. After reaction was completed the precipitated succinimide was removed by filtration. The filtrate was washed with sodium hydrosulfite, sodium bicarbonate and saturated salt solution, dried and evaporated to leave bromoketone **23** as an oil which was used in the next step without further purification. A sample of **23** was chromatographed (silica gel, benzene) for measuring spectra: IR (neat) 1720, 1585, 835 cm^{-1}; NMR τ (CCl_4) 8.80 (3H, s, CH_3), 8.76 (3H, s, CH_3), 5.02 (1H, d (J=3 Hz) of d (J=1.5 Hz), BrCH–), 3.78 (1H, d (J=6 Hz) of d (J=1.5 Hz), =CHCO), 2.42 (1H, d (J=6 Hz), of d (J=3 Hz), =CH–).

To a solution of crude bromoketone **23** (14 g) from four batches in 80 m*l* of acetic acid which was dried over phosphorus pentoxide, 18.5 g of silver acetate was added. The resulting mixture was heated at 110—115°C for 14 hr with stirring to precipitate silver bromide. The reaction mixture was then diluted with chloroform and filtered. The filtrate was neutralized with aqueous sodium carbonate solution, washed with saturated salt solution and dried. After removal of the solvent the residue was distilled to give 5.7 g of acetoxycyclopentanone **2** (42.5% from **22**): bp 92—94°C/10 mmHg; IR (neat) 3050, 1740, 1725, 1600, 1235 cm^{-1}; NMR τ (CCl_4) 9.05 (3H, s, CH_3), 8.83 (3H, s, CH_3), 7.93 (3H, s, AcO), 4.52 (1H, d (J=3 Hz) of d (J=1 Hz), AcOCH), 3.78 (1H, d (J=6 Hz) of d (J=1 Hz), =CHCO), 2.65 (1H, d (J=6 Hz) of d (J=3 Hz) =CH–).

Found: C, 64.51; H, 7.16%. Calcd for $C_9H_{12}O_3$: 64.27, H, 7.19%.

*5,5-Dimethyl-2,4-dicarbomethoxycyclopentanone (**24**).* This compound was prepared according to the method of Stork and Clarke[9] Two hundred and twenty grams of diester were obtained from 384 g of ethyl 2,3-dicyano-3-methylbutyrate (42% over 4 steps): bp 170—176°C/20 mmHg.

*5,5-Dimethyl-4-carboxycyclopentanone (**25**):* A mixture of 220 g of diester 24 and 1260 m*l* of 20% perchloric acid was refluxed for 7 hr until a homogeneous solution was obtained. The resulting solution was extracted with chloroform. The extract was washed with saturated salt solution and dried over anhydrous sodium sulfate and the solvent was distilled off. The crystalline residue was washed with hexane, 90 g (60%). A sample of product was recrystallized for analysis: mp 107°C; IR (Nujol) 1740, 1710 cm^{-1}; NMR ($CDCl_3$) 8.97 (3H, s, CH_3), 8.75 (3H, s, CH_3), 6.9—8.6 (5H, m, CH_2CH_2CH), −0.13 (1H, bs, CO_2H).

Found: C, 61.69; H, 7.88%. Calcd for $C_8H_{12}O_3$: C, 61.52; H, 7.75%.

*5,5-Dimethyl-4-carboxy-2-bromocyclopentanone (**26**).* The keto acid **25** (20 g) was dissolved in 200 m*l* of chloroform and 206 g of bromine was added with stirring under ice-cooling over a period of 1 hr. The chloroform solution was washed with water and dried over anhydrous sodium sulfate. Removal of the solvent left crude crystalline bromide (30 g). A small sample was recrystallized for analysis; mp 152—154°C; IR (Nujol) 1740, 1720 cm^{-1}.

Found: C, 40.65; H, 4.65%. Calcd for $C_8H_{11}O_3Br$: C, 40.53; H, 4.68%.

*2-Methyl-2-tosyloxymethylcyclopentanone Ethylene Ketal (**14**).* A solution of 29.2 g of 2-methyl-2-hydroxymethylcyclopentanone ethylene ketal (**8**)[7], 32.9 g of tosyl chloride and 30 g of pyridine in 180 m*l* of benzene was allowed to stand overnight in a refrigerator. The reaction mixture was poured into water and extracted with benzene. The extract was washed with aqueous sodium bicarbonate and saturated salt solution and dried. Evaporation of the solvent left 55 g (quantitative) of crude tosylate **14**. A sample of crude tosylate was recrystallized from carbon tetrachloride; mp 80°C, IR (Nujol) 1360, 1180 cm^{-1}.

Found: C, 59.03; H, 6.70%. Calcd for $C_{16}H_{22}O_5S$: C, 58.88; H, 6.80%.

Reduction of Tosylate ***14*** *with Lithium Aluminum Hydride.* To an ice-cooled solution of 750 mg of lithium aluminum hydride in 20 m*l* of dry ether was added dropwise with stirring a solution of 2.5 g of the tosylate **14** in 16 m*l* of dry ether. After refluxing for 7 hr the original tosylate was recovered. The recovered tosylate was dissolved in 25 m*l* of tetrahydrofuran and refiuxed with 750 mg of lithium aluminum hydride for 24 hr. The product obtained was the original alcohol **8** instead of dimethylcyclopentanone ethylene ketal.

*2-Methyl-2-tosyloxymethylcyclopentanone (****16****). A) By Tosylation of the Ketoalcohol* ***15***: The keto alcohol (141 g) was quantitatively converted by treatment with 209 g of tosylchloride and 87 g of pyridine in 500 m*l* of benzene to 310 g of tosylate **16**. A sample of the tosylate was recrystallized from carbon tetrachloride, mp 65—67°C; IR (Nujol) 1750, 1600, 1350, 1160 cm^{-1}.

B) By Deketalization of Tosylate ***14***: A solution of 2.5 g of ketal **14** and a pinch of *p*-toluenesulfonic acid in 100 m*l* of acetone was refluxed for 3 hr. The reaction mixture was concentrated under reduced pressure to remove most of acetone, and the residue was taken with ether. The ethereal phase was then washed with aqueous sodium bicarbonate solution and saturated salt solution and dried. Evaporation of ether left 1.6 g (74%) of tosylate **16**.

*2-Methyl-2-acetoxymethylcyclopentanone (****10****). A)* To a solution of 48 g of 2-methyl-2-hydroxymethylcyclopentanone ethylene ketal (**8**)[7] and 63 mg of *p*-toluenesulfonic acid in 480 m*l* of dry acetone was refluxed for 4.5 hr. After the reaction mixture was concentrated under reduced pressure at room temperature to remove most of acetone, benzene was added to the residue and the solution was washed with aqueous sodium bicarbonate solution and saturated salt solution and dried. The solvent was evaporated and the residue was distilled to give 26 g (73%) of ketone **15**, bp 93—98°C/6 mmHg, (lit,[6] 103—108°C/12 mmHg). Treatment of 10 g of the above alcohol with acetic anhydride and pyridine by the usual method gave 11.7 g (89%) of acetate **10**: bp 91—93°C/3 mmHg; IR (Neat) 1760, 1230 cm^{-1}.

Found: C, 63.32; H, 8.11%. Calcd for $C_9H_{14}O_3$; C, 63.53; H, 8.23%.

B): Ketal **8** (101 g) was acetylated by the usual method and treated with a pinch of *p*-toluenesulfonic acid in acetone to yield 80.2 g (80%) of acetoxy ketone **10**: bp 125—128°C/25 mmHg.

*5-Methyl-5-acetoxymethyl-2-bromocyclopentanone (****11****).* To a solution of 11 g of the acetoxy ketone **10** in 72 m*l* of chloroform was added dropwise a solution of 3.35 m*l* of bromine in 48 m*l* of the same solvent with stirring. The resulting mixture was washed with sodium bicarbonate solution and saturated salt solution and dried. The solvent was evaporated and the residue was distilled at 110—118°C/7 mmHg to give 145 g (90%) of bromoketone **11**. Formation of two configurational isomers might be expected. However, separation and examination of the ratio were not attempted. A sample of the bromo compound was redistilled and analyzed: IR (neat) 1750, 1735 cm^{-1}.

Found: C, 43.16; H, 5.27%. Calcd for $C_9H_{13}O_3Br$: C, 43.33; H, 5.22%.

*5-Methyl-5-acetoxymethyl-2-cyclopentenone (****12****).* A solution of 13 g of bromo compound **11** and 8.8 g of lithium chloride in 350 m*l* of dimethylformamide was heated at 150—160°C for 4 hr. The reaction mixture was then poured into ice-water and extracted several times with benzene. The combined extracts were washed successively with sodium bicarbonate and saturated salt solution, dried and distilled to yield 5.9 g (66%) of cyclopentenone; bp 94—100°C/4 mmHg, IR (neat) 1745, 1710, 1590, 1240 cm^{-1}; NMR τ (CCl_4) 8.91 (3H, s, CH_3), 8.07 (3H, s CH_3), 7.62 and 7.30 (2H, ABq, (J=19 Hz, each peak is split into J=2.5 Hz), CH_2) 6.07 (2H, s, CH_2OAc), 3.93 (1H, d (J=6 Hz) of t (J=2 Hz), =CHCO), 2.37 (1H, d (J=6 Hz) of t (J=2.5 Hz), =CH–).

Found: C, 64.23; H, 7.33%. Calcd for $C_9H_{12}O_3$: C, 64.28; H, 7.14%.

*5-Methyl-*t*-5-acetoxymethyl-*r*-4-acetoxy-2-cyclopentenone (****3****).* The compound (44.5 g 70%) was prepared from 52.2 g of cyclopentenone **12** by the same treatment as in the conversion of **22** into **2**. Bp 134—160°C/20 mmHg. A sample of ketone **3** was subjected to preparative vpc. A column of DEGS (3 m) was used at 170°C employing helium as a carrier gas (100 m*l*/min). The *cis* isomer **3b** appeared at 52 min (retention time) and the *trans* isomer **3a** at 62 min with a weight ratio of *ca.* 1 : 2.5. *cis*-5-Acetoxymethyl-4-acetoxy isomer (**3b**): IR (neat) 1745, 1725, 1595 and 1235 cm^{-1}; NMR τ (CCl_4) 8.80 (3H, s, CH_3), 8.05 (3H, s, AcO), 7.95 (3H, s, AcO), 6.23 and 5.77 (2H, ABq, J=2 Hz), HCOAc), 3.70 (1H, d (J=2 Hz) of d (J=6 Hz), =CHCO), 2.57 (1H, d (J=6 Hz) of d (J=3 Hz), -CH=). *trans*-5-Acetoxymethyl-4-acetoxy isomer (**3a**): IR (neat) 1745, 1725, 1595 and 1235 cm^{-1}; NMR τ (CCl_4) 9.05 (3H, s, CH_3), 8.05 (3H, s, AcO), 7.89 (3H, s, AcO), 5.99 and 5.89 (2H, ABq, J=11 Hz), 4.22 (1H, d (J=3 Hz) of d (J=2 Hz), HCOAc), 3.73 (1H, d (J=6 Hz) of d (J=3 Hz), –CH=), 2.56 (1H, d (J=6 Hz) of d (J=3 Hz), –CH=).

*2-Methyl-*c*-2-acetoxymethyl-*c*-3-acetoxy-*r*-1-cyclopentanol (****27****).* A sample (940 mg) of cyclopentenone **3b** was dissolved in 25 m*l* of ethanol. The solution was cooled in an ice bath and 315 mg of sodium borohydride was added with stirring. After stirring for 40 min, a small amount of acetic acid was added and the reaction mixture was poured into water and extracted with ethyl acetate. The extract was washed with saturated salt solution and dried. Removal of the solvent left 904 mg of reduced product: IR (neat) 3450, 1740, 1725, 1040 cm^{-1}.

Found: C, 57.18; H, 7.86%. Calcd for $C_{11}H_{18}O_5$: C, 57.38; H, 7.88%.

Treatment of 60 mg of alcohol with acetic anhydride and pyridine by the usual method gave 49 mg of pure triacetate; IR (neat) 1745, 1238, 1038 cm^{-1}; NMR τ (CCl_4) 8.90 (3H, s, CH_3), 8.00 (9H, s, 3×AcO), 5.99 (2H, s, CH_2OAc), 5.10 (2H, m, 2×HCOAc).

*2-Methyl-*r*-2-acetoxymethyl-*c*-3-acetoxycylcopentanone (****28****).* To a solution of 904 mg of alcohol derived from **3a** in 45 m*l* of acetone 0.7 m*l* of Jones reagent was added dropwise over a period of 80 min with ice cooling. After standing at room temperature for 20 min a small amount of ethanol was added and the precipitate was filtered off. The solvent was evaporated and the residue was extracted with ether. The extract was washed with saturated salt solution, sodium bicarbonate solution and then saturated salt solution and dried. Evaporation of the solvent left ketone which was chromatographed on silica gel to give 515 mg of ketone **28**: IR (neat) 1750, 1240, 1050, cm^{-1}; NMR τ(CCl_4) 8.88 (3H, s, CH_3), 8.03 (3H, s, AcO), 8.00 (3H, s, AcO), 5.94 (2H, d (appearance) J=2.4 Hz CH_2OAc), 4.87 (1H, m, HCOAc); *m/e*; 228 (M^+).

*2-Methyl-*r*-2-acetoxymethyl-*c*-3-acetoxycyclopentanone Ethylene Thioketal (****29****).* To a solution of 200 mg of ketone **28** in 2.7 m*l* of acetic acid, 840 mg of ethanedithiol and then 1.1 m*l* of boron trifluoride etherate were added and stirrred. The reaction mixture was allowed to stand at room temperature for 24 hr and poured into almost the same quantity of

water and extracted with ether. The extract was washed with sodium carbonate solution and with saturated salt solution and dried. After evaporation of the solvent, the residual oil was purified by chromatography to give 134 mg of thioketal; IR (neat) 1750 1250, 1045 cm^{-1}; NMR τ (CCl_4) 8.79 (3H, s, CH_3), 8.02, (3H, s, AcO), 7.91 (3H, s, AcO), 6.79 (4H, s, SCH_2CH_2S), 5.45 and 6.14 (4H, ABq, J=11 Hz CH_2OAc), 5.10 (1H, m, HCOAc).

r-*1*-*Acetoxy*-*2*-*methyl*-c-*2*-*acetoxymethylcyclopentane* (***30***). To solution of 130 mg of thioketal **29** in 40 m*l* of ethanol, 2.5 g of Raney nickel W-2 was added. The reaction mixture was stirred at 85°C to make the solvent reflux for 24 hr. The Raney nickel used was removed through a short column of aluminum oxide and the solvent was evaporated. The residue was dissolved in ether and filtered to remove solid mass and washed with saturated salt solution and dried. After removal of the solvent the residual oil was chromatographed to yield 91 mg of diacetate **30**; IR (neat) 1750, 1245, 1050 cm^{-1}.

Found: C, 61.86; H, 8.18%. Calcd for $C_{11}H_{18}O_4$: C, 61.66; H, 8.47%.

BULLETIN OF THE CHEMICAL SOCIETY OF JAPAN, VOL. 45, 1144—1147 (1972)

Synthesis of 5,5-Dimethyl-4-acetoxy-2-cyclopentenone, an Intermediate in the Total Synthesis of Illudin M, through Sulfur Compounds. A Novel Intramolecular Migration of Ethylenedioxy Group

Takeshi MATSUMOTO, Haruhisa SHIRAHAMA, Akitami ICHIHARA, Hyonsobb SHIN, and Shohei KAGAWA

Department of Chemistry, Faculty of Science, Hokkaido University, Sapporo

(Received August 6, 1971)

5,5-Dimethyl-4-acetoxy-2-cyclopentenone, an intermediate in the total synthesis of illudin M, has been prepared from 1-methylsulfinyl-3,3-dimethyl-4,4-ethylenedioxy-2-pentanone as well as from 1,1-trimethylenedithio-3,3-dimethyl-4,4-ethylenedioxy-2-pentanone. An example of new intramolecular transketalization has been described.

A report was given on a total synthesis[1] of *dl*-illudin M. The synthesis was started from the Michael addition of a sulfoxide **1** to a cyclopentenone **2**. In the early stage[2] of this work, it was thought to be of interest to convert a sulfoxide **5** or a dithiane **10**, both similar in structure to **1**, into the cyclopentenone **2**.[3] If the conversion were possible, it would mean that illudin M can be synthesized from two structurally similar seven-carbon units.

The present paper describes the synthesis of the cyclopentenone **2** along this line.[4,5] At first, the carbonyl group of ethyl dimethylacetoacetate (**3**)[6] was masked with ethylene glycol in the usual manner (52% yield), and the ketal ester was treated with methylsulfinyl carbanion according to Corey's method[7]

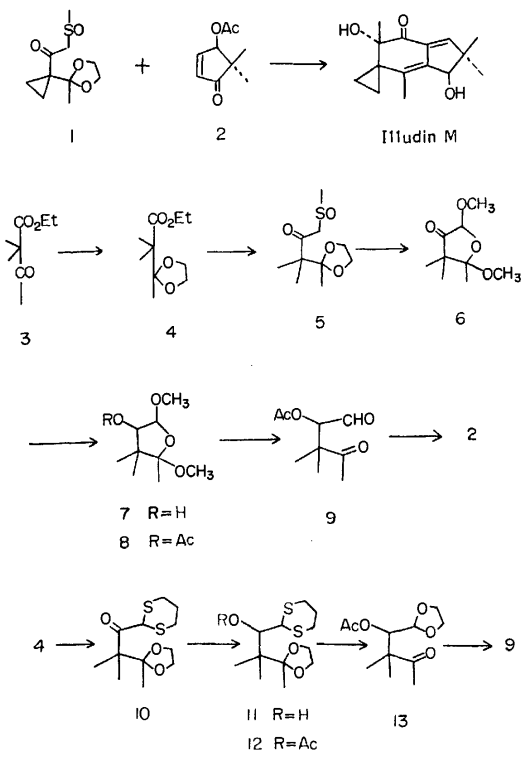

Fig. 1.

1) T. Matsumoto, H. Shirahama, A. Ichihara, H. Shin, S. Kagawa, F. Sakan, S. Matsumoto, and S. Nishida, *J. Amer. Chem. Soc.*, **90**, 3280 (1968).

2) T. Matsumoto, H. Shirahama, A. Ichihara, H. Shin, S. Kagawa, N. Ito, T. Hisamitsu, T. Kamada, and F. Sakan, *Tetrahedron Lett.*, **1967**, 4097.

3) T. Matsumoto, H. Shirahama, A. Ichihara, H. Shin, S. Kagawa, N. Ito, T. Hisamitsu, T. Kamada, K. Saito, S. Nishida, and S. Matsumoto, *icid.*, **1968**, 1925.

4) A part of the present paper was presented in the preliminary report.[1]

5) An alternative route: See T. Matsumoto, H. Shirahama, A. Ichihara, H. Shin, S. Kagawa, F. Sakan, S. Nishida, S. Matsumoto, K. Saito and H. Hashimoto, This Bulletin, **45**, 1140 (1972).

6) K. Folkers and H. Adkins, *J. Amer. Chem. Soc.*, **53**, 1416 (1931).

7) E. J. Corey and M. Chaykovsky, *ibid.*, **87**, 1345 (1965).

to give a β-ketosulfoxide **5**, mp 53—56°C, in 91% yield. It has been shown that in general β-ketosulfoxides gave α-ketoacetals on treatment with iodine in methanol.[8] Compound **5** was accordingly treated under these conditions to afford a mixture of an epimeric pair of tetrahydrofuranones **6** in moderate yield and minor products. By chromatography on silica gel the mixture was separated into four fractions. The first fraction obtained in a small amount as an oil was found to be a mixture of an epimeric pair of 2,3,3-trimethyl-2-methoxy-5-methylthiotetrahydro-4-furanone, on the basis of the NMR spectrum. The second and third fractions contained the main products of the reaction. NMR spectra indicated that each product was one of the epimeric pair of 2,3,3-trimethyl-2,5-dimethoxytetrahydro-4-furanone (**6**). The last fraction was a mixture of epimers of **6** and unidentified substances. Reduction followed by acetylation of each epimer of **6** afforded a single, but not identical, product: diastereoisomeric 2,3,3-trimethyl-2,5-dimethoxy-4-acetoxytetrahydrofuran (**8**), respectively. Both isomers of **8** gave the same compound, 2-acetoxy-3,3-dimethyl-4-ketopentanal (**9**, bis DNP mp 201—202°C) in moderate yield, on being dissolved in a mixture of 1 N hydrochloric acid and tetrahydrofuran (1/1). For the preparation of the final product, cyclopentenone **2**, the series of reactions (**5**→**9**) can be performed without purification of the intermediates. A crude product containing **9** was obtained in 47.5% yield from **5**. Vpc analysis revealed that one third of the product was the desired aldehyde **9**. The crude aldehyde **9** was cyclized to afford 5,5-dimethyl-4-acetoxy-2-cyclopentenone (**2**)[3] in 21% yield based on the crude product, on treatment with sodium hydride in a large amount of benzene under refluxing.

Pure aldehyde **9** was also obtained through a 1,3-dithiane derivative as follows. The addition reaction of an anion of 1,3-dithiane[9] to dimethylacetoacetic ester afforded 1,1-trimethylenedithio-3,3-dimethyl-4,4-ethylenedioxy-2-pentanone (**10**), mp 89—90°C. Reduction and acetylation of the dithiane **10** gave 1,1-trimethylenedithio-2-acetoxy-3,3-dimethyl-4,4-ethylenedioxypentane (**12**) which was treated with mercuric chloride and cadmium carbonate in aqueous acetone in order to remove the trimethylenedithio group.[10]

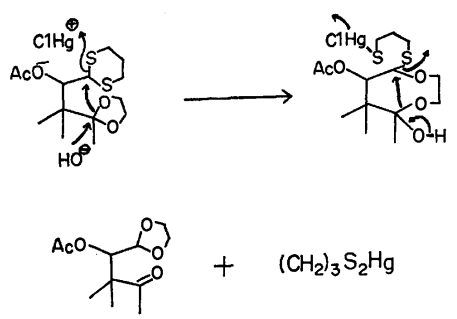

Fig. 2.

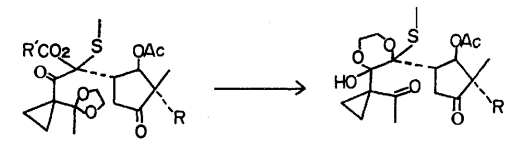

14 R=CH_3, R'=CH_3
15 R=CH_2OAc, R'=CH_3
16 R=CH_2OAc, R'=CH_2OCH_3

17 R=CH_3
18 R=CH_2OAc

Fig. 3.

The compound obtained lacked sulfur atom, but it was not the expected aldehyde and instead a ketone. The NMR spectrum showed signals for a *gem*-dimethyl group as singlets at τ 8.96 and 8.76, two acetyl groups as singlets at τ 7.89 and 7.81, an ethylenedioxy group as a rather sharp (W1/2=6Hz) multiplet at τ 6.31 and two methine groups as an AB quartet at τ 5.06 and 4.82 (J=7 Hz). Ethylenedioxy group was undoubtedly transferred to the γ-carbonyl group on the basis of the NMR spectrum and the structure of the product was expressed as 1,1-ethylenedioxy-2-acetoxy-3,3-dimethylpentanone (**13**). The reaction may be rationalized by a transition state containing as eight membered ring (Fig. 2). Similar rearrangements of ethylenedioxy group have been observed in our synthetic studies on illudin M[1] and S.[11,12] Methyl ketone **13** was readily converted into aldehyde **9** by a similar treatment to that for the deacetalization of **8**.

Experimental

Ethyl 2,2-dimethyl-3-ethylenedioxybutyrate (4). Ethyl 2,2-dimethyl-3-ketobutyrate (**3**)[6] was dissolved in 300 m*l* of benzene containing 27 g of ethylene glycol and 200 mg of *p*-toluenesulfonic acid. The mixture was heated at the reflux temperature of benzene. The water formed was removed by azeotropic distillation with a Dean-Stark separator and heating was continued until 4 m*l* of water was removed. The reaction mixture was washed three times with aqueous sodium carbonate and three times with water and dried. The solvent was removed and the residue was distilled to yield 27.2 g (52%) of **4**: bp 110°C/17 mmHg; IR (neat) 1730 cm^{-1} (CO); NMR τ ($CDCl_3$) 8.71 (3H, t, J=7 Hz, $CH_2\underline{CH_3}$), 8.80 (6H, s, 2×CH_3), 8.68 (3H, s, CH_3), 6.10 (4H, s, OCH_2CH_2O), 5.88 (2H, q, J=7 Hz, $\underline{CH_2}CH_3$).

1-Methylsulfinyl-3,3-dimethyl-4,4-ethylenedioxy-2-pentanone (5). The compound was prepared by the general method for preparation of β-ketosulfoxides according to Corey and Chaykovsky.[7] Ester **4** (27.2 g) was added dropwise to a dimethyl sulfoxide solution of methylsulfinyl carbanion prepared from 140 m*l* of dimethyl sulfoxide and 12.9 g of sodium hydride (50% mineral oil dispersion) under ice-water cooling and mechanical stirring in the atmosphere of nitrogen. The ice-water bath was removed, stirring was continued for 2 hr at room temperature and the reaction mixture was

8) T. L. Moore, *J. Org. Chem.*, **32**, 2786 (1967).
9) E. J. Corey and D. Seebach, *Angew. Chem.*, **77**, 1135 (1965).
10) A. G. Brook, J. M. Duff, P. F. Jones, and N. R. Davis, *J. Amer. Chem. Soc.*, **89**, 431 (1967).
11) T. Matsumoto, H. Shirahama, A. Ichihara, H. Shin, S. Kagawa, F. Sakan, and K. Miyano, *Tetrahedron Lett.*, **1971**, 2049.
12) In the course of studies on total synthesis of illudins,[1,11] reactions such as **14**→**17** and **16**→**18** (Fig. 3) were found. Warming compounds **14** and **16** in ethanol was enough to cause the transfer of the ethylenedioxy group but the rearrangement (**15**→**18**) did not occur under the same conditions.

then poured into 500 m*l* of water, wshed three times with benzenee, neutralized with dilute acetic acid to pH of 5—6 (pH paper), and extracted three times with chloroform. The combined extracts were washed three times with a saturated salt solution and dried over anhydrous sodium sulfate, and evaporated to yield 28.7 g (91%) of the ketosulfoxide **5** as a yellow crystalline solid. A small sample was recrystallized from carbon tetrachloride for analysis: mp 53—56°C; IR (nujol) 1700 cm^{-1}; NMR τ ($CDCl_3$) 8.77 (3H, s, $CH_3C\langle^{O}_{O}$), 8.75 (6H, s, CH_3CCH_3), 7.27 (3H, s, $SOCH_3$), 5.99 (4H, s, OCH_2CH_2O), 5.99 and 5.57 (2H, ABq, J=16 Hz, $SOCH_2CO$).

Found: C, 51.15; H, 7.65%. Calcd for $C_{10}H_{18}O_4S$: C, 51.27; H, 7.75%.

*2,3,3-Trimethyl-2,5-dimethoxytetrahydro-4-furanone (**6**).* Keto sulfoxide **3** (6.3 g) was dissolved in 120 m*l* of methanol containing 3.44 g of iodine. The solution was refluxed for 4 hr, and then allowed to cool. Most of the methanol was removed at room temperature on a rotary evaporator under reduced pressure. The dark residual oil was taken up in chloroform and washed twice with saturated sodium thiosulfate solution. The light yellow chloroform solution was dried with anhydrous sodium sulfate and the solvent was removed under reduced pressure. The residual oil was chromatographed on silica gel with benzene as a solvent and separated into four fractions.

The first fraction was 81 mg of an oil: IR (neat) 1765 cm^{-1}; NMR τ ($CDCl_3$) 8.90 (6H, s, CH_3CCH_3), 8.58 (3H, s, CH_3), 7.72 and 7.70 (3H, twin s, SCH_3), The qualitative analysis for sulfur was positive and the oil was converted into **6** by treatment with iodine in methanol. Thus, the oil should be a mixture of an epimeric pair of 2,3,3-tri methyl-2-methoxy-5-methylthiotetrahydro-4-furanone. The second fraction (877 mg): IR (neat) 1780 cm^{-1}; NMR ($CDCl_3$) 8.91, 8.86 and 8.57 (each 3H, s, 3×CH_3), 6.67 and 6.42 (each 3H, s, 2×OCH_3), 5.36 (1H, s, OCHO). The third fraction (1.338 g): IR 1780 cm^{-1}; NMR τ ($CDCl_3$) 8.90 (6H, s, CH_3CCH_3), 8.60 (3H, s, CH_3), 6.68 and 6.42 (each 3H, s, 2×OCH_3), 5.04 (1H, s, -OCHO-). From these spectral data, it was deduced that each of the second and the third fractions contained an epimer of **6**. The fourth fraction (694 mg) was a mixture of **6** and unidentified substances.

*2,3,3-Trimethyl-2,5-dimethoxy-4-acetoxytetrahydrofuran (**8**).* Each epimer of furanone **6** was separately reduced with sodium borohydride and then acetylated with acetic anhydride and pyridine. The earlier eluted furanone **6** (877 mg) gave 609 mg of a single epimer of **8**: IR (neat) 1750, 1240 cm^{-1}; NMR τ (CCl_4) 9.00 (6H, s, CH_3CCH_3), 8.78 (3H, s, CH_3), 7.95 (3H, s, OAc), 6.80 and 6.68 (each 3H, s, OCH_3), 5.29 and 5.11 (2H, ABq, J=6 Hz, $AcOCHCH\langle^{O}_{O}$). The later eluted furanone **6** (40 mg) gave 23 mg of another epimer of **8**: IR (neat) 1740, 1240 cm^{-1}; NMR τ (CCl_4) 9.04, 8.98 and 8.82 (each 3H, s, CH_3), 7.92 (3H, s, OAc), 6.78 and 6.55 (each 3H, s, OCH_3), 5.24 and 5.01 (2H, ABq, J=6 Hz, $AcOCHCH\langle^{O}_{O}$).

*2-Acetoxy-3,3-dimethyl-4-ketopentanal (**9**).* Each epimer of **8** was separately converted into aldehyde **9**. A sample of acetoxyfuran was dissolved in about 20 times its volume of a mixture of 1 N hydrochloric acid and tetrahydrofuran and allowed to stand for 3 hr at room temperature. The reaction mixture was extracted with chloroform three times. The combined extracts were washed with water twice, dried and evaporated to leave aldehyde **9**. IR (neat) 1740, 1705, 1230 cm^{-1}; NMR τ (CCl_4), 8.75 (6H, s, CH_3CCH_3), 7.86 (6H, s, OAc and $COCH_3$), 5.06 (1H, s, AcOCH), 0.50 (1H, s, CHO). Bisdinitrophenylhydrazone: mp 201—202°C.

Found: C, 46.21; H, 4.20; N, 20.19%. Calcd for $C_{21}H_{22}N_8O_{10}$: C, 46.15; H, 4.06; N, 20.50%.

Crude aldehyde **9** can be prepared from sulfoxide **5** without purification throughout the process as follows. Treatment of 8.2 g of the sulfoxide **5** gave 4.5 g of a crude epimeric mixture of acetoxyfuran **8**, 2.4 g which was hydrolysed to give 1.65 g of a crude product. Gas chromatographic analysis revealed that one third of the product was the desired aldehyde **9**.

*5,5-Dimethyl-4-acetoxy-2-cyclopentenone (**2**).* The above crude product (800 mg) containing aldehyde **9** was refluxed under stirring with 300 mg of sodium hydride in 400 m*l* of benzene for 9 hr. The reaction mixture was filtered and the solvent was removed. The resulting oil was fractionated by preparative gas chromatography on DEGS column (3m, at 270°C, He: 100 m*l*/min, reteniton time: 10 min) to give 150 mg of the cyclopentenone. The IR spectrum was identical with that of the authentic sample.[2]

*1,1-Trimethylenedithio-3,3-dimethyl-4,4-ethylenedioxy-2-pentanone (**10**).* A solution of 11.7 g of *n*-butyl bromide in 15 m*l* of ether was added dropwise to 1.4 g of lithium covered with 35 m*l* of ether −30——40°C and the mixture was stirred for 1.5 hr at 0—10°C. The resulting solution was added dropwise to a stirred solution of 3 g of 1,3-dithian in 50 m*l* of tetrahydrofuran at −30——40°C. To the solution prepared above was added dropwise 5 g of ethyl dimethylacetoacetate ethylene ketal (**4**) at −20——30°C with stirring. The reaction mixture was allowed to stand at the same temperature range for 40 hr and then poured into water. The solution was acidified with dilute hydrochloric acid and extracted with ethyl acetate. The extract was washed with a saturated salt solution and dried over anhydrous sodium sulfate. After removal of the solvent, the residue was distilled to give 2 g (29.3%) of **10**, bp 152—152.5°C/4 mmHg, which crystallized soon and was recrystallized from isopropyl ether: mp 89—90°C; IR (nujol) 1690 cm^{-1}; NMR τ (CCl_4) 8.74 (9H, s, 3×CH_3), 8.0—7.4 and 6.8—6.2 (4H and 2H, m, $S(CH_2)_3S$), 6.01 (4H, s, OCH_2CH_2O), 5.30 (1H, s, SCHS).

Found: C, 52.07; H, 7.05%. Calcd for $C_{12}H_{20}O_3S_2$: C, 52.16; H, 7.30%.

*1,1-Trimethylenedithio-3,3-dimethyl-4,4-ethylenedioxy-2-pentanol (**11**).* Ketone **10** (1.375 g) was dissolved in anhydrous ether and 50 mg of lithium aluminum hydride was added. After standing overnight, another 50 mg of lithium aluminum hydride was added and the reaction mixture was refluxed for 6 hr, poured on ice-water and the product was extracted with ether. The extract was dried and the solvent was removed to leave 1.24 g (90%) of **11**. Crystalline mass was recrystallized from isopropyl ether and analyzed, mp 68—69°C: IR (neat) 3450 cm^{-1}; NMR τ (CCl_4) 8.97, 8.87 and 8.71 (each 3H, s, CH_3), 8.5—6.5 (6H, m, $S(CH_2)_3S$), 6.02 (4H, s, OCH_2CH_2O), 6.10 (1H, d, J=3 Hz, HOCH), 5.80 (1H, d, J=3 Hz, SCHS).

Found: C, 51.81; H, 7.86%. Calcd for $C_{12}H_{22}O_3S_2$: C, 51.79; H, 7.97%.

Alcohol **11** was acetylated with acetic anhydride and pyridine in the usual manner to give acetate **12**: IR (neat) 1745, 1235 cm^{-1}: NMR τ (CCl_4) 8.98, 8.90 and 8.70 (each 3H, s, CH_3), 7.89 (3H, s, OAc), 6.03 (4H, s, OCH_2CH_2O), 5.32 (1H, d, J=2 Hz, SCHS), 4.85 (1H, d, J=2 Hz, AcOCH).

*1,1-Ethylenedioxy-2-acetoxy-3,3-dimethylpentanone (**13**).*

Acetate **12** (127 mg) was dissolved in 10 m*l* of acetone and 630 mg of mercuric chloride, 917 mg of cadmium carbonate and 90 mg of water were added and the whole solution was stirred for 6 hr at room temperature. The acetone was removed and the residue was extracted with chloroform. After evaporation of the solvent, the extracted mass was chromatographed on silica gel column employing a mixture of ethyl acetate and benzene (1 : 9) as a solvent to give 28 mg (31%) of **13**: IR (neat) 1750, 1710, 1230 cm^{-1}; NMR τ (CCl_4) 8.96 and 8.76 (each 3H, s, CH_3) 7.89 and 7.86 (each 3H, s, OAc and $COCH_3$), 6.13 (4H, m, W1/2= 6 Hz, OCH_2CH_2O), 5.06 and 4.82 (2H, ABq, J=7 Hz, $AcOCHCH\langle^{O}_{O}\rangle$).

Hydrolysis of ***13***. To a solution of 17 mg of ketoacetal **13** in 1 m*l* of tetrahydrofuran was added five drops of 6 N hydrochloric acid and the solution was left to stand overnight at room temperature. After addition of 1 m*l* of water, the solution was kept for a few minutes under reduced pressure to remove most of the tetrahydrofuran and the residue was extracted with chloroform three times. The combined extracts were washed with a saturated salt solution, dried and evaporated to leave 9 mg of an oil whose IR spectrum was identical with that of the aldehyde obtained from **8**.

BULLETIN OF THE CHEMICAL SOCIETY OF JAPAN, VOL. 45, 1147—1152 (1972)

The Stereochemistry of Nucleophilic Addition. IV.[1] The Condensation of 2,2,6-Trimethylcyclohexanone with *t*-Butyl Acetate in the Presence of Lithium Amide

Takashi MATSUMOTO, Gojo SAKATA, Yakudo TACHIBANA, and Kenji FUKUI

Department of Chemistry, Faculty of Science, Hiroshima University, Higashi-sendamachi, Hiroshima

(Received August 23, 1971)

The stereochemistry of the condensations of 2,2,6-trimethylcyclohexanone with *t*-butyl acetate in the presence of lithium amide, with ethyl bromoacetate in the presence of zinc (Reformatsky reaction), and with ethylmagnesium iodide (Grignard reaction) was studied. The configurations of the products in these reactions were assigned on the basis of their chromatographic behavior, and on the basis of spectroscopic and chemical studies of them. From the present experiments it is evident that all of these nucleophilic addition reactions proceed in a similar fashion. Further, the treatment of *t*-butyl 1-hydroxy-2,2,*t*-6-trimethyl-*r*-1-cyclohexaneacetate (IIa) with potassium hydrogensulfate or with dilute sulfuric acid gave (±)-*cis*-tetrahydroactinidiolide (IX), which was isolated from the essential oil of cigar tobacco leaves by Kaneko and Hoshino, while the treatment of IIa with isopropenyl acetate in the presence of *p*-toluenesulfonic acid gave a mixture of IX and its *trans*-isomer (X).

In previous papers,[1-3] the present authors have reported on the stereochemistry of the Reformatsky reaction with carbonyl compounds possessing an asymmetic α-carbon atom. A similar aldol-type condensation of *t*-butyl acetate with carbonyl compounds in the presense of lithium amide has been reported by Hauser *et al.*[4,5] However, since this reaction has not been studied stereochemically, it is of interest to study the stereochemistry of the aldol-type condensation with carbonyl compounds possessing an asymmetric α-carbon atom, and to compare it with that of the Reformatsky and Grignard reactions. The present paper will describe the stereochemistry of these nucleophilic addition reactions with 2,2,6-trimethylcyclohexanone (I). The condensation of I with *t*-butyl acetate in ether in the presence of lithium amide gave a mixture of epimeric *t*-butyl 1-hydroxy-2,2,6-trimethyl-1-cyclohexaneacetates (IIa and IIb) in a 76% yield, accompanied by a small amount of dehydrated esters (3% yield, IIIa and IIIb). The separation of these esters was successively carried out by means of column chromatography on silica gel to give, in the order of elution, the oily IIIa, IIIb, IIa, and IIb esters in a 3 : 1 : 78 : 18 ratio. The structures of IIIa and IIIb were assigned on the basis of their spectral data, as will be shown in the Experimental section. The alkaline hydrolyses of IIa and IIb gave the corresponding crystalline β-hydroxy acids, IVa (mp 118.5—119.5°C) and IVb (mp 143.5—144°C) respectively. Sakan *et al.*[6], during the course of their synthetic work on dihydroactinidiolide, reported on the synthesis of ethyl 1-hydroxy-2,2,6-trimethyl-1-cyclohexaneacetate (V) by the Reformatsky reaction of I with ethyl bromoacetate, but the composition of the epimeric alcohols expected was not recorded. Therefore, the stereochemistry of this reaction was also studied in order to compare it with that of the above aldol-type condensation. A mixture of the epimeric β-hydroxy esters obtained (62% yield) by the Reformatsky reaction was also separated by means of column chromatography on silica gel into two oily ethyl esters

1) Part III. T. Matsumoto, Y. Tachibana, T. Ohno, and K. Fukui, *J. Sci. Hiroshima Univ., Ser., A.* **35**, 231 (1971). Although the formulas depicted represent only one enantiomer, they are taken to indicate a racemate.

2) T. Matsumoto and K. Fukui, This Bulletin, **44**, 1090 (1971).

3) T. Matsumoto, I. Tanaka, and K. Fukui, *ibid.*, **44**, 3378 (1971).

4) C. R. Hauser and W. H. Puterbaugh, *J. Amer. Chem. Soc.*, **73**, 2972 (1951); **75**, 1068, 4756 (1953).

5) C. R. Hauser and W. R. Dunnavant, *J. Org. Chem.*, **25**, 1296 (1960).

6) T. Sakan, S. Isoe, and S. Be Hyeon, *Tetrahedron Lett.*, **1967**, 1623.

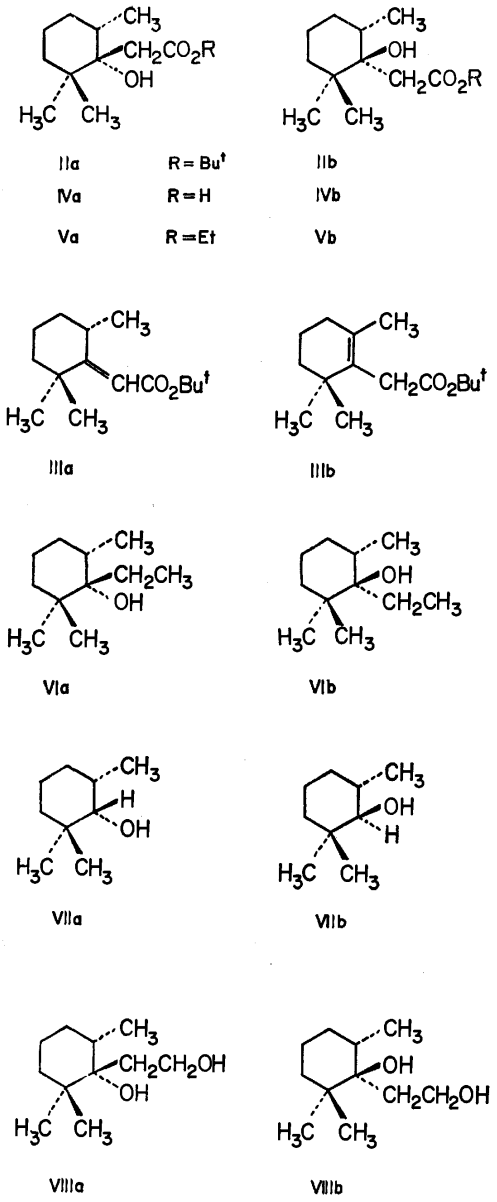

(Va and Vb) in a 76 : 24 ratio. These major (Va) and minor (Vb) esters were hydrolyzed with sodium hydroxide in methanol to give the corresponding acids (mp 117—119°C and mp 143—144°C), which were identified as IVa and IVb respectively. This finding means that the two reactions proceed on similar stereochemical courses. The NMR spectra of IIa, IIb, Va, and Vb are summarized in Tables 1 and 2. As is shown in these tables, the methylene protons alpha to the ester group in the major alcohols (IIa and Va) are observed as well-defined AB-type quartets in $CDCl_3$, while those in the minor alcohols (IIb and Vb) are observed as singlets. The pyridine-induced solvent shifts (Δ values[7]) of these methylene protons in IIa (−0.17 ppm) and Va (−0.13 ppm) are slightly larger than those in the corresponding epimers (IIb: −0.13 ppm and Vb: −0.08 ppm), although the differences (II: 0.04 ppm and V: 0.05 ppm) of these Δ values between the epimeric alcohols are smaller than those (0.10—0.14 ppm) in the cases of 2-monoalkylcyclohexylacetate derivatives which have been reported in previous papers[1,2] The above NMR spectral data suggest that the orientations of the $-CH_2CO_2R$ groups in the major (IIa and Va) and minor (IIb and Vb) alcohols are equatorial and axial respectively. These assignments are also supported by their IR spectra, because IIa and Va show the characteristic hydroxyl absorption bands, at 983 and 985 cm^{-1}, respectively, which suggest the presence of axial hydroxyl groups; on the other hand, in the cases of IIb and Vb their spectra (IIb: 1060 cm^{-1} and Vb: 1060 cm^{-1}) suggest the presence of equatorial hydroxyl groups. Recently, Demarco *et al.*[8] reported on the pyridine-induced solvent shift of a methyl group vicinally situated to a hydroxyl group; the extent of the deshielding is dependent upon the magnitude of the dihedral angle, θ,[9] subtended between the methyl and hydroxyl groups. As may be seen from Tables 1 and 2, the pyridine-induced solvent shifts[10] of the methyl groups at the 2 and 6 positions are observed to be in good accordance with the results of Demarco *et al.* That is, in the major alcohols (IIa and Va) one of three methyl groups is only slightly shifted in pyridine-d_5 (0.01—0.03 ppm), whereas the two other methyl groups experience strong deshielding effects (0.14—0.19 ppm). These pyridine-induced solvent shifts strongly suggest the presence of an axial hydroxyl, an axial methyl, and two equatorial methyl groups in IIa and Va. On the other hand, in the minor alcohols (IIb and Vb) all of the three methyl groups situated on the cyclohexane ring are shifted (0.10—0.13 ppm) in pyridine-d_5; this suggests the presence of an equatorial hydroxyl, an axial methyl, and two equatorial methyl groups.

Subsequently, the stereochemistry of the Grignard reaction of I with ethylmagnesium iodide in ether was also studied in order to compare it with that of the above aldol-type condensation and that of the Reformatsky reactions. The crude product obtained was then purified by means of column chromatography to give the epimeric alcohols (VIa and VIb) in a 58 : 42 ratio, accompanied by two by-products (VIIa and VIIb) in a 34 : 66 ratio.[11] The structures of VIIa (mp 62.5—63.5°C) and VIIb (mp 49—50°C) were confirmed by direct comparisons with the authentic 2,2,*c*-6- and 2,2,*t*-6-trimethyl-*r*-1-cyclohexanols[12] which had been prepared by the reduction of I with $LiAlH_4$ in ether, followed by the separation of a mixture of the epimers (30 : 70 ratio[11]) by means of column chromatography. The NMR spectra of VIIa and VIIb are summarized in Table 3; the preferred conformations of these alcohols may be assigned as

7) $\Delta_{ppm}=\delta$ in $CDCl_3-\delta$ in pyridine-d_5.

8) P. V. Demarco, E. Farkas, D. Doddrell, B. L. Mylari, and E. Wenkert, *J. Amer. Chem. Soc.*, **90**, 5480 (1968).

9) As θ decreases in magnitude, the Δ values increase; that is, when θ is 180°, 85°, and 60°, the reported Δ values are −0.03, −0.13, and −0.20— −0.27 ppm respectively.

10) The values observed in this series were somewhat smaller than those of Demarco *et al.*[8] See also Ref. 2.

11) Since VIIa and VIIb were easily sublimed during the evaporation of the solvent, the ratio was obtained by a NMR spectral analysis of the crude product.

Table 1. The NMR spectra of IIa and IIb

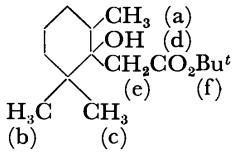

		a	b	c	d	e	f
IIa	$CDCl_3$	0.85 (d, J=6 Hz)	0.91 (s)	0.94 (s)	4.65 (s)	2.26 (d, J=16 Hz) 2.49 (d, J=16 Hz)	1.48 (s)
	Py-d_5	1.02 (d, J=6 Hz)	1.10 (s)	0.97 (s)	—	2.45 (d, J=16 Hz) 2.65 (d, J=16 Hz)	1.45 (s)
	Δ[7]	−0.17	−0.19	−0.03	—	−0.17	+0.03
IIb	$CDCl_3$	0.91 (d, J=6.5 Hz)	0.91 (s)	1.04 (s)	5.15 (s)	2.44 (s)	1.48 (s)
	Py-d_5	1.01 (d, J=6.5 Hz)	1.02 (s)	1.15 (s)	—	2.57 (s)	1.47 (s)
	Δ[7]	−0.10	−0.11	−0.11	—	−0.13	+0.01

Table 2. The NMR spectra of Va and Vb

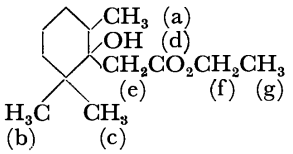

		a	b	c	d	e	f	g
Va	$CDCl_3$	0.85 (d, J=6 Hz)	0.93 (s)	0.93 (s)	4.31 (s)	2.37 (d, J=16 Hz) 2.54 (d, J=16 Hz)	4.14 (q, J=7 Hz)	1.26 (t, J=7 Hz)
	Py-d_5	1.01 (d, J=8 Hz)	1.07 (s)	0.94 (s)	—	2.59 (s)	4.09 (q, J=7 Hz)	1.15 (t, J=7 Hz)
	Δ[7]	−0.16	−0.14	−0.01	—	−0.13	+0.05	+0.11
Vb	$CDCl_3$	0.90 (d, J=6 Hz)	0.88 (s)	1.04 (s)	4.84 (bs)	2.51 (s)	4.14 (q, J=7 Hz)	1.27 (t, J=7 Hz)
	Py-d_5	1.02 (d, J=6 Hz)	1.01 (s)	1.16 (s)	—	2.59 (s)	4.12 (q, J=7 Hz)	1.16 (t, J=7 Hz)
	Δ[7]	−0.12	−0.13	−0.12	—	−0.08	+0.02	+0.11

Table 3. The NMR spectra of VIIa and VIIb

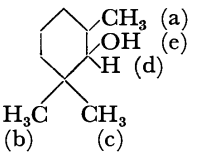

		a	b	c	d	e
VIIa	$CDCl_3$	0.93 (d, J=6.5 Hz)	0.96 (s)	0.91 (s)	3.15 (bs)	1.39 (s)
	Py-d_5	1.09 (d, J=6.5 Hz)	1.14 (s)	0.93 (s)	3.28 (bs)	—
	Δ[7]	−0.16	−0.18	−0.02	−0.13	—
VIIb	$CDCl_3$	0.98 (d, J=5 Hz)	0.98 (s)	0.88 (s)	2.83 (d, J=9 Hz)	1.44 (s)
	Py-d_5	1.13 (d, J=7 Hz)	1.14 (s)	1.07 (s)	2.95 (d, J=9 Hz)	—
	Δ[7]	−0.15	−0.16	−0.19	−0.12	—

follows. The magnitude of the coupling constant between the protons at the 1 and 6 positions suggests that the orientations of these vicinal protons in VIIa and VIIb are equatorial-axial[13] and diaxial respectively. The pyridine-induced solvent shifts of the methyl groups also suggest that the orientations of the hydroxyl groups in VIIa and VIIb are axial and equatorial respectively. Subsequently, the correlation of the β-hydroxy esters (II and V) with the alcohols (VIa and VIb) was also carried out in the following manner. The reduction of IIa and Va with $LiAlH_4$ in ether gave the same VIIIa diol (mp 46—46.5°C). On the other hand, the VIIIb diol (mp 51.5—52.5°C) was also obtained by the similar reduction of IIb or Vb. The VIIIa and VIIIb diols were subjected to tosylation with *p*-toluenesulfonyl chloride in pyridine; the reduction of the resulting tosylates with $LiAlH_4$ in tetrahydrofuran gave 1-ethyl-2,2,*c*-6-trimethyl-*r*-1-cyclohexanol and its *t*-6-isomer, which were shown to be identical with VIa and VIb respectively by comparisons of their IR and NMR spectra.

From the present study, it is evident that all of the aldol-type condensation and the Reformatsky reaction and the Grignard reaction with I proceed in a similar fashion. Furthermore, it is well known[2,14] that isomers with equatorial hydroxyl groups can be expected to be adsorbed more strongly on chromatography and that, therefore, they can be expected to be more difficult to elute than the isomers with more hindered axial hydroxyls. In this study, the isomers (IIa, Va, VIa, and VIIa) were eluted first in each instance on column chromatography. This behavior also supports the presence of the axial hydroxyl groups in these alcohols.

Finally, the tre2tment of IIa with potassium hydrogensulfate at 210—226°C or with dilute sulfuric acid under refluxing afforded a γ-lactone (mp 79.5—80.5°C). From the physical and spectral data which are shown in the Experimental section, the structure of the above lactone was deduced to be (±)-*cis*-tetrahydroactinidiolide (IX). The preparation of the optically-active or inactive IX by different methods had already been reported by Sakan *et al.*[6] and by other workers.[15-19] On the other hand, the treatment of IIa in toluene with isopropenyl acetate in the presence of *p*-toluenesulfonic acid gave a mixture of γ-lactones; the components were successfully separated by means of column chromatography on silica gel to give IX and a *trans*-γ-lactone (X), mp 71.5—74.5°C. The NMR spectrum of X in $CDCl_3$ showed signals at δ 0.92, 0.95, and 1.32 ppm due to three methyl groups. In contrast with the *cis*-lactone (IX), the lactone X was easily hydrolyzed with methanolic sodium hydroxide to give the corresponding γ-hydroxy acid (XI), mp 105—107°C; the preparation of this substance by a different method had also been reported by Ohloff and Schade.[15]

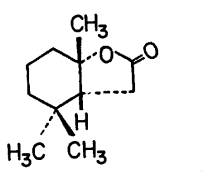

IX

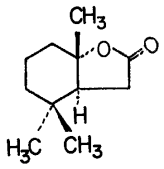

X

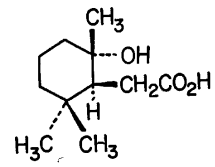

XI

Experimental

All the melting and boiling points are uncorrected. The NMR spectra were taken on a Hitachi Model R-20 NMR spectrometer (60 MHz), using tetramethylsilane as the internal standard. Their chemical shifts are presented in terms of δ values; s: singlet; bs: broad singlet; d: doublet; t: triplet; q: quartet. The column chromatography was performed on Merck silica gel (0.08 mm).

The Condensation of 2,2,6-Trimethylcyclohexanone (I) with t-Butyl Acetate. A solution of *t*-butyl acetate (49.5 g: 0.426 mol) in dry ether (45 m*l*) was stirred, drop by drop over a 15-min period, into a lithium amide solution which had been freshly prepared from lithium (2.96 g: 0.423 mol) and liquid ammonia (*ca.* 150 m*l*), with cooling in a dry ice–acetone bath. After the ammonia had evaporated, the residual syrup was diluted with dry ether (60 m*l*). To this solution there was then added, drop by drop, a solution of I[20] (15 g: 0.017 mol) in dry ether (30 m*l*) at room temperature over a 20-min period. The mixture was refluxed for 60 min, cooled, decomposed with dilute hydrochloric acid (3 N: 30 m*l*), and then extracted with ether. The extract was successively washed with aqueous sodium hydrogencarbonate (10%) and water, and then dried over sodium sulfate. After the removal of the solvent, the residue was distilled under a vacuum to give an oil (28.5 g); bp 123—148°C/14 mmHg. A part (4.00 g) of the above distilled oil was chromatographed on silica gel (200 g), using benzene as the eluent. The first fraction gave an oil (IIIa; 73 mg) which showed no hydroxyl absorption band in its IR spectrum. IR in $CHCl_3$: 1696 (C=O), 1622 cm^{-1} (C=C). NMR

12) G. Barraud, R. Cornubert, and A. M. Lemoine-Tressont, *Bull. Soc. Chim. Fr.*, **1957**, 1499. These authors had prepared VIIa (mp 61—62°C) and VIIb (mp 54°C) from I by catalytic hydrogenation in the presence of platinum and by reduction with sodium in ethanol respectively.

13) The possibility of its being diequatorial is rejected on the basis of the result of the pyridine-induced solvent shift of the methyl group at the 6 position.

14) S. Winstein and N. Holness, *J. Amer. Chem. Soc.*, **77**, 5562 (1955).

15) G. Ohloff and G. Schade, *Chem. Ber.*, **91**, 2017 (1958).

16) W. C. Bailey, Jr., A. K. Bose, R. M. Ikeda, R. H. Newman, H. V. Secor, and C. Varsel, *J. Org. Chem.*, **33**, 2819 (1968).

17) F. Demole and P. Enggist, *Helv. Chim. Acta*, **51**, 481 (1968).

18) M. Ribi and C. H. Eugster, *ibid.*, **52**, 1732 (1969).

19) H. Kaneko and K. Hoshino, *Agr. Biol. Chem. (Jap.)*, **33**, 969 (1969). The above authors had reported the isolation of tetrahydroactinidiolide from the essential oil of cigar tabacco leaves. The reported IR spectrum of the natural sample is identical with that of the synthetic (±)-IX.

20) C. L. Stevens and A. J. Weinheimer, *J. Amer. Chem. Soc.*, **80**, 4072 (1958).

in $CDCl_3$: 1.10 and 1.16 (each 3H and s, 2-CH_3), 1.24 (3H, d, J=7 Hz, -$CHCH_3$), 1.47 (9H, s, -$C(CH_3)_3$), 5.65 (1H, s, -C=$CHCO_2Bu^t$). UV: λ_{max}^{EtOH} 223 nm (ε=11900).

Found: C, 75.59; H, 11.02%. Calcd for $C_{15}H_{26}O_2$: C, 75.58; H, 11.00%.

The hydrolysis of IIIa in ethanol with aqueous sodium hydroxide gave the corresponding acid as colorless crystals; mp 101—102°C (from ether containing petroleum ether). IR in $CHCl_3$: 1680 (CO_2H), 1620 cm^{-1} (C=C).

Found: C, 72.53; H, 10.12%. Calcd for $C_{11}H_{18}O_2$: C, 72.49; H, 9.96%.

The second fraction gave an oil (IIIb: 35 mg) which also showed no hydroxyl absorption band in its IR spectrum and no absorption maximum in the 210—250 nm region of its UV spectrum. IR in $CHCl_3$: 1725 cm^{-1} (C=O). NMR in CCl_4: 0.96 (6H, s, 2-CH_3), 1.42 (9H, s, -$C(CH_3)_3$), 1.57 or 1.46 (3H, s, -C=CCH_3), 2.88 (2H, s, -$CH_2CO_2Bu^t$).

Found: C, 75.46; H, 11.14%. Calcd for $C_{15}H_{26}O_2$: C, 75.58; H, 11.00%.

The third fraction gave IIa as an oil (2.364 g). IR in $CHCl_3$: 3450 (OH), 1702 cm^{-1} (C=O).

Found: C, 70.11; H, 10.89%. Calcd for $C_{15}H_{28}O_3$: C, 70.27; H, 11.01%.

Further elution was carried out with benzene containing 3% ether; the fourth fraction gave IIb as an oil (0.550 g). IR in $CHCl_3$: 3440 (OH), 1702 cm^{-1} (C=O).

Found: C, 70.39; H, 11.01%. Calcd for $C_{15}H_{28}O_3$: C, 70.27; H, 11.01%.

The Reformatsky Reaction of I with Ethyl Bromoacetate. A solution of ethyl bromoacetate (16.0 g: 0.092 mol) in dry benzene (15 m*l*) was stirred; drop by drop at 85—88°C, into a mixture of I (6.50 g: 0.046 mol), purified zinc powder[21] (6.40 g: 0.092 mol), and dry benzene (2.0 m*l*). After the addition was complete, the mixture was refluxed for 30 min and then treated in the usual manner. The crude product was distilled under a vacuum to give an oil; bp 137—138°C/10 mmHg; yield, 7.0 g. A part (1.520 g) of the above oil was chromatographed on silica gel (100 g), using benzene as the eluent. The first fraction gave a dehydrated ester (10 mg). The second fraction gave Va as an oil (1.006 g).

Found: C, 68.52; H, 10.65%. Calcd for $C_{13}H_{24}O_3$: C, 68.38; H, 10.59%.

The third fraction gave Vb as an oil (0.333 g).

Found: C, 68.46; H, 10.43%. Calcd for $C_{13}H_{24}O_3$: C, 68.38; H, 10.59%.

*1-Hydroxy-2,2,*t*-6-trimethyl-*r*-1-cyclohexaneacetic Acid (IVa) and Its* c*-6-Isomer (IVb).* *a*) The hydrolysis of Va (1.00 g) in methanol with aqueous sodium hydroxide for 2 hr gave IVa as colorless crystals; mp 118.5—119.5°C; yield, 0.570 g. NMR in $CDCl_3$: 0.90 (3H, d, J=5 Hz -$CHCH_3$), 0.98 (6H, s, 2-CH_3), 2.47 and 2.67 (2H, each d and J=16 Hz, -CH_2CO_2H).

Found: C, 65.89; H, 10.09%. Calcd for $C_{11}H_{20}O_3$: C, 65.97; H, 10.07%.

Similarly, IIa was also hydrolyzed with aqueous sodium hydroxide for 5 hr to give IVa; mp 118.5—119.5°C.

b) The Vb ester (295 mg) was treated by a method similar to that used for IVa. The product (260 mg) was recrystallized from ether containing petroleum ether to give IVb as colorless crystals; mp 143.5—144°C; yield, 150 mg. NMR in $CDCl_3$: 0.96 (3H, d, J=6.5 Hz, -$CHCH_3$), 0.98 and 1.06 (each 3H and s, 2-CCH_3), 2.65 (2H, s, -CH_2CO_2H).

Found: C, 66.16; H, 10.01%. Calcd for $C_{11}H_{20}O_3$: C, 65.97; H, 10.07%.

Similarly, IIb was hydrolyzed to give IVb; mp 143.5—144°C.

Reduction of I with $LiAlH_4$. A solution of I (1.25 g) in dry ether (10 m*l*) was stirred, drop by drop over 20 min and at room temperature, into a suspension of $LiAlH_4$ (500 mg) in dry ether (10 m*l*). The mixture was refluxed for 3 hr, cooled, poured into a mixture of ice and dilute hydrochloric acid (10%: 25 m*l*), and then extracted with ether. The extract was washed with a saturated sodium chloride solution, dried over sodium sulfate, and then evaporated under a vacuum to give an oil (1.20 g) which showed no carbonyl absorption band in its IR spectrum. The NMR spectrum of the crude oil showed the presence of epimeric alcohols in a 30 : 70 ratio. The crude oil was chromatographed on silica gel (90 g), using benzene as the eluent. The first fraction gave VIIa[22] (327 mg), which was recrystallized from ether containing petroleum ether to give colorless crystals; mp 62.5—63.5°C (lit,[12] mp 61—62°C): Found: C, 75.91; H, 12.73%.

The second fraction gave VIIb[22] (502 mg) as colorless crystals, mp 49—50°C (lit,[12] mp 54°C): Found: C, 75.84; H, 12.80%. A mixed fusion with VIIa showed *ca.* 25°C.

The Grignard Reaction of I with Ethylmagnesium Iodide. A solution of I (1.400 g) in dry ether (5.0 m*l*) was added, drop by drop over 15 min at room temperature, to the Grignard reagent which had been prepared from magnesium (360 mg) and ethyl iodide (2.600 g) in dry ether (7.0 m*l*). The mixture was refluxed for 4 hr, allowed to stand overnight at room temperature, and then worked up in a usual manner to give a crude product which showed the presence of VIIa and VIIb in a 34 : 66 ratio upon NMR spectrum analysis. The crude product was purified by means of column chromatography on silica gel (150 g). Elution was carried out with benzene to give four fractions. The first fraction gave VIa (401 mg) as an oil.

Found: C, 77.51; H, 13.11%. Calcd for $C_{11}H_{22}O$: C, 77.58; H, 13.02%.

The second fraction gave VIb (290 mg) as an oil.

Found: C, 77.63; H, 13.09%. Calcd for $C_{11}H_{22}O$; C, 77.58; H, 13.02%.

The third fraction gave colorless crystals (139 mg.[22] mp 62.5—63.5°C),which were shown to be identical with authentic VIIa by a mixed-melting-point determination and by a comparison of their spectra.

The fourth fraction gave colorless crystals (236 mg:[22] mp 49—50°C) which were also shown to be identical with authentic VIIb by a comparison of their IR spectra.

Reduction of IIa, IIb, Va, and Vb with $LiAlH_4$. *a) From IIa and Va:* A solution of IIa (1.550 g) in dry ether (20 m*l*) was reduced with $LiAlH_4$ (500 mg). The crude product (1.402 g) was purified by means of column chromatography on silica gel (70 g), using benzene containing 20% ether as the eluent. The first fraction gave the recovered IIa (673 mg). The second fraction gave a diol (VIIIa: 737 mg), which was then recrystallized from ether containing petroleum ether to give colorless crystals; mp 46—46.5°C.

Found: C, 71.08; H, 12.10%. Calcd for $C_{11}H_{22}O_2$:

21) R. L. Shriner, "Organic Reactions," Coll. Vol. I, p. 16 (1942).

22) A part of the substance was lost by sublimation during the removal of the benzene.

C, 70.92; H, 11.90%.

Similarly, the ethyl ester (Va: 1.500 g) was also reduced with $LiAlH_4$ (500 mg) to give VIIIa (889 mg: mp 46—46.5°C).

b) *From IIb and Vb*: The esters (IIb and Vb) were also both reduced with $LiAlH_4$ to give VIIIb; mp 51.5—52.5°C. A mixed-melting-point determination with VIIIa showed 32—34°C.

Found: C, 71.14; H, 12.01%. Calcd for $C_{11}H_{22}O_2$: C, 70.92; H, 11.90%.

1-Ethyl-2,2,c-6-(VIa) and 1-Ethyl-2,2,t-6-trimethyl-r-1-cyclohexanol (VIb). *a*) A solution of VIIIa (400 mg), *p*-toluenesulfonyl chloride (440 mg), and dry pyridine (3.0 m*l*) was allowed to stand at room temperature for 60 hr. After a usual work-up, the crude product (420 mg) was dissolved in dry tetrahydrofuran (11.0 m*l*) and then reduced with $LiAlH_4$ (300 mg) for 3.5 hr under refluxing. The product was chromatographed on silica gel (40 g), using benzene containing 10% ether as the eluent. The first fraction gave an oil (126 mg) which was shown to be identical with VIa by a comparison of their IR spectra. The second fraction gave the recovered VIIIa (230 mg).

b) The diol VIIIb (573 mg) was treated by a method similar to that described in *a*) to give an oil (163 mg) which was identical with VIb. The starting VIIIb (253 mg) was also recovered.

2-Hydroxy-2,6,6-trimethyl-1-cyclohexaneacetic Acid γ-Lactones (IX and X). *a*) A mixture of IIa (3.40 g) and fused potassium hydrogensulfate (3.0 g) was heated at 210—226°C for 30 min in an oil bath. After cooling and the subsequent addition of water, the mixture was extracted with ether; the extract was washed with water, dried over sodium sulfate, and then evaporated. The crude product (2.04 g) was chromatographed on silica gel (200 g), using benzene containing 10% ether as the eluent, to give a *cis*-γ-lactone (IX: 1.66 g) ((±)-tetrahydroactinidiolide), which was then recrystallized from ether containing petroleum ether to give colorless crystals; mp 79.5—80.5°C (lit,[17] mp 77—79°C); Found: C, 72.25; H, 10.05%. The IR and NMR spectra of IX were in good accrodance with those in the literature.[6,16-18]

A mixture of the above *cis*-lactone (IX: 1.10 g) and aqueous sodium hydroxide (5%: 20 m*l*) was stirred and heated on a steam bath for 1 hr. The clear solution, after cooling, was acidified with dilute sulfuric acid to give the starting IX (0.95 g).

b) A mixture of IIa (429 mg) and dilute sulfuric acid 30%: 8.0 m*l*) was refluxed for 3 hr. After a usual work-up, the crude product (297 mg) was chromatographed on silica gel (25 g), using benzene containing 3% ether as the eluent, to give the *cis*-lactone (IX: 256 mg).

c) A mixture of IIa (635 mg), isopropenyl acetate (1.0 m*l*), and *p*-toluenesulfonic acid (40 mg) in dry toluene (12 m*l*) was refluxed for 3 hr, and then, after cooling, solid sodium hydrogencarbonate (140 mg) was added. The mixture was stirred at room temperature for 10 min and filtered; the filtrate was then evaporated under a vacuum to give a crude product which was chromatographed on silica gel (60 g). Elution was carried out with benzene containing 3% ether. The first fraction gave a *trans*-γ-lactone (X: 70 mg) which was recrystallized from ether containing petroleum ether to give colorless crystals; mp 71—74.5°C (softened at 66°C). A mixed-melting-point determination with the *cis*-γ-lactone (IX: mp 79.5—80.5°C) showed 50—55°C; it softened at room temperature.

Found: C, 72.63; H, 10.22%. Calcd for $C_{11}H_{18}O_2$: C, 72.49; H, 9.96%.

The second fraction gave the *cis*-γ-lactone (IX: 33 mg), the identity of which was established by an IR spectral comparison.

Hydrolysis of trans-γ-Lactone (X) with Alkali. A solution of X (50 mg) and aqueous sodium hydroxide (5%; 1.0 m*l*) in methanol (5.0 m*l*) was refluxed for 1 hr. After a usual work-up, the crude product was recrystallized from ether containing petroleum ether to give an acid (XI) as colorless crystals; mp 105—107°C (lit,[15] mp 113—115.5°C); Found: C, 66.16; H, 10.31%; yield, 40 mg. NMR in $CDCl_3$: 0.81 and 0.94 (each 3H and s, $-\dot{C}(C\underline{H}_3)_2$), 1.19 (3H, s, $-\dot{C}(OH)C\underline{H}_3$), *ca.* 6.0 (2H, bs, $-CO_2\underline{H}$ and $-O\underline{H}$).

Carbon-13 Magnetic Resonance Chemical Shifts in Alkylbiphenyls[1)]

Hideo HASEGAWA,* Mamoru IMANARI,** and Kazuhiko ISHIZU***

*JEOL (U.S.A.), Inc., 235 Birchwood Avenue, Cranford, N.J. U.S.A.

**JEOL, Akishima, Tokyo.

***Department of Chemistry, Faculty of Science, Ehime University, Bunkyo, Matsuyama, Ehime.

(Received September 9, 1971)

Carbon-13 NMR spectra were observed for the seventeen alkyl biphenyls. For the *meta*- and *para*-alkyl derivatives, the observed ring carbon-13 chemical shifts could be adequately understood in terms of the Karplus-Pople's formula by taking into account the hyperconjugative effect of the substituents. The observed chemical shifts of aliphatic carbon were in good agreement with the values of the corresponding alkylated benzenes within the limits of experimental error. For the *ortho*-derivatives, the conformation of substituents in the hindered biphenyls was particularly discussed in relation to the observed alkyl carbon-13 chemical shifts. In the cases of 2,2′-dimethylbiphenyl and 2,2′,6,6′-tetramethylbiphenyl, the chemical shifts of methyl carbons at the *ortho*-position revealed a high field shift of about 1 ppm, but that of 2,4,6-trimethylbiphenyl indicated only 0.4 ppm. The different shifts of the *ortho*-methyl carbons in the two cases suggested a spece interaction between the two methyl groups. This interaction may arise an orbital overlap between the methyl groups, which were considered to approach one another to take the *cis*-conformation.

Interest in the molecular structures of numerous biphenyl derivatives has often been focused on their stereochemistry. In particular, the substituents at the *ortho*-positions may cause a large steric effect; hence, two phenyls in *ortho*-substituted biphenyl derivatives are incapable of taking a planar structure in a solution. Regarding the conformation of the phenyl groups in the *ortho*-alkylated biphenyl, Suzuki[2)] has already proposed a correlation between the rotation angle of the two planar phenyl groups and the wavelength of the ultraviolet obsorption maxima. Furthermore, Mislow *et al.*[3)] and Ōki *et al.*[4)] have also reported that a similar relationship holds between the twisted angle of biphenyls and the NMR chemical shifts of the alkyl protons at the *ortho*-position. In this case, the chemical shifts of the alkyl protons were reasonably explained in terms of an increased diamagnetic shielding effected by the ring current of the rotating phenyl groups. In the case of NMR studies of aromatic protons, however, the assignment of their chemical shifts becomes more or less difficult because of the superimposed structures caused by the various spin-spin couplings of the ring protons. In this work, the carbon-13 NMR measurement of both ring and the alkyl carbon-13 were carried out for the seventeen alkylbiphenyls, and the hyperconjugative and steric effects due to the higher alkyl groups were investigated.

The observed ring carbon-13 chemical shifts are discussed in terms of the Karplus-Pople's formula, taking into account the hyperconjugative effect of the substituents. Finally, the conformation of the hindered biphenyls is considered in relation to the observed alkyl carbon-13 chemical shifts.

Experimental

Each alkylated biphenyl was synthesized and identified in the manner reported in previous papers.[5-7)] Samples containing carbon-13 in its natural abundance, 1.1%, were dissolved in tetrahydrofuran (THF). The carbon-13 magnetic resonance spectra were recorded using a JNM-4H-100 type NMR spectrometer at 25 MHz. A JNM-IS-100 proton decoupler was used in order to enchance the carbon-13 signal due to the nuclear Overhauser effect and to remove the splitting due to the spin-spin coupling between carbon-13 and proton spins.[8)] Benzene was used as the external primary reference for the ring carbon-13 chemical shifts in biphenyl, and the shift of the β-carbon of THF was taken as the internal secondary reference. For the aliphatic carbon-13 chemical shifts of the alkyl group, cyclohexane was used as the primary reference.

Results and Disusssion

Chemical Shifts of Aromatic Ring Carbon Para- *or* Meta-*Alkylated Biphenyls.* The aromatic carbon-13 NMR spectrum of 4,4′-diethylbiphenyl is shown in Fig. 1. The observed spectrum consists of four lines; their integrated intensity ratios are about 1 : 1 : 2 : 2, which easily distinguishes $\Delta\sigma_1$ and $\Delta\sigma_4$ from $\Delta\sigma_2$ and $\Delta\sigma_3$.[9)]

The chemical shift of each aromatic carbon-13 is calculated according to the additivity rule[10)] based on the experimental values of both biphenyl and ethylbenzene, and the observed $\Delta\sigma_i$ value is assigned to each ring carbon, with reference to the results of the

1) Presented at the 24th Annual Meeting of the Chemical Society of Japan, Osaka, April, 1971.

2) H. Suzuki, This Bulletin, **32**, 1350, 1357 (1959); *ibid.*, **33**, 109 (1960).

3) K. Mislow, M. A. W. Glass, H. B. Hopps, E. Simon, and G. H. Wahl, *J. Amer. Chem. Soc.*, **86**, 1710 (1964).

4) M. Ōki, H. Iwamura, and N. Hayakawa, This Bulletin, **37**, 1865 (1964).

5) K. Ishizu, H. Hasegawa, H. Chikaki, H. Nishiguchi, and Y. Deguchi, *Kogyo Kagaku Zasshi*, **68**, 1522 (1965).

6) K. Ishizu, K. Mukai, H. Hasegawa, K. Kubo, H. Nishiguchi, and Y. Deguchi, This Bulletin, **42**, 2808 (1969).

7) K. Ishizu, Y. Inui, K. Mukai, H. Shikata, and H. Hasegawa, *ibid.*, **43**, 3956 (1970).

8) E. G. Paul and D. M. Grant, *J. Amer. Chem. Soc.*, **86**, 2977 (1964).

9) The general sturcture of a biphenyl is

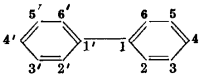

where $\Delta\sigma_1$, $\Delta\sigma_2$, $\Delta\sigma_3$, and $\Delta\sigma_4$ indicate both the positions and the chemical shifts.

10) G. B. Savitsky, *J. Phys. Chem.*, **67**, 2723 (1963).

Fig. 1. The aromatic carbon-13 NMR spectrum of 4,4'-diethylbiphenyl. (Solvent: THF).

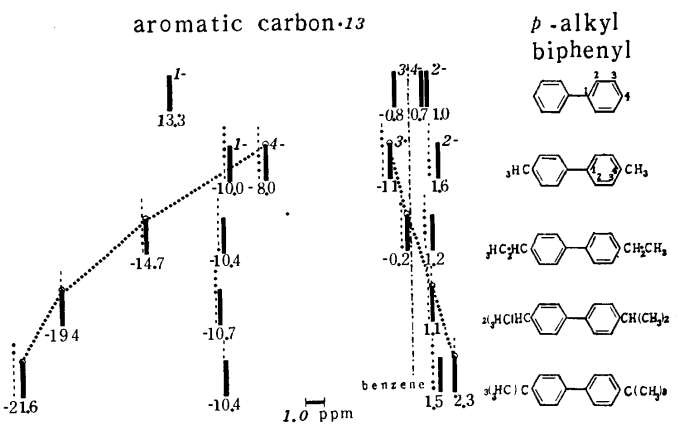

Fig. 2. The observed values and the calculated results of the aromatic carbon-13 chemical shifts for the *para*-alkylated biphenyls.[11] (Solvent: THF).

additivity calculations.

The observed and the calculated values of the aromatic carbon-13 chemical shifts for the *para*- and *meta*-alkylated biphenyls are summarized in Figs. 2 and 3. A satisfactory agreement can be seen between the observed values of the carbon-13 chemical shifts and those predicted by the additivity calculations.

In all cases, the hyperconjugative effect gives rise to a drastic lower-field shift for the ring carbon atoms ($\Delta\sigma_4$ and $\Delta\sigma_3$) bonded to the alkyl groups in the order of $CH_3<CH_3CH_2<CH(CH_3)_2<C(CH_3)_3$. At the same time, an alternative higher-field shift of the next neighboring carbon atoms of the alkyl groups can be observed; that is, in the case of 4,4'-dialkylbiphenyl, the ring carbons at the *meta*-position reveal a chemical shift in the directions opposite to the chemical shift of the *para*-positions.

This is probably due to the *ortho-para* conjugation

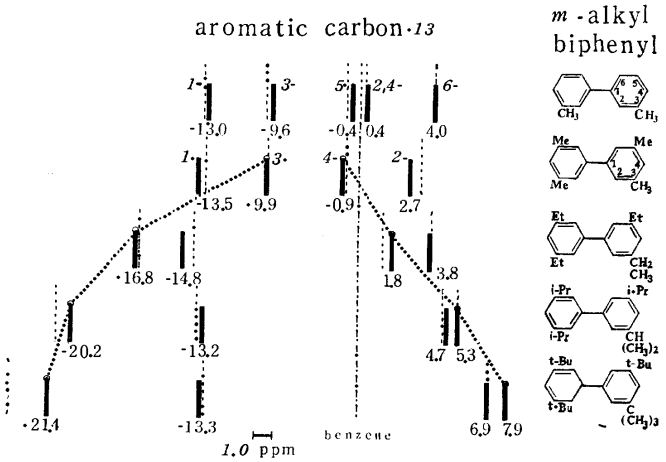

Fig. 3. The observed values and the calculated results of the aromatic carbon-13 chemical shifts for the *meta*-alkylated biphenyls.[11] (Solvent: THF).

or to the inductive effect of the alkyl groups. The large value of the chemical shift at the *para*-position in the *meta*-alkylated biphenyl is a result of this effect being enhanced by the neighboring two alkyl groups.

HMO Calculation of Carbon-13 Chemical Shifts in Aromatic Ring Carbon. In order to put the present experimental results on a more rigorous theoretical base, the aromatic carbon-13 chemical shifts ($\Delta\sigma_i$) were calculated using the Karplus and Pople's equation[12] expressed as follows; $\Delta\sigma_{i\,\mathrm{PPM}}=(86.7+46.0\lambda_H)(\rho-1)+46.0(F-0.399)$, where both the π-electron density (ρ) and the free valence (F) were calculated by the HMO method, and where the contribution due to the λ_H (polarity parameter of the C–H bond) is disregarded. For the treatment of the methyl group in the HMO calculation, we used two different models, the inductive (I) and the hyperconjugative models (II).

In the inductive model, any conjugative effect of the methyl group is disregarded, and the carbon to which the methyl group is attached is made somewhat more electropositive. The values of the Coulomb integral of these carbons, α_{CH_3} is estimated to be $\alpha_{CH_3}=\alpha-0.2\beta$.

The hyperconjugation model has been proposed by Coulson and Crawford[13]; in it a linear combination of the hydrogen 1*s* orbitals is taken to give the pseudo π-orbital conjugating with the ring system. The parameters used in the HMO calculation of the methyl group ($>C_1-C_2\equiv H_3$) are;

$$\alpha_2=\alpha-0.1\beta,\quad \alpha_{H_3}=\alpha-0.5\beta$$
$$\beta_{C_1-C_2}=0.7\beta,\quad \beta_{C_2\equiv H_3}=2.5\beta.$$

The results of 4,4'-dimethylbiphenyl, 3,3'-dimethylbiphenyl, and 3,3',5,5'-tetramethylbiphenyl are given in Table 1. It may be seen that the hyperconjugative model gives a more or less satisfactory prediction of the aromatic carbon-13 chemical shift, except for the *para*-position of the 3,3',5,5'-tetramethylbiphenyl, although the tendency of the observed chemical shift

11) Bold lines indicate the observed chemical shifts of the aromatic carbons and dotted lines correspond to the values of the chemical shifts calculated on the basis of the assumption of additivity rule. The chemical shifts are indicated such that positive ppm is to high field (to the right hand in each figure) of the shift from that of the carbon atoms of benzene (0 ppm) as an reference.

12) M. Karplus and J. A. Pople, *J. Chem. Phys.*, **38**, 2803 (1963).

13) C. A. Coulson and V. A. Crawford, *J. Chem. Soc.*, **1953**, 2052 (1953).

Table 1. The observed and calculated aromatic carbon-13 chemical shift of 4,4'-dimethylbiphenyl, 3,3'-dimethylbiphenyl and 3,3',5,5'-tetramethylbiphenyl (ppm)

4,4'-Dimethylbiphenyl

Position	Obsd	Calculated		
		Additivity	Inductive	Hyperconjugative
1	−10.0	−10.3	−11.1	−12.3
2	+1.6	+1.8	+1.8	+1.7
3	−1.1	−1.5	+2.6	+0.7
4	−8.0	−8.4	−6.1	−7.4

3,3'-Dimethylbiphenyl

Position	Obsd	Calculated		
		Additivity	Inductive	Hyperconjugative
1	−13.0	−13.2	−12.7	−12.7
2	+0.4	+0.3	+4.6	+2.6
3	−9.6	−9.9	−6.8	−7.6
4	−0.4	0.0	+3.3	+1.4
5	−0.4	−0.7	−0.3	−0.2
6	+4.0	4.0	+3.4	+2.1

3,3',5,5'-Tetramethylbiphenyl

Position	Obsd	Calculated		
		Additivity	Inductive	Hyperconjugative
1	−13.5	−13.5	−12.8	−12.7
2	+2.7	+3.3	+6.3	+3.0
3	−9.9	−9.8	−7.0	−8.0
4	−0.9	−0.7	+6.0	+2.3

can also be qualitatively understood using the inductive model. It is interesting to see how the tendency of the observed ring carbon-13 chemical shift can be understood in terms of the HMO calculation for higher alkylated biphenyls.

For the sake of simplicity, we carried out the HMO calculation taking the Coulomb integral of the aromatic carbon, α_R, bonded to the higher alkyl group (R), $\alpha_R=\alpha-\delta\beta$.

The relation between the calculated carbon-13 chemical shift and the value of δ is plotted in Fig. 4 and Fig. 5.

In the case of the *para*-derivatives (Fig. 4), the theoretical value of the aromatic carbon-13 chemical shift of the *para*-position ($\Delta\sigma_4$) shows an increased lower-field shift with an increment of δ, while, conversely, a higher-field shift is predicted for the *meta*-position. The tendency of the observed ring carbon-13 chemical shift resulting from the higher alkyl substitution is also well explained for *meta*-derivatives (Fig. 5) in terms of the inductive parameter, which increases in the order of methyl, ethyl, isopropyl, and *t*-butyl groups.

These calculations thus support the idea that the hyperconjugative effect not only gives drastic lower-field shifts for the ring carbon atoms bonded to the

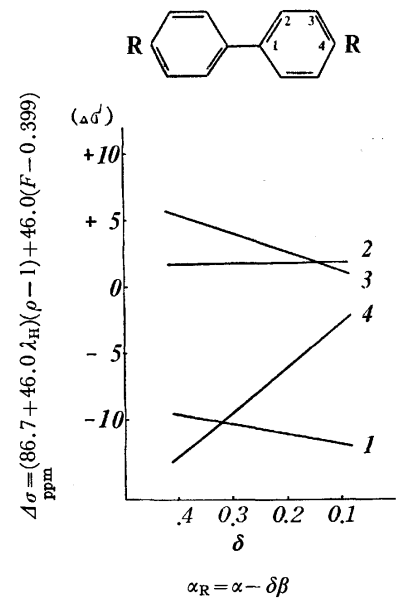

Fig. 4. The relation between the HMO carbon-13 chemical shift and the value of δ in 4,4'-dialkylated biphenyls.

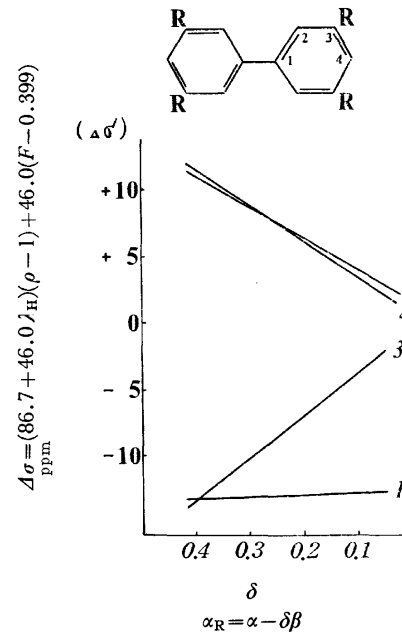

Fig. 5. The relation between the HMO carbon-13 chemical shift and the value of δ in 3,3',5,5'-tetraalkylated biphenyls.

alkyl groups, but also results in an auxiliary alternative shift on the next-nearest ring carbon atoms.

Ortho-*alkylated Biphenyls*. The observed chemical shifts of the ring carbons in several *ortho*-substituted biphenyls are given in Table 2. The analysis of the spectra of *ortho*-derivatives is much more difficult than *para*- or *meta*-derivatives, because we cannot make a quantitative assignment using the additivity rule such as was done for the *para*- and *meta*-derivatives. The HMO calculations of the aromatic carbon-13 chemical shift were carried out for the 2,2',6,6'-tetramethylbiphenyl, where the Coulomb integrals of the *ortho*-ring carbon atoms were taken as $\alpha-0.2\beta$ and were the resonance integral of the 1–1' bond was estimated to be

Table 2. The observed aromatic carbon-13 chemical shift of 2,2'-dialkylated biphenyl

Substrate	Position					
	1	2	3	4	5	6
2,2'-dimethylbiphenyl	−13.2	−7.2	−1.7	−1.2	+2.3	+0.9
2,2'-diethylbiphenyl	−12.7	−13.6	−1.7	−0.1	+2.7	+0.5
2,2'-diisopropylbiphenyl	−12.3	−18.6	+3.0	−1.7	+3.0	+0.4
2,2'-di-*t*-butylbiphenyl	−12.8	−18.0	+4.2	−4.3	+1.4	−0.6

Table 3. The observed and calculated aromatic carbon-13 chemical shift of 2,2',6,6'-tetramethylbiphenyl

Position	Obsd	Additivity	Calculated			
			$\theta=0°$	30°	45°	60°
1	−11.7	−14.7	−8.2	−7.0	−5.2	−2.6
2	−7.2	−8.0	−4.8	−5.2	−5.9	−6.3
3	+0.3	+1.5	+4.5	+4.5	+4.6	+4.6
4	+0.8	+0.7	+0.7	+0.5	+0.2	−0.1

There are large discrepancies between the observed values and those calculated; however, this will probably means that the contribution of the σ orbital should be taken into account.

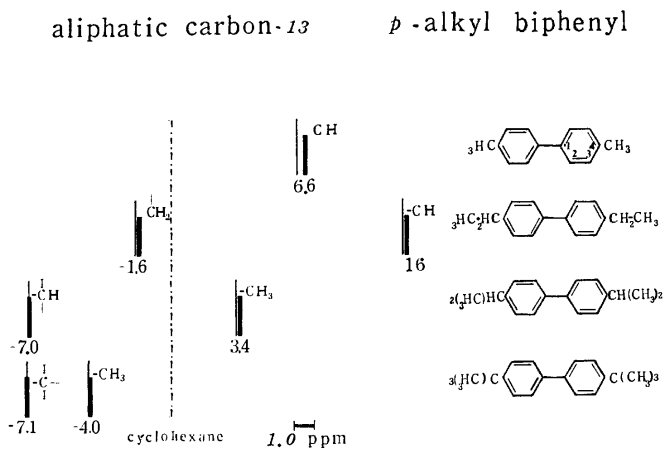

Fig. 6. The observed values of aliphatic carbon-13 chemical shifts for the *para*-alkylated biphenyls.[14] (Solvent: THF)

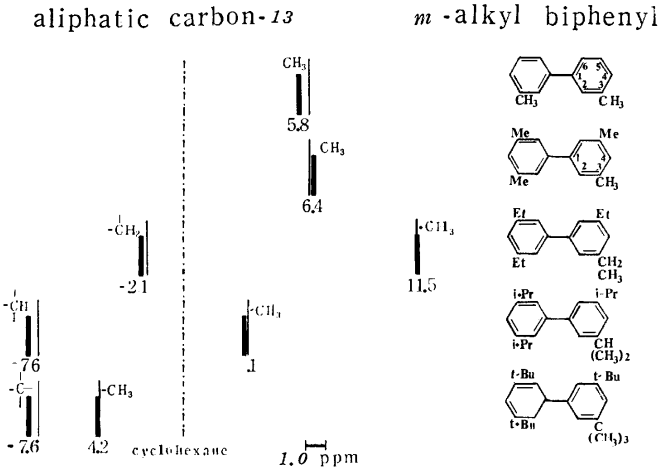

Fig. 7. The observed values of aliphatic carbon-13 chemical shifts for the *meta*-alkylated biphenyls.[14] (Solvent: THF)

$\beta\cos\theta$ as a function of the twisting angle (θ) of the two phenyl rings. The results are shown in Table 3. The calculations of the chemical shifts by the foregoing inductive model, however, could not be related to the observed values in the same manner as the *meta*- and *para*-alkylated biphenyls were. Therefore, these assignments are only qualitative.

Chemical Shifts of Aliphatic Carbon. The chemical shifts of aliphatic carbon-13 atoms for *para*-, *meta*-, or *ortho*-alkylated biphenyls are presented in Figs. 6—9. In the cases of *para*- or *meta*-alkylated biphenyls, the observed chemical shifts of the aliphatic carbon agree with the values of the corresponding alkylated benzenes within the limits of experimental error. In the case of *ortho*-alkylated biphenyls, such as 2,2'-dimethylbiphenyl (II) and 2,2',6,6'-tetramethylbiphenyl (III)

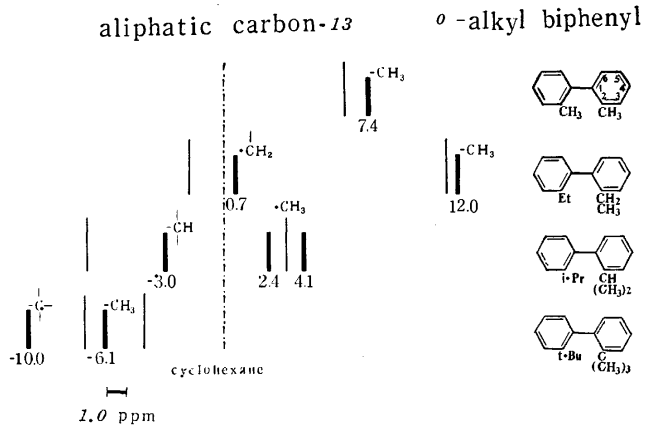

Fig. 8. The observed values of aliphatic carbon-13 chemical shifts for the *ortho*-alkylated biphenyls.[13] (Solvent: THF).

14) The bold lines indicate the observed chemical shifts and the narrow lines indicate those of aliphatic carbons in alkylated benzene. The chemical shifts were indicated in units of positive ppm to high field (to the right hand in each figure) taking the shift of the carbon atoms of cyclohexane (0 ppm) as a reference.

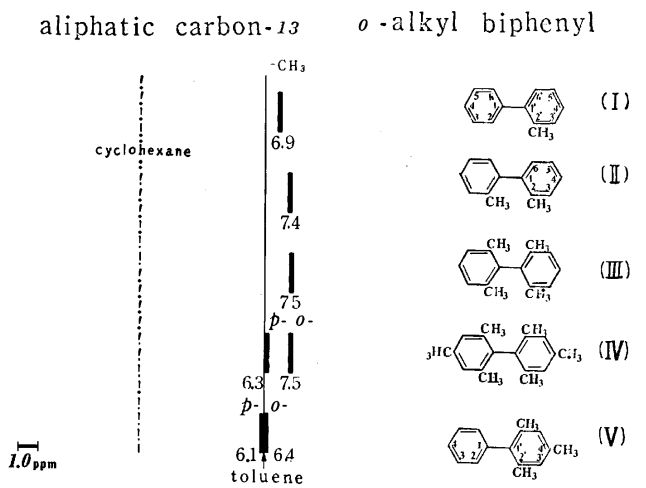

Fig. 9. The observed values of aliphatic carbon-13 chemical shifts for the *ortho*-methyl biphenyls. (Solvent: THF).

in Fig. 9, however, the chemical shifts of the methyl carbons shows a field shift higher by about 1 ppm than that of the corresponding toluene.

A similar higher-field shift is noted in the methyl protons, as is shown in Fig. 10; that is, the proton chemical shifts in the *ortho*-methyl groups also increase by about 0.4 ppm, thus exceeding the value for the methyl protons of toluene. These facts have already been understood in terms of the effect of the ring current[15] induced by the rotating biphenyl group[3,4]. It should be noticed, however, that a similar explanation is not always valid in all cases of the present investigation; a definite difference in the chemical shifts of carbon-13 NMR at the *ortho*-methyl groups is explicitly observed between the 2,4,6-tri-

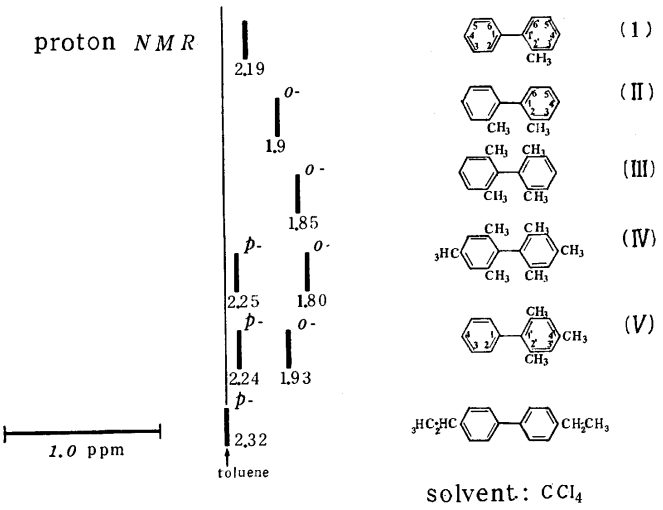

Fig. 10. The observed values of aliphatic proton chemical shifts for the *ortho*-methyl biphenyls. (Solvent: CCl_4).

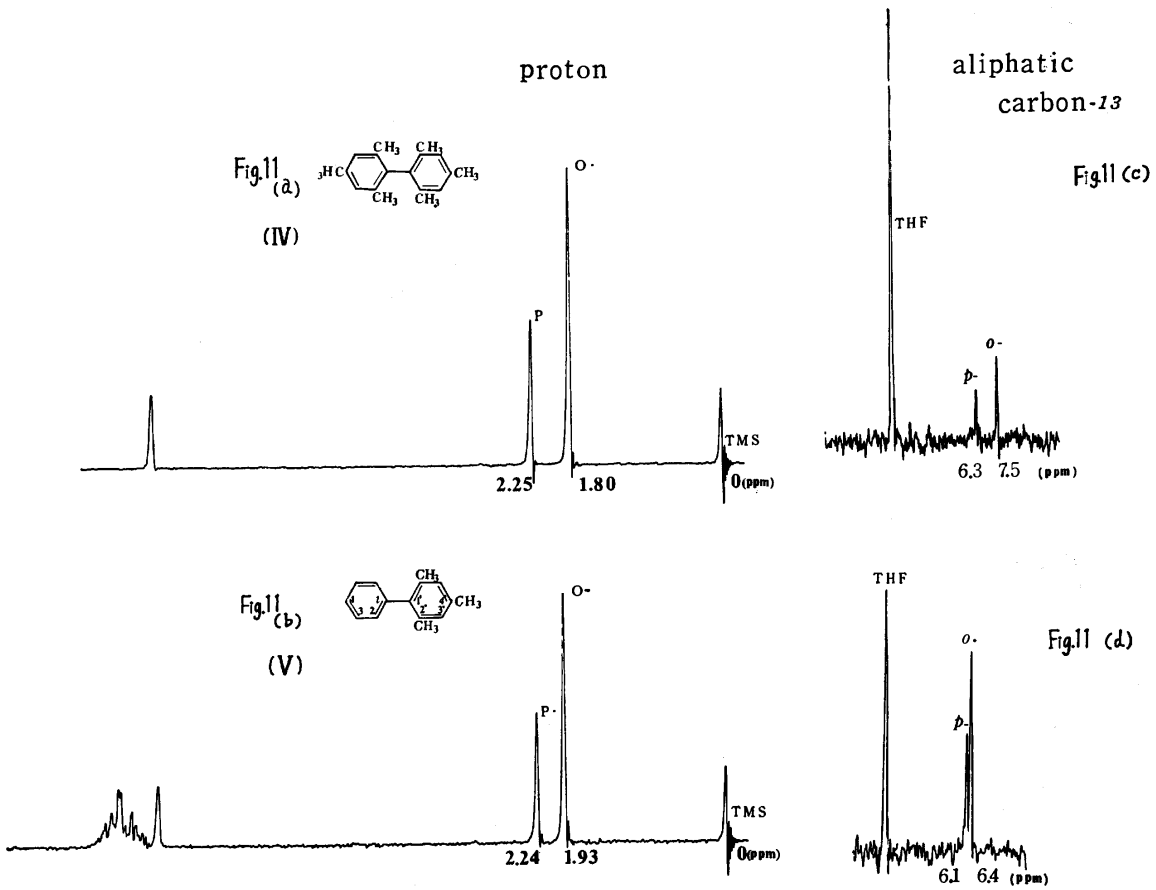

Fig. 11. The proton and carbon-13 NMR spectrum of 2,2′,4,4′,6,6′-hexamethylbiphenyl (IV) and 2,4,6-trimethylbiphenyl (V).

15) C. E. Johnson, Jr., and F. A. Bovey, *J. Chem. Phys.*, **29**, 1012 (1958).

methylbiphenyl (V) and the 2,2′,4,4′,6,6′-hexamethylbiphenyl (IV), as is shown in Figs. 11-c and d. The results of these anomalous carbon-13 chemical shifts cannot be explained only on the basis of the ring-current model, since the effect of the ring current can be expected to be nearly the same in both cases.

On the basis of the present results, one may speculate that the difference in the chemical shifts of the *ortho*-methyl groups is responsible for that in the short-range interaction across the neighboring 2,2′-dimethyl groups. If this is the case, the interaction may arise from an orbital overlap between the methyl groups, which will approach one another to take the *cis*-conformation, because, in the case of V, one cannot expect such interactions. On the other hand, for IV two pairs of *ortho*-methyl groups can be accessible through a rotation around the central C–C bond of the biphenyl ring. From this point of view, the chemical shifts of the aliphatic carbon-13 of the other 2,2′-substituted derivatives cited in Fig. 8 may be reasonably understood by assuming a space interaction between the two alkyl groups. The present results for carbon-13 NMR lead to the assumption that the 2,2′-alkyl biphenyls are likely to take the *cis*-conformation rather than the *trans*-form, as was previously proposed by Suzuki.[2] If the two methyl groups in the molecular structure of II have the *trans*-conformation, the chemical shifts for the methyl groups will have values near the chemical shift which V indicates.

We are grateful to Miss Keiko Suzuki for her HMO calculations.

BULLETIN OF THE CHEMICAL SOCIETY OF JAPAN, VOL. 45, 1158—1161 (1972)

Olefin Disproportionation by Rhenium, Tungsten, and Molybdenum Based Catalysts. Effect of the Addition of Oxygen

Yasuzo UCHIDA, Masanobu HIDAI, and Takashi TATSUMI

Department of Industrial Chemistry, Faculty of Engineering, The University of Tokyo, Hongo, Tokyo

(Received September 11, 1971)

$ReCl_5$ was activated with Et_3Al and oxygen to give a catalyst effective for the disproportionation of α-olefins as well as internal olefins. The catalyst species was deactivated by excess oxygen. The catalyst system consisting of either WCl_6 or $MoCl_5$ and Et_3Al exhibited disproportionation activity in a short range of Al/M (M=W or Mo) molar ratio. The activity decreased with the increase in the Al/M ratio, but was restored by the introduction of oxygen.

A number of Ziegler-Natta type catalysts have been reported to be effective for olefin disproportionation. These catalysts were derived from WCl_6–$EtAlCl_2$,[1,2] WCl_6–$EtAlCl_2$–EtOH,[1),2)] WCl_6–*n*-BuLi,[3)] and nitrosyl complexes $L_2Cl_2(NO)_2M$ (M=Mo or W; L=Ph_3P, C_5H_5N, Ph_3PO, *etc.*)-alkylaluminum halides.[4,5)] We wish to report a disproportionation catalyst consisting of $ReCl_5$, Et_3Al, and oxygen, which effected the disproportionation of α-olefins as well as internal olefins. The catalyst system of WCl_6 and Et_3Al, reported to convert 2-pentene into unknown oligomers,[3)] exhibited disproportionation in a short range of Al/W molar ratio. Though disproportionation activity decreased with the increase in the ratio, it was restored by the introduction of oxygen. $MoCl_5$ behaved like WCl_6 upon treatment with Et_3Al and oxygen. Catalysts consisting of rhenium oxide on alumina are notable for their disproportionation activity at relatively low temperatures.[6,7)] Ziegler-Natta type catalysts containing rhenium compounds do not seem to have been reported in detail, although a patent[8)] has been claimed.

Experimental

Materials and Procedures. All the reactions were carried out with a Schlenk-type tube under nitrogen. The reaction mixtures were stirred at room temperature and atmospheric pressure. Analysis by gas-liquid partition chromatography(glpc) was performed on a Shimadzu Model GC-3AH chromatograph, using a 3 m stainless-steel tube column packed with Silicone SE 30 fluid on 60—80 mesh Diasolid M.

Chlorobenzene and benzene were dried and distilled under a nitrogen stream. Organoaluminum compounds were used after dilution to about 8 wt%. All the transition metal chlorides were commercially obtained. WCl_6 was used after removal of more volatile contaminants, $WOCl_4$ and WO_2Cl_2, by sublimation under a nitrogen stream at about 180°C. Molybdenum(III) acetylacetonate was prepared by the method of Larson and Moore.[9)] Commercial olefins were used after degassing in a vacuum. When olefins purified by distillation in the presence of WCl_6 were

1) N. Calderon, H. Y. Chen, and K. W. Scott, *Tetrahedron Lett.*, **1967**, 3327.

2) N. Calderon, E. A. Ofstead, J. P. Ward, W. A. Judy, and K. W. Scott, *J. Amer. Chem. Soc.*, **90**, 4133 (1968).

3) J. L. Wang and H. R. Menapace, *J. Org. Chem.*, **33**, 3794 (1968).

4) E. A. Zuech, *Chem. Commun.*, **1968**, 1182.

5) E. A. Zuech, W. B. Hughes, D. H. Kubicek, and E. T. Kittleman, *J. Amer. Chem. Soc.*, **92**, 528 (1970).

6) British Petroleum Co. Ltd., Neth. Appl. 6610196 (1967).

7) J. C. Mol, J. A. Moulijn, and C. Boelhouser, *Chem. Commun.*, **1968**, 633.

8) D. Medema, W. Brunmayer-Schilt, and R. V. Helden, Brit. 1193943 (1970).

9) M. L. Larson and F. W. Moore, *Inorg. Chem.*, **1**, 856 (1962).

used, the catalytic activity was higher than that with unpurified olefins.

Reaction of 2-Pentene with $ReCl_5$–Et_3Al–O_2. $ReCl_5$ (0.1 mmol) and 2 m*l* of chlorobenzene were treated with 0.4 mmol of Et_3Al (chlorobenzene solution) at *ca.* −30°C. The reduction was carried out for 30 min at ambient temperature and then 9.3 mmol (0.65 g) of 2-pentene purified by adding WCl_6 was injected by a syringe. The reaction mixture was degassed and a calculated amount of oxygen was introduced. Reaction times given in the tables were estimated from the time of introduction of oxygen. After 30 min, the reaction vessel was filled with nitrogen. Glpc analysis was carried out at 75°C and 20 cc/min of helium flow rate employing a chlorobenzene standard, and indicated the presnece of 2-butene, 3-hexene, and unreacted 2-pentene in the reaction mixture. All peaks in the chromatograms were identified by comparison of their retention times with those of authentic samples. The olefin yield in the tables is mol% of each olefin to the staritng olefin.

Reaction of 1-Pentene with $ReCl_5$–Et_3Al–O_2. The catalyst was prepared as described above except that oxygen was introduced 16 hr after the addition of Et_3Al. Glpc analysis showed the presence of olefins ranging from C_2 to C_8. The analytical conditions were the same as described above. Mass spectral data confirmed identification.

Reaction of 2-Pentene or 1-Pentene with WCl_6–Et_3Al (–O_2). A mixture of 0.1 mmol of WCl_6, 2 m*l* of chlorobenzene, and either 9.3 mmol of 2-pentene or 9.1 mmol of 1-pentene was treated with Et_3Al at *ca.* −30°C. Oxygen was subsequently introduced in some cases.

Reaction of 2-Pentene or 1-Pentene with $MoCl_5$–Et_3Al (–O_2). The catalyst was prepared as described above except that $MoCl_5$ was used in place of WCl_6.

Results and Discussion

Catalyst from $ReCl_5$. Treatment of $ReCl_5$ with Et_3Al in chlorobenzene gave a reddish brown solution, to which 2-pentene and oxygen were added. During the reaction a black precipitate was gradually deposited. Glpc analysis after 2 hr indicated the presence of 2-butene, 3-hexene, and unreacted 2-pentene; no additional products other than ethylene were detected. In order to determine the optimum O_2/Re ratio and to obtain information on the stoichiometry of the catalyst-formation reaction, a series of runs was made increasing the amount of added oxygen while the concentrations of $ReCl_5$ and Et_3Al were kept constant. At Al/Re=4, good results were obtained at O_2/Re=6—10. The Al/Re molar ratio was varied without adding oxygen. No disproportionation took place. The products after 20 hr consisted 25% of 2-butene, 50% of 2-pentene, and 25% of 3-hexene, indicating that a thermodynamic equilibrium was reached in each experiment. The data are collected in Table 1. At O_2/Re≧3.5, the catalytic activity disappeared after 20 hr. It seems that at such large O_2/Re molar ratios, the disproportionation catalyst species was destroyed by excess oxygen.

When α-olefins were used as substrates, two competing processes occurred, namely disproportionation and double-bond migration. As shown in Table 2, 1-pentene gave a mixture of olefins ranging from C_2 to C_8. Only double-bond migration occurred before

Table 1. $ReCl_5$-Et_3Al-O_2 catalyst with 2-pentene[a)]

Olefin yield, mol%	O_2/Re molar ratio					
	2 hr					20 hr
	2.6	5.0	7.3	9.3	12.5	2.6—12.5
C_4H_8	16	23	25	24	22	25
C_5H_{10}	67	54	51	52	56	50
C_6H_{12}	16	23	25	24	21	25
$(C_4+C_6)/C_5$	0.48	0.85	0.98	0.92	0.77	1.0

a) Al/Re=4, 2-pentene/Re=93. 1-Pentene was purified by adding WCl_6.

Table 2. $ReCl_5$-Et_3Al-O_2 catalyst with 1-pentene[a)]

Al/Re Molar ratio	O_2/Re Molar ratio	Reaction time, hr	Olefin yield,[b)] mol%				
			C_4	C_5	C_6	C_7	C_8
4.0	2.0	2	3.5	93	2.1	1.1	0.0
	5.2		7.9	77	7.0	3.3	1.1
	11.4		15	53	14	5.9	3.6
4.0	1.0	72	1.0	98	1.0	0.2	0.0
	2.0		14	59	14	5.5	1.3
	2.5		20	25	18	12	7.3
	3.5		23	29	20	11	4.4
	5.2		20	42	17	9.4	4.4
	15.3		15	54	15	6.5	1.5
7.0	4.0	76	9.5	73	8.4	3.9	0.9
	5.1		18	43	17	7.3	4.3
	7.6		7.0	79	7.0	2.7	1.2

a) 1-Pentene/Re=60.
b) Ethylene and propylene were also detected.

the addition of oxygen. In this catalyst system the disproportionation of internal olefins proceeded at a fairly higher rate than the disproportionation and double-bond migration of α-olefins. Glpc analyses after 72 hr showed that at Al/Re=4, good results for disproportionation were obtained at O_2/Re=*ca.* 2.5. At Al/Re=4 and O_2/Re=2.6, the catalyst system was still active in the disproportionation of additional 1-pentene after 72 hr. This indicates that at a small O_2/Re ratio, the catalyst was probably long-lived. Thus 1-pentene was continually disproportionated little by little and 2-pentene which resulted from the slow double-bond migration of 1-pentene was rapidly disproportionated. But at a large O_2/Re ratio, the disproportionation catalyst was deactivated by excess oxygen present in the system before 2-pentene was gradually formed and the slow disproportionation of 1-pentene proceeded to a considerable extent. According to analyses after 72 hr, good results were obtained at relatively small O_2/Re ratios. At Al/Re=7, the optimum ratio was larger than that at Al/Re=4. At Al/Re=1 and O_2/Re=1, alkylation products were exclusively formed. The first three experiments in Table 2 indicate that in the early stage of the reaction, the high conversion of 1-pentene was attained at relatively large O_2/Re molar ratios. It seems that this was due to the slow catalyst-formation at small molar ratios. The result that large ratios are preferred (Table 1) could be similarly elucidated.

Glpc analyses of the 2-pentene reaction solutions after 96 hr showed the presence of small amounts of C_7 olefins (1—2%), which can be attributed to double-bond migration followed by disproportionation. This catalyst in combination with 1-hexene afforded a mixture of olefins ranging from C_2 to C_{10}. 2-Hexene gave a mixture of olefins ranging from C_4 to C_8 (Table 3). The formation of each olefin, as described in Tables 2 and 3, requires the interaction of a combination of α- and internal olefins.

In these catalyst systems olefins should be added after the reduction of $ReCl_5$ by Et_3Al, since $ReCl_5$ tself can promote the moderate alkylation of aromatic compounds and the oligomerization of olefins.[10] Aromatic compounds were suitable as solvent. Olefins were not disproportionated with tetrahydrofuran as a solvent. When three moles of PPh_3 per mole of $ReCl_5$ were present in the system before oxygen was introduced, the system showed no disproportionation activity. $ReCl_3$ showed none upon treatment with Et_3Al and oxygen.

TABLE 3. $ReCl_5$-Et_3Al-O_2 CATALYST WITH 1-HEXENE OR 2-HEXENE[a]

Olefin yield, mol%	Reactant	
	1-Hexene	2-Hexene
Al/O_2/Re Molar ratio	4/2/1	4/2/1
Reaction time, hr	74	64
C_4H_8	b)	19
C_5H_{10}	12	7.0
C_6H_{12}	52	45
C_7H_{14}	12	6.8
C_8H_{16}	1.5	20
C_9H_{18}	8.3	
$C_{10}H_{20}$	3.6	

a) Olefin/Re=50.
b) Ethylene, propylene, and butene were present. However, they were not estimated.

Catalyst from WCl_6. Wang and Menapace[3] reported that with a WCl_6–Et_3Al catalyst system, 100% conversion into unknown oligomers was obtained. The catalyst system WCl_6 and Et_3Al, however, exhibited disproportionation activity for 2-pentene in a short range of Al/W molar ratio. The optimum ratio was *ca.* 0.5. Though the catalyst activity decreased with the increase in the ratio, it was restored by the introduction of oxygen into the system. At Al/W=2.6, good results were obtained at O_2/W=1.2—1.7. Traces of oligomerization and Friedel-Crafts alkylation products were observed in the reaction mixture.[11] Glpc analyses after 96 hr indicated the presence of C_7 olefins.

In the reaction of α-olefins by the catalyst system of WCl_6–Et_3Al, unknown oligomerizasion took place considerably accompanied by disproportionation and double-bond migration. Although both oligomerization and disproportionation activities disappeared with the increase in the Al/W ratio and the double-bond migration activity was not much influenced, introduction of oxygen into this system recovered only the disproportionation activity. Addition of PPh_3 to WCl_6–Et_3Al system also suppressed the oligomerization activity and effected disproportionation and double-bond migration. The results are given in Table 4. The disproportionation activity of the catalyst WCl_6–Et_3Al–O_2 was dependent on the mixing order of the catalyst components. Preparation of the active catalyst was favored by the presence of olefin when WCl_6 was treated with Et_3Al and then oxygen.

Catalyst from Molybdenum Compounds. The catalyst system of $MoCl_5$ and Et_3Al also exhibited catalytic activity for olefin disproportionation in a narrow range of Al/Mo ratio. This system appeared to be less active than the tungsten system. The disproportion activity was reduced by the increase in the Al/Mo ratio but restored by the introduction of oxygen into the system. In the reaction of α-olefins with $MoCl_5$–Et_3Al, oligomerization occurred accompanied by disproportionation and double-bond migration. The results are summarized in Table 5.

Molybdenum(III) acetylacetonate also exhibited disproportionation activity for 1-pentene upon treatment with Et_3Al and oxygen. At Al/Mo=7 and O_2/Mo=2, the system exhibited a slight activity. At Al/Mo=4, only double-bond migration and dimerization were observed with a change of O_2/Mo.

As a reducing agent, other organoaluminum compounds were also investigated. Several systems were found to form disproportionation catalysts. Pertinent data are given in Table 6.

10) J. Tsuji, T. Nogi, and M. Morikawa, This Bulletin, **39**, 714 (1966).

11) J. R. Graham and L. H. Slaugh, *Tetrahedron Lett.*, **1971**, 787.

Table 4. WCl_6-$Et_3Al(-O_2)$ catalyst[a]

Reactant	Al/W Molar ratio	O_2/W Molar ratio	Reaction time, hr	Olefin yield,[c] mol% C_4	C_5	C_6	C_7	C_8
2-Pentene	0.6[b]	0	0.5	24	49	25		
	0.5	0	2	20	43	20		
	2.6	0	2	0	98	0		
	2.6	1.2	2	22	56	22		
	2.6	4.5	2	14	73	13		
1-Pentene	0.7	0	2	2.6	21	3.0	1.1	0.1
	2.6	0	12	0.9	96	0.6	3.0	0.0
	2.6	2.3[d]	2	11	59	11	5.3	3.5
	1.2	1.0[e]	44	19	26	20	11	4.4

a) 2-Pentene/W=93, 1-pentene/W=91.
b) In this reaction 2-pentene purified by adding WCl_6 was used. 2-Pentene/W=270.
c) When the reactant was 1-pentene, ethylene and propylene were also present. Although chlorophenylpentane was detected, the amount of alkylation products was so small that we could employ chlorobenzene as an internal standard in the glpc analysis.
d) Oxygen was added 12 hr after the reduction by Et_3Al.
e) PPh_3 was used in place of O_2. 1-Pentene was purified by adding WCl_6.

Table 5. $MoCl_5$-$Et_3Al(-O_2)$ catalyst[a]

Reactant	Al/Mo Molar ratio	O_2/Mo Molar ratio	Reaction time, hr	Olefin yield,[b] mol% C_4	C_5	C_6	C_7	C_8
2-Pentene	0.3	0	20	4.7	86	4.8		
	2.1	0	48	0.5	95	0.5		
	2.1	1.7[c]	2	5.1	86	4.8		
1-Pentene	0.3	0	20	0.3	18	0.4	1.0	0.0
	2.0	1.6[d]	2	4.0	71	4.0	3.1	0.2

a) 2-Pentene/Mo=93, 1-pentene/Mo=91.
b) Traces of chlorophenylpentane were also detected. When the reactant was 1-pentene, ethylene and propylene were present.
c) Oxygen was added 48 hr after the reduction by Et_3Al and the reaction was continued for another 2 hr.
d) Oxygen was added 12 hr after the reduction.

Table 6. MCl_n-$Et_2AlCl(-O_2)$ catalyst with 2-pentene[a]

Metal chloride	Al/M Molar ratio	O_2/M Molar ratio	Reaction time, hr	Olefin yield,[b] mol% C_4	C_5	C_6
WCl_6	3	0	24	0.7	59	0.7
$MoCl_5$	6	4	22	3.8	75	3.5
$ReCl_5$	7	5	24	1.0	80	1.0

a) 2-Pentene/M=93.
b) Traces of phenylpentane were also detected.

The Reaction Intermediate. Wang and Menapace[3] described the disproportionation of 2-pentene by a catalyst system of WCl_6 and *n*-BuLi. They reported that a conversion of 50% and a selectivity of 100% were obtained at Li/W=2, results not being good with other ratios. Thus they suggested a W-(IV) catalytic intermediate. Hughes[12] proposed a zero-valent molybdenum compound as the active species in the $L_2Cl_2(NO)_2Mo$–R_xAlCl_{3-x} catalyst.

In our catalyst systems starting metal chlorides, which demonstrate moderate Friedel-Crafts alkylation activity,[10,11] can be reduced to various oxidation states according to an added amount of Et_3Al. At Al/W=*ca.* 0.6, WCl_6 can be reduced to an appropriate oxidation state and exhibits disproportionation activity. Subsequently added oxygen can re-oxidize the low-valent complex and realize a favorable oxidation state for disproportionation. If oxygen was present in excess, the activity species would be further oxidized and destroyed. When three moles of PPh_3 per mole of $ReCl_5$ were present in the system before the introduction of oxygen, PPh_3 could stabilize the low-valent metal species and prevent it from re-oxidation. However, it is difficult to assume the precise oxidation state of the active species.

12) W. B. Hughes, *J. Amer. Chem. Soc.*, **92**, 532 (1970).

Studies on Hydroxy Amino Acids. IV.[1] Syntheses of Several Peptides Containing Aziridinecarboxylic Acid Derived from the Corresponding Hydroxy Amino Acid Derivatives

Yasuo NAKAGAWA,* Takashi TSUNO, Kiichiro NAKAJIMA, Michio IWAI, Haruki KAWAI, and Kenji OKAWA

Department of Chemistry, Faculty of Science, Kwansei Gakuin University, Nishinomiya

(Received September 13, 1971)

The β-elimination reaction of the *O*-tosyl β-hydroxy amino acid peptide derivative was thoroughly investigated. The *N*-tosyl-L-serylglycine ester and the *N*-tosyl-L-threonylglycine ester gave the *N*-tosyl-L-aziridinecarbonylglycine ester and the *N*-tosyl-3-methyl-L-aziridinecarbonylglycine ester as the resulting products respectively by the elimination reaction. On the other hand, the *N*-carbobenzoxyglycyl-L-serylglycine ester was not converted into the aziridine peptide derivative; only the dehydroalanine peptide was obtained. However, the *N*-tosyl-L-phenylalanyl-L-threonylglycine ester and the *N*-carbobenzoxyglycyl-L-threonylglycine ester were converted into the corresponding aziridine peptide, and the *N*-tosyl-L-phenylalanyl-3-methyl-L-aziridinecarbonylglycine ester and the *N*-carbobenzoxyglycyl-3-methyl-L-aziridinecarbonylglycine ester were obtained respectively. It was concluded that the peptides containing threonine were easily converted into the aziridine peptides and not the serine peptides by the β-elimination reaction.

The typical β-elimination reactions of the *N*-acylated hydroxy amino acid esters, such as serine or threonine derivatives, usually gave dehydroalanine derivatives as the resulting products. For example, the *N*-carbobenzoxy-*O*-tosyl-L-serine ethyl ester (IIe) was converted into the *N*-carbobenzoxydehydroalanine ester (IIIe) by the elimination reaction described by Photaki.[2] The above result was also supported by the present investigation; that here is, the *N*-carbobenzoxyglycyl-*O*-tosyl-L-serine ethyl ester (IIf) and the *N*-carbobenzoxyglycyl-*O*-tosyl-L-threonine ethyl ester (IIk) were also converted into the corresponding *N*-carbobenzoxyglycyldehydroamino acid ester derivatives (IIIf, IIIk).

In the case of the *N*-alkylated serine ester, however, the aziridine ring is formed by the elimination reaction, even though the carboxyl group is replaced by the ester group. For example, the *N*-trityl-L-aziridinecarboxylic acid methyl ester (IVa) was obtained from the *N*-trityl-*O*-mesyl-L-serine methyl ester (IIa), as has been described by Smrt.[3]

On the other hand, as has been described in a previous paper[4], an aziridinecarboxylic acid derivative, *N*-tosyl-3-methyl-aziridinecarboxylic acid anilide(IVi), was obtained instead of the dehydroalanine derivative from the *N,O*-ditosyl-L-threonine anilide(IIi). We will use "Azyline" as the name of aziridinecarboxylic acid and "Azy" as an abbreviation of azyline.

In the present investigation, we have systematically tried to clarify the structural influences of the substituent group on the formation of the aziridine ring by the elimination reaction of the hydroxy amino acid peptide derivatives, as is shown in Table 1. As the first experiments, the substituent effects of the ester and amide groups of *N*-tosylated hydroxy amino acid in the elimination reaction were investigated. It was found that, the *N,O*-ditosyl-L-serine ethyl ester (IIb) was converted into the *N*-tosyldehydroalanine ester (IIIb), while the aziridine derivative was not obtained at all. On the other hand, *N,O*-ditosyl-L-serylglycine esters (IIc, IId), in which carboxyl groups of serine were protected by the amide group, gave only aziridine peptides derivatives (IVc, IVd).

In the case of the threonine derivatives, however, the *N,O*-ditosyl-L-threonine ethyl ester (IIh) was converted into both the *N*-tosyl-3-methyl-L-azylylglycine ester (IVh) and the *N*-tosyl-α-amino-crotonic acid ester (IIIh).

On the other hand, in the case of the amide derivative of threonine, the *N*-tosyl-3-methyl-L-azylylglycine ethyl ester (IVj) was obtained from the *N,O*-ditosyl-L-threonylglycine ethyl ester (IIj), as had been expected on the basis of the results of a previous investigation.

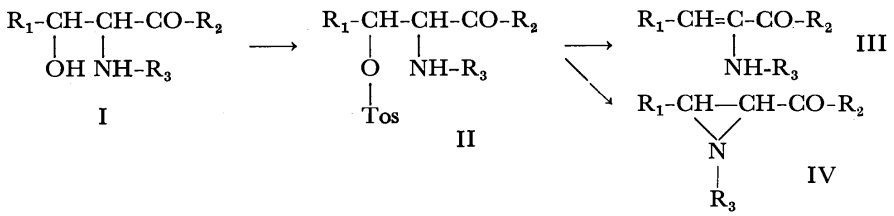

1) Part III: M. Iwai, K. Nakajima, A. Uno, S. Hase, I. Takeuchi and K. Okawa, This Bulletin, **43**, 3246 (1970). The abbreviations used for the amino acid residues, peptides, and other abbreviations are based on the proposals by: E. Schröder and K. Lübke, "The Peptides", Academic Press, New York, (1965).

* Present address: Research Center of Tekkosha and Co., Ltd. Musashino, Tokyo.

2) I. Photaki, *J. Amer. Chem. Soc.*, **85**, 1123 (1963).

3) J. Smrt, J. Beranek, and J. Sicher, *Chem. Abstr.*, **55**, 10468i (1961); U.S. 2958691 Nov. 1. 1960.

4) K. Okawa, T. Kinutani, and K. Sakai, This Bulletin, **41** 1353 (1968).

Table 1. Reaction products by the β-elimination reaction of the O-tosylated hydroxy amino acid derivatives.[a]

I, II	Protecting groups			Products (Yield%)	
	R_1	R_2	R_3	III	IV
a	H	-OMe	Tri-	—	80.2[b]
b	H	-OEt	Tos-	90	—
c	H	-Gly-OEt	Tos-	—	80.6
d	H	-Gly-OMe	Tos-	—	80
e	H	-OEt	Z-	63[c]	—
f	H	-OEt	Z-Gly-	95	—
g	H	-Gly-OEt	Z-Gly-	67	—
h	CH_3	-OEt	Tos-	29	64
i	CH_3	-NH-C_6H_5	Tos-	—	65[d]
j	CH_3	-Gly-OEt	Tos-	—	96 (oil)
k	CH_3	-OEt	Z-Gly-	87.5	—
l	CH_3	-Gly-OBzl	Z-Gly-	—	80
m	CH_3	-Gly-OEt	Tos-L-Phe-	—	60

a) Elimination reactions were carried out in tetrahydrofuran solution in the presence of triethylamine, but some of the cases, benzene-methanol or acetonitrile was used as the solvent and *N*-ethylpiperidine was used as the base.
b) *N*-Tri-*O*-Mesyl-L-serine methyl ester is used as the starting material in literature.[3]
c) This value shows the yield of the free acid in literature.[4]
d) This result was published in the previous paper.[4]

As the next experiments, the substituent effects of the *N*-acyl masking group of the hydroxy amino acid amide derivatives were investigated. It was found that the *N*-carbobenzoxyglycyl-*O*-tosyl-L-serylglycine ethyl ester (IIg) was converted into the corresponding *N*-carbobenzoxyglycyldehydroalanylglycine ethyl ester (IIIg), but no aziridine derivatives were obtained. However, the *N*-carbobenzoxyglycyl-*O*-tosyl-L-threonylglycine benzyl ester (IIl) and the *N*-tosyl-L-phenylalanyl-L-threonylglycine ethyl ester (IIm) were converted into the *N*-carbobenzoxyglycyl-3-methyl-L-azylylglycine benzyl ester (IVl) and *N*-tosyl-L-phenylalanyl-3-methyl-L-azylylglycine ethyl ester (IVm). These were the first synthetic peptides in which aziridinecarboxylic acid was placed at the middle position in the peptide linkage.

On the basis of the above experiments, it was concluded that threonine peptides and their derivatives (R_1=–CH_3) are relatively more easily converted into the corresponding aziridine derivatives than the serine peptides derivatives (R_1=–H). The replacement of the ester group (R_2) of the hydroxy amino acid by an amide group, such as the anilide or glycine ester, increased the tendency of the ring formation. The aminoacyl group (R_3) did not promote the tendency of the ring formation; only aziridine peptides derivatives were synthesized in the case of threonine peptipdes (R_1=–CH_3).

It is a matter of course that the aziridine derivatives preserved their optical activity throughout the β-elimination reaction, unlike the dehydroamino acid derivatives, which did not show any optical activity at all. The X-ray crystallographic analysis of the compound, *N*-tosyl-L-azylylglycine, also supported the above results; that is, the original configuration on the α-carbon atom was retained during the elimination procedure. (Fig. 1). The results of the X-ray crystallographic analysis will be published in This Bulletin soon.

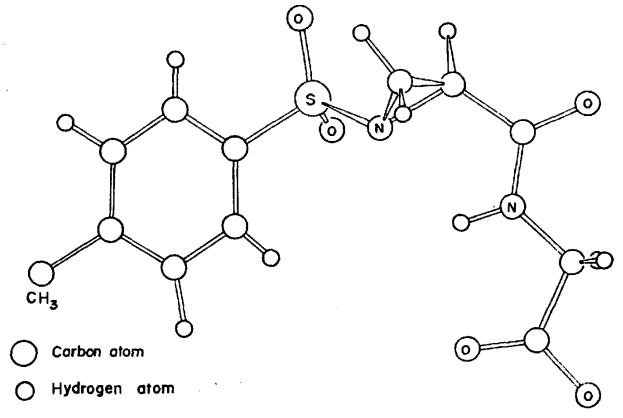

Fig. 1. The molecular structure of *N*-tosyl-L-azylylglycine as determined by X-ray analysis.

The *O*-tosylations of hydroxy amino acid derivatives were carried out in a dry pyridine solution with freshly-prepared *p*-toluenesulfonyl chloride at −5—−10°C. The *O*-tosylated products (II) thus obtained were gradually decomposed, especially in the solution, and were stored in a refrigerator.

The optimum conditions for a good yield of the aziridine derivative were also investigated by using the *N,O*-ditosyl-L-serylglycine ethyl ester (IIc). The results are summarized in Table 2.

The most satisfactory results were obtained when the solution of *N,O*-ditosyl derivatives in tetrahydrofuran was treated with 1.0—1.2 equivalent amounts of triethylamine at the refluxing temperature for a short time. Consequently, in the present investigation, tetrahydrofuran and triethylamine were mainly used as the solvent and the base respectively.

TABLE 2. THE REACTION CONDITION AND THE YIELD OF *N*-TOSYL-L-AZYLYLGLYCINE ETHYL ESTER (IVc)

Solvents[a]	Concentration of IIc (g/m*l*)	Bases[b]	Eq. amt. of bases	Reaction temp. (°C)	Reaction time	Yield (%)
THF	0.10	EP	1.0	38	10 hr	18
THF	0.10	EP	2.0	35	19 hr	15
THF	0.10	DEA	1.0	38	17 hr	18
THF	0.10	TEA	1.1	37	24 hr	27
CH_2Cl_2	0.16	TEA	1.2	37	16 hr	11
$CHCl_3$	0.16	TEA	1.1	37	16 hr	44
AcOEt	0.16	TEA	1.1	37	16 hr	46
MeCN	0.16	TEA	1.1	37	16 hr	50
THF	0.20	TEA	1.1	reflux	30 min	80
MeCN	0.16	TEA	1.0	reflux	30 min	81
DMSO	0.16	TEA	1.1	70	20 min	87

a) THF: tetrahydrofuran, DMSO: dimethyl sulfoxide. b) EP: *N*-ethylpiperidine, DEA: diethylamine, TEA: triethylamine.

Experimental

All the melting points are uncorrected. The NMR spectra were obtained with a Hitachi R-20B High Resolution NMR spectrometer, while the chemical shifts are given from TMS as the internal reference.

N-*Tosyl-*L*-serine Ethyl Ester (Ib).* Ib was prepared from *N*-tosyl-L-serine[5] (20.0 g, 77 mmol) by the method of Stevens[6] in a 92% (20.4 g) yield; mp 103—104°C. $[\alpha]_D^{23}$ −8.2° (*c* 2.2, EtOH).

Found: C, 49.98; H, 5.96; N, 5.06; S, 11.45%. Calcd for $C_{12}H_{15}O_5N_5$: C, 50.16; H, 5.96; N, 4.88; S, 11.16%.

N-*Tosyl-*L*-serylglycine Ethyl Ester (Ic).* Into a solution of *N*-tosyl-L-serine hydrazide[5] (27.4 g, 0.10 mol) in acetic acid (11 m*l*) and N hydrochloric acid (200 m*l*), we added 3N sodium nitrite (50 m*l*), drop by drop, under cooling at −5——10°C. After the solution had been stirred for 10 min, the product was extracted with ice-cold ethyl acetate (200 m*l*); the organic layer was neutralized with ice-cold saturated aqueous sodium bicarbonate and immediately cooled under −5°C. A solution of glycine ethyl ester hydrochloride[7] (41.9 g, 0.30 mol) and triethylamine (41.8 m*l*, 0.30 mol) in ethyl acetate (50 m*l*) was then added, drop by drop, to the azide solution. The stirring was continued for 4 hr at −5°C. After the reaction mixture had then been allowed to stand overnight in a refrigerator, the mixture was washed with N hydrochloric acid, N sodium bicarbonate, and water, and was dried over anhydrous sodium sulfate. The solution was concentrated under reduced pressure. The Ic produced was collected and recrystallized from ethyl acetate. The crystals were obtained in an 85% yield (29.3 g); mp 108—109°C. $[\alpha]_D^{23}$ −24.3° (*c* 2.0, EtOH).

Found: C, 48.74; H, 5.75; N, 8.19; S, 9.16%. Calcd for $C_{14}H_{20}O_6N_2S$: C, 48.82; H, 5.85; N, 8.14; S, 9.31%.

N-*Tosyl-*L*-serylglycine Methyl Ester (Id).* Id was prepared from *N*-tosyl-L-serine hydrazide[5] (27.4 g, 0.10 mol) and the glycine methyl ester (from hydrochloride[8] (37.8 g, 0.30 mol)) by the above azide procedure in an 84% (28.9 g) yield; mp 107—108°C. $[\alpha]_D^{23}$ −20.7° (*c* 2.0, EtOH).

Found: C, 47.07; H, 5.51; N, 8.45; S, 9.93%. Calcd for $C_{13}H_{18}O_6N_2S$: C, 47.26; H, 5.49; N, 8.48; S, 9.71%.

N-*Carbobenzoxyglycyl-*L*-serine Ethyl Ester (If).* *N*-Carbobenzoxyglycine hydrazide[9] (22.3 g, 0.10 mol) was coupled with the L-serine ethyl ester (from hydrochloride[10] (17.0 g, 0.10 mol)) in ethyl acetate by the above azide procedure. Recrystallization from hot ethyl acetate gave a pure material (24.8 g (76.4%)); mp 112.5°C. $[\alpha]_D^{23}$ +17.0° (*c* 2.1, dioxane).

Found: C, 55.36; H, 6.16; N, 8.59%. Calcd for $C_{15}H_{20}O_6N_2$: C, 55.55; H, 6.21; N, 8.64%.

N-*Tosyl-*L*-threonine Ethyl Ester (Ih).* Ih was prepared from *N*-tosyl-L-threonine[11] (109 g, 0.4 mol) by the method of Brenner[12] in a 98% (118 g) yield; mp 106°C. $[\alpha]_D^{23}$ −4.4° (*c* 2.0, MeOH).

Found: C, 52.05; H, 6.55; N, 4.92; S, 10.52%. Calcd for $C_{13}H_{19}O_5NS$: C, 51.81; H, 6.35; N, 4.65; S, 10.64%.

N-*Tosyl-*L*-threonylglycine Ethyl Ester (Ij).* *N*-Tosyl-L-threonine hydrazide[12] (14.41 g, 50 mmol) was coupled with the glycine ethyl ester (from hydrochloride[7] (20.9 g, 150 mmol)) by the above azide procedure in an 84% (15.0 g) yield. Recrystallization from ethyl acetate-*n*-hexane gave a pure material; mp 116—116.5°C. $[\alpha]_D^{23}$ −23.2° (*c* 2.0, MeOH).

Found: C, 50.02; H, 5.86; N, 7.91; S, 9.05%. Calcd for $C_{15}H_{22}O_6N_2S$: C, 50.26; H, 6.19; N, 7.82; S, 8.95%.

N-*Carbobenzoxyglycyl-*L*-threonine Hydrazide.* The *N*-carbobenzoxyglycyl-L-threonine ethyl ester[13] (30 g, 88 mmol) was dissolved in 80% hydrazine hydrate (37.3 g, 0.62 mol) in absolute methanol (40 m*l*). After the reaction mixture had been allowed to stand overnight in a refrigerator, a crude precipitate was collected and recrystallized from hot methanol. The yield was 27.9 g (97.5%); mp 172—173°C.

N-*Carbobenzoxyglycyl-*L*-threonylglycine Benzyl Ester (Il).* *N*-Carbobenzoxyglycyl-L-threonine hydrazide (27.4 g, 84 mmol) was coupled with the glycine benzyl ester (from tosylate[14] (26.4 g, 0.168 mol)) by the above azide procedure. Recrystallization from hot methanol gave a pure material;

5) K. Hofmann, A. Jöhl, A. E. Furlenmeier, and H. Kappler, *J. Amer. Chem. Soc.*, **79**, 1636 (1957).
6) C. M. Stevens and R. Watanabe, *ibid.*, **72**, 725 (1950).
7) R. W. Chambers and F. H. Carpenter, *ibid.*, **77**, 1522 (1955).
8) T. Curtius and F. Goebel, *J. Prakt. Chem.*, (2) **37**, 150 (1888).
9) B. F. Erlanger and E. Brand, *J. Amer. Chem. Soc.*, **73** 3508 (1951).
10) G. Riley, J. H. Turnbull, and W. Wilson, *J. Chem. Soc.*, **1957**, 1373.
11) M. Brenner, K. Rüfenacht, and E. Sailer., *Helv. Chim. Acta*, **34**, 2102 (1951).
12) M. Brenner, E. Sailer, and K. Rüfenacht, *ibid.*, **34**, 2096 (1951).
13) S. Sakakibara, K. H. Shin, and G. P. Hess, *J. Amer. Chem. Soc.*, **84**, 4921 (1962).
14) L. Zervas, M. Winitz, and J. P. Greenstein, *J. Org. Chem.*, **22**, 1515 (1957).

27.8 g (72%); mp 156—157°C. $[\alpha]_D^{23}$ −15.7° (*c* 2.0, dioxane).

Found: C, 60.35; H, 6.03; N, 9.34%. Calcd for $C_{23}H_{27}O_7N_3$: C, 60.38; H, 5.95; N, 9.19%.

N-*Tosyl-*L*-phenylalanyl-*L*-threonine Hydrazide.* The *N*-tosyl-L-phenylalanyl-L-threonine ethyl ester was prepared from *N*-tosyl-L-phenylalanine[15] and L-threonine ethyl ester hydrochloride[16] by the succinimide-ester method,[17] and was directly used for the next step without purification. The crude acyl peptide ester (15.9 g, 35 mmol) was treated with 80% hydrazine hydrate (43 m*l*) in methanol (20 m*l*) at room temperature for 44 hr. The crystals which appeared were collected and recrystallized from hot methanol in a 75% yield (from the ester) (11.4 g); mp 193°C.

Found: C, 55.48; H, 6.10; N, 12.62; S, 7.40%. Calcd for $C_{20}H_{26}O_5N_4S$: C, 55.28; H, 6.03; N, 12.89; S, 7.38%.

N-*Tosyl-*L*-phenylalnyl-*L*-threonylglycine Ethyl Ester (Im).* *N*-Tosyl-L-phenylalanyl-L-threonine hydrazide (11.3 g, 26 mmol) was coupled with the glycine ethyl ester (from hydrochloride[7]) (10.5 g, 75 mmol) by the above azide procedure. The yield of the crude product was 63.5% (8.4 g). Recrystallization from hot ethyl acetate–*n*-hexane gave a pure material; mp 162—163°C. $[\alpha]_D^{23}$ −65.3° (*c* 1.0, EtOH).

Found: C, 57.20; H, 6.20; N, 8.44; S, 6.53%. Calcd for $C_{23}H_{31}O_7N_3S$: C, 57.01; H, 6.18; N, 8.31; S, 6.34%.

O-*Tosylation of Hydroxy Amino Acid Derivatives.*

N,O-*Ditosyl-*L*-serine Ethyl Ester (IIb).* *p*-Toluenesulfonyl chloride (28.6 g, 105 mmol) in dry pyridine (45 m*l*) was stirred, drop by drop, into a solution of Ib (21.5 g, 75 mmol) in pyridine (150 m*l*) at −10°C over a 30-min period. The mixture was stirred for 1 hr at 0°C and then for an additional several hours at room temperature. The reaction mixture was poured into crushed ice (500 g) and allowed to stand overnight in a refrigerator. The precipitated products were dissolved in ethyl acetate, washed with water, and dried over anhydrous sodium sulfate. After the solution had been evaporated under reduced pressure, IIh was obtained as white crystals. Recrystallization from ethyl acetate-*n*-hexane gave pure crystals in a 52% (17 g) yield; mp 117—118°C. $[\alpha]_D^{23}$ +21.7° (*c* 1.0, MeOH).

Found: C, 51.64; H, 5.26; N, 3.04; S, 14.18%. Calcd for $C_{19}H_{23}O_7NS_2$: C, 51.68; H, 5.25; N, 3.17; S, 14.53%.

N,O-*Ditosyl-*L*-serylglycine Ethyl Ester (IIc).* IIc was prepared from Ic (10.3 g, 30 mmol) and *p*-toluenesulfonyl chloride (11.4 g, 50 mmol) in a dry pyridine (30 m*l*) solution by the above tosylation procedure. The crude product was obtained in a 92% (13.8 g) yield. The crude materials were recrystallized from ether-ethyl acetate; mp 107—108°C. $[\alpha]_D^{23}$ −2.7° (*c* 2.2, EtOH).

Found: C, 50.51; H, 5.15; N, 5.68; S, 12.76%. Calcd for $C_{21}H_{26}O_8N_2S_2$: C, 50.59; H, 5.26; N, 5.62; S, 12.86%.

N,O-*Ditosyl-*L*-serylglycine Methyl Ester (IId).* IId was prepared from Id (10.3 g, 30 mmol) and *p*-toluenesulfonyl chloride (11.4 g, 50 mmol) in a dry pyridine solution (30 m*l*) by the above tosylation procedure in an 85% (12.7 g) yield; mp 114—115°C. $[\alpha]_D^{23}$ −4.8° (*c* 2.0, $CHCl_3$).

Found: C, 49.58; H, 4.97; N, 5.61; S, 13.24%. Calcd for $C_{20}H_{24}O_8N_2S_2$: C, 49.58; H, 4.99; N, 5.78; S, 13.23%.

N-*Carbobenzoxyglycyl-*O*-tosyl-*L*-serine Ethyl Ester (IIf).* IIf was prepared from If (3.2 g, 10 mmol) and *p*-toluenesulfonyl chloride (3.8 g, 20 mmol) in dry pyridine (10 m*l*) by the above tosylation procedure in a 71.3% (3.5 g) yield. Recrystallization from ethyl acetate-ether gave a pure material; mp 109°—110°C. $[\alpha]_D^{23}$ +22.5° (*c* 2.0, dioxane).

Found: C, 54.97; H, 5.40; N, 5.79; S, 6.58%. Calcd for $C_{22}H_{26}O_8N_2S$: C, 55.22; H, 5.48; N, 1.85; S, 6.70%.

N,O-*Ditosyl-*L*-threonine Ethyl Ester (IIh).* IIh was prepared from Ih (15.1 g, 50 mmol) and *p*-toluenesulfonyl chloride (19.1 g, 100 mmol) in dry pyridine (45 m*l*) by the above tosylation procedure. Recrystallization from ethyl acetate–*n*-hexane gave a pure material in a 71% (16.1 g) yield; mp 118—119°C. $[\alpha]_D^{23}$ +20.3° (*c* 2.0. MeOH).

Found: C, 52.62; H, 5.41; N, 3.01; S, 14.20%. Calcd for $C_{20}H_{25}O_7NS_2$: C, 52.73; H, 5.53; N, 3.08; S, 14.08%.

N,O-*Ditosyl-*L*-threonylglycine Ethyl Ester (IIj).* IIj was prepared from Ij (17.9 g, 50 mmol) and *p*-toluenesulfonyl chloride (19.0 g, 100 mmol) in dry pyridine (30 m*l*) by the aobve tosylation procedure. Recrystallization from ethyl acetate–petroleum ether gave a pure material in an 85% (22.2 g) yield; mp 122—122.5°C. $[\alpha]_D^{23}$ +18.1° (*c* 2.0, MeOH).

Found: C, 51.36; H, 5.45; N, 5.31; S, 12.26%. Calcd for $C_{22}H_{28}O_8N_2S_2$: C, 51.55; H, 5.51; N, 5.47; S, 12.51%.

N-*Carbobenzoxyglycyl-*O*-tosyl-*L*-threonine Ethyl Ester (IIk).* IIk was prepared from the *N*-carbobenzoxyglycyl-L-threonine ethyl ester[13] (3.4 g, 10 mmol) and *p*-toluenesulfonyl chloride (3.8 g, 20 mmol) in dry pyridine (10 m*l*) by the above tosylation procedure. When the crude products were recrystallized from ether, fine crystals were obtained in a 71.4% (3.5 g) yield; mp 79—80°C. $[\alpha]_D^{23}$ +21.3° (*c* 1.0, EtOH).

Found: C, 55.93; H, 5.74; N, 5.70; S, 6.43%. Calcd for $C_{23}H_{28}O_8N_2S$: C, 56.08; H, 5.73; N, 5.69; S, 6.51%.

N-*Carbobenzoxyglycyl-*O*-tosyl-*L*-threonylglycine Benzyl Ester (IIl).* IIl was prepared from Il (4.6 g, 10 mmol) and *p*-toluenesulfonyl chloride (3.8 g, 20 mmol) in dry pyridine (25 m*l*) by the above tosylation procedure. Recrystallization from ethyl acetate-ether gave a pure material in a 77.6% (4.8 g) yield; mp 115—116°C. $[\alpha]_D^{23}$ −11.8° (*c* 1.0, THF).

Found: C, 58.83; H, 5.41; N, 6.78; S, 4.95%. Calcd for $C_{30}H_{34}O_9N_3S$: C, 58.83; H, 5.59; N, 6.86; S, 5.23%.

N-*Tosyl-*L*-phenylalanyl-*O*-tosyl-*L*-threonylglycine Ethyl Ester (IIm).* IIm was obtained from Im (7.8 g, 15.5 mmol) and *p*-toluenesulfonyl chloride (5.9 g, 31 mmol) in dry pyridine (24 m*l*) by the above tosylation procedure. Recrystallization from ethanol–ether gave a pure material in a 52% (5.3 g) yield; mp 121.3—122.5°C. $[\alpha]_D^{23}$ +7.9° (*c* 1.0, THF).

Found: C, 56.44; H, 5.69; N, 6.33; S, 9.47%. Calcd for $C_{31}H_{37}O_9N_3S_2$: C, 56.43; H, 5.65; N, 6.37; S, 9.72%.

β-Eliminations of O*-tosylated Hydroxy Amino Acid Derivatives.*

N-*Tosyldehydroalanine Ethyl Ester (IIIb).* A solution of IIb (2.2 g, 5 mmol) in tetrahydrofuran (18 m*l*) and triethylamine (0.7 m*l*, 5 mmol) was stirred for 9 hr at 35°C and then for 18 hr at room temperature. The reaction mixture was evaporated under reduced pressure, and the residue was dissolved in benzene; this benzene solution was washed with water three times, dried over anhydrous sodium sulfate, and concentrated under reduced pressure. The residual oily material was crystallized by scratching and then recrystallized from ether–petroleum ether; a pure material was obtained in a 90% (1.2 g) yield; mp 73—75.5°C.

Found: C, 52.69; H, 5.44; N, 5.40; S, 12.12%. Calcd for $C_{12}H_{15}O_4NS$: C, 53.51; H, 5.61; N, 5.20; S, 11.91%. NMR (DMSO-d_6): δ 5.33 ppm (1H(s) CH_2=), 5.52 ppm (1H(s) CH_2=).

N-*Tosyl-*L*-azylylglycine Ethyl Ester (IVc).* A solution of IIc (5.0 g, 10 mmol) and triethylamine (1.4 m*l*, 10 mmol) in tetrahydrofuran (30 m*l*) was refluxed for 30 min. After the removal of the solvent, water was added to the residue.

15) E. A. Popenoe and V. du Vigneaud, *J. Amer. Chem. Soc.*, **76**, 6202 (1954).
16) D. F. Elliott, *J. Chem. Soc.*, **1949**, 589.
17) G. W. Anderson, J. E. Zimmerman, and F. M. Callakan, *J. Amer. Chem. Soc.*, **86** 1839 (1964).

The reddish-brown mass was then dissolved in chloroform. The solution was washed with water, dried over anhydrous sodium sulfate, and concentrated under reduced pressure. The residue was recrystallized from chloroform-ether in an 80.6% (2.6 g) yield; mp 147—148°C. $[\alpha]_D^{23}$ −59.1° (*c* 2.3, dioxane).

Found: C, 51.76; H, 5.74; N, 8.58; S, 9.82%. Calcd for $C_{14}H_{18}O_5N_2S$: C, 51.52; H, 5.56; N, 8.58; S, 9.84%. NMR ($CDCl_3$): δ 2.43 ppm (1H(d), J_{trans}=4.2 Hz Azy; -CH_2-, 2.77 ppm (1H(d), J_{cis}=7.7 Hz Azy; -CH_2-), 3.32 ppm (1H(q), J_{trans}=4.2 Hz, J_{cis}=7.7 Hz Azy; α-proton).

N-Tosyl-L-azylylglycine Methyl Ester (IVd). IVd was obtained from IId (4.8 g, 10 mmol) and triethylamine (1.4 m*l*, 10 mmol) in tetrahydrofuran (40 m*l*) by the above elimination reaction procedure (IVc). Recrystallization from chloroform–ether gave a pure material in an 80% (2.6 g) yield; mp 116—117°C. $[\alpha]_D^{23}$ −55.7° (*c* 2.0, dioxane).

Found: C, 49.95; H, 5.23; N, 8.76; S, 10.49%. Calcd for $C_{13}H_{16}O_5N_2S$: C, 49.99; H, 5.16; N, 8.97; S, 10.27%.

N-Carbobenzoxyglycyldehydroalanine Ethyl Ester (IIIf). IIIf was prepared from IIf (2.4 g, 5 mmol) and triethylamine (1.4 m*l*, 10 mmol) in tetrahydrofuran (20 m*l*) by the above elimination reaction procedure (IVc). Recrystallization from ethyl acetate-ether gave a pure material in a 95% (1.5 g) yield; mp 81—81.5°C.

Found: C, 58.93; H, 5.96; N, 9.15%. Calcd for $C_{15}H_{18}O_5N_2$: C, 58.82; H, 5.92; N, 9.15%.

NMR ($CDCl_3$): δ 5.87 ppm (1H(d), J_{gem}=1.2 Hz, CH_2=), 6.53 ppm (1H(s), CH_2=).

N-Carbobenzoxyglycyldehydroalanylglycine Ethyl Ester (IIIg). A solution of the *N*-carbobenzoxyglycyl-*O*-tosyl-L-seryl-glycine ethyl ester[18] (5.4 g, 10 mmol) and *N*-ethylpiperidine (1.1 g, 10 mmol) in acetonitrile was incubated at 37°C for 24 hr. The solvent was then removed under reduced pressure, and the residue was dissolved in ethyl acetate. The solution was washed with water, dried over anhydrous sodium sulfate, and concentrated under reduced pressure. The resulting product was crystallized from ethyl acetate–ether. IIIg was thus obtained in a 67% (2.4 g) yield; mp 130—132°C.

Found: C, 56.07; H, 5.87; N, 11.53%. Calcd for $C_{17}H_{21}O_6N_3$: C, 56.19; H, 5.83; N, 11.56%.

NMR (DMSO-d_6): δ 5.58 ppm (1H(*q*), J=0.7, J=1.1 Hz, CH_2=), 6.25 ppm (1H(d), J=0.7 Hz, CH_2=).

N-Tosyl-α-amino-crotonic Acid Ethyl Ester (IIIh). *N-Tosyl-3-methyl-L-azyline Ethyl Ester (IVh).* Into a solution of IIh (9.1 g, 20 mmol) in benzene-methanol (50 : 1 v/v, 51 m*l*), we added *N*-ethylpiperidine (2.76 m*l*, 20 mmol). The solution was refluxed for 8.5 hr and then allowed to stand overnight. The reaction mixture was washed with water three times, dried over anhydrous sodium sulfate, and concentrated under reduced pressure; when the crystals thus produced were filtered off, IIIh (1.23 g) was obtained. The mother solution was chromatographed on silica gel (150 g) with benzene-chloroform (1 : 1 v/v) to yield the reaction products, IIIh and IVh respectively. The R_f values of IIIh and IVh were 0.24 (0.42 g) and 0.46 (3.62 g) respectively. The collected crystals of IIIh amounted to 1.65 g (29%); they were recrystallized from ethyl acetate–*n*-hexane; mp 93—94°C.

Found: C, 55.37; H, 6.00; N, 4.89; S, 11.23%. Calcd for $C_{13}H_{17}O_4NS$: C, 55.10; H, 6.05; N, 4.94; S, 11.32%.

NMR ($CDCl_3$): δ 2.02 ppm (3H(d), J=7.2 Hz, CH_3-CH=), 6.93 ppm (1H(q), J=7.2 Hz, CH_3-CH=). IVh was obtained in a 64% (3.62 g) yield; mp 56—56.5°C. $[\alpha]_D^{23}$ −40.2° (*c* 2.0, MeOH).

Found: C, 55.12; H, 6.01; N, 4.88; S, 11.52%. Calcd for $C_{13}H_{17}O_4NS$: C, 55.10; H, 6.05; N, 4.94; S, 11.32%.

NMR ($CDCl_3$): δ 1.31 ppm (3H(d), J=5.5 Hz Azy; CH_3-CH-), 3.13 ppm (1H(q), J=5.5, J_{cis}=7.5 Hz Azy; CH_3-CH-), 3.36 ppm (1H(d), J=7.5 Hz Azy; α-proton).

N-Tosyl-3-methyl-L-azylylglycine Ethyl Ester (IVj). The solution of triethylamine (2.8 m*l*, 20 mmol) and IIj (10.3 g, 20 mmol) in tetrahydrofuran was incubated at 50°C for 25 hr. The solvent was removed under reduced pressure, and the residue was dissolved in ethyl acetate. The solution was washed with water and dried over anhydrous sodium sulfate. After the evaporation of the solvent under reduced pressure, an oily product (IVj) was obtained in a 96% (7.0 g) yield. All efforts at crystallization failed.

N-Tosyl-3-methyl-L-azylylglycine. A solution of IVj (7.0 g) in acetonitrile (15 m*l*) and water (15 m*l*) was treated with N sodium hydroxide (22 m*l*) at 5°C for 1 hr and then allowed to stand at room temperature for 4 hr. After the acetonitrile had been removed under reduced pressure, the reaction mixture was acidified with 1 M citric acid (22 m*l*). The crystals which appeared were collected (6.0 g, 96%) and recrystallized from ethyl acetate–*n*-hexane (5.6 g); mp 138—139°C. $[\alpha]_D^{23}$ −52.3° (*c* 2.1, MeOH).

Found: C, 50.20; H, 4.97; N, 8.78; S, 10.29%. Calcd for $C_{13}H_{16}O_5N_2S$: C, 49.99; H, 5.16; N, 8.97; S, 10.26%.

NMR ($CDCl_3$): δ 1.23 ppm (3H(d), J=5.5 Hz Azy; CH_3-CH-), 3.02 ppm (1H(q), J=5.5, J_{cis}=7.5 Hz Azy; CH_3-CH-), 3.40 ppm (1H(d), J_{cis}=7.5 Hz Azy; α-proton).

N-Carbobenzoxyglycyl-α-amino-crotonic Acid Ethyl Ester (IIIk). A solution of IIk (3.5 g, 7.1 mmol) in tetrahydrofuran (15 m*l*) was treated with triethylamine (1.0 m*l*, 7.1 mmol) at 60°C for 4 hr, after which the solution was allowed to stand at room temperature for 15.5 hr. The solvent was then removed under reduced pressure; oily products were obtained and crystallized by the addition of *n*-hexane. IIIk was obtained in an 87.5% (2.1 g) yield; mp 86—88°C.

Found: C, 58.50; H, 6.33; N, 8.37%. Calcd for $C_{16}H_{20}O_5N_2 \cdot 1/2\,H_2O$: C, 58.35; H, 6.43; N, 8.50%.

NMR ($CDCl_3$): δ 1.73 ppm (3H(d), J=6.8 Hz, CH_3-CH=), 6.79 ppm (1H(q), J=6.8 Hz, CH_3-CH=).

N-Carbobenzoxyglycyl-3-methyl-L-azylylglycine Benzyl Ester (IVl). A solution of IIIl (610 mg, 1 mmol) and triethylamine (0.28 m*l*, 2 mmol) in absolute tetrahydrofuran (10 m*l*) was refluxed for 20.5 hr. The solvent was then removed under reduced pressure, and the residue was dissolved in ethyl acetate. The solution was washed with water, dried over anhydrous sodium sulfate, and concentrated under reduced pressure. The residual oil was crystallized by the addition of isopropyl ether. Recrystallization from acetone–isopropyl ether gave pure material in an 80% (350 mg) yield; mp 114—116°C. $[\alpha]_D^{23}$ −35.7° (*c* 1.0, THF).

Found: C, 62.66; H, 5.71; N, 9.68%. Calcd for $C_{23}H_{25}O_6N_3$: C, 62.86; H, 5.73; N, 9.56%.

NMR (DMSO-d_6): δ 1.01 ppm (3H(d), J=6.3 Hz Azy; CH_3-CH-), 4.49 ppm (1H(m), Azy; CH_3-CH-), 4.80 ppm (1H(d), J_{cis}=11.9 Hz Azy; α-proton).

N-Tosyl-L-phenylalanyl-3-methyl-L-azylylglycine Ethyl Ester (IVm). A solution of IIIm (1.30 g, 2 mmol) and triethylamine (0.28 m*l*, 2 mmol) in tetrahydrofuran (8 m*l*) was incubated at 40—50°C for 53 hr. The solvent was then removed under reduced pressure, and the residue was dissolved in ethyl acetate. The solution was washed with water, dried over anhydrous sodium sulfate, and concentrated under reduced pressure. The residual oily material

18) I. Photaki and V. Bardakos, *ibid.*, **87** 3489 (1965).

was chromatographed on silica gel (140 g) with chloroform–ethyl acetate (1 : 1 v/v) to yield a pure product. IVm was obtained as crystals from ethyl acetate–*n*-hexane in a 60% (0.59 g) yield; mp 118—121.5°C. $[\alpha]_D^{23}$ −52.0° (*c* 1.0, MeOH).

Found: C, 58.85; H, 5.84; N, 8.57; S, 6.86%. Calcd for $C_{24}H_{29}O_6N_3S$: C, 59.12; H, 6.00; N, 8.62; S, 6.58%.

NMR ($CDCl_3$): δ 1.16 ppm (3H(d), J=6.0 Hz Azy; CH_3–CH–), 4.20 ppm (1H(m) Azy; CH_3–CH–), 4.32 ppm (1H(d), J_{cis}=10.2 Hz Azy; α-proton).

The authors wish to express their deep thanks to the staff of the Fujisawa Pharmaceutical Co., Ltd., for their elemental microanalyses, and to Dr. Tokunosuke Watanabe, Professor of Kwansei Gakuin University, for his X-ray crystallographic analysis.

BULLETIN OF THE CHEMICAL SOCIETY OF JAPAN, VOL. 45, 1167—1169 (1972)

Stereochemical Studies and Synthetic Applications of Bis-β-keto Sulfoxides

Yasusi YAMAMOTO and Hitosi NOZAKI

Department of Industrial Chemistry, Kyoto University, Yosida, Sakyo-ku, Kyoto

(Received September 23, 1971)

Bis-β-keto sulfoxides of the $MeSOCH_2CO(CH_2)_nCOCH_2SOMe$ ($n=7$, 8, or 10) type are prepared. The *dl* and *meso* isomers are isolated, and the stereochemistry of bis-β-keto sulfoxides ($n=8$) is established by means of the asymmetric synthesis of the resolvable isomer from an optically-active ester, (−)-menthyl-O-$CO(CH_2)_8$-CO-O-(−)-menthyl, and methylsulfinylcarbanion. It is concluded that the higher-melting one is the meso isomer and that the lower-melting one is racemic. The condensation of bis-β-keto sulfoxides, $MeSOCH_2CO(CH_2)_8COCH_2SOMe$, and allyl bromide in the presence of a base and the subsequent desulfurization give the olefinic ketone, $(CH_2=CHCH_2CH_2CO(CH_2)_4)_2$. Optically active sulfoxide, $MeSOCH_2COPh$, is obtained from (−)-menthyl benzoate and methylsulfinylcarbanion.

Sulfoxides (R_1R_2SO) are chiral and are configurationally stable enough under ordinary conditions to be resolvable into enatiomeric forms.[1] Hence, bis-β-keto sulfoxide, $MeSOCH_2CO$-X-$COCH_2SOMe$,[2] may be expected to exist in *dl* and *meso* forms. Though Corey and his co-workers have obtained bis-β-keto sulfoxide from dimethyl azelate and methylsulfinylcarbanion ($DMSO^-$), they have described nothing about the separation of diastereomers.[2a] The present paper will report that the bis-β-keto sulfoxides are separable into two isomers, whose stereochemistry is established by means of asymmetric synthesis.

Dimethyl sebacate was treated with a carbanion solution obtained from sodium hydride and dimethyl sulfoxide (DMSO) at room temperature. A subsequent work-up gave bis-β-keto sulfoxide I ($X=(CH_2)_8$) in a 55% yield. The recrystallization of I from chloroform gave crystals which melted at 145.5—147°C (Ia), whereas the treatment of the mother liquor with ether, followed by purification, gave crystals melting at 131—132°C (Ib). As a mixture of Ia and Ib showed a mp of 125—142°C, the two are different from each other. The IR spectra are shown in Fig. 1, in which the points of clear difference are enlarged.

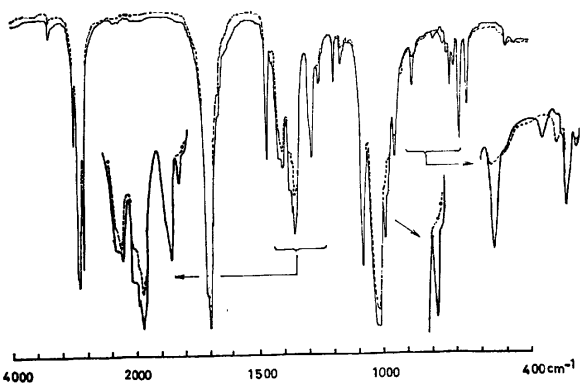

Fig. 1. IR spectra of bis-β-keto sulfoxides, Ia (——) and Ib (----) (KBr).

The higher homolog, II ($X=(CH_2)_{10}$), was similarly prepared (76%) and separated into isomers melting at 145—147°C (IIa) and at 125—127°C (IIb). A mixed-melting-point depression and IR differences were observed as in I. Bis-β-keto sulfoxides (III, $X=(CH_2)_7$) (19%) obtained from dimethyl azelate were also separated into two isomers, melting at 138—140°C and at 116—118°C (IIIb).

The independent reduction of each isomer (Ia or Ib) by means of an aluminum amalgam[2a,3,4] in aqous THF gave the same, single diketone, dode-

1) a) M. Axelrod, P. Bickart, J. Jacobus, M. M. Green, and K. Mislow, *J. Amer. Chem. Soc.*, **90**, 4835 (1968) and Refs. cited; b) K. K. Anderson, *Tetrahedron Lett.*, **1962**, 93; c) A. C. Cope and E. A. Caress, *J. Amer. Chem. Soc.*, **88**, 1711 (1966).

2) a) E. J. Corey and M. Chaykovsky, *ibid.*, **87**, 1345 (1965) and Refs. cited. For β-keto sulfoxides see: b) H.-D. Becker, G. J. Mikol, and G. A. Russell, *ibid.*, **85**, 3410 (1963); c) G. A. Russell and L. A. Ochrymowycz, *J. Org. Chem.*, **34**, 3618 (1969).

3) E. J. Corey and M. Chaykovsky, *J. Amer. Chem. Soc.*, **86**, 1639 (1964).

4) G. A. Russell and G. J. Mikol, *ibid.*, **88**, 5498 (1966).

cane-2,11-dione. Both sulfoxides, IIa and IIb, similarly yielded a single diketone, tetradecane-2,13-dione.

On the basis of these results, it may be concluded that the separated bis-β-keto sulfoxides, Ia and Ib or IIa and IIb, are diastereoisomers.

The Ia-Ib pair of diastereomers showed no percetible difference in NMR spectra (Fig. 2) even in the presence of shift reagents such as tris(dipivalomethanato)Eu(III) ($Eu(DPM)_3$).[5]

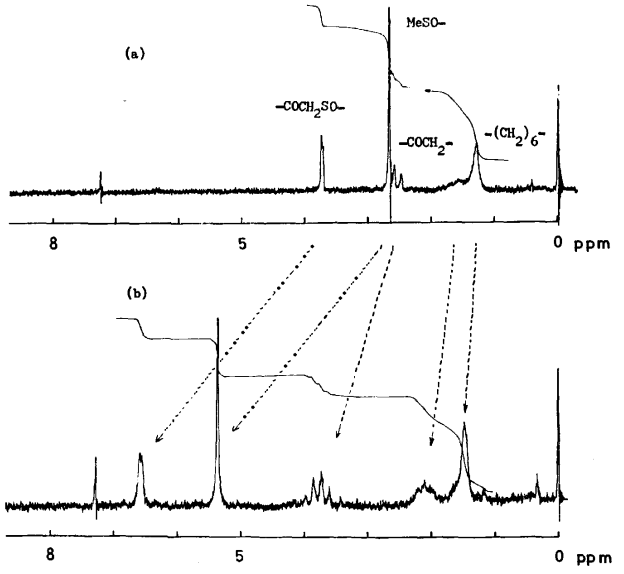

Fig. 2. NMR spectra of (a) sulfoxide Ia and (b) Ia (32 mg, 0.1 mmol) in $CDCl_3$ (0.75 m*l*) containing $Eu(DPM)_3$ (48 mg, 0.068 mmol),

The stereochemical assignment was finally established by means of an asymmetric synthesis of the resolvable isomers. Di-(−)-menthyl sebacate (IV), prepared from sebacoyl chloride and (−)-methnol, was treated with lithium methylsulfinylcarbanion in THF - hexane.[6] The resulting products were separated into two isomers by the method described above.

The sulfoxide melting at 141—143°C was optically inactive, $[\alpha]_D$ 0.0° (*c* 3.98, $CHCl_3$), whereas the other one, melting at 120—122°C, showed a specific rotation of $[\alpha]_D$ +1.22° (*c* 6.08, $CHCl_3$). Obviously, the higher-melting Ia is the *meso* isomer, while the lower-melting Ib is the *dl* isomer. Incidentally, the reaction of (−)-menthyl benzoate (V)[7] gave optically active methyl phenacyl sulfoxide (VI) $[\alpha]_D$ −1.68° (*c* 8.00, $CHCl_3$), of an unknown optical purity.

The condensation of I with allyl bromide in the presence of sodium hydride yielded an intractable oil. The subsequent desulfurization of this oil by means of an aluminum amalgam gave olefinic ketone ($CH_2=CHCH_2CH_2CO(CH_2)_4-)_2$ (21%). The bis-β-keto sulfoxides, such as I and II, are apparently useful in preparing long, straight chain compounds.

Experimental

All the mps are uncorrected. The microanalyses were performed by Mrs. K. Fujimoto of this department. The NMR spectra were obtained on a 60 MHz instrument (JEOL C-60H spectrometer) in deuteriochloroform, with tetramethylsilane as the internal standard. The mass spectra were taken on a Hitachi RMU-6L spectrometer.

The Reaction of Dimethyl Sebacate with DMSO⁻. A carbanion solution was obtained from sodium hydride (4.8 g, 0.20 mol) and DMSO (80 m*l*) under N_2. This was diluted with THF (50 m*l*), and then a solution of dimethyl sebacate (11.5 g, 0.05 mol) in THF (30 m*l*) was added, drop by drop in the course of 30 min under stirring and cooling in an ice bath. The ice bath was then removed, and stirring was continued at room temperature for 3 hr. The reaction mixture was then poured into water, acidified with diluted hydrochloric acid to a pH of about 5—6 (pH paper), and extracted with chloroform. The subsequent evaporation of chloroform *in vacuo* yielded I (8.95 g, 55%). The recrystallization of this product from chloroform gave the sulfoxide Ia (1.31 g, 8%); mp 145.5—147°C. The treatment of the mother liquor with ether and recrystallization from chloroform - ether (trace) gave the sulfoxide Ib (0.15 g, 1%); mp 131—132°C.

The Reaction of Dimethyl Dodecanedioate with DMSO⁻. The treatment of the ester (12.9 g, 0.05 mol) with a carbanion prepared from sodium hydride (4.8 g, 0.20 mol) and DMSO (80 m*l*) in THF (80 m*l*) at room temperature for 4 hr gave bis-β-keto sulfoxide II (13.3 g, 76%). This sulfoxide was separated into two isomers, IIa (1.24 g, 7%), mp 145—147°C, and IIb (0.68 g, 4%), mp 125—127°C.

Dimethyl azelate gave bis-β-keto sulfoxides (III) (19%), which were also separated into two isomers, IIIa (1%), mp 138—140°C, and IIIb (2%), mp 116—118°C. A mixed-melting-point depression and IR differences were observed as in I and II.

The Reduction of Ia with an Aluminum Amalgam. Bis-β-keto sulfoxide Ia (1.61 g, 0.005 mol) was dissolved in THF (40 m*l*) and water (30 m*l*), and then $HgCl_2$-pretreated aluminum foil (2.7 g) was stirred into the solution at room temperature. Stirring was continued at 60—70°C for 5 hr, during which time an additional amount of a mixed solvent (THF : water = 1 : 1) was added in order to overcome the difficulty in stirring due to the formation of aluminum hydroxide. The reaction mixture was then filtered with suction, and the residual solids were washed with chloroform. The combined organic solutions were washed with water and dried (Na_2SO_4). Upon the evaporation of the solvent, we obtained dodecane-2,11-dione (0.89 g, 90%), mp 68—69°C(lit,[8] 68—68.5°C). IR (Nujol): 1705 cm^{-1} (C=O). MS: 198 (M^+). NMR ($CDCl_3$): δ 1.00—1.90 (m, 12H, $-(CH_2)_6-$), 2.13 (s, 6H, COMe) and 2.42 (t (*J*=7 Hz), 4 H, $-CH_2CO$).

5) a) K. J. Eisentraut and R. E. Sievers, *J. Amer. Chem. Soc.*, **87**, 5254. (1965); b) J. K. M. Sanders and D. E. Williams, *Chem. Commun.*, **1970**, 422; c) R. R. Fraser and Y. Y. Wigfield, *ibid.*, **1970**, 1471; d) K. K. Anderson and J. J. Uebel, *Tetrahedron Lett.*, **1970**, 5253; e) G. M. Whitesides and D. W. Lewis, *J. Amer. Chem. Soc.*, **92**, 6979 (1970).

6) For a recent review in asymmetric synthesis, see: a) T. D. Inch, *Synthesis*, **1970**, 466; b) J. D. Morrison and H. S. Mosher, "Asymmetric Organic Reactions," Prentice, Inc., Englewood Cliffs, New Jersey (1971).

7) R. W. Taft, Jr., M. S. Newman, and F. H. Verhoek, *J. Amer. Chem. Soc.*, **72**, 4511 (1950).

8) Y. L. Goldfarb, M. A. Kalik, and M. L. Kirmalova, *Zhur. Obsch. Khim.*, **29**, 2034 (1959); *Chem. Abstr.*, **54**, 8776 (1961).

The sulfoxide Ib yielded the same diketone (97%).

The reduction of II under conditions similar to those used for I gave tetradecane-2,13-dione (90%), mp 72.5—74.5°C (lit,[9] 76—77°C). IR (Nujol): 1705 cm^{-1} (C=O). MS: 226 (M^+). NMR ($CDCl_3$): δ 1.00—1.90 (m, 16 H, $-(CH_2)_8-$), 2.14 (s, 6 H, -COMe), and 2.43 (t(J=7 Hz), 4 H, $-CH_2CO-$).

The Reaction of Di-(−)-menthyl Sebacate (IV) with Lithium Methylsulfinylcarbanion. Lithium methylsulfinylcarbanion was prepared by adding a hexane solution of *n*-butyllithium (1.50 N, 107 m*l*, 0.16 mol) to a stirred mixture of DMSO (12.8 g, 0.16 mol) in THF (70 m*l*) under ice cooling. The lithium salt separated as fine white precipitates. To this suspension, a solution of the ester IV (9.40 g, 0.02 mol) in THF (20 m*l*) was added at −30°C over a period of 30 min, after which the reaction mixture was stirred at −30——15°C for 2 hr. A work-up followed by the separation of the isomers gave sulfoxides Ia and Ib. The sulfoxide Ia, mp 141—143°C, showed $[\alpha]_D$ 0.0° (*c* 3.98, $CHCl_3$), and Ib, mp 120—122°C, showed $[\alpha]_D$ +1.22° (*c* 6.08, $CHCl_3$).

The Reaction of (−)-Methyl Benzoate (V) with Lithium Methylsulfinylcarbonion. The treatment of (−)-menthyl benzoate (2.7 g, 0.01 mol) with lithium methylsulfinylcarbanion prepared from a hexane solution of *n*-butyllithium (1.15 N, 35 m*l*, 0.04 mol) and DMSO (3.2 g, 0.04 mol) in THF (20 m*l*) gave methyl phenacyl sulfoxide VI (0.74 g, 41%). The sulfoxide VI showed a mp of 85—88°C (lit,[2a] 86—86.5°C); $[\alpha]_D$ −1.68° (*c* 8.00, $CHCl_3$).

The Condensation of I and Allyl Bromide in the Presence of Sodium Hydride. The treatment of I (3.23 g, 0.01 mol) with sodium hydride (0.48 g, 0.02 mol) in DMSO (15 m*l*) at 40°C for 1 hr gave a brown solution. To this, allyl bromide (2.42 g, 0.02 mol) in DMSO (15 m*l*) was added, after which the reaction mixture was stirred at 60°C for 3 hr. A work-up gave an intractable oil. This oil was dissolved in THF (40 m*l*) and water (30 m*l*), and this solution was treated with Hg_2Cl_2-pretreated aluminum foil (5.4 g) at 60—70°C for 3 hr. Subsequent distillation and chromatography on a Silicagel column gave octadeca-1,17-diene-5,14-dione (0.59 g, 21%), mp 68—71°C. IR (Nujol): 1710 cm^{-1} (C=O) and 1640, 995 and 915 cm^{-1} ($-CH=CH_2$). NMR ($CDCl_3$): δ 0.80—1.85 (m, 12 H, $-(CH_2)_6-$), 1.85—2.80 (m, 12 H, $-CHCH_2CH_2COCH_2-$), 4.80—5.25 (m, 4 H CH_2-) 1.85—2.80 (m, 12 H, $=CHC\underline{H}_2C\underline{H}_2COC\underline{H}_2-$), 4.80—5.25 (m, 4H, $CH_2=$) and 5.50—6.20 (m, 2 H, =CH-).

Found: C, 77.9; H, 10.8%. Calcd for $C_{18}H_{30}O_2$: C, 77.7; H, 10.9%.

The authors are grateful to Professor K. Sisido for his generous help. The financial support from the Ministry of Education, the Japanese Government, and from the Toray Science Foundation is also acknowledged with pleasure.

9) E. G. Hawkins and D. P. Young, *J. Chem. Soc.*, **1950**, 2804.

BULLETIN OF THE CHEMICAL SOCIETY OF JAPAN, VOL. 45, 1169—1175 (1972)

Photochemical Reactions of Aromatic Compounds. IX.[1] Photochemical Reactions of Dimethylaniline with Halobenzenes[2]

Chyongjin Pac, Takafumi Tosa, and Hiroshi Sakurai

The Institute of Scientific and Industrial Research, Osaka University, Suita-shi, Osaka

(Received September 23, 1971)

Irradiation of methanolic solutions of DMA containing halobenzenes (chlorobenzene, bromobenzene and iodobenzene) and triethylamine (TEA) gave TEA hydrohalides in quantitative yields along with benzene (II), diphenyl, *N*-methylaniline, *o*- and *p*-dimethylaminodiphenyls (IV and V). From the properties of the products and spectroscopic and kinetic data, it was suggested that the reactions took place by way of electron transfer from DMA to halobenzenes. The electron transfer reactions were classified into a short range type (chlorobenzene and bromobenzene) and a long range type (iodobenzene) on the basis of the product ratio (IV+V)/II and the proportion of benzene-d_1 in the benzene fraction obtained from the photoreactions of DMA-d_6 with halobenzenes. From the kinetic and fluorescence data, an exciplex mechanism was suggested for the photoreactions with chlorobenzene and bromobenzene, and a direct electron transfer mechanism in the case of iodobenzene.

Photochemical bimolecular electron transfer reactions (ETR) are of physicochemical interest and have been investigated in connection with decay of exciplexes.[3–5] Except for ETR of triplet aromatic ketones with amines,[1,6] however, mechanistic details have not been fully investigated, although various photo-induced ETR have been published.[7–10]

In a series of works on photochemical ETR,[1,2,11]

1) Part VIII, C. Pac, H. Sakurai, and T. Tosa, *Chem. Commun.*, **1970**, 1311.

2) A preliminary report, T. Tosa, C. Pac, and H. Sakurai, *Tetrahedron Lett.*, **1969**, 3635.

3) A. Weller, *Pure Appl. Chem.*, **16**, 115 (1968); H. Knibbe, D. Rehm, and A. Weller, *Z. Bunsenges. Physik. Chem.*, **72**, 257 (1968).

4) N. Mataga, T. Okada, and N. Yamamoto, *Chem. Phys. Lett.*, **1**, 119 (1967).

5) H. Yamashita and M. Koizumi, This Bulletin, **41**, 2313 (1968).

6) S. G. Cohen and H. M. Chao, *J. Amer. Chem. Soc.*, **90**, 165 (1968); R. S. Davidson and P. F. Lambeth, *Chem. Commun.*, **1969**, 1098.

7) T. Latowski, *Z. Naturforsch.*, **23a**, 1127 (1968).

8) M. T. McCall, G. S. Hammond, O. Yonemitsu, and B. Witkop, *J. Amer. Chem. Soc.*, **92**, 6991 (1970).

9) J. A. Barltrop and R. J. Owers, *Chem. Commun.*, **1970**, 1462.

10) R. S. Davidson, *ibid.*, **1969**, 1450.

11) C. Pac and H. Sakurai, *ibid.*, **1969**, 20; *Tetrahedron Lett.*, **1969**, 3829.

we published ETR from excited singlet dimethylaniline (DMA) to ground state anilinium salts.[12] The suggested mechanism was speculative, since spectroscopic investigation was limited on account of insolubility of anilinium salts in non-polar and less polar solvents. In an attempt to obtain more information on photochemical ETR mechanism, halobenzenes (chlorobenzene, bromobenzene and iodobenzene) were used as electron acceptors instead of anilinium salts, since they are soluble in most organic solvents.

In the present paper, we report the product distribution, spectroscopic and kinetic results. Qualitative discussion is given on the ETR distance depending on halobenzenes.

Results

Product Distribution. Irradiation of a methanolic solution of DMA containing a halobenzene in the presence of triethylamine (TEA),[13] by means of a Pyrex filter with a high pressure mercury arc, gave TEA hydrohalide in a quantitative yield along with benzene, diphenyl, *N*-methylaniline, *o*- and *p*-dimethylaminodiphenyls (Table 1).

$$\mathrm{DMA} + \mathrm{PhX} \xrightarrow[\mathrm{TEA}]{h\nu} \underset{\mathrm{I}}{\mathrm{TEA{\cdot}HX}} + \underset{\mathrm{II}}{\mathrm{PhH}} + \underset{\mathrm{III}}{\mathrm{Ph\text{-}Ph}} + \underset{\mathrm{IV}}{o\text{-}\mathrm{Ph\text{-}C_6H_4N(CH_3)_2}} + \underset{\mathbf{V}}{p\text{-}\mathrm{Ph\text{-}C_6H_4N(CH_3)_2}} + \mathrm{PhNHCH_3}$$

The structures of the products were confirmed by direct comparison of the physical and spectroscopic (NMR, UV, and IR) data with those of the corresponding authentic samples.

TABLE 1. PRODUCT DISTRIBUTION IN PHOTOCHEMICAL REACTIONS OF DMA WITH HALOBENZENES IN THE PRESENCE OF TEA[a]

PhX	Yields (mmol)					Conversion[b] (%)
	I	II	III	IV	V	
X=Cl	12.6	4.4	trace	5.3	0.7	35
X=Br	12.8	5.8	trace	4.0	0.5	50
X=I	12.0	11.3	trace	1.1	0.4	85

a) Irradiation of methanolic solutions (30 m*l*) containing 4 g DMA, 4 g halobenzenes and 5 m*l* TEA in a Pyrex tube with a high pressure mercury arc at room temperature.

b) Consumption of halobenzenes determined by vpc analyses.

Chlorobenzene and bromobenzene were stable in the absence of DMA and gave only a trace of benzene by irradiation for a long time. Iodobenzene was photolyzed to some extent, decomposition being considerably enhanced in the presence of DMA.

Control experiments showed that I, II, IV, and V increased linearly with irradiation time. Diphenyl could not be detected. However, all the products were stable under the reaction conditions and are considered to be primary products. The products ratios (IV+V)/II and IV/V were determined at 10—15% conversion and found to be dependent on halobenzenes used (Table 2).

TABLE 2. PRODUCT RATIOS (IV+V)/II AND IV/V[a]

	PhX		
	X=Cl	X=Br	X=I
(IV+V)/II	1.8±0.17	1.1±0.1	0.24±0.07
IV/V	3.8±0.7	3.5±0.5	2.2 ±0.2

a) Irradiation of methanolic solutions (5 m*l*) containing 1.0 M DMA, 0.1 M TEA and 0.1 M halobenzenes at 313 nm. Mean values for every three runs.

It should be noted that the products except TEA hydrohalides were the same as those obtained from the photochemical reactions of DMA with trimethylphenylammonium halides.

Sensitized Decomposition of Halobenzenes by Carbonyl Compounds. Enhanced decomposition of halobenzenes by DMA could be interpreted as being caused by electronic energy transfer from an excited DMA to halobenzenes leading to decomposition of halobenzenes into phenyl radical and halogen atoms. If so, selected sensitizers would result in sensitized decomposition of halobenzenes. Sensitization with carbonyl compounds was thus carried out in order to confirm the possibility of triplet excitation transfer.

The 0–0 transition of DMA phosphorescence at 77°K was reported to lie at 26650 cm^{-1} (76.2 kcal/mol).[14] If triplet excitation transfer from DMA to halobenzenes take place, acetone (E_T 80 kcal/mol),[15] acetophenone (E_T 74 kcal/mol in non-polar solvents and 76.3 kcal/mol in polar solvents)[16] and propiophenone (E_T 75 kcal/mol in non-polar solvents)[16] can sensitize the decomposition of halobenzenes.

However, propiophenone- and acetophenone-sensitized decomposition did not occur for chlorobenzene and bromobenzene, and was not clear in the case of iodobenzene. Acetone was effective for decomposition of bromobenzene and iodobenzene, but entirely ineffective for chlorobenzene (Table 3). The results for chlorobenzene are understandable, since the lowest triplet state lies at 82 kcal/mol above the ground state.[17] Thus, the triplet energies of

12) C. Pac and H. Sakurai, *Tetrahedron Lett.*, **1968**, 1865; *Kogyo Kagaku Zasshi*, **72**, 230 (1969).

13) In the absence of TEA, the photoreactions were complicated on account of the formation of DMA hydrohalides, since DMA was photochemically reactive with DMA hydrohalides.[12] For example, the photolysis of a methanolic solution containing DMA and bromobenzene gave crystal violet and bis(*p*-dimethylaminophenyl)methane along with II—V, while the photolysis in the presence of TEA gave a clean solution without the formation of the above two products.

14) Y. Gondo and Y. Kanda, *Mem. Fac. Kyushu Univ.*, **C5**, 133 (1964).

15) R. F. Borkman and D. R. Kearns, *J. Chem. Phys.*, **44**, 945 (1966); *J. Amer. Chem. Soc.*, **88**, 3467 (1967).

16) W. G. Herkstroeter, A. A. Lamola, and G. S. Hammond, *ibid.*, **86**, 4537 (1964).

17) S. P. McGlynn, T. Azumi, and M. Kasha, *J. Chem. Phys.*, **40**, 507 (1964).

Table 3. Sensitized decomposition of halobenzenes with carbonyl compounds[a)]

PhX	Ketones	E_T (kcal/mol)	Yields of benzene (mg)
X=Cl	—		0
	Acetophenone	76.3[b)]	0
	Propiophenone	75.0[b)]	0
	Acetone	−80[c)]	>2
X=Br	—		>2
	Acetophenone		>2
	Propiophenone		>2
	Acetone		50
X=I	—		7.5
	Propiophenone		7.5
	Acetone		17.5

a) Irradiation of *t*-butanol solutions containing 0.1 M ketones and 0.1 M halobenzenes in a Pyrex tube for 10 hr with a high pressure percury arc.
b) See Ref. 16.
c) See Ref. 15.

bromobenzene and iodobenzene can be estimated to be in the range 77—80 kcal/mol.

The triplet excitation transfer mechanism can be eliminated for DMA-induced decomposition of chlorobenzene and bromobenzene, and is considered to be also unfavorable in the case of iodobenzene.

Fluorescence Spectra of DMA in the Presence of Halobenzenes. A cyclohexane solution of DMA showed a structureless fluorescence spectrum with a maximum at 334 nm. On addition of chlorobenzene and bromobenzene into a cyclohexane solution of DMA, however, the fluorescence was quenched with bathochromic shift of the spectra. When chlorobenzene and bromobenzene were used as solvents, very weak and red-shifted new emissions appeared with respective maxima at 373 and 412 nm along with total quenching of DMA fluorescence (Fig. 1).[26] Appearance of new

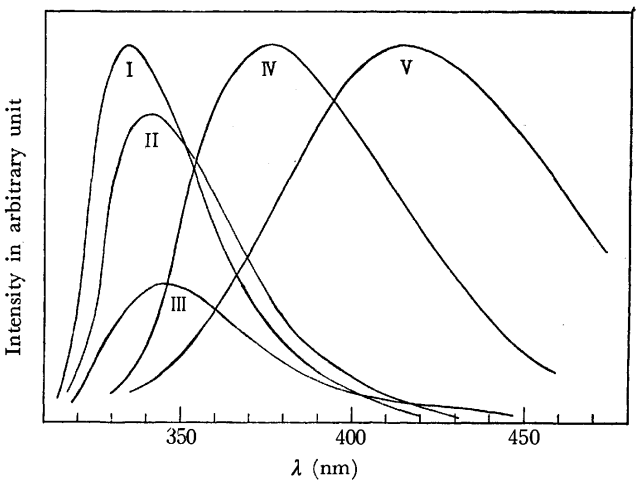

Fig. 1. The fluorescence spectra of DMA solutions in cyclohexane (curve I), in cyclohexane in the presence of 1 M PhCl (II), in cyclohexane in the presence of 0.1 M PhBr (III), in chlorobenzene (IV) and in bromobenzene (V). The spectra I—III were recorded with the same sensitivity, but the spectra IV and V with much higher sensitivities.

Table 4. Fluorescence maxima of aromatic amines in chlorobenzene and bromobenzene[a)]

Amines	Benzene	Solvent PhCl (nm)	PhBr	IP[b)] (eV)	Excitn[e)] light (nm)
Aniline	328	370	388	7.76	298
DMA	346	373	412	7.44	305
m-DMT[c)]	343	397	407	7.35	304
p-DMT	352	412	414	7.33	310
p-DMAN[d)]	369	428	429		319

a) Uncorrected maxima for air saturated solutions 10^{-3} -10^{-2} M amines.
b) Ionization potentials reported by P. G. Farrel and J. Newton.[28b)]
c) *N,N*-dimethyltoluidine.
d) *N,N*-dimethylanisidine.
e) Excitation spectra were about the same.

emissions was general for chlorobenzene and bromobenzene solutions of aromatic amines. New very weak emission maxima for aniline, *N,N*-dimethyl-*p*-anisidine, *N,N*-dimethyl-*p*- and -*m*-toluidines are given in Table 4.

In contrast, fluorescence quenching with iodobenzene was not accompanied with any bathochromic shift of the spectrum or new emissions even in non-polar solvents. Moreover, solvent-dependency of quenching constant $k_r\tau$ also differed in the two groups of halobenzenes. In the case of iodobenzene, $k_r\tau$ was dependent on solvent viscosity rather than solvent polarity (Table 5). On the other hand, fluorescence quenching with chlorobenzene was more effective in a polar solvent than in a non-polar solvent; the half-value concentration was 0.2 M in methanol, about 10 times lower than that in benzene (*ca.* 2 M).[18]

Table 5. Solvent dependency of fluorescence quenching with iodobenzene[a)]

Solvents	η at 20°C (cpoise)	Rel. $1/\eta$	Rel. k_r
n-Hexane	0.32	2.0	1.5
Acetonitrile	0.59	1.1	1.2
Benzene	0.65	1.0	1.0
Methanol	0.611	1.06	0.98

a) Fluorescence quenching for the solutions containing 0.1 M DMA and 10^{-3}—5×10^{-2} M iodobenzene.

For methanolic solutions, however, fluorescence quenching with any halobenzene was accompanied with no change of shape of the spectra, bathochromic shift or appearance of new emissions.

Kinetic Results. Quantum yields for the formation of halide anions at 313 nm at room temperature were determined by potassium ferrioxalate actinometry.[19] Quantitative analyses for chloride and bromide anions were titrimetrically carried out by a

18) Since the shape of the fluorescence spectra in the presence of chlorobenzene were changed, the half-value concentration could not be explicitly determined.
19) C. G. Hatchard and C. A. Parker, *Proc. Roy. Soc.* (London), **A235**, 518 (1956).

modified Vorhard's method[20] and for iodide anion by Jamieson's method.[21] The conversion was maintained below 10% for all the kinetic runs. Reciprocals of the quantum yields changed linearly with reciprocals of concentrations of halobenzenes (Fig. 2).

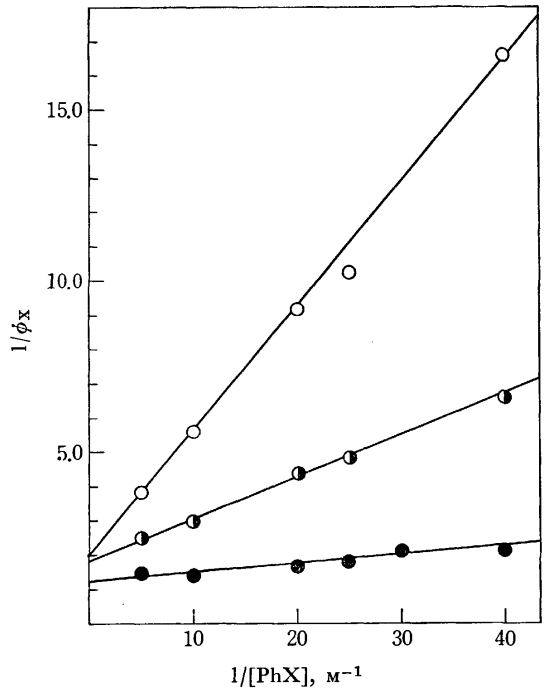

Fig. 2. The plots of reciprocals of quantum yields *vs.* reciprocals of concentrations of PhCl (-○-), PhBr (-◑-) and PhI (-●-).

Since fluorescence quenching for methanolic solutions was accompanied with no change of shape of the spectra, relative intensities of the fluorescence maximum at 352 nm in the absence and presence of halobenzenes (F_0/F) were plotted with concentrations of halobenzenes. Linear Stern-Volmer plots were obtained (Fig. 3). Table 6 lists the fluorescence quenching constants ($k_r\tau$, the slopes of the plots in Fig. 3), the rate ratios k_r/k_d ($=k_r\tau$, the intercept-to-slope ratios of the straight lines in Fig. 2) and k_n/k_e (the intercepts).

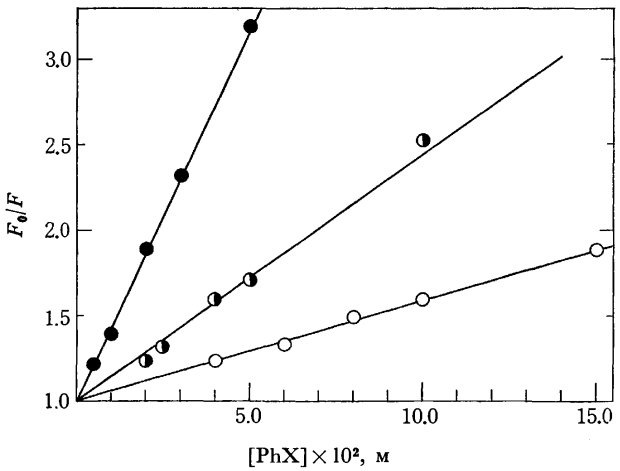

Fig. 3. The Stern-Volmer plots for the quenching of DMA fluorescence with chlorobenzene (-○-), bromobenzene (-◐-) and iodobenzene (-●-).

20) M. A. Rosanoff and A. E. Hill, *J. Amer. Chem. Soc.*, **29**, 269 (1907).
21) G. S. Jamieson, L. H. Lavy, and H. L. Wells, *ibid.*, **30**, 760 (1908)

TABLE 6. FLUORESCENCE QUENCHING CONSTANTS AND THE RATE RATIOS OBTAINED FROM QUANTUM YIELD MEASUREMENTS

Rate ratios	PhX		
	X=Cl	X=Br	X=I[a]
k_r/k_d (M^{-1})[b]	5.7	15.8	62.5
k_n/k_e[b]	1.0	0.8	0.25
$k_r\tau$ (M^{-1})[c]	5.2	13.6	42.0

a) The rate ratio k_n/k_e is replaced by k_q/k_r' and $k_r=(k_r'+k_q)$.
b) Mean values for every three runs within ±10% error.
c) The slopes of Stern-Volmer plots for the solutions containing 0.1 M DMA and 10^{-3}–0.15 M halobenzenes which were not affected appreciably by the presence of 0.1 M TEA.

Discussion

The products obtained from the photochemical reactions can be interpreted by ETR mechanism; electron transfer from excited DMA to ground state halobenzenes led to DMA radical cation and halobenzene radical anions. Since halobenzenes are dis-

$$\text{DMA} \xrightarrow{h\nu} {}^1\text{DMA} \quad (1)$$

$${}^1\text{DMA} \xrightarrow{k_d} \text{DMA} \quad (2)$$

$${}^1\text{DMA} + \text{PhX} \xrightarrow{k_r} \text{"exciplex"} \quad (3)$$

$$\text{"exciplex"} \xrightarrow{k_n} \text{DMA} + \text{PhX} \quad (4)$$

$$\text{"exciplex"} \xrightarrow{k_e} (\text{DMA}^+ + \text{Ph}\cdot + \text{X}^-) \quad (5)$$

Cage Reaction

$$(\text{DMA}^+ + \cdot\text{Ph}) \longrightarrow \text{PhH} + \text{PhN(Me)CH}_2^+ \quad (6)$$

$$(\text{DMA}^+ + \cdot\text{Ph}) \longrightarrow \text{IV and V} + \text{H}^+ \quad (7)$$

$$(\text{DMA}^+ + \cdot\text{Ph}) \longrightarrow \text{DMA}^+ + \text{Ph}\cdot \quad (8)$$

Free Radical Reaction

$$\text{Ph}\cdot + \text{Hydrogen Donors} \longrightarrow \text{PhH} \quad (9)$$

$$\text{Ph}\cdot + \text{DMA} \longrightarrow \text{IV and V} + \text{H} \quad (10)$$

Further Reactions

$$\text{PhN(Me)CH}_2^+ + \text{H}_2\text{O} \longrightarrow \text{PhNHMe} + \text{CH}_2\text{O} + \text{H}^+ \quad (11)$$

$$\text{NEt}_3 + \text{HX} \longrightarrow \text{NEt}_3\cdot\text{HX} \quad (12)$$

$$\text{DMA}^+ \longrightarrow \text{Polymeric products and others} \quad (13)$$

$$1/\phi_X = \left(1+\frac{k_d}{k_r[\text{PhX}]}\right)\left(1+\frac{k_n}{k_e}\right) \quad (14)$$

$$F_0/F = 1 + k_r\tau[\text{PhX}] \quad (15)$$

Scheme 1.

sociative in electron capture in vapor phase,[22a] it can be expected that the radical anions, if formed, are simultaneously decomposed into phenyl radical and halide anions in liquid phase. Phenyl radical abstracts hydrogen atom from solvent molecules, TEA, DMA radical cation and neutral DMA to give benzene, while the dimethylaminodiphenyls (IV and V) are formed by addition of phenyl radical to DMA and DMA radical cation. Thus the mechanism in Scheme 1 is suggested, from which rate equation (14) and the Stern-Volmer expression (15) for fluorescence quenching are derived.

Let F_0, F, and ϕ_X denote the fluorescence intensities in the absence and in the presence of halobenzenes and the quantum yields for the formation of halide anions, respectively in the rate equations. As is shown in Table 6, the rate ratios k_r/k_d are in good agreement with the quenching constants $k_r\tau$ within experimental errors for respective halobenzenes. Since k_d equals $1/\tau$, the agreement strongly supports the view that the photochemical reactions occur in the lowest excited singlet state of DMA (^{1}DMA).

It is noteworthy that the product ratios (IV+V)/II and IV/V change with halobenzenes. The photochemical reaction with iodobenzene leads to a remarkably low ratio of (IV+V)/II, *i.e.* dominant formation of benzene. In contrast, the dimethylaminodiphenyls are formed 1.8 times greater than benzene in the reaction with chlorobenzene. In the case of bromobenzene, the formation of the dimethylaminodiphenyls competes with that of benzene and the ratio (IV+V)/II is similar to the case of chlorobenzene rather than to the case of iodobenzene.

The results cannot be interpreted by means of a single mechanism, and suggest a competitive reaction mechanism. By assuming that ETR distance is dependent on halobenzenes, it can be predicted that the fraction of the radical pair (DMA radical cation and phenyl radical) in solvent cage increases with the decrease of distance and thus cage reaction plays a more important role in competition with free radical reaction. The product distribution is therefore expected to change with halobenzenes.

Since free phenyl radical is well known to abstract hydrogen from molecules having labile hydrogen atoms, free radical reaction affords benzene as an exclusive product. The photochemical reaction with iodobenzene is considered to fit the case. On the other hand, cage reaction may occur essentially between phenyl radical and DMA radical cation; bond formation of the radical pair giving IV and V may be competitive with hydrogen transfer from DMA radical cation to phenyl radical giving benzene. In the case of chlorobenzene and bromobenzene, therefore, the results suggest that the cage reaction plays important or dominant roles.

In order to clarify the above assumption and obtain information on ETR distances, the photochemical reactions were carried out with *N,N*-di(trideuteriomethyl)aniline (DMA-d_6) instead of DMA-h_{11}, and the contents of benzene-d_1 in benzene fraction of the products were estimated by vpc-mass spectrometry. Deuterium purity of DMA-d_6 was confirmed to be over 98% by NMR.

When the ETR distance is short, the cage reaction is dominant. When ETR takes place in a sufficiently long distance, the fraction of free phenyl radical will increase. The cage reaction might afford largely benzene-d_1 by deuterium transfer from DMA-d_6 radical cation to phenyl radical while free phenyl radical might abstract hydrogen atom from solvent molecules for the most part. Thus, it is reasonable to predict that the proportion of benzene-d_1 reflects a measure for the ETR distance.[22b]

$$(\overset{+\cdot}{\mathrm{PhN}}(\mathrm{CD_3})\mathrm{CD_3} + \cdot\mathrm{Ph})_{\mathrm{cage}} \rightarrow \mathrm{PhN}(\mathrm{CD_3})\mathrm{CD_2}^+ + \mathrm{PhD}$$

$$\mathrm{Ph}\cdot + \text{Hydrogen donor} \rightarrow \text{largely PhH}$$

Table 7 shows the proportions of benzene-d_1 obtained from the photochemical reactions of DMA-d_6 with halobenzenes which increase in the order: iodobenzene, bromobenzene, and chlorobenzene. In the case of iodobenzene, however, it should be noted that the proportion of benzene-d_1 is remarkably low in comparison with the other two cases, in analogy with the ratio (IV+V)/II. The low proportion of benzene-d_1 might be evidence of the free radical nature of the phenyl radical generated by electron transfer to iodobenzene and suggests that ETR occurs in a long range type[23] between ^{1}DMA and iodobenzene. On the other hand, a high proportion of benzene-d_1 is obtained from the photochemical reaction with chlorobenzene. This indicates that the cage reaction is dominant in the formation of benzene and suggests that ^{1}DMA donates the electron to chlorobenzene in close contact, *i.e.* in a short range type.[23] Since the proportion of benzene-d_1 obtained from the reaction with bromobenzene is nearer the case of chlorobenzene than iodobenzene, it can be suggested that the ETR distance for bromobenzene is in somewhat shorter range, but longer than the distance for chlorobenzene.

The results are in good parallelism with electron affinities of halobenzenes. The electron affinity of iodobenzene is the highest (0.5_7 eV) in the three halobenzenes,[24] while the electron affinities of chloro-

Table 7. Contents of benzene-d_1 obtained from photoreactions of DMA-d_6 with halobenzenes

	m/e	C_6H_6	PhX		
			X=Cl	X=Br	X=I
Rel. intensities	78	100	15	25	34.5
	79	8.2	22.8	17.9	10.2
Benzene-d_1	(%)	—	66	42	12

22) a) J. A. Stockdale and G. S. Hurst, *J. Chem. Phys.*, **41**, 255 (1964); W. E. Wetworth, R. S. Becker, and R. Tung, *J. Phys. Chem.*, **71**, 1652 (1967). b) This suggests only a qualitative measure, since the proportion of benzene-d_1 cannot represent the fraction of the cage reaction; the phenyl radical in the solvent cage might abstract the hydrogen atom of the wall of the solvent cage even in small proportions, while free phenyl radical might also abstract the deuterium atom from DMA-d_6.

23) T. Okada, H. Oohari, and N. Mataga, This Bulletin, **43**, 2750 (1970).

24) G. Briegleb, *Angew. Chem.*, **76**, 326 (1964).

benzene and bromobenzene are identical (0.4 eV)[24] or similar.[25] It is resonable to expect that ETR takes place in a long range type for iodobenzene with a high electron affinity,[23] while the acceptors having similar electron affinities may abstract electron from a donor in similar distances.

As regards quenching behavior to DMA fluorescence, halobenzenes are classified into two groups, one involving chlorobenzene and bromobenzene, and the other iodobenzene. It is of interest to note that the same classification of halobenzenes is made from both fluorescence data and product distribution.

With chlorobenzene and bromobenzene, exciplex formation in non-polar solvents is evident from the following observations; 1) appearance of new emissions,[2-4] 2) endothermic and dynamic property of the fluorescence quenching[26] and 3) solvent dependency of the fluorescence quenching on solvent polarity.[27] Moreover, the charge-transfer character of the emission entities is supported by the fact that the new emission maxima are shifted to longer wavelength with the decrease of ionization potentials of the aromatic amines (Table 4).[28] It might be suggested that the fluorescence quenching with chlorobenzene and bromobenzene is ascribed to the formation of the exciplexes between ^{1}DMA and the ground state halobenzenes, at least in non-polar solvents.

On the other hand, the exciplex formation with iodobenzene is negative. Therefore, the fluorescence quenching with iodobenzene is governed by a different mechanism from an exciplex one even in non-polar solvents. If a complex were assumed, it would have a configuration differing from the exciplexes discussed above and might be totally non-emissive as in the case of pyrene-tetracyanoethylene.[23] In polar solvents, in particular, no exciplex mechanism can be suggested, since exciplexes even if formed in non-polar solvents are non-existent[3] or quite shorter-lived[4] in polar solvents. A direct electron transfer mechanism is preferred for the fluorescence quenching. Since the kinetic data show the identity of the mechanism between the fluorescence quenching and the photochemical reaction, the mechanism is supported by the long range type character of the reaction deduced from the product distribution. It is unreasonable to assume that a long range type electron transfer

$$^1\text{DMA} + \text{PhI} \begin{cases} \xrightarrow{k_r'} \text{DMA}^+ + \text{Ph}\cdot + \text{I}^- & (16) \\ \xrightarrow{k_q} \text{DMA} + \text{PhI} & (17) \end{cases}$$

$$1/\phi = \left(1 + \frac{k_q}{k_r'}\right) + \frac{k_d}{k_r'}\frac{1}{[\text{PhI}]} \quad (18)$$

$$F_0/F = 1 + (k_r' + k_q)\tau[\text{PhI}] \quad (19)$$

$$k_r'/k_d = 50\ \text{M}^{-1},\quad k_q/k_r' = 0.25$$

$$(k_r' + k_q)\tau = k_r\tau = 42\ \text{M}^{-1}$$

Scheme 2.

takes place by way of a discrete intermediate such as an exciplex. The direct electron transfer mechanism is shown in Scheme 2.

On the other hand, all the results clearly show that the mechanism for chlorobenzene and bromobenzene differs from the case of iodobenzene. The short range character of ETR suggested from the product distribution may imply such a close contact intermediate as an exciplex or an ion pair shown in Scheme 1. The fluorescence data on the formation of exciplexes suggest an exciplex intermediacy, though the exciplex formation in non-polar solvents may exhibit no direct evidence for the exciplex intermediacy in methanol.[29]

For mechanistic elucidation, the rate data obtained from the quantum yield measurements will be briefly discussed. Although the life of ^{1}DMA has not been reported, it can be approximately replaced with the singlet life of aniline (3.2 nsec in ethanol).[30] If this is the case, the reaction rates (k_r and k_r') for chlorobenzene, bromobenzene and iodobenzene can be estimated to be respectively 1.8×10^9, 5.1×10^9 and 19×10^9 $\text{M}^{-1}\,\text{sec}^{-1}$, which are close to the diffusion rate in methanol (ca. 10^{10} $\text{M}^{-1}\,\text{sec}^{-1}$). Since it is well established that the formation of exciplexes and ETR occur in a diffusion or a near diffusion rate,[2-4,23] the rate data can support also the mechanisms in Schemes 1 and 2. The fact that k_r increases in the order of chlorobenzene, bromobenzene, and iodobenzene may reflect the order of the electron affinities of the halobenzenes.

Singlet excitation transfer, if it occurs, is endothermic, since the absorption of DMA appears at a longer wavelength than in any halobenzenes. If this is the case, near diffusion rates cannot be obtained, and the singlet excitation transfer mechanism can be excluded. A triplet excitation transfer mechanism can be also ruled out by sensitization experiments (*vide supra*).

Experimental

General. Spectroscopic analyses of the organic products were carried out as follows; the NMR spectra with a high Hitachi Perkin-Elmer R-20 spectrophotometer, IR

25) The electron affinities might correlate with polarographic half-wave potentials $E_{1/2}$. If this is the case, the electron affinities of bromobenzene will be slightly higher than that of chlorobenzene, since the half-wave potentials are reported to be -2.58 V for chlorobenzene and -2.32 V for bromobenzene; M. F. Thomas and B. Stevens, "Molecular Luminescence," ed. by E. C. Lim, W. A. Benjamin, Inc., New York (1969), p. 158.

26) No evidence could be obtained on the formation of EDA-complexes in the ground state. The UV spectra of DMA were the same in both the presence and the absence of 0.1 M halobenzenes. Even though chlorobenzene and bromobenzene were used as solvent, the maximum of ^1L_b band shifted only 2—3 nm to longer wavelength, and no new absorption could be observed.

27) K. Kaneta and M. Koizumi, This Bulletin, **40**, 2254 (1967).

28) a) Since all of the fluorescence spectra were uncorrected, no explicit first order correlation between ionization potentials and the emission maxima could be obtained. b) P. G. Farrel and J. Newton, *J. Phys. Chem.*, **69**, 3506 (1965).

29) The fluorescence quenching mechanism in polar solvents has not been established satisfactorily. Weller stated direct electron transfer mechanism,[3] while Mataga suggested exciplex mechanism for a short range type of ETR.[4,23]

30) I. B. Berlman, "Handbook of Fluorescence Spectra of Aromatic Molecules," Academic Press, New York and London (1965), p. 60.

spectra with a Hitachi EPI-S2 spectrophotometer, UV spectra with a Hitachi 124 spectrophotometer, fluorescence spectra with a Hitachi MPF-2A spectrofluorometer and mass spectra with a Hitachi RMS-4 spectrometer. Yields and the product ratios were determined by vpc with a Simadzu GC-2C under the conditions described previously.[12] Solvents were purified as usual. TEA was refluxed over potassium hydroxide and distilled. Chlorobenzene and bromobenzene were washed three times with concentrated sulfuric acid, three times with water, dried over anhydrous calcium chloride and distilled through a column packed with stainless steel helices. Iodobenzene was washed twice with a dilute aqueous solution of sodium thiosulfate, three times with water, dried over calcium chloride and distilled through the column. The tertiary aromatic amines were refluxed with an excess of acetic anhydride and acidified with hydrochloric acid. The acidified solutions were treated five times with ether and basified with sodium hydroxide. The amines separated from the aqueous layers were then treated as usual. All of the amines were distilled under nitrogen stream *in vacuo* before use. Acetone was purified by the ordinary method.[31] Acetophenone and propiophenone were purified by fractional distillation under reduced pressure.

Quantum Yields. Methanolic solutions (5 m*l*) containing 1.0 M DMA, 0.1 M TEA and 0.025—0.2 M halobenzenes were degassed and sealed in 10 mm o. d. Pyrex tubes, which were then irradiated on a merry-go-round apparatus at room temperature through a filter solution with a path length of 1 cm containing 0.2 g potassium chromate made up to 1 *l* with distilled water with a high pressure mercury arc. After the relative quantum yields were determined, the quantum yields at 0.2 M chlorobenzene, 0.2 M bromobenzene and 0.025 M iodobenzene were determined to be 0.26_4, 0.41_3, and 0.49 by potassium ferrioxalate actinometry,[19] respectively. The values were constant at 0.5—10% conversion within 10% experimental errors.

Sensitization Studies. Samples of *t*-butyl alcohol solutions containing 0.1 M halobenzenes and 0.1 M ketones were prepared, degassed and irradiated through a Pyrex glass with a high pressure mercury arc. The amounts of benzene formed and halobenzenes consumed were determined by vpc.

Photochemical Reaction in Preparative Scale. As a typical run, the photochemical reaction of DMA with bromobenzene will be described. A methanolic solution (30 m*l*) containing 4 g DMA, 4 g bromobenzene and 5 m*l* TEA in a Pyrex tube was irradiated for 45 hr with a high pressure mercury arc. The amounts of the products and of bromobenzene consumed were determined by vpc analyses of an aliquot of the photolysate (5 m*l*). It was found that 450 mg of benzene, 790 mg of *o*-dimethylaminodiphenyl and 96 mg of *p*-dimethylaminodiphenyl were formed at about 50% consumption of bromobenzene. After removal of the solvent fraction under reduced pressure at room temperature, 5 m*l* of benzene was added to the residue and cooled on an ice bath. TEA hydrobromide (2.32 g) was then filtered off, washed with benzene and recrystallized from 2-propanol. Found: C, 39.67; H, 9.09; N, 7.68; Br, 43.70%. Calcd for $C_6H_{16}NBr$: C, 39.59; H, 8.85; N, 7.69; Br, 43.90%.

After removal of benzene and the unreacted materials from the filtrate, further distillation gave crude *o*-dimethylaminodiphenyl, which was redistilled, bp 80°C/1 mmHg; $\tau(CCl_4)$ 7.5 (s, 6H) and 3.1—2.3 (m, 9H). The product was converted into its picrate, mp 184—186°C (dec.). Found; C, 56.72; H, 4.12; N, 13.09%. Calcd for $C_{20}H_{18}N_4O_7$; C, 56.34; H, 4.26; N, 13.14%.

Finally, the residue was chromatographed on silica gel. After *o*-dimethylaminodiphenyl was eluted with 10% of benzene in hexane, further elution with 1 : 1-mixture of benzene - hexane gave *p*-dimethylaminodiphenyl, which was recrystallized from methanol, mp 118—119°C. Found: C, 85.30; H, 7.63; N, 6.84%. Calcd for $C_{14}H_{15}N$: C, 85.24; H, 7.66; N, 7.10%.

Preparation of DMA-d_6. DMA-d_6 was obtained by alkylation of aniline[32] with perdeuterated trimethyl phosphate prepared from methanol-d_4 and phosphorus oxychloride, and purified by preparative vpc on a 3 m Apiezon column at 160°C, bp 84°C/15 mmHg. The IR spectrum showed a characteristic absorption of aromatic C–H bond at 3030 cm^{-1} and aliphatic C–D bond at 2000—2200 cm^{-1} (4 peaks), while absorption of aliphatic C–H at 2900 cm^{-1} region could not be observed. The NMR spectra showed only the signals of aromatic protons at τ 2.8—3.7 as a multiplet.

Photochemical Reaction of DMA-d_6. A methanolic solution containing 0.7 M DMA-d_6, 0.7 M TEA and 2 M chlorobenzene or bromobenzene was prepared. In the case of iodobenzene, the concentration was set in 0.2 M in order to avoid direct photolysis of iodobenzene. The samples (4 m*l*) were degassed and irradiated in the same way as in the quantum yield measurements. The photolysates were subjected directyl to vpc-mass spectrometric analyses. The vpc was operated with an 1 m ODPN column plus an 1 m PEG-200 column at 70°C. Table 7 lists the relative intensities at *m/e* 78 and 79 of benzene-h_6 and of the benzene fractions obtained from the photolyses, from which the contents of benzene-d_1 were determined.

31) A. Bramley, *J. Chem. Soc.*, **59**, 10 (1916).

32) J. H. Billman, A. Radike, and B. W. Mundy, *J. Amer. Chem. Soc.*, **64**, 2977 (1942); D. G. Thomas, T. H. Billman, and C. E. Davis, *ibid.*, **68**, 895 (1964).

The Photochemical Reaction of Some Ketoximes and Their Derivatives

Tadashi SATO, Takeshi INOUE, and Koichi YAMAMOTO
Department of Applied Chemistry, Waseda University, Shinjuku-ku, Tokyo
(Received October 8, 1971)

The photochemical reaction of mesityl oxide oxime was investigated. In protic solvents, the reaction *via* oxaziridine proceeded, while in aprotic solvents, *syn-anti* isomerization was the main reaction pattern. A cyclobutanol formation, which is a new type of reaction in the oxime system, was observed. The photochemical reactions on some other ketoximes and their derivatives were also investigated.

Recently several workers have investigated the photochemistry of oximes and their derivatives. The reactions can be classified into four types; (1) *syn-anti* isomerization,[1] (2) photo-Beckmann rearrangement,[2] (3) nitrile formation,[3] and (4) ketone formation.[4] deMayo[2a,5] proposed a mechanism *via* the oxaziridine formed for the polar state of oxime for the photo-induced conversion of benzaldehyde oxime into benzamide with an intramolecular oxygen migration. The reaction scheme through the intermediacy of the oxaziridine for the photo-Beckmann rearrangement and ketone formation from oximes has been confirmed in an indirect way by Mukai *et al.*[2d,6] These authors have also discussed possible states of excited states in the photochemistry of some α,β-unsaturated ketoximes.

We investigated photochemical reactions on several ketoximes and their *O*-methyl ethers, thus disclosing several new results.

Results

When mesityl oxide oxime (**1a**, a mixture of *anti*[7] 78% and *syn* 22%) containing 5% of isomesityl oxide oxime (**2a**) was irradiated with Pyrex-filtered light in methanol, mesityl oxide (**1b**), isomesityl oxide (**2b**), a cyclobutanol, **3**, and two amides, **4** and **5**, were obtained. Product identification was carried out spectroscopically with samples collected by preparative gas chromatography. The yields of the products were obtained by gas-chromatographic analysis; they are plotted against irradiation time in Fig. 1. It was confirmed that the irradiated reaction mixture was stable upon further standing under the present reaction conditions, but without the light. Since **2a** is supposed to be stable to the Pyrex-filtered light, in view of the lack of reactivity of the saturated ketoximes (such as cyclohexanone oxime) to this light source, the **2a** present in the starting material as a contaminant was used as the internal reference in the analysis by gas chromatography. It was found that the products and product distribution obtained from the photolysis

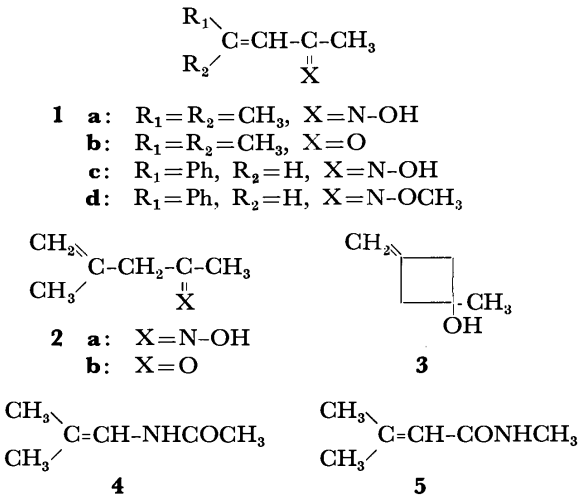

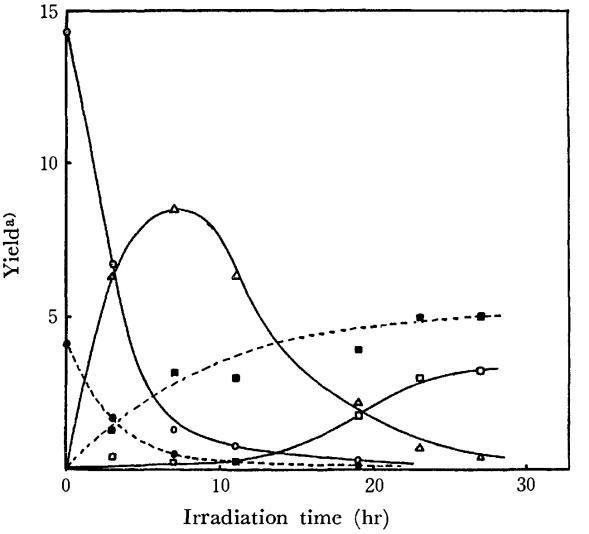

Fig. 1. Conversion of oximes and yields of products as a function of irradiation time.
—○— *anti*-**1a** —□— **3** --●-- *syn*-**1a**
--■-- **4**+**5** —△— **1b**
a) Figures refer to the relative area under each peak on the gas chromatogram, that of isomesityl oxide oxime (**2a**) being assigned an arbitrary value of 1.

1) G. Ciamician and P. Silber, *Ber.*, **36**, 4268 (1903).
2) a) J. H. Amin and P. de Mayo, *Tetrahedron Lett.*, **1963**, 1585. b) R. T. Taylor, M. Douek, and G. Just, *ibid.*, **1966**, 4143. c) G. Just and L. S. Ng, *Can. J. Chem.*, **46**, 3381 (1968). d) T. Oine and T. Mukai, *Tetrahedron Lett.*, **1969**, 157. e) H. Suginome and H. Takahashi, *ibid.*, **1970**, 5119. f) H. Izawa, P. de Mayo, and T. Tabata, *Can. J. Chem.*, **47**, 51 (1969). g) B. L. Fox and H. M. Rosenberg, *Chem. Commun.*, **1969**, 1115.
3) a) T. Sato and H. Obase, *Tetrahedron Lett.*, **1967**, 1633. b) G. Just and C. Pace-Asciak, *Tetrahedron*, **22**, 1069 (1966). c) A. Slojiljković and R. Tasovac, *Tetrahedron Lett.*, **1970**, 1405.
4) J-P. Vermès and R. Beugelmans, *ibid.*, **1969**, 2091.
5) P. de Mayo, "Solvay Institute 13th Chemistry Conference, Reactivity of Photoexcited Organic Molecule," Interscience Publishers, New York, N. Y. (1967), p. 320.
6) T. Oine and T. Mukai, Abstracts of papers presented at the 3rd ICHC, Sendai, August, 1971, p. 145.
7) The prefix *anti* implies that the oxime hydroxyl group and the C–C double bond are on the other side of the C–N double bond.

Table 1. Photolysis of ketoximes and their derivatives

Oximes	Solvent		Irr. time (hr)	Filter	Method[a] of work-up	Product[b] (relative ratio)
1a 1.3 g	MeOH	130 ml	c)	Pyrex	A	c)
1a 0.054 g	MeOH AcOH	6 ml 0.07 ml	20	Pyrex	A	**1b** (22), **3** (1), **4** (77)
1a 0.02 g	Ether	4 ml	106	Pyrex	A	*anti*-**1a** (53), *syn*-**1a** (28), **1b** (8), **4** and **5** (4), **13**[d] (2), **14**[e] (5)
1a 0.6 g	*n*-Hexane	60 ml	72	Pyrex	A	*anti*-**1a** (39), *syn*-**1a** (19), **1b** (21), **3** (3), **4** (6), **5** (14)
1c 1 g	Ether	100 ml	22	Pyrex	B	*trans-anti*-**1c** (70) *cis-anti*-**1c** (30)
1d 0.1 g	MeOH	10 ml	8	Pyrex	B	*trans*-anti-**1d** (68) *cis*-anti-**1d** (32)
8 0.9 g	MeOH	100 ml	7	none	C	**7**
9 1 g	MeOH AcOH	100 ml 2 ml	18	none	D	Camphor, **10**, **11**

a) A: The solvent was removed through a column under an ordinary pressure, and the residue was analyzed by gas chromatography. B: The solvent was removed *in vacuo* and the residue was analyzed by gas chromatography. C: The solvent was removed *in vacuo*, the residue was distilled under a reduced pressure, and the distillate was analyzed by gas chromatography. D: The solvent was removed *in vacuo*, the residue was diluted with ether and washed with an aqueous sodium bicarbonate solution, the ether was removed, and the residue was fractionated on an alumina column with chloroform.

b) Identification was carried out on pure samples obtained by preparative gas chromatography, except for samples marked with an asterisk, which contained the isomer indicated in the parentheses. **1b**, **2b**, **7**, **10**, and camphor: the retention times as shown by gas chromatography and the IR spectra were identical with those of the authentic samples. **3**: MS: *m/e* 98 (P). The IR and NMR spectra showed peaks identical with the reported values.[13] **4**: MS: *m/e* 113 (P). IR (CCl_4): 3300 (s), 1660 (vs) and 1505 cm^{-1} (vs). NMR (CCl_4): δ 1.67 (s, 6H), 2.07 (s, 3H), 6.56 (d, $J=12$ Hz, 1H) and 8.65 (bs, 1H). **5*** (containing **4**): NMR ($CDCl_3$): δ 1.80 (s, 3H), 2.10 (s, 3H), 2.73 (d, $J=5$ Hz, 3H), 5.47 (bs, 1H) and 5.82 (bs, 1H). *cis-anti*-**1c*** (containing *trans*-anti-**1c**): NMR ($CDCl_3$): δ 1.73 (s, 3H), 6.10 and 6.40 (AB type q, $J=12$ Hz, 2H), 6.85 (m, 5H) and 7.73 (bs, 1H). *cis-anti*-**1d**: IR (neat): 1054 (s), 895 (s), 775 (m) and 695 cm^{-1} (m). NMR ($CDCl_3$): δ 1.76 (s, 3H), 3.82 s, 3H), 6.25 and 6.54 (AB type q, $J=12$ Hz, 2H) and 7.15 (s, 5H). **11**: mp 133—136°C. IR ($CHCl_3$): 3400 (w) and 1660 cm^{-1} (vs). Found: C, 71.91; H, 10.55; N, 8.29%. Calcd for $C_{10}H_{17}NO$: C, 71.81; H, 10.25; N, 8.38%.

c) See Fig. 1.

d) Isobutyl methyl ketone.

e) Unidentified.

of **1a** were greatly solvent-dependent. The results are summarized in Table 1. Evidently, *syn-anti* isomerization became the major reaction pattern in nonpolar solvents, while only one amide, **4**, was obtained selectively in an acidic solvent. Compounds **1c**, **1d**, **8**, and **9** were also irradiated under the conditions specified in Table 1. The structure **11** was assigned to the product from **9** in view of the results of the elemental analysis, the amide carbonyl band in the IR spectrum at 1660 cm^{-1}, and the absence of an olefinic proton signal in the NMR spectrum. The

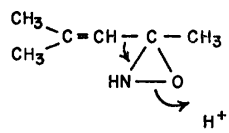

6

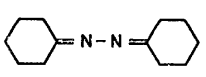

7

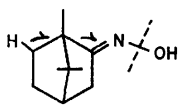

9

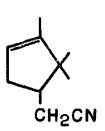

10

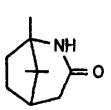

11

melting point (133—136°C) of this compound was lower than that of the reported value (156—160°C)[8] for **11**, but the possibility of the alternative structure of α-camphidone was excluded in view of the still higher melting point of α-camphidone (230—232°C).

Discussion

Oxime Disappearance. Figure 1 shows that the amount of mesityl oxide (**1b**) increases to reach a maximum and then decreases during the last stages of the reaction. As it has already been pointed out,[9] and has been confirmed in the present study, that **1b** is stable to the Pyrex-filtered light under various conditions, the decrease in the amount of **1b** upon prolonged irradiation can be explained by assuming that the curve is actually a plot of the amount of a photolabile intermediate from which the ketone is formed during the work-up of the reaction mixture. In view of the previous proposals, oxaziridine, **6**, is the most probable

8) M. Nakazaki and K. Naemura, This Bulletin, **37**, 532 (1964).

9) N. C. Yang and M. J. Jorgensen, *Tetrahedron Lett.*, **1964**, 1203.

candidate for the intermediate; this is consistent with the proposed scheme that the oxaziridine intermediate is formed in the initial step of the irradiation of oxime.

The formation of these products (**1b**, **2b**, **3**—**5**), which can be assumed to be secondary products from **6**, was greatly depressed when the photolysis was carried out in ether; the *syn-anti* isomerization became a major reaction pattern, instead (Table 1). Similarly, the amide formation from benzylideneacetone oxime (**1c**) upon the irradiation in methanol[2d] was replaced by an exclusive *cis-trans* isomerization when the irradiation was carried out in ether. Benzylideneacetone oxime *O*-methyl ether (**1d**) also underwent only *cis-trans* isomerization, even in methanol. These findings definitely support the argument by de Mayo[5] that an ionic dissociation of oxime hydrogen might be a necessary step in the formation of an oxaziridine intermediate. In a similar sense, the formation of 6-hexanelactam and hexanamide from cyclohexanone oxime upon irradiation (quartz) in methanol[2b] was greatly retarded, and an azine, **7**, became the main product upon the irradiation (quartz) of cyclohexanone oxime *O*-methyl ether (**8**) in methanol. Probably homolytic N–O bond fission, followed by dimerization, became dominant in this case. Both isomerizations (*cis-trans* and *syn-anti*) seemed to proceed through singlet states, because the reactions were not affected by the presence of piperylene in the range of quencher concentrations of 0.1—1M. **1a** indicates a weak n–π^* band at 310 nm (π–π^* at 235 nm) in the UV spectrum, while the n–π^* bands of **1c** and **1d** are completely covered with strong π–π^* bands at 284 nm. It seems reasonable to assume that the π–π^* state induces a *cis-trans* isomerization, while the n–π^* state induces a *syn-anti* isomerization.

Amide Formation. We found that the amide formation is also subject to a solvent effect. In contrast with the formation of two amides, **4** and **5**, upon the irradiation of **1a** in methanol, only one amide, **4**, was obtained upon the photolysis of **1a** in methanol *containing acetic acid.* Evidently a selective migration of the olefinic group occurs in methanol - acetic acid, while both alkyl and olefinic migrations occur non-selectively in methanol. We interpret the present result in terms of the difference in degree of protonation to the intermediate oxaziridine. That is, in an acidic solvent, protonation to an excited state of the oxaziridine would be effective, and this would induce a heterolytic N–O bond fission, as is shown in **6**, giving rise to a selective migration of the olefinic group; this seems likely in view of the preferential migratory aptitude of the olefinic group over the alkyl group in the reaction involving electron-deficient nitrogen.[10] However, in methanol, the proton-donating power of the solvent is weak and homolytic N–O bond fission in the excited oxaziridine would become dominant, thus inducing a non-selective migration of olefinic and alkyl groups. In contrast with the results obtained above, an exclusive migration of olefinic group in methanol has been reported in the styryl ketone oxime system;[2d] this result was also confirmed with **1c** in the present study. These results seem reasonable because, in this system, the phenyl group would effectively stabilize the transition state for the olefinic-group migration, thus favoring the heterolytic N–O bond fission even in a non-acidic solvent.

We also observed that the acidic solvent greatly favors the Beckmann-type rearrangement. Previously we investigated the photolysis of camphor oxime (**9**) in methanol and obtained Beckmann-fragmentation products (for instance, **10**) as well as camphor.[3a] It is probable that the Beckmann-fragmentation products arise through a homolytic cleavage of the N–O bond, as is shown in **9**, while camphor arises from the oxaziridine intermediate, which, because of the thermal unstability due to the ring strain, decomposes into camphor before it can be subject to a photochemical reaction. On the contrary, a lactam, **11**, was the product when the irradiation was carried out in an acidic solvent. Probably the Beckmann–type rearrangement became preferable because of the protonation of the excited state of the oxaziridine intermediate. The same type of reaction has been reported with the adamantanone oxime system.[11]

Cyclobutanol Formation. Although the γ-hydrogen abstraction in excited carbonyl compounds is a well-known type-II reaction, mesityl oxide is photostable under the conditions examined so far.[9] This lack of reactivity has been attributed to the assumption that the lowest state is the π–π^* triplet, which exhibits substantially reduced reactivity in intramolecular hydrogen abstraction.[12] Therefore, it is notable that a cyclobutanol, **3**, which is an expected but not realized product from mesityl oxide, was obtained from the oxime.

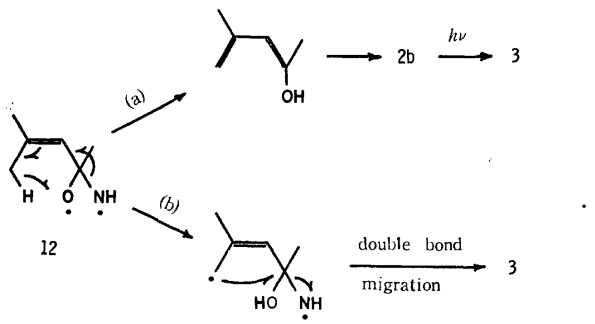

As the possible routes for the formation of **3**, we propose mechanisms (a) and (b) from a radical derived from oxaziridine (**12**). A scheme through an intermediacy of **12** was deduced from the fact that the formation of **3** was accompanied by the formation of two amides, **4** and **5**. When the irradiation was carried out in an acidic medium, where the possibility of a heterolytic cleavage of the N–O bond has been speculated about (*vide supra*), the formation of **3** was negligible (<1%). We consider that the mechanism (a),

10) T. Sato, H. Wakatsuka, and K. Amano, *Tetrahedron*, **27**, 5381 (1971).

11) T. Sasaki, S. Eguchi, and T. Toru, *Chem. Commun.*, **1970**, 1239.

12) P. J. Wagner, *Accounts Chem. Res.*, **4**, 168 (1971). Experiments questioning this assumption has been reported: R. A. Schneider and J. Meinwald, *J. Amer. Chem. Soc.*, **89**, 2023 (1967).

which involves isomesityl oxide (**2b**) as an intermediate, is preferable to (b) in view of the long induction period for the formation of **3** as compared with the formation of amides (Fig. 1). Isomesityl oxide was actually identified in the reaction mixture, but its quantitative analysis was unsuccessful because the peak on the gas chromatography overlapped with that of an unidentifiable component. The photochemical transformation of isomesityl oxide into cyclobutanol, **3**, has been established.[13] The reaction corresponding to the well-known type-II reaction in carbonyl compounds is a new type of reaction in the oxime system.

Experimental

The IR spectra were measured on a Hitachi EPI-G3 spectrometer, while the NMR spectra were obtained on a JEOL MH-60 (60 MHz) spectrometer, using TMS as the internal reference. The mass spectra were determined on a Hitachi RMS-4 mass spectrometer, using an ionization energy of 70 eV.

Mesityl Oxide Oximes. The material prepared by the method reported by Harries[14] was a mixture of *anti* (66%), *syn* (21%), and isomesityl oxide oxime (13%), as judged from the results of gas-chromatographic and NMR-spectroscopic analysis. Isomesityl oxide oxime and a mixture of *anti* and *syn* were isolated in preparative gas chromatography. The mixture of *anti* and *syn* isomers: IR (CCl_4): 3370 (s), 1670 (m) and 968 cm^{-1} (s). NMR (CCl_4): δ 1.76—2.15 (m), 5.65 (m) for the olefinic proton of the *anti*-isomer,[15] 6.03 (m) for the olefinic proton of the *syn*-isomer and 9.67 (bs). Isomesityl oxide oxime: IR (CCl_4): 3250 (s), 1655 (m), 945 (m) and 896 cm^{-1} (s). NMR (CCl_4): δ 1.70 (s, 3H), 1.82 (s, 3H), 2.90 (s, 2H), 4.93 (s, 2H) and 8.63 (bs, 1H).

The material was further fractionated, and a mixture of *anti* (75%), *syn* (20%), and isomesityl oxide oxime (5%) was used for the photoreaction.

trans-anti-*Benzylideneacetone Oxime* O-*Methyl Ether* (**1d**). Into a solution of *trans-anti*-benzylideneacetone oxime (16 g, mp 116°C, lit,[16] mp 113—115°C) in anhydrous benzene (50 m*l*), we added sodium amide (4 g) at 30°C. The mixture was stirred for 15—16 hr, and then the solid was collected on a glass filter. The material was washed with benzene and dried *in vacuo*. The solid was suspended in ether (50 m*l*), methyl iodide (43 g) was added, and the mixture was refluxed for 20 hr under a slight pressure (with a mercury seal). The mixture was then filtered from a solid, the solvent was removed, and the residue was distilled. Bp 110—115°C/2—3 mmHg. IR (neat): 1053 (s), 965 (m), 750 (m) and 690 cm^{-1} (m). NMR (CCl_4): δ 1.96 (s, 3H), 3.88 (s, 3H), 6.67 (s, 2H) and 7.18 (m, 5H).

Camphor Oxime. Mp 117.5°C. (lit,[17] mp 117.5—118°C).

Cyclohexanone Oxime O-*Methyl Ether.* Bp 50—51°C/10 mmHg. (lit,[18] bp 50°C/12 mmHg.)

Photolysis. The irradiation was carried out with a Riko high-pressure UVL-100P ultraviolet mercury lamp. The results are summarized in Table 1.

13) N. C. Yang and D-M. Thap, *Tetrahedron Lett.*, **1965**, 3671.
14) C. Harries, *Ann. Chem.*, **330**, 192 (1904).
15) G. Slomp and W. J. Wechter, *Chem. Ind.*, **1962**, 41.
16) B. Unterhalt, *Arch. Pharm.*, **299**, 274 (1966). Cf. S. Goszezynski and W. Zielinski, *Zeszyty Nauk. Politech. Slask., Chem.*, No. **24**, 239 (1964); *Chem. Abstr.*, **63**, 11298 (1965).
17) Beilsteins Handbuch der Organischen Chemie. Vol. VII, Verlag von Julius Springer, Berlin, p. 112 (1925).
18) L. G. Donaruma, *J. Org. Chem.*, **22**, 1024 (1957).

BULLETIN OF THE CHEMICAL SOCIETY OF JAPAN, VOL. 45, 1179—1183 (1972)

The Preparation and Deamination of 1-*t*-Butyl-3-amino-, 1-*t*-Butyl-3-aminomethyl-, and 1-*t*-Butyl-2-aminomethylazetidine

Teng-Yueh CHEN, Mu-Huang HUNG, Po-Tau CHEN, and Masaki OHTA*

Institute of Chemistry, National Tsing Hua University, Hsinchu, Taiwan, China

**Laboratory of Organic Chemistry, Tokyo Institute of Technology, Ookayama, Meguro-ku, Tokyo*

(Received October 11, 1971)

1-*t*-Butyl-3-amino-, 1-*t*-butyl-3-aminomethyl-, and 1-*t*-butyl-2-aminomethylazetidine were prepared by the ammonolysis of 1-*t*-butyl-3-azetidinyl tosylate, and by the reduction of 1-*t*-butyl-3-cyano, and 1-*t*-butyl-2-cyano-azetidine respectively. In the deamination, both of the first two azetidines gave only the corresponding alcohols, 1-*t*-butyl-3-azetidinol and 1-*t*-butyl-3-hydroxymethylazetidine, while the last one was found to afford two products, 1-*t*-butyl-2-hydroxymethylazetidine and 1-*t*-butyl-3-hydroxypyrrolidine. The deamination products were identified as the corresponding acetates.

Rearrangements involving carbonium ions in small-ring compounds[1] or involving the nucleophilic participation of the amino group in strainless alicyclic amines[2] are already known. With regard to the highly strained azetidines, reactions which closely resemble the above rearrangements have also been reported very recently by Gaertner,[3] Deyrup and Moyer,[4]

1) Review: R. Breslow, in "Molecular Rearrangements," ed. by P. de Mayo, Part One, Interscience Publishers, New York, N. Y. (1963), pp. 233—294.

2) R. C. Fuson and C. L. Zirkle, *J. Amer. Chem. Soc.*, **70**, 2760 (1948); R. H. Reitsema, *ibid.*, **71**, 2041 (1949); E. G. Brain, E. P. Doyl, and M. D. Mehta, *J. Chem. Soc.*, **1961**, 633.

3) V. R. Gaertner, *Tetrahedron Lett.*, **1968**, 5919; V. R. Gaertner, *J. Org. Chem.*, **35**, 3952 (1970).

4) J. A. Deyrup and C. L. Moyer, *Tetrahedron Lett.*, **1968**, 6179.

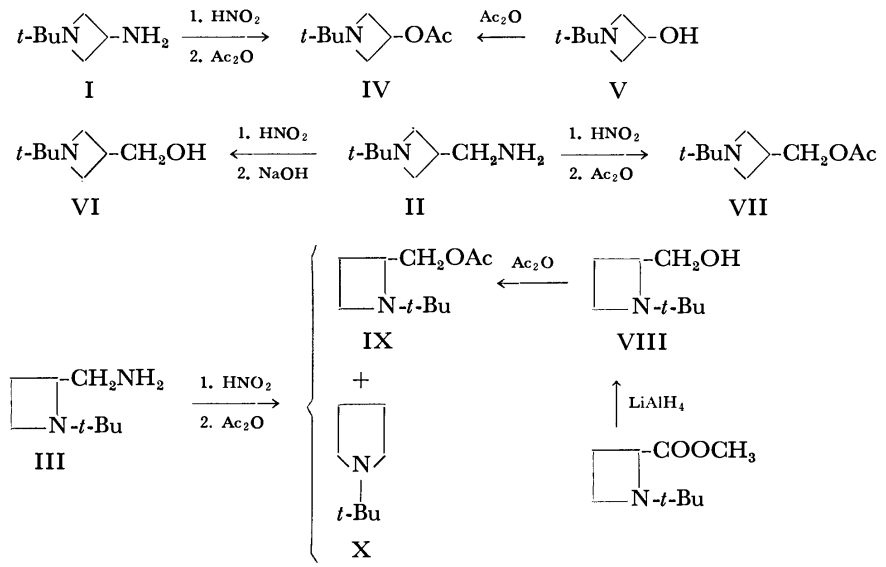

and Masuda *et al.*[5] Here, we will present the results of the deamination of the title compounds.[6] It is of interest to see if the cation so generated can be attacked by the nitrogen atom in the ring to give ring-contraction or ring-expansion products.

1-*t*-Butyl-3-aminoazetidine (I) was prepared according to a method reported before.[7] 1-*t*-Butyl-3-aminomethylazetidine (II) was prepared by the lithium aluminum hydride reduction of 1-*t*-butyl-3-cyanoazetidine.[8] The reduction of 1-*t*-butyl-2-cyanoazetidine[9] with lithium aluminum hydride offered a third amine, 1-*t*-butyl-2-aminomethylazetidine (III).[10] The infrared spectrum of the undistilled amine, II, shows the characteristic bands of a primary amino group at 3360 and 3290 cm^{-1} and an NH bending band at 1590 cm^{-1}, while that of the product III shows bands at 3360, 3280, and 1590 cm^{-1}. The results of the elemental analyses and spectroscopic studies of the dipicrates and phenylthioureas derived from the amines were completely consistent with the structures I, II, and III respectively (see Experimental). The homogeneity of the amines was also examined by vpc before deamination.

The amine I was allowed to react with sodium nitrite in aqueous acetic acid; the reaction mixture was then acetylated with acetic anhydride and analyzed by tlc and vpc. Only one product, 1-*t*-butyl-3-acetoxyazetidine (IV), was detected. The product, IV, isolated by vpc was found to be identical (IR, tlc, and vpc) with the authentic sample synthesized independently from the reaction of 1-*t*-butyl-3-azetidinol (V) and acetic anhydride.[6,11] The results of the elemental analysis were in agreement with the structure.

The deamination of the amine II was carried out in the same way, and the reaction mixture was analyzed before being treated with acetic anhydride. The mixture, which contained nearly equal amounts of 1-*t*-butyl-3-hydroxymethylazetidine (VI) and its acetate (VII) (detected by vpc), was then hydrolyzed to give VI as its only product. The infrared spectrum shows a broad absorption between 3500—3100 cm^{-1} for the hydroxyl group; the results of elemental analysis also coincided with the structure VI. For the purpose of confirmation, the deamination of II was performed again, and the reaction product was identified after acetylation. This time, only 1-*t*-butyl-3-acetoxymethylazetidine (VII) was obtained. The infrared spectrum of the product shows a strong ester carbonyl absorption at 1745 cm^{-1}. The NMR spectrum (CCl_4) exhibits a singlet at τ 9.10 (9H, *t*-Bu), a singlet at 8.03 (3H, CH_3CO), a multiplet between 7.67 and 7.25 (1H, ring methine), a triplet at 7.09 (2H, ring methylene), a triplet at 6.79 (2H, with the center split, ring methylene) and a doublet at 5.90 (2H, J= 6.8 Hz, methylene adjacent to ester oxygen). The results of the elemental analysis of the product and its picrate also agreed with the proposed structure, VII.

According to the same procedure, the amine III, in the deamination, was found to produce 1-*t*-butyl-2-acetoxymethylazetidine (IX) and the ring-expansion product, 1-*t*-butyl-3-acetoxypyrrolidine (X), in a vpc ratio of 45.6 : 54.6. The component with the shorter vpc retention time was spectrally (IR and NMR: Fig. 1) identical with the authentic sample of 1-*t*-butyl-2-acetoxymethylazetidine IX (see Experimental) prepared by the acetylation of the 1-*t*-butyl-2-hydroxymethylazetidine (VIII) which had been

5) T. Masuda, A. Chinone, and M. Ohta, This Bulletin, **43**, 3287 (1970).

6) Some of the results have been taken from the Ph. D. thesis of T. Chen, Tokyo Institute of Technology, March (1968).

7) T. Chen, H. Kato, and M. Ohta, This Bulletin, **41**, 712 (1968).

8) T. Chen, T. Sanjiki, H. Kato, and M. Ohta, *ibid.*, **40**, 2401 (1967).

9) T. Masuda, A. Chinone, and M. Ohta, *ibid.*, **43**, 3281 (1970).

10) The amines II and III were not purified by distillation because, unexpectedly, both of them bubble over the distillation flask by heating up to 80—90°C/19 mmHg and were confirmed by spectra and their derivatives (see Experimental).

11) V. R. Gaertner, *Tetrahedron Lett.*, **1966**, 4691; V. R. Gaertner, *J. Org. Chem.*, **32**, 2972 (1967).

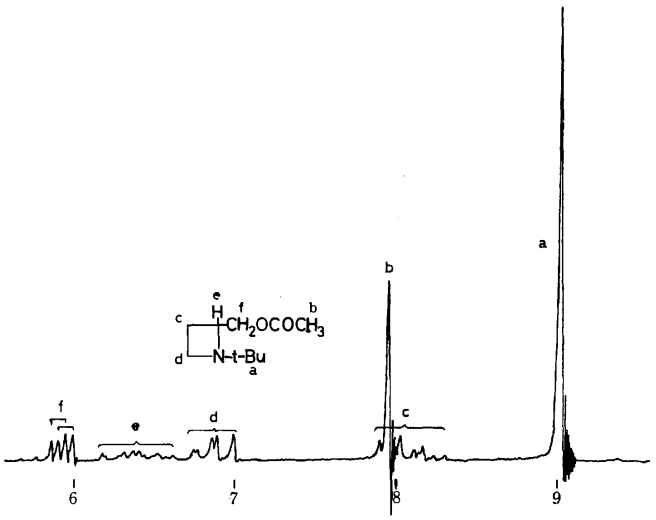

Fig. 1. The NMR spectrum of 1-*t*-butyl-2-acetoxymethylazetidine.

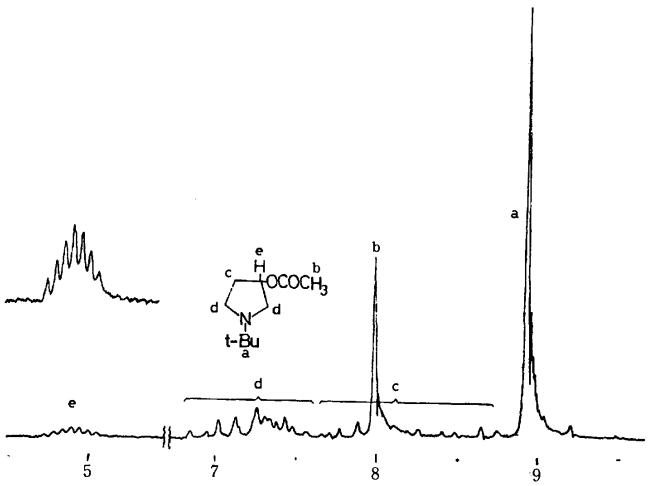

Fig. 2. The NMR spectrum of 1-*t*-butyl-3-acetoxypyrrolidine.

obtained by the reduction of 1-*t*-butyl-2-methoxycarbonylazetidine[5] with lithium aluminum hydride. The second compound isolated by vpc was considered to be 1-*t*-butyl-3-acetoxypyrrolidine (X) by the use of the spectroscopic method and by elemental analysis. The general pattern of the infrared spectrum of X is markedly different from that of IX; it has a strong absorption at 1740 cm^{-1} for the ester carbonyl group. The NMR spectrum ($CDCl_3$, Fig. 2) of X exhibits a singlet at τ 8.93 (9H, *t*-Bu), a singlet at 8.01 (3H, CH_3CO), a multiplet between 8.29 and 7.65 (2H, the methylene on the 4-carbon of the ring), a multiplet between 7.50 and 6.81 (4H, the two methylenes adjacent to the ring nitrogen), and a septet centered at 4.90 (1H, J=3.1 Hz, the asymmetric methine proton on the 3-carbon of the ring). A similar splitting of the methine proton in 1-*t*-butyl-2-aminomethylazetidine has also been observed by Rodebaugh and Cromwell.[12]

The fact that the ring contraction was not observed in the deamination of the amine I is in fair agreement with most previously-reported causes of replacement reactions involving 3-azetidinium cations, XI, which have a tendency to keep the ring unchanged rather than to contract it, though there are a few exceptions.[3,7,8] In the case of the amine II, 3-acetoxymethylazetidine, VII, should be formed from either the azabicyclo[1.1.1]pentyl cation, XIV (nitrogen atom participation), or the azetidinylmethyl cation, XIII. The formation of the ring-expansion product X by the deamination of the amine III may be expansion product X by the deamination of the amine III may be explained by the participation of the nitrogen atom (*via* the azabicyclo[2.1.0]pentyl cation, XVII) or, alternatively, by a simple 1,2-sigmatropic rearrangement of the 2-azetidinylmethyl cation, XV→ XVI. The absence of a ring-enlargement product in the deamination of II lends support to the probable nitrogen atom participation.

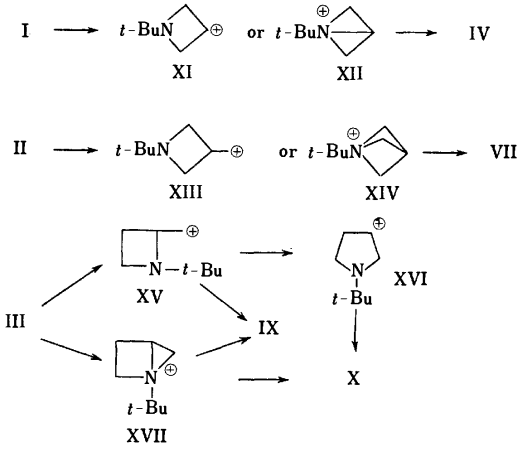

Experimental[13]

1-t-Butyl-3-aminoazetidine (I). This compound was prepared from 1-*t*-butyl-3-azetidinyl tosylate and a saturated methanolic solution of ammonia.[7] The fraction boiling at 71°C/20 mmHg was taken for the deamination. IR: 3370, 3290, 1600, 1390, 1365 cm^{-1}. Vpc: Carbowax 20 M on Diasolid A 4 mm × 225 cm 90°C, He 60 m*l*/min, retention time, 16 min; SE30 on Varaport 30, 1/4 in × 5 ft 75°C, N_2 60 m*l*/min, retention time, 3.8 min.

Dipicrate of I: Mp 198—200°C (decomp.).

Found: C, 39.15; H, 3.85; N, 19.32%. Calcd for $C_{19}H_{22}N_8O_{14}$: C, 38.91; H, 3.78; N, 19.10%.

1-*t*-Butyl-3-phenylthioureidoazetidine: Mp 141°C.

Found: N, 16.16%. Calcd for $C_{14}H_{21}N_3S$: N, 15.95%.

1-t-Butyl-3-cyanoazetidine. This was prepared in a 73% yield (3.5 g) from 10 g of 1-*t*-butyl-3-azetidinyl tosylate and 6.8 g of potassium cyanide in 100 m*l* of methanol.[8] Bp 46—47°C/2 mmHg. IR: 2240, 1390 and 1365 cm^{-1}. Vpc: Porapak Q 1/8 in × 5.7 ft 75°C, N_2 35 m*l*/min, reten-

12) R. M. Rodebaugh and N. H. Cromwell, *J. Heterocycl. Chem.*, **8**, 19 (1971).

13) All melting and boiling points are uncorrected. The melting points were measured on a micro hot state. The infrared spectra were taken on neat liquid or on KBr tablets, and the NMR spectra were determined on Varian A 60-D at 60 MHz, tetramethylsilane being used as the internal standard. The vpc were run on Shimadzu Type GC-1B Gas Chromatograph, Varian Aerograph Series 1200, Varian Aerograph Model 705, and Varian Model 90-F-3 alternatively.

tion time, 10.2 min; SE30 on Varaport 30,1/4 in × 5 ft 80°C, N_2 60 ml/min, retention time, 12 min.

Found: C, 69.78; H, 10.03; N, 20.21%. Calcd for $C_8H_{14}N_2$: C, 69.52; H, 10.21; N, 20.27%.

Picrate Mp 203—205°C.

1-t-Butyl-3-aminomethylazetidine (II). The reduction of 2.9 g (0.021 mol) of 1-*t*-butyl-3-cyanoazetidine with 0.9 g of lithium aluminum hydride in 80 ml of absolute ether yielded 2.2 g (74%) of a pale yellow liquid which could not be purified by distillation since it bubbled vigorously over the distillation flask when heated up to 90°C/19 mmHg. This crude product was found homogeneous by vpc and was used in the deamination. IR: 3360, 3290, 1590, 1390, and 1364 cm^{-1}. n_D^{25} 1.4645. vpc: SE30 on Varaport 30, 1/8 in × 6 ft 70°C, N_2 30 ml/min, retention time, 7.2 min.

Dipicrate of II: Mp 230°C (decomp.).

Found: C, 40.26; H, 4.20; N, 18.88%. Calcd for $C_{20}H_{24}N_8O_{14}$: C, 40.01; H, 4.03; N, 18.66%.

1-*t*-Butyl-3-phenylthioureidomethylazetidine: Mp 99—100.5°C. IR: 3470, 3150, 1600, and 1530 cm^{-1}.

Found: C, 64.72; H, 8.28; N, 15.45%. Calcd for $C_{15}H_{23}N_3S$: C, 64.94; H, 8.36; N, 15.15%.

1-t-Butyl-2-cyanoazetidine.[9] This compound was obtained by the reaction of 6.8 g of 1-*t*-butylazetidine-2-carboxamide and a solution of triphenylphosphine dibromide (prepared from 13.8 g of triphenylphosphine, 8.4 g of bromine, and 10.6 g of triethylamine) in 75 ml of acetonitrile. A colorless oil (3 g, 50% yield) was obtained. Bp 43°C/1 mmHg. $n_D^{24.5}$ 1.4482. IR: 2240, 1385, and 1355 cm^{-1}.

Picrate: Mp 150—151°C.

Found: C, 46.00; H, 4.50; N, 19.14%. Calcd for $C_{14}H_{17}N_5O_7$: C, 45.78; H, 4.69; N, 19.07%.

1-t-Butyl-2-aminomethylazetidine (III).[12] The reduction of 3 g (0.022 mol) of 1-*t*-butyl-2-cyanoazetidine with 1 g of lithium aluminum hydride in 140 ml of absolute ether gave 2.5 g (80%) of a pale yellow liquid; this liquid was not purified by distillation for the same reason as has been given above. IR: 3360, 3280, 1590, 1388, and 1362 cm^{-1}. $n_D^{24.5}$ 1.4666. Vpc: SE30 on Varaport 30, 1/8 in × 6 ft 70°C, N_2 30 ml/min, retention time, 6 min.

Dipicrate of III: Mp 196.5—197.5°C.

Found: C, 39.72; H, 4.14; N, 18.81%. Calcd for $C_{20}H_{24}N_8O_{14}$: C, 40.01; H, 4.03; N, 18.66%.

1-*t*-Butyl-2-phenylthioureidomethylazetidine: Mp 105—105.5°C. IR: 3220, 3160, 1600, 1540 cm^{-1}.

Found: C, 64.66; H, 8.19; N, 15.43%. Calcd for $C_{15}H_{23}N_3S$: C, 64.94; H, 8.35; N, 15.14%.

1-t-Butyl-3-acetoxyazetidine (IV) from 1-t-Butyl-3-azetidinol (V).[6,11] This was prepared by the acetylation of 5.6 g (0.043 mol) of V with 6 g (0.059 mol) of acetic anhydride at room temperature for 5 hr. After neutralization with sodium carbonate, by extraction with ether an subsequent distillation 6.7 g (91% yield) of a colorless liquid boiling at 30—31°C/0.5 mmHg were obtained. n_D^{24} 1.4383. IR: 1745, 1377, and 1365 cm^{-1}. NMR (CCl_4; τ): 9.08 (9H, singlet), 8.04 (3H, singlet), 7.02 (2H, triplet), 6.60 (2H, triplet), 5.35—5.07 (1H, multiplet). Tlc: Tōyō (Japan) thin-layer chromatosheet (silica gel), R_f=0.38 (acetone). Vpc: Apiezon Grease L on Diasolid A 4 mm × 300 cm 152°C, He 60 ml/min, retention time, 5.2 min; Carbowax 20 M on Diasolid A 4 mm × 300 cm 162°C, He 60 ml/min, retention time, 5 min; SE30 on Varaport 30, 1/4 in × 5 ft, 75°C, N_2 60 ml/min, retention time, 9.8 min.

Found: C, 62.39; H, 9.76; N, 7.81%. Calcd for $C_9H_{17}NO_2$: C, 63.13; H, 10.00; N, 8.18%.

Picrate of IV: Mp 150.5—152.5°C.

Found: C, 44.71; H, 4.82; N, 14.28%. Calcd for $C_{15}H_{20}N_4O_9$: C, 45.00; H, 5.04; N, 14.00%.

1-t-Butyl-2-hydroxymethylazetidine (VIII).[5] From 14.4 g (0.09 mol) of 1-*t*-butyl-2-methoxycarbonylazetidine and 2.5 g of lithium aluminum hydride in absolute ether, 8.3 g (68.8% yield) of a colorless oil, bp 38—40.5°C/0.5 mmHg, were obtained. n_D^{21} 1.4624. IR: a broad peak at 3500—3200, 1380 and 1360 cm^{-1}.

Found: C, 66.86; H, 12.11; N, 9.08%. Calcd for $C_8H_{17}NO$: C, 67.29; H, 11.95; N, 9.07%.

Picrate of VIII: Mp 190—191°C (decomp.).

Found: C, 45.09; H, 5.25; N, 15.32%. Calcd for $C_{14}H_{20}N_4O_8$: C, 45.16; H, 5.41; N, 15.05%.

1-t-Butyl-2-acetoxymethylazetidine (IX) from VIII. The acetylation of 3 g (0.021 mol) of VIII with 2.3 g (0.022 mol) of acetic anhydride gave 3 g (77.3% yield) of a colorless oil. Bp 88.5—89.5°C/19 mmHg. $n_D^{25.4}$ 1.4450. IR: 1750, 1390 and 1370 cm^{-1}. NMR ($CDCl_3$, τ): (Fig. 1), 9.03 (9H, singlet), 7.96 (3H, singlet), 8.34—7.85 (2H, multiplet), 7.04—6.65 (2H, multiplet), 6.64—6.17 (1H, multiplet), 5.95 (1H, doublet, $J\simeq$5.6 Hz), 5.9 (1H, doublet, J=5.5 Hz). Vpc: SE30 on Varaport 30, 1/8 in × 6 ft 70°C, N_2 30 ml/min, retention time, 17.3 min; SE30 on Varaport 30, 1/4 in × 5 ft 80°C, N_2 60 ml/min, retention time, 11. 6 min.

Found: C, 64.58; H, 10.04; N, 7.46%. Calcd for $C_{10}H_{19}NO_2$: C, 64.83; H, 10.33; N, 7.56%.

Picrate of IX: Mp 129—130°C (decomp.).

Found: C, 46.36; H, 5.13; N, 13.78%. Calcd for $C_{16}H_{22}N_4O_9$: C, 46.37; H, 5.35; N, 13.52%.

Deamination of 1-t-Butyl-3-aminoazetidine (I). A solution of 1.1 g (0.015 mol) of sodium mitrite in 6 ml of water was slowly stirred into a solution of 1.2 g (0.01 mol) of I in 7.2 g of 50% acetic acid cooled with ice-salt. After 5 hr, the reaction mixture was made alkaline with sodium carbonate and was extracted with ether. After the subsequent removal of the ether, 2 ml of acetic anhydride were stirred into the deamination mixture with cooling and the stirring was continued at room temperature for five hours. Then the solution was made alkaline with excess sodium carbonate, extracted with ether, and dried over magnesium sulfate overnight. The ether was removed, and the residue was analyzed by vpc and tlc. Only one component, with a R_f value of 0.38 (acetone) was detected by tlc (similar to the authentic sample, IV, under the same conditions). Vpc: SE30 on Varaport 30, 1/4 in × 5 ft 75°C, N_2 60 ml/min, retention time, a very small peak at 2.6 min and a main peak at 9.8 min, with a peak area ratio of 6 : 94. The other vpc data were identical with those of IV. The fraction corresponding to the smaller peak, isolated by vpc, did not form a picrate and may be not an amine. The IR spectrum of the main product isolated by vpc was completely identical with that of the authentic sample of IV.

Picrate of the main product: Mp 150—152°C.

Found: C, 44.91; H, 4.76%. Calcd for $C_{15}H_{20}N_4O_9$: C, 45.00; H, 5.04%.

Deamination of 1-t-Butyl-3-aminomethylazetidine (II). (A) The amine II (1.4 g, 0.01 mol) was deaminated with 1.5 g (0.02 mol) of sodium nitrite in 50% acetic acid in a manner similar to that described above (omitting the acetylation in this experiment). The deamination mixture, which consisted of nearly equal amounts of 1-*t*-butyl-3-hydroxymethylazetidine (VI) and its acetate (VII) (detected by vpc), was then warmed with aqueous sodium hydroxide at 55°C for 3 hr and extracted with ether. After the removal of the ether, a part of the crude product was reserved for vpc analysis, and the remainder was distilled *in vacuo* to give 0.5 g of pure VI. Bp 66—68°C/0.5 mmHg, n_D^{25} 1.4626. IR: 3500—3100(broad), 1385 and 1360 cm^{-1}.

Vpc: only one compound presented; SE30 on Varaport 30, 1/8 in ×6 ft 70°C, N_2 30 m*l*/min, retention time, 8.8 min; SE30 on Varaport 30, 1/4 in × 5 ft 80°C, N_2 60 m*l*/min, retention time, 13.6 min.

Found: C, 66.81; H, 11.72; N, 9.48%. Calcd for $C_8H_{17}NO$: C, 67.08; H, 11.97; N, 9.78%.

Picrate of VI: Mp 143—144°C.

Found: N, 15.51%. Calcd for $C_{14}H_{20}N_4O_8$: 15.05%.

(B) The deamination of II was carried out again with 2 g (0.014 mol) of II and 1.5 g (0.022 mol) of sodium nitrite in 50% acetic acid; the deamination product was then allowed to react with acetic anhydride as in the deamination of I, and then it was analyzed. Both the crude product and the distilled product consist of only 1-*t*-butyl-3-acetoxymethylazetidine (VII), a colorless liquid boiling at 57—58°C/0.5 mmHg, n_D^{25} 1.4421. IR: 1745, 1390 and 1370 cm^{-1}. NMR: see the Discussion. Vpc: SE30 on Varaport 30, 1/4 in × 5 ft 80°C, N_2 60 m*l*/min, retention time, 29.8 min.

Found: C, 64.90; H, 10.60; N, 7.85%. Calcd for $C_{10}H_{19}NO_2$: C, 64.83; H, 10.34; N, 7.56%.

Picrate of VII: Mp 114°C.

Found: C, 46.10; H, 5.40; N, 13.82%. Calcd for $C_{16}H_{22}N_4O_9$: C, 46.38; H, 5.35; N, 13.52%.

*Deamination of 1-*t*-Butyl-2-aminomethylazetidine (III).* The amine III (2 g, 0.014 mol) in 10 m*l* of 50% acetic acid was allowed to react with 1.6 g (0.025 mol) of sodium nitrite in 10 m*l* of water; the products were similarly identified as their acetates. Vpc analyses showed that both the crude substance and the distilled (the fraction boiling between 40—78°C/18 mmHg was collected) substance were composed of two products in the ratio of 45.6 : 54.4 (vpc peak area).

The first product was isolated by vpc: SE30 on Varaport 30, 1/8 in × 6 ft 70°C, N_2 30 m*l*/min, retention time, 17.3 min; SE30 on Varaport 30, 1/4 in × 5 ft 80°C, N_2 60 m*l*/min, retention time, 11.6 min. The IR and NMR spectra and the results of the vpc analyses showed this compound to be identical with the authentic sample of IX prepared from VIII.

Found: C, 64.61; H, 10.17; N, 7.81%. Calcd for $C_{10}H_{19}NO_2$: C, 64.83; H, 10.33; N, 7.56%.

The second product (X) was also isolated by vpc: SE 30 on Varaport 30, 1/8 in × 6 ft 70°C, N_2 30 m*l*/min, retention time, 22.6 min; SE30 on Varaport 30, 1/4 in × 5 ft 80°C, N_2 60 m*l*/min, retention time, 14.7 min. IR: 1740, 1393 and 1370 cm^{-1}. NMR: see Fig. 2.

Found: C, 64.93; H, 10.07; N, 7.38%. Calcd for $C_{10}H_{19}NO_2$: C, 64.83; H, 10.33; N, 7.56%.

The authors are indebted to Professor Hiroshi Kato of Shinshu University, Japan, for his invaluable discussions and to Professor Yu-shia Cheng of National Taiwan University for allowing us to use the gas chromatograph there.

One of the authors, Teng-yueh Chen, wishes also to thank the National Council for the Science Development of China for a research grant.

BULLETIN OF THE CHEMICAL SOCIETY OF JAPAN, VOL. 45, 1183—1191 (1972)

Palladium-catalyzed Reactions of 1,3-Dienes with Active Methylene Compounds. IV.[1] Palladium-diphosphine Complex Catalysts

Kuniyuki TAKAHASHI, Akihisa MIYAKE, and Go HATA

Basic Research Laboratory, Toray Industries, Inc., Tebiro, Kamakura, Kanagawa-ken

(Received October 18, 1971)

Active methylene compounds, such as acetylacetone and ethyl acetoacetate, reacted with 1,3-butadiene in the presence of palladium-diphosphine complex catalysts to yield two 1 : 1 adducts, **1** and **2**. Primary and secondary amines also afforded two 1 : 1 adducts, **10** and **11**. Isoprene, 1,3-pentadiene, and 2,4-hexadiene also reacted with the active methylene compounds and the amines in a manner similar to that of 1,3-butadiene. The most effective and easily available catalyst is the combination of $PdBr_2(Ph_2PCH_2CH_2PPh_2)_2$ and sodium phenoxide.

Recently, the reactions of 1,3-butadiene with active hydrogen compounds by means of palladium catalysts have been reported to afford 2,7-octadienyl derivatives of active hydrogen compounds.[2-5] For example, the addition of 1,3-butadiene to active methylene compounds to which two electronegative groups are attached gives the corresponding 2,7-octadienyl derivatives.[5] In the reactions, tertiaryphosphine complexes of palladium are quite effective catalysts or catalyst components. The reactions seem to proceed through the coordination of the two molecules of 1,3-butadiene to the metal atom. A coordination of a bidentate donor is expected to have an effect on the number of the coordinated 1,3-butadiene molecule. We have investigated the catalytic behavior of bidentate phosphine complexes of palladium in the reactions of 1,3-dienes with active hydrogen compounds such as active methylene compounds, and with primary and secondary amines. In contrast to the reaction catalyzed by the unidentate phosphine complexes of palladium,[4,5] this reaction has been found to give 1 : 1 adducts. In the iron- or cobalt-catalyzed reaction of

1) For paper III in this series, see K. Takahashi, A. Miyake, and G. Hata, *Chem. Ind.* (London), **1971**, 488.

2) S. Takahashi, T. Shibano, and N. Hagihara, *Tetrahedron Lett.*, **1967**, 2451.

3) E. J. Smutny, *J. Amer. Chem. Soc.*, **89**, 6793 (1968).

4) S. Takahashi, T. Shibano, and N. Hagihara, This Bulletin **41**, 454 (1968).

5) G. Hata, K. Takahashi, and A. Miyake, *Chem. Ind.* (London), **1969**, 1836.

1,3-butadiene with ethylene,[6] the coordination of bidentate diphosphine ligands such as $PhPCH_2CH_2PPh_2$ was found to have a drastic effect on the catalytic behavior as a result of the decrease in the number of coordination sites for the 1,3-dienes, thus yielding 1,4-hexadiene quite selectively. The reaction reported in this paper is another example of the change in the catalytic behavior by the coordination of the bidentate diphosphine ligands.

A part of this work has been reported in a preliminary communication.[1] The present paper will describe the reaction in detail.

This type of reaction has been applied to active methylene compounds, such as acetylacetone and ethyl acetoacetate, and to primary and secondary amines. Substituted 1,3-butadienes, such as isoprene, 1,3-pentadiene, and 2,4-hexadiene, reacted with the active hydrogen compounds to afford 1 : 1 adducts. However other active hydrogen compounds, such as alcohols, phenols, and carboxylic acids, did not give 1 : 1 adducts in the reaction with 1,3-dienes.

An active and easily available catalyst can be prepared by mixing $PdBr_2(Ph_2PCH_2CH_2PPh_2)_2$ and sodium phenoxide. A combination of palladium chloride, $Ph_2PCH_2CH_2PPh_2$ or $Ph_2PCH_2CH_2CH_2PPh_2$, and sodium phenoxide, one of palladium acetate and $Ph_2PCH_2CH_2PPh_2$, and a zerovalent palladium complex, $Pd(Ph_2PCH_2CH_2PPh_2)_2$, are also effective catalysts. In the reactions of amines, the presence of phenol has been found to enhance the catalytic activity.

The reaction products were identified by means of elemental analysis, molecular-weight measurements, vpc, and IR and NMR spectroscopies.

The reaction of 1,3-butadiene with active methylene compounds gave two 1 : 1 adducts, **1** and **2**, and 1 : 2 adducts, **3**. The 1 : 2 adducts were not isolated, but they were confirmed not to be 2,7-octadienyl derivatives[5] by a comparison of their vpc retention times with those of the octadienyl derivatives.

$$\mathrm{R^1_{R^2}}\!\!>\!\!CH_2 + CH_2{=}CH{-}CH{=}CH_2 \rightarrow$$

$$\mathrm{R^1_{R^2}}\!\!>\!\!CH{-}\underset{\displaystyle CH_3}{\underset{|}{CH}}{-}CH{=}CH_2 \quad \textbf{1}$$

$$+\ \mathrm{R^1_{R^2}}\!\!>\!\!CH{-}CH_2CH{=}CHCH_3 \quad \textbf{2}$$

$$+\ \mathrm{R^1_{R^2}}\!\!>\!\!C\!\!<\!\!\begin{matrix}C_4H_9\\C_4H_9\end{matrix} \quad \textbf{3}$$

	R^1	R^2
a	$COCH_3$	$COCH_3$
b	$COCH_3$	$COOC_2H_5$
c	$COOC_2H_5$	$COOC_2H_5$

The results of the reactions of 1,3-butadiene with the active methylene compounds catalyzed by $PdBr_2(Ph_2PCH_2CH_2PPh_2)_2$ and sodium phenoxide are summarized in Table 1. The infrared spectrum of **1** shows absorptions due to the out-of-plane deformation of $-CH{=}CH_2$ near 920 and 998 cm^{-1}, while that of **2** exhibited an absorption due to the out-of-plane deformation of *trans* $-CH{=}CH-$ near 965 cm^{-1} and no absorption due to *cis* $-CH{=}CH-$.

These reactions proceeded fairly rapidly at 150°C. The reaction of acetylacetone with 1,3-butadiene in the presence of $PdBr_2(Ph_2PCH_2CH_2PPh_2)_2$ and sodium phenoxide gave **1a**, **2a**, and **3a**. In the presence of a large excess of 1,3-butadiene, **3a** was the major product. Ethyl acetoacetate and diethyl malonate reacted with the diene to give **1b**, **2b**, and **3b**, and **1c** and **2c**, respectively. The reactivity of diethyl malonate was smaller than that of acetylacetone. No 1 : 2 adduct of diethyl malonate and 1,3-butadiene was observed.

2-Oxocyclododecanecarbaldehyde reacted with 1,3-butadiene to afford 2-oxo-2-(2-butenyl)cyclododecanecarbaldehyde. The reaction was accompanied by the partial elimination of the formyl group of the product.

The combination of $PdBr_2(Ph_2PCH_2CH_2PPh_2)_2$ and sodium phenoxide was the most efficient catalyst. The diphosphine complex, $PdBr_2(Ph_2PCH_2CH_2PPh_2)_2$, showed no catalytic activity. The addition of sodium phenoxide activated the palladium complex. A combination of palladium acetate and $Ph_2PCH_2CH_2PPh_2$, and one of $Pd(NO_2)_2(NH_3)_2$ and $Ph_2PCH_2CH_2PPh_2$, were effective catalysts without any sodium phenoxide. A diphosphine complex of Pd(0), $Pd(Ph_2PCH_2CH_2PPh_2)_2$, also catalyzed the reaction, although the activity was low. The presence of phenol or sodium phenoxide increased the catalytic activity of the complex of Pd(0) remarkably. The chain length of the ditertiaryphosphines, $Ph_2P(CH_2)_nPPh_2$ (n=1,2,3,4), was found to have a great effect on the catalytic behavior in the reaction of ethyl aectoacetate with 1,3-butadiene, as is shown in Table 3. It is clear that $Ph_2P(CH_2)_nPPh_2$ (n=2,3) is favorable ligand for the formation of the 1 : 1 adducts. The reaction using $Ph_2P(CH_2)_4PPh_2$ as a catalyst component gave mainly a 1 : 2 adduct, ethyl 2-acetyl-4,9-decadienoate, plus a small amount of the 1 : 1 adducts. The former diphosphines would form stable chelate rings with the palladium atom. However, the chelation of the latter diphosphine is much less favored, for the diphosphine behaves like a unidentate ligand.[5] α,α'-Dipyridyl and 2-(diphenylphosphine)-ethyl phenyl sulfide, $Ph_2PCH_2CH_2SPh$, showed a ligand effect on the products similar to that of $Ph_2P(CH_2)_nPPh_2$ (n=2,3).

Isoprene reacted with acetylacetone to give three kinds of 1 : 1 adducts with unidentified 2 : 1 adducts. The first product to emerge in the vpc (Silicone DC 550 column) was identified as **4** by IR and NMR-spectroscopic measurements.

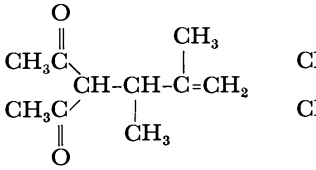

4

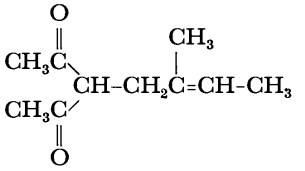

5

6) a) A. Miyake, G. Hata, M. Iwamoto, and S. Yuguchi, "Proceedings of the 7th World Petroleum Congress, Panel Discussion," Vol. 22, (1967), p. 37. b) M. Iwamoto and S. Yuguchi, *J. Org. Chem.*, **31**, 4290 (1966). c) G. Hata and A. Miyake, This Bulletin, **41**, 2762 (1968).

Table 1. Reactions of active methylene compounds with 1,3-butadiene catalyzed by $PdBr_2(DPE)_2$ and PhONa

Active methylene compound (mol)	BD[a] mol	Catalyst mmol $PdBr_2(DPE)_2$[b]	Catalyst mmol PhONa	Temp. °C	Time hr	Products[c] (%)[d]
$CH_3COCH_2COCH_3$ (0.2)	0.3	0.25	2.5	140—151	2	$CH_3COCHXCOCH_3$(17), $CH_3COCHYCOCH_3$(43) $CH_3COC(C_4H_7)_2COCH_3$(5)
$CH_3COCH_2COCH_3$ (0.1)	0.3	0.25	2.5	133—148	1	$CH_3COCHXCOCH_3$(10), $CH_3COCHYCOCH_3$(7) $CH_3COC(C_4H_7)_2COCH_3$(62)
$CH_3COCH_2CO_2C_2H_5$ (0.2)	0.3	0.25	2.5	142—154	2	$CH_3COCHXCO_2C_2H_5$(35), $CH_3COCHYCO_2C_2H_5$(36) $CH_3COC(C_4H_7)_2CO_2C_2H_5$(1)
$CH_3COCH_2CO_2C_2H_5$ (0.1)	0.15	0.25	2.5	90	0.5	——
$CH_3COCH_2CO_2C_2H_5$ (0.1)	0.15	0.25	0.25	150	0.5	——
$CH_3COCH_2CO_2C_2H_5$ (0.1)	0.15	0.25	0.75	150	0.5	$CH_3COCHXCO_2C_2H_5$(8), $CH_3COCHYCO_2C_2H_5$(6)
$CH_2(CO_2C_2H_5)_2$ (0.2)	0.3	0.25	2.5	145—148	2	$CHX(CO_2C_2H_5)_2$(18), $CHY(CO_2C_2H_5)_2$(18)

a) BD=1,3-butadiene, b) DPE=$Ph_2PCH_2CH_2PPh_2$, c) X=-$CH(CH_3)CH{=}CH_2$, Y=-$CH_2CH{=}CHCH_3$, C_4H_7=mixture of X and Y
d) Based on the active methylene compounds employed.

Table 2. Reaction of ethyl acetoacetate with 1,3-butadiene catalyzed by Pd-DPE catalysts

Catalyst[a] mmol	$CH_3COCH_2CO_2C_2H_5$ mol	BD mol	Temp. °C	Time hr	Products[b] %[c] $CH_3COCHXCO_2C_2H_5$	$CH_3COCHYCO_2C_2H_5$	$CH_3COC(C_4H_7)_2CO_2C_2H_5$
$PdBr_2(DPE)_2$ 0.25	0.1	0.15	140—150	16	—	—	—
$PdBr_2(DPE)_2$-PhONa 0.25 2.5	0.2	0.3	142—154	2	35	36	1
$PdCl_2$ DPE 0.5 1.25	0.1	0.15	140—150	16	—	—	—
$PdCl_2$-DPE-PhONa 0.2 0.5 2.5	0.1	0.15	150—152	2	28	33	1
$Pd(NO_2)_2(NH_3)_2$-DPE 0.5 1.25	0.1	0.15	142—150	1	22	25	4
$Pd(OCOCH_3)_2$-DPE 0.2 0.5	0.1	0.15	140—152	16	35	40	18
$Pd(acac)_2$-DPE 0.2 0.5	0.1	0.15	150—152	5	16	22	3
$Pd(DPE)_2$ 0.25	0.1	0.15	140—150	2	12	15	—
$Pd(DPE)_2$-PhOH 0.25 2.5	0.2	0.3	140—150	2	32	40	16
$Pd(DPE)_2$-PhONa 0.25 2.5	0.1	0.15	141—148	2	37	37	16

a) DPE=$Ph_2PCH_2CH_2PPh_2$, acac=acetylacetonate, b) X=-$CH(CH_3)CH{=}CH_2$, Y=-$CH_2CH{=}CHCH_3$, C_4H_7=mixture of X and Y
c) Based on ethyl acetoacetate employed.

Table 3. Comparison of effect of bidentate donors in the reaction of ethyl acetoacetate with 1,3-butadiene[a,b]

Bidentate donor	Time hr	Products[c] % [d]			
		$CH_3COCHXCO_2C_2H_5$	$CH_3COCHYCO_2C_2H_5$	$CH_3COC(C_4H_7)_2CO_2C_2H_5$	$CH_3COCHZCO_2C_2H_5$
$Ph_2PCH_2PPh_2$	2	trace	trace	—	—
$Ph_2PCH_2CH_2PPh_2$	2	28	33	1	—
$Ph_2P(CH_2)_3PPh_2$	1	29	49	7	7
$Ph_2P(CH_2)_4PPh_2$	1	7	4	—	53
$Ph_2PCH_2CH_2SPh$	20	5	9	—	—
α,α'-Dipyridyl	20	6	25	2	14

a) Catalyst; $PdCl_2$ 0.2 mmol, PhONa 2.5 mmol, bidentate donor 0.5 mmol.
b) Temperature 150°C.
c) X=$-CH(CH_3)CH=CH_2$, Y=$-CH_2CH=CHCH_3$, C_4H_7=mixture of X and Y, Z=$-CH_2CH=CH(CH_2)_3CH=CH_2$.
d) Based on ethyl acetoacetate employed.

Table 4. Reactions of active methylene compounds with 1,3-dienes catalyzed by $PdBr_2(Ph_2PCH_2CH_2PPh_2)_2$ and PhONa[a]

Active methylene compound mol	1,3-Diene mol	Temp. °C	Time hr	Products[b] %[c]
$CH_3COCH_2CO_2C_2H_5$ 0.1	isoprene 0.15	141—150	1	$CH_3COCHRCO_2C_2H_5$, 12; $CH_3COCHSCO_2C_2H_5$, 46; $CH_3COC(C_5H_9)_2CO_2C_2H_5$, 23
$CH_3COCH_2COCH_3$ 0.1	isoprene 0.15	136—146	2	$CH_3COCHRCOCH_3$, 7; $CH_3COCHR'COCH_3$, 60; $CH_3COC(C_5H_9)_2COCH_3$, 6
$CH_3COCH_2CO_2C_2H_5$ 0.1	1,3-pentadiene 0.15	137—148	15	$CH_3COCH[CH(CH_3)CH=CHCH_3]CO_2C_2H_5$, 61; $CH_3COCH(CH_2CH=CHCH_2CH_3)CO_2C_2H_5$, 7
$CH_3COCH_2CO_2C_2H_5$ 0.1	2,4-hexadiene 0.15	140—150	20	$CH_3COCH[CH(CH_3)CH=CHCH_2CH_3]CO_2C_2H_5$, 45

a) Catalyst; $PdBr_2(Ph_2PCH_2CH_2PPh_2)_2$ 0.25 mmol, PhONa 2.5 mmol.
b) R=$-CH(CH_3)C(CH_3)=CH_2$, R'=mixture of $-CH_2C(CH_3)=CHCH_3$ and $-CH_2CH=C(CH_3)CH_3$, C_5H_9=mixture of R and R'.
c) Based on the active methylene compounds employed.

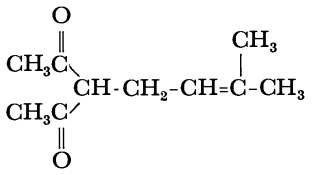

6

The compound **4** showed an IR absorption at 884 cm^{-1} due to the out-of-plane deformation of $>C=CH_2$, and NMR signals at 9.05 (3H, d, J=6.0 Hz), 8.30 (3H, s), 7.75 and 7.99 (6H, two s), 6.7—7.3(1H, m), 6.22(1H, d, J=11.0 Hz), and 5.25(2H, s). The spectrum of the second product to emerge showed a pair of triplet signals at 6.43 and 6.23 (J=7.5 Hz) due to the active methine hydrogen atom. This indicates that the product consists of two components. The IR spectrum exhibited no absorption characteristic of the $>C=CH_2$ or $-CH=CH_2$ bond, indicating that the products are not derived from the 1,2-addition of the active methylene to isoprene, but from the 1,4-addition. From the above spectral characteristics, the product can reasonably be estimated to be a mixture of **5** and **6**.

Ethyl acetoacetate also reacted with isoprene to give products similar to those derived from the 1,2- and 1,4-addition of the active methylene to isoprene.

The addition of 1,3-pentadiene to ethyl acetoacetate yielded two 1 : 1 adducts, **7** and **8**, in 61 and 7% yields respectively.

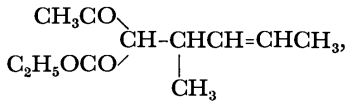

7

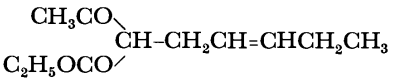

8

The reaction of 2,4-hexadiene with ethyl acetoacetate afforded a 1 : 1 adduct, **9**, selectively. The reactivity of the diene was much lower than those of 1,3-butadiene and isoprene. The results of the reaction

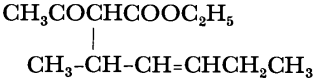

9

of active methylene compounds with substituted 1,3-butadienes are summarized in Table 4.

Primary and secondary amines also reacted with 1,3-butadiene in the presence of palladium-diphosphine complex catalysts to afford two 1 : 1 adducts, **10** and **11**. The results are shown in Table 5. The catalytic activity was remarkably enhanced by the addition of a small amount of phenol.

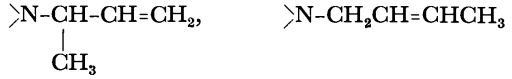

10 **11**

A change in the amount of phenol affected the yields of the products and the ratio of **11** to **10**, which was investigated in the reaction of piperidine with 1,3-butadiene. In the presence of a large amount of phenol, *N*-(2-butenyl)piperidine was the predominant product, as is shown in Table 5.

It is interesting to note that the reactivity of amines was associated with their basicity.[7] The more basic amines are more reactive. The reaction of morpholine (pK=9.61) and aniline (pK=9.42) gave the 1 : 1 adducts in 79 and 67% yields respectively. On the other hand, the reaction of less basic amines, such as *n*-butylamine (pK=3.39) and piperidine (pK=2.80), afforded the 1 : 1 adducts in 19 and 29% yields respectively.

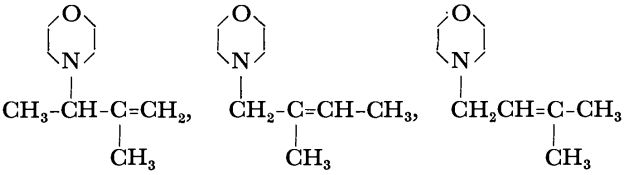

12 **13** **14**

The addition of isoprene to morpholine in the presence of $PdBr_2(Ph_2PCH_2CH_2PPh_2)_2$, sodium phenoxide, and phenol resulted in a formation of 1 : 1 adducts, **12**, **13**, and **14**, in 9, 30, and 16% yields respectively.

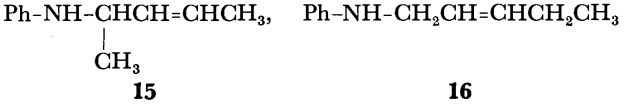

15 **16**

The reaction of 1,3-pentadiene with aniline gave two kinds of 1 : 1 adducts, **15** and **16**, in 52 and 5% yields respectively. No 2 : 1 adduct was formed.

The addition of 2,4-hexadiene to aniline also afforded a 1 : 1 adduct, **17**.

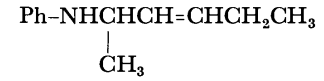

17

Experimental

Reagents. $Ph_2P(CH_2)_nPPh_2$,[8] $PdBr_2(Ph_2PCH_2CH_2PPh_2)_2$,[9] $Pd(Ph_2PCH_2CH_2PPh_2)_2$,[9] $Pd(OCOCH_3)_2$,[10] $Pd(acac)_2$,[11] and $Pd(NO_2)_2(NH_3)_2$[12] were prepared by the previously-reported methods.

Acetylacetone, ethyl acetoacetate, diethyl malonate, and amines were purified by distillation. 2-Oxocyclododecanecarbaldehyde[13] was prepared according to the procedure

7) N. A. Lang, Ed., "Handbook of Chemistry," McGraw-Hill Book Company, Inc., New York, N.Y. (1961), p. 1202.

8) a) W. Hewertson and H. R. Watson, *J. Chem. Soc.*, **1962**, 1490. b) K. Issleib and D. W. Miller, *Chem. Ber.*, **92**, 3175 (1959).

9) J. Chatt, F. A. Hart, and H. R. Watson, *J. Chem. Soc.*, **1962**, 2537.

10) T. Matsuda, T. Mitsuyasu, and Y. Nakamura, *Kogyo Kagaku Zasshi*, **72**, 1751 (1969).

11) A. A. Grenberg and L. K. Simonova, *Zhur. Prikl. Khim.*, **26**, 880 (1953); *Chem. Abstr.*, **47**, 11060 (1953).

12) J. C. Bailar, Jr., Ed., "Inorganic Syntheses," Vol. IV, McGraw-Hill Book Company, Inc., New York, N.Y. (1953), p. 179.

13) V. Prelog, L. Ruzicka, and O. Metzler, *Helv. Chim. Acta.*, **30**, 1882 (1947).

Table 5. Reactions of amines with 1,3-dienes

Amine[a]	1,3-Diene[b]	Catalyst[c] mmol	Temp. °C	Time hr	Products[d] %[e]		Residue g
$PhNH_2$	BD	$PdBr_2(DPE)_2$, 0.25 PhONa 2.5	155—158	20	PhNHX 18	PhNHY 13	1.7
$PhNH_2$	BD	$PdBr_2(DPE)_2$, 0.25 PhONa, 2.5 PhOH 2.5	155—162	0.5	PhNHX 44	PhNHY 15	3.1
$PhNH_2$	BD	$PdBr_2(DPE)_2$, 0.25 PhONa, 2.5 PhOH 5.0	85	3	PhNHX 57	PhNHY 10	1.3
cyclo-$C_6H_{11}NH_2$	BD	$PdBr_2(DPE)_2$, 0.25 PhONa, 2.5 PhOH 2.5	141—146	20	cyclo-C_6H_{11}NHX 18	cyclo-C_6H_{11}NHY 23	1.3
$(C_2H_5)_2NH$	BD	$Pd(DPE)_2$ 0.25 PhOH 2.5	144—148	5	$(C_2H_5)_2$NY 21		1.0
n-$C_4H_9NH_2$	BD	$PdBr_2(DPE)_2$, 0.25 PhONa, 2.5 PhOH 2.5	130—139	5	*n*-C_4H_9NHX 12	*n*-C_4H_9NHY 7	0.9
$PhCH_2NH_2$	BD	$PdBr_2(DPE)_2$, 0.25 PhONa, 2.5 PhOH 2.5	145—153	3	$PhCH_2$NHX 10	$PhCH_2$NHY 2	5.0
p-$CH_3C_6H_4NH_2$	BD	$PdBr_2(DPE)_2$, 0.25 PhONa, 2.5 PhOH 2.5	85	3	*p*-$CH_3C_6H_4$NHX 32	*p*-$CH_3C_6H_4$NHY 6	0.9
	BD	$PdBr_2(DPE)_2$, 0.25 PhONa, 2.5 PhOH 2.5	138—147	2	10	19	2.2
	BD	$PdBr_2(DPE)_2$, 0.25 PhONa, 2.5 PhOH 5	150	1	10	26	—[f]
	BD	$PdBr_2(DPE)_2$, 0.25 PhONa, 2.5 PhOH 10	150	1	6	50	—[f]
	BD	$Pd(DPE)_2$ 0.25	136—160	20	4	64	1.4
	BD	$Pd(DPE)_2$ 0.25 PhOH 2.5	141—152	1	5	65	1.3
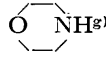 [g]	BD	$PdBr_2(DPE)_2$, 0.25 PhONa, 2.5 PhOH 2.5	143—152	1	32	47	2.4
[h]	IP	$PdBr_2(DPE)_2$, 0.25 PhONa, 2.5 PhOH 2.5	140—146	2	9 16	30	2.4
$PhNH_2$	1,3-PD	$PdBr_2(DPE)_2$, 0.25 PhONa, 2.5 PhOH 2.5	130—140	24	PhNH-CH(CH_3)CH=$CHCH_3$, 52	$PhNHCH_2CH$=$CHCH_2CH_3$ 5	1.7
$PhNH_2$	2,4-HD	$PdBr_2(DPE)_2$, 0.25 PhONa, 2.5 PhOH 2.5	136—143	24	PhNH-CH(CH_3)CH=$CHCH_2CH_3$ 9		1.4

a) 0.1 mol, b) 0.15 mol BD=1,3-butadiene, IP=isoprene, 1,3-PD=1,3-pentadiene, 2,4-HD=2,4-hexadiene, c) DPE=$Ph_2PCH_2CH_2PPh_2$, d) X=$-CH(CH_3)CH=CH_2$, Y=$-CH_2CH=CHCH_3$, e) Based on amine employed, f) Not measured, g) *N*-(2,7-octadienyl)morpholine was formed in an 11% yield, h) *N*-(dimethyl-2,7-octadienyl)-morpholine was formed in a 7% yield.

Table 6. Physical and analytical data of the products—1

Product[a]	Bp °C/mmHg	n_D^{25}	Empirical formula	Calcd			Found		
				C%	H%	Mol wt	C%	H%	Mol wt[b]
X-CH($COCH_3$)$_2$	199	1.4479	$C_9H_{14}O_2$	70.10	9.15	154	69.66	9.12	161
Y-CH($COCH_3$)$_2$	202	1.4602	$C_9H_{14}O_2$	70.10	9.15	154	70.30	9.23	155
X-CH($COCH_3$)$CO_2C_2H_5$	215	1.4372	$C_{10}H_{16}O_3$	65.19	8.70	184	65.18	8.75	183
Y-CH($COCH_3$)$CO_2C_2H_5$	220	1.4422	$C_{10}H_{16}O_3$	65.19	8.70	184	64.94	8.48	184
X-CH($CO_2C_2H_5$)$_2$	233	1.4330	$C_{11}H_{18}O_4$	61.66	8.47	214	61.76	8.39	207
Y-CH($CO_2C_2H_5$)$_2$	235	1.4346	$C_{11}H_{18}O_4$	61.66	8.47	214	61.83	8.37	214
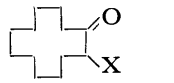	128/2	1.4880	$C_{16}H_{28}O$	81.29	11.94	236	80.92	12.21	227
R-CH($COCH_3$)$_2$	64/5	1.4538	$C_{10}H_{16}O_2$	71.39	9.59	168	71.57	9.65	168
R-CH($COCH_3$)$CO_2C_2H_5$	228	1.4443	$C_{11}H_{18}O_3$	66.59	9.15	198	66.79	9.18	199
CH_3CH=$CHCH(CH_3)CH$-($COCH_3$)$CO_2C_2H_5$	62/1	1.4414	$C_{11}H_{18}O_3$	66.59	9.15	198	66.50	9.08	201
CH_3CH_2CH=$CHCH_2CH$-($COCH_3$)$CO_2C_2H_5$	—	1.4448	$C_{11}H_{18}O_3$	66.59	9.15	198	67.35	9.08	191
CH_3CH_2CH=$CHCH(CH_3)CH$-($COCH_3$)$CO_2C_2H_5$	96—8/5	1.4460	$C_{12}H_{20}O_3$	67.89	9.50	212	67.81	9.52	206

a) X=-$CH(CH_3)CH$=CH_2, Y=-CH_2CH=$CHCH_3$, R=-$CH(CH_3)C(CH_3)$=CH_2.
b) Measured by vapor pressure osmometry.

described before.

The purification of 1,3-butadiene was accomplished by the vaporization of the liquid diene containing triethylaluminum. Isoprene, 1,3-pentadiene, and 2,4-hexadiene were distilled under an argon atmosphere.

General Procedure for the Reaction of Active Methylene Compounds and Amines with 1,3-Butadiene. A 100 m*l* stainless steel autoclave was charged with an active methylene compound or amine and catalyst components. The liquid 1,3-butadiene was vaporized in order to condense it in an autoclave chilled with dry ice and methanol which had been evacuated beforehand. The reaction was carried out by stirring at 140—150°C. The reaction mixture was distilled and analyzed by vpc. The products were separated by fractional distillation and by the use of preparative gas chromatography. The analytical and physical data of the products are listed in Tables 6 and 7.

Reaction of Acetylacetone with 1,3-Butadiene. A mixture of 0.2 mol of acetylacetone, 0.3 mol of 1,3-butadiene, 0.25 mmol of $PdBr_2(Ph_2PCH_2CH_2PPh_2)_2$, and 2.5 mmol of sodium phenoxide was stirred at 140—151°C for 2 hr. The products consisted of **1a** (5.3 g, 17%), **2a** (13.2 g, 43%), **3a** (2.1 g, 5%), and a residue (1.6 g). The spectroscopic data of the products are as follows: **1a** ν_{max} 1722 and 1700 cm^{-1} (β-diketone), 1644, 998 and 922 cm^{-1} (-CH=CH_2); τ 9.03 (d, J=6.5 Hz, CH_3-C-C=), 7.95 and 7.87 (CH_3CO-), 6.7—7.3 (m, CO-C-CH-), 6.45 (d, J=10.0 Hz, CO-CH-CO) and 4.0—5.2 (m, olefinic protons), **2a** ν_{max} 1725, 1701 and 1605 cm^{-1} (β=diketone), 968 cm^{-1} (*trans* -CH=CH-); 8.36 (d, J=6.0 Hz, CH_3-C=), 7.95 and 7.92 (CH_3CO-), 7.70—7.35 (br. t, CO-C-CH_2-C=, keto form), 7.09 (br, s, CO-C-CH_2-C=, enol form), 6.40 (t, J=7.0 Hz, CO-CH-CO, keto form), and 4.8—4.4 (m, olefinic protons).

Reaction of 2-Oxocyclododecanecarbaldehyde with 1,3-Butadiene. A mixture of 0.036 mol of 2-oxocyclododecanecarbaldehyde, 0.1 mol of 1,3-butadiene, 0.18 mmol of $PdBr_2(Ph_2PCH_2CH_2PPh_2)_2$, and 1.8 mmol of phenoxide was stirred at 138—142°C for 15 hr. The distillation of the resultant solution gave 4.9 g of a fraction boiling at 168—170°C/3 mmHg. The IR spectrum of the fraction showed an absorption due to the out-of-plane deformation of *trans* -CH=CH- near 960 cm^{-1}, and no absorptions due to the out-of-plane deformation of -CH=CH_2. The intensity of the NMR signal due to -CHO corresponded to only about 0.2 H (τ 1.39, s). This fact indicates that the decarbonylation from the aldehyde group of the first formed product, 1-(2-butenyl)-2-oxocyclododecanecarbaldehyde, takes place. The treatment of the fraction with sodium ethoxide in ethanol gave 2-(2-butenyl)cyclododecanone. It exhibited the following spectral characteristics: ν_{max} 1708 cm^{-1} (>C=O) and 965 cm^{-1} (*trans* -CH=CH-); τ 4.8—4.3 (m, olefinic protons).

Reaction of Acetylacetone with Isoprene. A mixture of 0.1 mol of acetylacetone, 0.15 mol of isoprene, 0.25 mmol of $PdBr_2(Ph_2PCH_2CH_2PPh_2)_2$, and 2.5 mmol of sodium phenoxide was stirred at 136—146°C for 2 hr to afford **4** (1.1 g, 7%) and a mixture of **5** and **6** (10.1 g, 60%). The product **4** showed the following spectral characteristics: ν_{max} 1710 and 1700 cm^{-1} (β-diketone), 1644 and 898 cm^{-1} (>C=CH_2); τ 9.05 (d, J=6.0 Hz, CH_3-C-C=), 8.30 (s, CH_3C=), 7.99 and 7.75 (CH_3CO-), 7.3—6.7 (m, -CH-C-CO-), 6.22 (d, J=11.0 Hz, -CH-CO-), and 5.25 (s, CH_2=C-).

Reaction of Ethyl Acetoacetate with 1,3-Pentadiene. A mixture of 0.1 mol of ethyl acetoacetate, 0.15 mol of 1,3-pentadiene, 0.25 mmol of $PdBr_2(Ph_2PCH_2CH_2PPh_2)_2$, and 2.5 mmol of sodium phenoxide was stirred at 137—148°C for 15 hr to yield **7** (12.0 g, 61%) and **8** (1.4 g, 7%). The product **7** showed the following spectral characteristics: ν_{max} 1745 and 1715 cm^{-1} (keto ester), 970 cm^{-1} (*trans* -CH=CH-); 9.05 and 9.01 (two d, J=6.5 Hz, CH_3-C-C=), 8.80 and 8.76 (two t, J=7.0 Hz, CH_3C-O-), 8.41 (d, J=5.0 Hz, CH_3-C=), 7.95 and 7.91 (two s, CH_3CO-), 6.81 (d, J=10.0 Hz, -CO-CH-CO-), 5.92 and 5.87 (two q, J=7.0 Hz, -O-CH_2-C), and 4.9—4.3 (m, olefinic protons). Two kinds of signals due to acetyl, ethyl, and one of the methyl groups on the side chain indicate that the compound is a mixture of the *erythro* and *threo* isomers. The product **8**

Table 7. Physical and analytical data of the products—2

Product[a)]	Bp °C/mmHg	n_D^{25}	Empirical formula	Calcd %			Found %		
				C	H	N	C	H	N
PhNH-X	98/12	1.5451	$C_{10}H_{13}N$	81.45	8.90	9.51	81.43	8.93	9.62
PhNH-Y	113/12	1.5537	$C_{10}H_{13}N$	81.45	8.90	9.51	81.38	8.83	9.75
cyclo-C_6H_{11}NH-X	187	1.4598	$C_{10}H_{19}N$	78.36	12.49	9.14	78.07	12.38	9.09
cyclo-C_6H_{11}NH-Y	209	1.4701	$C_{10}H_{19}N$	78.36	12.49	9.14	78.27	12.25	8.62
$(C_2H_5)_2$N-Y	57—58/42	1.4313	$C_8H_{17}N$	75.52	13.47	11.09	75.44	13.27	10.72
n-C_4H_9NH-X	143	1.4220	$C_8H_{17}N$	75.52	13.47	11.09	75.46	13.46	11.01
n-C_4H_9NH-Y	164	1.4332	$C_8H_{17}N$	75.52	13.47	11.09	75.22	13.58	11.01
$PhCH_2NH$-X	218	1.5102	$C_{11}H_{15}N$	81.94	9.38	8.68	81.82	9.38	8.87
$PhCH_2NH$-Y	240	1.5192	$C_{11}H_{15}N$	81.94	9.38	8.68	82.03	9.48	8.71
p-CH_3-C_6H_4-NH-X	237	1.5380	$C_{11}H_{15}N$	81.94	9.38	8.68	81.97	9.53	8.87
p-CH_3-C_6H_4-NH-Y	260	1.5455	$C_{11}H_{15}N$	81.94	9.38	8.68	82.03	9.48	8.71
	169	1.4607	$C_9H_{17}N$	77.64	12.37	9.99	77.46	12.35	10.04
	180	1.4634	$C_9H_{17}N$	77.64	12.37	9.99	77.47	12.37	10.08
	171	1.4601	$C_8H_{15}NO$	68.04	10.71	9.92	67.99	10.80	9.92
	187	1.4633	$C_8H_{15}NO$	68.04	10.71	9.92	67.98	10.69	9.86
	193	1.4620	$C_9H_{17}NO$	69.63	11.04	9.02	69.93	11.12	8.89
	197	1.4635	$C_9H_{17}NO$	69.63	11.04	9.02	69.56	11.03	9.03
	240	1.4681	$C_9H_{17}NO$	69.63	11.04	9.02	69.55	11.12	8.88
PhNH-$CH(CH_3)$C=$CHCH_3$	74—76/2	1.5418	$C_{11}H_{15}N$	81.94	9.38	8.68	82.05	9.35	8.46
PhNH-CH_2CH=$CHCH_2CH_3$	92—93/2	1.5412	$C_{11}H_{15}N$	81.94	9.38	8.68	82.00	9.35	8.68
PhNH-$CH(CH_3)$CH=$CHCH_2CH_3$	94—95/2.5	1.5353	$C_{12}H_{17}N$	82.23	9.78	7.99	81.96	9.68	8.12

a) X=-$CH(CH_3)CH=CH_2$, Y=-$CH_2CH=CHCH_3$.

showed the following spectral characteristics: ν_{max} 1745 and 1715 cm^{-1} (keto ester), 1648 and 967 cm^{-1} (*trans* -CH=CH-); τ 9.05 (t, $J=7.5$ Hz, CH_3C-C=), 8.75 (t, $J=7.0$ Hz, CH_3C-O-), 8.20—7.75 (m, C-CH_2-C=), 7.90 (s, CH_3CO-), 7.56 (t, $J=7.0$ Hz, -CO-C-CH_2-C), 6.68 (t, $J=7.0$ Hz, -CO-CH-CO-), 5.87 (q, $J=7.0$ Hz, -O-CH_2-C), and 4.9—4.3 (m, olefinic protons).

Reaction of Ethyl Acetoacetate with 2,4-Hexadiene. The reaction was carried out for 24 hr under the same conditions as those used in the reaction of ethyl acetoacetate with 1,3-pentadiene. The product (9.6 g, 45%) was identified as **9**: ν_{max} 1745 and 1715 cm^{-1} (keto ester), 1650 and 968 cm^{-1} (*trans* -CH=CH-); τ 9.1—8.8 (m, CH_3-C-C= and CH_3-C-C-CO), 8.68 and 8.66 (two t, $J=7.0$ Hz, -O-C-CH_3). 8.1—7.7 (m, C-CH_2-C=), 7.81 and 7.76 (two s, CH_3CO-), 7.4—6.8 (m, C-CH-C=), 6.60 (d, $J=10.0$ Hz, -CO-CH-CO-), 5.80 and 5.75 (two q, $J=7.0$ Hz, -O-CH_2-C), and 4.8—4.2 (m, olefinic protons).

Reaction of Aniline with 1,3-Butadiene. A mixture of 0.1 mol of aniline, 0.15 mol of 1,3-butadiene, 0.25 mmol of $PdBr_2(Ph_2PCH_2CH_2PPh_2)_2$, 2.5 mmol of sodium phenoxide, and 2.5 mmol of phenol was stirred at 85° for 3 hr to afford *N*-(1-methyl-2-propenyl)aniline (8.4 g, 57%) and *N*-(2-butenyl) aniline (1.4 g, 10%). The former product showed the following spectral characteristics: ν_{max} 3430 cm^{-1} (N-H), 1644, 992, and 915 cm^{-1} (-CH=CH_2); τ 8.77 (d, $J=7.0$ Hz, CH_3-C-C=), 6.60 (s, -NH-), 6.3—5.8 (m, -N-CH-), 5.15—4.27 (m, -CH=CH_2), and 3.65—2.75 (m, phenyl protons). *N*-(2-Butenyl)aniline exhibited the following spectral characteristics: ν_{max} 3410 cm^{-1} (N-H), 963 cm^{-1} (*trans* -CH=CH-); 8.35 (d, $J=5.0$ Hz, CH_3-C=), 6.55 s, N-H), 6.5—6.25 (m, -N-CH_2-C=), 4.8—4.1 (m, olefinic protons), and 3.65—2.75 (m, phenyl protons).

Reaction of Morpholine with Isoprene. A mixture of 0.1 mol of morpholine, 0.15 mol of isoprene, 0.25 mmol of $PdBr_2(Ph_2PCH_2CH_2PPh_2)_2$, 2.5 mmol of sodium phenoxide, and 2.5 mmol of phenol was stirred at 140—146°C for 2 hr to yield **12** (1.4 g, 9%), **13** (4.7 g, 30%), **14** (2.4 g, 16%), and a small amount of *N*-(dimethyl-2,7-octadienyl)morpholine. The products showed the following spectroscopic data: **12**: ν_{max} 1653 and 896 cm^{-1} (>C=CH_2); τ 8.93 (d, $J=6.5$ Hz, CH_3-C-C=), 8.36 (s, CH_3-C=), 7.7 and 6.45 (protons of morpholine), 7.34 (q, $J=6.5$ Hz, C-CH-C=), 5.29 and 5.22 (olefinic protons); **13**: ν_{max} 1674 (>C=C<); τ 8.44 (d, $J=3.0$ Hz, CH_3-C-N-), 8.42 (s, CH_3-C=), 7.55 and 6.45 (morpholine protons), 7.28 (s, -N-CH_2-C=), and 4.85—4.5 (m, -C=CH-); **14**: ν_{max} 1676 cm^{-1} (>C=C<); τ 8.40 and 8.31 (two s, =$C(CH_3)_2$), 7.70 and 6.50 (morpholine protons), 7.18 (d, $J=7.0$ Hz, -N-CH_2-C=), and 4.85 (t, $J=7.0$ Hz, -N-C-CH=).

BULLETIN OF THE CHEMICAL SOCIETY OF JAPAN, VOL. 45, 1191—1198 (1972)

Phenolyses of 1-Adamantyl Chloride, Bromide, and *p*-Toluenesulfonate in Binary Mixtures of Phenol with Benzene. The Rates and the Product Distribution

Kunio Okamoto, Kôichi Matsubara, and Tomomi Kinoshita

Department of Hydrocarbon Chemistry, Faculty of Engineering, Kyoto University, Sakyo-ku, Kyoto

(Received October 25, 1971)

Adamantyl derivatives, the bridgehead substrates, have been chosen as the reference compounds in the assessment of the ionizing power of phenolic solvents in the S_N1-type solvolysis. The S_N1-phenolyses of 1-adamantyl chloride, bromide, and *p*-toluenesulfonate have been studied at several temperatures in binary mixtures of phenol with benzene; the enthalpies and entropies of activation have been calculated. Phenolysis has also been made on *t*-butyl chloride in order to estimate the Grunwald-Winstein *Y* values for the phenol-benzene solvents. The solvolysis rates of 1-adamantyl compounds, including the literature values, have been correlated with the *Y* values and also with the dielectric constants ($(D-1)/(2D+1)$). A significant deviation is found for the phenolic solvents in both correlations; this deviation is discussed in terms of the electrophilic assistance by hydrogen-bonding of the phenolic solvents to the leaving group. The isolated phenolysis products have been characterized as 1-adamantyl phenyl ether, *o*-, and *p*-1-adamantylphenols. The product compositions for the reactions of the ion-pair intermediate with the phenol molecule and with the phenoxide ion have been estimated on the basis of the variation in the overall product compositions, caused by the increase in the concentrations of the added phenoxide or amine.

In previous studies of the phenolysis rates for *t*-butyl halides,[1] benzyl chloride,[1] 1-phenylethyl derivatives,[2] and benzhydryl bromide,[1] it has been demonstrated that phenol is a typical solvolytic solvent and that it is prominent[3] in giving hydrogen-bonding electrophilic assistance to the ionization of these substrates. However, little study has been made of the quantitative assessment of its solvolytic ionizing power.

Because the adamantyl system has no possibilities for elimination or for rear-side solvent attack, and because, consequently, its solvolysis rate exactly reflects the rate of the ionization process, Schleyer and his collaborators[4] recently suggested the use of 1-adamantyl bromide as a reference compound for the assessment of the ionizing power of a solvolytic solvent.

In the present paper we will report on the results of the assessment of the ionizing power of the phenolic

1) H. Shingu and K. Okamoto, *Nippon Kagaku Zasshi*, **81**, 111 (1960).

2) K. Okamoto, T. Kinoshita, and H. Shingu, This Bulletin, **43**, 1545 (1970), and the references cited therein.

3) K. Okamoto and H. Shingu, *ibid.*, **34**, 1131 (1961).

4) D. J. Raber, R. C. Bingham, J. M. Harris, J. L. Fry, and P. v. R. Schleyer, *J. Amer. Chem. Soc.*, **92**, 5977 (1970).

solvent by the use of this new reference system, including 1-adamantyl chloride, bromide, and *p*-toluenesulfonate; we will also report on the distribution of 1-adamantyl phenyl ether, *o*-, and *p*-1-adamantylphenols in the phenolysis products.

Results

Phenolysis Rate in Binary Mixtures of Phenol with Benzene. The rates of phenolysis for 1-adamantyl chloride, bromide, and *p*-toluenesulfonate (0.05 M for each) were determined titrimetrically in the presence of 0.05 M triethylamine at several temperatures between 25 and 100°C for binary mixtures of 10, 20, 30, 50, and 70 wt% phenol with benzene. A good first-order behavior was observed for each run. The results are tabulated in Table 1.

Table 1. First-order rate constants for phenolyses of 1-adamantyl derivatives in the presence of 0.05 M Et_3N in phenol-benzene solvents

Temp. (°C)	$k_1 \times 10^6$ (sec^{-1}) PhOH wt% 70	50	30	20	10
	1-Adamantyl *p*-toluenesulfonate				
25.0			39000	13000	1360
	1-Adamantyl bromide				
100.0		1830	200		
75.0	1790	397	51.3		
50.0	299	59.7	8.18		
25.0	29.4	8.18	1.19[a]		
	1-Adamantyl chloride				
100.0	201	151			
75.0	20	38.9			
50.0		5.75			
25.0		0.832[a]			

a) Extrapolated from data at the other temperatures.

Table 2. First-order rate constants for phenolyses of *t*-butyl chloride in the presence of 0.05 M Et_3N in phenol-benzene solvents

Temp. (°C)	$k_1 \times 10^6$ (sec^{-1}) PhOH wt% 90	70	50	30	20	10
100.0					418	47.0
86.0						20.5
75.0					110	9.60
60.0			633			3.12
50.0			288		12.8	1.30
45.0	1740					
40.0	1100					
35.0	675					
25.0	248[a]	117	24.6	6.16	1.74[a]	0.153[a]
Y[b]	+1.427	+1.101	+0.425	−0.192	−0.711	−1.791

a) Extrapolated from data at the other temperatures.
b) k_1 (80% aq. EtOH, 25.0°C) = 9.26×10^{-6} (sec^{-1}) (A. H. Fainberg and S. Winstein, *J. Amer. Chem. Soc.*, **78**, 2770 (1956)).

For the evaluation of the Grunwald-Winstein Y values[5] for these phenolic solvents, the phenolysis rates of *t*-butyl chloride in various phenol-benzene mixtures were also determined in the presence of triethylamine at several temperatures between 25 and 100°C; the results are presented in Table 2, along with the Y values.

The activation parameters for the adamantyl system, calculated from the data of Table 1, are presented in Table 3. The $\Delta H^{\neq}$ values for the phenolic solvents are smaller than those (19—27 kcal/mol) observed for such other hydroxylic solvents[4,6] as aqueous ethanol, aqueous methanol, aqueous dioxane, aqueous tetrahydrofuran, aqueous dimethyl sulfoxide, acetic acid, and formic acid; the $\Delta S^{\neq}$ values are more negative than the $\Delta S^{\neq}$ values (−2——18 eu) for the other hydroxylic solvents.[4,6] The activation parameters for *t*-butyl chloride are also presented in Table 3.

In order to examine the effect of the triethylamine concentration upon the first-order rate constant, the phenolysis rate for 1-adamantyl bromide was determined in a 50 wt% phenol-benzene solvent with variable triethylamine concentrations between 0.00 and 0.10 M at 50.0°C. The results are presented in Table 4. The rate constants are almost invariant in the concentration range employed.

Table 3. Enthalpies ($\Delta H^{\neq}$) and entropies ($\Delta S^{\neq}$) of activation for phenolyses of 1-adamantyl chloride, 1-adamantyl bromide, and *t*-butyl chloride in binaryl mixtures of phenol with benzene

Solvent	$\Delta H^{\neq}$ (kcal/mol)	$\Delta S^{\neq}$ (eu, 25°C)
	1-Adamantyl chloride	
50 wt% PhOH	15.2	−35.4
	1-Adamantyl bromide	
30 wt% PhOH	15.1	−35.1
50 wt% PhOH	15.5	−29.9
70 wt% PhOH	16.3	−24.4
	t-Butyl chloride	
10 wt% PhOH	16.7	−33.9
20 wt% PhOH	16.1	−31.0
50 wt% PhOH	17.7	−20.2
90 wt% PhOH	17.6	−16.0

Table 4. Effect of added triethylamine upon the phenolysis rate for 1-adamantyl bromide in 50 wt% phenol-benzene solvent at 50.0°C

Et_3N (M)	RBr (M)	$k_1 \times 10^5$ (sec^{-1})
0.000	0.052	3.51
0.0040	0.0040	5.72
0.011	0.0080	5.77
0.020	0.016	5.71
0.050	0.040	5.92
0.100	0.080	5.94

5) E. Grunwald and S. Winstein, *ibid.*, **70**, 846 (1948).
6) D. N. Kevill, K. C. Kolwyck, and F. L. Weitl, *ibid.*, **92**, 7300 (1970).

The Product Distribution for the Phenolysis. The reaction mixture from the phenolysis of 1-adamantyl bromide in 50 wt% phenol-benzene at 50°C was chromatographed over silica gel after a usual work-up. The structures of the isolated products (1-adamantyl phenyl ether, *o*-, and *p*-1-adamantylphenols) were assigned on the basis of the elemental compositions and the NMR and IR spectra. The details of the physical constants for these products are described in Table 8 (see Experimental section).

The runs for the product distribution analysis were carried out in a base concentration about ten times greater than the substrate concentration; the composition was assayed by gas chromatography. The effects of added triethylamine and sodium phenoxide upon the product compositions are tabulated in Tables 5 and 6.

Table 5. Effect of added triethylamine upon the product distribution for the phenolysis of 1-adamantyl compounds

Et_3N (M)	RX (M)	Product distribution %[a]		
		ROPh	*o*-RPhOH	*p*-RPhOH
1-Adamantyl chloride (50 wt% PhOH-Benzene, 100.0°C)				
0.00625	0.005	91.5	7.9	0.8
0.0125	0.010	91.5	7.9	0.8
0.025	0.020	91.5	7.9	0.8
0.028	0.025	90.7	8.5	0.8
0.050	0.005	91.7	7.6	0.7
0.100	0.010	89.3	9.6	1.1
0.200	0.050	89.1	9.6	1.3
0.300	0.030	88.9	10.0	1.1
1-Adamantyl bromide (50 wt% PhOH-Benzene, 50.0°C)				
0.0000	0.052	0.0[b]	39.0	61.0
0.00625	0.005	89.4	9.1	1.5
0.0125	0.010	89.3	9.7	1.0
0.025	0.020	90.8	8.0	1.2
0.050	0.040	90.3	8.3	1.4
1-Adamantyl *p*-toluenesulfonate (30 wt% PhOH(-Benzene), 25.0°C)				
0.010	0.0010	89.4	9.0	1.6
0.030	0.0030	88.0	10.3	1.7
0.200	0.002	86.3	11.0	2.7

a) (ROPh+*o*-RPhOH+*p*-RPhOH) % = 100%
b) In the absence of triethylamine, the phenyl ether was undergone the rapid rearrangement to afford *o*- and *p*-1-adamantylphenols, owing to liberation of hydrogen bromide in the course of the phenolysis.

Table 6. Effect of added sodium phenoxide upon the product distribution for the phenolysis of 1-adamantyl chloride in 50 wt% phenol-benzene solvent at 100.0°C

NaOPh (N)	RCl (M)	Product distribution %[a]		
		ROPh	*o*-RPhOH	*p*-RPhOH
0.005	0.0005	89.3	9.7	1.0
0.010	0.0010	86.8	11.4	1.8
0.020	0.0020	84.9	13.1	2.0
0.030	0.0030	83.0	14.2	2.8
0.050	0.0050	80.1	16.4	3.5
0.100	0.010	75.9	19.3	4.8
0.150	0.015	72.3	21.9	5.8

a) (ROPh+*o*-RPhOH+*p*-RPhOH) % = 100%

Rearrangement of 1-Adamantyl Phenyl Ether. It has been known that the *sec*- or *tert*-alkyl phenyl ether readily undergoes rearrangement to give *o*- and *p*-alkylphenols under an acidic catalyst.[7] In fact, in the absence of triethylamine, no phenyl ether was found in the phenolysis products of 1-adamantyl bromide, because of the rapid rearrangement of the phenyl ether to the *o*- and *p*-1-adamantylphenols, a rearrangement caused by the liberated HBr under the phenolysis conditions (Table 5). Therefore, the possibility of the rearrangement for 1-adamantyl phenyl ether could not be eliminated even with the acidity of the solvent phenol. However, we observed no rearrangement of the phenyl ether in the 50 wt% phenol-benzene solvent at 100°C in a 20-hr reaction.

Discussion

The S_N1 Character of the Phenolysis of 1-Adamantyl Derivatives. The effect of added triethylamine upon the titrimetric first-order rate constants for 1-adamantyl bromide are illustrated in Fig. 1 (see also Table 4). The rate constants are almost independent of the concentrations of triethylamine except in the concentration range lower than 0.0050 M. This constancy obviously indicates the S_N1 character of this phenolysis. However, a definite decrease in the rate constant in the absence of an added base indicates that there exists a small amount of "return" in the course of the ionization,[6] one of the simplest reaction schemes to account for the return process may be described as follows:

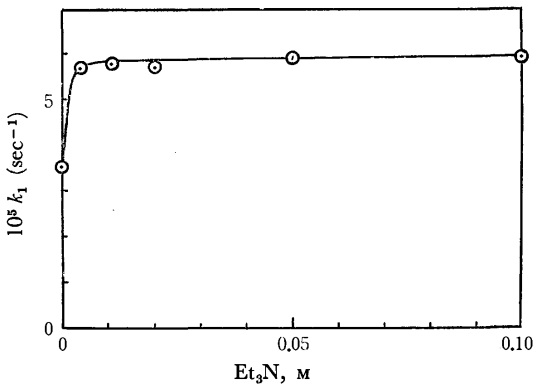

Fig. 1. The effect of added triethylamine upon the titrimetric first-order rate constants for 1-adamantyl bromide in the 1 : 1 (by wt.) Phenol-benzene solvent at 50.0°C.

$$RX \underset{k_{-1}}{\overset{k_1}{\rightleftharpoons}} [\text{Ion-pair Intermediate}] \xrightarrow{k_2[PhOH]+k_{2'}[PhO^{\ominus}]} \text{Products}$$

7) *Cf.* C. K. Ingold, "Structure and Mechanism in Organic Chemistry," 2nd ed., Cornell University Press, Ithaca and London (1969), pp. 904—906.

According to this scheme, we can express the total rate constant, $k_{obs.}$, by Eq. (1);

$$k_{obs.} = \frac{k_1(k_2[PhOH]+k_2'[PhO^{\ominus}])}{k_{-1}+k_2[PhOH]+k_2'[PhO^{\ominus}]} \quad (1)$$

When the magnitude of $(k_2[PhOH]+k_2'[PhO^{\ominus}])$ in Eq. (1) becomes much greater than that of k_{-1} at higher concentrations of $PhO^{\ominus}$, $k_{obs.}$ will virtually agree with k_1 (an ionization rate constant); on the contrary, in the absence of the phenoxide ion ($[PhO^{\ominus}]=0.00$), $k_{obs.}$ is expressed by Eq. (2);

$$k_{obs.} = \frac{k_1k_2[PhOH]}{k_{-1}+k_2[PhOH]} \quad (2)$$

Thus, if these equations apply to this phenolysis, we can calculate the rate ratio k_{-1}/k_2 to be 3.43 for the phenolysis of 1-adamantyl bromide in the 50 wt% phenol-benzene solvent at 50°C, assuming that $k_{obs.}$ at the 0.10 M triethylamine concentration is practically equal to k_1 (see Fig. 1).

In the phenolysis of 1-phenylethyl chloride, we observed a similar decrease in the titrimetric rate constant, k_t, at the lower concentrations of the added base.[8] In this case, the polarimetric rate constant, k_α, was found to be greater than the k_t value are the whole range of base concentrations; furthermore, the gap between k_α and k_t actually widened as the base concentration increased. From this fact we suggested the existence of two successive S_N1 intermediates in the phenolysis of 1-phenylethyl chloride.

In view of the observation for the 1-phenylethyl system, we can not exclusively rule out the possibility of the existence of two successive intermediates for the 1-adamantyl phenolysis, although we have tentatively treated the 1-adamantyl case as a phenolysis with a single ion-pair intermediate in the above reaction scheme. In order to work out a final solution for this problem, we would have to measure directly an intrinsic ionization rate constant, k_1, which may be afforded by the assessment of the oxygen-18 scrambling rate in the phenolysis, using the substrate containing the oxygen-18 atom in the carboxylic-leaving group; this remains a topic for future study.

Ionizing Power for the Phenol-Benzene Solvent. A plot of the logarithms of the rate constants (25°C) for 1-adamantyl bromide and *p*-toluenesulfonate *vs.* the Grunwald-Winstein *Y* values[5] is shown in Fig. 2. The open circles represent the values for the phenol-benzene solvents; the closed circles for 1-adamantyl bromide and *p*-toluenesulfonate designate, respectively the values cited by Schleyer *et al.*[4] and by Kevill *et al.*[6]

It is immediately obvious that the points for phenol-benzene solvents show significant deviations for both bromide and tosylate. Among the reported values, the points for aqueous trifluoroethanol[4] (1-adamantyl bromide) and for acetic acid (1-adamantyl tosylate) also deviate significantly. These anomalies may be ascribed to the results of the specific-substrate and leaving-group interaction.[4] If the extent of the ion-pair return for these phenolysis conditions is not significantly high, the high deviation of the phenolic solvent may be attributed to its high ability of hydrogen-bonding to the leaving group. This feature of the phenolic solvent has been suggested on the basis of the fact[3] that the substantial rate acceleration by *p*-nitrophenol in the acetolysis of *t*-butyl bromide is completely lost in the case of *o*-nitrophenol, the *intermolecular* hydrogen-bonding power of which is reduced or prevented by its *intramolecular* hydrogen-bonding.

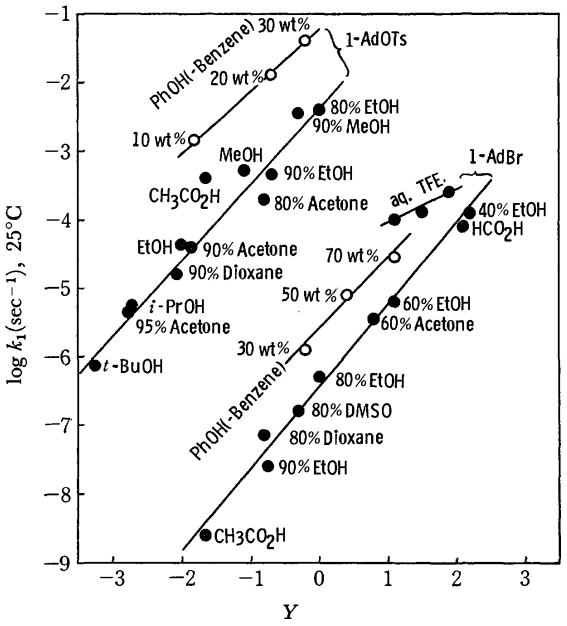

Fig. 2. Correlations of the 1-adamantyl solvolysis rates with Grunwald-Winstein *Y* values.

Since the role of the solvolytic solvent is generally ascribed to the electrostatic stabilization of the transition state,[4,9] it is of interest to express this general solvent effect on the solvolysis rates for 1-adamantyl and *t*-butyl systems by the use of a measure for the electrostatic solvation energy.

When we assume the transition state for the solvolysis to be a polarized molecule with a strong dipole moment, it is convenient to use a dielectric constant as a measure of the electrostatic solvation energy and to use the Eyring-Laidler treatment[10] in the assessment of the general solvent effect.

When we denote, following their treatment, the free-energies for the electrostatic solvation process for the molecule (RX) in the initial state and the molecule (RX^*) in the transition state by the expression proposed by Kirkwood,[11] the rate constants of the S_N1 solvolysis can be expressed as follows:[9]

$$\ln k_{obs.} + C = \left(\frac{N}{RT}\right)\left(\frac{D-1}{2D+1}\right)\left(\frac{\mu_{RX}^2}{r_{RX}^3} - \frac{\mu_{RX^*}^2}{r_{RX^*}^3}\right) + \frac{\Phi_{RX}-\Phi_{RX^*}}{RT} \quad (3)$$

8) K. Okamoto, K. Takeuchi, and H. Shingu, This Bulletin, **35**, 525 (1962).

9) H. Shingu and K. Okamoto, *Nippon Kagaku Zasshi*, **78**, 558 (1958).

10) K. J. Laidler and H. Eyring, *Ann. N. Y. Acad. Sci.*, **39**, 303 (1940).

11) J. G. Kirkwood, *J. Chem. Phys.*, **2**, 351 (1934).

where N is the Avogadro number, μ and r are the dipole moment (Debye unit) and the molecular radius (Å), respectively, D is the dielectric constant of the solvent, and the Φ's are non-electrostatic terms for the solvation process of RX and RX*.

Provided that the non-electrostatic terms are negligibly small or independent of the nature of the solvents, a plot of $\ln k_{obs.}$ (or $\log k_{obs.}$) *vs.* $(D-1)/(2D+1)$ should give a straight line. The plots of the $\log k_{obs.}$'s for 1-adamantyl derivatives and for *t*-butyl chloride *vs.* $(D-1)/(2D+1)$ for various solvents are shown in Figs. 3, 4, and 5. Among a variety of solvents, the phenol - benzene solvent and also the acetic acid solvent deviate far from the points expected for the linear relation between $\log k$ for the other hydroxylic solvents *vs.* $(D-1)/(2D+1)$, indicating that the non-electrostatic terms for these solvents are quite different in nature from the other solvents; thus, the gap from the straight line would mostly be a reflexion of the electrophilic acceleration by hydrogen-bonding, the existence of which has been suggested from the dispersion of the phenolic solvent and the acetic acid solvent in the $\log k$ *vs.* Y correlation (Fig. 2).

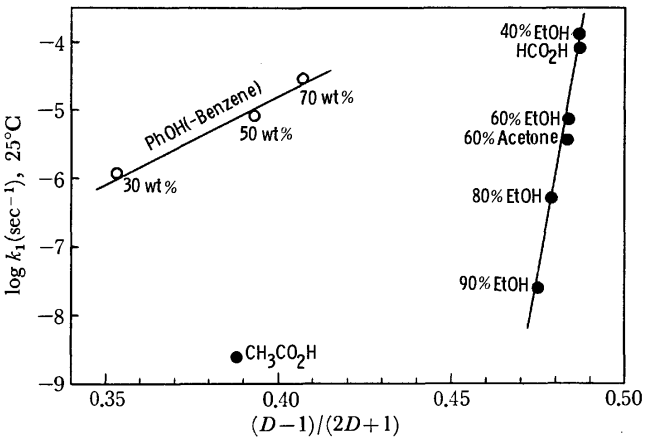

Fig. 3. The correlation of 1-adamantyl bromide solvolysis rates with $(D-1)/(2D+1)$.

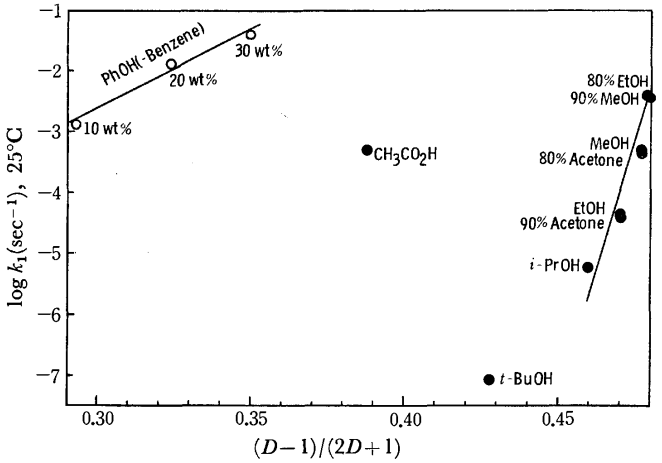

Fig. 4. The correlation of 1-adamantyl tosylate solvolysis rates with $(D-1)/(2D+1)$.

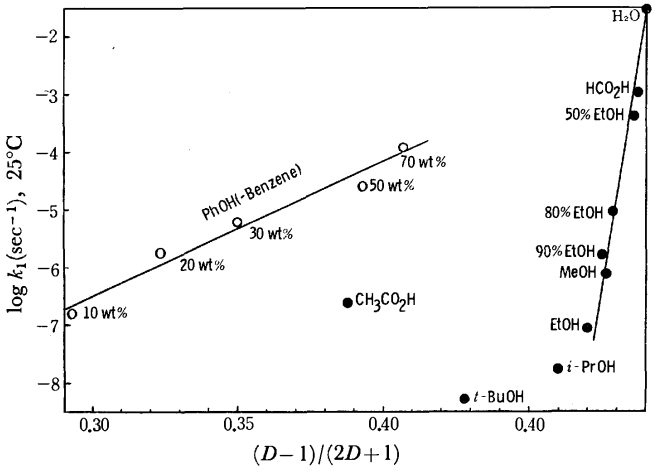

Fig. 5. The correlation of *t*-butyl chloride solvolysis rates with $(D-1)/(2D+1)$.

The Product Distribution for the Phenol and the Phenoxide Reactions. As is presented in the above reaction scheme, in the reaction media which contain sodium phenoxide (or triethylamine), there probably exist two kinds of nucleophiles, the phenol molecule and the phenoxide ion (or its ion-pair); it is of interest to estimate the distribution of the products with regard to each nucleophile.

The distribution for the products which stem from the reaction of the phenol molecule with the S_N1 intermediate can be graphically estimated by plotting the product compositions (r_{ether}, r_{ortho}, and r_{para}) *vs.* the concentrations of the added sodium phenoxide or triethylamine, and subsequently by extrapolating the r values (%) to a zero concentration of the added nucleophile. This is illustrated in Fig. 6 for the phenolysis of 1-adamantyl chloride in the 50 wt% phenol-benzene solvent at 100°C.

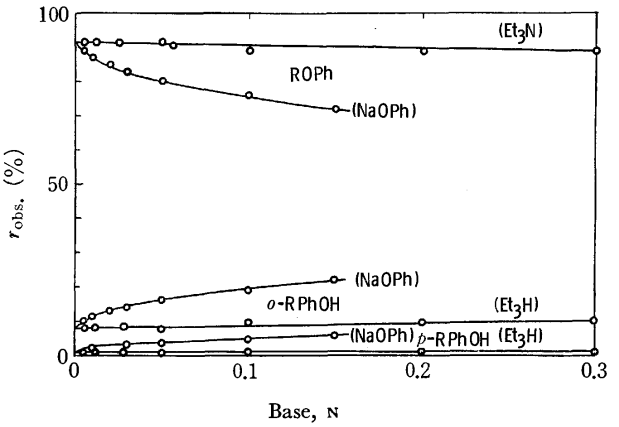

Fig. 6. The product distribution for 1-adamantyl chloride phenolysis in the presence of sodium phenoxide or triethylamine at 100.0°C.

The results of such estimations for chloride, bromide, and tosylate are tabulated in Table 7. The product distributions for the three substrates are in fair agreement with each other, irrespective of the nature of the leaving group and the reaction temperature; this may indicate the structural resemblance of the ion-pair intermediate for each substrate.

For the phenolysis with triethylamine, the product composition is less affected by the increase in the amine

Table 7. Product distributions for the reactions of the phenol molecule and tme phenoxide ion

Substrate	Temp. (°C)	Product distribution %		
		ROPh	*o*-RPhOH	*p*-RPhOH
	The reaction of the phenol molecule			
RCl	100.0	91.5	8	0.5
RBr	50.0	90	9	1.0
ROTs	25.0	90	9	1.0
	The reaction of the phenoxide ion			
RCl[a)]	100.0	70	23	9.0

a) The (k_2'/k_2) values for ROPh, *o*-RPhOH, and *p*-RPhOH are respectively 128, 134, and 56.

concentration compared with case of sodium phenoxide (Fig. 6). This can probably to be attributed to the lower dissociation degree of the phenol-triethylamine adduct into the free phenoxide ion.

The distribution of the products derived from the reaction of the phenoxide ion with the intermediate can be estimated by the following procedure. Provided that the phenoxide-ion concentrations are virtually constant at high ratios (>10) of the phenoxide concentration and the substrate concentration, we can derive the following equations (Eqs. (4), (5), and (6)) which express the relationships between the observed overall distributions of the products ($r_{obs.,\ ether}$, $r_{obs.,\ ortho}$, and $r_{obs.,\ para}$) and the estimated proportions of the products for the phenoxide reaction ($r_{i,\ ether}$, $r_{i,\ ortho}$, and $r_{i,\ para}$) and for the phenol reaction ($r_{m,\ ether}$, $r_{m,\ ortho}$, and $r_{m,\ para}$). The inferior letters, i, m, ether, *ortho*, and *para*, denote the phenoxide ion, the phenol molecule, 1-adamantyl phenyl ether, *o*-1-adamantylphenol, and *p*-1-adamantylphenol, respectively.

$$\mathrm{RX} \underset{k_{-1}}{\overset{k_1}{\rightleftharpoons}} [\text{Ion-pair intermediate}] \longrightarrow \begin{cases} \xrightarrow{k_2[\mathrm{PhOH}]} \underset{r_{m,\ ether}}{\mathrm{ROPh}} + \underset{r_{m,\ ortho}}{o\text{-RPhOH}} + \underset{r_{m,\ para}}{p\text{-RPhOH}} \\ \xrightarrow{k_2'[\mathrm{PhO}^{\ominus}]} \underset{r_{i,\ ether}}{\mathrm{ROPh}} + \underset{r_{i,\ ortho}}{o\text{-RPhOH}} + \underset{r_{i,\ para}}{p\text{-RPhOH}} \end{cases}$$

$$r_{obs.,\ ether} \equiv \frac{[\mathrm{ROPh}]_\infty}{[\mathrm{ROPh}]_\infty + [o\text{-RPhOH}]_\infty + [p\text{-RPhOH}]_\infty} = \frac{k_2[\mathrm{PhOH}] \times r_{m,\ ether} + k_2'[\mathrm{PhO}^{\ominus}] \times r_{i,\ ether}}{k_2[\mathrm{PhOH}] + k_2'[\mathrm{PhO}^{\ominus}]} \quad (4)$$

$$r_{obs.,\ ortho} \equiv \frac{[o\text{-RPhOH}]_\infty}{[\mathrm{ROPh}]_\infty + [o\text{-RPhOH}]_\infty + [p\text{-RPhOH}]_\infty} = \frac{k_2[\mathrm{PhOH}] \times r_{m,\ ortho} + k_2'[\mathrm{PhO}^{\ominus}] \times r_{i,\ ortho}}{k_2[\mathrm{PhOH}] + k_2'[\mathrm{PhO}^{\ominus}]} \quad (5)$$

$$r_{obs.,\ para} \equiv \frac{[p\text{-RPhOH}]_\infty}{[\mathrm{ROPh}]_\infty + [o\text{-RPhOH}]_\infty + [p\text{-RPhOH}]_\infty} = \frac{k_2[\mathrm{PhOH}] \times r_{m,\ para} + k_2'[\mathrm{PhO}^{\ominus}] \times r_{i,\ para}}{k_2[\mathrm{PhOH}] + k_2'[\mathrm{PhO}^{\ominus}]} \quad (6)$$

Eqs. (4), (5), and (6) are transformed into Eq. (7), in which x denotes ether, *ortho*, or *para*.

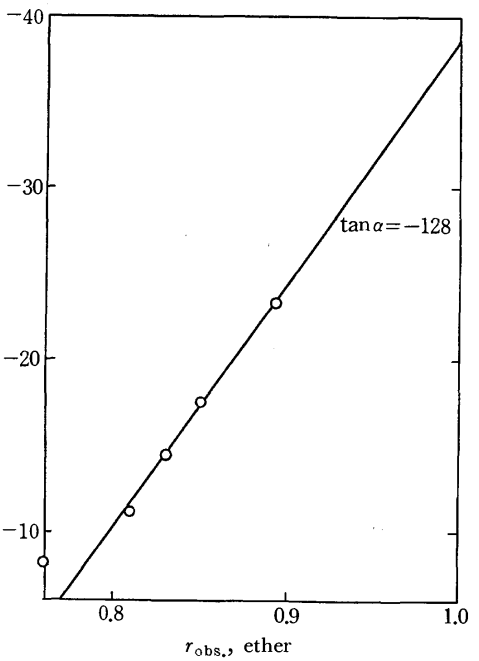

Fig. 7. Examination of the correlation shown in Fig. (6) for the distribution of 1-adamantyl phenyl ether in the 1-adamantyl chloride phenolysis products.

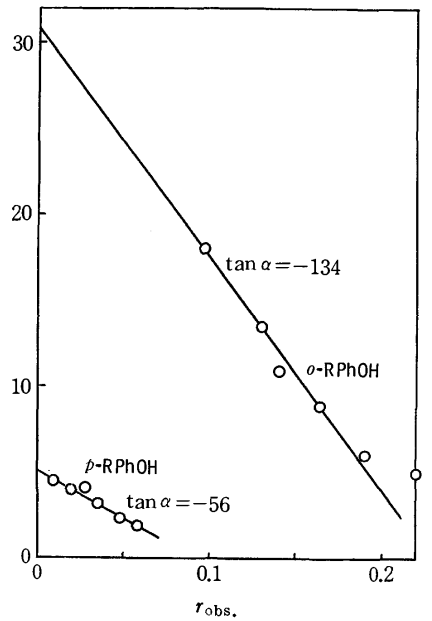

Fig. 8. Examination of the correlation shown in Eq. (6) for the distribution of *o*- and *p*-adamantylphenols in the 1-adamantyl chloride phenolysis products.

$$\frac{(r_{obs.,\ x} - r_{m,\ x})}{([\mathrm{PhO}^{\ominus}]/[\mathrm{PhOH}])} = \left(\frac{k_2'}{k_2}\right) r_{obs.,\ x} + \left(\frac{k_2'}{k_2}\right) r_{i,\ x} \quad (7)$$

In the reaction medium, the phenoxide ion may be dissolved as an ion-pair or as an aggregate at somewhat higher concentrations. However, in the lower concentrations we may consider that the phenoxide ion almost completely dissociates and that the ion concentration may be approximately equal to that of the added sodium phenoxide. Thus, using Eq. (7), we can evaluate the values for $r_{i,\ x}$ and for (k_2'/k_2) from the observed values for $r_{obs.,\ x}$, $r_{m,\ x}$ and $([\mathrm{PhO}^{\ominus}]/$

[PhOH]); a graphical procedure for the estimation of $r_{i,x}$'s is illustrated in Figs. (7) and (8) by plotting the amounts of the left side of Eq. (7) against $r_{obs\cdot,x}$ (see Table 6) for 1-adamantyl chloride. The results thus obtained for $r_{i,x}$ values are presented in Table 7. As is shown in Table 7, the sum of the $r_{i,x}$ values amounts to 102%. Therefore, the expected error limits for this estimation may be about 2% or less. The larger amount of carbon alkylation observed in the phenoxide reaction is in marked contrast to the results for the phenol reactions.

Experimental[12)]

Materials. 1-Adamantyl chloride mp 165.0—166.0°C (lit,[13)] 165°C), 1-adamantyl bromide mp 118.5—119.0°C (lit,[14)] 119—120°C), and 1-adamantyl *p*-toluenesulfonate mp 76—79°C (lit,[6)] 72—79°C) were prepared by the reported methods.[6,13)] Phenol, benzene, and triethylamine were fractionated just prior to use. Titration with a Karl Fischer reagent indicated the water content of phenol to be less than 10^{-2} M. The sodium phenoxide was prepared by refluxing the toluene solution of phenol with sodium metal.

Rate Measurement. Most of the measurements were carried out by a sealed ampoule technique; for the reactions which were rapid at lower temperatures, an aliquot method was employed. For the more rapid reactions of 1-adamantyl tosylate, a single sample for a specified reaction time was prepared as follows. A benzene solution of the tosylate and a triethylamine solution in 45 wt% phenol-(-benzene) were each temperature-equilibrated at 25°C, then they were mixed in a glass-stoppered reaction vessel at 25°C to make 30 wt% phenol (-benzene) solution; after a specified length of time, the reaction was interrupted by the addition of a large quantity of acetone, which had been cooled in Dry Ice-methanol, to the reaction vessel. For the phenolysis of 1-adamantyl bromide, carried out in the absence of a base, the free-space in the ampoule was filled with the HBr liberated in th course of the phenolysis. In that case, the ampoule had been cooled in liquid-nitrogen before it was opened in a large quantity of acetone which contained a small amount of aqueous NaOH.

The titrating solutions were, for the titration in acetic acid used as a stop-solvent, 0.05 N perchloric acid in acetic acid and, for the titration in an acetone solution, 0.01 N aqueous HCl. The indicators used were respectively crystal violet (in acetic acid) and lacmoid (in EtOH). All the rate data were treated graphically, and in each case the reaction was followed to at least 70% reaction and a smooth linear first-order relationship was obtained.

1-Adamantyl Bromide Phenolysis Products. 1-Adamantyl bromide (1.505 g, 7.00 mmol) was dissolved in 68 m*l* of a 1 : 1 (by wt.) mixture of phenol and benzene, containing triethylamine (1 m*l*, 7.17 mmol). After 28 hr (about 10 half-lives) at 50°C, the solution was diluted with 200 m*l* of ether, washed with 10% aqueous NaOH (25 m*l*×5) and 20% aqueous NaCl (100 m*l*×2), and dried ($MgSO_4$); most of solvent was then removed by distillation. A part (1/22 by wt.) of the residual liquid was examined by gas chromatography. The remainder was evaporated and separated by chromatography on silica gel (50 g) to give 0.866 g of 1-adamantyl phenyl ether (the eluent, 2 : 1 (by vol.) hexane-benzene), a 1 : 1 mixture (0.691 g) of 1-adamantyl phenyl, ether and *o*-1-adamantylphenol (1 : 2 hexane-benzene), and 0.048 g of *p*-1-adamantylphenol (20 : 1 benzene-ether). A mixture of the phenyl ether and the *ortho*-phenol was rechromatographed on alumina to give pure *o*-1-adamantylphenol (the eluent, 1 : 1 ether-ethanol). The structures of these products were assigned on the basis of the following spectral data and elemental compositions (Table 8). The gas-chromatographical analysis of a part of the reaction mixture, which had been taken out before the column chro-

Table 8. Melting points, spectral data, and elemental compositions for the phenolysis products

	1-Ad-OPh	*o*-1-Ad-PhOH	*p*-1-Ad-PhOH
mp °C (corr.)	113.5—114.0[a)]	146.9—147.5[b)]	182.4—182.8[a)]
IR (cm^{-1})[c)]			
ν_{C-H}	2940 2870	2920 2880	2920 2880
$\nu_{arom.\ ring}$	1597	1597 1580 1500	1615 1595 1510
ν_{O-H}		3580	3240
NMR (τ, J Hz)[d)]			
ring proton	2.35—3.02 (m, 5H)	2.44—3.27 (m, 4H)	2.68 (d, $2H_a$, 8.7) 3.14 (d, $2H_b$, 8.7)
β-H	8.09 (6H)	7.82 (9H)	8.12 (6H)
γ-H	7.77 (3H)		7.90 (3H)
δ-H	8.32 (6H)	8.17 (6H)	8.21 (6H)
OH		5.15 (s, 1H)	6.45 (s, 1H)
Elemental composition[e)]			
Found C%	84.41	83.92	84.22
Found H%	8.96	8.92	9.10

a) Recrystallized from methanol.
b) Recrystallized from *n*-hexane.
c) In CCl_4.
d)

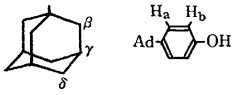

e) Calcd: C, 84.16; H, 8.83% (for each compound).

Table 9. The dielectric constants of phenol - benzene mixtures

Phenol wt%	*D* (25.0°C)
70.0	7.60
50.0	6.51
30.0	4.52
20.0	3.76
10.0	3.13
0.0	2.27[a)]

a) A. S. Brown, P. M. Levin, and E. W. Abrahamson, *J. Chem. Phys.*, **19**, 1226 (1951).

12) A. Shimadzu Model GC-2B gas chromatographic instrument, equipped with a thermal conductivity detector, a Hitachi Model 023—6003 gas chromatographic instrument, with a flame ionization detector, a Shimadzu Model IR-27 spectrophotometer, and a Japan Electronic Optics 60 MHz NMR instrument were used for the analytical work. Microanalyses were performed by the Elemental Analysis Center, Kyoto University.

13) H. Stetter, M. Schwarz, and A. Hirshhorn, *Chem. Ber.*, **92**, 1629 (1959).

14) St. Landa, S. Kriebel, and E. Knobloch, *Chem. Listy*, **48**, 61 (1954).

matography, revealed the presence of 1-adamantyl phenyl ether, *o*-, and *p*-1-adamantylphenols in the ratio of 88.9 : 8.2 : 2.9 (see below).

Product Distribution Analysis by Gas Chromatography. To several mg of an adamantyl compound, placed in a 2-m*l* ampoule, we added 1 m*l* of a phenol - benzene (1 : 1 by wt.) mixture which also contained a specified amount of triethylamine or sodium phenoxide. The sealed ampoule was kept at a reaction temperature for 10 half-lives. The reaction mixture was diluted with 30 m*l* of benzene, washed with 10% aq. NaOH (3 m*l*) and 10% aq. NaCl (10 m*l*), dried ($MgSO_4$), and distilled to leave 0.3—0.5 m*l* of the residual liquid, which was analyzed by gas chromatography using a 2-m Apiezon Grease column at 200°C.

Measurement of the Dielectric Constant. A resonance method was used; the frequency of the oscillator was 1 MHz, and the calibration of the test condenser, equipped with two circular platinum plates, was carried out using water, acetic acid, and acetic anhydride as the standard liquids. The results are presented in Table 9.

BULLETIN OF THE CHEMICAL SOCIETY OF JAPAN, VOL. 45, 1198—1205 (1972)

The Substituent Effect. I. Normal Substituent Constants from the Hydrolysis of Substituted-benzyl Benzoates

Yasuhide YUKAWA, Yuho TSUNO, and Masami SAWADA

The Institute of Scientific and Industrial Research, Osaka University, Suita, Osaka

(Received October 28, 1971)

The rates of the alkaline hydrolyses of 24 *m*- and *p*-substituted-benzyl benzoates were measured in 70% (v/v) aqueous acetone at 25°C. The given set of σ^0 constants was precisely identical with our standard set derived from *m*- and *p*-substituted ethyl phenylacetates. The general utility of σ^0 constants is demonstrated for unexalted and exalted resonance reactivities as the reference scale in our LArSR equation:

$$\log k/k_0 = \rho(\sigma^0 + r^+\Delta\bar{\sigma}_R^+ + r^-\Delta\bar{\sigma}_R^-)$$

The accommodation of extensive data makes it evident that the Hammett equation in its original form[1] fails to correlate the substituent effect of *para* electron-releasing groups on the electrophilic reactivity with the same line, such as *meta* substituents.[2-4] The resonance theory clearly anticipates that the conjugatively electron-releasing *para* substituents can interact strongly by resonance with the electron-deficient reaction center and that, in consequence, such *para* substituents deviate from the correlation line of the uninteracting substituents.[2-7] The effect of the resonance interaction can vary with reactions, depending on the degree of electron deficiency of the reaction site at the transition state relative to the ground state (or the final to initial state). The effect of *meta* substituents is approximately independent of such an interaction, so as to give generally satisfactory correlations with the Hammett σ_m values.[6,7] It is, therefore, necessary to introduce an additional term for *para* substituent effects taking this interaction into account in order to improve the Hammett relation for these reactions.

With this point in mind, we proposed Eq. (1) for correlating the effect of substituents on the electrophilic reaction of benzene derivatives;[8,9]

$$\log k/k_0 = \rho(\sigma^0 + r\Delta\bar{\sigma}_R^+) \quad (1)$$

where r is the variable describing the degree of resonance, and where the parameter, $\Delta\bar{\sigma}_R^+$, which corresponds to $\sigma^+ - \sigma^0$ in Brown and Okamoto's scale,[3] is the substituent constant measuring the capacity of substituents to donate electrons by resonance.

σ^0 is the substituent constant defined originally by Taft[5,6] as the measure of the insulated substituted phenyl polar effect; we practically determined a set of reliable σ^0 values from the substituent effects on the alkaline hydrolysis of ethyl phenylacetates.[9]

The generality of this linear aromatic substituent reactivity (LArSR) relationship (1) was demonstrated by applying it to about 70 representative reactions with excellent precision.[9] Thereafter, our LArSR Eq. (1) has been utilized to describe the substituent effects on various electrophilic reactions and to elucidate the mechanism of reactions by a number of investigators.[9]

The same type of treatment has been shown to apply to the effects of conjugatively electron-attracting (+R) substituents on σ^--type nucleophilic reactions.[9] Eq. (1) can be thus modified as a generalized form to Eq. (2);

$$\log k/k_0 = \rho\sigma^0 + \phi^{\pm} \quad (2)$$

$$\phi^+ = \rho r^+\Delta\bar{\sigma}_R^+ \text{ and } \phi^- = \rho r^-\Delta\bar{\sigma}_R^-$$

1) L. P. Hammett, *J. Amer. Chem. Soc.*, **59**, 96 (1937); "Physical Organic Chemistry", McGraw-Hill, New York (1940), Chapt. 7.
2) Y. Tsuno, T. Ibata, and Y. Yukawa, This Bulletin, **32**, 960 (1959); Y. Yukawa and Y. Tsuno, *ibid.*, **32**, 965 (1959).
3) H. C. Brown and Y. Okamoto, *J. Amer. Chem. Soc.*, **79**, 1914 (1957); *ibid.*, **80**, 4979 (1958); H. C. Brown, "Advances in Physical Organic Chemistry", Vol. 1, Academic Press, New York (1963), Chap. 2.
4) P. R. Wells, *Chem. Rev.*, **63**, 171 (1963).
5) R. W. Taft, Jr., *J. Phys. Chem.*, **64**, 1805 (1960).
6) R. W. Taft, Jr., and I. C. Lewis, *J. Amer. Chem. Soc.*, **80**, 2436 (1958); *ibid.*, **81**, 5343 (1959); R. W. Taft, Jr., S. Ehrenson, I. C. Lewis, and R. E. Glick, *ibid.*, **81**, 5354 (1959).
7) H. van Bekkum, P. E. Verkade, and B. M. Wepster, *Rec. Trav. Chim.*, **78**, 815 (1959).
8) Y. Yukawa and Y. Tsuno, This Bulletin, **32**, 971 (1959).
9) Y. Yukawa, Y. Tsuno, and M. Sawada, *ibid.*, **39**, 2274 (1966).

where $\Delta\bar{\sigma}_R$ is defined in the same way as $\Delta\bar{\sigma}_R^+$ by the quantities, $\sigma^- - \sigma^0$, for *para* +R substituents. Eq. (2) is essentially a separation of the general substituent effect on benzene reactivities into the insulated aryl polar effect, $\rho\sigma^0$, and additional pi-resonance exaltation effects, ϕ^+ and ϕ^-.

In view of the importance of the σ^0 constant as the standard of our LArSR relationship, and also of other relevant equations, it is necessary to examine more critically the generality of our set of σ^0 constants in practical reactivity correlations. In this connection, we have derived a set of σ^0-type substituent constants from the substituent effect on the alkaline hydrolysis of substituted benzyl esters of benzoic acid, where additional pi-electronic interaction of substituents with the reaction center is precluded structurally by an intervening methylene group.

The present paper will be mainly concerned with a comparison of this new set of substituent constants with our standard set of σ^0 constants, and also with a statistical examination of the applicability and limitation of these substituent constants.

Experimental

Materials. Almost all of the *meta*- and *para*-substituted-benzyl benzoates were successfully prepared by the esterification of benzoyl chloride with the corresponding carbinols in pyridine.[10] Carbinols were obtained from the appropriate ethyl or methyl benzoates by the $LiAlH_4$ reduction[11] except for nitro derivatives. *m*- and *p*-Nitrobenzyl alcohols were obtained by the Meerwein-Ponndorf reduction[12] of the corresponding aldehydes. Next, five benzyl esters were obtained as follows.

m- *or* p-*Methylsulfonylbenzyl Benzoate*: A mixture of *m*- or *p*-methylmercaptobenzyl benzoate (7 g), glacial acetic acid (40 m*l*), and 30% aq. hydrogen peroxide (11 m*l*), was heated under reflux for 4 hr. After the usual procedure, the crude methylsulfonylbenzyl benzoate (6 g) obtained was recrystallized from benzene - hexane or benzene - ligroin.

p-*Methylsulfinylbenzyl Benzoate*: *p*-Methylmercaptobenzyl benzoate (6 g) and 30% aq. hydrogen peroxide (11 m*l*) in acetone (200 m*l*) were allowed to stand at room temperature for 6 days. After the removal of the solvent, the residue was taken up in benzene and ether. The organic layer was washed with an aq. Na_2CO_3 solution and dried. A solid product (5.5 g) was recrystallized from aq. EtOH or benzene - ligroin to give colorless needles.

m- *or* p-*Cyanobenzyl Benzoate*: A solution of *m*- or *p*-bromobenzyl benzoate and cuprous cyanide in DMF was refluxed for 4 hr. The hot solution was then treated by Friedman's method.[13] Recrystallization from ligroin - benzene or 80% aq. EtOH gave pure esters.

All of the esters were purified by fractionation or recrystallization. The physical constants and the elemental analysis

Table 1. Physical constants and analytical data of arylcarbinyl benzoates

Substituent	Bp (mmHg) or Mp	Carbon		Hydrogen		Other	
		Found	Calcd	Found	Calcd	Found	Calcd
H	111.5 (0.3)[a]	79.40	79.23	5.82	5.70		
p-CH_3	169—171 (5)	79.98	79.62	6.60	6.24		
m-CH_3	143.5 (0.7)	79.97	79.62	6.61	6.24		
p-C_2H_5	156.5 (1)	79.77	79.97	6.80	6.71		
p-*i*-Pr	159.5—160.5 (0.6)	80.18	80.28	7.13	7.13		
p-*t*-Bu	170.5 (3), 46	80.71	80.56	7.55	7.51		
p-CH_3O	158 (1.3)[b]	74.68	74.36	5.55	5.83		
p-C_6H_5O	202—204 (1.5)	78.92	78.93	5.26	5.30		
p-CH_3S	203—203.5 (5)	70.41	69.74	5.46	5.46	12.56	12.41 (S)
m-CH_3S	203—205 (5)	69.90	69.74	5.42	5.46	12.47	12.41 (S)
p-F	127 (0.7)						
p-Cl	59[c]	67.90	68.16	4.68	4.49	14.15	14.37 (Cl)
m-Cl	153—154 (1.1)	68.40	68.16	4.78	4.49	14.37	14.37 (Cl)
p-Br	47—48[d]	58.02	57.76	4.10	3.81	27.20	27.45 (Br)
m-Br	154—155 (0.8)	57.97	57.76	3.38	3.81	27.73	27.45 (Br)
p-NO_2	88.5[e]	65.40	65.37	4.31	4.31	5.62	5.44 (N)
m-NO_2	71	65.18	65.37	4.16	4.31	5.45	5.44 (N)
p-CN	64.5—65.5	75.86	75.94	4.56	4.67	5.78	5.90 (N)
m-CN	44.5—45	76.02	75.94	4.57	4.67	6.10	5.90 (N)
p-$SOCH_3$	70.5—71	65.73	65.67	5.14	5.14	11.42	11.69 (S)
p-SO_2CH_3	96.0—96.5	61.87	62.05	4.79	4.86	11.13	11.04 (S)
m-SO_2CH_3	78.5—79	61.78	62.05	4.84	4.86	11.13	11.04 (S)

a) "Organic Syntheses", Coll. Vol. 1, p. 104. b) B. Gastambide and J. Blanc, *Bull. Chim. Soc. France*, **1962**, 2064; *C. A.*, **58**, 12455d (1963). c) T. Suehiro, S. Hibino, and T, Saito, This Bulletin, **41**, 1707 (1968). d) B. A. Fiekers and E. M. DiGeronimo, *J. Amer. Chem. Soc.*, **70**, 1654 (1948). e) E. J. Bourne, M. Stacey, J. C. Tatlow, and J. M. Tedder, *J. Chem. Soc.*, **1949**, 2976.

10) M. L. Bender, H. Matsui, R. J. Thomas, and S. W. Tobey, *J. Amer. Chem. Soc.*, **83**, 4193 (1961).
11) W. G. Brown, "Organic Reactions", Vol. 6, John Wiley and Sons, New York, (1942), Chapt. 10.
12) A. L. Wilds, "Organic Reactions", Vol. 2, Chapt. 5.
13) L. Friedman and H. Shechter, *J. Org. Chem.*, **26**, 2522 (1961).

data of these esters are listed in Table 1.

Solvent. Acetone which had been treated with potassium permanganate was distilled, dried over potassium carbonate, and fractionated. The stock solution of 70% aqueous acetone was made up by mixing 70 parts (by volume) of acetone with 30 parts (by volume) of freshly-boiled, deionized water.

Kinetic Measurements. The rates of the alkaline hydrolyses of all the arylcarbinyl benzoates were determined in a 70% (v/v) aqueous acetone solution at 25.00°C±0.01 by means of the usual titration method. The procedure employed for those measurements was essentially the same as that described in the literature.[14] The aqueous acetone solution of sodium hydroxide was freshly prepared and standardized frequently. The reaction was started by mixing up solutions containing exactly equimolar amounts of the ester and alkali to give an initial concentration of about 0.02 mol/*l* in the final mixture. Ten m*l* samples were withdrawn from the reaction flask at appropriate intervals, quenched with 10 m*l* of a HCl solution of a known concentration (about 0.03—0.04 N) and about 10 m*l* of acetone, and back-titrated with a standardized NaOH solution of about 0.02 N, bromothymol blue being used as the indicator. The end point was obtained by comparison with the color standard of sodium benzoate in 70% aq. acetone containing the same amount of indicator as was used in the titration. For nitro, cyano, methylsulfinyl, and methylsulfonyl derivatives, a low initial concentration of about 0.01 mol/*l* was employed because of the higher reaction rate to be followed by titration, and a 15 m*l* aliquot was utilized in each titration.

The initial titer, C_0, was determined by the use of the alkaline solution alone. All runs which involved more than 11 measurements followed the second-order kinetic law, covering up to an 80% reaction. The bimolecular rate constant, k_2, was obtained from the plot of $(C_x-C_0)/t$ against C_x, where C_x was the titer at $t=X$. The experimental uncertainty of a run was estimated to be much better than 2%, and the rate constants from repeated runs agreed within ±2% or better.

Results and Discussion

Table 2 lists the rate constants of the hydrolyses of 24 *m*- and *p*-substituted-benzyl benzoates in 70% (v/v) aqueous acetone at 25°. A precise Hammett relation was followed only by *meta* substituted and *para* +R substituted derivatives. The reaction constant, ρ_m, was obtained by fitting a regression line to log k against σ_m for *meta* substituents (including unsubstituted one); $\rho_m=0.981$, $(\log k_0)_{calc}=-2.169$; correlation coefficient, 0.999, and standard deviation, ±0.005.[15] From the structural features of the present system, it can be expected that the substituent effect can be described in terms of the σ^0 constants.

The plot of log k/k_0 against σ^0 gives an excellent straight line for all *meta* and *para* substituents, as is shown in Fig. 1. The ρ value obtained by least-squares fitting was 0.978 with a satisfactorily high precision; correlation coefficient, 0.999, and standard deviation, ±0.010.[16] The correlational parameters are identical

TABLE 2. RATE CONSTANTS OF ALKALINE HYDROLYSIS OF ARYLCARBINYL BENZOATES IN 70% (v/v) AQ. ACETONE AT 25°C

Substituent	$10^3\times k_2$ a)	Substituent	$10^3\times k_2$ a)
H	6.74	*p*-F	10.7
p-Me	5.13	*p*-Cl	12.8
m-Me	5.77	*m*-Cl	15.8
p-Et	5.02	*p*-Br	13.2
p-*i*-Pr	4.88	*m*-Br	16.6
p-*t*-Bu	4.56	*p*-NO_2	43.2
p-MeO	4.79	*m*-NO_2	33.3
p-PhO	7.57	*p*-CN	33.9
p-MeS	7.57	*m*-CN	29.8
m-MeS	8.88	*p*-SOMe	24.7
p-Ph	7.35	*p*-SO_2Me	36.8
2-Naph b)	7.74	*m*-SO_2Me	32.7

a) $l\cdot mol^{-1}\cdot sec^{-1}$. b) 2-Naphthyl group.

to the above ρ_m and intercept within the precision on the order of experimental uncertainty. These facts indicate that alkaline hydrolysis of arylcarbinyl benzoates is a typical σ^0 reactivity in which any additional resonance effect of the direct conjugation between aryl groups and the reaction center is completely absent.

As has been pointed out frequently, most of σ^0 reactivities available are comparatively less sensitive to the substituent change because of the attenuating effect by intervening methylene. Naturally, the uncertainty involved in the derived set of substituent constants is inevitably larger. The fact that the present reaction resulted in an excellent σ^0 plot with a relatively high ρ value is highly appreciated; thus, this reaction may be utilized as the secondary reference in the determination of σ^0 constants. Apparent

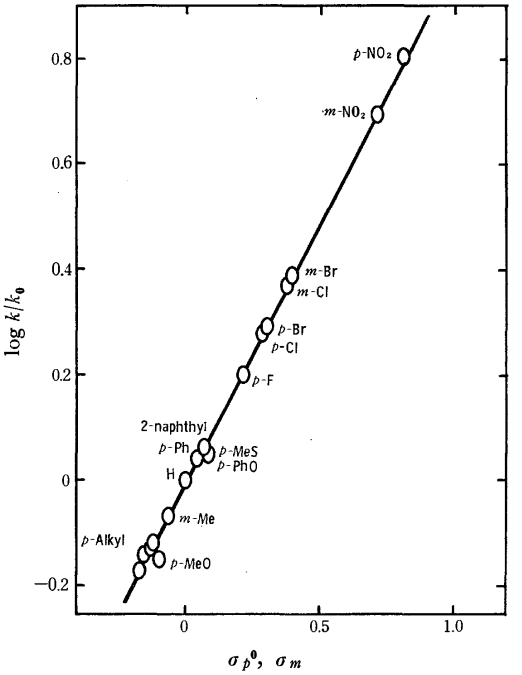

Fig. 1. σ^0 plot of the alkaline hydrolysis of substituted-benzyl benzoates.

14) D. P. Evans, J. J. Gordon, and H. B. Watson, *J. Chem. Soc.*, **1937**, 1430.

15) n(numbers of substituents)=5.

16) n=15.

Table 3. Comparison of various sets of σ^0 and σ

Substituent	σ^0			σ[d]	Substituent	σ^0			σ[d]
	Previous[a]	Present[b]	Taft's[c]			Previous[a]	Present[b]	Taft's[c]	
p-Me	−0.124	−0.123	−0.15	−0.170	*m*-Me	−0.069	−0.070	−0.07	−0.069
p-Et	−0.131	−0.133		−0.151	*m*-F	0.337		0.35	0.337
p-i-Pr	−0.156	−0.145			*m*-Cl	0.373	0.375	0.37	0.373
p-t-Bu	−0.174	−0.175		−0.197	*m*-Br	0.391	0.397	0.38	0.391
p-MeO	−0.100	−0.152	−0.12	−0.268	*m*-MeS		0.120		
p-PhO	0.076	0.049		(−0.061)	*p*-CN		0.714	0.69	0.653 (0.720)
p-MeS	0.083	0.049		(−0.047)	*p*-SOMe		0.573		(0.564)
p-F	0.212	0.203	0.17	0.062	*p*-SO_2Me		0.749		(0.721)
p-Cl	0.281	0.282	0.27	0.227	*p*-NO_2	0.778	0.821	0.82	0.778
p-Br	0.30	0.296	0.26	0.232	*m*-CN		0.655	0.62	0.607 (0.671)
p-Ph	0.039	0.037			*m*-SO_2Me		0.697		(0.659)
2-Naph	0.062	0.059		0.042	*m*-NO_2	0.710	0.705	0.70	0.710

a) Previous set of σ^0 derived from hydrolysis of ethyl phenylacetates (Ref. 9). For *meta* substituents σ_m values are taken. b) Apparent σ^0 calculated by $\rho_m = 0.981$. c) Ref. 5. d) Hammett σ constants. In parentheses the apparent σ calculated from hydrolysis rates of ethyl benzoates in 85% aq. ethanol (Ref. 17).

Table 4. Summary of correlations of σ^0 type reactivities[a]

No.	Reaction	ρ	s[1]	R[2]	n[3]	Ref.[4]
1	Saponification, ethyl arylacetates, 60% acetone, 25°	0.978			21	5
2	Saponification, X-benzyl benzoates, 70% acetone, 25°	0.978	0.010	0.9992	15	6
3	pK_a, Phenylacetic acids, water, 25°	0.480	0.012	0.9966	11	7
4	Saponification, benzyl acetates, 60% acetone, 25°	0.796	0.017	0.9984	8	8
5	Phenylacetic acids with diphenyldiazomethane. EtOH, 36°	0.353	0.011	0.9975	6	9
6	Saponification, ethyl arylacetates, 88% EtOH, 30°	1.021	0.023	0.9984	7	10
7	Saponification, ethyl arylacetates, 85% EtOH, 25°	1.104	0.036	0.9965	10	11
8	Saponification, ethyl arylpropionates, 88% EtOH, 30°	0.638	0.012	0.9988	11	12
9	Saponification, ethyl arylpropionates, 88% EtOH, 30°	0.635	0.011	0.9989	6	13
10	pK_a, Benzylammonium ions, water, 25°	1.089	0.033	0.9958	11	14
11	Saponification, ethyl arylcyclopropylcarboxylates, 88% EtOH, 30°	0.882	0.020	0.9982	8	13
12	pK_a, *trans*-Arylcyclopropylcarboxylic acids, 50% EtOH, 25°	0.517	0.016	0.994	7	15
13	pK_a, *N*-(2,4-dinitrophenyl)-X-benzylammonium ions, water, 25°	1.703	0.055	0.9956	9	16
14	Benzylamines with 2,4-dinitrochlorobenzene, azeotropic EtOH, 45°	−0.761	0.027	0.994	12	17

a) The Hammett type correlation based on the standard set of σ_p^0 and σ_m. Reference numbers in the last column refer to those below the table rather than those in the text.

1) Standard deviation. 2) Correlation coefficient. 3) The number of substituents involved in the calculation. 4) Reference numbers refer to the following rather than those cited in the text. 5) Ref. 9 in the text. 6) Present study. 7) J. F. J. Dippy and J. E. Page, *J. Chem. Soc.*, **1938**, 357; J. F. J. Dippy, S. R. C. Hughes, and J. W. Laxton, *ibid.*, **1934**, 1470; *ibid.*, **1954**, 4102; J. F. J. Dippy and F. R. Williams, *ibid.*, **1934**, 161; J. F. J. Dippy and R. H. Lewis, *ibid.*, **1937**, 1426. 8) E. Tommila and C. N. Hinshelwood, *ibid.*, **1938**, 1801; E. Tommila, *Ann. Acad. Sci. Fennicae*, Ser. A 59, No. 4, 3 (1942); *Chem. Abstr.*, **38**, 6172[9] (1944). 9) R. M. O'Ferrall and S. I. Miller, *J. Amer. Chem. Soc.*, **85**, 2440 (1963). 10) K. Kindler, *Ann. Chem.*, **452**, 90 (1927); A. Fischer, J. Packer, J. Vaughan, A. F. Wilson, and E. Wong, *J. Org. Chem.*, **24**, 155 (1959). 11) J. G. Watkinson, W. Watson, and B. L. Yates, *J. Chem. Soc.*, **1963**, 5437. 12) R. Fuchs and J. A. Caputo, *J. Org. Chem.*, **31**, 1524 (1966). 13) R. Fuchs and J. J. Bloomfield, *ibid.*, **28**, 910 (1963). 14) L. F. Blackwell, A. Fischer, R. D. Topsom, and J. Vaughan, *J. Chem. Soc.*, **1964**, 3588. 15) R. Fuchs, C. A. Kaplan, J. J. Bloomfield, and L. F. Hatch, *ibid.*, **27**, 733 (1962). 16) A. Fischer, M. P. Hartshorn, O. M. Senanayake, and J. Vaughan, *J. Chem. Soc., B*, **1967**, 833. 17) A. Fischer, R. S. H. Hickford, G. R. Scott, and J. Vaughan, *ibid., B*, **1966**, 466.

σ^0 values calculated by using the ρ_m value of 0.981 are given in Table 3, together with our previous set of σ^0 values, which were determined by the alkaline hydrolysis of ethyl phenylacetates.[9] Taft's values[5] are also given for the sake of comparison. The present set agrees generally with our previous set of σ^0 values within ±0.01 in σ unit. Good agreement is also found between ours and Taft's set of σ^0 values within the usual limits of precision of substituent constants.

In the last column of the table, the standard set of σ values is also included for further comparison. The difference between σ^0 and σ is significant for conjugatively electron-releasing (−R) *para* substituents; the σ^0 values are less effectively electron-releasing than the σ values for all these *para* groups. This, of course, arises from the effective through-conjugation of these −R groups with the reaction center, COOH, in the σ-reference reaction, pK_a of benzoic acids. On the other hand, no significant difference between the two sets is observed in conjugatively electron-attract-

TABLE 5. COMPARISON OF APPARENT σ^0 VALUES[a]

X[b] / Y[c]	1[d]	2	3	4	5	6	7
p-Me	−0.124	−0.122	−0.112	−0.113		−0.113	−0.130
m-Me	−0.074	−0.069		−0.067			
p-MeO	−0.100	−0.151[e]	−0.093	−0.112	−0.14[e]	−0.117	−0.100
m-MeO					0.06		−0.005[e]
p-F	0.212	0.206	0.142[e]	0.209			0.193
m-F	0.352						
p-Cl	0.281	0.285	0.261	0.302	0.28	0.320	0.298
m-Cl	0.336	0.379	0.365		0.41		0.344
p-Br	0.30	0.299	0.267	0.284			0.327
m-Br	0.351	0.400					
p-I			0.288	0.286	0.33		0.315
m-I			0.325	0.266	0.45		0.328
p-NO_2	0.808	0.825		0.806	0.77	0.761	0.758
m-NO_2	0.713	0.710	0.728	0.679			0.753
p-CN		0.718					
m-CN		0.660					
p-NH_2					−0.33	−0.364	−0.323
p-Et	−0.131	−0.131	−0.118				
p-i-Pr	−0.156	−0.143	−0.158				
p-t-Bu	−0.174	−0.174	−0.212				

X[b] / Y[c]	8	9	10	11	12	13	14
p-Me	−0.127	−0.132	−0.123	−0.112		−0.086	−0.102
m-Me	−0.052		−0.040			−0.098	−0.091
p-MeO	−0.130	−0.092	−0.095	−0.139	−0.11		−0.152[e]
m-MeO	0.047		0.107			0.131	0.067
p-F	0.196		0.097[e]			0.084[e]	0.172
m-F	0.317		0.336			0.397	0.360
p-Cl	0.290	0.287	0.244	0.278	0.32	0.260	0.326
m-Cl	0.373	0.398	0.364	0.403	0.35		0.375
p-Br			0.253	0.301	0.31	0.254	0.296
m-Br			0.391		0.35	0.378	0.422
p-NO_2	0.790	0.763	0.832	0.768	0.89	0.812	0.732[e]
m-NO_2	0.719		0.694	0.702	0.73	0.707	0.711
p-CN						0.736	0.681
m-CN						0.654	0.635
p-NH_2	−0.332						

a) Evaluated from the correlational parameters in Table 4. b) Substituent. c) Reaction number in Table 4.
d) $\sigma^0_{p\text{-COMe}} = 0.491$, $\sigma^0_{m\text{-COMe}} = 0.389$.
e) Values which are not included in the derivation of averaged σ^0 (Table 8).

ing (+R) *para* substituents where no through-conjugation with the conjugatively electron-attracting reaction center, COOH, is effectively operative in σ-reactivities.

In *para* electron-attracting groups, the nitro group gives a slightly higher σ_p^0 value, 0.82, than the σ_p value, but for others the σ_p values appear to be generally applicable as substitute for the σ^0 values. The σ^0 values for $SOCH_3$ and SO_2CH_3 do not appear to have been well-examined, but the obtained values are practically in accord with the corresponding σ values. *Meta*- and *para*-cyano groups give slightly higher values than the corresponding σ values, but consistent behavior was observed for the cyano groups in the hydrolysis of ethyl benzoates in aqueous ethanol.[17]

The apparent σ^0 value for the *p*-methoxy group, −0.15, is obviously different from the standard σ^0 value, −0.10. Taft has statistically derived dual σ^0 constants for this group, −0.16 in non-aqueous solutions and −0.12 in aqueous solutions.[5] The substituent constant for the methoxy group is considerably sensitive to the solvent change; this variation may be due to the change in the degree of the hydrogen-bonding interaction of the solvent with the basic oxygen of the methoxy group. In the case of the *p*-phenoxy group, the solvent interaction with the substituent will be less effective because of the lower basicity of the oxygen and because of the highly-crowded circumstances around it.

The solvent effect on the substituent constants may be expected to operate more or less effectively for all

17) Y. Yukawa, Y. Tsuno, and M. Sawada, unpublished.

polar substituent groups, not only for electron-releasing groups but also for electron-attracting groups. Despite the minor variation due mostly to the solvent modification of the nature of the substituent groups, a set of finite substituent constants appears to be practically determined for most of the substituent groups.

Before we determine the most reliable set of σ^0 constants, it appears necessary to check more critically the applicability of these constants to general σ^0-type reactivities. As far as we are aware, not many more than a dozen sets of data on σ^0 reactivities in which the through-conjugation is precluded by the structure are available in the literature. Table 4 includes the correlational parameters for these sets of reactivities, obtained by the least-squares application with σ^0 constants, while Table 5 lists the sets of apparent σ_0 values obtained from the respective reactions using the correlation parameters shown in Table 4. In these calculations, we have employed the selected σ^0 values given in the first column of Table 3 as the primary standard. For well-behaving *para* substituents, σ_p^0 values taken in principle from our standard set were employed, but for *meta* substituents the standard σ_m values were employed instead of σ_m^0.

The correlations resulted are excellent, as measured by correlation coefficients higher than 0.99, in all cases. The uncertainty in the apparent σ^0 value is estimated to be within 0.02 σ-unit for most of the substituents in each series, although it depends largely upon the magnitude of ρ's.

If the σ^0 values were applicable only to precise correlations of the reactivities of the specified structure insulated by intervening methylene, their utility would be so limited as to be of little value. However, their exist a substantial number of reactivities which are practically correlated by σ^0 values within the limits of the usual precision of fit. Table 6 shows the results of σ^0 correlations for such a class of reactivities of interest. The results are of practical importance not only in examining the generality of σ^0, but also in estimating the σ^0 values for substituents other than those involved in the σ^0 resorting, since the substituents involved in the former specified class of reactivities are limited in fact to the substituents of the so-called

Table 6. Summary of correlations of apparent σ^0-type reactivities[a]

No.	Reaction	ρ	S	R	n	Ref.
15	Benzoic acids with diphenylguanidine, benzene, 25°	2.127	0.032	0.9988	13	18
16	pK_a, Ar-PO_3H^-, water, 25°	1.129	0.037	0.9966	10	19
17	Alkaline hydrolysis, phenoxytriethylsilanes, 51% aq. ethanol, 25°	1.977	0.016	0.9994	6	20
18	pK_a, phenoxyacetic acids, water, 25°	0.304	0.014	0.9900	8	21
19	1-Cl, 2-NO_2-Benzenes with sodium thiophenoxide, methanol, 35°	5.203	0.14	0.996	14	22
20	Alkaline hydrolysis, phenyl tosylates	1.845	0.036	0.9989	9	23
21	Alkaline hydrolysis, phenyldinitrophenyl ethers	1.009	0.024	0.9977	15	24
22	pK_a, thiophenols, 48% aq. ethanol, 25°	2.605	0.037	0.9990	10	25
23	pK_a, phenols, water, 25°	2.247		0.9983		26

a) The Hammett type correlation based on the standard set of σ_p^0 and σ_m. In entries 19—23, the correlation is based on *meta* and $-R$ *para* substituents. Reference numbers in the last column refer to those below the Table.

18) M. M. Davis and H. H. Hetzer, *J. Res. Nat. Bur. Stand. A*, **60**, 596 (1958). 19) H. H. Jaffé, L. D. Freedman, and G. O. Doack, *J. Amer. Chem. Soc.*, **75**, 2209 (1953). 20) E. Aekerman, *Acta, Chem. Scand.*, **11**, 373 (1957). 21) N. V. Hayes and G. E. K. Branch, *J. Amer. Chem. Soc.*, **65**, 1555 (1943). 22) A. M. Porto, L. Altieri, A. J. Castro, and J. A. Brieux, *J. Chem. Soc., B*, **1966**, 963. 23) V. M. Maremae and V. A. Palm, "Organic Reactivity", Vol. 1, **2**, 85 (1964). 24) A. V. Ivanov, A. J. Kaminski, S. S. Gitis, and Z. A. Kosina, *ibid.*, Vol. 4, 290 (1967); S. S. Gitis, A. V. Ivanov, A. J. Kaminski, and Z. A. Kosina, *ibid.*, Vol. 3, **3**, 142 (1966). 25) F. G. Bordwell and H. H. Andersen, *J. Amer. Chem. Soc.*, **75**, 6019 (1953); G. Schwarzenbach and H. A. Egli, *Helv. Chim. Acta*, **17**, 1176 (1934). 26) Y. Tsuno, M. Fujio, and Y. Yukawa, unpublished results.

Table 7. Comparison of apparent σ^0 values[a]

X[b] / Y[c]	15	16	17	18	19	20	21	22	23
p-Me	−0.111	−0.126	−0.113	−0.099	−0.115	−0.116	−0.152	−0.106	−0.136
p-MeO	−0.160[d]		−0.110	−0.093	−0.098	−0.105	−0.120	−0.110	−0.113
p-F	0.166[d]			0.181			0.198		
p-Cl	0.262	0.308	0.280	0.270	0.269	0.267	0.302	0.281	0.257
p-Br	0.283	0.237			0.290		0.313	0.304	0.267
p-I	0.277								0.290
p-NO_2	0.719	0.769		0.961[d]		0.895[d]	0.856[d]		
p-CN	0.597			0.833[d]					
p-NH_2	−0.382	−0.382			−0.396	−0.371	−0.34		
p-NMe_2						−0.41	−0.388		
p-OH	−0.151	−0.134						−0.213	

a) Evaluated from the correlational parameters in Table 6. b) Substituent. c) Reaction number in Table 6.
d) Values which are not included in the derivation of averaged σ^0 (Table 8).

well-behaving category. The apparent substituent constants derived are given in Table 7.

The substituent constant, σ^0, is a measure of the substituent effect referred to the special case of Eq. (2), where both ϕ^+ and ϕ^- are diminished to zero (i.e., $r^+=r^-=0$). These reactivities may be classified as the apparent σ^0 class reactivity, regardless of the reaction mechanism or the interaction mechanism of substituents and the reaction center. Davis's data on the ion-pair formation of substituted benzoic acids with diphenylguanidine (Entry 15) are highly instructive. The course of the reaction may be compared with that of the acid dissociation of benzoic acids, where −R *para* substituents exhibit a substantial pi-resonance exaltation to give Hammett σ values ($r^+=0.27$). The excellent fit to the σ^0 of the −R *para* groups in the ion-pair formation may perhaps be due to the cancellation of the exalted resonance interactions of substituents and the reaction center between the initial and final states. In Entry 18 (the pK_a of phenoxyacetic acids), −R *para* groups such as cyano and nitro groups indicate the exalted contribution to a considerable extent (see Table 7). In this system, the through-conjugation with the reaction site is, of course, inhibited by the intervening methylene, while the insulated pi-system is extended to the phenoxy lone-pair orbital with which the direct resonance interaction of +R *para* groups is possible. Thus, the conjugative electron-withdrawal of +R groups can be relatively exalted as compared with that of the same groups attached to the insulated benzene pi-system.

In general reactivities, both ϕ^+ and ϕ^- terms, or, often, either one of them, are exalted to varying extents, as is evidenced by the wide applicability of Eq. (2). The extent of contributions from both terms varies continuously, depending upon reactions, but the relative importance of the two terms is independent of each other. As a general trend, however, a significant contribution of one of them is accompanied by an insignificant or, usually, a minimized contribution of the other. The effect of −R substituents in the σ^--type reactivities may be minimized to follow σ^0 constants, regardless of the exalted resonance contribution from +R *para* substituents, since no significant additional resonance interaction can be expected between −R *para* substituents and the electron-donative reaction center. The reactivities which correspond to the case of $r^->0$ and $r^+=0$ in Eq. (2) can thus be utilized to examine the significance of σ^0 values for −R *para* substituents.

Entry 22 is a typical example of such a case. In this reaction, +R *para* substituents give a high r^- value of 0.52 characteristic of σ^--type nucleophilic reactivities, which −R *para* substituents fit the ρ_m line with σ_p^0 values. The −R group in more strongly σ^--type reactivities, such as the pK_a of phenols, may be expected to give good correlations with the σ_p^0 values. This is actually true for weak −R *para* substituents in the reaction (Entry 23); however, the examination of the effect of strongly electron-releasing groups suffers from the levelling effect.

The entries of Table 6 thus consist of two classes of reactivities; one corresponds to the case of $r^+=r^-=0$ (Entries 15—18), and the other, to $r^+=0$ but $r^->0$ (Entries 19—23). The former class reactivities are correlated with the σ^0 values in closely the same way, otherwise noted, as for the specified class of reactivities given in Table 4. The latter class satisfies the partial σ^0 correlations, and the correlational data of this class are based upon all *meta* substituents and only −R *para* substituents.

It is clear that the σ^0 values for the respective substituents in the specified σ^0 reactivity class (in Table 5) are not different from those in the apparent σ^0 reactivity class, and that, furtheremore, there is no essential difference in the apparent σ^0 values for −R substituents between the class $r^+=0$ but $r^->0$ and the above two classes. The constancy of the apparent σ^0 values appears to be of a comparable order for *meta* and *para* substituents, or a little better for the former substituents. The respective values are all in good agreement with those of our sets given in Table 3. A set of averaged σ^0 values is given for the respective substituents in the first column of Table 8. The average deviation is less than ±0.02 for all the substituents. The values marked in Tables 5 and 7 were not included in the averaging. As has been mentioned before,

TABLE 8. COMPARISON OF AVERAGED AND RELIABLE σ^0

Substituent	Averaged σ^0	n	Reliable σ^0
p-NMe_2	−0.40	2	−0.48
p-NH_2	−0.358	9	−0.36
p-OH	−0.16	3	−0.16
p-MeO	−0.108	17	−0.100
	−0.15	5	−0.152
p-Me	−0.124	20	−0.124
p-Et	−0.127	3	−0.131
p-*i*-Pr	−0.153	3	−0.156
p-*t*-Bu	−0.187	3	−0.174
p-Ph	0.038	2	0.039
p-PhO	0.063	2	0.07
p-MeS	0.066	2	0.083
p-F	0.196	8	0.212
p-Cl	0.284	23	0.281
p-Br	0.287	16	0.296
p-I	0.298	6	
p-COMe	0.491	1	(0.502)
p-CN	0.682	4	0.653
p-SOMe	0.573	1	(0.573)
p-SO_2Me	0.749	1	
p-NO_2	0.800	14	0.808
m-Me	−0.070	7	−0.069
m-MeO	0.082	5	
m-MeS	0.120	1	(0.120)
m-F	0.352	5	0.337
m-Cl	0.372	11	0.373
m-Br	0.382	6	0.391
m-I	0.342	4	
m-COMe	0.389	1	0.376
m-CN	0.648	3	0.607
m-SO_2Me	0.697	1	
m-NO_2	0.713	11	0.709

the *p*-methoxy group appears to require also another special value, −0.15, for the reactivity in a non-aqueous solution or in a less aqueous one as well as the usual value of −0.100. For the *p*-fluoro group, a constant value, 0.20, is obtained from these entries except for the dissociations of benzylammonium ions, for which another σ^0 value, 0.09, appears to be required.

All the *meta* substituents gave values of σ^0 identical with the corresponding σ_m values. As is shown in Table 3, the present reaction results in considerably higher σ^0 values for both *meta* and *para* cyano groups. The average set gives the same value for *meta* cyano group, but for *p*-cyano group gives a value rather close to the σ_p value. However, the considerably large average deviation and the insufficient number of entries make this conclusion less significant.

As a summary of these results, the set in the last column of Table 8 can be proposed as the most reliable set of σ^0 constants. The values for representative *meta* substituents are taken from the standard σ_m values, which are derived by definition from the pK_a's of benzoic acids in water (25°C). For several substituents of which the standard σ values are unknown, σ^0 values from our studies are selected. The values for *para* substituents are generally taken from our previous set of $\sigma_p{}^0$ values derived from the alkaline hydrolysis of ethyl phenylacetates. Although the set of averaged values might also be taken as the standard, we prefer to define the standard set by a single set of data since the averaged value is subject to change depending on the number of data entries. This definition is reasonable since the agreement of the set with the averaged set is well within the practical limits of uncertainty of Hammett-type substituent constants.

This set of σ^0 values may, we believe, be reliable to the order of 0.01 σ-unit for most of the substituents. The σ^0 values for *p*-NMe_2 and *p*-OH are not, however, regarded as equally reliable as those for other groups because of the insufficient number of existing data. Further examination for these substituents is now in progress. The σ^0 constants selected for +R *para* substituents are not well-established except for the *p*-nitro group. For *p*-SO_2Me and *p*-SOMe, even their standard σ values have not yet been well-established; additional data must be obtained.

Our proposed set of σ^0 values is not intended for direct application to the limited class of σ^0 reactivities, but for general use as a reference substituent constant in our LArSR equation; the σ^0 constants are referred to the unexalted substituent effect (*i.e.*, $r^+=r^-=0$), and they give, by definition, the resonance substituent constants, $\Delta\bar{\sigma}_R^+$ or $\Delta\bar{\sigma}_R^-$, as the increments from σ^+ or σ^-.

In general applications of our LArSR equation as well as in the derivation of σ^0, σ^+, and σ^- constants, the determination of appropriate ρ values should be required. Since the effect of *para* substituents usually involves a certain extent of resonance exaltation, the ρ value must be practically determined by the correlation of the *meta*-reactivities with the σ_m values. That is, the ρ value and all these treatments are based primarily upon the assumption of the reaction independency of the *meta*-substituent effects, or on the assumption of the constancy of σ_m values. This is the reason why we have selected the standard σ_m values for the above set of σ^0 values for well-behaving *meta* substituents.

The set of $\sigma_p{}^0$ values is derived from the data in aqueous organic solvents. Since the standard σ values are given by the changes in the pK_a values of benzoic acids in pure water, we have to take into account the solvent change of substituent constants when we compare the present set with the corresponding σ values. However, the substituent constants obtained in aqueous organic solutions appear to be practically of a wider application in describing the substituent effects on general organic reactivities, because most of the data are obtained not in purely aqueous solutions, but in aqueous organic solutions.

The Substituent Effect. II. Normal Substituent Constants for Polynuclear Aryls from the Hydrolysis of Arylcarbinyl Benzoates

Masami SAWADA, Yuho TSUNO, and Yasuhide YUKAWA

The Institute of Scientific and Industrial Research, Osaka University, Suita, Osaka

(Received October 28, 1971)

The rates of the alkaline hydrolysis of 9 polynuclear arylcarbinyl benzoates were measured in 70% (v/v) aqueous acetone at 25°C. The new set of σ^0 values for polynuclear aryls was obtained, using the ρ_m value established by the hydrolysis of *m*- and *p*-substituted-benzyl benzoates. In the present reaction, it is possible to assume that the peri-hydrogen steric effect is practically absent, bacause *o*-tolyl derivative gives a σ^0 value comparable with that of *p*-tolyl, and 1-naphthyl with that of 2-naphthyl. The set thus obtained can be successfully described in terms of two components; self-atom polarizability and Streitwieser's inductive index, $\sum r_{ij}^{-1}$.

The correlation of the reactivities of polynuclear aromatic hydrocarbon systems with various molecular orbital reactivity indices is very significant as a connection of the empirical results with the theory.[1] Almost all of the previous comparisons have been based on a neglect of the contribution of substantial inductive effects of polynuclear aryls.[2] In a more exact approach, a consideration of this effect is required. In order to obtain empirically information about the inductive effect, it is useful to introduce the concept of a normal substituent constant,[3] σ^0, for polynuclear aryls, an insulated aryl polar effect relative to the parent phenyl group.

In our previous papers,[4,5] it has been shown that the LArSR relationship is generally applicable to the electrophilic reactivities of the substituted benzene system:

$$\log k/k_0 = \rho(\sigma^0 + r^+ \Delta\bar{\sigma}_R^+)$$

Therefore, it can naturally be expected that the above treatment can be extended without any modification to a correlation of the polynuclear aryl reactivities.[6] In view of the importance of the σ^0 constants as a standard for the above treatment, it is necessary first of all to examine the normal substituent constants for polynuclear aryls. Thus, we have studied the alkaline hydrolysis of polynuclear arylcarbinyl benzoates in 70% aqueous acetone, $ArCH_2OCOPh$. As has been described in the foregoing paper, it has been established that the hydrolysis of *m*- and *p*-substituted-benzyl benzoates under the same conditions[5] can be correlated by σ^0, giving a comparatively large ρ_m of 0.981.

The rate constants obtained for polynuclear aryl derivatives are given in Table 1. The σ^0 constant represents the total electronic effect of substituted phenyl groups arising in response to the perturbation due to the change in the reaction site within the aryl pi-framework; this effect is in turn transmitted to the site without any additional pi-delocalization. This concept of σ^0 definition may be extended without modification to polynuclear aryl residues as well as to substituted phenyl groups. It is, then, quite reasonable to derive a set of σ^0 constants for polynuclear aryl moieties from the present insulated system. The apparent substituent constants for polynuclear aryl groups are calculated in the same way as for *m*- and *p*- substituted phenyl groups, using the ρ_m value of 0.981 and $\log k_0 = -2.169$ for the unsubstituted phenyl group. They are given in Table 1. From the uncertainty involved in the σ^0 values for substituted phenyl groups, the value may be estimated to be reliable to the order of ± 0.01.

TABLE 1. RATE CONSTANTS OF HYDROLYSIS OF ARYLCARBINYL BENZOATES AND σ^0 VALUES FOR POLYNUCLEAR ARYLS

Aryl	$10^3 \times k_2$ [a]	σ^0
Phenyl	6.74	0.000
p-Tolyl	5.13	−0.124[b]
o-Tolyl	4.97	
4-Biphenylyl	7.35	0.039[b]
3-Biphenylyl	6.85	0.005
2-Fluorenyl	6.78	0.001
1-Naphthyl	7.54	0.048
2-Naphthyl	7.74	0.062[b]
2-Phenanthryl	9.12	0.131
3-Phenanthryl	8.67	0.109
9-Phenanthryl	8.74	0.113
9-Anthryl	6.84	0.004

a) $l \cdot mol^{-1} \cdot sec^{-1}$. b) Ref. 4.

The σ^0 values obtained are positive for all the polynuclear aryls, that is, all electron-attracting as compared with the reference, the unsubstituted phenyl group. It is worthy of note that the value of σ^0 appears to change mainly dependent upon the number of rings. Naphthyls give nearly the same values of σ^0 around 0.05; this is in clear contrast with the results obtained in the other typical insulated reactivities, such as the alkaline hydrolysis of ethyl arylacetates.[7] Similarly, phenanthryl indicates σ^0 values of the same order of magnitude for three positions.

1) A. Streitwieser, Jr., "Molecular Orbital Theory for Organic Chemists," John Wiley and Sons, New York, (1964).

2) A. Streitwieser, Jr., H. A. Hammond, R. H. Jagow, R. M. Williams, R. G. Jesaitis, C. J. Chang, and R. Wolf, *J. Amer. Chem. Soc.*, **92**, 5141 (1970); B. G. von Leuwen and R. J. Ouellette, *ibid.*, **90**, 7056 (1968); E. Berliner and N. Shieh, *ibid.*, **79**, 3849 (1957); L. Verbit and E. Berliner, *ibid.*, **86**, 3307 (1964); L. Altschuler and E. Berliner, *ibid.*, **88**, 5937 (1966).

3) R. W. Taft, Jr., *J. Phys. Chem.*, **64**, 1805 (1960).

4) Y. Yukawa, Y. Tsuno, and M. Sawada, This Bulletin, **39**, 2274 (1966); Y. Yukawa and Y. Tsuno, *ibid.*, **32**, 971 (1959).

5) Y. Yukawa, Y. Tsuno, and M. Sawada, This Bulletin, **45**, 1198 (1972).

6) Y. Yukawa, Y. Tsuno, and M. Sawada, *ibid.*, **45**, 1210 (1972).

A very interesting feature in the hydrolysis of arylcarbinyl benzoates is that the 1-naphthyl derivative gives a rate comparable with that of the 2-naphthyl derivative and the *o*-tolyl one comparable with that of the *p*-tolyl one. In the case of the hydrolysis of ethyl arylacetates in aqueous ethanol,[7] the 2-naphthyl group gives an identical apparent σ^0, while the 1-naphthyl group gives a completely different value (−0.35) from the value in the present reaction. These seems to be a clear difference between the present data and those of the hydrolysis of arylacetic esters. The 1-/2-naphthyl and *o*-/*p*-tolyl rate ratios of insulated reactivities and also the other relevant reactivities are listed in Table 2. The dependency of the ratio on the reaction appears to be nearly the same for both naphthyl and tolyl derivatives, as is to be expected from the geometrical similarity. The different dependency can be reasonably attributed to the structural feature of the present system. As compared with arylacetic esters, the reaction site carbonyl of the arylcarbinyl benzoate is located one oxygen atom far from the aryl moiety.

Berliner *et al.* have recently reported the rates of the alkaline hydrolysis of methyl arylacetates.[8] Figure 1 shows the plots of log $k/k_{(Ph)}$ in aqueous methanol at 25°C against the σ^0 values. Unhindered aryls apparently fall on or close to a line, whereas the deviations are significant for hindered 1-naphthyl and 9-phenanthryl, and twice as much remarkable for 9-anthryl, which possesses two peri-hydrogens. The disposition can be, of course, attributable to the difference in the locations of the reaction site carbonyls of the two systems. The steric hindrance with peri-hydrogen to the attacking hydroxide ion is significantly operative in the arylacetates, but it should be far less effective in the present system. This is evident from the comparison shown in Table 2.

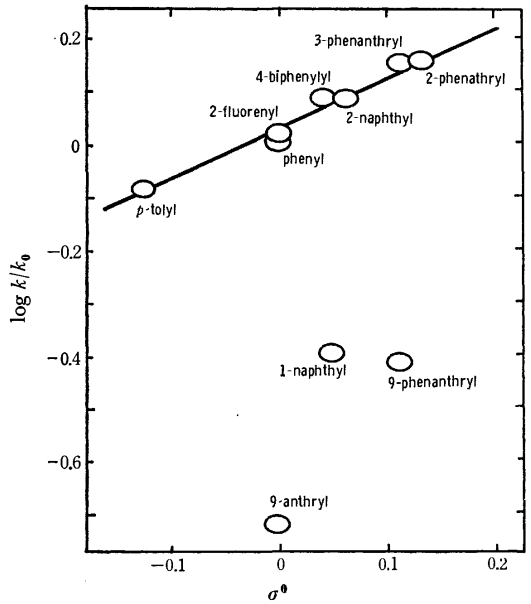

Fig. 1. Plots of the rates of hydrolysis of methyl arylacetates against σ^0.

It is perhaps not unreasonable to presume that the steric hindrance with peri-hydrogen is effectively absent in the present system. The present set of σ^0 values for polynuclear aryl groups might be regarded as parameters measuring only electronic effects and practically including no steric effect. As has been mentioned before, the steric effect does not appear to be practically effective in the dissociation of arylacetic or arylpropionic acids; the reactivity ratio of α-/β-naphthyl, 1.05, is comparable with that in the present reaction.[9] Unfortunately, no data for further comparison are available; indeed, even if they will be, the experimental uncertainty would outweigh the minor variation in σ^0 due to the structural changes of

Table 2. Rate ratios (k^1/k^2 for naphthyl and k^o/k^p for tolyl) of insulated and other relevant reactivities

Reaction	k^1/k^2	k^o/k^p
Benzyl benzoates+OH^- in 70% aq. acetone	0.97[a]	0.97[a]
Ethyl phenylacetates+OH^- in 85.4% aq. EtOH	0.35[b], 0.38[c]	0.40[d]
Ethyl phenylacetates+OH^- in 60% aq. acetone	0.28[e,f]	0.34[d,e]
Phenylacetic acids, pK_a in water	1.05[g]	1.05[h]
Benzoic acids, pK_a in water	2.93[i]	2.91[j]
Ethyl benzoates+OH^- in 85% aq. EtOH	0.32[k]	0.27[l]
Ethyl benzoates+OH^- in 60% aq. acetone	0.28[c,m]	0.29[n]

a) Present study. b) Y. Ohtsuji, T. Kubo, and E. Imoto, *Nippon Kagaku Zasshi* **80** 1300 (1959). c) J. Fischer, J. Packer, J. Vaughan, A. F. Wilson, and E. Wong, *J. Org. Chem.*, **24**, 155 (1959). d) J. G. Watkinson, W. Watson, and B. L. Yates, *J. Chem. Soc.*, **1963**, 5437. e) Ref. 4. f) Y. Yukawa, Y. Tsuno, and M. Sawada, unpublished results. g) J. F. J. Dippy, S. R. C. Hughes, and J. W. Laxton, *J. Chem. Soc.*, **1954**, 4102. h) J. Frederick, J. F. J. Dippy, and R. H. Lewis, *ibid.*, **1937**, 1008. i) J. F. J. Dippy, S. R. C. Hughes, and J. W. Laxton, *ibid.*, **1954**, 1470. j) J. F. J. Dippy and R. H. Lewis, *ibid.*, **1937**, 1426; J. Frederick, J. F. J. Dippy, and R. H. Lewis, *ibid.*, **1936**, 644. k) M. Adam-Briers, P. J. C. Fierens, and R. H. Martin, *Helv. Chim. Acta*, **38**, 2021 (1955). l) D. P. Evans, J. J. Gordon, and H. B. Watson, *ibid.*, **1937**, 1430. m) J. Packer, J. Vaughan, and E. Wong, *J. Org. Chem.*, **23**, 1373 (1958). n) E. Tommila and C. N. Hinshelwood, *J. Chem. Soc.*, **1938**, 1801; E. Tommila, *Ann. Acad. Sci. Fennicae*, Ser. A57, No. 13, 3 (1941); *Chem. Abstr.*, **38**, 6171[9] (1944).

7) A. Fischer, J. Packer, J. Vaughan, A. F. Wilson, and E. Wong, *J. Org. Chem.*, **24**, 155 (1959); K. Kindler, *Ann.*, **452**, 90 (1927).

8) N. Acton and E. Berliner, *J. Amer. Chem. Soc.*, **86**, 3312 (1964).

9) See Table 2.

polynuclear aromatic hydrocarbons, for the extremely small ρ value of the dissociation.

The noticeable features of the present system, the structurally insulated reactivity with a relatively large ρ value and practically no steric effect with peri-hydrogen, may sufficiently justify our attempt to determine an extended set of σ^0 values for polynuclear aryl groups on the basis of the present data. The derivative set of σ^0 values probably consists of idealized substituent constants, especially for hindered aryl moieties. Since the steric effect with peri-hydrogen is generally severe in the existing reactivity data, as may be seen in the hydrolysis of arylacetic esters, the present set of σ^0 values is not expected to serve widely as a reference for the simple linear free energy relationship, even for σ^0 reactivity data,

$$\log k/k_{(\mathrm{Ph})} = \rho\sigma^0$$

but instead the set will serve as a reference in estimating the importance of the peri interaction of given systems from the deviations of the hindered derivatives from the $\rho\sigma^0$ correlations.

It appears certain that the set has another important advantage in comparing the empirically derived electronic effects with theory at the various sites in the polynuclear aryl pi-system. As the theory predicts, the electronically most active site in the aryl pi-system being in common the hindered position, a reliable comparison of the electronic effects covering a significant extent of the variation in the theoretical index is possible with the present data, which include the reactivities of hindered sites.

Attempts have been made in vain by various investigators to ascertain the linear free energy relationship for the reactivities of polynuclear aromatic hydrocarbon derivatives, and further attempts have been also made to correlate them with the numerical index from simple MO theory.

As has been described in a previous paper on the analysis of substituent effects in *m*- and *p*-substituted phenyl derivatives, the standard substituent constant can be given by the combination of two intrinsic terms, inductive and pi-electronic effects.[10]

$$\sigma^0 = \sigma_i + \sigma_\pi$$

The σ^0 constant for polynuclear aryls might be similarly separable into the corresponding two terms. The inductive effect (σ_i) for polynuclear aryls might be referable to the electronegativities of additional sp^2-carbon atoms and might, then, have an electron-attracting character. Therefore, this might depend not only on the size, but also on the position of the site, of the respective aryls. The pi-electronic effect (σ_π) is the effect of only pi-electrons; it should be compared with the reactivity indices obtained by the simple MO theory.

As a theoretical scale measuring the σ_π effect involved in σ^0, self-atom polarizability, π_{rr}, (or free valence) would appear to be the most suitable,[1] for this theoretical index corresponds to the perturbation within the pi-electron framework of the aromatic system without reflecting the exo-conjugation interaction with the reaction site.

On the other hand, there seems to exist no appropriate theoretical indices of the inductive strength of polynuclear aryl groups. Streitwieser and Lawler recently proposed, as the inductive index, the relative quantity, Σr_{ij}^{-1}, in which r_{ij} denotes the distance of every carbon atom in the aromatic system from the carbon carrying the reaction site or from the side chain to which the reaction site is attached.[11] The plots of σ^0 against this set of inductive indices, as is shown in Fig. 2, resulted in a scattered pattern. Un-

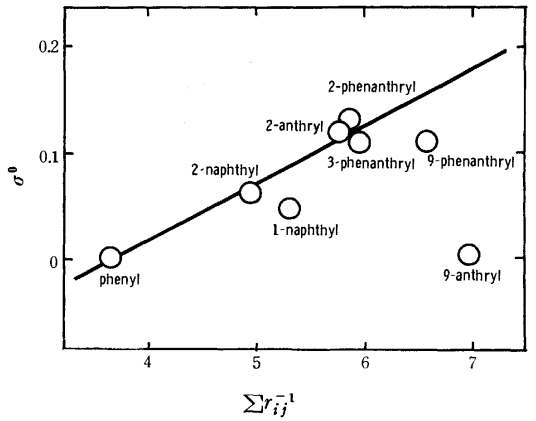

Fig. 2. σ^0 plotted against Streitwieser's inductive indices.

hindered aryls apparently lie close to a line, whereas a serious deviation is observed here also for hindered 9-anthryl and less significant deviations are noted for 1-naphthyl and 9-phenanthryl groups. Since no steric hindrance with peri-hydrogen is assumed, as has been mentioned above, the disposition of these groups may be attributable mainly to the substantial change in their pi-electronic effect. It is apparent that the groups which fall along the correlation line have π_{rr} values of the same magnitude, while, on the other hand, 1-naphthyl and 9-phenanthryl groups have relatively large π_{rr} values and fall below the line. The 9-anthryl group, which possesses an extremely high π_{rr} value, exhibits a serious deviation. The deviations from the line are apparently proportional to the differences in the corresponding π_{rr} values. On least-squares fitting, the σ^0 values can be correlated with both indices by the equation:

$$\sigma^0 = 0.06\Delta(\Sigma r_{ij}^{-1}) + 1.51\pi_{rr} + 0.06$$

The correlation[12] is rather surprisingly significant; standard deviation=±0.011, and correlation coefficient=0.984.

While this treatment is actually no more than a crude approximation, it suggests the possibility of the empirical separation of the σ^0 values for polynuclear aryls into inductive polar and pi-electronic effects. Polynuclear aryl groups in σ^0 reactivities apparently

10) Y. Yukawa and Y. Tsuno, *Nippon Kagaku Zasshi* **86**, 873 (1965).

11) A. Streitwieser, Jr., and R. G. Lawler, *J. Amer. Chem. Soc.*, **87**, 5388 (1964); *ibid.*, **85**, 2854 (1963).

12) In this calculation, σ^0 for 2-anthryl group is included (n=8). The σ^0 value is estimated to be approximately 0.12 from Ref. 8.

exert an electron-attracting inductive contribution by their intrinsic electronegativity of additional rings, but instead they exert the electron-donative pi-electronic contribution by additional pi-system to a considerable extent. These groups could be treated practically in the range from σ^0- to σ^+-type reactivities, as has been done successfully with the +I, —R-type substituents, such as the *p*-phenyl substituent. The treatment of the effect of the polynuclear aryl derivatives on the electrophilic reactivities will be discussed in another paper.[6]

Experimental

Materials. All the polynuclear arylcarbinyl benzoates were prepared by the esterification of benzoyl chloride with the corresponding carbinols in pyridine. The carbinols were obtained from the appropriate ethyl or methyl carboxylates by $LiAlH_4$[13] or $NaBH_4$[14] reduction, except for the 9-anthryl derivative, which was derived from the corresponding aldehyde. All of the esters were purified by fractionation or recrystallization. The physical constants and the elemental analysis data are listed in Table 3.

Kinetic Measurements. The rates of the alkaline hydrolyses of all the arylcarbinyl benzoates were determined in a 70% (v/v) aqueous acetone solution at 25°C. The procedure employed for these measurements was generally the same as that described in the previous paper.[5] For less soluble esters, such as 2-fluorenyl, 2- and 3-phenanthryl, and 9-anthryl derivatives, a low initial concentration, 0.01 mol/*l*, was employed, and a 15 m*l* aliquot was utilized in each titration. Since the 9-phenanthryl ester was hardly soluble under these conditions, a more diluted initial concentration, 0.005 mol/*l*, and a larger aliquot, 20 m*l*, was utilized. When the rate determination was carried out for *m*-nitro derivative under these conditions, no concentration effect was observed. As the 1- and 2-anthryl esters were insufficiently soluble even under more diluted conditions, the rate constants of these compounds could not be determined practically.

All runs which involved more than 12 measurements followed the second-order kinetic law, covering reactions up to an extent of 80%. The experimental uncertainty of a run was estimated to be much less than 2%, and the bimolecular rate constants from repeated runs agreed within ±2% or better.

Table 3. Physical constants and analytical data of arylcarbinyl benzoates

Aryl	Mp or Bp (mmHg)	Carbon		Hydrogen	
		Found	Calcd	Found	Calcd
o-Tolyl	144.5(2)	79.81	79.62	6.16	6.24
3-Biphenylyl	58—58.5	83.48	83.31	5.48	5.59
4-Biphenylyl	61.5—62	83.22	83.31	5.60	5.59
2-Fluorenyl	98—98.3	84.28	83.98	5.33	5.37
1-Naphthyl	183.5—184.5(0.15)[a]	82.24	82.42	5.28	5.38
2-Naphthyl	63.5—64[b]	82.47	82.42	5.29	5.38
2-Phenanthryl	95.5—96	84.50	84.59	4.98	5.16
3-Phenanthryl	86.5	85.02	84.59	4.64	5.16
9-Phenanthryl	125—126	84.80	84.59	4.51	5.16
9-Anthryl	93.5—94	84.37	84.59	5.27	5.16

a) C. W. Hyde and L. Young, *Biochem. J.*, **107**, 519 (1968).
b) R. N. Chakravarti and R. N. Adhya, *Bull. Calcutta School Trop. Med.*, **6** No. 4, 161 (1958); *Chem. Abstr.*, **54**, 2282b (1960).

13) W. G. Brown, "Organic Reactions", Vol. 6, John Wiley and Sons, New York, (1942), Chap. 10, p. 469.

14) S. W. Chaikin and W. G. Brown, *J. Amer. Chem. Soc.*, **71**, 122 (1949).

The Substituent Effect. III. The Basicities of Polynuclear Aryl Methyl Ketones

Yasuhide YUKAWA, Yuho TSUNO, and Masami SAWADA

The Institute of Scientific and Industrial Research, Osaka University, Yamadakami, Suita, Osaka

(Received October 28, 1971)

The basicities of nine polynuclear aryl methyl ketones have been determined spectrophotometrically in various aqueous sulfuric acid solutions. The electronic effects of unhindered polynuclear aryls on pK_{BH^+} can be successfully correlated with our LArSR equation,

$$\log k/k_0 = \rho(\sigma^0 + r\Delta\bar{\sigma}_R^+),$$

using ρ and r values established from *meta*- and *para*-substituted acetophenones. The applicability of this equation to polynuclear aryls is also shown for some other electrophilic reactivities. The $\Delta\bar{\sigma}_R^+$ parameters for polynuclear aryls are derived empirically from the solvolysis of α-arylethyl chlorides; these show a good linearity with the theoretical reactivity indices of the localization energies.

In our continuing studies of the substituent effect on chemical reactivities, it has been established that the linear aromatic substituent reactivity (LArSR) relationship (1)[1-3] is generally applicable with an excellent precision to electrophilic reactions of substituted benzene derivatives;

$$\log k/k_0 = \rho(\sigma^0 + r\Delta\bar{\sigma}_R^+) \quad (1)$$

where r is the variable characteristic of the reaction system describing the degree of the resonance exaltation and where $\Delta\bar{\sigma}_R^+$ is the substituent constant to donate electron by resonance. This equation is a bisecting description of the substituent effect in terms of the unexalted polar effect of substituted phenyl groups and the aryl resonance exaltation effect. Eq. (1) is immediately followed by Eq. (2):

$$1/\rho \log k/k_0 = \sigma^0 + r\Delta\bar{\sigma}_R^+ \quad (2)$$

As has been shown in previous papers,[1,3] the apparent substituent constants of a given *para* substituent generally exhibit a linear correlation, with a substantial slope, against r values for varying reactions. 4-Biphenylyl derivatives satisfy the above equation over a wide range of r. For 2-fluorenyl derivatives we obtained a similar plot with a slope of −0.49 and an intercept of 0.00, as is shown in Fig. 1. These findings mean that the apparent substituent constants for both derivatives can be successfully described in terms of the unexalted aryl polar effect, σ^0, and the exalted resonance effect, $r\Delta\bar{\sigma}_R^+$.

Even for condensed polynuclear aromatic hydrocarbons, such as naphthalene and phenanthrene, the above treatment can be also applicable as is shown in Fig. 2. The changes in the apparent substituent constants of 2-naphthyl are found to be a linear function of r, while those of 1-naphthyl do not satisfy the linear dependence on r. The random scatterings of the latter suggest that the steric interaction of peri-hydrogen with the reaction site depends on the nature of reactions. The linearity of the former is an evidence for the constancy of the resonance substituent constant for the 2-naphthyl group. Therefore, it might be expected that Eq. (1) can be extended so as to correlate the reactivity changes of polynuclear aromatic hydrocarbons, besides those with peri-hydrogen interaction, using ρ and r values established from a series of substituted benzene reactivities.

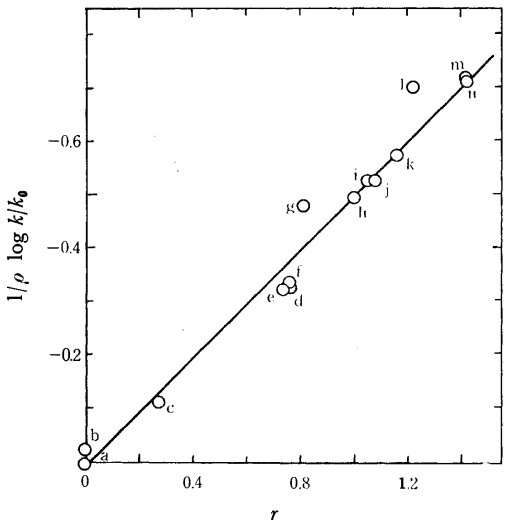

Fig. 1. Relation between apparent substituent constants for 2-fluorenyl group and r values.
Most ρ and r values are quoted from the previous paper, Ref. 1. a) Alkaline hydrolysis, arylcarbinyl benzoates, Ref. 31. b) Alkaline hydrolysis, methyl arylacetates, N, Acton and E. Berliner, *J. Amer. Chem. Soc.*, **86**, 3312 (1964). c) Alkaline hydrolysis, ethyl benzoates, Ref. 34. d) Basicity, aryl methyl ketones, present study. e) Protodesilylation in MeOH-aq. $HClO_4$, C. Eaborn, *J. Chem. Soc.*, **1956**, 4858. f) Protodesilylation in AcOH-aq. H_2SO_4, F. B. Deans and C. Eaborn, *ibid.*, **1959**, 2299. g) Acetylation, H. C. Brown, and G. Marino, *J. Amer. Chem. Soc.*, **84**, 1658 (1962). h) Solvolysis, Brown and Okamoto's σ^+, H. C. Brown and Y. Okamoto, *ibid.*, **80**, 4979 (1958). i) Mercuration, H. C. Brown, and G. Goldman, *ibid.*, **84**, 1650 (1962). j) Acetolysis, α-arylethyl chlorides, Y. Yukawa, Y. Tsuno, Y. Kusuyama, and N. Shimizu, unpublished. ($\rho = -4.70$ and $r = 1.08$). k) Solvolysis, α-arylethyl chlorides, Ref. 29. l) Molecular chlorination, L. M. Stock and H. C. Brown, *J. Amer. Chem. Soc.*, **84**, 1661 (1962). m) Molecular bromination, L. M. Stock and H. C. Brown, *ibid* **84**, 1661 (1962). n) Molecular bromination, L. Altschuler and E. Berliner, *ibid.*, **88**, 5837 (1966). From the linearity with the above bromination, ρ and r in this bromination are calculated to be −9.87 and 1.42, respectively.

As a more simplified treatment, Streitwieser has proposed a Hammett-type equation (3) for polynuclear aryl reactivities, in which the reference reaction in the solvolysis of polynuclear arylcarbinyl chlorides in 80% aq. ethanol.[4]

$$\log k/k_0 = \rho\sigma_{Ar} \quad (3)$$

1) Y. Yukawa, Y. Tsuno, and M. Sawada, This Bulletin, **39**, 2274 (1966).

2) Y. Tsuno, T. Ibata, and Y. Yukawa, *ibid.*, **32**, 960 (1959); Y. Yukawa and Y. Tsuno, *ibid.*, **32**, 965 (1959); **32**, 971 (1959).

3) Y. Yukawa and Y. Tsuno, *Nippon Kagaku Zasshi*, **86**, 873 (1965).

4) A. Streitwieser, Jr., "Molecular Orbital Theory for Organic Chemists", John Wiley & Sons, (1964), Chap. 12.

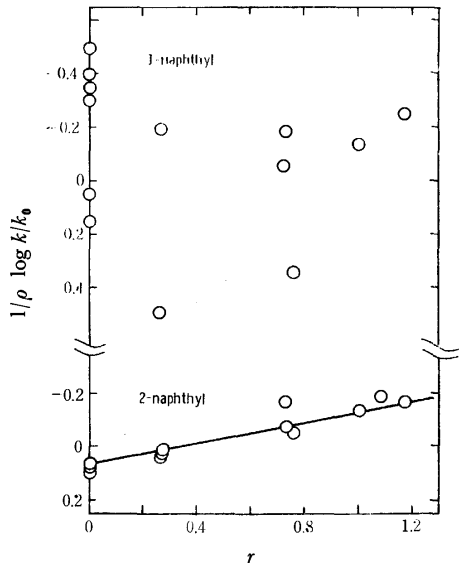

Fig. 2. Relation between apparent substituent constants for 1-naphthyl or 2-naphthyl group and r values.

He has shown a good applicability of Eq. (3) for some solvolysis reactions through a carbonium-ion intermediate. Several authors have utilized this equation and have derived revised or secondary σ values for polynuclear aryls.[5,6] However, the application of this equation is limited to the reaction system analogous to the reference system. This limitation probably arises from the neglect of the varying contribution of the resonance component to the electronic effect of polynuclear aryls.

In a previous paper, a set of σ^0 values for polynuclear aryl moieties was determined by the hydrolysis of arylcarbinyl benzoates and a set of $\Delta\bar{\sigma}_R^+$ values (in Brown Okamoto's σ^+ scale), from the solvolysis of α-arylethyl chlorides, the r value of which was 1.16. According to the LArSR approach, the solvolysis of the polynuclear $ArCH_2X$ system is treated with an extremely high r value of *ca.* 1.6 (see Discussion).

In order to verify this treatment, it is necessary and of interest to study the polynuclear reactivity changes which give the r of an intermediate value. From this point of view, the basicities of aryl methyl ketones was chosen because the r had been established to be 0.76 from that of substituted acetophenones. We have determined the dissociation constants for the conjugate acids of some polynuclear aryl methyl ketones, and have examined whether the electronic effects of polynuclear aryls on pK_{BH^+} could be treated by means of Eq. (1).

Experimental

Materials. The 1-naphthyl and 2-naphthyl methyl ketones were obtained commercially. The former was purified by recrystallization of the picrate, followed by fractional distillation of the regenerated ketone. No impurity was detected by vapor-phase chromatography. The other ketones were prepared by the method described in the literature. The 4-biphenylyl,[7] 2-fluorenyl,[8] 3-phenanthryl,[9] and 1-anthryl[10] methyl ketones were prepared by the Friedel-Crafts acetylation of the corresponding hydrocarbons. The 2-phenanthryl methyl ketone was obtained by the dehydrogenation of (9,10-dihydro) phenanthryl methyl ketone with sulfur.[11]

The 9-phenanthryl isomer was prepared from 9-carbomethoxyphenanthrene by the method of Mosettig and Kamp.[12] The 2-anthryl compound was derived from 9-anthryl ketone by isomerization with $AlCl_3$.[13]

Each isomer of the phenanthryl or anthryl methyl ketone was purified by column chromatography with Al_2O_3, followed by repeated recrystallizations from the appropriate solvents. The absorption spectra (λ_{max} and $\log \varepsilon$) in 95% EtOH were identical with those given in the organic electronic spectral data. The physical properties and analytical data are listed in Table 1.

Sulfuric Acid. Twenty stock solutions of different concentrations of sulfuric acid, ranging from 41.9% to 93.7 % by weight, were prepared by dilution with freshly-distilled water of sulfuric acid which had been purified by three re-solidifications on cooling. In these solutions no optical impurities were observed in the range of wavelengths measured.

The concentrations of the solutions were determined by titrating weighed samples with a satndard NaOH aqueous solution of about 1 N. The H_0 values of the above solutions were obtained by interpolation from a standard curve constructed using the revised values evaluated by Jorgenson and Hartter.[14]

Spectrophotometric Measurements. The method adopted for preparing the appropriate concentration of a ketone in aq. sulfuric acid was essentially the same as that described by Stewart and Yates.[15] A sample weighed on a microbalance was dissolved in 250 m*l* of anhydrous acetone, from which 0.5 m*l* aliquots were pipetted into a 10 m*l* volumetric flask. After the acetone had been carefully evaporated under a moderately reduced pressure, the flask was made up to volume with appropriate acid solutions. The concentration of the sample solution was about 10^{-5} mol/*l*. In the cases of 2- and 9-phenanthryl and 2-anthryl ketones, the solubilities into diluted acids were not so sufficient enough that the step-by-step dilution method was employed in these diluted acids.

The extinction coefficients were measured at room temperature with covered quartz cells of a 1 cm path length using a Hitachi Perkin-Elemr UV-VIS spectrophotometer. A solvent blank of the same concentration of acid as that containing a ketone was employed.

The pK_{BH^+} values were determined by the isosbestic-point method.[16] The isosbestic point was selected as an

5) A. Streitwieser, Jr., H. A. Hammond, R. H. Jagow, R. M. Williams, R. G. Jesaitis, C. J. Chang, and R. Wolf, *J. Amer. Chem. Soc.*, **92**, 5141 (1970).

6) B. G. von Leuwen and R. J. Ouellette, *ibid.*, **90**, 7056 (1968).

7) The method is the same as "Organic Syntheses," Coll. Vol. 1, p. 109.

8) "Organic Syntheses," Coll. Vol. 3, p. 23.

9) E. Mosettig and J. van de Kamp, *J. Amer. Chem. Soc.*, **52**, 3704 (1930).

10) P. H. Gore, *J. Org. Chem.*, **22**, 135 (1957).

11) A. Burger and E. Mosettig, *J. Amer. Chem. Soc.*, **58**, 1857 (1936); B. Riegel, M. H. Gold, and M. A. Kubico, *ibid.*, **64**, 2221 (1942).

12) E. Mosettig and J. van de Kamp, *ibid.*, **55**, 3442 (1933)

13) E. G. E. Hawkins, *J. Chem. Soc.*, **1957**, 3858.

14) M. J. Jorgenson and D. R. Hartter, *J. Amer. Chem. Soc.*, **85**, 878 (1963).

15) R. Stewart and K. Yates, *ibid.*, **80**, 6355 (1958).

16) L. A. Flexser, L. P. Hammett, and A. Dingwall, *ibid.*, **57**, 2103 (1935).

TABLE 1. PHYSICAL CONSTANTS AND ANALYTICAL DATA OF POLYNUCLEAR ARYL METHYL KETONES

Aryl	Mp or Bp(mmHg)	Carbon		Hydrogen	
		Found	Calcd	Found	Calcd
4-Biphenylyl	122[a,b]	85.50	85.64	5.94	6.04
2-Fluorenyl	130.5—131[a]	87.00	86.52	5.49	5.81
1-Naphthyl	127(1)[c]	84.88	84.64	5.85	5.92
2-Phenanthryl	146.5—147[a,d]	87.30	87.25	5.11	5.49
3-Phenanthryl	75.8—76[a,d,e]	87.53	87.25	5.21	5.49
9-Phenanthryl	74—74.8[a,d,f]	87.33	87.25	5.29	5.49
2-Anthryl	194[a,g,h]	87.20	87.25	5.50	5.49
1-Anthryl	109.5—110[a,g,i]	87.52	87.25	5.33	5.49

a) Ref. 30. b) W. F. Huber, M. Renoll, A. G. Rossow, and D. T. Mowry, *J. Amer. Chem. Soc.*, **68**, 1109 (1946); L. M. Long and H. R. Henze, *ibid.*, **63**, 1939 (1941); H. C. Brown, Y. Okamoto, and T. Inukai, *ibid.*, **80**, 4964 (1958). c) Y. Okamoto and H. C. Brown, *ibid.*, **79**, 1903 (1957). d) Ref. 12. e) Ref. 9. f) H. Lund, *Ber.*, **70**, 1520 (1937). g) Ref. 10; E. G. E. Hawkins, *J. Chem. Soc.*, **1957**, 3858; M. Martynoff, M. Chauvin, M. Grumez, and N. Lefevre, *Bull. Soc. Chim. Fr.*, **1958**, 164. h) Ng. Ph. Buu-Hoi and P. Cagniant, *Rec. Trav. Chim.*, **62**, 713 (1943). i) H. F. Bassilios, M. Shawky, and A. Y. Salem, *ibid.*, **81**, 679 (1962); *ibid*, **82**, 298 (1963); S. Akiyama and M. Nakagawa, This Bulletin, **33**, 1291 (1960); E. D. Bergmann and D. Katy, *J. Chem. Soc.*, **1958**, 3216.

intersecting point of two absorption curves for the sulfuric acid of the appropriate concentration, at which a ketone was protonated by approximately 50% (see Table 3). After one series of absorption curves had been shifted laterally to its point, the wavelength for the maximum peak of the fully protonated ketone in the visible wavelength region was taken as a reading wavelength. The extinction coefficients in various acids were measured at the above wavelength, chosen on the basis of the shifted curves, and were used to determine pK_{BH^+}.

Results

In the spectrum of each ketone at a higher concentration of acid, we observed a strong absorption band in the visible wavelength region (around 350—600 mμ); it seemed that this might possibly be a *P*-band characteristic of the π-π^* transition of polynuclear aromatic compound. This resulted in a large red shift and a change in the intensity of the *P*-band in going from the neutral ketone to the conjugated acid. We took note of the behavior of this terminal *P*-band and determined the pK_{BH^+} values by means of the isosbestic-point method. Stewart and Yates[15] had employed the method of Davis and Geissman[17] to obtain the pK_{BH^+} values of *m*- and *p*-substituted acetophenones. As a preliminary experiment, we chose the 2-naphthyl ketone and followed their procedure to determine the pK_{BH^+} value from their reported wavelength pair. The derived value agreed with theirs. However, the different choice of wavelength pair gave rather different pK_{BH^+} value. As would be anticipated, the spectra of polynuclear aryl ketones in aq. sulfuric acid had some characteristic bands in the UV and visible regions, which were not sufficiently separated. In such spectra the pK_{BH^+} value based on the Davis approach appeared to be less reliable because of the inclusion of a different kind of band.

To take the highest concentration of acid utilized, as a reference of the 100% protonation, would be

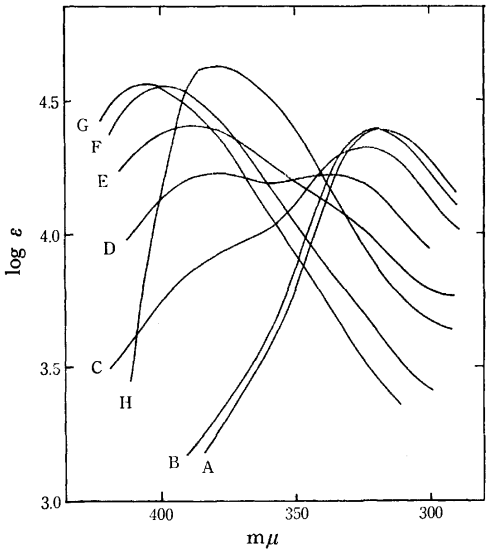

Fig. 3. UV spectra of 2-fluorenyl methyl ketone in various aq. sulfuric acid.
A; 47.2%, B; 52.7%, C; 61.1%, D; 66.8%, E; 71.6% F; 81.1%; G; 89.0%, H; 93.7% aq. H_2SO_4

at best unappropriate in determining the pK_{BH^+} by the isosbestic-point method, because it seems possible that aromatic hydrocarbon is subject to sulfonation and/or deacylation with higher concentrations of acid.[18] A typical example is shown in Fig. 3, which represents the spectra of the 2-fluorenyl methyl ketone. In the range from 47.2 to 89.0% acid, regular lateral changes were observed, while in 93.7% acid the absorption peak moved suddenly toward the lower wavelength. At concentrations higher than 89.0%, the initial yellow solutions were appreciably decolorized as time went on, and the higher the concentration of sulfuric acid, the faster the rate of change. These findings might be ascribed to certain reactions of the aromatic ketone with sulfuric acid, but not to a simple medium effect on the spectra. Similar features were

17) C. T. Davis and T. A. Geissman, *J. Amer. Chem. Soc.*, **76**, 350 7(1954).

18) W. M. Schubert and H. K. Labourette, *ibid.*, **74**, 1829 (1952).

Table 2. Mean pK_{BH^+} values and spectrophotometric data in aqueous H_2SO_4 for polynuclear aryl methyl ketones

Aryl	H_2SO_4 % for 100% protonation	Isosbestic point			Reading wavelength mμ	Slope	Mean pK_{BH^+}
		mμ	$\varepsilon \times 10^{-3}$	H_2SO_4 % inspection			
4-Biphenylyl	93.7	320	15.3	69.3—71.6	355	0.70	−6·03
2-Fluorenyl	89.0	343	15.3	66.8—69.3	380	0.72	−5.51
2-Naphthyl	93.7	309	9.18	71.6—74.2	333	0.65	−6.25
1-Naphthyl	93.7	352	4.60	71.6—77.7	406.5	0.75	−6.45
2-Phenanthryl	89.0	338.5	11.6	71.6—74.2	373	0.71	−6.22
3-Phenanthryl	89.0	373	6.97	71.6—74.2	420	0.60	−6.08
9-Phenanthryl	93.7	356.5	6.55	71.6—74.2	400	0.76	−6.56
2-Anthryl	89.0	305	31.8	69.3—74.2	320	0.70	−5.92
1-Anthryl	84.8	450	2.80	71.6—74.2	530	0.87	−6.02
Phenyl						(0.73[a])	(−6.36[b])

a) K. Yates and H. Wai *Can. J. Chem.*, **43**, 2131 (1965). b) Ref. 33.

also obtained for several of the other ketones studied. The reference concentrations chosen, at which a ketone would be completely protonated free from unfavorable reactions, are listed in Table 2. Stewart *et al.* were unable to determine the pK_{BH^+} values of 2-fluorenyl and 4-biphenylyl ketones because of their odd-shaped plots.[15] Their failure might be due to the unappropriate choice of 95% acid as the reference of complete protonation.

The plot of the extinction coefficient chosen *vs.* H_0 showed a good sigmoid titration curve, with flat arms in each ketone (see Fig. 4). Although, in the case of some other weak bases, vertical shifts on spectra due to the medium effect of higher concentrations of acid had been observed,[19] such shifts appeared to be small at the higher concentrations of sulfuric acid

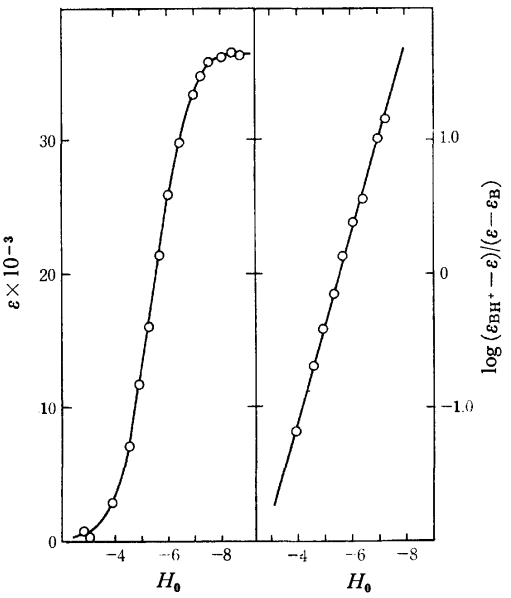

Fig. 4. Extinction coefficient ($\varepsilon \times 10^{-3}$) and $\log(\varepsilon_{BH^+}-\varepsilon)/(\varepsilon-\varepsilon_B)$ plotted against H_0 for 2-fluorenyl methyl ketone.

studied. The pK_{BH^+} value was determined graphically to read the H_0 value, giving $1/2(\varepsilon_{BH^+}+\varepsilon_B)$ on the basis of the sigmoid curve, where ε_{BH^+} and ε_B were the averaged extinction coefficients of completely protonated and unprotonated ketones respectively at the wavelength chosen. The H_0 value of the sulfuric acid, in which the ε value was taken as ε_{BH^+} or ε_B, was at least 2 H_0 units below or above the H_0 corresponding to 50% protonation.

As required by the Hammett-base equation,[20] the logarithms of the ionization ratios must be linear functions of H_0 with intercept equal an to pK_{BH^+}:

$$pK_{BH^+} = H_0 + \log [BH^+]/[B]$$

The other method to determine pK_{BH^+} is to find the intercept by least-square calculations. The ionization ratio, $[B]/[BH^+]$, was calculated by $(\varepsilon_{BH^+}-\varepsilon)/(\varepsilon-\varepsilon_B)$. The extinction coefficients used were the same as those in the former method. The plot thus obtained showed a good linearity in the region corresponding to $\log [B]/[BH^+] = \pm 1.0$ (see Fig. 4). The two methods gave identical pK_{BH^+} values within the limits of experimental uncertainty of 0.02 pK unit. The mean values are listed in Table 2. The values of 1-naphthyl and 1-anthryl ketones were slightly different from the previously-reported data.[21] This is probably due to a different choice of the acid concentration for complete protonation.

However, the values of the obtained slopes were equivalent to 0.72. If polynuclear aryl methyl ketones are to follow precisely the Hammett-base postulate, the slope should be equal to unity. This discrepancy might be mostly caused by the failure of the assumption on activity coefficients.[20] Similar findings have been reported for other non-charged weak bases,

19) D. C. Noyce and M. J. Jorgenson, *ibid.*, **84**, 4132 (1962); C. C. Greig and C. D. Johnson, *ibid.*, **90**, 6453 (1968).

20) M. A. Paul and F. A. Long, *Chem. Rev.*, **57**, 1 (1957); E. M. Arnett, "Progress in Physical Organic Chemistry," Vol. 1, John Wiley & Sons, (1963), p. 223.

21) G. Culbertson and R. Pettit, *J. Amer. Chem. Soc.*, **85**, 741 (1963); A. C. Hopkinson and P. A. H. Wyatt, *J. Chem. Soc., B*, **1967**, 1333.

such as substituted dimethylanilines,[22] benzamides,[23] benzophenones,[24] and diphenyl sulfoxides.[25,26] In view of the fact that the acidity function of the H_0 type depends strongly on the functional base, this result may indicate the possibility that a new acidity function applied to the protonation equilibria of aryl methyl ketones can be constructed.

Discussion

To examine the applicability of our LArSR Eq. (1), it is necessary first of all to evaluate the $\Delta\bar{\sigma}_R^+$ values for polynuclear aryls using the same scale as those for substituted benzenes. The numercial values of $\Delta\bar{\sigma}_R^+$ for substituted benzenes were defined by the subtraction of σ^0 from Brown and Okamoto's σ^+.[1] Since rate data are not available for polynuclear aryls in Brown's σ^+ series,[27] we have chosen the solvolysis of α-arylethyl chlorides in 80% aq. acetone as the secondary reference reaction. From our rate data[29] and Berliner's,[30] the $\Delta\bar{\sigma}_R^+$ values can be derived, using the precise ρ and r values established and, in addition, the σ^0 for polynuclear aryls already reported.[31] The resulting $\Delta\bar{\sigma}_R^+$ parameters, which are measures of the electron-releasing ability of polynuclear aryls by resonance relative to the parent benzene nucleus, are listed in Table 3 together with σ^0.

TABLE 3. σ^0 AND $\Delta\sigma_R^+$ PARAMETERS FOR POLYNUCLEAR ARYLS

Aryl	σ^0 a)	$\Delta\bar{\sigma}_R^+$
Phenyl	0.000	0.000
4-Biphenylyl	0.039	−0.218[d]
2-Fluorenyl	0.001	−0.484[e]
1-Naphthyl	0.048	
2-Naphthyl	0.062	−0.197[d]
2-Phenanthryl	0.131	−0.243[f]
3-Phenanthryl	0.109	−0.301[f]
9-Phenanthryl	0.113	
2-Anthryl	(0.12)[b]	(−0.42)[f]
9-Anthryl	0.004	
2-(9,10-Dihydro)-phenanthryl	(0.06)[c]	(−0.37)[c]

a) Refs. 1 and 31.
b) Data taken from N. Acton and E. Berliner, *J. Amer. Chem. Soc.*, **86**, 3313 (1964).
c) See text.
d) Already reported value in Ref. 1.
e) Data taken from Ref. 29.
f) Data taken from Ref. 30.

In a previous paper,[1] we have mentioned that the literature data on the pK_{BH^+} of *m*- and *p*-substituted acetophenones, which were obtained using Paul's H_0 scale,[20] can be correlated rather excellently by means of Eq. (1). Since the present data are based upon Jorgenson's recent H_0 scale,[14] correction of the published pK_{BH^+} values is required to compare the two series of ketones on the same recent scale.[32] The corrected pK_{BH^+} values for twelve *m*- and *p*-substituted acetophenones can be also correlated satisfactorily by Eq. (1). Using the method of least squares, ρ and r are calculated to be 2.58 and 0.76 respectively. Even when the present polynuclear aryl methyl ketones are included in the least-square calculations, no significant change is observed in ρ, r, and the correlation coefficient (2.57, 0.74, and 0.997 respectively). The total correlation is illustrated in Fig. 5. In order to visualized the degree of the contribution of the resonance component in this protonation, the quantities, $1/\rho \log k/k_0 - \sigma^0$, are plotted against $\Delta\bar{\sigma}_R^+$ in Fig. 6. The correlation line determined by the points of polynuclear aryls is in complete agreement with that of

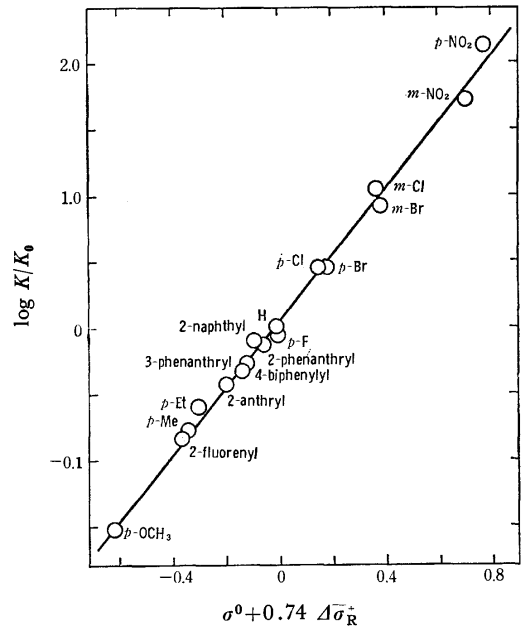

Fig. 5. The LArSR plot for dissociation of conjugate acids of aryl methyl ketones.

22) E. M. Arnett and G. W. Mach, *J. Amer. Chem. Soc.*, **86**, 2671 (1964).
23) K. Yates, J. B. Stevens, and A. R. Katritzky, *Can. J. Chem.*, **42**, 1957 (1964); A. R. Katritzky, A. J. Waring, and K. Yates, *Tetrahedron*, **19**, 465 (1963).
24) T. G. Bonner and J. Phillip, *J. Chem. Soc., B*, **1966**, 650. 1957 (1964).
25) S. Oae, K. Sakai, and N. Kunieda, This Bulletin, **42**, 1964 (1969).
26) K. Yates and H. Wai, *Can. J. Chem.*, **43**, 2131 (1965); P. Haake, R. D. Cook, and G. H. Hurst, *J. Amer. Chem. Soc.*, **89**, 2650 (1967).
27) Brown *et al.* have evaluated σ^+ values for some polynuclear aryls on the basis of the linearity between the solvolysis of aryldimethylcarbinyl chlorides and that of arylmethylcarbinyl chlorides.[28] However, according to our calculations, r of the latter is 1.16 and is slightly different from that of the former being 1.00 by definition. So, their values are not so adequate.
28) H. C. Brown and T. Inukai, *J. Amer. Chem. Soc.*, **83**, 4825 (1961).
29) Y. Yukawa, Y. Tsuno, Y. Kusuyama, and T. Fujii, To be published in this Bulletin.
30) E. Berliner and N. Shieh, *J. Amer. Chem. Soc.*, **79**, 3849 (1957).
31) M. Sawada, Y. Tsuno, and Y. Yukawa, This Bulletin, **45**, 1206 (1972).
32) A convenient method of converting previous pK_{BH^+} to the one in recent scale was described in the literature. On the basis of plotted curve of recent H_0 *vs.* previous H_0, the previous pK_{BH^+} could be directly converted to the recent one. In order to check the applicability of this procedure, pK_{BH^+} for the present ketones with previous scale was converted in the above method. The converted pK_{BH^+} agreed closely with the pK_{BH^+} based on the recent scale within 0.02 pK unit.

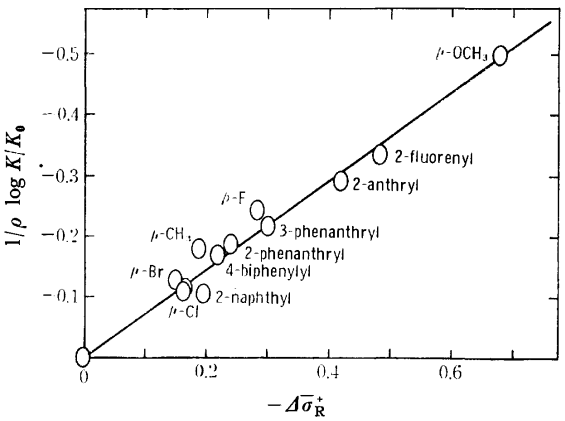

Fig. 6. Resonance contribution in the dissociation of the conjugate acids of aryl methyl ketones.

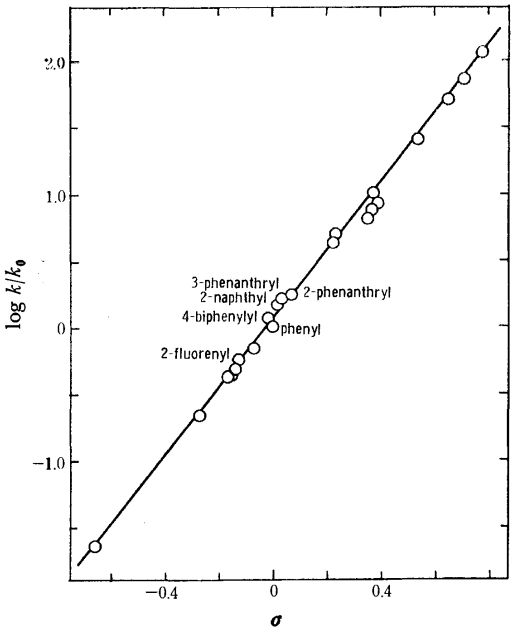

Fig. 7. Hammett plot for the alkaline hydrolysis of ethyl arylcarboxylates in 85% aq. ethanol.

p-substituted benzenes. The identical correlations indicate that the relative basicities of polynuclear aryl methyl ketones can be described by Eq. (1).

Such a treatment of polynuclear aryls has been also applied successfully to our recent data on the alkaline hydrolysis of ethyl arylcarboxylates in 85% aq. EtOH.[34] Since the apparent substituent constants of *para* electron-releasing groups for the above hydrolysis have been analyzed to have a r value of 0.25. The resulting points for polynuclear aryls fall on the line given by the *m*- and *p*-substituents, as is clear in Fig. 7.

It might be expected that the present treatment could be naturally applied to the correlation of reactivity changes for the solvolysis of the $ArCH_2X$ system.[4,5,35] Unfortunately, the definite ρ value and, in consequence, the definite r value can not be estimated for this reaction system.[1,5] However, the relative reactivities for polynuclear aryls in this system can be correlated using the approximate r value of 1.6.

Reactivity data for 2-naphthalene-like polynuclear aryls measured under the same experimental conditions (solvent, temperature, etc.) as those used for *m*- and *p*-substituted benzenes are very scarce in the literature; only the reactions the correlational data of which are summarized in Table 4 are available. The ρ and r values listed are mostly quoted from the results in our previous report.[1] The values of $1/\rho \log k/k_0$ for the 2-, 3-phenanthryl, and 2-anthryl[36] reactivities are plotted against r, as Fig. 8 shows. Satisfactory linear correlations are obtained for the respective unhindered polynuclear aryls. The most important features are that the three straight lines cover a wide variation in r values (0.0—1.6) and that, consequently, the $\Delta\bar{\sigma}_R^+$ values for the respective aryls remain constant in spite of the considerable variations in ρ and r. These facts indicate that Eq. (1) can be generally applicable to correlate polynuclear aryl reactivities as well as substituted benzene reactivities.

A similar linearity appears to be obtained for the 2-(9,10-dihydro)phenanthryl group. There are few reported data other than those for the protodesilylation of aryltrimethylsilane[37] and the solvolysis of α-arylethyl

Table 4. Summary of electrophilic reactivities for unhindered polynuclear aryls measured under the same experimental conditions as those for substituted benzenes

Reaction	ρ	r
Alkaline hydrolysis, $ArCH_2OCOPh$, 70% aq. acetone, 25°C[a]	0.978	0.000
Alkaline hydrolysis, ArCOOEt, 85% aq. EtOH, 25°C[b]	2.59	0.25
pK_{BH^+}, $ArCOCH_3$[c]	2.58	0.76
Protodesilylation, $ArSiMe_3$, aq.-MeOH, $HClO_4$, 50°C[d]	−5.32	0.73
Solvolysis, ArCHClMe, 80% aq. acetone, 45°C[e]	−4.96	1.16
Solvolysis, $ArCH_2OTs$, acetic acid, 40°C[f]	(−3.71)[g]	(1.65)[g]

a) Ref. 31. b) Ref. 34. c) Present study and Ref. 15. d) R. O. C. Norman and R. Taylor, "Electrophilic Substitution in Benzenoid Compounds," Vol. 3, Elsevier (1965), Chap. 9. e) Refs. 29 and 30. f) Ref. 5. g) These values are the total correlational parameters of substituted benzenes and polynuclear aryls. *p*-F derivative is not included in this calculation ($n=11$).

33) K. Yates and B. F. Scott, *Can. J. Chem.*, **41**, 2320 (1963).
34) Y. Yukawa, Y. Tsuno, and M. Sawada, unpublished.
35) B. G. von Leuwen and R. J. Ouellette, *J. Amer. Chem. Soc.*, **90**, 7056 (1968).
36) Data for 2-anthryl reactivities are not so adequate because of experimental difficulties due to low solubilities.
37) Data taken from R. O. C. Norman and R. Taylor, "Electrophilic Substitution in Benzenoid Compounds", Vol. 3, Elsevier, (1965), Chap. 9.

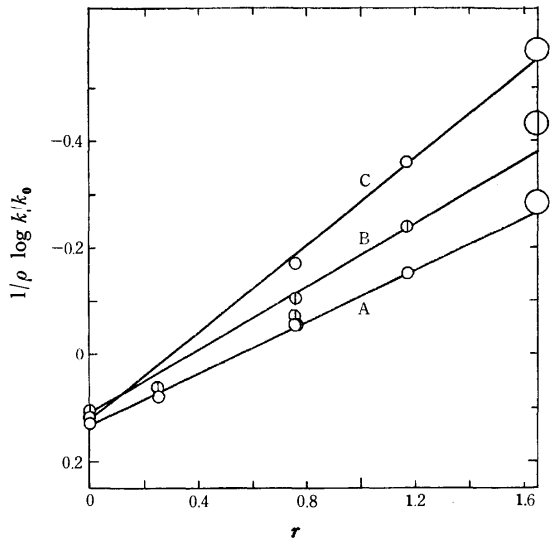

Fig. 8. Linear relationship between apparent substituent constants and r values.
A; 2-phenanthryl, B; 3-phenanthryl, C; 2-anthryl group.

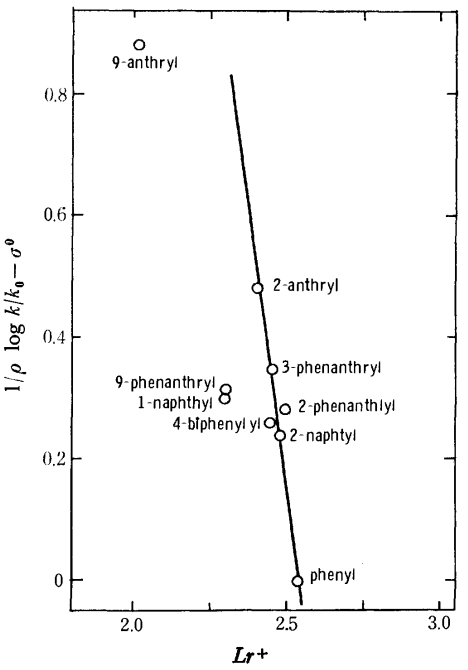

Fig. 9. Linear relationship between $1/\rho \log k/k_0 - \sigma^0$ and Lr^+ for solvolysis of arylmethylcarbinyl chlorides in 80% aqueous acetone at 45°.

chloride.[29] Although additional data should be necessary to examine the numerical value, the $\Delta\bar{\sigma}_R^+$ value for this group can be estimated to be approximately −0.37 on the basis of the above treatment. It is worth noting that the capabilities of biphenyl-type compounds for electron-donation by resonance, $\Delta\bar{\sigma}_R^+$, increase in the order: 4-biphenylyl<2-(9-10-dihydro)phenanthryl<2-fluorenyl. This order can be clearly explained on the basis of the increasing coplanarity between both benzene rings of the biphenyl component.

In the treatment of the reactivity data with theoretical reactivity indices derived from molecular orbital calculations, various authors have directly compared the logarithmus of the relative rates for polynuclear aryl derivatives with various simple MO indices.[4,5,10,38] We consider their approachs to be based on a neglect of the changes in the electronic energy due to the σ-framework effect for the respective polynuclear aryls. We have ourselves successfully separated the substituent effects of substituted benzene reactivities into two terms, the reaction-independent σ-inductive effect and the reaction-variable π-electronic effect.[3,39] On the basis of the same sort of consideration, it may be reasonable to say that the electronic effect on polynuclear aryls also contains the contribution of the σ-inductive effect as well as that of the π-electronic effect. The former may be referable to the electronegativities of the sp^2-carbon σ-framework; it should be characteristic of the reacting position, and also of the size of the polynuclear aromatic ring. On the other hand, the simple MO reactivity index depends on the nature of only the π-electron framework. Therefore, it would be more reasonable to compare a MO index with the quantity that the σ-inductive effect is removed from the observed electronic effect. Such quantities would correspond to $1/\rho \log k/k_0 - \sigma^0$ or residual $r\Delta\bar{\sigma}_R^+$ in our treatment, if the contribution of the σ-inductive effect of polynuclear aryls is independent of the reactions and remain constant.

For the solvolysis of α-arylethyl chlorides,[29,30] a plot of $1/\rho \log k/k_0 - \sigma^0$ against the localization energy, Lr^+,[4] derived from the simple HMO method, is shown in Fig. 9 as a typical example. In practise, 2-naphthalene-like groups show a remarkable linear correlation, and 1-naphthalene-like groups, large deviations. The latter feature is naturally due to peri-hydrogen steric effects. More precisely, the points of 4-biphenylyl and 2-phenanthryl deviate slightly from the correlation line. The minor deviation of the former can presumably be ascribed to the unpreferable Lr^+ value itself, because the different bond order or bond length on the pivot bond in biphenyl is not reflected in the HMO calculations. On the other hand, there is no plausible explanation of the minor deviation of the latter.[40] Of course, the same sorts of features are obtained in such a plot of the present basicity data and other reactivity data on the reactions listed in Table 4. The obtained linear correlation, which indicates a linearity between $\Delta\bar{\sigma}_R^+$ and Lr^+, may be sufficient to indicate a theoretical justification of our analysis of the electronic effect on polynuclear electrophilic reactivities.

38) L. Verbit and E. Berliner, *J. Amer. Chem. Soc.*, **86**, 3307 (1964); N. Acton and E. Berliner, *ibid.*, **86**, 3312 (1964); L. Altschuler and E. Berliner, *ibid.*, **88**, 5937 (1966); M. K. Hoffman and E. Berliner, *J. Org. Chem.*, **35**, 745 (1970).

39) Y. Yukawa and Y. Tsuno, *Mem. Ins. Sci. and Ind. Res., Osaka Univ.*, **23**, 71 (1966).

40) When the localization energy derived from advanced MO method which has been recently proposed by Dewar[41] is adopted for comparison, 2-phenanthryl falls on the correlational line, but 2-anthryl deviates in this plot.

41) M. J. S. Dewar and C. C. Thompson, Jr., *J. Amer. Chem. Soc.*, **87**, 4414 (1965).

The Base-catalyzed Condensation of α-Haloaldehydes with Dichloroacetates

Akira TAKEDA, Sadao TSUBOI, Satoshi WADA, and Hiroshi KATO

Department of Synthetic Chemistry, School of Engineering, Okayama University, Tsushima, Okayama

(Received October 29, 1971)

The reaction of aliphatic α-haloaldehydes with methyl dichloroacetate in the presence of sodium methoxide was carried out. α-Chloroaldehydes afforded 2,4-dichloro-2,3-epoxyalkanoates (**5**), whereas α-bromoaldehydes gave 2,2-dichloro-3,4-epoxyalkanoate (**7**). The attempted epoxy-carbonyl rearrangement of **5** with hydrogen chloride or thionyl chloride failed. The thermal decomposition of methyl 2,4-dichloro-2,3-epoxynonanoate (**5c**) at 300—400°C afforded methyl 3-chloro-2-oxo-3-nonenoate (**9c**), and the similar treatment of methyl 2,4-dichloro-4-methyl-2,3-epoxypentanoate (**5a**) afforded a mixture of methyl 3,4-dichloro-4-methyl-2-oxopentanoate (**6a**), methyl 3-chloro-4-methyl-2-oxo-3-pentenoate (**9a**), and methyl 3-chloro-4-methyl-2-oxo-4-pentenoate (**10**). The treatment of **5** with thiourea in methanol gave the thiazole derivative (**15**), but neither sodiomalonate nor sodioacetoacetate reacted with **5**.

The base-catalyzed condensation of aldehydes with the dichloroacetic ester has been reported by several authors.[1-4] It is known that the reaction affords α-chloroglycidic esters (**1**) and the α-chloropyruvic ester (**2**). Compound **2** is produced by the epoxy-carbonyl rearrangement of **1**:[4]

$$RCHO + Cl_2CHCO_2R' \longrightarrow R\text{-}\underset{\diagdown O \diagup}{CH\text{-}C}(Cl)\text{-}CO_2R' \quad \mathbf{1}$$

$$\longrightarrow R\text{-}CH(Cl)C(=O)CO_2R' \quad \mathbf{2}$$

Aliphatic aldehydes with a longer chain, such as heptanal, hexanal, and nonanal, usually give rearranged products (**2**). On the contrary, acetaldehyde and propionaldehyde yield the corresponding α-chloroglycidates (**1**) predominantly. Furthermore, 2-chloro-2,3-epoxyisocaproate resists the epoxy-carbonyl rearrangement with hydrogen chloride.[4] As an extension of previous work,[4] we carried out the Darzens-type condensation of aliphatic α-haloaldehydes with methyl dichloroacetate in the presence of sodium methoxide in order to establish a synthetic route to obtain 2-chloro-4-halogeno-2,3-epoxyalkanoate (**5**) and 3-chloro-4-halogeno-2-oxoalkanoate (**6**). The present report will describe the results of this reaction and will discuss the chemical properties and the structural chacacterization of the products. The yields, boiling points, and analytical results of the products are listed in Table 1.

Two pathways can be postulated for the elimination of the halogen atom of the possible intermediate (**4**), as is shown in Scheme 1. One involves the formation of the glycidates, **5**, which might further undergo an epoxy-carbonyl rearrangement to **6** (Route 1). In the other, the halogen atom originating from α-haloaldehyde is eliminated to produce 2,2-dichloro-3,4-epoxyalkanoate (**7**) (Route 2).

TABLE 1. PRODUCTS FROM THE REACTION OF α-HALOALDEHYDES WITH METHYL DICHLOROACETATE

α-Haloaldehyde RR′C(X)–CHO			Products[a]		Yield, %	Bp, °C/mmHg	Found, %		Calcd, %	
R	R′	X	Code	Structure			C	H	C	H
CH_3	CH_3	Cl	**5a**	$(CH_3)_2CClCH(O)CClCO_2Me$	34	86—89/3	39.51	4.70	39.46	4.73
C_2H_5	H	Cl	**5b**	$C_2H_5CH(Cl)CH(O)CClCO_2Me$	56	94—97/4	39.65	5.01	39.46	4.73
n-C_5H_{11}	H	Cl	**5c**	$C_5H_{11}CH(Cl)CH(O)CClCO_2Me$	40[b]	119—126/3	47.34	6.46	47.07	6.32
C_2H_5	H	Br	**7b**	$C_2H_5CH(O)CHCl_2CO_2Me$	10	98— 99/7	39.28	4.57	39.45	4.73
n-C_5H_{11}	H	Br	**7c**	$C_5H_{11}CH(O)CHCl_2CO_2Me$	15	107—112/2	46.77	6.39	47.07	6.32

a) All the compounds listed here are new.
b) Obtained as the mixture of **5c** and **7c** (92: 8). See experimental part.

1) V. F. Martynov and M. I. Titov, *Zh. Obschch. Khim.*, **32**, 319 (1962); *Chem. Abstr.*, **57**, 12373c (1962).
2) R. N. McDonald and P. A. Schwab, *J. Org. Chem.*, **29**, 2459 (1964).
3) A. Takeda, S. Wada, and T. Uno, *Mem. School Eng., Okayama Univ.*, **2**, 80 (1967).
4) A. Takeda, S. Wada, M. Fujii, and H. Tanaka, This Bulletin, **43**, 2997 (1970).

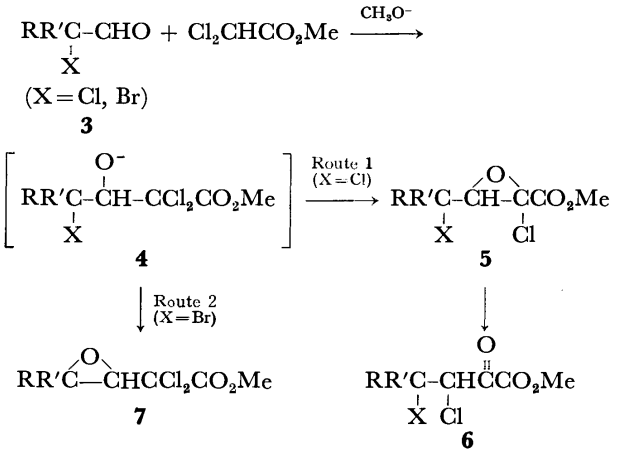

Scheme 1

The reaction of α-chloroaldehyde with dichloroacetates usually gave 2,4-dichloro-2,3-epoxyalkanoate (**5**) in a 30—55% yield. α-Chloroheptanal, however, gave a small amount (8% yield) of methyl 2,2-dichloro-3,4-epoxynonanoate (**7c**) in addition to methyl 2,4-dichloro-2,3-epoxynonanoate (**5c**). This indicates that the halogen atoms at the α and γ positions in the intermediacy (**4c**) compete as leaving groups. Indeed, α-bromoaldehydes afforded only 2,2-dichloro-3,4-epoxyalkanoate (**7**) under the same reaction conditions, even though in poor yields (10—15%), without the formation of **5**. Both compounds, **5** and **7**, were stable enough to be distillable under reduced pressure. For the structural assignment of these compounds, the NMR spectra, especially the multiplet (1H) at τ 5.8—6.2 (**5c**, C_4-methine proton) and the multiplet (1H) at τ 6.73 (**7c**, C_4-epoxide methine proton), were instructive.

The esters **5** were treated with dry hydrogen chloride in ether at 0°C in order to investigate their facility at undergoing epoxy-carbonyl rearrangement, but the starting material was recovered unchanged, without any formation of pyruvates, **6**. Furthermore, the treatment of methyl 2,4-dichloro-2,3-epoxynonanoate (**5c**) with dry hydrogen chloride in ether at the reflux temperature, or even with excess thionyl chloride at the reflux temperature, still had no effect on its transformation to **6**. The hydrolysis of **5c** with 10% H_2SO_4 afforded only 2,4-dichloro-2,3-epoxynonanoic acid (**8**). Since the acidic hydrolysis of glycidate usually causes decarboxylative elmination thus producing ketone or aldehyde,[5,6] it is rather surprising that the acid **8** can be isolated as stable crystals. The acid **8** was again transformed to **5c** with diazomethane. The larger stability of the esters **5** as compared to α-monochloroglycidate (**1**) under treatment with hydrogen chloride or thionyl chloride may be accounted for by assuming that the migration of the chlorine atom at C_2 is hindered by the electrical repulsion which the chlorine atom attached to C_4 exerts.

The transformation of **5** to **6** was performed pyrolytically; it was usually accompanied by a secondary elimination of hydrogen chloride. The distillation of **5c** at 300—400°C (oven temperature) under an atmosphere of nitrogen gave only methyl 3-chloro-2-oxo-3-nonenoate (**9c**). The IR bands of **9c** at 1740, 1690, and 1610 cm^{-1} are characteristic of the α,β-unsaturated ketoester. The triplet at τ 2.8 (J=7 Hz) in the NMR spectrum of **9c** represents the signal from the C_4-vinyl proton. These data all support the structure of **9c**. For the formation of **9c**, the rearranged product, **6c**,

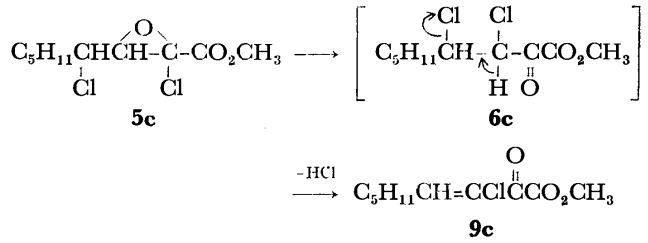

Scheme 2

might be the intermediate from which the more acidic hydrogen at C_3 is eliminated. This mechanism is supported by the pyrolysis of 4-methyl-2,4-dichloro-2,3-epoxypentanoate (**5a**), where the rearranged product **6a** has been isolated. The distillation of **5a** at 300—350°C gave a mixture of three components, methyl 3,4-dichloro-4-methyl-2-oxopentanoate (**6a**, 17%), methyl 3-chloro-4-methyl-2-oxo-3-pentenoate (**9a**, 9%), and methyl 3-chloro-4-methyl-2-oxo-4-pentenoate (**10**, 72%). The reaction sequence is shown in Scheme 3. The treatment of **6a** with triethylamine resulted in the formation of **9a** (37%).

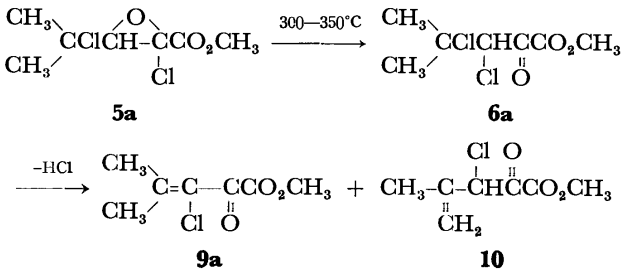

Scheme 3

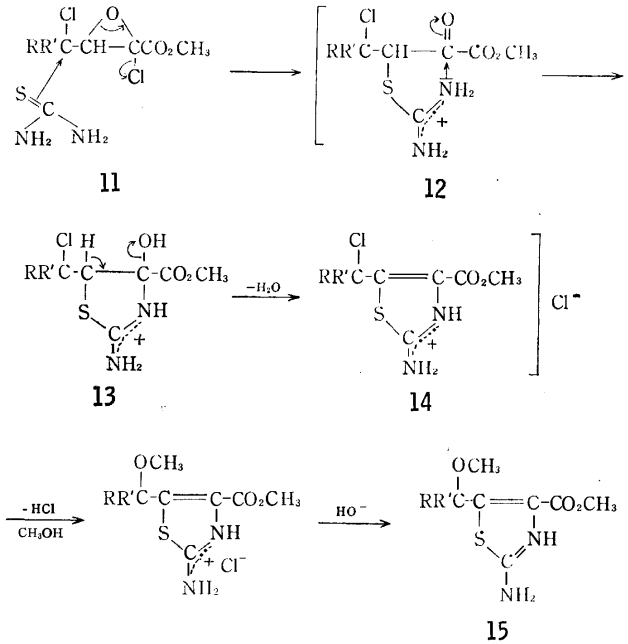

Scheme 4

5) M. Mousseron and R. Granger, *Compt. Rend.*, **218**, 358 (1944).
6) G. Darzens, *ibid.*, **195**, 884 (1932).

Although carbanions, such as sodiomalonate and sodioacetoacetate, were unreactive with **5** in methanol or dioxane, thiourea reacted with **5** in methanol to give the corresponding thiazole derivative (**15**). The possible pathway of the formation of **15** is shown in Scheme 4. Since 2-chloro-2,3-epoxyalkanoate has been known to produce the thiazole derivative readily,[4] it is reasonable to assume that the chlorinated thiazole derivative (**14**), which was formed intermediately, readily underwent solvolysis with methanol.

Experimental

The melting points and boiling points are uncorrected. The microanalyses were carried out by Mr. Eiichiro Amano of our laboratory. The analytical determinations by glpc were performed on a Hitachi K-53 model gas chromatograph (3 mm o.d.×1 m, 10% Apiezon Grease L on Chromosorb W), and the preparative isolations by glpc were performed on a Yanagimoto GCG-550T model gas chromatograph (3 mm o.d.×2.25 m, 10% Apiezon Grease L on Chromosorb W). We are indebted to Dr. Akira Suzuki and Mr. Shigezo Shimokawa, both of Hokkaido University, and to Mr. Hiroshi Ooyama, Hokko Chemical Industry Co., Ltd., for the NMR measurements.

The α-chloroaldehydes used in this experiment were prepared by the method of Stevens[7,8] by treating aldehydes with sulfuryl chloride: α-chloroisobutanal, bp 86—90°C (lit,[7] bp 86—88°C), yield 38%; α-chlorobutanal, bp 36—37°C/50 mmHg (lit,[8] bp 104—110°C), yield 27%; α-chloroheptanal, bp 76—79°C/24 mmHg (lit,[8] bp 36—38°C/2 mmHg), yield 78%. The α-bromoaldehydes were obtained by the direct bromination of aldehydes with bromine:[9,10] α-bromoheptanal, bp 75—78°C/4 mmHg (lit,[9] bp 81—82°C/3 mmHg), yield 40%; α-bromobutanal, bp 47—50°C/21 mmHg (lit,[10] bp 33°C/15 mmHg), yield 10%.

The following experiments are shown as typical runs.

Methyl 2,4-Dichloro-2,3-epoxy-4-methylpentanoate (5a). Powdered sodium methoxide (5.5 g, 0.1 mol) was added with caution to a mixture of freshly-distilled α-chloroisobutanal (10.6 g, 0.1 mol) and methyl dichloroacetate (14.3 g, 0.1 mol) dissolved in 60 m*l* of dry ether, at 5—10°C. After the addition had been completed, the heterogeneous reaction mixture was allowed to warm up to room temperature and then refluxed for 1.5 hr. The ethereal extract was washed several times with water and dried over Na_2SO_4. After the removal of the solvent, it was distilled to give 7.2 g (34%) of **5a**: bp 86—89°C/3 mmHg; IR (cm^{-1}, liquid) 1750 (ester C=O); NMR (τ, $CDCl_3$) 6.15 (s, 3H, $-COOCH_3$), 6.27 (s, 1H, $-CH(O)-CCl-$), 8.23 (s, 6H, $(CH_3)_2CCl-$).

Methyl 2,4-Dichloro-2,3-epoxynonanoate (5c). Powdered sodium methoxide (6.8 g, 0.125 mol) was added with caution to a mixture of freshly-distilled α-chloroheptanal (14.8 g, 0.1 mol) and methyl dichloroacetate (14.3 g, 0.1 mol) dissolved in dry ether (30 m*l*), at 0±1°C. The mixture was stirred for 1.5 hr at room temperature and then treated with water. The ethereal layer was separated, washed several times with water, and dried over Na_2SO_4. After the removal of the solvent, it was distilled giving 10.3 g (40% yield)[11] of the liquid, which was collected at 119—126°C/3 mmHg. Glpc analysis showed it to consist of two components. The peaks, retention times (min), and integrated percentages[12] are as follows: 1, 15.5, 8; 2, 17.1, 92. Component 1 was collected by preparative glpc and was identified as methyl 2,2-dichloro-3,4-epoxynonanoate (**7c**) by a comparison of its IR data and retention time with those of an authentic sample (see next section). Component 2 (**5c**) was purified similarly and analyzed: IR (cm^{-1}, liquid) 1760 (ester C=O); NMR (τ, $CDCl_3$) 6.08 (s, 3H, $-COOCH_3$), 5.8—6.2 (m, 1H, $-(CH_2)_4C\underline{H}(O)Cl-$), 6.4 (d, 1H, $-CH(O)-C(Cl)-$), 8.0—8.8 (m, 8H, $CH_3(C\underline{H}_2)_4-$), 9.03 (t, 3H, J=5 Hz, $C\underline{H}_3(CH_2)_4-$).

Methyl 2,2-Dichloro-3,4-epoxynonanoate (7c). Into a solution of α-bromoheptanal (15.0 g, 0.077 mol) and methyl dichloroacetate (11.0 g, 0.077 mol) in dry ether (30 m*l*), sodium methoxide (5.1 g, 0.096 mol) was stirred at 0±1°C. After the addition had been completed, the reaction mixture was allowed to warm up to room temperature. Stirring was continued for 1.5 hr. After the subsequent addition of water, the ethereal layer was separated, washed several times with water, dried over Na_2SO_4, and concentrated. A residual, thick yellow oil was distilled to give 3.0 g (15%) of **7c**: bp 107—112°C/2 mmHg; IR (cm^{-1}, liquid) 1750, 1760 (ester C=O); NMR (τ, $CDCl_3$) 6.1 (s, 3H, $-COOCH_3$), 6.52 (d, 1H, J=2.5 Hz, $-CH(O)-C\underline{H}CCl_2-$), 8.2—8.9 (m, 8H, $CH_3(C\underline{H}_2)_4-$), 9.09 (d, 3H, $C\underline{H}_3(CH_2)_4-$). A considerable amount of an undesirable resinous material was formed in this reaction and was discarded as a residue.

2,4-Dichloro-2,3-epoxynonanoic Acid (8). In a 50-m*l* three-necked, round-bottomed flask equipped with a dropping funnel, a mechanical stirrer, and a reflux condenser fitted with a drying tube, were placed dry methanol (20 m*l*) and sodium (0.46 g, 0.02 mol). While the mixture was being stirred at 0°C, 5.0 g (0.02 mol) of methyl 2,4-dichloro-2,3-epoxynonanoate (**5c**) and then 0.5 m*l* of water were added slowly. The solution was allowed to warm up to room temperature and then stirred for 3 hr. The sodium salt of the acid, **8**, precipitated in the solution was collected by filtration and washed with absolute methanol and ether. The salt was treated with a mixed solution of 2 m*l* of concentrated hydrochloric acid and 10 m*l* of water. The organic layer was extracted with ether, washed with water, and dried over Na_2SO_4. After the removal of the solvent, white needles were obtained. Recrystallization from *n*-hexane gave 1.5 g (31%) of white needles; mp 36—37°C; IR (cm^{-1}, liquid[13]) 2650 and 2500 (acid OH), 1738 (acid C=O).

Found: C, 44.43; H, 5.83%. Calcd for $C_9H_{14}Cl_2O_3$: C, 44.83; H, 5.83%.

The esterification of the above acid, **8** (1.7 g, 0.0071 mol), was carried out with diazomethane in ether. The removal of the solvent left a thick yellow liquid which, on distillation, gave 0.9 g of a clean oil: bp 126—127°C/5 mmHg. It was identified as **5c** by a comparison of IR and glpc with those of an authentic sample.

Thermal Decomposition of Methyl 2,4-Dichloro-2,3-epoxynonanoate (5c). The distillation of **5c** (2.5 g, 0.0098 mol) was carried out by heating it at 300—400°C with a mantle heater under an atmosphere of nitrogen. A thick yellow oil (2.0 g)

7) C. L. Stevens and B. T. Gillis, *J. Amer. Chem. Soc.*, **79**, 3448 (1957).
8) C. L. Stevens, E. Farkas, and B. Gillis, *ibid.*, **76**, 2695 (1954).
9) F. Ramiraz and A. F. Kirly, *ibid.*, **75**, 6026 (1953).
10) A. Kirrmann, *Compt. Rend.*, **184**, 525 (1927).
11) Estimated as compound **5c**.
12) Observed on a 1-m 10% Apiezon Grease L on Chromosorb W column. Column temp., 150°C; carrier gas, N_2 (0.5 kg/cm², 42 ml/min); detector, FID.
13) The IR spectrum of **8** was measured on warm NaCl prisms.

was distilled at 240—250°C under the evolution of hydrogen chloride. The glpc analysis of the oil showed two peaks.[12] The peaks, retention times (min), and integrated percentages are as follows: 1, 11.6, 62; 2, 17.2, 38. Component 1 (major constituent), collected by preparative glpc, was identified as methyl 3-chloro-2-oxo-3-nonenoate (**9c**): IR (cm^{-1}, liquid) 1740 (ester C=O), 1690 (conjugated keto C=O), 1610 (conjugated C=C).

Found: C, 54.89; H, 6.98%. Calcd for $C_{10}H_{15}ClO_3$: C, 54.92; H, 6.91%.

The spectral data of component 2 (minor constituent) were identical with those of **5c**.

Thermal Decomposition of Methyl 2,4-Dichloro-2,3-epoxy-4-methylpentanoate (5a). The distillation of **5a** (7 g, 0.033 mol) was carried out in the same manner as in the foregoing experiment on **5c**. A thick yellow oil (5.6 g) came out at 200—210°C under the evolution of hydrogen chloride. It gave a clean oil (5.1 g) on distillation under reduced pressure: bp 119—124°C/44 mmHg. Glpc analysis[14] showed three peaks, with retention times (min) of 4.5, 8.0, and 9.5 respectively, and in an area ratio of 72: 10: 18. The crude product was fractionated into components by preparative glpc. The spectral data and analyses of these components are as follows (components, retention times,[14] IR, NMR, analysis): Component 1: 4.0 min; IR (cm^{-1}, liquid) 1750 (ester C=O), 1735 (keto C=O), 1640, 1610 (C=C); NMR (τ, $CDCl_3$) 4.38 (s, 1H, $-\underset{\underset{H}{|}}{C}ClCOCO_2CH_3$), 4.78 (s, 2H, $CH_3-\overset{\overset{CH_2}{||}}{C}-$), 6.11 (s, 3H, $-COOCH_3$), 8.13 (s, 3H, $C\underline{H}_3-\overset{\overset{CH_2}{||}}{C}-$). Found: C, 47.29; H, 4.95%. Calcd for $C_7H_9ClO_3$: C, 47.61; H, 5.14%. Component 2: 5.6 min; IR (cm^{-1}, liquid) 1740 (ester C=O), 1685 (conjugated keto C=O) and 1590 (conjugated C=C); NMR (τ, $CDCl_3$) 6.12 (s, 3H, $-COOCH_3$), 7.76 (s, 3H, $C\underline{H}_3-\overset{\overset{CH_3}{|}}{C}=CCl-$) and 7.88 (s, 3H, $CH_3-\overset{\overset{C\underline{H}_3}{|}}{C}=CCl-$). Found: C, 47.32; H, 5.24. Calcd for $C_7H_9ClO_3$: C, 47.61; H, 5.14. Component 3: 7.2 min; IR (cm^{-1}, liquid) 1760 (ester C=O) and 1740 (keto C=O); NMR (τ, $CDCl_3$) 3.98 (s, 1H, $-\underset{\underset{H}{|}}{C}Cl-CO-$), 6.12 (s, 3H, $-COOCH_3$), 8.35 (s, 3H, $C\underline{H}_3-\underset{\underset{CH_3}{|}}{C}ClCHCl-$) and 8.48 (s, 3H, $CH_3-\underset{\underset{C\underline{H}_3}{|}}{C}ClCHCl-$). Found: C, 39.80; H, 4.67%. Calcd for $C_7H_{10}Cl_2O_3$: C, 39.46; H, 4.73%. On the basis of these data, components 1, 2, and 3 are identified as methyl 3-chloro-4-methyl-2-oxo-4-pentenoate (**10**), methyl 3-chloro-4-methyl-2-oxo-3-pentenoate (**9a**), and methyl 3,4-dichloro-4-methyl-2-oxopentanoate (**6a**) respectively. The conjugation of the double bond with the keto carbonyl group is obvious in compound **9a**, while it is not in compound **11**. Compound **9a** has no double bond.

Dehydrochlorination of 6a with Triethylamine. To a solution of gas-chromatographically-pure sample of **6a** (12 mg, 5.6×10^{-5} mol) in dry ether (0.1 m*l*), was added triethyl amine (0.0145 g, 1.4×10^{-4} mol) at room temperature. After the solution had been shaken upon occasion for 30 min, the excess of triethylamine was removed by evaporation. The glpc analysis of the residual oil showed two peaks which corresponded to **9a** and **6a** in retention times, *i.e.*, 8.0 min and 9.5 min respectively. By referring to the peak areas it can be estimated that 37% of the starting material (**6a**) has been transformed to **9a**.

2-Amino-4-methoxycarbonyl-5-(1-methoxyhexyl)thiazole (15c). A solution of **5c** (1.2 g 0.0047 mol) and thiourea (0.36 g, 0.0047 mol) in methanol (10 m*l*) was refluxed for 18 hr. The mixture was diluted with water and made alkaline with aqueous ammonia. The organic layer was extracted with ether, washed with water, and dried over Na_2SO_4. After the removal of the solvent, 0.9 g of a brownish-green oil (**15c** of *ca.* 80% purity by thin layer chromatography[15]) was obtained. A pure sample of **15c** was collected by preparative tlc for microanalyses and spectra determinations: R_f 0.2; IR (cm^{-1}, liquid) 3400, 3300, 3110, 2920, 1707, 1620, 1540, 1220; NMR (τ, $CDCl_3$) 4.1 (s, 2H, $-NH_2$), 4.9 (t, 1H, $J=6$ Hz, $C_5H_{11}-C\underline{H}OCH_3-$), 6.18 (s, 3H, $-COOCH_3$), 6.71 (s, 3H, $-OCH_3$), 8.1—8.9 (m, 8H, $CH_3(C\underline{H}_2)_4-$), 9.1 (t, 3H, $J=4.5$ Hz, $C\underline{H}_3(CH_2)_4-$).

Found: C, 52.98; H, 7.32; N, 10.08%. Calcd for $C_{12}H_{20}N_2O_3S$: C, 52.92; H, 7.40; N, 10.28%.

2-Amino-4-methoxycarbonyl-5-(1-methoxyisopropyl)thiazole (15a) A solution of **5a** (2.1 g, 0.01 mol) and thiourea (0.76 g, 0.01 mol) in methanol (15 m*l*) was refluxed for 15 hr. By treating the mixture in ways similar to those used in the case of **15c**, 0.9 g of a pale yellow oil (**15a** of *ca.* 80% purity by tlc[15]) was obtained. The analytical sample of **15a** was prepared by tlc: R_f 0.15; IR (cm^{-1}, liquid) 3400, 3320, 3120, 2960, 1610, 1620, 1540, 1215; NMR (τ, $CDCl_3$) 4.02 (s, 2H, $-NH_2$), 6.12 (s, 3H, $-COOCH_3$), 6.71 (s, 3H, $-OCH_3$,) 8.33 (s, 6H, $2CH_3-$).

Found: C, 46.84; H, 6.15; N, 11.84%. Calcd for $C_9H_{14}N_2O_3S$: C, 46.94; H, 6.13; N, 12.16%.

14) Column temp., 110°C.

15) On silica gel G (E. Merck AG, Darmstadt) with acetone–*n*-hexane (1: 3 v/v).

The Accelerated Reaction of 2,2-Diphenyl-1-picrylhydrazyl with Cupric 3-(1-Butenyl)-2,4-pentanedionate in Frozen Solutions and Its ESR Spectra[1]

Kaku UEHARA, Kiyohiro KAMEI, Makoto TANAKA, and Niro MURATA

Department of Applied Chemistry, College of Engineering, University of Osaka Prefecture, Sakai-shi, Osaka

(Received November 1, 1971)

The rate enhancements upon freezing in the reaction of 2,2-diphenyl-1-picrylhydrazyl (DPPH) with cupric 3-(1-butenyl)-2,4-pentanedionate (3-α-butenylacetylacetonate) were studied in benzene, dioxane, and cyclohexane. It was observed that the degree of the rate enhancements in frozen solutions varied remarkably with the kind of solvent. The order of the accelerating effect was as follows: benzene>dioxane>cyclohexane. Upon freezing, the hyperfine structure in the ESR spectra of DPPH collapsed into a single line, but the peak-to-peak line width (ΔH_{pp}) changed appreciably with the solvents used. The order of the values of ΔH_{pp} was as follows: cyclohexane >dioxane>benzene. These results suggest that the enhancement of the rate in a frozen solution is due to the increased concentration of reactants in the liquid region existing among the crystalline solvents.

Metal acetylacetonate reacts with a stable free radical, 2,2-diphenyl-1-picrylhydrazyl (DPPH), to yield 2,2-diphenyl-1-picrylhydrazine (DPPH-H); the reaction gives first-order kinetics for each reactant.[2] In an earlier

$$\text{DPPH} + \text{Cu(R-acac)}_2 \xrightarrow{k} \text{DPPH-H} + \text{other product}$$

paper,[3] it has been reported that this reaction is remarkably accelerated when a benzene solution of the reactants is frozen. This study was undertaken in an attempt to elucidate the frozen effect in more detail.

Enhanced rates in frozen solutions for the catalytic hydrolysis of the penicilline β-lactam and some other reactions have been reported, and several possible explanations have been offered for the frozen effect.[4-13] Pincock *et al.* have reported that there are highly concentrated liquid regions among the crystalline solvents when a dilute solution containing two reactants is frozen and that the reaction between the two reactants might be markedly accelerated by the concentration effect.[4-9] Grant *et al.* have described how the acceleration of the reaction in frozen solutions can be attributed to other effects, including the higher proton mobility, the imposition of a favorable positional orientation between reactants, the participation of the ice crystal surface as a replacement for a catalyst molecule, and the change in the dielectric constant of the reaction media upon freezing.[10-13]

In the reaction of DPPH with cupric 3-α-butenylacetylacetonate, the rate of the reaction was observed to be remarkably accelerated in benzene, but not appreciably so in cyclohexane, when the solutions were frozen. This solvent effect on the frozen reaction was considered on the basis of the ESR spectra of DPPH in these frozen solvents.

Experimental

Materials. DPPH and cupric 3-α-butenylacetylacetonate were prepared in the way shown in a preceding paper.[2] The solvents were purified by the ordinary method and were distilled before use.

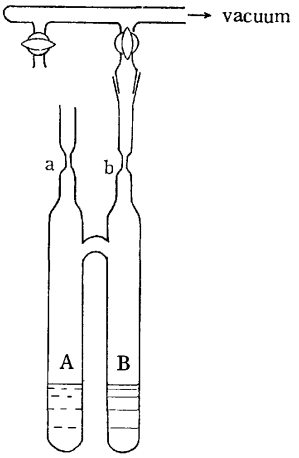

Fig. 1. Schematic drawing of the apparatus.

Apparatus and Procedure. The H-shaped tubes illustrated in Fig. 1 were used as the reaction cells. The solution of DPPH in A and the solution of the cupric chelate in B were simultaneously frozen in liquid nitrogen. The H-shaped tube was joined to a high-vacuum line after the tube had been sealed at the neck (a). Each solution was out-gassed by three freeze-thaw cycles under 10^{-5} mmHg, and then the H-shaped tube was sealed at (b). The solutions in A and B were warmed to room temperature and mixed thoroughly. The sealed tube was then immersed quickly into a dry ice–methanol mixture. The tube was allowed to remain submerged for a period of time to ensure complete freezing.

1) Paper XV in a series of "Catalytic Behavior of Metal Chelate Compounds".

2) K. Uehara, K. Kamei, M. Tanaka, and N. Murata, This Bulletin, **45**, 540 (1972).

3) K. Uehara, M. Tanaka, and N. Murata, *ibid.*, **41**, 3034 (1968).

4) A. R. Butler and T. C. Bruice, *J. Amer. Chem. Soc.*, **86**, 313 (1964).

5) R. E. Pincock and T. E. Kiovsky, *ibid.*, **87**, 2072, 4100 (1965).

6) R. E. Pincock and T. E. Kiovsky, *ibid.*, **88**, 51 (1966).

7) R. E. Pincock and T. E. Kiovsky, *ibid.*, **88**, 4455 (1966).

8) T. E. Kiovsky and R. E. Pincock, *ibid.*, **88**, 4705 (1966).

9) I. Kaetsu, Y. Nakase, and K. Hayashi, *J. Markomol. Sci. Chem.*, **A 3**, 1525 (1969).

10) N. H. Grant, D. E. Clark, and H. E. Alburn, *J. Amer. Chem. Soc.*, **83**, 4476 (1961).

11) T. C. Bruice and A. R. Butler, *ibid.*, **86**, 4104 (1964).

12) H. E. Alburn and N. H. Grant, *ibid.*, **87**, 4174 (1965).

13) N. H. Grant, D. E. Clark, and H. E. Alburn, *ibid.*, **88**, 4071 (1966).

Kinetic Method. The reaction was followed by the photometric measurement of the DPPH concentration using a EPS-3T Hitachi spectrometer. After having been removed from the dry ice–methanol bath, the reaction tube was placed in a methanol–water bath thermostated at the desired temperature. Upon warming to the temperature, the solutions remained solidly frozen. The tube was withdrawn from the bath after a certain lapse of time. To determine the concentration of DPPH, the frozen sample was melted at 25°C and the optical density of the solution at 525 mμ was measured as soon as possible after the tube was opened.

ESR Spectra. The ESR spectra of DPPH or cupric chelate in frozen solutions were recorded by means of a JES-3BX ESR spectrometer of Japan Electron Optics, using the X-band at the temperature of liquid nitrogen. Before measurement, the cubet containing the solution was immersed into a dry ice–methanol mixture for a period of time in a manner similar to that in the kinetic run.

Results and Discussion

The effect of the solvent on the reaction rate in frozen solutions was studied. In Fig. 2, the plots of the reaction rate against the reaction temperature in a few solvents are shown. The rate has a maximum at −3°C for benzene (mp 5.5°C), at 8°C for dioxane (mp 11.7°C), and at 3°C for cyclohexane (mp 6.5°C). The maximum rates in these solvents appeared not at the freezing points of these solvents, but 3—9°C below them.

Pincock and Kiovsky[5-8] have also observed the appearance of the maximum rate several degrees below the freezing points of the solvents in some frozen systems and have explained it on the basis of the concentration effect. The maximum rate described above seems to result from a decrease in the rate constant and an increase in the concentration of the solute in the liquid region as the temperature is lowered.

The rate enhancement on freezing for a few solvents is shown in Table 1. The order of the rate enhancement is as follows:

benzene (24.1)>dioxane (5.39)>cyclohexane (2.42).

The values in parentheses show the ratio between the rate in the frozen solution at the temperature of the maximum rate and the rate determined by the extrapolation of the Arrhenius plot in liquid solutions to the

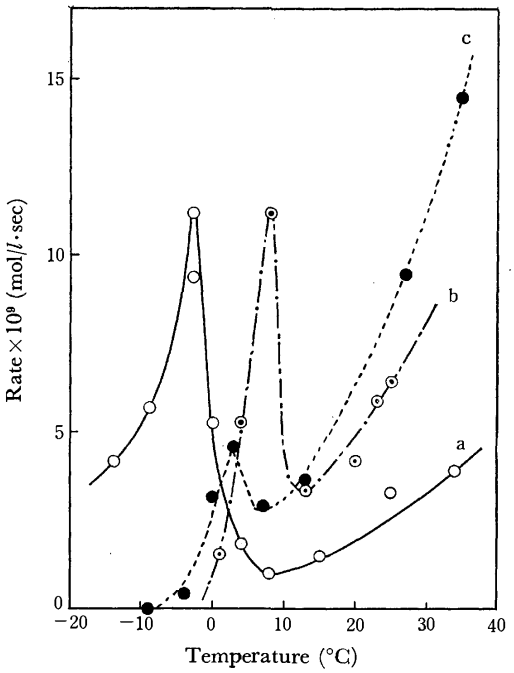

Fig. 2. Plots of rate *versus* temperature in a few solvents.
[DPPH]=0.545×10⁻⁴ mol/*l*,
[Cu(3-α-butenyl-acac)₂]=4.68×10⁻⁴ mol/*l*
a: benzene, b: dioxane, c: cyclohexane

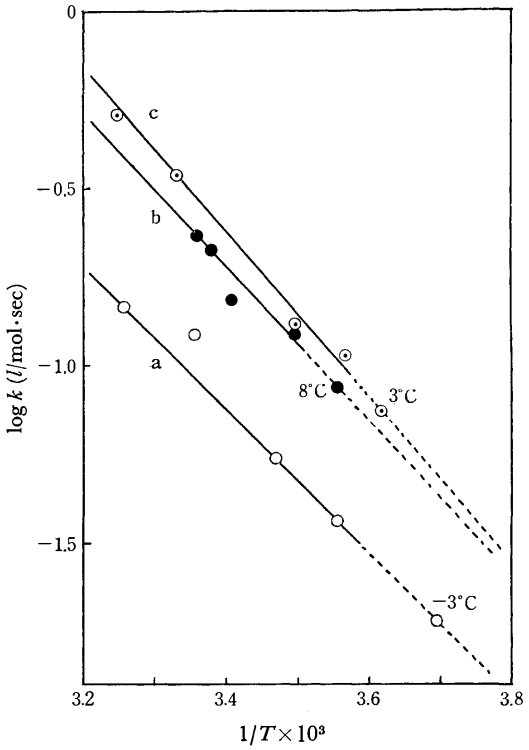

Fig. 3. Plots of log *k* *versus* 1/*T* in liquid solution.
[DPPH]=0.545×10⁻⁴ mol/*l*,
[Cu(3-α-butenyl-acac)₂]=4.68×10⁻⁴ mol/*l*
a: benzene, b: dioxane, c: cyclohexane

TABLE 1. THE EFFECTS OF THE SOLVENTS ON THE REACTIONS IN FROZEN SOLUTIONS
[DPPH]=0.545×10⁻⁴ mol/*l*, [Cu(3-α-butenyl-acac)₂]=4.68×10⁻⁴ mol/*l*

Solvent			Temperature of maximum rate (°C)	Rate in frozen solution at the temp. of max. rate (×10⁹mol/*l*·sec)	Rate in liquid solution extrapolated to the temp. of max. rate (×10⁹mol/*l*·sec)	Rate ratio (frozen/liquid)
	Mp (°C)	K_f				
Benzene	5.5	5.12	−3	11.7	0.485	24.1
Dioxane	11.7	4.95	8	11.7	1.88	5.39
Cyclohexane	6.5	20.0	3	4.55	2.17	2.42

temperature of the maximum rate (Fig. 3).

Several recent papers have referred to the ESR spectra of DPPH and the spatial distribution of DPPH in frozen solutions. Roggin *et al.*[14] measured the ESR spectra of DPPH in a frozen benzene solution and reported that, upon freezing, the hyperfine structure of DPPH collapsed into a single line with a total width significantly less than that of the hyperfine spread and approximately equal to that observed for the concentrated polycrystalline DPPH. They have explained this phenomenon on the basis of the fact that DPPH is concentrated in small crystallites in which exchange interaction, which averages out the hyperfine structure, can occur. Ayscough *et al.*[15] studied the ESR spectra of deaerated frozen solutions of DPPH in various solvents and found that there were wide differences in line width, hyperfine splittings, and saturation behavior. They showed that the ESR spectra could be divided into three groups: (a) strong, exchange-narrowed line spectra (width from peak to peak, ΔH_{pp}=2—4 gauss); (b) broader, unresolved line spectra (ΔH_{pp}=10—20 gauss); (c) poorly resolved, five-line spectra. It has been explained that the spectra of group (b) result from some DPPH in the form of crystallites and some in a solid solution.

From these papers, it is clear that there is some correlation between the ESR spectra and the spatial distribution of DPPH in frozen solutions. Therefore, an investigation by means of the ESR spectra was carried out in order to obtain a possible explanation of the above solvent effects on the rate enhancements upon freezing.

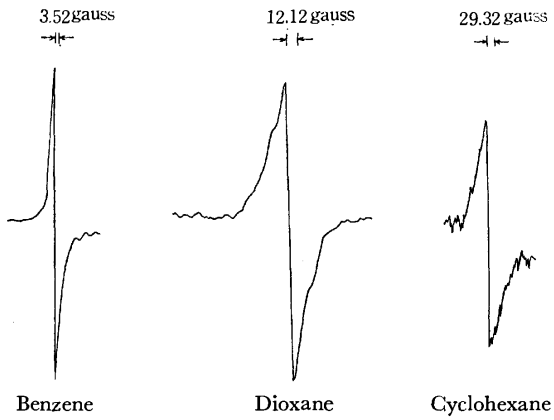

Fig. 4. ESR spectra of DPPH in the frozen solutions and peak to peak line width ΔH_{pp} (gauss).

The ESR spectra of DPPH in frozen solutions for the three solvents, benzene, dioxane, and cyclohexane, at the temperature of liquid nitrogen are shown in Fig. 4. The spectra in frozen benzene belonged to Group (a), as had been reported. On the other hand, the spectra in frozen dioxane and cyclohexane were found to belong to Group (b) in Ayscough's classification. The order of the magnitude of the ΔH_{pp} of DPPH in the frozen solution for the three solvents was as follows:

benzene (3.52 gauss)<dioxane (12.12 gauss)<cyclohexane (29.32 gauss).

The value of ΔH_{pp} in frozen benzene agreed with that of powder DPPH.[16] This proves that, in the benzene solution, DPPH is highly concentrated in small crystallites upon freezing. On the other hand, the value of ΔH_{pp} in frozen cyclohexane was remarkably large. This suggests that, in frozen cyclohexane solution, DPPH is scarcely concentrated at all in the form of crystallites and that almost all of the DPPH is in solid solution.

It was found that the ΔH_{pp} value of the ESR spectra in frozen solutions are closely related to the rate enhancement upon freezing in the reaction of DPPH with cupric 3-α-butenylacetylacetonate. That is, the smaller ΔH_{pp} value, the larger will be the rate enhancement upon freezing. This relationship between the ΔH_{pp} value and the rate enhancement suggests that the rate enhancement upon freezing in the reaction of DPPH with metal acetylacetonates is to be explained by the concentration effect mentioned by Pincock and Kiovsky.[5-8]

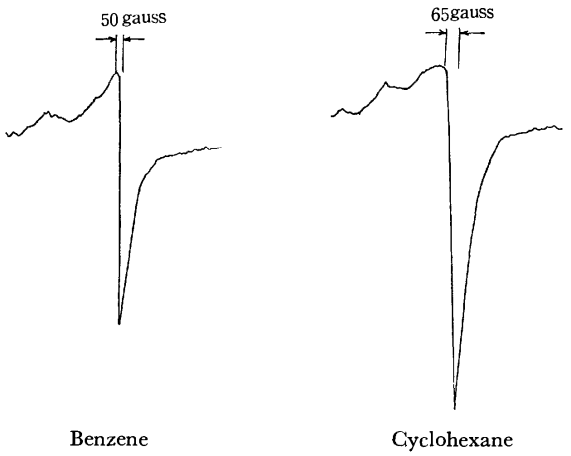

Fig. 5. ESR spectra of Cu(3-α-butenyl-acac)$_2$ in frozen solutions.

The ESR spectra of cupric 3-α-butenylacetylacetonate were also measured in a few frozen solutions, but they can not be discussed in detail. As is shown in Fig. 5, the ΔH_{pp} of the cupric chelate in a frozen benzene solution seems to be more narrow than that in frozen cyclohexane. Tominaga and Fujiwara[17] have reported that, in a frozen benzene solution containing 0.2M Co(acac)$_3$ at the temperature of dry ice, the most solute molecules are precipitated as microcrystals.

The facts presented above suggest that the reaction of DPPH with metal acetylacetonate in these frozen solutions is accelerated by the concentration of both reactants in the liquid region among the crystalline solvents upon freezing.

14) A. van Roggin, L. van Loggin, and W. Gordy, *Phys. Rev.*, **105**, 50 (1957).
15) P. B. Ayscough, H. E. Evans, and A. P. McCann, *Nature*, **203**, 1378 (1964).
16) N. W. Lord and S. M. Blinder, *J. Chem. Phys.*, **34**, 1693 (1961).
17) T. Tominaga and K. Fujiwara, This Bulletin, **43**, 2279 (1970).

Oxygen Exchange of Benzenesulfinic Acids in Water[1]

Michio KOBAYASHI, Hiroshi MINATO, and Yoshikuni OGI

Department of Chemistry, Tokyo Metropolitan University, Fukazawa, Setagaya, Tokyo

(Received November 9, 1971)

When arenesulfinic acids were heated in water ($H_2{}^{18}O$, 1.52 atom%) at 90—100°C for several hours, the ^{18}O contents of the disproportionation products (thiolsulfonate and sulfonic acid) and the sulfinic acid recovered were approximately the same. The rate of oxygen exchange of *p*-toluenesulfinic acid was much faster than that of methyl phenyl sulfoxide, whereas the rate of oxygen exchange of benzoic acid was much slower than that of benzaldehyde. A mechanism consistent with the kinetic results is proposed for the oxygen-exchange reaction, involving the formation of the sulfinic anhydride (sulfinylsulfone) as an intermediate.

It has long been known that a benzenesulfinic acid yields a thiolsulfonate and a benzenesulfonic acid by disproportionation.[2]

$$3ArSO_2H \longrightarrow ArSO_2SAr + ArSO_3H$$

Kice and his co-workers investigated the mechanism of this reaction in detail; they proposed that the initial step of this multi-step reaction is reversible formation of a sulfinylsulfone.[3]

$$2ArSO_2H \underset{+H_2O}{\overset{-H_2O}{\rightleftharpoons}} Ar\text{-}S(=O)\text{-}S(=O)\text{-}Ar$$

Carbonyl compounds such as aldehydes or carboxylic acids undergo oxygen exchange in water *via* a tetrahedral intermediate, and the rate is first order in the carbonyl compound.[4]

$$R\text{-}C(=O)\text{-}R \underset{-H_2O}{\overset{+H_2O}{\rightleftharpoons}} R\text{-}C(OH)_2\text{-}R$$

Since the nature of the oxygen exchange of sulfinic acids appears to be so different from that of the well-known oxygen exchange of carbonyl compounds, a detailed study of this interesting reaction has been carried out, and the results will be described in this paper.

Experimental

Disproportionation of Arenesulfinic Acid in Water-^{18}O. *p*-Bromobenzenesulfinic acid was precipitated by mixing its sodium salt and dilute sulfuric acid in water, the crystals thus formed were washed well with water and dried. An ampoule containing 1.2 g of *p*-bromobenzenesulfinic acid and 3 m*l* of water (^{18}O content, 1.52%) (not all sulfinic acid dissolved in the water at room temperature) was heated at 90±5°C for 12 hr. Crystals of the thiolsulfonate appeared after 2 hr of heating. After 12 hr the crystals of thiolsulfonate were filtered off while the solution was still hot, recrystallized twice from benzene, identified by infrared spectroscopy, and then subjected to the ^{18}O analysis which will be described below.

When the mother liquor was cooled, unchanged sulfinic acid precipitated as white crystals; these crystals were filtered and then converted to the acid's sodium salt by addition of a sodium hydrogen carbonate solution. The well-dried sodium sulfinate was converted, by heating it in an ampoule with 2 g of benzyl bromide, into *p*-bromophenyl benzyl sulfone, which was recrystallized from hexane and then subjected to the ^{18}O analysis.

$$BrC_6H_4SO_2Na + PhCH_2Br \longrightarrow BrC_6H_4\text{-}S(=O)_2\text{-}CH_2Ph$$

When an aqueous solution of *S*-benzylisothiuronium chloride was added to the filtrate from the mother liquor, crystals of *S*-benzylisothiuronium *p*-bromobenzenesulfonate appeared; these crystals were filtered, recrystallized from hexane, and then subjected to the ^{18}O analysis. The products of disproportionation of *p*-toluenesulfinic acid and *p*-nitrobenzenesulfinic acid under similar conditions were separated and analyzed by the same procedure.

Rates of Oxygen Exchange of p-*Bromobenzenesulfinic Acid and* p-*Toluenesulfinic Acid.* Sodium salts of the sulfinic acids were converted to the corresponding sulfinic acids by the method described above. By the use of purified dioxane and water (^{18}O content, 1.52 mol %), 1.131M solution of *p*-bromobenzenesulfinic acid and 1.324M solution of *p*-toluenesulfinic acid in 30% (v/v) aqueous dioxane were prepared. Aliquots (4 m*l* each) of these solutions were sealed in ampoules, which were then placed in a constant-temperature bath.

After suitable intervals, ampoules were removed from the bath and the reaction was stopped by cooling the ampoules in ice-water and by then converting the acids to sodium sulfinates. By separate experiments it was established that no oxygen exchange of sulfinic acids took place in alkaline media. Evaporation of the solvent *in vacuo* yielded white crystals of sodium sulfinate and excess sodium carbonate. These crystals were dried well *in vacuo* at 90—100°C, and were then allowed to react with benzyl bromide at 105—110°C for 7—10 hr. Then, 50 m*l* of water and 50 m*l* of ether were added to the mixture, and the ethereal solution containing an aryl benzyl sulfone was dried over magnesium sulfate. Evaporation of the ether yielded crude crystals of the sulfone, which were then recrystallized from hexane. From each ampoule, 200—400 mg of a sulfone was obtained.

Synthesis of p-*Bromobenzenesulfinic Acid-^{18}O.* *p*-Bromobenzenesulfinic acid (5 g) was heated in 15 m*l* of water (^{18}O, 1.52 mol %) at 90°C for 2 hr. The solution was cooled with ice, and the crystals thus obtained were filtered. In order to remove completely any *p*-bromobenzenesulfonic acid which might be present in these crystals, the crystals were quickly recrystallized from ordinary water and then

1) Organic Sulfur Compounds, Part XXIX.

2) R. Otto, *Ann.*, **145**, 13,317 (1868).

3) a) J. L. Kice and K. W. Bowers, *J. Amer. Chem. Soc.*, **84**, 605 (1961). b) J. L. Kice, G. Guaraldi, and C. G. Venier, *J. Org. Chem.*, **84**, 605 (1961). c) J. L. Kice and G. Guaraldi, *J. Amer. Chem. Soc.*, **88**, 5242 (1966).

4) E. S. Gould, "Mechanism and Structure in Organic Chemistry," Henry Holt and Co., New York (1959), p. 539.

thoroughly dried. The excess oxygen-18 content was 1.232 atom %.

Comparison of the Rates of Oxygen Exchange between p-*Toluenesulfinic Acid and Methyl Phenyl Sulfoxide.* In 19 ml of 30% (v/v) aqueous ($H_2{}^{18}O$, 1.52 atom %) dioxane, 3 g of methyl phenyl sulfoxide and 1.7 g of *p*-toluenesulfinic acid were mixed; the solution was then divided into two ampoules, which were placed in a bath at 60°C. One ampoule was removed after 5 hr of heating, while the other was removed after 23.3 hr.

The reaction was stopped by addition of a 5% sodium carbonate solution, after which the sulfoxide was extracted by chloroform. The chloroform solution was dried over magnesium sulfate; the subsequent evaporation of the solvent yielded crude sulfoxide, which was then purified by distillation under reduced pressure (102°C/2 mmHg). The sodium sulfinate present in the aqueous layer was analyzed in a manner similar to that described above.

Comparison of the Rates of Oxygen Exchange between Benzoic Acid and Benzaldehyde. Into 10 ml of 30% (v/v) aqueous ($H_2{}^{18}O$, 1.52 atom %) dioxane, 2.5 g of benzoic acid and 1 g of benzaldehyde were mixed; an ampoule containing the solution was then heated at 60°C for 5 hr. Then a 5% sodium carbonate solution was added, and the benzaldehyde was extracted with 50 ml of benzene. The benzene solution was dried over anhydrous magnesium sulfate; the subsequent evaporation of the solvent yielded benzaldehyde, which was then purified by distillation under reduced pressure. The aqueous layer was acidified with a dilute hydrochloric acid solution, and the benzoic acid was extracted with ether. The ethereal solution was dried over anhydrous magnesium sulfate; the subsequent evaporation of the solvent yielded crude benzoic acid, which was then recrystallized from hexane.

Analysis of Samples Containing Oxygen-18. By the method reported by Rittenberg,[5] a sample was pyrolyzed in the presence of mercuric chloride and mercuric cyanide at 400°C for 4 hr; the carbon dioxide thus obtained was analyzed by mass spectrometry.

Results and Discussion

At 90°C a 1.25M aqueous solution ($H_2{}^{18}O$, 1.52 atom %) of *p*-bromobenzenesulfinic acid was heated in an ampoule for 12 hr. Similar reactions were carried out with a 4.0M aqueous solution of *p*-toluenesulfinic acid at 100°C for 2 hr and with a 1.5M aqueous solution of *p*-nitrobenzenesulfinic acid at 100°C for 5 hr. The results of the mass-spectrometric analyses of the sulfinic acid recovered are summarized in Table 1.

Table 1. Incorporation of ^{18}O in the sulfinic acids recovered and the products formed on heating in $H_2{}^{18}O$

	Excess oxygen-18 atom %		
	p-BrC_6H_4-SO_2H	*p*-$CH_3C_6H_4$-SO_2H	*p*-$O_2NC_6H_4$-SO_2H[a]
Recovered RSO_2H	1.38	1.02	1.04
Products			
RSO_3H	1.29	0.95	1.15
RSO_2SR	1.31	1.04	1.14

a) No incorporation of ^{18}O in NO_2 group.

5) D. Rittenberg and L. Ponticorvo, *Int. J. Appl. Radiat. Isotopes.*, **1**, 208 (1956).

The fact that both the sulfinic acid and the reaction products contain approximately the same amount of oxygen-18 indicates that the rate of oxygen exchange is considerably faster than that of disproportionation.

Carbonyl compounds such as carboxylic acids or aldehydes undergo oxygen exchange in water in the presence of an acid, and the rate is first order in the substrate. The rates of oxygen exchange of benzoic acid and benzaldehyde and those of *p*-toluenesulfinic acid and methyl phenyl sulfoxide were determined, the results are summarized in Table 2.

Table 2. Comparison of the rates of oxygen exchange[a]

	Excess oxygen-18 atom %	
	5 hr	23.3 hr
p-$CH_3C_6H_4SO_2H$	0.06	0.28
CH_3–S–Ph ‖ O	0.03	0.03
Ph–CO_2H	0.01	—
Ph–CHO	0.80	—

a) In 30% (v/v) aqueous ($H_2{}^{18}O$) dioxane, at 60°C.

In the pair of the carbonyl compounds, the rate of oxygen exchange of the aldehyde was much faster than that of the acid, whereas in the pair of the sulfinyl compounds the rate of oxygen exchange of the acid was much faster than that of the sulfoxide, which underwent almost no exchange of oxygen even when it was heated at 60°C for 23.3 hr.

These findings suggest that the mechanism of oxygen exchange of a sulfinic acid is quite different from that of a carbonyl compound.

Kice and his co-workers proposed that the initial step of the disproportionation of a benzenesulfinic acid is reversible formation of a sulfinylsulfone,[2] the following reaction scheme seems plausible as the mechanism for incorporation of oxygen-18 in the sulfinic acid recovered:

$$RSO_2H + RSO_2H \underset{k_{b'}+H_2O}{\overset{k_{f'}-H_2O}{\rightleftharpoons}} RSO_2SOR \underset{k_{f'}-H_2O}{\overset{k_{b'}+H_2O^*}{\rightleftharpoons}} RSO_2^*H + RSO_2H$$

$$\Big\downarrow k_d$$

disproportionation products

The rate of increase of the labelled sulfinic acid, RSO_2^*H, is expressed by the following:

$$\frac{d[RSO_2^*H]}{dt} = k_b[RSO_2SOR][H_2O^*] - k_f[RSO_2^*H][RSO_2H]_T \quad (T = \text{total})$$

By a steady-state assumption for the sulfinylsulfone, the following equations are obtained:

$$\frac{d[RSO_2SOR]}{dt} = k_f[RSO_2H]_T{}^2 - k_b[RSO_2SOR][H_2O]_T - k_d[RSO_2SOR] = 0$$

$$\frac{d[RSO_2^*H]}{dt} = \frac{k_f k_b[H_2O^*]}{k_d + k_b[H_2O]_T}[RSO_2H]_T{}^2 - k_f[RSO_2^*H][RSO_2H]_T$$

When $k_b[H_2O]_T \gg k_d$,

$$\frac{d[RSO_2^*H]}{dt} = k_f[RSO_2H]_T^2\left(\frac{[H_2O^*]}{[H_2O]_T} - \frac{[RSO_2^*H]}{[RSO_2H]_T}\right)$$

$$\frac{d([RSO_2^*H]/[RSO_2H]_T)}{dt} = k_f[RSO_2H]_T\{([H_2O^*]/[H_2O]_T) - ([RSO_2^*H]/[RSO_2H]_T)\}$$

Since both $[RSO_2H]_T$ and $([H_2O^*]/[H_2O]_T)$ are approximately constant under mild conditions,

$$k_f = (1/[RSO_2H]_T \cdot t) \ln [([H_2O^*]/[H_2O]_T)/\{([H_2O^*]/[H_2O]_T) - ([RSO_2^*H]/[RSO_2H]_T)\}]$$

The rates of increase of oxygen-18 in the sulfinic acids recovered were measured, and found to follow the first-order equation described above. The results are shown in Table 3.

TABLE 3. RATES OF ^{18}O-INCREASE IN BENZENESULFINIC ACIDS IN 30% (v/v) AQUEOUS DIOXANE

Sulfinic Acid		*p*-$MeC_6H_4SO_2H$	*p*-$BrC_6H_4SO_2H$	$PhSO_2H$
$[RSO_2H]_0$ (mol/*l*)		1.32	1.13	1.30
$H_2{}^{18}O$ (atom %)		1.52	1.52	1.52
$10^7 \times k_f$ (M^{-1} sec^{-1})	20.0°C	1.37	2.49	1.42
	40.0°C	12.9	17.4	8.28
	60.0°C	110	—	35.5
	65.0°C	—	133	—
E_a (kcal/mol)		21.5	17.4	15.6
$\Delta S^{\neq}$ (e. u.)		−21.9	−31.3	−29.4

It is often desirable to prepare ^{18}O-labelled benzenesulfinic acids, which can easily be converted to ^{18}O-labelled sulfoxides and other derivatives; for this purpose the rate constants in Table 3 are valuable for predicting the rates of ^{18}O-incorporation. Under mild conditions, k_d is much smaller than $k_b[H_2O]_T$, and $k_f[RSO_2H]^2$ is approximately equal to the rate of production of the ^{18}O-labelled sufinic acids.

Kice and his co-workers observed that the exchange of oxygen was first-order in a sulfinic acid when a sulfinic acid-^{18}O was subjected to oxygen exchange in acetic aicd containing sulfuric acid as the catalyst or in 60% aqueous dioxane containing perchloric acid and sodium bromide.[6] However, their experimental conditions are quite different from those of the present investigation; the concentration of the mineral acid added as the catalyst was greater than, or equal to, the concentration of a sulfinic acid, and the concentration of a sulfinic acid was very low. Under such highly acidic conditions, it seems likely that the oxygen exchange takes place through a reaction between a protonated sulfinic acid and water, thus it is understandable why the rate was first-order in the sulfinic acid under their conditions.

If the oxygen exchange under our reaction conditions is due to the direct reaction between a sulfinic acid and $H_2{}^{18}O$, the rate of increase in the ^{18}O-content in the sulfinic acid must be independent of the initial concentration of the sulfinic acid. If the oxygen exchange takes place *via* the sulfinylsulfone formed by bimolecular dehydration of the sulfinic acid, the rate of increase in the ^{18}O-content must be greater when the initial concentration of the sulfinic acid is greater.

TABLE 4. INCREASE OF ^{18}O-CONTENT IN BENZENESULFINIC ACID IN 30% (v/v) AQUEOUS DIOXANE[a]

$[PhSO_2H]_0$ (mol/*l*)	Excess oxygen-18 atom % in $PhSO_2H$				
	40°C		60°C		
	24 hr	72 hr	5 hr	7 hr	10 hr
0.649	0.297	0.423	—	0.335	0.371
1.298	0.419	0.551	0.302	—	0.402

a) $H_2{}^{18}O$ atom %, 1.52.

The rates of oxygen exchange were determined in solutions of different sulfinic acid concentrations; the results are summarized in Table 4. The rates of exchange are faster in the solutions with greater sulfinic acid concentrations, this finding made unlikely any direct reaction between the sulfinic acid and water under our experimental conditions.

6) J.L. Kice, private communication.

Aminosugars. XIX. On the Structure of 2-Deoxy-2-guanidino-D-glucose[1]

Juji YOSHIMURA, Tetsuo SEKIYA, and Takao IIDA

Laboratory of Chemistry for Natural Products, Faculty of Science, Tokyo Institute of Technology, Meguro-ku, Tokyo

(Received November 25, 1971)

It was found that 2-deoxy-2-guanidino-D-glucose prepared by guanidination of 2-amino-2-deoxy-D-glucose with cyanamide exists mainly as α-D-glucofurano[1′,2′;4,5]-2-imino-imidazolidine (*5*) which is easily converted into 2-imino-4-(D-*arabino*-tetrahydroxybutyl)imidazoline-4 (*6*) under alkaline conditions. Acetylation of *5* and *6* gave the corresponding hexa- and heptaacetate (*7* and *8*), respectively. Warming of *7* in alcohols gave addition compounds of alcohols to the imino double bond, and deacetylation with sodium alcoholate at a room temperature yielded 2-acetamido-4-(D-*arabino*-tetrahydroxybutyl)imidazole (*10*). Similar treatment of *8* in ethanol at elevated temperature gave an unknown addition compound in which two *N*-acetyl groups were eliminated, and deacetylation with a small amount of sodium methylate yielded a mixture of (2*R*,*S*)-2-acetamido-2-methoxy-4-(D-*arabino*-tetraacetoxybutyl)imidazoline-4 and tetra-*O*-acetyl derivative of *10* which was also obtained by acetylation of *10*.

Several natural guanidino-compounds such as streptidine,[2] viomycidine,[3] and tetrodotoxin[4] are known about their strong biological activities. Among them, the aminal ring between the guanidino and aldehyde group in tetrodotoxin is interesting in the structural feature. Odo and Kono[5] reported that 2-deoxy-2-guanidino-D-glucose hydrochloride which was obtained by guanidination of 2-deoxy-2-amino-D-glucose hydrochloride with cyanamide exists in an equilibration between the usual lactol (**1**) and the imidazoline ring structures (**2**) in aqueous solutions.

In this paper, the authors have found that 2-deoxy-2-guanidino-D-glucose exists mainly as α-D-glucofurano-[1′,2′;4,5]-2-imino-imidazolidine (**3**) which is easily converted to 4-(D-*arabino*-tetrahydroxybutyl)imidazoline-4 (**4**) under alkaline conditions, and examined a few chemical properties of them.

Results and Discussion

A neutral solution of 2-amino-2-deoxy-D-glucose hydrochloride and cyanamide in water was heated at 60°C for 7 hr, and then picric acid in methanol was added to the reaction mixture. After standing at 0°C for 2 days, the known picrate of needles (**3**)[5]; mp 180°C, and a new granular picrate (**4**); mp 178°C, were obtained in 23.6% and 15.4% yield, respectively. These picrates were then converted into hydrochlorides (**5** and **6**), respectively. Both of them were negative to ninhydrin, Fehling, and Sakaguchi reactions, and distinguishable each other in specific rotations and C–O stretching absorptions in the region between 1000—1100 cm^{-1} in IR spectra. No mutarotation of them indicated the absence of **1** in solutions.

Moreover, in UV spectrum, **5** showed no absorption other than end absorptions (<210 nm), but **6** had a maximum at 212 nm (ε 1.057×10^4). NMR spectra of **5** and **6** showed two characteristic doublets at 3.55 and 5.07 τ, and two singlets at 2.77 and 4.60 τ, respectively. These facts indicated a glucofurano-configuration for the former and a heterocyclic structure for the latter. Furthermore, the conversion of **5** to **6** was found in alkaline conditions. The doublet at 3.55 τ in NMR spectrum of **5** instantly disappeared by addition of alkali, and a singlet at 2.89 τ appeared, which is shifted to 2.77 τ by acidification. A maximum at 208 nm was also observed in UV spectrum of **5** at pH 10.4. Such a conversion was also occured by adjustment of the pH of a solution of **5** with Amberlite IRA-410, and in fact, **6** was isolated by acidification in 80% yield. Further conversion of **6** to an unknown compound by standing the alkalline solution for 2 or 3 days was indicated with the disappearance of characteristic singlet, however, no definite compound could be isolated.

In order to clarify the structures, **5** and **6** was respectively acetylated with acetic anhydride in pyridine to the corresponding hexaacetate (**7**) and heptaacetate (**8**) in 83.3 and 50% yields. Both compounds showed UV absorptions of λ_{max}^{EtOH} 219 nm (ε 1.5×10^4) and 253 nm (ε 3.4×10^3), respectively. The NMR spectrum of **7** (Fig. 1) assigned by double resonance technique gave a very similar pattern of the ring-proton signals to 3′,5′,6′-tri-*O*-acetyl-α-D-glucofurano[1′,2′;4,5]-*N*-acetyloxazolidine-2-thion,[6] indicating the presence of α-D-glucofuranose configuration, and two acetyl signals appeared in lower field than other four acetyl signals are assignable to imino-acetyl and N_3-acetyl also by analogy to this compound. Therefore, **7** was determined to be 3′,5′,6′-tri-*O*-acetyl-α-D-glucofurano[1′,2′;4,5]-2-acetylimino-1,3-diacetylimidazolidine. It is interesting that such a ring formation in **7** as in glycosylamines is also seen in viomycidine[2] or anhydrotetro-

1) Part XVIII; This Bulletin, **43**, 2966 (1970).

2) R. U. Remieux and M. L. Wolfrom, "Advances in Carbohydrate Chemistry", Vol. 3, ed. by M. L. Wolfrom, Academic Press, (1948) p. 337.

3) T. Takita and K. Maeda, *J. Antibiot.* (Tokyo), **21**, 512 (1968).

4) K. Tsuda, C. Tamura, R. Tachikawa, K. Sakai, O. Amakasu, M. Kawamura, and S. Ikuma, *Chem. Pharm. Bull. Japan*, **12**, 634, 642 (1964); T. Goto, Y. Kishi, S. Takahashi, and Y. Hirata, *Tetrahedron Lett.*, 779, 1831 (1964); R. B. Woodward, *Pure, Appl. Chem.*, **9**, 49 (1964).

5) K. Odo, K. Kono, and K. Sugino, *J. Org. Chem.*, **23**, 1319 (1958).

6) J. C. Jochims, A. Seelinger, and G. Taigel, *Chem. Ber.*, **100**, 845 (1967); J. Yoshimura and H. Hashimoto, This Bulletin, **41**, 261 (1968).

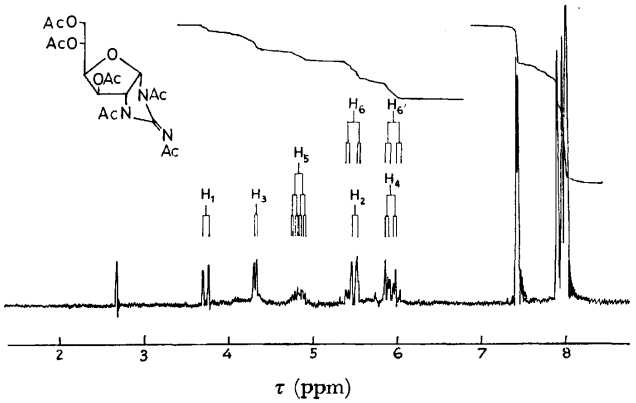

Fig. 1. The NMR spectrum of **7**.

dotoxin.[3]

On the other hand, the NMR spectrum of **8** (Fig. 2) showed again a closely similar pattern of sugar-chain protons to 2-methoxycarbonyl-4-(D-*arabino*-tetraacetoxybutyl)imidazole obtained by the reaction of 2-amino-2-deoxy-D-glucose and the corresponding iminoether,[7] indicating the presence of a five-membered heterocyclic structure. However, the difference of UV absorption between 8 and this compound (λ_{max} 260 nm; ε 1.05×10^4) and the presence of three acetyl groups in the heterocyclic part indicate a non-conjugated system. Consequently, **8** was concluded to be 2-acetylimino-1,3-diacetyl-4-(D-arabino-tetraacetoxybutyl)imidazolin-4.

Transformation of **1** to **3** or **4** mentioned above will be explained as follows (Scheme 1). Dehydration between the guanidino and aldehyde groups in the oxo-form of **1** give easily the intramolecular Schiff base which is equilibrating with the more stable imidazolidine structure at the pH region lower than 7. At a higher pH region, a prototropic shift is caused by the action of hydroxide ions to give the imidazoline derivative irreversibly. At the end of the condensation reaction of 2-amino-2-deoxy-D-glucose with cyanamide, the pH of the solution adjusted to 7 at the biginning has changed to 8.3. This change will be attributed to the reason for the formation of **3** and **4** at the same time. The participation of lone-paired electrons of nitrogen in the intramolecular Schiff base to the resonance stabilization of the imidazoline ring will accerelate the prototropic shift in the convesion into **4**.

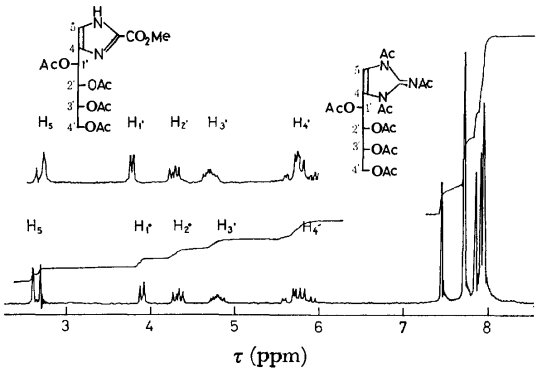

Fig. 2. The NMR spectrum of **8**.

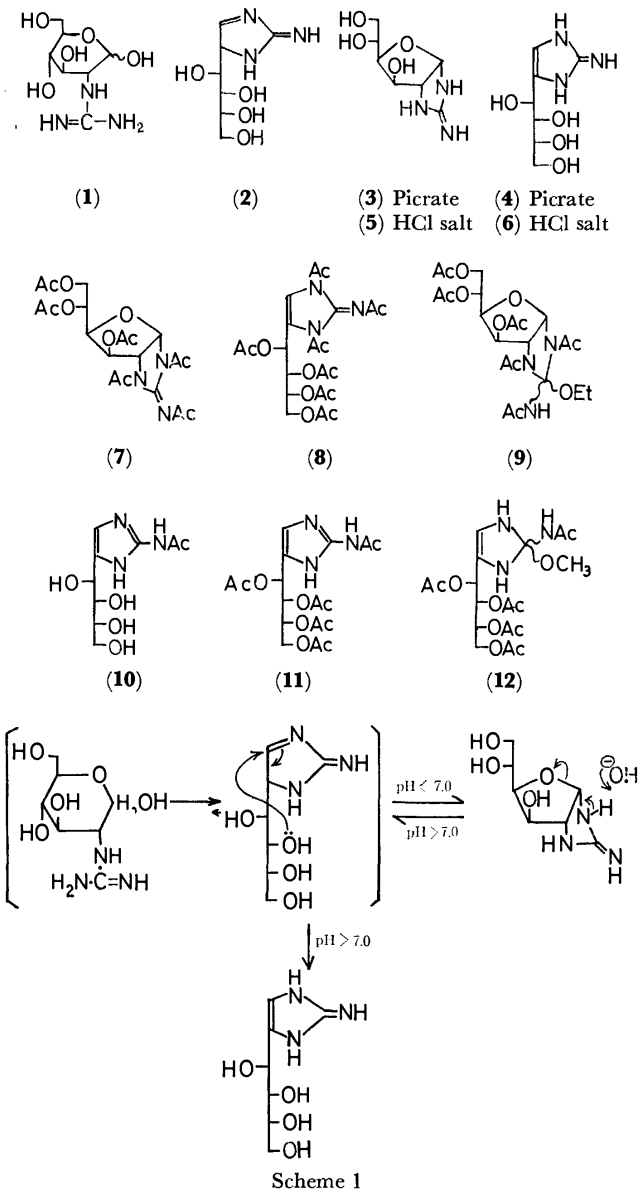

Scheme 1

On the other hand, it was found that **7** was converted to an addition product of ethanol (**9**) in 66% yield by heating it in ethanol at 60°C for 4 hr. IR spectrum of **9** showed the appearrance of characteristic absorptions of N–H (3250, 3200, and 1540 cm^{-1}), and the NMR spectrum two kinds of ethyl signals (C–CH_3 at 8.78 and 8.84 τ; O–CH_2– at 6.31 and 6.89 τ), indicating the addition of ethanol to the 2-imino bond from the both side. Formation of analogous addition compound of methanol or isopropyl alcohol were also ascertained with NMR spectra. A similar reaction was reported in the case of triacetyl-2-imino-imidazolidine.[8] Similar treatment of **8** in ethanol at an elevated temperature gave also an addition compound in which elimination of two *N*-acetyl groups was indicated by NMR spectrum, however, no definite compound could be isolated.

Moreover, an attempted deacetylation of **7** with sodium methoxide at a room temperature gave 2-acetamido-5-(D-*arabino*-tetrahydroxymethyl)imidazole

7) J. Yoshimura, K. Fujimori, Y. Sugiyama, and H. Ando, *ibid.*, **44**, 3131 (1971).

8) R. Greenhalgh and R. A. B. Bannard, *Can. J. Chem.*, **39**, 1017 (1961).

(**10**) in 80% yield. Reacetylation of **10** by the usual method gave a mixture of the corresponding *N,O*-pentaacetate (**11**) and another product. The presence of two kind of C_4- and C′-proton signals indicate that the structure of the latter is similar to the former. One attempted acetylation of **6** gave incidentally **11** as the main product, from which pure sample was isolated by preparative thin layer chromatography. Comparatively large molecular coefficency of the absorption of **11** [λ_{max}^{EtOH} 246 nm (ε 7.08×10^3)] and the presence of characteristic absorptions of secondary amide (1675 and 1520 cm^{-1}), esters (1745 cm^{-1}), monoacetylguanidine (1595 cm^{-1})[8] in IR spectrum indicated the presence of imidazole structure in **11**. Because of its insolubility NMR and UV spectrum of **10** could not be examined, however, the IR spectrum showed absorptions of secondary amide (1675 and 1530 cm^{-1}), monoacetylguanidine (1600 cm^{-1}), and characteristic C–O stretching in the region between 1000—1100 cm^{-1} as was observed that of **4** and **6**.

For the transformations of **7** to **10** and **10** to **11**, the following considerations will be given; (i) treatment of **7** with sodium methoxide caused the elimination of feasible *N*-acetyl groups attached to guanidine-type structure[9] as well as de-*O*-acetylation, and moreover, the skeletal conversion as shown in Scheme 1 is accompanied with the shift of *exo*-double bond to give more stable imidazole structure. Thus, the usual 2-acetamido group in **10** is remained intact. (ii) Because *N*-acetylation of heterocycles such as imidazole can be accomplished only by refluxing with acetic anhydride,[10] the usual acetylation of **10** gave the *N,O*-pentaacetate.

Similar deacetylation of **8** with a small amount of sodium methoxide gave again a mixture of **11** and another addition compound of methanol. From the integration of NMR spectrum the latter was deduced to be (2*R,S*)-2-acetamido-2-methoxy-4-(D-*arabino*-tetraacetoxybutyl)imidazoline-4 (**12**). The analitical data of the mixture consisted with that a mixture of them in the ratio estimated from the NMR spectrum. Treatment of **11** with excess amounts of ethoxide gave again crude **10**. These results indicate that guanidine-type *N*-acetyl groups are more labile than *O*-acetyl groups, and nucleophilic additions to the *exo*-double bond in **8** are also possible depending on condition used.

Many works on electrophillic reactions of triheterocarbonium ions including oxygen, nitrogen and sulfur as heteroatoms[11] have been done, but, the trinitrogen-system of guanidines has been considered to be rather stable than others. The result obtained in this work seems likely to suggest that *N*-acylation activates this system, and more simple model compound will be suitable to study for this aspect.

9) R. Greenhalgh and R. A. B. Bannard, *ibid.*, **37**, 1810 (1959).
10) L. Birkofer, *Chem. Ber.*, **76**, 769 (1943); J. A. Montgomery *J. Amer. Chem. Soc.*, **78**, 1928 (1956).
11) H. Prinzbach and E. Futter, "Advances in Heterocyclic Chemistry", Vol. 7, ed. by A. R. Katritzky and A. J. B. Boulton, Academic Press, (1967) p. 103; A. H. Land, "Heterocyclic Compounds", Vol. 5, ed. by R. C. Elderfield, John Wiley & Sons Inc., (1967) p. 484; T. Nakai, *Yuki Gosei Kagaku Kyokai Shi*, **28**, 708 (1970).

Experimental

All melting points are uncorrected. The solutions were evaporated under diminished pressure at a bath temperature not exceeding 45°C. Specific rotations were measured in a 0.5-dm tube, with a Carl Zeiss LEP Al Polarimeter. The IR spectra were recorded with a Hitachi Model EPI-GS grating IR spectrophotometer. The NMR spectra were taken with a JMN-4H-100MHz Spectrometer in deuteriochloroform unless otherwise stated, using tetramethylsilane as an internal standard. Chemical shifts and coupling constants were recorded in τ and Hz units, and IR frequencies in cm^{-1}.

α-D-Glucofurano[1′,2′;4,5]-2-iminoimidazolidine picrate (3) and 2-imino-4-(D-arabino-tetrahydroxybutyl)imidazoline picrate (4). A solution of D-glucosamine hydrochloride (4.30 g, 20 mmol) and cyanamide (1.26 g, 30 mmol) in water (20 m*l*) was neutralized with 5N-sodium hydroxide to pH 7.0, stirred at 60°C for 7 hr, and then picric acid (10.2 g) in methanol (140 m*l*) was added to the reaction mixture. After standing this solution at 0°C for 2 days, picrate of needle crystal (**3**) was obtained in 23.6% yield (2.02 g). Mp 180°C; IR: 1670 (C=N), 1560 (NO_2).

Found: C, 35.96; H, 3.70; N, 19.38%. Calcd for $C_{13}H_{16}N_6O_{11}$: C, 36.13; H, 3.73; N, 19.44%.

The mother liquor was suitably concentrated, and the precipitate appeared was gathered. This powder (8.50 g) was washed three times with benzene (25 m*l*) at 60°C to remove excess picric acid. The residue was recrystallized from hot water to give granular picrate (**4**) (1.33 g) in 15.4% yield. Mp 178°C; IR: 1680 (C=C), 1668 (C=N), 1550 (NO_2).

Found: C, 35.96; H, 3.76; N, 20.47%. Calcd for $C_{13}H_{16}N_6O_{11}$: C, 36.13; H, 3.73; N, 19.44%.

α-D-Glucofurano[1′,2′;4,5]-2-iminoimidazolidine hydrochloride (5). To a solution of **3** (1.4 g) in water (30 m*l*) was added 10% hydrochloric acid (10 m*l*) at 50°C, kept at the same temperature for ten minutes and then cooled to room temperature. After separating picric acid by filteration, the mother liquor was extracted several times with ether (15 m*l*× 5) to remove the picric acid. The water solution was adjusted to pH 5.0 with Amberlite IRA-410, decolorized with active carbon, concentrated, and the residual sirup was crystallized by addition of ethanol to give 0.6 g (77%) of colorless prisms which was recrystallized from water-ethanol. IR: 1674 (C=N); NMR (D_2O): 3.55 ($H_{1'}$; d, $J_{1,2}$=6.3); 5.07 ($H_{2'}$; d); 5.17 (1H; s) and 5.5—6.0 (4H; m), ($H_{3'}$, $H_{4'}$, $H_{5'}$, $H_{6'a}$, $H_{6'b}$). $[\alpha]_D^{23}$ −25.4° (*c* 1.0, water).

Found: C, 35.08; H, 6.07; N, 17.46%. Calcd for $C_7H_{14}N_3O_4Cl$: C, 35.07; H, 5.89; N, 17.53%.

2-Imino-4-(D-arabino-tetrahydroxybutyl)imidazoline-4 hydrochloride (6). The picrate **4** (1.0 g) was treated by the same method as mentioned above, and the corresponding hydrochloride was obtained as colorless needles in 72% (0.4 g) yield. Mp 171°C; $[\alpha]_D^{23}$ −11.7° (*c* 1.0, water); IR: 1664 and 1575 (C=N and C=C); NMR (D_2O): 2.77 (H_5; s); 4.60 ($H_{1'}$; s); 5.6—5.9 ($H_{2'}$, $H_{3'}$, $H_{4'a}$, $H_{4'b}$, m).

Found: C, 34.48; H, 5.59; N, 17.69%. Calcd for $C_7H_{14}N_3O_4Cl$: C, 35.07; H, 5.89; N, 17.53%.

Conversion of 5 into 6. A solution of **5** (1.00 g) in water (30 m*l*) was adjusted to pH 11.8 with Amberlite IRA-410 and kept at room temperature for thirty minutes. After checking the appearrance of the UV absorption (λ_{max} 208 nm) the solution was adjusted to pH 4.8 with 4N-HCl (*ca.* 8 m*l*), and evaporated to give a sirup which was crystallized by addition of ethanol. Yield, 0.8 g (80%). Physical properties of this crystals consisted with the authentic specimen.

3′,5′,6′-Tri-O-Acetyl-α-D-glucofurano[1′,2′;4,5]-2-acetylimino-1,3-diacetylimidazolidine (7). To a suspension of **5** (1.20 g, 5.0 mmol) in pyridine (8.0 m*l*) was added acetic anhydride

(6.0 ml, 64 mmol) with stirring under cooling at 0°C. After standing the reaction mixture at room temperature for 2 days, it was poured into ice-water (30 ml) with stirring to give white crystals, which was gathered on a filter paper, washed with cold water, and then recrystallized from chloroform–petroleum ether. Yield, 1.89 g (83.3%); mp 155°C; $[\alpha]_D^{23}$ +26.0° (*c* 2.00, chloroform); IR: 1745 (OAc), 1685 (C=N), 1640 (*tert.* amide); NMR: 3.73 ($H_{1'}$; d, $J_{1',2'}=6.5$), 5.49 ($H_{2'}$; d), 4.32 ($H_{3'}$; d, $J_{3',4'}=3.0$), 5.91 ($H_{4'}$; q, $J_{4',5'}=10.0$), 4.82 ($H_{5'}$; oct, $J_{5',6'a}=3.0$), 5.47 ($H_{6'a}$; q, $J_{6'a,b}=12.5$), 5.94 ($H_{6'b}$; q, $J_{5',6'b}=5.5$), 7.42 and 7.44 (N_3-Ac and imino-Ac), 7.90, 7.96, and 8.01 (N_1-Ac and 3×OAc).

Found: C, 50.01; H, 5.89; N, 9.23%. Calcd for $C_{19}H_{25}N_3O_{10}$: C, 50.11; H, 5.53; N, 9.23%.

*2-Acetylimino-1,3-diacetyl-4-(*D-arabino-*tetraacetoxybutyl)imidazoline-4 (**8**).* To a suspension of **6** (0.6 g, 2.5 mmol) in pyridine was added acetic anhydride (3.0 ml), and the reaction mixture was treated by the usual method to give the heptaacetate (0.65 g) in 50% yield, which was recrystallized from chloroform-petroleum ether. Mp 151°C; $[\alpha]_D^{23}$ −13.6° (*c* 1.01, chloroform); IR: 1740 (OAc), 1720 (NAc); NMR: 2.61 (H_5; s), 3.89 ($H_{1'}$; d, $J_{1',2'}=4.5$), 4.32 ($H_{2'}$; q, $J_{2',3'}=8.5$), 4.77 ($H_{3'}$; sex, $J_{3',4'a}=3.0$, $J_{3',4'b}=6.0$), 5.66 ($H_{4'a}$; q, $J_{4'a,b}=12.0$), 5.86 ($H_{4'b}$; q), 7.45 (-NAc), 7.72 (2 NAc), 7.86, 7.92, and 7.95 (4 OAc).

Found: C, 49.85; H, 5.41; N, 9.02%. Calcd for $C_{21}H_{27}N_3O_{11}$: C, 50.11; H, 5.53; N, 9.23%.

*3',5',6'-Tri-*O*-acetyl-α-*D*-glucofurano[1',2';4,5]-(2*R,S*)-2-acetamido-1,3-diacetyl-2-ethoxyimidazolidine (**9**).* A solution of **7** (0.45 g, 1.0 mmol) in ethanol (5 ml) was heated at 60°C for 4 hr, and the crystals appeared was filtered to give colorless crystals (0.33 g) in 66% yield. Mp 225°C (decom); IR: 3250, 3200, 1540 (NH).

Found: C, 50.00; H, 6.13; N, 8.52%. Calcd for $C_{21}H_{31}N_3O_{11}$: C, 50.29; H, 6.13; N, 8.78%.

*2-Acetamido-5-(*D-arabino-*tetrahydroxybutyl)imidazole (**10**).* To a solution of **7** (470 mg, 1.04 mmol) in aboslute methanol was added two drops of 2N-sodium methoxide at room temperature, and then white solid precipitated was filtered, washed with absolute methanol to give 0.2 g (79%) of the monoacetate. Mp 200°C (decomp). It was insoluble in methanol, water and DMSO. IR: 1675 and 1530 (*sec*-amide), 1600 (mono-acetylguanidine).

Found: C, 44.10; H, 6.72; N, 17.63%. Calcd for $C_9H_{17}N_3O_6$: C, 44.08; H, 6.17; N, 17.14%.

*2-Acetamido-5-(*D-arabino-tetraacetoxybutyl)imidazole (**11**).*

*i) From **6**;* To a suspension of **6** (0.48 g, 2 mmol) in pyridine was added acetic anhydride (0.3 ml) under cooling at 0°C. After stirring at room temperature for two days on a magnetic stirrer, the warm reaction mixture was poured into ice water (30 ml). As any crystals could not be obtained, the resulted solution was extracted four times with chloroform (40 ml), and the extracts were washed with 2N-sulfuric acid (30 ml), saturated aqueous sodium bicarbonate (30 ml) and water. The extract was then evaporated to give a sirup (0.53 g). This sirup showed three bands on preparative tlc (Wakogel B-5 UA; 10% methanol in benzene), and the main band which had the greatest R_f value was collected, and eluted with chloroform to give a sirup in 21% (0.17 g) yield. $[\alpha]_D^{23}$ −10.8° (*c* 0.52, ethanol); UV: λ_{max}^{EtOH} 246 nm (ε 7.08×10³); IR: 1740 (OAc), 1680 and 1520 (*sec*-amide), 1595 (monoacetylguanidine); NMR: 3.22 (H_4; s), 3.96 ($H_{1'}$; d, $J_{1',2'}=4.8$), 4.47 ($H_{2'}$; q, $J_{2',3'}=7.0$), 4.12 ($H_{3'}$; m), 5.76 ($H_{4'a}$; q, $J_{3',4'a}=3.5$, $J_{4'ab}=13.0$), 5.90 ($H_{4'b}$; q, $J_{3',4'b}=5.8$), 7.73 (NAc), 7.92, 7.96, and 7.98 (OAc).

Found: C, 49.72; H, 6.05; N, 9.53%. Calcd for $C_{17}H_{24}N_3O_9$: C, 49.27; H, 5.84; N, 10.14%.

*ii) From **10**;* To a solution of **10** (0.11 g, 0.45 mmol) in pyridine (1 ml) was added acetic anhydride (1 ml) at room temperature, and the reaction mixture was kept for three days with stirring, poured into ice–water. The resulted solution was extracted with benzene, and the extract was evaporated to give a sirup. This sirup showed the presence of two kinds of products in the NMR spectrum in which a series of proton chemical shifts of the main product consisted with that of **11**. Another one showed H_5-proton signal at 2.98 τ (s) and $H_{1'}$ at 4.03 τ (d, $J_{1',2'}=5.0$), respectively.

*Attempted deacetylation of **8** with sodium methoxide.* To a solution of **8** (0.5 g, 1 mmol) in absolute methanol (2 ml) was added five drops of 2N-sodium methoxide at room temperature. After standing overnight, the reaction mixture was neutralized with five drops of 2N-acetic acid and evaporated. A solution of the resulted sirup in chloroform (10 ml) was washed three times with water, dried and evaporated. The resulted sirup showed two bands on a preparative tlc (Wakogel B-5 UA; 10% methanol in benzene), and the main band which had larger R_f value was collected. The NMR sepctrum of the resulted sirup indicated the presence of two products in which the proton chemical shifts of the main product consisted with that of **11**. Another one showed H_5-proton signal at 3.23 τ (s), $H_{1'}$ at 4.01 τ (d, $J_{1',2'}=4.8$), OCH_3 at 6.79 τ (s) indicating the presence of the addition product of methanol. The ratio of the both compounds was deduced to be 3: 1 from intensities of OCH_3 and other proton signals. UV spectrum of the mixture showed at 247 nm. (Found: C, 48.78; H, 5.58; N, 9.52%. Calcd as 3: 1 mixture of the both compounds: C, 49.39; H, 5.95; N, 9.88%).

The authors are indebted to Mr. K. Fukukawa and H. Matsumoto for NMR measurments, and members of Laboratory of Organic Analysis for microanalysis.

Ionic Decomposition of Phenylazotriphenylmethane in Trifluoroacetic Acid[1]

Nobumasa KAMIGATA, Michio KOBAYASHI, and Hiroshi MINATO

Department of Chemistry, Faculty of Science, Tokyo Metropolitan University, Fukazawa, Setagaya, Tokyo

(Received December 13, 1971)

Acid-catalyzed decomposition of phenylazotriphenylmethane was studied in mixtures of benzene and large excess concentration of trifluoroacetic acid. The decomposition was of first order and the rate was much faster than that in pure aromatic solvents. The values of activation energy (E_a=22.3 kcal/mol) and activation entropy ($\Delta S^{\neq}$=−5.2 e.u.) fit the isokinetic relationship established for the ionic decomposition of benzenediazonium tetrafluoroborate in aprotic polar solvents and of phenylazo *p*-tolyl sulfone in mixtures of benzene and trifluoroacetic acid. The reaction products were benzene, biphenyl, benzophenone, triphenylmethane, triphenylmethyl alcohol and nitrogen. Orientations and partial rate factors for the phenylation of monosubstituted benzenes indicated that not phenyl radical but phenyl cation was produced as an intermediate. Further, the UV spectrum of PAT in benzene and trifluoroacetic acid shows λ_{max} at 403 mμ (log ε 4.48) and λ_{max} at 427 mμ (log ε 4.48). However, the UV spectrum of PAT in benzene and in the absence of trifluoroacetic acid has no absorption in this range. The formation of triphenylmethyl alcohol and the UV spectra of PAT in acid solution indicate that triphenylmethyl cation was formed as an intermediate. A plausible mechanism was discussed.

Benzenediazonium salts in aprotic polar solvents spontaneously decompose, yielding phenyl cation;[2] but they can generate phenyl radical when nitrite ion,[3] hydroxide ion[4] or pyridine[5] are added.

Phenylazo *p*-tolyl sulfone decomposes homolytically when such basic agents as pyridine, quinoline, and magnesium oxide are present,[6] but in the absence of such basic agents autocatalytic ionic decomposition takes place, yielding phenyl cation.[7]

However, there have been no papers reporting on the heterolytic decomposition of phenylazotriphenylmethane (PAT), which has been considered to be a good dependable source for phenyl radical.[8]

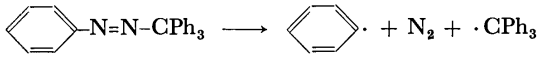

More recently, Takeuchi, Nagai, and Tokura reported that triphenylmethyl radical generated from PAT was converted to triphenylmethyl cation when SO_2 and O_2 were present in the reaction system.[9]

During a systematic investigation on the decomposition of arylazo compounds in our laboratories, it has been found that PAT decomposes quite rapidly with evolution of nitrogen under strongly acidic conditions. In order to determine whether this fast decomposition is homolytic or heterolytic, products of the decomposition have been analyzed and isomer distributions for phenylation of substituted benzenes have been studied.

In this papar, the results of this investigation will be described, and the mechanism of the reaction will be discussed.

Results and Discussion

Kinetic Studies. When a solution of PAT (1.00 g) in benzene (15.6 g) was mixed with trifluoroacetic acid (35.0 g), rapid evolution of nitrogen took place. The decomposition was of first order in PAT as shown in Fig. 1. The rate constants determined were compared with those for the decomposition of PAT in pure benzene,[10] and the results are summarized in Table 1. The values of the activation parameters were calculated (E_a=22.3 kcal/mol, $\Delta S^{\neq}$=−5.2 e.u.). These

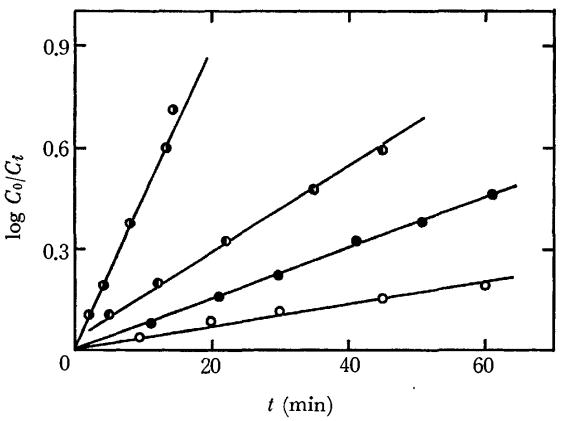

Fig. 1. First order rate plots for the decomposition of PAT in C_6H_6–CF_3CO_2H.
◑ 50.0°C, ◐ 40.0°C, ● 35.0°C, ○ 30.0°C

1) Cationic Arylation. IV.

2) a) R. A. Abramovitch and F. F. Gadallah, *J. Chem. Soc., B*, **1968**, 497; M. Kobayashi, H. Minato, E. Yamada, and N. Kobori, This Bulletin, **43**, 215 (1970).

3) M. Kobayashi, H. Minato, N. Kobori, and E. Yamada, *ibid.*, **43**, 1131 (1970).

4) N. Kamigata, T. Kurihara, H. Minato, and M. Kobayashi, *ibid.*, **44**, 3152 (1971).

5) R. A. Abramovitch and J. G. Saha, *Tetrahedron*, **21**, 3297 (1965).

6) M. Kobayashi, H. Minato, M. Kojima, and N. Kamigata, This Bulletin, **44**, 2501 (1971); C. G. Overberger and A. J. Rosenthal, *J. Amer. Chem. Soc.*, **82**, 108, 117 (1960).

7) M. Kobayashi, H. Minato, and N. Kobori, This Bulletin, **43**, 219 (1970).

8) For exsample: D. H. Hey, C. J. M. Stirling, and G. H. Williams, *J. Chem. Soc.*, **1955**, 3963; D. H. Hey, M. J. Perkins, and G. H. Williams, *ibid.*, **1965**, 110; W. A. Pryor, J. F. Echols, Jr., and K. Smith, *J. Amer. Chem. Soc.*, **89**, 1189 (1967); C. M. Camaggi, R. Leardimi, M. Tiecco, and A. Tundo, *J. Chem. Soc., B*, **1969**, 1251; M. Harada, R. Ito, T. Migita, and O. Simamura, *Kogyo Kagaku Zasshi*, **69**, 962 (1966).

9) H. Takeuchi, T. Nagai, and N. Tokura, This Bulletin, **43**, 1747 (1970).

10) S. G. Cohen and C. H. Wang, *J. Amer. Chem. Soc.*, **75**, 5504 (1953); T. Yamamoto, *Nippon Kagaku Zasshi*, **83**, 844 (1962); T. Yamamoto, *ibid.*, **85**, 691 (1964).

TABLE 1. FIRST ORDER RATE CONSTANTS FOR THE DECOMPOSITION OF PAT IN C_6H_6–CF_3CO_2H

T (°C)	$k_1 \times 10^4$ (sec^{-1})	
	C_6H_6–CF_3CO_2H	C_6H_6
30.0	0.92	
35.0	1.82	
40.0	4.04	
50.0	8.09	
43.30		0.60[9]
53.35		2.25[9]

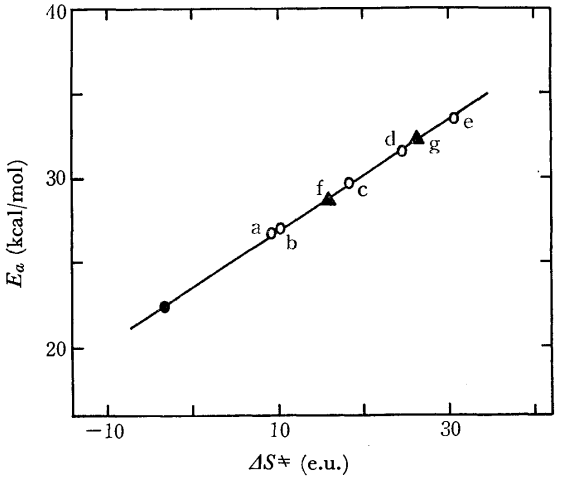

Fig. 2. Isokinetic relationship for the decom_osition of PAT, PhN_2BF_4 and p-TsN_2Ph.
●: Decomposition of PAT in C_6H_6–CF_3CO_2H
○: Decomposition of PhN_2BF_4 in aprotic polar solvents[10]
(a: in $Me_2C{=}O$, b: in DMSO, c: in CH_3CN, d: in DMF, e: in CH_3NO_2)
▲: Decomposition of p-TsN_2Ph in C_6H_6–CF_3CO_2H[6]
(f: p-TsN_2Ph/CF_3CO_2H=5.89 mol/mol, g: p-TsN_2Ph/CF_3CO_2H=2.95 mol/mol)

activation parameters fit surprisingly well the isokinetic relationship established for the decomposition of benzenediazonium tetrafluoroborate in various aprotic polar solvents[11] and for the decomposition of phenylazo p-tolyl sulfone in a mixture of benzene and trifluoroacetic acid,[7] as shown in Fig. 2 (β=311°K). The activation parameters are quite different from those reported[10] for the homolytic decomposition of PAT (E_a=27 kcal/mol, $\Delta S^{\neq}$=5 e.u.). These findings suggest that the decomposition of PAT in this medium is not homolysis but heterolysis. The fact that the activation parameters found fit the isokinetic relationship established for the decomposition of benzenediazonium ions suggests that benzenediazonium ion is an intermedate in this system and the rate-determining step is the decomposition of the diazonium ion.

$$Ph\text{-}N{=}N\text{-}CPh_3 \xrightarrow{CF_3CO_2H} PhN_2^+ \xrightarrow{\text{rate-determining step}} Ph^+ + N_2$$

Products Studies. PAT was decomposed in a mixture of benzene and trifluoroacetic acid at 40°C and the reaction products are summarized in Table 2. Evolution of nitrogen was almost quantitative (93—95%) and the yield of benzene was high in contrast to low yield of biphenyl and triphenylmethane; these results are quite different from those reported for homolysis of PAT.[8] In addition, a trace of benzophenone and a considerable amount of triphenylmethyl alcohol were produced, but no triphenylmethyl peroxide was found though the reaction was carried out under air. The formation of triphenylmethyl alcohol suggests that triphenylmethyl cation was produced as the intermediate, and then converted to triphenylmethyl alcohol.

$$Ph\text{-}N{=}N\text{-}CPh_3 \xrightarrow{CF_3CO_2H} Ph_3C^+ \xrightarrow{H_2O} Ph_3COH$$

Kinetic studies and product studies described above show that benzenediazonium ion and triphenylmethyl cation were formed as the intermediates from PAT. These results are abnormal and very surprising.

$$Ph\text{-}N{=}N\text{-}CPh_3 \longrightarrow Ph^+ + N_2 + Ph_3C^+$$

TABLE 2. DECOMPOSITION PRODUCTS OF PAT (40°C)

Products (mol/mol of PAT)	in $C_6H_6+CF_3CO_2H$[a]	in CF_3CO_2H[b]
N_2	0.93	0.95
PhH	—	0.74
Ph_2	0.16	0
Ph_3CH	0.24	0.26
Ph_3COH	0.53	0.57
PhCOPh	trace	trace

a) PAT (1.51g) was dissolved in C_6H_6 (23.5g) and CF_3CO_2H (50.0g): (Expt. 1).
b) PAT (1.42g) was dissolved in CF_3CO_2H (44.2g): (Expt. 2).

UV Spectra of PAT in Benzene and Trifluoroacetic Acid. In order to ascertain the formation of trityl cation in this medium, the UV spectrum of PAT was measured in benzene and trifluoroacetic acid at room temperature. The spectrum is shown in Fig. 3. The values of log ε at 403 mμ and 427 mμ were 4.48; no absorptions were observed in this range, when trifluoroacetic acid was absent. The UV absorptions reported for trityl cation are as follows:

Trityl chloride:[12] $\lambda_{max}^{98\%H_2SO_4}$ 430 mμ (log ε 4.58)
Gomberg's trityl:[13] $\lambda_{max}^{H_3PO_4}$ 400 mμ and 440 mμ(log ε 4.5)
Gomberg's trityl:[13] $\lambda_{max}^{POCl_3}$ 420 mμ and 440 mμ(log ε 4.2)

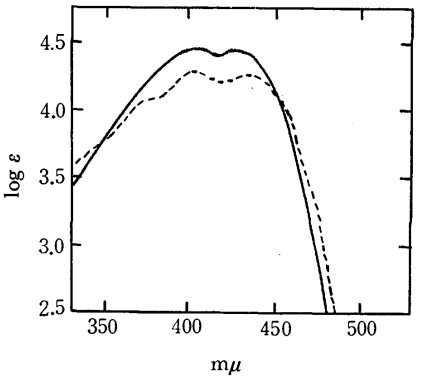

Fig. 3. The absorption spectrum of PAT in C_6H_6–CF_3CO_2H
—— PAT in C_6H_6–CF_3CO_2H
- - - Gomberg's trityl in liq. SO_2–O_2[9]

11) K. Ishida, N. Kobori, M. Kobayashi, and H. Minato, This Bulletin, **43**, 285 (1970).
12) A. G. Evans, J. A. G. Jones, and G. O. Osborne, *J. Chem. Soc.*, **1954**, 3803.
13) T. L. Chu and S. I. Weissman, *J. Chem. Phys.*, **22**, 21 (1954).

Therefore, the peaks at 403 mμ and 427 mμ in trifluoroacetic acid are ascribable to the presence of trityl cation in this medium. The values of log ε in our experiments are quite similar to the value reported[12] (log ε 4.58), and this means that PAT in trifluoroacetic acid is transformed to trityl cation to the same extent as the trityl chloride in 98% sulfuric acid.

Table 3. Orientation (%) and partial rate factors for the phenylation of PhX with PAT in CF_3CO_2H at 40°C

X in PhX	Orientation (%)			Partial rate factors		
	o-,	*m*-,	*p*-,	k_o/k	k_m/k	k_p/k
OMe	57.6	10.9	31.5	1.52	0.28	1.66
Et	31.5	16.1	52.4	1.80	0.92	5.99
Cl	69.1	12.4	18.5	0.89	0.16	0.48
NO_2	33.7	63.1	3.2	0.18	0.34	0.03

Phenylation of Substituted Benzenes with PAT in Trifluoroacetic Acid. Isomer distributions and partial rate factors for the phenylation of substituted benzenes with PAT in trifluoroacetic acid were determined at 40°C. The results are summarized in Table 3. The MeO, Et, and Cl groups behaved as *o,p*-directors and accelerated the phenylation, whereas the NO_2 group behaved as a *m*-director, and retarded the phenylation. These results are quite different from the results of phenylation with phenyl radicals generated from benzoyl peroxide[14] or *N*-nitrosoacetanilide[15] but similar to the phenylation with phenyl cations generated from benzenediazonium tetrafluoroborate in aprotic polar solvents[2] and phenylazo *p*-tolyl sulfone in trifluoroacetic acid.[7] Figure 4 is the Hammett plots for the phenylation *versus* σ^+, which followed a good straight line except for the points for *p*-OMe and *m*-NO_2 groups. In the case of the phenylation of PhX with phenyl

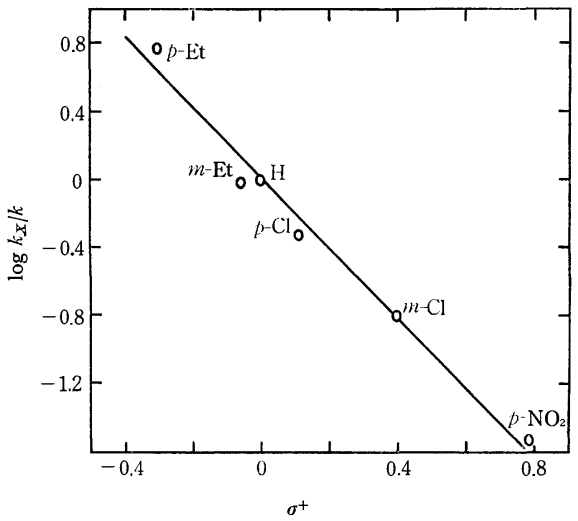

Fig. 4. The Hammett plots for the phenylation of PhX with PAT in CF_3CO_2H at 40°C.
$\rho = -2.1$

cation generated from benzenediazonium tetrafluoroborate, the points for *p*-OMe and *m*-NO_2 also deviated from a straight line in the Hammett plots.[2] The ρ value ($\rho = -2.1$) is a larger negative value than those obtained for the phenylation with benzenediazonium tetrafluoroborate ($\rho = -0.82$)[1] or phenylazo *p*-tolyl sulfone ($\rho = -0.10$).[7] This means that the decomposition of benzenediazonium ion in trifluoroacetic acid is more sensitive to the electron supply of substituents. Brown and Wirkkala reported that the relative rate of bromination of toluene and benzene (k_T/k_B) was 605 in 85% CH_3CO_2H and 2580 in CF_3CO_2H.[16]

Plausible Reaction Mechanism. Since the formation of trityl cation was instantaneous and almost quantitative upon addition of trifluoroacetic acid, trityl ion must be present before the rate-determining step. The red color of trityl cation did not fade when such nucleophiles as water was absent in the medium. When water was added to the mixture, the red color disappeared instantaneously.

It is of interest to determine what kind of chemical species are present in the mixture when the mixture changed from yellow to red upon addition of trifluoroacetic acid. When water was added about 20 sec after addition of trifluoroacetic acid, the products isolated from the benzene layer contained more triphenylmethane and less triphenylcarbinol, whereas the main product was triphenylcarbinol when water was added about 60 sec after addition of trifluoroacetic acid. The results are shown in Table 4.

Table 4. Products of hydrolysis of PAT–C_6H_6–CF_3CO_2H mixture

	Time interval between addition of CF_3CO_2H and that of H_2O	Products (mol/100 mol PAT)		
		Ph_3CH	Ph_3COH	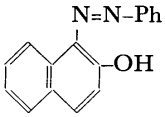
Expt. 7	about 20 sec	58.9	30.9	45
Expt. 8	about 60 sec	2.9	86.0	54

When the aqueous layer was separated and added to a 10% sodium β-naphthoxide solution, the coupling product was produced in good yield, indicating the presence of benzenediazonium ion in the mixture.

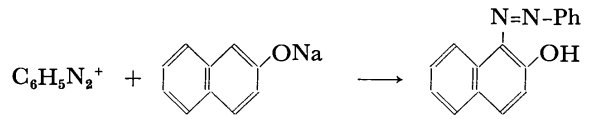

A mechanism which is consistent with these results is shown below.

The mechanism shown requires that the reaction between phenyl cation and triphenylmethane produces benzene and triphenylmethyl cation. Taft[17] and Abramovitch[18] proposed that phenyl cation is in equi-

14) G. H. Williams, "Homolytic Aromatic Substitution," Pergamon Press, Oxford (1960), p. 73.
15) R. Ito, T. Migita, N. Morikawa, and O. Simamura, *Tetrahedron*, **21**, 955 (1965).
16) H. C. Brown and R. A. Wirkkala, *J. Amer. Chem. Soc.*, **88**, 1447 (1966).
17) R. W. Taft, *ibid.*, **83**, 3350 (1961).
18) R. A. Abramovitch and J. G. Saha, *Can. J. Chem.*, **43**, 3269 (1965); R. A. Abramovitch and F. F. Gadallah, *J. Chem. Soc., B*, **1968**, 1497.

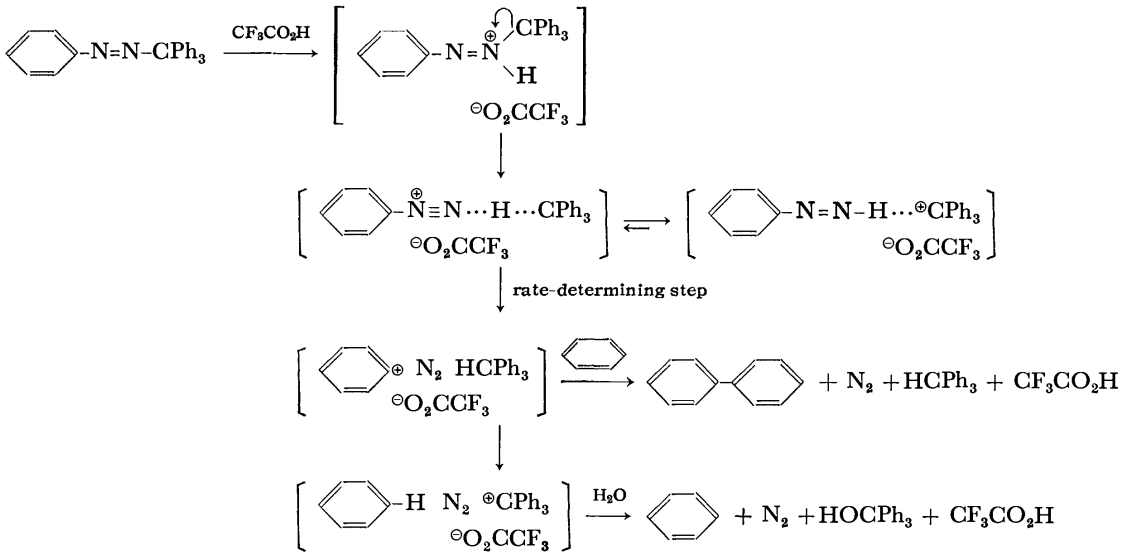

librium with a diradical cation.

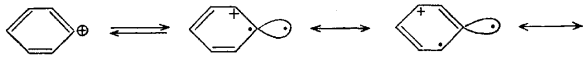

other canonical forms

The formation of triphenylmethyl cation from triphenylmethane would be better explained in terms of hydrogen abstraction by a diradical cation rather than hydride transfer.

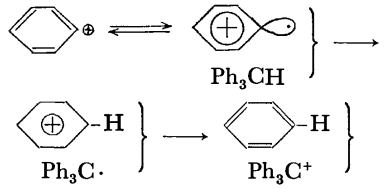

In order to prove that phenyl cation can oxidize triphenylmethane to triphenylmethyl cation, the phenyl cation produced from another source, benzenediazonium tetrafluoroborate (Exp. 3) or phenylazo *p*-tolyl sulfone (Exp. 4), were let to react with triphenylmethane in benzene-trifluoroacetic acid. Triphenylmethyl alcohol was found indeed as one of the products, though its yield was not so high (0.023 and 0.027 mol per mol of the benzenediazonium tetrafluoroborate and phenylazo *p*-tolyl sulfone, respectively). The lower yield in comparison with the yield in the case of the PAT–CF_3CO_2H system can be ascribed to the occurrence of the reaction in cage in the case of the PAT–CF_3CO_2H system. The yield must have been lowered by the reaction between phenyl cation and benzene, which was used to dissolve the triphenylmethane.

In an attempt to produce a system which resembles a mixture of PAT and trifluoroacetic acid, benzenediazonium trifluoroacetate was synthesized and dissolved in benzene containing triphenylmethane and trifluoroacetic acid. However, only a trace amount of triphenylcarbinol was found as a product by glc. These findings show that the tertiary hydrogen of triphenylmethane is very efficiently abstracted by phenyl cation in a cage, but much less efficiently in a system formed by simply mixing a diazonium ion and triphenylmethane.

According to the mechanism proposed, the amount of diphenyl produced must be comparable to that of triphenylmethane, and the amount of triphenylcarbinol must be comparable to that of benzene. The results in Table 2 are approximately in agreement with this mechanism.

Experimental

Materials. Phenylazotriphenylmethane was prepared by the bromine-water oxidation of phenylhydrazotriphenylmethane,[19] which was synthesized from the reaction between phenylhydrazine and triphenylmethyl chloride in ether.[20] Crude PAT was recrystallized from benzene–ethanol, mp 111—112°C (decomp.). Benzenediazonium tetrafluoroborate,[21] phenylazo *p*-tolyl sulfone[22] and benzenediazonium trifluoroacetate[23] were prepared according to the method described in the literature. Benzene, ethylbenzene, and chlorobenzene were washed with concentrated sulfuric acid and water successively, dried over calcium chloride, and distilled. Boiling points were 80, 135.5, and 131°C, respectively. Anisole was washed with an aqueous sodium hydroxide solution and water, dried over calcium chloride, and then distilled; bp 153°C. Nitrobenzene was washed repeatedly with a potassium dichromate solution and water, dried over calcium chloride, and distilled; bp 95.5°C/18 mmHg. Trifluoroacetic acid of Wako Pure Chemical Industries Limited was used without further purification. Isomeric ethylbiphenyls, methoxybiphenyls, chlorobiphenyls, and nitrobiphenyls were prepared as the reference compounds by the methods described in the literature.[24] They were purified by elution chromatography, distillation or recrystallization, and their melting points and boiling points agreed with the values reported in the literature. Triphenylmethane was prepared by lithium aluminum hydride reduction of

19) M. Gomberg and H. W. Berger, *Ber.*, **36**, 1088 (1903).
20) C. R. Hauser and B. E. Hudson, Jr., "Organic Syntheses," Coll. Vol. III, p. 842 (1955).
21) E. B. Starkey, "Organic Syntheses," Coll. Vol. II, p. 225 (1943).
22) A. Hantzsch and M. Singer, *Ber.*, **30**, 312 (1897).
23) M. R. Pettit, M. Stacey, and J. C. Tatlow, *J. Chem. Soc.*, **1953**, 3081.
24) R. Adams, "Organic Reactions," Coll. Vol. II, John Wiley and Sons, Inc., London (1957); P. E. Fanta, *Chem. Rev.*, **64**, 613 (1954).

triphenylmethyl chloride in ether and recrystallized from methanol, mp 92°C. Triphenylcarbinol was prepared by hydrolysis of triphenylmethyl chloride with an aqueous sodium hydroxide solution, and recrystallized from ethanol, mp 164°C.

Kinetic Measurements. PAT (1.00 g) was dissolved in benzene (15.6 g) and trifluoroacetic acid (35.0 g), and was decomposed in a water bath, the temperature of which was regulated within ± 0.1°C. The rate of decomposition was followed by measuring the evolution of nitrogen gas by use of a gas burette, and the total yield of nitrogen was determined.

Products of Decomposition of PAT in C_6H_6-CF_3COOH. Experiment 1: PAT (1.51 g) was decomposed in benzene (23.5 g) and trifluoroacetic acid (50.0 g) at 40°C. After the decomposition was over, the reaction mixture was washed successively with water, a 5% sodium hydrogen carbonate solution and water, and then dried over anhydrous magnesium sulfate. The nitrogen gas evolved was identified by gas chromatography with a Shimadzu GC-3AH (Molecular Sieve 5A 1m Column). The amounts of diphenyl, benzophenone, and triphenylmethane produced were determined by a Hitachi Gas Chromatograph K-53 on a column packed with 10% Apiezon L on Chromosorb W, on the basis of the comparison with the gas chromatograms of authentic samples. Triphenylmethyl alcohol was isolated by elution chromatography (alumina–benzene), identified by means of its IR spectrum and its melting point (164°C), and the weight was determined.

Products of Decomposition of PAT in CF_3COOH. Experiment 2: PAT (1.42 g) was decomposed in trifluoroacetic acid (44.2 g) at 40°C. The amount of benzene produced was determined by gas chromatography. The amounts of benzophenone, triphenylmethane and triphenylmethyl alcohol were determined according to the methods described above.

Phenylation of Monosubstituted Benzenes with PAT. PAT (1.00 g) was dissolved in an equimolar mixture of benzene and a substituted benzene (total aromatics, 50 mol per mol of PAT), and trifluoroacetic acid (35.0 g) was added to this solution. The flask containing the solution was placed in a bath at 40 ± 0.1°C, and the decomposition was followed by measuring the rate of evolution of nitrogen. After the evolution of nitrogen ceased, the reaction mixture was washed with water, a 5% sodium hydrogen carbonate solution and water, and dried over anhydrous magnesium sulfate, and then the amounts of substituted biphenyl isomers were determined by a Hitachi Gas Chromatograph K-53 (Apiezon L 10% on Chromosorb W).

Since the presence of a great quantity of a substituted benzene made the gas chromatographic determination of substituted biphenyls unreliable due to the tailing, the determination was made after about 70% of aromatic solvents were evaporated. Biphenyl isomers were identified by comparison of their retention times with those of the authentic samples.

Not benzene but chlorobenzene was used as the standard for the competitive phenylation, since unsubstituted biphenyl easily sublimes during the evaporation of substituted benzenes. The reactivity of each position of substituted benzenes was calculated relative to the reactivity of the *ortho* position of chlorobenzene. The partial rate factor of the *ortho* position of chlorobenzene was determined by an experiment carried out without evaporation of aromatic solvents. The partial rate factors of various substituted benzenes were calculated by the following equation.

$$k_x/k = (k_x/k_{o\text{-Cl}}) \times (k_{o\text{-Cl}}/k)$$

where,

k_x/k: partial rate factor for phenylation of PhX at the x (*o*-, *m*-, or *p*-) position

$k_x/k_{o\text{-Cl}}$: relative rate of phenylation at the x position of PhX against the *ortho* position of chlorobenzene

$k_{o\text{-Cl}}/k$: partial rate factor for phenylation at the *ortho* position of chlorobenzene

Spectra Measurements. UV and IR spectra were recorded with a Hitachi EPS-3T and Hitachi EPU-S2 spectrophotometer, respectively.

Decomposition of Benzenediazonium Tetrafluoroborate in the Presence of Triphenylmethane. Experiment 3: Benzenediazonium tetrafluoroborate (1.866 g) and triphenylmethane (0.650 g) were dissolved in a mixture of benzene (20 g) and trifluoroacetic acid (30 g). The diazonium salt was decomposed at 40°C overnight. The reaction mixture was washed successively with water, a 5% aqueous sodium carbonate solution and water. Triphenylmethyl alcohol was determined by gas chromatography (SE 30 on Chromosorb W). Yield, 58 mg (0.023 mol per mol of the diazonium salt).

Decomposition of Phenylazo p-*Tolyl Sulfone in the Presence of Triphenylmethane. Experiment 4*: Phenylazo *p*-tolyl sulfone (1.16 g) and triphenylmethane (0.94 g) were dissolved in a mixture of benzene (25 g) and trifluoroacetic acid (30 g). The azosulfone was decomposed for 20 hr in a water bath regulated at 40°C. The reaction mixture was washed successively with water, a 5% aqueous sodium carbonate solution and water. Triphenylmethyl alcohol was isolated by elution chromatography and identified by comparison of its IR spectrum with that of an authentic sample. Yield, 32 mg (0.027 mol per mol of the azosulfone).

Decomposition of Benzenediazonium Trifluoroacetate in the Presence of Triphenylmethane. Experiment 5: Benzenediazonium trifluoroacetate (2.0 g) and triphenylmethane (0.576 g) were dissolved in benzene (10 g) and trifluoroacetic acid (13 g) and stirred vigorously. The diazonium acetate was decomposed at room temperature overnight. The reaction mixture was treated in the manner described in Expt. 1, and triphenylmethyl alcohol was analyzed by glc; a trace of triphenylmethyl alcohol was detected.

Experiment 6: Benzenediazonium trifluoroacetate (2.0 g) and triphenylmethane (0.618 g) were dissolved in benzene (11 g), and stirred vigorously. The diazonium acetate was decomposed at room temperature overnight. The reaction mixture was treated in the manner described in Expt 2, and triphenylmethyl alcohol was analyzed quantitatively by glc; a trace of triphenylmethyl alcohol was detected.

Products of Hydrolysis of PAT–C_6H_6–CF_3CO_2H Mixture. Experiment 7: About 20 sec after the addition of CF_3CO_2H (30 g) to a benzene (20 g) solution of PAT (1.69 g), ice water was added. The aqueous layer was added to a 10% NaOH solution containing β-naphthol (1.4 g), and α-phenylazo-β-naphthol formed was filtered and dried; 0.508 g (45%).

The organic layer was treated in the manner described in Expt. 1, and the amounts of triphenylmethane and triphenylmethanol were determined by glc. Results are shown in Table 4.

Experiment 8: About 60 sec after the addition of CF_3CO_2H (30 g) to a benzene (20 g) solution of PAT (1.55 g), ice water was added. Evolution of nitrogen before addition of water was very little. The mixture was treated in the manner described in Expt 7. Results are shown in Table 4.

NOTES

BULLETIN OF THE CHEMICAL SOCIETY OF JAPAN, VOL. 45, 1236—1237(1972)

Properties of Polysarcosine Dodecylamide of Low Molecular Weight

Asahi SUZUKI*

Department of Biology, Faculty of Science, Osaka University, Toyonaka, Osaka

(Received July 5, 1971)

Properties of polysarcosine dodecylamide (*N*-dodecylpolysarcosineamide) in aqueous solution vary systematically with the degree of polymerization of the polymer, since the hydrophilic part of this amphiphilic polymer is proportional to the degree of polymerization.[1] However, unexpected properties were observed with polysarcosine dodecylamide of low molecular weight, which was synthesized (degree of polymerization: 5) and its properties examined. *N,N'*-dimethyldiketopiperazine was prepared and its properties were compared with that of polysarcosine dodecylamide of low molecular weight synthesized by Izumi *et al.*[1] From the results, it is concluded that the abnormal properties of polysarcosine dodecylamide of low molecular weight reported previously are caused by the presence of *N,N'*-dimethyldiketopiperazine in the products of polymerization.

Experimental

Polysarcosine dodecylamide was prepared by polymerization of *N*-carboxy-sarcosine anhydride in dioxane with dodecylamine as initiator.[1] *N*-carboxy-sarcosine anhydride was made from sarcosine by the phosgene method.[2] A solution of 0.483 g of dodecylamine in dioxane (59 m*l*) was added with vigorous stirring to a solution of 1.5 g of *N*-carboxy-sarcosine anhydride in dioxane (100 m*l*) at room temperature. The molar ratio of anhydride to initiator, [A]/[I], was chosen to be 5. The reaction mixture was put to stand overnight at room temperature. The polymer was precipitated by pouring the reaction mixture into ethyl ether. A white waxy solid was obtained. This polymer is denoted by PSD-5S.

Found: C, 54.64; H, 9.39; N, 15.44%. Calcd for $C_{27}H_{52}N_6O_5$: C, 59.97; H, 9.69; N, 15.54%.

N,N'-dimethyldiketopiperazine was obtained by heating sarcosine at 215°C for about 3 hr.[3] The product was recrystallized 3 times from ethanol and obtained as clear needles, mp 144°C, molecular weight 142 (by mass spectrum).

Needle-like crystals were extracted from the materials denoted by PSDA-5[1] with ethanol. 0.637 g of PSDA-5 was dissolved in 12 m*l* of ethanol. A trace amount of white powder was removed from the solution by filtration. The filtrate was evaporated to about 2 m*l* under reduced pressure, and needle-like crystals, mp 144°C, molecular weight 142 (by mass spectrum), were obtained at about −15°C. The crystals showed no melting point depression (144°C) on being mixed with *N,N'*-dimethyldiketopiperazine.

Found: C, 50.42; H, 7.09; N, 19.70%. Calcd for $C_6H_{10}N_2O_2$: C, 50.69; H, 7.09; N, 19.71%.

Surface tension was measured by the drop-weight method. Measurements of electric conductance were performed with an AC-bridge (Yokogawa, 4225A). The cell constant was 0.535, as calibrated with 0.01M potassium chloride. All measurements were carried out at 25°C. NMR spectra were recorded with a Varian A-60 apparatus. Polymers were dissolved in D_2O at a concentration of 10 wt%. IR spectra were determined in KBr pellet with a Yamaco ISG-25 spectrometer. Mass spectra were measured with a Hitachi RMU-6E operating at 70 eV.

Results and Discussion

The surface tension (γ) *vs.* concentration (c) curve for PSD-5S in aqueous solution is shown in Fig. 1. The results obtained by Izumi *et al.*[1] are also shown in Fig. 1. The critical micelle concentration (CMC) of PSD-5S was found to be 0.033 g/d*l*. The present preparation gave a much clearer CMC and a much smaller surface tension than those calculated from the γ-c curve obtained by Izumi *et al.*[1] The specific conductance (κ) *vs.* concentration (c) curve for PSD-5S is shown in Fig. 2. The value of κ_0 obtained by extrapolating the concentration to zero is in accord with the value of water. The CMC value at the bend in

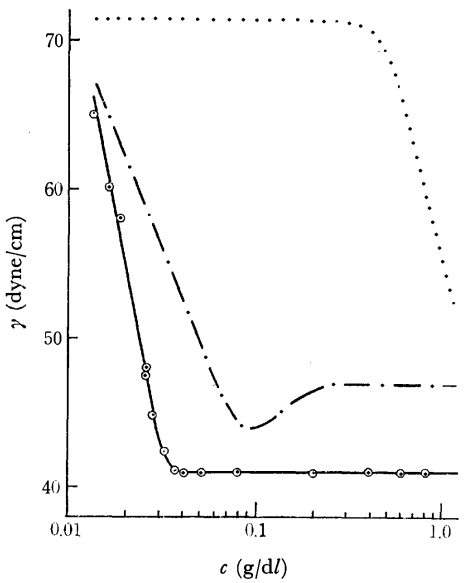

Fig. 1. Surface tension (γ) *vs.* concentration (c) curve for PSD-5S (-⊙-⊙-) at 25°C
(PSDA-5; ·····, PSDA-10; -·-·-, reported by Izumi *et al.*)

* Present address; Department of Applied Chemistry, Faculty of Engineering, Tokushima University, Tokushima.

1) T. Izumi, A. Suzuki, and T. Isemura, presented at the 21st Symposium on Colloid and Surface Chemistry, Chemical Society of Japan, Kyoto, 1968.

2) T. Isemura, S. Ikeda, F. Tokiwa, and J. Noguchi, This Bulletin, **34**, 1236 (1961); E. R. Blout and R. H. Karlson, *J. Amer. Chem. Soc.*, **78**, 941 (1956).

3) F. Mylieus, *Ber.*, **17**, 286 (1884); E. Fischer, *ibid.*, **39**, 530 (1906); *ibid.*, **65**, 1182 (1932).

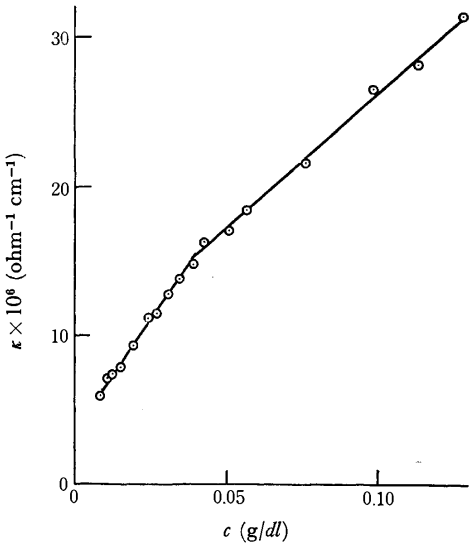

Fig. 2. Specific conductance (κ) *vs.* concentration (c) curve for PSD-5S at 25°C.

the κ-c curve was 0.04 g/d*l*. The NMR spectrum for PSD-5S is shown in Fig. 3. The degree of polymerization was found to be 5.2 from the ratio of the integrated signal from the dodecylamine residue and that from the sarcosine residue. This approximately corresponded to the ratio of anhydride to initiator.

With aqueous solution of *N,N'*-dimethyldiketopiperazine of concentration up to 1 g/d*l*, no decrease in surface tension was observed and the value of the specific conductance was $(2.5—2.8)\times10^{-6}$ ohm^{-1}cm^{-1}, which corresponds to that of water. The NMR spectrum of *N,N'*-dimethyldiketopiperazine had two single peaks, as shown in Fig. 3. The spectrum is similar

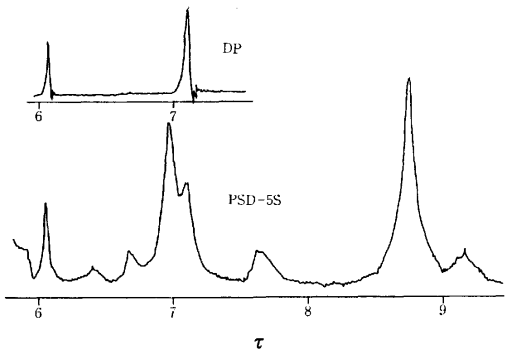

Fig. 3. NMR spectra of polysarcosine dodecylamide (PSD-5S) and *N,N'*-dimethyldiketopiperazine (DP) in D_2O at 60MHz.

to that for PSDA-5.[1]

The fragmentation pattern in the mass spectrum of needle-like crystals extracted from PSDA-5 was in accord with that of *N,N'*-dimethyldiketopiperazine and molecular weights of these compounds were estimated to be 142. The IR spectrum of needle-like crystals was similar to that of *N,N'*-dimethyldiketopiperazine. The compound extracted from PSDA-5 was proved to be identical with *N,N'*-dimethyldiketopiperazine by the mixed melting point, elemental analysis, and studies of its IR, NMR, and mass spectra.

Thus, it is concluded that the materials reported to be polysarcosine dodecylamide, (PSDA-5) are composed mainly of *N,N'*-dimethyldiketopiperazine. The formation of *N,N'*-dimethyldiketopiperazine during polymerization of PSDA-5 might depend on the conditions for polymerization; the initiator was added to the reaction mixture in a very high concentration and at a high temperature of about 80°C.

BULLETIN OF THE CHEMICAL SOCIETY OF JAPAN, VOL. 45, 1237—1238(1972)

The ^{60}Co Recoil Reactions in the Benzene Solutions of Tris(nitrosonaphtholato)cobalt(III)

Takeshi TOMINAGA and Takuhiko SAKAI

Department of Chemistry, Faculty of Science, The University of Tokyo, Hongo, Tokyo

(Received July 30, 1971)

While several works had been reported on the hot-atom chemistry of organic solutions of organometallic compounds[1,2] the hot-atom reactions of irradiated organic solutions of metal complexes had not been studied before our preliminary work on the tris(acetylacetonato)cobalt(III) benzene solutions.[3] We have thus far investigated the ^{60}Co and ^{51}Cr recoil reactions in neutron-irradiated benzene solutions of tris(acetylacetonato)cobalt(III)[3,4] and tris(acetylacetonato)chromium(III)[5] and found that metallic salts can well be used as scavengers to suppress the thermal reactions.

In the present article we will report that a similar scavenger effect of metallic salts can be observed in the irradiated benzene solutions of other chelate complexes, such as tris(nitrosonaphtholato)cobalt(III), and that the apparently high retentions in solid tris(nitrosonaphtholato)cobalt(III)[6] may be ascribed to the thermal reactions taking place in the solutions of the irradiated solid complexes.

1) I. C. Yang and D. R. Wiles, *Can. J. Chem.*, **45**, 1357 (1967).
2) U. Zahn, *Radiochim. Acta*, **7**, 170 (1967).
3) T. Tominaga and K. Fujiwara, This Bulletin, **43**, 2279 (1970).
4) T. Tominaga, T. Sakai, and K. Fujiwara, *ibid.*, **44**, 3036 (1971).
5) T. Tominaga and Y. Nishi, *Radiochem. Radioanal. Lett.*, **8**, 151 (1971).
6) N. Saito, T. Tominaga, and H. Sano, This Bulletin, **35**, 1739 (1962).

Experimental

The procedures used in preparing the solutions with various scavengers and the conditions of irradiation are similar to those described previously.[3,4]

The 0.01 M solutions of tris(α-nitroso-β-naphtholato)cobalt(III) and tris(β-nitroso-α-naphtholato)cobalt(III) in benzene containing 10% (by volume) of ethanol and various amounts of metallic salts as scavengers were prepared and irradiated with thermal neutrons (flux: 5×10^{11} n/cm^2·sec) for 5 min at room temperature in a TRIGA Mark II reactor. Solid samples of the above complexes were irradiated with thermal neutrons for 5 min in dry ice and then dissolved in benzene containing 10% (by volume) of ethanol and metallic salts. The irradiated benzene solution or the solution of the irradiated solid was diluted to 5 m*l* with benzene and extracted with three 5-m*l* portions of (1: 1) nitric acid.[6] The radioactivity of each fraction was measured with a well-type NaI scintillation counter at least one week after the neutron irradiation. The ^{60}Co retention, or the radiochemical yield of the parent chemical form, was obtained as a percentage of the total ^{60}Co activity found in the organic phase. No significant decomposition of the target complexes was observed during irradiation.

Results and Discussion

The effects of the scavenger salts on the ^{60}Co retention are summarized in Figs. 1 and 2.

The ^{60}Co Retention in the Irradiated Solutions. While the apparent ^{60}Co retentions in the irradiated 0.01 M solutions of both complexes were as high as 80—90% in the absence of scavengers, they decreased sharply with an increase in the concentration of the salts of such metals as cobalt and copper.[7] The nickel salt appeared to be less effective as a scavenger, and the magnesium salt had practically no effect on the retention. As in the case of the acetylacetone complexes,[4,5] it seems that salts of the metals which can form more stable complexes with free nitrosonaphthols work as more effective scavengers. Carbon tetrachloride showed a slight scavenger effect.

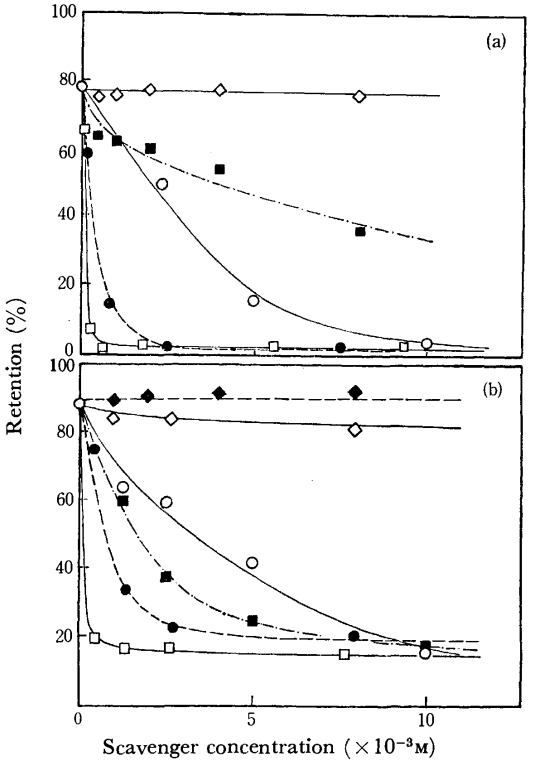

Fig. 1. Scavenger effect of various metallic salts on ^{60}Co retention (a) in the irradiated 0.01 M solutions of tris(α-nitroso-β-naphtholato)cobalt(III) and (b) in the 0.01 M solutions of irradiated solid tris(α-nitroso-β-naphtholato)cobalt(III).
—□— $CoCl_2$; —○— $CuCl_2\cdot2H_2O$;
--●-- $Cu(CH_3CO_2)_2\cdot H_2O$; -·-■-·- $NiCl_2\cdot6H_2O$;
—◇— $MgCl_2\cdot6H_2O$; --◆-- $ZnCl_2$;
--◪-- $MnCl_2\cdot4H_2O$. (Symbols common to Figs. 1 and 2).

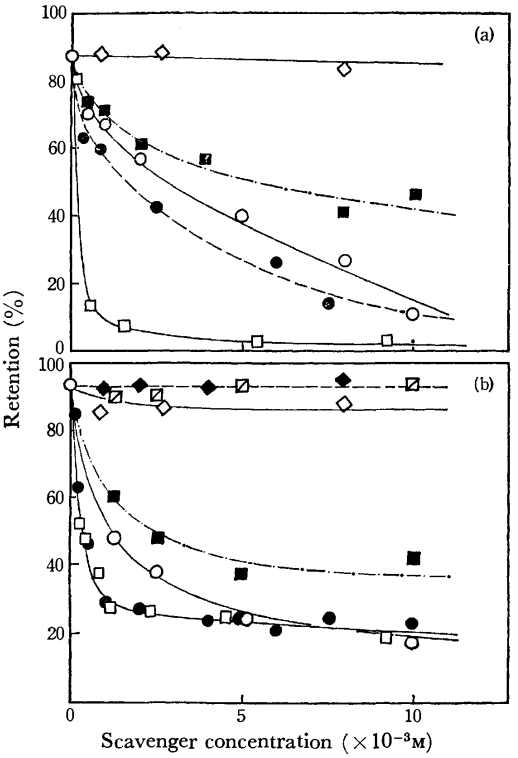

Fig. 2. Scavenger effect of various metallic salts on ^{60}Co retention (a) in the irradiated 0.01 M solutions of tris(β-nitroso-α-naphtholato)cobalt(III) and (b) in the 0.01 M solutions of irradiated solid tris(β-nitroso-α-naphtholato)-cobalt(III).

The ^{60}Co Retention in the Irradiated Solid. The apparent retentions in the irradiated solids were nearly 90% when dissolved in scavenger-free benzene, whereas they decreased to 15—20% when dissolved in benzene containing cobalt or copper salts. This indicates that the thermal reactions after the dissolution of the irradiated solid contribute greatly to the apparently high retentions in solids. The nickel salt was a less effective scavenger, and the magnesium, zinc, and manganese salts had no scavenger effects. The effects of the scavenger salts on the retention in solids seem essentially similar to those observed in the irradiated solutions.

In conclusion, it has been confirmed that the use of adequate scavengers (such as metallic salts) which can suppress the thermal reactions will be useful in determining the primary retention in irradiated solutions or the true retention in irradiated solids.

The authors wish to thank Professor Nobufusa Saito of the University of Tokyo for his encouragement and support during this work.

7) The lowest retention observed in the well-scavenged solutions was 1.1—1.6%.

BULLETIN OF THE CHEMICAL SOCIETY OF JAPAN, VOL. 45, 1239—1240(1972)

The Nonstoichiometry of Gadolinium Ditelluride

Koichi NIIHARA, Toetsu SHISHIDO, and Seishi YAJIMA

The Research Institute for Iron, Steel, and Other Metals, Tohoku University, Sendai

(Received August 13, 1971)

The following compounds are found in the rare earth-tellurium system:[1-3] LnTe, Ln_3Te_4, Ln_2Te_3, Ln_4Te_7, $LnTe_2$, $LnTe_3$, and $LnTe_4$, where Ln=rare earth elements. In these tellurides, the ditellurides have the tetragonal lattice (Fe_2As type). In the La–Te[2] and Nd–Te[4] systems, the ditellurides are stable over a large homogeneity range. The *a* parameter of the ditellurides, in both systems, increases monotonously with the increase in Te content in the homogeneity range represented by the $LnTe_{2\pm x}$ formula. The *c* parameter of the lanthanum ditelluride decreases in the monotone with the increase in the content, but in the neodymium ditelluride it has a minimum value at the composition of $NdTe_{1.96}$.

In the case of heavier rare earth elements than gadolinium, there have been few investigations of the nonstoichiometric properties of the ditellurides. In this article the preparation of pure gadolinium ditellurides and their nonstoichiometric properties will be described.

Experimental

The gadolinium was prepared in our laboratory by the calcium reduction of GdF_3 in tantalum containers under a purified argon atmosphere, and was then refined by arc-melting and electron-beam melting. The purity of the gadolinium obtained by this method was approximately 99.9%. Tellurium of 99.999% purity was obtained from Wako Chemical Industies, Ltd., Tokyo. The gadolinium ditellurides were prepared in double-compartment quartz tubes.

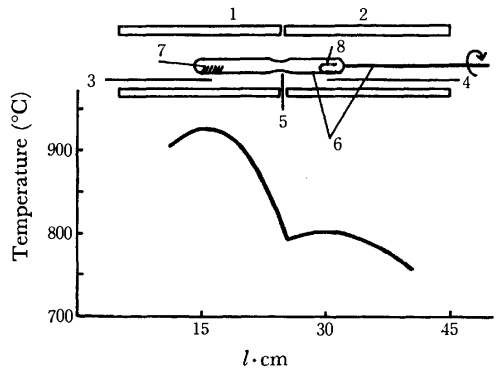

Fig. 1. Temperature distribution in the separate two-zone furnace. 1, 2) furnace; 3, 4, 5) thermocuples; 6) quarz tube and bar; 7) tellurium; 8) Ta boat and gadolinium metal

Finely-ground gadolinium was placed in one side and tellurium in the other side. Gadolinium was placed in tantalum crucibles in order to avoid direct contact with the quartz tube. In this way, the direct contact of gadolinium and tellurium, which might cause an explosion, was avoided. After the evacuating of the quartz tube to 10^{-5} mmHg, the tube was sealed and placed in a horizontal tublar furnace which had two heating zones. A sketch of the reaction apparatus and the temperature distribution in the separated two-zone furnace are shown in Fig. 1. The sealed quartz tube in the furnace was rotated at the rate of 50—100 rpm/min. The temperature of the gadolinium part was raised to 800°C from room temperature at a heating rate of 200°C/hr. The temperature of the tellurium part was 100—150°C higher than that of the gadolinium side. The quartz tube was held under the given conditions for 7—10 hr, until the tellurium had completely reacted, and was then cooled slowly to room temperature. The samples were investigated by chemical and X-ray analysis. The prepared powder was homogenous in its external appearance. The X-ray powder patterns were taken with a Debye-Scherrer camera using FeK_α radiation. These patterns were used to identify the phase present in polyphase samples and to determine the lattice parameters. The densities of the samples were determined by means of a pycnometer.

Results and Discussion

The powder of $GdTe_2$ shows a dark-violet color. From the X-ray diffraction pattern of $GdTe_2$, this phase appeared to be isostructural with the previously-reported tetragonal $GdTe_2$[3] (Fe_2As type). The lattice parameters of the stoichiometric $GdTe_2$ were $a=4.317$ Å, $c=8.951$ Å, and $c/a=2.073$.

In order to determine the range of the homogeneity of $GdTe_{2\pm x}$, samples were synthesized in the composition range of $GdTe_{1.7}$–$GdTe_{2.2}$ (63 at% to 68.7 at% of Te). For the gadolinium-rich side, the limit of the homogeneity phase was situated at approximately $GdTe_{1.77}$ (63.8 at% Te). A sample containing 63.6% Te ($GdTe_{1.75}$) was composed of two phases, a rhombic lattice (Gd_2Te_3) and a tetragonal lattice ($GdTe_2$). A sample containing 64.0 at% Te ($GdTe_{1.78}$) was constituted of pure $GdTe_{2-x}$ with a tetragonal lattice. On the tellurium-rich side, the limit of homogeneity was located at the composition of $GdTe_{2.10}$ (67.7 at% Te). In more tellurium-rich side, both phases, $GdTe_{2+x}$ and $GdTe_3$, appeared. These experimental results make it clear that the homogeneity range of $GdTe_{2\pm x}$ is situated from $GdTe_{1.77}$ to $GdTe_{2.10}$. The lattice parameter varied conspicuously with the variation in the nonstoichiometric composition, but the relation between them was not linear. The variations in the lattice parameters and *c*/*a* ratio are plotted against the Te/Gd atomic ratio in Fig. 2. The figure shows that the lattice parameter, *a*, increases with an increase in the

1) N. Kh. Abrikosov and V. Sh. Zargaryan, *Izv. Akad. Nauk SSSR, Neorg. Mat.*, **1**, 1462 (1965).

2) A. A. Eliseev, E. I. Yarembash, V. G. Kuznetsov, L. I. Antonova, and Z. P. Stoyantsova, *Izv. Akad. Nauk SSSR, Neorg. Mat.*, **1**, 1027 (1965).

3) J. Flahaut and D. Laruelle, "Proceeding in the Science and Technology of Rare Earths Vol. 3," ed, L. Eyring. Pergamon Press New York 1968, p. 149.

4) W. Lin, H. Steinfink, and E. J. Weiss, *Inorg. Chem.*, **4**, 877 (1965).

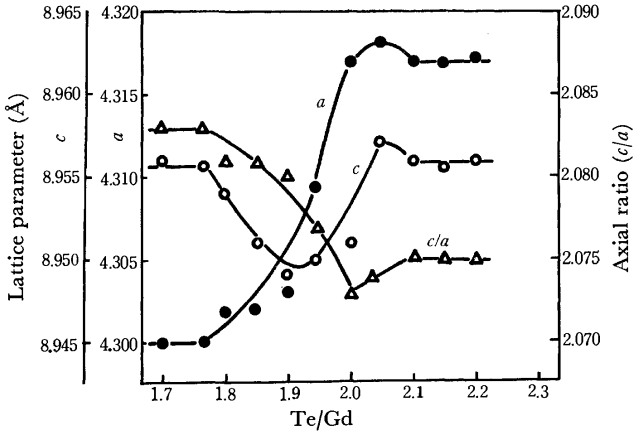

Fig. 2. The variation of the lattice parameters and the axial ratio against Te/Gd ratio in gadolinium detelluride.

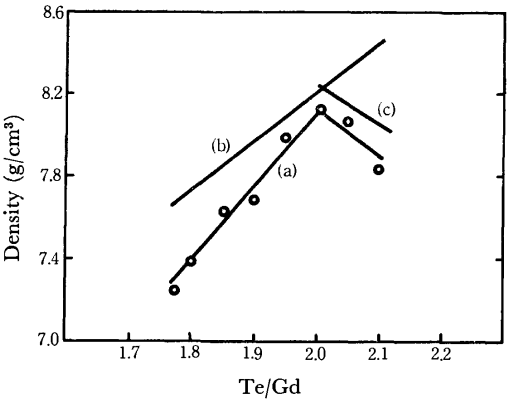

Fig. 3. The variation of density against nonstoichiometric composition of gadolinium ditelluride. (a): experimental value, (b) and (c): X-ray density calculated on the assumption of $GdTe_{2\pm x}$ or $Gd_{1-x}Te_2$, respectively.

tellurium concentration and that the lattice parameter, c, reaches its minimum value at the composition of $GdTe_{1.92}$. The relation between the axial ratio, c/a, and concentration ratio, Te/Gd, shows an anomaly at the composition of $GdTe_{2.0}$. From these facts, it may be seen that the types of defects in the crystal structures are different between the two regions of Te/Gd$<$2 and Te/Gd$>$2.

In Fig. 3 the variation in the densities in the homogeneity range is plotted against the Te/Gd ratio. The line (a) shows the experimental values. The lines (b) and (c) are the densities calculated on the assumption that the nonstoichiometric composition can be indicated by the $GdTe_{2\pm x}$ formula and the $Gd_{1-x}Te_2$ formula respectively. The experimental results show the same tendency as the values of the line (b) in the region of Te/Gd$<$2 and the same as the values of the line (c) in the region of Te/Gd$>$2.

From these variations in the lattice parameters, the axial ratio, c/a, and the densities, it seems probable that tellurium vacancies form in the region of Te/Gd$<$2 and that gadolinium vacancies from in the region of Te/Gd$>$2. Therefore, the homogeneity range of the gadolinium ditelluride is located form $GdTe_{1.77}$ to $Gd_{0.95}Te_2$.

Lin and Steinfink[4] investigated the neodymium ditelluride. According to their work, the variation in the lattice parameters of neodymium ditelluride appeared in the homogeneity range of $NdTe_{1.75}$ to $NdTe_{2.10}$. The tendency of the variation in the lattice parameters is similar to that of gadolinium ditelluride, which was studied in our experiment. It may be seen that the homogeneity range of the neodymium ditelluride is located from $NdTe_{1.75}$ to $Nd_{0.95}Te_2$.

BULLETIN OF THE CHEMICAL SOCIETY OF JAPAN, VOL. 45, 1240—1242(1972)

Photochemical Reactions of Diphenylacetylene with Enaminoesters[1)]

Mituyosi KAWANISI, Kinjiro MATSUNAGA, and Norioki MIYAMOTO

Department of Industrial Chemistry, Faculty of Engineering, Kyoto University, Yoshida, Kyoto, 606

(Received August 13, 1971)

As a consequence of our continuing interest in the behavior of enamines in photochemistry[2,3)] we have investigated the photochemical reaction of diphenylacetylene (I) with 3-alkylaminocrotonate (II) or 3-dialkylaminocrotonate (III), and found that the reaction resulted in the formation of heterocyclic compounds. This unprecedented result is the subject of this note.

When a benzene solution of I and IIa was irradiated by means of a high pressure Hg lamp and the reaction mixture was chromatographed on an alumina column, the following compounds were obtained: 4,5-diphenyl-1,6-dimethyl-2-pyridone (IVa) (19%), ethyl 4,5-diphenyl-1,2-dimethylpyrrole-3-carboxylate (Va) (4%), a mixture of photodimers of I[4)] along with some unidentified materials (trace).

The structure of IVa was assigned by spectroscopic methods and the conclusive evidence for the structure was obtained by the following chemical transformations. Hauser reported that the reaction of benzyl methyl ketone with benzoylacetonitrile in the presence of PPA gave a pyridone whose structure was estimated as VII

1) A part of this work was presented at the 24th Annual Meeting of the Chemical Society of Japan (1971).

2) M. Kawanisi, K. Kamogawa, T. Okada, and H. Nozaki, *Tetrahedron*, **24**, 6557 (1968).

3) N. Miyamoto, M. Kawanisi, and H. Nozaki, the 24th Annual Meeting of the Chemical Society of Japan, Osaka (1971).

4) G. Büchi, C. W. Perry, and G. W. Robb, *J. Org. Chem.*, **27**, 4016 (1962).

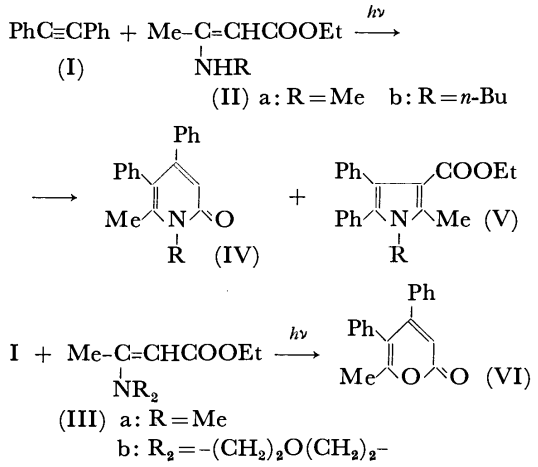

or VIII.[5] We have reinvestigated this reaction, and the pyridone obtained was scrutinized by means of NMR for the benzylic protons, but there was none. Thus the structure VII was established for the reaction product.

Methylation of VII with dimethyl sulfate in alkaline medium[6] proceeded in a selective manner giving an *N*-methylated pyridone which was identical in all respects with the photochemical product IVa.

The structure of Va was established by spectroscopic methods as well as the independent synthesis described by Huisgen from *N*-acetyl-*N*-methylphenylglycine and ethyl phenylpropiolate.[7]

The reaction of IIb proceeded similarly and IVb was obtained in 28% yield. The spectroscopic data for IVb were essentially identical with those of IVa. In this case no Vb was isolated probably due to the difficulty in separation.

When a mixture of I and IIIa or IIIb was treated similarly, 4,5-diphenyl-6-methyl-2-pyrone (VI) (8% and 2%, respectively) was obtained. The structure of VI was established by spectroscopic methods as well as by the independent synthesis.[8]

Although the intermediate products are not identified yet, the mechanism for the formation of IV, V, and VI is tentatively considered as follows. The reactions of some electrophilic acetylenes with enamines or enaminoesters have been well documented,[9] whereas the electrophilic nature of excited simple acetylenes such as I have been demonstrated in the cycloaddition of I with dihydropyran.[10] Consequently it may be safely stated that the photoexcited I might react with II in two ways giving a) a cyclobutene IX and b) an ionic intermediate XI. Ring opening of IX to X followed by reclosure may give IV, while proton shift in XI followed by aromatization will afford V.

On the other hand the cycloaddition of the photoexcited I with III might give XIII, ring opening and hydrolysis followed by reclosure will lead to VI. The reason why hydrolysis takes place in the case of XIII and does not in the case of X is still obscure. However, we feel that NH-hydrogen seems to be responsible to some extent for the reaction.

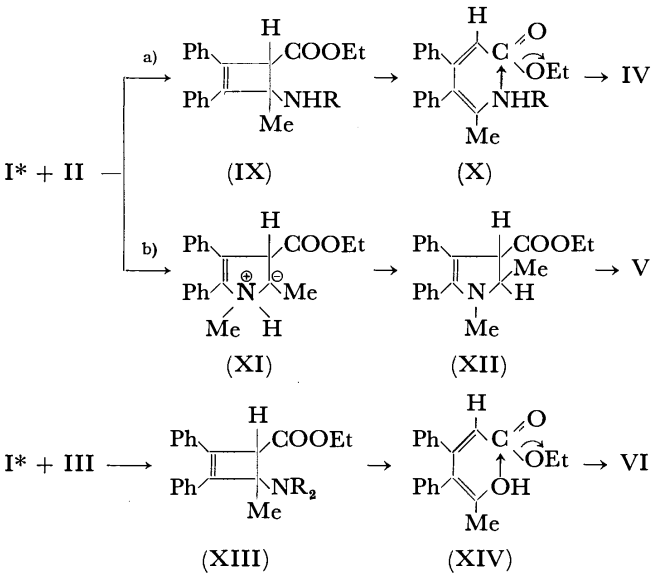

Experimental

All boiling and melting points are uncorrected. Microanalyses were performed at the Elemental Analyses Center of Kyoto University. The IR spectra were recorded in neat liquid film or as KBr pellets on a Shimadzu IR-27G spectrometer. The NMR spectra were taken on a JOEL C-60-H spectrometer in CCl_4 solutions and TMS as an internal standard. The UV spectra were obtained in ethanol solutions on Shimadzu MPS-50L spectrophotometer.

Reagents. The starting materials I, IIa, and IIIa were prepared according to the published methods and have following properties; I, mp 64—66°C (lit.[11,12] mp 60—61°C), IR: 1600, 1490, 1070, 910, 760, 690 cm^{-1}, NMR: δ 7.1—7.5 (10H), UV: λ_{max} 265 nm (ε=21800), 275 (24100), 280 (31900), 289 (23000), 297 (28000). IIa, bp 107—108°C/17 mmHg (lit.[13] bp 105—106°C/15 mmHg), IR: 3310, 2990, 1950, 1650, 1610, 1265, 1160, 780 cm^{-1}, NMR: δ 1.2 (t, 3H), 1.9 (s, 3H), 2.9 (d, 3H), 4.0 (q, 2H), 8.4 (1H), UV: λ_{max} 282 nm (ε=16600). IIIa, bp 87—89°C/3 mmHg (lit.[14] bp 131.2—132.2°C/15 mmHg), IR: 1695, 1585, 1140 cm^{-1}, NMR: δ 1.2 (t, 3H), 2.4 (s, 3H), 2.9 (s, 6H), 3.95 (q, 2H), 4.4 (s, 1H), UV: λ_{max} 284 nm (ε=28200).

5) C. R. Hauser and C. J. Eby, *J. Amer. Chem. Soc.*, **79**, 728 (1957).
6) R. Adams and A. W. Schrecker, *ibid.*, **71**, 1186 (1949).
7) R. Hisgen, N. Gotthardt, H. O. Bayer, and F. C. Schaefer, *Angew. Chem. Int. Engl. Ed.*, **3**, 136 (1964); *Chem. Ber.*, **103**, 2581 (1970).
8) G. Traverso, *Boll. Sci. Fac. Chim. Ind. Bologna*, **13**, 53 (1955).
9) A.G. Cook, "Enamines: Synthesis, Structure, and Reactions," Marcel-Dekker, New York, (1969), p. 129.
10) H. M. Rosenberg and P. Servé, *J. Org. Chem.*, **33**, 1653 (1968).
11) L. F. Fieser, "Organic Experiments," D. C. Heath and Co., Boston, (1964), p. 222.
12) L. I. Smith and H. H. Hoehn, *J. Amer. Chem. Soc.*, **63**, 1180 (1941).
13) E. Knoevenagel and E. Reinecke, *Ber.*, **32**, 420 (1899), Anmerkung.
14) K. W. F. Kohlrausch and A. Pongratz, *Ber.*, **67**, 976 (1934).

3-Butylaminocrotonate (IIb): A mixture of ethyl acetoacetate (13 g, 0.1 mol) and *n*-butylamine (7.3 g, 0.1 mol) in benzene was refluxed for several hr and the water formed was removed continuously in a Dean-Stark apparatus. The reaction mixture was concentrated *in vacuo* and repeatedly distilled throuth Vigreaux column to give IIb quantitatively as a colorless liquid, bp 86.5—87°C/3.5 mmHg (lit.[15] bp 129.5—131°C/14 mmHg), IR: 3290, 2960, 2860, 1650, 1610, 1265, 1170, 1140, 780 cm^{-1}, NMR: δ 1.0—1.5 (10H), 1.9 (s, 3H), 3.2 (q, 2H), 4.0 (q, 2H), 4.3 (s, 1H), 8.5 (1H), UV: λ_{max} 300 nm (ε=23000).

3-Morpholinocrotonate (IIIb): A mixture of ethyl acetoacetate (19.5 g; 0.15 mol) and morpholine (16 g; 0.18 mol) and *p*-toluenesulfonic acid in benzene was refluxed and the water formed was removed continuously. The reaction mixture was concentrated *in vacuo* and distilled to give IIIb, bp 120—122°C/5 mmHg, IR: 1690, 1595, 1140, 1120 cm^{-1}, NMR: δ 1.2 (t, 3H), 2.35 (s, 3H), 3.05—3.25 (4H), 3.5—3.75 (4H), 4.0 (q, 2H), 4.65 (s, 1H), UV: λ_{max} 283 nm (ε=20500). Found: C, 60.05; H, 8.53; N, 6.7%. Calcd for $C_{10}H_{17}O_3N$: C, 60.28; H, 8.60; N, 7.03%.

UV Irradiation. Solutions of I (590 mg; 3.3 mol) and IIa, IIb (a, 720 mg; b, 920 mg; each 5 mmol) or IIIa, IIIb (a, 790 mg; b, 1.0 g; each 5 mmol) in benzene (20 m*l*) were irradiated by means of a high pressure Hg lamp for 150 hr and the solvent was removed by distillation *in vacuo*. The residues were chromatographed on an alumina column to give IV, V, and VI, respectively. 4,5-Diphenyl-1,6-dimethyl-2-pyridone (IVa), mp 166.5—169°C, obtained by photolysis had following properties. IR: 3060, 2960, 1650, 1580, 1515, 1490, 860, 770, 700 cm^{-1}, NMR: δ 2.1 (s, 3H), 3.5 (s, 3H), 6.4 (s, 1H), 7.0—7.1 (10H), UV: λ_{max} 243 nm (ε= 17500), 324 (5880). Found: C, 82.66; H, 6.21; N, 4.95%. Calcd for $C_{19}H_{17}ON$: C, 82.88; H, 6.22; N, 5.09%. 1-Butyl-4,5-diphenyl-6-methyl-2-pyridone (IVb), mp 191—192.5°C, obtained by photolysis had following properties. IR: 3060, 2970, 1650, 1515, 1495, 865, 770, 705, 700 cm^{-1}, NMR: δ 1.0 (t, 3H), 1.3—2.0 (4H), 2.3 (s, 3H), 4.2 (t, 2H), 6.6 (s, 3H), 1.3—2.0 (10H), UV: λ_{max} 244 nm (ε=19000), 323 (6200). Found: C, 83.15; H, 7.11; N, 4.33. Cacld for $C_{22}H_{23}ON$: C, 83.24; H, 7.30; N, 4.41%. Ethyl 4,5-diphenyl-1,2-dimethylpyrrole-3-carboxylate (V), mp 116.5—117.5°C, obtained by photolysis had following properties. IR: 3060, 2930, 1690, 1600, 1280, 1160, 750, 690 cm^{-1}, NMR: δ 0.9 (t, 2H), 2.5 (s, 3H), 3.35 (s, 3H), 3.9 (q, 2H), 6.9—7.1 (10H), UV: λ_{max} 230 nm (ε=28900), 277 (15400), MS: *m/e* 319 (M^+), 290 (M^+-29), 274 (M^+-45). The MS supports the structure of IV. The authentic specimen prepared by the published method[7] had spectral properties quite identical with those of the photochemical product (V), and showed no depression of the mixed mp. 4,5-Diphenyl-6-methyl-2-pyrone (VI), mp 136—136.5°C (lit.[7] 135°C) obtained by photolysis had following properties. IR: 3060, 1720, 1630, 1530, 1495, 860, 770, 700 cm^{-1}, NMR: δ 2.2 (s, 3H), 6.2 (s, 1H), 6.85—7.25 (10H), UV: λ_{max} 233 nm (ε=16200), 282 (6800), 314 (5800).

Methylation of VII. A sample (1.82 g; 6.9 mmol) of V, mp 258—262°C (lit[4] mp 264—266°C), was dissolved in a warm, freshly prepared solution of sodium (0.8 g) in methanol (20 m*l*). After cooling to room temperature, dimethyl sulfate (5 g; 0.04 mol) was added with stirring in the course of 15 min. After refluxing for 12 hr, the solution was made strongly alkaline by adding aqueous sodium hydroxide (25%), and the mixture was poured into ice water. The precipitates were collected by filtration and recrystallized from ether, mp 169—171°C. The spectra of the compound was completely superimposable with the one of IVa obtained photochemically.

The authors wish to thank Professor Hitosi Nozaki for help and stimulating discussion.

15) G. R. Allen, Jr., C. Pidacks, and M. J. Weiss, *J. Amer. Chem. Soc.*, **81**, 2536 (1966).

BULLETIN OF THE CHEMICAL SOCIETY OF JAPAN, VOL. 45, 1242—1243(1972)

Biogenesis of the Essential Oils in Camphor Trees. XXX.[1] On the Components of the Essential Oil of *Cinnamomum reticulatum* Hay. in Taiwan[2]

Yasuji FUJITA and Shin-ichi FUJITA*

Government Industrial Research Institute, Osaka, Midorigaoka, Ikeda-shi, Osaka

**College of Education, Mukogawa Women's University, Ikebiraki-cho, Nishinomiya-shi, Hyogo*

(Received August 16, 1971)

Cinnamomum reticulatum Hay. [*Mat. Fl. Formos.* 239 (1911); *Icon. Pl. Formos.*, **5**, 160, f. 53, e (1915)] (Japanese name, *Hamagusu*) of the Lauraceae is an endemic plant growing only on the Hengchun (Kōsyun) Peninsula in Taiwan. It is a small tree which grows at low altitudes.[3]

We have examined the essential oil of this rare and very interesting plant. The yield of the oil is 0.56% in the fresh shoots, the chemical composition of the oil is in Table 1.

The characteristics of this oil are an abundance of *l*-linalool (as much as 97% of the oil), and an absence of camphor and phenol ethers.

These phenomena show that this plant may be a relic of the nearest species to the mother plant of the genus *Cinnamomum*, at least as seen from the viewpoint of the chemical systematics.[4] The existence of a small

1) Part XXIX: Y. Fujita, S. Fujita, and Y. Akama, *Nippon Nogeikagaku Kaishi*, **46**, 17 (1972).

2) Presented at the 24th Annual Meeting of the Chemical Society of Japan, Osaka, April, 1971.

3) R. Kanehira, "Formosan Trees," revised, Department of Forestry, Government Research Institute, Formosa, Yōkendo, Tokyo (1936), p. 211.

4) Y. Fujita, *Bot. Mag. Tokyo*, **80**, 261 (1967).

Table 1. The composition of the essential oil of *Cinnamomum reticulatum* Hay.

Peak No.	Compound	%	Remark
Monoterpenoids and other low boiling compounds			
1	α-Pinene	0.1	Rt.
2	Camphene	0.3	Rt.
3	β-Pinene	0.5	Rt.
4	Limonene	0.2	Rt.
5	1,8-Cineole	0.4	Rt.
6	*p*-Cymene	0.2	Rt.
7	*cis*-β,γ-Hexenol (?)	0.1	
8	*trans*-Linalooloxide	trace	Rt.
9	*cis*-Linalooloxide	trace	Rt.
10	**l-Linalool**	**96.8**	Rt., IR[a]
11	unidentified alcohol	0.1	
12	Terpinen-4-ol	trace	Rt.
13	α-Terpineol	0.3	Rt.
14	Citronellol	trace	Rt.
15	Nerol	trace	Rt.
16	Geraniol	0.1	Rt.
17	unidentified alcohol	0.1	
Sesquiterpene hydrocarbons (0.4% to the oil)[b]			
18	α-Cubebene (?)	3	
19	Copaene	8	IR,[c]
20	β-Cubebene	4	IR
21	β-Elemene	2	IR
22	Caryophyllene	5	Rt., IR
23	unidentified	6	
24	α-Humulene	5	Rt., IR
25	β-Bisabolene (?)	7	IR
26	δ-Cadinene	54	Rt., IR
27	unidentified	4	
28	Calamenene	2	IR
Sesquiterpene alcohols (0.2% to the oil)[d]			
29	Nerolidol	15	Rt.
30	Elemol	7	Rt.
31	unidentified	4	
32	unidentified	7	
33	unidentified	7	
34	α-Cadinol	60	Rt., IR

a) This linalool (99.5% purity) isolated from the fractions II and III, had the following properties: d_4^{30} 0.8607, n_D^{30} 1.4582, $[\alpha]_D^{25}$ −20.03°. The specific optical rotation shows a perfect optical purity.
b) The sesquiterpene hydrocarbon part (about 50 mg) was separated from the fraction IV by chromatography on alumina, using *n*-hexane as the eluent.
c) Identification by IR spectra (J. A. Wenninger, R. L. Yates, and M. Dolinsky, *J. Ass. Offic. Anal. Chem.*, **50**, 1313 (1967)).
d) The compositions of sesquiterpene alcohols were calculated from the gas chromatogram of the oxygenated compounds, separated from the fraction IV by chromatography using ether as the eluent.

amount of nerolidol as a sesquiterpenoid compound is also accordant with this supposition.

Experimental

Material. On September 4, 1969, the material was gathered from a tree (diameter of trunk at a height of one meter: 15 cmφ; height of the tree: *ca.* 7 m) which had been transplanted from the seashore to the garden of the Hengchun Branch of the Forestry Institute of Taiwan. The material (2.0 kg; the average length of a shoot: 23 cm; its weight: 11.0 g, consisting of 82% leaves, and 18% branchlets; size of leaf: 30×50 mm) was brought to Japan by air, and on September 10 the half-dried sample (1.2 kg) was subjected to steam distillation. The distilled oil was extracted with ether and then dried over anhydrous sodium sulfate. The oil (11.2 g), obtained in a yield 0.56% of the fresh material, had the following properties: d_4^{30} 0.8493, n_D^{30} 1.4584, α_D^{27} −14.40°, A.V. 0.25, E.V. 4.60.

Gas-liquid Chromatographic Analysis. The gas-liquid chromatography (glc) was carried out with a Shimadzu GC-1B Model apparatus equipped with a thermal conductivity detector. A 150×0.5 cm stainless steel column was packed with PEG 6000 (30%) on celite 545 (100 mesh). Hydrogen was used as the carrier gas. The percentages of the constituents of the oil were calculated from the areas of the peaks of the gas chromatogram.

Separation and Identification of the Individual Components. The oil (10.0 g) was fractionated, by distillation under reduced pressure in a current of nitrogen with a Widmer column, into the following four fractions: I, −87°C/20 mmHg, 1.0 m*l*; II, 87—89°C/20 mmHg, 3.0 m*l*; III, 89°C/20 mmHg, 2.0 m*l*; IV, residual, 4.5 g.

Each fraction was then further separated into hydrocarbons and oxygenated compounds by alumina-column chromatography. The main components were isolated by preparative glc using a PEG 6000 column and were identified by a comparison of the IR spectra and retention times (*Rt.*) of glc with those of authentic samples. Some minor compounds were identified by a comparison of the *Rt*s. with those of authentic samples by the use of PEG 6000 and Silicone DC-550 columns.

The results are shown in Table 1.

Cordial thanks are due to Dr. Kōichi Koshimizu of Kyoto University, who brought the sample of *C. reticulatum* at our request on the occasion of his visiting Taiwan.

BULLETIN OF THE CHEMICAL SOCIETY OF JAPAN, VOL. 45, 1244—1245(1972)

Studies on the Derivatives of Thiiranes. I. Synthesis of Some New Sulfonyl Compounds from 2-Chloromethylthiirane

Tsunehiko KUWAMURA, Eiichi KAMEYAMA, and Motoki NAKAJIMA*

Department of Synthetic Chemistry, Faculty of Engineering, Gunma University, Tenjincho, Kiryu

(Received August 23, 1971)

A number of investigations have been published on the ring-opening reactions of unsymmetrical thiiranes.[1] In order to synthesize a reactive aliphatic suflonyl compound, we allowed 2-chloromethylthiirane (**1**) to react with hydrogen chloride and chlorine in water, and confirmed that ring-cleavage of **1** took place preferentially at the primary carbon-sulfur bond giving predominantly the normal products as shown in Scheme 1.[2] This is in accord with the result of Schwartz[3] but contrary to the earlier observations.[4,5]

We have investigated the reactions of 1,3-dichloropropane-2-sulfonyl chloride (**3**) with bases of various basicities, and obtained several new olefinic sulfonyl compounds and their derivatives as shown in Scheme 1. Physical properties and analytical data of these compounds are listed in Table 1. Vinyl compounds **4** and **5** obtained in high yields in these reactions have two reactive substituents which differ from each other in reactivity. They could be used as new monomers for synthesis of reactive polymers and interesting intermediates for derivatives of sulfonic acid.

Experimental

All the boiling points and melting points are uncorrected. The NMR spectra were taken on a Varian A-60D or HA-100 Spectrophotometer in carbon tetrachloride unless otherwise stated. Chemical shifts are presented in terms of δ value. All the liquid products were purified by fractional distillation *in vacuo* in a stream of N_2 to obtain a single peak on glc.

Material. Compound **1** was prepared by the method of Culvenor and his coworkers,[6] bp 79—81°C/114 mmHg, n_D^{10} 1.5297, d_4^{10} 1.2277.

Addition of Hydrogen Chloride to 1. Into **1** (40 g) was gradually introduced gaseous HCl with stirring at 5—10°C. After an equimolar amount (13.1 g) of HCl had been taken out, bubbling was continued at 10°C for 1 hr. Removal of excess HCl and distillation of the residue gave 38.8 g of **2**, bp 104—106°C/88 mmHg, n_D^{10} 1.5301, d_4^{10} 1.3338.

Found: C, 25.12; H, 4.18; Cl, 49.7; S, 22.0%. Cacld for $C_3H_6Cl_2S$; C, 24.82; H, 4.17; Cl, 48.9; S, 22.1%.

IR (neat), 2580 (SH), 1425, 1285, 870, and 845 cm^{-1}; 100 MHz NMR, 2.10 (d, 1H, *sec* SH), 1.63 (t, small, *prim* SH), 3.20 (m, 1H, CH), 3.70 (q, 2H, CH_2), 3.94 (q, 2H,

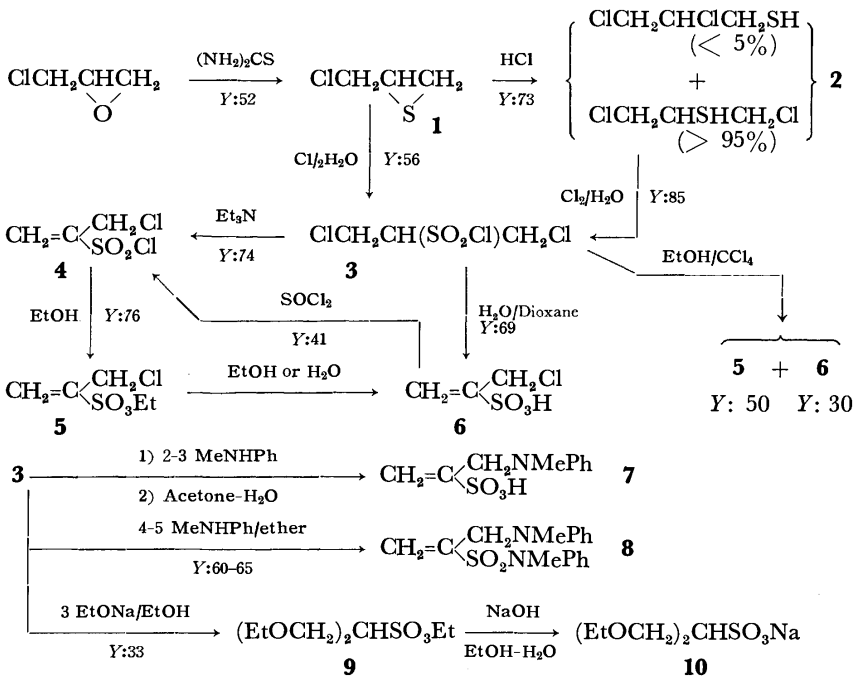

Scheme 1.

* Present address: Kao Sorp Co. Ltd., Sumidaku, Tokyo.

1) M. Sander, *Chem. Rev.*, **66**, 297 (1966).

2) T. Kuwamura, E. Kameyama, M. Nakajima, S. Mishiba, and Y. Onoguchi, presented at the Annual Meetings of the Chemical Society of Japan, March, 1967 (Tokyo), Lect. No. 4S111.

3) N. V. Schwartz, *J. Org. Chem.*, **33**, 2895 (1968).

4) W. Davies and W. E. Savige, *J. Chem. Soc.*, **1951**, 774.

5) J. M. Stewart, *J. Org. Chem.*, **29**, 1655 (1964).

6) C. C. J. Culvenor, W. Davies, and K. H. Pausacker, *J. Chem. Soc.*, **1952**, 1050.

TABLE 1. PHYSICAL PROPERTIES AND ANALYTICAL DATA OF THE SULFONYL COMPOUNDS

Compound	No.	Bp (°C/mmHg)	Mp (°C)	n_D^{20}	Elementary analysis (calcd)				
					C%	H%	N%	S%	Cl%
$(ClCH_2)_2CHSO_2Cl$	**3**	85 — 87/1	—	1.5140	17.26	2.45	—	15.0	49.0
					(17.04)	(2.38)	—	(15.1)	(50.3)
$CH_2=C(CH_2Cl)(SO_2Cl)$	**4**	89.0/15	—	—	20.76	2.64	—	17.7	39.1
					(20.59)	(2.30)	—	(18.3)	(40.5)
$CH_2=C(CH_2Cl)(SO_3Et)$	**5**	87.5— 88.5/0.5	—	1.4665	32.20	4.66	—	17.6	—
					(32.53)	(4.91)	—	(16.9)	—
$CH_2=C(CH_2Cl)(SO_3H)$	**6**	142 —143.5/1.5	—	1.4927	23.28	3.44	—	19.2	22.5
					(23.01)	(3.22)	—	(20.5)	(22.6)
$CH_2=C(CH_2Cl)(SO_3Na)$	—	—	—	—	—	—	—	17.6	20.1
					—	—	—	(17.9)	(19.9)
S-Benzyl thiuronium salt of **6**	—	—	85.2— 86.0 (from $ClCH_2CH_2Cl$)	—	41.43	4.71	8.37	—	—
					(40.93)	(4.68)	(8.68)	—	—
$CH_2=C(CH_2NMePh)(SO_3H)$	**7**	—	182.5—183.5 (from ethanol)	—	—	—	6.17	14.3	—
					—	—	(6.16)	(14.1)	—
$CH_2=C(CH_2NMePh)(SO_3Na)$	—	—	—	—	—	—	5.60	12.3	—
					—	—	(5.62)	(12.9)	—
S-Benzyl thiuronium salt of **7**	—	—	149 —150 (from acetone)	—	55.00	5.99	10.8	16.2	—
					(54.94)	(5.89)	(10.7)	(16.3)	—
$CH_2=C(CH_2NMePh)(SO_2NMePh)$	**8**	—	97.2— 97.5 (from ether)	—	—	—	8.75	10.0	—
					—	—	(8.85)	(10.1)	—
$(EtOCH_2)_2CHSO_3Et$	**9**	118.5—120/2	—	1.4419[a]	44.83	8.07	—	12.9	—
					(44.98)	(8.39)	—	(13.3)	—
$(EtOCH_2)_2CHSO_3Na$	**10**	—	—	—	—	—	—	13.8	—
					—	—	—	(13.7)	—

a) At 10°C.

CH_2). From the NMR spectrum the ratio of 2-thiol *vs.* 1-thiol in the product was determined to be 98: 2. By treatment of **1** with concd. HCl,[4] **2** containing 5 mol% of 1-thiol was obtained in 50—55% yields.

1,3-Dichloropropane-2-sulfonyl Chloride (3). The reaction of **1** and **2** containing 2% 1-thiol with chlorine in water was carried out under similar conditions to those of the method of Stewart[5] for the oxidation of **1**. From both materials the identical product **3** (d_4^{20} 1.6014) was obtained in good yields. IR (neat), 1379 (SO_2), 1169 (SO_2), 774 (C–S) cm^{-1}; 100 MHz NMR (in benzene), A 3.04 (m, 1H, CH), B 3.40 (q, 2H, CH_2), C 3.57 (q, 2H, CH_2), J_{BC}=12.5, J_{AB}=6.0, J_{AC}=4.0 Hz.

3-Chloropropene-2-sulfonyl Chloride (4). To an ether solution of **3** cooled to −75°C was added dropwise an equimolar amount of triethylamine. The mixture was stirred for 2 hr and filtered. Distillation of the filtrate gave **4** in 74% yield. IR (neat), 3126, 1375 (SO_2), 1182 (SO_2), 1154, 974, 758 (C–S) cm^{-1}; 60 MHz NMR, A 4.41 (q, 2H, $C\underline{H}_2Cl$), B 6.35 (m, 1H, CH_2=C *cis* proton against $-CH_2Cl$), C 6.58 (m, 1H, CH_2=C *trans*), J_{AB}=1.7, J_{BC}=2.0, J_{AC}=1.0 Hz. An identical product was also obtained in 41% yield by the treatment of **6** with an excess of thionyl chloride.

Ethyl 3-Chloropropene-2-sulfonate (5). Ethanolysis of **4** in ether gave **5** in 76% yield. IR (in CCl_4), 3114, 1636 (C=C), 1369 (SO_2), 1133—1191 (SO_2), 1001 (C–O), 915 (S–O) cm^{-1}; 60 MHz NMR, A 4.16 (q, 2H, $C\underline{H}_2CH_3$), B 4.30 (q, 2H, CH_2Cl), C 6.25 (q, 1H, CH_2=C *cis* proton against $-CH_2Cl$), D 6.40 (q, 1H, CH_2=C *trans*), J_{BC}=1.5, J_{BD}=0.7, J_{CD}=1.9 Hz.

3-Chloropropene-2-sulfonic Acid (6). Hydrolysis of **3** in dioxane and distillation of the reaction mixture gave a heavy oil **6** in 69% yield, identical with the hydrolysis product of **5**. 60 MHz NMR (in $CDCl_3$), 4.13 (q, 2H, CH_2Cl), 6.17 (q, 1H, CH_2=C *cis* proton against $-CH_2Cl$), 6.41 (q, 1H, CH_2=C *trans*), 11.02 (s, 1H, SO_3H).

Ethanolysis of 3. A solution of **3** (10.6 g), ethanol (13.8 g) and carbon tetrachloride (23 m*l*) was refluxed for 20 hr. After removal of the solvent, the residue was fractionally distilled to yield two fractions, 4.5 g of **5** and 2.4 g of **6**.

Reaction of 3 with N-*Methylaniline.* Aniline (10.6 g) was added dropwise to an ether solution of **3** (7.0 g) cooled to −65°C. The mixture was gradually warmed up to room temperature, stirred for 10 hr and then filtered. Removal of ether from the filtrate gave a paste-like residue. The residue was dissolved in acetone–water (volume ratio, 10: 1), and the resulting solution was allowed to stand to give 5.0 g (45%) of **7**. IR (KBr), 3460 (OH), 3050, 2890, 1240 (SO_2), 1165 (SO_2), 1030, 725 (phenyl) cm^{-1}. 60 MHz NMR (in D_2O) of Na salt of *7*, 3.05 (s, 3H, NCH_3), 4.30 (s, 2H, CH_2N), 5.28 (s, 1H, CH_2=C *trans* proton against $-SO_2Na$), 5.88 (s, 1H, CH_2=C *cis*). In the case of a 4—5 molar ratio (the aniline: **3**), concentration of the filtrate from the reaction mixture gave another crystalline product **8** in 60—65% yield.

Reaction of 3 with Sodium Ethoxide. To a solution of **3** (21.2 g) in ethanol was added dropwise with stirring an ethanol solution of sodium ethoxide (7.13 g of metallic sodium) at −3—4°C. The mixture was neutralized, filtered and then distilled to yield 8.0 g (33%) of a colorless oil **9**. IR (neat), 1375, 1345 (SO_2), 1165 (SO_2), 1110 (C–O–C), 1000 (C–O), 920 (S–O) cm^{-1}. 60 MHz NMR (in $CDCl_3$), 1.17 (t, 6H, $C\underline{H}_3CH_2$–OCH_2), 1.31 (t, 3H, $C\underline{H}_3CH_2O_3S$), 3.50 (q, 4H, $CH_3C\underline{H}_2OCH_2$), 3.80 (d, 4H, $EtOC\underline{H}_2$), 3.43 (m, 1H, CH), 4.27 (q, 2H, $CH_3C\underline{H}_2O_3S$).

Hydrolysis of **9** with alcohol–NaOH gave **10**. IR (KBr), 1185 (broad, SO_2), 1110 (C–O–C), 1050 (S–O) cm^{-1}. 60 MHz NMR (in D_2O), 1.35 (t, 6H, CH_3), 3.41 (m, 1H, CH), 3.77 (q, 4H, $C\underline{H}_2CH_3$), 4.02 (d, 4H, $EtOC\underline{H}_2$).

The authors wish to thank Dr. M. C. Woods for providing facility for NMR measurement and his helpful advice on the analysis of NMR spectra. They are also indebted to E. Fuchita and N. Shimizu for their assistance in the experiment.

BULLETIN OF THE CHEMICAL SOCIETY OF JAPAN, VOL. 45, 1246—1247(1972)

Hydrogen-Deuterium Exchange in 1,4,5- and 1,3,5-Trimethyltetrazolium Iodides

Tyûzô Isida, Shin-ichirô Fujimori, Kiyoshi Nabika, Keiiti Sisido, and Sinpei Kozima*

Department of Industrial Chemistry, Faculty of Engineering, Kyoto University, Sakyo-ku, Kyoto, 606

**Department of Chemistry, College of Liberal Arts and Sciences, Kyoto University, Sakyo-ku, Kyoto, 606*

(Received August 25, 1971)

Considerable attentions are directed to the C–H/C–D exchange reaction of ring protons in azoles such as thiazoles,[1] thiazolium salt,[2] pyrazolium, and imidazolium salts,[3] 1,4-,[3-5] 1,3-,[6] and 2,3-disubstituted tetrazolium salts.[3] These investigations were focused on C–H bond which is sp^2 hybridized at carbon. The most acidic 1,4-disubstituted tetrazolium salt undergoes rapid hydrogen-deuterium exchange on the 5-carbon even in 2N-DCl *via* ylide formation.[3,5] As for the deuterium exchange of methyl protons of substituted azoles where C–H bonds are sp^3 hybridized at carbon, there has been a report concerning with 3- or 5-methylisothiazole.[7] This paper presents the C–H/C–D exchange of methyl protons of 1,4,5- and 1,3,5-trimethyltetrazolium iodides[8] in basic D_2O solutions containing pD buffer mixtures.

On standing a deuterium oxide solution of 1,4,5-trimethyltetrazolium iodide (**1**) at room temperature, deuterium exchange of the 5-methyl protons occurred slowly and the hydrogen was completely replaced by deuterium in a week. When the H/D exchange was carried out in D_2O at pD 8.40, 9.34, and 10.50, the rate of deuterium incorporation increased under more basic conditions; $t_{1/2}$ 50 min at pD 8.40, $t_{1/2}$ 15 min at pD 9.34, $t_{1/2}$ 12 min at pD 10.50. The half-life, $t_{1/2}$, of the exchange was measured by following the disappearance of the peak at δ 2.95 ppm in the NMR spectrum. There was found no exchange of the *N*-methyl protons of **1** under the above conditions.

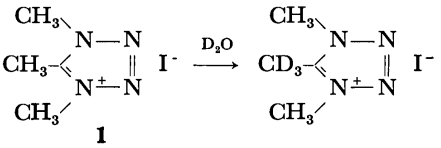

1

Under more basic condition (pD 13.50) the 1,4,5-trimethyl salt **1** underwent rapid decomposition with vigorous gas evolution. The gas was determined to be methylazide by the mass spectrum; a parent ion at *m/e* 57. When **1** was dissolved in deuterium oxide containing less than one-equivalent of potassium deuteroxide in an NMR tube, there appeared a couple of single peaks at δ 2.01 and 2.73 ppm assigned to acetyl and *N*-methyl protons of *N*-d_1-methylacetamide at the expense of the peaks at δ 2.95 and 4.27 ppm associated with **1**, and some amount of the original peaks at δ 2.95 and 4.27 ppm still remained maintaining the starting integral ratio of 1 : 2, respectively. This showed that the rapid hydrolytic decomposition occurred before H/D exchange. In the presence of excess potassium deuteroxide, the original peaks at δ 2.95 and 4.27 ppm disappeared showing complete decomposition of **1** into *N*-d_1-methylacetamide. On standing overnight, the acetyl protons of *N*-methylacetamide were exchanged with deuterium, which was displayed by the disappearance of the peak at δ 2.01 ppm associated with the acetyl protons, and further hydrolysis of the deuterated *N*-methylacetamide occurred slowly to give potassium d_3-acetate and *N*-d_2-methylamine whose peak was found at δ 2.30 ppm. This hydrolysis was also confirmed by following the change in the NMR spectrum of the authentic *N*-methylacetamide in potassium deuteroxide solution. These results showed that the reaction proceeded as follows:

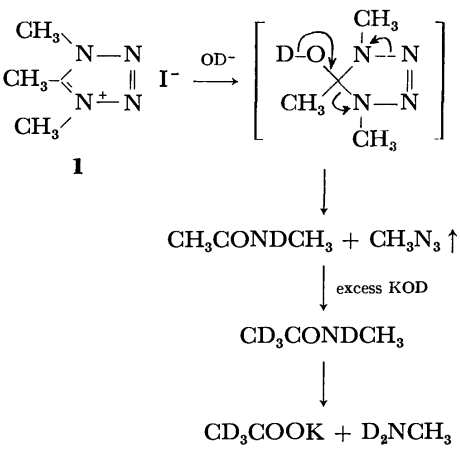

Duffin[9] reported the analogous hydrolytic decomposition of 1,5-dimethyl-4-phenyltetrazolium iodide in an aqueous 50% potassium hydroxide solution yielding phenylazide and methylamine.

In the case of 1,3,5-trimethyltetrazolium iodide (**2**), much slower H/D exchange was found even under fairly basic condition; $t_{1/2}$ 3115 min at pD 11.05. This is compatible with the easier deuterium exchange of the ring proton of 1,4-dimethyltetrazolium salt than the 1,3-dimethyl isomer.[6] When **2** was dissolved in more basic deuterium oxide, pD 13.50, there occurred no hydrolytic decomposition of **2**, but an additional H/D exchange of the 3-protons, $t_{1/2}$ 26 min, as well

1) R. A. Olofson, J. M. Landesberg, K. N. Houk, and J. S. Michelman, *J. Amer. Chem. Soc.*, **88**, 4265 (1966).

2) R. A. Olofson and J. M. Landesberg, *ibid.*, **88**, 4263 (1966).

3) R. A. Olofson, W. R. Thompson, and J. S. Michelman, *ibid.*, **86**, 1866 (1964).

4) T. J. Curphey, *ibid.*, **87**, 2064 (1965).

5) A. C. Rochat and R. A. Olofson, *Tetrahedron Lett.*, 3377 (1969).

6) W. P. Norris and R. A. Henry, *ibid.*, 1213 (1965).

7) J. A. White and R. C. Anderson, *J. Heterocycl. Chem.*, **6**, 199 (1969).

8) T. Isida, S. Kozima, S. Fujimori, and K. Sisido, This Bulletin to be published.

9) G. F. Duffin, *Chem. Ind.* (London), **1955** 1355.

as the rapid exchange of the 5-methyl protons (too fast to be measured). It must be notable that there was no exchange of the 1-methyl protons of **2** even under the strongly basic condition. Analogous selective deuterium exchange of the 3-methyl protons of 1,3-dimethyltetrazolium chloride was found by Norris and Henry.[6] The inertness of the 1-methyl protons of **2** as well as **1** could be attributed to the lower acidity of the 1-methyl protons than the 3-methyl ones. This might be brought about by the electron donation from the adjacent 5-carbon atom and the 5-methyl group into the 1-nitrogen atom, whereas, there might be comparatively less electron donation from the 2- and 4-nitrogen atoms to the 3-nitrogen atom.

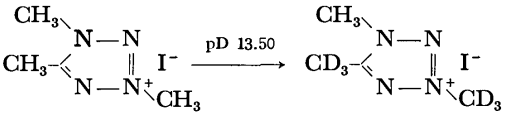

2

Experimental

1,4,5- and 1,3,5-Trimethyltetrazolium iodides were prepared by the reaction of 5-methyltetrazole with methyl iodide.[8]

The kinetics were run by following the changes in the NMR spectra at 23°C. The NMR spectra were determined at 60 MHz with a JEOL C-60HL spectrometer. The integral ratios were referred to an external standard acetonitrile kept in a capillary. The exchange was nicely first order over two half-lives, the substrate concentration was approximately 0.5 molar, and little rate variation was observed between 0.27—0.82M. D_2O buffer solutions of pD 8.40, 9.34, and 10.50 were made from Atkins-Pantin buffer mixture[10] (KCl–Na_2CO_3–H_3BO_3), and that of pD 11.05 from Menzel one[11] ($NaHCO_3$–Na_2CO_3). Measured pD values were uncorrected for differance between pH and pD. The buffer capacities were sufficient to maintain the same pD value on addition of the substrate. The mass spectrum was measured by Hitachi RMS-4 Mass Spectrometer.

10) W. R. G. Atkins and C. F. A. Pantin, *Biochem. J.*, **20**, 102 (1926).

11) H. Menzel, *Z. Phys. Chem.*, **100**, 276 (1921).

BULLETIN OF THE CHEMICAL SOCIETY OF JAPAN, VOL. 45, 1247—1248(1972)

The Formation of Solid Addition Compounds between Several *para*-Substituted Benzoic Acids and Piperidine

Setsuo KASHINO, Keiko KANEI, and Shigeo HASEGAWA

Department of Chemistry, Faculty of Science, Okayama University, Tsushima, Okayama

(Received August 27, 1971)

The formation of solid 1: 1 and 2: 1 addition compounds from benzoic acid and piperidine has previously been reported.[1]

This paper will describe the formation of the same type of addition compound from several *para*-substituted benzoic acids and piperidine, and will present some characteristic features of the infrared spectra of these compounds.

Experimental

Materials. The piperidine (GR-grade reagent) was used without further purification. The *p*-methyl-, *p*-chloro-, *p*-bromo-, and *p*-nitrobenzoic acids (each GR grade reagent) were recrystallized from benzene and dried over $CaCl_2$. Sodium salts of these substituted benzoic acids were prepared by the neutralization of the acids with a standard aqueous solution of sodium hydroxide. All the salts were dried at 110°C. The potassium hydrogen dibenzoate was prepared by the method described by Skinner *et al.*[2] The benzene was dried over metallic sodium and distilled.

The Addition Compound Formation. The 1: 1 addition compounds of *p*-methyl-, *p*-chloro-, *p*-bromo-, and *p*-nitrobenzoic acids with piperidine were prepared as follows: in a warm benzene solution of piperidine, an equimolar amount of the acid was dissolved. When the solution was then left to stand in a desiccator, crystals were separated out. They were recrystallized from benzene and then dried over $CaCl_2$.

p-Methylbenzoic acid–piperidine 1: 1 addition compound: mp 119°C.

Found: C, 70.45; H, 8.31; N, 5.86%. Calcd for $C_{13}H_{19}NO_2$: C, 70.56; H, 8.65; N, 6.33%.

p-Chlorobenzoic acid–piperidine 1: 1 addition compound: mp 121°C.

Found: C, 59.15; H, 6.46; N, 5.50%. Cacld for $C_{12}H_{16}NO_2Cl$: C, 59.63; H, 6.67; N, 5.80%.

p-Bromobenzoic acid–piperidine 1: 1 addition compound: mp 120°C.

Found: C, 50.16; H, 5.98; N, 4.82%. Calcd for $C_{12}H_{16}NO_2Br$: C, 50.37; H, 5.64; N, 4.89%.

p-Nitrobenzoic acid–piperidine 1: 1 addition compound: mp 158°C.

Found: C, 57.17; H, 6.25; N, 11.01%. Calcd for $C_{12}H_{16}N_2O_4$: C, 57.13; H, 6.39; N, 11.10%.

The 2: 1 addition compounds of *p*-methyl-, *p*-chloro-, and *p*-nitrobenzoic acids with piperidine were prepared by dissolving equimolar quantities of each acid and the 1: 1 addition compound in hot benzene, and by then allowing the solution to cool; they were recrystallized from benzene and then dried over $CaCl_2$.

p-Methylbenzoic acid-piperidine 2: 1 addition compound: mp 113°C.

Found: C, 70.75; H, 7.48; N, 3.98%. Calcd for $C_{21}H_{27}NO_4$: C, 70.56; H, 7.61; N, 3.92%.

p-Chlorobenzoic acid–piperidine 2: 1 addition compound: mp 140°C.

1) S. Kashino, This Bulletin, **41**, 248 (1968).

2) J. M. Skinner, G. M. D. Stewart, and J. C. Speakman, *J. Chem. Soc.*, **1954**, 180.

Found: C, 58.18; H, 5.20; N, 3.58%. Calcd for $C_{19}H_{21}NO_4Cl_2$: C, 57.30; H, 5.32; N, 3.52%.

p-Nitrobenzoic acid–piperidine 2: 1 addition compound: mp 177°C.

Found: C, 54.72; H, 4.88; N, 10.03%. Calcd for $C_{19}H_{21}N_3O_8$: C, 54.41; H, 5.05; N, 10.02%.

The Infrared Spectra. The infrared spectra were obtained by the usual KBr disk method at room temperature, using a Nihon-Bunko IR-S spectrophotometer.

Results and Discussion

In the infrared spectra of the 1: 1 addition compounds, no band characteristic of an un-ionized carboxyl group near 1700 cm^{-1} is observed, whereas antisymmetric and symmetric carboxylate stretching bands are observed near 1550 and 1400 cm^{-1} respectively. The peak positions of these bands are listed in Table 1, along with those of the corresponding sodium benzoates.

TABLE 1. THE CO_2^- STRETCHING FREQUENCIES OF THE *para*-SUBSTITUTED BENZOIC ACID-PIPERIDINE 1: 1 ADDITION COMPOUNDS (A) IN COMPARISON WITH THE CORRESPONDING SODIUM BENZOATES (B)

Substituent	Antisymmetric stretching ferquencies (cm^{-1})		Symmetric stretching frequencies (cm^{-1})	
	A	B	A	B
CH_3	1540	1540	1378	1414
H	1550[a]	1552[b]	1385[a]	1413[b]
Cl	1540	1436	1382	1406
Br	1525	1548	1375	1427
NO_2	1560	1578	—	—

a) Data from Ref. 1. b) Data from Ref. 3.

The spectra of the 1: 1 addition compounds were very similar to those of the corresponding sodium salts. Therefore, it may be concluded that the acid moiety in these 1: 1 addition compounds is almost fully ionized. However, it should be noted that the symmetric carboxylate stretchings of the addition compounds show lower values than those of the corresponding sodium salts. Since the vibrational frequency in a solid may be influenced by a number of factors,[3] no conclusive explanation of this behavior can be made. The X-ray crystallographic analysis of these adducts is now in progress.

3) J. H. S. Green, W. Kynaston, and A. S. Lindsey, *Spectrochim. Acta*, **17**, 486 (1961).

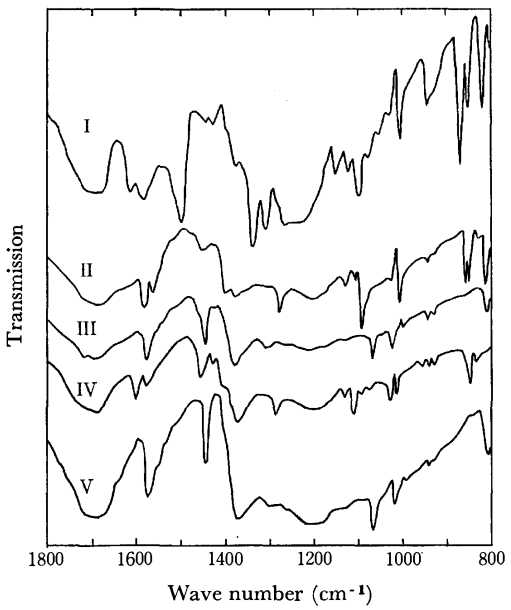

Fig. 1. Infrared spectra of the *para*-substituted benzoic acid-piperidine 2: 1 addition compounds (I—IV) and potassium hydrogen dibenzoate (V).
Substituent: I, NO_2; II, Cl; III, H; IV, CH_3

The infrared spectra of the 2: 1 addition compounds are shown in Fig. 1, along with those of potassium hydrogen dibenzoate.

The crystal structures of a series of acidic potassium salts of carboxylic acids have been studied by Speakman and his co-workers.[2,4-6] They have shown that, in many of these compounds, but not in potassium hydrogen di-*p*-nitrobenzoate,[4] the acid residues are joined to form dimers by a short and effectively symmetrical hydrogen bond.[2] According to Shrivastava and Speakman,[4] a characteristic feature of the infrared spectra of such compounds with a symmetrical hydrogen bond is a high background absorption spreading for several hundred wave numbers in the low-frequency region.

It may be noted here that all the present 2: 1 addition compounds apart from that of *p*-nitrobenzoic acid have a high background absorption in the region about 800—1100 cm^{-1}; these absorptions are very similar to those of the acidic potassium salts studied by Speakman and his co-workers.[2,5]

4) H. N. Shrivastava and J. C. Speakman, *J. Chem. Soc.*, **1961**, 1151.
5) H. H. Mills and J. C. Speakman, *ibid.*, **1963**, 4355.
6) J. C. Speakman, *Chem. Commun.*, **1967**, 32.

BULLETIN OF THE CHEMICAL SOCIETY OF JAPAN, VOL. 45, 1249—1250(1972)

Cyanomethylation Products of *dl*- and *meso*-Diphenylethylenediamines*

Tairoku YANO, Hiroshi KOBAYASHI, and Keihei UENO

Department of Organic Synthesis, Faculty of Engineering, Kyushu University, Hakozaki, Fukuoka, 812

(Received September 6, 1971)

During the course of investigation of syntheses and chelating behaviors of complexane-type ligands, we found that *dl*-diphenylethylenedinitrirotetraacetic acid was obtained by carboxymethylation of *dl*-diphenylethylenediamine, and the *meso*-isomer gave 2-oxo-5,6-diphenylpiperazine-1,4-diacetic acid, but not the expected *meso*-dinitrirotetraacetic acid.[1]

Kroll and Gordon reported the synthesis of cyclohexane-*cis*-1,2-dinitrirotetraacetic acid from *cis*-1,2-diaminocyclohexane *via* a cyanomethylated intermediate.[2]

In order to obtain the corresponding tetraacetic acid *via dl*- and *meso*-diphenyl-*N,N,N',N'*-tetrakis(cyanomethyl)ethylenediamines, cyanomethylation was attempted on the respective diamines using hydrocyanic acid and formaldehyde. However, the reaction products were not the tetrakiscyanomethylated compound, but the imidazolidine derivatives. In this paper we report on the structure with reference to the solvent effects in the proton chemical shifts of the compounds.

Results and Discussion

From the results of elemental analyses and spectroscopic data, the reaction products from *dl*- and *meso*-diphenylethylenediamines were found to be 4α,5β-diphenyl-1α,3β-bis(cyanomethyl)imidazolidine (I) and 4α,5α-diphenyl-1β,3β-bis(cyanomethyl)imidazolidine (II), respectively.

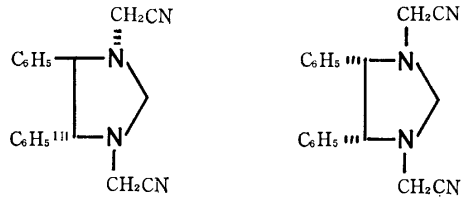

Structure (I) and (II)

NMR spectral data of (I) and (II) in various solvents and at various temperatures are summarized in Table 1. The patterns of the NMR spectrum of (I) at −30°C are the same as those at 80°C except for slight shifts in signals.

It is of interest to note that two cyanomethyl protons show a quartet signal centered at 3.55 and 3.59 ppm with J=17.7 and 17.5 Hz in deuteriochloroform for (I) and (II), respectively. However, the protons in benzene solution show a singlet at 2.72 and a broad one at 2.77 ppm for (I) and (II), respectively. The results suggest that two cyanomethyl groups are equivalent in a magnetic field but not the two protons on each cyanomethyl group due to the asymmetric effect

Table 1. Proton chemical shifts of (I) and (II) in various solvents (δ, ppm)

Solute	Proton	$CDCl_3$	C_6H_6	C_6H_5Br	C_5H_5N
(I)	$-CH_2CN$[a]	3.55[b] (3.58[c])	2.72[b] (2.78[d])	3.13[b] (3.00[d])	3.71[b] (3.65[d])
	$>CH_2$	3.85 (3.89)	3.76 (3.75)	3.79 (3.79)	4.04 (4.00)
	$-CH<$	4.28 (4.33)	3.78 (3.83)	4.03 (4.05)	4.38 (4.34)
	$-C_6H_5$	7.28 (7.33)			
(II)	$-CH_2CN$[a]	3.59[b]	2.77[b]	3.18[b] (3.22[e])	3.81[b] (3.71[e])
	$>CH_2$[a]	4.09	3.57	3.81 (3.86)	4.21 (4.21)
	$-CH<$	4.29	3.99	4.12 (4.13)	4.48 (4.42)
	$-C_6H_5$	6.97			

a) The center of AB quartet pattern signals was taken as the chemical shift.
b) at 38°C. c) at −30°C. d) at 80°C. e) at 90°C.

Table 2. Difference between the shifts in solvents and in $CDCl_3$ at 38°C (Hz)[a]

Solvent	(I)			(II)		
	$-CH_2CN$	$>CH_2$	$-CH<$	$-CH_2CN$	$>CH_2$	$-CH<$
C_6H_6	+49.5	+ 5.5	+29.9	+48.7	+31.1	+18.0
C_6H_5Br	+25.2	+ 3.4	+13.9	+24.0	+17.6	+ 9.9
C_5H_5N	−10.1	−11.3	− 6.0	−14.0	− 7.6	−11.3

a) Positive: high-field shift. Negative: low-field shift.

* Contribution No. 255 from the Department of Organic Synthesis, Kyushu University.

1) N. Okaku, Y. Toyota, Y. Moriguchi, and K. Ueno, This Bulletin, **40**, 2326 (1967).
2) H. Kroll and M. Gordon, *Ann. N.Y. Acad. Sci.*, **88**, 341 (1960).

of the imidazolidine ring nitrogen to which the cyanomethyl group attached, while in a benzene solution the asymmetric effect of nitrogen was suppressed owing to the association of the benzene molecule to the solute molecule.

A singlet signal at 3.85 ppm and a quartet one centered at 4.09 ppm with $J=3.4$ Hz for (I) and (II), respectively, can be attributed to the methylene protons interposed between two nitrogens on the ring. The methine protons appeared as a singlet at 4.28 and 4.29 ppm for (I) and (II), respectively.

The solvent-induced shift for protons are shown in Table 2. The solvent affected the methine proton to a greater extent than the methylene proton on the ring for (I), whereas the methylene protons in (II) were more affected than the methine proton. The difference was considered to be due to the fact that the benzene molecule is associated to the solute molecule in a different manner for (I) and (II) because of the different configurations of (I) and (II).

Superimposed proton signals for each pair of the substituents on the imidazolidine ring of (I) and (II), and splitting of the methylene protons interposed between two ring nitrogens of (II) indicated C_2 and σ symmetries effectively in NMR time scale for (I) and (II), respectively. Study with a molecular model showed significant steric hindrance between the phenyl and the cyanomethyl groups, favoring *trans* configuration for the substituents concerned.

A question remains whether cyanomethylation took place after the imidazolidine ring was formed[3] or a tricyanomethylated diamine once formed liberated hydrocyanic acid to form the imidazolidine ring.[4] The actual reaction conditions suggest that the former process is more probable.

Experimental

Chemical shifts were measured on a Varian A-60 spectrometer using TMS as an internal reference. The concentrations of the sample solution were approximately 10%.

Material. *dl*- and *meso*-Diphenylethylenediamines were synthesized from benzaldehyde according to the method in literature.[5-7]

4α,5β-Diphenyl-1α,3β-bis(cyanomethyl)imidazolidine (I). An aqueous 36% formaldehyde (1.4 g, 0.019 mol) and 0.93 g (0.019 mol) of sodium cyanide were added successively to a cold solution of 1.34 g (0.0047 mol) *dl*-diphenylethylenediamine dihydrochloride in 1.2N hydrochloric acid and the resulting mixture was kept in a pressure bottle. The mixture was allowed to stand for 3 days at room temperature. The precipitate obtained was recrystallized from methanol. $\nu_{C\equiv N}$, 2220 cm^{-1}; mp 130—131°C, yield 60%.

Found: C, 75.49; H, 5.99; N, 18.54%. Calcd for $C_{19}H_{18}N_4$: C, 75.50; H, 5.96; N, 18.54%.

4α,5α-Diphenyl-1β,3β-bis(cyanomethyl)imidazolidine (II) was synthesized in a similar manner to that described above. A methanol soluble fraction of the product was recrystallized from ethanol. $\nu_{C\equiv N}$, 2230 cm^{-1}; mp 163—164°C, yield 36%.

Found: C, 75.32; H, 5.83; N, 18.87%.

3) For example: T. Yano, H. Kobayashi, and K. Ueno, This Bulletin, **43**, 3167 (1970).

4) Unpublished data.

5) I. Lifschitz and J. G. Bos, *Rec. Trav. Chim. Pays-Bas*, **59**, 173 (1940).

6) S. Tripett, *J. Chem. Soc.*, **1957**, 4407.

7) W. H. Mills and T. H. H. Quibell, *ibid.*, **1935**, 839.

BULLETIN OF THE CHEMICAL SOCIETY OF JAPAN, VOL. 45, 1250—1251(1972)

An Interpretation of Mass Spectra by Simple LCAO MO Calculation. II. Derivatives of Benzene and Chlorobenzene

Susumu TAJIMA, Yoshio NIWA, Nobuhide WASADA, and Toshikazu TSUCHIYA

Government Chemical Industrial Research Institute, Tokyo, Honmachi, Shibuya-ku, Tokyo

(Received September 10, 1971)

Other than the well-known quasi-equilibrium theory,[1] several methods for the theoretical interpretation of the mass spectra of larger organic compounds have been reported.[2-5] In a previous paper,[6] we described that a simple relation was found between the summation of the intensities of certain peaks and the partial bond order, as calculated by simple LCAO MO method, for a frontier electron of the bond ruptured in the cases of the derivatives of aniline and anisole. The present note will report that the same relation holds for the derivatives of benzene and chlorobenzene.

The mass spectra were obtained with a CEC 21-103C mass spectrometer. The following derivatives of benzene were investigated: phenol, anisole, aniline, benzaldehyde, toluene, benzoic acid, and nitrobenzene; the following *o*-, *m*-, and *p*-derivatives of chlorobenzene were also investigated: hydroxychlorobenzene, methoxychlorobenzene, aminochlorobenzene, chlorobenzaldehyde, methylchlorobenzene, chlorobenzoic acid, and

1) H. M. Rosenstock and M. Krauss, "Mass Spectrometry of Organic Ions," ed. by F. W. McLafferty, Academic Press, New York (1963), Chapter 1.

2) K. Fueki and K. Hirota, *Nippon Kagaku Zasshi*, **81**, 212 (1960); K. Hirota and Y. Niwa, *Tetrahedron Lett.*, **1966**, 5757.

3) M. V. Gur'ev and M. V. Tikhomirov, *Zh. Fiz. Khim.*, **32**, 2731 (1958); M. V. Gur'ev, *ibid.*, **34**, 475 (1960).

4) R. C. Dougherty, *J. Amer. Chem. Soc.*, **90**, 5780 (1968).

5) H. Nakata and A. Tatematsu, *Tetrahedron Lett.*, **1969**, 4303.

6) S. Tajima, N. Wasada, and T. Tsuchiya, This Bulletin, **44**, 884 (1971).

nitrochlorobenzene. All the samples studied were of a research grade, were obtained from the Tokyo Kasei Co., Ltd., and were used without further purification. The experimental conditions have been described previously.[6]

The following daughter ions are produced from the molecular ion, $R\text{-}C_6H_4\text{-}X^+$, by electron impact:

$$R\text{-}C_6H_4\text{-}X^+ \longrightarrow R\text{-}C_6H_4^+ + X, \text{ and } R\text{-}C_6H_4 + X^+ \quad (1)$$

where R denotes the common substituent, H or Cl, in the derivatives of benzene or chlorobenzene respectively, and where X denotes the other substituent, such as OH or OCH_3.

We examined the correlation between the ion intensity, I, given by Eq. (2), and the partial bond order, P^h, of the bond between the aromatic moiety and the substituent, X, for a frontier electron.

$$I = 100 \times (R\text{-}C_6H_4^+ + X^+)/\sum I_i \quad (2)$$

$\sum I_i$ denotes the summation of the total ion intensities. The parameters used in the calculation of P^h were quoted from the accepted values in the literature.[7,8]

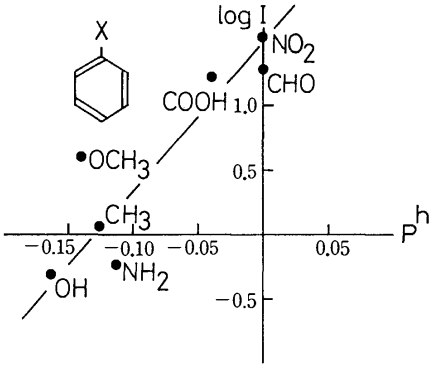

Fig. 1. log I *versus* partial bond order, P^h, of the frontier electron for benzene derivatives.

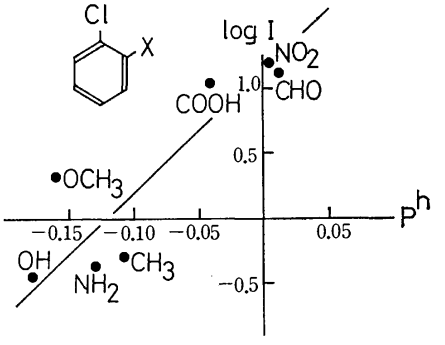

Fig. 2. log I *versus* partial bond order, P^h, of the frontier electron for *o*-chlorobenzene derivatives.

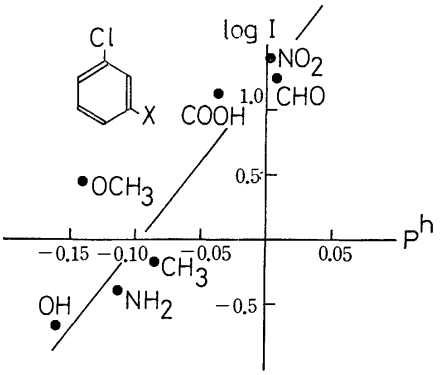

Fig. 3. log I *versus* partial bond order, P^h, of the frontier electron for *m*-chlorobenzene derivatives.

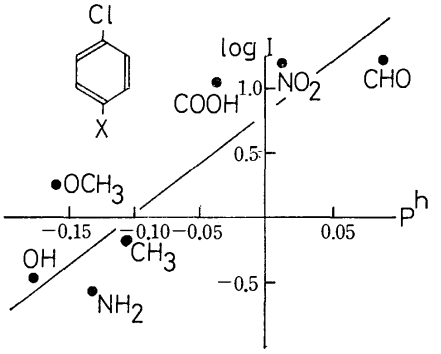

Fig. 4. log I *versus* partial bond order, P^h, of the frontier electron for *p*-chlorobenzene derivatives.

In Figures 1—4, plots of log I *versus* P^h for the derivatives of benzene and for the *o*-, *m*-, and *p*-derivatives of chlorobenzene are plotted. From each figure, we can see a simple relation: the larger the value of P^h, the larger the log I, just as in a previous paper.[6]

Almost every compound studied here exhibited a metastable peak corresponding to the decomposition $M^+ \rightarrow R\text{-}C_6H_4^+ + X$. This means that the half-life of the molecular ions of these compounds is about 10^{-5}—10^{-6} sec.[1] The life time of an ion in its excited states is considered to be less than 10^{-8} sec.[9,10] Therefore, at least a part of the ions shown in Eq. (1) may be considered to be produced by the following mechanism: a molecular ion in its excited state is not decomposed immediately after its production by electron impact, but the ion falls into its ground state by radiationless transitions; then it decomposes eventually to the daughter ions. The correlations indicated in Figs. 1—4 can be explained in the same way as in the previous report.[6]

7) L. E. Orgel, T. L. Cottrel, W. Dick, and L. E. Sutton, *Trans. Faraday Soc.*, **47**, 113 (1951).
8) H. H. Jaffé, *J. Chem. Phys.*, **20**, 279 (1952).
9) H. Sponer, *Radiat. Res. Suppl.*, **1**, 558 (1959).
10) M. A. Linotengarten, *Bull. Acad. Sci. USSR, Phys. Ser.*, **24**, 1050 (1960).

BULLETIN OF THE CHEMICAL SOCIETY OF JAPAN, VOL. 45, 1252—1253(1972)

Reactions of 2,4,4,6-Tetrabromo-2,5-cyclohexadien-1-one with Alkenes in the Presence of Weak Bases[1]

Motohiro TSUBOTA, Masaki Iso, and Kazuo SUZUKI

Department of Industrial Chemistry, Faculty of Engineering, Utsunomiya University, Ishii-cho, Utsunomiya

(Received September 14, 1971)

Schmidt and his co-workers[2] reported on the formation of 1-bromo-2-methoxycyclohexane by the reaction of 2,4,4,6-tetrabromo-2,5-cyclohexadien-1-one (**1**) with cyclohexene in methanol. As with other 4-bromo-2,5-cyclohexadien-1-ones,[3] one of the bromine atoms at the 4-position in **1** is presumed to react as a bromonium species in the reaction. This paper deals with the reaction of **1** with alkenes in the presence of several weak bases.

β-Bromo-α-methoxyethylbenzene (**3a**) was obtained in good yield by the reaction of **1** with styrene in methanol. Under similar conditions, β-bromo-α-methoxyethyl *n*-butyl ether (**3b**) and 4-bromo-3-methoxy-3-methyl-1-butene (**3c**) were obtained from *n*-butyl vinyl ether and isoprene, respectively. The reaction conditions and the results are summarized in Table 1.

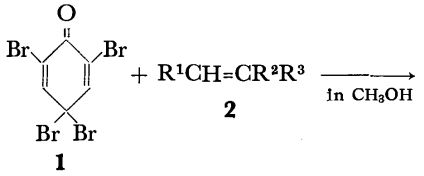

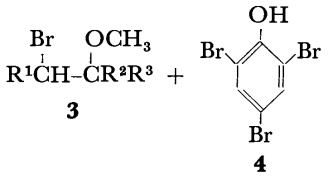

	2a,3a	**2b,3b**	**2c,3c**
R^1	C_6H_5	*n*-C_4H_9O	H
R^2	H	H	CH_3
R^3	H	H	$CH{=}CH_2$

It can be assumed that in the addition process a transitory bromonium species is formed in the initial step by the attack of a nucleophilic reagent under mild conditions, and then the bromonium species reacts with the double bond in alkenes.

The above addition reaction was further applied to the preparation of some bifunctional adducts of cyclohexene, which can be used for syntheses.

trans-1-Bromo-2-hydroxycyclohexane (**6a**),[4] *trans*-1-bromo-2-chlorocyclohexane (**6b**), *trans*-1,2-dibromocyclohexane (**6c**), and *trans*-1-acetoxy-2-bromocyclohexane (**6d**) were obtained by the reaction of **1** with cyclohexene in the presence of various bases (see Table 1).

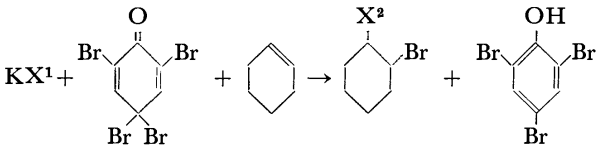

	a	**b**	**c**	**d**
X^1	*p*-$CH_3C_6H_4SO_3$	Cl	Br	CH_3CO_2
X^2	OH	Cl	Br	CH_3CO_2

These reactions are suitable for the preparation of bifunctional adducts of alkenes in view of simple procedure, mild conditions, and high yield.

Experimental

All melting points and boiling points are uncorrected. The mass spectra were measured with a Hitachi RMU-6L spectrometer; ionizing voltage: 70 eV, evaporation temperature: 95°C. The NMR spectra were obtained with a Japan

TABLE 1. SUMMARY OF THE REACTIONS OF **1** WITH ALKENES

Alkene	(mmol)	**1** (mmol)	Nucleophile (mmol)		Temp. (°C)	Time (hr)	**3** or **6**	Bp (°C/mmHg)	**3** or **6** Yield[a] (%)	**4** Yield[a] (%)
2a	2.6	1.3	CH_3OH[b]		−2— 4	1.5	**3a**	116—119/17	91	92
2b	3.0	1.5	CH_3OH[b]		4	1.5	**3b**	84— 86/15	88	100
2c	6.0	3.0	CH_3OH[b,f]		2	2.5	**3c**	71— 76/24	67	97
5	1.0	1.0	*p*-$CH_3C_6H_4SO_3K$[c]	1.0	4	2.5	**6a**	93/18	53	62
5	2.2	2.0	KCl[c,e]	3.0	5—21	4.0	**6b**	87— 89/18	29	95
5	2.2	2.0	KBr[c,f]	3.0	3— 7	2.5	**6c**	99—101/16	75	97
5	2.2	2.0	CH_3CO_2K[d]	3.0	26	72	**6d**	115—117/19	76	94

a) Based on **1**. b) Used as a reacting solvent. c) A dioxane-water mixture (3: 1) (40 m*l*) was used as a solvent. d) Acetic acid (30 m*l*) was used as a solvent. e) Concentrated hydrochloric acid (2 m*l*) was added. f) *p*-Toluenesulfonic acid monohydrate was added per mol of **1**.

1) Presented at the 24th Annual Meeting of the Chemical Society of Japan, Osaka, April, 1971: Preprints, III, p. 1585.

2) E. Schmidt, A. Aschel, and W. von Knilling, *Ber.*, **59**, 1876 (1926).

3) B. Miller, *J. Org. Chem.*, **28**, 345 (1963).

4) The hydroxy group in **6a** (in this case) is presumably a result of the addition of solvent water.

Electron Optics, JNM-6C spectrometer, using TMS as an internal standard. The IR spectra were recorded in neat liquid using a JASCO model IR-G spectrophotometer (Japan spectroscopic Co., Ltd.). The GLC data were obtained with a GCG-550T apparatus (Yanagimoto Mfg. Co., Ltd.), using a column containing 5% silicone SE-30 on Celite 545 AW.

Materials. Compounds **3a**—**c** were characterized by NMR and mass spectra.

3a: NMR (in CCl_4): 6.68 (CH_3, s), 6.54 (CH_2, q), 5.63 (CH, t), 2.65 (C_6H_5, s): Mass: *m/e* 216, 214 ($C_6H_5CH(OCH_3)$-CH_2Br), 185, 183 ($C_6H_5CHCH_2Br$), 121 ($C_6H_5CHOCH_3$): (Found: Br, 36.7%).

3b: NMR (in CCl_4): 9.05 (CH_3, m), 8.52 (CH_2, m), 6.70 ($BrCH_2$, d), 6.65 (OCH_3, s), 6.45 (OCH_2, m), 5.41 (OCH, t): Mass: *m/e* 181, 179 ($BrCH_2CHOC_4H_9$-*n*), 139, 137 ($BrCH_2CHOCH_3$), 117 ($CH_3OCHOC_4H_9$-*n*): (Found: Br, 36.2%).

3c: NMR (in CCl_4): 8.65 (CH_3, s), 6.83 ($BrCH_2$, s), 6.72 (OCH_3, s), 4.85, 4.70, 4.43 ($CH{=}CH_2$): Mass: *m/e* 165, 163 ($CH_2{=}CHC(OCH_3)CH_2Br$), 99 ($CH_2{=}CHC(OCH_3)$-$(CH_3)CH_2$), 85 ($CH_2{=}CHC(OCH_3)CH_3$), 55 ($CH_2{=}CHCH$-CH_3).

The structures of **6a**—**d** were confirmed by direct comparison of their retention times in GLC and IR spectra with those of authentic samples.[5-7]

2,4,4,6-Tetrabromo-2,5-cyclohexadien-1-one (1). Bromine (8.0 g, 5 mmol) was added in small portions to a solution of 2,4,6-tribromophenol (12.3 g, 4 mmol) in methanol-acetic acid (1:1) (60 m*l*) at 2—3°C. After 1 hour, 10% aqueous sodium carbonate solution (50 m*l*) was added. The yellow precipitates were collected, washed with water and methanol, and dried over anhydrous phosphorus pentoxide in a vacuum desiccator. Yield, 15.0 g (90%), mp 136°C (dec.) (lit.[8] 125°C (dec.)).

Reaction of 1 with an Alkene. As a typical example, the reaction of 1 with styrene is described: (for details, see Table 1). To a well-stirred solution of styrene (**2a**) (2.6 mmol) in methanol, **1** (1.3 mmol) was added at −2—4°C. Stirring was continued for 1.5 hr (solid **1** disappeared), the reaction mixture was poured into 10% aqueous sodium carbonate solution, and the aqueous layer was extracted with *n*-hexane. The organic layer was washed with water and dried over anhydrous potassium carbonate. After *n*-hexane was evaporated, the residue was distilled under reduced pressure to afford **3a** (91%), bp 116—119°C/17 mmHg. The carbonate solution was acidified with concentrated hydrochloric acid, and the precipitates were filtered and washed with water to give 2,4,6-tribromophenol, mp 91—93°C (92%).

5) S. Winstein and R. E. Buckles, *J. Amer. Chem. Soc.*, **64**, 2780 (1942).
6) H. L. Goering and L. L. Sims, *ibid.*, **77**, 3465 (1955).
7) H. R. Snyder and L. A. Brooks, "Organic Syntheses," Coll. Vol. II, p. 171 (1943).
8) R. Benedikt, *Ann. Chem.*, **199**, 127 (1879).

BULLETIN OF THE CHEMICAL SOCIETY OF JAPAN, VOL. 45, 1253—1254(1972)

p-Nitrophenyl Formate as a Reagent for Preparing *N*-Formyl-hexosamines[1]

Kazuhiko YAMAMOTO

Department of Chemistry, College of Science, Osaka University, Toyonaka, Osaka

(Received September 16, 1971)

In the course of a study of the substrate specificity of *N*-acetyl-β-D-glucosaminidase [EC. 3.2.1.30], *N*-formyl derivatives of *p*-nitrophenyl 2-amino-2-deoxy-β-D-glucopyranoside (I), 2-amino-2-deoxy-D-glucose (II), and 2-amino-2-deoxy-D-galactose (III) were required. The *N*-formylation of derivatives of II is usually achieved by a reaction in a mixture of formic acid and acetic anhydride,[2] by the pyrolysis of amine-formate,[3] or by the O→N acyl exchange of the formyl ester with sodium methoxide as the catalyst.[4] However, these known methods could not be applied to quite labile I because of their drastic conditions.

An attempt was made to use the active formyl ester for the *N*-formylation of I. *p*-Nitrophenyl formate, which had been used in the preparation of *N*-formyl amino acid,[5,6] was examined and found to be a suitable reagent. Further application of this reagent to II or III was also successful in the preparation of *N*-formyl-derivatives of II and III under milder conditions and by a simpler procedure.

After reporting[7] the use of *p*-nitrophenyl formate in the preparation of *p*-nitrophenyl 2-formylamino-2-deoxy-β-D-glucopyranoside, Pal and Mukerjee[8] reported the *N*-acylation of II using the *p*-nitrophenyl esters of acetic acid, benzoic acid, and stearic acid as the active esters. Active esters such as the *p*-nitrophenyl esters of organic acids seem to be very suitable for use in the *N*-acylation of D-hexosamines and their derivatives, as the reaction is performed under mild conditions. The further reaction of *p*-nitrophenyl formate with *p*-nitrophenyl 3,4,6-tri-*O*-acetyl-2-amino-2-deoxy-β-D-glucopyranoside hydrochloride[9] yielded the corresponding *N*-formyl derivative.

1) A part of the results was presented at the 22nd Annual Meeting of the Chemical Society of Japan (Tokyo, April, 1969).
2) C. G. Greig, D. H. Leaback, and P. K. Walker, *J. Chem. Soc.*, **1961**, 879.
3) A. Neuberger and R. U. Pitt Rivers, *Biochem. J.*, **33**, 1580 (1939).
4) W. Meyer zu Reckendorf and W. A. Bonner, *Chem. Ber.*, **94**, 3293 (1961).
5) M. Bodansky, *Nature*, **175**, 685 (1955).
6) K. Okawa and S. Hase, This Bulletin, **36**, 754 (1963).
7) K. Yamamoto, Preprint for the 22nd Annual Meeting of the Chemical Society of Japan, Part III, p. 1954 (1969).
8) H. Mukerjee and P. R. Pal, *J. Org. Chem.*, **35**, 2042 (1970).
9) E. L. May and E. Mosettig, *ibid.*, **15**, 890 (1950).

Experimental

The melting point was measured by means of a micro-melting-point apparatus (Yanagimoto Seisakusho) and was not corrected. The optical rotation was measured by means of a Rudolph (Model-200) photoelectric polarimeter at room temperature.

p-Nitrophenyl formate was prepared by the method of Okawa and Hase[6] and showed a mp of 74—76°C (lit, mp 75—77°C).

p-*Nitrophenyl 2-Formylamino-3,4,6-tri*-O-*acetyl-2-deoxy-β*-D-*glucopyranoside.* To a solution of *p*-nitrophenyl 2-amino-3,4,6-tri-*O*-acetyl-2-deoxy-β-D-glucopyranoside hydrochloride[7] (300 mg) in 30 m*l* of dimethylformamide, 0.1 m*l* of triethylamine was added, and then *p*-nitrophenyl formate (400 mg) in 15 m*l* of tetrahydrofuran was added, drop by drop. After the reaction mixture had been stirred in ice-bath for 3 hr, the slightly yellow solution was concentrated *in vacuo* (1—3 mmHg) to a syrup. The syrupy residue, dissolved in 100 m*l* of chloroform, was washed with a cold saturated sodium bicarbonate solution and finally with water. The chloroform layer which had been dried over anhydrous magnesium sulfate was evaporated *in vacuo* to dryness. The crystallization of the colorless residue from ethanol afforded 220 mg of *p*-nitrophenyl 2-formylamino-3,4,6-tri-*O*-acetyl-2-deoxy-β-D-glucopyranoside, which melted at 216—218°C. $[\alpha]_D^{19°} = -47.0$ (*c* 0.477, in acetone). Found: C, 50.05; H, 4.87; N, 6.16%. Calcd for $C_{19}H_{22}O_{11}N_2$: C, 50.22; H, 4.88; N, 6.16%.

2-Formylamino-2-deoxy-D-*glucose.* 2-Amino-2-deoxy-D-glucose hydrochloride (500 mg) was dissolved in 10 m*l* of water containing 10 m*l* of Dowex-1 (carbonate form) under cooling in an ice bath.[10] After the mixture had then been stirred for 1 hr, the ion exchange resin was removed by filtration. To the filtrate (10 m*l*) we then added 40 m*l* of tetrahydrofuran and 1.0 m*l* of pyridine, and then *p*-nitrophenyl formate (1000 mg) in 20 m*l* of tetrahydrofuran, drop by drop. After the reaction had been continued in an ice bath for 3 hr under stirring, the tetrahydrofuran was evaporated *in vacuo* and the residual aqueous solution, freed form the precipitate, was passed through a Dowex-50 (acidic from) column. The effluent was washed three times with chloroform and neutralized with Dowex-1 (carbonate form). The solution was then evaporated *in vacuo* to dryness, and the residual solid was crystallized from ethanol and ether to give 370 mg of 2-formylamino-2-deoxy-D-glucose, which melted at 112—118°C. $[\alpha]_D^{25°} = +30.9$ (Reading after 2 hr; *c* 0.905, in water). Found: C, 40.25; H, 6.33; N, 6.60%. Calcd for $C_7H_{13}O_6N$: C, 40.58; H, 6.33; N, 6.76%.

2-Formylamino-2-deoxy-D-*galactose.* A treatement of 2-amino-2-deoxy-D-galactose hydrochloride (500 mg) similar to that of 2-amino-2-deoxy-D-glucose gave 300 mg of 2-formylamino-2-deoxy-D-galactose, which melted at 162—164°C (dec.). $[\alpha]_D^{25°} = +80.8$ (Reading after 2 hr, *c* 1.06, in water). Found: C, 40.53; H, 6.45; N, 6.57%. Calcd for $C_7H_{13}O_6N$; C, 40.58; H, 6.33; N, 6.76%.

The author expresses his deep gratitude to Professor Y. Matsushima (Faculty of Science, Osaka University) for the continued interest and support throughout this work and to Dr. S. Sakakibara (Institute for protein research, Osaka University) for suggestion and advice relating to this work.

10) S. Roseman and J. Ludowieg, *J. Amer. Chem. Soc.*, **76**, 301 (1954).

BULLETIN OF THE CHEMICAL SOCIETY OF JAPAN, VOL. 45, 1254—1256 (1972)

Oxazolidone Derivatives of Hydroxyamino Acids. VII.[1] Syntheses and Properties of DL-*trans*-3-Benzoyl-5-methyl-2-oxo-oxazolidine-4-carboxylic Acid and Its Derivatives.

Toshishige INUI

Institute of Chemistry, College of General Education, Osaka University, Toyonaka, Osaka

(Received September 18, 1971)

Threonine (I) was cyclized by the reaction with phosgene to give an oxazolidonecarboxylic acid (II).[2] It was thought to be of interest to study the reaction of phosgene with *N*-benzoylthreonine. The reaction

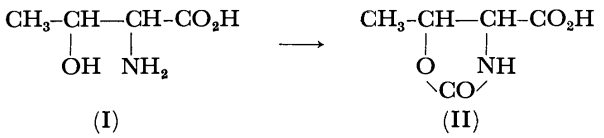

(I) (II)

of II with benzoyl chloride as well as the formation of *trans*-*N*-benzoylmethyloxazolidonecarboxylic acid (IVa) by direct cyclization of *N*-benzoyl-DL-threonine (IIIa) with phosgene in alkaline solution were unsuccessful. According to the method given previously,[1] IIIa was treated with phosgene in benzene in the presence of *N*,*N*-dimethylaniline. The expected *O*-chlorocarbonyl compound (Va) was obtained. Cyclization of this intermediate Va to IVa was not achieved and an azlactone VI was obtained.

In a similar way, methyl *N*-benzoyl-DL-threoninate (IIIb) was treated with phosgene to give *O*-chlorocar-

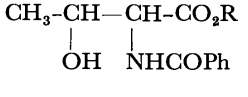

(III)

a: R=H b: R=CH_3
c: R=CH_2Ph

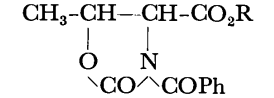

(IV)

a: R=H b: R=CH_3
c: R=CH_2Ph

1) Part VI: T. Inui, S. Tanaka, and M. Takino, This Bulletin, **43**, 1582 (1970).

2) T. Kaneko and T. Inui, *Nippon Kagaku Zasshi*, **82**, 1075 (1961); T. Inui and T. Kaneko, *ibid.*, **82**, 1078 (1961).

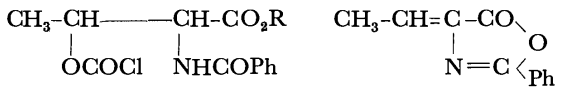

(V) (VI)

a: R=H b: R=CH_3
c: R=CH_2Ph

bonyl derivative Vb. Compound Vb was cyclized to methyl DL-*trans*-3-benzoyl-5-methyl-2-oxo-oxazolidine-4-carboxylate (IVb) when refluxed in xylene for 1—2 hr. When IVb was hydrolyzed in alkaline medium, elimination of the benzoyl group took place and DL-*trans*-5-methyl-2-oxo-oxazolidine-4-carboxylic acid (II) was obtained in the place of IVa. From this finding, the selective cleavage of threonine peptides is suggested.[3]

Benzyl *N*-benzoyl-DL-threoninate (IIIc) was converted with phosgene into the corresponding oxazolidone ester IVc through its *O*-chlorocarbonyl intermediate Vc. Catalytic hydrogenation of IVc with 5% palladium on carbon gave an acidic IVa. Treatment of IVa with thionyl chloride in benzene gave acid chloride (VII) which was converted into methyl ester IVb. VII was treated with aniline to give its an ilide. It is expected that this result will be useful for the synthesis of peptides containing modified threonine residues.

Experimental[4]

Reaction of N-*Benzoyl-*DL-*threonine (IIIa) with Phosgene. a) In Alkaline Solution*: To a solution of IIIa[5] (5.5 g, 0.025 mol) in 10% aqueous potassium hydroxide solution (60 m*l*, 0.107 mol) was added a solution of phosgene (3.0 g, 0.030 mol) in toluene (10 m*l*) at 0°C for 35 min and the reaction mixture was stirred at 0°C for 2 hr. After the organic layer had been removed, IIIa was recovered on acidification of the aqueous layer with concentrated hydrochloric acid. Yield, 3.9 g (recovery 71%), mp 146—147°C. A mixed melting point with an authentic sample showed no depression. The IR spectra were also identical with those of an authentic sample.

b) In Benzene Solution: Phosgene was passed through a suspension of IIIa (4.5 g, 0.02 mol) and *N,N*-dimethylaniline (1.0 g, 0.008 mol) in benzene (70 m*l*) at 5—8°C for 30 min. The reaction mixture was stirred for 4 hr below 20°C. Carbon dioxide (or nitrogen) was passed through the solution to remove excess phosgene. The benzene solution was washed with dilute hydrochloric acid and water. The dried solution was evaporated *in vacuo* to give Va. Yield, 3.9 g (67%), mp 125—126°C (decomp.) after recrystallization from ethyl acetate - petroleum ether (50—90°C).

Found: C, 50.94; H, 4.43; N, 5.02; Cl, 12.21%. Calcd for $C_{12}H_{12}O_5NCl$: C, 50.45; H, 4.23; N, 4.96; Cl, 12.41%.

N-Benzoyl-2-aminocrotonic Acid Azlactone (VI). A solution of Va (0.3 g, 0.001 mol) in xylene (3 m*l*) was refluxed for 1.3 hr and evaporated *in vacuo* to give VI. Yield, 0.15 g (76%). It gave a negative Beilstein's test. Its IR spectra were identical with those of an authentic sample.[6]

Methyl N-*Benzoyl-*O-*chlorocarbonyl-*DL-*threoninate (Vb)*. In a similar way to that for the preparation of Va, phosgene was passed through a suspension of IIIb[7] (4.7 g, 0.02 mol) and *N,N*-dimethylaniline (2.4 g, 0.02 mol) in benzene (70 m*l*) at 5—8°C for 30 min. Vb was obtained as crystals from the reaction mixture. Yield, 4.9 g (83%), mp 81—82°C after recrystallization from benzene - petroleum ether (50—90°C).

Found: C, 52.35; H, 4.67; N, 4.97; Cl, 12.34%. Calcd for $C_{13}H_{14}O_5NCl$: C, 52.09; H, 4.71; N, 4.70; Cl, 11.84%.

Methyl DL-trans-*3-Benzoyl-5-methyl-2-oxo-oxazolidine-4-carboxylate (IVb)*. A solution of Vb (6.0 g, 0.02 mol) in xylene (60 m*l*) was refluxed for 1.5 hr. The solution was evaporated *in vacuo* to give IVb as crystals. Yield, 4.0 g (75%), mp 115—117°C and 116—117°C after recrystallization from ethyl acetate - petroleum ether (50—90°C). IR (Nujol mull): 1800, 1780 (C=O in the oxazolidone ring), 1750 (C=O in the ester group), 1680 cm^{-1} (C=O in the benzoyl group).

Found: C, 59.36; H, 5.03; N, 5.16%. Calcd for $C_{13}H_{13}O_5N$: C, 59.31; H, 4.98; N, 5.32%.

Hydrolysis of IVb with hydrochloric acid (1 : 1, v/v) gave DL-threonine. The properties of this sample were identical with those of an authentic sample.

DL-trans-*5-Methyl-2-oxo-oxazolidine-4-carboxylic Acid (II)*. To a suspension of IVb (1.3 g, 0.005 mol) in methanol (5 m*l*) was added 1N methanolic potassium hydroxide solution (6.0 m*l*, 0.006 mol) and the reaction mixture was kept for 3.5 hr at room temperature. After diluting with water, the separated oil was extracted with ethyl acetate. Methyl benzoate was isolated from the extract as a sweet-smelling oil. Yield, 0.5 g (70%). Its IR spectra were identical with those of an authentic sample.

The aqueous layer separated from ethyl acetate extract was acidified with concentrated hydrochloric acid and evaporated *in vacuo* to dryness. The residue was extracted three times with hot ethyl acetate, and the evaporation of the combined extracts gave II. Yield, 0.5 g (70%), mp 126—127°C after recrystallization from ethyl acetate; lit,[2] mp 127—128°C. A mixed melting point with an authentic sample showed no depression.

Benzyl N-*Benzoyl-*O-*chlorocarbonyl-*DL-*threoninate (Vc)*. In a similar way to that for the preparation of Va, phosgene was passed through a suspension of IIIc[8] (12.5 g, 0.04 mol) and *N,N*-dimethylaniline (4.8 g, 0.04 mol) in benzene (140 m*l*) at 5°C for 30 min. Vc was obtained as crystals from the reaction mixture. Yield, 12.4 g (83%), mp 82—83°C after recrystallization from benzene - petroleum ether (50—90°C).

Found: C, 60.96; H, 4.92; N, 3.43; Cl, 9.23%. Calcd for $C_{19}H_{18}O_5NCl$: C, 60.72; H, 4.83; N, 3.73; Cl, 9.43%.

Benzyl DL-trans-*3-Benzoyl-5-methyl-2-oxo-oxazolidine-4-carboxylate (IVc)*. A solution of Vc (10.0 g, 0.026 mol) in xylene (100 m*l*) was refluxed for 2 hr. IVc was obtained from the solution. Yield, 7.1 g (76%), mp 69—70°C after recrystallization from benzene - petroleum ether (50—90°C). IR (Nujol mull): 1800 (C=O in the oxazolidone ring), 1755 (C=O in the ester group), 1680 cm^{-1} (C=O in the benzoyl group).

Found: C, 69.67; H, 5.34; N, 3.62; sol., 9.53%. Calcd for $C_{19}H_{17}O_5N \cdot 1/6C_6H_6$: C, 69.83; H, 5.33; N, 3.70; sol., 10.32%.

Drying over phosphorus pentoxide *in vacuo* raised the melting point to 79—80°C.

3) T. Kaneko and T. Inui, This Bulletin, **36**, 1541 (1963); T. Kaneko, S. Kusumoto, T. Inui, and T. Shiba, *ibid.*, **41**, 2155 (1968).

4) All melting points are uncorrected.

5) H. D. West and H. E. Carter, *J. Biol. Chem.*, **119**, 109 (1937).

6) H. E. Carter, P. Handler, and D. B. Melville, *ibid.*, **128**, 359 (1939).

7) K. Pfister, C. A. Robinson, A. C. Shabica, and M. Tishler, *J. Amer. Chem. Soc.*, **70**, 2297 (1948); **71**, 1101 (1949).

8) T. Inui, *Science Reports Osaka Univ.*, **18**, 19 (1969).

DL-trans-*3-Benzoyl-5-methyl-2-oxo-oxazolidine-4-carboxylic Acid (IVa).* A suspension of IVc (5.7 g, 0.016 mol) and 5% palladium on carbon (0.7 g) in a mixture of methanol (150 m*l*) and water (50 m*l*) was shaken for 2.5 hr in an atmosphere of hydrogen. After the catalyst had been removed, the filtrate was evaporated *in vacuo* to provide an oil which was crystallized by seeding. Yield, 6.5 g (86%), mp 151—153°C and 154—155°C after recrystallization from water. IR (Nujol mull): 1805 (C=O in the oxazolidone ring), 1730 (C=O in the carboxyl group), 1675 cm^{-1} (C=O in the benzoyl group).

Found: C, 57.90; H, 4.47; N, 5.58%. Calcd for $C_{12}H_{11}O_5N$: C, 57.83; H, 4.45; N, 5.62%.

DL-trans-*3-Benzoyl-5-methyl-2-oxo-oxazolidine-4-carboxylic Chloride (VII).* A suspension of IVa (1.5 g, 0.006 mol) in a mixture of thionyl chloride (3 m*l*) and benzene (10 m*l*) was warmed on a water bath for 2.5 hr. The resulting solution was evaporated *in vacuo* to give crystals. Yield, 1.6 g (100%), mp 67—70°C. IR (Nujol mull): 1810, 1795 (C=O in the oxazolidone ring and the acid chloride group), 1690 cm^{-1} (C=O in the benzoyl group).

Treatment of VII with methanol gave IVb in good yield, mp 113—115°C. Its IR spectra were identical with those of the product obtained from Vb by the cyclization process.

Treatment of VII with aniline in benzene gave DL-*trans*-3-benzoyl-5-methyl-2-oxo-oxazolidine-4-carboxanilide in a yield of 70%, mp 122—123°C after recrystallization from dioxane-petroleum ether (50—90°C).

Found: C, 63.28; H, 6.34; N, 6.37%. Calcd for $C_{18}H_{16}O_4N_2 \cdot 1.5C_4H_8O_2$: C, 63.14; H, 6.18; N, 6.14%.

BULLETIN OF THE CHEMICAL SOCIETY OF JAPAN, VOL. 45, 1256—1257(1972)

The Addition of Ferrocenylpalladium Chloride to Conjugated Dienes

Akira KASAHARA and Taeko IZUMI

Department of Applied Chemistry, Faculty of Engineering, Yamagata University, Yonezawa-shi, Yamagata

(Received September 22, 1971)

The addition reactions of conjugated dienes with various transition-metal compounds have been studied by many workers. For example, cobalt hydrocarbonyl,[1] methyl or acetylcobalt tetracarbonyl,[2] manganese hydrocarbonyl,[3] methyl-manganese pentacarbonyl,[4] and palladium chloride[5] add to butadiene to form π-allyl metal complexes by way of 1,4 addition reactions. Furthermore, Heck[6] has reported that arylpalladium chlorides, prepared *in situ* from aryl-mercury compounds and lithium palladium chloride, react with conjugated dienes to form 1-arylmethyl-π-allyl-palladium chloride dimers in moderate yields. We have now found that ferrocenylpalladium chloride will also add to conjugated dienes.

The reactions of conjugated dienes with ferrocenylpalladium chloride, prepared *in situ* from ferrocenylmercuric chloride and lithium palladium chloride in acetonitrile, gave 1-ferrocenylmethyl-π-allylpalladium chloride derivatives, plus a small amount of biferrocenyl (III). The products were isolated by evaporating the solvent and by then chromatographing the crude products on alumina. Butadiene, isoprene, and 2,3-dimethylbutadiene all gave the expected π-allylpalladium chlorides (IIA, IIB, and IIC). However, the reaction of methyl sorbate with ferrocenylpalladium chloride resulted in the formation of methyl 5-ferrocenyl sorbate (IV); this reaction seems to proceed though the π-allylic intermediate (V). The evidence for the nature of the organic ligand in the binuclear π-allylic palladium chloride complexes comes from NMR and IR spectra, and the chloro-bridged binuclear structure for these compounds is supported by the conversion into the mononuclear acetylacetonate derivatives, pyridine derivatives, and triphenylphosphine derivatives.

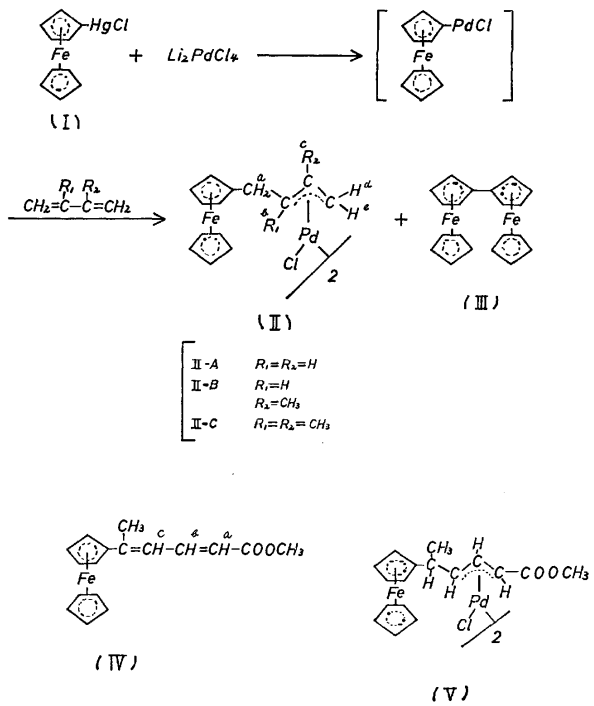

Fig. 1

1) R. F. Heck and D. S. Breslow, *J. Amer. Chem. Soc.*, **83**, 1097 (1961).
2) R. F. Heck, *ibid.*, **85**, 3381 (1963).
3) W. R. McClellan, H. H. Hoehn, H. N. Cripps, E. L. Mutterties, and B. W. Howk, *ibid.*, **83**, 1601 (1961).
4) W. D. Bannister, M. L. H. Green, and R. N. Haszeldine, *Proc. Chem. Soc.*, **1964**, 370.
5) S. D. Robinson and B. L. Shaw, *J. Chem. Soc.*, **1963**, 4306.
6) R. F. Heck, *J. Amer. Chem. Soc.*, **90**, 5542 (1968).

Experimental[7]

Materials. The ferrocenylmercuric chloride was prepared according to the method described by Fish and Rosenblum.[8]

The Preparation of Chloro-π-allylic Palladium Complexes. Lithium palladium chloride solutions were prepared by stirring 0.42 g (10 mmol) of anhydrous lithium chloride with 1.77 g (10 mmol) of anhydrous palladium chloride overnight at room temperature in 100 m*l* of acetonitrile. Into this lithium palladium chloride solution, a mixture of 4.20 g (10 mmol) of ferrocenylmercuric chloride and diolefins in a fourfold equivalent amount was then stirred at room temperature. In the reaction with butadiene, butadiene was added, by bubbling, to the reaction mixture under atmospheric pressure. The products were isolated by filtering to remove the solvent. The residue was dissolved in methylene chloride; subsequent recrystallization from ethanol afforded yellow crystals (mp 228—229°C, 6—10% yields), which were identified as biferrocenyl[9] by a comparison of the IR spectrum and by a mixed-melting-point determinations with an authentic sample. Further elution with methylene chloride and recrystallization from benzene-cyclohexane afforded the yellow product.

1-Ferrocenylmethyl-π-allylpalladium Chloride Dimer (II A). Mp 145—147°C (dec.). Yield, 35%. IR spectrum: 237, 255 cm^{-1} (Pd–Cl bridge). NMR sepctrum: 2.67 (d, J= 6.0 Hz, H_a), 2.70 (d-d, J=11.0 and 0.3 Hz, H_e), 3.65 (d-d, J=7.0 and 0.3 Hz, H_d), 3.80 (d-t, J=11.0 and 6.0 Hz, H_b), 4.09 (s, ferrocene ring protons), 5.32 ppm (m, H_c).

Found: C, 44.22; H, 4.08%. Calcd for $C_{28}H_{30}Fe_2Pd_2Cl_2$: C, 44.12; H, 3.96%.

1-Ferrocenylmethyl-2-methyl-π-allylpalladium Chloride Dimer (II B). Mp 157—159°C (dec.). Yield, 24%. IR spectrum: 237, 255 cm^{-1} (Pd–Cl bridge). NMR spectrum: 2.11 (s, CH_3), 2.67 (d, J=0.5 Hz, H_e), 2.72 (d, J=5.5 Hz, H_a), 3.70 (d, J=0.5 Hz, H_d), 3.93 (t, J=5.5 Hz, H_b), 4.08 ppm (s, ferrocene ring protons). Found: C, 45.65; H, 4.45%. Calcd for $C_{30}H_{34}Fe_2Pd_2Cl_2$: C, 45.60; H, 4.33%.

1-Ferrocenylmethyl-1,2-dimethyl-π-allylpalladium Chloride Dimer (II C). Mp 127—129°C. Yield, 29%. IR spectrum: 237, 255 cm^{-1} (Pd–Cl bridge). NMR spectrum: 2.13 (s, CH_3 on the terminal carbon atom of the π-allyl group), 2.18 (s, CH_3 on the central carbon atom of the π-allyl group), 2.65 (d, J=0.5 Hz, H_e), 2.70 (s, H_a), 3.78 (d, J=0.5 Hz, H_d), 4.08 (s, ferrocene ring protons).

Found: C, 47.10; H, 4.77%. Calcd for $C_{32}H_{38}Fe_2Pd_2Cl_2$: C, 47.04; H, 4.68%.

The Preparation of π-Allylic Palladium Acetylacetonate Complexes. The corresponding chloro-complex (0.4 g) in benzene was mixed with a solution of thallium acetylacetonate (5% excess) in benzene and kept at room temperature for 30 min. After the thallous chloride had then been filtered off, the filtrate was evaporated to dryness; the residue was recrystallized from benzene - light petroleum to give pale yellow crystals.

1-Ferrocenylmethyl-π-allylpalladium Acetylacetonate. Mp 93—94°C (dec.). Found: C, 51.47; H, 5.01%. Calcd for $C_{19}H_{22}OFePd$: C, 51.31; H, 4.94%.

1-Ferrocenylmethyl-2-methyl-π-allylpalladium Acetylacetonate. Mp 140—141°C (dec.).

Found: C, 52.62; H, 5.38%. Calcd for $C_{20}H_{24}OFePd$: C, 52.36; H, 5.27%.

1-Ferrocenylmethyl-1,2-dimethyl-π-allylpalladium Acetylacetonate. Mp 69—70°C (dec.).

Found: C, 53.50; H, 5.65%. Calcd for $C_{21}H_{26}OFePd$: C, 53.35; H, 5.54%.

The Preparation of Chloro-(π-allyl)-pyridine-palladium Complexes. A solution of the chloro-bridged palladium complex (0.10 g) in methylene chloride was treated with a solution of pyridine (5% excess) in ether. After 10 min, the solvent was removed under reduced pressure; the residue was then recrystallized from benzene - cyclohexane to give pale yellow crystals.

Chloro-(1-ferrocenylmethyl-π-allyl)-pyridine Palladium. Mp 116—118°C (dec.).

Found: C, 49.81; H, 4.45; N, 3.17%. Calcd for $C_{19}H_{20}NFePdCl$: C, 49.59; H, 4.38; N, 3.04%.

Chloro-(1-ferrocenylmethyl-2-methyl-π-allyl)-pyridine Palladium. Mp 118—120°C (dec.).

Found: C, 50.83; H, 4.69; N, 3.11%. Calcd for $C_{20}H_{22}NFePdCl$: C, 50.65; H, 4.67; N, 2.97%.

Chloro-(1-ferrocenylmethyl-1,2-dimethyl-π-allyl)-pyridine Palladium. Mp 110—112°C.

Found: C, 51.70; H, 4.99; N, 2.98%. Calcd for $C_{21}H_{24}NFePdCl$: C, 51.66; H, 4.95; N, 2.86%.

The Preparation of Chloro-(π-allyl)-triphenylphosphine-palladium Complexes. To a solution of the chloro-bridged complex (0.10 g) in warm benzene (20 m*l*), a solution of triphenylphosphine (5% excess) in benzene was added; the resultant mixture was rapidly cooled to *ca.* 8°C. Pale yellow crystals were then filtered off and recrystallized from benzene - cyclohexane.

Chloro-(1-ferrocenylmethyl-π-allyl)-triphenylphosphine Palladium. Mp 142—144°C.

Found: C, 59.91; H, 4.79%. Calcd for $C_{32}H_{30}PFePdCl$: C, 59.73; H, 4.70%.

Chloro-(1-ferrocenylmethyl-2-methyl-π-allyl)-triphenylphosphine Palladium. Mp 103—105°C.

Found: C, 60.22; H, 5.13%. Calcd for $C_{33}H_{32}PFePdCl$: C, 60.29; H, 5.05%.

Chloro-(1-ferrocenylmethyl-1,2-dimethyl-π-allyl)-triphenylphosphine Palladium. Mp 107—109°C.

Found: C, 60.87; H, 5.21%. Calcd for $C_{34}H_{34}PFePdCl$: C, 60.82; H, 5.10%.

Methyl 5-Ferrocenyl Sorbate (IV). A mixture of 4.2 g (10 mmol) of ferrocenylmercuric chloride, 4.8 g (40 mmol) of methyl sorbate, and a lithium palladium chloride solution (prepared from 1.77 g of palladium chloride, 0.42 g of lithium chloride, and 100 m*l* of acetonitrile) was stirred at room temperature for 12 hr; the products were then isolated as in the preparation of chloro-π-allylic palladium complexes. The products were chromatographed on alumina. First elution with methylene chloride afforded yellow crystals (mp 228—229°C, 10% yields), which were identified as biferrocenyl. Further elution with methylene chloride and recrystallization from benzene - cyclohexane afforded yellow crystals (mp 44—45°C, 28% yields), which were identified as methyl 5-ferrocenyl sorbate on the basis of their IR and NMR spectra.

IR spectrum: 1712, 1641, 1620 cm^{-1}. NMR spectrum: 2.08 (s, CH_3), 3.69 (s, OCH_3), 4.05, 4.29, 4.40 (ferrocene ring protons) 5.80, 6.48, 7.68 ppm (ABX pattern, H_a, H_c, and H_b).

Found: C, 68.58; H, 5.81%. Calcd for $C_{17}H_{18}O_2Fe$: C, 68.56; H, 5.72%.

7) All melting points are uncorrected. The NMR spectra were measured on a Hitachi H-60 spectrometer at 60 MHz in $CDCl_3$, using tetramethylsilane as the internal reference. The chemical shifts are given in ppm.

8) R. Fish and M. Rosenblum, *J. Org. Chem.*, **30**, 1253 (1965).

9) H. Shechter and J. H. Helling, *ibid.*, **26**, 1034 (1961).

BULLETIN OF THE CHEMICAL SOCIETY OF JAPAN, VOL. 45, 1258—1259(1972)

Alkoxysilanes. VI. The Preparation of Alkoxysiloxy Derivatives of Zirconium and Tin

Yoshimoto ABE,* Kiyoshi HAYAMA, and Ichiro KIJIMA

Department of Industrial Chemistry, Faculty of Engineering, Science University of Tokyo Kagurazaka, Shinjuku-ku, Tokyo

(Received October 6, 1971)

Tetrakis(tri-*t*-butoxysiloxy)zirconium (I) or tin (III), bis(tri-*t*-butoxysiloxy)diisopropoxyzirconium (II) or di-*t*-butoxytin (IV), and bis(tri-*t*-butoxysiloxy)bis(acetylacetonato)zirconium (V) or tin (VI) were prepared in the same way as in the cases of antimony[1] and titanium:[2]

$$M(OR)_4 + n(Bu^tO)_3SiOH \longrightarrow [(Bu^tO)_3SiO]_nM(OR)_{4-n} + nROH$$

where M=Zr, $n=4$ (I); $n=2$ (II) and M=Sn, $n=4$ (III); $n=2$ (IV)

$$(Acac)_2M(OR)_2 + 2(Bu^tO)_3SiOH \longrightarrow [(Bu^tO)_3SiO]_2M(Acac)_2 + 2ROH$$

where M=Zr (V) and M=Sn (VI).

The results of the elemental analysis and of the measurements of the IR and NMR spectra are given in Table 1. As compared to the cases of silicon[3] and titanium, (I) and (III) were more easily formed, probably indicating that the increase in the atomic radii of these metals led to an easy introduction of the tri-*t*-butoxysiloxy group. The results of the molecular-weight determination indicated that (I) and (II) are dimeric.[4] They may have an associated structure built up by a zirconosiloxane bridge similar to the alkoxy bridge in metal alkoxide.[5] It was observed that the absorption peaks due to the Si–O–M bond[6] shifted toward higher wave numbers with an increase in the atomic weight of the metals (Ti<Zr<Sn), and that the proton signals of the *t*-butyl group shifted toward an appreciably lower field in the sequence of Ti<Zr<Sn. (V) was very stable and could be distilled, while the other products were decomposed at relative low temperatures.

The preparation of a polymeric substance with Si–O–M bond was attempted; the reaction of zirconium tetraisopropoxide with di-*t*-butoxysilanediol in the molar ratio of 1:2 or 1:3 (alkoxide: silanediol) gave a glassy solid with a relatively low decomposition point (140—150 or 120—130°C). With bis(tri-*t*-butoxysiloxy)silanediol, a highly viscous liquid was obtained. On the other hand, the reaction of tin tetra-*t*-butoxide with this diol gave a white crystal which was identified as having a unit structure $[-Sn(OBu^t)_2-O-Si[O-Si(OBu^t)_3]_2-O-]_n$. The reaction of bis(acetylacetonato)-diisopropoxyzirconium with di-*t*-butoxysilanediol afforded polybis(acetylacetonato)zirconosiloxane, which was confirmed to have the structure of $[-Zr(Acac)_2-O-Si(OBu^t)_2-O-]_n$ ($n \fallingdotseq 4$). In order to compare the thermal stability of this compound with that of polytitanosiloxane,[2] the TGA curve was measured. The results showed that the polyzirconosiloxane was more stable than the polytitanosiloxanes; the weight loss of

Table 1. Tri-*t*-butoxysiloxy derivatives of Zr and Sn

Compd	IR (cm^{-1}) Si–O–M	NMR (τ)		Mp[d] Bp°C/mmHg	Yield (%)	Anal, Found (Calcd) (%)			
		Bu^t and Me	=CH–			C	H	Si	M
I[a]	940	8.68		150—160	75	45.98 (46.31)	8.43 (8.68)	9.36 (9.03)	7.80 (7.35)
II[b]	960	8.69, 8.22 8.73 (sh)	5.30—5.91[e] (sep)	166—170	65	48.49 (48.95)	9.57 (9.24)	8.09 (7.64)	12.50 (12.40)
III	1005	8.65		121—122	24	48.74 (49.23)	9.62 (9.29)	9.22 (9.56)	10.14 (10.10)
IV[c]	—	8.48		161	19	48.44 (48.55)	9.33 (9.16)	6.97 (7.09)	14.51 (14.81)
V	930	9.80, 9.95 9.83 (sh)	5.69 (s)	69—70 210—215/1	84	50.60 (50.10)	8.43 (8.35)	6.57 (6.88)	11.03 (11.17)
VI	930 904 (sh)	8.75 8.02, 7.97 (d)	4.59 (s)	115	56	48.32 (48.40)	8.41 (8.12)	6.59 (6.66)	13.89 (14.07)

Mol wt for a, b, and c; Found: 2400, 1280, and 795; Calcd: 1145, 734, and 792.

d: Decomposed; Recrystallized from *n*-hexane.

e: $-\overset{|}{\underset{|}{C}}H-$; methyne proton.

sh: shoulder, s: singlet, d: doublet, sep: septet

* Present address: Faculty of Science and Technology, Science University of Tokyo, Noda, 278.

1) Y. Abe and I. Kijima, This Bulletin, **42**, 1148 (1969).
2) Y. Abe and I. Kijima, *ibid.*, **43**, 466 (1970).
3) Y. Abe and I. Kijima, *ibid.*, **42**, 1118 (1969).
4) D. C. Bradley and I. M. Thomas, *J. Chem. Soc.*, **1959**, 4304.
5) W. Wardlow, *ibid.*, **1952**, 2027, 4204, 5020.
6) H. Schmidbaur and M. Schmidt, *J. Amer. Chem. Soc.*, **83**, 2963 (1961).

the former was about 30% at 200°C, whereas that of the latter was about 50% at the same temperature.

The reaction of the zirconium or tin acetylacetonato chelate with bis(tri-*t*-butoxysiloxy)silanediol, on the other hand, gave recrystallizable products with a Si–O–M bond. Although the molecular weight was not measured, the results of the elemental analysis and a study of the IR and NMR spectra indicated that the structure may correspond to:

$$\begin{matrix} \text{Acac} & \text{OR} \\ (\text{-M—O—Si-O-})_n & (\text{R}=(\text{Bu}^t\text{O})_3\text{Si}). \\ \text{Acac} & \text{OR} \end{matrix}$$

Experimental

Materials. The alkoxysilanols were prepared by a method previously described.[2,3] Zirconium tetraisopropoxide was obtained by the distillation of a commercially-available zirconium tetraisopropoxide isopropyl alcohol adduct (bp 195—196°C/3 mmHg).[7] Bis(acetylacetonato)diisopropoxyzirconium was afforded by the distillation of the reaction mixture after a mixture of zirconium tetraisopropoxide, acetylacetone, andbenzene had been refluxed for 1 hr (bp 140—142°C/2 mmHg). Tin tetra-*t*-butoxide (bp 82—83°C/1 mmHg) was prepared by the reaction of tin tetrachloride with *t*-butyl alcohol in the presence of diethylamine. The isolation of bis(acetylacetonato)di-*t*-butoxytin was attempted, but the attempt failed because of its decomposition upon distillation (at about 160°C/1—2 mmHg). The refore, the unpurified tin chelate obtained by the reaction of tin tetra-*t*-butoxide with acetylacetone in benzene was used as the starting material.

Preparation of Compounds (I)—(IV). A mixture of metal tetraalkoxide or bis(acetylacetonato)dialkoxymetal, tri-*t*-butoxysilanol (the molar ratio of the silanol to metal alkoxides was 2: 1 or 4: 1),[8] and benzene was refluxed for 1 hr. After the solvent had been removed along with the alcohol formed, the residue was distilled or recrystallized. The compounds thus obtained are given in Table 1.

The Reaction of Zirconium Tetraisopropoxide with Di-t-butoxysilanediol. A mixture of 4.5 g (0.0137 mol) of the alkoxide, 5.7 g (0.0274 mol) of the diol, and 40 m*l* of ethyl ether was refluxed for 1 hr. The removal of the solvent *in vacuo* gave 7.3 g of a pale yellow solid; mp 140—150°C (decomposed). Found: C, 31.40; H, 6.80; Si, 9.73; Zr, 29.42%. On the other hand, the reaction of 3.2 g (0.098 mol) of the alkoxide and 8.2 g (0.391 mol) of the diol gave 8.1 g of a pale yellow solid; mp 120—130°C (decomposed). Found: C, 30.06; H, 6.75; Si, 15.31; Zr, 15.93%. These polymeric substances were very soluble in common organic solvents.

Polybis(acetylacetonato)zirconosiloxane. A mixture of bis(acetylacetonato)diisopropoxyzirconium, di-*t*-butoxysilanediol, and toluene was refluxed for 1 hr. After the solvent had been removed at 100°C *in vacuo*, the residue was further heated for 2 hr to give a dark brown solid; mp 80—90°C. Found: C, 42.65; H, 6.45; Si, 5.43%; mol. wt, 2000. Calcd for $C_{18}H_{32}O_8SiZr$: C, 43.60; H, 6.52; Si, 5.76%; mol. wt, $495\times n$.

The Reaction of Bis(acetylacetonato)diisopropoxyzirconium or di-t-butoxytin with Bis(tri-t-butoxysiloxy)silanediol. A mixture of 8.2 g (0.0201 mol) of bis(acetylacetonato)diisopropoxyzirconium, 11.9 g (0.0201 mol) of the diol, and 40 m*l* of toluene was refluxed for 1 hr. After the solvent had been removed at 160°C, the subsequent evaporation of the solvent *in vacuo* yielded 17.6 g of a dark yellow solid, which was then recrystallized from *n*-hexane to give 10.6 g (56%) of white granular crystals; mp 222—223°C. Found: C, 45.85; H, 7.97; Si, 10.03%. Calcd for $(C_{34}H_{68}O_{14}Si_3Zr)_n$: C, 46.60; H, 7.82; Si, 9.61%. IR: 960 and 925 (shlouder) ($\nu_{Si-O-Zr}$) cm^{-1}. NMR: 8.72 (Bu^t), 8.06 (Me), and 4.52 (=CH–)τ.

On the other hand, the reaction between bis(acetylacetonato)di-*t*-butoxytin (5.3 g, 0.0112 mol) and the diol (6.6 g, 0.0112 mol) in 50 m*l* of benzene gave 3.2 g of white needle crystals; mp 138—145°C (recrystallized from *n*-hexane; decomposed at 185—190°C). Found: C, 46.27; H, 8.26; Si, 9.48; Sn, 13.19%. Calcd for $(C_{34}H_{68}O_{14}Si_3Sn)_n$: C, 46.84; H, 7.86; Si, 9.67; Sn, 13.61%. IR: 960, 934, and 904 (shoulder) ($\nu_{Si-O-Zr}$) cm^{-1}. NMR: 8.72 (Bu^t), 8.82 (Me), and 4.76 (=CH–, doublet) τ.

Analysis. The silicon was determined by a method described in a previous report. The zirconium was determined to be zirconium dioxide after a weighed sample had been hydrolyzed by means of an aqueous alcohol solution. The tin was determined by iodometry after a weighed sample had been decomposed in concentrated hydrochloric acid containing lead under a carbon dioxide atmosphere.

The authors wish to thank Professor Yojiro Tsuzuki for his helpful advice and interest.

7) The authors wish to thank the Matsumoto Pharmaceutical Co. for supplying the zirconium tetraisopropoxide isopropyl alcohol adduct.

8) Reagents for (I): 6.3 g (0.0193 mol, $Zr(OPr^i)_4$), 21.1 g (0.0799 mol, $(Bu^tO)_3SiOH$; (II): 11.2 (0.0343), 18.8 (0.0712); (III): 5.8 (0.0141, $Sn(OBu^t)_4$), 14.9 (0.0564); (IV): 9.4 (0.0229), 12.1 (0.0458); (V): 9.6 (0.0236, $(Acac)_2Zr(OPr^i)_2$), 12.5 (0.0473); (VI): 5.9 (0.0128, $(Acac)_2Sn(OBu^t)_2$, 7.1 (0.0269).

BULLETIN OF THE CHEMICAL SOCIETY OF JAPAN, VOL. 45, 1260—1261(1972)

The Effect of the Temperature on the Formation of Solvated Electrons and Hydrogen in the Photolysis of a Methanolic Solution of Potassium Iodide

Hiroshi SEKI, Hiroo ISHIDA, and Masashi IMAMURA
The Institute of Physical and Chemical Research, Wako, Saitama

(Received October 18, 1971)

In a previous paper[1] we reported the photochemical formation of the solvated electron and its reactions in methanolic solutions of potassium iodide. The solvated electrons in methanol decompose with a rate constant of 5.4×10^5 sec^{-1} to form hydrogen. Hydrogen is also produced from UV-irradiated CH_3OD solutions; its isotopic composition was found to be nearly 100% HD. It was concluded, therfore, that the reaction:

$$e^-_{solv} \longrightarrow H + CH_3O^- \qquad (1)$$

does occur in methanolic solutions, followed by:

$$H + CH_3OH \longrightarrow H_2 + CH_2OH \qquad (2)$$

Reaction (1) had been assumed to occur in the radiolysis of methanol;[2-4] our previous result gave a sound basis to this assumption.

The temperature dependence of the rate constant of Reaction (1) has been determined with the radiolytic system by somewhat indirect procedures.[3] In this study, we determined the quantum yields of hydrogen from UV-irradiated methanolic solutions of potassium iodide at temperatures between −15 and 85°C, as well as those of the solvated electrons scavengeable by nitrous oxide. Both quantum yields were found to fit the Arrhenius equation, the energies of activation being obtained.

Experimental

The chemicals and procedures were essentially the same as those previously reported.[1] UV-irradiations at temperatures lower and higher than room temperature were carried out by placing irradiation ampoules in a Dewar vessel equipped with quartz windows. For experiments above 0°C, the ampoule was immersed in water thermostated at the desired temperatures. For experiments below 0°C, dry nitrogen gas which had been cooled with liquid nitrogen to the desired temperatures was blown into the Dewar vessel through copper tubing.

The concentrations of N_2O in methanolic solutions at various temperatures were calculated by using Bunsen absorption coefficients estimated by extrapolating the existing data in pure methanol.[5] All the solutions contained 0.1 M KI and were irradiated with UV light centered at 254 nm, as previously.[1]

Results and Discussion

Table 1 lists the quantum yields of N_2 from 0.1 M KI solutions containing N_2O and those of H_2 in the absence of N_2O at various temperatures.

Table 1. Temperature dependence of $\Phi(N_2)$ and $\Phi(H_2)$

Temp °C	$\Phi(N_2)$[a]	$\Phi(H_2)$[b]
−15	0.46±0.01 (6—9)	0.13±0.01
3	0.51±0.01 (5—6)	0.22±0.01
25	0.58±0.01 (1—5)	0.35±0.01
60	0.69±0.02 (3—4)	0.57±0.02
85	0.78±0.01 (3—4)	0.69±0.01

a) The quantum yields at N_2O concentrations in 10^{-2} M given in parentheses
b) The quantum yields for 0.1 M KI solutions not containing N_2O

As has been reported previously,[1] with an increase in the concentration of N_2O, $\Phi(H_2)$ decreases rapidly to null at about 5×10^{-4} M N_2O and $\Phi(N_2)$ reaches a plateau value of 0.59 above 1.2×10^{-2} M at 25°C. The same plateau value as for $\Phi(N_2)$ was obtained for $\Phi(H_2)$ with acid solutions. (Hydrogen ions react with e^-_{solv} to produce H atoms.) We have, therefore, concluded that N_2 is produced solely by the reaction of N_2O with e^-_{solv} in a stoichiometric ratio of $N_2/e^-_{solv}=1$. Furthermore, $\Phi(N_2)$ was observed to keep its plateau value of 0.59 over the N_2O concentration range studied ($(1—5)\times10^{-2}$ M).

These results may indicate that N_2O scavenges, in these concentration ranges, all the e^-_{solv} produced by the reaction:

$$I^{-*}_{solv} \longrightarrow I_{solv} + e^-_{solv} \qquad (3)$$

competing with the deactivation process:

$$I^{-*}_{solv} \longrightarrow I^-_{solv} + \text{energy} \qquad (4)$$

The quantum yields of N_2 in Table 1 were obtained at N_2O concentrations of $(1—9)\times10^{-2}$ M; therefore, these values may be regarded as the limiting quantum yields of e^-_{solv} produced by Reaction (3).

Thus, $\Phi(e^-_{solv})$ may be expressed by:

$$\Phi(e^-_{solv}) = \Phi(N_2) = \frac{k_3}{k_3+k_4} \qquad (i)$$

Since the deactivation of I^{*-}_{solv} is a collisional process, k_4 may be expected to be proportional to $T^{1/2}$. On the other hand, k_3 should be regulated by the rate of rotational movements in methanol and should, therefore, be proportional to the fluidity. Since the temperature dependence of the viscosity is given by $\eta = A'\exp(B/\boldsymbol{R}T)$, k_3 may be expressed by:

1) H. Seki and M. Imamura, This Bulletin, **44**, 1538 (1971).
2) J. H. Baxendale and F. W. Mellows, *J. Amer. Chem. Soc.*, **83**, 4720 (1961).
3) K. N. Jha and G. R. Freeman, *J. Chem. Phys.*, **48**, 5480 (1968).
4) F. S. Dainton, G. A. Salmon, and P. Wardman, *Proc. Roy. Soc.* (London), *A*, **313**, 1 (1969).
5) A. Seidell, "Solubilities of Inorganic and Metal Organic Compounds," Vol. 2, 4th Ed., American Chemical Society, Washington, D. C. (1965), p. 802.

$$k_3 = A_3\exp(-E_3/\boldsymbol{R}T) \quad \text{(ii)}$$

where E_3 is expected to be equal to B.

From Eqs. (i) and (ii), it seems that the temperautre dependence of $\Phi(e^-_{solv})$ can be approximately expressed by Eq. (iii):

$$\ln\left(\frac{1}{\Phi(e^-_{solv})}-1\right)=\ln\frac{k_4}{A_3}+\frac{E_3}{\boldsymbol{R}T} \quad \text{(iii)}$$

From the plot according to Eq. (iii) shown in Fig. 1, E_3=2.7 kcal/mol is obtained. This value is close to the constant, B, for methanol (2.3 kcal/mol) in the same temperature range as that used in this study. In aqueous solutions the corresponding value of 4.7± 0.5 kcal/mol has been obtained (B=4.5 kcal/mol).[6]

Previously we have not decided whether or not all the e^-_{solv} scavengeable with N_2O (Φ=0.59) are free and participate in the H_2-formation process in the absence of N_2O. Figure 2 shows the homogeneous-kinetics plot of the data obtained at room temperature (25°C) according to this equation:

$$\frac{1}{\Phi(N_2)}=\frac{1}{\Phi(e^-_{solv})}\left(1+\frac{k_1+k_x[X]}{k_{N_2O}[N_2O]}\right) \quad \text{(iv)}$$

Here, X represents the reactive species (toward e^-_{solv}) not producing H atom (*i.e.*, I or I_2^- and/or impurity, if any). The straight line connecting points at low N_2O concentrations (10^{-4}M) can be extrapolated to $1/\Phi(N_2)=1.7$ or $\Phi(N_2)=0.59$, which is in agreement with the plateau value of $\Phi(N_2)$ obtained at (1—5)× 10^{-2}M N_2O. These results indicate that all the e^-_{solv} scavengeable with N_2O at concentrations of (1—5)× 10^{-2}M are free and can produce H_2 in the absence of N_2O.[7]

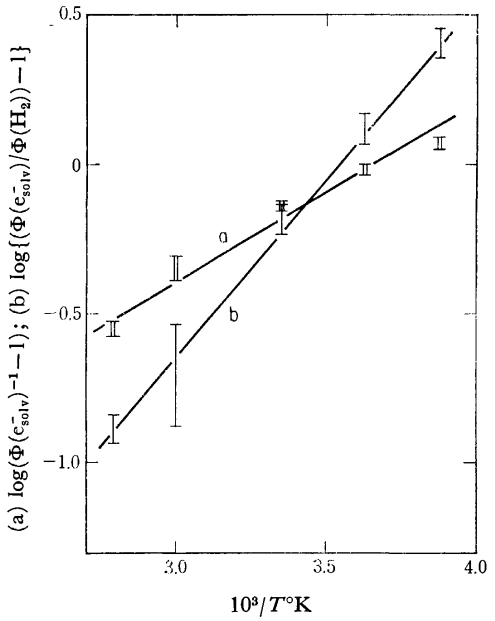

Fig. 1. Arrhenius plots for (a) $\Phi(e^-_{solv})$ and (b) $\Phi(H_2)$ according to Eqs. (iii) and (v).

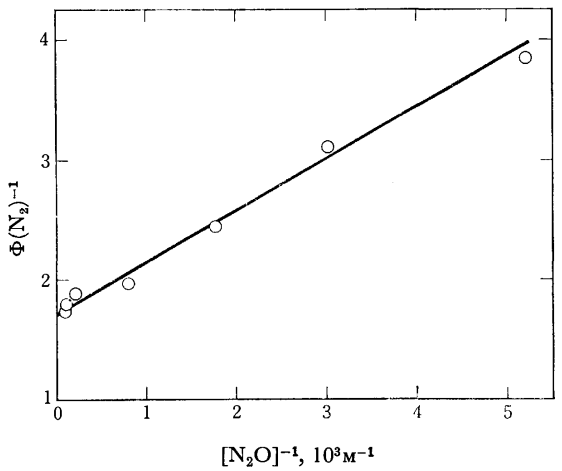

Fig. 2. A homogeneous-kinetics plot of $\Phi(N_2)$ for KI solutions containing N_2O at 25°C according to Eq. (iv).

Since H_2 is produced solely by Reactions (1) and (2), and since the rate of the latter reaction is about 100 times faster than the former, $\Phi(H_2)$ at each temperature is expressed by:

$$\Phi(H_2)=\Phi(e^-_{solv})\times\frac{A_1\exp(-E_1/\boldsymbol{R}T)}{A_1\exp(-E_1/\boldsymbol{R}T)+A_x\exp(-E_x/\boldsymbol{R}T)[X]}$$

or:

$$\ln\left(\frac{\Phi(e^-_{solv})}{\Phi(H_2)}-1\right)=\ln\frac{A_x}{A_1}[X]+\frac{E_1-E_x}{\boldsymbol{R}T} \quad \text{(v)}$$

The plot according to Eq. (v) is shown in Fig. 1, from which E_1-E_x=5.4 kcal/mol. As has been stated above, X is a general expression for reactive species toward e^-_{solv}; therefore, its rate constant, k_x, may be regarded as very close to a diffusion-controlled one. If we take $E_x\simeq$2.8 kcal/mol,[3] $E_1\simeq$8 kcal/mol is obtained. The entropy of activation, ΔS^*, can be estimated from the values of k_1[1] and E_1 to be −6 cal/deg·mol.

The value of E_1 estimated by Jha and Freeman[3] is 3.7 kcal/mol, lower than the present one. They estimated E_1 from the temperature dependence of the rate-constant ratio, $k(e^-_{solv}+N_2O)/k_1$, obtained from plots of $1/G(N_2)$ *vs.* $1/[N_2O]$ at −97, 25, and 150°C. There is, however, an ambiguity about the N_2O concentration at 150°C that was estimated by a long extrapolation of the Bunsen coefficient. Furthermore, their value of the rate-constant ratio of 1.1×10^4M^{-1} at 25°C is too low. This value can be expected to be $(2—3)\times10^4$M^{-1} on the basis of the reasonable values of $k(e^-_{solv}+N_2O)=1.3\times10^{10}$M^{-1} sec^{-1} [1,4,8] and $k_1=(4—6)\times10^5$ sec^{-1};[1,3,9] in fact, we have ourselves obtained 2.4×10^4M^{-1} for $k(e^-_{solv}+N_2O)/k_1$ in a previous paper.[1] The present disagreement in E_1 may be in part due to such reasons, though no quantiative accounts are available at this moment.

It does not seem that the value of E_1 is necessarily equal to that of the dielectric relaxation, as was suggested by Jha and Freeman.[3] Since E_1 should be used not only to rearrange the solvent structure but also to form an activated state producing CH_3O^- and H, E_1 may be expected to be higher than the activation energy of the dielectric relaxation.

6) F. S. Dainton and S. R. Logan, *Proc. Roy. Soc.* (London), *A*, **287**, 281 (1965).

7) This conclusion does not necessarily rule out the effect of the solvent cage in which geminate recombination may take place since the concentration of N_2O employed was not high enough.

8) H. Seki and M. Imamura, *J. Phys. Chem.*, **71**, 870 (1967).

9) F. S. Dainton, J. P. Keene, T. J. Kemp, G. A. Salmon, and J. Teplý, *Proc. Chem. Soc.*, **1964**, 265.

BULLETIN OF THE CHEMICAL SOCIETY OF JAPAN, VOL. 45, 1262—1263(1972)

Kinetic Studies of Association and Dissociation Reactions of Congo Red by the Temperature-Jump Method

Tatsuya YASUNAGA and Sadakatsu NISHIKAWA

Department of Chemistry, Faculty of Science, Hiroshima University, Higashisenda-machi, Hiroshima

(Received October 20, 1971)

The association of dye in an aqueous solution has been widely studied through the application of the polarograghic[1] or spectroscopical methods.[2-7] However, there is little information available concerning the kinetics of the association and dissociation reactions of dye.[8] The present study was undertaken in order to obtain kinetic and thermodynamic information concerning the association and dissociation of congo red by the use of the temperature-jump method.

Experimental

The techniques and apparatus used were fully described in a previous paper.[9] The temperature-jump, of about 4°C, was caused by discharging a 0.1 μF capacitor, charged to approximately 20 kV, through the solution. The wavelength of observation was 500 mμ. The congo red was kindly provided in an extremely pure form by Professor Suzawa.* The inoic strength of the solution was adjusted to $\mu=0.1$ by the addition of NaCl. All the solutions were prepared using distilled, air-free water in order to prevent the formation of air bubbles upon the discharge of the capacitor. The reciprocal relaxation time, τ^{-1}, was calculated from the plots of $-\log \Delta C$ *vs.* the time, where ΔC is the deviation of the concentration from its equilibrium value. The method of least-squares was employed to calculate the most probable values of the rate constants.

Results and Discussion

Table 1 shows the mean reciprocal relaxation times obtained from this study in the concentration range of 10^{-6} to 10^{-5}M at various temperatures. The dependence of the relaxation time on pH was not observed. This means that the observed relaxation phenomena are not associated with the hydrogen ion. Now, let us assume the following association-dissociation equilibrium at a low concentration of the dye:

$$2A \underset{k_2}{\overset{k_1}{\rightleftharpoons}} A_2 \qquad (1)$$

Table 1. THE RECIPROCAL RELAXATION TIME AT VARIOUS TEMPERATURES

$C_0\times 10^6$	$(1/\tau)_{av}$, sec^{-1}		
	13°C	17°C	22°C
1	—	93	—
2	62	118	—
3	69	142	182
4	66	133	183
5	67	162	213
6	62	153	231
7	68	141	244
8	67	174	259
9	73	171	253
10	89	196	—

where A and A_2 are the monomer and the dimer of the dye, and where k_1 and k_2 are the forward and backward rate constants respectively. The rate of association for this system is, then, given by:

$$\frac{d[A_2]}{dt} = k_1[A]^2 - k_2[A_2] \qquad (2)$$

The reciprocal relaxation time is related to the rate constants and the monomer concentration at equilibrium, $[A]_0$, as follows:

$$\tau^{-1} = 4k_1[A]_0 + k_2 \qquad (3)$$

Equation (3) can be rewritten in terms of the total concentration, C_0, by the use of the $C_0=[A]_0+2[A_2]_0$ and $k_2/k_1=[A]_0^2/[A_2]_0=K$ relationships. Therefore,

$$\tau^{-2} = 8k_1k_2C_0 + k_2^2 \qquad (4)$$

where K is the equilibrium constant. Figure 1 shows plots of τ^{-2} *vs.* C_0. The rate constants were calculated from the intercepts and slopes using the least-squares method. These values are listed in Table 2.

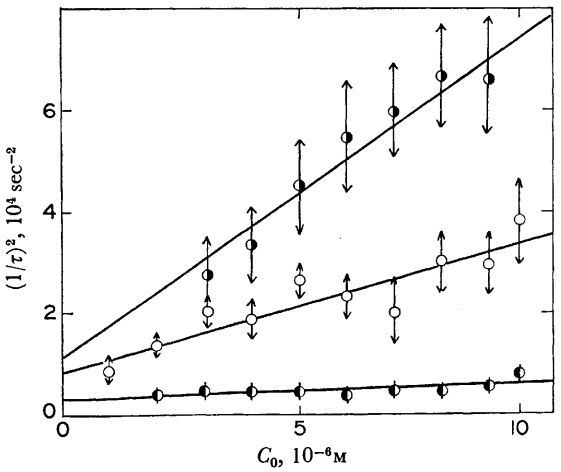

Fig. 1. The plots of $(1/\tau)^2$ *vs.* C_0 at various temperatures: ◐, 13°C; ○, 17°C; ◑, 22°C.

1) P. J. Hillson and R. B. Makay, *Trans. Faraday Soc.*, **61**, 374 (1965).
2) M. Hida, A. Yabe, H. Murayama, and M. Hayashi, This Bulletin, **41**, 1776 (1968).
3) M. E. Lamm and D. M. Neville, Jr., *J. Phys. Chem.*, **69**, 3872 (1965).
4) K. K. Rohatgi and G. S. Singhal, *ibid.*, **70**, 1695 (1966).
5) V. Zanker, *Z. Phys. Chem.*, **199**, 225 (1952).
6) TH. Förster and E. König, *Z. Elektrochem.*, **61**, 344 (1957).
7) E. Rabinowitch and L. F. Epstein, *J. Amer. Chem. Soc.*, **63**, 69 (1941).
8) G. G. Hammes and C. D. Hubbard, *J. Phys. Chem.*, **70**, 1615 (1966).
9) T. Yasunaga and S. Harada, This Bulletin, **42**, 2165 (1969).

* Department of Applied Chemistry, Faculty of Engineering, Hiroshima University, Hiroshima.

Table 2. The kinetic values for the association and dissociation reaction of congo red at various temperatures

	13°C	17°C	22°C
k_1, 10^6 sec^{-1} M^{-1}	0.70±0.16	3.5 ±0.8	6.7 ±1.5
k_2, 10^2 sec^{-1}	0.55±0.05	0.92±0.10	1.2 ±0.2
K, 10^{-4} M	0.79±0.26	0.26±0.09	0.17±0.05

According to Eyring's rate theory, the rate constant, k_i, is related to the activation energy, the activation enthalpy and the activation entropy as is the next equation:

$$k_i = PT\exp\left(-\frac{\Delta F_i^*}{RT}\right) = PT\exp\left(-\frac{\Delta H_i^* - T\Delta S_i^*}{RT}\right) \quad (5)$$

where P is the constant, R is the gas constant, T is the absolute temperature, ΔF_i^* is the activation energy, ΔH_i^* is the activation enthalpy, and ΔS_i^* is the activation entropy. Figure 2 shows the plots of $\ln(k_i/T)$ *vs.* $1/T$. The activation enthalpies were obtained from the slopes, while the enthalpy change was calculated from

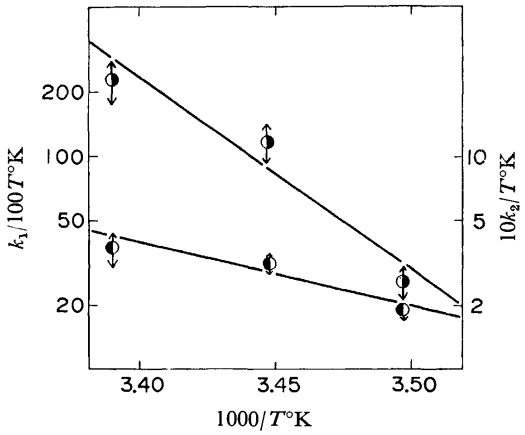

Fig. 2. Temperature dependence of rate constants in the association and dissociation reaction of congo red: ◑, k_1; ◐, k_2.

the difference between the activation enthalpies in the two states. Furthermore, the changes in the free energy and the entropy were calculated by the use of the $\Delta F = -RT\ln K$ and $\Delta F = \Delta H - T\Delta S$ relationships. These values are $\Delta H_1^* = 41$ kcal/mol, $\Delta H_2^* = 15$ kcal/mol, $\Delta H = \Delta H_1^* - \Delta H_2^* = 26$ kcal/mol, $\Delta F = \Delta F_1^* - \Delta F_2^* = -5.4$ kcal/mol at 13°C, -6.1 kcal/mol at 17°C, -6.5 kcal/mol at 22°C, and $\Delta S \cong 110$ cal/mol·deg.

The single relaxation phenomena and the linearity of the plots of τ^{-2} *vs.* C_0 show that the relaxation phenomena obtained in this study are attributable to the disturbance of the monomer-dimer equilibrium of congo red in the concentration range of 10^{-6} to 10^{-5}M. This proves that only the monomer and dimer of congo red exist in this concentration range at $\mu = 0.1$. In general, it has been reported that the polymerization of dyestuffs does not stop at the dimeric state, but often proceeds to trimers and higher polymers. Though even in the more concentrated solutions the relaxation spectra could be observed, they were not characterized by a single relaxation time. This shows that the higher polymers exist in the solutions of more than 10^{-5}M.

Only a few reports have been published containing thermodynamic information about the association of dyes.[4,7] It is, however, noteworthy that the changes in enthalpy and entropy obtained for the monomer-dimer equilibrium of congo red are large when compared with those obtained for other dyes.[4,7] The large change in entropy shows that the association and dissociation reactions of congo red are entropy-controled. The positive entropy change for dimer formation must be a consequence of the decreased structuring of the solvent about the dimers, and consequently the dimeric state must be stabilized with an increase in the temperature. As the congo red molecule, however, has a very complex structure, it is difficult to determine how dyes aggregate structurally. Further studies of analogous systems by relaxation methods will lead to a clarification of the aggregation mechanism of congo red.

BULLETIN OF THE CHEMICAL SOCIETY OF JAPAN, VOL. 45, 1264—1265(1972)

The Mass Spectra of Several Ferrocenoyl Compounds

Hiromu IMAI

Faculty of Engineering, Kansai University, Senriyama, Suita-shi, Osaka

(Received November 10, 1971)

Since 1955, beginning with the work of Friedman *et al.*,[1] some reports on the mass spectra of ferrocene[2-4] and its derivatives[5,6] have appeared. The fragmentation of disubstituted ferrocenoyl compounds has never been reported, however, though the mass spectra of some monosubstituted ferrocenoyl compounds has examined by Mandelbaum and Cais.[6] In this paper, it is my purpose to report on the fragmentation of several ferrocenoyl compounds, 1,1'-diacetylferrocene (I), 1,1'-ferrocenedicarboxylic acid (II), and mono- and 1,1'-bisacetoacetylferrocene (III) and (IV).

1,1'-Diacetylferrocene (I). I was ascertained to be cleavaged at *m/e* 199 by the following two paths: (a) the *m/e* 270→255→199 sequence was indicated by the appearance of metastable peaks at *m/e* 240.8 and 155.3, while (b) the *m/e* 270→227→199 sequence was suggested by the metastable peaks at *m/e* 190.8 and 174.4. The fragmentation described above is shown in Scheme 1.

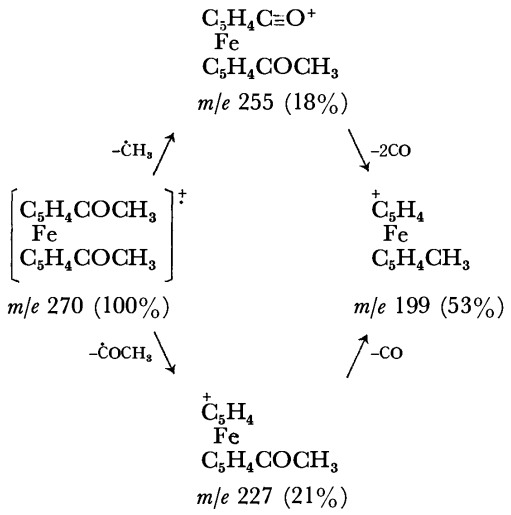

Scheme 1

The *m/e* 163 ($Fe^+C_5H_4COCH_3$), which appeared in the spectrum of monoacetylferrocene,[6] was also observed (relative intensity 19%) in the spectrum of I. This fragment ion might be produced by the loss of $\dot{C}_5H_4COCH_3$ from the molecular ion or by that of C_5H_4 from the *m/e* 227.

1,1'-Ferrocenedicarboxylic Acid (II). The following fragmentation was observed from the spectrum of II: (a) a sequence of *m/e* 274→256 (molecular ion of anhydride of II)→212, supported by the metastable peaks at *m/e* 239.2 and 175.6, corresponding to the loss of water and carbon dioxide in that order, and (b) the *m/e* 230 corresponding to the molecular ion of ferrocenemonocarboxylic acid and the rearrangement ion, *m/e* 210, produced from the *m/e* 274 by the loss of carbon dioxide and C_5H_4 respectively. This *m/e* 230 might be transferred to the fragment ion of $Fe^+C_5H_4COOH$ (*m/e* 165, 39%) and $HOFeC_5H_5$ (*m/e* 138, 25%), as has been reported by Mandelbaum and Cais.[6] The main paths of the fragmentation are shown in Scheme 2.

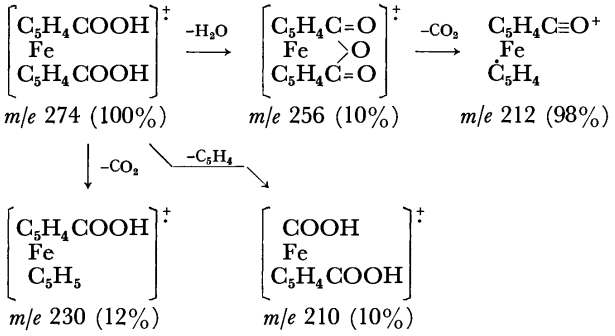

Scheme 2

Mono- and 1,1'-Bisacetoacetylferrocene (III) and (IV). There are three routes for the cleavage of III: (a) the *m/e* 270→205→163 sequence was supported by the metastable peaks at *m/e* 155.6 and 129.6, (b) the *m/e* 228 appeared upon the loss of $COCH_2$ from the *m/e* 270 (a metastable peak at *m/e* 192.5), (c) the rearrangement ion, *m/e* 178, appeared upon the loss of C_5H_4CO from

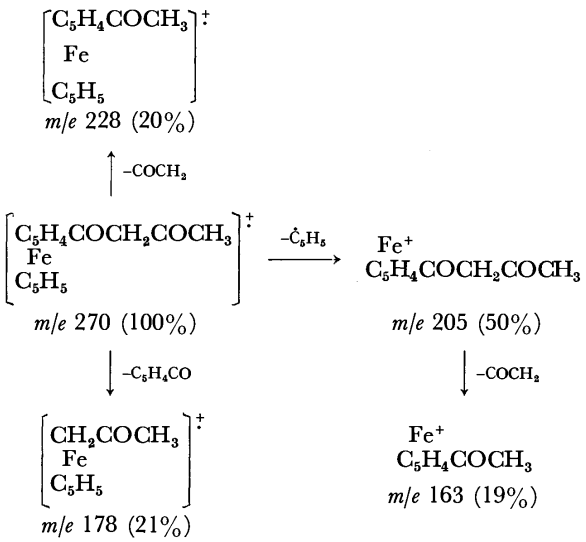

Scheme 3

1) L. Friedman, A. P. Irsa, and G. Wilkinson, *J. Amer. Chem. Soc.*, **77**, 3689 (1955).
2) E. Schumacher and R. Taubenest, *Helv. Chim. Acta*, **47**, 1525 (1964).
3) R. G. Denning and R. A. D. Wentworth, *J. Amer. Chem. Soc.*, **88**, 4619 (1966).
4) J. Mueller and L. D'or, *J. Organometal. Chem.*, **10**, 313 (1967).
5) D. T. Roberts, W. F. Little, and M. M. Bursey, *J. Amer. Chem. Soc.*, **89**, 4917, 6156 (1967).
6) A. Mandelbaum and M. Cais, *Tetrahedron Lett.*, **51**, 3847 (1964).

the *m/e* 270 (a metastable peak at *m/e* 117.3). These results are given in Scheme 3.

It can be presumed that the *m/e* 228 corresponding to molecular ion of monoacetylferrocene is decomposed to $C_5H_5FeC_5H_4C{\equiv}O^+$ (*m/e* 213, 12%) or $Fe^+C_5H_4CO\text{-}CH_3$ (*m/e* 163, 19%) upon the loss of $\dot{C}H_3$ or $\dot{C}_5H_5$,[6] while the *m/e* 178 resulting from the rearrangement is decomposed to $Fe^+CH_2COCH_3$ (*m/e* 113, 5.2%).

The fragmentation of IV can be explained as follows: (a) the *m/e* 354→297→205 sequence was supported by the metastable peaks at *m/e* 249.2 and 141.5, while the *m/e* 205 was formed by the loss of $\dot{C}_5H_4COCH_2\text{-}COCH_3$ from the *m/e* 354 (a metastable peak at *m/e* 118.7), and (b) both rearrangement ions, *m/e* 290 and 262, were formed from the *m/e* 354 by the loss of C_5H_4 and C_5H_4CO respectively (a metastable ion at *m/e* 235.9 for 354→290 and *m/e* 193.9 for 354→262). These results are shown in Scheme 4.

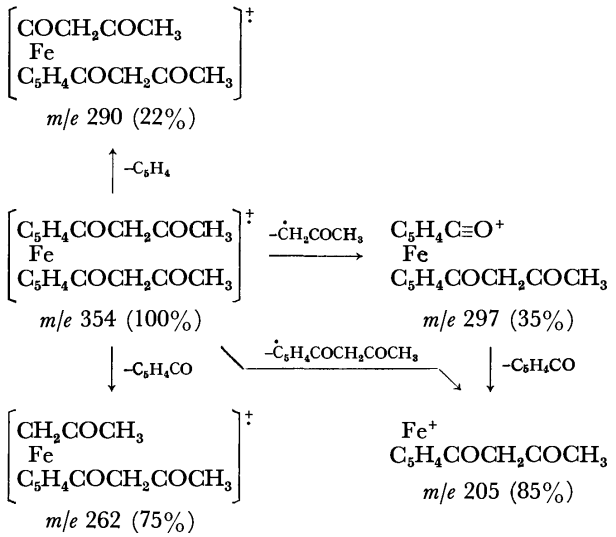

Scheme 4

Both ions of *m/e* 290 and 262 might be also transferred to *m/e* 205. This *m/e* 205 would seem to be further decomposed by a path similar to that shown in Scheme 3 because of the appearance of the *m/e* 163 (46%). As the other fragment ions, the *m/e* 270 (12%), corresponding to the molecular ion of I or III, and the *m/e* 178 (20%), which was confirmed by the cleavage of III, were observed in the spectrum.

The above results can be summarized as follows. (1) For the mono- and 1,1′-di-substituted ferrocenoyl compounds, II, III, and IV, but not I, the common mechanisms by which the rearrangement ions appear are given by:

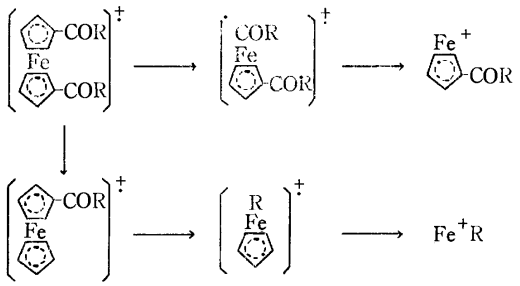

(R=OH or CH_2COCH_3)

(2) The fragment ions, such as $C_5H_5Fe^+C_5H_4$ (*m/e* 185), $\dot{C}_5H_4Fe^+C_5H_4$ (*m/e* 184), $Fe^+C_5H_5$ (*m/e* 121), $Fe^+\dot{C}_5H_4$ (*m/e* 120), and Fe^+ (*m/e* 56), observed by Mandelbaum *et al.*[6] were also observed by the cleavages of the fragment ions shown in Schemes 1, 2, 3, and 4.

Experimental

The mass spectra were obtained by means of a Japan Electron Optics Co., Ltd., JMS-01SG Mattauch-Herzog double-focussing mass spectrometer, at an ionizing voltage of 75 V, an emission current of 100 μA, and an accelerating voltage of 6.4 kV. The oven was maintained at 150°C.

1,1′-Diacetylferrocene (I). I was prepared from ferrocene by the method of Rosenblum and Woodward.[7] Recrystallization from benzene yielded a product with a mp of 130—131°C (lit,[7] mp 130—131°C).

1,1′-Ferrocenedicarboxylic Acid (II). II was prepared from I using the iodine-oxidation method.[8] The refined product decomposed at about 250°C (lit,[8] at more than 240°C decomp.).

Monoacetoacetylferrocene (III). III was prepared by the condensation of ethyl acetate with monoacetylferrocene in the presence of sodium amide.[9] Recrystallization from *n*-hexane yielded a product with a mp of 97—98°C (lit,[10] mp 97.5—98.5°C).

1,1′-Bisacetoacetylferrocene (IV). IV was prepared from I by the same method as III. Recrystallization from benzene yielded a product with a mp of 143—144°C (lit,[11] mp 142.5—144°C).

7) M. Rosenblum and R. B. Woodward, *J. Amer. Chem. Soc.*, **80**, 5443 (1958).
8) K. Yamakawa, H. Ochi, and K. Arakawa, *Chem. Pharm. Bull.*, **11**, 905 (1963).
9) H. Imai and Y. Yachashi, *Nippon Kagaku Zasshi*, **91**, 452 (1970).
10) L. Wolf and M. Beer, *Naturwissenschaften*, **44**, 442 (1957).
11) C. E. Cain, T. A. Mashburn, and C. R. Hauser, *J. Org. Chem.*, **26**, 1030 (1961).

BULLETIN OF THE CHEMICAL SOCIETY OF JAPAN, VOL. 45, 1266—1267(1972)

Multiple-Quantum Transitions in the EPR Spectra of Atomic Sulfur

Mamoru JINGUJI, Yuji MORI, and Ikuzo TANAKA

Department of Chemistry, Tokyo Institute of Technology, Ohokayama, Meguro-ku, Tokyo

(Received November 20, 1971)

The multiple-quantum transitions of atoms[1,2] and diatomic molecules[3] in the gas-phase EPR spectra have been reported and have attracted the attention of several scientists both theoretically and experimentally. The two-quantum transitions[1] in the EPR of $O(^3P_2)$ in the gas phase were among the first multiple-quantum transitions to be observed. The three- and four-quantum transitions to be observed. The three- and four-quantum transitions of $O(^3P_2)$ and the two-quantum transitions of $O(^3P_1)$ were observed by McDonald.[4] The EPR multiple-quantum transitions of S atoms have not yet been reported, however, in spite of the observation of the single-quantum transitions of S atoms by Brown[5] in 1966.

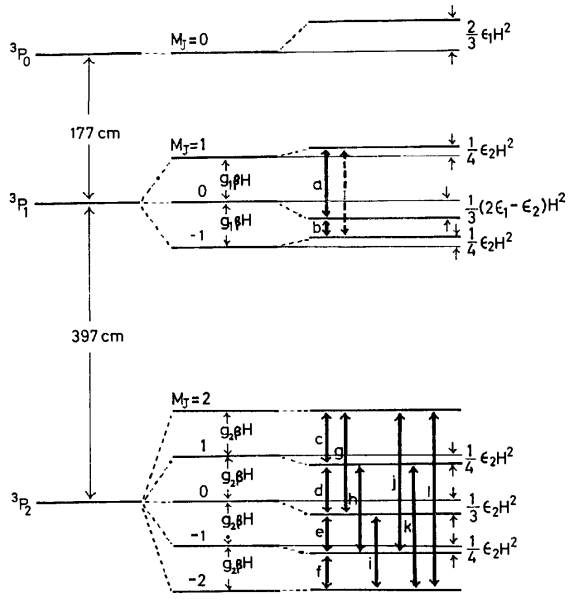

Fig. 1. Magnetic energy levels of the ground ^3P term in S atom (not to scale).
$\varepsilon_1=\beta^2/(177\ hc)$, $\varepsilon_2=\beta^2/(397\ hc)$ erg gauss^{-2}.

We have now observed the multiple-quantum transitions of $S(^3P_2)$ atoms. S atoms were produced in a 10-mm-i.d. quartz tube which passed through the center of a TE_{011}-mode EPR cavity resonant at 9168.64 MHz. A microwave discharge (2450 MHz, 100 W) was maintained in the flowing of wet H_2 40 cm upstream from the center of the cavity. Hydrogen sulfide was introduced at a point 5 cm upstream.

It is well known that the ground state of S atoms is the ^3P state and that it splits into three levels, $^3P_0$, $^3P_1$, and $^3P_2$, as a result of the spin-orbit interaction in the same manner as the O atom. The energy differences[6] are 177 cm^{-1} ($^3P_0$—$^3P_1$) and 397 cm^{-1} ($^3P_1$—$^3P_2$). The energy level diagram is schematically shown in Fig. 1. In the middle the diagram represents the linear Zeeman effect, while the quadratic level displacements are shown on the right side. The observed spectrum of the single-quantum transitions of S atoms is shown in Fig. 2, together with the spectrum of $O(^3P_2)$ for comparison. The four lines of $S(^3P_2)$ and the two lines of $S(^3P_1)$ are labeled from *a* though *f*, corresponding to the transitions shown in Fig. 1. The total pressure was kept at 0.05 Torr in order to achieve a better resolution of the spectra. The information required for its analysis may be obtained from the work of Radford and Hughes[7] on the spectrum of O atoms. As is shown in Table 1, the measured quadratic field splittings are in fair agreement with the spin-orbit coupling predictions, in spite of the possible errors in the measurement of the fine-structure separations of Fig. 1. The magnetic field was measured relative to the line positions of the spectrum of O atoms. The observed *g* factors for the $^3P_1$ and $^3P_2$ states of the S atom were the same as those reported by Brown.[5]

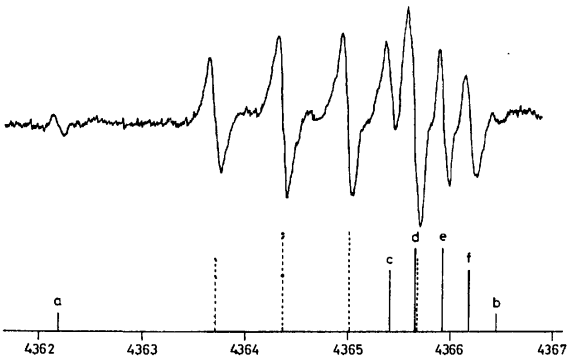

Fig. 2. EPR spectrum of S atom. O atom $J=2$ lines are shown for comparison.

We wish to report on an experiment demonstrating the multiple-quantum transitions among the Zeeman

Table 1. Comparison of measured quadratic field splittings with LS coupling theory

	Observed (gauss)	Calculated (gauss)
H_b—H_a	4.262±0.01	4.225
H_f—H_c	0.782±0.005	0.766
H_e—H_d	0.262±0.005	0.256

1) V. W. Hughes and J. S. Geiger, *Phys. Rev.*, **99**, 1842 (1955).
2) G. J. Wolga, *ibid.*, **127**, 805 (1962).
3) A. Carrington, D. H. Levy, T. A. Miller, and J. S. Hyde, *J. Chem. Phys.*, **47**, 4859 (1967).
4) C. C. McDonald, *ibid.*, **39**, 3159 (1963).
5) R. L. Brown, *ibid.*, **44**, 2827 (1966).
6) W. L. Wiese, M. W. Smith, and B. M. Miles, "Atomic Transition Probabilities," NSRDS-Natl. Bur. Std. (U. S.) 22, Vol. II (1969), p. 133.
7) H. E. Radford and V. W. Hughes, *Phys. Rev.*, **114**, 1274 (1959).

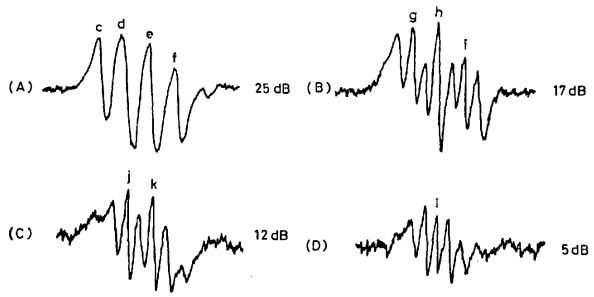

Fig. 3. EPR spectra of $S(^3P_2)$ showing the multiple-quantum transitions at increasing values of incident microwave power. Lines are labeled to correspond with Fig. 1.

levels of $S(^3P_2)$. At the pressure of 0.05 Torr, the spectrum was changed continuously as the microwave power was increased from a 25 to a 5 dB attenuation. The spectra showing the stages of these changes are presented in Fig. 3. At the 25-dB attenuation, only the single-quantum transitions (Fig. 3(A)) were detected. At this pressure, the linewidth of the single-quantum transition was 87 mG, corresponding to the relaxation time of 1.0 μsec. When the power was increased, the single-quantum transitions showed saturation broadening, and three new lines appeared between each two of the four lines of $S(^3P_2)$; the width of these new lines was approximately half the linewidth of the single-quantum transitions. The three new lines were assigned to the two-quantum transitions ($\Delta M_J=\pm 2$), which were more predominant in the spectrum at the 17-dB attenuation (Fig. 3(B)). A further increase in the microwave power produced two additional lines between the three lines of the two-quantum transitions, which could be interpreted as the three-quantum transitions ($\Delta M_J=\pm 3$). The single-quantum transitions vanished in the noise level, and the two-quantum transitions showed saturation broadening. At the 12-dB attenuation, the three-quantum transitions gave the strongest lines in the spectrum (Fig. 3(C)). Finally, between each two of the three-quantum transitions the four-quantum transition ($\Delta M_J=\pm 4$) could be detected at the 5-dB attenuation (Fig. 3(D)). Thus, by virtue of the different saturation properties of the various transitions, all the possible multiple-quantum transitions of $S(^3P_2)$ were observed. The two-quantum transitions of $S(^3P_1)$ were expected to be observable, but they could not be detected, probably because of the lower concentration of $S(^3P_1)$.

The theory of the multiple-quantum transitions in O atoms was developed by Hughes and Geiger,[1] it may be applied here to the case of S atoms. The linewidths of the multiple-quantum transitions were noticeably smaller than those of the single-quantum transitions, as would be expected from their theory. We estimated the minimum linewidths of the single-, two-, three-, and four-quantum transitions to be 87, 45, 35, and 33 mG respectively, though no completely-resolved lines were observed because of the rapid onset of pressure broadening. The three- and four-quantum transition lines may have been less sharpened experimentally than would theoretically be expected because of the 100 kHz modulation. It can also be expected from the theory that the intensities of the two- and three-quantum transitions are proportional to the square and cube of the microwave power respectively. This relation is confirmed by the experimental results shown in Fig. 4 (A) and (B).

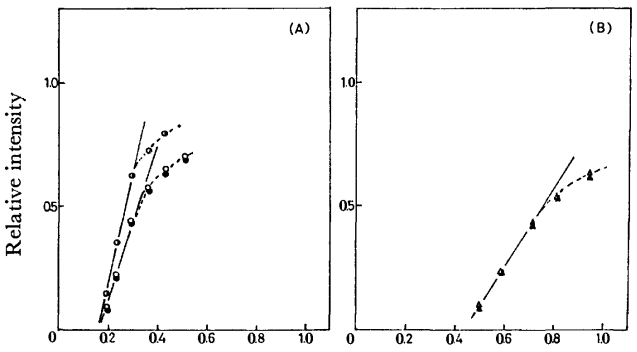

Fig. 4. The microwave power dependence of the intensities of the multiple-quantum transitions of $S(^3P_2)$.
(A) two-quantum transition.
○: $M_J=-2\rightarrow 0$, ◑: $M_J=-1\rightarrow 1$, ●: $M_J=0\rightarrow 2$.
(B) three-quantum transition.
△: $M_J=-2\rightarrow 1$, ▲: $M_J=-1\rightarrow 2$.

BULLETIN OF THE CHEMICAL SOCIETY OF JAPAN, VOL. 45, 1268—1269(1972)

Tracer Study of the Reaction of *p*-Toluenesulfinyl Chloride-^{36}Cl with Chloramine-T[1)]

Shigeru OAE, Mamoru NAKAI,* Naomichi FURUKAWA, and Reiko KIRITANI**

Department of Applied Chemistry, Faculty of Engineering, Osaka City University, Sumiyoshi-ku, Osaka

***Department of Chemistry, Radiation Center of Osaka Prefecture, Sakai, Osaka*

(Received May 26, 1971)

Recently, *N*-arenesulfonylareneiminosulfonyl chlorides were synthesized by the reaction of arenesulfinyl chlorides with dry *N*-arenesulfonyl chloramide,[2)] while *N*-alkaneiminosulfonyl chlorides were also prepared by treating the corresponding sulfinyl chlorides with *N,N*-dichloramine.[3)] However, the mechanism of the formation of these compounds has not been clarified. Therefore, in order to understand the nature of the reaction a tracer study on the reaction of *p*-toluenesulfinyl chloride-^{36}Cl with chloramine-T was carried out both in benzene and in THF solutions. This paper describes a detailed account and implications of the tracer experiments.

Results and Discussion

Following three mechanistic routes *i.e.* (1), (2), and (3) may be conceivable for this reaction.

(1) Initial Halogenation and Subsequent Nucleophilic Replacement.

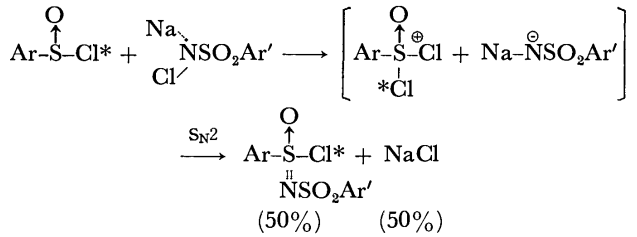

(2) Initial S_N2 Process Followed by Rearrangement of Chlorine Atom.

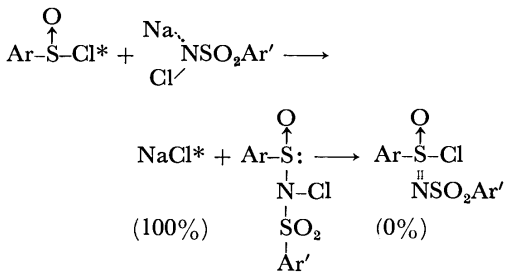

(3) Nitrene Mechanism.

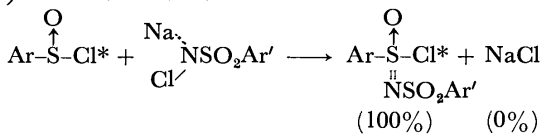

According to the first mechanism the sulfinyl chloride is chlorinated first by chloramine-T to form the dichlorosulfoxonium cation intermediate which upon nucleophilic attack of sulfonyl amide anion gives the product. Since the two chlorine atoms in the cation intermediate are equivalent, the iminosulfonyl chloride thus formed will retain 50% of the original ^{36}Cl-activity. The second mechanism which involves the initial nucleophilic attack of *N*-chlorosulfonyl function on sulfinyl chloride to form *N*-chlorosulfonylsulfineamide intermediate and the subsequent intramolecular migration of chlorine is quite reasonable and requires the final product to contain no ^{36}Cl-activity. The last mechanism which assumes the initial nitrene formation from chloramine-T will give the final product holding all the ^{36}Cl activity.

p-Toluenesulfinyl chloride-^{36}Cl was synthesized by the scheme outlined in Eq. (1).

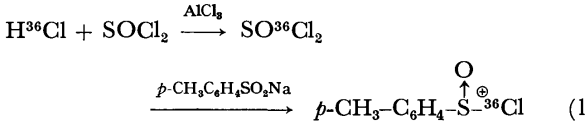

The reaction between *p*-toluenesulfinyl chloride-^{36}Cl thus obtained and dry chloramine-T was carried out in refluxing dry benzene or in dry THF at room temperature (Eq. 2). Since chloramine-T is insoluble in benzene, the reaction mixture is heterogeneous in benzene, while that in THF is homogeneous. In order to measure the ^{36}Cl activity, *p*-toluenesulfinyl chloride-^{36}Cl was oxidized to *p*-toluenesulfonyl chloride-^{36}Cl which was used as the standard sample. Meanwhile, the activity of the product, *N*-*p*-toluenesulfonyl-toluene-iminosulfonyl chloride-^{36}Cl, without further treatment, was measured with a liquid scintillation counter.

Furthermore, in order to check the possible chlorine atom exchange between the original sulfinyl chloride and iminosulfinyl chloride or sodium chloride obtained, an equimolar mixture of the ^{36}Cl-labeled sulfinyl chloride (4.85×10^4 dpm/mmol), the inactive iminosulfonyl chloride and sodium chloride was treated under the same condition as described above. Then it was found that the recovered iminosulfonyl chloride was incorporated with very little ^{36}Cl activity (1.21×10^2 dpm/mmol only, 0.25%), probably by the contamination during work up, indicating that actually ^{36}Cl-exchange between the starting material and the products did not take place. The above experimental results are summarized in Table 1.

The reaction proceeds faster in THF than in benzene and the value of the ^{36}Cl-activity of the product formed in THF is only 7.3%, while that formed in benzene is 23.7%. Perhaps, the sodium atom of chloramine-T

* Present address: Ube Industries Ltd., Ube, Yamaguchi-ken.

1) Sulfilimine and Sulfoximine Part VIII. Part VII. S. Oae, T. Aida, K. Tsujihara, and N. Furukawa, *Tetrahedron Lett.*, **1971**, 1145.

2) E. S. Levchenko, N. Ya. Derkash, and A. V. Kirsanov, *Zh. Obshch. Khim.*, **30**, 1971 (1960).

3) C. R. Johnson and E. U. Joneson, *J. Amer. Chem. Soc.*, **92**, 3815 (1970).

Table 1. The ^{36}Cl-counting data

Solvent	Condition	^{36}Cl-activity (dpm/mmol) $CH_3-C_6H_4-\overset{+}{S}(\rightarrow O)-{}^*Cl$	^{36}Cl-activity (dpm/mmol) $CH_3-C_6H_4-S(\rightarrow O)(=NTs)-{}^*Cl$
benzene	reflux 1 hr heterogeneous	4.85×10^4 (100%)	1.15×10^4 (23.7%)
THF	room temp. 1 hr homogeneous	4.85×10^4 (100%)	0.352×10^4 (7.3%)

is better solvated by THF than in benzene and hence the initial nucleophilic substitution of chloramine-T anion on the *p*-toluenesulfinyl chloride is facilitated, while the subsequent cleavage and migration of chlorine from the N-atom to the S-atom of the *N*-chlorosulfonyl-sulfinyl amide would also be faster in THF than in benzene. On the other hand, the reaction in benzene ought to be slow and somewhat different since the reaction mixture is heterogeneous and hence the reaction of the sulfinyl chloride would have to react with unionized chloramine. Therefore, it is somewhat complicated, though the main pathway would be a simple S_N2 process.

Thus the second mechanism which involves the initial nucleophilic attack of chloramine-T anion on the sulfinyl chloride and the subsequent chlorine migration seems to be the most plausible.

Experimental

The Preparation of Toluenesulfinyl Chloride-^{36}Cl. A small amount of aluminum chloride and sodium sulfate was added to 10 m*l* of thionyl chloride, then to this solution added 0.1 m*l* of active 3.55N hydrochloric acid-^{36}Cl (about 0.3 mCi/m*l*). After two hours, the solution was diluted with inactive thionyl chloride and then distilled twice.

p-Toluenesufinyl chloride-^{36}Cl was prepared by the same way as in the previous case[3] from the reaction of 19 m*l* of freshly distilled thionyl chloride-^{36}Cl with 7.4 g of sodium salt of toluenesulfinic acid.[5]

Oxidation of p-*Toluenesulfinyl Chloride-^{36}Cl.* An aliquote (about 0.2 m*l*) of *p*-toluenesulfinyl chloride-^{36}Cl was added to a solution of 1 g of anhydrous chromic acid in 5 m*l* of acetic acid. After half an hour, the reaction mixture was quenched into water, and then extracted twice with ether. The crude *p*-tosyl chloride-^{36}Cl thus obtained was recrystallized from ethanol - water.

The Reaction of p-*Toluenesulfinyl Chloride-^{36}Cl with Chloramine-T.* The reaction in benzene was carried out according to the procedure used by Levchenko and his co-workers.[2] The reaction in tetrahydrofuran was carried out at room temperature for one hour. The subsequent treatment of the product was performed in the same way as in benzene. The crude *N*-*p*-toluenesulfonyl-*p*-toluenеiminosulfonyl chloride thus obtained was recrystallized twice, from methanol, yield 70%, mp 76—77°C.

Measurement of the Activities. All the compounds were counted by a liquid scintillation counter (TRI-CARB), in toluene solution using POPOP and POP as scintillators.

We wish to thank Dr. M. Hamada of the Radiation Center of Osaka Prefecture, for his advices and affording facilities for the measurement of the activities.

4) I. B. Douglass and R. V. Norton, *J. Org. Chem.*, **33**, 2104 (1968).

5) H. Gilman, "Organic Synthesis," Coll. Vol. I (1941), p. 492.

SHORT COMMUNICATIONS

p-Quinols from the Nitration Product of Dihaloprehnitenes

Hitomi SUZUKI and Kiyomi NAKAMURA

Department of Chemistry, Faculty of Science, Kyoto University, Sakyo-ku, Kyoto

(Received December 27, 1971)

Nitration of halopentamethylbenzenes and dihalotetramethylbenzenes with fuming nitric acid gives, as a major product, benzyl nitrate or bis(nitro-oxymethyl)-benzene.[1,2] The crude product usually contains small amounts of carbonyl by-products arising from the oxidation of the nitro-oxymethyl compounds.[3] In a previous paper,[2] it was reported that 5,6-dihaloprehnitenes (5,6-dihalo-1,2,3,4-tetramethylbenzenes) are unusual in their ability to form a substantial amount (*ca.* 10—15%) of carbonyl compounds, the major component of which is now identified as 6-halo-4-nitro-2,3,4,5-tetramethyl-2,5-cyclohexadien-1-one (II), a new class of anomalous nitration product.

When 5,6-dichloroprehnitene was treated with fuming nitric acid (d=1.5) in dichloromethane at −5—0°C and the product mixture was subjected to chromatographic separation over alumina, using light petroleum, benzene and diethyl ether as eluents, the fractions eluted with a mixture of benzene and diethyl ether gave a carbonyl compound melting at 178—179°C as large prisms. The result of elemental analysis was consistent with the composition $C_{10}H_{13}ClO_2$ (Found: C, 60.0; H, 6.8; Cl, 17.3; O, 16.0%. Calcd for $C_{10}H_{13}ClO_2$: C, 59.8; H, 6.5; Cl, 17.5; O, 16.2%), and its infrared spectrum (in Nujol) showed prominent peaks at 766, 774, 902, 1073, 1083 (C–OH), 1224, 1270 (C–C=O), 1612 (C=C), 1636 (C=O), and 3400 cm^{-1} (OH). The possibility that the product is benzaldehyde or benzoic acid was immediately ruled out by its ^1H NMR spectrum (100 MHz, $CDCl_3$), which exhibited signals of four methyl groups (8.61, 8.19, 7.94, and 7.80 τ) and a hydroxyl group (*ca.* 7.0 τ). Ultraviolet spectrum (in CH_3OH) showed absorptions at 246—247 nm (log ε=4.08) and 286—287 nm (log ε= 3.34), which are characteristic of cross-conjugated cyclohexadienones. Comparison of the chemical shifts of its methyl groups with those of known polymethylcyclohexadienones readily revealed the presence of chlorine atom at a position next to the carbonyl group. The mass spectrum had a molecular ion peak at m/e 200, and fragment ion peaks at m/e 185 (M−CH_3), 165 (M−Cl), 157 (M−CH_3−CO), and 137 (M−Cl−CO). These spectral evidences permit the formulation of the ketonic product as *6-chloro-4-hydroxy-2,3,4,5-tetramethyl-2,5-cyclohexadien-1-one* (I, X=Cl). Since the infrared and ^1H NMR spectra of the original mixture had no indication of the presence of I, the quinol seems to be derived from the initially formed *6-chloro-4-nitro-2,3,4,5-tetramethyl-2,5-cyclohexadien-1-one* (II, X= Cl) through hydrolysis during the chromatographic treatment over alumina. The nitro group at 4-position of these systems is known to be subject to a facile hydrolysis.[4]

6-Bromo-4-hydroxy-2,3,4,5-tetramethyl-2,5-cyclohexadien-1-one (I, X=Br; mp 190—191°C) was similarly obtained from 5,6-dibromoprehnitene. IR: 739, 1070, 1085, 1216, 1260, 1607, 1637, and 3420 cm^{-1}; NMR: 8.64, 8.20, 7.98, 7.80 (CH_3), and *ca.* 7.3 τ (OH); UV: 248—249 (log ε=4.06) and 284—287 nm (log ε=3.30). Found: C, 49.0; H, 5.4%. Calcd for $C_{10}H_{13}BrO_2$: C, 49.0; H, 5.4%.

We suggest that the unusual product I is formed by the reaction sequence depicted in the Scheme. As the reaction seems to possess some synthetic potentials, the scope of the anomaly is being investigated.

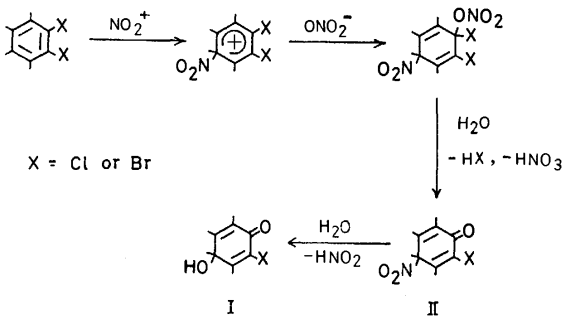

1) L. I. Smith and J. W. Horner, *J. Amer. Chem. Soc.*, **62**, 1349 (1940); H. Suzuki, This Bulletin, **43**, 481 (1970).

2) H. Suzuki, K. Nakamura, and M. Takeshima, *ibid.*, **44**, 2248 (1971).

3) H. Suzuki and K. Nakamura, *ibid.*, **43**, 473 (1970); H. Suzuki, *ibid.*, **43**, 879 (1970).

4) E. Müller, A. Schick, and K. Scheffler, *Chem. Ber.*, **92**, 474 (1959).

A Long-range Effect of Weaker π-Accepting Ligands, $M(C_6H_5)_3$ (M=P, As, and Sb), on the ^{119}Sn-Mössbauer Quadrupole Splitting in the R_3Sn-$Mn(CO)_4M(C_6H_5)_3$ Compounds

Satoru ONAKA and Hirotoshi SANO*,**

Department of Chemistry, Nagoya Institute of Technology, Showa-ku, Nagoya
**Department of Chemistry, Faculty of Science, Ochanomizu University, Bunkyo-ku, Tokyo*

(Received December 10, 1971)

We have recently reported that $(C_6H_5)_{3-x}X_xSn$–$Mn(CO)_5$ compounds show a smaller quadrupole splitting than their methyl analogues, $(CH_3)_{3-x}X_xSn$–$Mn(CO)_5$ (X=Cl and Br).[1] This finding has been interpreted in terms of the π-delocalizing effect of the phenyl group in $(C_6H_5)_{3-x}X_xSn$–$Mn(CO)_5$. It has also been pointed out that the π-interaction between tin and manganese atoms may affect the quadrupole splitting (Q.S.) in the ^{119}Sn-Mössbauer spectra of these compounds. The present studies were undertaken in order to provide evidence of the π-delocalizing effect of the phenyl group upon the Q. S. and to elucidate the π-interaction between tin and manganese atoms. For this purpose, the effect of the substitution of the CO group in R_3Sn–$Mn(CO)_5$ with a weaker π-accepting ligand L (L= $P(C_6H_5)_3$, $As(C_6H_5)_3$, or $Sb(C_6H_5)_3$) was studied.[2,3]

$(C_6H_5)_3Sn$–$Mn(CO)_4P(C_6H_5)_3$ and $(C_6H_5)_3Sn$–$Mn(CO)_4As(C_6H_5)_3$ were prepared by the method of Gorsich.[4] The other compounds not found in the literature were prepared by the direct replacement of CO with a ligand, L. The ^{119}Sn–Mössbauer spectra were measured against a barium stannate source moving in a constant acceleration mode at room temperature. The sample was used as an absorber and was kept at 79°K in a cryostat.

As is shown in Table 1, such a replacement causes no appreciable change in the isomer shift (I.S.), but it does cause a remarkable decrease in the Q.S. in methyl compounds; *i.e.*, $(CH_3)_3Sn$–$Mn(CO)_5$ gives a clearly-resolved quadrupole split spectrum, whereas $(CH_3)_3$-Sn–$Mn(CO)_4L$ gives a non-resolved spectrum, as is illustrated in Fig. 1. These results mean that the

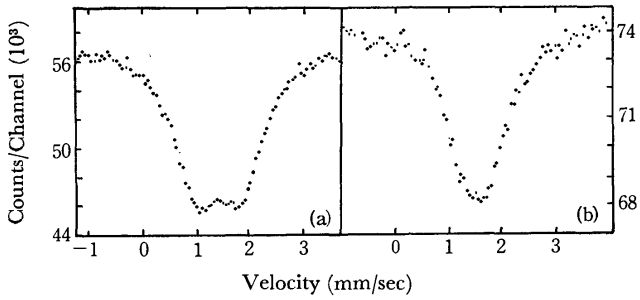

Fig. 1. Mössbaure spectra of (a) $(CH_3)_3Sn$–$Mn(CO)_5$ and (b) $(CH_3)_3Sn$–$Mn(CO)_4P(C_6H_5)_3$.

σ-characters of the Sn–Mn bond are not affected enough to be detected by the Mössbauer spectroscopy. It seems reasonable to conclude that the origin of the change in the electron distribution around the tin nucleus for methyl derivatives is due to the change in the π-interaction between tin and manganese atoms.[5]

IR spectroscopic study shows that these compounds have two peaks in the CO stretching region. The IR data and the results of the single crystal X-ray diffraction analysis for $(C_6H_5)_3Sn$–$Mn(CO)_4P(C_6H_5)_3$ indicate a *trans* configuration for all the substituted compounds; *i.e.*, the ligand, L, is coordinated to the manganese atom at the *trans* position with regard to the tin atom. In this *trans* configuration, the tin atom is supposed to compete with the ligand, L, for the d_π-electrons of the manganese atom. As the π-accepting ability of the ligand, L, is weaker than that of the substituted CO,[2,3] the d_π-electrons of manganese atom are forced to enter both the vacant 5*d* orbitals of the tin atom and the CO π-antibonding orbitals.[6] Thus, the π-accepting ability of the ligand, L, influences the efg around the tin nucleus through the π-electrons of the manganese atom. Such a long-range effect through the π-interaction should not be overlooked, although it has not yet been reported.[7]

The reason why the zero quadrupole splitting in $(C_6H_5)_3Sn$–$Mn(CO)_5$ is not affected by the replacement of CO with L may well be explained in terms of the predominant π-delocalizing effect of the phenyl groups attached to the tin atom.[1]

TABLE 1. ^{119}Sn-MÖSSBAUER PARAMETERS

Compound	I.S.[a] (mm/sec)	Q.S. (mm/sec)
$(CH_3)_3Sn$–$Mn(CO)_4P(C_6H_5)_3$	1.27	~0
$(CH_3)_3Sn$–$Mn(CO)_4As(C_6H_5)_3$	1.28	~0
$(CH_3)_3Sn$–$Mn(CO)_5$	1.33	0.61
$(C_6H_5)_3Sn$–$Mn(CO)_4(C_6H_5)_3$	1.43	0
$(C_6H_5)_3Sn$–$Mn(CO)_4As(C_6H_5)_3$	1.38	0
$(C_6H_5)_3Sn$–$Mn(CO)_4Sb(C_6H_5)_3$	1.40	0
$(C_6H_5)_3Sn$–$Mn(CO)_5$	1.41	0

a) All the isomer shifts are with respect to $BaSnO_3$ at room temperature.

** Present address: Department of Chemistry, Faculty of Science, Tokyo Metropolitan University, Fukazawa, Setagaya-ku Tokyo.

1) S. Onaka, Y. Sasaki, and H. Sano, This Bulletin, **44**, 726 (1971).
2) S. Onaka, *ibid.*, **44**, 2135 (1971).
3) F. Basolo and R. G. Pearson, "Mechanisms of Inorganic Reactions," Chapter VII, John Wiley & Sons, New York (1967).
4) R. D. Gorsich, *J. Amer. Chem. Soc.*, **84**, 2468 (1962).
5) X-ray analyses for $(C_6H_5)_3Sn$–$Mn(CO)_5$, $(CH_3)_3Sn$–$Mn(CO)_5$, and $(C_6H_5)_3Sn$–$Mn(CO)_4P(C_6H_5)_3$ indicate that the bond angles around the tin atom of $(CH_3)_3Sn$–$Mn(CO)_4L$ are not greatly distorted from the tetrahedral angle through the replacement; H. P. Weber and R. F. Bryan, *Acta Crystallogr.*, **22**, 822 (1967); R. F. Bryan, *J. Chem. Soc., A*, **1967**, 172; *ibid.*, **1968**, 696.
6) The increase in the π-characters between the manganese atom and the remaining CO is substantiated by their IR spectra, since the corresponding absorption peaks of ν(CO) shift to lower wave numbers in the substitution of *trans* CO.[2,3]
7) We have previously reported a similar long-range effect in ^{55}Mn–NMR for $Mn(CO)_5SnL_3$. S. Onaka, T. Miyamoto, and Y. Sasaki, This Bulletin, **44**, 1851 (1971).

Ionic Photodissociation of Some Weak Charge Transfer Complexes of Tetracyanoethylene with n-Type Donor Molecules

Yohji Achiba, Shunji Katsumata, and Katsumi Kimura

Physical Chemistry Laboratory, Institute of Applied Electricity Hokkaido University, Sapporo

(Received December 27, 1971)

During the last few years, several reports have appeared on ionic dissociation by photo-excitation of weak charge transfer (CT) complexes.[1-6] Potashnik *et al.*[4] and Masuhara *et al.*[5] studied spectroscopically the mechanisms of the ionic photo-dissociation process of some weak CT complexes composed of π-type donors and acceptors. We here report on preliminary results of the steady-state UV photolysis and flash photolysis of several weak CT complexes of tetracyanoethylene (TCNE) with tetrahydrofuran (THF), dioxane, acetonitrile, benzene and hexamethylbenzene. It is known that TCNE forms CT complexes with ether,[7] THF,[8] and dioxane[8] as n-type donors in nonpolar solvents at room temperature. We recently found that a weak CT complex is formed between donor acetonitrile and acceptor TCNE with an equilibrium constant of 1.86 *l*/mol at 25°C.[6]

Table 1. Wavelengths of the CT-band maxima (in nm units) of several TCNE complexes

Electron Donor	at 25°C			at 77°K	
ether	335[a]	335[b]	335[d]	320[a]	320[b]
THF	320[a]		318[e]	295[a]	
dioxane	345[a]		350[e]	325[a]	
acetonitrile	360[a]			325[a]	
benzene		380[c]	384[f]		380[c]
hexamethylbenzene		525[c]	545[f]	528 and	562[c]

a) The donor was used as a solvent. b) In ether-isopentane (1:1 and 1:2). c) In methylcyclohexane-isopentane (1:2). d) In ether (Ref. 7). e) In chloroform (Ref. 8). f) In dichloromethane (Ref. 7).

Ether, THF, dioxane, and acetonitrile were used as rigid solvents at 77°K. Since these rigid matrices are somewhat opaque, we used a 0.1-cm quartz cell capable of measuring absorption spectra with a Cary spectrophotometer, Model 15. Low-temperature photolyses of the rigid solutions were carried out with a high-pressure mercury lamp through Toshiba filter glasses UV-31 and -35 with which lights of wavelength shorter than 310 and 350 nm, respectively, are cut off. When ether, THF, dioxane, and acetonitrile were used as donor molecules, the CT bands are significantly enhanced and shifted to a shorter wavelength by freezing the solutions, as shown in Table 1. For the TCNE complexes with benzene and hexamethylbenzene, however, no such blue shifts were observed by freezing the solutions. The observed remarkable blue shifts seem to be a characteristic of the n-type CT complexes. The large blue shift (3000 cm^{-1}) observed for the CT band of the TCNE-acetonitrile system suggests that acetonitrile molecule acts as an n-type donor for TCNE.

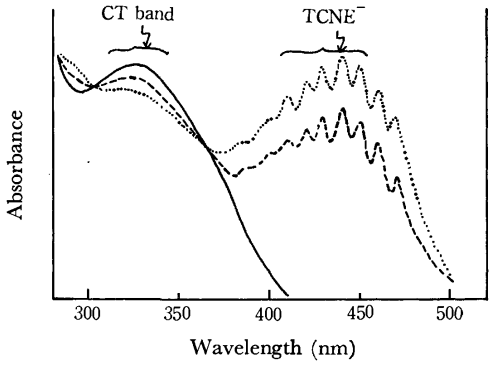

Fig. 1. Electronic absorption spectra showing the formation of TCNE⁻ by excitation of the CT band of the TCNE-dioxane complex in a dioxane rigid matrix at 77°K. Curve (——): before irradiation, and curves (·····) and (------): after irradiation through UV-31 and -35 respectively.

When a dioxane rigid matrix containing TCNE (10^{-3}M) was irradiated at 77°K by exciting the CT band of the TCNE-dioxane complex, the rigid matrix turned yellow, showing a new broad absorption band with vibrational structure exactly the same as that reported for the TCNE anion ($TCNE^-$), as shown in Fig. 1.

The same stable $TCNE^-$ species can be produced by the CT-band excitation in the cases of ether, THF and acetonitrile matrices at 77°K. We thus conclude that the ionic photodissociation takes place in the excited states of these complexes. It should be mentioned that in the case of the TCNE complexes with benzene and with hexamethylbenzene, no stable $TCNE^-$ species was formed by exciting their CTbands in a methylcyclohexane-isopentane matrix at 77°K.

Further photolytical experiments were performed with deaerated solutions containing TCNE (10^{-4}M) and one of the donors (about 1M) in dichloromethane by means of the flash spectroscopic technique. As a result, the transient $TCNE^-$ absorption spectrum was observed within 50 μsec in all the cases.[9] It should be mentioned that either in the absence of these donors or in the presence of oxygen no transient absorptions were detected.

1) C. Lagercrantz and M. Yhland, *Acta Chem. Scand.*, **16**, 1043, 1799, 1807 (1962).
2) D. F. Ilten and M. Calvin, *J. Chem. Phys.*, **42**, 3760 (1965).
3) W. C. Meyer, *J. Phys. Chem.*, **74**, 2119, 2122, 2127 (1970).
4) R. Potashnik, C. R. Goldschmidt, and M. Ottolenghi, *ibid.*, **73**, 3170 (1969).
5) H. Masuhara, M. Shimada, and N. Mataga, This Bulletin, **43**, 3316 (1970).
6) K. Kimura, Y. Achiba, and S. Katsumata, to be published.
7) R. E. Merrifield and W. D. Phillips, *J. Amer. Chem. Soc.*, **80**, 2778 (1958).
8) R. Vars, L. A. Tripp, and L. W. Pickett, *J. Phys. Chem.*, **66**, 1754 (1962).
9) The formation of long-lived $TCNE^-$ species by flash irradiation of rather concentrated solutions of TCNE in ether and acetonitrile has been reported by M. Sofue and S. Nagakura, This Bulletin, **38**, 1048 (1965).

Observation of Triplet-Triplet Absorption Spectra of Nitronaphthalenes by Means of Flash Excitation Technique

Nobuaki KANAMARU, Shigeo OKAJIMA, and Katsumi KIMURA

Physical Chemistry Laboratory, Institute of Applied Electricity, Hokkaido University, Sapporo

(Received December 31, 1971)

Aromatic hydrocarbons with the nitro group are known to have some peculiar characteristics in electronic structure and photochemical reactivity. Phosphorescence life times of nitrosubstituted aromatics are considerably shorter than those of non-substituted aromatics in spite of the nature of π-π^* type of the lowest triplet states of the aromatics having the nitro group.[1-4] Nitrobenzene is the only exception whose lowest triplet state is assigned to n-π^* type.[2,3] In order to obtain further information on characteristics of the triplet states of nitroaromatics, it seems important to measure their triplet-triplet (T-T) absorption spectra. So far, no reports have been published on T-T absorption spectra of nitroaromatics. This might be attributed to the short life times of their lowest triplet states and also to their reactivities. We report for the first time the T-T absorption spectra of some nitroaromatics obtained with a flash spectroscopic technique.[5]

Flash experiments of 1- and 2-nitronaphthalenes were carried out with various deaerated solutions (in n-hexane, liquid paraffin, ethanol, ether, and tetrachloromethane) at room temperature, and also with an ether–isopentane–alcohol (EPA, 5: 5: 2) glass at 77°K, giving transient absorption spectra in all cases. It was found that the transient absorption spectra are almost independent of the solvents. Typical spectra obtained with ethanol solutions of 1- and 2-nitronaphthalenes (1×10^{-4}M) are shown in Fig. 1. Each of the transient absorption spectra could be ascribed to only one sort of intermediate in either 1- or 2-nitronaphthalene. Life times of the transient absorptions in various solutions at room temperature were too short for an accurate measurement of decay curves. Intrinsic life times of the transient absorptions seem to be at most about 10 μsec at room temperature. It should be mentioned that the addition of oxygen remarkably reduces the intensities of the transient absorptions.

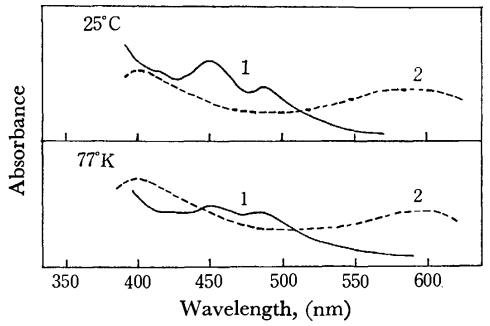

Fig. 1. Transient absorption spectra observed immediately (~0 μsec) after the flash irradiation of 1-nitronaphthalene (curve 1) and of 2-nitronaphthalene (curve 2) in deaerated ethanol solutions at room temperature and in EPA glasses at 77°K.

Transient absorption spectra obtained in the EPA glass at 77°K which are very similar to those obtained at room temperature are compared in Fig. 1. The decay curves of the transient absorptions observed at 77°K could be analyzed in terms of 60 ± 10 msec and 242 ± 10 msec for 1- and 2-nitronaphthalenes respectively in EPA at 77°K.

In order to compare the life time of the transient absorptions with that of phosphorescence under the same conditions, we also measured the phosphorescence life time for 1- and 2-nitronaphthalenes in EPA at 77°K with a Hitachi MPF-2A fluorescence spectrophotometer. As a result, we obtained a phosphorescence life time of 50 ± 2 msec for 1-nitronaphthalene, which is in good agreement with the reported values of 50 msec[1] and 47 msec[3], while a life time of 240 ± 6 msec was obtained for the phosphorescence of 2-nitronaphthalene.[6] Since the phosphorescence life times we obtained are in agreement with those of the transient absorptions within experimental limits of error, we conclude that the transient absorption spectra observed at room temperature as well as at 77°K can be assigned to the absorption spectra due to T-T transitions of 1- and 2-nitronaphthalenes.

1) D. S. McClure, *J. Chem. Phys.*, **17**, 905 (1949).
2) R. Hurley and A. C. Testa, *J. Amer. Chem. Soc.*, **90**, 1949 (1968).
3) R. Rusakowicz and A. C. Testa, *Spectrochim. Acta*, **27A**, 787 (1971).
4) E. C. Lim and J. Stanislaus, *Chem. Phys. Lett.*, **6**, 195 (1970).
5) The duration times of photolysisflash and spectroflash lamps are 5.0 and 3.5 μsec, respectively, quartz cells 10 cm long and 1 cm long being used at room temperature and 77°K, respectively. The output energy was about 400 joules. Transient absorption spectra were recorded photographically and their decay curves were followed photoelectrically.
6) The value 240 ± 6 msec differs somewhat from that reported by Rusakowicz and Testa who obtained a value of 206 msec in EPA at 77°K.[3] The difference might be attributed to the difference in experimental methods: We measured the decay curve of phosphorescence after cutting off stationary exciting light, while they employed the method of flash excitation.[3]

Stereospecific Dehydrobromination of *dl*- and *meso*-2,3-Dibromobutanes over Solid Catalysts

Makoto Misono and Yukio Yoneda

Department of Synthetic Chemistry, Faculty of Engineering, The University of Tokyo, Hongo, Bunkyo-ku, Tokyo

(Received December 20, 1971)

We have observed that the elimination of hydrogen bromide from the isomeric 2,3-dibromobutanes occurs in a stereospecific manner over some basic solid catalysts, giving products expected to be obtained by *anti*-elimination.

Elimination reactions in homogeneous liquid phase in the presence of basic catalyst usually proceeds stereospecifically by *anti*-elimination in *E*2 mechanism.[1] However, very few such stereospecific eliminations have been observed in the case of vapor phase elimination over solid catalyst. Non-catalytic debromination of 2,3-dibromobutanes with zinc was reported to give products expected by *anti*-elimination.[2] Pines and Manassen[3] postulated *anti*-elimination on the basis of the distribution of products obtained from the dehydration of cyclic alcohols such as menthol and neomenthol over alumina. Andreu *et al.*[4] reported that the dehydrobromination of 2,3-dibromobutanes over calcium chloride, sulfate and phosphate proceeded in a completely non-stereospecific way, leading them to propose an *E*1-like mechanism. If the elimination takes place by an *E*2-like mechanism as suggested by Pines and Manassen,[3] two sites on the surface of catalyst should simultaneously attack a reactant molecule, one from one side of the molecular plane and the other from the opposite side. It is of interest, also in this sense, to determine the steric course of reaction over solid catalyst.

We studied the products from the reaction of *meso*- and *dl*-2,3-dibromobutanes over sodium hydroxide and carbonate supported on silica gel (*ca.* 5 wt%) by a pulse technique at 120—200°C using hydrogen as a carrier gas. *dl*-2,3-Dibromobutane was prepared from *cis*-2-butene and bromine in methylene chloride. *meso*-2,3-Dibromobutane was prepared from *trans*-2-butene under the same conditions. Catalysts were prepared by impregnation on silica gel (Wako Chemicals, Q-12) from aqueous solution of each salt. Hydrogen was deoxygenated by a "Deoxo" purifier and dried by a dry ice trap. Products were analyzed by a glpc which was directly connected to a reactor and equipped with double columns, a dimethylsulfolane column for butene analysis and an Apiezon-grease column for the analysis of the rest. When necessary, products were analyzed after being collected with a trap inserted between the reactor and the glpc.

Table 1 Products from the elimination reaction of *dl*- and *meso*-2,3-dibromobutanes at 170°C

Catalyst	Reactant 2,3-Dibromobutane	% Conversion to 2-bromo-2-butene (-HBr) *trans*	2-bromo-2-butene (-HBr) *cis*	2-butene (-Br_2) *trans*	2-butene (-Br_2) *cis*
NaOH-SiO_2	*dl*-	6.3	<0.3	<0.1	0.6
	meso-	<0.3	5.3	0.8	<0.1
Na_2CO_3-SiO_2	*dl*-	8.0	<0.3	<0.1	0.8
	meso-	<0.5	6.5	1.1	<0.1

Typical results are given in Table 1. No reaction of 2-bromo-2-butenes or butenes was detected under these conditions. Stereospecific *anti*-elimination is clearly seen in this table; *dl*-2,3-dibromobutane gave *trans*-2-bromo-2-butene and *meso*-2,3-dibromobutane gave *cis*-2-bromo-2-butene. The stereoselectivity was higher than 90% for both cases in the temperature range investigated. Butene, coming from minor reaction of debromination, also showed a stereospecific *anti*-elimination. In addition, it was noted that *dl*-2,3-dibromobutane reacted faster than *meso*-2,3-dibromobutane in dehydrobromination, while the latter reacted faster in debromination, indicating favorable formation of *trans*-olefins in both reactions. This is likely due to an eclipsing effect between two methyl groups at the transition state.

Over silica gel, which was slightly acidic, no bromobutenes were formed, but formation of butenes expected by *anti*-debromination was observed together with a small amount of butadiene.

Financial support in part by the Kawakami Foundation is gratefully acknowledged.

1) J. F. Bunnett, "Survey of Progress in Chemistry," Vol. 5, Academic Press, New York (1969), p. 53.
2) M. Gordon and J. V. Hay, *J. Org. Chem.*, **33**, 427 (1968).
3) H. Pines and J. Manassen, "Advance in Catalysis," Vol. 16, Academic Press, New York (1966), p. 49.
4) P. Andreu, S. S. Zerain, and H. Noller, *An. Quim.*, **55**, 141 (1969); *Chem. Abstr.*, **71**, 2785z (1969).

Electrochemical Fluorination of *N*-Nitrosodiethylamine[1]

Nobuatsu WATANABE, Masatake HARUTA, and Byongte CHANG

Department of Industrial Chemistry, Faculty of Engineering, Kyoto University, Yoshida, Sakyo-ku, Kyoto

(Received May 31, 1971)

The fluorination of $(C_2H_5)_2N$–NO at a nickel anode under a variety of operating conditions resulted in the formation of liquid products such as $(CF_3)_2C_2F_5N$, $(C_2F_5)_2CF_3N$, $(C_2F_5)_3N$, and the compounds containing C–N groups together with gaseous fragmentation products such as CF_4, C_2F_6, CHF_3, NF_3, and N_2. Current efficiency of total gaseous products increased appreciably as the concentration of substrate and current density became higher. Effect of electrolysis temperature was so characteristic as observed in the fluorination of triethylamine that there existed the temperature at which a maximum value of current efficiency was given. On the basis of both the experimental results on the effects of operating conditions and the electrochemical measurements in hydrogen fluoride solutions of Et_2N–NO, mechanism of the fluorination reaction was discussed and compared with those of diethylamine and triethylamine.

Our previous work on the electrochemical fluorination of *n*-propyl, diethyl and triethyl amines[2] has shown that these amines underwent not only substitution reaction of hydrogen for fluorine but also simultaneous fragmentation reaction of C–N and C–C bonds in the molecule, and that the fragmentation reaction was appreciably affected by various operating conditions. Since it is reasonably expected that these substitution and fragmentation reactions are subject to an influence of a substituent in an amine molecule as well as the operating conditions, Et_2N–NO was chosen as a substrate to examine effect of *N*-nitroso group on the fluorination reaction. Many studies have been done on chemical or electrochemical fluorination of a series of representative amines, but no work on the fluorination of nitroso amine has yet been done. Effects of substrate concentration, electrolysis temperature and current density on the fluorination of Et_2N–NO were investigated by means of the method reported previously.[2]

Experimental

Materials. Et_2N–NO was prepared from diethylamine hydrochloride and sodium nitrite by the usual method.[3]

$$(C_2H_5)_2NH\cdot HCl + NaNO_2 \xrightarrow{2N\text{-HCl aq. soln.}} (C_2H_5)_2N\text{-}N{=}O + NaCl + H_2O$$

The prepared material was identified by its known infrared spectrum. The purity was checked up to be more than 99.5% by gas chromatography. The anhydrous hydrogen fluoride (purity 99.9%) was supplied by Daikin Co. Ltd.

Method. The apparatus and experimental methods used here were virtually identical with those described before.[2] The electrolytic cell used in the present study was an iron cylindrical vessel having a capacity of 700 m*l*, containing a pack of alternate nickel anodes and cathodes (99.9% in purity and 1 mm in thickness, effective anode area 3 dm^2). The liquid products collected in a dry ice–methanol trap were rectified in a low temperature precision still. Preparative separation of each fraction obtained by rectification was carried out with gas chromatography using Porapack R as column packing.

Results

Gaseous products. Results of the electrofluorination of *N*-nitrosodiethylamine under a variety of operating conditions are given in Table 1. Et_2N–NO yielded C_2F_6, NF_3, CF_4, CHF_3, N_2, and CO_2 as principal gaseous products and relatively small amounts of imperfectly fluorinated CHF_2CF_3, CHF_2CHF_2, and CH_2F_2. The current efficiency of each product was calculated according to the equation based on a discharge of fluorine ion as follows.

$$F^- \longrightarrow F\cdot + e \quad (1)$$

$$\rangle N\text{-}NO + 2F\cdot \longrightarrow N_2 + OF_2 \quad (2)$$

$$\rangle N\text{-} + 3F\cdot \longrightarrow NF_3 \quad (3)$$

$$\rangle C\langle + 2H_2O + 4F\cdot \longrightarrow CO_2 + 4HF \quad (4)$$

$$-C_2H_5 + 13F\cdot \longrightarrow 2CF_4 + 5HF \quad (5)$$

$$-C_2H_5 + 11F\cdot \longrightarrow C_2F_6 + 5HF \quad (6)$$

$$-C_2H_5 + 9F\cdot \longrightarrow 2CHF_3 + 3HF \quad (7)$$

$$-C_2H_5 + 5F\cdot \longrightarrow 2CH_2F_2 + HF \quad (8)$$

$$-C_2H_5 + 9F\cdot \longrightarrow CHF_2CF_3 + 4HF \quad (9)$$

$$-C_2H_5 + 7F\cdot \longrightarrow CHF_2CHF_2 + 3HF \quad (10)$$

The products obtained were identified by their known infrared spectra[4] except for CHF_2CHF_2 and N_2. N_2 was identified by gas chromatography equipped with Molecular Sieve 5A. CHF_2CHF_2 was identified by infrared and mass spectra as its spectral data were not given in the literature. Its infrared spectrum shows a strong absorption band at 8.9 μ and its mass spectrum is shown in Table 2.

The current efficiency for F_2 and OF_2 evolution was 0.3—1.0% for 2.4 mol% solution and 0.7—1.5% for 0.3 mol% solution, which indicated a tendency to increase with decreasing concentration. The current efficiency for dissolution of nickel electrode, calculated from the weight change before and at the end of electrolysis assuming that nickel dissolved as Ni^{2+} ion,

1) Presented at the Annual Meeting of the Chemical Society of Japan, April, 1971.

2) B. Chang, H. Yanase, K. Nakanishi, and N. Watanabe, *Electrochim. Acta*, **16**, 1179 (1971).

3) A.H. Blatt, "Organic Syntheses", Coll. Vol. II, 1950, p. 211.

4) J. H. Simons, "Fluorine Chemistry", Academic Press, New York, (1954), Vol. 2.

TABLE 1. OPERATING CONDITIONS FOR ELECTROCHEMICAL FLUORINATION OF Et_2N–NO

Concn. (mol%)	Temp. (°C)	C.d. (mA/cm²)	Cell voltage (V)	Current efficiency (%)									
				N_2	CF_4	NF_3	CO_2	C_2F_6	CHF_3	CH_2F_2	CHF_2CF_3	CHF_2CHF_2	Total
0.3	5±1	10	5.1	4.2	1.5	1.9	2.8	13.3	2.0	0.2	3.1	0.4	29.4
2.4	4±1	2	5.0	6.8	2.4	1.7	4.8	14.3	3.2	0.3	1.4	0.5	35.4
2.4	5±1	5	5.3	4.5	3.8	3.0	3.4	23.3	3.3	0.3	1.8	0.5	43.8
2.4	5±1	10	5.4	3.2	4.9	4.9	5.2	31.9	3.0	0.2	2.4	0.9	56.6
2.4	6±1	20	5.6	2.2	4.1	5.9	4.1	40.7	2.7	0.2	1.8	0.8	62.5
2.4	7±1	30	5.8	1.8	4.4	6.7	3.7	47.0	2.2	0.2	2.7	1.0	69.7
12.7	−25±2	20	6.9	3.4	5.1	7.0	2.2	51.8	1.0	—	1.6	0.9	73.0
12.7	−15±2	20	6.4	2.8	8.6	8.2	3.3	58.6	0.5	0.2	2.2	—	84.4
12.7	−2±2	20	5.9	3.2	9.1	8.4	4.3	58.5	1.6	—	1.7	0.2	87.0
12.7	9±1	20	5.6	3.4	8.6	8.2	4.7	57.6	1.6	—	2.5	0.6	87.2
12.7	19±2	20	5.5	3.9	8.2	6.7	4.9	45.6	2.0	—	2.4	0.5	74.2

TABLE 2. MASS SPECTRUM OF CHF_2CHF_2

m/e	Pattern coefficient	+Ion
51	100	CHF_2
83	44.3	CHF_2CHF
101	13.4	CHF_2CF_2
102	6.6	CHF_2CHF_2

amounted to 0.85%. This value is about three times as large as those in the fluorinations of diethylamine and triethylamine.

1) Effect of Substrate Concentration: In Fig. 1 are given the total current efficiencies of both anode and cathode gaseous products at three different concentrations 0.3, 2.4, and 12.7 mol% under the constant electrolysis temperature 5±1°C and current density 10 mA/cm². The current efficiency of total gases produced at the anode increases linearly with the logarithm of substrate concentration. The current efficiency for hydrogen evolution also increases with concentration but it does not exceed 40% at 0.3 mol%. Such a low value would be due to the recombination of hydrogen with fluorine which cannot be used for fluorination because of low concentration. On the assumption that the difference of current efficiency between gaseous anode products and hydrogen evolved at cathode is associated with the current efficiency of high boiling liquid products, it would be relatively advantageous to set up concentration around 2.5 mol% for the formation of liquid products less subject to the cleavage reaction. Figure 2 shows a trend that the molar formation ratios of imperfectly fluorinated CHF_2CF_3 and CHF_3 decrease with increasing concentration whereas those of C_2F_6, NF_3, and CF_4 increase. Molar ratio of NF_3 to N_2 is 0.31, 0.65, and 0.97 for 0.3, 2.4, and 12.7 mol% solution, respectively, which shows an increasing trend with concentration. Therefore, it is readily understood that concentration contributes to an acceleration of rate of fluorination. Molar ratio of C_2F_6 to NF_3 is about two, irrespective of substrate concentration, which is similar value as observed in the electrofluorination of diethylamine. The molar ratio of fluorinated ethanes C_2F_6, CHF_2CF_3, and CHF_2CHF_2 to fluorinated methanes CF_4, CHF_3, and CH_2F_2 increases with concentration; 2.18, 2.23, and 3.67 at 0.3, 2.4, and 12.7 mol%, respectively. This indicates that the higher the concentration is, the more readily C–N bonds are cleaved than C–C bonds.

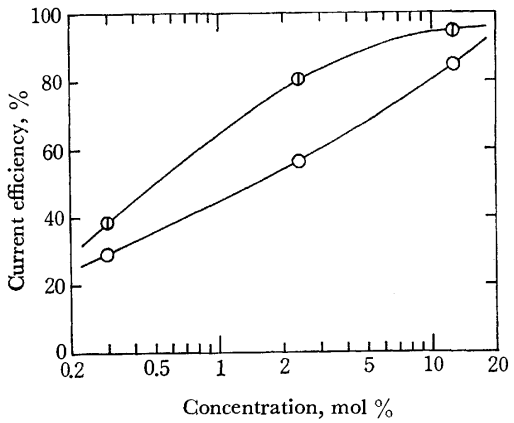

Fig. 1. Effect of concentration on the total current efficiency of gaseous products.
○: anode, ⓘ: cathode temperature: 5±1°C current density: 10 mA/cm²

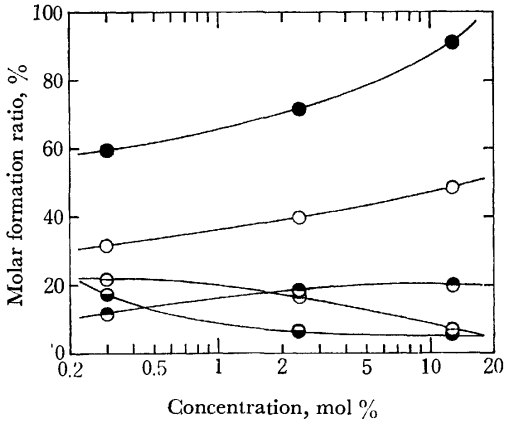

Fig. 2. Dependence of molar formation ratios of principal gaseous products on concentration.
●: C_2F_6, ○: NF_3, ◓: CF_4, ⊖: CHF_3, ◒: C_2HF_5
temperature: 5±1°C current density: 10 mA/cm²

2) Effect of Electrolysis Temperature: Figure 3 shows the effect of electrolysis temperature on the total current efficiency of gaseous products under constant concentration and current density. The total current efficiency increases rapidly in the range of −15—6°C at 2.4 mol%. On the other hand, there exists the tem-

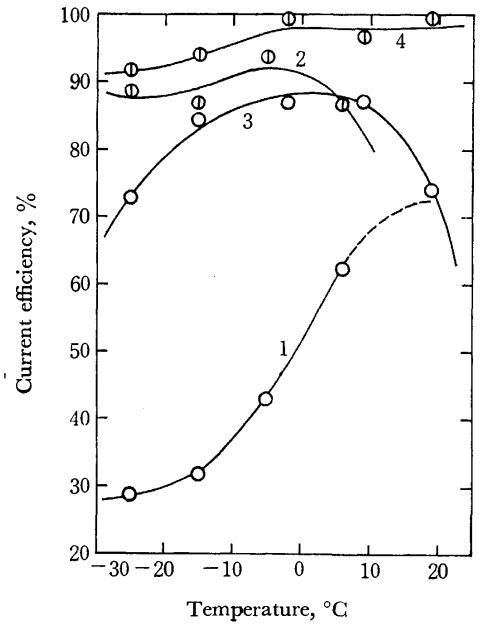

Fig. 3. Effect of temperature on the total current efficiency of gaseous products.
○: anode, ⓘ: cathode current density: 20 mA/cm²
1 and 2: 2.4 mol%, 3 and 4: 12.7 mol%

perature at which a maximum value of current efficiency is given at 12.7 mol%. It is obvious that the temperature dependence of current efficiency is not due to the recombination of fluorine with hydrogen, since the current efficiency of hydrogen evolution always exceeds 90%. The current efficiency of gaseous products for 12.7 mol% solution is always very high in the temperature range investigated and the maximum value reaches 87.2%, which implies that fragmentation takes place vigorously in the liquid phase. The relation is given in Fig. 4 between the current efficiencies of principal gaseous products and temperature for 2.4 mol% solution. The current efficiencies of NF_3 and CF_4 increased slightly while that of CHF_2CF_3 decreased slightly. An appreciable increase in the current efficiency was observed only for C_2F_6. It is also

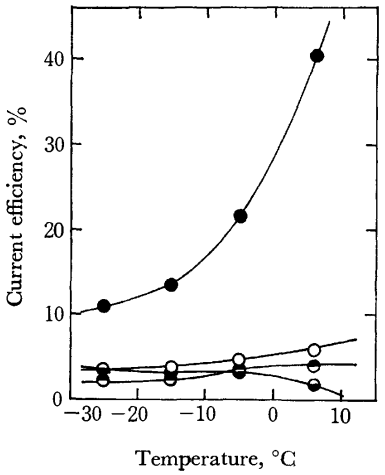

Fig. 4. Effect of temperature on the current efficiencies of principal gaseous products.
●: C_2F_6, ○: NF_3, ◓: CF_4, ◒: C_2HF_5
concentration: 2.4 mol% current density: 20 mA/cm²

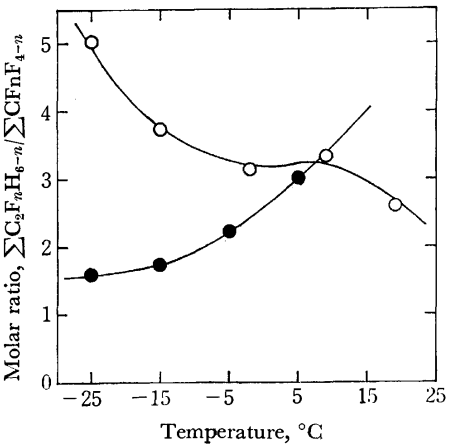

Fig. 5. Dependence of molar ratio of fluorinated ethanes to fluorinated methanes on temperature.
●: 2.4 mol%, ○: 12.7 mol%
current density: 20 mA/cm²

observed for 12.7 mol% solution that the current efficiency of C_2F_6 determines the temperature dependence of the total current efficiency of gaseous products. Since the molar formation ratios of CHF_3 and CHF_2-CF_3 decrease with temperature whereas that of C_2F_6 noticeably increases, it is evident that rate of fluorination is accelerated with increasing temperature. Figure 5 shows that molar ratio of C_2F_6 and CHF_2CF_3 to CF_4 and CHF_3 increases with temperature for 2.4 mol% solution, whereas it decreases for 12.7 mol% solution. As the boiling points of hexafluoroethane and pentafluoroethane are low compared with the electrolysis temperature, −78 and −23°C, respectively, it may scarecely occur that these fluorinated ethanes are subjected to further fluorination to yield fluorinated methanes. The fluorinated methanes may be produced from the scisson of C–C bonds before the breaking of C–N bonds occurs. Since most of the cleavage of C–C bonds would be thought to take place before C–N bonds are cleaved as stated above, the more readily C–N bonds are cleaved, the larger becomes the molar ratio of fluorinated ethanes to fluorinated methanes. Therefore, in order to restrain the breaking of C–N bonds, low concentration of Et_2N–NO and low temperature are prefered. But, if concentration is high, high temperature is prefered to low temperature.

In the case of Et_3N there existed the temperatures at which maximum values of current efficiency were given for both 2 and 10 mol% solutions, but only for 12.7 mol% solution in the case of Et_2N–NO. The fact that the temperature at the maximum value of current efficiency for 2 mol% solution of Et_3N was shifted to 7°C from −25°C for 10 mol% solution implies that the maximum value of current efficiency for 2.4 mol% solution of Et_2N–NO would be given at temperature higher than 15°C. Thus, it can also be concluded for the electrofluorination of Et_2N–NO that temperature has two opposing factors affecting the cleavage of bonds in a molecule: Solubilities of fluorinated products in HF solution is high at low temperature, and more likely to be exposed to further attack by fluorine. Low temperature makes, on the other hand, the fluorination reaction proceed mildly by taking away a large amount

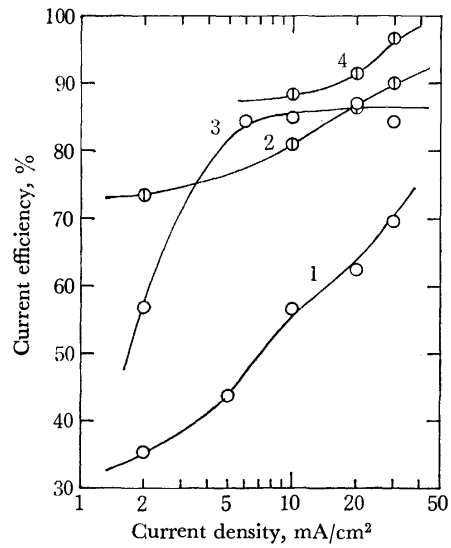

Fig. 6. Effect of current density on the total current efficiency of gaseous products.
○: anode, ◫: cathode
1 and 2: 2.4 mol%, 3 and 4: 12.7 mol%
temperature: 7±2°C

of heat of reaction. At high temperature, the reverse is the case.

3) Effect of Current Density: Effect of current density on the total current efficiency of gaseous products is shown in Fig. 6. A remarkable increase in current efficiency is observed for 2.4 mol% solution, while for 12.7 mol% solution it comes up to such a high value as 85% after a remarkable increase in the range of 2—5 mA/cm². The current efficiency for hydrogen evolution also shows an upward tendency with current density. It was observed that the increase in total current efficiency was mainly due to an increase in that of C_2F_6. Therefore it is understood that cleavage of C–N bonds occurs as current density becomes higher. Figure 7 shows the dependence of molar formation ratios of principal gaseous products on current density. C–N bonds are more readily cleaved than C–C bonds as current density is increased, since the ratio of C_2F_6 and CHF_2CF_3 to CF_4 and CHF_3 increases with current density. A tendency was observed that molar formation ratios of C_2F_6 and NF_3 increased with current density, while those of CHF_3 and CHF_2CF_3 decreased. This tendency is due to the fact that an increase in current density leads to higher concentration of fluorine and then to an acceleration of fluorination rate. The acceleration of rate of fluorination by increasing current density is also evidenced by the change of molar ratio of NF_3 to N_2; 0.17, 0.45, 0.65, 1.8, and 2.5 at 2, 5, 10, 20, and 30 mA/cm², respectively.

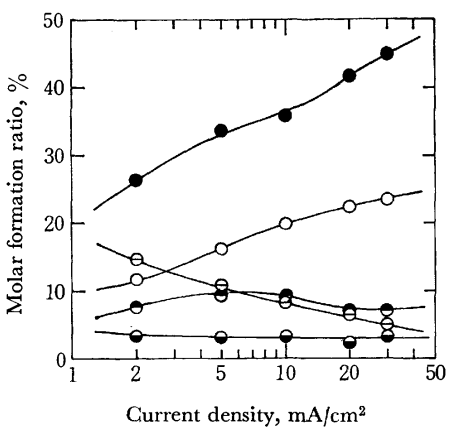

Fig. 7. Dependence of molar formation ratios of principal gaseous products on current density.
●: C_2F_6, ○: NF_3, ◓: CF_4, ⊖: CHF_3, ◒: C_2HF_5
concentration: 2.4 mol% temperature: 7±2°C

Liquid Products. Et_2N–NO fluorinated electrochemically gave a large number of liquid products together with the gaseous products descrbied above. Identification was carried out only on five principal liquid products, since the other liquid products were not obtained in sufficient amounts. Three of the principal liquid products were perfluorinated alkylation products $(C_2F_5)_2CF_3N$, $(C_2F_5)_3N$, and $(CF_3)_2C_2F_5N$. The first two were identified by their infrared spectra.[5] The last one was identified by its spectral data obtained in our laboratory.[2] Structural determination of the other two liquid products was unsuccessful. Nevertheless, some significant information on their structures was obtained by their infrared and ^1H NMR spectra. Their boiling points are above 70°C. Infrared spectrum of the lower boiling product (I) exibited absorption bands at 5.25 and 5.48 μ besides in the C–F stretching region, while that of the higher boiling one (II) exibited at 5.56 μ. These infrared absorptions may be assigned to the C=N stretching vibration.[6] The ^1H NMR spectra showed that both of them contained five hydrogen atoms. From the ^{19}F and ^1H NMR spectra the structure of II is supposed to be $CH_2FCH{=}NCH_2CF_3$, to which that of I would be analogous. These unsaturated compounds probably resulted from decomposition of the partially fluorinated dialkyl nitrosamines condensed in cold trap according to the following reaction;

$$R_1CHF\diagdown \atop R_2\diagup N\text{–}NO \xrightarrow{\text{decomposition at room temperature}} R_1CH{=}NR_2 + NOF \qquad (11)$$

Young *et al.*[7] described that although the dialkyl nitrosamines were reasonably stable thermodynamically and hydrolytically, the fluorinated compounds were unstable and lost the nitroso group readily due to increasing electronegativity of the alkyl groups. The formation of partially fluorinated dialkyl nitrosamines seemed to be apparent by appearance of a blue color presumably due to NO in liquid products condensed in cold trap.[7]

Electrochemical Measurements in HF–Et_2N–NO Solutions. The anodic behavior of nickel in liquid hydrogen fluoride (HF) containing Et_2N–NO has been investigated. The electrolytic cell and experimental procedures used in this study were essentially the same as those described in the preceding paper.[8] The reference electrode was Hg/Hg_2F_2, and potentials are reported *vs.* Hg/Hg_2F_2 at

5) C. M. Sharts, *J. Org. Chem.*, **33**, 1008 (1968).
6) J. B. Hynes, B. C. Bishop, P. Bandyopadhyay, and L. A. Bigelow, *J. Amer. Chem. Soc.*, **85**, 83 (1963).
7) J. A. Young, S. N. Tsuokalas, and R. D. Dresdner, *ibid.*, **82**, 396 (1960).
8) N. Watanabe, B. Chang, and K. Nakanishi, *Denki Kagaku*, **36**, 600 (1968).

0°C. Galvanostatic anodic polarization data were obtained on nickel electrodes in 2.5 and 10 mol% solutions in the current density range 0.01—50.0 mA/cm². Tafel-like region was observed in the range of 0.1—2.0 mA/cm² with slopes of about 440 and 280 mV/decade at the concentrations of 2.5 and 10 mol%, respectively. These values of Tafel slope are themselves unusually high, but relatively much smaller than the values obtained for diethylamine, triethylamine,[2] acetonitrile, and malononitrile.[9]

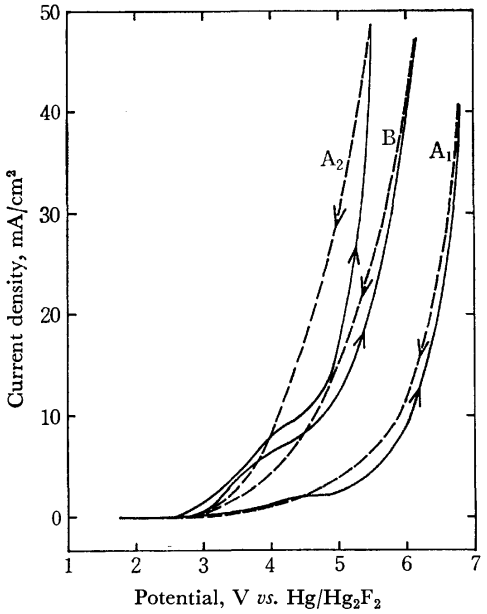

Fig. 8. Polarization curves for nickel in HF solutions of Et_2N–NO obtained by potential sweep method
A_1: new nickel in 10 mol% solution
A_2: nickel anodically polarized at 4.5V for 12 hr in 10 mol% solution
B: new nickel in 2.5 mol% solution
temperature: 0°C scan rate: 1V/min

Figure 8 shows polarization curves obtained by potential sweep method. Curves A_1 and B give the polarization curves on new nickel anodes in 10 and 2.5 mol% solutions, respectively. Compared the curve A_1 with B, it is evident that overpotential in HF solution is increased with increasing concentration of Et_2N–NO. It is also evident that nickel electrode is fairly activated when anodically biased at high potential, since an appreciable decrease in overpotential is observed on the nickel electrode anodically biased at 4.5 V for 12 hr, as shown in curve A_2 in Fig. 8. A plateau appeared around 4 V in all the curves, which is always observed for the anodic behavior of nickel in HF solution.

Figure 9 shows a polarization curve obtained by sweeping potential from 4.5 V with a scan rate of 0.2 V/sec. Cathodic current is observed below 2.4 V in curve 1, while a sharp increase in anodic current is observed above 2.6 in curve 2. The reversible fluorine potential in anhydrous hydrogen fluoride at −20°C has been reported to be +2.62 V *vs.* Hg/Hg_2F_2 by Hackerman *et al.*[10] Assuming that the cathodic current is a reduction current of fluorine adsorbed on the nickel anode, the cathodic charge required to reduce the fluorine is estimated to be about 1.3 mcoul/cm². This value is close to that in HF solution containing triethylamine.[2]

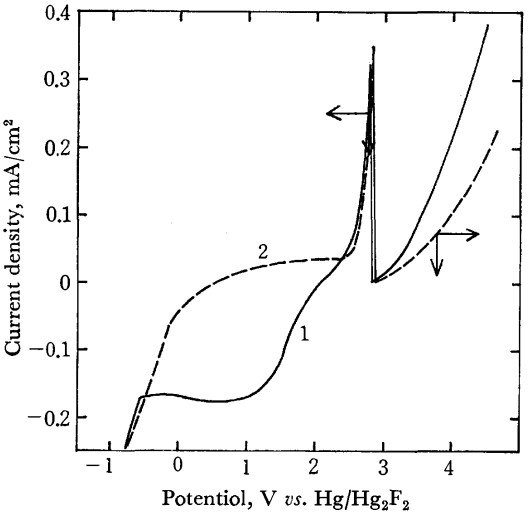

Fig. 9. Cathodic reduction curve of anodically polarized nickel electrode in 10 mol% solution.
scan rate: 0.2V/sec. temperature: 0°C

Discussion

In the present investigation on the electrochemical fluorination of Et_2N–NO, formation of the five liquid products and nine gaseous products was confirmed. However, nitrosyl fluoride which had been reasonably expected to be produced was not found in the products under any electrolysis conditions. This would be attributable to the following three reasons. Firstly, nitrosyl fluoride which is produced on the anode reacts with water contained a little in HF solution.[11]

$$2NOF + H_2O \longrightarrow NO + NO_2 + 2HF \qquad (12)$$

Secondly, it reacts with metal, rubber, or glass within the system before reaching the cold trap.[7] Finally, it reacts with hydrogen fluoride to form complexes.[12]

$$NOF + nHF \longrightarrow NO^+F(HF)_n^- \qquad (13)$$

Since the anhydrous hydrogen fluoride used was dried by pre-electrolysis passing a periodic reverse current and neither NO (bp, −151.8°C) nor NO_2 (bp, 21.3°C) was detected, and since fluorination was performed at relatively low temperature, the first and second reasons would not be essential. The last one would be a chief reason for the fact that formation of NOF was not confirmed. Although NOF is formed, it remains as complex with hydrogen fluoride in HF solution and can not be detected outside the electrolytic cell.

Figure 10 shows the total current efficiencies of gaseous products in the fluorination of Et_2NH, Et_2N–NO, and Et_3N under the same operating condition. The total current efficiency of gaseous products with

9) N. Watanabe, B. Chang, Y. Suhara, and K. Nakanishi, *ibid.*, **40**, 143 (1972).
10) N. Hackerman, E. S. Snavely, Jr., and L. D. Fiel, *Electrochim. Acta*, **12**, 535 (1967).
11) C. J. Hoffmann, R. G. Neville, *Chem. Rev.*, **62**, 1 (1962).
12) F. Seel, W. Birnkraut, and D. Werner, *Chem. Ber.*, **95**, 1264 (1962).

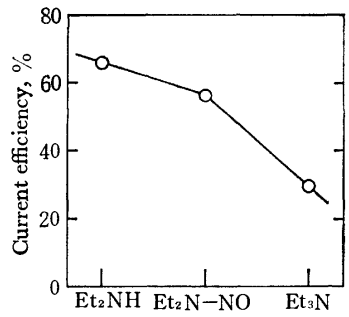

Fig. 10. Total current efficiencies of gaseous products in the fluorination of Et_2NH, Et_2N–NO, and Et_3N under the same operating conditions.
concentration: 2.2 ± 0.2 mol%
temperature: 5 ± 2°C
current density: 10mA/cm²

Et_2N–NO is slightly less than that with Et_2NH, but about twice as high as that with Et_3N. Since the total current efficiency of gaseous products is dependent upon the amount of cleavage, it may be concluded that the fluorination of Et_2NH and Et_2N–NO is accompanied with violent fragmentation, on the other hand fragmentation is noticeably restrained in the fluorination of Et_3N. Relation between substrate concentration and molar ratio of fluorinated ethanes to fluorinated methanes is given in Fig. 11 for Et_2N–NO and Et_3N. The

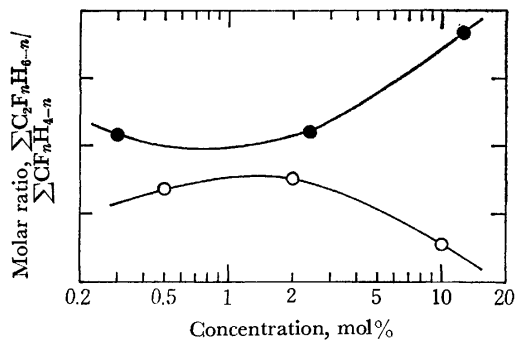

Fig. 11. Dependence of molar ratio of fluorinated ethanes to fluorinated methanes on concentration.
●: Et_2N–NO, ○: Et_3N temperature: 5 ± 1°C
current density: 10mA/cm²

values for Et_2N–NO are higher at any concentrations, which indicates that Et_2N–NO undergoes degradation more readily by the cleavage of C–N bonds than Et_3N. As concentration becomes higher, the molar ratio for Et_2N–NO increases while that for Et_3N decreases. This is indicative that C–N bonds are cleaved more preferentially than C–C bonds with increasing concentration in the fluorination of Et_2N–NO, on the contrary less preferentially in the fluorination of Et_3N. Thus it could be attributed to the stable C–N bonds against cleavage that the fluorination of Et_3N resulted in the formation of significant amounts of liquid products having the structure of the parent molecule. Et_2NH, on the other hand, did not yield detectable amounts of liquid products, since C–N bonds were almost completely cleaved. Et_2N–NO characteristically yielded as alkylation products the three completely fluorinated tertiary amines. In addition to them, the partially fluorinated dialkyl nitrosamines free from the cleavage of N–N bonds were thought to be formed. Formation of the above liquid products in the fluorination of Et_2N–NO indicates significant effects of *N*-nitroso group on the fluorination of dialkyl amines. Difference between the fluorination reaction of Et_2N–NO and that of Et_2NH also appeared in the effect of temperature on the formation of gaseous products. The maximum value of total current efficiency of gaseous products was not found at any temperatures ranged from −40 to +30°C in the fluorination of Et_2NH, whereas it was given around 5°C for 12.7 mol% solution in the fluorination of Et_2N–NO. In view of temperature effect on the formation of gaseous products, Et_2N–NO lies between Et_2NH and Et_3N. Assuming that the temperature effect is mainly due to steric hindrance by a substituent, effect of steric hindrance is in the order $H < NO < C_2H_5$, which is consistent with experimental results.

Although the fluorination of Et_2N–NO seems to proceed simultaneously by numerous routes, a representative mechanism is postulated which accounts for the scission and alkylation observed during the fluorination. During the replacement of hydrogen by fluorine a part of partially fluorinated dialkyl nitrosamines are bubbled out of a cell;

$$\text{cold trap} \xleftarrow{\text{decomposition}} CF_3CH_2N{=}CHCH_2F \quad \text{(II)}$$
$$\uparrow \text{bubbled out}$$
$$(C_2H_5)_2N\text{-}N{=}O \xrightarrow{\cdot F} (CF_3CH_2)(CH_2FCHF)N\text{-}N{=}O \qquad (15)$$

Most of the partially fluorinated dialkyl nitrosamines are followed by further fluorination since they still remain in the liquid phase because of their high solubilities in HF solution and high boiling points. During the fluorination at this stage, they are subjected to scission of bonds in molecules. Under milder operating conditions, especially at low concentration of substrate and low current density, cleavage of C–N bonds by carbon attack favorably occurs;

$$(CF_3CF_2)(R_1)N\text{-}N{=}O \xrightarrow[\text{C-attack}]{\cdot F} C_2F_6 + R_1F + N_2 + OF_2 \qquad (16)$$
(R_1; fluorinated alkyl group)

This is evidenced by the small molar ratio of NF_3 to N_2 at low concentration and low current density. As the operating conditions become vigorous, especially at the current density of 20—30 mA/cm², cleavage of N–N bonds takes place more readily than that of C–N bonds;

$$(CF_3CF_2)(R_1)N\text{-}N{=}O \xrightarrow[\text{N-attack}]{\cdot F} (CF_3CF_2)(R_1)N\cdot + NOF \qquad (17)$$
$$\downarrow HF$$
$$NO^+(FHF)^-$$

The fluorinated dialkyl amine radicals are successively attacked by fluorine until NF_3 is formed;

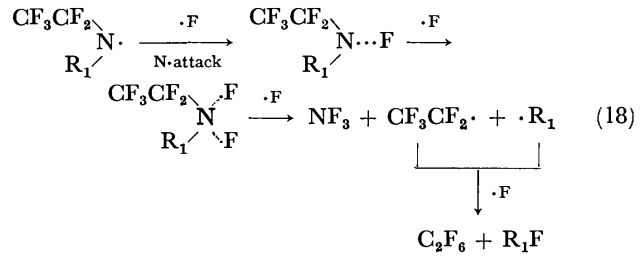

(18)

Fluorinated primary and secondary amines were completely absent in the products obtained in the fluorination of Et_2N–NO, which had been claimed as one of the characteristic features in electrochemical fluorination of nitrogen-containing compounds.[13] Nitrogen in an amine molecule is specifically oriented to Ni electrode, so that it is preferentially attacked by fluorine. NF_3 is formed probably through the transient state of fluorinated secondary and primary amines which are adsorbed on the nickel anode, as described in equation 18. This process would be explained well if fluorination took place between a loose complex of NiF_2 and ·F or F_2 and the substrate adsorbed on the anodic film.[14] The perfluoro dialkyl amine radicals are alkylated at nitrogen with perfluoro carbon radicals to produce perfluoro tertiary amines;

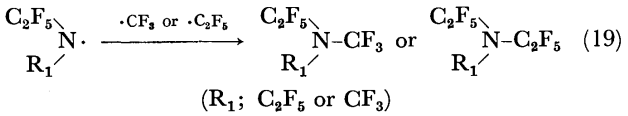

(19)

(R_1; C_2F_5 or CF_3)

We wish to express our appreciation to Dr. K. Nakanishi, assistant professor of Kyoto University, for his valuable suggestions in connection with this paper. We are also indebted to Dr. S. Nagase, Dr. H. Muramatsu and Mr. Baba, Government Industrial Research Institute in Nagoya, for a low temperature precision still and the measurement of ^{19}F NMR, and to Daikin Co. Ltd. for supplying anhydrous hydrogen fluoride.

13) J. A. Young and R. D. Dresdner, *J. Amer. Chem. Soc.*, **80**, 1889 (1958).

14) L. G. Spears and N. Hackerman, *J. Electrochem. Soc.*, **115** 452 (1968).

BULLETIN OF THE CHEMICAL SOCIETY OF JAPAN, VOL. 45, 1281—1288(1972)

Magnetic Circular Dichroism Studies on High-intensity Bands of d^8 Square-planar Metal Halides

Hajime KATÔ

Department of Chemistry, Faculty of Science, Kobe University, Kobe

(Received July 6, 1971)

The magnetic circular dichroism (MCD) of certain d^8 square-planar metal halides is studied theoretically on the basis of the molecular orbital theory. The ground state wavefunctions of $PtCl_4^{2-}$ and $PdCl_4^{2-}$ are calculated by the semi-empirical ASMO SCF MO method for valence electron systems. The line shape of the MCD of the allowed transition is investigated in detail; the calculated line shape is in good agreement with the observed line shape. The results strongly suggest that the transitions at 43400 cm^{-1} and 46200 cm^{-1} in $PtCl_4^{2-}$ are $^1A_{1g}\rightarrow{}^1A_{2u}(b_{2u}—3b_{1g}$ and $3a_{1g}—2a_{2u})$ and $^1A_{1g}\rightarrow{}^1E_u(5d—6p)$ respectively, and that the transition at 44900 cm^{-1} in $PdCl_4^{2-}$ is $^1A_{1g}\rightarrow{}^1E_u(1)$.

The electronic spectra of the d^8 square-planar metal halide complexes have been studied by many investigators,[1] and the spectrum has been assigned variously depending on the choice of the ordering of the orbital energy.[2-5] Interest has been focused on the absorption spectrum of $PtCl_4^{2-}$, the assignment of which has many different possibilities. The weak absorption spectrum of a single crystal of K_2PtCl_4 below 36000 cm^{-1} was observed with light polarized parallel to and normal to the symmetry axis of the $PtCl_4^{2-}$ ion.[3] The results of these observations have narrowed the assignment possibilities considerably. However, the polarized spectrum for the high-intensity band has not been reported because of the experimental difficulties.

The MCD spectra below 36000 cm^{-1} for a solution of K_2PtCl_4 in dilute HCl were first reported by Martin, Foss, and their coworkers.[6] The MCD spectra of $PtCl_4^{2-}$, $PdCl_4^{2-}$, $PdBr_4^{2-}$, $AuCl_4^-$, $AuBr_4^-$, and $Pd(NH_3)_4^{2+}$ in solution and K_2PtCl_4 crystal at 4°K

1) a) A. J. Cohen and N. Davidson, *J. Amer. Chem. Soc.*, **73**, 1955 (1951); b) A. J. Cohen and R. A. Plane, *J. Phys. Chem.*, **61**, 1096 (1957); c) G. H. Ayres and B. L. Tuffly, *Anal. Chem.*, **24**, 949 (1952); d) J. Chatt, G. A. Gamlen, and L. E. Orgel, *J. Chem. Soc.*, **1958**, 486, e) *Ibid.*, **1959**, 1047; f) J. G. Fraser, F. E. Beamish, and W. A. E. McBryde, *Anal. Chem.*, **26**, 495 (1954); g) S. Kida, This Bulletin **33**, 587 (1960); h) A. K. Gangopadhayay and A. Chakvavorthy, *J. Chem. Phys.*, **35**, 2206 (1961); i) C. K. Jφgensen, *Advan. Chem. Phys.*, **5**, 119 (1963).

2) R. F. Fenske, D. S. Martin, Jr., and K. Ruedenberg, *Inorg. Chem.*, **1**, 441 (1962); J. R. Miller, *J. Chem. Soc.*, **1965**, 713.

3) a) D. S. Martin, Jr., M. A. Tucker, and A. J. Kassman, *Inorg. Chem.*, **5**, 1298 (1966); *Ibid.*, **4**, 1682 (1965); b) D. S. Martin, Jr., and C. A. Lenhardt, *Ibid.*, **3**, 1368 (1964); c) H. B. Gray and C. J. Ballhausen, *J. Amer. Chem. Soc.*, **85**, 260 (1963); d) P. Day, A. F. Orchard, A. J. Thomson, and R. J. P. Williams, *J. Chem. Phys.*, **42**, 1973 (1965).

4) H. Basch and H. B. Gray, *Inorg. Chem.*, **6**, 365 (1967).

5) F. A. Cotton and C. B. Harris, *ibid.*, **6**, 369 (1967).

6) D. S. Martin, Jr., J. G. Foss, M. E. McCarrvulle, M. A. Tucker, and A. J. Kassman, *Inorg. Chem.*, **5**, 491 (1966).

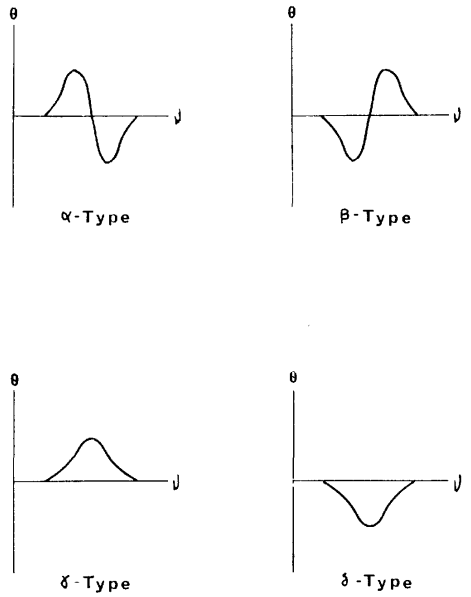

Fig. 1. The characteristic behavior of MCD in the vicinity of wave number corresponding to electronic absorption bands.

over the visible-UV spectral region were reported by McCaffery, Schatz, and Stephens.[7] The MCD curve exhibits its most striking characteristics in the vicinity of wavelengths corresponding to the electronic absorption bands. Some characteristic curves are shown in Fig. 1; we shall call them α-type, β-type, γ-type, and δ-type curves. The main features of the MCD curve around the absorption bands have been outlined previously,[8-10] and it has been shown that the MCD changes sign (α- or β-type) at the absorption maximum only when the excited state or the ground state is degenerate. However, the information which can be obtained from the difference between the α-type and β-type curves has not yet been used sufficiently. Further efforts in these areas are important, and considerable studies are expected.

In this paper, theoretical studies will be carried out on the MCD of the high-intensity bands of d^8 square-planar metal halides from the viewpoint of the MO theory. The line-shape of the MCD is studied in detail, and the observed bands are assigned on the basis of the line-shape analysis. As we will show later, this assignment does not depend strongly on the ordering of the calculated orbital energies. We give a quantitative discussion of the MCD intensity in $PtCl_4^{2-}$ and $PdCl_4^{2-}$, and it is then extended to the interpretation of the high-intensity bands in $PdBr_4^{2-}$, $AuCl_4^-$, and $AuBr_4^-$.

Calculations

A. Theory and MO Formulation. The quantum mechanical theory of MCD was developed around 1930,[11-14] and recently the quantitative expressions for the dispersion have been reported.[9,15,16] The contributions of the $a\rightarrow j$ transition to the MCD of molecules under a longitudinal magnetic field, H_s, along the z-axis are expressed as molar ellipticities in degrees deciliter decimeter^{-1} mole^{-1} gauss^{-1};[9]

$$[\theta(a\rightarrow j)]_M = \frac{18N}{\pi N_a^{(0)} H_s}\theta(a\rightarrow j) \tag{1}$$

where N is Avogadro's number, $N_a{}^{(0)}$, the number of molecules in the unperturbed state, a^0, per unit of volume, and $\theta(a\rightarrow j)$, the observed ellipticity in radians cm^{-1} given by:

$$\theta(a\rightarrow j) = -\frac{4\pi N_a}{\hbar c}\frac{\omega^3\Gamma_{ja}}{(\omega_{ja}^2-\omega^2)^2+\omega^2\Gamma_{ja}^2}Q(a\rightarrow j) \tag{2}$$

$$\begin{aligned}\theta(a\rightarrow j) = Im\{&\langle\Phi_a{}^0|m_x|\Phi_j{}^0\rangle\langle\Phi_j{}^0|m_y|\Phi_a{}^0\rangle \\ &+ H_s\sum_{k\neq a}(\langle\Phi_k{}^0|\mu_z|\Phi_a{}^0\rangle^*\langle\Phi_k{}^0|m_x|\Phi_j{}^0\rangle\langle\Phi_j{}^0|m_y|\Phi_a{}^0\rangle \\ &+ \langle\Phi_k{}^0|\mu_z|\Phi_a{}^0\rangle\langle\Phi_j{}^0|m_y|\Phi_k{}^0\rangle\langle\Phi_a{}^0|m_x|\Phi_j{}^0\rangle)/\hbar\omega_{ka}^0 \\ &+ H_s\sum_{k\neq j}(\langle\Phi_k{}^0|\mu_z|\Phi_j{}^0\rangle^*\langle\Phi_k{}^0|m_y|\Phi_a{}^0\rangle\langle\Phi_a{}^0|m_x|\Phi_j{}^0\rangle \\ &+ \langle\Phi_k{}^0|\mu_z|\Phi_j{}^0\rangle\langle\Phi_a{}^0|m_x|\Phi_k{}^0\rangle\langle\Phi_j{}^0|m_y|\Phi_a{}^0\rangle)/\hbar\omega_{kj}^0\},\end{aligned} \tag{3}$$

where $\boldsymbol{m}=\sum_i e_i\boldsymbol{r}_i$, $\boldsymbol{\mu}=\sum_i\frac{e_i}{2m_ic}[(\boldsymbol{r}_i\times\boldsymbol{p}_i)+2\boldsymbol{s}_i]$, N_a is the number of molecules in the state, a, per unit of volume in the presence of H_s, and Γ_{ja} is the band width at the half-maximum height of the $a\rightarrow j$ spectral line. The wavefunctions, $\Phi_a{}^0$, $\Phi_j{}^0$, and $\Phi_k{}^0$, are the eigenfunctions of the unperturbed states. If the a^0 and j^0 states are m-fold and n-fold degenerate respectively, the $\theta(a\rightarrow j)$ is given by $\theta(a\rightarrow j)=\sum_{m=1}^{m}\sum_{n=1}^{n}\theta(a_m\rightarrow j_n)$, and the degenerate state wavefunctions are required to diagonalize the magnetic moment, μ_z, in each degenerate state.

For the electronically-allowed transition $a\rightarrow j$ (that is, $\langle\Phi_a|\boldsymbol{m}|\Phi_j\rangle\neq 0$) of a complex with O_h, D_{4h}, and D_{4d} symmetry, the matrix elements, $\langle\Phi_a|\mu|\Phi_j\rangle$ and $\langle\Phi_a|\boldsymbol{\xi}|\Phi_j\rangle$ (where $\boldsymbol{\xi}=\sum_i e_i^2/(4m_ic^2)[\boldsymbol{r}_i(\boldsymbol{r}_i\cdot\boldsymbol{H}_s)-\boldsymbol{H}_s(\boldsymbol{r}_i\cdot\boldsymbol{r}_i)]$), are always equal to zero, because of symmetry properties.

In the present studies of d^8 square-planar metal halides, we choose the Cartesian coordinate system with its origin at the position of the metal atom and with the z-axis perpendicular to the molecular plane. In these complexes, the first term in Eq. (3) is non-zero only when the external magnetic field, $\boldsymbol{H}_s$, is applied in the z-direction. The ground state, a^0, is non-degenerate. Averaging over all the molecular orientations,[9] we obtain:

$$\begin{aligned}[\theta(a\rightarrow j)]_M = -\frac{720N}{\hbar c}\sum_{n=1}^{n}&\frac{\omega^3\Gamma_{j_na}}{(\omega_{j_na}^2-\omega^2)^2+\omega^2\Gamma_{j_na}^2} \\ &\times\{Q_A(a\rightarrow j_n)/H_s+Q_B(a\rightarrow j_n)\}\end{aligned} \tag{4}$$

where:

7) A. J. McCaffery, P. N. Schatz, and P. J. Stephens, *J. Amer. Chem. Soc.*, **90**, 5730 (1968).
8) P. J. Stephens, *J. Chem. Phys.*, **43**, 4444 (1965).
9) A. D. Buckingham and P. J. Stephens, *Ann. Rev. Phys. Chem.*, **17**, 399 (1966).
10) P. J. Stephens, *J. Chem. Phys.*, **52**, 3489 (1970).
11) L. Rosenfeld, *Z. Physik.*, **57**, 835 (1929).
12) H. A. Kramers, *Proc. Acad. Sci. Amsterdam*, **33**, 959 (1930).
13) R. Serber, *Phys. Rev.*, **41**, 489 (1932).
14) T. Carroll, *Phys. Rev.*, **52**, 822 (1937).
15) M. P. Groenewege, *Mol. Phys.*, **5**, 541 (1962).
16) P. J. Stephens, Theoretical Studies of Magneto-optical Phenomena (Doctoral thesis, Oxford Univ., Oxford 1964).

$$Q_A(a\to j_n) = \frac{1}{3}Im\{\langle\Phi_a^0|m_x|\Phi_{j_n}^0\rangle\langle\Phi_{j_n}^0|m_y|\Phi_a^0\rangle\} \quad (5)$$

and:

$$Q_B(a\to j_n) = \frac{1}{3}Im\{\langle\Phi_a^0|\boldsymbol{m}|\Phi_{j_n}^0\rangle\cdot\sum_{k\neq a}\frac{1}{\hbar\omega_{ka}^0}\langle\Phi_k^0|\boldsymbol{m}|\Phi_{j_n}^0\rangle \times\langle\Phi_k^0|\mu|\Phi_a^0\rangle + \langle\Phi_a^0|m|\Phi_{j_n}^0\rangle \cdot\sum_{k\neq j}\frac{1}{\hbar\omega_{kj_n}^0}\langle\Phi_k^0|\mu|\Phi_{j_n}^0\rangle\times\langle\Phi_k^0|m|\Phi_a^0\rangle\} \quad (6)$$

The wavefunctions for the ground state, a^0, and the excited state, j^0, can be constructed from the normalized anti-symmetrized product functions:

$$\Phi_a{}^0 = |a\bar{a}b\bar{b}|,\ \Phi_j{}^0 = \frac{1}{\sqrt{2}}\{|j\bar{a}b\bar{b}| - |\bar{j}ab\bar{b}|\} \quad (7)$$

where a and $\bar{a}$ denote the molecular orbitals, φ_a, with the spin functions of α and β respectively. The excited-state wavefunction, $\Phi_k{}^0$, must satisfy the conditions; $\langle\Phi_a{}^0|\boldsymbol{m}|\Phi_k{}^0\rangle\neq 0$ and $\langle\Phi_k{}^0|\boldsymbol{\mu}|\Phi_j{}^0\rangle\neq 0$.

Hence, the wavefunctions must be written as;

$$\Phi_k{}^0(a\to k) = \frac{1}{\sqrt{2}}\{|k\bar{a}b\bar{b}| - |\bar{k}ab\bar{b}|\}$$

or

$$\Phi_k{}^0(b\to j) = \frac{1}{\sqrt{2}}\{|a\bar{a}j\bar{b}| - |a\bar{a}\bar{j}b|\} \quad (8)$$

Then, in the molecular orbital form:

$$Q_A(a\to j) = \frac{2}{3}Im\{\langle a|m_x|j\rangle\langle j|m_y|a\rangle\} \quad (9)$$

and:

$$Q_B(a\to j) = \frac{2}{3}Im\left\{\langle a|\boldsymbol{m}|j\rangle\cdot\sum_k^{vac}\frac{1}{\hbar\omega_{k(a\to k)a}}\langle k|\boldsymbol{m}|j\rangle\times\langle k|\boldsymbol{\mu}|b\rangle + \langle a|\boldsymbol{m}|j\rangle\cdot\sum_{k\neq j}^{vac}\frac{1}{\hbar\omega_{k(a\to k)j}}\langle k|\boldsymbol{\mu}|j\rangle\times\langle k|\boldsymbol{m}|a\rangle\right\} - \frac{2}{3}Im\left\{\langle a|\boldsymbol{m}|j\rangle\cdot\sum_{b\neq a}^{occ}\frac{1}{\hbar\omega_{k(b\to j)a}}\langle a|\boldsymbol{m}|b\rangle\times\langle j|\boldsymbol{\mu}|b\rangle + \langle a|\boldsymbol{m}|j\rangle\cdot\sum_b^{occ}\frac{1}{\hbar\omega_{k(b\to j)j}}\langle a|\boldsymbol{\mu}|b\rangle\times\langle j|\boldsymbol{m}|b\rangle\right\} \quad (10)$$

B. Molecular Orbitals. Yonezawa and his coworkers[17] have proposed a semi-empirical SCF molecular orbital treatment for valence electron systems and have successfully applied it to various small molecules. The present MO calculation is similar to their treatment, but the previous method is improved so as to make it applicable to metal complexes. In the present MO treatment, all valence electrons in a compound are taken into account and all the overlap integrals are considered.

The molecular orbitals, φ's, are expressed as linear combinations of all the valence atomic orbitals, χ_r's, centered on the various atoms of the molecule:

$$\varphi_i = \sum_r C_{ir}\chi_r.$$

We take as χ_r the Slater-type atomic orbital, while the orbital exponents, ζ's, are taken from the tabulations of Clementi.[18] For a closed-shell molecule, the Roothaan SCF equation[19] is written as follows:

$$\sum_r C_{ir}(F_{rs}-S_{rs}\varepsilon) = 0 \quad (s = 1, 2, \cdots) \quad (11)$$

where:

$$F_{rs} = H_{rs} + \sum_{t,u}P_{tu}\{(rs|tu) - 0.5(rt|su)\}, \quad (12)$$

$$S_{rs} = \int\chi_r\chi_s d\tau, \quad (13)$$

$$H_{rs} = \int\chi_r(\mu)H_\mu^{core}\chi_s(\mu)d\tau_\mu, \quad (14)$$

$$(rs|tu) = \int\chi_r(\mu)\chi_s(\mu)\frac{1}{r_{\mu\nu}}\chi_t(\nu)\chi_u(\nu)d\tau_\mu d\tau_\nu, \quad (15)$$

$$P_{tu} = 2\sum_i^{occ}C_{it}C_{iu}. \quad (16)$$

The atomic integrals in the above equations are evaluated by the following approximations. For the electron repulsion integrals, $(rs|tu)$, the Mulliken approximation is adopted;[20]

$$(rs|tu) = 0.25S_{rs}S_{tu}\{(rr|tt) + (rr|uu) + (ss|tt) + (ss|uu)\}.$$

The one-center and two-center Coulomb repulsion integrals are calculated by means of:[21,22]

$$(rr|rr) = I_p{}^r - E_A{}^r,\ (rr|ss) = \frac{1}{R+a}$$

where $2/a = (rr|rr) + (ss|ss)$ and where R is the distance between the centers of r and s. The valence-state electron affinity, E_A, is assumed to be equal to the

Table 1. Molecular orbital energies(eV) and orbital characters for $PtCl_4^{2-}$

	Present method	SCCC-MO[a] Basch and Gray	Extended Hückel[b] Cotton and Harris
	$31.44e_u$	$14.8a_{1g}$	8.51
	$21.59a_{1g}$	$11.0e_u$	4.21
	$5.76a_{2u}$; $6p_z$	$-3.6a_{2u}$: $6p_z$	$-4.70a_{2u}$: $6p_z$
L.V.	$1.28b_{1g}$: $5d_{x^2-y^2}$	$-8.0b_{1g}$: $5d_{x^2-y^2}$	$-6.76b_{1g}$: $5d_{x^2-y^2}$
H.O.	$-7.88b_{2g}$: $5d_{xy}$	$-11.5b_{2g}$: $5d_{xy}$	$-10.49b_{2g}$: $5d_{xy}$
	$-7.96e_g$: $5d_{xz,yz}$	$-12.3e_g$: $5d_{xz,yz}$	$-10.68e_g$: $5d_{xz,yz}$
	$-8.02a_{1g}$: $5d_{z^2}$	$-13.3a_{1g}$: $5d_{z^2}$	$-10.98a_{1g}$: $5d_{z^2}$
	$-9.79b_{1g}$	$-13.6b_{2u}$	$-13.49b_{1g}$
	$-9.84e_u$	$-13.6a_{2g}$	$-13.83e_u$
	$-10.00a_{2g}$	$-13.7e_u$	-14.18
	$-10.32b_{2u}$	$-13.7a_{2u}$	-14.58
	$-10.52e_g$	$-14.9e_g$	-14.71
	$-11.35b_{2g}$	$-15.0e_u$	-14.82
	$-11.44a_{2u}$	$-15.2b_{2g}$	-15.09
	$-11.47e_u$	$-16.5a_{1g}$	-15.41
	$-11.77a_{1g}$	$-16.7b_{1g}$	-16.10
	$-18.94b_{1g}$	$-25.4e_u$	-23.29
	$-19.46e_u$	$-25.8b_{1g}$	-23.50
	$-20.06a_{1g}$	$-26.0a_{1g}$	-24.04
Charge on Pt	$=+0.31$	$+0.24$	$+0.44$
Pt–Cl bond order	$=0.489$		0.403

a) Ref. 4, b) Ref. 5.

17) T. Yonezawa, K. Yamaguchi, and H. Kato, This Bulletin **40**, 535 (1967), H. Kato, H. Konishi, and T. Yonezawa, *ibid.*, **40**, 1017 (1967).

18) E. Clementi and D. L. Raimondi, *J. Chem. Phys.*, **38**, 2686 (1963).

19) C. C. J. Roothaan, *Rev. Mod. Phys.*, **32**, 69 (1951).

20) R. S. Mulliken, *J. Chem. Phys.*, **46**, 497, 675 (1949).

21) R. Pariser, *J. Chem. Phys.*, **21**, 568 (1953), R. Pariser and R. G. Parr, *ibid.*, **21**, 767 (1953).

22) N. Mataga and K. Nishimoto, *Z. Physik. Chem. N.F.*, **13**, 140 (1957).

experimental value, and the valence-state ionization potential, I_p, is assumed to be equal to the valence orbital ionization potential (*VOIP*).[23] The values used are given in eV as follows; $(3s3s|3s3s)_{Cl}=9.57$, $(3p3p|3p3p)_{Cl}=11.30$, $(5s5s|5s5s)_{Pd}=7.56$, $(5p5p|5p5p)_{Pd}=3.85$, $(4d4d|4d4d)_{Pd}=8.51$, $(6s6s|6s6s)_{Pt}=8.73$, $(6p6p|6p-$

Table 2a. Molecular orbital for $PtCl_4^{2-}$

MO	Coefficients												
	$6s$	$6p_x$	$6p_y$	$6p_z$	$5d_{xz}$	$5d_{yz}$	$5d_{xy}$	$5d_{x^2-y^2}$	$5d_{z^2}$	$3s^1$	$3p_x^1$	$3p_y^1$	$3p_z^1$
$1a_{1g}$	0.21	0	0	0	0	0	0	0	−0.01	0.44	0.01	0	0
$1e_u$	0	0.14	0	0	0	0	0	0	0	0.65	0.04	0	0
	0	0	0.14	0	0	0	0	0	0	0	0	0.02	0
$1b_{1g}$	0	0	0	0	0	0	0	−0.03	0	0.50	−0.04	0	0
$2a_{1g}$	−0.24	0	0	0	0	0	0	0	0.15	0.12	0.43	0	0
$2e_u$	0	−0.20	0	0	0	0	0	0	0	0.13	0.41	0	0
	0	0	−0.20	0	0	0	0	0	0	0	0	−0.49	0
$1a_{2u}$	0	0	0	0.26	0	0	0	0	0	0	0	0	0.44
$1b_{2g}$	0	0	0	0	0	0	0.21	0	0	0	0	0.47	0
$1e_g$	0	0	0	0	0.22	0	0	0	0	0	0	0	0.69
	0	0	0	0	0	0.22	0	0	0	0	0	0	0
b_{2u}	0	0	0	0	0	0	0	0	0	0	0	0	−0.50
a_{2g}	0	0	0	0	0	0	0	0	0	0	0	−0.51	0
$3e_u$	0	−0.10	0	0	0	0	0	0	0	0.01	0.50	0	0
	0	0	−0.10	0	0	0	0	0	0	0	0	0.50	0
$2b_{1g}$	0	0	0	0	0	0	0	0.29	0	0.03	−0.47	0	0
$3a_{1g}$	−0.15	0	0	0	0	0	0	0	−0.98	0.04	0.07	0	0
$2e_g$	0	0	0	0	−0.98	0	0	0	0	0	0	0	0.18
	0	0	0	0	0	0.98	0	0	0	0	0	0	0
$2b_{2g}$	0	0	0	0	0	0	−0.98	0	0	0	0	0.13	0
$3b_{1g}$	0	0	0	0	0	0	0	0.97	0	−0.07	0.21	0	0
$2a_{2u}$	0	0	0	1.03	0	0	0	0	0	0	0	0	−0.29
$4a_{1g}$	1.27	0	0	0	0	0	0	0	−0.16	−0.40	0.35	0	0
$4e_u$	0	0	1.42	0	0	0	0	0	0	0	0	−0.25	0
	0	−1.42	0	0	0	0	0	0	0	0.67	−0.48	0	0

Table 2b. Molecular orbital and orbital energy(eV) for $PdCl_4^{2-}$

	MO Symmetry	Orbital energy	$5s$	$5p_x$	$5p_y$	$5p_z$	$4d_{xz}$	$4d_{yz}$	$4d_{xy}$	$4d_{x^2-y^2}$	$4d_{z^2}$	$3s^1$	$3p_x^1$	$3p_y^1$	$3p_z^1$
1	$1a_{1g}$	−19.83	0.19	0	0	0	0	0	0	0	−0.01	0.44	0.01	0	0
2	$1e_u$	−19.31	0	0.13	0	0	0	0	0	0	0	0.65	0.04	0	0
3			0	0	0.13	0	0	0	0	0	0	0	0	0.02	0
4	$1b_{1g}$	−18.85	0	0	0	0	0	0	0	−0.02	0	−0.50	−0.04	0	0
5	$2a_{1g}$	−11.64	−0.24	0	0	0	0	0	0	0	0.15	0.12	0.42	0	0
6	$2e_u$	−11.35	0	−0.20	0	0	0	0	0	0	0	0.12	0.41	0	0
7			0	0	−0.20	0	0	0	0	0	0	0	0	−0.48	0
8	$1a_{2u}$	−11.26	0	0	0	0.25	0	0	0	0	0	0	0	0	0.44
9	$1b_{2g}$	−11.20	0	0	0	0	0	0	0.20	0	0	0	0	0.48	0
10	$1e_g$	−10.37	0	0	0	0	0.21	0.01	0	0	0	0	0	0	0.69
11			0	0	0	0	−0.01	0.21	0	0	0	0	0	0	−0.02
12	b_{2u}	−10.18	0	0	0	0	0	0	0	0	0	0	0	0	−0.50
13	a_{2g}	− 9.83	0	0	0	0	0	0	0	0	0	0	0	−0.51	0
14	$3e_u$	− 9.70	0	−0.05	−0.08	0	0	0	0	0	0	0	0.27	0.43	0
15			0	−0.08	0.05	0	0	0	0	0	0	0	0.42	−0.27	0
16	$2b_{1g}$	− 9.46	0	0	0	0	0	0	0	0.26	0	0.04	−0.48	0	0
17	$3a_{1g}$	− 8.39	0.12	0	0	0	0	0	0	0	0.99	−0.03	−0.06	0	0
18	$2e_g$	− 8.36	0	0	0	0	−0.74	0.64	0	0	0	0	0	0	0.13
19			0	0	0	0	0.64	0.74	0	0	0	0	0	0	−0.11
20	$2b_{2g}$	− 8.32	0	0	0	0	0	0	−0.98	0	0	0	0	0.12	0
21	$3b_{1g}$	0.44	0	0	0	0	0	0	0	0.97	0	−0.05	0.19	0	0
22	$2a_{2u}$	5.72	0	0	0	1.03	0	0	0	0	0	0	0	0	−0.28
23	$4a_{1g}$	20.15	1.26	0	0	0	0	0	0	0	−0.12	−0.38	0.34	0	0
24	$4e_u$	28.27	0	−0.21	1.37	0	0	0	0	0	0	0.09	−0.07	−0.24	0
25			0	−1.37	−0.21	0	0	0	0	0	0	0.59	−0.48	0.04	0

23) H. Basch, A. Viste, and H. B. Gray, *J. Chem. Phys.*, **44**, 10 (1966).

TABLE 3. CALCULATED EXCITATION ENERGIES AND TRANSITION MOMENTS

Transition $i \rightarrow j$	$\delta E(i \rightarrow j)$ (eV)	$\lvert\langle \Psi_i \lvert r \rvert \Psi_j \rangle\rvert^2$ (a_0^2)	$\delta E(i \rightarrow j)$ (eV)	$\lvert\langle \Psi_i \lvert r \rvert \Psi_j \rangle\rvert^2$ (a_0^2)
	$PtCl_4^{2-}$		$PdCl_4^{2-}$	
$^1A_{1g} \rightarrow {}^1E_u$ (1) : $[3e_u - 3b_{1g}]$	7.391	1.166	6.367	0.682
$^1A_{1g} \rightarrow {}^1E_u$ (2) : $[2e_u - 3b_{1g}]$	8.755	0.639	7.794	0.434
$^1A_{1g} \rightarrow {}^1E_u$ $(d-p)$: $[2e_g - 2a_{2u}]$	7.673	0.414	8.357	0.313
$^1A_{1g} \rightarrow {}^1A_{2u}$ (1) : $[b_{2u} - 3b_{1g}]$	7.628	0.010	6.671	0.004
$^1A_{1g} \rightarrow {}^1A_{2u}$ $(d-p)$: $[3a_{1g} - 2a_{2u}]$	7.603	0.757	8.281	0.472

$6p)_{Pt}=4.56$, and $(5d5d|5d5d)_{Pt}=8.60$.

The H_{rr} is given by:

$$H_{rr} = U_{rr} + \sum_{B \neq A} (B|rr) \tag{17}$$

where:

$$U_{rr} = \int \chi_r(\mu) \left\{ -\frac{1}{2} \Delta(\mu) - \frac{Z_A}{r_{\mu A}} \right\} \chi_r(\mu) d\tau_\mu,$$

$$(B|rr) = -\int \chi_r(\mu) \frac{Z_B}{r_{\mu B}} \chi_r(\mu) d\tau_\mu$$

and where Z_A is the number of the valence electrons on the A atom. The molecular integrals, U_{rr} and $(B|rr)$, are approximated by:

$$U_{rr} = -I_r - (N_r - 1)(rr|rr) - \sum_{r' \neq r} N_{r'}(rr|r'r'), \tag{18}$$

$$(B|rr) = -Z_B(s_B s_B|rr), \tag{19}$$

where s_B refers to the valence s-orbital on the B atom.

The $H_{rs(r \neq s)}$ is approximated by:

$$H_{rs} = KS_{rs}(H_{rr} + H_{ss}) \tag{20}$$

where K is a constant taken to be 0.54 in the present calculations.

The molecular orbital energies of $PtCl_4^{2-}$ calculated by the present method are compared with the results of the other MO calculations in Table 1. The lowest vacant (*L.V.*) and the highest occupied (*H.O.*) orbital energies obtained by the present calculation are in good accordance with the values of the electron affinities and the ionization potentials. The obtained d-orbital ordering, $x^2-y^2 > xy > xz, yz > z^2$, is in agreement with the results obtained by others,[4,5] and this ordering is found to be invariant with a variation in the constant K (in Eq. (20)) from 0.53 to 0.56. The orbital energies of the occupied MO's are very close to each other, but this is not serious in the present studies of the MCD of d^8 square-planar complexes. The total charge distribution on Pt is calculated to be +0.310; the details of the electron distribution are $(5d)_{Pt}$; 8.212, $(6s)_{Pt}$: 0.960, $(6p)_{Pt}$: 0.618. The Pt–Cl bond order is calculated to be 0.489.

Calculations were carried out also on $PdCl_4^{2-}$. The MO energies and MO coefficients are presented in Tables 2*a* and 2*b*. The results on $PdCl_4^{2-}$ are nearly equal to those found for $PtCl_4^{2-}$, and the ordering of the MO energies is exactly the same as those of $PtCl_4^{2-}$.

C. Analysis of MCD. As may easily be found from the character table of D_{4h}, the transitions from the ground state, $^1A_{1g}$, to the excited states, $^1A_{2u}$'s or ^1E_u's, are the only allowed transitions. The allowed transitions the calculated excitation energy of which is less than 10 eV are presented in Table 3. The possible allowed transitions, considered previously as the observed high-intensity bands, are all included in the following five transitions: $^1A_{1g} \rightarrow {}^1E_u(1)$: $[3e_u - 3b_{1g}]$, $^1A_{1g} \rightarrow {}^1E_u(d\text{-}p)$: $[2e_g - 2a_{2u}]$, $^1A_{1g} \rightarrow {}^1E_u(2)$: $[2e_u - 3b_{1g}]$, $^1A_{1g} \rightarrow {}^1A_{2u}(1)$: $[b_{2u} - 3b_{1g}]$, and $^1A_{1g} \rightarrow {}^1A_{2u}(d\text{-}p)$: $[3a_{1g} - 2a_{2u}]$. The calculations of Q_A and Q_B by Eq. (9) and (10) were made for these five possible transitions of $PtCl_4^{2-}$; the results are shown in Table 4. The molecular integrals, $\langle k|\boldsymbol{m}|l\rangle$ and $\langle k|\boldsymbol{\mu}|l\rangle$, are accurately evaluated.

TABLE 4. CALCULATED VALUES OF Q_A AND Q_B FOR EACH TRANSITION IN $PtCl_4^{2-}$

Transition	Zeeman energy[a] (cm^{-1})	Q_A $((ea_0)^2)$	Q_B $\left(\frac{(ea_0)^2 \times}{\mu_B/eV}\right)$
$^1A_{1g} \rightarrow {}^1E_u$ (1)	2.669	−0.1943	0.3082
	−2.669	0.1943	0.3082
$^1A_{1g} \rightarrow {}^1E_u$ (2)	2.578	0.1062	−0.1803
	−2.578	−0.1062	−0.1803
$^1A_{1g} \rightarrow {}^1E_u$ $(d\text{-}p)$	2.214	0.0690	−0.8153
	−2.214	−0.0690	−0.8153
$^1A_{1g} \rightarrow {}^1A_{2u}$ (1)	0.0	0.0	−0.3158
$^1A_{1g} \rightarrow {}^1A_{2u}$ $(d\text{-}p)$	0.0	0.0	1.8064

a) Values at H_s=50000 gauss

It should be noted that the molecular integrals, $\langle \chi_A|\boldsymbol{\mu}|\chi_B\rangle$'s, are not Hermitian in some cases if χ_A and χ_B are not atomic orbitals centered on the same atom. In order to eliminate this difficulty, alternative approximate calculations were made. In these approximate calculations, we neglected the $\langle \chi_A|\boldsymbol{\mu}|\chi_B\rangle$ integral if χ_A and χ_B were on different atoms. A comparison of accurately and approximately calculated values of the Zeeman energies and Q_B for each transition in $PtCl_4^{2-}$ is shown in Table 5. The difference between these results is small and is not very important in interpreting the present MCD spectrum.

TABLE 5. COMPARISON OF EXACT AND APPROXIMATELY CALCULATED VALUES OF ZEEMAN ENERGY AND Q_B FOR EACH TRANSITION IN $PtCl_4^{2-}$

Transition	Zeeman energy[a] (cm^{-1})		Q_B $((ea_0)^2\mu_B/eV)$	
	exact	*approx.*	*exact*	*approx.*
$^1A_{1g} \rightarrow {}^1E_u$ (1)	2.669	2.426	0.3082	0.3162
$^1A_{1g} \rightarrow {}^1E_u$ (2)	2.578	3.007	−0.1803	−0.1519
$^1A_{1g} \rightarrow {}^1E_u$ $(d\text{-}p)$	2.214	2.228	−0.8153	−0.8632
$^1A_{1g} \rightarrow {}^1A_{2u}$ (1)	0.0	0.0	−0.3158	−0.1107
$^1A_{1g} \rightarrow {}^1A_{2u}$ $(d\text{-}p)$	0.0	0.0	1.8064	1.6182

a) Values at H_s=50000 gauss

TABLE 6. CALCULATED VALUES Q_A AND Q_B FOR EACH TRANSITION IN $PdCl_4^{2-}$

Transition	Zeeman energy[a] (cm^{-1})	Q_A ($(ea_0)^2$)	Q_A ($(ea_0)^2\times$ / μ_B/eV)
$^1A_{1g}\rightarrow{}^1E_u$ (1)	2.668	−0.1136	0.3923
	−2.668	0.1136	0.3923
$^1A_{1g}\rightarrow E_u$ (2)	2.928	0.0724	−0.2252
	−2.928	−0.0724	−0.2252
$^1A_{1u}\rightarrow{}^1E_u$ (*d-p*)	2.230	0.0521	−0.5824
	−2.230	−0.0521	−0.5824
$^1A_{1g}\rightarrow{}^1A_{2u}$ (1)	0.0	0.0	−0.0301
$^1A_{1g}\rightarrow{}^1A_{2u}$ (*d-p*)	0.0	0.0	1.1102

a) Values at $H_s=50000$ gauss

Then, we calculated the Zeeman energies and Q_B for each transition in $PdCl_4^{2-}$ by the alternative approximate method described above; the calculated results of Q_A and Q_B are shown in Table 6. The values of the corresponding transitions in $PdCl_4^{2-}$ and $PtCl_4^{2-}$ are very similar to each other. In the above calculations, the effect of spin-orbit coupling is not considered. The atomic constants defined by Condon and Shortley[24] determine the magnitude of the effect. The values of the spin-orbit coupling constant, ζ, for the Cl, Pd, and Pt atoms are listed by McClure[25] as $\zeta_{3p}^{Cl}=587$ cm^{-1}, $\zeta_{4d}^{Pt}=1410$ cm^{-1}, and $\zeta_{5d}^{Pt}=4060$ cm^{-1}. The perturbed ground-state wavefunction is given approximately by:

$$\Phi_{A_{1g}}=\Phi^0_{A_{1g}}-\frac{\langle\Phi^0_{A_{2g}:[2b_{2g}-3b_{1g}]}|\zeta^{Pt}_{5d}|\Phi^0_{A_{1g}}\rangle}{\delta E(2b_{2g}-3b_{1g})}\Phi^0_{A_{2g}:[2b_{2g}-3b_{1g}]}-\frac{\langle\Phi^0_{E_g:[2e_g-3b_{1g}]}|\zeta^{Pt}_{5d}|\Phi^0_{A_{1g}}\rangle}{\delta E(2e_g-3b_{1g})}\Phi^0_{E_g:[2e_g-3b_{1g}]} \quad (21)$$

The order of magnitude of the mixing coefficient can be easily estimated; the numerator is, at most, of the order of magnitude of 4000 cm^{-1} ($=\zeta_{5d}^{Pt}$), and the denominator is larger than 20000 cm^{-1}, as may esaily be found from the observed bands. Therefore, the mixing coefficients are smaller than 0.2. Hence, the effect of spin-orbit coupling on the ground-state wavefunction is not significant in the present calculations. The excited-state wavefunctions are also perturbed, but in order to interpret the electronic transition it is not necessary to include this effect in the calculation of high-intensity bands.

Discussion

The theoretical calculations of Q_A and Q_B are necessary in order to interpret the MCD spectrum. The value of Q_A determines whether the observed MCD curve is α-type or β-type; if the value of Q_A for a lower component of the excited state split by the Zeeman energy is positive, then the observed MCD curve is β-type. The values of Q_A and the Zeeman energy can be simply determined by the character of the state wavefunctions; this situation does not depend strongly on the method of the MO calculation. Some of the observed MCD curves for d^8 square-planar metal halides are very similar to each other; this fact suggests that the common assignments hold for these bands. Especially, the higher energy bands of $PdCl_4^{2-}$, $PdBr_4^{2-}$, $AuCl_4^-$, and $AuBr_4^-$ show strongly β-type MCD. Gray and Ballhausen[3c] identified the higher energy band as $^1A_{1g}\rightarrow{}^1E_u(2)$, Jørgensen[1i] suggested the band to be $^1A_{1g}\rightarrow{}^1E_u(2)$, and Basch and Gray[4] later adopted Jørgensen's assignment on the basis of their MO calculation. The results of the numerical calculation for $PdCl_4^{2-}$ shown in Table 6 predict the characteristic types of the MCD curves: the $^1A_{1g}\rightarrow{}^1E_u(1)$ transition is the β-type, the $^1A_{1g}\rightarrow{}^1E_u(2)$ and $^1A_{1g}\rightarrow{}^1E_u(d\text{-}p)$ transitions are both α-type, the $^1A_{1g}\rightarrow{}^1A_{2u}(1)$ transition is γ-type, and the $^1A_{1g}\rightarrow{}^1A_{2u}(d\text{-}p)$ transition is δ-type. The results of the numerical calculation for $PtCl_4^{2-}$ shown in Table 4 also predict the same characterstic types of MCD curves as those of the corresponding transitions for $PdCl_4^{2-}$. We may therefore assign the higher energy bands of $PdCl_4^{2-}$, $PdBr_4^{2-}$, $AuCl_4^-$, and $AuBr_4^-$ to the $^1A_{1g}\rightarrow{}^1E_u(1)$ transitions. We have calculated the line shape of the MCD by taking the center of MCD at the observed value; $\omega_{ja}\simeq44900$ cm^{-1}; the external magnetic field, $H_s=50000$ gauss, and the band width at half the height of the $a\rightarrow j$ spectral line; $\Gamma_{ja}=7000$ cm^{-1} (*cf.* Fig. 2). The agreement of the calculated MCD curve with the observed one is very good. We may conclude, therefore, that the theory and the experiment are in adequate agreement and the present study of the MCD spectra supports the assignment of the $^1A_{1g}\rightarrow{}^1E_u(1)$ transition. The main feature of the MCD line of shape is determined by Q_A, but the details of the contributions to Q_B from each mixing excited state are interesting; they are shown in Table 7. It should be noted that the magnitude of $Q_B(^1A_{1g}\rightarrow{}^1E_u(1))$ is mainly determined by the contribution from the perturbing excited state: $[2b_{2g}—3b_{1g}]$.

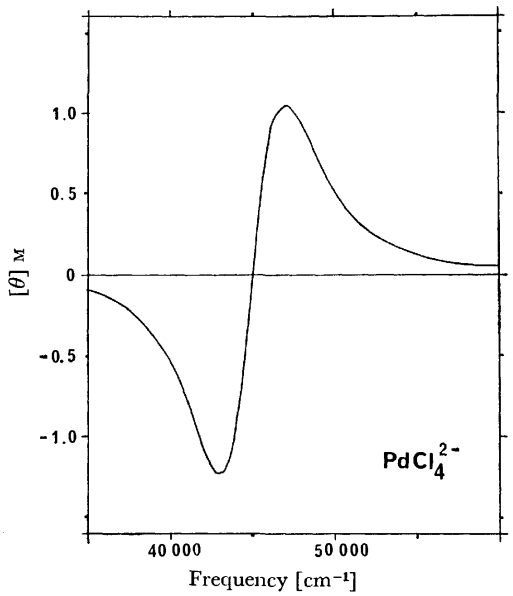

Fig. 2. Computed MCD of $PdCl_4^{2-}$ for $^1A_{1g}$—$^1E_u(1)$ transition

24) E. U. Condon and G. H. Shortley, "The Theory of Atomic Spectra," Cambridge University Press, London and New York 1951, p. 195.

25) D. S. McClure, *J. Chem. Phys.*, **17**, 905 (1949); *Solid State Phys.*, **9**, 399 (1959).

Table 7. Contribution to Q_B $(3e_u-2b_{1g})$ from various excited states in $PdCl_4^{2-}$

Excited state	Contribution to Q_B $((ea_0)^2\mu/eV)$
$[3e_u-4e_u]$	−0.0053
$[1b_{2g}-3b_{1g}]$	−0.0549
$[1e_g-3b_{1g}]$	0.0013
$[2e_g-3b_{1g}]$	0.0323
$[2b_{2g}-3b_{1g}]$	0.4545
$[1e_u-3b_{1g}]$	−0.0084
$[2e_u-3b_{1g}]$	−0.0272
Total	=0.3923

The weaker bands of $AuCl_4^-$ and $AuBr_4^-$ show the γ-type MCD line shape; we consider these bands to be due to only a $^1A_{1g}\rightarrow{}^1A_{2u}(1)$ transition. McCaffery, Schatz, and Stephens[7] suggested that they are composite $^1A_{1g}\rightarrow{}^1A_{2g}+{}^1E_u(1)$ transitions, but the observed intensity of the corresponding absorption band is too small. The present assignments are reasonable in that the magnitude of the calculated transition moment is in accordance with the observed intensity of the absorption band.

Unfortunately, the MCD of the lower energy band at 35800 cm^{-1} of $PdCl_4^{2-}$ has not been reported, but the MCD of $PdBr_4^{2-}$ gives as instructive information on the lower band. The MCD of the band at 30100 cm^{-1} of $PdBr_4^{2-}$ is α-type; it is possibly the $^1A_{1g}\rightarrow{}^1E_u(2)$ or $^1A_{1g}\rightarrow{}^1E_u(d\text{-}p)$ transition. The $^1A_{1g}\rightarrow{}^1E_u(2)$ transition will be on a higher energy side than the $^1A_{1g}\rightarrow{}^1E_u(1)$ transition. It thus seems reasonable to identify it as the $^1A_{1g}\rightarrow{}^1E_u(d\text{-}p)$ transition; this assignment is in agreement with the following assignment of the band at 46200 cm^{-1} in $PtCl_4^{2-}$.

The MCD of the relatively intense band of $PtCl_4^{2-}$ is more complicated than those of paradium halides. Gray and Ballhausen[3c] originally assigned the band to $^1A_{1g}\rightarrow{}^1A_{2u}(1)$, and later Basch and Gray[4] assigned the same band to the two allowed transitions, $^1A_{1g}\rightarrow{}^1A_{2u}(1)$ and $^1A_{1g}\rightarrow{}^1E_u(1)$. The MO calculations on $PtCl_4^{2-}$ by Cotton and Harris[5] predict the band to be the $^1A_{1g}\rightarrow{}^1A_{2u}(d\text{-}p)$ transition. McCaffery, Schatz, and Stephens[7] assigned the shoulder at 43400 cm^{-1} to the $^1A_{1g}\rightarrow{}^1A_{2u}(1)+{}^1E_u(1)$ transition on the basis of the common feature of the shapes of the MCD of this shoulder and on the basis of the lowest energy band in $PdBr_4^{2-}$, while the main band at 46200 cm^{-1} was assigned to the $^1A_{1g}\rightarrow{}^1A_{2u}(d\text{-}p)$ transition by them. However, the quantitative calculation does not support their assignments. The $^1A_{1g}\rightarrow{}^1E_u(1)$ transition is predicted in the above discussion to show strong β-type MCD curves, and the transition is expected to be in a higher energy region, though it is observed in $PdBr_4^{2-}$. The MCD of $PdBr_4^{2-}$ also suggests that the $^1A_{1g}\rightarrow{}^1E_u$ $(d\text{-}p)$ transition will be found among the lower energy bands. We assign the main band at 46200 cm^{-1} to the $^1A_{1g}\rightarrow{}^1E_u(d\text{-}p)$ transition. The $^1A_{1g}\rightarrow{}^1A_{2u}(1)$ transition which is assigned to the lowest energy band in $AuCl_4^-$ and $AuBr_4^-$ will be assigned to the shoulder band at 43400 cm^{-1}. In order to understand the MCD line shape, we should further assign the $^1A_{1g}\rightarrow{}^1A_{1u}(d\text{-}p)$ transitions to the same shoulder band. Taking the center of MCD at the observed point, the external magnetic field H_s=50000 cm^{-1}, the width at half the height of a band of the shape Γ_{ja}=5000 cm^{-1} for the 43400 cm^{-1} band and Γ_{ja}=7000 cm^{-1} for the 46200 cm^{-1} band, we have calculated the shape of the MCD; the results are shown in Fig. 3. The agreement with the observed MCD line shape is good. The details of the analysis of the contribution to $Q_B(2e_g-2a_{2u})$, $Q_B(b_{2u}-3b_{1g})$, and $Q_B(3a_{1g}-2a_{2u})$ from each mixing

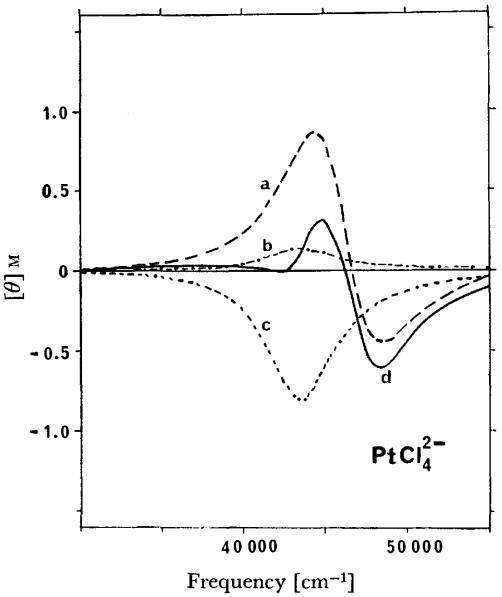

Fig. 3. Computed MCD of $PtCl_4^{2-}$ for $^1A_{1g}$—^1E_u $(d\text{-}p)$ transition: **a**, $^1A_{1g}$—$^1A_{2u}(1)$ transition: **b**, $^1A_{1g}$—$^1A_{2u}$ $(d\text{-}p)$ transition: **c**, and the composite band: **d**.

Table 8. Contribution to Q_B's from various excited states in $PtCl_4^{2-}$ $((ea_0)^2\mu_B/eV)$: unit

Excited state	Contribution to Q_B $(2e_g-2a_{2u})$	Excited state	Contribution to Q_B $(3a_{1g}-2a_{2u})$	Excited state	Contribution ot Q_B $(b_{2u}-3b_{1g})$
$[2e_g-4a_{1g}]$	0.0431	$[3a_{1g}-4e_u]$	0.0014	$[b_{2u}-4e_u]$	−0.0007
$[2e_g-4e_u]$	−0.0021	$[1e_u-2a_{2u}]$	−0.0010	$[1e_g-3b_{1g}]$	−0.2496
$[1e_u-2a_{2u}]$	0.0004	$[2e_u-2a_{2u}]$	−0.0067	$[2e_g-3b_{1g}]$	−0.0416
$[2e_u-2a_{2u}]$	0.0008	$[3e_u-2a_{2u}]$	−0.0100	$[1e_u-3b_{1g}]$	−0.0004
$[3e_{1g}-2a_{2u}]$	0.0007	$[1e_g-2a_{2u}]$	−0.0116	$[2e_u-3b_{1g}]$	−0.0587
$[1a_{1g}-2a_{2u}]$	0.0013	$[2e_g-2a_{2u}]$	1.8343	$[3e_u-3b_{1g}]$	0.0352
$[2a_{1g}-2a_{2u}]$	−0.0097	Total	= 1.8064	Total	= −0.3158
$[1e_g-2a_{2u}]$	−0.0102				
$[3a_{1g}-2a_{2u}]$	−0.8396				
Total	= −0.8153				

Table 9. Summary of the assignments

	Observed Transition		Assignment		McCaffery-Schatz[b]-Stephens
	(cm^{-1})	ε_{max}	Present method	Mason-Gray[a]	
$PtCl_4^{2-}$	43400	8500	$^1A_{2u}$ $(d-p)+{}^1A_{2u}$ (1)	$^1A_{2u}$ (1)	$^1A_{2u}$ (1)$+{}^1E_u$ (1)
	46200	10900	^1E_u $(d-p)$	^1E_u (1)	$^1A_{2u}$ $(d-p)$
$PdCl_4^{2-}$	35800	10400		$^1A_{2u}$ (1)$+{}^1E_u$ (1)	$^1A_{2u}$ (1)$+{}^1E_u$ (1)
	44900	28300	^1E_u (1)	^1E_u (2)	^1E_u (2)
$PdBr_4^{2-}$	30100	11500	$^1A_{2u}$ (1)$+{}^1E_u$ $(d-p)$	$^1A_{2u}$ (1)$+{}^1E_u$ (1)	$^1A_{2u}$ (1)$+{}^1E_u$ (1)
	40500	30800	^1E_u (1)	^1E_u (2)	^1E_u (2)
$AuCl_4^-$	32000	5300	$^1A_{2u}$ (1)	$^1A_{2u}$ (1)$+{}^1E_u$ (1)	$^1A_{2u}$ (1)$+{}^1E_u$ (1)
	44500	27500	^1E_u (1)	^1E_u (2)	^1E_u (2)
$AuBr_4^-$	26200	4400	$^1A_{2u}$ (1)	$^1A_{2u}$ (1)$+{}^1E_u$ (1)	$^1A_{2u}$ (1)$+{}^1E_u$ (1)
	39500	36300	^1E_u (1)	^1E_u (2)	^1E_u (2)

a) W. R. Mason and H. B. Gray, *J. Amer. Chem. Soc.*, **90**, 5721 (1968).
b) Ref. 7.

excited state are shown in Table 8. It may be noted that the magnitude of the above Q_B is mainly determined by the contributions from the mixing excited states, $[3a_{1g}-2a_{2u}]$, $[2e_g-2a_{2u}]$, and $[1e_g-3b_{1g}]$ respectively. Especially, we have used the observed values of 43400 cm^{-1} and 46200 cm^{-1} as the excitation energies to the excited states, $[3a_{1g}-2a_{2u}]$ and $[2e_g-2a_{2u}]$ respectively; these are the dominant mixing states.

The present study of the MCD line shape has clarified a number of problems with regard to the assignment of high-intensity bands in d^8 square-planar metal halides. The present assignments are summarized in Table 9, and they are there compared with the previous assignments of others. In some cases, the quantitative calculation is essential; then the MCD becomes the more useful method for understanding the electronic structures of molecules.

The author is grateful to Dr. T. Katô for a very instructive discussion of this article. He also wishes to thank Professor T. Yonezawa and Professor H. Kato for their generous support of this work.

BULLETIN OF THE CHEMICAL SOCIETY OF JAPAN, VOL. 45, 1288—1291(1972)

The Catalytic Oxidation of Carbon Monoxide on Zirconium Dioxide

Takuya HAMAMURA, Yoshito ONISHI, and Yasuo IIZUKA

Department of Chemistry, Faculty of Industrial Arts, Kyoto Technical University, Matsugasaki, Sakyo-ku, Kyoto

(Received July 19, 1971)

The catalytic oxidation of carbon monoxide on zirconium dioxide was kinetically examined in order to compare with the results of titanium dioxide. The experiment was carried out under gas pressures of 10^{-2}—100 mmHg at 400—550°C. The reaction rate was proportional to P_{CO} and did not depend upon P_{O_2}, and there was no retarding effect by carbon dioxide. The rate constant of this oxidation reaction almost agreed with that of the reduction of zirconium dioxide by carbon monoxide. The reaction mechanism could be explained in the same manner as that on titanium dioxide. The catalytic activity of zirconium dioxide for this reaction was almost the same as that of rutile. The activation energy was about 12.5 kcal/mol, and this value was intermediate between those of anatase and rutile. The same relation was obtained in the activation energies of the thermal desorption of surface oxygen from these catalysts.

The correlation between the crystal form and the catalytic activity of titanium dioxide has been examined in this laboratory using rutile and anatase.[1-4] It was found that both rutile and anatase showed the same reaction mechanism for the oxidations of carbon monoxide and hydrogen, but the activity of rutile was much larger than that of anatase for the two reactions. The activation energies of two reactions on anatase were larger by about 10 kcal/mol than those on rutile, and these differences almost coincided with that in activation energies of the thermal desorption of surface oxygen atoms from the catalysts between two crystal forms.

Zirconium, likewise titanium, belongs to the group IVA elements in the periodic table, and its electronic configuration (Kr core) $4d^25s^2$ is very similar to that of titanium (Ar core) $3d^24s^2$. Therefore, it is interesting to study the catalytic action of zirconium dioxide for comparison to that of titanium dioxide. The report about

1) Y. Onishi and T. Hamamura, This Bulletin, **43**, 996 (1970).
2) Y. Onishi, *ibid.*, **44**, 1460 (1971).
3) Y. Onishi, *ibid.*, **44**, 912 (1971).
4) Y. Onishi and T. Hamamura, *Memoirs of the Faculty of Industrial Arts, Kyoto Technical University, Science and Technology*, **19**, 44 (1970).

the carbon monoxide oxidation on zirconium dioxide can scarcely be found in the literature.[5]

Experimental

Two kinds of samples were used in the present investigation. One was obtained from the Nippon Gaishi Company (ZrO_2-1), and the other from the Zirconium Corporation of America (ZrO_2-2). Both samples are pure zirconium dioxide from which hafnia was separated. These samples were heated at 1200°C for 3 hr in a fused quartz tube to vaporize the volatile contaminants as well as to develop their crystal lattices. The BET surface areas of ZrO_2-1 and -2 were 3.8 and 1.0 m^2/g, respectively. Both of them were found to have the monoclinic crystal forms by the X-ray powder method.

Carbon monoxide and oxygen from commercial cylinders were purified by fractional distillation using liquid nitrogen. The apparatus used was essentially the same as before.[1] Since the formed carbon dioxide was caught in the trap, the rate of reaction was determined by measuring the total pressure. The experiments were carried out under the pressure range of 1—10 cmHg, and the pressure change was measured by using a mercury manometer. The McLeod gauge was used for the reaction at the gas pressure of about 10^{-2} mmHg. At such a low pressure the gas diffusion was thought to be so fast that the circulating pump was cut from the reaction system.

The sample of about 5 g was introduced into the apparatus and evacuated to 10^{-6} mmHg. Prior to the measurements, the sample was heated at 800°C in circulating oxygen of 5 cmHg for 3 hr to clean its surface.

Results and Discussion

Catalytic Activity. The oxidation rate of carbon monoxide on zirconium dioxide was measured by using a mixed gas with a composition of $CO/O_2=2/1$ in temperature range of 400—550°C and under pressures of 10^{-2}—100 mmHg. The oxidation rate is plotted against the total pressure in Fig. 1. The reaction is clearly of the first order with respect to the total pressure. In order to examine the effect of carbon dioxide, measurements were carried out by using a dry ice trap to mix the formed carbon dioxide into the reactant gas. However, no retarding effect by carbon dioxide was found. Therefore, the reaction rate can be expressed by the following equation:

$$d(CO_2)/dt = 2/3k \cdot P \qquad (1)$$

where k is a constant. The Arrhenius plots of k on ZrO_2-1 and -2 are given in Fig. 2 together with those on rutile and anatase. The ZrO_2-1 and -2 show almost the same values in their catalytic activities per unit of the surface area and in their activation energies, although they are different both in their specific surface areas and their conditions of formations.

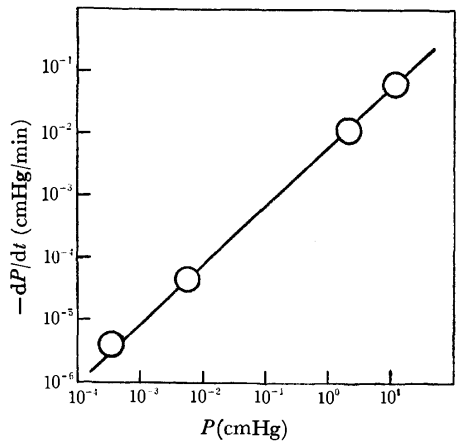

Fig. 1. Effect of total pressure on the reaction rate at 550°C on ZrO_2-1.

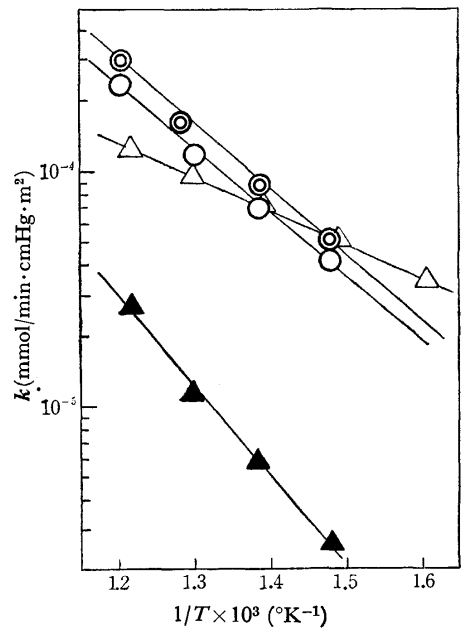

Fig. 2. Effect of temperature on the reaction rate constant.
○: ZrO_2-1 ◎: ZrO_2·2 ▲: Anatase △: Rutile

Comparing with titanium dioxide,[1] the catalytic activity of zirconium dioxide is approximately on the same level with that of rutile. As for the activation energy, zirconium dioxide shows the intermediate value of 12.5 kcal/mol between rutile, 6.7 kcal/mol, and anatase, 16.0 kcal/mol.

Effect of Partial Pressures of Carbon Monoxide and Oxygen on the Reaction Rate. To examine the effect of partial pressures of carbon monoxide and oxygen on the reaction rate, the reaction rate was measured keeping the initial partial pressure of oxygen constant and

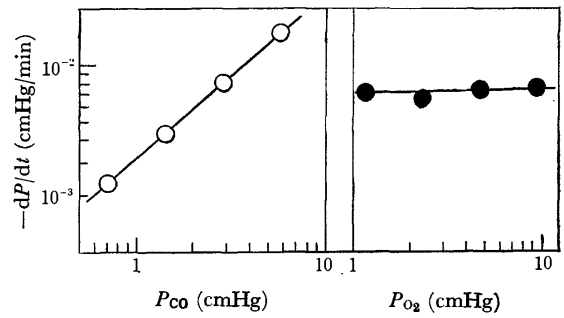

Fib. 3. Kinetics of the oxidation of carbon monoxide for ZrO_2-2 at 550°C. Open circles refer to constant O_2 pressure ($P_{O_2}=2.84$ cmHg) and varying CO pressures. Filled circles refer to constant CO pressure ($P_{CO}=2.35$ cmHg) and varying O_2 pressures.

5) C. J. Engelder and L. E. Miller, *J. Phys. Chem.*, **36**, 1345 (1932).

changing the partial pressure of carbon monoxide, or *vice versa*. The results are shown in Fig. 3. The reaction rate is nearly of the first order with respect to the carbon monoxide pressure P_{CO} and independent of the oxygen pressure P_{O_2}. Consequently, the reaction rate can be expressed by the following equation:

$$d(CO_2)/dt \simeq k \cdot P_{CO} \quad (2)$$

where k is a constant which is the same as that in Eq. (1).

Reaction of Carbon Monoxide with Surface Oxygen of Zirconium Dioxide. The catalyst pretreated in oxygen at 800°C for 3 hr was cooled to the reaction temperature and evacuated. When carbon monoxide, at a pressure of about 10^{-2} mmHg, was introduced into the reaction system, it reacted with the surface oxygen of the catalyst and the formed carbon dioxide was caught in the trap. It was confirmed that the amount of consumed carbon monoxide agreed well with that of the carbon dioxide caught in the trap. This fact shows that the amount of carbon monoxide which may be adsorbed on the surface of the catalyst is negligible compared with that of carbon monoxide oxidized to carbon dioxide and that the carbon dioxide formed on the surface of the catalyst immediately desorbs from there. The rate of formation of carbon dioxide was found to be proportional to P_{CO}:

$$d(CO_2)/dt = k_{CO} \cdot P_{CO} \quad (3)$$

where k_{CO} is the reduction rate constant of zirconium dioxide by carbon monoxide. The Arrhenius plots of k_{CO} on ZrO_2-1 are shown in Fig. 4 together with that of the oxidation rate constant k. It is obvious that k_{CO} almost agrees with k.

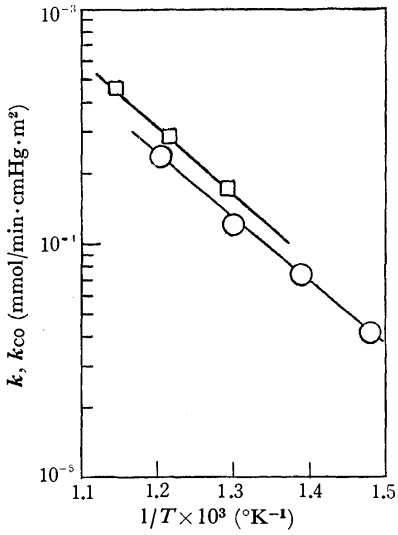

Fig. 4. Effect of temperature on the rate constant of oxidation of carbon monoxide k and that of reduction of ZrO_2 by carbon monoxide k_{CO}.
○: k □: k_{CO}

The catalyst was reduced by carbon monoxide of about 3 cmHg for 30 min, then oxygen of about 10^{-2} mmHg was introduced to measure the uptake rate of oxygen by the catalyst. It was found that the uptake rate of the reduced zirconium dioxide was far faster than the reduction rate of the catalyst by carbon monoxide.

Mechanism of the Oxidation of Carbon Monoxide on Zirconium Dioxide. Since 1) the reaction rate is proportional to P_{CO} and does not depend upon P_{O_2}, 2) the rate constant of the oxidation of carbon monoxide on zirconium dioxide almost agrees with that of the reduction of zirconium dioxide by carbon monoxide, and 3) the oxygen uptake rate of the reduced zirconium dioxide is much faster than the reduction rate of zirconium dioxide by carbon monoxide, the mechanism of this reaction can be explained in the same manner as that on titanium dioxide,[1,2] cupric oxide,[6] and nickel oxide.[7]

The reaction consists of two processes; 1) carbon monoxide which collides with the surface of the catalyst reacts with the surface oxygen of the catalyst and the carbon dioxide thus formed immediately desorbs, leaving an oxygen defect on the surface and 2) the oxygen defect thus formed is refilled with oxygen from the gas phase. Therefore, the reaction steps can be expressed as follows:

$$CO(g) + O(s) \longrightarrow CO_2(g) + (s) \quad (4)$$
$$(s) + 1/2O_2 \longrightarrow O(s) \quad (5)$$

where O(s) refers to the surface oxygen of the catalyst and (s) the oxygen defect on the surface. The step (5) is much faster than the step (4), so the overall reaction rate is proportional to P_{CO}.

Desorption of the Surface Oxygen. The catalyst pretreated in oxygen at 800°C was cooled down to 600°C and evacuated until the gas desorption became almost imperceptible. When the catalyst thus pretreated was heated to a temperature above 600°C, the oxygen desorption was detected and the desorption rate could be determined by measuring the pressure of oxygen, which was collected in a fixed volume by a compressing pump. The experimental results on zirconium dioxide are shown in Fig. 5 together with those on anatase

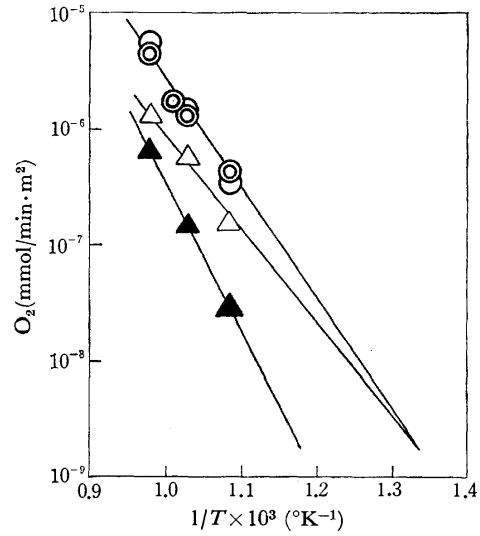

Fig. 5. Effect of temperature on the thermal desorption rate of surface oxygen.
○: ZrO_2-1 ◎: ZrO_2-2 ▲: Anatase △: Rutile

6) A. Kanome and T. Chitani, *Nippon Kagaku Zasshi*, **63**, 36 (1942); S. Nakata, *ibid.*, **63**, 41 (1942).

7) G. Parravano and M. Boudart, *Advan. Catal.*, **7**, 47 (1955); E. R. S. Winter, *J. Chem. Soc.*, **1955**, 2726; I. Matsuura, Y. Kubokawa, and O. Toyama, *Nippon Kagaku Zasshi*, **81**, 1003 (1960).

and rutile. The activation energy of the desorption of the surface oxygen of zirconium dioxide was about 44.0 kcal/mol. This value lies between those of anatase, 57.8 kcal/mol and rutile, 38.4 kcal/mol, which seems to correspond to the relation about the activation energies of the oxidation of carbon monoxide on these oxides. Furthermore, extrapolating the data to the temperature range of the oxidation reaction, it is found that zirconium dioxide shows almost the same level of the desorption rate of oxygen as rutile. This fact again seems to correspond to the resemblance between rutile and zirconium dioxide with respect to their catalytic activities. All these results indicate that there is a close relation between titanium dioxide and zirconium dioxide in their catalytic actions.

The authors wish to express their deep thanks to Professors Yasuro Nakazawa and Masayoshi Ihara of Kyoto Technical University for their kind advices and discussions.

BULLETIN OF THE CHEMICAL SOCIETY OF JAPAN, VOL. 45, 1291—1294(1972)

Molecular Structure of Propane

Takao IIJIMA

Department of Chemistry, Faculty of Science, Hokkaido University, Sapporo

(Received August 16, 1971)

The structure of propane has been investigated by gas electron diffraction. The thermal average distances r_g and r_a-angles determined with the estimated limits of error were: C–C = 1.532±0.003 Å, C–H = 1.107±0.005 Å, ∠CCC = 112±1°, and ∠HCH(CH_3) = 107±3°. By combining the diffraction results with the microwave data, the zero-point average structure has also been determined.

The structures of ethane and four *n*-hydrocarbons from butane to heptane were previously determined by gas-phase electron diffraction.[1,2] Somehow propane has been missing in this group of diffraction data. Lide investigated the microwave spectra of propane and its isotopic species,[3] and determined the substitution coordinates and the structure parameters. However, the C–C distance 1.526 Å he obtained was outside the range of the thermal average C–C distances 1.531—1.534 Å, of other *n*-hydrocarbons determined by electron diffraction, beyond the stated uncertainties. As was commented by Lide himself,[4] the existence of this difference was not surprising, in view of the different nature of the averaging over vibrational motions.

The present study was initiated for the purpose of filling up the list of the structure data of simple *n*-hydrocarbons. The C–C r_g distance has been determined to be 1.532±0.003 Å. Further by applying an appropriate correction for the vibrational effect, the microwave data have been combined with the diffraction result, and the structure parameters have been determined for the zero-point average configuration.

Electron Diffraction

The diffraction photographs were taken and analyzed by our routine procedures of recent sector-microphotometer method.[5] Experimental conditions were as follows: accelerating voltage was 42 kV, camera distance 109.3 mm, beam current 0.1 μA, and exposure time 4 min. Carbon disulfide was used as the reference substance. The results of the least-squares analysis for three best plates are summarized in Table 1. The indices of resolution were 0.94—0.98. All the nonbonded distances other than listed in the table were restricted under the geometrical constraint of r_a parameters. The HCH angle of the methylene group was assumed to be 106.1°, the value given by Lide.[3] The

Table 1. Results of the least-squares analysis of propane (in Å units)[a]

	r_{C-C}	$r_{C\cdots C}$	r_{C-H}[b]	$r_{C\cdots H}$[c]
r_a	1.5307	2.5421	1.1017	2.1886
σ_1	10	58	19	94
σ_2	6	21	2	26
r_g	1.5323	2.5440	1.1073	2.1940
limit of error	30	150	51	245
r°_a (r_z)[d]	1.5307	—	1.0956 (CH_3) 1.0941 (CH_2)	—
ϕ_a (CCC)	112.4°±1.2°,	ϕ_a (HCH; CH_3)	107°±3°	
ϕ_a (HCH; CH_2)	106.1° (assumed)			

a) Errors are in 10^{-4} Å units.
b) The r_a values of the methyl and the methylene C–H distances were assumed to be equivalent.
c) $r_{C\cdots H}$ is the distance between the central carbon atom and one of the methyl hydrogens.
d) Morse parameters were assumed to be 2.1 $Å^{-1}$ for C–C and 1.98 $Å^{-1}$ for C–H, respectively. The centrifugal stretching was assumed to be 0.0002 Å for C–C.

1) L. S. Bartell and H. K. Higginbotham, *J. Chem. Phys.*, **42**, 851 (1965).
2) a) R. A. Bonham and L. S. Bartell, *J. Amer. Chem. Soc.*, **81**, 3491 (1959); b) R. A. Bonham, L. S. Bartell, and D. A. Kohl, *ibid.*, **81**, 4765 (1959); c) K. Kuchitsu, This Bulletin, **32**, 748 (1959).
3) D. R. Lide, Jr., *J. Chem. Phys.*, **33**, 1514 (1960).
4) D. R. Lide, Jr., *ibid.*, **33**, 1519 (1960).
5) *e.g.*, S. Konaka and M. Kimura, This Bulletin, **43**, 1693 (1970).

C_{2v} symmetry of the whole molecule and the C_{3v} symmetry of the methyl tops were assumed. The conformation of the methyl hydrogens was taken as determined by Lide,[3] namely, the in-plane hydrogen is in the *trans* position to the C–C bond. All the mean amplitudes were fixed at the calculated values.

The present least-squares analysis did not follow an orthodox constrained procedure[6] but a more simplified method was employed. The four independent parameters were adjusted by the ordinary non-constrained least-squares routine, the dependent parameters being fixed. The dependent parameters were, however, recomputed and reset at every cycle of the least-squares iteration, by the use of the new values of the independent parameters. This method is practically useful but the standard deviations might be slightly larger than the values the exact constrained procedure would give.

The observed and calculated molecular intensity curves are shown in Fig. 1.[7]

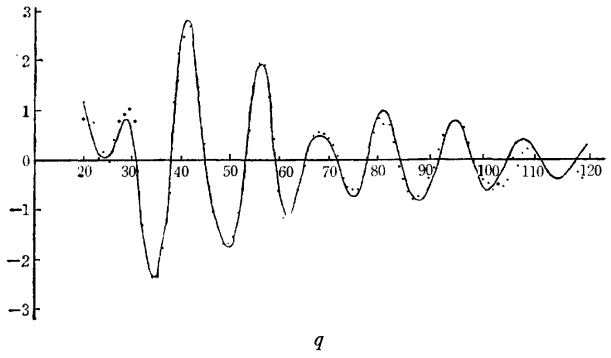

Fig. 1. Molecular intensity curve of propane calculated by the best-fit parameters. Dots indicate observed values.

The parallel and perpendicular mean amplitudes were calculated by the use of the force constants determined by Schachtschneider and Snyder.[8] Their constants were slightly readjusted to obtain better coincidence between the calculated and observed frequencies, because the structure parameters of the present study were not exactly the same as their values. Furthermore, the torsional constants were so adjusted as to give the frequencies determined by Hirota, Matsumura, and Morino.[9] For this purpose, an additional force constant which couples the two of the torsional internal coordinates had to be introduced. The calculated values of the mean amplitudes and the non-linear shrinkage correction Δ are listed in Table 2. The quantity $\Delta = r_a - r_\alpha$ was given by $(<\Delta\rho^2> - 2\,l^2)/2r$, where $<\Delta\rho^2>$ is the perpendicular mean amplitude of the atom pair concerned.[10]

Table 2. Mean amplitudes and shrinkage corrections of propane at 288°K (in 10^{-4} Å units)[a]

	l	Δ[b]		l	Δ[b]
C_1–C_2	496	4	$H_4\cdots H_5$	1299	78
$C_2\cdots C_3$	698	−15	$H_6\cdots H_7$	1283	355
$C_2\cdots H_6$	786	249	$H_4\cdots H_6$	1783	59
C_1–H_4	793	93	$H_4\cdots H_7$	1854	19
$C_1\cdots H_6$	1087	110	$H_4\cdots H_8$	1303	71
$C_2\cdots H_9$	1036	45	$H_6\cdots H_9$	1414	87
$C_2\cdots H_{10}$	1691	−12	$H_7\cdots H_{10}$	2448	2
$C_2\cdots H_4$	1075	20	$H_6\cdots H_{10}$	1784	32
			$H_7\cdots H_{11}$	2791	−244

a) The numbering of atoms are as follows: $C_1H_{4,5}$, methylene; $C_2H_{6,7,8}$, one methyl top; $C_3H_{9,10,11}$, the other methyl top. H_6 and H_9 lie on the CCC plane. H_7, H_4, and H_{10} are above the plane.
b) $\Delta = r_a - r_\alpha$.

Zero-point Average Structure

The effective moments of inertia of the normal species were converted to the zero-point moments of inertia, by applying the vibrational correction. The procedure has been established for ordinary molecules.[11] In the present study, the calculation was performed by an extended method applicable to a molecule containing internal rotors.[12] However, a recent investigation has revealed that the method used in the present study is not very exact but that a term proportional to the angular velocity of torsional motion should be added to the Eckart and Sayvetz conditions.[13] According to the rigorous treatment of a one-top problem the error due to the neglect of this term is of the order of 0.03 amu Å^2 for acetaldehyde.[13] Such an amount of error is not serious in the determination of the structure parameters with accuracy of 0.1% or so.

By assuming boldly that the same situation holds for propane, the zero-point average structure was de-

Table 3. Moments of inertia of propane (in amu Å^2 units)

	I_{obs}[a]	ΔI[b]	I_z[c]
a	17.3080	0.0634	17.371
b	59.8540	0.1053	59.959
c	67.7748	0.0427	67.818

a) Values observed by Lide.[3]
b) Correction for the vibrational effect.
c) Zero-point moments of inertia. $I_z = I_{obs} + \Delta I$.

Table 4. Zero-point average structure of propane (r_z in Å, I in amu Å^2 units)

r_z(C–C)	1.533_7	∠CCC	112.0°
r_z(C–H)(CH_3)	1.097_6	∠HCH(CH_3)	107.9°
r_z(C–H)(CH_2)	1.096_2	∠HCH(CH_2)	107.8°

$I_z(obs) - I_z(calc)$

a	+0.02	b	−0.02	c	0.00

6) K. Hedberg and M. Iwasaki, *Acta Crystallogr.*, **17**, 529 (1964).
7) Numerical experimental data of the leveled total intensity have been deposited with the Chemical Society of Japan (Document No. 7205). A copy may be secured upon request.
8) J. H. Schachtschneider and R. G. Snyder, *Spectrochim. Acta*, **19**, 117 (1963).
9) E. Hirota, C. Matsumura, and Y. Morino, This Bulletin, **40**, 1124 (1967).
10) Y. Morino, S. J. Cyvin, K. Kuchitsu, and T. Iijima, *J. Chem. Phys.*, **36**, 1109 (1962).
11) a) Y. Morino, K. Kuchitsu, and T. Oka, *ibid.*, **36**, 1108 (1962); b) K. Kuchitsu, *ibid.*, **49**, 4456 (1968).
12) T. Iijima and M. Kimura, Annual Meeting of the Chemical Society of Japan, Tokyo (April, 1970).
13) T. Iijima, S. Tsuchiya, and M. Kimura, *ibid.*, Tokyo (October, 1971).

termined from both moments of inertia given in Table 3 and the diffraction results in Table 1. The r_a^0 or r_z distances, C–C, C–H(CH_3), and C–H(CH_2) were varied along the direction of the possible uncertainty of the scale factor. For each set of these distances, the remaining structure parameters, ∠HCH(CH_3), ∠HCH(CH_2), and ∠CCC can be determined from the three moments of inertia. Thus further judgment for the reasonableness of the obtained set was made by requiring that the ∠HCH(CH_3) and ∠CCC should not be outside the rather large limits of error of the ϕ_a angles given by the diffraction results.

The best set of the structure parameters thus obtained are shown in Table 4. The uncertainties of the parameters are roughly assessed to be 0.2%.

It should be noted that the average structure of Table 4 corresponds to the state where the torsional motion is frozen. Therefore the mean amplitude corrections applied to obtain r_a^0 from r_g were calculated without the torsional freedom, while the amplitude-quantities listed in Table 2 include the torsional motion as well as the vibrational motions.

The author wishes to thank Professor Masao Kimura, Hokkaido University, for his encouragement throughout this work. Numerical calculations were carried out on a FACOM 230-60 of the Hokkaido University Computing Center and also on a FACOM 270-20 of Professor Kimio Ohno's laboratory, whom the author wishes to thank for allowing him to use the facilities.

BULLETIN OF THE CHEMICAL SOCIETY OF JAPAN, VOL. 45, 1293—1299(1972)

Bromination of Aliphatic Ketones with Copper(II) Bromide in Organic Solvents. I. The Reaction of Acetone with Copper(II) Bromide in Methanol

Yoshitane KOJIMA and Shinichi KAWAGUCHI

Department of Chemistry, Faculty of Science, Osaka City University, Osaka, 558

(Received August 16, 1971)

The reaction between acetone and methanol to form acetone dimethylacetal attains equilibrium quickly under the influence of copper(II) bromide. Reaction of both acetone and acetone dimethylacetal with copper(II) bromide thus proceed simultaneously to produce copper(I) bromide, hydrogen bromide, and brominated substrates. The mass balances of these reactions were established. On account of the retarding effect of copper(I) bromide and the enhancing effect of hydrogen bromide, the time course of reaction is too complicated to be analyzed, and the initial rate formula was determined. Two reaction pathways were suggested and copper(II) bromide was considered to play dual roles as a catalyst and a brominating agent in either case. The acid-catalyzed reactions were also found to follow a two-term rate law, one being independent of and the other first-order with respect to copper(II) bromide.

Copper(II) bromide is highly soluble in acetone and reacts with the solvent resulting in copper(I) bromide. Kosower, *et al.* reported halogenation reactions of various ketones with copper(II) chloride and bromide in dimethylformamide.[1] Castro and his coworkers also described halogenations of unsaturated compounds with copper(II) halides in boiling alcohols.[2] Kinetic studies of copper(II) chloride reactions were performed by Kochi[3] with acetone in aqueous solutions and by Lorenzini and Walling[4] with butylaldehyde and isobutylaldehyde in aqueous isopropyl alcohol. However, detailed kinetic studies of reactions between anhydrous copper(II) bromide and ketones in inert organic solvents have not been reported.

Reactivities of various organic solvents with copper(II) bromide have been examined, and methanol and dimethylformamide were found to be most suitable as unreactive solvents. Thus, we started the kinetic study of the reaction between copper(II) bromide and acetone in methanol. Unfortunately, however, this system has turned out to be complicated on account of the rapid acetal formation in the presence of copper(II) bromide.

Experimental

Materials. Organic solvents were purified by standard methods,[5] and their purities were checked by the vapor phase chromatography. The water contents of methanol and acetone were measured by the Karl-Fischer method to be 3.8×10^{-3} and 2.2×10^{-2}M, respectively. Anhydrous copper(II) bromide was supplied by Kishida Chemical Co. Ltd. The contaminant copper(I) bromide was checked by titration with a cerium(IV) ammonium sulfate solution. Found for two

1) (a) E. M. Kosower, W. J. Cole, G.-S. Wu, D. E. Cardy, and G. Meisters, *J. Org. Chem.*, **28**, 630 (1963); (b) E. M. Kosower and G.-S. Wu, *ibid.*, **28**, 633 (1963).

2) C. E. Castro, E. J. Gaughan, and D. C. Owsley, *ibid.*, **30**, 587 (1965).

3) J. K. Kochi, *J. Amer. Chem. Soc.*, **77**, 5274 (1955).

4) A. Lorenzini and C. Walling, *J. Org. Chem.*, **32**, 4008 (1967).

5) J. A. Riddick and E. E. Toops, Jr., "Organic Solvents", Vol. 7 of "Technique of Organic Chemistry" edited by A. Weissberger and E. S. Proskauer, 2nd ed., Interscience Publishers, New York (1955).

specimens: Cu, 28.60; Br, 71.38% and Cu, 28.34; Br, 71.58%. Calcd for $CuBr_2$: Cu, 28.45; Br, 71.55%.

Copper(I) bromide was prepared by reduction of copper(II) sulfate with sodium sulfite in an aqueous solution containing potassium bromide.[6] Sodium acetylacetonate was prepared by adding an aqueous solution of sodium hydroxide to a methanol solution of acetylacetone, and recrystallized from methanol. Commercial tetraethylammonium bromide was used without further purification. Dry methanol solutions of perchloric acid were prepared by passing dry methanol solutions of sodium perchlorate through a column of dried acid form cation exchange resin Dowex 50WX8 (100—200 mesh).[7] A stream of nitrogen was bubbled through boiling deionized water prior to use for quenching of the reaction mixture.

Identification and Determination of Reaction Products. After the desired period of reaction, volatile substances were distilled under reduced pressure. The residue was a mixture of copper(I) bromide and copper(II) bromide. To determine the copper(I) content, the whole residue was dissolved in a sulfuric acid solution containing iron(III) ammonium sulfate and iron(II) ions produced were titrated with an aqueous solution of cerium(IV) ammonium sulfate.[3] For the determination of total copper and bromine, the residue was dissolved in aqueous ammonia. Bromine was determined gravimetrically as silver bromide and copper by electrolysis.

The distillate was composed of methanol, acetone, and brominated substrates. Each component was identified by comparison of the gas-chromatogram with that of the authentic specimen and also by IR and NMR assays when possible. The combined quantity of hydrogen bromide and methyl bromide was measured by titration with an aqueous solution of sodium hydroxide using methyl red as an indicator. The amount of brominated substrates was determined by iodometry.[8]

Kinetics. A methanol solution of copper(II) bromide was thermostated (±0.02°C) in a three-necked flask equipped with a stirrer, a nitrogen gas inlet tube, and an outlet tube containing calcium chloride. The reaction started when thermostated acetone was added to this solution. At appropriate time intervals aliquots were withdrawn from the reacting mixture and quenched in cold sulfuric acid solutions of iron(III) ammonium sulfate. Iron(II) produced was determined by titration with a standardized sulfuric acid (0.5N) solution of cerium(IV) ammonium sulfate (0.01—0.05N).[3] The initial concentration of copper(II) bromide was determined in advance by the EDTA titration with murexide as an indicator.[9]

Equilibrium Determination of the Reaction between Acetone and Methanol. The reaction between acetone and methanol forming acetone dimethylacetal is quite slow, but it attains equilibrium fairly rapidly, within 5 min at the latest, in the presence of copper(II) bromide. The reaction mixture was poured into a methanol solution of sodium acetylacetonate cooled in a dry ice-methanol bath. The equilibrium was thus frozen by chelation of copper and neutralization of acid produced. The solution was then submitted to the gas-chromatographic separation through a column (3 m×4 mm in diameter) containing diglycerol (5%) and silicone grease (5%) carried on Neosorb NCS (63°C, hydrogen gas flow: 20 cc/min), and the equilibrium contents of acetone and acetone dimethylacetal were determined.

Results

Stoichiometry of Reactions of Copper(II) Bromide with Acetone and Acetone Dimethylacetal in Methanol. About 2 g of copper(II) bromide was dissolved in 20 ml of methanol, to which 4—5 ml of acetone or acetone dimethylacetal was added and allowed to react at room temperature for about 2 hr. The reaction mixtures were then analyzed by the method described in Experimental and the results are summarized in Table 1.

The distillation residue was composed of copper(I) bromide and copper(II) bromide, and the composition is given by the following equations:

$$CuBr = 2(\text{Total Cu}) - Br$$

$$CuBr_2 = Br - \text{Total Cu}$$

The mass balance is accounted for in the accuracy better than 95% in the case of acetone, but only around 90% for the acetal. Reactions occurring in the earlier stage of this system can thus be represented by the following equations:

$$(CH_3)_2CO + 2CH_3OH \overset{\text{fast}}{\rightleftharpoons} (CH_3)_2C(OCH_3)_2 + H_2O \quad (1)$$

$$(CH_3)_2CO + 2CuBr_2 \longrightarrow CH_3COCH_2Br + 2CuBr + HBr \quad (2)$$

$$(CH_3)_2C(OCH_3)_2 + 2CuBr_2 \longrightarrow CH_3(CH_2Br)C(OCH_3)_2 + 2CuBr + HBr \quad (3)$$

$$HBr + CH_3OH \overset{\text{fast}}{\rightleftharpoons} CH_3Br + H_2O \quad (4)$$

Monobromoacetone dimethylacetal was identified not only by IR and NMR assays but also by isolation as

Table 1. Products of reactions between copper(II) bromide and acetone or acetone dimethylacetal

Starting material			Residue			Distillate		
Acetone ml	Acetal ml	$CuBr_2$ mmol	Total Cu mmol	Br meq	Cu(I) mmol	HBr meq	Monobrominated substrate[a] meq	Dibrominated substrate[b] meq
4	0	6.90	6.83	10.83		1.42	1.46	
5	0	6.62	6.53	7.50		2.80	2.84	
0	5	7.19	7.17	8.60		2.66	1.65	0.92
0	5				4.41	2.05	1.70	0.28

a) Sum of monobromoacetone and monobromoacetone dimethylacetal
b) α, α′-dibromoacetone dimethylacetal

6) G. Brauer, "Handbuch der Preparativen Anorganischen Chemie," 2nd ed., Ferdinand Enke Verlag, Stuttgart (1962), Vol. 2, p. 888.
7) C. D. Ritchie and P. D. Heffley, *J. Amer. Chem. Soc.*, **87**, 5402 (1965).
8) F. P. Treadwell and W. T. Hall, "Analytical Chemistry," Vol. 2, 9th ed., J. Wiley, New York (1942), p. 583.
9) K. Ueno, "Chelate Tekiteiho (Methods of Chelate Titration)," Nankodo, Tokyo (1962), p. 254.

neat liquid. Found: C, 33.10; H, 5.98; Br (by iodometry), 45.2%. Calcd for $C_5H_{11}O_2Br$: C, 32.81; H, 6.06; Br, 43.2%. In the course of vacuum distillation of the reaction mixture from copper(II) bromide and acetone dimethylacetal, white needles separated out. Found: C, 23.08; H, 3.90%. Calcd for $C_5H_{10}O_2Br_2$: C, 22.93; H, 3.85%. NMR spectrum of this compound in CCl_4 shows CH_2Br signal at 3.72 τ and OCH_3 peak at 3.46 τ with the intensity ratio of 2: 3, but has no absorption assignable to CH_3. Thus the compound was identified as α,α'-dibromoacetone dimethylacetal, mp 61—63°C (lit. 63.5°C). The usual iodometric determination of bromine at room temperature was not useful for this compound, but disclosed about 90% of the theoretical value at around 50°C.

By means of the gas chromatographic measurements described earlier, the equilibrium constant of the acetal formation reaction (1), $K=[(CH_3)_2C(OCH_3)_2][H_2O]/[(CH_3)_2CO][CH_3OH]^2$, was determined to be 6.6×10^{-4}M^{-1} at 0°C and 5.5×10^{-4}M^{-1} at 8.15°C. These values are close to 6.5×10^{-4}M^{-1} at 10°C and 4.0×10^{-4}M^{-1} at 25°C obtained spectrophotometrically by Bell, *et al.*[10]

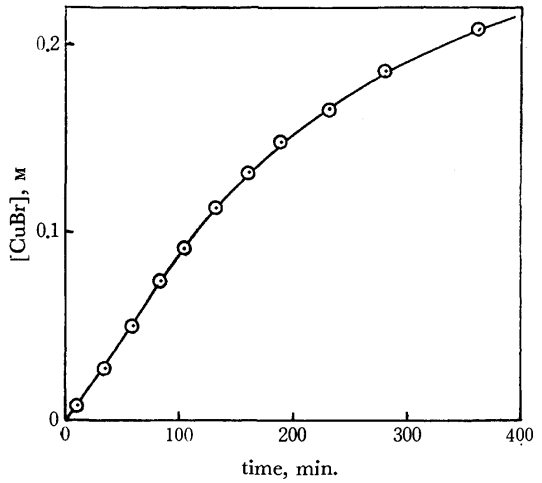

Fig. 1. A kinetic run of the reaction between copper(II) bromide and acetone in methanol at 0°C. Initial concentrations: $[CuBr_2]=0.234$M, $[acetone]=1.78$M.

The Rate Equation for the Reaction of Copper(II) Bromide with Acetone and Acetone dimethylacetal. A kinetic run of the title reaction shows complicated feature as illustrated by the curve in Fig. 1. The rate of decrease of copper(II) bromide can'not be formulated by a simple rate law concerning the concentration of copper(II) bromide. Complicating factors involve the retarding effect of copper(I) bromide and the accelerating effect of hydrogen bromide, both accumulating with the progress of reaction. Thus the complete analysis of each kinetic run was difficult and effects of various factors were examined on the initial rate (R_0) which was defined by the initial linear portion of the [CuBr] *vs.* time curve.

Plots of R_0/[acetone] *vs.* [acetal]/[acetone] gave straight lines at constant $[CuBr_2]$ as illustrated in

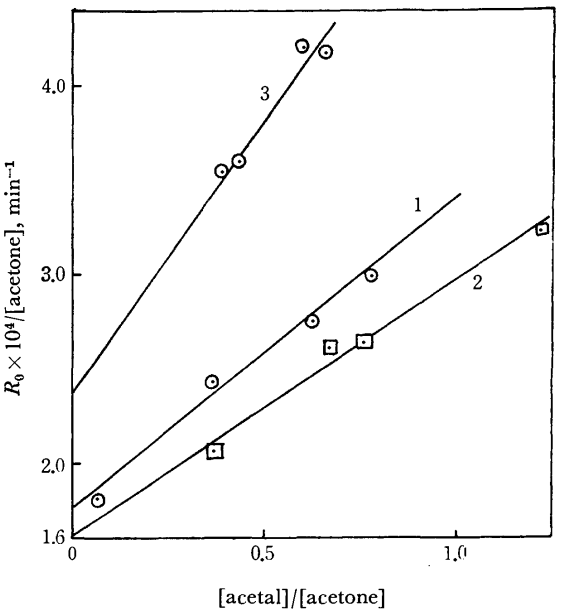

Fig. 2. Linear plots of initial rate data. Line 1: $[CuBr_2]=0.658$M, 0°C; line 2: $[CuBr_2]=0.368$M. 8.15°C; line 3: $[CuBr_2]=0.142$M, 22.05°C.

Fig. 2. Both of the intercept and the slope of these straight lines increase with the concentration of copper(II) bromide, conforming to the rate Eq. (5),

$$R_0 = (k_1'+k_2'[CuBr_2])[CuBr_2][acetone] + (k_1''+k_2''[CuBr_2])[CuBr_2][acetal] \quad (5)$$

where acetal stands for acetone dimethylacetal. The concentrations of acetone and acetal in the reaction mixture were measured at several time intervals and confirmed to be unchanged from the initial equilibrium value governed by the mixing ratio of acetone and methanol.

Table 2. Rate constants referring to the rate equation (5) for reactions of copper(II) bromide with acetone and acetone dimethylacetal

Temp. °C	$k_1'\times10^5$ M^{-1}sec^{-1}	$k_2'\times10^5$ M^{-2}sec^{-1}	$k_1''\times10^5$ M^{-1}sec^{-1}	$k_2''\times10^5$ M^{-2}sec^{-1}
0	~0	0.68	~0	0.62
8.15	0.12	1.73	0.04	1.52
22.05	1.10	13.5	1.19	12.4

Observed values of rate constants are summarized in Table 2. Activation energies referring to the third-order rate constants k_2' and k_2'' are both 22.0 kcal/mol, and frequency factors are 2.46×10^{12} and 2.29×10^{12}M^{-2} sec^{-1}, respectively. It is worth noting that the second-order rate constant is smaller than one tenth of the third-order rate constant in either case, vanishing at 0°C. Furthermore, the corresponding constants for acetone and acetone dimethylacetal lie quite close together. Taking into account the poor accuracy in gas chromatographic determinations of these two substrates, it might be allowed to presume that $k_1'=k_1''$ and $k_2'=k_2''$, that is, acetone and the acetal are brominated at equal rates. Then Eq. (5) is simplified as (6). In fact straight lines are obtained by plotting

10) J. M. Bell, D. G. Kubler, P. Sartwell, and R. G. Zepp, *J. Org. Chem.*, **30**, 4284 (1965).

$$R_0 = (k_1 + k_2[CuBr_2])([acetone] + [acetal])[CuBr_2] \quad (6)$$

$R_0/([acetone]+[acetal])[CuBr_2]$ against $[CuBr_2]$ as illustrated in Fig. 3, resulting in the rate constants as listed in Table 3.

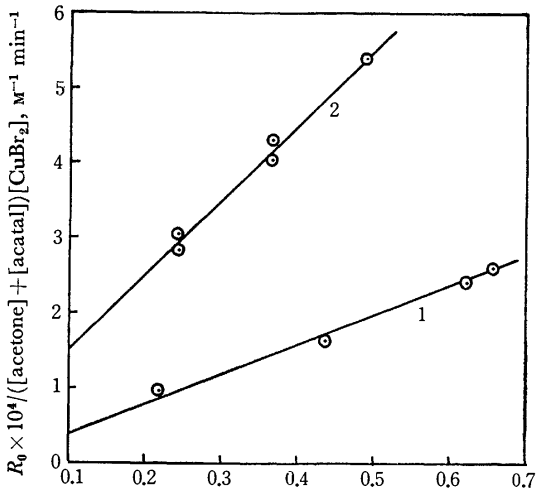

Fig. 3. Linear plots of initial rate data at 0° (line 1) and 8.15°C (line 2) referring to Eq. (6).

TABLE 3. RATE CONSTANTS REFERRING TO THE RATE EQUATION (6) FOR REACTIONS OF COPPER(II) BROMIDE WITH ACETONE AND ACETONE DIMETHYLACETAL

Temp. °C	$k_1 \times 10^5$M^{-1}sec^{-1}	$k_2 \times 10^5$M^{-1}sec^{-1}
0	~0	0.66
8.15	0.08	1.67
22.05	1.13	13.0

Retardation Effect of Copper(I) Bromide. Copper(I) bromide is insoluble in methanol and acetone, but it is dissolved appreciably in the solvents with the coexistence of copper(II) bromide. The solubilization of copper(I) halide is well known to be effected by halide ions forming complex ions. Similar effect may be brought about by the addition of copper(II) halide. McConnell and Davidson, for example, suggested the existence of Cu_2Cl_3 to interpret the interaction absorption of solutions containing copper(I), copper(II), and low concentrations of chloride ion.[11] In the present system, copper(I) bromide may also be considered to be solubilized by the interaction with copper(II) bromide as represented by Eq. (7),

$$CuBr + nCuBr_2 = CuBr \cdot nCuBr_2 \quad (7)$$

Addition of copper(I) bromide to the reaction mixture lowers the initial rate remarkably. If the retarding effect of copper(I) bromide is caused by the partial deactivation of copper(II) bromide according to Eq. (7), the reduced rate at 0°C may be represented by Eq. (8) since k_1 in Eq. (6) is zero at 0°C.

$$R_0 = k_2([acetone] + [acetal])([CuBr_2] - n[CuBr])^2 \quad (8)$$

If much less quantity of copper(I) bromide is added to copper(II) bromide, Eq. (8) can be approximated by

11) H. McConnell and N. Davidson, *J. Amer. Chem. Soc.*, **72**, 3168 (1950).

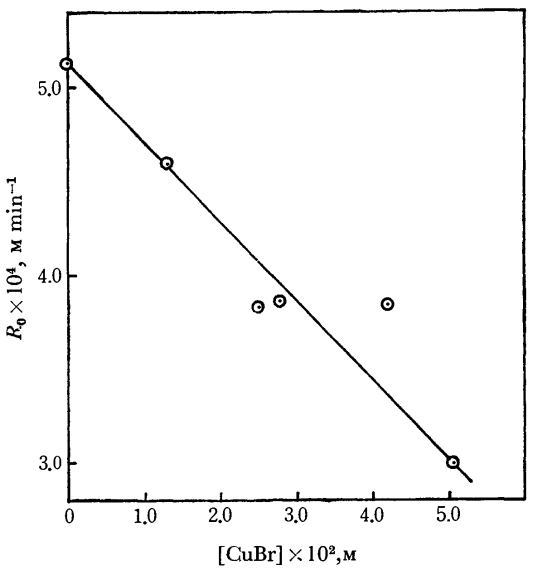

Fig. 4. The retarding effect of copper(I) bromide at 0°C. $[CuBr_2]=0.401$M, $[acetone]+[acetal]=7.47$M.

Eq. (9). In Fig. 4 are plotted the initial rates measured at constant concentrations of copper(II) bromide and acetone against the concentration of copper(I) bromide added. From the slope and the intercept of this straight line n was obtained as 1.6.

$$R_0 = k_2([acetone] + [acetal]) \times ([CuBr_2] - 2n[CuBr])[CuBr_2] \quad (9)$$

Addition of tetraethylammonium bromide also suppressed the bromination reaction of copper(II) bromide as shown in Table 4. This is probably caused by coordination of bromide ions to copper(II) forming complex anions such as $CuBr_3^-$ and $CuBr_4^{2-}$.

TABLE 4. RETARDATION EFFECT OF TETRAETHYLAMMONIUM BROMIDE ON THE REACTION OF COPPER(II) BROMIDE WITH ACETONE AND ACETONE DIMETHYLACETAL AT 0°C
$[CuBr_2]=0.0713$M, $[acetone]+[acetal]=2.38$M

Et_4NBr added, M	Initial rate $\times 10^6$, M sec^{-1}
0	5.25
0	4.72
0.020	4.72
0.059	4.20
0.079	4.20
0.136	1.83
0.194	1.27
0.291	0.65
0.933 (heterogeneous system)	0.00

Acid-catalyzed Reactions of Copper(II) Bromide with Acetone and Acetone Dimethylacetal. If dry acids such as hydrogen bromide, perchloric acid, and *p*-toluenesulfonic acid are added in advance, the initial rate of the reaction is increased linearly with the acid concentration. The initial rate of the acid-catalyzed reaction ΔR_0 was calculated as the difference between the initial rates in the presence and absence of an acid. Figure

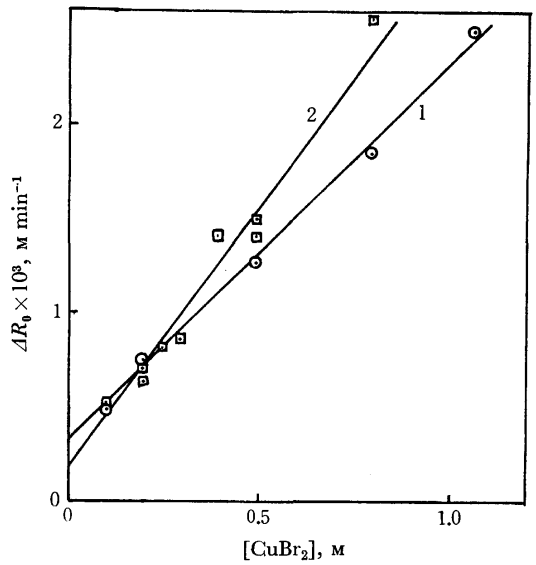

Fig. 5. The initial rate of acid-catalyzed reaction of copper(II) bromide with acetone and acetone dimethylacetal as a function of the concentration of copper(II) bromide at 0°C. Line 1: [$HClO_4$]=0.0318M, [acetone]+[acetal]=4.56M: Line 2: [*p*-toluenesulfonic acid]=0.0406M, [acetone]+[acetal]=4.56M.

5 shows the dependence of ΔR_0 upon the concentration of copper(II) bromide at constant concentrations of perchloric acid or *p*-toluenesulfonic acid and acetone. The linear relationship between ΔR_0 and [$CuBr_2$] reveals that there exist two reaction pathways, one being independent of and the other first-order with respect to copper(II) bromide. At constant concentrations of copper(II) bromide and perchloric acid ΔR_0 increased with the concentration of acetone. However, the interrelation was not linear but represented by a Langmuir-type curve as illustrated in Fig. 6.

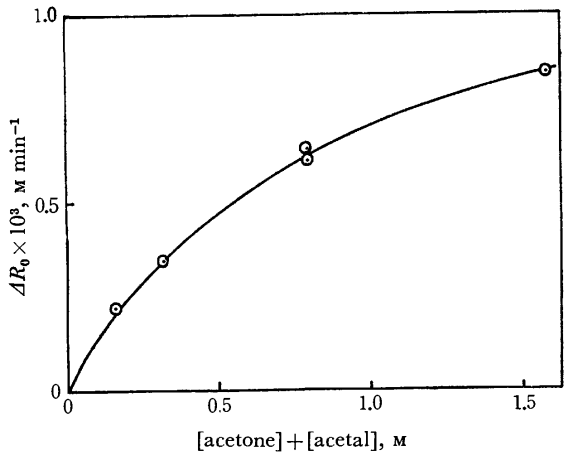

Fig. 6. The initial rate of acid-catalyzed reaction of copper(II) bromide with acetone and acetone dimethylacetal as a function of the combined concentration of acetone and the acetal at 0°C. [$HClO_4$]=0.034M, [$CuBr_2$]=0.659M.

Discussion

The reaction between acetone and methanol seemed troublesome for study of the reaction of copper(II) bromide with acetone, but fortunately the equilibria of acetal formation reactions are established so quickly in the presence of copper(II) bromide and the amount of hemiacetal is known to be so minute[10] that a single equilibrium (1) needs to be considered. Furthermore approximately equal rates of reactions of acetone and acetone dimethylacetal towards copper(II) bromide simplified the analysis of rate data.

It has been well established that the acid catalyzed halogenation of acetone in aqueous solutions is preceded by the rate-controlling enolization steps:[12]

$$\mathrm{CH_3C(=O)CH_3 + HA \rightleftharpoons CH_3C^{+}(OH)CH_3 + A^-} \quad (10)$$

$$\mathrm{CH_3C^{+}(OH)CH_3 + A^- \longrightarrow CH_3C(OH)CH_2 + HA} \quad (11)$$

By analogy, the first steps in reactions of copper(II) bromide with acetone and the acetal may be coordination of substrate molecules to copper atoms (Eqs. (12) and (13)). Partial ionizations of copper(II) bromide itself and of substrate complexes will be at rapid equilibrium, and both the neutral and charged complexes are conceivable to be equally effective in succeeding reactions.

$$\mathrm{(CH_3)_2CO + CuBr_2 \overset{K_1}{\rightleftharpoons} (CH_3)_2CO\cdot CuBr_2 \rightleftharpoons CH_3C(=O^{+}\cdot CuBr)CH_3 + Br^-} \quad (12)$$

(A)

$$\mathrm{(CH_3)_2C(OCH_3)_2 + CuBr_2 \overset{K_2}{\rightleftharpoons} (CH_3)_2C(OCH_3)_2\cdot CuBr_2 \rightleftharpoons CH_3C(OCH_3)(OCH_3)(^{+}CuBr)CH_3 + Br^-} \quad (13)$$

(B)

Although Kochi[3] reported that the initial rate of the reaction between acetone and copper(II) chloride in water was one-half order in gross copper(II), the observed initial rate Eq. (5) or (6) in the present study reflects the existence of two kinds of transition states for each substrate, one containing another copper(II) bromide and the other not. Thus steps (14) through (17) are presumed to be rate-controlling.

$$\mathrm{A + S \overset{k_3}{\longrightarrow} CH_3C(OCuBr)CH_2 + HS^+} \quad (14)$$

$$\mathrm{A + CuBr_2 \overset{k_4}{\longrightarrow} CH_3C(OCuBr)CH_2 + CuBr^+ + HBr} \quad (15)$$

$$\mathrm{B \overset{k_5}{\longrightarrow} CH_3C(OCH_3)CH_2 + CuBr^+ + CH_3OH} \quad (16)$$

$$\mathrm{B + CuBr_2 \overset{k_6}{\longrightarrow} CH_3C(OCH_3)CH_2 + CuBr(OCH_3) + CuBr^+ + HBr} \quad (17)$$

Here S stands for a proton acceptor which may be a methanol molecule. The detailed scheme for bromina-

12) R. P. Bell and Y. Yates, *J. Chem. Soc.*, **1962**, 1927.

tion of acetone dimethylacetal is very difficult to envisage, but is just assumed to involve an enolic ether as visualized in Eq. (16). In steps (15) and (17) copper(II) bromide is supposed to act as a proton acceptor in accordance with the second term with respect to copper(II) bromide in Eq. (5). Succeeding steps in which enolate intermediates are brominated by copper(II) bromide should be fast. Then the overall reaction rate is represented by Eq. (18),

$$\text{rate} = (k_3+k_4[CuBr_2])[A] + (k_5+k_6[CuBr_2])[B]. \quad (18)$$

Substituting equilibrium values of [A] and [B] derived from Eqs. (12) and (13) to Eq. (18),

$$\text{rate} = \{(k_3+k_4[CuBr_2])K_1[CuBr_2][\text{acetone}] + (k_5+k_6[CuBr_2])K_2[CuBr_2][\text{acetal}]\}/(1+K_1[\text{acetone}]+K_2[\text{acetal}]). \quad (19)$$

If $1 \gg (K_1[\text{acetone}]+K_2[\text{acetal}])$, the rate Eq. (19) reduces to the observed rate law (5) with $k_1'=k_3K_1$, $k_2'=k_4K_1$, $k_1''=k_5K_2$, and $k_2''=k_6K_2$.

Mechanisms of bromination of enolic molecules by copper(II) bromide in succeeding steps are not clear at all. Castro, *et al.*[2] obtained a rate equation independent of allyl alcohol, rate$=k[CuBr_2]^2$, for bromination of allyl alcohol by copper(II) bromide in refluxing methanol and attributed the rate expression to the reversible dissociation of copper(II) bromide to molecular bromine.

$$2CuBr_2 \rightleftarrows 2CuBr + Br_2$$

Similar possibility may not be denied for the present system although it seems less probable since the equilibrium concentration of bromine will be very low at 0°C. Alternatively copper(II) bromide itself might brominate an enolate molecule.

The retardation by copper(I) bromide was attributed to the association with copper(II) bromide invalidating 1.6 times as many molecules of the latter. Similar retarding effect of copper(I) chloride was also observed by Lorenzini and Walling[4] in reactions of copper(II) chloride with butyraldehydes in aqueous isopropyl alcohol and by Kochi[3] in the reaction of copper(II) chloride with acetone in water.

Bromide ions were found to act as a retarder in the present system. On the contrary, chloride ions were reported to stimulate reactions both by the Walling group and Kochi. This discrepancy is due to the difference in the reaction media. As discussed above copper(II) halide plays a dual function. The activity of copper(II) halide as a catalyst would be $CuX^+ > CuX_2 > CuX_3^-$, while effectiveness as a halogenating agent should be $CuX^+ < CuX_2 < CuX_3^-$. In aqueous solutions ionization of copper(II) halide (Eq. (20)) is extensive, and the halogenating capacity is rather

$$CuX_2 \rightleftarrows CuX^+ + X^- \quad (20)$$

poor. Addition of chloride ions reverts the equilibrium (20) to the left, increasing the chlorinating efficiency. On the other hand in methanol the ionization (20) is less significant and excess bromide ions added will enhance the addition equilibrium (21),[13]

$$CuX_2 + X^- \rightleftarrows CuX_3^- \quad (21)$$

thus diminishing the catalytic ability of copper(II). In reaction systems containing some acid the coordinative activation of an acetone molecule is effected by a proton, and copper(II) bromide only needs to function as a brominating agent. In such a case addition of bromide ions should increase the reaction rate. In fact, although the initial rate of reaction between copper(II) bromide (0.073M) and acetone (1.30M) in methanol containing perchloric acid (0.026M) was 9.7×10^{-7}M/sec at 0°C, addition of tetraethylammonium bromide in excess (0.27M) raised the rate to 5.8×10^{-6}M/sec. A methanol solution of copper(II) bromide at such a concentration shows a brown color, but changes to purple by addition of excess bromide ions[14] suggesting formations of $CuBr_3^-$ and $CuBr_4^{2-}$.

In analogy to Eqs. (10) and (11) for the reaction with bromine, the following scheme is presumed for the acid catalyzed reactions of copper(II) bromide with acetone and acetal. The concentration of acids employed was usually less than 0.15M and the complete

$$\mathrm{CH_3\!\!>\!\!C\!=\!O} + HS^+ \overset{K_7}{\rightleftarrows} \left[\mathrm{CH_3\!\!>\!\!C\!-\!OH}\right]^+ + S \quad (22)$$
(C)

$$\mathrm{CH_3\!\!>\!\!C(OCH_3)_2} + HS^+ \overset{K_8}{\rightleftarrows} \left[\mathrm{CH_3\!\!>\!\!C(H)(OCH_3)_2}\right]^+ + S \quad (23)$$
(D)

$$C + S \xrightarrow{k_9} \mathrm{CH_3\!\!>\!\!C\!-\!OH} + HS^+ \quad (24)$$

$$C + CuBr_2 \xrightarrow{k_{10}} \mathrm{CH_3\!\!>\!\!C\!-\!OH} + CuBr^+ + HBr \quad (25)$$

$$D \xrightarrow{k_{11}} \mathrm{CH_3\!\!>\!\!C\!-\!OCH_3} + CH_3OH_2^+ \quad (26)$$

$$D + CuBr_2 \xrightarrow{k_{12}} \mathrm{CH_3\!\!>\!\!C\!-\!OCH_3} + CH_3OH + CuBr^+ + HBr \quad (27)$$

dissociation could be assumed, HS^+ then standing for the protonated methanol molecule. From Eqs. (22) and (23) concentrations of protonated substrates C and D are represented by

$$[C] = K_7[HA]_0[\text{acetone}]/([\text{MeOH}]+K_7[\text{acetone}]+K_8[\text{acetal}])$$

$$[D] = K_8[HA]_0[\text{acetal}]/([\text{MeOH}]+K_7[\text{acetone}]+K_8[\text{acetal}])$$

where $[HA]_0$ stands for the total concentration of the acid employed. Then the rate of the acid-catalyzed reaction, namely the difference between rates in the presence and absence of an acid, can be written as

$$\Delta(\text{rate}) = \{(k_9+k_{10}[CuBr_2])K_7[\text{acetone}] + (k_{11}+k_{12}[CuBr_2])K_8[\text{acetal}]\}[HA]_0/([\text{MeOH}]+K_7[\text{acetone}]+K_8[\text{acetal}]) \quad (28)$$

If it is presumed that $k_9=k_{11}=k_a$, $k_{10}=k_{12}=k_b$, and $K_7=K_8=K$, Eq. (28) reduces to Eq. (29):

13) J. C. Barnes and D. N. Hume, *Inorg. Chem.*, **2**, 444 (1963).

14) S. Matsuo, *Nippon Kagaku Zasshi*, **83**, 1229 (1962).

$$\Delta(\text{rate}) = (k_a + k_b[CuBr_2])[HA]_0 K([\text{acetone}] + [\text{acetal}])/\{[\text{MeOH}] + K([\text{acetone}] + [\text{acetal}])\} \quad (29)$$

Braude[15] determined the equilibrium constants K_B^s of the proton-transfer reactions $SH^+ + B \rightleftarrows BH^+ + S$ between the solvated proton SH^+ and the proton-accepting indicator (B), *p*-nitroaniline. The value of K_B^s was 9, 20, 31, and 53 for water, dioxane, ethanol, and acetone, respectively, indicating that the basicity decreases in the order, water > dioxane > ethanol > acetone. The relative basic strengths of water, methanol, and ethanol were also reported[16] to be 1 : 0.13 : 0.33 or 1 : 0.13 : 0.22. These two sets of data indicate that the basicity of acetone is very similar to that of methanol, namely the equilibrium constant K_7 of the proton-transfer equilibrium (22) is close to one. K_8 will not be larger than K_7. Then, in the denominator of Eq. (29), [MeOH] is much larger than the second term in the concentration region of acetone employed (Fig. 5). Equation (29) may thus be approximated by Eq. (30),

$$\Delta(\text{rate}) = (k_a + k_b[CuBr_2])[HA]_0 K([\text{acetone}] + [\text{acetal}])/[\text{MeOH}] \quad (30)$$

The rate equation (30) for the acid-catalyzed reaction well conforms with observed dependences of the initial rate on the concentrations of acid (first order) and copper(II) bromide (Fig. 5), but contradicts the observed acetone dependence (Fig. 6). Equation (30) requires a straight line relationship as observed in Fig. 3, but actual data gave such a Langmuir-type curve. This discrepancy could be attributed to water formation in the reaction (1). As described in Experimental, the equilibrium constant of the acetal formation reaction (1) was determined to be 6.6×10^{-4}M^{-1} at 0°C. If it is put that $[H_2O] = [\text{acetal}]$, $[H_2O] = [\text{MeOH}]$ $(K[\text{acetone}])^{1/2}$ and takes rather large values as 0.2M when [acetone]=0.1 and [MeOH]=25M, and 0.6M when [acetone]=1 and [MeOH]=23M. Under such circumstances appreciable portions of protons are trapped by water molecules and the proton transfer equilibria to be taken into account are intractably complex. Qualitatively speaking, however, with the increase in the acetone concentration employed, the concentration of water is increased and the fraction of protons transferred to acetone moleculs is decreased. This might be concluded as the reason why the rate of the acid-catalyzed reaction is not enhanced in proportion to the acetone concentration (Fig. 6).

The authors are grateful to Dr. T. Ogura for his valuable discussion. Thanks are also due to Mr. J. Gohda for elemental analysis and IR measurements, and to Mr. K. Noda of the Osaka Municipal Technical Research Institute for NMR measurements.

15) E. A. Braude, *J. Chem. Soc.*, **1948**, 1971.
16) R. P. Bell, "The Proton in Chemistry," Cornell University Press, Ithaca, N. Y. (1959), p. 43.

BULLETIN OF THE CHEMICAL SOCIETY OF JAPAN, VOL. 45, 1299—1305(1972)

Ionization Energies and Rydberg States of Tetraaminoethylenes

Yoshihiro NAKATO, Masaru OZAKI,* and Hiroshi TSUBOMURA

Department of Chemistry, Faculty of Engineering Science, Osaka University, Toyonaka, Osaka

(Received September 13, 1971)

Absorption spectra and photo-ionization curves of tetrakis (dimethylamino) ethylene, (TMAE), and 1,1′,3,3′-tetramethyl-$\Delta^{2,2'}$-bi(imidazolidine), (TMBI), have been studied. It has been found that these compounds have very low ionization potentials (about 5.4 eV), which are even comparable with that of the lithium atom. The first ionization potentials of these compounds are nearly the same, although both their absorption spectra and their photo-ionization curves are considerably different from each other. These results can be explained semi-quantitatively by use of the results of simple, semi-empirical molecular orbital calculation with inclusion of direct interaction between four lone-pair orbitals on the N atoms, which was found to be important at the "perpendicular" structure. The first absorption bands of these molecules are assigned to the Rydberg bands, lying quite unusually near the visible region. The quantum defect δ is found to be 0.7 for the lowest Rydberg state of TMAE. The size of the Rydberg orbital for this state is estimated to be 2.9 Å from the maximum radial density, which is comparable with the core size. Higher Rydberg series are also observed for TMBI.

Ionization potentials of organic compounds are one of the key quantities in the studies of electronic processes in organic materials, such as organic semi-conductors, organic photo-conductors, and formation and reactions of electron-donor-acceptor complexes. The gas-phase ionization potentials of organic compounds reported so far lie in the range of about 7 to 12 eV.[1] Recently, we have found that tetrakis (dimethylamino)-ethylene, (TMAE), and 1,1′,3,3′-tetramethyl-$\Delta^{2,2'}$-bi-(imidazolidine), (TMBI), have extremely low ionization

* Present address: Asahi Chemical Industry Co., Ltd. Tokyo.

1) K. Watanabe, T. Nakayama, and J. Mottle, *J. Quant. Spectry. Radiative Transfer*, **2**, 369 (1962); F. I. Vilesov, *Usp. Fiz. Nauk. (SSSR)*, **81**, 669 (1963). English Translation, *Soviet Phys. USPEKHI*, **6**, 888 (1964).

potentials, about 5.4 eV, in spite of their relatively simple molecular structures.[2]

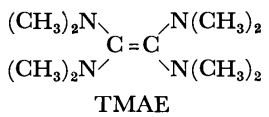

TMAE

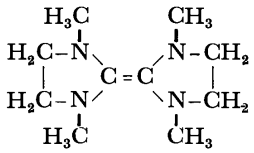

TMBI

The fact that dialkylamino groups have strong electron donating properties is well known. Tetraaminoethylenes have as many such groups as possible for a substituted ethylene, and hence are very strong electron-donors. The chemical properties of these interesting compounds have been studied extensively and they are characterized as electron-rich olefins[3] or as strong electron donors.[4]

The knowledge on the electronic structures of tetraaminoethylenes is, however, still rather limited. The electron donor strength, the bonding and the electronic spectra for TMAE were interpreted by a simple HMO calculation.[4] The electronic spectra were also explained qualitatively in terms of intramolecular charge transfer mechanism.[5]

There have been some difficulties, both experimental and theoretical, in the study of the electronic structure of the tetraaminoethylenes. In the first place, they are strongly reactive to oxygen, emitting strong luminescences. The experiments with them must, therefore, be made with extreme care. Secondly, there is some ambiguity as to their molecular conformations. It is expected that a large steric repulsion exists between four dialkylamino groups. This may prevent the tetraaminoethylenes from taking the "planar" structures and make their conformations more or less uncertain. The "non-planar" structure may lead to a breakdown of the π-electron approximation. Namely, the lone-pair orbitals on the N atoms overlap not only with the π-orbitals on the C atoms, but also directly with the other lone-pair orbitals, and with the σ-orbitals. Finally, the role of the molecular Rydberg states in the low-lying excited levels has been overlooked.

In the present paper, the results of measurements on the photo-ionization curves, ionization potentials and absorption spectra will be reported, together with the discussions on the electronic structures and ionization potentials of free molecules in the gas phase, based on the MO calculations of these molecules.

Experimental

Both TMAE and TMBI were prepared according to the literature.[6] Crude products were distilled in an atmosphere of nitrogen under reduced pressure. They were then degassed and distilled repeatedly in a vacuum line, and stored in evacuated glass ampoules with breakable seals. *n*-Pentane, isopentane, and methylcyclohexane were passed through silica gel columns, left overnight in contact with sodium wire and distilled. All the sample solutions were prepared by dissolving TMAE or TMBI through breakable seals into solvents after they had been completely deoxygenated. Absorption spectra of TMAE and TMBI at room temperature were measured by using various cells with pass length ranging from 1.0 to 10 cm.

Absorption spectra in the wavelength region longer than 190 nm were measured in a Cary Model 15 spectrophotometer. Both absorption spectra and photo-ionization curves in the wavelength region between 300 and 155 nm were measured by a 0.5 meter Nalumi vacuum monochromator. It has a Bausch and Lomb concave grating (concave radius 498.1 mm, ruled area 30 mm × 51 mm, 600 grooves/mm, blazed at 1500 Å, blaze angle 2°35′). The plate factor of the monochromator is calculated to be 28.3 Å/mm when the grating is used in the first order at $\lambda = 150$ nm. The slit width used was normally 200 μ. The light source used is a hot-cathode-type hydrogen-discharge lamp from Mitsubishi Electric Corp., operated at 0.9 A and 70 V, which emits photons of the wavelengths longer than 155 nm. A Toshiba 7696 photomultiplier (S-11 type) covered with a sodium salicylate thin film is used as a photon detector. Emission lines from mercury and hydrogen lamps were used to calibrate the wavelength scale. The stray light was found to be less than 3% of the total light from the exit slit around 160 and 180 nm.

Photon absorption and photocurrent were measured as functions of photon energy in the same run. A pyrex cell used has two quartz windows (transparent down to 155 nm) and two collecting-electrodes held parallel to each other by means of tungsten wire-pyrex seals, the resistance between which was 3×10^{15} ohms at 25°C. Photocurrent was measured by Takeda Riken vibrating reed electrometer, TR-84M. The applied voltage between electrodes was 5 to 10 V in normal use. In the above experimental conditions, the minimum photocurrent detected was about 2.0×10^{-15} A. Estimating the light intensity at some 10^9 photons/sec from the photomultiplier output, the photo-ionization yield ($= \sigma_i/\sigma$) can be measured to be at least 2×10^{-5}, if it is assumed roughly that one half the incident light was absorbed by the sample vapor (where σ and σ_i are absorption and photo-ionization cross sections, respectively).

Results

Absorption spectrum of TMAE in the vapor phase is shown in Fig. 1. At least four transitions may be involved in the spectrum which are centered at 29.0, 38.5, 44.8, and 53.0 kK. The first (29.0 kK) and the second (38.5 kK) bands agree closely with those reported by Winberg, Downing, and Coffman,[7] and the fourth (53.0 kK) agrees with that by Hori, Kimura, and Tsubomura.[5] Some structures are seen in the region around the fourth band. Near ultraviolet absorption spectra of TMAE in MP solutions, both at room temperature and 77°K, are given in Fig. 2 together with that in the gas phase, where MP is a mixed solvent consisting of methylcyclohexane and isopentane in a volume ratio of 1 : 1. Similar spectrum was ob-

2) Y. Nakato, M. Ozaki, A. Egawa, and H. Tsubomura, *Chem. Phys. Lett.*, **9**, 615 (1971).

3) R. W. Hoffmann, *Angew. Chem.*, **80**, 823 (1968); *Angew. Chem. Internat. Edit.*, **7**, 754 (1968).

4) N. Wiberg, *Angew. Chem.*, **80**, 809 (1968); *Angew. Chem. Internat. Edit.*, **7**, 766 (1968).

5) M. Hori, K. Kimura, and H. Tsubomura, *Spectrochim. Acta*, **24A**, 1397 (1968).

6) For TMAE, R. L. Pruett, J. T. Barr, K. E. Rapp, C. T. Bahner, J. D. Gibson, and R. H. Lafferty, Jr., *J. Amer. Chem. Soc.*, **72**, 3646 (1950). For TMBI, H. E. Winberg, U. S. 3239518, 3239519 (1966).

7) H. E. Winberg, D. R. Downing, and D. D. Coffman, *J. Amer. Chem. Soc.*, **87**, 2054 (1965).

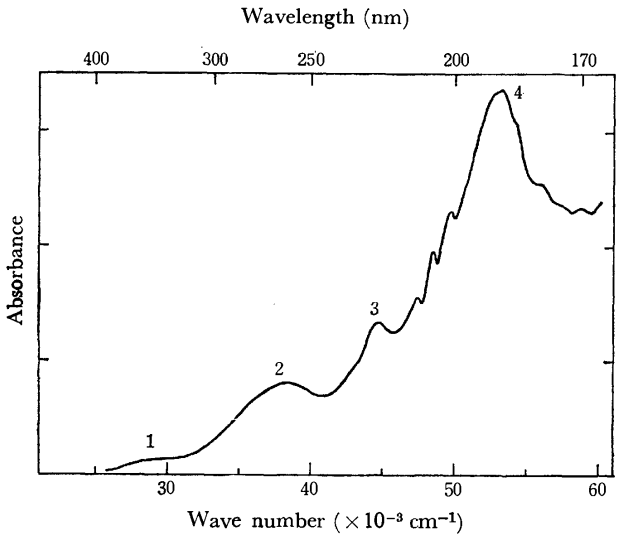

Fig. 1. The absorption spectrum of TMAE in the vapor.

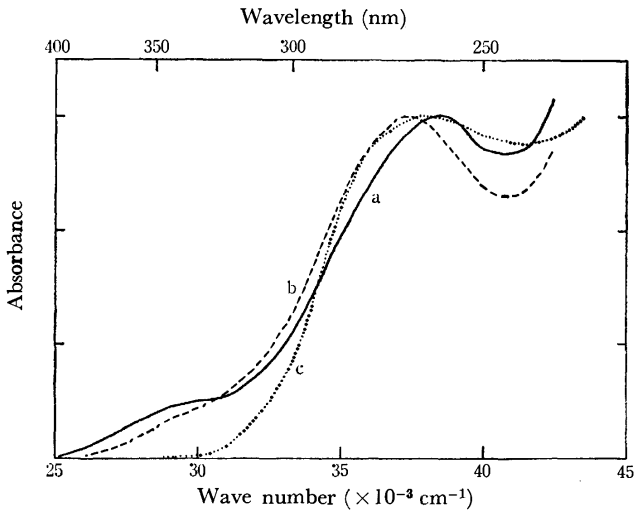

Fig. 2. The absorption spectra of TMAE in the near UV region; curve a (——) for the vapor, curve b(- - - - -) for an MP solution at room temperature and cruve c(·····) for the same solution as 77°K. The profile around the second band (38 kK) of cruve c is somewhat ambiguous, because the matrix became a little opaque.

tained in an *n*-pentane solution or in an ether solution, and a maximum was found at 45.5 kK. The absorption maxima previously reported are 37.3 kK in *n*-heptane, tetrahydrofuran and acetonitrile,[5] and 37.0 and 45.2 kK in *n*-decane.[8] The agreements are good.

Absorption spectra of TMBI both in the vapor and in an *n*-pentane solution are shown in Fig. 3. Vapor absorption begins at about 25.0 kK and increases towards higher wave numbers with a few inflexions (32.8 not clear, 35.7, 40.8 kK). The first peak is located at 50.5 kK. The second seems to exist at around 60 kK or higher.

It should be noted here that the first band of TMAE shifts to higher wave numbers in an MP solution at room temperature compared with that in the vapor although the second band shifts rather inversely. The first band is apparently missing at 77°K. The

8) C. A. Heller and A. N. Flechter, *J. Phys. Chem.*, **69**, 3313 (1965).

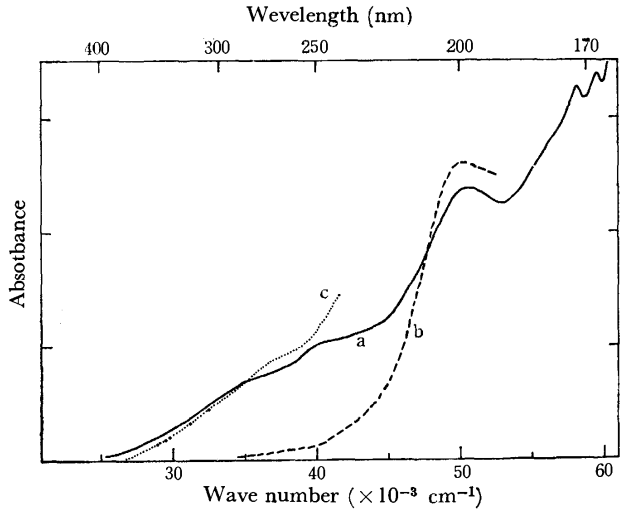

Fig. 3. The absorption spectra of TMBI; curve a (——) for the vapor, curve b (- - - - -) for an *n*-pentane solution at a low concentration of TMBI and curve c (·····) for the same one at a high concentration.

absorption spectrum at wave numbers lower than 45 kK for TMBI in the vapor is also apparently missing in an *n*-pentane solution.

Very recently, several studies concerning the Rydberg states in condensed media were made.[9,10] The main conclusion is that the Rydberg band is sensitive to the environments surrounding the molecule. It moves to shorter wavelengths when it is placed in the condensed phase or even in the gaseous state at high pressure.[11] The first band of TMAE and the bands in the near UV of TMBI show behaviors similar to the Rydberg bands reported in these papers, so that it may be concluded that they are Rydberg bands. It may also be concluded that the second and third bands of TMAE and the 50.5 kK band of TMBI are non-Rydberg bands from their insensitiveness to the environments. The fourth band of TMAE also seems to be non-Rydberg, because it is too strong to be assigned to the Rydberg band. This conclusion is supported by the molecular orbital calculation.

It must be pointed out here that the gas-phase absorption spectrum of TMAE seems to contain an underlying continuous absorption which increases in intensity towards higher wave numbers, as seen in Fig. 1. This may be concluded to correspond to the transitions to the higher Rydberg series and the ionization-continuum. A similar feature is seen for the gas-phase spectrum of TMBI in Fig. 3.

Figure 4 shows the photo-ionization curves for TMAE. Curve a shows the relative photo-ionization cross section, σ_i^{rel}, as a function of photon energy, E, and curve b is the first derivative curve ($d\sigma_i^{rel}/dE$ *vs.* E). σ_i^{rel} was calculated at every 10 Å by using the equation, $\sigma_i=\sigma\cdot i/(I_0-I)$, where σ, i, and I_0-I are the relative absorption cross section, photocurrent and relative light

9) B. Katz and J. Jortner, *Chem. Phys. Lett.*, **2**, 437 (1968), and the papers cited therein.

10) A. J. Merer and R. S. Mulliken, *Chem. Rev.*, **69**, 639 (1969).

11) M.B. Robin and N.A. Kuebler, *J. Mol. Spectrosc.*, **33**, 274 (1970).

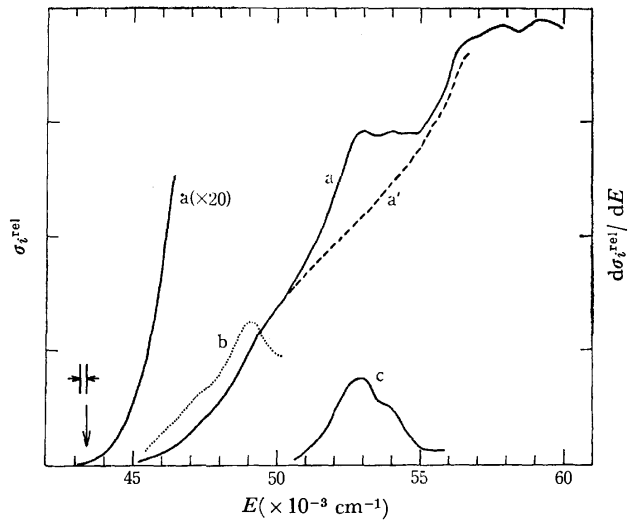

Fig. 4. Gas-phase photo-ionization of TMAE; curve a shows σ_i^{rel} *vs* E and curve b $d\sigma_i^{rel}/dE$ *vs.* E. Curve a is divided into curve a' and c in the energy region around 53 kK, which are estimated to correspond to the contributions of the direct ionization and the auto-ionization, respectively, (See text.). The threshold for photo-ionization is shown by an arrow. The energy spread of the photon beam at the threshold is also indicated.

intensity absorbed by the sample vapor, respectively. The onset of the ionization is rather gradual. Such a feature is common to those reported for aliphatic and aromatic amino compounds.[12,13] In such cases, it is difficult to determine the adiabatic ionization potentials accurately. We have, therefore, taken the point of appearence of σ_i^{rel} as an upper limit for the first adiabatic ionization potential.

Curve a has three steepest slopes at 49, 52, and 56 kK, and curve b has maxima at these positions, as shown only for the first steepest slope in Fig. 4. According to Morrison's method,[12] the first vertical ionization potential for TMAE can be determined to be 49.3 kK from the maximum of curve b. The second steepest slope at 52 kK, however, seems to be attributable to the auto-ionization from the fourth band of TMAE, rather than to the second (direct) ionization. The estimated curve for the direct ionization is shown as curve a' (a broken line) and the difference between the curves a and a' is shown as curve c, which corresponds to the contribution due to the auto-ionization. This interpretation may be supported by the fact that curve c agrees very well with the fourth band in Fig. 1. If this is the case, the second vertical ionization potential may be estimated to lie in 55—56 kK.

Photo-ionization curves for TMBI are shown in Fig. 5, from which the ionization potentials can be determined in the same way. The auto-ionization also seems to occur, but is not so clear. The first vertical ionization potential estimated to lie around 49 kK is, therefore, made somewhat uncertain. The second photo-ionization seems to start at about 57 kK.

Photo-ionization curves in the higher wave number regions ($\gtrsim$57—58 kK), both in Figs. 4 and 5, seem to be less reliable, because of the line spectrum of the hydrogen lamp used as the light source.

The observed ionization potentials are summarized in Table 1, together with those reported in the literature.

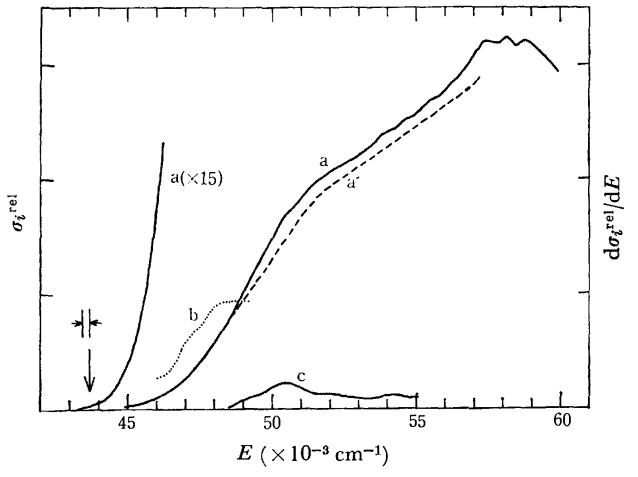

Fig. 5. Gas-phase photo-ionization of TMBI. Each curve and mark are indicated in the similar manner as in Fig. 4.

Table 1. Gas-phase ionization potentials

		the first *Ip*		the second *Ip*[c]
		adiabatic	veritcal	vertical
TMAE	this work	$\lesssim$5.36	6.11	*ca.* 6.9
	literature a)	<6.5		
	literature b)		6.27	
TMBI	this work	$\lesssim$5.41	~6.1	*ca.* 7.1

a) From the appearance potential of the parent ion in the mass spectrum; N. Wiberg and J.W. Buchler, unpublished.

b) Calculated from the difference in the charge-transfer absorption maxima for TMAE and dimethylaniline as the donors and nitrobenzene as the common acceptor, where 7.35 eV for the ionization potential of dimethylaniline was used; Ref. 15). This should be compared with the vertical value obtained by us.

c) These are only tentatively estimated values.

MO Calculations

In order to understand the experimental results, it seems worthwhile to make theoretical calculations of the electronic energies. For the purpose to find the orbital energies of filled π-MO's and to characterize the π-π^* type transitions, a simple semi-empirical molecular orbital calculation was made using only the $2p\pi$-AO's on the C atoms and the lone-pair AO's on the N atoms. Each of the lone-pair AO's is assumed to be one of the sp^3 hybrid orbitals of the nitrogen atom. The details of the method of calculation is given in the Appendix.

The molecular conformations of tetraaminoethylenes have not been fully established. The planar $N_2C{=}CN_2$ skeleton can at least be assumed for the ground state. The inspection of the molecular model shows that the

12) H. Hurzeler, M. G. Inghram, and J. D. Morrison, *J. Chem. Phys.*, **28**, 76 (1958).

13) M. Batley and L. E. Lyons, *Mol. Crystals*, **3**, 357 (1968).

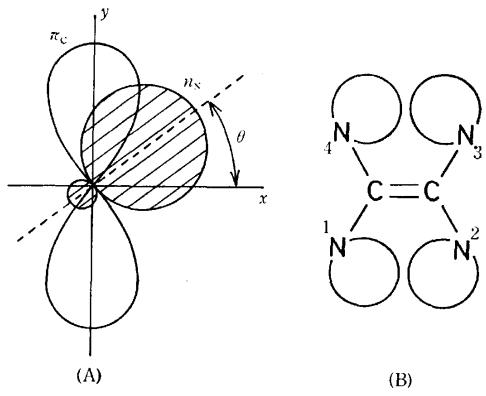

Fig. 6. (A), A projection of a nitrogen lone-pair AO and a carbon $2p\pi$-AO on the xy plane perpendicular to the C–N bond. The angle θ is indicated. (B), The "perpendicular" structure of tetraaminoethylenes. Only the $N_2C{=}CN_2$ skeleton and four lone-pair orbitals are illustrated.

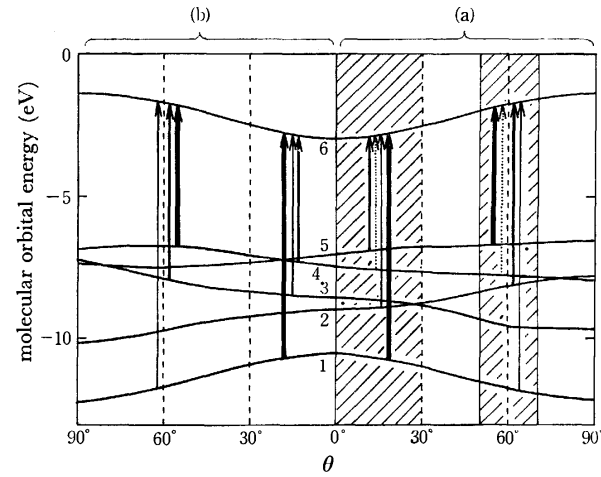

Fig. 7. Molecular orbital energies for tetraaminoethylenes. Each molecular orbital energy is plotted as a function of θ, for two types of conformations, (a) and (b). The Slater's parameter (μ) used is 1.80.

four dimethylamino groups have some freedom of twisting around each of the four C–N bonds. Let the direction of a C–N bond be the z-axis, and we draw the projectories of carbon $2p\pi$-AO and nitrogen lone-pair AO on the xy plane as shown in Fig. 6 (A). Then, the angle θ as shown in Fig. 6 (A) can be the best parameter to define the conformation of the dimethylamino group. The C–N resonance interaction (β_{CN} in the Appendix) makes the "planar" structure ($\theta=90°$ in Fig. 6 (A)) the most preferable, which is, however, more or less prevented by the mutual steric repulsion between the crowded methyl groups. The infrared absorption spectrum of TMAE shows no band in the $\nu_{C=C}$ regions,[14] whereas an intense $\nu_{C=C}$ band (1630 cm^{-1}) appears in the Raman spectra.[7] TMAE also gives only one sharp proton signal in the NMR spectrum.[7,14] All these results suggest that the molecular conformation is symmetric with respect to the C=C bond. At present, the most reasonable model for TMAE in the ground state seems to be a "perpendicular" structure ($\theta=0°$) under wobbly motion proposed by Hammond and Knipe,[15] in which the $(CH_3)_2N$ groups are vibrating about a position "perpendicular" to the $N_2C{=}CN_2$ plane. TMBI gives two sharp proton signals in the NMR spectrum. The steric repulsion between the methyl groups for TMBI seems to be much less than that for TMAE, but may still be large enough to prevent the complete "planar" structure.

The complexity of the problem arises from the fact that each of the four dimethylamino groups has a certain free domain of wobbly motion, and there are quite a number of possible conformations for TMAE. For TMBI, the situation is somewhat similar, although there is a geometrical restriction of cyclization for the twisting motions. In order to describe various conformations, we start from the "perpendicular" structure, in which all lone-pair orbitals lie on the $N_2C{=}CN_2$ plane in the manner as shown in Fig. 6 (B), and construct all other conformations by twisting dialkylamino groups about the C–N bonds with angles of θ_i, where $i(=1,2,3,4)$ is numbering of dialkylamino groups as shown in Fig. 6 (B). The angle θ_i is defined so as to have a positive value on twisting the lone-pair orbital upwards.

The calculation has been made for various possible conformations, *i.e.*, at various θ_i values each independent of others. Part of the results obtained is shown in Fig. 7. Here, the molecular orbital energies are plotted as a function of θ for two types of conformations: (a), $\theta_1=\theta_3=-\theta_2=-\theta_4$ $(=\theta)$ and (b), $\theta_1=\theta_4=-\theta_2=-\theta_3$ $(=\theta)$. Each of these two types of conformations, especially (a), is expected to have the least steric repulsion between the methyl groups. The orbital energies of the four lone-pair orbitals are split by the direct N–N interaction into those of four MO's at the "perpendicular" structure ($\theta=0°$). As the angle θ increases, this N–N interaction decreases, while the interaction between N and π_C becomes important. Consequently, somewhat complicated curves with several cross-points are obtained, as seen in Fig. 7.

Of the six MO's, which are numbered at $\theta=0°$ as shown in Fig. 7, the lower five are filled with electrons, and only the highest is vacant. Allowed transitions under the approximation described in the Appendix[16] are indicated by arrows in Fig. 7; those having strong transition moments by thick arrows and those having weak transition moments by thin arrows. Arrows with dotted lines indicate those with negligibly small transition probabilities. The transition probabilities are found to depend strongly on θ. From the consideration of steric hindrances, it is assumed that the allowable region of θ for TMAE is from 0° to 30° and that for

14) N. Wiberg and J. W. Buchler, *Z. Naturforsch.*, **19b**, 5 (1964).
15) P. R. Hammond and R. H. Knipe, *J. Amer. Chem. Soc.* **89**, 6063 (1967).

16) The transition moments calculated for the conformation (a) under the approximation described in the Appendix are as follows, $\mu(6\leftarrow5)^2$: $\mu(6\leftarrow4)^2$: $\mu(6\leftarrow2)^2$: $\mu(6\leftarrow1)^2=0.00$: 0.00: 0.00: 1.00 at $\theta=0°$; 0.69: 0.00: 0.29: 0.54 at $\theta=30°$; 1.29: 0.02: 0.54: 0.17 at $\theta=60°$; 1.45: 0.04: 0.56: 0.08 at $\theta=90°$, where $\mu(n\leftarrow m)^2$ indicates the square of the transition moment from the m-th MO to the n-th MO in Fig. 7 relatively. The transition, $6\leftarrow3$, is symmetry forbidden for the conformation (a). The transition moments change continuously with θ. Similar results are obtained for the conformation (b).

TMBI from 50° to 70°, which are marked by hatching for the conformation (a) in Fig. 7.

The results obtained are summarized as follows.

(1) The energy of the highest filled MO is nearly the same in the two regions; $\theta=0°$—$30°$ and $50°$—$70°$, as seen from Fig. 7. (Inversion of the highest filled MO's occurs for the conformation (b)). This result agrees with the observation that TMAE and TMBI have almost equal ionization potentials. The low ionization potentials of these molecules compared with the alkylamine and ethylene seem to be caused mainly by the direct N–N interaction for TMAE and mainly by the C–N resonance interaction for TMBI.[17]

(2) We have concluded in the previous section that the first band of TMAE (Fig. 1) is of Rydberg nature. From the results of calculation made for the conformation (a) in the region $0°\lesssim\theta\lesssim30°$, it is shown that the 6←1 transition indicated in Fig. 7 is mainly of the nature of π-π^* transition in the ethylenic group and is therefore very strong. The transitions, 6←5 and 6←2, are shown to be forbidden at $\theta=0°$ but become considerably strong near $\theta=30°$.[16] The theoretical predictions for the relative intensities of these three transitions agree fairly well with those observed for the second, third, and fourth bands in the TMAE absorption spectrum, though they are made somewhat ambiguous owing to the presence of the underlying continuum, as mentioned in the preceding section. The transition, 6←4, is predicted to be negligibly weak, and is probably hidden by other strong bands. Similar good agreements are also found for the conformation (b) in the region $0°\lesssim\theta\lesssim30°$.

(3) In the region $50°\lesssim\theta\lesssim70°$, the transition energies are much larger than the corresponding transition energies at $\theta=0°$—$30°$ both for the conformations (a) and (b). This explains very nicely the marked blue-shift of absorption bands observed for TMBI compared with those for TMAE, since it has been concluded in the previous section that the 50.5 kK band of TMBI corresponds to the lowest allowed valence transition (6←5 in Fig. 7(a) or 6←4 in Fig. 7(b)).

We have assumed that TMAE and TMBI take the structure represented by either the conformation (a) or the conformation (b). These two conformations are expected to be preferred owing to their least steric repulsions between methyl groups. It might be possible, however, that TMAE and TMBI take structures represented by mixtures of these two and other conformations with the less steric repulsions between the methyl groups. Even in such cases, the above-mentioned conclusion is not substantially altered.

Discussions

The above mentioned calculated and observed results seem to provide fairly convincing explanation as to the question why TMAE and TMBI have nearly the same ionization potentials (*Ip*'s), although they are expected to have different conformations.

Although the first vertical *Ip*'s of TMAE and TMBI are easy to determine from the σ_i^{rel} curves, only the upper limits are obtained for the adiabatic *Ip*'s. It seems, however, very likely from the following consideration that these observed limits lie close to the true adiabatic *Ip*'s. The nuclear configuration of TMAE in the Rydberg state is expected to be similar to that of the positive ion, as pointed out for ethylene.[11] Therefore, the difference between the adiabatic and vertical energies for the Rydberg transition will be nearly equal to that for the ionization. The difference between the vertical and adiabatic energies for the first Rydberg transition of TMAE is estimated fairly accurately to be about 0.6 eV, because the adiabatic energy for this transition can be obtained from the overlapping part of the absorption and fluorescence spectra. The difference between the observed limit for the adiabatic *Ip* and the vertical *Ip* determined in the present work for TMAE is about 0.7 eV as seen from Table 1, which is in fairly good agreement with the difference between vertical and adiabatic energies of the first Rydberg transition.

The large differences between the vertical and adiabatic *Ip*'s for both TMAE and TMBI should be attributable to large change of the molecular conformations upon ionization. It is suggested that $TMAE^+$ has nearly "planar" structure from the ESR studies.[4,18] It must also be pointed out that a large difference (~0.7 eV) was reported even for aliphatic amines,[13] possibly because of the change of the molecular shapes from the pyramidal structures to the planar.

We have assigned the first band of TMAE and a number of low-lying bands of TMBI to the Rydberg bands on the basis of their characteristic behaviors in solutions compared with those in the vapor. The higher series for TMAE may be covered by the stonger second band corresponding to the transition to the valence state. These unusually low-lying Rydberg states for tetraaminoethylenes are naturally expected from their very low *Ip*'s.

The term values of Rydberg states in molecules fall into a series, expressed in the form,

$$T = RZ^2/(n^*)^2 = RZ^2/(n-\delta)^2,$$

where, Z is the charge on the core, R the Rydberg constant, n^* the effective principal quantum number. From this equation, and using the adiabatic *Ip* and the wavelength at the center of the overlap between the first absorption band and the fluorescence spectrum, n^* is calculated to be 2.3. If this band is assumed to be the first member of the series ($n=3$), δ then becomes 0.7. The empirical δ-values reported for the Rydberg series of molecules built-up from atoms of the first period are 0.9—1.2 for *ns*-series, 0.3—0.5 for *np*-series and 0.1 for *nd*-series.[19] Deviation of the quantum defect, δ, for the first Rydberg state of TMAE from

17) Strictly speaking, the interaction with the σ-electrons must be included, especially at small θ. It is, however, expected from a simple consideration that this interaction causes little change for the highest filled MO in Fig. 7. R. Hoffmann, A. Imamura, and W. J. Hehre, *J. Amer. Chem. Soc.*, **90**, 1499 (1968).

18) K. Kuwata and D. H. Geske, *ibid.*, **86**, 2101 (1964).

19) G. Herzberg, "Molecular Spectra and Molecular Structure III. Electronic Spectra and Electronic Structure of Polyatomic Molecules," D. Van Nostrand Co., Inc., Princeton, N. J., (1966). p. 341.

either those for *ns* or *np*-series, as seen above, may be attributable to the large departure of the core potential from spherical symmetry. The size of the Rydberg MO can be roughly estimated from the equation, $r_0=(n-\delta)^2a_0/Z$, where a_0 is 0.529 Å and r_0 is the *r*-value at which the radial density has its maximum. We obtain $r_0=2.9$ Å for the first Rydberg state of TMAE. On the other hand, it is thought that the positive charge of the core is located mainly on the four equivalent N atoms, since the highest filled MO consists mainly of the four lone-pair orbitals on the N atoms. The size of the core is, therefore, comparable with r_0 obtained above, since the N–N distances of TMAE are about 2.7 and 2.4 Å.

A large Stokes' shift between the first absorption and fluorescence bands is observed for TMAE. This large Stokes' shift was attributed by some authors to the conformational change of the fluorescent state of TMAE from the ground state, in the former of which the two N_2C halves are assumed to be perpendicular to each other in the N_2C=CN_2 skeleton.[4,9] This explanation seems to assume that the first band is due to a π-π^* type transition. As discussed in the foregoing of this section, however, it seems more likely that the fluorescent state takes a structure similar to $TMAE^+$, in which the planarity of the skeleton is maintained.

Appendix

A simple LCAO MO theory is used in this work. Normalized symmetry orbitals, ξ_i, are first constructed as follows,

$$\begin{aligned}
\xi_1 &= (2+2S_{CC})^{-1/2}(\chi_{Ca}+\chi_{Cb})\\
\xi_2 &= (2-2S_{CC})^{-1/2}(\chi_{Ca}-\chi_{Cb})\\
\xi_3 &= 2^{-1}(\chi_{N1}+\chi_{N2}+\chi_{N3}+\chi_{N4})\\
\xi_4 &= 2^{-1}(\chi_{N1}+\chi_{N2}-\chi_{N3}-\chi_{N4})\\
\xi_5 &= 2^{-1}(\chi_{N1}-\chi_{N2}-\chi_{N3}+\chi_{N4})\\
\xi_6 &= 2^{-1}(\chi_{N1}-\chi_{N2}+\chi_{N3}-\chi_{N4})
\end{aligned}$$

where χ_{Ca} and χ_{Cb} indicate the two $2p\pi$-AO's on the C atoms of the C=C group and χ_{Ni} the lone-pair AO on the *i*-th N atom (Fig. 6(B)). The MO's of the whole molecule, ϕ, are, then, expressed as follows,

$$\phi = \sum c_i\xi_i$$

where c_i is a proper coefficient. The overlap integrals, S_{NN} and S_{CN}, are neglected, while S_{CC} is included and taken to be 0.257.

The two matrix elements, H_{11} and H_{22} ($H_{ii}=\int\xi_i H\xi_i d\tau$ where H indicates the effective one-electron Hamiltonian of the whole molecule), are assumed to be equal to -10.5 and -3.0 eV, respectively, empirically from the ionization potential and the excitation energy to the first excited singlet ($^1\sum_u^+$) state of ethylene. The four matrix elements, H_{33}, H_{44}, H_{55}, and H_{66}, are given as simple sums of the nitrogen Coulomb integral, α_N, and various resonance integrals between two nitrogen atoms, β_{NN}. α_N is taken to be -8.0 eV from the vertical ionization potential estimated for $N(C_2H_5)_3$. The β_{NN}'s are found to play an important role in the case of TMAE and included in the calculation, although they were neglected in the MO calculations made for TMAE previously.[4] These integrals are calculated from the equations of the type, $\beta_{NN}=S_{NN}(\beta_{CC}/S_{CC})$, where S_{NN} is the overlap integral between two nitrogen atoms, and β_{CC} and S_{CC} are taken to be -3.8 eV and 0.257, respectively. The calculation of S_{NN} is made by the use of Mulliken's table.[20] The Slater's parameter ($\mu=Z_{eff}/n^*$) for a nitrogen $2p$ AO calculated by ordinary Slater's rule is 1.95. However, a little smaller value may be more suited for a μ value of a nitrogen lone-pair AO. In the present work, calculations were made using two μ values of 1.95 and 1.80. It turned out that there was almost no substantial difference between the results obtained for the two μ values. The off-diagonal matrix elements, H_{ij} ($i\neq j$), are expressed in terms of β_{CN}, the resonance integral between the adjacent C and N atoms, which is calculated from the equation, $\beta_{CN}=0.8\beta_{CC}\sin\theta$, where β_{CC} is taken to be -2.5 eV by considering that the C–N distance is longer than the C=C distance of ethylene and θ is the twisting angle of the dialkylamino group defined before. The other parameters used are as follows; the bond distance, R(C=C)$=1.34$ Å, R(=C–N)$=1.37$ Å and the bond angle, $\angle$NCN$=\angle$NCC$=120°$.

Transition moments are calculated by assuming $\int\chi_p r\chi_q d\tau=0$ if $p\neq q$. The center of the charge density of the lone-pair AO is assumed to lie at 0.3 Å away from the nitrogen nucleus in the direction of the sp^3 hybrid orbital.

20) R. S. Mulliken, C. A. Rieke, D. Orloff, and H. Orloff, *J. Chem. Phys.*, **17**, 1248 (1949).

Radiolyses of Mixtures of Ammonia and Hydrocarbons. II. Formation of Hydrogen from Mixtures of Ammonia and Olefins (Ethylene, Propylene and Butadiene)

Kumao HAMANOUE, Jiro OKAMOTO, Okihiro TOKUNAGA, and Akibumi DANNO

Japan Atomic Energy Research Institute, Tokai Research Establishment, Tokai-mura, Naka-gun, Ibaraki-ken

(Received September 17, 1971)

γ-radiolyses of gaseous mixtures of ammonia and olefins (ethylene, propylene and butadiene) have been investigated over the whole composition range of mixtures, and consideration was given on the primary processes of hydrogen formation. From the extrapolated values of $G(H_2)$ obtained in the γ-radiolyses of the mixture of ammonia and olefins, it was found that the non-scavengeable $G(H_2)$ of ammonia, ethylene, propylene and butadiene were 0.68—0.72, 1.26, 1.06, and 0.33, respectively. Gas-phase radiolyses of ammonia–perdeuterated olefin mixtures have also been investigated. From kinetic calculation on the data of isotopic mixtures of hydrogen, the following results were obtained; 1) both thermal and non-scavengeable hydrogen molecules are produced by the γ-radiolysis of ammonia, and the non-scavengeable hydrogen molecules are produced for the most part by a unimolecular process, 2) almost all the hydrogen molecules produced by the γ-radiolyses of olefins (ethylene, propylene, and butadiene) are non-scavengeable; a unimolecular process plays an important role in the case of ethylene, and in other cases a bimolecular process. $G(H_2)$ of the butadiene radiolysis is very small compared with that of other olefins and with the calculated value of butadiene, *i.e.*, $G(H_2)<1$. The discrepancies can be interpreted in terms of the addition reaction of the "hot" hydrogen radicals to butadiene to form *t*-2-butene.

The radiolyses of olefins have been studied extensively. In particular, the primary process of hydrogen formation was investigated in detail by Hatano *et al.* on the simple olefins (ethylene, propylene, butene-1 and butene-2) under the action of the γ-ray radiation.[1-6] They concluded that almost all the hydrogen molecules produced were non-scavengeable and produced by the decomposition of the so-called "Super-excited state" proposed by Platzman.[7-12] Generally, it is well known that thermal hydrogen radical reacts quickly with olefins to form alkyl radicals, namely, the olefins are good radical scavengers.[13] Many works have also been carried out on the radiolysis of ammonia. The results have led to the conclusion that the G values of non-scavengeable hydrogen molecules are 0.64—0.84 and those of thermal (scavengeable) hydrogen radicals are 5—12.[14-20] It can be said that ammonia is a good donor of the thermal hydrogen radical.

Thus, it is interesting to study the γ-radiolysis of the mixture of ammonia and olefin. We have reported on the radiolysis of the gaseous mixture of ethylene and ammonia.[21] In this paper we will report on the results of γ-radiolyses of gaseous mixtures of ammonia and olefins (ethylene, propylene and butadiene). Consideration is given to the primary processes of hydrogen formation.

Experimental

Matheson pure-grade ammonia, ethylene, propylene and butadiene were purified by the same method as described in part I.[21] The purity of these purified gases was determined by gas chromatographic analyses to be greater than 99.9%. Ethylene-d_4, propylene-d_6, and butadiene-d_6, were purchased from Merck, Sharp and Dohme Ltd. (isotopic purity 98 at. %D), and were subjected to trap-to-trap distillation. The reactant gas, a mixture of ammonia and olefin, was led into a 3.1 m*l* pyrex glass ampoule at constant pressure of 4 atm. Irradiation was carried out at room temperature by Co-60 γ-rays at the exposure-dose rate of 6.0×10^5 R/hr. Unless otherwise stated, samples were irradiated to a total dose of 2.88×10^7 R. Analyses of products (hydrocarbon and hydrogen) were carried out by the same method as described in part I,[21] and those of isotopic hydrogens were carried out with a Hitachi RMS-4 mass spectrometer. We confirmed the formation of ethylamine in the mixture of ammonia and ethylene. No amines were observed in the mixtures of ammonia and propylene or butadiene.

Results

In the radiolyses of pure propylene and of a mixture of ammonia and propylene or butadiene, the yields of

1) Y. Hatano, S. Shida, and S. Sato, This Bulletin, **37**, 1854(1964).
2) Y. Hatano and S. Shida, *ibid.*, **39**, 456 (1966).
3) Y. Hatano and S. Shida, *J. Chem. Phys.*, **46**, 4784 (1967).
4) Y. Hatano, S. Shida, and M. Inokuti, *ibid.*, **48**, 940 (1968).
5) Y. Hatano, S. Shida, and S. Sato, This Bulletin, **41**, 1120 (1968).
6) Y. Hatano, *ibid.*, **41**, 1126 (1968).
7) R. L. Platzman, *J. Phys. Radium*, **21**, 853 (1960).
8) R. L. Platzman, *Vortex*, **23**, 372 (1962).
9) R. L. Platzman, *Radiation Res.*, **17**, 419 (1962).
10) R. L. Platzman and W. P. Jesse, *Nature*, **195**, 790 (1962).
11) R. L. Platzman, *J. Chem. Phys.*, **38**, 2757 (1963).
12) R. L. Platzman, "Radiation Research 1966, Proceedings of the Third International Congress of Radiation Research, Cortina d'Ampezzo, Italy 1966", p. 20, ed. by G. Silini, North-Holland Publ. Co., Amsterdam (1967).
13) K. Kikuchi, S. Sato, and S. Shida, *Nippon Kagaku Zasshi*, **84**, 561 (1963).
14) J. A. Eyre and D. Smithies, *Trans. Faraday Soc.*, **66**, 2199 (1970).
15) C. Willis, A. W. Boyd, and O. A. Miller, *Can. J. Chem.*, **47**, 3007 (1969).
16) G. R. A. Johnson and M. Simic, "Radiation Chemistry Vol. 2", p. 197, *Amer. Chem. Soc.*, (Washington D. C.), (1968).
17) F. T. Jones, T. J. Sworski, and J. M. Williams, *Trans. Faraday Soc.*, **63**, 2426 (1967).
18) M. Nishikawa and N. Shinohara, *Radiation Res.*, **33**, 194 (1968).
19) M. Nishikawa, K. Kuroda, and N. Matsuura, This Bulletin, **41**, 1276 (1968).
20) M. Nishikawa, K. Kuroda, and N. Matsuura, *ibid.*, **42**, 1783 (1969).
21) O. Tokunaga, K. Hamanoue, J. Okamoto, and A. Danno, *ibid.*, **45**, No. 3.

hydrogen increased linearly with irradiation doses up to at least 5.0×10^7 R. The same results were obtained in the case of pure ammonia and pure ethylene by Eyre and Smithies[14] and by Hatano *et al.*[5]

Figure 1 shows the pressure dependence of hydrogen formation. Pressure effects are very small in the range 1—4 atm.

The relationship between hydrogen formation and the concentration of olefin is shown in Fig. 2. It is obvious that $G(H_2)$ of ammonia is reduced rapidly by the addition of a small amount of ethylene or propylene, and then increases linearly with increasing concentration of the olefins. In the case of butadiene, a marked decrease is also observed by the addition of a small amount of butadiene. $G(H_2)$ is then reduced monotonously by the further addition of butadiene.

Figure 3 shows the relationship between the G values of the main products which seem to be formed from thermal hydrogen radicals, and the concentration of olefins.

The gas-phase radiolyses of ammonia–perdeuterated olefins mixtures (C_2D_4, C_3D_6, C_4D_6) have also been investigated. The isotopic compositions of HD are comparatively small, *i.e.*, 7—12% at most. The relationship between the concentrations of perdeuterated olefins and D_2/HD or H_2/HD are given in Figs. 4 and 5.

Figures 6 and 7 shows the temperature dependence of hydrogen formation in a mixture of C_3H_6–NH_3 and C_4H_6–NH_3, respectively. So far no explanation has been given on the maximum values near 0°C. Bp and mp denote the boiling and melting points of ammonia, propylene and butadiene, respectively.

Table 1. Effects of scavengers on hydrogen formation

System	Scavenger (%)	$G(H_2)$
C_3H_6	0.0	1.06
C_3H_6+NO	0.6	1.06
	1.2	1.04
	2.6	1.05
	5.6	1.11
C_3H_6+N_2O	0.7	1.06
	1.6	1.00
	2.9	1.16
	5.3	1.04
C_3H_6–NH_3(C_3H_6=30%)	0.0	0.82
C_3H_6–NH_3+NO	1.0	0.80
	1.9	0.80
	4.1	0.77
	6.5	0.86
C_3H_6–NH_3+N_2O	1.3	0.81
	2.3	0.85
	4.1	0.78
	7.1	0.79
C_4H_6–NH_3(C_4H_6=30%)	0.0	0.48
C_4H_6–NH_3+NO	1.4	0.45
	2.6	0.47
	9.8	0.48
	14.0	0.47
C_4H_6–NH_3+N_2O	1.4	0.50
	2.8	0.52
	10.0	0.48
	13.6	0.44

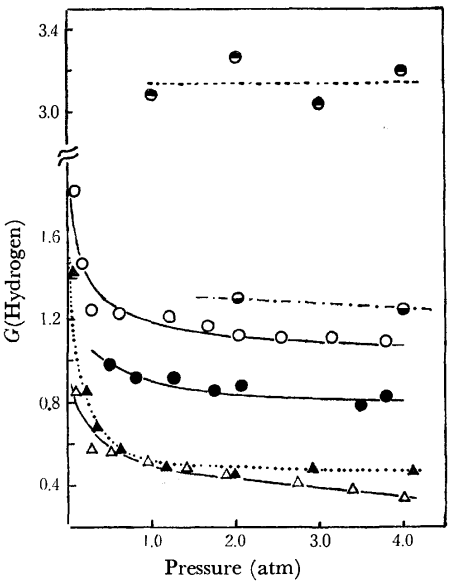

Fig. 1. Pressure-dependence of the formation of hydrogen
◓: NH_3, ◒: C_2H_4, ○: C_3H_6, ●: C_3H_6–NH_3 (C_3H_6=30%), △: C_4H_6, ▲: C_4H_6–NH_3(C_4H_6=30%).

Table 1 shows the effects of scavengers, nitric oxide and nitrous oxide, on the hydrogen formation. No effects were observed.

Discussion

It is obvious from Fig. 1 that there is little change in $G(H_2)$ in the gas-phase radiolysis of ammonia in the pressure range 1—4 atm, namely, $G(H_2)=3.14\pm0.11$. Willis *et al.* studied the radiolysis of ammonia by electron beams and found that $G(H_2)$ was constant, *i.e.*, $G(H_2)=3.58\pm0.08$, in the pressure range 1—2.25 atm.[15] The same results were obtained by Jones *et al.* in the pressure range 500—700 mmHg, but they found an increase at lower pressure.[17] Eyre and Smithies[14] studied the effects of pressure, temperature, dose and additives on the radiolysis of ammonia, and found that $G(H_2)$ is unaffected in the pressure range 100—700 mmHg. They obtained the G value of non-scavengeable hydrogen molecule and that of scavengeable hydrogen radical as follows.

$$G^*(H_2) = 0.70 \pm 0.02,\ G(H) = 7.0 \pm 0.6,$$

where $G^*(H_2)$ is the G value of non-scavengeable hydrogen molecule.

In our experiments in the radiolyses of pure olefins or of mixtures of ammonia and olefins, small pressure dependence of $G(H_2)$ above 1 atm can be observed. Marked increase in $G(H_2)$ at a lower pressure may presumably be attributed to the enhanced decrease of the collisional deactivation of excited state.

The initial sharp fall in $G(H_2)$ caused by the addition of a small amount of olefins is consistent with the fact that the olefins are good radical scavengers (Fig. 2). In the case of ethylene or propylene, $G(H_2)$ increased linearly with the increase of the concentration of olefins.

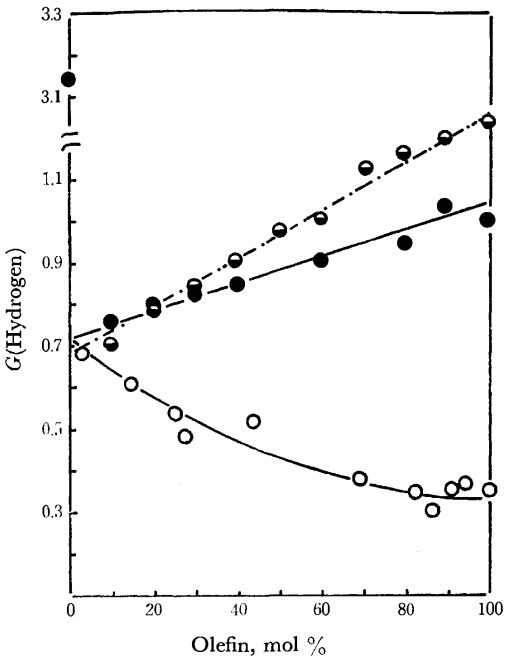

Fig. 2. Variation of hydrogen formation as a function of the concentration of C_2H_4, C_3H_6 and C_4H_6
◒: C_2H_4–NH_3, ●: C_3H_6–NH_3, ○: C_4H_6–NH_3

This suggests that they are due to non-scavengeable hydrogen from olefins. In the case of butadiene, the results is the opposite. However, the limiting values of $G(H_2)$, obtained by the extrapolation of the linear part of the curve to zero mol% olefins, namely 100 mol% ammonia, are nearly the same, *viz.*, $G_{NH_3}(H_2)=0.68$ with ethylene, 0.72 with propylene and butadiene. The values are in good agreement with the value of non-scavengeable hydrogen molecule ($G^*_{NH_3}(H_2)=0.70\pm0.02$).[14] The values obtained by extrapolating to 100 mol% olefins are 1.26, 1.06, and 0.33 for ethylene, propylene and butadiene, respectively. The data except for butadiene are in good agreement with those formerly obtained.[4-6,14,22-24]

Hatano *et al.* investigated the mechanism of hydrogen formation in the radiolysis of liquid olefins (RH_2).[1-6] They proposed a possible role of the superexcited state (RH_2**); hydrogen molecule is formed by the decomposition of RH_2** by reaction (1) or (2), either by a unimolecular process directly yielding molecular hydrogen or by a bimolecular process yielding hot hydrogen radical (H*) which abstracts hydrogen from the reactant.

$$RH_2^{**} \begin{cases} \longrightarrow H_2 + R & (1) \\ \longrightarrow H^* + RH & (2) \end{cases}$$

The G value of hydrogen formation by the decomposition of the superexcited state is derived by the optical approximation introduced by Platzman.[7-12]

$$G = \frac{100}{W}\frac{M_d^2}{M_i^2} \qquad (3)$$

where M_d^2 and M_i^2 are the dipole matrix elements squared for dissociation and for ionization, respectively. The calculated results show that the quantities M_d^2 and M_i^2 are directly proportional to the number of carbon atoms in the hydrocarbons. The G values were calculated from the results. The values obtained are in good agreement with those of experimental values for ethylene, propylene, butene-1 and butene-2. Thus we might conclude that the linear portion of Fig. 2 is due to non-scavengeable hydrogen molecule from olefin.

No report seems to have been published on the radiolysis of butadiene. However, if we assume that the hydrogen molecules produced by the radiolysis of butadiene are non-scavengeable like those of other olefins, then the G value, *i.e.*, $G(H_2)=0.33$, is much smaller than that of other olefins or that calculated by Hatano,[6] *i.e.*, $G(H_2)>1$. The discrepancies suggest that the "hot" hydrogen radical may partly react with butadiene to form a different product from hydrogen molecule.

In Fig. 3, it is obvious that the G values of products in the radiolyses of mixtures of ammonia and ethylene

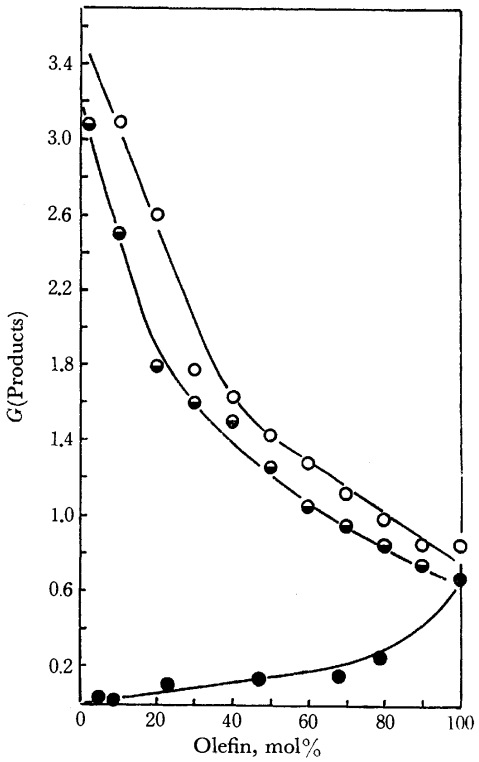

Fig. 3. Variation of the formation of major products as a function of the concentration of C_2H_4, C_3H_6 and C_4H_6
◒: $G(C_2H_6+n\text{-}C_4H_{10}+{}^1/_2C_2H_5NH_2)$ from C_2H_4–NH_3[21]
○: $G(C_3H_8)$ from C_3H_6–NH_3, ●: $G(t\text{-}2\text{-Butene})$ from C_4H_6–NH_3

22) Y. Hatano and S. Shida, 11th Symposium of Radiation Chemistry, p. 20, Tokyo, (1968).
23) R. A. Back, T. W. Woodward, and K. A. McLauchlan, *Can. J. Chem.*, **40**, 1380 (1962).
24) F. W. Lampe, *Radiation Res.*, **10**, 691 (1959).
25) The mechanism of the formation of *t*-2-butene is not known at present. Assuming that it may be formed by the following reaction in which one hot radical participates;

$C_4H_7^* + C_4H_6$ (or NH_3) $\rightarrow$ *t*-2-butene,

then, $G^*(H_2)$ is 0.99. An alternative explanation may be that two hot radicals participate in

$C_4H_7^* + C_4H_7^* \rightarrow$ *t*-2-butene,

in this case, $G^*(H_2)=0.33+2G(t\text{-}2\text{-butene})=1.65$.

or propylene decrease with the increase of the concentration of olefins. This can be explained from the fact that the G values of thermal hydrogen radical from olefins are comparatively small and from ammonia very large. In the case of propylene, the extrapolation of the curve to 100 mol% ammonia gives the value 3.5, the corresponding G value of hydrogen radical then being 7.0. This value agrees with the initial G value of hydrogen radical, $G(H)=7.0\pm0.6$[14] and $G(H)=7.2\pm0.5$.[16]

In the case of ethylene, if we take account of the formation of ethylamine, the corresponding value is 6.4 which shows also good agreement.

These results lead to the conclusion that the thermal hydrogen radicals produced by the γ-radiolysis add quickly to olefins in the case of ethylene and propylene. In the latter, the formation of amines is negligible. In contrast, the G value of *t*-2-butene which seems to be the main product from butadiene shows a different behaviour. If the product is formed by the reaction of thermal hydrogen radical and butadiene, G(*t*-2-butene) may decrease with the increase of the concentration of butadiene as in the case of ethylene and propylene. *t*-2-Butene should be formed by the reaction of hot hydrogen radical and butadiene, and the thermal hydrogen radical might react with butadiene to form higher hydrocarbon products.

Thus, we can explain the increase of G(*t*-2-butene) and the decrease of $G(H_2)$ to be due to increasing concentration of butadiene.

$G(H_2)$ of pure butadiene is 0.33, and it is obvious from Fig. 3 that G(*t*-2-butene) is 0.66. Assuming that $G^*(H_2)$ is equal to $G(H_2)+G$(*t*-2-butene), then $G^*(H_2)$ is 0.99,[25] which agrees well with the value calculated by Hatano[6] and with values of other olefins.

Tachikawa *et al.*,[26-28] and Tominaga and Rowland[29] investigated the hot-atom chemistry of recoil tritium, and found correlations between hot-yeilds of HT and bond-dissociation energies of hydrocarbons, halomethanes and amines. Thus it is reasonable to consider that the hydrogen abstraction reaction of hot hydrogen radicals produced by the γ-radiolyses might be affected by bond-dissociation energies.

In the radiolyses of mixtures of ammonia and perdeuterated hydrocarbons (C_2D_4, C_3D_6, C_4D_6), the isotopic composition of HD is comparatively small, *i.e.*, 7—12% at most. In the mixture of C_3H_6 and C_3D_6 (C_3H_6=50 mol%), the isotopic composition of HD is 15—16%. The lower value of HD in the system of NH_3–C_3D_6 than in the system of C_3H_6–C_3D_6 may indicate two posibilities; etiher a small G value of hot hydrogen radical from ammonia, or a larger bond-dissociation energy of ammonia than that of olefin.

Eyre and Smithies[14] proposed that the non-scavengeable hydrogen molecule probably arises for the most part from the decomposition of the excited ammonia molecule (NH_3**) *via* reaction (4):

$$NH_3^{**} \longrightarrow NH + H_2 \quad (4)$$

An alternative explanation is that some hot hydrogen radicals (H*) are formed and they may abstract hydrogen from ammonia:

$$NH_3^{**} \longrightarrow NH_2 + H^* \quad (5)$$

Thus, the hydrogen abstraction reaction in the mixed system of ammonia and olefin can be expressed as follows.

$$H^* + NH_3 \longrightarrow H_2 \quad (6)$$

$$H^* + RD_2 \longrightarrow HD \quad (7)$$

On the other hand, perdeuterated olefin (RD_2) might be decomposed by the following reactions.

$$RD_2^{**} \longrightarrow D_2 + R \quad (8)$$

$$RD_2^{**} \longrightarrow D^* + RD \quad (9)$$

$$D^* + RD_2 \longrightarrow D_2 \quad (10)$$

$$D^* + NH_3 \longrightarrow HD \quad (11)$$

Assuming the steady-state condition for the concentrations of the intermediate species H* and D*, we can derive the following equations by a simple kinetic treatment.

$$\lim_{[RD_2]\to 0} HD/D_2 = \frac{k_9}{k_8} + \frac{k_5k_7}{k_6k_8} \quad (12)$$

$$\lim_{[NH_3]\to 0} HD/H_2 = \frac{k_5}{k_4} + \frac{k_9k_{11}}{k_4k_{10}} \quad (13)$$

In the radiolysis of C_4D_6–NH_3 mixture, we have taken account of the following reaction besides reactions (10) and (11).

$$D^* + RD_2 \longrightarrow \text{No hydrogen molecule} \quad (14)$$

In this case, HD/D_2 is given by the same equation as that of Eq. (12), but HD/H_2 is given by the following equation.

$$\lim_{[NH_3]\to 0} HD/H_2 = \frac{k_5}{k_4} + \frac{k_9k_{11}}{k_4(k_{10}+k_{14})} \quad (15)$$

The results obtained from Figs. 4 and 5 and Eqs. (12), (13), and (15) are shown in Table 2. The values

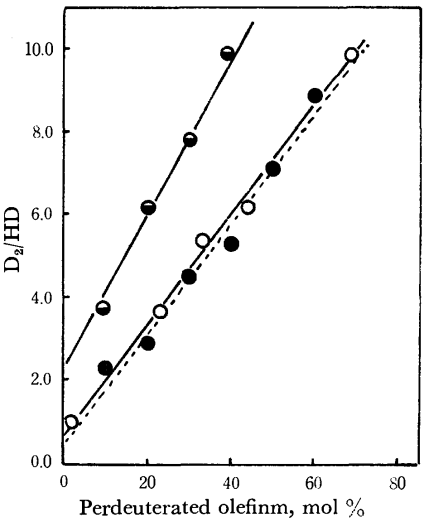

Fig. 4. D_2/HD *vs.* concentration of C_2D_4, C_3D_6 and C_4D_6
◒: C_2D_4–NH_3, ●: C_3D_6–NH_3 ○: C_4D_6–NH_3

26) E. Tachikawa and F. S. Rowland, *J. Amer. Chem. Soc.*, **90**, 4767 (1968).
27) E. Tachikawa, Y. N. Tang, and F. S. Rowland, *ibid.*, **90**, 3584 (1968).
28) E. Tachikawa and F. S. Rowland, *ibid.*, **91**, 559 (1969).
29) T. Tominaga and F. S. Rowland, *J. Phys. Chem.*, **72**, 1399 (1968).

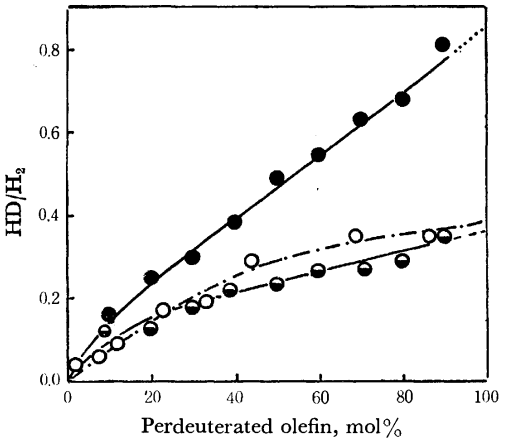

Fig. 5. HD/H_2 *vs.* concentration of C_2D_4, C_3D_6 and C_4D_6
◒: C_2D_4–NH_3 ●: C_3D_6–NH_3 ○: C_4D_6–NH_3

TABLE 2. LIMITING VALUES OF D_2/HD AND HD/H_2

Olefin	$\left(\frac{k_9}{k_8}+\frac{k_5k_7}{k_6k_8}\right)^{-1}$	$\frac{k_5}{k_4}+\frac{k_9k_{11}}{k_4k_{10}}$	$\frac{k_8}{k_9}$ [a]
C_2H_4	2.4	0.36	2.4
C_3H_6	0.4	0.86	0.4
C_4H_6	0.5	0.39[b]	

a) Ref. 5. b) $\frac{k_5}{k_4}+\frac{k_9+k_{11}}{k_4(k_{10}+k_{14})}$

of k_8/k_9 which were obtained by Hatano *et al.*[5] in the system of RH_2–RD_2 are also listed in the last column. Comparing our results with those of Hatano *et al.*, we obtain the following equations.

$$\frac{k_9}{k_8}=\frac{k_9}{k_8}+\frac{k_5k_7}{k_6k_8} \tag{16}$$

$$k_5 \simeq 0 \tag{17}$$

$$\frac{k_5}{k_4}<0.36 \tag{18}$$

The results lead to the following conclusions.

1) Non-scavengeable hydrogen molecules produced by the radiolysis of ammonia are mainly produced by reaction (4), or by a unimolecular process. Bimolecular processes like reaction (5) are much less important.

2) Almost all the hydrogen molecules produced by the γ-radiolyses of ethylene and propylene are non-scavengeable, 71% in the former and 29% in the latter are unimolecular processes.

3) Almost all the hydrogen molecules produced by the γ-radiolysis of butadiene are also non-scavengeable, and k_8/k_9 is 0.5. Consequently, 33% is due to a unimolecular process. Hot hydrogen radicals produced can react with butadiene not only by abstraction reaction of hydrogen, but also by addition reaction to butadiene.

We have assumed that the hot hydrogen radical can add to butadiene. This indicates that the energy of the hot hydrogen radical might not be so high, and the reaction in which this hot radical participates might be temperature dependent. As shown in Figs. 6 and 7, $G(H_2)$ changes with temperature. The change includes the effect of the change of phase of the reaction system.

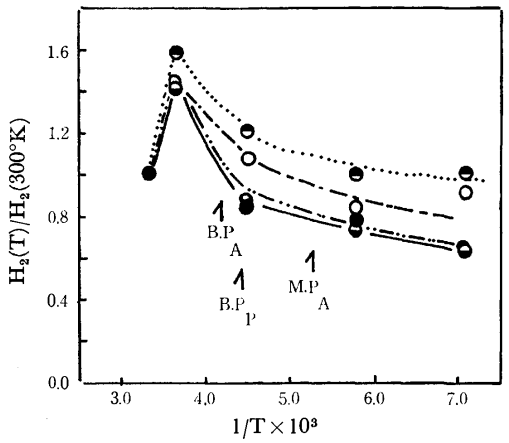

Fig. 6. Temperature-dependence of the formation of hydrogen in the mixture of C_3H_6–NH_3
●: (C_3H_6=100 mol%), ◒: (69.8%), ○: (50.0%), ◓: (30.0%)

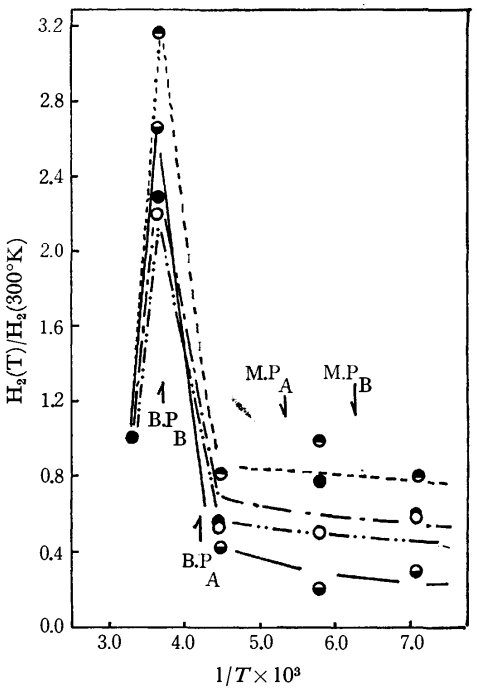

Fig. 7. Temperature-dependence of the formation of hydrogen in the mixture of C_4H_6–NH_3
◒: (C_4H_6=100 mol%), ○: (70%), ●: (50%), ◓: (30%)

The authors wish to express their sincere thanks to Prof. Keiichi Oshima, the University of Tokyo, for his valuable discussions and suggestions. They are also indebted to Mr. Kunihiro Matuzawa and Mr. Kikuo Kimura for their technical assistance in preparing the vacuum line.

The Effects of Pre-irradiation Treatments on the Chemical Behavior of ^{64}Cu Recoil Atoms in Neutron-irradiated Copper Phthalocyanine

Hiroshi KUDO

Japan Atomic Energy Research Institute, Tokai-mura, Ibaraki

(Received September 30, 1971)

The chemical behavior of ^{64}Cu recoil atoms was studied in copper phthalocyanine which had been quenched from an elevated temperature or exposed to ^{60}Co γ-rays before the neutron irradiation. In the quenched β-crystal, the initial retention was found to increase with an increase in the temperature of pre-irradiation heating, while the plateau retention of the post-neutron annealing reaction decreased. These results were compared with those for cadmium phthalocyanine and were understood in terms of "dislocation" in the crystal, the recoil atoms being assumed to be trapped and stabilized in the "dislocation." Although the variations were small, the irradiation with ^{60}Co γ-rays caused a change in the chemical behavior of the recoil atom. The role of some radiation-induced species were discussed.

A series of studies[1-5] have reported that the bulk properties of the target crystal have a marked influence on the chemical consequence of ^{64}Cu recoil atoms in neutron-irradiated copper phthalocyanine. Both the initial retention and the thermal-annealing process depended on the crystal structure, the size and shape of grains, and the concentration of defects in the solids.

The pre-irradiation treatments, involving quenching and irradiation with ionizing radiation, are well known to sensitize the material to the thermal-annealing reaction.[6-11] In the previous studies concerned with the chemical behavior of ^{115}Cd recoil atoms in cadmium phthalocyanine,[12,13] it was suggested that the central metal vacancies introduced in the target by quenching had a strong effect on the subsequent course of the thermal-annealing reaction of the recoil atom.

The present investigation was undertaken in order to see if a similar effect was observed for ^{64}Cu recoil atoms in copper phthalocyanine. The experiment was expected to provide some useful information for the understanding of the detailed scope of the chemical behavior of recoil atoms in the crystalline metal phthalocyanines.

Experimental

Target Material. α-Copper phthalocyanine from Dainippon Ink and Chemicals was carefully purified by recrystallization from sulfuric acid. The β-copper phthalocyanine was obtained by suspending the α-crystal in benzene at 80°C for 2 hr. The X-ray powder diffraction pattern, the electron micrograph, and the thermogram of the materials were recorded.

Irradiation. The neutron irradiation of copper phthalocyanine was performed at the temperature of dry ice (−78°C) for 10 sec in the nuclear reactor, JRR-2, of the Japan Atomic Energy Research Institute. The thermal neutron flux at the irradiation position was 5.7×10^{13} n/cm^2/sec, and the γ-ray dose rate was 1×10^8 R/hr.

For the pre-irradiation treatments with γ-rays, the target was irradiated by means of a 16 kCi ^{60}Co γ-ray source to a dose of 1.1×10^7 R or 1.0×10^8 R at temperatures of −78 and 20°C. The target was then irradiated in JRR-2 for 10 sec at the temperature of dry ice.

Chemical Treatments and Radioactivity Measurements. The procedures of the chemical separation and the thermal treatments used here were virtually identical with those described in the previous paper.[4]

In the quenching experiment, the targets were heated to a specified temperature for 5 hr in an electric furnace and then cooled quickly in liquid nitrogen. The target was stored in dry ice until the neutron irradiation.

The radioactivity was measured by means of a Baird Atomic single-channel γ-ray spectrometer, using the NaI(Tl) crystal as the detector.

Results

It has already been reported that the initial retentions[14] of ^{64}Cu recoil atoms in neutron-irradiated copper phthalocyanine are 5.5% for the α-crystal and 13.5% for the β-crystal,[1,2,4] and that the α-crystal is converted to the β-crystal by heating above 250°C.[4,15,16] The influence of heating the α-crystal prior to the neutron irradiation was examined. The results presented in Fig. 1 show that the initial retention increased, as would be expected, when the target was subjected to

1) K. Yoshihara and H. Ebihara, *J. Chem. Phys.*, **45**, 896 (1966).
2) M. H. Yang, H. Kudo, and K. Yoshihara, *Radiochim. Acta*, **14**, 52 (1970).
3) M. H. Yang, K. Yoshihara, and N. Shibata, *ibid.*, **14**, 16 (1970).
4) H. Kudo, This Bulletin, **45**, 389 (1972).
5) H. Kudo, *ibid.*, **45**, 392 (1972).
6) A. G. Maddock and J. I. Vargas, *Nature*, **184**, 1931 (1959).
7) A. G. Maddock, F. E. Treloar, and J. I. Vargas, *Trans. Faraday Soc.*, **59**, 924 (1963).
8) T. Andersen and A. G. Maddock, *ibid.*, **59**, 2362 (1963).
9) F. Baumgärtner and A. G. Maddock, *ibid.*, **64**, 714 (1968).
10) J. Shankar, A. Nath, and V. G. Thomas, *J. Inorg. Nucl. Chem.*, **30**, 1361 (1968).
11) I. G. Campbell and C. H. W. Jones, *Radiochim. Acta*, **9**, 7, 71 (1968).
12) H. Kudo and K. Yoshihara, *J. Inorg. Nucl. Chem.*, **32**, 2845 (1970).
13) H. Kudo, *ibid.*, **34**, 453 (1972).

14) The "initial retention" means the retention obtained in the target which has been irradiated at the temperature of dry ice and which led to a chemical separation without allowing the target to warm up.

15) H. H. Beynon and A. R. Humphries, *Trans. Faraday Soc.*, **51**, 1065 (1955).
16) V. C. Hamann and H. Wagner, *Z. Anorg. Allg. Chem.*, **373**, 18 (1970).

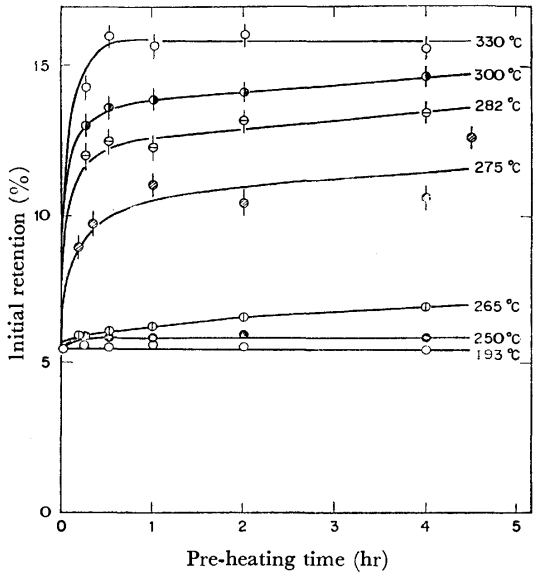

Fig. 1. The change in the initial retention of ^{64}Cu recoil atoms in α-copper phthalocyanine which has been heated before the neutron irradiation.

pre-irradiation heating (pre-heating) above 250°C, reflecting the α-β crystal structural transformation of copper phthalocyanine. The initial retention of the target pre-heated at 330°C reached a slightly higher value than that of the untreated β-crystal. This will be discussed further in the following section.

Table 1 lists the initial retentions of β-copper phthalocyanine pre-heated for 5 hr at various temperatures. It was found that the value increased with an increase in the temperature of pre-heating. Table 2 lists the thermal-annealing data of the pre-heated target in comparison with those of the untreated target. The annealing time of 5 hr was chosen because of the time at which the retention had reached the plateau. The data for the pre-heated α-crystal were the same as those observed for the pre-heated β-crystal. This may be attributed to the fact that the α-crystal has been completely transformed to the β-crystal by pre-heating, as is shown in Fig. 1.

Table 1. The initial retention of β-copper phthalocyanine heated for 5 hr before the neutron irradiation

Pre-heating temperature (°C)	Initial retention (%)
Untreated	13.5±0.2
195	13.7±0.2
300	14.6±0.4
330	16.0±0.3
350	17.2±0.5

Table 2. Comparison of the thermal annealing data between the quenched and the untreated copper phthalocyanine

Target	Retention (%)		
	Initial retention	Annealed at 196°C for 5 hr	Annealed at 300°C for 5 hr
α-Crystal			
Untreated	5.5±0.4	7.8±0.3	88.7±1.3
Quenched[a)]	14.6±0.3	19.9±0.3	25.5±0.5
β-Crystal			
Untreated	13.5±0.4	24.2±0.5	75.8±1.5
Quenched[a)]	14.6±0.2	19.8±0.4	24.2±0.5

a) The target was heated for 5 hr at 300°C and quenched before the neutron irradiation.

Table 3. The initial retention of α- and β-copper phthalocyanine exposed to ^{60}Co γ-rays before the neutron irradiation

Target	γ-Ray irradiation		Initial retention (%)
	Irradiation temperature (°C)	Radiation dose (R)	
α-Crystal	−78	1.1×10^7	5.3±0.5
	−78	1.0×10^8	5.4±0.5
	20	1.1×10^7	5.3±0.5
	20	1.0×10^8	5.3±0.5
		Untreated	5.5±0.3
β-Crystal	−78	1.1×10^7	13.2±0.3
	−78	1.0×10^8	15.2±0.3
	20	1.1×10^7	11.8±0.3
	20	1.0×10^8	11.0±0.3
		Untreated	13.5±0.3

The initial retentions of α- and β-copper phthalocyanine, which has been exposed to the ^{60}Co γ-rays before the neutron irradiation, are listed in Table 3. One can find almost the same initial retentions for the α-crystal between the untreated and the γ-irradiated targets. For the β-crystal, however, the initial retention was found to increase or decrease depending on the irradiation temperature of the γ-rays; the initial retention was a little higher at −78°C and lower at 20°C. Figure 2 shows the isothermal-annealing curve of ^{64}Cu recoil atoms in β-copper phthalocyanine which has been irradiated with γ-rays to dose of 1.0×10^8 R before the

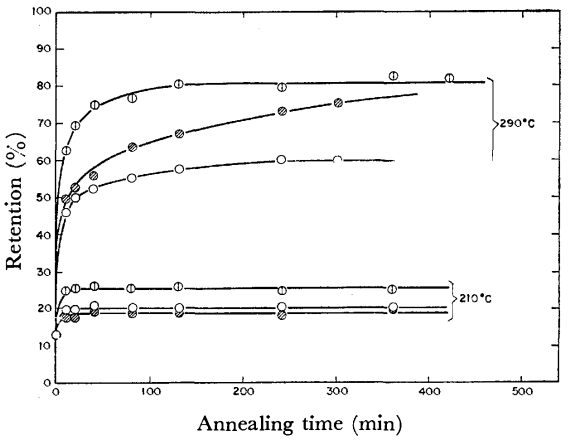

Fig. 2. The isothermal annealing curves for β-copper phthalocyanine which has been exposed to ^{60}Co γ-rays before the neutron irradiation.
○: Untreated sample; ◑: irradiated at −78°C to dose of 0.97×10^8R; ◍, irradiated at 20°C to does of 1.0×10^8R.

neutron irradiation, unlike the untreated target. The annealing curve at 290°C (Stage II) showed a different pattern from that of the untreated target—an increase in the plateau value of the retention. Only a small change in the annealing process was observed at 210°C (Stage I).

Discussion

As is shown in Tables 1 and 2, the heat treatment before the neutron irradiation (pre-heating) raised the initial retention and lowered the plateau of the post-neutron annealing curve in both Stage I and Stage II. It has been reported for tris-acetylacetonatocobalt(III) and -chromium(III) complexes[17] that heating the crystals before the neutron irradiation decreased the initial retention and reduced the thermal annealing reaction. In the case of pre-heating for cadmium phthalocyanine,[13] the initial retention was found to decrease, while the annealable portion increased. These results have been interpreted in terms of defects in the solids, but the role of the defects may vary from one compound to another.

The results obtained for cadmium phthalocyanine, from which the central metal was easily removed, were interpreted in terms of the central vacancy in the crystal, but this interpretation is not valid in the case of copper phthalocyanine, in which the bond strength between the central metal and the ligand is very strong. The central metal of copper phthalocyanine is quite stable under thermal treatment,[18-20] and the metal can not be removed from the central position of the complex. For ionic crystals[10,11] effects similar to those of copper phthalocyanine have been reported. The pre-irradiation heating raised the initial retention and decreased the annealable portion. These results were explained in terms of the thermal removal of defects from the lattice, suggesting that a small fraction of (n,γ)-activated recoils were stabilized only in a reduced state in the lattice by interaction with a "reducing" inherent crystal defect. However, this explanation does not seem applicable to the molecular crystal of copper phthalocyanine.

For copper phthalocyanine it seems possible that the effective crystal imperfection is not a point defect, as has been described for the ionic crystals, but a "dislocation" (a line defect) or a disorder of the molecular configuration, introduced through the recrystallization. Dislocations are thermodynamically unstable, since the enthalpy change associated with the formation of a dislocation is extremely large and since the entropy change is very small.[21] This kind of crystal imperfection can be removed from solids by heat treatment. In the electron micrograph of the α-crystal used here, a large number of "gaps" (separated from one another by some 100's of Å) were observed, while these gaps disappeared in the β-crystal which had been transformed from the α-crystal by heat treatment above 250°C. Dislocations being assumed to trap and stabilize the recoil atom, the results presented in Table 1 may be explained in connection with the "dislocation" in crystalline copper phthalocyanine. The decrease in the "dislocation" with the increase in the temperature of pre-heating should raise the initial retention of ^{64}Cu recoil atoms and reduce the annealable portion in copper phthalocyanine because of the reduction of diffusion processes controlled by the dislocation.

Contrary to the case of cadmium phthalocyanine,[13] the ionizing radiation caused a change in the chemical behavior of ^{64}Cu recoil atoms in copper phthalocyanine. Although the variations were small, the effect of irradiation with ^{60}Co γ-rays for β-copper phthalocyanine seems dependent upon the irradiation temperature of γ-rays. The irradiation at −78°C raised the initial retention and enhanced the thermal-annealing reaction. On the other hand, the initial retention of the target exposed to the ^{60}Co γ-rays at 20°C decreased slightly. The pattern of the isothermal annealing curve was different from that of the other case. An increase in the annealable portion in the Stage-II process (290°C) was seen in both cases.

The temperature dependence observed here may imply that the species produced by the ionizing radiation are different depending on whether the target is irradiated at 20°C or −78°C. The intermediate oxidized species might be produced in the solid under the γ-ray irradiation at 20°C. The intermediate species can be reversed to the parent complex by heat treatment,[22] so that the retention increases in the Stage-II annealing process. The decrease in the initial retention may be ascribed to the fact that the intermediate species stabilize the recoil atom placed in the interstitial position.

In the case of γ-ray irradiation at −78°C, the species which affect the behavior of recoil atoms may be some radiation-induced acceptor which can raise the initial retention. A previous investigation[5] has already revealed that the electron acceptor in the crystalline phthalocyanine is effective in increasing the initial retention of recoil atoms in the complex. However, more experimental data must be accumulated to clarify the effect of ionizing radiation, especially the radiation-induced acceptor.

The author wishes to express his thanks to Professor T. Shiokawa and Dr. K. Yoshihara of Tohoku University for their kind guidance throughout this study. He also wishes to thank Dr. H. Amano and Dr. H. Baba of the Japan Atomic Energy Research Institute for their useful suggestions and discussions.

17) J. C. Machado, R. M. Machado, and J. I. Vargas, "Chemical Effects of Nuclear Transformations," Proc. IAEA Symp., Vienna, Vol. II (1965), p. 195.

18) C. E. Dent, R. P. Linstead, and A. R. Lowe, *J. Chem. Soc.*, **1934**, 1027.

19) F. H. Moser and A. L. Thomas, "Phthalocyanine Compounds," Reinhold Pub. Corp., New York (1963).

20) A. B. P. Lever, "Advances in Inorganic Chemistry and Radiochemistry," Vol. 7, Academic Press, New York (1965), p. 27.

21) R. A. Swalin, "Thermodynamics of Solids," John Wiley & Sons, New York, London (1962).

22) T. Sekiguchi, E. Yamazaki, and K. Bansho, *Kogyo Kagaku Zasshi*, **70**, 503 (1967).

Polarographic Investigation of Biopolymers. II. Cu(II)-poly (α,L-Glutamic Acid) in the Helix-Coil Transition Region[1]

Senkichi INOUE, Kiwamu YAMAOKA,* and Masaji MIURA*

Department of Chemistry, Faculty of General Education,
**Department of Chemistry, Faculty of Science, Hiroshima University, Higashisenda-machi, Hiroshima*

(Received October 16, 1971)

The pH-induced helix-coil transition of the complex of Cu(II)-poly(α,L-glutamic acid) was studied with polarographic method. The diffusion current was found to change very sharply in a narrow range of pH and this change depended on the amount of Cu(II) ions. The half-wave potential of the complex was also dependent on pH and mixing ratio. The effect of Cu(II) ions on the secondary structure of the polymer was discussed from the viewpoint that the helix-coil transition of PGA is responsible for the change of the mode of binding interaction between Cu(II) ions and PGA sites. Based on the data of diffusion currents *versus* mixing ratios, the helical fractions of the complex at pH 3.4 and 4.0 were evaluated to be 0.37 and 0.11, respectively. From a value of the diffusion coefficient of the complex at pH 5.0, the molecular size in a random-coil form was calculated to be approximately 70 Å in diameter. The coordination number of the complex in the coiled form depended on the mixing ratio; the number was 3.4 in excess of polymer and 0.2—0.3 for the mixing ratio between 3.2 and 13. These values were discussed in terms of the possible mechanism of coordination. Finally, the activation energy of diffusion was obtained for complexes in helical and random-coil forms.

Biopolymers such as nucleic acids and proteins have been known to form specific and/or non-specific complexes with many physiologically important metallic ions. These complexes have been demonstrated to play significant roles in enzymatic or photosynthetic reactions *in vivo*. Towards the ultimate understanding of this complicated biological function, the elucidation of the mechanism of such complex formation *in vitro* has been attempted by means of various physico-chemical methods such as spectroscopy,[2] optical rotatory dispersion,[3] magnetic resonances,[4] potentiometric titration,[5] and polarography.[6]

Synthetic water-soluble homopolyamino acids have usually been employed, as the simplest model compound of natural proteins, to study the effects of secondary structures and conformational transitions upon the complex formation with metallic ions.[7] Among these polymers, the most frequently used one is poly(α,L-glutamic acid), PGA, which has ionizable carboxyl side chain groups and can undergo pH-induced helix-coil transitions. This polymer as such and complexes with metallic ions have also been investigated with aforementioned methods; however, very little has been unraveled regarding the ionic processes of the ligands (*i.e.*, polymer residues) from electrochemical points of view. Recently, some polarographic data of Cu(II)–PGA in the pH-induced helix-coil transition region were provided for the first time.[6]

Besides the numerous applications to metal–amino acids complex formation,[8] polarographic methods are useful in the study of (1) biopolymers which have intrinsic groups reducible at the dropping mercury electrode and (2) those to which some reducible metallic ions are attached extrinsically as a detecting probe. Earlier, Tanford reported that the polarographic limiting current of metallic ions decreased with increase in pH in the presence of bovine serum albumin.[9] He also noted that this observation was due to some complex formation between the protein and metallic ions. However, he was unable to elaborate his result in terms of the conformational transition of the protein. Saroff and Mark[10] also found similar results in the study of serum albumin in the presence of mercury or zinc. Rao and Lal[11] studied the complex formation of zinc and cadmium with native and chemically modified bovine serum albumin. Malik and his associates studied the interaction of copper[12] and lead[13] with transfusion gelatin. Recently, Malik and Jindal[14] reported the binding of copper(II) and cadmium with ovalbumin. Although these proteins are known to have a large fraction of helix,[15] none of these workers has attempted to correlate the secondary structure and the ability of binding to the metallic ions.

In the preliminary communication,[6] we have shown

1) The first of this series is Ref. 6.

2) G. Felsenfeld and S. Huang, *Biochim. Biophys. Acta*, **37**, 425 (1960); R. J. P. Williams, *Biopolymers, Symposia*, No. **1**, 515 (1964); J. Peisach, P. Aisen, and W. E. Blumberg, Ed., "The Biochemistry of Copper", Academic Press Inc., New York, N. Y., (1966).

3) D. D. Ulmer and B. L. Vallee, *J. Biol. Chem.*, **236**, 730 (1961); A. J. Adler, G. D. Fasman, and M. Tal, *Biochim. Biophys. Acta*, **213**, 424 (1970); M. Nakai, M. Yoneyama, and M. Hatano, This Bulletin, **44**, 874 (1971).

4) J. Ferretti, *Chem. Commun.*, **1967**, 1030; E. M. Bradbury, C. Crane-Robinson, and H. W. E. Rattle, *Nature*, **216**, 862 (1967); J. L. Markley, D. H. Meadows, and O. Jardetzky, *J. Mol. Biol.*, **27**, 25 (1967).

5) A. Wada, *Mol. Phys.*, **3**, 409 (1960); M. Nagasawa and A. Holtzer, *J. Amer. Chem. Soc.*, **86**, 538 (1964).

6) S. Inoue, K. Yamaoka, and M. Miura, This Bulletin, **44**, 1443 (1971).

7) H. Takesada, H. Yamazaki, and A. Wada, *Biopolymers*, **4**, 713 (1966).

8) M. Kodama and S. Takahashi, This Bulletin, **44**, 679 (1971); T. Nozaki, M. Kadowaki, D. Sagawa, and K. Orita, *Nippon Kagaku Zasshi*, **88**, 1168 (1967); **91**, 64 (1970).

9) C. Tanford, *J. Amer. Chem. Soc.*, **74**, 211 (1952).

10) H. A. Saroff and H. J. Mark, *ibid.*, **75**, 1420 (1953).

11) M. S. Narsinga Rao and Hira Lal, *ibid.*, **80**, 3222 (1958).

12) W. U. Malik and Salahuddin, *J. Electroanal. Chem.*, **5**, 147 (1963).

13) W. U. Malik and M. Muzaffaruddin, *ibid.*, **6**, 214 (1963).

14) W. U. Malik and M. R. Jindal, *ibid.*, **19**, 436 (1968).

15) E. R. Blout "Optical Rotatory Dispersion," ed. by C. Djerassi, McGraw-Hill Book Co., Inc., New York, N. Y., 1960, p. 272; E. Shechter and E. R. Blout, *Proc. Natl. Acad. Sci. (US)*, **51**, 794 (1964).

that the polarographic diffusion current of the Cu(II)–PGA complex changes with pH in the region between 3.6 and 6.0 and we noted that this change parallels the pH-induced helix-coil transition of PGA. In this paper, we present a further quantitative and detailed work on the pH-induced helix-coil transition of the Cu(II)–PGA complex in aqueous solutions. Our emphasis will lie on the following points: (1) the contribution of the Cu(II) ion to the conformational transition of PGA which can be established from the study of the effect of pH on the diffusion current, $(i_d)_p$, at various molar mixing ratios, R, of glutamic acid residue to Cu(II) ion, (2) the bonding models of Cu(II)–PGA complex which can be estimated from the relation between half-wave potential, $E_{1/2}$, and mixing ratio at various pH's, and (3) the interaction of Cu(II) ions with PGA in either helical or random-coil conformation which can be evaluated from the activation energy of diffusion calculated from the data of temperature effect on diffusion current of Cu(II)–PGA.

Experimental

Materials. PGA, which is in the form of sodium salt, was supplied from Ajinomoto Co., Inc. and used without further purification. An average degree of polymerization of 700-800 was estimated from the intrinsic viscosity in 2M sodium chloride solution at pH 7.0. The mean residue weight of sodium polyglutamate was taken to be 169.[16] Cupric chloride, sodium chloride, and hydrochloric acid were all of analytical grade.

Preparation of sample solutions. In order to maintain the ionic strength of the Cu(II)–PGA complex solution throughout this work at a constant level of 7.5×10^{-3} (which is equal to the final concentration of chloride ions in solution), the sample solution was prepared in such a way that a desired pH value was obtained by adding both hydrochloric acid and sodium chloride solution (which was employed as supporting electrolyte) in appropriate proportions. A stock PGA solution of 1.5 g/100 m*l* or 8×10^{-2}M was diluted prior to measurements. The molar mixing ratios, R, were controlled by varying the concentration of PGA at a constant Cu(II) concentration which was kept to be 5×10^{-4}M in all measurements.

Polarographic measurements. Polarographic limiting currents were measured with a Yanagimoto Model P-8 polarograph. Each current-potential curve was manually obtained by plotting the current at intervals of 10 mV potentials. Since the removal of dissolved oxygen is essential but the bubbling nitrogen gas through a sample solution at low pH causes a separation of fibrous Cu(II)–PGA, it was necessary to degas a hydrochloric acid-containing Cu(II) solution in a glass vessel, which has a narrow outlet and a gas inlet capillary, and a PGA solution in a polarographic cell individually before mixing. These two solutions were then mixed very slowly to avoid precipitation. The mixing order was always a Cu(II) solution to a PGA solution. With this method of mixing the sample solution was successfully prepared at a pH as low as 2.7. After 20 min of degassing, flushing of nitrogen gas was continued while current-potential plots were recorded. The value of $E_{1/2}$ was determined by plotting $\log[i/(i_d-i)]$ against dropping mercury electrode potential. Thus the intercept at $\log[i/(i_d-i)]=0$ yields $E_{1/2}$ and the slope of the plot is a measure of reversibility (see Discussion). A glass capillary, which has a flow rate of 1.0 mg/sec and a drop time of 8.0 sec, was used as dropping mercury electrode.

Verification of polarographic diffusion current. The polarographic limiting currents were measured at four different heights of a mercury column for both helical and coiled Cu(II)–PGA complex solutions. A strictly linear curve was obtained for each solution when the limiting current was plotted against the square root of the height of mercury column. These curves could be extrapolated to intercept the origin for both solutions. Therefore, the limiting current of Cu(II)–PGA solutions at such a low supporting electrolyte concentration as 7.5×10^{-3}M could be confirmed to be diffusion current.

Temperature was kept at 25±0.05°C except when the dependence of diffusion current on temperature was studied.

pH measurements were carried out with a Toa Electronics Model HM-5A pH-meter.

Results

Current-Potential Curves with Variation of pH. Current-potential curves obtained in the pH region between 3.0 and 6.0 with a fixed R value of 16 are shown in Fig. 1. All curves, whose half-wave potentials range from +0.01 to −0.07 V *vs.* S.C.E., are well-defined and reversible. In the pH region between 2.7 and 3.2, where PGA alone is known to be in a helical form, the current-potential curve is almost the same as that of a Cu(II) solution. As the pH of the Cu(II)–PGA solution is increased, the diffusion current decreases steadily. However, when the pH becomes higher than 4.5, the diffusion current approaches a finite value as can be seen from the figure. This polarographic behavior indicates that the formation of Cu(II)–PGA complex depends on pH.

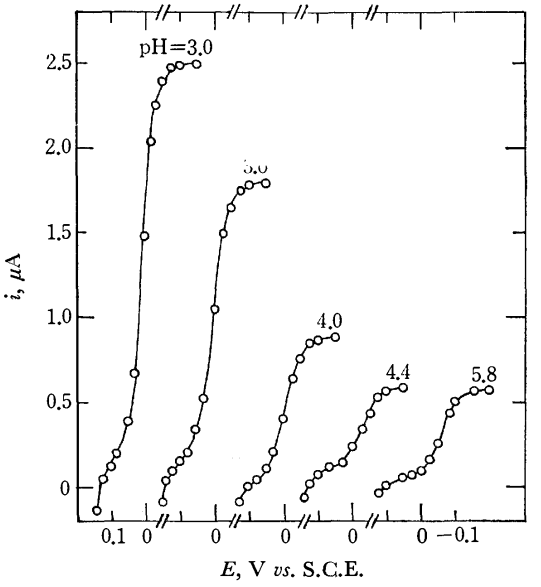

Fig. 1. The pH dependence of current-potential curves of Cu(II)–PGA at $R=16$. R=[PGA]/[Cu(II)]

The Relation between Diffusion Current and pH at Various Mixing Ratios. In Fig. 2, the diffusion currents are plotted against pH at various values of R. Each curve, which shifts toward high pH with decreasing R, shows a sharp decrease in $(i_d)_p$ that is confined in

16) K. Yamaoka, *Biopolymers*, **2**, 219 (1964).

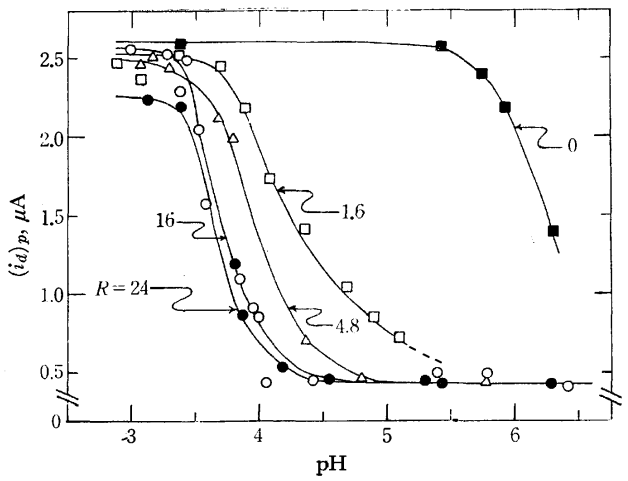

Fig. 2. The relation between diffusion current and pH for Cu(II)–PGA at various values of R as a parameter.[17]

a relatively narrow range of pH. No such change was observed for the Cu(II) aquocomplex solutions ($R=0$) in the same pH range between 3.0 and 5.4; however, the diffusion current gradually decreases as the pH value becomes higher than 5.4. This appears to be due to the formation of insoluble cupric hydroxide.[9] It should be noted here that the shape of the curves in Fig. 2 resembles very closely the pH-induced helix-coil transition of aqueous PGA and further that the shift of the curves as affected by the change in R is very similar to the trend induced by addition of various monovalent neutral salts.[17] This suggests that the Cu(II) ions coordinated with PGA ligands play an important role in the conformational transition of PGA. These conformational transition curves for R of 24, 16, and 4.8 are all similar in shape and approach a finite value which is independent of pH higher than 5.0. The measurements for R higher than 24 were not carried out, since the $(i_d)_p$–pH plot at $R=24$ could be almost superimposed upon that of $R=16$. On the other hand, as R decreases, not only the inflection point of each curve displaces for the higher pH, but also the slope becomes much more gradual (compare $R=24$ with 1.6). The polarographic measurement for $R=1.6$ was limited only up to pH around 5 due to the appearance of coagulated complex.

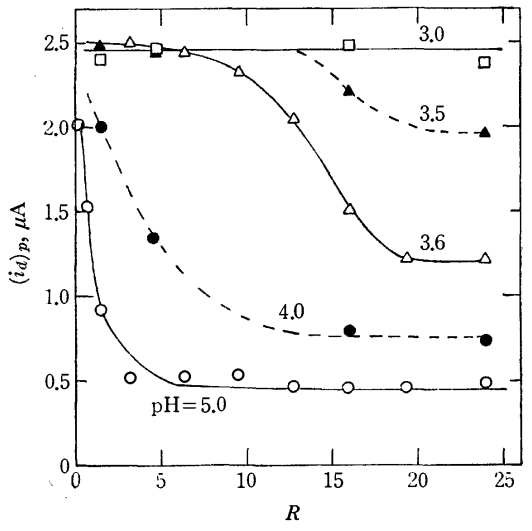

Fig. 3. The relation between diffusion current and mixing ratio at various pH's. Filled circles and triangles (dotted curves) are points read from the curves shown in Fig. 2.

The Relation between Diffusion Current and Mixing Ratio at Various pH's. In Fig. 3, the plots of $(i_d)_p$ *versus* R are shown at some representative pH's. Each of these curves shows its own characteristics. At pH 3.0, where the curves in Fig. 2 reach an upper plateau and apparently the Cu(II)–PGA complexes have the same gross conformation, presumably a rigid helix, the $(i_d)_p$–R curve is almost linear and independent of the values of R examined. At pH 3.6, where the complex may be a mixture of molecules in helical and in random-coil conformation or may possess the helical and random-coil segments in a single molecule, the $(i_d)_p$–R plot decreases gradually but steadily in the R region between 7 and 20, beyond which the curve levels off. Now, in the curve at pH 5.0, where the complex appears to be in a completely random-coil form as judged from $(i_d)_p$–pH curves in Fig. 2, the $(i_d)_p$ values decrease very sharply even at smaller values of R (between 0 and 3); beyond this, however, this curve approaches another plateau. It should be noted that this plateau is much lower than the one at pH 3.6 (see Discussion).

The Relation between Half-Wave Potential and Mixing Ratio at Two Extreme pH's. In Fig. 4, the effect of R on the half-wave potential is shown at the same two pH's as those in Fig. 3. The variation of $E_{1/2}$ with R is obvious at pH 5.0, but no such change is observed at pH 3.0 and 3.6 (not shown).

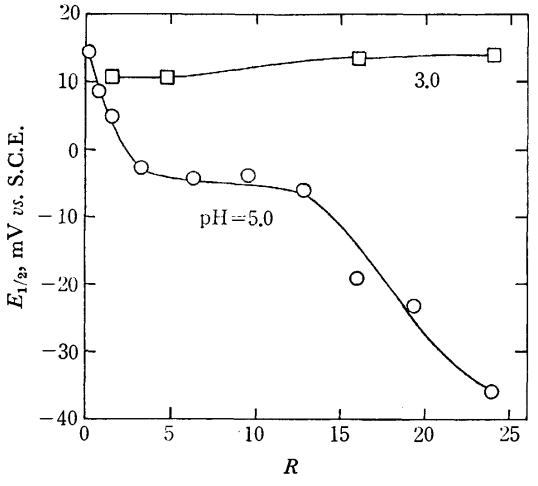

Fig. 4. The relation between the half-wave potential $E_{1/2}$ and the mixing ratio at pH's 3.0 and 5.0

The Effect of Temperature upon Diffusion Current at Two Extreme pH's. In order to obtain the activation energy of diffusion, Q_D, for the complexes in helical (pH 2.7) and random-coil (pH 5.0) conformations, diffusion currents were measured at four temperatures, 10, 20, 30, and 40°C. In Fig. 5, the plots of $\log[(i_d)_p/(m^{2/3}t^{1/6})]$ *versus* $1/T$ are shown at those pH's and at $R=16$. The slopes of the straight lines was found to be −470 and −760 (in degrees) at pH's of 2.7 (curve

17) Triton X-100 (0.01%) was used for the $R=0$ solution.
18) A. L. Jacobson, *Biopolymers*, **2**, 237 (1964).

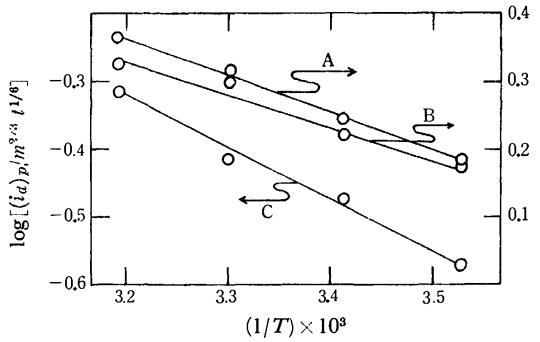

Fig. 5. The effect of temperature upon diffusion current.
Curve A: Cu(II) aquocomplex at pH 3.0;
Curve B: Cu(II)–PGA complex at pH 2.7;
Curve C: Cu(II)–PGA complex at pH 5.0.
Arrows indicate the ordinate to be referred to.

B) and 5.0 (curve C), respectively. A value of −550 was obtained for Cu(II) aquocomplex at pH 3.0 (curve A) for comparison. From these values the activation energy of diffusion can be calculated with the following equation derived by Vlček.[19]

$$\log\frac{(i_d)_p}{m^{2/3}t^{1/6}} = \log(0.627\cdot n\cdot C\cdot F\cdot D_0^{1/2}) - \frac{\frac{1}{2}Q_D}{2.3RT} \quad (1)$$

where C is the concentration of Cu(II) ions; F, the Faraday constant; D_0, a constant. The values of activation energy for Cu(II)–PGA complexes at two pH's and for Cu(II) aquocomplex at pH 3.0 are listed in Table 1.

Table 1. The activation energy of diffusion, Q_D

Sample	pH	R	Q_D (kcal)
Cu(II)–PGA (helical)	2.7	16	4.3
Cu(II)–PGA (random)	5.0	16	6.9
Cu(II) (aquo)	3.0	0	5.0

Discussion

The Role of the Cu(II) Ion in the Conformational Transition of PGA. The observed fact that the diffusion current of Cu(II)–PGA complexes at various values of R abruptly increases with decrease in pH, as shown in Fig. 2, should correspond to the pH-induced helix-coil transition of PGA. This conclusion on the behavior of $(i_d)_p$–pH curves of Cu(II)–PGA complexes is strongly supported by an independent experiment, under the conditions similar to those in this work, of the complex between Cu(II) and monomeric sodium glutamate which shows that the diffusion current does not change over the pH range between 3 and 7.[20] Moreover, the almost parallel shifts of the $(i_d)_p$–pH curves toward higher pH with decrease in R in Fig. 2 might be interpreted that the formation of such Cu(II)-rich complex stabilizes the secondary or helical structure of the polymer.[7]

It is interesting to compare the present results with the report by Takesada *et al.*[7] who noted that the pH-induced helix-coil transition curves in the presence of Cu(II) ions, studied by the method of optical rotatory dispersion, shifted in a similar manner. They observed that, although up to R larger than 20 the transition behavior of Cu(II)–PGA solutions was very close to that of a PGA solution, the slope of the pH-induced transition curves for values of R smaller than 6.6 became more gradual. They attributed their observation to the retention of a helical structure even at a relatively high pH region in the presence of a sufficient number of Cu(II) ions. The transition points in their work range from pH 6.3 to 7.1 (polymer concentration, 0.1 mg/m*l*), whereas the polarographic transition points in our study defined as the midpoint of the increment of diffusion currents, were confined between pH 3.7 and 4.5 (polymer concentration, 1.5 mg/m*l*). This discrepancy is beyond the experimental error and is unable to be attributed to the difference in concentration of polymer or neutral salt.[7] Whether or not it results from the difference in experimental methods employed remains to be resolved.

It is true, in fact, that the polarographic transition point is dependent on the concentrations of the Cu(II) ion and the ligand. As shown in the earlier paper,[6] the point was located at pH 4.2 for the Cu(II)–PGA complex in which the concentrations of the Cu(II) ion, PGA and NaCl were all kept at one-fifth of those employed in this work (in both cases R remained at 16). This is compared in Fig. 6 where the difference of one-half pH unit for two transition points is clearly noted. It should be stated here that the same trend was reported by Takesada *et al.*[7]

The Estimation of the Helical Content of the Complex at Various Values of R. Based on the plots in Fig. 3, it is possible to estimate the helical content of the Cu(II)–PGA complexes in a certain range of R at a

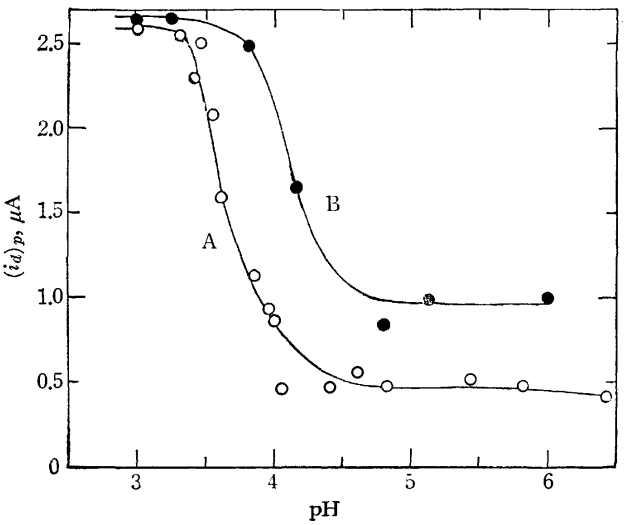

Fig. 6. The diffusion current *vs.* pH curves for two Cu(II)-GPA samples having the same R value of 16 but different concentrations for individual components.
Curve A: $[Cu(II)]=5\times10^{-4}$M, $[PGA]=8\times10^{-3}$M, $[NaCl]=7.5\times10^{-3}$M.
Curve B: $[Cu(II)]=10^{-4}$M, $[PGA]=1.6\times10^{-3}$M, $[NaCl]=1.5\times10^{-3}$M.
The scale of $(i_d)_p$ for curve B is expanded by a factor of 5. These data are taken from Ref. 6.

19) A. A. Vlček, *Collection Czechoslov. Chem. Commun.*, **24**, 3538 (1959).
20) To be published.

given pH. Here, we make the following assumptions. (1) The value of the diffusion current at pH 3.0, which is designated as $(i_d)_p^h$, represents the diffusion current of a Cu(II)–PGA helix. (2) Similarly the diffusion current of the complex at pH 5.0 in the range of R larger than 5 is due to random-coil PGA molecules which completely coordinate to all Cu(II) ions present in solution; this value is designated as $(i_d)_p^r$. The helical fraction, f_h, at a given pH and R, at which the observed diffusion current is $(i_d)_p$, is then given by the following expression

$$f_h = \frac{(i_d)_p - (i_d)_p{}^r}{(i_d)_p{}^h - (i_d)_p{}^r} \tag{2}$$

For a Cu(II)–PGA complex at pH 3.6, f_h is calculated to be about 0.37 in the range of R larger than 20 where $(i_d)_p$ is constant. Similarly an estimate is made for the complex at pH 4.0, in which f_h is 0.11 in the range of R larger than approximately 10.

Now, the question arises on what extent of helical fraction a complex possesses at a given pH and R where the diffusion current is continuously changing (*i.e.*, in the range of R between 5 and 18 for pH 3.6 and between 0 and nearly 10 for pH 4.0, *cf.* Fig. 3). There are two interpretations possible from the present data only. At first, the helical fraction of the complex at a fixed pH of 3.6 steadily increases as R becomes smaller, *i.e.*, the more Cu(II) ions are added, the more stable does the helix become. This is the view promoted by Takesada *et al.*[7] based on the results of an ORD study; however, this interpretation is not unique. An alternative is that the steady increase in $(i_d)_p$ for R smaller than 18 is in actuality the reflection of a chemical process in which the number of the bound Cu(II) ions remains constant at a certain level regardless of apparent values of R; in other words, the increase in $(i_d)_p$ is mostly due to free Cu(II) ions. If this is true, the notion that the presence of the Cu(II) ion in PGA facilitates or enhances the helical formation must critically be reexamined.

The Estimation of the Molecular Size of the Complex from Diffusion Currents. From analysis of diffusion currents, we are able to estimate the molecular size of Cu(II)–PGA complex in a random-coil conformation and to obtain some insight into the mechanism of the interaction between the Cu(II) ion and PGA in a helical conformation. Assuming that the Cu(II)–PGA complex at pH 5.0 is an impenetrable, rigid sphere and that the Stokes-Einstein equation (Eq. (3)) can be applied to the polarographic diffusion process prior to electrode reduction, the radius of such a sphere, r, can be estimated by

$$r = \frac{RT}{N}\frac{1}{6\pi\eta D} \tag{3}$$

where R is gas constant; N, the Avogadro number; T, the absolute temperature (=298°K); η, the viscosity of water ($=0.89\times10^{-3}$ g/cm·sec at 25°C). The diffusion coefficient, D, is calculated with the aid of Ilkovič's equation;

$$D = \left[\frac{(i_d)_p}{605\cdot n\cdot C\cdot m^{2/3}\cdot t^{1/6}}\right]^2 \tag{4}$$

where the following numerical values are adopted:

Table 2. Diffusion coefficients and other pertinent data

	Concentration (mM)	pH	Mixing ratio	$(i_d)_p$ μA	$D\times10^7$ cm²/sec
Cu(II)–PGA	0.5	5.0	16	0.37	7.36
Cu(II)–PGA	0.5	3.0	16	2.50	77.3
Cu(II)–PGA	0.1	5.0	16	0.20	9.00
Cu(II)–PGA	0.1	3.0	16	0.50	68.0
Cu(II)	0.5	3.0	0	2.60	78.0
Cu(II)	0.1	3.0	0	0.53	63.0
Cu(II)	—	—	—	—	72.0[a]
In(III)	1	—	—	—	96[b]

a) I. M. Kolthoff, and J. J. Lingane, "Polarography", Vol. 1, Interscience Publishers, New York, N. Y., (1952) p. 52.
b) S. Inoue, and H. Imai, This Bulletin, **33**, 149 (1960).

$(i_d)_p=0.37$ μA, $C=0.5$ mM, $n=2$, $m=0.989$ mg/sec, $t=8.14$ sec at pH 5.0. In Table 2 the diffusion coefficients of the complexes and other pertinent data are tabulated. As can be seen from Table 2, the diffusion coefficients calculated from our data are in good agreement with those of previous workers. The radius of the assumed sphere of the Cu(II)–PGA complex at pH 5.0 is then calculated to be 33 Å, the value of which yields a molecular volume of 1.5×10^5 Å³. This value is quite consistent with a calculated volume for PGA (details will be published in due course).

The Estimation of the Coordination Number of Cu(II)–PGA Complexes in a Random Conformation. If an electrode reaction proceeds reversibly[21] by the reduction of a complexed Cu(II) ion to a metallic state at the dropping mercury electrode, then the following expression can be applied to obtain the coordination number, j, of such a complex at a given temperature.[22]

$$\frac{d(E_{1/2})}{d(\log C_x)} = -j\frac{0.0591}{n} \tag{5}$$

Thus, from the slope of the $E_{1/2}$-log C_x curve, a value of j can be evaluated. To derive this expression the following assumptions are made:[21] (1) the diffusion current constants of both metallic ion and complex are independent of the respective concentrations, (2) a term containing the activity coefficients of chemical species in solution may be dropped out, and (3) C_x should be the concentration of the free ligands which, however, can be approximated as the total concentration of ligands.

In Fig. 4, the $E_{1/2}$ of Cu(II)–PGA complex was shown to vary in a distinctive manner with the value of R at pH 5.0 where the complex is in a random form, in contrast with the $(i_d)_p$ which, as shown in Fig. 3, remained constant for R larger than 5.0. The $E_{1/2}$ values were replotted in Fig. 7 against the logarithm of the total concentration of PGA in solution, C_x, which is equal to R times the concentration of the Cu(II) ion. Two linear portions cross at log $C_x=-2.2$. From the slope of the straight line A, a j value of 3.4 is yielded. Simi-

21) This assumption was verified by determining the slope of a plot of $\log[(i/(i_d)_p-i)]$ versus electrode potentials. A value of two was assumed for n.
22) D. R. Crow, "Polarography of Metal Complexes", Academic Press, London, 1969, p. 62.

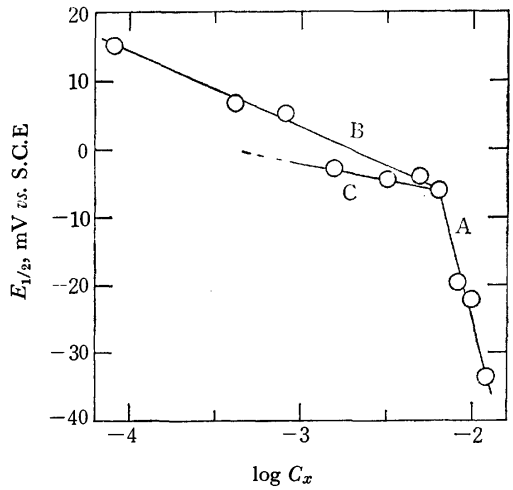

Fig. 7. The Relation between half-wave potential and logarithm of the total concentration of PGA at pH=5.0 and R=16. $C_x=R\cdot$[Cu(II)]

larly, the lines B and C result in j values of 0.34 and 0.17, respectively. It should be noted that the portions A and C correspond to the range of R (from 3 to 24) where $(i_d)_p$ remains unchanged (see Fig. 3). From these j values it is clear that the number of binding sites on each PGA residue changes with the value of R or the concentration of PGA. The coordination number of 3.4 (which reduces to 2.9 when the concentration of free ligands is taken for C_x) indicates that approximately three peptide residues coordinate to each Cu(II) ion as an average. Since each residue possesses three capable sites—amide nitrogen and oxygen atoms and a carboxyl side chain, nine binding sites at maximum are allowable to participate in complex formation. The exact number or stereochemistry, however, is undeterminable.

Assumed that the sharp increase in $(i_d)_p$ at pH 5.0 ($R<3$) shown in Fig. 3 is entirely due to the free Cu(II) ion released from the complex and, consequently, the line B has no meaning, the j value of 0.17 from line C should be interpreted as due to that each PGA residue apparently coordinates to about five Cu(II) ions. This result excludes the possibility that the same type of chelation as occurred in portion A also exists. Therefore, a most plausible mode of binding in portion C is an electrical or ionic pairing with PGA residue. However, if the entire portion of B is meaningful and the whole change in the $(i_d)_p$–R curve at pH 5.0 is assumed to be caused by the electrostatic interaction as described in Results, the j value of 0.34 means that each residue coordinates to three Cu(II) ions. The differentiation of these two ideas awaits a further study. In any case the data in Fig. 7 clearly show that the binding mode of Cu(II) ion to PGA residue changes with the mixing ratio even if the gross conformation of the complex is random-coil.

The Activation Energy of Cu(II)–PGA Complexes in Helical and Coiled Conformations. As can be seen in Figs. 3 and 4, the binding mode of Cu(II)–PGA complex in helical form should differ from that in coiled form. The data in these figures should reflect the difference of the diffusion of these complexes toward the electrode prior to electrode reduction. The difference between the value of Q_D of the Cu(II)–PGA complex at pH 2.7 and that of the complex at pH 5.0 listed in Table 1 clearly indicates that the mechanism of diffusion is affected by the secondary structure of Cu(II)–PGA complex. The finding that the Q_D value of the complex in helical conformation is almost the same as that of the free Cu(II) aquocomplex suggests that the interaction between Cu(II) ion and helical PGA molecule is weak, if any; hence, the loose interaction is likely to be ionic in nature. As the complex diffuses toward electrode, the loosely bound Cu(II) ions may be unsheathed or "zipped-off" to reduce at the electrode surface. The activation energy of diffusion for Cu(II)–PGA complex at pH 5.0 is 60% greater than that at pH 2.7. This means that Cu(II) ions are tightly or coordinately bound with PGA in the coiled region, and that the complex diffuses to the surface as a whole. Or alternatively, the amount of energy corresponding to break the bonds between Cu(II) ion and PGA is required to make unbound free aquo-ions diffuse.

Finally, from the present and earlier studies,[6] it is concluded that the relationship between the polarographic diffusion current and pH is clearly established and definitely reflects the pH-induced helix-coil transition of Cu(II)–PGA complex. These polarographic studies enable to provide rich information on characteristics of the complex in aqueous solutions such as molecular size, helical fraction, mode of coordination, and activation energy of diffusion.

Many thanks are due to our colleague, Dr. Y. Tadokoro of Hiroshima University, for determining the molecular weight of PGA and also for participating in discussion and reading this manuscript. The authors are indebted to Ajinomoto Co., Inc. for supplying PGA samples used in this work.

An MO-theoretical Study of the Nucleophilic Bimolecular Ring-opening of Ethylene Oxide

Hiroshi FUJIMOTO, Motohiro KATATA, Shinichi YAMABE, and Kenichi FUKUI

Faculty of Engineering, Kyoto University, Sakyo-ku, Kyoto

(Received October 30, 1971)

The results of an approximate molecular orbital (MO) calculation of the interaction energy of the ring-opening of ethylene oxide by a hydride ion are presented. The method of calculation is based upon the isolated-molecule approximation. The interaction energy was divided into the Coulomb, exchange, delocalization, and polarization interaction terms, and the changes in these four terms with the progress of the reaction were investigated. The wave function of the combined system of ethylene oxide and a hydride ion was obtained by the configuration interaction (CI) procedure. The changes in the electron populations of ethylene oxide and the hydride ion were calculated from the ground-state CI wave function. Among the unoccupied MO's of ethylene oxide, two low-lying unoccupied MO's were shown to be of special importance in the electron transfer from the attacking anion to ethylene oxide. The effect of the deformation of the molecular shape upon the interaction energy and the intermolecular bond formation is also discussed.

In order to elucidate the origin of the stereoselectivity in chemical reactions, several MO calculations of intermolecular interaction have been carried out.[1-5] These approaches have all intended to discuss the favorable path of several kinds of reaction in light of our knowledge of the MO's of the two reactants in an isolated state. Although the applications of these studies have been limited to the early stage of chemical interaction, they have been believed to be able to give rather detailed information about chemical reactions. The interaction energy between two systems can reasonably be divided into several terms,[4,6,7] to examine what kinds of interactions are important in a given reaction. We previously represented the interaction energy as approximately the sum of four terms, the Coulomb, exchange, delocalization, and polarization interaction energies.[8] Some succinct expressions for these terms were obtained by adopting LCAO SCF MO's. A discussion has also been presented on the role of each of these four terms in determining the favorable path of the bimolecular nucleophilic substitution reaction of methyl chloride, based upon the results of approximate numerical calculations.[9]

It is well known that the bimolecular nucleophilic ring-opening reaction of epoxides takes place stereoselectively, with the preferential occurrence of the inversion at the carbon atom to be attacked by the anion.[10] In the present paper we will discuss the effect of the four energy terms on the determination of the favorable path of the ring-opening of ethylene oxide. The attacking anion is simply represented by a hydride ion. A possible influence of the molecular deformation upon the ease of interaction will also be investigated.

Interaction Energy

The method of the present calculation is based on the concept of the isolated-molecule approximation. That is, the interaction energy between a hydride ion and ethylene oxide, and the changes in the electron populations due to the interaction, are expressed in terms of MO's, which are obtained with respect to each of the two species in the isolated state. We represent the wave function of the interacting system composed of a hydride ion and ethylene oxide as approximately (the symbols are the same as those in Ref. 8);

$$\Psi = C_0\Psi_0 + \sum_j^{\text{uno}} C_{h\to j}\Psi_{h\to j} + \sum_i^{\text{occ}}\sum_j^{\text{uno}} C_{i\to j}\Psi_{i\to j} \qquad (1)$$

where i and j denote the occupied and unoccupied MO's of ethylene oxide, and where h denotes the doubly-occupied orbital of the hydride ion. Although it may be interesting to include outer-shell orbitals, tentatively we do not regard unoccupied orbitals for the hydride ion. Then, the interaction energy, ΔW, between the two may be given approximately by:

$$\Delta W = \varepsilon_Q + \varepsilon_K - D - \Pi \qquad (2)$$

where ε_Q is the Coulomb interaction energy, ε_K is the exchange interaction energy, D is the delocalization interaction energy, and Π is the polarization interaction energy. The last two terms can be expressed in the second-order perturbation forms, provided the interaction is not yet strong.[8]

Calculation on Isolated Molecules

The MO's of ethylene oxide were obtained by a semi-empirical valence-electrons SCF MO method. The method of calculation and the approximations employed are the same as those used in the previous calculation.[9] In Fig. 1 are shown the MO levels.

1) a) R. B. Woodward and R. Hoffmann, *J. Amer. Chem. Soc.*, **87**, 2511 (1965). b) R. Hoffmann and R. B. Woodward, *ibid.*, **87**, 4388 (1965).
2) K. Fukui and H. Fujimoto, This Bulletin, **39**, 2116 (1966).
3) L. Salem, *J. Amer. Chem. Soc.*, **90**, 543, 553 (1968).
4) A. Devaquet and L. Salem, *ibid.*, **91**, 3797 (1969).
5) R. Sustmann and G. Binsch, *Mol. Phys.*, **20**, 1, 9 (1970).
6) J. N. Murrell, M. Randić, and D. R. Williams, *Proc. Roy. Soc.* (London), **A284**, 566 (1965).
7) G. Klopman, *J. Amer. Chem. Soc.*, **90**, 223 (1968).
8) K. Fukui and H. Fujimoto, This Bulletin, **41**, 1989 (1968).
9) a) H. Fujimoto, S. Yamabe, and K. Fukui, *ibid.*, **44**, 971 (1971). b) H. Fujimoto, S. Yamabe, and K. Fukui, *Tetrahedron Lett.*, **1971**, 439, 443.
10) See, for instance, E. S. Gould, "Mechanism and Structure in Organic Chemistry," Holt, Rinehart, and Winston, New York, N. Y. (1959).

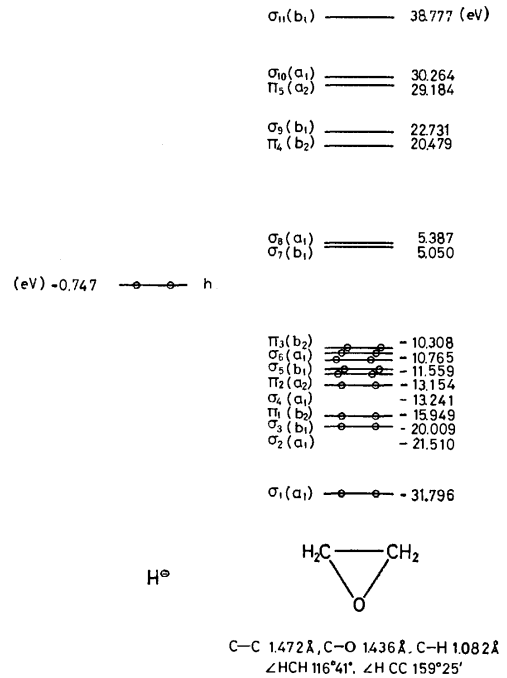

Fig. 1. MO energy levels of ethylene oxide and hydride ion.

The calculated ionization potential is 10.31 eV, showing a good agreement with the observed value, 10.562 eV.[11] There exist two relatively low-lying unoccupied MO's, having almost the same energy. Here, both of these two MO's may be regarded as the lowest unoccupied (LU) MO's. One of them belongs to the irreducible representation, a_1, and the other, to b_1, of the C_{2v} point group. The shapes of these two MO's are illustrated in Fig. 2. It is noted that both of these two MO's have nodes between carbons and oxygen. The energy level of the hydride ion was taken to be −0.747 eV, equal to the minus electron affinity value

Table 1. Calculated interaction energies

Model No.	(x, y, z)[a]	ε_Q, eV	ε_K, eV	D, eV	Π, eV
Ia	(3.3, 0.000, 0)	−0.815	0.138	0.128	0.104
IIa	(3.3, 0.368, 0)	−0.809	0.137	0.132	0.105
IIIa	(3.3, 0.736, 0)	−0.789	0.135	0.138	0.106
IVa	(3.3, 1.472, 0)	−0.715	0.111	0.116	0.104
Va	(3.3, 2.208, 0)	−0.608	0.066	0.061	0.091
Ib	(3.0, 0.000, 0)	−0.937	0.332	0.333	0.146
IIb	(3.0, 0.368, 0)	−0.929	0.331	0.347	0.147
IIIb	(3.0, 0.736, 0)	−0.905	0.324	0.367	0.149
IVb	(3.0, 1.472, 0)	−0.811	0.264	0.295	0.145
Vb	(3.0, 2.208, 0)	−0.677	0.149	0.135	0.122
Ic	(2.8, 0.000, 0)	−1.034	0.587	0.691	0.188
IIc	(2.8, 0.368, 0)	−1.025	0.586	0.726	0.190
IIIc	(2.8, 0.736, 0)	−0.997	0.573	0.776	0.193
IVc	(2.8, 1.472, 0)	−0.887	0.461	0.584	0.186
Vc	(2.8, 2.208, 0)	−0.729	0.254	0.233	0.152
VI	(−1.532, 3.316, 0)	0.228	0.386	0.281	0.162
VII	(−2.149, 2.948, 0)	0.553	0.262	0.283	0.156

a) in Å

11) A. Lowrey, III and K. Watanabe, *J. Chem. Phys.*, **28**, 208 (1958).

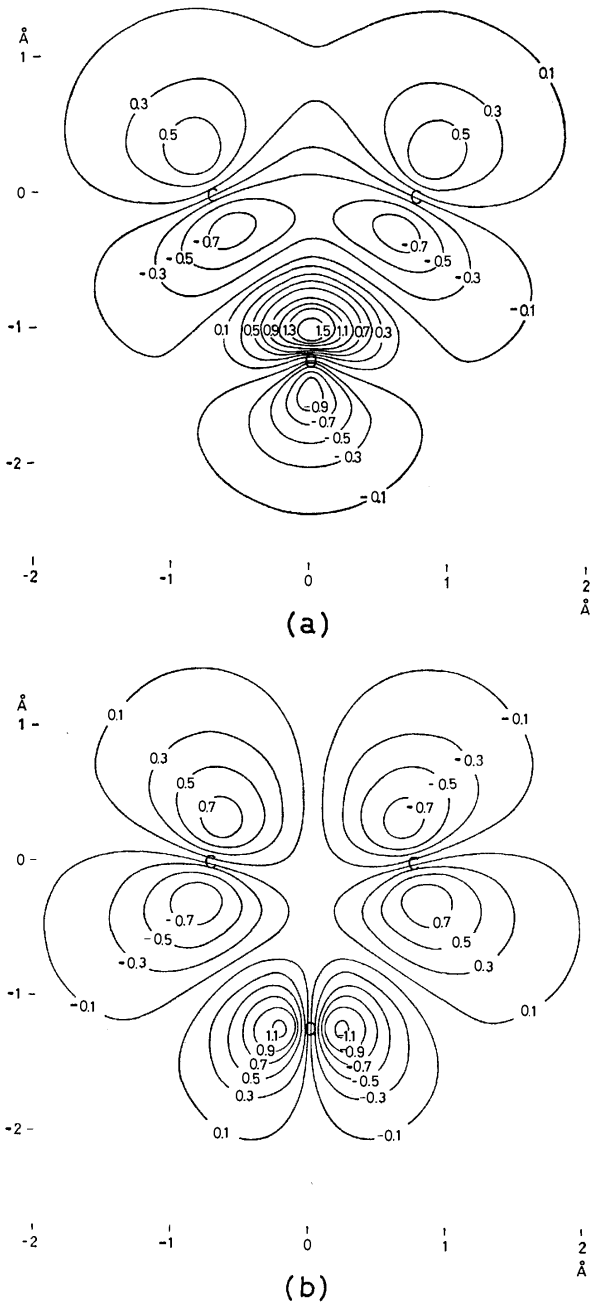

Fig. 2. The LUMO's of ethylene oxide. The figures indicate the values of the real MO's in the molecular plane.
(a): a_1 LUMO (b): b_1 LUMO

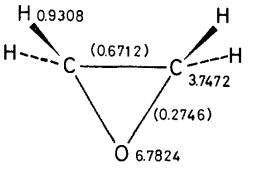

Fig. 3. The atomic populations and atomic bond populations of ethylne oxide.

of hydrogen atom. In Fig. 3 are shown the atomic populations and atomic-bond populations of ethylene oxide in an isolated state.

Calculation of the Interaction Energy

Table 1 gives the results of the calculation of the

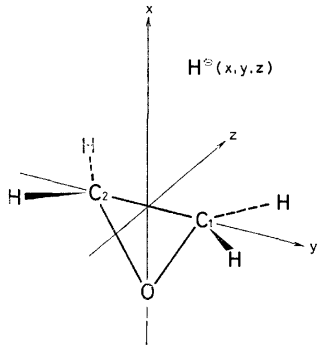

Fig. 4. A schematic representation of assumed reaction models.

interaction energy terms with respect to several assumed models. Each model corresponds to a location of the approaching hydride ion, as is indicated in Fig. 4. The interaction energies have been obtained in a manner similar to that used in previous calculations.[9,12] In the early stage of interaction, in which the hydride ion is distant, the Coulomb interaction term is dominant among the four energy terms. As the hydride ion gets near to ethylene oxide, the exchange and delocalization interaction terms rapidly increase. Because of the crudeness of the approximations employed, the relative magnitudes of the four energies are not trustworthy in a quantitative sense. The present calculation may, rather, be regarded as disclosing, only qualitatively, the possible directing effects of the four energy terms in this reaction. That is, it may be said that the Coulomb term favors the attack of the anion along the principal axis, while the other three require the approach of the anion apart from that axis. The delocalization interaction energy depends greatly on the nodal properties of the LUMO's. When the anion approaches ethylene oxide in a manner like Models Ia, Ib, Ic, ···, the 1*s* orbital of the hydride ion interacts with only one of the LUMO's with the a_1 symmetry, while in the course IIa, IIb, IIc, ···, or IIIa, IIIb, IIIc, ···, the hydride 1*s* orbital can overlap with both of the two LUMO's. The polarization interaction is found to be less important than the delocalization interaction as hydride comes nearer to ethylene oxide. The comparison of Models VI and VII with Models Ib—Vb seems to indicate the preference of inversion at the carbon atom to be attacked by the anion; this is in accordance with the experimental results.[10]

As the reaction proceeds, the initial molecular geometry of the reactant changes. The deformation in the molecular structure is accompanied by changes in the interaction energy terms through the changes in spatial functions and MO energy levels. In order to examine this problem, we have carried out further calculations

12) One-center core attraction integrals $v_{att}=\int t(1)(-Z_\alpha e^2/r_{\alpha 1})t(1)dv(1)$ (the AO t belongs to the nucleus α) were evaluated in a different way from the previous calculation. They were modified so as to make the quantity $\{v_{att}+\sum_{t'}^{\alpha} n_{t'}(t't'|t't')\}$ give the same value both for the non-empirically calculated and for the semi-empirically estimated cases, where $n_{t'}$ means the occupation number of the AO t' of the atom α.

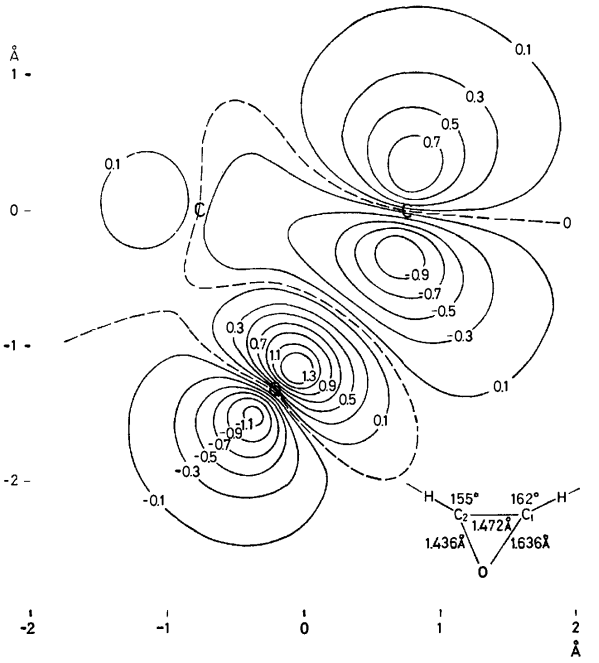

Fig. 5. The LUMO of ethylene oxide with a deformed nuclear configuration. The figures idicate the values of the real MO in the molecular plane.

Table 2. Calculated interaction energies

Model No.	(x, y, z)[a]	ε_Q, eV	ε_K, eV	D, eV	Π, eV
I′	(3.0, −0.736, 0)	−0.898	0.331	0.502	0.171
II′	(3.0, 0.000, 0)	−0.913	0.319	0.676	0.188
III′	(3.0, 0.736, 0)	−0.867	0.297	0.911	0.204
IV′	(3.0, 0.828, 0)	−0.858	0.292	0.917	0.205
V′	(3.0, 0.920, 0)	−0.848	0.287	0.914	0.205
VI′	(3.0, 1.472, 0)	−0.775	0.236	0.701	0.199

a) in Å

while altering the shape of ethylene oxide. Here, we tentatively stretch the C_1–O bond by 0.2 Å. Although this value is arbitrary, such a configuration would be rather in conformity with the deformation along the reaction path. By this deformation, the LUMO's, which are nearly degenerate in ethylene oxide of the symmetrical configuration, split by about 3.8 eV. The shape of the LUMO of the deformed ethylene oxide is shown in Fig. 5. Table 2 presents the results of the calculation of the interaction energy for some assumed locations of the approaching hydride ion with respect to the deformed ethylene oxide. The results in Table 2 seem to indicate that the departure of the hydride ion from the bisecting axis of the C–C bond is assisted by the deformation of the ring. We find the most significant influence of the molecular deformation on the energy term D. It is interesting that the delocalization energy is large when the hydride ion approaches from the direction of the maximum extension of the LUMO of ethylene oxide. The effect of the molecular deformation appears to be a matter of gerat significance in applying the isolated-molecule approximation.

Table 3. The coefficients of the ground-state CI wave functions

Model No.	C_0	$C_{h\to j}$						
		$j=\sigma_7$	$j=\sigma_8$	$j=\pi_4$	$j=\sigma_9$	$j=\pi_5$	$j=\sigma_{10}$	$j=\sigma_{11}$
IIa	0.9867	0.0332	0.1261	0	0.0019	0	0.0211	0.0022
IIIa	0.9860	0.0591	0.1193	0	0.0036	0	0.0213	0.0046
IVa	0.9881	0.0750	0.0929	0	0.0062	0	0.0215	0.0093
IIb	0.9654	0.0582	0.2077	0	0.0016	0	0.0239	0.0022
IIIb	0.9634	0.1024	0.1957	0	0.0030	0	0.0245	0.0050
IVb	0.9701	0.1248	0.1505	0	0.0056	0	0.0262	0.0117
VI	0.9655	0.1760	0.1205	0	0.0072	0	0.0182	0.0282
III′	0.8817	0.4247	0.0391	0	0.0021	0	0.0236	0.0005
IV′	0.8811	0.4262	0.0315	0	0.0025	0	0.0238	0.0012
V′	0.8813	0.4260	0.0246	0	0.0028	0	0.0241	0.0019
VI′	0.9008	0.3900	0.0025	0	0.0046	0	0.0268	0.0064

Table 4. The intermolecular AO bond populations of the AO's of ethylene oxide with hydride 1s orbital

Model No.	$1C_s$	$1C_x$	$1C_y$	$1C_z$	$2C_s$	$2C_x$	$2C_y$	$2C_z$
IIb	−0.0130	0.0197	−0.0006	0	−0.0075	0.0064	−0.0025	0
IIIb	−0.0138	0.0241	0	0	−0.0052	0.0022	−0.0027	0
IVb	−0.0111	0.0197	−0.0004	0	−0.0021	−0.0002	−0.0017	0
III′	−0.0172	0.0427	0	0	−0.0041	0.0020	−0.0026	0
V′	−0.0173	0.0427	0.0004	0	−0.0036	0.0015	−0.0025	0
VI′	−0.0151	0.0349	0.0007	0	−0.0015	0.0002	−0.0017	0

Electron Populations

The coefficients of Eq. (1) calculated for the lowest energy state of the combined system of two reacting species are shown in Table 3. We can see that the most contributing term to Ψ except Ψ_0 is the charge-transferred configuration from the hydride ion into the a_1 LUMO, and that the next contributing is that from the hydride orbital into the b_1 LUMO of the symmetrical-form ethylene oxide. The preferential contribution of a_1 MO to b_1 MO is attributable to the nodal properties of these MO's. The deformation of the nuclear configuration also promotes the mixing of charge-transferred states, as is clear from the comparison of Models IIIb and III′ in Table 3. In obtaining the wave functions, the locally-excited configurations of ethylene oxide were tentatively neglected, since they were thought to have little influence upon the intermolecular electron transfer.

The changes in the electron populations due to the interaction can be calculated by the use of Eq. (1).[13] The AO bond populations between the hydride 1s orbital and the AO's of the carbon atoms of ethylene oxide, obtained from the ground-state CI wave function, are shown in Table 4. The bond formation between the hydride ion and the carbon atom of ethylene oxide under attack is most effective in the model in which the delocalization interaction energy is the largest. The AO of the carbon atom 1, which plays the most dominant role in the formation of the intermolecular bond with the hydride ion, is the p_x orbital, which has its maximum extension in the direction of the approach of the anion. In order to calculate the AO populations of both reactants, we should divide the effused fraction of electrons over the intermolecular region through the overlapping of the AO's h of hydride and t of ethylene oxide into two parts, the one constituting a part of the AO population of the AO h, and the other, that of the AO t. This partitioning may be an extension of Mulliken's population analysis to intermolecular AO pairs.[14] The changes in the atomic populations and in the atomic-bond

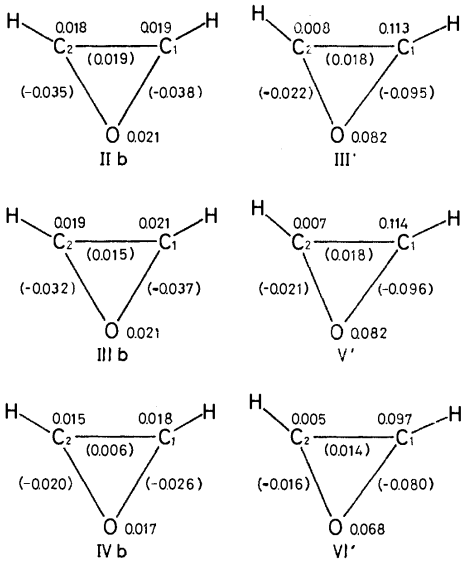

Fig. 6. The changes in the atomic populations and in the atomic bond populations of ethylene oxide due to the interaction with a hydride ion.

13) H. Fujimoto, S. Yamabe, and K. Fukui, This Bulletin, **44**, 2936 (1971).

14) R. S. Mulliken, *J. Chem. Phys.*, **23**, 1833, 1841, 2338, 2343 (1955).

populations of ethylene oxide are shown in Fig. 6 with respect to some of the models mentioned before. The figures in parentheses indicate the changes in atomic-bond populations from those in an isolated state. The atomic-bond populations of the C–O bonds decrease in the case of the interaction with the hydride ion. The results in Table 4 and in Fig. 6 demonstrate that both the formation of new bonds and the weakening of old bonds are accelerated by the molecular deformation. This result is consistent with our previous proposition that the cooperation of the electron delocalization with the change in the molecular shape is a possible driving force in chemical reactions.[15]

Conclusion

We have presented the results of a semi-empirical calculation of the chemical interaction energy and the bond interchange in the ring-opening reaction of ethylene oxide with a hydride ion. Because of the simplification of the reaction model and the crudeness of the calculation, we must refrain from drawing any decisive conclusion about the reaction path from our present results. We can only remark that the path of the approach of the hydride ion to ethylene oxide is very likely to be governed by a delicate balance of the four energy terms presented here. Among charge-transferred states, the one in which an electron of the hydride ion is transferred into the LUMO of ethylene oxide is most important. Molecular deformation along the reaction path appears to be of considerable significance, influencing the ease of the chemical interaction. The effect has been found to be striking in the delocalization interaction energy. The present calculation should not be looked upon as necessarily intending to search for the reaction coordinate leading to the transition state of this special reaction. They will better serve to provide a rough estimate of the directing effect of the four energy terms, and of the bond interchange with respect to some locations of the attacking anion, in the early stage of the reaction. We hope only that we can extend the calculations to a region of moderate interaction.

It is a pleasure to express our gratitude to the Data Processing Center, Kyoto University, for its generous permission to use the FACOM 230·60 computer.

15) K. Fukui and H. Fujimoto, This Bulletin, **42**, 3399 (1969).

BULLETIN OF THE CHEMICAL SOCIETY OF JAPAN, VOL. 45, 1324—1329(1972)

The Amine Sensitization of the Fluorescence of Tris-(dibenzoylmethano)europium(III)

Tadashi FUKUZAWA and Nozomu EBARA

College of General Education, The University of Tokyo, Tokyo

(Received July 8, 1971)

The effect of amines on the efficiency of fluorescence of tris(dibenzoylmethano)europium(III) has been investigated in a methanol solution. Amines with low pK_b values seem to form 1 : 1 complexes with the chelate, and the change in the fluorescence intensity of the chelate is due exclusively to the formation of a complex, which fluoresces more strongly than the chelate itself. It seems that the sensitization of the fluorescence is due to the change in the relaxation lifetime. In the case of amines with aromatic moieties, sensitization through energy transfer may also take place, but this never occurs unless the amine molecule is present in the complex. The structure of the complex and the mechanism of sensitization are discussed.

Fluorescence in rare-earth chelates has been a subject of extensive study[1-5] because of its prospective applicability in laser devices. The excitation of the chelates in a wavelength region where only the ligands absorb light results in high yields of a sharp emission characteristic of the rare-earth metal ions. The intramolecular energy-transfer process has been investigated by Crosby, Whan, and Alire,[6] who compared the fluorescence of several rare-earth chelates and concluded that the transfer of energy from the ligands to resonance levels of metals took place *via* the triplet states of the ligands. Bhaumik and El-Sayed[7] have studied the sensitization of the fluorescence of the chelates by benzophenone and supported the above mechanism.

On the other hand, the third-body effect on the fluorescence efficiency of chelates has been investigated by

1) N. E. Wolff and R. J. Pressley, *Appl. Phys. Lett.*, **2**, 152 (1963).

2) A. Lempicki and H. Samelson, *ibid.*, **2**, 159 (1963); *J. Chem. Phys.*, **39**, 110 (1963); *ibid.*, **40**, 2547 (1964); A. Lempicki, H. Samelson and C. Brecher, *Appl. Optics*, Suppl. on Chemical Lasers, 205 (1965).

3) E. J. Schimitschek, *Appl. Phys. Lett.*, **3**, 117 (1963).

4) H. Winston, O. J. Marsh, C. K. Suzuki, and C. L. Telk, *J. Chem. Phys.*, **39**, 267 (1963).

5) V. A. Brophy and C. Brecher, *ibid.*, **40**, 2553 (1965).

6) G. A. Crosby, R. E. Whan, and R. M. Alire, *ibid.*, **34**, 743 (1961).

7) M. L. Bhaumik and M. A. El-Sayed, *J. Phys. Chem.*, **69**, 275 (1965); see Y. Matsuda, S. Makishima, and S. Shionoya, This Bulletin, **41**, 1513 (1968).

several authors,[8,9] in the expectation that an increase in the fluorescence quantum yield might favor its laser activity. These authors found that the addition of several amines or alkylphosphine oxides greatly affected the quantum yields of the europium resonance fluorescence in the solid state. These investigations, however, lacked quantitative treatment and involved no apposite mechanism of sensitization. Systematic studies are required to account for the sensitization scheme in the fluorescence of europium chelates. The present paper will deal with the effect of several amines on the fluorescence yield of tris(dibenzoylmethano)europium(III) (EuD_3) in a methanol solution.

Experimental

Materials. Tris(dibenzoylmethano)europium(III) was prepared from europium oxide and dibenzoylmethane according to the method of Charles and Perrotto.[10] Yellow prisms, mp 231°C.

Tris(dibenzoylmethano)cobalt(III) was prepared from cobalt oxide and dibenzoylmethane according to the method of Ginestra and Marucci.[11] Green prisms, mp 232°C.

The amines used were G. R.-grade triethylamine, piperidine, octylamine, benzylamine, 4-aminopyridine, *N*-1-naphthylethylenediamine, 9-aminoacridine, pyridine, aniline, *N*-methylaniline, *N*,*N*-dimethylaniline, acridine, 1-naphthylamine, *N*,*N*,*N*′,*N*′-tetramethyl-*p*-phenylenediamine, and 2,5-diphenyloxazole; they were purified repeatedly by vacuum distilation or by recystallization.

Commercially-available spectrograde methanol, chloroform, and tetrahydrofuran were used as solvents without further purification.

Methods of Measurements. The absorption spectra were measured with a Hitachi EPS-2 type spectrophotometer, using 10 mm × 10 mm quartz cells. It is very important to note that the difference spectrum exhibited a marked irregularity when both the reference and sample solutions showed large extinctions. Therefore, care was taken to avoid this wavelength range.

The fluorescence excitation spectra were measured as follows. The sample solutions contained in a 1 mm × 10 mm quartz cell were excited with a 500 W Xenon arc through a Beckmann monochrometer. The radiation from the light source was modulated with a sector and was focused by a quartz lens at a normal incidence on the 10-mm surface of the cell. The fluorescence radiation emitted through the 1-mm surface of the cell was led into a photomultiplier, HTV 374, through several filters. The output of the photomultiplier was amplified with a PAR 122 Lock-in amplifier and displayed on a Toa EPR-2T recorder.

Results and Discussion

Complex Formation. Tris(dibenzoylmethano)europium(III) (EuD_3) and triethylamine were mixed at 15°C in a methanol solution, the concentration of the former being kept constant (7.67×10^{-5} mol/*l*), while that of the latter was varied. The solutions were left standing for more than 30 min, and then the difference spectra of the solutions were measured against a EuD_3 reference solution of the same concentration as that of the sample solutions (Fig. 1). A new peak appeared near 390 mμ, at which the amine did not absorb light, and the chelate absorption peak at 352 mμ seemed to shift gradually towards a shorter wavelength. The spectrum showed isosbestic points and indicated that a single complex was formed.

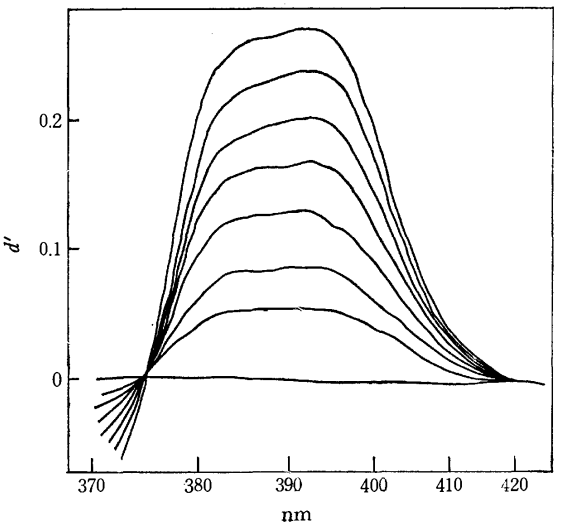

Fig. 1. Difference spectra of the mixtures of EuD_3 and triethylamine (reference EuD_3 solution)
EuD_3: 7.67×10^{-5} mol/*l*, amine: 3.37, 1.69, 0.843, 0.422, 0.211, 0.105 and 0.0527×10^{-2} mol/*l*

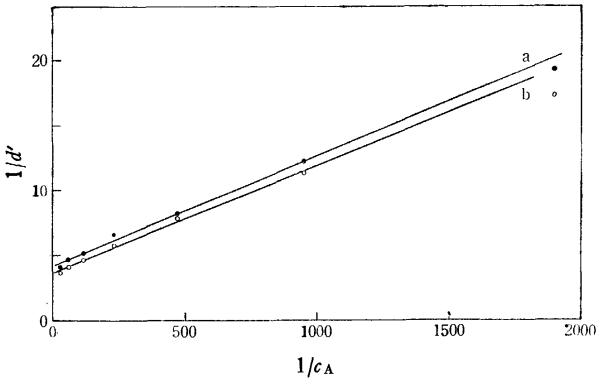

Fig. 2. Plot of $1/d'$ against $1/c_A$ for the mixtures of EuD_3 and triethylamine
a. at 384 mμ, b. at 396 mμ

The plot of $1/d'$ at several wavelengths against $1/c_A$ according to the following equation gave straight lines (Fig. 2), which showed that an equilibrium was reached between the chelate and the triethylamine to form a 1 : 1 complex[12];

$$1/d' = (1+1/c_EK)/(\varepsilon_C-\varepsilon_E)c_A + 1/(\varepsilon_C-\varepsilon_E)c_E$$

where d' is the optical density of the difference spectrum; c_E and c_A, the initial concentrations of the chelate and

8) R. G. Charles and R. C. Ohlmann, *J. Chem. Phys.*, **40**, 3131 (1964); *J. Inorg. Nucl. Chem.*, **27**, 119 (1965).

9) F. Halverson, J. S. Brinen, and J. R. Leto, *J. Chem. Phys.* **41**, 157 (1964).

10) R. G. Charles and A. Perrotto, *J. Inorg. Chem.*, **26**, 373 (1964).

11) A. L. Ginestra and G. Marucci, *Ann. Chim.*, (Rome), **54**, 891 (1964).

12) A 1 : 2 complex may as well be conceived provided no 1 : 1 complex is formed at all. However this is unlikely in a methanol solution.

amine respectively; ε_E and ε_C the molar extinction coefficients of the chelate and the complex respectively, and K, the equilibrium constant.

Similar plots gave similar straight lines when piperidine, octylamine, benzylamine, 4-aminopyridine, and *N*-1-naphthylethylenediamine were used instead of triethylamine (Fig. 3). The calculated equilibrium constants are listed in Table 1. In the case of 9-aminoacridine, the regular change in the spectrum indicated that a complex was formed, but the change was too small to allow an evaluation of the equilibrium constant.

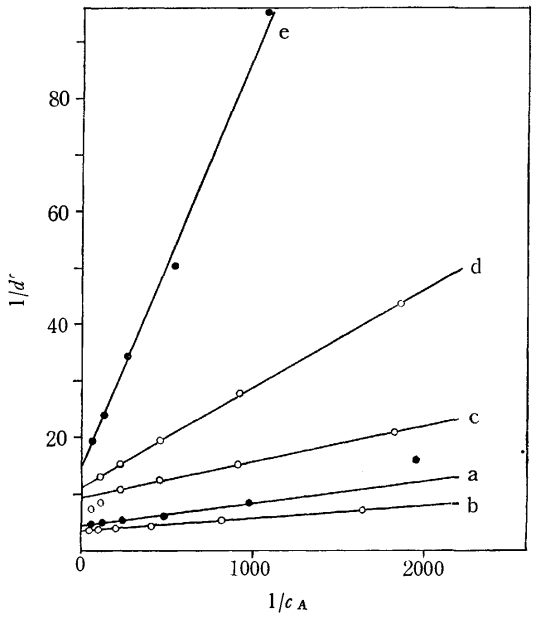

Fig. 3. Plots of $1/d'$ against $1/c_A$ for
a. piperidine: EuD_3 5.86×10^{-5} mol/*l*, c_A 1.64×10^{-2}—5.12×10^{-4} mol/*l*, b. octylamine: EuD_3 6.93×10^{-5} mol/*l*, c_A 1.95×10^{-2}—6.10×10^{-4} mol/*l*, c. benzylamine: EuD_3 5.06×10^{-5} mol/*l*, c_A 1.75×10^{-2}—5.48×10^{-4} mol/*l*, d. 4-aminopyridine: EuD_3 4.73×10^{-5} mol/*l*, c_A 8.95×10^{-3}—5.37×10^{-4} mol/*l*, e. N-1-naphthylethylenediamine: EuD_3 4.73×10^{-5} mol/*l*, c_A 1.48×10^{-3}—2.32×10^{-5} mol/*l*

TABLE 1. EQUILIBRIUM CONSTANTS AND FLUORESCENCE INTENSITY RATIOS OF EUROPIUM CHELATE-AMINE COMPLEXES

	Amine	pK_b	K	$F(C)^{a)}/F(E)$
I	triethylamine	3.13	480	11.4
	piperidine	2.88	510	12.6
	octylamine	3.35	1760	10.0
	benzylamine	4.65	1680	5.97
	aminopyridine	4.82	650	4.76
	naphthyl-ethylenediamine	4.04[b)]	2020	5.28
	aminoacridine	4.55	+	
II	pryidine	8.82		
	aniline	9.40		
	methylaniline	9.30		
	dimethylaniline	8.94		
	acridine	8.50		
	naphthylamine	10.08		
	tetramethyl-phenylenediamine	6.76		
	diphenyloxazole	—		

a) $F(C)$: calculated fluorescence intensity of the complex
b) value of ethylenediamine

On the other hand, aromatic amines such as pyridine, aniline, *N*-methylaniline, *N*,*N*-dimethylaniline, acridine, 1-naphthylamine, *N*,*N*,*N'*,*N'*-tetramethylphenylenediamine, and 3,5-dipehnyloxazole showed no evidence of forming complexes.

An inspection of Table 1 suggests that the ease with which the complex is formed is determined mainly by the following two factors:

1) Only amines with low pK_b values (lower than 5 in the present case) tend to form complexes. This parallelism is not consistent with the other properties of amines, such as the ionization potentials and the dipole moments.

2) The steric factor affects the equilibrium constant. The equilibrium constant is greater for primary amines and smaller for secondary or tertiary amines. In the case of 9-aminoacridine the equilibrium constant seems to be small, probably because of the dense steric disposition in the proximity of ring nitrogen.

Charles and Ohlmann[8] have prepared solid 1 : 2 complexes of EuD_3 with several amines involving pyridine and aniline (a 1 : 1 complex in the latter case) and have suggested that the amine is attached directly to the europium atom. This assumption has been supported by later workers[13-15] because of its consistency with current theory and with the experimental results, as exemplified by an X-ray analysis of a hydrated EDTA complex of lanthanum $LaAH_4\cdot7H_2O$ (AH_4 means the acidic form of EDTA) by Hoard *et al.*,[16] who showed that four of seven water molecules in the crystal were bonded directly to the La atom. They nevertheless did not reject the possibility that some of the complexes were formed by a van der Waals force (or a charge-transfer force) between the amine and the ligand. It is evident that the present result conforms to the assumption of Charles, in which a dative bond is formed between europium and nitrogen by the intrusion of amine molecules into the ligands.

To confirm the assumption more directly, we have prepared tris(dibenzoylmethano)cobalt(III) (CoD_3) and examined whether it could form complexes with amines in tetrahydrofuran or in chloroform. As the coordination number of Co(III) is six, and since it never exceeds six, the formation of a complex, if ever, must involve interaction between the amine and the ligand. Our experiment showed that CoD_3 formed no complex with triethylamine. It is hoped that the NMR chemical shift measurement of the NH proton in a complex of EuD_3 with a primary or secondary amine will reveal unambiguously the bonding aspect.[17-19]

The present experiment differed from that of Charles

13) L. R. Melby, N. J. Rose, E. Abramson, and J. C. Caris *J. Amer. Chem. Soc.*, **86**, 5117 (1964).
14) H. Bauer, J. Blanc, and D. L. Ross, *ibid.*, **86**, 5125 (1964).
15) E. L. Muetterties and C. M. Wright, *ibid.*, **87**, 4706 (1965).
16) J. L. Hoard, M. D. Lind, and B. Lee, *ibid.*, **87**, 1612 (1965).
17) J. K. M. Sanders and D. H. Williams, *Chem. Commun.*, **1970**, 422.
18) J. Briggs, G. H. Frost, F. A. Hart, G. P. Moss, and M. L. Staniforth, *ibid.*, **1970**, 749.
19) G. M. Whitesides and D. W. Lewis, *J. Amer. Chem. Soc.*, **92**, 6979 (1970).

in that the complex was 1: 1 rather than 1: 2 and in that pyridine and aniline formed no complex: this is not surprising, because the amine molecule had to replace the already-bonded solvent molecule to form a complex in the solution. In fact, the spectra of the mixture solutions of EuD_3 and aliphatic amines turned out to change within a short time after mixing, with the above consideration. The details of the time dependence will be presented elsewhere.

Fluorescence. The above mixed solutions of EuD_3 and amines have been subjected to the measurement of their fluorescence excitation spectrum. The excitation of the chelate in the ultraviolet region gave rise to a sharp red emission which peaked at 612 mμ; this was identified with the europium resonance fluorescence from $^5D_0$ to $^7F_2$.[2] In the case of amine which did not fluoresce, such as triethylamine, piperidine, or octylamine, the excitation spectra of the mixed solutions were measured with this emission peak alone. When amine itself fluoresced, as in 1-naphthylamine, the excitation spectra of a chelate solution (E), amine solutions (A) of various concentrations, and mixed solutions (M) in which the concentrations of the solutes were the same as in E and A were measured either with a 612 mμ emission (e) using Toshiba filters VR-60 and UV-39 or with an appropriate wavelength range (a) in which the amine fluorescence had an appreciable oscillator strength, but neither the amine nor chelate absorbed radiation. In the cases of 1-naphthylamine and *N*-1-naphthylethylenediamine, for example, the 422—520 mμ region using a combination of filters, UV-39, VV-42, and VY-44, was found to be appropriate.

For the sake of conciseness and clarification, the following notations are adopted:

F(A) and F(E)
fluorescence intensities of the amine solution and the chelate solution respectively

F(M)
fluorescence intensity of the mixed solution

F_A(M) and F_E(M)
parts of F(M) due to amine and europium respectively, so that $F_A(M)+F_E(M)=F(M)$

F^e and F^a as in F^e(A)
fluorescence intensities measured at 612 mμ (e) and at (a)

The excitation wavelength and the concentration of the amine are not specified.

The intensities were corrected for absorption and the emission of the partner molecules as follows:

1) The fluorescence of amine occasionally had a nonvanishing intensity, even at 612 mμ, at which point the europium fluorescence was to be measured (perhaps due to the low resolution of the filters). To obtain the intensity of the europium fluorescence at this wavelength in the mixture, F_E^e(M), the portion of the intensity due to amine, F_A^e(M), must be subtracted from the observed value, F^e(M). As the amine fluorescence was found to be affected strongly by the presence of a chelate, as will be shown later, F_A^e(M) can not be equated with F^e(A), but is obtained by:

$$F_A^e(M) = F^e(A) \times F^a(M)/F^a(A)$$

It is to be recalled that the effect of absorption on the above values has already been eliminated.

On the contrary, the observed fluorescence intensity, F^a(M), can be ascribed solely to amine, so that only the succeeding correction applies in this case.

2) The amine and chelate absorbed radiation at the same time in the exciting wavelength range, thereby reducing mutually the number of photons which, otherwise, were to be absorbed by the partner molecules. This was taken into account by multiplying the respective intensity values, F_E(M) or F_A(M), by:

$$f = (c\varepsilon+c'\varepsilon')[1-\exp(-c\varepsilon l)]/c\varepsilon[1-\exp\{-(c\varepsilon+c'\varepsilon')l\}]$$

where l is the cell length (0.1 cm). The other notations, c, c', ε, and ε', require some comment; c (c') represents the concentration, and ε (ε'), the extinction coefficient, at the exciting wavelength. When the fluorescence of the amine is going to be modified, the unprimed numbers, c and ε, refer to the chelate and the primed numbers, c' and ε', to the amine. Inversely, when the fluorescence of the chelate is going to be modified, the former refer to the amine, and the latter, to the chelate. In what follows, the intensity values, F_E(M) and F_A(M), are to be understood as already corrected for this factor.

3) The amine fluorescence was partly absorbed by the chelate. The extent of this factor could not be evaluated, but it seemed to be small and was disregarded.

A) Amines Which Do Not Form Complexes: Amines of the second group in Table 1 did not form complexes. The excitation spectrum of the EuD_3 solution F_E^e(E or M) did not change on the addition of these amines over the whole range of excitation wavelengths covering 370 mμ. In the case of 1-naphthylamine, for example, the radiation of 300 mμ excited the amine molecule almost exclusively, and F_E^e(M) was very weak. An increase in the amine concentration did not seem to affect the intensity, indicating that no transfer of energy from the amine to chelate took place. This also the case for aniline and pyridine, which were excited at 280 and 260 mμ respectively. It is concluded that free amine molecules, excited or unexcited, do not affect the fluorescence of the EuD_3 in solution.

B) Amines Which Form Complexes: Amines of the first group in Table 1 formed complexes. When these amines were added to the solution of EuD_3, the F_E^e(M) increased markedly on excitation at 370 mμ as the concentrations of amines increased. As most of the amines involved did not absorb any exciting radiation, excitation transfer from the amine molecule to the chelate molecule did not account for the sensitization. Moreover, the dielectric behavior of the solvent, which might affect the fluorescence intensity, did not change noticeably upon the addition of amine of such low concentrations. This is consistent with the fact that the addition of ketones, such as acetone or cyclohexanone, to a similar extent affected neither the absorption spectrum nor the fluorescence quantum yield.[20]

The fluorescence intensities, $F_E^e(M)/F^e(E)$, were plotted against the optical densities, d', of the difference spectra of the solutions near the peak of the band of the EuD_3-amine complex; they gave straight lines (Figs. 4

20) Unpublished data.

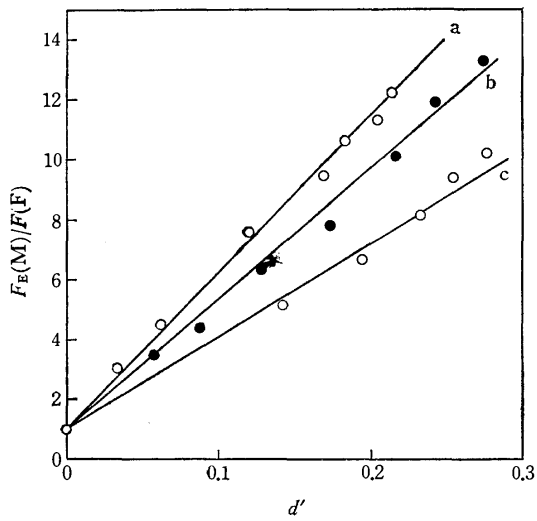

Fig. 4. Plots of $F_E(M)/F(E)$ against the optical density of the difference spectrum a. piperidine, b. triethylamine, c. octylamine concentrations are the same as in Figs. 1—3.

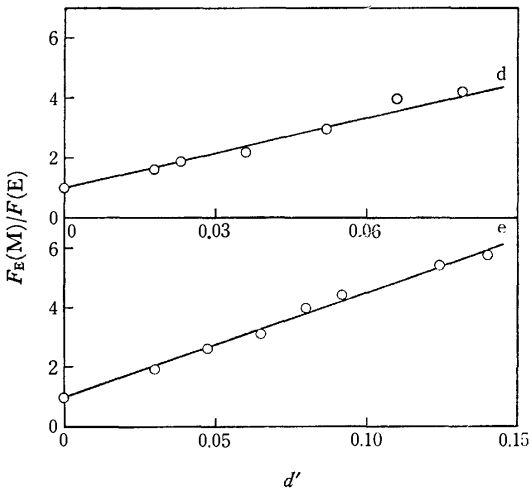

Fig. 5. Plots of $F_E(M)/F(E)$ against the optical density of the difference spectrum. The concentrations are the same as in Fig. 3. d. 4-aminopyridine, e. benzylamine

and 5). As d' is proportional to the concentration of the complex, as can be shown easily, the change in the fluorescence intensity, which is also proportional to it, should be attributed solely to the complex formation. The sensitization mechanism involving long-range interaction can again be ruled out. It follows, from our knowledge of the equilibrium constants and the intensity-optical density plits, that the fluorescence efficiencies of the complexes in a methanol solution are 4 to 12 times as high as that of the uncomplexed chelate (Table 1).

In the case of *N*-1-naphthylethylenediamine, the $F_E^e(M)/F^e(E)$ ratio was plotted at each of these excitation wavelengths, 370, 330, and 290 mμ. These wavelengths, were chosen for the following reasons. The radiation of 370 mμ excited almost exclusively the ligand of the chelate, the radiation of 290 mμ excited mainly the amine, and that of 330 mμ, excited both the chelate and amine. All of the plots showed a good linearity, but the slope was the greatest for the last plot (Fig. 6). As the slope of the plot for 370 mμ is a measure of the increase in the quantum yield of the fluores-

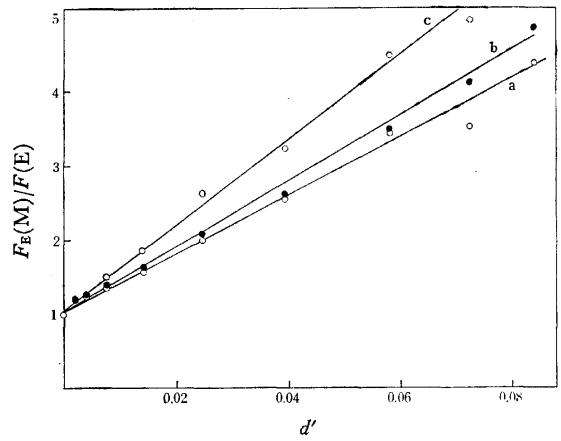

Fig. 6. Plots of $F_E(M)/F(E)$ for *N*-1-naphthylethylenediamine against the optical density of the difference spectrum.
a: excited at 370 mμ, b: 330 mμ, c: 290 mμ.

cence of the chelate by complex formation, it must be invariant under a change in the excitation wavelength, provided only that the ligand is excited at its first absorption band, as was the case for aliphatic amine complexes. Therefore, the increase in the slope should be attributed to the cooperative excitation-transfer process which took place from the amine to the chelate.

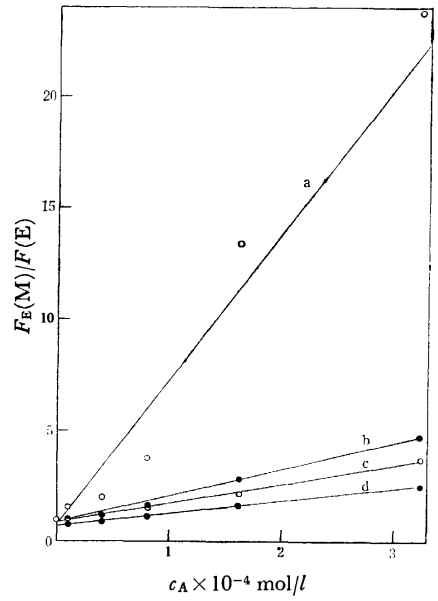

Fig. 7. Plots of $F_E(M)/F(E)$ for 9-aminoacridine against the concentration of amine.
a: excited at 410 mμ, b: 390 mμ, c: 370 mμ, d: 340 mμ

This was also the case for 9-aminoacridine. In Fig. 7, $F_E^e(M)/F^e(E)$ is plotted against the concentration of amine, as the optical density is not available because of the superposition of the amine absorption. The radiation of 370 or 340 mμ mainly excites the chelate, but that of 390 or 410 mμ mainly excites the amine. The latter two plots have larger slopes than the former.

The linearity of the $F_E^e(M)/F^e(E)$ ratio of *N*-1-naphthylethylenediamine against d', and the fact that naphthylamine, which failed to form a complex, did not affect the $F_E^e(M)$, suggest that the energy transfer takes place only from the amine molecule which is attached

to europium. Here again, the long-range or collisional-transfer mechanism can be discarded.

On the other hand, the excitation spectrum of the complex with benzylamine or aminopyridine fell to zero intensity near 260 mμ, although the amine absorbed radiation at this wavelength. It seemed, therefore, that the energy transfer did not take place in these complexes.

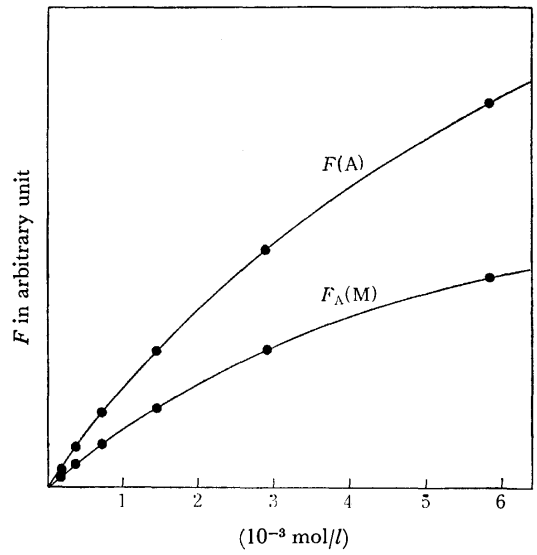

Fig. 8. Plots of $F_A(M)$ and $F(A)$ for aniline against the concentration of amine.

C) Fluorescence of Amine: Figure 8 shows the effect of the concentration on the fluorescence intensity of aniline, both in the absence and in the presence of the chelate, $F^a(A)$ and $F_A^a(M)$, on the excitation at 280 mμ, the peak of the excitation spectrum of aniline. Their ratio, $F_A^a(M)/F^a(A)$, is almost constant irrespective of the concentration of aniline: it amounts to 0.58. This suggests that the encounter-quenching mechanism accounts for the effect. The same is the case for tetramethylphenylenediamine on excitation at 330 mμ, the intensity ratio of which is 0.55 (Fig. 9).

When the amine forms a complex, the encounter-quenching mechanism applies only to free amine molecules and the $F_A^a(M)/F^a(A)$ ratio is expected to depend upon the concentration of amine, because the amount of the complex is most proportional to the latter. Unfortunately, in the cases of *N*-1-naphthylethylenediamine and 9-aminoacridine, both of which formed complexes, the expected concentration dependence could not be ascertained. Probably, the absorption of amine trailed into the transmission range of the filter with which the fluorescence was measured, and this precluded any exact determination of the fluorescence intensity. However, a comparison of 1-naphthylamine and *N*-1-naphthylethylenediamine showed that the fluorescence of naphthylamine was quenched to a somewhat smaller extent when the amine molecule was attached to the chelate.

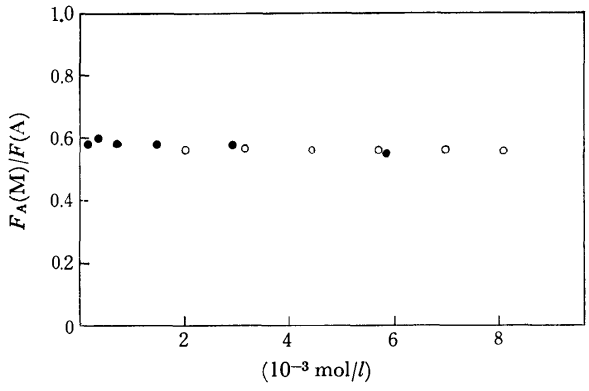

Fig. 9. Plots of $F_A(M)/F(A)$ against the concentration of amine.
●: aniline, ○: tetraemthylphenylenediamine

D) Mechanism of Sensitization: It seems to be established that the sensitization of the fluorescence of EuD_3 with amine take place solely by way of complex formation, and that two processes compete in the sensitization: sensitization involving energy transfer, and that not involving energy transfer. The following mechanisms are likely to hold.

1) Sensitization involving no energy transfer: There seem to be two concerted mechanisms; both serve to increase the relaxation lifetime of the chelate. Sensitization in the solid state, in which there is no participation of a solvent, suggests that the piling up of ligand molecules is responsible for it. The intrusion of amine molecules may restrict the free arrangement of ligand molecules so that the equilibrium structures of the ground state and the excited state of the complex become alike. This may reduce the Franck-Condon factor and suppress the radiationless process.

In solution, the fluorescence intensity of EuD_3 is a function of the nature of the solvent.[20] The solvent molecules seem to attach to the europium atom and exchange easily with other free solvent molecules. This may favor a radiationless transition by providing an energy continuum like that of predissociation near the energy levels of the chelate, thus invoking Fano configuration interaction,[21,22] or by bringing anharmonicity to the vibrational wavefunctions. Amines form comparatively rigid bonds and may interrupt this process.

2) Sensitization involving energy transfer: Excitation transfer takes place only from the ligand amine molecule, not from the free amine molecule. The collision of the free amine and the chelate only results in the quenching of the fluorescence of amine (but not of the fluorescence of the chelate). This suggests that the amine excitation energy is transferred directly to the europium atom, not through the ligand dibenzoylmethane molecule. This was strongly supported by the fact that 9-aminoacridine, the triplet and singlet levels of which lie below the corresponding levels of the ligand of the chelate, transfers its energy to the chelate, while the reverse process does not occur. This, in turn, gives support to the assumption that the complex is formed by an amine-europium bond.

The absence of energy transfer in benzylamine and in 4-aminopyridine still remains a problem. It may be due either to the intensity of the light source being too low to excite the amine to a detectable amount or to the energy separation being too large for crossing over to occur in the transfer process.

21) U. Fano, *Phys. Rev.*, **124**, 1866 (1961).
22) M. Bixon and J. Jortner, *J. Chem. Phys.*, **48**, 715 (1968).

Acidity and Acid Strength of Zeolite Catalysts

Misako IKEMOTO, Kazuo TSUTSUMI, and Hiroshi TAKAHASHI
Institute of Industrial Science, The University of Tokyo, Roppongi, Minato-ku, Tokyo
(Received August 17, 1971)

The influence of pretreatment temperature, silica-to-alumina mole ratio, the kind of cation and degree of cation exchange on the number of acid sites, and the acid strength of zeolite catalysts were examined by means of amine titration. Strong acid sites whose H_0 function is lower than -8.2 were analyzed by ultraviolet spectroscopy. Though H-zeolites have fairly strong acid sites ($-10.8<H_0<-8.2$), the number of acid sites decreases with the decrease of the silica-to-alumina mole ratio, as a result of the collapse of the zeolite structure. Ca-zeolites have an acid site distribution similar to that of H-zeolites only when the silica-to-alumina mole ratio is larger than 4.6. Only La-form Y-zeolite has strong acid sites ($H_0<-10.8$). When the degree of La-exchange exceeds 85 mol%, zeolite shows an acid coloration even with dinitrotoluene with $pK_a-12.8$.

In recent years, near-faujasite zeolite catalysts have been used in various reactions,[1] and their surface acidity has been investigated by means of infrared spectroscopy,[2-8] and titration with a base in nonaqueous solutions.[9,10] However, the nature of acid sites has not yet been clarified.

Hirshler measured the acidity of Linde Molecular Sieves 10X, 13X, and Li-X[11] by using Hammett indicators and H_R indicators, which form stable carbonium ions on the catalytic surface.[9] He showed that the acidity of 13X is very weak and only develops a red color with butter yellow, while both Li-X and Ca-X possess strong acid sites.

Otouma *et al.* studied the acid character of X and Y zeolites replaced by hydrogen, calcium and lanthanum ions by means of Hammett indicators,[10] and found characteristic features of the acid sites of zeolite catalysts. The number of acid sites is generally larger on the zeolites (2—3 meq/g) than on an amorphous silica-alumina cracking catalyst (0.5 meq/g). The acid strength is more widely distributed in the zeolites ($H_0=+3.3\sim-8.2$) than in silica-alumina ($H_0<-8.2$). The acid sites increase not only in number but also in strength with the advance of ion exchange.

The present investigation deals with a study of the effects of pretreatment temperature, the silica-to-alumina mole ratio, and the ion exchange on the surface acidity of faujasite-type zeolites. The nonaqueous titration method using Hammett indicators was applied for measurement of the acid sites.[12,13] Though it has been reported that zeolite has a strong acid character, little work has been carried out on the strong acid sites ($H_0<-8.2$). Information was obtained also on the strong acid centers on zeolite by a spectrophotometric method.

Experimental

Of the zeolite samples used in this study, Na–$X_{2.5}$[14] and Na–$Y_{5.0}$ were Linde Molecular Sieves 13X and SK-40, respectively, and Na–$Y_{3.25}$, Na–$Y_{3.85}$, and Na–$Y_{4.6}$ were synthesized from silica-alumina gel and sodium hydroxide. The calcium-, lanthanum-, or ammonium-exchange was performed by immersing the sodium-form zeolite in an aqueous solution of respective metal chlorides or ammonium chloride. Treatment was repeated several times in order to obtain a high degree of exchange. The samples were then collected by filtration, washed until no chloride ion was detected with silver nitrate and finally dried. The degree of exchange was determined by chemical analysis and flame photometry.

All the indicators were Wako Pure Chemicals Co. products. They were purified by recrystallization from benzene.

Cyclohexane was Dotite Spectrosol and was dried with a Linde Molecular Sieve 4A. *n*-Butylamine (Wako S grade) was purified by distillation and dried with a Linde Molecular Sieve 4A.

The Hammett indicators are listed, together with their pK_a's in Table I. Color changes of BY, DCA, BAP, and AQ are visible and the measurements were carried out with powdered samples. Since both acid and basic forms of absorbed PNT and DNT are colorless, the measurements were made by the aid of a spectrophotometer. Thin wafers were used as samples. Fifty mg of powdered zeolite was pressed into pellets between stainless steel blocks. The wafer "thickness" was 20 mg/cm^2.

The samples were placed in a vessel evacuated to 10^{-3}

Table 1. Indicators used in acid strength distribution measurements

Hammett indicators	pK_a
Butter yellow (BY)	+3.3
Diciannamalacetone (DCA)	−3.0
Benzalacetophenone (BAP)	−5.6
Anthraquinone (AQ)	−8.2
p-Nitrotoluene (PNT)	−10.8
2,4-Dinitrotoluene (DNT)	−12.8

1) P. B. Venuto and D. S. Landis, *Adv. Catal.*, **18**, 259 (1968).
2) J. L. Carter, P. J. Lucchesi, and D. J. C. Yates, *J. Phys. Chem.*, **68**, 1385 (1964).
3) J. B. Uytterhoeven, L. G. Christner, and W. K. Hall, *ibid.*, **69**, 2117 (1965).
4) J. R. Hughes and H. M. White, *ibid.*, **71**, 2192 (1967).
5) J. W. Ward, *J. Catal.*, **9**, 225, 396 (1967); **10**, 34 (1968); **11**, 238, 251 (1968); **13**, 364 (1969); **16**, 386 (1970); **17**, 355 (1970).
6) P. E. Eberly, Jr., *J. Phys. Chem.*, **72**, 1042 (1968).
7) H. Hattori and T. Shiba, *J. Catal.*, **12**, 111 (1968).
8) P. E. Eberly, Jr. and C. N. Kimberlin, Jr., Proc. 2nd Int. Conf. Molecular Sieve Zeolites, p. 283 (1970).
9) A. E. Hirschler, *J. Catal.*, **2**, 428 (1963).
10) H. Otouma, Y. Arai, and H. Ukihashi, This Bulletin, **42**, 2449 (1969).
11) This denotes the faujasite-type zeolite X with lithium ion.
12) H. A. Benesi, *J. Amer. Chem. Soc.*, **78**, 5490 (1956).
13) H. A. Benesi, *J. Phys. Chem.*, **61**, 970 (1957).
14) Zeolite with silica-to-alumina mole ratio 2.5.

Torr, and the temperature was then slowly raised to the desired temperature and kept constant for 5 hr under 10^{-5} Torr.

Acidity measurements were carried out as follows. The sample was transferred from the evacuated vessel to a test tube in a dry-box. Two m*l* of dry cyclohexane and a proper amount of a 0.1N solution of *n*-butylamine in cyclohexane were added. After the test tube was maintained at 60°C for 3 days, a few drops of 0.1% solution of the indicator in cyclohexane were added. After 2 days, it was determined whether the sample was basic or acidic to the indicator, either with the naked eye or by the use of a UV spectrophotometer.

Results and Discussion

Effect of Pretreatment Temperature. Figures 1 and 2 illustrate the correlation between the pretreatment temperature and the number of acid sites of the Ca- and NH_4-form zeolites at $H_0=+3.3$. The number of acid sites of Ca-zeolites increases to a maximum and then gradually decreases when the pretreatment temperature is raised. The number of acid sites of Ca-zeolite with a lower ratio of silica-to-alumina changes greatly with the pretreatment temperature, while that of Ca-zeolite with a higher ratio remains nearly constant. Since the zeolites with lower silica-to-alumina ratios have a relatively large number of Al atoms, the bond distance between Ca^{2+} and AlO_2^- ions is small. Thus, it is difficult to break the bonds and only a small number of acid sites was measured with the sample evacuated at a lower temperature.

As clearly shown in Fig. 2, the acidity of H-form zeolites[15] is greatly influenced by silica-to-alumina ratio.

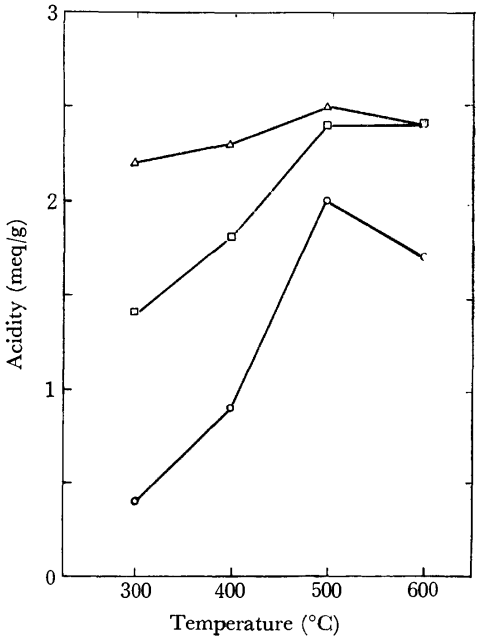

Fig. 1. Effect of pretreatment temperature on acidity of Ca-form zeolites ($H_0=+3.3$).
△: Ca-$Y_{5.0}$ (Ca^{2+}, 85 mol%)
□: Ca-$Y_{3.85}$ (Ca^{2+}, 90 mol%)
○: Ca-$X_{2.5}$ (Ca^{2+}, 99 mol%)

15) NH_4-form zeolites change into H-form zeolites with liberation of NH_3 during pretreatment at above 300°C.

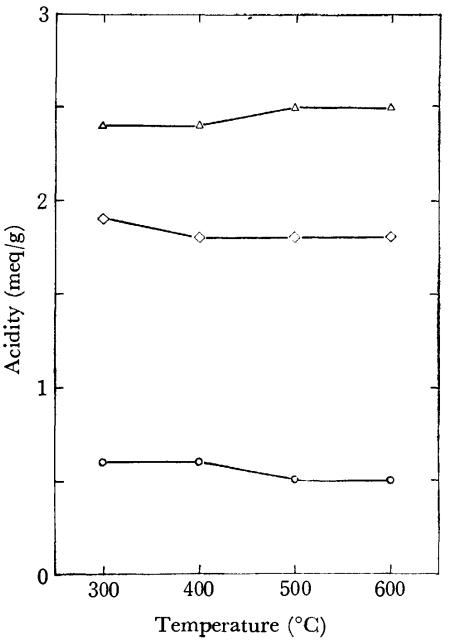

Fig. 2. Effect of pretreatment temperature on acidity of H-form zeolites ($H_0=+3.3$).
△: H-$Y_{5.0}$ (H^+, 92 mol%)
□: H-$Y_{4.6}$ (H^+, 89 mol%)
○: H-$X_{2.5}$ (H^+, 86 mol%)

The zeolite with a lower ratio showed a small number of acid sites at any pretreatment temperature, since it is thermally unstable and easily loses its crystallinity with heat treatment, when acid sites are lost. On the other hand, the zeolite with a higher ratio showed as many sites as Ca-zeolite because of its high thermal stability.

Effect of the Silica-to-Alumina Mole Ratio. The effects of the silica-to-alumina mole ratio on the acidity

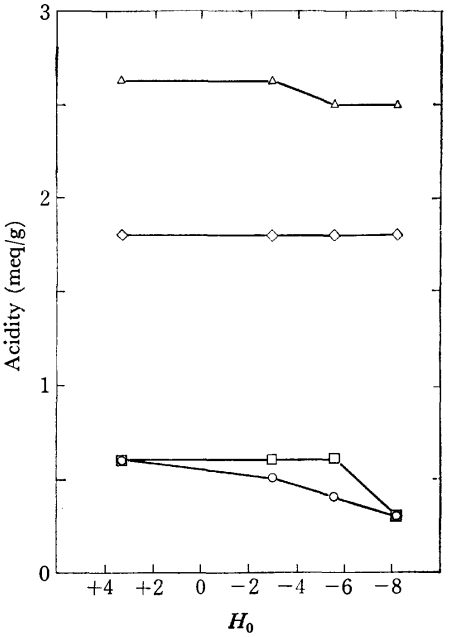

Fig. 3. Acid strength distributions of H-form zeolites.
△: H-$Y_{5.0}$ (H^+, 94 mol%), Pretreated at 500°C
◇: H-$Y_{4.6}$ (H^+, 89 mol%), Preatreated at 500°C
□: H-$Y_{3.86}$ (H^+, 86 mol%), Pretreated at 350°C
○: H-$X_{2.5}$ (H^+, 86 mol%), Pretreated at 350°C

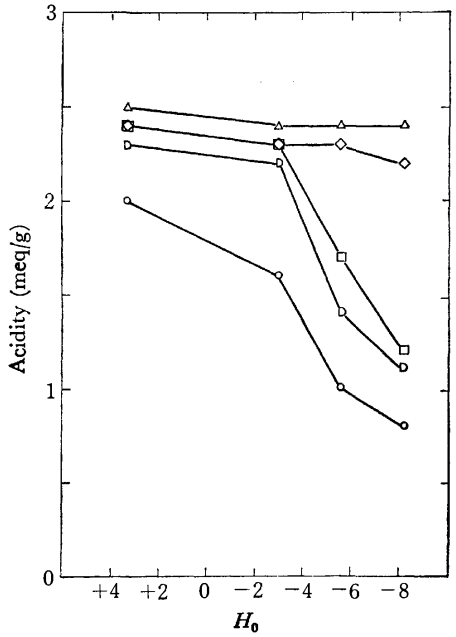

Fig. 4. Acid strength distributions of Ca-form zeolites pretreated at 500°C.
△: Ca-$Y_{5.0}$ (Ca^{2+}, 85 mol%)
◇: Ca-$Y_{4.6}$ (Ca^{2+}, 90 mol%)
□: Ca-$Y_{3.85}$ (Ca^{2+}, 90 mol%)
D: Ca-$Y_{3.25}$ (Ca^{2+}, 96 mol%)
○: Ca-$X_{2.5}$ (Ca^{2+}, 99 mol%)

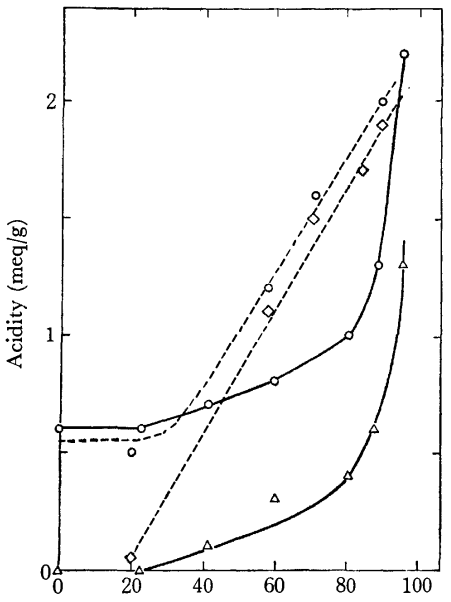

Fig. 5. Effect of Ca- and La-exchange on acidity of zeolites pretreated at 500°C.
——: Ca-$Y_{3.25}$, ----: La-$Y_{3.25}$
○: BY, △: BAP, ◇: AQ

of Ca- and H-zeolite were investigated. The distribution of acidity is shown in Figs. 3 and 4.

The maximum acidity in Ca-zeolite was 2.0 meq/g for Ca-$X_{2.5}$ and 2.5 meq/g for Ca-$Y_{5.0}$. The Ca-zeolites with silica-to-alumina mole ratios greater than 4.6 possess strong acid sites ($H_0 < -8.2$). However, the acid sites of Ca-zeolites with lower ratios of silica-to-alumina are distributed over a wide range of acid strength. The results agree with the fact that a strong electrostatic field is generated by heat treatment and easily produces H^+ ions in zeolites with a higher ratio of silica-to-alumina.[16] Though a decrease in the amount of alumina gives rise to a decrease in the number of cations, it makes the distance between cations and anions longer. As a result, separation between the positive and the negative charges becomes easier. Thus a strong electrostatic-field is generated and water is highly polarized.

On the other hand, H-zeolites with a higher ratio of silica-to-alumina possess acid sites as strong as those of Ca-zeolites. However, the number of acid sites of H-zeolites with a lower ratio is small due to the collapse of the structure resulting from the treatment. The higher the silica-to-alumina mole ratio, the less the number of anions in the zeolite structure. Protons with a low electric shield then become mobile and form strong acid sites.

Effect of Ion Exchange. Influence of the ion exchange of Ca^{2+} and La^{3+} ions on acidity was investigated. The acidity of Ca–Na–$Y_{3.25}$ and La–Na–$Y_{3.25}$ as a function of the degree of ion-exchange is shown in Fig. 5.

The number of acid sites of Ca–Na–$Y_{3.25}$ is nearly equal to that of Na–$Y_{3.25}$ when the Ca exchange is lower than 40%, but increases rapidly above 80%. When sodium ions are replaced by calcium ions, calcium ions enter energetically stable sites in the beginning and the formation of acid sites by heat treatment is difficult.[17] Since the number of acid sites with H_0 values higher than −5.6 is almost constant, independent of ion exchange, the acid centers formed through calcium ion exchange have H_0 values lower than −5.6.

The acidity property of low-exchange sample is consistent with the fact that the electrostatic-field strength and the cumene-cracking activity of these samples were almost the same as those of the Na-form zeolites.[17,18] The divalent cations strongly prefer the S_I cation sites connected to the large cavity through pores of about 2Å in diameter. As the pores are not large enough for the organic molecules to pass through, the cation-exchange does not influence the properties mentioned above.

In the case of the exchange with La^{3+} ion, the acidity measured with BY begins to increase in proportional to the degree of exchange above 20%. Since La^{3+} ion is highly charged, the bonds between La^{3+} and AlO_2^- ions are distorted remarkably, and many acid sites are formed even at lower exchange. Compared with the acidity measured with AQ, this acidity is distributed in a wider domain when the degree of exchange is 60% or less, and the acid sites with H_0 values lower than −8.2 are formed only above 60%.

Measurement of Strong Acid Sites. The UV spectra of PNT and DNT adsorbed on zeolites are shown in Figs. 6 and 7, respectively. The band at about 350 mμ in Fig. 6 is assigned to the acid form of PNT adsorbed

16) K. Tsutsumi and H. Takahashi, *J. Phys. Chem.*, **76**, 110 (1972).

17) K. Tsutsumi and H. Takahashi, *ibid.*, **74**, 2710 (1970).

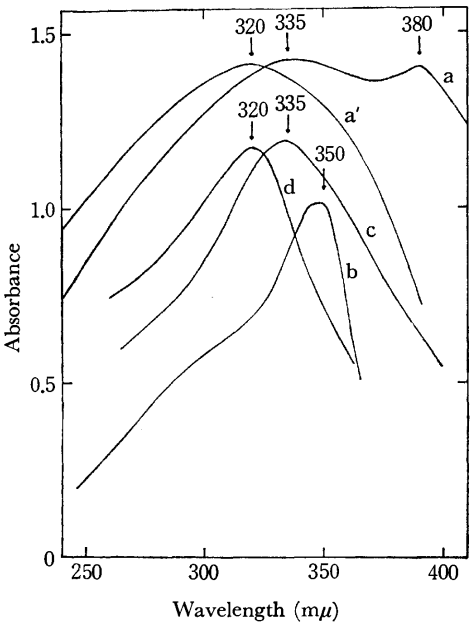

Fig. 6. UV spectra of PNT adsrobed on zeolites.
a: La-$Y_{3.25}$ (La^{3+}, 92 mol%)
a': Above+*n*-butylamine
b: La-$Y_{5.0}$ (La^{3+}, 85 mol%)
c: H-$Y_{4.6}$ (H^+, 85 mol%), H-$Y_{5.0}$ (H^+, 92 mol%)
d: Na-$Y_{3.25}$

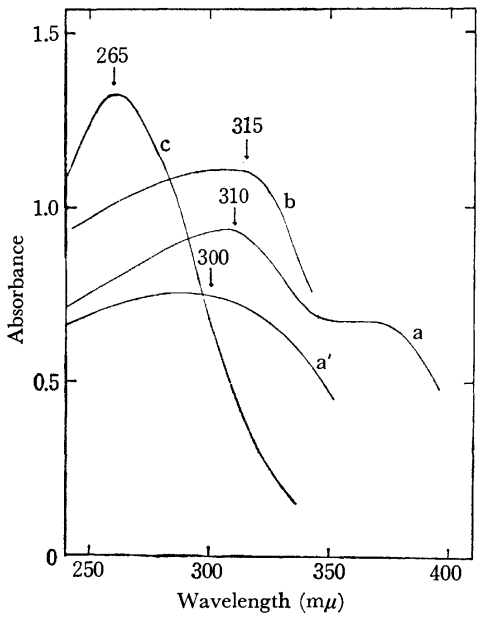

Fig. 7. UV spectra of DNT adsorbed on zeolites.
a: La-$Y_{3.25}$ (La^{3+}, 92 mol%)
a': Above+*n*-butylamine
b: La-$Y_{5.0}$ (La^{3+}, 85 mol%)
c: {H-$Y_{5.0}$ (H^+, 92 mol %) H-$Y_{4.6}$ (H^+, 85 mol %) Na-$Y_{3.25}$}

on the zeolite surface, and that at 310 mμ in Fig. 7 to that of DNT.

The absorption maxima of the indicators adsorbed on various samples are listed in Table 2, together with those of cyclohexane solution and sulfuric acid solution. The absorption maxima of the indicators adsorbed on two kinds of silica-alumina (HA; Al_2O_3 25% and LA; Al_2O_3 13%) are also shown.

Table 2. Absorption bands (mμ) of UV spectra of various indicators solved or adsorbed

	BY	BAP	PNT	DNT
Cyclohexane	400	300	260	<230
10 wt% H_2SO_4	515			
50 wt% H_2SO_4		435, 315	293	262
95 wt% H_2SO_4		435, 315	310	262
Fuming H_2SO_4			340, 288	327, 280, 255
Silica-Alumina (LA)			300	260
Silica-Alumina (HA)			300	260
Na-$Y_{3.25}$	460	310	320	265
H-$Y_{4.6}$(H^+, 85 mol%)	520	400, 310	335	265
+*n*-BA[a] (0.5 meq/g)	520	400, 310	335	265
+*n*-BA (1.0 meq/g)	480	310	330	
+*n*-BA (2.0 meq/g)	400	310		
+*n*-BA (3.0 meq/g)	400			
H-$Y_{5.0}$(H^+, 92 mol%)	520	400, 310	335	265
+*n*-BA (0.5 meq/g)	520			
+*n*-BA (1.0 meq/g)	520		330	
+*n*-BA (2.0 meq/g)	400			
La-$Y_{3.25}$(La^{3+}, 92 mol%)			380, 335	310
+*n*-BA (1.0 meq/g)		260	320	300
(La^{3+}, 85 mol %)		400	370	310
(La^{3+}, 71 mol %)			350	280
(La^{3+}, 67 mol %)			340	265
(La^{3+}, 49 mol %)			330	265
La-$Y_{5.0}$(La^{3+}, 85 mol %)			350	315
H-Mordenite (H^+, 92 mol %)	520	390, 315	310	265

a) *n*-butylamine

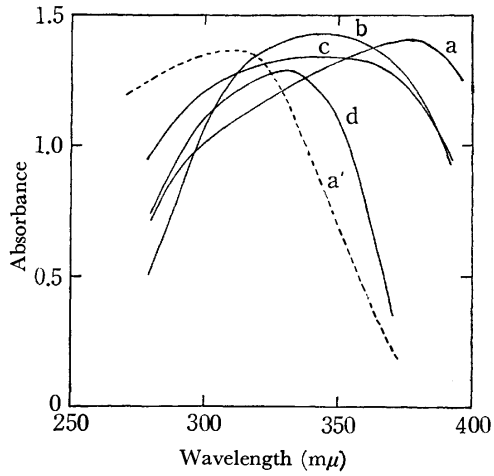

Fig. 8. UV spectra of PNT adsorbed on La-$Y_{3.25}$ having various degrees of La-exchange.
a: 85 mol%, a': Above+*n*-butylamine b: 71 mol%, c: 67 mol%, d: 49 mol%.

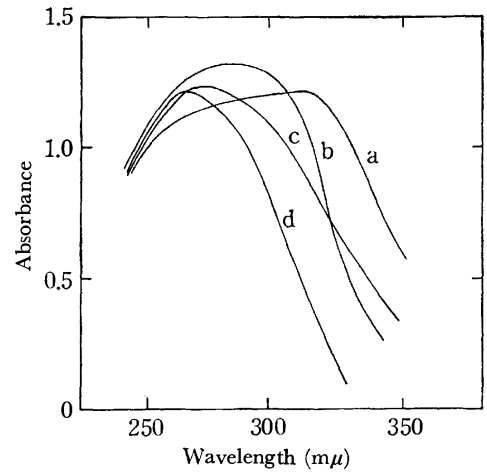

Fig. 9. UV spectra of DNT adsrobed on La-$Y_{3.25}$ having various degrees of La-exchange.
a: 85 mol%, b: 71 mol%, c: 67 mol%, d: 49 mol%

The results indicate that H–Y zeolite and H-mordenite which are considered to have a strong acid character, from the measurement with AQ, show basic colors of PNT and DNT. Their acid strength is therefore distributed in the H_0 range from −8.2 to −10.8. On the other hand, La–Y zeolites show acidic colors of both PNT and DNT as shown in Figs. 8 and 9. Thus, La–Y zeolites have very strong acid sites with H_0 values lower than −12.8. It is clear that the acid strength of La–Y is dependent on the degree of La-exchange. The La–Na–$Y_{3.25}$ showed an acid color of PNT when La-exchange exceeds 70% and even an acid color of DNT above 85%.

Such a strong acidity of La-form zeolite can be compared with that of fuming sulfuric acid. It turns out from this acidity that the cumene-cracking activity of La-form zeolite is much higher than that of H- and Ca-form zeolites.[18]

18) K. Tsutsumi and H. Takahashi, *J. Catal.*, **24**, 1 (1972).

A Theoretical Consideration of the Electron-scavenging Process In Liquid Hydrocarbons. III. Integral Transforms of the Distribution Functions

Hideo YAMAZAKI and Kyoji SHINSAKA

Laboratory of Physical Chemistry, Tokyo Institute of Technology, Meguro-ku, Tokyo

(Received September 16, 1971)

The relations of integral transforms between various distribution functions are discussed using the potential control approximation ignoring the diffusion term in the Smoluchowski equation; the initial spatial distribution of the electron-ion pair or the initial distribution of electrons from the central ion core in a spur, $\chi(r, 0)$; the relative G-value of electron recombination, $G(k_sC_s)$, as a function of the concentration of the scavenger and the rate constant; the time dependence of the electron concentration, $N(t)$, after pulse irradiation; and the relaxation time spectrum, $K(n)$, of the decay of the electron concentration after pulse irradiation or of the weight function, $K(n)$, in the initial exponential distribution of thermalized electrons in a spur are shown to be connected by the square diagram of Laplace transforms:

$$\begin{array}{ccc} K(n) & \xrightarrow{\text{Laplace Transform}} & \chi(r, 0) \\ \Big\downarrow \text{Laplace Transform} & & \Big\downarrow \text{Laplace Transform} \\ N(t) & \xrightarrow{\text{Laplace Transform}} & G(k_sC_s) \end{array}$$

By the use of this relation, the various distribution functions are evaluated from the empirical formulas of $G(k_sC_s)$ proposed by Schuler *et al.* and by Hummel.

Recently many experimental results of various methods of the radiolysis of liquid hydrocarbons have been accumulated, and it has been shown that the quantities measured are connected by the functional relations. Schuler *et al.*[1] proposed that the concentration dependence of the G-value of electron recombination and the change in ionic species after pulse radiolysis as a function of the time were related by the Laplace transform. Sato and Oka[2] and Tatsuya[3] found that the initial distribution of the electron-ion pair and the G-value of the electron recombination as a function of the scavenger concentration were interchangeable by the Laplace transform. In their studies, no information about the spatial distribution of electrons from the Smoluchowski equation is necessary in deriving these relations between functions. In a previous paper[4] the inverse Laplace transform was used by the present authors to obtain the lifetime spectrum in the decay function of the electron concentration, based on the Smoluchowski equation.

In this paper it is shown that, in addition to these rather phenomenological relations, the lifetime spectrum of the decay of the electron concentration is equivalent to the weight function of the superposition of the initial distribution. Four functions, $\chi(r,0)$, $G(k_sC_s)$, $N(t)$, and $K(n)$, which indicate the initial distribution of electrons from the central ion core in a spur, the concentration dependence of the G-value of the electron recombination, the time dependence of the electron concentration, and the relaxation time spectrum respectively, can be related by the Laplace transform by using the approximate solution ignoring the diffusion term of the Smoluchowski equation from the microscopic point of view. Thus, the experimental results are interconnected by these relations and depend on each other.

Theory

A. The Four Characteristic Functions and Their Transformations. Phenomenological treatment is possible for the relation between the relative G-value of the electron recombination as a function of the scavenger concentration, $G(k_sC_s)$, and the electron concentration after pulse irradiation, $N(t)$, and for that between $G(k_sC_s)$and the initial distribution of electrons, $\chi(r,0)$. However, the introduction of the distribution functions of the electron concentration as spatial and time functions is necessary in order to describe these relations in detail and to extend them. An extended form of the Smoluchowski equation is used to obtain the approximate distribution function of electrons and to treat the effect of the spur.

The extended form of Smoluchowski equation for the spatial distribution of electrons in a spherical spur is expressed by Eq. (1)[4]:

$$\frac{\partial C(r,t)}{\partial t} = D\frac{\partial^2 C(r,t)}{\partial r^2} + \left(\frac{2D}{r} + \frac{\alpha}{r_2}\right)\frac{\partial C(r,t)}{\partial r} - \beta C(r,t) \quad (1)$$

where r, t, D, and $C(r, t)$ refer to the radial distance, the time, the diffusion constant, and the distribution function of electrons, and where α and β are constants and are given by:

$$\alpha = N^+eu/\varepsilon \quad (2)$$

$$\beta = k_sC_s, \quad (3)$$

where N^+ is the average number of ions in the core, e is the electron charge, u is the mobility of electrons, ε is

1) S. J. Rzad, P. P. Infelta, J. M. Warman, and R. H. Schuler, *J. Chem. Phys.*, **52**, 3971 (1970).

2) S. Sato and T. Oka, This Bulletin, **44**, 856 (1971).

3) M. Tatsuya, The 13th Conference of Radiation Chemistry, October (1970), Tokyo.

4) H. Yamazaki and K. Shinsaka, This Bulletin, **44**, 2611 (1971).

the dielectric constant, k_s is the rate constant of scavenging, and C_s is the concentration of the scavenger. The successive approximation of the potential control case is convenient in obtaining the solution.[4] The solution of the zeroth order equation,

$$\frac{\partial \chi_0(r,t)}{\partial t} = \frac{\alpha}{r^2}\frac{\partial \chi_0(r,t)}{\partial r} - \beta\chi_0(r,t) \tag{4}$$

is given by:

$$\chi_0(r,t) = \int_0^\infty K_0(n)\exp(-\beta t - n\alpha t - nr^3/3)\mathrm{d}n \tag{5}$$

Thus, the approximate solution is given by the superposition of the exponential function with a weight function, $K_0(n)$. The initial distribution is expressed by:

$$\chi_0(\sqrt[3]{3\xi}, 0) = \int_0^\infty K_0(n)\exp(-n\xi)\mathrm{d}n \tag{6}$$

by the substitution of the distance by $\xi = r^3/3$. In Eq. (6) the initial distribution is expressed by the Laplace transform of $K_0(n)$. Therefore, the weight function in the spur distribution, $K_0(n)$, is evaluated by the inverse Laplace transform of the initial distribution function and is given by:

$$K_0(n) = \frac{1}{2\pi i}\int_{C-i\infty}^{C+i\infty}\chi_0(\sqrt[3]{3\xi}, 0)\exp(n\xi)\mathrm{d}\xi \tag{7}$$

The total number, $N_0(t)$, of the electrons is obtained by the integration of the distribution function of electrons over a spur and is expressed by:

$$N_0(t) = 4\pi\int_{R_0}^\infty \chi_0(r,t)r^2\mathrm{d}r \tag{8}$$

where R_0 is the reaction radius of the recombination between an electron and an ion. Then, $N_0(t)$ is evaluated by Eqs. (5) and (8):

$$N_0(t) = 4\pi\int_0^\infty K_0(n)g_0(n, R_0)\exp(-n\alpha t)\mathrm{d}n \tag{9}$$

where $g_0(n, R_0)$ is given by:

$$g_0(n, R_0) = \exp(-nR_0^3/3)/n \tag{10}$$

The lifetime spectrum of the electrons, $K_0(n)$, is evaluated by the inverse Laplace transform:[4]

$$K_0(n)g_0(n, R_0) = \frac{1}{8\pi^2 i}\int_{C-i\infty}^{C+i\infty} N_0(p/\alpha)\exp(np)\mathrm{d}p \tag{11}$$

The decay of the electron concentration after pulse irradiation was treated by Schuler *et al.*,[1] and for an infinitesimal short duration of pulse irradiation the relation between $N_0(t)$ and $G(\beta)$ was given by:

$$G(\beta) = -\int_0^\infty \frac{\mathrm{d}}{\mathrm{d}t}\left(\frac{N_0(t)}{N_0(0)}\right)\exp(-\beta t)\mathrm{d}t \tag{12}$$

where $G(\beta)$ is the portion of the G-value of electron recombination. Then, the inverse Laplace transform yields $N_0(t)$ by:

$$-\frac{\mathrm{d}}{\mathrm{d}t}\left(\frac{N_0(t)}{N_0(0)}\right) = \frac{1}{2\pi i}\int_{C-i\infty}^{C+i\infty} G(\beta)\exp(\beta t)\mathrm{d}\beta \tag{13}$$

A similar relation was obtained between the initial distribution of electrons and the G-value of the electron recombination or the scavenging process, if the effect of the diffusion term of electron is ignored, where the position of the electron at time t after pulse irradiation is determined by a time-distance relation.[5] $G(\beta)$ is expressed in terms of the Laplace transform of the initial distribution of electrons by:

$$G(\beta) = \frac{\int_0^\infty \chi_0(\sqrt[3]{3\xi + R_0^3}, 0)\exp(-\beta\xi/\alpha)\mathrm{d}\xi}{\int_0^\infty \chi_0(\sqrt[3]{3\xi + R_0^3}, 0)\mathrm{d}\xi} \tag{14}$$

where R_0 is the reaction radius. The inverse Laplace transform yields the initial distribution by:

$$\frac{\chi_0(\sqrt[3]{3\xi + R_0^3}, 0)}{\int_0^\infty \chi_0(\sqrt[3]{3\xi + R_0^3}, 0)\mathrm{d}\xi} = \frac{1}{2\pi i}\int_{C-i\infty}^{C+\infty t} G(\beta)\exp(\beta\xi/\alpha)\mathrm{d}\beta \tag{15}$$

As a summary of these transforms of the four characteristic functions, the flow chart of the transformations is given in Fig. 1.

Therefore, $G(\beta)$ is expressed in terms of $K_0(n)$ by using the double Laplace transform *via* $\chi_0(\sqrt{3\xi}, 0)$ or $N_0(t)$ in this flow chart:

$$G(\beta) = \frac{\int_0^\infty\int_0^\infty \exp\{-\beta\xi/\alpha - n(\xi + R_0^3/3)\}K_0(n)\mathrm{d}n\mathrm{d}\xi}{\int_0^\infty (K_0(n)/n)\exp(-nR_0^3/3)\mathrm{d}n} \tag{16}$$

The transforms in the higher-order approximations, including the effect of diffusion, are given in Appendix A.

B. Example of Distribution Functions. As the first example of this scheme, the superpositions of the δ-functions as $K_0(n)$ in Eqs. (6) and (9) are considered in Eq. (17).

The operations[6] of the Laplace transforms on $K_0(n)$ yield $\chi_0(\sqrt[3]{3\xi}, 0)$ and $N_0(t)$, and the double Laplace transform either *via* $\chi_0(\sqrt[3]{3\xi}, 0)$ or $N_0(t)$ in Fig. 1 yields $G(\beta)$:

$$K_0(n) = \sum_i f_i\delta(n - n_i) \tag{17}$$

where f_i are constants:

$$\frac{N_0(t)}{N_0(0)} = \sum_i (f_i/n_i)\exp(-R_0^3 n_i/3 - \alpha n_i t)\Big/ \sum_i (f_i/n_i)\exp(-R_0^3 n_i/3) \tag{18}$$

$$G(\beta) = \sum_i \frac{(f_i/n_i)\exp(-R_0^3 n_i/3)}{1 + \beta/\alpha n_i}\Big/\sum_i (f_i/n_i)\exp(-R_0^3 n_i/3) \tag{19}$$

$$\chi_0(r, 0) = \sum_i f_i \exp(-n_i r^3/3) \tag{20}$$

Equations (18) and (20) show that the decay function and the initial distribution can be expressed as a superposition of the exponential functions. Such a decay function of the electron concentration was observed by Yoshida[7] in hydrocarbon glass. In Eq. (19) the G-value of the recombination or the scavenging process is represented as a linear combination of functions of the Stern-Volmer or Langmuir type. Such a type of scavenger dependence was approximately verified in a previous paper.[8]

5) F. Williams, *J. Amer. Chem. Soc.*, **86**, 3954 (1964).
6) For example, H. Bateman, "Tables of Integral Transforms. I," McGraw-Hill Book Co. Inc., New York (1954).
7) H. Yoshida, *Ann. Repts. Reactor Inst. Kyoto Univ.*, **3**, 153 (1970).
8) H. Yamazaki and K. Shinsaka, This Bulletin, **43**, 2713 (1970).

As the second example, $G(\beta)$ as a function of the square root of the concentration of the scavenger was proposed by Schuler *et al.*[1] as in Eq. (21) for a wide range of scavenger concentrations:

$$G(\beta) = 1/(1+\sqrt{A\beta}) \quad (21)$$

where A is a constant. A comparison between Schuler's expression and the present one for $G(\beta)$ is given in Appendix B. The operations[6] of the inverse Laplace and double inverse Laplace transforms of Eq. (21) yield $N_0(t)$, $\chi_0(\sqrt[3]{3\xi}, 0)$ and $K_0(n)$ for the case of the square-root dependence on the scavenger concentration:

$$\frac{N_0(t)}{N_0(0)} = 1 - 2\sqrt{\frac{\alpha t}{\pi}} + \frac{1}{\sqrt{\alpha}}\int_0^t \exp(t/\alpha)\mathrm{Erfc}(\sqrt{t/\alpha})\mathrm{d}t \quad (22)$$

$$\chi_0(\sqrt[3]{3\xi+R_0^3}, 0)/\int_0^\infty \chi_0(\sqrt[3]{3\xi+R_0^3}, 0)\mathrm{d}\xi = \left\{\sqrt{\frac{1}{\pi\xi A\alpha}} - \frac{1}{A\alpha}\exp(\xi/A\alpha)\right\}\mathrm{Erfc}(\sqrt{\xi/A\alpha}) \quad (23)$$

and

$$K_0(n) = \frac{\sqrt{nA\alpha}}{\pi(1+nA\alpha)}\exp(nR_0^3/3) \quad (0<nR_0^3/3<1) \quad (24)$$

As the third example, Hummel's formula[9] for the G-value as the function of the concentration of the scavenger, corresponding to Eqs. (19) and (21), was expressed by:

$$G(\beta) = \exp(-\sqrt{A\beta}) \quad (25)$$

Similarly, $N_0(t)$, $\chi_0(\sqrt[3]{3\xi}, 0)$ and $K_0(n)$ can be obtained by using inverse Laplace transforms:[6]

$$\frac{N_0(t)}{N_0(0)} = 1 - \frac{1}{2}\sqrt{\frac{A}{\pi}}\int_0^t t^{-3/2}\exp(-A/4t)\mathrm{d}t \quad (26)$$

$$\frac{\chi_0(\sqrt[3]{3\xi+R_0^3}, 0)}{\int_0^\infty \chi_0(\sqrt[3]{3\xi+R_0^3}, 0)\mathrm{d}\xi} = \frac{1}{2}\sqrt{\frac{A\alpha}{\pi\xi^3}}\exp(-\alpha A/4\xi) \quad (27)$$

and

$$K_0(n) = \frac{1}{\pi}\sin(\sqrt{nA\alpha})\exp(nR_0^3/3) \quad (0<nR_0^3/3<1) \quad (28)$$

Discussion

The various measurements for obtaining $N_0(t)$, $G(\beta)$, $\chi_0(r, 0)$ and $K_0(n)$ are interconnected. In view of this relation, the experiment of the pulse radiolysis, the scavenging method with product analysis, and the relaxation time measurement of the ESR spectrum to get information on the spatial distribution are all needed under the same conditions. As to $K_0(n)$, the first term in the expansion of $K_0(n)$ in Eq. (28) as a power series of n gives the same term as that of Eq. (24). The actual calculation to obtain the initial distribution from the results of the scavenging method was carried out by Sato and Oka[2] on the basis of Freeman's method of calculation.[10] They obtained equations corresponding to Eqs. (23) and (27). According to their calculation, the initial distributions due to Schuler's and Hummel's expressions of the G-value are almost the same for large values of r; this corresponds to the fact that the weight functions, $K_0(n)$, for Schuler's and Hummel's expressions are approximated by the same equation for the small values of n. Thus, $\chi_0(r, 0)$ can be estimated indirectly from $G(\beta)$, because $G(\beta)$ has been obtained experimentally in the presence of various scavengers. A few experiments have been made to obtain direct information about $\chi_0(r, 0)$, for example, by relaxation-time measurement in liquid hydrocarbons. In a preliminary result of the measurement of the relaxation-time of ESR, the distribution of electrons showed heterogeneity in the glass state.[11]

In the present pulse radiolysis for the determination of $N_0(t)$, the electron-ion recombination process can be detectable at low temperatures[12,13] where the lifetime of the recombination increases over μ sec. At low temperatures, however, the equilibrium between bound and unbound electrons, e_t^- and e_m^-, must be considered, and this factor has to be added to the fundamental equation. If the rate of equilibration between e_t^- and e_m^- is fast, Eq. (1) can be rewritten as:

$$(1+K)\frac{\partial C_m}{\partial t} = D\frac{\partial^2 C_m}{\partial r^2} + \left(\frac{2D}{r} + \frac{\alpha}{r^2}\right)\frac{\partial C_m}{\partial r} - \beta C_m \quad (K = k_m/k_t = C_t/C_m) \quad (29)$$

where C_m and C_t are the distributions of unbound and bound electrons, k_m and k_t are the rate constants of equilibration between unbound and bound states, and K is an equilibrium constant between the bound and unbound states of electrons. The extremely small apparent values of the electron mobility, the diffusion constant, and the rate constant can be expected for a large values of K. Even when the coefficients in the equation are different, the equation remains in the same form in this approximation. In various types of distribution functions, the superposition of δ-functions for $K_0(n)$ and, therefore, the superposition of exponential functions for $N_0(t)$, are natural and reasonable, as is shown in the examples.

The square diagram of the Laplace transform in Fig. 1 was obtained by the zeroth order approximation, ignoring the diffusion term in the Smoluchowski equa-

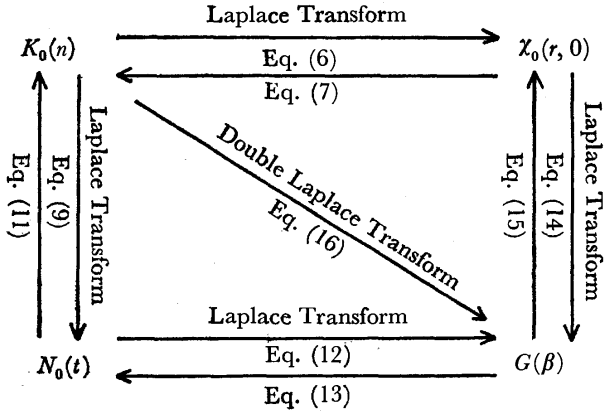

Fig. 1. Flow chart of the Laplace transorms of various distribution functions; $K_0(n)$, $\chi_0(r, 0)$, $N_0(t)$, and $G(\beta)$.

9) A. Hummel, *J. Chem. Phys.*, **49**, 4840 (1968).
10) G. R. Freeman, *ibid.*, **46**, 2822 (1967).
11) K. Oka, H. Yamazaki, and S. Shida, unpublished work.
12) I. A. Taub and H. A. Gillis, *J. Amer. Chem. Soc.*, **91**, 6507 (1969).
13) H. A. Gillis, N. V. Klassen, G. G. Teather, and K. H. Lokan, *Chem. Phys. Lett.*, **10**, 481 (1971).

tion. If the higher-order approximation including the diffusion term is used, the Laplace transform in the scheme should be replaced by a more complicated form of the integral transforms, as is shown in Appendix A. The validity of the potential control approximation can be discussed in the following two ways. In the first place, the Onsager radius has an order of magnitude of several hundreds Ångström in the liquid hydrocarbons, and most of the electrons ejected from the parent ions are within this region and are still localized in the range of the Coulomb field of the parent ions. Therefore, the potential term is more effective than the diffusion term for most of the electrons in the region inside of the Onsager radius. In the second place, it is most likely that the thermalized electrons do not show any sharp spatial distribution; this is because of diffused energy spectrum of the electrons ejected and because of the random collisions of thermalization. Moreover, the spatial distribution is broadened with time. The transport of the electrons by diffusional motion in one direction is quite small, because the second derivative of the electron distribution by the distance is negligibly small for the smoothed distribution.

The authors wish to thank Professor Shoji Shida and Dr. Shin Sato of Tokyo Institute of Technology and Dr. Kenji Fueki of Nagoya University for reading the preliminary manuscript of this paper and for their helpful discussions, and Dr. H. A. Gillis of the National Research Council, Ottawa, for his kind communication. The authors also wish to thank Misses Hisako Yamaguchi and Toshiko Kitagawa for typing the manuscripts of this series of reports.

Appendix

A. The Higher-order Approximation. The s-th order equation is given by a recurrent equation:

$$\frac{\partial \chi_s(r,t)}{\partial t} = D\frac{\partial^2 \chi_{s-1}(r,t)}{\partial r^2} + \frac{2D}{r}\frac{\partial \chi_{s-1}(r,t)}{\partial r} + \frac{\alpha}{r^2}\frac{\partial \chi_s(r,t)}{\partial r} - \beta\chi_s(r,t) \quad \text{(A-1)}$$

The s-th order of approximation can be written by:

$$\chi_s(r,t) = \int_0^\infty K_s(n)H_s(n,\alpha,D,r)\exp(-\beta t - n\alpha t - nr^3/3)\mathrm{d}n \quad \text{(A-2)}$$

where H_s is a function of n, α, D, and r; several examples of the explicit form are given by:

$$H_0(n,\alpha,D,r) = 1 \quad \text{(A-3)}$$

$$H_1(n,\alpha,D,r) = 1 + nDr^4/\alpha - n^2Dr^7/7\alpha \quad \text{(A-4)}$$

$$H_2(n,\alpha,D,r) = 1 + nDr^4/\alpha - n^2Dr^7/7\alpha - 4nD^2r^5/\alpha^2 + 5n^2D^2r^8/2\alpha^2 - 24n^3D^2r^{11}/77\alpha^2 + n^4D^2r^{14}/98\alpha^2 \quad \text{(A-5)}$$

In the case of a pure recombination, (β=0), the initial distribution can be expressed by:

$$\chi_s(\sqrt[3]{3\xi}, 0) = \int_0^\infty K_s(n)H_s(n,\alpha,D,\sqrt[3]{3\xi})\exp(-n\xi)\mathrm{d}n, \quad \text{(A-6)}$$

using the substitution, $r^3/3=\xi$, From Eqs. (8) and (A-2), $N_s(t)$ is given by:

$$N_s(t) = 4\pi\int_0^\infty K_s(n)g_s(n,\alpha,D,R_0)\exp(-n\alpha t)\mathrm{d}n \quad \text{(A-7)}$$

where $g_s(n,\alpha,D,R_0)$ is given by the integral of $H_s(n,\alpha,D,\sqrt[3]{3\xi})$:

$$g_s(n,\alpha,D,R_0) = \int_{R_0^3/3}^\infty H_s(n,\alpha,D,\sqrt[3]{3\xi})\exp(-n\xi)\mathrm{d}\xi \quad \text{(A-8)}$$

The relaxation time spectrum, $K(n)$, can be expressed by the use of the inverse Laplace transform of the dependence of the electron concentration in the system:

$$K_s(n)g_s(n,\alpha,D,R_0) = \frac{1}{8\pi^2 i}\int_{C-i\infty}^{C+i\infty} N_s(p/\alpha)\exp(np)\mathrm{d}p \quad \text{(A-9)}$$

Equations (12) and (13) are valid for the relation between the functions of $N_s(t)$ and $G_s(t)$ in the presence of diffusion, because this relation is phenomenological and does not need the Smoluchowski equation as a basis for discussion. However, the $\chi_s(r,0)$ and $G_s(\beta)$ functions are not directly connected by a Laplace transform, because the relation between t and r^3 can be held only by disregarding the diffusion term. A complicated relation can be obtained by the transforms *via* $K_s(n)$ and $N_s(t)$:

$$\chi_s(\sqrt[3]{3\xi},0) = \int_0^\infty \frac{N_s(0)H_s(n,\alpha,D,\sqrt[3]{3\xi})}{8\pi^2 i g_s(n,\alpha,D,R_0)}\exp(-n\xi) \times\left[\int_{C-i\infty}^{C+i\infty}\left\{\int_{p/\alpha}^\infty \frac{1}{2\pi i}\int_{C-i\infty}^{C+i\infty} G(\beta)\exp(\beta t)\mathrm{d}\beta\right\}\mathrm{d}t\right] \times\exp(np)\mathrm{d}p\Big]\mathrm{d}n \quad \text{(A-10)}$$

B. The Expressions for G(β). This equation is expressed by $G(p)=G_{ft}+G_{gt}\sqrt{A\beta}/(1+\sqrt{A\beta})$, where $G(p)$, G_{ft}, and G_{gt} are the G-values of the yields of the secondary products from the ionic reaction and those of free and germinate electrons respectively. A fraction, $F(c)$, undergoing the reaction of germinate pairs with the scavenger solute is expressed by:

$$F(c) = [G(p)-G_{ft}]/G_{gt} \quad \text{(B-1)}$$

where c is the concentration of the solute. $F(c)$ is represented using the Laplace transform of the life-time distribution, $f(t)$:

$$F(c) = 1 - \int_0^\infty \exp(-kct)f(t)\mathrm{d}t \quad \text{(B-2)}$$

where k is the rate constant with the solute. The life-time distribution is given by the differentiation of the fraction, $F(t)$, of the ion pair at time t, which is equal to the $N(t)/N(0)$ used in this paper:

$$f(t) = -\mathrm{d}F(t)/\mathrm{d}t \quad \text{(B-3)}$$

The relative G-value or fraction of recombination, $G(\beta)$, considered in this paper is expressed by:

$$G(\beta) = \frac{G_{gt}-G_{gt}\sqrt{A\beta}/(1+\sqrt{A\beta})}{G_{gt}} = 1/(1+\sqrt{A\beta}) \quad \text{(B-4)}$$

Equilibrium of Urea Synthesis. I.

Shigeru INOUE, Kazumichi KANAI, and Eiji OTSUKA

Central Research Laboratory (Ofuna) Mitsui Toatsu Chemicals, Inc., Totsuka-ku, Yokohama

(Received September 17, 1971)

A test of the equilibrium conversion of CO_2 to urea was carried out using a batch autoclave. Some results different from those reported by Frèjacques were obtained, as was expected from the latest data on commercial urea plants. The equilibrium conversion reached its maximum value at about 195°C by 5—15% higher than that reported by Frèjacques. On the contrary, at temperatures above 200°C the value was lower, and falled rapidly with the raise of temperature. This phenomenon may be due to the mechanism of the equilibrium of urea synthesis, and not to the experimental method, as our sampling was made directly from the liquid phase. The equilibrium conversion, x, may be expressed with respect to NH_3/CO_2, a, H_2O/CO_2, b, and temperature, t, as

$$x = \left(0.2616a - 0.01945a^2 + 0.0382ab - 0.1160b - 0.02732a\left(\frac{t}{100}\right) - 0.1030b\left(\frac{t}{100}\right) + 1.640\left(\frac{t}{100}\right) - 0.1394\left(\frac{t}{100}\right)^3 - 1.869\right) \times 100(\%)$$

Therefore, a limited conversion exists in the conventional urea process.

Many investigators have reported the values of actual conversion for commercial reactors by means of the Frèjacques nomograph,[1] and it seemed that the values thus obtained have been taken as the actual conversion in the process (not multiplied by a factor).

Howerver, from the analysis of data obtained with commercial scale reactors, it has become clear that the conversion for the reactor might well be higher than that reported by Frèjacques.

If this is true, the urea process should be improved. In order to confirm this possibility, the static equilibrium conversion should be examined.

For this purpose we measured the equilibrium conversion by an improved method using a batch autoclave, especially with regard to the method of sampling.

The original points of the present report are that, first, the sampling was made directly from the liquid phase and, second, it was made clear that the equilibrium conversion reaches its maximum value at a certain temperature.

The reason why "the direct sampling" must be emphasized is as follows: the popular interpretation of the existence of the maximum conversion depends on the effect of the loading density on the autoclave,[2] because the analyzed value for the equilibrium conversion is based not on the liquid phase, but on the total amount of $NH_4CO_2NH_2$ charged into the autoclave; otherwise, it is thought that a sampling operation might disturb the equilibrium. That is, the higher the temperature becomes in the autocalve at a certain loading density, the less $NH_4CO_2NH_2$ remains in the liquid phase because of the increased amount of NH_3 and CO_2 transferred into the gas phase. Thus, even though the conversion in the liquid phase increases because of the higher temperature, the amount of urea formed may become less above a certain temperature. Therefore, the (apparent) conversion based on the total amount of $NH_4CO_2NH_2$ charged into the autoclave reaches its maximum value at a certain temperature. Therefore, the larger the loading density is, the higher is the temperature of the maximum conversion.

Therefore, we think that this factor—the loading density—has caused the misunderstanding of the analysis or troubles in many cases. By our improved experimental method, the effect of the loading density can be removed; thus, the consideration of the equilibrium of urea synthesis becomes clearer than before.

In the present paper, our experimental results and a comparison with those of Frèjacques will be mainly described, while in the next paper some theoretical arguments will be presented.

Conventional Theory

Although urea synthesis has been developed on a large scale since 1950, the basic research on the equilibrium conversion was done long before, and many reports have been published.

The experimental method has been as follows: $NH_4CO_2NH_2$ (solid) is charged into a steel-made bomb or a glass tube, which is then sealed. After the contents had reached the equilibrium state, all of them in the bomb or in the tube were taken out as a sample for analysis; therefore, the eqiuilibrium conversion was calculated on the amount of urea formed relative to the total amount of $NH_4CO_2NH_2$ charged into the bomb or tube. Thus, the conversion was not a real value, but an apparent one.

In this case, the real value was estimated by an extrapolation (from various loading densities) or by a calibration for the gas phase. Even by these unsatisfactory methods, the effects of the excess NH_3, the excess water, and the temperature on the equilibrium conversion are rather clear for the most part.

Therefore, besides NH_3/CO_2, H_2O/CO_2, and the temperature, the parameter of the loading density is neces-

1) M. Frèjacques, *Chimie et Industrie*, **60**, No. 1, 22, (1948).

2) A. Baranski and A. Fulinski, *Chim. Ind. Gen. Chim.*, **99**, No. 11, 1605—1618 (1968).

sary to express the equilibrium conversion. Frèjacques, however, reported that the equilibrium conversion is dependent on NH_3/CO_2, H_2O/CO_2, and the temperature only as is expressed below:

$$\frac{x(x+b)(1+a+b-x)}{(1-x)(a-2x)^2} = K(t) \quad (1)$$

where a: molar ratio of NH_3/CO_2 in the total feed,
b: molar ratio of H_2O/CO_2 in the total feed,
K: equilibrium constant dependent on the temperature,
and x: conversion of CO_2 to urea, expressed in fractions of the total CO_2 in the total feed.

The equilibrium constant, $K(t)$, based on a stoichiometric mixture, was assumed also to be valid for a non-stoichiometric mixture; that is,

$$K(t) = \frac{x_{st}^2(3-x_{st})}{4(1-x_{st})^3} \quad (2)$$

where x_{st} is the equilibrium conversion when $a=2$, $b=0$ (for a stoichiometric mixture).
here $K(t)$ is an increasing, monotonous function with respect to the temperature.

Therefore, in most nonstoichiometric cases, the equilibrium conversion has also been supposed to increase as the temperature becomes higher.

Since his publication, no new basic research on the equilibrium conversion has been reported; interpretations have mainly been reported.

The actual conversion in a reactor effluent of an industrial scale was fairly consistent with Eq. (1) within the limits of the accuracy of measurement at that time, so it was thought that the equilibrium conversion obtained by means of Eq. (1) could be adopted for a reactor effluent in all processes.

Although the above description is sufficient for understanding fundamental matters, it will be convenient, in order to facilitate comparison with our results, that more details are given on the Frèjacques theory.

In Eq. (1) the equilibrium conversion is independent of $NH_4CO_2NH_2$, which is an intermediate in this equilibrium system, but, judging from the fact that, under a sufficient pressure, CO_2 converts to $NH_4CO_2NH_2$ completely either with excess NH_3 or without it, we think that the conversion of CO_2 to urea must be determined by the equilibrium between $NH_4CO_2NH_2$ and urea plus water; there is, then, some error in the expression of Eq. (1).

On the other hand, there has been an assumption that excess NH_3 decreases the activity of formed water since it promotes the reverse reaction. Next, with regard to the effect of temperature, it has been supposed that the equilibrium conversion increases as the temperature becomes higher unless by-products such as biuret and cyanuric acid (which are condensates of urea after deammoniation) are formed increasingly; however, considering that the temperature of the experiment at that time did not exceed 185°C, we think that the equilibrium conversion at temperatures higher than the above was estimated by extrapolation.

Nevertheless, the above trend seems reasonable, as the urea formation from $NH_4CO_2NH_2$ is an endothermic reaction.

The effect of excess NH_3 or water is deduced by a partial differentiation of x with respect to a or b as follows:

$$f(x, a, b) = x(x+b)(1+a+b-x) - K(t)(1-x)(a-2x)^2 = 0$$

$$\frac{\partial x}{\partial a} = -\frac{f_a(x, a, b)}{f_x(x, a, b)}, \quad \frac{\partial x}{\partial b} = -\frac{f_b(x, a, b)}{f_x(x, a, b)} \quad (3)$$

where the temperature is constant.

Under usual conditions, a is about 4.0, b is about 0.5 and the temperature is about 190°C; therefore, $\partial x/\partial a$ is about 0.08[3] and $\partial x/\partial b$ is about 0.16, a value which is not remarkably affected by b.

Experimental

The apparatus used was a batch autoclave with an induction heater which could heat up the contents rapidly, thus making it possible to measure the reaction velocity correctly.

As has been mentioned above, our measurement is characterized by its sampling method; that is, a direct sampling from the liquid phase was made with a rubber bladder.

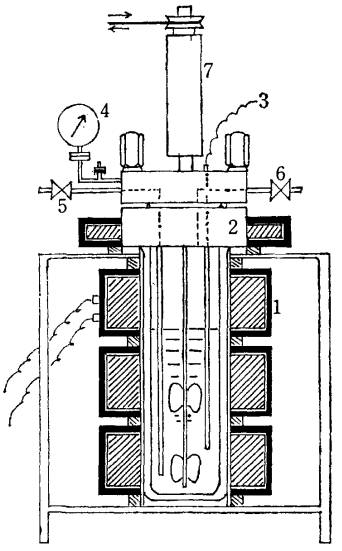

Fig. 1. Batch autoclave.
1: Induction heater, 2: Autoclave (Ti-lined), 3: Thermocouple, 4: Pressure gauge, 5: Sampling valve (liq.), 6: Sampling valve (gas), 7: Agitator

Apparatus. The apparatus is composed of the following three units: an autoclave with an agitator, an induction heater, and a temperature controller with its related meters.

Autoclave: As is shown in Fig. 1, this is a stainless steel batch autoclave lined with titanium; the inner volume is about 3 liters. All of the parts, such as the cover, the pipes, and the valves, are made of titanium alloy, because stainless steel is much corroded by the urea solution at higher temperatures. The agitator is a rotary type working by magnetic induction.

Heater and Others: This heater is composed of four induction coils, as is shown in Fig. 1 tightly fitted to the autoclave. The total output amounts to 35 kW. The temperature of the solution in the autoclave reaches 200°C from room temperature in only 12 min. The input current for heating is controlled with a pulse-type.

3) This figure corresponds to the increase in conversion when the excess of NH_3 is increased by 50%.

Table 1. Observed equilibrium conversions

Exp No	Temp.[a] (°C)	Press.[a] (kg/cm^2G)	NH_3/CO_2[b] (mol/mol)	H_2O/CO_2[b] (mol/mol)	Conv. (%)	R_F (%)	Remarks
R-63	161.5	99.0	3.95	0.13	76.1	117.3	Started with carbamate[c]
R-62a	161.5	93.0	3.88	0.43	68.8	118.09	
R-61	161.5	83.0	4.03	1.03	61.4	123.8	Started with carbamate
R-57	161.5	92.0	4.37	0.84	67.6	122.7	*ibid.*
R-63	171.5	116.0	3.94	0.11	78.1	115.9	*ibid.*
R-58	171.5	100.0	3.89	0.85	64.9	120.8	*ibid.*
R-56	171.5	111.0	4.49	0.75	69.8	116.3	*ibid.*
R-62	171.5	116.0	4.59	1.02	73.5	129.4	*ibid.*
V-11	176.5	120.0	4.01	0.09	78.6	113.2	
V- 8	176.5	113.0	4.06	0.53	70.8	115.0	
V-14	176.5	108.0	4.23	0.92	67.3	118.4	
V-23	176.5	130.0	5.07	0.13	83.4	111.0	
V-33	176.5	127.0	5.02	0.56	78.1	115.3	
V-25	176.5	118.0	5.00	0.86	74.6	118.2	
U-38	186.5	190.0	2.69	0.70	57.5	122.1	
U-11	186.5	148.0	4.00	0.06	79.2	110.0	
U- 7	186.5	145.0	4.04	0.28	75.4	111.0	
U-14	186.5	135.0	4.24	0.89	68.4	114.1	
U-28	186.5	177.0	5.14	0.13	83.2	107.3	
U-24	186.5	168.0	5.12	0.48	79.7	110.8	
U-25	186.5	155.0	4.95	0.84	74.5	113.3	
U-38	196.5	220.0	2.63	0.63	57.9	116.6	
U- 6	196.5	172.0	3.09	0.39	65.6	110.2	
U-12	196.5	183.0	3.93	0.07	79.5	108.3	
U-17	196.5	182.0	4.03	0.30	76.8	109.7	
R-24	196.5	180.0	3.88	0.56	74.5	115.5	Started with carbamate
U-15	196.5	172.0	4.16	0.94	68.2	111.4	
U-29	196.5	211.0	5.16	0.13	82.7	103.9	
R-46	196.5	210.0	5.36	0.39	80.4	104.8	Started with carbamate
R-51	196.5	198.0	5.09	0.76	76.5	108.9	*ibid.*
R-28	201.5	202.0	3.89	0.41	71.9	105.3	Started from 50% of conversion
U- 6	206.5	232.0	3.16	0.37	66.1	105.0	
U-11	206.5	224.0	3.93	0.04	79.5	104.6	
U-19	206.5	232.0	4.13	0.54	72.0	104.0	
U-15	206.5	225.0	4.22	0.95	67.6	105.3	
U-31	206.5	257.0	5.04	0.12	81.6	100.6	
U-34	206.5	245.0	5.04	0.58	75.8	101.5	
R-51	206.5	248.0	5.05	0.76	74.2	102.4	Started with carbamate
U-13	216.5	297.0	4.03	0.05	77.4	98.7	
U- 9	216.5	315.0	4.09	0.51	66.4	92.6	
U-16	216.5	304.0	4.24	0.94	64.5	96.2	
U-32	216.5	315.0	5.00	0.10	79.3	95.5	
R-53	216.5	324.0	5.17	0.90	65.1	88.1	Started with carbamate
U-13	226.5	378.0	4.07	0.05	72.5	90.0	
U-10	226.5	400.0	4.12	0.30	64.1	83.1	
U-16	226.5	415.0	4.21	0.91	51.8	74.3	
U-22	226.5	413.0	5.22	0.13	71.5	83.9	
R-54	226.5	447.0	5.16	0.81	61.0	79.1	Started with carbamate

a) Final value reached at the equilibrium state.
b) Molar ratio in a taken sample (equal to that in the liquid phase in the autoclave).
c) $NH_4CO_2NH_2$ was used as the starting material instead of urea plus water.

Procedure. For experimental convenience, the charge of materials into the autoclave in most cases was carried out as follows; at first urea plus water (1 : 1 molar ratio) was charged in instead of $NH_4CO_2NH_2$; next, excess water, and at last, excess NH_3 in the liquid state, was charged in. The total amount charged was about 2.1 kg, which corresponded to about 0.7 g/cc of the so-called loading density. In order to confirm the completion of the equilibrium, $NH_4CO_2NH_2$ was sometimes used as the starting material.

The autoclave was purged of air before the charge of liquid NH_3 by light evacuation. After the finish of the charge, heating was started, and then, after a given temperature of the autoclave had been reached, the autoclave was kept at the constant condition for 1—2 hr or longer. Then, after the confirmation of no change in pressure, a sample of liquid (also sometimes one of gas) was directly taken out from the liquid phase in the autoclave (also sometimes from the gas phase) using a weighed rubber bladder with water in it for dilution. About a 15 g sample was taken out and then analyzed by the following methods.

Analysis. After the above sampled solution had been diluted in a volumetric flask, each component was determined in aliquots by taking out a portion.

Urea: drying and weighing method

NH_3: back titration after the removal of CO_2 by excess H_2SO_4

CO_2: gravimetry as $BaCO_3$,[4] which is precipitated by $Ba(NO_3)_2$

Biuret: colorimetry by the cupric complex salt method.

The amount of pure urea is obtained by the subtraction of the amount of the biuret.

H_2O: a residue (assuming that the amount of any other component is negligible.)

In addition to the determinations of the above components, detections for cyanuric acid, melamine, *etc.* are carried out qualitatively if necessary.

Results

Although some experiments for reaction velocity were carried out, only the results on the equilibrium state will be shown in detail in this paper.

The periods of keeping the solution at a given temperature, was 1—2 hr when the temperature was above 180°C, and about 5 hr when it was below 180°C. The ranges of experimental conditions were as follows:

NH_3/CO_2 (mol) $\fallingdotseq 3$—5

H_2O/CO_2 (mol) $\fallingdotseq 0$—1.0

Temperature $\fallingdotseq 170$—220°C

The results are shown in Table 1 and in Figs. 2—6. The ratio, R_F, of the equilibrium conversion observed to that of Frèjacques is also shown by the percentages in Table 1.

Discussion

Experimental Data. First, the effects of three factors, NH_3/CO_2, H_2O/CO_2, and temperature, on the equilibrium conversion will be mentioned and compared with those reported by Frèjacques.

4) When volumetry by CO_2 gas evolution by means of conc. H_2SO_4 is used, the error caused by the hydrolysis of urea becomes a problem.

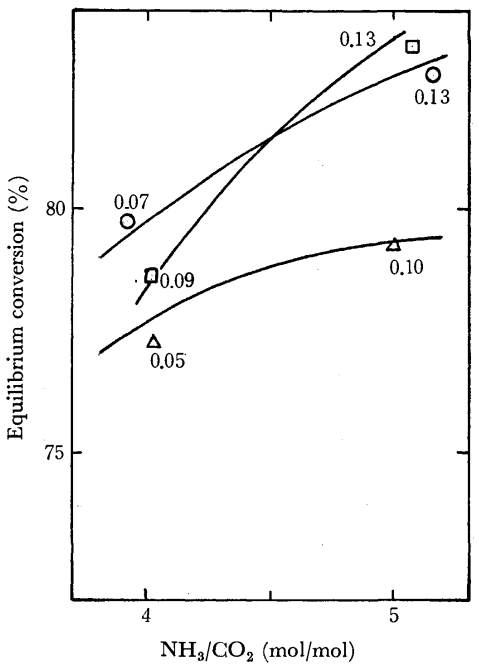

Fig. 2. Effect of NH_3/CO_2 on equil. conversion.
Each suffix shows H_2O/CO_2
-□- 176.5°C, -○- 196.5°C, -△- 216.5°C

Effect of NH_3/CO_2 (*Cf.* Fig. 2): The tendency for the rate of increase to become slower with an increase in the NH_3/CO_2 ratio is similar to that reported by Frèjacques. That is, $\partial^2 x/\partial a^2 < 0$, the increase in the equilibrium conversion is 1—1.5% per 0.2 of the increase in NH_3/CO_2 (corresponding to a 10% excess of NH_3), and at temperatures higher than 200°C the effect of NH_3/CO_2 is not so much as that reported by Frèjacques.

Effect of H_2O/CO_2 (*Cf.* Figs. 3, 4): In Fig. 3, some relations between the equilibrium conversion and H_2O/CO_2 are shown at several temperatures.

As is shown in Figs. 1—4, a reduction rate of the

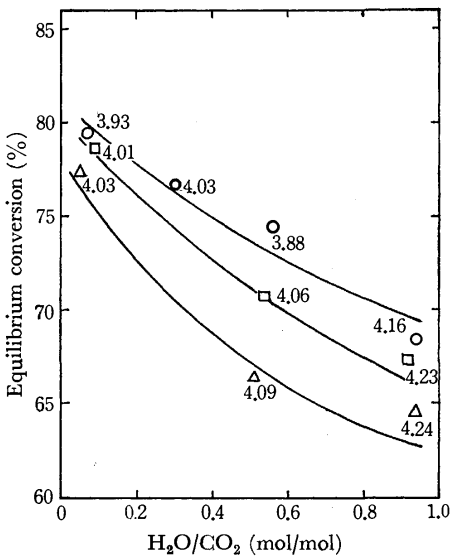

Fig. 3. Effect of H_2O/CO_2 on equil. conversion.
Each suffix shows NH_3/CO_2
-□- 176.5°C, -○- 196.5°C, -△- 216.5°C

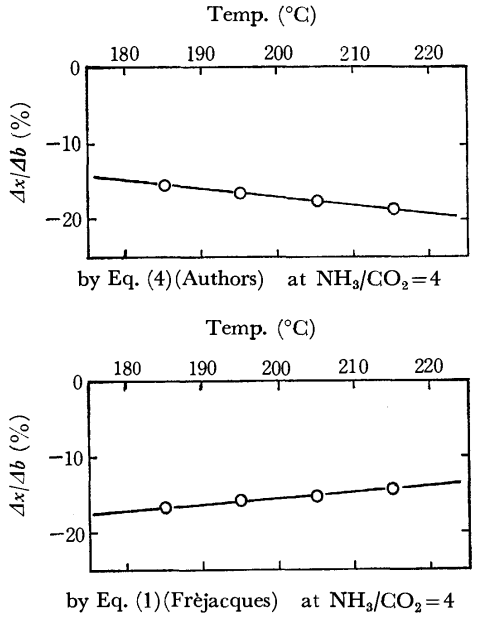

Fig. 4. Temperature dependence of reduction rate of equil. conversion.

equilibrium conversion per 1.0 of Δb becomes larger when the temperature rises, while, on the contrary, it gradually becomes smaller in Frèjacques' case.

Therefore, the ratio, R_F, is rather larger than 100% at higher H_2O/CO_2 ratios when the temperature is low, but, inversely, it is smaller when the temperature is high. The inversion temperature lies around 200°C.

Effect of Temperature (*Cf.* Fig. 5): This is the most important finding in this report. The equilibrium conversion has its maximum value at a temperature which lies between 190 and 195°C when NH_3/CO_2 is about 4.

Therefore, the observed equilibrium conversion is higher than that of Frèjacques at temperatures lower

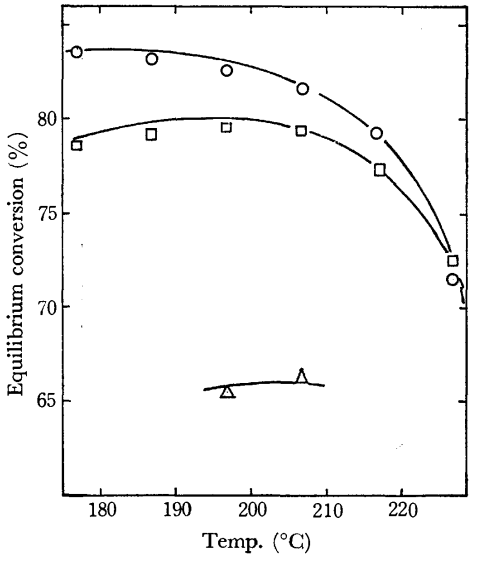

Fig. 5. Effect of temperature on equil. conversion.

	NH_3/CO_2	H_2O/CO_2
-△-	Ca 3.1	Ca 0.38
-□-	Ca 4.0	Ca 0.05
-○-	Ca 5.0	Ca 0.12

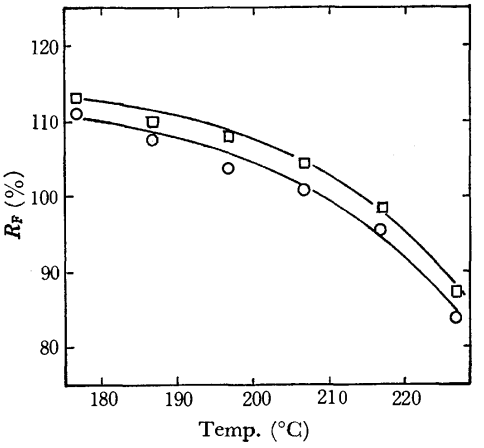

Fig. 6. Effect of temperature on R_F

	NH_3/CO_2	H_2O/CO_2
-□-	Ca 4.0	Ca 0.05
-○-	Ca 5.1	Ca 0.12

than about 200°C, while, on the contrary, it is lower at temperatures higher than 200°C.

In Fig. 6 the ratio, R_F of our conversion to that of Frèjacques at the equilibrium state is shown; the figure shows that the equilibrium conversion is higher by 5—15% under the conventional conditions of urea synthesis.

When NH_3/CO_2 changes to 5.0, the temperature giving the maximum equilibrium conversion seems to lie lower than 190°C.

By-products. It has been reported that the decrease in the equilibrium conversion is also due to the increased formation of by-products,[1] *e.g.*, biuret and cyanuric acid, besides the effect of the loading density. It is thought that this can, to some extent, be prevented by the addition of a large amount of excess NH_3; in order to confirm this, we determined the above by-products qualitatively or quantitatively. We found that biuret increases a little at higher temperatures and at lower NH_3/CO_2 ratios, but that, under other conditions, the quantity is far from that quantity which corresponds to the reduction of the equilibrium conversion, while no substantial amounts of cyanuric acid and melamine were detected. Furthermore, the amount of total carbon at the loading of materials was nearly equal to that indicated by analyzed value. Therefore, it can be concluded that the reduction of the equilibrium conversion is not due to the by-product formation.

Table 2. Effect of loading densities on the equilibrium conversion

	A	B	C
Loading density γ(g/cc)	0.8	0.5	0.3
Temp. (°C)	176.5	206.5	209.3
Press. (kg/cm²G)	152.0	245.0	231.0
NH_3/CO_2 (mol/mol)	(5.05)[a] 5.00	(4.25)[a] 3.98	(6.0)[a] 4.82
H_2O/CO_2 (mol/mol)	0.08	0.42	0.04
Conv. obsd (%)	83.6	73.0	83.9
Conv. estimated[b] (%)	83.2	72.8	81.5

a) Molar ratio of charged NH_3 to charged CO_2
b) Conversion estimated from those under near conditions at a loading density of $\gamma=0.7$

TABLE 3. COMPARISON OF EQUILIBRIUM CONSTANT WITH THAT OF FRÈJACQUES

Temp (°C)	NH_3/CO_2 (mol/mol)	H_2O/CO_2 (mol/mol)	$K_{Frèjacques}$	K_{obsd}
176.5	4.06	0.53	1.142	2.096
	4.99	0.86		2.353
196.5	4.03	0.30	1.561	2.593
	5.36	0.39		2.069
216.5	4.09	0.51	2.149	1.501
	5.17	0.90		1.241

Effect of the Loading Densities. As our data were based on the direct sampling from the liquid phase, it is thought that there is no effect of the loading density on the equilibrium conversion. However, in order to confirm this, some experiments with various loading densities were carried out; the results were nearly independent of the loading densities, as is shown in Table 2.

We also reconfirmed the existence of the temperature giving the maximum conversion using a continuous autoclave which was substantially filled with a urea solution.

Equilibrium Constant. According to the trends of our data, which are very different from the equation reported by Frèjacques, it is natural that the equilibrium constant obtained by Eq. (1) is also different from that of Frèjacques. Some examples are shown in Table 3.

Effect on Processes. From the above-mentioned results, no increase in the equilibrium conversion by raising the temperature can be expected; luckily, the urea reactors were operated at the temperature about 190°C for other reasons—to solve the problems of the reactor materials, pressure, the excess of NH_3, *etc.*

We think that the good equalities between the conversion in the process and that in Frèjacques' equation were due to such factors as the structure of the reactors and the operating conditions.

From another point of view, this means that actual conversion can approach equilibrium if we add some device to the reactor.

Of course economic considerations are necessary, and in this connection the design of the urea reactor would be assisted by reaction kinetics engineering.

Expansion of the Equation of the Equilibrium Conversion

As the equilibrium constant is also affected by the NH_3/CO_2 composition, a simple calculation from a equation like Eq. (1) is impossible. Therefore we obtained Eq. (4) by expansion with respect to a, b, and t, taking the character of our results into consideration. Thus, x is expressed:

$$x = C_1a + C_2a^2 + C_3ab + C_4b + C_5a\left(\frac{t}{100}\right) + C_6b\left(\frac{t}{100}\right) + C_7\left(\frac{t}{100}\right) + C_8\left(\frac{t}{100}\right)^3 + C_9 \quad (4)$$

Where C_i is a factor which was determined by the method of least squares using the data in Table 1. Each C_i value thus obtained is shown in Table 4.

TABLE 4. C_i's OF Eq. (4)

C_1	0.2616	C_6	−0.1030
C_2	−0.01945	C_7	1.640
C_3	0.0382	C_8	−0.1394
C_4	−0.1160	C_9	−1.869
C_5	−0.02732		

By $\partial x/\partial t=0$, the temperatures giving the maximum conversion are, found to be 192°C, 190°C, and 189°C for $a=3$, 4, and 5 respectively, where $b=0$ in all cases.

The differences between the calculated and the observed equilibrium conversions are within 2% in absolute error in 80% of all the data, as is shown in Fig. 7. Therefore, Eq. (4) is useful enough for a simple estimation of the equilibrium conversion.

Although the higher a is, the lower the said temperature seems to be, according to the above values, this is not certain because the data for low a values are few.

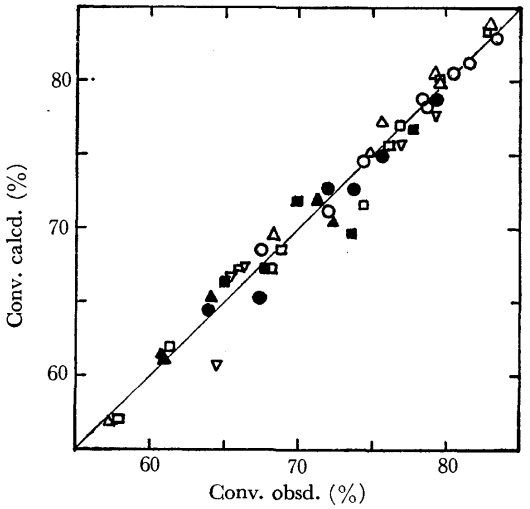

Fig. 7. Comparison of calcd. values with observed values for equil. conversion.

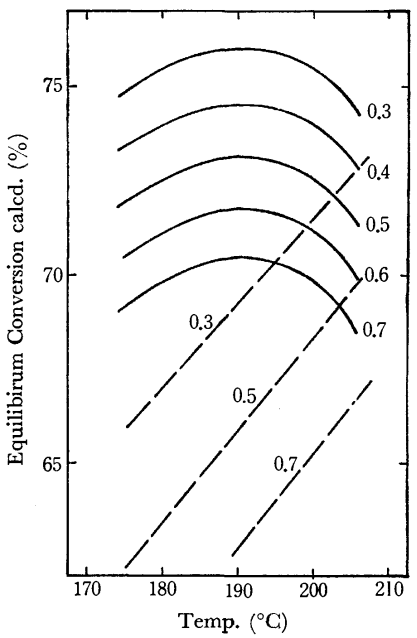

Fig. 8. Smoothed conversions for $NH_3/CO_2=4.0$
—— authors, ---- Frèjacques
Each suffix shows H_2O/CO_2

Table 5. Comparison of equilibrium conversions by various equations

t °C	a	b	x by Ref. (1)[a]	x by Ref. 5[b]	x by Eq. (4)
180	3.0	0.5	53.0	58.6	63.9
180	5.0	0.5	69.5	75.6	79.1
180	4.0	1.0	54.4	61.6	66.0
180	5.0	1.0	63.5	70.2	73.5

a) Values obtained by means of Frèjacques' monograph
b) Experimental values in Ref. 5

If this is true, however, it is a very interesting phenomenon.

An attempt like Eq. (4) was reported in Ref. 5 (*cf.* Eq. (5)), but the equilibrium conversion of this report lies between our data and those of Frèjacques; some examples are shown in Table 5. We suppose that the difference is due to a different experimental method.

The term of pressure in Eq. (5) is substantially not essential, from our point of view. The effects of NH_3/CO_2, H_2O/CO_2, and the temperature are very similar with our data, but this is supposed to be by chance because the highest temperature in Ref. 5 does not exceed 190°C.

$$x = 34.28\,a - 1.770\,a^2 - 29.30\,b + 3.699\,ab + 0.09129\,t - 0.07482\,at - 5.395\times10^{-6}\,t^3 + 0.002293\,P - 112.1 \quad (5)$$

In Fig. 8 smoothed curves of the equilibrium conversion for the case of $NH_3/CO_2=4.0$ are compared with those of Frèjacques.

The authors gratefully acknowledge, the help of their co-workers, Mr. Hironori Ito, Mr. Tomoyoshi Maekawa, Mr. Goro Komiya, and Mr. Katsumi Kagechika, who carried out all of the experiments.

5) V. I. Kucherryavyi, *Khim. Prom.* (3), 200 (1969).

BULLETIN OF THE CHEMICAL SOCIETY OF JAPAN, VOL. 45, 1345—1348(1972)

Infrared Intensities of Sodium, Calcium, and Potassium Hydroxide Crystals

Toshio KAMISUKI and Shiro MAEDA

Research Laboratory of Resources Utilization, Tokyo Institute of Technology, Meguro-ku, Tokyo

(Received October 5, 1971)

The absolute intensities of OH^- and OD^- stretching absorptions in Na, Ca, and K hydroxide crystals have been measured in the films formed on a quartz window. The thickness of the films was determined by chemical or flame photometric analysis of the solution in which the sample film had been dissolved. The expected difference between OH^- and OD^- in the dipole-moment derivative, $(d\mu/dr)_{OD}$—$(d\mu/dr)_{OH}$, was observed to be in excellent or moderate agreement with the theoretical value given from Ellison's equation for Na and Ca. This result also proves that the polarization of $d\mu/dr$ is in the O^-–$H^+(D^+)$ direction in these cases. As for K hydroxides, although the numeric results are rather dubious, the intensities are apparently by far greater than the two others, confirming the hydrogen-bond formation in this crystals, as suggested by the crystal structure and vibrational frequencies.

The infrared intensity of ionic species provides significant knowledge about the charge distribution in ions, but it has been scarcely investigated as yet except for the measurements of NH_4^+ by Ferriso and Hornig[1] and of BH_4^- by Shull and Schatz,[2] as far as we know. In the present investigation, the intensities of OH^- and OD^- stretching vibrations in Na, Ca, and K hydroxide crystals were measured; they have an unsymmetrical charge distribution, unlike the above two examples.

For a charged diatomic molecule, AB, with a net charge of Qe, Ellison[3] has derived the following expression for the dipole-moment derivative with respect to the vibrational coordinate:

$$(d\mu/dr)_e = e\{(1/2)[Q_a - Q_b - Q(M_a - M_b)/(M_a + M_b)] - N(d\bar{z}_{em}/dr)\}, \quad (1)$$

where M_α and eQ_α are the mass and the charge of a nucleus, α; where N is the number of electrons in a molecule, and where $\bar{z}_{em}$ is the averaged z coordinate (directed B→A) of an electron in the molecule relative to the midpoint between the nuclei.

Now, it can easily be seen from Eq. (1) that the difference in dipole-moment derivatives between isotopic molecules, AB and A′B, is given by:

$$(d\mu/dr)_{A'B} - (d\mu/dr)_{AB} = -eQM_b(M_a' - M_a)/[(M_a + M_b)(M_a' + M_b)], \quad (2)$$

where the subscript e representing the equilibrium value is omitted. For the hydroxide ion of $Q = -1$, it proves to be:

$$(d\mu/dr)_{DO} - (d\mu/dr)_{HO} = 0.251\text{D/Å}. \quad (3)$$

That is to say, the derivative for OD^- is always biased to the O^-–D^+ direction against the corresponding OH^- value by 0.251 D/Å, quite independently of the chemical or physical state of the ions. It is interesting, therefore,

1) C. C. Ferriso and D. F. Hornig, *J. Chem. Phys.*, **32**, 1240 (1960).

2) D. L. Shull, thesis, University of Virginia, Charlottesville, Va. (1961).

3) F. O. Ellison, *J. Chem. Phys.*, **36**, 478 (1962).

to see how closely this theoretical value is realized in experimental observations for typical metal hydroxides. On the other hand, such an experiment implies a means of estimating the amount of the net charge, Q, when sufficiently accurate measurements are possible.

Experimental

The infrared spectra were measured in thin solid films formed on the surface of a quartz window, which was transparent enough up to the wavelength of ν_{OD} absorption. In the preparation of Na and K hydroxides, the metal was deposited on the window in a vacuum infrared cell at first; then H_2O or D_2O vapour was introduced at a pressure of 10^{-1}—10^{-2} Torr for the reaction. The partial production of the hydrate was easily detected by observing the spectrum, and it was restored to an unhydrous one without difficultly by heating under evacuation. For Ca, separate apparatus equipped with a powerful heater was used for similar procedures, and the completed sample was transferred to the cell for the spectral measurements.

The infrared absorption measurements were limited to the OH^- and OD^- stretching bands because of absorption by the substrate. The spectrum was recorded at room temperature and at a low temperature with liquid N_2. The spectral slit width was chosen so as to be always less than one-third of the apparent band width; in that way the effect of the finite slit width on the integrated intensity could be neglected.

After recording the spectra, the Na and K hydroxide films were dissolved into a small amount of distilled water, and then its metal concentration was determined by flame photometry to give the thickness of the original films.[4] Ca hydroxide films were dissolved into dilute hydrochloric acid. After the residual HCl had been removed by evaporation to dryness, the remaining solid was dissolved in water again and titrated with EDTA.

Results and Discussion

Figure 1 shows the Beer's law plots of the experimental quantity:

$$B' = \int_{\text{band}} \ln (T_0/T) d\nu,$$

where T_0/T is the observed transmittance; the integrated absorption coefficient:

$$A = \int \alpha d\nu$$

was obtained as the limiting slope of these curves. The results are given in Table 1. It is noticeable that the OD^- *vs.* OH^- intensity ratio is definitely greater than the expected value for a neutral case, 1/2, in every case.

The good linearity of the Na and Ca plots in Fig. 1 shows that the thickness of the films was sufficiently uniform and had been determined accurately. The composite error may be estimated at about 15% in these two cases. On the other hand, the rather gross scatter in the K data, probably due to the poor uniformity of films because of its extremely hygroscopic nature, indicates a considerably greater composite error, one of some 30%.

NaOH, NaOD Let us consider the results for NaOH and NaOD first. Ernst[5] has shown by X-rays that the crystal has an orthorhombic lattice with Na and O positions, as is shown in Fig. 2. On the other hand, infrared[6,7] and Raman[6,8] investigations have shown that the two hydroxide ions present in a primitive unit cell are related to each other by a center of symmetry. The allignment of O–H axes has been concluded by Busing to be parallel to the c-axis after taking account of other factors, so that the

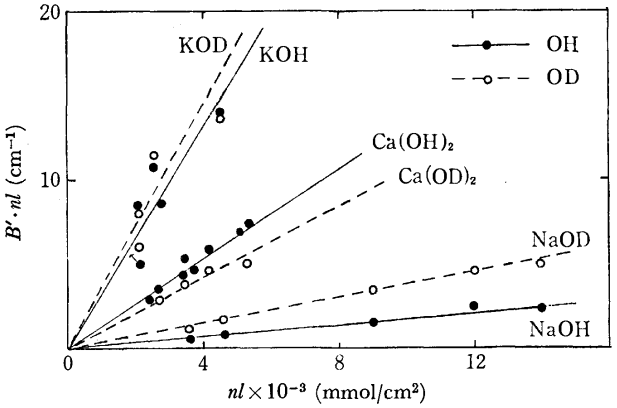

Fig. 1. Beer's law plots for intergrated intensities.

TABLE 1.

Substance	Frequency (cm^{-1}) 25°C	Frequency (cm^{-1}) −165°C	A(−165°C) (cm/mM)	$d\mu/dQ$ [a] ((D/Å)·amu$^{-1/2}$)	$d\mu/dr$ [a] (D/Å)
NaOH	3638	3643	3.8×10^2	0.262	0.255
NaOD	2680	2683	7.8×10^2	0.375	0.502
KOH	3595	3561, 3538 [b]	6.8×10^3	1.11	1.08
KOD	2655	2615, 2587 [b]	7.0×10^3	1.12	1.50
$Ca(OH)_2$	3645	3651	2.7×10^3	0.67	0.65
$Ca(OD)_2$	2686	2691	2.2×10^3	0.60	0.80

a) Values corrected by Polo-Wilson's equation. Since appropriate refractive index values are not available, they have been tentatively assumed at 1.47 for NaOH and KOH, and 1.57 for $Ca(OH)_2$ based on the existing data for visible light at room temperature.

b) Slight but appreciable shift from Ref. (15) (3556, 3533 cm^{-1}; 2609, 2592 cm^{-1}) may be due to the difference in the temperature of observation.

4) For the flame-photometric analysis, the authors are indebted to Professor Takashi Katsura of the Tokyo Institute of Technology.

5) T. Ernst, *Ang. Chem.*, **60A**, 77 (1948).

6) W. R. Busing, *J. Chem. Phys.*, **23**, 933 (1955).

7) R. A. Buchanan, *ibid.*, **31**, 870 (1959).

8) D. Krishnamurti, *Proc. Indian Acad. Sci.*, **50A**, 223 (1959).

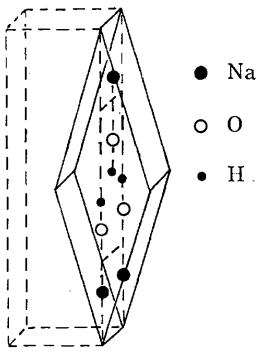

Fig. 2. Crystal structure of NaOH.

structure is described by the space group D_{2h}^{17}.

The infrared active mode of OH(OD) stretching vibration is represented by a unit-cell symmetry coordinate:

$$S_1 = (1/\sqrt{2})(r-r') \tag{4}$$

where r and r' are a pair of O–H(D) stretching coordinates in a unit cell. According to the crystal structure quoted above, the coordinate, S_1, may be allowed to mix only with a translational lattice vibration represented by a unit cell symmetry coordinate:

$$S_2 = (1/\sqrt{2})(R-R') \tag{5}$$

where R and R' are a pair of Na^+—OH^- coordinates in the unit cell. Slight as it may be, such a mixing of modes might influence the $\nu_{OH(OD)}$ intensity more or less significantly because the dipole-moment derivative, $\partial\mu/\partial S_2$, is apparently very great.

The symmetry coordinates above can be given in terms of unit-cell normal coordinates, Q_1 and Q_2, by:

$$\begin{aligned} S_1 &= L_{11}Q_1 + L_{12}Q_2 \\ S_2 &= L_{21}Q_1 + L_{22}Q_2 \end{aligned} \tag{6}$$

Then, the derivative with respect to the normal coordinate may be expressed as:

$$\begin{aligned} \partial\mu/\partial Q_1 &= L_{11}(\partial\mu/\partial S_1) + L_{21}(\partial\mu/\partial S_2) \\ &= \sqrt{2}\,[L_{11}(\partial\mu/\partial r) + L_{21}(\partial\mu/\partial R)], \end{aligned} \tag{7}$$

which is related to the observed intensity by:

$$A_t = \frac{N\pi}{3c^2n}\left(\frac{n^2+2}{3}\right)^2\left(\frac{\partial\mu}{\partial Q_i}\right)^2. \tag{8}$$

Equation (8) includes the correction factor given by Polo and Wilson[9] for the effective radiation field in a medium with a refractive index of n, where N is the number of molecules per cm^3, and c, the velocity of light in a vacuum.

Now, $\partial\mu/\partial R$ may be assumed to be roughly equal to the electronic charge, $e=4.80\times10^{-10}$esu. On the other hand, it can be shown straightforwardly from a fundamental equation that:

$$\frac{L_{21}}{L_{11}} = -\frac{(\mu_{Na}+\mu_{OH})f_{Rr}}{(\mu_{Na}+\mu_{OH})F_R-\lambda_1}, \tag{9}$$

where μ_M is the reciprocal of the mass of M, $\lambda_1=4\pi^2c^2\nu_1^2$ (ν_1 in cm^{-1}), and, where f_{Rr} and F_R are the force constants defined in the expression for the potential energy:

$$2V = F_r(r^2+r'^2) + F_R(R^2+R'^2) + 2f_{Rr}(rR+r'R'). \tag{10}$$

As it is certain that:

$$\lambda_1 \simeq (\mu_O+\mu_H)F_r \gg (\mu_{Na}+\mu_{OH})F_R \simeq \lambda_2, \tag{11}$$

Eq. (9) may be approximated as follows:

$$\frac{L_{21}}{L_{11}} \simeq \frac{f_{Rr}}{F_r}\left(\frac{\mu_{Na}+\mu_{OH(OD)}}{\mu_O+\mu_{H(D)}}\right) = \left(\frac{f_{Rr}}{F_r}\right)\times\begin{cases}0.096 & \text{(NaOH)}\\ 0.176 & \text{(NaOD)}\end{cases} \tag{12}$$

Although the lattice frequency concerned is not known, it may be reasonably approximated by the highest frequency of the translational mode estimated by Buchanan[7] based on the summation side band, *i.e.*, 296 cm^{-1} for NaOH and 286 cm^{-1} for NaOD. Force constants consistent with these frequencies, together with the observed ν_{OH} and ν_{OD} values, are obtained as follows:

$$F_r = 8.01,\ F_R = 0.46,\ f_{Rr} = 0.05 \text{ mdyne/Å}$$

Therefore, L_{11} may be almost exactly equal to $G_{11}^{1/2}=(\mu_O+\mu_{H(D)})^{1/2}$ ignoring L_{12} in Eq. (6). Therefore, it may be seen that $L_{21}(\partial\mu/\partial S_2)$ in Eq. (7) is no more than 0.005 D/Å for both OH^- and OD^-, so that the effect of lattice-mode mixing may be scarcely significant except when $|\partial\mu/\partial Q_1|$ is by far smaller than in the present observations.

Thus, we can now straightforwardly give $\partial\mu/\partial r$ as is shown in Table 1. The difference in the derivative between OD^- and OH^- is:

$$(\partial\mu/\partial r)_{OD} - (\partial\mu/\partial r)_{OH} = 0.247\ D/Å, \tag{13}$$

which is in very good agreement with the theoretical expectation, 0.251 D/Å. In addition, the positive value of (13) confirms that $\partial\mu/\partial r$ is of an O^-H^+(or O^-D^+) polarization in both OH^- and OD^-.

$Ca(OH)_2$, $Ca(OD)_2$ X-ray studies[10-12] have indicated that the crystal structure of $Ca(OH)_2$ has the hexagonal symmetry of the D_{3d}^3 space group, and that the hydrogen positions were determined to be as is shown in Fig. 3 by neutron diffraction.[13] The unit cell contains one $Ca(OH)_2$ "molecule," whose two OH^- ions are related to each other by a center of symmetry and are arranged in parallel with the

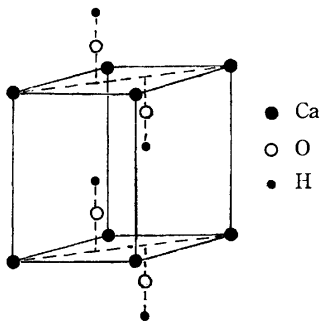

Fig. 3. Crystal structure of $Ca(OH)_2$.

9) S. R. Polo and M. K. Wilson, *J. Chem. Phys.*, **23**, 2376 (1955).

10) J. D. Bernal and H. D. Megaw, *Proc. Roy. Soc. (London)*, **A151**, 384 (1935).

11) H. E. Petch and H. D. Megaw, *J. Opt. Soc. Amer.*, **44**, 744 (1954).

12) H. E. Petch, *Phys. Rev.*, **99**, 1635 (1955).

13) W. R. Busing and H. A. Levy, *J. Chem. Phys.*, **26**, 563 (1957).

hexagonal axis. Therefore, the coupling between the O–H(D) stretching and translational lattice vibrations can be considered in essentially the same way as in NaOH. Thus, it is easily confirmed that the effect of lattice vibration on the $\nu_{OH(D)}$ intensity is no more than trivial in this case, too.

The quantity corresponding to (3) comes to be:

$$(\partial\mu/\partial r)_{OD^-} - (\partial\mu/\partial r)_{OH^-} = 0.15\ D/\text{Å}$$

which is appreciably smaller than the theoretically expected value, 0.251 D/Å, but still demonstrates the O^-H^+ (or O^-D^+) polarization of the derivatives. On the other hand, the values of $\partial\mu/\partial r$ are themselves definitely greater than those of the Na hydroxides. As the close proximity of the $\nu_{OH(OD)}$ frequencies for Na and Ca suggests little difference in the features of the O–H bonding electrons, the electronic condition of the metal···OH binding may be mainly responsible for the above difference in $\partial\mu/\partial r$. A possible inference is that the Ca···OH binding is of a slightly more covalent nature than Na···OH, so that the former has more vibronic coupling with the O–H stretching motion than the latter.

KOH, KOD Considerably greater intensities than the previous two were obtained for *K* compounds, confirming the formation of hydrogen bonds in this crystal, as suggested by the X-ray results[14] and the infrared frequency.[15] The poor agreement between the observed value,

$$(\partial\mu/\partial r)_{OD} - (\partial\mu/\partial r)_{OH} = 0.42\ D/\text{Å}$$

and the theoretical value, 0.251 D/Å, is probably due to experimental errors, as the scatter of the data was rather gross, as may be seen in Fig. 1. The appearance of the films, which was rather rough compared with that of the two others, suggests that the poor uniformity films caused such a scattering in this case.

A remarkable fact is the extreme dependence of the intensity on the temperature. Even the thickest sample recorded on Fig. 1 gives only a trace of absorption, about one-tenth of the low temperature value, at room temperature. This is in corespondence with the frequency shift caused by the temperature, as may be seen in Table 1, suggesting the temperature dependence of the hydrogen-bond strength.

Finally, mention may be made of the possible formation of the oriented crystals. For $Ca(OH)_2$, no appreciable orientation effect was found when the spectrum was recorded by tilting the sample film against the light beam by some 45°. The layer structure of this crystal suggests an orientation with *a*, *c*-axis perpendicular to the plate as most probable; for this, the above observation may be a sensitive test. For Na and K compounds, it was difficult to perform a similar test effectively, because of their hygroscopic natures. However, Busing[6] has concluded that the orientation effect is absent in NaOH by observing it with various substrate materials, and also by comparing it with a directly-evaporated NaOH film. The close agreement of the observed $(\partial\mu/\partial r)_{OD}-(\partial\mu/\partial r)_{OH}$ value with the theoretical value for randomly-oriented crystals seems to support the above conclusion.

14) J. A. Ibers, J. Kumamoto, and R. G. Snyder, *J. Chem. phys.*, **33**, 1164 (1960).
15) R. G. Snyder, J. Kumamoto, and J. A. Ibers, *ibid.*, **33**, 1171 (1960).

A Study on the Nature of the Electronic Absorption Bands of Formylpyrroles and Acetylpyrroles[1)]

Taku MATSUO and Hideto SHOSENJI*

Department of Organic Synthesis, Faculty of Engineering, Kyushu University, Hakozaki, Fukuoka

(Received October 11, 1971)

The electronic spectra of formyl- and acetylpyrroles were studied from both experimental and theoretical viewpoints. On the basis of the solvent effect and pH-dependence of the absorption spectra, the lowest energy transitions of 2- and 3-acetylpyrroles and the corresponding formylpyrroles, as well as the second lowest energy transitions of 3-acylpyrroles, were suggested to be accompanied by the electron-transfer from the pyrryl to carbonyl group. As to 1-acetylpyrrole (or 1-formylpyrrole), the longest wavelength absorption bands disappeared when the conjugation between the pyrryl and carbonyl groups were inhibited by steric hindrance. Solvent effects on the absorption band, however, were so small that the extent of electron-transfer was considered to change little during the transition. The results of VESCF MO calculations also supported the above suggestion based on experimental observations. The behaviors of the second lowest energy transitions of 1- and 2-acylpyrroles were too complicated to be accounted for straightforwardly.

Aside from pyrrole itself, no theoretical studies have been made on the electronic spectra of substituted pyrroles. In the case of monosubstituted benzenes, the composite-molecule method has been successfully applied to interpret electronic spectra. Taking the case of benzaldehyde, as an example, the absorption band at 43 kK was assigned to an intramolecular charge-transfer band from calculations based on the composite-molecule method.[2)] Similar treatment is expected to be successful also in the case of substituted pyrroles because the pyrryl group is known to be a good electron donor as can be seen in studies on charge-transfer complexes[3)] and the electronic spectra of 1-(*p*-substituted phenyl)-pyrroles.[4)] Since the ionization potential of a pyrryl group is lower than that of a phenyl group, the charge-transfer configuration is expected to make a significant contribution to the electronic structures of pyrrole derivatives with a carbonyl group. In fact, the internal rotation around the C–N bond in 1-acylpyrroles was found to be fairly restricted due to the presence of double bond character ascribed to the contribution of charge-transfer configurations.[5)]

In the present study, we investigated the characteristic absorption bands of formyl- and acetylpyrroles in the ultraviolet region which is usually accessible, to examine how well one can interpret the nature of these spectra on the basis of the electron transfer from the pyrryl to carbonyl group.

Results and Discussion

The lowest energy electronic transition of pyrrole is located at 47.6 kK. If an acyl group is attached to a pyrryl group, strong characteristic absorption bands are found for each isomer in the region between 35 and 45 kK (Fig. 1). The electronic spectra of formylpyrroles closely resemble those of the corresponding acetylpyrroles. The observed absorption maxima of these compounds together with their 1-methyl-substituted derivatives are listed in Table 1.

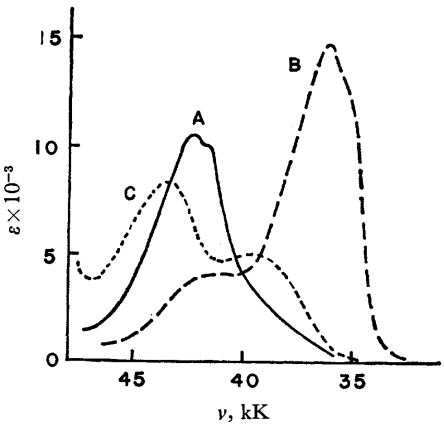

Fig. 1. The ultraviolet absorption spectra of acetylpyrroles in *n*-hexane.
A, 1-acetylpyrrole; B, 2-acetylpyrrole; C, 3-acetylpyrrole.

If the contribution of charge-transfer configurations in the electronic structure is more significant in an excited state than in the ground state, the corresponding absorption band should show an appreciable red-shift as the polarity of solvent increases. The behavior of the first absorption band of 2-acetylpyrrole is in accordance with this expectation. As an alternative explanation for the red-shift observed in the ethanol solution, the hydrogen bonding between pyrrole and ethanol molecules might be suggested. However, the absorption maximum of the first band of 1-methyl-2-acetylpyrrole is located very close to that of 2-acetylpyrrole not only in *n*-hexane but also in ethanol. The same situation is also encountered when we compare the first absorption bands of 2-formylpyrrole and 1-methyl-2-formylpyrrole. It is thus very unlikely that the hydrogen bonding plays an important role in the solvent-induced red-shift given in Table 1. The second absorption bands of 2-acetylpyrroles and 2-formylpyrroles, on the other hand, are not shifted appreciably by the change of solvent from *n*-hexane to alcohol.

* Present address: Department of Synthetic Chemistry, Faculty of Engineering, Kumamoto University, Kurokami-cho, Kumamoto.

1) Contribution No. 257 from the Department of Organic Synthesis, Faculty of Engineering, Kyushu University.

2) K. Kimura and S. Nagakura, *Theoret. Chim. Acta*, **3**, 164 (1965).

3) T. Matsuo and H. Shosenji, This Bulletin, **41**, 1068 (1968).

4) T. Matsuo, H. Shosenji, and R. Miyamoto, *ibid.*, **41**, 2849 (1968).

5) T. Matsuo and H. Shosenji, *Chem. Commun.*, **1969**, 501.

Table 1. Electronic absorption spectra of formylpyrroles and acetylpyrroles

Compound	in *n*-Hexane				in Ethanol			
	1st Band		2nd Band		1st Band		2nd Band	
	ν[a]	ε[b]	ν[a]	ε[b]	ν[a]	ε[b]	ν[a]	ε[b]
1-Formylpyrrole	38.0[c]	1.5	41.5[c]	9.5	38.0[c]	1.6	42.2	11.3
			42.4	11.2				
1-Acetylpyrrole	38.0[c]	2.0	41.6[c]	10.0	38.0[c]	2.0	41.9	10.6
			42.4	10.5				
2-Formylpyrrole	35.9	15.1	40.7	4.7	34.6	15.6	40.1[c]	4.4
1-Methyl-2-formylpyrrole	35.7	16.2	40.7	6.2	34.6	15.2	40.2	5.9
2-Acetylpyrrole	35.4[c]	12.7	40.7	4.1	34.8	14.9	41.2[c]	3.3
	36.2	14.7	41.8[c]	4.0				
1-Methyl-2-acetylpyrrole	36.0	15.5	40.8[c]	5.0	34.8	15.1	40.5[c]	4.5
3-Acetylpyrrole	38.6	4.3	43.6	7.9	35.8	4.8	41.0	9.4
1-Methyl-3-acetylpyrrole	38.2	5.3	41.5	8.6	d)		39.8	8.8

a) The values are in kK units. Errors are within 0.1 kK unless specified.
b) The values are in 10^3 *l*/mol·cm units. Errors are within 100 *l*/mol·cm except for the case of the shoulder of an absorption band, where the error may be twice as large as that for the case of a distinct peak.
c) The shoulder of an absorption band. Errors are estimated to be within 0.3 kK.
d) The absorption maximum could not be located on account of the band being hidden under the tail of the second absorption band.

In the case of 3-acetylpyrrole and its 1-methyl-substituted derivative, both the first and the second absorption bands show a red-shift when the solvent is changed from *n*-hexane to ethanol. In order to further investigate the electronic origin of the above described absorption bands of 2- and 3-acylpyrroles, we measured the electronic spectra in alkaline solutions. The results are shown in Figs. 2 and 3 for 2-formylpyrrole and 3-acetylpyrrole, respectively. In both cases, the longest wavelength absorption bands in 10N sodium hydroxide are found in a considerably longer wavelength region in neutral solutions. The spectra of 2-acetylpyrrole show a similar pH-dependence as observed in the case of 2-formylpyrrole. In alkaline solutions, these compounds are considered to exist as the anions as shown by structures (I) and (II).[6]

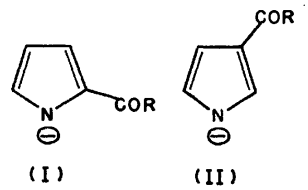

Since the ionization potential of the pyrryl anion should be considerably lower than that of neutral species, the large red-shift in alkaline solutions can be taken as sufficient evidence for assigning the absorptions to charge-transfer bands.

The longest wavelength absorption band of 1-acetylpyrrole is almost the same as that of 1-formylpyrrole, both of them being found in energy regions lower by about 5 kK than that of pyrrole. The absorption bands of 1-formylpyrrole, as well as those of 1-acetylpyrrole, consist of two components: a strong main peak (Band A) at about 42 kK and its shoulder (Band B) at approximately 38 kK. As to 1-formyl- and 1-acetylpyrrole, Band B is observed only as a small hump on the tail of Band A. On substitution of the proton at the 2-position by a methyl group, Band B appears clearly because

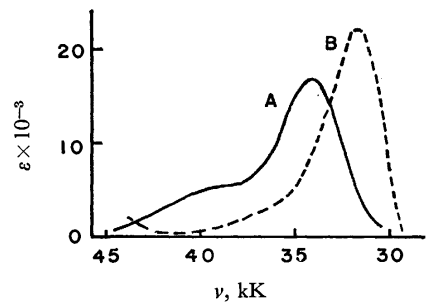

Fig. 2. The pH-dependence of the abosrption spectra of 2-formylpyrrole.
A, in water; B, in 10N aqueous sodium hydroxide solution.

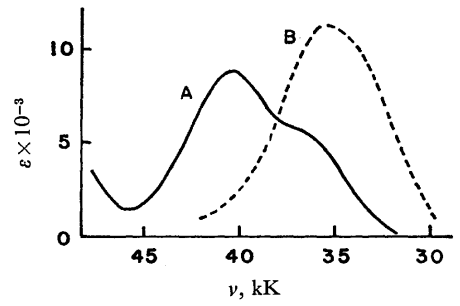

Fig. 3. The pH-dependence of the absorption spectra of 3-acetylpyrrole.
A, in water; B, in 10N aqueous sodium hydroxide solution.

6) Bonino and Mirone isolated the sodium salt of 2-formylpyrrole.[7] On inspecting the IR spectra, they concluded that the NH proton dissociated to yield the sodium salt. The evidence for the presence of anions (I) and (II) is also given by the fact that a methyl group is introduced to the nitrogen atom of 2-formylpyrrole,[8] 2-acetylpyrrole,[9] and 3-acetylpyrrole (present experiment), respectively, when the alkaline solutions are treated with dimethyl sulfate.

7) G. B. Bonino and P. Mirone, *Atti accad. Nazl. Lincei. Rend (Classe sci fis., mat. e nat.)*, **17**, 167 (1954); *Chem. Abst.*, **49**, 15488b (1955).

8) E. Fischer, *Ber.*, **46**, 2509 (1913).

9) P. Fournari, *Bull. Soc. Chim. France*, **1963**, 488.

a hypochromic effect is observed on Band A while Band B is slightly shifted to longer wavelength with no change in its intensity. The absorption maximum of 2-methyl-1-acetylpyrrole in the vapor phase is slightly shifted to longer wavelength in comparison with that in the solution, but the shapes of the spectra in the two phases are essentially the same. The intensity of Band B is rather weak ($f \sim 0.02$), but stronger than that of ordinary n-π^* absorption bands. The solution spectra are not affected even by the addition of trifluoroacetic acid. Thus we can disregard the possible contribution of the lone pair electrons of the carbonyl group to the appearance of the absorption bands. In other words, both Bands A and B are assigned to π–π^* transitions. In the case of 2,5-dimethyl-1-acetylpyrrole, the plane of the acetyl group is twisted to almost a perpendicular position to that of the pyrryl group. As a consequence, both Band A and B disappear as can be seen in Fig. 4. The above results are also summarized in Table 2. It is clearly understood that the conjugation between the pyrryl and carbonyl groups is definitely required for the presence of both Bands A and B. Introduction of methyl groups into the 3- and 4-positions of the pyrryl group causes a large red-shift (1.8 kK) of Band A of 1-acetylpyrrole. Band B, on the other hand, is not affected and almost concealed under the shifted Band A (Fig. 4). Considering the fact that the first charge-transfer band of the chloranil complex of 3-methylpyrrole is also shifted to a wavelength longer by 1.7 kK than that of the chloranil-pyrrole system,[3] we would like to assign Band A to the intramolecular charge-transfer band. However, on the basis of the solvent effects, it is difficult to assign either Band A or B to charge-transfer absorptions, because the absorption maxima of these bands of 2-methyl-1-acetylpyrrole are hardly shifted by the change of the solvent from n-hexane to ethanol.

The results are well accounted for if one assigns the longest wavelength absorption bands of 2- and 3-acetylpyrroles to charge-transfer bands. This is also true for 2- and 3-formylpyrroles. In the case of 1-acetyl- or 1-formylpyrrole, however, it is difficult to assign the longest wavelength absorption band to charge-transfer absorption straightforwardly.

In the NMR spectroscopic rate studies, on the other hand, the barrier to internal rotation in 1-formyl- or 1-acetylpyrrole has been found to be clearly higher than that in the isomers correspondingly substituted at the 2- or 3-position.[5,10] The result indicates that the ionic form (III) makes more significant contribution to the ground state of the 1-substituted pyrroles than the ionic forms (IV) and (V) to the ground states of 2- and 3-acylpyrroles, respectively.

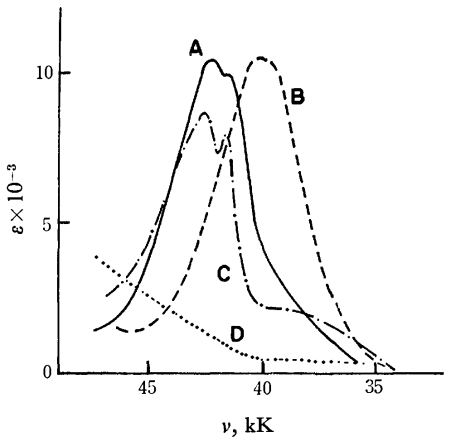

Fig. 4. The ultraviolet absorption spectra of methylsubstituted 1-acetylpyrroles in n-hexane.
A, 1-acetylpyrrole; B, 3,4-dimethyl-1-acetylpyrrole; C, 2-methyl-1-acetylpyrrole; D, 2,5-dimethyl-1-acetylpyrrole.

Table 2. Electronic absorption bands of methylsubstituted 1-acetylpyrroles[a]

Compound	Band A		Band B	
	ν[b]	ε[c]	ν[b]	ε[c]
1-Acetylpyrrole	41.6±0.1	10.0±0.1	38.0±0.5	2.0±0.2
	42.4±0.1	10.5±0.1		
3,4-Dimethyl-1-acetylpyrrole	40.2±0.1	10.5±0.1		d)
2-Methyl-1-acetylpyrrole	41.7±0.1	7.9±0.1	38.0±0.5	2.0±0.2
	42.6±0.1	8.7±0.1		

a) In n-hexane
b) Values in kK units
c) Values in 10^3 l/mol·cm units
d) The absorption maximum could not be located on account of the band being hidden under the tail of Band A.

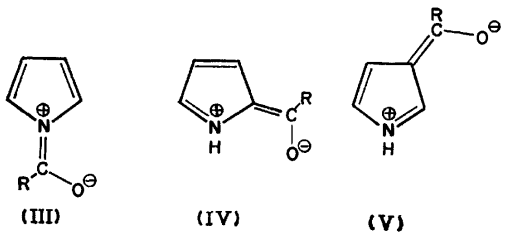

In order to explain the above results, spectroscopic differences between the isomers of formyl- or acetylpyrroles and the electronic structures of these molecules were examined by the use of pi-electron approximation. Brown and Heffernan's VESCF MO with CI was adopted for this purpose. Geometries of the investigated molecules were estimated from those of the closely related compounds.[11] The one-center electron repulsion integrals were calculated by the use of Paolini's approximation,[15] and the two-center integrals were

10) L. Arlinger, K.-I. Dahlqvist, and S. Forsén, *Acta Chem. Scand.*, **24**, 672 (1970).
11) The geometry of the pyrryl group was assumed to be the same as that of pyrrole itself.[12] Referring to the cases of acetamides[13] and acetaldehyde,[14] it was assumed that the bond between the pyrryl and carbonyl groups is either 1.36 Å (1-acylpyrroles) or 1.4 Å (2- and 3-acylpyrroles), and also that the bond bisects the angle between the adjacent two bonds in the pyrryl group. Similarly, the bond length of the carbonyl group was assumed to be 1.21 Å. The bond angles associated with the carbonyl carbon were taken to be those for the ideal sp^2 hybridization.
12) B. Bak, D. Christensen, L. Hansen-Nyagard and J. Rastrup-Andersen, *J. Chem. Phys.*, **24**, 720 (1956).
13) K. Kimura and M. Aoki, This Bulletin, **26**, 429 (1953).
14) D. P. Stevenson, H. D. Burnham, and V. Schomaker, *J. Amer. Chem. Soc.*, **61**, 2922 (1939).
15) L. Paolini, *Nuovo Cimento*, **4**, 410 (1956).

evaluated by the use of the Nishimoto and Mataga equation. The penetration integrals were not taken into consideration. Pariser and Parr's formula was used for the estimation of the core resonance integrals (H_{pq}), except for the case of $H_{C=O}$, where Tanaka's value for formamide (−3.35 eV)[16] was adopted. The valence ionization potentials were estimated by means of Brown's approximation based on the effective nuclear charges on the atoms.[17] The lower nine of the singly-excited configurations were included in the CI calculation. The values thus obtained for transition energy, oscillator strength and the electronic configurations mainly contributing to the relevant, low excited states of the acylpyrroles are given in Table 3. The coefficients for the $2p$ orbital of each atom in the relevant π orbitals are shown in Fig. 5. The results for only one conformer of each isomer are shown here, because no significant difference between the rotamers was found as far as the carbonyl group was assumed to be coplanar with the pyrryl group. Similarly, the difference between acetyl and formyl groups was also disregarded in the calculation, because the observed electronic spectra of formylpyrroles are almost the same as those of the corresponding acetylpyrroles in the investigated region.

The calculated π–π^* transition energies are higher than the values obtained experimentally by approximately 1 eV. It is clear that more advanced treatment is required to obtain a satisfactorily quantitative agreement between the observed and the calculated values. Several important features of the electronic spectra of acylpyrroles are noticed, however, even in the present results. On the basis of the data in Table 3, it is expected that two absorption bands for each isomer will be found in the energy region (200—300 mμ), and that the lowest energy transition of 2-acylpyrroles will be found at the longest wavelength side as a rather strong peak, which is distinctly separated from those of the other isomers. These predictions are in fair agreement with observations. On examination of the electron configurations concerned, it is easily found also that these low energy transitions are originated from the simultaneous excitation of both the pyrryl and the carbonyl groups. In other words, a strong conjugation between the two groups are theoretically required for the presence of the observed absorption bands, as was verified in the case of methylsubstituted 1-acetylpyrrole (Fig. 4).

TABLE 3. CALCULATED VALUES FOR THE TRANSITION ENERGY (ΔE_k), OSCILLATOR STRENGTH (f_k), AND WAVE FUNCTIONS (Φ_k) FOR LOW-EXCITED STATES OF ACYLPYRROLES

ΔE_k (eV)	f_k	Φ_k[a]
1-Acylpyrrole		
5.87	0.23	$0.875\Phi_{35}-0.446\Phi_{46}$
6.03	0.20	$0.997\Phi_{45}+0.045\Phi_{26}$
7.53	0.16	$0.828\Phi_{47}+0.387\Phi_{36}$
2-Acylpyrrole		
5.55	0.42	$0.902\Phi_{45}+0.372\Phi_{35}$
5.89	0.23	$0.751\Phi_{35}+0.468\Phi_{46}$
7.04	0.33	$0.748\Phi_{46}-0.459\Phi_{35}$
3-Acylpyrrole		
5.85	0.01	$0.765\Phi_{35}-0.540\Phi_{46}$
6.07	0.24	$0.942\Phi_{45}+0.251\Phi_{35}$
6.60	0.71	$0.781\Phi_{46}+0.561\Phi_{35}$

a) Φ_{ij} denotes an electronic configuration which is obtained by the promotion of a π electron from the ith MO to the jth MO, when the pi-electron approximation was adopted in the calculation. The most important two electronic configurations for each energy level are shown for the sake of simplicity.

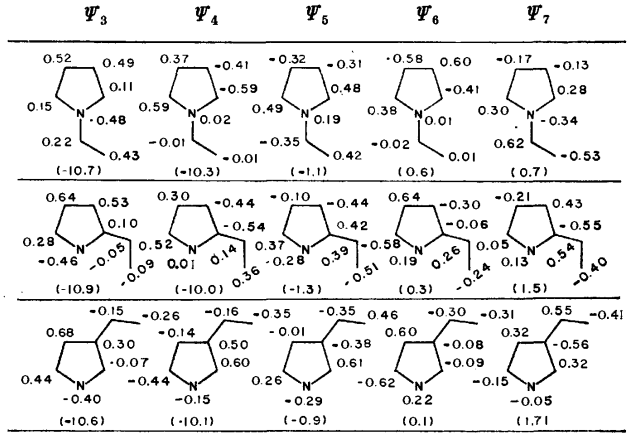

Fig. 5. The coefficients for the atomic orbitals in the relevant MO associated with the low energy transitions of acylpyrroles. The energy of each orbital, in eV units, is given by the numeral in parentheses under the corresponding structure.

TABLE 4. π-ELECTRON DENSITY ON THE CARBONYL GROUP OF ACYLPYRROLES IN THE GROUND STATE AND THE TWO LOW-EXCITED STATES

Compound	Ground State	1st Excited State	2nd Excited State
1-Acylpyrrole	0.065	0.056	0.383
2-Acylpyrrole	0.024	0.313	0.163
3-Acylpyrrole	0.026	0.162	0.226

The π electron densities on the carbonyl groups were evaluated in order to find an explanation for the different solvent-induced shifts of the absorption maxima of the acylpyrroles. The results are shown in Table 4. The extent of electron transfer in the ground state from the pyrryl to carbonyl group in 1-acylpyrrole is suggested to be larger than that in 2- and 3-acylpyrroles. This is in line with the fact that the barrier to internal rotation of carbonyl group in 1-acylpyrrole is higher than that in 2- and 3-acylpyrroles. In the first excited state, the π electron densities on the carbonyl groups of 2- and 3-acylpyrroles increase in comparison with those in the ground states. Thus, the first absorption bands of these compounds in ethanol are shifted to longer wavelength than those in n-hexane (Table 1). Similarly, the negligibly small solvent effects on the absorption bands of 1-acylpyrroles can be accounted for by the minute change in the calculated π electron density on the carbonyl group on going from the ground state to the first excited state.

The situation is much more complicated in the case

16) J. Tanaka, *Nippon Kagaku Zasshi*, **78**, 1636 (1957).
17) R. D. Brown and M. L. Heffernan, *Aust. J. Chem.*, **12**, 554 (1959).

of the second excited states of acylpyrroles. The correlation between the solvent-induced shift and the change in electron density at the carbonyl group is found only in the case of 3-acylpyrroles. From the values given in Table 4 we might expect a fairly strong solvent-dependence of the absorption due to the second lowest energy transition of 1-acylpyrrole. The experimental results are not in agreement with this expectation. Almost the same thing could be said with the second excited states of 2-acylpyrroles. It should be remembered that Band A of 1-acetylpyrrole shows an appreciable red-shift (1.8 kK) on the introduction of methyl groups at the 3- and 4-positions. A possible case might be where the π electron is actually transferred from the pyrryl to carbonyl group in the second excited state as indicated by calculation and also by the effect of methyl substitution at the 3- and 4-positions of 1-acetylpyrrole. The migration of π electrons thus induced might be counter-balanced by the polarization of σ electrons.

Experimental

Materials. The following compounds were prepared according to the method described in the literature given in parentheses or its modification: 1-formylpyrrole (Ref. 18, bp 81—83°C/60.5 mmHg), 1-acetylpyrrole (Ref. 19, bp 86.5°C/29 mmHg), 3,4-dimethyl-1-acetylpyrrole (Ref. 19, bp 120°C/27 mmHg), 2-methyl-1-acetylpyrrole (Ref. 20, bp 94—95°C/27.5 mmHg), 2,5-dimethyl-1-acetylpyrrole (Ref. 20, bp 110°C/23 mmHg), 2-formylpyrrole (Ref. 21, mp 44.4—44.9°C), 1-methyl-2-formylpyrrole (Ref. 21, bp 87—92°C/22 mmHg), 2-acetylpyrrole (Ref. 22, mp 92.0—92.7°C), 1-methyl-2-acetylpyrrole (Ref. 23, bp 92.3—94.0°C/22 mmHg), 3-acetylpyrrole (Ref. 24, mp 115.9—116.5°C), 1-methyl-3-acetylpyrrole (Ref. 9, bp 97.5—102.0°C/3 mmHg). All the above compounds were identified by elementary analyses, IR, and NMR spectra.

n-Hexane and ethanol were purchased from Wako Pure Chemicals Industries Ltd. They were repeatedly purified by the usual methods until they proved to be pure spectroscopically.

Spectroscopic Measurements. The electronic spectra were measured with a Bausch & Lomb Spectronic 505 Recording Spectrophotometer at temperatures between 17 and 19°C. The concentrations of the solutions were between 10^{-4} and 10^{-5} mol/*l*.

The authors are greatly indebted to the members of the Computer Center, Kyushu University, for their help in carrying out the VESCF MO calculations on a model OKITAC-5090H computer. Thanks are also due to Mr. Hajime Koga for his help in the study of the solvent effect on the spectra of 2-methyl-1-acetylpyrrole.

18) L. Alessandri, *Atti Accad Lincei*, **24**, **II**, 194 (1955); *Chem. Abst.*, **10**, 1350 (1916).
19) G. S. Reddy, *Chem. Ind.*, **1965**, 1426.
20) R. W. Guy and R. A. Jones, *Aust. J. Chem.*, **19**, 107 (1966).
21) R. M. Silverstein, E. E. Ryskiewicz, C. Williard, and R. C. Koehler, *J. Org. Chem.*, **20**, 668 (1958).
22) G. L. Ciamician and M. Dennstadt, *Ber.*, **16**, 2348 (1883).
23) A. Ermili, A. J. Castro, and P. A. Westfall, *J. Org. Chem.* **30**, 339 (1965).
24) H. J. Anderson and C. W. Huang, *Can. J. Chem.*, **45**, 597 (1967).

BULLETIN OF THE CHEMICAL SOCIETY OF JAPAN, VOL. 45, 1353—1357(1972)

The Isomerization of Propylene Oxide on Metal Phosphate Catalysts

Toshinobu IMANAKA, Yasuaki OKAMOTO, and Shiichiro TERANISHI
Department of Chemical Engineering, Faculty of Engineering Science, Osaka University, Osaka
(Received October 13, 1971)

The isomerization of propylene oxide was carried out on metal phosphate catalysts. The main products were allyl alcohol, propionaldehyde, acetone, and 1-propanol. It was found that allyl alcohol is produced by acid-base bifunctional catalysts, acetone, by basic-site catalysts only, and propionaldehyde, by acid-site catalysts. 1-Propanol may be produced by the hydrogen-transfer reaction of allyl alcohol. The conversion to propionaldehyde is proportional to the acidity of the catalyst, the strength of which is stronger than $H_0=+4.8$. The sum of the conversions to allyl alcohol, acetone, and 1-propanol correlate linearly with the observed basicity ($H_0 \geqq +7.2$) of the catalyst. The selectivity and activity are determined by the basic and acidic properties of the catalyst. The mechanisms of the propylene oxide isomerization are also discussed.

The activity and selectivity for a reaction on solid acids and bases are considered to be determined by the acidic and basic properties of the catalysts, and it is important to clarify the reaction between the acidic and basic properties of the catalysts and the selectivities and activities for the reactions. The relations between the activities and the observed acidities or basicities have already been reported by many workers.[1-4] However, as regards the relationship between the selectivity and the acidic and basic properties of the catalysts, little work has been done. Misono and his co-workers[5,6]

1) A. Tada, Y. Yamamoto, M. Ito, and A. Suzuki, Annual Meeting of the Chemical Society of Japan, 22nd, Tokyo, Preprints of Papers, No. 06421 (1969).
2) K. Tarama, S. Teranishi, K. Hattori, and T. Ishibashi, *Shokubai* (Tokyo), **4**, 69 (1962).
3) Y. Ogino, *ibid.*, **4**, 73 (1962).
4) K. Saito and K. Tanabe, *ibid.*, **11**, 206 (1969).
5) M. Misono, Y. Saito, and Y. Yoneda, *J. Catal.* **9**, 135 (1967).
6) M. Misono, Y. Saito, and Y. Yoneda, *ibid.*, **10**, 88 (1968).

have reported that the selectivities for the *n*-butene isomerization reaction over metal sulfates are determined by the acid strength of the catalyst. According to Niiyama and E. Echigoya[7] the selectivity for the dehydration and dehydrogenation of alcohols over acid-base bifunctional catalysts is controlled by the acid and base properties of catalysts. In our preceding paper,[8] the selectivity for the propylene-oxide isomerization on zeolite catalysts was determined by the acid strength of the catalysts. In this paper, the selectivity and activity for the propylene-oxide isomerization over metal phosphates will be investigated with respect to the acidic and basic properties of the catalysts.

Propylene oxide is generally isomerized to acetone, propionaldehyde, and allyl alcohol, but only a trace of allyl alcohol wasproduced on zeolite catalysts.[8] Fowler and Fitzpatrick[9] have reported that basic lithium phosphate has a high selectivity to allyl alcohol. It has been reported by Mathieu and co-workers[10,11] that propylene oxide is isomerized to allyl alcohol by basic sites on lithium phosphates and to propionaldehyde by acid sites on the 3.9 $Cr_2O_3 \cdot 1.1\ WO_3 \cdot 1.8\ H_2O$ catalyst.

The isomerization of propylene oxide on metal phosphates will be studied here. The relations between the selectivities and activities and the acidic and basic characteristics of catalysts are discussed. Moreover, a possible reaction mechanism of the isomerization is also discussed.

Experimental

Materials. The catalysts used were as follows: $NaLi_2PO_4$ (basic lithium phosphate), KLi_2PO_4, Na_2LiPO_4, K_2LiPO_4, $AlPO_4$, $Mg_3(PO_4)_2$, $Ca_3(PO_4)_2$, and Li_3PO_4. Basic lithium phosphate was prepared according to the method by Fowler and Fritzpatrick.[9] KLi_2PO_4, Na_2LiPO_4, and K_2LiPO_4 were prepared from potassium phosphate monobasic, sodium phosphate dibasic, and potassium phosphate dibasic respectively by neutralizing them with equivalent amounts of lithium hydroxide at 40°C. The following procedures were the same as those for basic lithium phosphate. The other reagents were commercial grade.

Procedures. The reactions were carried out using a usual pulse reactor in helium gas as the carrier. The catalysts (about 20 mg) were heated at a reaction temperature for about 2 hr in streaming helium before the reaction, The amount of reactant injected was 2 μl. Deactivation of the catalysts used was observed, and the material balance was found to hold approximately in this reaction.

The acidic and basic strengths of catalysts which had been heated at 300°C for 2 hr in air were measured by the conventional indicator method using a Hammett indicator. The acid and base contents were determined by the simple titration method, using *n*-butylamine and benzoic acid as the titers respectively.

Results and Discussion

The acid and basic strengths, the acidity ($H_0 \leq +6.8$ and $+4.8$), the basicity ($H_0 \geq +7.2$), and the surface area measured by the BET method are listed in Table 1 for each catalyst. Lithium phosphate has only acidic character, but Li_2MPO_4- and LiM_2PO_4-type phosphates (M=Na or K) have both basic and acidic properties. The product distributions of propylene oxide isomerization are shown in Table 2. The "other products" in the last column of Table 2 contain acrolein, polymers, and condensed products. Only small amounts of gaseous products and acetaldehyde, which may be products decomposed of propylene oxide and other products, are formed. High selectivities for allyl alcohol were obtained with sodium- or potassium-type lithium phosphates. The activation energies for allyl alcohol, acetone, propionaldehyde, 1-propanol, acetaldehyde, and gaseous products were 13.2, 6.1, 12.9, 12.0, 12.3, and 6.6 kcal/mol respectively over a basic lithium phosphate catalyst.

Generally, it is known[12-14] that when the oxygen atom of propylene oxide is attacked by a proton, the epoxide ring opens at the oxygen-α carbon linkage, and that when the β carbon is attacked by an anion, propylene oxide gives a product in which the oxygen-β carbon bond breaks. On the basis of these facts, it can be estimated that propionaldehyde is produced on acid

TABLE 1. ACIDIC AND BASIC PROPERTIES OF THE CATALYSTS

Catalyst	Surface area (m^2/g)	Maximum acid strength (H_0)	Acidity (mmol/g)[a]	Acidity (mmol/g)[b]	Maximum basic strength (H_0)	Basicity (mmol/g)[c]
Li_3PO_4	1	+4.8	0.020	0.006	—	—
Li_2NaPO_4	39	+6.8	0.025	—	+9.3	0.126
Li_2KPO_4	22	+6.8	0.014	—	+9.3	0.046
$LiNa_2PO_4$	15	+6.8	0.050	—	+9.3	0.040
Li_2KPO_4	19	+6.8	0.066	—	+9.3	0.016
$Ca_3(PO_4)_2$	54	+4.8	0.075	0.066	+7.1	0.052
$Mg_3(PO_4)_2$	8	+4.8	0.032	0.036	—	—
$AlPO_4$	28	+1.5	1.14	0.166	—	—

a) Measured at $H_0 = +6.8$ b) Measured at $H_0 = +4.8$ c) Measured at $H_0 = +7.2$

7) H. Niiyama and E. Echigoya, This Bulletin, **44**, 1739 (1971).
8) T. Imanaka, Y. Okamoto, and S. Teranishi, in press.
9) G. W. Fowler and J. Fitzpatrick, US 2426264.
10) M. Coudurier, M. N. Mathieu, M. Prettre, B. Imerik, and M. E. Degeorges, *Bull. Soc. Chim. Fr.*, **1968**, 1821.
11) G. France and M. B. Mathieu, *ibid.*, 2891 (1970).
12) F. C. Elderfield "Heterocyclic Compounds," Vol. 1 J. Wiley & Sons Inc., New York, London (1959).
13) A. Weissberger "Heterocyclic Compounds," Vol. 19 Part 1, Part 2, Interscience (1964).
14) M. Sander, *Chem. Rev.*, **66**, 297, 341 (1966).

Table 2. Product distributions on the propylene oxide isomerization

Catalyst	R. T. (°C)	Conv[a)] (%)	G. P. (%)	A (%)	PA (%)	AC (%)	1-PrOH (%)	AA (%)	O. P. (%)
Li_3PO_4	280	1.97	2.52	2.80	65.1	12.4	—	17.2	—
Li_2NaPO_4	260	28.7	0.14	1.11	4.78	2.76	2.79	86.0	2.40
Li_2KPO_4	240	28.2	0.17	1.09	13.3	10.3	2.54	71.2	1.45
$LiNa_2PO_4$	260	15.6	0.09	0.74	14.7	11.4	3.00	68.8	1.30
LiK_2PO_4	260	12.9	0.45	0.78	35.9	17.3	2.00	43.6	5.00
$AlPO_4$	280	42.7	0.14	0.10	91.7	—	0.72	4.44	2.92
$Mg_3(PO_4)_2$	260	20.0	0.71	0.42	75.2	4.70	1.95	15.8	1.31
$Ca_3(PO_4)_2$	260	40.2	0.59	0.59	37.3	13.5	15.0	20.3	11.5

a) Conversion (%)/10 mg cat.
G. P.: Gaseous products, A: Acetaldehyde, PA: Propionaldehyde, AC: Acetone, 1-PrOH: 1-Propanol, AA: Allyl alcohol, O. P.: Other products.

sites and that acetone is formed on basic sites. The poisoning effects of pyridine and dichloroacetic acid on the propylene oxide isomerization reaction were investigated in order to confirm these estimations. Figures 1a and 1b show the effects of pyridine injected with reactants over basic lithium phosphate. The conversions to propionaldehyde, allyl alcohol, and *n*-propanol decrease gradually with an increase in the amount of pyridine added, but those to acetone, acetaldehyde, and gaseous products increase with added pyridine. Without catalysts, only smallamounts of gaseous products and acetaldehyde were produced, and no effects of pyridine were observed. Hence, pyridine shows no catalytic effects in the gas phase. Consequently, it is considered that pyridine is adsorbed on acid sites and makes a basic site strong by means of an inductive effect.

Figures 2a and 2b show the effects of dichloroacetic acid on the reaction. The conversions to acetone, allyl alcohol, 1-propanol, and acetaldehyde decrease gradually with the addition of dichloroacetic acid, but those to propionaldehyde and gaseous products are un-

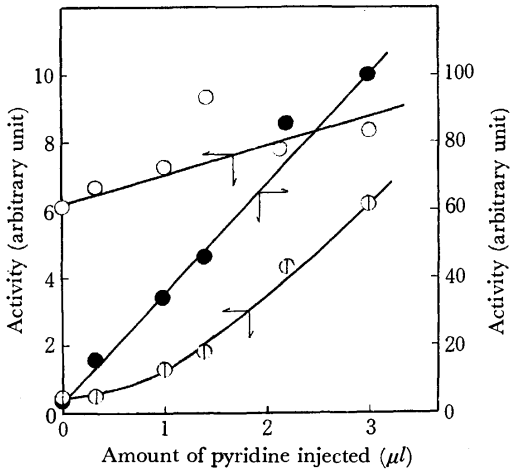

Fig. 1a. Effects of pyridine on the reaction
○: acetone, ●: acetaldehyde, ⦶: gaseous products

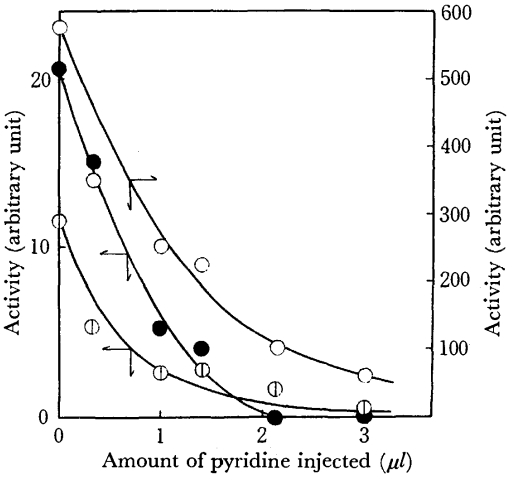

Fig. 1b. Effects of pyridine on the reaction
○: allyl alcohol, ●: propionaldehyde, ⦶: *n*-propanol

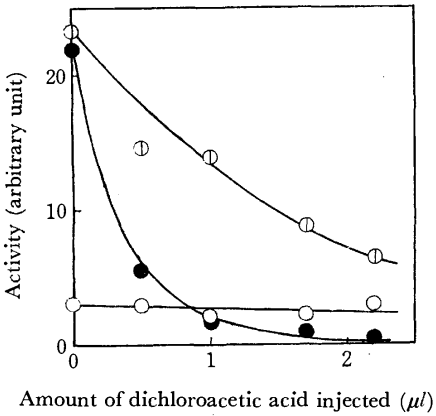

Fig. 2a. Effects of dichloroacetic acid on the reaction
○: gaseous products, ●: acetaldehyde, ⦶: acetone

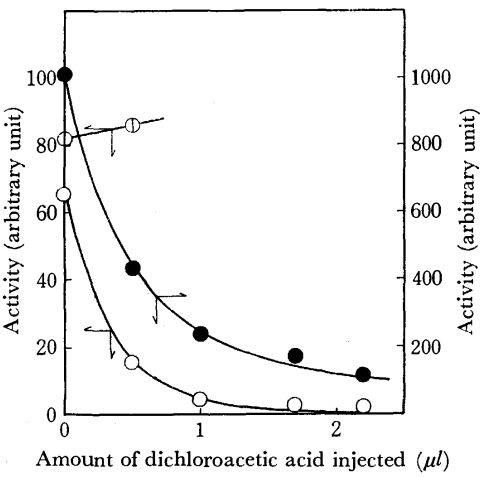

Fig. 2b. Effects of dichloroacetic acid on the reaction
○: 1-propanol, ●: allyl alcohol, ⦶: propionaldehyde

changed. Therefore, it may be concluded that propionaldehyde is produced on acid sites; acetone, acetaldehyde, and gaseous products, on basic sites, and allyl alcohol and 1-propanol, on acid-base bifunctional sites.

According to Table 2, a calcium phosphate catalyst produces larger amount of 1-propanol than do the other catalysts investigated. 1-Propanol is hydrogenated compound of propylene oxide, allyl alcohol, and propionaldehyde. The addition of water to the reaction system has no effect on the formation of 1-propanol. Moreover, in the case of the isomerization of propylene oxide, the amount of acrolein formed over calcium phosphate is 7.1% in the product distribution, but in the case of other catalysts, it is smaller than 1%. Hence, it is considered that the hydrogen atoms in 1-propanol come from the reactant and/or products by hydrogen-transfer reaction. The difference between the amount of 1-propanol and that of acrolein is deduced to be due to the fact that acrolein makes polymers easily. According to Figs. 1 and 2, the amount of 1-propanol gradually decreases as that of allyl alcohol does upon pyridine and dichloroacetic acid poisoning. Since the hydrogen-transfer reaction is considered to be catalyzed by basic sites, according to Schachter and Pines,[15] allyl alcohol must be at least concerned in the 1-propanol formation. Therefore, it may be deduced that 1-propanol and acrolein are produced by the hydrogen-transfer reactions between allyl alcohol and propylene oxide, propionaldehyde, and allyl alcohol.

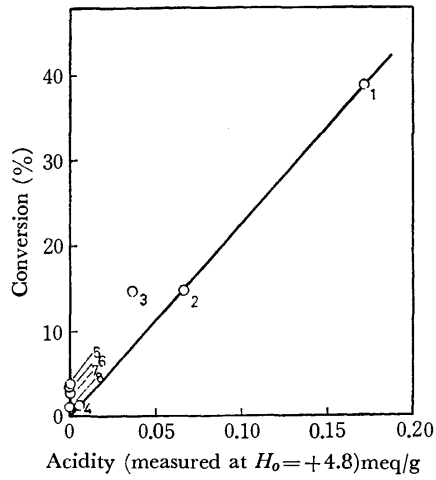

Fig. 3. Correlation between the conversion of propionaldehyde and the acidity measured at H_0=+4.8
1: $AlPO_4$, 2: $Ca_3(PO_4)_2$, 3: $Mg_3(PO_4)_2$, 4: Li_3PO_4, 6: KLi_2PO_4, 7: Na_2LiPO_4, 8: Li_2NaPO_4

The relationship between the conversion to propionaldehyde and the amount of the acid site, the strength of which is stronger than H_0=4.8, is shown in Fig. 3. However, there was no correlation when the acid content measured at H_0=+6.8 was taken into consideration. Therefore, it may be concluded that propionaldehyde is formed on stronger acid sites than H_0=+4.8. This conclusion is consistent with the results estimated from the propylene-oxide isomerization over a series of zeolite catalysts.[8] Figure 4 shows the

15) Y. Schachter and H. Pines, *J. Catal.*, **11**, 147 (1968).

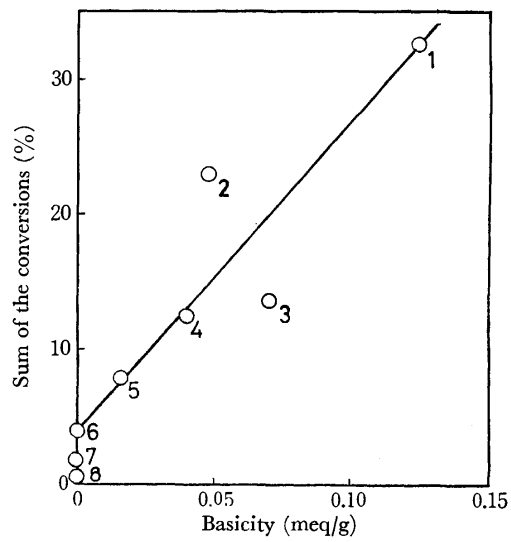

Fig. 4. Correlation between the sum of the conversions to allyl alcohol, acetone, and *n*-propanol and the basicity of the catalyst
1: Li_2NaPO_4, 2: KLi_2PO_4, 3: $Ca_3(PO_4)_2$, 4: Na_2LiPO_4, 5: K_2LiPO_4, 6: $Mg_3(PO_4)_2$, 7: $AlPO_4$, 8: Li_3PO_4.

relation between the observed basicity (H_0=+7.2) and the sum of the conversions to acetone, allyl alcohol, and 1-propanol. Acetaldehyde and gaseous products were disregarded in view of the small amounts of them formed. However, there were no good correlation between the basicity and the respective conversion to them. Consequently, acetone, allyl alcohol, and 1-propanol are considered to be formed competitively over basic sites.

The formation of allyl alcohol needs both acid and basic sites. However, the Li_2NaPO_4 catalyst, which is most active in allyl alcohol formation, has only weak acid (H_0=+6.8). Therefore, it may be concluded that the acid sites which are active for allyl alcohol production are weak ones. According to Fig. 1, the amount of propionaldehyde decreases more rapidly than that of allyl alcohol does. This fact supports our conclusion. As regards the selectivities of acetone and allyl alcohol, the strong base is considered to be favorable for allyl alcohol formation from the following facts. According to Table 1 and Table 2, the Li_2NaPO_4, Li_2KPO_4, $LiNa_2PO_4$, and LiK_2PO_4 catalysts have stronger basic sites and higher selectivities of acetone and propionaldehyde than do the other catalysts. Therefore, it can be concluded that the selectivity and the activity for the propylene oxide isomerization are controlled by the acidic and basic properties of the catalyst.

On the basis of these facts, the reaction mechanisms may be considered to be as follows. In the case of allyl alcohol formation, propylene oxide is adsorbed on the basic site, thus forming carbanion, the carbanion attacks acid sites and the epoxide ring is opened to produce allyl alcohol consequently. The rate-determining step of allyl alcohol formation is considered to be the proton-abstraction process on basic sites on the basis of the facts that the formation of allyl alcohol is controlled by the basicity of the catalyst. As regards acetone, the β carbon of propylene oxide attacks the basic site and the

oxygen-β carbon bond is broken. In the case of propionaldehyde, propylene oxide adsorbs with the oxygen atom on the acid site and the oxygen-α carbon linkage opens. The stronger the acid strength, the more easily the bond is broken, as was shown in the preceding paper.[8)]

BULLETIN OF THE CHEMICAL SOCIETY OF JAPAN, VOL. 45, 1357—1361(1972)

Intermolecular Hydrogen Transfer Reactions in the Excited States of EDA-Complexes of Benzophenone with Aromatic Amines at Low Temperature

Satoshi ARIMITSU* and Hiroshi TSUBOMURA

Department of Chemistry, Faculty of Engineering Science, Osaka University, Toyonaka, Osaka

(Received October 18, 1971)

Electronic absorption and emission spectra of the mixtures of benzophenone and aromatic amines have been studied in rigid solutions. From absorption spectral measurements, it has been concluded that benzophenone as an acceptor forms the molecular complexes with various aromatic amines as donors. Emission spectra different from those of the component molecules were observed at longer wavelengths in the same systems. The maxima of the anomalous emission spectra of these systems were found to shift slightly to lower frequencies with the decrease in the ionization potentials of donor molecules. On account of their decay times, the emissions may be ascribed to the phosphorescence of benzophenone-aromatic amine complexes. Photolysis of benzophenone-aromatic amine complexes in rigid matrices always resulted in the appearance of the visible absorption spectrum of benzoketyl radical, together with ESR spectra, the analysis of which indicated that there is an interacting pair of radicals which is in the combined triplet ($S=1$) state. From the evaluation of the zero field splitting constants, the average distances between the interacting radicals were estimated. These results suggest that intermolecular hydrogen atom transfer from aromatic amines to benzophenone occurs, yielding the ketyl and aromatic amine radicals which lie close to each other. The reaction was found to proceed by way of the lowest excited triplet state of benzophenone.

The photochemical reactions of aromatic ketones as correlated with the nature of their excited electronic structures have been an interesting subject in photochemistry. As the results of numerous investigations, it has been confirmed that ketones at the lowest $^3(n,\pi^*)$ state were photoreduced easily, while those at the lowest $^3(\pi,\pi^*)$ state were scarcely photoreduced.[1] The spectra of the photochemical reaction intermediates of these ketones, such as the triplet species and the ketyl radicals, have been obtained.[2-6]

Recently, Cohen and co-workers found that the yields of benzopinacol and related compounds from benzophenone and its derivatives get higher in aliphatic amines.[7] They proposed that the photoreduction may be facilitated by initial electron transfer from the amine to the excited ketones, leading to charge transfer complexes or pairs of ions, followed by proton transfer and electron redistribution. However, no evidence has been presented suggesting the formation of charge transfer complexes between aromatic ketones in the excited state and aliphatic amines in the ground state.

We have reported in a short communication that the photoreduction of benzophenone (BP) in *N,N*-dimethylaniline (DMA) and 2-methyltetrahydrofuran (2MTHF) mixed solvent occurs easily, producing ketyl radical at the temperature of liquid nitrogen.[8] Since no ketyl radical was found appreciably by the photolysis of BP in 2MTHF solution at 77°K, we pointed out that the charge transfer complex formation between BP and DMA, suggested by an electronic absorption measurement, is a prerequisite for the formation of ketyl radical.

In the present paper, more detailed studies on the BP-aromatic amine systems will be reported, and the photoreactivity and photoreaction mechanism of the charge transfer complexes of BP with aromatic amines will be discussed in relation with the electronic structure and the charge transfer interaction in the excited molecular complex.

Experimental

Materials. BP was purified by recrystallization from ethanol and sublimation twice in vacuum. Aromatic amines

* Present address: Sagami Chemical Research Center, 3100 Ohnuma, Sagamihara, Kanagawa.

1) P. J. Wagner and G. S. Hammond, *Advan. Photochem.*, **5**, 99 (1968); N. C. Yang and R. L. Dusenberg, *J. Amer. Chem. Soc.*, **90**, 5899 (1968); P. J. Wagner, A. E. Kemppainen, and H. N. Schott, *J. Amer. Chem. Soc.*, **92**, 5280 (1968).

2) D. S. McClure and P. L. Hanst, *J. Chem. Phys.*, **23**, 1772 (1955).

3) G. Porter and F. Willkinson, *Trans. Faraday Soc.*, **57**, 1686 (1961); G. Porter and P. Suppan, *ibid.*, **61**, 1664 (1965); G. Porter and R. M. Topp, *Proc. Roy. Soc.* (London), **315**, 163 (1970).

4) J. A. Bell and H. Linschitz, *J. Amer. Chem. Soc.*, **85**, 528 (1963).

5) H. Tsubomura, N. Yamamoto, and S. Tanaka, *Chem. Phys. Lett.* **1**, 309 (1967).

6) T. S. Godfrey, J. W. Hilpern, and G. Porter, *Chem. Phys. Lett.*, **1**, 490 (1967).

7) S. G. Cohen and J. I. Cohen, *J. Amer. Chem. Soc.*, **89**, 164 (1967); S. G. Cohen and R. J. Baumgarten, *ibid.*, **89**, 4571 (1967).

8) S. Arimitsu and H. Tsubomura, This Bulletin, **44**, 2288 (1971).

used were aniline (AN), *N*-methylaniline (NMA), *N,N*-dimethylaniline (DMA), *N,N*-diethylaniline (DEA), and *N*-methyldiphenylamine (NMDPA). Aniline and *N*-methylaniline were purified by distillation under reduced pressure. All other amines were refluxed with acetic anhydride for several hours, and purified by fractional distillation. The amines were kept in a deoxygenated condition. 2-Methyltetrahydrofuran (2MTHF) was dried with sodium and purified by distillation. The solvent used as a transparent organic matrix was a mixture of 2MTHF and aromatic amine (3: 1 by volume). The concentration of the solution of BP was about 5×10^{-3}M in most experiments. All samples studied were deaerated by the usual method with an evacuating system.

Apparatus. Photolysis was carried out by use of a 500-W super high-pressure mercury lamp, combined with Toshiba UV-D25 and UV-35 glass filters transparent in the wavelengths from 350 to 400 nm. The absorption spectra were measured with a Cary 15 spectrophotometer. The emission spectra were measured with an Amino-Bowman spectrophotofluorimeter equipped with a photomultiplier of RCA Type R213. The emission decay time was measured by using a Xe-flash lamp and the discharge from a tungsten air gap having duration times of *ca.* 10 μsec and 100 nsec, respectively. ESR spectra were measured at 77°K by a JES-3BX spectrometer of Japan Electron Optics using X-band with 100 kHz field modulation.

Results and Discussion

Absorption Spectra of Benzophenone - Aromatic Amines. The electronic absorption spectrum of BP in the near ultraviolet region shows vibrational structures at low temperature, assigned to the (n,π^*) transition (Fig. 1a). On the other hand, the spectrum of BP in *N,N*-diethylaniline (DEA) shows a quite different shape in the same region at 77°K as shown by spectrum b in Fig. 1, which was obtained by subtracting the absorption of DEA. The difference between these two spectra is obviously much greater than to be explained by the solvent effects, but seems to suggest a molecular complex formation between BP and DEA. The spectrum of Fig. 1b then may be interpreted as an (n,π^*) band of BP broadened by the coupling with the intermolecular vibration within the complex. From the electronic nature of benzophenone, it seems most probable that BP acts as an electron acceptor and *N,N*-diethylaniline (DEA) acts as a donor. Similar spectra, which suggest the formation of complex, have been observed for BP in various mixed solutions of 2MTHF and aromatic amines at 77°K. As the electronic absorption spectrum of BP in triethylamine solution does not change appreciably from that of BP in 2MTHF at 77°K, the interaction in this case seems to be very weak.

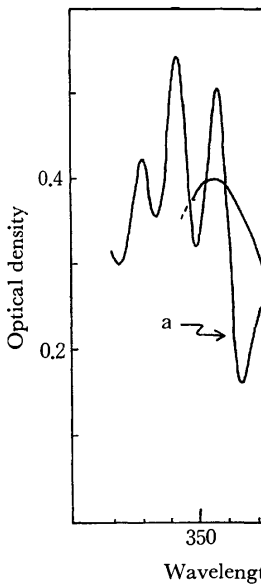

Fig. 1. Electronic absorption spectra of benzophenone in solvents at 77°K.
a: in 2-methyltetrahydrofuran, b: in *N,N*-diethylaniline

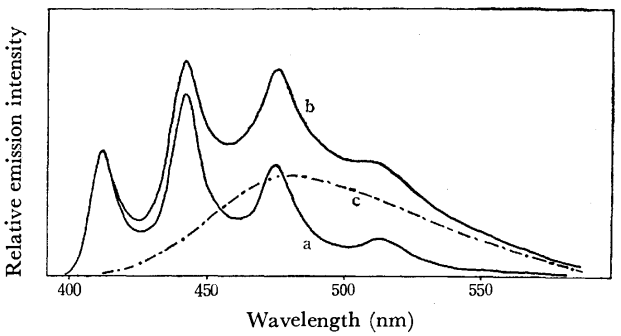

Fig. 2. Emission spectra of benzophenone and its complex with *N,N*-dimethylaniline at 77°K.
a: benzophenone in 2-methyltetrahydrofuran, b: benzophenone in 1 vol. *N,N*-dimethylaniline and 3 vol. 2-methyltetrahydrofuran, c: Emission of benzophenone-*N,N*-dimethylaniline complex obtained by subtracting spectrum a from b.

Emission Spectra of Benzophenone - Aromatic Amines. The phosphorescence spectrum of BP observed in 2MTHF solution at 77°K, having characteristic vibrational structures, is shown by spectrum a in Fig. 2. The emission spectrum of BP in a mixed solution (1 vol. DMA–3 vol. 2MTHF) at 77°K is shown by spectrum b in Fig. 2. From the comparison between these spectra, it may be seen that spectrum b is composed of spectrum a plus an additional emission lying at the longer wavelengths. Spectrum c is obtained by subtracting spectrum a from b. The emission spectrum c thus obtained is undoubtedly due to neither BP nor DMA. Moreover, the excitation spectrum obtained for the emission at 495 nm, where the emission is mostly composed of spectrum c, is fairly similar to that of the absorption of charge transfer complex of BP with DMA, while that observed for the emission at 412 nm is in good agreement with that of the absorption of BP at 77°K. Therefore, it may safely be concluded that the emission corresponding to curve c is due to BP–DMA complex.

The emission spectra of BP complexes with DMA, DEA, and NMDPA are shown in Fig. 3. The emission maxima show a tendency to shift to the longer wavelength with decreasing the ionization potentials of donor molecules. These results, together with the finding that these emission spectra shift to longer wavelengths with increase in the dielectric constant of the solvent indicate that the excited state of the BP complexes has the charge transfer nature.

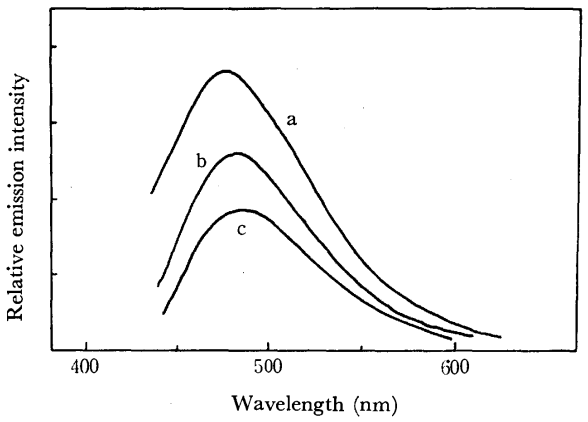

Fig. 3. Emission spectra of benzophenone complexes with various aromatic amines at 77°K.
a: *N,N*-dimethylaniline, b: *N,N*-diethylaniline, c: *N*-methyldiphenylamine

It was also found that the emission of the BP–DMA complex is quenched remarkably by ethanol used as a solvent instead of 2MTHF.

In order to get further information on the emission of the complexes, we also measured the emission decay-time. The phosphorescence of BP in 2MTHF decays exponentially with a decay time of 5 msec at 77°K. In the presence of aromatic amines at 77°K, the emission decay curve revealed that there are two components, one with a decay constant of 2.6 msec and another with a decay constant of *ca.* 10 μsec. The former may be assigned to an emission due to free BP, and the latter may be assigned to complexed BP, corresponding to the emission spectrum of Fig. 2c. It may be appropriate to conclude that the emission is due to the CT phosphorescence of the BP complex with the aromatic amine. The phosphorescent state of the complex may be mainly the locally excited $^3(n,\pi^*)$ configuration of BP mixed with the charge transfer configuration, since the peak positions of the phosphorescence spectra of complexes shift only slightly by changing the ionization potentials of donor molecules. The remarkable change of the phosphorescence life-time of BP-aromatic amine complex compared with that of free BP may be caused

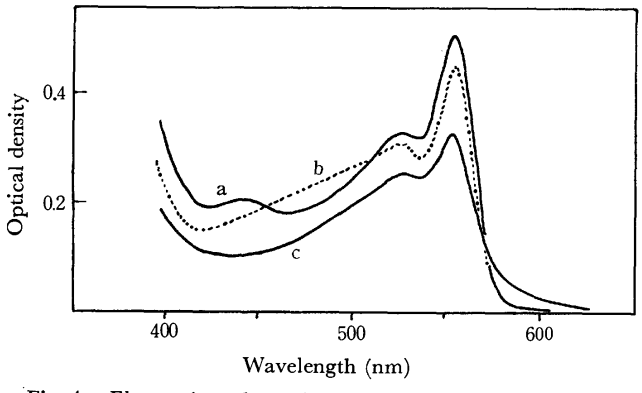

Fig. 4. Electronic absorption spectra of benzophenone complexes with aromatic amines irradiated at 77°K: a: benzophenone in *N*-methylaniline and 2-methyltetrahydrofuran, b: benzophenone in *N,N*-diethylaniline and 2-methyltetrahydrofuran, c: benzophenone in *N*-methyldiphenylamine and 2-methyltetahydrofuran

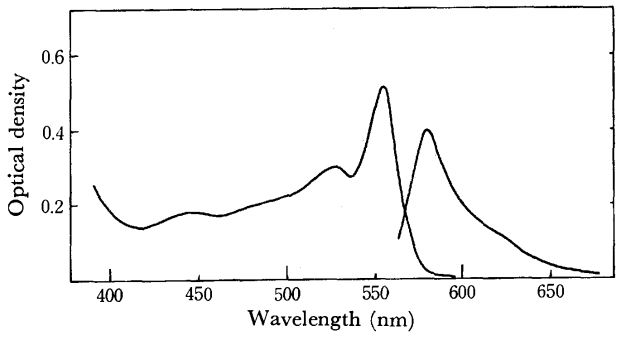

Fig. 5. Absorption and emission spectra of ketyl radical obtained by the photolysis of benzophenone-*N,N*-dimethylaniline complex at 77°K.

by the configuration interaction and spin-orbit coupling between the charge transfer and locally excited configurations. This problem is discussed in some detail by Iwata, *et al.*[9]

Hydrogen Abstraction of Benzophenone in Low Temperature Matrices. When the ternary solution of BP-aromatic amine-2MTHF was irradiated at the temperature of liquid nitrogen, the matrices colored red. The electronic absorption spectra after the photolysis of the solutions of BP–NMA, BP–DMA, BP–DEA, and BP–NMDPA in 2MTHF at 77°K are shown in Figs. 4 and 5. These absorption spectra disappeared after warming.

At a glance, these electronic absorption spectra are very similar to that of the ketyl radical obtained by flash photolysis of BP in ethanol or iso-pentane at room temperature.[5,6] Therefore, we may safely conclude that the main product is the ketyl radical. By more careful inspection of the spectra obtained, it is noticed that there is at least one more component, for instance, at about 445 nm in the case of DMA.

In the case of BP in a mixed solution of aniline and 2MTHF, the yield of ketyl radical was found to be about one tenth that for DMA and other aromatic amines mentioned above. It seems, therefore, that the presence of the alkyl group at the nitrogen atom is necessary for facilitating the hydrogen abstraction reaction.

The ketyl radical was also produced by the photolysis of BP in the solution of DMA and trichloro-trifluoroethane, the latter of which has no hydrogen atom to abstract. This result definitely indicates that the ketyl radical is produced as a result of hydrogen atom transfer from DMA to BP. The comparison of the absorption spectra shown in Figs. 4 and 5 with the absorption spectrum of ketyl radical obtained before[5] indicates that there are some components having absorptions in the region from 400 to 500 nm. In the case of the BP–DMA system, a clear peak is observed at 450 nm. In the present circumstances, these absorptions might be tentatively attributed to the radicals formed by the hydrogen abstraction from the alkyl group of the methylanilines; for example, $\phi\text{–N}\langle^{CH_3}_{CH_2}$, in the case of BP–DMA.

9) S. Iwata, J. Tanaka, and S. Nagakura, *J. Chem. Phys.*, **47**, 2203 (1967).

Since no ketyl radical was found noticeably by the photolysis of BP in the aniline-trichlorotrifluoroethane solution, it seems reasonable to assume that the hydrogen atom of the solvent is abstracted in the photoreduction of BP-aniline system.

These conclusions are confirmed by the measurement of ESR spectra and the excitation spectrum of the ketyl radical emission, which will be described in the following section.

When the solution of BP in a mixture of aliphatic amine, such as triethylamine, and ether was irradiated at 77°K, no ketyl radical was found appreciably. This result is in harmony with our observation of the absorption spectrum of the same system, which suggests no complex formation between BP and triethylamine in the ground state. It has also been found that photoreduction of BP proceeds only slightly in a solution of DMA and ethanol, contrary to the solution of DMA and 2MTHF.

Emission Spectrum of Ketyl Radical. We have tried to measure the luminescence spectrum of the ketyl radical using the photolysis products of BP complexes with aromatic amines. The emission spectrum observed in the case of the BP–DMA complex is shown in Fig. 5. The mirror symmetry relation between absorption and emission spectra can be seen. The excitation spectrum for the ketyl radical emission is in good agreement with the absorption spectrum of ketyl radical formed by the photolysis of BP–DMA complex, except that the absorption band with peak at 445 nm attributed to DMA radical was not found in the excitation spectrum.

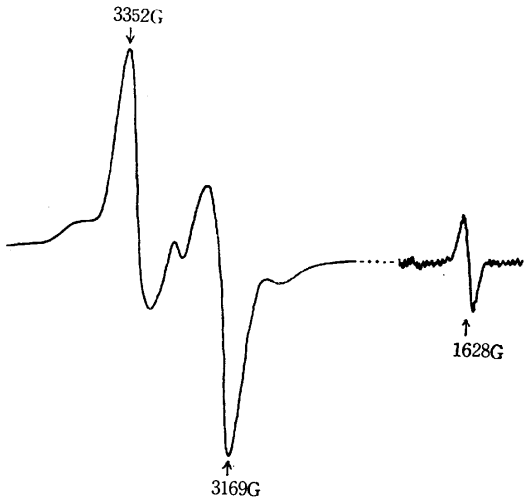

Fig. 6. ESR spectrum of benzophenone in *N*-methyldiphenylamine-2-methyltetrahydrofuran irradiated at 77°K: (ν= 9143 MHz).

ESR Spectra of Irradiated BP-Aromatic Amine Complexes. Figure 6 shows a typical ESR spectrum obtained after the photolysis of BP in NMDPA–2MTHF rigid glass at 77°K. This spectrum can be interpreted clearly on the basis of randomly oriented radical pairs in the triplet state ($S=1$).[10] In some cases, the absorption due to a free radical was observed slightly at the region of $g=2$ in addition to the spectrum as shown in Fig. 6. Photolysis of BP complexes with NMA, DMA, and DEA in 2MTHF also showed the similar ESR spectra. In case where the fine structure constant E is assumed to be zero, the ESR spectrum of a triplet radical pair is predicted to consist of a band due to the forbidden $\Delta m=\pm 2$ transitions at magnetic field strength $H=h\nu/2g\beta$, and two pairs of bands due to the allowed $\Delta m=\pm 1$ transitions having separations D and $2D$ with the center at the magnetic field strength $H=h\nu/g\beta$. D represents here the zero field splitting constant and ν the resonance microwave frequency.

TABLE 1. ZERO-FIELD SPLITTING CONSTANT (D) AND AVERAGE DISTANCE OF THE RADICAL PAIRS BETWEEN KETYL AND AROMATIC AMINE RADICALS, CALCULATED FROM OBSERVED ESR SPECTRA OF THE IRRADIATION PRODUCTS OF BENZOPHENONE-AROMATIC AMINE COMPLEXES

Aromatic Amine	D (gauss)	R (Å)
Aniline	<95	<6.64
N-methylaniline	162	5.55
N, *N*-dimethylaniline	154	5.64
N, *N*-diethylaniline	128	6.00
N-methyldiphenylamine	166	5.48

The ESR spectra obtained in the present work unambiguously lead to the conclusion that radical pairs in the triplet state are obtained. Although there have been some investigations on the ESR spectra of radical pairs made of equal radicals,[11] the studies on radical pairs composed of different species are rather scarce.[12] Table 1 shows the D values obtained from the experimentally observed separation corresponding to $2D$. One can see from Table 1 that the zero field splitting constants change from one to another. This result suports our previous conclusion that the ketyl radical is produced as a result of intermolecular hydrogen atom transfer from aromatic amine to BP, because, if the hydrogen atom is abstracted from the solvent molecule, the D values should be the same in all systems.

The ESR spectrum observed for photolyzed BP-aniline complex is somewhat different from that of BP–NMDPA complex at 77°K as shown in Fig. 7, the zero-field splitting constant being about 95 gauss, at most, which is fairly small compared with other values obtained in the present work. This small separation, together with the apparent absence of the weak absorption bands corresponding to the $2D$ separation, might arouse the suspicion that the spectrum is not due to the triplet species. However, it seems unlikely that this spectrum is due to separated free radicals ($S=1/2$), because a splitting of about 95 gauss is inadequately large for an ESR spectrum of any aromatic free radicals. Moreover, it was also confirmed that the spectrum is not ascribed to the solvent radicals produced by a

10) J. H. van der Waals and M. S. de Groot, *Mol. Phys.*, **2**, 333 (1954); W. A. Yager, E. Wasserman, and R. M. R. Cramer, *J. Chem. Phys.*, **37**, 1148 (1962).

11) Y. Kurita, *J. Chem. Phys.*, **41**, 3926 (1964); H. Ohigashi and Y. Kurita, This Bulletin, **40**, 704 (1967); D. A. Wierson and J. Kommandeur, *Mol. Phys.*, **13**, 241 (1967).

12) W. Gordy and R. Morehouse, *Phys. Rev.*, **151**, 207 (1966); M. C. R. Symons, *Nature*, **231**, 1226 (1967); S. Niizuma, H. Kokubun, and M. Koizumi, This Bulletin, **44**, 335 (1971).

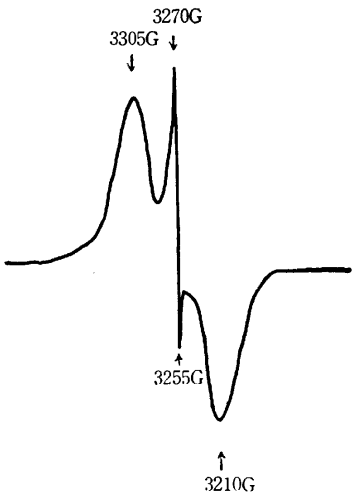

Fig. 7. ESR spectrum of benzophenone in aniline-2-methyltetrahydrofuran irradiated at 77°K: (ν=9135 MHz). The sharp ESR signal shown by arrows at 3270 G and 3255 G seems to be a radical species formed by dark reaction, because it was obtained for the BP-aniline-2MTHF mixture before irradiation.

photosensitization reaction. The most plausible interpretation for this spectrum is that the ketyl radical formed by direct hydrogen abstraction of BP from 2MTHF intracts with a 2MTHF radical. This is consistent with our experimental result described before that BP–AN complex in trichlorotrifluoroethane does not yield ketyl radical detectably.

The average distance R(Å) between radicals can be calculated using a point-spin-density approximation discussed by Kurita[13] as follows:

$$R^3(\text{Å}) = \frac{27800}{D(\text{gauss})}$$

The R values thus obtained are summarized in Table 1. In the case of BP–NMDPA complex, the average distance is the shortest of all cases. This might, however, be due to the theoretical approximation applied to a radical pair, because the unpaired electrons are distributed over the molecular framework of the component radicals, resulting in a slight underestimation of the average distance between radicals as the radicals get larger.

It seems curious that two radicals coexist stably at the temperature of liquid nitrogen within a short distance from each other as concluded in the present work. The reason for this may be attributed to a large resonance stabilization of these radicals owing to the delocalization of the unpaired electrons preventing a chemical bond formation or back transfer of hydrogen atom.

Photochemical Reaction Mechanism and Reactivity of BP Complexes. As is described in previous sections, we found that the photoreduction of BP undergoes easily in the solution of aniline derivatives and 2MTHF at 77°K. But the use of ethanol as the solvent instead of 2MTHF retards it to a great extent. Correspondingly, it has been found that the phosphorescence of BP complexes with aromatic amines is quenched remarkably by ethanol. This further gives support to the conclusion that photoreduction of the ketone in BP complexes undergoes through the triplet state of BP–aromatic amine complex.

In the case of BP–aniline complex, it has been concluded that hydrogen atom is abstracted from the solvent instead of aniline. As the yield of ketyl radical in this case is only about one tenth that in other cases, the hydrogen abstraction from solvent to BP is thought to be very slow. It seems plausible to attribute the difference in the photo-reactivity between aniline and other donors, to the presence of the *N*-methyl group. Although the reason for this effect of methyl group is not quite clear, it may be attributable to a steric circumstance for *N*-methylanilines, bringing a hydrogen atom at a closer position to the oxygen atom of BP in the complex.

The last question we have to answer is why photoreactivity of BP is much more enhanced in the molecular complex than in free BP. As mentioned before, the photoreduction of BP complexes undergoes most probably *via* the lowest triplet state, which is mainly of the locally excited $^3(n,\pi^*)$ character, with inclusion of a slight charge transfer character. That $^3(n,\pi^*)$ state is the state which undergoes hydrogen abstraction was demostrated by a paper by Porter and Suppan.[14] Our subsequent paper will give evidences for the necessary character of excited states for systems more directly related with the present problem. Therefore, the hydrogen abstraction reaction must essentially be a radical reaction and such a process as the electron transfer followed by proton jump from the aniline derivative to BP is unlikely. The reason why the hydrogen transfer is fascilitated by a comlpex formation between the anilines and BP may be as follows: 1) The binding of the complex may realize a geometric configuration where the hydrogen of the aniline derivative is situated at a position better for the abstraction reaction. 2) A slight mixing of the charge transfer character in the $^3(n,\pi^*)$ state may cause a change in the electron distribution, for example, a change in the orbital exponent of the oxygen n-orbital, which decreases the activation barrier for the hydrogen abstraction reaction.

The authors wish to thank Professor Koichi Ito for discussions on the interpretations of the ESR spectra.

13) Y. Kurita, *J. Chem. Phys.*, **41**, 3926 (1964).

14) G. Porter and P. Suppan, *Trans. Faraday Soc.*, **61**, **1965**, 1664.

Polarized Absorption Spectra of Crystals of Indole and Its Related Compounds

Yukio YAMAMOTO and Jiro TANAKA

Department of Chemistry, Faculty of Science, University of Nagoya, Chikusa-ku, Nagoya

(Received October 22, 1971)

The polarized absorption spectra of crystals of indole derivatives have been measured in order to confirm the presence of two types of electronic transitions, ^1L_b and ^1L_a, in the long-wavelength absorption region, and in order to determine the direction of their transition moments. The polarization spectra show that the ^1A—^1L_b electronic transition forms a sharp absroption band with vibrational structures lying below a broader absorption band of the ^1A—^1L_a transition. The transition memont direction of the ^1L_b makes an angle of 54° to the long axis of the molecule, while that of the ^1L_a lies at an angle of −38° to the same axis. These results were compared with the results of theoretical calculations of the P-P-P SCF MO-CI method.

The excited states of indole and its related compounds have been studied by many workers by means of absorption and emission spectral measurements in solution.[1-8] The absorption band of indole and tryptophan in the region of 40000—32250 cm^{-1} (250—310 nm) is composed of two different types of electronic transitions.[1,2] One is ^1A—^1L_b, with maxima at 34800 cm^{-1} (287 nm) and 35850 cm^{-1} (279 nm), while the other is the ^1A—^1L_a type forming a broad band with a maximum at 36200 cm^{-1} (276 nm). We have studied the polarized absorption spectra of crystals in order to clarify the vibrational structures of the ^1L_b and ^1L_a electronic levels and to find the direction of their transition moments. This study may be important in connection with the circular dichroism and chromophore interactions of tryptophan and its derivatives.

Experimental

The ultraviolet absorption spectrum of the solution was measured by means of a Carl-Zeiss PMQ-II-type spectrophotometer. The absorption spectra of crystals were obtained by the use of the microspectrophotometer described previously.[9]

Materials. The indole was of a special grade from the Tokyo Chemical Industry Co. and was purified by recrystallization from an ethanol-water mixture and by column chromatography. The crystal used for the spectral measurement was obtained from a methylcyclohexane solution. The 3-indolylacetic acid was purchased from the Nakarai Chemical Co. and was purified by recrystallization. The crystal obtained from chloroform had a form of diamond-shaped plates. The glycyl-L-tryptophan was of a pfs grade purchased from the Sigma Chemical Co. and was used without further purification. The glycyl-L-tryptophan dihydrate was obtained in the form of plate-like crystals from water-methylcellsolve solutions.

Results and Discussion

Absorption Spectra of Crystals. **1)** *Indole*: The crystal structure of indole has not yet been determined. The crystal used for the absorption measurement had an elongated plate-like shape and was thin enough to have an adequate optical density for the spectral measurement. Figure 1 shows the absorption spectrum of the indole crystal produced by a light polarized along the *X*-axis (the vibration direction of the faster ray), which shows maxima at 34250 cm^{-1} (292 nm), 35100 cm^{-1} (285 nm) and 36350—37000 cm^{-1} (275—270 nm), and one produced by a light polarized along the *Z*-axis (the vibration direction of the slower ray), which shows peaks at 34500 cm^{-1} (290 nm), 35350 cm^{-1} (283 nm) and 36650 cm^{-1} (273 nm). These vibrational peaks show a good correspondence to those of the solution spectrum.[1] The 0-0 absorption band of the indole

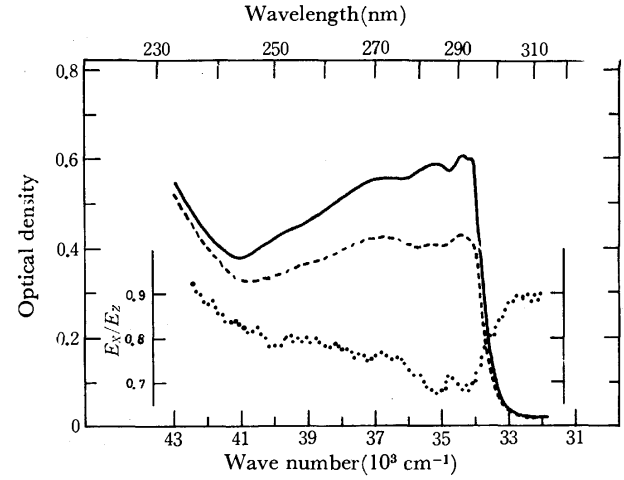

Fig. 1. The polarized absorption spectrum of the single crystal of indole.
The solid and broken lines show the spectrum parallel to the *Z*-axis and the *X*-axis in the crystals respectively. The dotted line indicates the polarization ratio (E_x:E_z). The polarization ratio in the 32400—33700 cm^{-1} region was obtained using a thicker plate which had the optical density of 0.75 at 33400 cm^{-1} for the absorption parallel to the *Z*-axis.

1) S. V. Konev, "Fluorescence and Phosphorescence of Proteins and Nucleic Acids", Plenum Press, New York, N. Y. (1967).
2) G. Weber, *Biochem. J.*, **75**, 335 (1960).
3) H. Zimmermann and H. Joop, *Ber. Bunsenges. Phys. Chem.*, **65**, 61 (1961).
4) H. U. Schutt and H. Zimmermann, *Z. Elektrochem.*, **67**, 54 (1963).
5) N. Mataga, Y. Torihashi, and K. Ezumi, *Theor. Chim. Acta* (Berl.), **2**, 158 (1964).
6) G. S. Kembrovskii, V. P. Bobrovich, and S. V. Konev, *Zh. Prikl. Spektrosk.*, **5**, 695 (1966).
7) J. Eisinger and G. Navon, *J. Chem. Phys.*, **50**, 2069 (1969).
8) P. S. Song and W. E. Kurtin, *J. Amer. Chem. Soc.*, **91**, 4892 (1969).
9) J. Tanaka, This Bulletin, **36**, 833 (1963).

crystal is red-shifted nearly 600 cm^{-1} relative to that of indole in *n*-hexane. In order to compare the absorption intensity produced by the light along the *X*-axis with that produced by the light along the *Z*-axis, the polarization ratio ($E_x : E_z$) as a function of the wavenumber was plotted. In the region of 32350 to 33500 cm^{-1} (309 to 298 nm), the polarization ratio has a higher value, 0.9. With an increase in the wavenumber, the polarization ratio is markedly reduced, having its minimum at 34100 cm^{-1} (293 nm). In the 35450—36750 cm^{-1} (283—272 nm) range, there is an increase in the polarization ratio and it has a maximum at 37000 cm^{-1} (270 nm). Thus, the variation in the polarization ratio suggests that the long-wavelength absorption band consists of two different electronic transitions, $^1A—^1L_b$ and $^1A—^1L_a$, and that the former transition forms a sharp absorption band lying below a broader absorption band due to the latter type of transition. The constancy of the polarization ratio in the 32350—33500 cm^{-1} region and in the 37000—40800 cm^{-1} region indicates that the absorptions in these regions are composed of mainly the $^1A—^1L_a$ transition. The reduction in the polarization ratio in the range from 33500 to 34100 cm^{-1} may be due to the increase in the contribution of the $^1A—^1L_b$ transition. Therefore, it is clear that the first two vibrational maxima at 34250 and 35100 cm^{-1} for the *X*-axis (34500 and 35350 cm^{-1} for the *Z*-axis) belong to the $^1A—^1L_b$ transition and that the broad band near 36350—37000 cm^{-1} for the *X*-axis (36650 cm^{-1} for the *Z*-axis) to the $^1A—^1L_a$ transition. These results are in good correspondence to the results obtained for the absorption polarization spectrum of the fluorescence of tryptophan and indole solutions.[1,2,10]

2) 3-Indolylacetic Acid: According to Karle *et al.*,[11] the crystal belongs to the space group of $P2_1/c$, with four molecules per unit cell. The (100) face develops, and the projection of molecules onto this face is shown in Fig. 2(a). The molecules form a dimeric structure with hydrogen bonds between the acid groups; the NH group in indole is not involved in any hydrogen bonding. The crystalline absorption spectrum was measured with the (100) face by a light polarized along the *b* axis and the *c* axis. Figure 2(b) shows the ^1L_b and ^1L_a absorption bands with six or more vibrational structures. The absorption peaks were clearly seen at 32940, 33550, 34600, 35400, 37250, and 38750 cm^{-1} (303.5, 298, 289, 282.5, 268.5, and 258 nm) in the absorption spectrum by means of the light polarized along the *b* axis, while they are clearly seen at 33000, 33620, 34540, 35340, 36950, and 38050 cm^{-1} (303, 297.5, 289.5, 283, 271, and 263 nm) in that along the *c* axis. The long-wavelength edge of the absorption band in the crystal is displaced by about 1500 cm^{-1} as compared with that in solution. At room temperature, it is difficult to guess accurately the band splitting: therefore, we have examined the peaks with care. The observed band splittings ($\nu_{//c}—\nu_{//b}$) are 60, 70, −60, −60, −300, and −700 cm^{-1} for the first, second, third, fourth, fifth, and sixth bands respectively. The experimental error is within 25 cm^{-1}. The band splittings of the higher bands are reversed in sign in comparison with the first two bands; this may suggest that the splitting of the band series is mainly due to the electronic transition of the $^1A—^1L_b$ type and that the higher bands may be affected by the $^1A—^1L_a$ electronic transition. The polarization ratio ($E_c : E_b$) against the wavenumber is shown in Fig. 2(b). In the 30600—32000 cm^{-1} (327—312 nm) region, the polarization ratio has a constant value of 0.9, which indicates that the absorption band in this region is due to the $^1A—^1L_a$ transition. The increase in the polarization ratio in the 32150—33200

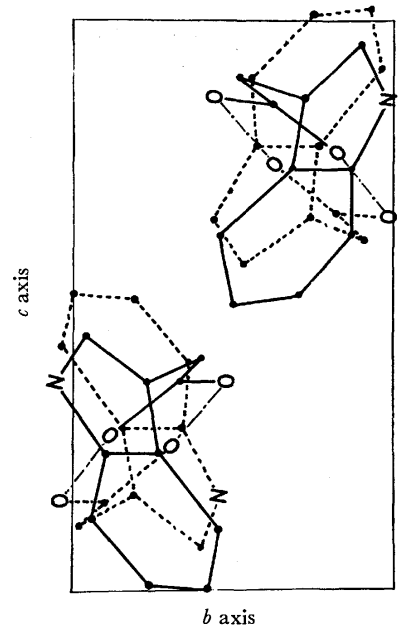

Fig. 2(a). Projection of the four molecules in the unit cell of 3-indolylacetic acid onto the (100) plane.

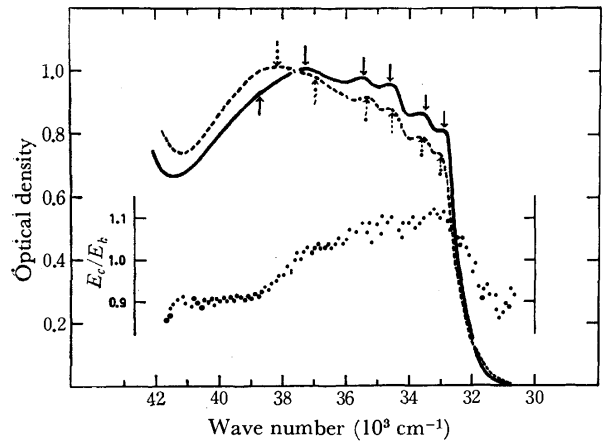

Fig. 2(b). The polarized absorption spectrum in the (100) plane of the single crystal of 3-indolylacetic acid.
The solid and broken lines show the spectrum parallel to the *c* axis and the *b* axis respectively.
The dotted line indicates the polarization ratio (E_c:E_d). The polarization ratio in the 30800—32200 cm^{-1} was obtained using a thicker plate which had the optical density of 0.62 at 32000 cm^{-1} for the absorption parallel to the a axis.

10) J. Lynn and G. D. Fasman, *Biopolymers*, **6**, 159 (1968).
11) I. L. Karle, K. Britts, and P. Gum, *Acta Crystallogr.*, **17**, 496 (1964).

cm^{-1} (311—301 nm) region reflects the gradual increase in the contribution of the ^1A—^1L_b transition, while the maximum at 32900 cm^{-1} (304 nm) corresponds to the 0–0 band of the ^1L_b transition. The increase in the ^1L_a transition may be responsible for the reduction in the polarization ratio from 34500 to 37700 cm^{-1} (from 290 to 265 nm). Above 37600 cm^{-1} (266 nm) the polarization ratio retains a nearly constant value of 0.9, which shows that the absorption band in this region may be predominantly due to the ^1A—^1L_a transition. The overlapping of the ^1A—^1L_b and ^1A—^1L_a transitions in the long-wavelength absorption band makes it difficult to determine the transition-moment directions of the ^1L_b and ^1L_a states. However, it may be possible to resolve the observed absorption spectrum into two types of electronic transitions, ^1A—^1L_b and ^1A—^1L_a, because the location and the vibrational structures of the ^1A—^1L_b transition have already been determined. The procedure of dividing the long-wavelength absorption band into the ^1L_b and ^1L_a bands was as follows. The absorption band below 32000 cm^{-1} and that above 37500 cm^{-1} may be due to only the ^1A—^1L_a transition; therefore the absorption band due to the ^1A—^1L_a transition was supposedly figured in the 32000—37500 cm^{-1} region to be linked with the absorption curves in the former and the latter regions. Thus, the *b*-axis polarized absorption band due to the ^1L_a transition was obtained. Then, the *c*-axis polarized absorption band originated from the same transition was obtained in the same way; the polarization ratio is 0.9 ($E_c : E_b$). The absorption band belonging to the ^1A—^1L_b transition was determined as the rest of the band after the ^1L_a band was subtracted from the observed spectrum. The thickness of the crystal could not be reliably estimated, and this made it impossible to obtain the oscillator strength. Nevertheless, it is possible to obtain the oscillator strength ratio (f_c^{exp}/f_b^{exp}) by integrating the observed absorption spectra parallel to the *b* and *c* axes. The direction of the transition moment of the ^1L_b and ^1L_a states was determined by the use of the corresponding oscillator strength ratios, namely, $f_c^{exp}(^1L_b)/f_b^{exp}(^1L_b)$ and $f_c^{exp}(^1L_a)/f_b^{exp}(^1L_a)$ respectively. The transition-moment direction of the ^1L_b state makes an angle of $+57$ or $-57°$ to the *b* axis, while that of the ^1L_a state lies at an angle of $+42$ or $-42°$ to the same axis.

3) Glycyl-L-tryptophan Dihydrate: The crystal structure of glycyl-L-tryptophan dihydrate has been determined by Pasternak.[12] The crystal is monoclinic, and the space group is $P2_1$, with two molecules per unit cell. The projection of the molecules in the unit cell onto the (001) plane, which is the developed face, is shown in Fig. 3(a). The optical properties of the crystal had been described in the literature,[12] and the axes were easily determined by a polarization microscope. The crystalline absorption spectra of glycyl-L-tryptophan dihydrate are shown in Fig. 3(b), together with the polarization spectrum. The crystalline absorption spectra obtained by the light polarized parallel to the *a* axis and the *b* axis have maxima at 33100, 34000, 35000, and 36100 cm^{-1} (302, 294, 285.5, and 277 nm), and

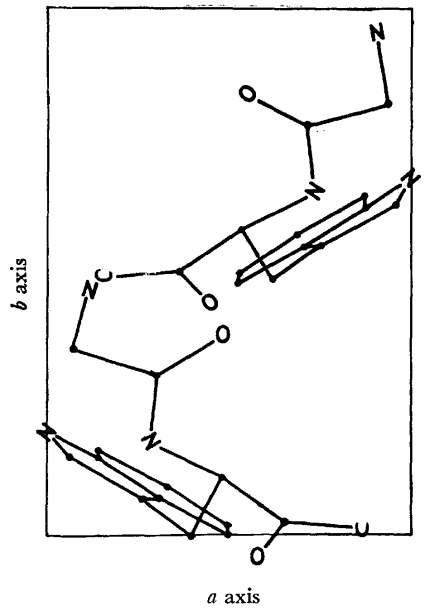

Fig. 3(a). Projection of the two molecules in the unit cell of glycyl-L-tryptophan dihydrate onto the (001) plane.

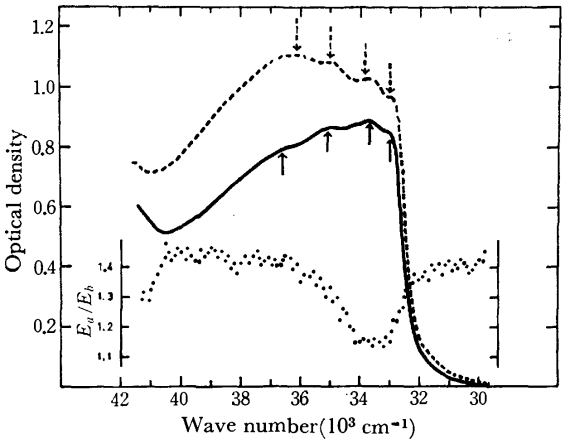

Fig. 3(b). The polarized absorption spectrum in the (001) plane of the single crystal of glycyl-L-tryptopahan dihydrate. The solid and broken lines show the spectrum parallel to the b axis and the a axis respectively. The dotted line indicates the polarization ratio (E_a:E_b). The polarization ratio in the 29800—32300 cm^{-1} was obtained using a thicker plate which had the optical density of 0.78 at 32000 cm^{-1} for the absorption parallel to the *a* axis.

33000, 33800, 35100, and 36750 cm^{-1} (303, 295.5, 285, and 272 nm) respectively. These absorption peaks are in good correspondence with those of the solution spectrum. The band splittings of the first two bands are reversed in sign compared with those of the higher bands, similar to the case of 3-indolylacetic acid. The polarization ratio (E_a: E_b) changes with the variation in the wavenumber, as is shown in the case of the indole or 3-indolylacetic acid crystal. In the 30000—31600 cm^{-1} (333—317 nm) region, the polarization ratio is calculated to be nearly 1.4. With an increase in wavenumber, the polarization ratio is sharply reduced; it has its minimum value of 1.15 at 33300 cm^{-1} (300 nm). In the range from 33900 to 36000 cm^{-1} (295 to 278 nm),

12) R. A. Pasternak, *Acta Crystallogr.*, **9**, 341 (1956).

there is an increase in the polarization ratio, and it has its maximum value of 1.4 at 36500 cm^{-1} (274 nm). Thus, the ^1A—^1L_b transition appears at from 31600 to 36350 cm^{-1} (316 to 275 nm), overlapping with the ^1A—^1L_a transition. This overlapping of the ^1L_b and ^1L_a transitions makes it difficult to determine the corresponding transition-moment directions. Therefore, the observed absorption spectrum was resolved into the bands due to the ^1A—^1L_b and the ^1A—^1L_a transitions in the same way as has been described in the case of the 3-indolylacetic acid crystal. With the use of the oscillator strength ratio of the ^1L_b transition ($f_a^{exp}(^1L_b)$: $f_b^{exp}(^1L_b)$) and that of the ^1L_a transition ($f_a^{exp}(^1L_a)$: $f_b^{exp}(^1L_a)$), the corresponding transition-moment directions were estimated. The direction of the transition-moment of the ^1L_b state makes an angle of +41 or −41° to the *a* axis, while that of the ^1L_a state lies at an angle of +30 or −30° to the same axis. When the transition-moment direction obtained from glycyl-L-tryptophan dihydrate was compared with that obtained from 3-indolylacetic acid, it was clear that the direction of the angle of −41 and −30° to the *a* axis in the former crystal coincides with the direction of the angle of −57 and +42° to the *b* axis in the latter crystal for the ^1L_b and ^1L_a states respectively. The experimental error is within 5°.

Determination of the Transition-moment Direction of the ^1L_b and ^1L_a States. According to the polarized absorption spectra of glycyl-L-tryptophan dihydrate and 3-indolylacetic acid crystals, the directions of the transition moments of the ^1L_b and ^1L_a states were determined to be as is shown in Fig. 4. The transition-moment direction of the ^1L_b and ^1L_a states determined from the 3-indolylacetic acid crystal, which is oriented −57 and +42° to the *b* axis, makes angles of +49 and −42° to the long axis of the indole molecule respectively. On the other hand, the orientations of −41 and −30° to the *a* axis, as determined from glycyl-L-tryptophan dihydrate crystal, corresponds to angles of +58 and −35° to the long axis of the indole molecule for the ^1L_b and ^1L_a states respectively. Thus, the orientation of the ^1L_b state makes an angle of +58 or +49° to the long axis of the molecule, while that of the ^1L_a state lies at an angle of −35 or −42° to the same axis. These results

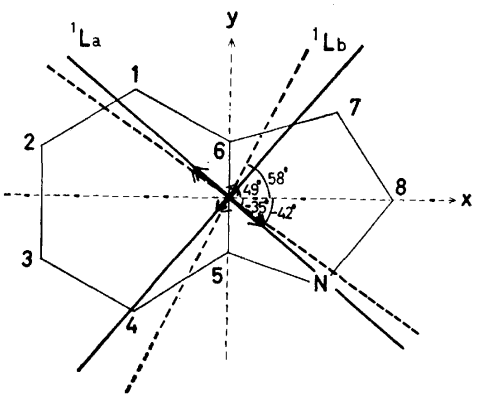

Fig. 4. Transition moments of the ^1L_b and ^1L_a states determined experimentally. The solid line was obtained by the ploarized absorption spectrum of 3-indolylacetic acid and the broken line by that of glycyl-L-tryptophan dihydrate.

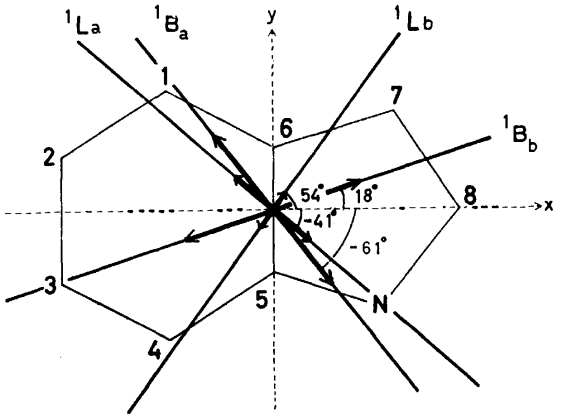

Fig. 5. The theroretical predictions of the transition moments of the four lowest excited singlet states (^1L_b, ^1L_a, ^1B_b, and ^1B_a) of indole.

are in satisfactory agreement with the theoretical orientations of +54 and −41° for the ^1L_b and ^1L_a states respectively, as is shown in Fig. 5. The mutual orientation angle between the ^1L_b and ^1L_a states is about 92° in both molecules, which is in reasonable agreement with the results obtained from the absorption polarization of the indole fluorescence.[1,8] The long-wavelength absorption spectrum of tryptophan in an aqueous solution is shown in Fig. 6, where the proposed resolution into the ^1A—^1L_b and ^1A—^1L_a bands is given. The location and absorption intensity of the ^1A—^1L_b transition were estimated with the help of the results described hitherto. The experimental oscillator strength (f^{exp}) may be obtained from the following equation, $f^{exp}=4.33\times10^{-9}\times\int\varepsilon(\sigma)\,d\sigma$, where $\varepsilon(\sigma)$ is a molar absorption coefficient and where σ means the wavenumber (cm^{-1}). Using the resolved absorption bands shown in Fig. 6, we have found the experimental oscillator strengths to be 0.010 and 0.112 for the ^1A—^1L_b and ^1A—^1L_a transitions. With these experimental oscillator strengths, the magnitude of the transition moments ($|r_{mn}|$) was estimated by means of this equation: $f=1.085\times10^{-5}\times\sigma\times|r_{mn}|^2$. They are 0.15 Å and

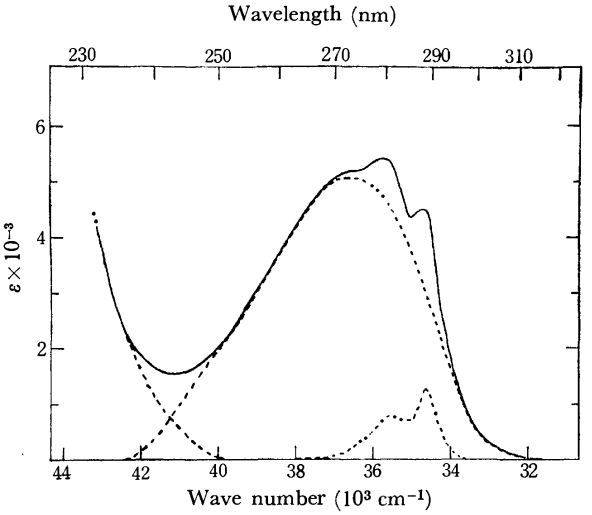

Fig. 6. The absorption spectrum of tryptophan in aqueous solution, showing the proposed resolution into the ^1L_b and ^1L_a absorption bands.

TABLE 1. THEORETICAL PREDICTIONS OF THE SINGLET EXCITED STATES OF INDOLE[a)]

State symbols	State energy[b)]	Transition-moment length		Oscillator strength	Orientation angle[d)]
		r_x[c)]	r_y[c)]		
^1L_b	4.51 (4.4)[e)]	0.161 Å	0.186 Å	0.024 (0.010)	54° (54°)
^1L_a	4.72 (4.6)	0.427 Å	−0.368 Å	0.133 (0.112)	−41° (−38°)
^1B_b	5.82 (5.8)	0.990 Å	0.320 Å	0.553 (0.680)	18°
^1B_a	6.49 (6.2)	0.668 Å	−0.864 Å	0.676	−61°

a) The calculated values were obtained by the P-P-P SCF MO-CI method.
b) The state energies are given in the electron volt (eV) unit.
c) The coordinate designations of x and y correspond to the long and short axis of the indole molecule, as is shown in Fig. 4 or 5.
d) The angle of the transition moment to the long axis (the x axis) of the molecule.
e) The values in the brackets are the experimental results.

0.54 Å for the ^1A—^1L_b and ^1A—^1L_a transitions respectively; these values are a little smaller than the results obtained from the theoretical calculations (0.25 Å and 0.57 Å).

Theoretical Calculation. The P-P-P SCF MO-CI calculations of indole has been done by many workers,[8,13-15] but their results were still not in satisfactory agreement with the experimental results. Momicchioli and Rastelli[13] used only four singly-excited configurations; later Song and Kurtin[8] employed a considerably larger number of configurations (20—25) in their P-P-P SCF MO-CI calculations. Their results on the polarizations are in reasonable agreement with the experimental results, but those on the transition energies and oscillator strengths are not so satisfactory. Recently, Evleth[15] made calculations employing 10 singly-excited and 5 additional doubly-excited configurations. His results on transition energies and oscillator strengths agree well with the observed ones; nevertheless, the transition-moment directions are inconsistent with the experimental results. We have considered all singly-excited configurations in the P-P-P SCF MO-CI calculation of indole and used the geometrical structure of the molecule taken from the data of the Xray analysis of glycyl-L-tryptophan dihydrate[12] or 3-indolylacetic acid crystal.[11] The Coulomb, resonance, and one-center repulsion parameters incorporated in this calculation were the same as have usually been used.[14] The values of the resonance integral at any distance were estimated by the following equation[16]:

$$\beta(r) = \beta^\circ \exp[4.599(1.397 - r)]$$

The results of our calculation for the four lowest singlet-excited states are listed in Table 1, where the state energies, the oscillator strengths, the transition-moment lengths, and the angles of the transition moments to the long axis of the molecule are presented. The calculated spectral features of the ^1A—^1L_b and ^1A—^1L_a transitions are in satisfactory agreement with the observed ones. Although the calculated energies of the ^1L_b and ^1L_a states are a little higher than the experimental ones, the values are in good agreement with the observed spectral characteristic that the ^1L_b and ^1L_a excited states are closely spaced. The experimental polarizations of the ^1A—^1B_b and ^1A—^1B_a transitions are still unknown; however, the calculated transition energies of the ^1B_b and ^1B_a states are reasonably correlated with the observed transition energies.

These calculations were carried out by the use of a computer program written by Dr. Masashi Tanaka of our laboratory, to whom our thanks are due. The calculation was carried out with the HITAC 5050E at the computation center of the University of Tokyo.

13) F. Momicchioli and A. Rastelli, *J. Mol. Spectrosc.*, **22**, 310 (1967).
14) F. Hjalmars and M. Sundbom, *Acta Chem. Scand.*, **22**, 607 (1968).
15) E. M. Evleth, *Thoer. Chim. Acta* (Berl.), **16**, 22 (1970).
16) T. Nakajima, "Molecular Orbitals in Chemistry, Physics, and Biology," ed. by P. O. Löwdin and B. Pullman, Academic Press, New York (1964), p. 454.

The Crystal and Molecular Structure of Bis(L-prolinamidato)-nickel(II) Dihydrate

Tomitake TSUKIHARA, Yukiteru KATSUBE, Kumiko FUJIMORI, and Yoshihisa ISHIMURA

Faculty of Engineering, Tottori University, Tottori

(Received November 1, 1971)

The crystal structure of bis(L-prolinamidato)nickel(II) dihydrate has been determined by three dimensional X-ray analysis. The crystals are vermilion needles and belong to the space group $P2_1$. . The unit cell has dimensions $a=10.915$, $b=7.319$, $c=9.445$ Å, $\beta=112.6°$ and contains two structure units. The structure has been solved using Patterson synthesis, minimum function and Fourier synthesis and refined by diagonal and block-diagonal least-squares methods on 1115 independent reflections. The final R value was 0.054. The nickel atom exhibits square planar coordination. Two proline-amide molecules are approximately related to each other by a two fold axis and these two ligand molecules coordinate to the central nickel atom in *trans* form. The oxygen atom of water does not coordinate to the nickel atom.

It is well known that nickel(II) complexes have octahedral, tetrahedral or square planar coordination. From the spectroscopic studies of the complexes of glycine-, L-alanine-, L-leucine-, and L-proline-amides, Komorita *et al.*[1,2] proposed that the nickel atom exhibits a square planar coordination and two ligand molecules are coordinated to the central nickel atom with four nitrogen atoms in *trans* form. The present study was undertaken to establish the configuration about the nickel of bis(L-prolinamidato)nickel(II) complex in solid state.

Experimental

The vermilion needle crystals of bis(L-prolinamidato)nickel-(II) dihydrate were kindly supplied by Dr. T. Komorita. Preliminary Weissenberg and oscillation photographs established that the crystal was monoclinic with the b axis along the needle axis. The systematic extinction of $(0k0)$ for k odd restricted the space group to $P2_1$. The crystal data are listed in Table 1.

TABLE 1. CRYSTAL DATA

Ni (L-$C_5H_9N_2O)_2\cdot 2H_2O$		M. W.=321.02
Monoclinic		$P2_1$
$a=10.915$ Å	$b=7.319$ Å	$c=9.445$ Å
$\alpha=\gamma=90.0°$	$\beta=112.6°$	
$D_{cal}=1.51$ g/cm³		
$D_{obs}=1.53$ g/cm³		(by floatation)

A nickel filtered Cu-K_α radiation was used to collect intensity data for all the reflections in the range $0°<\theta<60°$ within the octants (hkl) and $(\bar{h}kl)$. All the intensities were measured on a Rigaku Denki computer-controlled four-circle diffractometer. A crystal of approximate dimensions $0.03\times0.15\times0.04$ mm³ was used for the intensity measurement of 1115 reflections. The ω-2θ scan technique was employed with a scan speed 2°/min by ω, and the back grounds were measured for 10.0 sec at each start and end points of a scan range. A scan range of ω for each reflection was calculated by the formula $\Delta\omega=1.50°+0.15°\tan(\theta)$. Attenuators were automatically inserted when the maximum counting rate exceeded 8000 cps. The intensities were corrected only for Lorentz and polarization factors.

Measurement of the two reference reflections (500) and (060) was repeated for every thirty reflections. For 52 repetitions of the measurement, $|F_0(500)|=97.13\pm0.72$ and $|F_0(060)|=50.84\pm0.93$.

Structure Determination and Refinement

A trial structure derived from the three-dimensional

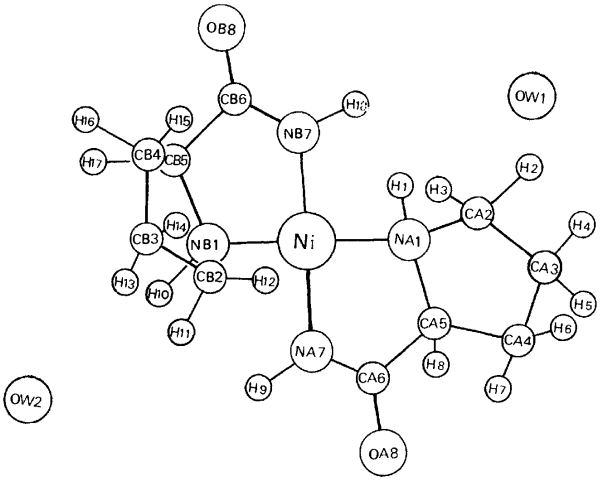

Fig. 1. Numbering of atoms in bis(L-prolinamidato)nickel(II) dihydrate.

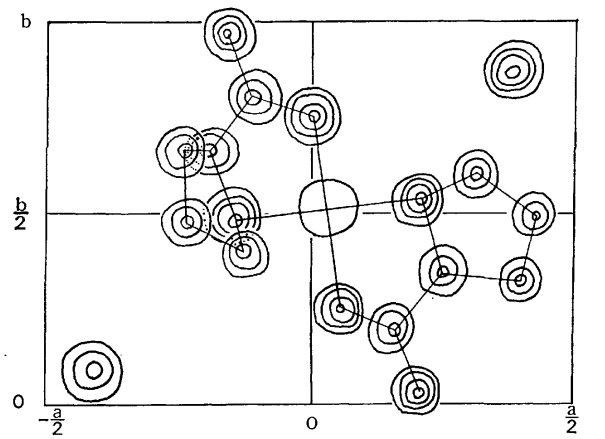

Fig. 2. The composite electron density map of bis(L-prolinamidato)nicel(II) dihydrate.

1) T. Komorita, J. Hidaka, and Y. Shimura, This Bulletin, **41**, 854 (1968).

2) T. Komorita, private communication.

Patterson synthesis, minimum function and Fourier synthesis was refined to $R=0.12$, ($R=\sum||F_o|-|F_c||/\sum|F_o|$), by using a diagonal least-squares program which minimizes the function $\sum(|F_o|-k|F_c|)^2$ with individual isotropic thermal parameters for all the non-hydrogen atoms. The atomic scattering factors were taken from International Tables for X-ray Crystallography (1962). Three cycles of block-diagonal least-squares refinement of the positional and the thermal parameters of all the non-hydrogen atoms with a program written by Dr. T.

TABLE 2. FINAL ATOMIC PARAMETERS

Atom	x	y	z	Atom	x	y	z
Ni	0.02838	0.50000	0.21031	OW1	0.37338	0.88067	0.07596
OW2	0.40278	0.58725	−0.11192	OA8	0.19271	0.02997	0.17173
OB8	−0.14625	0.97044	0.21276	NA1	0.20036	0.52841	0.19868
NA7	0.05503	0.24845	0.20255	NB1	−0.13714	0.47726	0.23624
NB7	0.00143	0.75010	0.21415	CA2	0.30052	0.60139	0.34425
CA3	0.42113	0.49388	0.37448	CA4	0.39207	0.32498	0.29409
CA5	0.25067	0.34078	0.17307	CA6	0.15923	0.19274	0.18222
CB2	−0.12229	0.40095	0.39062	CB3	−0.23866	0.47184	0.41912
CB4	−0.24645	0.67290	0.35965	CB5	−0.20616	0.65857	0.22192
CB6	−0.11038	0.80874	0.21661	H1	0.1891	0.6210	0.1082
H 2	0.3101	0.7525	0.3417	H3	0.2805	0.5184	0.4443
H 4	0.4925	0.5705	0.3515	H5	0.4815	0.4664	0.4891
H 6	0.4627	0.2733	0.2453	H7	0.4062	0.2043	0.3696
H 8	0.2643	0.3168	0.0770	H9	−0.0068	0.1608	0.2061
H10	−0.2135	0.3934	0.1481	H11	−0.1235	0.2677	0.3849
H12	−0.0261	0.4303	0.4830	H13	−0.3398	0.3999	0.3495
H14	−0.2222	0.4792	0.5235	H15	−0.3614	0.7343	0.3128
H16	−0.1907	0.7551	0.4528	H17	−0.3085	0.6738	0.1227
H18	0.0587	0.8482	0.2039				

Atom	$B_{11}\times10^4$	$B_{22}\times10^4$	$B_{33}\times10^4$	$B_{12}\times10^4$	$B_{13}\times10^4$	$B_{23}\times10^4$
Ni	72 (1)	91 (2)	121 (2)	1 (4)	84 (2)	21 (6)
OW1	169 (9)	146 (14)	214 (14)	24 (22)	187 (19)	− 75 (27)
OW2	127 (9)	302 (25)	408 (21)	−91 (24)	214 (23)	−254 (37)
OA8	113 (7)	101 (14)	229 (12)	42 (18)	173 (16)	− 10 (24)
OB8	105 (7)	27 (12)	266 (13)	− 3 (16)	163 (16)	− 4 (22)
NA1	81 (7)	85 (16)	140 (11)	25 (20)	95 (15)	37 (27)
NA7	76 (9)	165 (17)	174 (15)	− 2 (20)	131 (20)	11 (27)
NB1	64 (7)	134 (17)	122 (11)	−13 (22)	74 (14)	6 (28)
NB7	95 (9)	63 (14)	189 (14)	−23 (17)	133 (19)	10 (23)
CA2	90 (11)	188 (25)	270 (23)	−50 (29)	116 (26)	−227 (44)
CA3	135 (13)	583 (48)	431 (35)	241 (55)	−114 (36)	−650 (88)
CA4	84 (11)	173 (27)	376 (29)	20 (31)	27 (30)	−216 (50)
CA5	80 (10)	121 (21)	142 (16)	−72 (25)	113 (22)	−106 (31)
CA6	93 (11)	91 (17)	134 (16)	−13 (23)	102 (22)	2 (29)
CB2	127 (13)	152 (20)	167 (18)	91 (28)	175 (25)	139 (33)
CB3	133 (10)	100 (23)	176 (18)	47 (28)	180 (23)	47 (37)
CB4	122 (13)	137 (21)	183 (20)	−26 (27)	188 (27)	− 14 (34)
CB5	63 (9)	89 (18)	137 (15)	58 (22)	66 (20)	34 (28)
CB6	82 (10)	41 (14)	150 (16)	−17 (21)	76 (21)	27 (27)

Atom	B	e. s. d.	Atom	B	e. s. d.
H 1	6	3	H 2	2	2
H 3	3	2	H 4	7	3
H 5	5	3	H 6	4	3
H 7	6	3	H 8	1	2
H 9	1	2	H10	5	3
H11	4	2	H12	1	2
H13	2	2	H14	5	3
H15	2	2	H16	2	2
H17	4	3	H18	6	3

Temperature Factor $=\exp(-(B_{11}\times h^2+B_{22}\times k^2+B_{33}\times l^2+B_{12}\times hk+B_{13}\times hl+B_{23}\times kl))$
or $=\exp(-B(\sin\theta/\lambda)^2)$

Table 4. Intramolecular distances with their e. s. d.'s

Bond	Length	e. s. d.	Bond	Length	e. s. d.
Ni–NA1	1.929 Å	0.009 Å	Ni–NB1	1.918 Å	0.010 Å
Ni–NA7	1.872	0.008	Ni–NB7	1.855	0.008
NA1–CA2	1.509	0.015	NB1–CB2	1.532	0.014
NA1–CA5	1.493	0.013	NB1–CB5	1.459	0.013
CA2–CA3	1.455	0.025	CB2–CB3	1.493	0.015
CA3–CA4	1.416	0.026	CB3–CB4	1.540	0.015
CA4–CA5	1.535	0.018	CB4–CB5	1.534	0.014
CA5–CA6	1.494	0.013	CB5–CB6	1.535	0.013
CA6–NA7	1.313	0.012	CB6–NB7	1.323	0.013
CA6–OA8	1.267	0.012	CB6–OB8	1.245	0.012
NA1–H1	1.06	0.12	NB1–H10	1.11	0.12
CA2–H2	1.11	0.09	CB2–H11	0.98	0.09
CA2–H3	1.06	0.09	CB2–H12	1.10	0.08
CA3–H4	1.05	0.17	CB3–H13	1.17	0.09
CA3–H5	1.05	0.10	CB3–H14	0.93	0.13
CA4–H6	1.11	0.10	CB4–H15	1.24	0.09
CA4–H7	1.11	0.10	CB4–H16	1.05	0.08
CA5–H8	0.99	0.08	CB5–H17	1.16	0.11
NA7–H9	0.94	0.07	NB7–H18	0.98	0.10

Table 5. Intramolecular bond angles with their e. s. d.'s

Angle	degree	e. s. d.	Angle	degree	e. s. d.
NA1–Ni–NA7	85.8°	0.4°	NB1–Ni–NB7	84.8°	0.4°
NA1–Ni–NB7	94.0	0.4	NB1–Ni–NA7	95.5	0.4
Ni–NA1–CA5	110.6	0.6	Ni–NB1–CB5	113.8	0.7
Ni–NA1–CA2	111.4	0.7	Ni–NB1–CB2	113.0	0.7
Ni–NA1–H1	107.5	8.0	Ni–NB1–H10	115.6	5.9
CA2–NA1–CA5	107.9	0.8	CB2–NB1–CB5	107.0	0.8
H1–NA1–CA2	109.4	7.8	H10–NB1–CB2	102.7	5.9
NA1–CA2–CA3	104.7	1.2	NB1–CB2–CB3	103.9	0.8
NA1–CA2–H2	113.3	4.9	NB1–CB2–H11	108.5	5.4
NA1–CA2–H3	115.1	5.1	NB1–CB2–H12	112.8	4.7
H2–CA2–H3	103.9	7.0	H11–CB2–H12	105.0	7.1
H2–CA2–CA3	115.9	5.9	H11–CB2–CB3	113.1	5.4
H3–CA2–CA3	104.0	5.2	H12–CB2–CB3	113.7	4.7
CA2–CA3–CA4	111.6	1.6	CB2–CB3–CB4	102.2	0.9
CA2–CA3–H4	111.3	8.1	CB2–CB3–H13	113.1	4.6
CA2–CA3–H5	117.1	5.8	CB2–CB3–H14	112.9	7.7
H4–CA3–H5	92.3	9.8	H13–CB3–H14	116.5	9.1
H4–CA3–CA4	112.7	7.9	H13–CB3–CB4	109.0	4.6
CA3–CA4–CA5	106.8	1.3	CB3–CB4–CB5	104.1	0.8
CA3–CA4–H6	117.7	5.6	CB3–CB4–H15	112.6	4.3
CA3–CA4–H7	113.7	7.7	CB3–CB4–H16	109.2	4.7
H6–CA4–H7	92.8	9.8	H15–CB4–H16	104.2	6.4
H6–CA4–CA5	112.4	5.5	H15–CB4–CB5	108.7	4.3
H7–CA4–CA5	112.4	7.6	H16–CB4–CB5	118.3	4.9
CA4–CA5–NA1	105.5	0.9	CB4–CB5–NB1	107.0	0.8
CA4–CA5–CA6	113.6	0.9	CB4–CB5–CB6	113.3	0.8
CA4–CA5–H8	102.5	4.8	CB4–CB5–H17	99.6	5.5
H8–CA5–NA1	118.8	4.7	H17–CB5–NB1	117.0	5.5
H8–CA5–CA6	105.8	4.7	H17–CB5–CB6	111.6	5.5
CA5–CA6–OA8	118.3	0.8	CB5–CB6–OB8	119.4	0.8
CA5–CA6–NA7	115.1	0.8	CB5–CB6–NB7	114.3	0.8
OA8–CA6–NA7	126.6	0.9	OB8–CB6–NB7	126.3	0.9
CA6–NA7–Ni	117.4	0.7	CB6–NB7–Ni	118.1	0.7
CA6–NA7–H9	120.0	4.9	CB6–NB7–H18	114.7	7.3
H9–NA7–Ni	122.5	4.9	H18–NB7–Ni	126.9	7.3
NA1–CA5–CA6	109.9	1.0	NB1–CB5–CB6	108.4	0.8

Ashida gave a value of R of 0.09. To take into account the anomalous scattering by nickel atom, $\Delta f'(-3.1)$ and $\Delta f''(0.6)$ were included in the calculations of the refinement. An $(F_o—F_c)$ synthesis revealed all the hydrogen atoms in the complex. After several cycles of the refinement of the positional parameters, of the anisotropic thermal parameters for the non-hydrogen atoms and of the isotropic thermal parameters for hydrogen atoms, the R value decreased to 0.054. The final parameters of all atoms, and $|F_o|$ and $|F_c|$ are listed in Tables 2 and 3,[3] respectively. The standard deviations in positional parameters were: for Ni, 0.0015 Å, for O, N, and C, 0.012 Å and for H, 0.12 Å. The final composite electron density map is given in Fig. 2.

Molecular and Crystal Structure

The nickel atom exhibits four fold coordination, and lies on the plane formed by the four ligand atoms: two imino-nitrogen atoms and two amide-nitrogen atoms which exhibit sp^3 and sp^2 configuration, respectively (Fig. 3). The environment around the nickel atom indicates the coordination dsp^2 configuration. Two proline-amide molecules of the same complex are approximately related to each other by a two fold axis, so that the two ligand molecules coordinate to the central nickel atom in *trans* form. Two of the four bond distances between nickel and nitrogen atoms, Ni–NA1 and Ni–NB1, are significantly shorter than the other two, Ni–NA7 and Ni–NB7. These four bonds

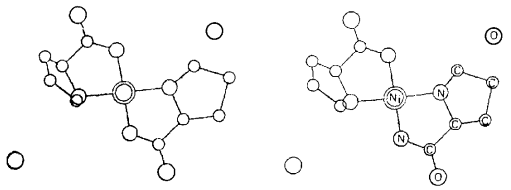

Fig. 3. The structure of bis(L-prolinamidato)nickel(II) complex shown by a stereo pair, illustrating the configuration.

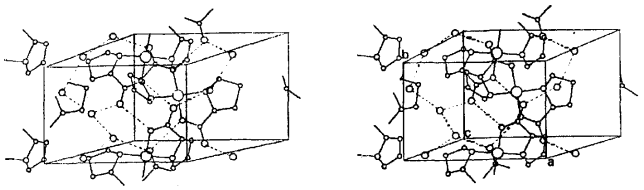

Fig. 4. The crystal structure of bis(L-prolinamidato)nickel(II) dihydrate shown by a stereo pair. Hydrogen bonds are indicated by broken lines.

Table 6. Equations of the least-squares planes through atoms

Equation	Atom	Deviation
$-0.0869X+0.0130Y+1.7701=Z$	NA1	−0.039Å
	NA7	0.039
	NB1	−0.040
	NB7	0.040
	*Ni	0.023
	*CA2	−1.346
	*CA3	−1.723
	*CA4	−1.038
	*CA5	0.110
	*CA6	0.105
	*CB2	−1.354
	*CB3	−1.475
	*CB4	−0.951
	*CB5	0.163
	*CB6	0.131
	*OA8	0.146
	*OB8	0.212
$0.9720X+0.7291Y-2.3724=Z$	NA1	0.089
	CA2	−0.121
	CA3	0.092
	CA4	−0.051
	CA5	−0.009
$-0.9129X-0.6485Y+2.411=Z$	NB1	0.156
	CB2	−0.259
	CB3	0.189
	CB4	−0.181
	CB5	0.093

Where $X=ax+cz\cos\beta$, $Y=by$, $Z=cz\sin\beta$
* Atoms not included in the least-squares calculations.

Table 7. Intermolecular atomic contacts

From atom	to atom	Distance	From atom	to atom	Distance
OW1	OW2 a	2.880 Å	OW1	OA8 c	2.696 Å
OW1	NB1 d	3.162	OW1	OW2 g	2.782
OW2	OW1 a	2.880	OW2	OB8 e	2.726
OW2	OW1 f	2.782	OA8	OW1 b	2.696
OA8	NB7 b	3.060	OB8	NA7 c	3.024
OB8	OW2 d	2.726	NA7	OB8 b	3.024
NB1	OW1 e	3.162	NB7	OA8 c	3.060

Key for the position of molecule

a (	x	y	z)	b (x	$-1.0+y$ z)
c (	x	$1.0+y$	z)	d ($-x$	$0.5+y$ $-z$)
e (	$-x$	$-0.5+y$	$-z$)	f (1.0$-x$	$-0.5+y$ $-z$)
g (1.0$-x$		$0.5+y$	$-z$)		

3) Table 3 which shows the calculated and observed structure factors has been submitted to, and is kept as Document No. 7203 by, the office of the Bulletin of the Chemical Society of Japan, 1-5 Kanda-Surugadai, Chiyoda-ku, Tokyo. A copy may be secured by citing the Document number and by remitting, in advance, ¥400 for photo prints. Pay by check or money order payable to: Chemical Society of Japan.

are shorter than those of $(Ni(H_2O)_2(pyridine\text{-}2\text{-}carboxamide)_2Cl_2$, (Ni–N, 2.02 Å),[4] in which the nickel atom exhibits octahedral coordination. Nawata *et al.*[5] reported the same observation in Ni(pyridine-2-carboxamidato)$_2$ dihydrate in which the nickel atom exhibited square planar coordination. The observations are consistent with theory. The bond angles around the nickel atom deviate from that of dsp^2 configuration by about five degrees. The distortion is not great from the viewpoint of molecular orbital theory.

Table 6 gives the equations of the least-squares planes and the distances of individual atoms from the planes. The two γ-carbon atoms of pyrrolidine ring, CA(3) and CB(3), are not displaced from the respective rings as much as those formed in acetyl-L-proline-*N*-methylamide[6] and other proline derivatives in which the nitrogen atom of pyrrolidine ring exhibits sp^2 configuration. Kim and Jeffey[7] compared the geometries of pyrrolidine rings with each other in which nitrogen atoms have sp^3 configuration. Both the two pyrrolidine rings in this crystal take the same puckered form as that in hydroxy-L-proline.[8]

4) A. Masuko, T. Nomura, and Y. Saito, This Bulletin, **40**, 511 (1967).
5) Y. Nawata, H. Iwasaki, and Y. Saito, This Bulletin, **40**, 515 (1967).
6) T. Matsuzaki and Y. Iitaka, *Acta Crystallogr.*, **B27**, 507 (1971).
7) H. S. Kim and G. A. Jeffey, *ibid.*, **B27**, 1123 (1971).
8) J. Donohue and K. N. Trueblood, *ibid.*, **5**, 414, 419 (1952).

Table 8. Intermolecular angles

Angle	degree
CA6 (a)...OA8 (a)...NB7 (b)	112.9°
OA8 (a)...NB7 (b)...Ni (b)	122.5
OA8 (a)...NB7 (b)...CB6 (b)	118.3
CA6 (a)...NA7 (a)...OB8 (b)	119.0
Ni (a)...NA7 (a)...OB8 (b)	122.4
NA7 (a)...OB8 (b)...CB6 (b)	114.7
OB8 (e)...OW2(a)...OW1(f)	127.5
OB8 (e)...OW2(a)...OW1(a)	96.1
OW1(a)...OW2(a)...OW1(f)	129.1
OW2(a)...OW1(a)...OW2(g)	100.4
OW2(a)...OW1(a)...OA8 (c)	141.0
OA3 (c)...OW1(a)...OW2(g)	117.4

The subscripts indicate the same operations as in Table 5.

The molecular packing in the crystal is shown in Fig. 4. Tables 7 and 8 give all the hydrogen bonding schemes with distances and angles. The two amide groups of neighbouring complexes are bound to each other through the two NH···O hydrogen bonds. The hydrogen bonds between non-equivalent water molecules, and those between water and imino carbonyl group of the complex construct the framework of this crystal structure. There are no intermolecular contact between nickel atom and oxygen atom of water.

The authors express their thanks to Dr. T. Komorita for valuable discussions.

BULLETIN OF THE CHEMICAL SOCIETY OF JAPAN, VOL. 45, 1371—1375(1972)

Thermodynamic Properties of an Aqueous Solution of Tetraethylene Glycol Diethyl Ether

Haruo NAKAYAMA

Department of Applied Chemistry, Faculty of Engineering, Yokohama National University, Ooka-machi, Minami-ku, Yokohama

(Received November 11, 1971)

The excess Gibbs energy of mixing, G^E; the excess enthalpy of mixing, H^E, and the excess volume of the mixing, V^E, of the tetraethylene glycol diethyl ether+water system have been measured as functions of the composition at 25°C. The G^E, which has been determined through the isopiestic measurement of the water activity, is positive over the entire range of composition and has its maximum at 40 mol% ether. As has been found for analogous systems, the *s*-curve of H^E is again found; that is, H^E is large and negative (exothermic) in the water-rich region and positive (endothermic) in the ether-rich region. The V^E is negative over the whole range of composition and has a minimum at 23 mol% ether. These results are discussed in the light of the structural modifications of water in the immediate neighborhood of the ether molecule.

That the structural modifications of water play an important role in the dissolution of hydrocarbons into water is now widely accepted. In order to investigate such a phenomenon, aqueous solutions of ethers are, in practice, probably the most convenient because the interaction between the polar group (ether oxygen) and water is not so strong, despite their elevated miscibility with water, that the effect of a polar group on the solution property can be minimized.

In a previous paper,[1] the enthalpies of the mixing of water with diethylene glycol diethyl ether and with some cyclic ethers were measured, and it was concluded that the water-water interaction persisted even in the ether-rich region (80 mol% ether, for example). In the present paper, the excess Gibbs free energy of mix-

1) H. Nakayama and K. Shinoda, *J. Chem. Thermodynamics*, **3**, 401 (1971).

ing, G^E; the excess enthaply of mixing, H^E; the excess entropy of mixing, S^E, and the excess volume of mixing, V^E, for the tetraethylene glycol diethyl ether+water system have been determined. The purpose of this paper is to see if the above-mentioned conclusion,[1] derived only from the concentration dependence of the partial molal excess enthalpy of water, H_1^E, is consistent with the behavior of the partial molal excess entropy of water, S_1^E, as well.

Tetraethylene glycol diethyl ether was chosen because the aqueous solution properties of such a compound can give fundamental information for many complicated systems, such as, for example, polyethylene glycol+water and a non-ionic surfactant with an oxyethylene chain as a hydrophilic group+water. Other advantages of this compound are its complete miscibility with water at room temperature and its low vapor pressure (less than 10^{-5} mmHg at 25°C), low enough to permit accurate determination of the water activity. No thermodynamic data for the present system have been reported.

Experimental

Materials. The tetraethylene glycol diethyl ether (3,6,9,12,15-pentaoxaheptadecane, which we will denote by TGDE hereafter) was synthesized by the condensation reaction (Williamson reaction) of β-ethoxy β′-chlorodiethyl ether ($ClCH_2CH_2OCH_2CH_2OCH_2CH_3$) (I) with the sodium salt of β-diethoxy ethyl alcohol ($NaOCH_2CH_2OCH_2CH_2OCH_2CH_3$) (II). Both reactants were prepared from commercially-available β-diethoxy ethyl alcohol (diethylene glycol monoethyl ether). The compound I was prepared according to the procedure of Hurd and others,[2] who synthesized β-ethoxy ethyl chloride. Some physical properties and analytical data for the compound I were as follows; bp 179.5—180.5°C/760 mmHg; n_D^{25} 1.4279.

Found: C, 47.12; H, 8.73; Cl, 23.45%. Calcd for $C_6H_{13}O_2Cl$: C, 47.22; H, 8.56; Cl, 23.23%.

The compound I was added, drop by drop, to the compound II dissolved in diethylene glycol monoethyl ether (reaction solvent), and then the mixture was heated under reflux for several hours at 110—130°C. After cooling, the organic layer was separated and distilled under reduced pressure. The crude product (120—125°C/2 mmHg) was re-distilled from sodium. The TGDE prepared in this way was further purified by fractional distillation under a vacuum. It was stored in an ampoule and then further distilled just before use. The analytical data and some physical properties of TGDE are summarized in Table 1.

Table 1. Analytical data and some properties of TGDE

Boiling point (°C)	124—125 at 2 mmHg
	159 at 11 mmHg[3]
	159 at 10 mmHg[4]
Refractive index (n_D)	1.4298 at 25°C
Density (g/cm³)	0.9712 at 25°C
Molal volume (cm³/mol)	257.8 at 25°C
Molecular weight (experimental)[a]	250.0
Molecular weight (theoretical)	250.3
Water content (wt%)[b]	less than 0.1
Analytical data	Found: C, 57.47; H, 10.58%
	Calcd for $C_{12}H_{26}O_5$: C, 57.58; H, 10.47%

a) determined by the cryoscopic method in benzene solution.
b) determined by the Karl Fischer titration method.

Vapor-pressure Measurements. The vapor pressure of the water of the aqueous solution of TGDE was determined by the isopiestic method. The apparatus was generally analogous to that used by Robinson and Stokes,[5] but with considerable simplifications. Four or six cylindrical glass dishes (20 mm in diameter and 50 mm deep) were put on a copper block (100 mm in diameter and 20 mm thick) placed within a cylindrical, separable flask (1000 m*l*). Small amounts of grease were placed between the block and each dish to maintain good thermal conact. The equilibrium concentration was determined by weight. At the same time, the amount of water was checked by the Karl Fischer titration method and by refractive-index measurements. Sodium chloride solutions (in the region less than 50 mol% TGDE) and calcium chloride solutions (in the region greater than 50 mol% TGDE) were used as reference solutions. The water activities were obtained by the graphical interpolation of the activity-concentration relation given by Robinson and Stokes.[6]

Enthalpy of Mixing Measurements. The calorimeter used to measure the enthalpies of mixing was the same as that described earlier.[1] At high mole fractions of TGDE, the enthalpies of mixing were determined by measuring the heat when the pure TGDE was mixed with an aqueous solution of TGDE of a known composition. The accuracy of measurement was $\pm 3\,J\cdot mol^{-1}$ at $x<0.5$ and $\pm 5\,J\cdot mol^{-1}$ at $x>0.5$ (x is the mole fraction of TGDE).

Density and Phase-separation Temperature Measurements. The density of the TGDE+water mixture was measured in a 10-m*l* pyknometer which had been calibrated with distilled water. The liquid - liquid phase separation temperature was

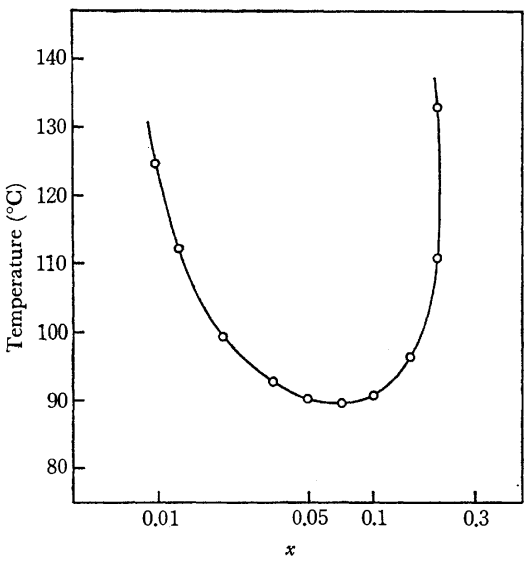

Fig. 1. The liquid-liquid phase diagram for the TGDE+water system.
x is the mole fraction of TGDE.

2) D. Hurd and G. W. Fowler, *J. Amer. Chem. Soc.*, **61**, 249 (1939).
3) P. Rempp, *Bull. Soc. Chim. Fr.*, **1957**, 844.
4) A. Kotera, K. Suzuki, K. Matsuura, T. Nakano, T. Oyama, and U. Kambayashi, This Bulletin, **35**, 797 (1962).
5) R. A. Robinson and R. H. Stokes, *J. Phys. Chem.*, **65**, 1954 (1961).
6) R. A. Robinson and R. H. Stokes, "Electrolyte Solutions," Butterworths, London (1959).

determined by heating (or cooling) solutions sealed in ampoules. The temperature shown in Fig. 1 is the average of the two temperatures; the temperature at which the phase separation occurred when the solution was heated slowly, and the one at which the solution became clear again upon slow cooling. The difference between the two temperatures was less than 1°C in all cases.

Results and Discussion

The liquid - liquid phase diagram for the TGDE+water system is shown in Fig. 1, in which the logarithms of x is plotted on the abscissa. This system has a lower critical solution temperature, one which is equal to 89.5°C. The critical concentration is about $x=0.072$. At 120°C, for example, a solution of $x\approx0.01$ is in equilibrium with a solution of $x\approx0.2$. The fact that the ether-rich phase still has a considerable amount of water indicates that the water molecules surrounding the ether molecule are appreciably stabilized. Four mixtures of mole fractions of 0.22, 0.33, 0.61, and 0.71 have been heated to 150°C. No separation of a second liquid phase is observed.

Table 2. Enthalpy of mixing H^E of tetraethylene glycol diethyl ether (TGDE) + water at 25°C. x is the mole fraction of TGDE

x	H^E/J·mol^{-1}	x	H^E/J·mol^{-1}
0.0106	−531.4	0.4383	−682.4
0.0346	−1323	0.4829	−577.0
0.0662	−1708	0.5168	−463.2
0.0973	−1813	0.5954	−242.7
0.1456	−1772	0.6881	−53.1
0.1962	−1662	0.7880	+48.5
0.2964	−1236	0.8865	+67.8
0.3708	−941.4		

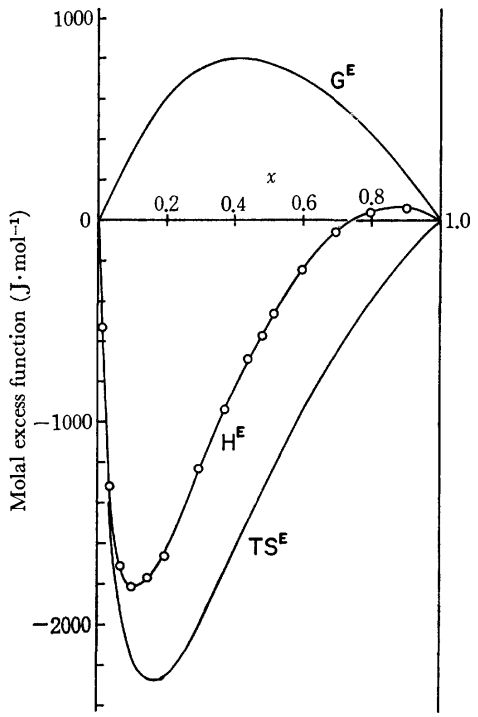

Fig. 2. The molal excess functions of the TGDE+water system at 25°C.

The enthalpies of the mixing, H^E, of the TGDE+water system at 25°C are presented in Table 2 and are shown in Fig. 2. The same general behavior as has been observed for the ethylene glycol dimethyl ether+water[7] and diethylene glycol diethyl ether+water[1] systems is also found for the present system; that is, the H^E is large and negative (exothermic) in the water-rich region and positive (endothermic) in the ether-rich region. However, the exothermicity is, as a whole, more remarkable in this system than in either of the systems cited above.

As has been mentioned earlier,[1] the exothermic heat of mixing in the water-rich region is probably attributable to the structural modifications of water around the ether molecule. The large exothermic heat of mixing observed in the present system, compared with that of diethylene glycol diethyl ether and of ethylene glycol dimethyl ether, is consistent with the prediction that the effect due to the structural modifications of water is more remarkable in an aqueous solution of large hydrocarbon molecules than in one of small ones, when compared at the same mole fraction.

Table 3. Isopiestic data at 25°C for the system TGDE + water

x	m_{NaCl}	m_{CaCl_2}	a_1	γ_1
0.0153	0.4823	—	0.9842	1.000
0.0313	1.049	—	0.9652	0.996
0.0473	1.598	—	0.9463	0.993
0.0727	2.241	—	0.9235	0.996
0.1048	2.742	—	0.903	1.009
0.1528	3.207	—	0.885	1.045
0.1878	3.451	—	0.875	1.078
0.2433	3.788	—	0.861	1.137
0.3021	4.108	—	0.847	1.214
0.3481	4.387	—	0.834	1.279
0.4015	4.849	—	0.813	1.360
0.4580	5.345	—	0.791	1.459
0.4675	—	2.896	0.763	1.434
0.5184	—	3.122	0.733	1.521
0.6306	—	3.822	0.647	1.753
0.6982	—	4.403	0.571	1.891
0.7511	—	4.990	0.500	2.008
0.8412	—	6.418	0.355	2.233

The isopiestic data for the TGDE+water system at 25°C are summarized in Table 3. The second and third columns give the isotonic concentration (in molality) of the reference solutions, which are in equilibrium with the aqueous solution of TGDE with the mole fraction x. The fourth column gives the activity of water, a_1, while the last column gives the activity coefficient of water, γ_1, which is defined by the relation: $\gamma_1=a_1/(1-x)$. The water activity shows a positive deviation from ideality over most of the composition range, though a negative deviation is observed in the water-rich region ($x<0.1$).

The activity coefficient of TGDE γ_2 is calculated by using the Gibbs-Duhem equation. From these results,

7) E. Tommila and V. Turkki, *Suom. Kemistilehti*, **40B**, 207 (1967).

the molal excess Gibbs energy of mixing, G^E, is obtained; it is plotted in Fig. 2. The G^E is defined by the following equation:

$$G^E = RT\{(1-x)\ln\gamma_1 + x\ln\gamma_2\}.$$

Figure 2 also includes the excess entropy of mixing multiplied by the absolute temperature, T, TS^E, which is merely the difference between H^E and G^E. The concentration dependence of these excess functions is similar to that of the 1,4-dioxane+water system.[8] As may be seen from Fig. 2, the concentration dependence of H^E (and of TS^E) is peculiar in contrast to that of G^E, which is positive over the entire range of composition and is approximately symmetrical with a relatively small maximum ($805\ J\cdot mol^{-1}$) at $x\approx0.4$. Thus, we can expect that information about the dissolution state of each component may be drawn from the analysis of H^E and (or) TS^E rather from than that of G^E.

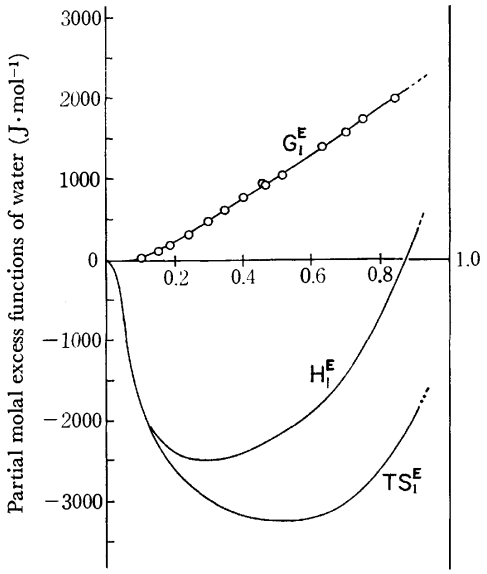

Fig. 3. The partial molal excess functions of water in the TGDE+water system at 25°C.

In Fig. 3, the partial molal excess functions of water in the TGDE+water system at 25°C are plotted against x. The G_1^E is calculated from the vapor-pressure data (Table 3) using the relation: $G_1^E = RT\ln\gamma_1$. The H_1^E is obtained by the graphical differentiation of the H^E *vs.* x curve (Fig. 2). The TS_1^E quantity is simply the difference between H_1^E and G_1^E.

In the previous paper,[1] as a reasonable explanation of the concentration dependence of H_1^E for the aqueous solution of diethylene glycol diethyl ether and of some cyclic ethers, it has been suggested that the hydrogen-bond formation between water molecules is dominant even in the ether-rich region, and that, with an increasing water concentration, the solvating layer of the ether molecule is gradually constructed through this water-water interaction. A similar explanation will hold for the present system, since the H_1^E *vs.* x curve is essentially similar to that of the previous systems. However, it is not only of interest, but also of importance, to see if the concentration dependence of the S_1^E is also consistent with this view. In conclusion, we can say that, judging from the following discussion, the behavior of S_1^E can also be interpreted in the same way.

In the initial stage, for instance $x>0.8$, added water molecules will form hydrogen bonds with the ether oxygen atoms. The value of S_1^E in this region will reflect the state of the water molecule, which is subject to the restraint of the ether. If such a hydrogen-bond formation continues until all of the oxygen atoms form at least one hydrogen bond with water, the value of S_1^E at a high mole fraction of ether would continue up to, say, $x=0.3$ or less. However, as may be seen from Fig. 3, the S_1^E decreases remarkably with an increase in the water concentration. This behavior is consistent with the above idea that an alternative, more ordered arrangement of the water molecule arises even at high mole fractions of the ether.

Now, some care must be taken in choosing an ideal entropy for the definition of an excess entropy of mixing. Since the TGDE molecule is a chain molecule whose chain length is comparable to that of heptadecane, it is reasonable to use, instead of $-R\ln(1-x)$ as before, the following expression for a partial molal excess entropy of water in an ideal solution, S_1^{ideal}:

$$S_1^{ideal} = -R\{\ln(1-\phi)+\phi(1-1/M)\}$$

where ϕ is the volume fraction of the TGDE and, where M is the ratio of the molal volume of the ether to that of water, which is equal to 14.3 at 25°C. However, the concentration dependence of this newly-defined S_1^E is essentially similar to that of the previous S_1^E, though the numerical value becomes much more negative. As a result of this, the above-mentioned interpretation of the S_1^E curve need not be changed.

The excess volume of mixing, V^E, is shown in Fig. 4, together with the partial molal excess volumes of the mixing of both components, V_1^E and V_2^E. The V_1^E and V_2^E are obtained by the graphical differentiation

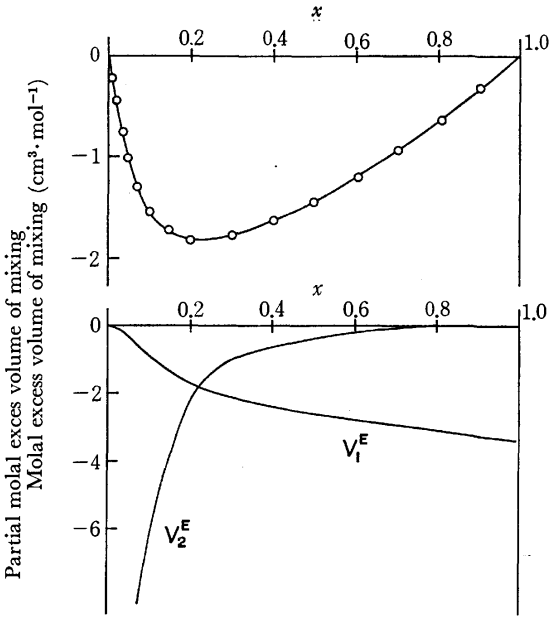

Fig. 4. The molal excess volume of mixing and the partial molal excess volume of mixing for the TGDR+water system at 25°C.

8) J. R. Goates and R. J. Sullivan, *J. Phys. Chem.*, **62**, 188 (1958).

of the V^E *vs.* x curve. The V^E is negative over the entire range of composition and has its minimum (-1.82 cm^3·mol^{-1}) at $x=0.23$. The V_2^E decreases appreciably with an increase in the water mole fraction and reaches about -23 cm^3·mol^{-1} at an infinite dilution. The V_1^E is about -3.4 cm^3·mol^{-1} at $x\rightarrow 1$, which means a 19% depression in the molal volume of normal water. This appreciable contraction may be ascribed to the breakdown of the bulky structure characteristic of liquid water when it is dissolved in a large amount of ether. In the intermediate region, ($0.2<x<0.8$, for instance) V_1^E is $-2\sim-3$ cm^3·mol^{-1}. This indicates that the water layer surrounding the ether is more dense than normal water. This observation is presumably related to the dense structure of water that would exist in the "iceberg" structure.

BULLETIN OF THE CHEMICAL SOCIETY OF JAPAN, VOL. 45, 1375—1380(1972)

On the Electron-transfer Reaction Rate between Different Molecular Species of Aromatic Hydrocarbons as Measured by ESR

Kosaku SUGA and Shigeru AOYAGUI*

Faculty of Engineering, Tokyo Institute of Technology, Meguro-ku, Tokyo

(Received December 9, 1971)

The rate constants of electron-transfer reactions between the anthracene anion radical and pyrene, and those between the former radical and 1,2-benzanthracene, were measured by the ESR method in tetrahydrofuran containing 20 mM of tetra-*n*-butylammonium perchlorate. In the analysis of the experimental results, correction of the ESR line width was made for the change in the radical concentration caused by the addition of neutral molecules. The rate constants thus obtained were $(2.0\pm0.4)\times10^{7}\,M^{-1}sec^{-1}$ and $(8.1\pm1.0)\times10^{7}\,M^{-1}sec^{-1}$ respectively at 25°C. Under the same experimental conditions, the rate constants of the electron exchange of anthracene and pyrene with their respective anions were about one-tenth of the rate constants of free anions. This fact led us to the supposition that the anion radicals had been combined with tetra-*n*-butylammonium ions into stable ion-pairs in our experiment. A semi-empirical method was proposed for the theoretical calculation of the rate constant according to the theory of R. A. Marcus. The agreement of the observed and the calculated rate constants was satisfactory. Further discussion of the dependence of the rate constant on the standard free energy of reaction was made in connection with the so-called "Linear Free Energy Relationship."

Kinetic studies of electron-transfer reactions in liquid solutions have been reported mainly on metal-complex ions. They have been summarized in several review articles.[1-3] The theoretical treatments have also been made by many investigators, and several excellent theoretical works have been presented, especially on the rate of electron-transfer reactions with outer-sphere mechanisms.[4-8]

However, there have been only a few experimental investigations of the kinetics of the electron-transfer reactions of organic compounds. Probably this is due to the difficulty in the measuring technique, which can be attributed to their large reaction rate and to the instability of the anion radicals. As to theoretical treatments of them, very few investigations have been done. The kinetic study of the electron-transfer reaction of organic compounds began with an electron spin resonance measurement of the rate of the electron exchange between naphthalene and its anion radical by Ward and Weissman;[9] this was followed by measurements of several kinds of anion radicals under various conditions. However, there has been no systematic experimental work which can be the basis for theoretical work. The difficulty is thought to be due to the formation of ion-pairs between anion radicals and cations.

It is known that the radical anions prepared by the reduction of aromatic hydrocarbons with alkali metals form ion-pairs with alkali metal ions in ethereal solvents with low dielectric constants, such as tetrahydrofuran (THF) and methyltetrahydrofuran. Further, the ion-pairs are in several different states, which are dependent on the nature of both the solvent and the cation.[10] These circumstances have troublesome influences on the analysis of the electron-transfer rate.

We have been engaged in experimental work to investigate the dependence of the rate of the electron transfer upon some of the physico-chemical parameters of the reaction, such as the standard free energy of the reaction (ΔG°), the dielectric constant of the solvent, the molecular radius of the reactants, and the temperature. The free anion radicals were expected to be generated by

* To whom correspondence should be addressed.

1) J. Halpern, *Quart. Rev.* (London), **15**, 207 (1961).
2) N. Sutin, *Ann. Rev. Nuclear Sci.*, **12**, 285 (1962).
3) R. A. Marcus, *Ann. Rev. Phys. Chem.*, **15**, 155 (1964).
4) R. A. Marcus, *J. Chem. Phys.*, **24**, 966 (1956).
5) R. A. Marcus, *Discuss. Faraday Soc.*, **29**, 21 (1960).
6) R. A. Marcus, *J. Phys. Chem.*, **67**, 853 (1963).
7) R. A. Marcus, *J. Chem. Phys.*, **43**, 679 (1965).
8) N. S. Hush, *Trans. Faraday Soc.*, **57**, 557 (1961).
9) R. L. Ward and S. I. Weissman, *J. Amer. Chem. Soc.*, **79**, 2086 (1957).
10) N. Hirota, *ibid.*, **90**, 3603 (1968).

the electrolytic reduction of hydrocarbons, in which tetraalkylammonium salt was used as a supporting electrolyte. However, it was found that, when tetra-*n*-alkylammonium perchlorate was added to the solution, the ESR spectrum of the solution of the radicals produced by the reduction with alkali metals did not have any hyperfine splittings due to alkali ions. This result suggested that the anion radicals could form stabler ion-pairs with tetraalkylammonium ions than those with alkali metal ions; this idea has been supported by other experiments.[11,12] Therefore, the investigation of the electron-transfer reaction of the free anion radical cannot be made in the presence of tetraalkylammonium ions. However, in this case, some new information may be obtained on the electron-transfer reaction of the stable ion-pairs themselves. The electron-transfer reaction of the ion-pairs of the hydrocarbon anion radicals with cations besides metal ions have never been investigated.

This paper will treat the electron-transfer rate from the ion-pairs of anthracene anions with tetra-*n*-butylammonium ions to hydrocarbons other than anthracene in order to examine its dependency on ΔG°. Until now the measurements of the electron-transfer rate by the ESR method have been carried out exclusively of the electron-transfer between the same species of molecules, *e.g.*, between naphthalene and its anion radical.[9] Measurements must be made for a couple of different molecular species for the dependence of the electron-transfer rate upon ΔG° to be investigated. Measurements on such a couple can, in principle, be made with the ESR method. In the following reaction of an anion radical, R_1^-, with a neutral molecule, R_2,

$$R_1^- + R_2 \underset{k_2}{\overset{k_1}{\rightleftharpoons}} R_1 + R_2^-$$

the rate constant, k_1, can be determined by the line-broadening of the spectrum of R_1^- after adding R_2, if the coexistence of R_2^- in the solution does not disturb the observation of the ESR spectrum of R_1^-. In practice, however, the measurement is possible only when ΔG° is positive, *i.e.*, when the position of the equilibrium of the reaction is located on the left-hand side of the equation. Moreover, there is another restriction on the value of ΔG°. When the ΔG° of the reaction is large, the equilibrium is located on far left-hand side of the reaction; consequently, the reaction rate is too slow to be measurable with this method. Hence, the ΔG° values of reactions the rates of which are measurable range within about 0—0.3 eV. The electron-transfer reactions dealt with in this paper are those between anthracene anion radicals and 1,2-benzanthracene, and those between anthracene anion radicals and pyrene, the ΔG° values of which are 0.052 eV and 0.113 eV respectively.[13]

Experimental

The aromatic hydrocarbons used, anthracene, pyrene, and 1,2-benzanthracene, were obtained by the recrystallization of the commercial reagents from benzene or ethyl alcohol.

Tetra-*n*-butylammonium perchlorate was prepared by adding an excess of perchloric acid to an aqueous solution of tetra-*n*-butylammonium iodide and then by filtering the precipitate. It was recrystallized from water first, and then from ethyl acetate. Tetra-*n*-butylammonium iodide was synthesized by the usual method from tri-*n*-butylamine and *n*-butyl iodide.

Tetrahydrofuran was used as a solvent throughout this investigation. It was refluxed over sodium metal, distilled, and then allowed to stand over sodium metal in a vaccum for a week. After the evolution of hydrogen gas had ceased, the solvent was distilled and stored in an ampoule containing anthracene and sodium metal in a vacuum in order to remove the trace of both oxygen and water. The stored solution was deep blue because of the presence of anthracene anion radicals. The solution of mono-negative ion radicals of hydrocarbons was prepared by the usual method, using a solvent redistilled from the stored solution.

The measurements of the ESR spectra were made with a JEOL JES-3BS spectrometer operated at about 9.7 kMHz, with 100 kHz field modulation and with a modulation amplitude of 0.03—0.08 gauss.

The rates of the electron-transfer reactions were determined from the increase in the linewidth of the ESR spectra of the radical anions after the addition of a known amount of neutral molecules. The measurements were carried out at 25°C.

The concentrations of the anion radicals were determined with a Shimadzu MPS-50L multipurpose autorecording spectrophotometer.

Results

The anthracene anion radicals prepared by the reduction of anthracene with sodium metal in THF yielded a rather unresolved ESR spectrum, as is shown in Fig. 1a. This spectrum evidently exhibited the hyperfine splittings due to a sodium nucleus, the coupling constant of which was about 0.5 gauss. On the other hand, no sign of hyperfine splittings due to sodium were seen in the spectrum of the solution of the anth-

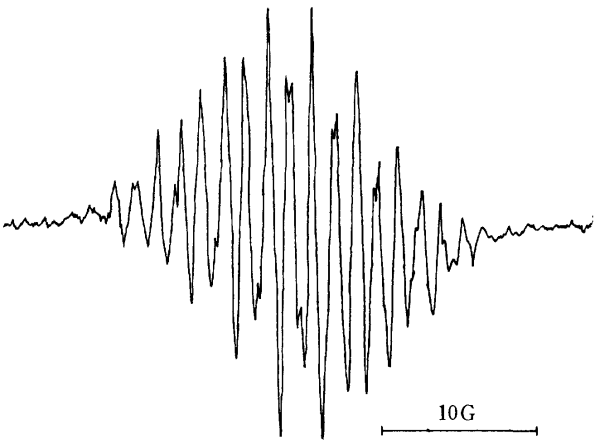

Fig. 1a. ESR spectrum of anthracene anion radical prepared by sodium reduction in THF. Radical concentration: 0.3 mM.

11) J. R. Bolton and G. K. Fraenkel, *J. Chem. Phys.*, **40**, 3307 (1964).
12) T. E. Hogen-Esch and J. Smid, *J. Amer. Chem. Soc.*, **88**, 307 (1966).
13) J. Chaudhuri, J. Jagur-Grodzinski, and M. Szwarc, *J. Phys. Chem.*, **71**, 3063 (1967).

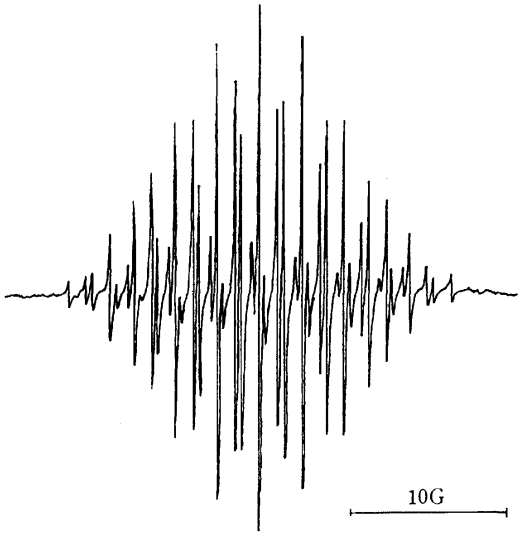

Fig. 1b. ESR spectrum of anthracene anion radical prepared by sodium reduction in THF and added by 20 mM of tetra-*n*-butylammonium perchlorate.

racene anion containing 20 mM of tetrabutylammonium perchlorate, though it was prepared in the way described above. The latter spectrum was a normal one with hyperfine splittings due to just three kinds of protons, as is shown in Fig. 1b. These results suggest that the sodium ion in the ion-pair had been replaced by the tetrabutylammonium ion.

The rates of electron-transfer reactions can be determined by measuring the increase in the linewidth after the addition of neutral molecules. However, this is the case only when the concentration of anion radicals is kept unchanged before and after the addition of neutral molecules. This is because a part of the linewidth of the ESR spectrum of anion radicals is caused by the spin-exchange interaction, the rate of which is dependent on the concentration of anion radicals. In the electron-transfer reactions between different molecular species, the initial concentration of the anion radical is decreased both by the following equilibrating reaction:

$$R_1^- + R_2 \underset{k_2}{\overset{k_1}{\rightleftharpoons}} R_1 + R_2^- \qquad (1)$$

and by the decomposition of the anion radicals, accompanied by the addition of neutral molecules. Accordingly, the linewidth should be corrected for the change in the concentration of anion radicals in this experiment.

It is necessary to examine the dependence of the linewidth upon the concentration of anion radicals in order to make a linewidth correction. Figure 2 shows this relation obtained experimentally. The concentration of anion radicals was determined by the use of the electronic spectra, the extinction coefficient by Balk *et al.* being used.[14] Figure 3 shows a typical spectrum of the anthracene anion radical; it is almost identical with that obtained by Balk *et al.* The plot of the observed linewidth against the radical concentration was linear, as is shown in Fig. 2. Such a dependence of the linewidth on the radical concentration is thought to be due to the spin-exchange interaction. The second-order rate constant of the spin-exchange process in solution can be calculated by the analysis of the relation in Fig. 2. It is 4.8×10^9M^{-1}sec^{-1}, a nearly diffusion-controlled value. The theoretical value of the diffusion-controlled rate constant in THF at 25°C[15] is 7.1×10^9M^{-1}sec^{-1}.

In our measurements of the rates by the ESR method, the concentration of anion radicals before the addition of the neutral molecules was determined by means of the relation shown in Fig. 2, and their concentration after addition, by means of the relative intensity of the central hyperfine lines. The intensity is defined here as the product of the derivative half amplitude (I) and the square of the peak-to-peak linewidth (ΔH_{pp}), on the

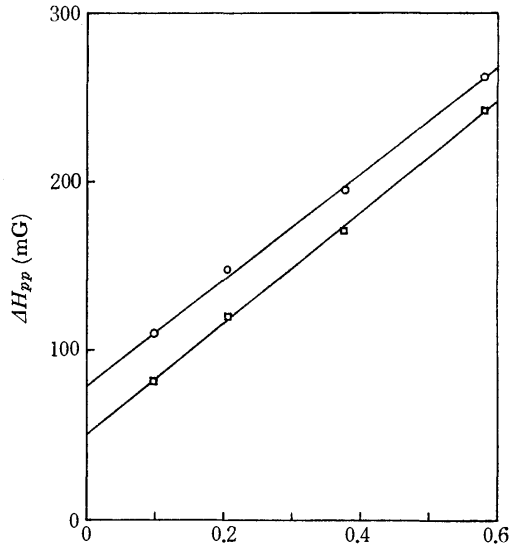

Fig. 2. Plots of linewidth against concentration of anthracene anion radical.
○: observed linewidth for the solution containing both anthracene and its anion radical ($A^- + A = 1$ mM), □: linewidth subtracted by the contribution of electron exchange between anthracene and its anion radical. ΔH_{pp}: peak-to-peak linewidth.

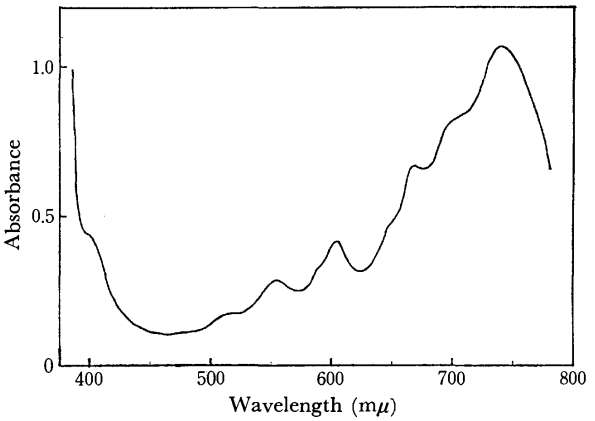

Fig. 3. Electronic spectrum of anthracene anion radical in THF containing 20 mM of tetra-*n*-butylammonium perchlorate.

14) P. Balk, G. J. Hoijtink, and J. W. H. Schreurs, *Rec. Trav. Chim. Pays-Bas*, **76**, 813 (1957).

15) M. P. Eastman, R. G. Kooser, M. R. Das, and J. H. Freed, *J. Chem. Phys.*, **51**, 2690 (1969).

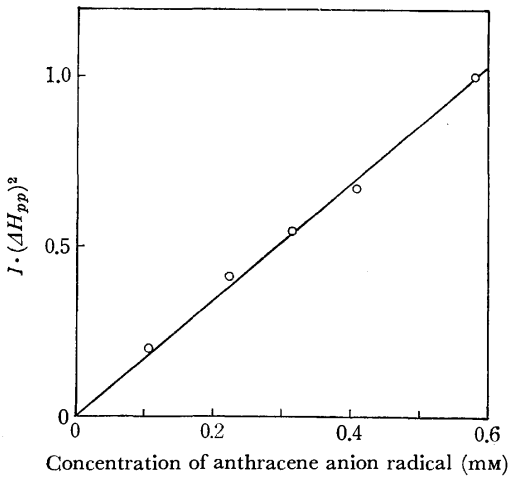

Fig. 4. Correlation between the relative intensity of ESR spectrum and the concentration of anthracene anion.

assumption that the Lorentzian line shape is unchanged after the addition of neutral molecules. It may be confirmed from Fig. 4 that the concentration obtained by the above method is in agreement with that determined spectroscopically.

When the equilibrium of the reaction (1) is attained, the linewidth, $\Delta H_{pp}(R_1^-)$, of the ESR spectrum of the anion radical, R_1^-, is given by the following equation:

$$\Delta H_{pp}(R_1^-) = c_1 + c_2[R_1^-] + c_3[R_1] + c_4[R_2^-] + c_5[R_2] \quad (2)$$

where $[R_1^-]$, $[R_1]$, $[R_2^-]$, and $[R_2]$ are the concentrations of the individual species. The five terms on the right-hand side of the equation are as follows: the first term is the linewidth intrinsic to the anion radical R_1^-; the second term is the linewidth due to the spin-exchange interaction between R_1^- ions; the third term is due to the electron transfer between R_1^- and R_1; the fourth term is due to the spin exchange interaction between R_1^- and R_2^-; the fifth term is due to the electron transfer between R_1^- and R_2. The c_1 and c_2 constants are obtainable from Fig. 2. The c_3 constant is estimated by means of the rate constant of the electron-transfer reaction between R_1^- and R_1. The fourth term in Eq. (2) is the linewidth due to the spin-exchange interaction between R_1^- and R_2^-, which may be diffusion-controlled, as is the interaction between R_1^- ions. Consequently, c_4 can be taken to be equal to c_2. It is c_5 that must be determined here. Its determination is feasible if $[R_1^-]$, $[R_2^-]$, $[R_1]$, and $[R_2]$ were known. Since $[R_1^-]$, $[R_1]$, and the added quantity of R_2 are already known, $[R_2^-]$ and $[R_2]$ can be evaluated by means of the mass action law, in which the equilibrium constant, K, is calculated from the difference in the standard reduction potential, ΔE°, between R_1 and R_2 by the use of the equation $K=\exp(\Delta E^\circ F/RT)$.

The contributions of each term in Eq. (2) to the linewidth are illustrated in Fig. 5. The symbolic notations A, P, and B means anthracene, pyrene, and 1,2-benzanthracene resectively. The uppermost plot in Fig. 5 is the plot of the observed linewidth against the concentration of added neutral molecules. The next lower plot indicates the linewidth due to the first four terms on the right-hand side of Eq. (2), each of them

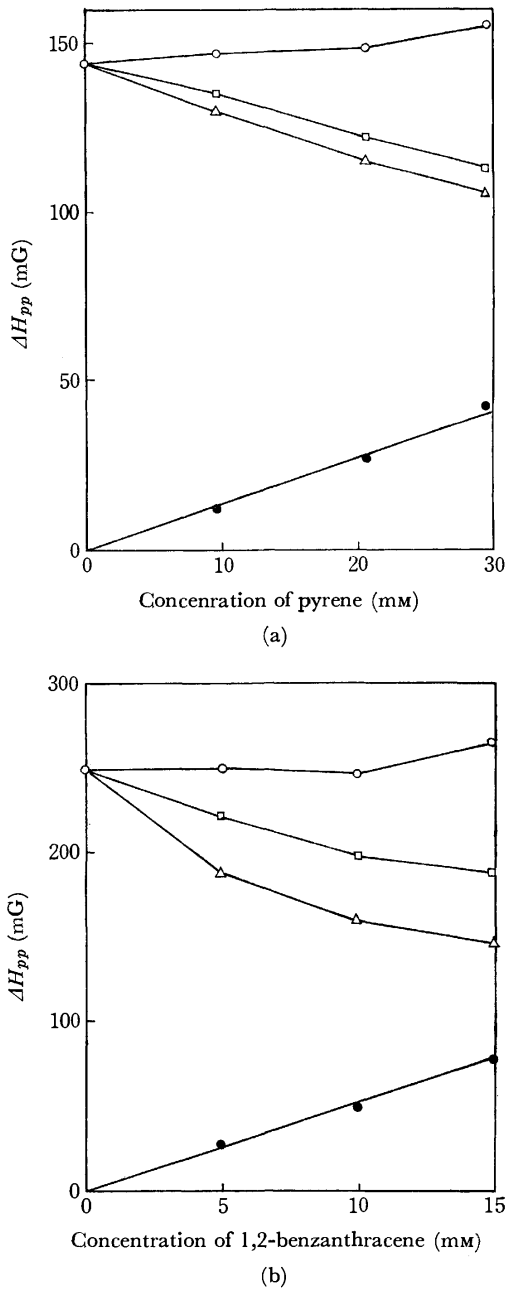

Fig. 5. Linewidth of ESR spectrum of anthracene anion radical plotted against the concentration of added neutral molecule of different kind from anthracene. ○: observed linewidth, □: the calculated contribution of first four terms in the right hand side of Eq. (2), △: the calculated contribution of first three terms of Eq. (2), ●: the difference between two upper plots, *i.e.*, the contribution of electron transfer reaction between different molecular species.
a) electron transfer reaction between A^- and P.
b) electron transfer reaction between A^- and B.

being evaluated by the above method. The third plot from the top shows the contribution of the first three terms of Eq. (2) to the linewidth. Accordingly, the difference between two upper plots is the linewidth attributed to the electron transfer between the different molecular species in question. This is shown as the lowermost plot in the figures. It was because of the cancelling effect of the decrease in the radical concentration of the linewidth that an increase in the measured

Table 1. Observed rate constants of electron transfer reactions in THF containing 20 mM of Bu_4NClO_4

Reaction	ΔG° (eV)	k_1 ($M^{-1}sec^{-1}$)
$A^- + A = A + A^-$	0	$(2.0\pm0.1)\times10^8$
$P^- + P = P + P^-$	0	$(2.3\pm0.2)\times10^8$
$A^- + B = A + B^-$	0.052	$(8.1\pm1.0)\times10^7$
$A^- + P = A + P^-$	0.113	$(2.0\pm0.4)\times10^7$

value of the linewidth was not observed when neutral molecules were added. The rate constants thus obtained are shown in Table 1, together with the ΔG° values of these reactions.

Figure 6 shows the similar plots for the couple of anthracene and its anion.

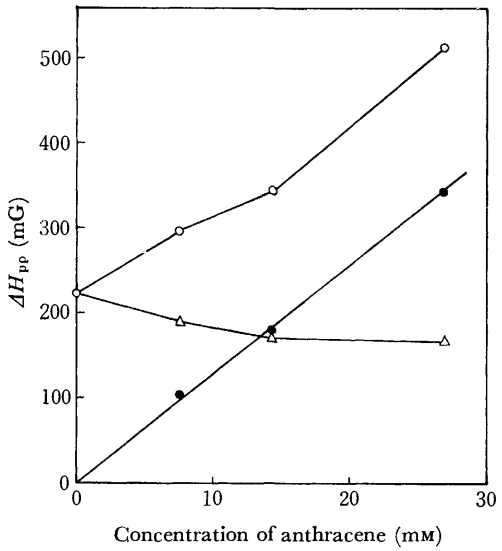

Fig. 6. Linewidth of ESR spectrum of anthracene anion radical plotted against the concentration of added parent molecule. ○: observed linewidth, △: the calculated linewidth with the exclusion of the contribution of electron transfer reaction, ●: the difference between two former plots, *i.e.*, the contribution of electron transfer reaction to the linewidth.

Discussion

The observed rate constants of the electron transfer between the same molecular species in Table 1 are seen to be about one-tenth of the rate constants for the free anions or their solvent-separated ion-pairs which were obtained with sodium metal in 1,2-dimethoxyethane (DME).[16] This suggests that A^- forms an ion-pair with the tetra-*n*-butylammonium ion (Bu_4N^+) in THF, although the ESR spectrum of A^- after the addition of tetrabutylammonium perchlorate does not have hyperfine splittings due to any of alkali ion, nitrogen atom, or protons in Bu_4N^+. The details of the effect of the ion-pairing of anion radicals with Bu_4N^+ ions on the electron-transfer rate will be reported later.

The rate constants of the electron-transfer reactions between different kinds of molecules are smaller for larger ΔG° values, as is shown in Table 1. The rate constant of the reaction between A^- and P was about one-tenth of that reported by Lyons *et al.*,[17] who worked with potassium and DME. The latter was $1.9\times10^8 M^{-1}sec^{-1}$. Although the extent of ion-pair formation between A^- and K^+ is not clear in their experiment, it is considered that the large rate constant is attributable to the large concentration of free ions or solvent-separated ion-pairs.[18]

The theories on the electron-transfer process which have been proposed should be examined in order to make a quantitative discussion of the ΔG° dependence of the electron-transfer rate. There have been several theoretical investigations of the electron-transfer processes of metal complex ions.[2-8] Marcus' work on those reactions which proceed with an outer-sphere mechanism and which are not accompanied by the formation or the rupture of the chemical bonds is thought to be the most outstanding.[4-7] The activation free energy of the electron-transfer reactions is obtained in this theory by calculating the energy of the reorientation of the solvent molecules in the vicinity of the discharging complex ions to form the activated complex, on the assumptions that the metal complex ions are the spheres of the conductor and that the solvent is a dielectrically unsaturated continuum. Moreover, the energy of the expansion and shrinkage of the inner coordination shell for the formation of the activated complex was also taken into consideration in the calculation of the activation free energy.[5-7]

According to the theory, the rate constant of the electron-transfer reaction, in which one of the reactants is neutral and the number of the transferring electron is one, is given by the following equation:[4-7]

$$k_1 = Z\exp(-\Delta G^*/RT) \tag{4}$$

where ΔG^* satisfies the equations:

$$\Delta G^* = (1/4)(1+\Delta G^\circ/\lambda)^2\lambda \tag{5}$$

$$\lambda = \lambda_0 + \lambda_i \tag{6}$$

$$\lambda_0 = e^2(1/2a_1 + 1/2a_2 - 1/r)(1/D_{op} - 1/D_s) \tag{7}$$

In these equations, Z is the bimolecular collision number of the hypothetical uncharged species in solution; e is the electric charge of the electron; λ_o and λ_i, the contributions to λ from the solvent and the inner coordination shell respectively; a_1 and a_2, the respective radii of the reactants; r, the distance between the centers of the reactants in the activated complex, and D_s and D_{op}, the static and the optical dielectric constants respectively.

In the present electron-transfer reaction of the organic ion radical, the model of Marcus is not consistent with the features of this reaction in two respects: the reactants are planar, and the anion radicals form ion-pairs. However, if λ is treated as a parameter which can be determined experimentally, no non-empirical estimation of those factors appearing in Eqs. (5) to (7)

16) N. Hirota, "Radical Ions," ed. by E. T. Kaiser, and L. Kevan, Interscience Publishers, New York, N. Y. (1968).

17) L. E. Lyons, J. E. Moore, and G. C. Morris, *Aust. J. Chem.*, **21**, 2789 (1968).

18) This value is inconsistent with our own unpublished data, $0.97\times10^8 M^{-1}sec^{-1}$, which was obtained with sodium metal and DME.

will be necessary. Accordingly, the examination of the dependence of the rate constants on ΔG° can be made by comparing the experimental value of the rate constant with that calculated by the above-mentioned method. In the electron-transfer reactions between the same species of molecules as those between anthracene and its anion radical, the ΔG° of the reaction is equal to zero and, accordingly, $\Delta G^* = \lambda/4$; therefore, the value of λ can be determined from the experimental value of the rate constant, if Z is given.

Generally, the value of λ is different for each reaction. As is shown in Table 1, however, the rate constants of the electron-transfer reactions between the ion-pair of the anion radical with the tetrabutylammonium ion and its parent molecule were nearly equal, *e.g.*, those of the reactions between $A^-Bu_4N^+$ and A, and between $P^-Bu_4N^+$ and P, were 2.0×10^8 and $2.3\times10^8 M^{-1}sec^{-1}$ respectively. If it is assumed that Z is 10^{11}, λ for $A^-Bu_4N^+$ and $P^-Bu_4N^+$ are of nearly equal values, *i.e.*, 14.7 and 14.4 kcal·mol^{-1} respectively. Because the λ of the cross electron-transfer reaction is thought to be equal to the mean value of the λ of the original reactions,[6] the λ values for the reactions $A^-+P=A+P^-$ and $A^-+B=A+B^-$ may be equal to that of $A^-+A=A+A^-$. Although there is some uncertainty in the value of Z, the value of 10^{11} proposed by Marcus[6] was taken here. ΔG° was calculated with the use of the data of the reduction potential of hydrocarbons by Chaudhuri *et al.*,[13] which were obtained in THF by means of potentiometric titration. The observed and the calculated values are both listed in Table 2; they

TABLE 2. COMPARISON OF THE OBSERVED AND THE CALCULATED VALUES OF RATE CONSTANT OF ELECTRON TRANSFER REACTIONS BETWEEN DIFFERENT MOLECULAR SPECIES

Reaction	ΔG°(eV)	k_1^{obs}($M^{-1}sec^{-1}$)	k_1^{theor}($M^{-1}sec^{-1}$)
$A^-+B=A+B^-$	0.052	8.1×10^7	7.0×10^7
$A^-+P=A+P^-$	0.113	2.0×10^7	1.9×10^7

are in agreement with one other. Although there is some difficulty in the non-empirical application of Marcus' theory to the electron-transfer reactions of organic ion radicals, the above results show that the ΔG°-dependence of the rate constants of those reactions

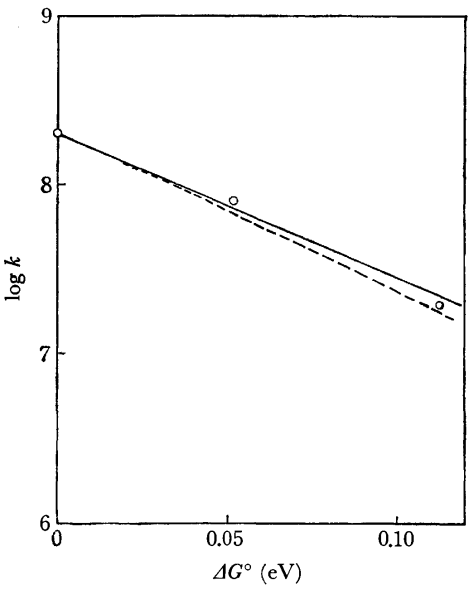

Fig. 7. Dependence of the rate constant of electron transfer reaction upon standard free energy of reaction (ΔG°). ○, observed value; ------, calculated value; ——, calculated value with the second order term in ΔG° being neglected.

can be calculated with this theory when λ is considered as a parameter.

It is known that there is a so-called "Linear Free Energy Relationship" between the rate constant of the chemical reaction and the standard free energy of the reaction; that is, there is a linear relation between ln k and ΔG°:

$$\ln k = A - \alpha\Delta G^\circ/RT \qquad (8)$$

where A and α are constants. The theory of Marcus shows that the quadratic term in ΔG° must also be included in the relation. If the quadratic term in the expansion of Eq. (4) is neglected, the value of 0.5 will correspond to the value of α in Eq. (8).[6] The plots of log k_1^{obs} and log k_1^{theor} against ΔG° are shown in Fig. 7, where a straight line drawn between log k and ΔG° by neglecting the quadratic term in Eq. (5) is also shown. On the basis of these results only it is difficult to decide whether or not the quadratic term in ΔG° contributes to the activation free energy. However, it is clear that the coefficient of the linear term is nearly equal to 0.5.

A Dilatometric Study of Compatible Polymer Mixtures

Saburo AKIYAMA

Department of Industrial Chemistry, Faculty of Technology, Tokyo University of Agriculture and Technology, Koganei, Tokyo

(Received April 15, 1971)

Polymer mixtures of poly(vinyl nitrate) ($PVONO_2$), and poly(vinyl acetate) (PVOAc), which had previously been concluded to be compatible with each other, were investigated by the dilatometric method. As a result, a characteristic behavior of the mixtures was observed. Each mixture showed a single glass-transition temperature (T_g) over the whole range of composition; this temperature was higher than those of pure polymers in the middle region of composition. The transition temperatures of the mixtures obeyed a modified Gordon-Taylor expression. The thermal expansion coefficients of the mixtures are discussed in relation to the effect of blending.

The investigation of compatible polymer mixtures is quite interesting as a means to know the possible behavior of polymer mixtures and to achieve a proper definition of compatibility.

There are only few polymer pairs which are compatible with each other. Especially, it is very difficult to make a compatible mixture with a pair of chemically-different polymers over a whole range of composition. Bohn[1] recently listed, from literature, thirteen examples of polymer pairs for which compatibility has been established, at least over a certain composition range. Among those polymers which are chemically quite different from each other, there are only a few pairs in which the compatibility is established over the whole range of their compositions. These are PVC(polyvinylchloride)/NBR(arcylonitile butadiene rubber)[2,3] and natural rubber/poly(butadiene)(Russian SKB).[4]

Other reports have shown by means of dynamic mechanical study[5] and by studying the heat of mixing[6,7] that PVOAc/nitrocellulose and PMMA (polymethyl methacrylate)/nitrocellulose are compatible pairs while the PIPA(polyisopropyl acrylate)/PIPMA(polyisopropyl methacrylate) pair has been established by dilatometric study[8] and the SBR(styrene butadiene rubber)/BR(butadiene rubber)[9] and phenol resin/NBR[10] pairs, by dynamic mechanical study.

We have studied the compatibility of mixtures of $PVONO_2$ and PVOAc. Several data, such as the temperature variation in the refractive indices and the mechanical properties ($T_{D\max}$), together with the observation under a phase-contrast microscope, have been taken to confirm the compatiblity of these mixtures, and it has been concluded that compatibility is observed in this pair with regard to these properties.[11,12]

In this paper, the thermal expansion of the polymer mixtures was investigated with dilatometers which are of the same type as that constructed by Bekkedahl.[13] In this dilatometric study, the present author also found that the glass-transition temperatures of the mixtures are slightly higher than those of the pure polymers. In addition, it is shown that the glass-transition temperatures of the mixtures satisfy the modified Gordon-Taylor equation introduced by Jenckel[14] and by Uematsu[15] for the copolymer system [Eq. (1)]:

$$T_{g12} = \frac{W_1\Delta\alpha_1 T_{g1} + W_2\Delta\alpha_2 T_{g2}}{W_1\Delta\alpha_1 + W_2\Delta\alpha_2} + \frac{W_1 W_2 \Delta k}{W_1\Delta\alpha_1 + W_2\Delta\alpha_2} \quad (1)$$

where T_{g12} is the glass-transition temperature of the mixture containing the weight fractions, W_1 and W_2, of two pure polymers, whose glass-transition temperatures are T_{g1} and T_{g2} respectively.

$$\Delta\alpha_1 = \alpha_{l1} - \alpha_{g1},\ \Delta\alpha_2 = \alpha_{l2} - \alpha_{g2} \text{ and } \Delta k = \bar{k} - k.$$

α_g and α_l are the volume expansion coefficients in the glassy and liquid states respectively. The 1 and 2 subscripts refer to two pure polymers, 1(PVOAc) and 2($PVONO_2$). $\bar{k}$ and k are parameters representing the volume change on mixing, as expressed by the following equations:

$$\bar{V} = W_1\bar{V}_1 + W_2\bar{V}_2 + \bar{k}W_1W_2$$
$$V = W_1V_1 + W_2V_2 + kW_1W_2 \quad (2)$$

where $\bar{V}$ and V are the specific volumes of a mixture in the glassy and liquid states respectively. The change in the specific volume with the temperature is assumed to be linear.

Experimental

The poly(vinyl nitrate) ($PVONO_2$) used for this work was obtained by the nitration[11] of a commercial sample of poly(vinyl alcohol) (PVA) with a degree of polymerization (DP) of 1700. The degree of nitration was 94.8 mol%. The poly(vinyl acetate) (PVOAc) used was a purified sample of a commercial product with a DP of 1800. Five specimens of polymer mixtures, BII-1, -3, -5, -7, and -9, were prepared from mixed solutions of $PVONO_2$ and PVOAc by evaporating the solvent. The mixing ratios of $PVONO_2$ to PVOAc in these samples were, in weight, 9/1, 7/3, 5/5, 3/7, and 1/9

1) L. Bohn, *Rubber Chem. Technol.*, **41**, 495 (1968).
2) L. E. Nielsen, *J. Amer. Chem. Soc.*, **75**, 1435 (1953).
3) M. Takayanagi, *Mem. Faculty Eng. Kyushu Univ.*, **23**, (1) 11 (1963).
4) G. M. Bartenev and G. S. Kongarov, *Vysokomolekul. Soedin*, **2**, 1962 (1960); *Rubber Chem. Technol.*, **36**, 668 (1963).
5) T. Koyama, Y. Inoue, and Y. Kobatake, *Kobunshi Kagaku*, **17**, 23 (1960).
6) S. Ichihara and T. Hata, *ibid.*, **26**, 249 (1969).
7) G. L. Slonimskii, *J. Polymer Sci.*, **30**, 625 (1958).
8) S. Krause and N. Roman, *ibid.*, **3**, 1631 (1965).
9) K. Fujimoto and N. Yoshimura, *Nippon Gomu Kyokaishi*, **38**, 284 (1965).
10) S. Nohara, *Kobunshi Kagaku*, **12**, 47 (1955).
11) S. Akiyama, N. Inaba, and R. Kaneko, *ibid.*, **26**, 529 (1969).
12) S. Akiyama and R. Kaneko, *ibid.*, **25**, 145 (1968).
13) N. Bekkedahl, *J. Research Natl. Bur. Standards*, **43**, 145 (1949).
14) E. Jenckel and R. Heusch, *Kolloid-Z.*, **130**, 89 (1953).
15) I. Uemastu and K. Honda, *Reports on Progress in Polymer Physics in Japan*, **9**, 245 (1966).

respectively, as is shown in Table 1. The conditions of preparation were given in detail in earlier reports.[11,12]

The specific volume of each specimen was measured at 25°C by the density gradient method. An aqueous solution of $CdCl_2$ was used for $PVONO_2$, BII-1, -3, and -5, and a $CaCl_2$ solution, for BII-5, -7, -9, and PVOAc. The temperature variation in the specific volume was determined by a method well-known in dilatometry.[13]

Dilatometry. The dilatometers were constructed of Pyrex glass and had a reservoir volume of about 20 cc. The measuring section was constructed of a precisely-bored capillary tube with a cross section of 0.01640—0.01642 cm^2. Each capillary was checked for uniformity and was calibrated with a mercury bead by the use of a travelling microscope. The volume of the reservoir was also determined by calibration with mercury. Tiny pieces of polymer samples without a void were cut off, weighed amounts of the tiny films were placed into the dilatometers, and then glass tubes were carefully shielded in order not to pyrolyze them. A special-grade commercial mercury was then charged on the top of the polymer samples while it was still under a vacuum. After breaking the vacuum, the mercury-filled dilatometers were allowed to rest for more than 24 hr at room temperature. They were then put into a water-ice bath maintained at 0——3°C. After a temperature equilibrium had been established, the temperature was raised at a rate of 20°C/hr and readings taken at 1°C intervals on a cathetometer which could be read to 0.005 cm. The glass-transition temperatures (T_g) and the volume-expansion coefficients below T_g (α_g) and above T_g (α_l) were obtained by this dilatometric measurement at the temperature elevation rate of 0.3—0.5 deg/min. The average standard estimations of the error in dv/dT were 1.5×10^{-6} cc/g°C in the glassy region and 3.0×10^{-6} cc/g°C in the rubbery region. The obtained T_g values were defined as the intersection of the straight-line portions of the plots of the specific volume *versus* the temperature.

Results and Discussion

Figure 1 shows the specific volume-*versus*-temperature curves obtained for $PVONO_2$, BII-1, BII-3, BII-5, BII-7, BII-9, and PVOAc. In the case of $PVONO_2$, it is noteworthy that the expansion does not show a linear increment above 55°C on account of the thermal degradation of $PVONO_2$. Table 1 summarizes the values of dv/dT, α_g, α_l, and T_g for the samples used. The calculated values for T_g were obtained from Eq. (1) using the following values:

$T_{g1} = 302.4$°K (PVOAc), $T_{g2} = 303.1$°K ($PVONO_2$),

$\alpha_1 = 2.88\times10^{-4}$, $\alpha_2 = 5.09\times10^{-4}$, and $\Delta k = 0.0097$.

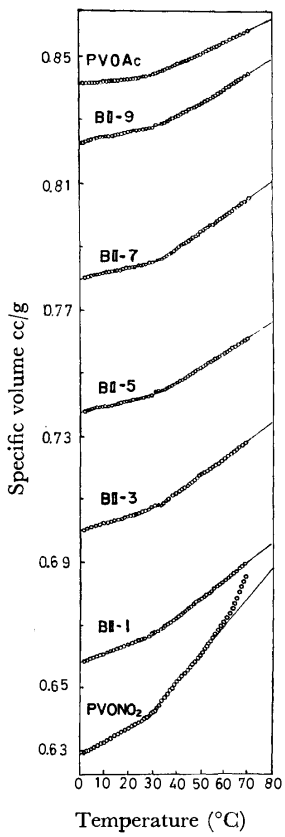

Fig. 1. Thermal expansion of $PVONO_2$, PVOAc, and mixtures.

To obtain the Δk value, we first read off a set of the values of the specific volume, $\bar{V}$ and V, say, at 0°C in the glassy state and at 50°C in the rubbery state, from the curves in Fig. 1. These values of $\bar{V}$ and V are plotted against W_1W_2 in Fig. 2. Then, we obtain, from the slopes of the straight lines, $\bar{k}=0.0205$ (cc/g) and $k=0.0108$; hence, the value of $\Delta k=0.0097$ is obtained [see Eq. (2)].

Figure 3 shows the glass-transition temperature, T_g, as a function of the weight fraction of PVOAc in the mixture. The full curve represents the calculated values of T_g given by Eq. (1), while the black and open circles are the experimental values obtained from the temperature dependencies of the refractive indices[11] and of the specific volumes respectively. It may be seen that the theoretical curve is in better agreement with the values obtained from the refractive indices.

TABLE 1. TRANSITION TEMPERATURES OF $PVONO_2$ AND PVOAc MIXTURES

Samples	Weight ratio of $PVONO_2$/PVOAc	Specific volume at 25°C cc/g	Expansion coefficient (dv/dT) cc/g°C: Below T_g $\alpha_g\times10^4$	Above T_g $\alpha_r\times10^4$	$(\Delta\alpha=\alpha_r-\alpha_g)\times10^4$	T_g^{dil}.°K[a]	$T_g^{n_D}$.°K[b]	T_g^{cal}.°K[c]
$PVONO_2$	10/0	0.6396	4.51	9.60	5.09	303.1	304.0	(303.1)
BII-1	9/1	0.6659	2.90	6.10	3.20	304.0	304.7	304.8
BII-3	7/3	0.7063	2.16	5.75	3.59	305.0	307.0	307.1
BII-5	5/5	0.7421	1.88	5.18	3.30	306.3	308.2	308.5
BII-7	3/7	0.7844	1.88	5.21	3.33	306.0	307.4	308.2
BII-9	1/9	0.8265	1.50	4.61	3.11	304.0	304.0	305.3
PVOAc	0/10	0.8431	1.10	3.98	2.88	302.4	302.4	(302.4)

a) Obtained by dilatometric measurements. b) Obtained by refractometric measurements.[11] c) Calculated T_g from Eq. (1).

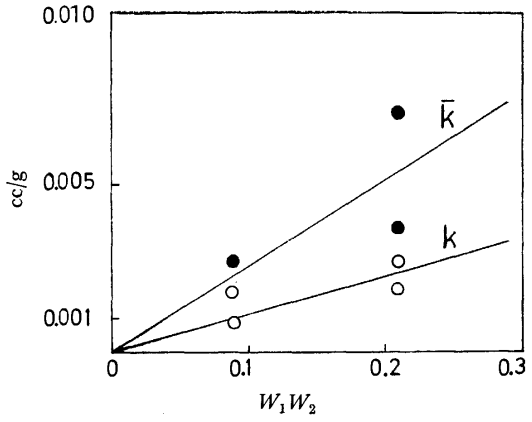

Fig. 2. Determination of $\bar{k}$ and k for $PVONO_2$ and PVOAc mixtures.
$\bar{V}-(W_1\bar{V}_2+W_2\bar{V}_2)$ and $V-(W_1V_1+W_2V_2)$ are plotted for W_1W_2 by Eq. (2).
From the slopes, $\bar{k}=0.0205$, $k=0.0108$ (cc/g).
(●, glassy state; ○, rubbery state)

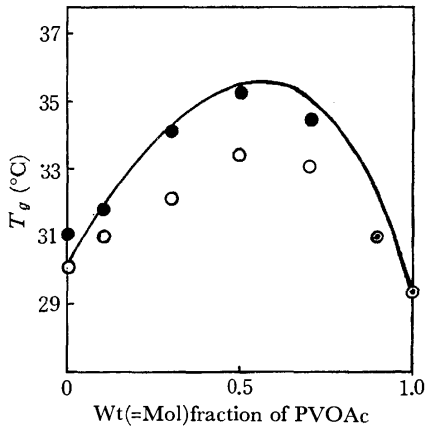

Fig. 3. Glass transition temperatures of PVOAc, $PVONO_2$, and their mixtures. The modified Gordon-Taylor expression is plotted using Eq. (1) (——). Experimental data obtained by means of refractometer (●) and by means of dilatometer (○).

Equation (2) appears to be insufficient to explain these experimental results completely. The small difference between the T_g values obtained by the two methods might be attributed to the errors due to the position of the thermometer and to the difference in experimental techniques (for example, the temperature-elevation rate). By the refractometric method we can avoid errors due to porosities in the samples better than by dilatometry; therefore, slightly higher values can be expected with the former method.

Figure 4 is a plot of the expansion coefficient as a function of the composition for the $PVONO_2$/PVOAc system. Small amounts of PVOAc can reduce the expansion of $PVONO_2$ quite effectively, but in the middle composition region, both α_g and α_l are nearly constant. It is clear that the α_g and α_l values of the mixtures deviate down from the straight lines. This depression in the expansion coefficients from additivity may result from an attractive interaction between the polar groups of the polymer pair.

By other measurements, such as those by means of a phase-contrast microscope, by mechanical damping (by

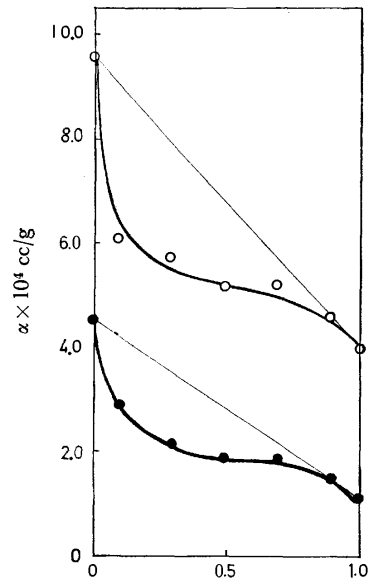

Fig. 4. Thermal expansion coefficients of $PVONO_2$, PVOAc, PVOAc, and their mixtures. (○, above T_g; ●, below T_g)

torsion pendulum[16]), and by the infrared spectra, the compatibility of this system has already been confirmed, and the characteristic behavior of the mixtures has been explained in forms of the interaction between the $-ONO_2$ and $-OCOCH_3$ polar groups. With the purpose of obtaining further evidence for this, studies of a low-molecular liquid mixtures of the nitric acid ester and the acetic acid ester, regarded as model compounds of the polymers, are now in progress by means of NMR and heat of mixing.

Recently Murakami[17] reported that a larger difference between the thermal-expansion coefficients of the homopolymers causes a rise in the T_g of the blend as a result of thermal stress. For the present compatible system, however it will be difficult to explain the results by this factor alone, although the large difference between the expansion coefficients may contribute to the rise in the T_g to some extent. As for the applicability of the Gordon-Taylor equation used for the copolymer in compatible mixtures, Koyama *et al.*[5] reported that, for the PVOAc/Nitrocellulose and PMMA/Nitrocellulose systems, the T_g varies with the composition according to this equation; Koleske and Lundberg[18] reported that the same was true for the poly ε-caprolactone/PVC system. However, Krause and Roman[8] found that, for PIPA/PIPMA mixtures, this equation was not applicable and argued that a new theoretical treatment was needed for their compatible mixtures. Therefore, by using only this equation it is quite difficult to determine whether or not they are compatible pairs.

By electron microscopic observations, Matsuo[19] re-

16) R. Kaneko, H. Shimizu, and S. Akiyama, *Kobunshi Kagaku* **23**, 97 (1966).
17) R. Murakami, *Kobunshi Kagaku*, **27**, 878 (1970).
18) J. V. Koleske and R. D. Lundberg, *J. Polymer Sci.*, **64**, 795 (1968).
19) M. Mastuo, C. Nozaki, and Y. Jou, *J. Electron Microscopy*, **17**, (1), 7 (1968).

cently showed that the PVC/NBR blends are not completely compatible and indicated that the micro heterogeneously-dispersed particles are less than 100 Å in diameter. Electron-microscopic observation will also be necessary to ascertain the morphology of this $PVONO_2$/PVOAc system accurately.

From the studies of the $PVONO_2$/PVOAc system, it is generally expected that the compatibility may be established when the intermolecular interaction between the mixed polymers has as strong an influence on the system as the intramolecular interaction.

Conclusions

By means of applying the dilatometric method to compatible mixtures of $PVONO_2$ and PVOAc, we arrived at the following conclusions:

(1) The mixtures showed higher glass-transition temperatures than both of the homopolymers.

(2) The transition data of the mixtures approximately obeyed the modified Gordon-Taylor equation.

(3) The fairly large depression of the expansion coefficients (Fig. 4) indicates the existence of a certain interaction between the polymer pairs.

The author wishes to express his thanks to Dr. Rokuro Kaneko of this University for his continued encouragement and discussions, and also to Teruo Iwanami and Satoshi Yamashita for their helpful assistance in carrying out the experiments.

BULLETIN OF THE CHEMICAL SOCIETY OF JAPAN, VOL. 45, 1384—1387(1972)

On the Long-range Interactions between Two Hydrogen Atoms and Two Helium Atoms

Tokio YAMABE, Shingo ISHIMARU, and Kenichi FUKUI
Department of Hydrocarbon Chemistry, Kyoto University, Kyoto
(Received November 11, 1971)

The numerical results of the interaction energy between two hydrogen atoms and two helium atoms are examined with the use of exact formulae of the second-order perturbation energy using the Unsöld approximation. It is found that the analytic expression gives a good long-range interaction energy between two hydrogen atoms comparable to the best variational results so far obtained. In the case of two helium atoms, the result lies in between experimental data for large nuclear distances; this seems to support the reliability of the present estimation. Finally, the effectiveness of the Unsöld approximation is remarked on.

In calculating the dispersion energy between two atoms, it happens that the multipole expansion of the perturbation leads to nonconvergent results.[1] To solve this difficulty, exact analytical expressions of the second-order perturbation energy within the framework of the Unsöld approximation have been derived by several authors for the hydrogen molecule ion[2] and for two hydrogen atoms and two helium atoms.[3] One particularly useful advantage is that they are so simple that one can use them for further calculations of the chemical or physical properties of atoms and molecules. On the other hand, a recent calculation[4] using the variation-perturbation technique, even though it avoided the divergence difficulty, is still given in expanded form in each angular component and is, as a consequence, too complicate to be applied to further calculations. Therefore, it is important to investigate whether or not the results obtained by the Unsöld approximation are numerically reliable, especially at a large separation. In the present paper, we will examine the numerical results with the use of the formulae previously obtained in two hydrogen and two helium cases[3] and will compare them with those of several authors.

On the interatomic force between two hydrogen atoms, many calculations have hitherto been carried out by both the variation and perturbation techniques. Among them, one of the most reliable techniques for the potential values in the range of $R>4.5$, where R is the interatomic separation in atomic units, is the variational technique proposed by Hirschfelder-Linnett with a nonexpanded Hamiltonian[5] for $4.5<R<8.0$, and another is that of Pauling and Beach,[6] with an expanded form for $9.0<R<12.0$. The present second-order perturbation energy is comparable to the above-mentioned values. Furthermore, the limit of the Unsöld approximation with the conventional asymptotic expansion is made clear numerically.

In the case of two helium atoms, the best theoretical potential curve is given by superimposing the results of Rosen, Margenau, and Page.[7] Unfortunately, the

1) F. C. Brooks, *Phys. Rev.*, **86**, 92 (1952).
2) G. M. Roe, *ibid.*, **88**, 659 (1952).
3) K. Fukui and T. Yamabe, *Intern. J. Quantum Chem.*, **2**, 359 (1968): This paper involves an error in one of the formulae, which has been corrected recently by the same authors.
4) H. Kreek and W. J. Meath, *J. Chem. Phys.*, **50**, 2289 (1969).
5) L. O. Hirschfelder and J. Y. Linnett, *ibid.*, **18**, 130 (1950).
6) L. Pauling and J. Y. Beach, *Phys. Rev.*, **47**, 686 (1935).
7) P. Rosen, *J. Chem. Phys.*, **18**, 1182 (1950); H. Margenau, *Phys. Rev.*, **56**, 1000 (1939); C. H. Page, *Phys. Rev.*, **53**, 426 (1938): These results are quoted and combined to one curve by J. O. Hirschfelder, C. F. Curtiss, and R. Bird, "Molecular Theory of Gasses and Liquids," John Wiley and Sons, Inc., New York, 1954, p. 1067.

curve lies under the experimental curves[8,9] for separations larger than 3.8 Å, although one has, of course, to consider the error involved in the experimental data. On the other hand, the interaction energy estimated in this paper lies between these values, at $R>4.0$ Å; this seems to support the present results. It seems that it would be of interest to examine whether or not this discrepancy is attributable to an essential error which is often brought about in the perturbation treatment. In this aspect, the dispersion energy is discussed in relation to that reported by Margenau and Page. Other theoretical calculations due to the molecular orbital theories have been made by several authors.[10,11] None of them gives satisfactory results in the van der Waals region.

In the last section of this paper, the theoretical foundation of the applicability of the Unsöld approximation is discussed with the use of a variational approach, which confirms the effectiveness of the Unsöld approximation, taking the ground-state energy of the system as the average excitation energy.

The Interaction Energy between Two Hydrogen Atoms

It is well known that, in the framework of the Unsöld approximation, the second-order perturbation energy $E_2(R)$, of the interaction between two hydrogen atoms in their ground states may be represented as follows:

$$E_2(R) = \frac{(H'^2)_{00} - (H')^2_{00}}{\langle \Delta E \rangle_{\mathrm{AV}}}. \tag{1}$$

$\langle \Delta E \rangle_{\mathrm{AV}}$ is an "average excitation energy" after Unsöld. $(H')_{00}$ and $(H'^2)_{00}$ are given by:

$$\begin{Bmatrix} (H')_{00} \\ (H'^2)_{00} \end{Bmatrix} = \iint \phi^2_{Ha}(1)\phi^2_{Hb}(2) \begin{Bmatrix} H' \\ H'^2 \end{Bmatrix} \mathrm{d}v_1 \mathrm{d}v_2, \tag{2}$$

where H' is the usual perturbation at an interatomic distance of R;

$$H' = \frac{1}{R} - \frac{1}{r_{1b}} - \frac{1}{r_{2a}} + \frac{1}{r_{12}} \text{ (in atomic units)},$$

ϕ_{Ha} and ϕ_{Hb} are the $1s$ functions of the a and b, hydrogen atoms and the exchange of two electrons, 1 and 2, is neglected.

In our previous paper,[3] Eq. (1) was evaluated exactly without resorting to a series expansion and was given in a closed analytical form applicable to an arbitrary interatomic distance, R, as follows:

$$(H')_{00} = \mathrm{e}^{-2R}\left(R^{-1} + \frac{5}{8} - \frac{3}{4}R - \frac{1}{6}R^2\right) \equiv U(R), \tag{3}$$

$$(H'^2)_{00} = V_{\mathrm{S}}(R) + V_{\mathrm{L}}(R) \equiv V(R), \tag{4}$$

$$V_{\mathrm{S}}(R) = V_1(R)\mathrm{e}^{-2R} + V_2(R)\mathrm{e}^{-4R} + \mathrm{e}^{2R}Ei(-4R)\left(4 - \frac{2}{R}\right), \tag{5}$$

$$V_{\mathrm{L}}(R) = \frac{1}{R^2} - \frac{7}{12} + \mathrm{e}^{2R}Ei(-2R)\left(\frac{11}{16R} - \frac{11}{8} - \frac{1}{2}R + \frac{1}{6}R^2\right) + \mathrm{e}^{-2R}\tilde{E}i(2R)\left(-\frac{11}{16R} - \frac{11}{8} + \frac{1}{2}R + \frac{1}{6}R^2\right), \tag{6}$$

where:

$$V_1(R) = -\frac{2}{R^2} + \left(4 + \frac{2}{R}\right)\log 4\gamma R - \frac{11}{4R} - \frac{9}{2} + \frac{5}{3}R,$$

$$V_2(R) = 2 + \frac{4}{R} + \frac{2}{R^2},$$

$$Ei(-x) = -\int_x^\infty \frac{\mathrm{e}^{-t}}{t}\mathrm{d}t, \quad \tilde{E}i(x) = -\int_{-x}^\infty \frac{\mathrm{e}^{-t}}{t}\mathrm{d}t$$

and where $\log \gamma$ is Euler's constant, 0.5772156649·····.

Some interesting features of the $V_{\mathrm{S}}(R)$ and $V_{\mathrm{L}}(R)$ functions presented above may be remarked on (Fig. 1). The $V_{\mathrm{S}}(R)$ function is the part of $V(R)$, which attenuates exponentially with increase in R, while the $V_{\mathrm{L}}(R)$ function is the origin of the well-known expression of asymptotic expansion in the inverse powers of R for large R values.

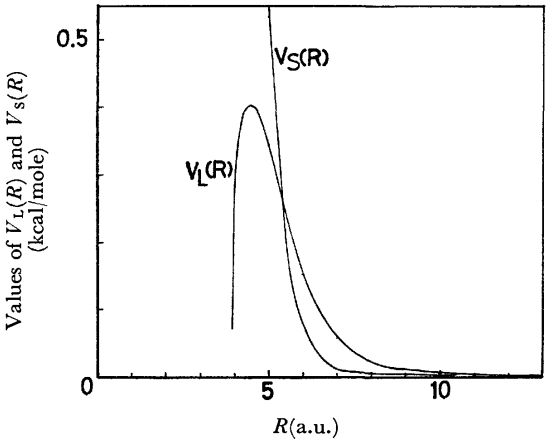

Fig. 1. The functions $V_{\mathrm{L}}(R)$ and $V_{\mathrm{S}}(R)$.

$$V_{\mathrm{L}}(R) \sim \frac{6}{R^6} + \frac{135}{R^8} + \frac{7875}{2}\cdot\frac{1}{R^{10}} + \cdots. \tag{7}$$

It may be seen in Fig. 1 that the value of $V_{\mathrm{S}}(R)$ prevails over $V_{\mathrm{L}}(R)$ at $R<5$, while at $R>7$ the latter is predominant. Therefore, Eq. (6) for $V_{\mathrm{L}}(R)$ or its asymptotic expansion, Eq. (7), with a limited number of terms, can not be a good approximation of the total interaction energy unless $R \gtrsim 8$. Moreover, it is noticeable that the $V_{\mathrm{L}}(R)$ has a maximum value of 0.40502 kcal/mol at $R=4.5$. Accordingly, the value of the interaction energy does not exceed *ca.* 0.4 kcal/mol so long as Eqs. (6) or (7) is adopted as the approximation of the total interaction energy.

In order to compare our results with the best potential energy curves previously obtained by Hirschfelder-Linnett[5] and Pauling-Beach,[6] we make the choice of $\langle \Delta E \rangle_{\mathrm{AV}}$, *i.e.* $\langle \Delta E \rangle_{\mathrm{AV}} = E_0 = -1.0$ a.u., as was previously suggested by Lennard-Jones.[12] Following this approximation, Eq. (1) and the total energy, E, are rewritten as:

$$E_2(R) = \frac{(H'^2)_{00} - (H')^2_{00}}{E_0} = U^2(R) - V(R), \tag{8}$$

8) W. G. Schneider and J. L. Yntema as quoted by P. Rosen, *J. Chem. Phys.*, **18**, 1182 (1950).

9) R. A. Buckingham, *Trans. Faraday Soc.*, **54**, 453 (1958).

10) S. Huzinaga, *Prog. Theoret. Phys.* (Kyoto), **20**, 631 (1958); P. Phillipson and R. S. Mulliken which was quoted by B. J. Ransil in Ref. 11.

11) B. J. Ransil, *J. Chem. Phys.*, **34**, 2109 (1961).

12) J. E. Lennard-Jones, *Proc. Roy. Soc.* (London), **A129**, 598 (1930).

$$E \sim E_0 + (H')_{00} + E_2(R). \quad (9)$$

As was pointed out by Dalgarno and Lewis,[13] the asymptotic form of Eq. (8) (equivalent to Eq. (7)) provides a good approximation to the variational calculation.[6] Moreover, the variational calculation gives $-6.49\,R^{-6}$ as the first leading term in its expanded form, while the present estimation gives $-6.00\,R^{-6}$ for the corresponding term. These facts imply that the above-mentioned choice of $<\Delta E>_{AV}$ is appropriate.

TABLE 1. THE INTERACTION ENERGY BETWEEN TWO HYDROGEN ATOMS (kcal/mol)

R (a.u.)	Present result	Pauling and Beach[a]	Hirschfelder and Linnett[b]
6.0	−0.2730	−0.1457	−0.3995
7.0	−0.07848	−0.0507	−0.09190
8.0	−0.02679	−0.0209	−0.02510
9.0	−0.01090		
10.0	−0.005130	−0.0049	−0.004380
11.0	−0.002687		
12.0	−0.001519	−0.0016	−0.001263

a) From Ref. 6. b) From Ref. 5.

In Table 1, the interaction energies between two hydrogen atoms at several interatomic separations larger than 6.0 are shown. Except for one case, at $R=12$, the present results give values below those of Pauling and Beach, which were obtained by the variational calculation taking the perturbation of the first three terms of the asymptotic expansion. Furthermore, at $6<R<7$, our results come close to the energy curve of Hirschfelder-Linnett obtained variationally by the use of the exact H' and by a trial function consisting of 1s functions with a variable exponent and corrected by considering all possible states of electron configurations and polarization effects. In the longer range, $8<R<12$, the present calculations give a lower energy curve than the previous results. As expected, the contribution of the first-order energy becomes negligibly small at all these distances.

The Interaction Energy between Two Helium Atoms

In the case of two helium atoms, the interaction energy was derived in a way analogous to the case of H_2, that is, by using the Unsöld approximation and by neglecting the electron exchange. The same discussion as that in the case of two hydrogen atoms is possible with respect to the $V(ZR)$ function, in which R is the distance between two helium nuclei in atomic units and in which Z is the effective nuclear charge of the isolated helium atom.

We chose the approximate wavefunction, $(Z^3/\pi)e^{-Z(r_1+r_2)}$, as the unperturbed state of an isolated helium atom in the ground state, where r_1 and r_2 are the distances from the nucleus of the 1 and 2 electrons respectively. This function gives the energy of $-Z^2$, and the optimum value of Z is 27/16. The second-order perturbation energy is obtained for two cases, in which $<\Delta E>_{AV}$ is approximated by the ground-state energy $(-Z^2)$ and by the ionization potential (-0.903695). These cases are denoted by $E_2{}^U$ and $E_2{}^L$ respectively. Following to Unsöld,[14] the value of $E_2{}^L$ is a lower limit to the second-order perturbation energy. The sum of the first- and second-order perturbation energies of these two cases are denoted by E^U and E^L respectively; they are tabulated in Table 2 together with the experimental and theoretical estimations. The present results give lower energy values than does the molecular orbital theory.[10,11] On the other hand, E^U gives higher values, over the whole range, than the combined results of Rosen, Margenau and Page (RMP), which consist of first- and second-order perturbation energies, including the electron exchange, and which are presumably the best theoretical potential energy curves so far obtained. However, in the $R>3.8$ Å range, the energies of RMP are always lower than both the experimental values,[8,9] whereas E^U lies between them. In this connection, it is worthwhile examining the dispersion energies obtained by these two theoretical approaches in the $4\text{ Å}<R<5\text{ Å}$ range in more detail. The results are indicated in Table 3. At $R=3.8$ Å, the difference be-

TABLE 3. THE DISPERSION ENERGY BETWEEN TWO HELIUM ATOMS (in 10^{-7} a.u.)

R (Å)	Present result		Margenau and Page
	$E_2{}^U$	$E_2{}^L$	
3.8	−54.0	−170.2	−129.6
4.0	−38.4	−121.0	− 94.0
4.2	−27.9	− 87.9	− 69.4
4.4	−20.7	− 65.2	− 52.0
4.6	−15.5	− 48.8	− 39.5
4.8	−11.8	− 37.2	− 30.3
5.0	− 9.1	− 28.7	− 23.6

TABLE 2. THEORETICAL AND EXPERIMENTAL DATA ON THE INTERACTION ENERGY BETWEEN TWO HELIUM ATOMS (in 10^{-7} a.u.)

R (Å)	Present calculation		Rancil[a]	RMP[b]	Schneider and Yntema[c]	Buckingham[d]	Corrected values
	E^U	E^L					
3.4	−90.1	−296.9	−41.3	−178	−178	−110	
3.8	−54.0	−170.2	− 9.2	−110	−100	− 32.1	−34.7
4.0	−38.5	−121.0	− 2.3	− 84.2	− 58.5	− 16.5	−28.6
4.5	−18.9	− 56.3					
5.0	− 9.1	− 28.7	0	− 22.0	− 19.3	− 0.5	− 7.5

a) From Ref. 11. b) From Ref. 7. c) From Ref. 8. d) From Ref. 9.

13) A. Dalgarno and J. T. Lewis, *Proc. Phys. Soc.* (London), **A69**, 57 (1956).

14) A. Unsöld, *Z. Phys.*, **43**, 374 (1927).

tween E_2^U and the value of Margenau and Page is 76×10^{-7}; this value is 56×10^{-7} at $R=4.0$ Å and 15×10^{-7} at $R=5.0$ Å. By adding these values to the interaction energies of RMP, one obtains the energies through the second-order perturbation energies, including the effect of electron exchange and lying at least between two experimental data. The corrected values of the interaction energy are shown in the last column of Table 2. In our previous paper, the present authors obtained the approximate dispersion energy of -1.63 R^{-6} (R in a.u.) for E_2^L. The value of the above coefficient is 0.517 for E_2^U, while Margenau reported 1.45. The former value is obviously too small, but the latter is in good agreement with the other results estimated by many authors over the last ten years.[15] However, as will be shown in the next section, the energy through E_2^U will give nearly an upper limit to the long-range interaction energy.

In the $R<4.0$ Å range, it is necessary to consider the electron exchange. Adding the approximate first-order exchange energy[16] to the above interaction energy gives an equilibrium distance of 3.2 Å, which roughly agrees with the experimental result of 2.8—3.0 Å.[8,9]

A Remark on the Applicability of the Unsöld Approximation

In the above discussions, in the cases of both two hydrogen and two helium atoms, it is clear that the analytical formula of the second-order perturbation energy on the basis of the Unsöld approximation gives a good descrpition of the long-range interaction. Here, a theoretical foundation may be required as to the applicability of the Unsöld approach.

For the sake of simplicity, we will discuss the case of the interaction of two hydrogen atoms. According to the variational principle,[17] and by the use of the variation function:

$$\psi = \phi_{Ha}(1)\phi_{Hb}(2)(1+AH'), \tag{10}$$

one obtains:

$$\begin{aligned} E \leqq E_0 &+ (H')_{00} + [(2A-E_0A^2)(H')_{00}-(H')_{00}^2 \\ &+A^2\{(H'H_0H')_{00}+(H'^3)_{00}-E_0(H')_{00}^2 \\ &-(H')_{00}(H'^2)_{00}\}]/[1+2A(H')_{00}+A^2(H'^2)_{00}], \end{aligned} \tag{11}$$

where A is the variational parameter, H_0 is the unperturbed Hamiltonian operator, and $(H'H_0H')_{00}$ and (H'^3) are integrals defined similarly to Eq. (2). At large separations, $(H')_{00}$ and $(H'^2)_{00}$ are small compared with unity (*e.g.*, at $R=8$ a.u., $(H')_{00}=-1.8\times10^{-6}$ and $(H'^2)_{00}=4.1\times10^{-5}$ a.u.); hence, they are negligible in the denominator of the third term in the right-hand side of Eq. (11), since A is found to be of the order of unity in the neibourhood of the minimum value of the righthand side of Eq. (11). Thus, Eq. (11) may be rewritten as:

$$\begin{aligned} E \lesssim E_0 &+ (H')_{00} + (2A-E_0A^2)\{(H'^2)_{00}-(H')_{00}^2\} \\ &+ A^2\{(H'H_0H')_{00}+(H'^3)_{00}\}. \end{aligned} \tag{12}$$

Up to the present, no exact evaluation of $(H'H_0H')_{00}$ or $(H'^3)_{00}$ has been found in the literature.

It may be permitted at large separations to estimate the relative magnitude of the integrals in Eq. (12) by the first leading terms of their asymptotic expansion.[18] The results are:

$$(H'^2)_{00} \sim -\frac{6}{R^6}, \tag{13}$$

$$(H'H_0H')_{00} \sim +\frac{45}{2}\frac{1}{R^8}, \tag{14}$$

$$(H'^3)_{00} \sim -\frac{2430}{R^{11}}. \tag{15}$$

At $R=8$, these one-term approximations give $(H'H_0H')_{00}\sim-0.0625\,\tilde{a}$ and $(H'^3)_{00}\sim+0.0124\,\tilde{a}$, while at $R=10$, $(H'H_0H')_{00}\sim-0.0375\,\tilde{a}$ and $(H'^3)_{00}\sim+0.0041\,\tilde{a}$ respectively. Where $\tilde{a}$ represents the values of $-6/R^6$ at each R. Consequently, if R is so large that the residual main term $(H'H_0H')_{00}$ can be neglected, Eq. (12) may be reduced to:

$$E \lesssim E_0 + (H')_{00} + (2A-E_0A^2)\{(H'^2)_{00}-(H')_{00}^2\}. \tag{16}$$

The right-hand side of this equation approaches approximately from the upper side to the upper limit of Eq. (11) with an increase in R. Now, we can easily find that Eq. (16) has a minimum with respect to the variation in A when $A=1/E_0$, in which case Eq. (16) becomes:

$$E \lesssim E_0 + (H')_{00} + \frac{(H'^2)_{00}-(H')_{00}^2}{E_0}. \tag{17}$$

The right-hand side of Eq. (17) agrees with Eq. (9). From the above discussions, it may be concluded that, if the energy of two isolated hydrogen atoms, E_0, is adopted for the value of $<\Delta E>_{AV}$ in the Unsöld approximation, the results give almost an upper limit for the energy; therefore, our previous result[3] and the numerical estimation presented in this paper are reliable. For a long-range interaction of two helium atoms, there is no essentially new problem and one will be able to treat it in the same way as in the case of two hydrogen atoms.

It becomes clear from the theoretical and numerical aspects that, if one uses the Unsöld approximation with the choice of the ground-state energy of the system considered as the average excitation energy, the resulting formula obtained analytically gives an energy value very close to the upper limit of the exact one. The evidence encourages us to investigate long-range forces between atoms and molecules, which are especially interesting in view of the chemical bond formation, in the simple manner described above.

The evidence reported in this paper may support the conclusion that the dispersion force is of the same nature as the chemical bond formation, being only a portion abstracted as acting at larger distances than ordinary bond lengths.

15) The data are summarized in the following paper: G. Starkshall and R. G. Gordon, *J. Chem. Phys.*, **54**, 663 (1971).

16) K. Fukui, "Quantum Chemistry," Asakura-Shoten, Inc., Tokyo 1968, p. 337.

17) L. I. Shiff, "Quantum Mechanics," second ed., McGraw-Hill Book Co., 1955, p. 179.

18) Mathematically, the integrals, $(H'H_0H')_{00}$ and $(H'^3)_{00}$ are infinite. However, one can avoid this difficulty in the manner previously developed by the present authors (This Bulletin, **43**, 2012 (1970)) and so find results not very different from those obtained by the use of the asymptotic expansion. A more detailed discussion of this point will be presented elsewhere.

The Behavior of Indium(III) Complexes in Several Distribution Systems. II. The Extraction of Indium(III) Halide and Thiocyanate Complexes into 4-Methyl-2-Pentanone, 4-Methyl-2-Pentanol, or Nitrobenzene

Yuko HASEGAWA, Hiroshi TAKEUCHI, and Tatsuya SEKINE

Department of Chemistry, Science University of Tokyo, Kagurazaka, Shinjuku-ku, Tokyo

(Received March 12, 1971)

The solvent extraction of indium(III) from a bromide, iodide, or thiocyanate solution into 4-methyl-2-pentanone(MIBK), 4-methyl-2-pentanol(hexol), or nitrobenzene was determined by using a ^{114m}In tracer. The extraction was, in general, most effective with MIBK and poorest with nitrobenzene, except from iodide solutions. The extraction with a certain solvent was always better from iodide solutions than from bromide solutions. The extraction from thiocyanate solutions was better than that from iodide solutions in some cases, but it was poorer in other cases, and it was better than that from bromide solutions except with nitrobenzene. Furthermore, it was found that the distribution ratio, determined as a function of the ligand concentration, was always poorer when the aqueous phase contained only the sodium salt of these ligands than when it was 4M Na(X, ClO_4) (where X denotes the ligand anion). The extractions from 4M Na(X, ClO_4) were analyzed by using the stability constants for the indium complexes with these ligands in the aqueous phase, and the extraction equilibria were determined. From these results, it was concluded that these polar solvents extract not only the uncharged complex, InX_3, but also the cationic and/or anionic indium complexes as ion-pairs, with the oppositely charged ions in the background salt, and that, in some cases, the solvent extracts only charged indium species. Thus, the difference in the distribution ratio in the presence and in the absence of the background sodium perchlorate was concluded to be caused not only by the change in the activities due to the change in the total salt concentration, but also by the extraction of ion-pairs of charged indium(III) species, which should be very much enhanced by the presence of the bulk perchlorate.

In Part I of this series,[1] it was reported that indium (III) forms complexes with various uninegative ligands and that the bromide, iodide, and thiocyanate complexes are extractable into hexane containing tributylphosphate (TBP). These extraction curves were explained in terms of a successive complex formation and the extraction of the uncharged complex, InX_3 (where X^- is a uninegative ligand), into this non-polar organic solvent containing a small amount of the coordinating extractant.

In the lower ligand-concentration region in these systems, an increase in the amount of extractable uncharged complex is caused by an increase in the ligand-concentration; consequently, it enhances the distribution ratio.

In the higher ligand-concentration region, where higher anionic complexes are formed, on the other hand, the distribution ratio decreases upon an increase in the ligand-concentration, because these charged complexes are usually unextractable into non-polar organic solvents. However, if the solvent is a polar one, it is supposed that the anionic complexes may also be extracted as ion-pairs with other cations in the aqueous phase, and the distribution ratio in such systems might increase, even in the higher ligand-concentration region.

The present paper will describe the results of experiments carried out along with this line. Three polar organic solvents, 4-methyl-2-pentanone(MIBK), 4-methyl-2-pentanol (hexol), and nitrobenzene, were employed as the organic solvents. The aqueous phases equilibrated with these organic solvents were similar to that in the previous study.[1]

The equilibrium constants at 25°C were determined by a successive approximation analysis of the distribution data graphically.

Experimental

Most of the experimental procedures were the same as those described in the previous study.[1] The indium-114*m* tracer was obtained from the Radio Chemical Center, England. The 4-methyl-2-pentanone and hexol were obtained from Kanto Kagaku Co. and the Tokyo Kasei Co. respectively; they were washed with 0.1M perchloric acid, water, and 0.1M sodium hydroxide successively, and then several times with water. The nitrobenzene was also obtained from the Kanto Kagaku Co. The sodium perchlorate was prepared from perchloric acid and sodium carbonate and was recrystallized three times from water. The other reagents were of an analytical grade and were used without further purification.

Aqueous solutions containing indium(III) labelled with the indium-114*m* tracer, and various amounts of the ligand and sodium perchlorate solutions, together with one of these solvents, were placed in stoppered glass tubes (volume, 20 m*l*). The initial volume of each phase was 5 m*l*, and the aqueous phase was adjusted to be a constant ionic medium of 4M sodium perchlorate, unless otherwise mentioned. The hydrogen-ion concentration was 1×10^{-2}M for the experiments on the bromide and iodide complexes, but it was about 1×10^{-3}M for the thiocyanate complexes, and the initial concentration of indium in the aqueous phase was about 2.5×10^{-6}M. All of the procedures were carried out in a thermostatted room at 25°C. The two phases in the tubes were agitated mechanically for about two hours and then centrifuged. The γ-radioactivity of these samples was measured with a scintillation counter (NaI), and the distribution ratio was calculated as;

$$D = \frac{\gamma\text{-count-rate per m}l\text{ of the org. phase}}{\gamma\text{-count-rate per m}l\text{ of the aq. phase}}$$

1) Y. Hasegawa, This Bulletin, **43**, 2665 (1970).

Results

Figures 1 to 3 give the extraction of indium(III) into the three organic solvents as a function of the ligand concentration in the aqueous phase, together with the extraction into hexane-containing TBP which has been

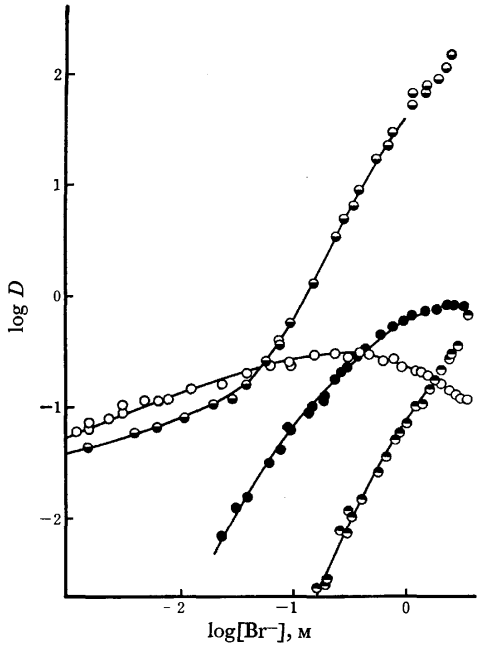

Fig. 1. The extraction of In(III) from 4M constant ionic medium containing bromide ions into various organic solvents.
◒: MIBK, ○: hexol, ●: 0.1M TBP-hexane taken from Ref. 1. ◓: nitrobenzene.

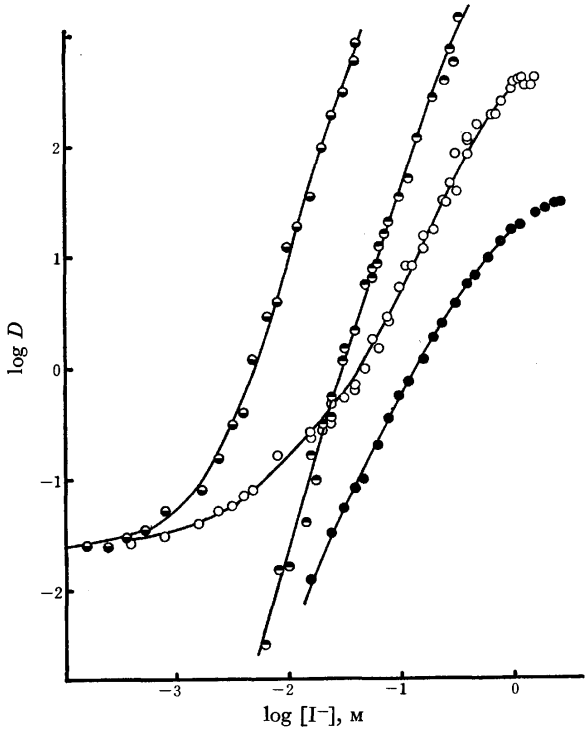

Fig. 2. The extraction of In(III) from 4M constant ionic medium containing iodide ions into various organic solvents.
◒: MIBK, ◓: nitrobenzene ○: hexol
●: 0.01M TBP-hexane taken from Ref. 1.

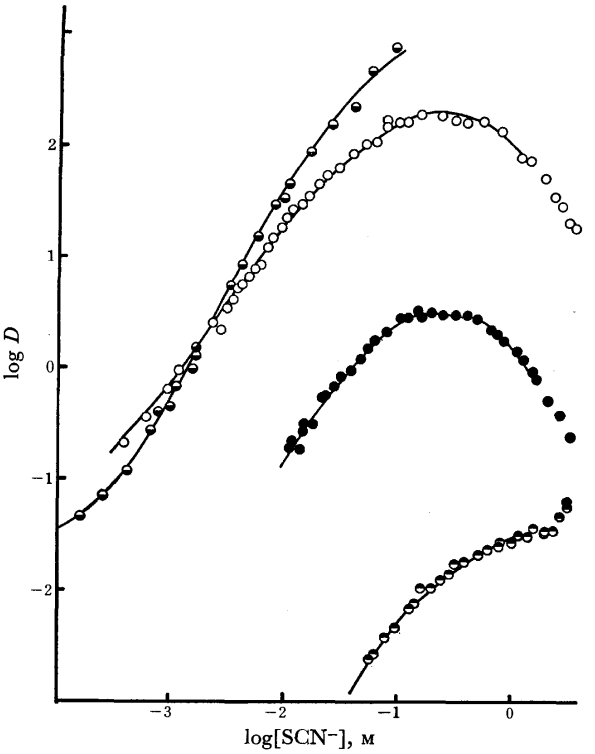

Fig. 3. The extraction of In(III) from 4M constant ionic medium containing thiocyanate ions into various organic solvents.
◒: MIBK, ○: hexol, ●: 0.01M TBP-hexane taken from Ref. 1. ◓: nitrobenzene

already given in Part I.[1] It will be seen from the figures that the distribution curves in the three polar organic solvent systems are rather different from that in the TBP-hexane system. As will be described later, this is due to the extraction of anionic complexes, such as InX_4^- and InX_5^{2-}, as well as to that of the uncharged complex; furthermore, that of cationic species is also assumed in some systems.

The following equilibrium was first assumed in order to explain the distribution ratio of the indium(III) measured experimentally (the complexes higher than the InX_5^{2-} were assumed to be very small, because they were found to be negligible under these conditions)[1]:

$$D = \frac{[\mathrm{In(III)}]_{org,t}}{[\mathrm{In(III)}]_{aq,t}} = \frac{[InX_3]_{org}+[InX_4]_{org,t}+[InX_5]_{org,t}}{[In^{3+}]+[InX^{2+}]+[InX_2^+]+[InX_3]+[InX_4^-]+[InX_5^{2-}]} \quad (1)$$

The stability constant of the "nth" indium complex with a uninegative ligand, X^-, is defined as:

$$\beta_n = \frac{[InX_n^{3-n}]}{[In^{3+}][X^-]^n} \quad (2)$$

The distribution constant for the uncharged complex is defined as:

$$K_{DM3} = \frac{[InX_3]_{org}}{[InX_3]} \quad (3)$$

The following constants were also defined for the extraction of the negatively-charged complexes:

$$K_{DM4} = \frac{[InX_4]_{org,t}}{[InX_4^-]} \quad (4)$$

$$K_{DM5} = \frac{[InX_5]_{org,t}}{[InX_5^{2-}]} \quad (5)$$

Here, the term $[InX_n]_{org,t}$ denotes the total concentration of those chemical species in the organic phase containing negatively-charged indium(III) complexes (*cf.* Eq. (15) or (16)), such as Na_2InX_5, $NaInX_5^-$, and InX_5^{2-}.

When the above-mentioned constants are introduced into Eq. (1), the following equation is obtained:

$$D = \frac{K_{DM3}\beta_3[X^-]^3 + K_{DM4}\beta_4[X^-]^4 + K_{DM5}\beta_5[X^-]^5}{1+\beta_1[X^-]+\beta_2[X^-]^2+\beta_3[X^-]^3+\beta_4[X^-]^4+\beta_5[X^-]^5} \quad (6)$$

An attempt was made to analyze the data in Figs. 1 to 3 graphically by using Eq. (6). However, it was not possible to explain by Eq. (6) the distribution behavior in the lowest ligand-concentration region because the distribution curves approach constant values in this region at these constant ionic medium solutions. This was assumed to be due to an extraction of positively-charged indium(III) species, InX_n^{3-n} (where $0 \leq n < 3$), most probably as ion-pairs with perchlorate ions. From this, the distribution ratio of indium(III) was assumed to be as follows:

$$D = \frac{[InX_0]_{org,t}+[InX_1]_{org,t}+[InX_2]_{org,t}+[InX_3]_{org}+[InX_4]_{org,t}+[InX_5]_{org,t}}{[In^{3+}]+[InX^{2+}]+[InX_2^+]+[InX_3]+[InX_4^-]+[InX_5^{2-}]} \quad (7)$$

Considering the extraction of these cationic indium(III) species, the following constants were also defined:

$$K_{DM0} = \frac{[InX_0]_{org,t}}{[In^{3+}]} \quad (8)$$

$$K_{DM1} = \frac{[InX_1]_{org,t}}{[InX_1^{2+}]} \quad (9)$$

$$K_{DM2} = \frac{[InX_2]_{org,t}}{[InX_2^+]} \quad (10)$$

A further detailed discussion of these constants will be given later. By introducing these constants and the constants in Eq. (6) into Eq. (7), the following equation could be obtained:

$$D = \frac{K_{DM0}+K_{DM1}\beta_1[X^-]+\cdots+K_{DM5}\beta_5[X^-]^5}{1+\beta_1[X^-]+\cdots+\beta_5[X^-]^5} \quad (11)$$

Equation (11) indicates that the distribution ratio in the lowest ligand-concentration or in the absence of the ligand ions can be denoted by K_{DM0} in Eq. (8). The value of K_{DM0} was very small in the extraction with nitrobenzene (log $D = \sim -4$), but the values were rather larger in the other two solvents.

However, the constancy of the distribution constant, K_{DM1} or K_{DM2}, should not be kept when the perchlorate concentration in the aqueous phase can not be regarded as 4M. Consequently, the following expression would be more reasonable than Eq. (11):

$$D = \frac{Kex_{0,3}[ClO_4^-]^3 + Kex_{1,2}[ClO_4^-]^2[X^-] + Kex_{2,1}[ClO_4^-][X^-]^2 + Kex_{3,0}[X^-]^3 + Kex_4[X^-]^4[Na^+] + Kex_5[X^-]^5[Na^+]^2}{1+\beta_1[X^-]+\beta_2[X^-]^2+\beta_3[X^-]^3+\beta_4[X^-]^4+\beta_5[X^-]^5} \quad (12)$$

where $Kex_{a,(3-a)}$ and Kex_b are the extraction constants of cationic or neutral species and anionic species respectively and where they are expressed as follows:

$$In^{3+} + aX^- + (3-a)ClO_4^- \rightleftarrows InX_a(ClO_4)_{3-a}(org) \quad (0 \leq a \leq 3)$$

$$Kex_{a,(3-a)} = \frac{[InX_a(ClO_4)_{3-a}]_{org}}{[In^{3+}][X^-]^a[ClO_4^-]^{3-a}} \quad (13)$$

$$In^{3+} + bX^- + (b-3)Na^+ \rightleftarrows Na_{b-3}InX_b(org) \quad (b \geq 3)$$

$$Kex_b = \frac{[Na_{b-3}InX_b]_{org}}{[In^{3+}][X^-]^b[Na^+]^{b-3}} \quad (14)$$

The effect of the dissociation of the ion-pairs in the organic phase will be considered later.

The graphic analysis of the distribution data in Figs. 1 to 3 was carried out as follows. The stability constants already determined in Part I[1] and the extraction constants of uncharged species were introduced into Eq. (12). The distribution ratio was calculated as a function of the ligand concentration. When a deviation of the calculated curve from the experimental data was observed, the constants were improved. This successive approximation was continued until the best-fit curve was found. The final equilibrium constants were determined from the best-fit curve. The solid curves in the figures are the extraction curves calculated by the use of the constants.

The equilibrium constants obtained by such a graphic analysis of the data in Figs. 1 to 3 are shown in Tables 1(a) to (d).

Figures 4(A) to 4(C) show the percentage distribution of each species in the organic phase and the aqueous phase calculated from the values in Tables 1(a) to (d). The equilibrium constants were determined by using the experimental data obtained when the ligand concentration is less than 1M. Thus, the calculated extraction curves in Figs. 1 to 3 are drawn only for the experimental data obtained in the ligand-concentration region below 1M. In some systems, however, the distribution ratio was too large to determine accurately when the ligand-concentration was lower than 1M (the extraction of iodide into MIBK or nitrobenzene, or that of thiocyanate into MIBK). In such systems, the graphic analysis of the data were made by using those in the $10^{-3} < D < 10^3$ region. The percentage of the indium (III) species in the organic phase in these systems was calculated in these ligand-concentration regions which are given in Figs. 4(A) to 4(C). The figures show that the extraction of indium species containing perchlorate ions is remarkable, especially into hexol.

In the present study, the salt concentration was kept at 4M by the use of sodium perchlorate. In usual experimental work in analytical chemistry, however, the ionic concentration changes with a change in the ligand-concentration. In order to ascertain the effect of added sodium perchlorate on the distribution behavior of indium(III), some experiments were carried out in the

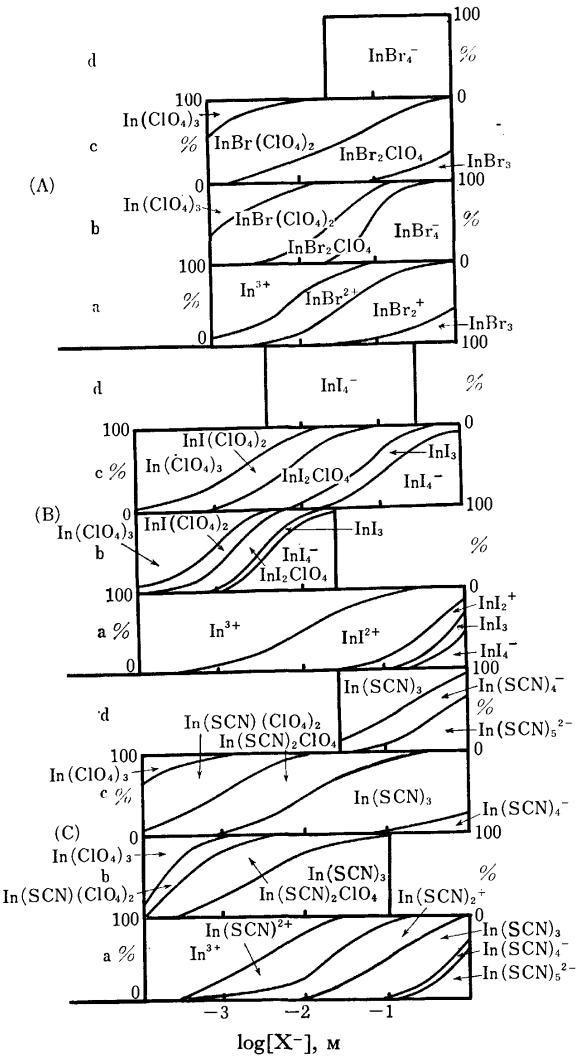

Fig. 4. The percentage distribution of In(III) species in 4M constant ionic medium containing bromide (A), iodide (B) or thiocyanate ions (C) and in the organic solvents equilibrated with the aqueous phase, within the ligand concentration range measured experimentally.
a: in aqueous phase, b: in MIBK, c: in hexol, d: in nitrobenzene

absence of perchlorate ions. Figures 5 to 7 give the distribution ratios in bromide, iodide, and thiocyanate systems where sodium perchlorate is absent in the aqueous phase. The solid curves in these figures are the extraction curves obtained in the 4M constant ionic medium; they have been taken from Figs. 1 to 3 in order to make a comparison with these experimental data. The distribution ratio decreases abruptly with a decrease in the ligand concentration when the ionic concentration changes. In other words, the distribution ratio of indium(III) is very much enhanced by the presence of the sodium perchlorate in the aqueous phase.

The results given above may be summarized as follows: i) The extraction curves into these three polar solvents are quite different from that into hexane containing a small amount of TBP, which could be regarded as an essentially non-polar solvent. This can be explained by saying that the only extractable species into hexane solutions is the uncharged complex, InX_3, while those extractable into polar solvents include not only the uncharged complex but also the ion-pairs of

Table 1. Extraction constants or distribution constants of indium(III) complexes from 4M constant ionic media into various organic solvents

(a) Aqueous phase: 4M $NaClO_4$

Solvent	MIBK	Hexol	Nitrobenzene
$\log Kex_{0,3}$	−3.41	−3.40	<−3
$\log K_{DM0}$	−1.60	−1.59	—

(b) Aqueous phase: 4M Na(Br, ClO_4)

Solvent	MIBK	Hexol	Nitro-benzene	0.1M TBP-hexane[1)]
$\log Kex_{1,2}$	0.04	0.38	—	—
$(\log K_{DM1})$	(−1.12)	(−0.78)	—	—
$\log Kex_{2,1}$	2.17	2.26	—	—
$(\log K_{DM2})$	(−0.39)	(∼−0.3)	—	—
$\log Kex_{3,0}$	—	2.47	—	3.35
$(\log K_{DM3})$	—	(−0.77)	—	(0.11)
$\log Kex_4$	4.53	—	1.81	—
$(\log K_{DM4})$	(2.95)	—	(0.23)	—

The stability constants for the bromide complexes in the aqueous phase employed for the analysis are[1)] $\log\beta_1=2.36$, $\log\beta_2=3.16$, $\log\beta_3=3.24$, and $\log\beta_4=2.18$.

(c) Aqueous phase: 4M Na(I, ClO_4)

Solvent	MIBK	Hexol	Nitro-benzene	0.01M TBP-hexane[1)]
$\log Kex_{1,2}$	0.00	−0.22	—	—
$(\log K_{DM1})$	(−0.77)	(−0.99)	—	—
$\log Kex_{2,1}$	3.61	2.61	—	—
$(\log K_{DM2})$	(2.03)	(1.03)	—	—
$\log Kex_{3,0}$	6.20	4.20	—	3.83
$(\log K_{DM3})$	(4.00)	(2.00)	—	(1.63)
$\log Kex_4$	8.6	4.8	6.1	—
$(\log K_{DM4})$	(6.70)	(2.85)	(4.23)	—

The stability constants for the iodide complexes in the aqueous phase employed for the analysis are[1)] $\log\beta_1=1.97$, $\log\beta_2=2.18$, and $\log\beta_3=2.20$. The formation of the fourth complex $\log\beta_4=\sim2.5$ is also assumed in this study in order to analyze the extraction data with hexol. However, this constant could be somewhat erroneous.

(d) Aqueous phase: 4M Na(SCN, ClO_4)

Solvent	MIBK	Hexol	Nitro-benzene	0.01M TBP-hexane[1)]
$\log Kex_{1,2}$	0.70	1.40	—	—
$(\log K_{DM1})$	(−0.54)	(0.16)	—	—
$\log Kex_{2,1}$	5.08	5.08	—	—
$(\log K_{DM2})$	(1.57)	(1.57)	—	—
$\log Kex_{3,0}$	8.25	7.59	2.90	5.80
$(\log K_{DM3})$	(3.15)	(2.49)	(−2.20)	(0.70)
$\log Kex_4$	—	6.51	3.00	—
$(\log K_{DM4})$	—	(2.54)	(−0.97)	—
$\log Kex_5$	—	—	2.70	—
$(\log K_{DM5})$	—	—	(−1.55)	—

The stability constants for the thiocyanate complexes in the aqueous phase employed for the analysis are[1)] $\log\beta_1=2.44$, $\log\beta_2=4.11$, $\log\beta_3=5.10$, $\log\beta_4=4.57$, and $\log\beta_5=5.45$.

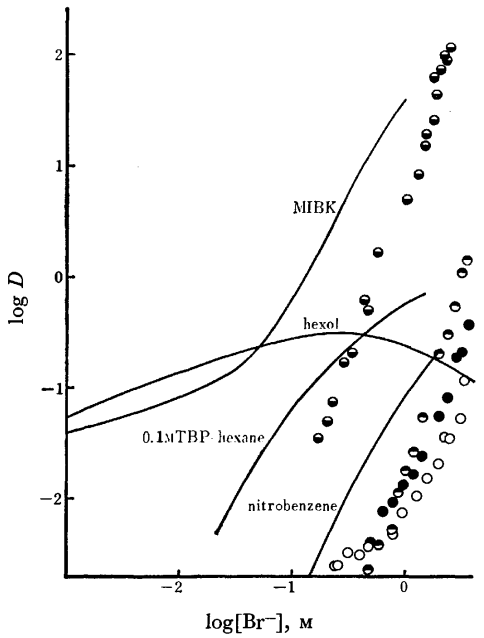

Fig. 5. The extraction of In(III) from aqueous solutions containing sodium bromide (ionic concentrations are varied) into various organic solvents. The solid curves indicate the extraction from 4M Na(Br, ClO_4).
◒: MIBK, ◓: nitrobenzene ●: 0.1M TBP-hexane, ○: hexol

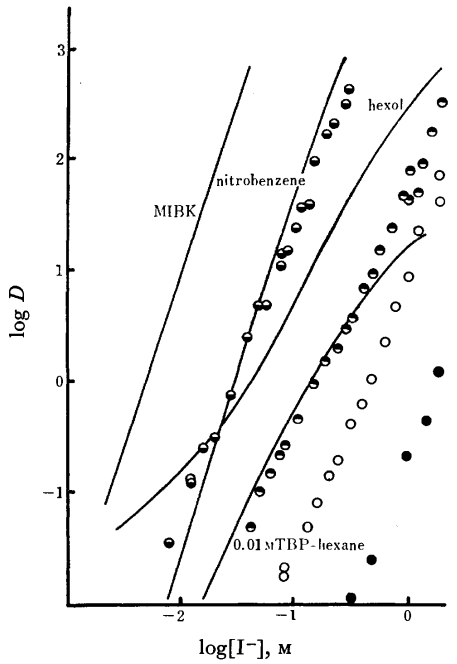

Fig. 6. The extraction of In(III) from aqueous solutions containing sodium iodide into various organic solvents. The solid curves indicate the extraction from 4M Na(I, ClO_4).
◒: MIBK, ◓: nitrobenzene, ○: hexol, ● 0.01M TBP-hexane

the cationic species and/or the anionic ones. ii) MIBK extracts both anionic and cationic species. The extraction of anionic thiocyanate species into MIBK was not confirmed in the ligand-concentration region studied. However, it is possible that the extraction of the anionic species occurs when the ligand concentration is higher

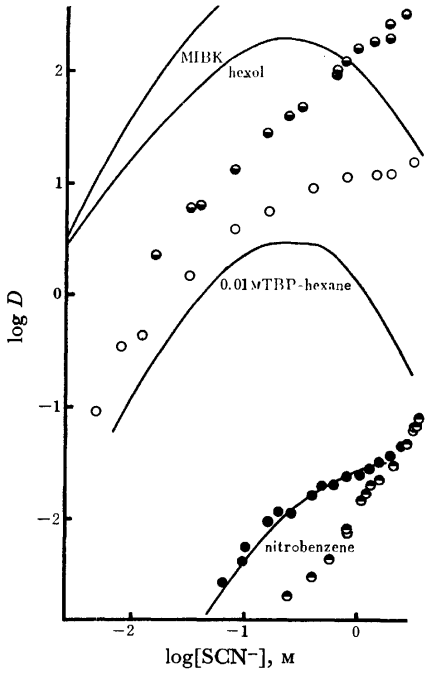

Fig. 7. The extraction of In(III) from aqueous solutions containing sodium thiocyanate into various organic solvents. The solid cruves indicate the extraction from 4M Na(SCN, ClO_4).
◒: MIBK, ◓: nitrobenzene, ○: hexol, ●: 0.01M TBP-hexane

(above 5×10^{-2}M). The extraction of indium(III) complexes from the 4M constant ionic media with MIBK is usually better than with the other two solvents. The extraction with MIBK is always the best when sodium perchlorate is absent in the aqueous phase. iii) Nitrobenzene, which has a much higher dielectric constant but a smaller solvation ability, extracts the ion-pairs of anionic complexes better than uncharged ones; furthermore, the extraction from the thiocyanate system is extremely inferior to that from other systems. iv) The distribution curves obatined by introducing the constants in Tables 1(a) to (d) as defined by Eqs. (2), (13), and (14), into Eq. (12) were found to fit with the data. Thus, it was concluded that the assumptions for the complex species in the two phases and the equilibrium constants for them listed in Tables 1(a) to (d) can explain the results within the limits of experimental accuracy.

Discussion

Not very much seems to know about the dissociation of ion-pairs in the organic phase of solvent extraction systems. However, the dissociation in the organic phase should be one of the most important factors to be taken into account in order to make a reasonable analysis of the experimental data. In the present study, this has been treated as follows.

As may be seen from Eqs. (4), (5), (8), (9), and (10), the concentration ratios of the charged species in the two phases are assumed to be constant, or it is assumed that Eq. (12) can be substituted for Eq. (7) only by using the extraction constant of the ion-pairs despite the

possibility of the dissociation of the ion-pairs in the organic phase. However, this should not be true from a general standpoint.

As has been pointed out,[2] the total concentration of the fourth or the fifth anionic complexes in the organic phase can be described as follows if the ion-pairs are partially dissociated in the organic phase:

$$[InX_4]_{org,t} = [NaInX_4]_{org} + [InX_4^-]_{org} \quad (15)$$

$$[InX_5]_{org,t} = [Na_2InX_5]_{org} + [NaInX_5^-]_{org} + [InX_5^{2-}]_{org} \quad (16)$$

The dissociation of the ion-pairs in the organic phase can be denoted as follows:

$$Na_{b-3}InX_b(org) \rightleftarrows (Na_{b-3-n}InX_b)^{n-}_{org} + nNa^+(org)$$

$$Kdiss_{b,n} = \frac{[Na_{b-3-n}InX_b^{n-}]_{org}[Na^+]^n_{org}}{[Na_{b-3}InX_b]_{org}} \quad (17)$$

where b is larger than 3.

By introducing Eqs. (14) and (17) into Eq. (15), the following equation is obtained:

$$[InX_4]_{org,t} = Kex_4[In^{3+}][X^-]^4[Na^+](1+Kdiss_{4,1}[Na^+]^{-1}_{org}) \quad (18)$$

Equation (18) shows that the concentration of the anionic complex in the organic phase is proportional to that of sodium ions in the aqueous phase if no dissociation of the ion-pairs occurs. On the other hand, when the ion-pairs dissociate and charged species are formed in the organic phase, the concentration of the ion-pairs is also dependent on the sodium concentration in the organic phase. In the present study, the aqueous sodium ion concentration was kept as 4M and the extraction of hydrogen or hydroxide ions could be disregarded. Thus, the sodium concentration in the organic phase could be described from the point of view of electrical neutrality as:

$$[Na^+]_{org} = [ClO_4^-]_{org} + [X^-]_{org} + [InX_4^-]_{org} + [NaInX_5^-]_{org} + 2[InX_5^{2-}]_{org} \quad (19)$$

According to the previous papers, the sodium concentration in nitrobenzene, MIBK, and hexol in an equilibrium with 4M sodium perchlorate are 4×10^{-4}M,[3] 6×10^{-2}M, and 1×10^{-2}M[4] respectively. The organic phases studied in this work could contain sodium ions which are produced by the dissociation of the extracted ion-pairs of anionic indium(III) complexes other than those produced by the dissociation of the sodium perchlorate. However, since the indium(III) concentration is very low (the initial aqueous concentration is about 3×10^{-6}M), the contribution of the sodium ions from the ion-pairs of the complexes to the total sodium ion concentration in the organic phase should be very small when the aqueous phase can be regarded as nearly a 4M sodium perchlorate solution.

From this, the total sodium ion concentration in the organic phase given in Eq. (19) can be regarded as constant; consequently, the values in parentheses in Eq. (18) should also be constant in the present study. Thus, it should be reasonable to assume that the ratio of the total concentrations of the fourth complex in the two phases denoted by K_{DM4} in Eq. (4) is a constant under the conditions employed here. For a similar reason, the concentration ratio of the fifth complex may also be assumed to be a constant, K_{DM5}, as is given in Eq. (5).

As may be seen from Eq. (19), the above assumption is not valid when the extraction of the ligand salt is no longer negligible, because the extraction of sodium salts as ion-pairs and their dissociation in the organic phase can be generally assumed when the anion is different. Thus, the extraction data in the higher ligand-concentrations could not be treated by assuming the constancy of K_{DM4} and K_{DM5}.

A similar problem is also present in the analysis of the extraction of ion-apirs with perchlorate ions. The problem of the extracted ion-pairs of cationic species with perchlorate ions should also be considered like the dissociation of sodium ions. When they partially dissociate in the organic phase, the total concentration of indium(III) species may be denoted as follows:

$$[InX_0]_{org,t} = [In(ClO_4)_3]_{org} + [In(ClO_4)_2^+]_{org} + [InClO_4^{2+}]_{org} + [In^{3+}]_{org} \quad (20)$$

$$[InX_1]_{org,t} = [InX(ClO_4)_2]_{org} + [InXClO_4^+]_{org} + [InX^{2+}]_{org} \quad (21)$$

$$[InX_2]_{org,t} = [InX_2ClO_4]_{org} + [InX_2^+]_{org} \quad (22)$$

The dissociation of the second ion-pair in the organic phase may be described as:

$$InX_2ClO_4(org) \rightleftarrows InX_2^+(org) + ClO_4^-(org)$$

$$Kdiss'_{2,1} = \frac{[InX_2^+]_{org}[ClO_4^-]_{org}}{[InX_2ClO_4]_{org}} \quad (23)$$

From Eqs. (13) and (23), Eq. (22) may be described as:

$$[InX_2]_{org,t} = Kex_{2,1}[In^{3+}][X^-]^2[ClO_4^-] \times (1+Kdiss'_{2,1}[ClO_4]^{-1}_{org}) \quad (24)$$

A similar but more complicated treatment is necessary for the term of $[InX_0]_{org,t}$ or $[InX_1]_{org,t}$.

Thus, like as the contribution of the sodium ions in the analysis of the extraction data of anionic complexes, the contribution of the perchlorate ions should be taken into account when the ion-pairs of cationic complexes with perchlorate ions dissociate in the organic phase. The concentration of perchlorate ions in the organic phase is dependent not only on the perchlorate concentration in the aqueous phase, but also on the total concentration of the dissociated ion-pairs of indium(III) species with perchlorate ions. However, for the same reason discussed in connection with the sodium concentration in the organic phase (that is, the concentration of indium(III) is much smaller than that of sodium perchlorate in the oragnic phase), it is possible to assume that the concentration ratio of cationic indium(III) species in the two phases denoted by Eq. (8), (9), or (10) is constant under the conditions employed in this study. Furthermore, the data obtained in solutions up to a ligand-concentration of 1M, where 25% of the perchlorate ions is replaced by the ligand anion, have been analyzed statistically. It seems to be very difficult to know if an aqueous solution containing 1M ligand salt in the 4M total salt can still be regarded practically as

2) T. Sekine and T. Ishii, This Bulletin, **43**, 2422 (1970).
3) T. Sekine and D. Dyrssen, *Anal. Chim. Acta*, **45**, 433 (1969).
4) Y. Hasegawa, T. Ishii, and T. Sekine, This Bulletin, **44**, 275 (1971).

a 4M sodium perchlorate solution in the above statistical analysis. The present authors, however, consider that this is not very unreasonable because the constants which have been determined on the above assumption seem to explain the experimental data well, as can be seen from Figs. 1 to 3. Actually, the data fit the calculated curve well, even in the highest ligand concentration region studied, except for the extraction of the thiocyanate complexes in the highest ligand-concentration region into nitrobenzene.

As can be seen from Figs. 5 to 7, the extraction curves from sodium salt solutions of the ligand anions containing no sodium perchlorate (the total concentration is not kept constant) were quite different from the extraction curves in the 4M constant ionic media systems. As has been shown in Figs. 4(A) to 4(C), the majority of the extracted indium(III) species from the 4M sodium perchlorate media consist of charged indium(III) species in these polar solvents: moreover, as may be seen from Eq. (13) or (14), the extraction of these charged species is dependent not only on the concentration of ligand anions, but also on the concentration of sodium ions or of perchlorate ions. In the aqueous solutions containing no sodium perchlorate, the concentration of perchlorate ions is zero and that of sodium ions is always lower than 4M. Thus, no extraction of ion-pairs with cationic species and perchlorate ions, and much less extraction of ion-pairs with the anionic species and sodium ions, should occur from these aqueous solutions; this should be one of the reasons for the poorer extractions of indium(III) from these aqueous solutions than from 4M sodium perchlorate constant ionic media.

However, the above explanation may not cover all the reasons for these poorer extractions. As can be seen from Eq. (12), the distribution ratio is also dependent on the stability constants of the aqueous complexes, β_n, and the distribution constants, K_{DMn}. When the ionic concentration changes, the activity coefficients of each species may be changed, and then the constants defined by the stoichiometric concentration scale should also be changed. These influences of the background salt on the distribution behavior of the indium(III) complexes will be reported on in a more quantitative manner in the following papers of this series.

The aqueous phase in analytical work usually contains only the ligand anions and no perchlorate ions. The extraction from constant ionic media is here different from the data of analytical experiments. For example, the extraction curve of indium(III) from 4M Na(SCN, ClO_4) into hexol or TBP-hexane has a peak where the ligand concentration is about 2×10^{-1}M; on the other hand, the extraction curves from thiocyanate solutions decrease with the decrease in the anion concentration, and also, according to the extraction of ion-pairs with perchlorate ions, the curves are very different from each other in the lower ligand-concentration region. The analysis of the equilibrium in such systems, in which the ionic concentrations are not kept constant, is very difficult.

The extraction of a charged indium(III) species which was negligible in quantity into hexane containing a small amount of TBP is very remarkable in these polar solvents. For the extraction of charged species as ion pairs, both solvation on the central metal ion and a polar nature (or a high dielectric constant) of the organic solvent are important. The solvation should be largest in MIBK, and this is probably the reason why MIBK shows the best extraction in most cases. The tendency for the large extraction of anionic complexes into nitrobenzene, which does not have a large ability for the solvation, may be due to the very high dielectric constant of this solvent. These properties in hexol are between those of these two organic solvents, and the intermolecular hydrogen bonds in this solvent must play an important role, although further information on the distribution equilibria of various species will be necessary before a detailed discussion of the extraction behavior will become possible.

The authors are grateful to Messrs. Shigeyoshi Ikegami and Hiroshi Iwasaki of the present laboratory for their experimental aids. Part of this work has been carried out in the Laboratory of Nuclear and Analytical Chemistry, Institute of Physical and Chemical Research. The authors are also grateful to Professor Nobufusa Saito, the head of that laboratory.

Fluorometric Determination of Aluminum and Gallium with Superchrome Garnet Y

Keizo HIRAKI

Department of Chemistry, Faculty of Science and Technology, Kinki University, Kowakae, Higashi-Osaka

(Received July 7, 1971)

A sensitive fluorometric determination of aluminum and gallium with Superchrome Garnet Y was described. The reagent reacts with aluminum and gallium to form complexes with reddish yellow fluorescence of emission maximum at 562 and 565 nm respectively. Several conditions for the determination, such as the pH of the solution, the reagent concentration, the time of standing *etc.* were investigated, and the composition of the complexes was determined. The maximum fluorescence intensity of the aluminum complex was found at pH 5 (heated for 10 min at 50°C), and that of the gallium complex, at pH 3. The fluorescence were stable at least for 2 hr. By using Superchrome Garnet Y, 0.02—4 μg of aluminum and 0.5—30 μg of gallium in 25 m*l* solution could be determined. Scandium and indium also formed fluorescent complexes. Iron(III), cobalt(II), copper(II), zirconium(IV), vanadate(V), and chromate(VI) ions interfered with the determination.

In the course of the investigation on the fluorometric determination of various metal ions with a series of *o,o'*-dihydroxyazo compounds, the author found that lumogallion [3-(2,4-dihydroxyphenylazo)-2-hydroxy-5-chlorobenzenesulfonic acid] (I) was a sensitive

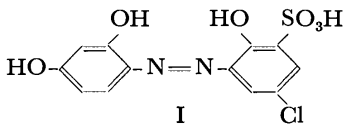

I

reagent for the determination of aluminum and gallium, appliciable to the determination of aluminum in sea water.[1-3]

Mordant Blue 31 [2-(2-hydroxy-5-sulfophenylazo)-1, 8-dihydroxynaphthalene-3,6-disulfonic acid] (II) was

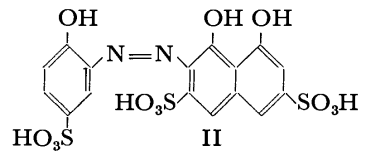

II

also a useful reagent for aluminum, gallium and scandium, and the fluorometric methods were proposed in a recent paper.[4]

Freeman and White[5] studied the configuration and the bond type of *o,o'*-dihydroxy azo compounds, which was favorable to form fluorescent metal complexes. According to their consideration, Superchrome Garnet Y [3-(2,4-dihydroxyphenylazo)-4-hydroxybenzenesulfonic acid] (III) seemed to be a very sensitive fluorescent reagent.

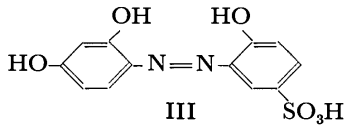

III

However, no quantitative investigation with this reagent has been carried out, except Powell and Saylor's research on the fluorometric determination of traces of fluoride using aluminum-Superchrome Garnet Y complex.[6]

The present author found that Superchrome Garnet Y was more sensitive than lumogallion for aluminum and gallium, and that scandium and indium also formed the fluorescent complexes, applicable to the fluorometric determination. In the present paper, the fundamental conditions for the determination of aluminum, gallium, scandium and indium with this reagent were described.

Reagent and Apparatus

Synthesis of Superchrome Garnet Y. 1-Amino-2-phenol-5-sulfonic acid dissolved in 6N hydrochloric acid was diazotized with an equivalent amount of sodium nitrite under ice-cooling. The cooled diazonium salt solution was added to resorcinol dissolved in about 6N sodium hydroxide under cooling below 5°C. The azo compound thus obtained was repeatedly recrystallized from 6N hydrochloric acid, and dried at room temperature in a desiccator on silica gel.

Solutions. Superchrome Garnet Y solution; 0.1 g of Superchrome Garnet Y was dissolved in redistilled water and diluted to a liter.

Standard solution of aluminum; 1.6803 g of alum was dissolved in water, and after 5 m*l* of concentrated hydrochloric acid was added, diluted to 100 m*l* with water. The stock solution was diluted with water to prepare a solution containing 1.00 μg of aluminum per m*l*.

Stock solution of gallium, scandium and indium were prepared by dissolving the 99.99%, 99.9%, and 99.99% pure oxides with 6N hydrochloric acid, respectively, and the standard solutions were prepared by suitable dilution from the stock solution.

Rhodamine B solution; 0.1 g of Rhodamine B was dissolved in water and diluted to 100 m*l*. The stock solution was diluted with water to make solutions containing 0.168 and 0.05 μg rhodamine B per m*l*. The former solution was sufficiently stable for several months, while the latter was unstable and must be freshly prepared every five days. These solutions were used as reference standards to adjust the sensitivity of the instrument.

All other chemicals used in the present work were special grade. Ethanol, hydrochloric acid and ammonia were dis-

1) Y. Nishikawa, K. Hiraki, K. Morishige, and T. Shigematsu, *Bunseki Kagaku*, **16**, 692 (1967).

2) Y. Nishikawa, K. Hiraki, K. Morishige, A. Tsuchiyama, and T. Shigematsu, *ibid.*, **17**, 1092 (1968).

3) T. Shigematsu, Y. Nishikawa, K. Hiraki, and N. Nagano, *ibid.*, **19**, 551 (1970).

4) K. Hiraki, This Bulletin, **45**, 789 (1972).

5) D. C. Freeman and C. E. White, *J. Amer. Chem. Soc.*, **78**, 2678 (1956).

6) W. A. Powell and J. H. Saylor, *Anal. Chem.*, **25**, 960 (1953).

tilled until the fluorescence disappeared. Redistilled water was used throughout the procedures.

Apparatus. Fluorescence spectra and the intensity were measured with a Hitachi spectrophotometer, Model G-3 (exciting source; 150 W Xenon lamp). A Hitachi-Horiba glass electrode pH meter, Model M-5, was used for the pH measurements.

Experimental

Fluorescence Spectra of the Metal Complexes of Superchrome Garnet Y. Superchrome Garnet Y reacted with aluminum, gallium, scandium, and indium to form complexes with orange fluorescence. Aluminum-Superchrome Garnet Y complex exhibited the excitation maxima at 365 and 485 nm and the fluorescence emission maximum at 562 nm; the gallium complex showed excitation maxima at 365 and 485 nm and the fluorescence maximum at 565 nm; the scandium complex had the excitation and the emission maximum at 482 and 575 nm respectively; and the indium complex, at 480 and 565 nm respectively. Spectra of Superchrome Garnet Y complexes are shown in Figs. 1 and 2.

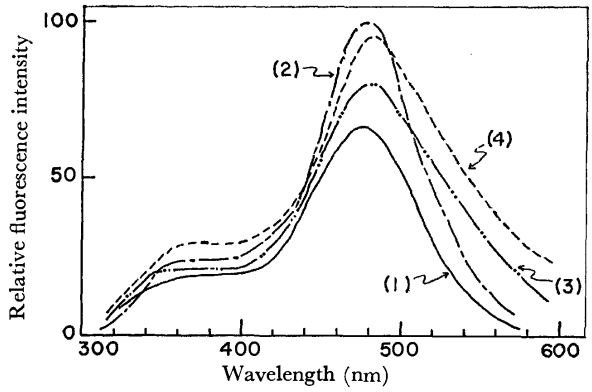

Fig. 1. Excitation spectra of aluminum, gallium, scandium and indium complexes.
(1): Al-Superchrome Garnet Y complex, emission spectrum measured at 562 nm; (2): Ga-Superchrome Garnet Y complex, emission spectrum measured at 565 nm; (3): Sc-Superchrome Garnet Y complex, emission spectrum measured at 575 nm; (4): In-Superchrome Garnet Y complex, emission spectrum measured at 565 nm.

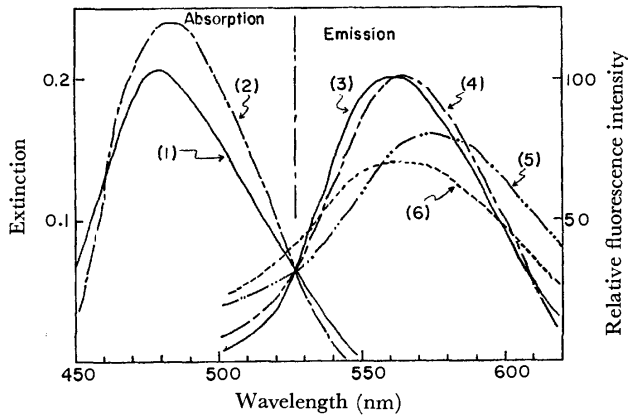

Fig. 2. Absorption and emission spectra of Superchrome Garnet Y complexes.
(1): Absorption spectrum of Al-Superchrome Garnet Y complex; (2): Absorption spectrum of Ga-Superchrome Garnet Y complex; (3): Emission spectrum of Al-Superchrome Garnet Y complex; (4): Emission spectrum of Ga-Superchrome Garnet Y; (5): Emission spectrum of Sc-Superchrome Garnet Y; (6): Emission spectrum of In-Superchrome Garnet Y complex.

Fluorescence Procedure for the Determination of Metals. 1) *Aluminum*: To 15—20 m*l* of the sample solution containing 0.1—4 μg of aluminum were added 0.7 m*l* of 0.01% Superchrome Garnet Y and 2 m*l* of 20% ammonium acetate and the pH was adjusted to 5 with dilute hydrochloric acid or ammonia. The solution was diluted to 25 m*l* with water and then kept at 50°C for 10 min. After cooling, the fluorescence intensity was measured by using a Rhodamine B solution as the reference standard.

2) *Gallium*: To the sample solution containing 0.5—30 μg of gallium were added 0.8 or 1.7 m*l* of 0.01% reagent and 2 m*l* of 20% ammonium acetate and the pH was adjusted to 3. The solution was diluted to 25 m*l* and then the fluorescence intensity was measured.

3) *Scandium and Indium*: Scandium (5—40 μg) was determined by the same procedure as in the case of gallium, but the pH was adjusted to 5.5. Indium (5—30 μg) was determined in the case of the same manner as aluminum, but 2 m*l* of the reagent solution was used.

Results and Discussion

Effect of Time of Standing. At room temperature, the aluminum and the indium complex needed 120 minutes' standing until they showed the full fluorescence. If the solutions were heated at 50°C, the fluorescence intensity readily reached the maximum. The fluorescence of the gallium and the scandium complex was fully developed within a few minutes after the preparation of the solutions.

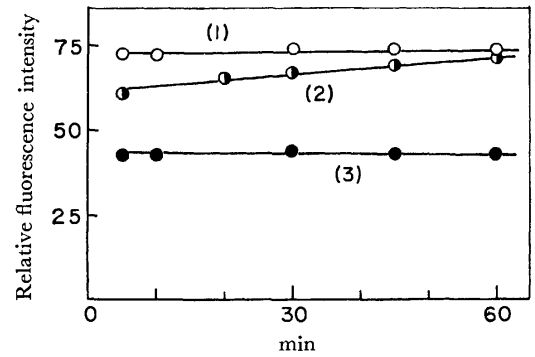

Fig. 3. Stability of fluorescence intensity of Superchrome Garnet Y complexes.
(1): Al 0.5 μg, digested at room temp., 485 nm/562 nm, fluorometer readings was setted at 40 div. with 0.168 μg rhodamine B/m*l* reference solution.
(2): Al 0.5 μg, digested at 50°C 10 min, 485 nm/562 nm, 40 div.
(3): Ga 5 μg, digested at room temp., 485 nm/565 nm, 20 div.

In all cases, the fluorescence was stable at least for 2 hr after reaching the maximum intensity. Figure 3 shows the stability of the fluorescent complexes of aluminum and gallium.

Effect of pH. The intensity of the fluorescence of metal complex was measured over a wide range of pH values. The results are shown in Fig. 4.

The aluminum and the indium complex showed maximum fluorescence intensity at pH 5, the scandium complex at pH 5.5, and the gallium complex showed

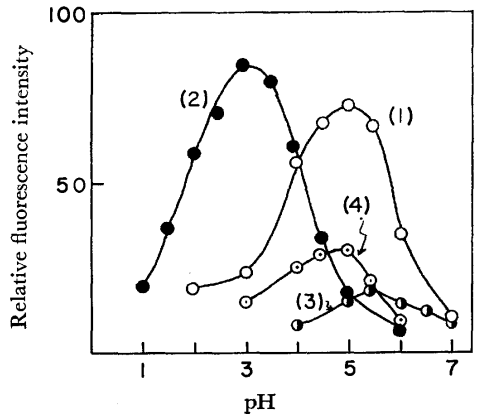

Fig. 4. Effect of pH on fluorescence intensity.
(1): Al 0.5 μg, 485 nm/562 nm, 40 div. *vis.* 0.168 μg Rhodamine B/m*l* standard solution:
(2): Ga 5 μg, 485 nm/565 nm, 40 div. *vis.* 0.168 μg Rhodamine B/m*l* standare solution;
(3): Sc 20 μg, 482 nm/575 nm, 60 div. *vis.* 0.168 μg Rhodamine B/m*l* standard solution;
(4): In 20 μg, 480 nm/565 nm, 60 div. *vis* 0.05 μg Rhodamine B standard solution.

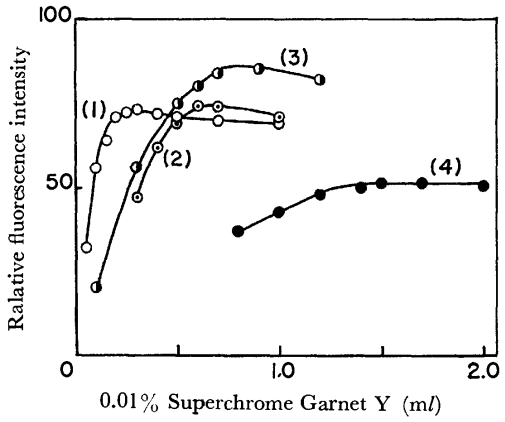

Fig. 5. Effect of reagent concentration.
(1): Al 0.5 μg, 485 nm/562 nm, 40 div. *vis.* 0.168 μg Rhodamine B standard solution;
(2): Al 3.5 μg, 365 nm/562 nm, 40 div. *vis.* 0.168 μg Rhodamine B standare solution;
(3): Ga 5 μg, 485 nm/565 nm, 40 div. *vis.* 0.168 μg Rhodamine B standard solution;
(4): Ga 25 μg, 485 nm/565 nm, 10 div. *vis.* 0.168 μg Rhodamine B standard solution.

the maximum in more acidic medium, near pH 3.

Effect of Concentration of Superchrome Garnet Y. The various amounts of Superchrome Garnet Y were added to the solutions containing 0.5 or 3.5 μg of aluminum, 5 or 25 μg of gallium, and the fluorescence intensity of the solution was measured at the optimum pH. Figure 5 shows the effect of the amounts of Superchrome Garnet Y on the fluorescence intensity.

The results indicated that 0.3 m*l* of 0.01% Superchrome Garnet Y solution was required for 0.5 μg of aluminum in 25 m*l* of solution and 0.7 m*l* for 3.5 μg of aluminum. In the case of gallium, 0.8 m*l* of the reagent solution was needed for up to 5 μg per 25 m*l* and 1.7 m*l* for 25 μg. For the determination of scandium and indium, 2 m*l* of 0.01% Superchrome Garnet Y solution was needed.

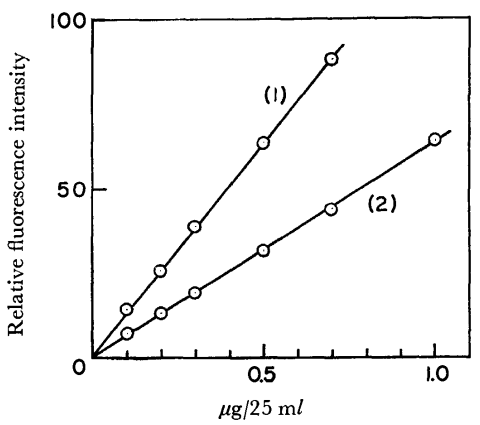

Fig. 6. Calibration curves for aluminum.
(1): 485 nm/562 nm, 40 div. *vis.* 0.168 μg Rhodamine B standard solution, 0.01% reagent solution 0.3 m*l*.
(2): 365 nm/562 nm, 30 div. *vis.* 0.168 μg Rhodamine B standard solution, 0.01% reagent solution 0.3 m*l*.

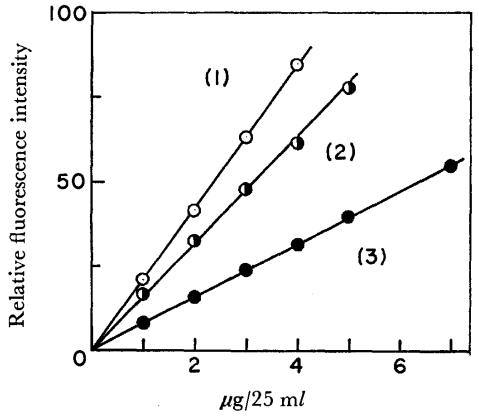

Fig. 7. Calibration curves for aluminum and gallium.
(1) Al: 485 nm/562 nm, 10 div. (0.168 μg Rhodamine B/m*l* standard solution), 0.01% reagent solution 0.7 m*l*.
(2) Ga: 485 nm/565 nm, 40 div. (0.168 μg Rhodamine B/m*l* standard solution), 0.01% reagent solusion 0.8 m*l*.
(3) Ga: 365 nm/565 nm, 30 div. (0.168 μg Rhodamine B/m*l* standard solution), 0.01% reagnet solution 0.8 m*l*.

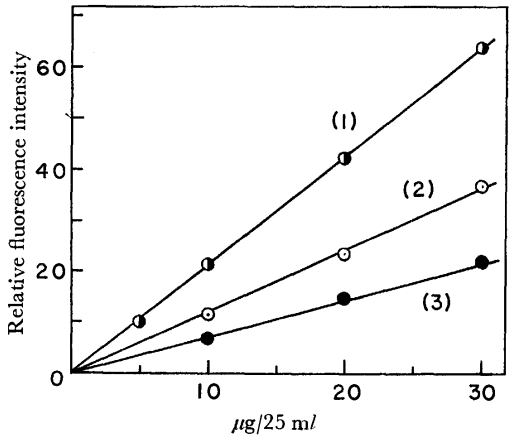

Fig. 8. Calibration curves for gallium, indium and scandium.
(1): Ga: 365 nm/565 nm, 10 div. (0.168 μg Rhodamine B/m*l* standard solution), 0.01% reagent solution 1.7 m*l*.
(2): In: 480 nm/565 nm, 60 div. (0.05 μg Rhodamine B/m*l* standard solution), 0.01% reagent solution 2 m*l*.
(3): Sc: 482 nm/575 nm, 60 div. (0.168 μg Rhodamine B/m*l* stadard solution), 0.01% reagent solution 2 m*l*.

Table 1. The conditions for the fluorometric determination of Al, Ga, Sc, and In

Ion	Al		Ga		Sc	In
Excitation wave length (nm)	365 485		365 485		482	480
λ_f max. (nm)	562		565		575	565
pH	5.0		3.0		5.5	5.0
Standing time	10 min., 50°C		10 min., room temp.		10 min., room temp.	10 min., 50°C
0.01%-reagent solution (ml)	0.3	0.7	0.8	1.7	2.0	2.0
Determinable range (μg/25 ml)	0.02—1.0	0.02—4.0	0.5—7.0	0.5—30	5—40	5—30
Fluorescence intensity at 60 div. per 1 μg	195		25.5		0.8	0.3
F. I. ratio {weight[a]	650		85		2.7	1
F. I. ratio {molar[b]	1463		494		1	10

a) This ratio was expressed in values relative to a fluorescence intensity of the indium complex for 1 μg In/25ml. (60 div., *vs.* 0.168 μg rhodamine B/ml)
b) This ratio was expressed in values relative to a fluorescence intensity of the scandium complex for 1 mol Sc/*l*. (60 div., *vs.* 0.168 μg rhodamine B/ml)

Calibration Curves. Figures 6, 7, and 8 show the calibration curves for aluminum, gallium, scandium and indium, respectively, which were obtained by the above-mentioned procedures. The sensitivity of the fluorometer was regulated by setting up the fluorescence of a standard Rhodamine B solution (0.168 μg/ml or 0.05 μg/ml) at an appropriate position of the reading (10—60 division). Aluminum, gallium, scandium, and indium can be determined in the following ranges with an average error of 3 percent; Al: 0.02—4 μg, Ga: 0.5—30 μg, Sc: 5—40 μg, In: 5—30 μg. A linear relationship exists between the fluorescence intensity and the metal ion concentration. The conditions for the fluorometric determination of these metal ions were summarized in Table 1.

For the determination of indium, 0.05 μg Rhodamine B per ml solution was used as the reference standard in order to raise the sensitivity of the fluorometer. Use of the dilute reference standard solution enabled the determination of aluminum, gallium, and scandium in lower concentrations, but the error was increased. The errors might be mainly due to two reasons; the lowering of the stability of the fluorometer resulting from the too high sensitivity, and the change of the concentration of Rhodamine B caused by the adsorption on the vessel wall that would be negligible in the concentrated standard.

Table 2. Effect of diverse ions

Ion	Added as	(μg)	Al found (μg)[a]	Diverse ion added (μg)	Ga found (μg)[b]
Be^{2+}	$Be(NO_3)_2$	10	0.5	20	5.3
Mg^{2+}	$MgSO_4$	10	0.5	20	4.8
Ca^{2+}	$CaCl_2$	10	0.5	20	5.0
Cu^{2+}	$CuSO_4$	10	0.0	20	1.6
Zn^{2+}	$ZnSO_4$	10	0.4	20	5.0
Sr^{2+}	$Sr(NO_3)_2$	10	0.5	20	5.0
Cd^{2+}	$CdSO_4$	10	0.5	20	5.3
Co^{2+}	$CoCl_2$	10	0.1	20	4.1
Ni^{2+}	$Ni(NO_3)_2$	10	0.4	20	4.8
Sc^{3+}	$ScCl_3$	10	0.4	20	5.0
Ga^{3+}	$GaCl_3$	10	0.4	—	—
Y^{3+}	YCl_3	10	0.5	20	4.8
Eu^{3+}	$EuCl_3$	10	0.5	20	5.0
In^{3+}	$InCl_3$	10	0.5	20	5.0
La^{3+}	$LaCl_3$	10	0.5	20	5.0
Tl^{3+}	$TlCl_3$	10	0.5	20	5.0
Fe^{3+}	$FeCl_3$	10	0.0	10	0.5
Zr^{4+}	$Zr(SO_4)_2$	10	0.0	20	3.4
Sn^{2+}	$SnCl_2$	10	0.4	20	4.8
V^{5+}	NH_4VO_3	10	0.0	10	0.4
Cr^{6+}	K_2CrO_4	10	0.0	10	0.0
Se^{4+}	Na_2SeO_3	10	0.5	20	4.8
Mo^{6+}	$(NH_4)Mo_7O_{24}$	10	0.5	20	3.6
Mn^{2+}	$MnSO_4$	10	0.4	20	5.0
UO_2^{2+}	$UO_2(CH_3COO)_2$	10	0.4	20	5.0
Th^{4+}	$Th(NO_3)_4$	10	0.5	20	5.0
Al^{3+}	$AlCl_3$	—	—	10	+

a) 0.5 μg of aluminum was taken.
b) 5.0 μg of gallium was taken.

Effect of Diverse Ions. The effects of 27 cations on the determination of aluminum and gallium were studied. The results are summarized in Table 2.

In the determination of aluminum, twentyfold amounts of cobalt(II), copper(II), iron(III), zirconium-

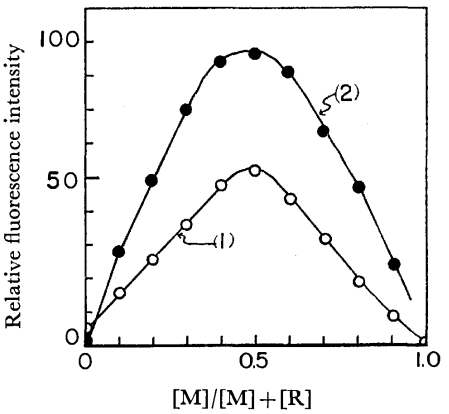

Fig. 9. Continuous variation method.
(1): M:Al, pH: 5.0, 485 mn/562 nm, 20 div. $[Al]+[R]=7.42\times10^{-5}$M
(2): M: Ga, pH: 3.0, 485 nm/565 nm, 30 div. $[Ga]+[R]=3.22\times10^{-4}$M

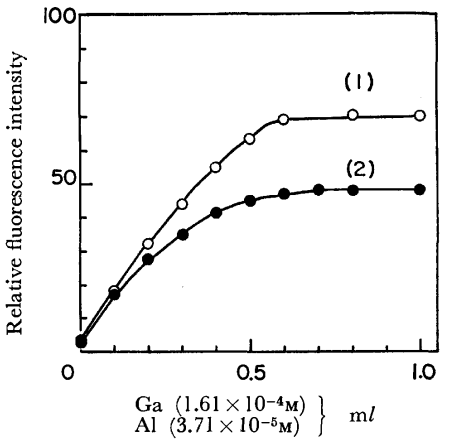

Fig. 10. Mole ratio method
(1): Al; [R]: 3.71×10^{-5}M 0.5 m*l*, 485 nm/562 nm, 60 div.
(2): Ga; [R]: 1.61×10^{-4}M 0.5 m*l*, 485 nm/562 nm, 30 div.

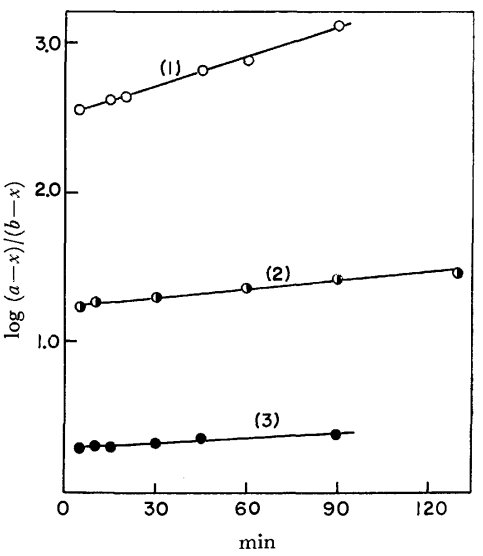

Fig. 11. Kinetics of chelate formation as indicated by fluorescence.
a is initial concentration of aluminum, *b* is initial concentration of Superchrome Garnet Y, and *x* is concentration of chelate as indicated by fluorescence.
(1) *a*: 10 μmol, *b*: 1 μmol;
(2) *a*: 1 μmol, *b*: 1 μmol;
(3) *a*: 1 μmol, *b*: 10 μmol'

(IV), vanadium(V), and chromate(VI) ions reduced the fluorescence intensity, but the following ions did not interfere; beryllium(II), calcium(II), cadmium(II), strontium(II), manganese(II), nickel(II), tin(II), magnesium(II), indium(III), gallium(III), scandium(III), lanthanum(III), yttrium(III), europium(III), thallium (III), zinc(II), selenium(IV), thorium(IV), molybdate (VI), and uranyl(VI) ions. In the determination of gallium, aluminum(III) gave positive error, and quadruple amounts of cobalt(II), copper(II), iron(III), zirconium(IV), vanadium(V), molybdate(VI), and chromate(VI) ions reduced the fluorescence, but other ions, presented in Table 1, did not interfere.

Determination of Metal to Ligand Ratio. The mole ratio of metal to ligand in the metal complexes of Superchrome Garnet Y was determined fluorometrically by the continuous variation method and the mole ratio method. Because the aluminum complex formed slowly at room temperature the metal to ligand ratio was also kinetically determined.

The results are shown in Figs. 9 (continuous variation method), 10 (mole ratio method) and 11 (kinetic method). Figures 9 and 10 indicate that both aluminum and gallium form the 1: 1 complex. Figure 11 shows that the formation of the aluminum complex follows the second-order kinetics, and therefore, supports the above-mentioned composition.

The author wishes to express his appreciation to Professor Tsunenobu Shigematsu (Institute for Chemical Research, Kyoto University) and Professor Yasuharu Nishikawa (Faculty of Science and Technology, Kinki University) for their kind advices and suggestions throughout the investigation.

The Nitration of Nickel(II)-, and Copper(II)-complexes of Bis(salicylaldehyde)ethylenediimine

Motonori TAMAKI, Isao MASUDA, and Koichiro SHINRA

Department of Applied Chemistry, Faculty of Engineering, Osaka University, Yamada-kami, Suita

(Received July 12, 1971)

The M(Salen) complexes (where M=Ni^{II}, Cu^{II}, Co^{II}-NO, and $V^{IV}O$, and where Salen=bis(salicylaldehyde)-ethylenediiminato dianion) were reacted with nitric oxide in organic solvents in the air. The free ligand can only form a compound with the formula of $SalenH_2 \cdot 2HNO_3$, while the complexes with M=Ni or Cu gave NO_2-substituted complexes, M(5,5'-dinitro-Salen), in almost quantitative yields. In the cases of Co(Salen)NO and VO(Salen), no substitution reaction on the phenyl ring took place, but they formed a nitric acid adduct, Co(Salen)NO$\cdot n HNO_3 \cdot n H_2O$ ($n=1$ and 2) and VO(Salen)$\cdot HNO_3 \cdot H_2O$. The reactions are thought to proceed by means of a process involving a nitric acid. The reactivity of the Ni- and Cu-Salen complexes is explained in terms of a π-electron localization at the 5- and 5'-positions of the phenyl rings resulting from $d_\pi \rightarrow p_\pi$ back bonding. A lack of a similar substitution reaction in Co(NO)- and VO-Salen complexes is explained as being due to the lower stability in the metal-Salen bonding.

In previous studies of the reaction of the transition metal complexes with nitric oxide, it has been reported that Ni(II), Cu(II), and Pd(II) complexes of bis(acetylacetone)ethylenediimine, and Pd(II) complexes of acetylacetone and its derivatives react at the γ-position of the metal chelate rings to form α-imine-oxime-type complexes,[1,2] whereas in the case of Co(II) complexes of bis(acetylacetone)ethylenediimine and bis(benzoylacetone)ethylenediimine, a nitrosyl complex binding NO as an axial ligand is obtained.[3]

The present work will deal with the reaction of NO with Cu(II) and Ni(II) chelates, including bis(salicylaldehyde)ethylenediimine,[4] to produce NO_2-substituted complexes, M(5,5'-dinitro-Salen) (M=Ni and Cu).

Experimental

Materials. $SalenH_2$ and its metal complexes were prepared according to the method described in the references.

Reaction with Nitric Oxide. In the following experiments, NO was bubbled through the solution in air.

Ni(5,5'-dinitro-Salen)$\cdot 1.5H_2O$. A 1.5 g portion of Ni(Salen)[5] was dissolved in 100 m*l* of acetonitrile. Bubbling NO through the solution at room temperature then resulted in the precipitation of an orange compound. After bubbling for two hours, the NO in the solution was driven off by N_2 gas; then the precipitates were collected by filtration. The compound was recrystallized from a large volume of acetonitrile to give fine crystals with an orange color (complex **1**). Complex **1** is soluble in acetonitrile and acetone. Yield, 1 g.

Found: C, 43.58; H, 3.21; N, 12.47%. Calcd for $NiC_{16}H_{15}N_4O_{7.5}$: C, 43.47; H, 3.43; N, 12.68%.

The complex **1** could also be obtained by a similar reaction in a chloroform solution. The greenish precipitates which separated were recrystallized from an acetonitrile solution to give orange crystals. The analytical and IR spectral data were consistent with those of the complex **1**.

Found: C, 43.85; H, 3.32; N, 12.41%. Calcd for $NiC_{16}H_{15}N_4O_{7.5}$: C, 43.47; H, 3.43; N, 12.68%.

Cu(5,5'-dinitro-Salen). One gram of Cu(Salen)[5] was dissolved in 150 m*l* of chloroform; when NO was then bubbled through this solution at room temperature for about three hours, brownish precipitates were separated. The NO in the solution was driven off by N_2 gas, and the precipitates were collected on a filter and washed with chloroform and then with ether. The precipitates were recrystallized from an anhydrous acetonitrile solution to give greenish-brown needles (complex **2**).

Found: C, 45.26; H, 2.87; N, 13.50%. Calcd for $CuC_{16}H_{12}N_4O_6$: C, 45.77; H, 2.86; N, 13.35%.

The same compound was also obtained by a reaction in an acetonitrile solution. The complex **2** including its water molecule, tends to crystallize when it is allowed to stand in a solution of an organic solvent in air; 2.5 hydrates are obtained from an acetonitrile solution, and 0.5 hydrates, from an acetone solution.

Co(Salen)NO$\cdot HNO_3 \cdot H_2O$. One gram of Co(Salen)NO[6] was dissolved in 150 m*l* of chloroform. NO gas was bubbled through this solution for five hours. The green complex thus precipitated was collected by filtration and was recrystallized from a mixed acetonitrile-ether solution as green crystals (complex **3**). Yield, 0.5 g.

Found: Co, 13.25; C, 44.41; H, 3.56; N, 13.02%. Calcd for $CoC_{16}H_{17}N_4O_7$: Co, 13.51; C, 44.04; H, 3.94; N, 12.84%.

Co(Salen)NO$\cdot 2HNO_3 \cdot 2H_2O$. The reaction that was carried out in an acetonitrile solution resulted in the precipitation of a brownish-green compound. This was then recrystallized from a mixed acetonitrile-ether solution.

Found: Co, 11.50; C, 37.11; H, 3.45; N, 13.81%. Calcd for $CoC_{16}H_{20}N_5O_{11}$: Co, 11.39; C, 37.14; H, 3.90; N, 13.54%.

VO(Salen)$\cdot HNO_3 \cdot H_2O$. A similar reaction of VO(Salen)[7] in a chloroform solution gave dark violet precipitates, which were then recrystallized from methanol.

Found: C, 46.85; H, 3.96; N, 10.03%. Calcd for $VC_{16}H_{17}N_3O_7$: C, 46.39; H, 4.10; N, 10.15%.

$SalenH_2 \cdot 2HNO_3$. Two grams of $SalenH_2$ were dissolved in 100 m*l* of chloroform; then NO was bubbled through the solution for about two hours. The white precipitates

1) I. Masuda, M. Tamaki, and K. Shinra, This Bulletin, **42**, 157 (1969).

2) D. A. White, *J. Chem. Soc., A*, **1971**, 233.

3) M. Tamaki, I. Masuda, and K. Shinra, This Bulletin, **42**, 2858 (1969).

4) The following abbreviations are used in the present paper. Salen: bis(salicylaldehyde)ethylenediiminato dianion, 5,5'-dinitro-Salen: bis(5-nitro-salicylaldehyde)ethylenediiminato dianion, and 3,3'-dinitro-Salen: bis(3-nitro-salicylaldehyde)ethylenediiminato dianion.

5) P. Pfeiffer, E. Breite, E. Lübbe, and T. Tsumaki, *Ann.*, **503**, 84 (1933).

6) A. Earnshaw, P. C. Hewlett, and L. F. Larkworthy, *J. Chem. Soc.*, **1965**, 4718.

7) H. J. Bielig and E. Bayer, *Ann.*, **580**, 135 (1953).

which resulted were washed with chloroform. Yield, 1.5 g.

Found: C, 47.95; H, 4.49; N, 14.40%. Calcd for $C_{16}H_{16}N_4O_8$: C, 48.21; H, 4.21; N, 14.28%.

The addition of $NiCl_2 \cdot 6H_2O$ to an aqueous alkaline solution of $SalenH_2 \cdot 2HNO_3$ resulted in the precipitation of reddish-orange crystals, which were then recrystallized from chloroform. The elementary analytical and IR spectral data indicated the compound to be Ni(Salen).

Found: C, 58.86; H, 4.41; N, 8.55%. Calcd for $NiC_{16}H_{14}N_2O_2$: C, 59.12; H, 4.35; N, 8.62%.

The recrystallization of the $SalenH_2 \cdot 2HNO_3$ from methanol or ethanol gave thin plates whose analytical data correspond to those of (ethylenediamine)$2HNO_3$. This compound is thought to be a hydrolytic product of $SalenH_2 \cdot 2HNO_3$.

Found: C, 13.00; H, 5.37; N, 30.22%. Calcd for $C_2H_{10}N_4O_6$: C, 12.90; H, 5.43; N, 30.10%.

In an acetonitrile solution, $SalenH_2$ reacted with NO to produce (ethylenediamine)$2HNO_3$.

Measurements. The IR spectra were measured in Nujol or in hexachlorobutadiene, using a Hitachi 225 grating spectrometer for the 4000—200 cm^{-1} region and a JASCO IR-G spectrometer for the 4000—400 cm^{-1} region. The magnetic susceptibilities were determined at room temperature by the Gouy method. The electronic absorption spectra were obtained with a Hitachi EPS-3 spectrophotometer. The conductance measurements were made at 25°C using a Universal Bridge Model 4225A, Yokogawa Electric Works, Ltd.

Results and Discussion

Ni(Salen) and Cu(Salen) reacted with NO in the air, in chloroform or in acetonitrile, to form an orange-colored compound (complex **1**) or a greenish-brown compound (complex **2**) respectively. As will be discussed below, these compounds have been confirmed to be 5,5′-dinitro-substituted complexes.

In general, it would not be reasonable to expect a remarkable difference in the IR spectra between metal complexes with 5,5′- and with 3,3′-dinitro-Salen.[4] However, it can clearly be seen in the spectra (Fig. 1) of the Ni(II)-complexes with 5,5′- and 3,3′-dinitro-Salen prepared as authentic compounds[8] that: i) of the two bands at about 1600 cm^{-1}, the one at the higher wave number is more intense than the one at the lower wave number for the 5,5′-dinitro-complex, while the former is weaker than the latter for the 3,3′-dinitro-complex, and ii) the band about 1300 cm^{-1} is broader for the 5,5′-dinitro-complex. The IR spectrum of the complex **2** exhibits the characteristic feature of the 5,5′-dinitro-complex (Fig. 1). Thus, the complex **1** can be considered to be Ni^{II}(5,5′-dinitro-Salen)$\cdot 1.5H_2O$. Similarly, an inspection of the IR spectrum (Fig. 2) leads us to conclude that the complex **2** can be formulated as: Cu^{II}(5,5′-dinitro-Salen).[9,10]

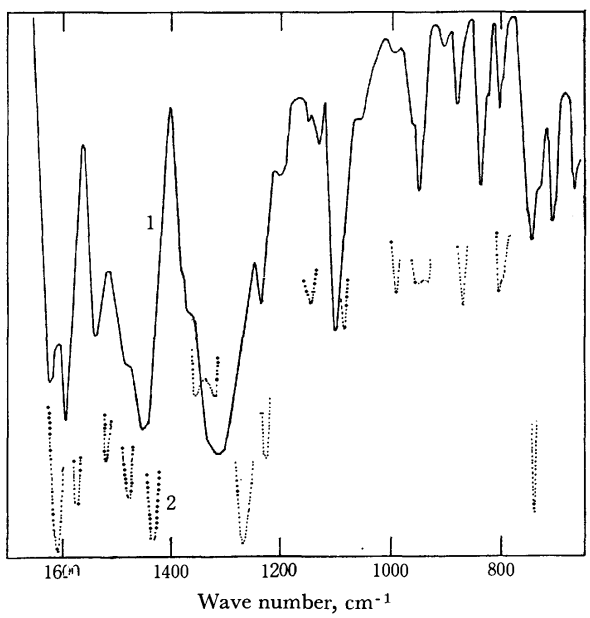

Fig. 1. IR spectra of Ni(5,5′-dinitro-Salen)$\cdot 1.5H_2O$[a]; ——, and Ni(3,3′-dinitro-Salen); ·····, in Nujol.
a) The frequencies of the complex **1** is identical to the curve 1.

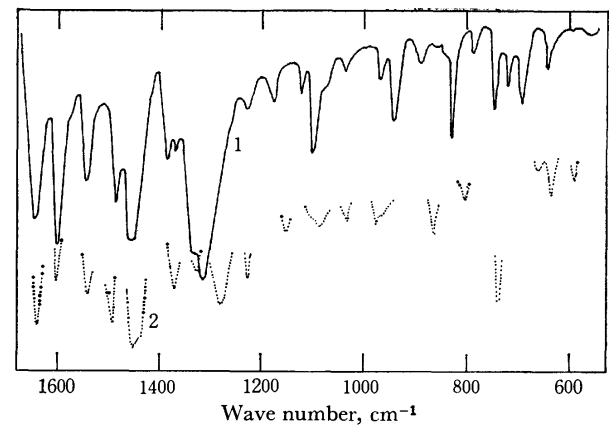

Fig. 2. IR spectra of Cu(5,5′-dinitro-Salen);[a] ——, and Cu(3,3′-dinitro-Salen); ·····, in Nujol.
a) The frequencies of the complex **2** is identical to the curve 1.

The reaction of the free ligand ($SalenH_2$) with NO in a chloroform solution produced neither a nitroso- nor a nitro-substituted compound, but only formed the precipitates of a compound corresponding to the $SalenH_2 \cdot 2HNO_3$ formula. This was characterized as a nitric acid adduct of the Schiff base by reaction with the Ni^{2+} ion in an aqueous solution, thus forming Ni(Salen), and by recrystallization from methanol or ethanol, by which it was converted into (ethylenediamine)$2HNO_3$ in an almost quantitative yield.

As has been described above, the reactions resulted in the formation of the nitric acid adduct of the free ligand and the nitro-substituted metal-Salen complex. Moreover, the reactions can not be observed to occur with pure NO; that is solutions of $SalenH_2$ or its Ni- and Cu-complexes did not react with NO in the absence of air. Thus, the reactions may be thought to proceed by means of a process involving a nitric acid. Further, it is likely that the complex formation of $SalenH_2$ with the Ni^{2+} or Cu^{2+} ion makes it easy for the nitration reaction to take place at the 5- and 5′-positions of the phenyl rings. In the complexes, this can tentatively

8) E. J. Olszewski and D. F. Martin, *J. Inorg. Nucl. Chem.*, **26**, 1577 (1964).

9) C. S. Marvel and N. Tarköy, *J. Amer. Chem. Soc.*, **77**, 5820 (1955).

10) T. Tanaka, *ibid.*, **80**, 4108 (1958); This Bulletin, **33**, 259 (1960).

be explained in terms of an electrophilic substitution reaction at the 5- and 5′-positions of the phenyl rings caused by a π-electron localization, as is shown in (a′).

(a) (a′)

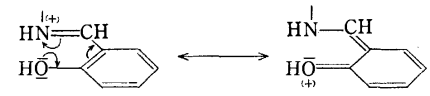

(b) (b′)

It is probable that the coordination bond between the nitrogen atom and the metal ion can participate in the mesomeric system through the $d_\pi \rightarrow p_\pi$ back donation, thus increasing π-localization on the 5- and 5′-positions.

On the other hand, the free $SalenH_2$ tends to form a proton-addition compound which may act to decrease the degree of π-localization on the 5- and 5′-carbons, as is shown in (b′).[11]

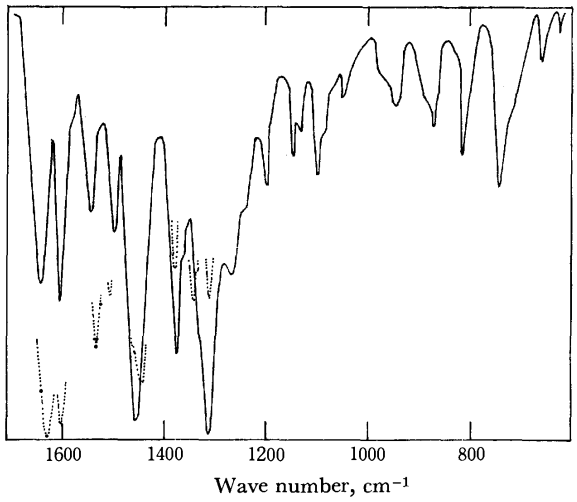

Fig. 3. IR spectra of $Co(Salen)NO \cdot HNO_3 \cdot H_2O$;——, and Co(Salen)NO;·····, in Nujol.

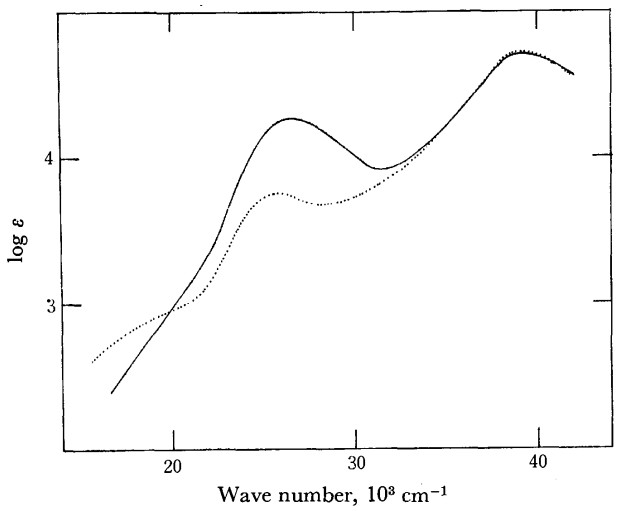

Fig. 4. Electronic spectra of $Co(Salen)NO \cdot HNO_3 \cdot H_2O$;——, and Co(Salen)NO;·····, in acetonitrile.

11) The adducts of Cu(Salen) with phenol and propionic acid are prepared by Tanaka, in Ref. 10.

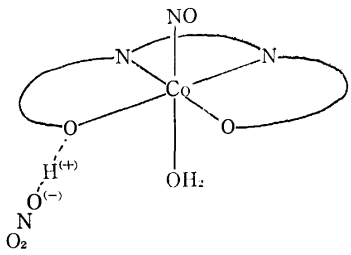

Fig. 5.

It should be noted that, in the case of the Co(Salen)-NO, no similar substitution reaction could be observed. It has already been reported that, by reaction with NO in organic solvents, Co(Salen) easily produces Co(Salen)-NO,[6] wherein the Salen is coordinated to the cobalt ion in the plane, as in the cases of Ni(II)- and Cu(II)-Salen. Hence, it seems possible to expect a similar nitration reaction to take place in the case of Co(Salen)NO. However, in fact, Co(Salen)NO afforded only a diamagnetic compound (complex **3**) which can be formulated as a nitric acid adduct, $Co(Salen)NO \cdot HNO_3 \cdot H_2O$. The IR spectrum of this adduct (Fig. 3) obviously differs from that of the Co(II) complexes with 5,5′- and 3,3′-dinitro-$SalenH_2$,[6] and possesses the characteristic absorptions for the NO group at 1640 cm^{-1} and for the NO_3^- group (ν_3) at about 1300 cm^{-1}.[12] The electronic absorption spectrum of this compound (Fig. 4) shows a maximum at 39.1×10^3 cm^{-1} which quite resembles Co(Salen)NO. On the other hand, in the $18—20 \times 10^3$ cm^{-1} region its spectrum differs remarkably from that of Co(Salen)NO and does not show the characteristic peak of penta-coordinate, diamagnetic Co(II) complexes.[3] Judging from these observations and the analytical data, a skeletal structure for this adduct is tentatively drawn in Fig. 5. When reacted in an acetonitrile solution, Co(Salen)NO binds two moles of HNO_3. In the case of VO(Salen), $VO(Salen) \cdot HNO_3 \cdot H_2O$ was separated by a similar reaction in a chloroform solution. The conductance data shown in Table 1 seem to be consistent with the formula of the adduct of the VO-complex. The adduct of the Co-complex shows less conductivity than would be expected for a 1 : 1 electrolyte.

The lack of a similar substitution reaction for Co(Salen)NO may be explained as follows. There seem to be no numerical data available for discussing the relative stabilities of a series of the metal-Salen com-

Table 1. Electric conductance; in acetonitrile

	Concn. (M)	Molar conductance ($cm^2/\Omega \cdot mol$)
$Co(Salen)NO \cdot HNO_3 \cdot H_2O$ (complex **3**)	1/250	2.43
$VO(Salen) \cdot HNO \cdot H_2O$	1/500	45.1
VO(Salen)	1/250	0.270
$[Co(dmgH)_2(py)_2]Cl$[a]	1/250	60.5

a) dmgH and py represent dimethylglyoximato monoanion and pyridine, respectively.

12) K. Nakamoto, "Infrared Spectra of Inorganic and Coordination compounds," John Wiley, & Sons, New York and London (1962), p.90.

plexes. However, judging from the common order of the stability constants,[13] Ni(II)- and Cu(II)-complexes may be expected to be the most stable of the Salen complexes used in the present work. When the bond of Co–N is more unstable, the degree of the $d_\pi \rightarrow p_\pi$ back donation is assumed to be more decreased in the metal complexes other than Ni and Cu. In the cases of the Co(NO)- and VO-complexes, the further formation of the bonding with the axial ligand may also cause a weakening of the bonding between metal and Salen.[14]

13) D. P. Mellor and L. Malay, *Nature*, **159**, 370; H. Irving *Proc. Intern. Conf. on Coordination Chem.*, Chem. Soc. London, (1959), p. 13.

14) T. Shigematsu, M. Tabushi, M. Matsui, and M. Munakata, This Bulletin, **41**, 2656 (1968).

BULLETIN OF THE CHEMICAL SOCIETY OF JAPAN, VOL. 45, 1403—1405(1972)

Trace Analysis of Metals by ESR. I. Microdetermination of Copper by Means of Solvent Extraction of Copper(II) Diethyldithiocarbamate

Daijiro YAMAMOTO, Tuneo FUKUMOTO, and Noriaki IKAWA
Faculty of Agriculture, Meiji University, Ikuta, Kawasaki-shi

(Received July 22, 1971)

A new method was developed for the direct determination of copper using ESR. Cupric diethyldithiocarbamate complex dissolved in benzene shows a unique ESR spectrum. The bivalent complex in benzene gave a very strong ESR signal with intensity sensitive to 0.005 ppm of Cu(II)-ion. Thus the ESR signal can be utilized for the trace analysis of Cu(II)-ion. The ESR signal intensity was linear in the ranges 1.0—0.1 γ/m*l* and 0.1—0.01 γ/m*l* of Cu(II)-ion. Mg^{2+}, Fe^{2+}, Ba^{2+}, Mn^{2+}, Zn^{2+}, Co^{2+}, Pb^{2+}, Ni^{2+}, I^-, Br^-, and NO_3^- did not interfere with the determination, while Hg^{2+} and CN^- did. Comparing this method with photometric determination, we see that a very low content of Cu(II)-ion can be determined with a very small amount of sample.

It is known that Cu(II) forms various paramagnetic Cu(II) complexes which show characteristic ESR spectra.[1-3] In a previous paper, ESR spectra of powder and solution of Cu(II) complexes were reported,[4] for which seventeen samples were prepared by the usual methods. In the present study, a new method was developed for the rapid solvent extraction and direct determination of Cu(II) using ESR. Powdered $(DDC)_2Cu$, the Cu(II) complex, showed the known broad absorption spectrum whereas hyperfine structure was observed in a benzene solution, *i.e.*, the ESR spectrum was split into four lines. In the case of cupric dithiocarbamates the ESR spectra were very narrow and sharp. The second signal, counted from higher magnetic field, was dominant and its height was proportional to the amount of Cu(II) in a certain concentration range. The signal could be found even in the very dilute solution of Cu(II)-ion. Thus the application of ESR signal to the trace analysis of Cu(II)-ion is possible.

Experimental

Apparatus. The ESR measurement was carried out with a Hitachi X-band spectrometer, Model MPU-3. The magnetic field was modulated at 100 kHz. A Hitachi-Perkin Elmer spectrophotometer, Model 139, was used for the absorption spectra and colorimetric analysis. The measurements were carried out with 1 cm glass cell.

Reagents. Sodium diethyldithiocarbamate(DDCNa) was of JIS special grade from Kokusan Kagaku Co., Ltd. A standard solution of Cu(II) was prepared by dissolving 78.592 mg of $CuSO_4 5H_2O$ of JIS special grade in 200 m*l* twice distilled water. Other reagents were of guaranteed grade from Kokusan Kagaku Co., Ltd. and used without further purification.

Preparation of the Sample Solution. One m*l* of 0.2% aqueous solution of DDCNa was added into 1 m*l* of the solution containing Cu(II)-ion. The pH was regulated to 1—2 with hydrochloric acid, and 1.0 m*l* of benzene was poured into the mixture. After shaking for a few minutes $(DDC)_2Cu$ was extracted entirely into the benzene layer, and 0.1 m*l* of the solution was taken for examination by ESR.

Results and Discussion

ESR spectrum of $(DDC)_2Cu$. $(DDC)_2Cu$ in benzene showed a unique ESR spectrum as shown in Fig. 1. Owing to the existence of nuclear spin (3/2) of ^{63}Cu and ^{65}Cu four splitting absorption bands appeared. The second signal counted from higher magnetic field was dominant, and its height was proportional to the amount of Cu(II)-ion in a certain range. Thus the second signal intensity was used for the determination of Cu(II)-ion concentration.

1) A. H. Maki and B. R. McGarvey, *J. Chem. Phys.*, **31**, 3135 (1958).
2) R. Rajan and T. R. Reddy, *ibid.*, **39**, 1140 (1963).
3) B. G. Malmström and T. Vänngård, *J. Mol. Biol.*, **2**, 118 (1960).
4) D. Yamamoto and T. Fukumoto, *Memoirs of Inst. of Sci. and Tech. Meiji Univ.*, **5**, 251 (1966).

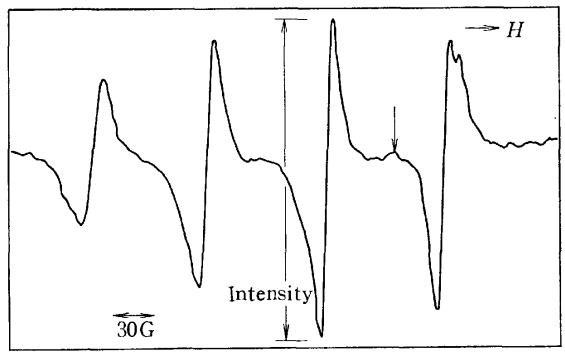

Fig. 1. ESR spectrum of $(DDC)_2Cu$ complex in benzene solution, at room temperature. The arrow indicates the resonance field of solid DPPH.

TABLE 1. COMPARISON OF SIGNAL INTENSITIES IN SOLVENTS

Organic solvent	Signal intensity
Benzene	100
Carbon tetrachloride	96.7
Carbon disulfide	94.8
Ethylbenzene	66.2
Xylene	62.3
Toluene	60.0

Signal intensity of $(DDC)_2Cu$ complex in benzene is taken as 100.

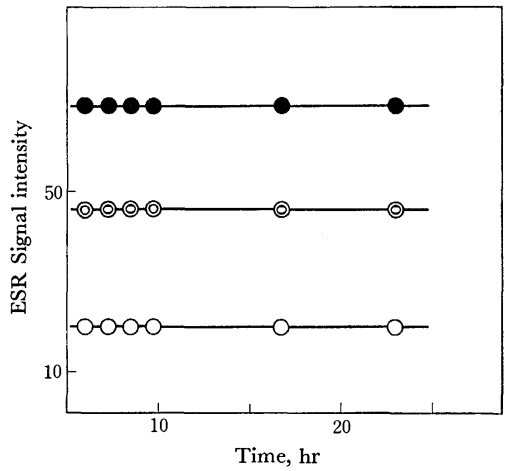

Fig. 2. Effect of time of standing.
●: 10.0γ/ml, ◎: 1.0γ/ml, ○: 0.1γ/ml.

Effect of Organic Solvents on Extraction. Extraction was carried out by the above procedure. ESR spectra of six solutions of $(DDC)_2Cu$ in different organic solvents were measured. The signal intensities are shown in Table 1. We see that the maximum ESR signal intensity is obtained in the benzene solution.

Effect of Time of Standing. The ESR signal intensity of the solution extracted at pH 2.0, was determined as a function of the time elapsed after the preparation of the solution. As shown in Fig. 2, no change was observed in the ESR signal intensities over a period of 24 hr.

Effect of pH on Extraction. The effect of pH on the extraction was examined. The signal intensities obtained from solutions of 0.1 γ/ml, 1.0 γ/ml, and 10.0 γ/ml Cu(II)-ion were constant in the pH range 1.0—7.0 as shown in Fig. 3. However, the range pH 1—2 was chosen to avoid the extraction of other metal ions such as Mn^{2+}, Fe^{2+}, Ni^{2+}.

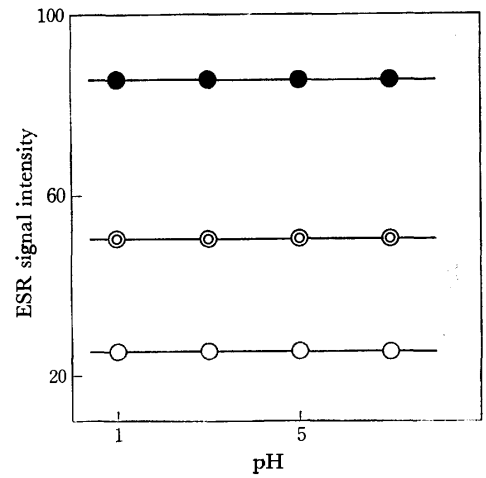

Fig. 3. Effect of pH on extraction.
●: 10.0γ/ml, ◎: 1.0γ/ml, ○: 0.1γ/ml.

TABLE 2. EFFECT OF DIVERSE IONS

Ion	Added as	0.1γ/ml Cu taken / Cu found	1.0γ/ml Cu taken / Cu found
Mg^{2+}	$MgCl_2$	—	—
Fe^{2+}	$FeCl_2$	—	—
Ba^{2+}	$BaCl_2$	—	—
Mn^{2+}	$MnCl_2$	—	—
Zn^{2+}	$ZnCl_2$	—	—
Co^{2+}	$CoCl_2$	—	—
Pb^{2+}	$Pb(CH_3COO)_2$	—	—
Ni^{2+}	$NiCl_2$	—	—
Hg^{2+}	$HgCl_2$	+	+
I^-	KI	—	—
Br^-	KBr	—	—
CN^-	KCN	+	+
NO_3^-	KNO_3	—	—

100 γ/ml of diverse ions added.
+) Interference —) No interference

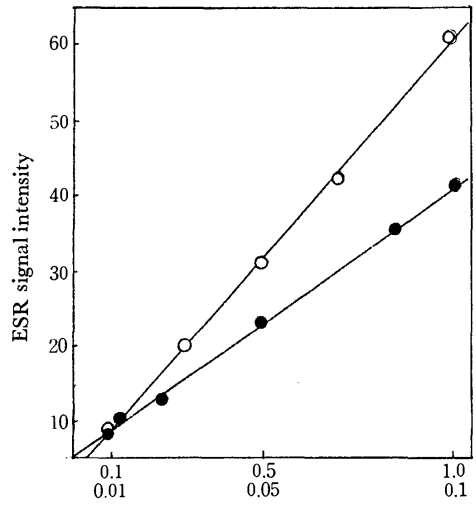

Fig. 4. Calibration curve.
●: 0.01—0.1γ/ml, ○: 0.1—1.0γ/ml.

Table 3. Comparison of esr method with photometric method. Cu contents in aluminum foil

Al-foil (g)	ESR method[a] (ppm)	Photometric method[b] (ppm)
0.0992	49.3	49.6
0.1014	56.6	56.4
0.1008	64.4	64.6
0.0998	28.0	28.5
0.1017	68.8	69.7

All values are means of five measurements.
a) 0.1 m*l* of 100 times diluted solution
b) 5.0 m*l* of 10 times diluted solution

Effect of Diverse Ions. The effect of 13 ions on the determination of Cu(II) was examined. The results are summarized in Table 2. CN^- and Hg^{2+} interfere with the determination.

Calibration Curve for the Determination of Cu(II). The calibration curve for the Cu(II)-ion was determined from the height of the second signal at different Cu(II)-ion concentrations. In Fig. 4, the ordinate is in an arbitrary scale.

Comparison with usual Photometric Determination. For the sake of comparison, the Cu content in aluminium foil were determined by the usual photometric and ESR methods. About 100 mg of aluminium foil was dissolved in 6N-HCl with a small amount of concd. nitric acid and diluted to 100 m*l* with water. The solution was used as a sample. Determination of Cu content was carried out by the usual photometric method.[5] Comparison of results from ESR and photometric methods is given in Table 3. We see that the ESR method can be used for the determination of a very low content of Cu(II)-ion with a very small amount of sample.

The authors are grateful to Dr. N. Iso for his interest and valuable suggestions.

5) *Cf.* IUPAC, Spectrophotometric Data for Colorimetric Analysis, Butterworths, London, 1963, pp. 150—156.

BULLETIN OF THE CHEMICAL SOCIETY OF JAPAN, VOL. 45, 1405—1407(1972)

Trace Analysis of Metals by ESR. II. Indirect Microdetermination of Mercury(II) with Tetraethylthiuram disulfide Copper(II) Complex[1]

Daijiro YAMAMOTO and Noriaki IKAWA
Faculty of Agriculture, Meiji University, Ikuta, Kawasaki-shi

(Received July 22, 1971)

A method was devised for the indirect microdetermination of mercury by means of ESR. Tetraethylthiuram disulfide(TET)-Cu(II) complex dissolved in benzene showed a characteristic ESR spectrum. Quantitative determination of a small amount of mercury(II) was made by application of the replacement reaction of TET-Cu(II) by mercury(II)-ion in a benzene solution:

$$\text{TET-Cu} + \text{Hg}^{2+} \rightarrow \text{TET-Hg} + \text{Cu}^{2+}$$

The ratio of metal to ligand was considered to be 1 : 1 in the complex. 1.0—0.1 γ/m*l* and 0.1—0.01 γ/m*l* of mercury was determined rapidly in the presence of Mg^{2+}, Fe^{2+}, Ba^{2+}, Mn^{2+}, Zn^{2+}, Co^{2+}, Pb^{2+}, Ni^{2+}, I^-, Br^-, NO_3^-, and Cl^- ions. CN^- interfered with the determination. From a comparison of this and photometric methods a very small amount of mercury(II) ion can be determined with a very small amount of sample.

Spectrophotometric determination of mercury(II) with dithizone, dithiocarbamates, and cupric diethyldithiocarbamate ($(DDC)_2Cu$)[2,3] has been reported. Determination with $(DDC)_2Cu$ was indirect and the following replacement reaction was used.

$$(DDC)_2Cu + Hg^{2+} \longrightarrow (DDC)_2Hg + Cu^{2+}$$

The decolorization which takes place in the solution by the replacement reaction was utilized in the spectrophotometric measurement. ESR spectra of $(DDC)_2Cu$ complex in various organic solvents have been reported.[4,5] A small amount of copper could be determined by means of ESR. $(DDC)_2Cu$ complex dissolved in benzene showed a characteristic ESR spectrum. The signal intensity was sensitive to 0.005 ppm of copper(II) ion.

In the present study, tetraethylthiuram disulfide (TET) was used in place of DDC, since TET-Cu(II) complex has the same structure as that of DDC-Cu(II),[6] and TET was cheaper than DDCNa. The TET-Cu(II) complex in benzene gave a strong ESR signal

1) Presented at the 19th Annual Meeting of the Chemical Society of Japan, Tokyo, April, 1966, and the 21st Annual Meeting of the Chemical Society of Japan, Osaka, April, 1968.

2) S. Komatsu and S. Kuwano, *Nippon Kagaku Zasshi*, **83**, 1262 (1962).

3) Y. Hamamoto and M. Kotaki, *Nippon Nogei Kagaku Kaishi*, **34**, 885 (1960); *ibid.*, **39**, 442 (1965). K. Takehara and T. Take shita, *Bunseki Kagaku*, **15**, 332 (1966).

4) D. Yamamoto and T. Fukumoto, *Memoirs of Inst. of Sci. and Tech. Meiji Univ.*, **5**, 251 (1966).

5) This Bulletin in press.

6) R. Petterson and T. Vänngård, *Arkiv. Kemi.*, **17**, 249 (1961).

and its intensity was sensitive to 0.005 ppm of Cu(II) ion. The ESR spectrum was split into four narrow lines. The intensity of the second signal, counted from higher magnetic field, was dominant and its height was proportional to the amount of Cu(II) in a certain concentration range. Thus the diminution of the ESR signal intensity could be used for the trace analysis of mercury(II).

Experimental

Apparatus. ESR measurements were carried out at room temperature with a Hitachi X-band spectrometer, Model MPU-3. The magnetic field was modulated at 100 KHz. Absorption spectra measurements and colorimetric analysis were carried out with a Hitachi-Perkin Elmer Spectrophotometer, Model 139 using a 1 cm glass cell.

Reagents. TET used in the experiments was of JIS special grade from Tokyo Kasei Kogyo Ltd. A pure TET was prepared by recrystallization in a hot mixture of ethanol and carbon tetrachloride. Standard mercury(II) solution was prepared as follows. Distilled mercury was dissolved in concd. nitric acid and diluted with water to the concentration 10 γ/ml. Other reagents were of guaranteed grade from Kokusan Kagaku Co., Ltd. and used without further purification.

Preparation of TET-Cu Complex. The complex was prepared by mixing 1.0% ethanolic solution of TET(ligand) and saturated cupric sulfate solution. Bluish brown precipitate was washed with water-ethanol mixture.

Results and Discussion

ESR Spectrum of TET-Cu Complex. TET-Cu complex in benzene showed a characteristic ESR spectrum.[4] This spectrum was the same as one of $(DDC)_2$-Cu in benzene.[4] The formation of TET-Cu might be as follows;

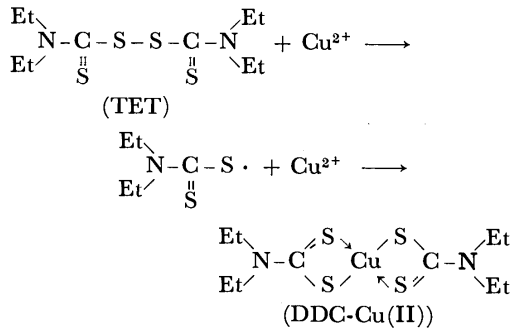

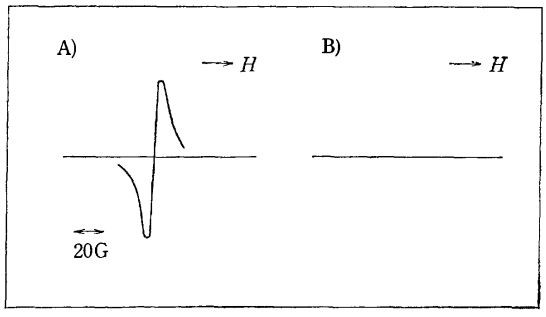

Fig. 1. ESR spectrum after replacement reaction of Hg(II) ion with Cu(II) in TET-Cu complex.
A): Before reaction, B): After reaction.

From the results we see that the second signal, counted from higher magnetic field, was dominant and its height is proportional to the amount of copper in certain

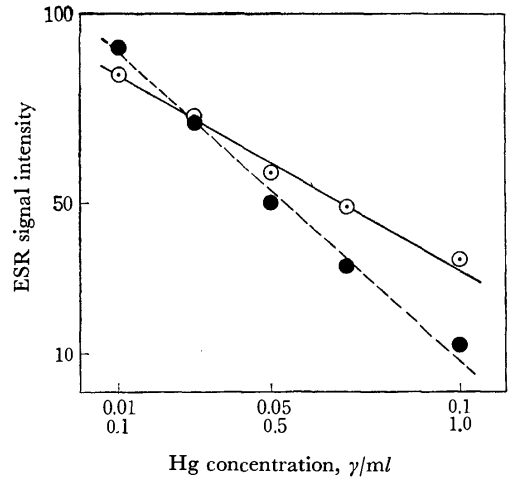

Fig. 2. Relations between mercury concentration and ESR signal intensity, 1.0 m*l* TET-Cu solution in benzene, pH 4.0, 1.0 m*l* mercury sample.
⊙: 1.0—0.1 γ/ml, ●: 0.1—0.01 γ/ml.

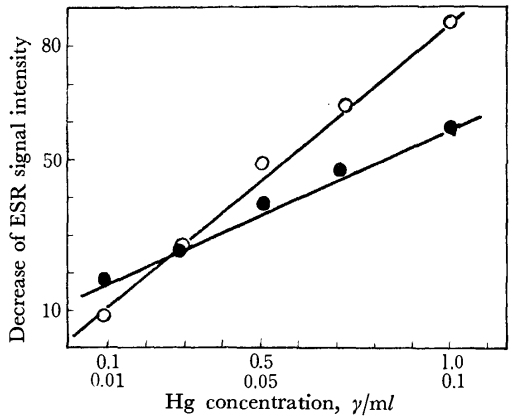

Fig. 3. Calibration curve.
●: 1.0—0.1 γ/ml, ○: 0.1—0.01 γ/ml.

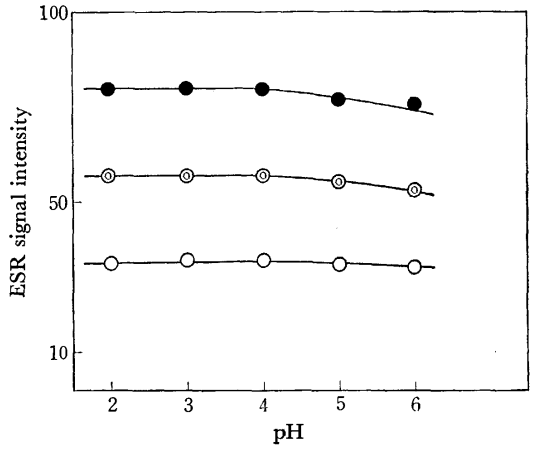

Fig. 4. Effect of pH.
●: 10.0 γ/ml, ◎: 1.0 γ/ml, ○: 0.1 γ/ml.

Table 1. Effect of diverse ions

Ion	Added as	1.0 γ/ml Hg taken	100 γ/ml Hg taken
Mg^{2+}	$MgCl_2$	—	—
Fe^{2+}	$FeCl_2$	—	—
Ba^{2+}	$BrCl_2$	—	—
Mn^{2+}	$MnCl_2$	—	—
Zn^{2+}	$ZnCl_2$	—	—
Co^{2+}	$CoCl_2$	—	—
Pb^{2+}	$Pb(CH_3COO)_2$	—	—
Ni^{2+}	$NiCl_2$	—	—
I^-	KI	—	—
Br^-	KBr	—	—
CN^-	KCN	+	+
NO_3^-	KNO_3	—	—
Cl^-	NaCl	—	—

100 γ/ml of diverse ions added.
+) Interference —) No interference

ranges. Thus the second signal intensity was used for the determination of copper(II) concentration.[5]

Replacement Reaction of Mercury(II) with Copper(II) in TET-Cu Complex. One ml of 0.00015M mercury-(II) solution was mixed with 1.0 ml of 0.00015M TET-Cu benzene solution. After shaking for a few minutes, the brownish yellow benzene layer disappeared completely showing the accomplishment of the replacement reaction.

One tenth ml of the benzene layer was taken for examination. The ESR spectrum after replacement reaction of mercury(II) with Cu(II) in TET-Cu complex in benzene (0.00015M, Cu(II) content) showed ESR spectrum as shown in Fig. 1. The spectrum disappeared when the benzene layer was taken. This shows the accomplishment of replacement reaction. The metal to ligand ratio of the complex was considered to be 1 : 1. Therefore, the overall replacement reaction between TET-Cu and mercury(II)-ion can be given by

$$\text{TET-Cu} + Hg^{2+} \longrightarrow \text{TET-Hg} + Cu^{2+}$$

Decrease of TET-Cu Concentration by Mercury(II) Ion. Decrease of TET-Cu concentration due to the replacement by mercury(II) ion was determined by ESR. The original concentration of copper(II) was 1.0 γ/ml or 0.5 γ/ml, and the mercury(II) concentration ranges were 0.1—0.01 γ/ml and 1.0—0.1 γ/ml. The intensity of the second signal peak height was used for the measurement. The results are given in Fig. 2.

Table 2. Comparison of ESR method with photometric method

Hg (γ/ml)	ESR method[a] (γ/ml)	Photometric[b] method (γ/ml)
100	102	101
250	252	253
500	503	501

All values are the means of five measurements.
a) 0.1 ml of 100 times diluted solution
b) 5.0 ml of 10 times diluted solution

Calibration Curve for the Determination of Mercury. From the results, calibration curves for the determination of mercury were prepared in the mercury(II) ion concentration ranges 0.1—0.01 γ/ml and 1.0—0.1 γ/ml, respectively. Figure 3 shows that the ESR signal intensities are linear in the above ranges.

Effect of pH on Solvent Extraction. The effect of pH on the replacement reaction was examined. The signal intensities of the solution of 0.1 γ/ml, 1.0 γ/ml, and 10.0 γ/ml mercury(II) were constant within experimental error in the pH range 1 to 7, as shown in Fig. 4.

Effect of Diverse Ions. The effect of diverse ions on the determination of mercury(II) was examined with 13 different ions. The results are summarized in Table 1. We see that CN^- interferes with determination of mercury(II).

Comparison with the Usual Photometric Method. For the sake of comparison the mercury(II) contents in $HgCl_2$ were determined by the usual photometric[2] and ESR methods. 135.4 mg $HgCl_2$ was dissolved in water and diluted to 100 ml. This was used as the sample. Comparison of the ESR and photometric methods is given in Table 2.

The authors are grateful to Dr. N. Iso for his interest and valuable suggestions.

Trace Analysis of Metals by ESR. III. Determination of Silver by Solvent Extraction with Tetraethylthiuram disulfide Silver(II) Complex[1]

Daijiro YAMAMOTO and Fumiaki OZEKI
Faculty of Agriculture, Meiji University, Ikuta, Kawasaki-shi

(Received July 22, 1971)

A new method was worked out for the determination of silver using ESR. Bivalent complex of silver with tetraethylthiuram disulfide extracted with carbon disulfide, benzene, carbon tetrachloride, xylene, ethylbenzene, toluene, chloroform, and organic solvents was stable. The complex in carbon disulfide gave a very strong ESR signal, the sensitivity being 0.1 ppb. The amount of solution required was 1 m*l*. Colorimetric method can also be applied. However, the sensitivity was lower than that of ESR method. Silver was determined photometrically at 620 nm as a complex with tetraethylthiuram disulfide. The absorption followed Beer's law in the range 10—100 ppm of silver concentration at 620 nm. Bivalent silver complex could be selectively extracted in the presence of several ions, except copper(II) and mercury(II). Results of the continuous variation method indicate that the silver(II) - tetraethylthiuram disulfide ratio in the complex is 1 : 1.

Bivalent silver (Ag(II)) compounds have long been known to be paramagnetic with electron configuration $4d^9$.[2-4] It is possible to infer the existence of this oxidation state from a study of the ESR spectra. Most measurements were carried out at 77°K under the irradiation of γ-ray or X-ray.[5-9] Studies of the ESR spectra at room temperature, however, have been only reported by McMillan, Ag^{2+} in nitric solution,[5] and by Vänngård, Ag(II)-thiuram disulfides.[10-12]

Many methods have been reported on the determination of silver. A spectrophotometric method using dithizone,[13] sodium diethyldithiocarbamate,[14] or *p*-dimethylaminobenzylidenerhodanine[15] has been reported. The sensitivities were in the order of ppm. The sensitivities of electoanalysis, atomic absorption spectrophotometrical analysis, emission spectrochemical analysis, and activation analysis were in the range 0.1—1 ppm.[16]

If silver is stable in Ag(II) complex and extracted in organic solvents, a minute amount of silver can be determined by ESR. Thus we attempted to prepare the stable complexes of Ag(II) and to extract them with organic solvents. Various Ag(II) complexes were prepared by oxidation with ammonium persulfate on Ag(I) complex. The ESR spectra of the solid Ag(II) complexes with dithizone, *o*-(1.10)phenanthroline, 8-hydroxyquinoline, picolinic acid, 2-aminopyrimidine, α-nitroso-β-naphthol, or ethylphenyldithiocarbamate could be observed at room temperature. However, these Ag(II) complexes could not be extracted in organic solvents. A Ag(II) complex which can be extracted with organic solvents was reported by Vänngård.[10] Ag(I) *N,N*-dialkyldithiocarbamates were mixed with the corresponding thiuram disulfides in benzene, and Ag(II) complexes were extracted in benzene layer. We found that Ag(II) complexes with tetraethylthiuram disulfide (TET), tetramethylthiuram disulfide (TMT), dipentamethylenethiuram tetrasulfide (DPTTS) and 2,2-dithio-bis-benzothiazole (DBT) prepared by mixing of Ag(I)-diethyldithiocarbamate complex with the above reagents, could be extracted with organic solvents.

Experimental

Reagents. A standard silver solution was prepared by dissolving 0.543 g of a silver nitrate in 100 m*l* of water distilled twice in a quartz apparatus. This solution was then diluted to the required concentration. 10^{-3}M solutions of TET, TMT, DBT, and DPTTS were prepared by dissolving the reagent in organic solvents. The 10^{-3}M solution of sodium diethyldithiocarbamate (DDCNa) was prepared by dissolving DDCNa in 100 m*l* of distilled water. The McIlvaine buffer solution was made from citric acid and Na_2HPO_4. The Menzel buffer solution was made from Na_2CO_3 and $NaHCO_3$. All reagents and organic solvents in the experiments were of JIS special grade and used without further purification.

Apparatus. The ESR spectra were measured in organic solutions at room temperature with a Hitachi X-band ESR spectrometer, Model MPU-3, equipped with a 100 KHz field modulation unit. Absorption spectra were measured with a Hitachi spectrophotometer, Model EPS-3, using a 1 cm glass cell.

Standard Procedure for Extraction. To 1 m*l* of sample

1) Presented at the 24th Annual Meeting of the Chemical Society of Japan, Osaka, April, 1971; at the 33rd Symposium of the Japan Society for Analytical Chemistry, Tokushima, June, 1971.

2) G. T. Morgan and S. Sugden, *Nature*, **128**, 31 (1931).
3) A. A. Noyes, K. S. Pitzes, and C. L. Dunn, *J. Amer. Chem. Soc.*, **57**, 1299 (1935).
4) E. G. Cox, W. Wardlaw, and K. C. Webster, *J. Chem. Soc.*, **1935** 775.
5) J. A. McMillan and B. Smaller, *J. Chem. Phys.*, **35**, 1968 (1961).
6) J. A. McMillan and W. S. Koski, *J. Amer. Chem. Soc.*, **85**, 2375 (1963).
7) F. K. Kneubukl, W. S. Koski, and W. S. Caughey, *ibid.*, **83**, 1607 (1961).
8) N. A. Ashford and G. A. Noble, *J. Chem. Phys.*, **49**, 4720 (1968).
9) N. A. Ashford and A. Snelson, *ibid.*, **51**, 532 (1969).
10) T. Vänngård and S. Akerstron, *Nature*, **187**, 183 (1959).
11) R. Pettersson and T. Vänngård, *Arkiv Kemi.*, **17**, 249 (1961).
12) R. Assa, R. Pettersson, and T. Vänngård, *Nature*, **190**, 258 (1961).
13) H. Friedeberg, *Anal. Chem.*, **27**, 305 (1955).
14) H. Bode, *Z. Anal. Chem.*, **114**, 164 (1955).
15) M. G. Lai and H. V. Weiss, *Anal. Chem.*, **34**, 1012 (1962).
16) Ref. L. L. Lewis, *ibid.*, **40**, No. 12, 28A (1968). E. B. Sandell; "Colorimetric Determination of traces of Metals," 3rd ed., Interscience-Wiley, New York, (1959).

solution containing 10^{-6}M of silver were added 1 m*l* of the DDCNa solution and 1 m*l* of the TET (or TMT, DBT, DPTTS) solution. After being shaken for one minute, and left to stand for ten minutes, 0.2 m*l* of the organic solvent layer was drawn off into an ESR cell. The ESR spectrum was measured with sweeping a rate 100 Gauss/15 min. Extraction for the measurement of absorption spectra was carried out in the same way, the volume of each solution being 5 m*l*.

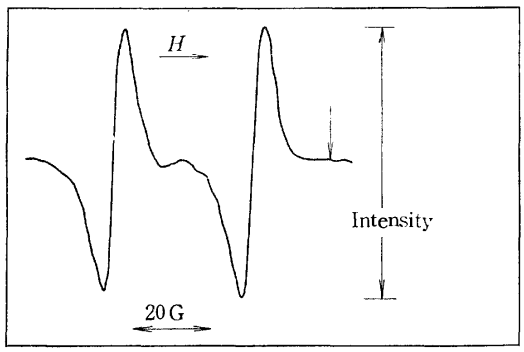

Fig. 1. ESR spectrum of TET-Ag(II) complex in organic solvent at room temperature. The perpendicular arrow in this figure indicates the resonacne filed of solid DPPH.

Results and Discussion

ESR Spectra and Absorption Spectra. Figure 1 shows a typical ESR spectrum obtained from carbon disulfide solution of TET-Ag(II) complex. The two lines of equal intensity ESR spectrum were due to the hyperfine interaction of the nuclear spin of 1/2. Super hyperfine splitting due to magnetic interaction with the nuclei of silver, ^{107}Ag and ^{109}Ag, which have the nuclear magnetic moment of −0.1130 and −0.1299, respectively, was not observed in the case of high field modulation such as 6—10 Gauss. The ESR spectra of the silver(II) complexes with TET, TMT, DBT, and DPTTS were almost the same. The *g*-values were 2.017, and both line widths were 4.7 Gauss. The ESR signal intensity was calculated by the signal height in the high magnetic field as shown in Fig. 1. The ESR signal intensity was proportional to silver concentration.

The typical absorption spectra shown in Fig. 2 were obtained for 10^{-4}M of silver solution. No absorbance maximum of the reagent (curve 2) exists in the wavelength range (Fig. 2). Appearance of the maximum in the absorption spectrum can be attributed to the formation of Ag(II) complex between the reagent cation and the complex anion.

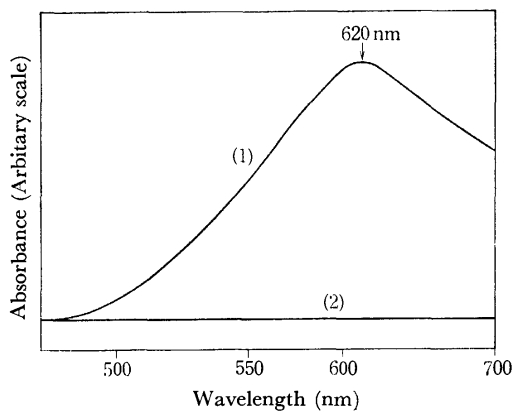

Fig. 2. Absorption spectra.
1) TET-Ag(II) complex in CS_2 solution.
2) TET in CS_2 solution.

Table 1. ESR signal intensities by the different combinations of solvents and reagents

	TET	TMT	DBT	DPTTS
CS_2	100.0	8.9	—	5.0
C_6H_6	27.2	4.4	—	—
CCl_4	12.1	1.3	—	—
$C_6H_5CH_3$	5.3	1.5	—	—
$C_6H_4(CH_3)_2$	4.5	1.1	—	—
$C_6H_5C_2H_5$	4.3	1.1	—	—

Signal intensity of TET-Ag(II) complex in carbon disulfide is taken as 100.0. — shows that ESR signal is obtained only at maximum ESR sensitivity.

Solvents and Reagents. The following solvents and reagents were examined for their ability to extract the Ag(II) complex; carbon disulfide, benzene, carbon tetrachloride, xylene, toluene, and ethylbenzene; TET, TMT, DBT, and DPTTS. The test solutions were made by extracting 10^{-6}M silver nitrate. The results are shown in Table 1. The carbon disulfide and TET pair was found to be the best for extracting the Ag(II) complex, and was thus chosen for the experiments.

Effect of Time of Standing. The stability of the TET-Ag(II) complex in the solvent was determined by measuring the ESR signal intensity. The ESR signal intensity of TET-Ag(II) complex of the solution remained almost constant for at least 8 hr after preparation.

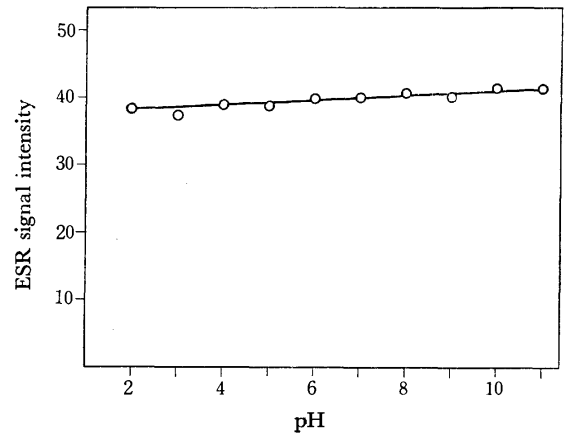

Fig. 3. Effect of pH on ESR signal intensity. Each test solution consists of 5 m*l* buffer solution and 10^{-6}M TET-Ag(II).

Effect of pH. Figure 3 shows a typical pH dependence of the extraction ability. The test solutions were made by extracting 10^{-6}M of silver nitrate in the pH range 2—11. The ESR signals are slightly larger on the alkaline side. The amount of buffer solution per 3 m*l* of the test solution was found to have no effect on the ESR signal intensity over the range 5—10 m*l*.

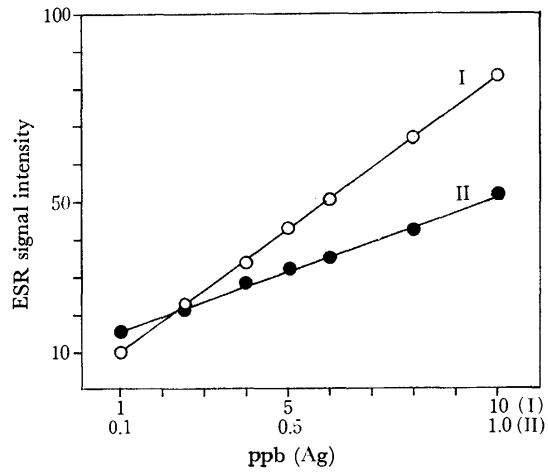

Fig. 4. Calibration curves by ESR method.

Calibration Curve for Silver and Sensitivity of the ESR method. The calibration curve for silver determination was prepared by the ESR signal intensity. Figure 4 shows typical calibration curves. We see that a linear relationship holds between the signal intensity and the silver concentration in the narrow ranges 1—0.1 ppb and 10—1 ppb. The sensitivity of the determination was 0.1 ppb. The total amount of sample solution required was only 1 m*l*.

Beer's Law and Spectrophotometric Sensitivity. The linearity between the absorbance of the TET-Ag II) complex and silver concentration was examined by varying the silver concentration and by measuring the absorbance at wavelength of 620 nm. The Ag(II) complex was found to follow Beer's law up to the silver concentration of at least 10 ppm at 620 nm.

TABLE 2. EFFECT OF DIVERSE IONS ON EXTRACTION OF Ag(II)

Ion	Added as	10	100	1000
Al^{3+}	$Al_2(SO_4)_3$	—	—	—
Zn^{2+}	$ZnCl_2$	—	—	—
Ba^{2+}	$BaCO_3$	—	—	—
Ni^{2+}	$NiCl_2 \cdot 4H_2O$	—	—	—
Mn^{2+}	$Mn(CH_3COO)_2 \cdot 4H_2O$	—	—	—
Mg^{2+}	$MgCl_2 \cdot 6H_2O$	—	—	—
Cd^{2+}	$Cd(NO_3)_2$	—	—	—
Fe^{2+}	$FeSO_4 \cdot 7H_2O$	—	—	—
Cu^{2+}	$CuSO_4 \cdot 5H_2O$	+	+	+
Hg^{2+}	Hg	—	+	+
I^-	KI	—	—	—
Br^-	KBr	—	—	—
Cl^-	KCl	—	—	—
NO_3^-	KNO_3	—	—	—
CN^-	KCN	—	—	—

Ag: 10^{-6}M, Ions: 10^{-3}M, 10^{-4}M, 10^{-5}M. 10, 100, and 1000 indicate that added diverse ion concentrations are of 10, 100, and 1000 times, respectively, to silver concentration. + Interference, — No interference

Effect of Diverse Ions. The effect of diverse ions was examined for a sample containing 10^{-6}M of silver nitrate. The results are shown in Table 2. Concentrations of the 1000—10 times of silver concentration ion were examined. Ag(II) complex could be selectively extracted in the presence of several ions. Mercury(II) and copper(II) ion interfered with extraction. Copper(II) could be separated, but not mercury(II).

Separation of Copper(II). The large solubility of $(DDC)_2Cu$ and very small solubility of DDC-Ag(I) in benzene were utilized for the separation of copper and silver. To 2 m*l* of the copper-silver mixture were added 10 m*l* of the 2% DDCNa, 20 m*l* of benzene and 1 m*l* of the 1N-HCl. The mixture was then shaken. After the organic layer was separated from the aqueous layer, 1 m*l* of a DDCNa solution and 1 m*l* of a TET-carbon disulfide solution were added to an aqueous solution. In the case of a large amount of copper the procedure was repeated several times. The ESR signal intensity was compared with that of standard TET-Ag(II) complex. The results are shown in Table 3. Copper(II) ion concentrations examined varied from 10000 to 100 times silver concentration. From the standard deviation shown in Table 3, we see that the interference of copper(II) ion diminished to some extent.

Composition of TET-Ag(II) Complex. The composition of the TET-Ag(II) complex was determined by the continuous variation method. The results are

TABLE 3. STANDARD DEVIATION

Ag^+ concn. (ppb)	Cu^{2+} concn. (ppm)	n	Standard Dev.
10	0	5	0.775
	10	5	0.894
	100	5	1.732
1.0	0	5	1.414
	1.0	5	2.000
	10	5	3.162
0.1	0	5	2.236
	0.1	5	2.645
	1.0	5	3.873

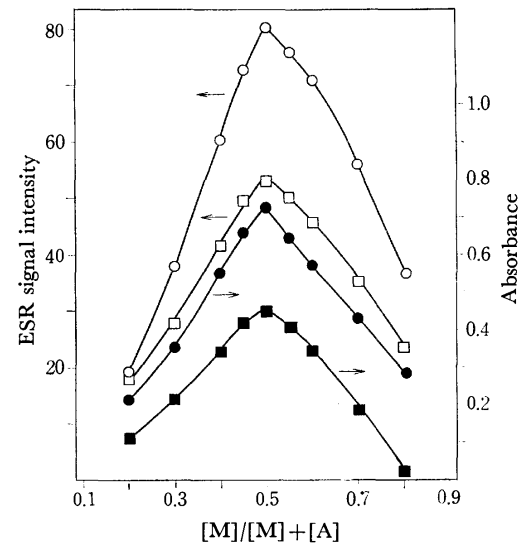

Fig. 5. Continuous variation method.
M: Ag, A: TET or TMT,
○: TET and Ag(II) by ESR,
●: TET and Ag(II) by absorbance at 620 nm,
□: TMT and Ag(II) by ESR,
■: TMT and Ag(II) by absorbance at 620 nm.

shown in Fig. 5. The curves were obtained by measuring the absorbance at 620 nm, and the ESR signal. The resulting curves have a maximum at 0.5 mol fraction of Ag(II), indicating TET-Ag(II) ion ratio 1 : 1, and TMT-Ag(II) ion ratio 1 : 1. Ag(II) complexes may have the following structure.

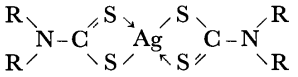

$R = C_2H_5$, CH_3

Reaction. When Ag(I) complex with DDC was mixed with TET, TMT, DBT, and DPTTS in organic solvent, the complexes with TET, TMT, DBT, and DPTTS were found to be extractable with organic solvents. Thus we assumed the mechanism of the complex formation. When DDCNa and TET were used, the reactions can be written as follows.

$$\text{DDCNa} + \text{Ag}^+ \longrightarrow \text{DDC-Ag(I)} + \text{Na}^+$$

$$\text{DDC-Ag(I)} + \text{TET} \longrightarrow \text{TET-Ag(II)} + \text{DDC}^-$$

The reaction of DDC-Ag(I) with TMT, DBT, or DPTTS was assumed to be same as that of DDCAg(I) with TET. These Ag(II) complexes gave strong ESR signal intensity.

When DDCNa and EDTA were used, and Ag(I) complexes with 2-aminopyrimidine, 8-hydroxyquinoline, α-nitroso-β-naphthol, dithizone, or *o*-(1.10)phenanthroline were mixed with TET-carbon disulfide solution, the products gave ESR spectra. Thus Ag(II) complexes were assumed to be prepared. Since it requires a long time for Ag(II) complexes to be stabilized and the ESR signal intensity obtained is weak, these complexes could not be used. The reaction, however, may be caused by the existence of DDC acid as impurity during the course of TET production.

The authors are grateful to Dr. N. Iso for his interest and valuable suggestions.

BULLETIN OF THE CHEMICAL SOCIETY OF JAPAN, VOL. 45, 1411—1417(1972)

Nickel(II) Complexes of 1,5-Dialkyl-2,4-pentanediones[1]

Isao Yoshida, Hiroshi KOBAYASHI, and Keihei UENO[2]

Department of Organic Synthesis, Faculty of Engineering, Kyushu University, Fukuoka

(Received September 2, 1971)

Bis(heptane-3,5-dionato)nickel(II) monohydrate [Ni(DNPM)$_2$·H$_2$O], bis(nonane-4,6-dionato)nickel(II) monohydrate [Ni(DNBM)$_2$·H$_2$O], bis(2,6-dimethylheptane-3,5-dionato)nickel(II) monohydrate [Ni(DIBM)$_2$·H$_2$O], bis(2,8-dimethylnonane-4,6-dionato)nickel(II) monohydrate [Ni(DIVM)$_2$·H$_2$O] and bis(tridecane-6,8-dionato)nickel(II) monohydrate [Ni(DNCM)$_2$·H$_2$O] were prepared, and a dimeric octahedral structure was proposed for each of them by means of spectroscopic studies. These dimeric chelates, (NiL$_2$·H$_2$O)$_2$ were stable in solid state, however they disproportionated in non-coordinating solvents to afford dimeric monohydrates, Ni$_2$L$_4$·H$_2$O, and monomeric dihydrates, NiL$_2$·2H$_2$O. DTA studies show that these monohydrates dehydrate in two steps and that the temperature of dehydration decreases in the order of the ligands, DNPM, DNBM, DIBM, DIVM, and DNCM. The dehydrated chelates are green in the neighborhood of room temperature while they changed into red at an elevated temperature. This thermochromism indicates that the chelates are in the trimeric octahedral form at low temperature and in monomeric tetra-coordinated square planar form at high temperature. On the other hand a nickel(II) chelate of 2,2,6,6-tetramethylheptane-3,5-dione (DPVM) was obtained as a penta-coordinated monodioxane adduct from aqueous dioxane. The coordinated dioxane was readily released to afford a monomeric tetra-coordinate square planar, red colored complex, Ni(DPVM)$_2$.

Extensive investigations have been worked out on nickel(II) chelates of pentane-2,4-dione, of which bis-(pentane-2,4-dionato)nickel(II) dihydrate can be most easily obtained. The coordination structure of this dihydrate is known to be similar to that of bis(pentane-2,4-dionato)cobalt(II) dihydrate,[3] in which two water molecules coordinate to the central cobalt ion in a planar bis(pentane-2,4-dionato)cobalt unit on both sides along z axis.[4]

It is also well known that the dehydration of this chelate affords the anhydrous trimeric chelate, in which nickel ion is octahedrally coordinated.[5] However, when the terminal methyl groups in pentane-2,4-dione are replaced with *t*-butyl groups, the steric hindrance among the substituents completely prevents trimerization and the chelate behaves as a spin-paired, red colored planar chelate.[6] This structure is maintained in solid state as well as in non-coordinating solvents.

In this connection, it is of great interest to investigate on the chelating behavior and the properties of the chelates of pentane-2,4-dione derivatives, in which the terminal methyl groups are replaced by various alkyl groups such as ethyl, *n*-propyl, isopropyl, isobutyl, *tert*-

1) Contribution No. 253 from the Departemnt of Organic Synthesis, Kyushu University.

2) To whom correspondences should be addressed.

3) R. H. Holm and F. A. Cotton, *J. Phys. Chem.*, **65**, 321 (1961).

4) G. J. Bullen, *Acta Crystallogr.*, **12**, 703 (1959).

5) G. J. Bullen, R. Mason, and P. Pauling, *Nature*, **189**, 291 (1961).

6) F. A. Cotton and J. P. Fackler, Jr., *J. Amer. Chem. Soc.*, **83**, 2818 (1961).

Table 1. Analyses of 1,3-dialkylsubstituted acetylacetone

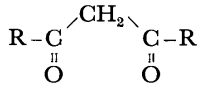

ligand	R	formula	C % found	C % calcd	H % found	H % calcd
DNPM	$-CH_2CH_3$	$C_7H_{12}O_2$	65.50	65.63	9.50	9.37
DNBM	$-CH_2-CH_2-CH_3$	$C_9H_{16}O_2$	69.00	69.24	10.31	10.25
DIBM	$-CH(CH_3)_2$	$C_9H_{16}O_2$	68.70	69.24	10.36	10.25
DIVM	$-CH_2-CH(CH_3)_2$	$C_{11}H_{20}O_2$	71.95	71.76	11.07	10.86
DPVM	$-C(CH_3)_3$	$C_{11}H_{20}O_2$	71.77	71.76	10.96	10.86
DNCM	$-CH_2-CH_2-CH_2-CH_2-CH_3$	$C_{13}H_{24}O_2$	73.62	73.61	11.51	11.32

Table 2. Elemental analyses, appearance, recrystalyzation solvents and percent yields of the bis(dialkylacetylacetonato)nickel(II) monohydrate

complex	molecular formula	Elemental analyses C % found	C % calcd	H % found	H % calcd	recrystalyzation solvent	appearance	Yield (%)
$Ni(DNPM)_2 \cdot H_2O$	$C_{14}H_{24}O_5Ni$	50.90	50.81	7.44	7.25	C_2H_5OH	light green needles	60
$Ni(DNBM)_2 \cdot H_2O$	$C_{18}H_{32}O_5Ni$	56.49	55.87	8.52	8.27	C_2H_5OH	light green[a] needles	95
$Ni(DIBM)_2 \cdot H_2O$	$C_{18}H_{32}O_5Ni$	56.03	55.87	8.70	8.27	C_2H_5OH	light green plates	85
$Ni(DIVM)_2 \cdot H_2O$	$C_{22}H_{40}O_5Ni$	60.40	59.66	9.21	9.03	C_2H_5OH	light green needles	100
$Ni(DPVM)_2 \cdot$dioxane	$C_{26}H_{46}O_6Ni$	60.62	60.87	9.05	8.97	C_2H_5OH+dioxane or dioxane	light blue needles	100
$Ni(DNCM)_2 \cdot H_2O$	$C_{26}H_{48}O_5Ni$	62.54	62.59	9.70	9.62	C_2H_5OH	light green[a] needles	95

a) These were exist as needles at the low temperature in the ethanol, however, melted at the room temperature.

butyl, and *n*-pentyl group.

Although these ligands are reported in the literature, and some of their nickel(II) chelates have been synthesized, very few detailed investigations have been carried out.[6] This paper is to report on the synthesis of nickel(II) chelates of the following six ligands; heptane-3,5-dione (or dipropionylmethane, DNPM), nonane-4,6-dione (or di-*n*-butyrylmethane, DNBM), 2,6-dimethylheptane-3,5-dione (or diisobutyrylmethane, DIBM), 2,8-dimethylnonane-4,6-dione (or diisovalerylmethane, DIVM), 2,2,6,6-tetramethylheptane-3,5-dione(or dipivaloylmethane, DPVM) and tridecane-6,8-dione(or di-*n*-caproylmethane, DNCM), and on the structural studies concerning these chelates chiefly by spectroscopic methods.

Experimental

Synthesis of Ligands. The ligands were synthesized by the standard procedure described by Adams and Hauser[7] with slight modifications. The corresponding methyl-ketone and ethyl ester were condensed in the presence of sodium amide, and the resulting crude diketone was isolated as a copper(II) chelate, from which the diketone was liberated by decomposing with 10% sulfuric acid, followed by extraction with ether and fractionation. The results of elemental analyses of the ligands are summarized in Table 1.

Preparation of Nickel(II) Chelates. All chelates were prepared by the procedure as described below. To a solution containing 1.5 g (0.005 mol) of nickel nitrate hexahydrate in 12 m*l* of water and 8 m*l* of methanol, was added a solution of 0.01 mol of a ligand in 5 m*l* of methanol. Then, 6 m*l* of 1.5M sodium hydroxide solution was added to the mixture with vigorous stirring, from which green complex precipitated immediately. The product was recrystallized from an appropriate solvent and was dried over phosphorous pentoxide in vacuum at room temperature. The appearance, solvent used for recrystallization, yield, and the result of elemental analyses of each chelate are summarized in Table 2.

A careful dehydration of the hydrated chelates at about 180°C in vacuum afforded the anhydrous chelates, which were also green and were hygroscopic.

Spectral Measurements. Solid reflectance spectra were measured with a Hitachi EPU-2A spectrophotometer with

7) J. T. Adams and C. R. Hauser, *J. Amer. Chem. Soc.*, **66**, 1220 (1944).

a diffuse reflectance attachment. Absorption spectra in visible and ultraviolet regions were measured with a Hitachi EPS-2 and Hitachi 124 spectrophotometer respectively. Visible absorption spectra of the anhydrous chelates in toluene at elevated temperature were measured with a Hitachi 139 spectrophotometer with a high temperature attachment. Infrared absorption spectra were measured with a JASCO-DS-403G spectrophotometer on Nujol mull samples.

Molecular Weight Measurement. Molecular weight of the chelates was determined in toluene at 37°C with a Mechlolab's 301A vapour pressure osmometer. The standard material for the caribration curve was $Cu(DNBM)_2$, which was analytically pure and it's molecular weight was checked previously using α-naphthol as a primary standard.

Results and Discussion

Structural Study on DNPM, DNBM, DIBM, DIVM-, and DNCM Chelates. The result of elemental analysis of the nickel(II) chelates (except dipivaloylmethanato-nickel to be described later) agrees well with a molecular formula of $NiL_2 \cdot H_2O$ where L represents a β-diketonato monoanion. A sharp, relatively strong absorption band in 3350—3400 cm^{-1} region is observed in IR spectra of these chelates as shown in Fig. 1, indicating the presence of coordinated water. Although the above results seem to suggest a penta-coordinate structure, the diffuse reflectance spectra of solid samples, which are shown in Fig. 2 and Table 3, are very much similar to that of bis(pentane-2,4-dionato)nickel(II) dihydrate which is a typical hexa-coordinate octahedral

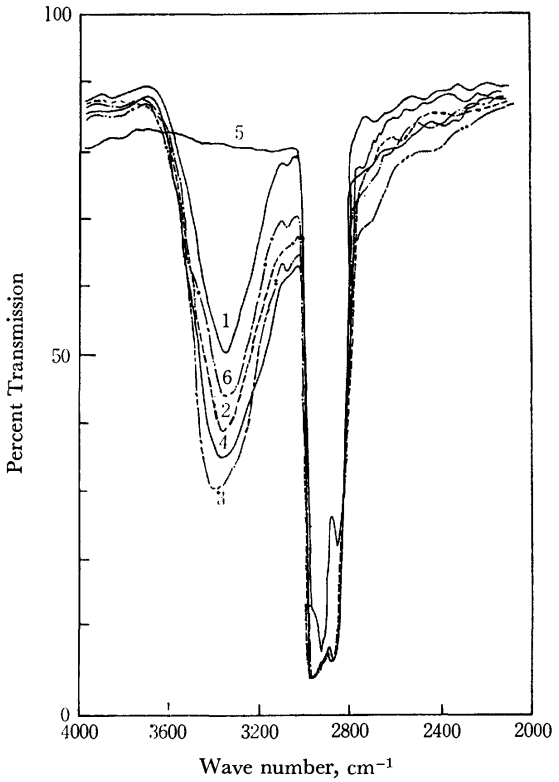

Fig. 1. Infrared spectra of the $Ni(DNPM)_2 \cdot H_2O$ (1), $Ni(DNBM)_2 \cdot H_2O$ (2), $Ni(DIBM)_2 \cdot H_2O$ (3), $Ni(DIVM)_2 \cdot H_2O$ (4), $Ni(DPVM)_2$·dioxane (5) and $Ni(DNCM)_2 \cdot H_2O$ (6) in 4000—2000 cm^{-1} region. (In Nujol mull)

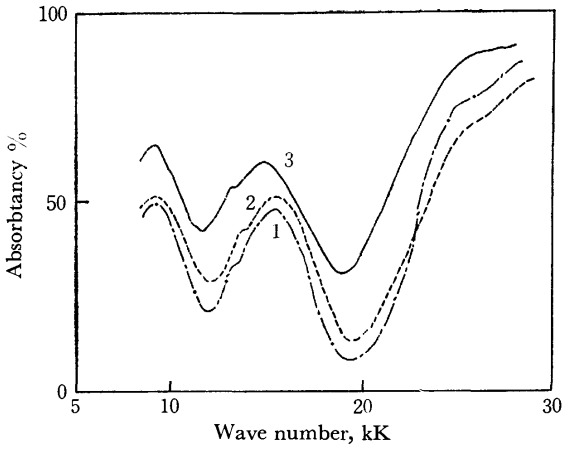

Fig. 2. Electronic reflectance spectra of the solid $Ni(DNPM)_2 \cdot H_2O$ (1), $Ni(DIBM)_2 \cdot H_2O$ (2) and $Ni(DIVM)_2 \cdot H_2O$ (3).

Table 3. Spectroscopic data for $NiL_2 \cdot H_2O$ (L=DNPM, DNBM, DIBM, DIVM) and NiL_2·dioxane (L=DPVM)

L	solid. ν_{max} (cm^{-1})	in toluene ν_{max} (cm^{-1})	ε_{max}
DNPM	9200	8340	6.9
	13000 (sh)	13200 (sh)	3.8
	15400	15300	6.3
DNBM		8320	5.8
		13300 (sh)	3.5
		15400	6.1
DIBM	9100	8340	3.9
	13300 (sh)	13200 (sh)	2.2
	15400	15400	4.3
DIVM	9100	8500	5.5
	12900 (sh)	13200 (sh)	3.7
	15300	15200	6.8
DNCM		8600	4.5
		13200 (sh)	2.9
		15200	4.9
DPVM	7900		
	10000 (sh)		
	11000		
	13500	18800	45.2
	16400		

nickel(II) chelate. Thus, it is reasonable to assume that the chelates are of dimeric structure, in which two $NiL_2 \cdot H_2O$ units are joined by two bridging oxygens as shown in Fig. 5 (I). Other possibility such as the double deck structure proposed for DNBM chelate of trimethyl platinum(IV),[8] can not be accepted in this case because the ionic radius of nickel(II) ion is too small in comparison with the van der Waals radius of terminal alkyl groups which prevents the approach of second unit from above or below of the nickel(II) ion in the first unit.

It has been known that the chloroform solution of trimeric bis(pentane-2,4-dionato)nickel(II) shows two bands in ultraviolet region at 33800 and 37700 cm^{-1}, and they merge into a single band at 34000 cm^{-1} when

8) A. G. Swallow and M. R. Truter, *Proc. Roy. Soc.* (London), **254A**, 205 (1960).

ethanol is added to the chloroform solution.[9] According to Cotton and Fackler,[6] this spectral change is related with the coordination of ethanol to nickel ion resulting in the depolymerization of trimeric nickel chelate to give a mononuclear $NiL_2 \cdot 2EtOH$. The two bands of the trimeric form are assigned to two types of chelate rings, *i.e.* one is the non-bridging chelate ring and the other the bridging chelate ring, respectively. The single band observed in the mononuclear ethanol-adduct is, as being obvious from its coordination structure, ascribable to the non-bridging chelate ring.

Table 4. Ultraviolet spectroscopic data for $NiL_2 \cdot H_2O$ (L=DNPM, DNBM, DIBM, DIVM) and $NiL_2 \cdot$dioxane (L=DPVN)

L	in cyclohexane		in 10% ethanol+ 90% cyclohexane	
	ν_{max} (cm^{-1})	ε_{max}	ν_{max} (cm^{-1})	ε_{max}
DNPM	33200	11500	33800	14200
	36600	10300		
DNBM	33000	12100	33700	13900
	36500	10600		
DIBM	33000	11600	36400	14600
	37200	16300		
DIVM	32700	14200	33600	17500
	36600	18200		
DPVM	37300	32600	36500	17000
$Ni(AA)_2$[7]	33800[a]	12400	34000[b]	23700
	37700	15200		

a) in chloroform. b) in ethanol.

As shown in Table 4, the UV spectra of the 1,5-dialkyl-2,4-pentanedionatonickel(II) chelates in cyclohexane solutions are very much similar to that of trimeric bis(pentane-2,4-dionato)nickel(II) in chloroform. The spectral change which is observed when ethanol is added to these cyclohexane solutions is also quite similar to that of the pentane-2,4-dionato chelate described above. The result, combined with their compositions and the spectral evidences in the visible and infrared regions, supports strongly the dimeric structure of bis(1,5-dialkyl-2,4-pentanedionato)nickel of type $NiL_2 \cdot H_2O$.

Table 5. Molecular weights of $NiL_2 \cdot H_2O$ in toluene at 37°C

molecular formula	calcd	found	found/calcd
$(Ni(DNPM)_2 \cdot H_2O)_2$	661.82	532	0.81
$(Ni(DNBM)_2 \cdot H_2O)_2$	773.82	588	0.77
$(Ni(DIBM)_2 \cdot H_2O)_2$	773.82	618	0.80
$(Ni(DIVM)_2 \cdot H_2O)_2$	885.86	575	0.65
$(Ni(DNCM)_2 \cdot H_2O)_2$	997.82	708	0.71

The molecular weights of these chelates, however, show somewhat odd values in toluene at 37°C as summarized in Table 5. The values are about 0.75± 0.1 of dimeric molecular weights. Thus, a certain kind of rearrangement of the chelate might occur even in a

9) R. H. Holm and F. A. Cotton, *J. Amer. Chem. Soc.*, **80**, 5658 (1958).

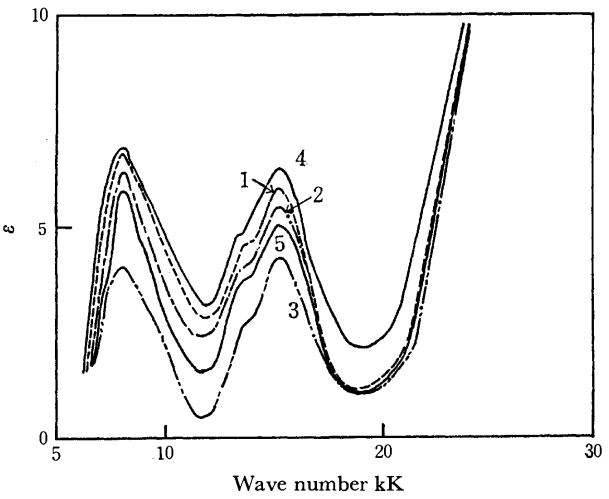

Fig. 3. Electronic absorption spectra of the $Ni(DNPM)_2 \cdot H_2O$ (1), $Ni(DNBM)_2 \cdot H_2O$ (2), $Ni(DIBM)_2 \cdot H_2O$ (3), $Ni(DIVM)_2 \cdot H_2O$ (4) and $Ni(DNCM)_2 \cdot H_2O$ (5) in toluene.

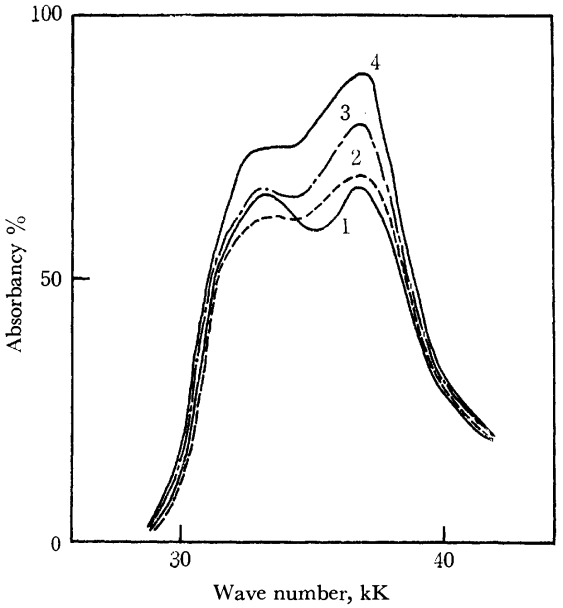

Fig. 4. Time dependency of UV absorbancy of the $Ni(DIVM)_2 \cdot H_2O$ in cyclohexane.
$Ni(DIVM)_2 \cdot H_2O = 9.56 \times 10^{-5}$M
1:3 min, 2:6 min, 3:17 min, 4:40 min

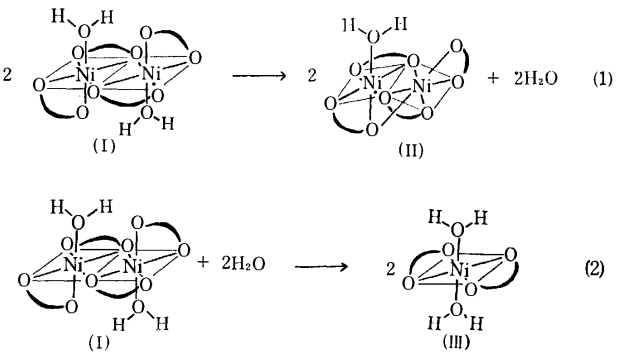

Fig. 5. Proposed dimeric structure and their rearrangements in non-coordinative solvents.

non-coordinating solvent such as toluene, while the octahedral structure is retained as suggested by the visible absorption spectra which are shown in Fig. 3. The structural change of the chelate after dissolution in such solvents can be traced also by observing the time dependence of the UV spectral change in cyclohexane which is also one of the non-coordinating solvents, as shown in Fig. 4. Although we are not successful in identifying the rearrangement products in solution, one of the possible scheme of the rearrangement may be such as shown in Fig. 5. As to the binuclear chelate (II) in Fig. 5, a similar structure was assigned to pyridine-tetrakis(pentane-2,4-dionato)dinickel, $[(NiL_2)_2 \cdot Py]$, which was isolated as a reaction intermediate when trimeric nickel chelate was dissolved in pyridine.[10] If it is assumed that the reactions (1) and (2) proceed until completion, three moles of $(NiL_2 \cdot H_2O)_2$ give each two moles of (II) and (III), thus the resulting solution giving an apparent molecular weight of three quarters of the formular weight of $(NiL_2 \cdot H_2O)_2$.

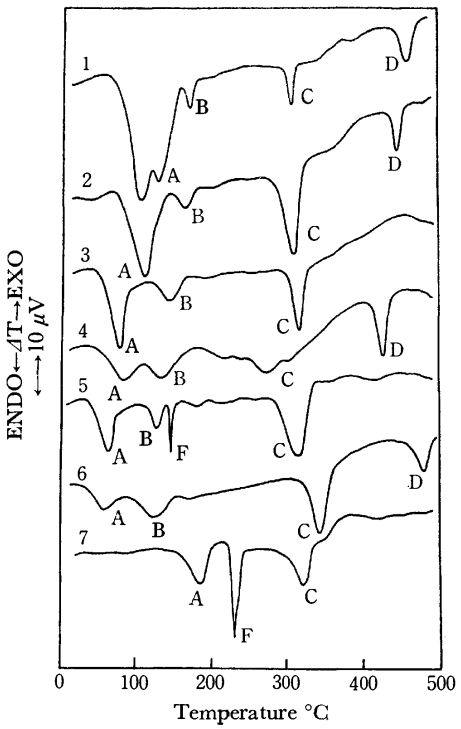

Fig. 6. DTA curves of nickel chelates in nitrogen atmosphere.
1: $Ni(AA)_2 \cdot 2H_2O$, 2: $Ni(DNPM)_2 \cdot H_2O$,
3: $Ni(DNBM)_2 \cdot H_2O$, 4: $Ni(DIBM)_2 \cdot H_2O$,
5: $Ni(DIVM)_2 \cdot H_2O$, 6: $Ni(DNCM)_2 \cdot H_2O$,
7: $Ni(DPVM)_2$·dioxane
Heating rate=15°C/min.

In addition to the structural change in solution, it is of interest to see if the dehydration of binuclear $NiL_2 \cdot H_2O$ chelate affords polymeric anhydrous nickel(II) chelate in solid state in a similar manner to the case of pentane-2,4-dionato chelate. In this connection, the dehydration process of the solid chelates was followed by differential thermal analysis (DTA) in nitrogen atmosphere with combined use of infrared spectroscopy. Although thermogravimetric analysis was also attempted, the present nickel chelates sublimed so easily, that no quantitative result on dehydration process could be obtained. As shown in Fig. 6, the DTA curves of the nickel chelates are characterized with four endothermic peaks, A, B, C, and D. When DTA was carried out in air, intense exothermic peak was observed generally in the range of 300—380°C which could be assigned to the oxidative decomposition of the sample. Of the four peaks, the first two seem to be related with the dehydration of the chelate, since the sample decreased the intensity of ν_{OH} band at 3300 cm^{-1} region when it was heated above the temperature corresponding to the peaks A and B. The resulting nickel chelate, which was still green, is considered to be polymeric structure such as trimeric bis(pentane-2,4-dionato)nickel(II). The latter two peaks, C and D, may be related with some sort of structural change of anhydrous chelates, however, little more informations could be obtained except that all four peaks were found to be irreversible ones. It is interesting to note, with this respect, that the respective temperatures corresponding to the peaks A and B decrease with increasing size of alkyl groups introduced to pentane-2,4-dione. This result may be interpreted as an effect of the hydrophobic nature of alkyl groups surrounding the coordinated water molecule. It is also safe to conclude that the replacement of terminal methyl groups of pentane-2,4-dione with higher alkyl groups except *t*-butyl group, is not a decisive factor to prevent the formation of an oxygen-bridged polymeric octahedral nickel chelate. An additional peak F of $Ni(DIVM)_2 \cdot H_2O$ and $Ni(DPVM)_2$·dioxane, was definitely due to the melting of samples as verified

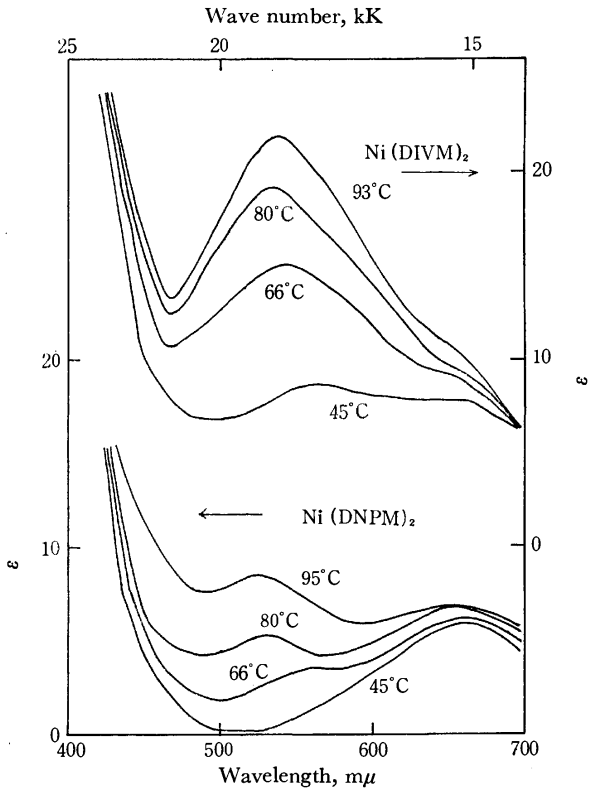

Fig. 7. Visible spectra of $Ni(DNPM)_2$ and $Ni(DIVM)_2$, in toluene at four temperatures, concentration about 1/100M.

10) J. P. Fackler, Jr., *J. Amer. Chem. Soc.*, **84**, 24 (1962).

by melting point measurement.

As described in the experimental section, the anhydrous octahedral green nickel(II) chelates could be obtained by heating the hydrated chelates in vacuum. Although the molecular weights of the anhydrous chelates at room temperature could not be determined because of the experimental difficulty, the spectral evidence for the octahedral structure and the metal-ligand ratio strongly suggest the polymeric structure similar to bis(pentane-2,4-dioanto)nickel(II).

Absorption spectra were measured on the anhydrous chelates of the present ligands in toluene over the temperature range of 45—95°C. Typical examples are illustrated in Fig. 7. The peak at 650 nm, which is observable at lower temperature, is most distinct for pentane-2,4-dionato chelate, and becomes less distinct when the terminal methyl groups are replaced with bulkier alkyl groups. With elevating temperature, a new peak becomes noticable at around 520 nm and overshadows the peak at 650 nm in the extreme case.

A similar thermochromic effect has been reported by Cotton and Fackler[6] with $Ni(DIBM)_2$, and was rationalized by reversible interconversion between polymeric octahedral and monomeric square planar structures.

The pentane-2,4-dionato- and dipivaloylmethanato chelates, however, show no spectral change in this temperature range; the former shows a single peak at 650 nm while the latter only at 520 nm throughout the temperature elevation. Of the remaining chelates, the spectral changes increase in the order of $Ni(DNPM)_2 < Ni(DNBM)_2 < Ni(DNCM)_2 < Ni(DIVM)_2 < Ni(DIBM)_2$, which parallels to the bulkiness of the terminal alkyl groups. These results clearly indicate that the peak at around 520 nm is assignable to the monomeric square planar structure, while the peak at 650 nm is due to the polymeric octahedral one, and that bulkier alkyl groups introduced on the 1- and 5-positions of pentane-2,4-dione favor the square planar configuration of the nickel chelates. In the extreme case of dipivaloylmethane, which has *t*-butyl groups on the both ends, the nickel chelate, $Ni(DPVM)_2$, takes a square planar structure even at room temperature.

Structural Study on DPVM Chelate. The properties of nickel DPVM chelate are different in many respects from those of other alkyl substituted pentane-2,4-dione. The result of elemental analysis on the light blue chelate agrees with a formula of NiL_2·dioxane. Infrared absorption spectrum also supports the existence of dioxane and the absence of water.

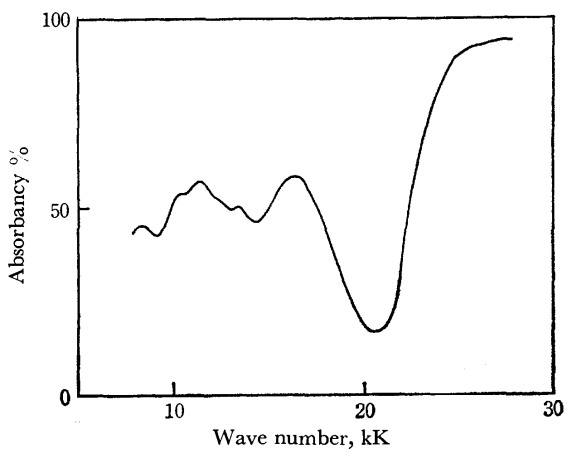

Fig. 8. Electronic reflectance spectrum of the solid $Ni(DPVM)_2$·dioxane.

A diffuse reflectance spectrum of the solid dioxane adduct in visible region which is shown in Fig. 8 and in Table 3, is quite different from the spectra which are typical to octahedral, tetrahedral or planar nickel(II) complexes. According to the result by Ciampolini who analyzed the energy levels of penta-coordinate nickel(II) complex of D_{3h} or C_{4v} symmetry,[11] the spectrum of $Ni(DPVM)_2$·dioxane is similar to that of C_{4v} symmetry, indicating that the chelate is monomeric penta-coordinate square pyramidal structure.

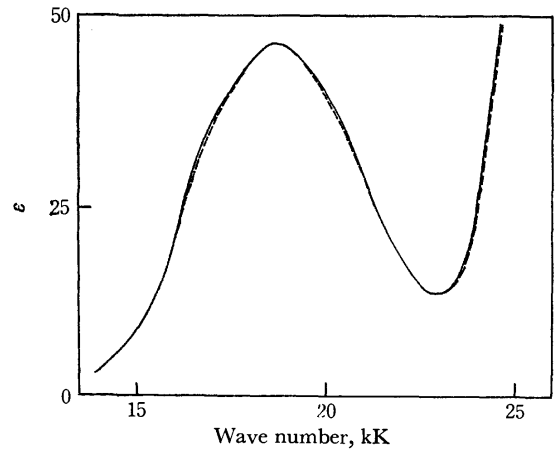

Fig. 9. Electronic absorption spectra of the $Ni(DPVM)_2$·dioxane (----) and $Ni(DPVM)_2$(——) in tolene.

When the light blue dioxane adduct is dissolved in toluene, it turned red, giving a spectrum as shown in Fig. 9. If the dioxane adduct is heated at 100°C in vacuum, it afforded a red chelate of the formula of $Ni(DPVM)_2$ with a monomeric molecular weight. The visible absorption spectrum of the toluene solution of red chelate was found to be identical with that obtained by dissolving light blue dioxane adduct in toluene as shown in Fig. 9. According to Cotton, this spectrum can be assigned to a diamagnetic tetra-coordinate square planar complex.[6] Thus, the dissolution of dioxane adduct in non-coordinating solvent at room temperature, results in the dissociation of coordinated dioxane, and no further rearrangement of the chelate could be observed.

Interestingly, $Ni(DPVM)_2$ does not accept coordinated water but does dioxane which is known to be much weaker ligand than water. A DTA study indicated that the coordinated dioxane dissociated at 188°C (peak A) and the resulting $Ni(DPVM)_2$ melted at 230°C (peak F). The preference of dioxane to water molecule as a secondary ligand to $Ni(DPVM)_2$ is again indicative that the hydrophobic dioxane molecule may receive less repulsion from the neighboring *t*-butyl groups than does water molecule. The relative easiness of dissociation in non-coordinating solvents, which is contrary to the result observed by DTA study, may be

11) C. Ciampolini, *Inorg. Chem.*, **5**, 35 (1966).

explained by the solvation of dissociated dioxane. The formation of red planar chelate after the dissociation of dioxane also suggests that the terminal *t*-butyl groups are bulky enough to prevent the formation of oxygen-bridged polymeric structure even at room temperature.

The authors are grateful to Ministry of Education for grant-in-aid for scientific researches.

BULLETIN OF THE CHEMICAL SOCIETY OF JAPAN, VOL. 45, 1417—1423(1972)

Reaction Rates and Mechanisms of the Formation of Gallium(III), Indium(III), and Thallium(III) Complexes with Semi-Xylenol Orange in Aqueous Solutions

Yoichi KAWAI, Tetsuro TAKAHASHI,* Katsuyuki HAYASHI,** Taira IMAMURA, Hiroaki NAKAYAMA,*** and Masatoshi FUJIMOTO

Department of Chemistry, Faculty of Science, Hokkaido University, Sapporo

(Received September 6, 1971)

The kinetics for the complex formation of Ga(III), In(III), and Tl(III) with Semi-Xylenol Orange (SXO) in acid solutions were studied by stopped-flow technique. Kinetic results are interpreted in terms of a two-step mechanism involving pre-equilibrium. The increase in the reaction rate with decreasing hydrogen ion concentration is interpreted as the sum of several parallel pathways including monohydroxo metal ions and a few charge types of the ligand. The mechanisms and the rates of the three different d^{10}-system metal ions are discussed. The phenomena of the slower increase in absorbance of Ga(III)-SXO complex after the rapid increase and the slow color fading of Tl(III)-SXO complex are also discussed.

Although there have been a large number of investigations on the kinetics of metal complex formation in aqueous solutions,[1,2] relatively meager kinetic data have been reported for trivalent d^{10}-system metal ions.[3-6] This arises mainly from the limited number of simple inorganic or organic ligands suitable for kinetic measurements for Ga(III), In(III), and Tl(III).

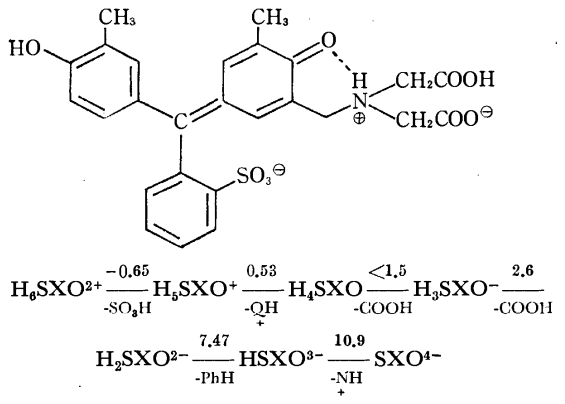

Fig. 1. Semi-Xylenol Orange (SXO) in the form of $[H_3SXO]^-$ and the acid dissociation constants (pK_a).[10]

In the present study, Semi-Xylenol Orange (SXO) has been chosen as a ligand, which forms 1 : 1 complexes with Ga(III), In(III), and Tl(III). The SXO complexes have absorption maxima in the visible range with sufficiently large absorption coefficients (see Fig. 1).

Characteristic rate constants for the water substitution in the inner coordination sphere of aquo-ions are listed[1] as 10^0—10^1, $10^{1.5}$—$10^{2.5}$, and 10^4—10^5 sec^{-1} for Ga(III), In(III), and Tl(III), respectively. These are obtained only from the extrapolation of the rate data for other charge types, by assuming that log k (k: rate constant) correlates linearly with the inverse of ionic radius for non-transition group and d^{10}-system ions. Though divalent d^{10}-metal ions were reported to satisfy the correlation, trivalent d^{10}-metal ions do not necessarily behave in the similar way, as is seen for the correlation of ionization potential and hydration energy with ionic radius.[7]

Experimental

Materials. The solution of Ga(III) perchlorate was prepared by dissolving metallic gallium (99.99% Wako) in perchloric acid (Reagent Grade, Wako). Aqueous In(III) perchlorate was prepared by dissolving indium oxide (Koso) in slight excess of perchloric acid. Aqueous Tl(III) perchlorate was made by electrolytically oxidizing Tl(I) perchlorate[8] which was prepared from thallium(I) acetate (BDH) and recrystallized.

* Present address: Yoshitomi Pharmaceutical Industries, Ltd., Osaka.

** Present address: Nisso Smelting Co., Bandai, Fukushima.

*** Present address: Kagawa Nutrition College, Sakado-machi, Saitama.

1) M. Eigen, *Pure Appl. Chem.*, **6**, 97 (1963).
2) A. McAuley and J. Hill, *Quart. Rev.*, **23**, 18 (1969).
3) G. Geier, *Ber. Bunsenges. Physik. Chem.*, **69**, 617 (1965).
4) J. Miceli and J. Stuehr, *J. Amer. Chem. Soc.*, **90**, 6967 (1968).
5) D. Fiat and R. E. Connick, *ibid.*, **88**, 4754 (1966).
6) N. D. Lukomskaya, T. V. Malikova, and K. B. Yatsimirskii, *Zh. Neorg. Khim.*, **12**, 2462 (1967).

7) Within a non-transition group the heat of hydration and the ionization potential vary inversely with the ionic radius. Crystal field correction acts well for the first transition series. On the other hand the correlation is almost worth nothing for trivalent d^{10}-system ions.

8) G. Biedermann, *Arkiv Kemi*, **5**, 441 (1953).

The concentration of each metal ion in the stock solution was standardized by titrating with EDTA.[9]

Sodium perchlorate (Reagent Grade, Koso) was dissolved in distilled water. In order to remove the trace amounts of impurities the concentrated aqueous solution was filtered through a quantitative filter paper after being kept several days. The concentration was determined by passing an aliquot of the solution through a column of cation-exchange resin (Dowex 50W-X8) in the hydrogen form and titrating the effluent with standard sodium hydroxide.

SXO was synthesized from *o*-Cresol Red, iminodiacetic acid and formaldehyde by the Mannich condensation and purified by means of cellulose column chromatography.[10] The acid form of SXO was obtained by passing the fraction of SXO through a column of cation-exchange resin in the hydrogen form. The purity of the SXO was checked by paper chromatography, and only one spot was observed. The elemental analysis agrees with the results of the previous workers.[10]

Found: C, 56.22; H, 5.39; N, 2.24; S, 4.90%. Calcd for $C_{26}H_{25}O_9NS \cdot H_2O$: C, 57.24; H, 4.99; N, 2.57; S, 5.89%.

Procedure. A Hitachi spectrophotometer model EPS-3T was used for spectral measurements. Yanagimoto SPS-1 Stopped-Flow apparatus with a 4-jet mixing chamber and 2 mm or 10 mm optical cell was used for kinetic measurements. The changes in absorbance were photographed on the storage screen of oscilloscope.

All measurements were made at 25.0±0.2°C. Hydrogen ion concentration and ionic strength were adjusted using $HClO_4$ and $NaClO_4$. The pH values were measured with a Horiba pH meter Model P calibrated with a standard buffer solution.

Results

Two forms of complexes of SXO with the metals M(III) were observed in the different pH region by the spectroscopic measurements. The composition of these complexes in solutions was determined to be 1 : 1 by means of the continuous variation method. Absorption maxima of the acid-form complexes are at 532 nm (pH=1.60), 529 nm (pH=3.10) and 538 nm ([H]=1.0M) for Ga(III), In(III), and Tl(III), respectively, and those of the alkaline-form complexes are at 470 nm (pH=4.0), 480 nm (pH=4.50), and 492 nm (pH=6.0) for Ga(III), In(III), and Tl(III), respectively. In order to minimize hydrolysis and polymerization of the metal ions, kinetic measurements were performed in the acid media by following the absorbance at the λ_{max} of the acid-form complex.

When metal(III) ion concentrations were at least in 10-fold excess over those of SXO, a pseudo-first-order kinetics was obeyed in most cases. Pseudo-first-order rate constants k_{obs} were evaluated from the slopes of such plots as

$$k_{obs} = -\mathrm{d} \ln (D_\infty - D_t)/\mathrm{d}t$$

where D_∞ and D_t represent the absorbances at the end of the reaction and at time t respectively. No significant dependence was observed for k_{obs} on the initial concentration of SXO. Plots of the observed pseudo-first-order rate constant k_{obs} against [M(III)] for Ga(III) and In(III) are not straight lines but curves (Figs. 2 and 3). Assuming the one step mechanism such plots should give a straight line with a slope k_f and an intercept k_r,

$$\mathrm{M(III)} + \mathrm{SXO} \underset{k_r}{\overset{k_f}{\rightleftharpoons}} \mathrm{M(III)SXO}$$

$$k_{obs} = k_f[\mathrm{M(III)}] + k_r \qquad (1)$$

The curves can thus be interpreted in terms of the two-

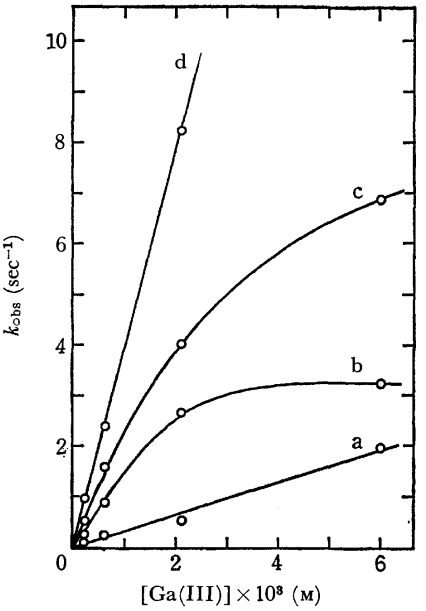

Fig. 2. Plot of k_{obs} *vs.* total concentration of Ga(III) at various hydrogen ion concentrations, 25.0°C and ionic strength of 0.1.
(a): pH=2.00±0.02; (b): pH=2.40±0.02; (c): pH=2.65±0.02; (d): pH=2.90±0.02.

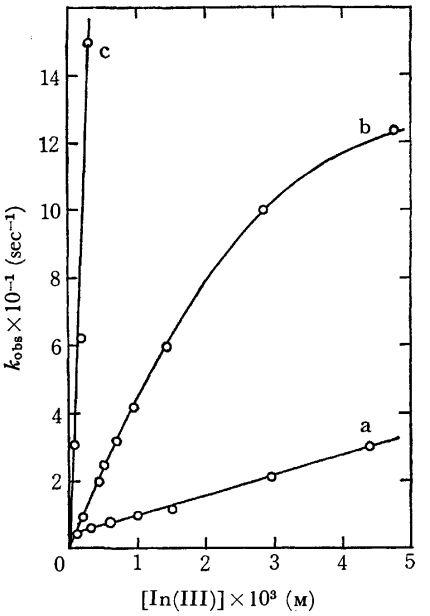

Fig. 3. Plot of k_{obs} *vs.* total concentration of In(III) at various hydrogen ion concentrations, 25.0°C and ionic strength of 0.1.
(a): pH=1.37±0.02; (b): pH=1.96±0.02; (c): pH=3.00±0.02.

9) G. Schwarzenbach and H. Flaschka, "Die Komplexometrische Titration," 5th ed., F. Enke, Stuttgart (1965).
10) M. Murakami, T. Yoshino, and S. Harasawa, *Talanta*, **14**, 1293 (1967).

step mechanisms.

$$M(III) + SXO \overset{K_p}{\rightleftharpoons} M(III)\cdots SXO$$

(K_p: pre-equilibrium constant)

$$M(III)\cdots SXO \underset{\overleftarrow{k}}{\overset{\vec{k}}{\rightleftharpoons}} M(III)SXO$$

Since the metal ion is in large excess over SXO, and is regarded as constant during the reactions, k_{obs} can be written as a function of [M(III)]

$$k_{obs} = \frac{\vec{k}K_p[M(III)]}{1+K_p[M(III)]} + \overleftarrow{k} \qquad (2)$$

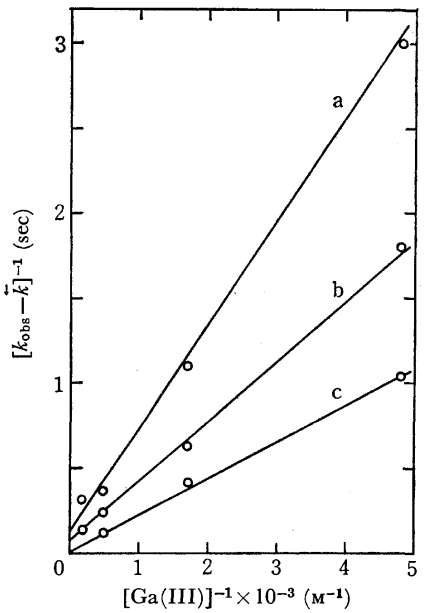

Fig. 4. Plot of $1/(k_{obs}-\overleftarrow{k})$ *vs.* inverse of the total concentration of Ga(III) for Ga(III)-SXO at various hydrogen ion concentrations.
(a): pH=2.40±0.02; (b): pH=2.65±0.02; (c): pH=2.90±0.02.

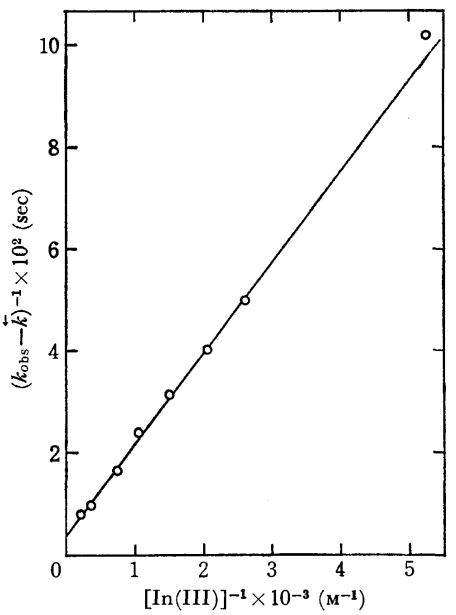

Fig. 5. Plot of $1/(k_{obs}-\overleftarrow{k})$ *vs.* inverse of the total concentration of In(III) for In(III)-SXO at pH=1.96±0.02.

Figures 4 and 5 show a linear plot of $1/(k_{obs}-\overleftarrow{k})$ *versus* $1/[M(III)]$ for Ga(III) and In(III) respectively. We have for the present no evidence of the actual structure of the intermediate M(III)···SXO; it may or may not be so-called ion pair.

If the M(III) concentration is sufficiently low, namely $1 \gg K_p[M(III)]$, Eq. (2) is reduced to Eq. (1) (namely $\vec{k}K_p = k_f$ and $\overleftarrow{k} = k_r$), and the plot of k_{obs} *versus* [M(III)] becomes linear. Actually in the case of Tl(III), plots of k_{obs} against [Tl(III)] were linear under the experimental condition (Fig. 6).

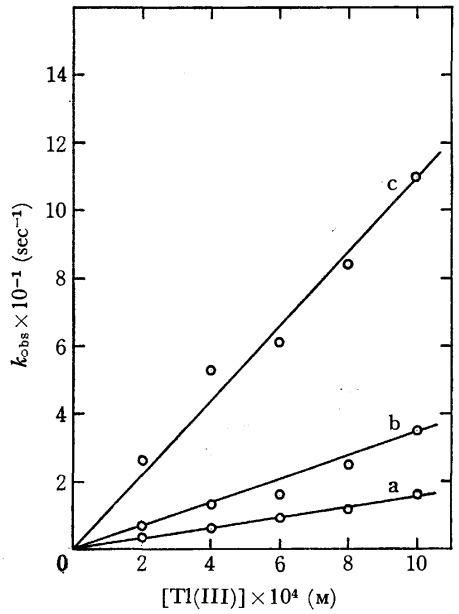

Fig. 6. Plot of k_{obs} *vs.* total concentration of Tl(III) at 25.0°C, ionic strength 2.0 and at various hydrogen ion concentrations.
(a): [H]=0.5M; (b): [H]=0.3M; (c): [H]=0.1M.

In the present work the values of k_f for Ga(III), In(III), and Tl(III) are discussed. It is difficult to discuss k_r, as the plots of k_{obs} *versus* [M(III)] have intercepts almost near the origin in most cases. This is consistent with the large value of apparent stability constants K_c=[M(III)SXO]/[M(III)][SXO]. The apparent stability constants are 1.4×10^5M (pH=2.1), 1.0×10^5M (pH=3.0), and 7.9×10^5M ([H]=5×10^{-2}M) for Ga(III), In(III), and Tl(III), respectively.

The increase of k_f with decreasing [H] is interpreted by considering the acid dissociation of aquo ion M^{3+} and SXO.

$$M(OH_2)_n^{3+} \rightleftharpoons M(OH_2)_{n-1}(OH)^{2+} + H^+ \qquad K_{a1}$$

$$M(OH_2)_{n-1}(OH)^{2+} \rightleftharpoons M(OH_2)_{n-2}(OH)_2^{+} + H^+ \qquad K_{a2}$$

$$H_6SXO^{2+} \rightleftharpoons H_5SXO^{+} + H^+ \qquad K_1$$

$$H_5SXO^{+} \rightleftharpoons H_4SXO + H^+ \qquad K_2$$

$$H_4SXO \rightleftharpoons H_3SXO^{-} + H^+ \qquad K_3$$

$$H_3SXO^{-} \rightleftharpoons H_2SXO^{2-} + H^+ \qquad K_4$$

All the possible chemical species and equilibria are summarized above, polynuclear hydroxo complexes being neglected under the experimental conditions.[12] Second-order rate constants are defined as follows;

$$\begin{cases} M^{3+} + H_6SXO^{2+} \xrightarrow{k_{11}} MOH^{2+} + H_6SXO^{2+} \xrightarrow{k_{21}} M(OH)_2^{+} + H_6SXO^{2+} \xrightarrow{k_{31}} \\ M^{3+} + H_5SXO^{+} \xrightarrow{k_{12}} MOH^{2+} + H_5SXO^{+} \xrightarrow{k_{22}} M(OH)_2^{+} + H_5SXO^{+} \xrightarrow{k_{32}} \\ M^{3+} + H_4SXO \xrightarrow{k_{13}} MOH^{2+} + H_4SXO \xrightarrow{k_{23}} M(OH)_2^{+} + H_4SXO \xrightarrow{k_{33}} \\ M^{3+} + H_3SXO^{-} \xrightarrow{k_{14}} MOH^{2+} + H_3SXO^{-} \xrightarrow{k_{24}} M(OH)_2^{+} + H_3SXO^{-} \xrightarrow{k_{34}} \\ M^{3+} + H_2SXO^{2-} \xrightarrow{k_{15}} MOH^{2+} + H_2SXO^{2-} \xrightarrow{k_{25}} M(OH)_2^{+} + H_2SXO^{2-} \xrightarrow{k_{35}} \end{cases}$$

The proton transfer of SXO was found to proceed fast as compared to the complex formation, as in the time range of complex formation no relaxation was observed by the pH-jump on mixing SXO with perchloric acid. The hydrolysis of M(III) is known to be fast as compared to the complex formation reactions.[11] Acid dissociation constants of SXO were reported to be $10^{+0.65}$, $10^{-0.53}$, $10^{-1.5}$, and $10^{-2.6}$M for K_1, K_2, K_3, and K_4 respectively (0.1M KNO_3, 25°C).[10]

Ga(III)-SXO. The acid dissociation constants of Ga(III) are reported to be $K_{a1}=10^{-2.8}$M and $K_{a2}=10^{-3.5}$M ($I\rightarrow 0$, 18°C).[12] H_4SXO, H_3SXO^-, and H_2SXO^{2-} are predominant charge types of the ligand under the experimental conditions. The contribution of $Ga(OH)_2^+$ was neglected. Following equation expresses k_f.

$$k_f = [k_{13}[H]^3 + (k_{14}K_3+k_{23}K_{a1})[H]^2 + (k_{15}K_3K_4 + k_{24}K_3K_{a1})[H] + k_{25}K_3K_4K_{a1}]/([H]+K_{a1}) \times ([H]^2+K_3[H]+K_3K_4)$$

In the Fig. 7 $k_f\times([H]+K_{a1})([H]^2+K_3[H]+K_3K_4)$ is plotted against [H][13] to give a straight line. The linearity can be interpreted by assuming that the rate constants k_{25}, and k_{24} and/or k_{15} are sufficiently larger than the others. The term of $k_{25}K_3K_4K_{a1}$ corresponds to the intercept, and the term of $(k_{15}K_3K_4+k_{24}K_3K_{a1})$ to the slope of the plots, so that the values of k_{15} and k_{24} are indistinguishable.[14,15] Following values of k_{15} and k_{24} have been calculated by attributing the slope only to the term $k_{15}K_3K_4$ and to $k_{24}K_3K_{a1}$ respectively: $k_{15}=6.9\times10^2$M^{-1}sec^{-1} and $k_{24}=1.1\times10^3$M^{-1}sec^{-1}. From the intercept k_{25} is obtained as 1.2×10^4M^{-1}sec^{-1}.

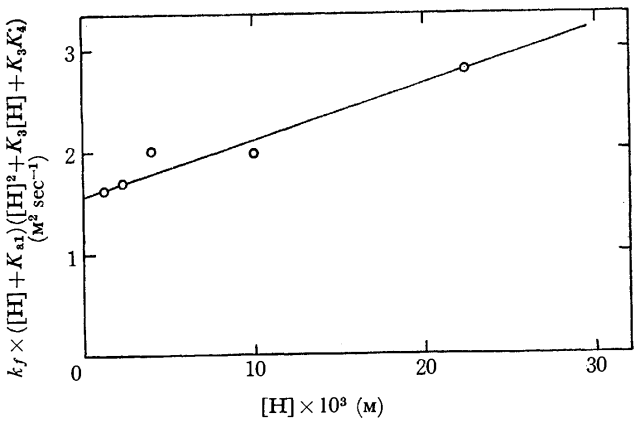

Fig. 7. Plot of $k_f([H]+K_{a1})([H]^2+K_3[H]+K_3K_4)$ *vs.* hydrogen ion concentration for Ga(III)-SXO at 25.0°C and ionic strength of 0.1.

In the case of Ga(III), we shall have to refer to the relatively slow increase in optical density. Exponential changes of optical density was really observed on the oscilloscope as mentioned above, but the absorbance of the complex usually still increases gradually even 2 hr after mixing. Under the extreme condition of high pH and high Ga(III) concentration, exponential signal was not observed as shown in Fig. 8.

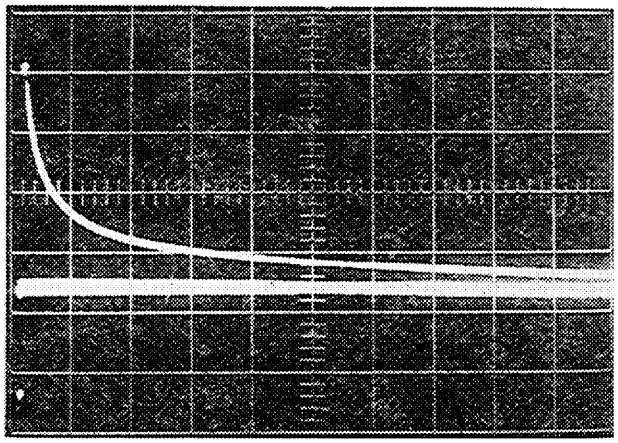

Fig. 8. Stopped-flow signal at 532 nm under the condition of $[Ga(III)]_0=6.0\times10^{-3}$M, $[SXO]_0=2.0\times10^{-5}$M, ionic strength 0.1, pH=2.9 and 25.0°C; vertical scale: absorbance 0.1/div; horizontal scale: 500 msec/div.

In(III)-SXO. The acid dissociation constants of In(III) are reported to be $K_{a1}=10^{-4.4}$M and $K_{a2}=10^{-3.9}$M (3M $NaClO_4$, 25°C).[12] Under the experimental conditions, $In(OH_2)_n^{3+}$ is the predominant chemical species of In(III), and H_4SXO, H_3SXO^-, and H_2SXO^{2-} are the predominant charge types of SXO. If the increase of k_f with decreasing [H] is attributed to the three charge types of the ligand, k_f is expressed as

$$k_f = \frac{k_{13}[H]^2+k_{14}K_3[H]+k_{15}K_3K_4}{[H]^2+K_3[H]+K_3K_4}$$

The plot of $k_f\times([H]^2+K_3[H]+K_3K_4)$ against [H] should show a second order increase, but shows a decrease as shown in Fig. 9. Therefore the reaction mechanism involving only $In(OH_2)_n^{3+}$ should be excluded, and the hydrolysis of $In(OH_2)_n^{3+}$ must be taken into account. The rate constant k_f is expressed

11) P. Hemmes, L. D. Rich, D. L. Cole, and E. M. Eyring, *J. Phys. Chem.*, **74**, 2859 (1970).
12) L. G. Sillén and A. E. Martell ed., "Stability Constants", Special Publication No. 17, The Chemical Society, London (1964).
13) Hydrogen ion concentrations [H] were calculated directly from the observed values of pH without correction of activity coefficients.
14) P. Seewald and N. Sutin, *Inorg. Chem.*, **2**, 643 (1963).
15) D. W. Carlyle and J. H. Espenson, *ibid.*, **6**, 1370 (1967).

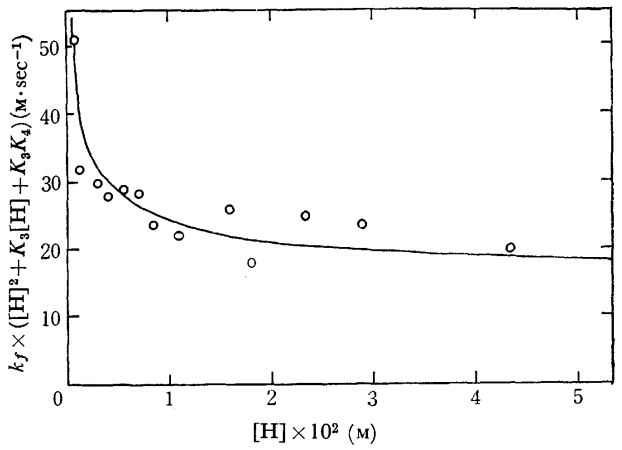

Fig. 9. Plot of $k_f([H]^2+K_3[H]+K_3K_4)$ *vs.* hydrogen ion concentration for In(III)-SXO at 25.0°C and ionic strength 0.1.

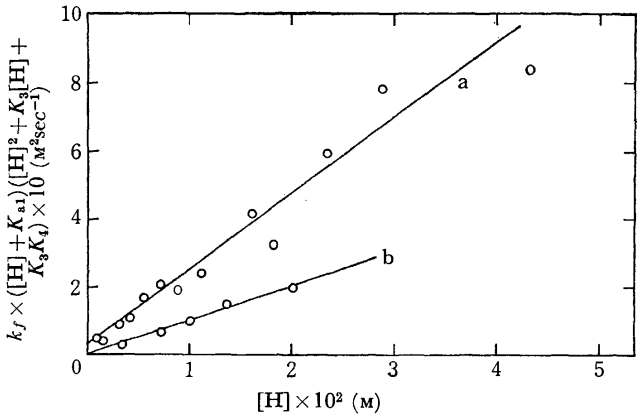

Fig. 10. Plot of $k_f([H]+K_{a1})([H]^2+K_3[H]+K_3K_4)$ *vs.* hydrogen ion concentration for In(III)-SXO at 25.0°C and ionic strength 0.1 (a) and 2.0 (b).

by the same equation as given for Ga(III). In Fig. 10, $k_f\times([H]+K_{a1})([H]^2+K_3[H]+K_3K_4)$ is plotted against [H]. The linearity of the plot is also interpreted by the same assumption as made for Ga(III). The values of k_{25}, k_{24}, and k_{15} are 3.1×10^6, 5.0×10^6, and 2.8×10^5M^{-1}sec^{-1} respectively.

In the case of In(III), absorbance of the complex, remains constant for more than 24 hr.

Tl(III)-SXO. The acid dissociation constants of Tl(III) are quite large as compared to Ga(III) or In(III), namely, $K_{a1}=10^{-1.14}$M and $K_{a2}=10^{-1.49}$M (3M $NaClO_4$, 25°C).[12] Measurements were necessarily made at high hydrogen ion concentrations, and ionic strength was adjusted to 2.0. Under the experimental conditions, H_5SXO^+, H_4SXO, and H_3SXO^- are the predominant charge types of SXO, and we neglected the contribution of $Tl(OH)_2^+$. The rate constant k_f is expressed as

$$k_f = [k_{12}[H]^3 + (k_{13}K_2+k_{22}K_{a1})[H]^2 + (k_{14}K_2K_3 + k_{23}K_2K_{a1})[H] + k_{24}K_3K_4K_{a1}]/([H]+K_{a1}) \times([H]^2+K_2[H]+K_2K_3).$$

Figure 11 shows the plot of $k_f\times([H]+K_{a1})([H]^2+K_2[H]+K_2K_3)$ against [H],[16] giving k_{24}, k_{23}, and k_{14}

16) These were calculated on the added acid concentrations.

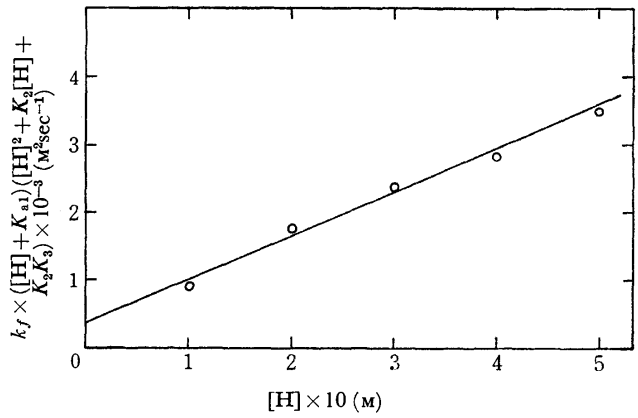

Fig. 11. Plot of $k_f([H]+K_{a1})([H]^2+K_2[H]+K_2K_3)$ *vs.* hydrogen ion concentration for Tl(III)-SXO at 25.0°C and ionic strength 2.0.

as 5.3×10^5, 3.0×10^5, and 7.0×10^5M^{-1}sec^{-1} respectively.

Unlike the case of Ga(III) or In(III), absorbance of the Tl(III)-SXO complex decreases gradually with time. The complex formation of Tl(III) is, however, much faster than the color fading, and the signals obtained on the screen of the oscilloscope are always exponential curves under the experimental conditions. The rate of color fading increases with decreasing hydrogen ion concentration.

Discussion

The non-linearity of the plot k_{obs} against [M(III)] was interpreted in terms of two-step mechanism including pre-equilibrium (Figs. 2 and 3). Apparent pre-equilibrium constant can be obtained from the slope and the intercept of the plot (Figs. 4 and 5), following the Eq. (2). Apparent pre-equilibrium constants for Ga(III)-SXO and In(III)-SXO are in the order of magnitude of 10^2M^{-1}. Although this value of K_p is relatively large, ion pair formation constant for 2+ and 2− ions is expected to be of the same order.

It will be difficult to discuss this apparent value of K_p precisely, because the rate equation is not so simple as Eq. (2), when several charge types of the ligand and the metal ions are taken into account; K_p is a function of [H] and k_f is not simply a product of K_p and a constant.

Only the rate constants k_{24} can be discussed among the three metal ions.[17] The order of the values of k_{24} is $InOH^{2+}>TlOH^{2+}>GaOH^{2+}$. The value of k_{24} for Tl(III) is obtained at ionic strength 2.0, whereas that for Ga(III) or In(III) is at ionic strength 0.1. Kinetic measurements for In(III) were also made at ionic strength 2.0. The results are shown in Fig. 10. The concentrations of hydrogen ion were determined by calibrating the measured pH values from ionic strength 2.0 ($NaClO_4$) to 0.1.

17) The value of k_{24} is indistinguishable from k_{15} as mentioned above, but it seems probable that k_{15} may be neglected. Generally speaking, the rate constants for MOH^{2+} are roughly 10^2 times larger than those for M^{3+} for the same charge type of ligands, as is shown for Fe(III).[14] The values of k_{15} obtained above are close to those of k_{25}. This will be improbable.

TABLE 1. KINETIC RESULTS FOR THE COMPLEX FORMATION OF Ga(III), In(III), AND Tl(III) WITH SXO, AT 25.0°C

	k_{25} M^{-1} sec^{-1}	k_{24} M^{-1} sec^{-1}	k_{15} M^{-1} sec^{-1}	k_{23} M^{-1} sec^{-1}	k_{14} M^{-1} sec^{-1}	I
Ga(III)	1.2×10^4	1.1×10^3	(6.9×10^2)			0.1
In(III)	3.1×10^6	5.0×10^6	(2.8×10^5)			0.1
	10^6	2.2×10^6	(1.3×10^5)			2.0
Tl(III)		5.3×10^5		3.0×10^5	(7.0×10^5)	2.0

In spite of the high $NaClO_4$ concentration, the pseudo-first-order rate constants k_{obs} are at most three times less than those obtained at ionic strength 0.1 and the results are summarized in Table 1. The order of the values of k_{24} is still that described above, namely, $InOH^{2+}>TlOH^{2+}>GaOH^{2+}$.

As SXO is a multidentate ligand, the complex formation process consists of several steps. The outer-sphere complex must be formed first, regardless of the successive mechanism. An inner-sphere coordinated water molecule is substituted by one of the coordinating groups of SXO next. The dissociation of the water molecule is the rate-determining, if the complex formation proceeds following the Eigen-Tamm mechanism.[1] It seems probable that the first coordination to the metal occurs through one of the carboxyl groups of SXO. The other carboxyl group, the nitrogen of the imino group and the oxygen of the phenol or quinone coordinate to the metal successively. If the pre-equilibrium constant K_p discussed above does not correspond to the ion-pair formation constant, the intermediate M(III)···L must be some species formed in these steps. As the coloration of the complex will be resulted from the coordination of the oxygen of the phenol or quinone which is directly connected with the π electron system of the ligand, the intermediate must be formed before the coordination of the phenol oxygen. Then the rate-determining step which may be S_N1 or S_N2 follows; for example the slow cleavage of the hydrogen bond between the imino nitrogen and the phenolic or the quinone oxygen was expected. The measurements of the rate of the proton dissociation reaction was tried by means of the temperature-jump technique. But no signal was observed in our experiment.

Kinetic data to date for trivalent d^{10}-system ions are summarized in Table 2. It is reported that the complex formation of Ga(III) proceeds *via* S_N2 mechanism.[4,5] Dividing the rate constant k_{25} for Ga(III)-SXO by ion-pair formation constant K_{ip}, that is assumed to be 80,[18] yields 10^2 sec^{-1}, which is less than the rate constant of the water exchange reaction. The rate constant for Ga^{3+} is lower than that for $GaOH^{2+}$ and then is much lower than that for water substitution reaction of Ga(III). This large difference between the water substitution and the complex formation rate for Ga(III) does not conflict with the S_N2 mechanism. But the fact that the complexing rate for Ga^{3+} is lower than that for $GaOH^{2+}$, which is also observed in the case of the complex formation with SO_4^{2-}, is inconsistent with the S_N2 mechanism from a coulombic point of view.

The complexing rate of $InOH^{2+}$ with SO_4^{2-} is reported to be $2.5\times10^7M^{-1}sec^{-1}$.[4] Assuming the ion-pair formation constant to be $80M^{-1}$, the rate of substitution is $3\times10^5sec^{-1}$.

The complexing rate of In^{3+} with murexide is reported to be $2\times10^6M^{-1}sec^{-1}$.[3] As the measurements are carried out at relatively high pH of 3.0—4.4, the contribution of $InOH^{2+}$ must be large. Attributing this rate constant to that for $InOH^{2+}$, and assuming the ion-pair formation constant to be $5M^{-1}$, first-order rate constant is 4×10^5 sec^{-1}. Estimating the value of ion-pair formation constant for k_{25} and k_{24} to be $80M^{-1}$ and $5M^{-1}$ respectively, we obtain the first-order rate constants 4×10^4 sec^{-1} and 1×10^6 sec^{-1} for k_{25} and k_{24} respectively. So the first-order rate constant for $InOH^{2+}$ is about 10^5 sec^{-1} in every case.

So far as we know, no data have been reported for the rate of complex formation of Tl(III). If the situations for $TlOH^{2+}$ is the same as those for $InOH^{2+}$ mentioned above, *viz.*, the elimination of the coordinated water molecule from the metal ion plays an important role, ionic radius will be a measure of coulombic factor of water elimination. But in effect the order of reactivity is different from that of ionic radius: despite of its larger ionic radius Tl(III) reacts relatively slowly as compared to In(III). This phenom-

TABLE 2. RATE CONSTANTS REPORTED FOR THE COMPLEX FORMATION OF Ga(III) AND In(III) WITH VARIOUS LIGANDS

M(III)	Ga(III)				In(III)			
Ligand	MTB[a] M^{-1} sec^{-1}	SO_4^{2-} [b] M^{-1} sec^{-1}		OH_2[c] sec^{-1}	Murexide[d] M^{-1} sec^{-1}		SO_4^{2-} [b] M^{-1} sec^{-1}	
k_f	22.4 (6°C)	Ga^{3+}	2.1×10^4	1×10^4	In^{3+}	2.0×10^6	In^{3+}	2.6×10^5
	40.9 (10°C)							
	77.1 (15°C)	$GaOH^{2+}$	1.0×10^5				$InOH^{2+}$	2.5×10^7
Condition		25°C		25°C	pH=3.0—4.4		25°C	
	pH=3.15	$I\rightarrow0$			12°C, I=0.1		$I\rightarrow0$	

a) Methylthymol Blue (MTB); Ref. 6. b) Ref. 4. c) Ref. 5. d) Ref. 3.

18) The values of K_{ip} used here were estimated by using the equation[19,20] $K_{ip}=(4Na^3/3000)\exp(-U(a)/\mathbf{R}T)$, where N is Avogadro's number, a the encounter complex separation assumed to be 5 Å and $U(a)$ the coulombic energy.

19) M. Eigen, *Z. Elektrochem.*, **64**, 115 (1960).

20) R. M. Fuoss, *J. Amer. Chem. Soc.*, **80**, 5059 (1958).

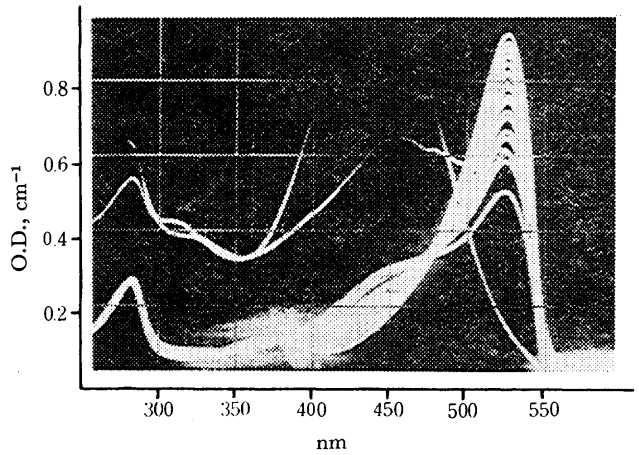

Fig. 12. Change in absorption spectra of Ga(III)-SXO during *ca.* 5 sec after mixing measured by the rapid-scan spectrometer. Each scan needs 300 msec. $[Ga(III)]_0=2.1\times10^{-3}$ M, $[SXO]_0=2.0\times10^{-5}$ M, pH=1.60, ionic strength 0.1, 25.0°C.

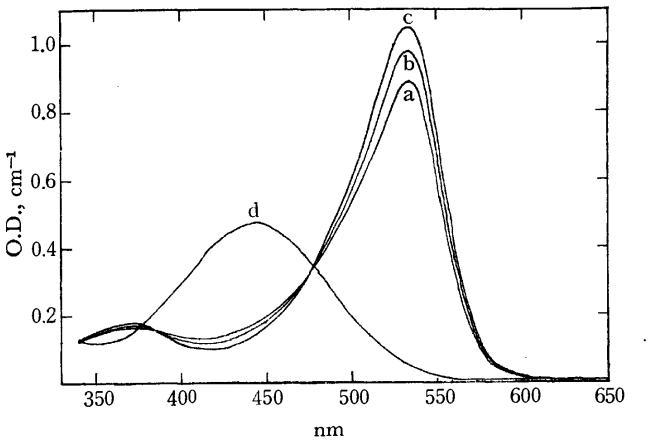

Fig. 13. Slow spectral change of Ga(III)-SXO system at (a): 2 min, (b): 20 min and (c): 600 min after mixing under the same conditions as those in Fig. 12, and (d): the spectrum of SXO.

enon may have some relation with the large electron affinity, large acid dissociation constant and relatively large hydration energy of Tl(III). All these properties are interpreted by the large electron attractive force of thallium(III) ion.

The slower increase in absorbance of Ga(III)-SXO complex after the rapid increase is an interesting phenomenon. Figures 12 and 13 show the change of absorption spectrum of Ga(III)-SXO system measured with a rapid-scan spectrophotometer and that measured with a usual spectrophotometer respectively. Isosbestic points are found at 340, 380, and 475 nm in both spectra, and no significant shift of spectra is observed. These results lead us to the mechanism involving only one final product and some slow processes for some of the reaction components. It would be reasonable to assume that some polymerized or aggregated forms of the reactants may cause such very slow process, though it was not experimentally ascertained. The similar slow processes were also observed in the complex formation between trivalent iron and SXO.

The slow decrease in absorbance in the visible region of Tl(III)-SXO complex is due to the oxidation of SXO by Tl(III), since the similar color fading were also found with the oxidizing agents as Fe(III), Co(III), and Ce(IV), and by anodic oxidation.

The authors wish to thank Professor H. Baba, Research Institute of Applied Electricity of our University, for his permission to use the rapid-scan spectrometer.

Ultraviolet and Infrared Spectra of Cupferron and Neocupferron

Tetsuhiko YOSHIMURA, Chie MIYAKE, and Shosuke IMOTO

Department of Nuclear Engineering, Faculty of Engineering, Osaka University, Suita, Osaka

(Received September 6, 1971)

N-nitroso-*N*-phenylhydroxylamine, *N*-nitroso-α-naphthylhydroxylamine, and their sodium salts have been prepared from the ammonium salt of *N*-nitroso-*N*-phenylhydroxylamine (cupferron) and the ammonium salt of *N*-nitroso-α-naphthylhydroxylamine (neocupferron) respectively. The measurements of the UV spectra in solution and the IR spectra with Nujol mull have been carried out on these compounds, including their ammonium salts. The solvent effect and the deuteration effect on the IR spectra have also been examined for the compounds with a hydroxyl group. The formation of a rather strong hydrogen bonding in these aromatic nitrosohydroxylamines has been confirmed from the deuteration effect on the IR spectra and from the solvent effect on the UV and IR spectra. These compounds and their salts have shown the absorption band considered to be a charge-transfer band in the UV spectra, and they have also shown the N=O stretching mode between 1450 and 1468 cm^{-1} corresponding to those of nitrosamines in the IR spectra with the HCB mull.

Ammonium salts of *N*-nitroso-*N*-phenylhydroxylamine and *N*-nitroso-α-naphthylhydroxylamine, which are called cupferron and neocupferron respectively, are well known as analytical reagents for various metallic ions, such as those of transition elements and rare earth elements.[1] They coordinate the metallic ion as a bidentate ligand, forming a chelate which is less soluble in water. In spite of their usefulness, however, few investigations have been made on the molecular structure and the spectroscopic properties of these compounds. For cupferron, some data on the ultraviolet and infrared spectra were reported by Piskorz and Urbanski, but without any detailed analysis.[2] On the other hand, the spectroscopic properties of other *N*-nitroso compounds, nitrosamine and nitrosohydroxylamine have been investigated by many workers. Haszeldine *et al.* carried out a systematic study of the ultraviolet and infrared spectra of *N*-nitroso compounds, and pointed out that the $n\rightarrow\pi^*$ band of the nitroso group usually observed with nitrosamines was absent in the ultraviolet spectra of *N*-alkyl-*N*-nitrosohydroxylamine.[3,4] Bellamy *et al.* and Williams *et al.* investigated the solvent effect of infrared absorption bands for various nitrosamines and assigned some absorption bands to the N=O, N–N, and C–N stretching vibrations.[5,6] Because there is a possibility of inter- or intra-molecular hydrogen bondings between the nitroso group and the hydroxyl group in nitrosohydroxylamines, the ultraviolet and infrared spectra may be very complicated.

The present paper will report on the ultraviolet and infrared spectra of cupferron, neocupferron, and related compounds, as well as on the deuteration effect for the hydroxyl group in *N*-nitrosophenylhydroxylamine and the solvent effect in various organic solvents on the infrared spectra.

1) F. J. Welcher, "Organic Analytical Reagents," Vol. III, Chap. XIII (1955), p. 354.
2) M. Piskorz and T. Urbanski, *Bull. Acad. Pol. Sci.*, **11**, 597 (1963).
3) R. N. Haszeldine and J. Jander, *J. Chem. Soc.*, **1954**, 691.
4) R. N. Haszeldine and B. J. H. Mattinson, *ibid.*, **1955**, 4172.
5) L. J. Bellamy, C. P. Conduit, R. J. Pace, and R. L. Williams, *Trans. Faraday Soc.*, **55**, 1677 (1959).
6) R. L. Williams, R. J. Pace, and G. J. Jeacocke, *Spectrochim. Acta*, **20**, 225 (1964).

Experimental

Materials. Cupferron, which will be designated by NH_4cupf hereafter (Nakarai Chemicals, Ltd., GR grade), was purified by recrystallization from methanol. Neocupferron, which will be designated by NH_4ncupf hereafter (Fluka AG. Buchs SG, Switzerland), was purified by recrystallization from a mixed solvent of methanol and ethyl ether. Since cupferron, neocupferron, and related compounds gradually decomposed in air and in solution at room temperature, all the operations during the syntheses and purification were carried out with the solutions kept at the temperature of ice. All the other reagents were of a GR grade and were used without further purification.

N-*Nitroso*-N-*phenylhydroxylamine (Hcupf)*: Ten milliliters of a 6N hydrochloric acid solution was added to an aqueous solution of NH_4cupf (10 g in 100 m*l* of H_2O). The white-colored precipitant was filtered and repeatedly washed with water. The product was purified several times by recrystallization from acetone and dried in a vacuum. The Hcupf thus obtained was very soluble in organic solvents, but was only slightly soluble in water. The Hcupf was very unstable in both air and organic solvents at room temperature.

Found: C, 51.88; H, 4.18; N, 20.29%. Calcd: C, 52.18; H, 4.38; N, 20.21%.

N-*Nitroso-α-naphthylhydroxylamine (Hncupf)*: The preparation of Hncupf was carried out in the same way as in the case of Hcupf. Hncupf was thus obtained as faint yellow-colored crystals and was less stable than Hcupf. The solubility of Hncupf in a solvent was found to be nearly same as that of Hcupf.

Found: C, 65.21; H, 4.14; N, 14.08%. Calcd: C, 63.82; H, 4.29; N, 14.89%.

Na Salt of Hcupf (Nacupf): NH_4cupf (1.6 g) was dissolved in a 1N NaOH solution (10 m*l*). The solution was heated for several hours at about 80°C and then cooled to room temperature. The white crystals thus precipitated were then recrystallized from a water-acetone mixed solvent. The Nacupf was very soluble in water, but was insoluble in organic solvents.

Found: C, 45.18; H, 3.13; N, 17.37%. Calcd: C, 45.01; H, 3.15; N, 17.50%.

Na Salt of Hncupf (Nancupf): The preparation of Nancupf was carried out in the same way as in the case of Nacupf. This salt was recrystallized from acetone. The Nancupf, obtaned as faintly-yellow-colored crystals, was very soluble in water, slightly soluble in polar organic solvents, such as acetone and methanol, and insoluble in non-polar solvents. The Nancupf was slightly hygroscopic. From the results of

chemical analysis and infrared spectroscopy, this salt was confirmed to be a hydrate.

Found: C, 55.13; H, 3.25; N, 12.98%. Calcd for Nancupf·$\frac{1}{2}H_2O$: C, 54.80; H, 3.68; N, 12.78%.

Deuteration of Hcupf. The deuteration of Hcupf was carried out by recrystallizing Hcupf seven times from an acetone-D_2O mixed solvent in an argon gas atmosphere while cooling in ice water. Before the deuteration, the acetone was dried by bubbling in argon gas. The product thus obtained was, however, partly deuterated Hcupf. D_2O (99.5%) by E. Merck was used.

Measurements. The ultraviolet spectra and infrared absorption spectra were recorded on a HITACHI ESP-3T type and a HITACHI-PERKIN-ELMER Model 225 type IR grating spectrophotometer respectively, where Nujol mull, HCB mull, and solution techniques were used. Most of the solvents in the UV and IR measurements were spectrograde reagents (E. Merck and Nakarai Chemicals, Ltd.). Since both the Hcupf and Hncupf were very unstable in solutions, it was impossible to determine the concentration of the solution in the IR measurements. Deuterated Hcupf was treated in a N_2 atmosphere.

Results and Discussion

UV Spectra. The ultraviolet spectra of Hcupf and Nacupf are shown in Figs. 1 and 2 respectively. In Table 1 are tabulated the wavelengths and molar extinction coefficients of the absorption maxima and minima observed with various solvents. The absorption spectra of Nacupf and NH_4cupf are similar to each other, but are different from those of Hcupf. The 290 mμ band observed with Nacupf and NH_4cupf shifts to 260 mμ for Hcupf, and the 220 mμ band of the former shifts to a shorter wavelength for the latter, where the band appears as a shoulder. The 220 mμ band of Nacupf and NH_4cupf and the 260 mμ band of Hcupf do not show any remarkable solvent effects, but the 290 mμ band of the former is sensitive to solvents, *i.e.*, it shows a blue shift with the change of the solvent from

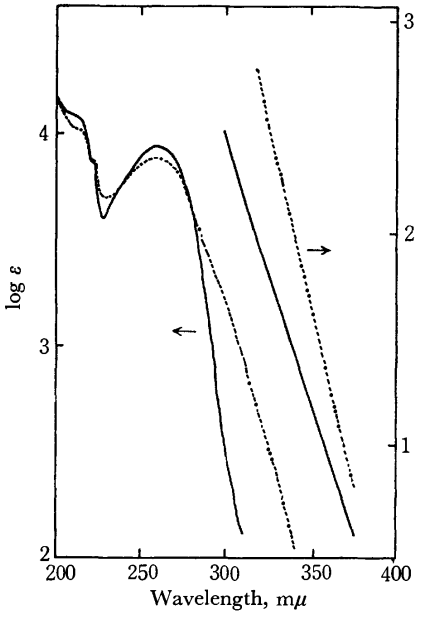

Fig. 1. UV spectra of Hcupf in *n*-heptane (——) and in methanol(- - - - -).

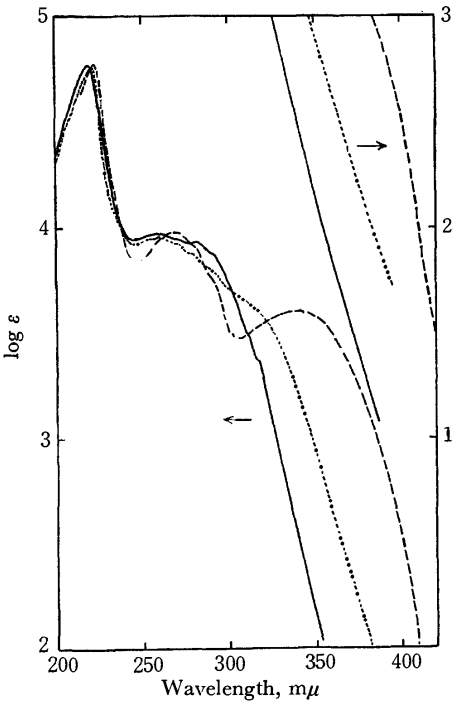

Fig. 2. UV spectra of Nancupf in water(——), in ethanol (·····), and in tetrahydrofuran(- - - -).

alcohol to water. The 260 mμ band of Hcupf or the 290 mμ band of NH_4cupf and Nacupf is not present in *N*-alkyl-*N*-nitrosohydroxylamine,[3] but it is too intense to be identified as originating only from the $A_{1g}\rightarrow B_{2u}$ transition band of benzene. Since the nitroso group is a strong electron acceptor,[7] and since the hydroxyl group as well as the phenyl ring are electron donors, this band is considered to be essentially a charge-transfer band generally sensitive to solvents. That it is insensitive to solvents for Hcupf is looked upon as being due to the presence of strong hydrogen bonding. The shoulder around the 210 mμ of Hcupf and the 220 mμ bands of NH_4cupf and Nacupf may be assigned to be the $A_{1g}\rightarrow B_{1u}$ transition band of the benzene ring, since it shows little solvent effect.

The spectra of Hncupf, Nancupf, and NH_4ncupf are very similar to each other and may all be considered to originate mainly from the naphthyl group, though the 339 mμ band for Nancupf in THF is not found in the others. The band around 220 mμ corresponds to the $A_{1g}\rightarrow E_{1u}$ transition; the band around 280 mμ with a structure to the $A_{1g}\rightarrow B_{1u}$ transition, and the 329 mμ band observed as a shoulder, to the $A_{1g}\rightarrow B_{2u}$. Though Hncupf is also considered to form hydrogen bonding, its effect upon the UV absorption spectra is not observed. For Nancupf and NH_4ncupf, a new band appears as a shoulder around 310 mμ when they are dissolved in ethanol; for Nancupf, this band is shifted to a longer wavelength as the polarity of the solvent decreases, finally resolving into a single peak at 339 mμ with THF. This band is considered to correspond to the 260 mμ band of Hcupf and can be assigned to the charge-transfer band. Thus the bands around 280 mμ

7) M. Tanaka, J. Tanaka, and S. Nagakura, This Bulletin, **39**, 766 (1966).

Table 1. Ultraviolet spectra of Hcupf, Hncupf, and their salts

Compounds	Solvent	λ_{max} in mμ (log ε)	λ_{min} in mμ (log ε)
Hcupf	*n*-heptane		227 (3.60)
		259.5 (3.95)	
	CCl_4	261 (3.96)	
	$CHCl_3$	260 (3.97)	
	THF		230 (3.68)
		260 (3.93)	
	C_2H_5OH		229 (3.68)
		258.5 (3.90)	
	CH_3OH		230 (3.70)
		259 (3.89)	
NH_4cupf	C_2H_5OH		212 (3.94)
		222 (4.00)	
			249 (3.56)
		298.5 (3.87)	
	CH_3OH	222 (4.03)	
			249 (3.35)
		293 (3.96)	
	H_2O	219 (4.03)	
			244 (3.50)
		284 (4.00)	
Nacupf[a)]	50% CH_3OH,		210 (3.98)
	50% H_2O	221.5 (4.06)	
			246 (3.43)
		289 (4.03)	
	H_2O		209.5 (4.00)
		219.5 (4.05)	
			244 (3.52)
		283.5 (4.02)	
Hncupf[a)]	*n*-heptane	218.5 (4.70)	265 (3.66)
		293 (3.80) str.	
	$CHCl_3$		268 (3.66)
		294 (3.77) str.	
	THF	218.5 (4.66)	
		291 (3.80) str.	
	CH_3OH	217.5 (4.74)	
			264 (3.74)
		282 (3.80) str.	
NH_4 ncupf[a)]	C_2H_5OH	219.5 (4.74)	
			250 (3.88)
		261 (3.89) str.	
	CH_3OH	220.5 (4.71)	
			247 (3.90)
		260 (3.92) str.	
	H_2O	219.5 (4.77)	
			245 (3.95)
		260 (3.97) str.	
Nancupf[a)]	THF	222.5 (4.78)	
			247 (3.83)
		269 (3.98) str.	
			306 (3.48)
		339 (3.61)	
	C_2H_5OH	221 (4.75)	
			245 (3.92)
		260 (3.96) str.	
	50% CH_3OH,	220.5 (4.75)	
	50% H_2O		246 (3.92)
		260 (3.94) str.	
	H_2O	219.5 (4.77)	
			244 (3.94)
		260 (3.97) str.	

a) The spectra of these compounds exhibited a structure between about 260 and 300 mμ, and in the table their absorption maxima are shown.
"str." is an abbreviation for the appearance of a structure in the absorption band.

of Hncupf, NH_4ncupf, and Nancupf seem to consist of the $A_{1g} \rightarrow B_{1u}$ transition of naphthalene superposed on the charge-transfer transition.

The Lack of $n \rightarrow \pi^*$ Bands in the UV Region. Hcupf and its salts are white in the polycrystalline state and colorless in solution. Hncupf and its salts are faintly yellow both in the polycrystalline state and in solution. *C*-nitroso compounds are also colorless or pale yellow in the crystalline form, in which they exist as a dimer, but their monomer in solution is green or blue. Most of the nitrosamine derivatives are known to be yellow in the liquid state.[3,4] The color of the monomer *C*-nitroso compounds and nitrosamine derivatives originates from the $n \rightarrow \pi^*$ transition bands of the nitroso group, which are observed in the nitrosamine derivatives around 350 mμ and in the monomer of *C*-nitroso compounds around 700 mμ.[8,9] Generally, in *N*-nitroso compounds there was no absorption band corresponding to the 700 mμ band appearing in monomer *C*-nitroso compounds, a band which is interpreted as one of the $n \rightarrow \pi^*$ transition bands that originate from the excitation of a non-bonding electron of the nitrogen atom to the anti-bonding π^* orbital. In order to explain this phenomenon, Haszeldin assumed that the non-bonding electron of the nitrogen atom in the nitroso group might be used to form the dimer, just as in the case of the dimer of *C*-nitroso compounds.[3,4] The presence of dimers in *N*-nitroso compounds, however, has been denied by Williams *et al.* and by Layne *et al.* on the basis of IR and UV measurements respectively.[6,10] Since it is impossible for cupferron, neocupferron, and their salts to be dimerized at the nitrogen atoms of nitroso groups because of the steric hindrance, the $n \rightarrow \pi^*$ transition band near 700 mμ could appear according to the assumption by Haszeldin *et al.* Nevertheless, no absorption bands are observed near 700 mμ in these compounds, just as in the case of other *N*-nitroso compounds.

In the spectra of Hcupf, Hncupf, and their salts, the $n \rightarrow \pi^*$ transition band around 350 mμ is also absent, although it is usually observed in nitrosamine derivatives. As for the reason why this is absent in the spectra of *N*-nitrosohydroxylamine, Haszeldin *et al.* suggested the possibility of inter- or intra-molecular hydrogen

8) B. G. Gowenlock and W. Luttke, *Quart. Rev.* (London), **12**, 321 (1958).
9) K. Nakamoto and R. E. Rundle, *J. Amer. Chem. Soc.*, **78**, 1113 (1956).
10) W. S. Layne, H. H. Jaffe, and H. Zimmer, *ibid.*, **85**, 435 (1963).

TABLE 2. INFRARED SPECTRA OF Hcupf, Hncupf, AND THEIR SALTS (Nujol and HCB mull)

Hcupf	NH_4cupf	Nacupf	Tentative assignment	Hncupf	NH_4ncupf	Nancupf	Tentative assignment
	1675 W, b			1598 M	1595 M	1597 M	ν(C=C)
1587 W	1589 M	1588 M	ν(C=C)	1506 M	1508 M	1510 M	
1487 S	1481	1481 S		1480 W			
1468 VS	1459 VS	1455 S	ν(N=O)	1460 sh	1460 sh	1460 W	
	1455 S			1450 S	1446 S	1440 W	ν(N=O)
	1422 S		$\nu_4(NH_4^+)$		1390 M	1396 M	
1397 sh			δ(OH)	1379 VS		1379 VW	
1382 S				1350 M	1351 VW	1357 M	
1338 M	1331 S	1341 VS			1324 M	1322 VS	
1303 S	1316 S	1312 S		1309 W			
1280 S	1264 VS	1265 VS			1295 VS	1297 S	
	1220 VS	1226 VS			1280 sh	1280 sh	
		1202 VW		1272 VW			
1167 M	1168 W	1166 M	phenyl	1256 S			
1158 M	1160 M			1217 W	1219 VS	1222 S	
1110 S	1104 VW	1105 VW	phenyl	1198 M	1190 M	1198 VS	
1097 W	1071 M	1073 M			1170 sh	1163 M	
1063 VS	1056 S	1058 S	ν(NH)	1149 VW	1148 VW	1143 W	
1019 VS	1020 M	1019 W	δ(CH)	1141 W	1125 M	1133 W	
1003 W				1081 sh			
993 VW				1069 VS	1064 W	1061 W	
	971 VW	967 W		1021 M	1019 W	1019 W	δ(CH)
922 VS	907 VS	907 VS	ν(N–O)	998 M	981 M	983 S	ν(NN)
		850 W		950 VW	943 VW		
	773 VW			911 S	905 VS	902 VS	ν(N–O)
763 VS	761 VS				895 M		
	755 VS	752 VS	γ(CH)		852 VW	853 VW	
742 S, b			γ(OH)	858 W	865 VW	864 VW	
713 S, b					817 M	815 S	γ(CH) 3 adj. H
	722 VW	720 VW		808 S	799 S	798 VS	
686 sh	695 sh	695 S		796 VS	789 VS	790 S	
680 VS	689 VS	683 VS		762 VS	769 VS	765 VS	γ(CH) 4 adj. H
647 S			δ(NNO)		758 S		
	615 VW	616 W		740 VW	735 VW	742 VW	
	581 M	584 S	δ(NNO)		721 VW	720 VW	
	514 W	522 M		684 S			γ(OH)
482 M	470 W	458 M		664 M			
406 W				654 S	662 M	663 M	δ(NNO)
393 M				630 W	636 W	647 W	
371 M	370 M	376 S		570 M	571 M	574 sh	
	305 VW	303 VW				530 S, vb	γ(OH)
	262 M	262 M		527 W	529 W		
				521 VW			
				463 VW			
				450 W	448 VW	453 W	
				430 W		425 W	
				413 M			

Abbreviations: V, very; S, strong; M, medium; W, weak; b, broad; sh, shoulder; ν, stretch; δ, in-plane deformation; γ, out-of-plane deformation.

bonding.[3] As will be discussed later, Hcupf and Hncupf are considered to form hydrogen bonding, but in Nacupf and Nancupf there is no possibility of forming hydrogen bonds. As a reason for the absence of the $n\rightarrow\pi^*$ transition band for *N*-nitrosohydroxylamine, there seems to be a possibility that the $n\rightarrow\pi^*$ band may be hidden by the intense bands of the shorter-wavelength side.

The Hcupf is very unstable in organic solvents; for example, it gradually decomposes into the green solution of *C*-nitroso compounds, meanwhile forming some colorless gas and a water-soluble precipitant. This solution exhibits absorption maxima at 283 mμ, 305 mμ, and 760 mμ, showing the formation of nitrosobenzene.[11,12]

11) C. N. R. Rao and K. R. Bhaskar, "The Chemistry of the Nitro and the Nitroso Groups," Part I, ed. by H. Feuer, Interscience Publishers, New York, Chap. III (1969), p. 137.

12) K. Tabei and S. Nagakura, This Bulletin, **38**, 965 (1965).

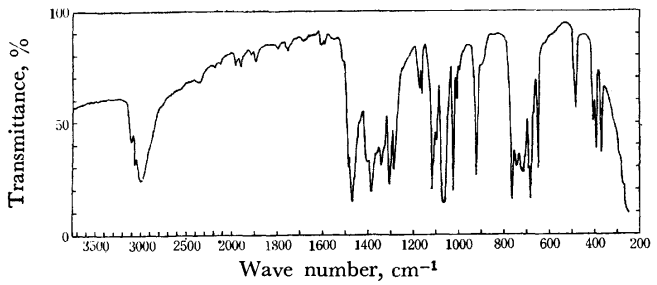

Fig. 3. IR spectrum of Hcupf. 200—1350, 1500—2700 cm^{-1}: Nujol mull, 1350—1500, 2700—4000 cm^{-1}: HCB mull.

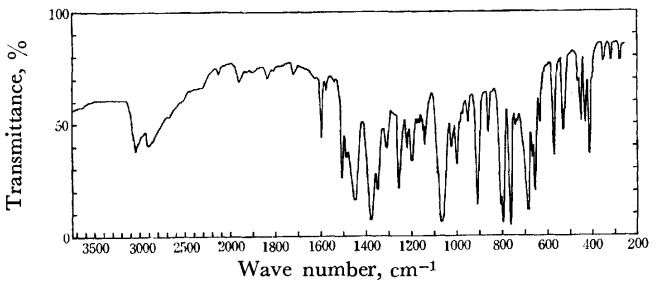

Fig. 4. IR spectrum of Hncupf. 200—1350, 1500—2700 cm^{-1}: Nujol mull, 1350—1500, 2700—4000 cm^{-1}: HCB mull.

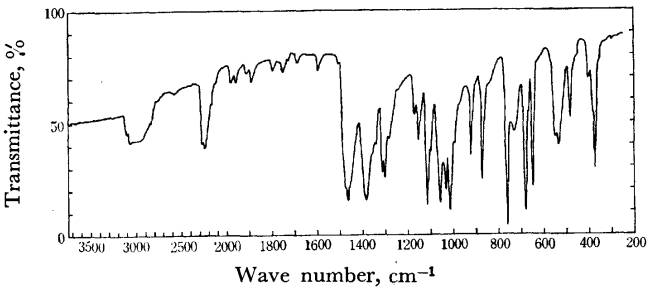

Fig. 5. IR spectrum of deuterated Hcupf. 200—1350, 1500—2700 cm^{-1}: Nujol mull, 1350—1500, 2700—4000 cm^{-1}: HCB mull.

It may be considered, therefore, that the strength of the N–N bond in Hcupf is relatively week.

IR Spectra. In Figs. 3—5 are shown the IR spectra of Hcupf, Hncupf, and partly deuterated Hcupf respectively. The peak wave numbers of the IR spectra and the tentative assignments of each band are tabulated in Table 2. All the compounds exhibited absorption bands corresponding to the vibrations of the aromatic ring, such as 690 and 750 cm^{-1} of the CH out-of-plane deformation, characteristic of the mono-substituted benzene. Particularly in the region between 1700 cm^{-1} and 1000 cm^{-1}, however, the spectra were very complicated by possible interactions between the substituent vibration and the aromatic-ring vibration. In this region, the spectra of the ammonium salts and sodium salts were very similar to each other, but the spectra of compounds with hydroxyl groups were different from those of the salts, just as was observed in the UV spectra. In the frequency region higher than 1700 cm^{-1} these appeared intense bands originating from the vibrations of CH stretching (benzene) and OH stretching, and from the NH_4^+ ion vibrations, which will be discussed later. Since Hcupf and Hncupf are soluble in various organic solvents, the measurement for solvent effects was carried out; the data obtained for the main peaks are shown in Tables 3 and 4, where it may be seen that most absorption peaks either shift to a slightly lower wave number side with the increasing polarity of solvents or are insensitive to solvents.

The bands around 1460 cm^{-1} and 1060 cm^{-1} of Hcupf and its salts were assigned to the N=O and the N–N stretching modes respectively, analogously with those of the nitrosamines. These bands of Hcupf were observed on a higher frequency side than the corresponding ones of Nacupf and NH_4cupf, and they scarcely shifted with the polarity of the solvents. This behavior is different from that of the nitrosamines, in which $\nu_{N=O}$ shifts to a lower frequency, and ν_{N-N}, to a higher frequency, with the increasing polarity of

Table 3. Frequencies, cm^{-1}, of Hcupf in various solvents

Solvent[a)]	Frequencies, (cm^{-1})									
Cyclohexane	—	—	—	—	1105	1067	—	920	753	—
Carbontetrachloride	1467	1388	1305	1273	1107	1066	1021	921	—	705
Carbondisulfide	—	1390	1305	1272	1105	1063	1022	920	759	700
Benzene	—	—	1305	1275	1105	—	—	920	756	—
Methyliodide	—	—	—	—	1106	1063	1020	—	762	706
Methylenechloride	—	1387	—	—	1106	1070	1022	921	—	—
Chloroform	1463	1387	1307	—	1107	1064	1021	919	—	—
Methylenebromide	1464	—	1304	1270	1100	1060	1020	921	763	—
Bromoform	1467	1388	1303	1266	—	1061	1020	921	762	—
Methyleneiodide	1464	—	1302	1265	—	—	—	920	762	—

a) The polarity of the solvent increases from cyclohexane to methylene iodide.

Table 4. Frequencies, cm^{-1}, of Hncupf in various solvents

Solvent[a)]								
Carbontetrachloride	1448	1250	1074	1062	998	912	—	656
Carbondisulfide	—	1254	1074	1062	998	911	766	656
Methylenebromide	1436	—	1070	1059	999	912	769	—
Methyleneiodide	1435	1252	—	—	998	912	768	657

a) The polarity of the solvent increases from carbon tetrachloride to methylene iodide.

solvents. According to Williams *et al.*,[6] the solvent effect of nitrosamines can be explained by assuming the following resonance structures:

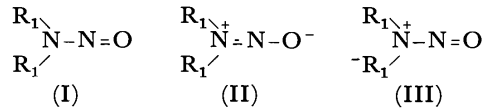

(I) (II) (III)

If the polarity of the solvents increases, the contribution of the structure II will increase, thus giving rise to a lowering of the frequency of N=O stretching vibration and a raising of the frequency for N–N. The reason why Hcupf, contrary to the case of nitrosamines, did not exhibit the solvent effect is considered to be that the relatively strong hydrogen bonding in Hcupf leading to a dimer may exclude the resonance structures which are sensitive to solvents. The large shift of the strong band assigned to the N–N=O deformation mode from 581 cm^{-1} for NH_4cupf and from 584 cm^{-1} for Nacupf to 647 cm^{-1} for Hcupf could also be due to the formation of hydrogen bonding in Hcupf.

In the partly-deuterated Hcupf, the intensity of the broad absorption bands at 713 and 743 cm^{-1} of Hcupf, which are absent in NH_4cupf and Nacupf, is much decreased and strong new broad bands are found at 531 and 548 cm^{-1}. Thus the bands at 713 and 743 cm^{-1} can be assigned to the γ_{OH} mode, and those at 531 and 548 cm^{-1}, to the γ_{OD} mode. The new band at 1030 cm^{-1} can be attributed to the δ_{OD} mode, and the corresponding δ_{OH} band, which is expected to appear near 1400 cm^{-1}, is observed as a shoulder at 1397 cm^{-1}. Deuteration also affects the frequency of the N–O stretching vibration, which appears as a strong and characteristic band at 922 cm^{-1} in Hcupf (at 907 cm^{-1} in NH_4cupf and Nacupf). In the deuterated Hcupf, the intensity of the band at 922 cm^{-1} was decreased and at 873 cm^{-1} there was found a strong new band which was considered to be the N–O band shifted to a lower frequency by the deuteration. A new band found at 1153 cm^{-1} has not yet been assigned.

In Hncupf and its salts, the bands of the CH out-of-plane deformation, being characteristic of α-substituted naphthalene, are found around 800 cm^{-1} and 750 cm^{-1}. The band at the former wave number is due to three adjacent ring hydrogen atoms, while the band at the latter is due to four adjacent ring hydrogen atoms. Each band of them is split into two or three subbands in the spectra measured with Nujol mull. As the splitting of the band around 800 cm^{-1} was observed even in the CS_2 solution, this splitting is considered not to be due to the inter-molecular interaction, but it may originate from the interaction between a ring hydrogen and substituents as follows:

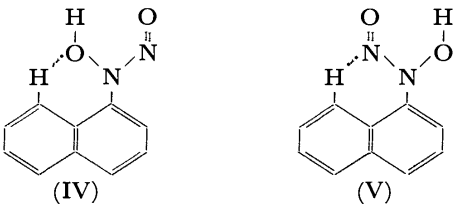

(IV) (V)

The bands around 1450 cm^{-1} and 990 cm^{-1} can be assigned to the N=O and N–N stretching modes respectively, just as in the case of cupferrons. In the neocupferrons, the band of N=O stretching mode is lowered in frequency and decreased in intensity compared to that of cupferrons. This behavior may be explained by a weakening of the double-bond character due to the increase in the electron-accepting property of the naphthyl group and the contribution of the structure V. The band of the N–O stretching mode is found around 900 cm^{-1} at nearly the same wave number as in the cases of the Hcupf and its salts.

IR Spectra in the Frequency Region Higher than 1700 cm^{-1}. Figure 6 shows the spectra of Hcupf and deuterated Hcupf between 2000 and 3500 cm^{-1} as measured with the HCB mull and in a CCl_4 solution. The broad band of Hcupf observed with the maximum at 2980 cm^{-1} (solid) can be assigned to the bonded OH stretching mode. In the deuterated Hcupf it is weakened, however, and a new band is found with maxima around 2240 and 2260 cm^{-1}. Both bands can be assigned to the bonded OD stretching mode. In a CCl_4 solution these ν_{OH} and ν_{OD} bands shift to a lower frequency side by 70 cm^{-1} and 100 cm^{-1} respectively. In the Hncupf, however, the broad band with the maximum at 2910

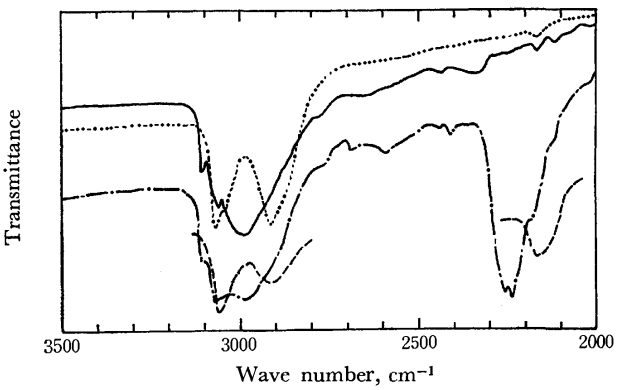

Fig. 6. IR spectra of Hcupf and deuterated Hcupf. ——; Hcupf with Nujol mull, ------; Hcupf in CCl_4, ·—·—; deuterated Hcupf with HCB mull, ----; deuterated Hcupf in CCl_4.

Table 5. The IR bands related to hydrogen bonding for Hcupf, deuterated Hcupf, and Hncupf

	ν(OX)		νN=O		δ(OX)		ν(N–O)		γ(OX)	
	A	B	A	B	A	B	A	B	A	B
Hcupf	2990	2915	1468	1467	1397	1388	922	921	713 742	705
Deuterated Hcupf	2240 2260	2160	1463	1467	1030	1049	873	870	531 548	528[c]
Hncupf	2910	2900[c]	1450	1448			911	912	684	703

a) X=H or D, b) A=solid, B=solution in CCl_4, c) Solution in CS_2.

cm^{-1} (solid), which corresponds to the 2980 cm^{-1} band of Hcupf, shifts to a frequency lower by only 10 cm^{-1} in CS_2 solution. The free OH stretching band was not found for either Hcupf or Hncupf not only in non-polar solvents, such as CCl_4 and CS_2, but also in proton donor solvents, such as $CHCl_3$ and $CHBr_3$. Since no change was ever observed with the bands related to the substituent in the proton-donor solvents, these compounds are considered not to form hydrogen bonding with solvents. Besides, the ν_{OH} bands are observed at relatively lower frequencies (2980 cm^{-1} for Hcupf), and the strong broad band of γ_{OH} mode is found at relatively higher frequencies (730 cm^{-1} for Hcupf and 685 cm^{-1} for Hncupf), so it is reasonable to conclude that Hcupf and Hncupf form a considerably strong hydrogen bonding, as is also to be expected on the basis of UV spectra and from the solvent effect upon the IR spectra in the frequency region lower than 1700 cm^{-1}. At present it is impossible to determine whether the hydrogen bonding is an intra-molecular type (VI) or an inter-molecular association type (VII), but the bimolecular type is considered to be more reasonable, as the stronger hydrogen bonding is sterically favored.

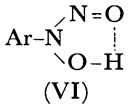

(VI)

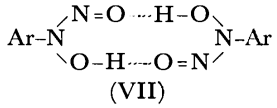

(VII)

The absorption bands related to hydrogen bonding for Hcupf, deuterated Hcupf, and Hncupf are summarized in Table 5.

BULLETIN OF THE CHEMICAL SOCIETY OF JAPAN, VOL. 45, 1430—1433(1972)

Spectrophotometric Study on The Extraction of The Ternary Complex Composed of Cobalt(II), 8-Hydroxyquinoline-5-sulphonic Acid and Zephiramine

Tomihito KAMBARA and Masao SUGAWARA

Department of Chemistry, Faculty of Science, Hokkaido University, Sapporo

(Received November 30, 1971)

8-Hydroxyquinoline-5-sulphonic acid (H_2QS) reacts with cobalt(II) in the presence of zephiramine (tetradecyl-dimethyl-benzyl-ammonium chloride) and gives a yellow green association complex. The ternary complex having an absorption maximum at 405 nm can be extracted into chloroform at pH 6.8—9.3. Beer's law holds for 2.73—33.0 μg of cobalt(II); molar absorptivity, 1.39×10^4 $cm^{-1}mol^{-1}l$. The composition of cobalt(II)-H_2QS complexes in water is 1:1 at pH 4.4, 1:2 at pH 5.8, and 1:3 at pH 7.6. The composition of the ternary complex is estimated to be $[Co^{2+}(QS^{2-})_2(HQS^-)(Z^+)_3]_o$. The equilibrium constant for the extraction

$$K=\frac{[Co^{2+}(QS^{2-})_2(HQS^-)(Z^+)_3]_o}{[Co^{2+}][(HQS^-Z^+)]_o^3[OH^-]^2}$$

was determined. It was found that $\log K=29.01\pm1.86$.

The solvent extraction of the ion-pair formed by the interaction of 8-hydroxyquinoline-5-sulphonic acid-metal chelate anions with cation of zephiramine (tetradecyl-dimethyl-benzyl-ammonium chloride) has been applied to the spectrophotometric determination of iron(III),[1] nickel(II),[2] and copper(II).[3] Matsuo *et al.*[4] proposed the extraction of thiocyanatocobaltate(II) complex anion with zephiramine into chloroform. In this paper, fundamental conditions for the spectrophotometric determination of cobalt(II) and the composition of the ternary complex formed are discussed: 8-hydroxyquinoline-5-sulphonic acid (H_2QS) reacts with cobalt(II)[5,6] and gives a water soluble chelate, which can be extracted into chloroform in the presence of zephiramine (Z^+Cl^-). The intensity of the yellow green coloration with an absorption maximum at 405 nm in chloroform is proportional to the amount of cobalt(II) in the aqueous layer.

Experimental

Reagents. *Cobalt(II) Standard Solution*: 2.3795 g of cobalt chloride (Wako Chemicals Co., guaranteed reagent) was dissolved into 10 m*l* of hydrochloric acid and diluted to 1 liter with deionized water. The solution was standardized with EDTA-titration using murexide as an indicator, and found to contain 586 μg of cobalt(II) per m*l*. The solution was diluted as required.

H_2QS Solution: 1.00×10^{-3}M solution was prepared by dissolving H_2QS (Wako Chemicals Co.) into water.

Zephiramine Solution: 5.00×10^{-3}M solution was prepared by dissolving Dotite zephiramine into water.

Buffer Solutions: Acetate buffer solution, pH 3.4—5.6;

1) T. Kambara, S. Matsumae, and K. Hasebe, *Bunseki Kagaku*, **19**, 462 (1970).
2) T. Kambara, M. Sugawara, and K. Hasebe, *ibid.*, **19**, 1239 (1970).
3) T. Kambara, M. Maeyama, and K. Hasebe, *ibid.*, **20**, 1249 (1971).
4) H. Matsuo, S. Chaki, and S. Hara, *ibid.*, **14**, 935 (1965).
5) C. F. Richard, R. L. Gustafson, and A. E. Martell, *J. Amer. Chem. Soc.*, **81**, 1033 (1959).
6) L. G. Sillén and A. E. Martell, Ed., "Stability Constants of Metal-Ion Complexes," The Chemical Society London (1964), p. 609.

Stock solutions of 0.1M sodium acetate and 0.1M acetic acid were prepared and mixed in appropriate proportions. Phosphate buffer solution, pH 6.3—8.3; Stock solutions of 0.1M disodium phosphate dihydrate and 0.1M potassium phosphate dibasic were prepared and mixed as required. Borate buffer solution, pH 9.1—10.5; 0.1M borax solution was mixed with 0.1M hydrochloric acid or 0.1M sodium hydroxide.

Chloroform and other reagents were all of analytical reagent grade.

Apparatus. Spectrophotometric measurements were carried out with a Shimadzu Model QV-5 spectrophotometer with 10-mm cells. The pH was measured with a Hitachi-Horiba, Model F-5, glass electrode pH meter. A shaker of Iwaki KM was used.

Established Procedure. Take 29.3 μg of cobalt(II) in a 100-m*l* separatory funnel and add 10 m*l* of the H_2QS solution and 3 m*l* of the zephiramine solution. Adjust pH to 7.3—7.5 with 15 m*l* of phosphate buffer solution and dilute to 50 m*l* with deionized water. Add 10 m*l* of chloroform, shake the mixture for 15 min and then allow the layers to separate for 10 min. Draw off the chloroform layer into a beaker containing anhydrous sodium sulphate and transfer the extract into a cell. Measure the absorbance at 405 nm against the reagent blank obtained in the same way.

Results and Discussion

Absorption Spectra. The absorption spectra of the aqueous layer and the organic extract obtained by the above procedure are given in Figs. 1 and 2, respectively. With increasing pH values, the absorption maxima of the cobalt(II)-H_2QS complexes in water shifted to longer wavelengths, *viz.*, 365 nm at pH 4.7, 370 nm at pH 5.3, and 375 nm at pH 7.9.

The ternary complex formed by the interaction of zephiramine with cobalt(II)-H_2QS complex anion had an absorption maximum at 405 nm both in the aqueous and organic layers (Figs. 1 and 2).

The bathochromic effect is probably due to the increment of molecular cross section caused by the combination with zephiramine. An ion-pair of H_2QS with zephiramine was also extracted but the absorbance at 405 nm was very low.

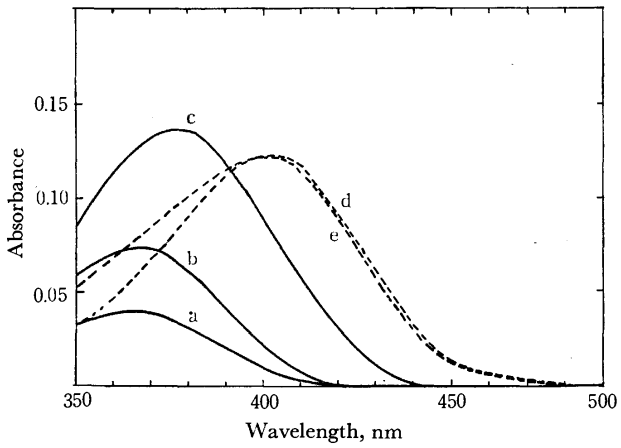

Fig. 1. Absorption spectra of Co(II)-QS and Co(II)-QS-Z complex in aqueous layer
Curve (a) $[Co(II)]_w=1.0\times10^{-5}$M, $[QS]_w=2,0\times10^{-4}$M, pH 4.7, (b) pH 5.3, (c) pH 7.9.
Curve (d) $[Co(II)]_w=1.0\times10^{-5}$M, $[QS]_w=2.0\times10^{-4}$M, $[Z]_w=3.0\times10^{-4}$M, pH 4.7, (e) pH 7.4.
Reference: Reagent blank.

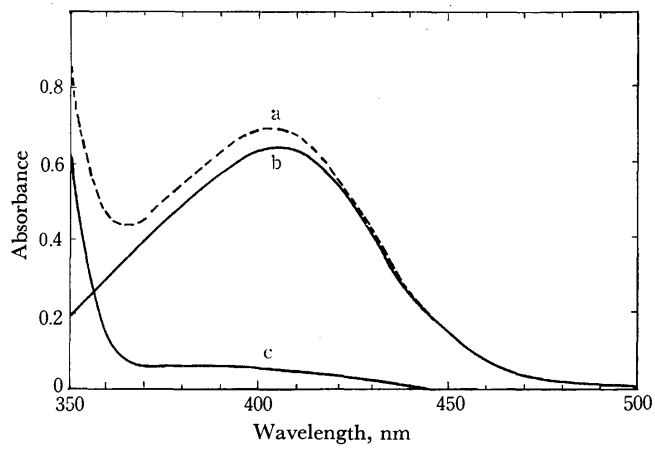

Fig. 2. Absorption spectra of the ternary complex Co(II)-QS-Z in chlorofrom
$[Co(II)]_w=1.0\times10^{-5}$M, $[QS]_w=2.0\times10^{-4}$M, $[Z]_w=3.0\times10^{-4}$M, pH 7.4, Volume of aq. layer $V_w=$ 50 m*l*, Volume of org. layer $V_o=10$ m*l*, Curve (a) *vs.* $CHCl_3$, (b) *vs.* reagent blank, (c) Reagent balnk *vs.* $CHCl_3$.

Effect of pH. The aqueous layer containing 29.3 μg of cobalt(II) was adjusted to various pH values and treated by the above procedure. It was found that the extraction of the ternary complex began at pH 3.0 and the pH range for the optimum extraction was 6.8—9.3 with phosphate and borate buffer solutions. Yamamoto[7] and Tôei[8] successfully employed nitrobenzene for the extraction of ion-pairs of tetracyanatonickelate(II) anion with bis(1,10-phenanthroline)iron(II) chelate cation and alkaline metals with picrate anion, respectively. Extraction with nitrobenzene was carried out by the above procedure. The absorbance measurement was made at 430 nm, the wavelength of the absorption maximum of the nitrobenzene extract. The optimum pH range was 7.6—8.3.

Effect of H_2QS Concentration. With the concentrations of cobalt(II) and zephiramine kept constant, various amounts of H_2QS were added and extraction was carried out by the above procedure. The absorbance of the organic layer was found to be constant and maximum in the concentration range 7—30-fold mol of H_2QS to cobalt(II). However, H_2QS in concentration higher than 30-fold of cobalt(II) lowered the absorbance of the extract. Therefore, the H_2QS concentration was kept to 20-fold to cobalt(II).

Effect of Zephiramine Concentration. The zephiramine concentration was varied for a series of extractions while the cobalt(II) and H_2QS concentrations were kept constant. The absorbance of the extract was measured against the reagent blank. It was found that the optimum molar concentration of zephiramine lies in 20—40-fold of cobalt(II). Further addition of zephiramine increases the absorbance of the extract gradually. Thus the concentration of zephiramine was kept to 30-fold of cobalt(II) throughout the procedure.

7) Y. Yamamoto, T. Kumamaru, S. Miura, and S. Kimura, *Nippon Kagaku Zasshi*, **92**, 64 (1971).
8) M. Yamane, T. Iwachido, and K. Tôei, This Bulletin, **44**, 745 (1971).

Effect of Shaking Time. The shaking time was varied from 30 sec to 30 min. Stable and constant absorbance of the extract was found for a shaking time longer than 10 min.

Extractability, Distribution Ratio, and Molar Absorptivity. Extractability under optimum conditions was determined by repetition of the extraction procedure on the same aqueous layer. A 50 m*l* portion of the aqueous layer containing 29.3 μg of cobalt(II) was shaken with 10 m*l* of chloroform. Twenty five milliliters of separated aqueous layer was again shaken with 5 m*l* of chloroform, followed by re-extraction on the 20 m*l* of the aqueous layer with 4 m*l* of chloroform. Absorbances A_1, A_2, and A_3 of each extract in sequence were measured. The extractability is then given by

$$E_{max} = \frac{A_1}{A_1+A_2+A_3} \times 100$$

$$= \frac{0.650}{0.650+0.038+0.002} \times 100 = 94.2\%$$

where A_i is the absorbance of each extract at 405 nm. Thus, distribution ratio D_{max} is

$$D_{max} = \frac{E_{max}}{100-E_{max}} \times \frac{V_w}{V_0} = 69.3$$

Molar absorptivity ε of the ternary complex calculated by using absorbance A_1 and E_{max} is

$$\varepsilon = 1.39 \times 10^4 \text{ cm}^{-1} \text{ mol}^{-1} \, l$$

The molar absorptivity is larger than 8500, that of the oxine complex $CoOx_2(C_4H_9NH_2)_2$.[9] In the case of the extraction with nitrobenzene, 98.5% of cobalt(II) was extracted by one extraction and the distribution ratio was 337.4. However, the molar absorptivity was 1.09×10^4.

Calibration Curve. Varying amounts of cobalt(II) were added to the aqueous layer and extraction was carried out. For the first extract, Beer's law holds for 2.73—33.0 μg of cobalt(II). Sandell's sensitivity for the absorbance of 0.001 is 0.0042 μg/cm^2. The relative standard deviation obtained by 7 measurements was 0.63% for the 29.3 μg of cobalt(II).

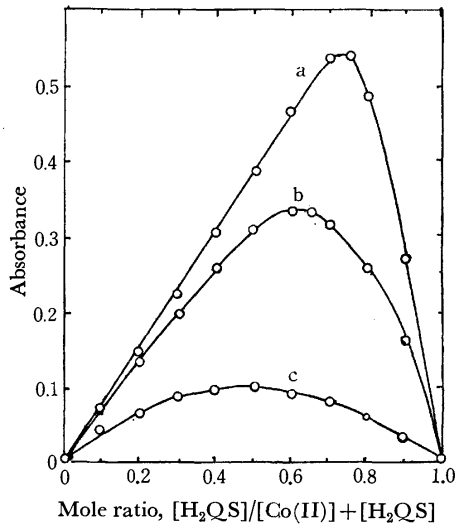

Fig. 3. Continuous variation method applied to Co(II)-H_2QS chelate in water
[Co(II)]+[H_2QS]=2.00×10^{-4}M,
Curve (a) pH 7.6, Wavelength: 375 nm,
(b) pH 5.8, Wavelength: 370 nm,
(c) pH 4.4, Wavelength: 365 nm.

Composition of Cobalt(II)-H_2QS Complexes. The results of continuous variation method (Fig. 3) indicate that molar ratios of H_2QS to cobalt(II) are 1:1 at pH 4.4, 2:1 at pH 5.8, and 3:1 at pH 7.6. The same results were obtained also by the mole ratio method. The results coincide with those by the potentiometric method.[5]

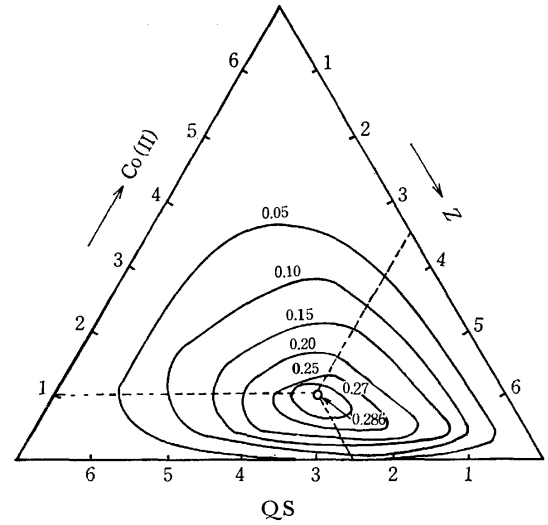

Fig. 4. Continuous variation method applied to the three-component system of Co(II)-QS-Z complex
V_w=50 m*l*, V_0=10 m*l*, [Co(II)]$_w$+[QS]$_w$+[Z]$_w$=7.00×10^{-5}M, pH 7.4, Wavelength: 405 nm,
Reference: Chloroform,
Numerals show the absorbance of organic layer.

Composition of the Ternary Complex. Determination of the composition of the ternary complex in the organic layer was attempted by means of the triangular coordinate method for three-component system.[1-3] The sum of the initial concentrations of cobalt(II), H_2QS and zephiramine in the aqueous layer being kept to 7.00×10^{-5}M, extraction was carried out at 74 points of various compositions. The absorbance of the extract was measured against chloroform. The contours in Fig. 4 show a composition of equal absorbance. The maximum absorbance was obtained in the composition of cobalt(II): H_2QS: zephiramine=1:2.5:3.5. However, results of the continuous variation method applied to the system of the cobalt(II)-H_2QS complex in the presence of excess zephiramine indicated that the composition of the ternary complex was cobalt(II): H_2QS: zephiramine=1:3:3. The same result was also obtained by applying the mole ratio method. We see that the contour which indicates the absorbance of 0.050 partially overlaps the QS-axis (Fig. 4). Deviation of the triangular method from continuous variation and mole ratio methods therefore seems to be due to the effect of absorption by the ion-pair of H_2QS with zephiramine. Thus, the composition of the ternary complex was estimated to be $[Co^{2+}(QS^{2-})_2(HQS^-)(Z^+)_3]_0$.

Equilibrium Constant For Extraction of The Ternary

9) F. Umland, *Z. Anal. Chem.*, **190**, 186 (1962).

Complex. When the ternary complex is extracted into chloroform, the extraction equilibrium is given as follows:

$$Co^{2+} + 3[(HQS^{-}Z^{+})]_o + 2OH^{-} = [Co^{2+}(QS^{2-})_2(HQS^{-})(Z^{+})_3]_o + 2H_2O \quad (1)$$

where suffix o indicates the organic layer. The equilibrium constant K is given by

$$K = \frac{[Co^{2+}(QS^{2-})_2(HQS^{-})(Z^{+})_3]_o}{[Co^{2+}][(HQS^{-}Z^{+})]_o^3[OH^{-}]^2} \quad (2)$$

The initial concentration of cobalt(II) in 50 m*l* aqueous layer is kept at *C, those of H_2QS and zephiramine at 3*C and the pH of the aqueous layer at 7.4, and the layer is shaken with 10 m*l* of chloroform. The absorbance of the organic layer is measured against chloroform after equilibrium is attained. The concentration of the ternary complex in the organic layer C_T is calculated from the molar absorptivity. Equation (2) is then expressed by

$$K = \frac{C_T}{\left[*C - \frac{10}{50}C_T\right]\left[\frac{50}{10}\times 3*C - 3C_T\right]^3[OH^{-}]^2} \quad (3)$$

The results obtained with various values of initial concentration *C are shown in Table I. The logarithm of the equilibrium constant is 29.01±1.86.

Table 1. Equilibrium constant of Co(II)-QS-Z ternary complex shown by Eq. (1)—(3)

*C (M)	Absorbance	C_T (M)	pH	log K
1.0×10^{-5}	0.256	1.84×10^{-5}	7.34	28.15
5.0×10^{-6}	0.095	6.83×10^{-6}	7.35	29.29
2.5×10^{-6}	0.035	2.52×10^{-6}	7.35	29.58

Ionic strength μ=0.064, Molar absorptivity $\varepsilon=1.39\times10^4$ cm^{-1} mol^{-1} l, Temp. 18.5°C, *C=Initial concn of Co(II) in 50-m*l* aqueous layer, 3*C=Initial concn. of H_2QS and Z^+ in 50-m*l* aqueous layer, C_T=Final concn. of the ternary complex in 10-m*l* $CHCl_3$-extract.

BULLETIN OF THE CHEMICAL SOCIETY OF JAPAN, VOL. 45, 1433—1438(1972)

The Reaction and Reaction Products of μ-O_2-Dicobalt Ammine Complexes with Nitrites, Thiocyanates, *etc.*[1]

Takashi SHIBAHARA and Masayasu MORI

Faculty of Science, Osaka City University, Sugimoto-cho, Sumiyoshi-ku, Osaka

(Received December 14, 1971)

In a neutral solution $[NH_3(en)_2CoO_2Co(en)_2NH_3]^{4+}$ was found to react with NO_2^- and SCN^- to give $[NO_2(en)_2CoO_2Co(en)_2NO_2]^{2+}$ and $[SCN(en)_2CoO_2Co(en)_2NCS]^{2+}$ respectively, without causing any cleavage of the O_2-bridge, while in an acid solution it was found to be oxidized by NO_2^- to a μ-superoxo (O_2^-) complex ion, $[NH_3(en)_2CoO_2Co(en)_2NH_3]^{5+}$. The latter is not affected by NO_2^-, in contrast with $[(en)_2Co(\mu\text{-}NH_2,O_2)Co(en)_2]^{4+}$, in which the O_2^--bridge is replaced by an NO_2^--bridge. The $[NO_2(en)_2CoO_2Co(en)_2NO_2]^{2+}$ formed as described reacts with CN^- to give $[Co_2(CN)_6(en)_2O_2]^{2-}$. The EPR spectra of some new μ-superoxo complexes which were synthesized by oxidizing some of the above μ-peroxo complexes were measured and compared with those of similar complexes. Infrared and electronic spectra were also taken.

The reactions of binuclear complexes of cobalt, in which two cobalt atoms are connected by both NH_2 and O_2 ligands, have been studied by many investigators, and various specific features have been found, as is shown by the following examples:

$$[(NH_3)_4Co^{NH_2}_{O_2}Co(NH_3)_4]^{4+} \xrightarrow[H^+]{NO_2^-}$$

μ-superoxo, green

$$[(NH_3)_4Co^{NH_2}_{NO_2}Co(NH_3)_4]^{4+} \quad (1)^{2}$$

orange

$$[(NH_3)_4Co^{NH_2}_{O_2}Co(NH_3)_4]^{4+} \xrightarrow[H^+]{SO_3^{2-}}$$

μ-superoxo, green

$$[(NH_3)_4Co^{NH_2}_{SO_4}Co(NH_3)_4]^{3+} \quad (2)^{3}$$

reddish violet

The reactions of the $[(NH_3)_5CoO_2Co(NH_3)_5]^{n+}$ complexes (n=4, 5), containing an O_2 single bridge, were also studied; in this case, the cleavage of the O_2-bridge and the formation of a mononuclear cobalt(III) ammine complex and/or a cobalt(II) ion is the usual mode of reaction:

$$[(NH_3)_5CoO_2Co(NH_3)_5]^{5+} \xrightarrow[H^+]{NO_2^-}$$

μ-superoxo, green

$$[CoOH_2(NH_3)_5]^{3+} + Co^{2+} \quad (3)^{4}$$

$$[(NH_3)_5CoO_2Co(NH_3)_5]^{4+} \xrightarrow[H^+]{}$$

μ-peroxo, brown

$$2Co^{2+} + O_2 + 10NH_3 \quad (4)^{5}$$

However, the last two examples do not seem to depend solely on the nature of the O_2 bridge, since the starting material itself is comparatively unstable. In this respect, the reaction of the more stable single-O_2-bridged

1) Presented at the 21st Conference on Coordination Chemistry of the Chemical Society of Japan, Nagoya, October (1971), Proceedings, p. 115.

2) A. Werner, F. Salzer, and M. Pieper, *Ann.*, **375**, 54 (1910).

3) A. G. Sykes and R. D. Mast, *J. Chem. Soc., A*, **1967**, 784.

4) A. G. Sykes, *Trans. Faraday Soc.*, **59**, 1325 (1963).

5) A. Werner and A. Mylius, *Z. Anorg. Chem.*, **16**, 245 (1898).

complex, $[NH_3(en)_2CoO_2Co(en)_2NH_3]^{n+}$, was thought to reflect the nature of the O_2 bridge more clearly. Therefore, we started to study the reaction of this complex with nitrites, thiocyanates, sulfites, etc. As a result, several new compounds with a peroxo or a superoxo bridge were obtained; they were examined by various spectroscopic techniques, such as UV, IR, and EPR.

Experimental

Reaction and Preparation. *1. μ-Peroxobis[amminebis(ethylenediamine)cobalt(III)] Triperchlorate Nitrate Dihydrate*: This compound was prepared by the method of Duffy *et al.*[6] Though they described the compound as a tetraperchlorate dihydrate, a definite amount of the nitrate ion has been detected in the sample even after multiple recrystallizations with sodium perchlorate. The nitrate ion was determined as follows: the anions were separated by passing a solution through cation-exchange resin in the Na-form (DIAION SK#1), the nitrate ion was reduced to ammonia using Devarda's alloy, and the ammonia which came over by distillation was titrated.

Found: Co, 14.18; C, 11.73; H, 4.89; N(total), 18.79; NO_3^-, 7.69%. Calcd for $[NH_3(en)_2CoO_2Co(en)_2NH_3](ClO_4)_3\cdot NO_3\cdot 2H_2O$: Co, 14.36; C, 11.71; H, 5.16; N(total), 18.78; NO_3^-, 7.56%.

2. Reaction of $[NH_3(en)_2CoO_2Co(en)_2NH_3]^{4+}$ with NO_2^- in an Acid Solution: Brown μ-peroxobis[amminebis(ethylenediamine)cobalt(III)] triperchlorate nitrate dihydrate was added to an acid solution (0.05N HCl) of sodium nitrite. The solution immediately turned green. The electronic spectrum of the green solution was identical with that of $[NH_3(en)_2CoO_2Co(en)_2NH_3]^{5+}$, which had been prepared by oxidizing the same starting 4+ ion with chlorine gas.

3. Reaction of $[NH_3(en)_2CoO_2Co(en)_2NH_3]^{4+}$ with NO_2^- in a Neutral Solution at Room Temperature: *3·1. Preparation of μ-Peroxobis[nitrobis(ethylenediamine)cobalt(III)] Dinitrate Tetrahydrate*: Thirty-three grams of μ-peroxobis[amminebis(ethylenediamine)cobalt(III)] triperchlorate nitrate dihydrate (2 above) was added to 500 ml of water containing 27 g of potassium nitrite. After this solution had been cooled in an ice bath, it was filtered and the precipitate (mainly potassium perchlorate) was discarded. The brown solution was evaporated almost to dryness using a rotary evaporator, while the temperature was kept at approximately 30°C. The product was washed successively with 50% ethanol, 95% ethanol, and ethyl ether. Yield, 20 g. This product will be named A. On the dissolution of 5 g of A in 80 ml of water at 40°C, followed by filtration and cooling, black crystals were precipitated. These crystals were washed with 95% ethanol and ethyl ether. Yield, 2 g.

Found: C, 14.21; H, 5.87; N, 24.95%. Calcd for $[NO_2(en)_2CoO_2Co(en)_2NO_2](NO_3)_2\cdot 4H_2O$: C, 14.19; H, 5.94; N, 24.80%.

3·2. Preparation of μ-Peroxobis[nitrobis(ethylenediamine)cobalt(III)] Dithionate Pentahydrate: Ten grams of sodium dithionate dihydrate was added to 10 g of A in 1 l of water. The brown precipitate that deposited was collected by filtration and washed successively with cold water, 95% ethanol, and ethyl ether, and then air-dried. Yield, 9.4 g. The sample (1 g) was recrystallized by dissolving it in 2 l of water at 30°C and by then adding 10 g of sodium dithionate dihydrate to the cooled, filtered solution. The brown crystalline material that was thus deposited was collected, washed, and dried as above. Yield, 0.3 g.

Found: Co, 16.38; C, 13.71; H, 5.81; N, 19.45%. Calcd for $[NO_2(en)_2CoO_2Co(en)_2NO_2]S_2O_6\cdot 5H_2O$: Co, 16.09; C, 13.12; H, 5.78; N, 19.15%.

3·3. Preparation of μ-Peroxobis[nitrobis(ethylenediamine)cobalt(III)] Dichloride Tetrahydrate: The A product (1 g; *cf.* 3·1), dissolved in 80 ml of water, was added to the top of the anion-exchange resin, Cl-form (DIAION SA#100), which was then washed with water. The effluent was evaporated to dryness with a rotary evaporator. The brown product was washed with 95% ethanol and ethyl ether. Yield, 0.1 g. It is very soluble in water.

Found: C, 15.91; H, 6.74; N, 22.64%. Calcd for $[NO_2(en)_2CoO_2Co(en)_2NO_2]Cl_2\cdot 4H_2O$: C, 15.37; H, 6.45; N, 22.56%.

4. The Oxidation Product of the μ-Peroxobis[nitrobis(ethylenediamine)cobalt(III)] Complex: *4·1. μ-Superoxobis[nitrobis(ethylenediamine)cobalt(III)] Triperchlorate Dihydrate*: Three grams of brown μ-peroxobis[nitrobis(ethylenediamine)cobalt(III)] dithionate pentahydrate (*cf.* 3·2) was stirred into 200 ml of a 0.2N hydrochloric acid solution, while a slow stream of chlorine gas was bubbled through the solution. As portions of the solid were added, the solution turned green. After about 5 min, the unreacted solid was filtered off and twenty grams of sodium perchlorate monohydrate was added to the ice-cooled filtrate. The green precipitate that deposited was collected by filtration and washed successively with water, 95% ethanol, and ethyl ether. Yield, 1.3 g. To recrystallize, as much of the sample as possible (1 g) was dissolved in 400 ml of water at 25°C, and then 5 g of sodium perchlorate monohydrate was added to the cooled filtered solution. The green crystalline material that was thus deposited was collected and washed as above. Yield, 0.8 g.

Found: Co, 14.25; C, 11.87; H, 4.42; N, 17.49%. Calcd for $[NO_2(en)_2CoO_2Co(en)_2NO_2](ClO_4)_3\cdot 2H_2O$: Co, 14.42; C, 11.78; H, 4.44; N, 17.17%.

4·2. μ-Superoxobis[nitrobis(ethylenediamine)cobalt(III)] Trithiocyanate Dihydrate: This complex was prepared similarly, using sodium thiocyanate instead of sodium perchlorate.

Found: Co, 17.04; C, 19.54; H, 5.25; N, 27.45; S, 14.66%. Calcd for $[NO_2(en)_2CoO_2Co(en)_2NO_2](SCN)_3\cdot 2H_2O$: Co, 17.03; C, 19.10; H, 5.24; N, 26.30; S, 13.88%.

4–3. μ-Superoxobis[nitrobis(ethylenediamine)cobalt(III)] Sesquisulfate Tetrahydrate: Five-tenths of a gram of the triperchlorate dihydrate (4·1 above) was dissolved in 60 ml of 6N sulfuric acid. Five hundred milliliters of ethanol was then stirred into the filtered solution. The green precipitate that was thus deposited was collected and washed successively with 95% ethanol and ethyl ether. Yield, 0.4 g. The sample (0.4 g) was recrystallized by dissolving it in 20 ml of a 0.5N sulfuric acid solution at room temperature and by then adding 50 ml of 95% ethanol to the filtered cooled solution. Yield, 0.2 g.

Found: Co, 16.58; C, 13.73; H, 5.29; N, 19.97%. Calcd for $[NO_2(en)_2CoO_2Co(en)_2NO_2]_2(SO_4)_3\cdot 8H_2O$: Co, 16.87; C, 13.75; H, 5.77; N, 20.05%.

5. Reaction of $[NO_2(en)_2CoO_2Co(en)_2NO_2]^{2+}$ with NO_2^- in a Neutral Solution at a High Temperature. The formation of trans-$[Co(NO_2)_2(en)_2]NO_3$: Twenty milliliters of water containing 0.7 g of μ-peroxobis[nitrobis(ethylenediamine)cobalt(III)] dinitrate tetrahydrate (*cf.* 3·1) and 1 g of sodium nitrite were warmed on a water bath at about 80°C for 2 hr. During the process, water was sometimes supplied. While hot, the solution was filtered, and a little 14N nitric acid was added to the filtered, cooled solution. The yellow crystals that

6) D. L. Duffy, D. A. House, and J. A. Weil, *J. Inorg. Nucl. Chem.*, **31**, 2053 (1969).

were thus deposited were filtered and washed with 95% ethanol and ethyl ether. Yield, 0.3 g.

Found: Co, 17.01; C, 14.38; H, 5.46; N, 29.13%. Calcd for $[Co(NO_2)_2(en)_2]NO_3$: Co, 17.68; C, 14.42; H, 4.84; N, 29.41%. The complex was concluded to be *trans* isomer by a comparison of its electronic spectrum with that of the known sample.

6. Reaction of $[NH_3(en)_2CoO_2Co(en)_2NH_3]^{4+}$ *with* SCN^-: Sixteen and four-tenths grams of μ-peroxobis[amminebis(ethylenediamine)cobalt(III)] triperchlorate nitrate dihydrate was added to a stirred solution of 15.6 g of potassium thiocyanate in 250 m*l* of water. The crude product (14 g) was obtained by the vacuum evaporation of this mixture, as in the case of 3·1. This product was named B. Five grams of B was dissolved in 250 m*l* of water at 40°C, and 50 g of sodium perchlorate monohydrate was added to the cooled filtrate. The brown precipitate that was thus deposited was collected by filtration and washed with 95% ethanol and ethyl ether. Yield, 3.6 g. The sample (3.6 g) was recrystallized by dissolving it in 250 m*l* of water at 40°C and by adding $NaClO_4 \cdot H_2O$ (50 g) to the cooled, filtered solution. The brown crystalline material that was thus deposited was collected and washed as above. Yield, 1.7 g.

Found: Co, 15.18; C, 16.09; H, 5.21; N, 18.36; S, 7.98%. Calcd for $[SCN(en)_2CoO_2Co(en)_2NCS](ClO_4)_2 \cdot 4H_2O$: Co, 15.16; C, 15.46; H, 5.18; N, 18.02; S, 8.25%.

7. Oxidation Product of $[SCN(en)_2CoO_2Co(en)_2NCS]^{2+}$: Ten milliliters of 14N nitric acid was added to 1 g of B (Exp. 6). The green solution obtained by this procedure was cooled in a refrigerator. The green crystals that deposited were washed with a little cold water, methanol, and ethyl ether. Yield, 0.1 g.

Found: C, 11.96; H, 5.21; N, 27.17%. Calcd for $[NH_3(en)_2CoO_2Co(en)_2NH_3](NO_3)_5 \cdot 2H_2O$: C, 12,46; H, 5.46; N, 27.13%.

8. Reaction of $[NO_2(en)_2CoO_2Co(en)_2NO_2]^{2+}$ *with* CN^-. *Preparation of* $K_2[Co_2(CN)_6(en)_2O_2] \cdot 5H_2O$: Two hundred milliliters of a solution containing 14 g of μ-peroxobis[nitrobis(ethylenediamine)cobalt(III)] dinitrate tetrahydrate and 26 g of potassium cyanide were warmed in a water bath at 35°C for 5 hr. Six hundred milliliters of methanol was added to the cooled, filtered solution. The precipitate that was thus deposited was filtered and washed with ethanol and ethyl ether. Yield, 7 g. The sample (7 g) was recrystallized by dissolution in 15 m*l* of water and filtration; this was followed by the successive addition of 20 m*l* of water and 200 m*l* of methanol. The precipitate that was thus deposited was again filtered and washed as above. Yield, 4.6 g. Recrystallization was repeated by dissolving this recrystallized sample (4 g) in 10 m*l* of water at 40°C and by stirring 10 m*l* of methanol (50°C) into the filtered solution. This solution was cooled in a refrigerator. The fragile, crystalline, red-brown precipitate that was thus deposited was washed with 60% methanol, pure methanol, and ethyl ether. Yield, 0.35 g.

Found: Co, 19.71; C, 20.40; H, 4.77; N, 23.71; K, 13.60%. Calcd for $K_2[Co_2(CN)_6(en)_2O_2] \cdot 5H_2O$: Co, 19.83; C, 20.21; H, 4.41; N, 23.59; K, 13.16%.

9. Oxidation Product of $[Co_2(CN)_6(en)_2O_2]^{2-}$. *The Preparation of* $H[Co_2(CN)_6(en)_2O_2] \cdot 4H_2O$: Five tenths of a gram of red-brown $K_2[Co_2(CN)_6(en)_2O_2] \cdot 4H_2O$ was added to 5 m*l* of water while a stream of chlorine gas was bubbled in. The violet solution obtained by this procedure was added to the cation-exchange resin in the H-form (DIAION SK#1) which had been washed with water. The effluent was then stirred into acetone (150 m*l*). The violet precipitate was washed with acetone. Yield 0.3 g.

Found: Co 23.40; C 25.23; H 5.18; N 28.34; H^+ (neutralization titration) 0.200%. Calcd for $H[Co_2(CN)_6(en)_2O_2] \cdot 4H_2O$: Co 23.62; C, 24.08; H, 5.05; N, 28.10; H^+, 0.201%.

10. Reaction of $[NH_3(en)_2CoO_2Co(en)_2NH_3]^{4+}$ *with* SO_3^{2-}: Sixteen and four-tenths grams of μ-peroxobis[amminebis(ethylenediamine)cobalt(III)] triperchlorate nitrate dihydrate was stirred into a solution of 25.2 g of potassium sulfite in 200 m*l* of water. A crude yellow product (25 g) was obtained by the vacuum evaporation of this mixture, as in the case of 3·1. The sample was recrystallized from a dilute sodium sulfite solution. The electronic spectrum was identical with that of *trans*-$[Co(SO_3)_2(en)_2]^-$, which was prepared from *trans*-$[CoCl_2(en)_2]^+$ by a known method.[7]

Apparatus. The visible and UV absorption measurements were carried out with a Hitachi EPS-3T spectrometer. IR spectra were recorded on a Jasco IR-E spectrometer, while the EPR spectra were recorded on a JEOL JES-3B spectrometer at room temperature. The pH measurements were carried out with a Hitachi-Horiba M-5 pH meter.

Results and Discussion

The reaction scheme elucidated in the present research is summarized in Chart 1. Some characteristic features will now be discussed in detail.

Reaction of $[NH_3(en)_2CoO_2Co(en)_2NH_3]^{n+}$ $(n=4, 5)$ *with* NO_2^-. As expected, $[NH_3(en)_2CoO_2Co(en)_2NH_3]^{n+}$ is far more stable than $[(NH_3)_5CoO_2Co(NH_3)_5]^{n+}$; in fact, the Co-$O_2$-Co linkage in the former showed a remarkable stability to various reagents in a neutral solution. Thus, at room temperature, the μ-peroxo complex $[NH_3(en)_2CoO_2Co(en)_2NH_3]^{4+}$ in a neutral solution reacts with NO_2^- to give a new μ-peroxo complex $[NO_2(en)_2CoO_2Co(en)_2NO_2]^{2+}$, without any cleavage of the O_2-bridge (Exp. 3). This is thought to be the first example in which the O_2-bridge remains intact in the reaction of the μ-O_2 complex with NO_2^- (Compare with the cases shown in Eqs. (1) and (3)). At about 80°C, $[NO_2(en)_2CoO_2Co(en)_2NO_2]^{2+}$ further reacts with NO_2^- to give *trans*-$[Co(NO_2)_2(en)_2]^+$ (Exp. 5), but it seems difficult to discuss the steric configuration of the starting material, since rearrangement may occur in the course of the reaction. Sasaki *et al.* reported that NH_3 in $[NH_3(en)_2CoO_2Co(en)_2NH_3]^{4+}$ is replaced comparatively easily, and that in water the complex is readily changed to $[(en)_2Co(\mu\text{-}OH,O_2)Co(en)_2]^{3+}$.[8] It thus seemed worthwhile to test if $[(en)_2Co(\mu\text{-}OH,O_2)Co(en)_2]^{3+}$ is the intermediate product in our reaction on the way from $[NH_3(en)_2CoO_2Co(en)_2NH_3]^{4+}$ to $[NO_2(en)_2CoO_2Co(en)_2NO_2]^{2+}$. This possibility was eliminated, however, since $[(en)_2Co(\mu\text{-}OH,O_2)Co(en)_2]^{3+}$, which had been prepared by the method of Foong *et al.*,[9] did not react with NO_2^- to give $[NO_2(en)_2CoO_2Co(en)_2NO_2]^{2+}$. However, it is still possible that an aquo-substituted complex, $[H_2O(en)_2CoO_2Co(en)_2OH_2]^{4+}$, is formed as an intermediate product.

7) M. E. Baldwin, *J. Chem. Soc.*, **1961**, 3123.

8) Y. Sasaki, J. Fujita, and K. Saito, the 20th Conference on Coordination Chemistry of the Chemical Society of Japan, Tokyo, November (1970), Proceedings, p. 17; This Bulletin, to be published.

9) S. W. Foong, J. E. Miller, and F. D. Oliver, *J. Chem. Soc.*, *A*, **1969**, 2848.

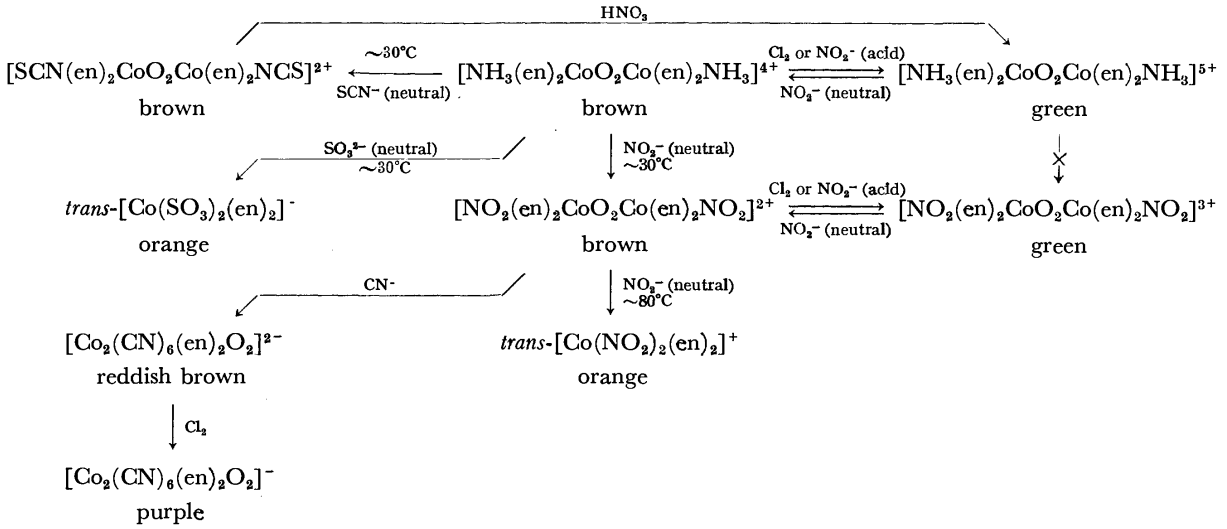

Chart 1. Reaction scheme of μ-O_2 dicobalt complexes

In an acid solution, the μ-peroxo complex $[NH_3(en)_2CoO_2Co(en)_2NH_3]^{4+}$ is easily oxidized by NO_2^- to the corresponding μ-superoxo complex $[NH_3(en)_2CoO_2Co(en)_2NH_3]^{5+}$ (Exp. 2), and the latter does not further react with NO_2^- to give $[NO_2(en)_2CoO_2Co(en)_2NO_2]^{3+}$. In other words, the NH_3 in the μ-superoxo complex $[NH_3(en)_2CoO_2Co(en)_2NH_3]^{5+}$ is not replaced by NO_2^-, in contrast with the NH_3 in the corresponding μ-peroxo (4+) complex (see above). Nor is the O_2-bridge in $[NH_3(en)_2CoO_2Co(en)_2NH_3]^{5+}$ replaced by NO_2^-. This is in contrast with the reaction of the double-bridged complex with NO_2^- cited in Eq. (1). Thus, the additional NH_2-bridge seems to play an important role in the transformation of the O_2-bridge to the NO_2-bridge. Davies *et al.* explained the easier reduction of $[(en)_2Co(\mu\text{-}NH_2,O_2)Co(en)_2]^{4+}$ by I^- by supposing that the presence of the NH_2-bridge places more strain on the O_2-bridge and places it more outside of the complex.[10] This idea may also explain the present situation.

The nitro-substituted μ-superoxo complex $[NO_2(en)_2CoO_2Co(en)_2NO_2]^{3+}$ may be obtained by the oxidation of the corresponding μ-peroxo (2+) ion described above by Cl_2 or even by NO_2^- (Exp. 4).

Reaction of $[NH_3(en)_2CoO_2Co(en)_2NH_3]^{4+}$ *with* SCN^-. In a neutral solution, $[NH_3(en)_2CoO_2Co(en)_2NH_3]^{4+}$ reacts with SCN^- to give $[SCN(en)_2CoO_2Co(en)_2NCS]^{2+}$ (Exp. 6) similarly to the case of $[NO_2(en)_2CoO_2Co(en)_2NO_2]^{2+}$. The preparation of the corresponding μ-superoxo complex has not yet been successful, for the reagents that oxidize the peroxo bridge to superoxo bridge also oxidize SCN^- to NH_3 (Exp. 7). The latter oxidation reaction is known to occur in mononuclear thiocyanato cobalt complexes as well. The above reaction shows that SCN^- coordinates to Co through the nitrogen atom.

Reaction of $[NO_2(en)_2CoO_2Co(en)_2NO_2]^{2+}$ *with* CN^-. $[NO_2(en)_2CoO_2Co(en)_2NO_2]^{2+}$ has been found to react with CN^- to give another new μ-peroxo complex $[Co_2(CN)_6(en)_2O_2]^{2-}$ (Exp. 8), which is then oxidized by chlorine gas to the corresponding μ-superoxo (1—) complex ion. The titration curve (Fig. 1) of $H[Co_2(CN)_6(en)_2O_2]\cdot 4H_2O$ (Exp. 9) showed it to be a strong acid. Analysis by the decomposition of $K_2[Co_2(CN)_6(en)_2O_2]\cdot 5H_2O$ with 12N hydrochloric acid, followed by the use of cation-exchange resin, showed that $[(CN)_5CoO_2Co(en)_2CN]^{2-}$ was the major component, accom-

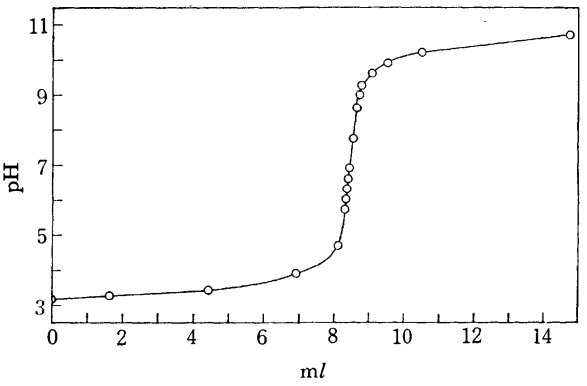

Fig. 1. Titration curve of $H[CO_2(CN)_6(en)_2O_2]\cdot 4H_2O$ solution (0.08890 mmol of complex in 30 m*l* of water) with 0.1043 N NaOH

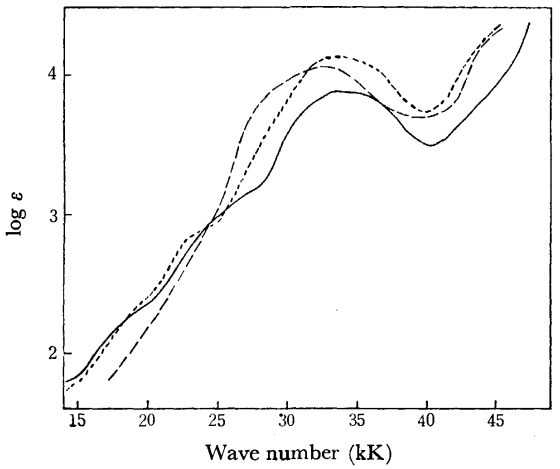

Fig. 2. Electronic spectra of several μ-peroxo dicobalt complexes in water.
——: $[NH_3(en)_2CoO_2Co(en)_2NH_3](ClO_4)_3\cdot NO_3\cdot 2H_2O$
----: $[NO_2(en)_2CoO_2Co(en)_2NO_2]S_2O_6\cdot 5H_2O$
·····: $[SCN(en)_2CoO_2Co(en)_2NCS](ClO_4)_2\cdot 4H_2O$

10) R. Davies and A. G. Sykes, *J. Chem. Soc., A*, **1968**, 2237.

TABLE 1. EPR PARAMETERS OF SEVERAL μ-SUPEROXO Co(III) COMPLEXES AT ROOM TEMPERATURES

Complex	Form	g	A_{Co}(Oe)
$[NO_2(en)_2CoO_2Co(en)_2NO_2](SO_4)_{3/2}\cdot 4H_2O$	40% H_3PO_4	2.026	10.5
$H[Co_2(CN)_6(en)_2O_2]\cdot 4H_2O$	H_2O	2.021	9.00
$[(NH_3)_5CoO_2Co(NH_3)_5](NO_3)_5$	50% H_2SO_4	2.025	11.4[11]
$[NH_3(en)_2CoO_2Co(en)_2NH_3](ClO_4)_4\cdot NO_3\cdot 3H_2O$	H_2O (slightly acid)	2.028	11.0[6]
$K_5[(CN)_5CoO_2Co(CN)_5]\cdot H_2O$	50% H_2SO_4	2.020	8.50[11]

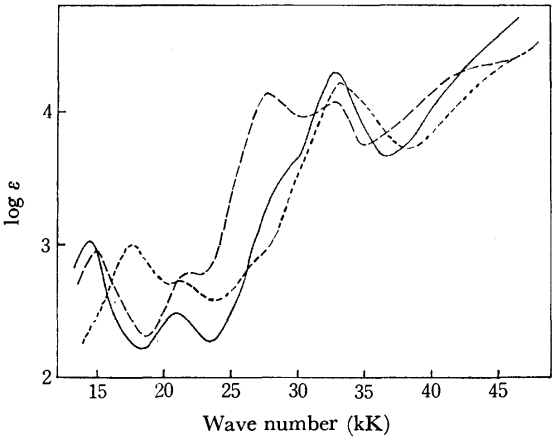

Fig. 3. Electronic spectra of several μ-superoxo dicobalt complexes in water
——: $[NH_3(en)_2CoO_2Co(en)_2NH_3](ClO_4)_4\cdot NO_3\cdot 3H_2O$ (in 0.3 N $HClO_4$)
----: $[NO_2(en)_2CoO_2Co(en)_2NO_2](ClO_4)_3\cdot 2H_2O$ (in 0.3 N $HClO_4$)
·····: $H[Co_2(CN)_6(en)_2O_2]\cdot 4H_2O$ (in water)

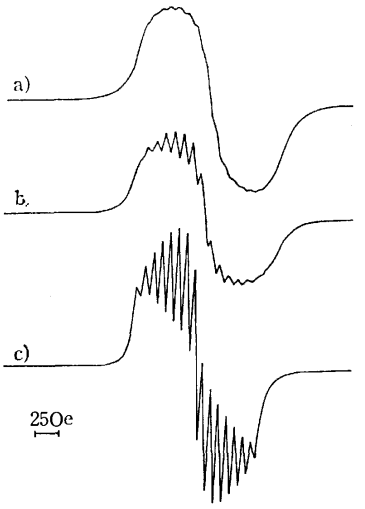

Fig. 4. EPR spectra of several μ-superoxo Co(III) complexes at room temperatures.
a): $[NO_2(en)_2CoO_2Co(en)_2NO_2](SO_4)_{312}\cdot 4H_2O$ in H_2O (slightly acid)
b): $[NO_2(en)_2CoO_2Co(en)_2NO_2](SO_4)_{312}\cdot 4H_2O$ in 40% H_3PO_4
c): $H[Co_2(CN)_6(en)_2O_2]\cdot 4H_3O$ in H_2O

panied by a small quantity of isomeric $[(CN)_3enCoO_2Coen(CN)_3]^{2-}$ (*cf.* Ref. 11).

Reaction of $[NH_3(en)_2CoO_2Co(en)_2NH_3]^{4+}$ *with* SO_3^{2-}. In a neutral solution at room temperature, $[NH_3(en)_2CoO_2Co(en)_2NH_3]^{4+}$ reacts with SO_3^{2-} to give *trans*-$[Co(SO_3)_2(en)_2]^-$ with a cleavage of the O_2-bridge; this is in contrast with the reaction of $[NH_3(en)_2CoO_2Co(en)_2NH_3]^{4+}$ with NO_2^-. Further experiments are in progress.

Electronic, IR, and EPR Spectra. The electronic spectra of the μ-peroxo and μ-superoxo complexes, obtained mainly in the present research, are shown in Figs. 2 and 3 respectively. The spectra of the μ-peroxo complexes (Fig. 2) have similar broad absorption peaks at about 33 kK; they have no clear peaks in the visible region, and the complexes are generally brown. On the other hand, every spectrum of the μ-superoxo complexes (Fig. 3) has characteristic absorption peaks in the visible and ultraviolet regions. The one lying in the 14—18 kK range has a log ε value of about 3, and its position change appreciably with the ligands in the order of the spectrochemical series. The positions of the peaks appearing at about 21 and 33 kK are not much affected by the change in ligands. Some assignments of the absorption bands of μ-superoxo complexes have been offered by several investigators,[12-15] but none of these seems to be conclusive, and further works will be required to explain the spectra satisfactorily. The strong absorption at 28 kK in the spectrum of $[NO_2(en)_2CoO_2Co(en)_2NO_2](ClO_4)_3\cdot 2H_2O$ (Fig. 3) is considered to be the specific absorption band due to NO_2^- ligands. The IR spectra in the NaCl region proved the existence of NO_2, SCN, and CN in related complexes.

The room-temperature EPR spectra are shown in Fig. 4 for the paramagnetic μ-superoxo complexes. The appearance of the hyperfine structure depends upon the experimental conditions, and, in the case of aqueous solutions, considerably concentrated solutions are required. Some of these results, together with those of other workers relevant to the following discussion, are collected in Table 1. It may be seen from the table that the change in ligands does not affect the Zeeman splitting factor, g, very sensitively, but that

11) M. Mori, J. A. Weil, and J. K. Kinnaird, *J. Phys. Chem.*, **71**, 103 (1967).

12) S. Yamada, Y. Shimura, and R. Tsuchida, This Bulletin, **26**, 72 (1953).

13) M. Linhard and M. Weigel, *Z. Anorg. Chem.*, **308**, 254 (1961).

14) J. Barrett, *Chem. Commun.*, **1968**, 874.

15) Y. Sasaki, J. Fujita, and K. Saito, This Bulletin, **42**, 146 (1969).

it does affect the cobalt hyperfine coupling consant, A_{Co}. The low A_{Co} values in cyano- and nitro-substituted complexes suggest that there is less spin density on the ^{59}Co nuclei in these complexes.[11] This may be explained in terms of the lowering of the t_{2g} orbitals caused by π-bonding, and by the subsequent decrease of the hole density therein.

The authors wish to thank Mr. Y. Miura for the EPR measurements and Mr. J. Goda for the elemental analyses.

BULLETIN OF THE CHEMICAL SOCIETY OF JAPAN, VOL. 45, 1438—1442(1972)

The Electrochemical Behavior of the Low-valent Transititon-metal Complexes. I. Nickel-2,2′-Dipyridyl Complexes.

Akira MISONO, Yasuzo UCHIDA, Takamichi YAMAGISHI, and Hironori KAGEYAMA

Department of Industrial Chemistry, Faculty of Engineering, The University of Tokyo, Hongo, Bunkyo-ku, Tokyo

(Received December 15, 1971)

The electrochemical behavior of zero-valent nickel-2,2′-dipyridyl complexes ($Ni(dipy)_2$, $Ni(CH_2CHCN)_2(dipy)$, and $Ni(NCCHCHCN)_2(dipy)$) was examined in a hexamethylphosphoric triamide solution by polarographic and ESR measurements. In the polarography, these complexes were first reduced at a very anodic potential ($E_{1/2}$: about -0.6——-0.8 V *vs.* Ag wire). At this reduction step, the anion radical of the complex was observed for all the complexes by means of ESR analysis. The spectra of the anion radicals and their *g*-values suggested the localization of an unpaired electron on the ligand side. The addition of 2,2′-dipyridyl to the solution increased the height of the second wave, the half-wave potential of which was also more anodic than that of free 2,2′-dipyridyl, and the anion radical of 2,2′-dipyridyl was observed at this reduction step. It was concluded that the dianion species formed at the second reduction step dissociated to give the 2,2′-dipyridyl anion radical, and that the anion radical of the complex was reproduced in the presence of excess 2,2′-dipyridyl.

2,2′-Dipyridyl, with a fairly cathodic reduction potential, are comparable to that of naphthalene,[1] easily coordinates to the transition metal of a high oxidation state as a strong donor. On the other hand, dipyridyl has an acceptor level, as well as a donor level, so as to make it possible to coordinate to the low-valent transition metal.

It seemed that it would be interesting to perform a study of the electrochemical behavior of low-valent transition-metal complexes in relation to the evaluation of the charge distribution on the complexes of lower oxidation state, and the stability of the reduced complex. In basic and polar media, transition-metal complexes of lower oxidation states, such as the anion radical or the dianion species, are expected to exist fairly stably. Hexamethylphosphoric triamide (HMPT), with a large basicity, has been reported to have a potential ability to solvate the alkali metals and anion radicals of aromatic compounds.[2] Therefore, HMPT is an appropriate solvent for the electrochemical study of low-valent transition-metal complexes. The present authors made a study of the electrochemical behavior of zero-valent nickel-dipyridyl complexes in the HMPT solution and found interesting phenomena using polarographic and ESR techniques.

Experimental

Materials. The examined complexes were bis(2,2′-dipyridyl)nickel, bis(acrylonitrile)(2,2′-dipyridyl)nickel, and bis(fumaronitrile)(2,2′-dipyridyl)nickel. The bis(2,2′-dipyridyl)nickel was obtained by de-ethylation from diethyldipyridylnickel in the presence of 2,2′-dipyridyl, which had itself been prepared by the reduction of nickel acetylacetonate with diethylaluminum mono ethoxide in the presence of excess dipyridyl in tetrahydrofuran.[3] After the solution had stood for a long time following the reduction, a dark green complex of bis(2,2′-dipyridyl)nickel precipitated from the solution.

Bis(acrylonitrile)nickel was prepared by the reaction of acrylonitrile with nickel tetracarbonyl in tetrahydrofuran.[4] This complex was treated with excess 2,2′-dipyridyl in ether, refluxing for several hours gave reddish-brown bis(acrylonitrile)(2,2′-dipyridyl)nickel.

The bis(fumaronitrile)(2,2′-dipyridyl)nickel (dark brown) was prepared similarly. 2,2′-Dipyridyl was purified by the sublimation of the reagent, followed by recrystallization from *n*-hexane. Acrylonitrile was fractionally distilled after drying calcium chloride.

Fumaronitrile was recrystallized from ether-hexane.

Tetra-*n*-butylammonium perchlorate was obtained by adding hydroperchloric acid to aqueous tetra-*n*-butylammonium bromide, and it was recrystallized from hot water three times after washing with cold water. HMPT was refluxed over calcium hydride for several hours and was then fractionally

1) B. J. Tabner and J. R. Yandle, *J. Chem. Soc., A*, **1968**, 381.

2) H. W. Sternberg, R. E. Markby, I. Wender, and D. M. Mohilner, *J. Amer. Chem. Soc.*, **89**, 186 (1967); *ibid.*, 91, 4191 (1969); M. Fontanille and P. Sigwalt, *C. R. hebd. Seances Acad. Sci., Ser. C*, **263**, 316 (1966); S. Boileau and P. Sigwalt, *ibid., C*, **262**, 1135 (1966); J. P. Pascault and J. Gole, *ibid., C*, **264**, 115 (1967).

3) T. Saito, Y. Uchida, A. Misono, A. Yamamoto, K. Morifuji, and S. Ikeda, *J. Amer. Chem. Soc.*, **88**, 5198 (1966).

4) G. N. Schrauzer, *ibid.*, **81**, 5310 (1959); **82**, 1008 (1960).

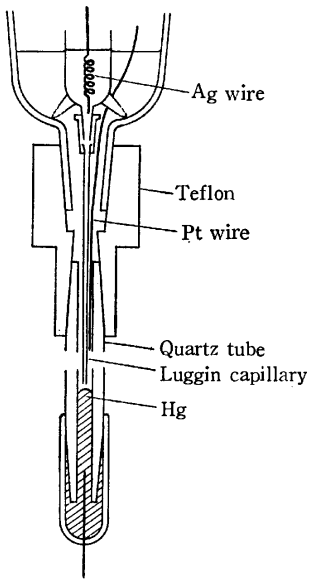

Fig. 1. Electrolytic cell for ESR measurement.

distilled under reduced nitrogen pressure.

Apparatus and Procedure. The polarographic analysis was performed using an H-type cell with a side arm to enable the insertion of an Ag-wire reference electrode.

The cathode was a dropping mercury electrode. The concentration of the complexes was generally 5.0×10^{-3} mol/*l*, while that of tetra-*n*-butylammonium perchlorate was 2.0×10^{-1} mol/*l*. The polarograph used was a Yanagimoto Model PB-105. For the ESR analysis, a electrolytic cell as is shown in Fig. 1 was used. The silver wire used as the reference electrode was dipped into a solution in a small reservoir equipped with a Luggin capillary, whose tip was set near the mercury surface to conduct the controlled potential electrolysis. A platinum wire was used as an anode, it was set about 3 cm from the mercury surface. The complex solution had the same composition as that used for the polarograghic analysis. The ESR spectra were recorded using a JEOL Model JS-3BS-X spectrometer. The electronic spectra of the complex in the HMPT solution were recorded using a Shimadzu MPS-50L spectrophotometer. The complexes to be examined were all air-sensitive, so the preparation and measurement of the complex solutions were performed under nitrogen purified by activated copper.

Results and Disscusion

Polarographic Results on the Complexes. The complexes were stable to only a small degree in solvents, such as acetonitrile, tetrahydrofuran, or ethyleneglycol dimethylether, but they were readily soluble in HMPT, giving strongly colored solutions, as is indicated in Table 1.

Table 1. The color of nickel-dipyridyl complexes

Complex	Solid state	HMPT solution (λ_{max} in mμ)
$Ni(dipy)_2$	dark green	dark green (680)
$Ni(AN)_2(dipy)$	reddish-brown	dark reddish-brown (570, 430, 340)
$Ni(FN)_2(dipy)$	dark brown	dark red (520)

AN: acrylonitrile FN: fumaronitrile

Table 2. Polarographic results on the complexes in HMPT

Compound	Half-wave potential $-E$ V *vs.* Ag wire	Wave height ratio
$Ni(dipy)_2$	0.73 1.00 1.25 1.60 2.05 (67.0) (73.1)[a)]	1.0 : 0.9 : 0.5 : 0.4 : 3.5
$Ni(AN)_2(dipy)$	0.67 1.32 1.94 (65.7) (115.0)	1.0 : 0.9 : 0.1
$Ni(FN)_2(dipy)$	0.87 1.68 2.25 (80.1) (93.7)	1.0 : 1.0 : 0.2
$Ni(AN)_2$	1.74	
$Ni(FN)_2$	1.93	
dipyridyl	2.37 2.80	1.0 : 0.7

a) Values in the parenthesis are the slope of the waves in the log-plott analysis.
Concentration of the compound 5×10^{-3} mol/*l*
$(C_4H_9)_4NClO_4$ concentration 2×10^{-1} mol/*l*

The complexes were stable in HMPT, the color of which did not change over a week under nitrogen.

The polarographic results are shown in Table 2. The first wave of three complexes lie in the range of -0.6——-0.8 V *vs.* Ag wire, which is far anodic than the first reduction wave of dipyridyl and also more anodic than those of acrylonitrile and fumaronitrile. For comparison, bis(acrylonitrile)nickel and bis(fumaronitrile)nickel were also examined. They were reduced at about -1.7——-1.9 V, indicating that the species to be reduced at -0.6——-0.8 V contained dipyridyl in the molecule, at least in the cases of nitrile-containing complexes. The stability of π-coordinated acrylonitrile or fumaronitrile in neutral complexes was affirmed by the CN stretching in the IR spectra of the solid complex, its HMPT solution, and the free nitrile in HMPT. The first reduction step was fairly reversible for $Ni(dipy)_2$ and $Ni(AN)_2(dipy)$.

For $Ni(FN)_2(dipy)$, the first step was less reversible than the former two. The electron to be transfered was supposed to be one from the slope of the reduction wave for all three complexes. The complexes were, therefore, considered to be reduced to form the anion radical.

At this reduction step, no color change was apparent except in $Ni(AN)_2(dipy)$ under prolonged reduction. In the case of $Ni(AN)_2(dipy)$, the solution turned a deep red from a dark reddish-brown as a result of one-electron transfer.

The 1 : 1 ratio of the heights of the first and the second waves in all the dipyridyl complexes indicates a one-electron transfer in the second wave as well as in the first, though the second wave is less reversible than the first. It has previously been reported that nickel complexes containing *o*-mercaptoaniline or thiobenzoylhydrazine readily undergo one-electron transfer steps to give mono- and dianions.[5)]

The bis(dipyridyl)nickel showed three more reduction waves with comparatively large wave heights, so a reduction state farther than the dianion may be expected. Tris(2,2'-dipyridyl)chromium has previously been reported to be reduced to the hexa-anion stage,

5) R. H. Holm, A. L. Balch, A. Davisdon, A. H. Maki, and T. E. Berry, *ibid.*, **89**, 2866 (1967).

$Ca_3[Cr(dipy)_3]\cdot 7NH_3$.[6]

For nitrile-containing complexes, the steps after the second are very small in height.

Since HMPT with a donor- and an acceptor-level can also coordinate to a low-valent transition metal, it is probable that coordinated dipyridyl is replaced by HMPT to lower the effective concentration of dipyridyl complexes below the calculated value. In the case of violet-colored bis(dipyridyl)iron, its HMPT solution slowly turned to brown from violet, and this color change was suppressed by the addition of more than 10-fold molar amount of dipyridyl to the complex solution.[7] The addition of dipyridyl to the nickel-dipyridyl complex solution, did not affect the height and potential of the first step.

This indicates that HMPT does not replace the coordinated dipyridyl of the examined neutral nickel-dipyridyl complexes.

The second wave increased in height upon the addition of dipyridyl, though the half-wave potential of this step scarcely changed in three complexes. Some steps after the second were also affected. The effect of the addition of dipyridyl is shown in Figs. 2 and 3 for $Ni(dipy)_2$ and $Ni(FN)_2(dipy)$. In the case of $Ni(dipy)_2$, dipyridyl addition increased the height of the second, fourth, and fifth waves, the third being left unchanged. Further, the waves became less reversible as their height was increased by dipyridyl addition. In Table 3, the change in the slope of the second wave is shown for $Ni(dipy)_2$. The change in the height and reversibility of the second wave suggests that added dipyridyl takes part in this reduction step and that its rate of coordination to the metal is slow.

In the presence of the complexes of 5×10^{-3} mol/l, the reduction waves with considerably cathodic potential could not be successfully observed because of the disturbance in the wave shapes. By decreasing the concentration of the complex, those waves were, however, observed in the case of $Ni(dipy)_2$, as is indicated in Fig. 4. The concentration of the complex was 3×10^{-4} mol/l, and that of added dipyridyl was 3×10^{-2} mol/l. The reduction wave of free dipyridyl was observed after the waves in which the complex was considered to take part. After a prolonged reduction (for

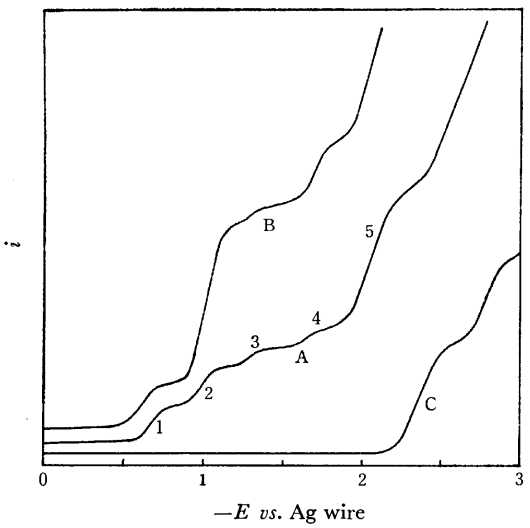

Fig. 2. Effect of dipyridyl addition on the reduction waves of $Ni(dipy)_2$ in HMPT.
A: $Ni(dipy)_2$
B: dipy: $Ni(dipy)_2$=3 : 1
C: free dipyridyl

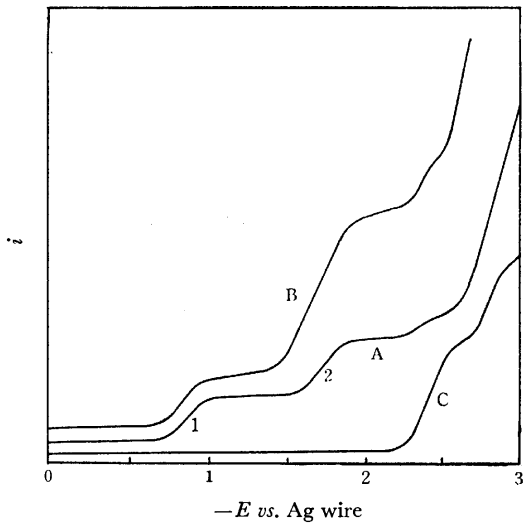

Fig. 3. Effect of dipyridyl addition on the reduction waves of $Ni(FN)_2(dipy)$ in HMPT.
A: $Ni(FN)_2(dipy)$
B: dipy: $Ni(FN)_2(dipy)$=3 : 1
C: free dipyridyl

Table 3. The effect of dipyridyl addition on the second reduction wave of $Ni(dipy)_2$

Molar ratio		Relative wave height	Slope[a] (mV)
dipy/$Ni(dipy)_2$	0	1.0	67.0
dipy/$Ni(dipy)_2$	3	2.3	81.2
dipy/$Ni(dipy)_2$	10	7.1	90.0

a) Values in the log-plott analysis.
$Ni(dipy)_2$, 5×10^{-3} mol/l; $(C_4H_9)_4NClO_4$, 2×10^{-1} mol/l.

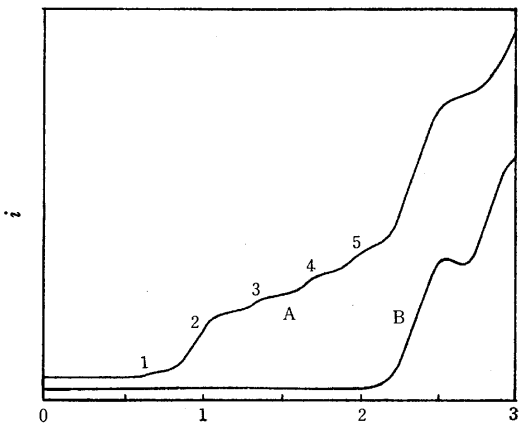

Fig. 4. Polarogram of $Ni(dipy)_2$ in the presence of large excess of dipyridyl
A: $Ni(dipy)_2$+100-fold dipyridyl
B: polarogram after the reduction at about −2.0 V for 20 min

6) S. Herzog, U. Grimm, and W. Waichenbauer, *Z. Chem.*, **7**, 355 (1967).
7) To be published in This Bulletin.

20 min) of this solution at about −2.0 V *vs.* Ag wire, the color of the solution (dark green) faded and the resulting polarogram showed only the reduction waves of dipyridyl. This result may be attributable to the unstability of the reduced species at −2.0 V in spite of the presence of a large excess of dipyridyl. As is shown in Figs. 2 and 4, the ratio of the second and fourth wave-heights in the polarogram of $Ni(dipy)_2$ is dependent on the concentrations of the complex and dipyridyl.

Fig. 5.

Fig. 6.

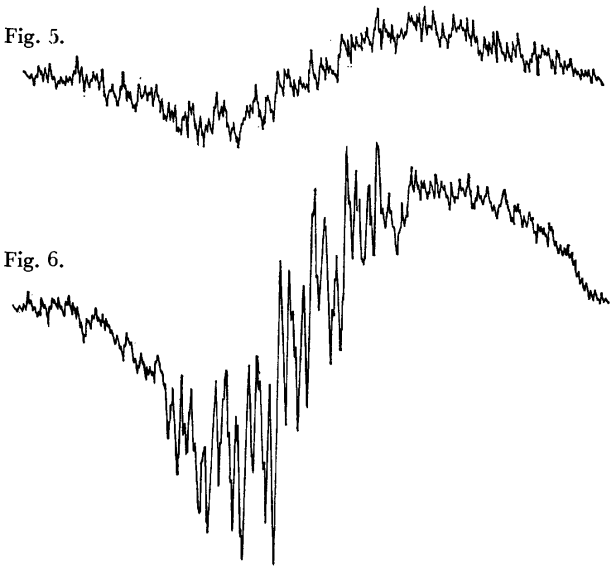

Fig. 5. ESR signal in the electrolysis of $Ni(dipy)_2$ at −0.8 V *vs.* Ag wire.

Fig. 6. ESR signal in the electrolysis of $Ni(dipy)_2$ at −1.1 V *vs.* Ag wire.

Fig. 7.

Fig. 8.

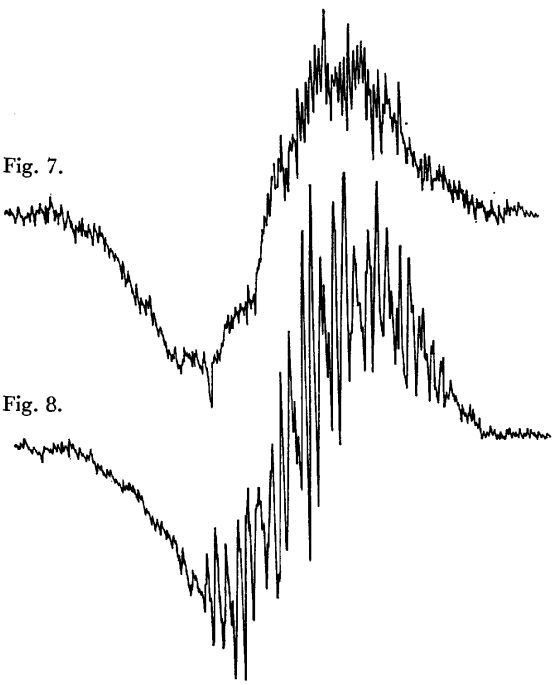

Fig. 7. ESR signal in the electrolysis of Ni $FN)_2$ dipy) at −1.07 V.

Fig. 8. ESR signal in the electrolysis of $Ni(FN)_2$(dipy) at −1.7 V.

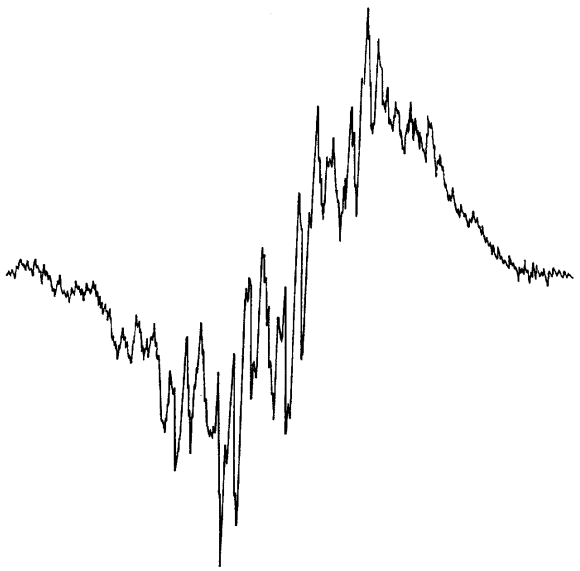

Fig. 9. ESR signal in the electrolysis of $Ni(AN)_2$(dipy) at −0.8 V.

ESR Measurements. In electrolysis at the potential sufficient cathodic to cause the first reduction step, the signal attributable to the anion radical of the complex was observed for all the nickel complexes, as is shown in Figs. 5, 7, and 9. The complexes before reduction, naturally, gave no ESR signal. Zero-valent nickel has a d^{10} configuration, so the unpaired electron of the complex anion radical seems to be mainly localized on the ligand side. For $Ni(dipy)_2$, no signal with a well-defined hyperfine structure could be obtained.

For $Ni(AN)_2$(dipy) and $Ni(FN)_2$(dipy), a comparatively well-defined structure was obtained. The spectra indicated the localization of the unpaired electron on the ligand side, compared with those obtained for the anion radicals of dipyridyl and dipyridyl metal carbonyl complexes.[8]

The *g*-values of the complex anion radicals were as follows; $Ni(dipy)_2$, 2.0036; $Ni(AN)_2$(dipy), 2.0009; $Ni(FN)_2$(dipy), 2.0013 (dipyridyl, 2.0023). They were close to that of the dipyridyl anion radical. This also indicates the spin localization of the ligand side.

It was noted that the electrolysis at the second reduction step produced the anion radical of dipyridyl.

The intensity of this signal increased upon the addition of dipyridyl to the solution. The set potential was more anodic by 0.6—1.3 V than the half-wave potential of free dipyridyl. In Figs. 6 and 8, the signal attributable to the anion radical of dipyridyl is shown. This dipyridyl anion radical was stable in HMPT and was observed to be overlapped with another signal with an ill-defined structure. Without excess dipyridyl, the first anion radical-signal of the complex was again observed by shifting the set potential to the first reduction step, but the signal intensity was lower than before.

Taking into account the polarographic results at the second step, it was concluded that the dianion species of

8) R. E. Dessy, R. B. King, and M. Waldrop, *J. Amer. Chem. Soc.*, **88**, 5112 (1966); R. E. Dessy, Intern. Symp. on the Synthetic and Mechanistic Aspects of Electro-organic Chemistry, 63 (1968).

the complex was formed by two one-electron transfer steps and that the dipyridyl anion radical was formed by the dissociation of this dianion species. To the authors' knowledge, this is the first time the dipyridyl anion radical has been formed at a far more anodic potential than the reduction potential of free dipyridyl in aprotic solvents.[9]

The polarographic results suggested the formation of the species with unpaired electron upon further reduction, for example, in the case of $Ni(dipy)_2$. Its ESR analysis was, however, impossible because of the presence of stable dipyridyl anion radical with a half-wave potential of about -2.8 V *vs.* Ag wire. This potential was more cathodic than the fifth reduction step in the polarography of $Ni(dipy)_2$. In the experiments with the complexes containing nitriles, the signal which corresponds to the anion radical of acrylonitrile or fumaronitrile was not detected. This suggests that π-coordinated acrylonitrile or fumaronitrile is stable in the complex dianion species.

The present authors also attempted the electrolysis of bis(dipyridyl)iron. The $Fe(dipy)_2$-HMPT solution was unstable and gave a disturbed polarogram, from which no clear-cut information was obtained, but the ESR analysis at the potential corresponding to the second step recorded the anion radical of dipyridyl. This potential was more anodic than the reduction potential of dipyridyl, too.

In the examined systems, the solvent HMPT was considered to have an important role. Its ability to solvate anions is greater than tetrahydrofuran or acetonitrile. The reduction potential to obtain the complex anion radical from $Ni(dipy)_2$ in HMPT was far anodic than that reported in acetonitrile.[10] The solvation mechanism of neutral complexes and derived complex anion radicals in HMPT is not yet clear and needs to be studied further.

The dissociation of dianion species produces a paramagnetic species containing a nickel atom, along with the formation of a dipyridyl anion radical, and the former coordinated by dipyridyl to reproduce complex anion radical species in the presence of excess dipyridyl.

Therefore, the degree of dissociation increases upon the addition of dipyridyl because of the difference in the stability between anion radicals and dianion species.

Were it not for the free dipyridyl in the solution, HMPT would coordinate to the above paramagnetic species.

The ill-defined signal in Figs. 6 and 8 may supposedly be ascribed to the complex anion radical and/or species derived from the previous paramagnetic species and HMPT.

As a mechanism of the electro-reduction of nickel-dipyridyl complexes, the following mechanism was proposed, for example, in the case of $Ni(dipy)_2$.

1st step

$$Ni(dipy)_2 + e^- \rightleftharpoons [Ni(dipy)_2]^-$$

2nd step

$$[Ni(dipy)_2]^- + e^- \rightleftharpoons [Ni(dipy)]^{2-}$$

$$[Ni(dipy)_2]^{2-} \rightleftharpoons [Ni(dipy)]^- + [dipy]^-$$

$$[Ni(dipy)]^- + dipy \rightleftharpoons [Ni(dipy)_2]^-$$

$$[Ni(dipy)]^- + HMPT \rightleftharpoons [Ni(dipy)(HMPT)]^-$$

9) N. Maki, T. Hirano, and S. Musha, This Bulletin, **36**, 756 (1963).

10) N. Tanaka and Y. Sato, *Inorg. Nucl. Chem. Letters*, **4**, 487 (1968).

Stereochemical Studies of Metal Chelates. IX.[1] The Preparation and Stereochemistry of Cobalt(III) Complexes Coordinated with the *meso*-Form of 3,6-Diaza-2,7-dimethyl-1,8-diaminooctane

Masahiko SABURI and Sadao YOSHIKAWA

Department of Synthetic Chemistry, Faculty of Engineering, The University of Tokyo, Hongo, Bunkyo-ku, Tokyo 113

(Received December 16, 1971)

The *meso*-form of 3,6-diaza-2,7-dimethyl-1,8-diaminooctane (*meso*-3,8-dimetrien), one of the triethylenetetramine derivatives, was prepared. Dinitro- and dichlorocobalt(III) complexes with this ligand were also prepared and characterized. The *Δ-cis-β(SS)* and/or the *Δ-cis-β(RR)* configuration were assigned to these complexes. The *trans*-dichlorocobalt(III) complex of *meso*-3,8-dimetrien derived from the *cis-β*-dichloro complex was determined to have the *meso-trans* configuration (the absolute configurations of the coordinated secondary nitrogen atoms were antimeric to each other, namely, *R* and *S*), on the basis of proton magnetic resonance measurements.

We have investigated the stereoisomerism of cobalt(III) complexes coordinated with triethylenetetramine (=trien) derivatives substituted with methyl groups at various carbon atoms of trien. Almost all of them were optically active enantiomorphs and showed a remarkable stereospecificity when coordinated.[2-5] The studies of complexes with substituted triens have occasionally served to elucidate the stereochemistry of the unsubstituted trien complex. The structures of the probable isomers so far proposed[3-7] are shown in Fig. 1. The structural features for these isomers have been discussed in detail in previous papers.[4,5] The presence of all the isomers except for the *meso-trans* form (*trans*-(*RS*)[8] form) has been proven for diacidocobalt(III) complexes with trien and/or its derivatives.[3-5]

Studies of trien derivatives[3-5] have pointed out the importance of the conformational rigidity attending to the chelate ring with the *C*-substituted methyl group, which tends to take the equatorial orientation with regard to the chelate ring. The 3,6-diaza-2(*S*),7(*S*)-dimethyl-1,8-diaminooctane (=(3*S*,8*S*)-dimetrien), for example, yielded the *Δ-cis-β(RS)* isomer,[4,5] among others. The isolation of the *Δ-cis-β(RS)* isomer was attributed to the effect of the methyl groups of the ligand used. It was difficult to obtain the *Δ-cis-β(RS)* and its enantiomeric forms in the case of trien complexes.[6] This suggests that any isomeric forms not isolated for unsubstituted trien might be obtained by employing trien derivatives substituted with methyl group(s) at the suitable position(s) and of the appropriate configuration(s).

As has been mentioned above, the *meso-trans* form is the only isomer not hitherto detected for complexes of trien or its derivatives. The most conspicuous characteristic of the *meso-trans* form is the fact that the two outer chelate rings have opposed conformations (*δ* and *λ*). This isomeric form might be obtained if methyl groups are introduced into a trien derivatives so that the two side chelate rings adopt the configurations opposed to each other. With this in view, we prepared the *meso*-form of 3,6-diaza-2,7-dimethyl-1,8-diaminooctane (*meso*-3,8-dimetrien), which is the epimer of (3*S*,

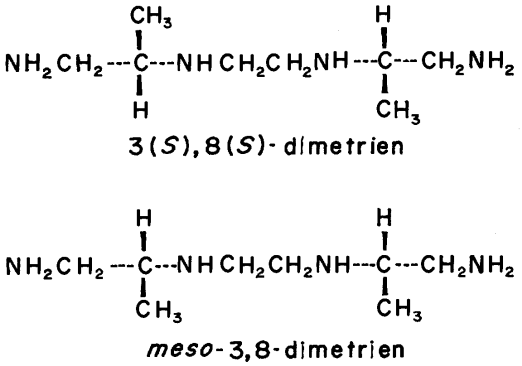

Fig. 2. Structures of Ligands.

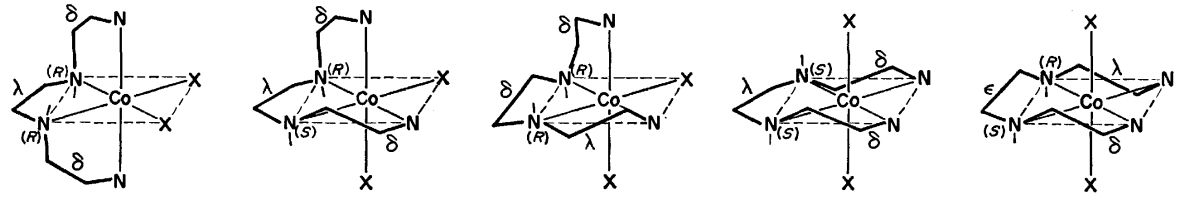

Fig. 1. Possible isomers of octahedral trien complexes; *Δ-cis-α-(RR)(δλδ)*, *Δ-cis-β(RS)(δλδ)*, *Δ-cis-β-(RR)(δδλ)*, *trans (SS)(δλδ)*, and *meso-trans(RS)(δελ)*.

1) Part VIII. M. Saburi, C. Hattori, and S. Yoshikawa, *Inorg. Chim. Acta*, in press.
2) S. Yoshikawa, T. Sekihara, and M. Goto, *Inorg. Chem.*, **6**, 169 (1967).
3) M. Goto, M. Saburi, and S. Yoshikawa, *ibid.*, **8**, 358 (1969).
4) M. Saburi and S. Yoshikawa, This Bulletin, **45**, 806 (1972).
5) M. Saburi, T. Sawai, and S. Yoshikawa, *ibid.*, **45**, 1086 (1972).
6) D. A. Buckingham, P. A. Marzilli, and A. M. Sargeson, *Inorg. Chem.*, **6**, 1032 (1967).
7) A. M. Sargeson and G. H. Searle, *ibid.*, **6**, 787 (1967).
8) *R* and *S* refer to the absolute configuration of the coordinated secondary nitrogen atoms, following the rules by R. S. Cahn, C. K. Ingold, and V. Prelog, *Angew. Chem. Intern. Edn.*, **5**, 385 (1966).

8*S*)-dimetrien, as is indicated in Fig. 2. Some cobalt(III) complexes with *meso*-3,8-dimetrien were prepared and characterized. It was decided that the *trans*-dichloro complex with this ligand had the *meso-trans* configuration.

Experimental

Racemic alanine amide was prepared by the usual method.[9] Oxalyl chloride was prepared by the method of Staudinger.[10]

Tetramide Mixture. Racemic alanine amide (46.0 g) and sodium carbonate (25.0 g) were dissolved in 200 m*l* of water, and the solution was cooled in an ice bath. Oxalyl chloride (27.6 g) dissolved in 150 m*l* of benzene was added dropwise with vigorous stirring using a blender. After the addition was completed, stirring was continued for 10 min; the resultant white precipitates were filtered off, washed with water, methanol, and ether, and dried under vacuum. Yield, 37.8 g.

Separation of meso- *and* racemic-*Tetramide.* 5.0 g of the tetramide mixture were dissolved in 100 m*l* of boiling acetic acid, and then the solution was cooled to room temperature. After 4 hr, the white crystals which separated were collected by decantation. The crystals were washed with methanol and air-dried. This fraction was almost pure *meso*-tetramide. Yield, 1.5 g. The decanted solution was stood at room temperature overnight; the crystals which appeared were filtered off, and then washed and dried, as in the case of the first fraction. Yield, 1.0 g. The second fraction was *meso*-tetramide containing a small portion of the racemic form; recrystallization from acetic acid gave the pure product.

racemic-Tetramide was recovered from the filtrate of the second crop by the evaporation of the solvent. The product was contaminated with a small amount of the *meso*-isomer.

Found for *meso*-tetramide: C, 41.66; H, 6.02; N, 23.94%. Found for *racemic*-tetramide: C, 41.74; H, 6.15; N, 23.37%. Calcd for $C_8H_{14}N_4O_4$: C, 41.74; H, 6.13; N, 24.34%.

Preparation of meso-*3,6-Diaza-2,7-dimethyl-1,8-diaminooctane (*meso-*3,8-dimetrien).* To 150 m*l* of anhydrous tetrahydrofuran were added 8.0 g of lithium aluminum hydride in small portions, followed by 6.9 g of well-pulverized *meso*-tetramide in small portions. The mixture was stirred and heated under reflux for 24 hr and then cooled to room temperature. 15.5 m*l* of water diluted with 30 m*l* of tetrahydrofuran was added dropwise to the mixture with vigorous stirring. The resultant slurry was stirred for 30 min, filtered off, and washed with tetrahydrofuran (100 m*l*). The residue was extracted by boiling with tetrahydrofuran (100 m*l*) for 1 hr and then filtered again. After this procedure had been repeated, the extracts and filtrates were combined and concentrated under reduced pressure. The oily residue was dissolved in 100 m*l* of ethanol, and the solution was saturated with dry hydrogen chloride gas. The white precipitates were collected and dissolved in warm water. Ethanol was added, while hot, until the solution became turbid, and then the solution was cooled to room temperature. The white crystals of the hydrochloride salt of the desired tetramine were collected, washed with ethanol and ether and dried under vacuum. Yield, 3.5 g. Found: C, 28.49; H, 8.48; N, 15.83%. Calcd for $C_8H_{22}N_4 \cdot 4HCl \cdot H_2O$: C, 28.41; H, 8.35; N, 16.57%.

Preparation of racemic-*3,6-Diaza-2,7-dimethyl-1,8-diaminooctane (*rac-*3,8-dimetrien).* This was prepared by the same procedures as were used for the *meso* form, but employing *racemic*-tetramide in place of *meso*-tetramide. The desired product was isolated as the hydrochroride. Found: C, 29.57; H, 7.88; N, 17.74%. Calcd for $C_8H_{22}N_4 \cdot 4HCl$: C, 30.02; H, 8.18; N, 17.50%.

cis-*β-Dinitro(*meso-*3,6-diaza-2,7-dimethyl-1,8-diaminooctane-cobalt(III) Chloride Sesquihydrate (*cis-*β-[Co(*meso-*3,8-dimetrien)(NO$_2$)$_2$]Cl·1.5H$_2$O).* To a solution of *meso*-3,8-dimetrien·4HCl (3.40 g) and $LiOH \cdot H_2O$ (1.25 g) in 40 m*l* of water, $CoCl_2 \cdot 6H_2O$ (2.38 g) and $NaNO_2$ (1.47 g) were added successively. The resultant solution was aerated with carbon dioxide-free air for 5 hr. The yellow-brown crystals which thus appeared were filtered off and washed with a small volume of cold water. Yield, 1.15 g. The second crop could be obtained by concentrating the combined filtrate and washings to a volume of 15 m*l*, followed by cooling in a refrigerator overnight. This crop was collected and washed with cold water and ethanol. Yield, 1.20 g. A further product was recovered from the filtrate. Total yield, 3.00 g. All the products were recrystallized from warm water. Found: C, 24.93; H, 6.56; N, 21.66%. Calcd for $[Co(C_8H_{22}N_4)(NO_2)_2]Cl \cdot 1.5H_2O$: C, 24.78; H, 6.50; N, 21.68%.

Resolution of cis-*β-*[*Co(*meso-*3,8-dimetrien)(NO$_2$)$_2$]Cl·1.5H$_2$O.* A 2 g sample of *cis-β-*[Co(*meso-*3,8-dimetrien)(NO$_2$)$_2$]Cl·1.5H$_2$O was dessolved in 15 m*l* of warm water. To the solution was added an aqueous solution of ammonium α-bromocamphor-π-sulfonate (1.60 g). Yellow precipitates began to separate immediately. After the mixture had stood at room temperature overnight, the precipitates were filtered off and washed with ethanol. Yield, 2.90 g. These crystals were dissolved in boiling methanol (150 m*l*), and the resultant solution was cooled and allowed to stand overnight. The crystals which separated were collected, washed with ethanol and ether, and air-dried. Yield, 1.25 g. $[\alpha]_D^{20}+147°$ ($c=0.2$, H_2O). The product was the pure diastereomer salt of the *Λ* isomer. Found: C, 33.21; H, 6.05; N, 12.53%. Calcd for $[Co(C_8H_{22}N_4)(NO_2)_2](C_9H_{14}BrO_4S) \cdot CH_3OH$: C, 32.98; H, 6.15; N, 12.82%.

The α-bromocamphor-π-sulfonate salt of the *Λ*-isomer obtained as above was ground with excess $NaClO_4$ and a small volume of water in a mortar. The yellow crystals thus obtained were collected and recrystallized from warm water. $[\alpha]_D^{20}+180°$ ($c=1.0$, H_2O). Found: C, 22.41; H, 5.33; N, 19.94%. Calcd for $[Co(C_8H_{22}N_4)(NO_2)_2]ClO_4$: C, 22.62; H, 5.38; N, 19.79%.

The *Δ* isomer which remains in the filtrate could not be isolated as the optically pure form.

cis-*β-Dichloro(*meso-*3,6-diaza-2,7-dimethyl-1,8-diaminooctane)-cobalt(III) Chloride Hemihydrate (*cis-*β-[Co(*meso-*3,8-dimetrien)Cl$_2$]·0.5H$_2$O).* 1.70 g of *meso*-3,8-dimetrien·4HCl and 0.625 g of $LiOH \cdot H_2O$ were dissolved in 20 m*l* of water, and then 1.19 g of $CoCl_2 \cdot 6H_2O$ was added. The resultant solution was aerated with carbon dioxide-free air for 7 hr. To the solution were added 10 m*l* of concentrated HCl, and the resultant solution was then evaporated on a water bath below 50°C. When a small portion of purple crystals began to separate, heating was stopped and ethanol (20 m*l*) was added. After the mixture had stood in a refrigerator overnight, the purple crystals which separated were filtered off, washed with methanol, acetone, and ether, and dried under vacuum. The product was recrystallized from dilute HCl. Found: C, 27.51; H, 6.92; N, 15.86%. Calcd for $[Co(C_8H_{22}N_4)Cl_2]Cl \cdot 0.5H_2O$: C, 27.56; H, 6.65; N, 16.07%.

trans-*Dichloro(*meso-*3,6-diaza-2,7-dimethyl-1,8-diaminooctane)-cobalt(III) Perchlorate (*trans-[*Co(*meso-*3,8-Dimetrien)Cl$_2$]ClO$_4$).* A 0.2 g sample of *cis-β-*[Co(*meso-*3,8-dimetrien)Cl$_2$]Cl·0.5H$_2$O was added to 100 m*l* of anhydrous methanol, and the mixture

9) P.S. Yang and M.R. Rising, *J. Amer. Chem. Soc.*, **53**, 3183 (1931).

10) H. Staudinger, *Ber.*, **41**, 3563 (1908).

was heated under reflux for 6 hr. The resultant red-brown solution was filtered and concentrated in a rotary evaporator almost to dryness. To the residue were added 3 m*l* of methanol and a excess amount of solid $LiClO_4$, and the mixture was scratched with a glass rod. The crystals which appeared were collected and washed with ethanol and ether. The product thus obtained was the desired complex contaminated with perchlorate salt of the unchanged *cis-β* isomer. This crude product was treated with 20 m*l* of methanol with gentle heating, after which the sparingly soluble *cis-β* form was removed by filtration. The pure *trans* isomer was obtained from the filtrate after concentration in a rotary evaporator. The product was filtered off, and washed with ethanol and ether. The product was recrystallized from concentrated HCl. Found: C, 23.46; H, 5.63; N, 13.84%. Calcd for $[Co(C_8H_{22}N_4)Cl_2]ClO_4$: C, 23.81; H, 5.50; N, 13.88%.

trans-*Dichloro(*racemic-*3,6-diaza-2,7-dimethyl-1,8-diaminooctane)cobalt(III) Perchlorate* (trans-[*Co(*rac-*3,8-dimetrien)*Cl_2]-ClO_4). A 1.60 g sample of *rac*-3,8-dimetrien·4HCl and 0.625 g sample of $LiOH \cdot H_2O$ were dissolved in 25 m*l* of water, and then 1.19 g of $CoCl_2 \cdot 6H_2O$ were added. The solution was aerated with carbon dioxide free air for 7 hr, and then 10 m*l* of concentrated HCl were added. The resultant solution was concentrated on a water bath below 50°C. When a small quantity of dark green crystals began to form, heating was stopped and the mixture was cooled in a refrigerator overnight. The dark green crystals which thus separated were filtered off, washed with methanol, acetone, and ether, and dried under vacuum. The dark green crystals were dissolved in hot methanol (100 m*l*), and the solution was refluxed for 2 hr. To the resultant green solution were added an excess amount of solid $LiClO_4$, and the methanol was removed under reduced pressure. The green crystals which separated were the desired complex. The products were collected, washed with methanol and acetone, and air-dried. Found: C, 24.27; H, 5.67; N, 13.82%. Calcd for $[Co(C_8H_{22}N_4)Cl_2]ClO_4$: C, 23.81; H, 5.50; N, 13.88%.

Measurements. The visible and ultraviolet absorption spectra were obtained with a Shimadzu MPS-50L spectrophotometer. The circular dichroism spectrum was measured with a JASCO J-20 automatic spectropolarimeter. The absorption spectrum for the *cis-β* dichloro isomer was obtained in a concentrated HCl solution in order to avoid the aquation of the complex. The absorption spectra for the *trans*-dichloro isomers were obtained in a methanol solution, while the absorption and CD spectra for the dinitro complex were obtained in an aqueous solution. The proton magnetic resonance spectra for the *trans*-dichloro complexes were obtained with a JNM C-60 spectrometer in a hexadeuterodimethyl sulfoxide solution immediately after dissolution. Sodium 2,2-dimethyl-2-silapentane-5-sulfonate was used as the internal standard reference. The infrared spectra were obtained with a JASCO DS-301 spectrophotometer by means of the KBr disk method.

Results and Discussion

(3*S*,8*S*)-Dimetrien has been prepared by the lithium aluminum hydride reduction of a tetramide obtained by the reaction of *S*-alanine amide (2 mol) with oxalyl chloride (1 mol) (designated hereafter as *SS*-tetramide).[4] If the *meso*-tetramide (or *RS*-tetramide), which contains an *S*-alanine moiety on one branch and an *R*-alanine moiety on the other, is available, the desired trien derivative, *meso*-3,8-dimetrien, may be readily prepared by the same procedure.

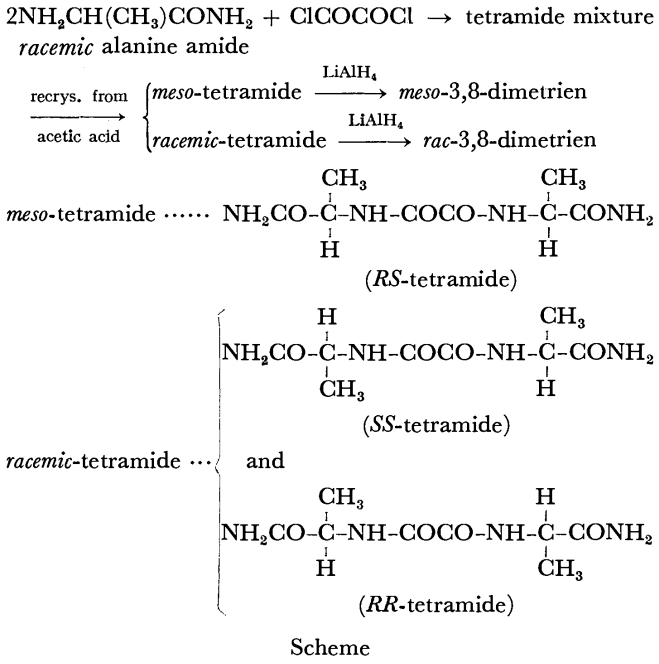

Scheme

However, the reaction of racemic alanine amide (2 mol) with oxalyl chloride (1 mol) must give a "tetramide mixture" composed of *SS*-, *RR*-, and *RS*-tetramide (See Scheme). The *SS*- and *RR*-tetramide are enantiomeric to each other, and an equimolar mixture of them may be designated as *racemic*-tetramide. The *RS*-tetramide is, on the other hand, diastereoisomeric with the racemic form. The above "tetramide mixture" must contain the *racemic*- and *meso*-tetramide in equal amounts.

The separation of the tetramide mixture into the *meso* and the *racemic* forms can be achieved by fractional crystallization from hot acetic acid. The more soluble and the less soluble parts fractionated as above showed infrared spectra evidently different to each other. Further, both fractions were distinguished in thin-layer chromatography, using cellulose powder (MN 300, Macherey, Nagel & Co.) as the absorbent and a pyridine - water mixture (82: 12) as the developing solvent. The R_f value for the less soluble fraction was nearly zero, while that for the more soluble fraction was 0.83. The *SS* tetramide, which was expected to have the same R_f value as the *racemic*-tetramide, showed a chromatogram identical with that of the more soluble fraction. Therefore, the more soluble and the less soluble fraction were identified as the *racemic*- and the *meso*-tetramide respectively.

The *meso*-3,8-dimetrien was obtained by the lithium aluminum hydride reduction of the *meso*-tetramide. In a similar way, the *rac*-3,8-dimetrien was prepared for the sake of comparison. The distinction of these ligands will be clarified by the differences in their complexes, such as *trans*-dichlorocobalt(III) complexes.

Among the possible isomers of trien complexes shown in Fig. 1, there are two isomers which adopt opposed conformations with respect to both of the outer chelate rings, *i.e.*, *Δ-cis-β(RR)* (and its antipodes) and *meso-trans* (*trans(RS)*) form. It was expected that the com-

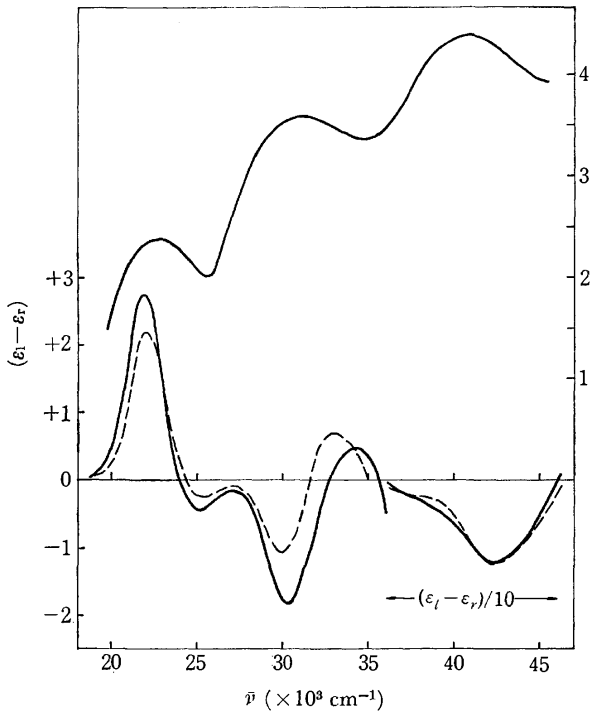

Fig. 3. Absorption and CD curves of *Λ-cis-β*-Co(*meso*-3,8-dimetrien)$(NO_2)_2^+$ ion (——) and CD curve of *Λ-cis-β*(*SS*)-Co(trien)$(NO_2)_2^+$ ion (----).

plexes with *meso*-3,8-dimetrien might give rise to these two geometries stereoselectively, since the present ligand prefers the λ conformation for one arm (the *R* absolute configuration site) and the δ conformation for the other (the *S* configuration site). However, the *meso-trans* geometry must be less stable than the *cis-β* form. In the former structure, the central chelate ring adopts an eclipsed envelope conformation, while all the three chelate rings take gauche conformations in the latter case. Therefore, the most preferred structure for *meso*-3,8-dimetrien complexes may be the *cis-β* configuration (*Δ-β*(*RR*) and *Λ-β*(*SS*)).

The dinitrocobalt(III) complex of *meso*-3,8-dimetrien showed the absorption spectrum given in Fig. 3. The second absorption band was found at 31,250 cm^{-1}, indicating the *cis* configuration of the complex. The absorption maxima for the *cis* isomers of the $Co(N)_4(NO_2)_2^+$ type were found at about 31,000 cm^{-1}, while those of the *trans* isomers were found in the vicinity of 29,000 cm^{-1}.[11] Such a tendency of absorption spectra was also observed in the case of dinitro complexes with some trien derivatives.[12]

The Co(*meso*-3,8-dimetrien)$(NO_2)_2^+$ ion was resolved into the optically active form using ammonium α-bromocamphor-π-sulfonate as the resolving agent. The $(+)_D$-enantiomorph isolated from the less soluble diastereoisomer salt showed the CD curve given in Fig. 3. This curve has a dominant positive CD peak ($\Delta\varepsilon = +2.75$), along with a minor negative peak ($\Delta\varepsilon = -0.46$), in the first absorption band region, indicating the *Λ* absolute configuration.[5] Further, this CD curve

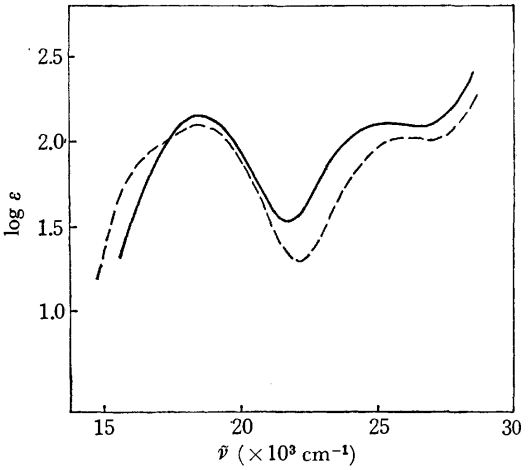

Fig. 4. Absorption curves of *cis-β*-Co(*meso*-3,8-dimetrien)Cl_2^+ ion (——) and *Λ-cis-α*-Co(3*S*, 8*S*)-dimetrien)Cl_2^+ion (----).

markedly resembles that of the *Λ-cis-β*-(*SS*)-Co(trien)-$(NO_2)_2^+$ ion, as shown in Fig. 3. The dinitro complex of some trien derivatives which have configurations other than the *Λ-β*(*SS*) or *Δ-β*(*RR*) geometry (*i.e.*, the *Λ-α*-(*RR*) and *Δ-β*(*RS*) forms) showed CD patterns different from this (*Λ-β*(*SS*)) geometry.[5] Hence, it was established that the dinitrocobalt(III) complex of *meso*-3,8-dimetrien have the *Λ-β*(*SS*)[13] and *Δ-β*(*RR*) configurations, as expected previously.

The dichlorocobalt(III) complex of *meso*-3,8-dimetrien prepared by the usual method was purple and showed the visible absorption curve given in Fig. 4. It has been recognized that the *cis-α* isomers of dichloro complexes with trien or its derivatives have a shoulder on the shorter wave number side of the first absorption band. The absorption curve of the *Λ-cis-α*-Co((3*S*,8*S*)-dimetrien)Cl_2^+ ion is shown for the sake of comparison in Fig. 4. For the *cis-β* configuration, such a shoulder has not been detected in the corresponding region in spite of the geometry of the *cis-β* isomers (*Λ-β*(*SS*) and

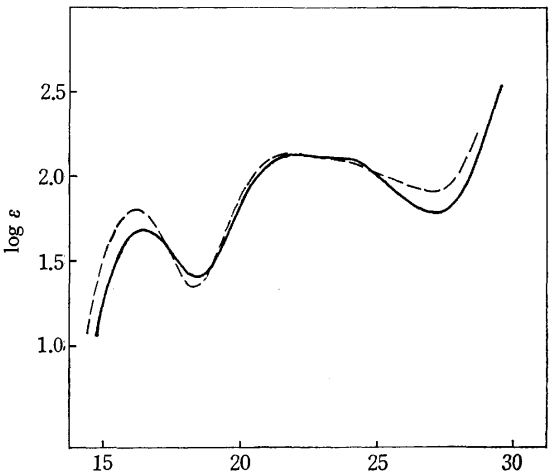

Fig. 5. Absorption curves of *trans*-Co(*meso*-3,8-dimetrien)Cl_2^+ ion (——) and *trans*-Co(*rac*-3,8-dimetrien)Cl_2^+ ion (----).

11) F. Basolo, *J. Amer. Chem. Soc.*, **72**, 4393 (1950).
12) M. Goto, A. Okubo, T. Sawai, and S. Yoshikawa, *Inorg. Chem.*, **9**, 1488 (1970).
13) The absolute configuration of the coordinated secondary nitrogen center is represented by *R* and *S*, neglecting the substituted methyl groups. See ref. (4) and (5).

Λ-β(RS) or their enantiomorphs).[4] No shoulder was observed in the first absorption band of the *meso*-3,8-dimetrien complex either (Fig. 4). Therefore, the present complex should have the *cis*-β configuration. Further, this complex ion probably takes the Λ-β(SS) and/or Λ-β(RR) configurations in the same manner as the corresponding dinitro complex.

When this *cis*-β dichloro complex suspended in methanol was heated under reflux, a red-brown solution was obtained, from which the *trans*-dichloro isomer of *meso*-3,8-dimetrien was isolated. The absorption spectra of this *trans* isomer and of the *trans*-Co(*rac*-3,8-dimetrien)-Cl_2^+ ion are shown in Fig. 5. These curves are apparently different from each other, reflecting the difference in the structures of the ligands. The absorption curve of the *rac*-3,8-dimetrien complex was identical with that of the (3S,8S)-dimetrien complex,[4] as expected.

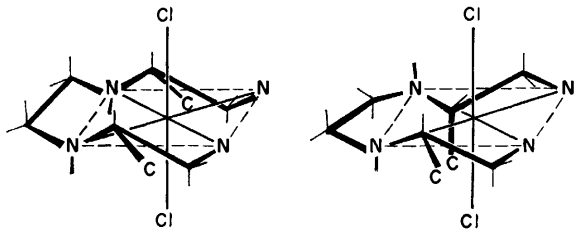

Fig. 6. Possible structures of *trans*-Co(*meso*-3,8-dimetrien)Cl_2^+ ion; (a) *meso-trans* and (b) *racemic-trans* (*SS* enantiomer).

There are two possible structures for the *trans* complexes of *meso*-3,8-dimetrien; they are illustrated in Fig. 6. In the *meso-trans* configuration, both of the methyl groups are situated equatorially. On the other hand, one of the methyl groups has the axial, and the other has the equatorial orientation for the *racemic-trans* configuration. (One of the enantiomers, the *trans*(SS) isomer, is represented in Fig. 6).

The PMR measurements may be useful in determining the actual structure of the *trans*-Co(*meso*-3,8-dimetrien)-Cl_2^+ ion. If the complex takes the *meso-trans* configuration, the PMR signals for the methyl groups should be observed as only one doublet. On the contrary, the methyl signals would be, in principle, observed as two doublets of equal intensity for the *racemic-trans* form.

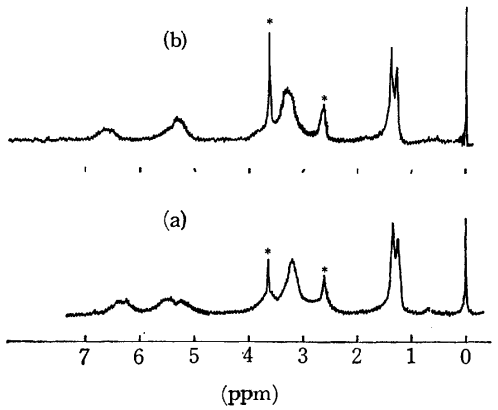

Fig. 7. PMR spectra of *trans*-Co(*meso*-3,8-dimetrien)Cl_2^+ ion (a) and *trans*-Co(*rac*-3,8-dimetrien)Cl_2^+ ion (b) in DMSO-d_6 (* are due to DMSO-d_6).

The PMR spectrum of the *trans*-dichloro complex of *meso*-3,8-dimetrien is shown in Fig. 7. The methyl signals were observed as a single soublet at about 1.3 ppm, indicating that the present complex has the *meso-trans* geometry. The PMR spectrum of the *rac*-3,8-dimetrien complex is given for the sake of comparison. The present complex also showed a single doublet for the methyl signals. However, the difference between the *meso*- and *rac*-3,8-dimetrien complexes was revealed clearly in the region of the N-bonded proton signals, which were found in the region of 5—7 ppm as broad peaks.

It was concluded, therefore, that the *trans*-dichloro complex of *meso*-3,8-dimetrien has the *meso-trans* configuration. Thus, it was clarified that the steric effects of methyl groups introduced into the trien backbone with appropriate configurations make it possible to obtain specific geometrical isomer(s) which would not be obtained in the case of non-substituted trien complexes.

Intramolecular Hydrogen Bonding in α-Keto and α-Alkoxy Carboxylic Acids. VIII. o-Methoxy-Substituted Phenoxyacetic and Phenylthioacetic Acids

Minoru HIROTA and Go HIRANO

Department of Applied Chemistry, Faculty of Engineering, Yokohama National University, Minami-ku, Yokohama

(Received June 24, 1970)

The infrared spectra in the O–H stretching region of several *ortho*-substituted phenoxyacetic and phenylthioacetic acids were determined in dilute carbon tetrachloride solutions. The O–H stretching absorption of phenoxyacetic acids carrying *o*-methoxy-substituents shows three absorption maxima, all of these being attributed to the monomeric species, and they are assigned to the free O–H group, the O–H group hydrogen bonded with α-phenoxy oxygen atom and the O–H group hydrogen bonded with methoxyl oxygen atom in the order of decreasing frequency. The O–H stretching absorption at the lower frequency of *o*-methoxyphenylthioacetic acids is also assigned to the hydrogen bonded monomeric species in which the chelation occurs between the carboxylic O–H group and the methoxyl oxygen atom.

From the previous investigations of the present authors,[1-9] the existence, as well as the steric and electronic behaviors, of the intramolecular hydrogen bonding (shown in (**1**)) in some carboxylic acids has become definite. The conclusion of these investigations shows (i) that only the acids with α-alkoxy groups ($n=1$) can form intramolecular hydrogen bonds in the homologous sereis $RO(CH_2)_nCOOH$, and (ii) that the occurrence of the hydrogen bonding is limited only when the hydrogen accepting group is an alkoxy, aryloxy, or oxo group.

In this paper, the intramolecular hydrogen bonding of the titled compounds is discussed, and it is shown that the methoxy groups at the *ortho* positions of phenoxyacetic and phenylthioacetic acids can participate as hydrogen acceptors in the COOH···O hydrogen bonding.

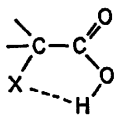

(1)

Expreimental

Preparation of Materials. All phenols employed in the preparation of phenoxyacetic acids are known and were prepared by the methods described previously.[10] Substituted phenoxyacetic acids were prepared either by the condensation of the phenol with chloroacetic acid in strongly alkaline aqueous medium,[11] or by the action of ethyl chloroacetate on the sodium phenoxide without the presence of solvents[12] followed by saponification. The following phenoxyacetic acids (shown in Table 1) were thus prepared and used in the further investigations. Most of the benzenethiols were prepared from the corresponding anilines by the action of potassium ethylxanthate,[13] and the others by the reduction of the corresponding benzenesulfonyl chlorides.[14] The phenylthioacetic acids were prepared by the methods similar to those of phenoxyacetic acids. The physical properties and the elementary analyses are shown in Table 2. Phenylpropionic acids and other materials were either prepared by the methods described or purchased commercial products, and used after appropriate purification.

Measurement of Infrared Spectra. The infrared spectra were recorded on a Perkin Elmer 112G grating infrared spectrophotometer in the O–H stretching region. The measurement was carried out in a carbon tetrachloride solution at a concentration less than 0.002 mol/*l*. The dimeric association of the carboxylic acids were not significant in this concentration range. To distinguish the absorption bands due to the dimer from those of the monomer, the concentration dependences of their absorption intensities were also measured with some typical acids.

The wave numbers, the extinction coefficients, and the half-widths of the overlapping bands were obtained by the least square calculations employing an NEAC 2230 computer.

Results and Discussion

The O–H stretching spectra are listed in Table 3 for phenoxyacetic acids, in Table 4 for phenylthioacetic acids and in Table 5 for some related compounds, and some typical spectra were illustrated in Figs. 1 and 2.

The intramolecular hydrogen bonding in aryloxyacetic acids without *ortho* substituent has been studied by the present authors,[2-5] and it has been shown that the acids have two absorptions in the O–H stretching region. The envelope of each absorption band could be approximated with the Lorentz function within experimental errors. The typical of them is phenoxyacetic acid (Fig. 1a) which has two O–H stretching absorptions at 3527 cm^{-1} and 3488 cm^{-1}. These absorptions are assigned to the free monomeric form **2** and intramolec-

1) M. Ōki and M. Hirota, This Bulletin, **33**, 119 (1960).
2) M. Ōki and M. Hirota, *ibid.*, **34**, 374 (1961).
3) M. Ōki and M. Hirota, *ibid.*, **34**, 378 (1961).
4) M. Ōki and M. Hirota, *Spectrochim. Acta*, **17**, 583 (1961).
5) M. Ōki and M. Hirota, This Bulletin, **36**, 290 (1963).
6) M. Ōki and M. Hirota, *ibid.*, **37**, 209 (1964).
7) M. Ōki and M. Hirota, *ibid.*, **37**, 213 (1964).
8) M. Ōki, M. Hirota, and S. Hirofuji, *Sepctrochim. Acta*, **22**, 1537 (1966).
9) M. Ōki and M. Hirota, *Nippon Kagaku Zasshi*, **86**, 115 (1965).
10) a) R. C. Huston and M. M. Ballard, "Organic Syntheses," Coll. Vol. II, p. 97 (1943); b) T. Mazima and Y. Okazaki, *Ber.*, **49**, (1916); c) Kalle & Co., D. R. P. 95337, 16721 (1945).
11) P. Fritzsche, *J. Prakt. Chem.*, [2] **20**, 269 (1879).
12) J. Grundy, *J. Chem. Soc.*, **1954**, 2649.
13) C. M. Sutar and H. L. Hansen, *J. Amer. Chem. Soc.*, **54**, 4102 (1932).
14) R. Adams, "Organic Syntheses," Coll. Vol. I, p. 504 (1941).

TABLE 1. PHENOXYACETIC ACIDS. 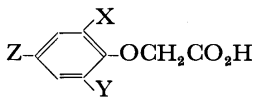

Substituents			Melting points (°C)		Analyses			
					Found		Calcd	
X	Y	Z	Obsd	Lit	C(%)	H(%)	C(%)	H(%)
H	H	H	98.2	98				
CH_3	H	H	153.5	153				
Cl	H	H	146.5	146				
Br	H	H	140.3	143				
Br	H	CH_3	142.7		44.23	3.72	44.11	3.70
Br	Br	CH_3	175.9		33.51	2.39	33.37	2.49
Br	CH_3	CH_3	150.5		46.08	4.25	46.35	4.28
NO_2	H	H	156.4	156.5				
CH_3	CH_3	H	137.5		66.75	6.65	66.65	6.71
OCH_3	H	H	121.5	129	59.34	5.72	59.33	5.53
OCH_3	CH_3	H	102					
OCH_3	Br	CH_3	129.5		43.42	4.00	43.66	4.03
OC_6H_5	H	H	100.0		68.73	4.97	68.84	4.95

TABLE 2. PHENYLTHIOACETIC ACIDS. 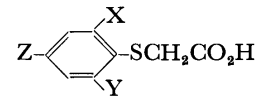

Substituents			Melting points (°C)		Analyses			
					Found		Calcd	
X	Y	Z	Obsd	Lit	C(%)	H(%)	C(%)	H(%)
H	H	H	61.7	62				
H	H	CH_3	75.1		59.50	5.57	59.33	5.53
OCH_3	H	H	118.1		54.76	5.27	54.53	5.09
OCH_3	OCH_3	H	88.5		52.75	5.39	52.62	5.30
Br	H	CH_3	119.3		41.60	3.69	41.39	3.47
Br	Br	CH_3	135.1		32.02	2.45	31.80	2.37

ularly hydrogen bonded monomeric form **3**, respectively. The O–H absorptions of *ortho*-substituted phenoxyacetic acids are essentially the same as the unsubstituted ones when the *ortho*-substituents are not hydrogen acceptors. Thus, *o*-methylphenoxyacetic acid has two absorptions at 3529 and 3485 cm^{-1} attributable to the free and hydrogen bonded monomeric forms, respectively.

However, a third absorption band (band IV of *ortho*-methoxy-derivatives) is observed when the *ortho*-substituent can act as hydrogen acceptor. The bands IV of *o*-methoxy-substituted acids appear at frequencies between 3400 and 3300 cm^{-1} and their halfwidths $\Delta\nu_{1/2}$, about 100 cm^{-1}, are by far larger than the absorption bands I and II. The *o*-methoxyphenylthioacetic acids also absorb at about 3330 cm^{-1} (as exemplified by the absorption band at 3352 cm^{-1} of *o*-methoxyphenylthioacetic acid (No. 16) and the one at 3333 cm^{-1} of 2,6-dimethoxyphenylthioacetic acid (No. 17)) and the halfwidths of these absorption bands are again near 100 cm^{-1}. Thus, the bands IV of *o*-methoxy substituted phenoxyacetic acids and the bands at the similar frequencies of *o*-methoxy-substituted phenylthioacetic acids might be absorption bands caused by the same kind of molecular interaction. The arylthioacetic acid without *o*-methoxy groups has only one absorption band attributable to the free monomeric form in the O–H stretching region. As the absorption has been assigned to the monomeric species the only plausible assignment for the band at a lower frequency is that it arises from the carboxylic hydroxyl group intramolecularly hydrogen bonded to the oxygen atom of the *o*-methoxyl group.

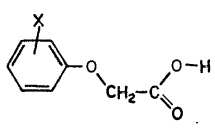

(2)

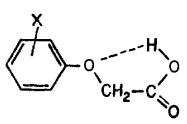

(3)

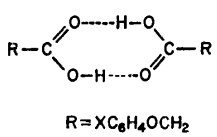

(4)

The authors have concluded that the existence of the COOH···O hydrogen bond of alkoxy- or aryloxy-acetic acid was limited to the case in which the acid forms a five-membered chelate ring by the hydrogen bond formation. The result above shows that an eight-membered chelate ring will be formed by the COOH··· O hydrogen bond, and is an exception of the earlier generalization. But the *o*-methoxy-substituents of these acids are located at a close distance from the carboxyl

TABLE 3. THE O–H STRETCHING ABSORPTIONS OF SUBSTITUTED PHENOXYACETIC ACIDS IN DILUTE CARBON TETRACHLORIDE SOLUTIONS

No.	Substituents X	Y	Z	i	ν_{max} (cm^{-1})	ε_{max}	$\Delta\nu_{1/2}$	$A\times10^{-3}$ (l/mol cm^2)	A_i/A_I	A_{IV}/A_{II}	$\Delta\nu_{max}$ (cm^{-1})
1	H	H	H	I	3527	49.5	31.7	5.68			
				II	3488	25.1	29.7	2.70	0.48		39
2	Me	H	H	I	3529	49.0	33.1	5.87			
				II	3485	24.0	33.9	2.94	0.50		43
3	Cl	H	H	I	3529	47.6	30.3	5.22			
				II	3480	47.5	47.3	8.13	1.56		49
4	NO_2	H	H	I	3525	—[a]	29.2	—			
				II	3430	—[a]	101.0	—	4.46		95
5	Me	Me	H	I	3530	44.4	31.3	5.03			
				II	3457	75.0	39.6	10.7	2.14		73
6	OMe	H	H	I	3527	46.0	33.8	5.63			
				II	3463	69.1	39.5	9.87	1.75		64
				IV	3355	51.6	116.9	21.8	6.97	2.21	172
7	OMe	Me	H	I	3532	18.5	28.7	1.94			
				II	3453	56.0	49.7	10.1	5.24		79
				III	3406	13.6	42.9	2.11	1.10		126
				IV	3318	67.1	131.9	32.0	16.6	3.18	214
8	OMe	Br	Me	I	3531	14.6	40.8	2.16			
				II	3454	77.0	57.6	16.0	7.44		77
				III	3417	17.1	38.6	2.39	1.11		114
				IV	3350	68.4	102.6	25.4	11.8	1.58	181
9	OC_6H_5	H	H	I	3530	29.4	30.2	3.21			
				II	3461	45.0	47.8	7.78	2.42		69
				IV	3395	24.0	82.0	7.12	2.22	0.92	135

a) Measured in a saturated solution

TABLE 4. THE O–H STRETCHING ABSORPTIONS OF SUBSTITUTED PHENYLTHIOACETIC ACIDS IN DILUTE CARBON TETRACHLORIDE SOLUTIONS

No.	Substituents X	Y	Z		ν_{max} (cm^{-1})	ε_{max}	$\Delta\nu_{1/2}$	$A\times10^{3}$ (l/mol cm^2)	A_b/A_f	$\Delta\nu_{max}$ (cm^{-1})
10	H	H	H	f	3528	61.5	33.6	7.48		
11	H	H	Me	f	3527	60.0	29.7	6.45		
12	OMe	H	H	f	3530	53.5	27.5	5.30		
				b	3352	21.5	122.0	9.49	1.79	178
13	OMe	OMe	H	f	3533	29.5	28.6	3.05		
				b	3333	77.2	85.6	23.9	7.83	200
14	Br	H	Me	f	3527	65.7	29.6	7.04		
15	Br	Br	Me	f	3529	69.8	24.2	6.11		

TABLE 5. THE O–H STRETCHING ABSORPTIONS OF SOME RELATED ACIDS

Acid	ν_{max} (cm^{-1})	ε_{max}	$\Delta\nu_{1/2}$ (cm^{-1})	$A\times10^{-3}$ (l/mol cm^2)
cis-*o*-Methoxycinnamic	3537	77.1	27.4	7.64
trans-*o*-Methoxy-cinnamic	3543	65.7	26.2	6.21
β-(*o*-Methoxyphenyl)-propionic	3534	64.9	21.7	5.08
β-Phenylpropionic	3532	59.4	24.0	2.24

group when the molecule takes a suitable conformation, and the hydrogen bond formation is not so unusual if the hydrogen bonding is mainly controlled by the steric accessibility of the donor hydroxyl group and an oxygen acceptor.

The fact that the band IV arises from the unassociated monomeric species is verified by the measurement of the concentration dependence of the O–H spectra carried out with some of these acids. An example is shown in Fig. 3 in which the O–H spectrum of 2,6-dimethoxyphenylthioacetic acid is illustrated at three different concentrations. In Fig. 3, the molar extinction coefficients of both the 3533 cm^{-1} band (band I) and the 3333 cm^{-1} band (band IV) increase as the concentration decreases. The increase in intensity can be interpreted that the monomeric species is more favorable at lower concentrations. The absorption due to the dimer lies in the frequency range between 3200 and 2500 cm^{-1}, and the isosbestic point near 3275 cm^{-1} indicates the

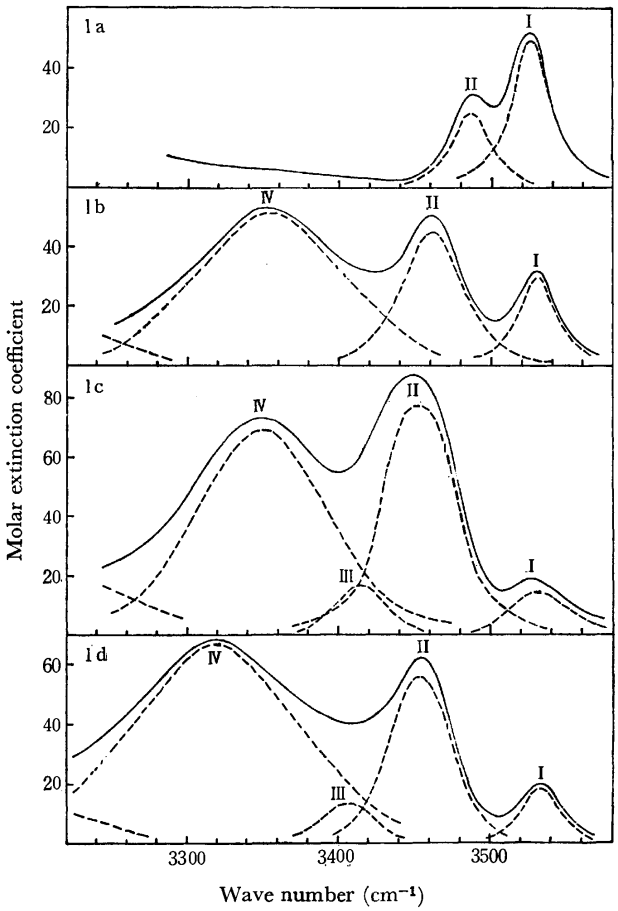

Fig. 1. The O–H Stretching Absorptions of *p*-Methoxyphenoxyacetic Acids in dilute Carbon Tetrachloride Solution.
1a: Phenoxyacetic Acid,
1b: 2-Methoxyphenoxyacetic Acid,
1c: 2-Methoxy-4-methyl-6-bromophenoxyacetic Acid and
1d: 2-Methoxy-6-methylphenoxyacetic Acid

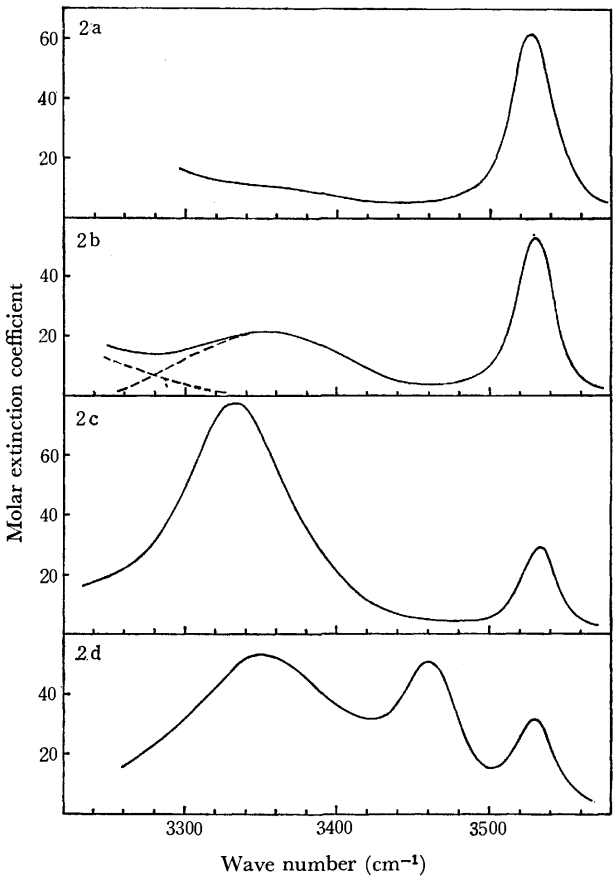

Fig. 2. The O–H Stretching Absorptions of *o*-Methoxyphenylthioacetic Acids in Dilute Carbon Tetrachloride Solution.
2a: Phenylthioacetic Acid,
2b: 2-Methoxyphenylthioacetic acid,
2c: 2,6-Dimethoxyphenylthioacetic Acid and
2d: 2-Methoxyphenoxyacetic Acid (for Comparison)

existence of the monomer-dimer equilibrium.[15]

To determine the extent of the existence of the COOH···OCH_3 hydrogen bond of this type, the O–H stretching absorptions of *o*-methoxy-substituted *β*-phenylpropionic and *cis*-cinnamic acids were observed, and the absence of the COOH···OCH_3 hydrogen bond was concluded because no absorption bands other than the free monomeric species appear in the O–H stretching region (as shown in Table 5).

The ultraviolet spectral studies on *cis*-cinnamic acids show that their aromatic rings and ethylenic linkages do not lie in the same plane, and angles between the two chromophores are estimated to be about 40° by comparison of the absorption intensities of the *cis* and the *trans* isomers.[16] In *cis-o*-methoxycinnamic acid, a much larger angle between the aryl and the ethylenic groups is expected from is lower intensity in π-π^* transition, though the calculation of the exact value for this angle is meaningless because the approximation does not hold in a case of such large steric hindrance.[17] Anyhow, the deviation of the aryl ring from the planar conformation increases the distance between the *o*-methoxy and the carboxyl groups in *cis-o*-methoxycinnamic acid and makes it difficult to form the intramolecular hydrogen bond.

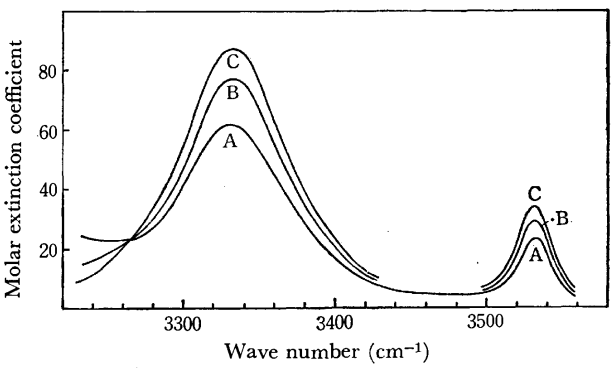

Fig. 3. Concentration Dependence of the O–H Absorption Bands of 2,6-Dimethoxyphenylthioacetic Acid. Spectra A, B, and C are measured in carbon tetrachloride at concentrations 3.048×10^{-3}, 1.016×10^{-3}, and 5.08×10^{-4} mol/*l*, respectively.

15) The measurement of the infrared spectra was carried out at a concentration less than 0.002 mol/*l* in order to lessen the effect of concentration. Nevertheless, the absolute values of the intensity are less significant quantities than their ratios.

16) Y. Urushibara and M. Hirota, *Nippon Kagaku Zasshi*, **82**, 354, 358 (1961).

17) E. A. Braude and F. Sondheimer, *J. Chem. Soc.*, **1955**, 3754,

The absence of the intramolecular hydrogen bond in β-(*o*-methoxyphenyl)propionic acid is explained in the following way. Difference in conformation between aryloxyacetic acids and β-aryloxypropionic acids may arise from the absence of the β-hydrogen atoms and aryl-oxygen conjugation in the former compound. The former factor restricts the conformations of the rotamers about the C_β-C_α bond of the β-arylpropionic acid, and may affect unfavorably on the hydrogen bond formation. The aryl-oxygen conjugation in phenoxy group enforces the essentially planar Ar–O–C conformation (either (**5**) or (**6**)) to the *o*-methoxyphenoxyacetic acid.[18] Thus the carboxyl group is located in the neighborhood of the *o*-methoxyl group in the conformation (**5**). The freedom of the rotation about the phenyl-β-carbon bond in β-aryloxypropionic acid may act as an entropically unfavorable factor to the hydrogen bond formation.

The other fact to be interpreted is why the intramolecular hydrogen bond is present in *o*-methoxyphenoxyacetic acid while it is absent in β-methoxypropionic acid.[1] The presence of the eight-membered intramolecular hydrogen bond is understood if the carboxyl group can form hydrogen bond maintaining the energetically favorable *cis*[19]-conformation (which is about 2 kcal/mol more stable than the *trans*).[20] The β-methoxypropionic acid should take the *trans*[19] conformation to form the intramolecular hydrogen bond. The *cis* conformation of the carboxyl group is very probable from the spectral data of the same compounds in the carbonyl stretching region.

The integrated intensity ratio A_{IV}/A_I corresponds to the ratio of the COOH···OCH_3 hydrogen bonded species to the free monomeric species, which represents how favorable the hydrogen bonded conformation is, and $\Delta\nu$ is assumed to be linear with the energy of hydrogen bond formation.[21] The parallel relation between the A_{IV}/A_I and $\Delta\nu$ is observed with the *o*-methoxyphenoxyacetic acids (No. 6—9) in Table 3 as expected from their definitions. In this series of carboxylic acids, the A_{IV}/A_I, as well as $\Delta\nu$ values indicate that the intramolecular hydrogen bond becomes more favorable in the following order of 6-substituent: H<Br<CH_3. The bulky 6-substituent presumably favors the intramolecular hydrogen bond of this type by preventing the carboxylic acid to take the "*s-trans*" conformation[25] (**6**) which is unfavorable for the hydrogen bond formation.

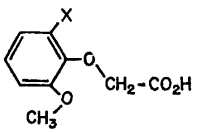

"*s-cis*" conformation
(**5**)

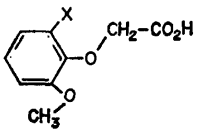

"*s-trans*" conformation
(**6**)

Another weak absorption (band III in Table 3) may exist at about 3440 cm^{-1}. But the existence and the assignment is not certain and to be further investigated.

The authors are grateful to Prof. M. Ōki of the University of Tokyo and to Prof. H. Kakiuchi of Yokohama National University for their valuable advice. The authors also wish to express their hearty thanks to Prof. T. Shimanouchi and Prof. I. Nakagawa of the University of Tokyo for their useful suggestions and their kind permission to use infrared spectrophotometers.

18) The coplanarity is supported by comparing the ultraviolet spectra of the *o*-methoxyphenoxyacetic acid (λ_{max} 276.5 nm, ε_{max} 2790) with catechol dimethyl ether (λ_{max} 277 nm, ε_{max} 2920). Assuming the angle between the phenyl and the C–O–C planes (20°) as estimated from UV data and that the carboxyl O–H group lies 30° above the O=C–O plane in the *cis* conformation,[22] the conformation (**5**) of the hydrogen bonded species were plausible, from the Stewart's molecular models. In the assumed conformer the ArO and the carboxyl C=O grous take the most stable eclipsed conformation.[23]

19) On the nomenclature of the carboxyl conformation, see Ref. 22.

20) T. Miyazawa and K. S. Pitzer, *J. Chem. Phys.*, **30**, 1076 (1959).

21) G. C. Pimentel and A. L. McClellan, "The Hydrogen Bond," W. H. Freeman & Co., San Francisco (1960), p. 82.

22) C. P. Smyth, "Dielectric Behavior and Structure" McGraw Hill, New York (1954), p. 305.

23) M. Hirota and T. Mizuno, Unpublished data.

24) E. L. Eliel, N. L. Allinger, S. J. Angyal, and G. A. Morrison, "Conformational Analysis," Interscience, New York (1965), p. 19.

25) The term "*s-trans*" and *s-cis*" refers to the conformations in which the methoxyl and carboxymethyl groups are the opposite and the same sides with respect to the C_{Ar}–O_{CH_2} bond, respectively. They are indifferent to the *cis* and *trans* conformations of carboxyl groups.

Photooxidation of 1,4-Dihyropyridines

Oyo MITSUNOBU, Shozo MATSUMOTO, Makoto WADA, and Hiroaki MASUDA

Department of Chemistry, College of Science and Engineering, Aoyama Gakuin University, Megurisawa-cho, Setagaya-ku, Tokyo

(Received July 3, 1971)

1,4-Dihydropyridines were successfully photooxidized to corresponding pyridines under suitable conditions. The substituents of the dihydropyridines, reaction mediums, and atmospheres affect the course of the reactions. When diethyl 2,6-dimethyl-1,4-dihydropyridine-3,5-dicarboxylate (**1a**), diethyl 1,4-dihydropyridine-3,5-dicarboxylate (**1b**), 2,6-dimethyl-3,5-diacetyl-1,4-dihydropyridine (**1c**), and 3,5-diacetyl-1,4-dihydropyridine (**1d**) were irradiated by a super high pressure mercury lamp with filter in ethanol under air or oxygen, corresponding pyridines, diethyl 2,6-dimethylpyridine-3,5-dicarboxylate (**2a**), diethyl pyridine-3,5-dicarboxylate (**2b**), 2,6-dimethyl-3,5-diacethylpyridine (**2c**), and 3,5-diacetylpyridine (**2d**) were formed in good yields. Irradiation of **1a**, **1c**, and **1d** in acetonitrile afforded **2a**, **2c**, and **2d** irrespective of their atomosphere, oxygen or nitrogen. On the other hand, photolysis of **1b** by the same lamp and filter in ethanol or acetonitrile in an atmosphere of nitrogen resulted in the formation of photodimer (**3**) which on irradiation by low pressure mercury lamp in acetonitrile dissociated to **1b** followed by photooxidation giving **2b**. Diethyl 1-acetyl-1,4-dihydropyridine-3,5-dicarbolxyate (**4e**) and 1,3,5-triacetyl-1,4-dihydropyridine (**4f**) afforded **2b** and **2d** in fairly good yields when the photolyses were carried out in an atmosphere of air in ethanol or acetonitrile.

The pyridine nucleotides, with their reduced forms, play a role in biological oxidation-reduction process and in biological hydroxylation of substrates by molecular oxygen.[1,2] For the chemical models of the process, the non-photochemical reaction of 1,4-dihydropyridine derivatives with a variety of hydrogen acceptor compounds has been widely investigated.[1,3]

Recently, Abelson, *et al.*[4] have examined the photolysis of reduced nicotinamide-adenine dinucleotide (NADH) and have speculated as to biological significance of the photoproducts. There are few reports, however, of the photochemical reactions of 1,4-dihydropyridines and NADH.[5-7] Eisner *et al.*[8] have demonstrated that on irradiation with medium pressure mercury lamp through a Pyrex filter in an atmosphere of nitrogen, diethyl 1,4-dihydropyridine-3,5-dicarboxylate in *t*-butyl alcohol afforded photodimer as a main product.

In the course of the investigation on the reactions coupled to oxidation-reduction systems, it was found that on irradiation of 1,4-dihydropyridines (**1**) under appropriate conditions the corresponding pyridines were formed in good yields.[9]

Irradiation of 1,4-Dihydropyridines in Ethanol under Oxygen Atmosphere. When diethyl 2,6-dimethyl-1,4-dihydropyridine-3,5-dicarboxylate (**1a**) in ethanol was irradiated under air, the oxidized product, diethyl 2,6-dimethylpyridine-3,5-dicarboxylate (**2a**) was formed as indicated by UV spectrum and thin layer chromatography (tlc) (Fig. 1). As shown in Fig. 1, isosbestic points were observed at 219 mμ, 265 mμ, and 300 mμ. Under similar conditions (ethanol, irradiation under air), diethyl 1,4-dihydropyridine-3,5-dicarboxylate (**1b**) and 2,6-dimethyl-3,5-diacetyl-1,4-dihydropyridine (**1c**) gave diethyl pyridine-3,5-dicarboxylate (**2b**) and 2,6-dimethyl-3,5-diacetylpyridine (**2c**), respectively (Fig. 2, 3).

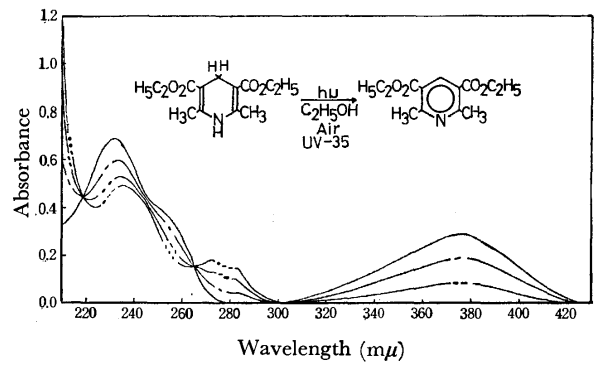

Fig. 1. Photolysis of diethyl 2,6-dimethyl-1, 4-dihydropyridine-3,5-dicarboxylate (**1a**). —— Before irradiation, —— after 15 min, —·— after 40 min, ——— after 130 min.

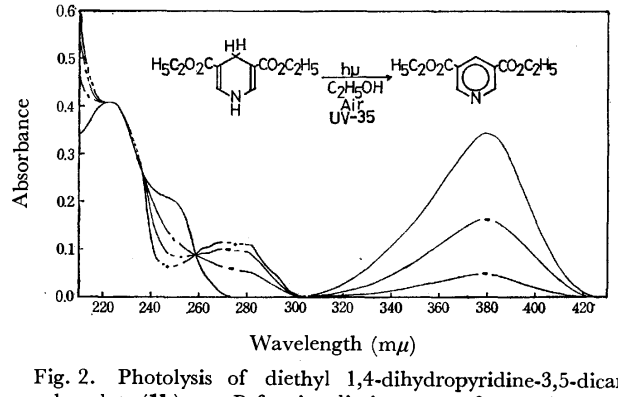

Fig. 2. Photolysis of diethyl 1,4-dihydropyridine-3,5-dicarboxylate (**1b**)—— Before irradiation,—·— after 2 min,—·—· after 5 min,—···— after 15 min.

1) T. C. Bruice and S. J. Benkovic, "Bioorganic Mechanisms," Vol. 2; W. A. Benjamin, Inc. New York (1966), p. 301.

2) M. Florkin and E. H. Stotz (Ed.), "Comprehensive Biochemistry," Vol. 14, Elsevier Publishing Co. Amsterdam (1966).

3) K. A. Schellenberg and F. H. Westheimer, *J. Org. Chem.*, **30**, 1859 (1965) and refs. cited therein; E.A. Braude, J. Hannah, and R. Linstead, *J. Chem. Soc.*, **1960**, 3249, 3257.

4) D. Abelson, E. Parthé, K. W. Lee, and A. Boyle, *Biochem. J.*, **96**, 840 (1965).

5) J. A. Berson and E. Brown, *J. Chem. Soc.*, **77**, 447 (1955).

6) J. L. Kurz, R. F. Hutton, and F. H. Westheimer, *ibid.*, **83**, 584 (1961).

7) A. A. Krasnovskii and G. P. Brin, *Ul'trafiolet Izluch*, No. 4, **50** (1966); *Chem. Abstr.*, **68**, 35938 (1968).

8) U. Eisner, J. R. Williams, B. W. Matthews, and H. Ziffer, *Tetrahedron*, **26**, 899 (1970).

9) Unless otherwise stated, the photolyses were carried out in a quartz vessel by use of super high pressure mercury lamp with Toshiba UV-31 or UV-35 filter.

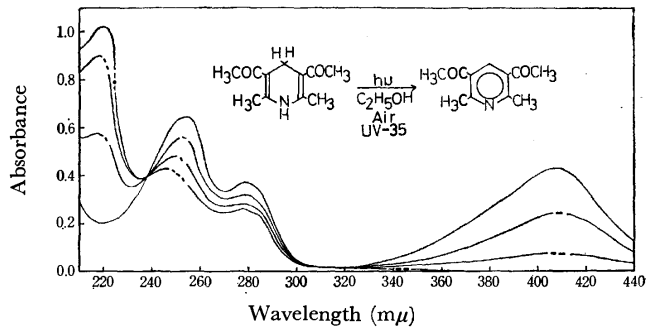

Fig. 3. Photolysis of 2,6-dimethyl-3,5-diacetyl-1,4-dihydropyridine(**1c**).—— Before irradiation,—·— after 20 min,—··— after 60 min,—·—·— after 120 min.

When oxygen was bubbled throughout the reaction, practically same results were obtained except that strong absorption intensity due to charge-transfer interaction between oxygen and ethanol[10] were observed in the short wavelength region.

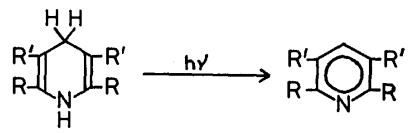

1 **2**

a: R=CH_3, R′=$COOC_2H_5$ **b**: R=H, R′=$COOC_2H_5$
c: R=CH_3, R′=$COCH_3$ **d**: R=H, R′=$COCH_3$

When 3,5-diacetyl-1,4-dihydropyridine (**1d**) in ethanol was irradiated in an atmosphere of oxygen, a new absorption maximum was appeared at 313 mμ as decrease of a maximum at 397 mμ of **1d**. Further irradiation caused a decrease of the new peak and 3,5-diacetylpyridine (**2d**) was simultaneously formed (Fig. 4). The appearance of the absorption maximum at 313 mμ may be attributed to the formation of an intermediate.

Irradiation of 1,4-Dihydropyridines in Ethanol under Nitrogen Atmosphere. Similar to the results obtained by Eisner *et al.*,[8] the irradiation of **1b** or **1c** in ethanol under nitrogen atmosphere resulted in the formation of

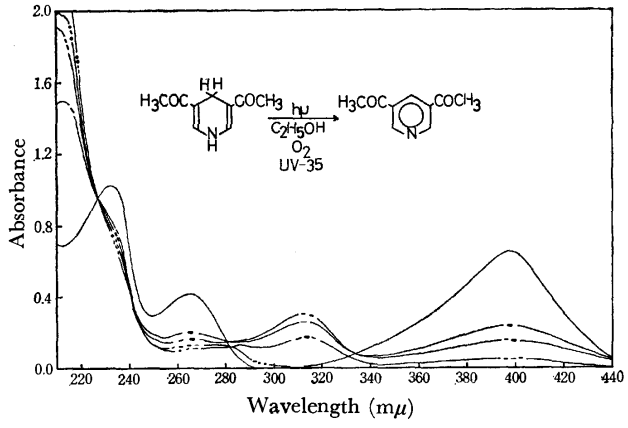

Fig. 4. Photolysis of 3,5-diacetyl-1,4-dihydropyridine (**1d**). —— Before irradiation,—·— after 10 min,—··— after 20 min, —·—·— after 40 min,—·—··— after 460 min.

10) H. Tsubomura and R. S. Mulliken, *J. Amer. Chem. Soc.*, **82**, 5966 (1960).

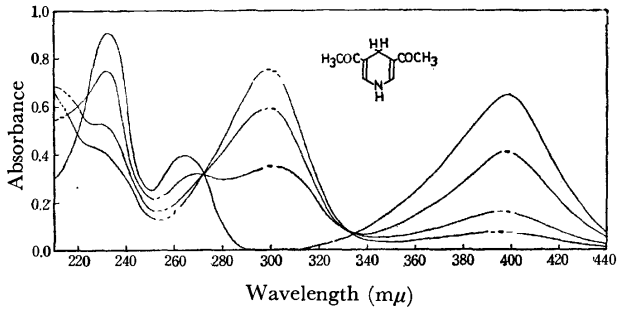

Fig. 5. Photolysis of 3,5-diacetyl-1,4-dihydropyridine (**1d**) in ethanol under an atomosphere of nitrogen using 100W immersion lamp.—— Before irradiation,—·— after 70 hr,—··— after 150 hr,—·····— after 300 hr. A new peak at 298 mμ may due the formation of photodimer.

a photodimer (**3**, λ_{max} 279 mμ) or 3-acetyl-2,6-dimethyl-5-α-hydroxyethylpyridine, respectively. The photodimer was isolated in an 81% yield. Under similar conditions, **1d** gave a new product (λ_{max} 298 mμ) which we presumed to be corresponding dimer as judged by its UV spectrum (Fig. 5). The attempt to isolate and confirm the structure of the compound was not made.

Photolysis of **1a** under similar conditions showed little spectral change; irradiation for 12 hr resulted in a decrease in the absorption maximum no less than 17% of the initial extinction.

Irradiation of 1,4-Dihydropyridines in Acetonitrile under Nitrogen or Oxygen. When acetonitrile was used as the solvent in the above experiments, **1a**, **1c**, and **1d** were oxidized to **2a**, **2c**, and **2d** irrespective of their atmosphere, nitrogen or oxygen. On irradiation of **1d** in acetonitrile under nitrogen atmosphere, **2d** was isolated in a 74% yield. Irradiation of **1b** under oxygen led to the formation of **2b**, while irradiation of **1b** under nitrogen led to dimerization to **3** which was isolated in a 74% yield.

It was noteworthy that when a solution of **3** in acetonitrile was irradiated without filter under an atmosphere of nitrogen, the solution fluoresced a blue color and new absorption maxima were appeared at 372 mμ and 220 mμ. Further irradiation caused disappearance of the peak at 372 mμ and **2b** was formed as indicated by UV spectrum (Fig. 6). This result suggests that the **3** is rather stable toward ultraviolet light of wavelength

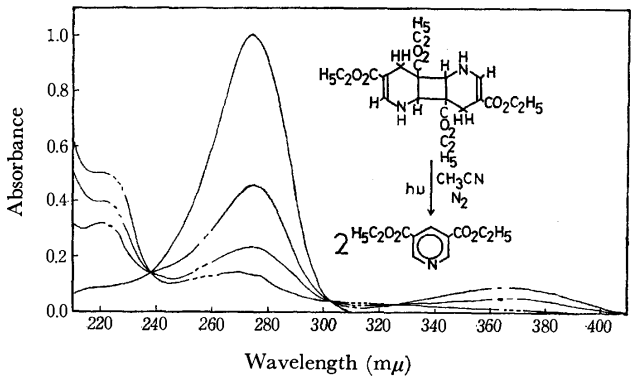

Fig. 6. Photolysis of tetraethyl 1,5,8,8bβ-tetrahydrocyclobuta [1,2-**b**:3,4-**b**′] dipyridine-3, 4aβ 7, 8aβ(4*H*, 4*bβH*) tetracarboxylate.—— Before irradiation,—·— after 8 min,—··— after 23 min,—·····— after 75 min.

TABLE 1. PHOTOLYSIS OF 1,4-DIHYDROPYRIDINES

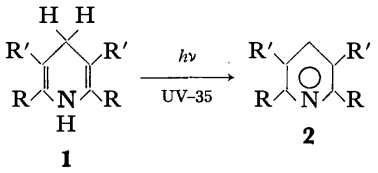

a: R=CH_3 R′=$COOC_2H_5$
b: R=H R′=$COOC_2H_5$
c: R=CH_3 R′=$COCH_3$
d: R=H R′=$COCH_3$

1 **2**

Atmosphere		Solvent: Ethanol				Solvent: Acetonitrile			
		1a	**1b**	**1c**	**1d**	**1a**	**1b**	**1c**	**1d**
O_2	Concentration of **1** $\times 10^5$ mol/*l*	4.33	6.71	5.53	6.82	4.69	6.70	5.34	7.04
	Product	**2a**	**2b**	**2c**	**2d**	**2a**	**2b**	**2c**	**2d**
N_2	Concentration of **1** $\times 10^5$ mol/*l*	4.30	4.52 $\times 10^3$	5.53	1.04 $\times 10^3$	4.35	1.73 $\times 10^3$	5.41	5.00 $\times 10^2$
	Product	a)	**3**	b)	c)	**2a**	**3**	**2c**	**2d**

a) The rate of the formation of **2a** was very slow.
b) 3-Acetyl-2, 6-dimethyl-5-α-hydroxyethylpyridine; λ_{max} 282, 243 mμ (lit[8]) λ_{max} 280, 240 mμ)
c) Presumably corresponding photodimer

above 310 mμ, whereas the **3** dissociated to **1b** followed by oxidation to **2b** by ultraviolet light of wavelength below 310 mμ. This assumption was proved by a separate experiment in which **1b** was oxidized to **2b** on irradiation with low pressure mercury lamp.

Contrary to the photolysis of the **3** in acetonitrile, the irradiation of the **3** in ethanol resulted in the formation of only a small amount of **2b** along with many side products as indicated by tlc.[11]

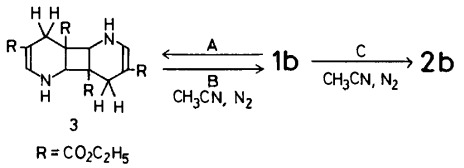

3
R=$CO_2C_2H_5$

A: high pressure Hg lamp with UV-35 filter
B: high pressure Hg lamp without filter
C: low pressure Hg lamp without filter

These results are summarized in Table 1.

Photolysis of 1-Substituted-1,4-dihydropyridines. Loev and Snader[12] have demonstrated that in the nitrous acid oxidation of 1,4-dihydropyridines, the most likely mechanism is that involves initial attack at 1-position. Thus, 1-methyl, 1-benzyl, and 1-acetyl-1,4-dihydropyridines were irradiated in order to investigate the influence of the substituents at 1-position.

When diethyl 1,2,6-trimethyl-1,4-dihydropyridine-3,5-dicarboxylate (**4a**), diethyl 1-methyl-1,4-dihydropyridine-3,5-dicarboxylate (**4b**), 1-methyl-3,5-diacetyl-1,4-dihydropyridine (**4c**), and 1-benzyl-3,5-diacetyl-1,4-dihydropyridine (**4d**) were irradiated and the reaction mixtures were monitored by tlc, only small amounts of the corresponding pyridines were formed along with many side products under the conditions examined (in ethanol or acetonitrile; under an atmosphere of nitrogen or oxygen). Although the possibilities of the formation of 1-alkylpyridinium salts could not be excluded, further attempts to isolate and determine the structures of the products were not be made.

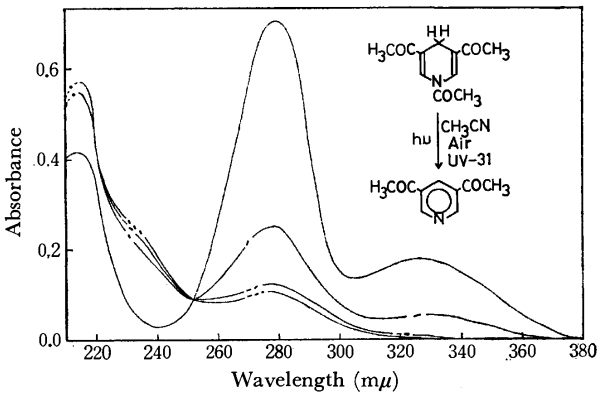

Fig. 7. Photolysis of 1,3,5-triacetyl-1,4-dihydropyridine (**4f**).
—— Before irradiation, ——— after 10 min, —·— after 25 min, —··— after 45 min.

Contrary to the cases of 1-alkyl-1,4-dihydropyridines diethyl 1-acetyl-1,4-dihydropyridine-3,5-dicarboxylate (**4e**) and 1,3,5-triacetyl-1,4-dihydropyridine (**4f**) afforded corresponding pyridines in fairly good yields when the photolyses were carried out in an atmosphere of air in ethanol or acetonitrile (Fig. 7). While **4e** is stable in ethanol at room temperature, **4f** decomposed to 3,5-diacetyl-1,4-dihydropyridine during blowing oxygen or nitrogen through the reaction vessel before irradiation. This result suggests that **4f** is an active acylating reagent. The use of 1-acyl and 1-phosphoryl-1,4-dihydropyridines for the acylation and phosphorylation of active hydrogen compounds are now under investigation.

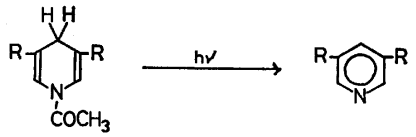

4e: R=$COOC_2H_5$ **2b**: R=$COOC_2H_5$
4f: R=$COCH_3$ **2d**: R=$COCH_3$

11) The photolysis was carried out by means of super high pressure mercury lamp without filter under an atmosphere of nitrogen or oxygen.
12) B. Loev and K. M. Snader, *J. Org. Chem.*, **30**, 1914 (1965).

Being irradiated under nitrogen atmosphere, **4e** and **4f** gave no expected pyridines, **2b** and **2d** but many side products were formed as indicated by tlc irrespective of their solvents, ethanol or acetonitrile. The results are summarized in Table 2.

Table 2. Photolysis of 1-acetyl-1,4-dihydropyridines

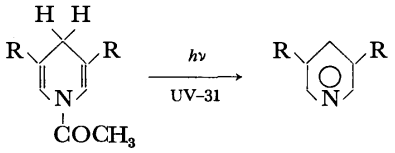

4e: R=$COOC_2H_5$ **2b**: R=$COOC_2H_5$
4f: R=$COCH_3$ **2d**: R=$COCH_3$

Atmosphere		Solvent and Reactant: Ethanol 4e	Ethanol 4f	Acetonitrile 4e	Acetonitrile 4f
O_2	Concentration of **4** $\times 10^5$ mol/*l*	3.55	4.07	3.62	3.44
	Product	**2b**	a)	**2b**	**2d**
Air	Concentration of **4** $\times 10^5$ mol/*l*	3.55	4.12	3.43	3.44
	Product	**2b**	**2d**	**2b**	**2d**
N_2	Concentration of **4** $\times 10^5$ mol/*l*	3.54	4.24	3.43	4.89
	Product	b)	a)	b)	b)

a) **4f** decomposed to 3,5-diacetyl-1,4-dihydropyridine during the oxygen was bubbled through the reaction vessel before irradiation.

b) Only small amount of the corresponding pyridines were formed along with many side products.

The results reported in this paper indicate that the photooxidation of 1,4-dihydropyridines to pyridines depends on the atmosphere and solvents used and under certain conditions, corresponding pyridines were formed in good yields. As have been pointed out by Eisner *et al.*[8] the substituents at 2,6-position also affect the course of the reaction. 1,4-Dihydropyridines without substituents at 2,6-positions such as diethyl 1,4-dihydropyridine-3,5-dicarboxylate afforded corresponding dimers on irradiation with ultraviolet light of wavelength above 310 mμ (N_2, in ethanol or acetonitrile). While, photolysis by means of ultraviolet light of short wavelength, **1b** was oxidized to diethyl pyridine-3,5-dicarboxylate (**2b**; N_2, in acetonitrile).

Further investigation on the photoreduction of various classes of substrates by means of 1,4-dihydropyridines are in progress.

Experimental

The UV spectra were obtained with a Hitachi EPS-3T spectrometer. The IR spectra were taken at Nippon Bunko IR-G spectrometer (KBr disk). The thin layer chromatograms were prepared on silica gel PF_{254} (Merck) and developed with chloroform, ethyl acetate or acetonitrile.

Diethyl 2,6-dimethyl-1,4-dihydropyridine-3,5-dicarboxylate (**1a**),[13] diethyl 1,4-dihydropyridine-3,5-dicarboxylate (**1b**),[14] 2,6-dimethyl-3,5-diacetyl-1,4-dihydropyridine (**1c**),[15] 3,5-diacetyl-1,4-dihydropyridine (**1d**),[16] diethyl 1,2,6-trimethyl-1,4-dihydropyridine-3,5-dicarboxylate (**4a**),[14] diethyl 1-methyl-1,4-dihydropyridine-3,5-dicarboxylate (**4b**),[14] 1-methyl-3,5-diacetyl-1,4-dihydropyridine (**4c**),[14] and 1,3,5-triacetyl-1,4-dihydropyridine (**4f**),[17] were prepared by known procedures. Acetonitrile was purified by distilling from phosphorus pentoxide.[18] Ethanol was dried and purified by known procedure.[19]

*Preparation of 1-Benzyl-3,5-diacetyl-1,4-dihydropyridine (**4d**).* 3,5-diacetyl-1,4-dihydropyridine (0.0696 g) and sodium hydride (0.0683 g) in dimethoxyethane (8 m*l*) were stirred for 30 min at room temperature. Benzyl chloride (0.5 m*l*) was added and stirring was continued for an additional 5 hr. The solution was filtered through a hyflo-super-cel and the filtrate was evaporated to dryness under reduced pressure. After two crystallization from ethyl acetate, the dihydropyridine was obtained yellow crystals, mp 159—160°C. Found: C, 74.43; H, 6.51%. Calcd for $C_{16}H_{17}NO_2$: C, 75.27; H, 6.61%.

*Preparation of Diethyl 1-Acetyl-1,4-dihydro-3,5-dicarboxylate (**4e**).* Under nitrogen atmosphere, diethyl 1,4-dihydropyridine-3,5-dicarboxylate (0.5 g) and sodium hydride (0.6 g) in dimethoxyethane (50 m*l*) were stirred for 30 min at room temperature. Acetyl chloride (6 m*l*) was added and stirring was continued for an additional 2 hr. The mixture was filtered through a hyflo-super-cel and the filtrate was evaporated to dryness under reduced pressure. After recrystallization from acetonitrile, the dihydropyridine was obtained as white crystals, mp 113—114°C. Found: C, 59.68; H, 6.44%. Calcd for $C_{13}H_{17}NO_5$; C, 58.42; H, 6.41%.

General Photolysis Procedures. A solution of 1,4-dihydropyridine (**1**) in ethanol or acetonitrile in a quartz vessel (5 cm×5 cm diameter) was irradiated by super high pressure mercury lamp (Ushio Electric Co., Type SH-250) with UV-35 (Toshiba Electric Co., opaque below 325 mμ, 50% transmission at 350 mμ, 80% transmission above 400 mμ) or UV-31 filter (opaque below 250 mμ, 50% transmission at 310 mμ, 90% transmission above 350 mμ). Nitrogen or oxygen was bubbled throughout the reaction and aliquots of 4 m*l* were removed after appropriate time intervals followed by spectrophotometric measurement.

When the photolyses were carried out in air, the solutions were placed in an absorption spectrum quartz cell of optical path 1.0 cm and irradiated through the filter.

The pyridines produced were identified by comparison of R_f values of tlc with those of authentic samples after the reaction mixtures were concentrated to a small volume.

For the preparative scale experiments, the reactions were carried out in a three necked flask using a 100 W high pressure immersion lamp (Osawa, Type NY-2).

*Photolysis of 3,5-Diacetyl-1,4-dihydropyridine (**1d**) in Acetonitrile under an Atmosphere of Nitrogen.* A solution of **1d** (0.330 g) in acetonitrile (400 m*l*) was stirred for 21 hr while irradiating with a 100 W high pressure immersion mercury lamp. Nitrogen was bubbled throughout the reaction. After the solution was evaporated to dryness under reduced pressure, the residue

13) A. Singer and S. M. McElvain, "Organic Syntheses," Coll. Vol. II, p. 214 (1948).

14) P. J. Brignell, U. Eisner, and P. G. Farrell, *J. Chem. Soc. B*, **1966**, 1083.

15) M. Scholtz, *Ber.*, **30**, 2295 (1897).

16) J. Kuthan and E. Janeckova, *Coll. Czechoslov. Chem. Commun.*, **31**, 2618 (1966).

17) F. Micheel and H. Dralle, *Ann.*, **760**, 57 (1963).

18) A. Weissberger and E. S. Proskauer (First Ed.); J. A. Riddick and E. E. Toops, Jr. (Second Ed.), "Technique of Organic Chemistry" Vol. VII, "Organic Solvents," Interscience Publisher, Inc., New York (1955).

19) L. F. Fieser, "Experiments in Organic Chemistry," D. C. Heath & Company, Boston (1955).

was extracted with *n*-hexane. The extract was evaporated to give 3,5-diacetylpyridine in 74.2% (0.242 g) yield, mp 67—68°C. The melting point and IR spectrum were identical to those of an authentic sample.

*Photolysis of Diethyl 1,4-Dihydropyridine-3,5-dicarboxylate (**1b**) in Ethanol under an Atmosphere of Nitrogen.* A solution of **1b** (0.77 g) in ethanol (77 m*l*) placed in a quartz vessel (5 cm×5 cm diameter) was irradiated with super high pressure mercury lamp through UV-35 filter for about 60 hr. A stream of nitrogen was bubbled throughout the reaction. After removal of the solvent *in vacuo*, there was obtained pale green crystals which was recrystallized from ethyl acetate to give an 81% (0.62 g) of photodimer (**3**) as a white crystals, mp 226—228°C. The melting point, elemental analysis, UV, IR, and NMR spectra were identical to those of tetraethyl 1,5,8,8bβ-tetrahydrocyclobuta[1,2-*b*: 3,4-*b'*]dipyridine-3,4aβ, 7,8aβ(4*H*,4*b*β*H*)tetracarboxylate.[8]

We thank Professor N. Hata and Mr. Y. Kamura for their helpful advices.

BULLETIN OF THE CHEMICAL SOCIETY OF JAPAN, VOL. 45, 1457—1460(1972)

Dimerization and Isotopic Mixing of Ethylene by a Palladium Complex Catalyst

Taketsugu KITAMURA, Ken-ichi MARUYA, Yoshihiko MORO-OKA, and Atsumu OZAKI

Research Laboratory of Resources Utilization, Tokyo Institute of Technology, Meguro-ku, Tokyo

(Received July 5, 1971)

Dimerization and accompanied isotopic exchange of ethylene were studied with dichlorobis(benzonitrile)-palladium(II) complex in benzene solution. Dimerization as well as isotopic exchange take place simultaneously after an induction period, the extent of which is reduced by the presence of hydrogen releasing olefin such as 3-methyl-1-butene. Kinetics of dimerization is of first order in ethylene, but the dimerization rate does not immediately respond to the change in ethylene pressure. The results are interpreted in terms of a preformed palladium hydride complex.

The dimerization of olefin catalyzed by palladium salts has been studied by a number of workers[2-7] since its discovery by Gemert and Wilkinson.[1] Although the catalyst species were varied among palladium chloride or its complex with benzonitrile and di-μ-chlorobis-(ethylene)palladium, *etc.*, the real active species in the dimerization seem to be a monomeric palladium-olefin complex[2] soluble in organic solvents. The following information has been obtained on the dimerization reaction: The rate of dimerization is proportional to concentrations of palladium salt and ethylene.[4] Co-dimerization of ethylene takes place in the presence of other olefin,[6,7] although ethylene is most reactive in the dimerization.[7] There is a remarkable solvent effect.[3,5,7] It is also known that the palladium catalyst catalyzes the isomerization of olefin.[7]

The mechanisms of dimerization so far proposed[2-7] can be summarized into two schemes: (1) A palladium hydride intermediate as adopted for butene isomerization by Cramer and Lindsey is assumed, according to the mechanism proposed by Barlow *et al.*[7] (2) A five co-ordinate hydride complex(II) as an intermediate is assumed according to the mechanism proposed by Ketley *et al.*[2] and is shown in the following. A detailed study was made by Kawamoto, Tatani, Imanaka, and Teranishi[6c] by means of solvent effect and deuterium labeled reactant, styrene-d_3.

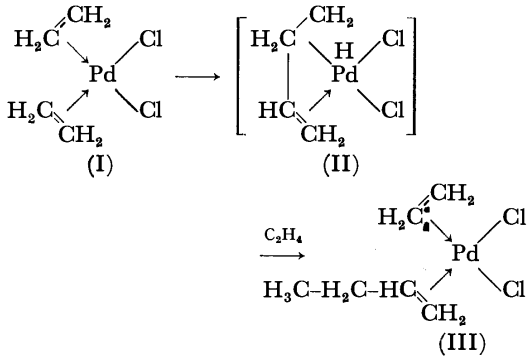

On the other hand in the study of the mechanism of ethylene dimerization with nickel oxide-silica catalyst,[9] it was found that a rapid isotopic mixing in ethylene takes place prior to the dimerization and both the isotopic mixing and dimerization are simultaneously poisoned by a very small amount of CO. Since both

1) J. T. van Gemert and P. R. Wilkinson, *J. Phys. Chem.*, **68**, 645 (1964).

2) A. D. Ketley, L. P. Fisher, A. J. Berlin, C. R. Morgan, E. H. Gorman, and T. R. Steadman, *Inorg. Chem.*, **6**, 657 (1967).

3) Y. Kusunoki, R. Katsuno, H. Hasegawa, and S. Kurematsu, This Bulletin, **39**, 2021 (1966).

4) K. Kawamoto, T. Imanaka, and S. Teranishi, *Nippon Kagaku Zasshi*, **89**, 639 (1968).

5) K. Kawamoto, T. Imanaka, and S. Teranishi, *ibid.*, **91**, 39 (1970).

6) K. Kawamoto, T. Imanaka, S. Teranishi a) *Kogyo Kagaku Zasshi*, **72**, 1612 (1969); b) This Bulletin, **43**, 2512 (1970); c) *ibid.*, **44**, 1239 (1971).

7) M. G. Barlow, M. J. Bryant, R. N. Haszeldine, and A. G. Mackie, *J. Organometal Chem.*, **21**, 215 (1970).

8) R. Cramer and R. V. Lindsey, *J. Amer. Chem. Soc.*, **88**, 3534 (1966).

9) A. Ozaki, H. Ai, and K. Kimura, Int. Congr. Catal, 4th, Moscow, prepr. **40** (1968); K. Kimura, H. Ai, and A. Ozaki, *J. Catal.*, **18**, 271 (1970).

reactions commonly require an intermolecular hydrogen transfer, the results suggest that the ability of the catalyst to cause the isotopic mixing in ethylene is a requisite for the dimerization catalyst and the dissociation of ethylene to form a nickel hydride is involved in the path way of dimerization.

Thus it is of interest to study the isotopic mixing during the course of dimerization by different catalysts in a homogeneous system. This paper deals with such a study of ethylene dimerization by the benzonitrile-palladium complex.

Experimental

Materials. Dichloro-bis-benzonitrile-palladium(II) complex was prepared by the method of Kharasch.[10] Benzene was treated with metallic sodium prior to distillation in dry nitrogen stream and was preserved and transferred in dry nitrogen. C_2D_4 was prepared by deuterogenation of C_2D_2 at room temperature over a Girdler (58A) Pd catalyst and separated from impurities by means of gas chromatography using a silica gel column. C_2D_2 was obtained by reaction of D_2O with CaC_2 which had been evacuated at 400°C for 150 hr.

Procedures. The reactions were carried out in a small flask with stirring under constant pressure at 36°C. The ethylene concentration in the solvent was confirmed to be proportional to the ethylene pressure. The rate of dimerization was determined from the amount of ethylene absorbed into the catalyst solution. Isotopic analyses were carried out by mass spectrometry with an ionization voltage of 10 eV.

Results

1. The Effect of Ethylene Concentration on the Rate of Dimerization. Ethylene dimerization by the palladium complex is much slower in benzene than in polar solvents,[6] but benzene was chosen as solvent because the slow reaction was convenient for studying the effects of reaction conditions. Figure 1 shows the time course of absorption of ethylene where 0.5 mmol of $PdCl_2(\phi CN)_2$ complex was used. In the initial period, 0.5 mmol of ethylene which is equimolar to the amount of catalyst is absorbed to form the ethylene complex. The amount of initial absorption is independent of ethylene pressure as shown by runs A and B. The absorption due to the dimerization begins after a few hours of induction period, which decreases with the increase in ethylene pressure. The rate of absorption increases with time and attains a steady value about 15—18 hr after the introduction of ethylene into the reactor. The steady rate of absorption is taken as the rate of dimerization of ethylene.

The reaction product was exclusively butenes with a composition of 1-butene 4%, *cis*-2-butene 36%, and *trans*-2-butene 60% which is close to the value corresponding to the equilibrium of isomerization.

According to Kawamoto *et al.*,[4] the kinetics of the dimerization by $Pd_2Cl_4(C_2H_4)_2$ complex in dioxane is as follows:

$$\text{Rate} = k[\text{Pd complex}]^{1.0}[C_2H_4]^{1.0} \quad (1)$$

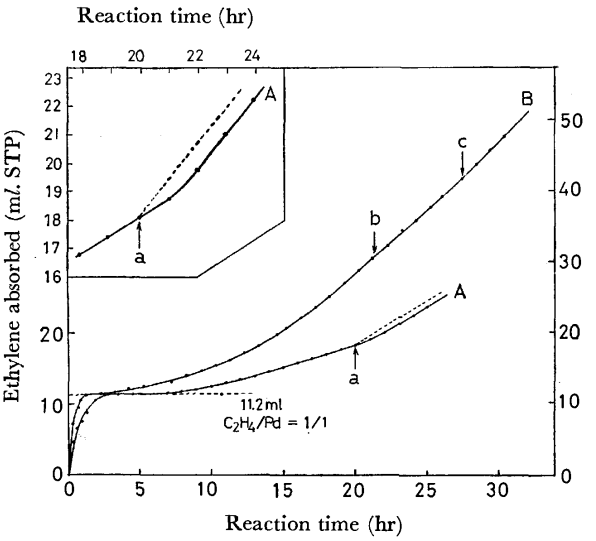

Fig. 1. Time course of ethylene dimerization by $PdCl_2(CN)_2$ catalyst (0.5 mmol) in benzene (50 m*l*) at 36°C under following pressures.
A: 168 mmHg changed to 579 mmHg at a
B: 596 mmHg changed to 131 mmHg at b and to 596 mmHg at c.

The present results is in line with this equation with respect to ethylene concentration as deduced from the results in Fig. 1, where about 3.5 times difference in the ethylene pressure causes a 3.0 times difference in the steady rate. Proportionality with the concentration of Pd complex was confirmed by separate runs.

A further study of the kinetic behavior of the dimerization was made by a pressure jump method as shown at point "a", Fig. 1, where the ethylene pressure was jumped up to about 3.5 times the initial level. However, as we see from the magnified scale, there is no immediate response in the reaction rate, which stays at the initial value for about 1 hr before beginning to increase and attains another steady value about 3 hr later. The response is further delayed in the case of pressure drop (point "b") where the ethylene concentration is reduced to about three tenths. The reaction rates in the following 6 hr is completely unchanged and the pressure jump up to the previous value made again after 6 hr (point "c") causes little change in the rate of absorption. This slow response of the reaction rate to the sudden change in ethylene pressure was further confirmed by repeated changes in the range of 131 to 600 mmHg which corresponded to ethylene concentration of 2.14×10^{-2} to 9.64×10^{-2} mol/*l*. This result demonstrates that the apparent first order kinetics with respect to ethylene does not directly reflect the kinetic nature of the rate determining step for the ethylene dimerization.

2. Isotopic Exchange between Olefins. A mixture of C_2H_4 and C_2D_4 was introduced into the reaction vessel under the reaction conditions of dimerization, and the isotopic distribution in the remaining ethylene was followed by intermittent analyses. Figure 2 shows the time course of individual isotopic species. It is clear that the palladium complex is activated for the isotopic exchange after a while of induction period and that ethylene exchanges one hydrogen atom at a time. It is

10) M. S. Kharasch, R. C. Seyler, and T. R. Mayo, *J. Amer. Chem. Soc.*, **60**, 882 (1938).

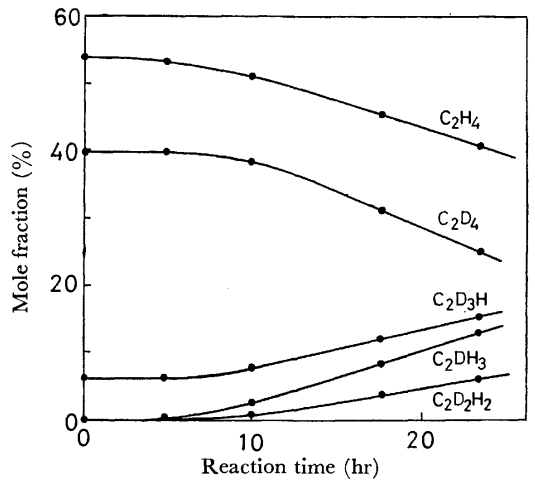

Fig. 2. C_2H_4–C_2D_4 exchange reaction by $PdCl_2(\phi CN)_2$ (0.5 mmol) in benzene (50 ml) at 36°C.

noteworthy that the induction period for the exchange is in agreement with that for the dimerization. That is, both reactions set in simultaneously. This demonstrates that a common active species, possibly a hydride, is responsible for the two reactions. It is also suggested that the hydride might be formed by reacting with ethylene.

3. The Effect of added Olefin on the Rate of Ethylene Dimerization. If the dimerization is promoted by a hydride complex whose hydrogen is provided by ethylene, the rate of dimerization would be enhanced by the presence of an olefin whose hydrogen is readily dissociated. Thus the runs of ethylene dimerization

Table 1. Effects of added olefins on the extent of induction period and rate of dimerization at 36°C and 150 mmHg of ethylene pressure

Added olefin (mmol)		Induction Period (hr)	Rate of Dimerization (ml STP/hr)
None		15—20	~0.9
1-Butene	0.05	17	0.9
1-Butene	0.2	10	0.95
1-Butene	0.5	8	1.0
1-Butene	0.8	5	1.1
trans-2-C′$_4$	0.6	17	~0.9
3-Me-1-C′$_4$	0.14	7	1.4
3-Me-1-C′$_4$	0.6	5	2.8

C′$_4$: butene, Me: methyl

were carried out in the presence of olefins which were mostly about equimolar to the amount of catalyst. The results are shown in Table 1. It is revealed that the hydrogen-releasing olefins such as 3-methyl-1-butene and 1-butene give rise to a decrease in the induction period with the extent increasing with the amount of added olefin. This decrease in the induction period is accompanied by a remarkable increase in the rate of ethylene dimerization in the case of 3-methyl-1-butene which is known to be most liable to release its hydrogen. The extent of enhancement is nearly proportional to the amount of 3-methyl-1-butene added. *trans*-2-Butene which is less liable to release hydrogen gives rise to no decrease in the induction period. In view of this fact, the rather small extent in the enhancement by butene-1 as compared with the decrease in the induction period may be due to the isomerization of added 1-butene to 2-butene.

Product analyses showed no formation of codimer or dimer of the added olefin. This is reasonable because the amount of added olefin is rather small, and ethylene is most reactive in dimerization among olefins.[7]

Discussion

The results are summarized as follows. (1) Although the rate of ethylene dimerization is consistent with the first order kinetics with respect to ethylene, the response of the rate to the ethylene pressure change is considerably delayed.

(2) The palladium-benzonitrile complex is activated after a while of induction period for two reactions simultaneously, ethylene dimerization and isotopic exchange in ethylene.

(3) The presence of hydrogen-releasing olefin decreases the extent of induction period and enhances the rate of dimerization without formation of codimer.

The observed delay in the response to pressure change seems to be caused by the step responsible for the induction period. The delayed response and the apparent first order kinetics can be understood if the equilibrated concentration of active intermediate formed in the induction period is proportional to ethylene pressure and the steady rate of dimerization is proportional to the concentration of this active intermediate.

The kinetics of ethylene dimerization by palladium complex in dioxane has been interpreted in terms of the following scheme:[4]

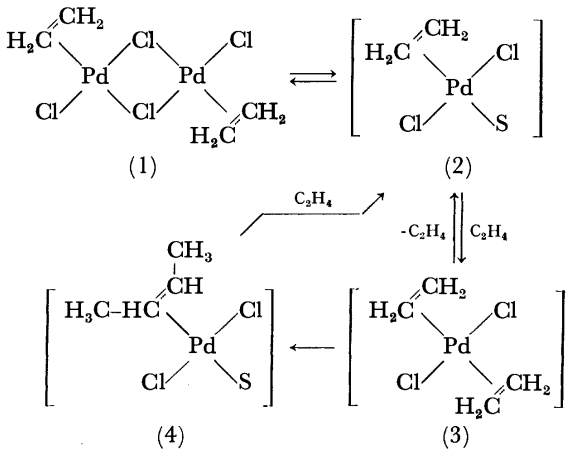

where a steady state of dimerization is attained by cyclic reactions (2)→(3)→(4)→(2), steps (3)→(4) being rate-determining. However, this scheme is inadequate for the present case because it is inconsistent with the delayed response.

Kawamoto *et al.*[6c] proposed a mechanism with a

hydride shift between coordinated olefins, on the basis of a tracer study of codimerization of styrene-d_3 with light ethylene. However, we found that the isotopic exchange between reacting olefins takes place ahead of the dimerization. Since this kind of exchange cannot be ignored in the case proposed by Kawamoto *et al.*, the interpretation of the tracer work seems to be open to question.

On the other hand the results (2) and (3) suggest that a palladium hydride complex whose hydrogen is provided by olefin is responsible for the ethylene dimerization. The observed effects of added olefin could not be due to the formation of codimer. Since 3-methyl-1-butene which is most effective both in decreasing the induction period and enhancing the rate of dimerization is admittedly liable to liberate its tertiary hydrogen, the observed effects of added olefin can be interpreted to be formation of an active hydride complex which catalyzes both the dimerization and the isotopic exchange. The scheme implies that the hydride complex responsible for the dimerization is necessarily preformed by a reaction of the palladium complex with olefin. The ready isomerization of 1-butene as demonstrated by the attainment of isomerization equilibrium in the dimerization product is also consistent with the presence of preformed hydride complex. In the case of five-coordinate hydride scheme[2] or concerted hydride shift scheme[6c] for dimerization, a separate scheme is required for the isomerization and isotopic exchange, whereas the preformed hydride can account for all of three reactions in terms of palladium alkyl intermediate,[7,8] as follows:

$$\begin{array}{l} \qquad\qquad\qquad\qquad\qquad\qquad \mathrm{PdD} + \mathrm{C_2D_3H}\ \text{(exchange)} \\ \qquad\qquad\qquad\qquad\qquad\qquad\quad \uparrow \\ \mathrm{Pd\text{-}H} + \mathrm{C_2D_4} \longrightarrow \mathrm{Pd\text{-}C_2D_4H} \xrightarrow{C_2H_4} \mathrm{Pd\text{-}C_2H_4\text{-}C_2D_4H} \\ \qquad\qquad\quad \longrightarrow \mathrm{Pd\text{-}H} + \mathrm{C_4H_4D_4}\ \text{(dimerization)} \end{array}$$

$$\begin{array}{l} \mathrm{Pd\text{-}H} + \text{1-}\mathrm{C_4H_8} \longrightarrow \mathrm{Pd\text{-}C_4H_9} \longrightarrow \\ \qquad\qquad\qquad\qquad\qquad\qquad \mathrm{PdH} + \text{2-}\mathrm{C_4H_8}\ \text{(isomerization)} \end{array}$$

If the preformed hydride is necessary for the dimerization, the observed induction period should be ascribed to the slow formation of the hydride complex from olefin. The delayed response of the dimerization rate to pressure change is reasonable if the equilibrium concentration of hydride complex is proportional to olefin concentration. Thus the mechanism of hydride formation is important. The present results seem to suggest a dissociation of olefin to form a hydride. The palladium hydride is known to exist[11] although it is unstable.

11) E. H. Brooks and F. Glocking, *J. Chem. Soc., (A)*, **1967**, 1030.

Synthesis of N^{δ}-Hydroxyornithine

Yoshikazu Isowa, Toshiyuki Takashima, Muneki Ohmori, Hideaki Kurita, Masanari Sato, and Kaoru Mori

Sagami Chemical Research Center, Ohnuma, Sagamihara, Kanagawa

(Received August 5, 1971)

N^{δ}-Tosyl-N^{δ}-benzyloxy-DL-ornithine was synthesized starting from γ-(N-tosyl-N-benzyloxy)-aminopropyl bromide and diethyl acetamidomalonate and resolved enzymatically to give the L- and D-isomers. Removal of one or both of protecting groups gave N^{δ}-benzyloxyornithine or N^{δ}-hydroxyornithine. The reduction product of N^{δ}-hydroxy-L-ornithine was identical with authentic L-ornithine.

N^{δ}-Hydroxyornithine is one of the most commonly found constituents of naturally occurring peptides.[1] In these compounds the α-amino and the carboxyl group of a N^{δ}-hydroxyornithine residue are linked by amide bonds to form a cyclic hexapeptide and the hydroxyamino group is present in the form of a hydroxamic acid derivative. These peptides, for example, ferrichrome[2] and albomycin[3] have been found to have potent microbial growth factor or antibiotic activities.

Synthesis of N^{δ}-hydroxyornithine have been attempted by two group of workers, but the amino acid was not isolated.[4,5]

This paper presents the successful synthesis of N^{δ}-hydroxyornithine *via* optical resolution of N^{δ}-tosyl-N^{δ}-benzyloxy-DL-ornithine and subsequent removal of the tosyl and benzyl groups.

O-Benzylhydroxylamine(I) was first converted into the tosyl derivative(II), which was alkylated with 1,3-dibromopropane to γ-(N-tosyl-N-benzyloxy)-aminopropyl bromide(III). This was allowed to react with diethyl sodio-acetamidomalonate, and the product was heated with concentrated hydrochloric acid–acetic acid to yield racemic N^{δ}-tosyl-N^{δ}-benzyloxyornithine(DL-V).

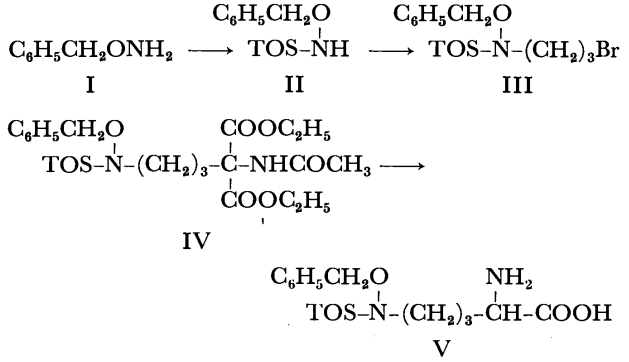

Fig. 1

Optically active N^{δ}-tosyl-N^{δ}-benzyloxy-L-ornithine and its D-isomer were prepared by enzymatic resolution of the N^{α}-acetyl-N^{δ}-tosyl-N^{δ}-benzyloxy-DL-ornithine (DL-VI) with aniline in the presence of papain. The resulting N^{α}-acetyl-N^{δ}-tosyl-N^{δ}-benzyloxy-L-ornithine anilide (L-VII) and N^{α}-acetyl-N^{δ}-tosyl-N^{δ}-benzyloxy-D-ornithine (D-VI) showed $[\alpha]_D^{25}$ −53.4° and $[\alpha]_D^{25}$ −18.1° in chloroform solution. N^{δ}-Tosyl-N^{δ}-benzyloxy-L-ornithine and its D-isomer (L–V and D–V) were prepared by acid hydrolysis in hydrochloric acid–acetic acid solution. The amino acid (L-V and D-V) thus obtained exhibited optical rotation of $[\alpha]_D^{23.5}$ +20.7° and $[\alpha]_D^{25}$ −21.0°, respectively, in acetic acid solution.

DL-VI was also obtained by racemization of D-VI using acetic anhydride or acetic anhydide–acetic acid.

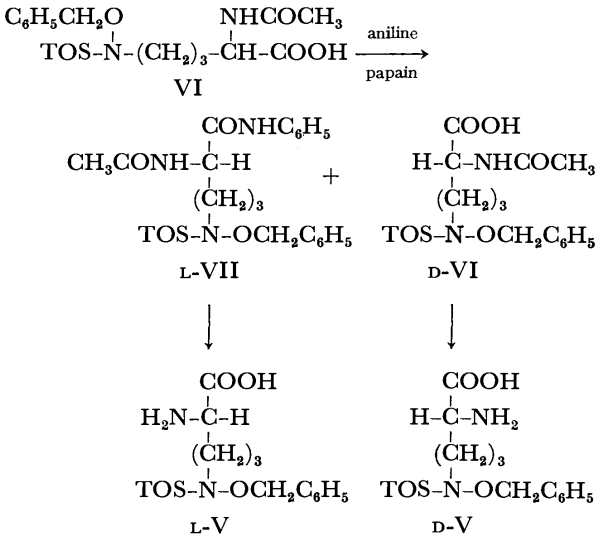

Fig. 2

As a mild method for the removal of a tosyl group in the synthesis of relatively unstable compounds, Weisblat *et al.*[6] used 30% hydrogen bromide in acetic acid in the presence of phenol at room temperature. They described detosylation of *N*-substituted sulfonamides, such as TOS–NRR′; R,R′=H, alkyl, aryl, acyl or alkoxycarbonyl. However similar condition has never been applied for detosylation of tosylhydroxamate series, TOS–N(OR)R′; R=$CH_2C_6H_5$, R′=alkyl. The removal of a tosyl group from the amino acid (V) was accomplished by the

1) W. Keller-Schierlein, V. Prelog, and H. Zähner, "Fortshritte der Chemie Organischer Naturstoffe XXII," Springer-Verlag, Wien (1964), p. 279—316.

2) J. B. Neilands, *J. Amer. Chem. Soc.*, **74**, 4846 (1952); J. A. Garibaldi and J. B. Neilands, *ibid.*, **77**, 2429 (1955); S. J. Rogers and J. B. Neilands, *Biochemistry*, **3**, 1850 (1964); S. J. Rogers, R. A. J. Warren, and J. B. Neilands, *Nature*, **200**, 167 (1963).

3) J. Turkova, O. Mikes, and F. Sorm, *Experientia*, **19**, 633 (1963).

4) S. J. Rogers, *Dissertation Abstr.* **25** (**10**), 5538 (1965); S. J. Rogers, University Microfilms, Inc., Ann Arbor, Michigan, order No 65-3073.

5) L. G. Makevnina and N. A. Poddubunaya, *Zh. Obsch. Khim.*, **36** (**10**), 1755 (1966).

6) D. I. Weisblat, B. J. Magerlein, and D. R. Myers, *J. Amer. Chem. Soc.*, **75**, 3630 (1953).

action of 36% hydrogen bromide in acetic acid in the presence of phenol at room temperature for 50 hr to give N^{δ}-benzyloxy-DL-ornithine monohydrobromide (DL-VIII·HBr). Similar treatment of the D- and L-amino acid (D- and L-V) with this reagent gave the corresponding D- and L-N^{δ}-benzyloxy derivatives (D- and L-VIII).

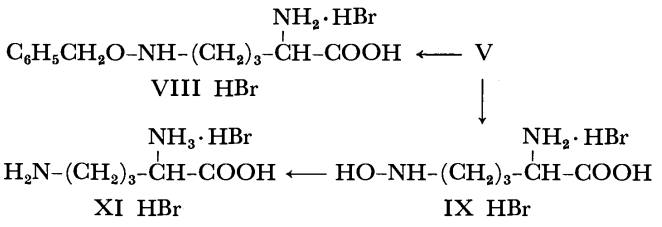

Fig. 3

Simultaneous cleavage of the tosyl and benzyl group from the amino acid (D-, L-, and DL-V) was carried out by the action of the above described reagent at room temperature for 10 days to give N^{δ}-hydroxyornithine monohydrobromide (D-, L-, and DL-IX), which showed blue color with ninhydrin and gave red color with the triphenyltetrazolium reagent.[7] The salt (X) of N^{δ}-hydroxy-DL-ornithine with one mole of 2-nitro-1,3-indanedione was obtained from DL-IX HBr by the procedure of Rogers.[4]

L- and D-IX were hydrogenated to give L- and D-ornithine monohydrobromide (L- and D-XI) in the presence of palladium charcoal.

It was demonstrated by measurements of the melting point, infrared spectrum, optical rotation, and elemental analysis that the L-isomer(XI) was identical with authentic L-ornithine monohydrobromide.

Experimental

Melting points were all determined with a Yanagimoto electric micromelting point apparatus and are uncorrected, and optical rotations were measured with a Yanagimoto automatic polarimeter OR-50.

O-Benzylhydroxylamine (I). It was prepared by the method described by Fuller and King.[8]

O-Benzyl-N-tosylhydroxylamine (II). To a chilled solution of *O*-benzylhydroxylamine (246 g, 2.0 mol) in pyridine (300 m*l*), a solution of *p*-toluenesulfonyl chloride (381 g, 2.0 mol) in pyridine was added slowly during 2 hr. The solution was stirred at room temperature for 2 hr and allowed to stand overnight. The material precipitated was filtered off and the filtrate was evaporated *in vacuo*. The residual oil was extracted with ethyl acetate (1.2 *l*) and the organic layer was washed with 2N hydrochloric acid and water, dried over sodium sulfate, and then evaporated *in vacuo*. The residual oil was solidified by adding petroleum ether. The product was recrystallized from ethyl acetate–petroleum ether; yield 454 g (82%), mp 93—97°C.

Found: C, 60.79; H, 5.45; N, 4.92%. Calcd for $C_{14}H_{15}NO_3S$: C, 60.64; H, 5.45; N, 5.05%.

γ-(N-Tosyl-N-benzyloxy)-aminopropyl Bromide (III). To a solution of sodium (23 g, 1.0 g-Atom) in ethanol (1.2 *l*) was added II (277 g, 1.0 mol) with vigorous stirring at 70°C. After a clear solution was obtained, trimethylene dibromide (404 g, 2.0 mol) was added. The mixture was refluxed for 8 hr, and evaporated *in vacuo* to give oily material, which was extracted with ethyl acetate and the organic layer was thoroughly washed with water and dried over sodium sulfate. Evaporation of the solvent afforded oily product which was crystallized from ethyl acetate–*n*-hexane; yield 350 g (88%), mp 73—77°C.

Found: C, 51.36; H, 5.11; N, 3.69%. Calcd for $C_{17}H_{20}O_3NSBr$: C, 51.26; H, 5.06; N, 3.51%.

Diethyl γ-(N-Tosyl-N-benzyloxy)-aminopropyl Acetamidomalonate (IV). To a solution of sodium (18.4 g, 0.8 g-Atom) in ethanol (1.5 *l*) was added diethyl acetamidomalonate (174 g, 0.8 mol) while stirring. After 5 min, III (319 g, 0.8 mol) was added and the mixture was refluxed for 8 hr. The solvent was then removed *in vacuo* and the residue was extracted with chloroform. The chloroform solution was successively washed with water, dilute hydrochloric acid and water, dried over magnesium sulfate, and evaporated *in vacuo*. The oily residue was crystallized from ethyl acetate–petroleum ether and then from ethanol; yield 299 g (70%), mp 135—138°C.

Found: C, 58.68; H, 6.12; N, 4.99%. Calcd for $C_{26}H_{34}N_2O_8S$: C, 58.42; H, 6.41; N, 5.24%.

N^{δ}-Tosyl-N^{δ}-benzyloxy-DL-ornithine (DL-V). A solution of IV (160 g, 0.3 mol) in a mixture of acetic acid (1.2 *l*) and concentrated hydrochloric acid (480 m*l*) was heated under gentle reflux for 8 hr. The solution was evaporated *in vacuo* and 14% aqueous ammonia was added to the residue. The resulting solid was collected by filtration, washed with water, and recrystallized from acetic acid–water; yield 106 g (90%), mp 207—210°C (decomp.).

Found: C, 57.84; H, 6.04; N, 6.89%. Calcd for $C_{19}H_{24}N_2O_5S$: C, 58.15; H, 6.17; N, 7.14%.

N^{α}-Acetyl-N^{δ}-tosyl-N^{δ}-benzyloxy-DL-ornithine (DL-VI). DL-V (70 g, 0.18 mol) was mixed with glacial acetic acid (420 m*l*) and warmed with gentle stirring to give a clear solution. The solution was cooled for several minutes and acetic anhydride (26 m*l*, 0.25 mol) was carefully added. The resulting solution was warmed to 80°C with stirring, held at this temperature for 5 hr and then evaporated *in vacuo*. The syrupy residue was taken up in a minimum quantity of ethyl acetate and the solution was chilled. After standing for 2 hr at 5°C, the crystals separated. Recrystallization from ethyl acetate gave colorless crystals; yield 58 g (75%), mp 142.5—144.0°C.

Found: C, 57.93; H, 6.01; N, 6.29%. Calcd for $C_{21}H_{26}N_2O_6S$: C, 58.05; H, 6.03; N, 6.45%.

Resolution of N^{α}-Acetyl-N^{δ}-tosyl-N^{δ}-benzyloxy-DL-ornithine (DL-VI). a) N^{α}-Acetyl-N^{δ}-tosyl-N^{δ}-benzyloxy-L-ornithine Anilide (L-VII). DL-Acetylamino acid (DL-VI) (74 g, 0.171 mol) was dissolved in 0.75N sodium hydroxide (600 m*l*) and the solution adjusted to pH 6.05—6.20 with 0.5M citric aicd. The solution was diluted with distilled water to the final volume of 1.2 *l*. Papain (20 g) was added to the solution together with freshly distilled aniline (20 m*l*) and cysteine hydrochloride monohydrate (10 g). The mixture was incubated for 36 hr at 38°C; the anilide deposited was filtered off, washed with water, 7% aqueous ammonia and water.

Recrystallization from *n*-propyl alcohol gave colorless crystals; yield 40 g (92%), mp 203—205°C, $[\alpha]_D^{25}$ −53.4° (*c* 1, chloroform).

Found: C, 63.25; H, 6.07; N, 8.14%. Calcd for $C_{27}H_{31}N_3O_5S$: C, 63.64; H, 6.13; N, 8.25%.

7) G. A. Snow, *J. Chem. Soc.*, **1954**, 2588.
8) A. T. Fuller and H. King, *ibid.*, **1947**, 963.

b) N^{α}-*Acetyl*-N^{δ}-*tosyl*-N^{δ}-*benzyloxy*-D-*ornithine (*D-*VI).* The above filtrate, combined with the washings was adjusted to pH 2 with 5N hydrochloric acid. Then the precipitated material was filtered off, washed with water and dried. Recrystallization from ethyl acetate gave colorless crystals; yield 32.4 g (88%), mp 131.0—133.5°C, $[\alpha]_D^{25}$ −18.1° (*c* 1, chloroform).

Found: C, 58.00; H, 5.91; N, 6.06%. Calcd for $C_{21}H_{26}N_2O_6S$: C, 58.05; H, 6.03; N, 6.45%.

N^{δ}-*Tosyl*-N^{δ}-*benzyloxy*-L-*ornithine (*L-*V).* L-VII (40 g, 78.7 mmol) was dissolved in glacial acetic acid (300 m*l*) while gently warming and concentrated hydrochloric acid (120 m*l*) was carefully added. After refluxing for 8 hr, the solution was evaporated *in vacuo* and aqueous ammonia was added to the residue. After standing for 2 hr at 5°C, the deposits were filtered off with suction, washed with water, and dried. Recrystallization from dilute acetic acid gave 25.8 g (83%), mp 222.5—224.8°C (decomp.), $[\alpha]_D^{23.5}$ +20.7° (*c* 3, acetic acid).

Found: C, 57.98; H, 6.46; N, 7.38%. Calcd for $C_{19}H_{24}N_2O_5S$: C, 58.15; H, 6.16; N, 7.14%.

N^{δ}-*Tosyl*-N^{δ}-*benzyloxy*-D-*ornithine (*D-*V).* This was obtained from D-VI by the method described above. Yield 86%, mp 220—223°C (decomp.) (from dilute acetic acid), $[\alpha]_D^{25}$ −21.0° (*c* 2, acetic acid).

Found: N, 7.25%. Calcd for $C_{19}H_{24}N_2O_5S$: N, 7.14%.

N^{δ}-*Benzyloxy*-L-*ornithine Monohydrobromide (*L-*VIII HBr).* To 18 m*l* of a solution of 36% hydrogen bromide-acetic acid and phenol (2.5 g) in a glass-stoppered bottle, L-V (3.92 g, 10 mmol) was added at room temperature. After stirring for 50 hr, the solution was evaporated to dryness *in vacuo* at 35°C. The residual oil was triturated several times with ether and dissolved in water (50 m*l*). The solution was washed repeatedly with ether and then kept in a refrigerator overnight, the crystals deposited was removed by filtration and the filtrate was evaporated *in vacuo* at 35°C. The above residue was dissolved in water (5 m*l*). The solution was adjusted to pH 4—5 with pyridine, and addition of ethanol (30 m*l*) and ether (50 m*l*) yielded crystals, which were purified by dissolving them in water and adding ethanol-ether. D- and DL-V were treated in the same manner to yield the corresponding D- and DL-VIII·HBr. The results are summarized in Table 1.

Table 1. Melting points, yields, optical rotations and elemental analyses of VIII

Compd.		L-VIII	D-VIII	DL-VIII
Mp (°C)		155—157 (decomp.)	155—156 (decomp.)	149—150 (decomp.)
Yield (%)		30	32	52
$[\alpha]_D$ (°)		+9.0 (*c* 1, H_2O, 27°C)	−8.4 (*c* 1, H_2O, 22°C)	—
Formula		$C_{12}H_{19}N_2O_3Br$	$C_{12}H_{19}N_2O_3Br$	$C_{12}H_{19}N_2O_3Br$
Calcd	C	45.15	45.15	45.15
	H	6.00	6.00	6.00
	N	8.78	8.78	8.78
Found	C	44.68	45.13	44.88
	H	6.08	6.06	6.12
	N	8.86	8.85	8.84

N^{δ}-*Benzyloxy*-DL-*ornithine (*DL-*VIII).* This was obtained from V by the method described above, except that the solution was adjusted to pH 8 by adding aqueous ammonia. The solution was evaporated to dryness again. The residue was crystallized from water-ethanol (Yield 53%), mp 195—203°C (decomp.). It gave positive ninhydrin test and negative Beilstein test. For the analysis, the product was recrystallized from water-ethanol.

Found: C, 60.43; H, 7.57; N, 11.58%. Calcd for $C_{12}H_{18}N_2O_3$: C, 60.48; H, 7.61; N, 11.76%.

N^{δ}-*Hydroxyornithine Monohydrobromide (IX·HBr).* To a mixture of 36% hydrogen bromide-acetic acid (18 m*l*) and phenol (2 g) in a glass-stoppered bottle, V (3.92 g, 10 mmol) was added at room temperature. After stirring for 10 days at room temperature, the solution was evaporated *in vacuo* at 50°C. The residual oil was triturated with ether. The residue was dissolved in water (50 m*l*) and the solution was washed repeatedly with ether and then evaporated *in vacuo* below 50°C. The residual oil was dissolved again in water (2 m*l*), the solution was adjusted to pH 4—5 with pyridine, and addition of ethanol deposited crystals. For analysis, the product was recrystallized from water-ethanol. Ninhydrin, triphenyltetrazolium, and Beilstein tests were all positive. The results are summarized in Table 2.

Table 2. Melting points, optical rotations, and elemental analyses of IX.

Compd.		L-IX	D-IX	DL-IX
Mp (°C)		174—176 (decomp.)	175—177 (decomp.)	199—201 (decomp.)
$[\alpha]_D^{25}$ (°)		+8.3 (*c* 2, H_2O)	−8.2 (*c* 2.5, H_2O)	—
Formula		$C_5H_{13}N_2O_3Br$	$C_5H_{13}N_2O_3Br$	$C_5H_{13}N_2O_3Br$
Calcd	C	26.21	26.21	26.21
	H	5.72	5.72	5.72
	N	12.23	12.23	12.23
Found	C	26.36	26.38	26.39
	H	5.69	5.70	5.88
	N	12.04	12.06	12.03

N^{δ}-*Hydroxy*-DL-*ornithine Mono-2-nitro-1,3-indanedione (X).* This compound was obtained from DL-IX by the procedure of Rogers.[4] Yellow needles, mp 212—219°C (decomp.). (lit,[4] mp 210—212°C (decomp.)).

Found: C, 49.60; H, 5.00; N, 12.38%. Calcd for $C_{14}H_{17}N_3O_7$: C, 49.56; H, 5.05; N, 12.38%.

Catalytic Reduction of L-*IX.* A solution of L-IX (0.5 g, 2.2 mmol) in water was hydrogenated in the presence of 5% palladium charcoal catalyst (0.5 g) at room temperature. After 20 hr, the catalyst was removed and the filtrate was evaporated *in vacuo*. The residual crystalline product was recrystallized from water-ethanol (Yield 74%). The corresponding D-isomer (D-XI·HBr) was obtained in the same

Table 3. Melting points, optical rotations and elemental analyses of XI.

Compd.		L-XI	D-XI	Authentic L-XI
Mp (°C)		243—246 (decomp.)	244—246 (decomp.)	245—247 (decomp.)
$[\alpha]_D$ (°)		+9.9 (*c* 2, H_2O, 23°C)	−9.5 (*c* 1.75, H_2O, 26°C)	+9.8 (*c* 2, H_2O, 23°C)
Formula		$C_5H_{13}N_2O_2Br$	$C_5H_{13}N_2O_2Br$	$C_5H_{13}N_2O_2Br$
Calcd	C	28.18	28.18	28.18
	H	6.15	6.15	6.15
	N	13.15	13.15	13.15
Found	C	28.13	28.21	28.41
	H	5.95	6.22	6.15
	N	12.91	13.34	13.23

manner with a 72% yield. This was positive to ninhydrin test and negative to triphenyltetrazolium test. The results are summarized in Table 3.

Racemization of N^{α}-*acetyl*-N^{δ}-*tosyl*-N^{δ}-*benzyloxy*-D-*ornithine (*D-*VI).* *a)*: A solution of D-VI (21.7 g, 0.05 mol) in acetic anhydride (40 m*l*) was heated at 120°C for 2 hr, and then evaporated *in vacuo*. The residual pale yellow syrup was dissolved in acetone (30 m*l*) and water (10 m*l*) was added. The mixture was stirred for 2 hr at room temperature and evaporated *in vacuo*. The residual syrup was dissolved in hot ethyl acetate (30 m*l*), and the racemic compound (VI), which precipitated on standing in a deep freezer, was collected, yield 16.4 g, mp 137—139°C. Recrystallization from ethyl acetate raised the melting point to 139.5—141°C. The product was optically inactive in chloroform solution.

b): A solution of D-VI (21.7 g) in a mixture of acetic acid (30 m*l*) and acetic anhydride (7 m*l*) was refluxed for 75 min, and then evaporated *in vacuo*. DL-VI was obtained with the same treatment as described above. Yield 16.1 g, mp 136°C. Recrystallization from ethyl acetate raised the melting point to 139—140°C. The product showed no optical rotation.

BULLETIN OF THE CHEMICAL SOCIETY OF JAPAN, VOL. 45, 1464—1466(1972)

Acylation of N^{δ}-Benzyloxyornithine

Yoshikazu Isowa, Toshiyuki Takashima, Muneki Ohmori,
Hideaki Kurita, Masanari Sato, and Kaoru Mori
Sagami Chemical Research Center, Ohnuma, Sagamihara, Kanagawa

(Received August 5, 1971)

Acetylation of N^{δ}-benzyloxyornithine monohydrobromide (I·HBr) with acetic anhydride gave the N^{δ}-acetylated product, which yielded N^{δ}-acetyl-N^{δ}-hydroxyornithine by catalytic reduction. On the other hand, acetylation or alkoxycarbonylation of N^{δ}-benzyloxyornithine(I) proceeded through N^{α}-acetylation, followed by spontaneous cyclization to form lactams, which yielded cyclic hydroxamic acids on catalytic reduction. These hydroxamic acid and N^{δ}-acetyl-N^{δ}-hydroxyornithine were readily hydrolyzed to give N^{δ}-hydroxyornithine.

In the preceding paper,[1] it was shown that N^{δ}-tosyl-N^{δ}-benzyloxyornithine gave N^{δ}-benzyloxyornithine(I) by detosylation under mild conditions. Since its benzyloxyamino-group may be converted into a hydroxamic group, I is expected to be used as a starting material for the synthesis of amino acid derivatives and peptides such as N^{δ}-acetyl-N^{δ}-hydroxyornithine,[2] rhodotorulic acid[3] and ferrichrome.[4] The present paper reports the behavior of I toward acylation.

Treatment of optically active or racemic N^{δ}-benzyloxyornithine monohydrobromide (L-, D-, and DL-I·HBr) with acetic anhydride in water yielded a viscous oily product (II), which gave, on catalytic hydrogenation with palladium on charcoal, optically active or racemic N^{δ}-acetyl-N^{δ}-hydroxyornithine (L-, D-, and DL-III). The results are summarized in Table 1.

Table 1. N^{δ}-Acetyl-N^{δ}-hydroxyornithine (III)

		L	D	DL
Mp (°C)		194—197 (decomp.)	195—197.5 (decomp.)	193—195.5 (decomp.)
Yield (%)		64	69	79
Found	C	44.01	44.20	44.16
	H	7.62	7.62	7.70
	N	14.51	14.62	14.46
Calcd for $C_7H_{14}N_2O_4$	C	44.20	44.20	44.20
	H	7.41	7.41	7.41
	N	14.73	14.73	14.73

NMR (D_2O) for DL-III: δ; 3.70 ppm (3H, δ-methylene and α-methine), 2.13 (3H, acetyl methyl protons), 1.80 (4H, β, γ-ethylene protons).

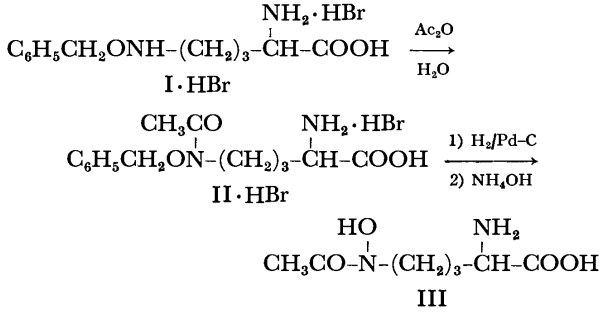

Fig. 1

Since these products gave positive ninhydrin- and ferric-test and negative triphenyltetrazolium reaction, their structure is established as formulated III in Fig. 1. Emery considered N^{δ}-acetyl-N^{δ}-hydroxy-L-ornithine (L-III) as a precursor in ferrichrome biosynthesis and prepared it from N^{δ}-hydroxyornithine obtained by the hydrolysis of fusarinine.[2] The melting point of our synthetic L-III was the same as that of Emery's product. No racemization occurred during the above mentioned synthesis of III, because hydrolysis and subsequent catalytic reduction of D-III gave D-ornithine monohydrochloride (D-V·HCl), $[\alpha]_D^{22}$ −12.2° (c 1, water), the optical activity of authentic L-isomer monohydrochloride obtained commercially being $[\alpha]_D^{22}$ +12.2° (c 1, water).

1) Y. Isowa, T. Takashima, M. Ohmori, H. Kurita, M. Sato, and K. Mori, This Bulletin, **45**, 1461 (1972).
2) T. Emery, *Biochemistry*, **5**, 3694 (1966).
3) C. L. Atkin and J. B. Neilands, *Biochemistry*, **7**, 3734 (1968).
4) J. B. Neilands. *J. Amer. Chem. Soc.*, **74**, 4846 (1952).

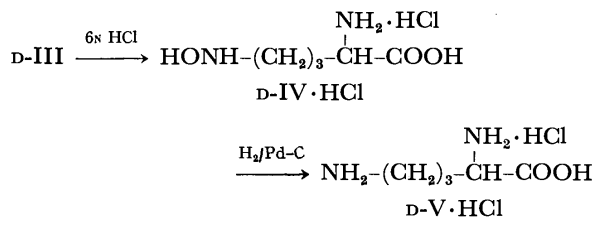

Fig. 2

It should be mentioned that N^{δ}-hydroxyornithine monohydrochloride (L-, and D-IV·HCl) has not been obtained previously, although isolation of the corresponding monohydrobromide was described in the preceding paper.[1] Further, L- and D-IV gave salts with 2-nitroindane-1,3-dione (L- and D-VI) by the procedure of Rogers.[5] Treatment of free I with two and a half equivalents of acetic anhydride in acetic acid afforded 1-benzyloxy-3-acetaminopiperidone (VII), instead of the expected product, N^{α}-acetyl-N^{δ}-acetyl-N^{δ}-benzyloxyornithine (VIII). The lactam (VII) was also obtained from I by treatment with one equivalent of *p*-nitrophenyl acetate in the presence of benzyltrimethylammonium hydroxide (Triton B) in dioxane followed by neutralization. Analogous lactam deivatives (IX and X) were obtained from free I. Attempted N^{α}-acylation of N^{δ}-benzyloxyornithine always resulted in spontaneous cyclization to give lactams.

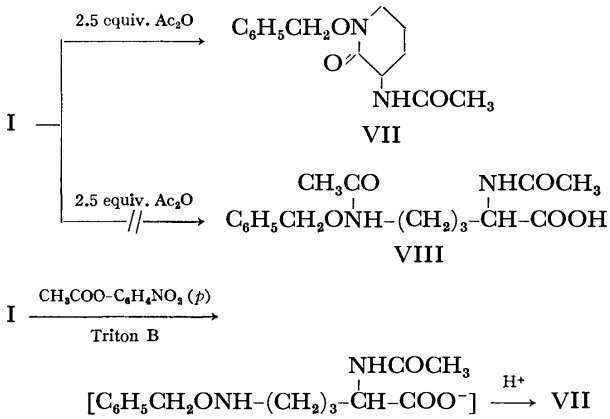

Fig. 3

It was found that the lactam (VII) reacts with hydrazine monohydrate to give N^{α}-acetyl-N^{δ}-benzyloxyornithine hydrazide (XI). Catalytic hydrogenation of VII and IX with palladium on charcoal yielded 1-hydroxy-3-acylaminopiperidones, XII and XIII. Treatment of D-XIII with 2N hydrochloric acid in dioxane afforded D-1-hydroxy-3-amino-2-piperidone monohydrochloride (XIV·HCl). It melted at 177—179°C. This is the same melting point as that of the monohydrochloride obtained from fusarinine,[4] although the latter is probably the optical enantiomorph (L-form). Finally, hydrolysis of D-XIV·HCl with 6N hydrochloric acid yielded N^{δ}-hydroxy-D-ornithine monohydrochloride.

5) S. J. Rogers, Univ. Microfilm (Ann Arbor, Mich.) Order No. 65—3073, Dissertation (1964).

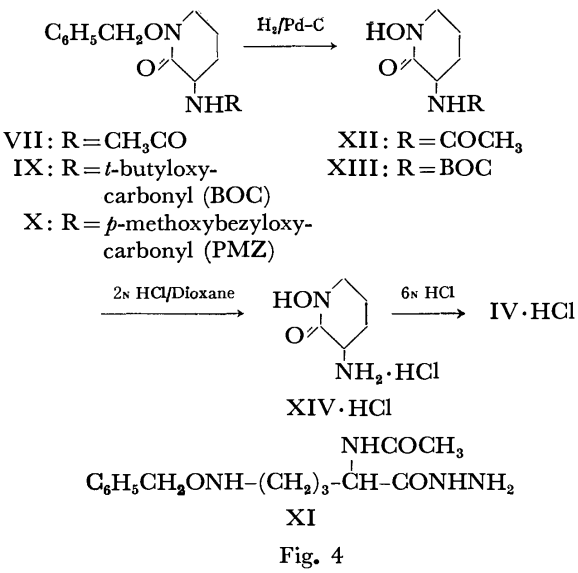

Fig. 4

Experimental

Melting points were all determined with a Yanagimoto electric micromelting point apparatus and are uncorrected, and optical rotations were measured with a Yanagimoto automatic polarimeter OR-50. Nuclear magnetic resonance spectra were taken on a Hitachi Perkin-Elmer R-20 High Resolution NMR spectrometer using tetramethylsilane as an internal standard.

N^{δ}-Benzyloxyornithine (I). This compound was prepared as monohydrobromide by the procedure described in the preceding paper.[1]

L-I·HBr: mp 155—157°C (decomp.), $[\alpha]_D^{27}+9.0°$ (*c* 1, water)
D-I·HBr: mp 155—157°C (decomp.), $[\alpha]_D^{22}-8.4°$ (*c* 1, water)

Free amino acid was obtained from monohydrobromide by treatment with aqueous ammonia. L-I: mp 198—202°C (decomp.), D-I: mp 198—205°C (decomp.).

N^{δ}-Acetyl-N^{δ}-benzyloxy-D-ornithine Monohydrobromide (D-II·HBr). To a solution of D-I·HBr (0.957 g, 3 mmol) in water (5 m*l*), acetic anhydride (0.375 m*l*) was added at room temperature. After it had been stirred for 1 hr at 50°C, the reaction mixture was evaporated *in vacuo*. The residual oil was used for subsequent operation without further purification.

The DL- and L-isomer were obtained as oily products in the same manner.

N^{δ}-Acetyl-N^{δ}-hydroxy-D-ornithine (D-III). A solution of D-II in methanol (15 m*l*) was hydrogenated in the presence of 5% palladium charcoal (0.15 g) at room temperature for 17 hr. The filtrate obtained from the reduction mixture was evaporated *in vacuo*. The residual oil was dissolved in water (0.15 m*l*), the solution was adjusted to pH 8—9 with aqueous ammonia, and addition of ethanol to the solution yielded crystals. Recrystallization from water-ethanol gave colorless crystals. The DL- and L-isomer were obtained in the same manner. The results are summarized in Table 1. Ninhydrin- and ferric chloride tests were positive and triphenyltetrazolium test was negative with these products.

N^{δ}-Hydroxy-D-ornithine Monohydrochloride (D-IV·HCl). D-III (0.37 g, 1.95 mmol) was hydrolyzed with 6N hydrochloric acid (15 m*l*) at 100°C, until ferric test became negative. The reaction mixture was evaporated to dryness *in vacuo* and the treatment was repeated after the addition of water. The residue was dissolved in water, the solution was adjusted to pH 4—5 with pyridine and evaporated to dryness *in vacuo*.

The residue was crystallized from water-ethanol-ether. Yield 78%, mp 179—181°C (decomp.), $[\alpha]_D^{19}-11.6°$ (*c* 1, water), positive triphenyltetrazolium, ninhydrin, and negative ferric chloride tests.

Found: C, 32.98; H, 6.78; N, 15.20%. Calcd for $C_5H_{13}N_2O_3Cl$: C, 32.52; H, 7.10; N, 15.18%.

L-Isomer (L-IV·HCl) was obtained from L-III bv the same procedure. Mp 178—180°C (decomp.), $[\alpha]_D^{19}+11.4°$ (*c* 0.5, water).

Found: C, 32.62; H, 7.29; N, 15.05%. Calcd for $C_5H_{13}N_2O_3Cl$: C, 32.52; H, 7.10; N, 15.18%.

N^{δ}-Hydroxy-D-ornithine Mono-2-nitro-1,3-indanedione (D-VI). This was obtained from D-IV by the procedure of Rogers.[5] Bright yellow crystals, mp 220—227°C (decomp.).

Found: C, 49.38; H, 5.11; N, 12.14%. Calcd for $C_{14}H_{17}N_3O_7$: C, 49.56; H, 5.05; N, 12.38%.

The L-isomer (L-VI) was obtained from L-IV by the same procedure. Bright yellow crystals, mp 221—227°C (decomp.).

D-Ornithine Monohydrochloride (D-V·HCl). A solution of D-IV (0.239 g, 1.3 mmol) in water (5 m*l*) was hydrogenated in the presence of 10% palladium charcoal (0.1 g) at room temperature, until the tetrazolium test became negative. The filtrate from the reduction mixture was evaporated *in vacuo* to give a crystalline product. Recrystallization from water-ethanol gave the desired product. Yield 92%, mp 242—245°C (decomp.), $[\alpha]_D^{22}-12.2°$ (*c* 1, water). (L-Ornithine monohydrochloride (obtained commercially). Mp 240—245°C (decomp.), $[\alpha]_D^{22}+12.2°$ (*c* 1, water)).

Found: C, 35.48; H, 7.84; N, 16.33%. Calcd for $C_5H_{13}N_2O_2Cl$: C, 35.61; H, 7.77; N, 16.62%.

DL-1-Benzyloxy-3-acetylaminopiperidone (DL-VII). DL-I (2.23 g, 0.01 mol) was dissolved in acetic acid (10 m*l*) by boiling and after the solution was allowed to cool for 1—2 min acetic anhydride (2.5 m*l*) was added in portions. The resulting solution was heated under reflux for 2 min and allowed to cool to room temperature. The reaction mixture was evaporated *in vacuo* and the evaporation was repeated after addition of water to the residue. The resulting crystals were taken up in ethyl acetate and the solution was washed repeatedly with water. The organic layer was dried over sodium sulfate and evaporated to dryness. The resulting crystalline residue was purified by recrystallization from ethyl acetate. Yield 46%, mp 151—152°C, ninhydrin, tetrazolium, and ferric chloride tests negative.

NMR (DMSO-d_6): δ; 8.10 ppm (1H, *N*-proton), 7.40 (5H, phenyl protons), 4.87 (2H, *O*-methylene protons), 4.30 (1H, C_3-proton), 3.45 (2H, C_6-protons), 1.86 (7H, C_4, C_5, and acetyl protons).

Found: C, 63.98; H, 6.77; N, 10.62%. Calcd for $C_{14}H_{18}N_2O_3$: C, 64.10; H, 6.92; N, 10.68%.

DL-1-Benzyloxy-3-t-butyloxycarbonylaminopiperidone (IX). To a suspension of DL-I (0.476 g, 2 mmol) in methanol (5 m*l*), 40% benzyltrimethylammonium hydroxide (0.94 m*l*) was added and the mixture was stirred until the suspension went into a clear solution. The resulting solution was evaporated *in vacuo* and the residue was evaporated successively with ethanol and benzene. To a solution of the residue in *t*-buthanol (4 m*l*), *t*-butyl 2,4,5-trichlorophenyl carbonate (0.601 g, 2.02 mmol) was added and stirred for 15 hr at 50—55°C. The reaction mixture was evaporated *in vacuo* and the residue was taken up in water. The solution was washed repeatedly with ether and was adjusted to pH 3.0—3.5 with solid citric acid. The deposit was extracted with ethyl acetate and the extract was washed with water, dried over sodium sulfate and evaporated *in vacuo*. The residue was crystallized from ethyl acetate-*n*-hexane; yield 50%. For analysis, the product was recrystallized from *n*-hexane, mp 116—117°C, ninhydrin, tetrazolium, and ferric chloride tests negative.

Found: C, 63.75; H, 8.10; N, 8.55%. Calcd for $C_{17}H_{24}N_2O_4$: C, 63.72; H, 7.55; N, 8.75%.

D-1-Benzyloxy-3-p-methoxybenzyloxycarbonylaminopiperidone (D-X). The product was obtained from D-I by the method described above, except that *p*-methoxybenzyl 2,4,5-trichlorophenyl carbonate and dioxane as solvent were used. The product was recrystallized from ethyl acetate-*n*-hexane. Yield 61%, mp 112—114°C, $[\alpha]_D^{24}-43.2°$ (*c* 1, ethyl acetate).

Found: C, 65.58; H, 6.33; N, 7.23%. Calcd for $C_{21}H_{24}N_2O_5$: C, 65.61; H, 6.29; N, 7.29%.

N^{α}-Acetyl-N^{δ}-benzyloxy-DL-ornithine Hydrazide (DL-XI). A solution of DL-VII (0.262 g, 1 mmol) and hydrazine monohydrate (0.1 m*l*) in dioxane (10 m*l*) was warmed for 2 hr at 100—110°C and evaporated *in vacuo*. The residue was crystallized from ethanol-ether. Yield 83%. For analysis, the product was recrystallized from ethanol-ether, mp 101—105°C, ninhydrin, tetrazolium, and ferric chloride tests negative.

Found: C, 57.37; H, 7.26; N, 18.90%. Calcd for $C_{14}H_{22}N_4O_3$: C, 57.12; H, 7.54; N, 19.04%.

DL-1-Hydroxy-3-acetylaminopiperidone (DL-XII). A solution of DL-VII (0.262 g, 1 mmol) in methanol (5 m*l*) was hydrogenated in the presence of 5% palladium charcoal (0.05 g) at room temperature for 24 hr. The filtrate from the reduction mixture was evaporated *in vacuo*. The residual crystalline product was recrystallized from methanol. Yield 76%, mp 203—205°C, negative ninhydrin, and tetrazolium tests, and positive ferric chloride test.

Found: C, 48.92; H, 7.22; N, 16.17%. Calcd for $C_7H_{12}N_2O_3$: C, 48.82; H, 7.03; N, 16.27%.

D-1-Hydroxy-3-amino-2-piperidone Hydrochloride (D-XIV·HCl). A solution of D-IX (1.46 g, 4.55 mmol) in methanol (20 m*l*) was hydrogenated in the presence of 5% palladium charcoal (0.25 g) at room temperature for 14 hr. The filtrate from the mixture was evaporated *in vacuo* (ferric positive and ninhydrin test negative). The resulting oily residue was treated with 2N hydrogen chloride-dioxane (44 m*l*) for 2 hr at room temperature. The reaction mixture was evaporated *in vacuo* and the residual oil crystallized from ethanol. Recrystallization from methanol-ethanol gave colorless crystals. Yield 51%, mp 208—215°C (decomp.), $[\alpha]_D^{24}-0.8°$ (*c* 0.83, water), ferric positive and tetrazolium test negative. The ninhydrin test gave yellow color.

Found: C, 36.08; H, 6.44; N, 16.56; Cl, 21.48%. Calcd for $C_5H_{11}N_2O_2Cl$: C, 36.04; H, 6.66; N, 16.82; Cl, 21.28%.

N^{δ}-Hydroxy-D-ornithine Monohydrochloride (D-IV·HCl). D-XIV (0.25 g, 1.5 mmol) was hydrolyzed with 6N hydrochloric acid (15 m*l*) at 100°C for 30 min, when the mixture gave negative ferric test. The reaction mixture was evaporated to dryness *in vacuo* and the evaporation was repeated after the addition of ethanol. The residue was crystallized from water-ethanol. The crystals were collected by filtration and recrystallized from water-ethanol. Yield 54%, mp 177—179.5°C, $[\alpha]_D^{24}-12.0°$ (*c* 1, water), tetrazolium and ninhydrin tests positive and ferric chloride test negative.

Found: C, 32.63; H, 6.92; N, 15.08%. Calcd for $C_5H_{13}N_2O_3Cl$: C, 32.52; H, 7.10; N, 15.18%.

Synthesis of Rhodotorulic Acid

Yoshikazu Isowa, Toshiyuki Takashima, Muneki Ohmori,
Hideaki Kurita, Masanari Sato, and Kaoru Mori
Sagami Chemical Research Center, Ohnuma, Sagamihara, Kanagawa

(Received August 5, 1971)

Rhodotorulic acid (I) was synthesized by a series of reaction starting from N^{δ}-tosyl-N^{δ}-benzyloxy-L-ornithine. Detosylation and acetylation of intermediate, cyclo-di-N^{δ}-tosyl-N^{δ}-benzyloxy-L-ornithyl (LL-IX), afforded cyclo-di-N^{δ}-acetyl-N^{δ}-benzyloxy-L-ornithyl (LL-XI), which, on reductive debenzylation, gave rhodotorulic acid.

Rhodotorulic acid was first obtained by Atkin and Neilands[1] from supernatants of iron-deficient culture of a red yeast, *Rhodotorula pilimanae*. They found a potent growth-factor activity in this compound in assays with Arthrobacter species and determined its structure to be cyclo-di-N^{δ}-acetyl-N^{δ}-hydroxy-L-ornithyl (LL-I). We have succeeded in synthesizing rhodotorulic acid (LL-I); the DD-isomer was also prepared.

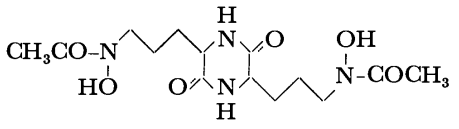

LL-I

Fig. 1

The synthetic route is shown in Fig. 2.

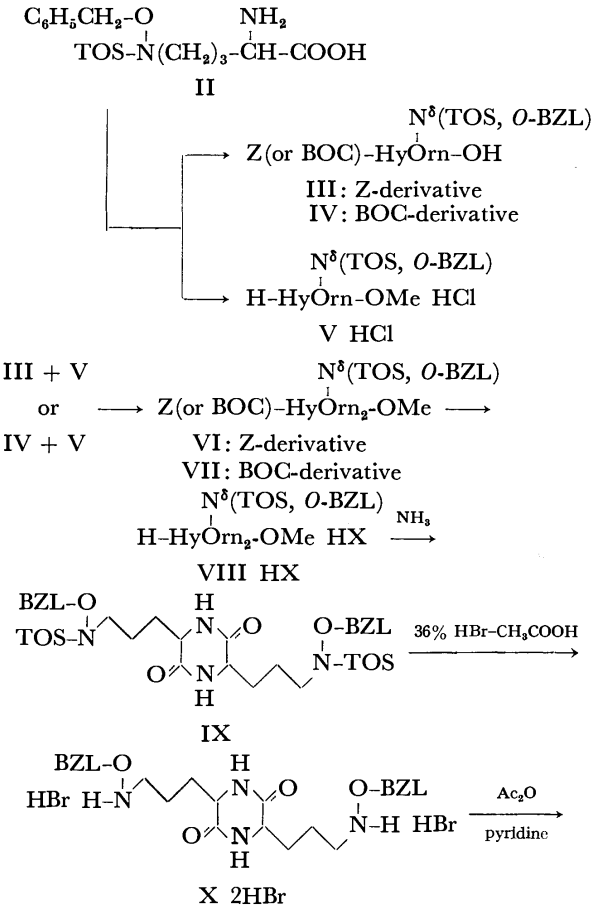

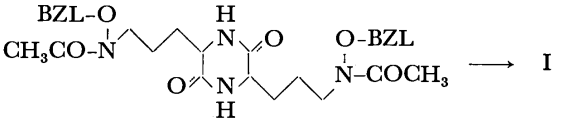

XI

Z=$C_6H_5CH_2OCO$-, BOC=$(CH_3)_3COCO$-,
TOS=p-$CH_3C_6H_4SO_2$-, BZL=$C_6H_5CH_2$-

Fig. 2. The abbreviations which are not listed in *Biochemistry* **5**, 1445 (1966), are H-HyOrn-OH for N^{δ}-hydroxyornithine and H-HyOrn-OH for N^{δ}-tosyl-N^{δ}-benzyloxyornithine.
N^{δ}-(TOS, *O*-BZL)

N^{α}-Benzyloxycarbonyl-N^{δ}-tosyl-N^{δ}-benzyloxy-L-ornithine (L-III) was obtained by benzyloxycarbonylation of N^{δ}-tosyl-N^{δ}-benzyloxy-L-ornithine (L-II).[2] A *t*-butyloxycarbonyl derivative (L-IV) was prepared by the reaction of L-II with *t*-butyl 2,4,5-trichlorophenyl carbonate in the presence of benzyltrimethylammonium hydroxide. By the reaction of the methyl ester (L-V) with the carbobenzoxy or *t*-butyloxycarbonyl amino acid (L-III or L-V) *via* the mixed anhydride, benzyloxycarbonyl-N^{δ}-tosyl-N^{δ}-benzyloxy-L-ornithyl-N^{δ}-tosyl-N^{δ}-benzyloxy-L-ornithine methyl ester (LL-VI) or the corresponding N^{α}-*t*-butyloxycarbonyl-dipeptide methyl ester (LL-VII) was obtained. Treatment of LL-VI or LL-VII with an excess of hydrogen bromide - acetic acid or hydrogen chloride - ethyl acetate, N^{δ}-tosyl-N^{δ}-benzyloxy-L-ornithyl-N^{δ}-tosyl-N^{δ}-benzyloxy-L-ornithine methyl ester hydrobromide or hydrochloride (LL-VIII HX) was obtained. Cyclo-di-N^{δ}-tosyl-N^{δ}-benzyloxy-L-ornithyl (LL-IX) was formed by the action of excess of ammonia on LL-VIII HX in methanol at

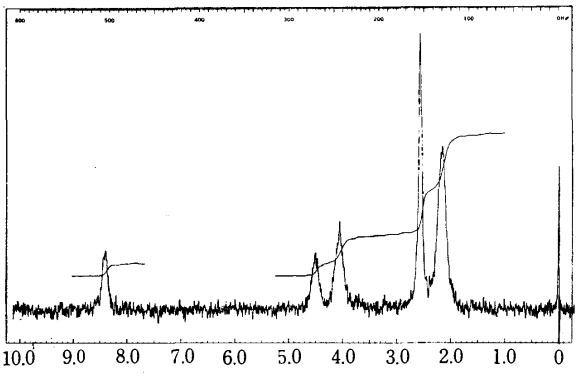

Fig. 3. NMR spectrum of synthetic rhodotorulic acid in trifluoroacetic acid.

1) C. L. Atkin and J. B. Neilands, *Biochemistry*, **7**, 3734 (1968).
2) Y. Isowa, T. Takashima, M. Ohmori, H. Kurita, M. Sato, and K. Mori, This Bulletin, **45**, 1461 (1972).

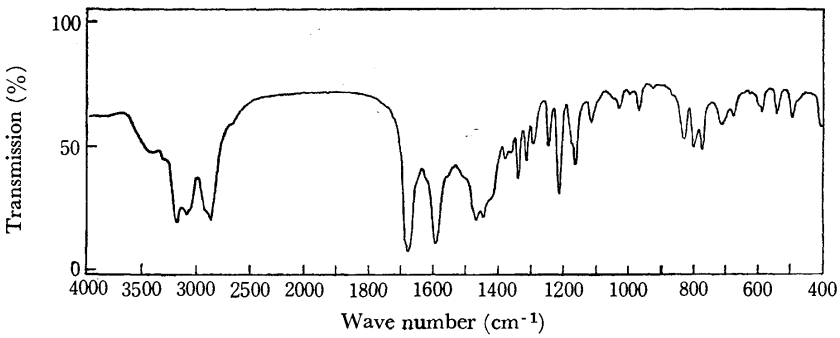

Fig. 4. IR spectrum of synthetic rhodotorulic acid.

room temperature.[3] The tosyl group of LL-IX was removed by treatment with 36% hydrogen bromide-acetic acid and phenol for 50 hr at room tempeature to yield cyclo-di-N^{δ}-benzyloxy-L-ornithyl dihydrobromide (LL-X 2HBr). LL-X 2HBr was converted into the acetyl derivative (LL-XI) with an excess of acetic anhydride in pyridine. Hydrogenation of LL-XI in methyl alcohol in the presence of palladium charcoal at room temperatue gave cyclo-di-N^{δ}-acetyl-N^{δ}-hydroxy-L-ornithyl; rhodotorulic acid (LL-I). The DD-isomer of rhodotorulic acid, DD-I, was also prepared in a similar manner. The synthetic rhodotorulic acid and its DD-isomer, LL-I and DD-I, exhibited specific rotations of $-28.5°$ (*c* 1, water, at 25°C) and $+28.0°$ (*c* 0.6, water, at 24°C) respectively. These products gave a positive ferric chloride test. The identity of the synthetic rhodotorulic acid with natural rhodotorulic acid[1] was substantiated through spectral comparison (IR and NMR) (Fig. 3 and 4).

The synthetic rhodotorulic acid was hydrogenated in the presence of Raney nickel catalyst to cyclo-di-N^{δ}-acetyl-L-ornithyl (LL-XII), which was identified by comparison of the melting points, optical rotations, IR and NMR spectra with authentic sample (XXIII) prepared from L-ornithine (Fig. 6).

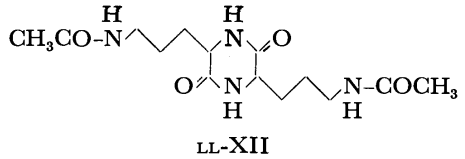

LL-XII

Fig. 5

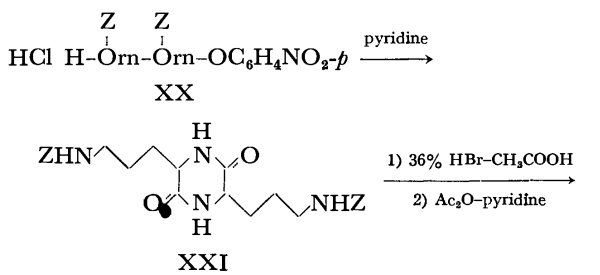

cyclo-di-N^{δ}-acetyl-L-ornithyl

XXIII

Fig. 6

3) E. Fischer and K. Raske, *Ber.*, **39**, 3981 (1906); N. Izumiya, T. Kato, Y. Fujita, M. Ohno, and M. Kondo, This Bulletin, **37**, 1809 (1964).

Experimental

Melting points of all the synthetic compounds were determined with a Yanagimoto electric micromelting point apparatus and are uncorrected. Optical rotations were measured with a Yanagimoto automatic polarimeter OR-50. Nuclear magnetic resonance spectra were run on a Hitachi Perkin-Elmer R-20 High Resolution NMR spectrometer, using tetramethylsilane as an internal standard. Molecular weight was determined with a Hitachi Perkin-Elmer 115 molecular weight apparatus.

N^{δ}-*Tosyl*-N^{δ}-*benzyloxyornithine (*L-*II and* D-*II).* The compound was prepared by the procedure described in the previous paper.[2]

L-II: mp 222.5—224.8°C (decomp.), $[\alpha]_D^{23.5}$ $+20.7°$ (*c* 3, acetic acid);

D-II: mp 217—223°C (decomp.), $[\alpha]_D^{25}$ $-21.0°$ (*c* 2, acetic acid).

N^{α}-*Benzyloxycarbonyl*-N^{δ}-*tosyl*-N^{δ}-*benzyloxy*-L-*ornithine (*L-*III).* It was obtained from L-II by the usual procedure, using a mixture of tetrahydrofuran and water as the solvent. The colorless oily product solidified to a glass. Yield 93%, $[\alpha]_D^{23}$ $-2.0°$ (*c* 2, acetic acid).

Found: N, 5.24%. Calcd for $C_{27}H_{30}N_2O_7S$: N, 5.32%.

N^{α}-t-*Butyloxycarbonyl*-N^{δ}-*tosyl*-N^{δ}-*benzyloxy*-L-*ornithine (*L-*IV).* To a suspension of L-II (15.7 g, 40 mmol) in methanol (80 m*l*), 40% benzyltrimethylammonium hydroxide (Triton B) (18.8 m*l*) was added. After stirring for 2 hr at room temperature, the solution was evaporated *in vacuo* at 50°C. The residue was then evaporated twice more with dimethylformamide *in vacuo* at 50°C in order to remove traces of water. The resulting syrup was dissolved in *t*-butanol (80 m*l*) and *t*-butyl 2,4,5-trichlorophenyl carbonate (11.9 g, 40 mmol) was added. After gentle stirring for 20 hr at 50—55°C, the reaction mixture was evaporated *in vacuo* and the residue taken up in water (70 m*l*). The solution was washed repeatedly with ether and acidified with M citric acid to about pH 3. The oily material thus deposited was extracted with ethyl acetate (600 m*l*). The extract was washed with water, dried over magnesium sulfate and evaporated *in vacuo*. The residue was crystallized from ethyl acetate - petroleum ether. Yield 18.5 g (94%), mp 58—66°C, $[\alpha]_D^{25}$ $+11.2°$ (*c* 1, ethanol).

Found: C, 58.74; H, 6.54; N, 5.40%. Calcd for $C_{24}H_{32}N_2O_7S$: C, 58.52; H, 6.55; N, 5.69%.

N^{α}-t-*Butyloxycarbonyl*-N^{δ}-*tosyl*-N^{δ}-*benzyloxy*-D-*ornithine (*D-*IV).* It was prepared in the same manner as described for the preparation of L-IV. Yield, 97.5%, mp 59—65°C and $[\alpha]_D^{25}$ $-9.0°$ (*c* 2, ethanol).

Found: C, 58.59; H, 6.75; N, 5.68%. Calcd for $C_{24}H_{32}N_2O_7S$: C, 58.52; H, 6.55; N, 5.69%.

N^{δ}-*Tosyl*-N^{δ}-*benzyloxy*-L-*ornithine Methyl Ester Hydrochloride (*L-*V HCl).* It was prepared from L-II by the usual

procedure. Recrystallization was effected from methanol - ether. Yield 83%, mp 151—152.5°C, $[\alpha]_D^{25}$ +18.9° (*c* 2, methanol).

Found: C, 54.18; H, 6.46; N, 6.14%. Calcd for $C_{20}H_{27}N_2O_5SCl$: C, 54.23; H, 6.14; N, 6.33%.

N^{δ}-*Tosyl*-N^{δ}-*benzyloxy*-D-*ornithine Methyl Ester Hydrochloride (*D-*V HCl)*. D-V HCl was obtained through the same method as described above. Yield 96%, mp 149—150°C and $[\alpha]_D^{24.5}$ −19.3° (*c* 1, methanol).

N^{α}-*Benzyloxycarbonyl*-N^{δ}-*tosyl*-N^{δ}-*benzyloxy*-L-*ornithyl*-N^{δ}-*tosyl*-N^{δ}-*benzyloxy*-L-*ornithine Methyl Ester (*LL-*VI)*. To a chilled solution of L-III (4.90 g, 9.3 mmol) and triethylamine (1.31 m*l*) in tetrahydrofuran (45 m*l*), isobutyl chloroformate (1.26 m*l*, 9.3 mmol) was added at −10°C. After 20 min, a mixture of V HCl (4.24 g, 9.3 mmol) and triethylamine (1.31 m*l*) in *N,N*-dimethylformamide (25 m*l*) was added to the above solution. The mixture was stirred overnight at room temperature. After the mixture had been evaporated *in vacuo*, the product was dissolved in ethyl acetate (50 m*l*). The solution was washed successively with N hydrochloric acid, water, 0.5M sodium bicarbonate, and water, and dried over anhydrous sodium sulfate. The filtered solution was evaporated to dryness *in vacuo*. The residual colorless oil resisted to attempt to crystallization. Yield 8.4 g, (98%).

Found: C, 61.59; H, 6.12; N, 6.25%. Calcd for $C_{47}H_{54}N_4O_{11}S_2$: C, 61.70; H, 5.95; N, 6.13%.

N^{δ}-*Tosyl*-N^{δ}-*benzyloxy*-L-*ornithyl*-N^{δ}-*tosyl*-N^{δ}-*benzyloxy*-L-*ornithine Methyl Ester Hydrobromide (VII HBr)*. To a solution of LL-VI (8.3 g, 9.1 mmol) in acetic acid (6.5 ml), 36% hydrogen bromide - acetic acid (8.2 m*l*) was added. After 90 min, the solution was evaporated *in vacuo*. The reisdual oil was triturated with ether. Yield of the oily product, 6.3 g (79%).

N^{α}-t-*Butyloxycarbonyl*-N^{δ}-*tosyl*-N^{δ}-*benzyloxy*-L-*ornithyl*-N^{δ}-*tosyl*-N^{δ}-*benzyloxy*-L-*ornithine Methyl Ester (*LL-*VII)*. This compound was prepared by coupling L-IV with L-V by the mixed anhydride method as described above; yield 96.7%, mp 63—69°C, $[\alpha]_D^{25}$ +1.1° (*c* 1, ethyl acetate).

Found: C, 60.09; H, 6.65; N, 6.10%. Calcd for $C_{44}H_{56}N_4O_{11}S_2$: C, 59.98; H, 6.41; N, 6.37%.

N^{δ}-*Tosyl*-N^{δ}-*benzyloxy*-L-*ornithyl*-N^{δ}-*tosyl*-N^{δ}-*benzyloxy*-L-*ornithine Methyl Ester Hydrochloride (*LL-*VIII HCl)*. To a solution of LL-VII (18.76 g, 21.3 mmol) in ethyl acetate (30 m*l*), 3N hydrogen chloride in ethyl acetate (80 m*l*) was added. The solution, being allowed to stand at room temperature for 2 hr, was evaporated *in vacuo* and the oily residue crystallized by addition of ether. Yield 16.10 g (92.5%), mp 100—105°C, $[\alpha]_D^{25}$ +12.10° (*c* 1, methanol).

Found: C, 56.98; H, 6.24; N, 6.58%. Calcd for $C_{39}H_{49}N_4O_9S_2Cl$: C, 57.30; H, 6.04; N, 6.85%.

N^{α}-t-*Butyloxycarbonyl*-N^{δ}-*tosyl*-N^{δ}-*benzyloxy*-D-*ornithyl*-N^{δ}-*tosyl*-N^{δ}-*benzyloxy*-D-*ornithine Methyl Ester (*DD-*VII)*. DD-VII was obtained by the same procedure as described above. Yield 90.3%, mp 63—69°C and $[\alpha]_D^{25}$ −1.4° (*c* 1, ethyl acetate).

Found: C, 60.01; H, 6.69; N, 6.03%. Calcd for $C_{44}H_{56}N_4O_{11}S_2$: C, 59.98; H, 6.41; N, 6.37%.

N^{δ}-*Tosyl*-N^{δ}-*benzyloxy*-D-*ornithyl*-N^{δ}-*tosyl*-N^{δ}-*benzyloxy*-D-*ornithine Methyl Ester Hydrochloride (*DD-*VIII HCl)*. This compound was prepared from DD-VII by the same method as that described for the corresponding LL-dipeptide ester hydrochloride LL-VIII HCl.

Cyclo-di-N^{δ}-*tosyl*-N^{δ}-*benzyloxy*-L-*ornithyl (*LL-*IX)*. This compound was prepared according to the general procedure.[3]

(a) From LL-*VIII HBr*: A solution of LL-VIII HBr (3.95 g, 4.59 mmol) in methanol (50 m*l*), previously saturated with dry ammonia at 0°C, was stored in a glass-stoppered bottle at room temperature for 2 days. A mass of crystals deposited was collected. The mother liquor was concentrated to dryness and crystalline residue was filtered with the aid of water. Recrystallization from methanol gave colorless crystals. Yield 1.9 g (54%), mp 197—199°C, $[\alpha]_D^{25.5}$ −31.5° (*c* 2, dimethylformamide).

Found: C, 61.15; H, 5.85; N, 7.48; S, 8.59%. Calcd for $C_{38}H_{44}N_4O_8S_2$: C, 60.94; H, 5.92; N, 7.48; S, 8.56%.

(b) From LL-*VIII HCl*: Similar treatment of LL-VIII HCl with ammonia gave LL-IX. Yield 47.7%, mp 174—175°C, $[\alpha]_D^{25.5}$ −31.3° (*c* 2, dimethylformamide).

Cyclo-di-N^{δ}-*benzyloxy*-L-*ornithyl Dihydrobromide (*LL-*X 2HBr)*. To a solution of 36% hydrogen bromide - acetic acid (20 m*l*) and phenol (5 g) in a glass-stoppered bottle, LL-IX (1.88 g, 2.5 mmol) was added at room temperature. After stirring for 50 hr at room temperature, the solution was evaporated *in vacuo* at 30°C. The residual oil was crystallized by addition of ether. Crystals were filtered off and washed with ethanol and ether. Yield 0.78 g (52%). The product was recrystallized from water - ethanol, mp 183—186°C, $[\alpha]_D^{22}$ −12.0° (*c* 0.5, methanol).

Found: C, 47.51; H, 5.81; N, 9.10%. Calcd for $C_{24}H_{32}N_4O_4$ 2HBr: C, 47.85; H, 5.69; N, 9.30%.

Cyclo-di-N^{δ}-*acetyl*-N^{δ}-*benzyloxy*-L-*ornithyl (*LL-*XI)*. LL-X 2HBr (0.78 g, 1.3 mmol) was mixed with pyridine (6.5 m*l*) and acetic anhydride (6.5 m*l*). After stirring for 20 hr at room temperature, the reaction mixture was evaporated to a syrup *in vacuo*. The residue was evaporated twice with water in order to decompose any acetic anhydride present. The final residue was taken up in ethyl acetate (30 m*l*) and the solution was repeatedly washed with water. The organic layer was dried over anhydrous sodium sulfate and evaporated to dryness *in vacuo*. The residue was triturated with ether to yield a crude crystalline product, which was purified from ethanol - ether. Yield 68%, mp 97—99°C, $[\alpha]_D^{20}$ −16.4° (*c* 1, ethanol).

Found: C, 63.97; H, 6.86; N, 10.62%. Calcd for $C_{28}H_{36}N_4O_6$: C, 64.10; H, 6.92; N, 10.68%.

Cyclo-di-N^{δ}-*acetyl*-N^{δ}-*hydroxy*-L-*ornithyl*; *Rhodotorulic Acid (*LL-*I)*. A solution of LL-XI (0.46 g, 0.88 mmol) in methanol (25 m*l*) was hydrogenated in the presence of 5% palladium charcoal (0.75 g) for 20 hr at room temperature. After the addition of methanol (25 m*l*), the reaction mixture was warmed to 70°C and the catalyst was filtered off while hot. The filtrate was evaporated *in vacuo* at room temperature. The residual crystals were recrystallized from boiling water. Yield 0.2 g (66%), mp 217—218.5°C, (decomp.), $[\alpha]_D^{25}$ −28.8° (*c* 1, water).

Found: C, 48.81; H, 7.07; N, 16.18%. Calcd for $C_{14}H_{24}N_4O_6$: C, 48.83; H, 7.03; N, 16.27%.

The substance gave negative ninhydrin- and triphenyltetrazolium tests and positive ferric chloride test. NMR spectrum; Fig. 3, IR spectrum; Fig. 4.

DD-IX, DD-X 2HBr, DD-XI, and DD-I were prepared by the same methods as described for the preparation of the corresponding LL-isomers.

Cyclo-di-N^{δ}-*tosyl*-N^{δ}-*benzyloxy*-D-*ornithyl (*DD-*IX)*. Yield 38.8%, mp 173—175°C, $[\alpha]_D^{25.5}$ +32.1° (*c* 2, dimethylformamide).

Found: C, 60.75; H, 5.90; N, 7.27%. Calcd for $C_{38}H_{44}N_4O_8S_2$: C, 60.94; H, 5.92; N, 7.48%.

Cyclo-di-N^{δ}-*benzyloxy*-D-*ornithyl Dihydrobromide (*DD-*X 2HBr)*. Yield 33.4%, mp 183—185°C (decomp.), $[\alpha]_D^{22}$ +12.8° (*c* 0.5, methanol).

Found: C, 47.88; H, 5.64; N, 9.35%. Calcd for $C_{24}H_{34}N_4O_4Br_2$: C, 47.85; H, 5.69; N, 9.30%.

Cyclo-di-N^{δ}-*acetyl*-N^{δ}-*benzyloxy*-D-*ornithyl (*DD-*XI)*. Yield

20.7%, mp 97—99°C, $[\alpha]_D^{20}$ −16.7° (*c* 0.3, ethanol).

Found: C, 63.93; H, 6.86; N, 10.74%. Calcd for $C_{28}H_{36}N_4O_6$: C, 64.10; H, 6.92; N, 10.68%.

*Cyclo-di-*N$^{\delta}$*-acetyl-*N$^{\delta}$*-hydroxy-*D*-ornithyl (*DD*-I)*; DD*-Isomer of Rhodotorulic Acid.* Yield 35%, mp 216—218.5°C (decomp.), $[\alpha]_D^{24}$ +28.0° (*c* 0.6, water).

Found: C, 48.72; H, 6.88; N, 16.05%. Calcd for $C_{14}H_{24}N_4O_6$: C, 48.83; H, 7.03; N, 16.27%.

*Catalytic Reduction of Rhodotorulic Acid (*LL*-I) to Cyclo-di-*N$^{\delta}$*-acetyl-*L*-ornithyl (*LL*-XII).* A suspension of LL-I (0.15 g, 0.44 mmol) in methanol (100 m*l*) was hydrogenated in the presence of Raney nickel (1 spatula) under atmospheric pressure at room temperature. After 6 days, the reaction mixture was warmed to 70°C in order to dissolve the precipitated product and filtered. The filtrate was evaporated *in vacuo* and the remaining crystals were recrystallized from boiling methanol. Yield 65 mg (48%), mp 270—275°C (decomp.), (lit,[1] mp *ca.* 265°C) and $[\alpha]_D^{25}$ −34.8° (*c* 0.5, water).

NMR (CF_3COOH): δ; 8.75 ppm (2H, side-chain amide protons), 8.33 (2H, ring-amide protons), 4.42 (2H, ring-carbon protons), 3.67 (4H, side-chain methylene protons adjacent to nitrogen), 2.52 (6H, acetyl methyl protons), 2.09 (8H, ethylene protons).

Found: C, 53.86; H, 7.95; N, 17.89%. Calcd for $C_{14}H_{24}N_4O_4$: C, 53.83; H, 7.74; N, 17.94%.

N$^{\alpha}$*-t-Butyloxycarbonyl-*N$^{\delta}$*-benzyloxycarbonyl-*L*-ornithine (XIII).*

a): XIII was obtained as a syrup according to the same procedure for the D-isomer[4] from N^{δ}-benzyloxycarbonyl-L-ornithine using *t*-butyloxycarbonyl azide as *t*-butyloxycarbonylating reagent, except that magnesium oxide was used instead of sodium bicarbonate. Yield 41%, $[\alpha]_D^{25}$ +10.1° (*c* 1, ethyl acetate), (lit,[5] BOC-L-Orn(δ-Z)-OH, $[\alpha]_{578}^{18-25}$ −8.9° (*c* 1, acetic acid)).

b): XIII was also prepared according to the method of Broadbent *et al.*,[6] using *t*-butyl 2,4,5-trichlorophenyl carbonate. Yield 84%.

N$^{\alpha}$*-t-Butyloxycarbonyl-*N$^{\delta}$*-benzyloxycarbonyl-*L*-ornithine* p*-Nitrophenyl Ester (XIV).* This compound was obtained from XIII and *p*-nitrophenol according to the same procedure for the D-isomer,[4] except that ethyl acetate was used as the solvent. Yield 86%, mp 113—114.5°C (from ethyl acetate-petroleum ether), $[\alpha]_D^{25}$ −20.4° (*c* 1, ethyl acetate).

Found: C, 59.31; H, 6.29; N, 8.50%. Calcd for $C_{24}H_{29}N_3O_8$: C, 59.13; H, 6.00; N, 8.62%.

N$^{\delta}$*-Benzyloxycarbonyl-*L*-ornithine* p*-Nitrophenyl Ester Hydrochloride (XV).* To a suspension of XIV (9.74 g, 0.02 mol) in ethyl acetate (80 m*l*) was added 5N hydrogen chloride in ethyl acetate (40 m*l*). After 1 hr, crystals were collected with the aid of dry ether. Yield 8.3 g (98%), mp 164.5—167.5°C, $[\alpha]_D^{25}$ +27.3° (*c* 1, methanol).

Found: C, 53.74; H, 5.44; N, 10.05%. Calcd for $C_{19}H_{22}N_3O_6Cl$: C, 53.84; H, 5.23; N, 9.92%.

N$^{\alpha}$*-t-Butyloxycarbonyl-*N$^{\delta}$*-benzyloxycarbonyl-*L*-ornithyl-*N$^{\delta}$*-benzyloxycarbonyl-*L*-ornithine Methyl Ester (XVI).* *a)*: To a stirred mixture of XIII (9.86 g, 26.9 mmol) and Woodward reagent K (7.08 g, 28 mmol) in dimethylformamide (70 m*l*) was added triethylamine (4.1 m*l*, 30 mmol) at 0°C. After 2 hr, N^{δ}-benzyloxycarbonyl-L-ornithine methyl ester hydrochloride (8.51 g, 26.9 mmol) and triethylamine (4.1 m*l*) were added. The reaction mixture was stirred for 20 hr and then evaporated. The residual semi-solid was dissolved in ethyl acetate, and the solution was washed successively with water (three times), M sodium bicarbonate, water, 10% citric acid and water (three times), dried and evaporated. The oily residue was solidified by addition of petroleum ether. Recrystallization from ethyl acetate-petroleum ether gave XVI. Yield 10.9 g (67%), mp 73.0—74.5°C, $[\alpha]_D^{25}$ −10.7° (*c* 1, methanol).

Found: C, 60.98; H, 7.31; N, 8.89%. Calcd for $C_{32}H_{44}N_4O_9$: C, 61.13; H, 7.05; N, 8.91%.

b): To a stirred suspension of N^{δ}-benzyloxycarbonyl-L-ornithine methyl ester hydrochloride (7.03 g, 22.2 mmol) in chloroform (100 m*l*) was added triethylamine (4.48 g, 44.4 mmol) at 0°C. After 10 min, XIV (10.8 g, 22.2 mmol) was added. The mixture was stirred at 0°C for 15 min and at room temperature for 20 hr. Chloroform (100 m*l*) was added and the mixture was treated as described above except that the chloroform layer was washed with M sodium bicarbonate for the removal of the resultant *p*-nitrophenol. Yield 10 g (74%), mp 70—74°C, $[\alpha]_D^{25}$ −11.5° (*c* 1, methanol).

Found: C, 60.96; H, 7.20; N, 9.16%. Calcd for $C_{32}H_{44}N_4O_9$: C, 61.13; H, 7.05; N, 8.91%.

N$^{\delta}$*-Benzyloxycarbonyl-*L*-ornithyl-*N$^{\delta}$*-benzyloxycarbonyl-*L*-ornithine Methyl Ester Hydrochloride (XVII).* This compound was obtained through the same method as described above.

a): *From XVI-a*, mp 102—117°C, $[\alpha]_D^{25}$ +8.4° (*c* 1, methanol).

Found: N, 10.13%. Calcd for $C_{27}H_{37}N_4O_7Cl$: N, 9.92%.

b): *From XVI-b*, $[\alpha]_D^{25}$ +8.2° (*c* 1, methanol).

N$^{\alpha}$*-t-Butyloxycarbonyl-*N$^{\delta}$*-benzyloxycarbonyl-*L*-ornithyl-*N$^{\delta}$*-benzyloxycarbonyl-*L*-ornithine (XVIII).* To a stirred solution of XVI (6.28 g, 0.01 mol) in dioxane was added N sodium hydroxide (12 m*l*). The mixture was stirred overnight and acidified with 2N hydrochloric acid. The separated oil was extracted with ethyl acetate. Ethyl acetate layer was dried and evaporated to an oil. Yield 5.7 g (93%), $[\alpha]_D^{25}$ −3.5° (*c* 1, methanol).

Found: C, 60.08; H, 6.78; N, 8.86%. Calcd for $C_{31}H_{42}N_4O_9$: C, 60.57; H, 6.89; N, 9.12%.

N$^{\alpha}$*-t-Butyloxycarbonyl-*N$^{\delta}$*-benzyloxycarbonyl-*L*-ornithyl-*N$^{\delta}$*-benzyloxycarbonyl-*L*-ornithine* p*-Nitrophenyl Ester (XIX).* *a)*: A mixture of XVIII (3.15 g, 5.13 mmol) and di-*p*-nitrophenyl sulfite (1.07 g, 5.5 mmol) in pyridine was stirred at 0°C for 12 hr and at room temperature for 2 days. Resultant pale yellow solution was poured into N hydrochloric acid (150 m*l*). Semisolid precipitated was extracted with ethyl acetate. The organic layer was washed with saturated sodium chloride solution, dried and evaporated to give crystals. Yield 1.58 g (42%), mp 113.5—116°C, $[\alpha]_D^{25}$ −23.1° (*c* 1, methanol). Recrystallization from methanol-ether gave an analytical sample.

Found: C, 60.40; H, 6.28; N, 9.66%. Calcd for $C_{37}H_{45}N_5O_{11}$: C, 60.41; H, 6.12; N, 9.52%.

b): To a mechanically stirred mixture of XIII (7.7 g, 21 mmol) and XV (8.92 g, 21 mmol) in acetonitrile (200 m*l*), was added triethylamine (2.9 m*l*, 21 mmol) at 0°C. After 40 min, dicyclohexylcarbodiimide (4.4 g, 22 mmol) in a small portion of acetonitrile was added and the mixture was stirred overnight at room temperature. The deposits were collected and extracted with hot tetrahydrofuran (350 m*l*). The tetrahydrofuran was evaporated and the remaining crystals were collected with the aid of dry ether. Yield 7.21 g (47%), mp 116.5—118.5°C, $[\alpha]_D^{25}$ −26.2° (*c* 1, methanol).

N$^{\delta}$*-Benzyloxycarbonyl-*L*-ornithyl-*N$^{\delta}$*-benzyloxycarbonyl-*L*-ornithine* p*-Nitrophenyl Ester Hydrochloride (XX).* To a suspension of XIX (2.94 g, 4 mmol) in ethyl acetate (10 m*l*) was added 5N hydrogen chloride in ethyl acetate (28 m*l*). After 2 hr, the ethyl acetate was evaporated and the remaining crystals were collected with the aid of dry ether. Yield 2.36 g (88%),

4) T. Kato and N. Izumiya, This Bulletin, **39**, 2242 (1966).
5) E. Schnabel, *Ann. Chem.*, **702**, 188 (1967).
6) W. Broadbent, J. S. Morley, and B. E. Stone, *J. Chem. Soc., C*, **1967**, 2632.

mp 124—128°C, $[\alpha]_D^{25}$ +27.3° (*c* 1, methanol).

Found: N, 10.53%. Calcd for $C_{32}H_{38}N_5O_9Cl$: N, 10.42%.

*Cyclo-di-*N$^{\delta}$*-benzyloxycarbonyl-*L*-ornithyl (XXI).* XX (2 g, 2.98 mmol) in the mixture of dimethylformamide (40 m*l*) and acetic acid (10 m*l*) was dropped over a period of 3 hr in the preheated pyridine (500 m*l*) at 70°C under vigorous stirring. Stirring was continued overnight at room temperature and the pyridine was evaporated. To the residue was added water and crystals were collected, 1.0 g (68%), mp 236—239°C (from dimethylformamide), $[\alpha]_D^{25}$ −19.5° (*c* 1, dimethylformamide). IR (KBr): 3325, 3175, 1690, 1550 cm^{-1}.

Found: C, 62.98; H, 6.32; N, 11.16; mol wt 470. Calcd for $C_{26}H_{32}N_4O_6$: C, 62.90; H, 6.50; N, 11.29%; mol wt 496.

*Cyclo-di-*L*-ornithyl Dihydrobromide (XXII).* XXI (10 g, 20.4 mmol) was treated with 20% hydrogen bromide in acetic acid (100 m*l*) with occasional shaking. A clear solution resulted and soon after a copious mass precipitated. After 6 hr, 20% hydrogen bromide in acetic acid (100 m*l*) was added again. After standing overnight, dry ether was added. The precipitate was collected and washed with ether. Yield 7.41 g (95%), mp 240—250°C (decomp.), $[\alpha]_D^{25}$ −28.1° (*c* 1, water).

Found: C, 30.36; H, 5.92; N, 13.80%. Calcd for $C_{10}H_{22}N_4O_2Br_2$: C, 30.78; H, 5.68; N, 14.36%.

*Cyclo-di-*N$^{\delta}$*-acetyl-*L*-ornithyl (XXIII). a)*: XXII (390 mg, 1 mmol) in pyridine (5 m*l*) was stirred at 50°C for 25 min. Thereafter acetic anhydride was added and stirring was continued for 5 hr at 50°C. The crystals were collected and washed successively with methanol, water and again methanol. Yield 250 mg (80%), mp 277—279°C (lit,[1] mp *ca.* 265°C), $[\alpha]_D^{21}$ −33.5° (*c* 1, water). IR (KBr): 3290, 3195, 3090, 1680, 1630, 1550 cm^{-1}.

Found: C, 53.89; H, 7.99; N, 17.75%. Calcd for $C_{14}H_{24}N_4O_4$: C, 53.83; H, 7.74; N, 17.94%.

b): To a stirred suspension of XXII (390 mg) in pyridine (5 m*l*) was added triethylamine (0.28 m*l*). After 30 min, *p*-nitrophenyl acetate (724 mg, 4 mmol) was added at room temperature. After one day, the crystals were collected. Yield 190 mg (61%), mp 278—279°C (from methanol), $[\alpha]_D^{21.5}$ −34.6° (*c* 1, water).

c): To a stirred solution of sodium bicarbonate (168 mg, 2 mmol) in water (1 m*l*) was added XXII (390 mg). After 10 min, acetic anhydride (0.3 m*l*) was added at 0°C. The homogeneous solution was stirred for 10 min at 0°C and then for 90 min at room temperature. The deposited crystals were collected. Yield 120 mg (38%), mp 278—281°C (from methanol), $[\alpha]_D^{22}$ −36.2° (*c* 1, water).

BULLETIN OF THE CHEMICAL SOCIETY OF JAPAN, VOL. 45, 1471—1473(1972)

Preparation and Thermal Decomposition of 1,4,5- and 1,3,5-Trimethyltetrazolium Iodides

Tyûzô Isida, Sinpei Kozima,* Shin-ichirô Fujimori, and Keiiti Sisido

Department of Industrial Chemistry, Faculty of Engineering, Kyoto University, Sakyo-ku, Kyoto

**Department of Chemistry, College of Liberal Arts and Sciences, Kyoto University, Sakyo-ku, Kyoto*

(Received August 14, 1971)

1,4,5- and 1,3,5-Trimethyltetrazolium iodides were prepared by the reaction of methyl iodide with 1,5- and 2,5-dimethyltetrazoles, and the reaction of methyl iodide with 5-methyltetrazole. The latter method is more facile for the preparation of these iodides. Upon thermal decomposition of the 1,3,5-trimethyl salt at 130°C, the 1-methyl group was eliminated predominantly to yield 2,5-dimethyltetrazole. When the 1,4,5-trimethyl salt was decomposed at 270°C, a mixture of 1,5- and 2,5-dimethyltetrazole was obtained in 74% and 21% yields, respectively. For the formation of 2,5-dimethyltetrazole from the 1,4,5-trimethyl salt, there has been shown an intermolecular methylation scheme that the 1,4,5-trimethyl salt methylated 1,5-dimethyltetrazole being formed *in situ* to give the 1,3,5-trimethyl salt.

In our previous paper,[1] quantitative isomerization of 1-alkyl-5-phenyltetrazole into the 2-alkyl isomer in the presence of alkyl iodide has been reported. The study of thermal decomposition of 1,3- and 1,4-dialkyl-5-phenyltetrazolium iodides revealed that 2-alkyl-5-phenyltetrazole was produced predominantly from the 1,3-dialkyl salt. The 1,4-dialkyl salt, more stable than the 1,3-dialkyl salt, was decomposed at 130°C to produce 1-alkyl-5-phenyltetrazole. As an extention of the preceding work, this paper presents a study of the preparation and thermal decomposition of 1,4,5- and 1,3,5-trimethyltetrazolium iodides.

As for the study of 5-methyltetrazolium iodides, there has been only one patent[2] in which was reported the preparation of 1,4,5-trimethyltetrazolium iodide (**1**) by the reaction of 1,5-dimethyltetrazole (**2**) with methyl iodide. In view of the formation of 1,3-dimethyl-5-phenyltetrazolium iodide as well as the 1,4-dimethyl salt from 1-methyl-5-phenyltetrazole,[1] formation of 1,3,5-trimethyltetrazolium iodide (**3**) from **2** was expected. However, in the reaction of **2** with methyl iodide carried out at 100°C for 2 hr or at room temperature for 10 days, the 1,4,5-trimethyl salt **1** was produced selectively without the formation of the other isomeric tetrazolium salts. The selective methylation at 4-nitrogen in 1,5-dimethyltetrazole might be

1) T. Isida, S. Kozima, K. Nabika, and K. Sisido, *J. Org. Chem.*, **36**, 3807 (1971).

2) H. R. J. Waddington, G. F. Duffin, and J. S. Kendall, Brit. 785334 (1957); *Chem. Abstr.*, **52**, 6030i (1958).

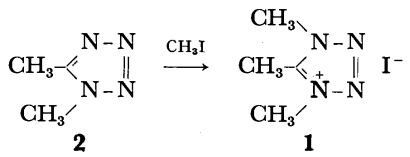

2 **1**

attributed to more electron-donating property of the 5-methyl group than that of the 5-phenyl group. The structure of the colorless crystals **1**, (mp 266°[3] decomp) has been identified by the NMR spectrum which has two singlets at δ 4.27 ppm assigned to a couple of equivalent *N*-methyl protons and δ 2.95 ppm to 5-methyl protons.

Preparation of 1,3,5-trimethyltetrazolium iodide (**3**) was carried out by the reaction of 2,5-dimethyltetrazole (**4**)[4] with methyl iodide at room temperature for a long time (90 days).

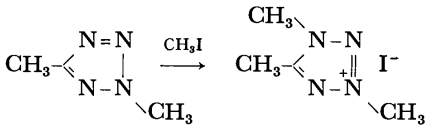

4 **3**

In the NMR spectrum of **3** prepared herewith, there were three singlets at δ 2.82, 4.34 and 4.62 ppm which could be assigned to the 5-, 1-, and 3-methyl protons, respectively. The similar assignment was reported with 1,3-dimethyltetrazolium iodide[5] and 1,3-dimethyl-5-phenyltetrazolium iodide.[1]

The above preparation of the 1,4,5-trimethyl salt **1** or the 1,3,5-trimethyl salt **3** from 1,5-dimethyltetrazole **2** or 2,5-dimethyltetrazole **4**, respectively, however, is not a convenient method, compared with the following facile one using readily prepared 5-methyltetrazole (**5**) as the starting material. When **5** was heated in an excess of methyl iodide at 40°C for 10 days, a mixture of **1** and **3** (68:32) was obtained in 77% yield together with hydrogen iodide, methane and iodine. Separation of **1** and **3** was carried out by the selective extraction of **3** from the mixture with acetone. The remaining crystals undissolved in acetone were identified as pure **1**. The crystalline **3** was precipitated by the addition of diethyl ether to the acetone extract. In the first step of this reaction there might be formed 1,5- and 2,5-dimethyltetrazole hydrogen iodides, $CH_3CN_4(CH_3)HI$, as intermediates. These compounds not isolated yet are considered to be unstable under the reaction condition and eliminated readily hydrogen iodide to produce **2** and **4** which reacted with methyl iodide to give **1** and **3**, respectively. A part of the liberated hydrogen iodide reduced methyl iodide to give iodine and methane.[6]

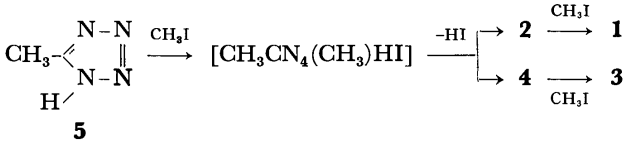

5

Thermal decomposition of tetrazolium salts has never been studied in detail until our recent investigation[1] of 1,3-dimethyl-5-phenyltetrazolium iodide (**6**) and the 1,4-dimethyl-5-phenyl salt (**7**). In the case of the 5-phenyltetrazolium salts, the 1,3-dimethyl salt **6** decomposed at a lower temperature (dp below 70°C) than the 1,4-dimethyl salt **7** (dp 130°C). The analogous relation has been found between the 1,3,5-trimethyl salt **3** (dp 130°C) and 1,4,5-trimethyl salt **1** (dp 266°C).

Thermal treatment of 1,3,5-trimethyltetrazolium iodide at 135°C for 30 min gave a mixture of 1,5-dimethyltetrazole **2** and 2,5-dimethyltetrazole **4** in a ratio of 15:85. 1-Methyl group was liberated predominantly to yield **4**. This is consistent with the selective elimination of the 1-methyl group in the thermal decomposition of **6**.[1] When decomposition of **3** was carried out at 180°C and 270°C, there were obtained mixtures of **2** and **4** in ratios of 42:58 and 60:40, respectively. The selectivity in the elimination of methyl iodide decreased with the elevation of the decomposition temperature.

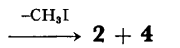

Thermal decomposition of 1,4,5-trimethyltetrazolium iodide **1** was carried out at 270°C, a slightly higher temperature than the decomposition point 266°C, for 3 min to afford 2,5-dimethyltetrazole **4** in 21% yield as well as 1,5-dimethyltetrazole **2** (74%) together with methyl iodide. The product **4** should be formed in the course of the thermal decomposition

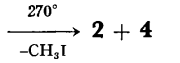

of **1**, since there was no formation of **4** when pure **2** was heated at 270°C. For the formation of **4**, the following experiment showed an intermolecular methylation scheme: 1,5-dimethyltetrazole **2** formed *in situ* from 1,4,5-trimethyl salt **1** was methylated by the remaining **1** to give intermediate **3**, whose decomposition products were **2** and **4** as described above.

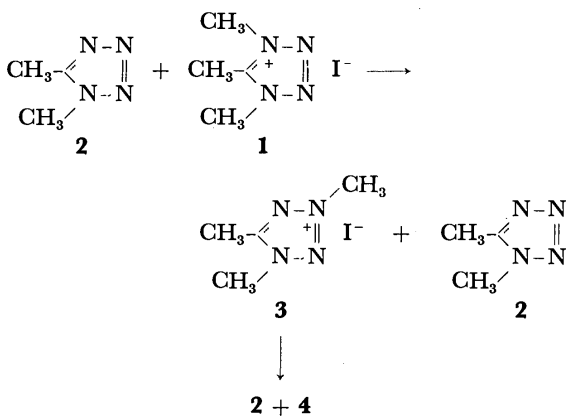

When thermal decomposition of **1** was carried out in the presence of 1-methyl-5-phenyltetrazole (**8**) at 270°C, there were obtained 2-methyl-5-phenyltetrazole (**9**) (23% yield based on **8**) together with **2** and **4**. It has already been established[1] that **9** was obtained from 1,3-dimethyl-5-phenyltetrazolium iodide (**6**) which was formed by the reaction of **8** with methyl iodide, and that in the absence of methyl iodide there was no

3) The reported decomposition point was 216°C.[2]

4) J. H. Markgraf, W. T. Bachman, and D. P. Hollis, *J. Org. Chem.*, **30**, 3472 (1965).

5) W. P. Norris and R. A. Henry, *Tetrahedron Lett.*, **1965**, 1213.

6) A. Butlerow, *Ann. Chem.*, **144**, 36 (1867); R. A. Ogg, Jr., *J. Amer. Chem. Soc.*, **56**, 526 (1934).

formation of **9** from **8**. Thus **8** was apparently methylated by **1** to produce **6** which liberated the 1-methyl group predominantly to yield **9** under the reaction condition. This result presented a sufficient support for the intermolecular methylation by the quaternary salt **1**.

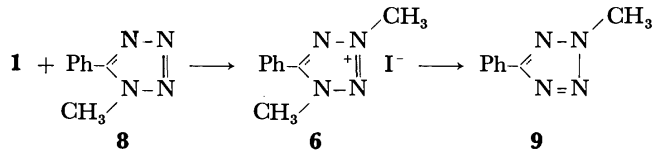

8 **6** **9**

Experimental

Reaction of 1,5-Dimethyltetrazole (2) with Methyl Iodide. A solution of 0.125 g (1.30 mmol) of **2**[4] in 10 m*l* of methyl iodide was heated in a sealed glass bottle at 100°C for 5 hr. Upon cooling to room temperature, colorless needles were precipitated. The crystals isolated by filtration were identified as 1,4,5-trimethyltetrazolium iodide (**1**), by the elemental analysis and the NMR spectrum, 0.239 g (77.2%), dp (decomposition point) 266°, (lit,[2] dp 216°). NMR [D_2O, sodium 2,2-dimethyl-2-silapentane-5-sulfonate (DSS) was used as an internal standard] δ 2.95 (s, 3H, 5-methyl protons), δ 4.27 ppm (s, 6H, 1,4-dimethyl protons), IR (Nujol) 1590 (vs), 1540 (m), 1355 (w), 1330 (w), 1240 (w), 1213 (w), 1043 (sh), 1030 (vs), 766 (vs), 618 cm^{-1}(m).

Found: C, 20.00; H, 3.78; N, 23.34%. Calcd for $C_4H_9N_4I$: C, 20.01; H, 3.78; N, 23.34%. Evaporation of methyl iodide of the filtrate gave 0.011 g (8.8%) of **2** recovered unchanged.

Reaction of **2** with methyl iodide was also carried out at room temperature in an NMR tube. After 10 days, a singlet at δ 4.05 ppm assigned to the 1-methyl protons of **2** disappeared completely. Colorless needles precipitated were identified as pure **1** by the mixed decomposition point determination and by the IR and NMR spectra.

Reaction of 5-Methyltetrazole (5) with Methyl Iodide. To a methanol solution of 1.378 g (16.4 mmol) of **5**[4,7] was added a large excess of methyl iodide. After 10 days heating at 40°C, the reaction mixture was cooled to precipitate yellowish crystals which were filtered and washed with acetone twice to give 1.795 g of pure **1**. The collected filtrate was evaporated off to dryness *in vacuo* without heating. To the residual crystals was added 10 m*l* of acetone to give additional 0.225 g of **1** insoluble in acetone (in total, 2.020 g (51.2%) of **1**), and to the acetone solution was added 100 m*l* of dry ether to precipitate 1.04 g (26.4%) of crystals. By the additional reprecipitation procedure there were obtained colorless crystals, dp 130°C, whose structure was determined as 1,3,5-trimethyltetrazolium iodide (**3**) by the NMR spectrum (D_2O, DSS): δ 2.82 (s, 3H, 5-methyl protons), δ 4.34 (s, 3H, 1-methyl), δ 4.62 ppm (s, 3H, 3-methyl), IR (Nujol) 1554 (vs), 1336 (m), 1293 (m), 1077 (m), 1038 (s), 1026 (m), 808 cm^{-1} (vs). Elemental analysis was given up because of its highly deliquescent property.

Reaction of 2,5-Dimethyltetrazole (4) with Methyl Iodide. A solution of **4**[4] in methyl iodide was kept at room temperature in an NMR tube. After 90 days, two singlets at δ 2.53 and δ 4.30 ppm assigned to the 5- and the 2-methyl protons of **4** disappeared. A pale yellowish oily substance insoluble in methyl iodide was separated by decantation, dissolved in 1 m*l* of acetone followed by the addition of dry ether to precipitate colorless needles which were identified as **3** by the NMR and the IR spectra.

Thermal Decomposition of 1,4,5-Trimethyltetrazolium Iodide (1). Thermal decomposition of 1.2354 g (5.14 mmol) of crystalline **1** was carried out at 270°C for 5 min in a small Claisen flask heated in a molten metal bath. Methyl iodide, **4** and a part of **2** were distilled out to be trapped through a cold condenser. After pyrolysis the condenser was rinsed with additional amount of methyl iodide to collect the whole distillate. It was calculated from the total weight and the integral ratio of the NMR spectrum that the distillate contained 0.024 g of **2** and 0.102 g (21.3%) of **4**. Pure **4** was isolated by preparative gas chromatography, bp 97—98°C /760 mmHg (lit.,[4] bp 57—57.2°C/13 mmHg). The chemical shifts of **4** in the NMR spectrum were coincided with the reported ones.[4] To the residue (0.5025 g) in the flask was added 20 m*l* of acetone to separate the starting ingredient **1** unchanged. The insoluble **1** (0.090 g) was removed by filtration, and the acetone of the filtrate was evaporated *in vacuo* to give 0.3466 g of pure **2**. In total, 0.370 g (73.5%) of **2** was obtained by the pyrolysis.

Thermal decomposition of **1** was also carried out in an NMR tube. To the top of the tube was attached an effective condenser made of a long (30 cm) needle of a syringe. The needle was cooled outside by dry-ice, and the syringe was packed with granulated calcium chloride. Crystalline **1** (0.0718 g) was heated in the tube at 270°C for 3 min. After cooling the tube in an ice bath, 0.4 m*l* of deuterochloroform was added through the needle, and NMR spectrum was measured. The starting iodide **1** was completely decomposed. The distribution of **2** and **4** produced was found to be 72: 28. This is in good agreement with the former isolation results indicating little loss of vaporizable **4** in this micro-procedure. Analogous equipments were used in the following experiments.

Thermal Decomposition of 1 in the Presence of 1-Methyl-5-phenyltetrazole (8). A mixture of 0.067 g (0.279 mmol) of **1** and 0.011 g (0.069 mmol) of **8** was heated at 270°C for 3 min in an NMR tube with the cooled needles as described above. After the mixture was cooled to room temperature, methyl iodide and 2,5-dimethyltetrazole **4** were evaporated off *in vacuo*, since the chemical shifts of **4** in the NMR spectrum was close to those of 2-methyl-5-phenyltetrazole (**9**). After evaporation of **4**, the residue was dissolved in deuterochloroform and the NMR spectrum was measured. The ratio of **8** and **9** was determined as 23: 77 by the integral ratio of the peaks at δ 4.18 and 4.38 ppm,[1] respectively.

Thermal Treatment of 2 at 270°C. In an NMR tube was heated 0.0464 g of **2** at 270°C for 30 min. After the tube was cooled in an ice bath, 0.4 m*l* of deuterochloroform was added through the needle, and NMR spectrum was measured. There was not detected even a trace of **4** in the NMR spectrum indicating no formation of **4** from **2** on heating at the decomposition condition at 270°C.

Thermal Decomposition of 1,3,5-Trimethyltetrazolium Iodide (3). On heating **3** at 135°C for 30 min in an NMR tube as described above, a mixture of **2** and **4** was obtained in a ratio of 14: 86 which was determined by NMR analysis. Analogous decompositions of **3** at 180°C for 15 min and at 270°C for 3 min gave mixtures of **2** and **4** in ratios of 42: 58 and 60: 40, respectively.

7) R. M. Herbst and K. R. Wilson, *J. Org. Chem.*, **22**, 1142 (1957).

Structures of Three Isomeric Dimers of 2,4,5-Triphenylimidazolyl[1]

Hideo TANINO, Tadao KONDO, Kunisuke OKADA, and Toshio GOTO
Department of Agricultural Chemistry, Nagoya University, Chikusa, Nagoya
(Received August 23, 1971)

In addition of the piezochromic and the photochromic (dimer A) dimers of 2,4,5-triphenylimidazolyl, two new isomeric dimers were prepared; one (dimer B) being photochromic and the other (dimer C) non-photochromic. Several *p*-substituted derivatives of the dimers were also prepared. By comparison of their NMR and IR spectra, structures (a), (b), and (c) were assigned to the dimers A, B, and C, respectively. On treatment with hydrochloric acid in ethanol, dimer A underwent heterolytic cleavage and gave a mixture of 2-ethoxy-2*H*- and 4-ethoxy-4*H*-2,4,5-triphenylisoimidazole, and 2,4,5-triphenylimidazole.

2,4,5-Triphenylimidazole (lophine) (I) is one of the well-known chemiluminescent substances[2-5] and the recent studies[3-7] on the luminescence mechanism suggested that the lophyl radical is the first intermediate of the luminescence. Another interesting feature of this compound is that it forms on oxidation a photochromic and a piezochromic dimer.[4,8,9] Thus, oxidation of lophine with ferricyanide produces violet lophyl radical which rapidly dimerizes to give the unstable piezochromic dimer. This dimer, when dissolved in benzene, isomerizes rapidly to the photochromic dimer (dimer A) (IA). Photochromism and piezochromism of these dimers have been assumed to be due to the reversible dissociation of these dimers to lophyl radical.[4,8-10]

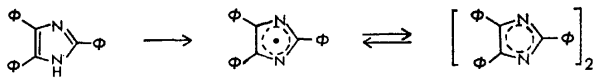

(I) radical dimer

Although initially the hydrazine structure (d) was suggested *a priori* for the dimer A.[4,11] White and Sonnenberg[9] pointed out the possibility of six dimer structures (a—f)[12] provided that the imidazole rings are linked together, and assigned the structures (f) and (a) for the piezochromic dimer and dimer A, respectively, mainly by comparisons of infrared spectra of these compounds measured in solid states with the model compounds. This assignments, however, would not be considered conclusive and require further confirmation.[13]

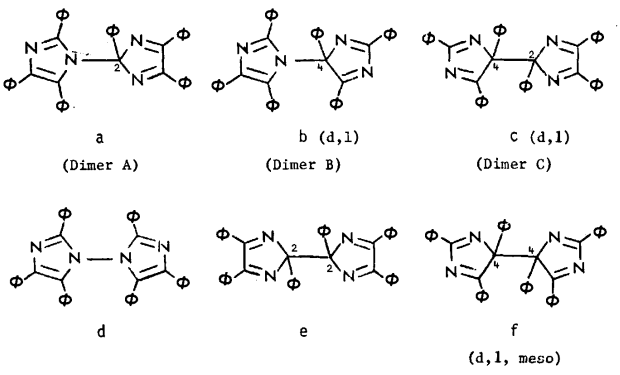

Besides these two dimers we have succeeded in preparing further two new dimers; one (dimer B) (IB) is photochromic and the other (dimer C) (IC) is non-photochromic. Thus, piezochromic dimer of I, when refluxed in benzene in the dark, afforded an equilibrium mixture of the three dimers, A, B, and C, which were separated by means of tlc on silica gel. Photochromic dimers, A and B, are interconvertible by UV irradiation, while dimer C is not affected by the light.

While NMR spectrum of the piezochromic dimer could not be measured due to its instability in solutions,

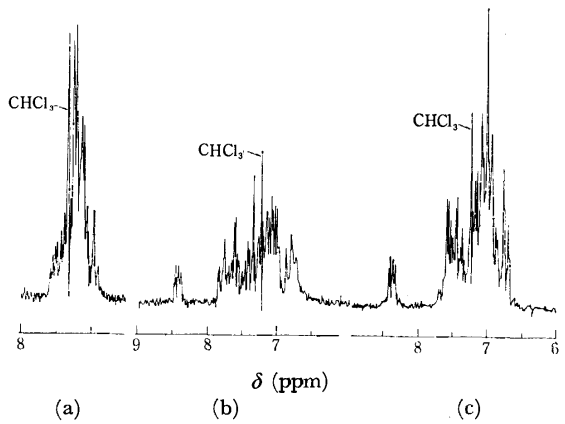

Fig. 1. NMR spectra of dimers of 2,4,5-triphenylimidazolyl in $CDCl_3$.
(a) Dimer A (IA); (b) Dimer B (IB); (c) Dimer C(IC).

1) Studies on Chemiluminescence of Organic Compounds. Part I. Presented at The 9th NMR Symposium (Kanazawa, Oct. 1970).
2) B. Radziszewski, *Ber.*, **10**, 70 (1877).
3) T. Hayashi and K. Maeda, This Bulletin, **35**, 2057 (1962).
4) E. H. White and M. J. C. Harding, *Photochem. Photobiol.*, **4**, 1129 (1965); and references cited hirein.
5) F. McCapra, *Quart. Rev.*, **20**, 485 (1966).
6) J. Sonnenberg and D. M. White, *J. Amer. Chem. Soc.*, **86**, 5685 (1964).
7) E. H. White and M. J. C. Harding, *ibid.*, **86**, 5687 (1964).
8) T. Hayashi and K. Maeda, This Bulletin, **33**, 565 (1960).
9) D. M. White and J. Sonnenberg, *J. Amer. Chem. Soc.*, **88**, 3825 (1966).
10) K. Maeda and T. Hayashi, This Bulletin, **42**, 3509 (1969); **43**, 429 (1970); T. Hayashi and K. Maeda, *Nippon Kagaku Zasshi*, **90**, 325 (1969).
11) H. Baumgärtel and H. Zimmermann, *Z. Naturforsch.*, **18b**, 406 (1963).
12) Structures (b) and (c) have one asymmetric center and hence dimer B and C must be a *dl* form, whereas structure (f) has a pair of such asymmetric centers, and *d*, *l*, and meso forms are possible.
13) A. R. Forrester, J. M. Hay, and R. H. Thomson, "Organic Chemistry of Stable Free Radicals" Academic Press, London (1968), p. 132.

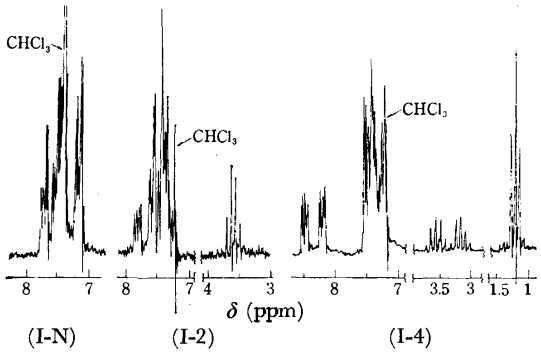

Fig. 2. NMR spectra of *N*-methyl-2,4,5-triphenylimidazole (I-N), 2-ethoxy-2,4,5-triphenyl-2*H*-isoimidazole (I-2) and 4-ethoxy-2,4,5-triphenyl-4*H*-isoimidazole (I-4) in $CDCl_3$.

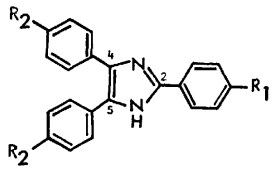

(I) $R_1=R_2=H$
(II) $R_1=CH_3$, $R_2=H$
(III) $R_1=H$, $R_2=CH_3$
(IV) $R_1=R_2=CH_3$
(V) $R_1=Cl$, $R_2=H$
(VI) $R_1=H$, $R_2=Cl$
(VII) $R_1=R_2=Cl$
(VIII) $R_1=CH_3O$, $R_2=H$
(IX) $R_1=H$, $R_2=CH_3O$

Table 1. Properties of dimers of 2,4,5-triphenylimidazolyl and substituted 2,4,5-triphenylimidazolyls

Compd.	Substituents 2-*p*-	Substituents 4,5-di-*p*-	Recryst.[a] solvent	Cryst. form	Mp °C (dec.)	Formula	C% Found	C% Calcd	H% Found	H% Calcd	N% Found	N% Calcd
IA	H	H	B–H	W–P	194—197[c]	$C_{42}H_{30}N_4$	85.74	85.40	5.07	5.12	9.26	9.49
IB	H	H	B–H	Y–P	178—179	$C_{42}H_{30}N_4\cdot 1/2C_6H_6$	85.97	85.82	5.06	5.28	9.14	8.90
IC	H	H	B–H	W–P	207—209	$C_{42}H_{30}N_4$	85.64	85.40	4.83	5.12	9.19	9.49
IIA	CH_3	H	B–H	LY–P	175—176[d]	$C_{44}H_{34}N_4$	85.31	85.41	5.24	5.54	8.96	9.05
IIB	CH_3	H	B–H	Y–Pl	178—179	$C_{44}H_{34}N_4\cdot 1/2C_6H_6$	85.74	85.81	5.79	5.67	8.78	8.52
IIC	CH_3	H	B–H	Y–P	172—173	$C_{44}H_{34}N_4$	85.64	85.41	5.66	5.54	8.92	9.05
IIIA	H	CH_3	B–H	LY–P	155—157	$C_{46}H_{38}N_4$	85.53	85.42	5.92	5.92	8.45	8.66
IIIB	H	CH_3	B–H	Y–R	145—147	$C_{46}H_{38}N_4\cdot 1/2C_6H_6$	85.92	85.81	6.27	6.03	8.29	8.17
IIIC	H	CH_3	B–H	Y–P	177—178	$C_{46}H_{38}N_4$	85.36	85.42	6.25	5.92	8.38	8.66
IVA	CH_3	CH_3	B–H	YG–P	161—162[d,e]	$C_{48}H_{42}N_4$	85.54	85.43	6.39	6.27	8.40	8.30
IVB	CH_3	CH_3	B–H	Y–P	187—188	$C_{48}H_{42}N_4$	85.25	85.43	6.28	6.27	8.22	8.30
IVC	CH_3	CH_3	B–H	Y–P	183—185	$C_{48}H_{42}N_4$	84.99	85.43	6.41	6.27	8.03	8.30
VA	Cl	H	B–H	C–R	206—207[c,e]	$C_{42}H_{28}N_4Cl_2\cdot 1/2C_6H_6$	77.41	77.36	4.15	4.47	8.04	8.02
VB	Cl	H	B–H	LY–P	200—202	$C_{42}H_{28}N_4Cl_2\cdot 1/2C_6H_6$	77.21	77.36	4.40	4.47	8.07	8.02
VC	Cl	H	B	W–P	179—180	$C_{42}H_{28}N_4Cl_2$	76.89	76.48	4.01	4.28	8.26	8.50
VIA	H	Cl	C–H	C–N	163—165	$C_{42}H_{26}N_4Cl_4\cdot 1/2CHCl_3$	65.34	64.76	3.64	3.39	6.95	7.11
VIB	H	Cl	B–H	Y–N	151—153	$C_{42}H_{26}N_4Cl_4\cdot 1/2C_6H_6$	70.39	70.72	4.19	3.81	7.29	7.30
VIC	H	Cl	E	LY–R	190—191	$C_{42}H_{26}N_4Cl_4$	69.40	69.25	3.42	3.60	7.77	7.69
VIIA	Cl	Cl	B–H	Y–P	207—208[c,e]	$C_{42}H_{24}N_4Cl_6$	63.72	63.29	3.18	3.03	6.82	7.03
VIIB	Cl	Cl	B–H	Y–P	179—181	$C_{42}H_{24}N_4Cl_6$	63.82	63.29	3.03	3.03	6.87	7.03
VIIC	Cl	Cl	B–H	Y–R	~155	$C_{42}H_{24}N_4Cl_6\cdot 1/2C_6H_6$	64.53	64.62	3.36	3.25	6.81	6.70
VIIIA	OCH_3	H	B–H	Y–N	120—122	$C_{44}H_{34}N_4O_2$	81.35	81.21	5.04	5.27	8.48	8.61
VIIIB	OCH_3	H	CH	Y–P	130—131	$C_{44}H_{34}N_4O_2\cdot C_6H_{12}$	81.63	81.71	6.12	6.32	7.47	7.62
VIIIC	OCH_3	H	E	Y–P	197—199	$C_{44}H_{34}N_4O_2$	81.27	81.21	5.23	5.27	8.64	8.61
IXA	H	OCH_3	B–H	Y–N	176—177	$C_{46}H_{38}N_4O_4\cdot 1/2C_6H_6$	78.33	78.54	5.28	5.51	7.25	7.47

a) B: benzene; H: *n*-hexane; C: chloroform; E: ethanol; CH: cyclohexane.
b) W: white; Y: yellow; LY: light yellow; YG: yellow-green; C: colorless; P: powder; Pl: plates; R: rods; N: needles.
c) D. M. White and J. Sonnenberg, *J. Amer. Chem. Soc.*, **88**, 3825 (1966): IA, mp 202—202.5°C; VA, mp 203—205°C; VIIA, mp 209—210°C.
d) H. Baumgärtel and H. Zimmermann, *Z. Naturforsch.*, **18b**, 406 (1963): IIA, mp 190°C; IVA, mp *ca.* 180°C; VIIIA, mp 146°C.
e) K. Maeda and T. Hayashi, This Bulletin, **43**, 429 (1970): IA: mp 199—201°C; IVA, mp 194—195°C; VA, mp 219—220°C; VIIA, mp 213—214°C.

Table 2. Characteristic NMR signals (δ in ppm; solvent $CDCl_3$)

Compound	Dimer A Signal at >8	Dimer B Signal at >8	Dimer B Broad signal	Dimer C Signal at >8	N[a] Signal at >8	2[b] Signal at >8	4[c] Singals at >8	
I	no	8.43*	6.80	8.35*	no	no	8.47*	8.18*
II (Me)	no	8.31°	6.7	8.22°				
III (Me_2)	no	8.32*	6.39	8.34*	no			
IV (Me_3)	no	8.20°	6.39	8.23°			8.36°	8.12°
V (Cl)	no	8.35°	6.7	8.26°	no		8.41°	8.19*
VI (Cl_2)	no	8.39*	6.63	8.37*	no		8.45*	8.13°
VII (Cl_3)	no	8.34°	6.72	8.22°	no		8.38°	8.10°
VIII (OMe)	no	8.39°	6.80	8.39°	no	no	8.44°	8.21*

* Signals corresponding to A_2 part of A_2X_2Y pattern.
° Signals corresponding to A_2 part of A_2X_2 pattern.
a) *N*-Methyltriarylimidazole
b) 2-Ethoxy-2,4,5-triaryl-2*H*-isoimidazole
c) 4-Ethoxy-2,4,5-triaryl-4*H*-isoimidazole

Table 3. Characteristic IR bands and R_f values

Compound	Dimer A IR[a]	Dimer A R_f[b]	Dimer B IR	Dimer B R_f	Dimer C IR	Dimer C R_f	N[c] IR	2[d] IR	4[e] IR
I	1604 m	0.25	1610 s	0.33	1613 vs	0.40	1605 m	1607 w	1612 vs
II (Me)	1602 m	0.21	1608 vs	0.30	1613 vs	0.35			
III (Me_2)	1610 m	0.22	1609 vs	0.29	1616 vs	0.38			
IV (Me_3)	1613 m	0.21	1605 vs	0.30	1618 vs	0.39			
V (Cl)	1605 m	0.35	1609 vs	0.38	1619 vs	0.42	1603 m		1610 vs
VI (Cl_2)	1600 m	0.36	1608 s	0.39	1621 vs	0.49	1605 vw		1613 vs
VII (Cl_3)	1600 m	0.38	1605 s	0.43	1620 s	0.47	1600 vw		1612 vs
VIII (OMe)	1609 m	0.09	1604 s	0.15	1611 s	0.23	1611 m	1609 m	1611 vs

a) ν (KBr) cm^{-1}; w: weak, m: medium, s: strong, v:very.
b) R_f value on silica gel tlc (Merck Kieselgel $PF_{254+366}$; benzene:ethyl acetate=20:1)
c) *N*-Methyltriarylimidazole
d) 2-Ethoxy-2,4,5-triaryl-2*H*-isoimidazole
e) 4-Ethoxy-2,4,5-triaryl-4*H*-isoimidazole

other three dimers, A, B, and C, could give their NMR spectra, but these spectra were too complicated to be analyzed (Fig. 1). Therefore, we have synthesized lophines (II–IX) having mono-, di-, and tri-*p*-substituents on the phenyl groups; each compound in turn has been oxidized to the three dimers corresponding to the lophyl dimers, A, B, and C, as shown in the Table 1. The structural correlation of these dimers to the parent lophyl dimers has been carried out by careful comparisons of the chemical shifts and coupling patterns of their NMR spectra, characteristic IR bands between 1400 and 1700 cm^{-1}, R_f values on tlc, and photochromic property. Some of the characteristic properties of the three series of dimers are as follows. Dimer A series gives no NMR signal at a lower field than 8 ppm, whereas a two-proton signal appears around 8.3 ppm in the NMR spectra of dimer B and C series. Furthermore, NMR spectra of dimer B series show a characteristically broad signal around 6.5 ppm. Dimer B and C series give a very strong IR band around 1600 cm^{-1}; a compound which belongs to the latter series always gives a bond at a higher frequency than that of the corresponding compound in the former series. Dimer A series of compounds also gives IR band around 1600 cm^{-1}, but intensity of this band is distinctly lower than those of other series. The data are summerized in Tables 2 and 3. The *p*-substituted phenyl groups gave A_2X_2 or A_2B_2 type NMR signals which could be analyzed fairly easily, and at the same time, the signals of the substituents such as CH_3 and OCH_3 could also be used for the structural elucidation. Selection of suitable compounds and suitable NMR conditions (temperature, solvents, *etc.*) made analysis of the signals possible. The results are as follows:

(1) Since the NMR spectrum of dimer B of 2,4,5-tri(*p*-tolyl)imidazolyl (IVB) shows well separated six A_2X_2 patterns of the tolyl grops (Fig. 3b;[14] all of the ortho coupling constants are 8.5 Hz) and six methyl singlets (solvent, $CDCl_3$; δ 1.98, 2.14, 2.17, 2.22, 2.35, and 2.48 ppm), dimer B has six magnetically different phenyl groups and hence the structure (b)[12] must be assigned for the dimer B.

14) The NMR spectrum of dimer B of tri(*p*-tolyl)imidazolyl (IVB) at room temperature shows a broad signal at 6.39 (in $CDCl_3$) ppm, which is spin coupled with the doublet at 7.48 ppm. This broad signal becomes a doublet by elevation of the measuring temperature to 60°C. This phenomenon would be attributable to the restricted rotation of a phenyl group about the C–C bond between the phenyl and the imidazole ring. This characteristic broad band can be used for identification of a series of dimer B (Table 2). Further discussion on this phenomenon will be reported elsewhere.

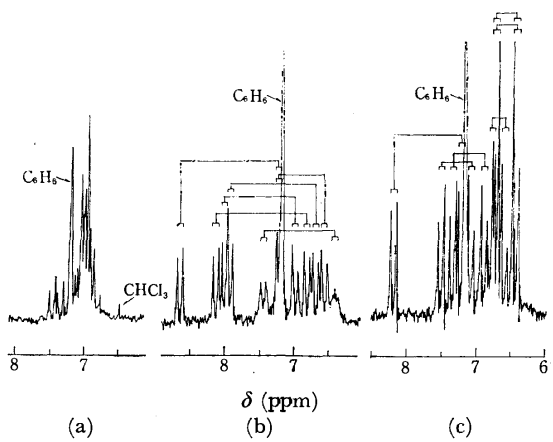

Fig. 3. NMR spectra of dimers of 2,4,5-triarylimidazolyl.
(a) Dimer A of 2.4,5-tri(*p*-chlorophenyl)imidazolyl (VIIA) in C_6D_6+$CDCl_3$ (3:2).
(b) Dimer B of 2,4,5-tri(*p*-tolyl)imidazolyl (IVB) in C_6D_6; the spin couplings indicated were confirmed by spin decoupling experiments.
(c) Dimer C of 2,4,5-tri(*p*-chlorophenyl)imidazolyl (VIIC) in C_6D_6; the spin couplings indicated (except one) were confirmed by spin decoupling experiments.

(2) The NMR spectrum of dimer C of 2,4,5-tri(*p*-chlorophenyl)imidazolyl (VIIC) in benzene-d_6 (Fig. 3c) shows in addition to well separated four A_2X_2 (or A_2B_2) patterns, each of which corresponds to four protons, an A_2B_2 pattern corresponding to eight protons, which indicates the presence of a pair of magnetically equivalent *p*-chlorophenyl groups (all of the ortho coupling constants are 8.5 Hz). This was further confirmed by analysis of the methyl signals of tri(*p*-tolyl)imidazolyl dimer C (IVC) (Fig. 4); there always exists a singlet signal corresponding to two methyl groups. Hence, the possible structures for dimer C are restricted to (a) or (c).[15]

(3) Dimer B and C have a low-field signal (δ *ca.* 8.4 ppm in $CDCl_3$) (Fig. 1 and Table 2), which is attributable to two ortho-protons of one of the two 2-phenyl groups, since the low-field signal becomes A_2X_2 pattern by introduction of a *p*-substituent on the 2-phenyl group of the dimer B and C (Table 2). Such a low-field signal exists in the NMR spectrum of 3-ethoxy-2,4,5-triphenyl-4*H*-isoimidazole (I-4), but not in those of 2-ethoxy-2,4,5-triphenyl-2*H*-isoimidazole (I-2) and *N*-methyl-2,4,5-triphenylimidazole (I-N) (Fig. 2), indicating that the signal is due to the 2-phenyl group of 4*H*-isoimidazole ring. Incidentally, the signal at δ 8.18 ppm in the NMR spectrum of the 4-ethoxy derivative (I-4) corresponds to the ortho protons in the 4-phenyl group, since (V-4) and (VI-4) gave in this region a signal having A_2 part of A_2X_2Y and A_2X_2 patterns, respectively; the low-field shift of this signal being attributable to the attachment of oxygen atom at 4-position. Dimer B and C, therefore, have a 2,4,5-triphenyl-4*H*-isoimidazolyl group linked at C_4; thus, possible structures being (b), (c), and (f). Since the structure of dimer C is already restricted to (a) or (c), above results indicate that the structure of dimer C must be represented by (c).[12]

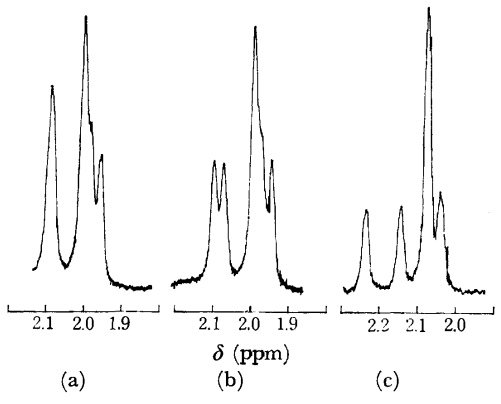

Fig. 4. Methyl signals in the NMR spectra of dimer C of 2,4,5-tri-(*p*-toyl)imidazolyl (IVC).
(a) in C_6D_6; (b) in C_6D_6+$CDCl_3$ (4:1); (c) in C_6D_6+$CDCl_3$ (4:5).

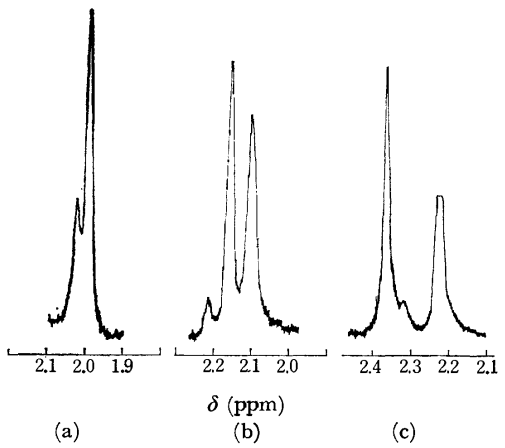

Fig. 5. Methyl signals in the NMR spectra of dimer A of 2-phenyl-4,5-di(*p*-tolyl)imidazolyl (IIIA). (a) in C_6D_6; (b) in C_6D_6+$CDCl_3$ (1:1); (c) in $CDCl_3$.

(4) The NMR signals of dimer A (Fig. 1a) appears in a narrow range (6.8—7.7 ppm in $CDCl_3$) and not well resolved, but analysis of the methyl signals of dimer A of 4,5-di(*p*-tolyl)-2-phenylimidazolyl (IIIA) indicates that two of the four methyl groups are in a magnetically identical environment (Fig. 5), whereas each of other two methyl groups is in a different environment from others. Since 4*H*-isoimidazolyl moiety is not involved in this dimer, structure (a) must be assigned to dimer A. This assignment is also supported by the NMR spectrum of the dimer A of 2,4,5-tri(*p*-chlorophenyl)imidazolyl (Fig. 3a), which indicates that at least the symmetrical structures, (d), (e), and (f), can be excluded (two-proton doublets at 7.34 and 7.46 ppm).

Infrared spectra also support these assignments (Fig. 6 and Table 3). The 4-ethoxy compound (I-4) has a very strong IR band at 1612 cm^{-1}, whereas 2-ethoxy (I-2) and *N*-methyl (I-N) compounds have only a medium but sharp band around 1600 cm^{-1}; thus, the strong band at 1612 cm^{-1} indicates the presence of 4*H*-isoimidazole ring. Dimer B and C, which have a

15) Structure (c) has an asymmetric carbon atom, and hence two phenyl groups at the 4 and 5 positions of 2*H*-isoimidazolyl group is in principle magnetically non-equivalent, but magnetic influence of the asymmetric center would be negligibly small, since it is far apart from the phenyl groups.

Table 4. Properties of *N*-methyl-2,4,5-triarylimidazoles, and 2-ethoxy- and 4-ethoxy-2,4,5-triarylisoimidazoles

Compd.	Substituents 2-*p*-	4,5-di-*p*-	Recryst.[a] solvent	Cryst.[b] form	Mp °C	Formula	C% Found	C% Calcd	H% Found	H% Calcd	N% Found	N% Calcd
I-N	H	H	CH	C–N	143[c]	$C_{22}H_{18}N_2$	85.35	85.13	5.93	5.85	9.17	9.09
I-2	H	H	E	C–R	138	$C_{23}H_{20}N_2O$	81.03	81.15	5.83	5.92	8.23	8.23
V-N	Cl	H	EA	C–N	194	$C_{22}H_{17}N_2Cl$	76.15	76.62	4.82	4.98	8.07	8.13
V-4	Cl	H	E	C–P	130—131	$C_{23}H_{19}N_2OCl$	73.52	73.97	4.96	5.12	7.47	7.47
VI-N	H	Cl	E	Y–N	188—189	$C_{22}H_{16}N_2Cl_2$	69.75	69.66	4.25	4.26	7.48	7.39
VI-4	H	Cl	E	C–P	130	$C_{23}H_{18}N_2OCl_2$	67.46	67.97	4.53	4.44	6.71	6.85
VII-N	Cl	Cl	E	Y–Pl	204—205	$C_{22}H_{15}N_2Cl_3$	63.70	63.86	3.56	3.66	6.81	6.77
VII-4	Cl	Cl	E	C–N	148—149	$C_{23}H_{17}ON_2Cl_3$	62.06	62.25	3.61	3.86	6.44	6.31
VIII-N	OCH_3	H	EA	C–N	174—175	$C_{23}H_{20}N_2O$	81.38	81.15	5.68	5.92	8.28	8.23
VIII-2	OCH_3	H	E	C–Pl	134—136	$C_{24}H_{22}N_2O_2$	78.15	78.81	6.06	5.99	7.60	7.56
VIII-4	OCH_3	H	E	C–P	145—146	$C_{24}H_{22}N_2O_2$	77.86	77.81	6.07	5.99	7.56	7.56

a) and b): see footnotes of Table 1; EA: ethyl acetate.
c) D. M. White and J. Sonnenberg, *J. Org. Chem.*, **29**, 1926 (1964): I-N: mp 143.5—144.5°C.

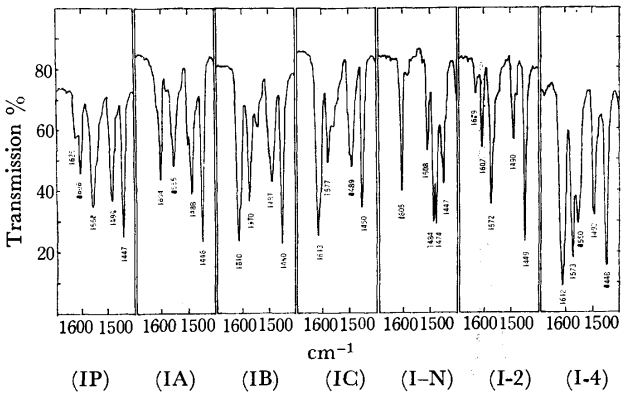

Fig. 6. IR spectra between 1400 and 1700 cm^{-1} in KBr disc. IP: piezochromic dimer of I; IA: dimer A of I; IB: dimer B of I; IC: dimer C of I; I-N: *N*-methyltriphenylimidazole; I-2: 2-ethoxytriphenylisoimidazole; I-4: 4-ethoxytriphenylisoimidazole.

4*H*-isoimidazole ring, indeed show a strong band at *ca.* 1610 cm^{-1}. On the other hand, a sharp medium band is present at 1604 cm^{-1} in the IR spectrum of dimer A indicating the absence of 4*H*-isoimidazole ring and the presence of 2*H*-iso- and/or imidazole ring.[16]

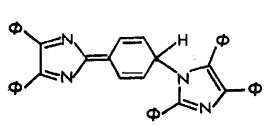
g

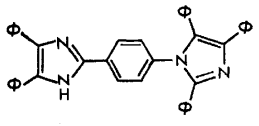
h

Since these three dimers can be prepared without difficulty from tri-*p*-substituted lophines, the structures involving the linkage at the *p*-position of one of the phenyl groups such as structure (g) are excluded.[17] Furthermore, since they show no NH band in their IR spectra as indicated by White and Sonnenberg[9] and since they can be interconverted thermally, the structures such as (h), in which a triphenylimidazole is substituted at a *p*-position of a phenyl group of another triphenylimidazole, are excluded.

It is of interest to note that the photochromic dimers, A and B, have the central C–N bond, whereas non-photochromic dimer C has the central C–C bond. In the former case the excitation energy is transferred from the aromatic imidazole ring to the central C–N bond, which is directly attached to the aromatic ring, whereas in the latter case, it is not, since the central C–C bond is separated by an sp^3 carbon atom from the conjugated systems.

2-Ethoxy-2*H*- (I-2) and 4-ethoxy-4*H*-2,4,5-triphenylisoimidazole (I-4) were prepared from lophyl dimer A (IA) by dissolving in ethanol and treating with dilute hydrochloric acid; the central C–N bond of this dimer being cleaved heterolytically. The 4-ethoxy compound

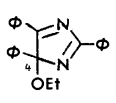
(I-4)

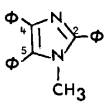
(I-N)

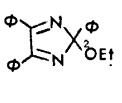
(I-2)

(I-4) has an asymmeric carbon atom and hence its NMR spectrum (Fig. 2) shows non-equivalence of the methylene protons in the ethoxy group, whereas only a quartet signal was observed for the methylene protons in the case of 2-ethoxy compound (I-2). Derivatives of these ethoxy compounds are listed in Table 4. The 4-ethoxy compound (VIII-4) seems to be more stable

16) The piezochromic dimer is rapidly converted to dimer A by dissolving it in organic solvents such as benzene, ethyl acetate, chloroform, acetone, and ether and followed by immediate evaporation at room temperature. Hence, its NMR, UV, and IR spectra in solutions could not be obtained. IR spectrum taken in KBr disc is only the available physical data for structural analysis. Although White and Sonnenberg[9] suggested the structure (f) for the piezochromic dimer by analysis of its IR spectrum; the piezochromic dimer shows only a medium band at 1606 cm^{-1} with a shoulder at 1625 cm^{-1}, and hence the structure (e) (or less probably (d)) would be more probable than (f). The piezochromic dimers obtained from other lophine derivatives may be impure compounds contaminated with the starting lophine derivative and the corresponding dimer A.

17) The structure of dimer of triphenylmethyl has recently been revised from the symmetric hexaphenylethane to the asymmetric structure similar to (g). H. Lankamp, W. Th. Nauta, and C. MacLean, *Tetrahedron Lett.*, **1968**, 249; H. A. Staab, H. Brettschneider, and H. Brunner, *Chem. Ber.*, **103**, 1101 (1970).

than 2-ethoxy compound (VIII-2), since the latter isomerizes to the former by treatment with acid.

N-Methyllophine (I-N) was prepared by treatment with dimethyl sulfate and potassium carbonate in boiling acetone. Synthesized derivatives of the *N*-methyl compound are listed in Table 4.

Experimental

All melting points are uncorrected. IR spectra were recorded on a JASCO IR-G grating spectrophotometer and NMR spectra on a JEOL 4H-100 (100 MHz) spectrometer. Chemical shifts are expressed in ppm from internal tetramethylsilane (δ-value) and coupling constants in Hz.

Lophine (I) and Substituted Lophines (II-IX). These compounds were synthesized by the method of Davidson *et al.*[18] by refluxing the appropriate benzil with the appropriate aldehyde and ammonium acetate in acetic acid for *ca.* 1 hr. The reaction mixture was then poured into ice-water and the precipitated product was collected. (Solvent in parentheses was used for crystallization) Lophine (I), colorless needles (methanol), mp 275—276°C, lit, 274—275°C.[19] 2-*p*-Tolyl-4,5-diphenylimidazole (II), needles (methanol), mp 233—237°C, lit, mp 234—235°C.[19] 2-Phenyl-4,5-di(*p*-tolyl)imidazole (III), needles (ethanol), mp 269—271°C. Found: C, 85.31; H, 6.18; N, 8.62%. Calcd for $C_{23}H_{20}N_2$: C, 85.15; H, 6.21; N, 8.64%. 2,4,5-Tri(*p*-tolyl)-imidazole (IV), pale yellow needles (methanol), mp 237—240°C, lit,[20] 234°C. 2-*p*-Chlorophenyl-4,5-diphenylimidazole (V), colorless needles (ethanol), mp 264—265.5°C, lit, 284—286°C.[19] (Found: C, 76.54; H, 4.24; N, 8.46%). 2-Phenyl-4,5-di(*p*-chlorophenyl)imidazole (VI), colorless needles (ethyl acetate), mp 294—295°C. Found: C, 68.48; H, 3.61; N, 7.74%. Calcd for $C_{21}H_{14}N_2Cl_2$: C, 69.06; H, 3.86; N, 7.67%. 2,4,5-Tri(*p*-chlorophenyl)imidazole (VII), pale yellow needles (ethyl acetate), mp 276—278°C, lit, 275—275.5°C.[21] 2-*p*-Anisyl-4,5-diphenylimidazole (VIII), colorless needles (ethanol), mp 232—233°C, lit, 233—233.5°C.[4] 2-Phenyl-4,5-di(*p*-anisyl)imidazole (IX), pale yellow plates (ethanol), mp 99—100°C, lit, 197°C,[4] 99°C.[22] Found: C, 70.40; H, 6.26; N, 6.62%. Calcd for $C_{23}H_{20}N_2O_2 \cdot 2H_2O$: C, 70.39; H, 6.16; N, 7.14%.

Piezochromic Dimers of Lophine and Substituted Lophines. According to the method of White and Sonnenberg,[9] to a solution of lophine (2 g) in 95% ethanol (200 m*l*) containing potassium hydroxide (24 g) was added under ice cooling at 5—10°C with stirring 1% aqueous potassium ferricyanide (900 m*l*) in a period of 3 hr and the mixture was stirred for additional 1 hr. The precipitated solid was collected on a filter, washed with water and dried over phosphorus pentoxide to give piezochromic dimer as pale violet powder, mp *ca.* 141°C (yield 95%), lit, 187.5—188.5°C,[9] 191—192°C.[10] Piezochromic dimers from substituted lophines (II—IX) were also prepared in a similar way, but IR spectra indicated that they may be impure and contaminated with the corresponding dimer A and starting material. Melting points (decomp.) are as follows: piezochromic dimer from II, mp 109—112°C; from III, 128—132°C; from IV, mp *ca.* 122°C; from V, mp 110—124°C, lit, 195—200°C,[9] 205—207°C;[10] from VII, mp *ca.* 123°C, lit, 105—115°C;[9] from VIII, mp *ca.* 111°C; from IX, mp *ca.* 125°C.

Dimer A of Lophine and Substituted Lophines (IA—IXA). The dimers, IA, VA, VIA, VIIA, VIIIA, and IXA, were prepared by crystallization of the corresponding piezochromic dimer from benzene–*n*-hexane (Table 1). The *p*-methyl derivatives, IIA, IIIA, and IVA, could not be obtained in a pure state from the corresponding piezochromic dimer by crystallizations, and hence they were prepared from the corresponding dimer B in the following way. A solution of IIB (200 mg) in benzene (15 m*l*) was irradiated with a fluorescent lamp (National High-light, 15 W) at room temperature for 13 hr and then evaporated to dryness *in vacuo*. Dimer A was separated from the remaining solid by means of silica gel tlc as a dark brown amorphous solid, which was crystallized from benzene–*n*-hexane yielding IIA (136 mg) as a crystalline powder. IIB (7 mg) was also recovered.

Dimers B and C of Lophine and Substituted Lophines. A solution of piezochromic dimer of lophine (300 mg) in benzene (15 m*l*) was refluxed for 20 hr and then evaporated to dryness *in vacuo* to give a yellow amorphous solid. The solid was subjected to silica gel tlc (Kieselgel $PF_{254+366}$; benzene: ethyl acetate = 20: 1) in the dark to afford three dimers, A, B, and C, each of which was purified by crystallization from a suitable solvent. The fraction of dimer A was usually contaminated with the monomer and this method was not suitable for preparation of dimer A. Dimers B and C of substituted lophines (II—VIII) were prepared in a similar way from the appropriate piezochromic dimer (Table 1).

Preparation of Three Dimers, A, B, and C, by Oxidation with Lead Dioxide. A mixture of lophine (2 g) and lead dioxide (8 g), which was freshly prepared from lead tetraacetate by treatment with water, in benzene (150 m*l*) was refluxed with stirring for 20 hr and filtered while in hot through Hyflo-supercel. The filtrate on evaporation to a small volume precipitated white crystals (195 mg, lophine), which were filtered off. The filtrate was evaporated to dryness *in vacuo* and the residue was subjected to tlc as described above to give three components, which were identical with the dimers, A, B, and C. Yields (crude) were 475 mg (dimer A), 340 mg (dimer B), and 809 mg (dimer C). Lophine (195 mg) was also recovered.

*2-Ethoxy-2,4,5-triphenyl-2*H*-isoimidazole (I-2) and 4-Ethoxy-2,4,5-triphenyl-4*H*-isoimidazole (I-4) and Their Derivatives.* A solution of the dimer IA (1 g) in dichloromethane (80 m*l*) and ethanol (160 m*l*) was treated with a drop of concentrated hydrochloric acid and the mixture was refluxed for 3 hr. After neutralization with dil. aqueous sodium hydrogen carbonate, the reaction mixture was evaporated to dryness *in vacuo* and the residue was extracted with chloroform. The chloroform extract was evaporated and the residue was subjected to tlc on silica gel (benzene: ethyl acetate = 20: 1) to give 4-ethoxy compound (I-4) (112 mg), 2-ethoxy compound (I-2) (115 mg), lophine (I) (276 mg) and recovered IA (271 mg) (Table 4). 4-Ethoxy compound (I-4) could not be crystallized but mass (*m/e* 340), NMR (Fig. 2), and IR (Fig. 6) spectra indicate its identity. Other 2-ethoxy and 4-ethoxy compounds of substituted lophines listed in Table 4 were prepared in a similar way from the appropriate dimer A.

*Conversion of 2-Ethoxy-2-anisyl-4,5-diphenyl-2*H*-isoimidazole (VIII-2) to 4-Ethoxy-2-anisyl-4,5-diphenyl-4*H*-isoimidazole (VIII-4).* A solution of VIII-2 (30 mg) in ethanol (3 m*l*) was treated with a drop of hydrochloric acid in ethanol (concentrated HCl: ethanol = 1: 9) and the mixture was allowed to stand at room temperature for 3 days. After neutraliza-

18) D. Davidson, M. Weiss, and M. Jelling, *J. Org. Chem.*, **2**, 319 (1957).
19) G. E. Philbrook, M. A. Maxwell, R. E. Taylor, and J. R. Totter, *Photochem. Photobiol.*, **4**, 1175 (1965).
20) L. Gattermann, *Ann. Chem.*, **347**, 367 (1906).
21) D. M. White and J. Sonnenberg, *J. Org. Chem.*, **29**, 1926 (1964).
22) Gevaert, Photo-Producten, N. V., *Chem. Abstr.*, **58**, 2530 (1963).

tion with aqueous sodium hydrogencarbonate, the mixture was evaporated to dryness *in vacuo* and the residue was subjected to silica gel tlc (benzene: ethyl acetate=20: 1) to give 4-ethoxy compound (VIII-4) (16 mg) and 2-ethoxy compound (VIII-2) (4 mg). The similar treatment of 4-ethoxy compound (VIII-4) gave no 2-ethoxy compound (VIII-2).

N-*Methyl-2,4,5-triphenylimidazole and Its Derivatives.* To a solution of lophine (1 g) and dimethyl sulfate (640 mg) in acetone (45 m*l*) was added powdered anhydrous potassium carbonate (700 mg) and the mixture was refluxed with stirring for 5 hr. After cooling, the mixture was poured into water (150 m*l*) and the precipitated white crystals were collected by filtration and recrystallized from *n*-hexane to give colorless needles (522 mg), mp 143°C.[21] Other *N*-methyl derivatives listed in Table 4 were prepared in a similar way; yields being about 50%.

The authors wish to thank Mr. Eiji Fukuoka and Mr. Hiroaki Morikawa for their assistance in some of the synthetic experiments.

BULLETIN OF THE CHEMICAL SOCIETY OF JAPAN, VOL. 45, 1480—1482(1972)

The Biosynthesis of Linalool in *Cinnamomum Camphora* Sieb. *var. linalooliferum* Fujita[1)]

Takayuki SUGA, Tsuyoshi SHISHIBORI, and Michie BUKEO

Department of Chemistry, Faculty of Science, Hiroshima University, Higashisenda-machi, Hiroshima

(Received September 9, 1971)

The labelling pattern in linalool biosynthesized from [2-^{14}C] mevalonic acid in *Cinnamomum Camphora* Sieb. *var. linalooliferum* Fujita was found to be consistent with the predicted biosynthetic pathway involving the condensation of isopentenyl pyrophosphate with 3,3-dimethylallyl pyrophosphate. The radioactivities at C-4 and C-8 (and/or C-10) were about equal, in contrast to the asymmetric pattern of labelling observed for bicyclic monoterpenes, which contained a tracer predominantly in one position of the skeleton derived from isopentenyl pyrophosphate. The efficiency of the incorporation of the tracer into linalool was almost independent of the season of the examination, although a slight increase was observed in the season of the active growth of the plant.

The biosynthesis of monoterpenes from mevalonic acid (MVA) involves the condensation of isopentenyl pyrophosphate (IPP) (I) with 3,3-dimethylallyl pyrophosphate (DMAPP) (II) directed towards the formation of geranyl pyrophosphate (GPP) (III) or neryl pyrophosphate, the presumed precursors of acyclic and cyclic monoterpenes respectively.[2)] Recently, thujane derivatives and camphor biosynthesized from [2-^{14}C] MVA were shown[3,4)] to contain their tracer to a great extent at one ring position derived from such a tracer-containing precursor as IPP (I), but not DMAPP (II). Such examples of preferential labelling being detected for one of the participating C_5-units have also been reported on sesquiterpenes, coriamyrtin and tutin,[5)] though other investigators[6)] have observed an equal distribution of labelling in tutin. In order to clarify the generality of these unexpected results, we have tested the labelling pattern and its seasonal variation in linalool biosynthesized from [2-^{14}C] MVA in *Cinnamomum Camphora* Sieb. *var. linalooliferum* Fujita (Hōsho in Japanese). In the biosynthesis of linalool, which is an acyclic monoterpene probably derived from GPP (III) in the initial stages, the situation was different from those observed for the bicyclic monoterpenes.[3,4)]

Results

Efficiency of the Incorporation of a Tracer. In order to test the seasonal variation of the incorporation of the tracer, [2-^{14}C] MVA was applied by stem-feeding into the leaves at three different seasons, April, July, and November. The results of the incorporation of the tracer into linalool are shown in Table 1.

TABLE 1. SEASONAL VARIATIONS OF ESSENTIAL OIL AND LINALOOL AND OF THE INCORPORATION OF [2-^{14}C] MVA INTO LINALOOL

	April	July	November
Essential oil (w/w%)[a)]	0.48	1.20	1.64
Linalool (w/w%)[a)]	0.27	0.60	0.85
Incorporation (%)	0.013	0.022	0.012

a) Of the plant

Labelling Patterns. The selective hydrogenation of linalool (IV) on platinum oxide afforded 1,2-dihydrolinalool, which was degraded to acetone containing a tracer from C-7, C-8, and C-10, and to 4-methyl-4-hexanolide (V) containing a tracer from C-1 to C-6 and

1) Preliminary communication: T. Suga, T. Shishibori, and M. Bukeo, *Phytochemistry*, **10**, 2725 (1971).

2) J. H. Richards and J. B. Hendrickson, "The Biosynthesis of Steroids, Terpenes, and Acetogenins," Benjamin, New York (1964), p. 173 and references cited therein.

3) a) D. V. Banthorpe and K. W. Turnbull, *Chem. Commun.*, **1966**, 177; b) D. V. Banthorpe, J. Mann, and K. W. Turnbull, *J. Chem. Soc., C*, **1970**, 2689.

4) a) D. V. Banthorpe and D. Baxendale, *Chem. Commun.*, **1968**, 1553; b) D. V. Banthorpe and D. Baxendale, *J. Chem. Soc., C*, **1970**, 2694.

5) M. Biollaz and D. Arigoni, *Chem. Commun.*, **1969**, 633.

6) A. Corbella, P. Gariboldi, G. Jommi, and C. Scolastico, *ibid.*, **1969**, 634.

C-9, by permanganate-periodate oxidation.[7,8] Acetone was degraded to iodoform containing a tracer from C-8 and C-10 and to acetic acid. Acetic acid thus produced was further cleaved to methylamine and to carbon dioxide containing a tracer originating from C-7. The lactone (V) was subjected to Kuhn-Roth oxidation[9] to obtain acetic acid containing a tracer from C-1 to C-3 and C-9. Linalool and all its degradation products were converted into barium carbonate by Van Slyke-Folch oxidation[10] in order to determine their specific activities. The results are shown in Table 2.

Table 2. Specific radioactivities of linalool and its degradation products

Compounds (Carbons originated from IV)	Specific radioactivity, dpm/mM (%)		
	April	July	November
Linalool (C-1—C-10)	5717	6169	607
Iodoform (C-8 and/or C-10)	1025(17.9)	1335(21.6)	124(20.4)
Acetic acid (C-7, 8, and /or C-7, 10)	1206(21.1)	1524(24.7)	154(25.3)
Methylamine (C-8 and/or C-10)	972(17.0)		
Carbon dioxide (C-7)	114(2.0)		
4-Methyl-4-hexanolide (C-1—C-6, and C-9)	3167(55.4)	3274(53.1)	331(54.4)
Acetic acid (C-1—C-3, and C-9)	363(6.3)	265(4.3)	26(4.2)

Seasonal Variation in Labelling Patterns. The labelling patterns of linalool obtained from the feeding experiments were determined at three different seasons of growth; the results are shown in Table 2.

Discussion

Both the yield of the essential oil and the content of linalool increased with the growth of the plant, as is shown in Table 1. A similar trend has previously been reported[11] in the same plant. Though a slight increase in the incorporation of the tracer into linalool was observed in July, which is the actively-growing season of *C. Camphora*, the efficiency of incorporation was judged to be almost independent of the season, as the increment was too small to discuss any seasonal dependence. The incorporations are, although low, similar to the values found in analogous experiments.[3,4,12]

The extensive degradation of linalool, obtained from feeding in July, revealed the location of 46% of the

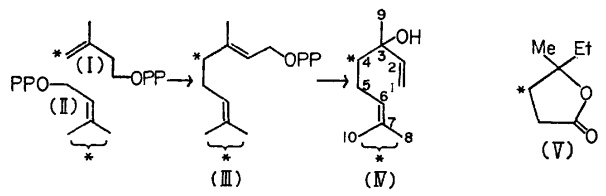

* indicates ^{14}C; OPP indicates a pyrophosphate group.

incorporated tracer on acetone and that of the residual activities (54%) on the lactone (V). Acetic acid derived from the lactone (V) showed, unfavorably, a small activity. This is presumably attributable to the incorporation of the C_1-pool which resulted from the degradation of a small amount of the applied MVA.[13,14] Thus, the main site of labelling on the lactone (V) was, on biogenetic grounds, considered to be the position which corresponds to the C-4 of linalool (IV). With respect to the pattern of labelling, the results obtained above have made us conclude as follows: (a) The pattern of labelling observed for linalool is consistent with the biosynthetic mechanism shown in the Scheme. (b) The specific activities at C-4 and C-8 (and/or C-10), originating from IPP (I) and DMAPP (II) respectively, are nearly equal. The almost balanced pattern of labelling in linalool, an alicyclic monoterpene, is in contrast with the asymmetric pattern of labelling observed for some cyclic monoterpenes.[3,4] The equality of the labelling means that the skeleton results from the condensation of IPP (I) with DMAPP (II), both of which have the same specific activities. It thus appears that the formation of DMAPP (II) in the plant under these conditions is caused by the isomerization of the radioactive IPP (I) generated from the applied [2-^{14}C] MVA. (c) The methyl group and the terminal methylene of IPP (I) are non-equivalent, in the same manner as they are in the biosynthesis of other mono- and higher-terpenes.[15,16]

It has been supposed[3] that the season affects the amount of enzymes, which in turn cause the asymmetrical labelling in thujone. We have now examined the seasonal effect on the radioactivities at C-4 and C-8 of linalool biosynthesized in *C. Camphora*. The specific radioactivities in July and November were comparable for the two carbon atoms (Table 2), but they were slightly unbalanced in April, the sprouting season of this plant. These facts seem to indicate that the active enzyme catalyzing the conversion of IPP (I) to DMAPP (II) may not be sufficient in the sprouting season. Thus, the condensation of the labelled IPP (I) with the unlabelled DMAPP (II) derived from the metabolic pool would lead to the low radioactivities in the part of the skeleton originating from DMAPP (II). However, the unbalance of radioactivities in April was very slight as compared with that in the cases of thujane derivatives[3] and camphor.[4] Although it has been suggested[3,4] that the asymmetrical labelling may be general for the biosynthesis of monoterpenes in leaves of higher plants, the

7) R. U. Lemieux and E. von Rudloff, *Can. J. Chem.*, **33**, 1701 (1955).
8) T. Suga and E. von Rudloff, *J. Sci. Hiroshima Univ., A-II.* **34**, 69 (1970).
9) E. Müller, "Methoden der Organischem Chemie," Bd. 2, Analytische Methoden, Georg Thieme Verlag, Stuttgart (1953), p. 273.
10) D. D. Van Slyke and J. Folch, *J. Biol. Chem.*, **136**, 509 (1940).
11) Y. Fujita, S. Fujita, and S. Nishida, Abstract of the 21st Annual Meeting of the Chemical Society of Japan (1968), Preprints III, p. 2206.
12) W. Sandermann and W. Schweors, *Tetrahedron Lett.*, **1962**, 257 and 259.
13) H. Geoggel and D. Arigoni, *Chem. Commun.*, **1965**, 538.
14) D. A. Yeowell and H. Schmid, *Experientia*, **20**, 250 (1964).
15) J. W. Cornforth, *Biochem. J.*, **66**, 10 (1957).
16) A. J. Birch, R. J. English, R. A. Massay-Westrop, and H. Smith, *J. Chem. Soc.*, **1959**, 369.

radioactivities derived from [2-^{14}C] MVA, on the contrary, were found to be almost equally distributed between the C-4 and C-8 of linalool, an alicyclic monoterpene.

Experimental

Materials. Specimens of *C. Camphora* were grown from young trees obtained from the experimental farm of the Soda Perfumery Co., Kagoshima Prefecture, Japan. Feeding experiments were carried out on small terminal branches (*ca.* 15 cm long) of three-year-old plants, from April to November. *C. Camphora* sprouts from March to April; the growth is more active in July than in November.

Administration of the Labelled Compound. A phosphate buffered solution (40 m*l*, pH 7.38) of [2-^{14}C] MVA (0.1 mCi, 17 μM), and ATP (0.1 mM) was fed through a cut-stem into small twigs (*ca.* 150 g). Immediately before use, the MVA lactone was converted into the potassium salt of MVA by a potassium hydroxide solution. After the solution had been fed in, the foliage was maintained in a phosphate-buffered solution (pH 7.38) for one day before harvesting.

Isolation of Radioactive Linalool. The harvested leaves and stems were subjected to steam distillation. The oil thus obtained (0.71 g) was subjected to column chromatography on silica gel (less than 0.08 mm, Merck). Elution by a mixture of *n*-hexane with increasing amounts of ethyl acetate afforded radioactive linalool (0.40 g), which was judged to be pure by analytical tlc and glc.

Degradation of Linalool. Linalool (598 mg) in methanol (3 m*l*) was selectively hydrogenated on Adams platinum oxide (4 mg) to 1,2-dihydrolinalool (600 mg). The dihydrolinalool (200 mg) was oxidized with a permanganate-periodate reagent[7,8] for 24 hr. After the excess oxidant had been reduced with a minimum of sodium bisulfite, the weakly alkaline solution was steam-distilled. The ether extraction of the acidified residual solution afforded 4-methyl-4-hexanolide (V) (98 mg; its *S*-benzylthiouronium salt, mp 132—133°C, lit,[17] mp 132—132.5°C). The aqueous distillate was subjected to hypoiodite oxidation. Iodoform (369 mg) filtered off was purified by sublimation at reduced pressure. The filtrate was acidified with sulfuric acid and treated with silver sulfate to remove iodine. The mixture was then steam-distilled. The evaporation of the neutralized distillate afforded acetic acid as the sodium salt (38 mg). The salt was purified by means of the addition of dry ether to its dry ethanol solution. The Schmidt reaction[18] of the purified salt afforded carbon dioxide and methylamine, which were then converted to barium carbonate and its hydrochloride respectively. The Kuhn-Roth oxidation[9] of 4-methyl-4-hexanolide (V) (71 mg) gave acetic acid as the sodium salt (94 mg); this was then refined as above.

Radioassay. Linalool and all its degradation products were converted to barium carbonate by Van Slyke-Folch oxidation, and aliquots of barium carbonate were counted on planchets at an infinite thickness under a Aloka TDC R 1361 2π-gas-flow detector. The counting error for the values shown in Tables 1 and 2 is about $\pm$3%.

The authors are thankful to Professor Emeritus T. Matsuura of Hiroshima University for his encouragement, to the Soda Perfumery Co., Ltd., Tokyo, for its gift of the plant, and to the Takasago Perfumery Co., Ltd., Tokyo, for its gift of linalool.

17) Chin-Te Chang, *Formosan Sci.*, **16**, 127 (1962); *Chem. Abstr.*, **59**, 3873a (1963).

18) H. Wolff, "Organic Reactions," (R. Adams, Ed-in-Chief) Vol. III, Wiley, New York (1946), Chapt. 8.

BULLETIN OF THE CHEMICAL SOCIETY OF JAPAN, VOL. 45, 1482—1484(1972)

Chlorination of Olefins with Thallium(III) Chloride Tetrahydrate[1)]

Sakae UEMURA, Osamu SASAKI, and Masaya OKANO
Institute for Chemical Research, Kyoto University, Uji, Kyoto

(Received September 13, 1971)

In CCl_4, $TlCl_3 \cdot 4H_2O$ reacted with mono- and diolefins to give *vic*-dichlorinated compounds (I) in 20—41% yields together with monochlorinated ones (II). The yields of I were intensely increased by adding $CuCl_2 \cdot 2H_2O$ or $FeCl_3$ and bubbling oxygen into the reaction system, although such additives alone gave none of I in CCl_4. In acetic acid, the reaction gave diacetoxylated compound. As to the *vic*-dichlorination, it was proposed that the reacting species was a polarized form of dimeric $TlCl_3$ and not free chlorine evolved from $TlCl_3 \cdot 4H_2O$.

Compared to a number of studies on the reactions of aromatic compounds with Lewis acid halides of metals or metalloids,[2)] the study on the behavior of olefins toward such chlorides is limited to only two cases using $CuCl_2$[3-7)] and $SbCl_5$[8)] in liquid or gas phases. Recently, we have found that aromatic carboxylation and chlorination occur by heating aromatic compounds with $TlCl_3 \cdot 4H_2O$ in CCl_4 solvent.[9)] An attempt to

1) Presented at the 24th Annual Meeting of the Chemical Society of Japan, Osaka, April, 1971.
2) "Friedel-Crafts and Related Reactions," Vol. IV, ed. by G. A. Olah, Interscience Publisher, New York, N. Y. (1965), Chapter 48.
3) J. K. Kochi, *J. Amer. Chem. Soc.*, **84**, 2121 (1962).
4) M. L. Spector, H. Heinemann, K. D. Miller, *Ind. Eng. Chem. Process Des. Develop.*, **6**, 327 (1967).
5) K. Ichikawa, S. Uemura, T. Hiramoto, and Y. Takagaki, *Kogyo Kagaku Zasshi*, **71**, 1657 (1968) and references therein.
6) T. Koyano, This Bulletin, **43**, 1439 (1970).
7) P. P. Nicholas and R. T. Carroll, *J. Org. Chem.*, **33**, 2345 (1968).
8) S. Uemura, O. Sasaki, and M. Okano, *Chem. Commun.*, **1971**, 1064 and unpublished data.
9) S. Uemura, O. Sasaki, and M. Okano, *ibid.*, **1970**, 1139.

Table 1. Chlorination of olefins with $TlCl_3 \cdot 4H_2O$ (25 mmol) in CCl_4 solvent (100 ml) at 77°C

Olefin	(mmol)	React. time (hr)	Addeudum (mmol)	Products (mmol) I	Products (mmol) II	Tl^{1+}[a] (mmol)
Oct-1-ene	100	2		6.42	13.9[b]	15.7
Oct-2-ene[c]	100	2		5.14[d]	18.2[e]	18.9
cis-Oct-2-ene	50	2		1.46[f]	8.2[e]	15.9
Cyclohexene	100	2		4.35[g]	13.7	22.7
Cyclohexene	100	2	NaOAc (20)	trace	0.1	1.4
Cyclohexene	100	10	$CuCl_2 \cdot 2H_2O$(10)[h]	49.9[i]	17.0	—[j]
Cyclohexene	100	10	$FeCl_3$(10)[h]	16.0[k]	13.1	—[j]
Styrene	100	2		1.25[l]	0	15.6
Cyclooctene	100	2		trace	19.3	22.4
Cycloocta-1,5-diene	100	1		2.58[m]	—[j]	23.5
Buta-1,3-diene[n]	56	2		4.72[o]	trace	13.0

a) The amount of consumed Tl^{3+} was determined by iodometry. b) 2-Chlorooctane. c) Mixture of *cis* and *trans* isomers. d) *Erythro* 1.86 mmol, *threo* 3.28 mmol. e) Three components in which 2-chlorooctane is the major one. f) *Erythro* 0.29 mmol, *threo* 1.17 mmol; *i.e.*, *trans*/*cis*=4.05. g) *Trans* 4.25 mmol, *cis* 0.1 mmol; *i.e.*, *trans*/*cis*=42.5[8]. h) Oxygen was bubbled into the reaction mixture at a rate of 1 ml/sec throughout the reaction. i) *Trans* 46.6 mmol. *cis* 3.3 mmol. j) Not determined. k) *Trans* 16.0 mmol, *cis* trace. l) 1,3-Diphenyl-1-butene (11.5 mmol) was formed. m) *Trans* 1.73 mmol, *cis* 0.85 mmol. n) Buta-1,3-diene gas was bubbled into the reaction mixture for 2 hr. o) 1,2-Isomer 2.58 mmol, *cis*-1,4-isomer 0.51 mmol, and *trans*-1,4-isomer 1.63 mmol.

extend this reaction to olefins resulted in the formation of only chlorinated compounds. The characteristics of this chlorination of olefins are described in this report, with a comparison to the results of the reaction using $CuCl_2$ or $SbCl_5$. Although the fact has been known that $TlCl_3 \cdot 4H_2O$ can be used as a catalyst for the synthesis of propylene chlorohydrin from propylene in aqueous medium,[10] this is the first report of the chlorination of olefins with $TlCl_3 \cdot 4H_2O$.

Results and Discussion

The reaction was carried out by adding or bubbling olefinic hydrocarbons into a stirred CCl_4 solution containing $TlCl_3 \cdot 4H_2O$ at refluxing temperature (77°C). Because of the low melting point (37°C) and the insolubility into CCl_4 of $TlCl_3 \cdot 4H_2O$, the solution was heterogeneous with the molten thallium salt. Dichlorinated (I) and monochlorinated hydrocarbons (II) were obtained as organic products, but none of hydrocarbons chlorinated at allylic position were found. Some typical data are summarized in Table 1. Because of the thallium(III) chloride-catalyzed hydrolysis of CCl_4,[11] this reaction accompanied the evolution of hydrogen chloride and phosgene regardless of the addition of olefinic component. I and II may be formed through Eqs. 1 and 2, respectively.

The formation of I occurred rather smoothly with 1- and 2-octenes, cyclohexene and buta-1,3-diene, and the

$$>C{=}C< + TlCl_3 \longrightarrow \underset{Cl\ \ Cl}{>C{-}C<}\ (I) + TlCl + 4H_2O \quad (1)$$

$$\left.\begin{aligned} CCl_4 + TlCl_3 \cdot 4H_2O &\longrightarrow \\ & COCl_2 + 2HCl + TlCl_3 \cdot 2H_2O \\ >C{=}C< + HCl &\longrightarrow \underset{H\ \ Cl}{>C{-}C<}\ (II) \end{aligned}\right\} \quad (2)$$

yields of which were 41, 27, 19, and 36%, respectively, on the basis of the amounts of the consumed Tl^{3+} salt. In the reaction with styrene, dimerization to yield 1,3-diphenyl-1-butene was the main reaction even at 50°C. In cases of cyclooctene and 1,3- and 1,5-cyclooctadienes, considerable amounts of II were formed but the yields of I were very poor. When buta-1,3-diene was used as a substrate, both 1,2- and 1,4-additions occurred and their ratio (1,4-dichloro-2-butene/3,4-dichloro-1-butene) was 0.83 for 2 hrs' reaction at refluxing temperature. It is premature to consider this ratio as a consequence of kinetic control, since a separate experiment showed that in this reaction condition 1,2-dichloroisomer readily converted to 1,4-one.[13] It must be noted here, however, that the 1,4-dichlorinated compound is consisted of *cis*- and *trans*-isomers in *ca.* 1: 3 ratio, although usual chlorination with chlorine gas gives only stable *trans*-isomer.[14] This may suggest the participation of the species other than Cl_2 molecule. The formation of the *cis*-isomer was also observed in the chlorination of buta-1,3-diene with $SbCl_5$ in CCl_4.[8] In addition, both facts have been known that free chlorine is not involved in aromatic chlorination using $TlCl_3 \cdot 4H_2O$ in CCl_4[15] and that $TlCl_3 \cdot 4H_2O$ does not evolve chlorine gas by heating at 110°C.[16] Hence, it seems very unlikely that this

10) K. Tanaka, G. Inoue, and N. Kominami, presented at the 22nd Annual Meeing of the Chemical Society of Japan, Tokyo, April, 1969, Vol. IV, p. 2549.

11) In one experiment using 25 mmol of $TlCl_3 \cdot 4H_2O$ and 100 ml of CCl_4 with stirring for 2 hr at 77°C, 29.7 mmol of phosgene and 141 mmol of hydrogen chloride were obtained. Details on the catalytic hydrolysis of trichloromethyl compounds were reported separately.[12]

12) S. Uemura, F. Tanaka, O. Sasaki, and M. Okano, *Bull. Inst. Chem. Res. Kyoto Univ.*, **49**, 97 (1971).

13) A 6:1 mixture of 1,2- and 1,4-dichloroisomers (0.64 g) changed to a *ca.* 1:1 mixture (0.50 g) by heating at 77°C for 40 min in 50 ml of CCl_4 in the presence of $TlCl_3 \cdot 4H_2O$ (3 mmol) and TlCl (4 mmol).

14) K. Mislow and H. M. Hellman, *J. Amer. Chem. Soc.*, **73**, 244 (1951); H. M. Hellman, J. W. Hellman, and K. Mislow, *ibid.*, **76**, 1075 (1954).

15) S. Uemura, O. Sasaki, and M. Okano, to be submitted.

16) F. M. McClenahan, *Amer. J. Sci.* (4), **18**, 104 (1904); J. W. Mellor, "A Comprehensive Treatise on Inorganic and Theoretical Chemistry," Vol. 5, Longmans, Green and Co., London (1924), p. 443.

reaction proceeds through addition of free chlorine evolved from $TlCl_3 \cdot 4H_2O$. The configurational analyses of I from cyclohexene and *cis*-2-octene (see Table 1) showed that this chlorination proceeds mainly in *trans* fashion as in the case of $CuCl_2$ chlorination in acetic acid or acetonitrile solvent.[5] Although a detailed mechanistic study was not carried out, a route involving the initial attack of a polarized $TlCl_3$ (probably in its dimeric form) on olefin would be reasonable.[17]

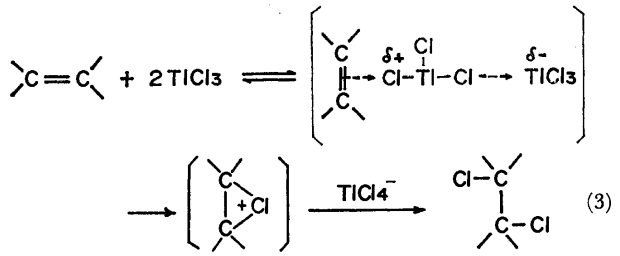

(3)

As thallium(III) chloride is reduced to thallium(I) chloride in this reaction, it is expected that the yield of I would increase if Tl^{1+} can be oxidized to Tl^{3+} by other metal salts. Thus, in the chlorination of cyclohexene with $TlCl_3 \cdot 4H_2O$, the addition of $CuCl_2 \cdot 2H_2O$ or $FeCl_3$ and the introduction of oxygen into the reaction system resulted in a significant increase in yields of I. Separate experiments showed that $CuCl_2 \cdot 2H_2O$ or $FeCl_3$ alone gave none of I in CCl_4 solvent, and it can safely be said that these chlorides oxidized Tl^{+1} to Tl^{+3} state as shown in Eq. 4. Since Cu^{1+} or Fe^{2+} salt formed here was readily oxidized to Cu^{2+} or Fe^{3+} state by oxygen respectively, probably under the coexistence of hydrochloric acid (see Eq. 2), the addition of an equivalent amount of these chlorides would not be required. As shown in Table 1, $CuCl_2 \cdot 2H_2O$ is more effective oxidant than $FeCl_3$ to TlCl.

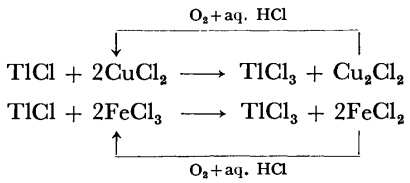

(4)

Although chlorination with $CuCl_2$ proceeded smoothly in acetic acid containing sodium acetate, alcohol or acetonitrile,[5] the reaction using $TlCl_3 \cdot 4H_2O$ in such solvents did not give any chlorinated product. In acetic acid containing sodium acetate (20 mmol) and $TlCl_3 \cdot 4H_2O$ (25 mmol), cyclohexene gave only a mixture of *cis*- and *trans*-1,2-diacetoxycyclohexane (8.75 mmol) for 2 hrs' reaction at 117°C. Similarly, styrene gave 1,2-diacetoxy-1-phenylethane (1.35 mmol), 1,3-diphenyl-1-butene (1.0 mmol) and a large amount of resinous residue. The formation of these products can be explained by the oxidation of olefins with thallium(III) acetate which might be formed in this reaction system. In acetonitrile, the formation of a complex $[TlCl_2(CH_3CN)_4TlCl_4]$[18] from $TlCl_3 \cdot 4H_2O$ and the solvent stopped the reaction.

Experimental

Materials. The organic materials were commercial products of the purest grade and were distilled and checked by gas chromatography. The inorganic metal chlorides were also commercial materials of an analytical grade and were used without purification.

Experimental Procedure. Olefinic substrates were added to mixtures of carbon tetrachloride and thallium(III) chloride tetrahydrate at refluxing temperature (77°C). After removing the evolved hydrogen chloride and phosgene by the stream of nitrogen into an ethereal solution of aniline, the reaction mixture were filtered from the resulting inorganic materials, and the filtrate was washed with water, dried over Na_2SO_4 and concentrated to *ca.* 10 m*l* by distillation of the solvent. The yields of the chlorinated products were calculated on the basis of the glc analysis of this residue using cyclohexanone or tetrachloroethylene as an internal standard. The amount of remaining Tl^{3+} salt was determined by iodometry.

Authentic Samples for Glc Analysis. Chlorocyclohexane, 3,4-dichloro-1-butene and 1,4-dichloro-2-butene were commercial products. 1,2-Dichlorooctane, 2,3-dichlorooctane (*erythro-threo* mixture), *trans*-1,2-dichlorocyclohexane, α,β-dichloroethylbenzene,[5] 1,2-dichlorocyclooctane, 5,6-dichlorocyclooctane (*trans-cis* mixture),[19] and α,β-diacetoxyethylbenzene[20] were prepared by the reported methods. 2-Chlorooctane was prepared from 2-octanol and thionyl chloride in pyridine;[21] bp 67—67.5°C/22 mmHg. *Threo*-2,3-dichlorooctane was prepared from the reaction of *cis*-2-octene with chlorine in chloroform; bp 104°C/25 mmHg, NMR τ 5.6—6.2 (m, 11H), 9.1 (t, 3H). *cis*-1,2-Dichlorocyclohexane was prepared from the reaction of *trans*-2-chlorocyclohexanol (bp 102—103°C/47 mmHg, prepared from cyclohexene[22]) and thionyl chloride in pyridine;[23] bp 68°C/6 mmHg, NMR: τ 5.5—5.8 (m, 2H), 7.5—8.8 (m, 8H). Chlorocyclooctane was isolated from the distillate (bp 82—90°C/21 mmHg) by preparative glc [PEG 6000 (25%)-Chromosorb-W 1.5 m column; carrier gas, He 120 m*l*/min at 150°C]; NMR: τ 5.6—6.0 (m, 1H), 7.75—8.2 (m, 4H), 8.2—8.65 (m, 10H). *cis*-1,4-Dichloro-2-butene was prepared as a mixture with *trans*-isomer (*trans*/*cis*=*ca.* 2) by the reaction of buta-1,3-diene with $SbCl_5$ in CCl_4;[8] bp 51—53°C/22 mmHg (Found: C, 37.64; H, 4.72%. Calcd for $C_4H_6Cl_2$: C, 38.44; H, 4.84%). NMR of *cis-trans* mixture: τ 3.95—4.3 (m, 2H), 5.8—6.0 (m, 4H). 1,2-Diacetoxycyclohexane (*trans-cis* mixture) was prepared as a mixture with cyclopentyl diacetoxymethane by heating cyclohexene and thallium(III) acetate in acetic acid at 70°C for 2 hr; bp 101—105°C/7 mmHg (reported[24] bp 112—120°C/12 mmHg).

Analytical Instruments. The IR and NMR spectra were measured with a Hitachi EPI-S2 apparatus and a Varian A-60 apparatus respectively. Gas chromatographies were carried out by Shimadzu 5APTF and 4APT [PEG 6000 (25%)-Chromosorb-W 3 m and Apiezon-L (30%) 1 m columns] apparatus.

17) See Ref. 2, p. 113. In the aromatic chlorination with this salt under similar conditions, we have recently obtained some results suggesting that an ionized form, $TlCl_2^+$, is preferable to the unionized one as actual attacking species.

18) B.F.G. Johnson and R.A. Walton, *Inorg. Chem.*, **5**, 49 (1966).

19) S. Uemura, A. Tabata, Y. Kimura, and K. Ichikawa, This Bulletin, **44**, 1973 (1971).

20) S. Uemura and K. Ichikawa, *Nippon Kagaku Zasshi*, **88**, 893 (1967).

21) F. C. Whitmor and F. A. Karnatz, *J. Amer. Chem. Soc.*, **60**, 2533 (1938).

22) M. S. Newmann, *ibid.*, **67**, 233 (1945).

23) B. Carrol, D. G. Kubler, H. W. Davis, and A. M. Whaley, *ibid.*, **73**, 5382 (1951).

24) H. J. Kabbe, *Ann. Chem.*, **656**, 204 (1962).

The Base-catalyzed Condensation of *o*-Nitropropiophenone*

Takeo SAKAN, Shoji HAYASHI, and Toshio MIWA
Faculty of Science, Osaka City University, Sumiyoshiku, Osaka
(Received September 22, 1971)

Treatment of *o*-nitropropiophenone with sodium acetylide in liquid ammonia at −70°C gave a yellow phenol, $C_{18}H_{18}O_3N_2$, as a major product. The permanganate oxidation of the phenol gave 2-(1-carbamoylethyl)-2-methyl-3-indolinone, which was synthesized independently. From this result and the spectral data, the structure of the phenol was postulated to be 1-(*o*-hydroxyphenyl) derivative of the above indolinone. The neutral fraction of the reaction mixture gave three new compounds: 3-(*o*-Nitrophenyl)-1-pentyn-3-ol, 2-methyl-2-(2-methyl-3-indolinon-2-yl)-3(2*H*)-benzofuranone, and 3,3a-dihydro-2-hydroxy-3,3a-dimethyl-2-(*o*-nitrophenyl)-4(2*H*)-isoxazolo[2,3-*a*]indolone. Their structures were assigned from their spectral data. A mechanism for the formation of these products as well as for the base-catalyzed condensation of *o*-nitroacetophenone is discussed.

A previous paper[1] from this laboratory reported that *o*-nitroacetophenone underwent a peculiar *o*-substituent interaction to form an orange-red product, compound A, along with *o*-nitrobenzoic acid when the ketone was treated with sodium acetylide in liquid ammonia at a temperature of −70°C. Compound A was proved to be 1,3-dihydroxy-3-methyl-2-(*o*-nitrophenacylidene)-indoline.[2] The base-catalyzed condensation of *o*-nitropropiophenone was studied in order to inquire into the mechanism of the formation of compound A. This paper deals with the elucidation of the structure of the condensation products of *o*-nitropropiophenone.

o-Nitropropiophenone was previously prepared either by the nitration of propiophenone[3] or by the reaction of *o*-nitrobenzaldehyde with diazoethane.[4] We prepared the ketone by the acylation of di-*t*-butyl methylmalonate with *o*-nitrobenzoyl chloride followed by decarboxylative hydrolysis in 57% overall yield based on *o*-nitrobenzoic acid. The purity of the ketone was confirmed both by gas-chromatography and by NMR spectroscopy.

Treatment of *o*-nitropropiophenone with sodium acetylide under the same condition as that in the condensation of *o*-nitroacetophenone[1] gave yellow crystals, $C_{18}H_{18}O_3N_2$, melting at 214°C, in a yield of 54—56%. The formation of the compound by the use of sodium amide instead of sodium acetylide indicated that the acetylide did not participate in the reaction. The yellow product will be referred to as compound C in this paper.

Compound C is a weakly acidic compound (pK_a 9.5) soluble in 2N sodium hydroxide solution; it is also soluble in concentrated hydrochloric acid. The weak acidity of compound C may be attributed to a phenolic hydroxyl. The presence of the function was not detected by the ferric chloride test, but inferred from a positive ferricyanide test[5] and from the coupling reaction with *p*-nitrobenzenediazonium salt.[6] The methylation of compound C with diazomethane gave a monomethyl ether, $C_{19}H_{20}O_3N_2$; the acetylation with acetic anhydride and pyridine at a room temperature led to a monoacetyl derivative, $C_{20}H_{20}O_4N_2$, whereas heating with acetic anhydride in the presence of sodium acetate gave a diacetyl derivative, $C_{22}H_{22}O_5N_2$.[7]

The IR spectrum of compound C shows the presence of the carbonyl group and the absence of the nitro group in the molecule. Its 3000-cm^{-1} region contains a broad band of a bonded hydroxyl group besides two sharp peaks at 3520 and 3405 cm^{-1}. The disappearance of the broad band by methylation or acetylation as well as the appearance of a new band at *ca.* 1760 cm^{-1} by acetylation allowed to assign the phenolic hydroxyl to the broad band.

The ultraviolet spectra of compound C and its derivatives reveal an absorption band at 400 nm characteristic of the pseudoindoxyl.[8] A bathochromic shift by 25 nm of the maximum of compound C by the addition of alkali suggests that the phenolic function may be associated with the pseudoindoxyl system. The carbonyl bands in the infrared spectra of these compounds are also compatible with those of pseudoindoxyls.[8a] The fact that the characteristic absorption band at 400 nm remained unchanged on diacetylation requires that the indoxyl ring be substituted at the nitrogen atom.[9]

The NMR spectrum[10] of compound C shows the presence of a tertiary methyl (singlet at 1.38 ppm), a secondary methyl (doublet at 1.42 ppm), and a methine

* Dedicated to Professor Munio Kotake on the celebration of the seventy-seventh anniversary of his birthday (Kiju).

1) T. Sakan, K. Kusuda, and T. Miwa, This Bulletin, **37**, 1678 (1964).
2) T. Sakan, K. Kusuda, and T. Miwa, *ibid.*, **38**, 18 (1965).
3) L. A. Elson, C. S. Gibson, and J. D. A. Johnson, *J. Chem. Soc.*, **1930**, 1128; B. L. Zenitz and W. H. Hartung, *J. Org. Chem.*, **11**, 444 (1964); J. R. Keneford and J. C. E. Simpson, *J. Chem. Soc.*, **1948**, 354.
4) C. W. Warner, E. J. Walsh, and R. F. Smith, *ibid.*, **1962**, 1232.
5) N. D. Cheronis and J. B. Entrikin, "Semimicro Qualitative Organic Analysis," Interscience Publishers, New York (1957), p. 230.
6) F. Wild, "Estimation of Organic Compounds," Cambridge University Press, New York (1953), p. 96.
7) This compound is apparently an *N*-acetyl amide; the C=O absorptions at 1734 and 1696 cm^{-1} correspond to this grouping. The values, 1743—1747 and 1690—1698 cm^{-1}, are given in the literature: T. Uno and K. Machida, This Bulletin, **35**, 1226 (1962).
8) a) B. Witkop, *J. Amer. Chem. Soc.*, **72**, 614 (1950); B. Witkop and A. Ek, *ibid.*, **73**, 5664 (1951). b) J. Kerble, H. Schmid, P. Waser and P. Karrer, *Helv. Chim. Acta*, **36**, 102 (1953).
9) *N*-Acetylation of a pseudoindoxyl causes a hypsochromic shift to 340 nm[8a])
10) The NMR spectrum of this compound was measured on a Varian model A-60 instrument at the Shionogi Research Laboratory. We are indebted to Doctor Ken'ichi Takeda, the Director of the Laboratory.

(quartet at 2.88 ppm) group. The complicated bands between 6.3 and 7.7 ppm correspond to eight aromatic protons. The phenolic proton appears at 10.9 ppm, the location of a rather low-magnetic field being due to a hydrogen bonding.[11] A broad band near 6 ppm (2 protons) suggests the presence of a primary amide group, to which two sharp peaks in the 3000-cm^{-1} region of the infrared spectrum (see above) may be attributed.

The presence of the amide group was confirmed by the acid hydrolysis of compound C followed by the identification of ammonium ion by paper chromatography.[12] On the other hand, no evolution of carbon dioxide in the hydrolysis indicated that the carbamoyl group was not attached to the α-carbon atom of the indoxyl nucleus directly. Any definite organic compounds were not characterized from the hydrolysis product.

The hydrogenation of compound C either over Raney nickel under high pressure or in the presence of platinum oxide under atmospheric pressure gave a tetrahydro-compound. Tetrahydro-compound C is a phenol (pK_a 9.0), giving a positive reaction with *p*-nitrobenzenediazonium salt. This compound gave a monomethyl ether on methylation with diazomethane. The ultraviolet absorption spectra of tetrahydro-compound C and its methyl ether show no absorption band of the pseudoindoxyl system at 400 nm, but possess a new maximum at 330 nm. The spectral data of these compounds correspond to those of *N*-aryl-β-acylvinylamines (λ_{max} near 340 nm).[13] The survival of the phenolic function during the hydrogenation of the pseudoindoxyl system[8a] allowed to locate the hydroxyl group on the *N*-phenyl nucleus. From these observations structure I was postulated for compound C.

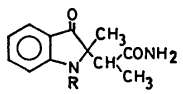

I: R=*x*-Hydroxyphenyl II: R=H

The carbon skeleton of the indoxyl nucleus was verified by the oxidative degradation of compound C. The permangenate oxidation of compound C gave a neutral compound, $C_{12}H_{14}O_2N_2$, mp 228°C. This was identified with 2-(1-carbamoylethyl)-2-methyl-3-indolinone (II), which was synthesized as follows.

Giovannini *et al.*[14] reported that the Dieckmann condensation of *N*-(*o*-ethoxycarbonylphenyl)alanine ethyl ester under atmospheric oxygen yielded 2,2'-dimethyl-[2,2'-bisindoline]-3,3'-dione (VI) instead of the expected 2-methyl-3-indolinone. In the absence of oxygen, this reaction should give the enolate anion (IV) of 2-methyl-3-indolinone, which would be alkylated with α-bromopropionate to give the ester V corresponding to the amide II. Actually, the alkylation of the Dieckmann condensation product of the dimethyl ester III[15] under the atmosphere of nitrogen occurred expectedly to give the ester V along with the *o*-alkylation product VII, the latter being not isolated but detected by the NMR spectrum of the crude product. Chromatography of the crude product gave the ester V as a crystalline state. The ester V was heated with ammonia in a sealed tube at 100°C for 8 hr to give the amide II.

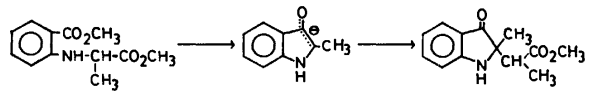

III IV V

VI VII

Although no direct proof was obtained about the position of the hydroxyl group on the *N*-phenyl nucleus, the existence of an intramolecular hydrogen bonding of the phenolic hydroxyl group inferred from the IR and NMR spectra may sufficiently allow to locate the group at the *ortho* position to the nitrogen. Hence, the structure of compound C was postulated to be 2-(1-carbamoylethyl)-1-(*o*-hydroxyphenyl)-2-methyl-3-indolinone (I, *x*=*o*).[16]

Chromatography on silicic acid of the neutral fraction of several runs of the condensation gave an oil, $C_{11}H_{11}O_3N$, and two crystalline products, $C_{18}H_{16}O_5N_2$ and $C_{18}H_{15}O_3N$, along with the unchanged ketone.

The IR spectrum of the oil revealed the presence of the hydroxyl, terminal alkyne, and nitro functions, but no carbonyl groups in it. Therefore, the oil was assumed to be 3-(*o*-nitrophenyl)-1-pentyn-3-ol (VIII), the expected product of the condensation of *o*-nitropropiophenone with sodium acetylide. The NMR spectrum of this compound is compatible with this structure. The permanganate oxidation of this compound gave a crystalline acid, $C_{10}H_{11}O_5N$, mp 154—156°C, which was assumed to be 2-hydroxy-2-(*o*-nitrophenyl)propionic acid (IX).

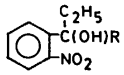

VIII: R=C≡CH IX: R=CO_2H

One of the crystalline products, $C_{18}H_{15}O_3N$, melting at 206—207°C, was assigned the structure of 2-methyl-2-(2-methyl-3-indolinon-2-yl)-3(2*H*)-benzofuranone (X) from its spectral data. The ultraviolet absorption spectrum of this compound showed maxima at 229, 335, and 390 nm and a shoulder at 255 nm. The absorption band at 390 nm is that characteristic of the psuedoindoxyl system and the band at 335 nm may be attri-

11) A. L. Porte, H. S. Gutowsky and I. M. Hunsberger, *J. Amer. Chem. Soc.*, **82**, 5057 (1960).

12) A. E. Steel, *Nature*, **173**, 315 (1954).

13) K. Bowden, E. A. Braude, E. R. Jones, and B. C. L. Weedon, *J. Chem. Soc.*, **1946**, 45.

14) E. Giovannini, F. Farkas, and J. Rosales, *Helv. Chim. Acta*, **46**, 1326 (1963).

15) O. Neuenhöffer and G. Lehmann, *Chem. Ber.*, **94**, 2960 (1961).

16) Attempt was made to determine the location of the hydroxyl group by the analysis of the aromatic region of the 100-MHz NMR spectrum of tetrahydro-compound C in DMSO-d_6; however, the pattern was too complicated to assign *o*-substituted benzene. The authors thank the Japan Electron Optics Laboratories for the measurement.

buted to the coumaranone system.[17] The infrared spectrum revealed the absorptions corresponding to the N–H (3400 cm^{-1}) and carbonyl (1700 cm^{-1}) groups. The existence of the two methyl groups was confirmed by two singlets (1.65 and 1.75 ppm) in the NMR spectrum.

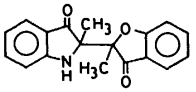

X

2,2-Dimethyl-3-indolinone shows its methyl signal at 1.32 ppm.[18] The methyl signal of the biindoxyl VI appears at 1.17 ppm, indicating a shielding effect by the keto group on the other nucleus. On the other hand, the methyl signals of the compound X is shifted extensively downfield, suggesting that the methyl groups are deshielded by the keto group on the other nucleus. These observations may be explained by postulating that the biindoxyl is a *meso* compound and the compound X is a racemoid, assuming conformations as shown in XI and XII, respectively. The conformation XII is apparently due to the compensation of the steric hindrance of two ethyl groups and of the dipole-dipole interaction between two keto groups.

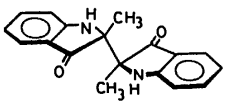

XI

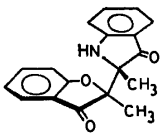

XII

Another crystalline product, $C_{18}H_{16}O_5N_2$, decomposing at 150°C, was tentatively postulated to be 3,3a-dihydro-2-hydroxy-3,3a-dimethyl-2-(*o*-nitrophenyl)-4-(2*H*)-isoxazolo[2,3-*a*]indolone (XIII) from the spectral data. Its infrared spectrum suggested the presence of the hydroxyl, carbonyl, and nitro groups. The NMR spectrum showed the existence of a tertiary methyl (1.58 ppm, singlet) and a secondary methyl (1.24 ppm, doublet) in accordance with the structure. The ultraviolet spectrum with maxima at 240, 310, and 360 nm needs some comments. 1-Hydroxy-2,2-dimethyl-3-indolinone has an absorption band at 381 nm;[19] the hypsochromic shift compared with that of 2,2-dimethyl-3-indolinone (391 nm[18]) may be due to the electrostatic attraction for the lone electron pair on the nitrogen atom exerted by the electro-negative oxygen. The *cis*-fusion of the isoxazolidine ring in the compound XIII would force the nitrogen atom to assume an sp^3-like configuration unfavorable for the unshared electron pair to conjugate with the carbonyl group, causing hence a hypsochromic shift of the absorption characteristic of the pseudoindoxyl system. This assumption is supported by the fact that the isoxazoloindolone XIV possesses an absorption band at 313 nm corresponding to the band at 310 nm of compound XIII and shows no absorption maximum over 350 nm.[20]

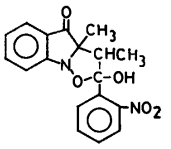

XIII

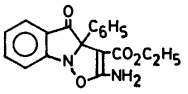

XIV

Treatment of the compound XIII with sodium amide in liquid ammonia yielded the compound X as a major product.

This observation and the fact that every crystalline product in this condensation was obtained as a single isomer, as inferred from the results of NMR spectroscopy, require the mechanism for the reaction to involve stereochemical consideration.

It has been pointed out[21] that the base-catalyzed condensation of *o*-nitrobenzoyl derivatives undergo cyclization to isatogens. In our case, 2-methylisatogen XVI is to be formed in the first step. Such isatogens are susceptible to nucleophilic addition at the carbon-nitrogen double bond.[22] The attack of another molecule of the enolate anion XV will produce either of the diastereoisomeric anions XVII. The attacking enolate anion should have the conformation as shown in XX because of the steric repulsion between the methyl and phenyl groups, on the one hand, and of the dipole-dipole repulsion between the carbonyl and nitro groups, on the other. The addition through the transition

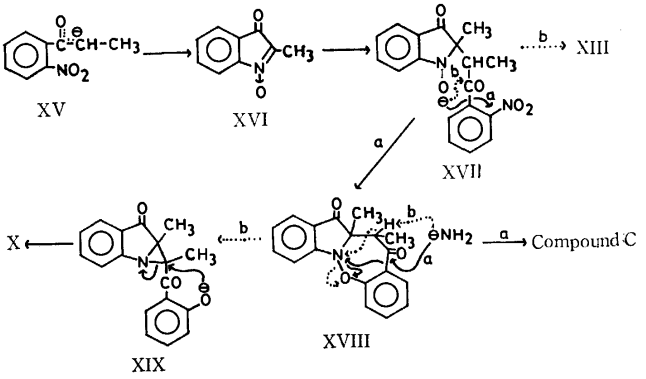

XV XVI XVII XIX XVIII

state XXI will be followed by the replacement of the nitro group by the *N*-oxide anion to form a seven-membered ring intermediate XVIII with two methyl groups in *trans*-relationship. On the other hand, the addition through the transition state XXII will cause the attack of the *N*-oxide anion on the carbonyl group rather than on the nitro group to give the compound XIII with two methyl groups in *cis* configuration.

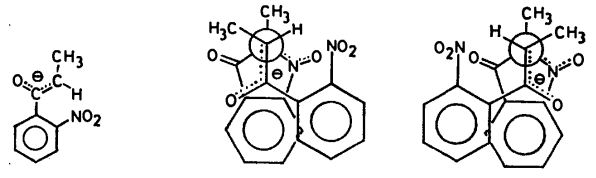

XX XXI XXII

17) P. McClockey, *J. Chem. Soc.*, **1958**, 4732.
18) R. T. Sundberg and T. Yamazaki, *J. Org. Chem.*, **32**, 290 (1967).
19) K. Nishimura and T. Miwa, unpublished work.
20) J. E. Bunney and M. Hooper. *Tetrahedron Lett.*, **1966**, 3857.
21) J. D. Loudon and G. Tennant, *Quart. Rev.*, **18**, 389 (1964).
22) D. A. Patterson and D. G. Wibberley, *J. Chem. Soc.*, **1965**, 1706.

Inspection of the framework molecular models of the intermediate XVIII proposes the conformation XXIII as the most favorite one.[23] Although the compound XIII was isolated as a by-product, the compound also may be transformed into the intermediate XVIII on prolonged exposure to sodium amide. In this case, the intermediate XVIII should have two methyl groups in *cis* relationship as shown in XXIV. The abstraction of the equatorial α-proton of the carbonyl group in XXIII will be more difficult than that of the axial α-proton in XXIV because of the stereoelectronic effect. In the former case, the attack of the amide anion to the carbonyl becomes prevailing and the reaction will proceed through the course a in XVIII to give compound C.[24] On the basis of these assumptions, compound C is expected to have two methyl groups in such a relative configuration as shown in XXV.

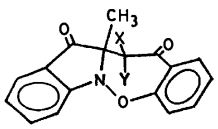

XXIII: X=H, Y=CH_3
XXIV: X=CH_3, Y=H

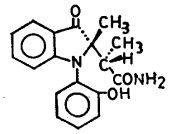

XXV

When the abstraction of the α-proton of the carbonyl group is assisted by the stereoelectronic effect, the resulting carbanion will attack on the nitrogen atom to form an aziridine intermediate XIX with liberation of a phenoxide anion,[25] which will cleave the aziridine ring to give the compound X. Since the stereochemistry of the compound X was proposed to be XII, these transformation would take a stereochemical course as shown in formulas XXVI to XXVII.

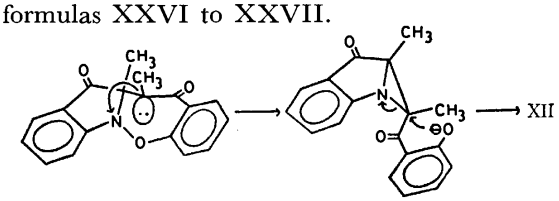

XXVI XXVII

Now, the attention is turned to the mechanism for the formation of compound A (see above). In this case, the first step of the reaction is assumed to be the aldol condensation of *o*-nitroacetophenone.[26] The product XXVIII will undergo a cyclization similar to that of *o*-nitropropiophenone to give a nitrone XXIX,[27] which will be transformed into an *N*-hydroxyindoline XXX by the addition of another mole of the enolate anion of *o*-nitroacetophenone. The oxidative deacylation of the indoline will give compound A.

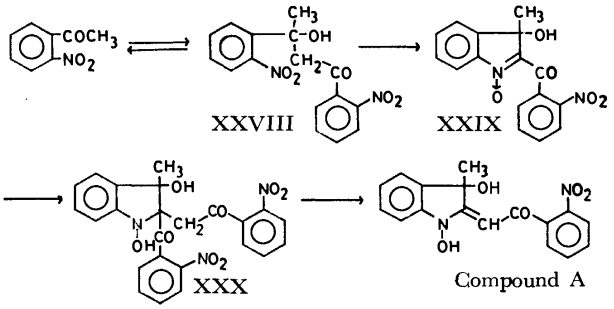

XXVIII XXIX XXX Compound A

The final step needs further comment. The simple Haller-Bauer reaction[28] of XXX with base should give aliphatic carboxylic acid derivatives as observed in the case of compound C. The formation of *o*-nitrobenzoic acid in this reaction requires another type of cleavage with simultaneous oxidation. This cleavage is well interpreted by the partial structures shown in Chart 1. The participation of *o*-nitroacetophenone in this oxidation was verified by the isolation of *o,o'*-azoxyacetophenone from the neutral fraction of the reaction. This compound was identified with an authentic sample synthesized according to a procedure for the preparation of *p,p'*-azoxyacetophenone.[29]

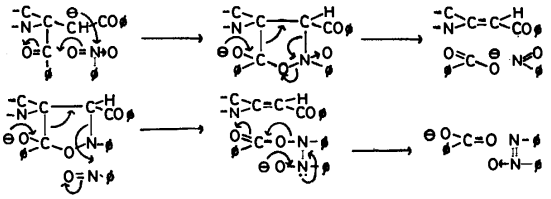

φ=*o*-Acetyl- or *o*-nitrophenyl
Chart 1

In conclusion, it is noteworthy that no alkynol was obtained from the neutral fraction of the condensation of *o*-nitroacetophenone in contrast with the formation of the alkynol VIII in the case of *o*-nitropropiophenone.

Experimental[30]

o-Nitropropiophenone. A mixture of 66.6 g (0.289 mol) of di-*t*-butyl methylmalonate[31] and 19.0 g (0.433 mol) of

23) The possibility for the nitrogen atom to assume an sp^3-like configuration cannot be precluded; however, in this case also, the environment around the carbonyl group in the seven-membered ring is not changed so much.

24) Methoxyamine reacts with Grignard compounds to give corresponding amines. R. Brown and W. E. Jones, *J. Chem. Soc.*, **1946**, 781.

25) O. C. Dermer and G. E. Ham, "Ethyleneimine and Other Aziridines," Academic Press, New York (1969), p. 59.

26) With *o*-nitropropiophenone also, the aldol condenstion may be possible; however, the condensate corresponding to XXVIII cannot be cyclized to an isatogen and will be reversed to the original ketone in this case.

27) Both of the nitro groups have the opportunity to react with the methylene group. The triagonal carbon of the keto group might prevent the formation of a five-membered ring. Actually, 1,3-bis(*o*-nitrophenyl)-1-propanone gave 1-hydroxy-2-(*o*-nitrobenzoyl)indole rather than 2-benzylisatogen (N. Nakatsuka and T. Miwa, unpublished work).

28) K. E. Hamlin and A. W. Weston, "Organic Reactions," Vol. IX, John Wiley, New York (1957), p. 1.

29) V. M. Clark, J. B. Hobbs, and D. W. Hutchinson, *Tetrahedron*, **25**, 4241 (1949).

30) All melting points are not corrected. Unless otherwise noted, UV, IR, and NMR spectra were measured in solution in 95% ethanol, chloroform, and deuteriochloroform, and presented in λ_{max} nm (log ε), ν_{max} cm^{-1}, and δ ppm, respectively. The instruments used for the measurements are a Hitachi model EPS-2 recording spectrophotometer, a Hitachi model EPI-2 infrared spectrophotometer, and a JEOLCO model C-60 spectrometer. The authors are much indebted to Mr. Jun'ichi Goda for the elemental analyses.

31) Pure material of this ester (bp 94—95°C/7 mmHg) was prepared from the corresponding acid (mp 134—136°C) and isobutylene in *ca.* 60% yield according to a general method for the *t*-butyl ester [R. E. Strube, "Organic Syntheses," Vol. 37, p. 34 (1957)].

54.4% sodium hydride dispersed in mineral oil (washed several times with benzene) in 1500 m*l* of dry benzene was heated under reflux with stirring for 2 hr. To the mixture was added a solution of *o*-nitrobenzoyl chloride, prepared from 48.3 g (0.289 mol) of *o*-nitrobenzoic acid and 57.9 g (0.289 mol) of phosphorus pentachloride, in 60 m*l* of dry benzene at room temperature over a period of 1 hr. The mixture was refluxed for 2 hr and then left to stand overnight. The excess of sodium hydride was decomposed by the addition of *p*-toluenesulfonic acid monohydrate. The salts were removed by filtration and the solvent was distilled off completely. The residue was heated under reflux with 75 m*l* of acetic acid, 9 m*l* of concentrated sulfuric acid and 50 m*l* of water for 5 hr. After cooling, the reaction mixture was made alkaline with 20% aqueous sodium hydroxide and extracted with ether. After drying and evaporation of the solvent, the residue was distilled under reduced pressure to give 29.7 g (57.3%) of *o*-nitropropiophenone boiling at 144—145°C/8 mmHg. Gas chromatography of this sample on silicone grease showed a single peak. UV: 259 (3.70). IR: 1704 (C=O); 1531, 1348, 855 (NO_2). NMR (CCl_4): 1.17^t (3H), 2.75^q (2H), $7.35—8.25^m$ (4H). (Found: C, 59.68; H, 5.28; N, 7.37%).

The Condensation of o-*Nitropropiophenone by Sodium Acetylide.* A mixture of 0.77 g (0.033 mol) of sodium and 150 m*l* of liquid ammonia was saturated with acetylene. The mixture was cooled to −70°C and a solution of 9 g (0.05 mol) of *o*-nitropropiophenone in 15 m*l* of dry ether was added in one portion. A violent reaction took place and the temperature of the mixture reached −50°C. After stirring at −70°C for 1 hr, 1.5 g (0.028 mol) of ammonium chloride was added and the liquid ammonia evaporated while about 150 m*l* of ether was added. The resulting yellow crystals were filtered and washed with water. Recrystallization of the crystals from ethanol gave 2.2 g of compound C, melting at 213—214°C. The filtrate was washed successively with 5% aqueous sodium hydrogen carbonate, 2N hydrochloric acid and 2N aqueous sodium hydroxide. The neutral fraction was processed as described below. The washing with 2N aqueous sodium hydroxide was acidified with sulfuric acid and extracted with ether. The ethereal extract was dried and evaporated to give 2.1 g of compound C, melting at 206—209°C. Total yield was 55.6%. Several recrystallization from ethanol gave a pure sample melting at 214°C. UV: 232 (4.54), 260^{sh} (4.07), 281^{sh} (3.90), 400 (3.69). UV (0.5N NaOH–EtOH): 237 (4.51), 300 (3.93), 425 (3.53). IR: 3520, 3405 (NH); 3300—2800 (OH); 1687 (C=O). NMR: 1.38^s (3H), 1.42^d (3H), 2.88^q (1H), $5.57—6.13^b$ (2H), $6.38—7.64^m$ (8H), 10.90^s (1H).

Found: C, 69.93; H, 5.97; N, 9.05%; C-Methyl group[32] 0.65; mol wt (Rast), 279. Calcd for $C_{18}H_{18}O_3N_2$: C, 69.66; H, 5.85; N, 9.03%; mol wt, 310.

The above-mentioned neutral fraction from several runs were combined and treated with benzene. After removal of insoluble material by filtration, the solvent was distilled off under reduced pressure. The residue (*ca.* 30 g) was chromatographed on 200 g of silicic acid (Mallincrodt, 100 mesh AR) and eluted with methylene chloride-benzene (2.5: 1, v/v). Fractions 1 to 5 were collected in each 200 m*l*. Fraction 2 gave pure *o*-nitropropiophenone. Fraction 6 to 13 were collected in each 300 m*l*. Fraction 6 gave the alkynol VIII. High-vacuum distillation of this fraction gave a yellow oil, bp 90°C (bath temperature)/10^{-3} mmHg. IR (neat)[33]: 3580 (OH); 3310 (≡CH); 2340 (C≡C); 1540, 1360, 860 (NO_2). NMR: 1.04^t (3H), 2.12^q (2H), 2.50^s (1H), 7.05^b (1H), $7.2—7.8^m$ (4H).

Found: C, 64.27; H, 5.51; N, 6.69%. Calcd for $C_{11}H_{11}O_3N$: C, 64.38; H, 5.40; N, 6.83%.

Fraction 8 gave yellow crystals, which, after recrystallization from ethanol, melted to a red liquid at 206—207°C. UV: 229 (4.44), 251^{sh} (4.16), 335 (3.62), 390 (3.51). IR:[33] 3400 (NH); 1700 (C=O). NMR: 1.65^s (3H), 1.75^s (3H), 4.50^s (1H), $6.5—7.8^m$ (8H).

Found: C, 73.54; H, 5.21; N, 4.80%. Calcd for $C_{18}H_{15}O_3N$: C, 73.70; H, 5.15; N, 4.78%.

Fraction 13 gave faintly colored crystals, which, after two recrystallizations from benzene-hexane, decomposed at 150°C. UV: 236 (4.40), 310 (3.32), 360 (3.23). IR:[33] *ca.* 3500 (OH); 1710 (C=O); 1540, 1355, 860 (NO_2). NMR: 1.24^d (3H), 1.58^s (3H), 3.12^q (1H), 3.37^s (1H), $7.0—7.7^m$ (8H).

Found: C, 63.65; H, 4.90; N, 8.10%. Calcd for $C_{18}H_{16}O_5N_2$: C, 63.52; H, 4.74; N, 8.23%.

The condensation using sodium amide instead of the acetylide under the same condition gave 46.4% yield of compound C.

Methylation of Compound C. Into a solution of 1.0 g (3.2 mmol) of compound C in a mixture of each 100 m*l* of ether and methanol was added ethereal solution of diazomethane prepared from 10 g of *N*-nitrosomethylurea. After being left to stand overnight, the mixture was treated with acetic acid to decompose excess of diazomethane and the solvent evaporated under reduced pressure, giving 867 mg (87%) of pale yellow crystals, which, after recrystallization from aqueous methanol, melting at 224.5—225°C. UV: 230.5 (4.48), 281 (3.77), 393 (3.66). IR: 3510, 3402 (NH); 1684 (C=O).

Found: C, 70.42; H, 6.21; N, 8.57%. Calcd for $C_{19}H_{20}O_3N_2$: C, 70.35; H, 6.22; N, 8.64%.

Acetylation of Compound C. *a) With Acetic Anhydride and Sodium Acetate*: A mixture of 300 mg (0.97 mmol) of compound C, 9 m*l* of acetic anhydride and 90 mg of anhydrous sodium acetate was boiled under reflux for one hour. After decomposition of the excess anhydride with water, the separated crystals were filtered and dried, to give 244 mg (64%) of yellow needles, mp 195—197°C. Recrystallization from aqueous methanol gave pure sample, mp 196.5°C. UV: 231 (4.48), 386 (3.64). IR: 3380, 3245, 3200, 3140 (NH); 1758, 1734, 1696 (C=O).

Found: C, 67.03; H, 5.56; N, 7.25%. Calcd for $C_{22}H_{22}O_5N_2$: C, 66.99; H, 5.62; N, 7.10%.

b) With Acetic Anhydride and Pyridine: A solution of 75 mg (0.26 mmol) of compound C in 0.5 m*l* of pyridine was treated with 0.08 m*l* of acetic anhydride and left to stand at room temperature for 2 hr, during which almost colorless crystals separated out. After the addition of ether, the solvent was decanted; the crystals were washed with ether and recrystallized from aqueous ethanol, giving pure sample melting at 229—230°C. IR: 3550, 3410 (NH); 1765, 1690 (C=O).

Found: C, 68.06; H, 5.88; N, 7.90%. Calcd for $C_{20}H_{20}O_4N_2$: C, 68.17; H, 5.72; N, 7.95%.

Acid Hydrolysis of Compound C. A mixture of 300 mg (0.97 mmol) of compound C and 15 m*l* of 6N hydrochloric acid was refluxed under the atmosphere of nitrogen for one and a half hours. No carbon dioxide was evolved during the reaction. After filtration from a solid material which could not be led to any crystalline derivatives, the filtrate, after concentration, was chromatographed on "Toyo" No. 51 filter paper, using ethanol - concentrated hydrochloric acid - water (7: 1: 2 v/v) as solvent. Detection of spots was made accord-

32) E. J. Eisenbraun, S. M. McElvain, and B. F. Aycock, *J. Amer. Chem. Soc.*, **76**, 607 (1954).

33) IR spectra of these compounds are taken on a spectrophotometer Model IR-E of Japan Spectroscopic Co.

ing to Steel.[12] The R_f value was 0.36.

Hydrogenation of Compound C. *a) Under High Pressure*: A mixture of 200 mg of compound C, 2 m*l* of Raney nickel and 40 m*l* of ethanol was hydrogenated at a hydrogen pressure of 80 atm and 110°C for 2 hr. After filtration of the catalyst, the solvent was removed under reduced pressure to give crystals, which, after recrystallization from aqueous ethanol, melted at 243°C. UV: 285 (3.50), 330 (4.06). IR: 3500, 3395 (NH); 3300—2800 (OH); 1660 (C=O).

Found: C, 69.00; H, 7.18; N, 8.76%. Calcd for $C_{18}H_{22}O_3N_2$: C, 68.77; H, 7.05; N, 8.91%.

b) Under Atmospheric Pressure: A solution of 200 mg of compound C in 10 m*l* of glacial acetic acid was hydrogenated in the presence of 100 mg of platinum oxide until the solution had lost the yellow color. After filtration, the solvent was evaporated under reduced pressure. Trituration of the residue with aqueous alcohol caused crystallization. The crystals were identified with the above mentioned tetrahydro-compound C by IR spectroscopy.

Methylation of Tetrahydro-compound C. Methylation of the tetrahydro derivative with diazomethane under the same condition as that of compound C gave a methyl ether melting at 223—224°C. UV: 285 (3.31), 330 (4.04). IR: 3480, 3376 (NH); 1671 (C=O).

Found: C, 68.92; H, 7.51; N, 8.70%. Calcd for $C_{19}H_{24}O_3N_2$: C, 69.49; H, 7.37; N, 8.53%.

Permanganate Oxidation of Compound C. Into a stirred solution of 465 mg (1.5 mmol) of compound C in aqueous potassium hydroxide (1.0 g of potassium hydroxide in 200 m*l* of water) was added each 158 mg (1 mmol) of finely powdered potassium permanganate. On the addition of eighteen portions, the color of the permanganate remained for 2 hr. The color was discharged by the addition of 0.4 m*l* of 30% of hydrogen peroxide and manganese dioxide was filtered off. The filtrate was extracted several times with ether and the combined extracts were washed with 2N sodium hydroxide, dried and evaporated to give 32 mg of crystals, which, after recrystallization from ethanol, melted at 228°C. UV: 233 (4.40), 255^{sh} (3.80), 400 (3.60). IR: 3520, 3470, 3405, 3350 (NH); 1690^{sh}, 1676 (C=O).

Found: C, 66.12; H, 6.67; N, 12.18%.[34] Calcd for $C_{12}H_{14}O_2N_2$: C, 66.03; H, 6.47; N, 12.84%.

A little amount of this compound was heated with acetic anhydride under reflux for 4 hr. After removal of the solvent under reduced pressure, the residue showed UV maxima at 233 and 334 nm.

2-(1-Methoxycarbonylethyl)-2-methyl-3-indolinone. Into a suspension of 1.92 g (44 mmol) of 54.5% sodium hydride dispersed in mineral oil in 400 m*l* of benzene was added a solution of 9.5 g (40 mmol) of *N*-(*o*-methoxycarbonylphenyl)-alanine methyl ester[15] (bp 137—140°C/2 mmHg) in 10 m*l* of benzene under atmosphere of nitrogen. The mixture was refluxed for 6 hr, during which about 800 m*l* of hydrogen was evolved, and cooled with ice-water. Into the mixture was added 7.5 g (45 mmol) of methyl α-bromopropionate and the mixture was left to stand at room temperature for 21 hr and then refluxed for 7 hr. After addition of 0.5 m*l* of acetic acid, water and ether, the organic layer was separated, washed with 2N hydrochloric acid and 2N sodium hydroxide successively and dried over anhydrous sodium sulfate. The residue obtained by the evaporation of the solvent showed the presence of the desired ester V and the *O*-alkylated product VII[35] (*ca.* 10:8) as major products. The crude product dissolved in benzene was applied to a column of 160 g of active alumina (Wako) and eluted with 2 *l* of benzene.[36] After evaporation of the benzene, the residue (4.00 g) was chromatographed again on 100 g of alumina and eluted with benzene. The fractions were collected after a yellow band reached the bottom of the column. The first 100-m*l* fraction gave a yellow oil. Thereafter, thirteen 100-m*l* fractions gave yellow crystals, which, after recrystallization from hexane, gave 0.77 g of pure ester V, melting at 53—54°C. IR: 3460 (NH); 1722, 1693 (C=O). NMR: 0.93^d (3H), 1.30^s (3H), 2.95^q (1H), 3.72^s (3H), *ca.* 5^b (1H), 6.5—7.2^m (4H).

Found: C, 67.06; H, 6.75; N, 5.84%. Calcd for $C_{13}H_{15}O_3N$: C, 66.93; H, 6.48; N, 6.01%.

2-(1-Carbamoylethyl)-2-methyl-3-indolinone. A mixture of 0.21 g (0.9 mmol) of the above ester V and 2 m*l* of 28% aqueous ammonia was heated in a sealed tube in a boiling water bath for 10 hr. On cooling, crystals separated and they were washed with water and dried; mp 230°C (Found: C, 65.70; H, 6.35; N, 12.76%). IR spectrum was completely identical with that of the specimen obtained above by the permanganate oxidation of compound C.

Permanganate Oxidation of the Alkynol VIII. Into a solution of 1 g of the alkynol VIII contaminated by *o*-nitropropiophenone in acetone was added powdered potassium permanganate in small portions until the purple color remained. After 3 hrs' stirring at room temperature, the excess permanganate was decomposed with methanol and manganese dioxide was filtered off. The filtrate was evaporated under reduced pressure and the residue taken into ether and water. The separated aqueous solution was acidified with hydrochloric acid, extracted with ether. The evaporation of the ether solution, after drying, gave crystals, which, after recrystallization from hexane-ether, melted at 154—156°C.

Found: C, 53.36; H, 4.90; N, 6.15%. Calcd for $C_{10}H_{11}O_5N$: C, 53.33; H, 4.92; N, 6.22%.

The Reaction of Compound XI with Sodium Amide. Into a solution of sodium amide in liquid ammonia (prepared from 126 mg (5.5 mmol) of sodium and 20 m*l* of liquid ammonia) was added a solution of 213 mg (0.63 mmol) of compound XI in one portion at −70°C. The mixture was stirred for 30 min and 400 mg (7 mmol) of ammonium chloride was added. The liquid ammonia was evaporated while ether was added. Evaporation of the ether solution left 160 mg of a residue, which was chromatographed on 5 g of silicic acid and eluted with dichloromethane - benzene (2.5:1, v/v). Evaporation of the solvent gave 90 mg of crystals, which was identified with compound X by comparison of the infrared spectra.

o,o'-*Azoxyacetophenone.* *a) From the Reaction Mixture of o-Nitroacetophenone*: The neutral fraction of the reaction mixture of *o*-nitroacetophenone with sodium acetylide in liquid ammonia[1] was subjected to steam distillation. Essentially no distillate was obtained. The residue in the distillation flask was dissolved in ether, the solution washed with dilute sulfuric acid, and the solvent evaporated. The residue was

34) The poor result of this nitrogen analysis is apparently due to concomitant impurity; however, this substance is very difficult to purify, another sample, which was purified by repeated sublimations and recrystallizations, giving much worse results in the elemental analyses.

35) The following peaks in the NMR spectrum of the crude product are assigned to this compound: 1.58^d (3H), 2.26^s (1H), 3.69^s (3H), 4.71^q (1H), 8.6^{bs} (1H).

36) The *O*-alkylation product is slightly more polar on silicic acid than the desired ester. Prolonged contact with silicic acid seems to hydrolyze this by-product; no *O*-alkylation product was isolated after repeated chromatography on silicic acid.

distilled under a 7-mmHg pressure until the bath temperature reached 200°C to give *o*-nitroacetophenone as the distillate. The residue was dissolved in hot ethanol. After removal of a black resin which deposited immediately after cooling by decantation, the solution was treated with charcoal and left to stand overnight to separate brown crystals, which, after recrystallization from ethanol, melted at 117—119°C. IR (Nujol): 1688, 1676 (C=O); 1478 (azoxy).

Found: C, 68.24; H, 5.24; N, 9.90%. Calcd for $C_{16}H_{14}O_3N_2$: C, 68.07; H, 5.00; N, 9.92%.

b) Synthesis: This compound was prepared from *o*-nitroacetophenone following a procedure for the preparation of *p,p'*-azoxyacetophenone by Clark *et al.*[29] *o*-Nitroacetophenone ethylene ketal was obtained, after distillation (bp 98—100°C/0.05 mmHg) followed by trituration with methanol, in 65% yield, mp 67°C. IR: 1535, 1375, 860 (NO_2); 1040 (ketal). NMR (CCl_4): 1.76^s (3H), 3.4—4.1^m (A_2B_2, 4H), 7.2—7.7^m (4H). (Found: C, 57.23; H, 5.40; N, 6.49%. Calcd for $C_{10}H_{11}O_4N$: C, 57.41; H, 5.30; N, 6.70%). Refluxing the nitro ketal with alkaline zinc dust for 5 hr gave *o,o'*-azoxyacetophenone bis-ethylene ketal in 28% yield, mp 206°C. Prolonged refluxing did not improve the yield. IR: 1470 (azoxy); 1040 (ketal). (Found: C, 64.77; H, 6.07; N, 7.49%. Calcd for $C_{20}H_{22}O_5N_2$: C, 64.85; H, 5.99; N, 7.56%). The acid hydrolysis of the ketal gave *o,o'*-azoxyacetophenone in 64% yield, mp 116—118°C. The IR spectrum of this compound was completely identical with that of the specimen obtained in a).

BULLETIN OF THE CHEMICAL SOCIETY OF JAPAN, VOL. 45, 1491—1493(1972)

Hydrogen Transfer Polymerization of Malononitrile

Nariyoshi KAWABATA,* Chung Kuang CHEN, and Shinzo YAMASHITA
Department of Chemistry, Kyoto Institute of Technology, Matsugasaki, Sakyo-ku, Kyoto
(Received October 15, 1971)

Treatment of malononitrile with a catalytic amount of cuprous chloride and triethylamine under a nitrogen atmosphere resulted in the formation of solid polymer in high yield. The polymer was soluble in dimethyl sulfoxide, pyridine and hexamethylphosphoramide but insoluble in other organic solvents. The polymer was characterized by elemental analyses and IR and NMR spectra to have a mixed structure of an enamine form, $-[C(CN)=C(NH_2)]-_n$, and a ketimine form, $-[CH(CN)-C(=NH)]-_n$.

Only a few publications are available on the polymerization of malononitrile. Korshak *et al.*[1] made an attempt to polymerize malononitrile by the polyrecombination mechanism, *i.e.*,

$$CH_2(CN)_2 \xrightarrow{\cdot R} \left\{\begin{matrix} CN \\ | \\ C \\ | \\ CN \end{matrix}\right\}_n \quad (1)$$

but found the participation of nitrile group in the polymerization reaction.

$$CH_2(CN)_2 \xrightarrow{\cdot R} \left\{\begin{matrix} C=N \\ | \\ CH_2CN \end{matrix}\right\}_n \quad (2)$$

Whang *et al.*[2] followed up this reaction but obtained oily material from malononitrile. Jones[3] studied on the base-catalyzed polycondensation of mono- and dinitriles involving the reaction,

$$RCN \xrightarrow[\text{base}]{} \left\{\begin{matrix} C=N \\ | \\ R \end{matrix}\right\}_n \quad (3)$$

and obtained black, hard, and insoluble solid from malononitrile.

The authors have found the polymerization of malononitrile by the hydrogen transfer mechanism in the presence of cuprous chloride and triethylamine under a nitrogen atmosphere.

$$CH_2(CN)_2 \xrightarrow[\text{under } N_2]{Cu_2Cl_2,\ Et_3N} \left\{\begin{matrix} C=C \\ | \quad | \\ CN\ NH_2 \end{matrix}\right\}_n - \left\{\begin{matrix} CH-C \\ | \quad \| \\ CN\ NH \end{matrix}\right\}_{n'} \quad (4)$$

The mechanism of this polymerization might be related to the Thorpe reaction, *i.e.*, base-catalyzed condensation of nitrile.

$$RCH_2CN + R'CH_2CN \xrightarrow[\text{base}]{} R-\underset{\substack{| \\ CN}}{CH}-\underset{\substack{| \quad \| \\ CN\ NH}}{C}-CH_2R' \quad (5)$$

The Thorpe reaction gives mainly the dimer, β-iminonitrile, but in some cases trimer and its cyclized products. Condensation of malononitrile by the Thorpe reaction is also reported to give dimer, trimer, and cyclized trimers.[4] There appears to be, however, no report of the condensation of malononitrile to afford tetramer, higher oligomer nor polymer of the above type.

Experimental

Elemental analyses were performed at the Elemental Analyses Center of Kyoto University. IR spectra were recorded on a Japan Spectroscopic Co. Model 402G spectrometer. NMR spectra were obtained with a Japan Electron Optics Lab. Model 4H-100 spectrometer using tetramethylsilane as the external standard.

Materials. Malononitrile and triethylamine were puri-

* To whom inquiries should be directed.

1) S. L. Socin, V. V. Korshak, V. A. Vasnev, and E. L. Baranov, *Izv. Akad. Nauk SSSR, Ser. Khim.*, **1962**, 1644.

2) J. J. Whang, E. J. Sinke, and R. K. Graham, *Amer. Chem. Soc., Div. Polymer Chem., Preprints*, **5**, 312 (1964).

3) I. B. Jones, *ibid.*, **5**, 239 (1964).

4) a) R. Schenk and H. Finken, *Ann. Chem.*, **462**, 267 (1928); b) D. M. W. Anderson, F. Bell, and J. L. Duncan, *J. Chem. Soc.*, **1961**, 4705; c) H. Junek and H. Sterk, *Z. Naturforsh.*, B **22**, 732 (1967), and references therein.

fied by distillation. Guaranteed reagent of cuprous chloride was used without further purification. Nitrogen was purified by passing through a tube containing copper turnings in a furnace at 170°C followed by drying with silica gel and molecular sieves. Solvents were purified by the usual methods.[5] Other chemicals were commercially available and used without further purification.

Procedure. Polymerizations were carried out under a nitrogen atmosphere in pyrex test tubes with magnetic stirring. The polymer was recovered by pouring into a large excess of water, and was purified by reprecipitation from dimethyl sulfoxide - water system followed by drying under high vacuum over phosphorus pentoxide for prolonged periods. Viscosity measurements of polymer solutions were made in dimethyl sulfoxide at 30°C with a Ubbelohde-type dilution viscometer. Number average molecular weight of polymers was determined by ebullioscopy in pyridine using a Cottrell-type ebulliometer.

Results and Discussion

Malononitrile polymerizes easily in the presence of catalytic amount of cuprous salt and tertiary amine. For example, when 3.2 m*l* (50 mmol) of malononitrile was heated in 5.0 m*l* of tetrahydrofuran at 60°C in the presence of 1 mol% of cuprous chloride and 4 mol% of triethylamine under a nitrogen atmosphere for 19.5 hr, polymer was obtained in 91% yield. The polymer became a nearly colorless (slightly brown) powder after purification. Melting point of the polymer was higher than 300°C. The polymer was soluble in dimethyl sulfoxide, pyridine, and hexamethylphosphoramide, but insoluble in other organic solvents and water. The intrinsic viscosity of the polymer determined in dimethyl sulfoxide at 30°C was 0.044 d*l*/g. The number average molecular weight of the polymer determined in pyridine was about 1700,[6] *i.e.*, the degree of polymerization was about 26. Many experiments were carried out in order to increase both molecular weight and yield of the resulting polymer. Some of good results are given in Table 1. No catalyst more suitable than cuprous salt - tertiary amine system could be found for this polymerization reaction. Nitrogen atmosphere is desirable because the cuprous salt - tertiary amine system is a catalyst for air oxidation of organic compounds.

Table 1. Polymerization of malononitrile[a]

Solvent	(m*l*)	Et_3N/Cu_2Cl_2 mol ratio	Temp. (°C)	Time (hr)	Conv. (%)	$[\eta]$[b] (d*l*/g)
Dimethyl sulfoxide	4.5	2	50	43	82	0.043
Dimethyl sulfoxide	4.1	8	50	68	80	0.044
Dimethyl sulfoxide	4.0	4	50	43	82	0.041
Nitrobenzene	5.0	4	50	21	88	0.041
Tetrahydrofuran	5.0	4	60	19.5	91	0.044

a) Malononitrile, 3.2 m*l* (50 mmol); cuprous chloride, 0.1 g (1 mol% for the monomer); polymerizations were carried out under a nitrogen atmosphere.
b) Viscosity of polymalononitrile was measured at 30°C in dimethyl sulfoxide.

Elemental analyses of the polymer gave the following results; Found: C, 54.41, 54.88; H, 3.19, 2.91; N, 41.29, 41.23%. Calcd for $(C_3H_2N_2)_n$: C, 54.54; H, 3.05; N, 42.41%. These results indicate that the polymer has the same empirical formula as the monomer, *i.e.*, there would be no possibility of dehydrogenation nor hydrolysis during the polymerization.[7]

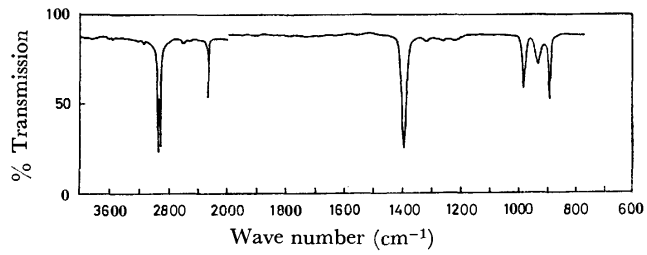

Fig. 1. IR spectrum of malononitrile monomer.

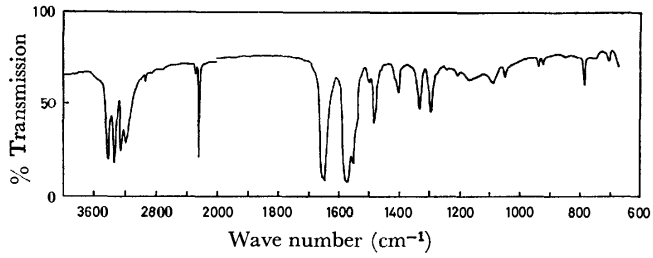

Fig. 2. IR spectrum of polymalononitrile in a KBr disk.

The IR spectrum of malononitrile monomer and that of the polymer in a KBr disk are shown in Figs. 1 and 2, respectively. The absorptions due to the methylene group of malononitrile monomer at 2938 and 2967 cm^{-1} disappeared during the polymerization. Absorptions between 3100—3500 cm^{-1} of the polymer are due to NH and/or NH_2 stretching vibrations, because the polymer has no oxygen as was pointed out by elemental analyses. The appearance of NH and/or NH_2 group together with the disappearance of the methylene group during the polymerization indicates the hydrogen transfer mechanism of the reaction. The authors concluded that the polymer has a mixed structure of an enamine form (I) and a ketimine form (II).

I II

As will be discussed later, IR and NMR spectra of the polymer are consistent with this conclusion. The absorptions at 3323 and 3399 cm^{-1} can be assigned to the NH_2 group of structure I, and those at 3167 and 3239 cm^{-1} to the NH group of structure II.[8] The absorptions of NH stretching vibration of ketimines are

5) J. A. Riddick and W. B. Bunger, "Organic Solvents," Wiley-Interscience, New York (1970).
6) Two experiments gave 1500 and 1900 as the number average molecular weight of the polymer.
7) The observed nitrogen content of the polymer is somewhat lower than the calculated value. However, this result is probably due to slightly difficult combustion of the polymer.
8) The reason of this splitting into two absorptions will be discussed later.

reported to appear in the range of 3205—3236 cm^{-1}.[9] The weak absorption at 2919 cm^{-1} can be assigned to the stretching vibration of methine group of II. The absorptions at 2219 and 2267 cm^{-1} can be attributed to nitrile groups of I and II, respectively. The absorption at 1647 cm^{-1} may be due to C=C group of I and C=N group of II. The absorption at 1573 cm^{-1} may be ascribable to deformation vibration of NH and NH_2 groups.

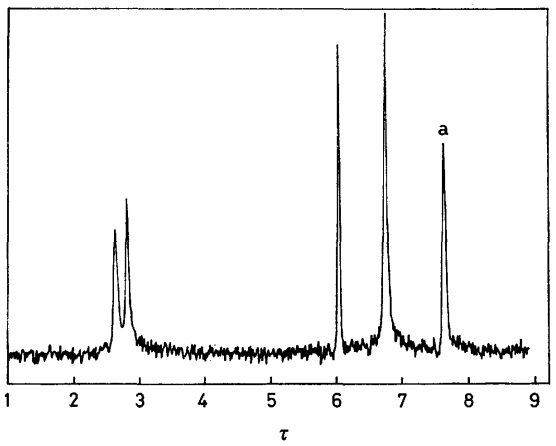

Fig. 3. Proton magnetic resonance spectrum of 5 wt % solution of polymalononitrile in dimethyl-d_6 sulfoxide. a: CH_3SOCH_3.

The NMR spectrum of the polymer obtained in dimethyl-d_6 sulfoxide is shown in Fig. 3. The peak at 6.04 τ can be assigned to NH_2 protons of structure I. The intensity of the peak at 6.75 τ is nearly equal to the total intensity of the two peaks at 2.63 and 2.82 τ. The former can be ascribable to CH proton and the latter two peaks to NH proton of structure II, respectively. Few data are available for NMR spectra of ketimines, but is reported to appear at 0.6 τ in the case of diphenylketimine.[10] The splitting of IR absorption

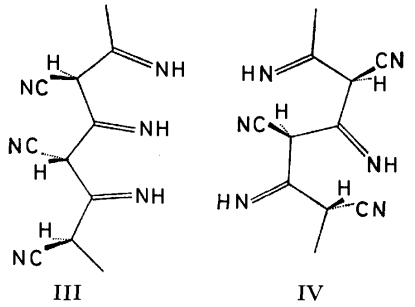

Fig. 4. Two types of possible steric circumstances around imino group of polymalononitrile.

of NH stretching vibration and that of NMR peak assigned to NH proton of structure II suggest that there are two types of imino groups in the polymer. Molecular model suggests the possibility of two types of steric circumstances around imino group, *i.e.*, *pseudo-isotactic* structure III and *pseudo-syndiotactic* structure IV with respect to the imino group, which are illustrated in Fig. 4.

The intensity ratio of the NMR absorption at 6.04 τ to that at 6.75 τ was 1 : 2.3. The ratio was not sensitive to change of concentration in the range of 1—10%. This result shows that in dimethyl sulfoxide solution, about 20% of monomer units have the enamine structure and the residual 80% the ketimine structure. This result consists with the general observation that the ketimine structure is more stable in the ketimine - enamine tautomerism.

Though the authors have no evidence concerning the mechanism of this polymerization, it would be reasonable to speculate as follows;

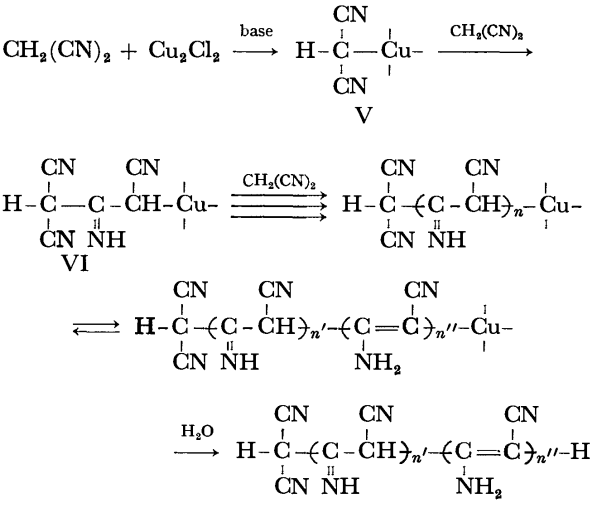

The formation of an organocopper compound V is conceivable, since the reaction of 1-hexyne with cuprous chloride and ammonia is reported to give 1-hexynylcopper.[11] The formation of VI by the reaction of V with malononitrile is also conceivable, because diethyl β-imino-α-cyano-α'-sodioglutarate VII is reported to be obtained by the following reaction.[12]

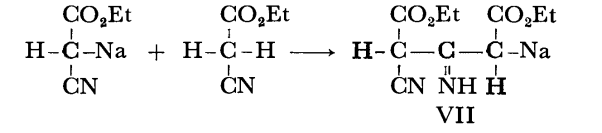

9) P. L. Pickard and G. W. Polly, *J. Amer. Chem. Soc.*, **76**, 5169 (1954).
10) J. B. Lambert, W. L. Oliver, and J. D. Roberts, *ibid.*, **87**, 5085 (1965).
11) W. J. Gensler and A. P. Mahadevan, *J. Org. Chem.*, **21** 180 (1956).
12) H. Baron, F. G. P. Remfry, and J. F. Thorpe, *J. Chem. Soc.*, **85**, 1726 (1904).

Intramolecular Hydrogen Bonding of *ortho*-Substituted Benzenethiols

Takahiro KOBAYASHI, Akihiko YAMASHITA, Yoshihiro FURUYA, Rumiko HORIE, and Minoru HIROTA

Department of Applied Chemistry, Faculty of Engineering, Yokohama National University, Minami-ku, Yokohama

(Received November 1, 1971)

From the infrared, NMR, and dipole moment measurements on several substituted benzenethiols, the intramolecular hydrogen bonding in *o*-halo, *o*-methoxy, *o*-nitro, and *o*-carbomethoxybenzenethiols is verified. Five-membered S–H···X hydrogen bonds cause remarkable enhancements of their S–H stretching absorptions without considerable frequency shifts. The favorable *s-cis* conformations in these thiols are also proved by comparing their experimental dipole moments with theoretical values. By far stronger hydrogen bond is observed in *o*-carbomethoxybenzenethiols which can form six-membered chelate ring by the intramolecular hydrogen bonding.

Several investigations on the hydrogen bonding of thiols have been reported and the hydrogen donating properties of the sulfhydryl groups have been discussed.[1-9] From these investigations, it is assumed that the hydrogen donating power of the S–H group is rather weak and that thiols behave as softer acids than alcohols and phenols in case of hydrogen bond formation. The existence of such weak hydrogen bonds can be best investigated by NMR spectroscopy. Thus the S–H···S intermolecular hydrogen bond in ethyl mercaptan[2] and the S–H···O intramolecular hydrogen bond[10] have been verified by this method. The present authors also reported on the PMR spectra of *o*-methoxy- and 2,6-dimethoxy-benzenethiols, and concluded the existence of the intramolecular hydrogen bonds by the comparison with the behaviors of the corresponding phenols.[11]

In order to establish the extent and the limit of the existence of the S–H···X intramolecular hydrogen bonds and to compare their relative strengths for various hydrogen acceptors, the PMR, IR, and dipole moments of several *ortho*-substituted benzenethiols were determined and the existence of the intramolecular hydrogen bonds were concluded in benzenethiols carrying alkoxy-, halogeno-, nitro-, alkoxycarbonyl-substituents at the *ortho*-positions.

Experimental

Materials. *p*-Toluenethiol, *p*-methoxybenzenethiol, *o*-toluenethiol, 2-bromo-4-methylbenzenethiol, *o*-iodobenzenethiol, *o*-methoxybenzenethiol, and 2,6-dimethoxybenzenethiol were prepared according to the method reported by Sutar.[12] *o*-Nitrobenzenethiol was obtained by the reduction of 2,2′-dinitrodiphenyl disulfide.[13] All of these thiols were known compounds and were purified by repeated recrystallization or fractional distillation until their physical constants agree with those reported in literatures.[12-16]

All solvents used were commercially available spectro-grade ones or were purified by the usual methods. The solvents were dried over appropriate desiccants and re-distilled when necessary.

Spectral and Dielectric Measurements. Infrared spectra in the S–H stretching region were measured with a Perkin-Elmer 112G infrared spectrophotometer. The measurements were carried out on a dilute solution of the thiol in carbon tetrachloride or chloroform employing a quartz cell of 2 cm in path length.

Proton magnetic resonance spectra were determined with a JEOL JNM-C60H spectrometer. The spectra were obtained over a wide range of concentrations (0.1 to 100% of solute) in carbon tetrachloride and chloroform-*d* to ascertain the existance of the intramolecular hydrogen bonds.

Dielectric constants of the benzene or carbon tetrachloride solution of the thiols were determined at 25°C, except the case of temperature dependence measurement, using a heterodyne apparatus. The dipole moment values were calculated by employing the method of Halverstadt and Kumler[17] from the dielectric constants of the solutions at varying concentrations. The molar refraction was calculated from the bond refraction values in the literature.[18]

Results and Discussion

Infrared S–H stretching absorptions and chemical shifts of the S–H protons at infinite dilution are given in Table 1. The thiols No. 1 to 4 are those without intramolecular hydrogen bonds, and intermolecular hydrogen bonding is also excluded by the measurement

1) L. H. Meyer, A. Saika, and H. S. Gutowsky, *J. Amer. Chem. Soc.*, **75**, 4567 (1953).
2) S. Fórsen, *Acta Chem. Scand.*, **13**, 1472 (1959).
3) A. S. N. Murthy, C. N. R. Rao, B. D. N. Rao, and P. Venkateswarku, *Trans. Faraday Soc.*, **58**, 855 (1962).
4) A. S. N. Murthy, C. N. R. Rao, and P. Venkateswarku, *Canad. J. Chem.*, **40**, 963 (1962).
5) W. Stacy and J. F. Harris, *J. Amer. Chem. Soc.*, **85**, 963 (1963).
6) S. H. Marcus and S. I. Miller, *J. Phys. Chem.*, **68**, 331 (1964).
7) H. B. Evans, Jr., A. R. Tarpley, and J. H. Goldstein, *ibid.*, **72**, 2552 (1968).
8) S. S. Dharmatti, M. M. Dhingra, G. Govil, and C. L. Khetrapal, *Proc. Nucl. Phys. Solid State Phys. Symp.*, **1964**, 405.
9) M. J. Copley, C. S. Marvel, and E. H. Ginsberg, *J. Amer. Chem. Soc.*, **61**, 3161 (1939).
10) F. Duus, E. B. Pedersen, and S. O. Lawesson, *Tetrahedron*, **25**, 5703 (1969).
11) M. Hirota and R. Hoshi, *ibid.*, **25**, 5953 (1969).
12) C. M. Sutar and H. L. Hansen, *J. Amer. Chem. Soc.*, **54**, 4102 (1932).
13) D. G. Foster and E. E. Reid, *ibid.*, **46**, 1936 (1924).
14) H. Kauffman *et al.*, *Ber.*, **37**, 726 (1904); **40**, 4001, 4006 (1907).
15) R. Adams, "Organic Syntheses," Col. Vol. I, p. 504 (1941).
16) K. Fries, *Ann. Chem.*, **346**, 166 (1906).
17) a) I. F. Halverstadt and W. D. Kumler, *J. Amer. Chem. Soc.*, **64**, 2988 (1942). b) C. P. Smyth, "Dielectric Behavior and Structure," McGraw-Hill Book Co., Inc., N. Y., (1955).
18) A. I. Vogel, W. T. Cresswell, G. H. Jeffery, and J. Leicester, *J. Chem. Soc.*, **1952**, 514.

TABLE 1. INFRARED AND PROTON MAGNETIC RESONANCE SPECTRA OF VARIOUS BENZENETHIOLS

Substituent	No. of compd.	Carbon tetrachloride solution				Chloroform solution			
		S–H stretching band			PMR spectra	S–H stretching band			PMR spectra
		$\nu(cm^{-1})$	$\varepsilon(l/mol\cdot cm)$	$A(10^2 l/mol\cdot cm^2)$	δ_{SH}(ppm from TMS)	$\nu(cm^{-1})$	$\varepsilon(l/mol\cdot cm)$	$A(10^2 l/mol\cdot cm)^2$	δ_{SH}(ppm from TMS)
4-CH_3	(1)	2588	3.2	2.58	3.17	2586	6.9	5.23	3.36
4-CH_3O	(2)	2583	3.4	3.44	3.14	—	—	—	3.33
2-CH_3	(3)	2582	2.1	2.13	3.06	—	—	—	3.23
2-Cl	(4)	2587	14.2	6.76	3.82	2586	17.9	9.07	3.90
2-Br-4-CH_3	(5)	2579	17.1	7.99	3.80	2584	16.4	10.7	3.92
2-I	(6)	2560	14.4	6.74	4.02	2558	12.2	7.51	—
2-CH_3O	(7)	2593	18.9	10.3	3.66	2592	17.3	12.5	3.79
2,6-$(CH_3O)_2$	(8)	2595	24.5	13.8	3.75	2592	28.4	16.5	4.00
2,6-Br_2-4-CH_3	(9)	2572	36.0	13.0	4.77	2569	32.4	15.9	4.72
2-NO_2	(10)	2598	27.4	15.9	4.05	2601	8.60	7.59	
2-$COOCH_3$	(11)	2534	33.3	65.1	5.26	2546	15.9	49.5	4.75

in extremely dilute solution of inert solvents. Their S–H absorption have rather low intensities ($\varepsilon_{max}=3$ in CCl_4) and not affected considerably by the introduction of *ortho* and *para* substituents, if the *ortho* substituents are incapable of forming intramolecular hydrogen bonds. On the other hand, the introduction of the hydrogen accepting substituents at the *ortho* position causes a remarkable increase in intensity as shown in Table 1. The absolute values of the integrated intensity is larger in chloroform than in carbon tetrachloride, while the intensity enhancement is more predominant in latter solvent. In contrast to the remarkable increase in intensity, the S–H absorption frequencies are not affected by the introduction of the hydrogen accepting substituents except the case of *o*-carbomethoxybenzenethiol. The introduction of a methyl group forming no intramolecular hydrogen bond to the *ortho*-position does not strengthen the S–H intensity, and the steric effect caused by the *ortho*-substituent might not be responsible for the intensity enhancement. The possibility of the electronic effect (mesomeric effect) is excluded by the fact that the intensity of the S–H absorption is little affected by the methoxy substituent in *p*-methoxybenzenethiol. In analogy with the substituent effect on the ν_{O-H} intensities of substituted phenols,[19] the electron donating character of the methoxy group at the *ortho*- or *para*-position is expected to decrease the intensity of S–H absorption. Thus the observed increase in intensity cannot be explained by the electronic effect.

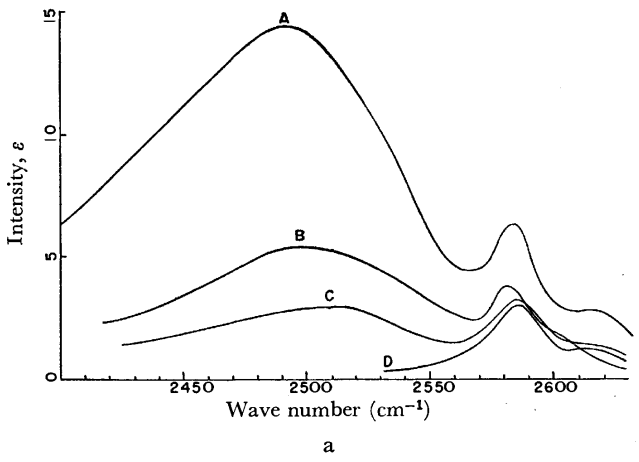

a

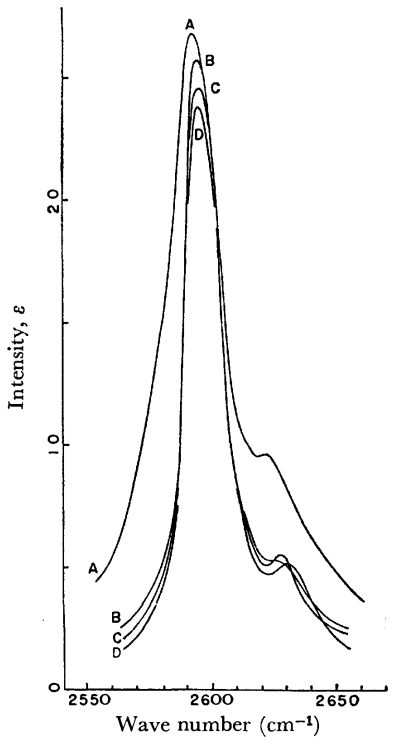

b

Fig. 1. The S–H stretching absorptions of *p*-toluenethiol (1a) and 2,6-dimethoxybenzenethiol (1b) in carbon tetrachloride–dimethyl sulfoxide mixtures.
A: 5.24 wt% DMSO in CCl_4, B: 1.36 wt% DMSO in CCl_4, C: 0.686 wt% DMSO in CCl_4, D: 100 wt% CCl_4.

In conclusion, the enhancement of the intensity might be attributed to the intramolecular hydrogen bond formation. Such an evidence was obtained by the investigation on the intermolecular interaction of the thiols with some solvents having proton accepting ability. The ν_{SH} intensities of *p*-toluenethiol (1) and 2,6-dimethoxybenzenethiol (8) are recorded in several sol-

19) G. A. Stone and H. W. Thompson, *Spectrochim. Acta*, **10**, 16 (1957).

TABLE 2. S–H STRETCHING BAND INTENSITIES AND HALF WIDTHS OF THE TWO TYPICAL BENZENETHIOLS

Thiol		Solvent			
		CCl_4	$CHCl_3$	$(CH_3)_2CO$	DMSO (8%) in CCl_4
p-$CH_3C_6H_4SH$	ε(*l*/mol·cm)	3.2	6.9	30.0	14.6
	$\Delta\nu_{1/2}$ (cm^{-1})	51.4	48.3	76.5	*ca.* 110
2,6-$(CH_3O)_2$-C_6H_3SH	ε(*l*/mol·cm)	34.5	28.4	29.0	26.7
	$\Delta\nu_{1/2}$ (cm^{-1})	35.8	37.0	42.5	29.0

vents and listed in Table 2. The thiols selected in Table 2. are the typicals of the intermolecular and intramolecular hydrogen bonded ones, respectively. Of the usual benzenethiols without *ortho*-hydrogen acceptor (1), the S–H absorption band tend to be more intense and broader when measured in hydrogen accepting solvents. (See also Fig. 1) However, the S–H absorption of 2,6-dimethoxybenzenethiol (8) is not remarkably affected by such solvents. In this compound, the S–H group is shielded by the two methoxy groups, and the solvent molecules are hardly accessible to the S–H group. Hence, the intermolecular hydrogen bonding might not disturb the intramolecular hydrogen bond of the latter thiol to a considerable extent. The increase in intensity is quite general with the intramolecularly hydrogen-bonded compounds carrying O–H and N–H groups.[20] Some experiments also showed that the S–H groups participating in the hydrogen bonds have stronger S–H absorptions.[21]

In the case of rather weak hydrogen bond, both the hydrogen bonded and the free X–H absorption bands must be observed. However, only one absorption band assigned to the S–H stretching vibration can be observed in most cases, though some weak bands whose origins are uncertain appear in the spectra of some thiols. The spectra in Fig. 2 show that the ν_{S-H} bands are intensified remarkably by the introduction of the additional hydrogen accepting substituent to the 6-positions of the 2-methoxy- and 2-bromobenzenethiols. This means that the hydrogen bonded form is increased by the introduction of the second substituent, and the existence of free *s-trans* form (II) is expected in the benzenethiol carrying one hydrogen accepting substituent at the *ortho* position. Because of the absence of the remarkable hydrogen bond shift, weaker S–H absorptions of the free species might be masked by the stronger S–H absorptions of the intramolecularly hydrogen bonded species. The S–H stretching spectrum of *o*-carbomethoxybenzenethiol in Fig. 3 shows the appearance of an additional band of low intensity in normal S–H stretching region, which can be assigned to the free S–H stretching vibration.

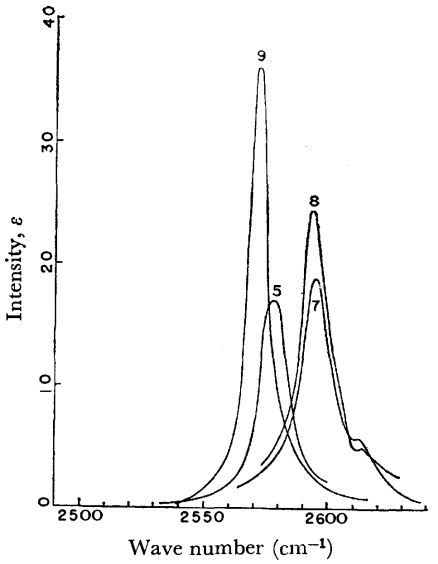

Fig. 2. The S–H stretching absorptions of 2-X- and 2,6-di-X-benzenethiols in carbon tetrachloride.

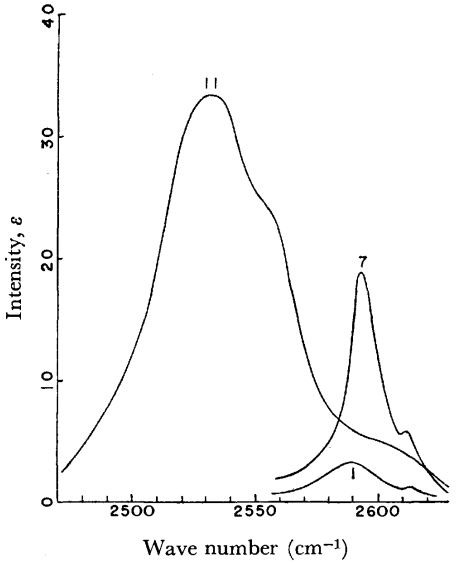

Fig. 3. The S–H stretching absorptions of the typical benzenethiols with five-membered and six-membered hydrogen bonded chelates (in carbon tetrachloride).

The PMR chemical shifts of the S–H protons in very dilute solutions are also given in Table 1. As reported previously by the present authors,[11] the PMR spectra are useful in the discussion of the hydrogen bonding of thiols and the chemical shifts of S–H protons at infinite dilution displace to considerably lower fields when the thiols exist as the intramolecularly hydrogen bonded forms. Thus, the usual thiols ((1) to (3) in Table 1) have δ_{SH} values ranging 3.0 to 3.3 ppm in carbon tetrachloride and 3.2 to 3.4 ppm in chloroform-*d*, while the thiols carrying *ortho* hydrogen accepting substituents have δ_{SH} values ranging 3.6 to 5.3 ppm and 3.7 to 4.8 ppm, respectively, in the above solvents. The ν_{S-H} intensity *vs.* δ_{SH} plot is illustrated in Fig. 4, and a fairly good linear relation is observed even though no correction for the magnetic anisotropy effect by the substituents are taken into accounts.

Additional evidence for the intramolecular hydrogen

20) G. C. Pimentel and A. L. McClellan, "The Hydrogen Bond," W. H. Freeman & Co., San Francisco (1960) p. 167.
21) A. Wagner, H. J. Becker, and K. G. Kottenhahn, *Chem. Ber.*, **89**, 1708 (1956).

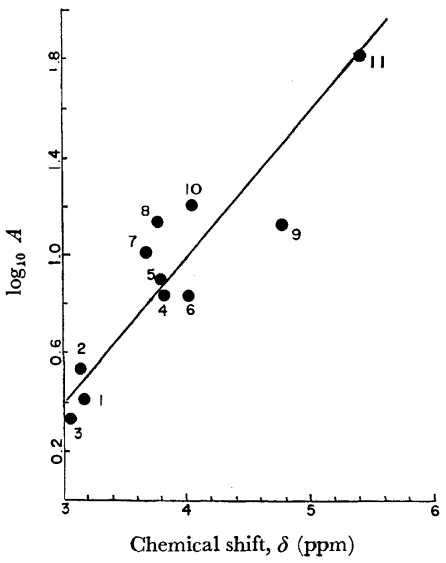

Fig. 4. Integrated intensity (A_{SH}) *vs.* SH chemical shift (δ_{SH}) plot.

bonding in benzenethiols with *ortho*-substituents of hydrogen accepting ability is supplied by the dipole moment data given in Table 3. The theoretical dipole moment for each conformation is calculated from the group moments in Table 4.[22] When *o*-halo- and *o*-nitrobenzenethiols form intramolecular hydrogen bond, the *s-cis* conformation (I) of these thiols should exist more favorably than the corresponding *s-trans* conformation. To obtain the ratios of *s-cis* and *s-trans* conformations, the experimental dipole moment values of the thiols are assumed to be expressed as the resultants of the mean squares of the theoretical dipole moments of the two conformers, and the following equation is employed,

$$\mu^2 = \frac{\mu_t^2 N_t + \mu_c^2 N_c}{N_t + N_c}$$

where μ_t and μ_c, N_t and N_c are the theoretical dipole moments and the numbers of the molecules of *s-trans* and *s-cis* conformers, respectively. Thus the experimental dipole moment 0.90 D of *o*-toluenethiol (3) in benzene solution at 25°C gives the result that 87% of the molecules take *trans* conformation and the rest of them have *cis* conformation. This means that *cis* conformation is unfavorable, and might be due to the steric hindrance between the methyl and sulydrylfh hydrogen atoms. On the other hand, the observed dipole moments of *o*-chloro-, 2-bromo-4-methyl-, and *o*-nitrobenzenethiols are closer to the theoretical values for *s-cis* conformations. When dissolved in benzene, 85%, 84%, and 76% of them, respectively, exist as *cis* conformations, and the proportions of *cis* conformers increase further when dissolved in carbon tetrachloride. The conclusions on the conformations obtained from the dipole moment measurements again supports the existence of intramolecular hydrogen bonding. Increased population of *s-trans* conformers in benzene solutions is explained by the stabilization caused by the S–H···π intermolecular interaction with the solvent molecules, as illustrated by (III).

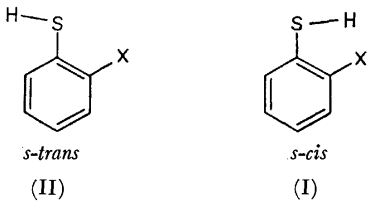

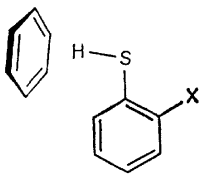

(III)

The dipole moment of *o*-methoxybenzenethiol does not agree with the favorable *s-cis* conformation. This may arise from the smaller difference of the theoretical dipole moments between *s-cis* and *s-trans* conformers and from the ambiguity of the direction of methoxy group moment caused by the rotation around the C–O bond.

In conclusion, the intramolecular S–H···X hydrogen bonds exist in some *ortho*-substituted benzenethiols forming both five-membered and six-membered chelate rings. Similar to the corresponding phenols, benzenethiols with *o*-methoxy-, *o*-chloro-, *o*-bromo-, *o*-iodo-, *o*-

TABLE 3. DIPOLE MOMENTS OF VARIOUS BENZENETHIOLS

Substituent	No. of compound	Dipole moment (D) Theoretical *s-cis*	Theoretical *s-trans*	Experimental	Abundance (%) *s-cis*	Abundance (%) *s-trans*
a) Benzene solution at 25°C						
None	(12)	—	—	1.21[a)]	—	—
4-CH_3	(1)	—	—	1.51[a)]	—	—
2-CH_3	(3)	1.35	0.81	0.90	13±10	87±10
2-Cl	(4)	1.72	2.73	1.91	85±5	15±5
2-Br-4-CH_3	(5)	2.08	2.96	2.25	84±6	16±6
2-CH_3O	(7)	—	—	2.25	—	—
2-NO_2	(10)	3.90	5.14	4.24	76±4	24±4
b) Carbon tetrachloride solution at 25°C						
2-Cl	(4)	1.72	2.73	1.78	95±5	5±5
2-Br-4-CH_3	(5)	2.08	2.96	2.05	97±6	3±6

a) Calculated dipole moments of benzenethiol and *p*-toluenethiol are 1.19D and 1.50D, respectively. These are obtained from the group moments employed in this investigation.

TABLE 4. THE GROUP DIPOLE MOMENT VALUES

Group (X)	μ_{C-X}	θ
SH	1.19	44°
CH_3	0.4	180°
Cl	1.58	0°
Br	1.54	0°
OCH_3	1.28	108°
NO_2	4.01	0°

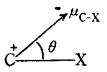

22) a) L. E. Sutton, "Determination of Organic Structures by Physical Methods," ed. by E. A. Braude and F. C. Nachod, Academic Press Inc., N. Y. (1955) p. 373. b) T. Shimozawa, "Interpretation of Dielectric Constant," Kyoritsu Shuppan Co., Tokyo (1967) p. 55.

nitro-, and *o*-methoxycarbonyl-substituents form intramolecular S–H···X hydrogen bonds, and it would be foreseen that the benzenethiols with *o*-acyl, *o*-formyl, and other hydrogen accepting substituents also form the intramolecular hydrogen bonds.

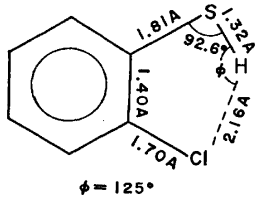

Fig. 5. Geometry of the planar *s-cis* conformation of *o*-chlorobenzenethiol (4).

Table 5. Molecular geometries of some *o*-substituted benzenethiols

Substituent	*d* (H···X) Å	(∠S–H···X)
2-Cl	2.16	125°
2-Br	2.20	130°
2-I	2.25	135°
2-OCH_3	2.16	117°
2-NO_2	1.15	140°
2-$COOCH_3$	1.35	151°

Then, some discussions will be given on the stereochemistry of the intramolecular hydrogen bond of this type. The H···X distances *d* and S–H–X angles were calculated by assuming the geometry in Fig. 5 for the *cis* conformers and the results were listed in Table 5.

23) Bond lengths and bond angles employed were taken from a) "Kagaku Benran," Fundamental Volume II, ed. by Chem.Soc. Japan, Maruzen Book Co., Tokyo (1966) p. 1209 and b) "Kagaku Benran," ed. by Chem. Soc. Japan, Maruzen Book Co., Tokyo (1958) p. 966.

The main factors determining the strength of the intramolecular hydrogen bond are i) the kinds of the hydrogen donating and accepting groups, ii) the linearity of the hydrogen bond, and iii) the distance between the donor and the acceptor atoms. In the discussion on the stereochemistry, the latter two factors play important roles. The hydrogen bond becomes stronger when the hydrogen atom comes closer to the accepting atom and when the S–H···X arrangement is nearer to the linear one. In these points of view, the six-membered chelation is stronger than the five-membered one, which is in agreement with the above results. The most suitable S–H···X distance values are rarely found in the previous investigations. However, the O–H···X distances are reported by many authors[24] and the O–H···Cl and the O–H···O distances in hydrogen bonded molecules are 3.1 to 3.2 Å and 2.5 to 2.8 Å, respectively. The H···X distances are then 1.5 to 1.8 Å and 2.1 to 2.2 Å. The calculated X···H distances in Table 5 are mostly within these ranges, but the H···O distance in *o*-nitrobenzenethiol[10] is rather too short, and the repulsive force between the atoms may cause the deviation from the planar six-membered ring. This could be a reason why the intramolecular hydrogen bond in (10) is weaker than expected.

The authors are grateful to Prof. H. Kakiuchi of Yokohama National University for his kind and valuable advice and to Prof. T. Shimozawa of Saitama University for his useful advice and kind guidance in constructing the apparatus for dielectric constant measurement. They also wish to express their hearty thanks to Prof. T. Shimanouchi and Prof. I. Nakagawa of the University of Tokyo for their kind permission to use infrared spectrophotometers.

24) p. 255 of Ref. 20.

Reactions of Aryloxycopper(I) with Organic Halides

Takao KAWAKI and Harukichi HASHIMOTO*

Department of Synthetic Chemistry, Faculty of Engineering, The University of Tokyo, Bunkyo-ku, Tokyo
**Department of Applied Chemistry, Faculty of Engineering, Tohoku University, Sendai*

(Received August 23, 1971)

Some aryloxycoppers were synthesized by the interaction of phenylcopper with phenols and then characterized. The reaction of aryloxycopper and organic halide in diglyme generally gave the corresponding ether. From these and other results, it is suggested that aryloxycopper(I) is an intermediate in the Ullmann condensation, *etc.*

A number of reactions utilizing cuprous salts have been reported by numerous investigators. However, the preparations and reactions of alkoxy- or aryloxycopper(I), as well as of $CuOCOCH_3$, Cu(acac) and $CuNO_3$, have not been studied thoroughly, though Costa[1] reported the preparation of unstable methoxycopper(I) and its decomposition reaction. Aryloxycopper(I) has been assumed to be an intermediate of some copper-promoted reaction.[2,3] Weingarten[4,5] reported that aryloxycopper(I) is an intermediate of the Ullmann condensation reaction. In the oxidative coupling reaction of substituted phenols, this compound was also reported by Hay and his co-workers[6] to play an important role. The aim of this work is to examine the preparation of aryloxycopper(I) and its reactivity.

Results and Discussion

Preparation and Properties of Phenoxycopper(I). Phenoxycopper(I) was prepared by adding a small excess of phenol to phenylcopper suspended in anhydrous diethyl ether; the details will be specified in the Experimental section. Phenoxycopper(I) is a violet micro-crystalline, oxygen-sensitive compound; it is soluble in dyglime and DMF and insoluble in benzene and ether.

Group Ib metal halides in the low oxidation state are well known to form stable complexes with triphenylphosphine (PPh_3). Recently, several investigators have reported halogenocopper(I) complexes with PPh_3.[7,8] Phenoxycopper(I) also formed a complex with the composition of $Cu(OPh)(PPh_3)_3$ by refluxing with PPh_3 in benzene. This complex is a white crystalline compound, stable to oxygen and soluble in an organic solvent.

Reactions of Aryloxycopper(I) with Organic Halides. Cuprous salts promoted the reaction of aryl halide with alkali metal phenoxide to give aryl ether.[5,9] This reaction was suggested, from the study of the ESR, to be a nucleophilic replacement reaction of the ate complex of phenoxycopper(I) on aryl halide. It appeared to be interesting to investigate the reactions of aryloxycopper(I) with organic halides in connection with the Ullmann condensation reaction. Table 1 shows the results of the reactions between aryloxycopper(I) and some organic halides. It is obvious that, under mild conditions, these reactions do not proceed successfully, but under rigorous conditions they proceed to obtain the corresponding ethers. In the reaction of No. 2, diphenyl ether was obtained from bromobenzene in a 38% yield. This result gives some support to the

Table 1. Reaction of CuOAr with organic halides in diglyme

No.	Ar in CuAr	Halide	Temp. (°C)	Time (hr)	Product	Yield (%)
1	Ph	PhBr	100	4	PhOPh	6.8
2	Ph	PhBr	124	17	PhOPh	38
3	Ph	CH_3I	40	17	$PhOCH_3$	20
4	Ph	$PhCH_2Cl$	100	4	$PhOCH_2Ph$	16
5	Ph	$CH_2=CH-CH_2Cl$	r.t.	0.5	$PhOCH_2-CH=CH_2$	3.8
					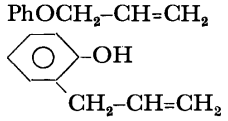	17[a]
6	*p*-CH_3-C_6H_4	PhBr	125	17	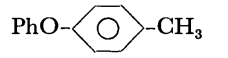	28
7	*p*-NO_2-C_6H_4[b]	PhBr	125	17	—	
8	*p*-CH_3O-C_6H_4[b]	PhBr	125	17	—	
9	*o*-Br-C_6H_4	PhBr	125	17	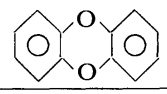	trace

a) Plus several unidentified high-boiling products. b) Heterogeneous reaction.

1) G. Costa, *J. Inorg. Nucl. Chem.*, **27**, 281 (1965).
2) R. G. Bacon and H. A. O. Hill, *Quart. Rev.*, **19**, 95 (1965).
3) R. G. Bacon and O. J. Stewart, *J. Chem. Soc., C*, **1969**, 301.
4) H. Weingarten, *J. Org. Chem.*, **29**, 977 (1964).
5) H. Weingarten, *ibid.*, **29**, 3624 (1964).
6) H. Finkbeiner, A. S. Hay, H. S. Blanchard, and G. F. Endres, *ibid.*, **31**, 549 (1966).
7) G. Costa, E. Reisenhofer, and L. Sefanni, *J. Inorg. Nucl. Chem.*, **27**, 2581 (1965).
8) F. H. Jardine, L. Rule, and A. G. Voba, *J. Chem. Soc., A*, **1970**, 238.
9) R. G. R. Bacon and O. J. Stewart, *ibid.*, **1965**, 4953.

hypothesis that aryloxycopper(I) is an intermediate of the Ullmann condensation reaction.

To investigate the substituent effects, *p*-methyl-, *p*-nitro-, and *p*-methoxyphenoxycopper(I) were prepared and reacted with bromobenzene, but only *p*-methylphenoxycopper(I) gave the corresponding ether. The result may be due to the fact that *p*-nitro- and *p*-methoxyphenoxycopper(I) were insoluble in diglyme. The reaction of phenoxycopper(I) with allyl chloride is abnormal with respect to producing *o*-allylphenol and several high-boiling by-products at room temperature. The formation of *o*-allylphenol can not be attributed to a Claisen rearrangement of the resulting allyl phenyl ether under very mild reaction conditions used.

TABLE 2. THE EFFECT OF LIGANDS IN THE REACTION OF CuOPh WITH PhBr AT 125°C FOR 17 hr IN DIGLYME

Ligand	Ligand/CuOPh (mol/mol)	Yield of PhOPh(%)
—	0	38
Pyridine	3	46
PPh_3	3	8.2

The effect of the addition of pyridine or PPh_3 in the reaction of phenoxycopper(I) and bromobenzene is shown in Table 2. The addition of pyridine increased the yield of diphenyl ether, and that of PPh_3 decreased significantly the yield of diphenyl ether. Bacon and his co-worker[2] proposed the following four-centered mechanism for the halogen exchange of ary halide with cuprous salts:

$$ArX + CuY \rightleftharpoons \left[\begin{matrix} & X & \\ Ar & & Cu \\ & Y & \end{matrix}\right] \longrightarrow ArY + CuX$$

X; Y=Cl, Br, I

The above reaction of phenoxycopper(I) with bromobenzene may be thought to proceed through a similar process.

Reactions of Phenoxycopper(I) with Acyl Halides. Phenoxycopper(I) as well as other metal alkoxides reacted with acyl halides very rapidly at room temperature to form the corresponding ester. For example, phenoxycopper(I) was reacted with benzoyl chloride and acetyl chloride in ether at room temperature for 2 hr to produce phenyl benzoate (74% yield) and phenyl acetate (64% yield) respectively.

Oxidation of 2,6-Di-t-butylphenoxycopper(I). 2,6-Di-*t*-butylphenoxycopper(I) was prepared by the same method as phenoxycopper(I) and was oxidized by passing air through its suspension in ether to give only 2,2′,6,6′-tetra-*t*-butyldiphenoquinone as the reaction product. It has been reported[6] that the oxidative coupling of 2,6-di-*t*-butylphenol catalyzed with cuprous chloride and pyridine also gave 2,2′,6,6′-tetra-*t*-butyldiphenoquinone. It seems from the results of this experiment that aryloxycopper(I) is an intermediate of the oxidative coupling of phenols catalyzed with copper salts.

Experimental

Preparation of Phenoxycopper(I). Phenlycopper was prepared according to the directions of Costa.[10] Phenyllithium (0.02 mol) was added to cuprous bromide (0.02 mol) suspended in absolute ether at −10°C under a nitrogen atmosphere. The resulting white precipitate of phenylcopper was washed several times with ether under the applied pressure of nitrogen.

To the above phenylcopper (0.02 mol) suspended in fresh ether at room temperature, we added a slight excess of phenol under nitrogen; the mixture was then stirred for 2 hr. The resulting violet solid of CuOPh was washed several times with ether and dried under nitrogen. The IR spectra showed the absorption bands of a trace of unreacted phenylcopper, which had little influence on the following reactions. The other aryloxycoppers were prepared in a similar way.

Preparation of Cu(OPh)(PPh_3)$_3$. PPh_3 (0.04 mol) was added to CuOPh (0.01 mol) suspended in benzene, after which the mixture was refluxed for 5 hr. The reaction mixture was then concentrated to deposit Cu(OPh)(PPh_3)$_3$.

Found: C, 76.16; H, 5.25; Cu, 6.38%. Calcd for $C_{60}H_{50}OP_3Cu$: C, 76.62; H, 5.25; Cu, 6.70%.

Reactions of Aryloxycopper with Organic Halides. All the reactions were carried out *in situ* without any drying of the aryloxycoppers prepared as described above. Organic halide (0.02 mol) was added to CuOAr (0.02 mol) suspended in ether under nitrogen, after which the mixture was heated under the conditions shown in Table 1. The yields of the products were determined by gas chromatography.

Reactions of Phenoxycopper(I) with Acyl Halides. Acetyl chloride or benzoyl chloride (0.02 mol) was added to phenoxycopper(I) (0.02 mol) suspended in ether as described above, and the mixture was stirred at room temperature for 2 hr.

Oxidation of 2,6-Di-t-butylphenoxycopper(I). Oxygen was bubbled into a suspension of 2,6-di-*t*-butylphenoxycopper in ether at room temperature for 10 hr. The mixture was hydrolyzed with dilute hydrochloric acid, and then the ether layer was separated. The ether was subsequently removed to give solid 2,2′,6,6′-tetra-*t*-butyldiphenoquinone in a yield of 16%; this substance was identified by elemental analysis, IR, and NMR and by its failure to depress the melting point of an authentic sample.

10) G. Costa, A. Camns, L. Gatti, and N. Marsich, *J. Organometal. Chem.*, **5**, 568 (1966).

The Synthesis and Configuration of Fukiic Acid Derivatives[1)]

Takashi MATSUMOTO, Kazuo HIDAKA, Teruko NAKAYAMA, and Kenji FUKUI

Department of Chemistry, Faculty of Science, Hiroshima University, Higashi-sendamachi, Hiroshima

(Received October 1, 1971)

The methylation of 3,4-dimethoxyphenylpyruvic acid (II) gave the corresponding methyl ester (III), which was then subjected to a Wittig reaction with carbomethoxymethylenetriphenylphosphorane to give the corresponding fumaric (IVa) and maleic (IVb) acid derivatives in a 1: 3 ratio. The *cis*-hydroxylation of IVa and IVb with an aqueous solution of potassium permanganate and magnesium sulfate gave methyl (±)-*threo*-2,3-dihydroxy-4-(3,4-dimethoxyphenyl)-3-methoxycarbonylbutyrate (Va) and its (±)-*erythro*-isomer (Vb) respectively. The dimethyl esters, (±)-Va and (±)-Vb, were converted to the corresponding monomethyl esters, (±)-VIIa and (±)-VIIb respectively, *via* two dicarboxylic acid derivatives, (±)-VIa and (±)-VIb. The resolution of (±)-VIIb with brucine gave (+)-VIIb and (−)-VIIb, which were then converted to (+)-Vb and (+)-VIb and to (−)-Vb and (−)-VIb respectively. The synthetic (+)-Vb was shown to be identical with the natural *O,O'*-dimethylfukiic acid dimethyl ester by a mixed fusion and by comparisons of their IR and NMR spectra. From the present study it is evident that natural fukiic acid has an *erythro* configuration.

Recently a new polyphenol, fukinolic acid, was isolated from the leaves, leaf stems, and flower stalks of *Petasites japonicus* by Sakamura *et al.*[2)] They have also been reported that the alkaline hydrolysis of fukinolic acid gave caffeic acid and a new acid, named fukiic acid, in a molar ratio of 1: 1. Although no physical properties of fukiic acid have been reported except the *Rf* value on paper chromatography, its structure was proposed to be 2,3-dihydroxy-4-(3,4-dihydroxyphenyl)-3-carboxybutyric acid (I) on the basis of the analytical and spectroscopic studies of its derivatives. Two racemic modifications (*threo* and *erythro*) are possible for I. However, since the stereochemistry of fukiic acid has not yet been reported, the present authors attempted a total synthesis of fukiic acid derivatives in order to confirm the proposed structure and to elucidate the stereochemistry of fukiic acid. The present paper will describe a stereospecific synthesis of fukiic acid derivatives and their stereochemistry. For their synthesis, 3, 4-dimethoxyphenylpyruvic acid (II) was chosen as the starting substance, and the acid (II) was methylated with one equivalent of diazomethane to give the corresponding methyl ester (III). The Wittig reaction[3)] of III with carbomethoxymethylenetriphenylphosphorane afforded a 96% yield of a mixture of geometric isomers, which were then successfully separated, by means of

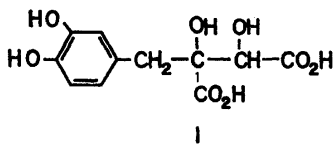

I

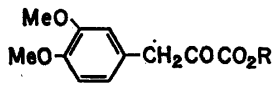

II R=H
III R=Me

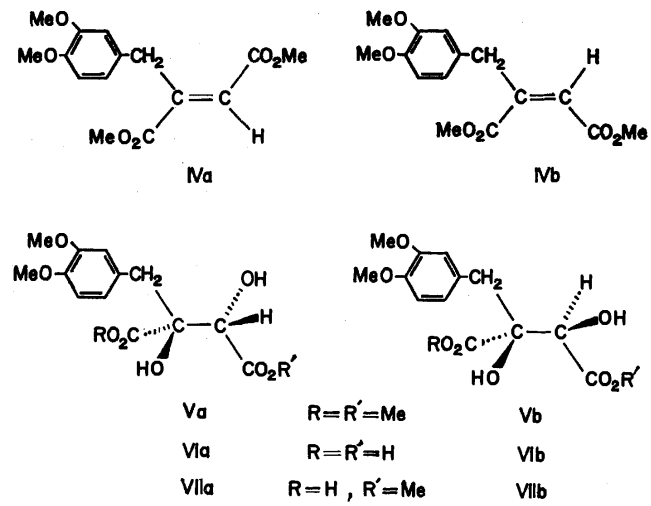

column chromatography on silica gel, into two crystalline esters in a 1: 3 ratio. It is well known that the ylids stabilized by an adjacent carbonyl function yield, as the predominant product, the isomer in which the carbonyl function is *trans* to the larger group at the beta carbon atom. In the NMR spectra it is also known that the signal of a *cis*-vinyl proton to the methoxycarbonyl group is to be found at a field lower than that of the corresponding *trans*-vinyl proton. The chemical shifts of the olefinic protons in the above minor (mp 49—50°C) and major (mp 56.5—57°C) esters were observed at δ *ca.* 6.8 ppm and at δ 5.67 ppm respectively. Therefore, the structures of the minor and major esters were identified as the 1-(3,4-dimethoxybenzyl)fumaric acid dimethyl ester (IVa) and the 1-(3,4-dimethoxybenzyl)maleic acid dimethyl ester (IVb) respectively. These assignments were further supported by the chemical shifts of the methylene protons in IVa and IVb. That is, IVa showed the signal of the methylene protons at δ 4.12 ppm, suggesting the presence of a *cis*-methoxycarbonyl group relative to the methylene protons, because IVb showed the corresponding signal at δ 3.61 ppm. The hydroxylation of IVa and IVb in methanol with an aqueous solution of potassium permanganate and magnesium sulfate at −20°C gave the corresponding diols, (±)-Va (mp 93—94°C) and (±)-Vb (mp 142°C) respectively. Since it is well

1) A preliminary communication concerning this work appeared in *Chem. Lett.*, **1972**, 1.

2) S. Sakamura, T. Yoshihara, and K. Toyoda, *Agr. Biol. Chem.* (Tokyo), **33**, 1795 (1969).

3) A. Maercker, "Organic Reactions," Vol. 14, Wiley, New York (1965), p. 270.

known that an aqueous solution of potassium permanganate reacts with olefins to add two hydroxyl functions to the double bond in a *cis* manner, the structures of the above diols were identified as methyl (±)-*threo*-2,3-dihydroxy-4-(3,4-dimethoxyphenyl)-3-methoxycarbonylbutyrate for Va and its (±)-*erythro*-isomer for Vb. The dimethyl esters, (±)-Va and (±)-Vb, were then hydrolyzed with aqueous potassium hydroxide to the corresponding dicarboxylic acid derivatives, (±)-VIa and (±)-VIb, which were subsequently methylated back into (±)-Va and (±)-Vb with diazomethane. This proved that there was no configurational change during the hydrolyses of (±)-Va and (±)-Vb. The NMR spectra of (±)-Vb in $CDCl_3$ and of (±)-VIb in $(CD_3)_2CO$ showed signals due to the methylene protons at δ 3.05 and 3.27 ppm, and at δ 3.06 and 3.26 ppm, respectively as well-defined AB-type quartets, while the spectra of (±)-Va in $CDCl_3$ and (±)-VIa in $(CD_3)_2CO$ showed the corresponding signals at δ 3.07 ppm as a singlet, and at δ 3.16 ppm as a slightly separated doublet, respectively. In the NMR spectrum of the natural fukiic acid monomethyl ester in $(CD_3)_2CO$, Sakamura *et al.*[2] had reported that the signal of the methylene protons was observed at δ 2.94 and 3.14 ppm as an AB-type quartet. From the similarity of these NMR spectra in the synthetic and natural compounds, it seemed that fukiic acid had an *erythro* configuration.

To obtain further confirmation by a direct comparison of the optically-active synthetic compound with the corresponding natural sample, the resolution of the synthetic racemate was carried out as follows. Since an attempt at the resolution of (±)-VIb was not encouraging, it was converted to the corresponding monomethyl ester, (±)-VIIb (mp 185—186°C), by treatment with methanol containing a small amount of concentrated hydrochloric acid. The (±)-VIIb acid in methanol was successfully resolved by means of brucine, and one of the diastereomeric salts (mp 185—186°C dec.) was decomposed with dilute hydrochloric acid to give (+)-VIIb, mp 138—139°C, $[\alpha]_D$+40.8° (methanol). The mother liquor, after the separation of the above brucine

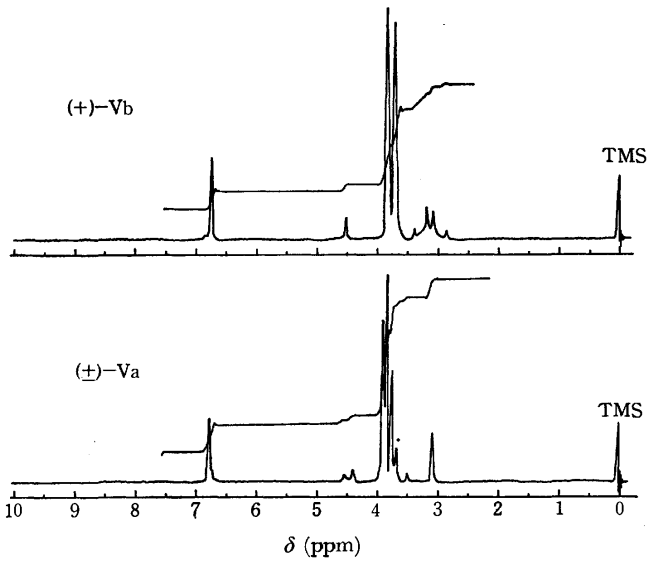

Fig. 1. NMR spectra of synthetic (+)-Vb and (±)-Va in $CDCl_3$.

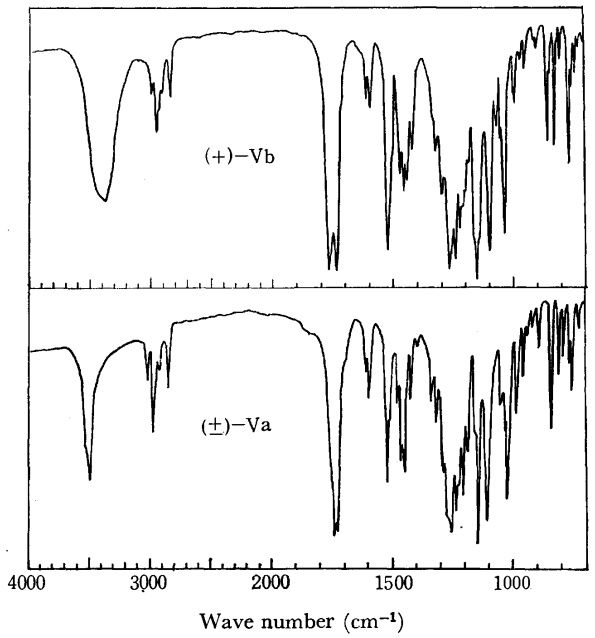

Fig. 2. IR spectra of synthetic (+)-Vb and (±)-Va in KBr.

salt, was also treated with dilute hydrochloric acid to give (−)-VIIb, mp 138—139°C, $[\alpha]_D$−38.0° (methanol). The alkaline hydrolyses of (+)-VIIb and (−)-VIIb gave (+)-VIb, mp 104—106°C, $[\alpha]_D$+40.3° (methanol) and (−)-VIb, mp 104—106°C, $[\alpha]_D$−40.5° (methanol), respectively. The methylation of (+)-VIb or (+)-VIIb with diazomethane gave (+)-Vb, mp 116—117°C, $[\alpha]_D$+40.5° (methanol), which was shown to be identical with the natural *O,O'*-dimethylfukiic acid dimethyl ester by a mixed-melting-point determination and by comparisons of their IR and NMR spectra. The acids, (−)-VIb, and (−)-VIIb, were also methylated with diazomethane to (−)-Vb, mp 116—117°C, $[\alpha]_D$−39.7° (methanol). (±)-VIa was also converted to the corresponding monomethyl ester, (±)-VIIa, mp 159—160°C.

From the present study, it is evident that natural fukiic acid has an *erythro* confiugration.[4]

Experimental

All the melting points are uncorrected. The NMR spectra were taken on a Hitachi Model R-20 NMR spectrometer (60 MHz), using tetramethylsilane as the internal standard. Their chemical shifts are presented in terms of δ values; s: singlet; d: doublet; dd: double doublet; t: triplet; m: multiplet. The optical rotation measurements were carried out by the use of a Yanagimoto OR-50 direct-reading polarimeter. The length of the cell used was 1 cm. The column chromatography was performed on Merck silica gel (0.08 mm).

Methyl 3,4-Dimethoxyphenylpyruvate (III). An ether solution (34 m*l*) containing diazomethane (0.56 g: 0.0134 mol) was stirred into a suspension of 3,4-dimethoxyphenylpyruvic

4) In a recent private communication from Professor S. Sakamura, he stated that his group also reached the same conclusion on the basis of a different synthesis of the (±)-*O,O'*-dimethylfukiic acid dimethyl ester, and that they also have identified the absolute configuration of fukiic acid; the details of their work were submitted to *Tetrahedron Lett.* and *Agr. Biol. Chem.* (Tokyo).

acid (II) (3.00 g: 0.0134 mol) in acetone (20 m*l*) with cooling in an ice–water bath. After the addition was complete, the mixture was filtered to remove a small amount of the starting acid (II), and then the filtrate was immediately evaporated under a vacuum. The residue was recrystallized from aqueous methanol to give pale yellow crystals (III); mp 99—102°C; yield, 2.10 g. NMR in $CDCl_3$: 3.89 (9H, s, 2-OC$\underline{H}_3$ and -$CO_2C\underline{H}_3$), 6.42 (2H, dd, J=1.5 and 8 Hz, -C$\underline{H}_2$-), 6.85 (1H, d, J=8 Hz), 7.28 (1H, dd, J=1.5 and 8 Hz), 7.49 (1H, d, J=1.5 Hz).

Found: C, 60.77; H, 5.93%. Calcd for $C_{12}H_{14}O_5$: C, 60.50; H, 5.92%.

1-(3,4-Dimethoxybenzyl)fumaric Acid Dimethyl Ester (IVa) and 1-(3,4-Dimethoxybenzyl)maleic Acid Dimethyl Ester (IVb). A mixture of the ester (III: 10.0 g), carbomethoxymethylenetriphenylphosphorane (14.6 g), and dry benzene (200 m*l*) was refluxed for 2 hr under a stream of nitrogen and then evaporated under a vacuum. The residue was extracted with ether, and the extract, after the removal of the ether, was chromatographed on silica gel, using benzene containing 7% and then 50% ether as the eluents. The first fraction gave IVa (2.943 g), which was recrystallized from ether containing petroleum ether to give pale yellow crystals; mp 49—50°C. NMR in $CDCl_3$: 3.74 and 3.79 (each 3H and s, 2-$CO_2C\underline{H}_3$), 3.82 (6H, s, 2-OC$\underline{H}_3$), 4.12 (2H, s, -C$\underline{H}_2$-), 6.78—6.95 (4H, m, aromatic (3H) and olefinic (1H) protons).

Found: C, 61.46; H, 6.35%. Calcd for $C_{15}H_{18}O_6$: C, 61.21; H, 6.17%.

The second fraction gave IVb (8.876 g) which was also recrystallized from ether containing petroleum ether to give colorless crystals; mp 56.5—57°C. A mixed-melting-point determination with the above IVa (mp 49—50°C) gave 34.5—36°C. NMR in $CDCl_3$: 3.61 (2H, d, J=1.5 Hz, -C$\underline{H}_2$-), 3.70 and 3.78 (each 3H and s, 2-$CO_2C\underline{H}_3$), 3.85 (6H, s, 2-OC$\underline{H}_3$), 5.67 (1H, t, J=1.5 Hz, =C$\underline{H}CO_2CH_3$), 6.68—6.83 (3H, m, aromatic protons).

Found: C, 61.16; H, 6.15%. Calcd for $C_{15}H_{18}O_6$: C, 61.21; H, 6.17%.

Methyl (±)-threo- (Va) and Methyl (±)-erythro-2,3-Dihydroxy-4-(3,4-dimethoxyphenyl)-3-methoxycarbonylbutyrate (Vb). *a)*: A solution of potassium permanganate (6.12 g) and magnesium sulfate heptahydrate (9.55 g) in water (270 m*l*) was stirred, drop by drop, into a solution of IVb (8.80 g) in methanol (255 m*l*) for 110 min at −20±2°C. The mixture was further stirred for 3 hr at this temperature, and then aqueous sodium bisulfite was added. The mixture was evaporated under a vacuum to remove the methanol, saturated with sodium chloride, and extracted with ethyl acetate, which was then washed with a saturated sodium chloride solution. After drying over sodium sulfate and removing the solvent, the residual solid was recrystallized from acetone to give methyl (±)-*erythro*-2,3-dihydroxy-4-(3,4-dimethoxyphenyl)-3-methoxycarbonylbutyrate (Vb) as colorless crystals; mp 142°C; yield, 4.17 g. NMR in $CDCl_3$: 3.28 (1H, s, -O$\underline{H}$), 3.28 (1H, d, J=8.5 Hz, -CH(O$\underline{H}$)-), 3.05 and 3.27 (2H, each d and J=14 Hz, -C$\underline{H}_2$-), 3.74 and 3.82 (each 6H and s, 2-$CO_2C\underline{H}_3$ and 2-OC$\underline{H}_3$), 4.54 (1H, d, J=8.5 Hz, -C$\underline{H}$(OH)-), 6.72 (3H, s, aromatic protons).

Found: C, 54.84; H, 6.10%. Calcd for $C_{15}H_{20}O_8$: C, 54.87; H, 6.14%.

b): A solution of IVa (1.09 g) in methanol was also hydroxylated with an aqueous potassium permanganate solution by a method similar to that used for (±)-Vb. The crude product was recrystallized from ether containing petroleum ether to give methyl (±)-*threo*-2,3-dihydroxy-4-(3,4-dimethoxyphenyl)-3-methoxycarbonylbutyrate (Va) as colorless crystals; mp 93—94°C; yield, 708 mg. NMR in $CDCl_3$: 3.07 (2H, s, -C$\underline{H}_2$-), 3.58 (1H, d, J=9 Hz, -CH(O$\underline{H}$)-), 3.71 (3H), 3.81 (6H), and 3.84 (3H) (each s, 2-$CO_2C\underline{H}_3$ and 2-OC$\underline{H}_3$), 4.43 (1H, d, J=9 Hz, -C$\underline{H}$(OH)-), 6.75 (3H, s, aromatic protons).

Found: C, 55.10; H, 6.16%. Calcd for $C_{15}H_{20}O_8$: C, 54.87; H, 6.14%.

(±)-threo- (VIa) and (±)-erythro-2,3-Dihydroxy-4-(3,4-dimethoxyphenyl)-3-carboxybutyric Acid (VIb). *a)*: A mixture of (±)-Vb (1.10 g) and aqueous potassium hydroxide (5%: 15 m*l*) was stirred on a steam bath for 40 min. After cooling, the mixture was acidified with dilute hydrochloric acid, saturated with sodium chloride, and then extracted with ethyl acetate. The extract, after having been washed with a saturated sodium chloride solution, was dried over sodium sulfate and then evaporated under a vacuum. The residue was recrystallized from acetone containing petroleum ether to give (±)-*erythro*-2,3-dihydroxy-4-(3,4-dimethoxyphenyl)-3-carboxybutyric acid (VIb) as colorless crystals; mp 179—180.5°C; yield, 830 mg. NMR in $(CD_3)_2CO$: 3.06 and 3.26 (2H, each d and J=13 Hz, -C$\underline{H}_2$-), 3.73 (6H, s, 2-OC$\underline{H}_3$), 4.57 (1H, s, -C$\underline{H}$(OH)-), 6.78 and 6.83 (3H, aromatic protons).

Found: C, 52.30; H, 5.54%. Calcd for $C_{13}H_{16}O_8$: C, 52.00; H, 5.37%.

The above (±)-VIb in acetone was methylated with diazomethane to give, after crystallization, colorless crystals (mp 142°C), which were shown to be identical with (±)-Vb by a mixed-melting-point determination and by a comparison of their IR spectra.

b): The dimethyl ester, (±)-Va, was also hydrolyzed with aqueous potassium hydroxide by a method similar to that used for (±)-VIb. The crude product was recrystallized from acetone to give (±)-*threo*-2,3-dihydroxy-4-(3,4-dimethoxyphenyl)-3-carboxybutyric acid (VIa) as colorless crystals; mp 112—115°C.

Found: C, 49.22; H, 5.81%. Calcd for $C_{13}H_{16}O_8 \cdot H_2O$: C, 49.06; H, 5.70%.

The above crystals were dissolved in acetone containing benzene, and the solution was then evaporated to dryness under a vacuum. The residue was recrystallized from acetone containing petroleum ether to give colorless crystals; mp 188—190°C. NMR in $(CD_3)_2CO$: 3.16 (2H, slightly separated d, -C$\underline{H}_2$-), 3.75 (6H, s, 2-OC$\underline{H}_3$), 4.43 (1H, s, -C$\underline{H}$(OH)-), 6.81 and 6.87 (3H, aromatic protons).

Found: C, 51.70; H, 5.37%. Calcd for $C_{13}H_{16}O_8$: C, 52.00; H, 5.37%.

The methylation of (±)-VIa with diazomethane gave (±)-Va.

Methyl (±)-threo- (VIIa) and Methyl (±)-erythro-2,3-Dihydroxy-4-(3,4-dimethoxyphenyl)-3-carboxybutyrate (VIIb). *a)*: A solution of (±)-VIb (200 mg) in methanol (3.0 m*l*) containing one drop of concentrated hydrochloric acid was allowed to stand at room temperature for 2 hr and then evaporated under a vacuum. The residue was recrystallized from a mixture of acetone and petroleum ether to give the corresponding monomethyl ester, (±)-VIIb (mp 185—186°C) as colorless crystals; yield, 110 mg. NMR in pyridine-d_5: 3.60 (9H, s, -$CO_2C\underline{H}_3$ and 2-OC$\underline{H}_3$), 3.62 and 3.83 (2H, each d, and J=14 Hz, -C$\underline{H}_2$-), 5.26 (1H, s, -C$\underline{H}$(OH)-).

Found: C, 53.52; H, 5.80%. Calcd for $C_{14}H_{18}O_8$: C, 53.50; H, 5.77%.

b): A mixture of (±)-VIa (1.20 g), concentrated hydrochloric acid (1.2 m*l*), and methanol (20 m*l*) was allowed to stand overnight at room temperature and was then evaporated under a vacuum. The residue was purified by means of column chromatography. A column was prepared from

a suspension of silica gel (100 g) in a mixture of benzene (400 ml) and acetone (140 ml) containing dilute sulfuric acid (20%: 6.0 ml). Elution was carried out with benzene containing 30% acetone to give a solid (1.02 g), which was then recrystallized from a mixture of acetone and petroleum ether to give the monomethyl ester, (±)-VIIa, as colorless crystals; mp 159—160°C; yield, 863 mg. NMR in $(CD_3)_2CO$: 3.04 (2H, s, $-C\underline{H}_2-$), 3.71 (6H) and 3.76 (3H) (each s, $-CO_2C\underline{H}_3$ and 2-$OC\underline{H}_3$), 4.40 (1H, s, $-C\underline{H}(OH)-$), 6.78 and 6.88 (3H, aromatic protons).

Found: C, 53.63; H, 5.73%. Calcd for $C_{14}H_{18}O_8$: C, 53.50; H, 5.77%.

Resolution of (±)-VIIb with Brucine. a): Brucine dihydrate (595 mg) was dissolved in a hot solution of (±)-VIIb (433 mg) in methanol (8.0 ml), after which the solution was allowed to stand at room temperature. The precipitates were collected, washed with acetone, and then recrystallized from methanol to give colorless crystals; mp 185—186°C dec.; yield, 490 mg. A mixed-melting-point determination with (±)-VIIb (mp 185—186°C) showed 175—178°C.

Found: C, 61.15; H, 6.13; N, 3.81%. Calcd for $C_{37}H_{44}O_{12}N_2 \cdot H_2O$: C, 61.00; H, 6.38; N, 3.86%.

A suspension of the above brucine salt (255 mg) in dilute hydrochloric acid (2N: 5.0 ml) was extracted with ethyl acetate. The extract was washed with water, dried over sodium sulfate, and then evaporated under a vacuum. The residue (132 mg) was recrystallized from a mixture of acetone and petroleum ether to give (+)-VIIb as colorless crystals; mp 138—139°C, $[\alpha]_D^{28}$+40.8° (*c* 1.25, methanol); yield, 114 mg.

Found: C, 50.82; H, 6.20%. Calcd for $C_{14}H_{18}O_8 \cdot H_2O$: C, 50.60; H, 6.07%.

b): The mother liquor in *a)*, after the separation of the brucine salt (490 mg: mp 185—186°C dec.), was evaporated under a vacuum. The residue was suspended in dilute hydrochloric acid (2N: 5.0 ml) and then treated by a method similar to that used for (+)-VIIb. The crude product was recrystallized from a mixture of acetone and petroleum ether to give (−)-VIIb as colorless crystals; mp 138—139°C, $[\alpha]_D^{28}$−38.0° (*c* 0.72, methanol); yield, 104 mg.

Found: C, 50.68; H, 5.98%. Calcd for $C_{14}H_{18}O_8 \cdot H_2O$: C, 50.60; H, 6.07%.

Hydrolyses of (+)-VIIb and (−)-VIIb. a): (+)-VIIb (245 mg) was hydrolyzed with aqueous potassium hydroxide (5%: 3.0 ml) by a method similar to that used for (±)-VIb. The crude product was recrystallized from a mixture of acetone and petroleum ether to give (+)-VIb as colorless crystals; mp 104—106°C, $[\alpha]_D^{28}$+40.3° (*c* 0.72, methanol); yield, 124 mg.

Found: C, 49.18; H, 5.75%. Calcd for $C_{13}H_{16}O_8 \cdot H_2O$: C, 49.06; H, 5.70%.

b): Similarly, (−)-VIIb was also hydrolyzed to (−)-VIb; mp 104—106°C, $[\alpha]_D^{25}$−40.5° (*c* 0.79, methanol).

Found: C, 49.27; H, 5.81%. Calcd for $C_{13}H_{16}O_8 \cdot H_2O$: C, 49.06; H, 5.70%.

(+)- and (−)-O,O'-Dimethylfukiic Acid Dimethyl Ester (Vb). a): The treatment of (+)-VIb or (+)-VIIb with diazomethane gave (+)-Vb as colorless crystals; mp 116—117°C, $[\alpha]_D^{26}$+40.5° (*c* 0.78, methanol).

Found: C, 54.89; H, 6.11%. Calcd for $C_{15}H_{20}O_8$: C, 54.87; H, 6.14%.

The synthetic (+)-Vb was shown to be identical with the natural *O,O'*-dimethylfukiic acid dimethyl ester (mp 117—118°C) by a mixed-melting-point determination and by comparisons of their IR and NMR spectra.

b): Similarly, (−)-VIb or (−)-VIIb was also methylated with diazomethane to (−)-Vb; mp 116—117°C, $[\alpha]_D^{26}$−39.7° (*c* 0.78, methanol).

Found: C, 55.04; H, 6.08%. Calcd for $C_{15}H_{20}O_8$: C, 54.87; H, 6.14%.

The authors are grateful to Professor S. Sakamura, Department of Agricultural Chemistry, Faculty of Agriculture, Hokkaido University, for his permission to publish this work and for the generous supply of a sample and copies of IR and NMR spectra of natural *O,O'*-dimethylfukiic acid dimethyl ester. Thanks are also due to Assistant Professor S. Yasuda, Department of Chemistry, Faculty of General Education of this University, for the measurements of the optical rotation.

Oxidation by Transition Metal Complexes. III. Oxidation of Cinnamaldehyde Catalyzed by Rhodium Compounds

Kiyotomi TAKAO, Masami WAYAKU, Yuzo FUJIWARA,
Toshinobu IMANAKA, and Shiichiro TERANISHI
Department of Chemical Engineering, Faculty of Engineering Science, Osaka University, Osaka
(Received November 4, 1971)

The catalytic activity of $RhCl(PPh_3)_3$ and $RhCl(CO)(PPh_3)_2$ for oxidations of styrene and cinnamaldehyde has been studied. Under oxygen atmosphere, these complexes can cause catalytically oxidation of cinnamaldehyde to give benzaldehyde, glyoxal, benzene and styrene. The reaction is complicated because decarbonylation reaction takes place with oxidation, and the carbonyl complex formed plays a catalytic role for the oxidation.

In previous papers,[1,2] we reported on the catalytic oxidation of styrene and methylstyrenes with some rhodium compounds under oxygen stream to produce the corresponding aldehydes and ketones.

In connection with this work, the catalytic oxidation of cinnamaldehyde by the rhodium complexes was investigated. It was found that some rhodium complexes have catalytic functions for oxidation, but the reaction is complicated because decarbonylation reaction also takes place at the same time. Cinnamaldehyde gave benzaldehyde and glyoxal by oxidation, and styrene and benzene by decarbonylation. It becomes apparent that the oxidation reaction might proceed *via* the carbonyl complex, $RhCl(CO)(PPh_3)_2$ formed by decarbonylation of the starting aldehyde. In the present paper we wish to report on the oxidation of cinnamaldehyde with rhodium complexes.

Results and Discussion

Catalytic oxidation of styrene with iridium and rhodium complexes under oxygen atmosphere[1,2] give benzaldehyde and acetophenone. The complex $RhCl(PPh_3)_3$ is known to be an efficient catalyst for decarbonylation of aldehydes.[3-6]

In order to investigate the relation between oxidation and decarbonylation, the relation between product concentrations and the time for the oxidation of styrene in toluene was examined.

The result is given in Fig. 1. We see that the concentration of benzaldehyde increases with reaction time very slowly during the first hour and then increases rapidly. After 8 hr, the yield of benzaldehyde became almost constant and reached 213%.[7]

Acetophenone was also formed in 13% yield. A 3% yield of benzene was attained by the decarbonylation of benzaldehyde.

From the fact that both oxidation and decarbonylation reactions take place simultaneously, we examined the decarbonylation of cinnamaldehyde with a $RhCl(PPh_3)_3$ catalyst before studying the oxidation of cinnamaldehyde.

Mixtures of the reactant cinnamaldehyde and $RhCl(PPh_3)_3$ in toluene were heated at 80°C for 8 hr under nitrogen stream.

Figure 2 shows that cinnamaldehyde easily undergoes decarbonylation to give styrene.

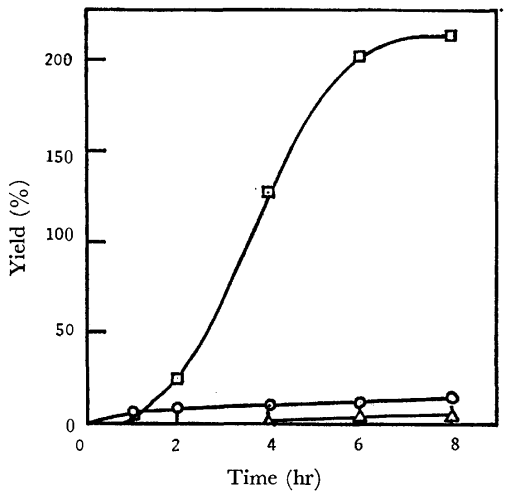

Fig. 1. Oxidation of styrene with $RhCl(PPh_3)_3$ in toluene: □: Benzaldehyde, ○: Acetophenone, △: Benzene

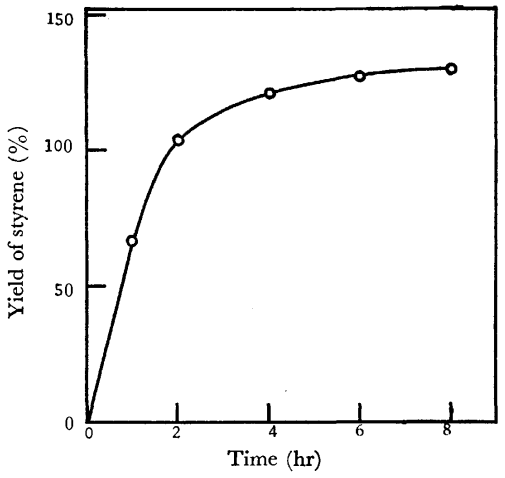

Fig. 2. Decarbonylation of cinnamaldehyde with $RhCl(PPh_3)_3$ in toluene under nitrogen stream.

1) K. Takao, Y. Fujiwara, T. Imanaka, and S. Teranishi, This Bulletin, **43**, 1153 (1970).
2) K. Takao, M. Wayaku, T. Fujiwara, T. Imanaka, and S. Teranishi, *ibid.*, **43**, 3898 (1970).
3) J. Tsuji and K. Ohno, *Tetrahedron Lett.*, **1965**, 3969.
4) Idem., *ibid.*, **1967**, 2173.
5) K. Ohno and J. Tsuji, *J. Amer. Chem. Soc.*, **90**, 99 (1968).
6) M. C. Baird, C. T. Nyman, and G. Wilkinson, *J. Chem. Soc.*, *A*, **1967**, 1347.
7) Yields are based on the catalyst used.

Table 1. Oxidation of cinnamaldehyde (Reaction temp. 80°C, Reaction time 8 hr)

Catalyst	Solvent	Products and yields,[a] %			
		Benzene	Styrene	Benzaldehyde	Acetophenone
$RhCl(PPh_3)_3$	Toluene	45	97	248	trace
$RhCl(PPh_3)_3$	Ethanol	trace	127	trace	8
$RhCl(CO)(PPh_3)_2$	Toluene	9	30	968	trace

a) Yields are based on the catalyst used.

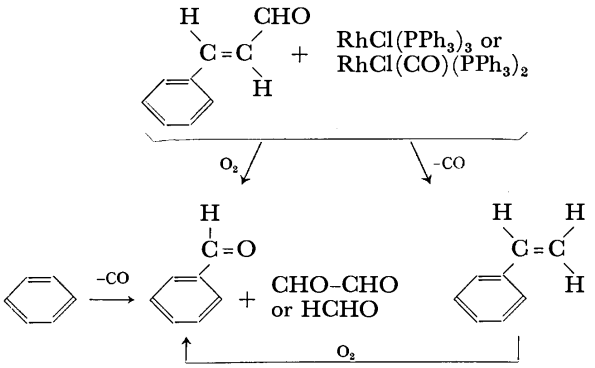

Scheme 1. Reaction scheme in the oxidation of cinnamaldehyde.

Oxidation reaction of cinnamaldehyde was then carried out under constant bubbling of oxygen (Table 1 and Scheme 1). The products were benzaldehyde (248%), styrene (97%), benzene (45%), glyoxal, and formaldehyde. The relation between the product concentration and the time for the oxidation reaction is given in Fig. 3.

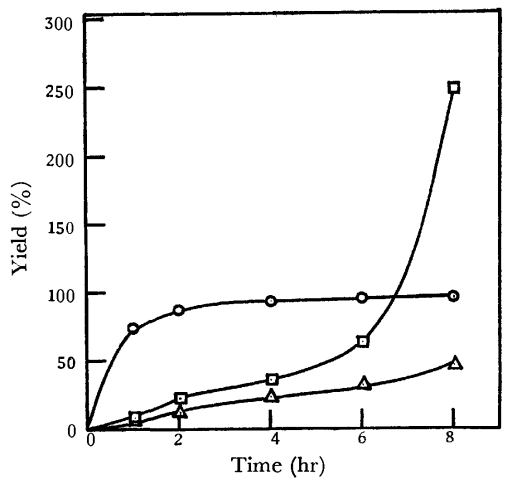

Fig. 3. Oxidation of cinnamaldehyde with $RhCl(PPh_3)_3$ in toluene.
□: Benzaldehyde, ○: Styrene, △: Benzene

It can be said that benzaldehyde is produced from the C=C double-bond cleavage of both cinnamaldehyde and styrene derived from the decarbonylation of cinnamadehyde. The fact that oxidation of both styrene and cinnamaldehyde has an induction period and involves decarbonylation reaction suggests that some rhodium carbonyl complexes formed play an important role for the oxidation catalyst. $RhCl(CO)(PPh_3)_2$ was obtained from the reaction mixtures. We therefore, examined the catalytic activity of the rhodium complex $RhCl(CO)(PPh_3)_2$ for oxidation reaction. Oxidation of cinnamaldehyde was carried out in the presence of $RhCl(CO)(PPh_3)_2$ under similar conditions. It was found that the carbonyl complex has remarkably high activity for the oxidation catalyst. A plot of the yields of products *versus* reaction time is given in Fig. 4.

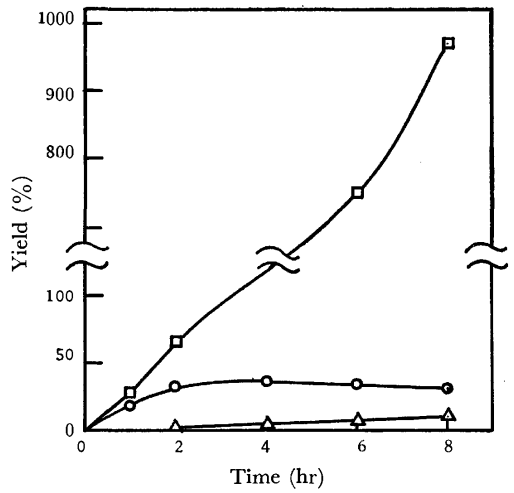

Fig. 4. Oxidation of cinnamaldehyde with $RhCl(CO)(PPh_3)_2$ in tolune.
□: Benzaldehyde. ○: Styrene. △: Benzene

The yield of benzaldehyde increased with reaction time and reached 968% after 8 hr.

On the other hand decarbonylation of aldehydes is very slow. The yield of styrene (30%) hardly changed with time and benzene derived from benzaldehyde was obtained in only 9% yield. The product distribution in the $RhCl(PPh_3)_3$ catalyst after the induction period (one hour) is very similar to that in the $RhCl(CO)(PPh_3)_2$ catalyst.

These results show that the $RhCl(PPh_3)_3$ catalyzed oxidation might proceed *via* the carbonyl complex, $RhCl(CO)(PPh_3)_2$.[8]

We reported that the catalytic oxidation of styrene with rhodium complexes undergoes a remarkable solvent effect.[2] Such an effect was also observed in the oxidation of cinnamaldehyde.

The catalytic oxidation of cinnamaldehyde with $RhCl(PPh_3)_3$ in ethanol gave styrene (127%) and acetophenone (8%).

8) $RhCl(CO)(PPh_3)_2$ liberates carbon monoxide during the catalytic decarbonylation.[5]

Alcohol is not a good solvent for the C=C double-bond cleavage.

Experimental

Materials and Analysis. All temperatures were uncorrected. Vpc analysis was made by a Yanagimoto G-8 gas chromatograph using Apiezon-L, Silicone OV-17 or Diethyl phthalate columns. Toluene and ethanol were purified as mentioned previously.[1] Cinnamaldehyde was dried over anhydrous magnesium sulfate and distilled.

Preparation of Rhodium Complexes. Chlorotris(triphenylphosphine)rhodium(I), $RhCl(PPh_3)_3$ and chlorocarbonylbis(triphenylphosphine)rhodium(I), $RhCl(CO)(PPh_3)_2$ were prepared by the method of Osborn *et al.*[9]

General Procedure for Oxidation by the Rhodium Complexes. The rhodium complex and cinnamaldehyde were dissolved in a solvent such as toluene. Under constant bubbling of oxygen the solution was heated at 80°C for 8 hr. After evaporation of the solvent, isolation of the products was carried out by gas or column chromatography.

9) J. A. Osborn, F. H. Jardine, J. F. Young, and G. Wilkinson, *J. Chem. Soc., C*, **1966**, 1711.

Oxidation of Cinnamaldehyde by Rhodium Complexes. In a flask similar to that described previously[1] was placed a mixture containing 2.83 g (3.06 mmol) of $RhCl(PPh_3)_3$, 15.5g (0.117 mol) of cinnamaldehyde and 150 m*l* of toluene as a solvent. The oxidation reaction was carried out at 80°C with constant bubbling of oxygen for 8 hr. At appropriate intervals, a portion of the solvent was analyzed as usual. After evaporation of the solvent under reduced pressure, the residual material was chromatographed on a silica-gel column (30 g). Elution with one liter of ether gave triphenylphosphine oxide. In addition, elution with 500 m*l* of methanol gave dark brown complexes. The complexes were further chromatographed on a silica-gel column to give a considerable amount of carbonyl complex $RhCl(CO)(PPh_3)_2$ and unidentified complexes (mp 210—213°C (decomp.)) which gave no carbonyl absorption. From vpc analysis and isolation of the solvent cinnamaldehyde, 0.97 g (248%) of benzaldehyde, 0.31 g (97%) of styrene, 0.11 g (45%) of benzene, glyoxal, and formaldehyde were obtained. From vpc analysis (activated carbon column) of the outlet gas, carbon monoxide was determined. In the case of the reaction in ethanol as solvent, we obtained cinnamaldehyde, 0.39 g (127%) of styrene and 0.03 g (8%) of acetophenone. The complex $RhCl(CO)(PPh_3)_2$ was isolated from the reaction mixtures.

BULLETIN OF THE CHEMICAL SOCIETY OF JAPAN, VOL. 45, 1507—1515(1972)

Mercaptoacetate Derivatives. I. Reaction of Thiocyanatoacetic Esters with Aldehydes[1)]

Toshio HAYASHI

The Institute of Physical and Chemical Research, Wako, Saitama

(Received October 5, 1971)

An equimolar reaction of thiocyanatoacetic esters with aromatic aldehydes in the presence of sodium hydride, followed by treatment with hydrogen chloride, led to a mixture of 4-alkoxycarbonyl-5-aryl-2-imino-1,3-oxathiolane hydrochloride (**3**) and α-(*S*-carbamoylthio)-β-chlorodihydrocinnamic ester (**4**). When excess aldehyde was used in the reaction, a small amount of 2,10-bis(α-chlorobenzyl)-4,8-dioxo-6-phenyl-5,7-diaza-3,9-dithiaundecanedioate (**5**) was obtained, together with the products **3** and **4**. The NMR studies revealed that product **3** isolated exists all in one isomer which has the 4-ester and 5-aryl groups *cis* about a single bond in the ring. It was suggested that product **4** was formed by rearrangement of the *trans* isomer of **3**.

In a previous paper[2)] it was shown that the reaction of thiocyanatoacetic esters (**1**) with aldehydes occurs in the presence of potassium carbonate or fluoride to give a mixture of 5-substituted-*N*-carbamoyl-2-imino-4-alkoxy carbonyl-1,3-oxathiolanes (**2**) and α,β-unsaturated esters. In the course of study, it was found that sodium hydride is also an effective condensing agent for this reaction. The reaction of **1** with an aromatic aldehyde in the presence of sodium hydride, when followed by treatment with dry hydrogen chloride, led to a mixture of 2-imino-4-alkoxycarbonyl-5-aryl-1,3-oxathiolane hydrochloride (**3**) and two unexpected compounds (**4** and **5**).

1) Presented in part at the Autumn Meeting of the Chemical Society of Japan, Sapporo, August 29th (1970).

2) S. Kambe, T. Hayashi, H. Yasuda, and H. Midorikawa, This Bulletin, **44**, 1357 (1971).

Results and Discussion

An equimolar reaction of **1** and an aromatic aldehyde in the presence of sodium hydride at room temperature, on prolonged standing, produced cinnamic ester exclusively. However, the reaction, when conducted at −5°C and followed by treatment with dry hydrogen chloride, afforded a mixture of two solid compounds **3** and **4** in good yield. These compounds could be separated easily by utilizing the difference of the solubility in acetone. The ratios of the two components, as evaluated from the integration of the area under the appropriate NMR signals, varied widely with aldehydes used. The yields and physical properties of **3** and **4** are summarized in Tables 1 and 2, respectively. When excess aldehyde was used in the reaction, a small amount of high-melting compound (**5**), along with **3** and **4**, was

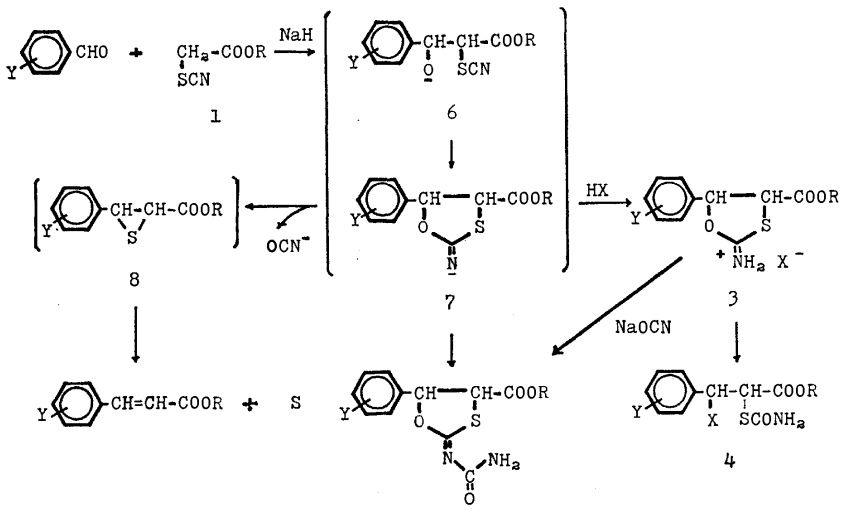

Scheme 1. [2]

Table 1. 2-Imino-4-alkoxycarbonyl-5-aryl-1,3-oxathiolane hydrochloride (**3**)

No.	R	X	Y	Yield (%)	Mp (°C)	Formula	Anal. Found (Calcd) C (%)	H (%)	N (%)	S (%)	Cl (%)	Br (%)
3b	Et	Cl	H	7	158—159	$C_{12}H_{14}NO_3SCl$	50.24 (50.08)	4.98 (4.90)	4.91 (4.87)	11.48 (11.15)	12.29 (12.32)	
3c	Et	Br	H	23	145—146	$C_{12}H_{14}NO_3SBr$	43.20 (43.38)	4.27 (4.25)	4.15 (4.22)	9.72 (9.65)	23.95 (24.06)	
3d	*t*-Bu	Cl	H	17	154—155	$C_{14}H_{18}NO_3SCl$	53.39 (53.24)	5.85 (5.74)	4.54 (4.27)	10.21 (10.15)	11.32 (11.23)	
3f	Et	Cl	*p*-Cl	trace (38)[a]	166—166.5	$C_{12}H_{13}NO_3SCl_2$	44.48 (44.73)	4.11 (4.07)	4.27 (4.35)	9.57 (9.96)	21.82 (22.00)	
3h	Et	Cl	*p*-Br	24 (10)[a]	163—164	$C_{12}H_{13}NO_3SBrCl$	39.14 (39.31)	3.55 (3.57)	3.78 (3.82)	8.46 (8.75)	9.60 (9.67)	21.64 (21.80)

a) Potassium carbonate was used as a catalyst (see the experimental section).

Table 2. α-(*S*-carbamoylthio)-β-aryl-β-chlorodihydrocinnamic esters (**4**)

No.	R	X	Y	Yield (%)	Mp (°C)	Formula	Anal. Found (Calcd) C (%)	H (%)	N (%)	S (%)	Cl (%)	Br (%)
4a	Me	Cl	H	32	129—130	$C_{11}H_{12}NO_3SCl$	48.22 (48.26)	4.44 (4.42)	5.33 (5.12)	11.57 (11.71)	13.01 (12.95)	
4b	Et	Cl	H	85	158—158.5	$C_{12}H_{14}NO_3SCl$	49.98 (50.08)	4.85 (4.90)	4.88 (4.87)	11.35 (11.15)	12.18 (12.32)	
4c	Et	Br	H	53	148—149	$C_{12}H_{14}NO_3SBr$	43.63 (43.38)	4.25 (4.25)	4.17 (4.22)	9.75 (9.65)		23.99 (24.06)
4d	*t*-Bu	Cl	H	45	125—126	$C_{14}H_{18}NO_3SCl$	53.32 (53.24)	5.75 (5.74)	4.49 (4.44)	10.22 (10.15)	10.83 (11.23)	
4e	Me	Cl	*p*-Cl	85	159—161	$C_{11}H_{11}NO_3SCl$	43.12 (42.87)	3.66 (3.60)	4.47 (4.55)	10.48 (10.40)	23.20 (23.01)	
4f	Et	Cl	*p*-Cl	95	152—153	$C_{12}H_{13}NO_3SCl_2$	44.67 (44.73)	4.03 (4.07)	4.25 (4.35)	9.72 (9.96)	21.85 (21.99)	
4g	Et	Cl	*o*-Cl	65	132—133	$C_{12}H_{13}NO_3SCl_2$	44.72 (44.73)	4.01 (4.07)	4.51 (4.35)	9.85 (9.96)	22.10 (22.01)	
4h	Et	Cl	*p*-Br	73	148—150	$C_{12}H_{13}NO_3SBrCl$	39.31 (39.31)	3.55 (3.57)	3.80 (3.82)	8.70 (8.75)	9.75 (9.67)	21.98 (21.80)
4i	Et	Cl	*p*-CN	50	137—138	$C_{13}H_{13}N_2O_3SCl$	50.12 (49.92)	4.21 (4.64)	9.09 (8.96)	9.30 (10.25)	11.30 (11.34)	
4j	Et	Cl	*p*-NO_2	50	149—149.5	$C_{14}H_{17}N_2O_5SCl$	46.55 (46.60)	4.64 (4.75)	7.80 (7.77)	9.00 (8.89)	9.67 (9.83)	
4k	Et	Cl	*p*-CH_3	38	142—143	$C_{13}H_{16}NO_3SCl$	51.62 (51.73)	5.31 (5.34)	4.89 (4.64)	10.51 (10.63)	11.82 (11.75)	
4l	Et	Cl	*p*-CH_3O	12	70— 73	$C_{13}H_{16}NO_4SCl$	49.35 (49.13)	5.34 (5.07)	4.62 (4.41)			

TABLE 3. PRODUCTS 5

No.	R	X	Y	Mp (°C)	Formula	Anal. Found (Calcd) C (%)	H (%)	N (%)	S (%)	Cl (%)
5b	Et	Cl	H	190—191	$C_{31}H_{32}N_2O_6S_2Cl_2$	56.06 (56.10)	4.86 (4.86)	4.33 (4.22)	9.87 (9.66)	10.36 (10.69)
5d	*t*-Bu	Cl	H	161	$C_{35}H_{40}N_2O_6S_2Cl_2$	58.49 (58.40)	5.48 (5.60)	3.92 (3.89)	8.78 (8.91)	9.78 (9.85)
5c	Et	Cl	*p*-Cl	194—195	$C_{31}H_{29}N_2O_6S_2Cl_5$	48.31 (48.56)	3.87 (3.81)	3.54 (3.65)	8.74 (8.36)	22.27 (23.11)
5h	Et	Cl	*p*-Br	196—196.5	$C_{31}H_{29}N_2O_6S_2Br_3Cl_2$	41.49 (41.35)	3.26 (3.25)	3.22 (3.11)	6.85 (7.12)	

obtained. The yield and physical properties of **5** are summarized in Table 3. As can be seen from the Table, the yields of **3** and **4** are extremely low, when benzaldehydes having an electron-donating substituent are used. Aliphatic aldehydes and ketones did not give any solid compound. In contrast, the reactions with benzaldehydes having an electron-attractive group produced **3** and **4** in fair to excellent yield. It was found that the esters **4** with an electron-donating group on the benzene nucleus decompose gradually in solid state and more rapidly in the solutions.

The structural assignments were made on the basis of elemental analysis, spectral studies, and chemical reactivity. As shown in the Tables, **3** and **4** have the

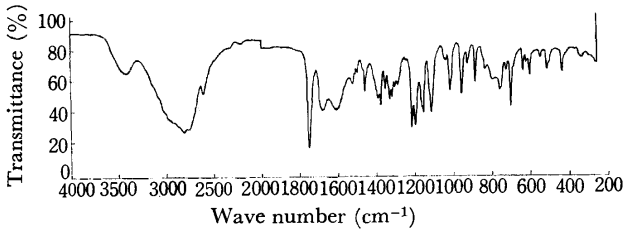

Fig. 1. IR spectrum of 2-imino-4-ethoxycarbonyl-5-phenyl-1, 3-oxathiolane hydrochloride (**3b**) (KBr pellet).

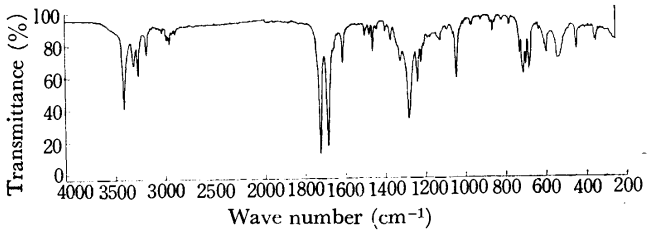

Fig. 2. IR spectrum of ethyl α-(S-carbamoylthio)-β-chlorodihydrocinnamate (**4b**) (KBr pellet).

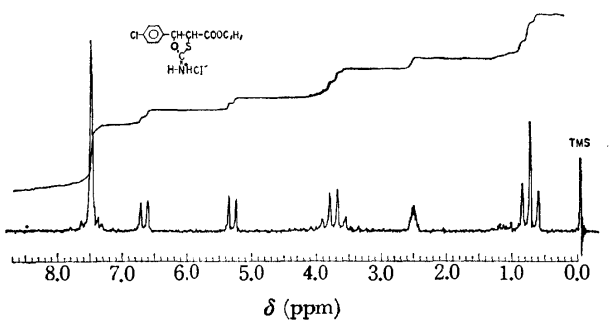

Fig. 3. NMR spectrum of 2-imino-4-ethoxycarbonyl-5-(*p*-chlorophenyl)-1,3-oxathiolane hydrochloride (**3f**) in DMSO-d_6 (60 MHz).

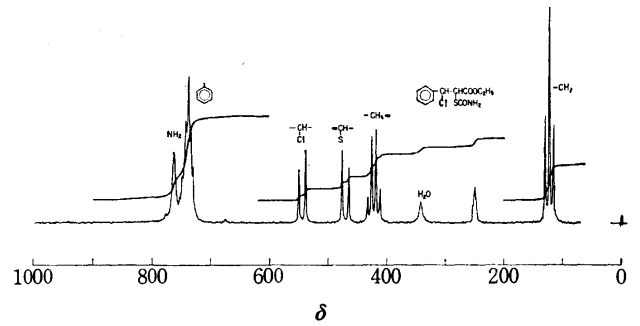

Fig. 4. NMR spectrum of ethyl α-(*S*-carbamoylthio)-β-chlorodihydrocinnamate (**4b**) in acetone-d_6 (100 MHz).

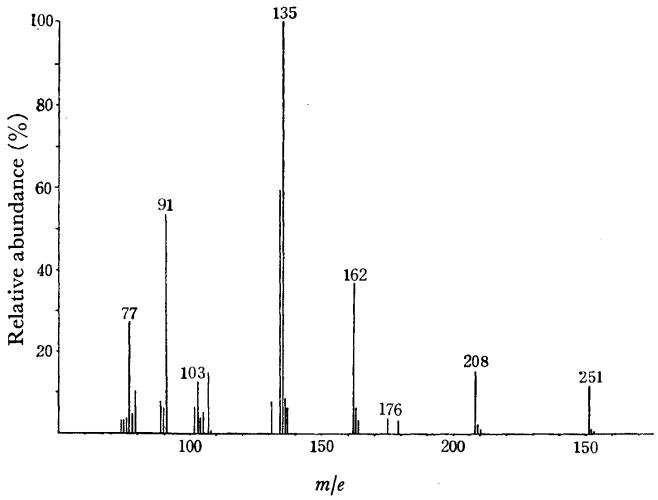

Fig. 5. Mass spectrum of 2-imino-4-ethoxycarbonyl-5-phenyl-1,3-oxathiolane hydrochloride (**3b**).

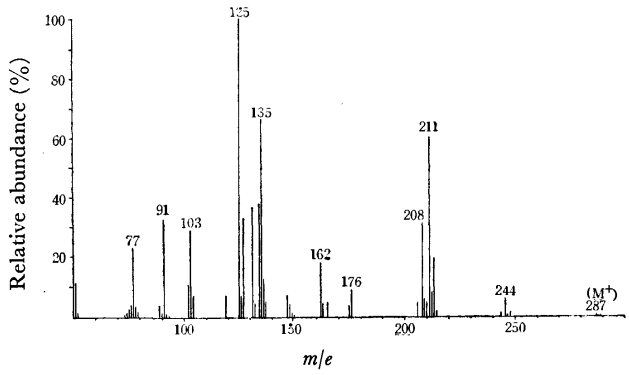

Fig. 6. Mass spectrum of ethyl α-(*S*-carbamoylthio)-β-chlorodihydrocinnamate (**4b**).

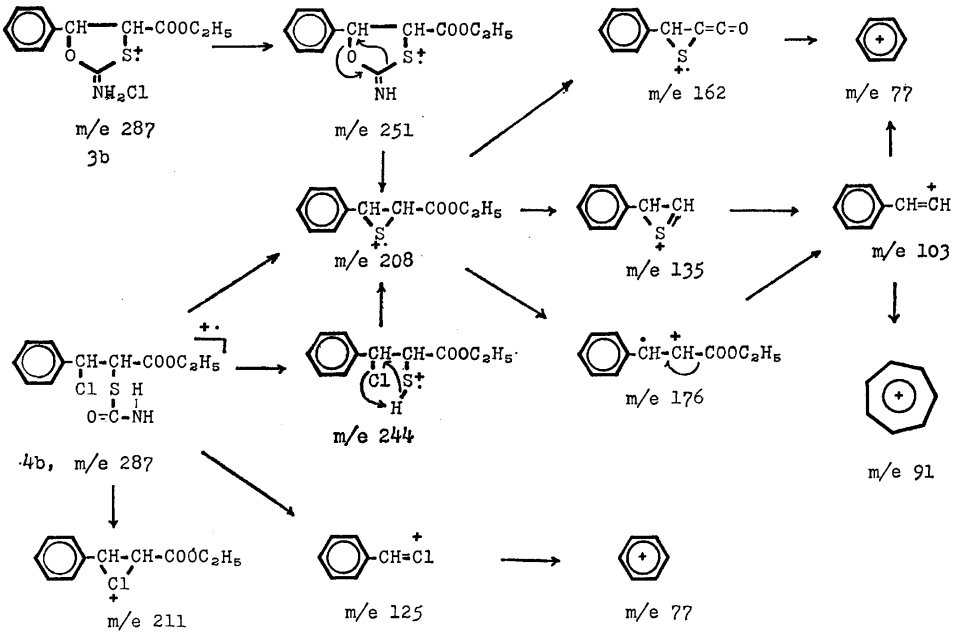

Scheme 2.

Table 4. IR data of products **3** in KBr (cm^{-1})

No.	NH_2 stretching	νC=O	νC=N	δNH_2
3b	3420 br 2800 br	1750 s	1680 s	1610 m
3c	3420 br 2860 br	1750 s	1670 s	
3d	3420 br 2840 br	1754 s	1680 s	1615 m
3f	3450 br 2860 br	1745 s	1680 s	1615 m
3h	2850 br	1745 s	1680 s	1610 m

br=broad, s=strong, m=medium.

same molecular formula, but their IR, NMR, and mass spectra showed marked differences (Figs. 1 to 6). In the IR spectrum of **3b** (KBr pellet), a complex series of absorptions between 3500 and 2500 cm^{-1} suggests the presence of the imine hydrochloride, while with **4b**, rather sharp bands in the ranges 3410—3182 cm^{-1} are due to the NH_2 stretching vibrations. These assignments may be supported by the following facts: **3**'s were readily soluble in water and when treated with silver nitrate reagent, showed a positive test for chloride ion. Convincing evidence for the structure of **3** may be supplied by the fact that **3b**, when treated with an equimolar amount of potassium cyanate, produced *N*-carbamoyl-2-imino-4-ethoxycarbonyl-5-phenyl-1,3-oxathiolane (**2b**), which was synthesized alternatively in previous papers.[2,3] Hence, the structure of **3** was determined to be 2-imino-4-alkoxycarbonyl-5-aryl-1,3-oxathiolane hydrochloride. The NMR and mass spectra support this assignment. In the mass spectrum of **3b** (Fig. 5), one observed a M–HCl ion as the highest mass peak, which is not seen in the spectrum of **4b**. Subsequent fragmentations may proceed in the way shown in Scheme 2. The base peak appears at *m/e* 135, which may correspond to C_6H_5–C_2H_2S.

Table 6. IR data of products **3** in KBr (cm^{-1})

No.	νNH_2	Ester νC=O	Amide νC=O	δNH_2
4a	3440 s, 3340 s, 3300 s, 3190 s	1730 vs	1685 vs	1610 m
4b	3410 s, 3312 s, 3272 s, 3185 s	1726 vs	1687 vs	1611 m
4c	3410 s, 3315 s, 3270 s, 3185 s	1730 vs	1690 vs	1613 m
4d	3410 s, 3310 s, 3270 s, 3180 s	1722 vs	1695 vs	1610 m
4e	3400 s, 3292 s, 3230 s, 3160 s	1724 vs	1694 vs	1605 m
4f	3408 s, 3290 s, 3230 s, 3170 s	1720 vs	1690 vs	1605 m
4g	3365 s, 3305 s, 3235 s, 3180 s	1730 vs	1680 vs	1625 m
4h	3415 s, 3320 s, 3282 s, 3190 s	1720 vs	1692 vs	1610 m
4i	3410 s, 3350 s, 3292 s, 3170 s	1723 vs	1687 vs	1608 m
4j	3410 s, 3315 s, 2372 s, 3187 s	1730 vs	1692 vs	1610 m
4k	3400 s, 3305 s, 3265 s, 3183 s	1730 vs	1690 vs	1611 m

Table 5. NMR data of products **3** in DMSO-d_6 (δ-values from TMS)

No.	H_α	H_β	$J_{\alpha\beta}$ (Hz±0.1)	COOR		NH	Aromatic protons
				CH_3	CH_2		
3b	5.30 d	6.65 d	6.1	0.70 t	3.73 q	11.75 br	7.45 s
3c	5.34 d	6.72 d	6.1	0.70 t	3.72 q	11.75 br	7.45 s
3d	5.24 d	6.65 d	6.0	1.02 s		11.75 br	7.42 s
3f	5.31 d	6.67 d	6.1	0.75 t	3.77 q	11.75 br	near 7.57 m
3h	5.30 d	6.62 d	6.1	0.75 t	3.78 q	11.75 br	*ca.* 7.35 *ca.* 7.67

s=singlet, d=doublet, t=triplet, q=quartet, m=multiplet, br=broad

3) T. Hayashi, M. Akano, T. Yokono, J. Uzawa, S. Kambe, and H. Midorikawa, This Bulletin, **45**, 578 (1972).

Table 7. NMR data of products **4** in acetone-d_6 (δ-values from TMS)

No.	H_α	H_β	$J_{\alpha\beta}$ (Hz±0.1)	COOR		NH_2	Aryl protons
				CH_3	CH_2		
4a	4.84 d	5.36 d	11.3	3.78 s		6.98 br	7.45 m
4b	4.83 d	5.33 d	11.3	1.27 t	4.25 q	6.98 br	7.45 m
4c[a)]	4.89 d	5.54 d	12.0	1.26 t	4.27 q	7.66 br	near 7.50 m
4d	4.74 d	5.30 d	11.3	1.50 s		7.92 br	7.47 m
4e	4.81 d	5.35 d	11.3	3.78 s		7.00 br	7.40 m, 7.46 m
4f	4.76 d	5.34 d	11.3	1.27 t	4.24 q	6.99 br	7.40 m, 7.46 m
4g	4.88 d	5.80 d	11.3	1.28 t	4.27 q	7.04 br	7.30—7.80 m
4h	4.76 d	5.34 d	11.3	1.27 t	4.24 q	6.97 br	near 7.46 m
4i	4.80 d	5.47 d	11.3	1.28 t	4.28 q	7.00 br	7.77 m
4j	4.82 d	5.54 d	11.3	1.28 t	4.28 q	7.03 br	7.80 m, 8.25 m
4k	4.80 d	5.30 d	11.3	1.27 t	4.24 q	6.96 br	7.32 s
4l[a)]	4.67 d	5.49 d	11.3	1.23 t	4.21 q	7.66 br	near 7.28 m

a) in DMSO-d_6

Table 8. IR data of products **5** in KBr (cm^{-1})

No.	NH	Ester νC=O	Amide νC=O	δNH	No.	NH	Ester νC=O	Amide νC=O	δNH
5b	3300 m	1744 vs	1676 vs	1605 w	**5e**	3315 m	1750 vs	1675 s	1603 w
5d	3306 m	1738 vs	1680 s	1590 w	**5h**	3405 m	1742 vs	1661 s	1601 w

Table 9. NMR data of products **4** and **5** in DMSO-d_6 (δ-values from TMS)

No.	H_α	H_β	$J_{\alpha\beta}$(Hz)	H_γ	$J_{\gamma NH}$(Hz)	COOR		Aryl protons		NH	$J_{\gamma NH}$(Hz)
						CH_3	CH_2				
5b	4.75 d	5.47 d	11.3	6.35 t	7.6	1.19 t	4.19 q	6.94 m	7.60 m	9.00 d	7.6
5b′	4.78 d	5.44 d	11.3	6.35 t	7.6	1.26 t	4.25 q	6.94 m	7.60 m	9.12 d	7.6
4b	4.71 d	5.44 d	11.3			1.22 t	4.22 q		7.45 m	7.62 br	
5d	4.63 d	5.39 d	11.3	6.33 t	7.6	1.43 s		6.94 m	7.33 m	8.94 d	7.6
5d′	4.64 d	5.37 d	11.3	6.33 t	7.6	1.49 s		6.94 m	7.33 m	9.07 d	7.6
4d	4.71 d	5.32 d	11.3			1.50 s			7.47 m	7.92 br	
5e	4.68 d	5.52 d	11.3	6.23 t	7.6	1.24 t	4.24 q	6.72 m	7.40 m	9.15 d	7.6
4e	4.66 d	5.55 d	11.3			1.24 t	4.23 q		7.43 m	7.70 br	
5h	4.64 d	5.42 d	11.3	6.23 t	7.6	1.16 t	4.16 q	6.70 m	7.46 m	9.08 d	7.6
5h′	4.67 d	5.48 d	11.3	6.23 t	7.6	1.29 t	4.25 q	6.70 m	7.46 m	9.29 d	7.6
4h	4.59 d	5.45 d	11.3			1.23 t	4.22 q		7.46 m	7.70 br	

In the spectrum of **4b**, a rearrangement peak (M–HOCN) is observed at *m/e* 244, which may arise by the four-center mechanism from the molecular ion. Similar rearrangement peak has been observed in the case of *S*-methyl phenylthiocarbonate[4] and *S*-(2-chloropropyl)-thiocarbamate.[5] The base peak at *m/e* 125 and an abundant peak at *m/e* 211 evidently contain a chloride atom, because the peaks are accompanied by a +2 isotope peak amounting to about a third of the intensity. Other abundant peaks appear at the same positions as observed in the case of **3b**. A plausible explanation for these fragmentation processes is depicted in Scheme 2. It is postulated that **4b** has the structure of ethyl α-*S*-carbamoylthio-β-chloro-dihydrocinnamate. The IR and NMR spectra of **4b** (Figs. 2 and 4) are in agreement with this assignment. The spectral data of **4** are summarized in Tables 6 and 7. The chemical shifts of the α-protons are in the ranges 4.67 to 4.89 ppm and those

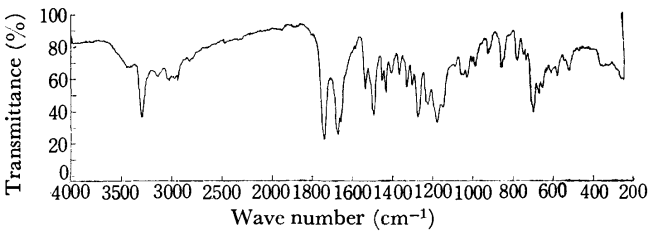

Fig. 7. IR spectrum of **5b** (KBr pellet).

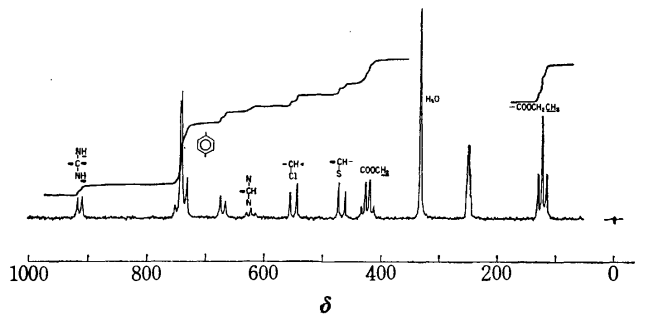

Fig. 8. NMR spectrum of **5f** in DMSO-d_6 (100 MHz).

4) J. B. Thomson, P. Brown, and C. Djerassi, *J. Amer. Chem. Soc.*, **88**, 4049 (1966).

5) See the experimental section.

of the β-protons are in the ranges 5.30 to 5.54 ppm, except for **4g**.

The analytical and spectral data of the high-melting solid products (**5**) are summarized in Tables 3, 8, and 9. The NMR spectrum revealed that the condensation occurred between the NH_2 groups of **4** and the C=O group of an aldehyde. In the spectrum of **5e** (Fig. 8), a triplet at 6.23 ppm and a doublet at 9.15 ppm (J= 7.6 Hz), whose coupling was confirmed by double resonance experiment, are attributable to the proton at the 6-position and the two NH protons, respectively, this being indicative of the NH–CH–NH system. This assignment may be supported by the fact that **5** was alternatively synthesized by treating a mixture of **4** and an aldehyde (mole ratio=2: 1) with dry hydrogen chloride. In Table 9, the chemical shifts of the corresponding **4**'s

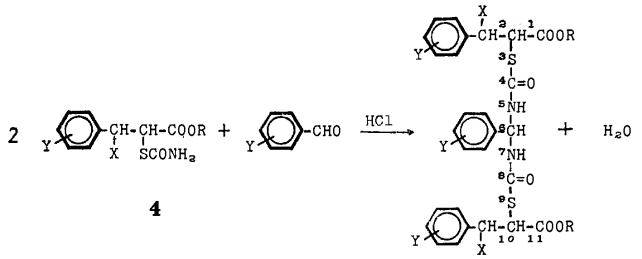

4 **5**

are given along with those of **5**'s for comparison. The signals of the H_α, H_β, and alkoxycarbonyl protons for **5** appeared at almost the same positions as those for **4**. The IR spectrum showed a single absorption band in the NH stretching frequency region (Fig. 7 and Table 8). On the basis of the above data, the structure of **5** was determined to be 2,10-bis(α-chlorobenzyl)-4,8-dioxo-6-phenyl-5,7-diaza-3,9-dithiaundecanedioate.

Geometric Configurations. 2-Imino-4-alkoxycarbonyl-5-aryl-1,3-oxathiolane hydrochlorides (**3**) can exist in two isomeric forms, relative to arrangements of the aryl and alkoxycarbonyl groups about a single bond in the ring. The isolated **5**, which proved to contain

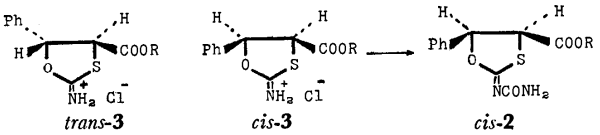

trans-**3** *cis*-**3** *cis*-**2**

only one isomer, when treated with an equimolar amount of sodium cyanate, led to the *cis* isomer of the corresponding *N*-carbamoyl drivative (**2**), whose geometric configuration was established in a previous paper.[3] It may be safely assumed that the geometric configuration is retained during the conversion of **3** to **2**. Therefore, **3** has the *cis* configuration. Further supports for this may be supplied by the fact that the alkoxycarbonyl protons of **3** are located at higher field by *ca.* 0.50 ppm rather than those of the corresponding ester **4**, and that the $J_{\alpha\beta}$ values for **3** are in the ranges 6.1±0.1 Hz. It was established in a previous paper[3] that the *cis* forms for **2** have the alkoxycarbonyl signals at higher field by *ca.* 0.50 ppm than the *trans* forms, whose alkoxycarbonyl protons appear at almost the same positions as the ordinary esters, and that the $J_{\alpha\beta}$ values for the *cis* forms are in the range of 6.0 to 6.4 Hz. Presumably, the conformations of **3** do not differ too greatly from those of **2**.

The product **4** can exist in two diastereoisomeric forms as shown below. However, the NMR spectra revealed that all the products **4** obtained in the

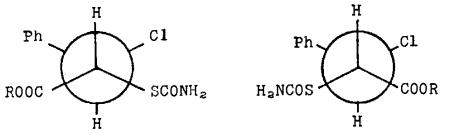

threo-s *erythro*-s

present work consisted of single diastereomer. The vicinal $J_{\alpha\beta}$ values for **4** are consistently 11.3±0.1 Hz except for **4c**. It was reported that the $J_{\alpha\beta}$ values for *erythro*- and *threo*-α,β-dichlorodihydrocinnamic esters are 11.0 and 8.6 Hz, respectively[6] and that the $J_{\alpha\beta}$ value for methyl *erythro*-*p*-methoxy-α,β-dibromodihydrocinnamate is 12.0 Hz.[7] The *erythro* forms of α,β-dihalodihydrocinnamic esters are considered to be heavily populated in a conformation having the two protons in *trans* position as shown.[8] Since the electro-

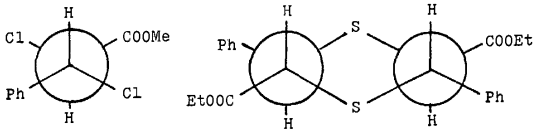

9

negativities of the carbamoylthio group and the chlorine atom are estimated to be almost the same,[9] the displacement of the α-chlorine atom by the carbamoylthio group should not lead to any significant effect on the magnitude of the $J_{\alpha\beta}$ value. Therefore, the Karplus rule[10] suggests that products **4** may be present predominantly in a conformation with the two protons in *trans* positions as shown above, whether *threo*-s or *erythro*-s.[11] If the steric requirement of the alkoxycarbonyl group would be larger than that of the carbamoylthio group, **4** might have the *erythro*-s configuration, and if the reverse would be true, the *threo*-s.[12] If the carbamoylthio group would be bulkier than the alkoxycarbonyl group, the displacement of the ethoxycarbonyl by the bulkier group should lead to the decrease in the $J_{\alpha\beta}$ value. However, the introduction of the *tert*-butyl group into the ester moiety made no change on the $J_{\alpha\beta}$

6) M. C. Cabaleiro and M. D. Johnson, *J. Chem. Soc., B*, **1967**, 565.

7) G. P. Newsoro and S. Sternhell, *Aust. J. Chem.*, **21**, 7471 (1968).

8) L. M. Jackman and S. Sternhell, "Applications of Nuclear Magnetic Resonance Spectroscopy in Organic Chemistry," Pergamon Press, New York, N. Y. (1969), p. 291.

9) Estimated from the equation of Dailey and Shoolery; B. P. Dailey and J. N. Shoolery, *J. Amer. Chem. Soc.*, **77**, 3977 (1956); J. R. Cavanaugh and B. P. Dailey, *J. Chem. Phys.*, **34**, 1099 (1961).

10) M. Karplus, *J. Chem. Phys.*, **30**, 11 (1959).

11) The suffix s indicates that the definition of *erythro* and *threo* is based on the size of groups; H. E. Zimmerman and W. Chang, *J. Amer. Chem. Soc.*, **81**, 3634 (1959).

12) M. Hanack, "Conformational Theory," Academic Press, New York, N. Y. (1965), p. 331.

value. Barbieux and Martin[13] reported that in the case of ethyl α,β-dialkyl-*p*-methoxydihydrocinnamates, the $J_{\alpha\beta}$ values are not a reliable indication of configurations, but that the chemical shifts of the ester protons are located at higher field for the *threo* forms by *ca.* 0.27 to 0.33 ppm than for the *erythro* forms, presumably due to the long-range shielding of the benzene ring. Examination of available data on α,β-dihalodihydrocinnamic esters also demonstrates that the ester protons resonate at higher field for the *threo* isomers by *ca.* 0.3 ppm than for the *erythro* isomers. On the other hand, it is interesting to observe that the chemical shifts of the ester protons for 2,5-diphenyl-3,6-diethoxycarbonyl-1,4-dithiane (**9**) appear at higher field by *ca.* 0.30 ppm than those of the ordinary ester. Since the $J_{\alpha\beta}$ value (10.5 Hz) indicates that the protons are in the axial conformation, the phenyl and ester groups should be present in the *equatorial* conformation. Therefore, as shown above, the spatial relationships of the phenyl and ester groups are the same for the dithiane **9** and the *threo*-s form of **4**. Consequently, if **4** has the *threo*-s configuration, the ester protons should resonate at higher field by *ca.* 0.3 ppm rather than the ordinary ester protons. However, the observed chemical shifts for the ester protons of **4** are at almost the same position as the ordinary ester, this being suggestive of the *erythro*-s configuration. All attempts to detect the *threo*-s form were unsuccessful and the solvent effects on the $J_{\alpha\beta}$ value for **4** were not observed.

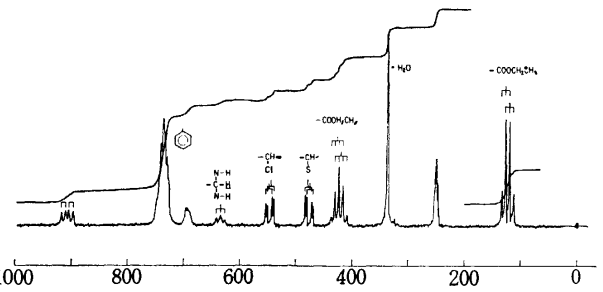

Fig. 9. NMR spectrum of **5b** in DMSO-d_6 (100 MHz).

One further problem to explain concerns the NMR spectra of product **5** (Table 9 and Fig. 9). As can be seen from Fig. 9, all the signals are duplicated with almost equal intensities. This is not due to the magnetic non-equivalence of the two cinnamate moieties in a molecule of **5**, because in the case of **5d**, two sets of signals with unequal intensities (**5d**: **5d'**=2.1: 1) were observed. Therefore, this duplication should be attributed to the presence of two chemical species. A plausible explanation is that the two enantiomers of **4** condenced with an aldehyde to give new diastereomers, which showed slightly different chemical shifts.

Reaction Mechanism. A possible mechanistic pathways for the reaction of the ester **1** with aldehydes are proposed in Scheme 1. There is little doubt that the reactions proceed through the intermediacy of α-thiocyanato-β-hydroxydihydrocinnamic ester (**6**) and 2-imino-4-alkoxycarbonyl-5-aryl-1,3-oxathiolane (**7**). The pathway leading to α,β-epithio-ester (**8**) is analogous to the route established by van Tamelen[14] for the conversion of oxiranes to thiiranes. Accordingly, this reaction has been at first considered to be a convenient one-step synthetic route to unknown α,β-epithio-esters.[15] However, the α,β-epithio-esters are unstable and readily lose sulfur, forming cinnamic esters.[16] In fact, when the reactions were conducted at room temperature and followed by prolonged standing, cinnamic esters were exclusively obtained.

The most probable route leading to ester **4** from hydrochloride **3** would be considered to be the molecular rearrangement of the hydrochloride **3**. It is known that 2-imino-1,3-oxathiolane hydrochloride readily isomerize on heating or prolonged standing into *S*-alkyl thiocarbamate.[17,18] However, it is suprising that

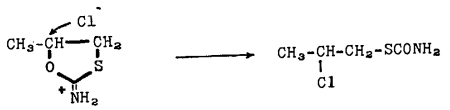

hydrochloride **3** resisted all our attempts to effect ring-opening, only starting material being recovered. Under the more drastic conditions, cinnamic esters and unidentified decompsotion compounds were obtained. A possible explanation may be offered as follows. There is a marked difference in the reaction rates between the *cis* and *trans* isomers of **3**, presumably due to the steric reason. Similar stereoselectivity has been observed before in the case of three-membered ring.[19] All attempts to detect the *trans* isomer of **3** have failed, but when the reaction mixture was neutralized carefully with hydrogen chloride gas at low temperature, *trans*-*N*-carbamoyl derivative **2** was obtained in 10% yield. Since it was confirmed that *cis*-**2** could not be isomerized into *trans*-**2**,[3] this means that *trans*-**7** should exist in the reaction mixture. Presumably, *trans*-**3** may be attacked very rapidly at the 5-position by halide ion to give the ester **4**, whereas *cis*-**3** may resist to be attacked by the halide ion and therefore, can be isolated as the hydrochloride **3**. This speculation may be supported by the fact that *trans*-**2**, when treated with hydrochloric acid, is readily converted into α-(ureidocarbonylthio)-β-chlorodihydrocinnamic ester (**10**), whereas *cis*-**2** does not undergo the ring-opening under the similar conditions.

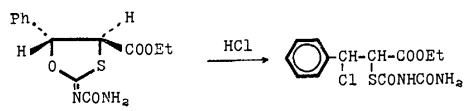

trans-**2b** **10b**

13) M. Barbieux and R. H. Martin, *Tetrahedron Lett.*, **1965**, 2919.

14) E. E. van Tamelen, *J. Amer. Chem. Soc.*, **73**, 3444 (1951).

15) M. Sander, *Chem. Rev.*, **66**, 297 (1966); C. C. Tung and A. J. Speziale, *J. Org. Chem.*, **29**, 1577 (1964).

16) T. C. Owen, C. L. Gladys, and L. Field, *J. Chem. Soc.*, **1962**, 501, 656.

17) P. G. Sergeev and B. S. Kolychev, *J. Gen. Chem.* (USSR), **7**, 1390 (1937): *Chem. Abstr.*, **32**, 2534 (1938); P. G. Sergeev, B. S. Kolychev, and V. S. Kolychev, *J. Gen. Chem.* (USSR), **7**, 2863 (1937): *Chem. Abstr.*, **32**, 2940 (1938).

18) T. Wagner-Jauregg and M. Haering, *Helv. Chim. Acta*, **61**, 377 (1958).

19) T. A. Foglia, L. M. Gregory, G. Maerker, and S. F. Osman, *J. Org. Chem.*, **36**, 1068 (1971).

Furthermore, if *trans*-**3** would undergo an S_N2-type ring opening reaction, as in the case of the reaction of aziridines with hydrochloric acid,[20] only the *erythro*-s isomer should be produced as shown below. If the reaction would proceed by an S_N1-type mechanism, a mixture of two diastereomers should be obtained. The results suggest that the rearrangement of *trans*-**3** to **4** might be an S_N2-type reaction. Further studies on the mechanism for this are now in progress.

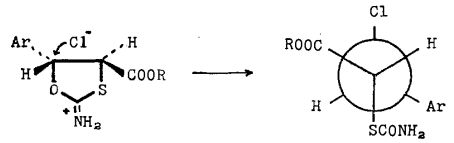

trans-**3** *erythro*-s-**4**

Experimental

All the melting points are uncorrected. NMR spectra were obtained with Varian HA-100D and JEOL C-60 spectrometers in DMSO-d_6, acetone-d_6, and $CDCl_3$ solutions using tetramethylsilane as internal standard. IR spectra were determined in KBr pellet using a Perkin-Elmer 521 spectrophotometer. Mass spectra were taken with a JMS-01SG instrument operating at 75 eV.

Preparation of Thiocyanatoacetic Esters (1). The esters were prepared by a modification of Heintz's method.[21] A mixture of chloroacetic ester (1 mol) and ammonium thiocyanate (1.5 mol) in 200 m*l* of ethanol was stirred at 50°C for 3 hr. After cooling the mixture, the precipitated ammonium chloride was removed by filtration, and the filtrate was concentrated under reduced pressure. The deposited ammonium chloride was again removed by filtration and washed with ether. The filtrate and the washings were combined and washed with a small amount of water. The ethereal solution was subjected to distillation, bp 108—109°C/12 mmHg for methyl ester, 108—111°C/8 mmHg for ethyl ester, and 110—112°C/8 mmHg for *tert*-butyl ester. *tert*-Butyl ester is a new compound. IR (neat): 2160 (νSC≡N), and 1736 cm^{-1} (νC=O).

Found: C, 48.61; H, 6.41; N, 7.72; S, 18.04%. Calcd for $C_7H_{11}NO_2S$: C, 48.56; H, 6.41; N, 8.09; S, 18.52%.

Reaction of Thiocyanatoacetic Esters (1) with an Aldehyde in the Presence of Sodium Hydride. General Procedure: In a three-necked round-bottomed flask fitted with an apparatus specially designed for addition of sodium hydride, a thermometer, and a reflux condenser protected with a calcium chloride tube, was placed thiocyanatoacetic ester (0.03 mol), an aldehyde (0.03 mol) and 40 m*l* of dried glyme. After the air in the flask was replaced with dry nitrogen, the flask was cooled to −5°C in a freezing mixture. Sodium hydride (0.03 mol) was slowly added to the solution so that the temperature did not rise over −2°C. After the addition of sodium hydride was over, the solution was stirred at −5°C for additional 30 min. Dry hydrogen chloride gas was passed through the solution below 0°C for 10 min, and the resulting sodium chloride was removed by filtration. The solvent was removed under reduced pressure and the residue was washed with ether repeatedly, until colored materials were removed. A fraction of the solid products was subjected to the NMR analysis for the measurement of the ratio of **3** to **4**. The solid products were dissolved in 15 m*l* of acetone and the insoluble material was collected on a filter. The filtrate was concentrated on a steam bath to yield a purple-tinged white needles (**4**). The acetone-insoluble material obtained above was dissolved in ethanol and an insoluble solid was removed by filtration. The filtrate was concentrated under reduced pressure to give almost pure hydrochloride **3**.[22]

Reaction of Thiocyanatoacetic Esters (1) with Excess Aldehyde in the Presence of Sodium Hydride. A solution of thiocyanatoacetic ester (0.03 mol) and an aldehyde (0.05 mol) in 40 m*l* of dry glyme was treated with 0.03 mol of sodium hydride, as described above. The reaction mixture was saturated with dry hydrogen chloride, the resulting sodium chloride was removed by filtration, and the filtrate was concentrated under reduced pressure. The residues were washed with ether and then dissolved in 20 m*l* of acetone. The insoluble materials were washed with 20 m*l* of ethanol and recrystallized from glyme–ethanol (1:1) to give compound **5**. The washings were concentrated to yield hydrochloride **3**. The acetone solution obtained above, when the solvent was removed, gave ester **4**, which was recrystallized from ethanol.

Reaction of Thiocyanatoacetic Esters (1) with an Aldehyde in the Presence of Potassium Carbonate. A mixture of thiocyanatoacetic ester (0.03 mol) and an aldehyde (0.03 mol) in 20 m*l* of moist ether was stirred in the presence of potassium carbonate (5.0 g) at room temperature for 4 hr. After the catalyst was removed by filtration and washed with 20 m*l* of acetone, the filtrate and the washings were combined and then saturated with dry hydrogen chloride. The solvents were removed by blowing air on the solution and the resulting solid products were washed with ether. Hydrochloride **3** and ester **4** were separated and purified as described above. It was found that this method gave a higher yield of **3** than the method using sodium hydride.

Conversion of Hydrochloride 3 to Ester 4. To a solution of hydrochloride **3** (1.5 g) in 3 m*l* of water was added a solution of sodium cyanate (0.4 g) in 2.0 m*l* of water and the solution was allowed to stand at room temperature for 10 min. The resulting precipitate was recystallized from ethanol, mp 159—160°C. The mixture of this crystals with an authentic sample of *trans*-**2b** did not show a depression in melting point.

Preparation of Compound 5 from Ester 4 and an Aldehyde. General Procedure: A mixture of ester **4** (0.01 mol) and an aldehyde (0.005 mol) in 10 m*l* of glyme was saturated with dry hydrogen chloride and then allowed to stand overnight in a refrigerator. The resulting crystals were collected on a filter, washed with ether, and then recrystallized from glyme–ethanol mixture (1:1). In some cases, crystals did not appear in the solutions, but concentration and cooling of the solution yielded the product **5**.

Conversion of 2-Imino-5-methyl-1,3-oxathiolane Hydrochloride into S-(2-chloropropyl)thiocarbamate. 2-Imino-5-methyl-1,3-oxathiolane hydrochloride was prepared according to the method of Price and Kirk.[23] The white needles were very hygroscopic, mp 115—118°C (lit,[23] 112—115°C). IR (KBr) 3100—2800 cm^{-1} (νNH_3), 1660 (νC=N); NMR (DMSO-d_6) δ 1.56 (CH_3, d, J_{ab}=6.6 Hz), 3.95 (CH_a, J_{ab}=11.4, J_{ax}=5.9 or 8.6), 3.97 (CH_b, m, J_{ab}=11.4, J_{bx}=8.6 or 5.9), 5.48 (CH_x, m), and 11.85 (NH_3, broad); Mass spectra, molecular

20) O. C. Dermer and G. E. Ham, "Ethylenimine and Other Aziridines," Academic Press, New York, N. Y. (1969), p. 208, and references listed therein.

21) A. Heinz, *Ann. Chem.*, **136**, 223 (1865).

22) Although the hydrochlorides **3** might be formed in all the experiments, only five of them (**3b**, **3c**, **3d**, **3f**, and **3h**) have been isolated pure. The yields of other hydrochlorides **3** have also not been measured.

23) C. C. Price and P. F. Kirk, *J. Amer. Chem. Soc.*, **75**, 2396 (1953).

ion *m/e* 153, base peak *m/e* 117, and a peak at *m/e* 74.

2-Imino-5-methyl-1,3-oxathiolane hydrochloride (2.0 g) was heated to 120°C for 30 min. The solid was recrystallized from ether–carbon tetrachloride mixture (1: 1), mp 92°C. IR (KBr) 3380, 3320, 3210, 3180 cm^{-1} (ν NH_2), and 1655 (ν C=O). NMR ($CDCl_3$) δ 1.57 (CH_3, d, J=6.6 Hz), 3.26 (CH_2, d, J=6.0), 5.17 (CH, m), and 5.87 (NH_2, broad); molecular ion, *m/e* 153, 117 (M−HCl), 110 (M−HOCN), and base peak *m/e* 74.

Found: C, 31.08; H, 5.12; N, 9.33; S, 20.64; Cl, 23.06%. Calcd for C_4H_8NOSCl: C, 31.27; H, 5.25; N, 9.12; S, 20.87; Cl, 23.08%.

Attempted Rearrangement of cis-**3b** *to* **4b**. *a)*: A solution of 0.5 g of *cis*-**3b** in 5 m*l* of glyme was bubbled with dry hydrogen chloride gas for five min, and then allowed to stand at room temperature for two days. Concentration of the solution gave the starting material only.

b): In a round-bottomed flask was placed 0.3 g of *cis*-**3b** and then heated to the melting point for five min. The solid mass was washed with ether and then recrystallized from ethanol. The melting point measurement and IR spectrum of the crystals were in agreement with those of *cis*-**3b**. The residue obtained from the washings proved to be ethyl cinnamate by glc.

c): A solution of 0.3 g of *cis*-**3b** in 5 m*l* of 99% ethanol was saturated with hydrogen chloride gas and then refluxed for 30 min. Concentration of the solution gave a high-melting product, which did not melt at 250°C. The structure of this product remains unsolved.

Conversion of trans-**2b** *to* **10b**. Dry hydrogen chloride was passed through 5.0 m*l* of glacial acetic acid for five min, and then 0.5 g of *trans*-*N*-carbamoyl-2-imino-4-ethoxycarbonyl-5-phenyl-1,3-oxathiolane (*trans*-**2b**) was dissolved. The solution was kept at 100°C for three min and then acetic acid was removed under reduced pressure. The residue was recrystallized from ethanol to give 0.3 g of **10b** melting at 167—168.5°C. IR spectrum (KBr pellet) 3397, 3320, 3215 cm^{-1} (ν NH_2 and ν NH), 1748 (ester C=O), 1730 (carbamoyl C=O), 1674 (allophanate C=O), and 1620 cm^{-1} (δ NH_2). NMR spectrum (acetone-d_6) 1.27 ppm (ester CH_3, t), 4.25 (ester CH_2, q), 4.85 (H_α, d, J=11.0 Hz), 5.39 (H_β, d, J=11.0), 6.80 (NH_2, br), 7.40 (C_6H_5, m), and 9.70 (NH, br).

Found: C, 46.90; H, 4.58; N, 8.49; S, 9.61; Cl, 10.13%. Calcd for $C_{13}H_{15}N_2O_4SCl$: C, 47.20; H, 4.57; N, 8.47; S, 9.69; Cl, 10.72%.

Attempted Conversion of cis-**2b** *to* **10b**. Dry hydrogen chloride was passed through 5.0 m*l* of glacial acetic acid for five min, and then 0.5 g of *cis*-*N*-carbamoyl-2-imino-4-ethoxycarbonyl-5-phenyl-1,3-oxathiolane (*cis*-**2b**) was dissolved. The solution was kept at 100°C for five min, and then acetic acid was removed under reduced pressure. The residue was recrystallized from ethanol to give the starting material.

The author wishes to express his thanks to Dr. Hiroshi Midorikawa of this institute and Mr. Satoshi Kambe of Oyama Technical College for fruitful discussions of the problems. Thanks are also due to Messrs. Tetsuro Yokono and Ko-ichi Iyama and Miss Makiko Akano for generous assistance in carrying out the experiments.

BULLETIN OF THE CHEMICAL SOCIETY OF JAPAN, VOL. 45, 1515—1518(1972)

Reinvestigation of the Nitration of Ethylmesitylene and *n*-Propylmesitylene. Revision of Early Works.[1]

Hitomi SUZUKI,* Mikio SAWAKI,** and Reiji SAKIMOTO**

**Department of Chemistry, Faculty of Science, Kyoto University, Sakyo-ku, Kyoto*

***Research Institute, Nihon Soda Co. Ltd., Kohdzu, Odawara*

(Received October 22, 1971)

Ethylmesitylene reacts with fuming nitric acid in dichloromethane at −5—0°C to give mononitroethylmesitylene, 3,5-dimethyl-4-ethylbenzyl nitrate, 2-nitro-3,5-dimethyl-4-ethylbenzyl nitrate and a dinitroethyltrimethylcyclohexenone, while on nitration with mixed acid it yields mono and dinitro derivatives as the major products, together with minor quantities of 2-nitro- and 2,6-dinitro-3,5-dimethyl-4-ethylbenzyl nitrates, diphenylmethanes, and unidentified nitro-carbonyl compounds, possibly nitrobenzaldehydes. Similar results are obtained from the nitration of *n*-propylmesitylene. If the hydrocarbons are nitrated by adding into a large excess of the nitrating agent, the major product is 2,6-dinitro-3,5-dimethyl-4-alkylbenzyl nitrate soon after the reaction, or 2,6-dinitro-3,5-dimethyl-4-alkylbenzaldehyde when the mixture is left to stand at room temperature. The nitro compound melting at 123°C, obtained by Smith and Kiess[2] from the nitration of ethylmesitylene and described as trinitro-4-ethyl-*o*-xylene, is identified as 2,6-dinitro-3,5-dimethyl-4-ethylbenzyl nitrate. An uncharacterized nitration product (mp 135°C) from *n*-propylmesitylene, obtained by Töhl and Tripke,[3] is found most likely to be 2,6-dinitro-3,5-dimethyl-4-*n*-propylbenzyl nitrate (mp 139—140°C).

Action of electrophilic reagent upon polyalkylbenzenes sometimes results in the migration of alkyl groups, giving products of orientation quite different from those predicted by the ordinary substitution rules. Such anomalies are frequently met and well documented

1) The Reaction of Polysubstituted Aromatics. XXIV. Part XXIII: This Bulletin, **44**, 2871 (1971).

2) L. I. Smith and M. A. Kiess, *J. Amer. Chem. Soc.*, **61**, 989 (1939). Also *cf.* D. V. Nightingale, *Chem. Rev.*, **40**, 117 (1947).

3) A. Töhl and H. Tripke, *Ber.*, **28**, 2459 (1895).

particularly in the sulfonation and acylation.[4] Meanwhile, the nitration of polyalkylbenzenes has generally been recognized not to involve such alkyl rearrangement, and therefore, their polynitro derivatives have been widely used for the characterization of isomeric series of polyalkylbenzenes.

Literature so far contains one exception which seems to involve both displacement and intramolecular migration of alkyl groups during the nitration. Töhl and Tripke[3] nitrated ethylmesitylene (2-ethyl-1,3,5-trimethylbenzene) with fuming nitric acid and obtained the product melting at 123°C, to which they assigned the dinitro structure on the basis of elemental analysis. Their claim was later re-examined by Smith and Kiess,[2] who showed that the hydrocarbon can afford two different nitro compounds depending on the nitrating conditions employed. When ethylmesitylene dissolved in chloroform was thoroughly stirred with sulfuric acid and slowly nitrated with fuming nitric acid at 0°C, the product was white needles melting at 110—111°C. Elemental analysis and chemical behavior were consistent with its formulation as dinitroethylmesitylene. However, treatment of the hydrocarbon with mixed acid (H_2SO_4 - HNO_3, 2: 1 v/v) at 0°C furnished the nitro compound of Töhl and Tripke, mp 123°C, which showed a large depression in melting point on admixture with the above nitro compound of mp 110—111°C. It did not afford on reduction with stannous chloride the expected diamino compound but gave an unidentified yellow substance melting at 255°C. Elemental analysis was close to that of a trinitroethylxylene, but the substance was found neither to be trinitro-4-ethyl-*m*-xylene (mp 129°C) nor trinitro-2-ethyl-*m*-xylene (mp 181°C), which could arise from ethylmesitylene through the displacement of one of methyl groups by nitro group. Hence they suggested the higher melting nitro compound as trinitro-4-ethyl-*o*-xylene (mp 121°C) on the evidences obtained from analysis and mixed melting determination. The formation of trinitro-4-ethyl-*o*-xylene from ethylmesitylene requires the intramolecular migration of at least one alkyl group during the nitration. In the lights of our present knowledge, such isomerization of polyalkylbenzenes seems to be quite unusual. Thus we have re-examined the early workers' results with the aims to solve the discrepancies in the literature as well as to ascertain if the nitration of ethylmesitylene can in fact lead to the claimed rearrangement of alkyl groups.

When a solution of ethylmesitylene in dichloromethane was treated with excess of fuming nitric acid (d=1.5) at −5—0°C, a dark red oily substance was obtained, which showed strong infrared bands due to benzyl nitrate at 1532 and 1364 (NO_2); 1648, 1272, and 844 cm^{-1} (ONO_2); a prominent PMR peak due to CH_2ONO_2 at 4.75 τ. Weak infrared bands due to carbonyl and hydroxyl groups were also observed at around 1700 and 3400—3500 cm^{-1}. Chromatography on alumina of the product mixture gave besides unchanged hydrocarbon (17%) mononitroethylmesitylene (42%) from light petroleum eluates, bis(4-ethyl-3,5-dimethylbenzyl) ether (3%) and nitro-carbonyl compounds (*ca.* 7%) from light petroleum - benzene mixture eluates, and 3,5-dimethyl-4-ethylbenzyl alcohol (7%) from ether eluates.[5] Bis-benzyl ether and benzyl alcohol were probably the secondary products from benzyl nitrate formed during the elution through activated alumina.

Chromatography on silica gel of the same product mixture proved to be unsatisfactory for the separation of nitro compounds from nitrooxymethyl compounds. However, a new alicyclic nitro-ketone, 5,6-dinitro-2,4,6-trimethyl-3-ethyl-3-cyclohexen-1-one (mp 140—141°C, crude yield 3—4%) was obtained as fine needles from the nitro-carbonyl fractions eluted with benzene-light petroleum mixture. The proof of structure for this unexpected product will be treated in the subsequent paper.[6]

When the nitration of the hydrocarbon was conducted by adding into the large excess of fuming nitric acid at −5—0°C, the major product which readily deposited from the dark reaction mixture was white needles melting at 120—122°C, the product described by Töhl and Tripke as dinitroethylmesitylene and by Smith and Kiess as trinitroethylxylene. The result of C, H analysis was quite close to that of trinitroethylxylene, as had been reported by American workers. However, its infrared spectrum contained prominent bands due to $-ONO_2$ group at 1645, 1270, and 843 cm^{-1} besides the expected absorptions of nitro group at 1530 and 1363 cm^{-1}, while PMR spectrum depicted the presence of one ethyl group (3H, 8.83 t; 2H, 7.21 q; J=8 Hz), two equivalent methyl groups (6H, 7.71 s) and one methylene group (2H, 4.67 s). These spectral evidences unambiguously show that the nitro compound melting at 123°C is not trinitro-4-ethyl-*o*-xylene but 2,6-dinitro-3,5-dimethyl-4-ethylbenzyl nitrate. In spite of its narrow melting range and brilliant crystalline form, the PMR spectrum revealed that the benzyl nitrate was usually accompanied by a small amount of dinitroethylmesitylene. It was quite tedious to remove this minor impurity without a considerable loss of the material. Obviously, the earlier workers have taken the less pure nitrate for trinitroethylxylene, since the presence of the dinitro derivative as impurity can contribute to the increase in the carbon content of the product. We can therefore conclude that the nitration of ethylmesitylene does not involve any rearrangement of alkyl groups under the ordinary conditions of the reaction.

Action of mixed acid (H_2SO_4 - HNO_3, 1:1 w/w) upon ethylmesitylene in dichloromethane at −5—0°C gave an oily substance, which on alumina chromatography gave besides unchanged starting material (*ca.* 4%) mononitro and dinitro derivatives (24 and 26%, respectively) as the major products from light petro-

4) For sulfonations, H. J. Shine, "Aromatic Rearrangements," Elsevier, London (1967), p. 48; H. Cerfontain, "Mechanistic Aspects in Aromatic Sulfonation and Desulfonation," Interscience, London (1968), p. 221; for acylations, P. H. Gore in "Friedel-Crafts and Related Reactions," Vol. III, Part I, ed. by G. A. Olah, Interscience, London (1964), p. 1, and S. Sethna in the same book, p. 911.

5) Yields are expressed in weight percentage calculated on the basis of the amount of product mixture, which was subjected to chromatographic separation.

6) H. Suzuki, M. Sawaki, and R. Sakimoto, This Bulletin, in press.

leum eluates, diphenylmethane and nitro-carbonyl compounds (less than 4%) from light petroleum-benzene eluates, and a mixture of nitrobenzyl alcohols (8%) from ether eluates. Diphenylmethane was probably formed by the sulfuric acid-catalyzed condensation of 2-nitro-3,5-dimethyl-4-ethylbenzyl nitrate with mononitroethylmesitylene.[7] The main component of the nitro-carbonyl fractions was presumably nitrobenzaldehydes, which could arise from nitrobenzyl nitrates under the influence of sulfuric acid.[8]

In connection with the present work, the nitration of *n*-propylmesitylene was re-examined with the expectation that the uncharacterized compound melting at 135°C, obtained by Töhl and Tripke[3] in the nitration of *n*-propylmesitylene, might be also a benzyl nitrate. A solution of the hydrocarbon in dichloromethane was treated with fuming nitric acid at −5—0°C to give a dark yellow oil, which on chromatography over alumina was separated into unchanged hydrocarbon (2%), mononitro-*n*-propylmesitylene (59%), impure bis(3,5-dimethyl-4-*n*-propylbenzyl) ether (3%), nitro-carbonyl compounds (*ca.* 5%), and 3,5-dimethyl-4-*n*-propylbenzyl alcohol (4%) and its nitro derivatives (2%).

When the nitration was conducted by dissolving the hydrocarbon into a large excess of cold fuming nitric acid, appreciable amounts of crystalline product were soon precipitated from the reaction mixture, which was immediately collected on a glass filter and recrystallized from a mixture of ligroin and dichloromethane. Colorless plates thus obtained melted at 139—140°C and had the formula $C_{12}H_{16}N_3O_7$. It showed infrared bands for nitro group at 1530 and 1361 cm^{-1} and those for nitrooxy group at 1644, 1277, and 857 cm^{-1}. Its PMR spectrum contained peaks due to one *n*-propyl group (3H, 8.95 t, J=7 Hz; 2H, 8.37—8.62 m; and 2H, 7.28 t, J=7 Hz), two equivalent methyl groups (6H, 7.72 s), and one methylene group (2H, 4.69 s). These analytical and spectral data were only compatible with the formulation of the product as 2,6-dinitro-3,5-dimethyl-4-*n*-propylbenzyl nitrate. Since there is no reason to believe that *n*-propylmesitylene behaves on nitration differently from ethylmesitylene, the product of Töhl and Tripke seems most likely to be the above nitrate although the original paper contains no detail to confirm its structure. If the hydrocarbon was dissolved into excess of fuming nitric acid in a ice-salt bath and the mixture was allowed to stand overnight without adding further amounts of ice, the well crystallized solid which separated on the surface of the acid medium was mainly 2,6-dinitro-3,5-dimethyl-4-*n*-propylbenzaldehyde. The initially formed benzyl nitrate was no doubt converted into the aldehyde under the influence of acid reagent.

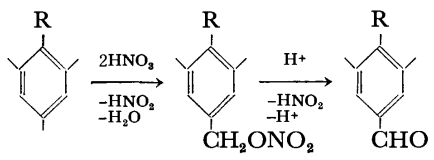

R: Et or *n*-Pr

The syrupy product obtained by the nitration of *n*-propylmesitylene with mixed acid gave by similar chromatographic treatment unchanged hydrocarbon (3%), mononitro and dinitro derivatives (5 and 33%, respectively), diphenylmethane and nitro-carbonyl compounds (less than 2%), and a mixture of nitrobenzyl alcohols (11%). The last compounds were secondary reaction products of nitrobenzyl nitrates formed during the chromatographic treatment over activated alumina.

Experimental

Ethylmesitylene [bp 104—105°C/25 mmHg. PMR: ethyl (3H 8.96 t, 2H 7.48 q, J=8 Hz), methyl (3H 7.84 s; 6H 7.80 s), and aromatic H (2H 3.36 s)] and *n*-propylmesitylene [bp 117—119°C/28 mmHg. PMR: *n*-Pr (3H 9.04 t, J=7 Hz; 2H 8.39—8.71 m; 2H 7.53 t, J=7 Hz), Me (3H 7.86 s; 6H 7.80 s), and aromatic H (2H 3.38 s)] were prepared by the Friedel-Crafts acylation of mesitylene, followed by the Clemmensen reduction of the corresponding mesitoyl ketones.[9,10]

Infrared spectra were measured on Nujol mulls with a Jasco 402G spectrophotometer and only prominent peaks are recorded. PMR spectra were determined in deuteriochloroform or carbon tetrachloride solutions with a Varian A-60A spectrometer and a JEOLCO PS-100 spectrometer against internal TMS.

The representative results obtained from the nitration with fuming nitric acid and mixed acid are shown below.

Nitrations with Fuming Nitric Acid. a): Fuming nitric acid (d=1.50, 8.4 g) was added dropwise to a magnetically stirred solution of ethylmesitylene (7.4 g) in dichloromethane (30 m*l*) at −5—0°C over a period of 30 min, and after the end of addition, the mixture was stirred at room temperature for additional 1 hr. The mixture was diluted with water and the organic part was thoroughly washed with water and dilute aqueous sodium bicarbonate. After drying over anhydrous sodium sulfate, the solvent was evaporated to give a yellow oily mixture (*ca.* 10 g), part of which (7.0 g) was subjected to chromatographic resolution over alumina using light petroleum as eluant to give unchanged hydrocarbon (bp 97—98°C/22 mmHg, 1.2 g) and *2-nitro-4-ethyl-1,3,5-trimethylbenzene* (3.0 g). The latter was a pale yellow liquid boiling at 113—114°C/3 mmHg: IR: 792, 847, 869, 1022, 1038, 1059, 1183, 1369, and 1530 cm^{-1}; PMR (CCl_4): Et (3H 8.90 t, 2H 7.38 q; J=8 Hz), Me (6H 7.84 s; 3H 7.72 s), and aromatic H (1H 3.20 s). It gave on reduction with stannous chloride a liquid amine, which was treated with acetic anhydride to give *2,4,6-trimethyl-3-ethylacetanilide*, mp 161—162°C.

Found: C, 76.07; H, 9.34%. Calcd for $C_{13}H_{19}NO$: C, 76.10; H, 9.27%.

The benzene eluates gave an impure bisbenzyl ether as a pale yellow oil (0.2 g) and a mixture of nitro-carbonyl compounds as a light brown syrup (0.5 g). The major component of the former was identified as *bis(4-ethyl-3,5-dimethylbenzyl) ether* by infrared absorptions (786, 863, 1010, 1092, 1061, and 1140 cm^{-1}) and PMR peaks (CCl_4; Et (3H 8.92 t; 2H 7.42 q; J=8 Hz), Me (6H 7.74 s), $-CH_2O-$ (2H 5.71 s), and aromatic H (2H 3.17 s)), although it could not be ob-

7) H. Suzuki and K. Nakamura, *ibid.*, **43**, 473 (1970); H. Suzuki, *ibid.*, **42**, 2618 (1969).

8) S. D. Ross, E. R. Coburn, and M. Finkelstein, *J. Org. Chem.*, **33**, 585 (1968).

9) O. R. Noller and R. Adams, *J. Amer. Chem. Soc.*, **46**, 1889 (1924).

10) P. H. Gore and J. A. Hoskins, *J. Chem. Soc., C*, **1971**, 517.

tained in pure form. The latter mixture showed a complicated pattern of infrared spectrum with prominent carbonyl bands at 1750, 1720, and 1677 cm^{-1}. No attempt was made to resolve them.

Further elution with ether gave colorless needles (0.5 g) melting at 72—74°C, identified as *4-ethyl-3,5-dimethylbenzyl alcohol* by analysis, infrared spectrum (730, 866, 998, 1046, 1143, and 3220 cm^{-1}), and PMR spectrum (CCl_4; Et (3H 8.93 t, 2H 7.41 q; $J=7$ Hz), Me (6H 7.74 s), OH (1H, 8.56 broad), CH_2 (2H 5.62 s), and aromatic H (2H 3.18 s)).

Found: C, 80.58; H, 9.52%. Calcd for $C_{11}H_{16}O$: C, 80.49; H, 9.76%.

b): Similar treatment of the nitration product (7.0 g) from *n*-propylmesitylene gave unchanged hydrocarbon (bp 110—111°C/19 mmHg, 0.15 g) and *2-nitro-4-n-propyl-1,3,5-trimethylbenzene* (113—114°C/2 mmHg, 4.1 g) from light petroleum eluates. The latter was slightly yellow oil, which readily solidified to large prisms (mp 34—35°C) and had infrared bands at 798, 840, 869, 1035, 1367, and 1521 cm^{-1}; PMR peaks at 8.99 (Me t, $J=8$ Hz), 8.42—8.67 (CH_2, m), 7.84 (2Me, s), 7.74 (Me, s), and 3.23 τ (aromatic H, s). It gave on reduction with stannous chloride and the subsequent treatment with acetic anhydride *3-n-propyl-2,4,6-trimethylacetanilide*, mp 163—164°C (lit,[3] mp 161°C).

Impure *bis(4-n-propyl-3,5-dimethylbenzyl) ether* (0.2 g) and a mixture of nitro-carbonyl compounds (0.35 g) were obtained from benzene eluates. The former product could not be isolated in crystalline form and had infrared bands at 862, 1091, and 1140 cm^{-1}; PMR peaks (CCl_4) at 9.01 (Me, t, $J=8$ Hz), 8.64—8.42 (CH_2, m), 7.75 (2Me, s), 5.73 (CH_2O, s), and 3.19 τ (aromatic H, s).

Elution with ether gave *4-n-propyl-3,5-dimethylbenzyl alcohol* (0.3 g), which crystallized from ethanol as white needles and melted at 68—69°C. IR: 732, 867, 1002, 1039, and 3200—3300 cm^{-1}; PMR (CCl_4): *n*-Pr (3H 9.00 t, $J=8$ Hz; 2H 8.40—8.76 m; 2H 7.48 t, $J=8$ Hz), OH (1H 8.44 broad), Me (6H 7.74 s), CH_2 (2H 5.63 s), and aromatic H (2H 3.18 s).

Found: C, 81.04; H, 10.41%. Calcd for $C_{12}H_{18}O$: C, 80.90; H, 10.11%.

c): Ethylmesitylene (7.4 g) was added dropwise to the fuming nitric acid (20 m*l*) during the course of 30 min at −5—0°C and the mixture slurried with precipitated crystals was rapidly filtered through a sintered glass filter to leave a white crystalline cake, which was crystallized from a mixture of *n*-hexane and dichloromethane as white needles, mp 120—122°C. It was identified as *2,6-dinitro-3,5-dimethyl-4-ethylbenzyl nitrate* on the basis of elemental analysis and spectral properties. IR: 727, 749, 759, 843, 860, 962, 993, 1059, 1270, 1363, 1530, and 1645 cm^{-1}.

Found: C, 44.27; H, 4.55%. Calcd for $C_{11}H_{14}N_2O_4$ (dinitroethylmesitylene): C, 55.46; H, 5.88%. Calcd for $C_{10}H_{11}N_3O_6$ (trinitroethylxylene): C, 44.61; H, 4.09%. Calcd for $C_{11}H_{13}N_3O_7$ (dinitrodimethylethylbenzyl nitrate): C, 44.15; H, 4.35%.

When the reaction mixture was quenched by pouring into excess of water, the precipitated nitrate was accompanied by appreciable amounts of dinitroethylmesitylene, and complete removal of the latter by simple recrystallization was quite difficult to effect.

d): A similar treatment of *n*-propylmesitylene gave *2,6-dinitro-3,5-dimethyl-4-n-propylbenzyl nitrate* as large plates, mp 139—140°C. IR: 754, 857, 873, 993, 1277, 1361, 1530, and 1644 cm^{-1}.

Found: C, 46.51; H, 4.96%. Calcd for $C_{12}H_{15}N_3O_7$: C, 46.01; H, 4.83%.

If the reaction mixture was left to stand at room temperature for a day or two, a large quantity of a crystalline solid was obtained. On recrystallization from a mixture of ligroin and dichloromethane, it gave colorless fine needles which began to sinter at around 135—140°C and melted away at 152—162°C. Elemental analysis and spectral properties agreed with the structure of *2,6-dinitro-3,5-dimethyl-4-n-propylbenzaldehyde*. IR: 743, 787, 862, 913, 1028, 1057, 1288, 1360, 1455, 1528, 1545, and 1709 cm^{-1}; PMR ($CDCl_3$): *n*-Pr (3H 8.92 t, $J=7$ Hz; 2H 8.35—8.58 m; 2H 7.28 t, $J=7$ Hz), Me (6H 7.70 s), and CHO (1H 0.26 s).

Found: C, 54.60; H, 5.52; N, 10.46%. Calcd for $C_{12}H_{14}N_2O_5$: C, 54.15; H, 5.30; N, 10.52%.

On storage under diffused light, it gradually became greenish yellow.

Nitrations with Mixed Acid. a): Ethylmesitylene (7.4 g) was dissolved in dichloromethane (30 m*l*) and the solution was stirred thoroughly with concentrated sulfuric acid (11.7 g) at −5—0°C. Fuming nitric acid (11.7 g, $d=1.5$) was introduced during the course of 30 min and the reaction mixture was worked up as usual to yield an oil (10.5 g), part of which (5 g) was chromatographed on alumina to give unchanged hydrocarbon (0.18 g), 2-nitro-4-ethyl-1,3,5-trimethylbenzene (1.2 g), and *2,6-dinitro-4-ethyl-1,3,5-trimethylbenzene* (mp 110—111°C, 1.3 g) from light petroleum eluates. The dinitro compound showed the PMR peaks at 8.85 (Me t, $J=7$ Hz), 7.79 (2Me s), 7.29 (CH_2 q, $J=7$ Hz), and 7.90 τ (Me s), and IR bands at 762, 781, 807, 856, 866, 1045, 1202, 1369, and 1529 cm^{-1}. Benzene eluted a diphenylmethane (mp 186—188°C, *ca.* 0.1 g) and nitro-carbonyl compounds (0.2 g). The former product had peaks at 8.87 (Me t), 7.95 (Me s), 7.83 (Me s), 7.64 (3Me s), 7.36 (CH_2 q), 6.13 (CH_2 s), and 3.77 τ (aromatic H s) in the PMR spectrum, and was probably a dinitropentamethyldiethyldiphenylmethane, although no attempt was made to clarify its structure. Ether eluted a mixture of mono and dinitroethyldimethylbenzyl alcohols as a dark glassy substance (*ca.* 0.4 g). *2-Nitro-3,5-dimethyl-4-ethylbenzyl alcohol* had IR bands: 755, 795, 849, 878, 1006, 1048, 1368, 1529, and 3360—3380 cm^{-1}, and PMR peaks: Et (3H 8.92 t, 2H 7.45 q; $J=7$ Hz), Me (3H, 7.84 s; 3H 7.71 s), CH_2 (2H 5.69 s), and aromatic H (1H 2.96 s).

b): On a similar treatment of the nitration product (7.0 g) from *n*-propylmesitylene gave unchanged hydrocarbon (*ca.* 0.2 g), 2-nitro-4-*n*-propyl-1,3,5-trimethylbenzene (0.35 g), and *2,6-dinitro-4-n-propyl-1,3,5-trimethylbenzene* (mp 117—118 °C; lit,[3] mp 93—94°C, 2.3 g) from light petroleum eluates. The dinitro compound had IR bands: 741, 797, 854, 864, 886, 1023, 1055, 1363, and 1521 cm^{-1}, and PMR peaks: *n*-Pr (3H 8.95 t, 2H 8.30—8.68 m, 2H 7.34 t), and Me (3H 7.88 s; 6H 7.78 s). Benzene eluted a small amount of a diphenylmethane (0.1 g) and nitro-carbonyl compounds (0.1 g). The former showed PMR peaks at 8.98 (Me t, $J=8$ Hz), 8.64—8.42 (CH_2 m), 7.98 (Me s), 7.87 (Me s), 7.78 (Me s), 7.41 (CH_2 t), 6.18 (CH_2 s), and 3.88 τ (aromatic H s), and was probably a dinitropentamethyldi-*n*-propyldiphenylmethane, although it could not be obtained in quantity sufficient for positive identification. Further elution with ether gave a mixture of nitrodimethyl-*n*-propylbenzyl alcohols as a dark red glass, which had PMR peaks due to *n*-propyl group at 9.01 (3H t, $J=7$ Hz), 8.46—8.77 (2H m), and 7.47 (2H t, $J=7$ Hz); those due to two methyl groups at 7.88 and 7.75; and those due to hydroxyl, methylene, and ring protons at 6.41 (broad), 5.74, and 2.98 τ, respectively.

The Substituent Effect. IV. Proton NMR Chemical Shifts of Phenols

Yuho Tsuno, Mizue Fujio, Yoshio Takai, and Yasuhide Yukawa
Institute of Scientific and Industrial Research, Osaka University, Yamada-kami, Suita, Osaka

(Received October 28, 1971)

NMR chemical shifts of the hydroxyl proton of *m*- and *p*-substituted phenols were determined in aprotic DMF and DMSO solutions. The effect of substituents on the hydroxy chemical shift was correlated much more excellently with our LArSR relationship, $\Delta\delta=\rho(\sigma^0+r\Delta\bar{\sigma}_R^-)$, than with simple Hammett equation, $\rho\sigma^0$ or $\rho\sigma^-$. The correlation resulted in $\rho=1.655$ and $r=0.639$ in DMF with correlation coefficient 0.9992 and $\rho=1.530$ and $r=0.673$ in DMSO with a correlation coefficient 0.9990. Anisotropy effect of any substituent was not significant. The deviations of particular substituents were ascribed to the modification of the electronic characters of substituents due to strong substituent-solvent interactions in DMF (or DMSO). The inductive and resonance substituent constants, $(\sigma_i)_{DMF}$ and $(\Delta\bar{\sigma}_R^-)_{DMF}$, were determined, on the basis of the assumption that the solvent-modification of a given substituent is practically the same at both *meta* and *para* positions.

As described in foregoing papers,[1,2] it had been established that the *Linear Aromatic Substituent-Reactivity* (LArSR) *relationship* (1) could be generally applicable to the substituent effect on both the chemical reactivities, log k/k_0, and physical properties, $P-P_0$, of *meta*- and *para*-substituted benzene derivatives.

$$\log(k/k_0) \text{ or } P-P_0=\rho\bar{\sigma}=\rho(\sigma^0+r^+\Delta\bar{\sigma}_R^++r^-\Delta\bar{\sigma}_R^-) \quad (1)$$

σ^0 is the standard substituent constant which does not involve any additional π-electronic interaction with the reaction center. $\Delta\bar{\sigma}_R^+$ and $\Delta\bar{\sigma}_R^-$ are the resonance substituent constants describing the capabilities for π-electron delocalization (resonance) of conjugatively electron releasing ($-R$) and electron attracting ($+R$) *para* substituents respectively. r^+ and r^- are the resonance reaction constants measuring the extents of effectively exalted resonance interactions of $-R$ and $+R$ substituents in a given system.

This equation implies that the apparent substituent constant $\bar{\sigma}$ can be given by the combination of three terms in bracket at right hand, when a unique ρ value is determined for a given system. Either of the two additional terms plays a significant role in the chemical reactivities in which the benzene conjugation system could be extended fully or partially to the reaction center. In general chemical reactivities, r^+ and r^- are not necessarily equivalent in a given system but are usually independent of each other. The requirement of independent r^+ and r^- values is a characteristic of our LArSR relationship, which subsequently requires the separate statistical applications to conjugatively electron releasing and attracting *para* substituents respectively.

It is believed that the generality of the LArSR Eq. (1) to the effect of electron releasing substituents in electrophilic exalted conjugation reactions, *i.e.*, the applicability of the second term in bracket, has been examined well by ourselves[2-4] and also by many investigators.[2,5-7] Whereas, practical role of the third term for the electron attracting substituent in nucleophilic exalted conjugation systems has not yet been examined enough, for the lack of appropriate data covering over a wide variety of substituents.[2,8] It has been thus highly desirable to obtain the reactivity data and physical data which would enable further testing of the applicability of the last term in the Eq. (1).

In the course of our continuing study of the substituent effect in aromatic derivatives, we have treated several series of NMR chemical shifts of *meta* and *para*-substituted benzene side-chain protons in terms of Hammett-type substituent parameters.[9] The treatment by means of Eq. (1) has appeared to be generally successful for existing data. However, it is rather common that the Hammett-type correlation of proton NMR chemical shifts suffers from the difficulties due to relatively significant role of specific magnetic effects from particular substituents. Our previous results were

1) a) Y. Yukawa and Y. Tsuno, *Nippon Kagaku Zasshi*, **86**, 873 (1965). b) Y. Yukawa and Y. Tsuno, This Bulletin, **32**, 971 (1959); Y. Tsuno, *Memoir, ISIR, Osaka Univ.*, **16**, 197 (1959).

2) Y. Yukawa, Y. Tsuno, and M. Sawada, This Bulletin, **39**, 2274 (1966).

3) a) Y. Yukawa and Y. Tsuno, *Memoir, ISIR, Osaka Univ.*, **23**, 71 (1966); b) Y. Yukawa, Y. Tsuno, and M. Sawada, This Bulletin, **45**, 1198 (1972).

4) T. Imamoto, Y. Tsuno, and Y. Yukawa, *ibid.*, **44**, 1632, 1639, 1644, 2776 (1971).

5) C. Eaborn and K. C. Pande, *J. Chem. Soc.*, **1961**, 297; C. Eaborn and J. A. Waters, *ibid.*, **1961**, 542; R. Baker, R. W. Bott, C. Eaborn, and P. P. M. Greasley, *ibid.*, **1964**, 627; R. W. Bott, C. Eaborn, and D. R. M. Walton, *ibid.*, **1965**, 384; R. Taylor, G. G. Smith, and W. H. Wetzel, *J. Amer. Chem. Soc.*, **84**, 4817 (1962); R. Taylor and G. G. Smith, *Tetrahedron*, **19**, 937 (1963); L. A. Singer and D. J. Cram, *J. Amer. Chem. Soc.*, **85**, 1080 (1963); M. Sheehan and D. J. Cram, *ibid.*, **91**, 3553 (1969); T. Inukai, This Bulletin, **35**, 400 (1962); K. Miyazaki, *Tetrahedron Lett.*, **1968**, 2793.

6) W. P. Jencks, "Progress in Physical Organic Chemistry," Vol. II, Interscience, New York (1964), p. 110; T.I. Crowell, C.E. Bell, Jr., and D. H. O'Brien, *J. Amer. Chem. Soc.*, **86**, 4973 (1964); R. O. C. Norman and G. K. Radda, *Tetrahedron Lett.*, **1962**, 125; R. W. Bott and C. Eaborn, *J. Chem. Soc.*, **1963**, 2139; M. R. Bridge, D. H. Davis, A. Maccoll, R. A. Ross, B. Stephenson, and O. Banjoko, *ibid., B*, **1968**, 805; J. E. Dubois and A. F. Hegarty, *ibid.*, **1969**, 638; T. Fueno, T. Okuyama, and J. Furukawa, This Bulletin, **39**, 569 (1966); S. Clementi and P. Linda, *Tetrahedron*, **26**, 2869 (1970).

7) T. Yokoyama, G. R. Wiley, and S. I. Miller, *J. Org. Chem.*, **34**, 1859 (1968); J. Niwa, This Bulletin, **42**, 1926 (1969).

8) M. Yoshioka, R. Hamamoto, and T. Kubota, *ibid.*, **35**, 1723 (1962); J. J. Ryan and A. A. Humffray, *J. Chem. Soc. B*, **1966**, 842; *ibid.*, **1967**, 468; *ibid.*, **1967**, 1300; *ibid.*, **1969**, 1138; Kuang-Chih Tseng, *Acta Chim. Sinica*, **32**, 107 (1966).

9) a) Y. Yukawa and Y. Tsuno, "Kagaku no Ryoiki," sp. ed. No. 85, Spectrochem. 68B, Chap. 4, Nankodo (1969), p. 87; b) Y. Yukawa and H. Yamada, *Nippon Kagaku Zasshi*, **85**, 501 (1964); H. Yamada, Y. Tsuno, and Y. Yukawa, This Bulletin, **43**, 1459 (1970); Y. Yukawa, Y. Tsuno, and H. Yamada, *Memoir, ISIR, Osaka Univ.*, **23**, 79 (1966).

also not quite free from these effects enough to permit the critical test of the applicability of Eq. (1). Our recent data on the chemical shift of ring protons of substituted benzenes in various solvents were correlated with Eq. (1) satisfactorily, but several nagging qualitative problems have still remained.[10]

Among a number of recent communications on the subject, Ouellette[11] reported that the hydroxyl proton resonance of *meta* and *para*-substituted phenols in dimethylsulfoxide solution exhibited remarkably magnified substituent chemical shifts and pointed out that the substituent chemical shifts were linearly correlated by Hammett σ^- constants with impressive accuracy. However, upon the Hammett-type treatment including our preliminary data, we arrived at somewhat different conclusions regarding the correlation of substituent contributions in this system. The hydroxyl chemical shifts were not so satisfactorily correlated, as had been reported, with a single set of ordinary σ^- parameters, but were found to be treated much more excellently with an aid of our LArSR Eq. (1).[12] As far as we were aware, this series of substituent chemical shifts appeared to be most precisely described by means of the reactivity substituent parameters. From these facts, we directed our attention to obtain more extensive data for the substituent effect on the NMR chemical shifts of the hydroxyl proton of *meta* and *para*-substituted phenols in various solvents.

The present paper mainly concerns the general treatment based on our LArSR equation of substituent effects on the hydroxyl chemical shifts of phenols in dimethylformamide. Later, Traynham and Tribble have reported a new set of data for phenol-hydroxyl chemical shifts in DMSO solution,[13] and our shift values, in cases where direct comparison is possible, agree well with data reported by these investigators. However, substituents involved in their determination are still insufficient for our purpose. Then, a full set of our data in DMSO are also included in this paper, in order to permit direct comparison of data obtained in a single study.

Experimental

Phenols. All the phenols used were thoroughly purified by repeated fractionations or recrystallizations from appropriate solvents, and for some phenols purification was effected by further sublimations of purified samples. The mps and other physical constants agreed well with established values.

About a half of *m*- and *p*-substituted phenols used in this series of studies were obtained from commercial sources except those given below.

Following phenols were prepared by the usual diazonium method from corresponding anilines available in pure form. Diazonium sulfates were decomposed by dropwise addition to 36% aqueous sulfuric acid solution at about 80°C and the phenols produced were steam-distilled or extracted by appropriate solvents; m-*Bromophenol*, bp 94—96°C/6 mmHg, lit,[14] bp 135—140°C/12 mmHg; m-*Fluorophenol*, bp 90°C/58 mmHg, lit,[14] bp 108°C/70 mmHg; m-*Trifluoromethylphenol*, bp 73—74°C/15 mmHg, lit,[15] bp 85.5—86.5°C/25 mmHg; m-*Phenoxyphenol*, bp 148°C/4 mmHg, lit,[14] bp 150°C/4.5 mmHg; p-*Fluorophenol*, mp 45—45.5°C recrystallized from *n*-hexane, lit,[14] mp 46.5°C; m-*Iodophenol*, mp 38.5—39.5°C recrystallized from benzene - *n*-hexane, lit,[14] mp 40°C; *3,5-Dichlorophenol*, mp 66°C recrystallized from *n*-hexane, lit,[14] mp 68°C.

p-*Trifluoromethylphenol* (bp 60°C/15 mmHg, lit,[16] bp 71.5—72°C/8 mmHg) was obtained from *p*-trifluoromethylaniline, which was prepared according to the direction of Jones[16] by fluorine-exchange of *p*-tribromomethylnitrobenzene with SbF_5 into trifluoromethylnitrobenzene followed by reduction with $SnCl_2$ in ethanol-hydrochloric acid solution.

p-N,N-*Dimethylaminophenol* was derived from *p*-anisidine. Methylation of anisidine with dimethyl sulfate gave dimethylaminoanisole (bp 146°C/38 mmHg), which was demethylated by boiling with conc. hydroiodic acid to the phenol and purified by recrystallizations from ligroin, mp 77°C, lit,[17] mp 77.5—78°C.

m-Aminophenol was converted into m-*Acetaminophenol* by the acetylation in aqueous acetic acid with acetic anhydride and purified by recrystallizations from water, mp 148—149°C, lit,[18] mp 148°C.

p-Aminophenol was converted into p-*Iodophenol* (mp 92.5—93.5°C recrystallized from ligroin, lit,[19] mp 93—94°C), by literature method and also into p-*Cyanophenol* (mp 111—112°C recrystallized from benzene, lit,[20] mp 113°C) by the Sandmeyer reaction of the diazonium salt with cuprous cyanide.

m-*Cyanophenol* (mp 80°C from benzene - *n*-hexane, lit,[21] mp 82°C) was obtained according to the procedure of Clemm by the dehydration of m-*Hydroxybenzaldoxime* (mp 89.5°C from benzene, lit,[21] mp 87.5°C) with acetic anhydride followed by the hydrolysis of the acetate.

p-*Hydroxybenzylidenaniline* was prepared by the condensation of *p*-hydroxybenzaldehyde with aniline in ether solution (mp 197—198°C, recrystallized from ethanol, lit,[22] mp 194—195°C). p-*Benzylidenaminophenol* was similarly prepared from benzaldehyde and *p*-aminophenol, mp 189—190°C, recrystallized from ethanol, lit,[23] mp 181°C.

Hydroxybenzophenones were obtained by the cleavage of the methyl ether of methoxybenzophenones by heating under reflux for 12 hr with hydrobromic acid - acetic acid mixture (3 vol. Ac_2O, 5 vol. AcOH, and 5 vol. 48% aqueous HBr). m-*Hydroxybenzophenone*, mp 117°C from benzene - ethanol and petroleum ether, lit,[14] mp 116°C; p-*Hydroxybenzophenone*, mp 133°C from benzene, lit,[14] mp 130—132°C.

p-*Phenoxyphenol* was obtained in the similar way from *p*-methoxydiphenyl ether and recrystallized from benzene - *n*-hexane, mp 85—86°C, lit,[14] mp 84—85°C.

m-*Methylmercaptophenol* was prepared by the ether-cleavage of *m*-methoxyphenyl methyl sulfide with hydrobromic acid

10) Y. Yukawa, Y. Tsuno, and N. Shimizu, This Bulletin, **44**, 2843 (1971).
11) R. J. Ouellette, *Can. J. Chem.*, **43**, 707 (1965).
12) Presented in part at the Hammett Symposium (1967) at Kyoto, Japan.
13) J. G. Traynham and G. A. Knesel, *J. Org. Chem.*, **31**, 3350 (1966); M. T. Tribble and J. G. Traynham, *J. Amer. Chem. Soc.*, **91**, 379 (1969); G. Socrates, *Trans. Faraday Soc.*, **66**, 1052 (1970).
14) Dictionary of Organic Compounds (1953).
15) J. K. Wolfe, US. 2547679; *Chem. Abstr.*, **45**, 9081g (1951).
16) R. G. Jones, *J. Amer. Chem. Soc.*, **69**, 2346 (1947).
17) F. G. Bordwell and P. J. Boutan, *ibid.*, **78**, 87 (1956).
18) F. Reverdin and A. de Luc, *Ber.*, **47**, 1537 (1914).
19) A. H. Blatt, "Organic Syntheses," Coll. Vol. II, p. 355 (1956).
20) F. Ahrens, *Ber.*, **20**, 2952 (1887).
21) A. Clemm, *ibid.*, **24**, 826 (1891).
22) A. Seiner and R. B. Forster, *J. Chem. Soc.*, **105**, 2462 (1914).
23) C. Philipp, *Ber.*, **25**, 3247 (1892).

in acetic acid solution (bp 141.5°C/8 mmHg, lit,[24] bp 154—156°C/17—18 mmHg). *m*-Methoxyphenyl methyl sulfide was obtained from anisidine by the modification of the direction given by Grice[25] for *m*-methylmercaptobenzoic acid, bp 125.5°C/17 mmHg. Oxidation of *m*-methylmercaptophenyl acetate, mp 39°C (lit,[24] mp 40—41°C), with hydrogen peroxide in acetic acid according to the direction of Bordwell gave *m*-methylsulfonylphenyl acetate, which yielded on hydrolysis with 10% aqueous sodium hydroxide m-*Methylsulfonylphenol*, in good yield (mp 81—82°C recrystallized from benzene - chloroform, lit,[24] mp 83—84°C). p-*Methylsulfonylphenol* was similarly obtained from methylmercaptophenol (mp 85°C from light petroleum, lit,[24] mp 84—85°C) by oxidation of the acetate with hydrogen peroxide in acetic acid, followed by hydrolysis of *p*-methylsulfonylphenyl acetate resulted; mp 92°C from benzene - chloroform mixture, lit,[24] mp 95—96°C.

p-*Thiocyanophenol* was prepared by the usual procedure given by Bordwell and was purified by recrystallizations from benzene - *n*-hexane, mp 61°C, lit,[26] mp 62—63°C.

Hydroxynitrostyrenes were prepared by condensation of corresponding hydroxybenzaldehydes with nitromethane; m-*Hydroxynitrostyrene*, mp 141—141.5°C from benzene - ethanol, lit,[27] mp 136—137°C; p-*Hydroxynitrostyrene*, mp 166—167°C from benzene - ethanol, lit,[28] mp 165—166°C.

m-Hydroxybenzaldoxime was converted by Field's direction[29] with nickel acetate into m-*Hydroxybenzamide*, mp 171—172°C from benzene - ethanol, lit,[30] mp 169—170°C.

Ethyl p-*hydroxycinnamate* (mp 76°C recrystallizations from benzene - *n*-hexane) was prepared by the condensation of *p*-hydroxybenzaldehyde with malonic acid, followed by esterification of cinnamic acid produced.[31] m-*Isomer* (mp 66.5—67.5°C, recrystallizations from benzene - *n*-hexane, lit,[32] mp 70—71°C) was also prepared by the similar procedure.[31]

Solvent. Dimethylsulfoxide was dried for 4 days, boiled under reflux for one day over calcium hydride and fractionally distilled under reduced pressure. The middle fraction bp 100.5°C at 39 mmHg was stored over molecular sieve and distilled before use.

Dimethylformamide which had been prepurified by the literature method was treated with molecular sieve and fractionated under reduced pressure, bp 58°C at 25 mm.

NMR Spectra. The proton resonance spectrum of the phenol hydroxyl group was recorded on a Hitachi-Perkin Elmer R-20 spectrometer, operating at 60 MHz. The probe temperature was maintained at 34.0°C. The measurement was made by freshly prepared DMF or DMSO solutions at the concentration in the range 1.0—0.05M. The solvent peak provided a convenient reference signal. The low field ^{13}C–H satellite of DMF or DMSO solvent main peak was utilized as the general internal standard throughout the series of chemical shift measurement. The shift value was determined by direct counting of peak to peak frequency differences from the standard satellite peak, and calibrated to the shift value from TMS in the usual way. At the concentration range studied, the line width of the hydroxyl resonance signal was generally 1.5 Hz or less, but in some cases was a little broader (2—3 Hz). The broad signal of hydroquinone, 7—8 Hz at 0.5M, was the worst case, and appeared to be diffused more on dilution. The shift values were determined repeatedly at least three different concentrations in the range lower than 0.5M, using independently prepared solution. The values were reproducible to ±0.2 Hz at a given concentration for all samples. Resonance position of a given phenol generally tended to shift very slightly toward high field on dilution, but mostly approached to or remained a constant within ±0.2 Hz at the concentration below 0.25M, independent of concentrations covering over more than 4 folds dilution. A minor dilution shift was apparent in 6 derivatives among 50 substituted phenols to an extent of 2.0—2.5 Hz through a wide range of the concentration 0.5—0.05M in either DMF or DMSO solution. To approximate actual chemical shift values at infinite dilution conditions, the measurement was extended to that in high dilute solutions possible

Table 1. Chemical shifts of hydroxyl protons of *m*, and *p*-substituted phenols

No.	Subst.	DMF		DMSO	
		$\Delta\delta_p^{TMS}$	$\Delta\delta_m^{TMS}$	$\Delta\delta_p^{TMS}$	$\Delta\delta_m^{TMS}$
1	NO_2	11.212	10.558	10.963	10.353
2	CN	10.768	10.372	10.540	10.140
3	CHO	10.733	10.053	10.533	9.878
4	SO_2CH_3	10.728	10.330	10.510	10.160
5	$SOCH_3$	10.203		10.010	
6	SO_2NH_2	10.380		10.187	
7	SCN	10.368		10.140	
8	COC_6H_5	10.572	9.955	10.373	9.793
9	$COCH_3$	10.455	9.848	10.250	9.703
10	$COOCH_3$	10.432	9.897	10.257	9.765
11	COOEt	10.418	9.888	10.238	9.737
12	$CONH_2$	10.077	9.718	9.877	9.531
13	CF_3	10.430	10.212	10.220	10.027
14	$CH{=}CHNO_2$	10.567	9.942	10.340	9.716
15	CH=CHCOOEt	10.148	9.730	9.936	9.556
16	$CH{=}NC_6H_5$	10.235		10.068	
17	$N{=}CHC_6H_5$	9.608		9.437	
18	$N{=}NC_6H_5$	10.438		10.247	
19	C_6H_5	9.632		9.480	
20	H	9.392		9.253	
21	I	9.812	9.882	9.613	9.690
22	Br	9.805	10.013	9.623	9.813
23	Cl	9.773	10.005	9.600	9.810
24	F	9.438	9.963	9.288	9.798
25	SCH_3	9.548	9.567	9.370	9.425
26	OC_6H_5	9.447	9.730	9.266	9.527
27	NHAc	9.217	9.385	9.078	9.262
28	NHC_6H_5	9.117	9.282	8.947	9.120
29	*t*-Bu	9.180	9.212	9.038	9.115
30	C_2H_5	9.162		9.021	
31	CH_3	9.138	9.265	9.002	9.140
32	OCH_3	8.945	9.408	8.828	9.295
33	OH	8.683	9.217	8.535	9.077
34	NMe_2	8.643	9.022	8.535	8.928
35	NH_2	8.400	8.875	8.267	8.755
36	$(CH_3)_2$		9.123		9.018
37	Cl_2		10.582		10.358

24) T. Zincke and C. Ebel, *Ber.*, **47**, 1100 (1914); F. G. Bordwell and P. J. Boutan, *J. Amer. Chem. Soc.*, **79**, 717 (1957).
25) R. Grice and L. N. Owen, *J. Chem. Soc.*, **1963**, 1947.
26) F. G. Bordwell and P. J. Boutan, *J. Amer. Chem. Soc.*, **78**, 854 (1956).
27) F. G. P. Remery, *J. Chem. Soc.*, **99**, 282 (1911).
28) R. Stewart and L. G. Walker, *Can. J. Chem.*, **35**, 1561 (1957).
29) L. Field, P. B. Hughmark, S. H. Shumaker, and W. S. Marshall, *J. Amer. Chem. Soc.*, **83**, 1984 (1961).
30) L. A. Cohen and W. M. Jones, *ibid.*, **85**, 3402 (1963).
31) K. C. Pandya and T. A. Vahidy, *Proc. Indian Acad. Sci.*, **4A**, 134 (1936), *Chem. Abstr.*, **30**, 8149 (1936); E. Fischer, *Ber.*, **50**, 619 (1917).
32) H. Ley, *Z. Phys. Chem.*, **94**, 405 (1920).

to give no further shift exceeding over a measurement error of ± 0.2 Hz by additional dilution with an equal volume of solvent. It can be then estimated that in nearly all instances the discrepancy from the infinite dilution value does not exceed ± 0.4 Hz, even for the least favorable case. Results are summarized in Table 1.

Result

In either dimethylsulfoxide (DMSO) or dimethylformamide (DMF) solution, phenols carrying various *meta* and *para*-substituents resulted in the stabilized NMR resonance signals of hydroxyl protons. As mentioned by previous workers,[11-13] the concentration dependence of the shift was not significant in these solvents in contrast to the dilution shift as much as 1 ppm observed in carbon tetrachloride solution.[33]

Table 1 lists the chemical shift values of the hydroxyl protons of *meta* and *para*-substituted phenols at approximately infinite dilution in DMF and DMSO solutions. It may be estimated that the uncertainty in the listed values of chemical shifts does not exceed ± 0.005 ppm. The hydroxyl chemical shift varies in either solution over a range of 2.7 ppm with respect to substituent changes. Then, the experimental uncertainty is effectively regarded as being negligible in comparison with the divergent chemical shift variation due to substituent changes. The present results in DMSO solution are generally in good agreement with those reported by Traynham[13] and Ouellette.[11] The latter author reported consistently lower (less shielded) values by *ca.* 0.04 ppm than the present data, but the relative substituent chemical shift values agree well with the present values within usual experimental error.

One of the important facts, as seen in the result in Table 1, is the proportionality between the substituent shifts in both DMF and DMSO solvents. The correlation is given by

$$\Delta\delta_{\mathrm{DMSO}} = 0.951\Delta\delta_{\mathrm{DMF}}$$

The precision can be measured by the standard deviation ± 0.022 and the correlation coefficient 0.9992. The similar linearity is observed for literature data of the phenol substituent chemical shifts in HMPA (Hexamethylphosphoramide)[35]

$$\Delta\delta_{\mathrm{HMPA}} = 1.1\Delta\delta_{\mathrm{DMF}}$$

In addition, a series of our recent data in acetonitrile can be also correlated linearly to the shift data in DMF with a coefficient of 0.68.[34] The variation of the chemical shift in a series of substituted phenols are appreciably magnified in either of these solvents as compared with those in carbon tetrachloride. The slope of these correlations appears qualitatively to vary in parallel to the low-field shift of hydroxyl resonance position of a given phenol in respective solvents, and the susceptibility of hydroxyl shifts to substituent changes varies dependent upon the solvent basicity or the hydrogen bond acceptor strength of solvents. Nevertheless, it is clear that the apparent substituent constant $\bar{\sigma}$ remains practically the same in either of these solvents, to a precision on the order of experimental error. Any particular effect on substituent constants is not significant among these solvents. Accordingly, the discussion followed will treat the results in DMF solution conveniently as a representative series of the substituent effects on the hydroxyl chemical shift in these solvents.

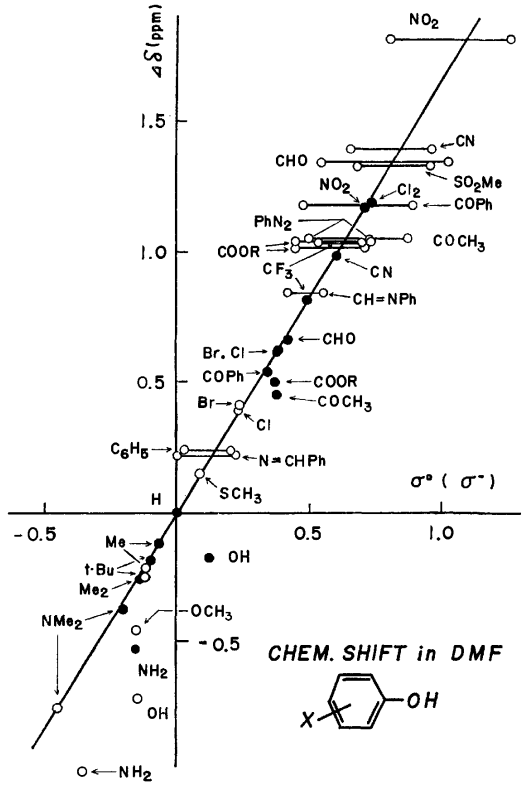

Fig. 1. Hammett plot of hydroxyl chemical shifts of phenols in DMF; open circle for *para* and closed circle for *meta* substituents.

In Fig. 1, the relative substituent chemical shifts of hydroxyl proton are plotted against corresponding σ^0 and σ_p^- constants. Contrary to the results reported by Ouellette[11] considerable scatterings are observed as a whole figure. Deviations from the σ^0 correlation line are more significant in *para* than in *meta*-substituents, while they appear to be rather systematic. The direct employment of any other ordinary set of substituent constants does not improve significantly the overall correlation. However, it should be noticed that most of the *m*-substituent chemical shifts are excellently described by σ_m constants. This is in clear contrast to the behavior of the *meta* ring proton of mono-substituted benzenes which provide apparently a better correlation with σ_p^0 values[10] and the ^{19}F shielding parameters for *meta*-substituted fluorobenzenes[36] which correlate with σ_I constants alone. Among 30 *meta*-substituents examined,

33) W. G. Paterson and N. R. Tipman, *Can. J. Chem.*, **40**, 2122 (1962); C. M. Huggins, G. C. Pimentel, and J. N. Shoolery, *J. Phys. Chem.*, **60**, 1311 (1956).

34) Y. Yukawa, Y. Tsuno, and M. Fujio, unpublished.

35) M. W. Dietrich, J. S. Nash, and R. E. Keller, *Anal. Chem.*, **38**, 1479 (1966).

36) R. W. Taft, E. Price, I. R. Fox, I. C. Lewis, K. K. Andersen, and G. T. Davis, *J. Amer. Chem. Soc.*, **85**, 709 (1963); J. Hirst and S. J. Una, *J. Chem. Soc., B*, **1969**, 646.

deviations are obvious only for amino, acetamino, and hydroxy, and detectable to a minor extent for methoxy, acetyl and carboalkoxy groups.[37] These deviations do not appear to be similar to the characteristic deviations observed in the chemical shift of the usual side-chain or ring protons at *meta* position.

Table 2. Standard substituent constants[3b]

Subst.	σ_p^0	σ_m^0	$\Delta\bar{\sigma}_R^-$
NO_2	0.810	0.709	0.455
CN	0.653	0.607	0.309
SO_2CH_3	0.686 (0.749)	*0.64* (0.697)	0.302
SO_2NH_2	*0.65*	0.622	0.246
CHO	*ca. 0.53*	0.415	0.465
COC_6H_5	0.490	0.357 (0.3)	0.387
$COCH_3$	0.491	0.376 (0.30)	0.365
$COOCH_3$	0.460	0.36 (0.32)	0.30
COOEt	0.453	0.38 (0.31)	0.28
$CONH_2$	*0.38*	0.32	0.24
$CH{=}CHNO_2$	*ca. 0.50*	*0.38*	*ca. 0.37*
$CH{=}NC_6H_5$	*0.42*		*0.14*
$N{=}CHC_6H_5$	*0.00*		*0.22*
$N{=}NC_6H_5$	0.40	*0.29*	0.31
CF_3	0.505	0.493, 0.476	0.196
SCN	0.493		0.12
C_6H_5	0.039		0.16
NH_2	−0.36	−0.15	
NMe_2	−0.48	−0.21	
OH	−0.16	0.122	
OCH_3	−0.100 (−0.152)	0.115 (0.06)	
NHAc	0.0	0.12	
CH_3	−0.124	−0.069	
C_2H_5	−0.131		
t-Bu	−0.174	−0.100	
SCH_3	0.083	0.120	
OC_6H_5	0.076	*0.252*	
F	0.212	0.337	
Cl	0.281	0.373	
Br	0.296	0.391	
I	*0.298*	0.352	

Values in bracket are the values to be used for the data in aqueous organic solutions, and given in italic are less reliable.

The hydroxy chemical shift for *meta* substituents diverges along a straight line for σ_m over a range of 1.5 ppm, which will be wide enough to determine the reliable ρ_m-line as a standard for the discussion of substituent effect. The substituent parameter values utilized in the following calculations are listed in Table 2. Nineteen well-behaving *meta*-substituents give a precise straight correlation, on employment of the method of least squares,

$$\Delta\delta_{DMF}^{OH} = 1.656\sigma_m - 0.019$$

the standard deviation being ±0.016 and the correlation coefficient 0.9994. On the basis of this ρ_m value, a set of apparent substituent constants can be determined from this series. They are listed in Table 3. A comparable set can be derived also from the shift data in DMSO solution, where *meta* substituents provide similarly ρ_m value of 1.529 ($s=\pm0.022$ and $R=0.9987$), and the apparent $\bar{\sigma}$ values for all *meta* substituents coincide precisely with the values derived from DMF data.

Table 3. Apparent substituent constants in DMF

No.	Subst.	$\bar{\sigma}_p$	$\bar{\sigma}_m$
1	NO_2	1.110	0.716
2	CN	0.843	0.603
3	CHO	0.822	0.411
4	SO_2CH_3	0.819	0.578
5	$SOCH_3$	0.502	
6	SO_2NH_2	0.608	
7	SCN	0.597	
8	COC_6H_5	0.724	0.351
9	$COCH_3$	0.653	0.287
10	$COOCH_3$	0.639	0.316
11	COOEt	0.632	0.312
12	$CONH_2$	0.425	0.209
13	CF_3	0.638	0.507
14	$CH{=}CHNO_2$	0.721	0.344
15	CH=CHCOOEt	0.469	0.243
16	$CH{=}NC_6H_5$	0.520	
17	$N{=}CHC_6H_5$	0.142	
18	$N{=}NC_6H_5$	0.644	
19	C_6H_5	0.156	
20	H	0.011	
21	I	0.265	0.307
22	Br	0.261	0.387
23	Cl	0.242	0.382
24	F	0.040	0.357
25	SCH_3	0.106	0.117
26	OC_6H_5	0.045	0.216
27	NHAc	−0.094	0.007
28	NHC_6H_5	−0.155	−0.055
29	*t*-Bu	−0.117	−0.097
30	C_2H_5	−0.127	
31	CH_3	−0.141	−0.065
32	OCH_3	−0.258	0.022
33	OH	−0.416	−0.094
34	NMe_2	−0.440	−0.212
35	NH_2	−0.587	−0.301
36	$(CH_3)_2$		−0.150
37	Cl_2		0.730

The apparent substituent constants $\bar{\sigma}_p$ for conjugatively electron attracting ($+R$) *para* substituents all lie in between corresponding σ^0 and σ^- values. The resonance contribution of these *para* substituents to the hydroxyl chemical shift appears to be relatively less effective than that in the phenol dissociation measured by σ^- constants. It may be expected that our LArSR Eq. (1) will enable to correlate the hydroxyl chemical shifts of these groups.

On the least squares application of Eq. (1) to the hydroxyl chemical shifts for these groups including well-behaving *meta*-substituents (total number 31), an excellent linear correlation (Fig. 2) is resulted in

$$\Delta\delta_{DMF}^{OH} = 1.655(\sigma^0 + 0.639\Delta\bar{\sigma}_R^-) - 0.016 \quad (2)$$

The standard deviation from the regression line is ±0.022 and the correlation coefficient 0.9992. The ρ

37) The latter three substituents could be fitted closer to the line by the use of σ_m values given for aqueous organic solution.

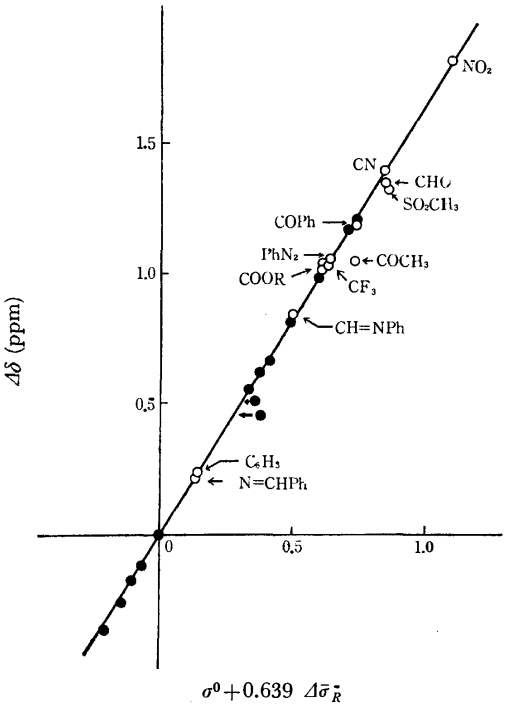

Fig. 2. LArSR plot for hydroxyl proton chemical shifts in DMF; open circle for $+R$ *para* substituents and closed circle for *meta* substituents.

value derived is identical with that obtained from *meta* substituents alone. The same treatment can be applied also to the shifts in the latter solution with analogous precision.[38]

$$\Delta\delta^{OH}_{DMSO} = 1.530(\sigma^0+0.673\Delta\bar{\sigma}_R) - 0.004$$

It is evident from these results that the hydroxyl chemical shifts of substituted phenols in these solvents can be treated quite successfully by means of our LArSR Eq. (1) in the same way as the general chemical reactivity changes, at least as far as conjugatively electron attracting groups are concerned.

On the other hand, the analogous treatment of conjugatively electron releasing ($-R$) *para* substituents based on Eq. (1), unfortunately, does not appear to be successful. The fit to the Eq. (1) should imply the existence of a certain proportionality between the increments of apparent $\bar{\sigma}_p$ from σ^0_p values and the corresponding $\Delta\bar{\sigma}^+_R$ parameters throughout a series of *para* $-R$ substituents. However, the apparent enhancement, $\bar{\sigma}_p-\sigma^0_p$, is significant for amino, hydroxy, acetamino, and methoxy groups, but is not significant for the remainder. A contrast is clear in the comparison of the behaviors of *p*-amino and *p*-dimethylamino substituents, in spite of their comparable and potential resonance capabilities in general chemical reactivities. In practice, no clear-cut correlation was observed for these $-R$ substituents between the enhancements $\bar{\sigma}_p-\sigma^0_p$ and the corresponding $\Delta\bar{\sigma}^+_R$ values. It is however to be mentioned that the substituent which gives the anomalous resonance enhancement $\bar{\sigma}_p-\sigma^0_p$ at *para* position does exhibit the anomalous effect, the exalted electron donation, also at *meta* position.

38) Correlation coefficient $R=0.9990$ and standard deviation $s=\pm0.023$.

Discussion

It is frequently noted that the substituent effect on the NMR chemical shift is not described so successfully by the ordinary substituent parameters which were derived from chemical reactivities.[9b] Even in chemical reactivities, in general, a single set of Hammett-type substituent constants such as σ, σ^+, and σ^- can not always provide a good description of the actual substituent contribution. The degree of resonance contribution from substituents, relative to their polar or inductive contribution, depends evidently upon the structure of the system and of the detection center and also upon the nature of the detection variables. The susceptibility of the proton NMR chemical shift to the π-electronic (resonance) contribution relative to the σ-electronic (or field) effect from substituents may differ from the relative π-electronic contributions in the reactivity changes of similar structural system. Such the effect should be taken into account, as a first approximation, by the aid of our LArSR relationship or other relevant equations.[39]

A most serious problem we often have encountered with the treatment of substituent effects on proton NMR chemical shifts is the fact that the *meta* substituent chemical shifts do not apparently follow σ_m values, and furthermore, the different ρ-values are often required for respective series of *meta* and *para* substituent chemical shifts. These provide a difficulty in determining unique ρ-value for a given system as generally assumed in the correlation of chemical reactivities. It is then an appreciated feature of the present data that the *meta* substituent chemical shifts can be precisely correlated with σ_m values and most of *para* substituent chemical shifts are described by the combination of σ^0_p and $\Delta\bar{\sigma}_R$ parameters, giving the same ρ value for both series.

Another difficulty in the treatment of substituent chemical shifts is the serious deviations of certain substituents arising from their specific magnetic contributions. Although deviations are significant for several substituents in the present series, the direction and magnitude of deviations are dissimilar to those expected from the nature of anisotropic substituents. The difference in the nature of deviations is evident in the comparison with the α-proton of substituted toluenes. It is clear that any specific magnetic contributions are of little practical consequence and the effects, if present, are relatively unimportant in the chemical shifts of phenol protons in these solvents examined. The hydroxyl chemical shift should be predominantly controlled by the charge produced or the electron density at the hydroxyl oxygen atom, which in turn should be determined by the intramolecular electronic interaction with substituents.

The hydrogen-bonding interaction of the hydroxyl

39) P. R. Wells, *Chem. Rev.*, **63**, 171 (1963); C. D. Ritchie and W. F. Sager, "Progress in Physical Organic Chemistry," Vol. II, Interscience, New York (1964), p. 323; P. R. Wells, S. Ehrenson, and R. W. Taft, *ibid.*, Vol. IV (1968), p. 147; C. G. Swain and E. C. Lupton, Jr., *J. Amer. Chem. Soc.*, **90**, 4328, (1968); M. J. S. Dewar and P. J. Grisdale, *ibid.*, **84**, 3539 (1962).

function with a hydrogen-bonding acceptor solvent plays evidently an important role in magnifying the substituent chemical shifts and also in fitting to the Hammett-type relationship. The state of phenol molecules reflected on the hydroxyl chemical shift must closely resemble the intermediate state for the acid dissociation of phenols. Intramolecular electronic interactions of substituents with the acquired charge at the phenol oxygen in the present system may be close to those in the phenoxide-ion. The large positive value of ρ and high r-value for conjugatively electron attracting *para* substituents justify the above explanation. What is actually observed in the present system would be the substituent effect on the hydrogen bonding measured by the proton chemical shift as the detection variable. Thus, it is not surprising that the substituent effect in the present system can be treated in the same way as those in the general chemical processes.

In view of the significance of fit to the correlation (2) of well-behaving substituents, dispositions of certain particular substituents, especially of several electron releasing groups, should be significant. The deviations can not be referred to the experimental error, but it is evident that some extraneous effects are operating in these groups. The precision within 0.010 in σ-unit would be high enough to permit the quantitative discussion of the extraneous effects producing significant deviations.

It should be noticed here that the present data are obtained from the measurement in anhydrous aprotic solvents. Several workers have pointed out the importance of the solvent effects on the NMR chemical shift and have offered a variety of rationalizations for the phenomena.[40] Most of these rationalizations are based primarily on the intermolecular long range magnetic effect induced from the solvent molecule specifically oriented to solute molecule. It may be expected that the substituent-solvent interaction should take an important part of the solute-solvent interactions in usual aromatic molecules, since the substituent is one of the most polar sites of the solute molecule. The long range magnetic effect might not be so significant from the solvent molecule which coordinates to the substituent located far from the detecting function, while the effect of variation in the electronic nature of particular substituent due to strong interaction with solvent could not be neglected. The parameters of a given substituent should be subject to change by the modification of its electronic characters by the solvent-substituent interaction. Evidence has been accummulated which indicates that substituent effects on aromatic reactivities are not generally independent of solvents.[41,42] Since the standard sets of substituent parameters were derived from the measurement in water (or aqueous organic solutions) where donative hydrogen bonding to substituents is highly important, certain deviations of particular substituents might be produced in the correlation of the data in aprotic solvents, upon employment of definite sets of parameters. Thus, it might be plausible to refer the deviations observed in the above correlation primarily to the effect of solvent-modification of substituent effects.

We should examine, first of all, the effect of *meta* substituents where no significant change is expected in the relative contribution of resonance from one series to another. Among a series of *meta* substituents, hydroxyl and amino groups exhibit exceptionally large deviations from the correlation (2); the apparent σ_m values of these groups are more negative than the ordinary σ_m values. It is qualitatively expected that not only these two but all the substituent which possesses a lone electron pair on the α-atom would be more electron releasing in hydrogen-bond acceptor solvents than estimated from the σ values in aqueous solution, from which donative hydrogen-bonding is effective. As a matter of fact, however, this effect does not appear so serious for general $-R$ *meta* substituents (except the above two particular groups) in the present system. Perhaps the small but real deviation of *m*-methoxy group may be referred to this effect. The loss of hydrogen-bond donation in non-aqueous solution can also explain reasonably the deviations of *m*-acetyl and *m*-carboalkoxy groups. Amino and hydroxyl groups, on the other hand, behave as the effective hydrogen-bond donor to DMF and DMSO solvents. The negative charge at hydroxyl oxygen or amino nitrogen due to hydrogen bonding with an acceptor solvent can make these groups further electron releasing, while such an effect would not be significant in aqueous solutions. Ritchie has recently noted the similar behavior of these groups in the dissociation of substituted benzoic acids in DMF solution.[43]

From these facts, it appears necessary to utilize the substituent constant characteristic of a substituent in given solvents. It does not appear unreasonable, as a useful approximation, to assume that the apparent substituent constant in a given solvent is to be the ordinary effect characteristic of the "solvent-modified substituent," or of *the existing solvent-coordinated substituent species whose electronic character is effectively modified.* This assumption may be practically useful in view of facts that the modifications of parameters are required only for certain particular substituents and also that finite parameter values can be adopted to these groups for respective solvent classes, since for any particular substituent there is a consistent behavior in the range of solvents.

The effect of the solvent-modification should be operative with the same substituent at *para* position as well as *meta* position. This can be evidently shown in

40) J. Ronayne and D. H. Williams, *J. Chem. Soc., B*, **1967**, 540; R. J. W. Le Fevre, D. V. Radford, G. L. D. Ritchie, and P. J. Stiles, *ibid.*, **1968**, 148; R. E. Klinck and J. B. Stothers, *Can. J. Chem.*, **40**, 2329 (1962); N. E. Alexandrou and D. Jannakoudakis, *Tetrahedron Lett.*, **1968**, 3841; T. Ledaal, *ibid.*, **1968**, 1683; N. Nakagawa and S. Fujiwara, This Bulletin, **34**, 143 (1961); I. D. Roe and L. K. Dyall, *Aust. J. Chem.*, **19**, 835 (1966); Y. Nomura and Y. Takeuchi, *J. Chem. Soc., B*, **1970**, 956.

41) C. D. Ritchie and G. H. Megerle, *J. Amer. Chem. Soc.*, **89**, 1447 (1967); C. D. Ritchie and R. E. Uschold, *ibid.*, **90**, 3415 (1968); C. D. Ritchie and E. S. Lewis, *ibid.*, **84**, 591 (1962).

42) A. Fischer, G. J. Leary, R. D. Topsom, and J. Vaughan, *J. Chem., Soc. B*, **1967**, 846.

43) C. D. Ritchie and R. E. Uschold, *J. Amer. Chem. Soc.*, **90**, 2821 (1968).

Fig. 1 as the deviations of particular substituents at both *para* and *meta* positions. Either of these substituents brings about the deviations of the same direction and of a comparable order of magnitude from both positions (or of a little greater extent from *para* position). This might partly validate the present discussion based on "solvent-modified substituent." For the correlation of *para* substituents, it is necessary to determine characteristic r-values of the system. Conjugatively electron attracting substituents in the present system (in DMF) give an r^- value, 0.639, but it is difficult to determine a unique r^+ value for conjugatively electron releasing substituents as mentioned in Result. However, as apparent substituent constants for most of $-R$ substituents do not differ from their original σ^0 values within the order of experimental uncertainty, excluding the substituents carrying an acidic hydrogen at the α-atom, we may estimate the r^+ value for electron releasing resonance contribution being approximately zero.

Previous investigators[11,13] have employed the standard σ_p values (*i.e.*, more exalted resonance scale, $r^+=0.27$) for *para* substituents instead of σ_p^0 values ($r^+=0.00$). *p*-Amino and *p*-hydroxyl groups fall near the line when they are correlated with σ_p values, while the subsequent deviations are resulted in the other groups, and such the treatment offers a difficulty in explaining why the substituent carrying an active α-hydrogen exerts the enhanced electron donation especially at *meta* position. Since the strongly electron donative detection center $-\overset{\delta-}{O}\cdots\overset{\delta+}{H}$ should prevent the additional resonance interaction with *para* $-R$ substituents, no significant resonance exaltation is expected for these *para* substituents. It appears thus more likely to refer the apparent σ-values for $-R$ *para* substituents in the present system to the σ^0, or the substituent parameters closely in the σ^0 scale, of the solvent-modified substituents rather than to the standard σ value.

In contrast to the complicated behaviors of $-R$ substituents, the effect of conjugatively electron attracting *para* substituents can be treated rather successfully as mentioned above. Figure 3 demonstrates the correlation between apparent enhancements, $\bar{\sigma}_p-\sigma_p^0$, of $+R$ *para* substituents in DMF solution and the corresponding $\Delta\bar{\sigma}_R^-$ parameters. Most of substituents fall on or near the straight line with a slope corresponding to the r value of 0.64. Carbonyl and sulfonyl derivatives exhibit weaker electron attracting effects than expected from the correlation, and deviations are most serious in $CONH_2$ and SO_2NH_2 groups.

The standard $\Delta\bar{\sigma}_R^-$ parameters ($=\sigma_p^--\sigma_p^0$), should be the resonance parameters referable to the substituent groups effectively modified by water. To the contrary, the ordinate ($\bar{\sigma}_p-\sigma_p^0$), the apparent enhancement from the standard σ^0, should include the specific effect referable to the change in the solvent-substituent interaction in DMF (or DMSO) from that in water. This effect might cause substantial deviations for particular substituent, while the correlation in Fig. 2 or Fig. 3 is satisfactory for most of substituents, besides some carbonyl and sulfonyl groups which exert weaker electron attracting effect than expected. The reduction observed can be attributed to the fact that in aqueous

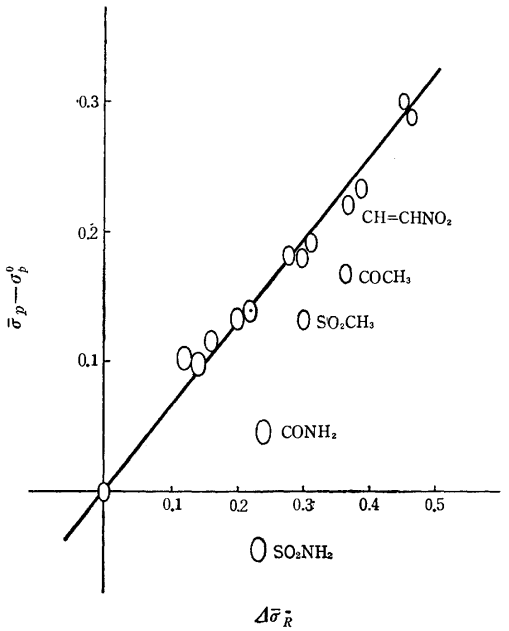

Fig. 3. The plot of the apparent resonance enhancements, $\bar{\sigma}_p-\sigma_p^0$, against standard $\Delta\bar{\sigma}_R^-$ values for $+R$ substituents.

solution the electron withdrawal of the carbonyl or sulfonyl is enhanced by virtue of its ability to disperse an acquired negative charge into the solvent through hydrogen bonding, but in either DMF or DMSO solution such an effect is inhibited. The consistent fact has been observed in the chemical reactivities.[42] The apparent σ_p^- value of *p*-acetyl group derived from the dissociation of phenols decreases from 0.87 in water to 0.80 in organic solvents, but no significant deduction is observed in σ_p^- of *p*-aldehyde group, in good accordance with the present result. The same effect may be also effective for other substituents. With $CONH_2$ and SO_2NH_2 groups, the similar effect discussed above for amino group could be also operative and hence the overall apparent effect is much more significant in these than the other carbonyl and sulfonyl groups.

The substituent-solvent interaction might afford the substantial changes in the inductive and then σ^0 parameters as well as in the resonance parameters of respective substituents. Therefore, the apparent enhancements from the standard σ^0 values, $\bar{\sigma}_p-\sigma_p^0$, are not merely referable to the exalted resonance contribution of substituents, but certain reflection of the change in the inductive component of solvent-modified substituents should be taken into consideration for the analysis of these parameters. Although the direct estimations of actual σ^0, inductive substituent constant σ_I, and resonance substituent constant σ_π, for solvent-modified substituents are not immediately possible, the following indirect methods may be applied as a useful approximation.

Inductive and π-Electronic Parameters in DMF

On the statistical analysis of the reaction-dependency of substituent constants, we have emphasized that the substituent effect on benzene reactivities could be sepa-

rable, to a first approximation, into the inductive σ_I and π-electonic σ_π effects. *Para* and *meta* substituent effects can be expressed generally by a *Linear Substituent Free Energy* (LSFE) *Relationship* (3),[1,3]

$$\log (k/k_0)_p = \rho\bar{\sigma}_p = \rho(\sigma_I + q_r^+\sigma_\pi^+ + q_r^-\sigma_\pi^-) \quad (3)$$

$$\log (k/k_0)_m = \rho\bar{\sigma}_m = \rho(1.17\sigma_I + 0.50\sigma_\pi^\pm) \quad (3')$$

σ_I is the inductive substituent constant, independent of the varying contribution of resonance effect. σ_π^+ and σ_π^- are the parameter measuring the capability of substituents to donate or withdraw electron through π-electronic delocalization. σ_π^+ corresponds numerically to 0.42 $\Delta\bar{\sigma}_R^+$ and σ_π^- to 0.73 $\Delta\bar{\sigma}_R^-$ in our LArSR Eq. (1).[44] q_r^+ and q_r^- are the characteristic variables of a given reaction or a given system, measuring the degree of π-electronic interaction with the detection center, and are in general mutually independent. Both q_r^+ and q_r^- are standardized in σ_p^0 scale to be unity; *i.e.*, $\sigma_p^0 = 1.00\ \sigma_I + 1.00\ \sigma_\pi^\pm$. As evident from the reaction-independence of σ_m values, the contribution of σ_π remains a constant, 0.50, in *meta* reactivities regardless of wide variations of reaction type. The fact that the inductive contribution from *meta* substituents is 1.17 times more effective, generally independent of reactions, than that from *para* substituents is a characteristic feature of our LSFE relationship. Combining both equations, can be derived the equations, in which the effect of inductive component is canceled out; for conjugatively electron attracting groups,

$$\log (k/k_0)_p - 0.85 \log (k/k_0)_m = \rho C^-\sigma_\pi^- \quad (4)$$

and for conjugatively electron releasing groups,

$$\log (k/k_0)_p - 0.85 \log (k/k_0)_m = \rho C^+\sigma_\pi^+ \quad (4')$$

where $C^\pm$ are practical constants corresponding to $q_r^\pm - 0.425$. Equation (4) is the *linear resonance free energy relationship* which can be practically utilized for the estimation of resonance parameters, without inquiring inductive parameters. If the operation of the same inductive contribution ratio might be assumed for the present system, this equation may be applied for the determination of resonance parameters of solvent-modified substituents. Equation (4) can be modified for ready applications for $+R$ substituents in the form;

$$1/\rho(\Delta\delta_p^{OH} - 0.85\Delta\delta_m^{OH}) = \bar{\sigma}_p - 0.85\bar{\sigma}_m = C_M^-(\sigma_\pi^-)_M = 0.73C_M^-(\Delta\bar{\sigma}_R^-)_M \quad (5)$$

C_M^- is a coefficient describing the effective resonance contribution of the system in a given medium M and should remain a constant for all $+R$ substituents. $(\sigma_\pi^-)_M$ or $(\Delta\bar{\sigma}_R^-)_M$ indicates the corresponding resonance parameter of the solvent-modified substituent in M. The same type of equation can be derived for $-R$ substituents; the right hand side of Eq. (5) is given by

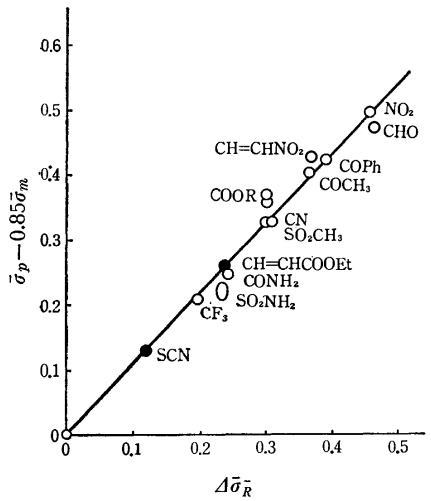

Fig. 4. The plot of the quantities, $\bar{\sigma}_p - 0.85\bar{\sigma}_m$, against standard $\Delta\bar{\sigma}_R^-$ values, for $+R$ substituents.

$$= C_M^+(\sigma_\pi^+)_M = 0.42C_M^+(\Delta\bar{\sigma}_R^+)_M \quad (5')$$

The coefficient C_M^+ is usually not equal to C_M^-.

In Fig. 4 the quantities $(\bar{\sigma}_p - 0.85\ \bar{\sigma}_m)$ for $+R$ substituents in DMF solution are plotted against the standard $\Delta\bar{\sigma}_R^-$. The correlation resulted is unexpectedly excellent. The significant deviations of acetyl and methylsulfonyl groups observed in Fig. 3 are not apparent, and it is really surprising that carbamido group just falls on the line. SO_2NH_2 group also appears to satisfy the correlation when the solvent-modified $\bar{\sigma}_m$ value derived from the NH proton chemical shifts of anilines and acetanilides is employed, though we were unable to prepare *m*-sulfonamido-phenol in pure form. The deviations from the line are at most within 0.05 in σ unit. A linear correlation with closely the same order of precision can be obtained for the corresponding quantities in DMSO solution.

It would be then concluded that the solvent-modification of substituent by DMF or DMSO does not affect significantly the resonance parameters so far as are concerned the conjugatively electron attracting substituents. The variation of the apparent substituent constants of these groups in aprotic DMF would be caused predominantly by the solvent-modification of the inductive nature of substituents. On the basis of the apparent slope of the above correlation line 1.09 which corresponds to 0.73 C_M^-, $(\Delta\bar{\sigma}_R^-)_{DMF}$ values can be derived. Since the slope 1.09 should correspond to 0.73 $(q_r^- - 0.425)$, according to Eqs. (3) and (5), $(\sigma_I)_{DMF}$ can be derived by using Eq. (6).

$$(\sigma_I)_{DMF} = \bar{\sigma}_p - 0.73q_r^-(\Delta\bar{\sigma}_R^-)_{DMF} = \bar{\sigma}_p - 1.40(\Delta\bar{\sigma}_R^-)_{DMF} \quad (6)$$

By the combination of $(\sigma_I)_{DMF}$ and $(\Delta\bar{\sigma}_R^-)_{DMF}$, we can calculate a set of $(\sigma^0)_{DMF}$ for $+R$ substituents modified by DMF solvent. These apparent sets of parameters are summarized in Table 4.

The new parameters for styryl derivative groups appear to be practically useful, even though certain but probably minor solvent-modification should be taken into account. As discussed in the above, the differences of $(\sigma_p^0)_{DMF}$ from the standard σ_p^0 are signifi-

44) $\Delta\bar{\sigma}_R^-$ values given in Table 2 and employed in this study are those derived from the most reliable set of σ_p^- values which have been determined from reliable pK_a values of phenols, anilines, and dimethylanilines in water. In a previous paper (Ref. 1a) we have noted preliminarily, on the basis of σ_p^- values in the literature, that σ_π^- corresponds to 0.81 $\Delta\bar{\sigma}_R^-$. However, detailed examination of the above new set of σ_p^- values indicates that σ_π^-, the π-electronic effect of $+R$ substituents in σ_p^0 scale should correspond to 0.73 $\Delta\bar{\sigma}_R^-$. Full data and relevant discussions will be published in the near future.

Table 4. Modified substituent parameters in DMF for $+R$ groups

Subst.	$(\Delta\bar{\sigma}_R^+)_{DMF}$	$(\sigma_I)_{DMF}$	$(\sigma_p^0)_{DMF}$
NO_2	0.459	0.467	0.802
CHO	0.434	0.214	0.531
CN	0.303	0.419	0.640
CF_3	0.191	0.371	0.510
$COCH_3$	0.375	0.128	0.402
COC_6H_5	0.391	0.177	0.462
$COOCH_3$	0.339	0.164	0.411
COOEt	0.337	0.160	0.406
SO_2CH_3	0.301	0.398	0.618
$CH=CHNO_2$	0.393	0.171	0.458
CH=CHCOOEt	0.240	0.133	0.308
$CONH_2$	0.226	0.109	0.274
SO_2NH_2	0.20	0.32	0.47

cant in carbonyl derivatives and remarkable in amide groups and they are clearly a reflection of the solvent-modification of the inductive components.

Evidences for the solvent-dependence of inductive parameters have been presented on the basis of various studies,[39] among which Taft's study of σ_I using ^{19}F NMR chemical shifts of substituted fluorobenzenes is the most practical and comprehensive.[36] He pointed out that ^{19}F substituent chemical shifts of *m*-substituted fluorobenzenes were correlated linearly with his σ_I parameters, derived from chemical reactivities. This is true in the case of the relative substituent chemical shifts in aqueous methanol, whereas the relative shift in DMF solution does not give so excellent plot against the σ_I.[41] The deviation might primarily arise as a result of solvent-modification in the inductive component of substituents. The analogous variation is expected to be involved in the present DMF system, and in fact $(\sigma_i)_{DMF}$ are found to correlate linearly with the ^{19}F *m*-substituent chemical shifts in DMF solution. If the substituent chemical shift of *m*-substituted fluorobenzenes, as Taft assumed, being a linear function of inductive parameters is valid, it is then suggested that the present set of $(\sigma_i)_{DMF}$ evaluates reasonably the inductive effect of the substituents solvated by DMF solvent, and subsequently, this may also offer an evidence justifying the above estimation of resonance parameters in DMF. Even though the test may not yet be regarded as critical, these treatments may have promising applicability to appropriate systems.

For conjugatively electron releasing ($-R$) substituents, the quantities $(\bar{\sigma}_p - 0.85\,\bar{\sigma}_m)$ are practically not proportional to the standard $\Delta\bar{\sigma}_R^+$ values. However, in view of the significance of the fit of $+R$ substituents to the above treatment (5), the *para*/*meta* inductive contribution ratio of 0.85 would be assumed for $-R$ substituents. It may be also assumed that the quantities $(\bar{\sigma}_p - 0.85\,\bar{\sigma}_m)$ for $-R$ groups in DMF solution are proportional to $(\Delta\bar{\sigma}_R^+)_{DMF}$. In order to practify the separation of substituent effect into σ_i and $\Delta\bar{\sigma}_R^+$ (or σ_π^+) contributions in the present system, it is necessary first to provide the C_{DMF}^+ scale of $(\Delta\bar{\sigma}_R^+)_{DMF}$ contribution. As discussed in the foregoing section, if the present set of apparent $\bar{\sigma}_p$ for $-R$ groups could be referable to the σ_p^0 for solvent-modified substituents in DMF solution, the scale of $(\Delta\bar{\sigma}_R^+)_{DMF}$ or the C_{DMF}^+ value for $-R$ substituents can be estimated to be 0.575 on the basis of *meta*/*para* σ_π-contribution ratio of 0.50 which is a characteristic of the σ^0 scale. Namely, the resonance contribution of these substituents might be roughly approximated by means of Eq. (7)

$$(\bar{\sigma}_p - 0.85\bar{\sigma}_m) = 0.242(\Delta\bar{\sigma}_R^+)_{DMF} \qquad (7)$$

This may lead to the crude estimation of $(\sigma_i)_{DMF}$ values for $-R$ substituents by

$$(\sigma_i)_{DMF} = \bar{\sigma}_p - 1.74(\bar{\sigma}_p - 0.85\bar{\sigma}_m)$$
$$= 1.48\bar{\sigma}_m - 0.74\bar{\sigma}_p$$

Table 5. Modified substituent parameters in DMF for $-R$ groups

Subst.	$(\Delta\bar{\sigma}_R^+)_{DMF}$	$(\sigma_i)_{DMF}$
I	0.02	0.26
Br	−0.28	0.38
Cl	−0.34	0.39
F	−1.09	0.50
SCH_3	−0.03	0.10
OC_6H_5	−0.57	0.29
NHAc	−0.41	0.08
NHC_6H_5	−0.45	0.03
t-Bu	−0.15	−0.06
CH_3	−0.36	0.01
OCH_3	−1.15	0.22
OH	−1.39	0.17
NMe_2	−1.07	0.01
NH_2	−1.37	−0.01

The results are summarized in Table 5. Although the crudeness of derivation does not permit the detailed discussion of these results, Table 5, as a whole, indicates that both $(\Delta\bar{\sigma}_R^+)_{DMF}$ and $(\sigma_i)_{DMF}$ derived are considerably modified from the standard values. This fact is in contrast with the result for conjugatively electron attracting substituents (Table 4). The solvent-modification of inductive effect appears serious for OH, NH_2, and $NHCOCH_3$ groups. The exaltation of π-electronic parameter is also most remarkable for these groups. The above treatment stands on the basis that the solvent-modification of substituents could be practically regarded as a minor perturbation as compared with the change in the electronic nature of the detection function, and the apparent nature of the modified substituent might be sufficiently invariable in *meta* and *para* positions in the system of interest. This may generally hold in usual chemical reactivities, while in the present case, especially of hydrogen-bond donor substituents, such as amino, hydroxyl and acetamino groups, the solvent-modification should no longer be a minor perturbation but a change of comparable importance with that of the detection function. There seems to be the possibility for these particular groups to result in the failure of the above treatment. Despite such the possible limitation of application, $(\sigma_i)_{DMF}$ values for most of $-R$ substituents including these particular groups can be correlated linearly with reasonable precision to $\Delta\Delta\delta_{m\text{-}X}^F$ values of *m*-substituted fluorobenzenes in DMF solution. This may suggest that the error induced from

this treatment could not be so serious.

Since related facts of interest have been available from our studies of the substituent chemical shifts of phenols and of amino protons of acetanilides and anilines in various aprotic solvents, the further discussion will be presented in accompanying papers.

BULLETIN OF THE CHEMICAL SOCIETY OF JAPAN, VOL. 45, 1529—1533(1972)

Location of the Sulfate Groups in κ-Carrageenan from *Gigartina Tenella*

Susumu HIRASE and Kyoko WATANABE

Department of Chemistry, Faculty of Industrial Arts, Kyoto Technical University, Matsugasaki, Kyoto

(Received November 8, 1971)

Location of the sulfate groups in κ-carrageenan from *G. tenella* has been re-investigated by adapting the method, which was devised by Bouveng for locating the acetyl groups in hemicellulose. In this method, the sulfate groups were replaced by methyl groups through a series of reactions consisting of blocking the free hydroxyl groups with phenylcarbamoyl groups, removing the sulfate groups and methylating the newly formed hydroxyl groups. The blocking substituents were then removed, and the positions of the methoxyl groups were investigated by the standard method. The results have shown, in accordance with the conclusion based on the methylation data, that one forth of the 1,4-linked 3,6-anhydro-D-galactose residues are 2-sulfated and that the 1,3-linked D-galactose residues are 4-sulfated. No evidence was obtained to indicate the presence of D-galactose 2,6-disulfate, which had been presumed by other workers. The problem concerning the acyl migration of the blocking groups during the process has also been discussed.

In our paper,[1] the structure of κ-carrageenan from *Gigartina tenella* has been investigated mainly by the methylation method. It has been concluded that the κ-carrageenan is composed of the residues of 1,3-linked β-D-galactose 4-sulfate (95 mol), 1,4-linked α-D-galactose 6-sulfate (5 mol), and 1,4-linked 3,6-anhydro-α-D-galactose (67 mol) and its 2-sulfate (24 mol), the 1,3- and 1,4-linked residues being repeated alternatingly to form a chain of the macro-molecule. This structure has been in approximate accordance with those reported by Anderson and his co-workers[2,3] for κ-carrageenans obtained from other species of *Gigartina* as well as from *Chondrus crisps*. The only difference is that they suggested the presence of a small amount of 1,4-linked D-galactose 2,6-disulfate residues in their polysaccharide samples. With this in mind, the location of the sulfate groups has been re-examined by the different method of investigation.

In the present work, the method devised by Bouveng for locating *O*-acetyl groups in hemicellulose[4,5] has been adapted for the purpose of locating sulfate groups. The method involves a series of reactions consisting of blocking the free hydroxyl groups with phenylcarbamoyl groups (I→II), removing the sulfate groups (II→III), methylating the newly formed hydroxyl groups (III→IV), removing the blocking groups (IV→V), breaking down the macro-molecule, and then identifying the fragments. The positions of methoxyl groups in the final products have been expected to indicate the positions of sulfate groups in the native polysaccharide.

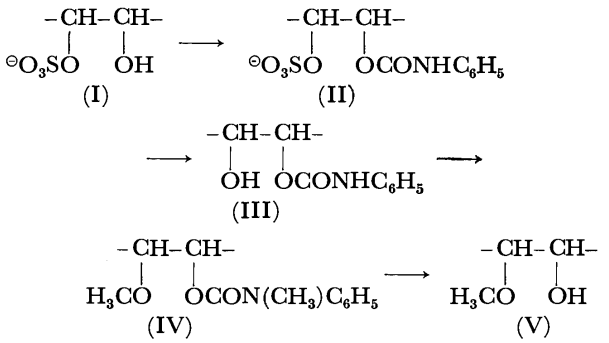

In applying the Bouveng's procedure to our own purpose, modification was needed in several respects. In the step I→II, κ-carrageenan in sodium or potassium salt was difficult to react with phenylisocyanate because of its insolubility in the reaction medium. This difficulty was overcome by converting the metal salt into cetyl pyridinium salt, which was found soluble in pyridine so that the complete phenylcarbamoylation was effected. For removing sulfate groups (the step II→III), on the basis of some preliminary experiments, the phenylcarbamoate(II) was heated in a mixture of dioxane and methanol containing 0.5% hydrogen chloride at 80°C for 3 hr. By this treatment, the sulfate groups were mostly released. But the macro-molecule was degraded by the concurrent methanolysis of the

1) S. Hirase and K. Watanabe, This Bulletin, **45**, No. 6 (1972) (in the press).
2) N. S. Anderson, T. C. S. Dolan, and D. A. Rees, *J. Chem. Soc., C*, **1968**, 596.
3) N. S. Anderson, T. C. S. Dolan, A. Penman, D. A. Rees, G. P. Mueller, D. J. Stancioff, and N. F. Stanley, *ibid.*, **1968**, 602.
4) H. O. Bouveng, *Acta Chem. Scand.*, **15**, 87 (1961).
5) H. O. Bouveng, *ibid.*, **15**, 96 (1961).

anhydro-galactoside linkages to form a mixture of oligosaccharide derivatives, whose average degree of polymerization was about six as determined by the methoxyl content. Examination of a part of the product by paper chromatography, after removal of the blocking substituents, showed the presence of carrabiose dimethyl acetal as well as higher oligosaccharide derivatives. The desulfated, partially degraded phenylcarbamoate(III) was next treated with trityl chloride to protect the primary hydroxyl groups, which might have been formed from galactose 6-sulfate residues, otherwise the phenylcarbamoyl groups would be migrated[4] from C_4 to C_6 during the succeeding step (III→IV) of methylation. The methylated product was then subjected to reductive removal of the blocking groups followed by detritylation and subsequent complete methanolysis.

TABLE 1. THE SUGARS IDENTIFIED IN THE FINAL PRODUCTS OF METHANOLYSIS

D-Galactose	Mol ratio[a]	3,6-Anhydro-D-galactose	Mol ratio[a]
non-methylated	1.0	non-methylated	1.0
3-*O*-methylated	0.66	2-*O*-methylated	0.24
4-*O*-methylated	1.64	5-*O*-methylated	0.84
3,4-di-*O*-methylated	2.44	2,5-di-*O*-methylated	0.38

a) The molar ratios are separately based on the respective non-methylated sugars.

The final product of methanolysis was a mixture of methyl glycosides or dimethyl acetals of the sugars listed in Table 1. These compounds were identified by isolation after separation on columns as well as by paper chromatography, thin layer chromatography, gas liquid chromatography and paper electrophoresis.

From these results, location of the sulfate groups in the polysaccharide is to be discussed. In the first place, the discussion is focussed to the distribution of the sulfate groups on anhydro-galactose residues. The methoxyl groups of C_5 in the final products are ascribed to the opening of pyranose rings during the process. When, as has already been described, anhydro-galactoside linkages were cleaved during the step II→III, the anhydro-sugar residues concerned would be undoubtedly changed from the pyranose structure to dimethyl acetal with the open chain structure,[6] forming thereby the free C_5-hydroxyl groups available for methylation in the succeeding step. While, the methoxyl groups on C_2 in the final products are ascribed to 2-sulfate groups. Thus, the relative yields of the anhydro-sugars (Table 1) show that non-sulfated and 2-sulfated anhydro-galactose residues exist in the proportion of 3: 1 in the native polysaccharide in exact agreement with the conclusion reported in our paper.[1] This agreement proves that the present carbamoylation-methylation analysis is effective in locating the sulfate groups on anhydro-galactose residues.

The discussion is now turned to the distribution of the sulfate groups on D-galactose residues. The presence of 3,4-di-*O*-methyl-D-galactose in the final products provides evidence that 1,3-linked D-galactose 4-sulfate residues exist in the polysaccharide in accordance again with the result reported in our paper.[1] In similar consideration, the positions of methoxyl groups in 3-*O*- and 4-*O*-methyl-D-galactoses may appear to indicate the positions of glycoside linkages and sulfate linkages, respectively, of D-galactose residues. However, no definite conclusion is obtainable from these mono-*O*-methyl-galactoses, because a part of the *O*-phenylcarbamoyl groups has been migrated between *cis* hydroxyl groups at C_3 and C_4 by the action of silver oxide during the methylation (III→IV). The occurrence of this migration has been proved by treating agarose from *Gelidium amansii* in exactly the same manner as in the case of κ-carrageenan. Since the agarose is a practically sulfate-free polysaccharide consisting of alternatingly repeated residues of 1,3-linked β-D-galactose and 1,4-linked 3,6-anhydro-α-L-galactose,[7] cleavage of the anhydro-galactoside linkages during the step II→III should produce free hydroxyl groups only at C_3 of D-galactose residues. Nevertheless, in the final products, a considerable amount of 4-*O*-methylgalactose was detected in addition to 3-*O*-methylgalactose. This result can be accounted for by the occurrence of migration of a part of the carbamoyl groups from C_4 to C_3. As for the non-methylated D-galactose in the final products from κ-carrageenan, the interpretation thereof is again ambiguous, because the sugar may be derived from any of the D-galactose non-sulfate, 4-sulfate and 6-sulfate residues, if these residues have survived the step II→III.

Thus the analysis by the present carbamoylation-methylation method seems to be of limited value as to the distribution of the sulfate groups on D-galactose residues. However, an important information would be obtainable as to the 2-sulfation of D-galactose residues. Anderson and his co-workers pointed out the presence of a small amount of the sugar sulfate residue, which formed 3,6-anhydro-galactose by alkaline treatment after periodate oxidation of their samples of κ-carrageenan.[2,3] They presumed this residue to be 1, 4-linked D-galactose 2,6-disulfate. Analysis of our polysaccharide sample by their method showed that there existed a very small amount of a similar residue. If this residue is presumed to be 1,4-linked D-galactose 2, 6-disulfate as Anderson and his coworkers did, 2-*O*-methylgalactose is then expected to be present in the final products of the carbamoylation-methylation method. In spite of careful examination, no trace of this sugar was detected. It follows from this result that neither galactose 2-sulfate nor 2,6-disulfate exist in our polysaccharide sample. The contradiction in the result between the two methods of analysis might be ascribed to an unavoidable experimental error of either method, because the amount of the residue under question is very small, if present. Another possible explanation is to presume the residue under question to be 1,4-linked D-galactose 3-sulfate, which would behave in the same manner as the 2,6-disulfate in periodate

6) C. Araki and S. Hirase, This Bulletin, **27**, 109 (1954).

7) C. Araki, Proceedings of the Fifth International Seaweed Symposium, Halifax, August 25—28, 1965, Pergamon Press-Oxford & New York, 1966.

oxidation followed by alkaline treatment, and which would not give 2-*O*-methylgalactose in the carbamoylation-methylation experiment. Further work will be needed to solve this problem.

Experimental

Abbreviation. For simplifying the description, the names of the compounds are abbreviated as shown in Table 2.

Table 2. Abbreviations of the names of compounds

Compounds	Abbreviations
3-*O*-methyl-D-galactose	3MG
4-*O*-methyl-D-galactose	4MG
3,4-di-*O*-methyl-D-galactose	34MG
3,6-anhydro-D-galactose	AG
2-*O*-methyl-3,6-anhydro-D-galactose	2MAG
5-*O*-methyl-3,6-anhydro-D-galactose	5MAG
2,5-di-*O*-methyl-3,6-anhydro-D-galactose	25MAG

General and Analytical Methods. General and analytical methods have been described in our paper[1] except those described below. The solvent I) benzene-ethyl acetate (3:2) was used for paper chromatography (pc), and L) benzene-ethyl acetate-water (40:15:trace) for thin layer chromatography (tlc), in addition to those (A—H and J—K, respectively) descrived before.

Gas Liquid Chromatography (glc). The columns used for glc were (a) 5% neopentylglycol succinate-chromosorb W, (b) 2.5% SE-30-chromosorb W and (c) 5% polyethylene glycol-chromosorb W, the length being 1 m unless otherwise stated. The final methanolysis product to be analysed was a complicated mixture consisting of methyl glycosides and dimethyl acetals of partially methylated galactoses and 3,6-anhydro-galactoses so that it was needed to analyse anhydro-galactose derivatives separately from galactose derivatives. For identifying the former derivatives was used the method B described in our paper,[1] in which anhydro-sugar derivatives were selectively converted into diethyl dithioacetal trimethylsilyl ethers. Analyses were carried out on the columns b at 160°C and c at 180°C as well as on the column a described before. For identifying galactose derivatives, the method D and E described below were devised. Furthermore, the method F described below was used for the sample of the relatively simple composition as in the case of a fraction obtained from column chromatography.

Method D: The sample to be analysed was hydrolysed with 1N-sulfuric acid at 100°C for 16 hr. During this treatment, anhydro-galactose derivatives were completely degraded. The remaining partially methylated galactoses were converted into diethyl dithioacetal trimethylsilyl ethers,[8] and analysed on the columns a at 160°C, b at 190°C and c at 180°C.

Method E: The partially methylated galactoses obtained in the method D were converted into diethyl dithioacetal acetates,[8] and analysed on the columns a at 215°C and b at 200°C.

Method F: Methyl glycosides or dimethyl acetals of partially methylated sugars were trimethylsilylated in the usual manner, and analysed on the columns a at 135°C, and b (2 m) at 160°C or 190°C.

Cetyl Pyridinium Salt of κ-Carrageenan. To a solution of κ-carrageenan (8 g) in water (240 m*l*), cetyl pyridinium chloride (8 g) in water was added with stirring. The precipitates, which formed, were collected by centrifugation, washed successively with water, methanol and again water, and dried *in vacuo*. The cetyl pyridinium salt was obtained as colorless powder (11.3 g). Found: N, 2.1%. Calcd for the polymer composed of galactose (1.0), 3,6-anhydro-galactose (0.91) and sulfate (1.24):[1] N, 2.26%.

Phenylcarbamoylation (I→II). To the cetyl pyridinium salt (11.3 g), which had been dried over phosphorus pentoxide at 40°C in vacuum overnight, dry pyridine (300 m*l*) and phenylisocyanate (25 g) were added. The mixture was heated at 100°C, when the salt was gradually dissolved within 1 hr. After being heated for 6 more hr, the reaction solution was left for 24 hr at room temperature. Ethanol (50 m*l*) was then added to destroy the excess of the reagent. The solution was centrifuged to remove small amounts of insoluble matter, and evaporated. The product was precipitated with 99% ethanol, the phenylcarbamoate (II) being obtained as slightly colored powder (14 g); $[\alpha]_D^{28}+75°$ (*c* 1.0 in pyridine). Found: SO_3, 8.9; N, 5.5%. Calcd for the phenylcarbamoate of the polymer with the composition described above: SO_3, 9.14; N, 5.04%.

Desulfation (II→III). A solution of the above-obtained phenylcarbamoate (14 g) in a mixture of dry dioxane (280 m*l*) and 1% methanolic hydrogen chloride (280 m*l*) was refluxed for 3 hr. The reaction mixture was neutralized with barium carbonate, filtered, evaporated to a small volume, and re-dissolved in chloroform. The solution was washed 3 times with water, dried with magnesium sulfate, and evaporated to a small volume, to which was added dry hexane. The product (III) was precipitated as powder (12.5 g); $[\alpha]_D^{24}+28.0°$ (*c* 0.78 in pyridine). Found: CH_3O, 3.3; SO_3, 0.5%. The methoxyl content indicated that the polymer was degraded to *O*-phenylcarbamoylated hexasaccharide dimethyl acetal in average. A portion of the product in dry dioxane was treated with lithium aluminum hydride to remove the phenyl-carbamoyl groups. Examination of the product by pc (solvent A, spray c) showed the presence of carrabiose dimethyl acetal as well as higher oligosaccharide derivatives.

Tritylation of III. The above-obtained product (12.5 g), which had been completely dried over phosphorus pentoxide, was dissolved in dry pyridine (75 m*l*). Trityl chloride (5.7 g) was added, and the mixture was left at 40°C for 2 days. After destroying the excess of the reagent by addition of water (10 m*l*), the mixture was disolved in chloroform, and the solution was washed successively with potassium hydrogen sulfate solution, sodium bicarbonate solution and water, dried with magnesium sulfate, and evaporated to a syrup, which was then dissolved in methanol and left aside in a refrigerator. Trityl carbinol, which crystallized, was filtered off, and the filtrate was evaporated to dryness (11.0 g); $[\alpha]_D^{24}+26.7°$ (*c* 0.72 in pyridine).

Methylation (III→IV). The tritylated product (11.0 g) obtained above in *N,N*-dimethylformamide[9] (130 m*l*) was shaken with iodomethane (50 g) and silver oxide (20 g) for 0.5—1.0 hr. Additional iodomethane (50 g) and silver oxide (20 g) were added, and the mixture was shaken for 24 hr. This methylation was repeated two more times. The reaction mixture was filtered, and evaporated at 90°C to a syrup, which was then dissolved in chloroform. The solution was washed successively with 10% potassium cyanide solution and water, dried with magnesium sulfate, and evaporated to a

8) Retention times of reference compounds and other experimental details will be published later.

9) R. Kuhn, H. Trischmann, and I. Löw, *Angew. Chem.*, **67**, 32 (1955).

thin syrup. Addition of hexane precipitated the product (IV) (8.4 g), which was filtered off, and dried *in vacuo* over phosphorus pentoxide at 40°C; $[\alpha]_D^{26}+30.8°$ (*c* 0.64 in pyridine).

Decarbamoylation (IV→V). The methylated product (8.4 g) obtained above was dissolved in dry tetrahydrofuran (200 m*l*), lithium aluminum hydride (3 g) added slowly, and the mixture was refluxed for 4 hr. Methanol (10 m*l*) and water (10 m*l*) were added slowly, and aluminum hydroxide was filtered off, and washed with methanol-water (1:1). The combined filtrate and washings were neutralized with dilute phosphoric acid and filtered again. The filtrate was extracted with hexane to remove an oily reduction product, and the residual solution was evaporated to dryness (7.0 g).

Detritylation and Methanolysis. The product (7.0 g) obtained above was refluxed with 1% methanolic hydrogen chloride (50 m*l*) for 2 hr, neutralized with silver carbonate and filtered. The filtrate was deionized with Amberlite IR-120 (70 m*l*) and IR-45 (150 m*l*), and evaporated to a syrup (3.6 g), $[\alpha]_D^{24}+9.3°$ (*c* 0.4 in methanol), which was again treated with 2% methanolic hydrogen chloride (50 m*l*) at 80°C for 22 hr. The reaction solution was treated in the usual manner, and the product was obtained as a syrup (3.4 g); $[\alpha]_D^{24}+60.1°$ (*c* 0.7 in water).

Analysis of the Methanolysis Products. Examination of the syrup obtained above by pc (solvent D, I, spray c) and tlc (solvent K) indicated the presence of dimethyl acetals of AG, 2MAG, 5MAG, and 25MAG and methyl glycoside of 2MAG. Quantitative determination was carried out by glc (method B, column a and b), and the result was expressed in the molar ratio (Table 1). On the other hand, a portion of the syrup was hydrolysed with 1N-hydrochloric acid at 100°C for 16 hr. The hydrolysate contained galactose, 3MG, 4MG, and 34MG as shown by pc (solvent A, B, C, E, G, and H, spray a and b), paper electrophoresis, and glc (method D and E). The results of quantitative determination by glc using the columns a, b and c were in good mutual agreement, and the mean values expressed in the molar ratio were given in Table 1.

Separation of the Methanolysis Products. A part of the methanolysis products (2.0 g), obtained above, was applied to a starch-Celite 545 column (5.5×46 cm), which was then eluted with butanol-water (6:1). The effuluents were checked by a resorcinol reagent, an anthrone reagent, pc (solvent D and I) and/or tlc (solvent J and K). Fractions showing similar contents were combined, and evaporated to give Fractions I, II, and III. These fractions were combined with similar fractions obtained from the remaining portion of the methanolysis products (1.4 g).

Fraction I. Yield 0.99 g. This fraction was shown to be a mixture of dimethyl acetals of 25MAG, 2MAG, and 5MAG and methyl glycoside of 2MAG by pc (solvent D and I, spray c) and tlc (solvent K and L). Separation and isolation of these components was achieved only when chromatography was repeated several times using different columns and different solvent mixtures. The yields were low mainly because of mechanical loss during the repeated treatment. Fraction I (0.99 g) was applied to a Dowex 1×4 column (OH form, 5×80 cm) and eluted by distilled water to give three fractions, I-1, I-2, and I-3 which were checked by pc (solvent D and I), tlc (solvent K and L) and glc (method F, column a, b and c).

Fraction I-1 (80 mg) was a mixture of dimethyl acetals of 25MAG and 5MAG. The mixture was separated on an alumina column (2×26 cm). 25MAG dimethyl acetal was eluted with benzene-ethanol (15:1), and obtained as a syrup (57 mg); $[\alpha]_D^{26}+22.9°$ (*c* 4.21 in water). It was converted into crystalline 3,6-anhydro-2,5-di-*O*-methyl-D-galactonic acid in the usual way;[10] mp and mmp 165—166°C, $[\alpha]_D^{25}+59.0°$ (*c* 0.64 in water). (Found: C, 46.42; H, 6.33; OCH_3, 30.18%). The alumina column was then eluted with benzene-ethanol (2:1) to give 5MAG dimethyl acetal (5 mg).

Fraction I-2 (0.44 g) was shown by pc to be 5MAG dimethyl acetal contaminated with a small amount of 2MAG dimethyl acetal. Seeding with a synthetic sample[11] afforded crystalline 5MAG dimethyl acetal, which was then recrystallized twice from ethyl acetate-benzene-hexane (1:1:2), yield 0.33 g; mp and mmp 53.5—54.5°C, $[\alpha]_D^{20}+42.6°$ (*c* 0.59 in water), (Found: C, 48.79; H, 8.23; OCH_3, 40.99%). This compound was further identified by conversion into its *p*-nitrobenzoate;[11] mp and mmp 143—145°C, $[\alpha]_D^{20}+66.1°$ (*c* 1.15 in chloroform), (Found: C, 52.92; H, 4.66; N, 5.26; OCH_3, 16.52%). The mother liquor of the crystallization showed the presence of 2MAG dimethyl acetal in addition to 5MAG dimethyl acetal by pc, tlc, and glc. Then the mixture was separated on a Sephadex LH-20 column (2×24 cm) with chloroform as a solvent. 5MAG (4 mg) was the faster-moving component, which was followed by 2MAG (15 mg); $[\alpha]_D^{28}+27.4°$ (*c* 1.48 in water). This compound was identified by conversion into crystalline 3,6-anhydro-2-*O*-methyl-D-galactonic acid in the usual manner; mp 142°C, $[\alpha]_D^{25}+65.2°$ (*c* 0.31 in water),[2] (Found: C, 42.98; H, 7.15%).

Fraction I-3 (53 mg) was a mixture of dimethyl acetal of 5MAG and methyl glycoside of 2MAG. The mixture was separated on an alumina column (2×26 cm) with benzene-ethanol (15:1) as solvent. The 2MAG derivative was the faster moving component, and was obtained as a syrup (13 mg), $[\alpha]_D^{26}-65.1°$ (*c* 1.06 in water), which was identified again by conversion into crystalline anhydro-2-*O*-methyl-3,6-D-galactonic acid;[2] mp and mmp 141.5°C, $[\alpha]_D^{25}+63.9°$ (*c* 0.15 in water).

Fraction II. Yield 1.32 g. This fraction was shown to be a mixture of dimethyl acetal of AG and methyl glycoside of 34MG by pc (solvent A, D and I) and tlc (solvent J and K). The mixture (1.32 g) was placed on a Dowex 1×4 (OH form, 3×30 cm) column. The methyl glycosides of 34MG were readily eluted with water, and obtained as a syrup (0.85 g); $[\alpha]_D^{29}+146°$ (*c* 1.2 in water). The syrup was hydrolysed with 1N-sulfuric acid at 100°C for 4 hr, and the product was twice recrystallized from methanol-ethyl acetate, 34MG being obtained as prisms;[12,13] mp and mmp 169—171°C, $[\alpha]_D^{21}+105.8°\rightarrow+126.3°$ (*c* 0.43 in water), (Found: C, 46.02; H, 7.65; OCH_3, 30.1%).

The Dowex column was then eluted with 0.2M-ammonium carbonate solution, and the effluent was deionized by Amberlite IR-120 and IR-45, and evaporated to dryness. AG dimethyl acetal was obtained as a syrup (0.45 g); $[\alpha]_D^{29}+38.9°$ (*c* 0.90 in water). It was converted into AG diphenyl hydrazone in the usual manner;[10] mp and mmp 154—156°C, $[\alpha]_D^{19}+24.5°$ (*c* 0.66 in methanol), (Found: C, 65.61; H, 6.24; N, 8.37%).

Fraction III. Yield 0.96 g. This fraction was shown to be a mixture of methyl galactosides and their mono-*O*-methyl derivatives and a small amount of oligosaccharide derivatives by pc (solvent A) and tlc (solvent J and K). The mixture (0.96 g) was hydrolysed with 1N-sulfuric acid for 4 hr in the usual manner to give a mixture of reducing sugars (0.92 g). Crystallization from methanol afforded D-galactose (0.36 g); mp and mmp 164—165°C, $[\alpha]_D^{20}+118.1°$—

10) C. Araki and S. Hirase, This Bulletin, **29**, 770 (1956).
11) S. Hirase and K. Watanabe, *ibid.*, **45**, No.6(1972) (in the press).
12) J. S. D. Bacon and D. J. Bell, *J. Chem. Soc.*, **1939**, 1869.
13) S. Hirase and K. Watanabe, This Bulletin, **45**, 1569 (1972).

+80.4° (*c* 0.91 in water), (Found: C, 40.14; H, 6.63%). The mother liquor was evaporated to a syrup (0.45 g), which was then separated on a starch-Celite 545 column (3×30 cm) with butanol-water (6:1). Three fractions III-1, III-2, and III-3 were obtained as checked by pc (solvent A, B, C, and E).

Fraction III-1 (42 mg) showed a single spot of 34MG by pc and crystallized on standing.

Fraction III-2 (0.19 g) was shown to be a mixture of 3MG and 4MG by pc (solvent A, E, G, and H), glc (method D, column a and b; method E, column a, and b), and paper electrophoresis. On standing, 4MG crystallized. It was recrystallized from water-methanol (36 mg);[14] mp and mmp 209—211°C, $[\alpha]_D^{29}$ +64.76→+89.46° (*c* 0.43 in water). (Found: C, 43.16; H, 7.20; OCH_3, 15.8%).

The mother liquor was evaporated to a syrup (0.14 g), which was then placed on a Dowex 1×4 (borate form, 2×16 cm) column. Elution with water afforded 4MG (13 mg). The eluant was then replaced by 0.03M-potassium borate solution. The effluent was treated with Amberlite IR-120 to remove potassium ion, and the resulting acidic solution was evaporated to dryness. Boric acid was removed by repeated addition of methanol to the residue followed by evaporation. The final product was obtained as a syrup (0.1 g); $[\alpha]_D^{31}$ +80.7° (*c* 0.82 in water). This syrup was indistinguishable in pc (solvent G, spray a and b), glc (method D, column a and b), and paper electrophoresis[15] from the sample of 3MG, which was synthesized by the method of Ball and Jones.[16] Crystallization of either of the syrup obtained above and the synthesized one was unsuccessful.

Fraction III-3 (0.14 g) was shown to be a mixture of galactose and a small amount of oligosaccharide by pc (solvent A, B and C). On standing, D-galactose crystallized (70 mg); mp and mmp 164—166.5°C.

Alkaline Treatment of κ-Carrageenan after Periodate Oxidation. According to the method of Anderson and his co-workers,[2] κ-carrageenan (0.5 g) was treated with 0.05M-sodium periodate solution (100 m*l*) at room temperature for 75 hr in the dark. After destroying the excess of the oxidant with ethylene glycol, potassium borohydride (1.5 g) was added. The solution was diluted to 500 m*l*, left for 2 days, and dialysed against running water. The dialysate was divided into two halves, one of which was used to analyse the sugars, and the other one was subjected to the treatment with potassium hydroxide at 80°C for 4 hr in the usual manner and subsequent analysis of the sugars. Comparison of the analytical results showed that 3% of the total galactose residues existed as the periodate-resistant sulfate residues, which were convertible into 3,6-anhydro-galactose by the alkaline treatment.

Experiments on Agarose from G. amansii. A series of reactions was performed in a similar manner to the case of κ-carrageenan. Dry agarose (2.0 g) suspended in dry *N*,*N*-dimethylformamide (70 m*l*) was heated with phenylisocyanate (10 m*l*) at 100°C for 10 hr. The phenylcarbamoate (4.6 g), obtained as powders, was treated with a boiling mixture of dioxane (40 m*l*) and 2% methanolic hydrogen chloride (40 m*l*) for 2 hr. The product (4.2 g), a part of which on removal of the carbamoyl group showed the presence of agarobiose dimethyl acetal as well as higher oligosaccharide derivatives by pc (solvent D, spray c), was methylated repeatedly by the Kuhn's method.[9] The methylated product (4.6 g) in dry tetrahydrofuran (50 m*l*) was refluxed with lithium aluminum hydride (1.0 g) for 4 hr, and the resulting decarbamoylated product (1.1 g) was subjected to complete methanolysis. The final product was obtained as a syrup (0.9 g).

Examination by pc (solvent D and I, spray c) and tlc (solvent K) showed the presence of dimethyl acetals of 3,6-anhydro-galactose and its 5-methyl ether. While, hydrolysis of the above final product followed by examination by pc (solvent C, E, G and H, spray a and b) showed the presence of galactose and its 3- and 4-methyl ether. Quantitative glc (method D, columns a, b and c) showed that galactose and its 3- and 4-methyl ethers existed in the molar proportions of 100:43:13.

The authors are grateful to the Ministry of Education for a Grant in Aid for Scientific Research.

14) S. Hirase, C. Araki, and K. Watanabe, *ibid.*, **40**, 1445 (1967).
15) H. Bouveng and B. Lindberg, *Acta Chem. Scand.*, **10**, 1283 (1956).
16) D. H. Ball and J. K. N. Jones, *J. Chem. Soc.*, **1958**, 905.

Studies of Acyl and Thioacyl Isocyanates. VIII.[1] Cycloaddition Reactions of Benzoyl and Thiobenzoyl Isocyanates with Carbodiimides

Otohiko Tsuge and Kazuko Sakai

Research Institute of Industrial Science, Kyushu University, Hakozaki, Fukuoka

(Received November 15, 1971)

The investigations of cycloaddition reactions of benzoyl and thiobenzoyl isocyanates with carbodiimides have shown that the adducts formed from benzoyl isocyanates and *N,N'*-dicyclohexylcarbodiimide are the corresponding (4+2) cycloadducts, and not the (2+2) cycloadducts proposed by Neidlein. The reaction of isocyanates with *N,N'*-diphenylcarbodiimide at 0°C gave (2+2) cycloadducts, which were thermally isomerized into the corresponding (4+2) cycloadducts. Benzoyl isocyanates reacted with *N*-cyclohexyl-*N'*-phenylcarbodiimide to give (4+2) cycloadducts of isocyanates to the cyclohexyl-N=C bond in the carbodiimide. On treatment with neutral alumina, (4+2) cycloadducts were easily isomerized into 1,3,5-triazines. Thiobenzoyl isocyanate reacted with both the N=C bonds of the carbodiimide to afford two isomeric (4+2) cycloadducts. It has been found that benzoyl isocyanates reacted with *N*-phenyl-*N'*-*o*-tolylcarbodiimide to yield the corresponding (4+2) cycloadducts of isocyanates to the *o*-tolyl-N=C bond and/or the isomeric 1,3,5-oxadiazin-6-ones, depending on the nature of the substituent in the isocyanate. Reaction paths for the formation of the product are also discussed.

During the last few years, cycloaddition reactions of carbodiimides with various reagents have been extensively investigated.[2]

Neidlein[3] reported that benzoyl isocyanate reacts with *N,N'*-dicyclohexylcarbodiimide to form a (2+2) cycloadduct, while Goerdeler and Schenk[4] reported that the cycloaddition of thiobenzoyl isocyanate to the same carbodiimide gave a (4+2) cycloadduct.

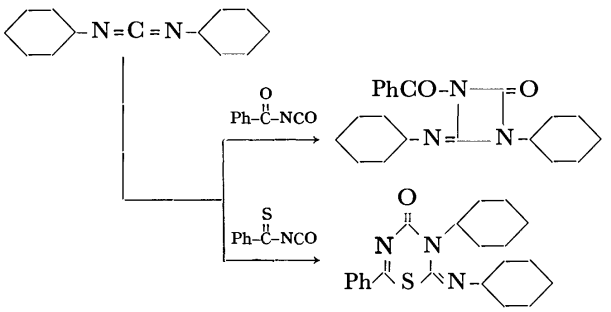

In the dimerization[5] and cycloaddition to anils,[6] benzoyl isocyanates gave (4+2) cycloadducts but no (2+2) cycloadducts. Formation of the (2+2) cycloadduct reported by Neidlein[3] would be the first example of (2+2) cycloaddition of benzoyl isocyanate to a C=N bond.

Acoordingly, the cycloaddition reactions of benzoyl isocyanates with carbodiimides were of special interest to us. This paper deals with the cycloaddition reactions of benzoyl and thiobenzoyl isocyanates with symmetrical and asymmetrical carbodiimides.

Results and Discussion

Cycloadditions to Symmetrical Carbodiimides. The reaction of benzoyl isocyanate (Ia) with an equimolar amount of *N,N'*-dicyclohexylcarbodiimide (II) in a benzene–diethyl ether solution at 0°C or at room temperature gave the 1:1 adduct IIIa of Ia and II. From a comparison of the melting point and UV spectrum of IIIa with those of the adduct reported by Neidlein,[3] the adduct IIIa obtained here was found to be the same one obtained by Neidlein.

The absorption bands in the range 1300—1750 cm^{-1} in the IR spectrum of IIIa are very similar to those in the spectra of 3-benzyl-2,6-diphenyl-2*H*-1,3,5-oxadiazin-4(3*H*)-one[6] and of the (4+2) cycloadduct[4] of thiobenzoyl isocyanate to II. The correlation between the intensities and the wave numbers of $\nu_{C=O}$ and $\nu_{C=N}$ in the three compounds is similar to that between the intensity and the wave number of $\nu_{C=O}$ and $\nu_{C=C}$ in γ-pyrone.[5]

Consequently, it can be assumed that IIIa is the (4+2) cycloadduct, 3-cyclohexyl-2-cyclohexylimino-6-phenyl-2*H*-1,3,5-oxadiazin-4(3*H*)-one, rather than the (2+2) cycloadduct proposed by Neidlein.[3]

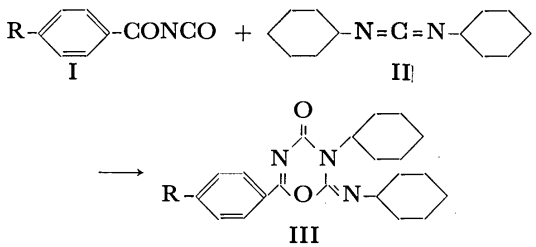

a: R=H, b; R=Cl, c: R=NO_2, d: R=OMe

Similar reactions of *p*-substituted benzoyl isocyanates (Ib—Id) with II gave the corresponding (4+2) cycloadducts (IIIb—IIId). The yields, physical properties and elemental analyses of III are summarized in Table 1.

On the other hand, with *N,N'*-diphenylcarbodiimide (IV) at 0°C, benzoyl isocyanate (Ia) gave the corre-

1) Part VII of this series; O. Tsuge, T. Itoh, and K. Sakai, *Nippon Kagaku Zasshi*, **90**, 1031 (1969).
2) H. Ulrich, "Cycloaddition Reactions of Heterocumulenes," Academic Press, New York, London 1967, p. 254.
3) R. Neidlein, *Arch. Pharm.* (Weinheim), **297**, 623 (1964).
4) J. Goerdeler and H. Schenk, *Chem. Ber.*, **98**, 3831 (1965).
5) O. Tsuge and R. Mizuguchi, *Kogyo Kagaku Zasshi*, **69**, 939 (1966).
6) O. Tsuge, M. Tashiro, R. Mizuguchi, and S. Kanemasa, *Chem. Pharm. Bull.* (Tokyo), **14**, 1055 (1966),

Table 1. Reaction of I with II[1]

	R	Yield (%)	Mp (°C)	λ_{max}^{EtOH} nm(log ε)	$\nu_{C=O}$[2] cm^{-1}	$\nu_{C=N}$[3] cm^{-1}		Analysis(%) Found(Calcd) C	H	N
IIIa	H	54 (82)[4]	142—143 (138—139)[5]	260(4.27) (256)[5]	1745	1670	1630	71.52 (71.36)	7.85 (7.70)	11.75 (11.89)
IIIb	Cl	76	122—123	271(4.32)	1740	1690	1630	64.89 (65.10)	6.94 (6.68)	10.85 (10.85)
IIIc	NO_2	87	139—140	271(4.44)	1740	1680	1640	63.34 (63.30)	6.45 (6.54)	14.22 (14.07)
IIId	OMe	64	157—158		1730	1675	1630	68.68 (68.90)	7.91 (7.62)	10.71 (10.96)

1) At room temperature for a few minutes.
2) Weak bands.
3) Very strong bands.
4) At 0°C for 15 hr.
5) Mp and λ_{max}^{EtOH} nm reported by R. Neidlein (lit.3).

Table 2. Reaction of I with IV at 0°C for 24 hr

	R	Yield (%)	Mp (°C)	λ_{max}^{EtOH} nm(log ε)	$\nu_{C=O}$ cm^{-1}		$\nu_{C=N}$ cm^{-1}	Analysis (%) Found (Calcd) C	H	N
Va	H	55	112—113 (decomp.)	238(4.62)	1880	1695	1740	74.05 (73.89)	4.41 (4.43)	12.34 (12.31)
Vb	Cl	72	115—116 (decomp.)	242(4.65)	1880	1695	1735	66.92 (67.20)	3.58 (3.72)	11.04 (11.18)
Vc	NO_2	50	102—103 (decomp.)	250(4.65)	1880	1695	1740	65.12 (65.28)	3.51 (3.65)	14.55 (14.50)

Table 3. Isomerization of V at 120°C for 1 hr

	R	Yield (%)	Mp (°C)	$\nu_{C=O}$ cm^{-1}	$\nu_{C=N}$ cm^{-1}		Analysis (%) Found (Calcd) C	H	N
VIa	H	59	179—179.5	1745	1690	1630	73.95 (73.89)	4.33 (4.43)	12.17 (12.31)
VIb	Cl	81	173—174	1745	1690	1630	67.40 (67.20)	3.48 (3.72)	11.33 (11.18)
VIc	NO_2	72	150—151	1740	1690	1635	65.04 (65.28)	3.93 (3.65)	14.67 (14.50)

sponding 1:1 adduct Va. From the characteristic $\nu_{C=O}$ at 1880 cm^{-1} in the IR spectrum as well as from the result of thermal isomerization, the structure of Va was established to be the (2+2) cycloadduct, 1-benzoyl-3-phenyl-2-phenylimino-1,3-diazetidin-4-one.

The (2+2) cycloadduct Va was thermally isomerized into the (4+2) cycloadduct, 3,6-diphenyl-2-phenylimino-2*H*-1,3,5-oxadiazin-4(3*H*)-one (VIa); a small amount of isomeric 1,3,5-oxadiazin-6-one VII was also formed.

Similar reactions of *p*-substituted benzoyl isocyanates (Ib—Ic) with IV at 0°C gave the corresponding (2+2) cycloadducts Vb and Vc, which on thermal isomerization afforded good yields of the corresponding (4+2) cycloadducts, VIb and VIc respectively.

The reaction of Ia with IV in a refluxing benzene–ether solution gave VIa and VII, but Va was not formed.

The proposed structures VI and VII were confirmed by spectral studies. The IR spectrum of VIa is similar to that of (4+2) cycloadducts III, while the absorption

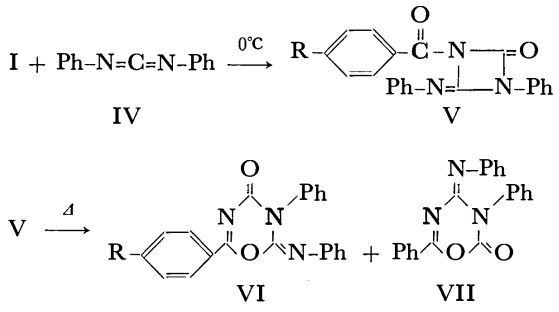

a: R=H, b: R=Cl, c: R=NO_2

bands in VII is similar to those of 2,4-diphenyl-1,3,5-oxadiazin-6-one.[5] Correlation between the intensity and wave number of $\nu_{C=O}$ and $\nu_{C=N}$ in the spectrum of VII is also similar to that between the intensity and wave number of $\nu_{C=O}$ and $\nu_{C=C}$ in α-pyrone.[5]

The physical properties and results of elemental analyses of V, VI, and VII are given in Tables 2 and 3 respectively.

Table 4. Reaction of I with VIII at 70°C

	R	Reaction time (hr)	Yield (%)	Mp (°C)	$\nu_{C=O}$ cm^{-1}	$\nu_{C=N}$ cm^{-1}	Analysis (%) Found (Calcd) C	H	N	MW (*m/e*)
IXa	H	1.5	75	128—129	1740	1685 1635	72.58 (72.60)	6.14 (6.09)	11.98 (12.10)	347
IXb	Cl	1.5	71	117—118	1740	1690 1630	66.25 (66.05)	5.30 (5.24)	11.04 (11.01)	381
IXc	NO_2	1.5	75	125—126	1740	1685 1640	64.45 (64.27)	5.07 (5.14)	14.37 (14.28)	392
IXd	OMe	5	66.5	123—124	1735	1680 1635	70.14 (70.01)	6.35 (6.14)	10.85 (11.13)	377

Cycloaddition to Asymmetrical Carbodiimides. The isocyanates would be expected to attack competitively both C=N bonds of asymmetrical carbodiimides.

The reactions of benzoyl isocyanates (I) with *N*-cyclohexyl-*N'*-phenylcarbodiimide (VIII) gave the corresponding 1:1 adducts IX of I and VIII in good yields.

From the similarity between the IR spectra of IX and the (4+2) cycloadducts III and VI, the structures of the adducts IX were assumed to be (4+2) cycloadducts.

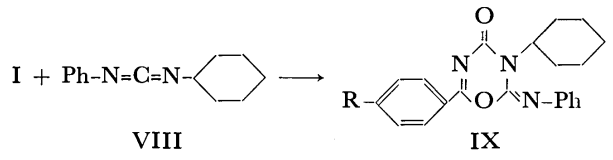

VIII IX

a: R=H, b: R=Cl, c: R=NO_2, d: R=OMe

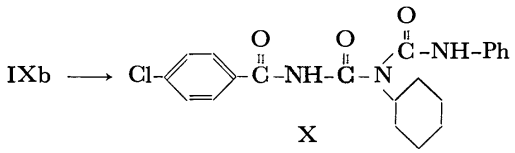

X

Hydrolysis of IXb with dilute hydrochloric acid gave 1-cyclohexyl-1-phenylcarbamoyl-3-*p*-chlorobenzoylurea (X). This indicates that the adduct IXb is 6-*p*-chlorophenyl-3-cyclohexyl-2-phenylimino-2*H*-1,3,5-oxadiazin-4(3*H*)-one, whose structure corresponds to the (4+2) cycloadduct of the isocyanate Ib to the cyclohexyl-N=C bond in VIII.

Thus, it could be concluded that all the adducts of IX are (4+2) cycloadducts of the isocyanates to the cyclohexyl-N=C bond of carbodiimide VIII.

The yields, physical properties and results of elemental analyses of IX are summarized in Table 4.

Treatment of the adducts IX with acidic alumina in chloroform gave the corresponding benzamide and 1-cyclohexyl-3-phenylurea, while similar treatment with neutral alumina afforded the isomeric 1,3,5-triazine-2,6-diones XI.

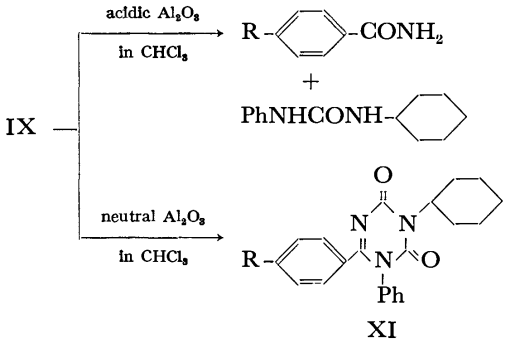

a: R=H, b: R=Cl, c: R=NO_2, d: R=OMe

The yields, physical properties, and results of elemental analyses of XI are given in Table 5.

Further confirmation of these assignments was provided by the mass spectral studies. The mass spectrum of IXb showed the parent peak (M^+) at *m/e* 381 and other peaks at *m/e* 299 (M^+-), 200 (M^+-ArCONCO), 181 (ArCONCO$^+$), 162 (299$^+-$ArCN), 139 (ArCO$^+$), 119 (PhNCO$^+$), and 118 (PhN=C=NH$^+$, base peak). In the mass spectrum of XIb, the parent peak (M^+) appeared at *m/e* 381, together with major peaks at *m/e* 300, 299 (M^+-), base peak), 257 (300$^+-$HCNO), 256 (299$^+-$HCNO), 215 (ArC=$\overset{+}{N}$HPh), 214 (Ar–C≡$\overset{+}{N}$–Ph), 163 (300$^+-$ArCN),

Table 5. Isomerization of IX

	R	Yield (%)	Mp (°C)	$\nu_{C=O}$ cm^{-1}	$\nu_{C=N}$ cm^{-1}	Analysis (%) Found (Calcd) C	H	N	MW (*m/e*)
XIa	H	32.4	225.5—226	1745 1690	1620	72.84 (72.60)	6.18 (6.09)	12.17 (12.10)	347
XIb	Cl	33	182 —183	1740 1680	1610	66.03 (66.05)	5.35 (5.24)	10.76 (11.01)	381
XIc	NO_2	44	142 —143	1745 1685	1620	66.91 (66.80)	5.52 (5.33)	12.99 (12.99)	392
XId	OMe	30	213	1740 1680	1610	70.52 (70.14)	6.25 (6.14)	10.91 (11.13)	377

Table 6. Reaction of I with XV

	R	Yield (%)	Mp (°C)	$\nu_{C=O}$ cm^{-1}	$\nu_{C=N}$ cm^{-1}	Analysis (%) Found (Calcd) C	H	N	MW (*m/e*)
XVIa	H	70[1]	154—155	1740[2]	1690 1640	74.07 (74.35)	4.92 (4.82)	11.49 (11.84)	355
XVIb	Cl	56	141—142	1740[2]	1690 1635	67.79 (67.80)	4.34 (4.12)	10.52 (10.78)	389
XVIc	NO_2	51	137—138	1740[2] 1720	1690 1640	66.31 (66.00)	4.04 (4.03)	13.64 (13.99)	400
XVIIa	H		194—195	1770[3]	1665 1640	74.54 (74.35)	4.81 (4.82)	11.85 (11.84)	355
XVIId	OMe	67.5[4]	151—152	1780[3]	1660 1640	71.54 (71.67)	5.19 (4.97)	10.66 (10.90)	385

1) Total yield of XVIa and XVIIa. 2) Weak bands. 3) Very strong bands. 4) Total yield of XVId and XVIId.

138 ($ArC\equiv\overset{+}{N}H$), and 119 ($PhNCO^+$).[7]

Thiobenzoyl isocyanate (XII) reacted with VIII to give two isomeric cycloadducts, XIII (mp 146.5—147.5°C) and XIV (mp 160°C), in 23 and 20% yields, respectively.

On the basis of IR and NMR spectra, structures XIII and XIV were assigned to (4+2) cycloadducts of the isocyanate to the cyclohexyl–N=C bond and to the phenyl–N=C bond of VIII, respectively.

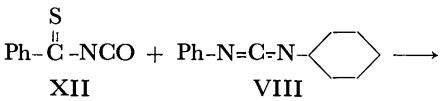

XII VIII

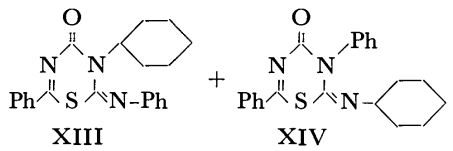

XIII XIV

In the NMR spectrum of (4+2) cycloadduct IXb the methine-proton of *N*-cyclohexyl ring appears at δ 4.4—5.0 ppm as a multiplet, and the spectrum of (4+2) cycloadduct IIIa gives two methine-protons at δ 3.4—4.0 $\left(=N-\underset{H}{\text{C}}<\right)$ and 4.3—5.0 ppm $\left(-\overset{|}{N}-\underset{H}{\text{C}}<\right)$. The spectra of XIII and XIV show a multiplet at δ 4.8—5.2 ppm $\left(-\overset{|}{N}-\underset{H}{\text{C}}<\right)$ and one at δ 3.2—3.9 ppm $\left(=N-\underset{H}{\text{C}}<\right)$.

Cycloadditions of benzoyl isocyanates (I) to *N*-phenyl-*N'*-*o*-tolylcarbodiimide (XV) were investigated; the results are given in Table 6. The products XVI and/or XVII were formed, depending on the nature of the substituents in the isocyanate. Crystals obtained from the reaction of Id with XV were found to be a mixture of XVId and XVIId by the IR spectrum. An attempt to separate XVId from the crystals by recrystallization was unsuccessful.

On the basis of the IR spectra, the adducts XVI were confirmed to be the corresponding (4+2)cycloadducts. It is evident from the results of chemical conversions that compounds XVI are the 6-aryl-2-phenylimino-3-*o*-tolyl-2*H*-1,3,5-oxadiazin-4(3*H*)-ones, whose structures correspond to the (4+2) cycloadducts of the isocyanates to the *o*-tolyl-N=C bond in XV.

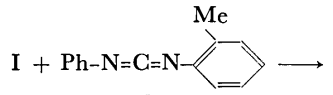

XV

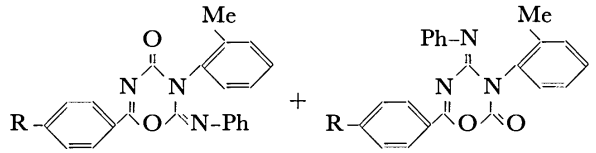

XVI XVII

a: R=H, b: R=Cl, c: R=NO_2, d: R=OMe

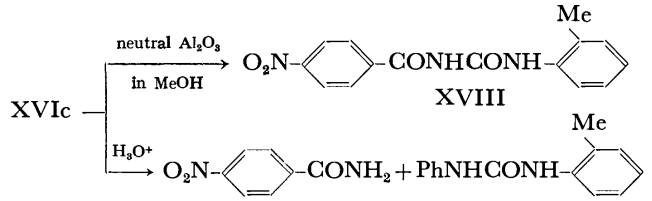

XVIII

Treatment of the adduct XVIc with neutral alumina in methanol gave 1-*p*-nitrobenzoyl-3-*o*-tolylurea (XVIII), while XVIc was hydrolyzed with dilute hydrochloric acid to afford *p*-nitrobenzamide and 1-phenyl-3-*o*-tolylurea.

Isomeric adducts XVIIa and XVIId were assumed from the similarity between the IR spectra of XVII and VII, to be the corresponding 1,3,5-oxadiazin-6-ones.

Formation Pathways of the Products. The reaction pathways of the isocyanates and carbodiimides can be considered as follows.

As shown in Scheme 1, the isocyanate reacts with the carbodiimide to give first (2+2) cycloadduct (**A**). In fact, (2+2) cycloadducts V were obtained in the reaction of isocyanates I with carbodiimide IV at 0°C. Since (2+2) cycloadduct (**A**) is thermally unstable, it is converted to (4+2) cycloadduct (**B**) through either isomerization (path a) or 1,4-cycloaddition after dissociation into its components (path b).

On the other hand, 1,3,5-oxadiazin-6-one (**C**) obtained by the thermal isomerization of (2+2) cycloadduct Va or from the reaction of isocyanates I with carbodiimide XV, might be formed through either

7) Ar represents the *p*-chlorophenyl group.

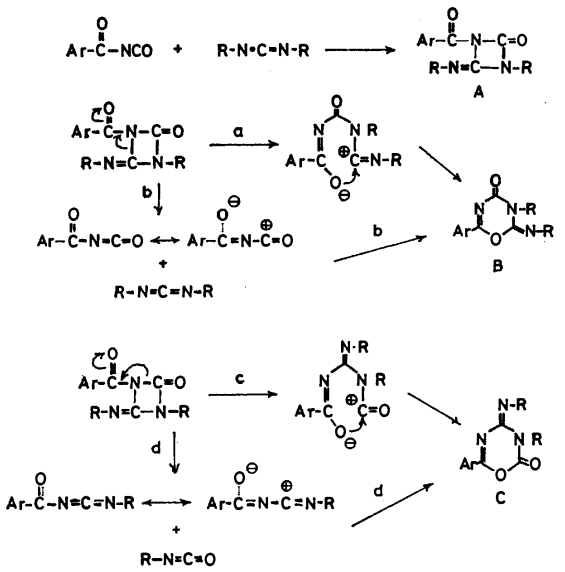

Scheme 1

isomerization (path c) or 1,4-cycloaddition after dissociation into aryl isocyanate and asymmetrical aroyl carbodiimide (path d).

However, isomerization paths a and c would seem to be more reasonable than the dissociation routes b and d. Indeed, no cross-over products, which would be expected from the reactions of isocyanate (Ar–C(=O)–NCO) with carbodiimide (Ar–C(=O)–N=C=N–R) and of isocyanate (RNCO) with carbodiimide (R–N=C=N–R), were formed in all the reactions.

Although the exact course of the formation of 1,3,5-triazine-2,6-diones XI from (4+2) cycloadducts IX and neutral alumina is not clear, we proposed the following sequence: if the ring opening of IX occurs, it would then recyclize to 1,3,5-triazine XI.

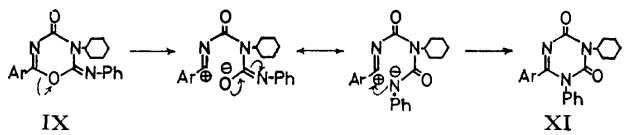

IX XI

A similar ring opening followed by recyclization was observed in the isomerization of the adduct of benzoylsulfene to carbodiimide.[8]

Experimental

All the melting points are uncorrected. The IR spectra were recorded on a Nippon Bunko IR-S spectrometer, and the UV spectra were measured with a Shimadzu SV-50A spectrophotometer. The NMR spectra were determined at 60 MHz with a Hitachi R-20 NMR spectrometer with TMS as the internal reference. The mass spectra were obtained on a Hitachi RMS-4 mass spectrometer with a direct inlet and an ionization energy of 70 eV.

Materials. *p*-Substituted benzoyl isocyanates (Ia—Id)[5] and thiobenzoyl isocyanate (XII)[9] were prepared by the methods reported previously.

N,N'-Dicyclohexylcarbodiimide (II), bp 155—156°C/10 mmHg (lit,[10] bp 148—152°C/11 mmHg), and *N,N'*-diphenylcarbodiimide (IV), bp 119—120°C/0.2—0.3 mmHg (lit,[11] bp 110—112°C/0.2 mmHg), were prepared according to the reported methods.

N-Cyclohexyl-*N'*-phenylcarbodiimide (VIII). The carbodiimide was obtained from *N*-cyclohexyl-*N'*-phenylthiourea by a method similar to that described by Iwakura and Noguchi.[12] A mixture of *N*-cyclohexyl-*N'*-phenylthiourea (38 g), commercial sodium hypochlorite (650 g), 40% aqueous sodium hydroxide solution (180 m*l*) and toluene (200 m*l*) was stirred at 70°C for 2 hr. After the reaction mixture was cooled, the aqueous layer was separated and then extracted with toluene. The combined toluene solution was washed with water and dried over anhydrous sodium sulfate. After evaporation of the toluene, the residue was distilled over active copper powder,[13] affording VIII (16 g), bp 139—140°C/4 mmHg. $\nu_{N=C=N}$: 2180 cm^{-1}. M$^+$: *m/e* 200.

N-Phenyl-*N'*-*o*-tolylcarbodiimide (XV). The carbodiimide was prepared according to a method similar to that described by Meakins and Moss.[14] Yellow mercuric oxide (35.6 g) was added in portions to a refluxing solution of *N*-phenyl-*N'*-*o*-tolylthiourea (20 g) and sulfur (0.2 g) in acetone (400 m*l*). After the reaction mixture was boiled for 20 min, the precipitate was collected and washed with acetone (100 m*l*). The combined acetone solution was dried over anhydrous sodium sulfate and concentrated *in vacuo*, leaving a residue. Since the residue was transformed into *N,N'*-diphenyl- and -di-*o*-tolylcarbodiimide on distillation, the residue was purified by chromatography on neutral alumina using petroleum benzine as an eluent. $\nu_{N=C=N}$ 2180 cm^{-1}. M$^+$: *m/e* 208.

Reaction of I with II. A solution of 0.7 g of II in 5 m*l* of benzene–diethyl ether mixture (1:1) was added dropwise to a solution of 0.5 g of Ia in 2 m*l* of benzene at 0°C. The reaction mixture was stirred at room temperature for a few minutes, during which time crystals were formed. Filtration gave colorless crystals, which on recrystallization from benzene–petroleum benzine (bp 45—60°C) mixture afforded (4+2) cycloadduct IIIa, mp 142—143°C, as colorless prisms. Yield, 0.6 g (54%).

Similar reactions of Ib—Id with II afforded the corresponding (4+2) cycloadducts IIIb—IIId. The results are given in Table 1.

Reaction of I with IV. *i)*: To a solution of 1.2 g of Ia in 10 m*l* of benzene was added dropwise a solution of 1.6 g of IV in 10 m*l* of benzene–diethyl ether mixture (1:1) at 0°C. After the reaction mixture was stirred at the same temperature for 24 hr, filtration gave colorless crystals. Recrystallization from dichloromethane–petroleum benzine (bp 35—45°C) mixture afforded 1.5 g (55%) of (2+2) cycloadduct Va, mp 112—113°C (decomp.), as colorless needles.

Similar reactions of Ib and Ic with IV gave the corresponding (2+2) cycloadducts Vb and Vc. The results are summarized in Table 2.

8) O. Tsuge and S. Iwanami, *Nippon Kagaku Zasshi*, **92**, 448 (1971).

9) O. Tsuge S. Kanemasa, and M. Tashiro, *Tetrahedron*, **24**, 5205 (1968).

10) N. F. Albertson, "Organic Reactions," Vol. 1, ed. by A. C. Cope, John Wiley & Sons, Inc., New York, London (1962), p. 212.

11) T. W. Campbell and J. J. Monagle, "Organic Syntheses," Vol. 43, (1963), p. 31.

12) Y. Iwakura and K. Noguchi, This Bulletin, **40**, 2383 (1967).

13) R. Q. Brewster and T. Groening, "Organic Syntheses," Coll. Vol. III, (1961), p. 445.

14) G. D. Meakins and R. J. Moss, *J. Chem. Soc.*, **1957**, 993.

ii): A solution of 1.0 g of Ia and 1.32 g of IV in a mixture of 15 m*l* of benzene and 5 m*l* of diethyl ether was stirred at room temperature for 2 hr, and then at 70°C for 5 hr. The reaction mixture was concentrated *in vacuo* to leave a residue, which crystallized on trituration with petroleum benzine (bp 40—50°C). The crystals were separated into more soluble and less soluble parts by fractional crystallization. The former was recrystallized from ethanol to give 0.69 g (30%) of 3,6-diphenyl-4-phenylimino-2*H*-1,3,5-oxadiazin-2-(3*H*)-one (VII), mp 204—205°C (decomp.), as yellow needles.

Found: C, 73.82; H, 4.43; N, 12.29%. Calcd for $C_{21}H_{15}O_2N_3$: C, 73.89; H, 4.43; N, 12.31%.

Recrystallization of the latter from ethanol afforded 0.29 g (12%) of (4+2) cycloadduct VIa, mp 179—179.5°C, as yellow prisms.

Thermal Isomerization of (2+2) Cycloadduct V. Thermal isomerization of V in the solid state was carried out in a test tube at 120°C (oil bath) for 2 hr. After cooling, the product was triturated with petroleum benzine (bp 40—50°C) to yield crystals. Recrystallization from ethanol afforded isomeric (4+2) cycloadduct VI. The results are given in Table 3.

Reaction of I with VIII. A solution of 0.7 g of Ia and 1.0 g of VIII in a mixture of 18 m*l* of benzene and 8 m*l* of diethyl ether was stirred at 70°C for 1.5 hr. The reaction mixture was then concentrated *in vacuo* to leave a residue, which crystallized on trituration with petroleum benzine (bp 35—50°C). Recrystallization from *n*-pentane afforded 1.3 g (75%) of (4+2) cycloadduct IXa, mp 128—129°C, as colorless needles.

Similar reactions of Ib—Id with VIII gave the corresponding (4+2) cycloadducts IXb—IXd. The results are summarized in Table 4.

Hydrolysis of IXb with Hydrochloric Acid. A suspension of 0.5 g of IXb in 5 m*l* of 1N hydrochloric acid was stirred at room temperature for 3 hr. The solution was filtered to give crystals. Recrystallization from methanol gave 0.36 g (69%) of 1-cyclohexyl-1-phenylcarbamoyl-3-*p*-chlorobenzoylurea (X), mp 131—132°C, as colorless needles.

Found: C, 63.12; H, 5.60; N, 10.62%. Calcd for $C_{21}H_{22}O_3N_3Cl$: C, 63.08; H, 5.51; N, 10.52%.

IR (KBr) cm^{-1}: ν_{NH} 3245, 3230. ν_{CO} 1715, 1680, 1660.

Isomerization of IX with Neutral Alumina. After a mixture of 0.65 g of IXa and 20 g of neutral alumina in 35 m*l* of chloroform was stirred at room temperature for 1 hr, the alumina was collected and washed with chloroform. The combined chloroform solution was concentrated *in vacuo* to leave crystals. Recrystallization from petroleum benzine (bp 60—90°C) gave 0.21 g (32.4%) of the 1,3,5-triazine-2,6-dione XIa, mp 255.5—256°C, as colorless prisms.

The results of similar isomerizations of IXb—IXd with neutral alumina are summarized in Table 5.

Reaction of XII with VIII. To a solution of XII generated *in situ* from 0.93 g of 2-phenylthiazoline-4,5-dione[15] in 20 m*l* of xylene was added 0.97 g of VIII. After the reaction mixture was stirred at room temperature for 3 hr, the xylene was evaporated *in vacuo* to leave crystals. Recrystallization from diethyl ether gave 0.36 g (20%) of the (4+2) cycloadduct XIV, mp 160°C, as colorless needles.

Found: C, 69.65; H, 5.68; N, 11.51%. Calcd for $C_{21}H_{21}ON_3S$: C, 69.40; H, 5.83; N, 11.56%. M^+: *m/e* 363.

IR (KBr) cm^{-1}: $\nu_{C=O}$ 1700 (sh), $\nu_{C=N}$ 1690, 1610.

The mother liquor was concentrated to leave a residue, which on chromatography on neutral alumina using chloroform as an eluent afforded crystals. Recrystallization from petroleum benzine (bp 60—90°C) gave 0.41 g (23%) of the isomeric (4+2) cycloadduct XIII, mp 146.5—147.5°C, as yellow prisms.

Found: C, 69.66; H, 5.65; N, 11.25%. Calcd for $C_{21}H_{21}ON_3S$: C, 69.40; H, 5.83; N, 11.56%. M^+: *m/e* 363.

IR (KBr) cm^{-1}: $\nu_{C=O}$ 1720 (sh), $\nu_{C=N}$ 1700, 1610.

Reaction of I with XV. A solution of 0.7 g of Ib and 0.8 g of XV in a mixture of 18 m*l* of benzene and 8 m*l* of diethyl ether was stirred at 70°C for 4 hr. The reaction mixture was then concentrated to leave a residue which was triturated with petroleum benzine (bp 35—50°C) to form crystals. Recrystallization from *n*-pentane gave 0.85 g (57%) of (4+2) cycloadduct XVI, mp 141—142°C, as yellow prisms.

Similar reactions of Ia and Id with XV gave a mixture of the corresponding (4+2) cycloadducts XVIa and XVId, and isomers XVIIa and XVIId. By repeated fractional recrystallization from *n*-pentane, XVIa, XVIIa, and XVIId were isolated in pure form but not XVId. The results are given in Table 6.

Hydrolysis of XVIc. A mixture of 0.5 g of XVIc and 15 g of neutral alumina in 30 m*l* of methanol was stirred at room temperature for 1.5 hr. The alumina was then collected and washed with methanol and the combined methanol solution concentrated *in vacuo* to leave a residue. Several recrystallizations from methanol gave 0.16 g (42.5%) of 1-*p*-nitrobenzoyl-3-*o*-tolylurea (XVIII), mp 232—233°C, which was identical with the authentic sample prepared from *p*-nitrobenzoyl isocyanate and *o*-toluidine.

Found: C, 60.45; H, 4.30; N, 14.34%. Calcd for $C_{15}H_{13}O_4N_3$: C, 60.19; H, 4.38; N, 14.04%.

IR (KBr) cm^{-1}: ν_{NH} 3240, 3170. $\nu_{C=O}$ 1720, 1690 (sh), 1670 (sh).

15) J. Goerdeler and H. Schenk, *Chem. Ber.*, **98**, 2954 (1965).

Preparation of Reinforcing Fillers from Japanese Acid Clays with Lime and by Calcination. I. Availability of Raw Materials for Preparing Hard Clay and the Properties of Products

Hideki RAI and Junkichi YAMADA*

Engineering Research Institute, Faculty of Engineering, The University of Tokyo, Yayoi, Bunkyo-ku, Tokyo

(Received May 11, 1971)

Reinforcing fillers for elastomers were prepared from three representative specimens of Japanese acid clay by treatment with hydrated lime (CaO 10%), subsequent calcination (600°C, 1.5 hr), and mechanical disintegration. Physicochemical properties of the products such as hygroscopicity, pH, diphenylguanidine (DPG) adsorption, specific gravity, and bulk density were determined in comparison with those of raw materials. Morphological and structural features were investigated by means of electron microscopy, X-ray diffraction, infrared and far infrared spectroscopy, DTA, and TGA. The reinforcing effects on SBR-1502 were compared with those of Dixie Clay and Silene EF. The following results were obtained. (1) Acid clays containing montmorillonite and α-cristobalite as principal constituents are suitable for the preparation of the fillers, but not the clay containing halloysite mineral as a major component in the randomly mixed-layers of kaolinite and montmorillonite with no excess silica. (2) Irreversible contraction as well as the formation of calcium silicates took place in montmorillonite minerals. Calcium silicate is formed in two states, one covering the surface of montmorillonite minerals and the other being set free. This gives rise to remarkable changes in adsorptivity, pH, swelling, bulk density, and specific gravity. Thus it becomes possible to use acid clays as reinforcing fillers. Hygroscopicity and the pH could be made about the same as those of Silene EF. The DPG adsorption capacities could be reduced as low as that of Dixie Clay. The products thus obtained greatly increased in bulk density and exhibited an average property of Dixie Clay and Silene EF in reinforcing SBR-1502.

Elastomer reinforcement with inorganic fillers seems to be influenced by their properties. Specific surface area and the available functional groups of the filler play the most important role.[1-3]

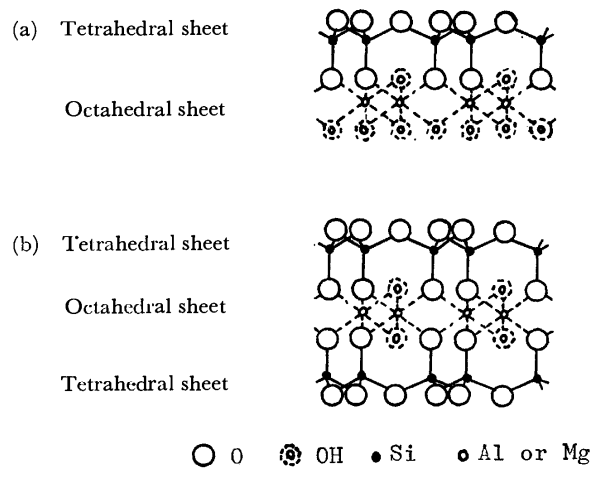

Fig. 1. Base structures of a two-sheet mineral (a) and a three-sheet mineral (b) (schematic).

Kaolinite is composed of a hydrated aluminum silicate with a two-layer type sheet structure as shown in Fig. 1-(a). Reinforcement of elastomers with kaolinite has been attributed to the effective hydroxyl groups of the external crystal surfaces and the fineness.[4]

Since kaolinite resource is small in Japan, we have attempted to prepare a reinforcing filler such as hard clay from Japanese acid clays. Acid clays generally contain montmorillonite minerals of three-layer type sheet structure as shown in Fig. 1-(b) accompanying some hydrous amorphous silica.[5] Their primary particles are finer than those of kaolinite.[6]

In view of the similarity in the constitutional units, fineness and functional groups between montmorillonite and kaolinite, the acid clays can be used as a material of reinforcing fillers. However, the structural factors[5c,7] such as substitutions in the tetrahedral and/or octahedral sheet, nonconformity in the layers, and lattice defects of montmorillonite give rise to too great adsorption, cation exchange, swelling, and catalytic activity.

If such surface activity could be controlled keeping fineness and effective hydroxyl groups unchanged, acid clays can be transformed into hard clay. Attempts were made from this viewpoint. Thermal treatment caused dehydroxylation as well as dehydration. Dehydroxylation gave rise not only to an irreversible contraction but also the polycondensation in the interlayers, reducing the adsorptivity noticeably. Caking or sintering of the minute particles which took place during the course of thermal treatment made it difficult for the products to be disintegrated mechanically or rehydroxylated even in wet milling. Thermal treat-

* Present address: AA Chemical Company, Tamagawa, Ota-ku, Tokyo.

1) S. Yamashita, *Kogyo Kagaku Zasshi*, **73**, 50 (1970).
2) G. Kraus, *Rubber Chem. Technol.*, **38**, 1070 (1965).
3) E. Suito, *J. Soc. Rubber Ind. Japan*, **34**, 441 (1962).
4) E. Suito and M. Arakawa, *ibid*, **36**, 704 (1963); *Kogyo Kagaku Zasshi*, **66**, 1616 (1963).
5) a) T. Mitsuda, *J. Mineral. Soc. Japan*, **4**, 342, 359 (1960); b) T. Sudo, "Mineralogical Study on Clays of Japan," Maruzen Co., Tokyo (1959), p. 194; c) Y. Otsubo, *Kagaku To Kogyo*, **4**, 229 (1951).
6) a) R. E. Grim, "Clay Mineralogy," 2nd Edt., MacGraw-Hill Ind. (1968), p. 165; b) E.C. Jonas and R.M. Oliber, "Proceedings of the 15th National Conference for Clay and Clay Minerals," Pergamon Press, New York (1967), p. 27.
7) R. E. Grim, Ref. 6a, p. 77.

Table 1. Characteristics of acid clays

Sample	Symbol	Mineralogical composition	Structural formula	Excess silica	Locality
Kuramitsu acid clay	**K**	More halloysite than montmorillonite in randomly mixed layers	$(Al_{1.60}Fe_{0.13}Mg_{0.26})(Si_4)$ - $O_{10}(OH)_2X_{0.33}$	<1%	Kuramitsu, Sugaya-mura, Kitakambara-gun, Niigata Prefecture
Matsune acid clay	**M**	Normal montmorillonite, only	$(Al_{1.48}Fe_{0.06}Mg_{0.50})(Si_4)$ - $O_{10}(OH)_2X_{0.33}$ - $3.36\,SiO_2\ 0.31\,H_2O$	34	Matsune, Kushibiki-mura, Higashitagawa-gun, Yamagata Prefecture
Nakajo acid clay	**N**	More abnormal montmorillonite than normal one	$(Al_{1.35}Fe_{0.15}Mg_{0.55})(Si_4)$ - $O_{10}(OH)_2X_{0.33}$ - $0.08\,SiO_2\ 0.48\,H_2O$	13	Nakajo-machi, Kitakambara-gun, Niigata Prefecture

ment diminished markedly the reinforcing effects of the fillers. Treatment with alkali only afforded alkali-montmorillonites and hydrous alkali silicates which still showed considerable rehydration. The surface activity did not decrease satisfactorily. Caking which took place on drying made it difficult for particles to be pulverized. The residual alkali caused an early scorching of loaded compound and poor aging resistance of the vulcanizate.

Treatment with a proper alkali such as hydrated lime and subsequent calcination caused the fixation of the applied cation in the cavities of the tetrahedral sheets as well as an irreversible contraction. Formation of calcium silicates with excess silica, covering external and internal surfaces of the montmorillonite crystallites or existing in an isolated state, improve the properties.

This paper describes the preliminary results on the preparation of reinforcing fillers from acid clays. Three representative specimens of acid clays, Nakajo (**N**), Matsune (**M**), and Kuramitsu (**K**) were first treated with lime (CaO 10%) and then calcined at 600°C for 1.5 hr. Their physicochemical properties such as hygroscopicity, pH, DPG adsorption, specific gravity, and bulk density were determined. The mineralogical features were investigated by means of electron microscopy, X-ray diffraction, infrared and far infrared spectroscopy, DTA, and TGA. The reinforcing effects on SBR-1502 were examined in comparison with those of Dixie Clay and Silene EF. Availability of the acid clays as a raw material for hard clay was discussed.

Experimental

Raw Materials. *Acid Clays*: Specimens from Mizusawa Chem. Ind. Co. were used (Table 1). Five kilograms of the air dried, massive specimens[8] of light yellowish gray (**N**) consisting of montmorillonites (the amount of abnormal montmorillonite is greater than that of normal one) containing excess silica (13%) were crushed in an iron mortar, sifted through a 6 mesh screen of Tylor standard sieves and then subjected to homogeneous mixing. The white powdery (**M**) consisting only of normal montmorillonite containing excess silica (34%) and light yellowish gray (**K**) containing halloysite as a major component in the randomly mixed-layers of kaolinite and montmorillonite with no excess silica were also studied.

Quick Lime: Calcium oxide of reagent grade with grain sizes 10—30 cm^3 was pulverized and grains smaller than 60 mesh were chosen.

8) grain size, *ca.* 30—120 cm^3.

Preparation of Reinforcing Fillers. Acid clay (150 g), water (1000 m*l*), and quick lime (CaO, 10% in wt. of the acid clay dehydrated at 110°C for 4 hr) were put into a porcelain ball mill of about 3 *l* containing 2 kg of porcelain balls of diameter 10 mm, and ground at 40 rpm for 1 hr at room temperature. The slurry of acid clay was filtered, dried at 110°C, and calcined at 600°C for 1.5 hr. The resulting product was subjected to wet milling at 40 rpm for 18 hr at room temperature. It was then diluted with water to about 10% slurry and passed through a 200 mesh sieve to remove coarse particles. After the finer particles obtained by filtration were dried at 110°C, the dehydrated product was pulverized with an atomizer.

Determination of Physicochemical Properties. The following properties were studied.

Hygroscopicity: One gram of the specimen which had been exposed to the air for 24 hr at room temperature was taken into a 10 m*l* weighing bottle and dried at 110°C in an electric oven to a constant weight. The loss in weight (%) before and after drying was determined as a measure of hygroscopicity.

pH: The value was determined by the JIS K 6221 (1960) method[9] with a pH meter with a glass electrode.

DPG adsorption: The adsorptivity for vulcanizing accelerator was estimated by means of a method which is a modification of the one for carbon black.[10] Reagents were prepared as follows: (a) 0.01N DPG ethanol solution. DPG (2.11 g) was dissolved in 1 *l* of ethanol (purity 99.7%) followed by filtration. (b) Bromophenol blue (BPB). 0.1% ethanol solution was prepared for the use as an indicator. Estimation of DPG adsorption was carried out as follows: Two grams of the specimen dried at 110°C for 3 hr just before assay was taken into a 200 m*l* conical flask with a stopper. After addition of 100 m*l* of the 0.01N DPG ethanol solution the flask was closed and the following treatment was carried out 5 times: Shaking of the flask for 1 min and then putting it to stand for 5 min. The resulting mixture was centrifuged for 10 min at 3000—3500 rpm. Ten milliliters of the supernatant liquid was then taken for titration with a 0.01N HCl standard solution in the presence of 3 drops of the BPB ethanol solution. The original blue solution turned green at the end of titration. Blank tests were carried out simultaneously. The amount S of the DPG adsorbed by 10 kg of the dehydrated filler was estimated by the following equation from the average of two measurements for each specimen.

$$S = \frac{211 \cdot f \cdot (B - C)}{W} \times 10^4$$

9) Japanese Industrial Standards (JIS) K 6221-60 (1960); American Standards for Testing Materials (ASTM) D 1512-57T (1957).

10) W. B. Wiegand and J. W. Snyder, *Ind. Eng. Chem.*, **23**, 646 (1931).

where

f = factor of the 0.01N HCl solution

B = volume (ml) of the 0.01N HCl solution consumed in the blank test

C = volume (ml) of the 0.01N HCl solution consumed in the test

W = weight (g) of the dehydrated filler applied

211 = molecular weight of DPG

Specific Gravity: One gram of the specimen was dried at 110°C for 2 hr, following the ASTM D 135-39 method A.[11] Kerosene (bp 70—100°C/2 mmHg) was used as an immersion liquid (D_4^{30} 0.7811).

Bulk Density: The measuring cylinder method[12] was applied.

Morphological and Structural Studies. The shape, size, and structural features both of the fillers and raw materials were investigated by means of electron microscopy, X-ray diffraction, infrared and far infrared spectroscopy, DTA, and TGA.

Electron Microscopy: Studies were carried out with a JEOL (Japan Electron Optics Laboratory Co.) JEM-6AS electron microscope operating at 50 kV.

X-Ray Diffraction: The patterns were obtained with a Rigaku Denki Geigerflex diffractometer using nickel filtered Cu-$K\alpha$ radiation, 30 kV, 12 mA, rate meter 16, multiplier 1, time constant 4 sec, slits 1°–1°–0.2 mm, scanning speed 2° (2θ)/min, chart speed 1 cm/min.

Infrared and Far Infrared Spectroscopy: Measurements were carried out with a JASCO Model DS-403G spectrophotometer through a KBr disc and Nujol mull in the regions 4000—200 and 4000—2800 cm^{-1}, respectively.

DTA and TGA. Thermal analyses were carried out with a Rigaku Denki Thermoflex differential thremogravimetric analyser up to 1300°C with a heating rate 10°C/min.

Structural formulas of the acid clays and the contents of excess silica were calculated by Otsubo's method[13] from the data of chemical analysis (Table 1).

Table 2. Constituents (PHR) of compounds

SBR-1502	100	Vulcanizing accelerator, DM	1.5
Zinc oxide	5	Vulcanizing accelerator, TT	0.25
Sulfur	2	Antioxidant, D	1.0
Stearic acid	2	Reinforcing filler	75

Compounding Test. A master batch containing elastomer (SBR-1502), zinc oxide, sulfur, stearic acid, dibenzothiazoyle disulfide (DM), tetramethylthiuram disulfide (TT), and phenyl-β-naphthylamine (D) was loaded with the reinforcing filler and masticated with a test-roll (6″×8″, frontroll) under the following conditions: Number of revolution 17 rpm; speed ratio of the front and back rolls 1 : 1; roll temperature 55±5°C. The constituents of the compounds are given in Table 2. A test piece (diameter 70 mm, thickness 3 mm) was made from this compound by vulcanization at 150±3°C under a pressure of 1500 lb/in² for 8, 12, and 16 min and tested according to the JIS K 6301-62 (1962) method.[14] Tensile strength (kg/cm²), modulus (300%, kg/cm²) and elongation (%) were measured with a Schopper tensile tester. Hardness after 30 sec was determined with a spring tester. Data were taken from the average of four measurements. Values not reaching 80% of the maximum value were discarded. When one value is exceptional the average of the three measurements was taken. If two values are abnormal one 80% value is added to the normal ones. If three values are abnormal two 80% values are added.

11) ASTM D 153-39 (1939).

12) S. Kuribayashi, "Methods of Examination for Rubber and Relating Materials," ed. by S. Kunisawa, Soc. Rubber Ind. Japan (1963), p. 651.

13) Y. Otsubo, Ref. 5c, p. 231; *ibid.*, **2**, 258 (1949).

14) JIS K 6301-62 (1962).

Results

Physicochemical Properties. Surface Properties: The hygroscopicity of the fillers became less than half of that of the specimens. The adsorptivity for the DPG became smaller than 1/3—1/5 of the original values. The pH values 4.52—5.95 turned 9.80—8.45 (Fig. 2).

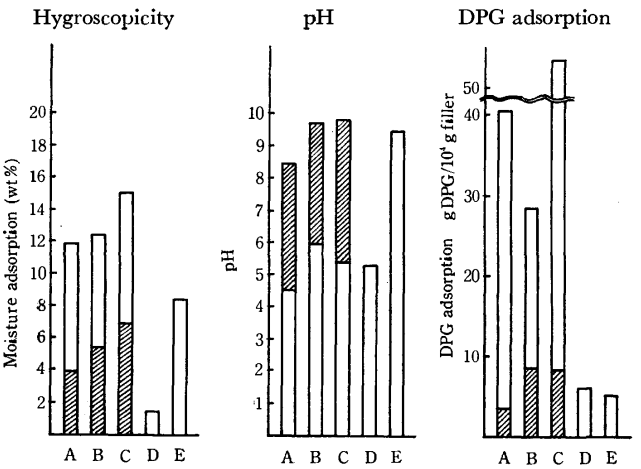

Fig. 2. Effect of treatment with lime (CaO 10%) and calcination (600°C, 1.5 hr) on hygroscopicity, pH, and DPG adsorption of the specimens in comparrison with those of Dixie Clay and Silene EF. Bar graphs indicate the results for original clays and reference fillers and hatched bars the prepared fillers.
A: Kuramitsu acid clay and **K** hard clay B: Matsune acid clay and **M** hard clay C: Nakajo acid clay and **N** hard clay D: Dixie Clay E: Silene EF

Table 3. Specific gravity and bulk density of the fillers in comparison with those of the original acid clays and reference fillers

Variety	Specific gravity		Bulk density cc/g
	Hard clay	Acid clay	
Kuramitsu-series	2.3946	2.4958	2.25
Matsune-series	2.2298	2.3891	3.02
Nakajo-series	2.3032	2.4755	2.54
Dixic Clay	2.5684	—	1.38
Silene EF	2.0989	—	4.05

Specific Gravity and Bulk Density: The maximum specific gravity of the specimens was in the order **K**<**N**<**M**. The prepared fillers showed the same order with 4—7% decrease in the values. The values of bulk density were also found to be in the same order **K**<**N**<**M**. This is in line with the amount of excess silica and the decrease in iron contents (**K** 2.93; **N** 2.75; **M** 0.79%) in the raw materials. The results agreed with the distribution observed by electron microscopy.

Morphological and Structural Features. Morphological Studies: *Shape and Size*: Hard clay **K** contains grains of maximum size, and hard clays **M** and **N**

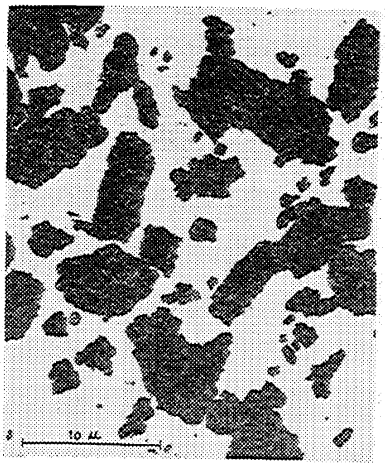

Plate 1: Kuramitsu acid clay ×4500

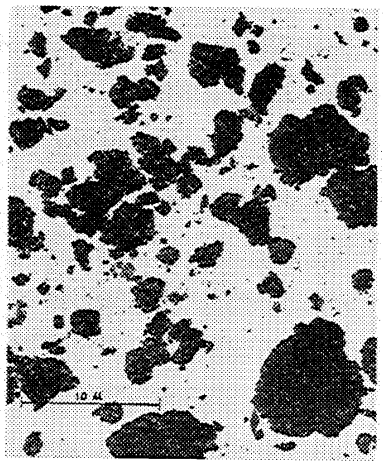

Plate 2: Matsune acid clay ×4500

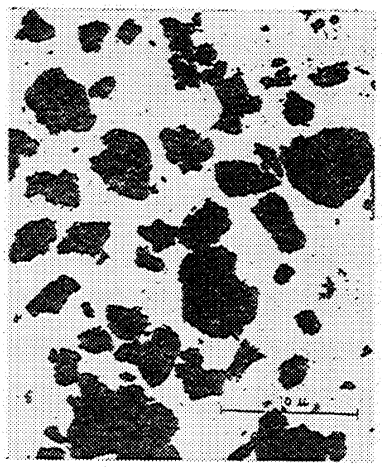

Plate 3: Nakajo acid clay ×4500

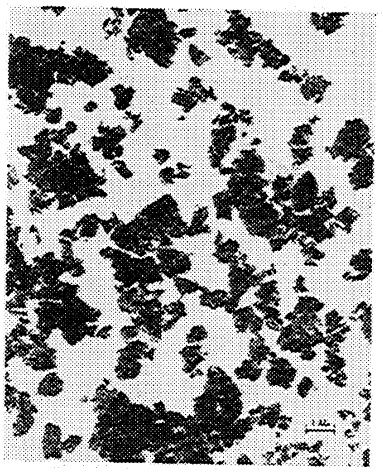

Plate 4: **K** hard clay ×9000

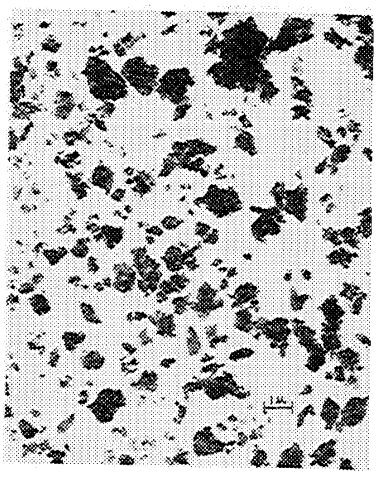

Plate 5: **M** hard clay ×9000

Plate 6: **N** hard clay ×9000

Fig. 3. Electron micrographs of the fillers (CaO 10%, calcined at 600°C for 1.5 hr) in comparison with those of original acid clays.

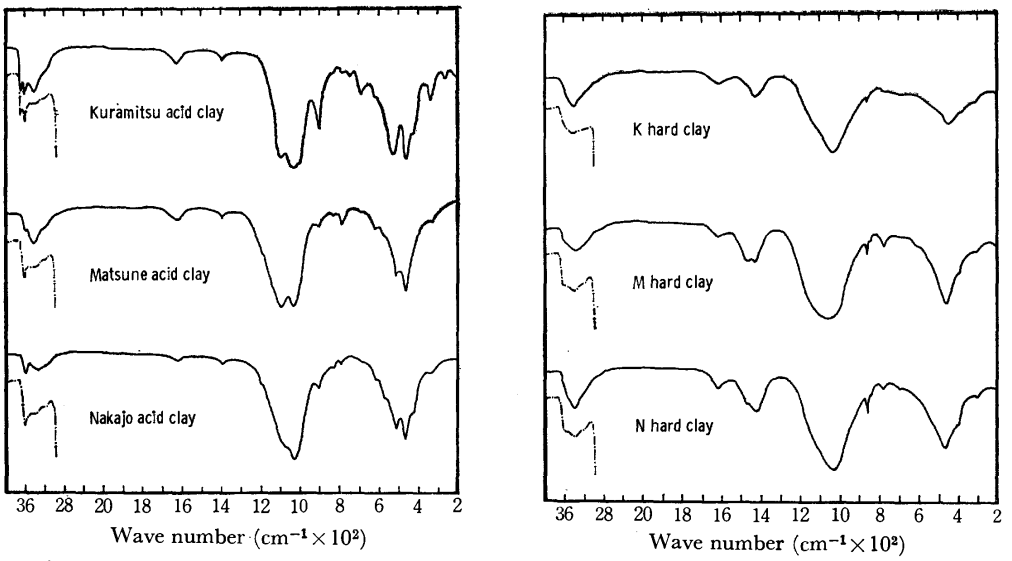

Fig. 4. Infrared and far infrared spectra of the fillers (CaO 10%, calcined at 600°C for 1.5 hr) in comparison with those of original acid clays.

contain small plate-shaped particles (Fig. 3). The grain size decrease with the increase of excess silica and the decrease of iron content.

New Minerals: A small amount of needle-like or cylindrical crystallites of calcium silicate hydrates[15] is contained in hard clays **M** and **N** but not in **K**. This was confirmed by selected-area electron diffraction. The less the content of excess silica, the less the formation of calcium silicate hydrates. However, the crystallites are large in size.

Investigation on Structural Features: *a) Infrared and Far Infrared Spectra*: The diagnostic bands[16] of montmorillonite in acid clays **M** and **N** changed with the treatment with lime and subsequent calcination as follows (Fig. 4). The bands around 3630 (νO–H, free), 3330—3420 (νO–H, hydrogen bonded), and 1630—1635 cm^{-1} (δO–H) diminished noticeably, and those around 913 (δAl^{3+}–O–H) and 838 cm^{-1} (δFe^{3+}–O–H) disappeared completely. Among the bands of layer-lattice silicates in the regions 900—1200 (νSi–O) and 400—650 cm^{-1}, the band around 1083—1100 cm^{-1} related to colloidal silica[17] and/or ion saturation[18] and the band 520 cm^{-1} related to (Si–O–Al^{VI})[19] decreased markedly. The bands around 1033—1036 (νSi–O) and 470 cm^{-1} (δSi–O) related to the skeletal vibrations of the tetrahedrons of montmorillonite shifted towards higher frequencies overlapping the adjacent bands, giving one single, strong, and broader band around 1055 and 475 cm^{-1}, respectively. The band at 795 cm^{-1} (δSi–O, hydrated amorphous silica)[17] became broader with a slight diminution in intensity and a shift towards 791 cm^{-1}. The other weak bands at 617—621, 568—574, 431, 355, and 340 cm^{-1} characteristic of montmorillonite almost disappeared. New distinct bands ascribable to calcium silicate (1483—1472 and 858—856 cm^{-1})[20] and calcite (1435, 875, 715, and 318 cm^{-1})[21] appeared. The intensity of the former increased and that of the latter decreased with the increase in the amount of excess silica.

In the case of hard clay **K** the bands at 3714 (νO–H, free in the halloysite lattices),[16] 3638 (νO–H, free in the montmorillonite lattices),[16] 3434 (νO–H, hydrogen bonded) and 1630 cm^{-1} (δO–H) diminished markedly, while the bands of kandite minerals at 912 (Al^{3+}–O–H), 791 and 751 (Si–O–Al^{VI}, in-plane and perpendicular, respectively), 698 and 436 (δSi–O), 342 and 272 cm^{-1} disappeared completely. The prominent bands of skeletal vibrations at 1100, 1030, and 1010 (νSi–O), 541 (Si–O–Al^{VI}) and 470 cm^{-1} (δSi–O) similarly turned to single bands and became less prominent at 1046 and 467 cm^{-1}, respectively. These bands were much broader and markedly smaller than those of the original acid clay and the other hard clays **M** and **N**. Feeble absorption bands of calcium silicate (1472 cm^{-1}) and calcite (1434, 875, 715, and 319 cm^{-1}) were observed. This suggests that a considerable sintering of the minute crystallites as well as the collapse of the layer-lattices took place during the course of treatment.

b) DTA and TGA Thermograms: In the DTA

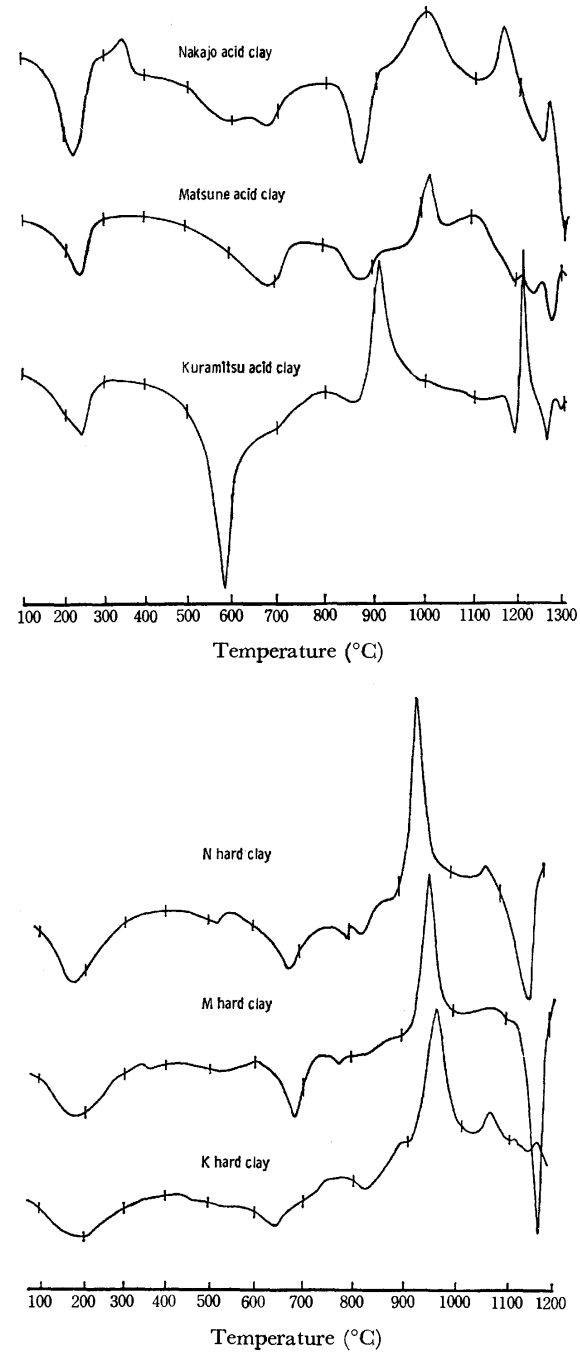

Fig. 5. DTA thermograms of the prepared fillers (CaO 10%, calcined at 600°C for 1.5 hr) in comparison with those of original acid clays.

15) a) J. A. Gard, "The Chemistry of Cement," Vol. 2, ed. by H. F. W. Taylor, Academic Press (1964), p. 256; b) H. F. W. Taylor, "Progress in Ceramic Sience," Vol. 1, ed. by J. E. Burke, Pergamon Press (1961), p. 89.

16) I. Oinuma and H. Kodama, "Clay Science Handbook," ed. by S. Iwao, Clay Sci. Soc. Japan, Gihodo (1967), pp. 65—75.

17) a) B. D. Mitchell, V. C. Farmer, and W. J. MacHardy, *Advan. Agr.*, **16**, 349 (1964); b) E. R. Lippincott, A. V. Valkenburg, C. E. Weir, and E. N. Bunting, *J. Res. Nat. Bur. Stand.*, **61**, 61 (1958); c) M. Field, I. K. Walker, and P. P. Williams, *New Zealand J. Sci. Tech.*, **38**, 31 (1956).

18) V. C. Farmer and J. D. Russel, *Spectrochim. Acta*, **20**, 1149 (1964).

19) V. Stubičan and R. Roy, *Z. Kristallogr.*, **115**, 200 (1961); *Amer. Mineral.*, **46**, 32 (1961).

20) a) E. Suito and M. Arakawa, *J. Soc. Rubber Ind. Japan*, **34**, 885 (1961); b) K. Fukui, *ibid.*, **37**, 858 (1964).

21) a) C. E. Weir and E. R. Lippincott, *J. Res. Nat. Bur. Stand.*, **65A**, 175 (1961); b) E. E. Angino, *Amer. Mineral.*, **52**, 137 (1967).

thermograms of the hard clays **M** and **N** prepared from the specimens containing montmorillonite and α-cristobalite as principal constituents, the diagnostic peaks of montmorillonite disappeared or diminished considerably (Fig. 5). Endothermic reactions: Dehydration (100—300°C, strong and sharp), dehydroxylation (500—750°C, strong and broad) and phase transition (820—910°C, strong or medium). Exothermic reactions: Oxidation of the organic matter adsorbed (around 350°C, medium), spinel or β-quartz (around 1000°C, strong and broad or sharp), β-cristobalite, mullite or cordierite (around 1150°C, medium). The fusion points of the specimens were observed to be around 1300°C and those of the fillers around 1170°C. Some new peaks appeared around 180 (due to the first endothermic reaction, very broad and strong), 678 (due to the second endothermic reaction, rather sharp and strong) and 930—950°C (due to the first exothermic reaction, very strong and sharp). They were attributed to calcium silicate hydrate.[23] No endothermic peak attributable to the decomposition of free alkali $Ca(OH)_2$ was found. However, a weak one ascribable to calcium carbonate[24] appeared around 795°C, suggesting the presence of a small amount of calcite. The amount estimated from the area of the endothermic peak was less than 3%. This seemed to decrease with the increase in the amount of excess silica.

In the case of hard clay **K** the characteristic peaks in the specimen also diminished or disappeared completely. Endothermic reaction: Dehydration (100—300°C, strong and broad), dehydroxylation of halloysite (586°C, very strong and sharp) and montmorillonite (around 695°C, strong and broad) and phase transition (855, 1190, and 1258°C, medium). Exothermic reaction: Phase transition related to halloysite (906 and 1208°C, very strong and sharp). The filler showed broad and strong endothermic peaks (195 and 639°C) and a relatively strong and sharp exothermic peak (953°C) which could be attributed to calcium silicate and aluminate, accompanied by several peaks (1053, 1109, and 1158°C).

The fillers exhibited similar profiles of TGA thermograms, which nearly corresponded to an intermediate of acid clay **M** and Silene EF. The former consists mainly of normal montmorillonite with excess silica, the latter being a hydrous calcium silicate (Fig. 6). The weight loss of hard clay **K** is greater than that of raw material. This suggests that dehydroxylation occurred to a greater extent during the course of calcination as compared with the rehydration during the course of wet milling. The weight loss of the other hard clays **M** and **N** decreased with the increase of the amount of excess silica in raw material due to the formation of hydrous calcium silicates.

The results agreed with those of infrared and far

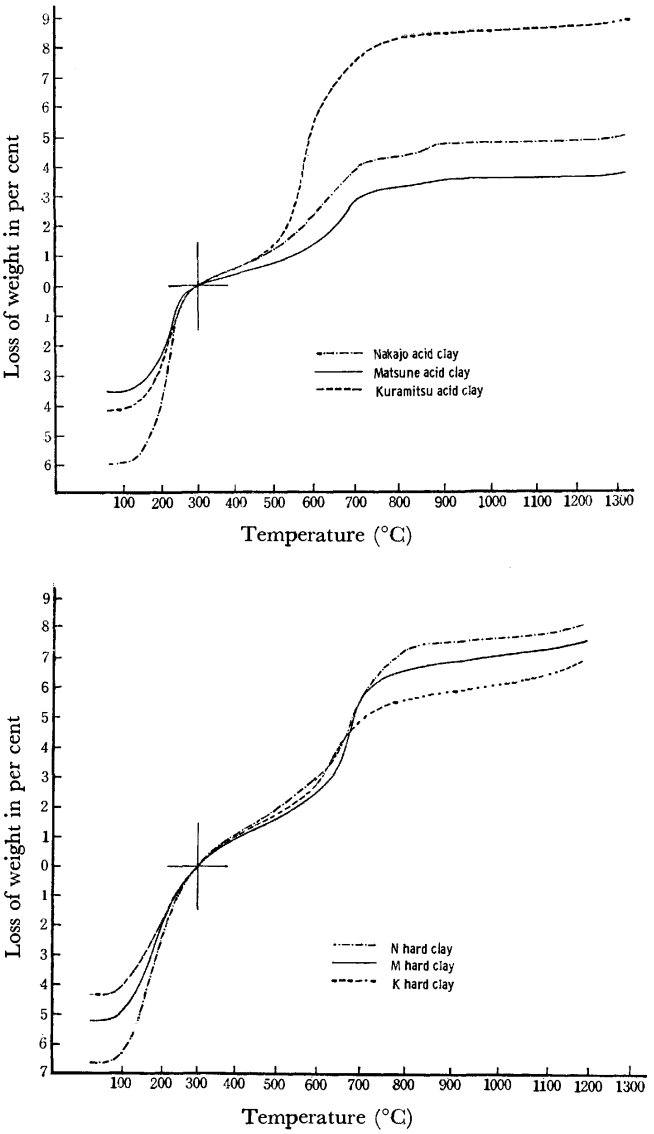

Fig. 6. TGA thermograms of the fillers (CaO 10%, calcined at 600°C for 1.5 hr) in comparison with those of original acid clays.

infrared spectroscopy and X-ray diffraction.

c) X-Ray Powder Diffraction Patterns:[25] The treatment of the original acid clays with hydrated lime (CaO 10%) caused a slight shift from 15.4 to 13.7 Å in the basal reflections as a result of the formation of Ca-montmorillonite. The intensities of the prominent basal reflections related to the amounts of interlayer water did not change much. New reflections appeared which were ascribed to the calcium silicate hydrates (3.03 and 2.72 Å) which are very similar to Taylor's CSH[15b] and calcite (3.83, 3.03, 2.53, and 2.28 Å).[26] A slight decrease in the intensities of the α-cristobalite was observed as well. Subsequent calcination (600°C, 1.5 hr) caused an irreversible contraction along *c*-axis in the montmorillonite and the disappearance of basal

22) a) R. G. Kelly, "The Differential Thermal Investigation of Clays," ed. by R. C. Mackenzie, Miner. Soc. London (1957), p. 140; b) R. E. Grim and Kulbicki, *Amer. Mineral.*, **46**, 1333 (1961).

23) S. Diamond, J. L. White, and W. L. Dolch, Caly and Clay Minerals, Proc. 12th Nat. Conf., Pergamon Press, New York (1964), p. 359.

24) a) S. Iwao ed., Ref. 15, p. 40, 395; b) R. C. Mackenzie ed., Ref. 22a, p. 331.

25) D.M.C. MacEwan, "The X-Ray Indentification and Crystal Structures of Clay Minerals," ed. by G. Brown, Miner. Soc. London (1961), p. 143.

26) H. E. Swanson and R. K. Fuyat, *NBS Circular 539*, **II**, 51 (1953); ASTM, X-Ray Powder Data File Card 5-0586.

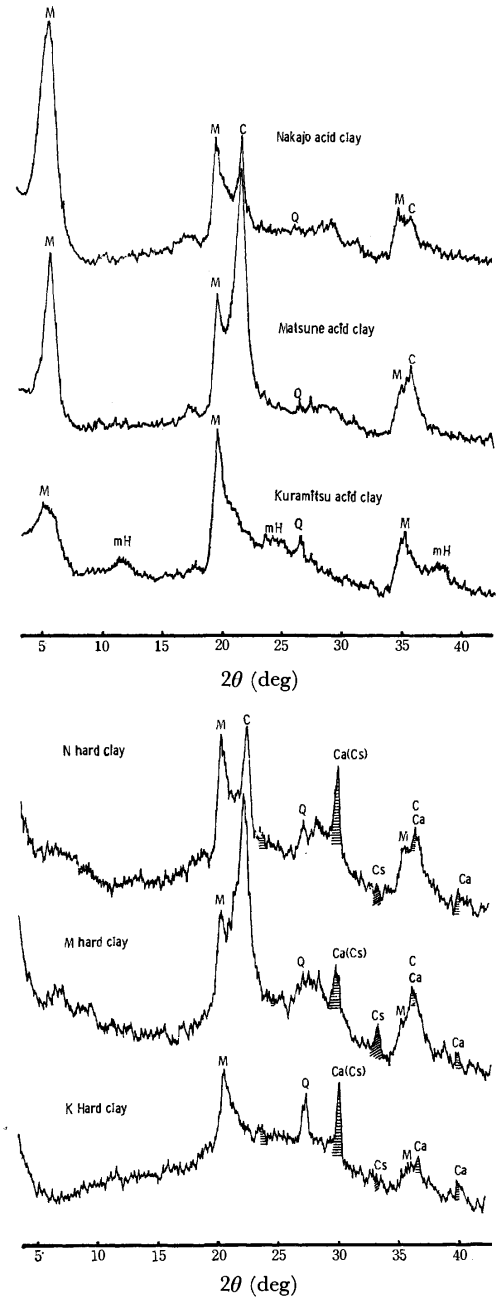

Fig. 7. X-ray powder diagrams of the prepared fillers (CaO 10%, calcined at 600°C for 1.5 hr) in comparison with those of their original acid clays. (Cu K_α radiation)
M: montmorillonite, mH: *meta*-halloysite, C: α-cristobalite, Q: quartz, Ca: calcite, Cs: calcium silicate hydrate

reflections. However, the crystal lattices remained with no serious collapse (Fig. 7). Amounts of calcium silicate hydrates and calcite estimated from the intensities of the X-ray reflections varied as follows. The former increased with an increase in the amount of excess silica α-cristobalite in raw material, and the latter decreased. This agreed with the results obtained for the structural features of fillers.

In hard clay **K** the distinct reflections of halloysite observable in the raw material disappeared almost completely, and those of montmorillonite diminished more markedly than in hard clays **M** and **N**. Only weak reflections of calcium silicate hydrate and calcite were observed together with that of unreacted quartz (3.34 Å).

Table 4. Reinforcing effects of the fillers on SBR-1502, derived from acid clays with lime (CaO 10%) and calcination (600°C, 1.5 hr)

Reinforcing filler	Vulcanization time, min	Tensile strength kg/cm²	300% Modulus kg/cm²	Elongation %	Hardness JIS
K hard clay	8	31.1	14.4	559	52
	12	34.9	13.9	559	52
	16	28.1	13.8	553	53
M hard clay	8	67.6	20.8	739	50
	12	59.4	20.9	732	52
	16	57.3	20.5	717	53
N hard clay	8	59.8	16.4	742	51
	12	59.3	16.4	726	52
	16	52.3	16.8	693	52
Silene EF	8	46.1	28.1	429	59
	12	50.7	26.7	486	61
	16	44.6	28.3	418	65
Dixie Clay	8	96.9	23.5	759	53
	12	93.0	25.3	720	55
	16	94.9	26.4	705	55

Reinforcing Effects on SBR-1502. The reinforcing effects of the fillers were compared with those of Dixie Clay and Silene EF (Table 4). The results obtained under the optimum vulcanizing conditions are given in Figs. 8 (a)—(b).

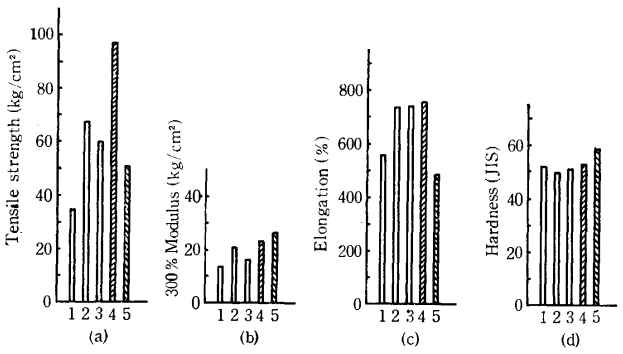

Fig. 8. Reinforcing effects of the prepared fillers (CaO 10%, calcined at 600°C for 1.5 hr) on SBR-1502 in comparison with those of Dixie Clay and Silene EF. Inscriptions are as follows:
(a): Tensile strength (kg/cm²), (b): 300% Modulus (kg/cm²)
(c): Elongation (%), (d): Hardness (JIS),
(1): **K** hard clay, (2): **M** hard clay, (3): **N** hard clay,
(4): Dixie Clay, (5): Silene EF

Tensile strength (kg/in²): The compounds obtained by loading hard clay **M** or **N** exhibited 70% or a little less tensile strength than that of Dixie Clay (Fig. 8-a). It is much greater than that of Silene EF. In the case of hard clay **K** only 35% value of Dixie Clay or one half of hard clay **M** was obtained.

Modulus (300%, kg/in²): The compounds obtained by loading the fillers gave lower modulus than those containing a reference filler Dixie Clay or Silene EF (Fig. 8-b).

Elongation (%): The compound obtained by loading the fillers exhibited fairly larger elongation as compared with those containing one of the reference fillers (Fig. 8(c)). Even the compound containing hard clay **K** showed much greater value than that of Silene EF. However, hardly any significant difference was observed between the compounds containing hard clay **M** and **N**.

Hardness: The compounds obtained by loading the fillers gave the hardness very close to that of Dixie Clay but smaller than that of Silene EF (Fig. 8-d).

The results show that the hard clays make the reinforcing effects on SBR-1502 increase with the increase in the amount of excess silica, the decrease in particle sizes, and the increase of the amount of remaining effective hydroxyl groups.

Discussion

The physicochemical and morphological studies on the fillers suggest that treatment with lime and subsequent calcination make the acid clays hydrophobic as well as basic. The fillers showed a noticeable diminution in their adsorptivity for the vulcanizing agent and moisture. Facility of crushing the products is closely related to both the mineralogical composition and the content of excess silica α-cristobalite.

Investigation of the structures of the fillers by X-ray diffraction, infrared and far infrared spectroscopy, and thermal analyses revealed the following. The above treatment caused an irreversible shrinkage along *c*-axis in montmorillonite as well as the formation of calcium silicate hydrates with the excess silica which covered the internal and external surfaces of the crystallites. This contributes in improving surface activity such as hygroscopicity, DPG adsorption capacity, swelling, and pH, and ease for the crushing of products. The formation of calcite is assumed to be originated from the carbonation of free alkali during the course of treatment.

Acid clay **K** containing halloysite as a major constituent in the randomly mixed-layers of kaolinite and montmorillonite with no excess silica, is considered to be more susceptible to treatment with lime and calcination than the acid clays **M** and **N** consisting mainly of normal and/or abnormal montmorillonites containing excess silica. This gives rise to an appreciable sintering as well as collapse in the layer lattices, which cause a glassification and caking of the minute crystallites or the primary particles due to the depression of fusion point by alkali treatment. The fact that hard clay **K** showed coarser particles, less bulk density, lower diminution in the specific gravity, greater decrease in the adsorptivity, and lower pH than those of the other two fillers **M** and **N**, can be attributed to its high susceptivility to the foregoing treatment.

The results on the reinforcement of SBR-1502 suggest that acid clays such as **M** or **N** can be used to prepare a reinforcing filler, but not an acid clay like **K**. Acid clay **M** (white) has the merit of providing a less colored product than that of acid clay **N** (light yellowish gray); the former contains less iron and more excess silica. The compound obtained by loading hard clay **M** gave much better reinforcing properties such as tensile strength, modulus, elongation, and hardness than that containing hard clay **N**. Thus acid clay **M** is considered to be a more suitable raw material.

Suito and Arakawa[4] reported on the reinforcing effects of hard clay on SBR-1502, a commercial reinforcing filler (kaolinite treated thermally up to 800°C). This suggests that the interaction between the hydroxyl radicals and the compounded elastomer molecules plays the most important role. The precise mechanism of the reinforcing effects has not been clarified. However, the markedly lower reinforcing effects of hard clay **K** as compared with those of the hard clays **M** and **N**, could be explained in terms of remarkable reduction of the specific surface area and the available hydroxyl groups.

The authors are greatly indebted to the late Prof. T. Kuwata and Associate Prof. J. Kumanotani for their encouragement, help, and valuable discussion, and Y. Sugawara, Mizusawa Chem. Ind. Co. for providing samples of acid clay. Thanks are also due Messrs. Y. Kubo, S. Yamamiya, H. Mitsui, and K. Adachi for their technical help in the experiments of X-ray diffraction, infrared and far infrared spectroscopy, and electron micrography, respectively.

NOTES

BULLETIN OF THE CHEMICAL SOCIETY OF JAPAN, VOL. 45, 1548—1549(1972)

Photocyclization of *o*-Terphenyl-Type Compounds and Reactivity Indices[1]

Takeo SATO and Toshifumi MORITA*

Department of Chemistry, Faculty of Science, Tokyo Metropolitan University, Setagaya, Tokyo
**Department of Chemistry, Faculty of Engineering, Gunma University, Kiryu, Gunma*

(Received March 12, 1971)

The photocyclodehydrogenation of stilbene and *o*-terphenyl type compounds has been throughly explored and is utilized as a synthetic means for a number of polycondensed aromatic and heteroaromatic compounds.[1,2]

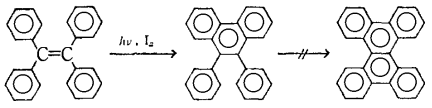

I II

For certain type of compounds, however, the photocyclization reaction did not take place: Mallory and co-workers[3] reported the failure to obtain dibenzo[*g,p*]chrysene (II) by the attempted photolysis reaction of 9,10-diphenylphenanthrene (I), although the formation of the latter was easily achieved by the irradiation of tetraphenylethylene in the presence of iodine. They attributed the inertness of I toward further cyclization reaction to a low electron density on the carbon atoms undergoing coupling. The failure of cyclization with 1,2,3-triphenylazulene,[4] 1,2,3,4- and 1,2,4,5-tetraphenylbenzenes[5] and 1,2,3-triphenylnaphthalene[5] was explained by steric reasons. 1,1′-Binaphthyl was also found to resist toward cyclization.[6] We have reported the failure of the attempted photocyclization of diphenylquaterphenyl (XVII),[1] although 2,2′-diphenylbiphenyl (XII) was smoothly converted to dibenzo[*fg, op*]naphthacene.[1,7]

For compounds where different way of cyclization is possible, some give more than one product but others result in a selective cyclization. The cyclization of 1,2-dipyridylethylene[8] or styrylpyridines[9] was shown to be possible in a dual way or more, whereas 1,2-di-β-naphthylethylene[10] gave only benzo[*g,h,i*]perylene, indicating that two other possible cyclization modes are unimportant.

When several routes are conceivable for the construction of a certain ring system the selection of the method is left to one's choice or is determined by the availability of the starting materials. For example, benzo[*g*]chrysene (III) will be produced from either IV,[11] V,[12] or VI (not tested).

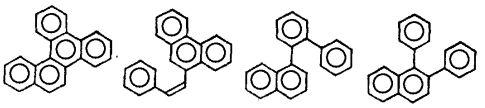

III IV V VI

In order to give a measure for the occurrence or otherwise of the cyclization reaction, to predict the product where several routes are conceivable, and to select the most efficient way to a given ring system, one can rely on the calculation of the reaction indices.

We have carried out the calculation of free valence numbers and localization energies for a series of *o*-terphenyl type compounds by the simple HMO method, expecting these figures be served as a criterion for the occurrence of the photocyclization reaction. Model compounds we studied are shown by a general formula A, where phenyl group(s) is introduced at W—Z positions. The *o*-terphenyl–triphenylene reaction is selected, since it is regarded as the basic reaction for the synthesis of polycondensed aromatics.[1,7,13,14]

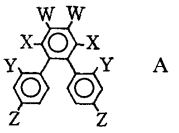

A

From these models we may learn both the electronic and steric effects of the phenyl substitution on the cyclization of *o*-terphenyl compounds. Phenyl group(s) at X or Y position is capable of entering into further cyclization reactions.

The sum of free valence numbers in the first excited state, $\sum Fr^*$, was calculated for the atoms undergoing photo-coupling, location of which being shown by a dotted line. These figures together with localization energies, L^*, are summarized in Table 1. Compounds

1) Photo-Aryl Coupling and Related Reactions. VIII. Part VII: T. Sato, S. Shimada, and K. Hata, This Bulletin, **44**, 2484 (1971).

2) For reviews see: F. R. Stermitz in O. L. Chapman ed, "Organic Photochemistry," Vol. 1, Marcel Dekker, Inc., New York (1967), p. 249; E. V. Blackburn and C. J. Timmons, *Quart. Rev.*, **23**, 482 (1969); T. Sato, *Yuki Gosei Kagaku Kyokai Shi*, **27**, 715 (1969).

3) F. B. Mallory, C. S. Wood, and J. T. Gordon, *J. Amer. Chem. Soc.*, **86**, 3094 (1964).

4) N. Kharasch, T. G. Alston, H. B. Reiris, and W. Wolf, *Chem. Commun.*, **1965**, 242.

5) W. H. Laarhoven, Th. J. H. M. Cuppen, and R. J. F. Niverd, *Rec. Trav. Chim., Pays-Bas*, **87**, 687 (1968).

6) M. Scholtz, F. Dietz, and M. Mühlstädt, *Z. Chem.*, **7**, 329 (1967).

7) T. Sato, S. Shimada, and K. Hata, *Chem. Commun.*, **1970**, 766.

8) H. -H. Herkampus and G. Kassebeer, *Ann., Chem.* **696**, 1 (1966).

9) P. Bortolus, G. Cauzzo, and G. Galiazzo, *Tetrahedron Lett.*, **1966**, 239, 3717.

10) M. Scholtz, M. Muhlstadt, and F. Dietz, *ibid.*, **1967**, 665.

11) W. Carruthers, *J. Chem. Soc. C*, **1967**, 1525.

12) W. A. Henderson, Jr. and A. Zweig, *J. Amer. Chem. Soc.*, **89**, 6778 (1967).

13) T. Sato, Y. Goto, and K. Hata, This Bulletin, **40**, 1994 (1967).

TABLE 1. FREE VALENCE NUMBERS IN THE FIRST EXCITED STATE, $\sum Fr^*$, AND LOCALIZATION ENERGIES, L^*, FOR A[a)]

	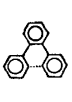 VII[1,13)]	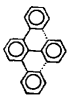 VIII[1,7)]	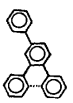 IX[1)]	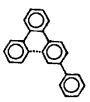 X[14)]	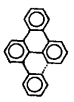 XI[1,7)]	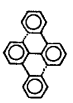 XII[1,7)]	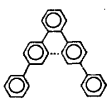 XIII[14)]	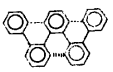 XIV	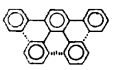 XV[5)]	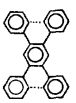 XVI[5)]	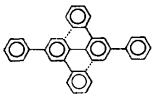 XVII[1)]
$\sum Fr^*$	1.027	1.003	0.981	0.967	0.962	0.949	0.949	--- 0.918 IIIII 0.926	IIIII 0.909 --- 0.955	0.955	0.925
L^*	3.320	3.349	3.427	3.458	3.369	3.423	3.537	--- 3.484 IIIII 3.485	IIIII 3.426 --- 3.421	3.601	3.589

a) Free valence numbers shown in the Table are the sum of the values obtained for the atoms undergoing coupling, the location of which being shown by --- or IIIII

I through XIII, listed in the order of decreasing $\sum Fr^*$, were successfully converted to the corresponding polycondensed aromatic compounds by the photolysis reactions using iodine as an oxidant.[1,7,13,14)]

Compounds XV and XVI were reported to be inert under the conditions studied.[5)] The reaction of XIV is not examined yet.

Critical values deduced from Table 1 are $\sum Fr^* > 0.95$ and $L^* < 3.54$, for which the cyclization is possible. Recently Laarhoven and co-workers[5)] proposed that the reaction is possible if $\sum Fr^* > 1$ and $L^* < 3.45$. They considered the photocyclization of tetraphenylethylene, $\sum Fr^* = 0.965$, to be exceptional, although from our results the conversion to I could be predictable. The Table by Laarhoven[5)] listing non-photocyclizing cases appear to contain those compounds of which inertness is explainable not by the free valence consideration but from two other reasons; 1) non-existence of the intermediate dihydro structures, and 2) steric inhibition by neighboring bulky groups.

The failure due to the first case include the lack of cyclization in α,α'-dinaphthyl,[6)] and a related compound.[5)] Assumably a steric factor becomes important when more than four benzene rings occupy vicinal position as in XV[5)] since 1,2,3-triphenylbenzene VIII is photocyclizable.[1,7)] A fused ring with a phenyl substitution is considered to cause a similar steric inhibition. This explains the inertness of II, 1,2,3-triphenylnaphthalene,[5)] 1,2,3-triphenylazulene *etc.*[4)]

In the cases of VIII and XII, a double cyclization reaction occurred and yet we could not trap intermediate XI. This is understood since XI is also a photocyclizable molecule.

The failure of XVI to undergo photocyclization, however, can not be explained and should be treated as exceptional.

More refined treatments considering the non-planarity of the molecule will make the situation clearer.

As far as the simple molecular orbital calculations concern, further accurate discussions could not be done. Some investigaters[15–17)] have made calculations to see if a relation exists for excited states between static and dynamic reactivity indices. However, they have not found out any correlation at all and the situation is the same in the present work as is seen in Fig. 1.

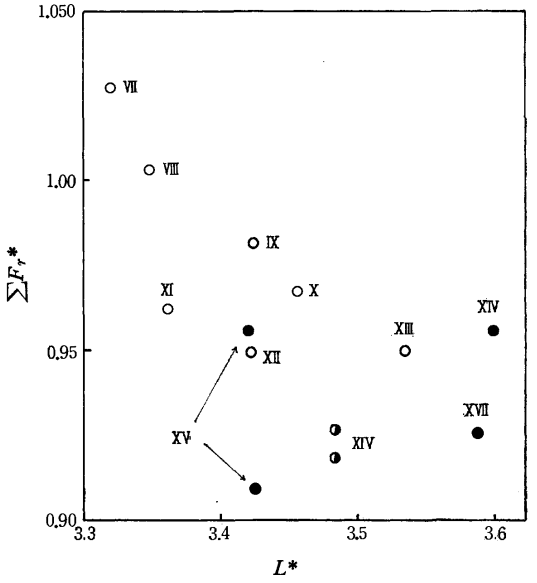

Fig. 1. The relation between $\sum Fr^*$ and L^* for those compounds that underwent photocyclization (○) and that did not (●). Compound XIV (◑) has not been examined.

The failure in obtaining a relationship between static and dynamic reactivity indices would be presumably due to the following factors: 1) Firstly, excited state molecular orbitals used in estimating reactivity indices are those obtained from minimization of ground state energy and not of excited state energy. 2) Secondly, localization energies are usually expressed in terms of π-electron energies. In discussing reactivity of molecules, localization energies should be expressed in terms of bond energies as pointed out by Dewar *et al.*[18,19)] Some improvements might be expected, if we do this.

14) T. Sato, S. Shimada, and K. Hata, *ibid.*, **42**, 766 (1969).

15) M. Trsic, G. Bessis, O. Chalvet, and R. Daudel, *C. R. Acad. Sci. Ser. C*, **263**, 386 (1966).

16) G. Bassis, O. Chalvet, and C. Polydoropoules, *ibid.*, **264**, 1368 (1967).

17) R. Daudel, *Advan. Quantum Chem.*, **5**, 1 (1970).

18) M. J. S. Dewar and C. C. Thompson, Jr., *J. Amer. Chem. Soc.*, **87**, 4414 (1965).

91) M. J. S. Dewar and T. Morita, *ibid.*, **91**, 796 (1969).

BULLETIN OF THE CHEMICAL SOCIETY OF JAPAN, VOL. 45, 1550—1551(1972)

A Theoretical Account of the Catalytic Behavior of Sulfonium Compounds in Oxidation Reactions

Katsutoshi OHKUBO and Hirokazu KANAEDA

Department of Synthetic Chemistry, Faculty of Engineering, Kumamoto University, Kurokami-machi, Kumamoto

(Received July 30, 1971)

In previous papers,[1,2] it has been emphasized that sulfonium compounds are the most effective catalysts in hydrocarbon oxidations among various onium compounds containing central atoms of C, N, O, P, S, As, Se, and Te, and that their catalytic activities are appreciably affected by the difference in counter anions and substituents attached to the central sulfur. This distinguished activity of the sulfonium compounds was well explained by their catalytic activations of molecular oxygen on the basis of the interaction between the partially-occupied sulfur *d*-orbitals and O_2: a strong $d\sigma$-$p\sigma$ type interaction between the sulfur d_{xz} (or d_{yz}) orbital and the $(1\pi_g)_z$-orbital of O_2, and a weak interaction between the sulfur d_{xy}-orbital and the $(1\pi_g)_y$-orbital of O_2.[3] The present study will try to clarify the catalytic behavior of the sulfonium compounds in oxidation reactions using an extended Hückel method[4] augmented by sulfur *d*-orbitals.

First, we will discuss the role of the counter anion and the substituents of the sulfonium compound in the catalytic activity. As Table 1 indicates, there is a parallelism between the catalytic activity (as estimated

TABLE 1. CORRELATION BETWEEN THE CATALYTIC ACTIVITY OF SULFONIUM COMPOUNDS AND THE AO POPULATIONS OF THE SULFUR *d*-ORBITALS UTILIZED FOR THE INTERACTION WITH $1\pi_g$-ORBITALS OF MOLECULAR OXYGEN

R_3SX[a]	S–X (Å)	M_{S-X}[b]	AO populations of S *d*-orbitals			$R_{max}\times 10^4$ [c] (mol/*l* sec)
			d_{xz}	d_{yz}	d_{xy}	
$(CH_3)_3SNO_3$	3.50	0.021	0.145	0.429	0.432	3.01
$(CH_3)_3SCl$	3.50	0.090	0.142	0.142	0.100	2.68
$CH_3)_3SBr$	3.80	0.071	0.142	0.142	0.100	2.60
$(CH_3)_3SI$	4.00	0.055	0.141	0.141	0.100	0.98
$(CH_3)_3SBF_4$	2.80	0.063	0.119	0.122	0.100	1.12
$(C_2H_5)_3SCl$	3.50	0.076	0.016	0.017	0.066	3.50
$(CH_3)_2C_6H_5SCl$	3.50	0.087	0.147	0.166	−0.011	2.52

a) ASMO SCF calculations on $(CH_3)_3SX$ demonstrated that the planar C_{3v} symmetrical sulfonium cation gave the most energetically stable $(CH_3)_3SX$[2].
b) Bond population of the S-X.
d) Maximum rates were estimated from O_2 absorbed (mol) which corresponds to the hydroperoxide formed (mol) in the cumene oxidation at 85°C (the amount of the sulfonium catalyst=3.0 mmol/*l*).

TABLE 2. CONTRIBUTIONS OF THE SULFUR *d*-ORBITALS TO THE ELECTRONIC PROPERTIES OF $(CH_3)_3S^+$ AND $(CH_3)_3SCl$

Compound	Atom population			Bond population		AO bond population					
						S–C[a]			S–Cl		
	S	C	Cl	S–C[a]	S–Cl	d_{xz}–p_z	d_{xy}–p_y	$d_{x^2-y^2}$–p_x	d_{xz}–p_x	d_{yz}–p_y	d_{z^2}–p_z
$(CH_3)_3S^+$ excluding S *d*-orbitals	6.379	3.748	—	0.576	—	—	—	—	—	—	—
$(CH_3)_3S^+$ including S *d*-orbitals	5.715	4.137	—	0.814	—	0.084	0.083	—	—	—	—
$(CH_3)_3SCl$ excluding S *d*-orbitals	5.260	4.255	7.995	0.699	−0.005	—	—	—	—	—	—
$(CH_3)_3SCl$ including S *d*-orbitals	5.773	4.145	7.919	0.815	0.092	0.092	0.083	0.004	0.007	0.007	0.054

a) S–C bond corresponds to 1S-2C bond of $(CH_3)_3SCl$ illustrated in the following figure:

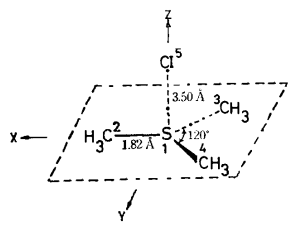

1) K. Fukui, K. Ohkubo, and T. Yamabe, This Bulletin, **42**, 312 (1969).
2) K. Ohkubo, *Tetrahedron Lett.*, **1971**, 2571, 2897.
3) K. Ohkubo and T. Yamabe, This Bulletin, **44**, 1183 (1971).
4) R. Hoffmann, *J. Chem. Phys.*, **39**, 1397 (1963); *ibid.*, **40**, 2474, 2480, 2745 (1964); the Coulomb integrals of the sulfur *d*-orbital and the oxygen 2*p*-orbital were taken to be −7.00 eV and −13.61 eV respectively.

by the maximum reaction rate, R_{max}) and the AO populations of the d_{xz}, d_{yz}, or d_{xy} sulfur orbital, with some irregularities caused by the gap between the configurations of the sulfonium compounds in the present calculations and those in the reaction system, or by some steric hindrances to the interaction between sulfonium compounds and O_2. This partial occupation of the sulfur *d*-orbitals is a result of the d–π interactions with the counter anion and the substituents, as can be seen from the electronic property of $(CH_3)_3SCl$ in Table 2, in which the electronic property of $(CH_3)_3S^+$ has been recorded in order to suggest the contribution of the counter chlorine. The counter anion and the substituents thus contribute to the partial occupation of the sulfur *d*-orbitals of the sulfonium compounds.

Second, let us discuss the interaction between the sulfonium compounds and molecular oxygen. The most likely mode of the interaction of molecular oxygen is parallel to the ligand plane of the sulfonium and occurs in the range of the distance between the sulfonium catalyst and O_2, 2.5—3.0 Å.[2] The d_{xz} (or d_{yz}) sulfur orbital of the sulfonium catalyst contributes predominantly to the catalytic activation of O_2 by means of interaction with the $(1\pi_g)_z$-orbital of O_2, as is shown in Fig. 1.[5]

Third, it is of interest to investigate the process of the hydrogen abstraction of the $(CH_3)_3SCl$–O_2 system

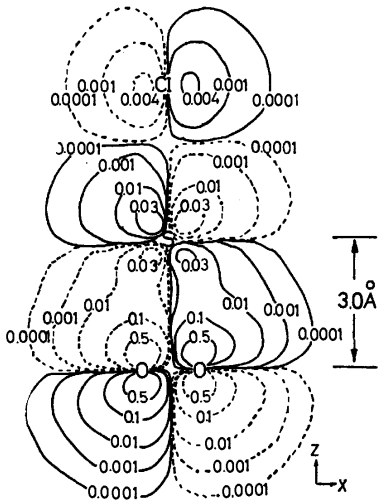

Fig. 1. The contour diagram for HO MO of the interacting system. This MO mainly comes from the interaction between $(1\pi_g)_z$ of O_2 and d_{xz} of $(CH_3)_3SCl$. (Solid and dotted curves indicate positive and negative MO-signs respectively.)

5) The contour diagram portrayed in Fig. 1 indicates the highest occupied molecular orbital (HO MO) of $(CH_3)_3SCl$–O_2. The $(1\pi_g)_z$-orbital of O_2 occupied most strongly the HO MO, in which, except for the d_{xz} orbital, the *p* and *d* orbitals of the central sulfur have negligible eigenvetors.

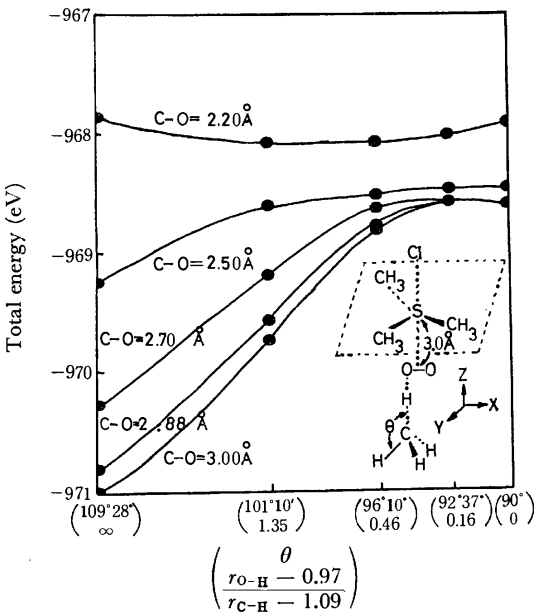

Fig. 2. Total energy changes in the process of hydrogen abstraction due to the stretching of the C–H and the variation of the bond angle of H–C–H (θ).

from hydrocarbons (CH_4 was used for the sake of simplicity of computation). The process was simulated by the stretching of the C–H in CH_4 (from C–H= 1.09 Å to H–O=0.97 Å), together with the change in the sp^3-hybrid structure of CH_4 to the sp^2-hybrid one, with the residual moiety retaining its equilibrium geometries (see Fig. 2). As Fig. 2 indicates, the transition state of the process seems to be situated near θ=92°37′, and the most plausible C–O distance falls in the range of 2.70—2.50 Å. The apparent activation energies calculated were 0.759 eV (2.50 Å), 1.652 eV (2.70 Å), 2.17 eV (2.88 Å), and 2.43 eV (3.00 Å), where the values in parentheses stand for the C–O distances. Some remarks should be here made: the activation energy in the other mode of interaction between the $(1\pi_g)_y$-orbital of O_2 and CH_4 was found to be higher than that in the interaction illustrated in Fig. 2 (for instance, 2.42 eV at C–O= 2.88 Å). In the hydrogen abstraction of O_2, O_2^-, and O_2^{2-} from CH_4 without sulfonium catalysts, the least activation energies were evaluated to be 2.04 eV (C–O=3.2 Å), 3.01 eV (C–O=3.5 Å), and 3.26 eV (C–O=3.8 Å) respectively; In other distances of C–O, the activation energies were higher. Sulfonium catalysts thus activate molecular oxygen and lower the activation energy required for the hydrogen abstraction from hydrocarbons.

The calculations were carried out on the FACOM 230.60 Computer at the Computation Center of Kyushu University.

BULLETIN OF THE CHEMICAL SOCIETY OF JAPAN, VOL. 45, 1552—1553(1972)

Conformations of the Ester. VII. The Conformations of Chloroformates[1)]

Michinori Ōki and Hiroshi Nakanishi

Department of Chemistry, Faculty of Science, The University of Tokyo, Hongo, Bunkyo-ku, Tokyo

(Received September 3, 1971)

In earlier papers from this laboratory, it has been shown that acetates[2)] and other carboxylate esters exist as *s-trans* conformers only, whereas two conformational isomers (*s-trans* and *s-cis*) exist in some formates,[3)] carbamates,[4)] carbonates,[5)] and monothiocarbonates.[1)]

In formates, the *s-trans* conformer is more stable than the *s-cis*, while in the others, which have an electronegative atom connected with the carbonyl group, the *s-cis* conformer is more stable than the *s-trans*.

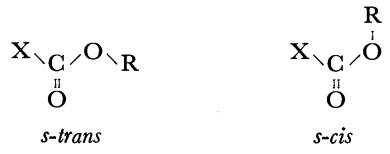

s-trans *s-cis*

X = CH_3, H, NR_2, OR, SR, Cl

Since the electronegativity of chlorine is greater than that of nitrogen and oxygen, it seemed that it would be of interest to study the case of chloroformates. Since the chlorine atom is larger than nitrogen and oxygen, the steric repulsion between X (N or O) and R in the *s-cis* conformation is expected to be smaller in carbamates and carbonates than that between Cl and R in chloroformates. Thus, the steric and electronic effects may counterbalance each other in chloroformates in determining the conformational preference to some extent.

As to the conformation of haloformates, several papers have been published. The haloformates had most commonly been reported to exist as *s-cis* conformers, judging from the data of dipole moments[6-8)] and NMR spectra.[8)] However, an exception has been reported by O'Gorman *et al.*,[9)] who postulated that the conformation is *s-trans*; they based their postulate on the electron scattering spectral data.

From our experience so far, it seems that the infrared spectral study may throw light on this problem. Thus, the infrared spectra of some chloroformates have been carefully observed, and NMR spectra have been measured at low temperatures.

Experimental

Methyl and ethyl chloroformates were of commercial origin. Isopropyl chloroformate was prepared from phosgene and isopropyl alcohol and phenyl chloroformate from phosgene and sodium phenoxide. The esters were purified by distillation before the measurements. The purity was checked by means of the NMR spectra and the infrared spectra. The spectra were measured with previously-described spectrometers.[5)]

Results and Discussion

Infrared Spectra. There have been several reports on the carbonyl stretching absorption of chloroformates, but no one has yet discussed the shape of the carbonyl absorption. The results obtained with carbon tetrachloride and acetonitrile solutions are shown in Table 1. Apparently, methyl, ethyl, and isopropyl chloroformates show two carbonyl absorptions. Since the solvent effect is not very large, the bifurcation of the carbonyl absorption may not originate from Fermi resonance,[10)] but from the existence of the *s-cis* and *s-trans* conformers.

Table 1. Carbonyl absorption of chloroformates $ClCO_2R$

Compound		Solvent: CCl_4 c=0.0004 mol/*l*		Solvent: CH_3CN c=0.02 mol/*l*	
I	Me	1770cm^{-1}	(266)	1767cm^{-1}	(277)
		1786	(613)	1786	(1363)
II	Et	1765	(36)	1768	(35)
		1778	(1161)	1779	(1021)
III	*i*-Pr	1761	(64)	1763	(64)
		1777	(1140)	1777	(1461)
IV	Ph	1790	(1477)	1788	(1106)

The dipole moments of the two conformers are calculated to be 1.6 D for the *s-trans* and 2.0 D for the *s-cis*. Since the *s-cis* conformer is more polar than the *s-trans*, the population of the former will become greater in the polar solvent than in the nonpolar. Table 1 shows that the intensity of the band at the higher frequency becomes larger in acetonitrile than in carbon tetrachloride, indicating that the band at the higher frequency may be assigned to the *s-cis* conformer. This assignment is also in accordance with the consideration of the arrangement of the bond dipoles (see the figure below): apparently, the stretching of the carbonyl bond in the *s-cis* conformation needs more energy. All of these results are consistent with the idea that the *s-cis* conformer is more stable than the *s-trans* in chloroformates.

1) Part VI: M. Ōki and H. Nakanishi, This Bulletin, in press.
2) M. Ōki and H. Nakanishi, *ibid.*, **44**, 3144 (1971).
3) M. Ōki and H. Nakanishi, *ibid.*, **43**, 2558 (1970).
4) M. Ōki and H. Nakanishi, *ibid.*, **44**, 3148 (1971).
5) M. Ōki and H. Nakanishi, *ibid.*, **44**, 3419 (1971).
6) S. Mizushima and M. Kubo, *ibid.*, **13**, 174 (1938).
7) E. Bock and D. Iwacha, *Can. J. Chem.*, **45**, 3177 (1967).
8) E. Bock, D. Iwacha, H. Hutton, and A. Queen, *ibid.*, **46**, 1645 (1968).
9) J. M. O'Gorman, W. Shand, Jr., and V. Shomaker, *J. Amer. Chem. Soc.*, **72**, 4222 (1950).
10) The solvent effect on the intensities of the carbonyl absorptions is very large if the bifuraction has its origin at the Fermi resonance. The detailed discussions were given in a previous paper.[2)]

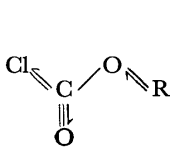

s-trans

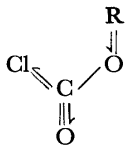

s-cis

Methyl chloroformate has two absorptions in the carbonyl overtone region, at 3538 cm^{-1} (ε=6.3) and 3506 cm^{-1} (ε=0.32), in crabon tetrachloride (c=0.01 mol/l). This result lends further support to the idea that there are two conformational isomers in chloroformates. If the origin of the bifurcation of the carbonyl band were Fermi resonance, there would have been only one absorption in the overtone region.

Nuclear Magnetic Resonance Spectra. The NMR spectra of methyl chloroformate were measured at various temperatures in CS_2–CH_2Cl_2. A sharp singlet of methyl protons at 3.95 ppm from TMS is observed at room temperature, whereas the peak height decreases as the temperature is lowered. The peak height at −100°C is about a half of that at 23°C, whereas the peak height of standard TMS remains almost unchanged. This broadening of the methyl peak can best be interpreted by assuming the existence of conformational isomers.

The results of the infrared and NMR spectra and the discussions given above clearly show that alkyl formates have two conformers and that the *s-cis* conformer is more stable than the *s-trans*. Since the chlorine atom (1.80 Å)[11] is larger than hydrogen (1.2 Å) and a little smaller than the methyl group (2.0 Å), the *s-trans* conformation should be favored over the *s-cis* in view of the steric requirement. Therefore, the fact that the *s-cis* conformer is more stable in reality suggests that the electronic effect is the most important factor in determining the conformational preference.

11) The numbers in parentheses refer to the van der Waals radii.

BULLETIN OF THE CHEMICAL SOCIETY OF JAPAN, VOL. 45, 1553—1554(1972)

The Reaction of α,β-Unsaturated Aldehydes with 1,3-Dienes in the Presence of Alkylaluminums

Shingo MIYAJIMA and Takashi INUKAI

The Central Research Laboratories, Chisso Corporation, Kamariya, Kanazawa-ku, Yokohama

(Received September 18, 1971)

The reaction mixture in suspension form, prepared from 3 $AlEt_3$–$TiCl_4$ in heptane, is known to catalyze the Diels-Alder reactions of α,β-unsaturated aldehydes with 1,3-dienes followed by the Tishchenko condensation of the resulting 3-cyclohexenecarboxaldehyde (I) to give the bicyclic ester (II).[1]

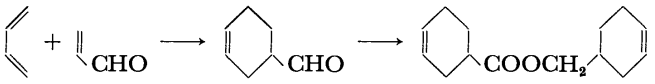

(I) (II)

On the other hand the solid catalyst, prepared from 2 $AlEt_2Cl$–$TiCl_4$ and washed with octane, was reported to be useful for preparation of I.[2] Although the question as to the chemical species of the catalytic activity is left open, these catalyzed Diels-Alder reactions are regarded as those related to general Lewis acid catalyzed reactions of dienophiles carrying carbonyl functions.[3] We now tried $AlEt_3$, $AlEt_2Cl$, and $AlEtCl_2$ as the catalysts for the reactions of acrolein, methacrolein, and crotonaldehyde with dienes in search of a more satisfactory catalyst than those so far known.[1,2,3c]

Results

The reactions between acroleins and dienes proceed with moderate rates at normal temperature and pressure in benzene solution in the presence of suitable aluminum compounds. The reaction conditions and results are summarized in Table 1.

It appears that $AlEt_3$ is too weak as a Lewis acid to catalyze the reaction and that the catalytic activity

Table 1. Reactions of α, β-unsaturated aldehydes with 1,3-dienes[a]

Diene	Dienophile	Catalyst	Yield[b], %
Butadiene	Acrolein	$AlEt_3$	none
		$AlEt_2Cl$	(19.4)[c]
		$AlEtCl_2$	41.4
—	Methacrolein	$AlEtCl_2$	42.9
		$AlCl_3$	19.8
—	Crotonaldehyde	$AlEt_2Cl$	3.5
		$AlEtCl_2$	48.0
		$AlCl_3$	47.0
Isoprene	Crotonaldehyde	$AlEtCl_2$	26.9

a) Reaction in benzene solution at room temperature for *ca.* 20 hr.
b) Yield of the isolated Diels-Alder adduct based on the dienophile charged.
c) Yield of the isolated Tishchenko ester II based on the dienophile charged.

1) E. F. Lutz, *J. Org. Chem.*, **28**, 912 (1963).
2) R. Robinson and G. I. Fray, Brit. 835840 (1960).
3) a) P. Yates and P. Eaton, *J. Amer. Chem. Soc.*, **82**, 4436 (1960); b) G. I. Fray and R. Robinson, *ibid.*, **83**, 249 (1961); c) E. F. Lutz and G. M. Bailey, *ibid.*, **86**, 3899 (1964); d) T. Inukai and M. Kasai, *J. Org. Chem.*, **30**, 3567 (1965).

increases as the acidity of catalysts increases by substitution with chlorine atoms. For acid sensitive acrolein and methacrolein, however, aluminum chloride seems to be too drastic, and brings about much tar formation, as in the cases with $SnCl_4 \cdot 5H_2O$.[3c,4] So far as we have experienced $AlEtCl_2$ is the generally recommendable catalyst for aldehyde dienophiles.[5]

$AlEt_2Cl$ is unique in that it leads to the Tishchenko condensation product II leaving not more than trace of I. An aluminum alkoxide compound, that is active in catalyzing Tishchenko condensation, is naturally assumed to form *in situ*.[6]

The reaction product formed from crotonaldehyde and butadiene by the present method is pure *trans*-6-methyl-3-cyclohexenecarboxaldehyde at the initial stage of the reaction, conforming to the well-known stereochemistry of the Diels-Alder reactions, but it undergoes acid-catalyzed transformation to a *ca.* 2.7: 1 mixture of the *trans* and *cis* isomers before synthetically acceptable yield is attained.

Experimental

General Procedure. Under exclusion of oxygen and moisture, an aldehyde (0.5 mol) solution in benzene (100 m*l*) was added dropwise into a solution or suspension (in the case of $AlCl_3$) of catalyst (0.05 mol) in benzene (500 m*l*) with stirring in 5 hr, and concurrently a slight excess of a diene was slowly bubbled into the reaction mixture which was kept at 20±1°C by external cooling. After standing overnight at room temperature the mixture was treated with water (250 m*l*), the benzene layer dried with anhydrous magnesium sulfate, and the reaction product isolated by fractional distillation under reduced pressure.

Reaction Products. 3-Cyclohexenecarboxaldehyde, 1-methyl-3-cyclohexenecarboxaldehyde, and 4,6-dimethyl-3-cyclohexenecarboxaldehyde were identified by agreement of physical properties of themselves and their crystalline derivatives with those of the authentic samples: semicarbazone of 1-methyl-3-cyclohexenecarboxaldehyde, mp 174°C, (Found: C, 59.7; H, 8.3; N, 23.1%. Calcd for $C_9H_{15}N_3O$: C, 59.64; H, 8.34; N, 23.18%.). 3-Methyl-3-cyclohexenecarboxaldehyde (III) obtained by the catalytic reaction showed the same bp (59.5—61°C/12 mmHg) and IR spectrum as the authentic sample,[7] but the glpc analysis with a tricresyl phosphate column showed two peaks in an area ratio of *ca.* 2.7: 1. The major peak coincided with that of pure *trans*-III[7] in the retention time, and the minor peak with that of *cis*-III formed by thermal isomerization[8] of *trans*-III. The identification was further supported by the fact that both the reaction product and *trans*-III gave the identical *trans* to *cis* peak ratio of 1.4: 1 after thermal isomerization at 240°C. 3-Cyclohexenylmethyl 3-cyclohexenecarboxylate (II), bp 109—112°C/0.56 mmHg (lit,[1] 108—109°C/0.6 mmHg), was identified by hydrolyzing it into 3-cyclohexenylcarbinol and 3-cyclohexenecarboxylic acid: *p*-nitrobenzoate of the carbinol, mp 60—61°C (lit,[9] 60—62°C); *p*-bromophenacyl ester of the acid, mp 81.5—82.5°C (lit,[1] 81.5—82°C).

4) Unpublished work.

5) $AlEtCl_2$ was recently reported to catalyze the Diels-Alder reaction of acrylonitrile too [J. Furukawa, E. Kobayashi, K. Haga, and Y. Iseda, *Polymer Journal*, **2**, 475 (1971)].

6) We are not in a position to study the reaction of alkylaluminums with acrolein, but it may be worth noting that $AlEt_2Cl$ reacts with acrolein to give off ethylene and from acid hydrolysis of the reaction mixture was isolated 0.3 mol of allyl alcohol per mol of $AlEt_2Cl$, indicating the formation of $CH_2{=}CH{-}CH_2OAl(Et)Cl$.

7) O. Diels and K. Alder, *Ann.*, **470**, 62 (1929).

8) G. P. Kugatova-Shemyakina and Yu. A. Ovchinnikov, *Tetrahedron*, **18**, 697 (1962).

9) E. G. E. Hawkins, D. J. G. Long, and F. W. Major, *J. Chem. Soc.*, **1955**, 1465.

BULLETIN OF THE CHEMICAL SOCIETY OF JAPAN, VOL. 45, 1554—1556(1972)

An Attempted Synthesis of 3,6-Epidithio-2,5-piperazinedione by Cyclization of *N,N'*-dialkyl-2,2'-dithiodicinnamamide

Juji YOSHIMURA and Yuichi SUGIYAMA

Laboratory of Chemistry for Natural Products, Faculty of Science, Tokyo Institute of Technology, Meguro-ku, Tokyo

(Received September 21, 1971)

It has been known that several antibiotics such as gliotoxin[1] and sporidesmin[2] have a characteristic partial structure of 3,6-epidithio-2,5-piperazinedione skeleton (**1**), and the numbers of analogous antibiotics are yet increasing.[3,4] Recently, Trown,[5] and Poisel and Schmidt[6] have reported the synthesis of 1,4-dimethyl-3,6-epidithio-2,5-piperazinedione (**1a**; R=R''=H, R'=R'''=CH_3) by substitution of 3,6-dibromo-1,4-dimethyl-2,5-piperazinedione with sodium thioacetate followed by hydrolysis and oxidation, however, that of the corresponding alkyl derivatives (**1b**; R=methyl, hydroxymethyl) has not yet appeared in literatures.

On the other hand, it is known that an amide group can be added to unsaturated carbons such as olefins[7]

1) M. R. Bell, J. R. Johnson, B. S. Wildi, and R. B. Woodward, *J. Amer. Chem. Soc.*, **80**, 1001 (1958).
2) S. Safe and A. Taylor, *J. Chem. Soc. C*, **1970**, 432.
3) R. Nagarajan, L. L. Huckstep, D. H. Lively, D. C. Delong, M. M. Marsh, and N. Neuss, *J. Amer. Chem. Soc.*, **90**, 2980 (1968).
4) D. Hauser, H. P. Weber, and H. P. Sigg, *Helv. Chim. Acta*, **53**, 1061 (1970).
5) P. W. Trown, *Biochem. Biophys. Res. Commun.*, **33**, 402 (1968).
6) H. Poisel and U. Schmidt, *Angew. Chem.*, **83**, 114 (1971).
7) Erf. A. S. Matlack, *Chem. Abstr.*, **49**, 3244 (1955).

and carbonyls,[8] and in fact, *N*-aryl-pyruvamide was dimerized to 1,4-diaryl-3,6-dihydroxy-3,6-dimethyl-2,5-piperazinedione[9] by treatment with aqueous ammonia. Therefore, it was considered that dimerization of 2-thiopyruvamide (or corresponding enthiol (**2**)) may offer the desired intermediate for the synthesis of **1b**.

In this paper, the authors attempted to synthesize **1b** by dimeriaztion of *N*-alkyl-2-mercaptocinnamamide (**2**), or by intramolecular additive cyclization of *N,N'*-dialkyl-2,2'-dithiodicinnamamide (**3**).

Results and Discussion

As an analogous conversion of β-keto-acidamide to β-thio-analogue,[10] *N*-cyclohexyl-phenylglyoxylamide[11] was treated with hydrogen sulfide in ethanol saturated with dried hydrogen chloride at −90°C for 3 days, but only *N*-cyclohexyl-2,2-diethoxy-2-phenyl-acetamide (Found: C, 70.60; H, 9.29; N, 4.77%. Calcd for $C_{18}H_{27}NO_3$: C, 70.79; H, 8.91; N, 4.59%.) was obtained in 79% yield, and the same reaction at −10—+6°C for 10 hr gave white powder ($C_{28}H_{36}N_2O_2S_3$) in 68% yield, which could not be characterized. Moreover, attempted elimination of hydrogen sulfide from 2,2'-tetrathiodipropionanilide by thermal degradation or by treatment with heavy metals were unsuccessful.

On the other hand, 2,2'-dithiodicinnamyl chloride was synthesized by treatment of the free acid[12] in chloroform with phophorus pentachloride. Treatment of this unstable chloride with alkylamine gave no expected **3**, however, dropwise addition of the chloride in benzene to alkylamine hydrochloride in dimethylformamide under cooling gave **3** (R=methyl, ethyl, propyl, isopropyl, *n*-butyl) in 14—41% yield.

Attempted reduction of **3** to **2** with acetic acid and zinc was unsuccessful. Considering that **3** and **2** might be unstable both in alkaline and acid condition, reductive insertion reaction was tried by use of cuprous oxide or mercuric dichloride in the presence of potassium metabisulfate. In the former case **3** was recovered, but in the latter, the corresponding mercaptide (**4**) was afforded quantitatively, by adding triethylamine dropwise. Treatment of **4** with hydrogen sulfide gave no desired product, however, only *N*-isopropyl-2-mercaptocinnamamide (**2a**) was obtained in 45% yield. **2a** was successfully oxidized to **3d** by air, but conversion of **2a** to **1b** was not tried, because of its unstability.

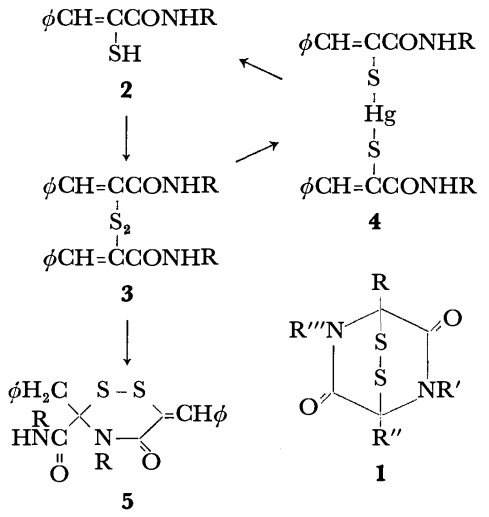

Scheme 1

Table 1. Physical constants and analytical data of new compounds

	R'	Mp (°C)	Yield (%)	Found (Calcd),% C	H	N	S
2a	Isopropyl	78	45	64.59 (65.14)	6.60 (6.83)	6.38 (6.33)	13.81 (14.47)
3a	Methy	138	14	63.52 (62.49)	5.89 (5.24)	7.38 (7.29)	16.10 (16.15)
3b	Ethyl	158	41	64.13 (64.06)	6.00 (5.87)	6.89 (6.79)	15.72 (15.52)
3c	Propyl	120	28	65.16 (65.44)	6.62 (6.41)	6.58 (6.36)	14.62 (14.53)
3d	Isopropyl	153	31	65.71 (65.44)	6.34 (6.41)	6.51 (6.36)	14.66 (14.53)
3e	*n*-Butyl	116	31	66.56 (66.65)	6.62 (6.88)	6.15 (5.98)	13.68 (13.67)
4a	Methyl	197	100	41.31 (41.05)	3.66 (3.45)	4.89 (4.79)	— —
4b	Ethyl	171	100	42.94 (43.11)	3.92 (3.95)	4.65 (4.56)	— —
4c	Propyl	163	100	45.00 (44.95)	4.45 (4.40)	4.36 (4.37)	— —
4d	Isopropyl	194	100	44.97 (44.95)	4.21 (4.40)	4.28 (4.37)	— —
4e	*n*-Butyl	154	100	46.89 (46.66)	4.84 (4.82)	4.22 (4.19)	— —
5a	Ethyl	234	10	64.00 (64.06)	6.07 (5.87)	6.60 (6.79)	15.33 (15.52)
5b	Isopropyl	240	1	65.72 (65.44)	6.37 (6.41)	6.38 (6.36)	14.26 (14.53)

In order to cyclize intramolecularly, **3b** and **3d** were treated with triethylamine to give 4-alkyl-3-alkylaminocarbonyl-3-benzyl-6-benzylidene-5-oxo-3,4',5,6-tetrahydro-1,2,4-dithiazine (**5a**; R=ethyl, **5b**; R=isopropyl) in 10 and 1% yield, respectively, accompanied with intractable sirup which seems to be intermolecular reaction products or degradated products. The structure of **5** was deduced from elemental analysis and the following facts. The existence of two triplet signals (τ 8.95, 9.35) of C-methyl protons of **5a** in NMR spectrum indicates that the two nitrogen atoms are in the different circumstances. Moreover, the presence of peaks *m/e* 379 (5a—SH) and 407 (5b—SH), and 308 (5a—$CONHC_2H_5$—S) and 322 (5b—$CONHC_3H_7$—S) in mass spectra of **5a** and **5b** (Fig. 1) indicated the presence of another intramolecular bond, in addition to a disulfide bond.

From these facts, it will be concluded that only one intramolecular cyclization was occured, because of a steric hindrance.

8) A. Kaneda and R. Sudo, This Bulletin, **43**, 2159 (1970).
9) A. Wohl and C. Oesterlin, *Ber.*, **34**, 1147 (1901).
10) J. Goerdeler and W. Mittler, *ibid.*, **96**, 944 (1963).
11) I. Ugi and U. Fetzer, *ibid.*, **94**, 1116 (1961).
12) P. L. Julian and B. M. Sturgis, *J. Amer. Chem. Soc.*, **57**, 1126 (1935).

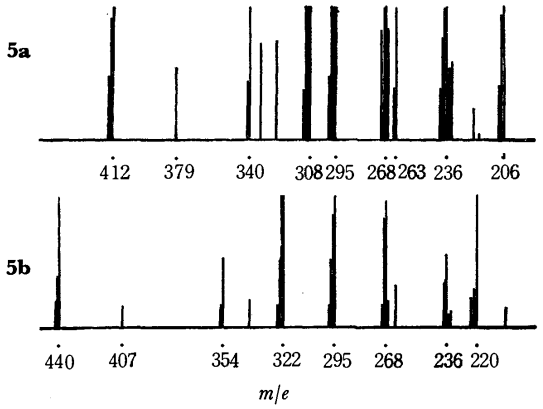

Fig. 1. Mass spectra of **5a** (R=ethyl, MW 412) and **5b** (R=Isopr., MW 440).

Experimental

All the melting points are uncorrected. The solutions were evaporated under reduced pressure at a bath temperature not exceeding 40°C. The infrared spectra were measured in KBr discs, and the NMR spectra were determined at 100 MHz with a JNM-100H spectrometer, using TMS as an internal reference. The mass spectra were obtained on a Hitachi RMU6E mass spectrometer, using a direct inlet and an ionization energy of 70 eV.

2,2′-Tetrathiodipropionanilide. Sulfur monochloride (0.34 g, 2.5 mmol) was added dropwise to 2-mercaptopropionanilide (0.9 g, 5 mmol)[13] in dried ether (100 m*l*) under cooling with ice-salt. This reaction mixture was allowed to stand for 1 day at room temperature, and white crystals deposited was filtered. Yield 0.9 g (73%); mp 134°C. Found: C, 50.92; H, 5.04; N, 6.68; S, 29.95%. Calcd for $C_{18}H_{20}N_2O_2S_4$: C, 50.94; H, 4.75; N, 6.60; S, 30.16%. IR (cm^{-1}): 3250 (N–H), 1650 (C=O).

General Synthesis of N,N′-*dialkyl-2,2′-dithiodicinnamamide (3).* A suspension of 2,2′-dithiodicinnamic acid (36 g, 0.1 mol) and excess amount of phosphorus pentachloride in chloroform mixed under cooling was stirred for 1 day at room temperature. After removal of phosphorus oxychloride, the resulted sirup was dissolved in water-free benzene, and then insoluble phosphorus pentachloride was filtered off. This filtrate was added dropwise into the dimethylformamide solution of alkylamine hydrochloride (0.2 mol) cooled with ice-salt. After standing for two hours at room temperature, this reaction mixture was neutralyzed with aqueous sodium bicarbonate and extracted with chloroform. The extract was washed with water, and concentrated to a viscous solution which gave white crystals. For example, *N*-ethyl derivative (**3b**) showed; IR (cm^{-1}): 3240 (N–H), 1620 (C=O). NMR (τ) in $CDCl_3$: 2.0 (s, 2H), 6.68 (m, 4H), 8.82 (t, 6H).

General Synthesis of Mercuric Biscinnamamide-2-thiolate (4). A suspended solution made by successive addition of water (100 m*l*) and potassium metabisulfate (2.0 g, 9 mmol) to a solution of **3** (4.5 mmol) and mercuric dichloride (2.0 g, 7.4 mmol) in methanol (500 m*l*), was stirred for 30 min. Further addition of a small amount of triethylamine gave white precipitates of **4**. After removal of methanol, precipitates were filtered and recrystallized from methanol to give white crystals.

N-*Isopropyl-2-mercaptocinnamamide (2a).* Hg thiolate (**4d**, 3.2 g, 4.9 mmol) and potassium sulfide (1 g, 9 mmol) were dissolved in water to give mercuric sulfide. After filtration, the filtrate was added into 5% solution of acetic acid in water (500 m*l*) to give **2a**, which was recrystallized from ethanol. IR (cm^{-1}): 3270 (N–H), 2550 (S–H).

4-Alkyl-3-alkylaminocarbonyl-3-benzyl-6-benzylidene-5-oxo-3,4,5,6-tetrahydro-1,2,4-dithiazine (5a and 5b). A solution of **3b** (1 g, 2.4 mmol) in chloroform was gradually added into the solution of triethylamine in chloroform for 30 min. After standing for 30 min at room temperature, the solution was concentrated, and the resulted powder was crystallized from chloroform–petroleum ether to give white crystals of **5a**. IR (cm^{-1}): 3300 (N–H), 1625 (C=O). NMR (τ) in DMSO (d_6): 8.95 (t, 3H), 9.35 (t, 3H). In the case of **5b**, it showed; IR (cm^{-1}): 3290 (N–H), 1620 (C=O).

The authors are indebted to Mr. K. Fukukawa for NMR measurements.

13) H. Beckurts and G. Frerichs, *J. Prakt. Chem.*, **66**, 190 (1902).

BULLETIN OF THE CHEMICAL SOCIETY OF JAPAN, VOL. 45, 1557—1559(1972)

An Approach for Calculation of n,π^* State Energies of Some Carbonyl Molecules Within the Framework of the Semi-Empirical SCF-MO-CI Method

Kozo INUZUKA and Ralph S. BECKER*

Department of Applied Science, Tokyo Electrical Engineering College, Kanda, Chiyoda-ku, Tokyo
**Department of Chemistry, University of Houston, Houston, Texas 77004, U.S.A.*

(Received September 25, 1971)

Electronic state energies (π,π^*) of many organic molecules have been calculated by the Pariser-Parr and Pople SCF–MO–CI methods.[1,2] Such approaches have proven successful for the electronic properties of π,π^* states, but their application to n,π^* state energy calculations is scarce. One reason is the difficulty of obtaining good values for the electronic repulsion integrals between n and π electrons. Lindner *et al.*[3] used the Ohno approximation[4] for such integrals to calculate n,π^* state properties of nitrogen-heterocyclics. However, the state energies were not in agreement with experiment. Sidman[5] carried out n,π^* state energy calculations for several carbonyl molecules within the framework of the P–P–P SCF–MO–CI method. The assumption was made that the n-orbital energy of the carbonyl molecules is constant, and the value, −10.50 eV, was assigned to it throughout the calculations. The electronic repulsion integral between n and π electrons was obtained by the Pariser-Parr approximation.[1] The assumption that the n-orbital energy of carbonyl group is constant appeared reasonable since it is known that there is not such a large variation in the n-orbital energy as in the π-orbital energy within similar carbonyl molecules. However, such an assumption may not give good calculated results when we use the SCF–MO's and the energies obtained using different approximations for the electronic repulsion integrals. In addition, it may not be valid for different values of the parameters such as resonance integral, ionization potential, electron affinity or effective nuclear charge of the atomic orbital.

On the other hand, Plotnikov[6] carried out SCF–MO calculation for n,π^* and π,π^* state energies of different kinds of organic molecules taking into account their n-orbital energies and using proper approximation for repulsion integrals between n and π electrons. His calculated results were in good agreement with experimental values. In view of the difficulties encountered in calculating n,π^* transition energies in agreement with experiment, we have examined different approximations for the two-center repulsion integrals in order to obtain better absolute agreement for the π,π^* and n,π^* state energies, particularly for the latter. In this paper, the n-orbital energies and n,π^* state energies were calculated using both Mataga-Nishimoto (M–N)[7] and Pariser-Parr (P–P)[1] approximations.

Methods of Calculation

All calculations were carried out by means of the usual semi-empirical SCF–MO–CI method:

$$\sum_{\nu} F_{\mu\nu} c_{i\nu} = \varepsilon_i c_{i\mu} \tag{1}$$

$$F_{\mu\mu} = -I_\mu + (1/2)P_{\mu\mu}\gamma_{\mu\mu} + \sum_{\nu\neq\mu}(P_{\nu\nu}-1)\gamma_{\mu\nu} \tag{2}$$

$$F_{\mu\nu} = \beta_{\mu\nu} - (1/2)P_{\mu\nu}\gamma_{\mu\nu} \tag{3}$$

$$\gamma_{\mu\mu} = I_\mu - A_\mu \tag{4}$$

where I_μ and A_μ are the ionization potential and electron affinity of atom μ, and $P_{\mu\mu}$ is the electron charge density on atom μ. $\beta_{\mu\nu}$ is the resonance integral for the nearest neighbor atoms μ and ν. Numerical values used for the skeletal structures of *trans*-acrolein,[8] *trans*-2,4-pentadienal, benzaldehyde, and *trans*-cinnamaldehyde were, respectively, 1.36 Å for the carbon double bond, 1.46 Å for the single bond, 1.22 Å for the carbonyl group, and 1.39 Å for the benzene ring. The value 120° was assigned to the C–C–C and C–C–O bond angles.

The n,π^* and π,π^* transition energies were calculated by the following equations.

$$^1E_{jk} = \varepsilon_k - \varepsilon_j - J_{jk} + 2K_{jk} \tag{5}$$

$$^3E_{jk} = \varepsilon_k - \varepsilon_j - J_{jk} \tag{6}$$

where ε_k is the energy of k-th molecular orbital, J_{jk} Coulomb integral over the MO's j and k, and K_{jk} an exchange integral. The n,π^* and π,π^* state energies were calculated including all singly excited configurations.

The SCF–MO's and π,π^* transition energies of these four molecules were calculated using the Pariser-Parr approximation[1] for the electronic repulsion integral between π electrons with Z_c=3.25 and Z_o=4.55. The resonance integral β_{co} of the carbonyl group was obtained by Kon's equation,[9] and the value −2.67 eV was used for the four molecules. The value of β_{cc} for the nearest neighbour carbon atoms was treated as a parameter and adjusted for each molecule to fit the calculated π,π^* state energy to the experimental value.

The n-orbital on the oxygen atom is assumed to be a pure $2p\pi$ atomic orbital. The n-orbital energy ε_n was obtained from the following equation.[3]

1) R. Pariser and R. G. Parr, *J. Chem. Phys.*, **21**, 466, 767 (1953).
2) J. A. Pople, *Trans. Faraday Soc.*, **49**, 1375 (1953).
3) P. Lindner, R. Manne, and O. Martensson, *Theor. Chim. Acta*, **5**, 406 (1966).
4) K. Ohno, *ibid.*, **2**, 219 (1964).
5) J. W. Sidman, *J. Chem. Phys.*, **27**, 429 (1957).
6) V. G. Plotnikov, *Opt. Spektrosk.*, **20**, 217 (1966).
7) N. Mataga and K. Nishimoto, *Z. Phys. Chem. N. F.*, **13**, 140 (1957).
8) H. Mackle and L. E. Sutton, *Trans. Faraday Soc.*, **47**, 691 (1951).
9) H. Koṇ, This Bulletin, **28**, 275 (1955).

TABLE 1. CALCULATED AND OBSERVED LOWEST SINGLET AND TRIPLET STATE ENERGIES AND CALCULATED *n*-ORBITAL ENERGIES OF CARBONYL MOLECULES (eV in unit)

Approx. for γ_{ij} integral	Config.	Sym.	Singlet		Triplet		ε_n
			Calcd	Obsd	Calcd	Obsd	
trans-Arcolein							
P–P	π-π^*	A'	5.960	5.96[a]	2.935	3.05[b]	
M–N	n-π^*	A''	3.917	3.71[a]	3.405	3.01[c]	−12.037
P–P	n-π^*	A''	3.292		2.771		−12.955
trans-2,4-Pentadienal							
P–P	π-π^*	A'	4.745	4.79[d]	2.048		
M–N	n-π^*	A''	3.801	3.81[d]	3.311		−11.897
P–P	n-π^*	A''	3.221		2.714		−12.783
Benzaldehyde							
P–P	π-π^*	A'	4.675	4.50[e]	3.082		
M–N	n-π^*	A''	3.900	3.66[f]	3.404	3.22[f]	−11.890
P–P	n-π^*	A''	3.286		2.780		−12.803
trans-Cinnamaldehyde							
P–P	π-π^*	A'	4.366	4.41[g]	2.314		
M–N	n-π^*	A''	3.822	3.49[h]	3.332		−11.874
P–P	n-π^*	A''	3.233		2.727		−12.757

a) See Ref. 13 and 17. b) See Ref. 13 and 16. c) See Ref. 12 and 13. d) See Ref. 18. e) See Ref. 19. f) See Ref. 15. g) See Ref. 20. h) The value was obtained in the *n*-hexane solution. It corresponds to λ_{max} value.

$$\varepsilon_n = U_n + \sum_{\mu \neq o}(P_{\mu\mu}-1)\gamma_{\mu n} + (P_{oo}-1)(\gamma_{no}-\delta_{no}/2) \quad (7)$$

where U_n is treated as a parameter for the *n*-electron, and the value −14.75 eV[10] was used. The two one-center integrals concerning the oxygen atom, γ_{no} and δ_{no} represent $\langle n_o\pi_o|r_{12}^{-1}|n_o\pi_o\rangle$ and $\langle n_o\pi_o|r_{12}^{-1}|\pi_o n_o\rangle$, respectively. The value 12.865 eV[5] was used for the former integral and the value 0.903 eV[11] for the latter one. The $\gamma_{\mu n}$ is a two-center atomic repulsion integral between the π-electron of the carbon atom μ and the *n*-electron of the oxygen atom. The $\gamma_{\mu n}$ was calculated by the usual Matage-Nishimoto and Pariser-Parr approximations.

Results and Discussion

The calculated results are shown in Table 1. The data show that the n,π^* state energies calculated by M–N approximation are higher than those by P–P approximation, and somewhat higher than the corresponding observed values. However, the calculated n,π^* state energies using the P–P approximation are lower than the corresponding observed values.

The lowest singlet state of the molecules is assigned as the n,π^* state as shown in Table 1. The relative order of the calculated lowest n,π^* and π,π^* singlet state by both approximations is in accordance with the observed order (*cf.* Table 1).

The observed lowest triplet states of acrolein[12–14] and benzaldehyde[15] are assigned to be n,π^* states. The calculated n,π^* triplet state energies by M–N approximation are higher than the calculated π,π^* triplet states, but the corresponding states by P–P approximation are lower than the calculated π,π^* triplet state energies. The relative order of n,π^* and π,π^* triplet states of acrolein and benzaldehyde using P–P approximation is in harmony with the observed order; however, the values of calculated n,π^* triplet states, 2.771 eV (acrolein) and 2.780 eV (benzaldehyde) differ slightly form the observed values 3.01 eV[12,13] and 3.22 eV[15] for acrolein and benzaldehyde, respectively. In the case of *trans*-2,4-pentadienal, the theoretical n,π^* triplet state energy by both approximations, M–N (3.311 eV) and P–P (2.714 eV) is higher than the corresponding π,π^* triplet state energy (2.048 eV). We can not compare the theoretical values with experimental values (no data) for 2,4-pentadienal. However, the theoretical result and the small energy difference between the n,π^* and π,π^* triplet states of acrolein[12,16] suggest that the lowest triplet state of polyenals with polyene chains longer than acrolein may be assigned to the π,π^* triplet state. It is interesting that our calculated n,π^* state energies of acrolein and 2,4-pentadienal using M–N approximation show a good correspondence with those of crotonaldehyde and sorbaldehyde by Plotnikov.[6] Parallel state energy ordering is obtained for *trans*-cinnamaldehyde (n,π^* states higher than π,π^* states). Judging from the present calculated results, the lower triplet state of cinnamaldehyde may be assigned to the π,π^* state.

10) H. A. Skinner and H. O. Pritchard, *Trans. Faraday Soc.*, **49**, 1254 (1953).
11) J. M. Parks and R. G. Parr, *J. Chem. Phys.*, **32**, 1657 (1960).
12) J. C. D. Brand and D. G. Williamson, *Discuss. Faraday Soc.*, **35**, 184 (1963).
13) R. S. Becker, K. Inuzuka, and J. King, *J. Chem. Phys.*, **52**, 5164 (1970).
14) W. H. Eberhardt and H. Renner, *J. Mol. Spectrosc.*, **6**, 483 (1961).
15) Y. Kanda, H. Kaseda, and T. Matumura, *Spectrochim. Acta*, **20**, 1387 (1964).
16) J. M. Hollas, *ibid.*, **19**, 1425 (1963).
17) K. Inuzuka, This Bulletin, **34**, 6 (1961).
18) E. L. Pippen and M. Nonaka, *J. Org. Chem.*, **23**, 1580 (1958).
19) J. Tanaka, *Nippon Kagaku Zasshi*, **79**, 1114 (1958).
20) K. Inuzuka, This Bulletin, **34**, 1557 (1961).

The calculated n-orbital energies of the molecules are shown in Table 1. The energies are almost the same for all molecules by means of either M–N or P–P approximation although the absolute values depend upon the choice of approximation. The result is in agreement with the assumption by Sidman[5] that the n-orbital energy in carbonyl group is approximately constant, although our absolute magnitude is greater.

If the value of U_n in Eq. (7) and/or the numerical values in the Mataga-Nishimoto and Pariser-Parr's electronic repulsion integrals between the n- and π-electrons are taken as parameters and adjusted properly, better calculated results for the n,π^* state energy and the n-orbital energy may be expected. The method is also applicable to n,π^* state energy calculations for N-heterocyclics.

This work was supported by the grants from Tokyo Electrical Engineering College (T. E. E. C.) Research Fund and the Robert A. Welch Foundation. One of the authors (K. I) wishes to acknowledge the assistance of the staff of T. E. E. C. Computing Center.

BULLETIN OF THE CHEMICAL SOCIETY OF JAPAN, VOL. 45, 1559—1560(1972)

Some Reactions of Hydrazino- and Aminophosphonium Bromides

Koh-ichi YAMADA and Naoki INAMOTO

Department of Chemistry, Faculty of Science, The University of Tokyo, Hongo, Tokyo

(Received October 1, 1971)

Hydrazonophosphorane has two reaction sites, P=N bond and amino group, and reacts with carbonyl compounds to give hydrazones[1] and phosphazines,[2] respectively.

A reaction at both sites being expected, excess amount of phenyl isocyanate was allowed to react with hydrazonotriphenylphosphorane (I) produced *in situ* from the corresponding phosphonium bromide and potassium *t*-butoxide. The product was *N*-(phenylcarbamoylazomethylene)aniline (II) (12%).

$$\underset{\text{I}}{Ph_3P{=}NNH_2} + 2PhNCO \xrightarrow{-Ph_3PO}$$

$$[PhN{=}C{=}NNHCONHPh] \longrightarrow \underset{\text{II}}{PhN{=}CH{-}N{=}NCONHPh}$$

Oxidation of I was carried out with mercuric oxide at −60°C, the formation of triphenyldiazophosphorane (III) being anticipated, but the reaction products isolated were triphenylphosphine (10%) and oxide (65%).

$$\underset{\text{I}}{Ph_3P{=}NNH_2} \xrightarrow{HgO} \underset{\text{III}}{[Ph_3PN_2]} \xrightarrow{-N_2} Ph_3P \xrightarrow{HgO} Ph_3P{=}O$$

Formation of triphenylphosphine strongly suggests the presence of III as an intermediate. However, III could not be trapped with styrene or diphenylacetylene. III seems to be too unstable to be isolated. Oxidation of I with bromine or lead tetraacetate gave analogous results.

No report has appeared on the reactivity of the amino group in aminotriphenylphosphonium bromide (IV). IV did not react with phenyl isocyanate, but in the presence of triethylamine gave *N*-phenylcarbamoyliminotriphenylphosphorane (V) in a good yield.

$$\underset{\text{IV}}{Ph_3\overset{+}{P}NH_2\ Br^-} + R{-}N{=}C{=}X \xrightarrow{Et_3N} Ph_3P{=}NCXNHR$$

V: R=Ph, X=O; VI: R=Ph, X=S
VII: R=*c*-C_6H_{11}, X=*c*-$C_6H_{11}N$

Phenyl isothiocyanate and dicyclohexyl carbodiimide reacted similarly, but *N*-sulfinylaniline gave only tarry material. Acyl and tosyl chlorides gave VIII—X

Table 1. *N*-Substituted iminotriphenylphosphoranes from IV

Reactant	Reac. temp. (°C)	$Ph_3P{=}N{-}R'$ R′	Yield (%)	Mp (°C) (lit. mp)
PhNCO	−40	PhNHCO (V)	95	181—182 (178—179)[3]
PhNCS	−40	PhNHCS (VI)	90	172—174 (174—176)[4]
(*c*-$C_6H_{11}N{=})_2C$	82	*c*-$C_6H_{11}N{=}C(c\text{-}C_6H_{11}NH)$- (VII)	70	138—142
PhCOCl	−40	PhCO (VIII)	93	193—194 (194—195.5)[5]
MeCOCl	−40	MeCO (IX)	40	161—163 (163—165)[6]
p-$MeC_6H_4SO_2Cl$	20	*p*-$MeC_6H_4SO_2$ (X)	30	175—177 (177)[7]

1) R. Appel and R. Schollhorn, *Angew. Chem.*, **76**, 991 (1964).
2) C. C. Walker and H. Shechter, *Tetrahedron Lett.*, **1965**, 1447.
3) G. I. Derkach and A. V. Narbut, *Zh. Obshch. Khim.*, **35**, 1006 (1965); *Chem. Abstr.*, **63**, 9857h (1965).
4) I. N. Zhmurova, A. P. Martynyuk, and G. I. Derkach, *Zh. Obshch. Khim.*, **38**, 163 (1968); *Chem. Abstr.*, **69**, 52209u (1968).
5) H. H. Wasserman and R. C. Koch, *Chem. Ind.* (London), **1956**, 1014.
6) G. I. Derkach, E. S. Gubnitskaya, V. A. Shokol, and A. V. Kirsanov, *Zh. Obshch. Khim.*, **32**, 1874 (1962); *Chem. Abstr.*, **58**, 6857f (1963).
7) F. G. Mann and E. J. Chaplin, *J. Chem. Soc.*, **1937**, 527.

similarly.

$$Ph_3\overset{+}{P}NH_2\ Br^- + R\text{-}Cl \xrightarrow{2Et_3N} Ph_3P{=}N\text{-}R$$

IV — VIII: R=PhCO; IX: R=MeCO; X: R=*p*-$MeC_6H_4SO_2$

The results are summarized in Table 1. The low yield of *N*-acetyl compound (IX) is attributable to easy hydrolysis.

These *N*-substituted iminophosphoranes are usually prepared from iminophosphorane[3,4,8] prepared from IV and sodium in liquid ammonia. In the present method, however, *N*-substituted iminophosphoranes are directly obtained from IV in high yields.

In the course of preparation of IV,[9] it was found that addition of triethylamine gave triphenyl(triphenylphosphoranylideneamino)phosphonium tribromide (XI), which differs from the corresponding bromide,[10,11] in the place of IV in 40% yield. Addition of triethylamine does more harm than good in the preparation of IV.

$$Ph_3PBr_2 \xrightarrow{NH_3} Ph_3\overset{+}{P}NH_2\ Br^- \xrightarrow[Et_3N]{Ph_3PBr_2} (Ph_3P{=}N\text{-}PPh_3)^+\ Br_3^-$$

IV — XI

Experimental

Materials. Hydrazinotriphenylphosphonium bromide was prepared according to literature,[12] mp 218—220°C (lit, 210—212°C). Aminotriphenylphosphonium bromide (IV) was prepared from triphenylphosphine dibromide and ammonia gas,[9] mp 242.5—244°C (lit, 243°C).

Reaction of Hydrazonotriphenylphosphorane (I) with Mercuric Oxide. To 0.05 mol of potassium *t*-butoxide in 200 m*l* of anhydrous ether was added 14.9 g (0.04 mol) of hydrazinotriphenylphosphonium bromide with stirring under nitrogen. After filtration of inorganic precipitate under nitrogen, 8.6 g (0.04 mol) of yellow mercuric oxide was added to the deep red filtrate (I) at −50——60°C. The mixture was stirred for 30 min and the temperature was gradually raised, during which time small bubbles evolved constantly. Precipitates were filtered off at room temperature and the filtrate was evaporated *in vacuo*. The residue was washed with ether to give 7.2 g (64.7%) of triphenylphosphine oxide, mp 153—155°C (from ether). The ethereal washings were evaporated to give 1 g (9.6%) of triphenylphosphine, mp 75—77°C (from petroleum ether).

Reaction of I with Phenyl Isocyanate. Phenyl isocyanate (3 g, 25.2 mmol) was added at room temperature to an ether solution (10 m*l*) of I, prepared from 3.73 g (10 mmol) of the phosphonium bromide, and the reaction mixture was chromatographed on alumina after concentration. After elution of triphenylphosphine oxide with benzene, elution with benzene - dichloromethane (1:1) gave 0.3 g (12%) of brown crystals (II), mp 185—186°C (dec) (from ethyl acetate-petroleum ether (1:3)). IR: 3320 (N–H), 3080 (C–H), 1670 (C=O), 1610 (C=N), and 1560 cm^{-1} (N–H, N=N). MS: *m/e* 252 (M^+).

Found: C, 66.94; H, 4.42; N, 22.41%. Calcd for $C_{14}H_{12}N_4O$: C, 66.66; H, 4.79; N, 22.21%.

Preparation of N-Substituted Iminophosphoranes. Typical procedures are described.

a) With Phenyl Isocyanate: Phenyl isocyanate (3.6 g, 0.03 mol) in acetonitrile (30 m*l*) was added dropwise to a suspension of 10.7 g (0.03 mol) of IV in 70 m*l* of acetonitrile containing 3.5 g (0.035 mol) of triethylamine with stirring at −30——40°C for 2 hr. The mixture was stirred at room temperature for one hour, then cooled to −40°C and 150 m*l* of ether was added. The precipitate thus obtained was washed three times with 200 m*l* of water, and dissolved in 200 m*l* of benzene to remove unchanged IV. The benzene solution was dried over anhydrous sodium sulfate. Removal of solvent gave 11.3 g (95%) of white crystals (V), mp 181—182°C (from ethanol).

b) With Dicyclohexyl Carbodiimide: A mixture of 5.3 g (0.015 mol) of IV, 3.1 g (0.015 mol) of the carbodiimide and 2 g (0.02 mol) of triethylamine was refluxed in 50 m*l* of acetonitrile for 6 hr, and 150 m*l* of ether was added at room temperature. After washing with 100 m*l* of water, removal of the solvent gave 5.1 g (70.4%) of iminophosphorane (VII), mp 138—142°C (from acetonitrile). IR: 3300 (N–H), 1610 (C=N), 1560 (N–H), 1305 (P=N), and 1110 cm^{-1} (P–Ph). VII was slowly hydrolyzed with moisture in air to triphenylphosphine oxide (mp 155°C) and dicyclohexylurea (mp 229—230°C). It was, therefore, difficult to obtain an analytically pure sample.

Triphenyl(triphenylphosphoranylideneamino)phosphonium Tribromide. Triethylamine (13.1 g, 0.13 mol) was added to a suspension of triphenyldibromophosphorane (42.2 g, 0.1 mol) in chlorobenzene (120 m*l*) at 95°C, ammonia gas being passed. After stirring for one hour, the mixture was treated in the usual manner. Orange-yellow crystals thus obtained (31 g, 39.8%), mp 170—175°C, were recrystallized twice from acetonitrile, mp 191.5—193.5°C.

Found: C, 56.01; H, 3.82; N, 1.87; Br, 30.14%. Calcd for $C_{36}H_{30}NP_2Br_3$: C, 55.56; H, 3.89; N, 1.80; Br, 30.80%.

8) I. N. Zhmurova and A. P. Martynyuk, *Zh. Obshch. Khim.*, **38**, 876 (1968); *Chem. Abstr.*, **69**, 59346v (1968).
9) L. Horner and H. Oediger, *Ann. Chem.*, **627**, 142 (1959).
10) R. Appel and A. Hauss, *Z. Anorg. Allg. Chem.*, **311**, 290 (1961).
11) R. Appel and G. Siegemund, *ibid.*, **361**, 203 (1968).
12) H. Zimmer and G. Singh, *J. Org. Chem.*, **29**, 1579 (1964).

BULLETIN OF THE CHEMICAL SOCIETY OF JAPAN, VOL. 45, 1561—1562(1972)

A Simple Preparation of 2,3-Dimethylenebicyclo[2.2.1]hept-5-ene

Takashi TODA, Tadanori OHYA, and Toshio MUKAI

Department of Chemistry, Faculty of Science, Tohoku University, Katahira-cho, Sendai-shi

(Received October 1, 1971)

2,3-Dimethylenebicyclo[2.2.1]hept-5-ene (I) is a compound possessing an interesting triene system and can be used as a starting material to synthesize many other polycyclic compounds. This compound was already synthesized by Alder and his co-workers;[1] however, their procedure contained multi-step of reactions and seems not to be suitable for large scale preparation. We have been interested in the chemistry of this triene compound and found a simple preparation method of I which was composed of two step reactions. This procedure is presented in this report.

Diels-Alder reaction of cyclopentadiene and *trans*-1,4-dichlorobut-2-ene gave *trans*-2,3-dichloromethyl-bicyclo-[2.2.1]hept-5-ene (II) accompanied with small amounts of isomeric products of II. Dehydrochlorination of II by Hock's method[2] which had been successfully applied to dehydrohalogenation of analogous compounds resulted in the recovery of the starting substance. After several fruitless trials, we found that treatment of II with potassium hydroxide in DMSO afforded the desired compound in 55—65% yield.

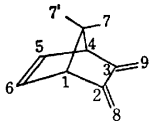

(I)

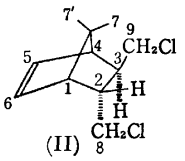

(II)

NMR spectra of I and II are shown in Table 1. The assignment of all hydrogens of I and II was done by double and triple resonance technique. H_7 of I shows a long-range coupling with H_5 and H_6 which nicely accords with W-rule[3] and this type long-range coupling is also observed between H_1 and H_5 (H_4 and H_6). The coupling constants ($J_{1,2}$ and $J_{3,4}$) of II can be explained from the fact that the dihedral angle between H_1 and H_2 and that between H_3 and H_4 are nearly 45° and 90° respectively, which values are agree with those of the Dreiding model of II. It should be noted that the spectrum indicated non-equivalency of methylene hydrogens of C_8 and C_9.

The mass spectrum of II shows a very intense peak at mass 66 and other peak's intensities are less 1/10 than that of the peak at 66: *m/e* (relative intensities); 190 (parent, 1.40), 105 (1.68), 91 (1.12), 67 (66+1, 6.20), 66 ($M-C_4H_6Cl_2$, 100), and 54 (1.07). The ratio of the intensities of the isotope peaks of the parent ion nicely accords with the reported values:[4] *m/e* (relative intensities); 190, 192, and 194 (100, 65, and 10). Therefore, *retro*-Diels-Alder type reaction is the most significant fragmentation of electron impact of II. On the other hand, the mass spectrum of I is as follows: *m/e* (relative intensities); 118 (parent, 76), 117 (M-1, 100), 103 ($M-CH_2$, 11), 91 ($117-C_2H_2$, 21), 78 (10), and 66 ($M-C_4H_4$, 61). In this case, a hydrogen was probably taken off from the methylene bridge and the base peak was formed. Although the main fragmentation is also *retro*-Diels-Alder type one, the intensity of mass 66 peak is not strong compared with that in the case of II. The reason of this may be due to the formation of unfavorable cummulene fragment. This property is parallel with thermally stable nature of I.[5]

Experimental[6]

trans-2,3-Dichloromethyl-bicyclo[2.2.1]hept-5-ene (II) A mixture of 8.26 g of 1,4-dichloro-2-butene, 5.26 g of freshly distilled cyclopentadiene and 6 ml of benzene in a sealed glass tube was heated in an autoclave which was also filled with benzene. An oil bath (or electric heater) used should be

TABLE 1[a]. δ values of the products (I and II)

	H_1	H_2	H_3	H_4	H_5	H_6	H_7	$H_{7'}$	H_8	H_9
I	2.23			3.23	6.11	6.11	1.56	1.73	4.87	4.87
									5.06	5.06
II	2.99	2.04	1.30	2.79	6.27	6.10	1.51	1.51	3.11	3.63
									3.40	4.45

J values of the products (I and II)

	$J_{1,2}$	$J_{1,5}$	$J_{1,6}$	$J_{1,7}$	$J_{2,3}$	$J_{2,8}$	$J_{3,4}$	$J_{3,9}$	$J_{4,5}$	$J_{4,6}$	$J_{4,7}$	$J_{5,6}$	$J_{5,7}$	$J_{6,7}$	$J_{7,7'}$	$J_{8,8'}$	$J_{9,9'}$
I		1.4	1.4	1.6					1.4	1.4	0		0.5	0.5	8.5	~0.3	~0.3
II	3.5	0	3.5	1.0	5.0	10.5	~0	6.5	3.5	~0	1.5	5.5	~0.3	~0.3		9.5	10.5

a) All chemical shifts are presented by ppm from internal standard TMS in CCl_4 at 100 MHz, and all coupling constants are presented by Hz.

1) K. Alder, S. Hartung, and O. Netz, *Chem. Ber.*, **90**, 1 (1957).
2) P. E. Hock and J. M. Clegg, *J. Amer. Chem. Soc.*, **81**, 5413 (1959).
3) S. Sternhell, *Rev. Pure Appl. Chem.*, **14**, 15 (1964).
4) R. M. Silverstein and G. C. Bassler, "Spectrometric Identification of Organic Compounds," John Wiley & Sons, New York (1963), p. 17.
5) When I was heated up to 500°C in vapor phase, I was recovered almost quantitatively; unpublished work.
6) All boiling points are uncorrected.

heated at 180°C before the reaction and the temperature should be kept at 180±5°C during the reaction. After cooling, the benzene was removed under reduced pressure and then the residue was distilled fractionally. II was obtained as a colorless oil (7.35 g), bp 117°C/16 mmHg; average yields of II are 50—60%. ν (oil neat); 3070, 2960, 2905, 1460, 1445, 1325, 1285, 1265, and 710 cm^{-1}.

Found: C, 56.84; H, 6.50%. Calcd for $C_9H_{10}Cl_2$: C, 56.56; H, 6.33%.

2,3-Dimethylenebicyclo[2.2.1]hept-5-ene (I). A solution of 6.65 g of II and 7.0 g of potassium hydroxide in 30 m*l* of DMSO which contained 3 m*l* of water was put in a Claisen flask and heated for 6 hr at 160±5°C under gentle stream of nitrogen. As the reaction proceeded, oily products were distilled out and collected in an flask cooled in an ice bath. The collected products were washed well with water, extracted with ether, and the combined ether layers were dried over sodium sulfate. After the drying reagent and the ether had been removed, the obtained products were distilled fractionally to give 2.63 g of I; bp 142°C (lit, bp 142°C);[1] average yields of I are 55—65%. λ_{MeOH}^{max}; 242 mμ (log ε, 3.97). ν (oil neat); 3060, 2957, 2855, 1640, 1420, 1308, 880, 792, 765, and 678 cm^{-1}.

The oily product afforded an adduct, mp 121°C, in 95% yield on reacting with maleic anhydride.

The mass spectra were measured at 70 eV by indirect method.

The authors are indebted to the Hitachi Chemical Co. for the gift of cyclopentadiene dimer.

BULLETIN OF THE CHEMICAL SOCIETY OF JAPAN, VOL. 45, 1562—1564(1972)

Hindered Rotation in [12]Paracyclophanes[1)]

Masao NAKAZAKI, Koji YAMAMOTO, and Susumu OKAMOTO

Department of Chemistry, Faculty of Engineering Science, Osaka University, Toyonaka, Osaka

(Received October 19, 1971)

In our preceding communication,[2)] we examined the rates of internal rotation of the benzene rings in a series of [*n*]paracyclophane derivatives with CH_2X side chains on the benzene nucleus, by taking advantage of the phenomenon that the diastereotopic methylene protons (H_A, H_B) become indistinguishable on rapid interconversion between the conformational enantiomers (**1**), (**2**) on NMR time scale.

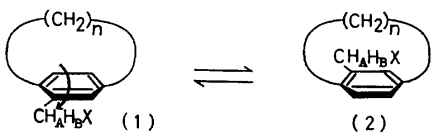

(1) (2)

In this communication, we report an NMR analysis of the hindered rotation in [12]paracyclophane deirvatives (**3**), (**4**) with substituents on benzylic positions of the bridges.

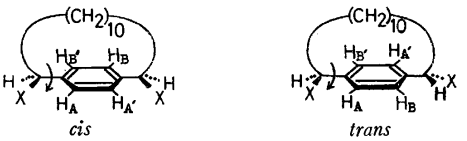

cis *trans*

(3) a,X=Br
b,X=OAc
c,X=OH

(4) a,X=Br
b,X=OAc
c,X=OH

Bromination of [12]paracyclophane[3)] with *N*-bromosuccinimide in carbon tetrachloride afforded a mixture of dibromides which could be separated by recrystallization from *n*-hexane into *cis*-1,12-dibromo[12]paracyclophane (**3a**), mp 172—173°C and *trans*-1,12-dibromo[12]paracyclophane (**4a**), mp 155—156°C. Each of these dibromides was converted into the *cis*-diacetate (**3b**), mp 64—65°C and the *trans*-diacetate (**4b**), mp 82—83°C. Alkaline hydrolysis of the diacetates (**3b**) and (**4b**) gave the *cis*-diol (**3c**), mp 180—181°C and *trans*-diol (**4c**), mp 174—175°C respectively.

Their *cis*- and *trans*-configurational assignments are based on the following observations of their NMR spectra[4)] (Fig. 1, 2).

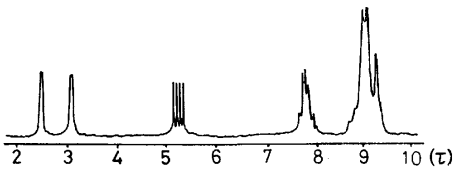

Fig. 1. 100-MHz NMR spectrum of *cis*-1,12-dibromo[12]-paracyclophane (**3a**) in CS_2 at +42°C.

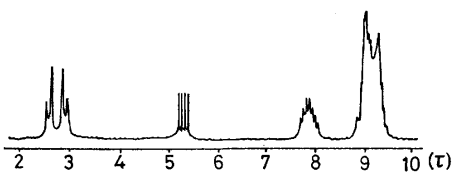

Fig. 2. 100-MHz NMR spectrum of *trans*-1,12-dibromo[12]-paracyclophane (**4a**) in CCl_4 at +25°C.

The *cis*-dibromide (**3a**) has C_s symmetry and its aromatic protons can be grouped into two enantiotopic pairs, $H_A/H_{A'}$ and $H_B/H_{B'}$, and the stereochemical

1) Presented in part before the 22nd Annual Meeting of the Chemical Society of Japan, Tokyo, March, 1969.

2) M. Nakazaki, K. Yamamoto, and S. Okamoto, *Tetrahedron Lett.*, **1969**, 4597.

3) D. J. Cram and H. Daeniker, *J. Amer. Chem. Soc.*, **76**, 2743 (1954); D. J. Cram, N. L. Allinger, and H. Steinberg, *ibid.*, **76**, 6132 (1954).

4) NMR spectra were taken on a Nucleomagnetic Resonance Spectrometer, JNM-4H-100, Japan Electron-Optics Laboratory Co., Ltd.

relationship between H_A and $H_{B'}$ (or between $H_{A'}$ and H_B) is diastereotopic.

C_2 symmetry of the *trans*-isomer (**4a**) generates two homotopic pairs $H_A/H_{A'}$ and $H_B/H_{B'}$: all the stereochemical relationships between these pairs in turn are diastereotopic.

Being proximate to the bromine atoms, the protons H_A and $H_{A'}$ are expected to be more heavily deshielded than H_B and $H_{B'}$ in both *cis*- and *trans*-dibromides. From their molecular geometries, the chemical shift difference between the diastereotopic set of protons H_A and H_B of the *cis*-isomer (**3a**) is expected much lager than that of the *trans*-isomer (**4a**). This consideration suggests that the dibromide (mp 172—173°C) with larger chemical shift difference (0.6 ppm) has the *cis*-configuration, and another dibromide (mp 155—156°C) exhibiting smaller chemical shift difference has the *trans*-configuration. This conclusion is further supported by their coupling patterns. In the *cis*-dibromide, it is safe to assume that the coupling constants J_{AB}(*para*) and $J_{AB'}$(*meta*) are negligibly small, and the same is also true for the coupling constants within the enantiotopic pairs, *i.e.* $J_{AA'}\approx 0$, $J_{BB'}\approx 0$. And these degeneracies explain a surprisingly simple resonance pattern of the *cis*-compound in aromatic region, which is otherwise expected to show a rather complicated AA'BB' pattern. In the same token, AA'BB' type[5] of spin coupling pattern in the *trans*-dibromide (**4a**) is reduced to become resemble a simple AB quartet due to the relatively large magnitudes of *ortho*-coupling constants (J_{AB}, $J_{A'B'}$) and negligibly small coupling constants between the protons in *para* and *meta* positions ($J_{AB'}\approx 0$, $J_{AA'}\approx 0$).

On warming, the benzene nucleus of the *cis*-dibromide (**3a**) becomes to rotate through the loop of the polymethylene bridge rendering the diastereotopic sets of protons ($H_AH_{A'}$ and $H_BH_{B'}$) indistinguishable on NMR time scale.

Figure 3 shows typical temperature dependence (71—148°C in diglyme) of the NMR spectrum in aromatic region of the *cis*-dibromide (**3a**), together with the calculated spectra generated for a range of values of the pre-exchange life time τ using the density matrix procedure,[6] in which approximation that all coupling constants are zero was made.

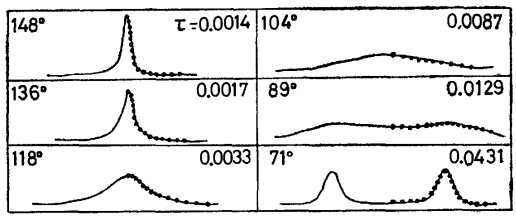

Fig. 3. Observed (——) and calculated (·····) spectra for the aromatic protons of *cis*-1,12-dibromo[12]paracyclophane (**3a**) as a function of temperature. (Solvent: diglyme)

5) These unique AA'BB' spin systems around a benzene nucleus are peculiar to these rather queer benzene derivatives with C_s and C_2 symmetry respectively.

6) C. S. Johnson, Jr., *Advan. Magnetic Resonance*, **1**, 35 (1965). These calculated spectra were made up with the aid of a program written for NEAC-2200 Computer, Osaka University Computation Center.

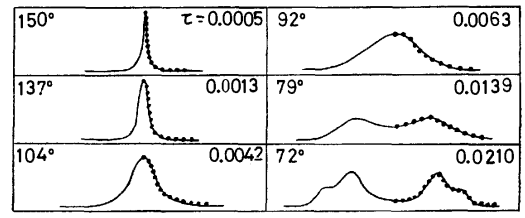

Fig. 4. Observed (——) and calculated (——) spectra for the aromatic protons of *trans*-1,12-dibromo[12]paracyclophane (**4a**) as a function of temperature. (Solvent: hexachloro-1,3-butadiene)

Also, in aromatic region of the *trans*-dibromide (**4a**) (in hexachlorobutadiene), the quartet changes to a broad doublet at 79°C, then coalesces into a broad singlet at 92°C which further transforms into a sharp singlet in higher temperature. In Fig. 4 are shown this temperature dependent NMR spectra with their calculated spectra which were computed on the approximation $J_{AB'}=0$ and $J_{AA'}=0$.

Table 1. Coupling constants and chemical shifts used in variable-temperature analysis

Compd	Solvent	Temp. range (°C)	δ_{AB} (Hz)	J_{AB} (Hz)	T_c (°C)	E_a (kcal/mol)
(**3a**)	c	20—159	50.5		104	12.8±0.8
	b	18—160	56.0		105	13.2±0.5
(**3b**)	c	19—158	29.7		113	13.1±0.6
	b	20—155	28.0		111	12.6±0.5
(**3c**)	c	21—161	55.0		136	18.5±1.0
(**4a**)	c	16—157	32.4	7.8	76	13.1±0.5
	a	15—160	33.8	8.1	79	13.4±0.4
(**4b**)	c	15—163	7.7	8.5	92	12.2±0.4
	a	14—151	10.8	8.4	91	12.8±0.6
(**4c**)	c	17—160	28.6	9.2	139	18.1±0.8

E_a: Arrhenius activation energy; T_c: coalescence temperature a: hexachloro-1,3-butadiene; b: nitrobenzene-d_5; c: diglyme

Arrhenius plots of these data afforded E_a listed in Table 1, which also lists the chemical-shift differences and coupling constants employed in these calculations. From Table 1, it is clear that each pair of *cis*- and *trans*-isomers shows relatively small differences in their activation energies of internal rotation. Remarkably high activation energies found in the *cis*-diol and *trans*-diol should be ascribed to intermolecular hydrogen bonds.

Experimental

cis-1,12-Dibromo[12]paracyclophane (3a) and trans-1,12-dibromo[12]paracyclophane (4a). A mixture of 5 g of [12]-paracyclophane,[3] 7.7 g of *N*-bromosuccinimide, and 1400 m*l* of carbon tetrachloride was refluxed for 10 hr. The warm solution was filtered to remove succinimide, and evaporated to dryness. The residue was refluxed for 3 hr with 200 m*l* of *n*-hexane, and the undissolved white solide was recrystallized 3 times from *n*-hexane–benzene to give 4.8 g (58%) of the *cis*-dibromide **3a**, mp 172—173°C. Found: C, 53.68; H, 6.50; Br, 39.80%. Calcd for $C_{18}H_{26}Br_2$: C, 53.75; H, 6.51; Br, 39.74%.

Evaporation of mother liquor gave a residue which was

recrystallized 4 times from *n*-hexane to give 0.6 g (7%) of the *trans*-dibromide **4a**, mp 155—156°C. Found: C, 53.61; H, 6.55; Br, 39.83%. Calcd for $C_{18}H_{26}Br_2$: C, 53.75; H, 6.51; Br, 39.74%.

cis-*1,12-Diacetoxy*[*12*]*paracyclophane* (***3b***). A mixture of the *cis*-dibromide **3a** (0.5g), 0.5 g of sodium acetate, and 5 m*l* of acetic acid was refluxed for 16 hr. The warm mixture was filtered to remove sodium bromide, and the filtrate was evaporated *in vacuo*. The residue was cooled, diluted with water, and extracted with ether. The ether layer was washed with water, diluted sodium bicarbonate, and water. The solution was dried, evaporated, and the residue was recrystallized 2 times from *n*-hexane to give 0.33 g (73%) of **3b**, mp 64—65°C. Found: C, 73.18; H, 8.88%. Calcd for $C_{22}H_{32}O_4$: C, 73.30; H, 8.95%.

cis-*1,12-Dihydroxy*[*12*]*paracyclophane* (***3c***). To a solution of 0.7 g of potassium hydroxide in 6 m*l* of ethanol was added 0.25 g of the *cis*-diacetate **3b**, and the mixture was refluxed for 10 hr. The reaction mixture was poured into 20 m*l* of water and extracted with chloroform. The chloroform layer was washed with water, dried and evaporated. The residual solid was recrystallized 3 times from benzene to give 0.11 g (57%) of **3c**, mp 180—181°C. Found: C, 78.08; H, 10.18%. Calcd for $C_{18}H_{28}O_2$: C, 78.21; H, 10.21%.

trans-*1,12-Diacetoxy*[*12*]*paracyclophane* (***4b***). Reaction of the *trans*-dibromide **4a** (0.5 g) with sodium acetate was carried out in a manner similar to that described for the preparation of *cis*-diacetate **3b**. Recrystallization from ethanol gave 0.32 g (71%) of **4b**, mp 82—83°C. Found: C, 73.43; H, 8.92%. Calcd for $C_{22}H_{32}O_4$: C, 73.30; H, 8.95%.

trans-*1,12-Dihydroxy*[*12*]*paracyclophane* (***4c***). Alkaline hydrolysis of 0.25 of the *trans*-diacetate **4b** was carried out in a manner similar to the preparation of *cis*-diol **3c**. Recrystallization from benzene gave 0.12 g (63%) of **4c**, mp 174—175°C. Found: C, 78.11; H, 10.19%. Calcd for $C_{18}H_{28}O_2$: C, 78.21; H, 10.21%.

BULLETIN OF THE CHEMICAL SOCIETY OF JAPAN, VOL. 45, 1564—1565(1972)

The Crystal Structure of *o*-Nitrobenzamide

Kumiko FUJIMORI, Tomitake TSUKIHARA, Yukiteru KATSUBE, and Jiro YAMAMOTO
Faculty of Engineering, Tottori University, Tottori

(Received October 27, 1971)

There are several types of molecular arrangement connected by hydrogen bonds[1-6] in the crystals of the derivatives of benzamide. It seems that a substituent group of benzamide influences the crystal structure. It is impossible, however, to discuss the effect of substituent on molecular arrangement at the present stage, because little is known about the crystal structure of the derivatives of benzamide. The present structure determination of *o*-nitrobenzamide has been undertaken as a part of a series of investigations on the crystal structures of aromatic carboxyamide.

Experimental

The crystal grown from alcohol solution was a transparent needle elongated along the *c* axis. The physical and crystal data are shown in Table 1. The unit cell dimensions were determined by the rotation and Weissenberg photographs about *b* and *c* axes. Intensities of 1494 independent reflections were measured visually on equi-inclination Weissenberg photographs of 0—3 layers around the *c* axis and of 0—8 layers around the *b* axis, with the use of Cu-K_α radiation. Intensities were corrected only for the usual Lorentz and polarization factors.

Table 1. Crystal data

$C_6H_4(NO_2)(CONH_2)$		M.W.=166.14
Monoclinic		$P2_1/a$
$a=12.01$Å	$b=12.79$Å	$c=5.03$Å
$\alpha=90.0°$	$\beta=97.5°$	$\gamma=90.0°$
$D_{cal}=1.44$g/cm^3		
$D_{obs}=1.43$g/cm^3	(by floatation)	

Structure Determination and Refinement

The orientation of the benzene ring was easily determined by the three-dimensional Patterson function. The three-dimensional coordinates of the atoms in the molecule for a probable orientation were at first determined by trial and successive Fourier methods. The coordinates of the atoms thus obtained were refined by the diagonal-matrix least-squares method with isotropic temperature factors. All the hydrogen atoms were revealed by (F_o-F_c) synthesis, at the stage of 0.15 of the *R* factor. Further refinements including hydrogen atoms were made by the block-diagonal-matrix least-squares method. The final *R* factor obtained was 0.136 for all the reflections but it was 0.108 excluding unobserved reflections. The atomic parameters are given in Table 2.

Structure Description and Discussion

The intramolecular bond lengths and angles are shown in Fig. 1. All the values seem to be reasonable.

1) B. R. Penfold and T. C. B. White, *Acta Crystallogr.*, **12**, 130 (1959).
2) S. Orii, T. Nakamura, Y. Takaki, Y. Sasada, and M. Kakudo, This Bulletin, **36**, 788 (1963).
3) Y. Sasada, T. Takano, and M. Kakudo, *ibid.*, **37**, 940 (1964).
4) T. Taniguchi, Y. Kato, Y. Takaki, and K. Sakata, *Mem. Osaka Gakugei Univ.*, **B14**, 56 (1965).
5) Y. Kataube, Y. Sasada, and M. Kakudo, This Bulletin, **39**, 2576 (1966).
6) Y. Harada, T. Taniguchi, Y. Takaki, and K. Sakurai, *Mem. Osaka Gakugei Univ.*, **18 III**, 1 (1969).

TABLE 2. FINAL ATOMIC COORDINATES AND THERMAL PARAMETERS

	x	y	z	$B_{11}\times10^5$	$B_{22}\times10^5$	$B_{33}\times10^4$	$B_{12}\times10^5$	$B_{13}\times10^4$	$B_{23}\times10^4$
C1	0.0769	0.3425	0.4306	476 (38)	359 (32)	239 (20)	24 (58)	−1 (13)	−1 (14)
C2	0.1295	0.4394	0.4522	780 (55)	382 (37)	494 (33)	−177 (74)	90 (21)	33 (18)
C3	0.2218	0.4522	0.6459	715 (57)	611 (50)	632 (41)	−436 (90)	40 (24)	−33 (24)
C4	0.2609	0.3709	0.8110	555 (49)	745 (55)	585 (38)	−339 (86)	−14 (21)	−82 (24)
C5	0.2091	0.2718	0.7816	501 (42)	573 (44)	388 (28)	−16 (71)	−33 (17)	27 (18)
C6	0.1164	0.2579	0.5908	483 (37)	276 (29)	236 (19)	105 (55)	21 (13)	−25 (13)
C7	0.0672	0.1506	0.5404	657 (43)	314 (31)	183 (18)	130 (61)	31 (14)	23 (13)
O1	−0.0303	0.3709	0.0212	1406 (62)	816 (42)	355 (21)	−0 (83)	−100 (18)	128 (16)
O2	−0.1080	0.2917	0.3302	557 (33)	741 (36)	503 (23)	−152 (58)	−52 (14)	8 (15)
O3	0.0442	0.1161	0.3125	1002 (40)	336 (23)	167 (13)	−137 (50)	25 (11)	−23 (9)
N1	−0.0276	0.3336	0.2465	755 (42)	340 (29)	309 (20)	331 (58)	−60 (14)	−12 (13)
N2	0.0547	0.0940	0.7588	923 (47)	410 (30)	190 (17)	−112 (63)	46 (14)	17 (12)
H1	0.107	0.485	0.296						
H2	0.254	0.537	0.630						
H3	0.328	0.380	0.982						
H4	0.223	0.229	0.934						
H5	−0.000	0.019	0.723						
H6	0.082	0.113	0.951						

Temperature factor=exp $\{-(B_{11}\times h^2+B_{22}\times k^2+B_{33}\times l^2+B_{12}\times hk+B_{13}\times hl+B_{23}\times kl)\}$

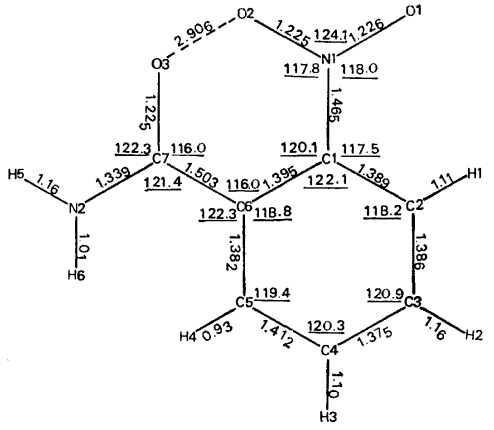

Fig. 1. Intramolecular distances (Å) and angles (°).

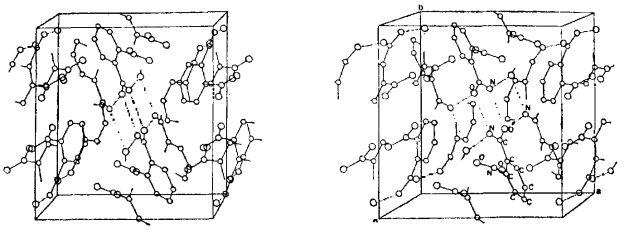

Fig. 3. The crystal structure of *o*-nitrobenzamide shown by a stereo pair, broken lines showing hydrogen bonds.

The average estimated standard deviation of bond lengths between non-hydrogen atoms is about 0.008 Å.

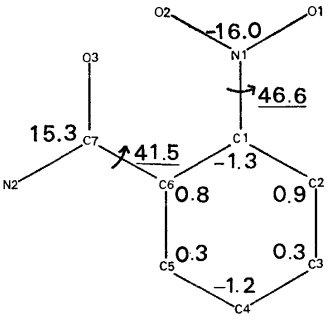

Fig. 2. The deviations ($\times10^2$Å) from the least-squares plane formed by the six carbon atoms of the benzene ring, and rotation angles of amide and nitro groups from the plane of the benzene ring.

The equation of the best plane of the benzene ring and the deviations of the atoms from the plane are given in Fig. 2. The planes of the amide and nitro groups rotate from that of the benzene ring at about 42 and 47 degrees, respectively. The arrangement of molecules in the unit cell is shown in Fig. 3 by a stereoscopic pair. There are two NH···O hydrogen bonds; the first set, 2.94 Å, forms a dimer across the center of symmetry, and the second set, 2.82 Å, links the dimers to form an endless chain extended along the *c* axis. A similar hydrogen bonding scheme has been found in the crystal of benzamide[1] and *m*-methylbenzamide.[2] The NO_2 group does not participate in the hydrogen bonds.

BULLETIN OF THE CHEMICAL SOCIETY OF JAPAN, VOL. 45, 1566(1972)

A Remark on the Importance of Particular Orbital Interaction in the Dimerization of Methylenes

Hiroshi FUJIMOTO, Shinichi YAMABE, and Kenichi FUKUI
Faculty of Engineering, Kyoto University, Sakyo-ku, Kyoto

(Received October 30, 1971)

Hoffmann discussed the mode of the approach of two singlet methylenes to form an ethylene molecule, suggesting the preference of a non-least-motion path to the least-motion path.[1] The dimerization of methylenes was also investigated by Kollmar using the CNDO MO method,[2] and by Sustmann and Binsch applying their perturbation calculation method.[3] In our own recent papers,[4,5] the interaction energy between two species has been discussed by dividing it into the Coulomb, exchange, delocalization, and polarization terms, and the important role of the delocalization interaction in representing the bond interchange in chemical reactions has been pointed out. In this note we will present the results of an approximate MO calculation on the dimerization of singlet methylenes.

Table 1 gives the four energies which have been obtained much as in our previous calculation.[6] The necessary variables in order to determine the relative positions of the two singlet methylenes are defined in Fig. 1. We see that Model III is the best among the three. It may also be noted that the superiority of Model III to Model I and to Model II is based mainly on the small unstabilization due to the exchange interaction and to the large stabilization due to the delocalization interaction. The contributions of the Coulomb interaction energy and the polarization interaction energy are both rather small, reflecting the fact that methylene is a neutral species. The exchange interaction energy is supposed to depend on the sum of the squares of the overlap integrals between the occupied MO's of two methylenes.[4] Such a relation can easily be confirmed by comparing the ε_K in Table 1 and the $\sum_i^{occ}\sum_k^{occ} S_{ik}^2$ in Table 2. The delocalization term comes from the mixing of charge-transferred electron configurations into the adiabatically interacting state. Among the various charge-transferred states, the one in which an electron is transferred from the highest occupied (HO) MO of one molecule into the lowest unoccupied (LU) MO of another molecule, and the converse, are usually the most important in governing the course of chemical reactions. In Table 2 are also presented the absolute values of the overlap integrals between the HOMO of one methylene and the LUMO of another. We find a close parallelism between the magnitudes of the energy, D, and the sums of the squares of the overlap integrals between these particular MO's.

Thus, the present calculation demonstrates that two singlet methylenes favor approaching in such a way as to make small the overlappings of occupied MO's and to gain an effective orbital interaction between the HOMO of one methylene and the LUMO of another. This seems to be a general feature of chemical interactions between two neutral systems.

TABLE 1. THE CALCULATED RESULTS OF THE INTERACTION ENERGIES

	Model I	Model II	Model III
ε_Q eV	0.102	0.067	0.054
ε_K eV	0.356	0.148	0.139
D eV	0.015	0.223	0.291
Π eV	0.010	0.004	0.003

ε_Q: Coulomb energy, ε_K: exchange energy, D: delocalization energy, Π: polarization energy

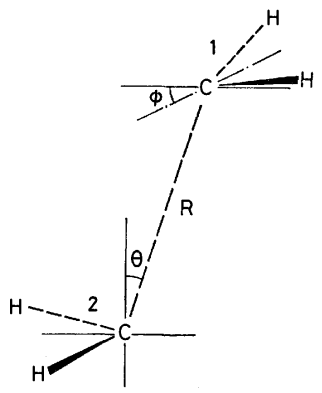

	Model I	Model II	Model III
R(Å)	3.0	3.0	3.0
θ(°)	90	44	6
ϕ(°)	0	0	78

Fig. 1. Assumed reaction models. (Model I corresponds to the least-motion path, and Model III to the non-least-motion path.[1])

TABLE 2. THE ORBITAL OVERLAPPINGS BETWEEN TWO METHYLENES

	Model I	Model II	Model III
$\sum_i^{occ}\sum_k^{occ} S_{ik}^2$	0.00668	0.00285	0.00279
$S_{HO^1,\,LU^2}$	0	0.0346	0.0575
$S_{HO^2,\,LU^1}$	0	0.0346	0.0112

HO^1 means the HOMO of methylene 1 and LU^2 the LUMO of methylene 2. (see Fig. 1) S_{ik} is the overlap integral between the ith MO of one methylene and the kth MO of another methylene. $\sum_i^{occ}\sum_k^{occ}$ implies the summation over all the combinations of occupied MO's of two methylenes.

1) R. Hoffmann, R. Gleiter, and F. B. Mallory, *J. Amer. Chem. Soc.*, **92**, 1460 (1970).
2) H. Kollmar, *Tetrahedron Lett.*, **1970**, 3337.
3) R. Sustmann and G. Binsch, *Mol. Phys.*, **20**, 1, 9 (1971).
4) K. Fukui and H. Fujimoto, This Bulletin, **41**, 1989 (1968).
5) H. Fujimoto, S. Yamabe, and K. Fukui, *ibid.*, **44**, 2936 (1971).
6) H. Fujimoto, S. Yamabe, and K. Fukui, *Tetrahedron Lett.*, **1971**, 439, 443.

BULLETIN OF THE CHEMICAL SOCIETY OF JAPAN, VOL. 45, 1567—1568(1972)

The Synthesis of the 3-Substituted 1,4,2-Dithiazine 1,1-Dioxides[1)]

Kiyoshi HASEGAWA and Syuzi HIROOKA

Department of Industrial Chemistry, Faculty of Engineering, Toyama University, Takaoka-shi

(Received November 1, 1971)

Our previous report[2)] has dealt with the synthesis, cleavage, and structural elucidation of a new heterocycle, 3-monoalkylamino-5-phenyl-1,1-dioxo-5, 6-dihydro-1,4, 2-dithiazine (**5**). This paper will describe the general procedures for the synthesis and cleavage of 3-sub-stituted 1,4,2-dithiazine-1,1-dioxides, which are outlined below:

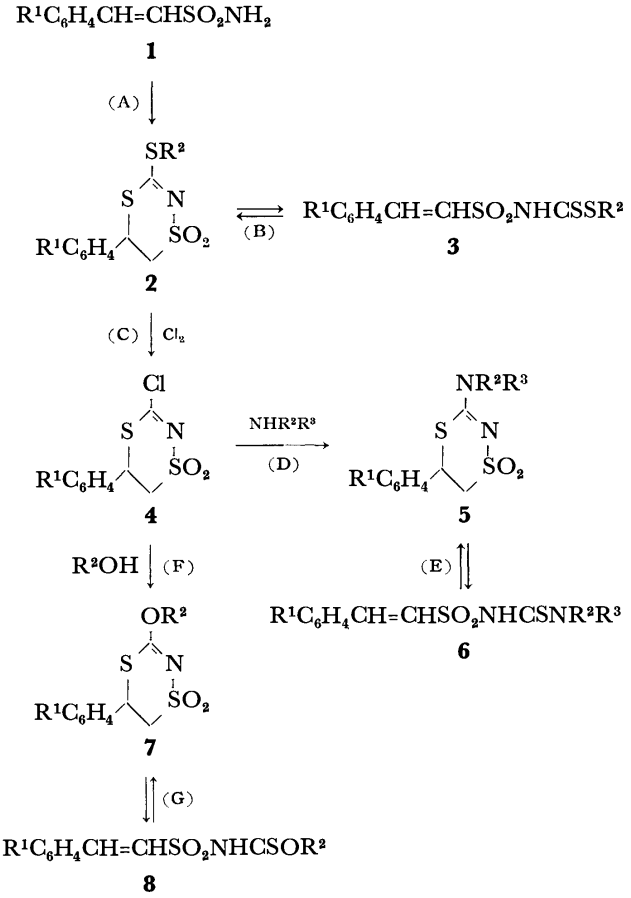

Results

The reaction of $R^1C_6H_4CH{=}CHSO_2NH_2$ with NaOH, CS_2, and R^2X yielded 3-alkylthio-5-phenyl-1,1-dioxo-5,6-dihydro-1,4,2-dithiazines (**2**). The mechanism is assumed to involve the intermediate of 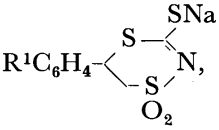 , which is an intramolecular Michael cycloadduct of $R^1C_6H_4CH{=}CHSO_2N{=}C(SNa)_2$ (Step (A)). The structure of **2** was confirmed by studying its IR, NMR, and mass spectra and by elemental analyses. The C–S bond in **2** could be split to yield *N*-(2-phenylethene-1-sulfonyl) dithiocarbamates, **3**, in strongly basic media (pH≥13.40). They tend to undergo ring-closure to **2** when preserved for long periods. Cycloadducts, **2**, were again obtained from **3** by intramolecular Michael cycloaddition in weakly basic media (pH≤12.55, Step (B)) and also by dissolving it in alcohol, even at room temperature. A mixture of **2** and **3** was obtained when the pH of the solution was between 12.55 and 13.40. The treatment of **2** with chlorine afforded 3-chloro derivatives, **4** (Step (C)). Ammonia, mono-, and dialkylamines attacked **4** at the chlorine atom to form **5** (Step (D)). They were also formed by the Michael cycloaddition of *N*-(2-phenylethene-1-sulfonyl)-*N'*,*N'*-dialkylthioureas, **6**, which are reverse Michael reaction products (Step (E)). *N'*-hydrogen derivatives of **6** are unstable and undergo rapid ring-closure, giving a rather impure product. Thioureas, **6b** and **6c**, were cycloadded upon melting, and **6a**, at 104—106°C before melting. Alcohols reacted with **4** to form 3-alkoxy derivatives, **7** (Step (F)). They were also prepared by the Michael cycloaddition of *O*-alkyl *N*-(2-phenylethene-1-sulfonyl)thiocarbamates, **8**, which are also reverse Michael reaction products of **7** (Step (G)). Solid **8** was stable at room temperature, but was easily cycloadded to give **7** when dissolved in warm alcohol. The results are summarized in Tables 1 and 2.

Experimental

*3-Methylthio-5-phenyl-1,1-dioxo-5,6-dihydro-1,4,2-dithiazine (**2a**).* *Step (A)*: To a stirred solution of 2-phenylethene-1-sulfonamide (18.3 g, 0.100 mol) in DMF (180 m*l*), we added NaOH (4.0 g, 0.100 mol) in water (8 m*l*) at room temperature, and then CS_2 (5.7 g, 0.075 mol) was added at 20—30°C. After 10 min, NaOH (4.0 g, 0.100 mol) in water (8 m*l*) and CS_2 (5.7 g, 0.075 mol) were added, and the mixture was stirred for 2 hr; then $(CH_3O)_2SO_2$ (25.2 g, 0.200 mol) was added, portion by portion, at 20—35°C. The yellow reaction mixture was stirred for 2 hr at room temperature, poured into ice water (1000 m*l*), and left to stand overnight. The yellow solid which formed was filtered to give 26.0 g (95%) of **2a**. Recrystallization from methanol gave colorless crystals. IR (KBr): 1535 ($\nu_{N=C}$), 1320 and 1135 cm^{-1} (ν_{SO_2}). NMR ($CDCl_3$): δ 2.58 (s, 3H, CH_3), 3.43 (q, 1H, H_A), 3.80 (q, 1H, H_C), 5.16 (q, 1H, H_B), J_{AC}= 14.0 Hz, J_{AB}=12.0 Hz, J_{BC}=3.6 Hz, 7.41±0.03 (5H, phenyl). MS: *m/e* 121 ($C_6H_5CS^+$), 273 (M^+).

Step (B): When **3a** (1.09 g, 0.004 mol) was dissolved in a warm 0.1M K_2CO_3 solution (40 m*l*, 0.004 mol), the **2a** began to separate out in a few minutes. After the mixture had then been kept overnight, it was filtered to give 0.98 g (90%) of **2a**.

*Methyl N-(2-Phenylethene-1-sulfonyl)dithiocarbamate (**3a**).* To **2a** (6.90 g, 0.025 mol) in acetone (100 m*l*), we added a 1.0N NaOH solution (50 m*l*, 0.050 mol), and then the mixture was stirred for 1 hr at room temperature. The acetone was

1) Presented at the 25th Annual Meeting of the Chemical Society of Japan, Tokyo, October, 1971.

2) K. Hasegawa and S. Hirooka, This Bulletin, **45**, 525 (1972).

TABLE I.

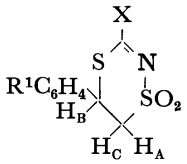

Compd	R^1	X	Yield (%) Method A, C D, F	Yield (%) Method B, E G	Mp (°C)	Calcd (%) C	Calcd (%) H	Calcd (%) N	Calcd (%) S	Found (%) C	Found (%) H	Found (%) N	Found (%) S
2a	H	SCH_3	95	90	157—158	43.96	4.06	5.13		44.07	4.10	5.31	
2b	H	SC_2H_5	93	91	125—126	46.00	4.56	4.88	33.43	46.00	4.32	4.87	33.11
2c	*p*-Cl	SCH_3	95	92	164—165	39.00	3.27	4.55	31.24	38.98	3.01	4.42	31.52
2d	*p*-CH_3	SCH_3	98	93	194—196	46.00	4.56	4.88	33.43	45.94	4.33	4.64	33.37
4a	H	Cl	94		158—160	41.30	3.08	5.35		41.16	3.10	5.41	
4b	*p*-Cl	Cl	87		112—113	36.49	2.38	4.76	21.65	36.36	2.13	4.54	21.89
4c	*p*-CH_3	Cl	60		142—143	43.55	3.66	5.08		43.25	3.41	4.83	
5a	H	NH_2	99		207—208	44.63	4.16	11.57	26.43	44.41	4.28	11.51	26.35
5b	H	$N(CH_3)_2$	98	89	185—186	48.89	5.22	10.37	23.68	48.61	5.17	10.33	23.54
5c	*p*-Cl	$N(CH_3)_2$	99	95	174—176	43.34	4.30	9.19	21.04	43.14	4.00	9.07	21.23
5d	*p*-CH_3	$N(CH_3)_2$	96	80	192—193	50.70	5.67	9.86	22.51	50.51	5.64	9.73	22.47
7a	H	OCH_3	96	90	176—178	46.70	4.31	5.45	24.88	46.86	4.49	5.67	24.93
7b	H	OC_2H_5	94	90	155—157	48.71	4.83	5.16	23.58	48.55	4.87	5.27	24.38
7c	*p*-Cl	OCH_3	92	83	174—175	41.16	3.45	4.80	21.98	41.40	3.64	4.87	22.04
7d	*p*-CH_3	OCH_3	57	57	188—190	48.71	4.83	5.16	23.58	48.45	4.63	4.91	23.50

TABLE 2. $R^1C_6H_4CH_B{=}CH_ASO_2NHCS{-}Y$

Compd	R^1	Y	Yield (%)	Mp (°C)	Calcd (%) C	Calcd (%) H	Calcd (%) N	Calcd (%) S	Found (%) C	Found (%) H	Found (%) N	Found (%) S
3a	H	SCH_3	98	106—108	43.96	4.06	5.13		44.09	4.01	4.84	
3b	*p*-Cl	SCH_3	94	114—117	39.00	3.27	4.55	31.24	39.11	3.30	4.38	30.63
6a	H	$N(CH_3)_2$	85	176—178	48.89	5.22	10.37	23.68	48.84	5.09	10.04	23.97
6b	*p*-Cl	$N(CH_3)_2$	95	119—120	43.34	4.30	9.19	21.04	43.31	4.36	9.23	20.77
6c	*p*-CH_3	$N(CH_3)_2$	99	121—123	50.70	5.67	9.86	22.51	50.85	5.72	9.98	22.16
8a	H	OCH_3	85	91— 92	46.70	4.31	5.45	24.88	46.51	4.27	5.21	24.44
8b	*p*-Cl	OCH_3	98	128—129	41.16	3.45	4.80	21.98	41.39	3.55	4.96	21.81
8c	*p*-CH_3	OCH_3	100	117—119	48.71	4.83	5.16	23.59	49.01	4.56	5.04	23.52

removed *in vacuo*, and the residual solution was acidified with concd. HCl to give 6.80 g (98%) of **3a**. Recrystallization from benzene–petroleum ether gave yellow crystals. IR (KBr): 3170 (ν_{NH}), 1620 ($\nu_{C=C}$), 1360 and 1150 cm^{-1} (ν_{SO_2}). NMR ($CDCl_3$): δ 2.59 (s, 3H, CH_3), 7.14 (d, 1H, H_A), 7.84 (d, 1H, H_B), J_{AB}=15.0 Hz, 7.48±0.03 (5H, phenyl).

3-Chloro-5-phenyl-1,1-dioxo-5,6-dihydro-1,4,2-dithiazine (4a). Excess chlorine was bubbled through a solution of **2a** (16.4 g, 0.060 mol) in chloroform (120 m*l*) cooled to 0—5°C over a 1-hr period. The colorless solution turned orange and yielded methanesulfenyl chloride. The chloroform was removed *in vacuo*, CCl_4 (20 m*l*) was added to the crystals, and the mixture was filtered to give 14.8 g (94%) of **4a**. Recrystallization from CCl_4 gave colorless crystals.

3-Dimethylamino-5-phenyl-1,1-dioxo-5,6-dihydro-1,4,2-dithiazine (5b). *Step (D)*: To **4a** (1.60 g, 0.006 mol) in chloroform (20 m*l*), we added 40% aqueous dimethylamine (1.37 g, 0.012 mol), after which the reaction mixture was stirred for 1 hr at room temperature. The chloroform was then removed *in vacuo*, and water (20 m*l*) was added to the residue. The cooled precipitate was filtered to give 1.62 g (98%) of **5b**. Recrystallization from methanol gave colorless crystals.

3-Methoxy-5-phenyl-1,1-dioxo-5,6-dihydro-1,4,2-dithiazine (7a). *Step (F)*: A solution of **4a** (2.62 g, 0.010 mol) in methanol (30 m*l*) was refluxed for 2 hr, diluted with water (10 m*l*), and then cooled overnight. The crystals which formed were filtered to give 2.47 g (96%) of **7a**. Recrystallization from methanol gave colorless crystals.

BULLETIN OF THE CHEMICAL SOCIETY OF JAPAN, VOL. 45, 1569(1972)

The Synthesis of 3,4-Di-*O*-methyl-D-galactose

Susumu HIRASE and Kyoko WATANABE

Department of Chemistry, Faculty of Industrial Arts, Kyoto Technical University, Matsugasaki, Kyoto

(Received November 6, 1971)

Partially methylated sugars are important for the structural investigation of polysaccharides. In the course of our studies on the polysaccharide from certain species of red seaweeds, 3,4-di-*O*-methyl-D-galactose has been needed as a reference compound. This partially methylated sugar was synthesized by Bacon and Bell.[1] But their method of synthesis has the disadvantages that the starting compound (methyl 3,4-*O*-isopropylidene-β-D-galactopyranoside) was obtained in a low yield,[2] and that the succeeding step involves the use of nitrogen pentoxide, which is inconvenient to handle. We have carried out the synthesis through the different route reported below.

1,6-Anhydro-3,4-*O*-isopropylidene-β-D-galactopyranose(I), prepared by the method of Hann and Hudson,[3] has been used as a starting compound. Its free hydroxyl group at C_2 was first blocked with a phenylcarbamoyl group (I→II). The *O*-isopropylidene group was then removed by methanolysis (II→III). The newly fromed hydroxyl groups at C_3 and C_4 were methylated (III→IV), and the blocking substituent was removed reductively with lithium aluminum hydride (IV→V).[4] Finally, the 1,6-anhydro-ring was opened. The product was identical in the physical constants with 3,4-di-*O*-methyl-β-D-galactose, which had been reported by Bacon and Bell. The intermediates (II—V) are the new compounds. Since these compounds crystallize well except IV, and the yield was considerably high in each step, the synthesis has been performed very easily.

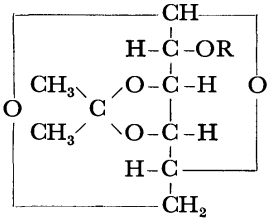

(I) R=H
(II) R=CONHC$_6$H$_5$

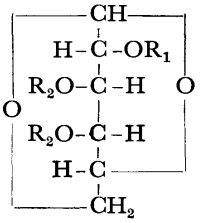

(III) $\begin{cases} R_1=CONHC_6H_5 \\ R_2=H \end{cases}$
(IV) $\begin{cases} R_1=CON(CH_3)C_6H_5 \\ R_2=CH_3 \end{cases}$
(V) $\begin{cases} R_1=H \\ R_2=CH_3 \end{cases}$

Experimental

Solutions were evaporated under reduced pressure in a rotary evaporator. Melting points were measured on a micro hot stage with Yanagimoto apparatus Model MP-S2.

1,6-Anhydro-3,4-O-isopropylidene-2-O-phenylcarbamoyl-β-D-galactopyranose(II). To a solution of I[3] (5.0 g) in dry pyridine (50 m*l*), phenylisocyanate (3.5 g) was added, and the mixture was heated at 100°C for 2 hr. Evaporation of the solution gave the crystalline II, which was triturated with ethanol and filtered; yield 7.9 g (100%), mp 226—228°C. It was recrystallized twice from ethanol (600 m*l*); needles, mp 229.5—230.5°C, $[\alpha]_D^{25}$ −30.0° (*c* 1.0 in chloroform).

Found: C, 59.87; H, 6.02; N, 4.38%. Calcd for $C_{16}H_{19}O_6N$: C, 59.80; H, 5.96; N, 4.36%.

1,6-Anhydro-2-O-phenylcarbamoyl-β-D-galactopyranose(III). A solution of II (7.0 g) in 1% methanolic hydrogen chloride (200 m*l*) was refluxed for 3 hr, neutralized with silver carbonate, and filtered. Evaporation of the filtrate gave crystalline III; yield 5.8 g (95%), mp 158—161°C. It was recrystallized twice from water; needles, mp 162—163°C, $[\alpha]_D^{25}$ +24.7° (*c* 0.85 in methanol).

Found: C, 55.55; H, 5.41; N, 5.05%. Calcd for $C_{13}H_{15}O_6N$: C, 55.51; H, 5.38; N, 4.98%.

1,6-Anhydro-3,4-di-O-methyl-2-O-(N-methyl-phenylcarbamoyl)-β-D-galactopyranose (IV). The compound III (3.0 g) was methylated twice with iodomethane (20 m*l*) and silver oxide (20 g) in *N*,*N*-dimethylformamide (30 m*l*) by the method of Kuhn and his coworkers.[5] The product was obtained as a slightly colored syrup; yield 2.8 g (82%), $[\alpha]_D^{25}$ +14.9° (*c* 0.75 in chloroform). (Found: OCH_3, 19.0%).

1,6-Anhydro-3,4-di-O-methyl-β-D-galactopyranose (V). According to the procedure of Bouveng,[4] IV (2.7 g) was treated with excess lithium aluminum hydride (0.7 g) in boiling tetrahydrofuran for 3 hr. The syrupy crude product obtained was purified by dissolution in water and extraction with hexane to remove an oily material. Evaporation of the aqueous solution gave crystalline V; yield 1.5 g (94%), mp 76—79°C. It was further purified by recrystallization twice from a mixture of ethyl acetate and hexane (3:5 v/v); tetragonals, mp 81°C, $[\alpha]_D^{25}$ −41.1° (*c* 0.90 in water).

Found: C, 50.52; H, 7.41%. Calcd for $C_8H_{14}O_5$: C, 50.56; H, 7.61%.

3,4-Di-O-methyl-β-D-galactose. The compound V (1.2 g) was hydrolysed with 4% hydrochloric acid (40 m*l*) at 100°C for 4 hr, at which time the optical rotation of the solution reached the constant value ($[\alpha]_D$ −41→+113°). The hydrochloric acid was removed by neutralization with silver carbonate and filtration. Evaporation of the filtrate afforded crystalline 3,4-di-*O*-methyl-β-D-galactose; yield 1.2 g (92%), mp 164—166°C. It was recrystallized from a small volume of methanol; mp 170—171°C, $[\alpha]_D^{20}$ +90.2→+117.3° (*c* 0.92 in water). Literature values are mp 164—166°C and $[\alpha]_D^{20}$ +95.7→+117.1° in water.[1] (Found: C, 46.10; H, 7.79; OCH_3, 22.0%).

We are grateful to the Ministry of Education for a Grant in Aid for Scientific Research.

1) J. S. D. Bacon and D. J. Bell, *J. Chem. Soc.*, **1939**, 1869.
2) F. Micheel, *Ber.*, **62**, 687 (1929).
3) R. M. Hann and C. S. Hudson, *J. Amer. Chem. Soc.*, **64**, 2435 (1942); R. W. Jeanloz and P. J. Stoffyn, "Methods in Carbohydrate Chemistry," Vol. I, ed. by R. L. Whistler and M. L. Wolfrom, Academic Press, New York and London (1960), p. 223.
4) H. O. Bouveng, *Acta Chem. Scand.*, **15**, 87 (1961).
5) R. Kuhn, H. Trischmann, and I. Löw, *Angew. Chem.*, **67**, 32 (1955).

BULLETIN OF THE CHEMICAL SOCIETY OF JAPAN, VOL. 45, 1570—1571(1972)

The Deacylation of β-Diketones in the Presence of Copper(II)-β-Diketonates in Methanol[1]

Kaku UEHARA, Seiichi SHIONOIRI, Makoto TANAKA, and Niro MURATA

Department of Applied Chemistry, College of Engineering, University of Osaka Prefecture, Sakai-shi, Osaka

(Received November 15, 1971)

In a previous paper[2] we reported that the copper(II) chelate of 3-α-butenylacetylacetone shows a high activity as an initiator of the radical polymerization of styrene and methyl methacrylate, that the polymerization proceeds *via* the reduction of Cu(II), and that the ligand is bound to the polymer chain. Furthermore, it has been found that the copper(II) chelate of 3-*n*-butylacetylacetone shows a moderate activity, while the chelate of acetylacetone, $Cu(acac)_2$, is an inefficient initiator.[2] We now wish to report a novel reaction of these β-diketones catalyzed by their copper(II) chelates.

When 3-α-butenylacetylacetone was heated with its copper(II) chelate in methanol under atmospheric air at 70°C, 4-hepten-2-one was obtained. In the course of the reaction, some metallic copper was precipitated. In the reaction carried out under pure oxygen, however, 4-hepten-2-one was formed without the precipitation of metallic copper. It was found that the copper(II) chelate decomposed in methanol to give 4-hepten-2-one, that metallic copper and/or cuprous oxide was precipitated when the solution was heated, and that the precipitation was delayed by the addition of a free ligand. It has also been reported that when the ligand is added to the metallic copper or cuprous oxide in hot methanol under atmospheric air, the copper(II) chelate is reformed.[3]

The deacylation of 3-α-butenylacetylacetone was very slow in tetrahydrofuran or benzene, and did not occur in the absence of the copper(II) chelate.

When 3-*n*-butylacetylacetone was heated with its copper(II) chelate in methanol, 2-heptanone was obtained. The reaction was slower than that of 3-α-butenylacetylacetone. When acetylacetone was heated with $Cu(acac)_2$ in methanol, however, no reaction occurred.

The experimental results in the present study suggest that the deacylation of β-diketones catalyzed by their copper(II) chelates proceeds *via* the reduction of Cu(II); the following cycle may be considered, although the reaction mechanism is yet unclear. The present reaction seems to be interesting as a new route of forming β,γ-unsaturated ketones.

Experimental

Materials. The 3-α-butenylacetylacetone, the 3-*n*-butylacetylacetone, and their copper(II) chelates were prepared in the way described in a previous paper.[2] The acetylacetone and $Cu(acac)_2$ were G.R.-grade reagents. The solvents were purified by the ordinary method and were distilled before use.

Deacylation of 3-α-butenylacetylacetone. A solution of 3-α-butenylacetylacetone (37 g, 0.24 mol) and its copper(II) chelate (3.6 g, 0.01 mol) in methanol (200 m*l*) was heated under reflux at 70°C for 24 hr, during which period metallic copper was gradually precipitated. The reaction mixture was then subjected to distillation. From the volatile fraction, methanol was recovered. From the second fraction (bp 52—55°C/18 mmHg, n_D^{25} 1.4297, d_4^{25} 0.8423), 4-hepten-2-one (**1**) was obtained in a yield of 31% (8.4 g).

Semicarbazone of **1**, mp 105.5°C; Found: C, 57.32; H, 9.09; N, 24.74%, Calcd for $C_8H_{15}ON_3$: C, 56.78; H, 8.93; N, 24.89%. 2,4-Dinitrophenylhydrazone of **1**, mp 121°C; Found: C, 52.77; H, 5.21; N, 19.45%, Calcd for $C_{13}H_{16}O_4N_4$: C, 53.42; H, 5.52; N, 19.18%. The IR spectrum of **1** showed sharp absorption peaks at 1714 cm^{-1} and 970 cm^{-1}. The former was attributed to the C=O group, and the latter, to the *trans* C=C group. The UV spectrum of **1** showed an absorption at 277 mμ (methanol). The NMR spectrum of **1** showed signals at 9.00 (3H, t, $CH_2C\underline{H}_3$), 7.95 (3H, s, $COC\underline{H}_3$), 7.90 (2H, m, $CH_3C\underline{H}_2CH$=), 6.98 (2H, d, $-C\underline{H}_2-CO-$), and 4.50 (2H, q, CH=CH). The mass spectrum of **1** showed the parent peak at *m/e* 112 and fragment peaks at *m/e* 97 $(CH_2CH{=}CHCH_2COCH_3)^+$, *m/e* 83 $(CH{=}CHCH_2COCH_3)^+$, *m/e* 69 $(CH_3CH_2CH{=}CHCH_2)^+$, *m/e* 55 $(CH_3CH_2-$

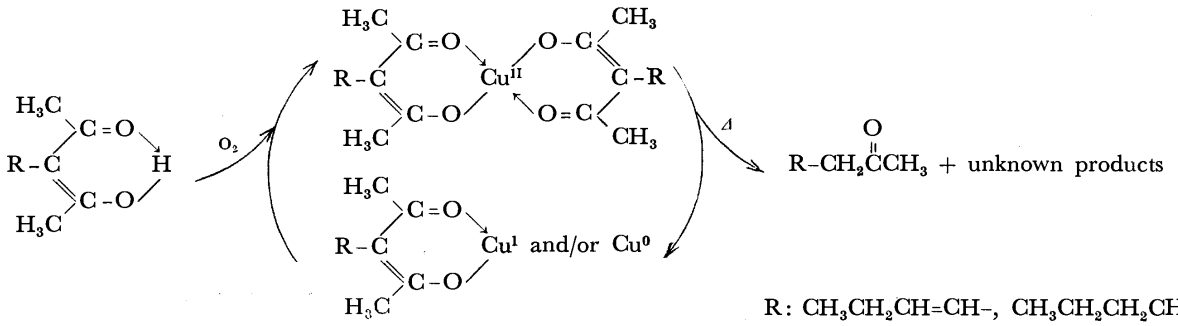

1) Paper XVI in a series of "Catalytic Behavior of Metal Chelate Compounds."

2) K. Uehara, T. Matsumura, T. Nishi, F. Tamura, and N. Murata, *Kogyo Kagaku Zasshi*, **69**, 2027 (1966); K. Uehara, T. Matsumura, Y. Murata, M. Tanaka, and N. Murata, *ibid.*, **72**, 1825 (1969).

3) K. Uehara, M. Tanaka, and N. Murata, *ibid.*, **70**, 1564 (1967).

$CH{=}CH)^+$, and *m/e* 43 $(CH_3CO)^+$.

Deacylation of Copper(II) Chelate of 3-α-Butenylacetylacetone. A 0.1-g portion of the copper(II) chelate of 3-α-butenylacetylacetone was dissolved in 5 m*l* of methanol, and then the mixture was heated under reflux at 70°C for 24 hr, during which period a mixture of metallic copper and cuprous oxide precipitated and the green color of the solution disappeared. After the precipitate had then been filtered off, the methanol was evapolated from the filtrate. The residue was analyzed by gas chromatography. 4-Hepten-2-one was identified by a comparison of its retention time with that of an authentic sample prepared above by means of a Shimadzu GC 4APT gas chromatograph using a silicon gum SE 52 column.

Deacylation of 3-n-Butylacetylacetone. A solution of 3-*n*-butylacetylacetone (15 g, 0.095 mol) and its copper(II) chelate (1.5 g, 0.006 mol) in methanol (500 m*l*) was heated under reflux at 70°C for 48 hr. The reaction mixture was then subjected to distillation. From the volatile fraction, methanol was recovered. From the second fraction (bp 47—50°C/18 mmHg, n_D^{25} 1.4189, d_4^{25} 0.8394), 2-heptanone (**2**) was obtained in a yield of 4.5% (1.0 g). Semicarbazone of **2**, mp 105.5°C; Found: C, 55.94; H, 9.54; N, 24.17%. Calcd for $C_8H_{17}ON_3$: C, 56.11; H, 10.00; N, 24.55%. The IR, UV, NMR, and mass spectra of **2** were closely analogous to those of an authentic sample of 2-heptanone (G.R.-grade reagent).

Spectral Measurements. The IR spectra were measured as a liquid film by means of a Hitachi Model EPI-S2 infrared spectrometer. The UV spectra were measured using a Hitachi recording spectrophotometer, Model EPS-3T. The NMR spectra were determined by means of a Hitachi Model R-20 spectrometer. Tetramethylsilane was used as the internal standard, and CCl_4 was used as the solvent. The mass spectra were recorded on a Hitachi Model RMU-6E mass spectrometer under the following conditions: chamber voltage 80 V, total emission current 80 μA, vacuum 2×10^{-6} mmHg, sample temp. 160°C.

BULLETIN OF THE CHEMICAL SOCIETY OF JAPAN, VOL. 45, 1571—1574(1972)

A Theoretical Account of the Correlation between the Electronic Properties of Onium Compounds and Their Catalytic Activities in the Liquid-phase Oxidation of Hydrocarbons

Katsutoshi OHKUBO and Hirokazu KANAEDA

Department of Synthetic Chemistry, Faculty of Engineering, Kumamoto University, Kurokami-machi, Kumamoto

(Received November 17, 1971)

Previous studies[1,2] have suggested that onium compounds catalyze the liquid-phase oxidation of hydrocarbons. The catalytic activity of onium compounds containing C, N, O, P, S, As, Se, and Te as their onium central atoms is directly affected by the difference in the central atoms and indirectly by that in the counteranions and the substituents attached to the central atom. The larger the alkyl groups possessing the electron-donor property employed as substituents, the higher the catalytic acitvity, while the counteranions of phosphate, sulfate, *etc.* are more active than those of halides. As has been suggested by the spectroscopic[3] and theoretical[4,5] investigations of the possible interaction between the onium compound and molecular oxygen, these experimental phenomena can be considered to be immediately related to the catalytic activation of O_2. The present theoretical study with a semiempirical ASMO SCF method and an extended Hückel method[6] including all the valence electrons in a molecule appeared significant in elucidating the correlation between the electronic properties of onium compounds and their catalytic activities in the liquid-phase oxidation of such hydrocarbons as cumene and α-pinene.[1,2] The silyl compound will also be considered in this report for the sake of comparison.

First, we will discuss the molecular geometries of onium compounds (trimethyl- or tetramethyl-onium chlorides were used) from the energetic point of view. According to the total energies of the compounds listed in Table 1, the stable geometries of the trimethyl onium chlorides (carbonium, oxonium, sulfonium, selenonium, and telluronium) were found in those taking the planar structures of onium cations, while tetramethylonium chlorides (ammonium, phosphonium, and arsonium chlorides) have cations with tetrahedral forms.

Some mention should be made here of the geometries of onium compounds. An experimental finding has

1) K. Fukui, K. Ohkubo, and T. Yamabe, This Bulletin, **42**, 312 (1969).

2) K. Ohkubo and T. Yamabe, *Bull. Japan Petrol. Inst.*, **12**, 130 (1970).

3) K. Ohkubo and T. Yamabe, *J. Org. Chem.*, **36**, 3149 (1971).

4) K. Ohkubo and T. Yamabe, This Bulletin, **44**, 1183 (1971).

5) K. Ohkubo, *Tetrahedron Lett.*, **1971**, 2571, 2897.

6) C. C. Roothaan, *Rev. Mod. Phys.*, **23**, 69 (1951) for the SCF MO; R. Hoffmann, *J. Chem. Phys.*, **39**, 1397 (1963); *ibid.*, **40**, 2474 (1964) for the extended Hückel MO. The valence orbital ionization potentials (and electron affinities) of the *d*-orbitals of P, S, As, Se, and Te were taken to be 6.53 eV (0.8 eV), 7.00 eV (2.40 eV), 4.00 eV (1.0 eV), 5.00 eV (2.0 eV), and 4.00 eV (2.1 eV) respectively on the basis of the following references: H. O. Prichard and H. A. Skinner, *Chem. Rev.*, **55**, 745 (1955); *Trans. Faraday Soc.*, **49**, 1254 (1953); T. Jordan, H. W. Smith, L. L. Lohr, Jr., and W. N. Lipscomb, *J. Amer. Chem. Soc.*, **85**, 846 (1963). Those of *s* and *p* orbitals of the atoms were cited from J. Hinze and H. H. Jaffé. *J. Amer. Chem. Soc.*, **84**, 540 (1962); *J. Chem. Phys.*, **67**, 1501 (1963). For the Coulomb repulsion integrals, ($pp|pp$) and ($pp|qq$)), ($pp|pp$) were estimated by the Pariser approximation (R. Pariser, *J. Chem. Phys.*, **21**, 568 (1953)), while ($pp|qq$) was evaluated by the Ohno approximation (K. Ohno, *Theoret. Chim. Acta*, **2**, 219 (1964)). For more details on the calculation method, see H. Kato, This Bulletin, **44**, 348 (1971), *etc.*

TABLE 1. THE RELATION BETWEEN TOTAL ENERGIES OF ONIUM COMPOUNDS AND THEIR MOLECULAR GEOMETRIES

Onium compound $(CH_3)_3ACl$ or $(CH_3)_4ACl$	Structure of onium cation	A–C (Å)	A–Cl (Å)	Dipole moment (D)	Total energies (eV)	
					EHMO	SCF MO
$(CH_3)_3CCl$	planar (C_{3v})	1.54	2.66	5.398	−548.34	−662.90
		1.54	2.00	3.308	−544.06	−617.41
		1.54	1.76[a]	2.696	−541.32	−591.46
$(CH_3)_4NCl$	planar (C_{3v})	1.47	3.30	9.483	−688.78	−699.61
	tetrahedral (T_d)	1.47	3.30	14.660	−699.22	−713.55
$(CH_3)_3OCl$	planar (C_{3v})	1.45	3.20	14.722	−604.29	−796.15
		1.45	3.00	12.850	−603.90	−782.81
		1.45	1.65[a]	4.207	−579.25	−655.21
	pyramidal (C_{3v})	1.45	1.65[a]	4.207	—	−683.03
$(CH_3)_3SiCl$	planar (C_{3v})	1.95	3.80	9.483	−541.25	−703.65
	pyramidal (C_{3v})	1.95	2.16[a]	3.124	−541.12	−659.21
$(CH_3)_4PCl$	planar (C_{4v})	1.87	3.70	6.007	−679.98	−852.00
	tetrahedral (T_d)	1.87	3.70	7.617	−683.88	−856.49
$(CH_3)_3SCl$	planar (C_{3v})	1.82	3.50	7.088	−541.25	−788.59
	pyramidal (C_{3v})	1.82	3.50	16.21	—	−769.11
$(CH_3)_4AsCl$	planar (C_{4v})	1.95	3.80	14.699	−680.89	−780.01
	tetrahedral (T_d)	1.95	3.80	13.212	−579.80	−787.44
$(CH_3)_3SeCl$	planar (C_{3v})	1.87	3.80	11.454	−576.16	−782.56
	pyramidal (C_{3v})	1.87	2.15[a]	2.97	−563.67	−728.40
$(CH_3)_3TeCl$	planar (C_{3v})	2.09	4.00	12.141	−575.08	−809.49
	pyramidal (C_{3v})	2.09	2.31[a]	5.661	−566.75	−756.49

a) Covalent bond lengths. Another values of A–C bond indicate ionic distances.

TABLE 2. THE CORRELATION BETWEEN THE AO POPULATIONS OF CENTRAL-ATOM ORBITALS UTILIZED FOR THE INTERACTION WITH $1\pi_g$-ORBITALS OF O_2 AND THEIR CATALYTIC ACTIVITIES

Onium compound $(CH_3)_3ACl$ or $(CH_3)_4ACl$	Bond population		AO population			$R_{max}\times 10^4$ [a] (mol/l sec)	
	A–C	A–Cl	p_z	d_{xz}	d_{xy}		
$(CH_3)_3CCl$	0.850	0.040	0.596	—	—	0.26	(0.52)
$(CH_3)_4NCl$	0.676	−0.001	1.235	—	—	0.34	(0.74)
$(CH_3)_3OCl$	0.536	0.000	1.939	—	—	0.67	(0.82)
$(CH_3)_3SiCl$	0.638	0.012	0.495	—	—		(0.75)
$(CH_3)_4PCl$	0.881	0.050	0.996	0.258	0.241		(0.89)
$(CH_3)_3SCl$	0.788	0.090	1.898	0.200	0.210	1.12	(0.97)
$(CH_3)_4AsCl$	0.480	0.003	1.085	0.142	0.118	0.22	
$(CH_3)_3SeCl$	0.536	0.052	1.962	0.105	0.162	1.04	
$(CH_3)_3TeCl$	0.339	0.021	1.980	0.073	0.153	0.45	

These data except bond populations were supplied by the ASMO SCF calculations on the most energetically stable onium chlorides: the bond populations were calculated by the extended Hückel method.

a) R_{max} and those in parentheses stand for the rates in cumene and α-pinene oxidations respectively. Without an onium catalyst, $R_{max}\times 10^4$ was 0.17 or 0.34 mol/l sec in cumene or α-pinene oxidation respectively.

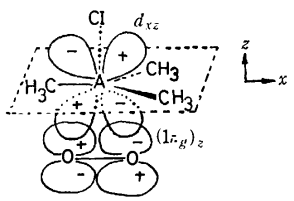

already demonstrated that the planar C_{3v} symmetry is the most plausible for the molecular geometry of the carbonium compound,[7] which is analogous with that of an oxonium compound. With respect to the bond length between the central atom and the counteranion, we can predict the ionic bond length on the baiss of the reaction system containing polar oxidation products, such as hydroperoxides and alcohols, although the present calculations on carbonium and oxonium chlorides do not provide the minimum values of their potential surfaces. Concerning the plausibility of the ionic bond length between the central atom and the counteranion, our previous detailed calculations on trimethylsulfonium chloride also supported this concept.[3-5] Therefore, the ionic bond length can be adopted for the other onium chlorides, though some

7) D. W. A. Sharp and N. Sheppard, *J. Chem. Soc.*, **1957**, 674.

TABLE 3. CONTRIBUTIONS OF THE NEIGHBORING ATOMS TO THE PARTIAL OCCUPATION OF d_{xz} OR d_{xy} ORBITAL OF ONIUM CENTRAL ATOM (A) IN $(CH_3)_3ACl$

Central atom (A)	d-π Overlap				AO bond population			
	A–C[a]		A–Cl		A–C[a]		A–Cl	
	d_{xz}-p_z	d_{xy}-p_z	d_{xz}-p_x	d_{yz}-p_y	d_{xz}-p_z	d_{xy}-p_y	d_{xz}-p_x	d_{yz}-p_y
S	0.399	0.399	0.070	0.070	0.082	0.083	0.007	0.007
Se	0.368	0.368	0.078	0.078	0.010	0.007	0.006	0.006
Te	0.344	0.344	0.062	0.062	−0.019	−0.024	0.002	0.002

These data were supplied by EHMO calculations.

a) A–C bond corresponds to 1A-2C bond of $(CH_3)_3ACl$ illustrated in the following figure:

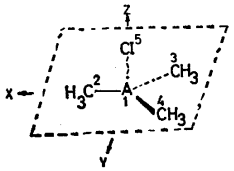

discrepancies yet remain in regard to the configuration of the silyl chloride. Moreover, the planar C_{3v} structure of trimethylsulfonium chloride[3-5] may also support the analogous structures (planar C_{3v} ones) of onium chlorides containing Group VI elements as onium central atoms.

Secondly, the discussion will be developed with respect to the correlation between the electronic properties of onium compounds and their catalytic activities as oxidation catalysts. The order of the activity was found to be as follows: carbonium<ammonium< oxonium; (silyl)<phosphonium≲sulfonium; arsonium≃(telluronium)<selenonium. Among these-onium compounds, third-row onium compounds are most effective. The relatively low activity of the second-row onium compounds is probably due to the fact that their onium central atoms possess only the $2p_z$-orbital utilized for the interaction with the $(1\pi_g)_z$-orbital of O_2; the $2p_z$-orbital may not be so effective as d_{xz} and d_{yz} orbitals, in view of the orbital energy and the orbital overlap with the $(1\pi_g)_z$-orbital of O_2 (as to the mode of the interaction between the onium catalyst and O_2, see the simple model[8] in Table 2). Another reason why the activity of the compound is low is that these onium compounds, especially the carbonium compound, are unstable and ionic. There exists, however, a parallelism between the catalytic activity of the second-row onium compounds and the atomic orbital (AO) population of the p_z-orbital of their central atoms (see Table 2). Some remarks should be here made. The catalytic activity is defined by the maximum reaction rate (R_{max} in Table 2), which is itself estimated from the quantity of O_2 absorbed (mol) in cumene (10 m*l*) or α-pinene (10 m*l*) oxidation at 85°C during the formation of a quantity of the hydroperoxides equal to that of the O_2 absorbed.

Concerning the electronic properties of third-, fourth-, and fifth-row onium compounds, they are characterized by their spatially far-reaching, partially-occupied d_{xz} (or d_{yz}) and d_{xy} orbitals utilized for the interaction with the $(1\pi_g)_z$ and the $(1\pi_g)_y$ of O_2 on the basis of a strong $d\sigma$-$p\sigma$ type overlap and a weak $d\pi$-$p\pi$ type overlap[4] respectively. The remarkable activity of sulfonium and phosphonium compounds is the result of the low-lying, partially-occupied $3d_{xz}$ (or $3d_{yz}$) and $3d_{xy}$ orbitals. The silyl compound, however, exhibits a low activity because of the vacant $3p_z$-orbital. The order of the activity is also in good agreement with that of the AO population of the d_{xz} (or d_{yz}) or the d_{xy}, as may be seen from Table 2. In the cases of phosphonium and arsonium compounds, some steric hindrances by the substituents of the interaction between the onium catalyst and O_2 should be taken into consideration. The partial electron occupation of the d-orbitals is the result of the d-π interactions between the d-orbitals of the central atom and the pi-orbitals of the counteranion or the substituents. From this point of view, the contributions of neighboring atoms (C and Cl) to the partial electron occupation of the d_{xz} or the d_{xy} are confirmed by the d-π overlaps recorded in Table 3.

The relatively low activity of the fourth- or fifth-row onium compounds may be ascribed to the diffuse $4d$ or $5d$ orbitals, especially $4d_{xz}$ or $5d_{xz}$, of their central arsenium, selenium, or tellurium. This diffuseness of the d-orbitals depresses their orbital overlaps with the $(1\pi_g)_z$-orbital of O_2 and is reflected in the orbital contour map of the next higher MO to the lowest unoccupied MO (LU+1 MO) of $(CH_3)_3TeCl$, as may

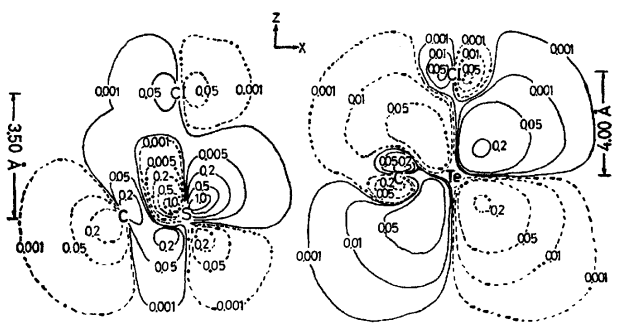

Fig. 1. Orbital contour maps of the LU+1 MOs of $(CH_3)_3SCl$ and $(CH_3)_3TeCl$. These MOs mainly come from the sulfur d_{xz}, carbon p_x and p_z, and chlorine p_x in the x-z cross section. (Solid and dotted curves indicate positive and negative MO-signs respectively.)

8) For detailed models of the interaction, see Ref. 4.

be seen when we compare the map with that of the LU+1 MO of $(CH_3)_3\overset{+}{S}Cl$ (see Fig. 1).

Finally, it may be concluded that the partially-occupied 3*d*-orbitals are most effective for the catalytic activation of molecular oxygen, and that onium compounds possessing them on their central atoms exhibit a catalysis analogous with those of transition-metal catalysts.

The calculations were carried out on a FACOM 230.60 computer at the computation center of the University of Kyushu.

BULLETIN OF THE CHEMICAL SOCIETY OF JAPAN, VOL. 45, 1574—1575(1972)

An MO Interpretation of the Chemical Shifts of the Binding Energies of Inner-shell Electrons. II. A Study of Intramolecular Shifts

Kazuhiro ISHIDA, Hiroshi KATO,* Hiroshi NAKATSUJI, and Teijiro YONEZAWA

Department of Hydrocarbon Chemistry, Faculty of Engineering, Kyoto University, Kyoto

**Department of General Education, Nagoya University, Nagoya*

(Received December 4, 1971)

The relationship between chemical shifts in the binding energies of inner-shell electrons and molecular-charge distributions has been pointed out.[1] For adenine and cytosine molecules, however, Barber and Clark[2] concluded that a "simple relationship between 'shifts' in binding energies and 'charge distributions' can be misleading." In a previous paper,[3] we have derived the following correlation formula between the chemical shifts and molecular-charge distributions within a MO framework:

$$\delta\Delta\varepsilon_s(X, Y) = [Q_A(X) - Q_A(Y)]\gamma_{AA} + \sum_{B(\neq A)}^{\text{in } X} Q_B(X)\gamma_{AB}(X) - \sum_{B(\neq A)}^{\text{in } Y} Q_B(Y)\gamma_{AB}(Y)$$

where $\delta\Delta\varepsilon_s(X,Y)$ denotes the chemical shifts of an inner-shell electron, s, on an atom, A, in a chemical environment, X, from that in another environment, Y. $Q_A(X)$, $Q_B(Y)$, and so on denote the net charges on the A, B, *etc.* atoms in the X, Y, *etc.* environments respectively. γ_{AA} denotes a one-center average Coulomb interaction between inner and valence electrons on an A atom. $\gamma_{AB}(X)$ denotes a two-center average Coulomb interaction between inner electrons on an A atom and valence electrons on a B atom in an X environment.

For inter-molecular shifts of simple molecules, the results by the above formula almost entirely accorded with the experimentally obtained values. In the present note, we will report an application of the above formula to the intra-molecular shifts of adenine and cytosine molecules. The results are shown in Table 1 for carbon 1s and nitrogen 1s. Figures 1 and 2 show the plots of the observed binding energies against the calculated $\Delta\varepsilon_s$[4] values for carbon 1s and for nitrogen 1s respectively. The figures illustrate that the correlations are fairly satisfactory. Especially, the correlation is quantitatively good for the carbon 1s of adenine in Fig. 1, in view of the fact that the solid line is drawn at 45 degree with respect to the horizontal axis. For the nitrogen 1s, the correlations are rather good, but not quantitative, as shown in Fig. 2. In view of the non-empirical calculations done on limited bases by Mely and Pullman[5] and by Clementi,[6] deviation of the observed binding energy from the calculated orbital energy can be not said to be constant (except for the carbon 1s of adenine). Therefore, the different slopes in Fig. 2 most probably arise from the fact that the above deviation is not constant.

TABLE 1. CALCULATED $\Delta\varepsilon_s$ AND OBSERVED BINDING ENERGIES

Molecule	1s Binding		
	Atom	Energy[a] (±0.3 eV)	$\Delta\varepsilon_s$ (eV)
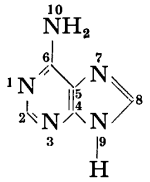	C-5	284.7	−0.44
	C-2	285.7	1.63
	C-8	286.2	1.88
	C-4	286.6	2.40
	C-6	287.8	3.04
	N-1	398.6	−5.98
	N-3	399.1	−4.68
	N-7	399.5	−2.67
	N-10	399.6	−4.73
	N-9	400.9	1.24
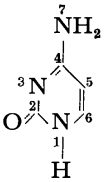	C-5	285.4	−0.28
	C-6	286.5	3.29
	C-4	287.9	4.75
	C-2	289.4	4.22
	N-3	399.6	−5.87
	N-7	400.5	−1.90
	N-1	401.4	−1.33

a) M. Barber and D. T. Clark, *Chem. Commun.*, **1970**, 22, 24.

1) *E.g.* K. Siegbahn *et al.*, ESCA "Atomic Molecular and Solid State Structure Studied by Means of Electron Spectroscopy," Almquist and Wiksells, Uppsala, (1967); D. M. Hercules, *Anal. Chem.*, **42**, 20A (1970).

2) M. Barber and D. T. Clark, *Chem. Commun.*, **1970**, 22.

3) H. Kato, K. A. Ishida, H. Nakatsuji, and T. Yonezawa, This Bulletin, **44**, 2587 (1971).

4) We calculated the $\Delta\varepsilon_s$ with $\Delta\varepsilon_s(X) = Q_A(X)\gamma_{AA} + \sum_{B(\neq A)}^{\text{in } X} Q_B(X)\cdot\gamma_{AB}(X)$, using approximate net charges which has been obtained by the CNDO/2 method.

5) B. Mely and A. Pullman, *Theor. Chim. Acta*, **13**, 278 (1969).

6) E. Clementi, *Int. J. Quant. Chem.*, **IIIs**, 179 (1969).

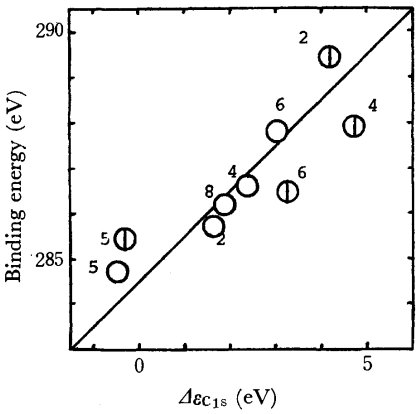

Fig. 1. Observed binding energy *vs.* calculated $\Delta\varepsilon_s$ plots for carbon 1*s* in adenine and cytosine.

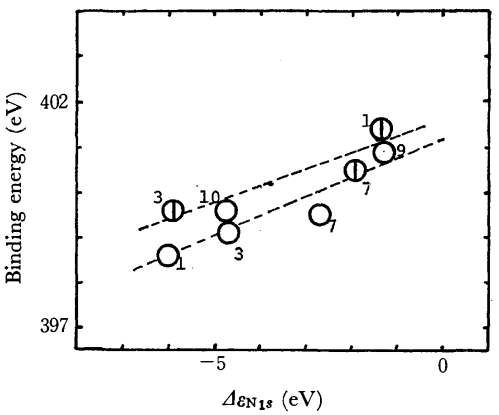

Fig. 2. Observed binding energy *vs.* calculated $\Delta\varepsilon_s$ plots for nitrogen 1*s* in adenine and cytosine.

The above formula means that the chemical shifts of the binding energies should be correlated with charge distributions, though not with simple local charges. Therefore, the previously-refered to suggestion by Barber and Clark is not valid in the present case.

From the above brief discussions we conclude that our formula is useful for the assignment of intra-molecular shifts so long as approximate net charges obtained by a semi-empirical method are used.

BULLETIN OF THE CHEMICAL SOCIETY OF JAPAN, VOL. 45, 1575—1576(1972)

The Polarization Measurement of He-Ne Laser Excitation Raman Lines of Liquid Acetone

Tsunetake FUJIYAMA and Takehiko SHIMANOUCHI

Department of Chemistry, Faculty of Science, The University of Tokyo, Hongo, Bunkyo-ku, Tokyo

(Received December 8, 1971)

Liquid acetone shows three Raman lines, near 530, 490, and 390 cm^{-1}, in the low-frequency region. These bands arise from the three deformation vibrations of the C–CO–C skeleton, namely, the CCC deformation (ν_8, a_1 species), the in-plane CO bending (ν_{18}, b_1 species), and the out-of-plane CO bending (ν_{23}, b_2 species). However, the assignments of these three lines have not yet been settled.[1] Some authors[2–4] assign ν_8 to the 490 cm^{-1} band, ν_{18}, to the 530 cm^{-1} band, and ν_{23} to the 390 cm^{-1} band, while others[5–7] reverse the assignments of ν_8 and ν_{23}.

Mikami-Abe[8] measured the infrared band envelopes of the 475, 409, and 320 cm^{-1} bands of acetone-d_6 in the gaseous state. The 409 cm^{-1} band shows the C-type envelope, which favors the second set of assignments. Alkins and Lippincott[9] measured the depolarization degree of Raman lines of liquid acetone using He–Ne laser excitation. The 490 cm^{-1} band was observed to be strongly polarized, thus supporting the first set of assignments.

TABLE 1. DEPOLARIZATION RATIOS

Compound	$\Delta\nu$ (cm^{-1})	ρ (Ref. 9)	ρ (present results)
Acetone	394	0.76	0.774
	489	0.18	0.770
	531	0.80	0.792
	788	0.11	0.123
Chloroform	262	0.76	0.746
	366	0.11	0.114
	668	0.03	0.041
Methylene iodide	121	0.26	0.284
	485	0.10	0.092

Recently we measured the depolarization degree of the Raman lines of basic compounds and found that the observed value of the 490 cm^{-1} band of liquid acetone was considerably different from that observed by Alkins and Lippincott, although those of the other bands are in good agreement (Table 1). This finding obviates the idea that the 490 cm^{-1} line belongs to the a_1 species.

1) T. Shimanouchi, Tables of Molecular Vibrational Frequencies, Part I, NSRDS-NBS and Consolidated Volume, NSRDS-NBS No. 189, in press.
2) A. Hadni, *Ann. Phys.*, **10**, 874 (1955).
3) J. Lecomte, M. L. Josien, and J. Lascombe, *Bull. Soc. Chim. Fr.*, **1956**, 163.
4) P. Cossee and J. H. Shachtschneider, *J. Chem. Phys.*, **44**, 97 (1966).
5) P. Mirone, *Spectrochim. Acta*, **20**, 1646 (1964).
6) G. Dellepiane and J. Overend, *ibid.*, **22**, 593 (1966).
7) M. T. Forel and M. Fouassier, *ibid.*, **23A**, 1977 (1967).
8) M. Mikami-Abe, Thesis (University of Tokyo, 1968).
9) J. R. Alkins and E. R. Lippincott, *Spectrochim. Acta*, **25A**, 761 (1969).

Experimental

Acetone was purified by vacuum distillation, and its purity was checked by gas chromatography. The Raman spectra were recorded by means of a laser Raman spectrophotometer which had been constructed in our laboratory.[10] A Spex 1401 double monochromator was used as part of the equipment.

The polarized spectra were measured by the standard 90° scattering method, in which the polarization direction of the post-sample analyzer is fixed perpendicular to the direction of the monochromator slit. The pre-sample half-wave plate was used to rotate the direction of the polarization of the incident light. The exciting laser beam was passed only once through the cubic sample-cell, the edges of which were covered with sheets of black paper. The observation of the aperture was confined within an arc of 12 degrees. The polarization ratios were calculated from the relative band areas corresponding to the incident lights polarized parallel to and perpendicular to the polarization direction of the post-sample analyser.

10) T. Fujiyama and M. Tasumi, *Bunko Kenkyu*, **20**, 27 (1971).

BULLETIN OF THE CHEMICAL SOCIETY OF JAPAN, VOL. 45, 1576—1578(1972)

Reduction of Some 7-Halonorcaranes with Tri-*n*-butyltin Hydride

Teiichi ANDO, Kiyotaka WAKABAYASHI, Hiroki YAMANAKA,* and Wataru FUNASAKA

Department of Industrial Chemistry, Faculty of Engineering, Kyoto University, Yoshida-Honmachi, Sakyo-ku, Kyoto

**Department of Chemistry, Kyoto Institute of Technology, Matsugasaki, Sakyo-ku, Kyoto*

(Received December 15, 1971)

It has been found that the reduction of 1-chloro-(or -bromo-)1-fluorocyclopropanes with tri-*n*-butyltin hydride at 0—135°C generally proceeds stereospecifically, *i.e.*, with a complete retention of the configuration.[1,2] Thus, 7-*exo*-chloro-7-*endo*-fluoronorcarane gives 7-*endo*-fluoronorcarane exclusively, and 7-*endo*-chloro-7-*exo*-fluoronorcarane gives 7-*exo*-fluoronorcarane exclusively. Since the reduction of organic halides with organotin hydrides is known to be a radical process,[3] this result must be interpreted as being due to the pyramidal structure of the intermediately-formed 7-fluoro-7-norcaryl radical and the slow rate of its inversion of configuration relative to its hydrogen abstraction.

As was mentioned in the previous paper,[2] the reduction of 7-bromo-7-chloronorcarane shows a lower degree of stereospecificity; one of its geometrical isomers, 7-*exo*-bromo-7-*endo*-chloronorcarane, gives a 76: 24 mixture of 7-*endo*- and -*exo*-chloronorcarane when reduced with tri-*n*-butyltin hydride at 0°C. Analogous results have very recently been reported by Altman and Baldwin.[4] Obviously, the inversion of the 7-chloro-7-norcaryl radical can compete with hydrogen abstraction even at 0°C, resulting in the decrease of stereospecificity.

In contrast, the reduction of the geometrical isomers of 1-bromo-1-trifluoromethyl-2-phenylcyclopropane with triphenyltin hydride has been reported to give a mixture of the two possible geometrical isomers of the same composition, irrespective of the geometry of the starting material.[5]

These experimental facts suggest that the configurational stability of cyclopropyl radicals is strongly affected by the nature of the substituent at the 1-position.

The present paper will deal with studies of the reduction of 7-methoxycarbonyl- and 7-cyano-substituted 7-chloro-(or -bromo-)norcarane with tri-*n*-butyltin hydride, carried out in order to ascertain the effect of substituents at the 7-position upon the configurational stability of 7-norcaryl radicals.

Results and Discussion

The norcarane derivatives employed for the present study, *i.e.*, methyl 7-chloro-(or -bromo-)norcarane-7-carboxylate (IV or IV′) and 7-chloro-(or -bromo-)-norcarane-7-nitrile (V or V′), were prepared from the corresponding carboxylic acids (III and III′), which had been synthesized by applying the method of Köbrich and Goyert[6] to 7,7-dichloro-(and -dibromo-)-norcarane (I and I′):

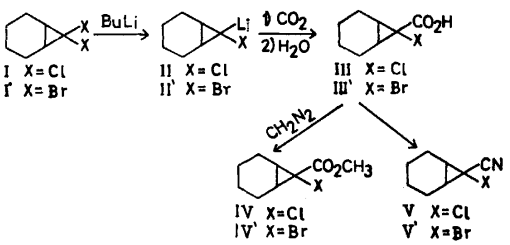

It was found that, although 7,7-dichloronorcarane (I) gave a mixture of the two geometrical isomers of the chloro acid (III), 7,7-dibromonorcarane (I′) gave little, if any, of the *endo*-bromo isomer of 7-bromo-norcarane-7-carboxylic acid (III′), even when the reaction (treatment with *n*-butyllithium followed by

1) T. Ando, F. Namigata, H. Yamanaka, and W. Funasaka, *J. Amer. Chem. Soc.*, **89**, 5719 (1967).

2) T. Ando, H. Yamanaka, F. Namigata, and W. Funasaka, *J. Org. Chem.*, **35**, 33 (1970).

3) L. W. Menapace and H. G. Kuivila, *J. Amer. Chem. Soc.*, **86**, 3047 (1964).

4) L. J. Altman and R. C. Baldwin, *Tetrahedron Lett.*, **1971**, 2531.

5) L. J. Altman and J. C. Vederas, *Chem. Commun.*, **1969**, 895.

6) G. Kobrich and W. Goyert, *Tetrahedron*, **24**, 4327 (1968).

Table 1. Properties of 7-substituted 7-halonorcaranes

Structure	Bp, °C/mmHg (Mp, °C)	n_D (°C)	$\nu_{C=O}$, cm^{-1} ($\nu_{C\equiv N}$, cm^{-1})	δ_{OCH_3}, ppm (δ_{OH}, ppm)	C % Found	C % Calcd	H % Found	H % Calcd	N % Found	N % Calcd
HOOC, Br (IIIa)	(110—111)	—	1705	(11.76)	44.09	43.85	5.31	5.07	—	—
CH_3OC O, Cl (IVa)	123—126/22	1.4892 (18)	1745	3.77	57.43	57.29	6.96	6.96	—	—
Cl, $COOCH_3$ (IVb)	123—126/22	1.5009 (18)	1730	3.73	57.23	57.29	6.90	6.96	—	—
CH_3OCO, Br (IV'a)	70—72/3	1.5080 (19)	1730	3.78	46.35	46.37	5.67	5.63	—	—
$N\equiv C$, Cl (Va)	118—120/20	1.4940 (22)	(2250)	—	61.60	61.34	6.55	6.45	8.70	8.94
Cl, $C\equiv N$ (Vb)	118—120/20	1.5007 (22)	(2250)	—	61.54	61.34	6.56	6.45	8.67	8.94
$N\equiv C$, Br (V'a)	119/13	1.5249 (16)	(2230)	—	47.76	48.02	5.05	4.73	6.72	7.00

carbonation) was conducted at −150 to −140°C. The assignment of the *exo*-bromo configuration to the isolated product was based on the methanolysis of the reaction mixture at the same temperature, which gave predominantly the *exo*-bromo isomer of 7-bromonorcarane.[7,8] Probably the *endo*-bromo lithium carbenoid (II', X=*endo*-Br), if formed, had reacted with the tetrahydrofuran solvent to form 7-*exo*-(2-tetrahydrofuryl)norcarane[6] before carbon dioxide was added to the reaction mixture. The possibility cannot be excluded, however, that the *endo*-bromo carbenoid isomerizes to the *exo*-bromo carbenoid under the reaction conditions.

Each of the geometrical isomers of 7-chloronorcarane-7-carboxylic acid (III), as well as 7-*exo*-bromonorcarane-7-*endo*-carboxylic acid (III'a), was converted to the corresponding methyl ester or nitrile by the usual methods. The assignment of configuration to the products is straightforward, since no configurational change should occur during these transformations.

The properties of the hitherto-unknown 7-substituted 7-chloro-(or -bromo-)norcaranes thus prepared are shown in Table 1.

The reduction of the chloro (or bromo) esters and nitriles was performed by treating them with a slight excess of tri-*n*-butyltin hydride under the variety of conditions shown in Table 2. The yields of the reduction product were about 90% for the esters and about 70% for the nitriles. The isomer distributions in the product, which were determined by vpc before distillation, are also listed in Table 2.

As is evident from Table 2, the isomer ratios in the product were nearly identical in all experimental runs. This implies that the 7-methoxycarbonyl- or -cyano-7-norcaryl radical, which would be intermediately formed in the process of the reduction, is either pyramidal but inverts its configuration so rapidly that it behaves as if it were planar, or is in fact planar. Very probably the p-π conjugation between the π-electrons in the methoxycarbonyl or the cyano group and the p-electron at the radical center lowers the energy barrier for the inversion of the configuration of these radicals.

7) D. Seyferth, H. Yamazaki, and D. L. Alleston, *J. Org. Chem.*, **28**, 703 (1963).

8) C. L. Osborn, T. C. Shields, B. A. Shoulders, C. G. Cardenas, and P. D. Gardner, *Chem. Ind.* (London), **1965**, 766.

Table 2. Reduction of 7-substituted 7-halonorcaranes

Compound reduced	Reaction condition: Catalyst	Temp., (°C)	Time, (hr)	Isomer ratio in product (*endo*-: *exo*-)
IVa	AIBN	80	8	93:7
	DTBP	140	4	92:8
IVb	AIBN	80	8	94:6
	DTBP	140	4	93:7
IV'a	None	0	2	95:5
	None	110	2	93:7
	None	170	2	90:10
Va	AIBN	80	8	93:7
	DTBP	140	4	92:8
Vb	AIBN	80	8	94:6
	DTBP	140	4	92:8
V'a	None	0	2	97:3
	None	110	2	94:6
	None	170	2	91:9

The predominant formation of the *endo*-substituted isomers in these reductions must be due to the greater steric repulsion in the hydrogen transfer from the tin hydride to the *endo* side of the radical than to the *exo* side. The increase in the relative amount of the *exo*-substituted product with the increase in the reaction temperature may be explained on the same ground.

Experimental

The proton NMR spectra were recorded on a JEOL C-60H spectrometer in carbon tetrachloride with tetramethylsilane (TMS) as the internal reference. The chemical shifts (δ) are expressed in ppm downfield from TMS. In vapor-phase chromatography (vpc), a Golay column of 0.5 mm × 45 m (BDS 45) was used for analytical purposes, and a column of 10 mm × 0.8 m (30% Silicone Grease on 60—80 mesh Celite 550), for preparative purposes. The isomer distributions in the products were determined from the peak areas in vpc before distillation.

Reduction of 7-Substituted 7-Halonorcaranes with Tri-n-butyltin Hydride. The reduction of chloro derivatives was effected by heating a mixture of an isomerically-pure substrate (IVa, IVb, Va, or Vb) and a slight excess of tri-*n*-butyltin hydride under nitrogen with stirring in the presence of a small amount

Table 3. Properties of the products

Structure	Bp, °C/mmHg	n_D (°C)	$\nu_{C=O}$, cm^{-1} ($\nu_{C\equiv N}$, cm^{-1})	δ_{OCH_3}, ppm	C %		H %		N %	
					Found	Calcd	Found	Calcd	Found	Calcd
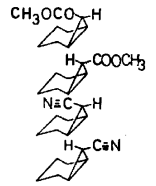	93— 95/18	1.4786 (18)	1735	6.93	69.78	69.65	9.20	9.09	—	—
	93— 95/18	1.4729 (26)	1720	6.43	69.51	69.65	8.95	9.09	—	—
	125—130/55	1.4930 (19)	(2250)	—	79.31	79.29	8.93	9.15	11.44	11.56
	109—111/22	1.4857 (25)	(2250)	—	79.56	79.29	9.30	9.15	11.75	11.56

of azobisisobutyronitrile (AIBN) or di-*t*-butyl peroxide (DTBP). For bromo derivatives (IV'a or V'a), tri-*n*-butyltin hydride was gradually added to a substrate kept at a constant temperature. The reaction conditions and the isomer distributions in the products are shown in Table 2. The identification of the products was made by preparing authentic samples of norcarane-7-*endo*- or -*exo*-carboxylic acid by the method of Skell and Etter,[9] converting them to the corresponding methyl esters or nitriles in the usual way and then comparing their physical properties (IR, NMR, and mass spectra as well as retention times in vpc) with those of the products. Generally, the *endo* esters or nitriles had a shorter retention time than the *exo* isomers. The properties of the products are summarized in Table 3, together with the results of elemental analyses.

9) P. S. Skell and R. M. Etter, *Proc. Chem. Soc.*, **1961**, 443.

SHORT COMMUNICATIONS

Hydrolysis of Adenosine 5′-Triphosphate in the Presence of Various Polyamines

Shinnichiro SUZUKI, Tadayoshi HIGASHIYAMA, Kazuko UEDA, and Akitsugu NAKAHARA
Institute of Chemistry, College of General Education, Osaka University, Toyonaka, Osaka
(Received January 31, 1972)

We have recently investigated the non-enzymatic hydrolysis of adenosine 5′-triphosphate (ATP) with various polyamines in order to find a clue to the ATPase function. We observed that ATP is hydrolyzed effectively and specifically with some amines.

Aqueous solutions of ATP (1×10^{-3}M) containing polyamine hydrochloride (1×10^{-3}M) adjusted at a series of pH values with small quantities of hydrochloric acid or sodium hydroxides, were heated at 60°C for 3 hr. The reaction products, orthophosphate (Pi)[1] and/or pyrophosphate (PPi),[1] were determined by the methods of Martin and Doty[2] and of Tetas and Lowenstein,[3] respectively. For some particularly important data on the amount of Pi and PPi, the results were re-examined on the basis of the amount of nucleotides such as ATP, ADP, and AMP by Cohn-Carter method,[4] showing a satisfactory coincidence with each other. The results of ATP hydrolysis with polyamines, *viz.*, $NH_2CH_2CH_2(NHCH_2CH_2)_nNH_2$ (n=0, 1, 2, 3, and 4) are given in Fig. 1.

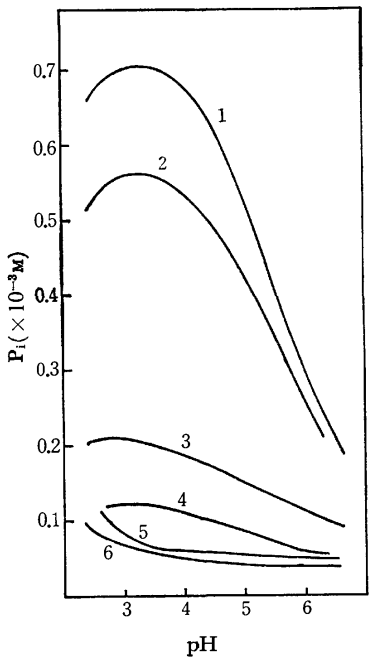

Fig. 1. The results of hydrolysis reactions of ATP with polyamines at various pH values.
1: pentaen (n=4), 2: tetraen (n=3), 3: trien (n=2), 4: dien (n=1), 5: en (n=0), 6: in the absence of amine
experimental error: within 2 to 3%

We see that hydrolyses with pentaen,[5] tetraen, trien, or dien show a maximum at pH range 3—4, and the behaviors of pentaen and tetraen show remarkably high activities. The reaction of ATP with pentaen or tetraen also exhibited excellent specificity, producing only ADP and Pi. Figure 2 shows plots of the yields of Pi against ATP-amine ratio. The breaks in the two curves which occur at a 1:1, amine: ATP system suggest that the intermediates in the hydrolysis reactions consist of equimolecular amounts of ATP and amine. Hydrolysis reactions in the presence of dien(N 2 N 2 N),[6] spmd(N 3 N 4 N), ditn(N 3 N 3 N), trien (N 2 N 2-N 2 N), spmn(N 3 N 4 N 3 N), and dheen (O 2 N-2 N 2 O) were also carried out in water–dioxane (3:2) mixture. The spmd and ditn, and spmn and dheen showed no reaction activities compared with dien and trien, respectively. Of special interest is the fact that no alcohol group in dheen molecule shows activity, and the number of the methylene chains between two nitrogen atoms in a polyamine is extremely important for the hydrolysis reaction.

It may be suggested that there are intermolecular hydrogen bondings between the amino groups of polyamine and the parts of adenine ring, ribose ring and phosphate chain in ATP to activate the phosphate group so that the hydrolytic attack of water molecule becomes easier.

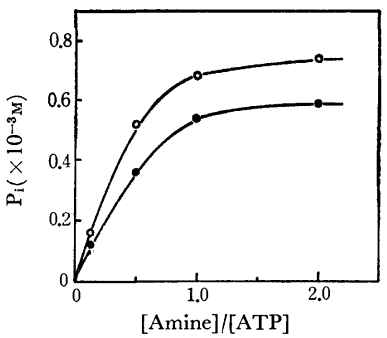

Fig. 2. The reaction activities against the ratio of polyamines.
(○: pentaen, ●: tetraen) to ATP (1×10^{-3}M).
The reactions were performed at pH 4.0 and at 60°C for 3 hr.

1) These products are shown in the following schemes.
ATP→ADP+Pi ADP: adenosine-5′-diphosphate
ATP→AMP+PPi AMP: adenosine-5′-monophosphate
2) J. B. Martin and D. M. Doty, *Anal. Chem.*, **21**, 965 (1940).
3) M. Tetas and J. M. Lowenstein, *Biochem.*, **1963**, 350.
4) W. E. Cohn and C. E. Carter, *J. Amer. Chem. Soc.*, **72**, 4273 (1950).

5) The polyamines and the alcohol derivative used are abbreviated as follows:
en: ethylenediamine; dien: diethylenetriamine; trien: triethylenetetramine; tetraen: tetraethylenepentamine; pentaen: pentaethylenehexamine; spmd: spermidine; spmn: spermine; ditn: dipropylenetriamine; dheen: *N,N′*-(di-2-hydroxyethyl)ethylenediamine.
6) The numerals 2, 3, and 4 symbolize the numbers of methylene chains; notation, for example, N 2 N 2 N and O 2 N 2 N 2 O show $NH_2CH_2CH_2NHCH_2CH_2NH_2$ and $HOCH_2CH_2NHCH_2CH_2NHCH_2CH_2OH$, respectively.

Evidence of a π-Allyl Intermediate in the Deuterium Propylene Exchange Reaction over $C_{24}K$

Toshihiko KONDO, Masaru ICHIKAWA, Shuji SAITO, and Kenzi TAMARU*

Sagami Chemical Research Center, Ohnuma, Sagamihara, Kanagawa

**Department of Chemistry, The University of Tokyo, Hongo, Bunkyo-ku, Tokyo*

(Received December 24, 1971)

The deuterium propylene exchange reaction was studied over the potassium graphite intercalation compound $C_{24}K$. The deep blue $C_{24}K$[1] was prepared by heating 2.0 g of spectroscopic powder graphite (Union Carbide Co.) with *ca.* 0.5 g of distilled potassium metal in *vacuo* at 380°C for 24 hr. A conventional closed circulating system was used to study the exchange reaction. Mass and microwave spectroscopic techniques[2] were used to determine the deuterium content and its distribution in the propylene.

Deuterium (*ca.* 200 mmHg) was circulated over $C_{24}K$ at 120°C for about 15 hr and the system was then evacuated for about 10 min. When a mixture of propylene and D_2 was introduced onto the catalyst at 120°C, simultaneous deuteration and exchange of the propylene took place. The amounts of the various propylenes d_1, d_2,$\cdots d_6$, were determined by mass spectrometry, using an ionization voltage of 10 V to avoid fragmentation. No propylene-d_6 was detected throughout the reaction. The hydrogen exchange reaction did not proceed through a multiple exchange process, but through successive single exchange steps.

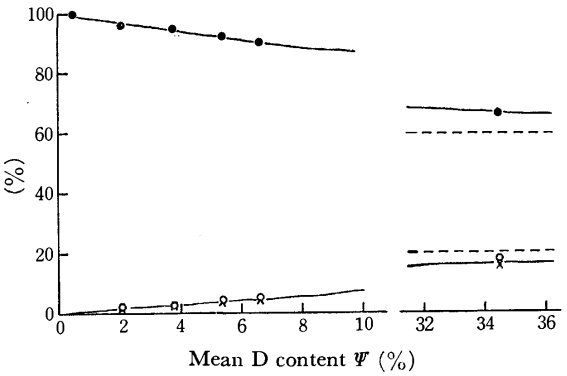

Fig. 1. Hyperfine deuterium distribution of propylene-d_1 at 120°C over $C_{24}K$.
Mean deuterium content Ψ is represented by the equation $\Psi=100(\sum_{i=1}^{6} id_i/6\sum_{i=0}^{6} d_i)$. ●: 3-$d_1$, ×: *cis*-1-$d_1$, ○: *trans*-1-$d_1$

The results of microwave spectroscopic measurements of propylene-d_1, C_3H_5D, as shown in Fig. 1, demonstrated that propylene-3-d_1, $CH_2DCH{=}CH_2$, was the only reaction product in the initial stage of the reaction. As the reaction proceeded, *cis*-1-d_1 and *trans*-1-d_1[3] propylene were formed. However, no propylene-2-d_1, $CH_3CD{=}CH_2$, was observed during the reaction. This indicates that the normal propyl species ($CH_3CH_2\overset{*}{C}H_2$) is not the intermediate of this exchange reaction. Also, the isopropyl species ($CH_3\overset{*}{C}HCH_3$) cannot be the intermediate since it should give a deuterium distribution of 60% 3-d_1, 20% *trans*-1-d_1, and 20% *cis*-1-d_1 which should not vary with reaction time. Accordingly, the intermediate of this exchange reaction cannot be of the half-hydrogenated state of propylene.

If the exchange reaction proceeded by the concerted mechanism (push-pull mechanism),[4] propylene-3-d_1 should predominate in the initial stage of the reaction and be followed by *cis*-1-d_1 and *trans*-1-d_1 propylene. The deuterium distribution of propylene-d_1 in the concerted mechanism shows good agreement with the results in Fig. 1.

TABLE 1. HYPERFINE DEUTERIUM DISTRIBUTION OF PROPYLENE-d_2 IN THE INITIAL STAGE OF THE REACTION ($\Psi=6.6\%$) AT 120°C OVER $C_{24}K$

1,1-d_2	3 (%)
cis-1,3-d_2	22
trans-1,3-d_2	25
3,3-d_2	50

However, the deuterium distribution of propylene-d_2, $C_3H_4D_2$, as shown in Table 1, cannot be explained by a concerted mechanism, because this mechanism would require an initial $C_3H_4D_2$ propylene distribution of 50% *cis*-1,3-d_2 and 50% *trans*-1,3-d_2. In contrast, the results in Table 1 show that the main product in the initial stage is propylene-3,3-d_2, $CHD_2{-}CH{=}CH_2$, (50%) and that the *cis*-1,3-d_2 and *trans*-1,3-d_2 propylene account for only 22% and 25%, respectively, of the total propylene-d_2. This initial distribution of propylene-d_2 indicates that in the reaction intermediate 1 and 3-carbons are equivalent.

The propylene-d_1 distribution shown in Fig. 1 can also be explained by a π-allyl intermediate ($CH_2{=}\overset{*}{C}H{=}CH_2$) mechanism.[5] The mechanism would predict an initial propylene-d_2 distribution of 50% 3,3-d_2, 25% *cis*-1,3-d_2, and 25% *trans*-1,3-d_2. The distribution is in good agreement with that given in Table 1. Other dissociative intermediates (*e.g.*, $CH_2{-}\overset{*}{C}H{=}CH_2$, $CH_3{-}\overset{*}{C}{=}\overset{*}{C}H_2$, $CH_3{-}\overset{*}{C}H{=}\overset{*}{C}H$) are also excluded by our results. It is thus concluded that the intermediate of the exchange reaction of propylene with deuterium over $C_{24}K$ is most probably the π-allyl species, and definitely neither an associative nor dissociative species and no concerted mechanism is involved.

1) D. E. Nixon and G. S. Parry, *Brit. J. Appl. Phys.*, **1968**, Ser. 2, Vol. 1, 291.

2) K. Hirota, Y. Hironaka, and E. Hirota, *Tetrahedron Lett.*, **1964**, 1645; K. Hirota, N. Yoshida, S. Teratani, S. Saito, *J. Catal.*, **15**, 425 (1969).

3) *Cis*-1-d_1 and *trans*-1-d_1 represent $\begin{matrix} CH_3 & D \\ & \diagdown\!\diagup \\ & C{=}C \\ & \diagup\!\diagdown \\ H & H \end{matrix}$ and $\begin{matrix} CH_3 & H \\ & \diagdown\!\diagup \\ & C{=}C \\ & \diagup\!\diagdown \\ H & D \end{matrix}$, respectively.

4) D. M. Brouwer, *J. Catal.*, **1**, 22 (1962).

5) S. Naito, Y. Sakurai, H. Shimizu, T. Onishi, and K. Tamaru, *Trans. Faraday Soc.*, **67**, 1529 (1971).

A Novel Cleavage of Carbon-Carbon Triple Bond

Hiroshi FUJITA, Rokuro ENDO, Keisuke MURAYAMA, and Takeshi ICHII
Central Research Laboratories, Sankyo Co., Ltd., Hiromachi, Shinagawa-ku, Tokyo

(Received December 25, 1971)

In our studies of phenylpropiolamidines, nucleophilic addition occurred predominantly at the β-carbon of the acetylenic bond in an acidic medium, and reactions with bifunctional nucleophiles (*e.g.* NH_2OH) afforded five membered heterocyclic compounds such as isoxazoles.[1)]

Although *N,N'*-diphenylphenylpropiolamidine (I) exhibited behavior similar to phenylpropiolate in the above cases, reaction of I with 4-methyl-*o*-phenylenediamine[2)] in boiling ethanolic hydrogen chloride proceeded characteristically to furnish 5-methyl-2-phenylbenzimidazole (II; mp 248—248.5°C), as a result of cleavage of the acetylenic bond.

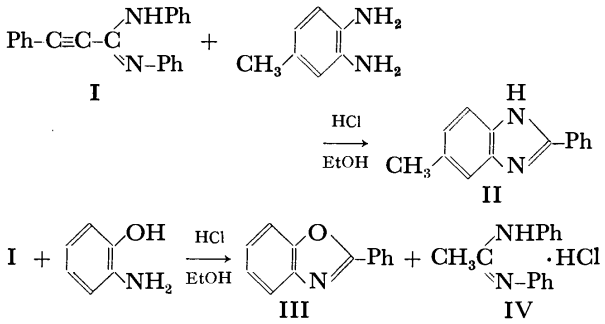

In the reaction of I with *o*-aminophenol in the presence of hydrogen chloride, *N,N'*-diphenylacetamidine was obtained as a hydrochloride (IV; mp 224—226°C), together with 2-phenylbenzoxazole (III; mp 103—104°C). The acetamidine formation indicated clearly that acetylenic bond fission had occurred.

o-Aminobenzenethiol reacted with I in ethanol to give 2-(*o*-aminophenylthio)-*N,N'*-diphenylcinnamamidine [V; mp 150—151°C. Found: C, 77.33; H, 5.62; N, 9.78; S, 7.66%. Calcd for $C_{27}H_{23}N_3S$: C, 76.93; H, 5.50; N, 9.97; S, 7.60%. NMR (δ in acetone-d_6): 5.54 (s, =CH–)]. Heating of V·HCl (mp 186.5—187°C) for a short time in dimethylformamide afforded 2-phenylbenzothiazole (VI; mp 114—115°C) and IV respectively, in good yields.

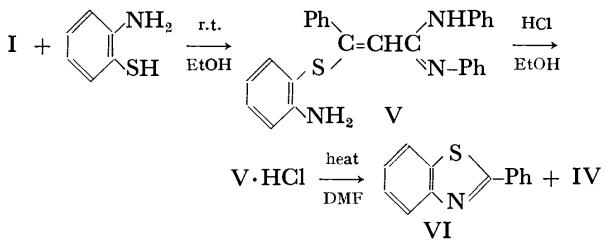

The reaction of I with toluene-3,4-dithiol gave 2-(*N,N'*-diphenylamidinomethyl)-5-methyl-2-phenyl-1,3-benzodithiol [VII; mp 139.5—141°C. Found: C, 74.61; H, 5.24; N, 6.22; S, 14.32%. Calcd for $C_{28}H_{24}N_2S_2$: C, 74.30; H, 5.34; N, 6.19; S, 14.17%. NMR (δ in $CDCl_3$): 3.52 (2H, s, CH_2). Mass (*m/e*): 452 (M^+), 243 (5-methyl-2-phenyl-1,3-benzodithiolium cation)].

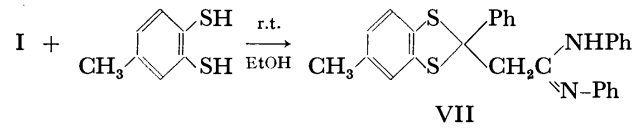

This reaction shows that a second nucleophilic attack can take place at the β-carbon of the acetylenic bond.

The mechanism of the cleavage of the triple bond followed by the formation of benzimidazole, benzoxazole, or benzothiazole can thus be considered as shown in Scheme 1.

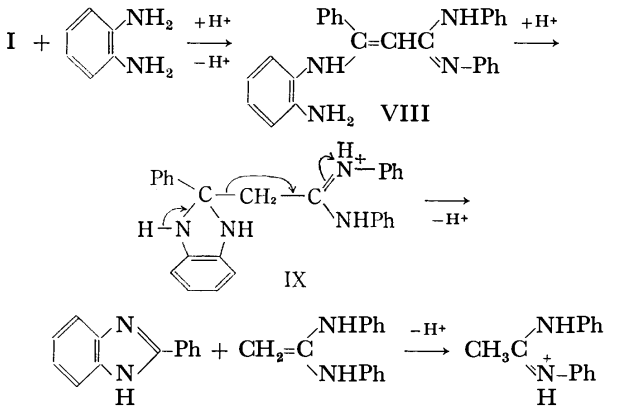

Scheme 1

The smooth fission of the carbon-carbon triple bond in the protonated propiolamidine system under such mild reaction conditions might be explained by successive nucleophilic additions at the β-carbon of the acetylenic bond, followed by a fragmentation process, which would be due to the stronger electron withdrawing character of the protonated amidine group. Although the stereochemical aspects of this reaction are not clear, it is presumed that an activated enediamine form of protonated VIII (X in Scheme 2) readily undergoes prototropic change to XI, which is attacked predominantly at the β-carbon by the second nucleophilic function, as shown in Scheme 2.

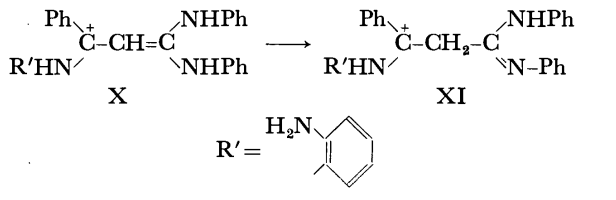

Scheme 2

1) H. Fujita, R. Endo, A. Aoyama, and T. Ichii, This Bulletin, in press.

2) For the reaction of diethyl acetylenedicarboxylate with 4-methyl-*o*-phenylenediamine, *cf.*, Y. Iwanami, *Nippon Kagaku Zasshi*, **83**, 161 (1962).

A New Route to Nitriles from Thioamides

Hiroshi FUJITA, Rokuro ENDO, and Keisuke MURAYAMA
Central Research Laboratories, Sankyo Co. Ltd., Hiromachi, Shinagawa-ku, Tokyo
(Received December 28, 1971)

In the preceding paper,[1] we reported that a new cleavage reaction of a carbon-carbon triple bond occurred in the protonated propiolamidine system. In this paper, a new kind of fragmentation reaction is described, involving reactions of phenylpropiolamidines with thioamides, thioureas, and thiosemicarbazides.

The reaction of *N,N'*-dicyclohexylphenylpropiolamidine (Ia) with thioacetamide in boiling ethanol gave *N,N'*-dicyclohexyl-*β*-mercaptocinnamamidine [IIa; mp 158—159°C. Found: C, 73.43; H, 8.65; N, 8.13; S, 9.39%. Calcd for $C_{21}H_{30}N_2S$: C, 73.64; H, 8.83; N, 8.16; S, 9.36%. NMR (*δ* in $CDCl_3$): 6.26 (1H, s, =CH–)] in 50% yield, while dimethyl acetylenedicarboxylate and methyl propiolate reacted with thioacetamide to give (1'-iminoethyl)thiodimethyl fumarate and *cis,cis*- and *cis,trans*-dimethyl-*β*-thiodiacrylic esters, respectively.[2] Subsequently, IIa afforded 5-cyclohexylamino-3-phenylisoxazole (mp 128—129°C)[3] by the reaction with hydroxylamine hydrochloride.

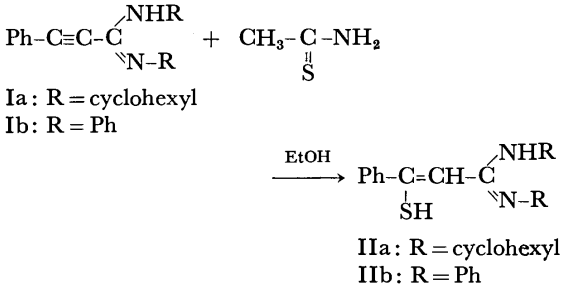

Ia: R = cyclohexyl
Ib: R = Ph

A reaction of Ia with thiobenzamide also gave IIa and benzonitrile in 53 and 65% yield, respectively. The reaction provided a convenient synthetic route to nitriles from thioamides under mild, neutral conditions.

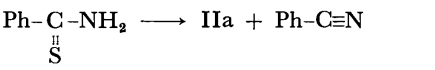

Both reactions of Ia with 1-phenylthiourea and with 1,3-diphenylthiourea gave IIa in 32 and 39% yield, respectively, but thiourea and 1,3-di-*n*-butylthiourea failed to react with Ia and the thioureas were predominantly recovered. This shows that the acidity of N–H in thioureas would be a factor influencing the reaction.

N,N'-Diphenylphenylpropiolamidine (Ib) reacted with 4-phenylthiosemicarbazide to afford *N,N'*-diphenyl-*β*-mercaptocinnamamidine [IIb: mp 162—164°C. Found: C, 76.43; H, 5.28; N, 8.60; S, 9.79%. Calcd for $C_{21}H_{18}N_2S$: C, 76.33; H, 5.49; N, 8.48; S, 9.70%. NMR (*δ* in $CDCl_3$): 6.47 (1H, s, =CH–)] in 16% yield: IIb was also obtained by reaction of Ib with thioacetamide, but in a poorer yield than IIa. The difference in yield suggests that the basicity of the amidine function plays an important role in the reaction. Addition of hydrogen chloride slightly improved the yield of IIb. Thiosemicarbazide also reacted with Ia to give IIa.

Thiol synthesis using thioamides is common and the cleavage of the C–S bond is usually carried out by alkaline hydrolysis. The facile fission of the C–S bond under such mild conditions as in the above cases may be attributed to the heterolytic fragmentation reaction. Although the proton source is not clear, we assume that the driving force of the fragmentation reaction would be due to the electron withdrawing character of the protonated amidine moiety, as shown in Scheme 1, since a thioamide could act as the proton source. This would also support the view that both the basicity of the amidine nitrogen and the acidity of N–H in the thioureas seem to be the important factors in promoting the reaction.

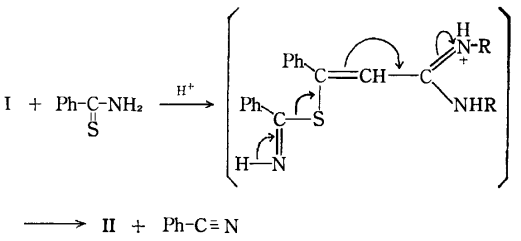

Scheme 1

1) H. Fujita, R. Endo, K. Murayama, and T. Ichii, This Bulletin, **45**, 1581 (1972).
2) J. W. Lown and J. C. N. Ma, *Can. J. Chem.*, **45**, 953 (1967); Y. Kishida and A. Terada, *Chem. Pharm. Bull.* (Tokyo), **16**, 1351 (1968).
3) H. Fujita, R. Endo, A. Aoyama, and T. Ichii, This Bulletin, in press.

Preparation and Properties of Methylcopper-triphenylphosphine Complexes[1)]

Akio YAMAMOTO, Akira MIYASHITA, Takakazu YAMAMOTO, and Sakuji IKEDA

Research Laboratory of Resources Utilization, Tokyo Institute of Technology, Ookayama, Meguro, Tokyo

(Received December 2, 1971)

Alkyl and aryl copper complexes are considered to be involved in various copper-catalyzed organic reactions.[2)] A number of reports have been given on the preparation of alkyl and aryl copper complexes by reactions of copper salts with alkyllithium,[3)] alkylzinc,[4)] Grignard reagents,[3,5)] and tetraalkyllead.[6)] Most of the complexes, however, have been prepared *in situ* and the unequivocal isolation of a pure alkyl copper complex free from the alkylating agent does not seem to have been reported so far.

Alkyl copper complexes are thermally unstable. Attempts to stabilize the copper-alkyl bond by addition of ligands such as triphenylphosphine and α,α′-dipyridyl have been unsuccessful.[4,5a)] These ligands are claimed to have no stabilizing effects and the methylcopper complexes with these ligands are reported to decompose explosively even at a low temperature.

We wish to report the preparation of moderately stable methylcopper complexes from copper acetylacetonate, dimethylaluminium ethoxide and triphenylphosphine (in a ratio of 1:3:4) below −10C° in toluene and diethyl ether under nitrogen in a similar way to that for the preparation of other alkyltransition metal complexes.[7)]

$$Cu(acac)_2 + Al(CH_3)_2OC_2H_5 + PPh_3 \xrightarrow{\text{toluene}} CuCH_3(PPh_3)_3\cdot C_6H_5CH_3 \quad (\mathbf{1})$$

$$Cu(acac)_2 + Al(CH_3)_2OC_2H_5 + PPh_3 \xrightarrow{\text{ether}} CuCH_3(PPh_3)_2\cdot {}^1/_2(C_2H_5)_2O \quad (\mathbf{2})$$

Complexes **1** and **2** isolated as light yellow needles and crystalline powder, containing toluene and ether as solvents of crystallization, were characterized by elemental analysis, IR and NMR spectroscopy and chemical reactions.

Found: C, 75.6; H, 6.0; Cu, 6.5; $P(C_6H_5)_3$,[8)] 77; $C_6H_5CH_3$,[9)] 10.3%; CH_3/Cu, 1.1. Calcd for $CuCH_3\{P(C_6H_5)_3\}_3C_6H_5CH_3$ (**1**): C, 77.7; H, 5.9; Cu, 6.6; $P(C_6H_5)_3$, 82; $C_6H_5CH_3$, 9.6%; CH_3/Cu, 1.0. IR (KBr): 2830, 2780 (C–H of CH_3–Cu); NMR (100 MHz in THF): τ 10.4 (s, 3H, CH_3–Cu), 7.7 (s, 3H, CH_3–C_6H_5), 2.7 (m, 50H, C_6H_5).

Found: C, 72.8; H, 5.8; Cu, 10.0; $P(C_6H_5)_3$,[10)] 81—88%; CH_3/Cu, 1.01; $(C_2H_5)_2O$/Cu, 0.43. Calcd for $CuCH_3\{P(C_6H_5)_3\}_2\cdot {}^1/_2(C_2H_5)_2O$ (**2**): C, 73.2; H, 6.0; Cu, 9.9; $P(C_6H_5)_3$, 82.0%; CH_3/Cu, 1.00; $(C_2H_5)_2$ O/Cu, 0.5. NMR: τ 10.3 (s, 3H, CH_3–Cu).

The methyl copper complexes are thermally moderately stable in contrast to the behavior of $CuCH_3(PPh_3)_3$ prepared by Costa *et al.*;[5a)] **1** decomposes gradually over 0°C and **2** can be kept at room temperature in the solid state in nitrogen in the dark. These methylcopper complexes are light-sensitive and are decomposed by UV light releasing methane. On alcoholysis and acidolysis **1** and **2** released quantitative amounts of CH_4; the reaction with D_2SO_4 yielded only CH_3D. The possibility of a structure with copper bonded to the *ortho*-carbon of a phenyl group of triphenylphosphine was excluded in view of the absence of deuterium introduced to triphenylphosphine after the acidolysis with D_2SO_4, as proved by mass spectrometric examination of water formed by degradative oxidation of the triphenylphosphine ligands in the presence of copper oxide. On pyrolysis at 85°C **1** gave CH_4 and C_2H_6 in a ratio of 1:2 and **2** released CH_4, C_2H_6, and C_2H_4 in a ratio of 1:4.5:0.5. Reaction of **1** with ethyl iodide gave methane and propane in a ratio of about 1:1; **2** reacted with ethyl iodide yielding methane and propane in a ratio of 3:2 with a trace of butane. Carbon monoxide was inserted into the methyl–copper bond affording acetone.

Vinyl monomers such as acrylonitrile, methacrylonitrile, methyl acrylate, methyl methacrylate and 2-vinyl pyridine were polymerized with **1**. In general complex **2** showed lesser polymerization activities for these monomers.[11)]

1) Presented partly at the Vth International Conference on Organometallic Chemistry, Moscow, 23rd August, 1971.

2) a) T. Saegusa, T. Tsuda, and Y. Ito, *Kogyo Kagaku Zasshi*, **72**, 1627 (1969); b) R. G. R. Bacon and H. A. O. Hill, *Quart. Rev.*, **19**, 95 (1965); c) K. Wada, M. Tamura, and J. Kochi, *J. Amer. Chem. Soc.*, **92**, 6656 (1970) and references cited therein.

3) a) H. Gilman, R. G. Jones, and L. A. Woods, *J. Org. Chem.*, **17**, 1630 (1952); b) H. O. House, W. L. Respess, and G. M. Whitesides, *ibid.*, **31**, 3128 (1966); c) H. O. House, and W. F. Fischer, Jr., *ibid.*, **33**, 949 (1968); d) G. M. Whitesides, W. F. Fischer, Jr., J. San Filippo, Jr., R. W. Bashe, and H. O. House, *J. Amer. Chem. Soc.*, **91**, 4871 (1969); e) G. M. Whitesides, E. R. Stredronsky, D.P. Casy, J. San Filippo, Jr., *ibid.*, **92**, 1426 (1970).

4) K. H. Thiele and J. Köhler, *J. Organometal. Chem.*, **12**, 225 (1968).

5) a) G. Costa, G. Pellizer, and F. Rubessa, *J. Inorg. Nucl. Chem.*, **26**, 961 (1964); b) M. Tamura and J. Kochi, *J. Amer. Chem. Soc.*, **93**, 1485 (1971).

6) a) G. Costa, G. De Alti, L. Stefani, and G. Boscarato, *Ann. Chim.*, **52**, 289 (1962); b) H. Gilman and L. A. Woods, *J. Amer. Chem. Soc.*, **65**, 435 (1943); c) C. E. H. Bawn and F. J. Whitby, *J. Chem. Soc.*, **1960**, 3926; d) C. E. H. Bawn and R. Johnson, *ibid.*, 4162 (1960).

7) A. Yamamoto, K. Morifuji, S. Ikeda, T. Saito, Y. Uchida, and A. Misono, *J. Amer. Chem. Soc.*, **87**, 4652 (1965); *ibid.*, **90**, 1878 (1968); T. Saito, Y. Uchida, A. Misono, A. Yamamoto, K. Morifuji, and S. Ikeda, *J. Organometal. Chem.*, **6**, 572 (1966); *J. Amer. Chem. Soc.*, **88**, 5198 (1966); K. Nishimura, H. Kuribayashi, A. Yamamoto, and S. Ikeda, *J. Organometal. Chem.*, in press.

8) Triphenylphosphine content of **1** was determined spectrophotometrically as methyltriphenylphosphonium iodide.

9) The amounts of toluene and ether contained in the methyl complexes were determined by gas chromatography of the thermal decomposition products of **1** and **2**.

10) The amount of triphenylphosphine in **2** was determined spectroscopically after hydrolysis of **2** with sulfuric acid and extraction of triphenylphosphine with hexane.

11) Polymerization of acrylonitrile and styrene by methyl- and ethylcopper has been reported by Bawn and Johnson;[6a)] Saegusa *et al.* also found the polymerization activity of copper complexes for acrylonitrile, T. Saegusa, Y. Ito, H. Kinoshita, and S. Tomita, This Bulletin, **43**, 877 (1970).

The Stereospecific Rearrangement of 1,3,5-Cycloheptatriene-7-carboxaldehyde Dimethyl Acetal to *cis*-β-Methoxystyrene

Haruki TSURUTA, Kazuyuki TOMISAWA, and Toshio MUKAI
Department of Chemistry, Faculty of Science Tohoku University, Sendai

(Received October 22, 1971)

During our continuing studies of the intramolecular addition of a carbene located at a side chain to the cycloheptatriene ring,[1] 1,3,5-cycloheptatriene-7-carboxaldehyde dimethylacetal (**1**)[2] has emerged as a promising potential precursor to generate 1,3,5-cycloheptatriene-7-methylene, because the 2,4-dinitrophenylhydrazone of the aldehyde was successfully synthesized from **1** in a high yield without any isolation of the aldehyde.[2,3] Thus, we tried to prepare the corresponding tosylhydrazone or hydrazone, which is a precursor of the carbene, from Compound **1** by the application of a similar manner; however, this attempt was unsuccessful. Instead, we found a curious rearrangement of **1** during the hydrolysis of **1** and wish to report the outlines of the result obtained.

Dimethylacetals of 1,3,5-cycloheptatriene-3-carboxaldehyde[4] and 1-formylbicyclo[3.2.0]hepta-3,6-diene,[5] upon treatment with methanolic hydrochloric acid, provided the corresponding aldehydes, whereas the dimethylacetal (**1**) on treatment with dilute hydrochloric acid, afforded only a rearranged product, phenylacetaldehyde.[2,3] On the other hand, when **1** was warmed in anhydrous acetic acid, a clean reaction took place and *cis*-β-methoxystyrene (**2a**) was mainly formed (the ratio of *cis* to *trans* was 5). The structure of **2a** was established on the basis of the NMR (J= 7.0 Hz, *cis* –CH=CH–) and by a comparison of the retention time in vpc with that of an authentic sample. The rearrangement was a first-order reaction $k = 1.46 \times 10^{-5}$ sec^{-1} at 40°C),[6] and the *cis*: *trans* ratio (about 5) was almost constant from 40 to 60°C. In addition, the prolonged heating of **1** under the same conditions (20 hr at 40°C) resulted in the slow formation of phenylacetaldehyde dimethylacetal (**3**).[3] The possibility of interconversion between *cis*- (**2a**) and *trans*-β-methoxystyrene (**2b**) and of the formation of **2a** or **2b** by the elimination of methanol from **3** could be excluded by the following control experiments. When the *cis*-isomer (**2a**) was subjected to the solvolysis at 60°C for 4 hr in the presence of one equivalent of methanol-d_4, deuterium incorporation took place only in **3**, and the formation of *trans*-isomer (**2b**) was not observed, indicating that **3** is a secondary product. Under the same conditions, the product (**3**) was stable, in addition, the *trans*-isomer (**2b**) was not converted into the *cis*-isomer (**2a**). These facts established that *cis*-β-methoxystyrene (**2a**) was directly formed from 1,3,5-cycloheptatriene-7-carboxaldehyde dimethylacetal (**1**) by stereospecific rearrangement.

In the solvolysis of 1,3,5-cycloheptatrien-7-ylmethylcarbinol 3,5-dinitrobenzoate, Sargent *et al.* observed a novel type of rate enhancement promoted by the participation of the cyclopropane ring which exists in its valence isomer, the norcaradiene form.[7]

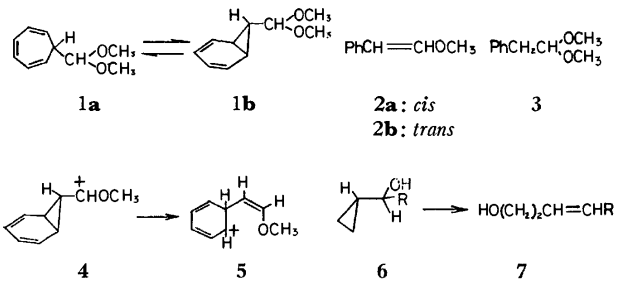

Similarly, the enhancement in the rate of the solvolysis of **1** can be attributed to the assistance of the cyclopropane ring of the corresponding norcaradiene form (**1b**). The styrene derivative (**2**) should be produced from the norcaradienylcarbinyl cation (**4**) by the cleavage of the cyclopropane ring to the homoallyl cation (**5**), followed by aromatization leading to β-methoxystyrene (**2**).[3,7,8] Thus, this rearrangement can be seen as an example of the general cyclopropylcarbinol-homoallyl carbinol rearrangement, as is shown from **6** to **7**. The geometry of the homoallyl carbinols obtained by this rearrangement has been widely studied.[9] For example, 1-cyclopropyl-1-methoxyethane[10] and (bicyclo[4.1.0]heptan-7-yl)benzyl alcohol,[11] upon solvolysis, rearranged to the corresponding *trans*-allyl derivatives, but not to *cis*-isomers. The preferable formation of *cis*-β-methoxystyrene (**2a**) from **1** is in sharp contrast to these examples. Therefore, the present results raise interesting questions concerning the conformation of the intermediate in the norcaradienylcarbinyl-styryl rearrangement (**4**→**5**), especially as to the location of the methoxy group in the transition state.

1) H. Tsuruta, K. Kurabayashi, and T. Mukai, *Tetrahedron Lett.*, **1967**, 3775; *J. Amer. Chem. Soc.*, **90**, 7167 (1968).
2) A. C. Cope, V. A. Nelson, and D. S. Smith, *ibid.*, **76**, 1100 (1954).
3) C. R. Ganellin and R. Pettit, *J. Chem. Soc.*, **1958**, 576.
4) Prepared by 1,5-hydrogen shift of (**1**); *cf.* A. P. ter Borg and H. Kloosterziel, *Rec. Trav. Chim.* Pays-Bas, **82**, 741 (1963).
5) Obtained by the irradiation of (**1**) through quartz; *cf.* G. W. Borden, O. L. Chapman, R. Swindell, and T. Tezuka, *J. Amer. Chem. Soc.*, **89**, 2979 (1965).
6) The kinetic measurement was carried out from 40° to 80° by using a Lauda Thermostat Model WB-20 and by checking on DC-11 (1 m×3 mm) at 90°, using β-methylnaphthalene as the internal standard. E_a=22.1 kcal/mol.
7) G. D. Sargent, N. Lowry, and S. D. Reich, *J. Amer. Chem. Soc.*, **89**, 5985 (1967).
8) J. A. Blair and C. J. Tate, *Chem. Commun.*, **1970**, 1319.
9) S. Sarel, S. Yovell, and M. Sarel-Imber, *Angew. Chem. Internat. Ed.*, **7**, 577 (1968).
10) R. G. Pearson and S. H. Langer, *J. Amer. Chem. Soc.*, **75**, 1065 (1953).
11) P. Besinet, M. R. Fraisse, R. Jacquier, and P. Viallefont, *Bull. Soc. Chim. Fr.*, **1960**, 1377.

The Determination of the Diffusion Coefficient and the Maximum Surface Concentration of Polyvinylpyrrolidone by Means of a Hanging Mercury Drop Electrode

Tadashi Yoshida, Tetsuya Ohsaka, and Shigemitsu Nomoto

Applied Electrochemical Laboratory, Graduate School of Science and Engineering, Waseda University, Nishi-okubo, Shinjuku-ku, Tokyo, 160

(Received April 20, 1971)

Subsequently to the previous work with a dropping mercury electrode (DME), the diffusion coefficient (D) and the maximum surface concentration (Γ_m) for polyvinylpyrrolidone (PVP) were determined in a 1N sulfuric acid solution by means of a hanging mercury drop electrode (HMDE). The values of D and Γ_m for PVP were obtained separately by means of the equation for a semi-infinite spherical diffusion for HMDE. The results for D were compared with the values evaluated from the Stokes-Einstein equation or with those previously published. The results for Γ_m are also shown in comparison with those values to be expected from the data obtained by the use of DME or HMDE on the assumption of linear diffusion and D, or in comparison with the results published by Jehring. It was also confirmed that the HMDE used by the authors is almost satisfactory for the determination of D and Γ_m in this case.

In most cases, the adsorption process of organic high polymers is mainly diffusion-controlled; such a process for PVP (polyvinylpyrrolidone)[1] has been discussed by the authors on the basis of the results obtained with the DME (dropping mercury electrode) in a previous paper.[2] It is necessary to assume the diffusion coefficient (D) of adsorbates in order to evaluate the maximum surface concentration (Γ_m) with the Koryta equation; however, the maximum surface concentration and the diffusion coefficient may be computed separately by using a equation based on the spherical diffusion for HMDE (hanging mercury drop electrode). Moreover, the results obtained by the use of HMDE under the diffusion-controlled adsorption will be reported in this paper with reference to the values of D and Γ_m published[3-5] or obtained[2] by the authors with the DME.

Experimental

Apparatus. The equipment used for the HMDE was made from Pyrex glass except for some parts of the microsyringe; it is sketched in Fig. 1. The differential capacity was measured at the frequency of 1 kHz with an impedance bridge of a transformer-connected type described in the previous paper.[2] A platinum wire ring[6] was used as the counter electrode, and all the potentials were measured and described with reference to the saturated calomel electrode (SCE). Further, almost all the measurements with the HMDE were made at −500 mV (SCE)[7] in an atmosphere of purified nitrogen kept at 20°C without stirring, except in the case shown in Fig. 3.

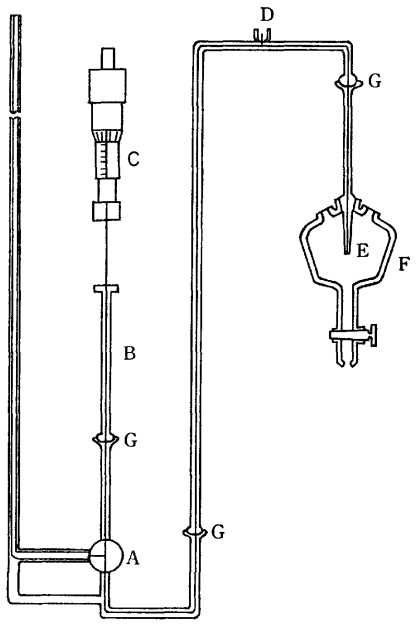

Fig. 1. Equipment for HMDE.
A: Cock, B: Microsyringe, C: Micrometer, D: Pt wire, E: Capillary, F: Cell, G: Ball-joint.

Materials. The mercury used in the present experiment was distilled twice *in vacuo* after being treated in the usual way. For the investigation, four kinds of the PVP prepared by BASF as chemical-grade reagents were used without any further purification; their mean molecular weights ($\bar{M}$) were 10000, 26000, 37000, and 750000 respectively. All the solutions were prepared with guaranteed reagents and triply-distilled water.

Purification of the Solution. Because of the fact that even a trace of impurities influences the results observed with the HMDE, the sulfuric acid solution, prepared as described above, was always standardized after treatment with granular active charcoal and then it was subjected to preelectrolysis over about 10 hours at −500 mV (SCE) in an atmosphere of purified nitrogen just before use.

Procedure for Observation with HMDE. The mercury drop ("E" in Fig. 1) of the HMDE was polarized at the potential of −500 mV (SCE) in a sulfuric acid solution which had been carefully purified and deaerated; then a definite

1) R. L. Davidson and M. Sittig, eds., "Water-Soluble Resins," Reinhold Pub. Corp., New York 1963, p. 110.
2) T. Yoshida, T. Ohsaka, and S. Tanaka, This Bulletin, **45**, 326 (1972).
3) L. E. Miller and F. A. Hamm, *J. Phys. Chem.*, **57**, 110 (1953).
4) W. Scholtan, *Makromol. Chem.*, **7**, 209 (1951).
5) H. Jehring, *Monatsber. Deut. Akad. Wiss. Berlin*, **10**, 295 (1968).
6) The ring-like electrode is prepared by winding the platinum wire which is *ca.* 50 cm in length and 0.3 mm in diameter.
7) The saturated adsorption of PVP was always attainable at this potential, as has been described in the previous paper.[2]

amount of mercury was forced out by means of a micrometer connected with the microsyringe (shown as "C" and "B" in Fig. 1), just before the observation was started in pursuit of the time dependence of the differential capacity at the mercury interface, the starting time of observation being put at zero. The surface area of a mercury drop for the HMDE was determined from its differential capacity with reference to the value per unit area of mercury obtained with the DME under the same conditions; the result was also compared with that derived from the volume of mercury forced out by the microsyringe ("B" in Fig. 1). The radius of a drop was found to be 0.047 cm.

Theoretical

Relation for the Semi-Infinite Linear Diffusion. In the case of the adsorption controlled by the diffusion of adsorbates, the surface concentration (Γ_t) at the time (t) on a planar electrode is given by:[8,9]

$$\Gamma_t = (2/\pi^{1/2})D^{1/2}at^{1/2} \quad (1)$$

where Γ_t, D, a, and t are the surface concentration of adsorbates at time t in mol/cm^2, its diffusion coefficient in cm^2/sec, its bulk concentration in mol/cm^3, and the time from the beginning of its adsorption in sec respcetively. By substituting the above expression for Γ_t into the relation introduced by Frumkin,[10] we obtain:

$$\theta = \Gamma_t/\Gamma_m = (C_0-C)/(C_0-C_1) \quad (2)$$

it may be written as follows:[9]

$$C = C_0 - 1.13(C_0-C_1)D^{1/2}\Gamma_m^{-1}at^{1/2} \quad (3)$$

where C is the differential capacity per unit of area in μF/cm^2; θ, the coverage; C_0 and C_1, the differential capacities for $\theta=0$ and $\theta=1$ respectively, and Γ_m, the maximum surface concentration in mol/cm^2, that is, the value of Γ_t at $\theta=1$.

Relation for the Semi-Infinite Spherical Diffusion. Fick's law for the diffusional process on a spherical electrode is written by:[11]

$$\partial a/\partial t = D\{\partial^2 a/\partial r^2 + (2/r)(\partial a/\partial r)\} \quad (4)$$

where r is the radius distance from the center of the spherical electrode. When the initial and boundary conditions are substituted in Eq. (4), Eq. (5)[12] is obtained by the Laplace transformation:

$$\Gamma_m = (2/\pi^{1/2})D^{1/2}at_m^{1/2} + Dat_m/r_0 \quad (5)$$

where t_m is the time required to form a monolayer in sec, and r_0, the radius of the spherical electrode in cm. It follows from the rearangement of the above equation that:

$$(at_m^{1/2})^{-1} = (2D^{1/2})/(\pi^{1/2}\Gamma_m) + (Dt_m^{1/2})/(r_0\Gamma_m) \quad (6)$$

where a plot of $(at_m^{1/2})^{-1}$ against $(t_m^{1/2})$ gives a linear relation with a slope of $(D/\Gamma_m r_0)$ and an intercept of $(2D^{1/2}/\pi^{1/2}\Gamma_m)$; therefore, the slope and the intercept are denoted by "K" and "L" respectively, for convenience. The values of Γ_m and D may be computed from K and L as follows, while the values of K and L are obtainable from the experimental data:

$$\left.\begin{aligned}\Gamma_m &= (4r_0K)/(\pi L^2) = D/(Kr_0)\\ D &= (4r_0^2K^2)/(\pi L^2)\end{aligned}\right\} \quad (7)$$

Results

Purification Effect for a Solution. The sulfuric acid solution to be observed was carefully purified as has been stated previously, because of the high sensitiveness of a HMDE for contamination compared with that of a DME. An example, illustrating the wide difference between the solutions prepared with or without the treatment, is given in Fig. 2. The results shown in Fig. 2 confirm that the active charcoal treatment is very effective in the purification; the differential capacity decreases rapidly with the time in the case of the blank 1N sulfuric acid solution prepared without treatment, whereas only a slight decrease with time was observed in the case of that purified with active charcoal.

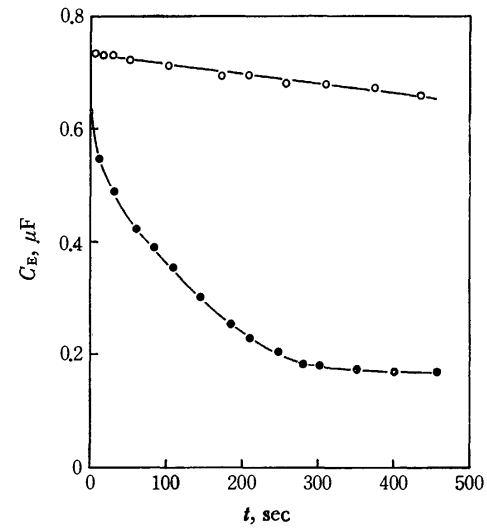

Fig. 2. Pretreatment effect with active charcoal.
20°C, Observed at −500 mV (SCE), 1N sulfuric acid solution,
-○-: Solution with pretreatment of charcoal,
-●-: Solution without pretreatment of charcoal.

Stirring Effect for a Solution. For the case observed with a 1N sulfuric acid solution containing 1.0 mg per litre of PVP ($\bar{M}$=10000), the variation in the differential capacity with the time is shown in Fig. 3, where the results were obtained with or without the stirring of the solution by nitrogen bubbling. When the bubbling was started, the differential capacity for the solution containing PVP decreased more rapidly until the minimum differential capacity was-attained than in the case without bubbling. It may be considered from the above that the process for PVP adsorption is mainly controlled by the diffusion until the saturated adsorption is achieved.

Differential Capacity vs. Time Relation. The C_E *vs.* t curves in Fig. 4-(a) were observed with extremely dilute solutions of PVP ($\bar{M}$=10000). It appears that the minimum differential capacity depends to some extent upon the bulk concentration and that the adsorp-

8) P. Delahay and I. Trachtenberg, *J. Amer. Chem. Soc.*, **79**, 2355 (1957).
9) D. W. Imhoff and J. W. Collat, *J. Phys. Chem.*, **71**, 3048 (1967).
10) A. N. Frumkin, *Z. Phys.*, **35**, 792 (1926).
11) I. Shain and K. J. Martin, *J. Phys. Chem.*, **65**, 254 (1961).
12) S. L. Phillips, *J. Electroanal. Chem.*, **12**, 294 (1966).

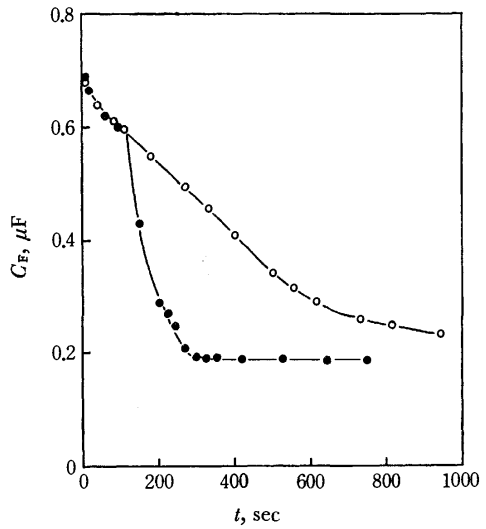

Fig. 3. Stirring effect for solution.
20°C, Observed at −500 mV (SCE), 1N sulfuric acid solution+PVP ($\bar{M}$=10000) 1.0 mg/l,
-○-: No stirring, -●-: Stirring with nitrogen bubble after 120 sec.

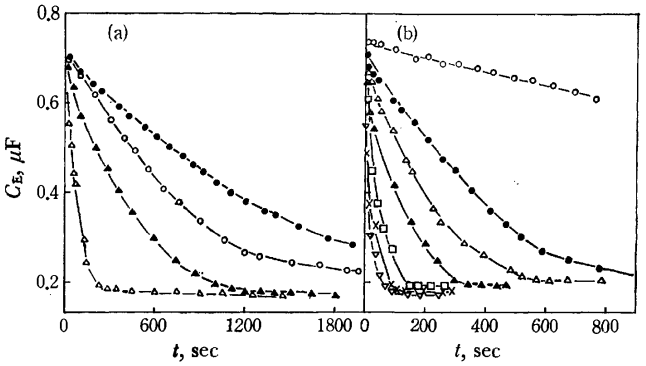

Fig. 4. Differential capacity *vs.* time curves.
20°C, Observed at −500 mV (SCE), 1N sulfuric acid solution+PVP ($\bar{M}$=10000),
(a) -●-: 0.2 mg/l, -○-: 0.4 ml/l, -▲-: 0.8 mg/l, -△-: 4.0 mg/l
(b) -○-: 0 mg/l, -●-: 1.0 mg/l, -△-: 2.0 mg/l, -▲-: 4.0 mg/l, -□-: 6.0 mg/l, -×-: 8.0 mg/l, -▽-: 10.0 mg/l.
Where C_E is the observed differential capacity (μF/electrode surface).

tion equilibrium may take place even for the condition of $\theta<1$ in this case. However, the minimum differential capacity for this case gradually decreased with the time. Therefore, for extremely dilute solutions of PVP, it is considered that the saturated adsorption of PVP may occur after a very long time, or that the differential capacity corresponding to an adsorption equilibrium may be slowly depressed by a trace of impurities left in the solution. On the other hand, in the case of Fig. 4-(b), observed with a relatively concentrated solution of PVP as compared with that of the above case, the minimum differential capacities were nearly constant, independently of the bulk concentration, although a slight dependence of the minimum capacity on the concentration was still observed. In a plot similar to the above, observed with PVP of $\bar{M}$=750000, the minimum differential capacities always reached a common value, regardless of the bulk concentration. The time required to attain the minimum capacity of the constant value for the PVP of $\bar{M}$=750000 was about two or three times that in the case with one of $\bar{M}$=10000, in the same bulk concentration in mg per litre.

Discussion

Application of the Semi-Infinite Linear Diffusion (C_E vs. $t^{1/2}$). Equation (3) makes it clear that the differential capacity for the solution containing adsorbates

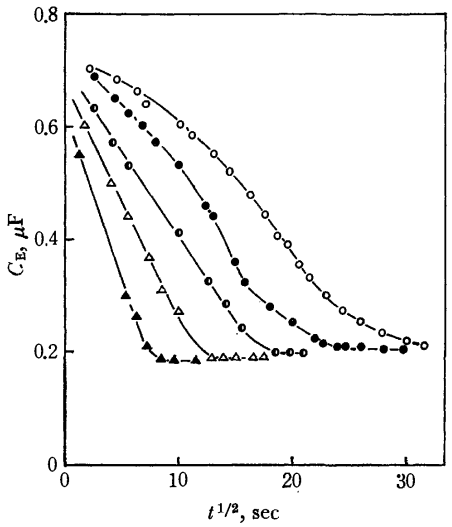

Fig. 5. Relation between differential capacity and square root of time.
20°C, Observed at −500 mV (SCE), 1N sulfuric acid solution+PVP ($\bar{M}$=10000),
-○-: 1.0 mg/l, -●-: 2.0 mg/ml, -◐-: 4.0 mg/l, -△-: 6.0 mg/l, -▲-: 10.0 mg/l.

decreases linearly with $t^{1/2}$ or a. In Fig. 5, the differential capacity decreases with $t^{1/2}$, until finally it shows a constant value for the saturated adsorption, regardless of the bulk concentration. The time required to form a complete monolayer (t_m) was obtained by extrapolating these two linear relations, as has been described in the previous paper.[2] In the case of relatively concentrated solution of PVP, nearly linear plots were obtained for the diffusion process within about 100 sec, as was to be expected from Eq. (3). However, in the case of the relatively dilute solution in this case, the curves were remarkably depressed and deviated from the linear relation of Eq. (3), especially after about 100 sec. The above deviation was not due to the relation expected from a spherical diffusion, shown in Fig. 6. Consequently, such a deviation is considered to be due to the convection besides the diffusion; therefore, the effect of the convection may be neglected within a relatively short time, such as about 100 sec.

Accordingly, the examination was made mainly on the basis of the data observed within a relatively short time, when the effect due to the convection may be neglected.

The value of the differential capacity at the starting time of t=0 should be a constant, independently of the concentration of PVP. The discrepancy nevertheless observed may be due to the slight difference

among mercury drops resulting from the different operations of the HMDE.

In the next place, by substituting the observed value of t_m into Eq. (3), we can evaluate Γ_m by assuming the diffusion coefficient of PVP; the results will be given later in comparison with the data derived in the other way.

Application of the Semi-Infinite Spherical Diffusion ($(at_m^{1/2})^{-1}$ *vs.* $t_m^{1/2}$). As has previously been stated, the values of Γ_m and D cannot be evaluated separately by the equation for the linear diffusion process unless one of them is determined or postulated; therefore, only the ratio of (D/Γ_m^2) is obtainable in this case. However, the value either for Γ_m or D can be evaluated separately using the relation for the spherical diffusion process, as is given by Eq. (6) in relation to a HMDE.

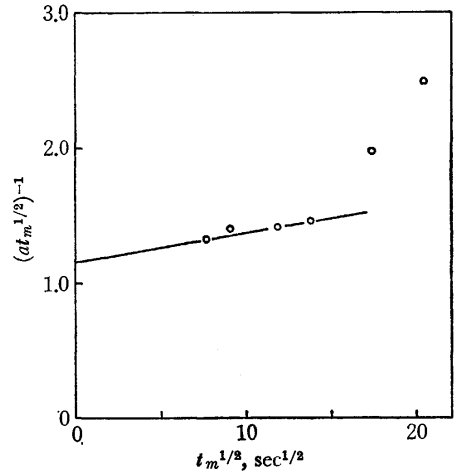

Fig. 6. Relation between $(at_m^{1/2})^{-1}$ and $t_m^{1/2}$.
20°C, Observed at −500 mV (SCE), 1N sulfuric acid solution+PVP ($\bar{M}$=10000).

The relation $(at_m^{1/2})^{-1}$ *vs.* $t_m^{1/2}$ based on Eq. (6) is illustrated in Fig. 6 for the PVP of $\bar{M}$=10000 as an example; it rises steeply from the saturation time (t_m) of about 200 sec. Such a deviation observed for a relatively long saturation time can be attributed mainly to the effect of the convection pointed out previously. Therefore, a linear relation obtained for a saturation time, of less than about 200 sec may be approximately regarded as a reasonable result for the purpose. Accordingly, the values of Γ_m and D were computed, respectively, from the slope and the intercept observed for the linear relation, as above.

Diffusion Coefficient of PVP. The diffusion coefficient of PVP has been measured by the electrophoresis[3] or diffusional sedimentation method,[4] while an approximate value for colloidal particles or large molecules was frequently estimated through the well-known Stokes-Einstein equation in the case of an unknown conductivity. Meanwhile, the Stokes-Einstein equation holds only in the case where the moving particles or molecules are nearly spherical and very large in size compared with the molecules of the solvent.

The results for D in this paper were derived from Eq. (6), related to a spherical diffusion, or from the Stokes-Einstein equation; these results are shown in Table 1 in comparison with the published values.[3,4] Further, the results obtained by Scholtan's relation[4] between D and $\bar{M}$ are also quoted in Table 1 for reference. As is shown in Table 1, the results obtained by the present authors seem to be reasonable apart from the case for the PVP of $\bar{M}$=37000.

Maximum Surface Concentration of PVP. The values of Γ_m for the PVP of several $\bar{M}$'s obtained directly by Eq. (6) are shown in Table 2 with reference to the results derived on the assumption of linear diffusion and the values of D; the D values[13] used in the previous paper[2] were also assumed for the case of the HMDE. The results by Jehring[5] are also quoted there for reference. The values resulting form the HMDE or DME[2] were always measured at −500 mV (SCE) in a 1N sulfuric acid solution at 20°C, whereas those by Jehring[5] were obtained at −1100 mV (SCE) in a 0.5M potassium chloride solution at 25°C.

Table 1. Diffusion coefficient of PVP
($\times 10^7$ cm²/sec)

$\bar{M}$	I[a]	II[b]	III[c]	IV[d]	V[e]
10000	10.3	10.5			10.0
12100				9.15	
13000			7.55		
21000			5.94 6.33		
23000			5.87		
25500				6.20	
26000	7.28	7.65			6.21
32000			4.81		
32500				6.00	
36000			4.24		
37000	9.52	6.78			5.21
39200				4.50	
41500			4.14		
55600				3.50	
584000				1.35	
750000	1.27	2.50			1.15
1129000				0.70	

a) The results derived from the equation for spherical diffusion [*cf.* Eqs. (5) and (6)].
b) The calculated results from the Stokes-Einstein equation, *i.e.* $D=2.96\times10^{-7}/(\eta V^{1/3})$, where η in dyn·sec·cm^{-2} and V in $\bar{M}$/density.
c) The values by the electrophoresis method (*cf.* Ref. 3).
d) The values by the sedimentation method (*cf.* Ref. 4).
e) The values calculated with $D=1.00\times10^{-4}\bar{M}^{-0.5}$ (cm²/sec) (*cf.* Ref. 4).

It was found previously[2] that the saturated adsorption of PVP is attained promptly at −500 mV (SCE) in a 1N sulfuric acid solution in the case of a relatively high bulk concentration, while Jehring[5] also investigated the Γ_m for PVP under conditions when the saturated adsorption was achieved easily. Accordingly, the values of Γ_m reported by Jehring[5] may be compared approximately with the present authors' results.

The data in Table 2 are illustrated in Fig. 7, where the results obtained with the DME[2] are approximately in agreement with those reported by Jehring.[5]

13) Here $D=10.3\times10^{-7}$ (cm²/sec) for $\bar{M}$=10000, 7.3×10^{-7} (cm²/sec) for $\bar{M}$=26000, 5.1×10^{-7} (cm²/sec) for $\bar{M}$=37000, and 1.2×10^{-7} (cm²/sec) for $\bar{M}$=750000.

Table 2. Maximum surface concentration of PVP ($\times 10^{12}$ mol/cm^2)

$\bar{M}$	HMDE[a)]	HMDE[b)]	DME[c)]	Jehring[d)]
10000	9.98	8.10	6.67	
11500				6.06
25000				3.29
26000	3.10	2.85	2.92	
37000	2.90	1.80	2.02	
38000				1.98
750000	0.101	0.075	0.090	0.089

a) The results obtained directly with the equation for spherical diffusion.
b) The results obtained on the assumption of linear diffusion and D (*cf.* Ref. 13).
c) The results by the previous paper.[2)]
d) The values[5)] by A.C. polarography observed at −1100 mV (SCE) in 0.5M potassium chloride kept at 25°C.

Therefore, it may be considered for PVP that the dependence of Γ_m upon the electrolyte and the polarized potential is almost negligible under the above conditions.

In Fig. 7, with reference to the results derived from the equation for linear diffusion, the values obtained by the HMDE are approximately in accordance with those obtained by the DME.[2)] On the other hand, the results obtained directly by the equation of spherical diffusion with regard to the HMDE are somewhat large as compared with both results mentioned above.

It is considered from the above results that nearly reliable values of the D or Γ_m of PVP were obtained by means of the HMDE shown in Fig. 1.

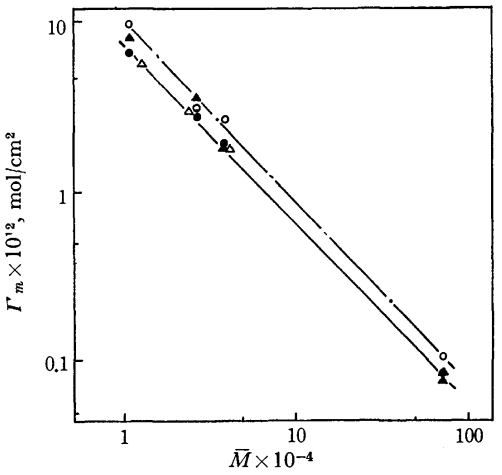

Fig. 7. Relation between Γ_m and $\bar{M}$.
-○-: Values with HMDE, derived from the equation for spherical diffusion.
▲: Values with HMDE, derived from the equation for linear diffusion.
-●-: Values with DME,[2)] derived from the assumption of D as described in the text.
△: Results by Jehring.[5)]

The authors would like to express their appreciation to Mr. Shoji Tanaka and Mr. Osamu Yoshioka for the earnest assistance.

BULLETIN OF THE CHEMICAL SOCIETY OF JAPAN, VOL. 45, 1589—1594(1972)

Electronic Structures of Thianthrene, Phenothiazine, and Related Heterocyclic Compounds

Mamoru KAMIYA
Shizuoka College of Pharmacy, Oshika, Shizuoka-shi

(Received July 29, 1971)

Systematic studies were made on thianthrene, phenoxathiin, diphenylene dioxide, phenothiazine, and phenoxazine for the correlation between the folded structure and electronic spectra in terms of the semiempirical SCF–MO–CI method. The calculated results are in good agreement with the experimental results, the folded structure being prominent in the sulfur-containing molecules. The dihedral angle dependency of the all valence-electronic energy and ionization potential was also studied by the extended Hückel method.

Electronic structures of the heterocyclic compounds thianthrene, phenoxathiin, diphenylene dioxide, phenothiazine, and phenoxazine are of interest since the data on dipole moment[1] and X-ray analysis[2] indicate that these compounds, sulfur-containing ones in particular, are of non-planar spacial configurations folded about the central axis joining the heteroatoms. Several molecular orbital studies have been undertaken in order to survey the correlations between the extent of the folded structure and various physico-chemical properties. As regards the Hückel MO studies, the best integral values for the thianthrene analogs were studied by Kuboyama referring to the energies of the charge-transfer bands.[3] The value of the dihedral angle of thianthrene was predicted by Chandra in terms of the

1) a) K. Higasi, *Sci. Papers Inst. Phys. Chem. Res.* (Tokyo), **38**, 331 (1941); b) N. J. Leonard and L. E. Sutton, *J. Amer. Chem. Soc.*, **70**, 1564 (1948); c) H. Musso, *Chem. Ber.*, **92**, 2881 (1959); d) H. Lumbroso and G. Montando, *Bull. Soc. Chim. France*, **9**, 2119 (1964).

2) a) H. Lyton and E. G. Cox, *J. Chem. Soc.*, 488 (1956); b) I. Rowe and B. Post, *Acta Crystallogr.*, **11**, 372 (1958); c) S. Hosoya, *ibid.*, **16**, 310 (1963); *ibid.*, **20**, 429 (1966); d) J. D. Bell, J. F. Blount, O. V. Briscol, and H. C. Freeman, *Chem. Commun.*, 1656 (1968).

3) A. Kuboyama, *J. Amer. Chem. Soc.*, **86**, 164 (1964).

electronic and strain energies.[4] The spacial configuration and electronic properties of phenothiazine were studied by Malrieu and Pullman,[5] and by Bloor *et al.*[6] from a biological viewpoint. With respect to the SCF MO study, Wratten and Ali performed a P–P–P type calculation on the neutral molecule and cation radical of diphenylene dioxide by making adequate allowance for non-planarity.[7] An analogous calculation was applied by the present author to a series of the related heterocyclic compounds.[8] It seems, however, that no systematic calculation has been published concerning at least the dihedral angle dependence of the electronic spectra and also the hybridization state of the heteroatoms.

The calculations in this paper have been performed in order to supply such deficient data.

Calculation Method

In the semiempirical SCF MO method (P–P–P approximation)[9] the valence-state ionization potential (I) and electron affinity (A) of the π-orbitals are taken as follows referring to the data given by Hinze and Jaffé.[10]

I(=C–) 11.16 eV, I(–O–) 32.90, I(–S–) 23.59, I(–$\overset{|}{\underset{|}{N}}$–) 26.70

A(=C–) 0.03 eV, A(–O–) 11.37, A(–S–) 10.54, A(–$\overset{|}{\underset{|}{N}}$–) 9.26

The two-center repulsion integral is obtained by the Nishimoto-Mataga formula.[11] For the sake of comparison the core-resonance integral is evaluated by the following two methods. In method I, the integral β_{rs} is evaluated for all atomic pairs by the equation $\beta_{rs}=-\frac{1}{2}S_{rs}(I_r+I_s)$, where the overlap integral S_{rs} is calculated on the basis of the Slater type atomic orbitals. In method II, β_{rs} is evaluated for neighbouring pairs by the variable β procedure,[12] where the parametrization is taken as follows.

$$\beta_{C-C} = -0.51P_{C-C} - 1.84$$
$$\beta_{C-O} = -0.56P_{C-O} - 2.20$$
$$\beta_{C-N} = -0.53P_{C-N} - 2.02$$
$$\beta_{C-S} = -0.33P_{C-S} - 1.80$$

Here, P_{rs} corresponds to the usual π-bond order, and to allow for non-planarity the β_{C-X} (X=heteroatom) is corrected by the equation $\beta_{C-X}(\alpha)=\beta_{C-X}(O)\cos\alpha$, where the $\beta_{C-X}(O)$ is the value for the planar structure, and the value of α is the distortion angle from planarity. In both methods all singly excited configurations are allowed to interact.

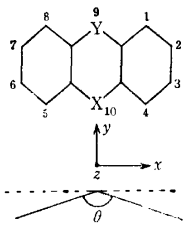

Fig. 1. Molecular geometry and structural formula

TABLE 1. DIHEDRAL ANGLE DEPENDENCE OF THE CALCULATED π-π^* TRANSITION ASSIGNED TO THE LOWEST OBSERVED BAND

θ[a]	method I		method II	
	ΔE_S(eV)[b]	f[c]	ΔE_S(eV)	f
a) Thianthrene (I)				
180°	2.487	0.600	3.815	0.163
170°	2.501	0.594	3.819	0.160
160°	2.539	0.579	3.830	0.153
150°	2.608	0.552	3.849	0.142
140°	2.716	0.510	3.875	0.127
130°	2.866	0.453	3.908	0.110
120°	3.086	0.379	3.948	0.091
b) Phenoxathiin (II)				
180°	3.202	0.529	3.787	0.172
170°	3.217	0.520	3.791	0.169
160°	3.261	0.495	3.803	0.162
150°	3.339	0.452	3.822	0.150
140°	3.459	0.391	3.849	0.134
130°	3.626	0.312	3.884	0.116
120°	3.858	0.212	3.925	0.096
c) Diphenylene Dioxide (III)				
180°	4.173	0.304	3.750	0.188
170°	4.187	0.297	3.754	0.186
160°	4.232	0.279	3.766	0.178
150°	4.308	0.249	3.786	0.165
140°	4.419	0.210	3.814	0.149
130°	4.560	0.163	3.850	0.129
120°	4.709	0.116	3.893	0.108
d) Phenothiazine (IV)				
180°	2.881	0.562	3.587	0.222
170°	2.895	0.555	3.591	0.219
160°	2.934	0.535	3.602	0.211
150°	3.003	0.502	3.621	0.198
140°	3.110	0.454	3.646	0.180
130°	3.260	0.394	3.679	0.159
120°	3.471	0.323	3.717	0.136
e) Phenoxazine (V)				
180°	3.729	0.397	3.540	0.250
170°	3.743	0.390	3.543	0.247
160°	3.785	0.370	3.555	0.238
150°	3.858	0.336	3.574	0.224
140°	3.967	0.289	3.600	0.205
130°	4.117	0.228	3.634	0.182
120°	4.309	0.147	3.674	0.157

a) Dihedral angle between the lateral benzene planes
b) Singlet π-π^* transition energy calculated with CI
c) Oscillator strength

4) A. K. Chandra, *Tetrahedron*, **19**, 471 (1963).
5) J. P. Malrieu and B. Pullman, *Theor. Chim. Acta*, **2**, 293 (1964).
6) J. E. Bloor, B. R. Gilson, R. J. Haas, and C. L. Zirkle, *J. Med. Chem.*, **13**, 922 (1970).
7) R. J. Wratten and M. A. Ali, *Mol. Phys.*, **13**, 233 (1967).
8) M. Kamiya, *Bull. Chem. Soc. Japan*, **43**, 3929 (1970).
9) R. Pariser and R. G. Parr, *J. Chem. Phys.*, **21**, 466, 767 (1953); J. A. Pople, *Trans. Faraday Soc.*, **49**, 1375 (1953).
10) J. Hinze and H. H. Jaffé, *J. Amer. Chem. Soc.*, **84**, 540 (1962).
11) K. Nishimoto and N. Mataga, *Z. Physik. Chem.*, **12**, 335 (1957).
12) K. Nishimoto and L. S. Forster, *Theor. Chim. Acta*, **4**, 155 (1966).

TABLE 2. COMPARISON BETWEEN THE EXPERIMENTAL AND THEORETICAL SPECTRA AROUND THE OPTIMUM DIHEDRAL ANGLE VALUES

a) Thianthrene (I)

Calcd.	$\theta=130°$ method I		$\theta=130°$ method II		$\theta=120°$ method I		$\theta=120°$ method II		Obsd.[b] ΔE_{max}(eV) ($\log\varepsilon_{max}$)		
	ΔE_S(eV)	f	ΔE_S(eV)	f	ΔE_S(eV)	f	ΔE_S(eV)	f			
	2.004	0.000	3.814	0.000	2.441	0.000	3.880	0.000			
	2.866	0.453	3.908	0.110	3.086	0.379	3.948	0.091	x	4.13	(2.9)
	3.534	0.055	4.097	0.009	3.593	0.072	4.117	0.012	z		
	4.234	0.283	4.908	0.133	4.359	0.272	4.908	0.123	y	4.81	(4.6)
	5.073	1.518	5.011	0.938	5.158	1.111	5.008	0.816	x	5.10	
	5.230	0.000	5.414	0.059	5.471	0.000	5.397	0.076	z		
	5.675	0.001	5.702	0.000	5.620	0.036	5.698	0.000			
	5.709	0.037	5.783	0.090	5.786	0.000	5.771	0.076	y		
	5.748	0.000	6.112	0.279	5.828	0.000	6.065	0.245	x	5.93	
	6.133	0.083	6.242	0.235	6.065	0.092	6.201	0.170	y		
	ΔE_T(eV)[a] 1.100		ΔE_T(eV) 1.838		ΔE_T(eV) 1.446		ΔE_T(eV) 1.859				

b) Phenoxathiin (II)

Calcd.	$\theta=130°$ method I		$\theta=130°$ method II		$\theta=120°$ method I		$\theta=120°$ method II		Obsd. ΔE_{max} (eV) ($\log\varepsilon_{max}$)		
	ΔE_S(eV)	f	ΔE_S(eV)	f	ΔE_S(eV)	f	ΔE_S(eV)	f			
	3.234	0.170	3.755	0.002	3.598	0.203	3.825	0.003	x		
	3.626	0.312	3.884	0.116	3.858	0.212	3.925	0.096	x	4.20	(3.60)
	3.853	0.085	4.103	0.010	3.954	0.088	4.121	0.012	y		
	4.926	0.191	5.008	0.122	4.992	0.180	5.007	0.114	y	5.14	(4.50)
	5.428	0.626	5.045	1.021	5.455	0.281	5.043	0.889	x	5.21	(4.50)
	5.835	0.078	5.497	0.052	5.741	0.073	5.477	0.065	y	5.64	
	6.062	0.062	5.728	0.003	6.170	0.004	5.725	0.003	x		
	6.219	0.005	5.810	0.070	6.214	0.479	5.797	0.058	y		
	6.306	0.252	6.189	0.281	6.367	0.478	6.140	0.252	x		
	6.457	0.117	6.298	0.309	6.412	0.097	6.255	0.211	y		
	ΔE_T(eV) 1.883		ΔE_T(eV) 1.795		ΔE_T(eV) 2.141		ΔE (eV) 1.820				

c) Diphenylene Dioxide (III)

Calcd.	$\theta=180°$ method II		$\theta=180°$ method I		$\theta=170°$ method II		$\theta=170°$ method I		Obsd. ΔE_{max}(eV) ($\log\varepsilon_{max}$)		
	ΔE_S(eV)	f	ΔE_S(eV)	f	ΔE_S(eV)	f	ΔE_S(eV)	f			
	3.508	—	3.861	—	3.515	0.000	3.885	0.000			
	3.750	0.188	4.173	0.304	3.754	0.186	4.187	0.297	x	4.13	
	4.079	—	4.500	—	4.080	0.000	4.505	0.001	z	4.29	(3.87)
	5.074	1.498	5.460	0.220	5.074	1.481	5.467	0.217	y	5.44	(4.73)
	5.109	0.136	5.631	1.351	5.109	0.135	5.635	1.323	x	5.58	(4.64)
	5.632	—	6.154	—	5.630	0.002	6.149	0.002	z	6.11	
	5.749	—	6.372	—	5.751	0.000	6.376	0.000			
	5.854	0.078	6.472	0.114	5.852	0.077	6.467	0.110	y		
	6.374	0.292	6.784	—	6.370	0.290	6.796	0.000			
	6.425	0.834	6.943	0.697	6.423	0.814	6.934	0.484	x		
	ΔE_T(eV) 1.668		ΔE_T(eV) 2.298		ΔE_T(eV) 1.671		ΔE_T(eV) 2.312				

d) Phenothiazine (IV)

Calcd.	$\theta=140°$ method I		$\theta=140°$ method II		$\theta=130°$ method I		$\theta=130°$ method II		Obsd. ΔE_{max} (eV) ($\log\varepsilon_{max}$)	
	ΔE_S(eV)	f	ΔE_S(eV)	f	ΔE_S(eV)	f	ΔE_S(eV)	f		
	2.352	0.025	3.303	0.042	2.632	0.026	3.354	0.042	x	
	3.110	0.454	3.646	0.180	3.260	0.394	3.679	0.159	x	3.87 (3.64)
	3.666	0.062	3.934	0.016	3.713	0.070	3.946	0.019	y	
	4.505	0.244	4.804	0.154	4.569	0.242	4.800	0.146	y	4.89 (4.65)
	5.133	1.347	4.870	1.042	5.183	1.074	4.863	0.922	x	
	5.534	0.024	5.356	0.041	5.693	0.019	5.336	0.057	y	
	5.809	0.035	5.611	0.037	5.740	0.040	5.607	0.038	x	
	5.897	0.051	5.749	0.089	5.935	0.035	5.738	0.082	y	
	5.952	0.006	6.119	0.260	5.998	0.007	6.078	0.235	x	
	6.239	0.124	6.203	0.269	6.205	0.130	6.169	0.212	y	
	ΔE_T(eV) 1.360		ΔE_T(eV) 1.684		ΔE_T(eV) 1.590		ΔE_T(eV) 1.710			

e) Phenoxazine (V)

Calcd.	$\theta=160°$ method II		$\theta=160°$ method I		$\theta=150°$ method II		$\theta=150°$ method I		Obsd. ΔE_{max}(eV) ($\log\varepsilon_{max}$)	
	ΔE_S(eV)	f	ΔE_S(eV)	f	ΔE_S(eV)	f	ΔE_S(eV)	f		
	3.129	0.025	3.288	0.052	3.161	0.025	3.411	0.057	x	
	3.555	0.238	3.785	0.370	3.574	0.224	3.858	0.336	x	3.89 (3.93)
	3.944	0.004	4.182	0.020	3.949	0.007	4.206	0.026	y	
	4.864	0.163	5.113	0.233	4.863	0.159	5.143	0.226	y	5.19 (4.66)
	4.906	1.303	5.459	1.212	4.904	1.222	5.476	1.065	x	
	5.439	0.022	5.992	0.032	5.427	0.031	5.959	0.040	y	
	5.638	0.057	6.190	0.060	5.638	0.057	6.225	0.079	x	
	5.801	0.063	6.376	0.035	5.796	0.060	6.356	0.062	y	
	6.265	0.271	6.379	0.075	6.244	0.265	6.429	0.023	x	
	6.326	0.556	6.710	0.225	6.310	0.488	6.714	0.308	y	
	ΔE_T(eV) 1.480		ΔE_T(eV) 1.985		ΔE_T(eV) 1.598		ΔE_T(eV) 2.104			

a) Lowest $^3(\pi,\pi^*)$excitation energy

b) The observed spectral data of I, II, and III are quoted from:
B. Lamatte *et al.*, *J. Chim. Phys.*, **63**, 369 (1966).
Those of IV from: R. J. Warren *et al.*, *J. Pharm. Sci.*, **55**, 144 (1966).
Those of V from: M. P. Olmsted *et al.*, *J. Org. Chem.*, **26**, 1901 (1961).
Here, the 4.13 eV band of I alone is taken from: L, Lang,
"Absorption Spectra in the Ultraviolet and Visible Region," Part II, Akadémiai Kiado, Budapest (1961).

In the extended Hückel method[13] parametrizations of the Coulomb integrals are done with the data by Pritchard and Skinner.[14]

All the bond lengths in the aromatic ring are assumed to be 1.395 Å, and the C–H and N–H bond lengths are taken to be 1.08 and 1.012 Å, respectively. The intramolecular coordinate axes and numbering of the related molecules are given in Fig. 1.

Results and Discussion

Electronic Spectra. In this calculation the dihedral angle is varied in the range 180—120°. Table 1 shows the dihedral angle dependency of the calculated results for the second π-π^* transition, since this transition can be correlated with the longest wavelength band of each spectrum. By method I the calculated value of the transition energy is in the order I<IV<II<V<III, and by method II in the order V<IV<III<II<I. We see that method I indicates more clearly the effects of the folded structure upon the calculated values of the transition energy and oscillator strength.

Table 2 shows the calculated results obtained in a proper range of the dihedral angle as compared to experimental data. It is known that method I gives superior results for molecules not containing the sulfur atom, and method II for the sulfur-containing molecules. As for thianthrene, all the observed values of the transition energies except the lowest value are in good agreement with the values calculated by method II at the dihedral angle 120—130°. The lowest observed bands of thianthrene and phenoxathiin appear to be correlated with both the second and third transi-

13) R. Hoffmann, *J. Chem. Phys.*, **39**, 1397 (1963); *ibid.*, **40**, 2745 (1964).
14) H. O. Pritchard and H. A. Skinner, *Chem. Rev.*, **55**, 745 (1955).

tions. In fact, the polarized excitation spectrum of phenoxathiin indicates that the lowest observed band consists of perpendicularly polarized transitions which may be assigned to the second and third transitions.[15] The observed bands of diphenylene dioxide except the band at 4.29 eV are in good accord with the transitions calculated by method I at the dihedral angle 180—170°. It should be mentioned that the third transition of diphenylene dioxide, which is forbidden at planar structure, is slightly enhanced by molecular deformation.

The lowest observed bands of phenothiazine and phenoxazine can be well correlated with the second transition. The second observed bands of these molecules are situated fairly close to both the fourth (y-polarized) and fifth (x-polarized) transitions. In fact, the polarized excitation spectra of these molecules indicate that the second observed bands are composed of two transitions with perpendicular polarization directions.[15] On the other hand, the calculated values of lowest $^3(\pi,\pi^*)$ excitation energy tend to become lower than the experimental values, *i.e.*, 2.4 eV for phenothiazine and 2.6 eV for phenoxazine.[16]

In conclusion, the present calculations on the electronic spectra show that the folded structure is prominently associated with the sulfur-containing molecules in line with the experimental results on dipole moment or crystal structure.[17] Thus, it can be said that the p-orbital model of the sulfur atom adopted is enough for explanation of the electronic spectra.

Table 3. Dihedral angle dependence of the all valence-electronic energies

	Thianthrene (I) eV	Phenoxathiin (II) eV	Diphenylene Dioxide (III) eV
180°	−1184.431	−1233.889	−1281.491
170°	−1185.215	−1234.233	−1281.468
160°	−1183.537	−1233.368	−1281.391
150°	−1181.336	−1231.310	−1281.007
140°	−1179.578	−1231.046	−1280.076
120°	−1170.391	−1227.691	−1279.784

	Phenothiazine (IV)
H intra	−1189.404 eV
H extra	−1189.193

All Valence-electronic Structures and Ionization Potentials. All the valence-electronic structures of the molecules treated herewith are considered to depend sensitively on the dihedral angle through the change in the hybridization state of the central heteroatoms. Hence, a comparative survey on the electronic structure of typical molecules is made using the extended Hückel

Table 4. Calculated and experimental results of ionization potentials

a) Calculated data by the EHT method.

Thianthrene (I)

	I_p(eV)	HOMO coefficients of the 10th heteroatom			
		S(3s)	S(3P_x)	S(3P_y)	S(3P_z)
180°	9.838	0.000	0.000	0.000	0.371
160°	9.812	0.026	0.000	−0.184	0.349
140°	9.808	0.035	0.000	−0.302	0.326

Diphenylene dioxide (III)

	I_p(eV)	HOMO coefficients of the 10th heteroatom			
		O(2S)	O(2P_x)	O(2P_y)	O(2P_z)
180°	12.225	0.000	0.000	0.000	−0.264
160°	12.265	0.010	0.000	0.042	−0.259
140°	12.380	0.018	0.000	0.087	−0.242

Phenothiazine (IV)

	I_p(eV)	HOMO coefficients of the heteroatoms							
		N(2S)	N(2P_x)	N(2P)$_y$	N(2P_z)	S(3S)	S(3P_x)	S(3P_y)	S(3P_z)
H intra	10.253	−0.053	0.000	−0.080	−0.167	0.063	0.000	0.492	−0.299
H extra	10.143	0.013	0.000	−0.249	−0.123	0.077	0.000	0.513	−0.236

b) Calculated data by the P–P–P method

Calcd. by the method I

	(I)	(II)	(III)	(IV)	(V)
180°	5.444 eV	6.494	7.962	6.093	7.342
160°	5.520	6.566	8.034	6.162	7.406
140°	5.767	6.799	8.267	6.387	7.612

Calcd. by the method II

	(I)	(II)	(III)	(IV)	(V)
180°	8.350 eV	8.395	8.435	8.077	8.090
160°	8.375	8.420	8.459	8.099	8.118
140°	8.449	8.494	8.533	8.164	8.183

c) experimental data

Thianthrene (I)	7.80 eV	
Phenoxathiin (II)	7.98	Taken from: B. Lamatte *et al.*, *J. Chim. Phys.*, **63**, 369 (1966).
Diphenylene dioxide (III)	8.10	
phenothiazine (IV)	7.28	Taken from: M.Kinoshita, This Bulletin, **35**, 1609 (1962).

15) H. H. Mantsch and J. Dehler, *Can. J. Chem.*, **47**, 3173 (1969).
16) J. M. Lhoste, M. Ptak, and D. Lexa, *J. Chim. Phys. Physicochim. Biol.*, **65**, 1876 (1968).
17) From a summary of the data in (1) and (2), it is known that diphenylene dioxide is nearly planar, and the dihedral angle for thianthrene and phenoxathiin is 120—130° and that for phenothiazine 140—150°.

theory (EHT). The valence angle of the heteroatoms in a non-folded molecule is tentatively taken to be 120°, since it is not known which value of the valence angle would be appropriate for this case.

Table 3 shows the dihedral angle dependency of the all valence electronic energy. The energy values for thianthrene and phenoxathiin are liable to yield a slight energy minimum around the dihedral angle 170°, but those for diphenylene dioxide go on increasing as the molecule folds. This theoretical finding appears to be in line with the fact that the former two molecules have appreciably folded structures. Conclusive remarks about the dihedral angle dependency of the stability of the folded structure should be avoided, because the strain energy term possibly due to the difference between the assumed and preferred values of the C–S–C bond angle is neglected.

EHT calculations on the two possible spacial configurations of phenothiazine, to be referred to as H intra and H extra according to the notation by Malrieu and Pullman,[5] indicate that the all valence electronic energy of H intra is by 0.2 eV lower than that of H extra in agreement with the ordering of the HMO energies they obtained.

Vertical ionization potentials calculated by Koopmans' theorem are given in Table 4. The values obtained by the EHT method are considerably higher than the experimental data. The dihedral angle dependency of the atomic orbital coefficients of the heteroatoms in the highest occupied molecular orbitals (HOMO) is also given for thianthrene, diphenylene dioxide and phenothiazine because these molecules are known to be typical electron-donors. The EHT ionization potential of thianthrene tends to diminish by molecular deformation. The decrease is accompanied by increase of the S($3P_y$) coefficient and decrease of the S($3P_z$) coefficient. On the other hand, the HOMO coefficient of the oxygen atom in diphenylene dioxide is largely concentrated upon the $2P_z$-orbital. This might indicate that the effect of the lone-pair orbital hybridization to electron donating property is associated with thianthrene to a greater extent than with diphenylene dioxide. The EHT ionization potential of phenothiazine is slightly lowered in going from H intra to H extra. This is followed by a remarkable increase of the N($2P_y$) orbital component in the HOMO. The ionization potentials calculated by the P–P–P method increase with the degree of folding of the molecules. The data calculated by method II well fit the relative ordering of the experimental data.

Chemical Reactivity. The P–P–P method has been found useful for explaining the observed electronic spectra. A brief comment is given on the chemical reactivities in terms of the reactivity indices obtained from the SCF MO coefficients. These heterocyclic molecules are characterized by enhanced electrophilic substitution reactions and ready formation of charge-transfer complexes. The frontier electron densities for electrophilic reaction ($f_r^{(E)}$) were calculated. The $f_r^{(E)}$ values do not change much by the change of dihedral angle (Table 5). The data on phenothiazine and phenoxazine calculated by method II well explain the fact that position 3 is a preferable site for electrophilic reagents in a number of electrophilic reactions. The calculated data on diphenylene dioxide and thianthrene indicate that the β-position is the preferable site for electrophilic attack. The calculated data on phenoxathiin can not explain the fact that electrophilic substitutions such as bromination, formylation or chloromethylation proceed at positions 2 or 8, *i.e.*, *para* to the oxygen atom. Such unexpected directing effects of the oxygen atom have been attributed by Mantsch and Dehler to the formation of a stable complex at the sulfur atom, such as evidenced by an isolable phenoxathiin-dibromide complex.[15]

TABLE 5. FRONTIER ELECTRON DENSITY VALUES FOR ELECTROPHILIC ATTACK CALCULATED WITH THE P–P–P METHOD

	position	method I		method II	
		$\theta=180°$	$\theta=120°$	$\theta=180°$	$\theta=120°$
Thianthrene (I)	1	0.077	0.042	0.017	0.013
	2	0.063	0.054	0.056	0.057
Phenoxathiin (II)	1	0.094	0.077	0.018	0.014
	2	0.020	0.014	0.061	0.061
	3	0.105	0.101	0.060	0.062
	4	0.008	0.000	0.018	0.013
Diphenylene	1	0.017	0.007	0.019	0.015
Dioxide (III)	2	0.064	0.065	0.065	0.067
Phenothiazine	1	0.027	0.010	0.037	0.033
(IV)	2	0.086	0.076	0.040	0.038
	3	0.034	0.029	0.068	0.069
	4	0.083	0.056	0.011	0.006
Phenoxazine (V)	1	0.047	0.040	0.038	0.035
	2	0.037	0.027	0.044	0.041
	3	0.079	0.080	0.071	0.072
	4	0.009	0.000	0.012	0.007

Calculations were performed with a HITAC 5020-E computer, the University of Tokyo. The author wishes to thank Professor Y. Akahori for useful suggestions. Thanks are also due to Mr. T. Mizokoshi for his collaboration.

The Infrared Spectra of Addition Compounds of Hydrogen and Deuterium Cyanides with Boron Tribromide

Isao KANESAKA, Yoshiyuki HASE, and Kiyoyasu KAWAI
Faculty of Literature and Science, Toyama University, Gofuku, Toyama
(Received August 10, 1971)

The infrared spectra of addition compounds of hydrogen and deuterium cyanides with boron tribromide have been measured in the frequency region from 4000 to 200 cm^{-1}, and the normal frequencies have been proposed on the basis of the C_{3v} symmetry for four isotopic compounds, HCN·$^{10}BBr_3$, HCN·$^{11}BBr_3$, DCN·$^{10}BBr_3$, and DCN·$^{11}BBr_3$. The force constants have been calculated on the assumption of a modified Urey-Bradley force field, and the shift of the vibrational frequencies by the coordination has been discussed.

The infrared spectra of the addition compounds of hydrogen and deuterium cyanides with boron trichloride have been studied previously, and the observed spectra have been assigned on the basis of the C_{3v} symmetry, the isotopic effect of H and D or of ^{10}B and ^{11}B being taken account of.[1] The force constants of those compounds have also been calculated.[2]

In many of the addition compounds of R–C≡N with metal halides, in which R is H, D, Cl, Br, CH_3, or C_6H_5, the C≡N stretching frequency has been found to become higher than that of the parent R–C≡N.[1,3-9] Purcell and Drago[8] have explained that the shift of the C≡N stretching frequency in the addition compounds of acetonitrile is due mainly to the increase in the C≡N stretching force constant by coordination. In the addition compounds of hydrogen and deuterium cyanides, however, it has been found that the shift is due mainly to the mechanical coupling and only partly to the increase in the force constant.[1,2] The vibrational spectra of the addition compounds of trimethylamine with boron trihalides have been studied in detail, and the vibrational assignments of the observed frequencies have been proposed on the basis of the isotopic shift and the trend of the frequencies.[10]

In the present paper, the infrared spectra of the addition compounds of hydrogen and deuterium cyanides with boron tribromide will be studied, and the force constants of those compounds will be calculated.

Experimental

The hydrogen cyanide, deuterium cyanide, and boron tribromide were prepared by the ordinary method and were purified by fractional distillation *in vacuo*. The addition compound, HCN·BBr_3 or DCN·BBr_3, was prepared by the reaction of boron tribromide dissolved in cyclopentane with hydrogen or deuterium cyanide, after the method described by Woolf[11] in his study of the addition compounds of cyanogen halides.

The addition compounds were covered with cyclohexane or carbon tetrachloride to prevent them from hydrolysis and were then dispersed on KRS-5 plates, and their infrared

TABLE 1. THE ASSIGNMENT OF THE INFRARED SPECTRA OF HCN·BBr_3 AND DCN·BBr_3 (cm^{-1})

Obsd		Assignment[a]
HCN·BBr_3	DCN·BBr_3	
3120 s	3120* w	ν(C–H)
	2594 s	ν(C–D)
2197 s	2200* w	ν(C≡N)
	1942 s	ν(C≡N)
1110 w		750+363=1113
	1089 w	776+317=1093
795 w		δ(HCN)
777 w	776 w	ν(N–^{10}B)
750 s	749 s	ν(N–^{11}B)
696 s	696 s	ν(^{10}B–Br) asym.
674 vs	674 vs	ν(^{11}B–Br) asym.
	656 m	δ(DCN)
662 vw		363+2×150=663
632 vw		2×318=636
560 vw		3×188=564
501 vw		318+188=506
	496 vw	350+150=500
	396 vw	2×198=396
375 vw		2×188=376
	372 vw	198+174=372
363 m	350 w	δ(CNB)
333 vw		188+150=338
318 s	317 s	ν(B–Br) sym.
300 vw	300 vw	2×150=300
207 vw	198[c]	δ(NBBr)sym.
188[c]	174[c]	δ(NBBr) asym.
150[c]	150[c]	δ(BrBBr) asym.

a: When the frequencies are same for the compounds of boron ten and boron eleven, boron atom is simply indicated as B.
c: Assigned from combination bands. *: Assigned to the impurity.
vs=very strong, s=strong, m=medium, w=weak, and vw=very weak.

1) K. Kawai and I. Kanesaka, *Spectrochim. Acta*, **25A**, 1265 (1969).
2) Y. Hase and I. Kanesaka, *Nippon Kagaku Kaishi*, to be published.
3) H. J. Coerver and C. Curran, *J. Amer. Chem. Soc.*, **80**, 3522 (1958).
4) W. Gerrard, M. F. Lappert, H. Pyszora, and J. W. Wallis, *J. Chem. Soc.*, **1960**, 2182.
5) D. S. Bystrov and B. K. Nazarov, *Dokl. Akad. Nauk SSSR*, **148**, 1335 (1963).
6) E. Allenstein and A. Schmidt, *Chem. Ber.*, **97**, 1863 (1964).
7) E. Oikawa and S. Kambara, *J. Polymer Sci., Part B*, **2**, 649 (1964).
8) K. F. Purcell and R. S. Drago, *J. Amer. Chem. Soc.*, **88**, 919 (1966).
9) K. Kawai and I. Kanesaka, *Spectrochim. Acta*, **25A**, 263 (1969).
10) R. L. Amster and R. C. Taylor, *ibid.*, **20**, 1487 (1964).
11) A. A. Woolf, *J. Chem. Soc.*, **1954**, 252.

spectra were recorded in the range from 200 to 4000 cm^{-1}. The observed frequencies are expected to be accurate within the limit of ± 5 cm^{-1} for the 4000—2000 cm^{-1} region and ± 2 cm^{-1} for the 2000—200 cm^{-1} region; their assignments are listed in Table 1, in which the two asterisked weak bands are attributable to the addition compound of hydrogen cyanide, which was present in deuterium cyanide as an impurity, with boron tribromide.

Assignments

On the basis of an examination of the structures of certain boron trihalide complexes, it seems reasonable to expect that the addition compound of hydrogen or deuterium cyanide with boron tribromide, $XCN \cdot BBr_3$, where X is H or D, possesses the C_{3v} symmetry. Accordingly, ten normal vibrations, of which five belong to A_1 species and five to E species, can be expected for each compound, and all of them can be expected to be active in the infrared spectra.

In the spectra of $HCN \cdot BBr_3$, six strong and one medium bands were observed. The two bands at 3120 and 2197 cm^{-1} are easily assigned to the C–H and C≡N stretching vibrations respectively. The isotopic shift of the ^{11}B–N and ^{10}B–N stretching frequencies is estimated to be about 30 cm^{-1} from the calculation of the normal frequencies of this type of compound. Taking account of this isotopic shift, the natural abundance of ^{11}B and ^{10}B, and the relative intensities of the observed bands, we assigned the band at 750 cm^{-1} to the ^{11}B–N stretching vibration and the weak band at 777 cm^{-1} to the ^{10}B–N stretching vibration. The isotopic shift of asymmetric ^{11}B–Br and ^{10}B–Br stretching frequencies is also estimated to be about 30 cm^{-1}; this shift has been found to be 29 cm^{-1} for $(CH_3)_3N \cdot BBr_3$.[10] Since the band at 662 cm^{-1} is too weak to assign to a normal vibration, and since this frequency was not observed in the spectra of $DCN \cdot BBr_3$, we assigned the two bands at 674 and 696 cm^{-1} to the asymmetric ^{11}B–Br and ^{10}B–Br stretching vibrations respectively. The band at 318 cm^{-1} was assigned to both the symmetric ^{11}B–Br and ^{10}B–Br stretching vibrations, and the medium band at 363 cm^{-1}, to C≡N–B bending vibration. In addition to those bands, several weak bands were observed. The two bands at 795 and 207 cm^{-1} may be assigned to the H–C≡N and N–B–Br bending vibrations respectively. The remaining weak bands were assigned as combination or overtone bands, for which we propose two normal frequencies, 188 and 150 cm^{-1}.

The bands observed in the spectra of $DCN \cdot BBr_3$ were assigned by comparing their frequencies with those assigned to the normal vibrations of $HCN \cdot BBr_3$ or $DCN \cdot BCl_3$.[1] The two strong bands at 2594 and 1942 cm^{-1} and the medium band at 656 cm^{-1} are easily attributable to the coordinated DCN group. From the tentative assignment of the weak bands as combination or overtone bands, three normal frequencies were proposed, as is shown in Table 1.

The normal frequencies thus assigned for four isotopic compounds, $HCN \cdot {}^{10}BBr_3$, $HCN \cdot {}^{11}BBr_3$, $DCN \cdot {}^{10}BBr_3$, and $DCN \cdot {}^{11}BBr_3$, are listed in Table 2.

Table 2. The normal frequencies of $XCN \cdot BBr_3$[a] (cm^{-1})

Species	Mode	$HCN \cdot {}^{10}BBr_3$	$HCN \cdot {}^{11}BBr_3$	$DCN \cdot {}^{10}BBr_3$	$DCN \cdot {}^{11}BBr_3$
A_1	ν_1 ν(C–X)[a]	3120	3120	2594	2594
	ν_2 ν(C≡N)	2197	2197	1942	1942
	ν_3 ν(N–B)	777	750	776	749
	ν_4 ν(B–Br)	318	318	317	317
	ν_5 δ(NBBr)	207	207	198	198
E	ν_6 δ(XCN)[a]	795	795	656	656
	ν_7 ν(B–Br)	696	674	696	674
	ν_8 δ(CNB)	363	363	350	350
	ν_9 δ(NBBr)	188	188	174	174
	ν_{10} δ(BrBBr)	150	150	150	150

a) X=H or D.

Normal Coordinate Analysis

In order to confirm the assignment of the observed frequencies and calculate the force constants, a normal coordinate analysis was carried out for the four isotopic compounds on the assumption of a modified Urey-Bradley force field which contains two bending-bending interaction constants, I[CNB,NBBr] and I[HCN,CNB] or I[DCN,CNB].

The interatomic distances were assumed to be B–Br= 1.95, N–B=1.56, C≡N=1.16, and C–H or C–D= 1.07 Å, and the valence angle was assumed to be tetrahedral for the $NBBr_3$ group.

Since the harmonic oscillator approximation was applied in this analysis, the C–H and C≡N stretching force constants of the addition compounds of hydrogen cyanide, K[C–H] and K[C≡N], were expected to be considerably different from the C–D and C≡N stretching force constants of the addition compounds of deuterium cyanide, K[C–D] and K[C≡N], as has been found for free hydrogen and deuterium cyanides or the addition compounds of those cyanides.[2] It may probably be assumed that the same values of force constants can be applied to the addition compounds with boron ten and those with boron eleven, and that F' (linear repulsive force constant) is $-0.1F$ (repulsive force constant) as usual. Accordingly, fourteen force constants were calculated from the normal frequencies listed in Table 2 by the least-squares method.

The numerical calculation was carried out by means of a computer program reported previously,[12] using an electronic computer HITAC 5020E, at the Computer Center of The University of Tokyo. The calculated force constants are listed in Table 3, along with those of the parent compounds[13] and those of the addition compounds of hydrogen and deuterium cyanides with boron trichloride, which are listed for the sake of comparison. The mean deviation of the calculated frequencies from the observed ones is 2.4 cm^{-1}, while the largest is 6.9 cm^{-1}.

The potential energy distributions (PED), defined as $(PED)_{ij}=(L_{ij})^2 \times (F_s)_{ii}/\lambda_j \times 100$, where λ_j is the jth

12) T. Shimanouchi, "Computer Program, BGLZ and LSMB," The University of Tokyo (1968).

13) K. Shimizu and H. Shingu, *Spectrochim. Acta*, **22**, 199 (1966).

Table 3. The force constants of $HCN \cdot BBr_3$, $DCN \cdot BBr_3$, $HCN \cdot BCl_3$, $DCN \cdot BCl_3$, BBr_3, HCN, and DCN (mdyne/Å)

	$HCN \cdot BBr_3$ ε $DCN \cdot BBr_3$	$HCN \cdot BCl_3$[2] ε $DCN \cdot BCl_3$	BBr_3[13]	HCN[b]	DCN[b]
K[C–H]	5.094	5.229		5.817	
K[C–D]	5.790	5.876			6.058
K[C≡N][h]	19.480	19.193		18.019	
K[C≡N][d]	17.698	17.680			17.721
K[N–B]	1.710	1.581			
K[B–X][a]	1.193	1.601	2.397		
H[H(D)CN]	0.261	0.241		0.261	0.247
H[CNB]	0.289	0.233			
H[NBX][a]	0.269	0.179			
H[XBX][a]	0.124	0.151	0.058		
F[X··X][a]	0.406	0.444	0.422		
F[N··X][a]	0.397	0.613			
I[CNB,NBX][a]	0.363	0.213			
I[H(D)CN,CNB]	0.040	0.050			

a) X is Br or Cl. b) The force constants calculated from the normal frequencies listed in reference 14. h or d refers to HCN or DCN, respectively.

Table 4. The potential energy distributions for $HCN \cdot {}^{10}BBr_3$

Species A_1	Calculated frequencies				
	3120	2197	780	321	203
C–H str.	91.19	8.73	0.05	0.03	0.00
C≡N str.	8.74	88.06	1.75	1.35	0.10
N–B str.	0.07	3.31	81.71	20.97	3.41
B–Br sym. str.	0.00	0.00	22.46	43.42	41.82
BrBBr sym. bend.	0.00	0.01	41.79	23.25	42.55

Species E	Calculated frequencies				
	800	700	368	185	150
B–Br asym. str.	0.10	81.06	12.78	15.13	4.05
NBBr asym. bend.	0.44	53.50	29.72	35.76	10.60
BrBBr asym. bend.	0.03	25.12	2.31	1.66	77.74
CNB bend.	5.87	13.91	91.41	15.05	0.25
HCN bend.	102.02	0.16	0.43	0.08	0.02

Table 5. The potential energy distributions for $HCN \cdot {}^{11}BBr$

Species A_1	Calculated frequencies				
	3120	2197	749	320	202
C–H str.	91.19	8.73	0.05	0.03	0.00
C≡N str.	8.74	88.09	1.76	1.32	0.10
N–B str.	0.07	3.27	82.85	19.93	3.35
B–Br sym. str.	0.00	0.00	21.97	44.50	41.23
BrBBr sym. bend.	0.00	0.01	40.73	23.72	43.14

Species E	Calculated frequencies				
	800	670	368	185	150
B–Br asym. str.	0.05	80.62	13.47	14.99	4.00
NBBr asym. bend.	0.54	54.17	28.92	35.91	10.49
BrBBr asym. bend.	0.01	24.79	2.45	1.65	77.95
CNB bend.	6.03	14.50	90.65	15.05	0.24
HCN bend.	102.09	0.08	0.43	0.08	0.02

Table 6. The potential energy distributions for $DCN \cdot {}^{10}BBr_3$

Species A_1	Calculated frequencies				
	2594	1942	777	316	202
C–D str.	65.45	34.27	0.17	0.11	0.01
C≡N str.	34.01	62.11	2.14	1.62	0.13
N–B str.	0.55	3.77	80.35	21.14	3.66
B–Br sym. str.	0.00	0.01	22.81	44.01	40.88
BrBBr sym. bend.	0.00	0.02	42.38	38.03	43.17

Species E	Calculated frequencies				
	701	649	344	176	149
B–Br asym. str.	80.41	1.30	13.92	14.50	3.00
NBBr asym. bend.	54.06	0.69	34.17	27.73	13.38
BrBBr asym. bend.	24.92	0.37	2.26	4.71	74.59
CNB bend.	15.12	15.26	76.07	19.01	1.01
DCN bend.	0.77	96.27	4.67	0.85	0.41

Table 7. The potential energy distributions for $DCN \cdot {}^{11}BBr_3$

Species A_1	Calculated frequencies				
	2594	1942	746	315	202
C–D str.	65.46	34.27	0.17	0.10	0.01
C≡N str.	34.01	62.16	2.13	1.58	0.13
N–B str.	0.55	3.71	81.47	20.16	3.59
B–Br sym. str.	0.00	0.01	22.35	45.05	40.30
BrBBr sym. bend.	0.00	0.01	42.36	22.46	43.75

Species E	Calculated frequencies				
	673	648	344	176	149
B–Br asym. str.	70.40	8.03	14.07	14.27	3.00
NBBr asym. bend.	58.12	0.45	34.01	27.95	13.30
BrBBr asym. bend.	22.27	2.46	2.27	4.83	74.66
CNB bend.	21.13	8.83	75.98	19.01	1.01
DCN bend.	7.38	89.55	4.67	0.85	0.14

frequency parameter, $(F_s)_{ii}$ is the ith diagonal element of the symmetry force constants, and L_{ij} is the L-matrix element, were also calculated; they are listed in Tables 4—7.

Discussion

From the values listed in Tables 4—7, it is found that the vibrational assignments listed in Table 2 are reasonable. The isotopic product ratios derived experimentally from the observed frequencies and theoretically from the masses of atoms and geometrical structure are shown in Table 8; it is also found that those four isotopic compounds obey the product rule.

In Table 9, the shifts of the C≡N stretching, C–H or C–D stretching, and H–C≡N or D–C≡N bending vibrations are summarized; they correspond to the difference between the frequencies of the parent hydrogen or deuterium cyanide,[14] that is, 2097, 3311, and 712, or 1925, 2630, and 569 cm^{-1}, and those of the

14) K. Nakamoto, "Infrared Spectra of Inorganic and Coordination Compounds", Van Nostrand 1962, p. 80.

TABLE 8. THE ISOTOPIC PRODUCT RATIOS IN $XCN \cdot BBr_3$[a]

	Species	Ratio	
		Obsd	Theoret
$HCN \cdot {}^{10}BBr_3/HCN \cdot {}^{11}BBr_3$	A_1	1.036	1.047
	E	1.033	1.047
$DCN \cdot {}^{10}BBr_3/DCN \cdot {}^{11}BBr_3$	A_1	1.036	1.047
	E	1.033	1.047
$HCN \cdot {}^{10}BBr_3/DCN \cdot {}^{10}BBr_3$	A_1	1.423	1.412
	E	1.358	1.356
$HCN \cdot {}^{11}BBr_3/DCN \cdot {}^{11}BBr_3$	A_1	1.429	1.412
	E	1.358	1.356

a) X=H or D.

TABLE 9. THE SHIFT OF THE FREQUENCIES OF HYDROGEN AND DEUTERIUM CYANIDES (cm^{-1})

	$\Delta\nu$(C≡N)	$\Delta\nu$(C–H)	$\Delta\delta$(HCN)
$HCN \cdot BCl_3$	92	−155	46
$HCN \cdot BBr_3$	100	−191	83
	$\Delta\nu$(C≡N)	$\Delta\nu$(C–D)	$\Delta\delta$(DCN)
$DCN \cdot BCl_3$	25	−23	42
$DCN \cdot BBr_3$	17	−36	87

addition compounds listed in Table 2 or, for the sake of comparison, those of the addition compounds with boron trichloride.[1] From Table 9, one may notice that the shifts of the frequencies are, on the whole, more significant in the addition compounds with boron tribromide than in those with boron trichloride. This may be caused by the difference between the Lewis acidity of the boron trichloride and boron tribromide: the latter exhibits a stronger acidity than the former.[15,16] This difference also appears in the N–B stretching force constants listed in Table 3; it is reasonably certain that the dative N–B bond in the addition compounds with boron tribromide is stronger than that in those with boron trichloride.

As has been found with regard to the force constants of the addition compounds of hydrogen and deuterium cyanides with boron trichloride,[2] there are indications that the K[C–H] or K[C–D] of the addition compounds of hydrogen or deuterium cyanide with boron tribromide is smaller than that of free cyanides, and that the K[C≡N] of the addition compounds is slightly larger than, or nearly the same as, that of the cyanides, as is shown in Table 3. This suggests that the shift of the C≡N stretching frequency is due not only to the increase in the force constant, but also to the mechanical coupling of this vibration with the C–H or C–D stretching vibration. The appearance of the C≡N stretching frequency in the lower-frequency region in the addition compounds of deuterium cyanide with boron tribromide than in those with boron trichloride may also be explained in terms of the mechanical coupling.

The B–Br stretching force constant of the addition compounds given in Table 3 is considerably smaller than that of free boron tribromide. This indicates that the strength of the B–Br bond in the addition compounds decreases considerably as a result of the change in the hybridization from sp^2 to sp^3 at the boron atom and as a result of the increase in the polarity in the bond as well as the C–H or C–D bond of the addition compounds.

The N–^{10}B or N–^{11}B stretching frequency has been found to be 720 or 689 cm^{-1} respectively in the addition compounds of trimethylamine with boron tribromide;[10] it seems reasonable to consider that the dative N–B bond in the addition compounds of hydrogen or deuterium cyanide is stronger than that in those of trimethylamine.

The authors wish to express their gratitude to Professor Hiromu Murata of Hiroshima University and to Dr. Isao Suzuki of The University of Tokyo for their useful suggestions.

15) H. C. Brown and R. R. Holmes, *J. Amer. Chem. Soc.*, **78**, 2173 (1956).

16) K. Tanabe and T. Takeshita, "Acid-Base Catalysis", Sangyo Tosho 1966, p. 99.

An Interstitial-Electron Model for the Structure of Metals and Alloys I. Description of Model for Metallic Binding

Oliver JOHNSON

Research Institute for Catalysis, Hokkaido University, Sapporo

(Received August 9, 1971)

Application of the Hellmann-Feynman Theorem to Metals has led to an interstitial-electron model in which there is some localization of itinerant electron density in octahedral or tetrahedral interstices of close-packed metal ion cores. A flat maximum of electron density at centers of interstices is proposed as well as preferential occupancy of either octahedral or tetrahedral interstices. Such occupancy is rather precisely determined by the requirements of minimum electron-electron repulsion and of opposite spins for electrons in adjacent interstices. Writing the interstitial-electron structure of a metal in terms of interstice occupancy thus includes electron correlation effects. The interstitial-electron structures are instantaneous pictures of electron density which are representative of the highly dynamic situation of electrons in metals. The model leads to localization of *d*-electrons on the metal-ion core when interstices are fully occupied by itinerant electrons, *i.e.* at M^{6+}. The presence of vacant interstices is required for metallic properties. On the basis of the model, chemical binding in metals differs from that in polyhedral molecules or metal cluster compounds only in the greater delocalization of electron density in metals. The concepts of the interstitial-electron model are closer to those of the method of pseudopotentials than to the Bloch Band Theory although all of these descriptions of metals can be considered equivalent.

The starting point of all discussions of chemical binding must be with electrons and positive nuclei. It is generally accepted that in the metallic state the valence electrons of the metal atom are given up to the whole metal structure as itinerant electrons ($\bar{e}$) which are relatively free to move throughout the lattice of positive ion cores. Intuitively, it seems likely that the maximum binding of such a lattice would be obtained by an optimum distribution of the itinerant electrons within the octahedral and tetrahedral interstices of the metal lattice, *i.e.* some localization of electron density rather than a uniform distribution of electron density. A model with uniform electron density is probably more appropriate for a liquid metal than a solid metal.

In the Band Theory of Metals the wave functions of the itinerant electrons are considered to be extended through the whole lattice and itinerant electrons are described as occupying energy bands. In this paper an interstitial-electron model is presented in which the itinerant electron density is considered to be localized in lattice interstices and presumably, itinerant electron wave functions are not associated with a single atomic core. Since the interstitial-electron model will be developed in terms of spatial location of electrons (*i.e.* electrons-in-interstices) it will not be possible to make direct comparisons to Band Theory which uses energy-momentum coordinates. However, it will be shown that the model can be related to some of the results of the method of pseudopotentials. The view is taken that the interstitial-electron description of metals is equivalent to that of electrons in energy bands, and where energies of electrons are involved, use will be made of Band Theory concepts such as Fermi level and Band width. The model will be presented with a minimum reference to Band Theory of metals since, there have been excellent recent reviews on the topic.[1-3]

1. Background of Interstitial-Electron Model

This paper will give the details of an interstitial-electron model for the structure of metals, and the model will be used in a following series of papers to formulate electronic structure for metals (Part II), to interpret properties of metals (III) including magnetic properties (IV), to explain the formation and structure of intermetallic phases (*e.g.* Cu_5Zn_8) (V) and to give a physical interpretation of superconductivity (VI).

It is difficult to give credit to the large number of investigators who have discussed some aspect of the importance of interstices in metals and related solids. The first proposal of electrons-in-interstices for metals was by Lorentz.[4] Electron pairs at positions of potential minima was proposed for noble metals by Fajans,[5] and Bent[6] has included metals in his tangent-sphere models with electron pairs occupying anionic positions. The model builds as well on important foundations laid by the essentially metallurgical approach of Hume-Rothery[7] and others. The new feature of the present paper is to take the interstitial-model as a definitive description of the metallic state which can incorporate all the quantum chemical aspects of chemical binding including electron correlation and spin. The detailed consideration of the geometry of the HCP and CCP close-packed metals and the BCC metals along with the pattern of interstices in these structures is an integral part of the model.

The Hellmann-Feynman viewpoint[8] offers a means of relating the idea of electron density in interstices to

1) W. M. Lomer, *Prog. Materials Sci.*, **14**, 99 (1969).
2) J. M. Sivertson and M. E. Nicholson, *ibid.*, **9**, 305 (1961). T. B. Massalski and H. W. King, *ibid.*, **10**, 5 (1961).
3) J. M. Ziman, *J. Res. N. Bur. Stand.*, **74A**, 241 (1970).
4) H. A. Lorentz, "Theory of Electrons", Teubner, Leipsig, 1906.
5) K. Fajans, *Ceram. Age*, **54**, 288 (1949); Gordon Conference Lecture, 1959.
6) H. Bent, *J. Chem. Educ.*, **42**, 348 (1965); *Amer. Chem. Soc. Lectures*, 1969—70.
7) W. Hume-Rothery, "The Structure of Metals and Alloys," Institute of Metals, London, (1947).
8) T. Berlin, *J. Chem. Phys.*, **19**, 208 (1951).

general discussions of chemical binding. Berlin and Fajans[9] pointed out clearly that a complete description of chemical binding in a diatomic molecule could be based on considerations of interactions of positively charged atomic cores and electrons. Berlin's[8] analysis of the Hellmann-Feynman Theorem was to point out that at equilibrium the classical coulomb forces exerted by the quantum-mechanical electron distribution on the nuclei must precisely balance the forces of nuclear-nuclear repulsion. The electron density between nuclei in homopolar molecules exerts an attractive force on each nucleus and pulls them together (*i.e.* exerts a binding force). Electron density outside of a critical nodal surface attracts the near nucleus so much more than the far nucleus that there is a net force tending to separate the nuclei, an anti-binding force.

Bader and Jones[10] have applied the Hellmann-Feynman Theorem to many molecules, and this viewpoint has been extended to polyatomic molecules by Bader *et al.*[11] and Bader and Preston.[12] Bader and co-workers have discussed chemical binding by comparing calculated electron densities in molecules with one electron wave functions and resultant electron densities for the constituent atoms. The Berlin analysis of the Hellmann-Feynman Theorem leads to the expectation of a triangular binding region for a triatomic molecule and to a pyramidal binding region for a tetratomic molecule; these are also the conclusions of Bader *et al.* for H_2O and NH_3 based on density difference diagrams.[11,12] Wannier[13] has recently applied the Hellmann-Feynman Theorem to the problem of cohesion in metals. The Hellmann-Feynman viewpoint has been extensively applied to molecules by Bader,[11] Roux and Daudel,[14] Pollisar and Harris,[15] Boyd[16] and Marron,[17] and it appears to be a very fruitful way to discuss chemical binding. The interstitial-electron model proposes a localization of electron density in interstices of a metal structure, and the Hellmann-Feynman Theorem provides a rigorous basis for treatment of forces between electrons and metal ion cores in this binding region.

In extending this viewpoint to metals it is convenient at the same time to define the positive ion core more precisely for a metal. Except for transition metals the ion cores are closed shells of electrons, equivalent to rare gas shells. Berlin[8] has shown that such electrons exert a binding force in molecules since they exert no net force on the nucleus to which they are symmetrical but attract the other nucleus. However, the valence electrons in metals hardly penetrate these ion cores, and the problem of wave functions for itinerant electrons is greatly simplified if it is assumed that the metal positive on cores are not penetrated by valence electrons. This places an additional restriction on the binding region for itinerant electrons in a metal. The binding region in metals is defined by the model as the interstices of the metal lattice, and it is proposed that there are $\bar{e}$ or $\bar{e}_2$ in the octahedral or tetrahedral interstices, *i.e.* electron density centered on the interstice. "Shapes of binding regions" in polyatomic molecules and metals have been discussed more in detail elsewhere.[17a]

Fajans[18] has developed the concept of binding regions in molecules in his Quanticule Theory in terms of quantization of electron or groups of electrons with respect to the positive field of a single nucleus or more than one nuclei. The electronic structure for the tetrahedral molecule B_4Cl_4 is written $[(4B^{3+})\ (\bar{e}_8),\ 4Cl^-]$ where the $(\bar{e}_8)$ group of electrons is termed a quanticule. In the Hellmann-Feynman viewpoint this corresponds to 8 electrons in the tetrahedral binding region which extends out from each triangular face of the tetrahedron. Gillespie[19] has proposed that there are 4 $(\bar{e}_2)$ on the triangular faces of the B_4Cl_4 molecule. When the requirements of electron repulsion and electron spin are imposed on the 8 electrons in the binding region, it seems very reasonable that electrons would be found in the 4 binding regions associated with the triangular faces of the tetrahedral molecule. Delocalization of electrons, as compared to $\bar{e}_2$ between ions, has been proposed by Fajans[18] for benzene and pyrrol and is a widely used concept in Molecular Orbital Theory.

The proposed model for the electronic structure of metals has been discussed thus far in terms of electron density of itinerant electrons in metal interstices. As projected such a model can treat metal properties in a qualitative or semiquantitative way on an electrostatic basis. It is of interest to consider what kind of wave function could represent electron density localized in metal interstice. Non-overlapping wave functions centered on an interstice could be the floating spherical gaussian functions such as used by Frost[20] and also recently by Linnett.[21] The similarity of the present model to Gillespie's[22] treatment of electrons in molecules extends as well to his specification of electron wave functions which are non-overlapping and not centered on atoms. The movement of electrons between such orbitals (or binding regions) will be discussed further in considering the average *vs.* instantaneous electron distribution.

2. Postulates of the Interstitial-Electron Model

The basic postulates of the interstitial-electron model will be given, and this will be followed by a complete

9) K. Fajans and T. Berlin, *J. Chem. Phys.*, **10**, 691 (1942).
10) R. F. W. Bader and G. A. Jones, *Can. J. Chem.*, **39**, 1253 (1961).
11) R. F. W. Bader, *J. Amer. Chem. Soc.*, **86**, 5070 (1964); R. F. W. Bader, I. Keaveny, and G. Runtz, *Can. J. Chem.*, **47**, 2308 (1969).
12) R. F. W. Bader and H. J. T. Preston, *Can. J. Chem.*, **44**, 1131 (1969).
13) G. H. Wannier, C. Misner, and G. Schay, Jr., *Phys. Rev.*, **185**, 983 (1969).
14) M. Roux and R. Daudel, *Compt. Rend.*, **240**, 90 (1955).
15) P. Pollisar and R. R. Harris, *J. Amer. Chem. Soc.*, **92**, 1834 (1970).
16) D. H. Boyd, *J. Chem. Phys.*, **52**, 4846 (1970).
17) M. T. Marron, *ibid.*, **52**, 3600, 3606 (1970).
17a) O. Johnson, Paper Submitted to *J. Chem. Educ.*
18) K. Fajans, "Quanticule theory of Chemical Binding", *Chimia*, **13**, 349 (1959), English Translation available from Ulrich's Book Store, Ann Arbor, Michigan.
19) R. G. Gillespie, Conference on Coordination Chemistry, Banff, British Columbia, (1969).
20) A. A. Frost, *J. Phys. Chem.*, **72**, 1289 (1968).
21) J. W. Linnett, Lecture, U. of California, Berkeley, 1970.
22) R. G. Gillespie, *Angew. Chem. (Int. Edit.)*, **6**, 819 (1967).

description of metal lattices which form the basis of the model. Each of the postulates will be discussed in detail and justifications offered.

I. In a metal the valence electrons belong to the whole structure as itinerant (or conduction) electrons, $\bar{e}$.

$$M \longrightarrow \underset{\text{ion core}}{M^{n+}} + n\bar{e}$$

II. Interstices of the close-packed metal structure are taken as the location of $\bar{e}$. Electron density is centered on an interstice, and there is a flat maximum at the interstice center. It can also be considered that the binding regions for metal electrons are the tetrahedral(tet) and octahedral(oct) interstices.

III. There is preferential $\bar{e}$ occupancy of oct or tet interstices depending on which interstice provides most effective screening from adjacent $\bar{e}$ by positive ion cores.

IV. There are opposite electron spins for $\bar{e}$ in the adjacent interstices with minimum screening. This corresponds to interstices joined by a triangle of metal ion cores.

V. Before the number of $\bar{e}$ reaches 6, the *d*-electrons are localized on the metal ion core, *e.g.* Mn^{7+} (d^5), $2\bar{e}$. The number 6 corresponds to the filling of the 2 tet and 1 oct interstice per M^{n+} with 2 electrons each.

VI. Itinerant electrons in interstices act as ligands and determine the degeneracy of the *d*-electrons localized on the ion core and, thus, their magnetic properties.

VII. For metallic properties there must be some vacant interstices in the metal structure.

VIII. The shape of the oct or tet binding region can change with occupancy since repulsion exerted by electrons in adjacent interstices defines the boundary of the binding region.[17a] Mutual polarization of itinerant electrons and ion cores also modify electron density and "shape of the binding region".

3. Description of the Interstitial-Electron Model

Metal structures have been traditionally discussed in terms of models of close-packed spheres. These are especially useful to show the positions of the tetrahedral(tet) and octahedral(oct) interstices, but it must be emphasized that the observed metal lattice is that of an array of metal ion cores and that the electron density at the periphery of the so-called close-packed spheres is very low. Except for transition metals the metal ion cores are closed shells (rare gas shells).

The interstitial-electron model is based on the postulate that in the array of metal ion cores the maximum attraction of these cores by the electrons is obtained when there is some degree of localization of the electron density in the interstices of the structure. A careful consideration of the geometry of each of the close-packed metal structures as well as the pattern of interstices within each structure shows that there are very important differences in interstice distance and arrangement. Each structure will be considered in detail to illustrate the proposed location of electrons according to the interstitial-electron model. The most complete discussion of interstices in crystal lattices has been given by Gehman[23] for Cubic Close Packing (CCP) and for Hexagonal Close Packing (HCP). Gehman emphasized that the occupancy of tetrahedral interstices was the key for understanding the CCP structure of compounds and that octahedral interstices were the key to HCP structures. The present discussion considers electrons in the interstices rather than anions or cations as in Gehman's paper and adds the Body Centered Cubic Structure (BCC). The placement of electrons in interstices offers a natural way to incorporate electron correlation which now becomes inherent in the symmetry of electrons in interstices.

The use of "electron-in-an-interstice" individualizes the electrons in a many-electron system. This is a good approximation[8] and a physically fruitful way to discuss electrons in a metal. This gives an *instantaneous picture* of electron density in oct and tet interstices and includes both occupied and vacant interstices. In the application of the interstitial-electron model it is considered that vacant interstices are required for metallic properties, *e.g.* electrical conductivity. The designation of electron occupancy of interstices (the interstitial-electron structure) is then an instantaneous picture of a highly dynamic situation in which the detailed arrangement is mobile, but the average situation is stationary with high correlation of electronic motion. The model and the interstitial-electron structures to be given are based on short-range correlation of electron position and motion, but the electrons in this arrangement are free to move because of absence of long range correlation of electron repulsions (see *e.g.* Lomer[1]). In the dynamic situation of rapid electron movement and lattice vibrations, the movement of electrons from one orbital to another with many energy states possible is not unlike the models discussed by Hubbard.

The average itinerant electron density is accurately represented by the instantaneous picture of electrons in interstices, and a time average picture results when the total number of electrons in an interstice type is fractionally distributed over the total number of interstices of that kind. In addition to localization of electron density in one interstice as compared to another (oct more than tet), there can be spatial localization of electron density within one type of interstice (maximum density in center *vs.* more complex distribution). The latter kind of localization may be more important in metal alloys and intermetallic phases and will be discussed in Part V.

Close-packed metal lattices have 2 tetrahedral and 1 octahedral interstice per metal ion core. The interstitial-electron model places electrons in these interstices in the way which gives the maximum screening of positive ion cores by electrons and the minimum electron-electron repulsion. The screening of the electrons from each other by the positive ion cores is very effective, and it is generally assumed[1] that effects of other electrons are screened out within 1 atomic cell. This is also taken to be the case for the interstitial-electron model, and the model can specify which adjacent electrons are least efficiently screened by consideration of geometry of lattices. It will now be

23) W. G. Gehman, *J. Chem. Educ.*, **40**, 54 (1963).

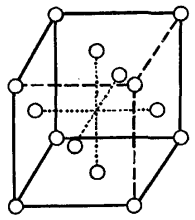

CCP Unit Cell

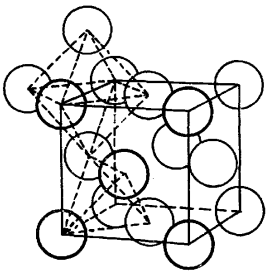

Location of oct and tet interstices
(The CCP unit cell of $4M^{n+}$ has 4 oct interstices per unit cell on centers of each edge and at the center of the unit cell. The 8 tet interstices per unit cell form a cube around each M^{n+}.)

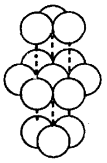

Packing of layers in CCP

Fig. 1. Structure and location of interstices in CCP metals.

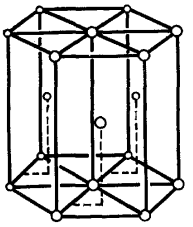

HCP unit cell

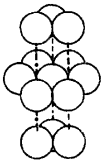

Packing of layers in HCP

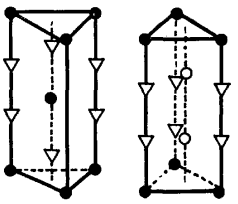

Location of oct and tet interstices (●=ion core, ○=oct, ▽=tet).
The HCP unit cell of $2M^{n+}$ has 2 oct interstices within the cell. Oct interstices form a trigonal prism around M^{n+}. The 4 tet intersices per unit cell are along the *c*-axis in pairs between all M^{n+}. They form a double set of tetrahedra around M^{n+} (C_{3h} symmetry).

Fig. 2. Structure and location of interstices in hexagonal close packed metals.

shown how the geometry and symmetry of the interstices can lead to definitive assignments of electrons to the interstices in different metal structures.

In the CCP structure shown in Fig. 1 there is a symmetrical arrangement of interconnected octahedral and tetrahedral interstices. The screening between octahedral electrons and tetrahedral electrons is by a triangle of close-packed metal ion cores. Tetrahedral and octahedral electrons are screened from each other by metal ion cores along a tetrahedral edge. Thus, the important distance establishing electron-electron repulsion is that between tetrahedral and octahedral interstices in CCP or 0.61 *a*, where *a* is the distance of closest approach. The maximum screening occurs between tet interstices. This comes about because an oct interstice is joined to 12 other oct interstices by 12 edges and to 6 tet by triangular faces while a tet interstice is joined to 6 adjacent tet interstices by edges and to four oct interstices by triangular faces. It can be concluded that in the absence of other controlling factors CCP metals will show a preference for tetrahedral occupancy of interstices by itinerant electrons. Interstice Distances for CCP, HCP, and BCC structures are given in Table 1.

The HCP structure shown in Fig. 2 has interconnected octahedral interstices in a line perpendicular to the layers. This is a consequence of the above arrangement of close-packed layers. The tetrahedral interstices occur in interconnected pairs which are screened from other pairs by an ion core. Thus, in the HCP metals all interstices are involved in mutual electron-electron repulsions. The distances between them are the following: oct-oct, 0.82 *a*; oct-tet, 0.61 *a*; tet-tet, 0.41 *a*. The latter, very short distance is only applicable when over 1/2 of the tet interstices are occupied. For low $\bar{e}$ occupancy there will be a preference for tet occupancy because with 1 $\bar{e}$ per tet there is screening by ion cores. With 2 $\bar{e}$ in tet there is strong $\bar{e}$-$\bar{e}$ repulsion in tet, and the greater interstice distance for oct-oct makes for a preference for octahedral interstice occupancy in HCP. These conclusions as to interstice preference agree with the conclusions of Gehman based on metal compounds.

The distorted HCP structures require special treatment. When the *c*/*a* ratio is greater than 1.633 *a* as in Zn or Cd there is an increase in oct-oct distance which is greater than the oct-tet increase. The octahedral preference is enhanced. However, when there is less than half occupancy of tet interstices as is the case for Zn, there is a stronger tet preference since these electrons are completely screened from each other by ion cores just as in Normal HCP. The HCP lattices with the opposite distortion, *c*/*a* less than 1.633 *a*, can be considered to have the pair of tet interstices changed to a single bi-pyramidal (bipyr) interstice.[24] This is the structure observed for Be, Sc, Y, and a few other metals. Since the structure now has 1 oct and 1 bipyr interstice per metal ion core, this structure differs greatly from the normal metal with 1 oct and 2 tet interstices per ion core. There are 2 factors influencing occupancy here; the tet interstices are the ones completely screened by an ion core but the oct-oct distance is much greater than oct-tet. Becasue of spin restrictions there appears to be a restriction on oct occupancy in this type of distorted HCP (see discussion below).

The BCC structures are not close-packed, but inter-

TABLE 1. INTERSTICE DISTANCES IN METAL STRUCTURES[a]

Distance	CCP	HCP	BCC
Unit Cell Edge	1.414	1[b]	1.155
tet-tet ($^1/_2$)	1	1	0.82
tet-tet	0.71	0.41	0.41,0.58
oct-oct	1	0.82	0.41,0.58
oct-tet	0.61	0.61	—
M^{n+}-oct	0.71	0.71	0.58,0.81
M^{n+}-tet	0.61	0.61	0.645[c]

a) Distances also given in S. Ho and B. E. Douglas, *J. Chem. Educ.*, **46**, 207 (1969).
b) Distance of closest approach taken as 1.
c) Distance to two nearest tet interstices.

24) A. Kjershus and W. B. Pearson in H. Reiss, Progress in Solid State Chemistry, Vol. I, Pergammon Press, Oxford, 1964.

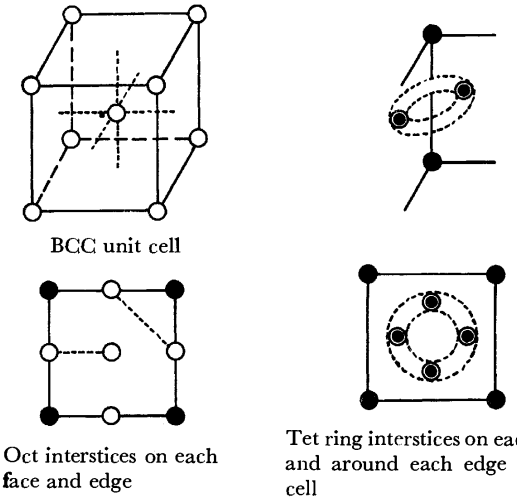

Fig. 3. Structure and location of interstices for body centered cubic metals.

stices can also be defined for BCC metals. The octahedral interstices shown in Fig. 3 are not symmetrical, *i.e.* there are 4 M^{n+} at 0.81 *a* and $2M^{n+}$ at 0.58 *a* (or *vice versa*). Such oct interstices are at centers of faces and the middle of edges of the unit cell. There are also tetrahedral interstices in the BCC structure. Tet interstices are formed by 2 body center M^{n+} and two corner M^{n+}, and 4 are located on each face at the (0,1/2,1/4) positions. Both types of interstices are joined by triangular faces of ion cores, so there is less screening of electrons by ion cores (and more volume between metal ion cores) in the BCC structure than in CCP or HCP structures. It is unlikely that both the closely spaced oct and tet interstices could be occupied by electrons. It is also expected in view of the similarity in energies of the BCC and close-packed structures that there would be the same number of interstitial electrons in BCC metals as CCP or HCP metals. Thus, the maximum number of electrons expected would be 2 electrons per face (one interstice) or two electrons per edge in octahedral interstices or 2 electrons per face in tetrahedral interstices. Any of these possibilities gives a total of 12 electrons per unit cell or 6 electrons per ion core as a maximum.

In comparing the screening of electrons by ion cores in BCC it was noticed that although both oct and tet interstices were joined through triangular faces, the orientation of tet interstices caused the binding regions of one tet interstice to extend well into an adjacent tet interstice. This observation along with the close proximity of the tet interstices makes it likely that the binding region is continuous for tet interstices on a face (and likewise around the corresponding interstices around an edge). This would place a ring of tetrahedral interstices on each face (f. tet) and likewise a ring of interstices centered on the middle of each edge (e. tet) and perpendicular to the face tet rings. The two sets of rings are interlocking. This interstitial-electron distribution for BCC metals[17a] corresponds to the areas of negative magnetization observed in neutron diffraction studies by Shull and Mock for BCC iron. This first physical explanation of these neutron diffraction observations is discussed further in Part IV. The CCP and HCP lattices had no comparable ring structure of interstices.

The symmetry of the tetrahedral interstices in BCC as well as the freedom of motion of electrons makes it more likely that tet interstices rather that oct interstices are occupied in BCC metals. Some possible exceptions will be noted for intermetallic phases as discussed in Part V.

As seen in Fig. 3 the distances for oct interstices vary from 0.8 for two oct edge interstices and 0.58 for an oct edge and oct face. The latter interstices are not effectively screened by ion cores. The distances for the interlocking rings of tet interstices have the same distances from centers of rings as those for oct (see Table 1). The distances are larger when all the tet rings are not occupied by 1 electron each. In BCC the symmetry of face tet and edge tet is identical, so there is no preference for occupancy of either type of tet interstice in this structure (see spin restrictions below, however.)

It is inherent in the interstitial-electron model that after 3 itinerant $\bar{e}$ are present there must be pairing of electrons in the interstices, and that after 6 electrons are present there must be localization of any additional electrons on the metal ion core as *d*-electrons or "bound" electrons. It has been postulated that vacancies in interstices are necessary for metallic properties so the localization is expected after 5 electrons are present. There is an additional possibility of some localization on cores after 3 electrons as an alternative to electron pairing in interstices. For transition metals past group 5 (*e.g.*,/V^{5+}, 5 $\bar{e}$/BCC), there will be localization of *d*-electrons. The interstitial-electron model will specify location of the itinerant electrons in these metals. Since the itinerant electrons in the instantaneous picture can be considered as ligands around the metal ion core, the degeneracy of the *d*-orbitals is determined and thus the magnetic properties of the transition metal. These structures are discussed in Part IV.

The intersitial-electron model leads to formulae for the electronic structure of metals which specify the metal ion core charge and the number of itinerant electrons in octahedral or tetrahedral interstices. It will be seen below that spin restrictions limit the electron preference for oct interstices in HCP and for tet interstices in CCP with the result that electron density differences in the two types of interstices are not large. In addition to this localization of electron density according to interstice type, there can be localization within the interstice. The model postulates that there will be a maximum of electron density at the centers of interstices. In view of rapid electron motion this probably will be a very flat maximum in electron density. Postulate VIII mentions variations in electron density with occupancy and with polarization effects; these will be discussed in Part III in connection with lattice distortions and properties of metals.

4. Restrictions on Metal Electrons Due to Electron-Spin

The model defines the binding region of electrons and location of electron density as corresponding to

octahedral or tetrahedral interstices in close packed metals and to the interlocking ring tet interstices in BCC metals. When electrons are in adjacent interstices which are not well screened by ion cores (*i.e.* adjacent interstices joined by triangular faces), greater repulsion is expected when the adjacent electrons have the same spin. Thus, in keeping with the Pauli Principle, it is postulated that electrons in such adjacent interstices have opposite spins. It follows then from the model that in CCP, electrons in tet interstices have opposite spins from electrons in oct interstices. In HCP the electron spins must alternate within both oct and tet interstices and between adjacent oct and tet as well because all these interstices are interconnected by triangular faces. In BCC structures adjacent electrons in tet rings will have opposite spins. It can be seen that because of these spin restrictions there is a correlation of electron motion due to spin as well as the correlation due to $\bar{e}$ repulsions and that both are determined by the symmetry of the ion cores and interstices.

Without motion of ion cores there could be a large number of electrons in the whole metal lattice with the same 4 quantum numbers. However, the lattice vibration gives rise to a large number of small energy variations. These energy differences also allow several electrons of the same spin around a given ion core. It should be noted that the restrictions due to electron spin became more important as the total number of itinerant electrons per metal ion core increases, *e.g.* with only 1 $\bar{e}$, spins can be random in BCC. When there are more than 3 electrons there must be pairing of electrons in some interstices for all metal structures. The details of such electron distribution is discussed in Part II for each metal. It will be assumed that at normal temperatures there are sufficient energy variations of $\bar{e}$ in interstices to make the most severe restrictions of the Pauli Principle inapplicable, *i.e.* all interstices can potentially be occupied by electrons. This is discussed further in Part VI on Superconductivity. The above interpretation of the Pauli Principle is similar to that of Bader and Preston[12] who discuss the relation of electron density to the usual orbital considerations in applying the Pauli Principle. Bent[6] has used the term "Pauli Mechanics" to emphasize the importance of the Pauli Principle in chemistry.

The restrictions on interstice occupancy due to electron spin can oppose the preference for tet occupancy in CCP and oct occupancy in HCP which was based on distance of electrons and their screening from adjacent electrons by ion cores. Since there is only low paramagnetism for most metals there must be roughly equal occupancy of oct and tet interstices for CCP metals to give equal spins of each kind. The preference for tet occupancy could only be satisfied in these cases by electron pairing in tet interstices. It will be seen in Part II that this probably occurs for some metals and in Part IV that unbalanced itinerant electron spins do occur in some of the ferromagnetic metals.

In regular HCP there is alternation of spins in both tet and oct interstices, so there is essentially no restriction on occupancy due to spin. However, in the HCP structures with c/a less than 1.633 the bipyramidal intersticies are in two sets which adjoin two oct interstices in a line. For this arrangement to give opposite spins in adjacent interstices only 1/2 oct can be occupied by single electrons if all the tet are occupied. Other ratios apply when a fraction of the tet interstices are occupied.

Since so many metals are weakly paramagnetic it must be assumed that the spin restrictions are more important than the interstice preference suggested by interstice distance and $\bar{e}$ screening by ion cores.

5. Occupancy of Interstices in Metals by Electrons

The criterion as to whether an interstice will be occupied by an itinerant electron ultimately must depend on relative energies of the electrons in the metal structure. An attempt will be made to list the various factors that determine electron energies in metals and to assess the effect of each. From the interstitial-electron model the following factors are expected to influence the energies of itinerant electrons: (1). The number, symmetry, and positive field strength of M^{n+} around an interstice. (2). The distance between neighboring M^{n+} and between itinerant electrons in interstices and M^{n+}. (3). Volume available for $\bar{e}$ in the interstice. (4). Distance of $\bar{e}$ neighbors and the extent of screening by M^{n+}. (5). Spins of neighboring $\bar{e}$ and their screening. (6). Extent of pairing of $\bar{e}$ in interstices. (7). Presence of localized *d*-electrons or bound electrons on M^{n+}. (8). Magnitude of lattice vibrations.

The attraction of $\bar{e}$ due to (1) must balance the repulsions of itinerant electrons and the ion-core repulsions. Similarly, there is a balancing of effects due to potential in the interstice and the volume (3). Presence of localized *d*-electrons affect both symmetry and field of M^{n+} and must be treated as special cases (See Part IV).

When comparing metals of approximately equal fields of M^{n+} and with equal numbers of itinerant electrons the decisive factors are then the $\bar{e}$-$\bar{e}$ repulsions (determined by the screening by ion cores and distance) and spin restrictions. Thus, in the majority of metals a decision as to interstice occupancy can be made on the basis of obtaining the minimum itinerant electron repulsion while at the same time balancing itinerant $\bar{e}$ spin. This is accomplished by a maximum spreading of $\bar{e}$ through the structure in preferred interstices while also satisfying the requirement for maximum screening of ion core repulsions.

Lattice vibrations have not been discussed in relation to the interstice occupancy. The instantaneous picture which will be used to specify electronic structures always has an imbalance of electron energies, since there is greater screening of ion core repulsions in a region where the interstice is occupied by an electron than when it is vacant. A rapid movement of electrons is expected to lead to a time-average picture in which

25) C. C. Shull and H. A. Mook, *Phys. Rev. Lett.*, **15**, 184 (1966).

there is electron density in all interstices. Lattice vibrations play an important role in this dynamic picture. At every change in positions of ion cores in the lattice vibration, all of the electron energies are shifted from equilibrium. Rapid movement of electrons is expected to restore equilibrium and optimum binding for the new state. As pointed out earlier the average electron density distribution in all the interstices can still retain the degree of preference for oct occupancy or tet occupancy, if this is present in the instantaneous picture of specific interstice occupancy, since the same correlation effects are in operation during electron motion.

Two examples will be given to illustrate the use of the interstitial-electron model in defining the electronic structure of a metal. Sodium metal has the BCC structure, and thus two Na^+ and two itinerant electrons per unit cell. Since there is no interstice preference in BCC these $\bar{e}$ are expected to occupy 1 f.tet and 1 e.tet ring (or 2 f.tet and 4 e.tet per unit cell).

$$|2Na^+,\ \bar{e}_{f.tet},\ \bar{e}_{e.tet}|BCC$$

The instantaneous picture of electron occupancy can be described as having $\bar{e}$ in tet rings on upper and lower horizontal faces and $\bar{e}$ in tet rings on 4 vertical edges. There is 1/6 occupancy of interstices, and since there is not likely to be interaction of electrons so widely spread, spins can be random. In the time-average picture there is equal electron density on all faces and edges. This is shown in Fig. 4a.

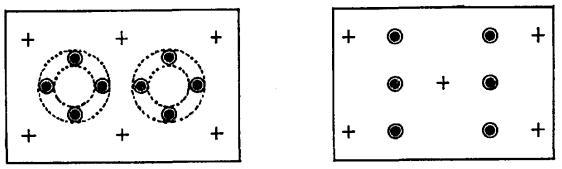

4a. Sodium Metal (100 plane) 4b. Na (110 plane)

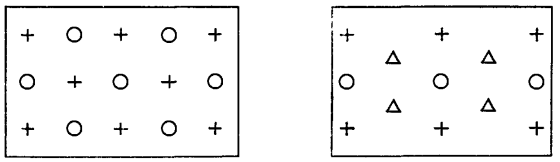

4c. Copper Metal (100 plane) 4d. Cu (110 plane)

Fig. 4. Electron density on different crystal planes of Na and Cu metals.
(⊙=tet rings, ○=oct interstices, △=tet interstices, +=ion cores)

Copper metal has the CCP structure in which $\bar{e}$ has tet preference. However, since copper is diamagnetic, there must be balancing of spins which can come about by equal occupancy of oct and tet interstices. The structure for Cu is written for the unit cell of 4 Cu^+ and 4 $\bar{e}$:

$$|4Cu^+,\ 2\bar{e}_{oct},\ 2\bar{e}_{tet}|CCP$$

This represents 1/2 occupancy of oct and 1/4 occupancy of tet by $\bar{e}$ and the average $\bar{e}$ density is shown in Fig. 4c.

All of the metals of Groups I—V will be treated in Part II and those of Groups VI—VIII in Part IV.

6. The Interstitial-Electron Model and Metal Alloys

Metallic structures for alloys of 2 or more metals can be written in the same way as for pure metals. There will be an array of M_a^{n+} and M_b^{m+} metal ion cores with $(n+m)$ itinerant electrons in interstices. When the electric fields around the ion cores of the two metals are similar there will be no disruption of the periodic potential of the lattice, so electrons will move freely throughout the structure, and no change in metallic properties in general is expected. A general formula for a CCP alloy with equal distribution of electrons in oct and tet would be:

$$|M_a^{n+},\ M_b^{m+},\ \frac{1}{2}(n+m)\bar{e}_{oct},\ \frac{1}{2}(n+m)\bar{e}_{tet}|CCP$$

Some degree of localization in interstices would be expected as m and n are further apart or as the size of M_a and M_b differs. The variety of alloys probably results from the possibility of this kind of localization of itinerant electrons. The intermetallic phases discussed in Part V have abnormally large localizations of electron density with formation of electron pairs in certain interstices.

7. Discussion

The interstitial-electron model emphasizes the spatial distribution of electrons in metal structures. This makes it possible to consider metal properties in terms of occupied or vacant interstices, and the "degree of localization" of electrons will be useful in discussing deviations from ideal metallic behavior. The high degree of interstitial delocalization of electron density in metals contrasts strongly with the high degree of localization in a solid structure such as diamond, with electron pairs between all of the ions. The $\bar{e}$ localization in metals proposed in the interstitial electron model is more closely related to the $\bar{e}$ localization in metal cluster compounds and metal complexes than to the electron distribution in polar or non-polar molecules. It may be clarifying to relate the interstitial-electron model to other models and theories of metals.

Raich and Good[26] have proposed an electrostatic-type model for metals using uniform electron density between cores, whereas the present model proposes some degree of interstitial localization of electron density. Wannier *et al.*[13] have recently demonstrated that application of the Hellmann-Feynmann theorem to metals makes some localization of electron density necessary in metals to account for cohesion. The magnitude of this localization is consistent with that suggested in this paper and for metals discussed in Part II. Girifalco[27] has suggested the kind of wave functions possible for a localized description of electron density in metals. Hubbard[28] has made proposals for considerations of structure in the electron density.

26) J. C. Raich and R. H. Good, Jr., *J. Phys. Chem. Solids*, **26**, 1061 (1965).
27) L. A. Girifalco, *Int. J. Quantum Chem.*, IIIS, 879 (1970).
28) J. Hubbard, *Proc. Roy. Soc.*, **A244**, 199 (1958).

The above authors provide some background and justification for the interstitial-electron model used in this paper. Further justification arises from purely classical considerations of electrons in metals. Harrison has pointed out that an itinerant $\bar{e}$ has its greatest velocity near an ion core, and thus spends most of its time in regions away from the ion cores. The present model defines this region as the center of interstices. Discussion of hydrogen in metal[19] places the hydrogen at the centers of interstices where there is greatest concentration of electron density. Thornber[30] has shown that "atomic" electron states are required to explain optical transitions rather than $\bar{e}$ in energy bands.

Other discussions of localized binding such as those of Pauling[31] and Engle-Brewer[32] appear to be further from band theory than the present model. It is of interest to consider how the highly successful Brewer-Engel Correlation might be related to the concepts of the interstitial-electron model. It is a possibility that the s, sp, and sp^2 (or d_xs, d_xsp, and d_xsp^2) binding proposed by Engel places electron density in spatial directions closely corresponding to the interstitial localization proposed in this paper. The orbital constructions of Trost[33] and the band structures proposed for transition metals by Goodenough[34] both emphasize the spatial extension of d-electrons in metals. The present model considers the itinerant electrons as ligands rather than the adjacent transition metal ion core, and is thus only indirectly related to the models of Trost and Goodenough. The differences will be treated in detail in the discussion of magnetic properties of metals in Part IV. The present model treats itinerant electrons in molecular orbitals (as does band theory) and not in atomic orbitals.

The method of pseudopotentials in metals[35] appears to be an extremely useful concept which has some striking similarities to the interstitial electron model. Ziman[3,36] has termed the screened ion core a "pseudo-atom". This ion core with its localized charge density interacts weakly with its neighbors. This appears the same as the manner ion cores are treated in the interstitial-electron model, and Ziman[3] emphasized that the method of pseudopotentials derives from and is entirely equivalent to band theory of metals. The "orthogonalization hole" in the method of pseudopotentials has its counterpart in the non-penetrable ion core postulated for the interstitial-electron model. The form factor[35] appears related in the two, while the structure factor in the interstitial-electron model would deal with the geometry of $\bar{e}$ in interstices rather than of the ion cores. It will be seen in Part II that the electronic structure of Al as derived from the interstitial-electron model has the same degree of localization of electron density in tet interstices as found by Harrison[35] in calculations of electron density for Al by the method of pseudopotentials. This is illustrated by data in Part II. Other models for metals in which there is some localization of electrons have also been discussed by Hubbard,[28] Cutler,[37] Szas and Mcguinn,[38] and Gombas.[39]

The concept of binding regions is useful in relating metallic binding to that in molecules and in non-metallic solids. For the tetrahedral and octahedral interstices shown in Fig. 1 and 2 there are single electrons or electron pairs in these interstices. For tetrahedral molecules, *e.g.* with 8 valence electrons, as discussed above there could be an $(\bar{e})_8$ closed shell or four electron pairs centered on triangular faces of the tetrahedron. For octahedral molecules with 12 valence electrons there can be electron pairs centered on 6 faces. There can be single electrons in these positions for metal clusters of these geometries in complexes containing metal clusters, and these can be considered intermediate between metals and polyatomic molecules. When the C.N. is low as in Silicon (diamond structure, tetrahedral arrangement), $(\bar{e})_2$ will be along edges of the tetrahedron to give the usual kind of binding in non-metallic solids, *i.e.*, electron pairs between all the ion cores. The increasing localization of electrons for these substances is as follows:

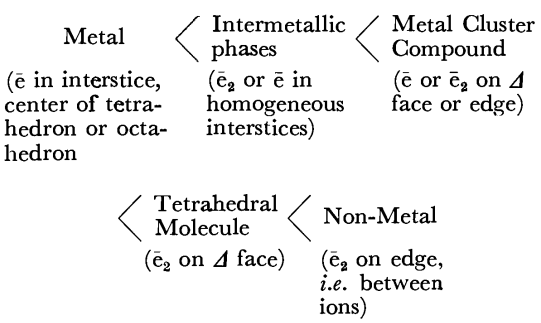

The interstitial-electron model thus treats metallic binding in the same way as other forms of chemical binding and shows that metallic binding is unique in its high degree of delocalization of $\bar{e}$ density.

The author wishes to thank the Japan Society for Promotion of Science for the invitation to Hokkaido University as a Visiting Scientist (1971—72) and to express appreciation to Professor Toya and the Staff of the Research Institute for Catalysis for valuable suggestions during Seminar discussions on this series of papers.

29) Y. Ebisuzaki and M. O'Keeffe, Ch. 5 in "Prog. in Solid State Chem.", Vol. 2, Ed. H. Reiss, Pergammon Press, London (1967).
30) K. K. Thornber, *Sci. Prog. Oxf.*, **57**, 149 (1969).
31) L. Pauling, *J. Amer. Chem. Soc.*, **69**, 542 (1947).
32) N. Engle, *Acta Metalurgica*, **15**, 557 (1966), *Powder Met. Bulletin*, **7**, 8 (1954) and earlier papers quoted there; L. Brewer, *Science*, **161**, 115 (1968).
33) W. A. Trost, *Can. J. Chem.*, **37**, 466 (1959).
34) J. B. Goodenough, *Phys. Rev.*, **120**, 67 (1966).
35) W. A. Harrison, "Pseudopotentials in the Theory of Metals", W. A. Benjamin, Inc, m New York, 1966.
36) J. M. Ziman, "Electron and Phonons", Oxford, Clarendon Press, 1968; *Adv. Phys.* **13**, 89 (1964).
37) M. Cutler, *J. Chem. Phys.*, **46**, 2044 (1967).
38) L. Szas and G. McGuinn, *ibid.*, **45**, 2898 (1966).
39) A. Gombas, *Phys. Lett.*, **24A**, 64 (1967).

An Interstitial-Electron Model for the Structure of Metals and Alloys II. Electronic Structure of Metals of Groups I—V

Oliver JOHNSON

Research Institute for Catalysis, Hokkaido University, Sapporo

(Received August 9, 1971)

The interstitial-electron model leads to metal structures which are instantaneous pictures of electron distribution written in terms of metal ion core charge M^{n+} (n=valency) and numbers of electrons in octahedral or tetrahedral interstices. On the average there are $\bar{e}$ in all interstices, and the degree of electron localization is small in metals. Decisions as to electron occupancy of interstices are primarily based on considerations of $\bar{e}$ spin and of screening of $\bar{e}$ by ion cores, but electronic heat capacity, Hall coefficient and anisotropy in magnetic susceptibility are of use in making decisions on electron occupancy of interstices. For univalent metals there is little localization of $\bar{e}$ because of the large excess of vacant interstices. This is also true when interstices approach full occupancy by $(\bar{e})_2$ as in M^{4+} and M^{5+}. Among divalent and trivalent metals the preferential occupancy of interstices leads to considerable localization of $\bar{e}$ density for Be, Sc, Y, and Tl. This high degree of localization is a consequence of mutual polarization of ion cores and $\bar{e}$; it accounts for the lattice distortion in these metals and leads to other unusual properties.

The interstitial-electron model for the structure of metals is described in detail in Part I.[1] In order to write such electronic structures for metals, the proper ion core charge (M^{n+}) or valency must be chosen as well as the interstice occupancy by these itinerant or conduction electrons ($\bar{e}$). The itinerant electrons will occupy preferentially the octahedral (oct) or tetrahedral (tet) interstice (I) which offers the maximum screening of its electron from neighboring $\bar{e}$ by positive ion cores and (2) which places $\bar{e}$ of parallel spin farthest away from each other. It turns out for CCP and HCP structures that $\bar{e}$ in adjacent interstices connected by a triangle of ion cores must have opposite spins.

There is a preference for tet occupancy in CCP, no preference in BCC, and a preference which depends on the number of $\bar{e}$ in HCP. For normal HCP lattices there is probably equal oct and tet preference for 1 $\bar{e}/M^{n+}$ since the $\bar{e}$ are widely separated. Since the second $\bar{e}$ in the tet paired interstice is at a short distance ($0.41a$) from the first, at $2\bar{e}$/ion core there will be 1 oct and 1 tet occupied. There will now be tet preference for a second $\bar{e}$ rather than pairing in oct so that at 3 $\bar{e}$ there will be 1 oct and 2 tet occupied. After 3 $\bar{e}$ there is oct preference, again because of the short interstice distance in tet paired interstices. These interstices are shown in Fig. 2 and in Part I. The same preferences for interstice occupancy are expected to hold for the HCP lattice with c/a greater than 1.633 (Zn and Cd).

For HCP lattices with c/a less than 1.633 (Li, Be, Sc) the tet preference is modified by special spin requirements. When all of the bipyramidal interstices (1 BP instead of 2 tet) are occupied, only 1/2 of the oct interstices can be occupied by unpaired electrons. Thus, after 1 1/2 $\bar{e}$, pairing must occur in BP interstices. Between 3 and 4 $\bar{e}$ there is probably pairing in both types of interstices. Figure 2 illustrates these interstices. The model provides for free movement of electrons between occupied and vacant interstices, but the average electron distribution retains a degree of localization of electron density. Electron correlation is a built-in feature of the model due to (1) the geometry of interstices, (2) the effects of screening of $\bar{e}$ repulsions by ion cores and (3) the spin restrictions based on type of interstice.

This paper will treat the metals of Group I—V and will propose electronic structures for all of them in terms of the metal ion core charge and numbers of electrons in oct and tet interstices. These will be illustrated by electron density diagrams for different crystal planes for representative metals. Metals beyond Group V have localized d-electrons and are discussed separately along with their magnetic properties in Part IV.

1. Interstitial-Electronic Structures of Metals

No attempt will be made to use the interstitial-electron model to predict types of lattice for various metals. The differences in energy between HCP and CCP, *e.g.*, are very small.[2] The model will be used to specify the spatial location of electrons in Group I—V metals, and it will be shown in Part III that such a description of a metal can give considerable insight into the many unusual gradations of metal properties.

In assigning electrons to interstices as discussed above the primary guides will be an assessment of screening of $\bar{e}$ by ion cores in a given structure and the restrictions on electron spin. Whenever unusual features such as lattice distortion or asymmetry in magnetic susceptibility indicate definite electron distributions, these data will be taken into account in assigning electrons to interstices. Since electron pairing in interstices requires considerable energy the minimum number of $(\bar{e})_2$ will be proposed for higher valent metals.

1.1 Alkali Metals. The BCC structure observed for Li, Na, K, Rb, and Cs at ordinary temperatures has 2 M^{n+} per unit cell and the 2 itinerant electrons are expected to occupy tet ring interstices (See Part I). The structure for potassium metal can be written

1) O. Johnson, This Bulletin, **45**, 1599 (1972).

2) W. R. Harrison, "Pseudopotentials in the Theory of Metals," W. A. Benjamin, Inc, N. Y., (1966).

$$|2K^+,\ 2\bar{e}_{tet.\ rings}|BCC.$$

An instantaneous picture of the electron distribution could be occupancy of 2 face tet and 4 edge tet per unit cell. On the average there would be 1/6 occupancy of the interstices by electrons where the interstices are the interlocking rings described in Part 1. To illustrate the electron densities indicated by the model, areas of electron concentration (flat maximum) are shown for different crystal planes on Fig. 1.

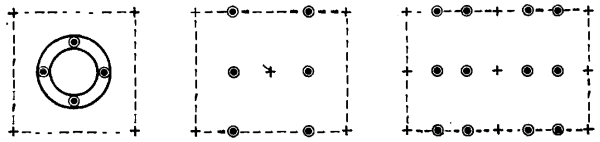

Fig. 1a. Location of interstitial electrons in BCC metals (100, 110, and 111 plane)
(⊙=electron in tetrahedral rings)

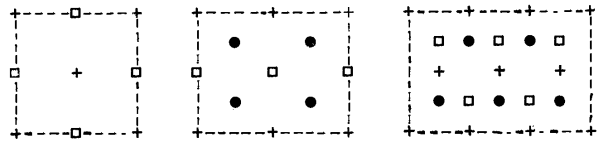

Fig. 1b. Location of interstitial electrons in CCP metals (100, 110, and 111 plane)
(□=oct interstices, ●=tet interstices, +=positive ion cores)

The same structures are expected for Na, Rb, and Cs as given for K. Lithium has certain unusual properties, *e.g.* a higher electronic heat capacity and magnetic susceptibility than Na, and a relatively large lattice displacement. These differences suggest a weaker field of the ion core for Li which might arise from some localization of electron density in one type of interstice or asymmetry of electron density in an interstice.

Both Na and Li form HCP structures at low temperatures. That for Na has a normal *c*/*a* ratio and is written with equal $\bar{e}$ distribution in oct and tet interstices:

$$|2Na^+,\ \bar{e}_{oct},\ \bar{e}_{tet}|HCP$$

On the average there is 1/2 occupancy of oct interstices and 1/4 occupancy of tet interstices. The HCP structure of Li has a *c*/*a* ratio of 1.563, and this distortion changes 2 tet interstices to a single bipyramidal (BP) interstice. The following structure suggests a greater number of $\bar{e}$ in BP interstices which give greater screening of $\bar{e}$ by ion cores than oct:

$$\left|2Li^+,\ \underset{BP}{\bar{e}_{1+n}},\ \underset{oct}{\bar{e}_{1-n}}\right|HCP$$

the value of n is believed to be small (0.1) since the relative preference for BP is reduced for all $\bar{e}$ over 1.

In view of the small ($1s^2$) ion core for Li^+, unusual properties are not unexpected. They occur as well for Li^+ in solution and for Li compounds and have been interpreted[3] as an especially strong local interaction of Li^+ with cations or solvent molecules. In Li metal, polarization of the $\bar{e}$ cloud could lead to asymmetry in $\bar{e}$ distribution in interstices. Any distortion from optimum $\bar{e}$ distribution would be equivalent to weaker binding forces for Li^+. The general nature of the distortion would be to increase $\bar{e}$ density around the cores. The lattice distortion observed represents the lowest energy arrangement for Li^+ ion cores and the polarized $\bar{e}$ cloud.

1.2 Noble Metals. Although there is a preference for tet occupancy in CCP metals the diamagnetism of Cu, Ag, and Au requires that there be equal numbers of itinerant electrons of each spin. The following structure is proposed for these metals with Cu as example:

$$|4Cu^{11+}(d^{10}),\ 2\bar{e}_{oct},\ 2\bar{e}_{tet}|CCP$$

Placement of electron pairs in tet interstices to satisfy the preference for tet occupancy in CCP is unlikely for a monovalent metal with so many vacant interstices. No properties of copper indicate any special localization. The differences between the alkali and noble metals arise mainly from the larger and more polarizable outer 18-electron shell of Cu, Ag, and Au. The ion core is written above to show the *d*-shell for copper. Because of the poor screening[4] provided by the *d* and *f* electrons the ion core for noble metals has a relatively stronger field than in alkali metals. Itinerant electrons can interpenetrate such ion cores, and the non-rare-gas shell ion core constitutes an exception to the proposed non-penetrability of ion cores. The way electrons are distributed on the (1,1,0) face of a copper unit cell is shown in Fig. 1. This can be considered to show $\bar{e}$ in binding regions as discussed in Part I. The extension of *d*-orbitals into interstitial regions should also be part of such diagrams. This aspect is treated fully in the discussion of magnetic properties in Part IV.

TABLE 1. ELECTRONIC STRUCTURE OF DIVALENT METALS

Be	$\|2Be^{2+},\bar{e}_{1\frac{1}{4}BP}(\bar{e}_2)_{3/4BP},\bar{e}_{1\frac{1}{4}oct}\|$HCP
Mg, Ca,[a] Sr[a]	$\|2M^{2+},2\bar{e}_{oct},2\bar{e}_{tet}\|$HCP
Ca, Sr	$\|4M^{2+},4,\bar{e}_{oct},4\bar{e}_{tet}\|$CCP
Ba	$\|2Ba^{2+},4\bar{e}_{tet\cdot rings}\|$BCC
Zn	$\|2Zn^{2+},1.8\bar{e}_{tet},1.8,\bar{e}_{oct},(\bar{e}_2)_{0.2\,oct}\|$HCP
Cd	$\|2Cd^{2+},1.6\bar{e}_{tet},1.6\bar{e}_{oct},(\bar{e}_2)_{0.4\,oct}\|$HCP

a) Structure at high temperature

1.3 Alkaline Earth Metals, Zinc, and Cadmium. All three lattice types are represented in the alkaline earth metals. As shown in Table 1 an equal distribution in oct and tet interstices is proposed for Ca, Mg, Sr, and Ba in the different lattices. The equal oct and tet preference is quite certain for CCP calcium; it then follows that similar distribution of $\bar{e}$ occurs in HCP and BCC structures since there is very little energy difference between these structures. Beryllium is the unusual metal in the alkaline earth group. Its HCP lattice with *c*/*a* of 1.567 has the same kind of distortion as Li in the HCP form. Also, Be is diamagnetic while the other alkaline earth metals have the usual weak paramagnetism of metals. Be has a large positive Hall coefficient,[5] which is discussed in Part III and

3) K. Fajans and O. Johnson, *T. Electrochem. Soc.*, **82**, 273 (1942).

4) O. Johnson, *J. Chem. Educ.*, **47**, 431 (1970).

5) R. J. Weiss, "Solid State Physics for Metallurgists," Pergammon, Oxford, (1963).

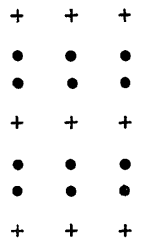

2a. Plane along c-axis

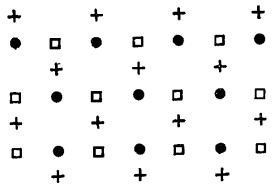

2b. Close-packed layer for HCP ($c/a<1.633$) ●=tet, in plane □=oct, above and below plane

2c. Row of tet interstices in Normal HCP

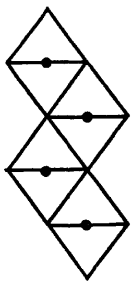

2d. Bipyramidal Interstices in Distorted HCP

2e. Row of oct interstices

Fig. 2. Interstitial electrons in HCP metals. (●=tet interstices, □=oct interstices)

connected with presence of electron pairs in the structure. Thus, a different structure is proposed for Be metal with $(\bar{e}_2)$ in BP interstices (See Fig. 2). This localization of electron density in BP interstices explains the above properties as well as the anisotropy of the diamagnetism. The hardness of Be also reflects localization of electron density.

The localization of $\bar{e}$ in one interstice in Be metal results from the requirement that only 1 unpaired $\bar{e}$ can be in the 2 oct Interstices adjacent to a BP interstice. As with Li the strong polarization of $\bar{e}$ by the $1s^2$ core of Be^{2+} leads to a distorted lattice to satisfy energy requirements. There is anisotropy of the diamagnetic susceptibility of Be with values of -21.4 parallel to c-axis and -7.2 perpendicular to c-axis (at 300°C).[6] This is probably the result of the greater density of Be^{2+} cores and $\bar{e}$ in the parallel direction.

Zinc and Cadmium form HCP structures with strong axial distortion ($c/a=1.856$ and 1.88, respectively). There are no restrictions on spin since there can be an alternation of spins in both oct and tet interstices as in the normal HCP lattice. The electronic structure for Zinc must also reflect the magnetic susceptibility of Zinc which when corrected for the diamagnetism of the core is weakly paramagnetic.[6]

The Zn^{2+} core contains d-electrons and in addition to its high+field this ion core is very deformable compared to rare gas shells (Mg^{2+}, Ca^{2+}) and there will be interpenetration of the $Zn^{12+}(d^{10})$ core by $\bar{e}$. This leads to a different localization or asymmetry of $\bar{e}$ in interstices than observed for Be. It is assumed in the structure written below that there is a small localization as $(\bar{e})_2$ in oct.

$$\left|2Zn^{12+}(d^{10}),\ 1.8\bar{e}_{tet},\ 1.8\bar{e}_{oct},\ (\bar{e}_2)_{\substack{0.2\\oct}}\right| HCP$$

As with Be the greater diamagnetic susceptibility[6] is observed for Zn in the direction parallel to the axis. In this case it must be the distortion of the ion core in this direction which leads to the small anisotropy. The smaller localization of $\bar{e}$ in tet is compatible with greater extension of d-orbitals along the c-axis.

Cadmium metal must have a very similar structure. The structure proposed below has greater electron localization than for Zn to account for the higher diamagnetic susceptibility of Cd *i.e.* diamagnetic when correction is made for the core diamagnetism.[4]

$$\left|2Cd^{2+},\ 1.6\bar{e}_{tet},\ 1.6\bar{e}_{oct},\ (\bar{e}_2)_{\substack{0.4\\oct}}\right| HCP$$

The anisotropy[6] of the diamagnetic susceptibility is very high for Cd and has a large decrease with decreasing temperature. This is expected for the more polarizable Cd and also is in keeping with greater localization of $\bar{e}$ in oct. Placement of electrons in unit cells are shown for some of these Group II metals in Fig. 2. Mercury is discussed in section 9 with other non-close packed metals.

1.4 Trivalent Metals. HCP structures are more prevalent for trivalent metals than CCP, and BCC structures are not observed. The CCP structure for Al can be specified rather closely. Because there are more itinerant electrons and because there must be equal numbers of single electrons in oct and tet interstices for balancing of electron spin, there will be electron pairs in all of the trivalent metals. For the CCP structure of Al the pairing is expected for tet interstices. The following structure has the minimum amount of electron pairing:

$$|4Al^{3+},\ 2(\bar{e}_2)_{tet},\ 4\bar{e}_{tet},\ 4\bar{e}_{oct}|\ CCP$$

This structure has 66% of the electron density in tet interstices. It is also important that the structure leaves some interstices vacant. A smaller fraction of pairs in tet would also require pairing in oct interstices which is not reasonable in CCP lattices. More pairs in tet would lead to some vacant tet interstices which is not reasonable considering the extra energy required for electron pairing. The above structure with 66% of electron density in tet then seems optimum for Al. This will have the same $\bar{e}$ distribution as Cu (Fig. 1). It is of interest that this is a very similar result to that of Harrison[2] who calculated electron density for CCP Al by the method of pseudopotentials. In Fig. 3 which is Harrison's electron density map for Al the tet interstices are indicated. These are regions of slightly greater electron density than the oct regions also indicated in Fig. 3. An estimate of electron density from the contour lines gives 60—70% of the interstitial electrons in the tet interstice region. This can be taken as an independent confirmation of the kind of localization of electrons proposed in the interstitial-electron model. Including $\bar{e}$ around cores, Harrison estimates a small interstitial localization.

Although indium has a tetragonally distorted CCP lattice ($a_0=3.244$, $c_0=4.938$), there is no property

6) W. M. Lomer and W. E. Gardner, *Prog. Metals Science*, **14**, 145 (1969).

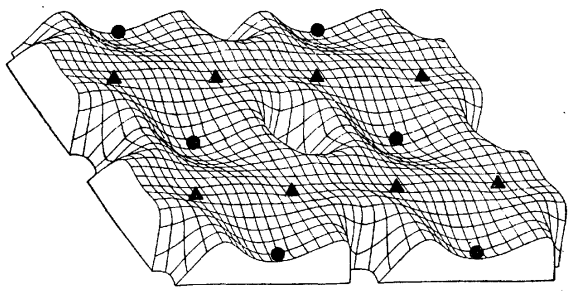

Fig. 3. Relative electron density on a (1, 1, 0) plane in aluminum.
(from W.A. Harrison, "Pseudopotentials in the Theory of Metals," W.A. Benjamin, Inc., New York, 1966)
(▲=$\bar{e}$ in tet interstices,
●=$\bar{e}$ in oct interstices from interstitial-electrom model.)

which indicates that the structure would differ markedly from that of Al. Since In^{3+} (or $In^{13+}(d^{10})$) has a deformable ion core like Zn, the distortion of the lattice is another example of a means of achieving the lowest energy structure.

The metals Sc and Y have relatively small ion cores ($3s^2$, $3p^6$) and are cations with strong positive field like Be and Li. If is not unexpected that they have HCP lattices with the same distortion ($c/a<1.633$). La is also classed with these metals although it has a more complex layer structure. Tl has an especially strong positive field because of the poor screening by its $4f$ electrons. This apparently puts it with Sc, Y, and La in spite of its deformable character.

The following structure is proposed for the metals Sc, Y, La, and Tl:

$$|2M^{3+}, \bar{e}_{1/2BP}, (\bar{e}_2)_{1\frac{1}{2}BP}, e_{1/2oct}, (\bar{e}_2)_{oct}|HCP$$

This structure has the maximum number of unpaired electrons compatable with spin requirements in this type of HCP lattice. An alternate structure would be:

$$|2M^{3+}, 2\bar{e}_{oct}, 4\bar{e}_{BP}|HCP$$

In this case the occupancy of BP could be considered as 2 $\bar{e}$ or as $(\bar{e})_2$. The high value of electronic heat capacity indicates electrons at high energy levels. The observed 30% greater diamagnetic susceptibility for Sc in the direction of the c-axis is expected for this type of lattice distortion. For Tl the anisotropy is even greater. Gallium metal is discussed in section 9.

The rare earth metals are predominantly trivalent and differ from other trivalent metals in having the $4f$ electron shell occupied. Arrott[7] has surveyed the properties of the f-shell containing metals and concluded that with the exception of Eu and Yb, the rare earth metals donate 3 $\bar{e}$ to the metal lattice as itinerant electrons. It is because of the unusual stability of the half filled and completely filled f-shell that only 2 $\bar{e}$ are itinerant for Eu and Yb. The reduced number of itinerant electrons is shown by greater atomic volume, the BCC structure instead of close-packed, lower MP and lower cohesive energy for Eu and Yb than the other rare earth metals. Kasuya[8] has discussed the differences in properties and structures of the heavy and light rare earth metals.

The interstitial electron structure for Eu and Yb below is proposed to be the same as that of BCC Ba, with difference in properties expected from the very different ion cores in RE

$$|2M^{2+}, 4\bar{e}_{tet.\ rings}|BCC$$

For Pr and Nd which have normal La type HCP structures and for Ce which has HCP at high temperature the following interstitial-electron structure is proposed (similar interstices exist for the La-type lattice):

$$|2M^{3+}, 2\bar{e}_{oct}, 2\bar{e}_{tet}, (\bar{e}_2)_{tet}|HCP$$

alternative structure: $|2M^{3+}, 2\bar{e}_{oct}, 4\bar{e}_{tet}|HCP$

For the heavy Rare Earth Metals (Gd, Tb, Dy, Ho, Er, Tm) which have c/a ratios in the range 1.57—1.59 the following structure (like Sc) is proposed:

$$|2M^{3+}, \bar{e}_{1/2BP}, (\bar{e}_2)_{1\frac{1}{2}BP}, \bar{e}_{1/2oct}, (\bar{e}_2)_{oct}|HCP$$

Variations in $\bar{e}$ distribution are anticipated and may be estimated from Hall coefficients or magnetic anisotropy but no attempt will be made to evaluate them at this time.

The CCP structures for Ce and Pr are proposed to be the same as that for Al. The detailed structures of rare earth metals which are ferromagnetic will be discussed in a separate paper.

1.5 Tetravalent Metals. At ordinary temperature the structures for Ti and Zr are HCP with c/a ratios of 1.593 and 1.581 respectively. This distortion leads to oct and bipyramidal interstices and 4 itinerant electrons in 2 interstices would lead to only pairs and complete occupancy. These metals are paramagnetic and have a negative Hall coefficient so there must be unpaired electrons in these metals. Since the distortion is very small for these metals the bipyr (or tet) electrons need not be paired as was suggested also for trivalent metals. The following structure formulates Ti and Zr in this way:

$$|2M^{4+}, 2(\bar{e}_2)_{oct}, 4\bar{e}_{tet}|HCP$$

This electronic structure is also in keeping with the large electronic heat capacity for these metals. The absence of $(\bar{e})_2$ in tet may imply some asymmetry in $\bar{e}$ distribution within the tet interstices.

There are BCC structures for Hf and for Ti and Zr at high temperatures. The structure written below with a minimum of electron pairs has 1/3 occupancy of interstices by 2 $\bar{e}$ per ring which probably act as electron pairs. Since polymorphic structures do not differ greatly in energy this is an additional reason for considering the HCP structures of Ti and Zr as above with only 1/2 occupancy by electron pairs.

$$|2M^{4+}, 8\bar{e}_{tet.\ rings}|BCC$$

The latter structure shows how the BCC lattice can accomodate more electrons without extensive pairing. This arises because there is equal preference for and equal numbers of the two kinds of interstices (rings around face and edge).

The CCP structures for Pb and Th are formulated as follows:

7) A. Arrott in G. T. Rado, and H. Suhl, "Magnetism," Vol. II B, Acad. Press, N. Y., 1966, p. 339.
8) T. Kasuya, *ibid.*, p. 230.

$$|4M^{4+}, 4(\bar{e}_2)_{tet}, 4\bar{e}_{tet}, 4\bar{e}_{oct}|\,CCP$$

These electronic structure for Pb and Th have 75% of the electron density in tet interstices. This strong localization of $\bar{e}$ density is probably counter-balanced by distortion of the very deformable ion cores which contain both *d* and *f* shells.[4]

1.6 Pentavalent Metals. V, Nb, and Ta all have the BCC structure and can be formulated as follows with the minimum number of electron pairs (2/3 occupancy):

$$|2M^{5+}, 10e_{tet.\ rings}|\,BCC$$

The possible electronic structures for Bi, As, and Sb are discussed in the following section along with other metals which do not have close packed structures.

2. Interstitial-Electron Structures for Non-close-packed Metals

Mercury is a liquid at room temperature, and gallium melts just above room temperature. Solid mercury has a rhombohedral structure and the CN of Hg^{2+} is 6. Compared to a simple cubic lattice the interaxial angle is 70° 1/2. *Gallium* has an orthorhombic structure with two identical axes of its pseudotetragonal unit. There are 8 atoms per unit cell, a_0 and b_0 (1.5107) and c_0 (7.6448). There are 2 neighbours at 2.71, 2 at 2.80, and 1 at 2.44 Å. Bent[9] has pointed out that gallium sulfide has 2 Ga-Ga at short distance and 6Ga-Ga larger distances with the suggestion of electrons pairs in gallium metal where anions are placed in the sulfide. The interstitial electron model cannot specify the location of electrons in Ga and Hg. There are likely to be $-Ga^{3+}\ (\bar{e})_2\ Ga-^{3+}$ units in the structure along with single electrons in interstitial positions. The combination of long range and short range order probably accounts for the liquid state at low temperatures.

White tin is tetragonal with a_0 of 5.8197 and c_0 of 3.1748. Each ion core is surrounded by a distorted tetrahedron of Sn neighbours at 3.02 Å with 2 more Sn in the axial positions at 3.17 Å. Although white tin deviates from a close packed structure the interstices are related to those of CCP, and the structure proposed is similar to that of lead:

$$|4Sn^{4+}, 4(\bar{e}_2)_{tet}, 4\bar{e}_{tet}, 4\bar{e}_{oct}|\,Tetrag.$$

Some asymmetry in the $\bar{e}$ distribution within oct and within tet interstices is expected from the lattice distortion. The slightly greater diamagnetic susceptibility in the direction perpendicular to the *c*-axis[10] is compatable with ion core distortion and greater core numbers in that direction.

Gray tin has the diamond structure and is non-metallic. It will be mentioned to illustrate the difference in chemical binding. The distance of 2.80 Å between Sn^{4+} is about 10% less than for white tin. Electron pairs ($\bar{e}_2$) between all Sn^{4+} tetrahedrally arranged are expected as in Ge or diamond as written below:

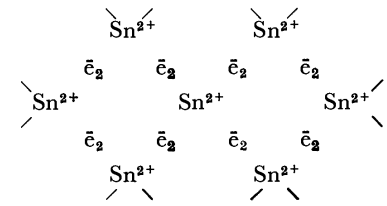

Bismuth crystallizes in a puckered layer lattice with a CN of 3. It is unusual in that it has the highest diamagnetic susceptibility of all the metals.[10] In the tetragonal Bi_2O_3 lattice each Bi^{3+} has 6 O^{2-} neighbours (related to Mn_2O_3 lattice). In bismuth metal there is the counterpart of the octahedral hole in the puckered layer and if all the octahedral interstices are filled there remains an $(\bar{e})_2$ per 2 Bi^{3+}. This may well be within the layers as follows:

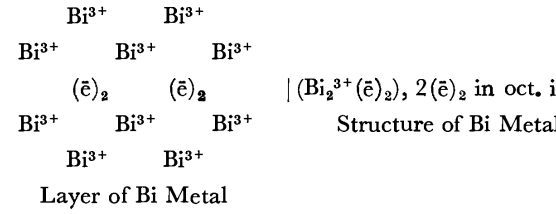

$|(Bi_2^{3+}(\bar{e})_2),\ 2(\bar{e})_2$ in oct. inter.|

Structure of Bi Metal

The filled octahedral interstices would explain the low electric conductivity and the $(\bar{e})_2$ associated with the layers can account for the very large diamagnetic susceptibility as well as the anisotropy of the diamagnetism.

The related elements As and Sb depart further from metallic behavior. The layer spacing increases from Bi to Sb to As and thus they deviate further than Bi from close-packed structures.

3. Conclusions

Electronic structures have been proposed for all the Group I—V metals. In most cases a precise electronic structure could be given in terms of $\bar{e}$ occupancy of interstices. In a few cases alternate structures or a range of possible occupancies was given. The areas of electron localization could also be indicated for various crystal faces in terms of the electron model. These represent electrons in the binding areas of the interstices in a metal and should be useful in interpreting both chemical and physical properties of metals.

The relation of $\bar{e}$ and $(\bar{e}_2)$ in metal interstices to a number of properties (*e.g.* Hall coefficient, magnetic susceptibility) has been used as a guide in formulating interstitial-electronic structures in some cases. It has been possible to correlate metal properties with the interstitial-electron distribution, and this is presented in detail in Part III. It may be possible to further refine the structures given in this paper on the basis of experimental data on metal properties.

The interstitial-electron structures proposed on the basis of simple rules for occupancy of interstices show the greatest localization of $\bar{e}$ density in just those HCP and CCP structures which are distorted from normal close packing. Ion cores with strong positive fields (*e.g.*, Li^+, Be^{2+}) are expected to polarize the itinerant $\bar{e}$ cloud. Ions containing *d* and *f* electrons[4] are expected also to have strong positive fields but these

9) H. Bent, *J. Chem. Educ.*, **45**, 768 (1968); **42**, 348 (1965).
10) L. F. Bates, "Modern Magnetism," Cambridge Univ. Press, Cambridge, 3rd Ed, (1951).

non-rare gas shells are deformable and will be penetrated by itinerant electrons. These polarizing effects of and on itinerant electrons are held to be the cause of the lattice distortion. These polarization and interpenetration effects are less important when there are few $\bar{e}$ and when there are predominantly ($\bar{e}_2$) in the interstices and thus predominate for divalent and trivalent metals.

BULLETIN OF THE CHEMICAL SOCIETY OF JAPAN, VOL. 45, 1612—1616(1972)

Convenient Quadratic Formulas for the Two-center Coulomb Repulsion Integrals in the Semiempirical LCAO-MO Method and the Significance of the Pariser-Parr Approximation[1)]

Yasuhiko GONDO and Yoshiya KANDA

Department of Chemistry, Faculty of Science, Kyushu University, Hakozaki, Fukuoka

(Received August 25, 1971)

The coefficients in the Pariser-Parr-type quadratic formulas for the two-center Coulomb repulsion integrals encountered in the planar as well as the non-planar conjugated systems have been expressed as linear functions of the effective nuclear charges of the $2p$ atomic orbitals involved. The formulas thus obtained are applicable to those conjugated systems consisting of carbon, nitrogen, and oxygen atoms, and may well be useful in variable-electronegativity self-consistent field calculations on these systems. With some illustrative applications to spin densities and phosphorescent-state energies, it has been shown that the Pariser-Parr approximation gives better results than the Nishimoto-Mataga one, although the latter is successful in the prediction of electronic transitions within the singlet manifold. Incidentally, this was also the case for the phosphorescent-state zero-field splittings (Y. Gondo and Y. Kanda, This Bulletin, **43**, 3943 (1970)). The electric dipole moments have also been discussed.

As is well known, in the Pariser-Parr-Pople method[2,3)] the two-center Coulomb repulsion integrals are evaluated semiempirically for smaller interatomic distances, and several kinds of approximations have been proposed for this purpose.[4,5)] Among them, the Nishimoto-Mataga approximation[6)] is distinctly different from the others in giving nearest-neighbor values smaller than those of the others by nearly 2 eV.[5)] As for the others, they are practically identical with each other; the Pariser-Parr approximation may be regarded as a prototype. The Nishimoto-Mataga approximation has been employed quite extensively and frequently because of its simplicity, its successful prediction of electronic transitions within the singlet manifold, and also its easy adaptability to variable-electronegativity self-consistent field (VESCF) calculations.[7,8)]

However, in the prediction of triplet-state zero-field splittings (ZFS), for example, a Pariser-Parr-type (PP-type) quadratic formula is much better than a Nishimoto-Mataga-type (NM-type) one, as has previously been pointed out by the present authors.[9)] In addition, a PP-type formula gives better results with regard to the phosphorescent-triplet-state energies of neutral molecules and the spin densities in the molecular ions than does a NM-type formula, as will be described later. The electric dipole moments of neutral molecules will also be discussed.

Thus, if we have a PP-type formula as simple as a NM-type formula, it can be invoked as extensively and frequently as the latter. In this paper, it will be shown that the coefficients appearing in the PP approximation are linearly dependent on the effective nuclear charges of the AO's involved, subject to the Paoloni-type approximations[10)] for the one-center Coulomb repulsion integrals. All the two-center Coulomb repulsion integrals encountered in the planar as well as the non-planar conjugated systems consisting of carbon, nitrogen, and oxygen atoms have been studied jointly. The formulas thus obtained are easily adaptable to the VESCF calculations of these systems.

Incidentally, the very difference of 2 eV for the nearest neighbors is significant, as is suggested by the clearly different results on the various molecular properties mentioned above. Since this may be closely associated with the problem of electronic correlation in molecules,[11,12)] it is desirable to accumulate as many results as possible with the PP approximation as well in

1) Presented in part at the 24th Annual Meeting of the Chemical Society of Japan, Osaka, April, 1971.

2) R. Pariser and R. G. Parr, *J. Chem. Phys.*, **21**, 466, 767 (1953).

3) J. A. Pople, *Trans. Faraday Soc.*, **49**, 1375 (1953).

4) K. Ohno, "Advances in Quantum Chemistry," Vol. 3, ed. by P. O. Löwdin, Academic Press, New York 1967, p. 239.

5) T. Anno, "Bunshi Kagaku Koza," Vol. 3, ed. by T. Nakajima, Kyoritsu, Tokyo 1966, p. 232.

6) K. Nishimoto and N. Mataga, *Z. Phys. Chem.* (Frankfurt), **12**, 335 (1957).

7) P. J. Black and C. A. McDowell, *Mol. Phys.*, **12**, 233 (1967).

8) R. D. Brown and B. A. W. Coller, *Theor. Chim. Acta*, **7**, 259 (1967).

9) Y. Gondo and Y. Kanda, This Bulletin, **43**, 3943 (1970).

10) L. Paoloni, *Nuovo Cimento*, **4**, 410 (1956).

11) P. O. Löwdin, "Advances in Chemical Physics," Vol. II, ed. by I. Prigogine, Interscience Publishers, New York 1959, p. 207.

12) *Ibid.*, Vol. XIV, ed. by R. Lefebvre and C. Moser (1969).

order to gain a better understanding of this interesting but intractable problem. In this context, the convenient formulas we have obtained might be of some use.

General Remarks

The symbols σ, π, and $\bar{\pi}$ stand for $2p\sigma$, $2p\pi$, and $2p\bar{\pi}$ respectively.[13] In the planar conjugated systems, every two-center Coulomb repulsion integral $(pp|qq)$ is of the $(\pi_p\pi_p|\pi_q\pi_q)$ type, whereas this is not the case for the non-planar systems. Thus, we have the following expression, in general:[14]

$$\begin{aligned}(pp|qq) = {} & \omega_1(\sigma_p\sigma_p|\sigma_q\sigma_q) + \omega_2(\sigma_p\sigma_p|\pi_q\pi_q) \\ & + \omega_3(\pi_p\pi_p|\sigma_q\sigma_q) + \omega_4(\pi_p\pi_p|\pi_q\pi_q) \\ & + \omega_5(\pi_p\pi_p|\bar{\pi}_q\bar{\pi}_q) + \omega_6(\pi_p\bar{\pi}_p|\pi_q\bar{\pi}_q) \\ & + \omega_7(\sigma_p\pi_p|\sigma_q\pi_q), \end{aligned} \quad (1)$$

where the coefficients ω_1, ω_2,$\cdots$are determined by the relative orientation of the $2p$ AO's involved.

According to Pariser and Parr,[2] for interatomic distances smaller than 2.8 Å each of the basic integrals in Eq. (1) may be evaluated by means of the quadratic extrapolation formula:

$$(\mu_p\mu_p'|\nu_q\nu_q') = C_0 + C_1R + C_2R^2, \quad (2)$$

where μ, μ', ν, and ν' stand for σ, π, or $\bar{\pi}$, and where R is the pertinent interatomic distance. In addition, C_0 is defined by the relation:

$$C_0 = [(\mu_p\mu_p'|\nu_p\nu_p') + (\mu_q\mu_q'|\nu_q\nu_q')]/2. \quad (3)$$

The one-center integrals in Eq. (3) can be obtained through the expressions listed under "Semiempirical" heading in Table 1; these expressions have been derived

Table 1. One-center coulomb repulsion integrals involving $2p$ atomic orbitals[a]

Integral	Theoretical[b]	Semiempirical
$(\sigma\sigma\,|\,\sigma\sigma)=(\pi\pi\,|\,\pi\pi)$	$5.325\,Z$	$3.294\,Z$[c]
$(\sigma\sigma\,|\,\pi\pi)=(\pi\pi\,|\,\bar{\pi}\bar{\pi})$	$4.751\,Z$	$2.939\,Z$
$(\sigma\pi\,|\,\sigma\pi)=(\pi\bar{\pi}\,|\,\pi\bar{\pi})$	$0.2870\,Z$	$0.1775\,Z$

a) Z stands for the effective nuclear charge.
b) Obtained with the Slater-type AO's and the formulas given by Roothaan.[13]
c) Paoloni's relation.[10]

on an assumption of the same proportionality between the theoretical and the semiempirical values for every type of basic integral[15] as that for $(\pi\pi|\pi\pi)$, which is in turn based on Paoloni's relation.[10] These theoretical one-center integrals have been obtained with the Slater-type AO's and the formulas of Roothaan.[13] The effective nuclear charges used are 3.25, 3.90, and 4.55 for carbon, nitrogen, and oxygen respectively.

For interatomic distances larger than 2.8 Å, the multipole expansion formula can be used without decomposing $(pp|qq)$ into the basic integrals.[16] It should be noted that the multipole expansion formula has a simple dependence on the effective nuclear charges of the AO's involved; hence, it is easily adaptable to the VESCF calculation.

The C_1 and C_2 Coefficients

The Use of Multipole Expansion Formulas for Obtaining the C_1 *and* C_2 *Coefficients.* The coefficients, C_1 and C_2, of Eq. (2) for every basic integral in Eq. (1) have been determined originally with the C_0 of Eq. (3) and with the corresponding two-center integrals, obtained at 2.8 and 3.7 Å with the multipole expansion formulas.[16] The largest deviation of the integrals obtained with these formulas from those obtained with the theoretical formulas of Roothaan[13] has been found for the basic integral $(\sigma\sigma|\sigma\sigma)$; it is, at most, for example, 1% for the C–C pair at 2.75 Å. For the second to fifth basic integrals in Eq. (1), however, the deviations are of the order of 0.01% at the same distance. As for the rest, they are intrinsically very small quantities, and practically no deviations are found down to three decimal places in electron-volts at the same distance as above. In addition, the coefficient multiplying $(\sigma\sigma|\sigma\sigma)$ in Eq. (1) is usually small. Therefore, the use of the multipole expansion formulas may be justified.

Linear Dependence of C_1 *and* C_2 *on the Effective Nuclear Charges.* The coefficients, C_1 and C_2, thus obtained have been found expressible as linear functions of the effective nuclear charges of the AO's involved, as is shown in Fig. 1, for example, for the basic integral

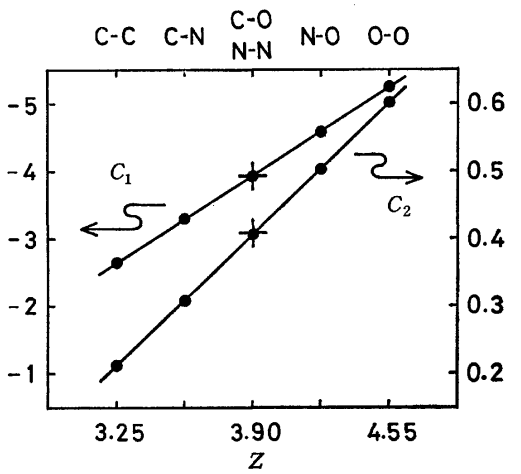

Fig. 1. Linear depencence of the C_1 and C_2 coefficients on the arithmetic mean of the effective nuclear charges of the AO's involved, Z, in the basic integral $(\pi\pi|\pi\pi)$. With Z=3.90, the crosses refer to the C–O pair.

$(\pi\pi|\pi\pi)$. The linear functions have been obtained through the method of least-squares; they are collected in Table 2. These results reproduce the integral values obtained with the original coefficients, C_1 and C_2, for example, at 1.5 Å within a margin of 0.3% for the first, 0.1% for the second to fifth, 0.4% for the sixth, and 1% for the last basic integral of Eq. (1). As has been mentioned above, in Eq. (1) the coefficient, ω_1, is usually small, and the last two basic integrals are of intrinsically very small quantity. Therefore, it may be concluded that the results collected in Table

13) C. C. J. Roothaan, *J. Chem. Phys.*, **19**, 1445 (1951).
14) Y. Gondo, *ibid.*, **41**, 3928 (1964).
15) R. Hoffmann, A. Imamura, and G. Zeiss, *J. Amer. Chem. Soc.*, **89**, 5215 (1967).
16) R. G. Parr, *J. Chem. Phys.*, **33**, 375 (1960).

TABLE 2. THE COEFFICIENTS IN THE QUADRATIC FORMULAS FOR THE TWO-CENTER COULOMB REPULSION INTEGRALS[a)]

Integral	C_0	C_1	C_2
$(\sigma\sigma \mid \sigma\sigma)$	$3.294\,Z$	$5.5778-2.2985\,Z$	$-1.1900+0.3748\,Z$
$(\sigma\sigma \mid \pi\pi)$	$2.939\,Z$	$4.4455-0.9999\,Z\sigma-0.8697\,Z\pi$	$-0.9112+0.1605\,Z\sigma+0.1291\,Z\pi$
$(\pi\pi \mid \pi\pi)$	$3.294\,Z$	$3.8360-1.9934\,Z$	$-0.7661+0.3004\,Z$
$(\pi\pi \mid \bar{\pi}\bar{\pi})$	$2.939\,Z$	$3.7923-1.7617\,Z$	$-0.7549+0.2639\,Z$
$(\pi\bar{\pi} \mid \pi\bar{\pi})$	$0.1775\,Z$	$0.0219-0.1158\,Z$	$-0.0056+0.0183\,Z$
$(\sigma\pi \mid \sigma\pi)$	$0.1775\,Z$	$0.0875-0.1293\,Z$	$-0.0224+0.0217\,Z$

a) Z stands for the arithmetic mean of the effective nuclear charges of the AO's involved. Lengths are given in angstroms, and energies, in electron-volts in Eq. (2).

2 reproduce the integral values calculated with the original coefficients within a margin of 0.1%.

Further Remarks on $(\pi\bar{\pi}|\pi\bar{\pi})$ and $(\sigma\pi|\sigma\pi)$. From the symmetry and R-dependence, the basic integrals, $(\pi\bar{\pi}|\pi\bar{\pi})$ and $(\sigma\pi|\sigma\pi)$, are distinguished from the rest. Since these integrals are themselves intrinsically very small, the relevant quadratic formulas sometimes give negative values, even for interatomic distances smaller than 3.0 Å, although they must be positive in principle. Further, the integral values are smaller than 0.02 eV at 3.0 Å. Therefore, it may be concluded that these basic integrals can be neglected if the interatomic distance is larger than 3.0 Å or if the calculated integral values are found to be negative.

Some Illustrative Applications

In this concluding section, as was mentioned in the introduction, some examples will be presented in order to illustrate the usefulness of the PP approximation through the use of the convenient formulas obtained in the preceding section, although these examples are chosen rather arbitrarily and are restricted to the planar conjugated systems. In what follows, the wavefunctions are calculated by means of a method described previously,[9,17] and by means of the effective nuclear charges of 3.25 and 3.90 for carbon and nitrogen respectively in the usual SCF scheme. In the VESCF calculations, the dependences of the effective nuclear charges and valence-state ionization potentials on the charge densities are incorporated by the use of the procedure adopted by Brown and Heffernan;[18] moreover, all the parameters are variable, unless otherwise specified.

The Energies of the Phosphorescent Triplet States. The excitation energies of the phosphorescent triplet states of some aromatic hydrocarbons and nitrogen heterocycles are predicted by the PP approximation much better than by the NM approximation, as is shown in Table 3. Tyutyulkov, Gochev, and Fratev[19] also noted this, and modified a NM formula in order to remedy this shortcoming. They stated that their formula was as simple as the original one and that it was successful in the prediction of singlet-singlet transitions. However, it hardly seems acceptable, not only in the sense that it has no correct asymptotic behavior for sufficiently large distances, such behavior as the original formula shows, but also in the sense that it gives significant deviations from the theoretical values at intermediate distances larger than 2.8 Å.

TABLE 3. THE EXCITATION ENERGIES OF THE PHOSPHORESCENT TRIPLET STATES (eV)

Compound[a)]	Calculated: Approximation for $(pp \mid qq)$[b)] NM	Calculated: Approximation for $(pp \mid qq)$[b)] PP	Obsd
Benzene	2.64	3.56	3.66[c)]
Naphthalene	1.82	2.53	2.64[c)]
Quinoline	1.73	2.49	2.69[e)]
Isoquinoline	1.77	2.50	2.63[d)]
Quinoxaline	1.54	2.31	2.65[e)]
Anthracene	1.09	1.67	1.85[e)]
Phenanthrene	1.85	2.56	2.69[e)]
1,10-Phenanthroline	1.78	2.55	2.74[f)]
5,6-Benzoquinoline	1.80	2.54	2.71[e)]
7,8-Benzoquinoline	1.81	2.56	2.70[e)]
Triphenylene	2.10	2.88	2.95[g)]

a) For the structural formulas, see Ref. 9.
b) For the abbreviations, see the text.
c) to g) Ref. 20 to 24 respectively.

Since the development of this kind of modification may be due to the need for a foumula as simple and useful as the NM one, the formulas proposed in this paper seem to acquire justification. In particular, any conjugated systems consisting of carbon, nitrogen, and oxygen atoms are within the scope of these formulas. Moreover, these are easily adaptable to the VESCF procedure, which has been demonstrated to be useful for the prediction of the electric dipole moments of various organic compounds.[8]

Incidentally, it should be noted that the approximation that gives better results on the state energies also leads to better results on the ZFS parameters.[9]

The Electric Dipole Moment of the Ground State of Azulene

17) Y. Gondo and A. H. Maki, *J. Chem. Phys.*, **50**, 3270 (1969).
18) R. D. Brown and M. L. Heffernan, *Trans. Faraday Soc.*, **54**, 757 (1958).
19) N. Tyutyulkov, A. Gochev, and F. Fratev, *Chem. Phys. Lett.*, **4**, 9 (1969).
20) S. P. McGlynn, T. Azumi, and M. Kinoshita, "The Triplet State," Prentice-Hall, Englewood Cliffs, New Jersey (1969), Chap. 4.
21) F. Dörr and H. Gropper, *Ber. Bunsenges. Phys. Chem.*, **67**, 193 (1963).
22) Y. Kanda and R. Shimada, *Spectrochim. Acta*, **15**, 211 (1959).
23) H. Gropper and F. Dörr, *Ber. Bunsenges. Phys. Chem.*, **67**, 46 (1963).
24) D. S. McClure, *J. Chem. Phys.*, **17**, 905 (1949).

and the Spin Densities in Its Anion. Azulene is chosen for two reasons—first, because it is a non-alternant hydrocarbon, and second, because the complex problem of a correct allowance of the electronic effects of hetero-atoms does not, of course, arise.[8] The first reason is based on the observation of Ruedenberg[25] that the results of calculations on the polycyclic alternant hydrocarbons are more strongly dependent on their topological matrix than on the choice of repulsion or resonance integrals.

Table 4. Calculated electric dipole moments of the ground state of azulene[a] (D)

Method[b]	Approximation for $(pp \mid qq)$[c]	
	NM	PP
S1	2.735	2.464
S2	2.170	2.039
V1	2.196	2.066
V2	1.698	1.648
W1	2.140	2.021
W2	1.652	1.608
Observed[d]	0.796 ± 0.014	

a) For the defined positive direction of the dipole moment, see Fig. 2.
b) S: SCF; V: VESCF; W: VESCF, except for $(pp|qq)$, for which the neutral-atom effective nuclear charges are used; 1 and 2: Core resonance integrals are taken into account up to nearest neighbors and next-nearest neighbors respectively.
c) For the abbreviations, see the text.
d) Ref. 26.

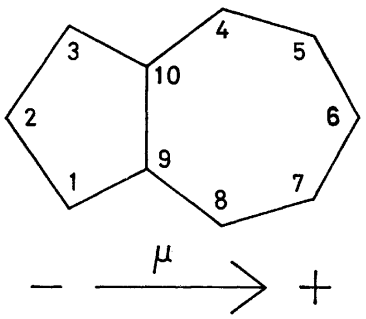

Fig. 2. The carbon skeleton of azulene and the defined positive direction of the electric dipole moment, μ, with the numbering of atoms.

The electric dipole moments obtained for the ground state by various methods are collected in Table 4, in which the contributions from the σ-electrons are not taken into account.[8] The molecular geometry adopted is based on the x-ray data after averaging according to the molecular symmetry.[27] As this table shows, the VESCF procedure and the inclusion of the next-nearest-neighbor resonance integrals[28] improve the results considerably.

Table 5. Calculated π-electronic charge densities in the ground state of azulene[a]

Atomic position	Approximation for $(pp \mid qq)$[b]	
	NM	PP
1,3	1.0643	1.0706
2	0.9993	0.9904
4,8	0.9575	0.9513
5,7	1.0019	1.0071
6	0.9682	0.9671
9,10	0.9926	0.9923

a) Obtained by means of the V2 method, as defined in Table 4.
b) For the abbreviations, see the text.

Brown and Coller[8] have stated that the PP approximation has a tendency to give larger π-moments than the NM. However, this does not seem to be confirmed even by their own results. The present results on azulene also contradict this statement. The most characteristic difference between the NM and PP approximations seems to be that the latter gives larger absolute values to the net charge densities than the former; that is, the alternation in the charge distribution derived through the latter is more distinct than that due to the former, as can be seen, for example, from the entries of Table 5. This is also found for furan, pyrrole, and pyridine.[8] In the VESCF procedure, this characteristic difference seems to be blurred to an appreciable extent, but it still survives, as may be seen in Table 5. Brown and Coller[8] did not incorporate the dependence of $(pp|qq)$ integrals on the effective nuclear charges in their VESCF scheme; their scheme is obviously an improvement, as is revealed by a comparison of the relevant entries in Table 4.

Table 6. Calculated spin densities and expectation values of $\mathbf{S}^2$ for azulene anion after single annihilation[a]

Atomic position	Approximation for $(pp \mid qq)$[b]		a^{Hc} (Gauss)
	NM	PP	
1,3	0.108	−0.020	0.274
2	0.055	0.140	3.948
4,8	0.375	0.223	6.219
5,7	−0.283	−0.083	1.338
6	0.442	0.359	8.829
9,10	0.051	0.131	
$\langle \mathbf{S}^2 \rangle$	0.694	0.748	

a) Based on the single-determinant UHF wavefunctions obtained with the V2 method, as defined in Table 4, and the same molecular geometry as was used for the neutral molecule. For the annihilation procedure, see Ref. 29.
b) For the abbreviations, see the text.
c) Absolute values of the experimental splitting constants. See Ref. 30.

25) K. Ruedenberg, *J. Chem. Phys.*, **34**, 1861 (1961).
26) H. J. Tobler, A. Bauder, and H. H. Günthard, *J. Mol. Spectrosc.*, **18**, 239 (1965).
27) J. M. Robertson, H. M. M. Shearer, G. A. Sim, and D. G. Watson, *Acta Crystallogr.*, **15**, 1 (1962).
28) R. D. Brown, F. R. Burden, and G. M. Mohay, *Aust. J. Chem.*, **21**, 1695 (1968).
29) T. Amos and L. C. Snyder, *J. Chem. Phys.*, **41**, 1773 (1964).
30) I. Bernal, P. H. Rieger, and G. K. Fraenkel, *ibid.*, **37**, 1489 (1962).

The spin densities and the expectation values of $\mathbf{S}^2$ in the azulene anion are predicted by the PP approximation much better than by the NM, as Table 6 shows. This has also been confirmed with various aromatic nitrogen heterocycles.[7,31] By multiplying these spin densities by the Q^{H}_{CH} value of −23G for a CH bond in an aromatic system,[30] those from the PP approximation are found to reproduce the experimental splitting constants very well, whereas with those of the NM approximation no reasonable correspondence can be found between the theoretical and experimental values. Since, by and large, this is also the case for the other methods described in Table 4, the PP approximation seems undoubtedly much better than the NM for the calculation of spin densities.

Finally, it should be noted that the above excellent agreement obtained with the PP approximation is lost if Q^{H}_{CH} values inclusive of their variations with the bond angle[30] are used in place of the above value of −23G. Although this is an interesting finding, we prefer to refrain from a presentation of detailed results and from detailed discussions;[31] here, we intend mainly to show the significance of the PP approximation through the use of the convenient formulas obtained.

The calculations have been carried out on the FACOM 230-60 computer at the Computer Center of Kyushu University.

31) Y. Gondo, M. Hirai, and Y. Kanda, to be published; M. Hirai, MS thesis submitted to Kyushu University, March, 1971.

BULLETIN OF THE CHEMICAL SOCIETY OF JAPAN, VOL. 45, 1616—1619(1972)

Equilibrium of Urea Synthesis. II.

Shigeru INOUE, Kazumichi KANAI, and Eiji OTSUKA
Central Research Laboratory (Ofuna) Mitsui Toatsu Chemicals, Inc., Totsuka-ku, Yokohama

(Received September 17, 1971)

In the preceding paper (This Bulletin, **45**, 1339 (1972)) it was reported that the existence of the maximum equilibrium conversion was not due to the experimental method. For this phenomenon, we have presented the following interpretation. While $NH_4CO_2NH_2$ is converted to urea and water, it dissociates into NH_3 and CO_2 in the solution (not in the gas phase), and the degree of the dissociation increases exponentially as the temperature becomes higher, while the conversion to urea gradually increases. Therefore, at a certain temperature, the equilibrium conversion reaches its maximum value. Although it is nearly impossible to prove analytically the dissociation of $NH_4CO_2NH_2$ in the solution, we are sure of it from the following facts: 1) The dissociation of $NH_4CO_2NH_2$ is a great endothermic reaction, even under the conditions of urea synthesis. 2) The value of NH_3/CO_2 which gives the minimum equilibrium pressure at a usual temperature is not always equal to 2.0, but varies with the temperature. 3) The effect of H_2O/CO_2 on the equilibrium pressure varies with the temperature; that is, when the temperature is lower than about 200°C, an increase in H_2O/CO_2 reduces the equilibrium pressure, but when the temperature is higher than 200°C, an increase in H_2O/CO_2 makes the equilibrium pressure higher.

The dissociation of $NH_4CO_2NH_2$ in a solution has never been proved by means of chemical analysis, because experimentally it is nearly impossible to separate CO_2 in the form of carbamate from free CO_2. This has already been reported in Ref. 1.

However, in view of the fact that we carried out experiments over a broader range than in Ref. 1, many facts may be thought to suggest the dissociation of $NH_4CO_2NH_2$ in the solution. This point will be discussed.

Mechanism of the Equilibrium

In the preceding paper[2] we reported that the equilibrium conversion is independent of the loading density if the composition in the liquid phase is constant; therefore, other points must be investigated.

Our interpretation is that part of the $NH_4CO_2NH_2$ dissociates into NH_3 and CO_2 in the solution, and that this causes the temperature which gives the maximum equilibrium conversion. Thus, we presume two kinds of chemical equilibria in the solution, as is shown in Eqs. (1) and (2):

$$NH_4CO_2NH_2(soln) \rightleftarrows 2NH_3(soln) + CO_2(soln) \quad (1)$$

$$NH_4CO_2NH_2(soln) \rightleftarrows (NH_2)_2CO(soln) + H_2O(soln) \quad (2)$$

The equilibrium constants, K_1 and K_2, are defined as follows (the solutions are assumed to be ideal);

$$K_1(T) = \frac{x_{NH_3}^2 \cdot x_{CO_2}}{x_{carb}} \quad (3)$$

$$K_2(T) = \frac{x_u \cdot x_{H_2O}}{x_{carb}} \quad (4)$$

The equilibrium constant, $K_F(T)$, for the Frèjacques equation then becomes:

$$K_F(T) = \frac{K_2(T)}{K_1(T)} = \frac{x_u \cdot x_{H_2O}}{x_{NH_3}^2 \cdot x_{CO_2}} \quad (5)^{3)}$$

1) S. Kawasumi, *Journal of the Society of High Pressure Gas Industry*; **20**, No. 2, 4 (1956).

2) S. Inoue, K. Kanai, and E. Otsuka, **45**, 1339 (1972).

3) Although Eq. (5) is apparently the same as the Eq. (1) of Frèjacques reported in the previous paper, $K_F(T)$ is not equal to $K(t)$, because the molar fractions for each component are not equal in the two equations.

where x_{NH_3}, x_{CO_2}, x_u, x_{H_2O}, and x_{carb} denote the molar fractions of NH_3, CO_2, urea, H_2O, and carbamate respectively.

If $K_1(T)$ increases exponentially above a certain temperature compared with $K_2(T)$, as is shown in Fig. 1, the equilibrium constant, $K(t)$, in the previous paper reaches its maximum value near the temperature which results in the maximum equilibrium conversion.

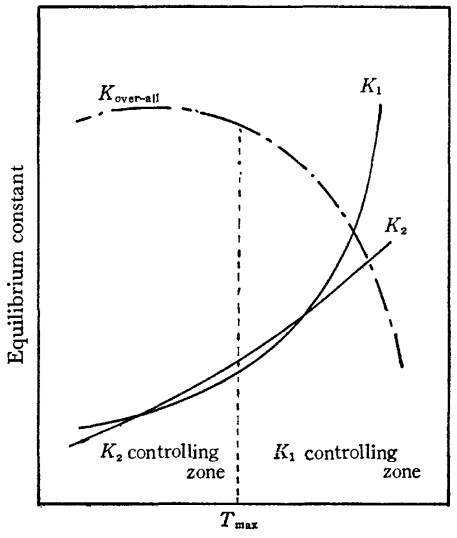

Fig. 1. Temperature dependence of $K_1(T)$, $K_2(T)$, and overall equilibirum constant.

Besides this, there is another presumption that when the urea formation of Eq. (2) change from an endothermic to an exothermic reaction at a certain temperature, the equilibrium conversion reaches its maximum value according to the Van't Hoff equation, because a high temperature—for example, 200°C—can not be easily attained in the urea reactor if the degree of dissociation of $NH_4CO_2NH_2$ is so large. However, our presumption seems to be true, judging from the following evidence.

Thermodynamic Discussion

Let the liquid composition be as follows before and after the reaction:

$$2NH_3 + CO_2 \overset{K_1(T)}{\rightleftarrows} \text{carb} \overset{K_2(T)}{\rightleftarrows} \text{urea} + H_2O \qquad (6)$$

before the reaction:

$$2m_N,\ 1,\ 0,\ 0,\ m_H,$$

after the reaction:

$$2(m_N - m_K - m_u),$$
$$m_c,\ m_K,\ m_u,\ m_u + m_H$$
$$\therefore\ \text{total} = 2m_N - 1 + 2m_c + m_u + m_H$$
$$(\because\ m_c + m_K + m_H = 1)$$

$$K_1(T) = \frac{(4m_N - 1 + m_c)^2 \cdot m_c}{(2m_N - 1 + 2m_c + m_u + m_H)^2(1 - m_u - m_c)} \qquad (7)$$

$$K_2(T) = \frac{m_u(m_u + m_H)}{(2m_N - 1 + 2m_c + m_u + m_H)^2(1 - m_u - m_c)} \qquad (8)$$

If it is assumed that $K_1(T)$ and $K_2(T)$ are dependent only on the temperature, the equilibrium conversion, m_u, can be obtained by solving Eqs. (7) and (8) at given NH_3/CO_2 ($=2m_N$) and H_2O/CO_2 ($=m_H$) ratios. Therefore, the temperature, T_{max}, giving the maximum equilibrium conversion is obtained by solving:

$$dm_u/dT = 0$$

However, neither m_c nor m_u is separable from the other in Eqs. (7) and (8), so it is difficult to obtain the derivative in a simple form.

On the other hand, it is doubtful whether or not the system or urea synthesis can be assumed to be ideal; therefore, we will show only the existence of the maximum conversion, using a simple model in the case of simultaneous equilibria.

Thus, let the following system be taken:

$$A \overset{K_A}{\rightleftarrows} C \overset{K_B}{\rightleftarrows} B$$

$a,\ 1-a-b,\ b,$ total $= 1$ mol

$$K_A = \frac{a}{1-a-b} \qquad (9)$$

$$K_B = \frac{b}{1-a-b} \qquad (10)$$

From Eqs. (9) and (10),

$$A = \frac{K_A(T)}{K_B(T)} \cdot b$$

We thus obtain:

$$b = \frac{K_B(T)}{1 + K_A(T) + K_B(T)} \qquad (11)$$

As b is dependent only on the temperature, the differentiation of b with respect to T affords:

$$K_B'(T)(1 + K_A(T)) = K_B(T) \cdot K_A'(T) \qquad (12)$$

Within a relatively narrow range of temperature, $K_A(T)$ and $K_B(T)$ may be expressed as follows:

$$A_0 - A_1 T = -RT \ln K_A,\ B_0 - B_1 T = -RT \ln K_B \qquad (13)$$

By the substitution of K_A and K_B in Eq. (12) with Eq. (13), and by solving Eq. (12) with respect to T, the temperature, T_{max}, giving the maximum conversion is obtained:

$$T_{max} = \frac{A_0}{R\left(\frac{A_1}{R} - \ln\frac{B_0}{A_0 - B_0}\right)} \qquad (14)$$

where $A_0 > B_0 > 0$.

If the logarithmic term is very small compared with the A_1/R, term:

$$T_{max} \doteqdot A_0/A_1 \qquad (15)$$

Therefore, T_{max} can be calculated if A_0, A_1, and B_0 are given. Now,

$$\Delta G = \Delta H - T\Delta S$$

By assuming ΔH and ΔS to be constant within a narrow range of temperature, A_0 or B_0 is replaced by ΔH, and also A_1 or B_1, by ΔS. Therefore, if ΔH and ΔS are given, T_{max} can be calculated.

Although it is very difficult to estimate these real values under the conditions of urea synthesis, if the values in Ref. 1 can be used, T_{max} can be obtained; that is,

$$A_0 = 15890,\ A_1 = 33.7,\ B_0 = 9160$$

$$\therefore\ T_{max} = \frac{15890}{33.7-4.575\log 1.36} = 482°K \quad (16)$$

$$\therefore\ t_{max} = 209°C$$

The value of T_{max} thus obtained is a little different from the actual one. This inconsistency is unavoidable in such a simple treatment.

We estimate the heat of dissociation of $NH_4CO_2NH_2$ in the solution at the temperature of urea synthesis, using a thermochemical cycle from the standard state of $NH_4CO_2NH_2$. It decreases with the rise in the temperature, but it does not turn out to be zero or minus, as is shown in Table 1. Therefore, it may be presumed that the dissociation of $NH_4CO_2NH_2$ in the solution takes place.

Table 1. Heat of dissociation of $NH_4CO_2NH_2$ (Estimated)

Temp	°C	160	180	200	220
ΔH	cal/mol	27074	24746	21993	20509

On the other hand, assuming that $K_1(T)$ and $K_2(T)$ are expressed as in Eq. (13), a value for A_0, which is approximately equal to the heat of the dissocation of $NH_4CO_2NH_2$ can be obtained in such a way that the optimum values of A_0, B_0, A_1, and B_1 are selected; the difference between the calculated and the observed conversion thus becomes a minimum when Eqs. (7) and (8) are solved simultaneouly for some given data. The value thus estimated is about 20 kcal/mol $NH_4CO_2NH_2$.

Discussion of the Equilibrium Pressure

The Minimum Equilibrium Pressure. The effect of NH_3/CO_2 (mol/mol) on the equilibrium pressure is shown in Fig. 2, where curves are drawn assuming a smoothed formula.

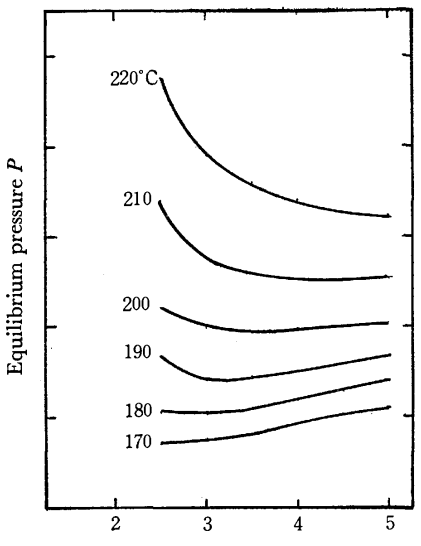

Fig. 2. Effect of NH_3/CO_2 on the equilibrium pressure.

The minimum equilibrium pressure at any temperature under the usual conditions of urea synthesis does not exist at 2.0 of NH_3/CO_2; as the temperature rises, the minimum point seems to move to higher values of NH_3/CO_2. Furthermore, the effect of NH_3/CO_2 on the equilibrium pressure at higher temperatures becomes slightly sensitive.

Table 2. Partial pressures of NH_3 and CO_2

Component	NH_3 [a]	CO_2 [b]	$NH_4CO_2NH_2$ [c] ($2NH_3+CO_2$)
mol/mol H_2O	1.0	0.022	1.0
Partial press. kg/cm²abs.	32.5	200	8.7 (5.8+2.9)

(at 120°C)
a) observed value by authors
b) Seidel's data collection
c) Calculated value by Raoult's law applied to the dissociation pressure by Frèjacques.

This can be understood according to the following explanation. Table 2 shows each partial pressure when NH_3, CO_2, or carbamate dissolves into one mole of H_2O.

It is evident that the partial pressure of CO_2, p_{CO_2}, is much greater than that of any other component because of physical absorption. As the partial pressure of H_2O, p_{H_2O}, is small compared to the total pressure, P: according to the mass action law and Raoult's law, the following equation is obtained:

$$P \doteqdot p_{NH_3} + p_{CO_2} \quad (17)$$

Then, by combining Eq. (17) with Eq. (18), Eq. (19) is obtained:

$$K_P(T) = (f_N p'_{NH_3})^2 (f_c p'_{CO_2}) \quad (18)$$

where p_{NH_3} and p_{CO_2} are actual partial pressures, and where p'_{NH_3} and p'_{CO_2} are ideal partial pressures;

$$P \doteqdot f_N p'_{NH_3} + K_P(T)/(f_N p'_{NH_3})^2 \quad (19)$$

therefore, f_N and f_C are factors which inidcate deviation from an ideal solution. By the partial differentiation of Eq. (19) with respect to p'_{NH_3}, Eq. (20) is obtained:

$$\frac{\partial P}{\partial p'_{NH_3}} = \frac{\partial f_N}{\partial p'_{NH_3}} \cdot p'_{NH_3} + f_N - 2\left(\frac{f_c p_{CO_2}}{f_N} \cdot \frac{\partial f_N}{\partial p'_{NH_3}} + \frac{f_c p'_{CO_2}}{p'_{NH_3}}\right) \quad (20)$$

Now, by supposing that f_N is independent of the p'_{NH_3}-compositions in the solution, and that $\partial f_N/\partial p'_{NH_3}=0$, at the minimum pressure, Eq. (20) becomes Eq. (21):

$$\frac{\partial P}{\partial p'_{NH_3}} = f_N - 2\frac{f_c p'_{CO_2}}{p'_{NH_3}} = 0 \quad (21)$$

$$p'_{NH_3}/p'_{CO_2} = 2f_c/f_N \quad (22)$$

As p'_{NH_3}/p'_{CO_2} is the ratio of the partial pressure of NH_3 to that of CO_2 in equilibrium with the solution, this is also the molar ratio of NH_3 to CO_2 in the solution. When we think that NH_3 dissolves by chemical absorption, while CO_2 dissolves by physical absorption, $f_c \gg f_N$.

Since NH_3/CO_2, which gives the minimum equilibrium pressure, is greater than 2, and since the effect

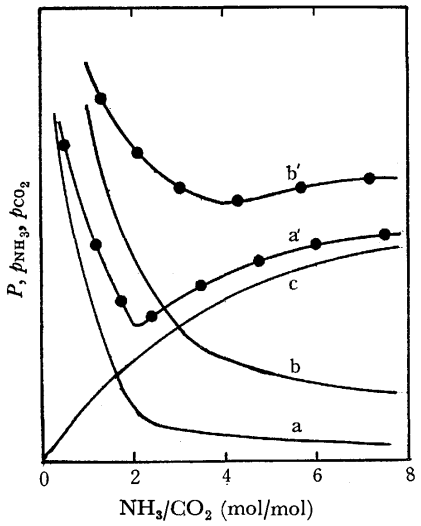

Fig. 3. Partial and total equilibrium pressure profile *vs.* NH_3/CO_2.
at const. temperature
a: p_{CO_2}, a': P when $fc=f_N$
b: p_{CO_2}, b': P when $fc>f_N$
c: p_{NH_3} of NH_3aq.

of the temperature on f_c is much greater than that on f_N, when the temperature becomes higher, the minimum equilibrium pressure moves to the side of higher NH_3/CO_2 ratios, we think.

If $NH_4CO_2NH_2$ does not dissociate into NH_3 and CO_2, and if the system is assumed to be ideal, the equilibrium pressure naturally reaches its minimum value when NH_3/CO_2 is just equal to 2. Figure 3 indicates the above state schematically.

However, NH_3 and CO_2 in the solution partially neutrallize each other, so p_{NH_3} and p_{CO_2} may be considered to be greatly reduced. Furthermore, the urea which is contained in the solution of urea synthesis is also a solvent for NH_3 and carbamate, so p_{NH_3} and p_{CO_2} are lower than in the case of no urea. From these considerations, the actual equilibrium pressure can be said not to be so great as was estimated from such data as those in Table 2.

Effect of H_2O/CO_2. While the increase in H_2O/CO_2, a solvent for carbamate, brings about a lowering of the equilibrium pressure, it also lowers the amount of urea to be formed, and urea is also a solvent for carbamate. Therefore, it is thought that the equilibrium pressure remains almost unchanged, or is reduced to some extent, with the increase in H_2O/CO_2, depending on the temperature.

The experimental data, however, show that, at a lower temperature, the equilibrium pressure is gradually reduced as H_2O/CO_2 increases and that, on the contrary, at a temperature higher than 200°C, it increases as H_2O/CO_2 increases (*cf.* Table 1 in the preceding paper).

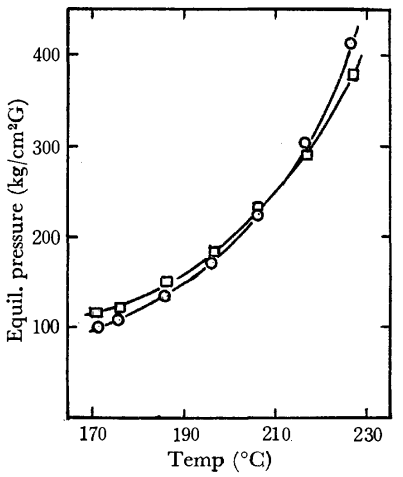

Fig. 4. Temperature dependence of the equilibrium pressure at various H_2O/CO_2.
at $NH_3/CO_2\fallingdotseq4$
-□- $H_2O/CO_2\fallingdotseq0.1$ -○- $H_2O/CO_2\fallingdotseq0.9$

Some examples are shown in Fig. 4. For this phenomenon we have the following interpretation. That is, when the temperature is low, the equilibrium pressure stays almost constat, or is reduced, with an increase in H_2O/CO_2 because of the low degree of dissociation of $NH_4CO_2NH_2$ in the solution.

When the temperature is high, however, the equilibrium pressure becomes higher because of the high degree of dissociation of $NH_4CO_2NH_2$ in the solution,[4] because the partial pressures of free NH_3 and CO_2 are much greater than the partial pressure of $NH_4CO_2NH_2$ in the solution.

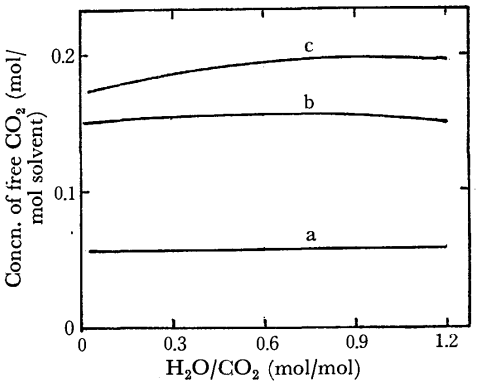

Fig. 5. Effect of H_2O/CO_2 on the conc. of free CO_2 in the solution.
a: 160°C, b: 190°C, c:220°C

The authors owed much computational aid to Mr. Kenji Yoshida. Here we gratefully acknowledge him.

4) Figure 5 shows the concentration of free CO_2 in the solution due to the dissociation of $NH_4CO_2NH_2$, when the solvent effect of formed urea are taken into consideration.

The Solvent Extraction of Iron(III) in Perchlorate Solutions Containing Chloride or Bromide Ions with 2-Thenoyltrifluoroacetone and Trioctylphosphine Oxide

Tatsuya SEKINE and Toshihiro TETSUKA

Department of Chemistry, Science University of Tokyo, Kagurazaka, Shinjuku-ku, Tokyo

(Received July 29, 1971)

Iron(III) in aqueous solutions, in which $[H^+]=1.0$M, $[Na^+]=3.0$M, and $[L^-]+[ClO_4^-]=4.0$M, where L^- is a chloride or bromide ion, was extracted with thenoyltrifluoroacetone (TTA) in carbon tetrachloride or with trioctylphosphine oxide (TOPO) in hexane. From the TTA extraction, it was concluded that iron(III) formed the first and the second complexes with both chloride ($\beta_1=10^{0.88}$ and $\beta_2=10^{0.80}$) and bromide ($\beta_1=10^{-0.10}$ and $\beta_2=10^{0.00}$) ions in the aqueous phase. The distribution data of iron(III) with TOPO were then explained in terms of the extraction of the ion-pairs, $Fe(ClO_4)_3$, $FeL(ClO_4)_2$, and $FeL_2(ClO_4)$, by using these stability constants. When the aqueous phase contained only chloride or bromide ions, and no perchlorate ion, the increase in the extraction with the increase in the halide ion concentration was much larger than that observed when the aqueous phase contained both halide and perchlorate ions. From the determination of the extraction of hydrogen ions and halide ions with TOPO, the extracted species in the absence of a perchlorate ion were identified as FeL_3 and/or $HFeL_4$. It was concluded that the difference in the extraction of iron(III) when a perchlorate ion was present and when it was absent is mainly caused by (i) the extraction of perchloric acid, which combines with TOPO in the organic phase and interferes with the extraction of the iron(III) halide complexes, and (ii) the extraction of iron(III) species containing one or more perchlorate ions which are large enough to be extractable with TOPO in the organic phase.

The solvent extraction of iron(III) in hydrochloric acid with diethylether was one of the earliest examples of the application of this experimental technique.[1,2] However, the chemical equilibria involved in such solvent extraction systems containing strong acids in the aqueous phase, and a polar solvent, such as an ether or a ketone, in the organic phase have not been analyzed very clearly, although Diamond and Tuck[3] and Marcus and Kertes[4] made comprehensive discussions of this problem.

The difficulties in the analysis of the thermodynamic equilibria involved in such systems are mainly due to the changes in the chemical properties of the organic phase caused by the extraction of the strong acid.

It has also been reported that iron(III) in hydrochloric acid is extractable with tributylphosphate (TBP)[5-9] or trioctylphosphine oxide (TOPO).[10,11] The chemical equilibria in these extraction systems, especially when the organic phase is a nonpolar solvent containing a small amount of one of these extractants, are assumed to be much simpler than those in extraction systems containing a polar solvent, because the extraction behavior of strong acids is much simpler when the organic solvent is nonpolar than when it is polar.

In the present investigation, the authors studied the chemical equilibria of iron(III) in aqueous sodium perchlorate solutions containing chloride or bromide ions and the extraction of iron(III) from these aqueous solutions into carbon tetrachloride containing TTA or into hexane containing TOPO. They determined the stability constants of these halide complexes in the aqueous phase and the chemical form of the extracted species in the organic phase. From these results, they discussed the role of perchlorate ions in the extraction of iron(III) in such systems.

Experimental

Tracer and Reagents. The iron-59 tracer was obtained from the Union Carbide Corporation, USA. It was purified as follows: a 6N hydrochloric acid solution of the tracer was shaken with the same volume of methylisobutylketone (MIBK), and then the tracer was extracted into the organic phase. The organic phase was washed with an equal volume of 4N hydrochloric acid, and then the tracer was back-extracted into the same volume of water. The solution thus prepared was diluted with 0.01N nitric acid and used as the stock solution. The concentration of chloride ions back-extracted together with the tracer into the final aqueous solutions was assumed to be very small[12] ($[Cl^-]$ is 4×10^{-4}M in the stock tracer solution and, consequently it is 7×10^{-6}M in the final solution). Furthermore, since only 0.1 m*l* of this tracer solution was added to 5 m*l* of the aqueous phase, the nitrate concentration in the latter solution was also very low (2×10^{-4}M). The effect of these ions was checked by changing the amount of the tracer solution added to the aqueous phase, but no change in the distribution ratio of iron(III) was thus observed. The TTA and the TOPO were obtained from the Dojin-Do & Co. The MIBK was

1) M. Hanroit, *Bull. Soc. Chim. Fr.*, (3) **7**, 171 (1892).
2) J. W. Rothe, *Chem. News*, **66**, 182 (1892).
3) R. M. Diamond and D. G. Tuck, *Progr. Inorg. Chem.*, **2**, 109 (1960).
4) Y. Marcus and A. S. Kertes, "Ion exchange and solvent extraction of metal complexes," Willy-Interscience, London 1969, p. 575.
5) S. K. Majumdar and A. K. De, *Talanta*, **7**, 1 (1960).
6) G. Weidmann, *Can. J. Chem.*, **38**, 459 (1960).
7) H. Specker and M. Cremer, *Z. Anal. Chem.*, **167**, 110 (1959).
8) A. Alian and R. Shabana, *Microchem. J.*, **12**, 427 (1967).
9) O. D. Lyakh, I. A. Sheka, and A. I. Porfil'ev, *Zh. Prikl. Khim.*, **39**, 1799 (1966).
10) W. J. Ross and J. C. White, U. S. At. Energy Comm. Rept. ORNL-2382 (1957).
11) J. Hibbits, W. F. Davis, and M. R. Menke, *Talanta*, **4**, 101 (1960).
12) T. Sekine, T. Fukushima, and Y. Hasegawa, This Bulletin, **43**, 2638 (1970).

obtained from the Tokyo Kasei Co. The MIBK was washed with 0.1N perchloric acid, water, and a 0.1N sodium hydroxide solution successively, and then several times with water. The sodium perchlorate was prepared from sodium carbonate and perchloric acid and recrystallized three times from water. The other reagents were of an analytical-grade and were used without further purification.

Procedures. All of the procedures were carried out in a thermostated room at 25°C. Stoppered glass tubes (volume, 20 m*l*) were used to equilibrate the two phases. A five-milliliter portion of an aqueous solution containing iron(III) (carrier-free iron-59 or a small amount of an iron(III) carrier prepared from an analytical-grade reagent and labelled by iron-59) and various amounts of the ligand and sodium perchlorate, and a 5-m*l* portion of carbon tetrachloride containing TTA or hexane containing TOPO were placed in the tubes. The aqueous phase contained 4M electrolytes, unless noted. The initial concentration of iron(III) ions in the aqueous phase was 2×10^{-4}M to 1×10^{-5}M in the TTA extraction system and about 10^{-8}M in the TOPO extraction system. The tubes containing the aqueous and organic phases were placed on a rotating framework, and the two phases were agitated mechanically (20 rpm) for 24 hr and then centrifuged. A four-milliliter portion was pipetted from each phase and transferred into a small test tube. The γ-radioactivity in the sample solutions was measured with a well-type (NaI) scintillation counter, and the distribution ratio of iron(III) was calculated as follows:

$$D = \frac{[\mathrm{Fe(III)}]_{org,total}}{[\mathrm{Fe(III)}]_{total}} = \frac{\gamma\text{-count-rate per m}l\text{ of the organic phase}}{\gamma\text{-count-rate per m}l\text{ of the aqueous phase}}$$

The titration of the hydrogen ion in the organic phase was made by using a standard barium hydroxide solution, with phenolphthalein as the indicator.

Statistical

The stability constants of iron(III) complexes with L^- in the aqueous phase may be described as follows;

$$\mathrm{Fe^{3+}} + n\mathrm{L^-} \rightleftarrows \mathrm{FeL}_n^{3-n}$$

$$\beta_n = \frac{[\mathrm{FeL}_n^{3-n}]}{[\mathrm{Fe^{3+}}][\mathrm{L^-}]^n} \quad (1)$$

The total iron(III) concentration in the aqueous solution may then be described as;

$$[\mathrm{Fe(III)}]_{total} = [\mathrm{Fe^{3+}}] + [\mathrm{FeL^{2+}}] + [\mathrm{FeL_2^+}] + \cdots + [\mathrm{FeL}_n^{3-n}] = [\mathrm{Fe^{3+}}](1+\sum\beta_n[\mathrm{L^-}]^n) \quad (2)$$

When iron(III) is extracted into the organic phase with an organophilic chelating acid, the distribution equilibrium may be described as;

$$\mathrm{Fe^{3+}} + 3\mathrm{HA(org)} \rightleftarrows \mathrm{FeA_3(org)} + 3\mathrm{H^+}$$

$$K_{ex} = \frac{[\mathrm{FeA_3}]_{org}[\mathrm{H^+}]^3}{[\mathrm{Fe^{3+}}][\mathrm{HA}]^3_{org}} \quad (3)$$

If no complex formation or no hydrolysis of iron(III) in the aqueous phase is assumed, the distribution ratio is given by (here the subscript "0" denotes no complex formation in the aqueous phase);

$$D_0 = \frac{[\mathrm{FeA_3}]_{org}}{[\mathrm{Fe^{3+}}]} = K_{ex}[\mathrm{HA}]^3_{org}[\mathrm{H^+}]^{-3} \quad (4)$$

However, when iron(III) forms complexes with L^-, in the aqueous phase, the distribution ratio is given from Eqs. (2) and (4) as;

$$D = \frac{[\mathrm{FeA_3}]_{org}}{[\mathrm{Fe^{3+}}]+[\mathrm{FeL^{2+}}]+[\mathrm{FeL_2^+}]+\cdots} = \frac{K_{ex}[\mathrm{HA}]^3_{org}[\mathrm{H^+}]^{-3}}{1+\beta_1[\mathrm{L^-}]+\beta_2[\mathrm{L^-}]^2+\cdots} \quad (5)$$

From Eq. (5), the following relation is obtained;

$$\log D[\mathrm{H^+}]^3[\mathrm{HA}]_{org}^{-3}K_{ex}^{-1} = -\log(1+\sum\beta_n[\mathrm{L^-}]^n) \quad (6)$$

As may be seen (*cf.* Fig. 1, Table 1(a)), the formation of only the first and the second complexes in the aqueous phase was assumed, and the data were found to be represented by the following equation;[13,14]

$$Y = -\log(1+\beta_1[\mathrm{L^-}]+\beta_2[\mathrm{L^-}]^2) \quad (7)$$

The plot may be fitted with a family of standard curves;

$$Y = -\log(1+pv+v^2),\ X = \log v \quad (8)$$

and the constants, β_1 and β_2, can be determined from the parameters of the "best-fit" standard curve.

It is possible that iron(III) in the aqueous phase is extracted with a neutral extractant, E, as various uncharged species containing the ligand anions, L^-, and/or perchlorate ions. The extraction equilibria can be described as follows;

$$\mathrm{Fe^{3+}} + a\mathrm{L^-} + (3-a)\mathrm{ClO_4^-} + e\mathrm{E}(org) \rightleftarrows \mathrm{FeL}_a(\mathrm{ClO_4})_{3-a}\mathrm{E}_e(org)$$

$$K_{ex'3-a.a} = \frac{[\mathrm{FeL}_a(\mathrm{ClO_4})_{3-a}\mathrm{E}_e]_{org}}{[\mathrm{Fe^{3+}}][\mathrm{L^-}]^a[\mathrm{ClO_4^-}]^{3-a}[\mathrm{E}]^e_{org}} \quad (9)$$

However, when the concentration of the extractant is kept constant throughout a series of experiments, the $[\mathrm{E}]^e_{org}$ term can be eliminated from the equation and the following equation can be used instead of Eq. (9);

$$K_{ex_{3-a.a}} = \frac{[\mathrm{FeL}_a(\mathrm{ClO_4})_{3-a}]_{org}}{[\mathrm{Fe^{3+}}][\mathrm{L^-}]^a[\mathrm{ClO_4^-}]^{3-a}} \quad (10)$$

It is also possible that ion-pairs of anionic iron(III) complexes with sodium in the background salt such as $\mathrm{Na^+Fe(ClO_4)_4^-}$ are extracted. However, as will be seen later, this type of extraction is negligible in the present study, and so it will not be considered here.

The distribution ratio under these conditions may, then, be described as;

$$D = \frac{[\mathrm{Fe(ClO_4)_3}]_{org}+[\mathrm{FeL(ClO_4)_2}]_{org}+[\mathrm{FeL_2(ClO_4)}]_{org}+[\mathrm{FeL_3}]_{org}}{[\mathrm{Fe^{3+}}]+[\mathrm{FeL^{2+}}]+[\mathrm{FeL_2^+}]+\cdots} \quad (11)$$

As will be seen, the data were found to be represented well if the formation of the first and the second complexes in the aqueous phase and the extraction of the ion-pairs with perchlorate ions, $\mathrm{Fe(ClO_4)_3}$, $\mathrm{FeL(ClO_4)_2}$, and $\mathrm{FeL_2(ClO_4)}$, were assumed (*cf.* Figs. 1, 3, and 4, Table 1); thus, by introducing the equilibrium constants, Eq. (11) can be rewritten as;

13) T. Sekine and M. Ono, This Bulletin, **38**, 2087 (1965).
14) T. Sekine and Y. Hasegawa, *ibid.*, **39**, 240 (1966).

$$D=\frac{K_{ex_{3,0}}[ClO_4^-]^3+K_{ex_{2,1}}[ClO_4^-]^2[L^-]+K_{ex_{1,2}}[ClO_4^-][L^-]^2}{1+\beta_1[L^-]+\beta_2[L^-]^2} \quad (12)$$

From Eq. (12), the following relation is obtained;

$$\log\frac{D(1+\beta_1[L^-]+\beta_2[L^-]^2)}{[ClO_4^-]^3} = \log K_{ex_{3,0}} + \log\left\{1+\frac{K_{ex_{2,1}}}{K_{ex_{3,0}}}\left(\frac{[L^-]}{[ClO_4^-]}\right)+\frac{K_{ex_{1,2}}}{K_{ex_{3,0}}}\left(\frac{[L^-]}{[ClO_4^-]}\right)^2\right\} \quad (13)$$

The plot may also be fitted with the following family of standard curves;[13,14]

$$Y=\log(1+pv+v^2),\ X=\log v \quad (14)$$

and the constants, $K_{ex_{3,0}}$, $K_{ex_{2,1}}$, and $K_{ex_{1,2}}$, can be determined from the curve-fitting.

Results

Rate of Extraction. In the present study, it was found that the extraction of iron(III) with TTA is a slow reaction, as had previously been reported.[15,16] It took almost 20 hr until the distribution equilibrium was reached under the conditions employed. The rate of the extraction of the uncharged species of iron(III) with TOPO was also small, especially when the ligand concentration in the 4M sodium perchlorate medium was very low (where only the $Fe(ClO_4)_3$ species is extracted). Thus, the mechanical agitation of the two phases was always carried out for 24 hr before they separated.

TTA Extraction from an Aqueous Phase Containing no Ligand. Since the hydrogen-ion concentration in most of the experiments in this work was 1.0M, the extraction of iron(III) from an aqueous solution containing 1.0M perchloric acid and 3.0M sodium perchlorate with TTA in carbon tetrachloride was determined as a function of the TTA concentration. It was found from these determinations that the $D_0[H^+]^3[HA]_{org}^{-3}$ values obtained are nearly constant (log K_{ex} is 3.99). Thus, as can be seen from Eq. (4), the TTA complexes in the aqueous phase are practically negligible in the aqueous phase. Since the hydrogen-ion concentration was kept constant, no information about the hydrolysis of iron(III) was obtained from these distribution data alone. However, as the previously reported values of the hydrolysis constants of iron(III) in 3M sodium perchlorate solutions[17] are $*K_1=[FeOH^{2+}][H^+]/[Fe^{3+}]=10^{-3.05}$, $*\beta_2=[Fe(OH)_2^+][H^+]^2/[Fe^{3+}]=10^{-6.31}$, and $*\beta_{22}=[Fe_2(OH)_2^{4+}][H^+]^2/[Fe^{3+}]^2=10^{-2.96}$, the hydrolysis in 4M sodium perchlorate media at hydrogen-ion concentrations higher than 1M can be regarded as negligible.

TTA Extraction from an Aqueous Phase Containing Chloride or Bromide Ions. Figure 1(a) gives the log $D[H^+]^3[HA]_{org}^{-3}K_{ex}^{-1}$ *vs.* log[L^-] plot (*cf.* Eq. (6)) when the aqueous phase contained chloride (open circles) or bromide (closed circles) ions in a 4M sodium perchlorate medium at the hydrogen-ion concentration of 1.0M. The stability constants were determined by

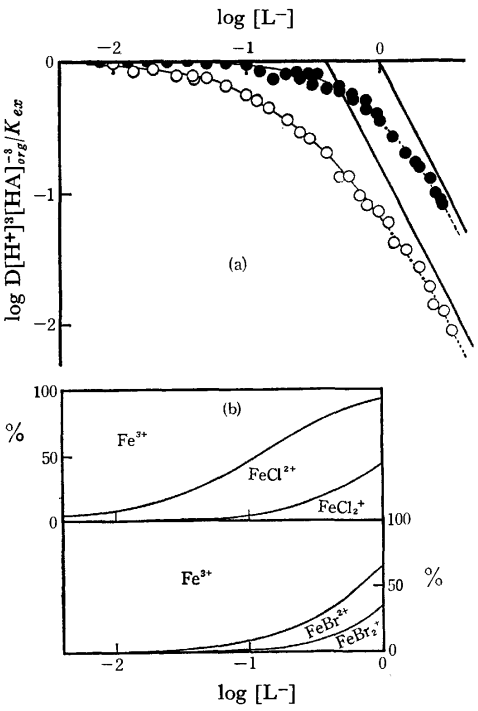

Fig. 1(a). Decrease in the TTA extraction of iron (III) as a function of the chloride (○) or bromide (●) concentration. Org. phase: carbon tetrachloride containing 0.1M TTA, Aq. phase: 4M perchlorate inoic medium in which $[H^+]=1.0$M, $[Na^+]=3.0$M, and $[L^-]+[ClO_4]=4.0$M. The solid cruves ($[L^-]<1.0$M) and the dotted lines ($[L^-]>1.0$M) are calculated by using the following equation and the stability constants in Table I(a):

$$\log D[H^+]^3[HA]_{org}^{-3}K_{ex}^{-1}=-\log(1+\beta_1[L^-]+\beta_2[L^-]^2)$$

1(b). The distribution of the chemical species in the aqueous phase as a function of the ligand concentration calculated by using the stability constants in Table 1(a).

Table 1. Equilibrium constants for iron(III) at 25°C

(a) Stability constants for iron (III) complexes in a 4M perchlorate ionic medium in which $[H^+]=1.0$M, $[Na^+]=3.0$M, and $[L^-]+[ClO^-]=4.0$M.

Ligand	Cl^-	Br^-
log β_1	0.88	−0.10
log β_2	0.80	0.00

(b) Extraction constants for iron (III) species with TOPO. Org. phase: hexane containing 0.03M TOPO, Aq. phase: aqueous solutions in which $[H^+]=1.0$M, $[Na^+]=3.0$M, and $[L^-]+[ClO^-_3]=4.0$M.

$K_{ex_{3,0}}=[Fe(ClO_4)_3]_{org}/[Fe^{3+}][ClO^-_4]^3$

$K_{ex_{2,1}}=[FeL(ClO_4)_2]_{org}/[Fe^{3+}][L^-][ClO_4^-]^2$

$K_{ex_{1,2}}=[FeL_2(ClO_4)]_{org}/[Fe^{3+}][L^-]^2[ClO_4^-]$

Ligand	Cl^-	Br^-
log $K_{ex_{3,0}}$	−1.31	
log $K_{ex_{2,1}}$	0.39	−0.01
log $K_{ex_{1,2}}$	0.53	0.21

15) R. A. Bolomey and L. Wish, *J. Amer. Chem. Soc.*, **72**, 4483 (1950).

16) A. Adin and L. Newman, *J. Inorg. Nucl. Chem.*, **32**, 3321 (1970).

17) A. Martell and L. G. Sillén, "Stability constants," the Chemical Society, London, spec. pub. No. 17 (1964).

using the data in the ligand-concentration region below 1.0M. By the curve-fitting, the stability constants for the first and the second complexes were determined to be as are listed in Table 1(a). The solid curves in Fig. 1(a) are the curves calculated from these constants. The dotted lines in Fig. 1(a) are calculated by using these constants for the ligand-concentration region above 1.0M.

Figure 1(b) gives the distribution of iron(III) complex species in the aqueous phase as a function of the ligand concentration.

TOPO Extraction from Aqueous Solutions Containing Chloride or Bromide Ions. The extraction of iron(III) with TOPO in hexane was reproducible only when the iron(III) concentration was very low; the distribution ratio was constant when the iron(III) concentration was changed between 10^{-8}M to 10^{-6}M, but it became lower than this value when the initial iron(III) concentration in the aqueous phase was above 10^{-5}M, the extraction being almost negligible when the iron(III) concentration was higher than 10^{-4}M. Thus, the initial iron(III) concentration in the aqueous phase was settled to be about 10^{-8}M.

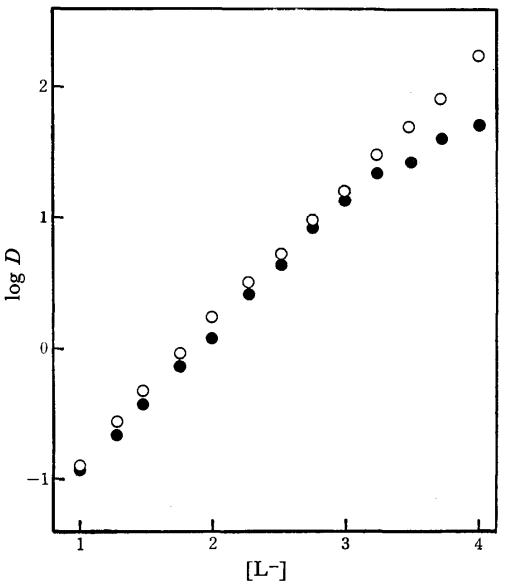

Fig. 2. TOPO extraction of iron (III) in the absence of perchlorate ions as a function of the chloride (○) or bromide (●) concentration in the aqueous phase. Org. phase: hexane containing 0.03 M TOPO, Aq. phase: aqueous solutions containing 1.0 M hydrohalic acid and various amounts of sodium halide but no perchlorate.

Figure 2 gives the extraction of iron(III) when the organic phase is hexane containing 0.03M TOPO and when the aqueous phase contains 1.0M hydrochloric acid and various amounts of sodium chloride, or when it contains 1.0M hydrobromic acid and various amounts of sodium bromide. The distribution ratio always increases with an increase in the halide concentration.

Figure 3 gives the extraction of iron(III) when the organic phase is also hexane containing 0.03M TOPO, but when the aqueous phase contains 1.0M hydrogen ions, 3.0M sodium ions and various amounts of perchlorate and chloride or bromide ions (prepared by mixing a solution containing 1.0M perchloric acid and

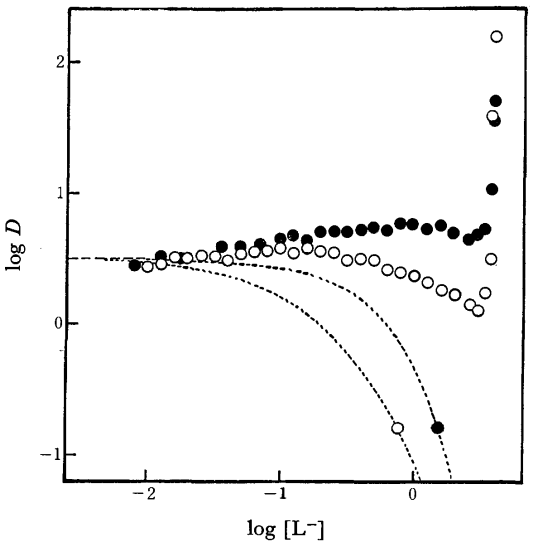

Fig. 3. TOPO extraction of iron(III) in the presence of perchlorate ions as a function of the chloride (○) or bromide (●) concentration. Org. phase: hexane containing 0.03M TOPO, Aq. phase: aqueous solutions in which $[H^+]=1.0$M, $[Na^+]=3.0$M, and $[L^-]+[ClO_4]=4.0$M. The broken line indicates the extraction in the absence of halide ions ($D=10^{0.50}$). The dotted lindes are the calculated curves (○: chloride system and ●: bromide system) assuming only the extraction of iron(III) perchlorate by using the equation, $\log D=\log K_{ex_{3,0}}[ClO_4^-]^3-\log(1+\beta_1[L^-]+\beta_2[L^-]^2)$ where β_1 and β_2 were taken from Table 1(a).

3.0M sodium perchlorate and a solution containing 1.0M hydrohalic acid and 3.0M sodium halide at various mixing ratios). The distribution ratio was $10^{0.50}$ (indicated by a broken line) when the aqueous phase was a perchlorate solution containing no halide ions.

As may be seen from Fig. 3, the distribution ratio is not changed very much by the halide ions when the

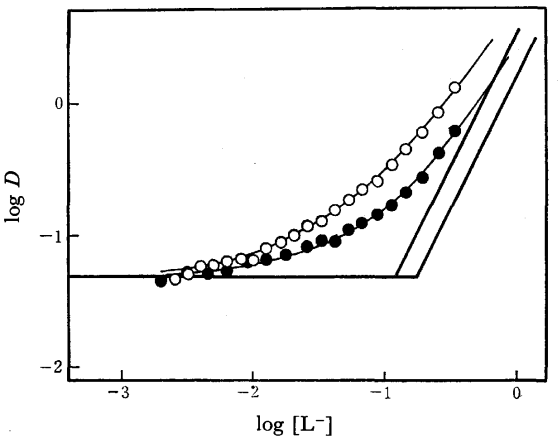

Fig. 4. Determination of the extraction constants (○: chloride and ●: bromide).
$K_{ex_{3,0}}=[Fe(ClO_4)_3]_{org}/[Fe^{3+}][ClO_4^-]^3$
$K_{ex_{2,1}}=[FeL(ClO_4)_2]_{org}/[Fe^{3+}][L^-][ClO_4^-]^2$
$K_{ex_{1,2}}=[FeL_2(ClO_4)]_{org}/[Fe^{3}][L^-]^2[ClO_4^-]$
Org. phase: hexane containing 0.03M TOPO, Aq. phase: aqueous solutions in which $[H^+]=1.0$M, $[Na^+]=3.0$M, and $[L^-]+[ClO_4^-]=4.0$M. The solid curves are calculated by using the following equation and the constants in Table 1.
$\log D(1+\beta_1[L^-]+\beta_2[L^-]^2)/[ClO_4^-]^3=$
$\log\{K_{ex_{3,0}}+K_{ex_{2,1}}[L^-]/[ClO_4^-]+K_{ex_{1,2}}([L^-]/[ClO_4^-])^2\}$

concentration is lower than 3M, but it increases drastically in the region between 3M and 4M.

In order to determine the equilibrium constants in these extractions, the data were analyzed on the basis of Eq. (12). Figure 4 gives the $\log D(1+\beta_1[L^-]+\beta_2[L^-]^2)[ClO_4^-]^{-3}$ *vs.* $\log[L^-][ClO_4^-]^{-1}$ plot. Since the limitting slope for the plot in Fig. 4 is 0 or +2, it was concluded from Eq. (13) that the extracted species were $Fe(ClO_4)_3$, $FeL(ClO_4)_2$, and $FeL_2(ClO_4)$ in the ligand-concentration region below 1.0M and when the TOPO concentration was 0.03M. The extraction constants were determined by the curve-fitting of the plot in Fig. 4: they are listed in Table 1(b). The extraction of ion-pairs of the iron(III) ion, $Fe(ClO_4)_3$, and the first and the second complexes, $FeL(ClO_4)_2$ and $FeL_2(ClO_4)$, seems to explain the results in Fig. 3 reasonably, for if only the extraction of the $Fe(ClO_4)_3$ ion-pair occurs, the distribution ratio should decrease due to the complex formation in the aqueous phase and due to the decrease in the perchlorate concentration as the halide concentration increases. The dotted lines in Fig. 3 give the calculated curves assuming only the extraction of the $Fe(ClO_4)_3$ species, that is, assuming $D=K_{ex_3,0}[ClO_4^-]^3/(1+\beta_1[L^-]+\beta_2[L^-]^2)$. However, as may be seen from Fig. 3, the data experimentally observed are higher than these except in the very low ligand-concentration region. This is probably due to the extraction of halide complexes as ion-pairs, as was pointed out above. The solid curves in Fig. 4 are the curves calculated by using the constants listed in Table 1.

It was observed that the extraction from a solution containing 4.0M perchlorate ions ($[H^+]=1.0$M) or one containing 3.0M perchlorate and 1.0M bromide ions ($[H^+]=1.0$M) is proportional to the 1.5th order of the TOPO concentration in the 2×10^{-3}M to 3×10^{-2}M range. It was also found that the extraction from the 4.0M perchlorate ionic medium containing halide ions is practically independent of the hydrogen-ion concentration between 0.1M and 1.0M. Thus, the extracted species from these solutions should not contain protons. On the other hand, the extraction from 4.0M chloride or bromide solutions containing no perchlorate ions is dependent on the hydrogen-ion concentration, the distribution ratio when the hydrogen-ion concentration is 1.0M is about ten times larger than the distribution ratio when it is 0.1M; thus the iron(III) extracted from these solutions should, at least some part of it, contain protons.

In order to obtain further information, the extraction of hydrogen ions into the organic phase was determined.

Extraction of Acids into the Organic Phase. Table 2 gives the hydrogen-ion concentration determined by titration with barium hydroxide. It may be seen from Table 2(a) that the extraction of perchloric acid into hexane containing 0.03M TOPO is practically independent of the acid concentration, whereas that of hydrohalic acid increases as the acid concentration increases. It may be seen from Table 2(b) that the extraction of hydrogen ion from the aqueous phase containing perchlorate and halide ions is also independent of the composition of the aqueous phase. Its extraction in the absence of perchlorate ions is also dependent on the salt concentration. It was also found in the organic phase that precipitates of silver halide were always formed by the addition of a silver nitrate solution if no perchlorate was present in the aqueous phase, but no precipitate was formed if perchlorate ions were present in the aqueous phase together with the halide ions.

This fact indicates that all of the acid extracted from the aqueous halide solutions is perchloric acid as long as the solution contains perchlorate ions, and that the organic phase is saturated with perchloric acid by the following extraction:

$$H^+ + ClO_4^- + 2TOPO(org) \rightleftarrows (HClO_4)(TOPO)_2(org) \quad (15)$$

Since extraction from an aqueous phase containing no sodium salt gives the same results (Table 2(a)), the extraction of sodium perchlorate under these conditions is negligible.

TABLE 2. EXTRACTION OF ACIDS WITH 0.03M TOPO IN HEXANE

(a) Extraction from an aqueous phase containing only an acid and no sodium salt

$[HClO_4]$	$[H^+]_{org}$	$[HCl]$	$[H^+]_{org}$	$[HBr]$	$[H^+]_{org}$
1.0M	1.4×10^{-2}M	1.0M	3.1×10^{-4}M	1.0M	1.4×10^{-3}M
2.0	1.5×10^{-2}	2.0	1.3×10^{-3}	2.0	5.6×10^{-3}
3.0	1.6×10^{-2}	3.0	3.7×10^{-3}	3.0	1.1×10^{-2}
4.0	1.5×10^{-2}	4.0	8.9×10^{-3}	4.0	1.6×10^{-2}

(b) Extraction from an aqueous phase at $[H^+]=1.00$M containing various amounts of sodium salt

$[HClO_4]$	$[NaClO_4]$	$[NaCl]$	$[H^+]_{org}$	$[HClO_4]$	$[NaClO_4]$	$[NaBr]$	$[H^+]_{org}$
1.0M	3.0M	0.0M	1.5×10^{-2}M	1.0M	3.0M	0.0M	1.5×10^{-2}M
1.0	2.0	1.0	1.5×10^{-2}	1.0	2.0	1.0	1.6×10^{-2}
1.0	1.0	2.0	1.5×10^{-2}	1.0	1.0	2.0	1.6×10^{-2}
1.0	0.0	3.0	1.5×10^{-2}	1.0	0.0	3.0	1.5×10^{-2}
$[HCl]$	$[NaClO_4]$	$[NaCl]$	$[H^+]_{org}$	$[HBr]$	$[NaClO_4]$	$[NaBr]$	$[H^+]_{org}$
1.0M	—	0.0M	3.1×10^{-4}M	1.0M	—	0.0M	1.4×10^{-3}M
1.0	—	1.0	1.1×10^{-3}	1.0	—	1.0	3.6×10^{-3}
1.0	—	2.0	1.6×10^{-3}	1.0	—	2.0	6.0×10^{-3}
1.0	—	3.0	2.3×10^{-3}	1.0	—	3.0	9.9×10^{-3}

Discussion

There have been several reports on the stability constants for iron(III) complexes with chloride or bromide ions.[17] The values reported for the chloride complexes ($\beta_1=10^{0.5}$ to $10^{1.0}$, $K_2\simeq10^{0.0}$) and for the bromide complex ($\beta_1\simeq10^{0.0}$) nearly agree with the present results. The higher complex, FeL_3 or FeL_4^-, may be very unstable, and the stability constants may be negligible even when the halide concentration is high.

The role of perchlorate ions and perchloric acid in the TOPO extraction system is remarkable. In the absence of perchlorate ions, the FeL_3 and the $HFeL_4$ (or $NaFeL_4$) species are possibly extracted into the organic phase, but these extractions are not remarkable when the halide concentration is lower than 2M (*cf.* Fig. 2). In the perchlorate ionic medium, the distribution of iron(III) is practically constant over a wide range of ligand concentration due to the extraction of ion-pairs, Fe^{3+}, FeL^{2+}, and FeL_2^+, with perchlorate ions.

Perchlorate solutions have often been used in order to control the activity of solutes in the aqueous phase. When such an aqueous phase is equilibrated with an organic phase, and when some portion of the anions is extracted together with hydrogen ion into the organic phase, the effect of the extracted acid should also be taken into account, because the extraction of the iron(III) species with TOPO combined with perchloric acid can be different from that with TOPO combined with hydrochloric or hydrobromic acid. However, under the conditions employed in the present study, the organic phase at equilibrium with the aqueous phase always contains 0.015M perchloric acid, even when 75% of the perchlorate ions is replaced by halide ions (*cf.* Table 2(b) and the fact that no halide ions were detected in these organic phases). Thus, the organic phase can be regarded as constant, even when the ligand ions are added to the aqueous phase. On the other hand, the extraction of the acid from the aqueous phase containing no perchlorate changes very much as the hydrogen ion or the salt concentration increases. Such changes in the composition in the aqueous phase should change not only the activity coefficients of the solutes in the aqueous phase, but also those in the organic phase.

The determination of the chemical form of the extracted species from chloride or bromide solutions containing no perchlorate seems to be difficult for the above reasons. However, from the observation described, the extracted species are assumed to be FeL_3 and/or $HFeL_4$. The extraction of these iron(III) halides seems to compete with the extraction of perchloric acid. Since the extraction of perchloric acid is effective, the addition of a small amount of perchlorate into the aqueous phase turns all the TOPO into the $(HClO_4)(TOPO)_2$ form. It is likely that the extraction of the FeL_3 and/or $HFeL_4$ species with this $(HClO_4)(TOPO)_2$ is much poorer than with free TOPO. This explains why the replacement of a small fraction of halide ions in the 4M halide solution by perchlorate ions causes a drastic decrease in the extraction of iron(III) (in the highest ligand-concentration range), as may be seen from Fig. 3.

The extraction of perchloric acid with TOPO in carbon tetrachloride was reported by Conocchioli, Tocher, and Diamond.[18] They described that the predominant species in the organic phase is the ion-pair $H_3O^+3TOPO\cdot ClO_4^-$ when the acid concentration is low enough, but for high concentrations of acid, the predominant species is $H^+TOPO\cdot ClO_4^-$. This does not agree with the present observation, which was made by using hexane as the diluent.

18) T. J. Conocchioli, M. I. Tocher, and R. M. Diamond, *J. Phys. Chem.*, **69**, 1106 (1965).

The Solvent Extraction of Zinc(II) in Sodium Perchlorate-halide Solutions with Trioctylphosphine Oxide

Hiromitsu MORIYA and Tatsuya SEKINE

Department of Chemistry, Science University of Tokyo, Kagurazaka, Shinjuku-ku, Tokyo

(Received September 28, 1971)

The solvent extraction of zinc(II) in 1M sodium perchlorate ionic media containing chloride, bromide, or iodide ions at 25°C was determined as a function of the halide-ion (X^-) concentration by using the zinc-65 tracer. From the extraction data with isopropyltropolone (IPT) in chloroform, the formation of the ZnX^+ complex was observed, but the stability constants of these complexes were not large ($ZnCl^+$: β_1 is $10^{0.00}$, $ZnBr^+$: β_1 is less than $10^{-0.5}$ and the formation of ZnI^+ is negligible), and the higher complexes were negligible in all cases. The extraction of zinc(II) from these media with methylisobutylketone (MIBK) was not effective, although the extracted species could be identified as ZnX_2. The extraction with trioctylphosphine oxide (TOPO) in hexane, on the other hand, was much better than that with MIBK. From the distribution ratio determined as a function of the halide and TOPO concentrations, the extracted species were concluded to be $Zn(ClO_4)_2(TOPO)_4$, $ZnX(ClO_4)(TOPO)_3$, and $ZnX_2(TOPO)_2$. The extraction constants for these species were determined by a graphic analysis of the data, and it was concluded that the extractabilities are larger in the order: iodide>bromide>chloride. From these data, it is clear that, if a suitable and effective neutral extractant is employed, the extractions of the above complexes are possible, even from aqueous solutions in which practically no complex is formed.

In a previous paper,[1] the present authors studied the solvent extraction of zinc(II) in 1M sodium perchlorate media containing various amounts of thiocyanate ions with trioctylphosphine oxide (TOPO) in hexane or methylisobutylketone (MIBK). They have reported, on the basis of these results, that zinc(II) in the aqueous phase forms the first, the second, and the third thiocyanate complexes, and that only the second one was extractable with TOPO in hexane, whereas both the second and the third complexes were extracted with MIBK.

After the above had been concluded, the authors desired to know further about the extraction of zinc(II) with the same extractants from aqueous solutions containing halide ions, which often form complexes somewhat similar to thiocyanate ions. The present paper will describe measurements of the stabilities and extractabilities of zinc(II) halide complexes from this standpoint. The results will be analyzed statistically, and some discussion will be made of the extraction of zinc(II) complexes, which are less stable in aqueous solutions than in organic solutions.

Experimental

The experiments were carried out in the same way described in the previous paper.[1] Zinc-65 was used for the determination of the distribution ratio of zinc(II). The organic solutions of the extractants and the aqueous solutions of the sodium salt were prepared in the manner described in the previous paper except that sodium chloride, bromide, or iodide solutions were prepared by dissolving an analytical-grade reagent and were added to the aqueous phase instead of sodium thiocyanate, as in the previous work. The concentrations of these ligand solutions were determined by gravimetry. The initial concentration of zinc(II) in the aqueous phase was 1×10^{-6}M, and the hydrogen-ion concentration at equilibrium was 10^{-4} to 10^{-5}M.

Statistical

As was also described,[1] the stability constants of zinc(II) complexes with an anionic ligand, X^-, in the aqueous phase can be determined from the decrease in the extraction of zinc(II) with a chelating extractant, HA, if the concentration of the extractant is kept constant:

$$D[H^+]^2/K = (1+\beta_1[X^-]+\beta_2[X^-]^2+\cdots) \quad (1)$$

where K is equal to $D_0[H^+]^2$ (D_0 is the distribution ratio in the absence of the ligand anions in the aqueous phase).

When the uncharged zinc(II) complex, ZnX_2, is extracted into the organic phase with e molecules of an organophilic extractant, E, the extraction equilibrium can be described as;

$$Zn^{2+} + 2X^- + eE(org) \rightleftarrows ZnX_2E_e(org)$$

$$K_{ex2,e} = \frac{[ZnX_2E_e]_{org}}{[Zn^{2+}][X^-]^2[E]^e_{org}} \quad (2)$$

However, if the concentration of the extractant, $[E]_{org}$, is kept constant over a series of experiments, this term can be eliminated, then;

$$K_{ex2} = \frac{[ZnX_2]_{org}}{[Zn^{2+}][X^-]^2} = K_{ex2,0} + K_{ex2,1}[E]_{org} + \cdots + K_{ex2,e}[E]^e_{org} \quad (3)$$

Furthermore, when zinc(II) species combining with perchlorate ions are extracted, the equilibrium can be described in the same manner as in Eqs. (2) and (3);

$$Zn^{2+} + X^- + ClO_4^- + eE(org) \rightleftarrows ZnX(ClO_4)E_e(org)$$

$$K_{ex1,e} = \frac{[ZnX(ClO_4)E_e]_{org}}{[Zn^{2+}][X^-][ClO_4^-][E]^e_{org}} \quad (4)$$

$$K_{ex1} = \frac{[ZnX(ClO_4)]_{org}}{[Zn^{2+}][X^-][ClO_4^-]} \quad (5)$$

$$Zn^{2+} + 2ClO_4^- + eE(org) \rightleftarrows Zn(ClO_4)_2E_e(org)$$

$$K_{ex0,e} = \frac{[Zn(ClO_4)_2E_e]_{org}}{[Zn^{2+}][ClO_4^-]^2[E]^e_{org}} \quad (6)$$

$$K_{ex0} = \frac{[Zn(ClO_4)_2]_{org}}{[Zn^{2+}][ClO_4^-]} \quad (7)$$

1) H. Moriya and T. Sekine, This Bulletin, 44, 3347 (1971).

It should be possible to evolve a general expression for the distribution ratios in such systems. However, in this study, the following equations are introduced, assuming that each zinc(II) species in the organic phase forms only one kind of solvate with the extractant and that it can be described as $Zn(ClO_4)_2E_{e0}$, $ZnX(ClO_4)E_{e1}$, or ZnX_2E_{e2}. The distribution ratio can then be described as;

$$D = \frac{[Zn(ClO_4)_2E_{e0}]_{org} + [ZnX(ClO_4)E_{e1}]_{org} + [ZnX_2E_{e2}]_{org}}{[Zn^{2+}] + [ZnX^+] + \cdots} \quad (8)$$

$$= \frac{K_{ex0,e0}[ClO_4^-][E]_{org}^{e0} + K_{ex1,e1}[X^-][ClO_4^-][E]_{org}^{e1} + K_{ex2,e2}[X^-]^2[E]_{org}^{e2}}{1 + \sum\beta_n[X^-]^n} \quad (9)$$

$$= \frac{K_{ex0}[ClO_4^-]^2 + K_{ex1}[X^-][ClO_4^-] + K_{ex2}[X^-]^2}{1 + \sum\beta_n[X^-]^n} \quad (10)$$

When a series of extractions are carried out at a certain concentration of the extractant, it is clear from Eq. (10) that;

$$Y = \left(\frac{D(1+\sum\beta_1[X^-]+\cdots)}{[ClO_4^-]^2} - K_{ex0}\right) \times \frac{[ClO_4^-]}{[X^-]}$$

$$= K_{ex1} + K_{ex2}\frac{[X^-]}{[ClO_4^-]} \quad (11)$$

The extraction constant, K_{ex0} or $K_{ex0,e0}$, can be determined from the extraction data in the absence of the ligand, and the other constants in Eq. (11) can be determined from the log$Y$ *vs.* log$[X^-]/[ClO_4^-]$ plot, by a curve-fitting method with the following standard curve, as has been described;[2-4]

$$Y = \log(1+v);\ X = \log v \quad (12)$$

When the extraction constants, K_{ex0}, K_{ex1}, and K_{ex2}, are determined at various concentrations of the extractant, the solvation number, $e0$, $e1$, and $e2$, can be determined from the slope of the log K_{exe} *vs.* log$[E]_{org}$ plot, because, for example, as the above assumption, Eq. (3) can be rewritten as;

$$\log K_{ex2} = \log K_{ex2,e} + e \log [E]_{org} \quad (13)$$

and K_{exe} can be obtained by a calculation based on Eq. (13).

Results

The results were reproducible, and the recovery of the zinc(II) tracer from the two phases was quantitative within the limit of experimental accuracy.

Extraction with IPT. As has been described,[1] the extraction of zinc(II) in 1M sodium perchlorate with IPT is proportional to the square of the hydrogen-ion concentration, and the value of K in Eq. (1) is $10^{-8.38}$ when the IPT concentration is 0.1M in chloroform. When the perchlorate ions in the aqueous phase were replaced with chloride ions, a decrease in the extraction of zinc(II) was observed. On the other hand, when they were replaced with bromide ions, the decrease was much smaller, and with iodide ions, the decrease was practically negligible in the ligand concentration range below 0.5M. The results in the chloride and the bromide systems are given in Fig. 1. From these

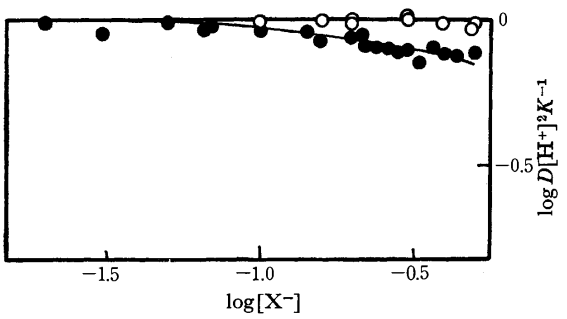

Fig. 1. Decrease in the IPT extraction of Zn(II) as a function of the ligand concentration.
Org. phase. $CHCl_3$ containing 0.1M TPT
Aq. phase. 1M Na(X, ClO_4) ●: Cl^- ○: Br^-
The solid curve indicates (K is defined by Eq. (1)
log$D[H^+]^2K^{-1}$=log $(1+1.0\times[Cl^-])$

results, the stability constants were determined by the curve-fitting method and were found to be;

$ZnCl^+$: $\log\beta_1 = 0.00$

$ZnBr^+$: $\log\beta_1 < -0.5$

ZnI^+: very small

The higher complexes were concluded to be negligible.

Extraction with MIBK. The extraction of zinc(II) in 1M sodium perchlorate solutions containing no ligand or in 1M Na(Cl,ClO_4) with MIBK was found to be very low. The distribution ratio was, in both cases, less than 10^{-3}. The extraction of zinc(II) from 1M Na(Br,ClO_4) or in 1M Na(I,ClO_4) was also poor. The distribution ratio was $10^{-2.3}$ and $10^{-1.6}$ when the aqueous phase contained 0.5M bromide and 0.5M iodide ions, respectively, (and consequently, in both cases, 0.5M perchlorate was also present). The extraction was proportional to the square of the ligand concentration. The following extraction constants in Eq. (3) were determined from these results;

Extraction of $ZnCl_2$: $\log K_{ex2} < -2.5$

Extraction of $ZnBr_2$: $\log K_{ex2} = -1.7$

Extraction of ZnI_2: $\log K_{ex2} = -1.0$

Extraction with TOPO in Hexane. Zinc(II) in 1M sodium perchlorate containing no ligand is extractable with TOPO in hexane, and the extraction is proportional to the fourth power of the TOPO concentration, as is given in Table 1.

The extraction of zinc(II) from 1M Na(X,ClO_4) with TOPO in hexane was determined as a function of the ligand concentration at certain TOPO concentrations.

2) F. J. C. Rossotti and H. Rossotti, "The Determination of Stability Constants," Mcgraw-Hill (1961).
3) T. Sekine and M. Ono, This Bulletin, **38**, 2087 (1965).
4) T. Sekine, M. Sakairi, and Y. Hasegawa, *ibid.*, **39**, 2141 (1966).

Table 1. Extraction of zinc(II) in 1M $NaClO_4$ with TOPO in hexane (for K_{ex0} and $K_{ex0,4}$ see Eqs. 6,7)

$[TOPO]_{org}$	D	$\log K_{ex0}$	$\log K_{ex0,4}$
5×10^{-2}	1.36	0.17	5.37
5×10^{-2}	1.25	0.13	5.34
3×10^{-2}	2.22×10^{-1}	−0.62	5.47
3×10^{-2}	1.74×10^{-1}	−0.72	5.37
2.4×10^{-2}	7.60×10^{-2}	−1.08	5.40
2×10^{-2}	4.70×10^{-2}	−1.29	5.50
2×10^{-2}	4.18×10^{-2}	−1.34	5.45
1.98×10^{-2}	3.52×10^{-2}	−1.42	5.42
1×10^{-2}	2.42×10^{-2}	−2.58	5.42
		av.	5.42

The slopes of the curves obtained at the same ligand concentration are larger in this order; iodide>bromide>chloride. Figure 2 gives the extraction with 1×10^{-2}M TOPO as an example of these experiments.

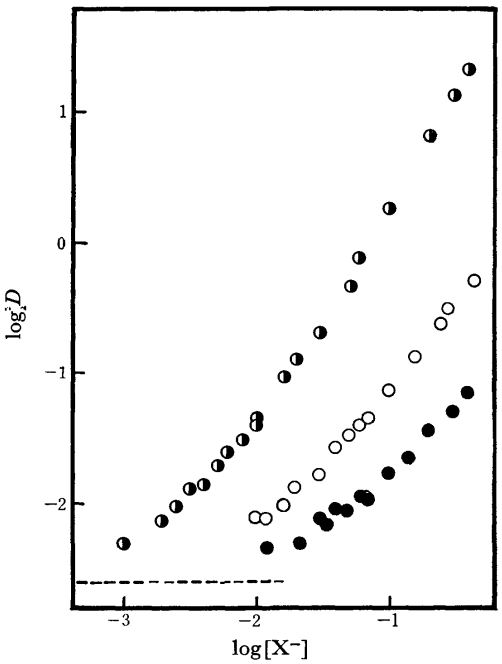

Fig. 2. Extraction of zinc(II) in 1M Na(X, ClO_4) with 1.0×10^{-2}M TOPO in hexane determined as a function of the ligand concentration.
(●: Cl^- ○: Br^- ◑: I^-)
The broken line indicates the extraction in the absence of halide ion ($\log D=-2.60$)

In order to determine the extraction constants in Eqs. (3), (5), and (7), the distribution ratio, the ligand concentration, the perchlorate concentration (that is, $1-[X^-]$M), and the K_{ex0} value in Table 1 were introduced into Eq. (11), and on the basis of the values thus calculated, the $\log Y$ *vs.* $\log[X^-]/[ClO_4^-]$ plot was made. It is given in Figs. 3, 4, or 5. The extraction constants were determined from these figures by the curve-fitting method. The solid curves in these figures show the best-fit curves. When a large part of the background perchlorate ions are replaced by the ligand anions, changes in the activity coefficients of solutes could occur. Thus, the extraction constants were determined by using the data in the ligand-concentration range below 0.5M. Thus, the fitted standard curves above this concentration, that is, at $\log[X^-]/[ClO_4^-]$ ratios higher than zero, are given by broken lines. The extraction constants thus obtained are given in Table 2. It was found that the slopes of the $\log k_{exe}$ *vs.* $\log[TOPO]_{org}$ plots were +4, +3, and +2 for K_{ex0}, K_{ex1}, and K_{ex2}, respectively, for all of the extractable complexes containing one of these three ligands. The extraction constants defined by Eqs. (2), (4), and (6) were determined from these data; they are also listed in Tables 1 and 2.

Discussion

The stability constants of zinc(II) halide complexes have been determined by many authors by using various

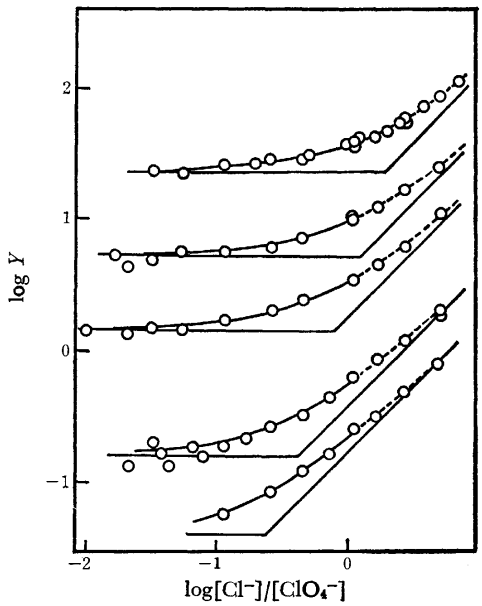

Fig. 3.

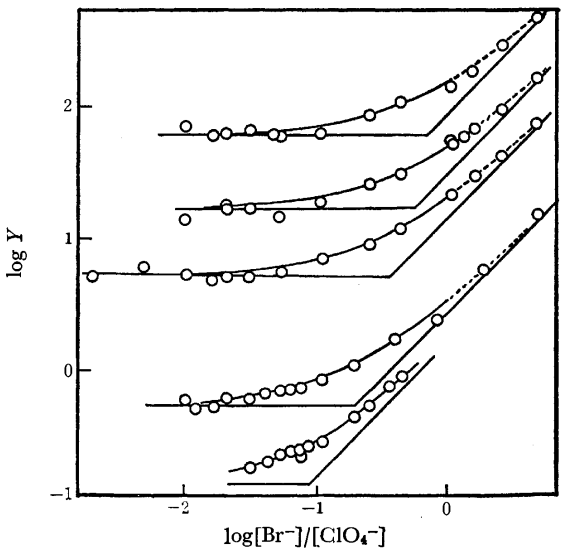

Fig. 4.

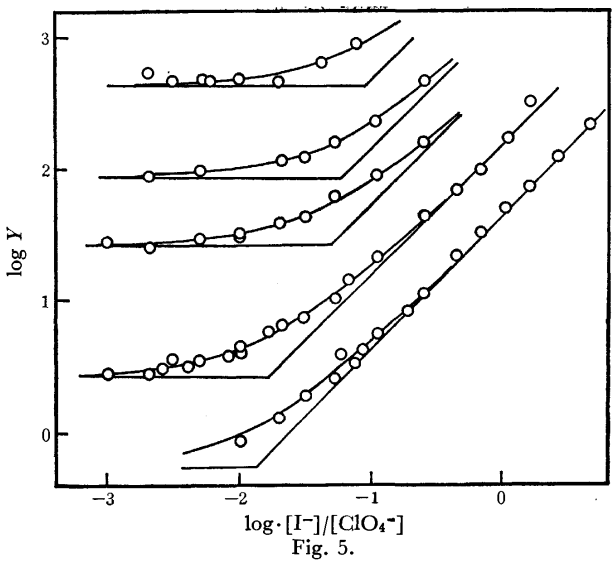

Fig. 5.

Fig. 3 to 5. Extraction of zinc(II) in 1M Na(X, ClO_4) with TOPO in hexane at various concentrations.
The data are plotted according to Eq. (11). The solid curves are $\log Y=\log(K_{ex1}+K_{ex2}[X^-]/[ClO_4])$ were K_{ex1} and K_{ex2} are taken from Table 2.
The aqueous phase contains chloride (Fig. 3), bromide (Fig. 4) or iodide ions (Fig. 5).
The concentration of TOPO in hexane is 5×10^{-2}M, 3×10^{-2}M, 2×10^{-2}M, 1×10^{-2}M or 6×10^{-3}M (top to bottom).

TABLE 2. EXTRACTION CONSTANTS OF ZINC(II) FROM 1M Na(X,ClO) WITH TOPO IN HEXANE
(cf. Eqs. (11), (13))

(a) Chloride system

$[TOPO]_{org}$	$\log K_{ex1}$	$\log K_{ex2}$	$\log K_{ex1,3}$	$\log K_{ex2,2}$
6×10^{-3}	−1.40	−0.78	5.27	3.66
1×10^{-2}	−0.80	−0.42	5.20	3.58
2×10^{-2}	0.16	0.26	5.26	3.66
3×10^{-2}	0.72	0.60	5.29	3.65
5×10^{-2}	1.36	1.07	5.26	3.67
		av.	5.26	3.64

(b) Bromide system

$[TOPO]_{org}$	$\log K_{ex1}$	$\log K_{ex2}$	$\log K_{ex1,3}$	$\log K_{ex2,2}$
6×10^{-3}	−0.87	0.16	5.80	4.60
1×10^{-2}	−0.27	0.41	5.73	4.41
2×10^{-2}	0.71	1.13	5.81	4.53
3×10^{-2}	1.22	1.46	5.77	4.51
5×10^{-2}	1.78	1.91	5.68	4.51
		av.	5.76	4.51

(c) Iodide system

$[TOPO]_{org}$	$\log K_{ex1}$	$\log K_{ex2}$	$\log K_{xe1,3}$	$\log K_{xe2,2}$
6×10^{-3}	−0.26	1.60	6.41	6.04
1×10^{-2}	0.43	2.19	6.43	6.19
2×10^{-2}	1.43	2.69	6.53	6.09
3×10^{-2}	1.94	3.12	6.51	6.17
5×10^{-2}	2.64	3.63	6.54	6.13
		av.	6.48	6.12

experiments methods.[5] The values determined in different ionic media are rather scattered. However, it is the general tendency for the stability constants for the first chloride complex at higher ionic concentrations to be around one ($\log\beta_1$ is −0.19 in 3M $NaClO_4$,[6] 0.30 in 4M $NaClO_4$,[7] and 0.2 in 1M $NaClO_4$[8]), and for those of the first bromide complex to be smaller than those of the chloride complex ($\log\beta_1$ is −0.60 in 3M $NaClO_4$[6]). These values practically agree with the present results. Some authors have also reported higher chloride or bromide complexes which are generally less stable than the first complex. However, the present authors could not determine any complexes higher than ZnX^+ from the results in Fig. 1. The stability constants determined by Morris and his coworkers in a 0.69M ionic medium by an ion-exchange method,[9] and in a 1M perchloric acid medium by a solvent extraction method with dinonylnaphthalene sulfonic acid[10] ($\log\beta_1=0.83$, $\log\beta_2=0.56$, $\log\beta_3=0.66$ for the chloride complexes and $\log\beta_1=0.10$, $\log\beta_2=-0.12$ for the bromide complexes), are obviously larger than the present results.

The extracted zinc(II) species with MIBK in the organic phase is assumed to be ZnX_2, and those with TOPO in hexane are assumed to be $Zn(ClO_4)_2$, $ZnX(ClO_4)$, and ZnX_2. Practically the only zinc(II) species in the aqueous phase, on the other hand, is the Zn^{2+} species in the bromide or iodide system, while the zinc(II) species are the Zn^{2+} and $ZnCl^+$ species in the chloride system. This indicates that the interaction between the metal ion and the ligand anions, or those between the metal ion and the perchlorate ions, are much stronger in the organic phase than in the aqueous phase, in which all the cations and anions are in a hydrated and uncomplexed form except for the $ZnCl^+$ species.

The dissociation of the extracted species in the organic phase should not be important in hexane, which is a low dielectric solvent, and it may be negligible in MIBK, which extracts only the $ZnBr_2$ or ZnI_2 complex.

No direct information is available on the nature of the bond in the extracted species from only the distribution data. However, the results in Table 2 indicate rather clearly the four coordination of znic(II) in the organic phase, although it is not possible to know if one or two molecules of water are coextracted with the metal species. Since the solvation numbers for the $Zn(ClO_4)_2$, $ZnX(ClO_4)$, and ZnX_2 species are four, three, and two, respectively, it can be assumed that the interaction between metal ion and the perchlorate ions are electrostatic and that those between the metal ion and the halide ions are coordinative. This also suggests that, among the four coordination positions of zinc(II), those unoccupied by the ligand anions are solvated with TOPO in the organic phase. The

5) A. E. Martell and L. G. Sillén "Stability Constants," The Chemical Society, London, spec, pub. **17**, (1964).

6) L. G. Sillén and B. Liljeguist, *Svensk, Kem. Tidsker.*, **56**, 85 (1944).

7) V. E. Mironov, F. Y. Kul'ba, and Y. E. Ivanov, *Russ. J. Inorg. Chem.*, **2**, 884 (1964).

8) S. Tribalat and C. Dutheil, *Bull. Soc. Chim. Fr.*, **1960**, 160.

9) E. L. Short and D. F. C. Morris, *J. Inorg. Nucl. Chem.*, **18**, 192 (1961).

10) D. F. C. Morris, D. T. Anderson, S. L. Waters, and G. L. Reed, *Electrochim. Acta*, **14**, 643 (1969).

extraction of the thiocyanate complex in the previous study was also estimated to be $Zn(SCN)_2(TOPO)_2$.[1]

Thus, it can reasonably be concluded that, for example, the extracted zinc(II) iodide is not an ion-pair of Zn^{2+} and the large iodide ions, but is a coordination complex which is stable only in these organic solvents and is completely dissociated in the aqueous phase.

In the previous paper,[1] the distribution ratio of zinc(II) between hexane containing TOPO and aqueous thiocyanate solutions was described in terms of the formation of zinc(II) complexes in the aqueous phase and the extraction of the uncharged complex species. This extraction was represented by the distribution constant;

$$K_{DM} = [ZnX_2]_{org,tot}/[ZnX_2] \quad (14)$$

As can be seen from Eqs. (3) and (14), the extraction constant of the second complex is the product of the stability constant of the ZnX_2 species in the aqueous phase and the distribution constant of this species, that is, $K_{ex_2}=K_{DM}\beta_2$. The extraction constant of the zinc-(II) thiocyanate complex with TOPO, $K_{ex_2,2}$ in Eq. (2), can be calculated from the constants in the previous paper[1] to be $10^{8.76}$. In the present study, however, the determination of the β_2 and K_{DM} was not possible. Thus, the extraction constant, K_{ex_2}, is used in order to describe the distribution equilibrium.

It is remarkable that the extractabilities of the complexes given in Figs. 2 to 5 or in Table 2 and in the previous paper[1] are larger in the order of; chloride$<$ bromide$<$iodide$<$thiocyanate. The most stable thiocyanate complex ($\log\beta_1=0.57$, $\log\beta_2=1.32$, and $\log\beta_3=1.18$) shows the highest extractability, but among the three halide complexes, the magnitude of the extractabilities shows an inverse order to the stability of the complexes in the aqueous phase.

Without any further information about these constants, it seems to be impossible to make a more detailed discussion of the extractability of these complexes. However, the fact that iodide, which forms the least stable complex (most probably the value of β_2 is also larger in the same order as β_1), is extracted better than bromide or chloride is probably due to the larger molecular size or the larger aquophobic tendency of the ZnI_2 species. The much higher extractability of the thiocyanate complex is probably mainly due to the greater stability of the $Zn(SCN)_2$ species than those of these bis-halide complexes.

It is remarkable that the extraction with the neutral extractant takes place even when no measurable amount of the extracted metal complexes are present in the aqueous phase. Such extractions, however, are very commonly observed when chelating extractants are employed for the metal extraction. Actually, in many metal extractions with chelating agents, HA, the distribution ratio can be denoted by $D=[MA_m]_{org}/[M^{m+}]$.

When the stability of the extractable species in the aqueous phase is low, the extraction of the species is obviously low. As has been pointed out,[11] the K_{DM} in Eq. (14) is the product of the distribution constant of the uncharged species between the diluent and the aqueous phase and the terms of the adduct formation constants between the metal complex and the extractant. From this point of view, the use of a strongly basic extractant such as TOPO is always suitable. However, the effect on its extractablilty of the stability and the molecular size of the complex is complicated. It seems to be common that the extractability of the larger halide complexes is higher than the smaller halide complexes if the stability constants of the former is larger. However, we have not found any general principle for the order of the extractability of halide complexes when the stabilities of the complexes of a smaller molecular size are higher than those of a larger molecular size.

Part of this study was carried out at the Laboratory of Nuclear and Analytical Chemistry, Institute of Physical and Chemical Research. The authors are grateful to Professor Nobufusa Saito, the head of the Laboratory.

11) T. Sekine and T. Ishii, This Bulletin, **43**, 2422 (1970).

Least-Squares Determination of Molecular Structures from Gaseous Electron-Diffraction Data. II. Polynomial Expression of Background

Shuzo Shibata
Department of Chemistry, Shizuoka University, Oya, Shizuoka, Japan
(Received October 6, 1971)

A new least-squares method has been devised for interpreting electron-diffraction data by comparison of an experimental background with a calculated background. The former is derived from an experimental total intensity by assuming a molecular model. The latter is approximated by a polynomial function. A computer program is written to refine structural parameters of a molecule so as to yield a smooth background. The characteristic of the present method is that it does not need any bias depending upon human judgement throughout an analysis. The distinctive features of the procedure are discussed, and the application of this method to structure determination of several molecules is also described.

Since a molecular intensity is not directly observable in electron-diffraction experiment, the procedure of drawing a background through an experimental intensity has been used as a bias to obtain a molecular intensity. In the past this background has often been frozen throughout an analysis; consequently, an uncertainty in the background probably leads to errors in final values of molecular parameters. Therefore, a method with no operator bias is desirable. In a previous paper[1] the criteria for smoothness of a background were presented and a least-squares method was given, that refines molecular parameters to make the background as smooth as possible. The purpose of this paper is to report another method which is based on quite the same viewpoint as the previous method. In the present method a background was expressed by a polynomial function, of which the parameters were allowed to vary freely in every iteration of the least-squares calculation. Bartell *et al.*[2] presented recently a least-squares analysis of total intensity, where a background was presented in terms of a polynomial with an exponential function. The present method does not essentially differ from it except that the best fit between experimental and calculated backgrounds, instead of that between total intensities, is sought by the refinements of molecular parameters and background parameters. Moreover, this method is mathematically rather simple and works without any initial guesses of background parameters.

Procedure

Criterion. An experimental total intensity is divided by an atomic background calculated by means of the scattering theory. Such leveling does not usually yield a horizontal background which cleaves molecular oscillations, but yields a considerably curved background because of imperfections of theory and experiment. However, it was found that this curved background can be approximated satisfactory in terms of a polynomial function, as described below.

A background I_b is provided from both a leveled experimental total intensity I_t and a molecular intensity M which is calculated for an assumed model by use of the relation (5) in Ref. 1. If a molecular model is strictly correct, the background should have no sudden fluctuation over the whole range of scattering angles. On the other hand, if the model is not correct, the background may have some fluctuations with a frequency similar to that of the molecular intensity. Thus, molecular parameters should be adjusted so as to make the background smooth. In the present method, the criterion for smoothness of a background is expressed as follows:

$$P_n = \sum_i w_i[I_b(q_i) - \sum_n a_n q_i^n]^2 = \text{minimum} \qquad (1)$$

Here w_i is a suitable weighting function, and $I_b = I_t/(1+RM)$, where R is an index of resolution. The equation means the minimization of the sum of the squares of the difference between an experimental and a calculated background over experimental points. Smoothness of the background is guaranteed by the degree of the polynomial. This method which we refer to as the *smooth-background method* differs from the usual method in that a background is never frozen and is refined with molecular parameters, and therefore it can determine values of molecular parameters without accompanying the uncertainties arising from a fixed background. The mathematical formulation of this method is omitted here since the details were described in other papers on the least-squares method.[3,4]

Sectional Smooth-background Method. The number of unknowns in a normal equation is generally equal to $(2m+1)+(n+1)$, if molecular parameters of interatomic distances and mean amplitudes with an index of resolution are varied independently to determine the structure of a molecule having m atomic pairs by use of a polynomial of nth degree. When a molecule consists of many atoms, the number of molecular parameters to be determined is large even if the symmetry of a molecule is taken into consideration. In the structure analysis of such a molecule, it seems difficult to solve the normal equation and get a good convergence of a standard deviation. This may be

1) S. Shibata and L. S. Bartell, *J. Mol. Structure*, **9**, 1 (1971).
2) L. S. Bartell, D. A. Kohl, B. L. Carroll, and R. M. Gavin, Jr., *J. Chem. Phys.*, **42**, 3079 (1965).
3) K. Hedberg and M. Iwasaki, *Acta Crystallogr.*, **17**, 529 (1964).
4) Y. Morino, K. Kuchitsu, and Y. Murata, *ibid.*, **18**, 549 (1965).

mainly attributable to the unreasonable expansion of parameters at the initial values and to the correlation among the parameters. To avoid such difficulty, a program has been written so as to first solve the normal equation for a part of molecular parameters with all of background parameters and other molecular parameters being fixed, and then to repeat this procedure alternatively with respect to another part of molecular parameters. After the initial values of the molecular parameters are improved sufficiently by the iteration of such block-diagram calculations, it is possible to obtain reasonable solutions of the complete normal equation with a good convergence. Correlation between molecular parameters should be taken into consideration with respect to the division of molecular parameters into groups. This sectional method can determine a structure of the molecule involving more than thirty interatomic distances as independent parameters, as described in the Application.

In contrast to the above analysis in which all interatomic distances are refined independently, a few parameters are allowed to vary with background parameters in consideration of geometric constrains. The geometrical consistency is maintained by the procedure in Ref. 5 at all stages through the analysis.

Fitting of Background. Some of the most probable backgrounds used for radial distributions are fitted in terms of various analytical functions, and a polynomial was found to be a good approximate function. In general, a background for a short camera range of $q \gtrsim 20$ is leveled fairly well; and it can be approximated satisfactory with the polynomials of low degree, *e.g.*, $n=5$, within an error of 0.3%. Significance test[6] shows that a fitting by lower degree polynomials may be rejected at 0.005 significance level. Nevertheless, a background for a long camera range of $q \gtrsim 10$ has often a hump in the range of small scattering angles and falls off rapidly inside this range; a fit of the jump by polynomials sometimes disturbs the remainder of the background curve. In such a case, however, polynomials of higher degree, *e.g.*, $n=7$, can fit the background within the above error. Moreover, the use of μ background cited in Ref. 1 is probably a better method because the fitting by the polynomial of higher degree causes a large correlation between molecular parameters, and the final parameters determined are usually accompanied by large errors.

Correlation Between Data Points. Correlation coefficients ρ_k between data points q_t and q_{t+k} are computed by the usual way with use of the residuals of backgrounds I_b with respect to data of various molecules, assuming that all the correlation coefficients for constant interval are equal and that all the standard deviations for data points are also equal. The result indicates that they can be expressed approximately by the function $\exp(-\gamma_n|k|\Delta q)$, where Δq is the interval between observations.[7] The correlation matrix can therefore be expressed as follows:

$$\begin{vmatrix} 1 & \rho_1 & \rho_2 & \rho_3 \cdots \\ \rho_1 & 1 & \rho_1 & \rho_2 \cdots \\ \rho_2 & \rho_1 & 1 & \rho_1 \cdots \\ \cdots & & & \rho_2 \quad \rho_1 \quad 1 \end{vmatrix} \tag{2}$$

where all off-diagonal elements are included. The values of the parameter γ_n is slightly dependent on the degree n of a polynomial used for a fit of the background. A higher degree polynomial gives a smaller correlation coefficient, but it can be estimated to be about 0.4 for ρ_1, *i.e.*, $\gamma \sim 1$ Å. However, if a background is manually drawn, a correlation between data points is often significantly increased to about 0.8 for ρ_1, *i.e.*, $\gamma \sim 0.2$ Å.

The inverse of the correlation matrix for which the $i\ j$ elements are $\exp(-\gamma_n|i-j|\Delta q)$ can be simply expressed as,

$$\begin{vmatrix} 1 & p & 0 & 0 & 0 \cdots 0 \\ p & 1 & p & 0 & 0 \cdots 0 \\ 0 & p & 1 & p & 0 \cdots 0 \\ 0 & 0 & 0 & 0 & 0 \cdots 0 \quad p \quad 1 \end{vmatrix} \tag{3}$$

where

$$\begin{aligned} p &= -\exp(-\gamma_n \Delta q)/[1+\exp(-2\gamma_n \Delta q)] \\ &= -\rho_1/(1+\rho_1^2) \end{aligned} \tag{4}$$

This form is identical with the relation (13) in Ref. 8, where the above form of the inverse matrix is assumed. The inverse matrix corresponds to the weight matrix w_{ij} in the following relation:

$$\begin{aligned} P_n' &= \sum_i \sum_j w_{ij}[I_b(q_i) - \sum_n a_n q_i^n][I_b(q_j) - \sum_n a_n q_j^n] \\ &= \text{minimum} \end{aligned} \tag{5}$$

where the diagonal weight matrix elements w_t in the Eq. (1) are taken to be unity for simplicity.

For example, in the data of water[9] for the camera distance of 11 cm, the values of correlation parameter γ_n are 0.90 and 1.05 Å for $n=5$ and 7, respectively. Table 1 lists the molecular parameters and their errors for water obtained by the smooth-background method. A consideration of the correlation between data points increased the errors by a factor of about 1.4, if γ_n of 0.9 Å, *i.e.*, p of -0.35 is used, as seen in the table.

Applications

An application of the smooth-background method for the determination of molecular structures is described, as examples, for carbon tetrachloride, water[9] and bis-(acetylacetonato)palladium(II).[10] The analysis of CCl_4 is illustrated in Fig. 1. The backgrounds were expressed by means of a polynomial of the 7th degree for both long and short camera distance data. The convergence of molecular parameters is shown in Fig. 2 for both data. The C–Cl and Cl–Cl distances were refined independently of each other.

In the analysis of H_2O by both long and short camera distance data, polynomials of various degree were used

5) K. Kuchitsu, T. Fukuyama, and Y. Morino, *J. Mol. Structure*, **1**, 463 (1967—1968).
6) W. C. Hamilton, *Acta Crystallogr.*, **18**, 502 (1965).
7) L. S. Bartell, *ibid.*, **A25**, Supplement, 76 (1969).
8) Y. Murata and Y. Morino, *ibid.*, **20**, 605 (1966).
9) S. Shibata and L. S. Bartell, *J. Chem. Phys.*, **42**, 1147 (1965).
10) S. Shibata, K. Ozaki, and K. Iijima, to be published.

to fit the background; however, it was found that the converged values of molecular parameters did not significantly depend upon the degree of the polynomial used and were in agreement with one another within

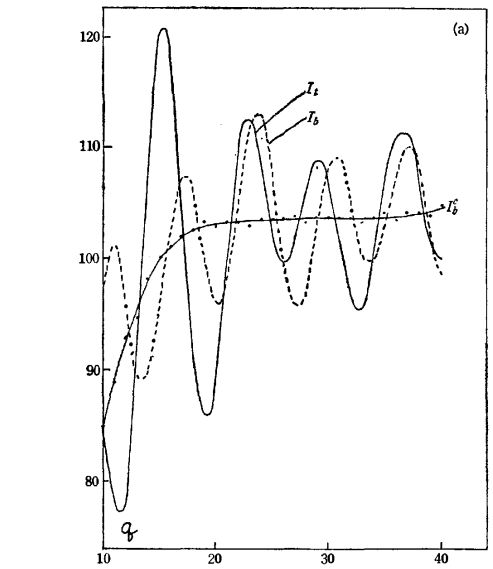

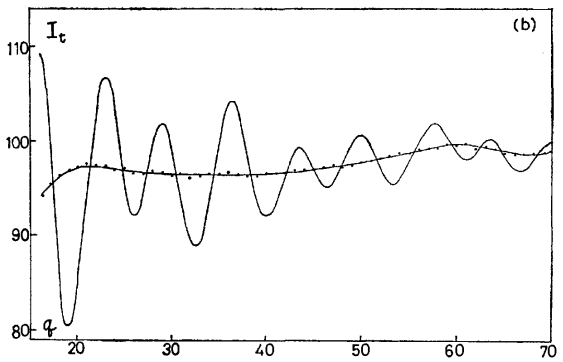

Fig. 1. Experimental leveled intensities I_t and calculated backgrounds I_b for CCl_4.

Figures a and b correspond to the long and short camera distance, respectively. The backgrounds I_b^s are obtained by the smooth-background method using the polynomial of the 7th degree. ------, I_b for input parametes; ····· I_b for output parameters from the 4th cycle.

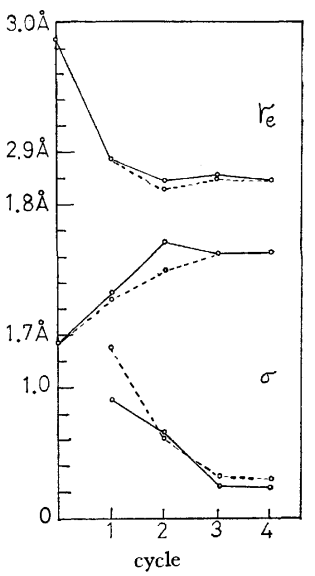

Fig. 2. Determination of the C–Cl and Cl–Cl distances o CCl_4 by the smooth-background method.
——, the short camera distance data; ------, the long camera distance data.

Table 1. Derived parameters for O–H in water from the smooth-background method.[a)]
(units; Å)

	P_5*(L)	P_7(L)	P_5(S)	P_7(S)	P_5'(S)	P_7'(S)
r_e	0.9609	0.9640	0.9605	0.9581	0.9605	0.9575
$r_g(1)$	0.9718	0.9765	0.9713	0.9704	0.9712	0.9702
$r_g(0)$	0.9765	0.9818	0.9760	0.9758	0.9758	0.9757
l_m	0.0672	0.0718	0.0669	0.0717	0.0666	0.0727
$\sigma(r)$	0.0004	0.0064	0.0004	0.0008	0.0005	0.0010
$\sigma(l)$	0.0008	0.0077	0.0006	0.0016	0.0009	0.0020

a) L and S mean long (21 cm) and short (11 cm) camera distance data, respectively. The ranges covered are seen in Fig. 3. The results for P_n were obtained by Eq. (1) by use of polynomials of the nth degree. For P_n* the method of μ background was used. The results for P_n' were obtained by Eq. (5) by use of −0.35 for p in Eq. (4). The Morse asymmetry constant of O–H was assumed to be 2.3 $Å^{-1}$, and w_t in Eq. (1) was taken to be unity. The errors σ do not include systematic errors.

Table 2. Correlation matrix of parameters for water[a)]

r_{O-H}	r_{H-H}	l_{O-H}	l_{H-H}	R	a_0	a_1	a_2	a_3	a_4	a_5
1.000	−0.047	−0.360	0.080	−0.269	0.485	−0.473	0.459	−0.442	0.425	−0.408
	1.000	0.291	0.014	0.445	0.313	−0.287	0.265	−0.247	0.233	−0.221
		1.000	0.279	0.885	0.046	−0.033	0.026	−0.025	0.027	−0.031
			1.000	0.304	0.119	−0.115	0.113	−0.111	0.111	−0.111
				1.000	0.057	−0.032	0.016	−0.005	0.000	−0.000
					1.000	−0.997	0.991	−0.982	0.971	−0.958
						1.000	−0.998	0.992	−0.984	0.974
							1.000	−0.998	0.993	−0.986
								1.000	−0.998	0.994
									1.000	−0.998
										1.000

a) Matrix elements are given by $\rho_{ij}=B^{-1}{}_{ij}/(B^{-1}{}_{ii}\,B^{-1}{}_{jj})^{1/2}$. This matrix corresponds to the analysis P_5(S) in Table 1. The notation in the above relation corresponds to that in reference 11.

11) O. Bastiansen, L. Hedberg, and K. Hedberg, *J. Chem. Phys.*, **27**, 1311 (1957).

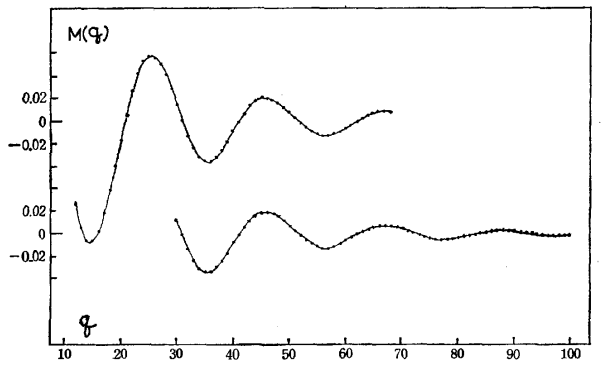

Fig. 3. Experimental and calculated molecular intesities M for H_2O.
The solid curves are the calculated molecular intensities obtained by the smooth-background method using the polynomials of the 5th degree. The upper curve corresponds to the long camera distance and the lower corresponds to the short camera distance. The dots are observations. Both curves correspond to P^*_5 (L) and P_5 (S) in Table 1, respectively.

the limits of errors. The derived parameters for O–H in H_2O are listed in Table 1, where the results obtained by use of the polynomials of 5th and 7th degrees are compared with each other. Table 2 shows the correlation matrix of parameters for water obtained from the analysis using the 5th degree polynomial as the background intensity. The use of higher degree polynomial resulted in larger correlation between molecular parameters, and consequently, increased errors in molecular parameters as seen in Table 1. This seems to be enhanced in the case of a long camera distance data, and therefore, the use of μ background is desirable, as shown in Table 1. Figure 3 shows the experimental and calculated molecular intensities.

As an example of the structure determination of a complex molecule, the structure analysis of Pd-$(C_5H_7O_2)_2$ is described. The three following calculations were compared with respect to the convergence of the standard deviation: 1) all of thirty-two interatomic distances were varied independently, 2) these distances were divided into four sets of eight distances and the least-squares calculation was performed successively by the use of the sectional method described above, 3) four interatomic distances and three bond angles were varied independently and other distances were changed according to the geometrical constraint remains. In these calculations it was assumed that

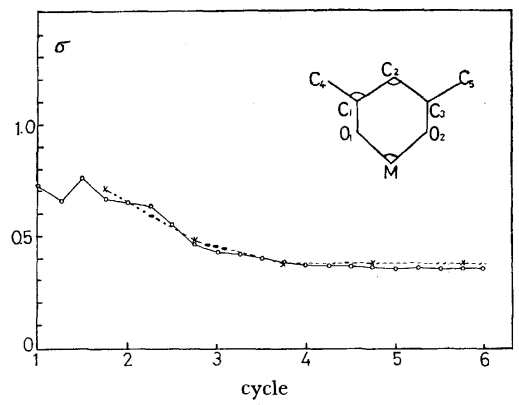

Fig. 4. The standard deviations at each cycle of the calculation for the analysis of $Pd(C_5H_7O_2)_2$.
——, case 2; -------, case 3 in the text. Independent parameters in the case 3 are as follows; interatomic distances of M-O_1, M-C_2, C_1-C_2, C_1-C_4 and bond angles of O_1MO_2, $C_1C_2C_3$, and $C_2C_1C_4$.

the molecule takes a planar form and the ligand of acetylacetone $C_5H_7O_2$ has the symmetry of C_{2v}. The first case could not give any convergence of the standard deviation. The second and third cases gave the good convergence given in Fig. 4; moreover, the computing time required for the second case was about twice for the third case. Generally, the present smooth-background method gave a relatively slow convergence of solutions in comparison with the previous method using the slope and curvature criteria.[1)]

Conclusion

The present method seems to be useful for the determination of interatomic distances and mean-amplitudes of vibrations because it is basically simple and straightforward. Electron-diffraction data are handled successively by a digital computer without manual processing of data. Numerical input data to the program routine are digital microphotometer readings. The present method does not need initial guess of background parameters, and thus it removes an operator bias from the analysis of molecular structure by the electron-diffraction method.

We are indebted to the Ministry of Education of Japan for a Scientific Research Grant supported this study. We are also indebted to Professor L.S. Bartell for his kind advice on this study.

Elimination Reactions of Ethylene Halohydrins on Solid Catalysts

Isao MOCHIDA, Yasuhide ANJU, Akio KATO, and Tetsuro SEIYAMA
Department of Applied Chemistry, Faculty of Engineering, Kyushu Universtiy, Fukuoka
(Received November 4, 1971)

Elimination reactions of ethylene chlorohydrin and ethylene bromohydrin were studied over solid acids, solid bases, and metals supported by silica gel at 300°C using a microcatalytic gas chromatographic technique in order to elucidate the relationship between the elimination selectivity and the nature of active sites. Acetaldehyde was exclusively formed on solid acids and MgO. However, ethylene oxide as well was formed on solid bases. The ratio seems to depend on the basic strength of the solid bases. On the metals, ethylene was formed in addition to acetaldehyde. The former was the principal product on Pd and Pt. From these results, it was concluded that acetaldehyde was formed on acidic sites by halide-ion abstraction; ethylene oxide, on basic sites by proton abstraction, and ethylene, on less polar sites of metals by halogen atom abstraction.

It has been reported in previous papers that the halogen anion and proton abstractions play important roles in the catalytic elimination of hydrogen halide from haloethanes on solid acids and bases respectively.[1] On the other hand, OH-group abstraction has been thought to be important in the dehydration of ethanol on solid acids.[2] The elimination reactions of halohydrins on solid acids and bases may be interesting because the roles of two functional groups, halogen and OH, can be investigated under the same conditions. In this elimination several kinds of reaction products can be expected. This selectivity should reflect the acid-base character of the catalysts.

On the other hand, olefins are formed from halohydrins by metals such as magnesium and zinc in an acidic medium.[3] This result means that the metal surface has another kind of active site for the reactant.[4]

In the present research, the eliminations of two halohydrins were observed on solid acids, solid bases, and metals supported by silica gel, using the microcatalytic gas-chromatographic technique, mainly at 300°C. The poisoning effect of *n*-butylamine was also examined. The mechanisms of the elimination and the function of the catalysts were deduced from the reactivities of the reagents and the activities and selectivities of the catalysts on the basis of linear-free-energy-relationships.[1]

Experimental

Reagents. The ethylene chlorohydrin and ethylene bromohydrin (G.R.) were obtained from the Tokyo Kasei Co. They were used without further purifucation.

Catalysts. The solid acids and bases used in this work were described in previous papers.[1,2] Their abbreviations are summarized in Table 1. The metal catalysts were obtained by impregnating silica gel (Wako) with 0.4 mg-atom/g of each metal salt (Cu, Ag, Co, Ni: nitrate, Au, Pd, Pt: chloride, Fe: hydroxide) and by then drying it at 120°C in the air. They were all reduced in the reactor at 300°C except for Fe, Co, and Ni (Fe, Co: 450°C, Ni: 400°C) by hydrogen gas before the reaction.

TABLE 1. CATALYSTS

No.	Symbol	Name	Remarks
1	A	alumina	calcined at 550°C
2	A–Na	sodium poisoned alumina	0.3 meq Na/g
3	MS	Molecular Sieve Y	proton type
4	AB	alumina boria	10% B_2O_3
5	SA	silica alumina	13% Al_2O_3
6	MgO	magnesium oxide	calcined at 600°C
7	CaO	calcium oxide	calcined at 900°C
8	SrO	strontium oxide	calcined at 850°C
9	Na–S	NaOH–SiO_2	0.3 meq Na/g
10	K–S	KOH–SiO_2	0.3 meq Na/g

Procedures. The reaction rates and selectivities were measured with the pulse technique with a hydrogen carrier in the temperature range from 200°C to 450°C. The hydrogenolysis of halohydrins on Pd, Pt, and Ni was observed, but it was small compared with the other eliminations. Polyethylene glycol (PEG 1000) was used in an analytical column (60°C, 2 m) to get the conversion data, and a 4-m portion of PEG 1000 was used at room temperature for the determination of the ethylene oxide/acetaldehyde ratio. The reaction rates (ml/g·min) were calculated by dividing the conversion with the contact time below its value of 20%. The details of the experiments were described in previous papers.[1,2]

Results

Elimination of Halohydrins on Solid Acids and Bases. Ethylene halohydrins may give vinyl halide upon dehydration; vinyl alcohol and its isomers, by dehydrohalogenation, and ethylene, by the use of dehypohaloic acid. Only acetaldehyde was formed from halohydrins on solid acids. Ethylene oxide and acetaldehyde were formed on all the solid bases except MgO. The formation of ethylene oxide has also been reported in elimination in an alkaline solution.[5]

1) The Reactivities of Ethylene Chlorohydrin and Ethylene Bromohydrin: The catalytic activities of solid acids and bases are shown in Fig. 1. The activities were cal-

1) a) I. Mochida, J. Take, Y. Saito, and Y. Yoneda, *J. Org. Chem.*, **32**, 2894 (1967); *ibid.*, **33**, 2161, 2163 (1968); I. Mochida, A. Kato, and T. Seiyama, *J. Catal.*, **18**, 33 (1970). b) I. Mochida, Y. Anju, H. Yamamoto, A. Kato, and T. Seiyama, This Bulletin, **44**, 3305 (1971).

2) I. Mochida, Y. Anju, A. Kato, and T. Seiyama, This Bulletin, **43**, 2245 (1970).

3) H. O. House and R. S. Ro, *J. Amer. Chem. Soc.*, **80**, 182 (1958).

4) I. Mochida, Y. Anju, H. Yamamoto, A. Kato, and T. Seiyama, This Bulletin, in press.

5) A. A. Frost and R. G. Person, "Kinetics and Mechanism" 2nd Edition, John Wiley and Sons, New York 1961, p. 288.

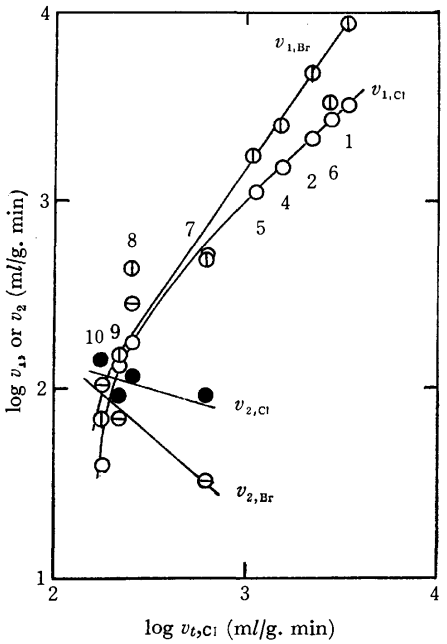

Fig. 1. Catalytic activities of solid acids and bases. (300°C)
The abscissa corresponds to the total elimination reactivities of ethylene chlorohydrin ($v_{t,Cl}$).
○; rates of acetaldehyde formation from ethylene chlorohydrin ($v_{1,Cl}$),
●; rates of ethylene oxide formation from ethylene chlorohydrin($v_{2,Cl}$),
⊕; rates of acetaldehyde formation from ethylene bromohydrin, ($v_{1,Br}$),
⊖; rates of ethylene oxide formation from ethylene bromohydrin. ($v_{2,Br}$).
Numbers refer to Table 1.

culated from the first pulse. The total elimination reactivities of ethylene chlorohydrin were taken in the abscissa, and the rates of acetaldehyde and ethylene-oxide formation from ethylene chlorohydrin and ethylene bromohydrin were taken in the ordinate. The rates of acetaldehyde formation from ethylene bromohydrin were larger than those from ethylene chlorohydrin throughout the solid acids and bases. In contrast, as to the rates of ethylene oxide formation, ethylene chlorohydrin was more reactive than ethylene bromohydrin except in the case of SrO.

The rate of acetaldehyde formation was larger on solid acids than on solid bases, except for the case of MgO. Among the so-called basic oxides, their activities for acetaldehyde formation increased with the decrease in the basicity (K_2O>Na_2O, and SrO> CaO>MgO), whereas the activity for ethylene-oxide formation was the reverse. The catalytic behavior of MgO was close to that of typical solid acids, as has also been observed in the dehydrohalogenation of 1,2-dibromoethane and isopropyl halides.[1b]

2) Poisoning Effect: The decrease in catalytic activities with regard to ethylene-oxide formation was very striking from pulse to pulse on solid bases, but not so with regard to acetaldehyde formation on either acidic or basic solids. In the former case, the activities were almost lost by the first pulse. This poisoning effect may be due to the adsorption of hydrogen halide, one of the elimination products, onto the basic site. The poisoning of catalysts with *n*-butylamine suppressed acetaldehyde formation very much on solid acids and bases, but it did not affect ethylene oxide formation at all. These poisoning effects, in accordance with the variation in activities shown in Fig. 1, indicate that acidic sites and basic sites play an important role in the acetaldehyde and ethylene-oxide formations respectively.

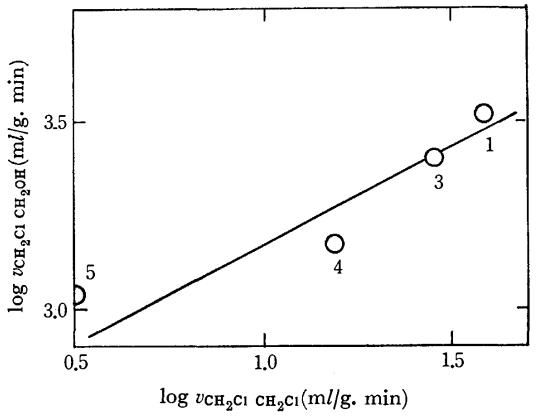

Fig. 2. Correlation between the rates of dehydrochlorination of 1,2-dichloroethane ($v_{CH_2Cl\ CH_2Cl}$) and ethylene chlorohydrin ($CH_2Cl\ CH_2OH$). The former are taken in the abscissa and the latter in the ordinate.
Numbers refer to Table 1.

3) A Comparison between the Dehydrochlorination Reactivities of 1,2-Dichloroethane and Ethylene Chlorohydrin: Between the reactivities of chlorohydrin and 1,2-dichloroethane on some solid acids, a certain correlation can be observed, as is shown in Fig. 2; this suggests a similarity in mechanism for the two dehydrochlorinations. The reactivity of ethylene chlorohydrin was larger than that of 1,2-dichloroethane by two orders of magnitude. Ethylene chlorohydrin was more reactive than 1,2-dichloroethane on solid bases, too. However, no correlation between the two reactivities could be found on solid bases.

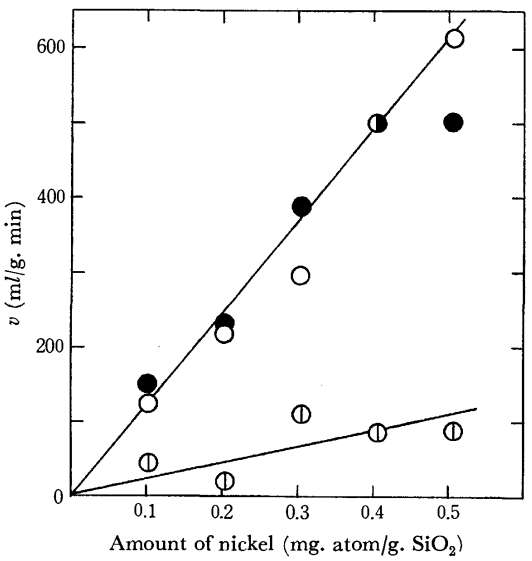

Fig. 3. The effect of the amount of nickel on catalytic activities for ethylene chlorohydrin at 300°C.
○; the rates of ethylene formation.
●; the rates of acetaldehyde formation.
⊕; the rates of ethanol formation.

Elimination of Halohydrins on Metals Supported by Silica Gel. *1) Catalytic Activities and Selectivities of Metals*: Acetaldehyde and ethylene were formed from halohydrins on metals supported by silica gel. The catalytic activity was increased, but the selectivity did not change, with the amount of metal mounted, as is shown in Fig. 3. Furthermore, the selectivities of non-supported metals (Cu, Ni, Pd) were equal to those of metals supported by silica gel, although the activity per unit weight of the supported metals was much larger than that of unsupported metals. These facts indicate that silica gel does not affect the catalytic selectivity. The catalytic activities of supported metals are shown in Fig. 4. Ethylene bromohydrin was more reactive for both product formations than ethylene chlorohydrin, as was observed for the acetaldehyde formation on solid acids. The selectivities (rate of ethylene formation/total rate of elimination) are shown as a function of the standard heats of the formation of metal chloride per chlorine atom (ΔH°_f)[6] in Fig. 5. There are volcano correlations, with the highest selectivity at Pt. Such a volcano relation has also been observed in the dechlorination of 1,2-dichloropropane.[4] Generally speaking, the more reactive bromohydrin was less selective for ethylene formation than was chlorohydrin.

The apparent activation energies for the acetaldehyde formation are larger than those for the ethylene formation, as is shown in Table 2.

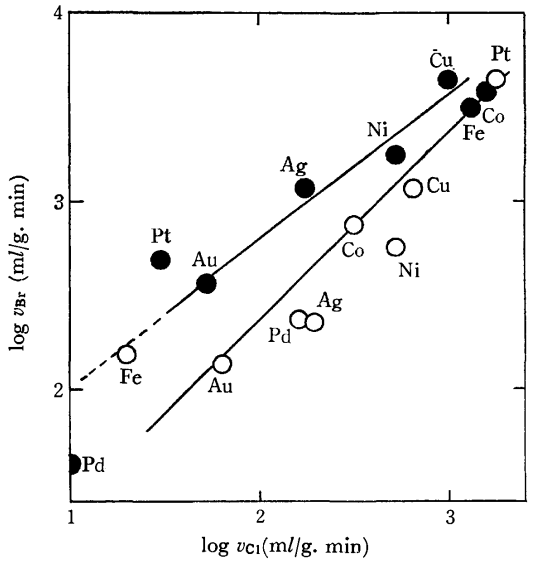

Fig. 4. Catalytic activities of metals at 300°C.
○; the rates of ethylene formation.
●; the rates of acetaldehyde formation.
log v_{Cl} (abscissa) is regarding ethylene chlorohydrin and log v_{Br} (ordinate) regarding ethylene bromohydrin.

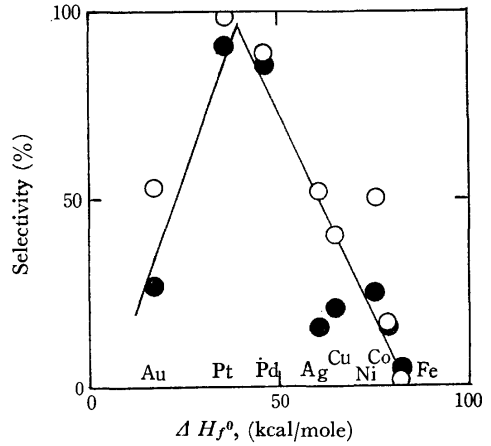

Fig. 5. The selectivities for ethylene formation of metals (rate of ethylene formation/total rate of elimination) at 300°C as a function of standard heats of formation of metal chloride per chlorine atom (ΔH_f°).
○; for ethylene chlorohydrin.
●; for ethylene bromohydrin.

Table 2. Apparent activation energies of HCl or HClO elimination from ethylene chlorohydrin on metals

Catalysts	Acetaldehyde (–HCl)	Ethylene (–HClO)
Cu–SiO_2	15 kcal/mol	4 kcal/mol
Ag–SiO_2	12	9
Au–SiO_2	21	15
Fe–SiO_2	14	a)
Co–SiO_2	12	9
Ni–SiO_2	14	14
Pd–SiO_2	a)	10.5
Pt–SiO_2	a)	10

a) Activity was too small to be measured.

2) The Poisoning Effect: The poisoning effect with *n*-butylamine was severe for the acetaldehyde formation, but was negligible for the ethylene formation, among all the metal catalysts examined.

The catalytic activities of all the metals except Pd and Pt for acetaldehyde and ethylene formations decreased to a half of the original activity upon a pulse injection. Pd and Pt showed no activity change from pulse to pulse.

3) A Comparison between the Dechlorination of 1,2-dichloroethane and Dehypochloric Acid of Ethylene Chloro-

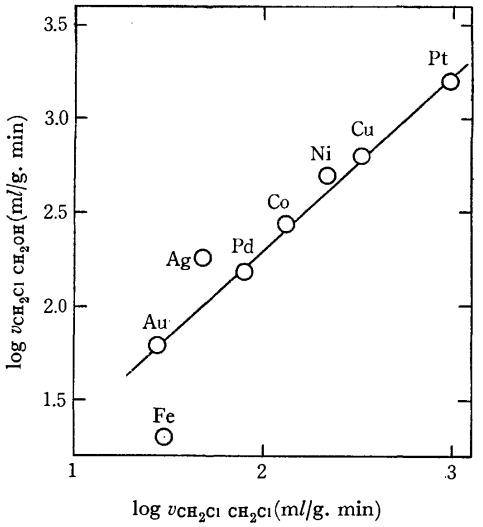

Fig. 6. Correlation between the rates of dechlorination of 1,2-dichloroethane ($v_{CH_2Cl\ CH_2Cl}$) and those of dehypochloric acid of ethylene chlorohydrin ($v_{CH_2Cl\ CH_2OH}$) at 300°C.
The former are taken in the abscissa and the latter in the ordinate.

6) "Kagaku Binran", Maruzen 1966, p. 817.

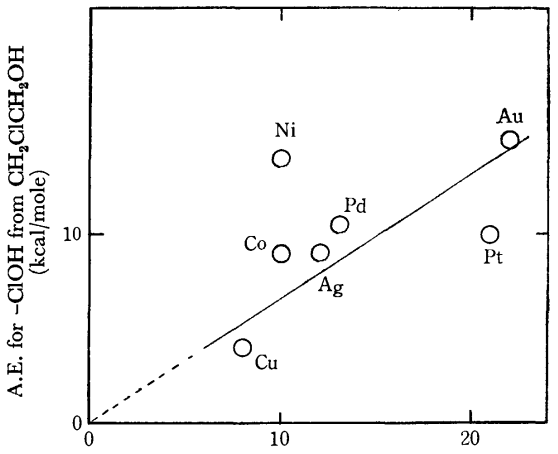

Fig. 7. Correlation of apparent activation energies between dechlorination of 1,2-dichloroethane and dehypochloric acid of ethylene chlorohydrin.

hydrin on Metals: A good correlation was recognized between the dechlorination-reactivities of 1,2-dichloroethane[4] and the dehypochloric-acid-reactivities of ethylene chlorohydrin, as is shown in Fig. 6. Furthermore, the activation energies of the two elimination reactions on the same metal were also correlated with each other, as is shown in Fig. 7. Both correlations were observed between the corresponding reactions of 1,2-dibromoethane and ethylene bromohydrin. Such correlations indicate that the ethylene formation from halohydrins proceeds through a mechanism similar to that of the dehalogenation of haloethanes.

Discussion

Acetaldehyde Formation. Acetaldehyde is formed on acidic sites, as has been described above. The following facts suggest that the halogen-abstraction step is important. 1) There is a good correlation between the reactivities of 1,2-dichloroethane and ethylene chlorohydrin on solid acids, as is shown in Fig. 2. 2) Bromohydrin, the C–Br bond of which is weaker than the C–Cl bond of ethylene chlorohydrin, was more reactive than chlorohydrin. From these findings, it seems that acetaldehyde formation may proceed through a mechanism by which the halogen is eliminated as an anion in the first stage, and then the β proton may leave through an $\alpha\beta$ elimination mechanism to give vinyl alcohol, which isomerizes immediately to acetaldehyde:

$$CH_2OHCH_2X \xrightarrow{-X^-} CH_2OHCH_2^+ \xrightarrow{-H^+} CHOH{=}CH_2 \longrightarrow CH_3CHO$$

As alumina had a higher catalytic activity than silica-alumina, it is difficult to assume only protonic acid as the active site for the acetaldehyde formation. Such a situation was also observed in the dehydration of ethanol.[2] The higher reactivity of halohydrin in comparison with that of 1,2-dichloroethane may be due to the interaction between the hydroxyl group of halohydrin with acid sites in the same manner as in the dehydration of ethanol, in addition to the difference in enthalpy changes between the two reactions.[7]

The linear correlation observed through solid acids and bases (Fig. 1) and the similar poisoning effect may indicate an analogous mechanism for the acetaldehyde formation on solid bases.

Similar poisoning effects of *n*-butylamine and the higher reactivity of ethylene bromohydrin than ethylene chlorohydrin were also observed for the reactions on metal catalysts as well as on solid acids, indicating a similar mechanism for acetaldehyde formation on metals. The acidic nature of the metal atom may be due to its vacant *d*- or *f*-orbitals.

Ethylene Oxide Formation. Ethylene oxide was formed on the catalysts which were located on the left side of Fig. 1, that is, the solid bases. The poisoning effect of HX was remarkable for the ethylene-oxide formation. Therefore, the active site for the ethylene-oxide formation may be basic. Basic sites may eliminate the proton from the hydroxyl group at first:

$$CH_2XCH_2OH \xrightarrow{-H^+} CH_2XCH_2O^- \xrightarrow{-X^-} CH_2{-}CH_2 \quad (O)$$

This scheme is the same one as that suggested for the reaction in basic media.[8] According to this scheme, the reactivity may depend on the acidity of the hydrogen atom to be eliminated. Thus, the reactivity difference between chloro- and bromohydrins can be understood. The higher acidity of the hydrogen in the OH group than in the CH group may also explain the higher reactivity of halohydrin in comparison with haloethanes on solid bases.

Ethylene Formation on Metals. The larger reactivity of bromohydrin than that of chlorohydrin suggested the importance of the halogen-abstraction step for the ethylene formation. The correlations of the activities and activation energies of metals for the ethylene formation with those for the dechlorination of 1,2-dichloroethane in Figs. 6 and 7 indicate the similarity of the rate-determining steps in these two reactions. The poisoning with *n*-butylamine does not affect the ethylene formation, in contrast to the acetaldehyde formation, which is considered to proceed through the ionic mechanism on metals described above. Therefore, the following mechanism is considered to hold for the ethylene formation on metals:

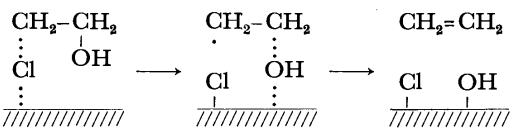

It is interesting that the less electronegative and higher back-donating metals, such as Pt and Pd, show a high selectivity for ethylene formation.

7) $\Delta Hf^\circ_{(298)} = -39.86$, -70.3, 8.4, and -31.0 (kcal/mol) for acetaldehyde, ethylene chlorohydrin, vinyl chloride, and 1,2-dichloroethane respectively. (D. R. Stull, E. F. Westrum, and G. C. Sinke, "The Chemical Thermodynamics of Organic Compounds," Wiley, New York 1968, p. 641.

8) S. Winstein and H. J. Lucas, *J. Amer. Chem. Soc.*, **61**, 1576 (1939); D. Porret, *Helv. Chim. Acta*, **30**, 701 (1947).

Intersystem Crossing Quantum Yields of Phthalazine and Pyridazine[1]

Takeshi TAKEMURA, Kohzaburo YAMAMOTO, Iwao YAMAZAKI, and Hiroaki BABA
Division of Chemistry, Research Institute of Applied Electricity, Hokkaido University, Sapporo
(Received November 15, 1971)

The quantum yields of $S_1 \rightarrow T_1$ intersystem crossing have been determined for phthalazine and pyridazine in EPA at 77°K by using the technique of T–T energy transfer. Phthalazine and pyridazine were used as the energy donor, and naphthalene-h_8 and naphthalene-d_8 as energy acceptor. The intersystem crossing quantum yields were found to be 0.49 for phthalazine and 0.24 for pyridazine. These values lead to the conclusion that the weakness or lack of phosphorescence in the compounds is due to an anomalously high rate of the radiationless transition from their phosphorescent triplet state as compared with the rate of the corresponding radiative transition.

The radiative and radiationless processes in nitrogen heterocyclic compounds have been studied extensively.[2-11] Although most of these compounds show strong phosphorescence, *ortho*-diazines such as pyridazine, phthalazine, and 9,10-diazaphenanthrene show either only very weak phosphorescence or none at all. Several attempts have been made to explain this phenomenon. El-Sayed proposed that the rate of $S_1 \rightarrow T_1$ intersystem crossing is low in pyridazine because the $^3(\pi,\pi^*)$ state lies above the lowest $^1(n,\pi^*)$ state and the only path for the intersystem crossing is $^1(n,\pi^*) \rightarrow {}^3(n,\pi^*)$, which should be slower than $^1(n,\pi^*) \rightarrow {}^3(\pi,\pi^*)$ by a factor of 10^3.[6] Cohen and Goodman attributed the lack of phosphorescence in pyridazine to an efficient intersystem crossing process from the phosphorescent triplet state to a low-lying excited singlet state.[7] Hochstrasser and Marzzacco suggested that the lack of phosphorescence is due to the fact that the $T_1 \rightarrow S_0$ radiationless process is much faster than the radiative one.[8] Thus, despite widespread interest the problem remains unsettled, little quantitative information being available concerning the radiationless transition.

We found recently that phthalazine gives no emission in hydrocarbon solvents, but it phosphoresces with a moderate intensity in polar solvents such as EPA.[2,3] It was suggested in addition that phthalazine has a high intersystem crossing quantum yield.[2]

With a view to elucidating the mechanism of excitation-energy relaxation in *ortho*-diazines, we measured quantitatively the intersystem crossing quantum yields of phthalazine and pyridazine in EPA rigid glass solution at 77°K, using the technique of T–T energy transfer.[12] Phthalazine and pyridazine were used as energy donor, and naphthalene-h_8 and naphthalene-d_8 as energy acceptor.

Experimental

Phthalazine (Aldrich Chemical Co.) was recrystallized from diethyl ether and then sublimed under reduced pressure. Pyridazine was purified by vacuum distillation. Naphthalene-h_8 and -d_8 (the latter was obtained from Merck, Sharp & Dohme of Canada) were purified by recrystallization or vacuum sublimation. Diethyl ether was carefully purified after the method described by Kanda and Shimada.[13] Isopentane was passed through a silica-gel column. Spectrograde ethyl alcohol was used without further purification. EPA (5:5:2 parts by volume of diethyl ether, isopentane and ethyl alcohol) was used as solvent. All the sample solutions were degassed by repeated freeze-thaw cycles.

Phosphorescence spectra were measured at 77°K with a Hitachi MPF-2A fluorescence spectrophotometer, equipped with a phosphoroscope.

The phosphorescence spectra were corrected for the spectral sensitivity of the system of monochromator and photomultiplier, using quinine sulfate in 1 N sulfuric acid and β-naphthol in acetic acid-sodium acetate buffer solution as standards.[14] The phosphorescence quantum yield of phthalazine was found to be 0.04 in a previous study,[3] and the quantum yields of naphthalene-h_8 and -d_8 were determined by comparing the corrected phosphorescence spectra of these compounds with the spectrum of phthalazine. In all systems of phthalazine-naphthalene-h_8 and -naphthalene-d_8, and pyridazine-naphthalene-d_8, excitation was carried out at 340 nm, where only the donor molecules show absorption.

Procedures

Intermolecular triplet-triplet excitation energy transfer is known to take place in systems where the energy levels of the lowest excited singlet state S_1^D and lowest triplet state T_1^D of the donor are bracketed by the same two levels of the acceptor, as illustrated in Fig. 1.

The present procedures for determining intersystem crossing quantum yields are based on the phenomenon of T–T energy transfer in rigid-glass solution. The following assumptions have been made: (1) The solute molecules are uniformly distributed in rigid-

1) Presented at the Symposium on Molecular Structure held by the Chemical Society of Japan at the University of Electro-Communications, Tokyo, 9—11 Oct. 1970.

2) H. Baba, I. Yamazaki, and T. Takemura, This Bulletin, **42**, 276 (1969).

3) H. Baba, I. Yamazaki, and T. Takemura, *Spectrochim. Acta*, **27A**, 1271 (1971).

4) S. K. Lower and M. A. El-Sayed, *Chem. Revs.*, **66**, 199 (1966).

5) S. P. McGlynn, T. Azumi, and M. Kinoshita, "Molecular Spectroscopy of the Triplet State," Prentice-Hall, Englewood Cliffs, New Jersey (1969).

6) M. A. El-Sayed, *J. Chem. Phys.*, **36**, 573 (1962); **38**, 2834 (1963).

7) B. J. Cohen and L. Goodman, *ibid.*, **46**, 713 (1967).

8) R. M. Hochstrasser and C. Marzzacco, *ibid.*, **45**, 4681 (1966); **46**, 4155 (1967).

9) E. C. Lim and J. M. H. Yu, *ibid.*, **49**, 3878 (1968).

10) E. C. Lim and J. Stanislaus, *ibid.*, **53**, 2096 (1970).

11) H. Baba, L. Goodman, and P. C. Valenti, *J. Amer. Chem. Soc.*, **88**, 5410 (1966).

12) V. L. Ermolaev, *Usp. Fiz. Nauk*, **80**, 3 (1963).

13) Y. Kanda and R. Shimada, *Spectrochim. Acta*, **15**, 211 (1959).

14) E. Lippert, W. Nägele, I. Seibold-Blankenstein, U. Staiger, and W. Voss, *Z. Anal. Chem.*, **170**, 1 (1959).

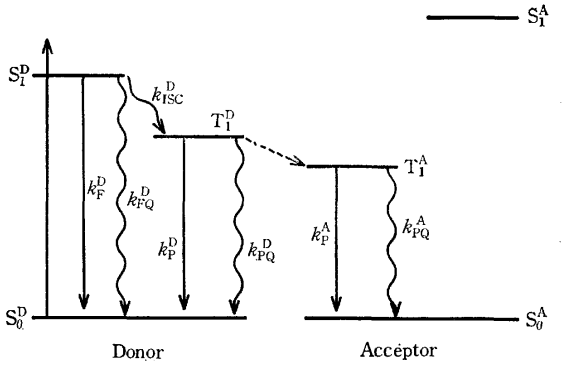

Fig. 1. Energy level scheme for triplet-triplet energy transfer experiment. The symbols k attached to the arrows are the rate constants of the corresponding processes. Solid straight-line arrows represent radiative processes corresponding to absorption or emission of light. Wiggly and dashed lines denote non-radiative and energy transfer processes, respectively.

glass solution. (2) All the unimolecular rate constants defined for the donor and acceptor (Fig. 1) are not affected by the presence of their respective partners, acceptor and donor. (3) The energy transfer from donor to acceptor occurs only through the path $T_1^D \rightarrow T_1^A$. These assumptions are generally recognized to be valid under the usual conditions.

In this study, two procedures A and B were employed according to two different cases; one where the emission can be observed from both donor and acceptor (Case A), and the other where the donor emission cannot be observed (Case B).

Procedure A. This is applicable only to Case A. A quantity called the quantum yield of sensitized phosphorescence γ_{SP} is available. The quantity was defined by Ermolaev[12] as

$$\gamma_{sp} = \frac{\Phi_{sp}^A}{\Phi_{PO}^D - \Phi_P^D} \quad (1)$$

where Φ_{SP}^A is the quantum yield of the sensitized phosphorescence of the acceptor, and Φ_{PO}^D and Φ_P^D are the quantum yields of the phosphorescence of the donor in the absence and in the presence of the acceptor, respectively. γ_{SP} can be obtained directly from the experiment. Equation (1) can be rewritten as[12]

$$\gamma_{sp} = \frac{\Phi_{ISC}^D}{\Phi_{PO}^D} \cdot \theta_P^A \quad (2)$$

with

$$\theta_P^A = \frac{\Phi_P^A}{\Phi_{ISC}^A} = \frac{k_P^A}{k_P^A + k_{PQ}^A} \quad (3)$$

where Φ_{ISC}^D and Φ_{ISC}^A are the intersystem crossing quantum yields of the donor and acceptor, respectively; Φ_{ISC}^D, for example, is given by

$$\Phi_{ISC}^D = k_{ISC}^D/(k_F^D + k_{FQ}^D + k_{ISC}^D)$$

Φ_P^A is the quantum yield of the phosphorescence of the acceptor, and θ_P^A represents the fraction of triplet molecules which phosphoresce.

Thus, if γ_{SP}, Φ_{PO}^D, and θ_P^A are known, Φ_{ISC}^D can be calculated from Eq. (2).

Procedure B. This is applicable to Cases A and B. If T–T energy transfer is assumed to be caused by the exchange mechanism, Φ_{SP}^A can be written in the form[12]

$$\Phi_{sp}^A = \Phi_{ISC}^D[1 - \exp(-VNC)]\theta_P^A \quad (4)$$

where V is the volume of the sphere of action of quenching, N the Avogadro number, and C the concentration of acceptor. It should be noted that $\exp(-VNC)$ represents the probability that there is no acceptor molecule in the volume V about an excited donor molecule, so that $\Phi_P^D/\Phi_{PO}^D = \exp(-VNC)$.

Differentiation of Φ_{SP}^A with respect to C leads to the form $d\Phi_{SP}^A/dC = \Phi_{ISC}^D\theta_P^A VN\exp(-VNC)$. Thus, we obtain

$$\ln(d\Phi_{sp}^A/dC) = \ln(\Phi_{ISC}^D\theta_P^A VN) - VNC \quad (5)$$

If Φ_{SP}^A as a function of C and θ_P^A are known, Φ_{ISC}^D and V can be obtained from a linear plot of $\ln(d\Phi_{SP}^A/dC)$ *vs.* C.

Results and Discussion

In order to determine the intersystem crossing quantum yield of phthalazine and pyridazine, we used these diazines as energy donor, and naphthalene-h_8

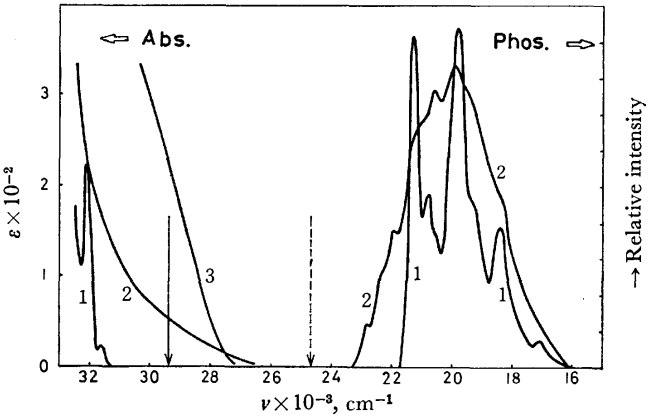

Fig. 2. Absorption and phosphorescence spectra of phthalazine and naphthalene-h_8, and absorption spectrum of pyridazine in EPA at 77°K. The phosphorescence spectra are uncorrected for the spectral sensitivity. 1,2 and 3 represent naphthalne-h_8, phthalazine and pyridazine, respectively.

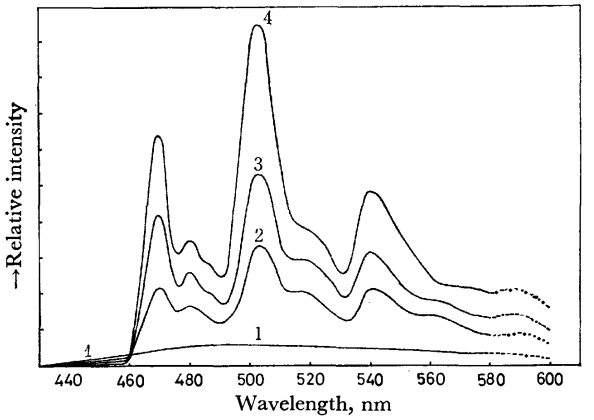

Fig. 3. Changes in the phosphorescence spectrum of phthalazine-naphthalene-d_8 system in EPA at 77°K caused by increase of the concentration of naphthalene-d_8. The concentrations of naphthalene-d_8: 1, 0; 2, 2.5×10^{-2}; 3, 5×10^{-2}; 4, 1×10^{-1} mol/l. The intensity of the phosphorescence spectra represents the relative quanta per unit wavelength interval.

and naphthalene-d_8 as energy acceptor. The absorption and phosphorescence spectra of phthalazine and naphthalene-h_8, and the absorption spectrum of pyridazine are shown in Fig. 2. The excitation frequency adopted throughout the T–T energy transfer experiments is indicated by a solid arrow, and the estimated position of electronic origin in the T_1 state of pyridazine by a dashed arrow. All the donor-acceptor combinations chosen satisfy the optimum conditions for the experiment of intermolecular T–T energy transfer.

Intersystem Crossing Quantum Yield of Phthalazine. The changes in the phosphorescence spectrum of phthalazine-naphthalene-d_8 system in EPA at 77°K caused by the increase in amount of naphthalene-d_8 are shown in Fig. 3. In the absence of phthalazine, no phosphorescence was observed from naphthalene-d_8 upon excitation at the frequency mentioned above. The spectral changes are therefore regarded as due solely to T–T energy transfer.

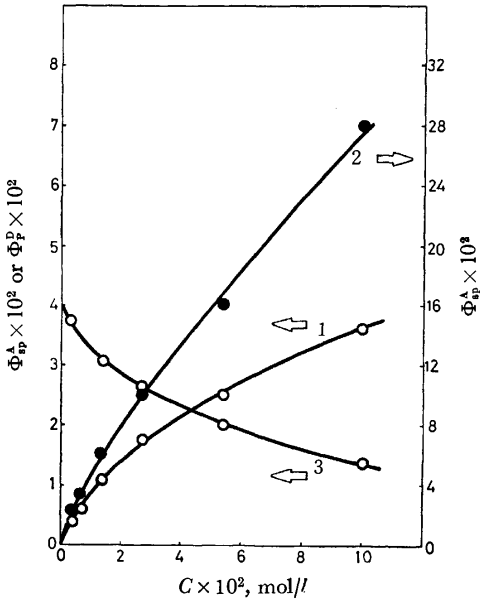

Fig. 4. Quantum yields of the sensitized phosphorescence Φ^A_{sp} of the acceptor, naphthalene-h_8 (1) or naphthalene-d_8 (2), as a function of the acceptor concentration C, and phosphorescence quantum yield Φ^D_p of the donor, phthalazine (3) as a function of C with naphthalene-d_8 as acceptor.

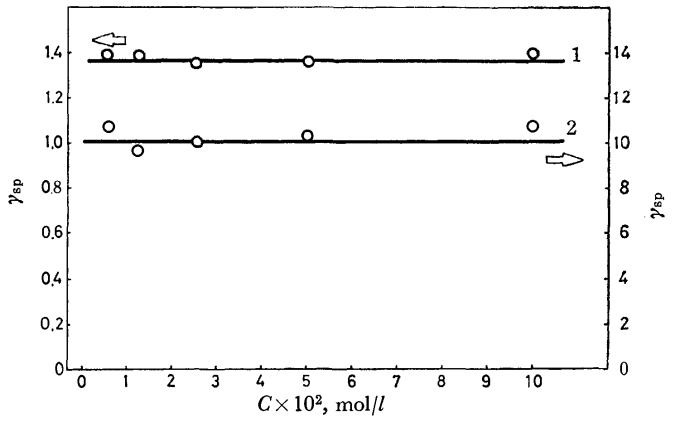

Fig. 5. Plots of γ_{sp} *vs.* C for donor-acceptor pairs: 1, phthalazine-naphthalene-h_8; 2, phthalazine-naphthalene-d_8.

TABLE 1. INTERSYSTEM CROSSING QUANTUM YIELDS OF PHTHALAZINE AND PYRIDAZINE

Donor	Acceptor	Procedure	Φ^D_{ISC}
Phthalazine	Naphthalene-h_8	A	0.45±0.05
Phthalazine	Naphthalene-d_8	A	0.50±0.05
Phthalazine	Naphthalene-h_8	B	0.51±0.05
Phthalazine	Naphthalene-d_8	B	0.48±0.05
Pyridazine	Naphthalene-d_8	B	0.24±0.05

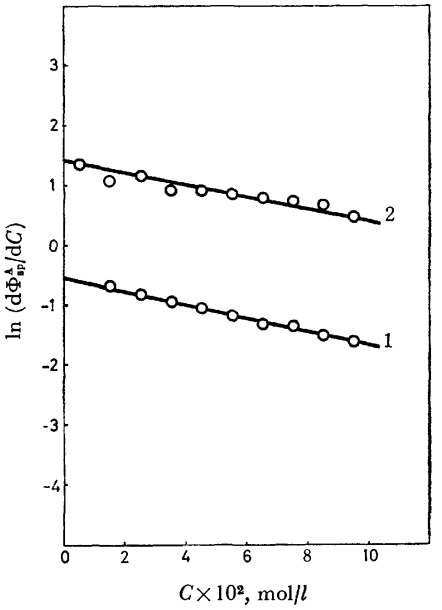

Fig. 6. Plots of $\ln(d\Phi^A_{SP}/dC)$ vs. C for donor-acceptor pairs: 1, phthalazine-naphthalene-h_8; 2, phthalazine-naphthalene-d_8.

The sensitized phosphorescence quantum yield Φ^A_{SP} of the acceptor, naphthalene-h_8 or naphthalene-d_8, as a function of C is shown in Fig. 4. A plot of the donor phosphorescence quantum yield *vs.* C with naphthalene-

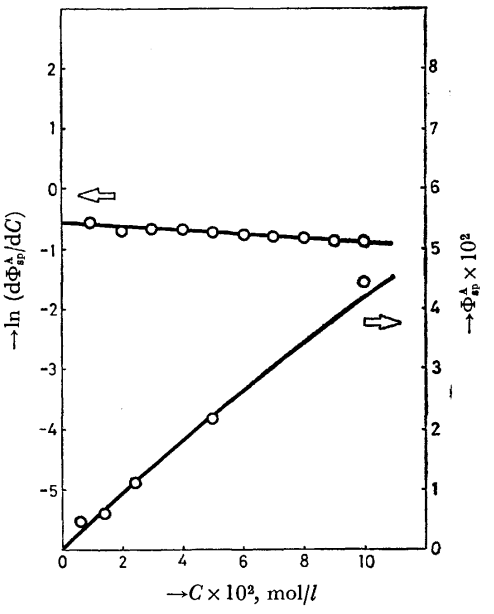

Fig. 7. Plots of Φ^A_{sp} and $\ln(d\Phi^A_{sp}/dC)$ *vs.* C for pyridazine-naphthalne-d_8 system.

d_8 as acceptor is also shown. Almost the same plot was obtained when naphthalene-h_8 was used as acceptor.

The sensitized phosphorescence quantum yields γ_{SP}, defined in Eq. (1), were calculated from the above data. Figure 5 shows plots of the resulting γ_{SP} values against the concentration of acceptor, C. As expected, γ_{SP} is independent of C, indicating the validity of the present treatment of the T–T energy transfer.

In EPA at 77°K, the phosphorescence quantum yield of phthalazine (Φ_{PO}^{D}) is known to be 0.04.[3] We found the phosphorescence quantum yields of naphthalene-h_8 and -d_8 to be 0.03 and 0.20, respectively. It has been reported that the intersystem crossing quantum yield is 0.25 for both naphthalene-h_8 and -d_8.[15] By using these values and the γ_{SP} values shown in Fig. 5, we determined the intersystem crossing quantum yield of phthalazine, Φ_{ISC}^{D}, in EPA at 77°K. The results are shown in Table 1.

On the other hand, $\ln(d\Phi_{SP}^{A}/dC)$ was plotted against C (Fig. 6). Analysis of the resulting straight lines by Eq. (5) also gives Φ_{ISC}^{D} (Table 1). The radius R of the sphere of action, defined by $V=(4\pi/3)R^3$, is found to be 15.8 Å.

From Table 1 we see that the Φ_{ISC}^{D} values for phthalazine obtained by Procedures A and B and with the use of naphthalene-h_8 and -d_8 agree within the limit of experimental error; the average value of Φ_{ISD}^{D} is 0.49. Also, the value of R, 15.8 Å, is seen to be reasonable in reference to the R values reported in the literature[12] for analogous donor-acceptor pairs involved in T–T energy transfer in rigid-glass solution, indicating that the excitation transfer occurs by the exchange mechanism.[12]

Intersystem Crossing Quantum Yield of Pyridazine. Although the lowest triplet state T_1 of pyridazine is not known, it should be of (n,π^*) type by the analogy of other monocyclic diazines. Then, the 0-0 band of the phosphorescence spectrum, if it appears at all, would be situated at about 400 nm (*cf.* Fig. 2).[7] Thus, with pyridazine as an energy donor, naphthalene can be chosen as an acceptor, as in the case of phthalazine. Because of the lack of phosphorescence, only Procedure B can be used for pyridazine.

The relation of Φ_{SP}^{A} to C for pyridazine-naphthalene-d_8 system is shown in Fig. 7, together with the relation of $\ln(d\Phi_{SP}^{A}/dC)$ to C. From these data and Eq. (5), $\Phi_{ISC}^{D}=0.24\pm0.05$ and $R=10$ Å are obtained immediately. This Φ_{ISC}^{D} value for pyridazine in EPA at 77°K is essentially the same as that reported by Cohen and Goodman,[7] although their value (0.2) was obtained from a photochemical measurement in fluid solution at room temperature. In addition, the R value mentioned above agrees with values in other analogous donor-acceptor systems.[12]

Thus, all the results obtained show that the excitation energy transfer from pyridazine to naphthalene-d_8 occurring under our experimental conditions is attributable to the exchange mechanism as in the case of phthalazine-naphthalene system.

Deactivation Path of Excitation Energy in Phthalazine and Pyridazine. The experimental results (Table 1) indicate that a fairly efficient intersystem crossing occurs between S_1^D and T_1^D to populate the T_1^D state in both phthalazine and pyridazine. The quantum yields of intersystem crossing in these *ortho*-diazines do not differ essentially from those of other diazines such as pyrazine, pyrimidine and quinoxaline. We are thus led to the conclusion that the deactivation of the excited *ortho*-diazine molecules occurs to a good extent *via* their phosphorescent triplet state, and that the weakness or lack of phosphorescence in the *ortho*-diazines is due to an anomalously fast rate of the radiationless transition from the triplet state.

15) S. G. Hadley and R. A. Keller, *J. Phys. Chem.*, **73**, 4356 (1969).

Liquid-phase Adsorption from Binary Solutions on Silica Gel. The Apparent Separation Factors and the Distribution of Adsorption Sites

Tsutomu KAGIYA, Yūzō SUMIDA, and Toshihiro TACHI
Faculty of Engineering, Kyoto University, Sakyo-ku, Kyoto
(Received November 15, 1971)

The liquid-phase adsorption equilibrium of a cyclohexane-benzene mixture on a silica-gel surface, containing various quantities of physically-adsorbed water, has been studied at 30°C. The apparent separation factors (α^{ap}) have been determined on the assumption that this liquid-phase adsorption is of the Langmuir-type. It was found that the values of α^{ap} were, in general, markedly affected not only by the composition of binary solvents, but also by the amounts of physically-adsorbed water. In order to discuss this point quantitatively, the theoretical equation for estimating the apparent separation factors on a complicated solid surface having two or more types of adsorption sites has been derived on the basis of the theory of chemical equilibrium. The following three types of adsorption sites have been assumed to exist on the silica-gel surface used in this experiment: the surface silanol (σ_1), the monolayer of water (σ_2), and the multilayer of water (σ_3). The separation factors of the σ_1 and σ_3 were experimentally measured as 17.1 and 2.5. By best-fitting the above theoretical equation for α^{ap} with the observed values, the separation factor of the σ_2 site was taken to be 3.7 and the distribution of each adsorption site on the surface was determined.

It is well known that a solid surface consists of the various adsorption sites with different adsorptive capacities. In this sense, studies of the adsorption phenomena offer fundamental and interesting information on the distribution of the adsorption sites and on the chemical reactions on solid catalyst surfaces. Quantitative investigations of the adsorption behavior and the chemical structures of solid surfaces have long been made by using gravimetric methods,[1,2] spectroscopic methods,[3,4] thermodynamic methods,[5,6] and so on.[7,8] However, the quantitative studies have been restricted to the gas-solid interface, and sufficient systematic studies of the liquid-phase adsorption have not been made.[9-11]

In a previous paper,[12] the present authors studied the adsorption equilibria of various binary solutions on chromatographic silica-gel, and determined the separation factors and the numbers of moles in the adsorbed-phase. On the basis of this information, the microscopic behavior of the liquid-phase adsorption was discussed in relation to the adsorption models proposed.

In this study, the adsorption equilibria of cyclohexane-benzene mixtures have been studied on silica-gel, on which a small quantity of water had previously been adsorbed. The purposes of this work are (1) to elucidate the relationships between the apparent separation factor and the composition of solvents and/or the quantity of physically-adsorbed water, and (2) to gain information on the distribution of adsorption sites on the silica-gel surface on the basis of the simple models of adsorption sites.

Experimental

Materials. The spectro-grade cyclohexane and benzene were used as the adsorbates. They were dried with silica-gel and were then used without further purification. The adsorbent was silica-gel (100—200 mesh) for thin-layer chromatography; this silica-gel was commercially obtained. The silica-gel was dried at 160°C for 6 hr in an electric furnace,[13] and various amounts of water were physically-adsorbed to prepare four kinds of adsorbents (SG-1, 2, 3, and 4), which were of the different adsorptive capacities on the surface. The silica-gel dried at 160°C had the following characteristics: B.E.T. (N_2) area = 380—420 m²/g, and pH of aqueous suspension = 7.0.

Adsorption Equilibrium. Portions (about 10 ml) of a cyclohexane(S_1)–benzene(S_2) solution of a known composition were added to about 4 g of an accurately-weighed adsorbent in a glass ampoule. The sealed ampoule was placed in a constant-temperature bath controlled at 30±0.2°C and then allowed to equilibrate while being stirred frequently. The analysis of the equilibrium mixture was made by means of a Shimadzu gas-chromatography, GC-4AIT.

Determination of Amounts of Physically-adsorbed Water. The amounts of water physically-adsorbed on silica-gel were weighed by means of a Shimadzu micro-thermobalance, MTB-50.

Analysis of Experimental Data

The overall adsorption equilibrium of a binary solution (S_1–S_2) can be expressed as follows:

1) G. J. Young, *J. Colloid Sci.*, **13**, 67 (1958).
2) M. L. Hair and W. Hertl, *J. Phys. Chem.*, **73**, 4269 (1969).
3) L. H. Little, "Infrared Spectra of Adsorbed Species," Academic Press Inc. (London) Ltd. (1966).
4) M. L. Hair, "Infrared Spectroscopy in Surface Chemistry," Marcel Dekker Inc., New York (1967).
5) V. Ya. Davydov, A. V. Kiselev, and B. G. Kuznetsov, *Zhur. Fiz. Khim.*, **39**, 2058 (1965).
6) P. A. Elkington and G. Curthoys, *J. Phys. Chem.*, **72**, 3475 (1968).
7) J. J. Fripiat and J. Uytterhoeven, *ibid.*, **66**, 800 (1962).
8) V. Ya. Davydov, A. V. Kiselev, and L. T. Zhuravlev, *Trans. Faraday Soc.*, **60**, 2254 (1964).
9) A. E. Hirschler and T. S. Mertes, *Ind. Eng. Chem.*, **47**, 193 (1955).
10) E. Funakubo, I. Moritani, N. Toshima, and T. Nagai., *Kogyo Kagaku Zasshi*, **66**, 237 (1963).
11) T. Yagi, K. Shimizu, K. Uchimoto, and S. Maeda, *ibid.*, **68**, 335 (1965).
12) T. Kagiya, Y. Sumida, and T. Tachi, This Bulletin, **44**, 1219 (1971).

13) As will be described after, the fact that the physically-adsorbed water is nearly completely removed by the prolonged evacuation at about 160°C has been supported by many investigators, on the basis of the experimental data by the spectroscopic[3,4] and gravimetric techniques.[1]

$$(S_1)^\sigma + (S_2)^l \overset{\alpha^{ap}}{\rightleftarrows} (S_1)^l + (S_2)^\sigma \quad (1)$$

where the σ and l superscripts represent the adsorbed-phase and the liquid-phase respectively. If the surface of the adsorbent is a heterogeneous one consisting of various adsorption sites, then the apparent separation factor (α^{ap}) is defined as follows:

$$\alpha^{ap} \equiv \frac{n_1{}^l n_2{}^\sigma}{n_2{}^l n_1{}^\sigma} = \frac{n_1{}^l \sum_i n_2{}^{\sigma_i}}{n_2{}^l \sum_i n_1{}^{\sigma_i}} \quad (2)$$

where σ_i is the i-th adsorption site on the adsorbent; where $n_1{}^l$ and $n_2{}^l$ are, respectively, the numbers of moles of S_1 and S_2 in the equilibrium mixture (mol); where $n_1{}^{\sigma_i}$ and $n_2{}^{\sigma_i}$ are, respectively, the numbers of moles of S_1 and S_2 adsorbed on the σ_i site (mol), and where $n_1{}^\sigma = \sum_i n_1{}^{\sigma_i}$ and $n_2{}^\sigma = \sum_i n_2{}^{\sigma_i}$.

The numbers of moles of S_1 and S_2 in the adsorbed-phase, namely, $\sum_i n_1{}^{\sigma_i}$ and $\sum_i n_2{}^{\sigma_i}$, can be related to the Gibbs surface excess (Γ), defined by Eq. (3), by means of the following Eq. (4):[14]

$$\Gamma_2 \equiv \frac{n^0}{mS} \Delta x_2{}^l \quad (3)$$

$$\Gamma_2 = \frac{1}{mS}(x_1{}^l \sum_i n_2{}^{\sigma_i} - x_2{}^l \sum_i n_1{}^{\sigma_i}) \quad (4)$$

In these equations, m is the weight of the adsorbent (g); S, the surface area per unit of mass of the adsorbent (m^2/g); n^0, the total number of moles of the original mixture (mol), and $\Delta x_2{}^l$, the change in the mole fractions of S_2 in the solutions between before and after the adsorption.

On the other hand, supposing that the adsorption is of the Langmuir-type and that the effective molecular occupancies (A) of the two components in the adsorbed-phase are known in advance, then the surface area should be given by:[15,16]

$$S = \frac{N_A}{m}(A_1 \sum_i n_1{}^{\sigma_i} + A_2 \sum_i n_2{}^{\sigma_i}) \quad (5)$$

As has been described in the previous paper,[12] it is known that the adsorption of a cyclohexane-benzene solution on silica-gel is of the Langmuir-type. If the surface is almost completely covered by the preferentially-adsorbed component (S_2=benzene), we have:

$$S = \frac{n_{m2}^\sigma}{m} A_2 N_A \quad (6)$$

where n_{m2}^σ is the number of moles of S_2 required to form a perfect monolayer.

Since the ratio of A_1 and A_2 is a constant ($\beta = A_2/A_1$), the following equations are derived from Eqs. (3), (4), (5), and (6):

$$\sum_i n_1{}^{\sigma_i} = \frac{\beta(n_{m2}^\sigma x_1{}^l + n^0 \Delta x_1{}^l)}{x_1{}^l + \beta x_2{}^l} \quad (7)$$

and

$$\sum_i n_2{}^{\sigma_i} = \frac{\beta n_{m2}^\sigma x_2{}^l + n^0 \Delta x_2{}^l}{x_1{}^l + \beta x_2{}^l} \quad (8)$$

Hence, the apparent separation factor should be expressed by Eq. (9):[17]

$$\alpha^{ap} = \frac{\left(\beta \frac{n_{m2}^\sigma x_2{}^l}{m} + \frac{n^0 \Delta x_2{}^l}{m}\right) x_1{}^l}{\beta\left(\frac{n_{m2}^\sigma x_1{}^l}{m} + \frac{n^0 \Delta x_1{}^l}{m}\right) x_2{}^l} \quad (9)$$

As is obvious from Eq. (9), one can easily determine the apparent separation factor (α^{ap}) from the observed values of $x_1{}^l$ and $x_2{}^l$, if the values of β and n_{m2}^σ/m can be measured in any way. The effective molecular occupancies of benzene derivatives and cyclic ethers have already been reported.[12]

The value of n_{m2}^σ/m may be evaluated from the B.E.T. (N_2) area according to Eq. (6). However, there is a possibility of overestimating the value of S, because the molecular size of benzene is quite large compared with that of the nitrogen molecule. In order to avoid this risk, it is desirable to estimate directly the n_{m2}^σ/m value from the same experimental data of liquid-phase adsorption.

According to Everett,[14] the behavior of a perfect binary solution in contact with a Langmuir-type adsorbing surface can be discussed on the basis of the following equation:

$$\frac{x_1{}^l x_2{}^l}{n^0 \Delta x_2{}^l / m} = \frac{m}{n^\sigma}\left(x_2{}^l + \frac{1}{\alpha^{ap} - 1}\right) \quad (10)$$

where $n^\sigma = \sum_i n_1{}^{\sigma_i} + \sum_i n_2{}^{\sigma_i}$. Equation (10) shows that a good linear relationship holds over an entire concentration range between $m x_1{}^l x_2{}^l / n^0 \Delta x_2{}^l$ and $x_2{}^l$ if the values of α^{ap} and m/n^σ are both constant. In general, a curvature is observed in a low concentration range of a preferentially-adsorbed component (S_2) because of the existence of the various adsorption sites, the difference in the effective molecular occupancies of adsorbed components, and so on. It can, however, be expected that a linear relationship exists over a wide concentration range of S_2 when the adsorption power of S_2 is so large in comparison with that of S_1 that the surface can be almost entirely covered by S_2. The slope is nearly equal to m/n_{m2}^σ:

$$\frac{m}{n^\sigma} \simeq \frac{m}{n_{m2}^\sigma} \quad (11)$$

By substituting the n_{m2}^σ/m values obtained from the Everett plots and the β values into Eq. (9), one can examine the dependence of the composition of binary solvents on the apparent separation factors.

Results

The amounts of water adsorbed physically on silica-gel were measured; they are listed in Table 1.

Table 1. Lists of experimental results of liquid-phase adsorption of cyclohexane-benzene solution on silica-gel surface

Adsorbent	ω (mmol/g)	n_{m2}^σ/m (mmol/g)	$\bar{\alpha}^{ap}$	$\alpha^{ap}(x_2^l=1.0)$	$\alpha^{ap}(x_2^l=0)$
SG-1	0	1.848	16.03	17.10	17.10
SG-2	1.12	1.854	11.36	15.70	8.10
SG-3	2.21	2.068	5.89	8.30	4.70
SG-4	4.14	1.799	3.56	5.05	3.00

14) D. H. Everett, *Trans. Faraday Soc.*, **60**, 1803 (1964); *ibid.*, **61**, 2478 (1965).

15) a) G. Schay, L. Gy. Nagy, and T. Szekrenyesy, *Periodica Polytechnica*, **6**, 91 (1962); b) L. Gy. Nagy, *ibid.*, **7**, 75 (1963).

16) S. K. Suri and V. Ramakrishna, *Trans. Faraday Soc.*, **65**, 1690 (1969).

17) A. V. Kiselev and V. V. Khopina, *ibid.*, **65**, 1936 (1969).

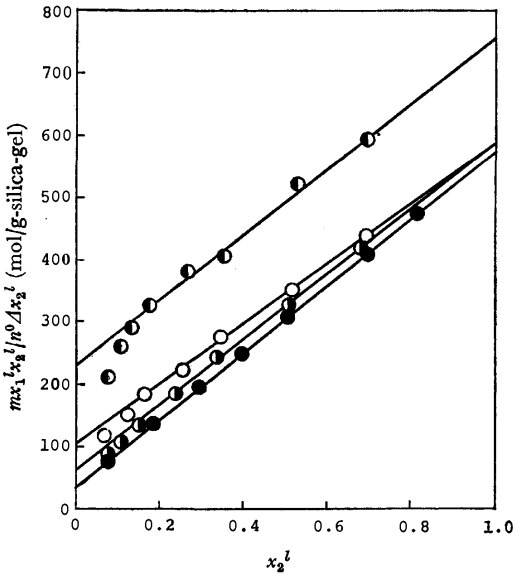

Fig. 1. Everett plots of $mx_1^l x_2^l/n^0 \Delta x_2^l$ *vs.* x_2^l for cyclohexane (S_1)-benzene (S_2) mixture on various silica-gel surfaces. Silica-gel surface: ●, SG-1; ◑, SG-2; ○, SG-3; ◐, SG-4.

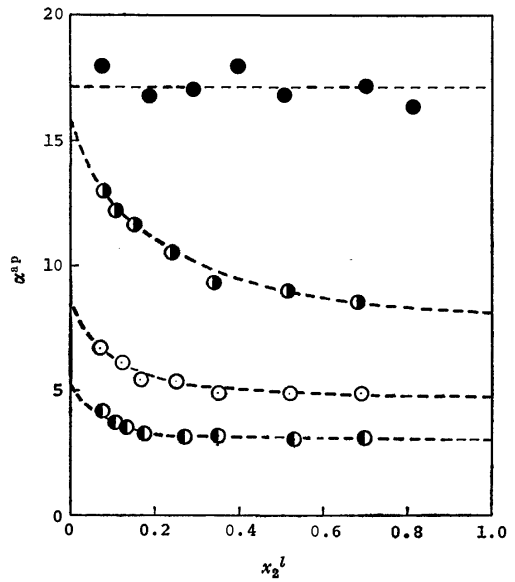

Fig. 2. Changes in apparent separation factors of cyclohexane (S_1)-benzene (S_2) mixture on various silica-gel surfaces. Silica-gel surface: ●, SG-1; ◑, SG-2; ○, SG-3; ◐, SG-4.

Figure 1 shows the analytical results for the adsorption of cyclohexane(S_1)-benzene(S_2) plotted according to Eq. (10). Although good linear relationships hold in the high concentration range of S_2, pronounced deviations are observed in the low concentration range. The degrees of deviations become larger as the amounts of adsorbed water increase. From the solpe and the intercept of the linear part in Fig. 1, the numbers of moles of adsorbed components in the high concentrations of S_2 were determined; they are listed in Table 1, together with the $\overline{\alpha^{ap}}$ values which correspond to the average values of the apparent separation factors at the high concentrations of S_2. It is obvious in Table 1 that the value of $\overline{\alpha^{ap}}$ decreases remarkably with the increase in the amount of adsorbed water, whereas the value of n_{m2}^{σ}/m is constant within the limits of experimental error. More noticeable is the fact that there exists a linear relationship over an entire concentration range when using silica-gel (SG-1) containing no physically-adsorbed water. As will be discussed below, the effective molecular occupancy of benzene is nearly equal to that of cyclohexane. Taking this fact into account, the correlation obtained for SG-1 may indicate that the α^{ap} value is to be regarded as a constant, independent of the composition of the solvents. In other words, it may be suggested that there is only one type of adsorption site on the surface of SG-1. Joining this suggestion with the results of the infrared-spectroscopic analysis of the structures of the silica-gel surface,[3,4] the surface of SG-1 is considered to be maximally hydroxylated.[1]

On the other hand, the effective molecular occupancy of benzene was reported in a previous paper to be 34.41 Å^2/molecule.[12] That of cyclohexane was calculated to be 38.46 Å^2/molecule from its molar volume on the assumption of a cube-shaped molecule. The β value is 0.895.

Using this β value and the n_{m2}^{σ}/m value in Table 1, the apparent separation factor in Eq. (9) was determined and plotted against the x_2^l, as is shown in Fig. 2. It was evident in Fig. 2 that the apparent separation factors (α^{ap}) decrease markedly with the increase in the quantity of adsorbed water. This corresponds to the fact that the adsorptive capacity of a site become small during the physical adsorption of water. Of interest is the fact that the α^{ap} value approaches the preferential coordination constant ($\alpha^{H_2O}=2.5$) of a cyclohexane-benzene solution to liquid water, which is the separation factor in the liquid-liquid interface.[18,19] It should also be noted that the α^{ap} values for SG-1 are constant, regardless of the solvent compositions,

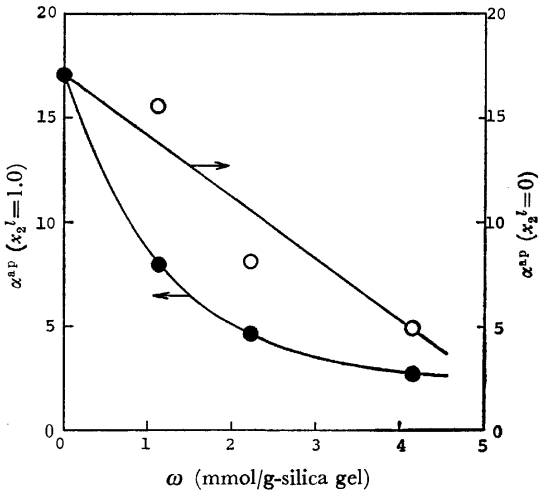

Fig. 3. Relationships between limited values of α^{ap} of cyclohexane (S_1)-benzene (S_2) mixture and amounts of physically-adsorbed water.
●, α^{ap} (x_2^l=1.0); ○, α^{ap} (x_2^l=0).

18) T. Kagiya, Y. Sumida, and T. Tachi, unpublished data.
19) T. Kagiya, Y. Sumida, T. Watanabe, and T. Tachi, This Bulletin, **44**, 923 (1971).

while the α^{ap} values for SG-2, 3, and 4 vary with the changes in the solvent compositions. This may imply the existence of two or more types of adsorption sites on the silica-gel surface of SG-2, 3, and 4, the adsorptive capacities of which differ from each other. This problem will be discussed in the next section in connection with the models of various adsorption sites.

By extrapolating the α^{ap}–x_2^l curves to $x_2^l \to 0$ and $x_2^l \to 1$, the limited values of α^{ap} were determined; they are summarized in the last two columns of Table 1. Figure 3 shows the relationships between these limited values and the amounts of adsorbed water (ω); the $\alpha^{ap}(x_2^l=1.0)$ value decreases exponentially with the increase in the ω value, while the $\alpha^{ap}(x_2^l=0)$ value decreases almost linearly.

When we define x_2^σ as the mole fraction of S_2 in the whole adsorbed-phase, the values of x_2^σ can be expressed as follows:

$$x_2^\sigma = \frac{\alpha^{ap} x_2^l}{x_1^l + \alpha^{ap} x_2^l} \tag{12}$$

The relationships of x_2^l *vs.* x_2^σ are demonstrated in Fig. 4. The non-symmetric curves for SG-2, 3, and 4 are obviously due to the fact that the α^{ap} values change greatly with the compositions of the binary solvents.[19]

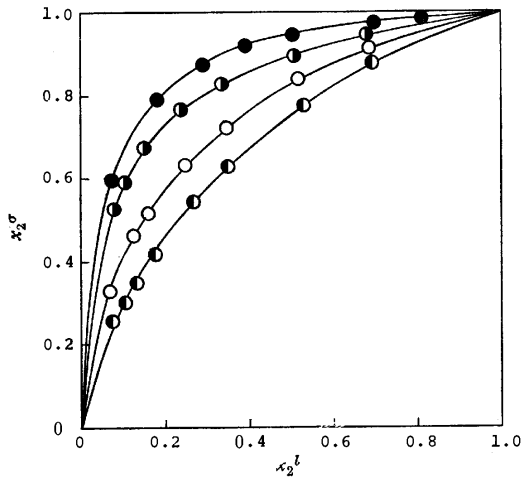

Fig. 4. Relationships between mole fractions of benzene in whole adsorbed-phase (x_2^σ) and mole fractions of benzene in equilibrium mixtures (x_2^l).
Silica-gel surface: ●, SG-1; ◑, SG-2; ○, SG-3; ◐, SG-4.

Discussion

Estimation of Apparent Separation Factors on the Basis of the Theory of Chemical Equilibrium. In the previous section, it has been indicated that the apparent separation factors are remarkably affected by both the quantity of physically-adsorbed water and the composition of the solvents. On the basis of the theory of chemical equilibrium, we examined first of all the dependence of both factors on the apparent separation factors.

In general, the silica-gel surface is well known to be a so-called heterogeneous adsorption surface, on which various adsorption sites with different adsorptive capacities are distributed. It can be considered, therefore, that the overall adsorption equilibrium of the binary solvents on such a solid surface can be expressed as the summation of the adsorption equilibria on all the adsorption sites:

$$\begin{array}{l} (S_1)^{\sigma_1} + (S_2)^l \overset{\alpha^{\sigma_1}}{\rightleftarrows} (S_1)^l + (S_2)^{\sigma_1} \\ (S_1)^{\sigma_2} + (S_2)^l \overset{\alpha^{\sigma_2}}{\rightleftarrows} (S_1)^l + (S_2)^{\sigma_2} \\ \vdots \quad\quad\quad \vdots \quad\quad\quad \vdots \quad\quad\quad \vdots \\ (S_1)^{\sigma_i} + (S_2)^l \overset{\alpha^{\sigma_i}}{\rightleftarrows} (S_1)^l + (S_2)^{\sigma_i} \\ \vdots \quad\quad\quad \vdots \quad\quad\quad \vdots \quad\quad\quad \vdots \end{array} \tag{13}$$

where $(S)^{\sigma_i}$ is the solvent component adsorbed on the adsorption site σ_i; $(S)^l$ is the solvent in the equilibrium mixture, and α^{σ_i} is the separation factor of the binary solvents on the σ_i site.

Each of the separation factors can be defined by:

$$\alpha^{\sigma_i} \equiv \frac{n_1^l n_2^{\sigma_i}}{n_2^l n_1^{\sigma_i}} \tag{14}$$

Hence, the apparent separation factor on the whole adsorption surface can be given as follows:

$$\alpha^{ap} = \frac{n_1^l \sum_i n_2^{\sigma_i}}{n_2^l \sum_i n_1^{\sigma_i}} = \frac{\sum_i n_2^{\sigma_i}}{\sum_i n_2^{\sigma_i}/\alpha^{\sigma_i}} \tag{15}$$

By using Eq. (14), the number of moles of adsorbed components on the σ_i site is:

$$n^{\sigma_i} = n_1^{\sigma_i} + n_2^{\sigma_i} = \left(1 + \frac{n_1^l}{\alpha^{\sigma_i} n_2^l}\right) n_2^{\sigma_i} \tag{16}$$

If the θ^{σ_i} is defined as the ratio of n^{σ_i} to the total number of moles of adsorbed components in the adsorbed-phase, then:

$$\theta^{\sigma_i} \equiv \frac{n^{\sigma_i}}{\sum_i n^{\sigma_i}} \tag{17}$$

Since the effective molecular occupancies of cyclohexane and benzene are nearly equal ($A_1 \simeq A_2$), the values of $\sum_i n^{\sigma_i}$ and n^{σ_i} can be approximated as follows:

$$\sum_i n^{\sigma_i} \simeq \frac{mS}{N_A A_2} \tag{18}$$

$$n^{\sigma_i} \simeq \frac{mS^{\sigma_i}}{N_A A_2} \tag{19}$$

where S^{σ_i} represents the surface area of the σ_i site, *i.e.*, $S = \sum S^{\sigma_i}$. Accordingly,

$$n_2^{\sigma_i} = \frac{\alpha^{\sigma_i} x_2^l}{x_1^l + \alpha^{\sigma_i} x_2^l} \theta^{\sigma_i} \frac{mS}{N_A A_2} \tag{20}$$

By substituting Eq. (20) into Eq. (15), we obtain:

$$\alpha^{ap} = \frac{\sum_i \alpha^{\sigma_i} \theta^{\sigma_i} / (x_1^l + \alpha^{\sigma_i} x_2^l)}{\sum_i \theta^{\sigma_i} / (x_1^l + \alpha^{\sigma_i} x_2^l)} \tag{21}$$

In Eq. (21), the α^{σ_i} value is the constant characteristic of the combination of the adsorption site and the binary solvent system, and the θ^{σ_i} is the factor (S^{σ_i}/S) depending on the distribution of the adsorption sites (or the adsorptive capacities) of the silica-gel surface. Therefore, even when using the same silica-gel and the same binary solvents, if there is a distribution of the adsorption sites on the surface, the apparent separation factor should change with the composition of the solvents. When x_2^l approaches 1.0, the α^{ap} values converge to a constant value:

$$\alpha^{ap}(x_2^l=1.0) = \frac{1}{\sum_i \theta^{\sigma}{}_i/\alpha^{\sigma}{}_i} \quad (22)$$

Similarly, by extrapolating to $x_2^l \to 0$:

$$\alpha^{ap}(x_2^l=0) = \sum_i \alpha^{\sigma}{}_i\theta^{\sigma}{}_i \quad (23)$$

Models of Adsorption Sites on the Silica-gel Surface. In order to discuss the analytical results obtained in Fig. 2 by using Eq. (21), we must determine the various types of adsorption sites on the silica-gel surface on which a small quantity of water has been previously adsorbed. Many experimental studies of the change in the silica-gel surface upon the adsorption of water have been made, and much reliable informations have been gathered.[3,20]

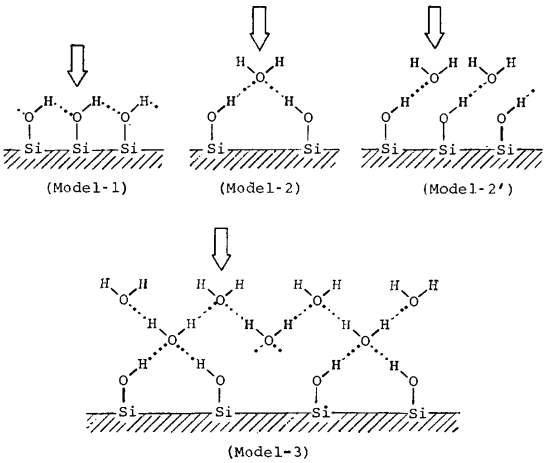

Fig. 5. Adsorption sites on silica-gel surface containing physically-adsorbed water.

From these combined infrared and gravimetric data,[1,3] it has been concluded that the physically-adsorbed water on silica-gel surface is almost completely removed by prolonged evacuation at 150—170°C, leaving a hydrogen-bonding surface formed between the adjacent silanol groups (Site Model-1 in Fig. 5). This has also been approximately, though not seriously, supported by Fripiat *et al.*[7] and Kiselev *et al.*[8] Moreover, Kiselev *et al.*[8] estimated, from their experimental results on the surface chemical reaction, that the number of surface hydroxyl groups is about 4.8 OH/100 Å^2, corresponding to one OH group per silicon atom on the surface. However, recent spectroscopic studies[21-23] have suggested the existence of three types of surface silanol, *i.e.*, the single, geminal, and paired silanol groups. In this study, the proper amounts of water were artifically adsorbed on silica-gel heated at 160°C. Therefore, the surface should be entirely covered with bridged silanol O–H groups.

The models of physically-adsorbed water have not been clear enough to permit the drawing of exact conclusions.[20] On the adsorption of a very small quantity of water, Kiselev *et al.*[7,24] proposed that a 1 : 2 hydrogen bonding was formed between one molecule of water and two adjacent surface silanols (Site Model-2), while Morimoto *et al.*[25] presented a 1 : 1 hydrogen bond mechanism (Site Model-2'). The 1 : 2 and 1 : 1 mechanisms may, of course, coexist on the surface.[20] If there are no clear-cut differences in the adsorptive capacities of the cyclohexane-benzene system on the 1 : 2 and 1 : 1 hydrogen-bonding surfaces, we can identify Model-2' with Model-2 with respect to the adsorptive capacity. This is almost certain, because the liquid-phase adsorptions on both Model-2 and Model-2' take place on the monolayer of water molecules bonded "directly" to the surface silanol.[26] A further physical-adsorption of water forms the multilayer coverage of water molecules (Site Model-3), where the liquid-phase adsorption occurs on the multilayer of water molecules bonded "indirectly" to the silanol.[26]

On the basis of such speculations, we conventionally classified the adsorption sites of silica-gel containing the physically-adsorbed water into the following three groups: Model-1 (the surface silanol, σ_1), Model-2 (the monolayer of water, σ_2), and Model-3 (the multilayer of water, σ_3).

Distribution of Adsorption Sites on the Silica-gel Surface. The next problem is to determine the separation factor

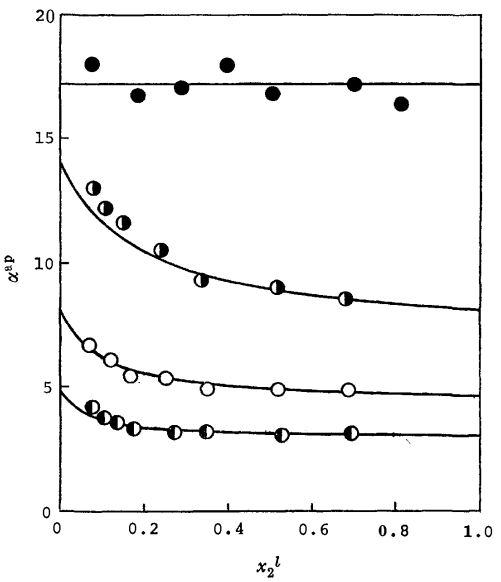

Fig. 6. Simulation of apparent separation factors of cyclohexane (S_1)-benzene (S_2) mixture on various silica-gel surfaces. Silica-gel surface:
●, SG-1; ◑, SG-2; ○, SG-3; ◐, SG-4.
The solid line represents the theoretical curve.

20) J. H. Anderson and K. A. Wickersheim, *Surface Sci.*, **2**, 252 (1964).
21) J. B. Peri and A. L. Hensley, Jr., *J. Phys. Chem.*, **72**, 2926 (1968).
22) J. Erkelens and B. G. Linsen, *J. Colloid & Interface Sci.*, **29**, 464 (1969).
23) C. G. Armistead, A. J. Tyler, F. H. Hambleton, S. A. Mitchell, and J. A. Hockey, *J. Phys. Chem.*, **73**, 3947 (1969).
24) A. V. Kiselev and V. I. Lygin, *Kolloid. Zhur.*, **21**, 581 (1959); A. V. Kiselev and V. I. Lygin, *Usp. Khim.*, **31**, 351 (1962), English Translation, *Russ. Chem. Rev.*, **31**, 175 (1962).
25) M. Nagao and T. Morimoto, paper presented at the 23rd Symposium on Colloid & Interface Chemistry, Tokushima (November, 1970), preprint, p. 138.
26) In the case of binary solvent system in which the proton-accepting power of solvent component is considerably large, compared with that of water, the solvent component may destroy the coverage of water molecules to adsorb "directly" to the surface silanol. However, the possibility can be neglected in the cyclohexane-benzene system employed here.

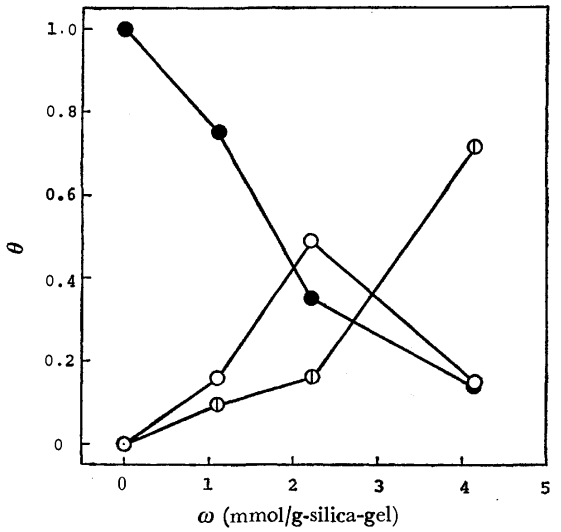

Fig. 7. Distribution of adsorption sites on silica-gel surfaces containing physically-adsorbed water.
Adsorption site: ●, σ_1; ○, σ_2; ⓘ, σ_3.

(α^{σ_i}) of cyclohexane-benzene on each adsorption site, σ_i. According to the above speculations, the surface of SG-1 is a so-called homogeneous σ_1 site. Therefore, the $\alpha^{\sigma}{}_1$ value can be taken to be 17.1 from the experimental data in Table 1. Supposing that, in Model-3, the silanol groups exert little influence on the adsorptive capacity of the adsorption surface, the value of α^{σ_3} on the multilayer of water may be considered to be approximately equal to the preferential coordination constant ($\alpha^{H_2O}=2.5$) to liquid water.[18,19]

The value of α^{σ_2} cannot be measured by the use of this experimental technique, since it is impossible to prepare artifically a complete monolayer of water molecules on the silica-gel surface. However, we calculated the α^{σ_2} value by using Eq. (21). That is, by simulating the experimental points of the apparent separation factors obtained from Eq. (9) with Eq. (21), in which the values of x_1^l, x_2^l, α^{σ_1}, and α^{σ_3} are known, the best-fitting α^{σ_2} value was determined, together with θ^{σ_1}, θ^{σ_2}, and θ^{σ_3} values. The value of α^{σ_2} was calculated to be 3.7. It is reasonable that the α^{σ_2} value is slightly larger than the α^{σ_3} value.

The agreement between the experimental results and the theoretical curves of Eq. (21) is shown in Fig. 6. Though slight deviations are observed in the low concentration range of benzene, they may be overcome by considering four or more types of adsorption sites. However, it can be considered, on the basis of the fairly good accordance, that the above speculation regarding adsorption sites is quite reasonable.

In Fig. 7, each of the calculated θ^{σ} values is plotted against the amounts of physically-adsorbed water (ω). The curves represent the distribution of the adsorption sites on the silica-gel surface. On the silica-gel surface (SG-2) containing a very small quantity of adsorbed water, the σ_1 site gradually decreases and the σ_2 and σ_3 sites gradually increase. On the surface of SG-3, the σ_2 site occupies about half of the adsorption surface. The further adsorption of water (SG-4) brings about decreases in the σ_1 and σ_2 sites and a prominent increase in the σ_3 site. These tendencies are also in harmony with chemical intuition.

On the basis of this discussion, it may be reasonable to conclude that Eq. (21) is useful in offering not only valuable information on the liquid-phase adsorption on complicated solid surface, but also microscopic information on the structures of the surface.

The Crystal and Molecular Structure of Dimethyltin Bis(*N,N*-dimethyldithiocarbamate)

Toshihide KIMURA, Noritake YASUOKA, Nobutami KASAI,* and Masao KAKUDO**

Department of Applied Chemistry, Faculty of Engineering, Osaka University, Yamadakami, Suita, Osaka

***Institute for Protein Research, Osaka University, Yamadakami, Suita, Osaka*

(Received November 22, 1971)

The crystal and molecular structure of dimethyltin bis(*N,N*-dimethyldithiocarbamate), $[(CH_3)_2Sn\{S_2CN(CH_3)_2\}_2]$, has been determined by single crystal X-ray diffraction. The crystals are orthorhombic; *Fdd*2; $a=25.478\pm0.008$, $b=35.323\pm0.011$, $c=6.936\pm0.006$ Å, $Z=16$. The tin atom has a distorted octahedral environment. The tin atom and the four sulfur atoms lie approximately on the same plane, with two Sn–S bond distances of 2.515 ± 0.008 and 2.497 ± 0.008 Å and two longer Sn–S distances of 2.954 ± 0.007 and 3.061 ± 0.008 Å, while the methyl groups are in *trans* positions; average Sn–C$=2.15\pm0.04$ Å. The SnSC(S)N skeletons on both sides of the tin atom are approximately planar, and the average bond distances are S–C$=1.72\pm0.03$, C–N$=1.31\pm0.03$, and N–C(Me)$=1.49\pm0.04$ Å.

Many structural investigations have been reported on transition metal complexes of dialkyldithiocarbamates. Most of them have a typical octahedral structure. On the other hand, only a few structures of non-transition metal complexes have been reported.[1]

As a part of the structural studies of organotin compounds, we have recently reported[2] the crystal and molecular structure of dimethyltin chloride *N,N*-dimethyldithiocarbamate (to be abbreviated as Me_2Sn-Cl(dtc) hereafter). It has been found that the coordination around the tin atom is a distorted trigonal bipyramid, the two methyl groups being in equatorial positions.

Dimethyltin bis(*N,N*-dimethyldithiocarbamate)(to be abbreviated as $Me_2Sn(dtc)_2$ hereafter) is the *N,N*-dimethyldithiocarbamate substitute for $Me_2SnCl(dtc)$, and this complex must have a hexa-coordinated structure. IR and PMR investigations[3] have shown that the complex has a distorted octahedral configuration, the two methyl groups being in *trans* positions. In order to determine the exact configuration, crystal structure analysis has been undertaken by means of X-rays.

The present investigation will also contribute to the understanding of the bonding nature of the tin atom in penta- and hexa-coordinated dimethyltin complexes. Schlemper has determined the structure of dimethyltin bis(8-hydroxyquinolinate);[4] he found that the Me–Sn–Me angle ($110.7\pm0.8°$) is remarkably close to the tetrahedral angle. With the aid of a qualitative MO approach, he proposed that the bonding could involve sp^3 hybrid orbitals on the tin participating in the methyl groups and three-center bonds in the oxinate groups. It would be very interesting to determine whether the structure of $Me_2Sn(dtc)_2$ can be understood in terms of such a bonding scheme or not.

Experimental

The crystals were recrystallized from a chloroform-ethanol solution to form colorless needles elongated along the *c* axis.

Approximate unit-cell dimensions were obtained from osillation and Weissenberg photographs taken around the *c* axis, while the accurate cell dimensions were determined on a Rigaku automated four-circle diffractometer.

Crystal Data. $C_8H_{18}N_2S_4Sn$, *F.W.*$=389.1$, orthorhombic, $a=25.478\pm0.008$, $b=35.323\pm0.011$, and $c=6.936\pm0.006$ Å, $U=6242$ Å^3, $D_m=1.650$ and $D_x=1.656$ g·cm^{-3} for $Z=16$. The systematic absences (*hkl*: $h+k\neq2n$, $k+l\neq2n$; 0*kl*: $k+l\neq4n$: *h*0*l*: $h+l\neq4n$; *hk*0: $h\neq2n$, $k\neq2n$; *h*00: $h\neq4n$; 0*k*0: $k\neq4n$, and 00*l*: $l\neq4n$) uniquely define the space group as *Fdd*2.

The three-dimensional intensity data for $2\theta\leq45°$ were collected on the diffractometer at room temperature, using Zr-filtered Mo$K\alpha$ radiation. The integrated intensity was recorded by the ω-2θ scan technique:

Range of scan (in 2θ)$=(2.0+0.70\tan\theta_c)°$ and

Starting angle of the scan$=(2\theta_c-1.0)°$,

where θ_c is the calculated value of the Bragg angle for $\lambda(\text{Mo}K\alpha_1)=0.70926$ Å. At each end of the scan, the background counts were measured for 10 sec by the stationary crystal-stationary counter technique. The intensity data were corrected for the background counts and for the usual Lorentz and polarization effects. No absorption correction was applied, since the linear absorption coefficient is not very large ($\mu=21.1$ cm^{-1} for Mo$K\alpha$). Finally, two sets of 1143 independent reflections, $F(hkl)$'s and $F(\bar{h}\bar{k}\bar{l})$'s, were collected in order to consider the anomalous dispersion effect.

Determination and Refinement of the Structure

The initial coordinates of the tin atom were easily determined from the three-dimensional Patterson function computed by using $F(hkl)$'s. The four sulfur atoms could also be located from the Patterson and the minimum function, but two of them were located about 3.0 Å from the tin atom. The first Fourier synthesis was computed with the phases based on the tin atom only, and the four sulfur atoms were found at the positions expected from the Patterson function. The two nitrogen atoms and the four carbon atoms were then found in the Fourier map with the phases based on the tin and the four sulfur atoms. The

* To whom any correspondence should be addressed.

1) S. Ooi, *Kagaku no Ryoiki*, **24**, 151 (1970) (in Japanese).

2) K. Furue, T. Kimura, N. Yasuoka, N. Kasai, and M. Kakudo, This Bulletin, **43**, 1661 (1970).

3) M. Honda, M. Komura, Y. Kawasaki, T. Tanaka, and R. Okawara, *J. Inorg. Nucl. Chem.*, **30**, 3231 (1968).

4) E. O. Schlemper, *Inorg. Chem.*, **6**, 2012 (1967).

remaining four carbon atoms were found in the successive Fourier maps. At this stage, the structure factor calculation gave a discrepancy facor, $R=\sum||F_o|-|F_c||/\sum|F_o|$, of 0.20 for the $F(hkl)$ reflections. The atomic-scattering factors used were taken from those of Hanson and his co-workers.[5]

The block-diagonal least-squares refinement was carried out on a HITAC 5020E computer at the University of Tokyo, and also on a FACOM 230-60 computer at the Kyoto University, with a program, HBLS IV, written by Dr. T. Ashida.[6] Eight cycles of the refinement with isotropic temperature factors for all non-hydrogen atoms gave the R value of 0.17 for a set of $F(hkl)$ data. The anisotropic temperature factors for all non-hydrogen atoms were then introduced, and three cycles of the refinement reduced the R value to 0.095.

At this stage, the corrections for the anomalous dispersion effect were introduced for the tin and the sulfur atoms (for Mo$K\alpha$, $\Delta f'=-0.60$, $\Delta f''=1.90$ for Sn, and $\Delta f'=0.1$, $\Delta f''=0.2$ for S).[7]

The structure was refined using the combined data of $F(hkl)$ and $F(\bar{h}\bar{k}\bar{l})$ by starting from the coordinates representing the molecules of one direction of the polar axis and also from those of the opposite direction. Through refinement, the following weighting scheme was applied;

$$w = 1 \quad \text{for } F_o > 0$$
$$w = 0.2 \quad \text{for } F_o = 0$$

After several cycles, the refinement converged; the values of the R and the residual (defined as $\sum w(|F_o|-|F_c|)^2$) were 0.089 and 7385, respectively, for the coordinates representing the molecules of one direction of the polar axis, while those of the opposite direction were 0.092 and 7638. The relatively small values of the correction for the anomalous scattering of Sn and S atoms might have given such a small difference. This difference might not be significant, but the former structure was chosen as the final result only because it gave the smaller discrepancy. All of the coordinates of this structure are in good agreement with those of the opposite structure within the range of the estimated

TABLE 1. (a) THE FINAL ATOMIC COORDINATES ALONG WITH THEIR ESTIMATED STANDARD DEVIATIONS IN PARENTHESES

Atom	x	y	z
Sn	0.06259(6)	0.08391(4)	0.0000(5)
S(1)	0.00683(24)	0.12223(16)	0.22686(10)
S(2)	0.05927(25)	0.03688(17)	0.2686(10)
S(3)	0.11276(25)	0.01039(17)	−0.0849(9)
S(4)	0.03680(24)	0.16488(19)	−0.1253(11)
N(1)	0.1024(6)	−0.0313(4)	0.232(3)
N(2)	−0.0229(6)	0.1915(4)	0.155(3)
C(1)	0.0917(8)	0.0012(6)	0.147(3)
C(2)	0.0049(8)	0.1635(6)	0.087(3)
C(3)	0.1291(9)	−0.0627(6)	0.133(4)
C(4)	0.0840(9)	−0.0387(7)	0.433(4)
C(5)	−0.0553(10)	0.1887(8)	0.334(5)
C(6)	−0.0218(10)	0.2294(7)	0.055(5)
C(10)	0.0081(10)	0.0692(8)	−0.227(4)
C(20)	0.1406(7)	0.1052(7)	0.017(5)

(b) THE ANISOTROPIC THERMAL PARAMETERS (EACH MULTIPLIED BY 10^4) OF THE FORM:
$\exp\{-(\beta_{11}h^2+\beta_{22}k^2+\beta_{33}l^2+\beta_{12}hk+\beta_{13}hl+\beta_{23}kl)\}$

Atom	β_{11}	β_{22}	β_{33}	β_{12}	β_{13}	β_{23}
Sn	14	9	162	−1	7	−1
S(1)	22	9	186	0	35	9
S(2)	24	10	182	4	40	−1
S(3)	23	9	172	4	46	−10
S(4)	18	12	234	0	35	4
N(1)	17	6	217	1	−22	3
N(2)	15	6	291	0	−39	−9
C(1)	16	8	208	1	−7	11
C(2)	13	8	199	−3	−5	−18
C(3)	26	7	318	−1	81	−39
C(4)	20	10	259	−2	18	15
C(5)	25	15	416	10	114	−22
C(6)	23	9	446	4	25	38
C(10)	22	16	204	7	−40	−6
C(20)	9	13	406	1	12	24

TABLE 3. GEOMETRY AROUND THE TIN ATOM (a) BOND DISTANCES AND ANGLES ALONG WITH THEIR ESTIMATED STANDARD DEVIATIONS IN PARENTHESES.

Bond distance (Å)		Bond angle (°)	
Sn–S(1)	2.515(8)	S(1)–Sn–S(2)	82.7(0.3)
Sn–S(2)	2.497(8)	S(1)–Sn–S(4)	63.5(0.2)
Sn–S(3)	2.954(7)	S(1)–Sn–C(10)	102.8(0.8)
Sn–S(4)	3.061(8)	S(1)–Sn–C(20)	108 (1)
Sn–C(10)	2.16 (3)	S(2)–Sn–S(3)	65.1(0.2)
Sn–C(20)	2.13 (4)	S(2)–Sn–C(10)	111.1(0.8)
		S(2)–Sn–C(20)	103 (1)
		S(3)–Sn–S(1)	147.4(0.3)
		S(2)–Sn–S(4)	145.7(0.3)
		S(3)–Sn–S(4)	149.1(0.2)
		S(3)–Sn–C(10)	85.5(0.8)
		S(3)–Sn–C(20)	85 (1)
		S(4)–Sn–C(10)	83.1(0.8)
		S(4)–Sn–C(20)	83 (1)
		C(10)–Sn–C(20)	136 (1)

(b) THE LEAST-SQUARES PLANE OF THE FIVE ATOMS, Sn, S(1), S(2), S(3), and S(4):
$-0.84637x-0.34451y-0.40615z+2.38101=0$,
Deviations from the least-squares plane (Å):

Sn	0.010
S(1)	0.107
S(2)	−0.103
S(3)	0.062
S(4)	−0.066

Angle between the least-squares plane and the Sn–C(10) bond: 67.3°,
Angle between the least-squares plane and the Sn–C(20) bond: 69.1°.

5) H. P. Hanson, F. Herman, J. D. Lea, and S. Skillman, *Acta Crystallogr.*, **17**, 1040 (1964).

6) "Universal Crystallographic Computation Program System," ed. by Tosio Sakurai, Crystallographic Society of Japan, Tokyo (1967).

7) "International Tables for X-ray Crystallography," Vol. III, The Kynoch Press, Birmingham 1962, p. 214.

standard deviations.

The final atomic coordinates and the anisotropic thermal parameters obtained by using the combined data are listed in Table 1. The observed and calculated structure factors are listed in Table 2.[8]

Results and Discussion

The Geometry Around the Tin Atom. The molecular structure and the numbering system of $Me_2Sn(dtc)_2$ are shown in Fig. 1. The bond distances and angles around the tin atom are given in Table 3.

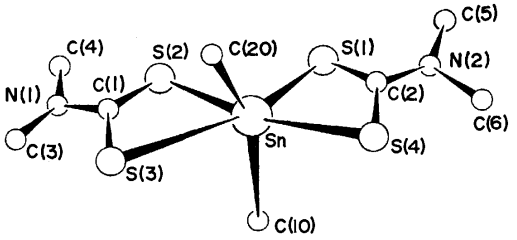

Fig. 1. Molecular structure of dimethyltin bis(*N*,*N*-dimethyldithiocarbamate) with the numbering of atoms.

The configuration about the tin atom could be described as a hexa-coordinated octahedron, with the two methyl groups attached to the tin atom in the *trans* positions. This configuration would be in agreement with the proposed structure. However this description would not correspond to that of the bonding nature.

It may be easily concluded by an inspection of Table 4, which lists the sulfur-metal bond distances and angles in some of the transition and non-transition metal complexes of dithiocarbamates, that there is a remarkable difference between them. In the transition metal complexes, all the sulfur-metal bond distances are almost equal, while there are two kinds of bond distances in the non-transition metal complexes.

In the present compound, the Sn–S(1) and Sn–S(2) bond distances (2.525(8) and 2.497(8) Å) are slightly longer than the sum of the covalent radii of Sn and S(2.44 Å);[22] they are nearly equal to those in $Me_3Sn(dtc)$[20,21] (2.47(1) Å) and the equatorial Sn–S bond in $Me_2SnCl(dtc)$[2] (2.48(1) Å). On the other hand, the Sn–S(3) and Sn–S(4) distances (2.954(7) and 3.061(8) Å) are significantly longer than the Sn–S(1) and Sn–S(2) bonds. These bonds might be considered as weak coordination bonds. Such weak metal-sulfur bonds have been found in other tin and arsenic complexes, but not in transition metal complexes. These facts suggest, that the bonding nature of the tin atom in the present complex is quite different from those in transition metal complexes. Furthermore, the C–Sn–C angle of 136(1)° shows an appreciable deviation from

8) Table 2 which gives a complete list of the observed and the calculated structure factors has been submitted to, and is kept as Document No. 7205 by, the office of the Bulletin of the Chemical Society of Japan, 1-5 Kanda-Surugadai, Chiyoda-ku, Tokyo. A copy may be secured by citing the Document number and by remitting, in advance, ¥300 for photo prints. Pay by check or money order payable to: Chemical Society of Japan.

22) L. Pauling, "The Nature of the Chemical Bond," 3rd ed., Cornell Univ. Press, Ithaca 1960, p. 246.

Table 4. Metal-sulfur bond distances and angles in some metal dithiocarbamates

Compound	M–S (Å)		∠S–M–S (°)	Ref.
$Fe(NO)(S_2CNEt_2)_2$	2.295(2)	2.298(2)	76.2(1)	9)
	2.394(2)	2.308(2)	75.8(1)	
$Co(S_2CNEt_2)_3$	2.255(3)	2.255(3)	76.8(2)	10)
	2.258(2)	2.260(3)	75.9(1)	
$Ni(S_2CNH_2)_2$	2.207(7)	2.224(15)	78.6(3)	11)
	2.210(7)	2.218(15)	78.4(2)	
$Ni(S_2CNEt_2)_2$	2.195(2)	2.207(2)	79.2(2)	12)
$(Cu(S_2CNEt_2)_2)_2$	2.297(2)	2.317(2)	77.3(2)[a]	13)
$(Cd(S_2CNEt_2)_2)_2$	2.547(4)	2.594(3)	70.9(1)[a]	14)
$(Zn(S_2CNMe_2)_2)_2$	2.333(6)	2.429(6)	76.4(2)[a]	15)
$(Zn(S_2CNEt_2)_2)_2$	2.355(3)	2.443(3)	75.8(2)[a]	16)
$Zn(S_2CNMe_2)_2(C_5H_5N)$	2.330(4)	2.598(4)	73.4(3)	17)
	2.325(4)	2.612(4)	72.9(3)	
$PhAs(S_2CNEt_2)_2$	2.330(6)	2.911(6)	67.8(2)	18)
	2.322(6)	2.835(6)	69.1(2)	
$As(S_2CNEt_2)_3$	2.351(3)	2.903(4)		19)
	2.336(2)	2.820(3)		
	2.358(3)	2.810(3)		
$Me_3Sn(S_2CNMe_2)$				
monoclinic	2.47(1)	3.16(1)	62(1)	20)
orthorhombic	2.47(1)	3.16(3)	63(1)	21)
	2.47(1)	3.33(1)	60(1)	
$Me_2SnCl(S_2CNMe_2)$	2.48(1)	2.79(1)	68.2(3)	2)
$Me_2Sn(S_2CNMe_2)_2$	2.515(8)	3.061(8)	63.5(2)	b)
	2.497(8)	2.954(7)	65.1(2)	

a) The metal-sulfur bonds in which the sulfur atom bridges between two metal atoms are omitted.
b) present work

Table 5. The PMR coupling constants, $J(^{119}Sn–CH_3)$, and the C–Sn–C bond angles in some dimethyltin compounds

Complex	$J(^{119}Sn–CH_3)$ (*cps*)	Ref.	∠C–Sn–C(°)	Ref.
$Me_2Sn(C_9H_6NO)_2$	71.5	22)	110.7	4)
$Me_2SnCl(dtc)$	74.0	3)	128	2)
$Me_2Sn(dtc)_2$	84.0	3)	136.5	present work
$Me_2SnCl_2 \cdot Me_2SO$	86	23)	172	25)

9) G. R. Davies, J. A. J. Jarvis, B. T. Kilbourn, R. H. B. Mais, and P. G. Owston, *J. Chem. Soc., A*, **1970**, 1275.
10) S. Merlino, *Acta Crystallogr.*, **B24**, 1441 (1968).
11) G. F. Gasparri, M. Nardelli, and A. Villa, *ibid.*, **23**, 384 (1967).
12) M. Bonamico, G. Dessy, A. Mariani, A. Vaciago, and L. Zambonelli, *ibid.*, **19**, 619 (1965).
13) M. Bonamico, G. Dessy, A. Mugnoli, A. Vaciago, and L. Zambonelli, *ibid.*, **19**, 886 (1965).
14) A. Domenicano, L. Torelli, A. Vaciago, and L. Zambonelli, *J. Chem. Soc., A*, **1968**, 1351.
15) H. P. Klug, *Acta Crystallogr.*, **21**, 536 (1966).
16) M. Bonamico, G. Mazzone, A. Vaciago, and L. Zambonelli, *ibid.*, **19**, 898 (1965).
17) K. A. Fraser and M. M. Harding, *ibid.*, **22**, 75 (1967).
18) R. Bally, *ibid.*, **23**, 295 (1967).
19) M. Colapietro, A. Domenicano, L. Scaramuzza, and A. Vaciago, *Chem. Commun.*, **1968**, 302.
20) G. M. Sheldrick, W. S. Sheldrick, R. F. Dalton, and K. Jones, *J. Chem. Soc., A*, **1970**, 493.
21) G. M. Sheldrick and W. S. Sheldrick *ibid.*, **1970**, 490.
23) Y. Kawasaki and R. Okawara, *J. Organometal. Chem.*, **6**, 249 (1966).
24) W. Kitching, *Tetrahedron Lett.*, **1966**, 3689.
25) N. W. Isaacs, C. H. L. Kennard, and W. Kitching, *Chem. Commun.*, **1968**, 820.

the angle in the exact *trans* position (180°).

From these observations it might be considered that the bonding on the tin atom could involve sp^3 hybrid orbitals participating in covalent bonds to the two methyl groups and two sulfur atoms, S(1) and S(2). Since there are two additional tin-sulfur interactions (Sn–S(3) and Sn–S(4)), which originate from the electronegativity of S(3) and S(4) and the electropositivity of Sn, the steric effects of S(3) and S(4) would increase the C–Sn–C angle from a tetrahedral one to 136(1)° and would decrease the S(1)–Sn–S(2) angle to 82.7(3)°. Such a conception could explain why the sp^3 tin atom occasionally takes an apparently hexa-coordinated octahedral configuration.

Another approach to this problem has been proposed by Schlemper.[4] With regard to the structure of $(CH_3)_2Sn(C_9H_6NO)_2$, he postulated that the sp^3 tin atom has two normal covalent bonds to the methyl

TABLE 6. GEOMETRY OF THE LIGAND, *N,N*-DIMETHYLDITHIOCARBAMATE GROUP.

(a) BOND DISTANCES AND ANGLES ALONG WITH THEIR ESTIMATED STANDARD DEVIATIONS IN PARENTHESES.

Bond distance (Å)		Bond angle (°)	
S(1)–C(2)	1.75(2)	Sn–S(1)–C(2)	96.8(0.8)
S(2)–C(1)	1.73(3)	Sn–S(2)–C(1)	96.0(0.9)
S(3)–C(1)	1.73(3)	Sn–S(3)–C(1)	81.1(0.8)
S(4)–C(2)	1.68(2)	Sn–S(4)–C(2)	80.1(0.8)
C(1)–N(1)	1.32(3)	S(1)–C(2)–S(4)	120 (1)
C(2)–N(2)	1.30(3)	S(2)–C(1)–S(3)	118 (1)
N(1)–C(3)	1.48(4)	S(2)–C(1)–N(1)	121 (2)
N(1)–C(4)	1.49(4)	S(3)–C(1)–N(1)	121 (2)
N(2)–C(5)	1.50(4)	S(1)–C(2)–N(2)	117 (2)
N(2)–C(6)	1.50(4)	S(4)–C(2)–N(2)	124 (2)
		C(1)–N(1)–C(3)	123 (2)
		C(1)–N(1)–C(4)	121 (2)
		C(2)–N(2)–C(5)	123 (2)
		C(2)–N(2)–C(6)	120 (2)
		C(3)–N(1)–C(4)	118 (2)
		C(5)–N(2)–C(6)	117 (2)

(b) THE LEAST-SQUARES PLANES OF THE LIGAND GROUPS AND DEVIATIONS FROM THE PLANES (Å):

(1)	$-0.80120x-0.32292y-0.50379z+2.26878=0$,	
	S(1)	−0.057
	S(4)	0.074
	C(2)	0.000
	N(2)	0.011
	C(5)	0.077
	C(6)	−0.096
(2)	$-0.87050x-0.35100y-0.34500z+2.41725=0$,	
	S(2)	0.003
	S(3)	−0.009
	C(1)	0.018
	N(1)	−0.022
	C(3)	0.013
	C(4)	−0.001

TABLE 7. COMPARISON OF THE S–C AND C–N BOND DISTANCES AND THE S–C–S ANGLE WITHIN THE DITHIOCARBAMATE GROUP IN VARIOUS COMPOUNDS.

compound	S–C (Å)		C–N (Å)	∠S–C–S (°)	Ref.
$Na^+(S_2CNEt_2)^-$	1.712(7)	1.729(6)	1.344(8)	120.4(4)	27)
$Fe(NO)(S_2CNEt_2)_2$	1.720(6)	1.726(6)	1.323(7)	110.7(3)	9)
	1.720(6)	1.740(6)	1.312(7)	109.7(3)	
$Co(S_2CNEt_2)_3$	1.714(8)	1.714(8)	1.304(15)	109.6(7)	10)
	1.695(9)	1.703(7)	1.327(10)	110.0(4)	
$Ni(S_2CNH_2)_2$	1.68(2)	1.70(3)	1.37(3)	111.9(11)	11)
	1.68(2)	1.70(3)	1.38(3)	111.6(12)	
$Ni(S_2CNEt_2)_2$	1.700(7)	1.713(7)	1.33(1)	110.6(6)	12)
$[Cu(S_2CNEt_2)_2]_2$	1.711(8)	1.713(8)	1.35(1)	114.6(7)[a]	13)
$[Cd(S_2CNEt_2)_2]_2$	1.714(14)	1.725(14)	1.33(2)	120.2(7)[a]	14)
$[Zn(S_2CNMe_2)_2]_2$	1.701(19)	1.748(19)	1.325(25)	120.2(12)[a]	15)
$[Zn(S_2CNEt_2)_2]_2$	1.722(10)	1.725(10)	1.34(1)	117.5(9)[a]	16)
$Zn(S_2CNMe_2)_2$ (C_5H_5N)	1.701(10)	1.727(10)	1.333(13)	118.3(15)	17)
	1.707(10)	1.732(10)	1.342(13)	117.3(15)	
$PhAs(S_2CNEt_2)_2$	1.652(2)	1.781(2)	1.35(3)	119(1)	18)
	1.687(2)	1.756(2)	1.34(3)	118(1)	
$As(S_2CNEt_2)_3$	1.678(6)	1.760(5)	1.338(7)[a]	—	19)
$Me_3Sn(S_2CNMe_2)$					
monoclinic	1.72(1)	1.75(1)	1.31(2)	117(1)	20)
orthorhombic	1.70(3)	1.80(3)	1.35(3)	117(2)	21)
	1.71(3)	1.78(3)	1.34(3)	119(2)	
$Me_2SnCl(S_2CNMe_2)$	1.68(4)	1.74(4)	1.32(5)	120(2)	2)
$Me_2Sn(S_2CNMe_2)_2$	1.68(2)	1.75(2)	1.30(3)	120(1)	b)
	1.73(3)	1.73(3)	1.32(3)	118(1)	

a) Bond distances and angles concering bridged groups are omitted.
b) present work

27) M. Colapietro, A. Domenicano, and A. Vaciago, *Chem. Commun.*, **1968**, 572.

groups, and the two 'three-center bonds' to the oxinate groups. In a way similar to Schlemper's,[4] the angles of C(10)–Sn–M(1), C(20)–Sn–M(1), C(10)–Sn–M(2), C(20)–Sn–M(2), and M(1)–Sn–M(2) were calculated to be 98, 94, 92, 95, and 153° respectively, where M(1) and M(2) are the midpoints of the lines connecting S(2) and S(3), and S(1) and S(4), respectively. None of these values is, however, a tetrahedral angle. It seems, then, that his conception can not be applied to the present compound.

The distortion of the tetrahedral configuration about the tin atom in $Me_3Sn(dtc)$,[20,21] in particular the widening of the average C–Sn–C angles (119(1) and 118(1)° respectively in monoclinic and orthorhombic forms) and the narrowing of the average C–Sn–S angle (95(1) and 95(1)°), can be well understood by the considerations described above. The short non-bonded Sn—S interactions (3.16 and 3.33 Å) affect the slight distortion of the tetrahedral configuration in $Me_3Sn(dtc)$. In $Me_2SnCl(dtc)$, the substitution of a methyl group by a chlorine atom results in an increase in the covalent character of the non-bonded Sn—S interaction, thus giving a shorter Sn—S distance (2.79(1) Å) and a higher distortion of the configuration about the tin atom. In the present complex, $Me_2Sn(dtc)_2$, the substitution of the methyl group by a (dtc) group changes the coordination number of the tin atom and gives a large distortion. The slightly longer Sn–S bond distances and the larger C–Sn–C angle in $Me_2Sn(dtc)_2$ may be due to the difference in the steric effect and the electronegativity of the ligand groups attached to the tin atom.

It has been suggested that a linear relation holds between the degree of *s*-character of the tin orbitals directed to the carbon atom and the PMR coupling constants.[26] The C–Sn–C bond angles and the coupling constants of some dimethyltin complexes are summarized in Table 5. As is shown in Table 5, however, the increase in the C–Sn–C angle is probably due not only to the *s*-character of the Sn–C bond, but also to the steric effect around the tin atom.

Geometry of the Ligand Group. The bond distances and angles in the ligand groups, *N,N*-Dimethyldithiocarbamate, are given in Table 6(a).

One of the two lignad groups is planar within ±0.03 Å; however, in the other group deviations from the least-squares plane are about ±0.1 Å (Table 6(b)). The dihedral angle between these planes is 10.1°.

The S(1)–C(2), S(4)–C(2), S(2)–C(1), and S(3)–C(1) distances are 1.75(2), 1.68(2), 1.73(3), and 1.73(3) Å respectively. These values are close to those in $Me_2SnCl(dtc)$, and also to those in other dialkyldithiocarbamates (Table 7). The differences in these bond distances are not significant within the limits of experimental error. The C(1)–N(1) and C(2)–N(2) distances of 1.32(3) and 1.30(3) Å are equal to those in other dithiocarbamate complexes. These values suggest that the carbon(sp^2)-nitrogen(sp^2) bond has a high double-bond character, as was to be expected from the IR studies; a similar conclusion was suggested for $Me_2Sn(dtc)_2$. The four N–C (alkyl) bond distances, 1.48(4), 1.49(4), 1.50(4), and 1.50(4) Å, are equal, within the limits of experimental error, to the N–C single-bond distance (1.48 Å).

Crystal Structure. The crystal structure of $Me_2Sn(dtc)_2$ projected onto the (001) plane is shown in Fig. 2. The short intermolecular atomic contacts less than 4.0 Å are summarized in Table 8. None of them is short enough to suggest any significant deviation from

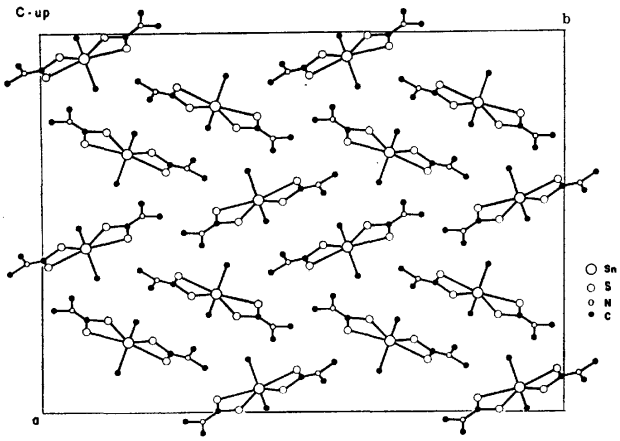

Fig. 2. Crystal structure of dimethyltin bis(*N,N*-dimethyldithiocarbamate) projected onto the (001) plane.

Table 8. The short intermolecular atomic contacts less than 4.0Å

From the unit No. 1,				
To the unit No. 2				
	S(2)–S(2)	3.99Å	S(2)–C(4)	3.82Å
	C(4)–S(2)	3.82		
To the unit No. 3				
	N(1)–C(6)	3.73	C(1)–C(6)	3.71
	C(20)–C(2)	3.72	C(20)–N(2)	3.85
	C(20)–S(4)	3.87		
To the unit No. 4				
	S(1)–C(3)	3.86	N(2)–C(3)	3.99
	C(2)–C(3)	3.69	C(20)–C(3)	3.89
To the unit No. 5				
	C(5)–C(6)	3.82	C(6)–C(6)	3.92
Key	No. 1	x,	y,	z
	2	$-x$,	$-y$,	$-z$
	3	$0.25+x$,	$0.25-y$,	$0.25+z$
	4	$0.25-x$,	$0.25+y$,	$0.25+z$
	5	$-x$,	$0.5-y$,	$0.5+z$

Table 9. Preliminary crystal data of dimethyltin bis(*N,N*-dimethyldiselenocarbamate)

$C_7H_{18}NSe_2Sn$
$F.W.=570.6$
Orthorhombic
Space group *Pnn*2
$a=14.0$Å
$b=18.1$
$c=7.5$
$V=1903$Å^3
$D=1.99$ g.cm^{-3}
for $Z=4$

26) J. R. Holmes and H. D. Kasez, *J. Amer. Chem. Soc.*, **83**, 3903 (1961).

the normal van der Waals interaction.

Besides the structure analysis of $(CH_3)_2Sn(S_2CN(CH_3)_2)_2$, preliminary X-ray examinations of $(CH_3)_2Sn(Se_2CN(CH_3)_2)_2$ have been carried out. The crystal data of the compound are listed in Table 9.

The authors wish to express their deep thanks to Professor Toshio Tanaka and to Professor Rokuro Okawara of this university for their kindness in supplying crystals.

BULLETIN OF THE CHEMICAL SOCIETY OF JAPAN, VOL. 45, 1654—1655(1972)

An ESR Study of Some Substituted Pyridine *N*-Oxide Copper(II) Complexes

Derek P. FREYBERG, Toshiyuki ISOBE, and Seizo MISUMI
Inorganic Chemistry Laboratory, Faculty of Science, Kyushu University, Fukuoka

(Received December 6, 1971)

The ESR (methanol solution, frozen solution, powder, and single crystal) spectra of $[CuL_4](ClO_4)_2$, where L=pyridine *N*-oxide, α-picoline *N*-oxide, β-picoline *N*-oxide, γ-picoline *N*-oxide, and 2,6-lutidine *N*-oxide, and of $[CuL_6](ClO_4)_2$, where L=pyridine *N*-oxide and γ-picoline *N*-oxide, have been obtained. The preparation of hexa(γ-picoline *N*-oxide) copper(II) perchlorate is reported. The solution and frozen solution spectra indicate a very similar bonding in all the complexes, with moderately ionic metal-oxygen. The powder spectra reveal all the tetrakis complexes to be axially symmetric; though tetra(γ-picoline *N*-oxide) copper(II) perchlorate shows a reversal of the usual order of the *g*-values. This is explained in terms of the packing interactions within the crystal structure, rather than metal-ligand interaction. All the single crystal spectra are characteristic of axially symmetric complexes. Hexa(pyridine *N*-oxide)copper(II) perchlorate gives an isotropic ESR spectrum, but this does not seem to be due to exchange interaction. Hexa(γ-picoline *N*-oxide)copper(II) perchlorate gives an axial ESR spectrum with a considerable tetragonal misalignment.

Although there has been considerable interest in transition metal complexes with aromatic amine *N*-oxides (particularly pyridine *N*-oxide) in recent years,[1] the principal interest lies in copper(II) in binuclear complexes formed with *e.g.* $CuCl_2$. We report here the ESR (methanol solution, frozen methanol solution (−150°C), powder, and single crystal) spectra of $[CuL_4](ClO_4)_2$ where L=pyridine *N*-oxide (pyNO), α-picoline *N*-oxide (αNO), β-picoline *N*-oxide (βNO), γ-picoline *N*-oxide (γNO), and 2,6-lutidine *N*-oxide (lNO); and $[CuL_6](ClO_4)_2$ where L=pyNO and γNO. The preparation of $[Cu(\gamma NO)_6](ClO_4)_2$ is reported for the first time.

Experimental

The aromatic amine *N*-oxide ligands were prepared from the amines by the method of Ochiai.[2] The chloroform extract, after removal of the chloroform by rotary evaporation, was used without further purification. The copper(II) complexes were prepared by the usual methods.[3,4] $[Cu(\gamma NO)_6](ClO_4)_2$ was prepared by the reaction of hot acetone[5] solutions of $Cu(ClO_4)_2 \cdot 6H_2O$ and γNO in 1:20 mole ratio. On cooling, pale lime-green needles separated. They were filtered off, washed with acetone and dried over silica gel. If the filtrate is allowed to stand further, dark green crystals of $[Cu(\gamma NO)_4](ClO_4)_2$ and not $[Cu(\gamma NO)_6](ClO_4)_2$ are formed. Analysis: found C; 47.2, H; 4.61, N; 9.18%; calcd for $CuC_{36}H_{42}N_6O_{14}Cl_2$ C; 47.1, H; 4.61, N; 9.19%.

Reflection spectra of powdered samples and absorption spectra were taken on Hitachi EPS-3T and EPS-2 spectrophotometers, respectively. ESR spectra were taken on a JEOL JES ME-3X spectrometer with a variable temperature attachment operating at about 9.3 GHz. Calibration was made with a Mn^{2+}/MgO powder standard ($g_4=1.981$). Solutions for absorption and ESR measurements were approximately 1:20 Cu:L in MeOH. Single crystal spectra were taken on a holder similar to that described by Hathaway and Billing,[6] except that it was made of silica rod. The same face of the crystal can be mounted (using silicone grease) onto two mutually perpendicular faces of the rod, and the rod rotated in the spectrometer cavity. The crystal was thus rotated about three orthogonal axes, and spectra were taken every 15° in each rotation.

Results

The *g*- and *A*-values obtained from ESR spectra of the solution and frozen solution samples together with absorption maxima of the solutions are shown in Table 1.

The lNO spectra show a rather large $g_\parallel$ and A^*, but a low g^*. This might be due to steric interaction involving the methyl groups of ligand molecules. The value of α^2, a measure of the covalency of the metal-ligand bond,[7] changes very little indicating that the bonding in all cases is similar.

1) R. G. Garvey, J. H. Nelson, and R. G. Ragsdale, *Coordin. Chem. Rev.*, **3**, 375 (1968).
2) E. Ochiai, *J. Org. Chem.*, **18**, 534 (1953).
3) J. V. Quagliano, J. Fujita, G. Franz, D. J. Phillips, J. A. Walmsley, and S. Y. Tyree, *J. Amer. Chem. Soc.*, **83**, 3770 (1961).
4) R. L. Carlin, *ibid.*, **83**, 3773 (1961).
5) S. J. Gruber, C. H. Harris, E. Kokot, S. T. Lenzer, T. N. Lockyer, and E. Sinn, *Aust. J. Chem.*, **20**, 2403 (1967).
6) B. J. Hathaway and D. E. Billing, *Coordin. Chem. Rev.*, **5**, 143 (1970).
7) V. C. Swett and E. P. Dudek, *J. Phys. Chem.*, **72**, 1244 (1968).

Table 1. Solution and frozen solution spectra

Ligand	$g_{\parallel}$	g^*	$g_{\perp}$	$A_{\perp}$(G)	A^*(G)	$A_{\perp}$(G)	ΔE(cm^{-1})	α^2
pyNO	2.320	2.160	2.080	138	52	9	12700	0.84
αNO	2.291	2.151	2.081	150	52	3	12300	0.86
βNO	2.300	2.161	2.082	150	60	15	12500	0.82
γNO	2.297	2.152	2.080	155	60	12	13200	0.86
lNO	2.393	2.126	2.043	149	80	45	12500	0.79

Notes: 1. $g_{\perp}=1/2(3g^*-g_{\parallel})$; $A_{\perp}=1/2(3A^*-A_{\parallel})$.
2. $g_{\parallel}$, $g^*\pm0.005$; $A_{\parallel}$, $A^*\pm3$G; $\Delta E\pm50$ cm^{-1}
3. Samples: $Cu(ClO_4)_2$+ligand 1:20 in MeOH at 25°C and −150°C.

Table 2. Powder spectra

Sample	$g_{\parallel}$	$g_{\perp}$	G	ΔE(cm^{-1})
$[Cu(pyNO)_4](ClO_4)_2$	2.240	2.065	3.7	14700
$[Cu(\alpha NO)_4](ClO_4)_2$	2.261	2.061	4.4	14900
$[Cu(\beta NO)_4](ClO_4)_2$	2.282	2.065	4.3	14500
$[Cu(\gamma NO)_4](ClO_4)_2$	2.066	2.172	—	14700
$[Cu(lNO)_4](ClO_4)_2$	2.241	2.054	4.5	15600
$[Cu(pyNO)_6](ClO_4)_2$	Isotropic	$g=2.189$	—	12300/9600sh
$[Cu(\gamma NO)_6](ClO_4)_2$	2.313	2.102	3.1	13000/10500sh

Notes: 1. $g_{\parallel}$, $g_{\perp}\pm0.005$; $\Delta E\pm50$ cm^{-1}
2. $G=(g_{\parallel}-2)/(g_{\perp}-2)$

The g-values obtained from ESR spectra of the powder samples together with reflection maxima of the complexes are shown in Table 2.

All the spectra are characteristic of axial symmetry[6] and the values of $g_{\parallel}$ and $g_{\perp}$ were obtained by the method of Kneubühl.[8] For the tetrakis complexes, the single crystal g-values were identical with the powder g-values within experimental error. The spectrum of $[Cu(\gamma NO)_6](ClO_4)_2$, despite analytical purity of the sample, displayed lines due to $[Cu(\gamma NO)_4](ClO_4)_2$ present as an impurity as well as to the hexakis complex. However, the g-value assignments were confirmed by the spectrum of $[Cu(\gamma NO)_6](ClO_4)_2$ diluted 1:500 in $[Zn(\gamma NO)_6](ClO_4)_2$, which gave $g_{\parallel}=2.326$, $A_{11}=110$ G, $g_{\perp}=2.087$, and $A_{\perp}=30$ G. The usual reason for the observation of an isotropic spectrum, as for $[Cu(pyNO)_6](ClO_4)_2$, is that the tetragonal axes are grossly misaligned. Exchange coupling[9] between local copper(II) ions does not seem to occur, as the spectrum of $[Zn(pyNO)_6](ClO_4)_2$ containing 1% Cu^{2+} is identical with that of the undiluted complex.

Discussion

The solution and frozen solution spectra display no unusual features; the ESR and solution spectra are very similar for all the complexes. Thus we can state that the bonding within a single unit is identical for all the complexes.

The powder spectra, on the other hand, show an unexpected feature, *viz.*, $g_{\perp}$ is greater than $g_{\parallel}$ for $[Cu(\gamma NO)_4](ClO_4)_2$ and not for any of the other complexes. The value of $G(=g_{\parallel}-2/g_{\perp}-2)$ has been used[9] to explain distortions from tetragonal symmetry. The result $G>4.0$ indicates good alignment of the tetragonal axes within the crystal, and $G<4.0$ indicates misalignment. Thus the αNO, βNO, and lNO complexes show aligned tetragonal axes and the pyNO complex shows misaligned ones. G has no meaning in the case where $g_{\perp}$ is greater than $g_{\parallel}$. Single crystal spectra of all the complexes followed the theoretical pattern for a complex with axial symmetry[10] *i.e.* $g^2=g_{\perp}^2\sin^2\theta+g_{\parallel}^2\cos^2\theta$ for rotations about two axes and $g=g_{\perp}$ for rotation about the third axis. These spectra confirmed the assignments of $g_{\parallel}$ and $g_{\perp}$ for the tetrakis complexes.

The reflection spectra of the five tetrakis complexes are all similar, and it is likely that the crystal environment is also similar. Hence, a reversal of the g-values for $[Cu(\gamma NO)_4](ClO_4)_2$ is unexpected. Usually, a value of $g_{\perp}$ greater than $g_{\parallel}$ indicates a d_z^2 ground state;[11] however, this gives a $g_{\parallel}$ close to the free electron value ($g=2.002$). In the present case, $g_{\parallel}=2.066$, a value considerably higher than is usual for d_z^2. Also, a d_z^2 ground state does not favour square planar coordination and is usually observed in trigonal complexes. For these reasons, and also because the solution and frozen solution spectra are similar to those of the other complexes, we conclude that the reversal of the g-values is not in the metal atom environment but in the crystal packing. This is supported by examination of structural models based on the crystal structure of $[Cu(pyO)_4](ClO_4)_2$ which has been described by Lee *et al.*[12] These models indicate that a methyl group in the α- or β-position does not significantly alter the size of the complex unit but γ-substitution does. It may be noted also, that the ESR spectrum of Cu^{2+} in $[Pd(\gamma NO)_4](ClO_4)_2$ is normal *i.e.* $g_{\parallel}>g_{\perp}$.

8) F. K. Kneubühl, *J. Chem. Phys.*, **33**, 1074 (1960).
9) I. M. Procter, B. J. Hathaway, and P. Nicholls, *J. Chem. Soc. A*, **1968**, 1678.
10) R. M. Golding, "Applied Wave Mechanics", Van Nostrand, London, (1969).
11) B. J. Hathaway and A. A. G. Tomlinson, *Coordin. Chem. Rev.*, **5**, 1 (1970).
12) J. D. Lee, D. S. Brown, and B, G. A. Melsom, *Acta Crystallogr.*, **B25**, 1378 (1969).

Transfer-hydrogenation and Transfer-hydrogenolysis. I. Transfer-hydrogenation of Cyclooctadienes Catalyzed by Dichlorobis(triphenylphosphine)iron(II)

Takeshi NISHIGUCHI and Kazuo FUKUZUMI

Department of Applied Chemistry, Faculty of Engineering, Nagoya University, Chikusa-ku, Nagoya

(Received December 9, 1971)

Hydrogen transfer from a number of organic compounds to olefins in a homogeneous system was studied. In the case of hydrogen transfer to 1,5-cyclooctadiene, using dichlorobis(triphenylphosphine)iron(II) as the catalyst, dihydroxybenzenes, such as pyrocatechol and hydroquinone, were much superior to *prim*- and *sec*-alcohols, 1-dodecanethiol, and cyclohexene as hydrogen donors.

In almost all catalytic hydrogenations of olefins, molecular hydrogen has been used as the hydrogen source. However, the hydrogenation in which hydrogen transfer from organic compounds takes place has also been reported;[1] it has been called transfer-hydrogenation,[2] transhydrogenation[3] or conjugated hydrogenation.[4] Transfer-hydrogenation has several advantages because it needs no hydrogen gas. For example, the experimental operation is easy, and a completely homogeneous system is made available. It has been reported that primary alcohols, secondary alcohols,[4,5] and six-membered cyclic olefins[2] donate hydrogen to olefins to give aldehydes, ketones, and aromatic compounds respectively in the presence of heterogeneous catalysts, such as metallic palladium and nickel. As for the reactions of homogeneous systems, Itatani and Bailar have reported that methyl linoleate[6] or soybean oil[7] are hydrogenated to monoenes selectively under the pressure of nitrogen gas when benzene–methanol is used as the solvent and platinum or palladium complexes as the catalysts. In this case, methanol is inferred to be the hydrogen souce. It has also been reported that the hydrogenation of methyl linoleate occurs in the presence of dihalobis(triphenylphosphine)nickel(II) as the catalyst and tetrahydrofuran or benzene as the solvent.[8] Studies of homogeneous transfer-hydrogenation have thus far been performed incidentally to hydrogenation by molecular hydrogen; no systmatic investigation of the reaction conditions or the reaction mechanism has yet been undertaken. We also found that the olefin linkages of methyl linoleate were reduced in 2-propanol in the presence of bis(2,4-pentanedionato)nickel(II) under an atmosphere of nitrogen; however, the reproducibility of the reaction was discouragingly bad, perhaps because the catalyst decomposed to give an insoluble substance.[9]

The work reported here was undertaken in order to study transfer-hydrogenation systematically; some of the results have been reported in a preliminary communication.[10] There it was shown that $FeBr_2(PPh_3)_2$ and $FeCl_2(PPh_3)_2$ are the most active catalysts of the $MX_2(PPh_3)_2$ complexes, where M is Fe(II), Co(II), or Ni(II), and where X is Cl, Br, or I, and that 1,5-cyclooctadiene (1,5-COD), which is presumed to have the strongest coordinating ability of all the cycloolefins attempted, is most readily reduced.

Results and Discussion

The experiments in this study were carried out under conditions such as follows, unless otherwise noted. For instance, a dioxane solution of 1,5-COD (concn., 0.5M), dichlorobis(triphenylphosphine)iron(II) (0.05M), and pyrocatechol (2.0M), sealed in a Pyrex glass tube under a vacuum (10^{-2} mmHg), was heated at 200±1°C for six hours. Though the catalyst did not dissolve completely at room temperature, it did so at once at the reaction temperature and gave no insoluble materials until the end of the reaction. In this reaction, not only the hydrogenation of 1,5-COD to cyclooctene (COE) and cyclooctane (COA), but also the isomerization to 1,4- and 1,3-cyclooctadiene (1,4-COD and 1,3-COD), occurred. From the composition of the reaction mixtures, the following reaction parameters were derived: the selectivity is the percentage of COE in the reduced products, and the percentage of hydrogenation was calculated on the assumption that both double bonds of cyclooctadienes (COD) are reduced. (See the footnotes of Table 1.) Therefore, if the selectivity is 100%, the reaction may be regarded as having been completed at 50% hydrogenation. The percentage of conversion is the percentage of the 1,5-COD consumed. A part of the results are summarized in Table 1.

Hydrogen Donors. At first, *prim*- and *sec*-alcohols, and cyclohexene, which have been reported as hydrogen donors, were examined, but their ability to donate hydrogen was quite weak. Then, taking a hint from

1) L. M. Jackman, "Advances in Organic Chemistry," Vol. II, ed. by P. A. Raphael, E. C. Taylor, and H. Wynberg, Interscience Publishers, New York (1960), p. 329.
2) E. A. Braude, R. P. Linstead, and P. W. D. Mitchell, *J. Chem. Soc.*, **1954**, 3578.
3) L. E. Brown, and G. A. Hamilton, *J. Amer. Chem. Soc.*, **92**, 7225 (1970).
4) H. N. Basu and M. M. Chakrabarty, *J. Amer. Oil Chemists, Soc.*, **43**, 119 (1966).
5) K. Sakai, T. Ito, and K. Watanabe, This Bulletin, **39**, 2230 (1966).
6) J. C. Bailar, Jr. and H. Itatani, *J. Amer. Chem. Soc.*, **89**, 1592 (1967).
7) H. Itatani and J. C. Bailar, Jr., *J. Amer. Oil Chemists' Soc.*, **44**, 147 (1967).
8) H. Itatani and J. C. Bailar, Jr., *J. Amer. Chem. Soc.*, **89**, 1600 (1967).
9) S. Nanya, M. Hanai, and K. Fukuzumi, *Kogyo Kagaku Zasshi*, **72**, 2005 (1969).
10) T. Nishiguchi and K. Fukuzumi, *Chem. Commun.*, **1971**, 139.

Table 1. Transfer-hydrogenation of 1,5-COD catalyzed by $FeCl_2(PPh_3)_2$[a]

No.	Gas in sealed tube	Hydrogen donor	React. temp. °C	Yield of products, %				% Conv.[b]	% Conv. of COD[c]	% Hyd.[d]	Selectivity[e] %
				COA	COE	1,3-COD	1,4-COD				
1	None	*o*-$C_6H_4(OH)_2$	160	5	6	1	5	16	11	8	53
2	None	*o*-$C_6H_4(OH)_2$	180	22	8	6	10	46	30	26	27
3	None	None	180	3	5	1	5	14	8	5	64
4	None	*o*-$C_6H_4(OH)_2$	200	57	9	22	9	97	66	62	14
5	O_2	*o*-$C_6H_4(OH)_2$	200	55	9	22	9	95	64	60	14
6	Air	*o*-$C_6H_4(OH)_2$	200	57	9	22	9	97	66	62	15
7	N_2	*o*-$C_6H_4(OH)_2$	200	58	9	22	8	97	67	64	13
8	CO_2	*o*-$C_6H_4(OH)_2$	200	57	9	20	9	95	66	62	15
9	None	1,2,3-$C_6H_3(OH)_3$	200	63	6	14	9	92	69	65	8
10	None	*p*-$C_6H_4(OH)_2$	200	53	8	24	10	96	61	57	13
11	None	2-C_3H_7OH	200	3	1	1	7	12	4	3	21
12	None	1-$C_8H_{17}OH$	200	3	8	1	8	20	11	6	73
13	None	2-$C_8H_{17}OH$	200	4	1	2	11	17	5	4	13
14	None	1-$C_{12}H_{25}OH$	200	3	1	1	7	11	3	3	16
15	None	1-$C_{12}H_{25}SH$	200	6	7	4	18	33	13	9	56
16	None	1-$C_{12}H_{25}NH_2$	200	1	1	1	5	6	1	1	f)
17	None	Cyclohexene	200	4	1	1	9	15	5	4	20
18	None	None	200	11	3	4	14	30	14	12	16
19	None	1,2,3-$C_6H_3(OH)_3$	240	75	23	2	1	99	98	87	22
20	None	*o*-$C_6H_4(OH)_2$	240	71	14	14	2	99	85	77	16
21	None	*p*-$C_6H_4(OH)_2$	240	68	15	13	3	98	83	75	18
22	None	1-$C_7H_{15}OH$	240	6	3	3	10	12	9	8	33
23	None	None	240	32	9	20	11	72	42	37	22

a) 1,5-COD (concn., 0.5M), hydrogen donors(2.0M) and the catalyst (0.05M) were heated in dioxane for 6 hr.
b) Conversion of 1,5-COD to COA, COE, 1,3-COD and 1,4-COD.
c) Conversion of COD to COA and COE.
d) This is given by $\frac{2\times COA+COE}{2}$.
e) Given by $\frac{COE}{COA+COE}\times 100$.
f) The yield was too low to evaluate.

the reaction in which *p*-benzoquinone abstracts hydrogen from organic compounds to form hydroquinone,[1] we tried to use polyhydroxybenzenes with hydroxyl groups at the *ortho* or *para* positions as hydrogen donors; we founs that they were much superior to the other organic compounds tried. That is, the percentage of hydrogenation was 64—57% in the case of the polyhydroxybenzenes (Nos. 4—10 in Table 1), while it was less than 10% in the cases of the other compounds (Nos. 11—18). The order of the ability to give hydrogen, based on the percentage of hydrogenation, was found to be as follows: pyrogallol>pyrocatechol>hydroquinone$\gg$*n*-dodecanethiol>1-octanol>cyclohexene>2-octanol>*n*-dodecanol>*n*-dodecyl amine.
When *prim*- or *sec*-alcohols were used, small amounts of aldehydes or ketones were detected by IR analysis. However, when the polyhydroxybenzenes were used, a tarry material was formed and no quinones were identified. This might be at least partly attributable to the thermal instability of the quinones, though further study is needed. In fact, *o*- and *p*-benzoquinone gave tarry substances when heated in dioxane at 200°C.

Unexpectedly, as is shown in Table 1 and Figs. 5 and 6, not only were COA and COE formed, even if no hydrogen donor was added especially, but also the percentage of hydrogenation was higher in these cases (Nos. 18 and 23) than in the cases where the alcohols, *n*-dodecanethiol, cyclohexene and *n*-dodecyl amine, were used (Nos. 11—17 and 23). Hydrogen transfer from the solvent, dioxane, to 1,5-COD was inferred, for the possibility of the disproportionation of the diene may be rejected on the following grounds: cyclooctatrienes, which would result from the disproportionation of the diene, were not detected by gas-chromatographic analysis, and the total amount of the detected eight-membered cyclic hydrocarbons was almost equal to the amount of 1,5-COD charged as a reactant.

Effect of Gases in the Sealed Tubes. It is well known that some metal complexes react with oxygen or nitrogen,[11] and that radical reactions are apt to be influenced by the presence of oxygen. Therefore, the experiments under atmosphers of oxygen, air, nitrogen, and carbon dioxide were carried out (Nos. 5—8), and compared with the one done under a vacuum. The results showed that the compositions of the reaction mixtures were identical within the limits of experimental error under any gas or in a vacuum.

Reaction Temperature. The percentage of conversion was 16% at 160°C, 46% at 180°C, 97% at 200°C, and more than 99% at 240°C. As the reac-

11) J. P. Collman, *Accounts Chem. Res.*, **1**, 136 (1968).

tion temperature was raised, the percentage of hydrogenation also increased, but the selectivity had almost no connection with the reaction temperature at relatively high conversions.

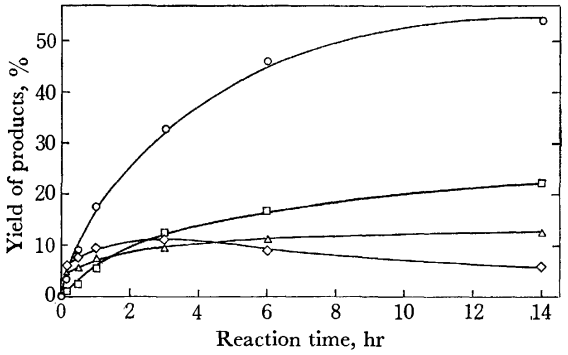

Fig. 1. Time dependence of the yield of the products.
○: COA, △: COE, □: 1,3-COD, ◇: 1,4-COD

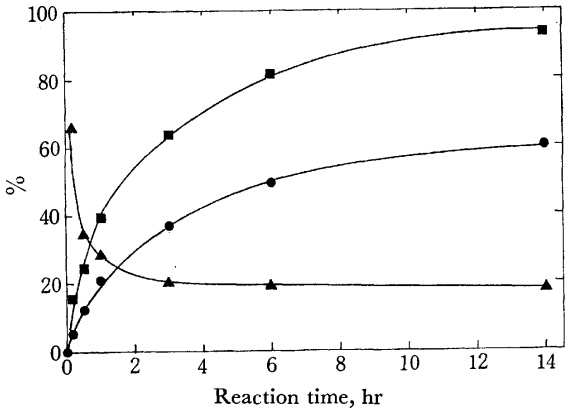

Fig. 2. Time dependence of the reaction parameters.
●: % Hydrogenation, ▲: Selectivity, ■: % Conversion

Reaction Time. At an early stage of the reaction, all the reaction parameters except that of the selectivity were in proportion to the reaction time (Figs. 1 and 2). The lack of an induction period suggests that the time for the formation of an active species is short, though induction periods have been reported in a few homogeneous hydrogenations.[12]

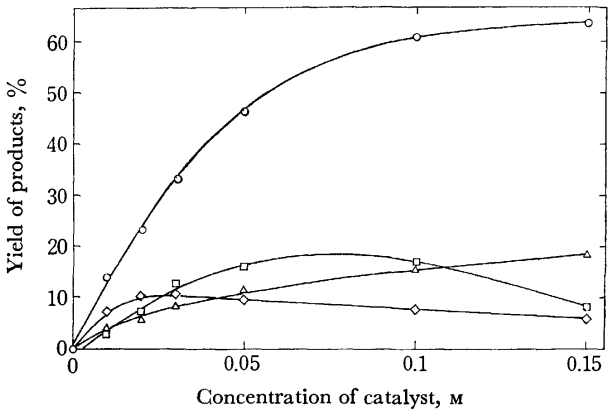

Fig. 3. Dependence of yield of the products on initial concentration of the catlyst.
○: COA, △: COE, □: 1,3-COD, ◇, 1,4-COD

12) P. S. Hallman, B. R. McGarvey, and G. Wilkinson, *J. Chem. Soc., A*, **1968**, 3143.

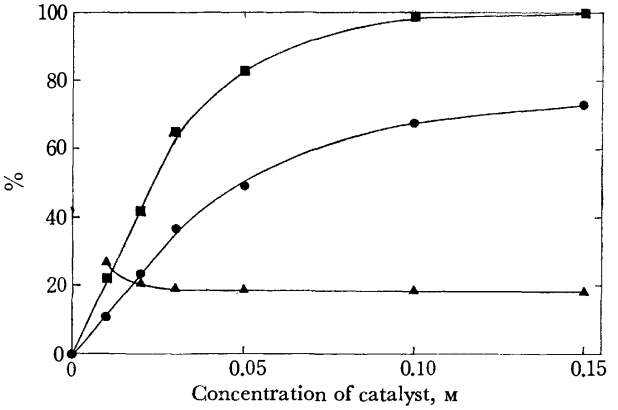

Fig. 4. Dependence of the reaction parameters on initial concenttation of the catalyst.
●: % Hydrogenation,
■: % Conversion, ▲: Selectivity

Concentration of the Catalyst. The percentage of hydrogenation and the percentage of conversion were proportional to the initial concentration of the catalyst below 0.05M (Figs. 3 and 4). This fact suggests that the rate of the hydrogenation is first order in relation to the initial concentration of the catalyst.

Concentration of Pyrocatechol. The influence of the

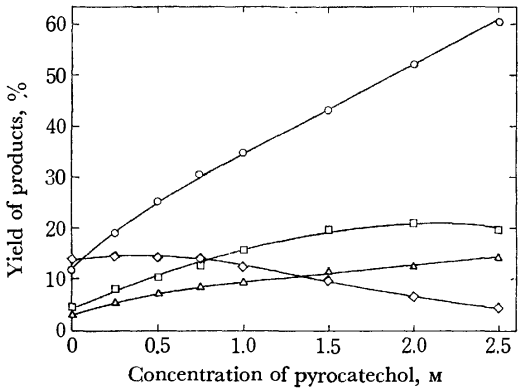

Fig. 5. Dependence of yield of the products on initial concentration of pyrocatechol.
○: COA, △: COE,
□: 1,3-COD, ◇: 1,4-COD

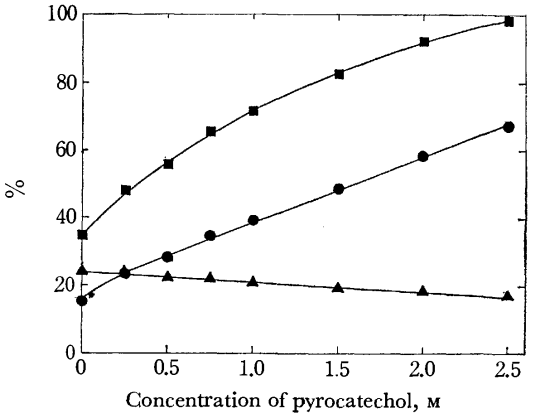

Fig. 6. Depencence of the reaction parameters on initial concentration of pyrocatechol.
●: % Hydrogenation,
■: % Conversion, ▲: Selectivity

initial concentration of a hydrogen donor was examined by the use of pyrocatechol, which has a strong ability to supply hydrogen and a high solubility (Figs. 5 and 6). The interpretation of the results was complicated by the fact that the solvent, dioxane, gave some hydrogen, as has been mentioned previously. If the hydrogen-donating capacity of the solvent is equal to that of pyrocatechol at a concentration of about 0.8M in the solvent, the percentage of hydrogenation and the percentage of conversion may have a linear relation to the initial concentration of pyrocatechol.

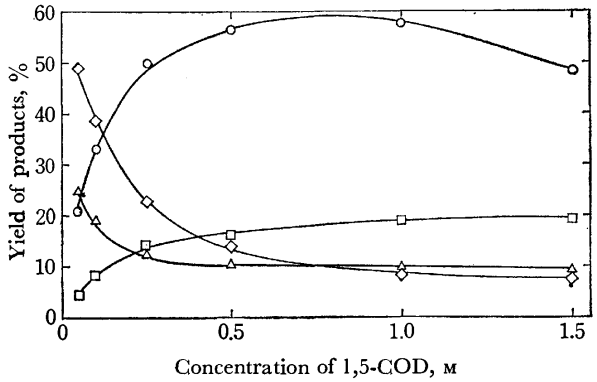

Fig. 7. Depencence of yield of the products on initial concentration of 1,5-COD.
○: COA, △: COE, □: 1,3-COD,
◇: 1,4-COD

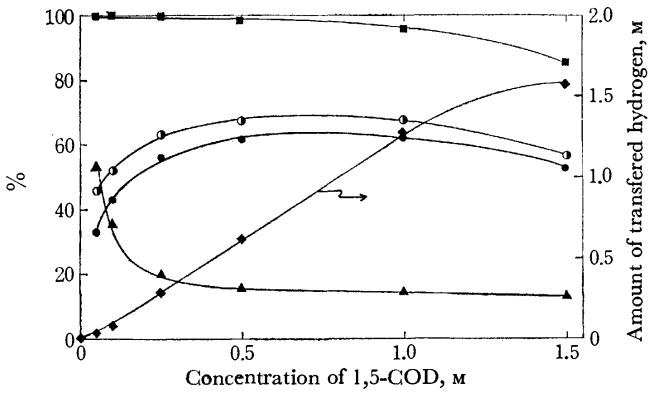

Fig. 8. Depencence of the reaction parameters and the amount of transfered hydrogen on initial concentration of 1,5-COD.
●: % Hydrogenation, ■: % Conversion,
◑: % Conversion of COD, ▲: Selectivity, ◆: Amount of transfered hydrogen which is given by [% Hydrogenation] ×[Initial concentration of 1,5-COD]×1/100

Concentration of 1,5-COD. The percentage of hydrogenation and the percentage of conversion of COD were found to have maximum values against the initial concentration of 1,5-COD (Figs. 7 and 8). That is, the higher the concentration, the larger the degree of the hydrogenation, until it decreased, perhaps because of the deficiency of the hydrogen donor. This fact suggests that at least two 1,5-COD molecules are involved in the reduction and that they act not only as hydrogen acceptors, but also as ligands having the function of co-catalysts, for if merely one molecule of 1,5-COD is involved, the lower values of the parameters at the lower concentration of 1,5-COD cannot be explained. Therefore, it is difficult to decide whether the susceptibility of 1,5-COD to the reduction is due to its nature as a hydrogen acceptor or as a ligand in activating the catalyst. The amount of transferred hydrogen which caused the reduction was roughly proportional to the initial concentration of 1,5-COD at concentrations from 0.3M to 1.0M.

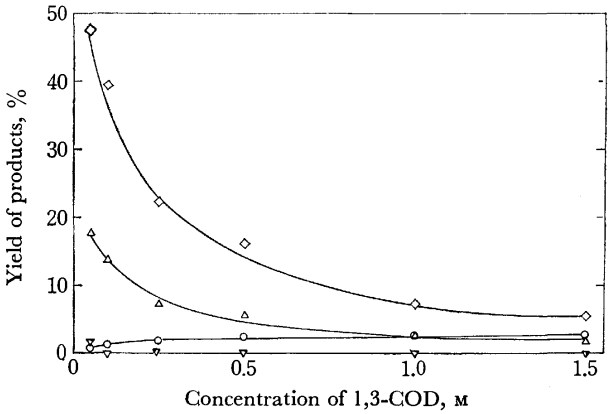

Fig. 9. Depencence of yield of the products on initial concentration of 1,3-COD.
○: COA, △: COE, ▽: 1,5-COD,
◇: 1,4-COD

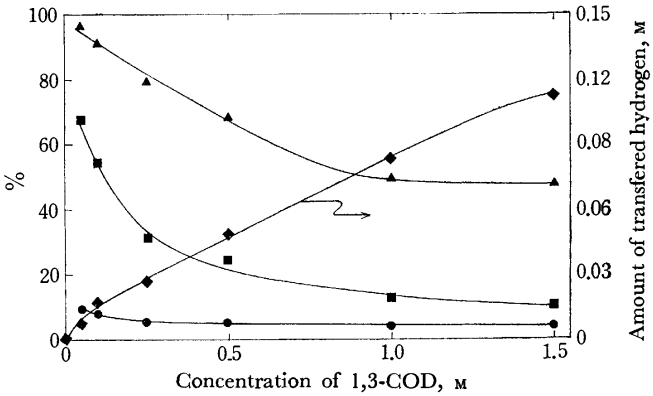

Fig. 10. Depencence of the reaction parameters and the amount of transfered hydgogen on initial concentration of 1,3-COD.
●: % Hydrogenation of 1,3-COD, ■: % Conversion of 1,3-COD, ▲: Selectivity, ◆: Amount of transfered hydgogen which is given by [% Hydrogenation]×[Initial concenration of 1,3-COD]×1/100

The lower the initial concentration of 1,5-COD, the higher the ratio of 1,4-COD in the reaction mixture. It can thus be inferred that the lower the concentration of COD at constant concentrations of the catalyst and the hydrogen donor, the easier it is to reach an equilibrium among COD. From this inference and our observations, the isomerization of 1,3-COD to 1,4-COD can be expected to occur more easily at a lower initial concentration of the conjugated diene; this expectation was confirmed (Figs. 9 and 10). 1,3-COD did not show such a co-catalystic action as 1,5-COD did, and the percentage of hydrogenation decreased constantly as the initial concentration of 1,3-COD increased.

General Discussion. It is well known that hydrido complexes are formed as active species not only in

homogeneous hydrogenation by molecular hydrogen, but also in the isomerization of olefins, where alcohols act as co-catalysts.[4,13] Moreover, hydrido complexes are obtained in the reaction of Rh(I), Os(I), Ir(I), and Pt(II) complexes with alcohols.[14] In analogy with these reactions, a hydrido complex is presumed to be involved as an active species in the transfer-hydrogenation.

It has been reported that alcohols give molecular hydrogen and carbonyl compounds when heated in the presence of catalysts in not only a heterogeneous but also in a homogeneous system.[15] Therefore, the evolution of molecular hydrogen during the transfer-hydrogenation reaction may not be so unreasonable. However, perhaps hydrogen is not transferred in the gaseous form in the reaction, for the evolution of molecular hydrogen from pyrocatechol was not observed upon heating at 200°C without the catalyst, and the hydrogenation of 1,5-COD by molecular hydrogen did not take place without the catalyst. Such a reaction as is shown in the following equation should not be regarded as a transfer-hydrogenation *via* molecular hydrogen.

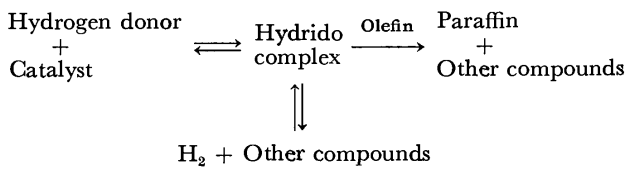

The mechanistic study of the transfer-hydrogenation is now in progress.

13) H. A. Tayim and J. C. Bailar, Jr., *J. Amer. Chem. Soc.*, **89**, 3420 (1967); *ibid.*, **89**, 4330 (1967); R. W. Adams, G. E. Batley, and J. C. Bailar, Jr., *ibid.*, **90**, 6051 (1968); J. F. Harrod and A. J. Chalk, *ibid.*, **86**, 1776 (1964).

14) J. Chatt and B. L. Shaw, *Chem. Ind.*, (London) **1961**, 290; L. Vaska, *ibid.*, **1961**, 1403; L. Vaska, *J. Amer. Chem. Soc.*, **83**, 756 (1961); *ibid.*, **86**, 1943 (1964); J. Chatt and B. L. Shaw, *J. Chem. Soc.*, **1962**, 5075; J. Chatt, B. L. Shaw, and A. E. Field, *ibid.*, **1964**, 3466; J. Chatt, R. S. Coffey, and B. L. Shaw, *ibid.*, **1965**, 7391; L. Vaska and J. W. DiLuzio, *J. Amer. Chem. Soc.*, **83**, 1262 (1961).

15) H. B. Charman, *J. Chem. Soc., B*, **1970**, 548; *ibid.*, **1967**, 629; J. Chatt and B. L. Shaw, *J. Chem. Soc., A*, **1966**, 1437; M. H. Saltza, J. Red, J. D. Dutcher, and O. Winterstein, *J. Amer. Chem. Soc.*, **83**, 2784 (1961).

Experimental

Materials. The dichlorobis(triphenylphosphine)iron(II) was prepared according to the method of Pignolet *et al.*[15] and was recrystallized from toluene. The dioxane, 1,5-COD, 1,3-COD and cyclohexene were purified by distillation over metallic sodium. The purified 1,5-COD was found to be contaminated with 0.2% of COA, 0.7% of COE, 0.5% of 1,3-COD, and 0.9% of 1,4-COD. The Pyrocatechol, hydroquinone, and pyrogallol were purified by recrystallization from benzene. All the other reagents were of a commercial G. R. grade. The mixture of cyclooctatrienes was prepared by the method of Cope and Hockstein.[16]

An Example of Transfer-hydrogenation. 1,5-COD (0.0541 g, 0.5 mmol), pyrocatechol (0.22 g, 2.0 mmol), and $FeCl_2(PPh_3)_2$ (0.0326 g, 0.05 mmol) were put into a Pyrex glass tube which had been sealed at one side. Into the mixture, dioxane was then stirred with a wire, and the total volume of the solution was made 1.0 m*l*. The solution was degassed with a Dry Ice-acetone bath and a vacuum line, and sealed in a vacuum (10^{-2} mmHg). The sealed tube was heated for 6 hr in a silicon-oil bath kept at 200±1°C. To analyze the reaction mixture, gas chromatography was performed at 80°C with a Hitachi Perkin-Elmer instrument equipped with a flame ionization detector. A 2 m×6 mm stainless steel column packed with 25% of 1,2,3-tris(2-cyanoethoxy)-propane on Celite 545 was used.

The other transfer-hydrogenations were carried out in the same way.

When the glass tubes were sealed under gases, the volume of the gases in the reaction vessels was three times that of the solution.

An Attempted Hydrogenation by Molecular Hydrogen without Catalysts. A dioxane solution of 1,5-COD (0.5M, 10 m*l*) was placed in a 50 m*l* stainless steel autoclave, and the air in the vessel was replaced with hydrogen of 10 atm. After being heated for 6 hr at 180°C, the solution was analyzed by gas chromatography.

An Examination to Test the Evolution of Hydrogen. A dioxane solution of pyrocatechol (1.0M) was sealed in a Pyrex glass tube under a vacuum and was then heated at 200°C for 4 hr. When the sealed tube was then broken in water, no evolution of gas was observed.

16) L. H. Pignolet, D. Forster, and W. D. Horrocks, Jr., *Inorg. Chem.*, **7**, 828 (1968).

17) C. Cope and F. A. Hochstein, *J. Amer. Chem. Soc.*, **72**, 2517 (1950).

Spectral Shift of Band Origins in the Near Ultraviolet Absorption Spectra of Some 2- and 3-Substituted Pyridines

G. S. KASTHA and S. C. BAG

Optics Department, Indian Association for the Cultivation of Science, Calcutta 32, India

(Received April 30, 1971)

The relative shifts in the position of band origin of the lowest singlet π-electron transition in some 2- and 3-substituted pyridines, and monosubstituted benzenes with similar substituents, with respect to those of the parent molecules have been calculated by the method of localized orbitals with configuration interaction. Under certain assumptions, the calculated relative shifts in the 2- and 3-substituted pyridines are found to bear a linear relationship with that of the corresponding monosubstituted benzenes. The experimental data are found to be in agreement with the theoretical expectation.

The close similarity between the near ultraviolet π-electronic absorption spectra of monosubstituted benzenes and similarly substituted pyridines is well known. From the available values of the position of the O–O band of the lowest singlet $\pi\rightarrow\pi^*$ transitions in these compounds in the vapour phase, it is seen that the shifts of the band origin in the near ultraviolet absorption spectra of 2- and 3-substituted pyridines from that of pyridine are closely parallel to those of corresponding monoderivatives of benzene with respect to that of benzene. The π-electronic energy levels of some monosubstituted benzene molecules have been calculated from localized orbital model with configuration interaction by Kimura, Tsubomura, and Nagakura[1] and by Kimura and Nagakura.[2] Similar calculations including inductive effect of the substituent have been made by Favini, Gamba, and Bellobono[3] in amino- and nitro-substituted pyridines. With reasonable values of the ionization potential of the substituent, the electron affinity of benzene and pyridine molecules to which the substituent is attached and the resonance integrals between the substituent and the carbon atom of the respective molecules, these authors have obtained fair agreement between the calculated and experimentally observed values of the π-electronic energy levels in these molecules. SCF calculations of the π-electronic energy level of monosubstituted benzenes have also been reported by several workers.[4–6]

We have applied the localized orbital model with configuration interaction to explain the observed parallelism of the shifts of band origins in the near ultraviolet absorption spectra of some monosubstituted benzenes and 2- and 3-substituted pyridines with the same substituent without going into the actual calculations of the lowest π-electronic energy levels of all these molecules.

Theoretical Considerations

a) Monosubstituted Benzenes. The energy of the lowest excited π-electronic level E_a^X of monosubstituted benzenes with substituent X corresponding to E_a the energy of the α-band in benzene has been obtained from an approximate solution of the 3×3 determinantal equation (which is equivalent to a second order perturbation calculation) of B-species given by Kimura and Nagakura[2] for monosubstituted benzenes, and is given by

$$E_a^X = E_a + \frac{\frac{1}{6}\beta_X^2}{E_a - E_{C.T,b}} \qquad (1)$$

where β_X is the resonance integral corresponding to $\beta+\beta'$ of Kimura and Nagakura[2] and $E_{C.T,b}=I_X-A-Q_2$ is the energy of the charge transfer state. All these quantities are given in electron volts and the notations used are those of Kimura and Nagakura.[2]

The validity of Eq. (1) is seen from Table 1 where a comparison of the exact values of this energy level in a number of monosubstituted benzene molecules calculated by Kimura and Nagakura[2] and those for the corresponding molecules obtained from Eq. (1) is given. All these values have been calculated with the parameters given by Kimura and Nagalura.[2]

TABLE 1. COMPARISON OF THE ENERGY OF THE LOWEST EXCITED STATE IN MONOSUBSTITUTED BENZENES

(All values in eV)

Substituent	F	Cl	Br	OH	NH_2
Kimura and Nagakura[2]	4.80	4.70	4.53	4.68	4.40
Equation (1)	4.80	4.71	4.53	4.68	4.35

If the lowering of the ground state energy is neglected, the shift in the position of α-band of benzene with substitution is given by:

$$\Delta E_a^X = E_a - E_a^X,$$

and from Eq. (1) we get

$$\beta_X^2 = 6\Delta E_a^X (E_{C.T,b} - E_a) \qquad (2)$$

b) Monosubstituted Pyridines. The method of calculating the lowest excited π-electron energy levels in 2- and 3-substituted pyridines is the same as that used by Favini, Gamba, and Bellobono[3] in the case of aminopyridines. But instead of solving the 7×7 determinantal equation exactly, an approximate solution as in the case of monosubstituted benzenes has been used for obtaining the energy of the lowest excited state in each of the 2- and 3-substituted pyridines with the

1) K. Kimura, H. T. Tsubomura, and S. Nagakura, This Bulletin, **37**, 1336 (1964).
2) K. Kimura and S. Nagakura, *Mol. Phys.*, **9**, 117 (1965).
3) G. Favini, A. Gamba, and I. R. Bellobono, *Spectrochim. Acta*, **23A**, 89 (1967).
4) B. R. Russell, R. M. Hedges, and W. R. Carper, *Mol. Phys.*, **12**, 283 (1967).
5) P. Knowlton and W. R. Carper, *ibid.*, **11**, 213 (1966).
6) J. D. Bene and H. H. Jaffé, *J. Chem. Phys.*, **49**, 221 (1968).

substituent X. These are respectively given by the following equations:
For 2-substituted pyridines:

$$E_1^{X(2)} = E_1 - 0.017I_\pi^X + \frac{0.166\beta_X^2}{E_1 - E_5^{(2)} - 0.132I_\pi^X} + \frac{0.011\beta_X^2}{E_1 - E_6^{(2)} - 0.27I_\pi^X} \quad (3)$$

and for 3-substituted pyridines:

$$E_1^{X(3)} = E_1 - 0.083I_\pi^X + \frac{0.171\beta_X^2}{E_1 - E_5^{(3)} - 0.157I_\pi^X} + \frac{0.042\beta_X^2}{E_1 - E_6^{(3)} - 0.33I_\pi^X} \quad (4)$$

where E_1 is the energy of the lowest excited state (A_1) of pyridine, $E_1^{X(2)}$ and $E_1^{X(3)}$ are those of 2- and 3-substituted pyridines, respectively, I_π^X is the inductive parameter of the substituent X given by Godfrey and Murrell,[7] the quantities containing β_X^2 are the square of the Hamiltonian matrix elements between the lowest excited state (A_1) of pyridine and the appropriate charge transfer state $T_D{}^4$ and $T_D{}^5$ according to the notations used by Favini, Gamba, and Bellobono.[3]

For the two types of substituted pyridines, the following are the energies of these two charge transfer states.

$$\left.\begin{aligned} E_5^{(2)} &= I^X - A - Q_5{}^{(5)}; \quad E_6^{(2)} = I^X - A - Q_6{}^{(2)} \\ E_5^{(3)} &= I^X - A - Q_5{}^{(3)}; \quad E_6^{(3)} = I^X - A - Q_6{}^{(3)} \end{aligned}\right\} \quad (5)$$

If the lowering of the ground state energy is neglected, the substitution of β_X^2 from Eq. (2) into Eqs. (3) and (4) yields, for the values of the shift of the lowest excited energy level for the two kinds of substituted pyridines, the following expressions:

$$\Delta E_2^X = E_1 - E_1^{X(2)} = 0.017I_\pi^X + \left[\frac{E_{C.T,b} - E_a}{E_5^{(2)} - E_1 + 0.132I_\pi^X} + \frac{0.066(E_{C.T,b} - E_a)}{E_6^{(2)} - E_1 + 0.27I_\pi^X}\right]\Delta E_a^X \quad (6)$$

and

$$\Delta E_3^X = E_1 - E_1^{X(3)} = 0.083I_\pi^X + \left[\frac{1.026(E_{C.T,b} - E_a)}{E_5^{(3)} - E_1 + 0.157I_\pi^X} + \frac{0.252(E_{C.T,b} - E_a)}{E_6^{(3)} - E_1 + 0.33I_\pi^X}\right]\Delta E_a^X \quad (7)$$

Assuming that the molecules of monosubstituted benzene and the two types of substituted pyridine as regular hexagons with bond distances 1.39 Å, the values for the bond lengths between the substituent and the substituted carbon atom as those given by Kimura and Nagakura[2] and a point charge approximation for the evaluation of the electrostatic energies Q, it is found $Q_5{}^{(2)} \approx Q_5{}^{(3)}$, $Q_6{}^{(2)} \approx Q_6{}^{(3)}$, and $Q_6 > Q_5 > Q_2$, Q_6 being greater than Q_5 by about 10% and Q_5 greater than Q_2 by the same amount.

If we assume that for a given substituent $I^X - A$ has the same value for the monosubstituted benzene and the corresponding 2- and 3-substituted pyridines and observing that $E_a \approx E_1$ the Eqs. (6) and (7) may be further simplified. The quantities $(E_{C.T,b} - E_a)/(E_5^{(2)} - E_1 + 0.132I_\pi^X)$ etc. will be somewhat larger than unity while though the terms like $(E_{C.T,b} - E_a)/(E_6^{(3)} - E_1 + 0.271_\pi^X)$ have values appreciably greater than unity their effects will be reduced because in each case they are multiplied by small quantities. Hence the coefficients of ΔE_a^X in Eqs. (6) and (7) will be a little larger than 1.066 and 1.278, respectively. These equations may, therefore, be written as

$$\Delta E_2^X = 0.017I_\pi^X + 1.1\Delta E_a^X \quad (8)$$

and

$$\Delta E_3^X = 0.083I_\pi^X + 1.3\Delta E_a^X \quad (9)$$

Further, if we assume that I_π^X for the different substituents may be represented by an average value I_π for both types of pyridine molecules considered, then it follows from Eqs. (8) and (9) that the plots of ΔE_2^X and ΔE_3^X *vs.* ΔE_a^X are straight lines with slopes 1.1 for the 2-pyridines and 1.3 for the 3-pyridines and the intercepts have values $0.017\,I_\pi$ and $0.083\,I_\pi$, respectively.

Comparison with Experiment

In order to find out how far the conclusions drawn from the theoretical considerations agree with the experimental data obtained by various workers[8–22] the shifts in the positions of O-O band (expressed in units of electron volt) for the 2- and 3-substituted pyridines with respect to that of pyridine are plotted against

TABLE 2. POSITION OF O–O BAND (cm^{-1}) IN THE NEAR ULTRAVIOLET ABSORPTION SPECTRA OF BENZENE, MONOSUBSTITUTED BENZENES, PYRIDINE, 2-SUBSTITUTED AND 3-SUBSTITUTED PYRIDINES

Substituent	Monosubstituted benzenes	2-Substituted pyridine	3-Substituted pyridine
H	38090[8]	38350[9]	
F	37819[10]	38000[11]	37320[11]
CH_3	37477[12]	37620[13]	37380[13]
Cl	37052[14]	37115[15]	36469[15]
Br	36996[16]	36958[17]	36300[17]
OH	36350[18]	36420[19]	36247[19]
NH_2	34035[20,21]	34324[22]	33854[22]

7) M. Godfrey and J. N. Murrell, *Proc. Roy. Soc., Ser. A*, **278**, 64 (1964).

8) H. Sponer, G. Nordheim, A. L. Sklar, and E. Teller, *J. Chem. Phys.*, **7**, 207 (1939).
9) H. Sponer and H. Strucklen, *ibid.*, **14**, 101 (1946).
10) S. H. Wollman, *ibid.*, **14**, 123 (1946).
11) H. P. Stephenson, *ibid.*, **22**, 1077 (1954).
12) N. Ginsburg, W. W. Robertson, and F. A. Matsenm *ibid.*, **14**, 511 (1946).
13) J. H. Rush and H. Sponer, *ibid.*, **20**, 1847 (1952).
14) H. Sponer and S. H. Wollman, *ibid.*, **9**, 816 (1941).
15) G. S. Kastha and S. C. Bag, *Indian. J. Pure Appl. Phys.*, (1971). (Communicated)
16) I. Wallerstein, *Phys. Rev.*, **59**, 924 (1941).
17) T. N. Misra, *Indian J. Phys.*, **34**, 381 (1960).
18) F. A. Matsen, N. Ginsburg, and W. W. Robertson, *J. Chem. Phys.*, **13**, 309 (1945).
19) S. C. Bag, (Unpublished data).
20) R. Titeica, *Bull. Soc. Roumaine Phys.*, **43**, 15 (1942).
21) N. Ginsburg and F. A. Matsen, *J. Chem. Phys.*, **13**, 167 (1945).
22) T. N. Misra, *Indian J. Phys.*, **35**, 420 (1961).

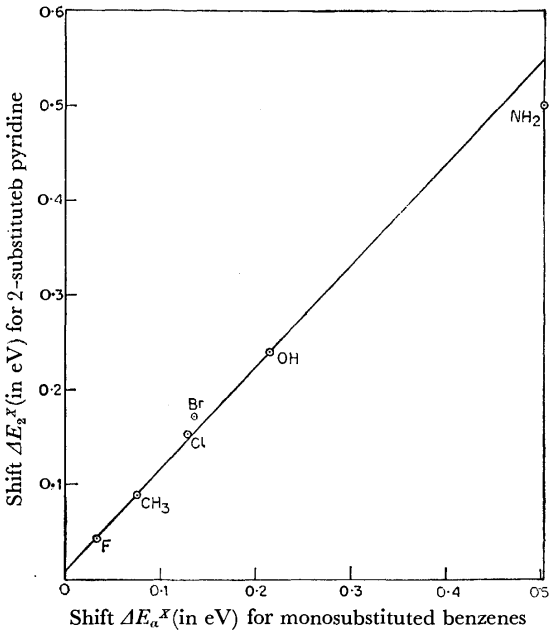

Fig. 1.

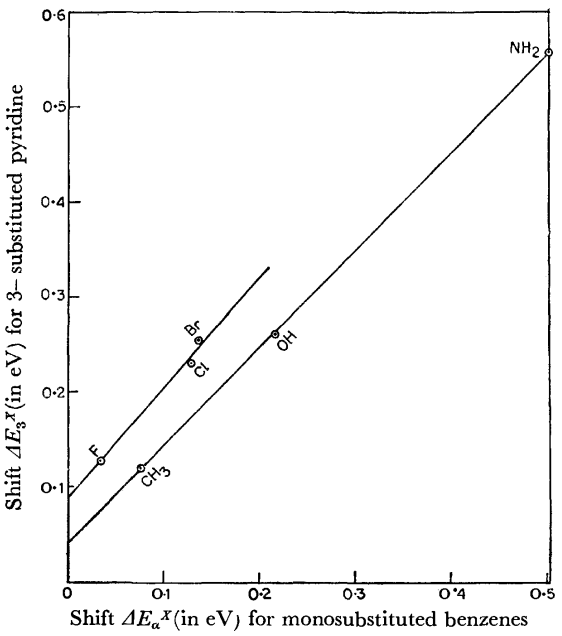

Fig. 2.

those of the corresponding monosubstituted benzene with respect to benzene in Figs. 1 and 2, respectively. For this purpose the positions of the O–O band in the near ultraviolet absorption spectra of monosubstituted benzenes and some 2- and 3-substituted pyridines with similar substitutions, taken from available data, are shown in Table 2.

It is seen from Figs. 1 and 2 that the plots of ΔE_2^X *vs.* ΔE_α^X and ΔE_3^X *vs.* ΔE_α^X give straingt lines. In the case of 2-substituted pyridines all the points corresponding to different substituents fall on the same line (Fig. 1) with a slope of 1.07 and an intercept of 0.01 eV. This value of the slope compares favourably with the expected value 1.1 of Eq. (8). The average value of I_π obtained from the same equation is about 0.6 eV. For the 3-substituted pyridines the points corresponding to F, Cl, and Br as substituents and those with CH_3, OH, and NH_2 as substituents fall on two different straight lines (Fig. 2). The former has an inclination of 1.16 and an intercept of 0.09 eV while for the latter these values are 1.02 and 0.04 eV, respectively. The value of the slope for either of the straight lines is smaller than 1.3 expected from Eq. (9) while the average values of I_π for the two groups of compounds are respectively about 1.0 and 0.5 eV. The value 0.6 eV of I_π obtained from 2-substituted pyridine compares favourably with the values 1.0 eV and 0.5 eV for this quantity in the case of 3-substituted pyridines. The values of I_π^X given by Godfrey and Murrell[7] for these substituents vary from 0.54 eV for the methyl group to 1.74 eV for the amino group. The values obtained in the present case lie within these limits.

Far Infrared Spectra and the Calculation of Lattice Vibrations of Benzoic Acid[1]

Shunsuke MESHITSUKA, Hiroaki TAKAHASHI, Keniti HIGASI, and Bernhard SCHRADER*

Department of Chemistry, School of Science and Engineering, Waseda University, Tokyo

**Institut für Spektrochemie und angewandte Spektroskopie, Dortmund, Germany*

(Received December 27, 1971)

Polarized far infrared spectra from 400 to 30 cm^{-1} of benzoic acid single crystals have been measured. Three bands polarized parallel to the C_2^5 screw axis *b* were observed at 104, 86, and 62 cm^{-1}, and three bands polarized parallel to the *a*-axis at 106, 76, and 65 cm^{-1}. The lattice vibrations of benzoic acid have been calculated assuming the rigidity of the molecule during the lattice vibrations and applying a simple force field. The bands at 104, 86, and 62 cm^{-1} were assigned to the rotational vibrations of A_u symmetry species: the O–H···O stretching, the ring torsional and the O–H···O out-of-plane bending modes, respectively, and the bands at 106, 76, and 65 cm^{-1} to those of B_u symmetry species. The force constant K(O···H) related to the hydrogen bonds in the cyclic dimer was calculated to be 0.35 mdyn/Å.

The far infrared spectra of carboxylic acid dimers in the vapor phase and in solutions have been studied by several investigators.[2–9] It has been well established in both formic and acetic acids[3,5,8] that the three infrared active vibrations associated with the hydrogen bonds in the cyclic dimer are, from the higher frequencies, the O···H stretching+O–H···O in-plane bending, the O–H···O out-of-plane bending and the ring torsional modes; they are approximately rotational vibrations of the monomers.

Only a few works have been carried out on the low frequency Raman spectra of dimeric carboxylic acids.[10,11] The three Raman active hydrogen-bond vibrations would be the O···H stretching, the O–H···O in-plane bending and the O–H···O out-of-plane bending modes; they can be regarded as translational vibrations of the monomers.

In crystalline solids, provided that the Bravais unit cell contains more than two dimers, translational vibrations of the dimers are also expected to appear in the far infrared spectra and rotational vibrations of the dimers in the low frequency Raman spectra. In such a crystalline state, the low frequency vibrational modes would become complicated due to the interactions between the rotational and translational motions.

Thus it is interesting to study the low frequency vibrational spectra of carboxylic acid dimers in crystalline solids. Simple carboxylic acids such as formic and acetic acids do not exist as hydrogen-bonded dimers in the crystal; they are chain polymers. Benzoic acid is a suitable sample for this purpose because its Bravais unit cell contains two dimers.

The low frequency vibrational spectra of benzoic acid single crystals have been studied by Stanevich,[6] Statz and Lippert,[9] and Maier and Schifferdecker.[12] Recently Wyncke *et al.*[13] measured polarized far infrared spectra of single crystals and proposed an assignment for the infrared active lattice vibrations. Their assignment is based on the assumption that the frequencies of the rotational vibrations of the monomers are in the inverse order of the corresponding moment of inertia. The assumption, however, is not appropriate in the case of benzoic acid because of the strong hydrogen bonds in the dimer.

More recently, Colombo and Furic[14] observed polarized Raman spectra and gave an assignment of the Raman active lattice vibrations. They separated translational vibrations of the monomers from rotational vibrations of the dimers by the difference in the temperature dependence of these two groups of vibrations. The separation, however, does not seem convincing.[15]

The purpose of this paper is to give an assignment for the lattice vibrations of benzoic acid based on the normal coordinate calculations as well as the polarized far infrared spectra of the single crystals.

Experimental

Single crystals of benzoic acid were grown from a saturated ethanol solution by slow evaporation at 30°C. The evaporation rate was adjusted so that crystals of centimeter dimensions were formed over a period of several weeks. The crystals were obtained as fine needles with *b* as needle axis, sometimes as small rectangular plates developed on (001).

X-Ray measurements were carried out with CuK_α radiation by using oscillation and Weissenberg photographic methods. Oscillation photographs indicated that the C_2^5

1) This work was supported in part by a research grant of the Kawakami Memorial Foundation.

2) R. C. Millikan and K. S. Pitzer, *J. Amer. Chem. Soc.*, **80**, 3515 (1958).

3) T. Miyazawa and K. S. Pitzer, *ibid.*, **81**, 74 (1959).

4) K. Hirota and Y. Nakai, This Bulletin, **32**, 769 (1959).

5) S. Kishida and K. Nakamoto, *J. Chem. Phys.*, **41**, 1558 (1964).

6) A. E. Stanevich, *Optics Spectrosc.*, **16**, 243 (1964).

7) G. L. Carlson, R. E. Witkowski, and W. G. Fateley, *Spectrochim. Acta*, **22**, 1117 (1966).

8) R. J. Jacobsen, Y. Mikawa, and J. W. Brash, *Spectrochim. Acta*, **23A**, 2199 (1967).

9) G. Statz and E. Lippert, *Ber. Bunsenges. Phys. Chem.*, **71**, 673 (1967).

10) L. Bonner and J. S. Kirby-Smith, *Phys. Rev.*, **57**, 1078 (1940).

11) J. O. Halford, *J. Chem. Phys.*, **14**, 395 (1946).

12) W. Maier and O. Schifferdecker, *Spectrochim. Acta*, **18**, 709 (1962).

13) B. Wyncke, A. Hadni, H. Wendling, X. Gerbaux, P. Strimer, and G. Marlot, *J. Phys.*, **29**, 851 (1968).

14) L. Colombo and K. Furic, *Spectrochim. Acta*, **27A**, 1773 (1971).

15) Still more recently Colombo *et al.* have given a newer assignment based on their normal coordinate analysis (private communication).

screw axis (b-axis) was always along the longer edge of the rectangular crystal plates. The cell dimensions obtained are: $a \cdot sin\beta = 5.44$, $b = 5.14$, and $c \cdot sin\beta = 21.8$ Å, which are in good agreement with the values reported by Sim *et al.*[16]

The infrared spectra were recorded with a Hitachi FIS-3 far infrared spectrometer. For the infrared polarization measurements a polarizer made up of a stack of polyethylene sheets was used and the sample, about 20 mm long, 10 mm wide and 0.2 mm thick, prepared by cleaving a suitable crystal plate, was attached to the slit 45° tilted with respect to the vertical in order to minimize the polarization effects in the spectrometer. The spectrum of the powder was recorded in a Nujol mull between silicon plates.

Calculation of Lattice Vibrations

The crystal structure of benzoic acid is monoclinic $P2_1/c-C_{2h}^5$, with two cyclic dimers in a Bravais unit cell (Fig. 1). The cell dimensions are: $a=5.52\pm0.02$, $b=5.14\pm0.02$, $c=21.90\pm0.05$ Å and $\beta=97°$.[16] The O···O distance of the two hydrogen bonds in the dimer is 2.65 Å. The bond length O–H and C–H were assumed to be 1.03 and 1.08 Å, respectively, in this frequency calculation.

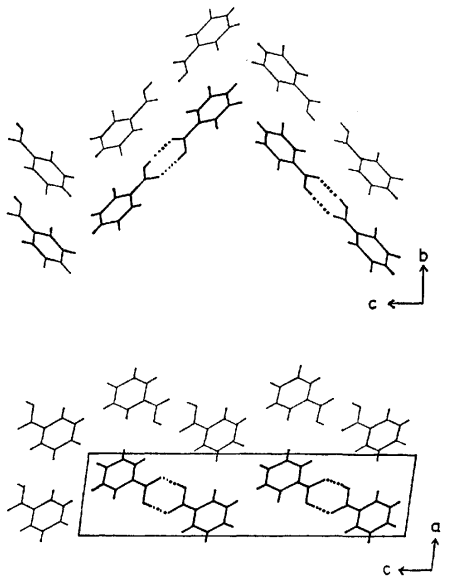

Fig. 1. Crystal structure of benzoic acid.

The calculation of the lattice vibrations has been carried out using the method developed by Shimanouchi *et al.*[17] and assuming that the molecule is not distorted during the vibrations. The intermolecular potential can be expressed as the sum of the potential associated with the hydrogen bonds in the dimer V_h, and the potential representing the interactions between the atoms of different dimers V_t. The interactions between atoms more than 3 Å apart were neglected,

$$V = V_h + V_t$$

$$V_h = (1/2)\sum_i K(\text{O}\cdots\text{H})\Delta q_i^2 + (1/2)\sum_i H_{//}(\text{O–H}\cdots\text{O}) r_{\text{OH}} q_{\text{OH}} \Delta\alpha_i^2 + (1/2)\sum_i H_{\perp}(\text{O–H}\cdots\text{O}) r_{\text{OH}} q_{\text{OH}} \Delta\beta_i^2 + (1/2)\sum_i H(\text{C=O}\cdots\text{H}) r_{\text{CO}} q_{\text{OH}} \Delta\gamma_i^2 + (1/2)\sum_i Y(\text{C=O})\Delta\tau_i^2 + \sum_{i\neq j} p(\text{O}\cdots\text{H, O}\cdots\text{H})\Delta q_i \Delta q_j$$

$$V_t = (1/2)\sum_i F_t(\text{O}\cdots\text{H})\Delta q_{1i}^2 + (1/2)\sum_i F_t(\text{C}\cdots\text{H})\Delta q_{2i}^2 + (1/2)\sum_i F_t(\text{H}\cdots\text{H})\Delta q_{3i}^2$$

where $Y(\text{C=O})$ is the force constant of the torsion around the C=O bond and $p(\text{O}\cdots\text{H, O}\cdots\text{H})$ is the force constant representing the resonance interaction between the two O···H bonds in the dimer.

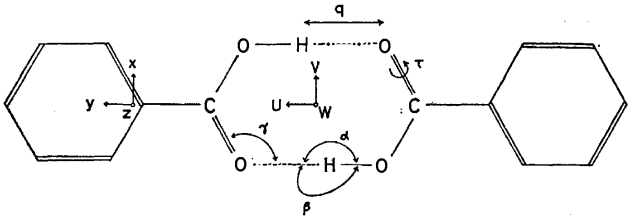

Fig. 2. Coordinates related to the hydrogen bonds in the cyclic dimer.

Results and Discussion

1. Infrared Active Lattice Vibrations. The far infrared spectrum from 400 to 30 cm^{-1} of benzoic acid powder suspended in Nujol is given in Fig. 3. The bands at 106, 78, and 63 cm^{-1} are reduced to weak and broad bands in the spectrum of cyclohexane solution, as shown in Fig. 4. These bands are therefore considered to be due to lattice vibrations. Although

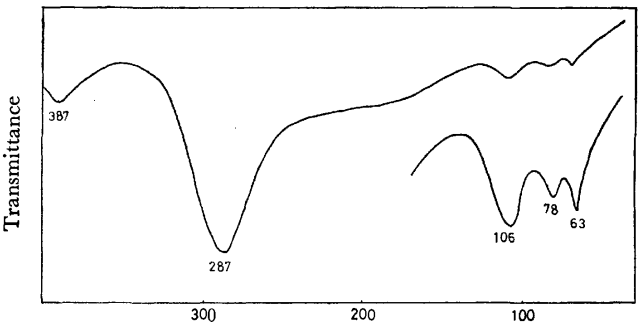

Fig. 3. Far-infrared spectrum of benzoic acid powder in Nujol mull.

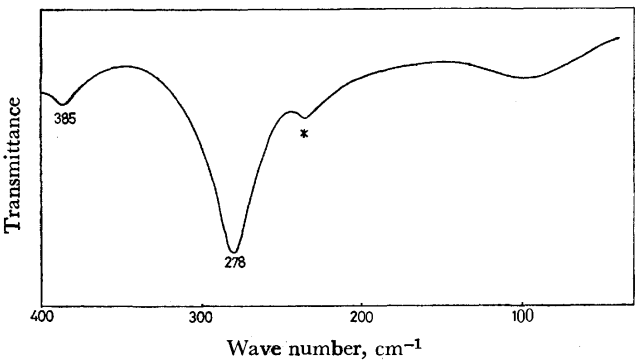

Fig. 4. Far-infrared spectrum of benzoic acid in cyclohexane solution. *band due to cyclohexane.

16) G. A. Sim, J. M. Robertson, and T. H. Goodwin, *Acta Crystallogr.*, **8**, 157 (1955).

17) T. Shimanouchi, M. Tsuboi, and T. Miyazawa, *J. Chem. Phys.*, **35**, 1597 (1961).

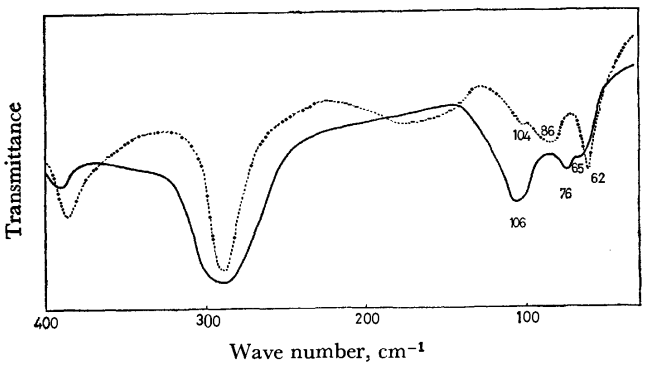

Fig. 5. Polarized far-infrared spectra of benzoic acid single crystals.
·····Electric vector parallel to the *b*-axis
——Electric vector perpendicular to the *b*-axis (parallel to the *a*-axis)

Wyncke *et al.*[13] reported two weak bands at 36 and 29 cm^{-1}, we could find no bands between 60 to 30 cm^{-1}.

In the polarized spectrum of the single crystal shown in Fig. 5, the lattice vibrations occur at 104, 86, and 62 cm^{-1}, when the electric vector of the incident light is parallel to the *b*-axis (C_2^s screw axis) and at 106, 76, and 65 cm^{-1}, when the electric vector is parallel to the *a*-axis. Thus the bands at 104, 86, and 62 cm^{-1} are assigned to the lattice modes of symmetry species A_u, while the bands at 106, 76, and 65 cm^{-1} to those of B_u species. The polarization measurement, however, does not agree with the observation of Wyncke *et al*;[13] their *a* and *b* axes correspond to our *b* and *a* axes, respectively.

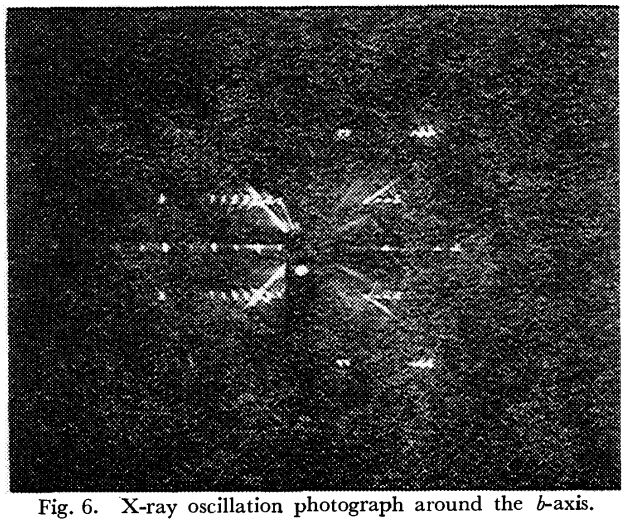

Fig. 6. X-ray oscillation photograph around the *b*-axis.

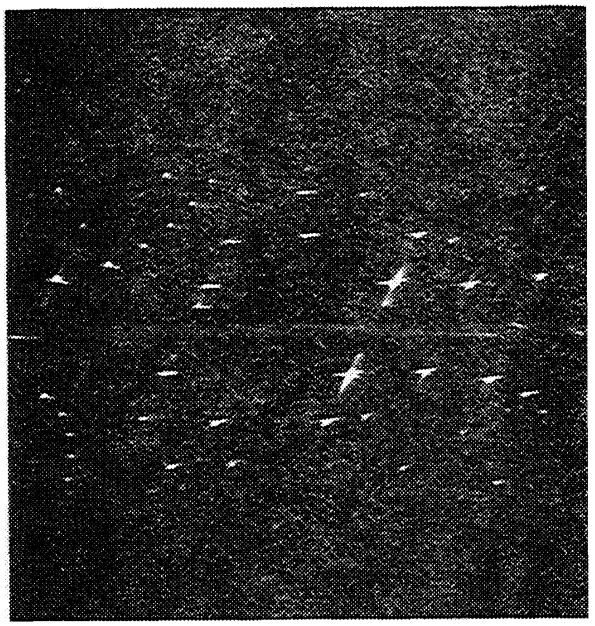

Fig. 7. Weissenberg photograph around the *b*-axis.

The X-ray oscillation photograph around our *b*-axis which is parallel to the longer edge of the rectangular crystal is given in Fig. 6. The photograph clearly shows that the screw axis C_2^s lies along our *b*-axis. Moreover, the cell dimensions, $a \cdot sin\beta = 5.44$, $b = 5.14$, and $c \cdot sin\beta = 21.8$ Å, calculated from this photograph and the Weissenberg photograph (Fig. 7) are in substantial agreement with the results $a = 5.52$, $b = 5.14$, $c = 21.90$ Å, and $\beta = 97°$ obtained by Sim *et al.*[16] This suggests that Wyncke's *a* and *b* axes should be interchanged.

Infrared active lattice vibrations of benzoic acid are approximately described as rotational vibrations of the monomers R_x, R_y, and R_z and translational vibrations of the dimers T_U, T_V, and T_W (Fig. 2). The former can be regarded as the O–H···O out-of-plane bending, the O–H···O torsional and the O···H stretching+O–H···O in-plane bending vibrations, respectively. The frequencies of the former depend mainly on the force constants related to the hydrogen bonds in the cyclic dimer, while the frequencies of the latter are determined mainly by interaction force constants between atoms of different dimers. Accordingly, the

TABLE 1. OBSERVED AND CALCULATED FREQUENCIES AND APPROXIMATE LATTICE MODES OF BENZOIC ACID SINGLE CRYSTSLS

Symmetry Species	Obsd. (cm^{-1})	Calcd. (cm^{-1})	Assignment
A_g	122	126	O···H stretch (T_y)
	114	113	O–H···O *i*-bend(T_x)
	93	100	O–H···O *o*-bend(T_z)
	74	59	R_U
	49	51	R_W
	45	34	R_V
B_g	126	122	O···H stretch(T_y)
	114	113	O–H··· O *i*-bend(T_x)
	96	100	O–H···O *o*-bend(T_z)
	72	60	R_U
	31	41	R_W
	27	20	R_V
A_u	104	108	O···H stretch+O–H···O *i*-bend (R_z)
	86	84	ring torsion(R_y)
	62	63	O–H···O *o*-bend(R_x)
	—	39	T_V
	—	9	T_W
B_u	106	110	O···H stretch+O–H···O *i*-bend(R_z)
	76	74	ring torsion(R_y)
	65	58	O–H···O *o*-bend(R_x)
	—	17	T_U

TABLE 2. HYDROGEN-BOND FREQUENCIES OF CARBOXYLIC ACID DIMERS (cm^{-1})

	Approximate Modes	$(HCOOH)_2$ vapor[7]		$(CH_3COOH)_2$ vapor[7]		$(C_6H_5COOH)_2$ solid	
						A_u	B_u
IR Active	O···H stretch+ O–H···O *i*-bend(R_z)	248		188		104	106
	O–H···O *o*-bend(R_x)	164		80[a]	79[c]	62	65
	ring torsion (R_y)	68		50		86	76
						A_g	B_g
Raman Active	O–H···O *o*-bend(T_z)	243[a]	260[c]	128[a]	130[c]	93	96
	O–H···O stretch(T_y)	221[a]	224[b]	193[a]	210[b]	122	126
	O–H···O *i*-bend(T_x)	103[a]	91[b]	95[a]	81[b]	114	114

a) Calculated values by Miyazawa and Pitzer[3]
b) Calculated values by Kishida and Nakamoto[5]
c) Calculated values by Jacobsen, Mikawa and Brash[8]

frequencies of rotational vibrations of the monomers are anticipated to be higher than those of translational vibrations of the dimers, because hydrogen bonding forces are usually stronger than non-bonding interaction forces.

The principal moment of inertia of the monomer are in the order $I_z>I_x>I_y$. If we assume that the force field around each monomer has spherical symmetry, *viz.*, the effective force constants for R_x, R_y, and R_z are approximately the same, the frequencies of the rotational vibrations of the monomer would be in the order $\nu(R_y)>\nu(R_x)>\nu(R_z)$. Actually the assumption is not acceptable because two monomers are combined together by strong hydrogen bonds to form a cyclic dimer in the crystal, and the largest hydrogen-bond force constant K(O···H) is almost solely effective for R_z. This suggests that the frequency of R_z is the highest in spite of the biggest moment of inertia I_z. It is not easy to tell, *a priori*, which frequency is higher, $\nu(R_x)$ or $\nu(R_y)$. The effective force constant for R_x might be slightly larger than that for R_y, whereas the moment of inertia for R_y is smaller than that for R_x.

2. Raman Active Lattice Vibrations. Raman active lattice vibrations of benzoic acid can be classified approximately into two groups: translational vibrations of the monomers T_x, T_y, and T_z, and rotational vibrations of the dimers R_U, R_V, and R_W. The former are in other expressions, the O–H···O in-plane bending, O···H stretching and the O–H···O out-of-plane bending vibrations, respectively. For the same reason as that for infrared active lattice vibrations, the frequencies of translational vibrations of the monomers are supposed to be higher than those of rotational vibrations of the dimers, and the highest frequency of these vibrations would be the O···H stretch $\nu(T_y)$.

The moment of inertia of the dimer is in the order

TABLE 3. INTER-MOLECULAR FORCE CONSTANTS OF BENZOIC ACID

Force Constants	mdyn/Å	Inter-atomic Distances (Å)
in Dimers		
K(O···H)	0.350	1.61
$H_{\parallel}$(O–H···O)	0.030	
$H_{\perp}$(O–H···O)	0.048	
H(C=O···H)	0.038	
Y(C=O)	0.010[a]	
p(O···H, O···H)	−0.060	
between Dimers		
F(O···H)	0.025	2.55
F(O···H)	0.020	2.62
F(C···H)	0.030	2.88
F(C···H)	0.025	2.94
F(C···H)	0.010	3.04
F(H···H)	0.038	2.43
F(H···H)	0.015	2.70
F(H···H)	0.008	2.75
F(H···H)	0.006	2.84
F(H···H)	0.004	3.03

a) in mdyn. Å

TABLE 4. HYDROGEN-BOND FORCE CONSTANTS OF CARBOXYLIC ACIDS (mdyn/Å)

Force Constants	HCOOH Ref. 3	HCOOH Ref. 5	CH_3COOH Ref. 3	CH_3COOH Ref. 5	succinic[18] and adipic[19] acid	C_6H_5COOH this work
K(O···H)	0.330	0.360	0.330	0.460	0.360	0.350
$H_{\parallel}$(O–H···O)	0.025	0.015	0.025	0.020	0.010	0.030
H(C=O···H)	0.012	0.010	0.012	0.005	0.010	0.038
$H_{\perp}$(O–H···O)	0.025	···	0.025	···	0.055	0.048
Y(C=O)[a]	0.012	···	···	···	0.024	0.010
p(O···H, O···H)	···	···	···	···	···	−0.060

a) in mdyn. Å

18) M. Suzuki and T. Shimanouchi, *J. Mol. Spectrosc.*, **28**, 394 (1968).
19) M. Suzuki and T. Shimanouchi, *ibid.*, **29**, 415 (1969).

$I_W > I_V > I_U$. The effective force constants for R R_V, and R_W would not differ much from each other, because it is highly improbable that some strong interaction forces are operative along particular directions between the dimers. Thus, the rotational vibrations of the dimers would be in the order $\nu(R_U) > \nu(R_V) > \nu(R_W)$.

3. Assignment of Lattice Modes. The observed and calculated frequencies along with their approximate lattice modes are listed in Table 1. The Raman frequencies (A_g and B_g species) are those measured by Colombo *et al.*[14] The calculated frequencies are in fairly good agreement with the observed. In the frequency calculation, it was assumed that the molecule of benzoic acid was not distorted during lattice vibrations; in other words, the coupling between intramolecular vibrations and lattice vibrations was ignored. This might be a good approximation when the frequencies of all the intra-molecular vibrations are high and are far apart from the frequencies of lattice vibrations. In the case of benzoic acid, the frequencies of the C–C torsion and the C–O torsion, which are intramolecular vibrations, are very low, presumably around 200 cm^{-1}, and the interactions between these two intramolecular vibrations and the lattice vibrations can not be neglected. This could be one reason why we see minor discrepancies between calculated and observed frequencies.

The lattice modes assigned to the observed and calculated frequencies are more or less approximate ones. The actual lattice mode should be expressed as a linear combination of these approximate modes. However, only the mode of largest weight or contribution is given in the table. Hydrogen-bond vibrations of several carboxylic acids are summerized in Table 2. We see that in formic and acetic acids $\nu(R_x)$ is higher than $\nu(R_y)$, while in benzoic acid $\nu(R_x)$ is lower than $\nu(R_y)$. This is probably attributed to the fact that in formic and acetic acids the difference between I_x and I_y is smaller than that in benzoic acid, and the effect of the difference in the force constants becomes important. Besides this, the frequencies of formic and acetic acids given in the table are those of isolated dimers in the vapor phase and are free from interaction forces between the dimers, while in benzoic acid crystals the effects of these interaction forces can no longer be neglected.

4. Force Constants. The intermolecular force constants obtained from the calculation of the lattice vibrations are shown in Table 3. The non-bonding interaction force constants F(H···H) and F(C···H) were fixed to the values reported for benzene and naphthalene.[20] Other force constants were determined by a least square method to get the best fit between observed and calculated frequencies.

A resonance interaction force constant p(O···H, O···H) between the two O···H bonds in the cyclic dimer was introduced in this calculation. The same type of force constant has been used in the calculation of 1-methylthymine ($p = -0.09$ mdyn/Å).[21] Without this force constant the Raman active O···H stretching (T_y) frequencies 122 and 126 cm^{-1}, and the infrared active O···H stretching+O–H···O in-plane bending (R_x) frequencies 104 and 106 cm^{-1} cannot be explained simultaneously. This resonance force constant is not used in the normal-coordinate calculation of formic and acetic acid dimers (Table 4). This is probably because the Raman active frequencies of these acids are not exactly known (Table 2), and the hydrogen-bond force constants were determined using infrared frequencies alone. The negative value of this force constant is consistent with the physical meaning of "resonance interaction", *i.e.* the potential energy of the configuration in which the two O···H distances in the cyclic dimer are lengthened or shortened simultaneously is lower than that of the configuration in which one O···H is lengthened while at the same time the other is shortened.

We thank Dr. Midori Goto of the Government Chemical Industrial Research Institute Tokyo for the measurement of X-ray photographs.

20) I. Harada and T. Shimanouchi, *J. Chem. Phys.*, **44**, 2016 (1966).
21) I. Harada and R. C. Lord, *Spectrochim. Acta*, **26A**, 2305 (1970).

The Abnormal Absorption Intensity of the C-H Stretching Vibration Band in Chloroform Vapor. II.

Tomoo MIYAZAKI and Hiroshi YAMAMOTO

Department of Applied Chemistry, Faculty of Science and Engineering, Waseda University, Nishi-Ohkubo, Shinjuku-ku, Tokyo

(Received January 18, 1972)

By CNDO calculations considering the 3*d* orbitals of the chlorine atom, the infrared absorption intensity of the C–H stretching vibration band in chloroform vapor has been discussed in comparison with those of methyl chloride and methylene chloride. The absolute intensities of the fundamental and the first-overtone bands of these compounds have been calculated in view of the mechanical and the electrical anharmoniciteis of the vibrating bond. From the results of these calculations, it was revealed that the contribution of the electrical properties of the vibrating bond to the abnormal absorption intensity of the C–H stretching vibration band in chloroform vapor is really greater than that of the mechanical anharmonicity.

In a previous paper,[1] the abnormal infrared absorption intensity of the C–H stretching vibration band in chloroform vapor was discussed in terms of the electrical properties of the vibrating bond. By CNDO calculations involving the 3*d* orbitals of the chlorine atom,[2] the absolute intensities of the fundamental and the first-overtone bands of the C–H stretching vibrations in CH_3Cl, CH_2Cl_2, and $CHCl_3$ were calculated from the values of the first and the second derivatives of the dipole moment with respect to the normal coordinates. The calculated relative intensities of the fundamental bands of these compounds were in satisfactory agreement with the observed values. The calculated absolute intensity of the first-overtone band of the C–H stretching vibration in chloroform was stronger than that of the fundamental band, and the $A^*_{1\leftarrow0}/A^*_{2\leftarrow0}$ ratio was 0.558, where $A^*_{1\leftarrow0}$ and $A^*_{2\leftarrow0}$ are the absolute intensities of the fundamental and the first-overtone bands in a harmonic oscillator approximation respectively. From the results of the calculations, it was learned that the electrical properties of the vibrating bond are the effective factors in bringing about the abnormal absorption intensity of the C–H stretching vibration band in chloroform vapor. However, the calculated absolute intensity of the first-overtone band in chloroform was smaller than the observed one. (The $A^*_{1\leftarrow0}/A^*_{2\leftarrow0}$ ratio calculated from the observed values has been reported to be 0.16—0.2.[3,4]) Therefore, in this paper, the fundamental and the first-overtone band intensities of the C–H stretching vibrations of CH_3Cl, CH_2Cl_2, and $CHCl_3$ have been calculated in view of the mechanical anharmonicity of the vibrating bond.

Methods of Calculation

The mechanical anharmonicity of the molecular vibration can be discussed on the basis of an analysis of the potential energy expanded by the normal coordinate. The treatment of the subject in this work is simplified because the normal modes considered are approximately equal to the pure C–H symmetric stretching modes, as has been described in the previous paper.[1]

The CNDO method, involving the 3*d* orbitals of the chlorine atom, used in this work was described in detail in the previous paper of this series.[1] From the results of the CNDO calculations for the molecules distorted in the manner dictated by the C–H symmetric coordinates (S_{CH}), the potential energy function for the C–H vibration was obtained by fitting the total energy of the molecule to a quartic function with respect to the S_{CH} coordinate. The potential energy functions thus obtained are as follows:

$$V_{CH}(CH_3Cl) = 62.1720 \times 10^4 S_{CH}^2 - 52.5935 \times 10^{12} S_{CH}^3 + 27.2339 \times 10^{20} S_{CH}^4, \quad (1)$$

$$V_{CH}(CH_2Cl_2) = 60.8290 \times 10^4 S_{CH}^2 - 61.2499 \times 10^{12} S_{CH}^3 - 1.59167 \times 10^{20} S_{CH}^4, \quad (2)$$

$$V_{CH}(CHCl_3) = 58.9394 \times 10^4 S_{CH}^2 - 83.4185 \times 10^{12} S_{CH}^3 + 31.8084 \times 10^{20} S_{CH}^4, \quad (3)$$

where the S'_{CH}s in Eqs. (1), (2), and (3) are equal to $(1/\sqrt{3})$ $(\Delta r'_{CH}+\Delta r''_{CH}+\Delta r'''_{CH})$, $(1/\sqrt{2})$ $(\Delta r'_{CH}+\Delta r''_{CH})$, and Δr_{CH} respectively. The units of the V_{CH} and the S_{CH} are [erg] and [cm] respectively. For our present object, the potential energy as a function of the normal coordinate (Q_k) alone will be sufficient; here the Q_k involves the C–H symmetric stretching vibration as the main constituent. Since there is a singularity about the vibration mode considered in this work, as has been described above, the energy functions can be obtained from Eqs. (1), (2), and (3) as a function of the normal coordinate, Q_k:

$$V_k(CH_3Cl) = (1/2) \times 7.60852 \times 10^{29} Q_k^2 - 2.51736 \times 10^{49} Q_k^3 + 1.01967 \times 10^{69} Q_k^4, \quad (4)$$

$$V_k(CH_2Cl_2) = (1/2) \times 7.65022 \times 10^{29} Q_k^2 - 3.05426 \times 10^{49} Q_k^3 - 0.062939 \times 10^{69} Q_k^4, \quad (5)$$

$$V_k(CHCl_3) = (1/2) \times 7.63400 \times 10^{29} Q_k^2 - 4.34747 \times 10^{49} Q_k^3 + 1.33405 \times 10^{69} Q_k^4, \quad (6)$$

where the units of the V_k and the Q_k are [erg] and [erg$^{1/2}$sec] respectively. In the above equations, the Q_ks differ from each other, but they are not distin-

1) T. Miyazaki, T. Shigetani, and H. Yamamoto, This Bulletin, **45**, 678 (1972).
2) D. P. Santry and G. A. Segal, *J. Chem. Phys.*, **47**, 158 (1967).
3) C. C. Robinson, S. T. Tare, and H. W. Thompson, *Proc. Roy. Soc.*, **A269**, 492 (1962).
4) I. Rossi, M. Nguyen-Van-Thanh, and C. Haeusler, *Can. J. Chem.*, **47**, 3319 (1969).

guished in expression in order to avoid complexity. In rewriting the above, the Ls(CH)'s were taken to be $1.00797\times\sqrt{N_A}$, $1.02183\times\sqrt{N_A}$, and $1.03698\times\sqrt{N_A}$ in [$g^{-1/2}$] units for CH_3Cl, CH_2Cl_2, and $CHCl_3$ respectively, where the Ls(CH)'s are the elements of the $\boldsymbol{L}$ matrix which relate the symmetry coordinate to the normal coordinate, and where the N_A is Avogadro's number. Unfortunately, however, the calculated potential energy for the stretching vibration by the CNDO method is not appropriate since the energy increase with the displacement from the equilibrium distance is too much larger than that generally found. In other words, the force constant of the stretching vibration calculated by the CNDO method is too large (2—3 times). Therefore, in order to determine the appropriate potential energy of the vibration considered, we assumed that each potential energy function of Eqs. (4)—(6) can be rewritten by multiplying the coefficients by the constant (α) determined in comparison with the observed frequency of the actual vibration. To determine the constant (α), trial calculations were performed until the difference between energy levels, which were calculated by the Rayleigh-Ritz method, as will be indicated below, coincided with the observed frequency of the fundamental band. In these calculations, the wave functions, ψ_v's, involving the mechanical anharmonicity were described as linear combinations of harmonic oscillator wave functions, φ_i^0's:

$$\psi_v = \sum_{i=0}^{n} c_{vi}\varphi_i^0. \tag{7}$$

The variational treatment of the coefficient, c_{vi}, leads to this equation:

$$\sum_j c_{vj}(H_{ij}-\varepsilon_v\delta_{ij}) = 0 \qquad i = 0, 1, 2, \cdots, n, \tag{8}$$

where:

$$H_{ij} = T_{ij} + V_{ij},$$
$$T_{ij} = \left\langle \varphi_i^0 \middle| -\frac{\boldsymbol{h}^2}{8\pi^2}\frac{\partial^2}{\partial Q_k^2} \middle| \varphi_j^0 \right\rangle, \tag{9}$$
$$V_{ij} = \left\langle \varphi_i^0 \middle| \frac{1}{2}\lambda_k Q_k^2 + g_k Q_k^3 + h_k Q_k^4 \middle| \varphi_j^0 \right\rangle.$$

In Eq. (8), ε_v is the energy for the wave function, ψ_v. H_{ij} is the matrix element of the Hamiltonian, including the kinetic (T_{ij}) and the potential (V_{ij}) energies for the vibrating system. The energies (ε_v's) are the roots of the secular equation. Practically, the n in Eq. (7) was taken to be 11, since the further addition of φ_i^0 no longer changed the eigenvalues (ε_0, ε_1, ε_2, and ε_3) within an order of six significant figures. It should also be noted that the constant (α) is set appropriately at the first step of this calculation. The calculated energies and wave functions are listed in Table 2, in which the potential energy functions are also indicated.

Dipole Moments and Their Derivatives. The formulas used to calculate the dipole moments, in view of the atomic polarization, were given in the previous paper.[1] The dipole moments were calculated for the molecules distorted in the manner dictated by the symmetry coordinate including the C–H symmetric stretching modes. The numerical values required to calculate the absorption intensity were obtained by fitting the calculated dipole moments to a quartic function with respect to the C–H distance, and by taking the first and the second derivatives at the C–H equilibrium distance. They are listed in Table 1, in which the dipole-moment derivatives at the observed and the calculated equilibrium distances are also indicated. Although there are two distinct evaluations of the numerical values required, this problem will be dealt with in the following discussion.

Absolute Absorption Intensities. The absolute absorption intensities of the fundamental and the first-overtone bands, in view of the mechanical and the electrical anharmonicities, can be calculated by the following equation:

$$A_{v+n\leftarrow v} = \frac{8\pi^3}{3c\boldsymbol{h}}\left(\frac{N_v}{N_t}-\frac{N_{v+n}}{N_t}\right)\nu_{v+n,v}\sum_{i=x,y,z}|(\mu_i)_v^{v+n}|^2, \tag{10}$$

$$N_v = N_0\exp\left(-(\varepsilon_v-\varepsilon_0)\right)/\boldsymbol{k}T, \tag{11}$$

$$N_t = N_0\sum_{v=0}^{\infty}\exp\left(-(\varepsilon_v-\varepsilon_0)\right)/\boldsymbol{k}T, \tag{12}$$

$$(\mu_i)_v^{v+n} = \left\langle \psi_v \middle| \mu_i^0 + \left(\frac{\partial\mu_i}{\partial Q_k}\right)_0 Q_k + \frac{1}{2}\left(\frac{\partial^2\mu_i}{\partial Q_k^2}\right)_0 Q_k^2 \middle| \psi_{v+n} \right\rangle, \tag{13}$$

where N_0 and N_v are the numbers of the molecules which are involved at the energy levels of ε_0 and ε_v respectively, and where N_t is the total number of molecules. Also, c is the velocity of light, $\boldsymbol{h}$ is Planck's constant, and $\boldsymbol{k}$ is Boltzmann's constant. In this calculation, the T was taken to be 300°K. μ_i^0 is the i-component of the dipole moment, and $\nu_{v+n,v}$ is the

Table 1. Dipole moments and their derivatives

Molecule		C–H Equilibrium distance (Å)	$\mu^0{}_z$ [a] (Debye)		μ'_z [a] $\left(\frac{\text{Debye}}{\text{Å}}\right)$	μ''_z [a] $\left(\frac{\text{Debye}}{\text{Å}^2}\right)$
CH_3Cl	Obsd.	1.0959[b]	1.857	(1.86)[c]	−0.3242	−0.3297
	Calcd.	1.1128	1.847		−0.3343	−0.3584
CH_2Cl_2	Obsd.	1.068[b]	2.004	(1.57)[c]	−0.1583	−0.4574
	Calcd.	1.1132	1.993		−0.1908	−0.5599
$CHCl_3$	Obsd.	1.073[b]	1.710	(1.01)[c]	0.0381	−0.6866
	Calcd.	1.1148	1.711		0.0099	−0.6802

a) $\mu^0{}_z$=dipole moment along the z-axis. $\mu'_z=\left(\frac{\partial\mu_z}{\partial S_{CH}}\right)_0$. $\mu''_z=\left(\frac{\partial^2\mu_z}{\partial S^2{}_{CH}}\right)_0$

b) "Interatomic Distances", Supplement, Special Publication No. 18, The Chemical Society (London).

c) Figures in parentheses are observed values.

transition energy in [sec^{-1}] units from the energy level (v) to the energy level ($v+n$). The summation in Eq. (12) was terminated under the condition that a further increase in the i no longer changed the absolute intensity (A), as calculated from Eq. (10), within an order of six significant figures. In the previous paper, since the vibration was approximated to be harmonic, the absolute intensity of the fundamental band, $A_{1\leftarrow 0}$*, was calculated by the summation of $A_{1\leftarrow 0}$, $A_{2\leftarrow 1}$, $A_{3\leftarrow 2}$, *etc.* In this calculation, however, we cannot treat the problem in the same way in view of the mechanical anharmonicity. Fortunately, the mechod of approach to this problem was simplified, since the values of $A_{2\leftarrow 1}$ and $A_{3\leftarrow 1}$ were negligibly small in comparison with the values of $A_{1\leftarrow 0}$ and $A_{2\leftarrow 0}$ respectively.

Results and Discussion

In the treatment of this work, there are some problems which have been left unsolved. In the first place, the equilibrium distance obtained by the total energy minimization disagrees with the observed one. Consequently, the dipole moment calculated in the observed geometry differs from that at the calculated equilibrium distance. It is the same in the dipole-moment derivatives. Generally, the theoretical dipole moment has been calculated by many investigators at the observed equilibrium distance. Also, in the previous paper we discussed the absolute infrared absorption intensity of the C-H stretching vibration band in chloroform by the use of the dipole-moment derivatives at the observed equilibrium distance. In this paper, however, the dipole-moment derivatives were calculated at both the observed and the calculated equilibrium distances. Between these values, a considerable discrepancy was noted in the first derivative of the dipole moment of $CHCl_3$ as is indicated in Table 1. However, as indicated in Table 3, the absolute intensities calculated by these values were not contradictory to each other

Table 2-a. Energy levels and wave functions of the vibration in CH_3Cl
(ε_v, and $\psi_v=\sum_i c_{vi}\psi_i^0$)

v	0	1	2	3
$\varepsilon\times10^{13}$ [erg]	2.96448	8.85940	14.71216	20.52596
c_{v0}	**0.99878**	−0.04771	0.00115	−0.01216
c_{v1}	0.04767	**0.98947**	−0.13361	0.01021
c_{v2}	0.00215	0.13333	**0.96002**	−0.23982
c_{v3}	0.01298	0.01274	0.23890	**0.89868**
c_{v4}	0.00137	0.02652	0.03578	0.35187
c_{v5}	0.00005	0.00577	0.04390	0.07388
c_{v6}	0.00036	0.00069	0.01463	0.06632
c_{v7}	0.00005	0.00100	0.00280	0.02933
c_{v8}	0.00000	0.00028	0.00224	0.00768
c_{v9}	0.00001	0.00004	0.00087	0.00453
c_{v10}	0.00000_3	0.00004	0.00018	0.00211
c_{v11}	0.00000	0.00001	0.00011	0.00054

$\Delta\varepsilon_{0,1}$=2968 cm^{-1} (Obsd. 2967.8 cm^{-1}),
$\Delta\varepsilon_{0,2}$=5914 cm^{-1}.
$V_k=(1/2)\times3.17276\times10^{29}\,Q_k^2-1.04974\times10^{49}Q_k^3+0.42520\times10^{69}Q_k^4$, where the units of V_k and Q_k are [erg] and [erg$^{1/2}$sec] respectively.

Table 2-b. Energy levels and wave functions of the vibration in CH_2Cl_2
(ε_v, and $\psi_v=\sum_i c_{vi}\psi_i^0$)

v	0	1	2	3
$\varepsilon\times10^{13}$ [erg]	3.01564	8.95298	14.72662	20.31040
c_{v0}	**0.99811**	−0.05953	−0.00232	−0.01351
c_{v1}	0.05847	**0.98284**	−0.17228	0.00615
c_{v2}	0.00746	0.16647	**0.93088**	−0.31897
c_{v3}	0.01689	0.03271	0.29976	**0.81365**
c_{v4}	0.00350	0.03855	0.08383	0.43092
c_{v5}	0.00082	0.01341	0.07316	0.16305
c_{v6}	0.00076	0.00433	0.03508	0.12642
c_{v7}	0.00027	0.00287	0.01454	0.07497
c_{v8}	0.00009	0.00135	0.00870	0.03778
c_{v9}	0.00006	0.00057	0.00467	0.02236
c_{v10}	0.00003	0.00032	0.00229	0.01299
c_{v11}	0.00001	0.00015	0.00112	0.00620

$\Delta\varepsilon_{0,1}$=2989 cm^{-1} (Obsd. 2989 cm^{-1}),
$\Delta\varepsilon_{0,2}$=5896 cm^{-1}.
$V_k=(1/2)\times3.32785\times10^{29}Q_k^2-1.32860\times10^{49}Q_k^3-0.02738\times10^{69}Q_k^4$, where the units of V_k and Q_k are [erg] and [erg$^{1/2}$ sec] respectively.

Table 2-c. Energy levels and wave functions of the vibration in $CHCl_3$
(ε_v, and $\psi_v=\sum_i c_{vi}\psi_i^0$)

v	0	1	2	3
$\varepsilon\times10^{13}$ [erg]	3.08859	9.11309	14.89067	20.39499
c_{v0}	**0.99631**	−0.08323	−0.00033	−0.01669
c_{v1}	0.08160	**0.96666**	−0.23734	0.02494
c_{v2}	0.01079	0.22860	**0.86799**	−0.42178
c_{v3}	0.02364	0.05164	0.39476	**0.65778**
c_{v4}	0.00562	0.05553	0.13255	0.51959
c_{v5}	0.00132	0.02302	0.10878	0.24281
c_{v6}	0.00140	0.00809	0.06144	0.18706
c_{v7}	0.00054	0.00554	0.02854	0.12803
c_{v8}	0.00018	0.00286	0.01758	0.07258
c_{v9}	0.00013	0.00125	0.01020	0.04470
c_{v10}	0.00006	0.00073	0.00530	0.02772
c_{v11}	0.00002	0.00035	0.00257	0.01340

$\Delta\varepsilon_{0,1}$=3033 cm^{-1} (Obsd 3033 cm^{-1}),
$\Delta\varepsilon_{0,2}$=5942 cm^{-1} (Obsd 5945 cm^{-1}).
$V_k=(1/2)\times3.51164\times10^{29}Q_k^2-1.99984\times10^{49}Q_k^3+0.61367\times10^{69}Q_k^4$, where the units of V_k and Q_k are [erg] and [erg$^{1/2}$ sec] respectively.

in terms of the general tendency of the problem. Second, the force constant calculated by the CNDO method is too large, as has been stated above. That is, the absorption bands calculated from the coefficients of Q^2 in Eqs. (4), (5), and (6) are by far larger than the observed values in frequency; therefore, we rewrote the potential energy by multiplying the coefficients of the function by the constant (α). The values of the constants for CH_3Cl, CH_2Cl_2, and $CHCl_3$ were 0.417, 0.435, and 0.460 respectively. In estimating the constants (α's), we made it a condition that the differences between energy levels of the vibration had to be in agreement with the observed values, where the energy levels were calculated by the variational method de-

TABLE 3. ABSOLUTE ABSORPTION INTENSITIES OF THE C–H VIBRATION OF CH_3Cl, CH_2Cl_2, AND $CHCl_3$ (at 300°K)

Molecule		Equilibrium distance (Å)	Absolute intensity [$cm^2\ sec^{-1}\ molecule^{-1}$] Fundamental band ($\times 10^{10}$) $A_{1\leftarrow 0}$	$A_{2\leftarrow 1}$	$A^*_{1\leftarrow 0}$ [a]	Obsd	1st overtone band ($\times 10^{10}$) $A_{2\leftarrow 0}$	$A_{3\leftarrow 1}$	$A^*_{2\leftarrow 0}$ [a]	Obsd.
CH_3Cl	Obsd.	1.0959	228.4	0.3×10^{-3}	(225)	1006[b]	0.0346	0.7×10^{-7}	(1.30)	
	Calcd.	1.1128	243.1	0.3×10^{-3}			0.0652	0.1×10^{-6}		
CH_2Cl_2	Obsd.	1.068	58.9	0.7×10^{-4}	(54.1)	333.5[b], 176[d]	0.908	0.1×10^{-5}	(2.89)	
	Calcd.	1.1132	85.6	0.1×10^{-3}			1.39	0.2×10^{-5}		
$CHCl_3$	Obsd.	1.073	1.45	0.3×10^{-6}	(3.19)	11.4[b], 8[c], 15[d]	6.37	0.8×10^{-5}	(5.71)	50[c], 80[d]
	Calcd.	1.1148	0.014	0.5×10^{-6}			5.53	0.7×10^{-5}		

a) The values were published in the previous paper[1] where the calculation was performed with consideration of the electrical anharmonicity alone.
b) M. M. Chalaye and G. Levi, C. R. Acad. Sci. Paris, t. 267, B-45 (1968).
c) From Ref. 4.
d) From Ref. 3.

TABLE 4. RELATIVE INTENSITIES BETWEEN THE FUNDAMENTAL AND THE OVERTONE BANDS

Molecule	Relative intensity ($A_{1\leftarrow 0}/A_{2\leftarrow 0}$) Calcd.	Obsd.
CH_3Cl	6601	
CH_2Cl_2	64.9	
$CHCl_3$	0.228	0.16–0.2[a]

a) From Refs. 3 and 4.

scribed in the method of calculation. The potential energies used in this calculation are indicated in Table 2. The frequencies of the fundamental and the first–overtone bands calculated from the energy levels for the C–H vibration of $CHCl_3$ were in good agreement with the observed values: Calcd. 3033 cm^{-1}, Obsd. 3033 cm^{-1} for the fundamental band, and Calcd. 5942 cm^{-1}, Obsd. 5945 cm^{-1} for the first–overtone band. The calculated energy levels and wave functions are listed in Table 2. Therefore, we consider that it is reasonable to calculate the absolute infrared absorption intensity by considering the mechanical anharmonicity for the C–H stretching vibration of $CHCl_3$ by the use of the wave functions associated with these energy levels. The calculated absolute intensities of the fundamental and the first–overtone bands are summarized in Table 3. It is sufficient to consider the values of $A_{1\leftarrow 0}$ and $A_{2\leftarrow 0}$ alone in order to obtain the fundamental and the first–overtone band intensities, because the values of $A_{2\leftarrow 1}$ and $A_{3\leftarrow 1}$ were quite small. The absolute intensity of the fundamental band of the C–H stretching vibration in chloroform is much weaker than those of the symmetric C–H stretching vibration bands of CH_3Cl and CH_2Cl_2. The absolute intensity of the first–overtone band of this vibration in $CHCl_3$ is stronger than those of CH_3Cl and CH_2Cl_2. The $A_{1\leftarrow 0}/A_{2\leftarrow 0}$ ratios for these compounds are indicated in Table 4. The ratio for chloroform is in good agreement with the observed one.

In Table 5, the absolute intensities calculated from the integrals, $\langle\psi_0|\mu_i^0+(\partial\mu_i/\partial Q_k)_0 Q_k|\psi_v\rangle$ and $\langle\psi_0|\mu_i^0+(\partial\mu_i^0/\partial Q_k)_0 Q_k+1/2\,(\partial^2\mu_i/\partial Q_k^2)_0 Q_k^2|\psi_v\rangle$, are compared with the previous results,[1] which are calculated on the basis of the electrical anharmonicity alone. This comparative table clarifies the contribu-

TABLE 5. COMPARISON BETWEEN ABSOLUTE INTENSITIES CALCULATED BY THE DIFFERENT APPROXIMATION

Molecule	Absolute intensity [$cm^2 sec^{-1} molecule^{-1}$] Fundamental band ($\times 10^{10}$) A[a]	$A(m)$[b]	(A)[c]	1st overtone band ($\times 10^{10}$) A[a]	$A(m)$[b]	(A)[c]
CH_3Cl	228.4	223.7	(225)	0.035	0.89	(1.30)
CH_2Cl_2	58.8	53.7	(54.1)	0.91	0.37	(2.89)
$CHCl_3$	1.45	3.15	(3.19)	6.39	0.042	(5.71)

a) Absorption intensity calculated with consideration of the mechanical and the electrical anharmonicities. (Calculated from the integral $\langle\psi_0|\mu^0+\left(\frac{\partial\mu}{\partial Q}\right)_0 Q+\frac{1}{2}\left(\frac{\partial^2\mu}{\partial Q^2}\right)_0 Q^2|\psi_v\rangle$.)
b) Absorption intensity calculated with consideration of the mechanical anharmonicity alone. (Calculated from the integral $\langle\psi_0|\mu^0+\left(\frac{\partial\mu}{\partial Q}\right)_0 Q|\psi_v\rangle$.)
c) The values of the previous calculation.[1] (Calculated with consideration of the electrical anharmonicity alone.)

TABLE 6. THE NUMERICAL VALUES OF THE EFFECTIVE TERMS IN CALCULATING THE ABSOLUTE INTENSITY

Molucule	Band		$\langle\psi_0\|Q\|\psi_v\rangle\times10^{41/2}$ [$erg^{1/2}sec$]	$\frac{\partial\mu}{\partial Q}\langle\psi_0\|Q\|\psi_v\rangle\times10^{20}$ [esu cm]	$\langle\psi_0\|Q^2\|\psi_v\rangle\times10^{41}$ [erg sec^2]	$\frac{1}{2}\frac{\partial^2\mu}{\partial Q^2}\langle\psi_0\|Q^2\|\psi_v\rangle\times10^{20}$ [esu cm]
CH_3Cl	Fundamental	($v=1$)	0.3065	−2.4579	0.0253	−0.0256
	1st overtone	($v=2$)	−0.0137	0.1100	0.1305	−0.1317
CH_2Cl_2	Fundamental	($v=1$)	0.3049	−1.2105	0.0317	−0.0455
	1st overtone	($v=2$)	−0.0181	0.0719	0.1272	−0.1829
$CHCl_3$	Fundamental	($v=1$)	0.3017	0.2921	0.0433	−0.0962
	1st overtone	($v=2$)	−0.0250	−0.0242	0.1210	−0.2689

tion of the mechanical anharmonicity of the vibration to the fundamental and the first–overtone band intensities. Furthermore, in Table 6, the numerical values of the terms effective in calculating the absolute absorption intensities are indicated. Thus, it is found that the abnormal absorption intensity of the C–H stretching vibration band in chloroform vapor arises, mainly, from the electrical properties of the vibrating bond.

Conclusion

The absolute infrared absorption intensities of the fundamental and the first–overtone bands of the C–H stretching vibration in chloroform were calculated in view of the mechanical and the electrical anharmonicities of the vibrating bond. These absolute infrared absorption intensities were then compared with those of the C–H symmetric stretching vibration bands in methyl chloride and methylene chloride. The contribution of the mechanical anharmonicity of the vibrating bond to the abnormal absorption intensity of the C–H stretching vibration band in chloroform vapor was compared with that of the electrical anharmonicity. From the results of these calculations, it was confirmed that the abnormal absorption intensity of the C–H stretching vibration band in chloroform vapor arises from the electrical properties of the vibrating bond.

The authors would like to acknowledge the continuing encouragement of Professor K. Higasi. They are also indebted to Professor H. Takahashi for drawing their attention to this problem. Several helpful discussions with Mr. H. Shinida are gratefully acknowledged. In their calculations, they were helped by "the university contribution" of I.B.M. Japan, Ltd.

BULLETIN OF THE CHEMICAL SOCIETY OF JAPAN, VOL. 45, 1673—1679(1972)

The n-π^* Absorption and Phosphorescnce of Terephthalaldehyde

Yoshio MURAKAMI, Ryoichi SHIMADA and Yoshiya KANDA

Department of Chemistry, Faculty of Science, Kyushu University, Hakozaki, Fukuoka

(Received December 17, 1971)

The $n\rightarrow\pi^*$ absorption spectrum of terephthalaldehyde (TPA) has been studied. The $f_{n\rightarrow\pi^*}$-value observed in cyclohexane at room temperature was 1.3×10^{-3}, which was 2.4 times that of benzaldehyde (BA). Vibrational analyses of the absorption and phosphorescence spectra of TPA indicate that the CHO-torsional, CHO-wagging, aldehyde H-wagging, and out-of-plane ring deformation vibrations are important in the vibronic perturbation between (n,π^*) and (π,π^*) states. The spectral structures and the results of CNDO computations of the $f_{n\rightarrow\pi^*}$-values of the $n\rightarrow\pi^*$ absorptions of TPA and BA suggest that the intensity enhancement in the TPA absorption is due to an increase in the vibronic perturbation between (n,π^*) and (π,π^*) states as well as to an increase in the electronically-allowed character in TPA in comparison with that in BA.

Since McMurry's study was published in 1941, a number of investigations have been carried out on the singlet-singlet electronic $n\rightarrow\pi^*$ systems of various aliphatic and aromatic carbonyls. Especially, the $n\rightarrow\pi^*$ absorptions of benzaldehyde and its derivatives have been a major object of interest.

It has been shown that the $n\rightarrow\pi^*$ transition of benzaldehyde is electronically allowed by the formal destruction of the C_{2v} symmetry of its parent molecule, formaldhyde, but a significant amount of the intensity is induced by $\pi\rightarrow\pi^*$ transitions through vibronic interaction between (n,π^*) and (π,π^*) states.

From the nature of the vibronic interactions, the out-of-plane vibrations of the CHO group are known to be important in promoting vibronic intensification.[1-4] Goodman *et al.* found out-of-plane CHO-torsional, CHO-wagging, and ring deformation vibrations in the $n\rightarrow\pi^*$ absorption and concluded that these vibrations are most effective in the intensification.[5-10]

It is interesting to study the $n\rightarrow\pi^*$ absorption of terephthalaldehyde(TPA), which is composed of a benzene ring and two CHO groups. TPA gives an absorption spectrum in the near ultraviolet region quite similar to that of benzaldehyde(BA), but the intensity of the $n\rightarrow\pi^*$ absorption is about 2.4 times greater than that of BA. Two main sources of the intensification of the $n\rightarrow\pi^*$ absorption in TPA may be considered to be (1) an increase in the intrinsic

1) E. C. Lim and Y. H. Li, *J. Chem. Phys.*, **50**, 4925 (1969).
2) E. C. Lim, "Molecular Luminescence," ed. by E. C. Lim, Benjamin, New York (1969), p. 469.
3) E. C. Lim, Y. H. Li, and R. Li, *J. Chem. Phys.*, **53**, 2443 (1970).
4) R. Shimada and L. Goodman, *ibid.*, **43**, 2027 (1965).
5) J. M. Hollas, E. Gregorek, and L. Goodman, *ibid.*, **49**, 1745 (1968).
6) R. Zwarich and L. Goodman, *Chem. Phys. Lett.*, **7**, 609 (1970).
7) R. Zwarich, J. Smolarek, and L. Goodman, *J. Mol. Spectry.*, **38**, 336 (1971).
8) M. Koyanagi, R. Zwarich, and L. Goodman, *Chem. Phys. Lett.*, **9**, 74 (1971).
9) M. Koyanagi and L. Goodman, *ibid.*, **9**, 636 (1971).
10) M. Koyanagi and L. Goodman, *J. Chem. Phys.*, **55**, 2959 (1971).

$n\rightarrow\pi^*$-allowed character and (2) an increase in vibronic interaction between the (n,π^*) and (π,π^*) states. TPA has two nearly degenerate (n,π^*) states; one gives an electronically-allowed transition, and the other, a forbidden $n\rightarrow\pi^*$ transition. The forbidden transition may be also perturbed by $\pi\rightarrow\pi^*$ transitions, and this perturbation may contribute to the intensity-enhancement of the $n\rightarrow\pi^*$ absorption.

The purpose of this paper is to discuss the nature of the $n\rightarrow\pi^*$ absorption of TPA and to show the probable sources for the intensification of the absorption.

The phosphorescence spectrum of TPA will also be studied because the absorption and phosphorescence are both due to the $n\rightarrow\pi^*$ transition and because their spectral structures are very similar to each other. The information obtained from the study of the phosphorescence spectrum of TPA will be useful in understanding the nature of the $n\rightarrow\pi^*$ absorptions.

Experimental

The TPA was prepared through the dehydration reaction of tetrabromo-*p*-xylene, which had been synthesized by means of *p*-xylene and bromine.[11] The crude TPA was purified by repeated recrystallization from 10% hot methanol and by repeated vacuum sublimation. Cyclohexane, methylcyclohexane, ethyl ether, isopentane, and ethanol were purified by ordinary methods.[12]

The near-ultraviolet absorption spectrum of TPA was studied in cyclohexane at room temperature and in EPA at 77°K with a Shimadzu multipurpose recording spectrophotometer MPS-50L and in the vapor with a recording spectrophotometer made of a Bausch & Lomb 500-mm grating monochromator, an RCA 1P28 photomultiplier tube, an RCA amplifier WV-84C, and a recorder. A 500-W xenon short-arc lamp and a tungsten lamp were used as the continuous-light sources. The vapor pressure of TPA in a vapor cell 45 cm in length was controlled by changing the temperature of the cell from 80 to 100°C. The infrared spectrum was recorded with a Hitachi-Perkin-Elmer infrared spectrophotometer, type 225, for the 200—4000 cm^{-1} region in the KBr disk. The Raman spectrum of the TPA crystal was recorded in the 250—4000 cm^{-1} region with a JRS-U1 laser Raman spectrophotometer equipped with a JEOL argon-ion laser, JLG-A4. The depolarization factor of the Raman lines was also measured in ethanol.

The phosphorescence spectra were studied in methylcyclohexane at 4.2 and 77°K with a Hilger E2 spectrograph. The degree of polarization of the phosphorescence was measured in EPA at 77°K by the usual method.[13]

Results and Discussion

Phosphorescence. The near-ultraviolet absorption spectra of TPA and BA[4] observed in EPA at 77°K are shown in Fig. 1. By analogy with the BA absorption, the three main absorption bands of TPA appearing in the 3900—3200, 3200—2800, and 2800—2300 Å

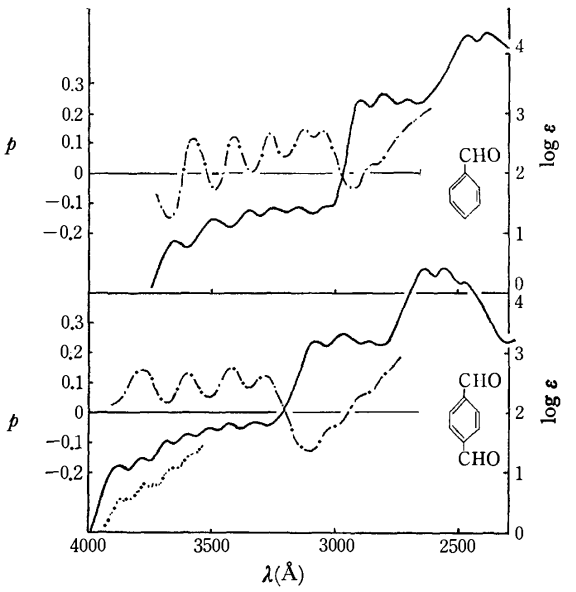

Fig. 1. The absorption spectra in EPA at 77°K (——) and the excitation polarization spectra (-·-·-) obtained relative to the O–O band of the phosphorescence of BA and TPA in EPA at 77°K. The $n\rightarrow\pi^*$ absorption spectrum of TPA observed in the vapor is also shown (------).

regions can be ascribed to $^1U(n,\pi^*)\leftarrow S_0$, $^1L_b(\pi,\pi^*)\leftarrow S_0$, and $^1L_a(\pi,\pi^*)\leftarrow S_0$ transitions respectively.

TPA emits a weak blue-green phosphorescence with a lifetime of 2.01×10^{-2} sec in EPA at 77°K. The phosphorescence is negatively polarized relative to the $^1L_b(\pi,\pi^*)$ excitation and positively polarized relative to the $^1L_a(\pi,\pi^*)$ excitation, as can be seen in Fig. 1. The polarized phosphorescence spectrum is shown in Fig. 2; it has been observed with respect to the excitation into the O–O band at 2700 Å of the $^1L_a(\pi,\pi^*)$ system in EPA at 77°K. The most remarkable feature of the spectrum is a progression of about 1700 cm^{-1}; this frequency can be assigned to the totally symmetric C=O stretching vibration. The shortest wavelength band at 4350 Å was taken as the O–O band. The separation between this band and the longest-wavelength band at 3880 Å in the S′←S absorption observed in EPA at 77°K, which was taken as the O–O band of the $^1U(n,\pi^*)\leftarrow S_0$ absorption system, is about 2600 cm^{-1}. These characteristic features of the phosphorescence are consistent with the lowest triplet state of TPA being a $^3U(n,\pi^*)$ state.

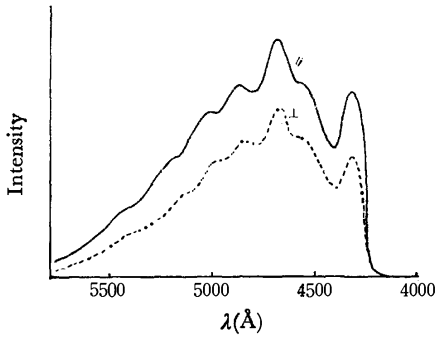

Fig. 2. The polarized phosphorescence spectrum of TPA in EPA at 77°K. Excitation was made into the O–O band of the $^1L_a(\pi,\pi^*)$ band.

11) J. M. Snell and A. Weissberger, "Organic Syntheses," Coll. Vol. III, (1955), p. 788.
12) Y. Kanda, "Zikken Kagaku Koza," 2nd Ser. Vol. XI, ed. by S. Nagakura, Maruzen, Tokyo (1965), p. 85.
13) Y. Murakami, R. Shimada, and Y. Kanda, "Molecular Luminescence," ed. by E. C. Lim, Benjamin, New York (1969), p. 119.

The phosphorescence spectrum was also observed in methylcyclohexane at 4.2°K. A part of the spectral structure is given in Fig. 3, along with the phosphorescence spectrum and the phosphorescence polarization spectra measured with respect to the excitation into the O–O bands of the $^1L_b(\pi,\pi^*)$ and $^1L_a(\pi,\pi^*)$ systems in EPA at 77°K. The phosphorescence observed in methylcyclohexane at 77°K gives almost the same spectrum as that observed in EPA at 77°K. The spectrum observed in methylcyclohexane at 4.2°K shows a well-resolved fine structure. The shortest-wavelength band at 4331.8 Å, which is the strongest in the spectrum, was taken as the O–O band of the system. The observed vibrational frequencies are given in Table 1, along with their intensities. The infrared and Raman spectral data are given in the same table. Clearly polarized Raman bands are indicated by a letter, *p*.

The prominent vibrational frequency of 1715 cm^{-1}, which constitutes the main progression in the phos-

Table 1. The vibrational analysis of the phosphorescence spectrum of TPA and the corresponding vibrational frequency in BA

IR		Raman			Phosphorescence			Assignment[15]	Corresponding vibrational frequency in BA[7,10]	
$\tilde{\nu}$(cm^{-1})	Int.	$\tilde{\nu}$ (cm^{-1})	Int.	Pol.	Design.	$\tilde{\nu}$ (cm^{-1})	Int.		IR & Raman $\tilde{\nu}$(cm^{-1})	Phos. $\tilde{\nu}$(cm^{-1})
						O–O	s			
					a	70	m			
					b	150	s	ϕ-CHO-torsion	133	141
					c	235	m	ϕ-CHO-wag	245	245
		257	m							
		326	w		d	320	vw			
400	w	392	m		e	405	vw	ν_{16a}	388	
474	m									
526	m									
		634	m							
		687	w	*p*						
		707	w		f	705	w	ν_4	688	685
774	s									
818	s				g	810	w	ν_{10a}	806	817
828	w*sh*	824	vw							
		872	s	*p*	h	870	w	ν_1	1004	1004
988	vw				i	970	m	ν_5	978	978
1009	m	1020	w		j	1010	m	aldehyde H-wag	1010	1008
1013	m									
1090	w									
1096	w				k	1105	vw			
		1150	s	*p*	l	1170	m	ν_{9a}	1164	
		1166	vw							
1197	s									
		1210	s	*p*						
1300	m	1298	w		m	1295	w	ν_{14}	1292	
1335	w									
1369	m									
1388	m									
1422	w*sh*	1408	m		n	1415	m	aldehyde C–H bend	1395	1412
1429	w									
1494	m*sh*	1491	vw							
1500	m									
		1586	m	*p*						
		1615	vs	*p*	o	1610	s	ν_{8a}	1601	1600
1633	s*sh*									
1658	s*sh*	1661	vw							
1689	vs									
1696	vs	1695	vs	*p*						
		1708	vs	*p*	p	1715	s	ν(C=O)	1694	1698
		1729	m*sh*							
1832	vw									
					q	1870	w	ν(C=O)+CHO-torsion		

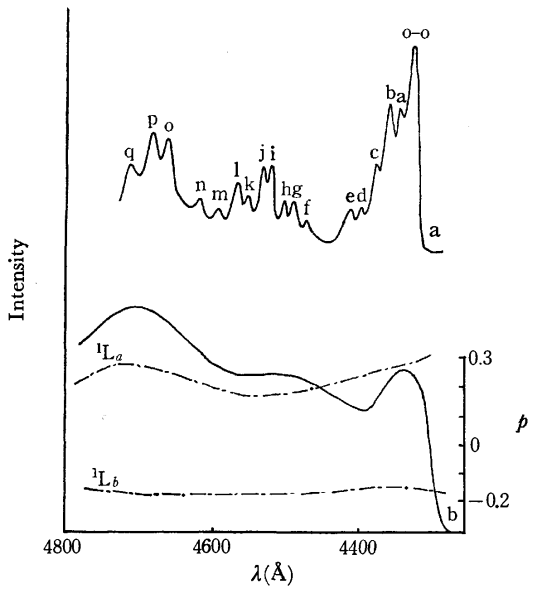

Fig. 3. A part of the phosphorescence spectra (——) of TPA at 4.2°K, a, and in EPA at 77°K, b. The phosphorescence polarization spectra (-·-·-) were obtained with respect to the O–O bands of the ^1L_a and ^1L_b bands.

phorescence spectrum, was assigned to the totally symmetric C=O stretching vibration. Two strong and polarized Raman bands were observed in the C=O stretching frequency region. These are 1695 and 1708 cm^{-1} in frequency and are nearly equal in intensity. This doublet was attributed to a Fermi resonance between a totally symmetric combination and the C=O stretching vibration. The in-plane CHO-bending vibration is expected to appear in the 230—240 cm^{-1} region. A combination of the overtone of this vibration and the ring-CHO stretching vibration, to which a strong and polarized Raman band of 1210 cm^{-1} was assigned, gives a frequency of about 1700 cm^{-1}. The C=O stretching vibration may be mechanically coupled with this combination vibration through the carbonyl carbon atom. Fermi resonances in the C=O stretching vibration are observed in various carbonyl compounds. The fairly strong bands at 150, 235, 970, and 1010 cm^{-1} were assigned to the out-of-plane CHO-torsional, CHO-wagging, ring deformation, ν_5,[14] and aldehyde H-wagging vibrations respectively. The other bands, at 870, 1170, 1415, and 1610 cm^{-1}, were ascribed to the totally symmetric vibrations, ν_1, ν_{9a}, aldehyde C–H bending, and ν_{8a} respectively. The degree of polarization of the phosphorescence, measured relative to the ^1L_b excitation, is negative and is approximately uniform throughout the phosphorescence region, while the degree of polarization measured relative to the ^1L_a excitation gives a minimum around the 1000 cm^{-1} region, although the overall value is positive, as can be seen in Fig. 3. This observation is consistent with the above vibrational assignment. Detailed vibrational analyses of the infrared and Raman spectra will be reported in the near future.

14) The notations of the normal modes of vibrations characteristic of the benzene ring are according to Langseth and Lord.[15]

15) A. Langseth and R. C. Lord, *Kgl. Danske Videnskab. Selskab. Math-Fys. Medd.*, **16**, 1 (1938).

It should be noted that only a few vibrational frequencies were observed in both the infrared and Raman spectra. Such a mutually exclusive relation between infrared and Raman spectra must hold only for the *trans*-form of this molecule. However, the distance between two CHO groups is long enough for there to be a possibility that TPA has both *trans*- and *cis*-conformations. In this connection, the two conformations are calculated to have almost the same ground-state energy, as can be seen in Table 2. Although the CHO plane may deviate from the plane of the benzene ring by repulsion between H atoms of the benzene ring and H and O atoms of the carbonyl group, the deviation may be minimized by the conjugation of the π-electrons. Thus, the TPA molecule may be assumed to have an almost planar structure in the ground state. The *trans*-form of the TPA molecule belongs to the C_{2h} point group and the *cis*-form belongs to the C_{2v} point group. The z axis was taken to be perpendicular to the molecular plane and the y axis to be along the long axis for the C_{2h} point group, while the z axis was taken to be along the C_2 axis and the y axis to be perpendicular to the molecular plane for the C_{2v}.

TPA has two low-lying $^3U(n,\pi^*)$ states, $^3A_u(n,\pi^*)$ and $^3B_g(n,\pi^*)$ states for the *trans*-form, and $^3B_2(n,\pi^*)$ and $^3A_2(n,\pi^*)$ states for the *cis*-form. The electronically-allowed $n\leftarrow\pi^*$ character of the phosphorescence clearly indicates that the lowest triplet state in the *trans*-form is a $^3A_u(n,\pi^*)$ state; thus, the lowest triplet in the *cis*-form is a $^3B_2(n,\pi^*)$ state. CNDO SCF CI calculations, which will be described later, suggest that the lowest $^3A_u(n,\pi^*)$ and $^3B_2(n,\pi^*)$ states are strongly perturbed by the $^1L_a(\pi,\pi^*)$ state, but that the perturbations by the $^1L_b(\pi,\pi^*)$ state are negligibly small, as can be seen in Table 3. In TPA, the $^3L_a(\pi,\pi^*)$ state is expected to be located just above the emitting $^3U_A(n,\pi^*)$ state; thus, the $^3U_A(n,\pi^*)$ state may be perturbed by the $^1U_A(n,\pi^*)$ state through second-order spin-orbit-vibronic coupling. The out-of-plane vibrations observed in the phosphorescence spectrum should be due to the strong vibronic coupling between the $^3L_a(\pi,\pi^*)$ and $^3U_A(n,\pi^*)$ states through b_g or a_2 vibrations. The same phenomenon was observed in the phosphorescence spectrum of BA.[8-10]

$n\rightarrow\pi^*$ Absorption. The near-ultraviolet absorption spectrum and the excitation polarization spectrum measured with respect to the O–O band of the phosphorescence spectrum of TPA in EPA at 77°K are shown in Fig. 1. The corresponding spectra of BA[4] are also given in the same figure. The $n\rightarrow\pi^*$ absorption spectrum of TPA consists of two main progressions. One starts from the longest-wavelength band, located at 3880 Å, with an interval of 1385 cm^{-1}, while the other starts from a band separated by 695 cm^{-1} from the 3880 Å band toward the shorter-wavelength side, with the same interval. The first progression has polarization minima requiring negative polarization, even though the sign of the observed polarization is positive, while the second progression shows positive polarization maxima. No band could be observed on the longer-wavelength side of the 3880 Å band at 77°K, even though a concentrated TPA solution was used. This definitely indicates that the 3880 Å band is a O–O

band of the $n\rightarrow\pi^*$ absorption.

The absorption spectrum of TPA observed in cyclohexane at room temperature is almost the same as that observed in EPA at 77°K. The oscillator strengths of the $n\rightarrow\pi^*$ and $\pi\rightarrow\pi^*$ absorption bands are given in Tables 2 and 3, together with the data for BA. A question immediately arises why the $f_{n\rightarrow\pi^*}$-value of TPA is 2.4 times that of BA. Three possible reasons for the intensification of the $n\rightarrow\pi^*$ absorption in TPA may be considered:

(1) The $n\rightarrow\pi^*$ absorption of TPA has a more electronically allowed character.

(2) The $n\rightarrow\pi^*$ absorption of TPA is more vibronically intensified by strong $\pi\rightarrow\pi^*$ absorptions.

(3) TPA has two CHO groups, and thus two $n\rightarrow\pi^*$ absorptions can be expected to be observed in this region, one electronically allowed and the other forbidden. The observed $n\rightarrow\pi^*$ absorption is the superposition of these two systems.

In order to study the nature of the $n\rightarrow\pi^*$ absorption of TPA in detail, the absorption spectrum was observed in the vapor phase. The $n\rightarrow\pi^*$ vapor absorption, which is given in Fig. 1, shows a rather simple spectral structure, and the individual bands are not sharp enough. The CHO plane may deviate from the plane of the benzene ring somewhat freely in the vapor phase, and this may cause the diffuseness of the spectral structure. The longest-wavelength band at 3857 Å was taken as the O–O band of the $n\rightarrow\pi^*$ absorption. A weak and diffuse band was observed at 3830 Å, separated by 180 cm^{-1} from the O–O band. This band may be ascribed to the superposition of the CHO-torsional and CHO-wagging vibrational bands, whose ground-state vibrational frequencies are 150 and 235 cm^{-1} respectively. The second band observed in the solution spectra splits into two bands in this vapor spectrum. The observed frequencies of 740 and 880 cm^{-1} were assigned to the out-of-plane ring deformation, ν_5, and aldehyde H-wagging vibrations, whose ground-state vibrational frequencies are 970 and 1010 cm^{-1} respectively. A rather strong band was observed at 3660 Å, separated by 1395 cm^{-1} from the O–O band corresponding to the third band of the solution spectra. A frequency of 1395 cm^{-1} was assigned to the totally symmetric C=O stretching vibration in the excited state.

It should be noted that the spectral structures of the n-π^* absorption and phosphorescence spectra are very similar to one another. This means that the $^1U_A(n,\pi^*)\leftarrow S_0$ transition is perturbed by the $^1L_a(\pi,\pi^*)\leftarrow S_0$ transition through exactly the same out-of-plane vibrations as are involved in the vibronic coupling between the emitting $^3U_A(n,\pi^*)$ and the low-lying $^3L_a(\pi,\pi^*)$ states. From the electronically-allowed character of the spectral structure, the $n\rightarrow\pi^*$ absorption of TPA can be ascribed to a $^1A_u(n,\pi^*)\leftarrow S_0$ transition for *trans*-TPA and to a $^1B_2(n,\pi^*)\leftarrow S_0$ transition for *cis*-TPA.

The intensities of the $n\rightarrow\pi^*$ absorptions of TPA and BA were calculated by the CNDO SCF CI method, using Pople's parameter.[16,17] In the CI calculations, seven higher-lying occupied molecular orbitals and seven lower-lying vacant molecular orbitals were employed. All the calculations were made on the basis of an assumption that the conformations of TPA and BA molecules were both planar. The geometries of the molecular structure used in the calculation were:

ring C–C = 1.396 Å, ring C–H = 1.084 Å,
ring – aldehyde C–C = 1.490 Å,
aldehyde C–O = 1.240 Å, aldehyde C–H = 1.114 Å,
ring ∠C–C–C = 120°, ring ∠H–C–C = 120°,
ring – aldehyde ∠C–C–C = 120°,
aldehyde ∠O–C–C = 123°, and
aldehyde ∠O–C–H = 120°.

The calculated state functions of the ^1L_a, ^1L_b, and ^1U ($=^3U$ in CNDO approximation) states for the *trans*- and *cis*-forms of TPA and BA are as follows:

for *trans*-TPA,

$$\Psi_{^1B_u(\pi,\pi^*);\,L_a} = 0.931(\phi_{24},\phi_{26}) - 0.293(\phi_{21},\phi_{27}) - 0.091(\phi_{24},\phi_{29}) + 0.067(\phi_{20},\phi_{31}) + 0.063(\phi_{23},\phi_{30}) + \cdots$$

$$\Psi_{^1B_u(\pi,\pi^*);\,L_b} = 0.761(\phi_{21},\phi_{26}) + 0.619(\phi_{24},\phi_{27}) - 0.187(\phi_{21},\phi_{29}) + \cdots$$

$$\Psi_{^1A_u(n,\pi^*);\,U_A} = 0.681(\phi_{25},\phi_{26}) + 0.600(\phi_{23},\phi_{28}) + 0.266(\phi_{20},\phi_{26}) + 0.259(\phi_{25},\phi_{29}) + 0.196(\phi_{20},\phi_{29}) + \cdots$$

$$\Psi_{^1B_g(n,\pi^*);\,U_F} = 0.698(\phi_{23},\phi_{26}) + 0.556(\phi_{25},\phi_{28}) + 0.355(\phi_{23},\phi_{29}) + 0.302(\phi_{20},\phi_{28}) + \cdots$$

for *cis*-TPA,

$$\Psi_{^1B_1(\pi,\pi^*);\,L_a} = 0.932(\phi_{24},\phi_{26}) - 0.294(\phi_{22},\phi_{27}) + 0.150(\phi_{19},\phi_{28}) - 0.091(\phi_{24},\phi_{29}) + \cdots$$

$$\Psi_{^1A_1(\pi,\pi^*);\,L_b} = 0.764(\phi_{22},\phi_{26}) + 0.617(\phi_{24},\phi_{27}) - 0.187(\phi_{22},\phi_{29}) + \cdots$$

$$\Psi_{^1B_2(n,\pi^*);\,U_A} = 0.692(\phi_{25},\phi_{26}) + 0.532(\phi_{23},\phi_{28}) - 0.273(\phi_{21},\phi_{28}) + 0.256(\phi_{25},\phi_{29}) + 0.251(\phi_{20},\phi_{26}) + 0.187(\phi_{20},\phi_{29}) + \cdots$$

$$\Psi_{^1A_2(n,\pi^*);\,U_F} = 0.633(\phi_{23},\phi_{26}) + 0.559(\phi_{25},\phi_{28}) - 0.306(\phi_{21},\phi_{26}) + 0.292(\phi_{23},\phi_{29}) + 0.287(\phi_{20},\phi_{28}) + \cdots$$

and for BA,

$$\Psi_{^1A'(\pi,\pi^*);\,L_a} = 0.868(\phi_{19},\phi_{21}) + 0.418(\phi_{17},\phi_{22}) - 0.150(\phi_{15},\phi_{23}) - 0.106(\phi_{17},\phi_{21}) - 0.100(\phi_{19},\phi_{23}) + \cdots$$

$$\Psi_{^1A'(\pi,\pi^*);\,L_b} = 0.703(\phi_{17},\phi_{21}) - 0.645(\phi_{19},\phi_{22}) - 0.231(\phi_{17},\phi_{23}) - 0.144(\phi_{15},\phi_{22}) + 0.108(\phi_{19},\phi_{21}) + \cdots$$

$$\Psi_{^1A''(n,\pi^*);\,U} = 0.776(\phi_{20},\phi_{21}) + 0.444(\phi_{20},\phi_{24}) - 0.351(\phi_{16},\phi_{21}) - 0.278(\phi_{16},\phi_{23}) + \cdots$$

16) J. A. Pople, D. P. Santry, and G. A. Segal, *J. Chem. Phys.*, **43**, S129 (1965).

17) J. A. Pople and G. A. Segal, *ibid.*, **43**, S136 (1965); *ibid.*, **44**, 3289 (1966).

Table 2. Observed and calculated intensities of the $^1U_A(n,\pi^*)\leftarrow S_0$ absorptions and the total energies of the ground states of TPA and BA

		$f^{obs.}_{n\to\pi^*}$	$\tilde{\nu}^{obs.}_{n\to\pi^*0\text{-}0}$ (cm^{-1})	$M^{calc.}_{n\to\pi^*}$ (D)		$f^{calc.}_{n\to\pi^*}$		Total energy of the ground state (eV)	
				Pople	Jaffé	Pople	Jaffé	Pople	Jaffé
TPA	*trans*	1.3×10^{-3}	25,750	0.193	0.141	4.52×10^{-4}	2.40×10^{-4}	−2665.8	−1273.7
	cis			0.209	0.143	5.31×10^{-4}	2.48×10^{-4}	−2665.8	−1273.7
BA		5.5×10^{-4}	27,300	0.158	0.104	3.22×10^{-4}	1.39×10^{-4}	−1973.7	− 933.4
TPA/BA	*trans*	2.4				1.4	1.7		
	cis					1.6	1.8		

Table 3. $f_{T\leftarrow S}$-values contributed from the two perturbing paths in TPA and BA

	Perturbing transition	$\tilde{\nu}^{obs.}_{\pi\to\pi^*0\text{-}0}$ (cm^{-1})	$f^{obs.}_{\pi\to\pi^*}$	Emitting triplet state	$f^{calc.}_{T\leftarrow S}$ a)
trans-TPA	$^1L_a(\pi,\pi^*)$-S_0	37,600	3.51×10^{-1}	$^3A_u(n,\pi^*)$	5.44×10^{-6}
	$^1L_b(\pi,\pi^*)$-S_0	32,450	2.47×10^{-2}	$^3A_u(n,\pi^*)$	1.22×10^{-9}
cis-TPA	$^1L_a(\pi,\pi^*)$-S_0	37,600	3.51×10^{-1}	$^3B_2(n,\pi^*)$	3.24×10^{-6}
	$^1L_b(\pi,\pi^*)$-S_0	32,450	2.47×10^{-2}	$^3B_2(n,\pi^*)$	1.43×10^{-9}
BA	$^1L_a(\pi,\pi^*)$-S_0	40,500	2.56×10^{-1}	$^3A''(n,\pi^*)$	2.93×10^{-6}
	$^1L_b(\pi,\pi^*)$-S_0	34,600	2.02×10^{-2}	$^3A''(n,\pi^*)$	1.18×10^{-8}

a) The $f^{calc.}_{T\leftarrow S}$-value was calculated with the following equations and observed values:

$$M_{T\leftarrow S}=M_{^1L_a \text{ or } ^1L_b\text{-}S_0}\frac{\langle\psi_{^1L_a \text{ or } ^1L_b}|H_{so}|\psi_{^3U_A}\rangle}{E_{^1L_a \text{ or } ^1L_b}-E_{^3U_A}}$$

$$f_{T\leftarrow S}=1.08\times10^{-5}\times\tilde{\nu}(cm^{-1})\times G\times M^2_{T\leftarrow S},$$

$E^{TPA}_{^3U_A}=23{,}100\ cm^{-1}$, and

$E^{BA}_{^3U}=25{,}150\ cm^{-1}$.

These state functions were used for the calculations of the transition moments of the $n\to\pi^*$ absorptions and the spin-orbit couplings between the $^3U_A(n,\pi^*)$ states and the $^1L_a(\pi,\pi^*)$ and $^1L_b(\pi,\pi^*)$ states for TPA and BA; the results are listed in Tables 2 and 3. The calculated $f_{n\to\pi^*}$-values of TPA and BA are listed in Table 2, together with the $f_{n\to\pi^*}$-values observed in cyclohexane at room temperature. The $f_{n\to\pi^*}$-values were also calculated by the use of Jaffé's parameter;[18] the results are given in the same table. Although Jaffé's parameter gives $f_{n\to\pi^*}$-values about one half of those obtained with Pople's parameter, the ratios of the calculated $f_{n\to\pi^*}$-values of TPA to those of BA are almost all the same. The values were 1.4 and 1.7 for *trans*-TPA and 1.6 and 1.8 for *cis*-TPA with Pople's and Jaffé's parameters respectively, as is shown in Table 2.

$$f_{n\to\pi^*}(\textit{trans}\text{-TPA})/f_{n\to\pi^*}(\text{BA})\approx 1.6 \text{ and}$$

$$f_{n\to\pi^*}(\textit{cis}\text{-TPA})/f_{n\to\pi^*}(\text{BA})\approx 1.7.$$

The calculation shows that *cis*-TPA gives an $f_{n\to\pi^*}$-value slightly greater than that of *trans*-TPA. The molecular extinction coefficients of the O–O bands of the $n\to\pi^*$ absorptions of TPA and BA measured in cyclohexane at room temperature are 18 and 11 respectively, the ratio being 1.6: 1. This value cannot be directly equal to the ratio of the electronically-allowed characteristics of the $n\to\pi^*$ absorptions of TPA and BA because the O–O band observed in solution generally involves non-totally symmetric vibrational bands of a low frequency, and the Frank-Condon factors of the n-π^* transitions of TPA and BA may be different. The calculated and experimental ratios both give values greater than unity. Hence, this leads to the conclusion that the $n\to\pi^*$ absorption of TPA has a fairly stronger electronically-allowed character than that of BA.

It is well known that the greater part of the observed intensity of the $n\to\pi^*$ absorption of BA is vibronically induced. The ratio of the observed $f_{n\to\pi^*}$-values of TPA and BA, 2.4: 1, may suggest that the $n\to\pi^*$ absorption of TPA is much more intensified vibronically than that of BA. This may be supported by the experimental fact that the second progression of the $n\to\pi^*$ absorption of TPA, which contains vibronic bands due to the out-of-plane ring deformation, ν_5, and aldehyde H-wagging vibrations, is remarkably enhanced in intensity compared with that of BA. This may result in an increase in the degree of polarization of the first band of the second progression of TPA to +0.15 from +0.10 for BA.

It should be noted that the degree of polarization of the first progression of TPA is markedly increased compared with that of BA. The degree of polarization of the first band of the progression of BA is −0.15, while that of TPA is +0.02. It was observed in the vapor absorption that the first band of TPA contains not only the O–O band, but also vibronic bands due to the CHO-torsional and CHO-wagging vibrations. These out-of-plane vibrations may increase the degree of polarization of the first progression of TPA. Since they increase the intensity of the first band of the first progression, the experimental ratio of $\varepsilon^{TPA}_{0\text{-}0}/\varepsilon^{BA}_{0\text{-}0}$, 1.6: 1, seems a little greater than the ratio in an ideal case where no out-of-plane vibrations are involved. The calculations of the transition densities between $^1U_A(n,\pi^*)$ and $^1L_a(\pi,\pi^*)$, and between $^1U_A(n,\pi^*)$ and $^1L_b(\pi,\pi^*)$ with the state functions given above suggest that the n-π^* transition in TPA is preferentially perturbed by $^1L_a(\pi,\pi^*)$. The ratio of intensity incre-

18) J. D. Bene and H. H. Jaffé, *J. Chem. Phys.*, **48**, 1807 (1968); *ibid.*, **48**, 4050 (1968); *ibid.*, **49**, 1221 (1968).

ments of the $n\rightarrow\pi^*$ absorptions due to the vibronic perturbation in TPA and BA is given by:

$$\frac{f^{\mathrm{TPA}}_{^1U_A(n,\pi^*)_{\mathrm{vib}}}}{f^{\mathrm{BA}}_{^1U(n,\pi^*)_{\mathrm{vib}}}} = \frac{f^{\mathrm{TPA}}_{^1L_a}}{f^{\mathrm{BA}}_{^1L_a}} \cdot \frac{E^{\mathrm{TPA}}_{^1U_A}}{E^{\mathrm{BA}}_{^1U}} \cdot \frac{E^{\mathrm{BA}}_{^1L_a}}{E^{\mathrm{TPA}}_{^1L_a}} \times \frac{\{E^{\mathrm{BA}}_{^1U} - E^{\mathrm{BA}}_{^1L_a}\}^2}{\{E^{\mathrm{TPA}}_{^1U_A} - E^{\mathrm{TPA}}_{^1L_a}\}^2} \frac{(W^{\mathrm{TPA}}_{^1U_A{}^1L_a})^2}{(W^{\mathrm{BA}}_{^1U^1L_a})^2} \approx 1.7 \times \frac{(W^{\mathrm{TPA}}_{^1U_A{}^1L_a})^2}{(W^{\mathrm{BA}}_{^1U^1L_a})^2}$$

where $W_{^1U^1L_a}$ is the vibronic interaction energy matrix element between ^1U and ^1L_a states.[19] The ratio of $W^{TPA}_{^1U_A{}^1L_a}/W^{BA}_{^1U^1L_a}$ is suggested to be greater than unity by a rough estimation of the value of the energy matrix element. Therefore, the above relation clearly explains the increase in the vibronic intensification of the $n\rightarrow\pi^*$ absorption of TPA.

The CNDO calculation indicates that the forbidden $n\rightarrow\pi^*$ transition is also strongly perturbed by the $^1L_a(\pi,\pi^*)\leftarrow S_0$ transition; thus, a_u or b_2 vibrations can be expected to appear in the $n\rightarrow\pi^*$ absorption. These vibronic bands give a positive polarization and should have different vibrational frequencies from those of the b_g or a_2 vibrations which are found in the allowed $n\rightarrow\pi^*$ absorption. Therefore, the observed $n\rightarrow\pi^*$ absorption and excitation polarization spectra can be expected to have very complicated patterns if a_u or b_2 vibrations are present. The $n\rightarrow\pi^*$ absorption spectrum of TPA was carefully studied in the vapor phase and in the crystal matrix at a low temperature in order to find the vibronic bands due to the electronically-forbidden $n\rightarrow\pi^*$ transition, but no positive evidence for the existence of these bands could be found. This indicates that the enhancement of the $n\rightarrow\pi^*$ absorptions due to the forbidden $n\rightarrow\pi^*$ transition is negligible.

19) J. A. Pople and J. W. Sidman, *J. Chem. Phys.*, **27**, 1720 (1957).

The authors wish to thank Mr. Anjin Matsuda for his very helpful collaboration, and Mr. Hajime Ishii for his help in the theoretical calculations. The authors are also grateful to the Japan Electron Optics Laboratory Co., Ltd., for the measurement of the Raman spectrum of TPA.

BULLETIN OF THE CHEMICAL SOCIETY OF JAPAN, VOL. 45, 1679—1682(1972)

Mössbauer Effect of ^{119}Sn in Tetracarbonylcobalt Derivatives of Tin(IV) Halides

Sumio Ichiba, Motomi Katada, and Hisao Negita
Department of Chemistry, Faculty of Science, Hiroshima University, Hiroshima

(Received October 18, 1971)

The ^{119}Sn Mössbauer effect was studied in tetracarbonylcobalt derivatives of tin(IV) halides, $X_nSn[Co(CO)_4]_{4-n}$, where X=Cl, Br or I, and $n=0\sim4$. The isomer shift in each halogen series increased as the halogen atom was successively replaced by the $Co(CO)_4$ group. The values of the isomer shift were between those of tin(IV) halides and $XSn[Co(CO)_4]_3$ and did not change lineraly with the number of halogen atoms. The values of the quadrupole splitting were smaller than those of the corresponding organotin halides, X_nSnR_{4-n}, and attained their maximum at dihalides. From the Mössbauer parameters, the chemical bonds in the compounds, especially the Sn–Co bond, were discussed.

A large number of compounds containing metal-metal bonds between a Group IV element and a transition element have been synthesized, and the nature of the bonds and chemical properties of the compounds have been investigated by many workers.[1-5] Recently, Mössbauer spectroscopy has become available for compounds containing tin atoms, and the compounds containing a Sn–M bond, such as Sn–Fe, Sn–Co, Sn–Mn, and Sn–Re, have been studied by this method.[6-13] In particular, compounds containing metalcarbonyl have been investigated in the studies of metal-metal bonding. Karasyov *et al.*[13] have studied $A_nSn(C_6H_5)_{4-n}$ ($A=Mn(CO)_5$, $Re(CO)_5$, or $Co(CO)_4$, and $n=1\sim3$) by Mössbauer spectroscopy and elucidated the electron-donating nature of $Mn(CO)_5$ and $Re(CO)_5$ and accepting nature of $Co(CO)_4$

1) D. J. Patmore and W. A. G. Graham, *Inorg. Chem.*, **5**, 1405 (1966); *ibid.*, **5**, 2222 (1966); *ibid.*, **7**, 771 (1968).
2) J. F. Young, "Advances in Inorganic Chemistry and Radiochemistry," Vol. 11, ed. by H. J. Emeleus and A. G. Sharpe, Academic Press, New York (1968), p. 91.
3) W. A. G. Graham, *Inorg. Chem.*, **7**, 315 (1968).
4) A. D. Berry, E. R. Corey, A. P. Hagen, A. G. MacDiarmid, F. E. Saalfeld, and B. B. Wayland, *J. Amer. Chem. Soc.*, **92**, 1940 (1970).
5) H. W. Spiess and R. K. Sheline, *J. Chem. Phys.*, **53**, 3036 (1970).
6) R. H. Herber and Y. Goscinny, *Inorg. Chem.*, **7**, 1293 (1968).
7) D. E. Fenton and J. J. Zuckerman, *J. Amer. Chem. Soc.*, **90**, 6226 (1968).
8) D. E. Fenton and J. J. Zuckerman, *Inorg. Chem.*, **8**, 1771 (1969).
9) C. Whyter and L. Chandler, This Bulletin, **43**, 2115 (1970).
10) S. Onaka, Y. Sasaki, and H. Sano, *ibid.*, **44**, 726 (1971).
11) S. R. A. Bird, J. D. Donaldson, A. F. Le C. Holding, B. J. Senior, and M. J. Tricker, *J. Chem. Soc., A*, **1971**, 1616.
12) B. A. Goodman, R. Greatrex, and N. N. Greenwood, *J. Chem. Soc., A*, **1971**, 1868.
13) "Chemical Applications of Mössbauer Spectroscopy," ed. by V. I. Goldanskii and R. H. Herber, Academic Press, New York (1968).

as compared to C_6H_5. Goldandkii *et al.*[13] have studied the A_nSnCl_{4-n}, $[C_5H_5Fe(CO)_2]_nSn(C_6H_5)_{4-n}$, and $[C_5H_5Fe(CO)_2]_nSnCl_{4-n}$ compounds and reported that in them metalcarbonyl groups act as electron acceptors. Onaka *et al.*[10] have studied $R_{3-n}X_nSn[Mn(CO)_5]$ and reported that the $Mn(CO)_5$ group is a stronger electron donor than the methyl, phenyl, and halogen groups. Spencer *et al.*[14] have studied $X_nSn[Co(CO)_4]_{4-n}$ and $R_nSn[Co(CO)_4]_{4-n}$ by ^{59}Co nuclear quadrupole resonance (NQR) and reported that there are Sn–Co π-interactions and that $Co(CO)_4$ is more electron-withdrawing than the methyl group. In the present studies, the Mössbauer effects of ^{119}Sn in $X_nSn[Co(CO)_4]_{4-n}$, where X=Cl, Br, or I, and n=0~4, were investigated in order to study the chemical bond, especially the Sn–Co bond.

Experimental

Materials. Tin(IV) halides and dicobalt octacarbonyl were obtained commercially. Tin(II) chloride was dehydrated completely by heating it in a nitrogen atmosphere. Tin(II) bromide was prepared by dissolving tin metal powder in concentrated hydrobromic acid. Tin(II) iodide was purified by sublimation in a nitrogen atmosphere. The purity of the tin(II) halides was checked by means of the Mössbauer spectrum.

Preparation of the Compounds. The compounds studied were prepared by the method of Patmore and Graham.[1] All the reactions were carried out under a nitrogen atmosphere because of their reactivity with air. The compounds were identified by their melting points and infrared spectra.

Measurements. The measurements were made as has been described previously.[15] The γ-ray source of barium stannate was used at room temperature, whereas the absorber was cooled with liquid nitrogen. The thickness of the absorber was about 20 mg/cm^2 for tin.

Results and Discussion

The Mössbauer spectrum of $Cl_3Sn[Co(CO)_4]$ is shown in Fig. 1, as an example. The solid line in the figure is the computer fit of the experimental points to the Lorentzian curve by the least-squares method. From the curves, the Mössbauer parameters, such as

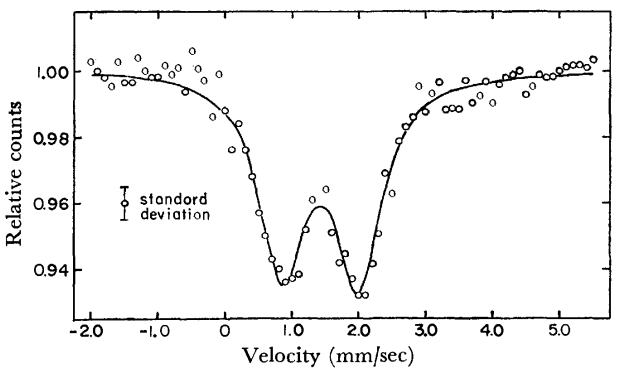

Fig. 1. The Mössbauer spectrum of $Cl_3Sn[Co(CO)_4]$.

Table 1. Mössbauer parameters for tin compounds

Compounds	δ[a] (mm/sec)	2ε (mm/sec)	Γ (mm/sec)
$SnCl_4$	0.86	0	1.08
$Cl_3Sn[Co(CO)_4]$	1.42	1.15	0.82
$Cl_2Sn[Co(CO)_4]_2$	1.74	1.40	0.86
$ClSn[Co(CO)_4]_3$	1.93	1.18	1.10
$SnBr_4$	1.01	0	1.35
$Br_3Sn[Co(CO)_4]$	1.49	1.28	1.23
$Br_2Sn[Co(CO)_4]_2$	1.81	1.46	0.86
$BrSn[Co(CO)_4]_3$	1.97	1.06	0.80
SnI_4	1.54	0	1.10
$I_3Sn[Co(CO)_4]$	1.73	0.71	1.09
$I_2Sn[Co(CO)_4]_2$	2.02	1.07	0.95
$ISn[Co(CO)_4]_3$	2.03	0.95	0.91
$Sn[Co(CO_4)]_4$[b]	1.96	0	—

a) Isomer shift with respect to $BaSnO_3$.
b) Ref. 8).

the isomer shift (δ), the quadrupole splitting (2ε), and the half width (Γ), were derived. The values of these parameters are summarized in Table 1.

Isomer Shift. According to Cordey-Hayes,[16] the isomer shift of tin (IV) compounds is lower than the value of gray tin, which is completely quadrivalent, with the hybridized configuration $(5s)(5p)^3$, and which is sensitive to the s-electron density at the tin nucleus in such a way that the decrease in the value is closely related to the increase in the partial ionic character of the bond. The screening effects of the s-electrons by the $5s$, $5p$ and, in some cases, $5d$ electrons are also taken into account.

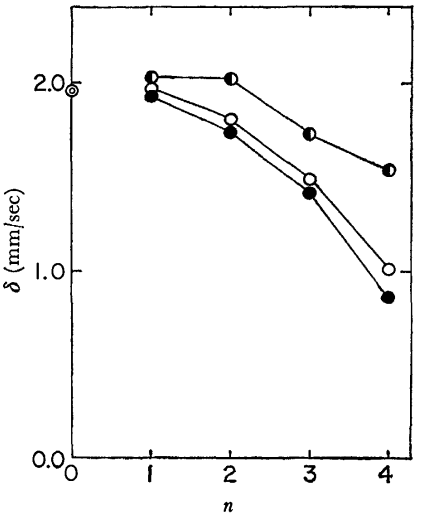

Fig. 2. The isomer shift *vs.* the number of halogens, n, in $X_nSn[Co(CO)_4]_{4-n}$ series.
●: Cl, ○: Br, ◐: I and ◎: $Sn[Co(CO)_4]_4$.

In Table 1, the values of the isomer shift of tin tetrahalides agree with the literature values,[13] and the values of the $X_nSn[Co(CO)_4]_{4-n}$ compounds (X=Cl, Br, or I, and n=1~3) increase as the electronegativities of the halogen atoms decrease. The plots of the values of the isomer shift *versus* the number of halogens, n,

14) D. D. Spencer, J. L. Kirsch, and T. L. Brown, *Inorg. Chem.*, **9**, 235 (1970).
15) S. Ichiba, M. Mishima, H. Sakai, and H. Negita, This Bulletin, **41**, 49 (1968).
16) M. Cordey-Hayes, *J. Inorg. Nucl. Chem.*, **26**, 915 (1964).

are shown in Fig. 2. Since the value of the isomer shift of $Sn[Co(CO)_4]_4$ is higher than that of each tin (IV) halide, the bonding character of the Sn–Co must be more covalent than those of Sn–X. The values of the isomer shift of the compounds in each series of halogen are between the values of $XSn[Co(CO)_4]_3$ and SnX_4. In each curve, it is observed that the changes in the isomer shift *versus* the number of halogens are not linear. That is, the change in the isomer shift becomes smaller as the number of halogens, n, decreases. On the other hand, it has been reported that the ionic character in the Sn–Cl bond increases with the decrease in the n, as is shown by the findings concerning the NQR due to ^{35}Cl in $Cl_nSn[Co(CO)_4]_{4-n}$ (n=2~4).[17-19] Thus, the electrons on the tin atom are more withdrawn to chlorine atoms as their number, n, decreases. Furthermore, according to Spencer *et al.*,[14] more π-electrons transfer to the tin atom from $Co(CO)_4$ and, in turn, decrease the isomer shift of tin, as their number, n, increases. The observed isomer shift must be the result of the competition of the ionic character in the Sn–X bond with the π-bonding in the Sn–Co bond as the number, n, changes.

The same tendency of the isomer shift has been observed in the $[C_5H_5Fe(CO)_2]_nSnCl_{4-n}$ and $[C_5H_5Fe(CO)_2]_nSn(C_6H_5)_{4-n}$ (n=0~3) series of compounds.[7]

Quadrupole Splitting. In tin(IV) compounds, large quadrupole splittings are generally observed when there is an unequal electron population at the three $5p$ or four $5sp^3$ orbitals. Sizable quadrupole splittings are observed in the $X_nSn[Co(CO)_4]_{4-n}$ compounds (X=Cl, Br, or I, and n=1~3), as is shown in Table 1. Thus, in these compounds there is an unequal electron population at the three $5p$ orbitals, so that the bonding characters of Sn–X and Sn–Co are considerably different. Many workers have studied the quadrupole splitting of organotin compounds of the type of X_nSnR_{4-n} (R=alkyl or aryl, X=halogen, and n=1~3).[13,20-22] The results show that the quadrupole splitting in the organotin compound becomes smaller as the electronegativity of the organic group, R, approaches that of the halogen atom. Because the quadrupole splittings of the $X_nSn[Co(CO)_4]_{4-n}$ compounds are smaller than the values of the corresponding organotin compounds, the $Co(CO)_4$ group is more electronegative than the alkyl or aryl group. This result agrees with the conclusions of the NQR study of the compounds by Spencer *et al.*[14] and the Mössbauer study of the $(C_6H_5)_nSn[Co(CO)_4]_{4-n}$ series by Karasyov *et al.*[13]

Bir'yukov *et al.*[23] reported that the Co–Sn–Cl angle in $ClSn[Co(CO)_4]_3$ is 104°, as determined by the X-ray diffraction method. Boer *et al.*[24] reported that, in $Cl_2Sn[Co(CO)_2C_7H_8]_2$ or $(C_6H_5)_2Sn[Co(CO)_2C_7H_8]_2$, the Co–Sn–Co angle is larger than Cl–Sn–Cl or C_6H_5–Sn–C_6H_5, as determined by the X-ray diffraction method. Patmore and Graham[25] reported that the Co–Sn–Co angle in $Cl_2Sn[Co(CO)_4]_2$ is larger than the tetrahedral angle, as determined by IR spectroscopy. They also studied the $(CH_3)_nSn[Co(CO)_4]_{4-n}$ compounds by NMR spectroscopy and showed, from the coupling constants, $J(^{117}Sn-CH_3)$ and $J(^{119}Sn-CH_3)$, that an increase in the s-character is observed in the Sn–Co bond. All those results may be summarized by Bent's rule,[26] which suggests that the s-character is concentrated in the orbitals directed toward more electropositive substituents. In the light of Bent's rule, it is plausible that the s-character is concentrated in the Sn–Co bonds, while the p-character is concentrated in the Sn–X bonds. In consequence, the Co–Sn–Co bond angle becomes larger than the tetrahedral angle, while the X–Sn–X angle becomes smaller. The resultant imbalance in p-electron populations is manifested by quadrupole splitting.

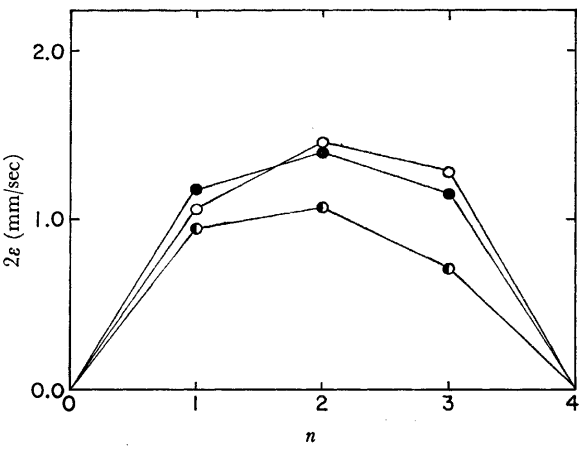

Fig. 3. The quadrupole splitting *vs.* the number of halogens, n, in $X_nSn[Co(CO)_4]_{4-n}$ series.
●: Cl, ○: Br, and ◐: I.

In Fig. 3, the values of the quadrupole splitting are plotted *versus* the number of halogen atoms, n. From the electronegativity of halogen, it can be expected that the values of the quadrupole splitting will decrease in the order of Cl>Br>I, but this is not true of bromine. The anomaly of bromine compounds seems to result from the distorted tetrahedral structure of tin tetrabromide,[27,28] in accordance with its broad line width.

The values of the quadrupole splitting attain their maximum at n=2 in all series of the compounds. An explanation of this phenomenon was attempted using a simple point-charge model. According to Parish and Platt,[21] the coordinates and arrangements of the

17) T. L. Brown, P. A. Edwards, C. B. Harris, and J. L. Kirsch, *Inorg. Chem.*, **8**, 763 (1969).
18) J. D. Graybeal and P. J. Green, *J. Phys. Chem.*, **73**, 2948 (1969).
19) J. D. Graybeal, S. D. Ing, and M. W. Hsu, *Inorg. Chem.*, **9**, 678 (1970).
20) H. A. Stöcker and H. Sano, *Trans. Fraday Soc.*, **64**, 577 (1968).
21) R. V. Parish and R. H. Platt, *Inorg. Chim. Acta*, **4**, 65 (1970).
22) J. J. Zuckerman, "Advances in Organometalic Chemistry," Vol. 9, ed. by F. G. A. Stone and R. West, Academic Press, New York (1970), p. 21.
23) B. P. Bir'yukov, E. A. Kukhtenkova, Yu. T. Struchkov, K. N. Anisimov, N. E. Kolobova, and V. I. Khandozhko, *J. Organometal. Chem.*, **27**, 337 (1971).
24) F. P. Boer, J. H. Tsai, and J. J. Flynn, Jr., *J. Amer. Chem. Soc.*, **92**, 6092 (1970).
25) D. J. Patmore and W. A. G. Graham, *Inorg. Chem.*, **6**, 981 (1967).
26) H. A. Bent, *Chem. Rev.*, **61**, 275 (1961).
27) K. Shimomura, *J. Phys. Soc. Japan*, **12**, 657 (1957).
28) Von P. Brand and H. Sackmann, *Acta Cryst.*, **16**, 446 (1963).

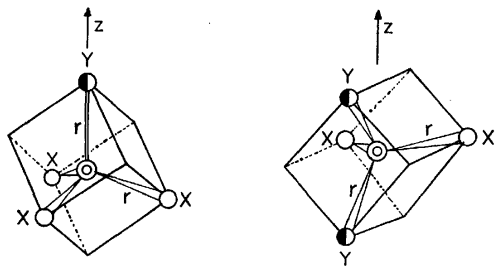

(a) X_3SnY(or $XSnY_3$) (b) X_2SnY_2

Fig. 4. Point-charge models of the tetrahedral bonding.

tetrahedral point-charge model of the X_nSnY_{4-n} type, in which X is the halogen atom and Y is the $Co(CO)_4$ group in the present case, are as is shown in Fig. 4.

The quadrupole splitting of ^{119}Sn, which has spin states of the excited and ground states of the nuclei, 3/2 and 1/2, is given by:

$$2\varepsilon = KV_{zz}(1+\eta^2/3)^{1/2} \quad (1)$$

Where V_{zz} is the electric-field gradient in the direction of the principal axis, which is taken as the z axis, and where the asymmetry parameter, η, is defined by:

$$\eta = \frac{V_{xx}-V_{yy}}{V_{zz}} \quad (2)$$

The electric-field gradients, V_{xx}, V_{yy}, and V_{zz}, can be expressed as follows:

$$\begin{aligned} V_{xx} &= \sum_L (3\sin^2\theta_L\cos^2\phi_L - 1)[L] \\ V_{yy} &= \sum_L (3\sin^2\theta_L\sin^2\phi_L - 1)[L] \\ V_{zz} &= \sum_L (3\cos^2\theta_L - 1)[L] \end{aligned} \quad (3)$$

where [L] represents the nature of the ligand contributing to the electric-field gradient, and where θ_L and ϕ_L are the polar and azimuthal angles of the ligand respectively. Using the three Eqs., (1), (2), and (3), the relative values of the quadrupole splitting for the tetrahedral point-charge model of X_nSnY_{4-n} ($n=1\sim3$) are calculated as follows:

X_3SnY	tetrahedral	$2\varepsilon\sim2[Y]-2[X]$
X_2SnY_2	tetrahedral	$2\varepsilon\sim1.15(2[Y]-2[X])(\eta=1)$
$XSnY_3$	tetrahedral	$2\varepsilon\sim-2[Y]+2[X]$

where [X] and [Y] are the parameters of the contributions to the electric-field gradient by the X and Y ligands.

In this interpretation, the dihalides should have a quadrupole splitting larger by 15% than that for the monohalide or trihalide, which have the same value but the opposite sign. The experimental data are consistent with the results of the point-charge treatment for the maximum value at dihalide. However, the values of $X_3Sn[Co(CO)_4]$ and $XSn[Co(CO)_4]_3$ are not equal. This can be explained on the basis of the deviation of the bond angle from the tetrahedral angle. As has been stated above, the X–Sn–Co bond angle is larger than the tetrahedral angle in $X_3Sn[Co(CO)_4]$ and is smaller in $XSn[Co(CO)_4]_3$. The electric-field gradient arises from the imbalances in the charges on the ligands as well as in the valence electron, but the latter is far more effective than the former. Therefore, the sign of the electric-field gradient in the tetrahedral compound, $XSn[Co(CO)_4]_3$, would be positive, because the valence shell of the tin atom will have more electron density concentrated in the x- and y-directions (Sn–Co) than in the z-direction (Sn–X), and the sign in $X_3Sn[Co(CO)_4]$ would be negative. The parameters of the quadrupole splitting are:

$2[X] - 2[Y] > 0$ in tetrahedral $XSn[Co(CO)_4]_3$

$2[Y] - 2[X] < 0$ in tetrahedral $X_3Sn[Co(CO)_4]$

If the X–Sn–Co bond angle were smaller than the tetrahedral angle in $XSn[Co(CO)_4]_3$ and larger in $X_3Sn[Co(CO)_4]$, the values of the parameter of the quadrupole splitting in both compounds would be decreased. However, the decreasing rate of the quadrupole splitting in $X_3Sn[Co(CO)_4]$ with the increase in the X–Sn–Co angle would be larger than that in $XSn[Co(CO)_4]_3$ with the decrease in the X–Sn–Co angle, because the value of $3(3\cos^2\theta-1)$ decreases more rapidly as θ increases in the neighborhood of the tetrahedral angle and [X]>[Y]. Furthermore, it is expected that the parameter, [X], of $XSn[Co(CO)_4]_3$ would become larger than that of $X_3Sn[Co(CO)_4]$. This is the case with the compounds of chloride and iodide.

When all the molecules in the series of the X_nSnY_{4-n} compound are obtained in an isolated state in solid or frozen solutions, the data of quadrupole splitting provide valuable information about the molecular structure, as is shown in the present study. In view of this, the Mössbauer studies of organic tin halides in a frozen solution would be interesting, for in that way all the molecules may be isolated, while it is difficult to discuss the molecular structure from the data in the solid state, where some association occurs.

Polarography of Uranyl Complex with *p*-Aminothiophenoxyacetic Acid in Dimethyl Sulfoxide Solution

Tsai-Teh LAI and Jan-Chin YANG

Department of Chemical Engineering, Cheng Kung University, Tainan, Taiwan, China

(Received September 22, 1970)

The polarography of uranyl ion in dimethyl sulfoxide (DMSO) was investigated in the DMSO concentration range 40—99 vol%. The complex species identified is $UO_2(DMSO)_6^{2+}$; it is transformed into $UO_2(DMSO)_2^+$ and UO_2^+ after the electrode reduction. In the presence of *p*-aminothiophenoxyacetic acid, the uranyl ion in the DMSO medium produces a two-step wave at lower pH and higher concentration of DMSO. The limiting current of the wave is controlled partially by the kinetics of the preceding chemical reaction and partially by the diffusion of the complex. The rate constant and diffusion coefficient of the reduction process were determined. At pH around 4, the formation of binuclear uranyl complexes was confirmed.

Gutman and Shoeber were the first to study the polarography of a number of inorganic ions in dimethyl sulfoxide solution.[1-3] They found that many polarographic reductions appeared to be irreversible in dimethyl sulfoxide. The polarography of uranyl complex with fumarate in a dimethyl sulfoxide concentration up to 40 vol% has been studied.[4]

Because of difficult solubility of *p*-aminothiopenoxyacetic acid in water, dimethyl sulfoxide was chosen as a solvent to study the complex of uranium(VI) with *p*-aminothiophenoxyacetic acid. The concentration range of dimethyl sulfoxide was 40—99 vol%.

Experimental

Apparatus. The polarograph and technique used in this work have been reported.[5] The capillary characteristics were: $m=1.307$ mg/sec and $t=4.88$ sec/drop at $H=67.3$ cm in 1.0 mM $UO_2(ClO_4)_2$, 70 vol% dimethyl sulfoxide, 0.08M *p*-aminothiophenoxyacetic acid, 0.15M $NaClO_4$ and 0.002% Triton X-100 at closed circuit. The hydrogen used for deaeration of the polarographic solution was presaturated with dimethyl sulfoxide by passing through a bottle filled with 70 vol% dimethyl sulfoxide solution. All polarograms were taken at 30±0.1°C.

Chemicals. *p*-Aminothiophenoxyacetic acid (P-ATPAA) was of research grade, Aldrich Chemical Co., and the solution was freshly prepared for each run.

Dimethyl sulfoxide (DMSO) was of chemical pure reagent (Wako Pure Chemical Industries Co.) and was not further purified.

All the polarograhic solutions contained 0.15M $NaClO_4$ as supporting electrolyte and 0.002% Triton X-100 as maximum suppressor.

Results and Discussion

Uranyl Ion in DMSO in the Absence of p-*ATPAA.* The polarographic behavior of uranyl ion in DMSO was studied in the DMSO concentration range 40—99 vol% over the pH range 2.40—5.25. Beyond this pH range, the waves become less well-defined. Above DMSO concentration 90 vol%, a strong maximum appears and the concentration of Triton X-100 must be increased from 0.002% to 0.03% to suppress the maximum.

TABLE 1. WAVE CHARACTERISTICS OF URANYL ION IN DMSO (1.0 mM $UO_2(ClO_4)_2$, 0.15M $NaClO_4$, 0.002% Triton X-100)

C_{DMSO} vol %	pH	$-E_{1/2}$ V *vs.* SCE	i_d μA	$E_{1/4}-E_{3/4}$
40	2.40	0.313	1.82	0.058
	3.30	0.312	1.66	0.057
	4.00	0.312	1.71	0.061
	5.00	0.312	1.61	0.062
60	2.50	0.366	1.83	0.055
	3.00	0.378	1.64	0.058
	4.30	0.378	1.44	0.059
	5.25	0.381	1.25	0.061
80	2.60	0.396	1.79	0.060
	3.70	0.420	1.65	0.059
	4.20	0.430	1.51	0.057
	4.78	0.430	1.30	0.061
99[a]	2.95	0.458	2.55	0.067
	3.50	0.474	1.82	4.060
	4.60	0.498	1.17	0.060
	4.95	0.492	1.14	0.066

a) 0.03% Triton X-100

The values of $E_{1/4}-E_{3/4}$ are in the range 0.055—0.067 (Table 1); the temperature coefficients of half-wave potential and diffusion current are −0.3 mV/°C and 1.5%/°C, respectively, in the temperature range 24—36°C. The results indicate that the electrode reductions are one-electron reversible and diffusion-controlled reduction process.

The dependence of the half-wave potential of uranyl ion on pH value in various concentrations of DMSO is shown in Fig. 1. The breaking point on the plots of $-E_{1/2}$ *vs.* pH is a function of the concentration of DMSO. Above 70 vol% DMSO, the breaking points are at pH 4.0; and at pH 3.0 for 50—60 vol% DMSO. However, below 40 vol% DMSO no breaking point appeared indicating that no hydrogen ion is invloved in the electrode reaction for any pH value of solution. The slope of the plots at pH<4.0 is also a function of DMSO concentration. The slope reaches 0.051 at 90 vol% DMSO. It indicates that one hydrogen ion is involved

1) V. Gutmann, P. Heilmayer, and G. Schoeber, *Monatsh, Chem.*, **92**, 240 (1961).
2) V. Gutmann and G. Schoeber, *Z. Anal. Chem.*, **171**, 339 (1959).
3) G. Gritzner, V. Gutmann, and G. Schoeber, *Monatsch, Chem.*, **96**, 1056 (1965).
4) T. T. Lai and T. Y. Chen, *Rev. Polarogr. Jap.*, **16**, 75 (1969).
5) T. T. Lai and T. Y. Chen, *J. Inorg. Nucl. Chem.*, **29**, 2975 (1967).

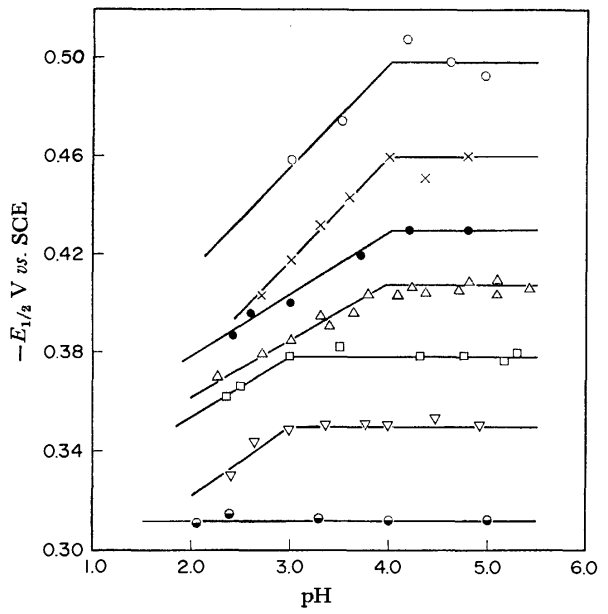

Fig. 1. Effect of pH on the half-wave potential of uranyl ion in DMSO.
1.0 mM $UO_2(ClO_4)_2$, 0.15 M $NaClO_4$, 0.002% Triton X-100 and various concentration of DMSO:
◒40 vol%; ▽50 vol%; □60 vol%; △70 vol%:
●80 vol%; ×90 vol%; ○99 vol%.

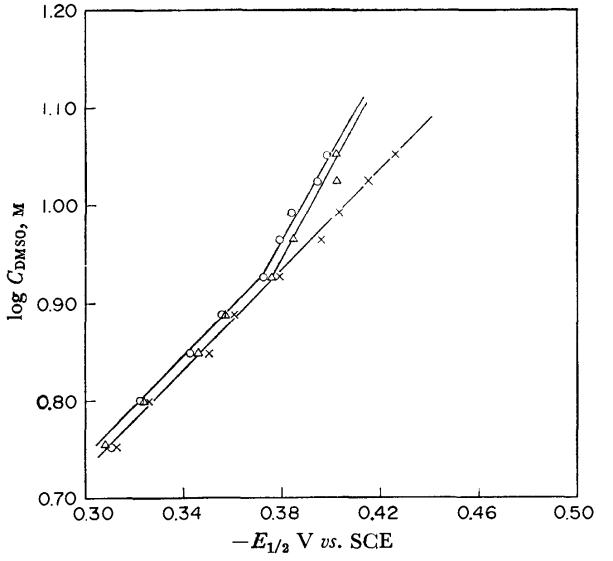

Fig. 2. Plots of log C_{DMSO} *vs.* $-E_{1/2}$ for uranyl ion in DMSO.
1.0 mM $UO_2(ClO_4)_2$, 0.15 M $NaClO_4$ and 0.002% Triton X-100.
× pH 4.00; △ pH 3.00; ○ pH 2.75.

in the electrode reaction. At pH>4.0 no hydrogen ion takes part in the electrode reaction for any concentration of DMSO.

Figure 2 shows the half-wave potential of uranyl ion in DMSO as a function of the lograrithmic concentration of DMSO. At pH≥4.0 and [DMSO]<80 vol%, a straight line with a slope 0.377 was obtained. At pH<4.0, breaking points were found; the slopes are 0.377 and 0.230 for 40 vol%<[DMSO]<60 vol% and 60 vol%<[DMSO]<80 vol%, respectively.

Introducing these values of slopes into the half-wave potential equation

$$(E_{1/2})_c = \text{const.} - (p-q)0.060 \log C_{DMSO} - 0.060a\,\text{pH} \quad (1)$$

for the electrode reaction

$$UO_2(DMSO)_p^{2+} + aH^+ + e = UO_2(DMSO)_q^+ + a\text{DMSO}\cdot H^+ + (p-q-a)\text{DMSO} \quad (2)$$

the values of (p-q) become equal to 6 at pH>4.0 and equal to 6 and 4 at pH<4.0.

The coordination between uranyl ion and DMSO has been proved by the donation of a lone pair of electrons on oxygen atom of DMSO of a monodentate ligand.[6]

Thus, it was inferred that the uranyl-DMSO complex species formed is $UO_2(DMSO)_6^{2+}$, proving that the uranyl ion is solvated completely by six molecules of DMSO in the presence of an excess DMSO. However, it is transformed into $UO_2(DMSO)_2^+$ and UO_2^+ after it undergoes the electrode reduction.

Uranyl Ion in DMSO in the Presence of p-*ATPAA.*

The polarographic behavior of the uranyl-DMSO-*p*-ATPAA system was studied systematically in the pH range 2.75—6.00 with DMSO concentration 65—99 vol% and *p*-ATPAA concentration 0.01—0.12M.

Typical current-potential curves for the polarographic solution containing 1.0 mM $UO_2(ClO_4)_2$, 0.08M *p*-ATPAA, 90 vol% DMSO, 0.15M $NaClO_4$ and 0.002% Triton X-100 at various pH values are presented in Fig. 3. At pH 4.80, a single well-defined wave was obtained; however, at pH<4.30, two-step waves were observed. The electrocapillary curves are shown in Fig. 4. A large decrease in the drop time of the capillary was observed by the addition of *p*-ATPAA proving the existence of adsorption of *p*-ATPAA on the dropping mercury electrode. The formation of two-step waves was attributed to the adsorption of *p*-ATPAA on the dropping mercury

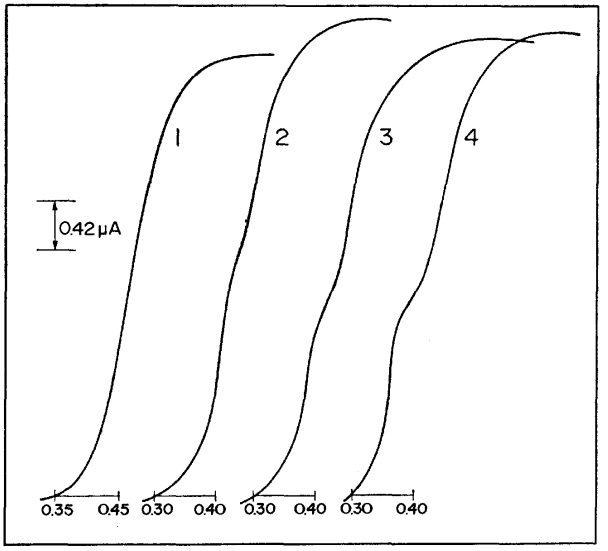

Fig. 3. Typical current-potential curves.
(1.0 mM $UO_2(ClO_4)_2$, 0.08 M *p*-ATPAA, 90 vol% DMSO, 0.15 M $NaClO_4$, 0.002% Triton X-100)
1. pH 4.80; 2. pH 4.30; 3. pH 3.72; 4. pH 3.30.

6) V. Krishnan and C. C. Potel, *Indian J. Chem.*, **2**, (10) 416 (1964).

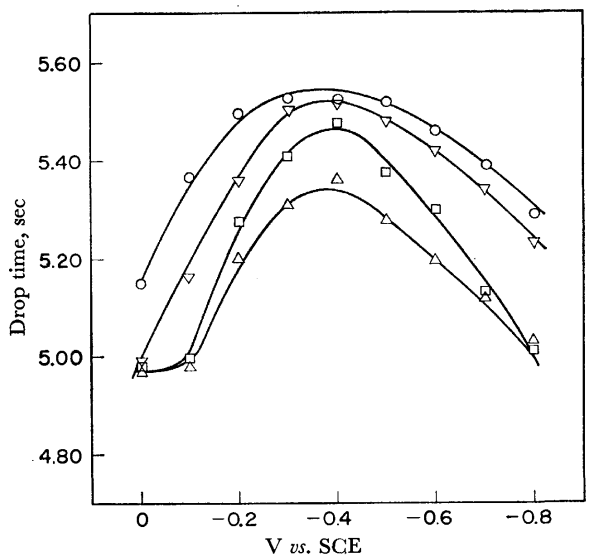

Fig. 4. Electrocapillary curve of mercury.
1 mM $UO_2(ClO_4)_2$, 0.15 M $NaClO_4$, 0.002% Triton X-100, 80 vol% DMSO at pH 4.00 and various concentrations of *p*-ATPAA: ○ 0 M; ▽ 0.02 M; □ 0.04 M; △ 0.08 M.

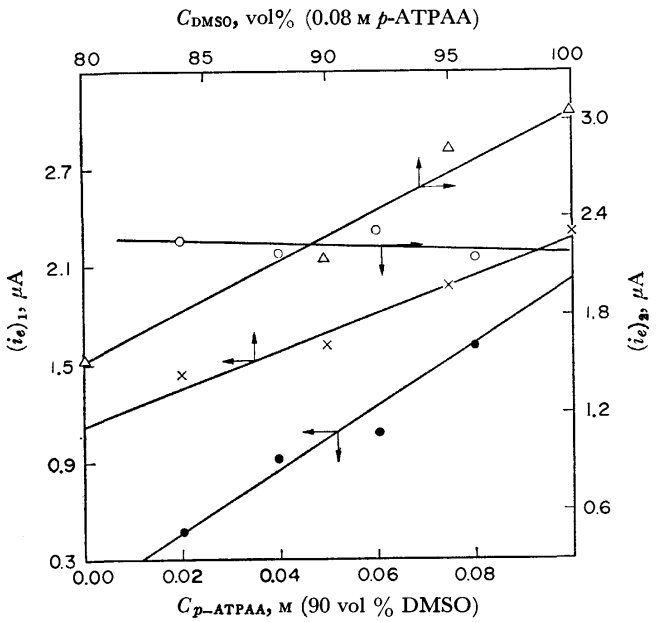

Fig. 5. Effect of concentrations of DMSO and *p*-ATPAA on the limiting currents of the two waves.
(1.0 mM $UO_2(ClO_4)_2$, 0.15 M $NaClO_4$, 0.002% Triton X-100, pH 3.3)

electrode.[7] The lower pH value and higher DMSO concentration favor the formation of two-step waves.

The effect of the concentration of DMSO and *p*-ATPAA on the limiting currents of the two waves is shown in Fig. 5 and the wave parameters of the two-step waves in Table 2. The limiting current of the first wave increases with the concentrations of DMSO and *p*-ATPAA; however, the limiting current of the second wave is independent of the concentration of *p*-ATPAA and increases with the concentration of DMSO.

7) J. Heyrovsky and J. Kuta, "Principles of Polarography," Interscience Publishers, New York, Vol. 1, 96, (1966).

Table 2. Wave parameters of the two-step waves (1.0 mM $UO_2(ClO_4)_2$, 0.08M *p*-ATPAA, 0.15M $NaClO_4$, 0.002% Triton X-100 at pH 3.30)

C_{DMSO} vol %	$-(E_{1/2})_1$ V *vs.* SCE	$-(E_{1/2})_2$ V *vs.* SCE	$(i_e)_1$ μA	$(i_e)_2$ μA
80	0.370	0.440	4.8	5.1
90	0.360	0.460	5.4	6.8
95	0.355	0.465	6.6	9.6

Nature of the Limiting Current. A preceding chemical reaction takes place between the $UO_2(DMSO)_6^{2+}$ complex and *p*-ATPAA producing a mixed ligand complex and reaches a chemical equilibrium; then an electrode reaction occurs to the mixed ligand complex.

In an attempt to determine both the kinetic parameter of the preceding chemical reaction and the nature of the limiting current of the polarogram of the mixed ligand complex, the following equation[8] was applied

$$\bar{i} = r \cdot 1255nm^{2/3}\tau^{2/3}\mathrm{Co}k\left[1 - \mathrm{erf}\left(k\sqrt{\frac{\tau}{D}}\right)\right]\exp\left[\frac{k^2\tau}{D}\right] \quad (3)$$

where k is the rate constant, r the ratio of the average limiting current to the maximum limiting current and a function of τ and $kD^{-1/2}$, and other notations have their usual meaning.

Introducing $m=m_0H$ and $\tau_0=\tau H$; Eq. (3) becomes;

$$i = r \cdot 1255nm_0^{2/3}\tau_0^{2/3}\mathrm{Co}k\left[1 - \mathrm{erf}\left(k\sqrt{\frac{\tau_0}{HD}}\right)\right]\exp\left[\frac{k^2\tau_0}{HD}\right] \quad (4)$$

and

$$\frac{\bar{i}}{\bar{i}_0} = \frac{r}{r_0}\frac{\left[1 - \mathrm{erf}\left(k\sqrt{\frac{\tau_0}{HD}}\right)\right]}{\left[1 - \mathrm{erf}\left(k\sqrt{\frac{\tau_0}{H_0D}}\right)\right]}\exp\left[\frac{k^2\tau_0}{HD} - \frac{k^2\tau_0}{H_0D}\right] \quad (5)$$

The plots of $\bar{i}/\bar{i}_0$ against mercury head H using $kD^{-1/2}$ as parameter are shown in Fig. 6, in which $\bar{i}_0$ is the average limiting current for the polarograms ob-

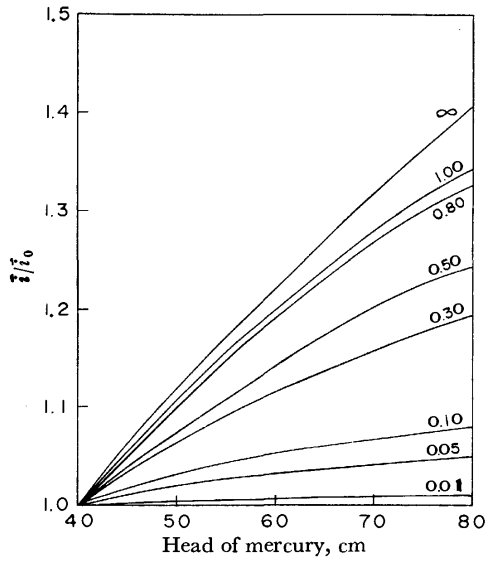

Fig. 6. Plots of the average limiting current ratio *vs.* head of mercury; $kD^{-1/2}$ as paramenser.
($\bar{i}_0$: average limiting current at H=40 cm and τ_0=2700 sec-mm/drop)

8) P. Delahay, *J. Amer Chem. Soc.*, **73**, 4944 (1951).

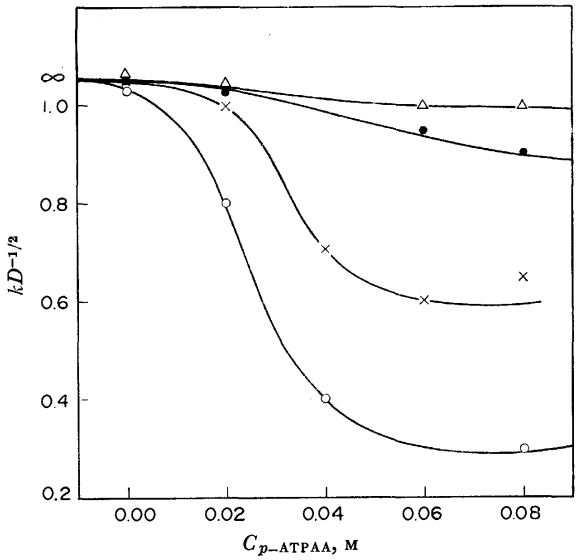

Fig. 7. Variation of $kD^{-1/2}$ value as a function of $C_{p\text{-ATPAA}}$ for different concentrations of DMSO.
(1.0 mM $UO_2(ClO_4)_2$, 0.15 M $NaClO_4$, 0.002% Triton X-100)
△ 70 vol% DMSO at pH 4.90; ●90 vol% DMSO at pH 4.90; × 70 vol% DMSO at pH 3.30; ○ 90 vol% DMSO at pH 3.30.

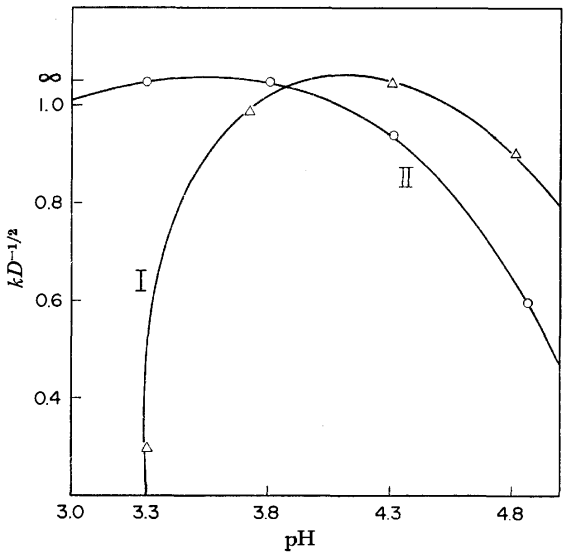

Fig. 8. Variation of $kD^{-1/2}$ values as a function of pH value.
(1.0 mM $UO_2(ClO_4)_2$, 90 vol% DMSO, 0.08 M *p*-ATPAA, 0.15 M $NaClO_4$ and 0.002% Triton X-100)
△ 30°C; ○ 37°C.

tained from a given polarographic solution at $H=$ 40 cm and $\tau_0=2700$ sec-mm/drop. We see that the limiting current is practically diffusion-controlled when $kD^{-1/2}$ is larger than 1.0 $sec^{-1/2}$. At $k=\infty$, the error function should be expanded into a series and Eq. (3) can be reduced to Ilkovic equation.[9] On the contrary, the limiting current is essentially rate-controlled when $kD^{-1/2}$ is smaller than 0.01 $sec^{-1/2}$. When $kD^{-1/2}$ is between 0.01 and 1.00 $sec^{-1/2}$, the limiting current is controlled partially by diffusion and partially by the rate of the preceding chemical reaction.

The variations of $kD^{-1/2}$ values as a function of the concentration of *p*-ATPAA and as a function of pH value are demonstrated in Figs. 7 and 8, respectively. The values of $kD^{-1/2}$ were evaluated by determining the $\bar{i}/\bar{i}_0$ values by varying mercury head and by applying Fig. 6.

It is obvious from Fig. 7 that in the absence of *p*-ATPAA, irrespective of the concentration of DMSO and the pH value, the value of $kD^{-1/2}$ is infinite, indicating that the electrode reduction of the uranyl-DMSO complexes is completely diffusion-controlled. This result is in accord with that obtained from the temperature coefficient of diffusion current. The $kD^{-1/2}$ value decreases with the increase of the concentration of *p*-ATPAA and DMSO. This reveals that the higher concentrations of DMSO and *p*-ATPAA enhance the rate-controlled character of the electrode reduction process of uranyl-DMSO-*p*-ATPAA complexes.

A complete diffusion-controlled reduction process of uranyl-DMSO-*p*-ATPAA complex is obtained in the pH range 3.7—4.5 at 30°C (Fig. 8). Polynuclear complexes are formed in the pH range and the increment of viscosity of the polarographic solution rendered the electrode reduction to be diffusion-controlled.[10] However, beyond this pH range, a rate-controlled character takes part in the reduction of the complex.

It can be expected that at higher temperature the adsorption is hindered and no rate-controlled phenomenon appeared even at pH<3.7 (curve II, Fig. 8).

Formation of Polynuclear Complexes. The temperature coefficient of the half-wave potential is determined to be 0.6 mV/°C in a polarographic solution containing 1.0 mM $UO_2(ClO_4)_2$, 70 vol% DMSO, 0.08M *p*-ATPAA, 0.15M $NaClO_4$, and 0.002% Triton X-100 at pH 4.30 in temperature range 18.0—39.5°C. This indicates that the electrode process is reversible. However, as shown in Table 3, in the vicinity of pH 4, the mean $E_{1/4}-E_{3/4}$ value is 0.039; the deviation of this value from the

Table 3. Evidence for the formation of binuclear complexes
(1.0 mM $UO_2(ClO_4)_2$, 70 vol % DMSO, 0.15M $NaClO_4$, 0.002% Triton X-100 and various concentrations of *p*-ATPAA)

pH	$\frac{E_{1/2}-E_{7/8}}{E_{1/8}-E_{1/2}}$	$E_{1/4}-E_{3/4}$	*a*	*b*
$C_{ATPAA}=0.02$M				
5.50	1.225	0.060	0.80	1.25
4.20	0.770	0.040	2.20	1.10
3.35	1.000	0.060	1.00	1.00
$C_{ATPAA}=0.08$M				
4.90	1.000	0.060	1.00	1.00
4.45	0.920	0.040	1.63	1.30
3.14	1.000	0.060	1.00	1.00
$C_{ATPAA}=0.12$M				
5.60	0.770	0.057	1.60	0.80
4.08	0.900	0.036	1.85	1.40
3.40	0.930	0.051	1.25	1.00

9) I. M. Kolthoff and J. J. Lingane, "Polarography" Interscience Publisher, New York, Vol. 1, 63 (1952).

10) Michel Boudart, "Kinetics of Chemical Processes" Prentice-Hall, Inc., United Kingdom, 145 (1968).

Table 4. Rate constants and diffusion coefficients of uranyl complexes
(1.0 mM $UO_2(ClO_4)_2$, 0.15M $NaClO_4$, 0.002% Triton X-100)

Complexing agent	pH	$kD^{-1/2}(sec^{-1/2})$	r	k (cm/sec)	D (cm^2/sec)
70 vol% DMSO	3.15	1.00	0.77	2.24×10^{-3}	5.00×10^{-6}
70 vol% DMSO; 0.08M *p*-ATPAA	4.90	1.00	0.77	2.43×10^{-3}	5.90×10^{-6}
90 vol% DMSO; 0.08M *p*-ATPAA	3.30	0.30	0.68	1.99×10^{-3}	4.42×10^{-5}

heoretical value of 0.057 V for one-electron reversible reduction was no doubt due to the asymmetry of the polarogram which arose from the polymerization effect.[11]

The polymerization degree for the polynuclear complexes formed was determined by the same method as described previously.[11] The results are shown in Table 3, in which a and b denote the polymerization degree of the oxidized and reduced form of the uranium complex, respectively. It is obvious from Table 3 that a binuclear uranyl complex was formed in the vicinity of pH 4.

Rate Constant and Diffusion Coefficient. The rate constant k of the preceding chemical reaction and the diffusion coefficient D of the uranyl complex can be determined by applying Eq. (4) for $m_0=2.734\times10^{-3}$ mg/sec-mm, $\tau_0=2.7\times10^3$ sec-mm/drop and $n=1$ values. Table 4 lists some data of k and D of the uranyl complexes. The $kD^{-1/2}=1.00$ and $k\gg D$ for uranyl-DMSO and uranyl-DMSO-*p*-ATPAA (70 vol% DMSO; 0.08M *p*-ATPAA) systems show again that the electrode reaction is diffusion-controlled. However, the data obtained for uranyl-DMSO-*p*-ATPAA (90 vol% DMSO; 0.08M *p*-ATPAA) system indicate a partial kinetic-controlled character. These results support the deduction.

The authous thank the National Science Council of Taiwan, China for financial support of this work.

11) T. T. Lai and B. C. Wang, *Anal. Chem.*, **36**, 26 (1964).

BULLETIN OF THE CHEMICAL SOCIETY OF JAPAN, VOL. 45, 1687—1695(1972)

Fluorescence Emission in the Gas Phase of Several Aromatic Hydrocarbons

Akira NAKAJIMA

Division of Chemistry, Research Institute of Applied Electricity, Hokkaido University, Sapporo

(Received December 13, 1971)

The fluorescence and excitation spectra of several condensed aromatic hydrocarbons were measured in the gas phase at low pressures. The emission from the second excited singlet state (S_2 emission) could be observed with some of the compounds studied, in which the first weak absorption band is located close to the second much stronger band. The relative yield of the S_2 emission always increased with the increase in the excitation wavenumber. It has been shown that the occurrence of the S_2 emission can be explained in a qualitative way by the state densities and the radiative rates. In coronene, an emission to be regarded as originating from the third excited singlet state was observed.

It is well known that radiationless transitions from higher excited singlet states to the first excited singlet state in most complex molecules occur with such a high efficiency that usually fluorescence arises solely from the lowest excited singlet state.[1-8] Recent theoretical studies[9-12] have indicated that, in large molecules, internal conversion can take place even in the isolated state. Although the emission from the second excited singlet state (S_2 emission) of a large molecule[8] has been considered to be extremely weak on account of the very fast internal conversion,[4-7] it may be detected in principle by means of a highly sensitive spectroscopic device and by the use of a favorable compound satisfying certain conditions.

The fluorescence originating from the second excited singlet state of pyrene in the gas phase at low pressures

1) M. Kasha, *Disc. Faraday Soc.*, **9**, 14 (1950).
2) C. Reid, "Excited States in Chemistry and Biology," Butterworths, London (1957).
3) J. G. Calvert and J. N. Pitts, Jr., "Photochemistry," John Wiley & Sons, New York (1966).
4) N. J. Turro, "Molecular Photochemistry," W. A. Benjamin, New York (1965).
5) D. M. Hercules, ed., "Fluorescence and Phosphorescence Analysis," John Wiley & Sons, New York (1966).
6) R. S. Becker, "Theory and Interpretation of Fluorescence and Phosphorescence," Wiley-Interscience, New York (1969).
7) J. B. Birks, "Photophysics of Aromatic Molecules," Wiley-Interscience, London (1970).
8) Here we will make an exception of azulene and its derivatives.
9) M. Bixon and J. Jortner, *J. Chem. Phys.*, **48**, 715 (1968).
10) J. Jortner, S. A. Rice, and R. M. Hochstrasser, "Advances in Photochemistry," Vol. 7, 149 (1969).
11) R. Englman and J. Jortner, *Mol. Phys.*, **18**, 145 (1970).
12) B. R. Henry and M. Kasha, *Ann. Rev. Phys. Chem.*, **19**, 161 (1968).

was found independently by Geldof *et al.*[13] and by the present author *et al.*[14] With the aid of a very sensitive emission spectrometer,[15] Geldof *et al.* observed anomalous emission bands in the short-wavelength region of the fluorescence spectrum of a rarified pyrene gas excited in the second absorption band; these bands are to be ascribed to the S_2 emission.[13] They also studied the effect of the inert gas and the temperature on the relative yield of this emission and estimated the rate constants for the internal conversion and the reverse process.[13] On the other hand, the present author *et al.* measured the fluorescence and excitation spectra of pyrene gas, paying special attention to the S_2 emission, and showed a very remarkable increase in its relative quantum efficiency with excitation into successively higher excited singlet states.[14]

It seems to be established that the 'anomalous' emission can be regarded as quite intrinsic and not due to impurities, because no impurity band was detected in the fluorescence and excitation spectra in the solutions of the highly purified sample employed, because its excitation spectrum corresponds well in wavenumber to the absorption spectrum of pyrene gas,[14,16] because its relative intensity is reduced by the vibrational relaxation on the addition of an inert (non-electronically-quenching) gas such as nitrogen[17] and cyclohexane,[16] and further, because such emissions have also been observed with deuteropyrene[17] and methylpyrenes.[18]

Moreover, it has been reported that fluorescence from the second excited singlet state can be observed with 3,4-benzpyrene[13,19] both in the gas phase and in solution, 1,2-benzanthracene[19] in solution, and 1,12-benzperylene[20] in plastics.

In particular, in all of these 'abnormal' molecules, as we can recognize, the very weak first absorption band is situated in the immediate vicinity of the much stronger second band. In this respect, the weakness of the first band should be regarded as more significant than would be desirable for reducing self-absorption.[13,19]

In view of these facts, the following empirical criteria for the occurrence of the S_2 emission may be proposed:

(1) The rate of emission from the second excited singlet is sufficiently large compared to that from the first excited singlet.

(2) The energy separation between the first and second excited singlets is relatively small.

The purpose of this work is to test these criteria on a number of condensed aromatic hydrocarbons by making attempts to detect S_2 emission in the short-wavelength tail of their 'normal' fluorescence spectra. In addition, the influence of the internal conversion rates on the behavior of the S_2 emission has been considered in connection with the vibrational level densities for the relevant states.

Experimental

Naphthalene and phenanthrene were recrystallized from ethanol and zone-refined. 1-Methoxynaphthalene was distilled under reduced pressure. 1-Naphthol was recrystallized from ethanol. Biphenyl was recrystallized from ethanol, zone-refined, and sublimed *in vacuo*. Anthracene was recrystallized from xylene, zone-refined, and sublimed *in vacuo*. Chrysene was recrystallized from benzene and zone-refined. Perylene was chromatographed and sublimed *in vacuo*. Triphenylene, tetracene, 1,2-benzanthracene, 20-methylcholanthrene, 1,12-benzperylene, and coronene were sublimed *in vacuo*. Spectroscopic-grade benzene was used as a solvent without further purification. The purities of the samples were carefully checked by observing the excitation spectra. If, unfortunately, an impurity band was found in the excitation spectrum, the emission spectra were not measured with excitation in the neighborhood of that band.

The fluorescence and excitation spectra were measured with a Hitachi MPF-2A spectrofluorometer, to which an electric furnace was attached in the cell compartment. The square, non-fluorescent quartz cell containing a small amount of the sample was evacuated and sealed off. The furnace in which the gas cell was placed was constructed of brass blocks and was covered with asbestine slates as insulators. It consists of a lower part with two quartz windows and an upper, windowless part; the temperatures of the two parts were separately controlled. The vapor pressure of the compound was assessed utilizing the published data,[21,22] with the temperature of the upper part always set at a somewhat lower temperature. The vapor pressures at which the experiments were carried out were 0.01—1 Torr, except for 1-methoxynaphthalene and biphenyl, whose pressures were raised to 5 Torr.

The fluorescence spectra were corrected for the spectral sensitivity of the instrument by the use of the standard fluorescence spectra of quinine sulfate, 2-naphthol, and phenol.[23-25] The excitation spectra were also corrected using rhodamine B as the standard substance.[25,26]

Results and Discussion

Since the experiments were made at such low vapor pressures that the lifetime of the excited molecule was considerably shorter than the time interval between molecular collisions, during the processes of internal conversion the excitation energy was conserved, with part of it reserved as excess vibrational energy. It may be assumed that the internal conversion to the second excited singlet state from a higher excited singlet state, in which the molecule is initially prepared by

13) P. A. Geldof, R. P. H. Rettschnick, and G. H. Hoytink, *Chem. Phys. Lett.*, **4**, 59 (1969).
14) A. Nakajima and H. Baba, This Bulletin, **43**, 967 (1970).
15) J. Langelaar, G. A. de Vries, and D. Bebelaar, *J. Sci. Instr.*, **46**, 149 (1969).
16) H. Baba, A. Nakajima, M. Aoi, and K. Chihara, *J. Chem. Phys.*, **55**, 2433 (1971).
17) A. Nakajima, unpublished data.
18) M. Aoi, unpublished data.
19) C. E. Easterly, L. G. Christophorou, R. P. Blaunstein, and J. G. Carter, *Chem. Phys. Lett.*, **6**, 579 (1970).
20) W. Dawson and J. L. Kropp, *J. Phys. Chem.*, **73**, 1752 (1969).
21) The Chemical Society of Japan, ed., "Kagaku Binran," (Handbook of Chemistry), Maruzen, Tokyo (1958).
22) H. Inokuchi, S. Shiba, T. Handa, and H. Akamatu, This Bulletin, **25**, 299 (1952); N. Wakayama and H. Inokuchi, *ibid.*, **40**, 2267 (1967).
23) E. Lippert, W. Nägele, I. Seibold-Blankenstein, U. Staiger, and W. Voss, *Z. Anal. Chem.*, **170**, 1 (1959).
24) C. A. Parker, *Anal. Chem.*, **34**, 502 (1959).
25) C. A. Parker, "Photoluminescence of Solutions," Elsevier, Amsterdam (1968).
26) W. H. Melhuish, *J. Opt. Soc. Amer.*, **52**, 1256 (1962).

photon absorption, occurs very rapidly and irreversively. The resultant molecule in the high vibronic levels of the second excited singlet state (S_2) either emits the S_2 emission or is isoenergetically converted into the high vibronic levels of the first excited singlet state (S_1), from which it may in turn emit the 'normal' S_1 emission or pass nonradiatively into the highly-excited vibrational levels of the triplet or ground state (S_0). If the radiative lifetime in the high vibronic levels of S_1 is relatively long, then the returning process from S_1 to S_2 can take place.[13] Thus, the yield of the S_2 emission can be considered to be composed of a direct, short-lived component occurring before internal conversion and an indirect, long-lived component derived from the reverse process.[13,16]

By a simple consideration of the kinetics based on this scheme,[16] the ratio of the quantum yield of the S_2 emission, Φ_2, to that of the S_1 emission, Φ_1, is obtained as follows:

$$\Phi_2/\Phi_1 = k_2(k_{1f}+k_{1q}+k_{rp})/k_{1f}k_{ic}, \quad (1)$$

where k_{1f} and k_2 are the rate constants for the emissions from S_1 and S_2 respectively, where k_{ic} and k_{rp} are those for the internal conversion and the reverse process respectively, and where k_{1q} is the overall rate constant for the nonradiative (quenching) processes from S_1.

The radiative rate constants, k_i, were estimated from the S_0—S_1 absorption spectra in solution, using the following well-known equation:[3,4,6,7]

$$k = 2.88 \times 10^{-9} n^2 \bar{\nu}_m^2 \int \varepsilon d\bar{\nu}, \quad (2)$$

or by the aid of a simpler expression:[27]

$$k \sim 8.6 \times 10^{-6} n^2 \bar{\nu}_m^2 \varepsilon_{max}, \quad (3)$$

where ε is the molar extinction coefficient, and n, the refractive index of the solvent.

The rate constant of internal conversion, k_{ic}, can be formulated as:[7,9-12,28]

$$k_{ic} = (2\pi/\hbar)v^2\rho_1, \quad (4)$$

where v is the coupling matrix element between the zero-order Born-Oppenheimer states for the perturbation inducing internal conversion and where ρ_1 is the density of the final vibronic states (in S_1) at resonance with the initial state (in S_2). For the reverse process, the rate constant, k_{rp}, is expressed in a similar form:[16]

$$k_{rp} = (2\pi/\hbar)v^2\rho_2, \quad (5)$$

where ρ_2 is the density of states in S_2.

Using these expressions, Eq. (1) can be reduced to:

$$\Phi_2/\Phi_1 = (k_2/k_1)(\rho_2/\rho_1) + k_2/k_{ic}\phi_1, \quad (6)$$

where ϕ_1 is the quantum yield of S_1 fluorescence caused by excitation in the first excited singlet or within high-pressure limits. It is assumed here that ϕ_1 can be approximated by the quantum yield in solution.

Internal conversion in a large molecule has been thought to occur in 10^{-11}—10^{-13} sec.[1,4-7] Recently, the rate constant, k_{ic}, was estimated for pyrene in the gas phase as $\sim 10^{12}$ sec^{-1} by Geldof *et al.*[13] and as 5.8×10^{11} sec^{-1} by us.[16,29] In the present study, no attempt was made to determine the value of k_{ic}, *e.g.*, by performing the inert-gas experiments[13,16] when S_2 emission could be observed. Instead, for all the molecules under consideration k_{ic} was assumed to take a value similar to that estimated for pyrene, *i.e.*, 10^{12} sec^{-1}.[1,4,7,12] Because of this large k_{ic} value, the contribution of the second term in Eq. (6) may be comparatively small for most 'abnormal' molecules.

The density of vibrational states, ρ, was computed by the use of Haarhoff's formula.[30] As we have no definite knowledge at the present stage about the effectiveness of the vibrational modes in giving rise to radiationless transitions, the contributions of all the modes are taken into account equally. Since the vibrational assignments are not available for most of the compounds studied, a scaling method has been adopted;[31,32] that is, for an aromatic hydrocarbon, C_mH_n, there are n degenerate CH stretching modes assigned at 3050 cm^{-1}, n in-plane CH bending modes at 1100 cm^{-1}, n out-of-plane CH bending modes at 900 cm^{-1}, $m-1$ ring stretching modes at 1500 cm^{-1}, $m-2$ in-plane ring deformation modes at 700 cm^{-1}, and $m-3$ out-of-plane ring deformation modes at 500 cm^{-1}. The values of ρ calculated by this method were compared with those obtained by direct calculation using the observed frequencies; the differences were only 15% for benzene,[33] less than 6 times for naphthalene,[34] and up to 100 times for anthracene[35] and pyrene.[36] Although the difference in ρ increases rapidly with the number of atoms, yet the difference in the ratio between ρ's is satisfactorily smaller, *e.g.*, within a factor of only two for anthracene. It should be kept in mind, however, that the value computed by Haarhoff's approximation becomes inaccurate at smaller energies.[30]

Below, the results of observations of the fluorescence and excitation spectra in the gas phase will be illustrated and the possibility of the appearance of S_2 emission will be investigated by means of the rate constants evaluated in the manner described above.

Naphthalene, 1-Naphthol, and 1-Methoxynaphthalene. Since the lowest excited singlet state (^1L_b), which gives rise to a weak absorption band, is located close to the

27) The half-width of an absorption band was taken as 6.0 kK, and the mean wavenumber, $\bar{\nu}_m$, and the maximum extinction coefficient, ε_{max}, were used.

28) G. W. Robinson and R. P. Frosch, *J. Chem. Phys.*, **37**, 1962 (1962); D. M. Burland and G. W. Robinson, *ibid.*, **51**, 4548(1969).

29) In this connection, it is of interest to note that k_{ic} seems to vary only slightly with the excess vibrational energy; despite the large difference between the excitation energies (10.5 kK), the value of k_{ic} obtained by Geldof *et al.* is not very different from ours. Since the term for electronic interaction, β, may be assumed to be constant, and since $v^2=\beta^2\bar{F}$,[7,9,28] the product of the averaged Franck-Condon factor, $\bar{F}$, and the density of states, ρ, can be considered as a relatively slowly-decreasing function of the excitation energy.

30) P. C. Haarhoff, *Mol. Phys.*, **6**, 337 (1963); **7**, 101 (1963).

31) R. J. Watts and S. J. Strickler, *J. Chem. Phys.*, **44**, 2423 (1966).

32) J. L. Richards and S. A. Rice, *Chem. Phys. Lett.*, **9**, 444 (1971).

33) N. Herzfeld, C. K. Ingold, and H. G. Poole, *J. Chem. Soc.*, **1946**, 316.

34) D. B. Scully and D. H. Whiffen, *Spectrochim. Acta*, **16**, 1393 (1960); J. M. Hollas, *J. Mol. Spectry.*, **9**, 138 (1962).

35) W. Bruhn and R. Mecke, *Z. Elektrochem.*, **65**, 543 (1961); E. R. Krainov, *Opt. Spectry.*, **16**, 532 (1964).

36) R. Mecke and W. E. Klee, *Z. Electrochem.*, **65**, 327 (1961).

second excited singlet state (^1L_a), which gives rise to a relatively strong band, naphthalene may be considered to meet the aforesaid criteria. The gas-phase fluorescence of naphthalene has thus far been studied by a number of workers,[31,37-39] some of whom attempted, but failed, to detect fluorescence from the second excited singlet state with ordinary exciting light sources.[31,38] The present author also examined the short-wavelength region of the fluorescence spectra, while varying the excitation wavelength, but no emission from an excited singlet state other than the first could be observed. The observed fluorescence and excitation spectra of naphthalene vapor, being similar to those already reported,[31,37,38] will not be presented here.

It can be expected that, by the substitution of an electron-donating group (-OH, -OCH_3) into the naphthalene ring, the ^1L_a state will come close in energy to the ^1L_b state, while the absorption intensities of the ^1L_b and ^1L_a bands and, hence, the associated radiative rates will also vary to some extent. In order to observe such substituent effects on the emissivity, the fluorescence spectra of 1-naphthol and 1-methoxynaphthalene were measured. As may be seen from Figs. 1 and 2, no emission from the ^1L_a state could be observed.

The reason why S_2 emission could not be found in these compounds can be considered in terms of the

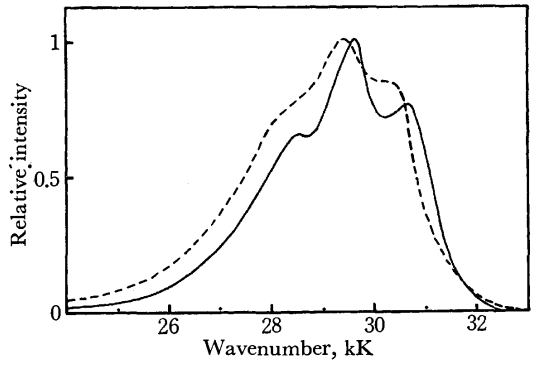

Fig. 1. The gas-phase fluorescence spectra of 1-naphthol. Excitations at 31.8 kK (——) and 35.7 kK (----). At 103°C (~1.7 Torr).

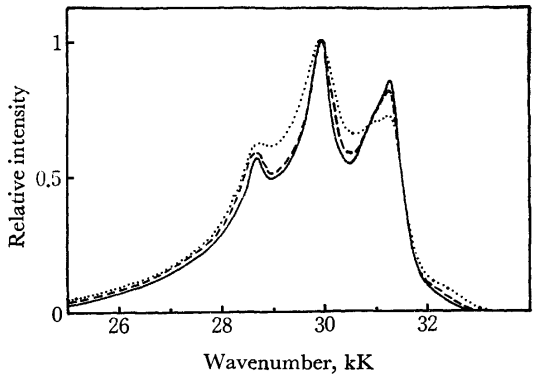

Fig. 2. The gas-phase fluorescence spectra of 1-methoxynaphthalene. Excitations at 32.3 kK (——), 34.5 kK (----), and 40.0 kK (·····). At 76°C (<5 Torr).

37) J. O. Uy and E. C. Lim, *Chem. Phys. Lett.*, **7**, 306 (1970).
38) J. M. Bondeau and M. Stockburger, *ibid.*, **8**, 436 (1971).
39) U. Laor and P. K. Ludwig, *J. Chem. Phys.*, **54**, 1054 (1971).

TABLE 1. THE VALUES GIVEN FOR NAPHTHALENE, 1-NAPHTHOL, AND 1-METHOXYNAPHTHALENE

	Naphthalene		1-Naphthol	1-Methoxy-naphthalene
S_1(kK)	32.0		31.3	31.4
S_2(kK)	36.0		34.1	35.8
k_1(sec^{-1})	5.2×10^6		5.4×10^6	5.8×10^6
k_2(sec^{-1})	4.8×10^7		4.8×10^7	1.1×10^8
ϕ_1[a]	0.19		0.17	0.36
$\bar{\nu}_{exc}$(kK)[b]	36.4	40.0	35.7	40.0
ρ_1(cm)	2.8×10^3	8.9×10^6	2.8×10^3	2.8×10^7
ρ_2(cm)	1.1×10^{-4}	9.5×10^2	2.5×10^{-1}	1.6×10^8
Φ_2/Φ_1 (calc.)	2.5×10^{-4}	1.2×10^{-3}	1.1×10^{-3}	1.4×10^{-3}

a) Ref. 7.
b) Hereafter, $\bar{\nu}_{exc}$ will denote the excitation wavenumber at which the actual observation of the emissions was made.

estimated values of the radiative rate constants, the densities of states, and the related parameters listed in Table 1. The values of ρ for 1-naphthol and 1-methoxynaphthalene were assumed to be the same as that for naphthalene. As is indicated in Table 1, the calculated quantum yield ratios are so small compared with those of 'abnormal' molecules (*vide infra*) that the intensity of the S_2 emission may be expected to be too weak to be observed with conventional instruments. However, a more sensitive technique may permit its detection. In fact, quite recently Wannier *et al.*[40] could observe the resonance fluorescence from the second excited singlet state of naphthalene in the gas phase by utilizing a laser excitation source. It should be added, however, that the emission mechanism considered by them is very different from ours.[16]

Biphenyl, Phenanthrene, Triphenylene, and Chrysene. The absorption spectrum of biphenyl in solution shows a structureless intense band at about 40.5 kK and a weak band observed as a slight inflection around 36 kK.[41] It is thus interesting to see whether or not S_2 emission occurs in the gaseous state. As is shown in Fig. 3, the 35—42 kK region of the fluorescence spectrum does not vary with an increase in the excita-

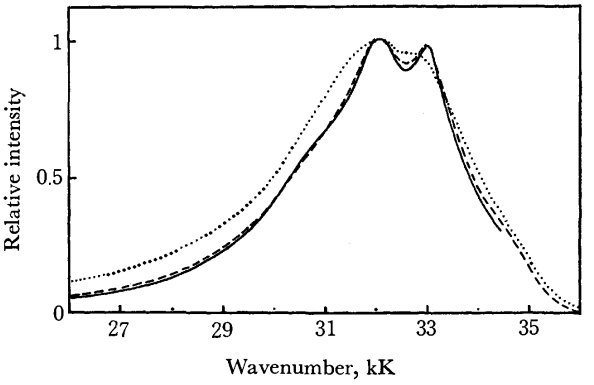

Fig. 3. The gas-phase fluorescence spectra of biphenyl. Excitations at 35.7 kK (——), 37.0 kK (----), and 40.0 kK (·····). At 85°C (~2.3 Torr).

40) P. Wannier, P. M. Rentzepis, and J. Jortner, *Chem. Phys. Lett.*, **10**, 193 (1971).

TABLE 2. THE VALUES GIVEN FOR BIPHENYL, PHENANTHRENE, TRIPHENYLENE, AND CHRYSENE

	Biphenyl	Phenanthrene			Triphenylene		Chrysene		
S_1 (kK)	~37	29.2			29.5		27.6		
S_2 (kK)	42	35.2			35.7		32.5		
k_1 (sec^{-1})	1.2×10^{7} a)	2.6×10^{6}			3.8×10^{6}		1.7×10^{6}		
k_2 (sec^{-1})	7.7×10^{8}	2.5×10^{8}			3.5×10^{8}		1.2×10^{8}		
ϕ_1 b)	0.15	0.16			0.07		0.12		
$\bar{\nu}_{exc}$ (kK)	45 c)	39.2	41.0	43.5	38.5	41.7	35.0	38.5	40.8
ρ_1 (cm)	4.1×10^{7}	8.8×10^{9}	3.1×10^{11}	2.5×10^{13}	1.5×10^{10}	2.3×10^{13}	2.3×10^{8}	1.3×10^{12}	1.8×10^{14}
ρ_2 (cm)	5.5×10	2.4×10^{3}	5.0×10^{5}	2.3×10^{8}	2.9×10	4.0×10^{6}	7.0	4.0×10^{6}	2.6×10^{9}
Φ_2/Φ_1 (calc.)	5.2×10^{-3}	1.6×10^{-3}	1.8×10^{-3}	2.5×10^{-3}	5.0×10^{-3}	5.0×10^{-3}	1.0×10^{-3}	1.2×10^{-3}	2.0×10^{-3}

a) This value, obtained assuming $\varepsilon_{max}\sim1000$, agrees with that estimated from the quantum yield and lifetime.
b) Ref. 7.
c) An assumed wavenumber at which no fluorescence spectrum was observed.

tion energy. The observed large Stokes shift (4 kK) may be due to the change in the molecular geometry in the excited state.[41] The absence of S_2 emission in biphenyl is considered to be ultimately ascribable to the small ρ_2/ρ_1 values arising from the somewhat large energy separation between the first and second singlet states (~5 kK), as may be seen from Table 2.

Phenanthrene exhibits fairly well-structured fluorescence spectra on low-energy excitation and considerably broadened and red-shifted spectra on high-energy excitation, as is illustrated in Fig. 4. The spectral changes observed are uniform and gradual. In the 29—35 kK range of these spectra, however, no trace of S_2 emission can be found. The fluorescence spectra of triphenylene with excitation at various wavelengths are shown in Fig. 5. As the excitation wavenumber increases, the spectrum gradually becomes broader, and in the 29—35 kK range no S_2 emission is found. The reason for the absence of S_2 emission in phenanthrene and triphenylene is that the energy difference between S_1 and S_2 is quite large (6.0 and 6.2 kK respectively), as is indicated in Table 2.

The emission spectra of chrysene excited at several wavenumbers are shown in Fig. 6. The whole spectrum

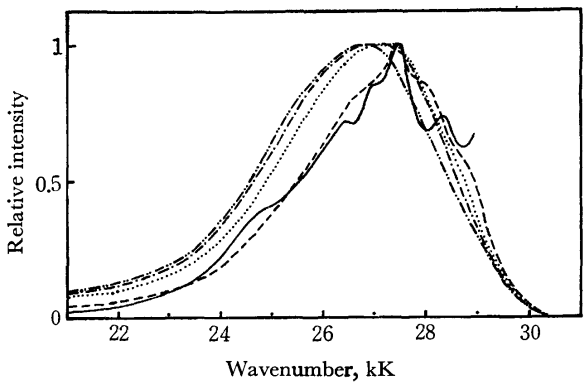

Fig. 4. The gas-phase fluorescence spectra of phenanthrene. Excitations at 30.3 kK (——), 35.2 kK (----), 39.2 kK (·····), 41.1 kK (-·-·), and 43.5 kK (-···-). At 113°C (~0.9 Torr).

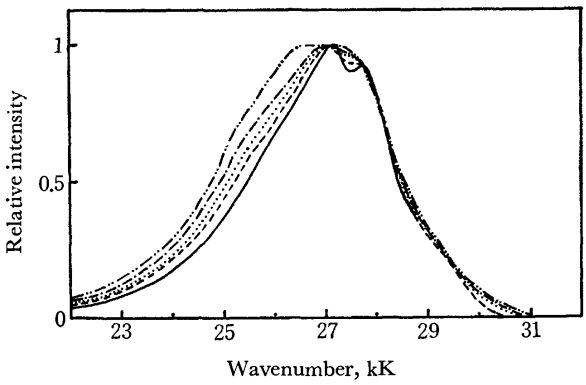

Fig. 5. The gas-phase fluorescence spectra of triphenylene. Excitations at 31.3 kK (——), 33.3 kK (----), 35.7 kK (·····), 38.5 kK (-·-·), and 41.7 kK (-···-). At 200°C (~0.032 Torr).

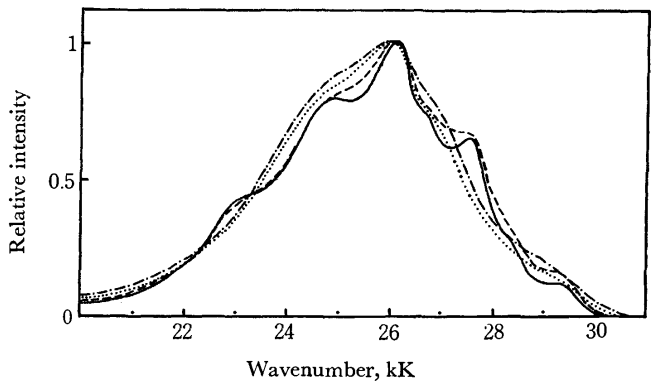

Fig. 6. The gas-phase fluorescence spectra of chrysene. Excitations at 32.5 kK (——), 35.0 kK (----), 38.5 kK (·····), and 40.8 kK (-·-·). At 212°C (~0.7 Torr).

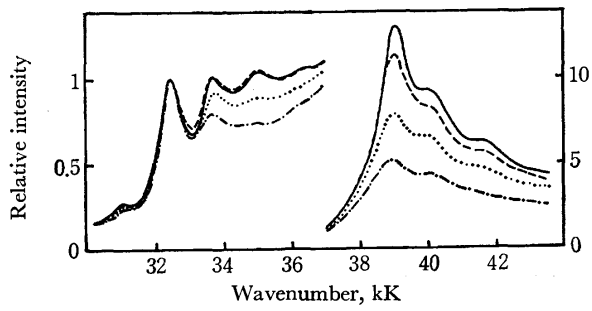

Fig. 7. The excitation spectra of chrysene gas. Emission observed at 25.0 and 26.3 kK (——), 27.5 kK (----), 28.6 kK (·····), and 29.2 kK (-·-·). At 210°C (~0.7 Torr).

41) H. Suzuki, "Electronic Absorption Spectra and Geometry of Organic Molecules," Academic Press, New York (1967).

becomes more diffuse on excitation at higher energies. The relatively well-resolved band at about 29.3 kK might be assigned to an S_2-emission band. However, this band is situated too far from the position of the second absorption band at about 32.5 kK; further, the behavior of the excitation spectrum is quite anomalous in that its relative intensity decreases with the increase in the monitoring wavenumber, as is shown in Fig. 7. Moreover, Table 2 indicates that the calculated Φ_2/Φ_1 values for chrysene are appreciably smaller than those of, for example, 1,2-benzanthracene (*vide infra*). This is also due to the large S_1—S_2 energy difference (4.9 kK). These facts imply that some impurity is possibly responsible for the emission observed around 29.3 kK.[42]

1,2-Benzanthracene and 20-Methylcholanthrene. As the criteria are well satisfied by 1,2-benzanthracene and its derivative, 20-methylcholanthrene, it is tempting to test the presence of S_2 emission in these molecules. The observation of the emission from the second excited singlet state of 1,2-benzanthracene in *n*-heptane solutions was reported by Easterly *et al.*[19] According to their interpretation. the emission arises from the thermal population of S_2 from S_1.[19] In the present study, the gas-phase fluorescence spectra of 1,2-benzanthracene and 20-methylcholanthrene were measured at various excitation wavenumbers; these are shown in Figs. 8 and 9. The observed spectra are relatively sharp and well-structured with low energy excitations. On excitation at higher wavenumbers, however, the spectrum broadens and shifts to the red, and the intensity on its short-wavelength tail increases appreciably. On the basis of its band position and spectral behavior, the emission appearing in the high-wavenumber region can be assigned to the S_2 emission.

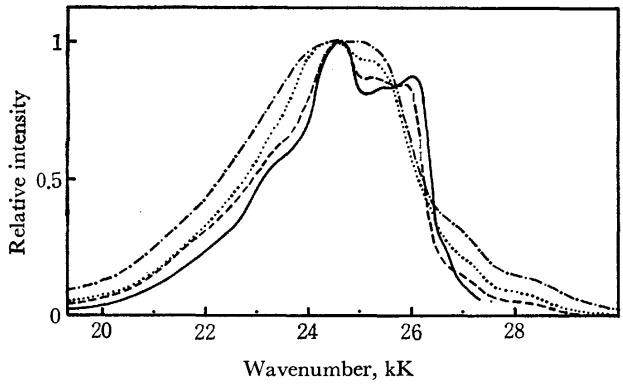

Fig. 8. The gas-phase fluorescence spectra of 1,2-benzanthracene. Excitations at 28.9 kK (——), 31.5 kK (——), 36.4 kK (·····), and 41.7 kK (-·-·). At 152°C (~0.01 Torr).

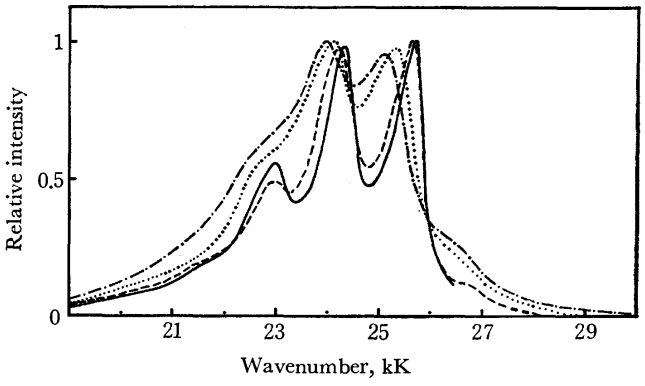

Fig. 9. The gas-phase fluorescence spectra of 20-methylcholanthrene. Excitations at 27.2 kK (——), 28.7 kK (——), 35.5 kK (·····), and 40.0 kK (-·-·). At 190°C (~0.065 Torr).

42) An alternative explanation may be that this band arises from the v—$v-1$ resonance fluorescence and that the anomaly in its excitation spectrum is caused by the considerable broadening of the band.

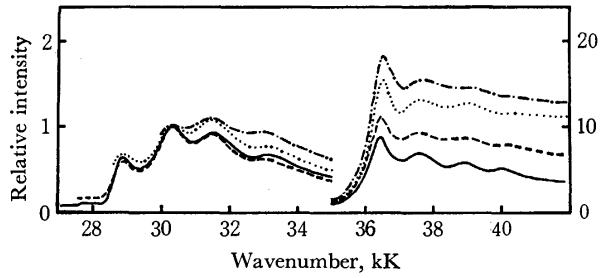

Fig. 10. The excitation spectra of 1,2-benzanthracene gas. Emission observed at 25.0 kK (——), 27.0 kK (——), 27.8 kK (·····), and 28.6 kK (-·-·). At 167°C (~0.024 Torr).

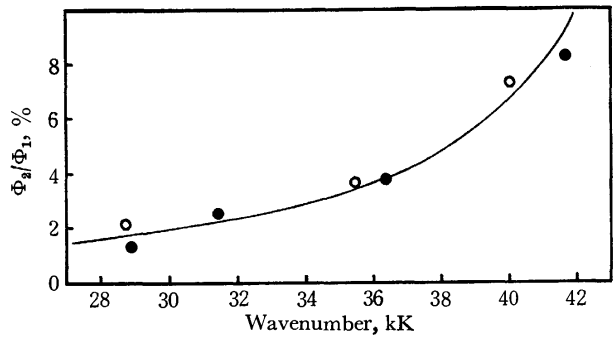

Fig. 11. The observed Φ_2/Φ_1 value *vs.* excitation wavenumber, for 1,2-benzanthracene (●) and 20-methylcholanthrene (○).

Figure 10 shows the excitation spectra of 1,2-benzanthracene, indicating that the relative intensity of the S_2 emission increases with the excitation energy. In Fig. 11, the observed ratio Φ_2/Φ_1 for 1,2-benzanthracene and 20-methylcholanthrene is plotted against the excitation wavenumber, showing the progressive increase in the former with the increase in the latter. Interestingly, the data on 20-methylcholanthrene give almost the same curve as those on 1,2-benzanthracene, as Fig. 11 shows.

The radiative rate constants, state densities, and related parameters are given in Table 3. The ρ values for 1,2-benzanthracene were substituted for those for 20-methylcholanthrene. As is shown in Table 3, the calculated relative yields of the S_2 emission are very large in these molecules, suggesting that the expectation regarding the appearance of the S_2 emission is quite realistic. The great enhancement of the S_2 emission by the substituent effects to be expected with 20-methylcholanthrene was not actually observed, however, as is shown in Fig. 9.

1,12-Benzperylene and Coronene. Dawson and Kropp reported an S_2 emission due to thermal repopulation

TABLE 3. THE VALUES GIVEN FOR 1,2-BENZANTHRACENE AND 20-METHYLCHOLANTHRENE

	1,2-Benzanthracene			20-Methylcholanthrene		
S_1 (kK)		26.2			25.7	
S_2 (kK)		28.9			27.1	
k_1 (sec^{-1})		3.3×10^{6}			4.1×10^{6}	
k_2 (sec^{-1})		1.1×10^{8}			1.4×10^{8}	
ϕ_1		0.19[a]			0.2[b]	
$\bar{\nu}_{exc}$ (kK)	31.5	36.4	41.7	28.7	35.5	40.0
ρ_1 (cm)	4.3×10^{5}	2.7×10^{11}	1.6×10^{16}	7.3×10	1.1×10^{11}	1.6×10^{15}
ρ_2 (cm)	1.1×10	3.0×10^{8}	8.0×10^{13}	4.5×10^{-2}	3.3×10^{9}	9.9×10^{13}
Φ_2/Φ_1 (calcd)	0.001	0.038	0.17	0.022	1.0	2.0
(obsd)	0.025	0.037	0.081	0.022	0.037	0.073

a) Ref. 7. b) The value assumed by reference to that for 1,12-benzanthracene.

with 1,12-benzperylene in a poly (methyl methacrylate) matrix.[20] 1,12-Benzperylene shows absorption spectra with a very weak first band, followed by a much stronger second band, well satisfying the criteria. In coronene, the first and second absorption bands are extremely weak and closely spaced (α-band), accompanied by an intense third band (p-band).[43] This assignment was made in view of the relatively complicated structure of the 'α-band' and the theoretical results.[44-46]

The fluorescence spectra of 1,12-benzperylene and coronene measured in the gas phase and in benzene solutions are shown in Figs. 12 and 13. In benzene solutions the spectra exhibit quite distinct vibrational structures, with an enhanced 0—0 band indicative of the so-called Ham effect recently studied by the present author;[47] this effect can be utilized in the assignment of the vibronic bands.

As may be seen from Fig. 12, the gas-phase fluorescence of 1,12-benzperylene has an interesting feature. On the short-wavelength side of the weak 0—0 band observed as a small peak at 24.6 kK, a band corresponding to the solution band around 25 kK appears at about 25.1 kK, with an appreciably high intensity. In addition to this, another relatively intense band can be observed around 26.4 kK upon excitation at higher wavenumbers.

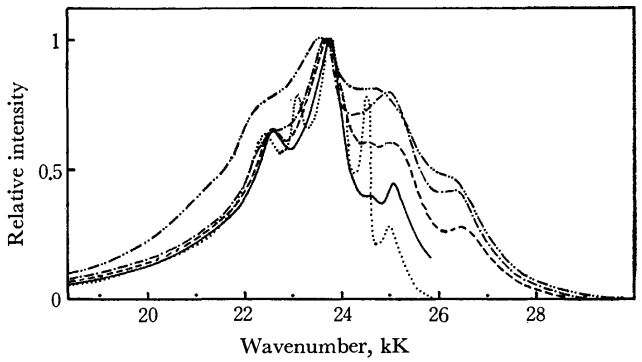

Fig. 12. The fluorescence spectra of 1,12-benzperylene. In the gas phase: excitations at 27.0 kK (——), 29.9 kK (----), 34.5 kK (-·-·), and 40.0 kK (-···-···-); at 210°C (~0.02 Torr). In the benzene solution: excitation at 28.6 kK (·····); at room temperature.

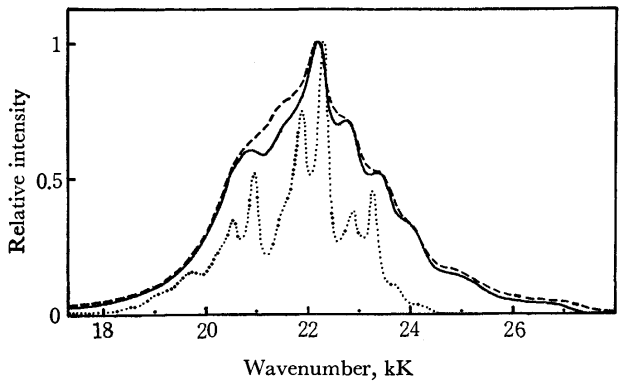

Fig. 13. The fluorescence spectra of coronene. In the gas phase: excitations at 30.1 kK (——) and 34.2 kK (----); at 285°C (~0.09 Torr). In the benzene solution: excitation at 29.5 kK (·····); at room temperature.

The excitation spectra monitoring on the three bands is shown in Fig. 14. Though these spectra differ considerably in relative intensity in the high-wavenumber region, their agreement with one another in wavenumber is very good, implying that these three bands originate from the same molecular species and not from impurities.

The emission observed around 25 kK in solution was

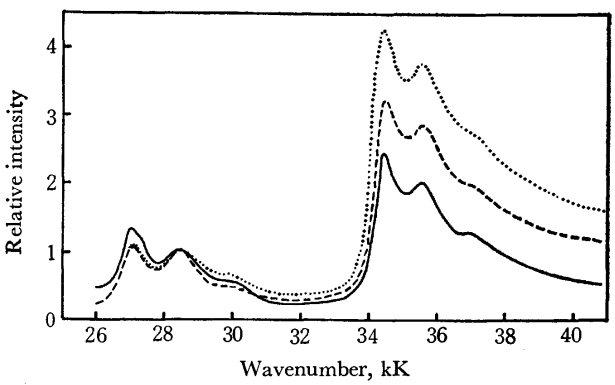

Fig. 14. The excitation spectra of 1,12-benzperylene gas. Emission observed at 23.7 kK (——), 25.0 kK (----), and 26.5 kK (·····). At 210°C (~0.02 Torr).

43) E. Clar, "Polycyclic Hydrocarbons," Academic Press, New York (1964).
44) R. L. Hummel and K. Ruedenberg, *J. Phys. Chem.*, **66**, 2334 (1962).
45) H. Gutfreund and W. A. Little, *Phys. Rev.*, **183**, 68 (1969); *J. Chem. Phys.*, **50**, 4468 (1969).
46) K. Ohno, T. Kajiwara, and H. Inokuchi, *Technical Report of ISSP*, Ser. A, No. 414 (1970).
47) A. Nakajima, This Bulletin, **44**, 3272 (1971); unpublished data.

TABLE 4. THE VALUES GIVEN FOR 1,12-BENZPERYLENE AND CORONENE

1,12-Benzperylene				Coronene		
S_1 (kK)		24.6		S_1 (kK)	23.5	
				S_2 (kK)	~25	
S_2 (kK)		27.0		S_3 (kK)	29.6	
k_1 (sec^{-1})		6.6×10^{6}		k_1 (sec^{-1})	1.4×10^{6}	
				k_2 (sec^{-1})	$\sim6\times10^{6}$	
k_2 (sec^{-1})		3.9×10^{8}		k_3 (sec^{-1})	3.4×10^{8}	
ϕ_1		0.36[a]		ϕ_1	0.3[b]	
$\bar{\nu}_{exc}$ (kK)	29.9	34.5	40.0	$\bar{\nu}_{exc}$ (kK)	30.1	34.3
ρ_1 (cm)	1.0×10^{6}	1.1×10^{12}	3.1×10^{17}	ρ_1 (cm)	1.4×10^{8}	2.8×10^{13}
ρ_2 (cm)	4.5×10	1.3×10^{9}	1.8×10^{15}	ρ_2 (cm)	6.8×10^{5}	5.0×10^{11}
				ρ_3 (cm)	10^{-7}	1.4×10^{5}
Φ_2/Φ_1 (calc.)	0.004	0.076	0.35	$(\Phi_2+\Phi_3)/\Phi_1$ (calc.)	0.022	0.079
(obs.)	0.24	0.37	0.38	(obs.)	0.097	0.11

a) Ref. 20. b) Ref. 7.

assigned by Kropp and Dawson[20] to the S_2 emission. If this is true, the bands appearing around 25.1 kK and 26.4 kK might be attributable to the S_2 and S_3 emissions respectively. However, the 0—0 absorption band of the second electronic transition is observed in the gas phase at 27.0 kK (see Fig. 14). Accordingly, it is preferable to assign the 26.4 kK band[48] to the S_2 emission. The 25 kK band, on the other hand, may be considered to be the 1—0 resonance emission band, overlapped by the higher vibrational components of the S_2 emission. This explanation seems to be consistent with the observation in the condensed phase by Kropp and Dawson of the temperature-dependent anti-Stokes band, which may, in our opinion, occur from an excited vibronic level.

The relative yields of the S_2 emission were estimated from the areas under the emission curves obtained on the assumption of a mirror-image relationship. The observed and calculated yield ratios are given in Table 4, showing that these ratios have appreciably large values and that they increase with the excitation energy.

The fluorescence spectra of coronene are also interesting, as is shown in Fig. 13. Excitation was made at the limited peaks (30.1 and 34.3 kK), because a weak impurity band was observed with excitation at lower wavenumbers and because the purification of coronene is notoriously difficult.[49] The fluorescence tail extending to the higher-energy region (24—29 kK) may be composed of S_2 and S_3 emissions. Since the relative intensities of these emissions could not be estimated separately, their yields were treated as a sum. As is shown in Table 4, the values of $(\Phi_2+\Phi_3)/\Phi_1$ observed are of a reasonable order of magnitude in comparison with those calculated in the manner described in the Appendix. The calculated value of Φ_3/Φ_1 was relatively small, of the order of 10^{-3}.

Anthracene, Tetracene, and Perylene. Since the second absorption band (^1L_b) in anthracene, tetracene, and perylene is quite weak compared to the first band (^1L_a), this is a case where the criteria are not satisfied. The gas-phase fluorescence spectra of these compounds were also measured, while varying the excitation wavelength, and the absence of any S_2 emission was shown. The spectral results were almost the same as those obtained by other workers[50-55] and so are not given in this paper. The failure of any S_2 emission to appear can be well understood by the very small values of Φ_2/Φ_1 calculated to be as is shown in Table 5.

TABLE 5. THE VALUES GIVEN FOR ANTHRACENE, TETRACENE, AND PERYLENE

	Anthracene	Tetracene	Perylene
S_1 (kK)	27.6	22.2	23.9
S_2 (kK)	~31	~26	~30
k_1 (sec^{-1})	9.1×10^{7}	1.1×10^{8}	4.8×10^{8}
k_2 (sec^{-1})	$\sim10^{7}$	$\sim10^{7}$	$\sim10^{7}$
ϕ_1[a]	0.30	0.17	0.78
$\bar{\nu}_{exc}$ (kK)	40	38.5	37.7
ρ_1 (cm)	9.0×10^{11}	7.0×10^{16}	2.5×10^{15}
ρ_2 (cm)	1.1×10^{9}	4.3×10^{13}	1.1×10^{9}
Φ_2/Φ_1 (calc.)	1.7×10^{-4}	1.2×10^{-4}	1.3×10^{-5}

a) Ref. 7.

Concluding Remarks

It has been shown that the density of states can play an important role in radiationless transitions; this is in contrast with the view of Siebrand,[56] who places more emphasis on the Franck-Condon factors. Despite our simple model, the tendency for the relative yield of the S_2 emission to increase with the excitation energy can be interpreted, though qualitatively, in terms of

48) The band seems to be affected by the reabsorption by the strong second absorption band.

49) S. Iwashima, K. Ohno, T. Kajiwara, and J. Aoki, *Nippon Kagaku Zasshi*, **90**, 884 (1969).

50) E. Bowen and S. Veljkovic, *Proc. Roy. Soc.*, **A236**, 1 (1956).

51) K. H. Härdtl and A. Scharmann, *Z. Naturforsch.*, **12a**, 715 (1957).

52) B. Stevens and E. Hutton, *Mol. Phys.*, **3**, 71 (1960).

53) R. Williams and G. J. Goldsmith, *J. Chem. Phys.*, **39**, 2008 (1963).

54) V. V. Gruzinski and N. A. Borisevich, *Opt. Spectry.*, **14**, 246 (1965).

55) W. R. Ware and P. T. Cunningham, *J. Chem. Phys.*, **43**, 3826 (1965).

56) W. Siebrand and D. F. Williams, *ibid.*, **46**, 403 (1967); W. Siebrand, *ibid.*, **46**, 440 (1967); **47**, 2411 (1967).

the appropriately evaluated values of the state densities and the radiative rate constants. All the results obtained have proved consistent with the criteria previously mentioned, which can be restated on the basis of the first term in Eq. (6) that the S_2 emission can occur because of the large values of k_2/k_{1f} and ρ_2/ρ_1, the latter of which depends strongly on the energy difference. The contribution of the second term in Eq. (6), on the other hand, has been estimated to be comparatively small ($\lesssim 5\times10^{-3}$). In the case of azulene, it can be considered that k_{rp}/k_{ic} is very small because of the anomalously large S_1—S_2 energy separation, but k_{ic} is nearly comparable to k_2 because of the small Franck-Condon factors, so that the large second term permits the fluorescence emission from S_2. According to our results, in the molecule whose Φ_2/Φ_1 value is evaluated to be larger than about 0.01, there is a possibility for the S_2 emission to occur; this emission is essentially of an indirect nature. A strong laser excitation source would, however, be very useful for detecting a much weaker S_2 emission in a variety of compounds, including those studied in this work.

The participation of the triplet state has been neglected, but the vibrational relaxation by molecular collisions is so fast and complete during the sufficiently long lifetime of the triplet state that the molecule resulting in this state may contribute only to the quenching process.

The discrepancy between the observed and calculated yield ratios and, especially, the too great dependence of the calculated Φ_2/Φ_1 values on the excitation energy may be improved to some extent by considering the differences in the Franck-Condon overlap integrals for the individual vibrational modes; this must be done in a more elaborate study, irrespective of the model assumed.

Attention should be called to the assignment of the S_2 emission, which is generally made on the basis of the observations that it occurs in the short-wavelength region of the normal fluorescence and that its excitation spectrum almost agrees with the absorption spectrum. As has been suggested in the case of 1,12-benzperylene (and chrysene[42]), such behavior can be exhibited by the v—v—i resonance fluorescence in the gas phase or the thermally-excited vibronic band (hot band) in the condensed phase. This possibility requires further investigations designed to establish a method for an unambiguous identification.

In view of the interesting spectral features observed in 1,12-benzperylene and coronene, it seems worthwhile to make further studies of their gas-phase emissions.

The author wishes to express his thanks to Professors Junji Aoki and Hiroo Inokuchi for the gift of the sample of 1,12-benzperylene. His tahnks are also due to Mr. Masakatsu Aoi for his helpful discussions.

Appendix

The kinetics involving the third excited singlet state is considered, in which it is assumed that the direct conversion process between S_1 and S_3 is negligible. In Fig. 15 the

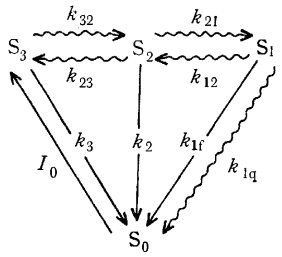

Fig. 15. Three-state scheme, with the rate constants for various radiative (——) and nonradiative (~~~) processes.

radiative and nonradiative processes concerned are represented, along with the definitions of the rate constants. According to this scheme, the rate equations can be expressed as follows:

$$dS_1/dt = k_{21}S_2 - (k_{1f}+k_{1q}+k_{12})S_1 \quad (7)$$

$$dS_2/dt = k_{32}S_3 + k_{12}S_1 - (k_2+k_{21}+k_{23})S_2 \quad (8)$$

$$dS_3/dt = I_0 + k_{23}S_2 - (k_3+k_{32})S_3 \quad (9)$$

where S_i is the concentration of the molecules in S_i. Under photostationary conditions, $dS_1/dt = dS_2/dt = dS_3/dt = 0$, from which the following formulae can be obtained:

$$\Phi_2/\Phi_1 = (k_2/k_{1f})(k_{12}/k_{21}) + k_2/k_{21}\phi_1 = \text{Eq. (1)} \quad (10)$$

$$\begin{aligned}\Phi_3/\Phi_1 &= (k_3k_{12}/k_{1f}k_{21})(k_{23}/k_{32}+k_2/k_{32}) + (k_3k_{23}/k_{21}k_{32} \\ &\quad + k_3k_2/k_{21}k_{32}+k_3/k_{32})(k_{1f}+k_{1q})/k_{1f} \\ &= (k_3/k_{1f})(\rho_2/\rho_1)(\rho_3/\rho_2+k_2/k_{32}) \\ &\quad + [(k_3/k_{21})(\rho_3/\rho_2)+k_2k_3/k_{21}k_{32}+k_3/k_{32}]/\phi_1, \end{aligned} \quad (11)$$

where the rate constants for the forward and backward conversion processes have been given by

$$k_{ij}/\rho_j = k_{ji}/\rho_i = (2\pi/\hbar)v_{ij}^2. \quad (12)$$

The Φ_2/Φ_1 ratio obtained by neglecting the S_1—S_3 conversion process and the quenching process from S_2 is identical to that given before for the two-state scheme, as is indicated by Eq. (10). On the basis of these expressions, the quantum-yield ratios for coronene are evaluated using the rate constants and state densities listed in Table 4. It was assumed that $k_{32}\sim k_{21}\sim 10^{12}$ (sec^{-1}).

Dielectric Dispersion at Meter Waves of 1-Hexanol and 1-Octanol in Cyclohexane Solutions

Hitoshi KOMOOKA

School of Pharmaceutical Sciences, Kitasato University, Shirokane, Minato-ku, Tokyo

(Received January 13, 1972)

The dielectric constants and losses of 1-hexanol and 1-octanol in cyclohexane solutions were measured in the frequency range 60—480 MHz at various temperatures. The values $\varepsilon_0-\varepsilon_\infty$ deviate widely from the linear dependence on concentration. The curve of $(\varepsilon_0-\varepsilon_\infty)/c$ plotted against concentration c falls rapidly as c decreases. Its value seems to be zero at the concentration of 1 mol/*l*. A comparison with the values of higher alcohols given in literature shows that the curve is almost uniquely determined for each temperature as a function of the concentration of hydroxyl group alone, irrespective of the length of C–C chain in alkyl group of alcohols. As shown by Ibbitson and Moore, there exist considerable amounts of dimers, trimers and cyclic polymers in the dilute solutions of 1% by weight. The cause for the large values of dielectric constant cannot be merely attributed to the formation of hydrogen-bonded aggregates of molecules. A possible structure of the aggregates is discussed.

Since Mizushima[1] investigated the dielectric dispersion of alcohols in 1927, studies in this field have been made by several authors with various methods. Lebrun[2] measured the dielectric constants and losses of 1-heptanol, 1-octanol, 1-nonanol, and 1-decanol at 20°C in the frequency range $1—9.5\times10^3$ MHz, obtaining two relaxation times. Garg and Smyth[3] measured those of ten normal alcohols from propyl through dodecyl in the wavelength range 30,000—0.22 cm. They analyzed the dispersion into three separate regions. The dispersion process with the longest relaxation time was attributed to the breaking of the hydrogen bonds in molecular aggregates followed by the rotation of alcohol molecules.

Measurements on dilute solutions of alcohols were carried out by Johari and Smyth.[4] It was shown that normal alcohols in dilute benzene solutions have two relaxation processes instead of three, lacking the one attributable to the associated molecules.

Theoretical studies on the dielectric constant of liquid were made by Onsager, Kirkwood[5] and others. Kirkwood succeeded at least qualitatively in explaining the large values for alcohol. His theory is by no means satisfactory. It does not take into account the existence of three relaxation processes in liquid alcohols. The lowest frequency relaxation process dominates in the dispersion region. A study on the process would help elucidate complicated problems with regard to liquid structure.

The dielectric constants and losses of alcohols have been determined. Cyclohexane was selected as a solvent among others, because the value $\varepsilon_0—\varepsilon_\infty$ for the solution of an alcohol is nearly equal to that of the other, if the concentrations of hydroxyl group are equal to each other, although the relaxation frequencies are quite different.

Experimental

Purification of Materials. 1-Hexanol was washed with a 10% solution of sodium hydroxide and distilled through a 50 cm column under reduced pressure. The middle portion was distilled fractionally through a 1 m column packed with Dixon packings at 30 Torr. About 20% of the distillates was separated off at a reflux ratio of 180: 1, in which at least four impurities were found to be present by gas chromatography with a column containing Silicone Oil SE-30 as a fixed phase liquid. Removal of one of them was difficult,[6] and seemed almost impossible by distillation at 50 Torr. In the middle fraction, there was no perceptible peak originating from impurity in its chromatogram. Molecular Sieve 5A was used as a drying agent.

1-Octanol was purified by the same method as described above except that it was distilled fractionally at 15 Torr. The gas chromatograms resembled those of 1-hexanol when the temperature of the column was elevated.

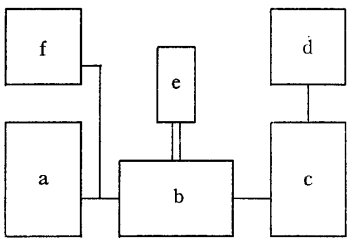

Fig. 1. Block diagram of the apparatus. a: signal generator hp 608C, b: VHF bridge hp 803A, c: VHF detector hp 417A, d: null detector hp 415E, e: sample holder, f: frequency counter.

Cyclohexane was washed with concentrated sulfuric acid, with mixed acid and again with sulfuric acid. It was distilled fractionally through a 1 m column packed with Helipack packings and dried with calcium hydride. Density 0.7738, n_D 1.4235, ε_0 2.016 at 25°C.

Apparatus. Dielectric constants and losses were measured with a Hewlet-Packard Type 803A VHF bridge which operates as a Byrne bridge. The setup for measurement is shown by a block diagram in Fig. 1. The error in the measurement of impedance, according to the specifications, may be within 2% in magnitude and within 1.2° in phase angle when the necessary corrections are made to the bridge readings.

The sample holder or cell is shown diagrammatically

1) S. Mizushima, *Physik. Z.*, **28**, 418 (1927).
2) A. Lebrun, *Ann. Phys.* (Paris), **10**, 16 (1955).
3) S. K. Garg and C. P. Smyth, *J. Phys. Chem.*, **69**, 1294 (1965).
4) G. P. Johari and C. P. Smyth, *J. Amer. Chem. Soc.*, **91**, 6215 (1969).
5) J. G. Kirkwood, *J. Chem. Phys.*, **7**, 911 (1939).
6) A. Weissberger, E. S. Proskauer, J. A. Riddick, and E. E. Toops, Jr., "Organic Solvents", second ed., Interscience Publishers, New York, N. Y. 1955, p. 354.

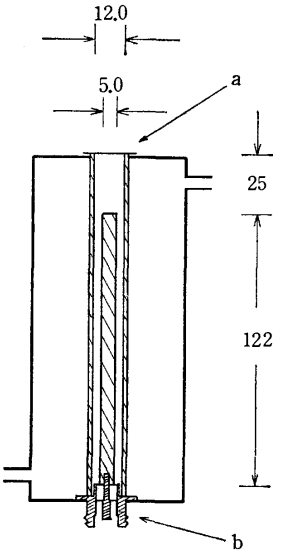

Fig. 2. Sample holder. a: thin glass plate, b: type-N jack. All dimensions in mm.

with dimensions in Fig. 2. Made of brass, it is an open-circuited coaxial line equipped with a N-female type connector at one end. As the outer conductor is 2.5 cm longer than the inner one, leakage of high frequency signals is effectively prevented. The electrical length and characteristic impedance of the cell were so determined that the measured values of the dielectric constant of cyclohexane, benzene and chlorobenzene agree with the values at low frequencies reported in various papers. The electrical length thus obtained is 12.5 cm, which is 0.3 cm longer than the physical length of the inner conductor. The characteristic impedance is 52.5Ω, which agrees with the value calculated from the dimensions of the cell.

The electrical length of the transmission line which connects the cell to bridge was about 9.2 cm. This showed slight variations with frequency within 0.1 cm.

Method of Calculations. The imput admittance Y of an open-circuited cell of coaxial type is given by

$$Y = i\frac{\sqrt{\varepsilon}}{Z_0}\tan\frac{2\pi\sqrt{\varepsilon}fl}{c} \tag{1}$$

if wall losses are neglected, where $\varepsilon(=\varepsilon'-i\varepsilon'')$ is the complex dielectric constant of a substance filled in the cell, c light velocity; Z_0 and l the characteristic impedance and electrical length of the cell, respectively. If we put

$$a = \frac{2\pi ifl Z_0}{c}Y \text{ and } z = \frac{2\pi i\sqrt{\varepsilon}fl}{c}, \tag{2}$$

a and z are complex numbers and fulfill the following equations:

$$a = z\tanh z \tag{3}$$

or

$$z = a\coth z. \tag{3'}$$

Equation (3') can be solved easily by means of successive approximations. If z_i is the i-th approximate value of z, the $(i+1)$-th approximation is given by

$$z_{i+1} = a - \frac{2z_i+\sinh 2z_i}{2a-1+\cosh 2z_i}. \tag{4}$$

Static value ε_0 and high frequency limit ε_∞ of dielectric constant and relaxation frequency f_r are calculated in the following way. By Debye's theory the following equations hold at each frequency f:

$$\varepsilon' = \varepsilon_\infty + (\varepsilon_0-\varepsilon_\infty)\frac{1}{1+(f/f_r)^2} \tag{5}$$

$$\varepsilon'' = (\varepsilon_0-\varepsilon_\infty)\frac{f/f_r}{1+(f/f_r)^2}. \tag{6}$$

From these equations, the relation

$$\varepsilon'' = \frac{1}{f_r}\varepsilon' f - \frac{\varepsilon_\infty}{f_r}f \tag{7}$$

can be derived. According to the method of least squares, we can choose $1/f_r$ and ε_∞/f_r so that the following expression is minimum:

$$\sum_i\left(\varepsilon_i'' - \frac{1}{f_r}\varepsilon_i' f_i + \frac{\varepsilon_\infty}{f_r}f_i\right)^2 = \min. \tag{8}$$

where ε_i' and ε_i'' are experimental values at frequency f_i. Then, ε_0 is calculated from

$$\sum_i(\varepsilon_i'-\varepsilon_\infty) = (\varepsilon_0-\varepsilon_\infty)\sum_i\frac{1}{1+(f_i/f_r)^2}. \tag{9}$$

Measurements. Dielectric constants and losses were measured at the frequencies 60, 80, 100, 150, 200, 250, 300, 400, and 480 MHz. Frequencies were controlled to be within ±0.1% of the specified values. Temperatures were kept constant by circulation of water from a thermostat through a jacket around the cell. No measurements were made for dilute solutions with relaxation frequency out of the frequency range.

Results

Some typical plots of complex dielectric constant $\varepsilon=\varepsilon'-i\varepsilon''$ for 1-hexanol and solutions are shown in Fig. 3. The plots for each liquid are on a semicircle within experimental error. It is sufficient if we consider a single dispersion process in each liquid in the frequency range where measurements are made. The observed dielectric constant and loss of 1-hexanol at 25°C are given in Table 1 with the calculated values from Eqs. (5) and (6).

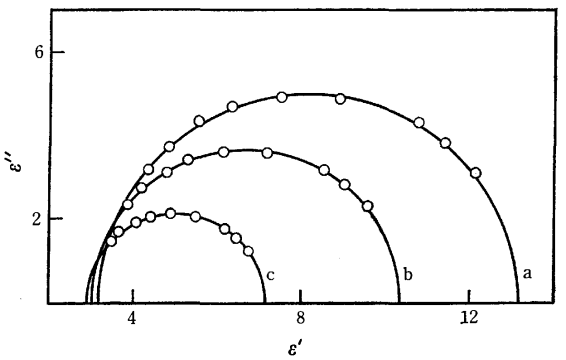

Fig. 3. Complex dielectric constants of 1-hexanol in cyclohexane soltuions at 25°C. a: 100%, b: 80.12%, c: 60.44%.

The dielectric parameters calculated from Eqs. (8) and (9) of pure 1-hexanol and 1-octanol and cyclohexane solutions are given in Tables 2 and 3, together with the refractive indices measured by use of a Pulfrich refractometer and with densities.

TABLE 1. OBSERVED AND CALCULATED DIELECTRIC CONSTANT AND LOSS OF 1-HEXANOL AT 25°C

f (MHz)	(obsd) ε'	(obsd) ε''	(calcd)[a] ε'	(calcd)[a] ε''
60	12.12	3.11	12.10	3.10
80	11.39	3.84	11.41	3.82
100	10.75	4.31	10.67	4.34
150	8.86	4.88	8.88	4.96
200	7.49	4.92	7.45	4.96
250	6.31	4.70	6.40	4.69
300	5.52	4.35	5.66	4.33
400	4.82	3.74	4.74	3.65
480	4.33	3.19	4.31	3.19

a) From Eqs. (5) and (6) with $\varepsilon_0=13.179$, $\varepsilon_\infty=3.160$, $f_r=172.9$ MHz.

TABLE 2. DIELECTRIC PARAMETERS, REFRACTIVE INDICES AND DENSITIES OF 1-HEXANOL IN CYCLOHEXANE SOLUTIONS

x (mol%)	ε_0	ε_∞	f_r (MHz)	n_D	d (g/cm³)
			15°C		
100.00	14.22	3.17	106	1.4198	0.8222
89.88	12.78	3.08	104	1.4201	0.8181
79.53	11.25	3.01	102	1.4206	0.8138
69.74	9.61	2.93	105	1.4211	0.8097
60.19	7.84	2.83	111	1.4217	0.8056
49.98	5.97	2.74	125	1.4224	0.8014
40.20	4.39	2.63	151	1.4231	0.7975
30.58	3.24	2.47	205	1.4241	0.7936
			20°C		
100.00	13.66	3.16	135	1.4180	0.8187
88.93	12.18	3.08	132	1.4182	0.8141
79.76	10.81	3.00	132	1.4187	0.8101
70.10	9.21	2.93	135	1.4190	0.8059
59.92	7.40	2.83	145	1.4196	0.8016
50.68	5.80	2.77	161	1.4201	0.7977
40.15	4.21	2.64	194	1.4209	0.7930
30.14	3.15	2.48	253	1.4230	0.7891
			25°C		
100.00	13.18	3.16	173	1.4161	0.8151
89.73	11.75	3.03	171	1.4163	0.8107
80.12	10.35	2.99	172	1.4166	0.8064
70.38	8.82	2.94	175	1.4170	0.8021
60.44	7.15	2.88	186	1.4174	0.7977
50.26	5.47	2.77	209	1.4179	0.7932
40.08	4.07	2.67	246	1.4185	0.7888
32.58	3.29	2.51	308	1.4192	0.7856
			30°C		
100.00	12.70	3.17	221	1.4140	0.8113
90.20	11.37	3.08	219	1.4141	0.8070
80.59	10.04	3.06	216	1.4144	0.8026
70.28	8.41	2.96	227	1.4146	0.7982
59.62	6.69	2.88	244	1.4150	0.7934
49.45	5.13	2.78	275	1.4154	0.7889
			35°C		
100.00	12.18	3.22	277	1.4122	0.8077
89.55	10.84	3.12	275	1.4121	0.8031
80.25	9.50	3.07	280	1.4121	0.7993
70.37	8.01	3.00	287	1.4124	0.7943
59.87	6.40	2.89	313	1.4127	0.7893
49.70	4.94	2.81	349	1.4132	0.7847

TABLE 3. DIELECTRIC PARAMETERS, REFRACTIVE INDICES AND DENSITIES OF 1-OCTANOL IN CYCLOHEXANE SOLUTIONS

x	ε_0	ε_∞	f_r	n_D	d
			20°C		
100.00	10.55	3.03	89	1.4294	0.8250
90.91	9.69	2.98	90	1.4290	0.8215
80.93	8.61	2.92	94	1.4284	0.8176
70.07	7.23	2.85	102	1.4276	0.8126
60.32	6.02	2.78	112	1.4271	0.8083
50.69	4.78	2.70	134	1.4267	0.8038
40.41	3.68	2.58	172	1.4263	0.7988
30.08	2.93	2.44	235	1.4258	0.7936
			25°C		
100.00	10.14	3.04	116	1.4275	0.8215
90.77	9.26	2.99	119	1.4270	0.8178
79.96	8.12	2.94	124	1.4262	0.8132
70.07	6.95	2.88	133	1.4256	0.8090
60.70	5.79	2.81	149	1.4251	0.8047
50.66	4.59	2.71	175	1.4244	0.7999
40.49	3.60	2.60	218	1.4239	0.7948
			30°C		
100.00	9.70	3.04	153	1.4196	0.8179
91.45	8.93	3.01	155	1.4190	0.8145
80.22	7.76	2.94	164	1.4183	0.8097
69.69	6.57	2.90	178	1.4175	0.8050
59.75	5.42	2.82	197	1.4168	0.8002
49.57	4.32	2.73	233	1.4162	0.7952
			35°C		
100.00	9.32	3.06	192	1.4237	0.8144
89.71	8.36	3.03	202	1.4228	0.8101
80.09	7.36	2.93	216	1.4221	0.8059
70.54	6.35	2.88	230	1.4216	0.8016
59.83	5.20	2.83	254	1.4208	0.7966

Discussion

The value $\varepsilon_0-\varepsilon_\infty$ decreases rapidly with the decrease in the concentration of alcohol, as seen from Table 2 or 3. The ratio $(\varepsilon_0-\varepsilon_\infty)/c$ at 25°C is plotted against concentration c for both alcohols in Fig. 4. We see a large dependence of $\varepsilon_0-\varepsilon_\infty$ on concentration. The two curves are situated closely to each other; especially at low concentration below 4 mol/l they coincide within experimental error. This indicates that the magnitude of $\varepsilon_0-\varepsilon_\infty$ is mainly determined by the concentration of

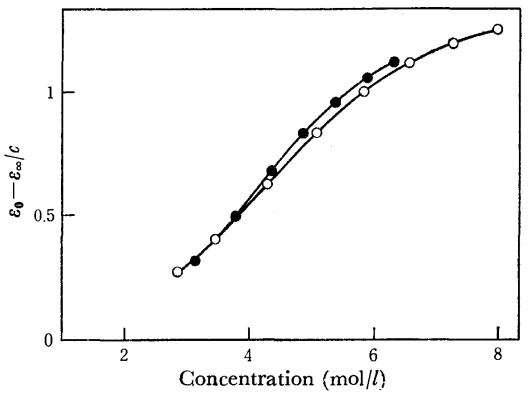

Fig. 4. Comparison of 1-hexanol and 1-octanol at 25°C. ○: 1-hexanol, ●: 1-octanol.

hydroxyl group irrespective of the length of C–C chain in alkyl group of alcohols. If it is proportional to the number of alcohol molecules per unit volume, these curves can be interpreted as representing the concentration dependence of the contribution of a molecule to dielectric dispersion. We see from Tables 2 and 3 that the variation of refractive indices of the solutions is so small that its influence can be ignored. It is suggested that a large change in the properties of alcohol molecules takes place in the concentration range 2—7 mol/*l*.

The situation stated above remains unchanged if we examine the concentration dependecne of

$$\frac{(\varepsilon_0-\varepsilon_\infty)(2\varepsilon_0+\varepsilon_\infty)\,T}{\varepsilon_0(\varepsilon_\infty+2)^2c}$$

according to Onsager's equation in which ε_∞ is used in place of n^2. The two curves plotted in Fig. 5 represent the relation. We cannot consider these curves to represent the concentration dependence of Kirkwood's *g*-factor. The value 31.6 for pure 1-octanol becomes 8.4 at the concentration of 2.4 mol/*l*; the ratio 31.6/8.4= 3.76 is much greater than the value 2.57 of *g*-factor calculated for normal alcohols.[7] Other equations for the dielectric constant of liquid will give the same conclusion.

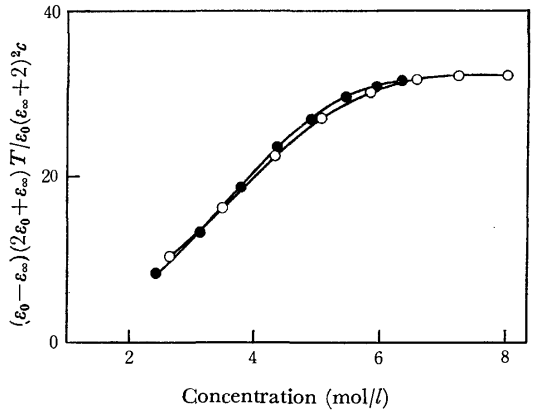

Fig. 5. Plots of $(\varepsilon_0-\varepsilon_\infty)(2\varepsilon_0+\varepsilon_\infty)T/\varepsilon_0(\varepsilon_\infty+2)^2c$ for 1-hexanol and 1-octanol at 20°C.

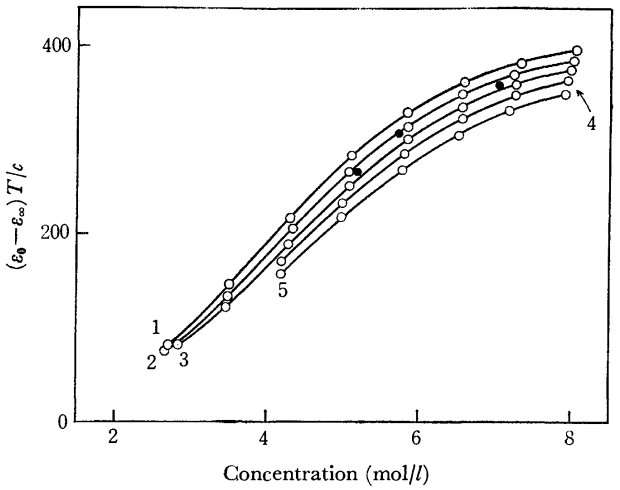

Fig. 6. Plots of $(\varepsilon_0-\varepsilon_\infty)T/c$ for 1-hexanol against concentration. 1: 15°C, 2: 20°C, 3: 25°C, 4: 30°C, 5: 35°C. ●: calculated from Lebrun's data at 20°C for 1-heptanol, 1-nonanol and 1-decanol (from right to left).

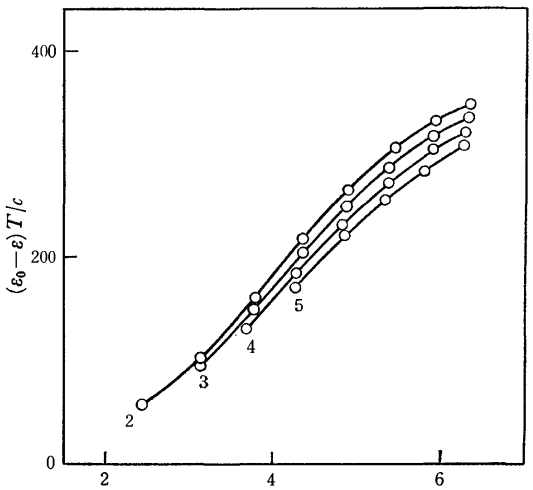

Fig. 7. Plots of $(\varepsilon_0-\varepsilon_\infty)T/c$ for 1-octanol against concentration.

In Figs. 6 and 7, the values $(\varepsilon_0-\varepsilon_\infty)T/c$ are plotted against *c* at various temperatures for 1-hexanol and 1-octanol in cyclohexane solutions, respectively. In order to facilitate comparison of the curves at different temperatures, the values in the ordinates are multiplied by the absolute temperature. The slope of these curves at middle concentration is steep at low temperature. With increasing temperature, it becomes gradual and the curve shifts toward high concentration side as a whole. If we extrapolate the curves to lower concentration, their values vanish in the vicinity of 1 mol/*l*.

The curves seem to indicate that the mechanism of association to hydrogen-bonded polymers which have an anomalously large dielectric constant is of co-operative nature. At sufficiently low concentration, the percentage of alcohol molecules which form the polymers will be zero; when the concentration reaches a certain value near 1 mol/*l*, the percentage will begin to increase; with increasing concentration, the percentage increases rapidly and finally it would attain a saturated value if the concentration increased further beyond that of pure alcohols. It is easy to explain the large temperature dependence of dielectric constant of the alcohols if we assume the mechanism of co-operative nature.

Ibbitson and Moore[8] reported that alcohols in the dilute solution of 1% by weight have two near infrared absorption bands besides the one attributable to monomers. The two bands were attributed to the presence of dimers, trimers and cyclic polymers. They also found that, with the appearance of the two bands, the solute polarization began to decrease from a constant value at lower concentrations. Therefore, we cannot expect a considerable amount of molecules to form the polymers with large dielectric constant at such concentration.

7) G. Oster and J. G. Kirkwood, *J. Chem. Phys.*, **11**, 175 (1943).

8) D. A. Ibbitson and L. F. Moore, *J. Chem. Soc B*, **1967**, 76.

The saturation property can be inferred from the values $(\varepsilon_0-\varepsilon_\infty)\,T/c$ for pure alcohols. The calculated values from the data by Saxton *et al.*[9] are 331 and 354 at 20°C for methanol and ethanol, respectively; 382 for 1-propanol, 395 for 1-butanol and 378 for 1-pentanol from the data tabulated by Brot, Magat, and Reinisch[10] at the same temperature. Smaller values for methanol and ethanol might be due to the smallness of their refractive indices.

The points for 1-heptanol, 1-nonanol, and 1-decanol calculated from Lebrun's experiments lie approximately on our curve as seen from Fig. 6.

The polymers are supposed to have the structure of nets composed of alcohol molecules bridged by hydrogen bonds. The two dimensional spread is necessary for co-operative phenomenon. It can be easily imagined that chain multimers and cyclic polymers join together to form a net when concentration increases.

The author is grateful to Professor Hideo Okabayashi for his kind guidance and encouragement throughout this work, and to Mr. Takei and Mr. Shinomiya for their advice.

9) J. A. Saxton, R. A. Bond, G. T. Coats, and R. M. Dickinson, *J. Chem. Phys.*, **37**, 2132 (1962).
10) C. Brot, M. Magat, and L. Reinisch, *Kolloid-Z.*, **134**, 101 (1953).

BULLETIN OF THE CHEMICAL SOCIETY OF JAPAN, VOL. 45, 1700—1704(1972)

Mass Spectrometric Analysis of Water-insoluble Yellow Monoazo Pigments

Kousuke KOBAYASHI and Kazutoyo HIROSE

Dai-Nippon Ink Institute of Chemical Research, Kamikizaki, Urawa, Saitama

(Received May 19, 1971)

Water-insoluble Yellow Monoazo Pigments were examined in order to establish a new analytical system using mass spectrometry. The characteristic ions observed were as follows: molecular ions, amine-component ions which are formed by the scission of the amide bond with hydrogen transfer and which are the most intense ones, ions at *m/e*: 43, and, in some cases, further-decomposed ions from the amine-component ions. A new analytical system was established on the basis of the analysis of the mass fragmentations of 27 samples, and applied to three unknown samples. The structure of these pigments can be deduced from the low-resolution mass spectra for those derived from substituted anilines, and from the high-resolution spectra for those derived from other amines.

Organic pigments have been widely used in many fields, such as printing inks, paints, plastics, and coatings. There have been many reports on the syntheses and physical properties of these pigments, but only a few on their analysis.[1] They are usually analysed by chemical methods, by infrared spectrometry, or by the X-ray diffraction method. The chemical analysis does not always give successful results in spite of its difficulty and its slowness. The latter two instrumental methods give information which can be compared with the known data, but not enough to elucidate their chemical structure.

On the other hand, mass spectrometry, developed recently in the field of organic chemistry, can be expected to give some information about the structure of organic pigments, because the pigments give molecular ions (as they have a long conjugated system in their structure) and because their chemical compositions can be practically determined by the high-resolution measurements. The final object of our research is to establish software for typing out the chemical structure of organic pigments after feeding the mass-spectrometric data into a computer. Some examples of such autoanalysis have already been reported in the cases of ketones[2] and fatty acid esters.[3] As the first step of our series of studies, we examined the mass-spectrometric analysis of Water-insoluble Yellow Monoazo Pigments (YMP) in order to find some characteristic peaks which differentiate them from other types of organic pigments, such as Water-insoluble Red Monoazo Pigments, and to determine the kind and location of the substituents.

Experimental

Apparatus and Measurement. The spectra were obtained using a JMS-O1SG double-focussing mass spectrometer (Japan Electron Optics Laboratory Co., Ltd.). Using 75 eV electrons at a regulated emission current of 200 μA, all the experiments were made by the electrical detection method under low-resolution conditions (*ca.* 1600); some results were also examined by the photo-plate detection method, using perfluoro kerosene under high-resolution conditions (*ca.* 20000), in order to confirm the elemental composition of the ions. Samples were introduced through a direct sample

1) A. McClure, J. Thomson, and J. Tannahill, *J. Oil Col. Chem. Assoc.*, **51**, 580 (1968).

2) A. M. Duffield, A. V. Robertson, C. Djerassi, B. G. Buchanan, G. L. Sutherland, E. A. Feigenbaum, and J. Lederberg, *J. Amer. Chem. Soc.*, **91**, 2977 (1969).

3) G. Schroll, A. M. Duffield, C. Djerassi, B. G. Buchanan, G. L. Sutherland, E. A. Feigenbaum, and J. Lederberg, *ibid.*, **91**, 7440 (1969).

inlet system at an ion-source temperature of 200—240°C and a sample-vaporizing temperature of 120—240°C.

Samples. The samples were all furnished by Dai-Nippon Ink and Chemicals, Inc., and were purified by recrystallization from nitrobenzene. The samples, with their various substituents, are shown in Table 1. The fundamental structure of YMP is shown by the following general formula:

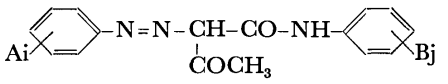

Table 1. Samples and their substituents

Samples	Substituents as Ai	Substituents as Bj
YMP-1	nothing	nothing
2	2-NO_2, 4-CH_3	nothing
3	2-NO_2, 4-Cl	2-Cl
4	2-NO_2, 4-Cl	4-OCH_3
5	2-NO_2, 4-Cl	2-OCH_3
6	2-NO_2, 4-Cl	2-$COOCH_3$
7	2-OCH_3, 4-NO_2	2-$COOCH_3$
8	2-NO_2, 4-OCH_3	2-$COOCH_3$
9	2-NO_2, 4-Cl	2,4-di-Cl
10	2-NO_2, 4-CH_3	2,4-di-Cl
11	2-NO_2, 4-OCH_3	2,4-di-Cl
12	2-NO_2, 4-Cl	2-CH_3, 5-Cl
13	2-NO_2, 4-OCH_3	2-CH_3, 5-Cl
14	2-NO_2, 4-CH_3	2-CH_3, 5-Cl
15	2-CH_3, 4-NO_2	2-OCH_3, 5-CH_3
16	2-NO_2, 4-OCH_3	2-OCH_3, 5-CH_3
17	2-NO_2, 4-Cl	2-OCH_3, 5-CH_3
18	2-NO_2, 4-CH_3	2-OCH_3, 5-CH_2
19	2-OCH_3, 4-NO_2	2-OCH_3, 5-CH_3
20	2-NO_2	2-OCH_3, 5-CH_3
21	4-NO_2	2-OCH_3, 5-CH_3
22	2-NO_2, 4-Cl	2-OCH_3, 5-Cl
23	2-NO_2, 4-CH_3	2,4-di-OCH_3
24	4-NO_2	2,5-di-OCH_3, 4-Cl
25	2-NO_2, 4-CH_3	2,5-di-OCH_3, 4-Cl
26	2,4-di-OCH_3, 5-$SO_2NHC_6H_5$	2-OCH_3, 5-$CONH_2$
27	2-NO_2, 4-OCH_3	2-OCH_3, 5-$CONH_2$

Results and Discussion

Fragmentation Process. Some examples of the mass spectra of YMP are shown in Fig. 1. In all cases except YMP-12, the most intense peak was the amine-component ion (Am^+) formed by the scission of the amide bond with hydrogen transfer. Furthermore, the molecular ion (M^+) and the ion at *m/e*: 43 ($Ac^+=CH_3CO^+$) were observed in every sample. When Am^+ has a methoxy or carbomethoxy group, a further-decomposed ion (Ad^+) was also observed at an appreciable intensity. The pattern coefficient, based on Am^+, and the sample-vaporizing temperature of each sample are shown in Table 2. The intensities of M^+, Ad^+, and Ac^+ were 10—50%, 10—40%, and 10—60%, respectively, based upon that of the base peak with some exceptions.

The fact that the scission of the amide bond with hydrogen transfer gives the most intense peak was also observed in *N,N*-diphenyl phenylacetamide.[4] In diphenyl acetanilide, an ion which arises from the scission of the amide bond with reverse hydrogen transfer was observed.[4] The cleavage of both sides of the carbonyl

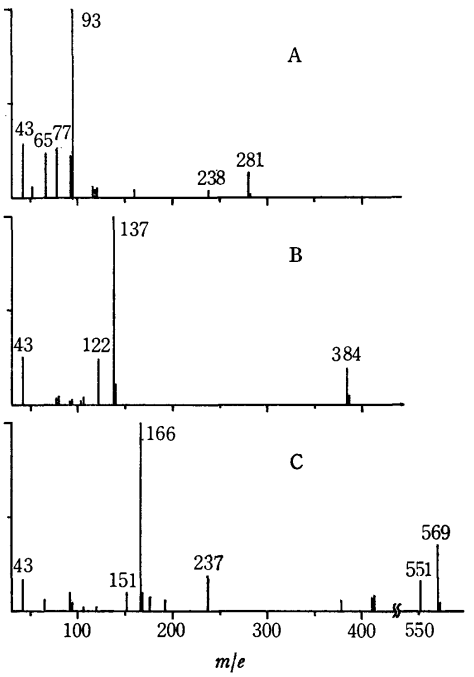

Fig. 1. Mass spectra of YMP.
A: YMP-1, B: YMP-15, C: YMP-26

Table 2. Relative intensities of M^+, Am^+, Ad^+, and Ac^+

Sample No.	Measured temp.	M^+		Am^+		Ad^+		Ac^+
		m/e	*R.I.*	*m/e*	*R.I.*	*m/e*	*R.I.*	*R.I.*
YMP-1	130°C	281	11	93	100	—	—	31
2	140	340	28	93	100	—	—	40
3	140	394	28	127	100	—	—	47
4	180	390	49	123	100	108	11	40
5	170	390	28	123	100	108	23	53
6	135	418	9	151	100	119	27	40
7	160	414	14	151	100	119	28	53
8	175	414	11	151	100	119	24	42
9	185	428	18	161	100	—	—	95
10	170	408	26	161	100	—	—	29
11	210	424	34	161	100	—	—	76
12	160	408	17	141	100	—	—	150
13	170	404	24	141	100	—	—	51
14	165	388	26	141	100	—	—	67
15	175	384	19	137	100	122	24	25
16	160	400	23	137	100	122	19	8
17	165	404	27	137	100	122	26	37
18	150	384	21	137	100	122	26	28
19	140	400	30	137	100	122	25	19
20	160	370	23	137	100	122	28	38
21	165	370	59	137	100	122	35	25
22	190	424	21	157	100	142	18	47
23	150	400	35	153	100	138	10	7
24	175	420	62	187	100	172	26	55
25	165	434	24	187	100	172	29	67
26	240	569	35	166	100	151	10	17
27	210	429	29	166	100	151	43	49

The observed values are the mean of triplicate of the measurements.

4) K. G. Das, P. T. Funke, and A. K. Bose, *J. Amer. Chem. Soc.*, **86**, 3729 (1964).

TABLE 3. HIGH RESOLUTION MASS MEASUREMENTS OF YMP-1 AND -10

Standard ion structure	YMP-1 Formula	YMP-1 Calcd mass	YMP-1 Obsd mass	YMP-10 Formula	YMP-10 Calcd mass	YMP-10 Obsd mass
Ar(Ai)–N=N–CH(COCH$_3$)–CO–NH$^{\cdot+}$–Ar(Bj)	$C_{16}H_{15}N_3O_2$	281.116	281.116	$C_{17}H_{14}N_4O_4Cl_2$	408.039	408.040
Ar(Bj)–NH$_2^{+\cdot}$	C_6H_7N	93.058	93.060	$C_6H_5NCl_2$	160.980	160.983
Ar(Ai)–N=N–CH(COCH$_3$)–CO$^+$	$C_{10}H_9N_2O_2$	189.066	189.069	$C_{11}H_{10}N_3O_4$	248.067	248.065
Ar(Bj)–N=C=O$^{+\cdot}$	C_7H_5NO	119.037	119.035	$C_7H_3NOCl_2$	186.962	186.960
Ar(Bj)–NH–CO$^+$	C_7H_6NO	120.045	120.043	$C_7H_4NOCl_2$	187.970	187.968
Ar(Ai)$^+$	C_6H_5	77.039	77.041	$C_7H_6NO_2$	136.040	—[a]
Ar(Ai)–N=N$^+$	$C_6H_5N_2$	105.045	105.047	$C_7H_6N_3O_2$	164.046	164.044
Ar(Bj)–NH–CO–CH(COCH$_3$)$^+$	$C_{10}H_{10}NO_2$	176.071	176.070	$C_{10}H_8NO_2Cl_2$	243.993	243.993
Ar(Ai)–NH$_2^{+\cdot}$	C_6H_7N	93.058	93.060	$C_7H_8N_2O_2$	152.058	152.057
Ar(Ai)–NH$^+$	C_6H_6N	92.050	92.048	$C_7H_7N_2O_2$	151.050	151.048

a) An ion of this formula was not observed.

group in β-diketone[5] and that of both sides of the azo group in substituted azo benzene[6] have also been reported.

All the apparent peaks in each spectrum were examined by the high-resolution method; some of them are shown in Table 3 in the cases of YMP-1 and -10. The mean intensities of the ions were as follows (the intensity obtained is shown in parentheses):

Ar(Ai)–N=N–CH(COCH$_3$)–CO$^+$ (1)
Ar(Ai)$^+$ (<1)
Ar(Ai)–N=N$^+$ (1)
Ar(Bj)–NH$_2^{+\cdot}$ (100)
Ar(Bj)–N=C=O$^{+\cdot}$ (5)
Ar(Bj)–NH$^+$ (<1)
Ar(Bj)–NH–CO–CH(COCH$_3$)$^+$ (1)
Ar(Bj)–NH–CO$^+$ (2)
(M–43)$^+$ (3)
Ac$^+$ (49)
(M–17)$^+$ (<1)
Ar(Ai)–NH$^+$ (2)
Ar(Ai)–NH$_2^{+\cdot}$ (3)

The last ion, Ar(Ai)–NH$_2^{+\cdot}$, is assumed to be produced from the enol form of M$^+$ with hydrogen scrambling.[7] The formation of these ions can be similarly explained by the scission described in the above literature.[4-6]

When Am$^+$ has a methoxy group at the *ortho* or *para* position, Ad$^+$ was observed in every case at a position of 15 mass units lower than Am$^+$. Compounds possessing a carbomethoxy group at the *ortho* position showed two typical ions at *m/e*: 119 and 146. The formation of these unusual ions can reasonably be explained by the fragmentation process shown in Scheme 1. The transformation of Am$^+$ (*m/e*: 151) into Ad$^+$ (*m/e*: 119) is known as the *ortho* effect.[8]

Analytical Method of YMP. As has been mentioned above, M$^+$, Am$^+$, Ad$^+$, and Ac$^+$ are typical ions in the mass spectra of YMP. Ac$^+$ is a specific ion by which YMP can be distinguished from other types of organic pigments. The only exceptions are Water-insoluble Yellow Disazo Pigments, but they can easily be differentiated by their high molecular weights (over 600).

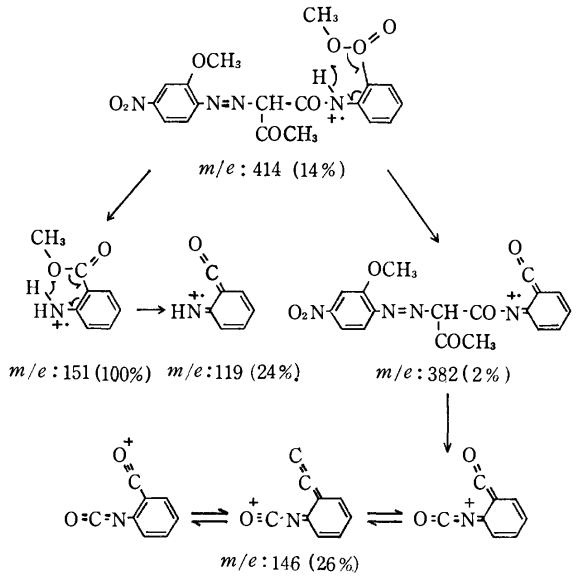

Scheme 1. Fragmentation process of YMP-7.

Usually YMP are synthesized from two aromatic amines. For example, a pigment with the general formula is synthesized from two amines, Ar(Ai)–NH$_2$ and Ar(Bj)–NH$_2$. If these amines are limited to substituted anilines, such as anisidine or toluidine, the structure of YMP can be decided on the basis of low-resolution mass-spectrometric measurements alone. The substituents, Ai and Bj, can be easily deduced from the following equations. The correlation in the mass among M$^+$, Am$^+$, and substituents is given by Eqs. (1) and (2), where M(X) represents the mass of X, and where m and n represent the number of substituents:

$$\sum_{i=1}^{m} M(\mathrm{Ai}) + \sum_{j=1}^{n} M(\mathrm{Bj}) = M(\mathrm{M}^+) - 281 + m + n \quad (1)$$

5) C. Beard, J. M. Wilson, H. Budzikiewicz, and C. Djerassi, *J. Amer. Chem. Soc.*, **86**, 248 (1964).
6) J. H. Bowie and G. E. Lewis, *J. Chem. Soc., B*, 621 (1967).
7) R. G. Cooks, I. Howe, and D. H. Williams, *Org. Mass Spectrom.*, **2**, 137 (1969).
8) H. Budzikiewicz, C. Djerassi, and D. H. Williams, "Mass Spectrometry of Organic Compounds," Holden-Day, San Francisco (1967), pp. 197, 279, 516, 636.

$$\sum_{j=1}^{n} M(\mathrm{Bj}) = M(\mathrm{Am}^+) - 93 + n \quad (2)$$

Equations (3) and (4) are obtained from Eqs. (1) and (2):

$$\sum_{j=1}^{n}(M(\mathrm{Bj})-1) = M(\mathrm{Am}^+) - 93 \quad (3)$$

$$\sum_{i=1}^{m}(M(\mathrm{Ai})-1) = M(\mathrm{M}^+) - M(\mathrm{Am}^+) - 188 \quad (4)$$

If Ai or Bj is the chlorine or bromine atom, the number and kind of these halogen atoms can be decided from the intensities of the isotope peaks of these ions. The methoxy or carbomethoxy group can be deduced from Ad^+, and the number of nitrogen atoms also be easily deduced by the application of the nitrogen rule.[9] If no appropriate combination can be found, the amines seem not to be simple substituted anilines. In this case, a precise mass determination would be very useful.

The position of the substituent cannot usually be decided on the basis of the mass spectrum, except in the cases of the methoxy and carbomethoxy groups mentioned above. However, the positions of the substituents are limited to some extent because of the difficulty of synthesis and the inferiority of the physical properties. We surveyed the literature and can now presume the position of the substituent from its structure with some statistical probability. In the case of the dimethylamino group, for example, *p-N,N*-dimethylaminoaniline alone has been used as the starting material.

Application to Unknown Samples (Fig. 2). *X-1*: M^+ and Am^+ were observed at *m/e*: 423 and 187 respectively. M^+ contains two chlorine atoms, and Am^+ contains one chlorine atom, showing that both substituents, Ai and Bj, contain one chlorine atom. Equations (3) and (4) give the following values:

$$\sum(M(\mathrm{Bj})-1) = 94, \quad \sum(M(\mathrm{Ai})-1) = 48$$

It is conclusively deduced that Ai consists of one chlorine atom and one methyl group, and that Bj consists of one chlorine atom and two methoxy groups, one of which is considered to be at the *ortho* of *para* position from the presence of Ad^+ at *m/e*: 172. The following structure was, then, considered most probable from the statistical viewpoint; it was confirmed by comparison with the compound synthesized.

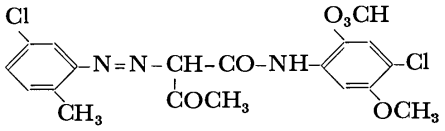

X-2: M^+ and Am^+ were observed at *m/e*: 378 and 121 respectively. Neither ion contains a halogen atom. As Ad^+ was not observed, the methoxy and carbomethoxy groups are absent. The summation of the mass of substituents may be given as follows:

$$\sum(M(\mathrm{Bj})-1) = 28, \quad \sum(M(\mathrm{Ai})-1) = 69$$

Obviously Bj consists of two methyl groups or one ethyl group, but ethyl aniline has never been used as a starting material. As an appropriate combination of substituents for 69 mass units could not be found, the amine, $Ar(Ai)–NH_2$, used as the starting material seemed not to be a simple substituted aniline. The elemental composition of M^+ was determined to be $C_{20}H_{18}N_4O_4$ (calcd: 378.135, obsd: 378.133) by a precise mass determination. Therefore, the 69 mass units corresponding to $C_2H_{-1}NO_2$ may be presumed to be an imide group or acetylene plus a nitro group. The latter can, however, be rejected because of the absence of the 2200 cm^{-1} band in its infrared spectrum. Thus, the –CO–NH–CO– grouping appears to be most probable. Although the positions of methyl groups cannot be decided on the basis of the experimental results, 2,4-dimethylaniline seemed to be the most probable starting material. The following structure was, then, suggested; it was confirmed by comparison with the compound synthesized.

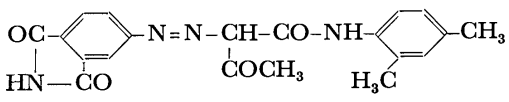

X-3: M^+ is an ion at *m/e*: 450 and contains two chlorine atoms. Am^+ is an ion at *m/e*: 221 or 194 and contains no chlorine atoms. Therefore, two chlorine atoms are contained in Ai. If Am^+ is an ion at *m/e*: 221, $\sum(M(\mathrm{Ai})—1)$ must be 41 mass units, which conflicts with the foregoing result. Therefore, Am^+ must be an ion at *m/e*: 194, and the mass numbers of the substituents may be calculated as follows:

$$\sum(M(\mathrm{Ai})-1) = 68, \quad \sum(M(\mathrm{Bj})-1) = 101$$

Ad^+ was observed at *m/e*: 166 and 165, which correspond to the loss of an ethylene and an ethyl radical from Am^+ respectively. From this fact, it was assumed that Am^+ contains an ethoxy group at the *ortho* or *para*

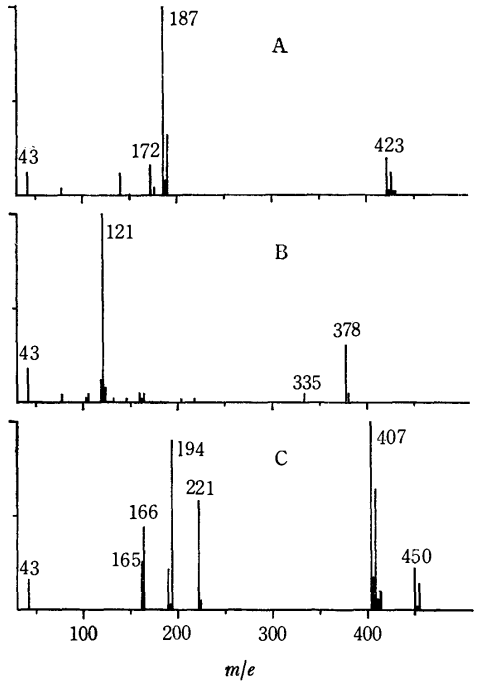

Fig. 2. Mass spectra of unknown samples.
A: X-1, B: X-2, C: X-3

9) R. M. Silverstein and G. C. Bassler, "Spectrometric Identification of Organic Compounds," John Wiley & Sons, New York (1963), p. 11.

TABLE 4. HIGH RESOLUTION MASS MEASUREMENT OF X-3

Observed mass	Formula	Calculated mass	Standard ion structure
450.032	$C_{10}H_{16}N_4O_3SCl_2$	450.032	M^+
221.040	$C_{10}H_9N_2O_2S$	221.038	$Ar(Bj)-NH-CO^+$
194.053	$C_9H_{10}N_2OS$	194.051	Am^+
166.019	$C_7H_6N_2OS$	166.020	$Ad^+:Am^+-C_2H_4$
165.010	$C_7H_5N_2OS$	165.012	$Ad^+:Am_+-C_2H_5$

position.[10] By subtracting the mass of the ethoxy group from 101, the total mass of Bj becomes 57 mass units, which corresponds to methyl plus an amide group. As the combination of ethoxy, methyl, and amide groups has never been used, the elemental composition of M^+ was examined. The elemental composition of M^+ was $C_{19}H_{16}N_4O_5Cl_2S$ (Table 4); the 57 mass units described above corresponded to $CH_{-1}NS$, suggesting a thioisocyanate or thiazole ring.

10) K. Kobayashi, unpublished work (1970).

The former was rejected on the basis of its high reactivity. The following structure was, then, proposed as the most probable one and was confirmed by comparison with the compound synthesized:

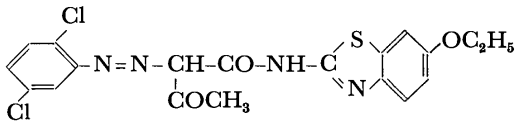

Ions at *m/e*: 407 and 211, corresponding to $(M—43)^+$ and $Ar(Bj)-NH-CO^+$ respectively, were observed as intense peaks in this case alone.

The authors wish to express their thanks to Mr. K. Kurihara for his technical assistance and to Mr. K. Takagi and Mr. H. Sakai of Dai-Nippon Ink and Chemicals, Inc., for their generous support of this work. We are also sincerely grateful to Professor T. Takeuchi of Nagoya University for his constant interest and encouragement.

BULLETIN OF THE CHEMICAL SOCIETY OF JAPAN, VOL. 45, 1704—1708(1972)

Activation Analysis of Arsenic, Copper, and Antimony in Sea Water

Shiro GOHDA

Atomic Energy Research Institute, Kinki University, Kowakae, Higashi-Osaka

(Received September 16, 1971)

Arsenic, copper, and antimony in sea water were determined by the thermal neutron activation analysis. Convenient pre- and post-irradiation procedures were proposed and some samples were analyzed. Arsenic, copper, and antimony were collected by the cocrystallization with thionalide, and were irradiated for 30 min in the neutron flux of 2×10^{13} n/cm^2/sec. After the thionalide complex was decomposed with nitric acid, the copper and antimony were separated from the arsenic by precipitating with oxine, and the arsenic in the filtrate was coprecipitated with ferric hydroxide. Gamma-ray spectra were obtained and the decays of the 0.44—0.67 MeV photo peak of ^{64}Cu plus ^{122}Sb and the 0.55 MeV peak of ^{76}As were followed. The arsenic, copper, and antimony contents in sea water were estimated to be 1.12—1.71 μg As/l, 1.49—3.35 μg Cu/l, and 0.22—0.57 μg Sb/l.

Many workers have studied on the amount of arsenic and copper in sea water. Gorgy *et al.*,[1] Rakestraw and Lutz.[2] and Ishibashi *et al.*[3] determined the total amount of arsenic in sea water by the arsenomolybdate blue method or Gutzeit method, and found 15—35 μg As/l, 6—28 μg As/l, and 3—6 μg As/l, respectively. However, these methods give generally high values, that may result from arsenic impurity contained in the zinc and the acid employed, which sometimes exceeds the amount of arsenic in sea water. Smales and Pate[4,5] stated that the activation analysis could minimize the errors caused by the contamination from the reagents, and they found 1.6—5 μg As/l in sea water. Portmann and Riley[6] also gave the value of 2 μg As/l in sea water spectrophotometrically by molybdenum blue method, after concentrating arsenic by the thionalide cocrystallization.

The copper content in sea water have been reported to be in the range 1—20 μg Cu/l. Riley[7] searched for the favorable method for the determination of copper in such a low concentration, and pointed out that much of the earlier works were unreliable because of the poor analytical technique and the contamination. Brooks *et al.*[8] applied the atomic absorption spectrophotometry, and found 0.7—1.5 μg Cu/l in sea water; the value was in good agreement with Riley and Shinhaseni's data.[9] On the antimony content in sea

1) S. Gorgy, D. L. Fox, and N. W. Rakestraw, *J. Marine Res.*, **7**, 22 (1948).
2) N. W. Rakestraw and F. B. Lutz, *Woods Hole Biol. Bull.*, **65**, 397 (1933).
3) M. Ishibashi, T. Shigematsu, Y. Nishikawa, and Y. Ishibashi, *Record Oceanog. Works Japan*, **5**, 66 (1960).
4) A. A. Smales and B. D. Pate, *Anal. Chem.*, **24**, 717 (1952).
5) A. A. Smales and B. D. Pate, *Analyst*, **77**, 188 (1952).
6) J. E. Portmann and J. P. Riley, *Anal. Chim. Acta*, **31**, 509 (1964).
7) J. P. Riley and G. Skirrow, "Chemical Oceanography," Vol. 2, Academic Press, London and New York, (1965), p. 295.
8) R. R. Brooks, B. J. Presley, and I. R. Kaplan, *Anal. Chim. Acta*, **38**, 321 (1967).
9) J. P. Riley and P. Shinhaseni, *Analyst*, **83**, 299 (1958).

water, a few reports[10-12] have been published. Portmann[10] analyzed the Irish sea water samples spectrophotometrically and estimated to be 0.13—0.40 μg Sb/l.

Since the concentration of arsenic, copper, and antimony in sea water are very low, as described above, a suitable concentrating technique and sensitive analytical method have been desired. The neutron activation coupled with the thionalide cocrystallization seems to be one of the most attractive techniques, because of the simple and rapid procedure, the high sensitivity, and the minimum contamination. But ^{64}Cu, ^{76}As, and ^{122}Sb, which are available radioactive nuclides for the analysis, show the gamma photo peaks in the similar energy region. Moreover, the half-lives of ^{64}Cu (12.8 h) and ^{76}As (26.5 h) are too close to be used in the decay curve analysis. In this research, a simple and convenient chemical procedure for the neutron activation analysis of arsenic, copper, and antimony in sea water was recommended. These elements were concentrated by means of the thionalide cocrystallization, and after the neutron irradiation, copper and antimony were precipitated with oxine, arsenic was coprecipitated with ferric hydroxide, and the ^{76}As, ^{64}Cu, and ^{122}Sb activities were measured by the gamma-ray spectrometry. Some sea water samples were analyzed by this method, and furthermore, to search on the dissolved form of these elements, the particle size distribution of the elements was also investigated.

Experimental

Materials. Thionalide solution, 2% (w/v); 2 g of thionalide (Thioglycollic-β-aminonaphthalide) was dissolved in acetone and diluted to 100 ml with acetone. The solution was freshly prepared as required.

Sulfuric acid, 6N; Arsenic-free sulfuric acid was diluted with water.

Standard solution of arsenic, 10 μg/ml; 0.1607 g of arsenic trioxide was dissolved in diluted sodium hydroxide solution, which was neutralized with diluted sulfuric acid and diluted to 100 ml with water. This stock solution (1 mg As per ml) was diluted to make a working standard solution containing 10 μg of arsenic per ml.

Standard solution of antimony, 10 μg/ml; 0.2669g of potassium antimonyl tartrate ($K[Sb(C_4H_2O_6)(H_2O)]$) was dissolved in sulfuric acid and diluted to 100 ml with 6N sulfuric acid. This stock solution (1 mg Sb per ml) was diluted with 6N sulfuric acid to make a standard solution containing 10 μg of antimony per ml.

Standard solution of copper, 10 μg/ml; 0.3929 g of copper sulfate ($CuSO_4 \cdot 5H_2O$) was dissolved in water, and after 5 ml of 6N sulfuric acid was added, diluted to 100 ml with water. The stock solution was diluted to get a solution containing 10 μg of copper per ml.

Oxine solution, 2% (w/v); 2 g of 8-quinolinol was dissolved in 7 ml of glacial acetic acid and diluted to 100 ml with water.

All the other reagents were the reagent grade, and employed without the further purification. Redistilled water was used in all the procedures.

Apparatus. Gamma-ray spectra were obtained with a well-type 3″×3″ NaI(Tl) scintillation detector connected to a Hitachi Gammascope, Model RAH-403 (a 400 channel pulse height analyzer), and the radioactivity measurements in the tracer experiments were made with a 2″×2″ NaI(Tl) detector connected to a Hitachi scalor, Model RC-2.

Procedure. *Pre-irradiation*: Immediately after the sampling, 1 l of sea water was successively filtered through a 8 μ pore-size Millipore filter and a 0.45 μ pore-size Millipore filter. To the filtered sample was added 0.3 g of ascorbic acid, and the solution was heated just under the boiling point, for 30 min (to reduce arsenic(V) to arsenic(III)). After 5 ml of 6N sulfuric acid and 8 ml of 2% thionalide acetone solution were added to the cooled solution with vigorous stirring, and the solution was boiled for about 30 min and then allowed to stand overnight at room temperature. The precipitate was filtered with a Millipore filter (pore size; 0.45 μ) and washed with water.

Irradiation: Two Millipore filters employed for the filtration of sea water sample and the filter including the thionalide precipitate were separately packed in three polyethylene capsule (8 mm long×12 mm in diameter), which were stuffed in a polyethylene rabbit tube. The sample and the standard material were irradiated for 30 minutes in a neutron flux of 2×10^{13} n/cm^2·sec in KUR.

Post-irradiation: After cooling a few hours, the irradiated sample was treated with 20 ml of nitric acid containing 5 mg of copper, 1 mg of arsenic, and 0.3 mg of antimony carriers, and was decomposed by fuming to almost dryness. The residue was dissolved with 3 ml of 1N nitric acid, and copper and antimony were precipitated as the oxinates by adding 5 ml of 2% oxine solution at pH 7—8. Arsenic remaining in the filtrate was coprecipitated with ferric hydroxide at pH 8 by adding 10 mg of ferric ion, after the excess oxine was removed as the copper chelate (10 mg of copper was added).

Radioactivity Measurement: The copper and antimony oxinates and the ferric hydroxide precipitates were used for the gamma ray spectrometry of ^{64}Cu, ^{122}Sb, and ^{76}As. For the hydroxide precipitate, the 0.55 MeV photo peak of the gamma rays following to the decay of ^{76}As was measured. For the oxinates precipitate, the decay of the photo peak area from 0.44 to 0.67 MeV, which was the sum of the 0.51 MeV annihilation gamma rays of ^{64}Cu and the 0.57 MeV gamma rays of ^{122}Sb, was followed for one week.

Results

Thionalide Cocrystallization of Copper, Arsenic, and Antimony. In order to establish the pre-irradiation procedure, the conditions for the cocrystallization, such as the acidity of sulfuric acid and the amount of thionalide, were studied by using the radioactive tracers, ^{64}Cu, ^{76}As, and ^{124}Sb.

The tracer and 5 μg of the carrier were added to 1 l of sea water, and the recovery of the cocrystallization with thionalide was obtained by comparing the gamma activity with that of the original tracer solution.

1) Effect of Sulfuric Acid Concentration: The effect of sulfuric acid concentration on the recovery is shown in Fig. 1.

Copper(II), arsenic(III), and antimony(III), (V) are

10) J. E. Portmann and J. P. Riley, *Anal. Chim. Acta*, **35**, 35 (1966).
11) I. Noddack and W. Noddack, *Ark. Zool.*, **1**, 32 (1940).
12) D. F. Schutz and K. K. Turekian, *Geochim. Cosmochim. Acta*, **29**, 259 (1965).

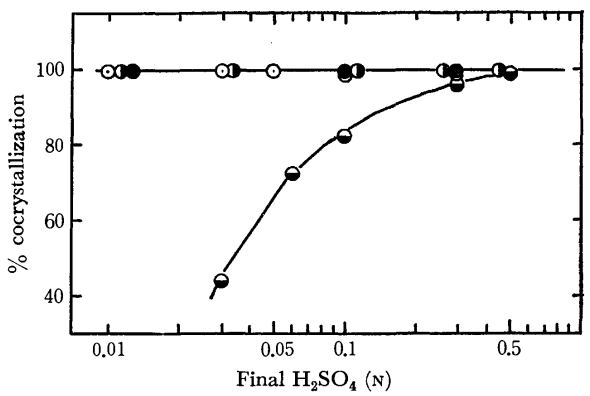

Fig. 1. Effect of sulfuric acid concentration on cocrystallization with thionalide (Thionalide: 160 mg/*l* of sea water).
⊙: As(III), ◒: As(V), ●: Sb(III), (V), ◑: Cu(II)

almost quantitatively recovered in the range from 0.01N to 0.5N sulfuric acid concentration, while the recovery of arsenic(V) is incomplete in this range, and reaches to a maximum value (about 97%) at 0.5N sulfuric acid. The volume of sulfuric acid used must be as small as possible, for minimizing the contamination from the acid, and therefore, arsenic(V) is reduced to arsenic(III) with ascorbic acid, and the acidity is maintained at 0.03N.

TABLE 1. RECOVERY OF ARSENIC, COPPER AND ANTIMONY USING VARIOUS VOLUME OF 2% THIONALIDE

Volume of thionalide added (m*l*)	% Recovery		
	As	Cu	Sb
3	62.8		
5	95.8	96.2	94.8
7	98.3	98.3	98.6
8	98.6	98.9	98.6
10	99.4		99.3
12	99.8	99.2	99.5
15	99.8		

2) Effect of the Amount of Thionalide on the Cocrystallization: The effect of the thionalide amount was studied by adding the different amount of 2% thionalide solution to 1 *l* of sea water containing the tracer, 5 μg of the carrier and ascorbic acid, which was kept at 0.03N with sulfuric acid. The results are presented in Table 1. The recovery of more than 98 per cent can be obtained by addition of 7 m*l* or more of 2% thionalide solution, and therefore, in the further experiments, 8 m*l* of 2% thionalide is employed per 1 *l* of sea water.

Chemical Separation with Oxine. Because ^{64}Cu and ^{76}As emit the gamma rays of the similar energies and have the half lives not so different from each other, neither the gamma ray spectrometry nor the decay curve analysis was successful to estimate the activity of each of the nuclides. The post-irradiation procedure, described above, was designed and preliminarily tested by the tracer experiments. The precipitate of oxinates was filtered with a glass filter, then dissolved into hydrochloric acid solution of a constant volume

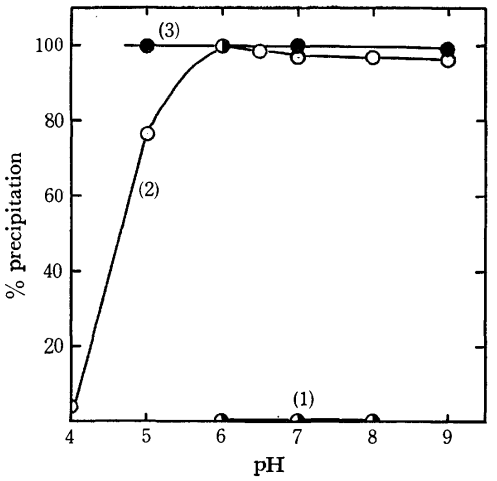

Fig. 2. Effect of pH on the precipitation of oxinates.
(1): As, (2): Sb-oxinate, (3): Cu-oxinate

and the gamma activity of the solution was compared with that of the same volume of original tracer solution. The percentage of precipitation *vs.* pH curves are shown in Fig. 2.

Copper and antimony are almost quantitatively precipitated in the pH range from 6 to 9, but arsenic remains in the solution, which is readily recovered by coprecipitation with ferric hydroxide at a pH between 6 and 9. The overall recovery in the pre- and post-irradiation procedures is to be 98.6±3.5%.

Analysis of Sea Water Samples. Sea water samples were collected from 11 stations, 137—139° E and 31—34° N. At the station No. 5, six samples were obtained from the surface to a depth of 500 m. Samples at stations No. 9, No. 10, and No. 11 were used for the study of the adsorption of arsenic, copper, and antimony on the vessel wall in the storage.

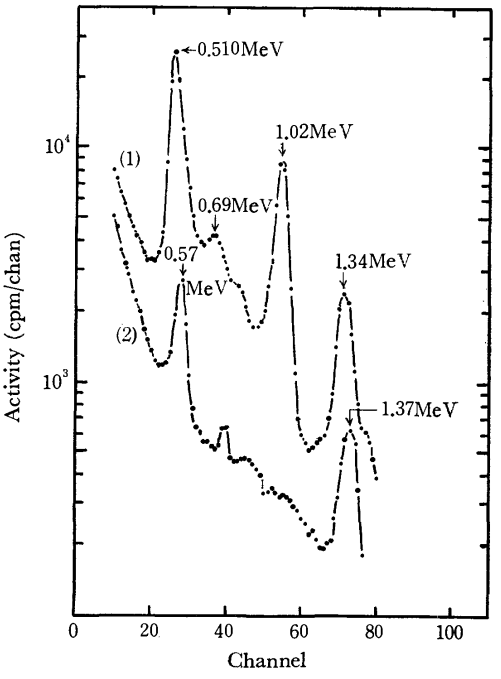

Fig. 3. Gamma-rays spectra of $^{64}Cu+^{122}Sb$ in sample (1): 10 h, (2): 125 h after irradiation.

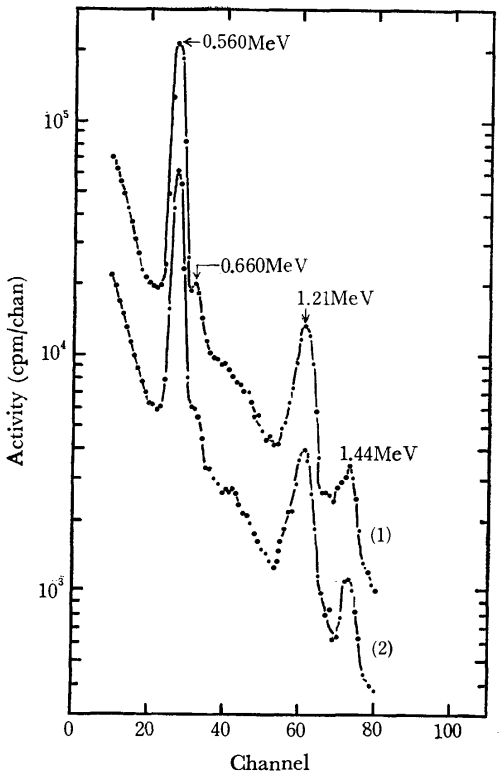

Fig. 4. Gamma-rays spectra of ^{76}As in sample (1): 10 h, (2): 25 h after irradiation.

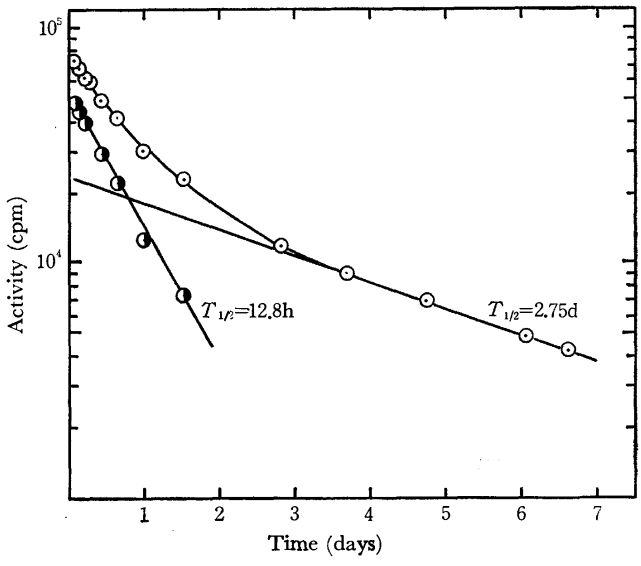

Fig. 5. Decay curves of $^{64}Cu(T_{1/2}=12.8\ h)$ and $^{122}Sb(T_{1/2}=2.75\ d)$.

These samples were analyzed according to the procedure described above. The typical gamma ray spectra of the copper and antimony fraction and the arsenic fraction are shown in Figs. 3 and 4, and the decay curves are presented in Figs. 5 and 6 respectively.

By the present procedures, 0.01 μg of arsenic, copper and antimony could be detected. However, the results of the blank test were as follows; As: 0.01—0.03 μg, Cu: 0.02 μg, Sb: 0.007—0.01 μg. The analytical results are summarized in Table 2. The relative error of the duplicated analysis was estimated to be within $\pm$5%.

Table 2. Analysis of arsenic, copper, and antimony in sea water

No.	Sampling date and station	Fraction	As (μg/l)	Sb (μg/l)	Cu (μg/l)
1	34°20.5′N	>8μ	0.09	<0.01	0.82
	138°00.5′E	0.45—8μ	0.01	<0.01	0.46
	22, Nov. 1969	Filtrate	1.40	0.44	0.22
	Surface	Total	1.50	0.44	1.50
2	33°40.8′N	>8μ	0.02	<0.01	0.97
	137°59.2′E	0.45—8μ	0.01	<0.01	0.69
	22, Nov. 1969	Filtrate	1.19	0.35	0.23
	Surface	Total	1.22	0.35	1.89
3	32°54.5′E	>8μ	<0.01	0.02	1.07
	138°01.5′E	0.45—8μ	<0.01	0.01	0.65
	23, Nov. 1969	Filtrate	1.28	0.27	0.46
	Surface	Total	1.28	0.30	2.18
4	32°21.0′N	>8μ	<0.01	0.01	0.42
	137°59.0′E	0.45—8μ	<0.01	0.01	0.89
	24, Nov. 1969	Filtrate	1.21	0.24	2.01
	Surface	Total	1.21	0.26	3.32
5-1	31°38.5′N	>8μ	0.20	0.04	0.55
	138°02.0′E	0.45—8μ	0.03	0.01	0.33
	24, Nov. 1969	Filtrate	1.35	0.26	0.67
	Surface	Total	1.58	0.31	1.55
5-2	31°38.5′N	>8μ	0.35	0.03	0.58
	138°02.2′E	0.45—8μ	0.02	0.07	0.24
	24, Nov. 1969	Filtrate	0.79	0.32	0.82
	Depth: 20m	Total	1.16	0.42	1.64
5-3	31°38.5′N	>8μ	0.04	0.04	0.26
	138°02.0′E	0.45—8μ	0.03	0.02	0.22
	24, Nov. 1969	Filtrate	1.17	0.20	0.61
	Depth: 100m	Total	1.24	0.26	1.06
5-4	31°38.5′N	>8μ	0.03	0.03	0.10
	138°02.0′E	0.45—8μ	0.03	0.02	0.16
	24, Nov. 1969	Filtrate	1.28	0.17	0.83
	Depth: 300m	Total	1.34	0.22	1.09
5-5	31°38.5′N	>8μ	0.05	0.03	0.18
	138°02.0′E	0.45—8μ	0.06	0.05	0.28
	24, Nov. 1969	Filtrate	1.59	0.22	0.76
	Depth: 500m	Total	1.70	0.30	1.22
6	32°15.0′N	>8μ	0.08	0.01	0.92
	139°13.0′E	0.45—8μ	0.01	0.01	0.49
	24, Nov. 1969	Filtrate	1.03	0.32	0.43
	Surface	Total	1.12	0.33	1.84
7	33°00.0′N	>8μ	<0.01	0.02	0.88
	139°56.5′E	0.45—8μ	<0.01	0.02	0.42
	25, Nov. 1969	Filtrate	1.40	0.39	0.35
	Surface	Total	1.40	0.43	1.65
8	34°29.9′N	>8μ	<0.01	0.04	0.94
	138°59.2′E	0.45—8μ	<0.01	0.04	0.41
	26, Nov. 1969	Filtrate	1.30	0.15	0.71
	Surface	Total	1.30	0.23	2.06

Discussion

The total contents of these elements in sea water are in the range of 1.12—1.71 μg As/l, 1.49—3.35 μg Cu/l, and 0.22—0.57 μg Sb/l. The concentration of arsenic well agrees with the value of Portmann and Riley,[6] and the content of antimony also agrees with

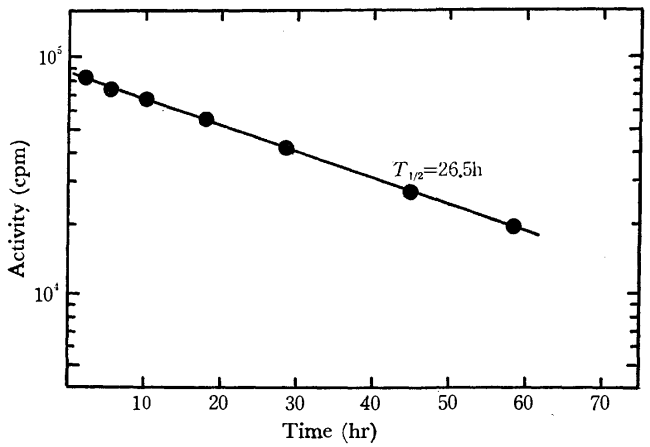

Fig. 6. Decay curve of $^{76}As(T_{1/2}=26.5$ h).

those of Noddack and Noddack,[11] Schutz and Turekian,[12] and Portmann and Riley.[10] The amount of copper is in the good agreement with the results of Fabricand *et al.*,[13] Riley and Shinhaseni.[9] and Brooks *et al.*[8]

The particle-size distribution suggests that the most parts of arsenic and antimony occur in soluble ionic state, passing through the 0.45 μ pore-size filter. 70—80% of copper exists in the particle species (about 50% distribution in the particles of larger than 8 μ, and 20—30%, in the particles of 0.45—8 μ), except for samples at station No. 4 and No. 5, in which about a half part of copper exists in the soluble ionic state. This phenomenon might be caused by the fact that the stations No. 4 and No. 5 were influenced by the Kuroshio Stream.

The vertical distributions of these elements were obtained at the station No.5. The total content and the particle size distribution slightly varried from the surface to 100 m depth, but in more than 100 m depth, they seemed to be almost changeless. After sample No. 9 was stored for 80 days, arsenic, copper, and antimony remaining in the solution and adsorbed on to the vessel wall were separately determined. For sample No. 10 and No. 11, the sample water was filtered with a 0.65 μ pore-size Millipore filter after the 30 days storage, and the analysis was made on the filtrate, the Millipore filter and the vessel wall. The results are shown in Table 3, from which it was deduced that the samples should be analyzed within a few days after the sampling.

TABLE 3. % ADSORPTION ONTO VESSEL WALL IN STORAGE OF SEA WATER

No.	Sampling date and station	Fraction	% distribution		
			As	Cu	Sb
9	33°58.5′N	Adsorpt.	5.31	40.66	17.65
	137°31.5′E		(0.07)	(1.24)	(0.09)
	31, July, 1969	Soln.	94.69	59.34	82.35
	Surface		(1.25)	(1.81)	(0.42)
10	33°29.0′N	Adsorpt.	5.06	25.77	10.86
	136°02.0′E		(0.07)	(0.84)	(0.05)
	10, Oct. 1969	>0.65μ	7.25	36.50	8.71
	Surface		(0.10)	(1.19)	(0.04)
		Filtrate	87.68	37.73	80.43
			(1.21)	(1.23)	(0.37)
11	33°29.5′N	Adsorpt.	5.67	33.22	8.51
	135°15.0′E		(0.08)	(1.01)	(0.04)
	10, Oct. 1969	>0.65μ	7.09	33.88	10.64
	Surface		(0.10)	(1.03)	(0.05)
		Filtrate	87.23	32.90	80.85
			(1.23)	(1.00)	(0.38)

No. 9: 80 days storage, No. 10, No. 11: 30 days storage.
The values in bracket were expressed the amount of the elements; (μg/l).

The author wishes to express his sincere thanks to Professor Tsunenobu Shigematsu, Institute for Chimical Research, Kyoto University, and Professor Yasuharu Nishikawa, Faculty of Science and Technology, Kinki University, for their kind advice and suggestion throughout this work. The author is deeply indebted to Hot Laboratory groups of Kyoto University for their helps in the irradiation operation, and also indebted to Professor Shiro Okabe, Faculty of Oceanography, Tokai University, for his kind help in the sampling of sea water.

13) B. P. Fabricand, R. R. Sawyer, S. G. Ungar, and S. Adler, *Geochim. Cosmochim. Acta*, **26**, 1023 (1962).

Spectrophotometric Studies and Analytical Applications of Vanadium(IV) Chelates with 4-(2-Pyridylazo)resorcinol and 1-(2-Pyridylazo)-2-naphthol

S. P. MUSHRAN, Om PRAKASH, and J. R. VERMA
Chemical Laboratories, University of Allahabad, Allahabad, India
(Received May 1, 1971)

Oxovanadium(IV), VO^{2+}, gives sensitive colour reactions with 4-(2-pyridylazo)resorcinol ($\varepsilon=2.54\times10^4$ at λ_{max} 550 nm) and 1-(2-pyridylazo)-2-naphthol ($\varepsilon=1.02\times10^4$ at λ_{max} 560 nm). The composition of the complexes VO^{2+}: PAN or PAR was established by the continuous variations, mole ratio, and Asmus straight line methods. Lambert-Beer's law range, Ringbom optimum range, pH stability range, photometric error, and stability constant values were also evaluated.

The formation of coloured chelates of VO^{2+} with Alizarin red S,[1] chrome azurol S,[2] Pyrocatechol violet,[3] and Pyrogallol red[4] have recently been reported. Pyridylazo dyes particularly 4-(2-pyridylazo)resorcinol (PAR) and 1-(2-pyridylazo)-2-naphthol (PAN) have assumed importance in analytical chemistry as metallochromic indicators and colorimetric reagents for the microdetermination of a number of metal ions.[5-8] The present paper describes spectrophotometric studies on the composition, stability and analytical applications of VO^{2+} chelates with PAR and PAN.

Experimental

The metal salt ($VOSO_4\cdot H_2O$, Anala R. B.D.H.) solution prepared in water was standardized by titration with permanganate. The solution was flushed with pure nitrogen to check aerial oxidation of the metal ion. The solutions of PAR and PAN (E. Merck) were prepared in doubly distilled water and ethanol, respectively. Acetate buffer of pH 5.0 and 4.4 was used in VO^{2+}-PAR and VO^{2+}-PAN systems, respectively. Ionic strength was adjusted to 0.1 in VO^{2+}-PAR system and 0.05 in VO^{2+}-PAN system by the addition of sodium perchlorate solution.

A Beckman (DU) spectrophotometer with 10 mm^2 quartz cells was used for all absorbance measurements. For pH measurements a Leeds and Northrup direct reading pH meter with glass-calomel electrode assembly was used.

All mixtures were flushed with pure nitrogen and kept at 12°C in a water bath for 15 minutes and then absorbance was recorded. The total volume was kept at 25 *ml*. The VO^{2+}-PAR system was studied in aqueous medium and VO^{2+}-PAN system in 30% ethanol.

Results and Discussion

At pH>3 a water soluble red VO^{2+}-PAR chelate is formed and at pH 5—7 the colour of the chelate is red-violet and is intensified by the addition of excess of metal ion. The VO^{2+}-PAN chelate formation starts at pH>2 and a red violet chelate is formed at pH>3.5. The reagents are coloured yellow under these conditions. The pH *versus* λ_{max} plots (Fig. 1) show that the VO^{2+}-PAR system is stable at pH 5—7 and VO^{2+}-PAN at pH 4.7.

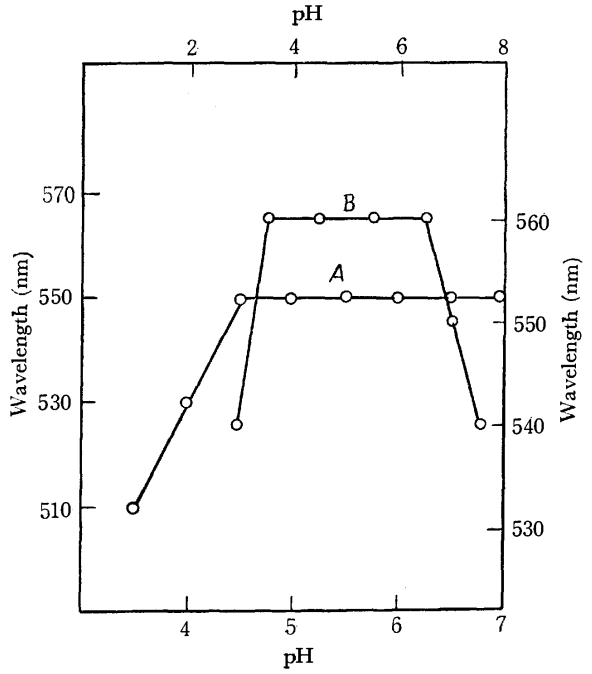

Fig. 1. Variation of λ_{max} of the chelates with pH; A, VO^{2+}-PAN chelate; B, VO^{2+}-PAR chelate.

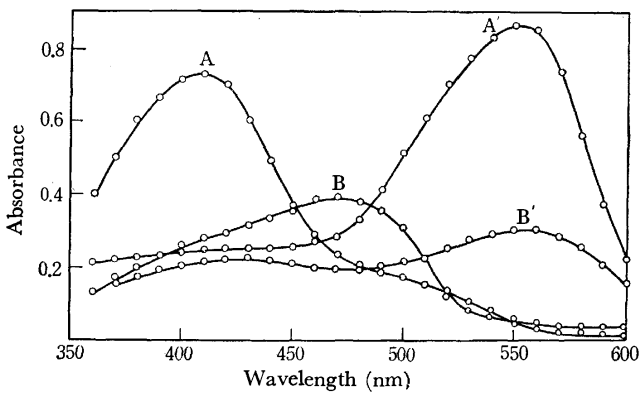

Fig. 2. Absorption spectra A, PAR (4.0×10^{-5}M); A', VO^{2+}-PAR chelate (CM=CR=4.0×10^{-5}M); B, PAN (4.0×10^{-5}M) B', VO^{2+}-PAN chelate (CM=CR=4.0×10^{-5}M).

1) P. Sanyal and S.P. Mushran, *Anal. Chim. Acta*, **35**, 400 (1966).
2) P. Sanyal and S. P. Mushran, *Mikrochim. Acta*, **5**, 959 (1965).
3) S. P. Mushran, O. Prakash, and J. N. Awasthi, *Anal. Chem.*, **39**, 1307 (1967).
4) S. P. Mushran, O. Prakash, and J. N. Awasthi, *Microchem. J.*, **14**, 29 (1969).
5) K. L. Cheng and R. H. Bray, *Anal. Chem.*, **27**, 782 (1955).
6) R. Pueschel, E. Lassner, and K. Katzengruber, *Z. Anal. Chem.*, **223**, 414 (1966).
7) P. Wehber, *ibid.*, **166**, 186 (1959).
8) F. J. Langmyhr and H. Kritiansen, *Anal. Chim. Acta*, **20**, 524 (1959).

The absorption curves for the reagents PAR and PAN and their chelates with VO^{2+} were obtained by the method of Vosburgh and Cooper[9] (Fig. 2). At pH 5.0 λ_{max} of PAR is 410 nm and of VO^{2+}-PAR chelate 550 nm. The λ_{max} of PAN and VO^{2+}-PAN chelate at pH 4.4 are 470 nm and 560 nm, respectively. The λ_{max} of the chelates remain unchanged in small excess of reagent or large excess of metal concentrations showing the existence of only one chelate.

The composition of the chelate was studied by continuous variations (Fig. 3), mole ratio (Fig. 4) methods. The composition 1 : 1 (VO^{2+}: PAR or PAN) was established by the above methods. Application of Asmus[10] straight line method as extended by Klausen and Langmyhr[11] shows straight line at $m=1$ and $n=1$ (Figs. 5 and 6, where m and n are the number of metal atoms and ligand molecules, respectively, in a chelate molecule) establishing the formation of only one mononuclear chelate in each system having the composition 1 : 1 (VO^{2+}: PAR or PAN).

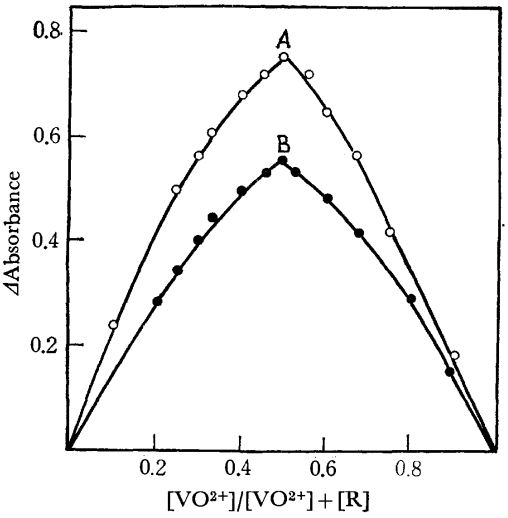

Fig. 3. Continuous variation plots, A, VO^{2+}-PAR chelate at pH 5.0, λ_{max} 550 nm (CM=CR=1.33×10^{-4}M); B, VO^{2+}-PAN chelate at pH 4.0, λ_{max} 560 nm (CM=CR=1.67×10^{-4}M).

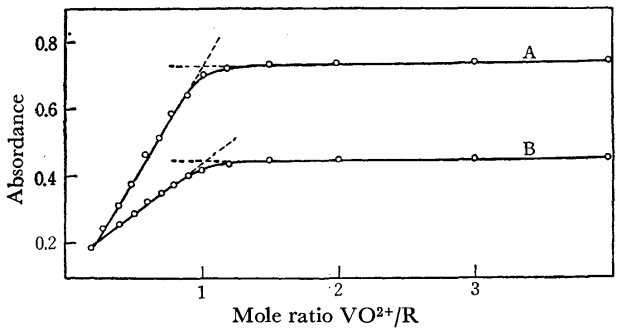

Fig. 4. Mole ratio plots, A, VO^{2+}-PAR chelate at pH 5.0, λ_{max}, 550 nm (CR=3.33×10^{-5}M); B, VO^{2+}-PAN chelate at pH 4.4, λ_{max} 560 nm (CR=5.0×10^{-5}M).

9) W. C. Vosburgh and G. R. Cooper, *J. Amer. Chem. Soc.*, **63**, 437 (1941).
10) E. Asmus, *Z. Anal. Chem.*, **178**, 104 (1960).
11) K. S. Klausen and F. J. Langmyhr, *Anal. Chim. Acta*, **28**, 501 (1963).

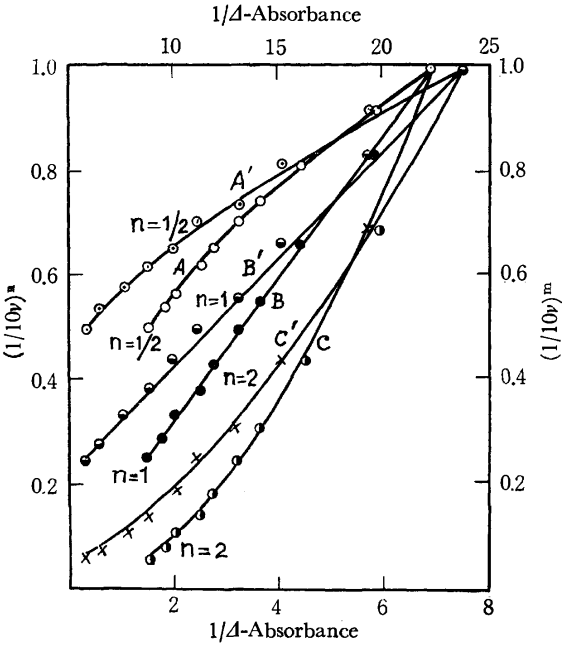

Fig. 5. Straight line plots, A, B, and C, VO^{2+}-PAR chelate in excess of $VOSO_4$ at pH 5.0, λ_{max} 550 nm, CM=2.0×10^{-3}M (1.0 ml), CR=2.0×10^{-3}M (0.1 —0.4 ml); A′, B′, and C′, VO^{2+}-PAN chelate in excess of $VOSO_4$ at pH 4.4, λ_{max} 560 nm, CM=1.0×10^{-3}M (1.0 ml), CR=1.0×10^{-3}M (0.1—0.4 ml).

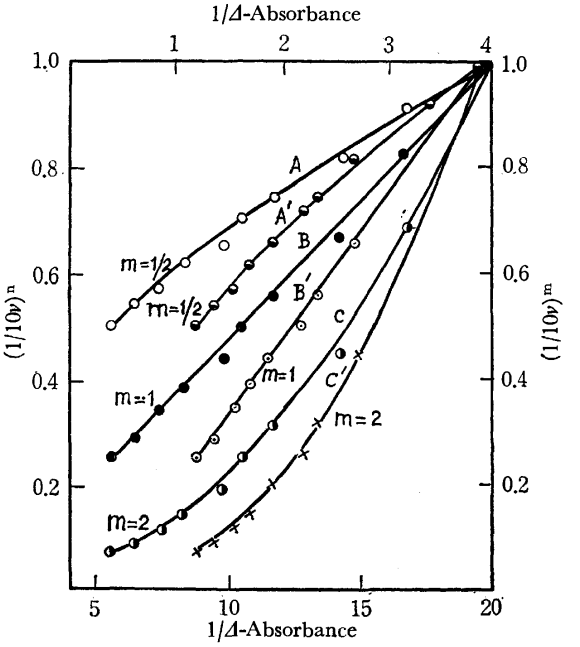

Fig. 6. Straight line plots, A, B, and C, VO^{2+}-PAR chelate in excess of $VOSO_4$ at pH 5.0, λ_{max} 550 nm, CR=2.0×10^{-3}M (1.0 ml), CM=2.0×10^{-3}M (0.1 —0.4 ml); A′, B′, and C′, VO^{2+}-PAN chelate in excess of $VOSO_4$ at pH 4.4, λ_{max} 560 nm, CM=1.0×10^{-3}M (1.0 ml), CR=1.0×10^{-3}M (0.1—0.4 ml).

The conditional stability constant values were evaluated by two different methods, (a) continuous variations using non equimolar solutions and (b) mole ratio. The stability constant (K) values along with the change in free energy of formation (ΔG) are summarised in the following table.

Table 1. Values of log K and ΔG of VO^{2+}-PAR and VO^{2+}-PAN chelates
(Temp., 12°C; μ=0.1 $NaClO_4$)

VO^{2+} complex with	Average log K	$\Delta G=-RT\log K$ (kcal/mol)	Method
PAR	6.3	−8.2	(a)
	7.2	−9.4	(b)
PAN	6.0	−7.8	(a)
	6.7	−8.7	(b)

For the photometric determination of vanadium(IV) with PAR and PAN, ranges of Beer's law were determined. These are VO^{2+}-PAR: 2.5—0.2 and VO^{2+}-PAN: 3.5—0.1 ppm of vanadium. For more accurate analysis the Ringbom[12] optimum range was determined by plotting log [V^{4+}] in ppm against % transmittance. The Ringbom optimum range of analysis for VO^{2+}-PAR system was found to be 2.0—0.3 and for VO^{2+}-PAN system it was computed as 3.0—0.6 ppm of vanadium. The photometric error was computed from the Ringbom plot using the Ayres[13] equation. The minimum % relative error per 1% photometric error was 0.3 for VO^{2+}-PAR system and 0.8 for VO^{2+}-PAN system. The sensitivity values in Sandell units are VO^{2+}-PAR 0.002 γ/cm^2 (at 550 nm) and VO^{2+}-PAN 0.005 γ/cm^2 (at 560 nm). The molar absorptivity values computed at the same wavelengths are 2.54×10^4 for the system VO^{2+}-PAR and 1.02×10^4 for the system VO^{2+}-PAN.

Procedure

For the determination of 2.0—0.3 ppm of vanadium(IV), take PAR in five times excess. Fix the pH at 5.0 using acetate buffer and flush with nitrogen. Measure the absorbance at 550 nm and compare with calibration plot. For the determination of vanadium(IV) in 3.0—0.6 ppm range, PAN is a suitable reagent. When using PAN, the mixture should contain at least-30% ethanol. The pH should be fixed at 4.4. The procedure is similar to that for PAR.

Effect of Diverse Ions

In the determination of vanadium (IV) with PAR at pH 5.0, V^{5+}, Nb^{5+}, Ta^{5+}, U^{6+}, Zr^{4+}, In^{3+}, Ga^{3+}, Al^{3+}, La^{3+}, Bi^{3+}, Y^{3+}, Sc^{3+}, Mn^{2+}, Zn^{2+}, Cu^{2+}, Co^{2+}, Ni^{2+}, Hg^{2+}, and Pb^{2+} give positive errors and Cr^{6+}, Mo^{6+}, W^{6+}, Th^{4+}, Cd^{2+}, Fe^{3+}, Mg^{2+}, Ca^{2+}, Ba^{2+}, Sr^{2+} do not interfere and interferences by Zr^{4+}, Y^{3+}, Al^{3+} are masked by adding 1 m*l* 0.4% fluoride solution.

In determination with PAN at pH 4.4, Mo^{6+}, W^{6+}, Os^{8+}, Nb^{5+}, Ta^{5+}, Ti^{4+}, Zr^{4+}, Th^{4+}, Al^{3+}, La^{3+}, Sc^{3+}, Y^{3+}, Fe^{3+}, Cr^{6+}, As^{3+}, Be^{2+}, Ca^{2+}, Ba^{2+}, Sr^{2+}, Mn^{2+}, Pb^{2+}, Cd^{2+}, Sn^{4+}, Mg^{2+}, Tl^{+} do not interfere while U^{6+}, V^{5+}, Ga^{3+}, In^{3+}, Bi^{3+}, Co^{2+}, Ni^{2+}, Hg^{2+}, Zn^{2+}, Cu^{2+} give positive errors.

In the determination of vanadium(IV) with PAR and PAN 100 fold excess of F^-, Cl^-, Br^-, I^-, SO_3^{2-}, NO_3^-, SCN^-, IO_3^-, NO_2^-, $S_2O_8^{2-}$, PO_4^{3-}, $B_4O_7^{2-}$ do not interfere.

The authors are grateful to the Council of Scientific and Industrial Research, New Delhi, for supporting the work and providing financial assistance to J.R.V.

12) A. Ringbom, *Z. Anal. Chem.*, **115**, 332 (1939).
13) G. H. Ayres, *Anal. Chem.*, **21**, 652 (1949).

Electron-transfer Reactions of Multidentate Ligand Cobalt(III) Complexes. IV. The Reductions of Cobalt(III) Complexes of Amino Acids by Iron(II) in Aqueous and Water-methanol Solutions

Kousaburo OHASHI, Katsumi YAMAMOTO, Ichiro HIRAKO, and Yoshimi KURIMURA*

Department of Chemistry, Ibaraki University, Mito

**College of General Education, Ibaraki University, Mito*

(Received September 17, 1971)

The kinetics of the Fe(II) reductions of *trans*(O,Cl)-Co(dien)(am)Cl^+ (am=glycine, α-alanine, β-alanine, leucine, and proline) and *trans*(N)-$Co(am)_2(ox)^-$ (am=glycine, α-alanine, β-alanine, ox=oxalate, and dien=diethylenetriamine) have been made spectrophotometrically in an aqueous solution. Except for the β-alanine complex, the reactivities of the Co(III) complexes are not very different when the amino acid is replaced by the other one. The greater reactivities of the β-alanine complexes may be due to the steric strain on the six-membered β-alanine chelate ring. The rates of the reductions of *cis*(N)-$Co(\alpha\text{-ala})_2(ox)^-$ and *cis*(N)-$Co(\beta\text{-ala})_2(ox)^-$ by Fe(II) are greatly affected by the addition of methanol to the aqueous solutions; the rate increases with an increase in the mol fraction of methanol. The replacement of water molecules in the solvation sphere of the reductant by the methanol molecules is considered to be one of the reasons for the greater rate in water-methanol solutions.

In the electron-transfer reactions of Co(III) complexes which proceed *via* the inner-sphere and outer-sphere activated states, the nonbridging ligand can appreciably affect the reaction rates.[1,6,7,9,10] The nonbridging ligand effect has been investigated mostly on the metal complexes with a uni-dentate bridging ligand.[1-10] Kinetic studies of the Fe(II) rdeuctions of Co(III) complexes, with oxalate ions as the bridging ligand, are very few, and the effects of amino acids as the nonbridging ligand in the Fe(II) reductions of Co(III) complexes have not been examined. In this connection, the Fe(II) reductions of *trans*(N)-$Co(am)_2(ox)^-$, and *trans*(O,Cl)-Co(dien)(am)Cl^+ were investigated.

The effect of organic solvents on the reduction rate of *cis*-$Co(en)_2NH_2CH_2CH_2OHCl^{2+}$ by Fe(II) was also examined previously.[11] In this study, we observed the increase in the rate upon the addition of such organic solvents as ethanol, acetone, dimethylformamide, and dimethylsulfoxide to the aqueous solutions. The reactivity of the Co(III) complex in an ethanol-water (0.5 mol fraction of ethanol) is about 10 times grater than that in an aqueous solution at $[H^+]=0.080$M. The reason for this grater reactivity is, however, yet uncertain. A further investigation of the Fe(II) reduction of Co(III) complexes in methanol-water was carried out using anionic Co(III) complexes such as *cis*(N)-$Co(\alpha\text{-ala})_2(ox)^-$ and *cis*(N)-$Co(\beta\text{-ala})_2(ox)^-$ in a methanol-water medium; those results will be also reported in this paper.

Experimental

Preparation of Complexes. The *trans*(O,Cl)-[Co(dien)(gly)Cl]ClO_4, *trans*(O,Cl)-[Co(dien)(α-ala)Cl]$ClO_4\cdot H_2O$, *trans*(O,Cl)-[Co(dien)(β-ala)Cl]ClO_4, *trans*(O,Cl)-[Co(dien)(leu)Cl]ClO_4, and *trans*(O,Cl)-[Co(dien)(pro)Cl]ClO_4[12] used as the oxidants were prepared by a method established by Ohkawa.[13] The configurations of these complexes with respect to diethylenetriamine were ascertained by means of the NMR spectra.[14] The coordinated chlorine atom in the *trans*(O,Cl)-Co(dien)(am)Cl^+ is located at the *trans*-positions to the coordinated oxygen atom of amino acid, and the diethylenetriamine occupies the *cis-trans* (mer) position in these complexes (Fig. 1).

The *trans*(N)-$K[Co(gly)_2(ox)]$,[15] *cis*(N)-,[16] and *trans*(N)-

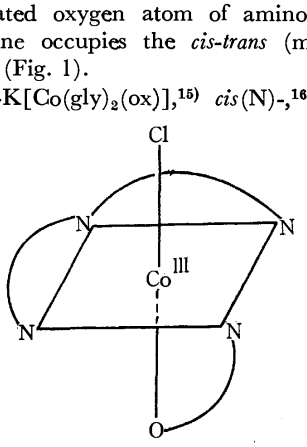

Fig. 1. The configuration of the *trans*(O,Cl)-[Co(dien)(am)-Cl]ClO_4.

1) P. Benson and A. Haim, *J. Amer. Chem. Soc.*, **87**, 3826 (1965).
2) H. Taube, *Adv. Inorg. Chem. Radiochem.*, **1**, 1 (1959).
3) H. Taube, *Can. J. Chem.*, **37**, 129 (1959).
4) R. T. M. Fraser, *Proc. Chem. Soc.*, **1963**, 262.
5) T. T. M. Fraser, *Inorg. Chem.*, **2**, 954 (1963).
6) Y. Kurimura, K. Ohashi, T. Ohtsuki, and K. Yamamoto, This Bulletin, **44**, 1293 (1971).
7) Y. Kurimura and K. Ohashi, *ibid.*, **44**, 1797 (1971).
8) Y. Kurimura, I. Meguro, and K. Ohashi, *ibid.*, **44**, 3367 (1971).
9) K. Ohashi, *ibid.*, **45**, 947 (1972).
10) R. C. Patel and J. F. Endicott, *J. Amer. Chem. Soc.*, **90**, 6364 (1968).
11) K. Ohashi, K. Yamamoto, T. Suzuki, and Y. Kurimura, This Bulletin, **44**, 3363 (1971).
12) The gly, ala, leu, pro, and dien abbreviation represent glycinate, alaninate, leucinate, prolinate ions, and diethylenetriamine respectively.
13) K. Ohkawa, Ph. D. Thesis, Osaka University, Japan, 1969.
14) K. Ohkawa, S. Yano, and J. Fujita, This Bulletin, **41**, 2224 (1968).
15) M. Matsuoka, J. Hidaka, and Y. Shimura, *ibid.*, **40**, 1868 (1967).
16) This complex has two geometrical isomers. The linear behavior of the log (A_t-A_∞) *vs.* time plot for the Fe(II) reductions of this complex in aqueous solution indicates that the reactivities of the two isomers with Fe(II) are of almost the same degree or that the content of one isomer is relatively small as compared with that of the other one.

Table 1. The microanalysis for *trans*(O,Cl)-[Co(dien)(am)Cl]ClO_4 and *trans*(N)-K[$Co(am)_2ox$]

Complex	Obsd. (%)			Calcd. (%)		
	C	H	N	C	H	N
trans(O,Cl)-[Co(dien)(gly)Cl]ClO_4	19.6	4.62	15.06	19.42	4.62	15.10
trans(O,Cl)-[Co(dien)(α-ala)Cl]$ClO_4 \cdot H_2O$	20.8	5.32	13.77	20.86	5.25	13.90
trans(O,Cl)-[Co(dien)(β-ala)Cl]ClO_4	22.31	5.32	14.63	22.81	4.98	14.55
trans(O,Cl)-[Co(dien)(leu)Cl]ClO_4	28.45	6.26	13.27	28.10	5.90	13.10
trans(O,Cl)-[Co(dien)(pro)Cl]ClO_4	26.37	5.20	13.77	26.29	5.17	13.63
trans(N)-K[$Co(gly)_2(ox)$]	21.37	2.20	8.21	21.67	2.49	8.41
trans(N)-K[$Co(α\text{-}ala)_2(ox)$]	26.24	3.18	7.58	26.52	3.33	7.73
trans(N)-K]$Co(β\text{-}ala)_2(ox)] \cdot 2H_2O$	26.90	3.40	7.68	26.86	3.35	7.77

a) gly=$CH_2(NH_2)COO^-$, α-ala=$CH_3CH(NH_2)COO^-$, β-ala=$CH_2(NH_2)CH_2COO^-$, leu=$(CH_3)_2CHCH_2CH(NH_2)COO^-$, pro=$NHCH_2CH_2CH_2CHCOO^-$, dien=$NH_2CH_2CH_2NHCH_2CH_2NH_2$, ox=$^-OOCCOO^-$

K[$Co(α\text{-}ala)_2(ox)$],[15] and *cis*(N)-,[16] and *trans*(N)-K[$Co(β\text{-}ala)_2(ox)$][17] compounds were prepared by the methods cited in the references. The purities and identities of the complexes were ascertained by microanalysis for carbon, hydrogen, and nitrogen and by comparing the absorption spectra with those reported in the literature.

The results of the microanalysis of carbon, hydrogen, and nitrogen for the complexes are presented in Table 1.

Materials. The preparation of the iron(II) solution and the determinations of the concentrations of the iron(II), hydrogen, and perchlorate ions in this solution were carried out by methods similar to those described in a previous paper.[6] Methanol of Tokyo Kasei, spectroscopic-grade, was distilled before use. The other chemicals used were G. R.-grade reagents. The concentration of the perchlorate anion in the reaction mixture was adjusted to 1.0M by the addition of sodium perchlorate.

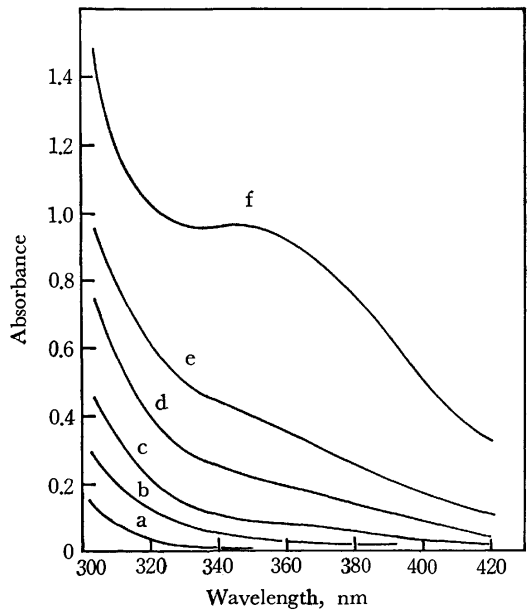

Fig. 2. Absorption spectra of ferric perchlorate in aqueous solution of methanol.
$[Fe(III)]=1.09\times10^{-3}$M, $\sum[ClO_4^-]=0.24$M, $[HClO_4]=0.24$M.
a: aqueous solution
b: 0.16 mole fraction of methanol
c: 0.32 mole fraction of methanol
d: 0.52 mole fraction of methanol
e: 0.64 mole fraction of methanol
f: 0.80 mole fraction of methanol

Measurement of Reaction Rate in Aqueous Solutions. The reduction rate was followed by the usual spectrophotometric method. The wavelengths used were the first absorption maxima of the complexes. For all the complexes, the kinetic runs were carried out under pseudo-first-order conditions.

Measurement of the Reaction Rate in Water-methanol Mixtures. The kinetic runs for *cis*(N)-$Co(α\text{-}ala)_2(ox)^-$ and *cis*(N)-$Co(β\text{-}ala)_2(ox)^-$ were carried out under pseudo-first-order and second order conditions respectively. The wavelengths used for the determinations of the rate constants were 535 nm for *cis*(N)-$Co(α\text{-}ala)_2(ox)^-$ and 550 nm for *cis*(N)-$Co(β\text{-}ala)_2(ox)^-$.

Absorption Spectra of Ferric Perchlorate in Methanol-water Mixtures. The absorption spectra of ferric perchlorate in aqueous solutions of methanol are represented in Fig. 2. The absorbances of the solutions in the near-ultraviolet region increase with an increase in the mol fraction of methanol. Such increases in absorbance were also observed previously by the addition of ethanol, acetone, dimethylsulfoxide, and dimethylformamide to an aqueous solution of ferric perchlorate.[11]

Results and Discussion

Reductions in Aqueous Solutions. The rate data obtained with $Co(dien)(am)Cl^+$ and $Co(am)_2(ox)^-$ listed in Table 2 show that; a) the β-alanine complexes have greater effectiveness than other complexes in the $Co(dien)(am)Cl^+$ and $Co(am)_2(ox)^-$ series; for example, the rate constants of the β-alanine complexes are greater than those of the corresponding α-alanine complexes by 114—140 times; b) the patterns of reactivity with respect to the amino acids are very similar in the two series; the ratios of the rate constant of the Co(III) complexes to the corresponding glycine complex (represented) by R values for α-alanine and glycine complex are in the ranges of 0.24—0.41 and 33—42 respectively; c) except for the β-alanine complexes, the reactivities of the amino acid complexes are not very different within the same series. The activation parameters for the reductions which were obtained from the temperature dependence of the rate constant are also listed in Table 2.

Since an oxalate-bridged mechanism has been demonstrated for the Fe(II) reductions of $Co(ox)_3^{3-}$ and

17) J. Hidaka and Y. Shimura, This Bulletin, **40**, 2312 (1967).

Table 2. Second-order rate constants and activation parameters for the iron(II) reductions of Co(III) complexes at 25°C

Complex ion	Rate constant $M^{-1}sec^{-1}$	R_1	R_2	$\Delta H^{\neq}$ kcal mol^{-1}	$\Delta S^{\neq}$ eu
trans(N)-Co(gly)$_2$(ox)$^-$	4.13×10^{-3} a)	1		14	−21
trans(N)-Co(α-ala)$_2$(ox)$^-$	1.01×10^{-3} a)	0.24		16	−24
trans(N)-Co(β-ala)$_2$(ox)$^-$	1.42×10^{-1} a)	33		12	−23
Co(dien)(gly)Cl$^+$	2.68×10^{-5} b)		1	17	−24
Co(dien)(α-ala)Cl$^+$	1.09×10^{-5} b)		0.41	18	−20
Co(dien)(β-ala)Cl$^+$	1.24×10^{-3} b)		42	16	−17
Co(dien)(leu)Cl$^+$	1.01×10^{-5} b)		0.38	20	−16
Co(dien)(pro)Cl$^+$	5.33×10^{-6} b)		0.20	22	−10

a) $[H^+]=0.20$M, $\sum[ClO_4^-]=1.0$M. b) *trans*(O,Cl)-Co(III) complex, $[H^+]=0.26$M, $\sum[ClO_4^-]=1.0$M.
c) R_1 and R_2 represent the ratios of the rate constants to the corresponding glycine complexes.

$Co(NH_3)_3(H_2O)(ox)^+$ by observing the spectrum of Fe(III) product and by determining its rate of formation and decay,[18] and since the reactivity of $Co(NH)_4(gly)^{2+}$ with Fe(II) is negligibly small as compared with that $Co(NH_3)_4(ox)^+$,[19] it is reasonable to assume that the Fe(II) reductions of the $Co(am)_2(ox)^-$ proceed *via* oxalate-bridged activated states. For Co(dien)(am)-Cl^+, since the rate of the $Co(NH_3)_4(am)^{2+}$ with Fe(II) can be again ignored as compared with that of Co-$(NH_3)_5Cl^{2+}$ ($k=1.6\times10^{-3}M^{-1}sec^{-1}$, 25°C, $\mu=1.7$),[20] there is little doubt that the Cl^- is the bridging ligand.

These results, (a)—(c), seem to indicate the effect of the nonbridging ligand on the electron-transfer reaction. It is interesting to note here that the reactivity of the β-alanine complex is remarkably greater than that of the corresponding glycine and α-alanine complexes. The greater reactivity of the Co(III) complex with a six-membered chelate ring as compared with that of a five-membered one may be due to strain on the six-membered ring. Such a steric strain on the six-membered ring would reduce the energy needed for the reorganization of the nonbridging ligand in the Co(III) complex for the electron-transfer. The smaller enthalpies of the activation for the β-alanine complexes relative to those for other amino acid complexes seem to be responsible for the smaller reorganization energy for the β-alanine complexes. A part of the energy may consist of the energy for stretching the nonbridging β-alanine ligand away from the Co(III) center.[1,6]

Reduction in an Aqueous Solution of Methanol. The reductions of *cis*(N)-Co(α-ala)$_2$(ox)$^-$ and *cis*(N)-Co(β-ala)$_2$(ox)$^-$ by Fe(II) in a methanol-water mixture obey the first order dependence of the Fe(II) and Co(III) concentrations respectively. In an aqueous solution of methanol, the reactivities of these complexes increase sharply upon the addition of methanol to the aqueous solution (Fig. 3). In the previous work, it was found that the reduction rates of the cationic Co(III) complex, *cis*-$Co(en)_2NH_2CH_2CH_2OHCl^{2+}$, with Fe(II) in aqueous solution is accelerated in the presence of such organic solvents as dimethylformamide, dimethylsulfoxide, ethanol, and acetone.[11] Such an increase in the rate in a mixed solvent medium is contrary to the trend of electron-transfer reactions, such as $Co(phen)_3^{2+}$–Co-

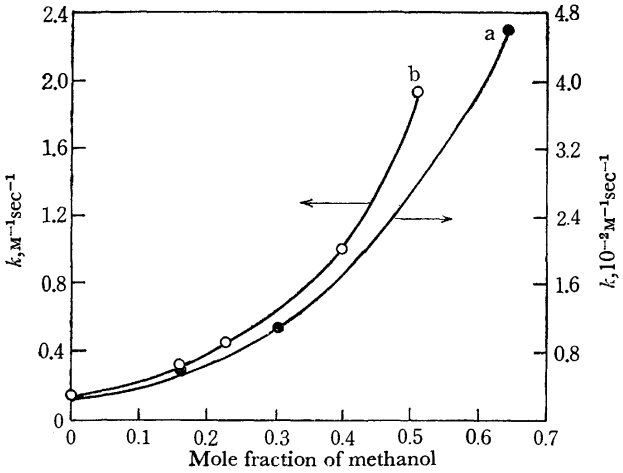

Fig. 3. The plots of the second-order rate constant *vs.* mole fraction of methanol.
$\sum[ClO_4^-]=0.43$M, $[H^+]=0.080$M, 25±0.1°C.
a) $[cis(N)\text{-}Co(\alpha\text{-}ala)_2(ox)^-]=7.43\times10^{-3}$M, $[Fe(II)]=0.173$M.
b) $[cis(N)\text{-}Co(\beta\text{-}ala)_2(ox)^-]=1.29\times10^{-2}$M, $[Fe(II)]=2.07\times10^{-2}$M.

$(phen)_3^{3+}$[21] and Fe^{2+}–Fe^{3+}.[22,23] The ratio of the rate constants in water (k_{H_2O}) and isopropanol (k_{alc}) for the Fe^{2+}–Fe^{3+} reaction was calculated by Sutin by assuming that the iron species are not changed in the two solvents. The obtained values of k_{alc}/k_{H_2O} are about 10^{-9} for the Fe^{2+}–Fe^{3+} reaction and about 10^{-6} for the Fe^{2+}–$FeOH^{2+}$ reaction.[22a] These values agree satisfactorily with that experimentally obtained when $[H^+]=0.01$M. However, Sutin pointed out that the predominat species may be quite different in the two solvents, as was suggested by the spectrophotometric measurements. If the reactants have larger differences in configuration in isopropanol than in water, the reorganization energy may be much greater in alcohol.[22a]

Though the formation of the mixed-ligand Fe(II), $Fe(H_2O)_{6-n}(CH_3OH)_n^{2+}$, has not been ascertained, the

18) A. Haim and N. Sutin, *J. Amer. Chem. Soc.*, **88**, 5343 (1966).
19) C. Hwang and A. Haim, *Inorg. Chem.*, **9**, 500 (1970).
20) H. Diebler and H. Taube, *ibid.*, **4**, 1029 (1965).
21) B. R. Baker, F. Basolo, and H. M. Neuman, *J. Phys. Chem.*, **63**, 371 (1959).
22) a) N. Sutin, *ibid.*, **64**, 1766 (1960); b) R. A. Horne, Ph. D. Thesis, Columbia University, New York, 1955.
23) L. Menashi, W. L. Reynolds, and G. Van Auken, *Inorg. Chem.*, **4**, 299 (1965).

progressive change in the absorption spectra of the Fe(III) perchlorate solution upon the addition of methanol to an aqueous solution (Fig. 2) would suggest the formation of a mixed-ligand complex such as $Fe(H_2O)_{6-n}(CH_3OH)_n^{2+}$.

The results of the present and of previous studies suggest that the rate increase with an increase in the concentration of organic solvents in the Fe(II) reductions of the cationic Co(III) complex, *cis*-$Co(en)_2NH_2CH_2CH_2OHCl^{2+}$, and anionic Co(III) complexes, *cis*(N)-$Co(\alpha\text{-ala})_2(ox)^-$ and *cis*(N)-$Co(\beta\text{-ala})_2(ox)^-$ proceed *via* the bridged activated states. In the organic substance-water media, the first coordination sphere of the ferrous ion may be changed from that in water; on the other hand, the replacement of the ligands in the Co(III) complex ions by the organic substance need hardly be considered because of the inertness of the complexes.

Consequently, the replacement of the water molecules in only the first coordination sphere of the reductant by organic solvent molecules is considered to be one of the most important reasons for the acceleration of the rate. However, no further discussion about the increase in the rate of electron-transfer reactions between the Co(III)-oxalate complexes and Fe(II) with an increase in the concentration of methanol in an aqueous solution could be made because of the present lack of much kinetic data on these effects.

BULLETIN OF THE CHEMICAL SOCIETY OF JAPAN, VOL. 45, 1715—1719(1972)

The Reactions of ^{80}Br Activated by the (n, γ) Process with Methane

Masakatsu SAEKI, Kenshi NUMAKURA,* and Enzo TACHIKAWA
Division of Chemistry, Japan Atomic Energy Research Institute, Tokai-mura, Ibaraki-ken

(Received September 20, 1971)

The reactions of ^{80}Br activated by the (n,γ) process with CH_4 have been examined. By assuming that the limiting yields of products at 1.0 m.f. of the Kr-moderator is due to thermal ionic processes, the kinetic yields were tentatively determined to be the 12.4% for total organic, 11.4% for $CH_3{}^{80}Br$, and 1.0% for $CH_2{}^{80}BrBr$. A similar treatment of the results from the reactions with CD_4 gives 5.1% for total organic, 3.9% for $CD_3{}^{80}Br$, and 1.2% for $CD_2{}^{80}BrBr$. When the $CH_3{}^{80}Br$ yield was compared with that from the reactions of ^{80}Br from the (I.T.) activation, a noticeable difference was noticed; it was roughly 3 times as large as in the latter system. Furthermore, the pressure effects on the $CH_3{}^{80}Br$ show that a fraction of $CH_3{}^{80}Br$ is highly excited and is able to decompose even at a pressure of 1920 mmHg. This suggests that the distribution of ^{80}Br in the reaction energy range extends to a higher energy than in the case of ^{80}Br activated by the (I.T.) process.

The ^{80}Br atom activated by isomeric transition has a charge distribution ranging from +1 to +14, with a peak at +7 and an excess kinetic energy, as a result of a molecular explosion.[1,2] In previous papers[3-5] it was concluded that, in the reactions with CH_4, both kinetic-energy and kinetic-energy-independent processes are involved in the formation of organic products.

The (n,γ) activation process, on the other hand, results in ^{80}Br atoms and ions of a maximum kinetic energy equal to 358 eV when the ^{79}Br is a free atom. The maximum energy of ^{80}Br depends principally on the mass of the radical to which ^{79}Br is bonded.[6,7] However, the partial cancellation of prompt gamma-cascade momenta could result in a distribution of ^{80}Br from zero to the maximum, although most of the ^{80}Br energies will probably be formed with energies in a large excess of the reaction energy range, 18% of which is in a singly-charged state.[8] Thus, the study of the reactions of ^{80}Br from the (n,γ) activation is interesting with a view to comparing the reactivity of ^{80}Br activated by the (I.T.) process.

Rack and Gordus[9] investigated the reactions of ^{80}Br from the (n,γ) activation with gaseous CH_4 in an attempt to determine whether the reaction occurs principally because of the positive charge or because of the γ-recoil kinetic energy acquired by the ^{80}Br. The conclusion reached was that the reactions with CH_4 occur principally, if not completely, as a result of the recoil kinetic energy acquired by the atom in the activation. Later, Spicer and Gordus[10] conducted a gas-chromatographic analysis of the products and observed that 89% of the organic activity was due to $CH_3{}^{80}Br$, and 11%, to $CH_2{}^{80}BrBr$, and that the limiting organic yields at zero m.f. of Br_2 were 10.7% $CH_3{}^{80}Br$ and 1.3% $CH_2{}^{80}BrBr$.

However, in Rack's experiments,[9] the highest m.f. of

* On leave of absence from the Faculty of Engineering, Ibaraki University, Hitachi-shi, Ibaraki-ken.

1) S. Wexler and G. Anderson, *J. Chem. Phys.*, **33**, 850 (1960).
2) S. Wexler, *ibid.*, **36**, 1992 (1962).
3) E. Tachikawa and T. Kahara, This Bulletin, **43**, 1293 (1970).
4) M. Yagi, K. Kondo, and T. Kobayashi, *ibid.*, **44**, 580 (1971).
5) K. Numakura, M. Saeki, and E. Tachikawa, presented at the 15th discussion meeting on radiochemistry, Kyoto, 1971, and submitted to This Bulletin.
6) C. Hsiung and A. A. Gordus, *J. Chem. Phys.*, **36**, 947 (1962).
7) A. A. Gordus and C. Hsiung, *ibid.*, **36**, 945 (1962).
8) S. Wexler and T. Davies, *ibid.*, **20**, 1688 (1952).
9) E. P. Rack and A. A. Gordus, *J. Phys. Chem.*, **65**, 944 (1961).
10) L. D. Spicer and A. A. Gordus, "Chemical Effects of Nuclear Transformations," Vol. I, IAEA, Vienna, (1965), p. 185.

the moderator reached was 0.7. The previous work[5] in the (I.T.) experiments suggested that their extrapolation of the yields of the products to 1.0 m.f. of the moderator did not necessarily reflect the real yield-curve in highly-moderated systems.

The prime object of this paper is to examine the product-distribution from the reactions of ^{80}Br from the (n,γ) activation with CH_4 over the whole m.f. range of an inert moderator, Kr. The results obtained will be discussed in comparison with those in the (I.T.) experiments. Some experiments have also been performed on the isotopic variation between CH_4 and CD_4.

Experimental

The methane and Kr were supplied by the Takachiho Chemical Co., while the deuterated methane was supplied by Merck of Canada (its nominal purity was 99%). Those gases were used without purification.

Samples prepared in 18.5 m*l* silica bubblets usually contained about 1—10 mmHg of Br_2. The total pressure was kept constant at 500 ± 10 mmHg, except in the series of experiments where the yield variations of the products were measured as a function of the total pressure. Energetic (n,γ) activated ^{80}Br was formed by irradiating the samples for 5—60 sec in the JRR-4 reactor. The thermal neutron flux at the irradiation port was 2×10^{12} n/cm^2/sec. After irradiation, the ampoule was dipped into liq. N_2 within 1 min in order to stop further reactions; this was followed by the isomeric transition of ^{80m}Br. After the sample had been thawed by inserting it into warm water, it was divided into two portions using a vacuum-line technique. One portion was used to measure the decay of activities in the sample to obtain the total ^{80}Br activity involved. The other was directly injected into radio-gas chromatography. The relative yields of the individual products were obtained by dividing the activities in the radio-gas chromatograms by the total ^{80}Br activity.

The total organic yield was measured with samples with no additive. Separation into organic and inorganic fractions was achieved by the usual solvent extraction method.[5] The organic phase contained an activity, of which at least 98% was ^{80}Br, thus indicating that a proper chemical separation was achieved. After applying decay corrections, the total organic yield, O.Y. = 100 × organic activity/(organic + inorganic activities), was calculated. All the relative yields of the individual products have been corrected to percentage yields, using a correction factor determined from the sum of the relative yields and the total organic yield found in the sample with no additive.

The concomitant irradiation of Kr added as a moderator yields various radioactive Kr-isotopes. However, the species which must be taken into account in the irradiation 5 to 60 sec in duration are ^{85m}Kr, ^{87}Kr, and ^{79}Kr, the relative activities of which are 1.00, 0.633, and 0.016. The uncertainty as to the total ^{80}Br activity caused by their simultaneous presence was not significant, less than a few percent.

A contamination of the results from the $^{80m}Br(I.T.)^{80}Br$ process can be anticipated. When the isomeric transition occurred while the sample was dipped in a liq. N_2 bath, the reaction of the newly-formed ^{80}Br with the reactant can be ignored because of the clamping effect.[11] Thus, the error resulting from the isomeric transition can be estimated to be less than 1%.

11) J. A. Merrigan, W. K. Ellgren, Jr., and E. P. Rack, *J. Chem. Phys.*, **44**, 174 (1966).

The most serious error in this work seems to result from the non-uniformity of the components among the two divided portions. The accuracy of the present results is usually limited to ±10%. For most of the samples, 2 to 3 samples were made and worked with. The data are usually consistent within the limits of experimental error.

Results

The radio-gas chromatographic analysis of samples has shown that the main products from the reactions of (n,γ)-activated ^{80}Br with CH_4 or CD_4 are $CH_3{}^{80}Br$ and $CH_2{}^{80}BrBr$ or their isotropic analogues, much as in the (I.T.) experiments.

Table 1. The total pressure effect on products from the ^{80}Br–CH_4 system

Total Pressure (mmHg)	$CH_3{}^{80}Br$ (%)	$CH_2{}^{80}BrBr$ (%)
55	11.1±1.1	1.1±0.1
110	11.5±1.2	1.1±0.1
210	10.5±1.1	1.2±0.1
310	—	1.5±0.2
500	12.3±0.4	1.6±0.3
710	12.9±0.4	1.8±0.2
890	—	2.5±0.3
930	13.8±1.4	1.9±0.2
1560	14.9±1.5	2.3±0.2
1920	15.8±0.6	2.1±0.2

Table 1 summarizes the yields of the individual products obtained under various total pressures. In all cases, the Br_2/CH_4 ratio is in the range from 0.02 to 0.03. The $CH_3{}^{80}Br$ yield increases with an increase in the total pressure, at least up to 1920 mmHg; $CH_2{}^{80}BrBr$ increases at the beginning, but a further increase in pressure has no measurable effect on it.

Table 2. The percentage yields of products from the Kr-moderated ^{80}Br–CH_4 and ^{80}Br–CD_4 systems

m.f. of Kr	Reactant CH_4		Reactant CD_4	
	$CH_3{}^{80}Br$ (%)	$CH_2{}^{80}BrBr$ (%)	$CD_3{}^{80}Br$ (%)	$CD_2{}^{80}BrBr$ (%)
0.00	12.3 ±0.4	1.5 ±0.4	4.6 ±0.4	1.7 ±0.2
0.10	8.5 ±0.9	0.82±0.07	3.8 ±0.4	1.5 ±0.15
0.19	9.4 ±0.9	1.4 ±0.2	2.0 ±0.2	0.87±0.09
0.24	6.4 ±0.6	0.95±0.10	—	—
0.30	6.7 ±0.7	—	1.6 ±0.2	0.80±0.08
0.42	3.7 ±0.4	0.96±0.10	1.6 ±0.2	0.90±0.09
0.51	2.2 ±0.2	0.66±0.07	—	—
0.60	1.7 ±0.6	0.81±0.28	0.88±0.09	0.88±0.09
0.71	1.1 ±0.1	0.51±0.05	0.69±0.07	0.83±0.08
0.80	0.78±0.08	0.47±0.05	0.60±0.06	0.64±0.06
0.90	0.93±0.10	0.54±0.08	0.72±0.07	0.47±0.05

The moderator effects of Kr in these products have been examined while keeping the Br_2/CH_4 ratio in the range from 0.02 to 0.05. The results obtained are summarized in Table 2. The yields of the total organic products and of the individual products in the ^{80}Br–CH_4 system were 13.8±0.6% total organic, 12.3±0.4% $CH_3{}^{80}Br$, and 1.5±0.2% $CH_2{}^{80}BrBr$. In the ^{80}Br–CD_4

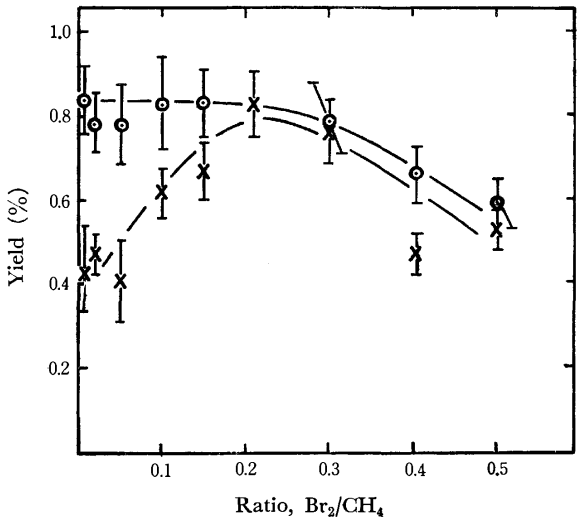

Fig. 1. Variations in $CH_3{}^{80}Br$ and $CH_2{}^{80}BrBr$ with the Br_2/CH_4 ratio in the reaction system in the constant presence of 100 mmHg of CH_4. (The total pressure was kept at 500±10 mmHg by adding Kr.)
⊙: $CH_3{}^{80}Br$, ×: $CH_2{}^{80}BrBr$

system, the yields were 6.3±0.6% total organic, 4.6±0.4% $CD_3{}^{80}Br$, and 1.7±0.2% $CD_2{}^{80}BrBr$. As the dilution of the reaction system by Kr proceeds, the yields decreased; the limiting values at 1.0 m.f. of Kr were 0.9±0.1% $CH_3{}^{80}Br$ and 0.5±0.1% $CH_2{}^{80}BrBr$, 0.7±0.1% $CD_3{}^{80}Br$ and 0.5±0.1% $CD_2{}^{80}BrBr$.

In order to make a comparison with the results obtained in the ^{80m}Br–CH_4 system,[5] the variation in $CH_3{}^{80}Br$ and $CH_2{}^{80}BrBr$ as a function of the ratio of Br_2/CH_4 has also been examined; the results are graphically depicted in Fig. 1. In all cases, the pressure of CH_4 was kept constant at 100 mmHg and Kr was added until the total pressure reached 500±10 mmHg. Under these conditions, the variation in Kr (400—350 mmHg) concomitantly with the increase in the Br concentration has no significant effect on the kinetic energy moderation of the energetic ^{80}Br, since Kr is as good a kinetic energy moderator as Br_2. Thus, the yield-curve of $CH_2{}^{80}BrBr$, showing a maximum, is related directly with the increase in Br_2, but not with the concomitant decrease in the amount of Kr in the system.

Discussion

The total organic yields found in the present work are in agreement with the values (12.0±1.0% from ^{80}Br–CH_4 and 6.4±1.0% ^{80}Br–CD_4) previously reported by Spicer and Gordus[10,12] and with the value of 13.3±0.5% from ^{80}Br–CH_4 reported by Rack and Gordus.[9,12] Furthermore, the percentage yields of individual products also show a reasonable agreement with the values,[10] 10.7% for $CH_3{}^{80}Br$ and 1.3% for $CH_2{}^{80}BrBr$, and 4.9% for $CD_3{}^{80}Br$ and 1.5% for $CD_2{}^{80}BrBr$. If one estimates the kinetic energy yield by simply subtracting the limiting yield at 1.0 m.f. of Kr from that obtained with no additive, 13.8−1.4=12.4% for the total organic products, 12.3−0.9=11.4% for $CH_3{}^{80}Br$, and 1.5−0.5=1.0% for $CH_2{}^{80}BrBr$ are obtained. A similar treatment of the results from the ^{80}Br–CD_4 system yields 6.3−1.2=5.1% for the total organic products, 4.6−0.7=3.9% for $CD_3{}^{80}Br$, and 1.7−0.5=1.2% for $CD_2{}^{80}BrBr$. The value of 12.3% for $CH_3{}^{80}Br$ is roughly 3 times that found in the (I.T.) experiments.[5] As has been discussed in a previous paper,[5] an additional formation of products due to the thermal ionic processes is possible in the highly Kr-moderated ^{80m}Br–CH_4 system. There is no "*a priori*" reason to believe that this additional formation does not occur in the present ^{80}Br–CH_4 or CD_4 systems. Thus, the values obtained for the kinetic energy yields in the above calculation should be taken to be minimum values.

Comparison of the Results with Those from the (I.T.) Experiments. The higher yield of $CH_3{}^{80}Br$ from the kinetic energy process in the (n,γ) experiment than in the (I.T.) experiments results from the difference in the physical nature of the ^{80}Br from the two types of activation. Since the ^{80}Br atom from the (n,γ) activation has a kinetic-energy distribution ranging up to E_{max}, while a fraction of the charged atom is of the order of 18%,[8] mostly singly-charged, the kinetic energy is a more important factor in the course of the reactions than is the positive charge. When products are formed *via* energetic processes, they are excited and so can undergo a secondary decomposition or isomerization, as detected by a pressure-dependent competition between the collisional deactivation and the unimolecular decomposition. The results in Table 1 agree with the above expectation, indicating that a fraction of $CH_3{}^{80}Br$ is highly excited and that it is subjected to a secondary decomposition, even under a total pressure of 1920 mmHg, although a large fraction is easily stabilized and is essentially pressure-independent. This is in great contrast with the results of the (I.T.) experiments, where $CH_3{}^{80}Br$ increases with the pressure at the beginning, but tends to level off at around 500 mmHg.[3] This is indicative that a fraction of the $CH_3{}^{80}Br$ in the (n,γ) experiment stays in somewhat higher excitation states than that in the (I.T.) experiment. Since the excitation energy of the products is a good measure of the energetic state of the reacting atom at the time of the reactions,[13] it may be pointed out that the possible collisions which can lead to energetic reactions of ^{80}Br are available to a higher energy in the present (n,γ) experiments, than in the (I.T.) experiments.

When one compares the $CH_2{}^{80}BrBr$ yield with that in the (I.T.) experiments, it is noticeable that a higher yield is obtained from the latter (2.1±0.2% in the (I.T.) experiments). This trend is very different from that found in $CH_3{}^{80}Br$ and implies that an appreciable amount of $CH_2{}^{80}BrBr$ is formed *via* a thermal ionic process in the (I.T.) experiments.

One attempt to evaluate the maximum yield of

12) These values were obtained by extrapolating to zero additive, while in the present work they are the percentage yields in the presence of 1—5 mmHg Br_2. However, the presence of this amount of Br_2 does not affect the yield beyond the range of experimental uncertainty. Thus, the direct comparison of the present values with the reported values is rather reasonable.

13) C. F. McKnight and J. W. Root, *J. Phys. Chem.*, **73**, 4430 (1971).

$CH_2{}^{80}BrBr$ in the (I.T.) experiments proceeds on the assumption that the energetic formations of $CH_3{}^{80}Br$ and $CH_2{}^{80}BrBr$ occur in the same energy range. On this assumption, the ratio of the yields of products, $CH_3{}^{80}Br/CH_2{}^{80}BrBr$, from the energetic reactions of ^{80}Br can be considered to be the same for both types of activation of ^{80}Br. The maximum value of the energetic yield of $CH_2{}^{80}BrBr$ in the (I.T.) experiments can, thus, be estimated by the calculation:

$$(CH_2{}^{80}BrBr/CH_3{}^{80}Br) \text{ in } (n,\gamma) \text{ work} \times (CH_3{}^{80}Br \text{ in (I.T.) work}) = (1.0/11.4) \times (3.9) = 0.34$$

The experimental uncertainty in the (I.T.) experiments[5] did not allow us to detect definitely the kinetic energy moderation of $CH_2{}^{80}BrBr$ by Kr, both because of its small yield and because of its additional formation in the Kr-moderated system. Although the above calculation does not involve any certainty, it may be considered that the kinetic energy formation of $CH_2{}^{80}BrBr$ is less important in the (I.T.) experiments.[4]

Another important observation regards the yields of products in the highly Kr-moderated system. While the limiting yields of $CH_3{}^{80}Br$ at 1.0 m.f. of Kr are $0.9\pm0.1\%$ for the (n,γ) activation and $0.5\pm0.1\%$ for the (I.T.) activation, a significant difference is noticed in the limiting yields of $CH_2{}^{80}BrBr$ between the two types of activations. In the (n,γ) activation, $CH_2{}^{80}BrBr$ decreases from 1.5% with the m.f. of Kr and can be extrapolated to 0.5% at 1.0 m.f. of Kr, but in the (I.T.) activation an additional, noticeable formation occurs when the m.f. of Kr exceeds 0.5 and can be extrapolated to 2.9%.[5]

The fraction of the charged ^{80}Br from the (n,γ) activation is mostly singly-charged. Thus, the thermal ionic yield of $CH_3{}^{80}Br$ and $CH_2{}^{80}BrBr$ must be due to the reactions of thermal Br^{1+}. If this species is also the most important reacting one in the limiting conditions of 1.0 m.f. of Kr in the (I.T.) experiments, there exists no plausible explanation of the higher yield of $CH_2{}^{80}BrBr$ and the lower yield of $CH_3{}^{80}Br$, relative to those in the (n,γ) experiments. A possible explanation, thus, would involve another kind of reacting species of ^{80}Br for the formation of products *via* kinetic-energy-independent processes in the (I.T.) experiments. This is very concievable when one considers that a large fraction of ^{80}Br is formed with multiple charges and little excess kinetic energy as a result of successive internal conversions.[14] As the dilution of the reaction system with Kr proceeds, the distribution of the charge and the energy tends to be controlled through collisions with Kr. At least the fractions of ^{80}Br may be in different charge and energy states from those in the (n,γ) experiments[15] and may react with CH_4 *via* a kinetic-energy-independent process. However, further study will be required before we can describe a real working process which can explain these results.

Formation of $CH_2{}^{80}BrBr$. The yield curve shown in Fig. 1 is very similar to that found in the (I.T.) experiments and can also be explained in terms of the competition of two types of reactions: 1) the formation of $CH_2{}^{80}BrBr$ through the reaction of $\cdot CH_2{}^{80}Br + Br_2 \rightarrow CH_2{}^{80}BrBr + Br$, and 2) the scavenging reaction of Br_2 for the reacting ^{80}Br atom.

However, the shift of the maximum from 0.08 to 0.2, a higher value of Br_2/CH_4 than in the (I.T.) experiments is indicative that the energy state of $\cdot CH_2{}^{80}Br$ is different in the two kinds of activation of ^{80}Br; $\cdot CH_2{}^{80}Br$ in the present (n,γ) activation is rather excited and is less sensitive to Br_2 than in the previous (I.T.) activation. This is possible if they are formed by different reaction processes. However, this is not the time to explore this problem further, although Kr may play a role in the formation of $\cdot CH_2{}^{80}Br$ in the (I.T.) activation.[16]

In the unmoderated systems, at least 2/3 of the $CH_2{}^{80}BrBr$ is formed *via* an energetic process of ^{80}Br. Thus, it is worthwhile to discuss its formation process on the basis of the model previously presented[17-19] by assuming that, in the energetic process, $\cdot CH_2{}^{80}Br$ exists as an intermediate in the formation of $CH_2{}^{80}BrBr$. Wolfgang[17] proposed a direct-double-displacement process to explain the formation of CH_2TI from the reaction of the recoil tritium atom with CH_4 in the iodine-scavenged systems. Later, Tang and Rowland[18] concluded that the process is of minor importance in the reaction of the recoil tritium atom. In the energetic reaction of ^{80}Br, however, the process is rather probable, since the greater the mass of the reacting species is, the larger is the linear momentum transfer into a product in collision, although some ambiguity concerning the time interval between the leaving of the two H atoms remains.[19] The following two reaction schemes can be suggested:

1) single-step double-replacement reaction

$$^{80}Br^* + CH_4 \longrightarrow \cdot CH_2{}^{80}Br + 2H$$

2) two-step single-replacement reaction

$$^{80}Br^* + CH_4 \longrightarrow (CH_3{}^{80}Br)^* + H$$
$$(CH_3{}^{80}Br)^* \longrightarrow \cdot CH_2{}^{80}Br + H$$

The implication of a double displacement occurring in a single step is that the entire reaction process is complete on a time scale comparable to that of the single-substitution processes, *i.e.*, $<10^{-13}$ sec. The two-step process, on the other hand, describes a situation in

14) E. Tachikawa, This Bulletin, **43**, 63 (1970).

15) This consideration is consistent with observations in the reactions of ^{80}Br and ^{82}Br activated by (I.T.) processes with CH_3Br. The moderator curve of the products from the reactions of ^{82}Br can be extrapolated to zero % at 1.0 m.f. of Kr, while those from the reaction of ^{80}Br can be extrapolated to some finite value. This difference can also be ascribed to the difference in the decay schemes of ^{80m}Br and ^{82m}Br: the latter decays to the ground state in a single transition, and the resulting ^{82}Br has a high excess kinetic energy as well as a high charge. Ref. T. Kobaysahi, unpublished data; J. Okamoto and E. Tachikawa, This Bulletin, **42**, 1504 (1969); D. W. Oates, R. L. Ayres, R. W. Helton, K. S. Schwartz, and E. P. Rack, *Radiochem. Radioanal. Lett.*, **4**, 123 (1970).

16) This is possible, since the ^{80}Br from the (I.T.) activation is highly ionized with a relatively low kinetic energy. In the ^{80m}Br–C_2H_6 system, the amount of one of the products, $CH_3{}^{80}Br$, very much depends upon the moderator used (see Ref. 21).

17) R. Wolfgang, *Progr. Reaction Kinetics*, **3**, 97 (1965).

18) Y. N. Tang and F. S. Rowland, *J. Phys. Chem.*, **72**, 707 (1968).

19) R. T. K. Baker and R. L. Wolfgang, *ibid.*, **73**, 3478 (1969).

which the excited molecule formed in the first step has sufficient time for some vibrations and/or rotations of individual groups in the molecule on prior to the bond breaking. The two-step mechanism is normally determined through the pressure dependence of the yields of the decomposition products relative to that of the single-displacement products. In the present case, if $CH_2{}^{80}BrBr$ is mainly formed by a two-step mechanism, the ratio of $CH_2{}^{80}BrBr/CH_3{}^{80}Br$ must decrease with an increase in the total pressure. This is in great contrast to the results shown in Fig. 2, which

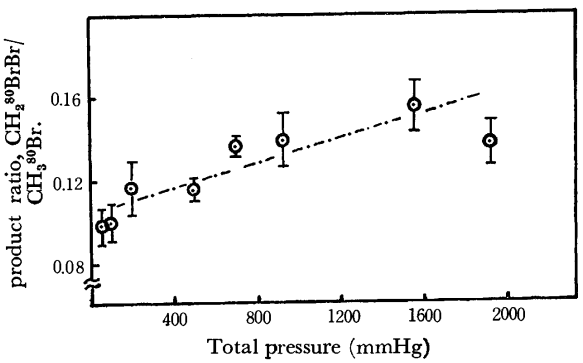

Fig. 2. The product ratio, $CH_2{}^{80}BrBr/CH_3{}^{80}Br$, as a function of the total pressure ($Br_2/CH_4=0.02$—0.03).

shows the plot of the $CH_2{}^{80}BrBr/CH_3{}^{80}Br$ ratio against the total pressure (using the results in Table 1). Although a quantitative treatment of the results requires a correct knowledge of the energetics of the individual reaction path as well as of a ^{80}Br-energy spectrum, qualitatively it is evident that the $\cdot CH_2{}^{80}Br$ radical is indeed formed largely by the one-step mechanism. However, the contribution, if any, by the two-step mechanism to the formation of this radical cannot be estimated.

Isotope Effect. The isotope effect has been observed in the $CH_3{}^{80}Br$–$CD_3{}^{80}Br$ pair; its value is 2.7 in the unmoderated system, decreases with the m.f. of Kr, and becomes close to unity when the m.f. of Kr becomes over 0.8. The difference in the yields between $CH_2{}^{80}BrBr$ and $CD_2{}^{80}BrBr$ does not exceed the experimental fluctuation over the range of the m.f. of Kr studied.

By tentatively identifying the kinetic energy yield of $CH_3{}^{80}Br$ and $CD_3{}^{80}Br$ as 11.4% and 3.9%, the value of 2.9 ± 0.3 can be obtained as the kinetic isotope effect. When one compares these results with those obtained in the (I.T.) experiments, the ratio is found to be comparable with the 2.7 ± 0.3 for $CH_3{}^{80}Br/CD_3{}^{80}Br$ in the latter experiments.[3] Furthermore, the non-existence of any isotope variation between $CH_2{}^{80}BrBr$ and $CD_2{}^{80}BrBr$ within the range of experimental uncertainty shows an agreement between them.[3] The present isotope effect is due to the reactivity integral isotope effect,[20] and the contribution of the moderator isotope effect is not significant, as has been discussed previously.[3]

The results in Table 2 show that at least 2/3 of the $CH_2{}^{80}BrBr$ is formed *via* an energetic process. Thus, if a similar value of isotope effects presents in the energetic formation of $CH_2{}^{80}BrBr$, the present experimental method will provide a method of detecting the isotopic variation between $CH_2{}^{80}BrBr$ and its isotopic analogue, contrary to the experimental results. The current set of experiments in our laboratory shows that the kinetic isotope effect in C_2H_6–C_2D_6[21] and C_3H_8-isotopic analogues[22] ranges from 1.3 to 1.5. These results suggest that the chemical and/or physical natures of the residual and leaving groups play a role in the isotope effect. If the kinetic isotope effect in the present $CH_2{}^{80}BrBr$–$CD_2{}^{80}BrBr$ remains in this range, the difference in the yields might be overshadowed by the experimental fluctuation. This is possible, since their formations will involve the breaks of two C–H or D bonds. In conclusion, it can only be said that the isotope effect in $CH_2{}^{80}BrBr$–$CD_2{}^{80}BrBr$, if it exists, is much less than that in the $CH_3{}^{80}Br$–$CD_3{}^{80}Br$ pair.

20) E. K. C. Lee, G. Miller, and F. S. Rowland, *J. Amer. Chem. Soc.*, **87**, 190 (1965).

21) K. Yanai and E. Tachikawa, presented at the 23rd annual meeting of the Chemical Society of Japan, Tokyo, 1970; *Radiochim. Acta*, in press.

22) K. Numakura and E. Tachikawa, presented at the 6th Informal International Hot Atom Symposium, Brookhaven, N.Y., U.S.A. (abstract only).

Crystal Growth of β-Hopeite on (0001) Plane of a Single Crystal of Zinc

Akitsugu OKUWAKI, Jinichi NINAGAWA, Taijiro OKABE, and Keiichi OMORI

Department of Applied Chemistry, Faculty of Engineering, Tohoku University, Sendai
**Institute of Mineralogy, Petrology and Economic Geology, Tohoku University, Sendai*

(Received September 22, 1971)

The epitaxy and the orientation of β-hopeite grown on the (0001) plane of a single crystal of zinc were studied. The epitaxy was found to be (0001)-Zn//(010)-β-hopeite, and the orientation was [10.0]//[100] or [12.0]//[100]. The nature of the chemical bond between β-hopeite and zinc is considered to be similar to that of the wurtzite type rather than to that of the wüstite type in view of the structure of the boundary surfaces.

One of the present authors previously studied the influence of impurities on the phosphatizing of steel,[1,2] the composition and the orientation of phsophate,[3] and also the electrochemical behavior of phosphatizing.[4] Machu,[5] Jaenicke and Lorenz,[6] and Khain[7] have studied the mechanism of phosphatization, and Neuhaus and Gebhardt[8–10] have presented a unique opinion on the epitaxies of phosphate coated on such base metals as Fe, Zn, and Cu.

From the above-mentioned investigations into the orientation of β-hopeite, $Zn_3(PO_4)_2 \cdot 4H_2O$, on iron and steel, it has become obvious that the (010) plane of β-hopeite combines with the metal surface. In those studies, however, since polycrystalline pieces have been used as the base metal, the experimental determination of the epitaxies between phosphate and metal was difficult. Consequently, their estimation was carried out from their lattice constants. In order to examine the orientation and epitaxy between coating and metal precisely, the use of a single crystal as the base metal is necessary. In the present paper the following investigations will be reported: the orientation and the epitaxy of β-hopeite grown on the (0001) plane of zinc single crystal were studied by a microscopic observation of the crystal growth of β-hopeite, based on our experimental results and the crystal structure of β-hopeite, an adhesive mechanism between β-hopeite and zinc was also investigated.

Experimental

Phosphatizing Solution. The phosphatizing solution was prepared from a 0.1 mol/*l* solution of phosphoric acid by adjusting its pH with anhydrous sodium carbonate.

Microscopic Observation of the Crystal Growth. A single crystal of zinc (3 mm × 3 mm × 100 mm) was prepared by a modification of the method of Czochralski', the *c*-axis of zinc in the single crystal is perpendicular to the base plane. It was split just before the experiment, and a split chip of 2 mm was dipped in the phosphatizing solution, and held in a crystallizing dish. Then, under a microscope whose object glass was immersed into the phosphatizing solution, the crystal growth was observed, photographed, and filmed using a FUJICA Single 8, Z 2-type 8 mm movie camera by means of the memo-motion technique.

Results and Discussion

Observation of the Growth Direction of β-Hopeite. Photographs of crystals grown on the (0001) plane of zinc treated with the phosphatizing solution at various pH's are shown in Figs. 1—4. At pH 3.5, β-hopeite did not form, except for the appearance of etch pits. In the pH range of 4.5—5.0, the growth of a relatively large crystal of β-hopeite was observed.

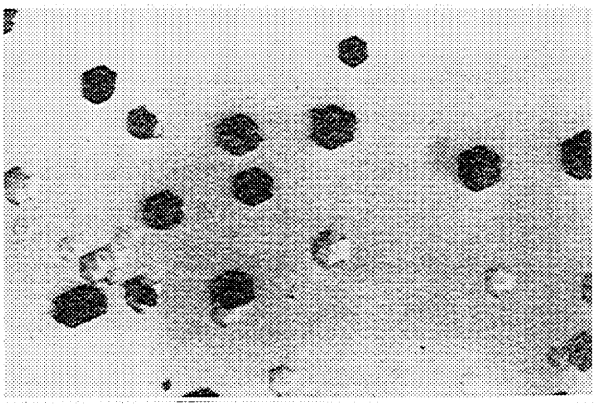

Fig. 1. Crystal growth of β-hopeite on the (0001)-Zn at pH 3.5 (45 min). (×180)

Fig. 2. Crystal growth of β-hopeite on the (0001)-Zn at pH 4.0 (45 min). (×180)

1) T. Umegaki, H. Ito, and T. Okabe, This Bulletin, **42**, 1555 (1968).
2) T. Umegaki, H. Ito, and T. Okabe, *ibid.*, **42**, 2364 (1969).
3) T. Umegaki, T. Okabe, and K. Omori, *ibid.*, **42**, 1304 (1969).
4) R. Shirakawa, S. Takeda, T. Umegaki, and T. Okabe, *ibid.*, **44**, 1007 (1971).
5) W. Machu, *Chem. Fabrik*, **13**, 461 (1940).
6) W. Jaenicke and B. Lorenz, *Werkstoffe u. Korrosion*, **10**, 681, **10**, 761 (1959).
7) I. I. Khain, *J. Appl. Chem. USSR*, **32**, 2531, 2542, 2662 (1959).
8) A. Neuhaus, E. Jumpertz, and M. Gebhardt, *Z. Elektrochem.*, **66**, 593 (1962).
9) A. Neuhaus and M. Gebhardt, *Naturwiss.*, **51**, 358 (1964).
10) M. Gebhardt, *Farbe Lack*, **74**, 217 (1968).

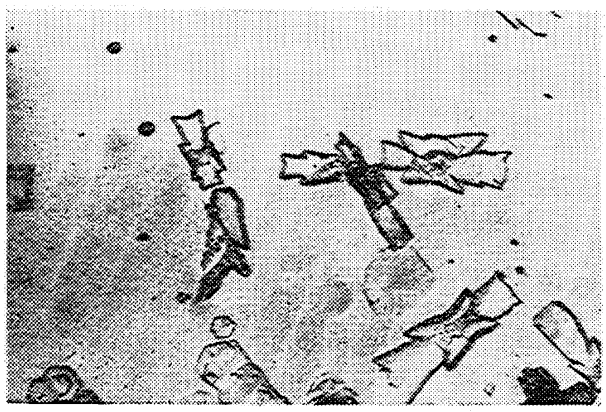

Fig. 3. Crystal growth of β-hopeite on the (0001)-Zn at pH 4.5 (45 min). (×180)

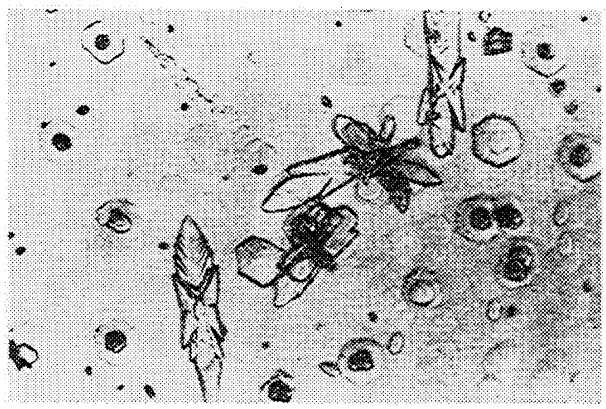

Fig. 4. Crystal growth of β-hopeite on the (0001)-Zn at pH 5.0 (45 min). (×180)

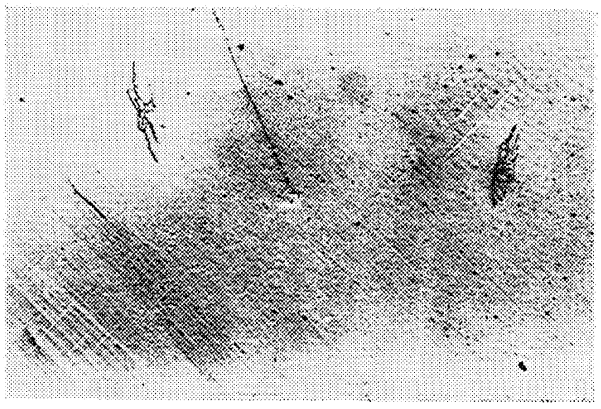

Fig. 5. Crystal growth of β-hopeite on the (0001)-Zn at pH 4.72 (10 min). (×180)

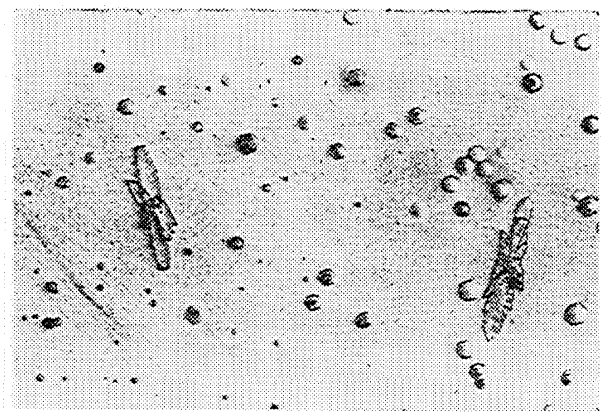

Fig. 6. Crystal growth of β-hopeite on the (0001)-Zn at pH 4.72 (20 min). (×180)

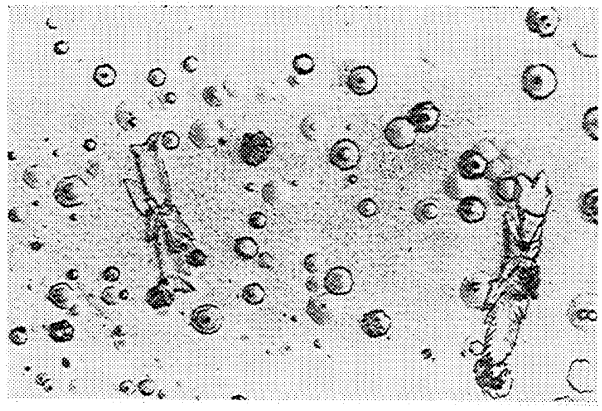

Fig. 7. Crystal growth of β-hopeite on the (0001)-Zn at pH 4.72 (30 min). (×180)

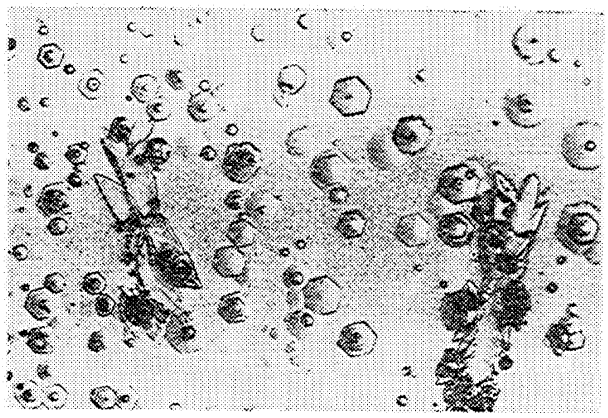

Fig. 8. Crystal growth of β-hopeite on the (0001)-Zn at pH 4.72 (40 min). (×180)

The series of microscopic photographs shown in Figs. 5 to 8 are the crystal growth of β-hopeite on the (0001) plane of zinc at pH 4.72, 20°C. The orientation of the *a*-axis on the (0001) plane of zinc can easily be recognized from the etch pits formed. Yamamoto and Watanabe[11] reported that etch pits appeared as regular hexagons when the (0001) plane of zinc was etched with a dilute hydrogen chloride solution. In these cases, the three *a*-axes of the zinc crystal are at right angles to the sides of the hexagon. When a zinc single crystal revealing a (0001) plane was dipped in the phosphatizing solution, etch pits with the same orientation as has been described above appeared, as is shown in Fig. 1. In Figs. 9 and 10, obtained by tracing Figs. 4 and 7 respectively, the directions of the crystal growth of β-hopeite are shown as dotted lines, and the three *a*-axes, a_1, a_2, and a_3, of the zinc crystal are drawn on an enlarged regular hexagon of the etch pit.

Two kinds of direction of the crystal growth can be observed in these figures; one of them coincides with the direction of the three *a*-axes, while the other makes an angle of 30° with the *a*-axes. From these results, it can be said that β-hopeite crystal grows along the [10.0] or [12.0] direction on the (0001) plane of zinc.

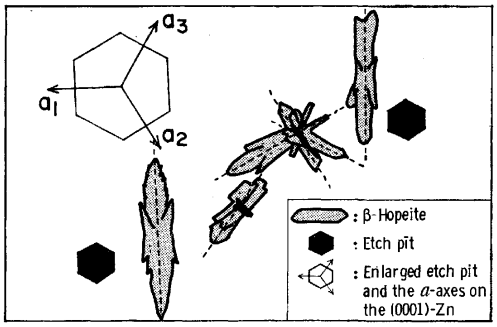

Fig. 9. Relation between the direction of crystal growth and that of the a-axes on the (0001)-Zn.

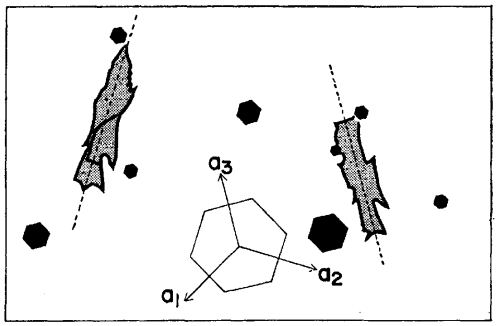

Fig. 10. Relation between the direction of crystal growth and that of the a-axes on the (0001)-Zn.
The illustrations of shapes are the same as in Fig. 9

Epitaxy. The epitaxies of β-hopeite on the (0001) plane of zinc are shown by two modes in Fig. 11 and Table 1. The black spots in Fig. 11 are zinc atoms on the (0001) plane, while the regular hexagon and the rectangle with perimeters of thick lines indicate an etch pit and the unit cell of β-hopeite projected on the (010) plane respectively.

The length of the a-axis in β-hopeite is equivalent to

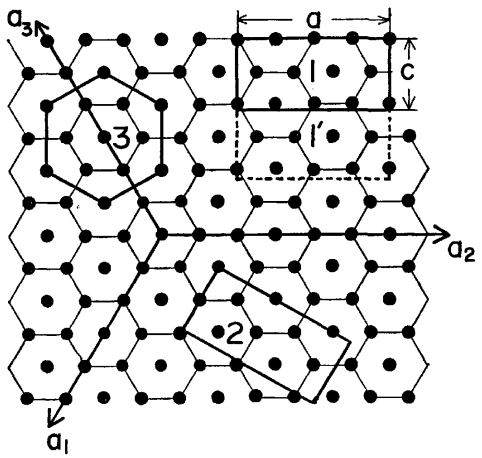

Fig. 11. The epitaxies of β-hopeite on the (0001)-Zn.
a_{1-3}: a-axes on the (0001)-Zn
a,c: lattice constant of β-hopeite

	Zn	β-Hopeite
1:	[10.0]	// [100]
1′:	[10.0]	// [100]
2:	[12.0]	// [100]
3:	etch pit	

β-Hopeite: a=10.64 Å, b=18.36 Å, c=5.04 Å, Zinc: a=2.665 Å, c=4.947 Å.

Table 1. Epitaxies between β-hopeite and zinc

Mode	Epitaxy Zinc	Epitaxy β-Hopeite	Period Zinc	Period β-Hopeite	Misfitting (%)
1	$[1\bar{2}10]$	// [100]	10.66	10.64	0
	$[10\bar{1}0]$	// [001]	4.62	5.04	+9
1′	$[10\bar{1}0]$	// [001]	10.01	10.08	+1
2	$[01\bar{1}0]$	// [100]	10.01	10.64	+6
	$[\bar{2}110]$	// [001]	5.33	5.04	−5

4 times the a-axis in zinc in the 1 mode. This mode of orientation accords with that published by Neuhaus and Gebhardt.[9] As for the direction of the c-axis in β-hopeite, considering zinc atoms on the (0002) plane in relation to such epitaxy as the 1′ mode, the misfitting in the epitaxy becomes smaller than that in the 1 mode, as is shown in Table 1. In the 2 mode, β-hopeite grows along the [12.0] direction; perhaps this relation is a new finding. Although, many other modes can be observed in the epitaxies between β-hopeite and zinc, the two modes described above seem to be the simplest ones, with the least misfitting.

The growth of crystals of a fin shape is observed in some figures of this paper; the crystal joins at an angle of about 30° with the [001] direction of β-hopeite. The angle between [100] and [101] in β-hopeite is smaller than 30°, that between [10.0] and [12.0] in zinc, therefore, the rate of crystal growth in the direction of [001] is more rapid than that in the direction of [101] in a β-hopeite crystal. Seemingly, the quantity of β-hopeite formed on the (0001) plane of zinc by the epitaxies of either mode, 1 or 1′, is larger than that formed by the epitaxy of the 2 mode, and the growth rate of the former is larger than that of the latter judging from an observation of Figs. 4—8 and several other photographs and movies, although some of them are not cited here. This may be due to the fact that the misfitting in the 1 or 1′ mode is smaller than that in the 2 mode.

Adhesive Mechanism. Neuhaus and Gebhardt have found that the (010) plane of β-hopeite usually combines with the surface of metals in phosphatization.[9] Such phenomena seem to be attributable to the crystal structure of β-hopeite, which was analysed by Gamidov and Galovachev.[12] The projection of the phosphate

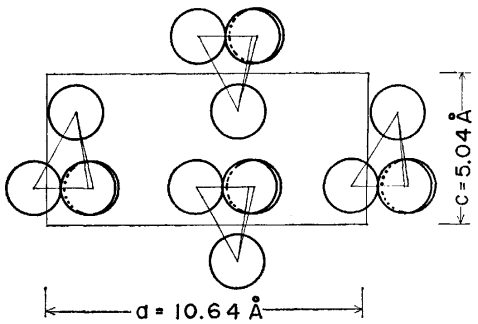

Fig. 12. The projection of phosphate ion on the (010) plane of β-hopeite.

11) M. Yamamoto and J. Watanabe, *J. Japan Inst. Metals*, **17**, 628 (1953).
12) R. S. Gamidov and V. P. Galovachev, *Dokl. Akad. Nauk. USSR*, **150**, 381 (1963).

ion to the (010) plane is shown in Fig. 12 in aid in the consideration of the adhesive mechanism.

As it is impossible to project all the atoms because of the mutual hindrance, only phosphate ions combined to metallic zinc are projected.

A brief explanation of the combination of the (010) plane of β-hopeite with a metal surface is given below from the standpoints of the density and the distribution of oxygen atoms, and the bond length and the coordination between metal and oxygen atoms of the phosphate ion in β-hopeite. On the (001) plane, all the oxygen atoms are located on the 1/4 and 3/4 *c* levels; therefore, it is difficult for this plane to combine with the metal surface. Similarly, on the (100) plane, the low density of the oxygen atom and its localization at one corner are observed. On the (010) plane, however, the density of the oxygen atom is the highest, and the distribution of these atoms is relatively uniform, as is shown in Fig. 12, consequently, the strongest combination is that between the (0001) plane of zinc and the (010) plane of β-hopeite occurs, as is indicated in Figs. 13 and 14.

The positions of the oxygen atom of phosphate in these figures were determined so that the bond distance between the oxygen and zinc atoms was about 2 Å. The lattices, however, combine with each other in a

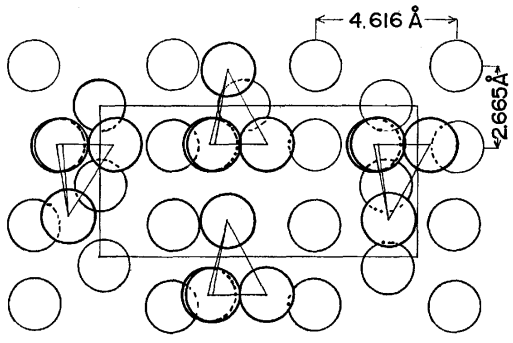

Fig. 13. Overlapped projection of the (010) plane of β-hopeite and the (0001) plane of zinc.

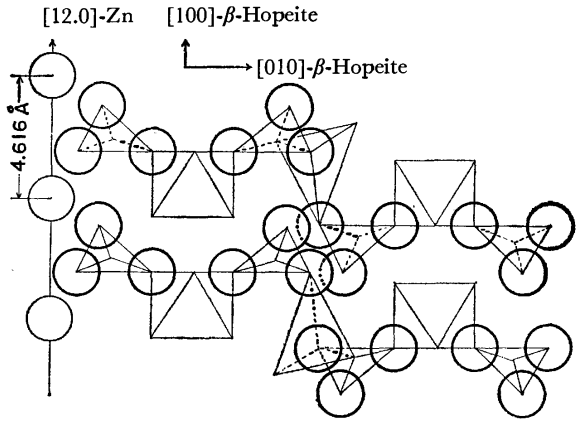

$Zn[PO_4][ZnO_2(H_2O)_4][PO_4][ZnO_4]$

Fig. 14. Side view of the overlapped projection.

rather distorted manner, and the nature of the chemical bond may be of a strong chemisorption. Neuhaus and Gebhardt[13] have proposed that the chemical bond between β-hopeite and the metal surface is of the wüstite type and that a mesomery exists between $Me^{(+)}\cdots O^{(-)}\cdots PO_3$ and $MeO^{(-)}\cdots P^{(+)}\cdots O_3$. It is, however, reasonable that the bond is not of an wüstite type but of an wurtzite one for the following reasons:

1. Zinc atoms are abundant on the boundary surface between β-hopeite and zinc, as is shown in Fig. 13. This may be analogous to an wurtzite enriched with zinc atoms, having an oxygen vacancy and behaving as a negative semiconductor. On the other hand, an wüstite enriched with oxygen atoms is positive.[14]
2. It is reasonable to say that zinc combined with the oxygen in the phosphate ion located at the boundary has a coordination number of 4, in the light of the crystal structures of β-hopeite and wurtzite.

13) A. Neuhaus, *Dechema Monograph.*, **51**, 119 (1964).
14) A. F. Wells, "Structural Inorganic Chemistry," Clarendon Press, (1962), p. 165.

The Characterization of Oligomeric Iron(II)-tetraoxime Complexes

Joseph BACKES, ISAO MASUDA, and Koichiro SHINRA

Department of Applied Chemistry, Faculty of Engineering, Osaka University, Yamada-kami, Suita, Osaka

(Received September 29, 1971)

Several polymeric iron(II) chelates with tetraoxime ligands,

$$CH_3C(NOH)C(NOH)-\overset{(\alpha)}{CH_2}-\overset{(\beta)}{CH_2}-(CH_2)_n-\overset{(\beta)}{CH_2}-\overset{(\alpha)}{CH_2}-C(NOH)C(NOH)CH_3,$$

where $n=2$ and 6, were characterized. They show a ligand-to-iron molar ratio of 1:1, corresponding to a planar arrangement of the ferrous ion and the four oxime nitrogens; two pyridine or methylpyridine substituents are axially coordinated to the central metal ion. The complexes are diamagnetic in the solid state, and their absorption spectra closely resemble those of the monomeric ferrous dimethylglyoxime compounds. The molecular weight, determined in a pyridine solution by vapor-pressure osmometry (2800 for $-(CH_2)_2-$ and 3100 for $-(CH_2)_6-$), corresponds to 5 or 6 Fe–N_4 units within the polymer chain. An NMR investigation including tetraoxime ligands with both aliphatic and aromatic linkages, as well as the corresponding chelates, shows that the protons in the α or in the β position to the oxime groups do not undergo any shift upon chelation. The electronic spectral data and NMR data provide no evidence that the Fe(II) chelate rings within the polymer chain are affected by one another.

In a recent work,[1] polymeric ferrous tetraoxime complexes with aromatic groups as linkage between the two α-dioxime ligand units have been synthesized and characterized. In the present study, two low-molecular-weight ferrous tetraoxime polymers with methylene bridges, $-(CH_2)_6-$ and $-(CH_2)_{10}-$, will be described. The molecular model shows that, because of the extended methylene chain, the α-dioxime groups are situated at random in space, this results in a structure far less rigid than the one incorporating phenyl- or similar bridging groups. An NMR study shows that the chelation of the oxime nitrogens does not cause any shift to the protons adjacent to the chelate ring. The polymer chain is thus considered to be formed of Fe–N_4 units independent of one another.

The properties and the structures of these new chelates are compared with those of the monomeric iron(II)-α-dioxime complexes, as well as with those of the previously-reported polymeric chelates.

Experimental

Preparation of the Tetraoxime Ligands. Dodecane-2,3,10,11-tetraone-tetraoxime, and hexadecane-2,3,14,15-tetraone-tetraoxime were prepared according to the methods described by Murahashi and Kubota.[2] The products obtained showed the following characteristics.

Dodecane-2,3,10,11-tetraone-tetraoxime. White crystals; soluble in DMSO, DMF, pyridine, and other organic solvents; mp 251—253°C. (Found: C, 50.41; H, 7.61; N, 19.33%.)

Hexadecane-2,3,14,15-tetraone-tetraoxime. White crystals; soluble in DMSO, DMF, and pyridine; insoluble in ethanol, methanol, *etc.*; mp 240—241°C. (Found: C, 56.18; H, 8.72; N, 16.28%.)

Preparation of the Complexes. One millimole of an iron(II) salt (Mohr's salt) was dissolved under nitrogen in 20 m*l* of water; to this solution we then added, at room temperature, a solution of 0.5 mmol of a tetraoxime ligand in 5 m*l* of the base (pyridine, methylpyridine). An intensely-red-colored precipitate immediately formed. The reaction mixture was stirred for five hours. The product was then filtered, washed extensively with water and ethanol, and then dried *in vacuo* at room temperature.

The red powders obtained were all soluble in pyridine. They were only slightly soluble in other organic bases and were extremely unstable in common organic solvents (DMF, DMSO, *etc.*). The yield was quantitative. The analytical data are shown in Table 1.

Apparatus and Procedures. The molecular weight was determined in a pyridine solution at 25°C, using a Mechrolab vapor-pressure osmometer, Model 302.

TABLE 1. ANALYTICAL DATA OF THE POLYMERIC IRON(II)-COMPLEXES WITH TETRAOXIMES, CH_3–C(NOH)–C(NOH)–$(CH_2)_n$–C(NOH)–C(NOH)–CH_3;[a] $n=6$, 10

Compound number		Dissociation temp. (°C)[b]	Found, %				Calcd, %			
			C	H	N	Py	C	H	N	Py
1	$(CH_2)_6TOH_2\cdot Fe\cdot(Py)_2$[c]	190	52.20	5.97	16.06	29.85	53.01	6.06	16.86	31.74
2	$(CH_2)_6TOH_2\cdot Fe\cdot(\beta\text{-Pic})_2$[c]	165	52.68	6.13	14.96		54.75	6.51	15.96	
3	$(CH_2)_6TOH_2\cdot Fe\cdot(\gamma\text{-Pic})_2$[c]	160	53.28	6.22	15.26		54.25	6.51	15.96	
4	$(CH_2)_{10}TOH_2\cdot Fe\cdot(Py)_2$	195	56.10	7.01	14.93	27.93	56.31	6.90	15.15	28.53
5	$(CH_2)_{10}TOH_2\cdot Fe\cdot(\beta\text{-Pic})_2$	160	56.39	7.16	14.21		57.73	7.26	14.42	
6	$(CH_2)_{10}TOH_2\cdot Fe\cdot(\gamma\text{-Pic})_2$	165	56.37	7.51	13.82		57.73	7.26	14.42	

a) Tetraoximes will be abbreviated as $(CH_2)_n$ TOH_4.
b) Temperature at which the compounds turn black without melting.
c) "Py," "β-Pic," and "γ-Pic" stand for pyridine, β-picoline, and γ-picoline respectively.

1) J. Backes, I. Masuda, and K. Shinra, This Bulletin, **45**, 1061 (1972).

2) S. Murahashi and H. Kubota, *ibid.*, **35**, 1465 (1962).

The NMR spectra were obtained with a Japan Electron Optics JNM-3H-60 spectrometer at 60 Mc/sec, using tetramethylsilane as the internal reference. Under a nitrogen atmosphere, equimolar amounts of the tetraoxime ligand and an iron(II) salt were dissolved in 1 m*l* of deuterated pyridine; the solution was kept at room temperature for 5 hours before recording. We used solutions of 10% for the ligands and up to 20% for the ferrous complexes. The addition of D_2O caused the disappearance of the oxime protons of the free ligands at a low field.

The apparatus and techniques concerning the infrared and electronic spectra, the thermogravimetric analyses, and the magnetic properties have been described previously.[1)]

Results and Discussion

Table 1 shows the anlytical data of the different chelate polymers. They indicate a tetraoxime ligand-to-iron molar ratio of 1 : 1, and thus a structure where two α-dioxime groups and the ferrous ion form a planar arrangement and where the pyridine ligands (pyridine and methylpyridine) are axially substituted. This structure is further supported by the following thermogravimetric and spectral data.

The thermogravimetric curve (*cf.* Fig. 1) shows the characteristic pattern expected for the release of two coordinated pyridine molecules. The weight loss observed (29.9%) is in fair agreement with the calculated value (31.7%).

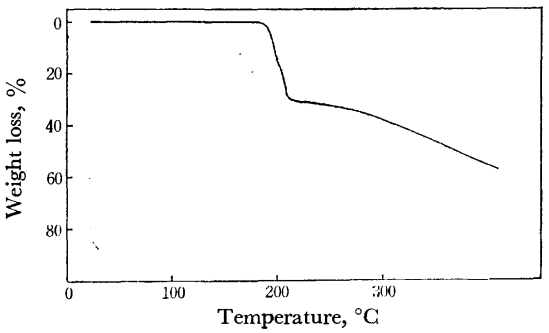

Fig. 1. Thermogravimetric analysis of $(CH_2)_6TOH_2\cdot Fe\cdot(Py)_2$ under nitrogen atmosphere.

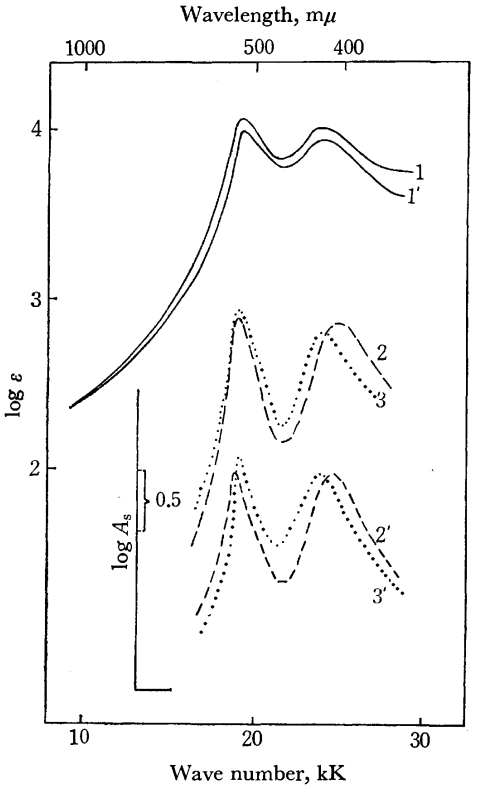

Fig. 2. Absorption spectra: 1: $(CH_2)_{10}TOH_2\cdot Fe\cdot(Py)_2$ in pyridine; 2: $(CH_2)_{10}TOH_2\cdot Fe\cdot(\gamma\text{-Pic})_2$ in γ-picoline;*) 3: $(CH_2)_{10}TOH_2\cdot Fe\cdot(\beta\text{-Pic})_2$ in β-picoline;*) 1′: $(CH_2)_6TOH_2\cdot Fe\cdot(Py)_2$ in pyridine; 2′: $(CH_2)_6TOH_2\cdot Fe\cdot(\gamma\text{-Pic})_2$ in γ-picoline;*) 3′: $(CH_2)_6TOH_2\cdot Fe\cdot(\beta\text{-Pic})_2$ in β-picoline.*)
*) Concentration inaccurate due to low solubility.

While, for the tetraoxime polymers with aromatic linkages, no pyridine and pyridine-like bases were found to be axially coordinated in the solid state,[1)] the present polymers readily underwent this axial substitution.

The polymers are soluble in pyridine. The absorp-

Table 2. Electronic absorption spectra

Complexes	ν_{max}, kK (log ε)		Solvents
$(CH_2)_6TOH_2\cdot Fe\cdot(Py)_2$	19.4 (4.00)	24.5 (3.95)	Py
$(CH_2)_6TOH_2\cdot Fe\cdot(\beta\text{-Pic})_2$	19.4	24.5	Py
$(CH_2)_6TOH_2\cdot Fe\cdot(\beta\text{-Pic})_2$	19.3	24.1	β-Pic
$(CH_2)_6TOH_2\cdot Fe\cdot(\gamma\text{-Pic})_2$	19.3	24.2	Py
$(CH_2)_6TOH_2\cdot Fe\cdot(\gamma\text{-Pic})_2$	19.1	24.7	γ-Pic
$(CH_2)_6TOH_2\cdot Fe\cdot(\gamma\text{-Pic})_2$	18.7		Aniline
$(CH_2)_6TOH_2\cdot Fe\cdot(\gamma\text{-Pic})_2$	18.6		Hydrazine Hydrate
$(CH_2)_6TOH_2\cdot Fe\cdot(\gamma\text{-Pic})_2$	17.9		Ethylenediamine
$(CH_2)_6TOH_2\cdot Fe\cdot(\gamma\text{-Pic})_2$	17.9		Piperidine
$(CH_2)_{10}TOH_2\cdot Fe\cdot(Py)_2$	19.4 (4.06)	24.0 (4.00)	Py
$(CH_2)_{10}TOH_2\cdot Fe\cdot(\beta\text{-Pic})_2$	19.3	24.0	Py
$(CH_2)_{10}TOH_2\cdot Fe\cdot(\beta\text{-Pic})_2$	19.3	24.0	β-Pic
$(CH_2)_{10}TOH_2\cdot Fe\cdot(\gamma\text{-Pic})_2$	19.3	24.2	Py
$(CH_2)_{10}TOH_2\cdot Fe\cdot(\gamma\text{-Pic})_2$	19.0	24.8	γ-Pic
$(CH_2)_{10}TOH_2\cdot Fe\cdot(\gamma\text{-Pic})_2$	18.7		Aniline
$(CH_2)_{10}TOH_2\cdot Fe\cdot(\gamma\text{-Pic})_2$	18.6		Hydrazine Hydrate
$(CH_2)_{10}TOH_2\cdot Fe\cdot(\gamma\text{-Pic})_2$	17.9		Piperidine
$(CH_2)_{10}TOH_2\cdot Fe\cdot(\gamma\text{-Pic})_2$	17.7		Ethylenediamine

Table 3. Comparision of the charge-transfer bands in the monomeric and the polymeric ferrous chelates

Complexes	Fe→Py CT	Fe→Oxime CT
$(DmgH)_2\cdot Fe\cdot(Py)_2$[4]	26.0 (kK)	19.6 (kK)
$(CH_2)_6TOH_2\cdot Fe\cdot(Py)_2$	24.5	19.4
$(CH_2)_{10}TOH_2\cdot Fe\cdot(Py)_2$	24.0	19.4
$(BzdH)_2\cdot Fe\cdot(Py)_2$[a),6)]	25.7	18.3(18.6,sh)
$(FrdH)_2\cdot Fe\cdot(Py)_2$[a),6)]	25.7	17.6(19.2,sh)
$(C_6H_4-O-C_6H_4)TOH_2\cdot Fe(Py)_2$[1)]	25.0	18.5
$(C_6H_4-C_6H_4)TOH_2\cdot Fe\cdot(Py)_2$[1)]	25.6	18.3
(2,6-Pyridyl)$TOH_2\cdot Fe\cdot(Py)_2$[1)]	24.8(27.5,sh)	18.4

a) BzdH and FrdH represent monoanions of α-benzildioxime and α-furildioxime respectively.
b) 'sh' stands for shoulder.

tion spectra in a pyridine solution (*cf.* Fig. 2) bear a close resemblance to those of the monomeric ferrous dimethylglyoxime compounds, $(DmgH)_2\cdot Fe\cdot(Py)_2$, for which two intense absorption bands are found at 19.6 and 26.0 kK; they are assigned to the Fe→oxime and the Fe→pyridine charge transfers respectively.[3,4,5] The absorption bands of the tetraoxime complexes with axial pyridine are found in the same region (*cf.* Table 3). In monomeric ferrous complexes involving aromatic dioxime ligands (*i.e.*, α-benzil-dioxime or α-furil-dioxime), as well as in the polymeric chelates with aromatic bridges, the Fe→oxime charge-transfer bands undergo almost the same shifts as the dimethylglyoxime compounds (Table 3). The fact that no considerable shifts occur upon the linking together of several of these $Fe-N_4$ units indicates further that the different chelate rings within the polymer chain are independent of one another and that the iron(II) $d\pi$-electrons do not engage into an extended π-delocalization in the case of aromatic linkage groups. The effect of substitution on the axially-coordinated pyridine is the same in the monomeric as in the polymeric compounds (*cf.* Table 2 and Ref. 4). The electronic states of the ferrous ion in the monomer and in the polymer may thus be considered to be quite similar.

The absorption spectra at different pH values, ranging ftom pH 8.9 to pH 4.9 fail to show one single isosbestic point; this indicates a two-step dissociation of the axial base. A look at the thermogravimetric curve supports this assumption.

The ferrous tetraoxime compounds with aromatic linkages were all paramagnetic in the solid state. Upon dissolution in pyridine, these compounds are considered to undergo spin-pairing to form octahedrally-substituted diamagnetic complexes.[1] The present tetraoxime chelates with axial pyridine substituents were all found to have negative susceptibilities at room temperature in the solid state; this indicates a low-spin ferrous ion in the complexes. This is consistent with the high extinction coefficient of the absorption bands in the visible region (Fig. 2).[3]

The infrared spectra of the ligands exhibit a broad absorption band between 1620 and 1680 cm^{-1}. Upon coordination with iron(II), a strong band appears in

Table 4. NMR spectral data[a] of the bis(α-ketoxime) ligands, $CH_3C(NOH)CO-R-COC(NOH)CH_3$ and $CH_3COC(NOH)CH_2-R'-CH_2C(NOH)COCH_3$

Compound	Chemical shift, τ					Solvent
	CH_3	CH_2	$CH_2-C=N$	Ring −CH=	=N−OH	
R:						
$C_6H_4-O-C_6H_4$	7.96		2.85	2.06	−2.37	$(CD_3)_2SO$
	(s, 6H)		(d, 4H, J: 9 cps)	(d, 4H, J: 9 cps)	(s, 2H)	
	7.58		2.91	1.73	−4.55	C_5D_5N
	(s, 6H)		(d, 4H, J: 9 cps)	(d, 4H, J: 9 cps)	(s, br, 2H)	
$C_6H_4-C_6H_4$	7.92		2.11		−2.46	$(CD_3)_2SO$
	(s, 6H)		(m, 8H)		(s, 2H)	
	7.55		2.34	1.75	−4.73	C_5D_5N
	(s, 6H)		(d, 4H, J: 8.75 cps)	(d, 4H, J:8.75 cps)	(s, 2H)	
R′:						
$(CH_2)_4$	7.68	8.74	7.6[b]		−2.21	$(CD_3)_2SO$
	(s, 6H)	(m, 8H)			(s, 2H)	
	7.52	8.53	7.2		−4.40	C_5D_5N
	(s, 6H)	(m, 8H)	(m, br, 4H)		(s, 2H)	
$(CH_2)_8$	7.70	8.78	7.5[b]		−2.20	$(CD_3)_2SO$
	(s, 6H)	(m, 16H)			(s, 2H)	
	7.50	8.75	7.1		−4.45	C_5D_5N
	(s, 6H)	(m, 16H)	(m, br, 4H)		(s, br, 2H)	

a) Parts per million downfield from tetramethylsilane; s=singlet, d=doublet, m=multiplet, br=broad.
b) Overlap with $(CD_3)_2SO$.

3) M. J. Cowan, J. M. F. Drake, and R. J. P. Williams, *Discuss. Faraday Soc.*, **27**, 217 (1959), and the references cited therein.
4) Y. Yamano, I. Masuda, and K. Shinra, This Bulletin, **44**, 1581 (1971).
5) The *d-d* bands of low-spin ferrous dimethylglyoxime complexs with axially-coordinated bases are predicted in a region between 15 and 25 kK, but they are believed to be obscured by the intense charge-transfer bands in the visible region (G. De Alti, V. Galasso, A. Bigotto, and G. Costa, *Inorg. Chim. Acta*, **3**, 533 (1969); the *d-d* bands of pyridine-substituted ferrous dimethylglyoxime complexes in ethanol could only be detected in the case of axial 3-methyl-pyridine at 14.0 and 15.4 kK ($\log\varepsilon$=2.0 and 2.16 respectively) (Ref. 4). In the present ferrous tetraoxime complexes, no *d-d* bands were detected.
6) T. Matsumoto, Y. Yamano, and K. Shinra, *Nippon Kagaku Zasshi*, **89**, 44 (1968).

TABLE 5. NMR SPECTRAL DATA[a] OF THE TETRAOXIME LIGANDS AND THEIR FERROUS POLYMER COMPLEXES, $CH_3C(NOH)C(NOH)$–R–$C(NOH)C(NOH)CH_3$ and $CH_3C(NOH)C(NOH)CH_2$–R′–$CH_2C(NOH)C(NOH)CH_3$

Compound	Chemical shift, τ					Solvent
	CH_3	CH_2	CH_2–C=N	Ring –CH=	=N–OH	
R:						
C_6H_4–O–C_6H_4 Ligand	7.95 (s, 6H)		3.05 (d, 4H, J: 9 cps)	2.80 (d, 4H, J: 9 cps)	−1.44 (s, 4H)	$(CD_3)_2SO$
	7.38 (s, 6H)		2.81 (d, 4H, J: 9 cps)	2.28 (d, 4H, J: 9 cps)	−3.50 (s, 2H) −3.80 (s, 2H)	C_5D_5N
	7.52 (s, 6H)		2.90 (d, 4H, J: 9 cps)	2.48 (d, 4H, J:9 cps)		$C_5D_5N/CDCl_3$ (1:1)
Complex	7.38 (s, 6H)		2.81 (d, br, 4H, J:9 cps)	2.28 (d, br, 4H, J:9 cps)		C_5D_5N
C_6H_4–C_6H_4 Ligand	7.88 (s, 6H)		2.73 (d, 4H, J:8.75 cps)	2.35 (d, 4H, J: 8.75 cps)	−1.55 (s, 4H)	$(CD_3)_2SO$
	7.32 (s, 6H)		2.12 (s, br, 8H)		−3.57 (s,2H) −3.86 (s, 2H)	C_5D_5N
Complex	7.33 (s, 6H)		2.15 (s, br, 8H)			C_5D_5N
R′:						
$(CH_2)_4$ Ligand	8.04 (s, 6H)	8.70 (m, 8H)	7.5[b]		−1.26 (s, 2H) −1.34 (s, 2H)	$(CD_3)_2SO$
	7.51 (s, 6H)	8.35 (m, 8H)	6.85 (m, br, 4H)		−3.45 (s, 4H)	C_5D_5N
Complex	7.52 (s, 6H)	8.35 (m, 8H)	6.88 (m, br, 4H)			C_5D_5N
$(CH_2)_8$ Ligand	8.07 (s, 6H)	8.73 (m, 16H)	7.5[b]		−1.29 (s, 2H) −1.36 (s, 2H)	$(CD_3)_2SO$
	7.47 (s, 6H)	8.73 (m, 16H)	6.82 (m, br, 4H)		−3.49 (s, 4H)	C_5D_5N
Complex	7.48 (s, 6H)	8.73 (m, 16H)	6.83 (m, br, 4H)			C_5D_5N

a), b): see Table 4.

the 1620 cm^{-1} region; its position changes only slightly from one chelate to another. This band is attributed to the C=N stretching mode within the chelate. In both the free ligands and the chelate compounds, the OH stretching vibrations are found around 3200 cm^{-1} indicating the presence of free end-group oximes in the latter.

The solubility of these ferrous tetraoxime polymers in pyridine permitted vapor-pressure osmometry measurements. For the chelates with $-(CH_2)_6-$, the molecular weight values were found at 2800 ± 50, and for the chelates with $-(CH_2)_{10}-$, at 3100 ± 50, thus indicating a chain-length of 5 to 6 units.

For neither of the coordination compounds could an X-ray diffraction pattern, indicating an inherent crystalline structure, be found; this is in agreement with the polymeric character of the complexes.

NMR Spectra. This investigation was carried out in order to determine whether the complexing of the four oxime nitrogens with a ferrous ion had an effect on the protons close to this chelate ring.

Compounds involving keto-oxime groups have been the subject of extensive NMR studies[7,8] because of their properties to form *syn-anti* isomers. In the case of α-ketoximes, several isomeric structures can be theoretically conceived; this number increases considerably when the tetraoxime compounds are considered. However, the results obtained for the present compounds show no evidence of the presence of different isomers.

The spectral data of the bis(α-ketoxime) compounds incorporating aromatic as well as methylene linkages are shown in Table 4. They are taken as a basis for assigning the protons in the tetraoxime compounds. The protons of the aromatic rings appear as two doublets in the region between 1 and 3 ppm (τ-scale); this pattern is characteristic of a *para*-substituted species.

7) L. M. Jackman and S. Sternhell, "Applications of Nuclear Magnetic Resonance in Organic Chemistry," Pergamon Press, (1969), p. 266, and the references cited therein.

8) M. Tanaka, T. Shono, and K. Shinra, *Anal. Chim. Acta*, **46**, 125 (1969).

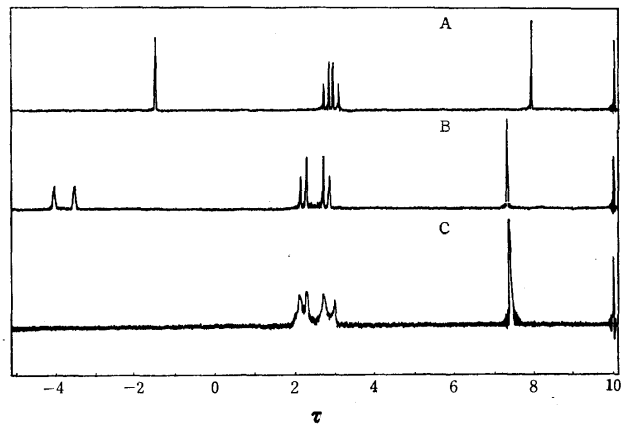

Fig. 3. NMR spectra.
A: C_6H_4–O–$C_6H_4TOH_4$ in $(CD_3)_2SO$
B: C_6H_4–O–$C_6H_4TOH_4$ in C_5D_5N
C: C_6H_4–O–$C_6H_4TOH_2$·Fe in C_5D_5N.

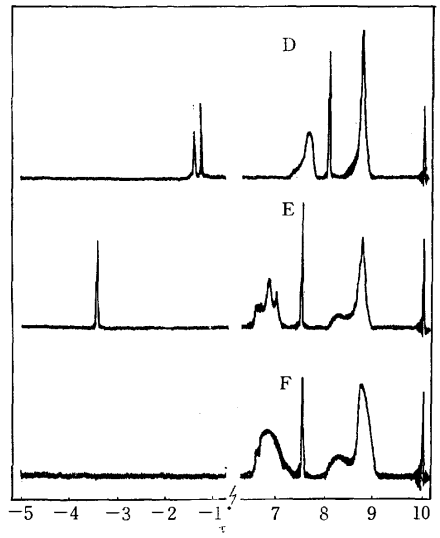

Fig. 4. NMR spectra.
D: $(CH_2)_{10}TOH_4$ in $(CD_3)_2SO$
E: $(CH_2)_{10}TOH_4$ in C_5D_5N
F: $(CH_2)_{10}TOH_2$·Fe in C_5D_5N

The oxime protons are found as sharp signals at a low field in DMSO; they are shifted to a lower field in pyridine. Through all of these spectra a common effect of the pyridine solvent is found, as all the signals undergo a shift, varying from 0.5 to 2.5 ppm toward a lower field than in the case of the spectra in DMSO. Further, the oxime protons appear as very sharp signals in DMSO, while in a pyridine solution the shape changes and the intensity decreases considerably.

The bis(α-ketoxime) compounds with methylene linkages show a broad absorption of the protons in the chain, extending over 1 ppm. The protons in the position α to the oxime C=N bond are shifted to a lower field. The oxime protons are found in the same region as those of the ketoximes with aromatic links. A similar solvent effect due to pyridine can be seen.

The spectra of the tetraoxime ligands are quite similar to those of the α-ketoxime compounds (*cf.* Table 5). The methyl protons appear as one sharp singlet (*cf.* Figs. 3 and 4). The oxime protons are found at a higher field than the monoxime compounds and appear either as a sharp singlet or as two less intense singlets, the latter at a lower field, in DMSO and in pyridine respectively.

Upon chelation in a pyridine solution, the position of neither the methyl protons nor the aromatic protons is altered (*cf.* Fig. 3); only the resolution decreases, and the oxime protons cannot be detected any more down to −20 ppm. For a series of monomeric Co(III) dimethylglyoxime compounds, the hydrogen-bond protons have been found to range between −8.1 and −8.5 ppm, depending on the nature of the complex.[9]

For the methylene-bridged tetraoxime chelate compounds, a similar spectral pattern is found (*cf.* Fig. 4). The positions of neither the methyl nor the methylene protons changes, while the oxime protons are no more detected down to −20 ppm.

The conclusion which can be drawn from these NMR data is that the protons in the α or in the β position relative to the oxime groups remain unaffected upon chelation with iron(II). Thus, no indication is found for an extended π-delocalization within the polymer chain involving the Fe(II)-*dπ* electrons.

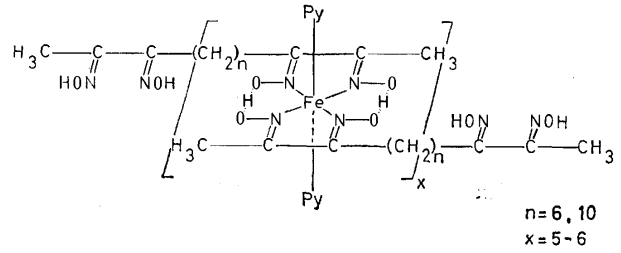

Fig. 5. Schematic representation of the pyridine-substituted, ferrous, methylene-bridged tetraoxime polymers.

Murahashi and Kubota[3] have suggested linear and cyclic structures for the nickel chelates of methylene- and phenyl-bridged tetraoximes. In a previous work we proposed a linear structure for the ferrous polymer chelates with aromatic linkages. This structure has been confirmed for the present methylene-bridged compounds (*cf.* Fig. 5). The infrared data as well as the molecular-weight data make it possible to eliminate the cyclic structures postulated by the above authors.

9) Y. Yamano, I. Masuda, and K. Shinra, *J. Inorg. Nucl. Chem.*, **33**, 521 (1970).

The Polarography of *N,N'*-Ethylenebis(acetylacetoniminato) and *N,N'*-Ethylenebis(salicylaldehydeiminato) Complexes of Cobalt(III), Nickel(II), and Copper(II) in an *N,N*-Dimethylformamide Solution

Mutsuo KODAMA, Yuki FUJII, and Mitsuo SAKURAI
Department of Chemistry, Ibaraki University, Bunkyo, Mito, Ibaraki

(Received September 30, 1971)

The polarographic behavior of *N,N'*-ethylenebis(acetylacetoniminato) (baen) and *N,N'*-ethylenebis(salicylaldehydeiminato) (bisaen) complexes of cobalt(III), nickel(II), and copper(II) in DMF solutions was studied thoroughly. At the dropping mercury electrode, these metal complexes give well-defined cathodic waves corresponding to the reduction of metal(II) to metal(I). A careful and systematic study of the polarographic behavior of *β-cis* and *trans* cobalt(III)-baen and -bisaen complexes of the general formulae: $CoZY^{1-a}$ and $CoZX_2^{1-2b}$, and that of nickel(II)- and copper(II)-baen complexes, revealed that the unusual stability of the metal(I)-baen and -bisaen complexes can be ascribed mainly to the stable square-planar nature of baen and bisaen. The effect of the replacement of the ligand by the halogen atom was also investigated.

Recently, Olson, and Vasilevskis[1-3] reported, in their polarographic investigation of cyclic amine complexes of nickel(II), copper(II), and cobalt(II), that these complexes give single well-defined polarographic steps corresponding to the reduction of metal(II) to metal(I), and that the unusual stability of cyclic amine complexes containing the metal formally in the +1 oxidation state can be ascribed to the cyclic nature of ligands. In our laboratory, a series of mixed *β-cis* and *trans* cobalt(III)-*N,N'*-ethylenebis(acetylacetoniminato) (baen) and -*N,N'*-ethylenebis(salicylaldehydeiminato) (bisaen) complexes containing ammonia, amino acids, acetylacetone, and 2,2'-dipyridyl were prepared by oxidizing the cobalt(II)-baen and -bisaen complexes, which have long been known to be oxygen carriers.[4-6] These baen and bisaen-cobalt(III) complexes and their cobalt(II) complexes in the *N,N*-dimethylformamide (DMF) give a reversible cathodic step corresponding to the reduction of cobalt(II) to cobalt(I), as in the cases of metal(II)-cyclic amine complexes. In this paper, we will study systematically the polarographic behavior of the mixed cobalt(III)-baen and -bisaen complexes in DMF and will discuss the nature of baen and bisaen, which can trap the metal ion in an uncommon oxidation state. Some comparisons will also be made between the cabalt and copper and nickel complexes in order to describe the precise nature of baen and bisaen as ligands.

Experimental

Reagents. The *N,N*-dimethylformamide (DMF) used for the polarographic work was purified by a procedure described by Fujinaga *et al.*[7] The supporting electrolyte, tetraethylammonium perchlorate (TEAP), was prepared by the method given by Fujinaga, Izutsu, and Takaoka.[8] Baen, bisaen, and their cobalt(II) complexes were prepared by the methods given by Morgan and Smith[9] and by Diehl and Hach.[10] The cobalt(III)-baen and -bisaen complexes used in this study were prepared by oxidizing the cobalt(II)-baen and -bisaen complexes with hydrogen peroxide in solutions containing ammonia, amino acids, acetylacetone, or 2,2'-dipyridyl. The detailed ways of preparing them, the determination of their stereochemical configuration, and the elemental analyses will be described in a future paper. All the other chemicals used were reagent-grade and were used without further purification.

Apparatus and Experimental Procedures. The DC polarographic waves were measured by using a manual polarograph similar to that of Kolthoff and Lingane[11] or Yanagimoto pen-recording polarograph PA-102. All the AC polarograms were also recorded automatically by employing the above pen-recording polarograph. The DC polarographic data given in this paper were corrected for the residual current and the ohmic drop of the cell circuit (4.1 kΩ). For all the measurements, we used three dropping mercury electrodes. They have *m* values of 0.7396, 0.9153, and 0.5836 mg/sec, and drop times, t_d's, of 4.10, 5.10, and 4.40 sec respectively, in an air-free DMF (0.15 M TEAP) solution at the mercury height of 70.0 cm and with an open circuit. A saturated calomel electrode (SCE) with a large area was used as the reference electrode and was connected to the cell solution through the salt bridge proposed by Takaoka.[12] In the AC polarographic measurements, a 200-μF condenser was used to minimize the effect of cell resistance.[13] All the polarographic studies were carried out at 20°C using sample solutions containing no free ligand. The oxygen dissolved in the sample solutions was removed by bubbling pure nitrogen gas saturated with pure DMF through the solution. All the free ligands, except *N,N'*-ethylenebis-(3-bromoacetylacetonimine) (baen-Br_2), used in this study were found to give no reduction wave under the present experimental conditions.

Results and Discussion

As is illustrated by the DC polaragrams in Figs. 1 and 2, the cobalt(III)-baen and -bisaen complexes in

1) D. C. Olson and J. Vasilevskis, *Inorg. Chem.*, **8**, 1611 (1969).
2) D. C. Olson and J. Vasilevskis, *ibid.*, **10**, 463 (1971).
3) J. Vasilevskis and D. C. Olson, *ibid.*, **10**, 1228 (1971).
4) T. Tsumaki, This Bulletin, **13**, 252 (1958).
5) M. Calvin and C. H. Barkelew, *J. Amer. Chem. Soc.*, **68**, 2254 (1946).
6) A. L. Crumbliss and F. Basolo, *ibid.*, **92**, 55 (1970).
7) T. Fujinaga, K. Izutsu, K. Umemoto, T. Arai, and K. Takaoka, *Nippon Kagaku Zasshi*, **89**, 105 (1968).
8) T. Fujinaga, K. Izutsu, and K. Takaoka, *J. Electroanal. Chem.*, **12**, 203 (1966).
9) G. T. Morgan and J. D. Smith, *J. Chem. Soc.*, **127**, 2030 (1925).
10) H. Diehl and C. C. Hach, *Inorg. Syn.*, III, p. 196.
11) I. M. Kolthoff and J. J. Lingane, "Polarography," Vol. 1, Interscience, New York (1952), p. 297.
12) K. Takaoka, *Rev. Polarography* (Japan), **14**, 63 (1966).
13) B. Breyer, F. Gutmann, and S. Hacobian, *Australian J. Sci. Res., Ser. A*, **4**, 595 (1951).

TABLE 1. THE DEPENDENCE OF LIMITING CURRENT ON THE HEIGHT OF MERCURY COLUMN
The concentration of Co(baen)(acac)^0=1.82 mM, 20°C
The TEAP concentration=0.15 M

h, cm	$h_c^{1/2}$	i_{l_1}, μA (−1.30 V)	i_{l_2}, μA (−2.00 V)	$i_{l_1}/h_c^{1/2}$	$i_{l_2}/h_c^{1/2}$
70.0	8.21	1.90_9	1.74_5	0.232	0.213
75.5	8.65	2.00_0	1.83_6	0.231	0.212
85.0	9.08	2.14_1	1.96_3	0.235	0.216

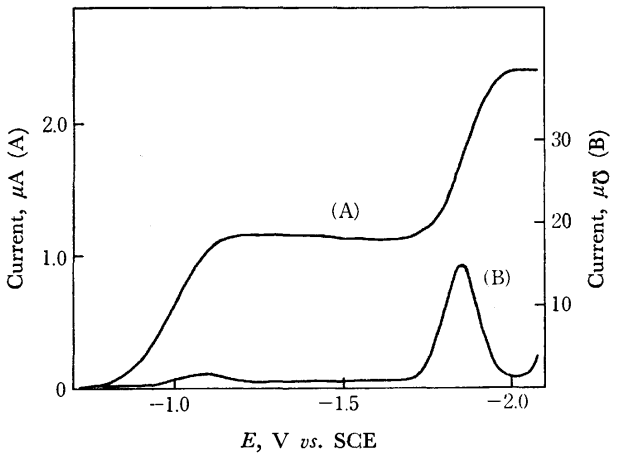

Fig. 1. DC and AC polarograms of K[Co(baen)(ala)$_2$]. 0.15 M TEAP, 20°C
The concentration of K[Co(bean)(ala)$_2$]=1.09 mM
A: DC polarogram, B: AC polarogram

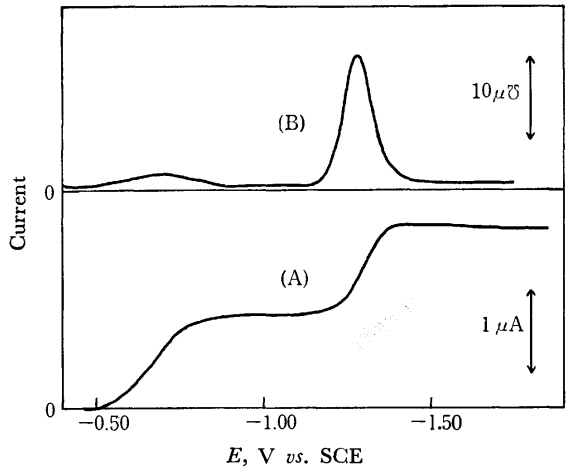

Fig. 2. DC and AC polarograms of K[Co(bisaen)(ala)$_2$]. 0.15 M TEAP, 20°C
The concentration of K[Co(bisaen)(ala)$_2$]=1.09 mM
A: DC polarogram, B: AC polarogram

TABLE 2. THE DEPENDENCE OF LIMITING CURRENT ON THE CONCENTRATION OF COMPLEX
The TEAP concentration=0.15 M, 20°C

Concentration of K[Co(baen)(ala)$_2$] C, mM	i_{l_1}, μA (−1.30 V)	i_{l_1}/C	i_{l_2}, μA (−2.00 V)	i_{l_2}/C
1.0	1.01_2	1.01	0.93_6	0.93_6
1.5	1.52_0	1.01	1.40_4	0.93_7
2.0	2.02_1	1.01	1.87_6	0.93_6
3.0	3.04_0	1.01	2.80_8	0.93_6

TABLE 3. DIFFUSION CURRENT CONSTANTS OF METAL COMPLEXES
0.15 M TEAP, 20°C

System[c]	I[a] 1st wave	I[a] 2nd wave
Co(acac)$_3^0$	1.21_5	—
(Et)$_4$NCoY2H$_2$O	1.24	—
Co(baen)(H$_2$O)$_2^0$	—	1.25
K[Co(baen)(ala)$_2$]·7H$_2$O	1.17_5	1.18
K[Co(baen)(val)$_2$]·8H$_2$O	1.20	1.20
K[Co(baen)(isoleu)$_2$]·8H$_2$O	1.17	1.16
K[Co(baen)(leu)$_2$]·8H$_2$O	1.24	1.22
K[Co(baen)(phenala)$_2$]·6H$_2$O	1.28	1.28
[Co(baen)(NH$_3$)$_2$]ClO$_4$	1.24	1.26
Co(baen)(acac)^0	1.21	1.22
Co(baen)(bzacac)^0	1.20	1.20
[Co(baen)(dip)]ClO$_4$	1.22	1.24
Co(baen-Br$_2$)(acac-Br)^0	1.13_5	1.16[b]
Co(bisaen)(H$_2$O)$_2$	—	1.26_3
K[Co(bisaen)(ala)$_2$]·12H$_2$O	1.18	1.19
[Co(bisaen)(NH$_3$)$_2$]ClO$_4$	1.20	1.20
[Co(bisaen)(dip)]ClO$_4$	1.16	1.18
Co(bisaen)(acac)^0	1.24	1.24
Cu(baen)^0	1.33	—
Cu(baen-Cl$_2$)^0	1.31	—
Cu(baen-Br$_2$)^0	1.33	—
Ni(baen)^0	1.22	—
Ni(baen-Cl$_2$)^0	1.21_5	—

a) $I=i_d/Cm^{2/3}t_d^{1/6}$
b) less accurate
c) acac; acetylacetonate anion, Y^{4-}; EDTA anion, ala; alanine, val; valine, leu; leucine, isoleu; isoleucine, phenala; phenylalanine, bzacac; benzylacetone, dip; 2,2-dipyridyl

a DMF solution give two cathodic waves, the limiting currents of which are exactly proportional to their bulk concentration and to the square-root of the effective pressure on the DME (Tables 1 and 2). The peak-heights of the AC polarograms in Figs. 1 and 2 show that the electrode reaction at the first step of these complexes is irreversible, but that at the second wave, reversible in a polarographic sense. Furthermore, the diffusion current constants, I_d's ($=i_d/C\ m^{2/3}\ t_d^{1/6}$), of both steps were found to be nearly identical to that for the reduction wave of the trisacetylacetonatocobalt(III) complex in the DMF solution (Table 3). It was also found that cobalt(II)-baen and -bisaen complexes give a single reversible reduction wave, the reduction potential of which agrees

TABLE 4. THE POLAROGRAPHIC DATA

System	1st wave			2nd wave			
	Log-plot slope $\left(\log\frac{i}{i_d-i}\right)$, mV	$E_{1/2}$ (V *vs.* SCE)	R[a]	Log-plot slope, mV $\left(\log\frac{i^n}{i_d-i}\right)$ $n=1$	$n=2$	$E_{1/2}$ or E_f[b] (V *vs.* SCE)	R[a]
$Co(acac)_3^0$	92	−0.410	0.51	—	—	—	—
$Et_4NCoY\cdot 2H_2O$	120	−0.518	0.75	—	—	—	—
$Co(baen)(H_2O)_2^0$	—	—	—	—	—	−1.845	7.20
$K[Co(baen)(ala)_2]\cdot 7H_2O$	107	−1.020	0.51	70	—	−1.845	7.20
$K[Co(baen)(val)_2]\cdot 8H_2O$	102	−0.972	0.37	70	—	−1.834	9.00
$[Co(baen)(NH_3)_2]ClO_4$	108	−0.750	0.68	72	—	−1.852	7.16
$Co(baen)(acac)^0$	119	−0.945	0.49	—	66	−1.826	8.56
$[Co(baen)(dip)]ClO_4$	125	−0.452	0.65	—	60	−1.832	7.70
$Co(bisaen)(H_2O)_2^0$	—	—	—	75	—	−1.280	5.77
$K[Co(bisaen)(ala)_2]\cdot 12H_2O$	115	−0.665	0.70	68	—	−1.279	7.50
$[Co(bisaen)(NH_3)_2]ClO_4$	114	−0.590	0.52	65	—	−1.287	6.00
$Co(bisaen)(acac)^0$	125	−0.400	0.90	—	64	−1.315	6.00
$[Co(bisaen)(dip)]ClO_4$	132	−0.104	0.92	—	56	−1.315	7.55
$Cu(baen)^0$	80	−1.541	2.55	—	—	—	—
$Cu(baen\text{-}Cl_2)^0$	68	−1.306	4.70	—	—	—	—
$Cu(baen\text{-}Br_2)^0$	70	−1.289	3.92	—	—	—	—
$Ni(baen)^0$	75	−2.004	7.10	—	—	—	—
$Ni(baen\text{-}Cl_2)^0$	80	−1.760	6.11	—	—	—	—

a) R: R is defined as $I_p/ni_dt_d^{1/2}$, where I_p is the peak-height of AC polarogram.
b) E_f: The potential where $\log(i^2/(i_d-i))$ is equal to zero.

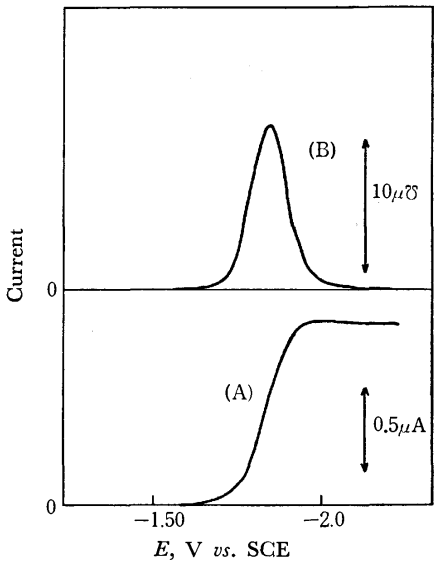

Fig. 3. DC and AC polarograms of $Co(bean)(H_2O)_2^0$.
0.15 M TEAP, 20°C
The concentration of $Co(baen)(H_2O)_2^0=1.10$ mM
A: DC polarogram, B: AC polarogram

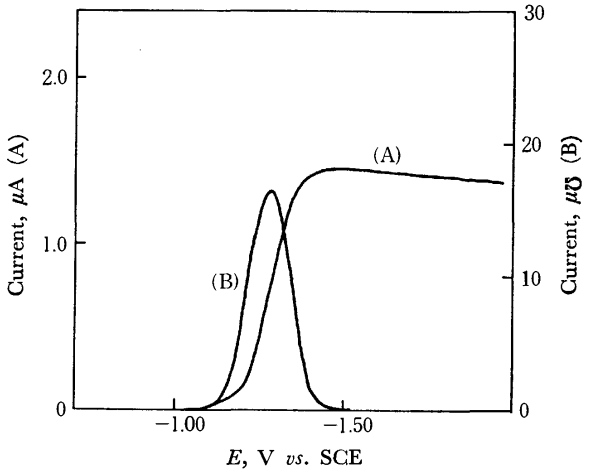

Fig. 4. DC and AC polarograms of $Co(bisaen)(H_2O)_2^0$.
0.15 M TEAP, 20°C
The concentration of $Co(bisaen)(H_2O)_2^0=1.40$ mM
A: DC polarogram, B: AC polarogram

well within several milivolts with that of the second step of the corresponding cobalt(III) complex, and that their I_d values are nearly identical to that of the cobalt(III) complex (Figs. 3 and 4). All the above polarographic evidence indicates that the first and second steps of cobalt(III) complexes correspond, respectively, to the one-electron reduction of cobalt(III) to cobalt(II) and that of cobalt(II) to cobalt(I). The polarographic data on cobalt(III)-baen and -bisaen complexes studied in this paper are summarized in Table 4, together with those on nickel(II) and copper(II)-bean complexes.

As is shown by the data in Table 4, the first waves of the *β-cis* complexes with the general formula $CoZY^{1-a}$ give log-plot (E *vs.* $\log(i/(i_d-i))$) slopes larger than those of *trans* complexes, $CoZX_2^{1-2b}$. Although the details of the determination of the configuration have not been described in this paper, the NMR study confirmed that all the cobalt(III) complexes of the general formula $CoZY^{1-a}$ have the *β-cis* configuration, and the $CoZX_2^{1-2b}$ complexes the *trans* configuration.

An electrode reaction accompanied by a change in the configuration of the reactant is generally believed to be slow.[14] Therefore, the above finding may imply that the electrode reaction at the first step of the *β-cis* complex is accompanied by a change in its configuration or by a loosening of its structure. This would also explain well the reversible property of the second reduction step of the *β-cis* complex. However, in the case of the irreversible polarographic reduction, from the theoretical point of view the log-plot examination can not be expected to provide many useful information on the electrode reaction mechanism or on the formula of the reduction product. Therefore, we can not describe more precisely the nature of the first wave on the basis of the log-plot examination. On the other hand, in the case of the second step, because of its perfect reversible nature, we can determine exactly the electrode reaction mechanism and, hence, formulate the reduction product by performing a careful log-plot examination (E *vs.* $\log(i^n/(i_d-i))$ plot). The polarographic data gives in Table 4 also indicate that the second waves of the mixed cobalt(III) complexes of baen and bisaen containing bidentate ligands give exclusively straight lines, with reciprocal slopes of about 65 mV, close to the theoretical value of 58 mV for the reversible one-electron reduction in the plot of the DC potential, E, against $\log(i^2/(i_d-i))$ (Fig. 5). As has been stated previously, the sample solutions used in this study contained no free ligand. Therefore, the above linear relation between E and $\log(i^2/(i_d-i))$ implies that one molecule of the ligand will be liberated in the course of the reduction of the complex. Considering the polarographic evidence that the second wave appears at the potential nearly identical to the reduction potential of the corresponding cobalt(II) complex, the ligand liberated in the course of the reduction may be concluded to be the bidentate one. Consequently, the electrode reactions for the reduction of the *β-cis* cobalt(III)-baen and -bisaen complexes at the DME can be formulated as:

$$CoZY^{1-a} + e^- \rightleftharpoons CoZY^{a-}$$

$$CoZY^{a-} + e^- \rightleftharpoons CoZ^- + Y^{a-}$$

On the other hand, in the polarography of a series of mixed cobalt(III)-baen and -bisaen complexes involving amino acids or ammonia (the general formula is $CoZX_2^{1-2b}$), which have the *trans* configuration, the plot of E against $\log(i/(i_d-i))$ for the second step gave straight lines, with slopes falling in the range from 60 to 70 mV, corresponding to the reversible one-electron reduction (Fig. 6). By the addition of lithium(I) perchlorate to the sample solution, the reduction step was shifted remarkably to less negative potentials, and the plot of E against $\log(i^3/(i_d-i))$ in place of $\log(i/(i_d-i))$ gave a straight line with a slope of 57 mV. A typical result is shown in Fig. 7. The above positive shift of the reduction potential and the linear relation between the E and $\log(i^3/(i_d-i))$ can be reasonably explained in terms of the interaction of a lithium(I) ion with the reduction product, the cobalt(I) complex, that is, the coordinative relaxation of the amino acid anion from the cobalt(I)-baen or -bisaen complex.[15] Although the dependence of the potential shift on the concentration of the lithium(I) ion was examined in only a qualitative way, because of the lack of an association constant in the DMF solu-

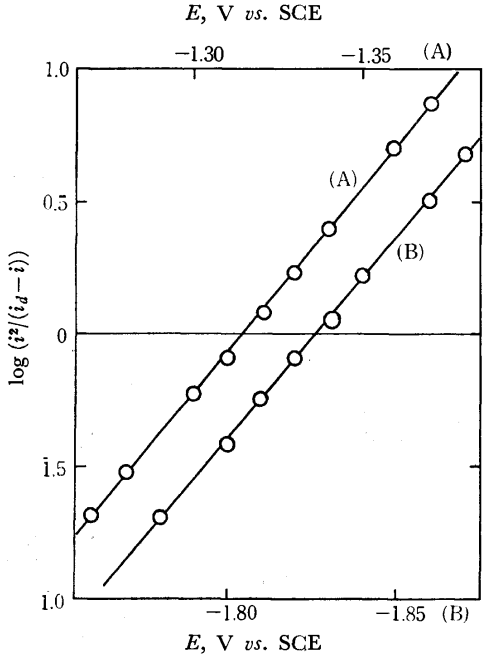

Fig. 5. The log-plot examination of the second wave.
0.15 M TEAP, 20°C
A: Co(bisaen)(acac)$^{\oplus}$, B: Co(bean)(acac)$^{\oplus}$

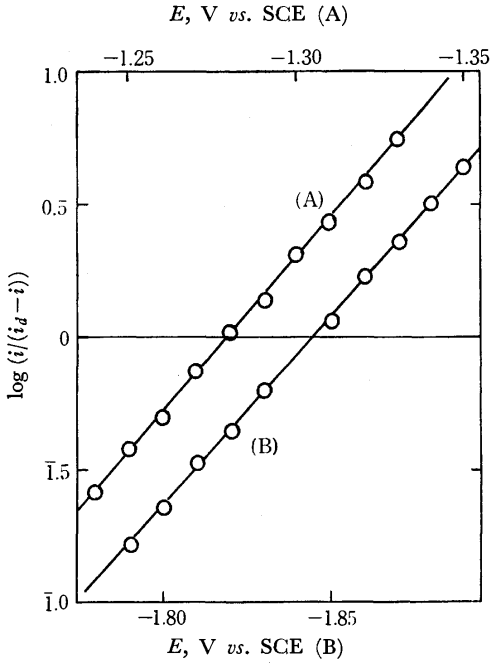

Fig. 6. The log-plot examination of the second wave.
0.15 M TEAP, 20°C
A: K[Co(bisaen)(ala)$_2$], B: K[Co(baen)(ala)$_2$]

14) A. A. Vlcek, "Mechanism of the Electrode Processes and Structure of Inorganic Complexes," pp. 356, 359, 364 of "Progress in Inorganic Chemistry," edited by F. A. Cotton, Interscience Publ. Inc., (1963).

15) R. W. Murray and L. K. Hiller, Jr., *Anal. Chem.*, **39**, 1221 (1967).

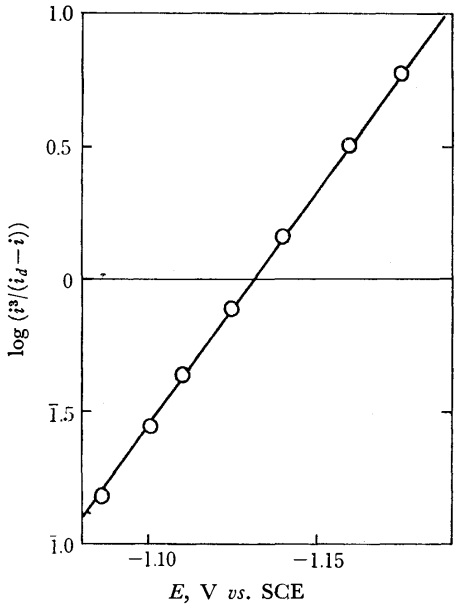

Fig. 7. The log-plot examination of the second wave of K[Co(bisaen)(ala)$_2$] in the presence of 0.10 M lithium(I) salt.
0.15 M TEAP, 20°C

tion, the finding that the reduction potential is shifted to less negative potentials with an increase in the lithium(I) ion concentration also supports the present authors' explanation. Thus, the above linear relation between E and $\log(i^3/(i_d-i))$ suggests the following reaction mechanism for the relaxation process:

$$CoZX_2^{2-} + e^- + 2Li^+ \rightleftharpoons CoZ^- + 2LiX$$

where Z^{2-} and X^- mean the baen or bisaen anion and the amino acid anion. Therefore, the reduction process of *trans* cobalt(III)-baen and -bisaen complexes involving amino acids or ammonia in solutions not containing lithium(I) salt can be formulated as:

$$CoZX_2^- + e^- \rightleftharpoons CoZX_2^{2-} \quad \text{irreversible}$$

$$CoZX_2^{2-} + e^- \rightleftharpoons CoZX_2^{3-} \quad \text{reversible}$$

The addition of calcium(II) salt to the trans cobalt(III)-baen and -bisaen complex solutions also caused a similar coordinative relaxation. That is, in the presence of the calcium(II) ion, the second wave gave a straight line with a slope of 60 mV between E and $\log(i^2/(i_d-i))$. Those results are not shown here.

We have mentioned earlier that a series of *trans* cobalt(III)-baen and -bisaen complexes with the general formula of $CoZX_2^{1-2b}$ all give the reduction product $CoZX_2^{-(1+2b)}$, which has an atomic configuration similar to that of $CoZX_2^{1-2b}$, in their polarographic reduction at the DME. On the other hand, a series of *β-cis* cobalt(III) complexes with the general formula of $CoZY^{1-a}$ are reduced to the cobalt(I) to give the CoZ^-, thus, liberating the bidentate ligand, Y^{a-}. The coordination of a bidentate ligand such as the acetylacetonate anion and 2,2′-dipyridyl to the metal ion force the baen and bisaen to take a *β-cis* configuration in the octahedral complex. Therefore, the dissociation of bidentate Y^{a-} from the metal will allow the baen and bisaen to be in a *trans* configuration, which has less strain than the *β-cis* configuration.

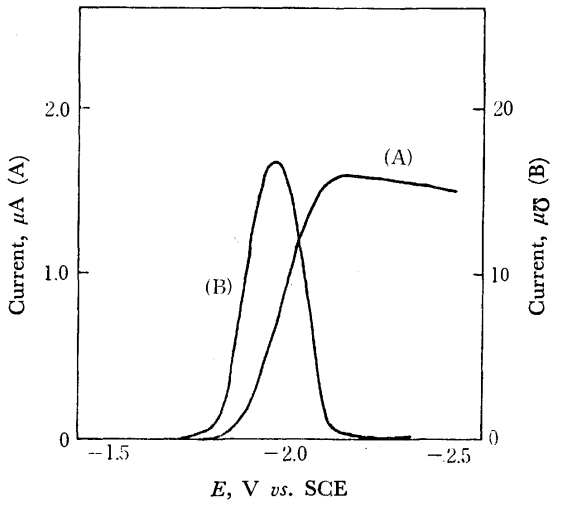

Fig. 8. DC and AC polarograms of Ni(baen)^0.
0.15 M TEAP, 20°C
The concentration of Ni(baen)^0 = 1.70 mM

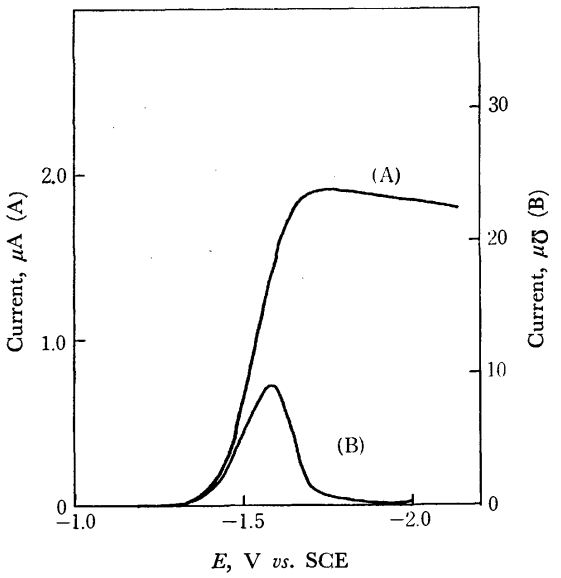

Fig. 9. DC and AC polarograms of Cu(baen)^0.
0.15 M TEAP, 20°C
The concentration of Cu(baen)^0 = 1.74 mM

Square-planar nickel(II) and copper(II)-baen complexes also gave single cathodic waves corresponding to the one-electron reduction of the metal(II) complex (see the I_d values in Table 3). Typical polarograms are reproduced in Figs. 8 and 9. The plot of E against $\log(i/(i_d-i))$ also gave linear relations, with slopes of about 70 mV, corresponding to the following reversible one-electron reduction:

$$MZ^0 + e^- \rightleftharpoons MZ^- \quad \text{reversible}$$

From the above experimental results and the discussion of them, it can be stated that the unusual stability of baen and bisaen complexes containing the metal ion formally in the +1 oxidation state is ascribable to the stable planar configuration of the ligands. The possibility of the formation of cobalt, nickel, and copper metals in the course of the reductions of baen, and bisaen complexes was disproved by the α-nitroso-β-naphthol, dimethylglyoxime, and ammonia tests of

aqueous solutions obtained by treating the mercury metal used in the polarographic study with concentrated hydrochloric acid and by then neutralizing the resulted solutions.

The influence of the replacement of the ligand by the halogen atom on the polarographic behavior of baen complexes was also studied. As is shown by the data in Tables 3 and 4, the introduction of the halogen atom on the ligand causes a remarkable positive shift of polarographic waves. However, *N,N'*-ethylene-bis(3-halogenoacetylacetoniminato) (baen-X_2) complexes also gave well-defined polarographic steps which correspond to the reversible reduction of M(II) to M(I). Although the influence of such a substitution on the coordinated ligand can be discussed from various points of view, as a first approximation the introduction of a halogen atom may be considered to have a remarkable effect on the delocalized π system of the ligand. In considering that the cobalt(III) ethylenediaminetetraacetate complex gives only one reduction step, corresponding to the reduction from Co(III) to Co(II) under the present experimental conditions (Table 4), we can not completely neglect the possibility that the delocalized π system of the baen or bisaen contributes to some extent to the stabilization of the M(I) oxidation state. Therefore, the finding that the metal(II)- baen-X_2 complexes also give polarographic steps which correspond to the reduction of M(II) to M(I) seems to indicate that the delocalized π system of the acetylacetone segment in the baen and bisaen plays only a minor role in the stabilization of the M(I) oxidation state. Furthermore, we can mention the following two facts (Table 4):

1) The first step of the *β-cis* cobalt(III)-baen or -bisaen complex appears at less negative potentials than that of the *trans* complex, $CoZX_2$[1-2b].

2) The reduction steps of the bisaen complexes appear at less negative potentials than those of corresponding baen complexes.

The former can be ascribed to the asymmetric structure of the *β-cis* complex and to the coordination of the bisentate ligand with a delocalized π system.[14] The latter fact, that the reduction wave of bisaen complex is located at a less negative potential than that of the baen complex, is ascribable to the benzene ring of bisaen.[14]

Olson and Vasilevskis[1-3] stated in their electrochemical and synthetic studies of cyclic amine complexes of nickel(II), copper(II), and cobalt(II) that probably the major factor responsible for the unusual stability of the cyclic amine complexes containing the metal ion in the +1 oxidation state is the cyclic nature of the ligands. However, all the experimental evidence obtained in this polarographic study of the metal complexes of noncyclic Schiff bases, baen and bisaen, leads to the conclusion that the unusual stability of metal(I) complexes can be attributed to the rigid and stable square-planar nature of tetradentate ligands. Here, we can not disregard the role played by the stable environment provided by the inert aprotic solvent, DMF.

Ionic Equilibria in Mixed Solvents. VII. Hydrolysis of Copper(II) Ion in Dioxane-Water Mixtures containing 3 M (Li)ClO_4 as an Ionic Medium

Hitoshi OHTAKI and Takayoshi KAWAI

Department of Electrochemistry, Tokyo Institute of Technology, O-okayama, Meguro, Tokyo

(Received October 2, 1971)

The hydrolytic reactions of copper(II) ion were studied at 25°C in water, in 0.1 and 0.5 mole fraction dioxane-water mixtures, each containing 3 M (Li)ClO_4 as an ionic medium. Emf measurements were carried out in the range of the total copper(II) concentration of 0.01125—0.07106 M (in water), 0.01548—0.1356 M (in the 0.1 mole fraction dioxane-water mixture), and 0.02257—0.1231 M (in the 0.5 mole fraction dioxane-water mixture), respectively. Species formed and their formation constants determined (log $*\beta_{p,q}$) are: CuOH (-7.54 ± 0.02), Cu_2OH (-6.22 ± 0.02), $Cu_2(OH)_2$ (-11.12 ± 0.05), and $Cu_3(OH)_2$ (-10.36 ± 0.05) in water; CuOH (-7.44 ± 0.02), Cu_2OH (-6.22 ± 0.02), $Cu_2(OH)_2$ (-11.35 ± 0.05), and $Cu_3(OH)_2$ (-10.12 ± 0.08) in the 0.1 mole fraction dioxane-water mixture; CuOH (-7.74 ± 0.02), and Cu_2OH (-6.40 ± 0.02) in the 0.5 mole fraction dioxane-water mixture.

From the hydrolytic reaction of beryllium ion in dioxane-water mixtures, Ohtaki and Kato[1,2] found that the composition and formation constants of hydrolyzed species of beryllium ions change little even though the dioxane concentration is varied from zero to 0.2 mole fraction (55.01 wt%). Thus, dissociation constants of aquated metal ions, which are weak acids, vary in different manner from those of carboxylic acids[3,4] and of ammonium ions[5,6].

In the present work, the hydrolytic reaction of copper(II) ion was studied by emf measurements in water, in 0.1 and 0.5 mole fraction dioxane-water mixtures, and the chemical species formed and their formation constants were determined.

If we neglect solvated solvent molecules and electric charges of the species for the sake of simplification, the hydrolytic reaction of copper(II) ions can be written as follows, no association of perchlorate ions with any species being assumed;

$$qCu + pH_2O = Cu_q(OH)_p + pH \qquad *\beta_{p,q} = [Cu_q(OH)_p][H]^p/[Cu]^q \qquad (1)$$

h Hydrogen ion concentration in equilibrium.
H Analytical excess of hydrogen ion concentration $=[ClO_4]=2B=[Li]$.
B Total concentration of copper(II) ion.
b Concentration of free copper(II) ion.
Z Average number of hydrogen ions set free per copper ion $=(h-H)/B$.
p Number of hydroxyl groups bound to hydrolyzed species.
q Number of copper atoms present in hydrolyzed species.
$*\beta_{p,q}$ Equilibrium constant for the formation of $Cu_q(OH)_p$.
E Emf.
[ ] Concentration.

The Method of Measurements. B was kept constant during the course of potentiometric titration. Lithium perchlorate was used as an ionic medium in order to keep the total ionic equivalent concentration constant (3 M). Potentiometric titrations were carried out by the following two methods.

1) Water and the 0.1 mole fraction dioxane-water mixture. Ordinary titration method was employed for the cases of water and the 0.1 mole fraction dioxane-water mixture. Thus a titrant was added from a buret to a test solution prepared as follows. Copper(II) perchlorate solution was neutralized with an alkaline solution prepared by electrolysis, until a certain amount of copper hydroxide was precipitated. The turbid solution was bubbled for several days with nitrogen gas which was presaturated with solvent vapor. The solution was then filtered through G3 and G4 glas filters covered with platinum powder, a clear test solution being obtained. The total concentration of copper(II) ion in this solution was determined by means of gravimetry with salicylaldoxime.[7] An acidic titrant with the same concentration of copper(II) ion as that of the test solution was added. The composition of the titrant was B M of $Cu(ClO_4)_2$, H_0 M of $HClO_4$ and $(3-2B-H_0)$ M of $LiClO_4$.

2) In a system of a 0.5 mole fraction dioxane-water mixture, hydrogen ions were generated coulometrically, because solubility of copper hydroxo complexes was so low that a fairly small amount of hydrogen ions had to be added for carrying out measurements and the solution was so viscous that addition of a titrant from a buret gave rise to erroneous results. The electric circuit for coulometry was as follows.

(−) Pt | 0.10 M $AgClO_4$, 2.90 M $LiClO_4$ in water | 3 M $LiClO_4$ in water | 3 M $LiClO_4$ in mixture | Test soln | Pt (+)

Neither precipitation nor turbidity was observed during the course of experiments. A constant emf was obtained within 10 min after addition of a titrant, and remained unchanged for at least 5 hours within the accuracy 0.1 mV.

1) H. Ohtaki, *Inorg. Chem.*, **6**, 808 (1967).
2) H. Ohtaki and H. Kato, *ibid.*, **6**, 1935 (1967).
3) T. Shedrovsky and R. L. Kay, *J. Phys. Chem.*, **60**, 151 (1956).
4) H. S. Dunsmore and J. C. Speakmann, *Trans. Faraday Soc.*, **50**, 236 (1954).
5) A. K. Covington and M. J. Tait, *Disscuss. Faraday Soc.*, **39**, 176 (1956).
6) M. H. Miles and E. M. Eyring, *J. Phys. Chem.*, **69**, 467 (1965).
7) F. J. Welcher, "Organic Anayltical Reagents," Vol. III. 2nd ed. D. Van Nostrand C., Inc., New York, N. Y. (1947), p. 262.

The hydrogen ion concentration was determined by means of the cell

$$\text{Ref} \mid \text{Test Solution} \mid \text{GE}, \qquad \text{(A)}$$

where GE denotes a glass electrode and Ref, the reference half cell (B)

$$\left|\begin{array}{l|l|l} 3.000\ \text{M}\ LiClO_4 & 2.990\ \text{M}\ LiClO_4 & \text{AgCl-Ag} \\ \text{in mixture} & 0.010\ \text{M}\ AgClO_4 & \\ & \text{in water} & \end{array}\right| \qquad \text{(B)}$$

The emf of cell (A) can be written (at 25°C) as

$$E = E_0' + 59.15 \log h + 59.15 \log f_H + E_j(h, B), \qquad (2)$$

where E_0' is a constant and f_H represents the activity coefficient of hydrogen ion. The standard state is so defined that f_H as well as the activity coefficients of the reacting species tends to unity as the composition approaches 3 M $LiClO_4$ in a given solvent. $E_j(h, B)$ denotes the liquid junction potential at the junction, test solution | 3 M $LiClO_4$ aqueous solution. The liquid junction potential at the other junction, 3 M $LiClO_4$ in the aqueous or mixed solvent | 2.99 M $LiClO_4$, 0.01 M $AgClO_4$ aqueous solution, can be assumed to be constant throughout the course of titration.

In such a case where the total ionic concentration B, and the solvent composition are kept constant, constancy of f_H can be assumed in the course of a series of potentiometric measurements. When h is small and the total copper ion concentration is kept $E_j(h, B)$ can be a constant and Eq. (2) may be written as follows[2].

$$E = E_0 + 59.15 \log h \qquad (3)$$

where

$$E_0 = E_0' + 59.15 \log f_H + E_j(h, B)$$

This was used to determine the hydrogen ion concentration from emf data.

Experimental

Reagents and Analysis. *Copper(II) perchlorate*: Reagent grade copper(II) nitrate recrystallized twice from water was heated under an infrared lamp until no evolution of NO_2 gas could be recognized, and then in an electric oven for 1 day at 800°C. The copper(II) oxide thus prepared was dissolved in a hot perchloric acid solution and then filtered. Copper(II) perchlorate crystals were obtained by recrystallization. The stock solution of copper perchlorate was prepared by dissolving the crystals in water. pH of the solution was about 2. The acid concentration in the stock solution was determined in the following way. An aliquot (about 50 ml) of aqueous 3 M $LiClO_4$ solution containing about 10^{-3} M $HClO_4$ was gradually neutralized coulometrically. As the volume change is negligible during the course of coulometric titration, the end point was located by plotting $10^{E/59.15}$ against microfaradays passed (Gran plot[8]). A small and known amount of the stock solution of copper(II) perchlorate was then added to the vessel from a weighing buret and the solution was gradually acidified by means of a coulometric generation of hydrogen ions. The amount of acid present in the solution could be estimated from a similar plot of $10^{E/59.15}$ *vs.* microfaradays.

The total perchloric acid concentration determined by the ion exchange method agreed satisfactorily with the sum of equivalent concentrations of copper(II) and hydrogen ions in the solution.

Lithium perchlorate was prepared by the method described by Biedermann and Ciavatta.[9]

Dioxane was purified by the method described elsewhere.[1]

Apparatus. *Glass electrode and pH meter*: Beckman No. 40498 glass electrodes were used in combination with Radiometer PHM-4d pH meter (Copenhagen).

The Wilhelm-type of the half-cell described by Forsling, Hietanen, and Sillén[10] was used for emf measurements.

A coulometric analyzer (Leeds & Northrup Co., Philadelphia, Pa.) was employed as a current power source. Constant currents of 0.643 and 6.43 mA were used; the currents were held constant within ±0.05 and ±0.1%, respectively. Emf measurements were carried out at 25.00±0.01°C in a paraffin oil thermostat in a room thermostated at 25±1°C.

Results

Values of Z and $-\log h$ in each series of B calculated from the emf data are represented graphically in Figs. 1, 2, and 3. The compositions and the formation constants of the species were evaluated on the basis of the data.

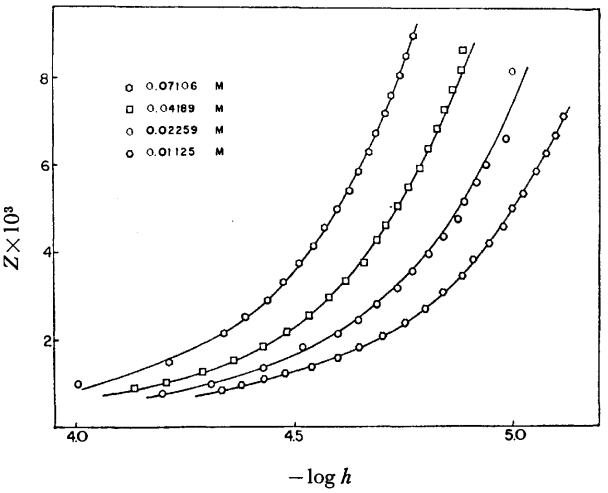

Fig. 1. Values of Z *vs.* $-\log h$ in the aqueous solution. Solid lines show calculated curves of Z with formation constants of $\log {}^*\beta_{1,1} = -7.54$, $\log {}^*\beta_{1,2} = -6.22$, $\log {}^*\beta_{2,2} = -11.12$ and $\log {}^*\beta_{2,3} = -10.36$.

The concentration of hydrogen ion set free by hydrolysis BZ is given by the general formula

$$BZ = \sum_p \sum_q p[Cu_q(OH)_p] = \sum_p \sum_q p {}^*\beta_{p,q} b^q h^{-p} \qquad (4)$$

In the case where maximum value of Z is very low, we can, without introducing any appreciable error, simplify the preliminary calculations by employing the approximation

$$[Cu^{2+}] = b \approx B \qquad (5)$$

Applying the approximation to Eq. (4) and rearrang-

8) G. Gran, *Analyst* (London), **77**, 661 (1952).

9) C. Berecki-Biedermann, *Ark. Kemi*, **9**, 175 (1955).

10) W. Forsling, S. Hietanen, and G. Sillén, *Acta Chem. Scand.*, **6**, 901 (1952).

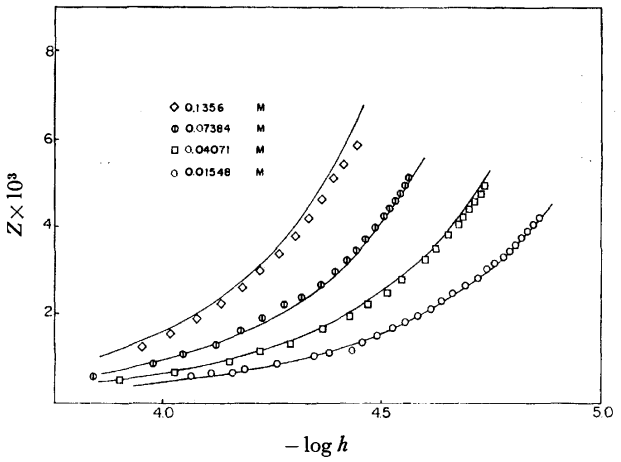

Fig. 2. Values of Z *vs.* $-\log h$ in the solution of a 0.1 mole fraction dioxane-water mixture. Solid lines show calculated curves of Z with formation constants of $\log {}^*\beta_{1,1}=-7.44$, $\log {}^*\beta_{1,2}=-6.22$, $\log {}^*\beta_{2,2}=-11.35$, and $\log {}^*\beta_{2,3}=-10.12$.

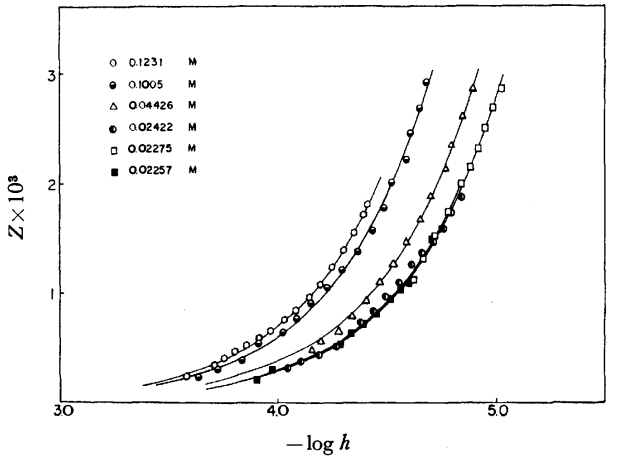

Fig. 3. Values of Z *vs.* $-\log h$ in the solution of a 0.5 mole fraction dioxane-water mixture. Solid lines show calculated curves of Z with formation constants of $\log {}^*\beta_{1,1}=-7.74$ and $\log {}^*\beta_{1,2}=-6.40$.

ing it, we have

$$Zh = \sum_p pK_p h^{-(p-1)} \tag{6}$$

where

$$K_p = \sum_q {}^*\beta_{p,q} B^{q-1} \tag{7}$$

By plotting Zh against h^{-1} we obtain sets of straight lines with various slopes in the system of water and a 0.1 mole fraction dioxane-water mixture, and a set of horizontal lines in the system of the 0.5 mole fraction dioxane-water mixture. We see that there are homoligandic complexes with one and two hydroxo groups in water and in the 0.1 mole fraction dioxane-water mixture, whereas homoligandic complexes with one hydroxo group are formed in the 0.5 mole fraction dioxane water mixture. Plots of $K_1=\sum_q {}^*\beta_{1,q}B^{q-1}$ *vs.* B gave a straight line in each solvent system, which showed that q is equal to 1 and 2 at $p=1$; thus, CuOH and Cu_2OH are present in all solvent compositions examined. The formation constants of the CuOH and Cu_2OH complexes can be obtained from the intercept and the slope of the plot in each solvent system.

The values of the slope ($K_2=2\sum_q {}^*\beta_{2,q}B^{q-1}$) are plotted against B in the case of water and a 0.1 mole fraction dioxane-water mixture. The plot gave a smooth curve with zero intercept. If values of K_2 divided by B were plotted against B, a straight line was obtained in both solvent systems. The result indicates that q is equal to 2 and 3 at $p=2$; the $Cu_2(OH)_2$ and $Cu_3(OH)_2$ complexes exist as dihydroxo complexes. From the intercepts and slopes of these plots the formation constants of the $Cu_2(OH)_2$ and $Cu_3(OH)_2$ complexes are obtained. No other complexes have been detected.

The species formed by hydrolysis of copper(II) ion are found to be CuOH, Cu_2OH, $Cu_2(OH)_2$, and $Cu_3(OH)_2$ in water and in the 0.1 mole fraction dioxane-water mixture, and CuOH and Cu_2OH in the 0.5 mole fraction dioxane-water mixture. Thus, Eq. (4) can be written as

$$BZ = {}^*\beta_{1,1}h^{-1}b + {}^*\beta_{1,2}h^{-1}b^2 + 2{}^*\beta_{2,2}h^{-2}b^2 + 2{}^*\beta_{2,3}h^{-2}b^3 \tag{8}$$

for the systems of water and 0.1 mole fraction dioxane-water mixture and,

$$BZ = {}^*\beta_{1,1}h^{-1}b + {}^*\beta_{1,2}h^{-1}b^2 \tag{8'}$$

for the system of 0.5 mole fraction dioxane-water mixture.

The data were treated by a generalized least-squares method with an electronic computer, HITAC 5020E, in order to make the error square sum $U=\sum(Z-Z_{\text{calcd}})^2$ a minimum for the set of formation constants ${}^*\beta_{p,q}$.

The final values of the constants obtained by computer calculation and their uncertainties estimated are collected in Table 1.

Discussion

Several workers[9,11,12] proposed the formation of $CuOH^+$ and $Cu_2(OH)_2^{2+}$ complexes in aqueous 3 M (Li or Na) ClO_4 solution. Pedersen[13] reported formation of the $CuOH^+$, Cu_2OH^{3+}, and $Cu_2(OH)_2^{2+}$ complexes. Mahapatra[14] confirmed the formation of higher polynuclear complexes.

In the present study we have found the formation of the $Cu_3(OH)_2^{4+}$ complex as well as complexes found by previous workers.[9,11-13] Addition of dioxane, however, prevents the formation of higher complexes.

The difference between $\log {}^*\beta_{1,1}$ and $\log {}^*\beta_{1,2}$ is close to that between $\log {}^*\beta_{2,2}$ and $\log {}^*\beta_{2,3}$. This shows that the stabilization of the Cu_2OH^{3+} complex formed by the combination of a copper ion with an OH^- group in the $CuOH^+$ complex is similar to that of the $Cu_3(OH)_2^{4+}$ complex formed by the combination of a copper ion with the $Cu_2(OH)_2^{2+}$ complex. This

11) H. Ohtaki, *Inorg. Chem.*, **7**, 1205 (1958).
12) H. Kakihana, T. Amaya, and M. Maeda, This Bulletin, **43**, 3155 (1970).
13) K. J. Pedersen, *Kgl. Danske Videnskab. Selskab, Mat. Fys. Medd.*, **20**, 1 (1939).
14) S. Mahapatra and R. S. Subrahmanya, *Proc. Indian Acad. Sci., Sect. A.*, **65**, 283 (1967).

Table 1. Formation constants ($\log {}^*\beta_{q,p}$)

Solvent	CuOH	Cu_2OH	$Cu_2(OH)_2$	$Cu_3(OH)_2$
water	-7.54 ± 0.02	-6.22 ± 0.02	-11.12 ± 0.05	-10.36 ± 0.05
0.1 m.f. dioxane-H_2O	-7.44 ± 0.02	-6.22 ± 0.02	-11.35 ± 0.05	-10.12 ± 0.08
0.2 m.f. dioxane-H_2O[11]	-7.60 ± 0.05	<-7.4	-10.98 ± 0.05	
0.5 m.f. dioxane-H_2O	-7.74 ± 0.02	-6.40 ± 0.02	—	—

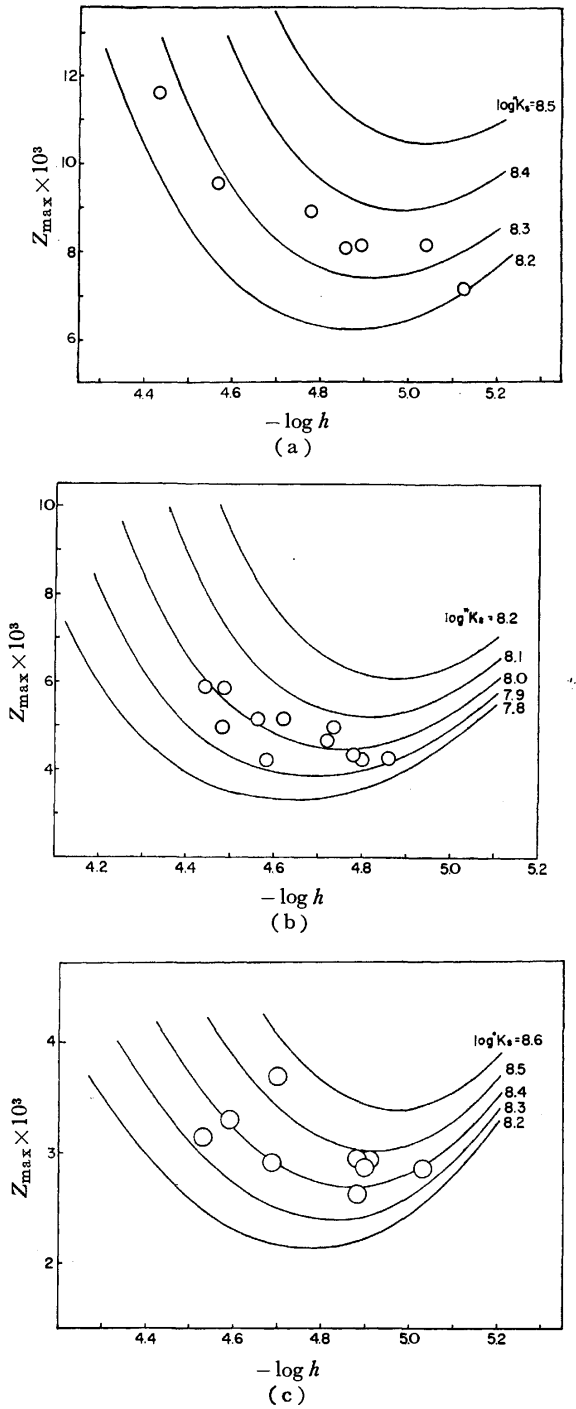

Fig. 4. Z_{max} plotted against $-\log h$. Solid lines are calculated curves of Z_{max} at various values of K_s. a) Water, b) the 0.1 mole fraction dioxane-water mixture, c) the 0.5 mole fraction dioxane-water mixture.

suggests that in the latter reaction the copper ion makes a bond with one OH^- group which is connected with only one copper atom, as in the case of a copper atom combining with one OH^- group in the Cu_2OH^{3+} complex in the former reaction. Thus, the $Cu_2(OH)_2^{2+}$ complex can take a linear form but not a ring form and the $Cu_3(OH)_2^{4+}$ complex can have two single OH^- bridges in the molecule.

In the range of concentration of dioxane up to 0.2 mole fraction, the composition of species produced and their formation constants were scarcely affected by solvent compositions. However, in the 0.5 mole fraction (83.5 wt%) dioxane-water mixture, dihydroxo complexes disappeared while monohydroxo complexes existed without appreciable change in formation constants.

The maximum value of Z, *i.e.*, Z_{max}, at a given B depends on the solubility product of copper hydroxide as well as the formation constants of the complexes in the solution, provided that the solution is equilibrated with copper hydroxide precipitates. If the solubility product ${}^*K_s$ is defined by

$$ {}^*K_s = [Cu^{2+}][H^+]^{-2} = bh^{-2} \simeq Bh^{-2} \quad (9) $$

we get the following equations by substituting this relation into Eqs. (8) and (8'), respectively;

$$ Z_{max} \simeq {}^*\beta_{1,1}h_{max}^{-1} + {}^*\beta_{1,2}{}^*K_s h_{max} + 2{}^*\beta_{2,2}{}^*K_s + 2{}^*\beta_{2,3}{}^*K_s{}^2 h^2{}_{max} \quad (10) $$

for systems of water and 0.1 mole fraction dioxane-water mixture, and

$$ Z_{max} \simeq {}^*\beta_{1,1}h_{max}^{-1} + {}^*\beta_{1,2}{}^*K_s h_{max} \quad (10') $$

for the system of 0.5 mole fraction dioxane-water mixture.

Some supplementary experiments have been achieved to determine Z_{max} at various values of B in these solvents. Since no appreciable increase in Z_{max} was observed when agitation of a solution with copper hydroxide precipitates was continued for 3—7 days, we regarded the solution as a saturated solution with copper hydroxide. Values of Z_{max} thus found are plotted against $-\log h$ in Fig. 4. They are compared with values of Z_{max} calculated by Eqs. (10) and (10') with various values of ${}^*K_s$. From these plots the most probable values of $\log {}^*K_s$ were estimated to be 8.3 ± 0.2 in the aqueous solution, 8.0 ± 0.2 in the 0.1 mole fraction dioxane-water mixture and 8.4 ± 0.2 in the 0.5 mole fraction dioxane-water mixture containing 3M $LiClO_4$ as an ionic medium. From these results it is seen that the solubility product of $Cu(OH)_2$ given in terms of ${}^*K_s$ is practically independent of solvent composition as is so the formation constant of the $Cu_q(OH)_p^{(2p-q)+}$ complex described in terms of ${}^*\beta_{p,q}$.

The authors thank Prof. M. Tanaka, Nagoya University, for his advice. They are indebted to Dr. M. Maeda for valuable discussions.

Interaction between Organoaluminum Compounds and Ditertiary Phosphines Studied by Proton Magnetic Resonance

Teruhiko KAGAWA and Harukichi HASHIMOTO*

Department of Synthetic Chemistry, The University of Tokyo, Bunkyo-ku, Tokyo

**Department of Applied Chemistry, Faculty of Engineering, Tohoku University, Sendai*

(Received October 14, 1971)

The adduct formation of triethylaluminum or diethylaluminum chloride with ditertiary phosphines ($Ph_2P(CH_2)_nPPh_2$ $n=1,2,3,4$, and 6) in benzene solution was investigated by PMR. The adducts have a composition of $(AlEt_3)_2$ (diphosphine) except in the case of $Ph_2PCH_2PPh_2$, which makes two kinds of adducts (1 : 1 and 2 : 1). Electronegativity of the complexed aluminum is also calculated from Dailey-Shoolery equation.

During the course of an investigation of the effect of ligands on butadiene-ethylene codimerization reaction catalyzed by $CoCl_2(Ph_2P(CH_2)_nPPh_2)$-$AlEt_3$,[1] it became desirable to study the interaction of ditertiary phosphine ligand with triethylaluminum. In such catalyst system, the organoaluminum compound may be considered not only to reduce the metal to low oxidation state, but also to activate the low oxidation state complex to make the coordination site(s) vacant.[2] Such activation may be caused by the interaction of ditertiary phosphine(Lewis base) with organoaluminum compound(Lewis acid).

On the other hand, interaction of Lewis bases such as ethers and tertiary amines with organoaluminum compounds has been extensively studied.[3] But much less is studied about the interaction with phosphines,[4] especially ditertiary phosphines.

The object of this paper is to describe the interaction of triethylaluminum or diethylaluminum chloride with ditertiary phosphines $Ph_2P(CH_2)_nPPh_2$ ($n=1,2,3,4$, and 6) by PMR and to discuss the effect of the methylene chain length of phosphines.

Experimental

All operations were performed under dry nitrogen atmosphere.

Reagent. $AlEt_3$ and $AlEt_2Cl$(Ethyl Corp., USA) were distilled under vacuum and ditertiary phosphines $Ph_2P(CH_2)_nPPh_2$ ($n=1,2,3,4,6$)[5] were synthesized according to the method of Hewertson and Watson,[6] and purified toluene and benzene were stored under dry nitrogen.

Procedure. An appropriate amount of 14.5 wt% benzene solution of triethylaluminum was mixed with an appropriate amount of ditertiary phosphine and a small amount of toluene as an internal standard, and this homogeneous solution was poured into 5.0 mm diameter pyrex tube by syringe and the tube was sealed off. Proton magnetic resonance spectra were run at room temperature on Hitachi Perkin-Elmer R-20A at 60 MHz.

Results and Discussion

PMR Spectra of Ditertiary Phosphines and Organoaluminum Compounds. Spectra of 1,1-bis(diphenylphosphino)methane and 1,2-bis(diphenylphosphino)-ethane in benzene solution were observed as a triplet due to the coupling between ^{31}P and ^{1}H, and the coupling constants were as follows; DPM: $|\,^2J_{PH}\,| = 1.8$ cps, DPE: $|\,^2J_{PH}+{}^3J_{PH}\,| = ca.$ 8.4 cps. The methylene proton resonaces of other longer methylene chain ditertiary phosphines occurred as a broad band and were not analysed further.

The signals of methyl and methylene protons of triethylaluminum, which has been analysed as A_2B_3 system,[7] were simply analysed as triplet and quartet respectively in this paper.

Ditertiary Phosphines-Organoaluminum Compounds Systems. Spectrum of ditertiary phosphine-$AlEt_3$ system consists of singnals due to methylene protons of ditertiary phosphine, a triplet of methyl protons and a quartet of methylene protons of $AlEt_3$. The chemical shift and the coupling constant (^1H-^{31}P) of ditertiary phosphines and the chemical shift of two kinds of protons of $AlEt_3$ vary with molar ratio of ditertiary phosphine/$AlEt_3$. This is considered to be a result of adduct formation by the interaction of diphosphine as a Lewis base with triethylaluminum as a Lewis acid in solution. Consequently, a composition of this adduct will be estimated from the variation of these parameters (namely chemical shift and coupling constant) with molar ratio.

The variation in the chemical shift of methylene protons of DPE, and of methyl and methylene protons of aluminum compounds with DPE/Al molar ratio in DPE-$AlEt_3$ or $AlEt_2Cl$ systems is shown in Fig. 1. The chemical shift of DPE is constant until the molar ratio becomes 0.5, but that of methyl- and methylene protons of aluminum are linearly increased. On the further addition of DPE a monotonous and nearly linear decrease in chemical shift of DPE is observed,

1) T. Kagawa, Y. Inoue, and H. Hashimoto, This Bulletin, **43**, 1250 (1970).

2) M. Iwamoto and S. Yuguchi, *Kogyo Kagaku Zasshi*, **71**, 233 (1968).

3) M. E. Coates, M. L. H. Green, and K. Wade, "Organometallic Compounds" Vol. 1, Third Edition, Methuen, London, (1967), p. 304.

4) a) B. M. Cohen, A. R. Cullingworth, and J. D. Smith, *J. Chem. Soc., A*, **1969**, 2193. b) A. R. Cullingworth, A. Pidcock, and J. D. Smith, *Chem. Commun.*, **1966**, 89. c) D. F. Clemens, H. H. Sisler, and W. S. Brey, Jr., *Inorg. Chem.*, **5**, 527 (1966). d) K. Issleib and F. Krech, *Z. Anorg. Allgem. Chem.*, **328**, 21 (1964).

5) Abbreviation:
$n=1$: DPM 1,1-bis(diphenylphosphino)methane
$n=2$: DPE 1,2-bis(diphenylphosphino)ethane, in a similar manner, $n=3$: DPP, $n=4$: DPB, $n=6$: DPH.

6) W. Hewertson and H. R. Watson, *J. Chem. Soc.*, **1962**, 1940.

7) a) O. Yamamoto, This Bulletin, **36**, 1463 (1963) b) O. Yamamoto, *ibid.*, **37**, 1125 (1964).

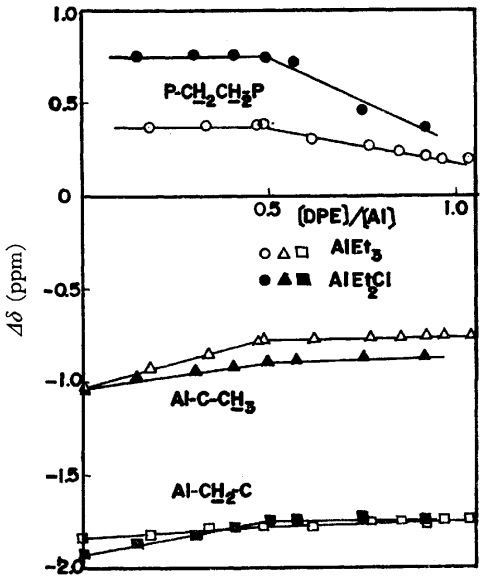

Fig. 1. The variation of chemical shift with molar ratio of DPE/$AlEt_3$ or $AlEt_2Cl$ system.

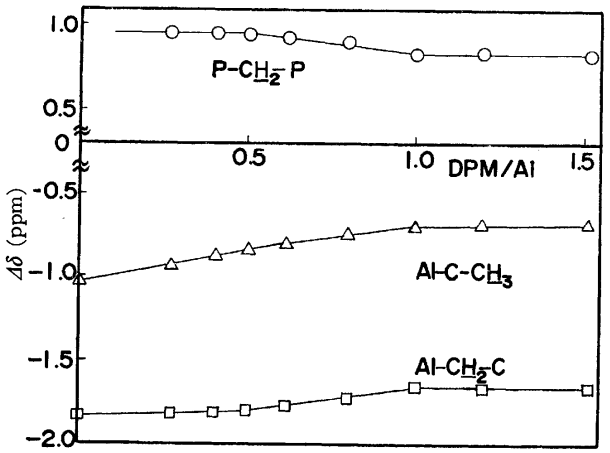

Fig. 2. The variation of chemical shift with DPM/Al of DPM-$AlEt_3$ system.
○ P-C$\underline{H}_2$-P, △ Al-C-C$\underline{H}_3$, □ Al-C$\underline{H}_2$-C

but the ethyl signals of aluminum part are almost constant. This may show that DPE and $AlEt_3$ form 1 : 2 adduct in solution. Similar behavior has been observed in a system of $AlEt_3$-PMe_3 by Cullingworth and co-workers[4b] and a change of chemical shift occurs at the molar ratio of 1 : 1. The variation of these parameters in the system of DPM-$AlEt_3$ is slightly different from that of DPE system and shown in Fig. 2. In this case the parameters vary at molar ratio of 0.5 and 1.0, and two kinds of adduct, *i.e.*, 1 : 2 and 1 : 1, may be present.

Other ditertiary phosphines (DPP, DPB, and DPH) were examined with combination of triethylaluminum and the results are the same as DPE system. Using triphenylphosphine as a monophosphine, chemical shifts of $AlEt_3$ vary at 1 : 1 molar ratio like PMe_3.

The coupling constants J_{PH} of DPE and DPM changed also with the molar ratio and this variation

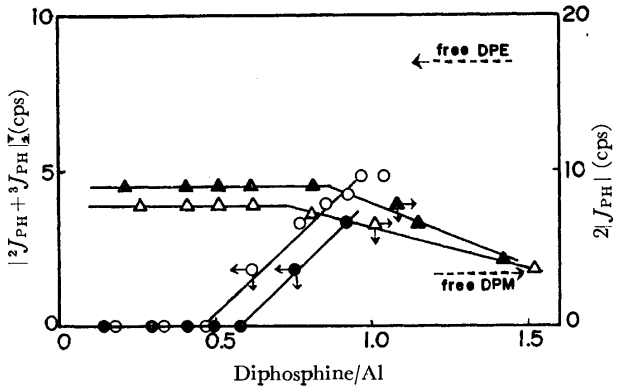

Fig. 3. Change in coupling constant ($^1H-^{31}P$) of DPM and DPE.
DPM: △ $AlEt_3$ ▲ $AlEt_2Cl$
DPE: ○ $AlEt_3$ ● $AlEt_2Cl$

is given in Fig. 3. As seen in Fig. 3, the change in DPE system occurs at the ratio of 0.5 in a similar manner to the chemical shift described above, and this is a piece of evidence in support of the formation of 1 : 2 adduct. But the changing point in the DPM system is at molar ratio of ca 0.8 and this may also show that there are two kinds of adduct in solution. The reasons why $|\,^2J_{PH}\,|$ of complexed DPM is larger than that of free one and why $|\,^2J_{PH}+{}^3J_{PH}\,|$ of complexed DPE is smaller than that of free ligand are not clear. It may be necessary to know the sign of coupling constants between ^1H and ^{31}P.

It is now concluded by the variations of chemical shift and the coupling constant with molar ratio that ditertiary phosphines ($Ph_2P(CH_2)_nPPh_2$, n=2,3,4,6) form 1 : 2 adduct with triethylaluminum in solution, while DPM forms 1 : 1 and 1 : 2 adducts. These results are similar to those of ditertiary amine-trimethylaluminum systems[10], in which $Me_2NCH_2NMe_2$ forms 1 : 1 complex, and $Me_2N(CH_2)_2NMe_2$ and $Me_2N(CH_2)_3NMe_2$ form 1 : 2 complex. The relationship between composition of the adduct and the methylene chain length*(n)* is same in both cases except n=1.

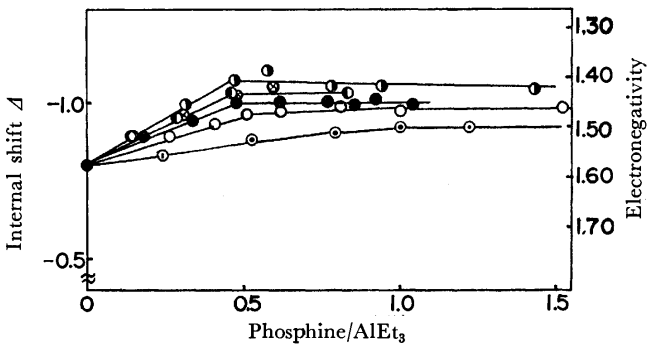

Fig. 4. Changes in electronegativity of aluminum by coordination of diphosphines.
$\chi = 0.62\Delta + 2.07$ $\Delta = \tau_{CH_3} - \tau_{CH_2}$
diphosphine-$AlEt_3$ system
○: DPM ●: DPE ◑: DPP
◐: DPB ⊗: DPH ⊙: PPh_3

8) R. K. Harris, *Can. J. Chem.*, **42**, 2275 (1964).
9) A. J. Carty and R. K. Harris, *Chem. Commun.*, **1967**, 234.
10) a) N. R. Fetter, B. Bartocha, F. E. Brinckman, Jr., and D. W. Moore, *Can. J. Chem.*, **41**, 1359 (1963) b) N. R. Fetter and D. W. Moore, *ibid.*, **42**, 885 (1964).

An empirical linear relationship between the electronegativity χ of a metal atom (CH_3CH_2M) and its internal shift Δ: a difference in the chemical shift of methylene and methyl protons, was known as Dailey-Shoolery equation and this equation has been useful in studying the change of electronegativity with coordination of donor molecules.[11]

$$\chi = 0.62\Delta + 2.07$$

11) T. Takeshita and W. E. Frankle, *Tetrahedron Lett.*, **1968**, 5913.

The Lewis acidity of aluminum coordinated with diphosphine was evaluated by application of Dailey-Shoolery equation to ditertiary phosphine-$AlEt_3$ system. The variation in the internal shift with the molar ratio of diphosphine/$AlEt_3$ was calculated from above data and shown in Fig. 4. As expected, the complex formation with phosphine results in decreasing the electronegativity of aluminum. The effect of the length of methylene chain in the ditertirary phosphines is not so remarkable but the following order of donor ability to aluminum was obtained: DPP>DPB≈DPH≳DPE>DPM.

BULLETIN OF THE CHEMICAL SOCIETY OF JAPAN, VOL. 45, 1741—1746 (1972)

The Dissolution of Olivine in Aqueous Solutions of Inorganic Acids[1)]

Isao SANEMASA, Minoru YOSHIDA, and Takejiro OZAWA

Department of Chemistry, Faculty of Science,
Tokyo Institute of Technology, Ookayama, Meguro-ku, Tokyo

(Received November 17, 1971)

The dissolution of olivine was studied in aqueous solutions of inorganic acids at temperatures of 35, 50, and 65°C in order to obtain basic information about the alteration and leaching processes in acid hot spring regions. The rates of dissolution have been determined by measuring the change in the concentrations of silica, magnesium, and the total iron leached in the solutions as a function of the time. Olivine dissolved in stirred aqueous solutions of 0.05—2N perchloric, hydrochloric, and sulphuric acids without any selective dissolution of components in the mineral. The rate at which olivine dissolved was found to be two-thirds of the reaction order with respect to the sample-powder (10—20 μ in diameter) weight (*i.e.*, first order with respect to the surface area) and to decrease in the order of $H_2SO_4 \gg HCl > HClO_4$. HSO_4^- enchanced the rate remarkably. The complexing affinity of the anions did not play an important part in the reaction with olivine powder.

Studies of the leaching of chemical elements from rocks and minerals from various points of view have been reported by many investigators.[2-5)] Olivine is a common and important rock-forming mineral; it is particularly characteristic of basic and ultrabasic igneous rocks. The minerals of the olivine group are very susceptible to hydrothermal alteration, low-grade metamorphism, and weathering.[6)] As a result, olivine has been observed to be more altered than magnetite, the glassy part, and pyroxene in natural altered rocks found in acid hot spring regions.[7)]

Heterogeneous reactions between inorganic materials and aqueous solutions are important in discussing the alteration and weathering of rocks and minerals and the formation of ores and thermal waters. The kinetics of the dissolution of ferric oxide[8,9)] and gibbsite[10)] in aqueous solutions have been studied, while silicate minerals,[11-13)] especially feldspars,[14,15)] have also been investigated, mainly from the practical point of view. It is somewhat difficult to study the rate at which silicate minerals go into a solution, since their structures are complicated.

The olivine group has a fundamental structure in silicate minerals, which consist of independent $[SiO_4]^{4-}$ tetrahedra linked by divalent ions in a six-fold coordination. Leaching and hydrothermal alteration experiments of olivine have been carried out in order to clarify the origin of chemical species in natural waters,[16)] the mechanism of weathering,[17)] and alteration at high temperatures.[18)]

The object of this paper is to obtain some basic information on the kinetic behavior of olivine in acid hot spring regions.

1) Read at the Symposium on Geochemistry of the Geochemical Society of Japan and the Chemical Society of Japan, Tokyo, Oct., 1971.

2) H. Kamiya, This Bulletin, **33**, 1731 (1960).

3) W. A. J. Mahon, *New Zealand J. Sci.*, **10**, 206 (1967).

4) A. J. Ellis and W. A. J. Mahon, *Geochim. Cosmochim. Acta*, **31**, 519 (1967).

5) A. J. Ellis, *ibid.*, **32**, 1350 (1968).

6) W. A. Deer, R. A. Howie, and J. Zussaman, "Rock-forming Minerals," Vol. 1, Longmans, London (1965), p. 18.

7) J. Ossaka and Y. Ōhira, Read at the Annual Meeting of the Volcanological Society of Japan, Fukuoka, Oct., 1968; abstract: *Kazan, Ser.* II, **13**, 151 (1968).

8) K. Azuma and H. Kametani, *Trans. Metall. Soc. AIME.*, **230**, 853 (1964).

9) J. Pryor and U. R. Evans, *J. Chem. Soc.*, **71**, 3330 (1949).

10) A. Packter and H. S. Dhillon, *ibid.*, (A), **1969**, 2588.

11) C. W. Correns, *Clay Minerals Bull.*, **4**, 249 (1961).

12) C. W. Correns, *Clays and Clay Minerals*, 10*th Conf.*, Pergamon Press, New York (1963), p. 443.

13) H. C. Helgeson, *Geochim. Cosmochim. Acta.* **35**, 421 (1971).

14) A. F. Frederickson, *Bull. Geol. Soc. Am.*, **62**, 221 (1951).

15) R. Wollast, *Geochim. Cosmochim. Acta*, **31**, 635 (1967).

16) T. Tarutani, *Mem. Fac. Sci., Kyushu Univ., Ser. C*, **5**, 47 (1962).

17) H. J. Hoppe, Dissertation, Göttingen, 1947 (cited in Ref. 12).

18) T. Kikuchi, *Ganseki Kōbutsu Kōshō Gakkai-shi*, **57**, 200 (1967).

Experimental

Materials. The olivine (Fo_{91}) sample used in the present study was separated from dunite[19] from Takashima, Karatsu, Saga Prefecture. The dunite was constituted of 94, 3, 3, and 0.1 vol% of olivine, spinels, clinopyroxene, and orthopyroxene respectively. The dunite was crushed in a steel Ellis mortar and powdered in an agate mortar. The fraction containing particles between 150 and 200 meshes was collected, washed with distilled water, and dried at 110°C. After this treatment, the olivine was separated by means of an iso-dynamic magnetic separator (S. G. Frantz Co., INC, Model L-1). This fraction will hereafter be called Sample A. This sample was further finely pulverized in an agate mortar again. This powder was sized by sedimentation in distilled water to 10—20 μ, and then dried at 110°C. This fraction will be called Sample B. The chemical composition of the olivine sample is given in Table 1. Accord-

Table 1. Chemical composition of olivine

Constituent	Content (%)
SiO_2	40.24
TiO_2	trace
Al_2O_3	0.24
Fe_2O_3	1.50
FeO	8.29
MnO	0.15
MgO	50.03
CaO	trace
Na_2O	trace
K_2O	trace
H_2O (−)	0.0
H_2O (+)	0.0
P_2O_5	trace
Total	100.45

ing to Dr. Kiyoshi Ishibashi, who examined this olivine sample microscopically, the spinel-group minerals (mainly chromite) and pyroxene comprized less than 3—4 vol%, while no hydrous minerals were observed as alteration products. The purity of the sample is sufficient for the present purposes.

Reagents. All the chemicals used were of analytical-reagent quality. Concentrated perchloric, hydrochloric, and sulphuric acid were diluted to the desired concentrations with redistilled water; the concentrations of the acid in the dilute solutions were determined by titration against a standard sodium carbonate solution. A sodium hydrogen sulphate solution (0.45 M) was prepared by adding a sodium hydroxide solution to a sulphuric acid standard solution in just half the volume required for neutralization.

Equipment. The reaction vessel was a 300-m*l* glass flask with four necks; the center neck was connected with a water-sealed stirring rod, while the other three were fitted with a nitrogen-introducing tube, a condenser, and a stopper. The stoppered neck was utilized to add the sample powder to the aqueous solution and to take out the sample solution. The container was placed on a water bath thermostated at from 35—65°C to 0.1°C.

Measurements of Reaction Kinetics. The sample powder, 200 mg for Sample A and 100 mg for B, was disperesed in 200 m*l* of an aqueous acid solution in the reaction vessel, into which nitrogen gas had previously been introduced continuously. The mixture was then stirred at about 1000 rpm. The preliminary experiments revealed that the stirring speed, over the range of about 200 to 2000 rpm, did not affect the rate of dissolution of the sample powder. After various times, 2-m*l* aliquots of the sample solution were withdrawn for analysis in the following manner. When Sample A was used, the stirring was stopped for 30 sec before each desired time. The sample particles were allowed to settle on the bottom of the reaction vessel; then the supernatant was pippetted off at the prescribed time, and it was submitted to chemical analysis. On the other hand, when Sample B was used, a portion of the reaction solution containing sample particles was pippetted off immediately at each desired time with continuous stirring. The mixture was then filtered and washed with redistilled water through a membrane filter(having a porous size of 0.45 μ) with suction into a 25-m*l* volumetric flask.

Chemical Analysis of the Reaction Solution. The silica was determined photometrically by the silico-molybdate yellow method.[20] We found no colloidal silica under the present experimental conditions. The total iron was estimated photometrically with α,α'-dipyridyl after the reduction of all the iron to the ferrous state using sodium thioglycolate. The magnesium was determined by the Xylidyl blue-II[21] photometric method,[22] with some modifications.

Results and Discussion

The Amount of Each Element Dissolved from Olivine. Tarutani[16] reported, in his leaching studies in the pH range from 1.5 to 10 with or without organic acid (EDTA and citric acid), that olivine dissolved in the same ratio as that in the mineral into a solution of pH 1.5 and into solutions with the organic acids except at pH 10. However, his experiments lacked sufficient data, since his major attention was devoted to the effects of organic acids on the leaching process. On the contray, Hoppe,[17] who studied the question from the view of the weathering of rocks, assumed the presence of a residual layer rich in iron.

Figures 1, 2, and 3 show how amounts of silica,

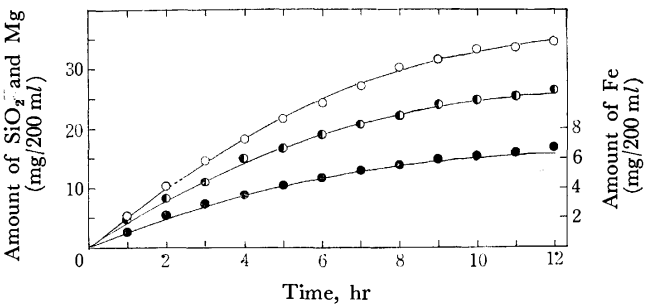

Fig. 1. Change in the amounts of silica, magnesium, and iron dissolved in a 0.1 N $HClO_4$ solution at 50°C with the time of reaction.
○: SiO_2 ◐: Mg ●: Fe

19) K. Ishibashi, *Mem. Fac. Sci., Kyushu Univ.*, **20**, 85 (1970).

20) T. Tarutani, *Nippon Kagaku Zasshi*, **77**, 743 (1956).

21) Xylidyl blue-II is a commercial product with the chemical formura of 1-Azo-2-hydroxy-3-(2,4-dimethylcarboxyanilido)-naphthalene-1′-(2-hydroxybenzene).

22) I. Iwasaki, M. Yoshida, S. Yoshida, H. Neriishi, and M. Sato, read at the 21st Annual Meeting of the Chemical Society of Japan, Osaka, Apr., 1968. (Preprints II, p. 896).

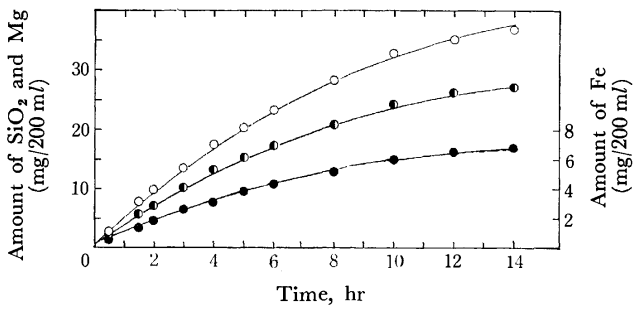

Fig. 2. Change in the amounts of silica, magnesium, and iron dissolved in a 0.1 N HCl solution at 50°C with the time of reaction.
○: SiO_2 ◐: Mg ●: Fe

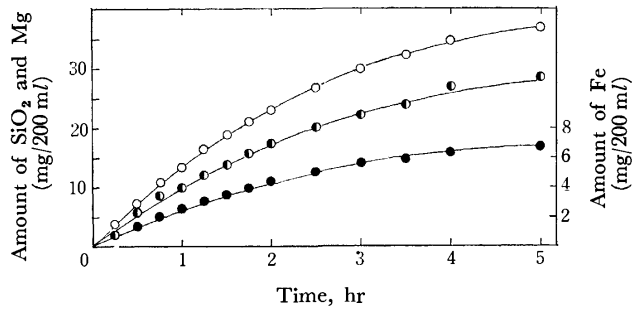

Fig. 3. Change in the amounts of silica, magnesium, and iron dissolved in a 0.1 N H_2SO_4 solution at 50°C with the time of reaction.
○: SiO_2 ◐: Mg ●: Fe

magnesium, and iron dissolved from olivine (Sample B) increase against the time of the reaction in 0.1 N perchloric, hydrochloric, and sulphuric acid solutions (200 ml) at 50°C.

The initial amount of each component presented in the olivine sample, W_0, can be calculated from Table 1, *i.e.*, 40.2 mg as SiO_2, 30.2 mg as Mg, and 7.49 mg as Fe for 100 mg of Sample B. Table 2 shows the amount of each component dissolved in a 0.1 N perchloric acid solution at different times, $(\Delta W)_{sol}$, and the ratios of each $(\Delta W)_{sol}$ to W_0. The amount of Fe is the sum of Fe^{2+} and Fe^{3+}. The $(\Delta W)_{sol}/W_0$ ratios for SiO_2, Mg, and Fe in solution are shown to be in fairly good agreement at any time of reaction. This suggests that olivine is dissolved in an acid inorganic solution without any selective dissolution of the components in the mineral, as was pointed out by Tarutani.[16] The selective dissolution of silica and magnesium, resulting in a residual layer rich in iron, was not observed under the present experimental conditions.

Table 2. Amount of each component dissolved
Reaction conditions: 0.1 N $HClO_4$, 200 ml, sample B, 100 mg, temp. 50°C

Time (hr)	Components					
	SiO_2		Mg		Fe	
	(a)	(b)	(a)	(b)	(a)	(b)
1	5.52	0.14	0.94	0.16	1.14	0.15
2	10.5	0.26	8.20	0.27	2.18	0.29
3	14.8	0.37	11.1	0.37	2.90	0.39
4	18.3	0.46	15.0	0.50	3.58	0.48
5	21.6	0.54	16.8	0.56	4.24	0.57
6	24.4	0.61	19.0	0.63	4.70	0.63
7	27.2	0.68	20.6	0.68	5.18	0.69
8	30.2	0.75	22.6	0.75	5.64	0.75
9	31.6	0.79	24.0	0.80	5.94	0.79
10	33.4	0.83	24.8	0.82	6.22	0.83
11	33.8	0.84	25.4	0.84	6.36	0.85
12	34.6	0.86	26.4	0.87	6.66	0.89

(a): $(\Delta W)_{sol}$, mg. (b): $(\Delta W)_{sol}/W_0$

Dissolution Rate of Olivine. When the reaction at the solid surface is the rate-determining step, the reaction rate, dw/dt, is said to be given by the following equation:[23]

$$-dw/dt = k_0SC \quad (1)$$

where w and S indicate, respectively, the weight and the surface area of the particles remaining at the reaction time, t, where k_0 is the rate constant per unit of surface area, and where C is the concentration of the reactant. Spherical particles of W_0 grams, the average radius of which is r_0, are used as the initial material. The rate can be shown by Equation (2):

$$-dw/dt = 3k_0W_0^{1/3}W^{2/3}C/r_0d_s \quad (2)$$

where d_s is the specific gravity of the solid. As $3k_0W_0^{1/3}C/r_0d_s$ is constant, we can obtain Equation (3) by integrating Eq. (2):

$$W_0^{1/3} - W^{1/3} = 1/3\,kt \quad (3)$$

where k is constant. By substituting Eq. (3) for $W=W_0(1-\alpha)$, we obtain:

$$1-(1-\alpha)^{1/3} = 1/3\,kW_0^{-1/3}t \quad (4)$$

Since $1/3\,kW_0^{-1/3}$ is a constant, we can obtain a straight-line relationship by plotting $1-(1-\alpha)^{1/3}$ *vs.* t.

From the definition of α, $\alpha=(W_0-W)/W_0=(\Delta W)_{t,sol}/W_0$, where $(\Delta W)_{t,sol}$ is the weight loss of the mineral into a solution at time t. Olivine, $(Mg, Fe)_2SiO_4$, dissolves into aqueous solutions of acids to form soluble aquo-magnesium and ferrous (ferric in part) cations and silicic acid.[24] Theoretical-

Table 3. The amount of each component dissolved and the weight loss of olivine

Run no.	Amount of each component dissolved (mg)				Weight loss of olivine (mg)
	SiO_2	MgO	FeO	Total	
I	15.59	18.90	3.87	38.36	39.05
II	45.45	60.53	12.35	121.33	125.05
III	22.25	28.30	5.84	56.39	58.05
IV	53.62	66.93	14.00	134.55	139.70

23) T. Kagiya, "Kinetic Studies in Chemical Reactions" (in Japanese), Kagakudojin, Tokyo (1970), p. 398.
24) E. Weitz, H. Frank, and M. Schuchard, *Chem. Ztg.*, **74**, 256 (1950).

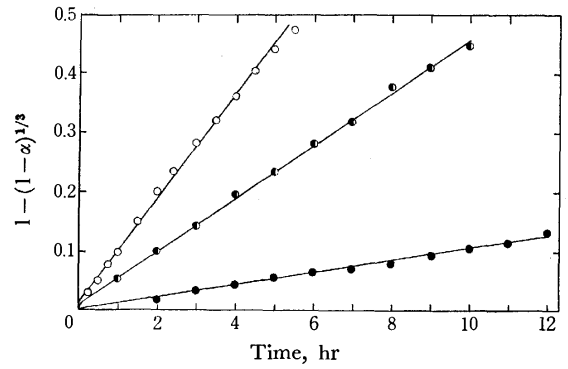

Fig. 4. Dissolution of olivine in a 0.1 N $HClO_4$ solution at 35, 50, and 65°C. Plots of $1-(1-\alpha)^{1/3}$ *vs.* time.
●: 35°C ◐: 50°C ○: 65°C

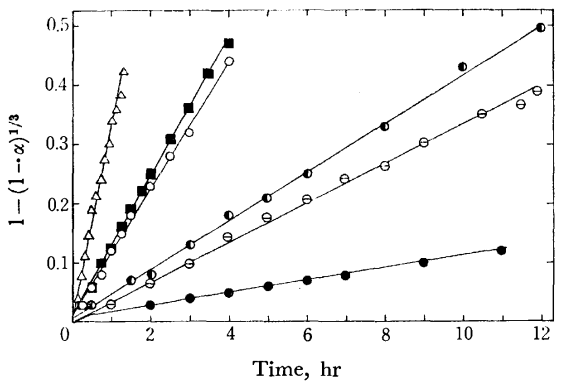

Fig. 5. Dissolution of olivine in 0.1 N HCl and H_2SO_4 solutions at 35, 50, and 65°C.
Plots of $1-(1-\alpha)^{1/3}$ *vs.* time.
●: 35°C, ◐: 50°C, ○: 65°C HCl
⊖: 35°C, ■: 50°C, △: 65°C H_2SO_4

ly, the sum of the components in a solution should be equal to the weight loss of the solid. The results obtained, given in Table 3, confirmed the material balance among them. Thus, $(\Delta W)_{t,sol}$ is equal to the sum of the amounts of each component dissolved in the solution at time t. The amounts of the other components in olivine are negligibly small compared with those of the three components. The plots of $1-(1-\alpha)^{1/3}$ against time t, in 0.1 N perchloric, hydrochloric, and sulphuric acid solutions at 35, 50, and 65°C, are shown in Figs. 4 and 5, which give straight lines up to about 85% dissolution. These results suggest that olivine powder (10—20 μ) reacts with well-stirred aqueous perchloric, hydrochloric, and sulphuric acid solutions according to a two-thirds reaction order with respect to the powder weight; that is, the reaction is first-order with respect to the surface area. It may be seen from Figs. 4 and 5 that the rate at which olivine goes into $HClO_4$ solutions is almost the same as that at which it goes into HCl solutions, but it is apparently enhanced in H_2SO_4 solutions under the same reaction conditions.

The Estimation of the Activation Energy. The relation between the slopes of the straight lines in Figs. 4 and 5 and the reaction temperatures is illustrated in Fig. 6 according to the Arrhenius plot. The apparent activation energy, 14 Kcal/mol, obtained for

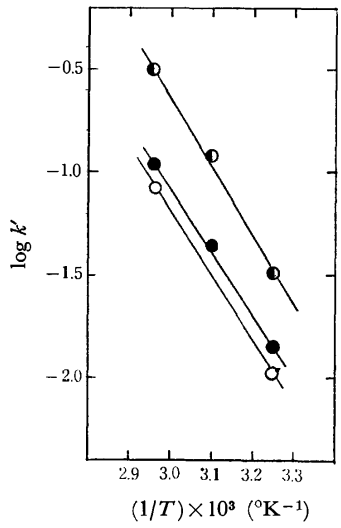

Fig. 6. Arrhenius plots for the dissolution of olivine in $HClO_4$, HCl, and H_2SO_4 solutions. k' corresponds to 1/3 $k\ W_0^{-1/3}$ in Eq. (4).
○: $HClO_4$, ●: HCl, ◐: H_2SO_4

the reaction with $HClO_4$ is similar to that for the reaction with HCl. For the reaction with H_2SO_4, it is somewhat higher, *i.e.*, 16 Kcal/mol. That is, the enhanced rate of the reaction with a sulphuric acid solution corresponds to the increase in the pre-exponential term in the Arrhenius equation.

In the subsequent experiments, Sample A was used; its particle size was larger than that of Sample B. The rate of the reaction was measured by estimating only the total iron dissolved in the solution at various times. The rate of dissolution was interpreted by comparing it with the slopes of straight lines for the range where a plot of the amount of total iron against the time is linear.

Effect of the HSO_4^- Ion. The dissolution curves at 50°C for $HClO_4$ with a concentration of 0.05—2 N, HCl with one of 0.05—1 N, and H_2SO_4 with one of 0.05—1 N are illustrated in Figs. 7, 8, and 9 respectively. The straight lines break early in the reaction at an about 5% dissolution. These breaks are also observed in the cases of silica and magnesium. No explanation for these bends can be offered at the

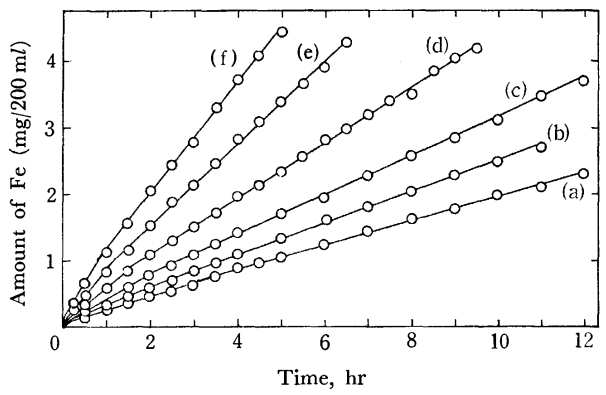

Fig. 7. Change in the amount of iron dissolved in $HClO_4$ solutions with various acid normalities at 50°C.
(a): 0.05, (b): 0.1, (c): 0.2, (d): 0.5, (e): 1, (f): 2

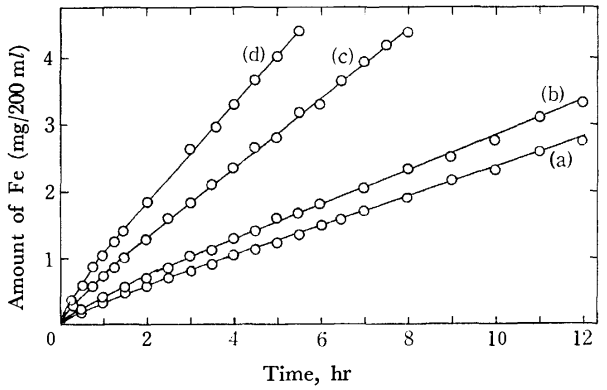

Fig. 8. Change in the amount of iron dissolved in HCl solutions of various acid normalities at 50°C.
(a): 0.05, (b): 0.1, (c): 0.5, (d):1

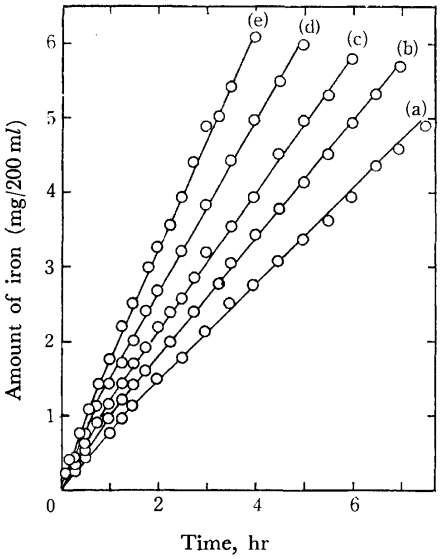

Fig. 9. Change in the amount of iron dissolved in H_2SO_4 solutions of various acid normalities at 50°C.
(a): 0.05, (b): 0.1, (c): 0.2, (d): 0.5, (e): 1

Table 4. Acid normalities and slopes of straight lines

N	Slopes of straight lines (mg/hr)		
	$HClO_4$	HCl	H_2SO_4
0.05	0.18	0.22	0.50
0.1	0.24	0.26	0.78
0.2	0.29		0.93
0.5	0.41	0.53	1.2
1	0.61	0.75	1.5
2	0.80		

present time. The slopes of these lines, ranging from about 5 to 35% dissolution at various acid normalities, are listed in Table 4. Table 4 shows that the values for HCl are somewhat greater than those for $HClO_4$, while those for H_2SO_4 are markedly greater than those $HClO_4$ and HCl with the same hydrogen-ion concentration.

In order to confirm the remarkable enhancement in the sulphuric acid solution, experiments were made in

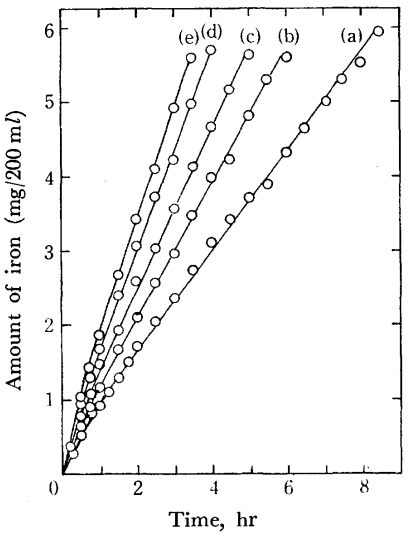

Fig. 10. Effect of the HSO_4^- ion on the dissolution of olivine at 50°C.
(a): 1 M $HClO_4$
(b): 1 M $HClO_4$+0.98×10^{-3} M $NaHSO_4$
(c): 1 M $HClO_4$+0.49×10^{-2} M $NaHSO_4$
(d): 1 M $HClO_4$+0.49×10^{-1} M $NaHSO_4$
(e): 1 M $HClO_4$+0.2 M $NaHSO_4$

solutions containing 1 M $HClO_4$ and $NaHSO_4$ in various concentrations. At such a high hydrogen-ion concentration, the dissociation of the HSO_4^- ion is negligible. The results obtained are shown in Fig. 10. It is apparent from Fig. 10 that the presence of the HSO_4^- ion in only one-thousandth the concentration of $HClO_4$ promotes the dissolution rate considerably.

According to the studies of the dissolution of hydrous ferric oxide by Furuichi *et al.*[25] and of α-ferric oxide by Pryor *et al.*[9] and Azuma,[8] each in aqueous acid solutions, the rate of dissolution is in accord with the order of decrease in the complexing affinity of the anions for the ferric ion, *i.e.*, $HCl > H_2SO_4 > HClO_4$. On the other hand, Packter *et al.*[10] observed that the rate of the dissolution of gibbsite in the H_2SO_4 solution was markedly enhanced as compared to those in the HCl and $HClO_4$ solutions. They attributed the promoting effect of sulphuric acid to dipole interaction between the HSO_4^- ion or $H^+\cdots SO_4^{2-}$ ion-paris and active sites on the solid surface. Our study of olivine showed the effect of sulphuric acid to be similar to the case of gibbsite.

Effect of Cl^- and ClO_4^- ions. The rate of dissolution was measured in 0.2 M $HClO_4$ solutions with varying NaCl concentrations, and was also measured in 0.1 M $HClO_4$ solutions containing an adequate amount of $NaClO_4$. The results are shown in Fig. 11 and 12. The rate of the dissolution of olivine was found to be greater in the solutions containing the ClO_4^- ion as well as Cl^- ion than in the solutions without them. The effects of the Cl^- and ClO_4^- ions were, however, very small compared with that of the HSO_4^- ion. The roles of each anion, HSO_4^-, Cl^-, and ClO_4^-, in the reaction of dissolution may be

25) R. Furuichi, N. Sato, G. Okamoto, and T. Takeuchi, *Kogyo Kagaku Zasshi*, **72**, 1455 (1969).

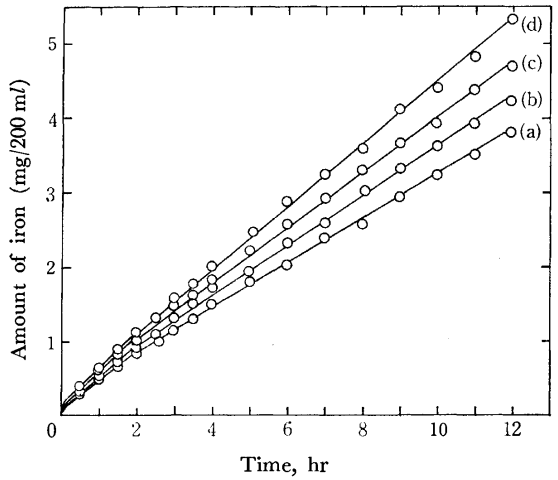

Fig. 11. Effect of the Cl^- ion on the dissolution of olivine at 50°C.
(a): 0.2 M $HClO_4$, (b): 0.2 M $HClO_4$+0.2 M NaCl
(c): 0.2 M $HClO_4$+0.5 M NaCl
(d): 0.2 M $HClO_4$+1.0 M NaCl

understood in terms of the structure of olivine, which consists of individual silicon-oxygen tetrahedra linked by magnesium and iron atoms, each of which has six nearest oxygen neighbours.

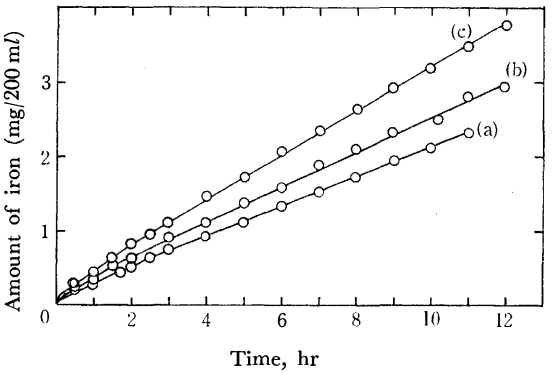

Fig. 12. Effect of the ClO_4^- ion on the dissolution of olivine at 50°C.
(a): 0.1 M $HClO_4$, (b): 0.1 M $HClO_4$+0.09 M $NaClO_4$
(c): 0.1 M $HClO_4$+0.36 M $NaClO_4$

The authors wish to express their deep gratitude to Professor Iwaji Iwasaki of Tōhō University for his guidance and encouragement throughout this work. The authors are also indebted to Dr. Kiyoshi Ishibashi of Kyushyu University, who examined the olivine sample microscopically and who gave us helpful advice from the mineralogical standpoint. Thanks are also due to Mr. Hiroshi Haramura, who Kindly analyzed the olivine sample.

BULLETIN OF THE CHEMICAL SOCIETY OF JAPAN, VOL. 45, 1746—1751 (1972)

Distribution Studies of the Potassium Salts with Hexanitrodiphenylamine and Analogous Acids

Tadashi IWACHIDO

College of Liberal Arts, Okayama University, Tsushima, Okayama

(Received December 16, 1971)

The association constants of potassium salts with 2,4,6,2′,4′,6′-hexanitrodiphenylamine (hexyl), *N*-(2,4,6-trinitrobenzo)-2,4-dinitro-1-naphthylamine (α-hexyl), and 1,3,7,9-tetranitrophenothiazine-5-oxide (thiohexyl) in the nitrobenzene phase were determined conductometrically. The distribution constants and the association constants of these salts in an aqueous phase were determined simultaneously by means of solvent extraction. The dissociation constants in the aqueous phase and the distribution constants of the acids were estimated from an analysis of the curve obtained by plotting the distribution ratios of the metal or the acids against the pH. The results show that these salts exist mainly in the dissociated form in both phases. The applicability of the proposed distribution mechanism was also discussed.

In a previous paper,[1] the extraction mechanism of the alkali metal picrates into nitrobenzene has been discussed. This paper will show that the distribution of alkali metals or picric acid can well be explained in terms of the association constants of the salts in both the aqueous and the nitrobenzene phases, in terms of the dissociation constant of picric acid in the aqueous phase, and in terms of the distribution constants of the salts.

The distribution ratio of the alkali metals increases with a decrease in the association constant in the nitrobenzene phase and with an increase in that in the aqueous phase. In an earlier work,[2] it has been shown that some amine derivatives have a high extractability for potassium (% E=60 or more), even in the presence of much greater amounts of lithium ions (added as a buffer solution, $[Li^+]/[K^+]=100—1000$), which is quite different from the case of potassium picrates (%E=2, when $[Li^+]/[K^+]=100$). The present paper will describe how the extraction mechanism established for alkali metal picrates is also useful for weak and bulky acids, such as hexyl, α-hexyl, and thiohexyl. The amounts of lithium ions in the aqueous phase are decisive for the determination of the

1) T. Iwachido, This Bulletin, **45**, 432 (1972).

2) T. Iwachido, *ibid.*, **44**, 1835 (1971).

distribution ratio of potassium, especially at an alkaline pH.

Experimental

Reagents. Potassium salt with hexyl was prepared by dissolving commercially-available hexyl into a hot aqueous solution containing potassium carbonate. The resultant precipitates were recrystallized three times from water containing a small amount of potassium carbonate. α-Hexyl was prepared by the nitration of the condensation product of picrylchloride with 1-naphthylamine[3], and thiohexyl, by the nitration of phenothiazine.[4,5] Potassium salts with these acids were prepared by dissolving these substances into a hot mixture of alcohol and water containing potassium carbonate; then the precipitates were recrystallized three times from such a mixture.

Acetic acid-lithium acetate buffers (0.01 M) and 0.01 M phosphoric acid-lithium phosphate buffers were used to adjust the pH values of the solution to pH 4—5.5 and pH 6—8 respectively. More alkaline solutions (pH 9—11) were prepared with a 0.005 M lithium carbonate solution and hydrochloric acid and a pH 12 solution, with a 0.01 M lithium hydroxide solution.

Extraction. Into a 50-m*l* centrifuge tube equipped with a stopper, 10 m*l* of a 0.01 M buffer solution and 10 m*l* of water were transferred; then 20 m*l* of a nitrobenzene solution containing potassium salts of these acids (1×10^{-3} M) was added. The resultant mixture of the aqueous and nitrobenzene solutions was shaken moderately for two hours at 25°C and then centrifuged at the same temperature. The preparation of the aqueous phase was slightly modified when the association constant and the distribution constant in the aqueous phase had been determined: 10 m*l* of an 8×10^{-4} M potassium hydroxide solution was mixed with 10 m*l* of a potassium chloride solution, the concentration ranging from 0 to 2×10^{-3} M. The resultant solutions were then treated as before.

Determination of Potassium, Lithium, and the Acids. The concentration of potassium remaining in the aqueous phase after equilibration and that of lithium extracted into nitrobenzene were determined using an atomic absorption spectrophotometer (Nippon Jarrell Ash, Type AA-1); the concentrations of the acids in the aqueous phase were determined spectrophotometrically (Hitachi Ltd.; Spectrophotometer, Type 124) using matched 50-mm cells at 425, 445, and 463 mμ for hexyl, α-hexyl, and thiohexyl respectively, while the solution was kept sufficiently alkaline (pH 13) to avoid the hydrolysis of the salts. The pH of the aqueous solution was also measured in order to analyse the distribution equilibria.

Conductance Measurements in the Nitrobenzene Solution. Nitrobenzene of a guaranteed-grade was washed with an aqueous solution of sodium carbonate and then distilled water, and subsequently dried over calcium chloride for two days. The nitrobenzene was then distilled under reduced pressure. A fraction boiling at 75°C/5 mmHg, with a specific conductance of 0.02 μ℧/cm, was collected. The specific conductance of the water-saturated or wet nitrobenzene was about 20 times that of the dry nitrobenzene. The conductance of the nitrobenzene solution placed in a jacketted vessel equipped with platinized platinum electrodes and a thermometer (a thermocouple; Cu-Con.) was measured by using a conductometer (Ando Electric Co. Ltd., LCR-10, Universal Bridge), while the temperature of the solution was kept at 25±0.005°C by circulating the thermostated water. In order to obtain the $\Lambda-\sqrt{C}$ plot, a dilution method using a weighing buret was adopted.

3) K. Tôei, *Nippon Kagaku Zasshi*, **76**, 106 (1955).
4) A. Bernthsen and H. Sattler, *Ann.*, **230**, 116 (1885).
5) F. Kehrmann and F. Ringer, *Ber.*, **46**, 3018 (1913).

Theoretical

By writing the formulae for the hexyl, α-hexyl, and thiohexyl acids and the potassium salts of these acids as HR and MR respectively, the equilibria involved can be represented schematically as in Fig. 1:

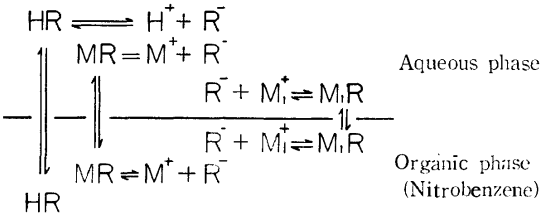

Fig. 1. Schematic representation of the equilibria involved in the extraction.

1) Dissociation of the Acids:

$$HR \rightleftharpoons H^+ + R^- \qquad K_a^{HR} = \frac{[H^+]_a[R^-]_a}{[HR]_a} \tag{1}$$

2) Association of Potassium Salts:

$$M^+ + R^- \rightleftharpoons MR \qquad K_a^{MR} = \frac{[MR]_a}{[M^+]_a[R^-]_a} \tag{2}$$

$$K_o^{MR} = \frac{[MR]_o}{[M^+]_o[R^-]_o} \tag{3}$$

$$M_I^+ + R^- \rightleftharpoons M_IR \qquad K_a^{M_IR} = \frac{[M_IR]_a}{[M_I^+]_a[R^-]_a} \tag{4}$$

$$K_o^{M_IR} = \frac{[M_IR]_o}{[M_I^+]_o[R^-]_o} \tag{5}$$

3) Distribution of the Neutral Molecules:

$$D^{HR} = \frac{[HR]_o}{[HR]_a} \tag{6}$$

$$D^{MR} = \frac{[MR]_o}{[MR]_a} \tag{7}$$

$$D^{M_IR} = \frac{[M_IR]_o}{[M_IR]_a} \tag{8}$$

In these equilibrium expressions, the subscripts a and o refer to the aqueous and the organic phases respectively; the brackets, to the molar concentration, and M_I^+, to a competing cation. As the competing cation, it is desirable to choose the lithium ion, because the extractability of the lithium salts with the acids is much lower than that of the potassium salts.

i) Association Constant, K_o^{MR}. The association constants of these salts in a nitrobenzene solution were determined by the method of Shedlovsky.[6] The conductances, Λ, were related to the concentration of the electrolytes, C, by the following equation:

$$\frac{1}{\Lambda S} = \frac{1}{\Lambda_\infty} + \frac{K_o^{MR}C\Lambda S f_o^2}{\Lambda_\infty^2} \qquad S \equiv \left[\frac{Z}{2} + \sqrt{1+\left(\frac{Z}{2}\right)^2}\right]^2 \qquad Z = \frac{\alpha\sqrt{C\Lambda}}{\Lambda_\infty^{3/2}} \tag{9}$$

where Λ_∞ refers to the limiting conductance; f, to the mean activity coefficient, and α, to the Onsager

6) T. Shedlovsky, *J. Franklin Inst.*, **225**, 739 (1938).

coefficient.

ii) Association Constant, K_a^{MR}, and Distribution Constant, D^{MR}. The distribution ratio of the acid, q^R, in a sufficiently alkaline solution can be written as:

$$q^R = \frac{[MR]_o + [R^-]_o}{[MR]_a + [R^-]_a} \tag{10}$$

In this case only, the pH of the solution was adjusted by the use of potassium hydroxide instead of the lithium buffers. Hence, the terms of lithium in neither phase appears in the expression (cf. Eq. (13)).

The combination of Eqs. (2), (3), and (7) leads to the following equation:

$$\frac{Y}{q^R} = \frac{1}{D^{MR}} + \frac{1}{D^{MR}K_a^{MR}f_a^2[M^+]_a}$$

$$Y = \frac{\sqrt{0.25 + C_oK_o^{MR}f_o^2} + 0.5}{C_oK_o^{MR}f_o^2} + 1 \tag{11}$$

The values of the mean activity coefficient, f, in both the aqueous (ε=78.54) and the nitrobenzene (ε=34.8) phases were approximated by the Debye-Hückel limiting law:

$$-\log f^2 = \frac{3.6494 \times 10^6 \sqrt{I}}{(\varepsilon T)^{3/2}} \tag{12}$$

where I denotes the ionic strength.

iii) Distribution of the Acids. The distribution ratio of the acid at equilibrium between the two phases can be written as:

$$q^R = \frac{[HR]_o + [MR]_o + [M_IR]_o + [R^-]_o}{[HR]_a + [MR]_a + [M_IR]_a + [R^-]_a} \tag{13}$$

The substitution of the equilibrium constants defined by Eqs. (1) to (8) into Eq. (13) gives this equation:

$$q^R = D^{HR}\frac{\left[1 + \left\{\left(1 + \frac{1}{K_o^{MR}[M^+]_o}\right)D^{MR}K_a^{MR}[M^+]_a + D^{M_IR}K_a^{M_IR}[M_I^+]_a\right\}\frac{K_a^{HR}}{D^{HR}[H^+]_a}\right]}{\left\{1 + \left(1 + K_a^{MR}[M^+]_a + K_a^{M_IR}[M_I^+]_a\right)\frac{K_a^{HR}}{[H^+]_a}\right\}} \tag{14}$$

iv) Distribution of Potassium. At equilibrium the distribution of potassium between the two phases can be written as:

$$q^M = \frac{[MR]_o + [M^+]_o}{[MR]_a + [M^+]_a} \tag{15}$$

The total concentrations of the reagent, C^R, and of potassium, C^M, are represented as:

$$C^R = [HR]_a + [HR]_o + [MR]_a + [MR]_o + [M_IR]_a + [M_IR]_o + [R^-]_a + [R^-]_o \tag{16}$$

$$C^M = [MR]_a + [MR]_o + [M^+]_a + [M^+]_o \tag{17}$$

The electroneutrality condition in the organic phase is expressed as:

$$[R^-]_o = [M^+]_o + [M_I^+]_o \tag{18}$$

Combining Eqs. (16), (17), and (18) and solving for $[R^-]_a$ gives:

$$\frac{1}{[R^-]_a} = \frac{1 + \frac{1 + D^{HR}}{K_a^{HR}}[H^+]_a + (1 + D^{M_IR})K_a^{M_IR}[M_I^+]_a}{C^R - C^M + [M^+]_a - [M_I^+]_o} \tag{19}$$

On the other hand, the rearrangement of Eq. (15) gives:

$$q^M = D^{MR}\left(\frac{1 + \frac{1}{K_o^{MR}[R^-]_o}}{1 + \frac{1}{K_a^{MR}[R^-]_a}}\right) \tag{20}$$

The substitution of Eq. (19) into Eq. (20) gives this useful expression:

$$q^M = D^{MR}\frac{\left(1 + \frac{1}{K_o^{MR}([M^+]_o + [M_I^+]_o)}\right)}{\left\{1 + \frac{1 + (1 + D^{HR})[H^+]_a/K_a^{HR} + (1 + D^{M_IR})K_a^{M_IR}[M_I^+]_a}{K_a^{MR}(C^R - C^M + [M^+]_a - [M_I^+]_o)}\right\}} \tag{21}$$

It must be noted that all the experiments were carried out under such a condition as $C^R - C^M = 0$, which can easily and exactly be realized by the use of the salt as the source of the reagent and the metal species. This is also advantageous in simplifing Eq. (21).

Results and Discussion

i) Equilibria Involved in the Extraction System. The equilibria shown in Fig. 1 are fundamental ones. Certainly, some other equilibria also exist in the two phases, such as the dissociation of the acids in nitrobenzene, the homoconjugation reaction (as has been mentioned in connection with picric acid in nitrobenzene),[7] the dimerization of the acids in both phases, *etc.* Lin[8] has suggested that the polymerization of hexylate ions in the aqueous phase does not occur until the concentration of hexylate exceeds 10^{-2} M.

7) I. M. Kolthoff, D. Stŏcesocá, and T. S. Lee, *J. Amer. Chem. Soc.*, **75**, 1834 (1953).

8) Z. F. Lin, *J. Chinese Chem. Soc.*, **9**, 115 (1962).

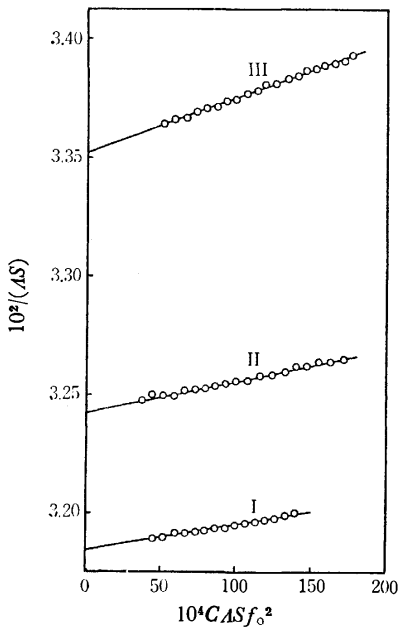

Fig. 2. Shedlovsky plot of the potassium salts in wet nitrobenzene,
I: Hexyl, II: α-Hexyl, III: Thiohexyl.

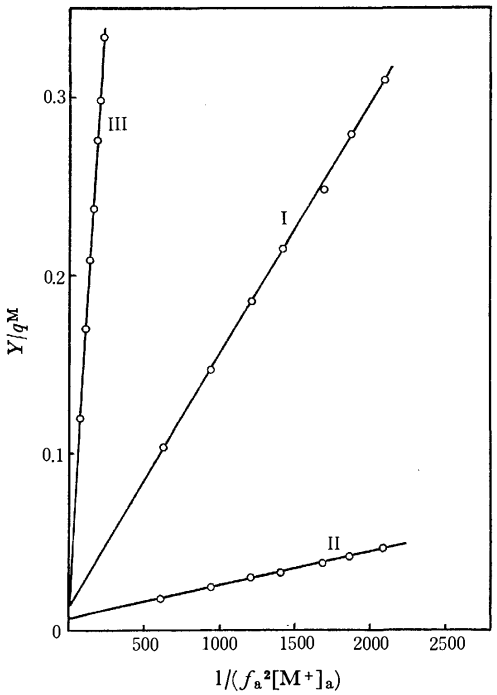

Fig. 3. The plot of Y/q^M *vs.* $1/f_a^2[M^+]_a$,
I: Hexyl, II: α-Hexyl, III: Thiohexyl.

The present studies of the distribution of potassium or the acids between the aqueous and the nitrobenzene phases show that the neglect of the reactions mentioned above does not cause any trouble in explaining the experimental results. This fact supports the idea that these equilibria are of minor importance.

ii) Association Constants of Potassium Salts in Nitrobenzene, K_o^{MR}. The conductance measurements were carried out with a cell devised for dilution runs, the concentrations ranging from about 0.5×10^{-4} to 7×10^{-4} M. A plot of Λ *vs.* $\sqrt{C}$ gives good straight lines, the intercepts on the Λ-axis for potassium salts with hexyl, α-hexyl, and thiohexyl being 31.42, 30.89, and 29.90 respectively, and the slope giving a value almost equal to Onsager's coefficient for each salt. The Shedlovsky plot (Fig. 2) was obtained by the the following calculations. First, z (Eq. (9)) is calculated from the Λ_∞ evaluated approximately by extrapolating the above linear $\Lambda-\sqrt{C}$ plot to the Λ-axis, and then the Shedlovsky plot is made by the help of Eq. (12). The reciprocal of the intercept of the plot on the $1/(\Lambda S)$-axis gives the second approximation for Λ_∞. The process is repeated until the Λ_∞ thus obtained is no longer altered. The final plots are shown in Fig. 2. The values of Λ_∞ and K_o^{MR} can be determined simultaneously from the plot. The value of K_o^{MR} in the wet nitrobenzene solution is calculated in the same manner, because the saturation of water (about 0.1 M) does not alter the dielectric constant of nitrobenzene (34.8) practically. Table 1 shows that the saturation of water causes about a 1.5-hold increase in Λ_∞ and a large decrease in K_o^{MR}. Taking into consideration the fact that the Λ_∞ values of potassium picrate are 34.7 and 40.3 for dry and the wet nitrobenzene solutions respectively, the sequence of Λ_∞ may well account for the bulkiness of the conjugate base, R^-.

iii) Distribution Coefficients, D^{MR}, *and Association Constants of Potassium Salts in the Aqueous Phase,* K_a^{MR}. The pH values of the aqueous solution were kept at pH 10.46±0.03, 10.14±0.02, and 11.67±0.01 for hexyl, α-hexyl, and thiohexyl respectively. A plot of Y/q^M *vs.* $1/(f_a^2[M^+]_a)$ (Fig. 3) shows a line in accordance with the theoretical requirements. However, the enlarged plot for thiohexyl shows that the line curves slightly downwards at the upper part.

For potassium picrate, it has been reported that the values of K_a^{MR} and D^{MR} are 44 and 0.014 respectively.[1] A comparison of the present results with those of the picrates shows that the structural difference (for example, in a functional group or bulkiness) be-

Table 1. Several constants obtained with hexyl, α-hexyl, and thiohexyl

Compound	Soln.	Λ_∞	K_o^{MR}	K_a^{MR}	D^{MR}	$K_a^{MR}D^{MR}/K_o^{MR}$	K_a^{HR}/D^{HR}	K_a^{HR}
Hexyl	Dry	29.72	32.65					
	Wet	31.41	10.32	112.5	78.55	$10^{1.466}$	$10^{-8.573}$	$10^{-4.75}$
α-Hexyl	Dry	29.27	31.29					
	Wet	30.84	12.48	418.4	160.5	$10^{1.865}$	$10^{-11.151}$	$>10^{-7}$
Thiohexyl	Dry	28.46	46.68					
	Wet	29.83	20.47	12.86	69.76	$10^{0.821}$	$10^{-11.481}$	$>10^{-9}$

tween the picrates and the acids much more significantly influences the value of D^{MR} than that of K_a^{MR}. It may, however, be difficult to point out such a correlation between K_a^{MR} or D^{MR} and the structural factors among these three acids.

iv) Distribution of Potassium, q^M. Figures 4, 5, and 6 show a plot of log q^M *vs.* pH by means of solid circles. Each curve consists of two constant-slope portions; that is, one is a line with a slope exactly 1/2, and the other, a horizontal line independent of the pH.

The appearance of the horizontal line can be explained from Eq. (21) by assuming that the potassium or lithium concentration in both phases attains a certain constant value characteristic of the acids in a sufficiently high pH region. The $(1+D^{HR})[H^+]_a/K_a^{HR}$ term is, of course, much smaller than unity and smaller than the $(1+D^{M_IR})[M^+]_a$ term. If the $[M^+]_a$ term can be assumed to be much larger than $[M_I^+]_o$, Eq. (21) reduces to a much simpler expression, as has been pointed out in the case of alkali metal picrates,[1] as:

$$(q^M)^2 = \frac{K_a^{MR} D^{MR}}{K_o^{MR}} \qquad (22)$$

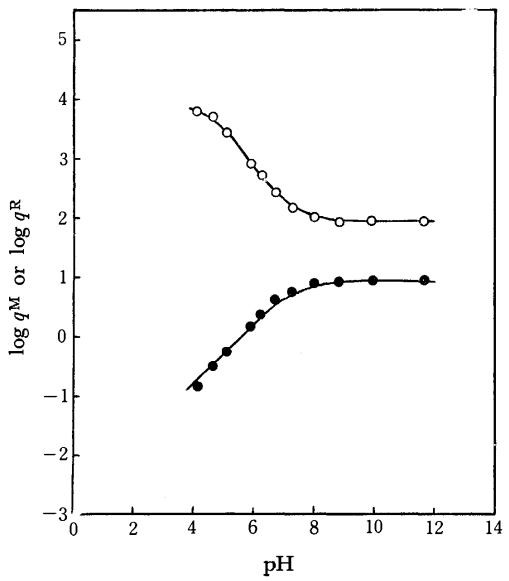

Fig. 4. The distribution of the potassium salt with hexyl,
Open circles: log q^R – pH curve
Solid circles: log q^M – pH curve.

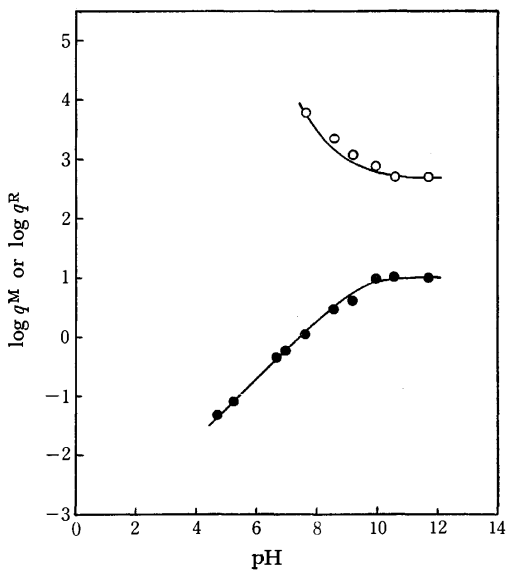

Fig. 5. The distribution of the potassium salt with α-hexyl,
Open circles: log q^R – pH curve
Solid circles: log q^M – pH curve.

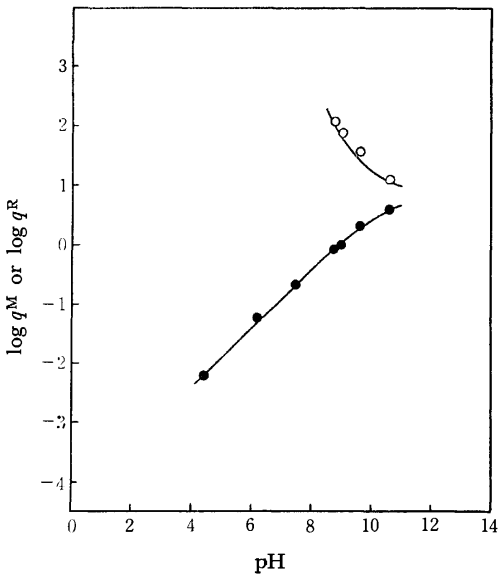

Fig. 6. The distribution of the potassium salt with thiohexyl,
Open circles: log q^R – pH curve
Solid circles: log q^M – pH curve.

Figures 4 and 5 show that the q^M values measured at sufficiently high pH values are considerably smaller than those to be expected from Eq. (22), as shown in Table 1. Such a result can well be understood by taking into account the effect of the concentration of the lithium extracted, $[M_I^+]_o$. In fact, the results of the atomic absorption spectrophotometric measurements show that the extractabilities of potassium salts by these acids are so high that the concentration of potassium in the aqueous phase, $[M^+]_a$, decreases to about 10^{-4} M. The value is only slightly larger than that of the lithium extracted, $[M_I^+]_o$, though the extractability of lithium ions still remains much lower than that of potassium. Therefore, the neglect of the $[M_I^+]_o$ term compared to the $[M^+]_a$ term causes a large deviation between the measured q^M values and q^M values estimated by means of the much simpler expression. An atomic absorption spectrophotometric method might not always be satisfactory in finding out such a small difference.

Thiohexyl reveals no horizontal line below pH 11.5. With a more alkaline solution (pH 12.69), a slightly small q^M value was obtained (log q^M=0.356). The decrease in q^M value can also be explained from Eq. (21) by taking into account the increased value of $[M_I^+]_o$. The log q^M value thus obtained is 0.3564. The good agreement between the measured and calculated q^M values may prove the usefulness of Eq. (21).

On the other hand, when the aqueous solution is acidic, potassium as well as lithium ions will remain

almost unextracted in the aqueous phase to satisfy the condition $[M^+]_a \gg [M_I^+]_o$. Accordingly, under such a condition a useful approximation for q^M may be obtained from Eq. (21) by making the following assumptions:

$$[M^+]_o \gg [M_I^+]_o,\ D^{M_IR} \ll 1,\ D^{HR} \gg 1, \text{ and } q^M \approx \frac{[M^+]_o}{[M^+]_a}$$

In this manner, Eq. (21) can be simplified to the following expression:

$$(q^M)^2 = \frac{[M^+]_o + \frac{1}{K_o^{MR}}}{[M^+]_a + \frac{1}{K_a^{MR}}\left(1 + \frac{D^{HR}}{K_a^{HR}}[H^+]_a + K_a^{M_IR}[M_I^+]_a\right)} \quad (23)$$

Under sufficiently acidic conditions, Eq. (21) is further simplified, yielding:

$$(q^M)^2 = \frac{D^{MR}K_a^{MR}K_a^{HR}}{K_o^{MR}D^{HR}} \cdot \frac{1}{[H^+]_a} \quad (24)$$

A plot of log q^M *vs.* pH gives a straight line with a slope of 1/2; the intercept on the Y/q^M-axis is given by $1/2(\log K_a^{MR}D^{MR}K_a^{HR}/K_o^{MR}D^{HR})$. In Figs. 4, 5, and 6, it is shown that the above relation holds well in the acidic region. The solid line in each figure was drawn by means of Eq. (21) so as to fit well with the experimental values (solid circles) by choosing an appropriate value for K_a^{HR}/D^{HR} (Table 1).

v) Distribution of the Acids, q^R. The dependence of the distribution ratio of the acid upon pH is expressed by Eq. (14). This equation may well be understood by dividing it into two equations on the basis of appropriate assumptions; that is, an equation which holds in a sufficiently alkaline pH:

$$q^R = \frac{\left(1 + \frac{1}{K_o^{MR}[M^+]_o}\right)D^{MR}K_a^{MR}[M^+]_a + D^{M_IR}K_a^{M_IR}[M_I^+]_a}{1 + K_a^{MR}[M^+]_a + K_a^{M_IR}[M_I^+]_a} \quad (25)$$

and one which holds in a sufficiently acidic pH:

$$q^R = D^{HR} \quad (26)$$

When the aqueous solution is sufficiently alkaline, the amounts of potassium in both phases attain a certain constant value, as has been mentioned before. Accordingly, from Eq. (25) it can be expected that log q^R will also attain a certain constant value. Figures 4 and 5 show that Eq. (25) holds well in such an alkaline solution. Thiohexyl (Fig. 6) does not show such a constant portion below pH 11.5.

On the other hand, when the aqueous solution is sufficiently acidic, it can be expected from Eq. (26) that the log q^R value will also attain a constant value. Only hexyl reveals incompletely the presence of such a constant. The distribution behavior in a more acidic region can be shown only when more sensitive methods than spectrophotometry are available for the determination of the acid in the aqueous phase.

When the pH value of the solution is comparable with that of pK_a^{HR} ($K_a^{HR}/[H^+]_a \approx 1$), no terms (except lithium terms) can be neglected. Therefore, it is impossible to make such an illustrative statement about the distribution curves.

When appropriate values for K_a^{HR} and D^{HR} are chosen, a theoretical q^R—pH curve which fits well with the experimental values should be obtained. In Figs. 4, 5, and 6 the calculated curves are shown by solid lines. The fit is the best for the hexyl salt. In the remaining two salts, the experimental q^R values are so few that the K_a^{HR} and D^{HR} values can not be determined exactly, because the data on q^R in the acidic region (which are lacking in the experiment) are dominant in determining these values. This can easily be understood from the fact mentioned above; that is, the q^R values in the alkaline region do not depend upon K_a^{HR} or D^{HR} (cf. Eq. (25)). The K_a^{HR} value thus obtained for hexyl agrees well with that reported by Lin[9] ($pK_a = 5.4$). It is noticeable, however, that the K_a^{HR} values reported by Grunwald,[10] Glover,[11] and O'Donnell[12] are much larger than that of the present work.

vi) Association Constants, $K_a^{M_IR}$, and Distribution Constants, D^{M_IR}, for the Lithium Salts. The values of $K_a^{M_IR}$ and D^{M_IR} for these salts have not been reported, except in the case of hexyl salt ($K_a^{M_IR} = 8.9$, $D^{M_IR} = 0.5$[13]). The atomic absorption spectrophotometric measurements proved that the distribution ratio of lithium was almost the same for hexyl and α-hexyl and was considerably smaller for thiohexyl. This fact supports the idea that the terms containing these constants are negligibly small, as is the case with hexyl. Therefore, for α-hexyl and thiohexyl the theoretical q^R—pH and the q^M—pH curves are calculated by means of Eqs. (14) and (21) respectively, disregarding these terms.

In conclusion, the present work has made it clear that the distribution mechanism proposed for alkali metal picrates is valid also for the acids which show a high extractability. However, it must be noted that the application of this method suffers some limitations from the properties of the acid used. The acids favorable for such distribution studies are sufficiently acidic in nature to prevent the hydrolysis of the salts in wet nitrobenzene. The hydrolysis makes it impossible to determine the association constant of the salt by conductometry. Another important requirement is that the acids must have a moderate q^R or q^M value. For example, with an acid having an extremely high q^R value the method fails to determine a dissociation constant and a distribution constant, as has been mentioned in connection with α-hexyl and thiohexyl.

The author wishes to express his gratitude to Professor Kyoji Tôei for his guidance throughout the course of this work.

9) K. Pan and Z. F. Lin, *J. Chinese Chem. Soc.*, **2**, 1 (1955).
10) D. W. Fon and E. Grunwald, *J. Phys. Chem.*, **73**, 3909 (1969).
11) D. J. Glover, *J. Amer. Chem. Soc.*, **87**, 5275 (1965).
12) R. Stewart and J. P. O'Donnell, *ibid.*, **84**, 493 (1962).
13) S. Motomizu, K. Tôei, and T. Iwachido, This Bulletin, **42**, 1006 (1969).

Kinetic Studies of the Nickel Malate Complex Formation in Solution by the Pressure-jump Method

Shoji HARADA, Katsuyoshi AMIDAIJI, and Tatsuya YASUNAGA

Department of Chemistry, Faculty of Science, Hiroshima University, Higashisenda-machi, Hiroshima

(Received December 21, 1971)

The nickel malate complex formation reaction in an aqueous solution, $Ni^{2+}+Mal^{2-} \underset{k_d}{\overset{k_f}{\rightleftharpoons}} NiMal$, where Mal^{2-} represents the malate ion, was studied by the pressure-jump method. The following rate constants and the equilibrium constant were obtained: $k_f=5.6\times10^5$ M^{-1} sec^{-1}, $k_d=17$ sec^{-1} and $K=3\times10^4$ M^{-1} at 25°C and $\mu\rightarrow0$. Studies at various temperatures between 12 and 30.5°C gave the thermodynamic parameters. In comparison with the results on other ligand complexes, the ligand effects seem to be found not in the formation rate constant, but in the dissociation rate constant. The results indicate that the rate-determining step of the complex formation is the release of the water molecule from the inner coordination sphere of the nickel ion.

The development of the relaxation method has made it possible to study kinetically the fast metal complex formation reactions.[1] Some of the complex formations of the nickel(II) ion have been studied by the flow method,[2] the temperature-jump method,[3] the pressure-jump method[4], and most recently by the pressure-shock method.[5] These studies have revealed that the step-by-step association picture proposed by Eigen[6] *et al.* for the complex formation reaction is valid and that the rate-determining step is the release of the water molecule from the inner coordination sphere of the nickel ion. In the case of the complex formation with a bidentate ligand, however, two water molecules on the nickel ion should be replaced, and the reaction mechanism is more complicated.

The present study was undertaken in order to obtain kinetic information on the nickel malate complex formation reaction and in order to compare the ligand effects on the kinetic parameters with those of other bidentate ligands. Another purpose was to test the operation of a newly-built device at the beginning of the pressure-jump study.

Experimental

All of the chemicals used were of a reagent grade. A stock solution of nickel malate was prepared by mixing a stoichiometric amount of $NiSO_4$ with malic acid, and then it was titrated with a solution of $Ba(OH)_2$ until all the sulfate ion had precipitated as $BaSO_4$. The solid $BaSO_4$ was removed by filtration. The concentration of the nickel malate of the resultant solution was determined by a dimethylglyoxime titration. Each solution studied was prepared by diluting the stock solution to the desired concentration. The pH values of the solutions were $\geq$6.5 where most of the ligand was in the dissociated form. In order to reduce the cavitation effects, the solutions were degassed by sonoration with a 400 KHz transducer under reduced pressure.

The pressure-jump apparatus used was a modification of that described by Macri and Petrucci.[7] The pressure-jump cell is shown in Fig. 1. N_2 gas was introduced from

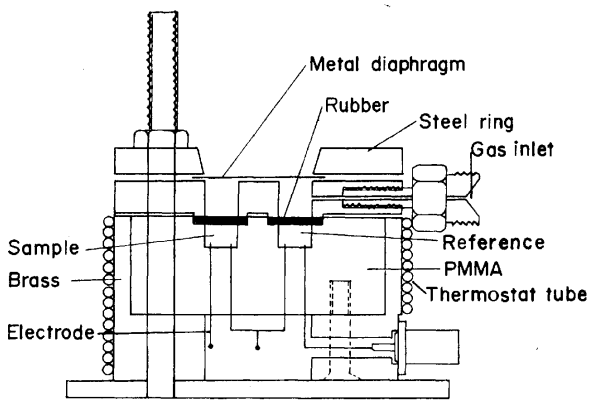

Fig. 1. Pressure-jump cell.

the gas inlet until a brass diaphragm burst at a pressure of approximately 25 atm. The pressure of the two cells, one containing the sample solution and the other containing the reference KCl solution, decreases abruptly from 25 to 1 atm. The concentration changes of the species were followed by means of the electric conductivity method; *i.e.*, the two cells were in separate arms of a Wheatstone bridge circuit fed from a 150 KHz oscillator. To calibrate the time constant of the apparatus, a 0.02 M $MgSO_4$ solution which exhibites a relaxation effect faster than 1 μsec was used. From the trace obtained (Fig. 2a), the apparatus has been proved to be useful for kinetic studies of reactions with relaxation times down to 100 μsec. The temperature of the sample cell was controlled to $\pm$0.5°C by circulating the water from a thermostat through a copper tube spiraled around the cell.

In all the nickel malate solutions, the relaxation spectrum was characterised by a single relaxation time. A representative relaxation spectrum is shown in Fig. 2b. The reciprocal relaxation time was calculated from a plot of $-\log \Delta C$ *vs.* the time, where ΔC is the deviation of the concentration from its equilibrium value. The quoted relaxation times and the rate constants are the mean values of several runs.

1) M. Eigen and L. DeMaeyer, "Technique of Organic Chemistry", Vol. VIII, 2nd Ed., S. L. Friess, Interscience Publishers Inc., New York, N. Y. (1963), Part 2, p. 895.
2) G. H. Nancollas and N. Sutin, *Inorg. Chem.*, **3**, 360 (1964).
3) G. G. Hammes and J. I. Steinfeld, *J. Amer. Chem. Soc.*, **84**, 4639 (1962).
4) J. L. Bear and C. T. Lin, *J. Phys. Chem.*, **72**, 2026 (1968).
5) H. Hoffmann and E. Yeager, *Ber. Bunsenges. Physik. Chem.*, **74**, 641 (1970).
6) M. Eigen and K. Tamm, *Z. Elektrochem.*, **66**, 93, 107 (1962).
7) G. Macri and S. Petrucci, *Inorg. Chem.*, **9**, 1009 (1970).

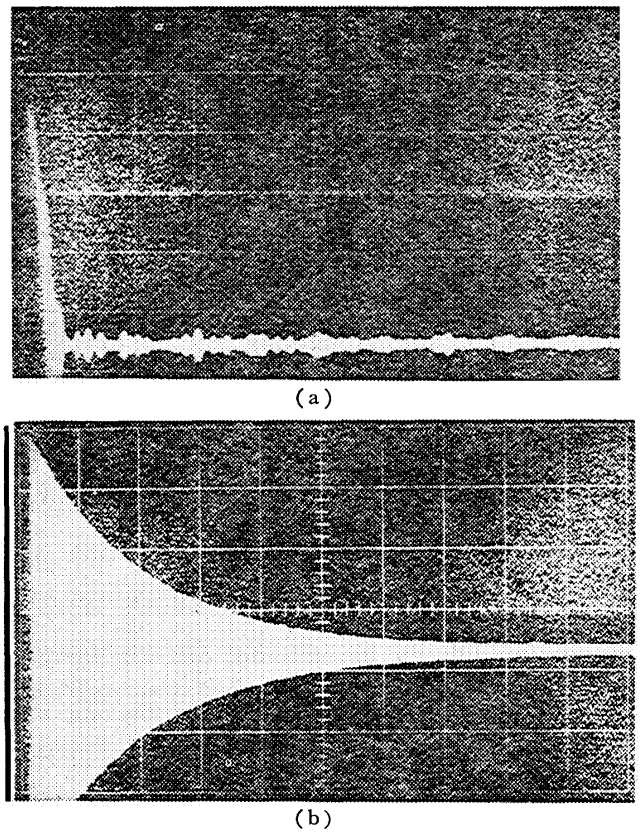

(a)

(b)

Fig. 2. Pressure-jump spectra.
(a) 0.02 M $MgSO_4$; sweep 200 μsec/division,
(b) 29.2×10^{-4} M Nickel malate; sweep 2 msec/division at 25°C.

Results

In the present studies, the complex formation reaction may be expressed as follows:

$$M^{2+} + L^{2-} \underset{k_d}{\overset{k_f}{\rightleftharpoons}} ML \qquad (1)$$

where M^{2+} is the metal ion, L^{2-} is the ligand, and ML is the complex. The rate constants are related to the relaxation time, τ, by the following equation:

$$1/\tau = k_d + k_f\gamma_{\pm}^2(C_M + C_L) \qquad (2)$$

where C_M and C_L are the concentrations of M^{2+} and L^{2-} respectively and where $\gamma_{\pm}$ is the mean activity coefficient of the free ions. The experimental conditions and the observed relaxation times at 25°C are shown in Table 1.

The complex formation constant, $K(=k_f/k_d)$, of nickel malate was not, unfortunately, given in the literature, so the values of k_f, k_d, and K were calculated from the kinetic data. As the first approximation, a value of K which had been roughly estimated from those of nickel malonate and succinate[8] was used to calculate the ionic concentrations. The activity coefficients of the ions were calculated by means of the Kielland equation.[9] The $1/\tau$ values were plotted against $\gamma_{\pm}^2(C_M+C_L)$ to give k_f and k_d from the slope and the intercept of the line respectively. Here, the ratio of k_f and k_d should coincide with the first estimated K value. The same procedures were repeated until a constant K value was obtained. The final results are shown in Fig. 3, and the following rate and equilibrium constants were obtained: $k_f=5.6\times10^5$ M^{-1} sec^{-1}, $k_d=17$ sec^{-1}, and $K=3\times10^4$ M^{-1} at 25°C $\mu\to0$.

8) R. M. Fuoss, *J. Amer. Chem. Soc.*, **80**, 5059 (1958).
9) J. Kielland, *ibid.*, **59**, 1675 (1937).

Table 1. Relaxation times and experimental conditions for the nickel malate system at 25°C

C_o[a] (10^{-4} M)	C_{Nimal} (10^{-4} M)	$C_{Ni}=C_{mal}$ (10^{-5} M)	μ (10^{-4})	$\gamma_{\pm}$	$1/\tau$ (sec^{-1})
6.8	5.5	13.0	5.2	0.90	136
9.8	8.2	15.8	6.3	0.90	160
19.5	17.2	22.8	9.1	0.88	206
29.2	26.4	28.2	11.3	0.86	284
39.0	35.7	32.8	13.1	0.85	310
58.5	54.4	40.5	16.2	0.84	348
78.0	73.3	47.0	18.8	0.83	371
117.0	111.2	57.8	23.1	0.82	445
156.0	149.3	67.0	26.8	0.80	510
195.0	187.5	75.0	30.0	0.79	576
234.0	225.8	82.3	32.9	0.79	585
273.0	264.1	89.0	35.6	0.78	626
312.0	302.5	95.3	38.1	0.77	700
351.0	340.9	101.2	40.5	0.77	670
390.0	379.3	106.8	42.7	0.76	635

a) C_o refers to the total stoichiometric concentrations of nickel malate.

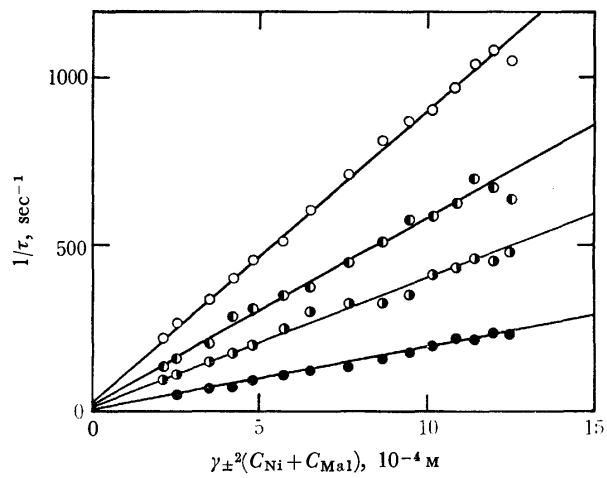

Fig. 3. $1/\tau$ *vs.* $\gamma_{\pm}^2(C_{Ni}+C_{Mal})$ plot at 12°C (●), 20°C (◑), 25°C (◐), and 30.5°C (○).

In order to determine the energies of activation, a series of experiments was run covering the temperature range from 12 to 30.5°C. The rate constants, k_f, and k_d, and the equilibrium constants at each temperature were obtained from Fig. 3. The Arrhenius energy of activation, $\Delta E_f^{\ddagger}$, was obtained from the plot of $\log k_f$ against $1/T$, as is shown in Fig. 4. The entropy of activation, $\Delta S_f^{\ddagger}$, the enthalpy of activation, $\Delta H_f^{\ddagger}$, and the free energy of activation, $\Delta G_f^{\ddagger}$, were calculated from the next

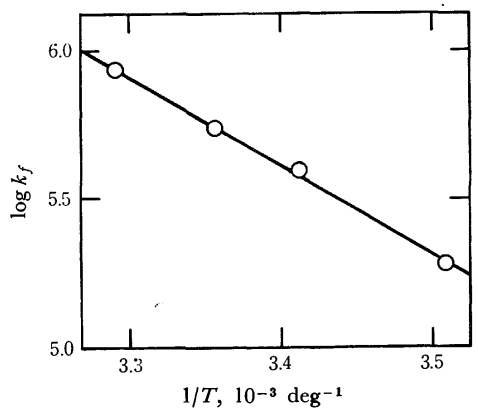

Fig. 4. Temperature dependence of k_f.

TABLE 2. KINETIC DATA FOR THE NICKEL MALATE COMPLEX FORMATION AT 25°C ($\mu \to 0$)

$$Ni^{2+} + Mal^{2-} \underset{k_d}{\overset{k_f}{\rightleftharpoons}} NiMal$$

K, M^{-1}	3×10^4
k_f, M^{-1} sec^{-1}	5.6×10^5
k_d, sec^{-1}	17
$E_f^{\neq}$, kcal mol^{-1}	14
$\Delta G_f^{\neq}$, kcal mol^{-1}	10
$\Delta H_f^{\neq}$, kcal mol^{-1}	13
$\Delta S_f^{\neq}$, cal deg^{-1} mol^{-1}	12
K_0, M^{-1}	25
k_{12}, sec^{-1}	22×10^3
ΔG_0, kcal mol^{-1}	-1.9
ΔH_0, kcal mol^{-1}	3
ΔS_0, cal deg^{-1} mol^{-1}	16
$\Delta H_{12}^{\neq}$, kcal mol^{-1}	10
$\Delta S_{12}^{\neq}$, cal deg^{-1} mol^{-1}	-4

equations; they are listed in Table 2.

$$\log A = \log \frac{eRT}{Nh} + \frac{\Delta S_f^{\neq}}{2.3R} \tag{3}$$

$$\Delta H_f^{\neq} = \Delta E_f^{\neq} - RT \tag{4}$$

$$\Delta G_f^{\neq} = \Delta H_f^{\neq} - T\Delta S_f^{\neq} \tag{5}$$

where A is the frequency factor.

Discussion

The kinetic data obtained for the nickel malate systems are compared with those for similar systems in Table 3. The values of k_f lie in approximately the same order, $\sim10^5$ M^{-1} sec^{-1}, irrespective of the nature of the ligand, and the ligand effects are found not in the value of k_f, but in the values of k_d and K.

Eigen and his co-workeers have proposed[6] a mechanism of complex formation reaction *via* rapid ion-pair formation, followed by the rate-determining loss of a water molecule in the inner coordination sphere of the metal ion:

$$\underset{\text{I}}{Ni(H_2O)_6^{2+} + Mal^{2-}} \overset{K_0}{\rightleftharpoons} \underset{\text{(II)}}{[(H_2O)_5Ni(H_2O)Mal]} \overset{k_{12}}{\underset{k_{21}}{\rightleftharpoons}} \underset{\text{(III)}}{[(H_2O)_5NiMal]} \overset{k_{23}}{\underset{k_{32}}{\rightleftharpoons}} \underset{\text{(IV)}}{[(H_2O)_4NiMal]} \tag{6}$$

where state (I) is the free ions, state (II) is the ion-pair, state (III) is the half-bonded intermediate, state (IV) is the bidentated complex, and K_0 is the ion-pair association constant.

On the assumptions that the intermediate state (III) is in a steady state and that $k_{23} \gg k_{21}$, the rate constant in Eq. (6) may be thus related to the formation rate constant in Eq. (1):

$$k_f = K_0 \cdot k_{12} \tag{7}$$

K_0 cannot be determined experimentally, so it has become customary to estimate it by means of the Fuoss equation.[3,8] For 2—2 electrolytes, K_0 can be calculated to be about 25 M^{-1}. The rate constant for the rate-determining process of Reaction (6), k_{12}, was, then, calculated to be 2.2×10^4 sec^{-1} by means of Eq. (7).

As may be seen in Table 4, this value has become of interest in comparison with the case of other ligand complexes, *i.e.*, the rate constants of the rate-deter-

TABLE 3. RATES AND COMPLEX FORMATION CONSTANTS OF NICKEL DICARBOXYLATE

Ligand	K, M^{-1}	k_f, M^{-1} sec^{-1}	k_d, sec^{-1}	t, °C	μ	Reference
Oxalate	2.1×10^4	7.5×10^4	3.6	25	0.1	2
Malonate	1.2×10^4	2.7×10^5	24	20	$\to 0$	4
Succinate	2.1×10^2	4.3×10^5	2.7×10^3	20	$\to 0$	4
Malate	3×10^4	5.6×10^5	17	25	$\to 0$	This work

TABLE 4. RATE CONSTANT OF THE RATE-DETERMINING PROCESS OF THE NICKEL COMPLEX FORMATION REACTION AT 25°C

Ligand	$k_{12}(10^3$ sec$^{-1})$	Ref.	Ligand	$k_{12}(10^3$ sec$^{-1})$	Ref.
Water	27	2	Triglycine	5	10
Imidazole	16	3	Oxalate	6	2
Sulfate[a]	15	6	Malonate[a]	11	4
Glycine	9	3	Succinate[a]	17	4
Diglycine	12	3	Malate	22	This work

a) At 20°C.

10) J. I. Steinfeld and G. G. Hammes, *J. Phys. Chem.*, **67**, 528 (1963).

mining process of the nickel complex formation lie approximately 10^3—10^4 sec^{-1} irrespective of the nature of the entering ligand. The small difference between them may be due to the approximation in calculating K_0. These facts indicate that the loss of a water molecule in the inner coordination sphere of the nickel ion is the rate-determining process of the complex fomration reaction.

Activation parameters can be reevaluated as follows for the detailed mechanism of complex formation in considering the variation in the free energy (ΔG_0), the entoropy (ΔS_0), and the enthalpy (ΔH_0) for the ion-pair formation:

$$\Delta G_0 = -RT \ln K_0 \tag{8}$$

$$\Delta S_0 = -19.4\, Z_- Z_+ / a = \Delta S^* - \Delta S_{12}^* \tag{9}$$

$$\Delta H_0 = \Delta G_0 + T\Delta S_0 = \Delta H^* - \Delta H_{12}^* \tag{10}$$

where Z is the valence of the ion and where a is the distance of the closest approach of the ion-pair partners (5Å). The results are listed in Table 2. In comparison with the complexes of other ligands, the thermodynamic parameters calculated are of the same order of magnitude, despite the large differences in the nature of the ligands, *e.g.*, the carbon number and the acidity. This fact also suggests that the rate-determining step of the complex formation is the release of the water molecule from the inner-sphere of the nickel ion.

In acid solutions, another path of the nickel malate complex formation can be proposed:

$$Ni^{2+} + HMal^- \rightleftharpoons NiMal + H^+ \tag{11}$$

In this experiment, however, the relaxation effect has become small with an increase in the concentration of $HMal^-$. Therefore, we could not obtain very precisely the dependency of τ on the hydrogen-ion concentration, as was done in the nickel malonate complex formation reaction.[11]

The authors wish to express their thanks to Mr. Takayasu Goto for the assistance he has given in the construction of the apparatus.

11) F. P. Cavasino, *ibid.*, **69**, 4380 (1965).

BULLETIN OF THE CHEMICAL SOCIETY OF JAPAN, VOL. 45, 1755—1759 (1972)

The Crystal Structure of $(-)_{589}$-Dinitrobis(ethylenediamine)cobalt(III) $(+)_{589}$-Bis(malonato)ethylenediaminecobaltate(III)

Keiji MATSUMOTO and Hisao KUROYA

Department of Chemistry, Faculty of Science, Osaka City University, Sumiyoshi-ku, Osaka

(Received December 24, 1971)

The crystal structure of $(-)_{589}$-[$Co(NO_2)_2en_2$] $(+)_{589}$-[Co mal_2 en] has been investigated by the X-ray method. Crystal data: triclinic, space group $P\bar{1}$; $a=10.58(2)$Å, $b=7.98(1)$Å, $c=7.99(1)$Å, $\alpha=122.8(2)°$, $\beta=105.3(2)°$, $\gamma=74.6(2)°$; $Z=1$. The crystal structure was determined by the Fourier technique and was refined by the least-squares method to an R factor of 0.101. The Δ configuration has been assigned to both the complex cation and anion, $(-)_{589}$-$[Co(NO_2)_2en_2]^+$ and $(+)_{589}$-[Co $mal_2en]^-$. The two Co-mal chelate rings are nearly planar. The O–Co–O angle in this ring is 96°, slightly larger than the N–Co–N angle observed in the cobalt(III)-trimethylenediamine chelate ring. All the ethylenediamine ligands in the two complex ions have the *ob*-conformation.

The absolute configuration of $(-)_{589}$-[Co $mal_2en]^-$ (mal=malonate ion) was studied by Douglas and his co-workers[1] by means of the ORD and CD spectra. They identified the lowest frequency CD peak with a positive sign as the A component by referring to the ORD and CD spectra of $(+)_{589}$-[Co $ox_2en]^-$ and $(-)_{546}$-[Co EDTA]$^-$; thus, they assigned the Δ configuration to $(-)_{589}$-[Co $mal_2en]^-$ on the basis of Mason's empirical rule.[2]

Recently, Judkins and Royer[3] measured the CD spectrum of $\Delta(+)_{589}$-[Co $tn_3]^{3+}$ in a signle crystal, showed that the relative positions of the E_a and A_2 bands in this complex are reversed as compared with those found in $\Delta(-)_{589}$-[Co $en_3]^{3+}$, and concluded that the sign of the Cotton effect should change when the coordination angle (θ) in the chelate ring goes from less than to greater than 90°, as had been predicted by Piper.[4] If such is the case with the Δtris(malonato)-cobalt(III) (possibly $\theta>90°$; this complex has not yet been prepared) and the Δtris(oxalato)coablt(III) complexes, the CD signs of their E_a components will be the opposite of each other. On the other hand, the rotational strength of the A component, $R(A)$, of the bis-complex seems to have a sign reflecting that of the R (E_a) of the parent tris-complex.[5] Therefore, the sign of the A component of $\Delta(-)_{589}$-[Co $mal_2en]^-$ should be the reverse of that of $\Delta(+)_{589}$[Co $ox_2en]^-$. These circumstances were not taken into account by Douglas *et al.* in making the assignment of the absolute configuration of $(-)_{589}$-[Co $mal_2en]^-$. In order to re-examine and determine its configuration directly,

1) B. E. Douglas, R. A. Haines, and J. G. Brushmiller, *Inorg. Chem.*, **2**, 1194 (1963).

2) S. F. Mason, *Quart. Rev.*, **17**, 20 (1963).

3) R. R. Judkins and D. J. Royer, *Inorg. Nucl. Chem. Lett.*, **6**, 305 (1970).

4) A. G. Karipides and T. S. Piper, *J. Chem. Phys.*, **40**, 674 (1964).

5) A. J. McCaffery, S. F. Mason, and B. J. Norman, *J. Chem. Soc.*, **1965**, 5094.

we carried out a crystal-structure analysis of $(-)_{589}$-$[Co(NO_2)_2en_2]$ $(+)_{589}$-[Co mal_2en].

Experimental

The complex compound, $(-)_{589}$-$[Co(NO_2)_2en_2]$ $(+)_{589}$-[Co mal_2en], was prepared following the method of Dwyer *et al.*[6]; subsequent recrystallization from an aqueous solution yielded brown crystals suitable for X-ray work. Using Cu$K\alpha$ radiation, the unit-cell dimensions were determined from higher angle reflections of Weissenberg photographs, on which aluminum powder diffraction lines were superimposed for calibration. Oscillation and Weissenberg photographs did not show any special symmetry or systematic absences, indicating that the space group is $P1$ or $P\bar{1}$. Only the former is, however, consistent with the optical activity of the specimen. The crystal data are as follows:

Triclinic
$a=10.58(0.02)$Å
$b=7.98(0.01)$Å
$c=7.99(0.01)$Å
$\alpha=122.8(0.2)°$
$\beta=105.3(0.2)°$
$\gamma=74.6(0.2)°$
Space group $P1$
$Z=1$ ($D_m=1.81$, $D_c=1.82$ g cm^{-3})
$\mu=35.9$ cm^{-1} for Ni$K\alpha$

Multiple-film, equi-inclination Weissenberg photographs were taken about the c (0 to 4th layers) and a axes (0 to 3rd layers) using Ni$K\alpha$ radiation. The intensities of 1442 independent reflections were estimated visually with the standard calibrated scales, but 71 of these were too weak to be measured: therefore, their intensities were assumed to be zero. The intensities were corrected for the usual L_p factor and spot shape,[7] but not for absorption. The crystal specimen used for the data collection had dimensions of $0.1\times0.04\times0.4$ mm.

Determination of the Crystal Structure

The positions of the two cobalt atoms were readily determined from the three-dimensional Patterson map. Their positional and thermal parameters were refined by the least-squares method. At this stage, the R factor was 0.411. The two nitro groups and one malonate ligand were found on the Fourier map phased by the two heavy atoms (Co_1 and Co_2). Then, the parameters of the 15 atoms thus obtained were refined and the structure factors were computed by their use. The subseuqent Fourier synthesis of the electron density showed the locations of all the remaining atoms. The five cycles of the least-squares refinement with an individual isotropic temperature factor reduced the R value to 0.101 for 1371 observed reflections. The weighting scheme employed was:

$w=0.3$ for $F_0<3.8$
$w=1.0$ for $3.8\leq F_0\leq 25.9$
$w=25.9/F_0$ for $F_0>25.9$

The atomic scattering factors were taken from the International Tables for X-ray Crystallography.[8] The real part of the anomalous disperison correction for Co was taken into account.[9] A subsequent refinement, in which anisotropic vibrations were permitted to the two cobalt atoms, improved neither the R factor nor the e.s.d.'s of the parameters. A difference synthesis computed at this stage did not show peaks corresponding to any of the hydrogen atoms. The final atomic coordinates, the temperature factors, and their e.s.d.'s are given in Table 1. The observed and calculated structure factors are preserved by the Chemical Society of Japan.[10]

The absolute configurations of the complex ions

TABLE 1. ATOMIC PARAMETERS AND THEIR e.s.d.'s[a]

Atom	x/a	y/b	z/c	B
Co_1	0.0	0.0	0.0	2.06(6)
O_1	−0.177(1)	0.074(2)	−0.095(2)	2.2(3)
O_2	0.057(1)	0.248(2)	0.098(2)	2.4(3)
O_3	−0.059(1)	0.100(2)	0.248(2)	2.3(3)
O_4	0.178(1)	−0.096(2)	0.078(2)	2.5(3)
O_5	−0.356(1)	0.295(2)	−0.079(2)	2.4(3)
O_6	0.041(1)	0.543(2)	0.124(2)	2.5(3)
O_7	−0.046(2)	0.118(2)	0.536(2)	3.5(3)
O_8	0.355(2)	−0.082(2)	0.294(2)	2.8(3)
C_1	−0.233(2)	0.257(3)	−0.055(3)	2.2(3)
C_2	−0.157(3)	0.418(4)	0.019(4)	5.1(6)
C_3	−0.010(2)	0.401(3)	0.080(3)	2.9(4)
C_4	0.008(2)	0.079(4)	0.399(4)	3.4(4)
C_5	0.147(3)	0.008(4)	0.411(4)	5.4(7)
C_6	0.230(2)	−0.052(3)	0.255(3)	2.7(4)
C_7	0.006(3)	−0.418(4)	−0.293(4)	4.2(5)
C_8	−0.003(2)	−0.305(3)	−0.406(4)	3.3(4)
N_1	−0.053(2)	−0.262(3)	−0.111(3)	3.2(4)
N_2	0.053(2)	−0.114(4)	−0.259(3)	2.3(3)
Co_2	0.5000(4)	0.3613(6)	0.3624(6)	2.24(6)
N_3	0.640(2)	0.151(3)	0.204(3)	2.5(3)
N_4	0.531(2)	0.210(2)	0.499(3)	2.2(3)
N_5	0.362(2)	0.198(3)	0.155(3)	3.3(4)
N_6	0.470(2)	0.501(3)	0.210(3)	2.7(3)
N_7	0.367(2)	0.552(3)	0.529(3)	2.4(3)
N_8	0.635(2)	0.525(2)	0.556(3)	2.2(3)
C_9	0.655(3)	−0.030(4)	0.221(4)	4.2(5)
C_{10}	0.648(2)	0.050(3)	0.446(3)	2.9(4)
C_{11}	0.345(2)	0.226(4)	−0.022(4)	3.3(4)
C_{12}	0.352(2)	0.449(4)	0.048(4)	3.5(4)
O_9	0.295(2)	0.491(3)	0.571(3)	3.9(3)
O_{10}	0.351(2)	0.735(2)	0.581(3)	3.8(3)
O_{11}	0.651(2)	0.584(3)	0.730(3)	4.2(4)
O_{12}	0.705(2)	0.573(3)	0.490(3)	4.1(4)

a) e.s.d.'s in parentheses

6) F. P. Dwyer, I. K. Reid, and F. L. Garvan, *J. Amer. Chem. Soc.*, **83**, 1285 (1961).
7) D. C. Philips, *Acta Crystallogr.*, **7**, 746 (1954).
8) "International Tables for X-ray Crystallography," Vol. III, Kynoch Press, Birmingham (1962), pp. 202, 214.
9) R. W. James, "The Optical Principles of the Diffraction of X-rays," G. Bell & Sons, London (1948), p. 608.
10) The complete data of the F_o-F_c table are kept as Document No. 7206 at the office of the Bulletin of the Chemical Society of Japan. A copy may be secured by citing the document number and remittimg, in advance, ¥200 for photoprints. Pay by check or money order payable to: Chemical Society of Japan.

Table 2. Calculated and observed intensities

$h\ k\ l$	$F_c^2(hkl)$	Obsd.	$\bar{h}\ \bar{k}\ \bar{l}$	$F_c^2(\bar{h}\bar{k}\bar{l})$
$\bar{1}\ 2\ 0$	576	>	$1\ \bar{2}\ 0$	196
$\bar{2}\ 2\ 0$	81	<	$2\ \bar{2}\ 0$	169
$\bar{1}\ 5\ 0$	225	>	$1\ \bar{5}\ 0$	121
$2\ 2\ 0$	144	>	$\bar{2}\ \bar{2}\ 0$	9
$4\ 1\ 0$	169	>	$\bar{4}\ \bar{1}\ 0$	49
$1\ 3\ 0$	484	>	$\bar{1}\ \bar{3}\ 0$	361
$7\ 1\ 0$	484	<	$\bar{7}\ \bar{1}\ 0$	784
$7\ 2\ 0$	676	<	$\bar{7}\ \bar{2}\ 0$	841
$0\ 3\ 0$	81	<	$0\ \bar{3}\ 0$	361
$\bar{2}\ 3\ 0$	256	>	$2\ \bar{3}\ 0$	9
$\bar{1}\ 4\ 0$	25	<	$1\ \bar{4}\ 0$	169
$0\ 6\ 0$	256	>	$0\ \bar{6}\ 0$	64

were determined by using the anomalous dispersion effects of the cobalt atoms for Cu$K\alpha$ radiation. The right-handed coordinate system was used in the indexing of the Weissenberg photographs throughout the present work. The intensities of the $hk0$ reflections were compared with those of $\bar{h}\bar{k}0$ on Weissenberg photographs around the c axis. The inequality relationships which were observed for some Bijvoet pairs are shown in Table 2. In this table the calculated intensities which were obtained by the use of the atomic coordinates shown in Table 1 are also listed. The values of $\Delta f'_{Co}$ and $\Delta f''_{Co}$ were taken from the International Tables for X-ray Crystallography.[8] A comparison of the observed inequality relationships with the calculated ones indicates that the set of the atomic coordinates shown in Table 1 represents the absolute structure of the crystal.

Results and Discussion

Projections of the crystal structure of an symmetric unit along the c and b axes are presented in Figs. 1 and 2 respectively. The crystal is composed of $(-)_{589}$-$[Co(NO_2)_2en_2]^+$ and $(+)_{589}$-$[Co\ mal_2en]^-$ ions, which are linked to each other by hydrogen bonds. In order to confirm the hydrogen bonds which exist between the amine groups of the coordinated ethylenediamine ligands and the oxygen atoms of the malonate ions, the positions of the hydrogen atoms were computed on the assumption that the $>NH_2$ groups have the tetrahedral geometry and the N–H bond distance is 1.03 Å.[11] The hydrogen bonds are summarized in Table 3. In the $(-)_{589}$-$[Co(NO_2)_2en_2]^+$ cation, all of the $H(NH_2)$'s of the ethylenediamine ligands participate in the hydrogen bonding. The N_4–H···O_8 and N_6–H···O_5 bonds seem to be stronger than the other six bonds. In the $(+)_{589}$-$[Co\ mal_2en]^-$ anion, only one hydrogen atom of the individual NH_2 group takes part in the hydrogen bonding; these N–H···O bonds are as strong as the N_4–H···O_8 and N_6–H···O_5 bonds.

11) K. N. Raymond, P. W. R. Corfield, and J. A. Ibers, *Inorg. Chem.*, **7**, 1362 (1968).

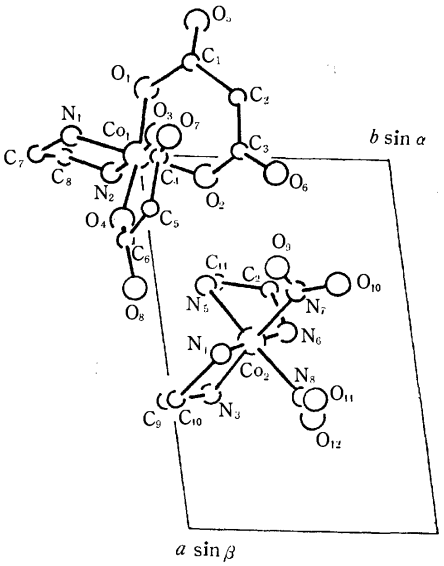

Fig. 1. The structure in an asymmetric unit, viewed along the c axis.

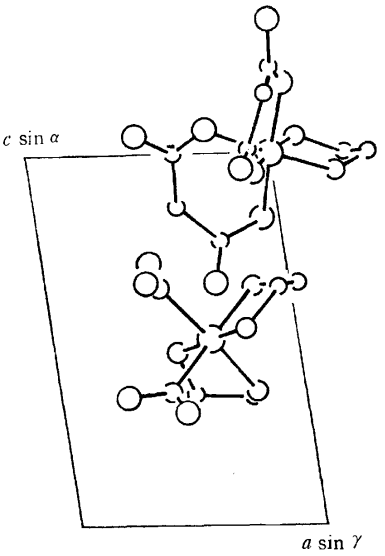

Fig. 2. Projection of the unit cell contents along the b axis.

Table 3. Possible hydrogen bonds with N···O distances less than 3.20Å

N	O	N···O	H···O	Angle around H
N_1 (1)	O_6 (5)	2.88Å	1.88Å	153°
N_2 (1)	O_7 (6)	2.93	1.92	166
N_3 (1)	O_5 (2)	3.05	2.34	125
N_3 (1)	O_3 (2)	3.05	2.19	140
N_4 (1)	O_5 (3)	3.02	2.18	137
N_4 (1)	O_8 (1)	2.85	1.92	149
N_5 (1)	O_8 (1)	3.01	2.34	122
N_5 (1)	O_2 (1)	3.09	2.24	139
N_6 (1)	O_8 (4)	2.98	2.15	136
N_6 (1)	O_5 (2)	2.82	1.89	148

(1) x, y, z (2) $1+x, y, z$ (3) $1+x, y, 1+z$ (4) $x, 1+y, z$ (5) $x, -1+y, z$ (6) $x, y, -1+z$

The perspectives of $(-)_{589}$-$[Co(NO_2)_2en_2]^+$ and $(+)_{589}$-$[Co\ mal_2en]^-$ are depicted in Fig. 3. It has been elucidated by the present work that both the complex ions have the same configuration, *i.e.*, Λ.[12]

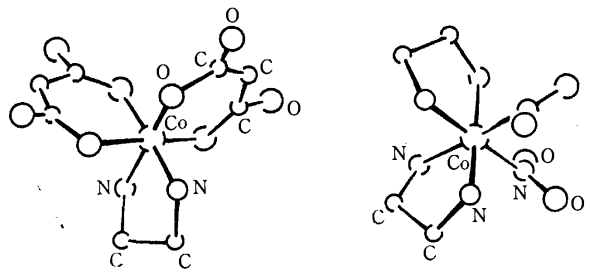

$(+)_{589}$-$[Co\ mal_2en]^-$ $(-)_{589}$-$[Co(NO_2)_2en_2]^+$

Fig. 3. The absolute configurations of the complex ions.

The absolute configuration of $(+)_{589}$-$[Co\ mal_2en]^-$ is consistent with the assignment made by Douglas *et al.*[1] Their spectral assignment of the *A* transition is possibly correct. On the other hand, if Piper's model is also applicable in the case of the tris(malonato)-coablt(III) complex,[4] the sign of the rotational strength, $R(A)$, of $\Lambda(+)_{589}$-$[Co\ mal_2en]^-$ should be reversed to that of $\Lambda(-)_{589}$-$[Co\ ox_2en]^-$, as has already been stated. Douglas *et al.* gave the negative sign to the rotational strengths of the *A* components of these two complexes. Therefore, their assignment of the *A* component is not entirely satisfactory.

The Λ configuration of $(-)_{589}$-$[Co\ (NO_2)_2en_2]^+$ established in the present work has already been assigned by some workers on the basis of the CD[5,13,14] and ORD[15] data. It is possible that the sign of the major CD peak in the first-absorption-band region is to be regarded as a diagnostic of the absolute configuration of the dissymmetric *cis*-$[CoL_2en_2]$ complexes (the ligands, L, are unidentate).[5,16,17]

The bond distances and angles in the complex ions are listed in Table 4. The approximate symmetry of $(-)_{589}$-$[Co(NO_2)_2en_2]^+$ and $(+)_{589}$-$[Co\ mal_2en]^-$ is C_2. All the ethylenediamine molecules in both com-

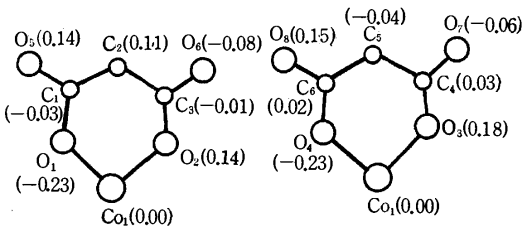

Fig. 4. Projection of the Co-mal six-membered chelate rings.
mal: malonate ion
Deviations of the atoms from the mean planes are given in parentheses.

TABLE 4. THE BOND LENGTHS AND BOND ANGLES IN THE COMPLEX IONS
Their e.s.d.'s are given in parentheses

Co_1-O_1	1.89(2) Å	O_1-Co_1-O_2	96(1)°	Co_2-N_3	2.00(2) Å	N_3-Co_2-N_4	85(1)°
Co_1-O_2	1.90(2)	O_3-Co_1-O_4	96(1)	Co_2-N_4	1.95(2)	N_5-Co_2-N_6	86(1)
Co_1-O_3	1.91(2)	Co_1-O_1-C_1	126(2)	Co_2-N_5	1.99(3)	Co_2-N_3-C_9	109(2)
Co_1-O_4	1.91(2)	Co_1-O_2-C_3	128(2)	Co_2-N_6	1.98(2)	Co_2-N_4-C_{10}	113(2)
Co_1-N_1	1.96(2)	Co_1-O_3-C_4	127(2)	Co_2-N_7	1.93(2)	Co_2-N_5-C_{11}	107(2)
Co_1-N_2	1.93(2)	Co_1-O_4-C_6	125(2)	Co_2-N_8	1.95(2)	Co_2-N_6-C_{12}	113(2)
O_1-C_1	1.31(3)	O_1-C_1-C_2	123(2)	N_3-C_9	1.49(4)	N_3-C_9-C_{10}	106(2)
O_2-C_3	1.30(3)	O_2-C_3-C_2	121(3)	N_4-C_{10}	1.48(3)	N_4-C_{10}-C_9	106(2)
O_3-C_4	1.30(3)	O_3-C_4-C_5	122(3)	N_5-C_{11}	1.51(4)	N_5-C_{11}-C_{12}	112(3)
O_4-C_6	1.26(3)	O_4-C_6-C_5	121(3)	N_6-C_{12}	1.51(4)	N_6-C_{12}-C_{11}	103(2)
C_1-O_5	1.24(3)	C_1-C_2-C_3	124(3)	C_9-C_{10}	1.57(4)	O_9-N_7-O_{10}	121(2)
C_3-O_6	1.22(3)	C_4-C_5-C_6	125(3)	C_{11}-C_{12}	1.57(4)	O_{11}-N_8-O_{12}	119(2)
C_4-O_7	1.22(3)	O_1-C_1-O_5	119(2)	N_7-O_9	1.20(3)	N_7-Co_2-N_8	90(1)
C_6-O_8	1.27(3)	O_2-C_3-O_6	122(3)	N_7-O_{10}	1.26(3)		
C_1-C_2	1.46(4)	O_3-C_4-O_7	121(3)	N_8-O_{11}	1.18(3)		
C_2-C_3	1.50(5)	O_4-C_6-O_8	118(3)	N_8-O_{12}	1.25(3)		
C_4-C_5	1.43(5)	C_2-C_1-O_5	119(3)				
C_5-C_6	1.51(5)	O_6-C_3-C_2	117(3)				
N_1-C_7	1.47(4)	C_5-C_4-O_7	117(3)				
N_2-C_8	1.49(4)	C_5-C_6-O_8	120(3)				
C_7-C_8	1.56(4)	N_1-Co_1-N_2	86(1)				
		Co_1-N_1-C_7	112(2)				
		Co_1-N_2-C_8	110(2)				
		N_1-C_7-C_8	103(3)				
		N_2-C_8-C_7	108(2)				

12) K. R. Butler and M. R. Snow, *Chem. Commun.*, **1971**, 550.
13) R. D. Gillard and G. Wilkinson, *J. Chem. Soc.*, **1965**, 1368.
14) G. A. Barclay, E. Goldschmied, N. E. Stephenson, and A. M. Sargeson, *Chem. Commun.*, **1966**, 540.
15) T. E. McDermott and A. M. Sargeson, *Aust. J. Chem.*, **16**, 334 (1968).
16) K. Matsumoto, S. Ooi, and H. Kuroya, This Bulletin, **43**, 3801 (1970).
17) K. Matsumoto, S. Ooi, and H. Kuroya, *ibid.*, **44**, 2721 (1971).

plexes are of the *ob*-conformation. The role of the hydrogen bonding in $(-)_{589}$-$[Co(NO_2)_2en_2]^+$ may be important in stabilizing the unstable *ob-ob* conformer.[11] The two Co-mal chelate rings are approximately planar (Fig. 4). The maximum deviation of the atom from mean plane is 0.23 Å. The presence of N–H···O hydrogen bonds seems to be significant in the formation of the nearly planar Co-mal chelate rings.[12] The average O–Co–O angle is 96°, slightly larger than the N–Co–N angle (94°) found in $(-)_{589}$-$[Co\ tn_3]^{3+}$.[18] The C–C–C angle (125°) is far from the tetrahedral angle, indicating that there is much strain in this bond angle. The C–O (coordinated to the Co atom) distances in the carboxyl groups are likely to be slightly larger than in the uncoordinated C–O bonds.

The authors wish to express their thanks to Mr. K. Hirotsu, who adapted the HBLS-4 and the RSSFR-3 computer programs to the FACOM 270—30 computer at Osaka City University. This research was aided in part by a Scientific Research Grant from the Ministry of Education, to which the authors' thanks are due. One of authors (K. M.) gratefully acknowledges the finacial support of the Matsunaga Science Foundation for his research.

18) T. Nomura, F. Marumo, and Y. Saito, *ibid.*, **42**, 1016 (1969).

BULLETIN OF THE CHEMICAL SOCIETY OF JAPAN VOL. 45, 1759—1764 (1972)

Binuclear Metal Complexes. III.[1] Preparation and Properties of Mononuclear and Binuclear Copper(II) and Nickel(II) Complexes of New Macrocycles and Their Related Ligands[2]

Hisashi Okawa and Sigeo Kida

Department of Chemistry, Faculty of Science, Kyushu University, Hakozaki, Fukuoka

(Received January 5, 1972)

The syntheses and properties of copper(II) and nickel(II) complexes of *N,N'*-alkylenebis(3-formyl-5-methylsalicylaldimine (alkylene=ethylene, propylene, or trimethylene) are described. By the reaction of these complexes with other alkylenediamines (ethylenediamine or trimethylenediamine), mononuclear copper(II) and nickel(II) complexes of new N_4O_2-type macrocycles have been synthesized. These complexes react with additional copper(II) or nickel(II) ions to form binuclear copper(II) or nickel(II) complexes. The geometries and properties of these new complexes are discussed.

It is known that the syntheses of macrocyclic, polydentate ligands are much facilitated by the template effect of metal ions.[3] In recent years considerable efforts have been directed towards syntheses of new macrocycles and their metal complexes. However, it appears that most of the work in this area dealt with mononuclear complexes of macrocycles, and only a few macrocycles making a binuclear metal complex have been reported.[4-7]

It is known that *N,N'*-ethylenebis(salicyclaldimino)-copper(II) reacts with copper(II) and other divalent metal ions to form a binuclear or trinuclear complex.[8] It is also well established that binuclear copper(II) complexes are obtained when copper(II) chloride or bromide is allowed to react with bis-(*N*-R-salicylaldimino)copper(II),[9] where R is an alkyl or a phenyl group attached to the imino nitrogen. Formation of these complexes is based on the fact that a phenolic oxygen atom can form bonds with two metal ions. Binuclear copper(II) complexes of 2,6-diformyl-4-4-methylphenol[10] and its Schiff base derivatives[10,11,12] have also been reported, where the phenolic oxygen acts as a bridge and the two formyl oxygens or imino nitrogens coordinate to copper(II) ions.

We have attempted to prepare new macrocycles which form a nearly planar, binuclear metal complex in such a way that two phenolic oxygens in the macrocyclic moiety bridge two metal ions. We prepared the copper(II) and nickel(II) complexes of *N,N'*-alkylenebis(3-formyl-5-methylsalicylaldimine) (alkylene=ethylene, propylene, or trimethylene) and then the mononuclear copper(II) and nickel(II) complexes of new N_4O_2-type macrocycles, using the above complexes as starting materials. The four macrocycles obtained are: 23,24-dihydroxy-10,21-dimethyl-3,6,14,17-tetraazatricyclo[17,3,1,$1^{8,12}$]tetracosa-1(23),2,6,8(24),9,11,13,17,19,21-decaene (abbreviated to

1) Part I: Ref. 9 and Part II: Ref. 10.

2) Presented at the 20th Symposium on Coordination Chemistry, Tokyo, Novermber, 1970. A part of this work has been reported by H. Okawa and S. Kida, *Inorg. Nucl. Chem. Lett.*, **7**, 751 (1971).

3) D. H. Busch, *Helv. Chim. Acta*, Fasciculus Extraordinarius Alfred Werner, 174 (1967).

4) N. F. Pilkington and R. Robson, *Aust. J. Chem.*, **23**, 2225 (1970).

5) R. W. Stotz and R. C. Stoufer, *Chem. Commun.*, **1970**, 1682.

6) K. Travis and D. H. Busch, *ibid.*, **1970**, 1041.

7) W. Rosen, *Inorg. Chem.*, **10**, 1832 (1971).

8) S. J. Gruber, C. M. Harris, and E. Sinn, *Inorg. Nucl. Chem. Lett.*, **4**, 107 (1968).

9) C. M. Harris and E. Sinn, *J. Inorg. Nucl. Chem.*, **30**, 2723 (1968).

10) H. Okawa, This Bulletin, **43**, 3019 (1970).

11) H. Okawa and S. Kida, *ibid.*, **44**, 1172 (1971).

12) R. Robson, *Inorg. Nucl. Chem. Lett.*, **6**, 125 (1970).

OK-2,2), 24,25-dihydroxy-10,22-dimethyl-3,6,14,18-tetraazatricyclo[18,3,1,$1^{8,12}$)]pentacosa-1(24),2,6,8(25),9,11,13,18,20,22-decaene (OK-2,3), 24,25-dihydroxy-4,10,22-trimethyl-3,6,14,18-tetraazatricyclo[18,3,1,$1^{8,12}$)]pentacosa-1(24),2,6,8(25),9,11,13,18,20,22-decaene (OK-2(pn),3), and 25,26-dihydroxy-11,23-dimethyl-3,7,15,19-tetraazatricyclo[19,3,1,$1^{9,13}$)]hexacosa-1(25),2,7,9(26),10,12,14,19,21,23-decaene (OK-3,3) (Fig. 1).

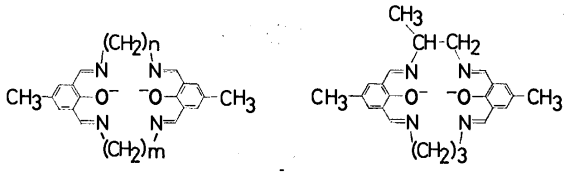

$m=2$, $n=2$: OK-2,2
$m=2$, $n=3$: OK-2,3
$m=3$, $n=3$: OK-3,3

OK-2(pn), 3

Fig. 1. Structures of macrocycles.

Three types of complexes have been prepared. The strucutral formulas are given in Fig. 2. The metal complexes of *N,N'*-alkylenebis(3-formyl-5-methylsalicylaldimine) (type 1) are abbreviated to Fsal-*m*-M, where *m* is 2 or 3 and M stands for copper or nickel. OK-*m,n*-M indicates the mononuclear metal complex of the macrocycles, in which *m* and *n* denote the number of methylene groups in the chelate ring and the number of the methylene groups in the bridge combining the two uncoordinated nitrogens, respectively. In the case where *l*-propylenediamine is included in the ligand instead of ethylenediamine, the macrocycle is abbreviated to OK-2-(*l*-pn),3. $[OK\text{-}m,n\text{-}M_2]^{2+}$ represents the binuclear metal complex of the macrocycle.

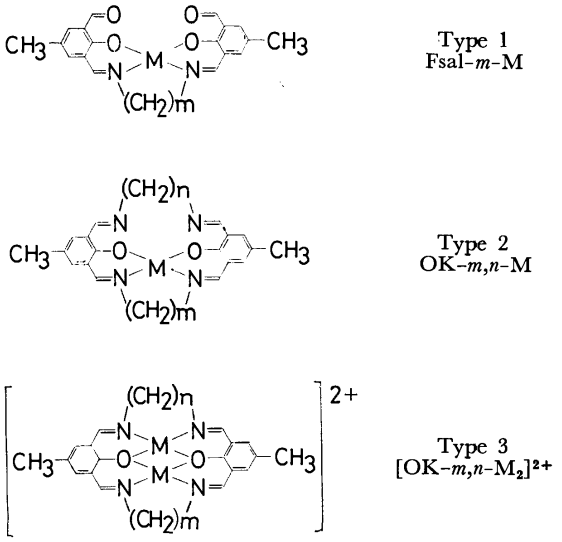

Type 1
Fsal-*m*-M

Type 2
OK-*m,n*-M

Type 3
$[OK\text{-}m,n\text{-}M_2]^{2+}$

Fig. 2. Structures of three types of complexes.

Experimental

Syntheses. 2,6-*diformyl*-4-*methylphenol*: Denton and Suschitzky's method[13] was modified for the preparation of 2,6-diformyl-4-methylphenol. *p*-Cresol (50 g) and hexamethylenetetramine (50 g) were mixed in a mortar. The pulverized mixture was added to polyphosphoric acid (500 g) at 160°C under vigorous stirring. The reaction mixture was cooled and hydrolyzed with water, and the product was isolated by steam distillation. Chameleon chemical grade polyphosphoric acid is suitable for this reaction. The yield was 8—11%, which is superior to that reported in literature.[13]

Fsal-2: 2,6-diformyl-4-methylphenol (9.85 g) and ethylenediamine (1.8 g) were mixed in ethanol. The orange prisms which separated were collected and recrystallized from dioxane to give yellow prisms with a melting point of 190—193°C.

Found: C, 68.05; H, 5.90; N, 8.49%. Calcd for $C_{20}H_{20}N_2O_4$: C, 68.17; H, 5.72; N, 7.95%.

Fsal-3: This compound was prepared by treating 2,6-diformyl-4-methylphenol (9.85 g) with 1,3-diaminopropane (2.22 g) in ethanol. The precipitate was collected and recrystallized from dioxane as yellow prisms. It melts at 144—147°C.

Found: C, 69.10; H, 6.02; N, 7.67%. Calcd for $C_{21}H_{22}N_2O_4$: C, 68.84; H, 6.05; N, 7.65%.

Fsal-m-M type Complexes: Copper(II) and nickel(II) complexes of Fsal-2 and Fsal-3 were synthesized. Methods of preparation for these complexes are the same in principle. A typical procedure is as follows. An aqueous solution of a slight excess of copper(II) acetate monohydrate was added to a solution of Fsal-2 in warm ethanol. Soon brown needles separated. They were collected and washed with ethanol.

The complexes can be prepared by treating stoichiometric amounts of 2,6-diformyl-4-methylphenol, diamine, and metal acetate in ethanol. Fsal-2(*l*-pn)-Cu was synthesized by this method.

Fsal-2-Cu and Fsal-2(*l*-pn)-Cu form greenish brown needles and Fsal-3-Cu green needles. The nickel(II) complexes form orange needles. Elemental analyses of the complexes are given in Table 1.

Table 1. Analyses of Fsal-*m*-M type complexes

	Found(%)			Calcd(%)		
Fsal-*m*-M[a]	C	H	N	C	H	N
Fsal-2-Cu	57.79	4.50	6.86	58.04	4.38	6.77
Fsal-2(*l*-pn)-Cu	58.81	4.78	6.39	58.94	4.71	6.55
Fsal-3-Cu	58.56	4.61	6.10	58.94	4.71	6.55
Fsal-2-Ni·1/2H_2O	57.18	4.53	6.60	57.46	4.58	6.70
Fsal-3-Ni	59.42	4.78	6.41	59.61	4.76	6.62

a) Fsal-2=$C_{20}H_{18}N_2O_4$; Fsal-2(*l*-pn) and Fsal-3=$C_{21}H_{20}N_2O_4$.

OK-m,n-M type Complexes: These were synthesized by the reaction of Fsal-*m*-M and ethylenediamine or 1,3-diaminopropane in *N,N*-dimethylformamide. The general synthetic method for macrocyclic complexes is given for OK-2,2-Cu as an example. Ethylenediamine (120 mg) was added to a vigorously stirred, hot solution of Fsal-2-Cu (828 mg) in *N,N*-dimethylformamide (800 m*l*) for thirty seconds. Stirring was continued for ten minutes and the reaction mixture was allowed to stand overnight. The brown prisms which separated were collected and washed with ethanol.

OK-2,3-Cu and OK-3,3-Cu form greenish brown and green prisms, respectively. OK-2,2-Ni and OK-2,3-Ni form orange prisms. The elemental analyses of the complexes are given in Table 2.

$[OK\text{-}m,n\text{-}M_2]^{2+}$ *type Complexes*: These were synthesized when an equimolar quantity of OK-*m,n*-M and M(II) salt

13) A. Denton and H. Suschitzky. *J. Chem. Soc.*, **1963**, 4741.

TABLE 2. YIELDS AND ANALYSES OF OK-*m*, *n*-M TYPE COMPLEXES

OK-*m*,*n*-M[a]	Yield %	Analysis					
		Found (%)			Calcd (%)		
		C	H	N	C	H	N
OK-2,2-Cu·H_2O	91	57.90	5.21	11.94	57.95	5.31	12.29
OK-2(*l*-pn), 3-Cu·H_2O	70	59.39	5.87	11.64	59.55	5.83	11.57
OK-2,3-Cu·H_2O	73	58.68	5.76	11.95	58.77	5.58	11.93
OK-3,3-Cu	97	61.56	5.62	11.73	61.58	5.62	12.02
OK-2,2-Ni·1/2H_2O	95	59.70	5.11	12.38	59.78	5.24	12.67
OK-2,3-Ni	75	61.65	5.50	12.29	61.68	5.41	13.53

a) OK-2,2=$C_{22}H_{22}N_4O_2$; OK-2,3=$C_{23}H_{24}N_4O_2$; OK-2(*l*-pn),3 and OK-3,3=$C_{24}H_{26}N_4O_2$.

TABLE. 3. ANALYSES OF $[OK\text{-}m,n\text{-}M_2]^{2+}$ TYPE COMPLEXES

$[OK\text{-}m,n\text{-}M_2]^{2+}$	Found (%)			Calcd (%)		
	C	H	N	C	H	N
$[OK\text{-}2,2\text{-}Cu_2]Cl_2\cdot C_2H_5OH\cdot 2H_2O$	44.15	4.36	8.60	44.04	4.93	8.56
$[OK\text{-}2,3\text{-}Cu_2]Cl_2\cdot 2H_2O$	44.76	4.42	8.71	44.38	4.53	9.00
$[OK\text{-}3,3\text{-}Cu_2]Cl_2\cdot H_2O$	46.61	4.54	9.11	46.61	4.56	9.06
$[OK\text{-}3,3\text{-}Cu_2]SO_4\cdot 2H_2O$	43.61	4.82	8.20	43.56	4.57	8.47
$[OK\text{-}2,2\text{-}Ni_2]Cl_2\cdot 3H_2O$	43.02	4.33	8.93	42.84	4.58	9.03
$[OK\text{-}2,3\text{-}Ni_2]Cl_2\cdot 2H_2O$	45.33	4.44	9.09	45.08	4.61	9.14

were treated in methanol. A typical procedure is given for $[OK\text{-}3,3\text{-}Cu_2]Cl_2\cdot H_2O$. Copper(II) chloride dihydrate (35 mg) was added to a suspension of OK-3,3-Cu (120 mg) in methanol (20 m*l*), and the mixture was heated on a water bath. A clean solution was filtered, concentrated to 5 m*l* and diluted with ethanol (5 m*l*) to give green needles. They were collected and washed with a small amount of ethanol.

The results of elemental analyses of binuclear complexes of macrocycles are given in Table 3.

Measurements. Electronic spectra were determined in solution and in solid with a Hitachi EPS-3T recording spectrophotometer. A reflectance attachment was used for the measurements on the solid samples. Infrared spectra were measured with a Hitachi EPI-S2 spectrophotometer in the region from 4000 to 650 cm^{-1}, using the KBr disk method. Magnetic susceptibilities were measured by the Gouy method at room temperature, where Pascal's constants were used for diamagnetic correction. Circular dichroism spectra were recorded with a JASCO ORD/SP optical rotatary dispersion recorder.

Results and Discussion

Fsal-m-M type Complexes. Condensation of two molecules of 2,6-diformyl-4-methylphenol with one molecule of ethylenediamine or 1,3-diaminopropane affords the monomeric Schiff base, Fsal-2 or Fsal-3, in quantitative yield with no formation of polymer. Copper(II) and nickel(II) complexes of Fsal-2 and Fsal-3 were synthesized. Their IR and visible spectral bands and magnetic moments are given in Table 4.

In the IR spectra, the bands around 1670 and 1635—1628 cm^{-1} can be assigned to the C=O and C=N stretching vibrations, respectively. A new band appeared around 1545 cm^{-1} upon complex formation. The band can be assigned to the skeletal vibration of the aromatic ring.[15]

The ligand field bands of Fsal-2-Cu and Fsal-3-Cu were observed at 17.5 and 16.6 kK, respectively. The *d-d* band for Fsal-3-Cu was found at a lower energy region than that for Fsal-2-Cu, which is thought to be a typical square-planarr copper(II) complex.[21-23] Since it is well established that the red shift in the d-d band takes place when the configuration around the copper(II) ion is distorted from planarity,[17,24-26] Fsal-3-Cu is assumed to possess a slightly distorted structure. The distortion of the configuration around the copper(II) ion in Fsal-3-Cu may also be demonstrated by its large magnetic moment of 2.01 B.M.

14) This band had previously been assigned to $\nu_{C=N}$[15], but it is known from N^{15} data that the band due to $\nu_{C=N}$ is located at a higher frequency.[16] Now the band around 1545 cm^{-1} is attributed to the phenolic C–O vibration[17] or the C–C vibration of the aromatic ring.[4] However, the former assignment is inconsistent with the assignment of the band near 1340 cm^{-1} to the phenolic C–O vibration.[4,18,19] Recently it has been reported that anilato complexes also show a similar band around 1530 cm^{-1}.[20] From this fact it seems reasonable to assign this new band to the skeletal vibration of the aromatic ring.

15) K. Ueno and A. E. Martell, *J. Amer. Chem. Soc.*, **60**, 1270 (1956).
16) E. P. Dudek and G. Dudek, *Inorg. Nucl. Chem. Lett.*, **3**, 241 (1967).
17) S. J. Gruber, C. M. Harris, and E. Sinn, *J. Inorg. Nucl. Chem.*, **30**, 1805 (1968).
18) B. Das Sarma and J. L. Bailar, Jr., *J. Amer. Chem. Soc.*, **77**, 5476 (1955).
19) P. Teyessie and J. J. Charette, *Spectrochim. Acta*, **19**, 1407 (1963).
20) M. Green and P. A. Tasker, *J. Chem. Soc. A*, **1970**, 3105.
21) S. M. Crawford, *Spectrochim. Acta*, **19**, 255 (1963).
22) R. S. Dawning and F. L. Urbach, *J. Amer. Chem. Soc.*, **91**, 5977 (1969).
23) K. S. Patel and J. C. Bailar, Jr., *J. Inorg. Nucl. Chem.*, **33**, 1399 (1971).
24) M. Honda and G. Schwarzenbach, *Helv. Chim. Acta*, **40**, 27 (1957).
25) R. L. Belford and T. S. Piper, *Mol. Phys.*, **5**, 251 (1962).
26) L. Sacconi, and M. Ciampolini, *J. Chem. Soc.*, **1964**, 276.

Table 4. Properties of Fsal-*m* and Fsal-*m*-M type complexes

	IR bands (cm^{-1})			*d-d* band (kK)		μ_{eff} (B.M.)
	C=O	C=N	Skeletal	in DMF	Powder	
Fsal-2	1688	1645				
Fsal-2-Cu	1670	1635	1540	17.5	17.5	1.80
Fsal-2-Ni·1/2H_2O	1670	1630	1545	18.2	18.2	diamag.
Fsal-3	1685	1645				
Fsal-3-Cu	1670	1631	1548	16.6	16.5	2.01
Fsal-3-Ni	1667	1629	1549	16.7	16.3	diamag.

Table 5. Properties of OK-*m*,*n*-M type complexes

	IR bands (cm^{-1})			*d-d* band (powder) (kK)	μ_{eff} (B.M.)
	C=N	C=N→M	Skeletal		
OK-2,2-Cu·H_2O	1645	1635	1540	17.5	1.80
OK-2,3-Cu·H_2O	1632		1543	17.3	1.81
OK-2(*l*-pn),3-Cu·H_2O	1635		1545	17.3	1.82
OK-3,3-Cu	1630	1625	1545	16.9	1.92
OK-2,2-Ni·1/2H_2O	1645	1627	1547	18.2	diamag.
OK-2,3-Ni	1628		1547	18.1	diamag.

as compared with 1.81 B.M. for Fsal-2-Cu, since it is well known that the distortion from planar towards tetrahedral configuration gives rise to an increase in μ_{eff} value.[17] The large magnetic moment of 2.01 B.M. for Fsal-3-Cu as compared with 1.90 B.M. for *N*,*N*′-1,3-propylenebis(salicylaldimino)copper(II)[17] can be attributed to the greater distortion caused by the steric repulsion between its formyl groups, which are in the ortho-position relative to phenol oxygen.

Fsal-2-Ni and Fsal-3-Ni are diamagnetic and have only one ligand field band at 18.2 and 16.7 kK, respectively (in DMF). Thus it is evident that these complexes have a planar configuration. This agrees with the fact that Ni-salen families (salen=*N*,*N*′-ethylenebis(salicylaldimine)) retain the planar structure even if the number of methylene groups is increased to 3, 4, or 5.[28,29] However, it appears that the configuration around the nickel(II) ion in Fsal-3-Ni is slightly distorted judging from the position of its d-d band which is lower in energy than that of Fsal-2-Ni.

OK-m,n-M type Complexes. In the case of Fsal-*m*-*M* type complexes, the two uncoordinated formyl groups are sufficiently close to each other to allow an intramolecular cyclization by treatment with other molecules such as ethylenediamine or 1,3-diaminopropane (kinetic template reaction). The complexes employed as starting matetials for the syntheses of OK-m,n-M were Fsal-2-Cu, Fsal-3-Cu and Fsal-2-Ni. Fsal-3-Ni was not used because of its limited amount. Since OK-*m*,*n*-M type complexes are sparingly soluble in any solvent, their molecular weight could not be determined. The yields of the macrocyclic complexes were nearly quantitative. Their IR and electronic specta and magnetic moments are given in Table 5.

The IR spectra show two bands in the region from 1645 to 1625 cm^{-1} in the case of the same methylene chain (*i.e.* $n=m$), and no band due to the $\nu_{C=O}$ mode. The bands can be attributed to the coordinated and uncoordinated azomethine groups, respectively. On the other hand, in the case of OK-2,3-Cu and OK-2,3-Ni the bands due to the coordinated and uncoordinated azomethine groups do not appear as well-resolved bands. No appreciable shift of the skeletal vibration of the aromatic ring was observed by clcyization.

The powder reflectance spectra of OK-2,2-Cu, OK-2,3-Cu and OK-3,3-Cu possess *d-d* bands at 17.5, 17.3 and 16.9 kK, respectively. The magnetic moments of OK-2,2-Cu, OK-2,3-Cu and OK-3,3-Cu are 1.92, 1.81, and 1.80 B.M., respectively. The sequences of these *d-d* bands and magnetic moments are compatible with each other and agreee in the order of distortion from a square planar configuration, which is effected by the increase in numbers, *n*(and *m*), of methylene groups. A similar trend in the *d-d* bands is found in the copper(II), nickel(II) and cobalt(II) complexes of N_4-macrocycles.[30]

OK-2,2-Ni and OK-2,3-Ni are undoubtedly planar complexes, since they are diamagnetic and have only one *d-d* band around 18.1—18.2 kK. They are insoluble in polar solvents such as pyridine. This implies that coordination bonds in the tetragonal plane are strong enough to exclude the fifth and sixth coordination of the solvent molecules in the axial position. A similar behavior has been observed in Ni-salen,[31] in Ni-amben series[32] (amben=*N*,*N*′-ethylenebis(*o*-aminobenzylideneimine) and in nickel-

27) G. E. Batley and D. P. Graddon, *Aust. J. Chem.*, **21**, 1473 (1968).
28) R. H. Holm, *J. Amer. Chem. Soc.*, **82**, 5632 (1960).
29) W. C. Hoyt and G. W. Everett, Jr., *Inorg. Chem.*, **8**, 2013 (1969).
30) M. Green and P. A. Tasker, *Inorg. Chim. Acta*, **5**, 65 (1971).
31) H. C. Clark and A. L. Odell, *J. Chem. Soc.*, **1955**, 3431.
32) M. Green and P. A. Tasker, *ibid.*, *A*, **1970**, 2531.

(II) complexes of N_4-macrocycles.[30]

In order to obtain „OK-3,2,-Cu" with 6-6-6 condensed ring system, Fsal-3-Cu and ethylenediamine were allowed to react in *N,N*-dimethylformamide. The product obtained, however, showed identical IR and visivle spectra and the same magnetic moment as OK-2,3-Cu. Thus it can be concluded that „OK-3,2-Cu" and OK-2,3-Cu are the same compound. It seems that the copper(II) ion migrates during the cyclization process to form a stable 6-5-6 condensed ring system. For the sake of confirmation, Fsal-2-(*l*-pn)-Cu, OK-2(*l*-pn),3-Cu and „OK-3,2(*l*-pn)-Cu" were prepared by using *l*-propylenediamine instead of ethylenediamine, and their CD spectra were compared (Fig. 3). The CD spectra of OK-2(*l*-pn),3-Cu and

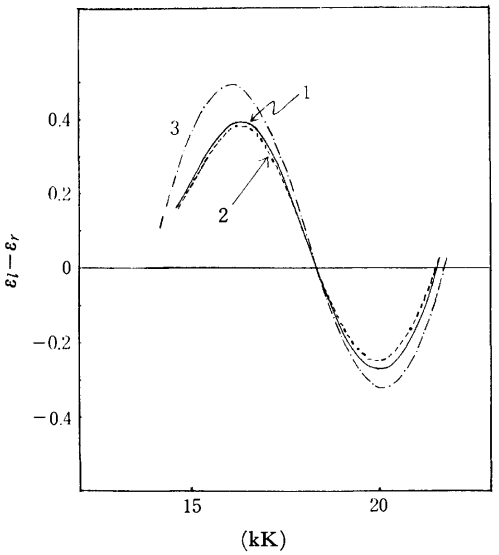

Fig. 3. CD spectra of OK-2(*l*-pn), 3-Cu(1), „OK-3,2(*l*-pn)-Cu"(2) and Fsal-2(*l*-pn)-Cu(3)(in *N,N*-dimethylformamide).

„OK-3,2(*l*-pn)-Cu" were found to be practically the same and very similar to that of Fsal-2(*l*-pn)-Cu in intensity as well as in sign. This indicates that they all possess the 6-5-6 condensed ring system, which is more stable than the 6-6-6 condensed ring system. Our results are consistent with the conclusion of Nakahara *et al.*[33] that *N,N'*-ethylenebis(salicylaldimino)-copper(II) is more stable than *N,N'*-1,3-propylenebis-(salicylaldimino)copper(II). It seems that the reaction carried out in hot N,N-dimethylformamide causes copper(II) ion migration.

[OK-m,n-M_2]$^{2+}$ type Complexes. The ligand field bands and some IR bands of complexes of this type are given in Table 6. Their magnetic moments were not measured because of limited amounts.

Infrared spectra show only one band for the C=N stretching vibration. The marked difference in IR spectra between OK-*m,n*-M and [OK-*m,n*-M_2]$^{2+}$ is seen in the frequencies of the skeletal vibration of the benzene ring; 1540 cm^{-1} for the former and 1560—1565 cm^{-1} for the latter with the exception of [OK-2,2-Cu_2]$Cl_2 \cdot C_2H_5OH \cdot 2H_2O$. A similar behavior was found in a complex where a phenolic oxygen atom bridges two copper(II) ion.[34,35] Thus such a behavior in the skeletal vibration appears to be characteristic of this type of binuclear structure. However, [OK-2,2-Cu_2]$Cl_2 \cdot C_2H_5OH \cdot 2H_2O$ shows a band due to a skeletal vibration of the aromatic ring at 1540 cm^{-1}, which is difficult to explain at present.

The reflectance and absorption spectra of [OK-2,2-Cu_2]$Cl_2 \cdot C_2H_5OH \cdot 2H_2O$ show one ligand field band at 18.1 and 17.4 kK, respectively, which are higher in energy than that of OK-2,2-Cu. In both the solid and solution spectra of [OK-2,3-Cu_2]$Cl_2 \cdot 2H_2O$ a very broad band was observed in the range from 15 to 18 kK. This may be due to the presence of two copper(II) ions with enivornments of different steric geometry. The reflectance spectra of [OK-3,3-Cu_2]$Cl_2 \cdot H_2O$ and [OK-3,3-Cu_2]$SO_4 \cdot 2H_2O$ show one ligand field band at 15.3 and 15.6 kK, respectively, while their solution spectra show a main peak at 16.5 kK and a discernible shoulder at the longer wavelength side of the main absorption band. Recently Pilkington and Robson[3] prepared $LCu_2Cl_2 \cdot 6H_2O$ and $LCu_2SO_4 \cdot 2H_2O$ (L is their abbreviation for OK-3,3) by another method. $LCu_2SO_4 \cdot 2H_2O$ and our

Table 6. IR and *d-d* bands of [OK-*m,n*-M_2]$^{2+}$ type complexes

	IR bands (cm^{-1})		*d-d* bands (kK)		
			Solutions		Powder
	C=N	Skeletal	MeOH	Py	
[OK-2,2-Cu_2]$Cl_2 \cdot C_2H_5OH \cdot 2H_2O$	1630	1540	18.1		17.4
[OK-2,3-Cu_2]$Cl_2 \cdot 2H_2O$	1641	1560	15—18		15—17.5
[OK-3,3-Cu_2]$Cl_2 \cdot H_2O$	1635	1565	16.5 (14.5)		15.3
[OK-3,3-Cu_2]$SO_4 \cdot 2H_2O$	1633	1563	16.5 (14.5)		15.6
[OK-2,2-Ni_2]$Cl_2 \cdot 3H_2O$	1633	1565	18.2	18.2	18.3
[OK-2,3-Ni_2]$Cl_2 \cdot 2H_2O$	1632	1563	18.0	18.1	18.2

Bands in parenthesis appear as a shoulder.

33) A. Nakahara, H. Yamamoto, and H. Matsumoto, This Bulletin, **37**, 1137 (1964).
34) C. M. Harris, J. M. James, P, J. Milham, and E. Sinn, *Inorg. Chim. Acta*, **3**, 81 (1969).
35) B. Coles, C. M. Harris, and E. Sinn, *Inorg. Chem.*, **8**, 2607 (1969).

$[OK\text{-}3,3\text{-}Cu_2]SO_4\cdot 2H_2O$ are undoubtedly the same complex, since they have the same composition and show very similar IR and visible spectra. Furthermore, $LCu_2Cl_2\cdot 6H_2O$ and $[OK\text{-}3,3\text{-}Cu_2]Cl_2\cdot H_2O$ are the same complex except for water of crystallization, because their IR and visible absorption peaks are practically the same. Pilkington and Robson[3] suggested on the basis of X-ray analysis that $LCu_2Cl_2\cdot 6H_2O$ has a square-pyramidal structure with a chlorine or a water molecule in apical positions. According to Ciampolini,[36] the copper(II) ion in a square pyramidal environment shows two distinguishable *d-d* bands, their main peak appearing on the shorter wave-length side with a shoulder on the longer wave-length side, but in the case of trigonal bipyramidal copper(II) complexes the band on the longer wave-length side is the main peak. Thus, $[OK\text{-}3,3\text{-}Cu_2]Cl_2\cdot H_2O$ and $[OK\text{-}3,3\text{-}Cu_2]SO_4\cdot 2H_2O$ probably keep a square-pyramidal, five-coordinate configuration in methanol solution.

36) M. Ciampolini, *Structure and Bonding*, **6**, 52 (1969).

$[OK\text{-}2,2\text{-}Ni_2]Cl_2\cdot 3H_2O$ and $[OK\text{-}2,3\text{-}Ni_2]Cl_2\cdot 2H_2O$ form orange prisms. Their visible spectra possess only one d-d band in the region from 18.3 to 18.0 kK. No absorption is found up to 2000 mμ. Thus it is expected that they are low-spin, square-planare binuclear complexes. It might be concluded that both complexes retain the planar geometry in a polar solvent such as pyridine, since there is no significant difference in electronic spectra between solid state, methanol solution and pyridine solution (Table 6). On the other hand, they differ from $LNi_2Cl_2\cdot 2H_2O$ (corresponding to „$[OK\text{-}3,3\text{-}Ni_2]Cl_2\cdot 2H_2O$") prepared by Pilkington and Robson,[3] in that the latter is dark-green and para-magnetic. Thus it can be concluded that nickel(II) ions in $[OK\text{-}2,2,\text{-}Ni_2]Cl_2\cdot 3H_2O$ and $[OK\text{-}2,3\text{-}Ni_2]Cl_2\cdot 2H_2O$ keep the square-planar configuration even in pyridine owing to the sufficiently strong ligand field, but that in $LNi_2Cl_2\cdot 2H_2O$ ($=[OK\text{-}3,3\text{-}Ni_2]Cl_2\cdot 2H_2O$) a chloride ion or water molecule can coordinate to apical positions, consistent with the decrease in the ligand field caused by an increase in the number of methylene groups.

BULLETIN OF THE CHEMICAL SOCIETY OF JAPAN, VOL. 45, 1764—1766 (1972)

Studies on Stable Free Radicals. XI. ESR Spectra of Stable Nitroxide Biradicals

Toshimasa TODA, Eiko MORI, and Keisuke MURAYAMA

Central Research Laboratories, Sankyo Co., Ltd., Shinagawa-ku, Tokyo

(Received October 5, 1971)

The ESR spectra of the triplet state of stable nitroxide biradicals, 1,9-diaza-2,2,8,8,10,10-hexamethyl-4-oxo-spiro[5.5]-undecane-1,9-dioxyl (III), cyclohexane-1-spiro-2′-(4′-oxoimidazolidine)-5′-spiro-4″-(2″,2″,6″,6″-tetramethylpiperidine)-1′,1″-dioxyl (IV) and cyclohexane-1-spiro-2′-(3′-oxoimidazolidine)-5′-spiro-4″-(2″,2″,-6″,6″-tetramethylpiperidine)-1′,1″-dioxyl (V) have been observed in a frozen MTHF glass. The biradicals have $2\mathbf{D} \simeq 500$ and $\mathbf{E} \simeq 0$ gauss. The distance ($r \simeq 5$ Å) between the two radical sites in these biradicals indicates that one piperidine ring can exist in chair form and the other in twisted form in III, and both in the twisted form in IV and V. The biradical, 2,2,6,6-tetramethylpiperidine-4-spiro-2′-(4′-oxoimidazolidine)-5′-spiro-4″-(2″,2″,-6″,6″-tetramethylpiperidine)-1,1″-dioxyl (VI) in a MTHF frozen glass shows no spectrum corresponding to a triplet state.

The electron spin resonance spectra of the stable biradicals and in particular nitroxide biradicals[2] with a small scalar electron spin-spin interaction are well known. However, cases of very large interaction are less common.[3] Calder and his co-workers[4] reported on the ESR spectrum of the nitroxide biradical (I) of this type. The crystalline samples of the triplet I undergoes a spontaneous topochemical change to the aminoquinone imine *N*-oxide (II).

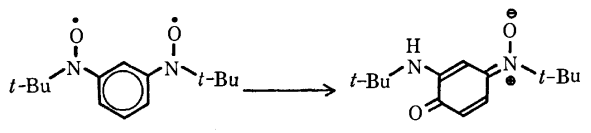

(I) (II)

We have isolated four stable nitroxide biradicals, III–VI.[5,6] They are very stable and no change have taken place on standing at room teaperature over several years.

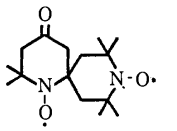

(III)

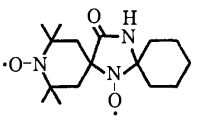

(IV)

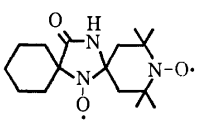

(V)

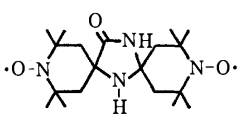

(VI)

1) Part X: T. Toda, E. Mori, H. Horiuchi, and K. Murayama, This Bulletin, **45**, 1802 (1972).

2) a) R. Briere, R. M. Dupeyre, H. Lamaire, C. Morat, A. Rassat, and P. Rey, *Bull. Soc. Chim. Fr.*, **1966**, 3290. b) E. G. Rozantsev, V. A. Golubev, V. I. Suskina, and M. B. Neiman, *Izv. Akad. Nauk SSSR, Ser, Khim.*, **1966**, 2192.

3) M. Itoh and E. M. Kosower, *J. Amer. Chem. Soc.*, **89**, 3655 (1967).

4) A. Calder, A. R. Forrester, P. G. James, and G. R. Luckhurst, *ibid.*, **91**, 3724 (1969).

5) K. Murayama, S. Morimura, O. Amakasu, T. Toda, and E. Yamao, *Nippon Kagaku Zasshi*, **90**, 296 (1969).

6) T. Toda, S. Morimura, E. Mori, H. Horiuchi, and K. Murayama, This Bulletin, **44**, 3445 (1971).

Since the molecular models of these nitroxide biradicals indicate that the two radical sites in the molecule can approach each other closely, and the molecules are relatively rigid, the direct intramolecular interactions of the two radical sites are expected to be larger than those of the nitroxide biradicals in which the two nitroxide radical subunits are connected to each other by flexible chains.[2a,7]

In this paper, we wish to report on the ESR spectra of the nitroxide biradicals III—VI.

After our work had been completed, Keana and Dinerstein[8] published a report on the ESR spectrum of stable nitroxide biradical (VII), which is compatible with ours.

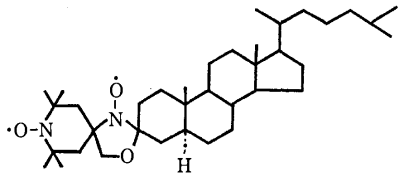

(VII)

Results and Discussion

The nitroxide biradical, 1,9-diaza-2,2,8,8,10,10-hexamethyl-4-oxo-spiro[5.5]undecane-1,9-dioxyl (III) in solution and frozen 2-methyltetrahydrofuran (MTHF) gave the spectra shown in Fig. 1. Since the spectrum in the transition of $\Delta m=\pm 2$ could be observed in a rigid glass state, the spectrum in Fig. 1-b gives a typical triplet state in a randomly oriented molecule.[9]

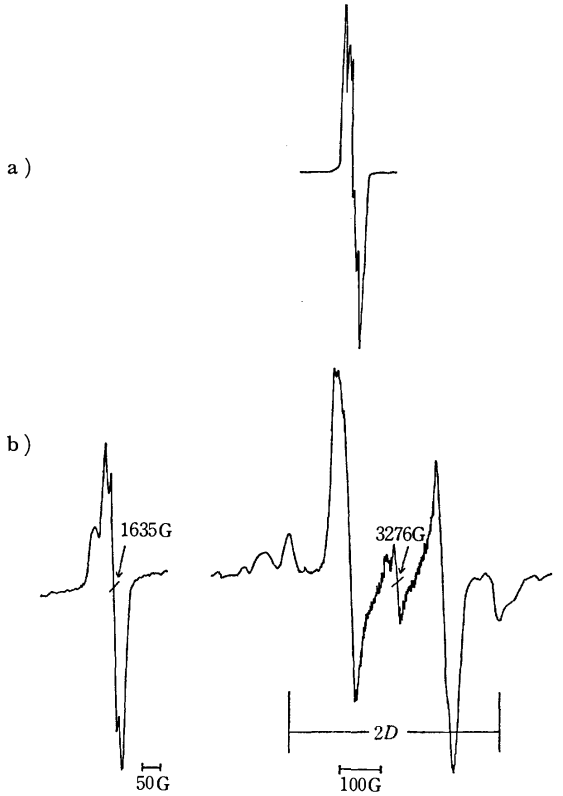

Fig. 1. ESR Spectra of III in 10^{-3} mol/l MTHF solution. a): at room temperature and b): at −196°C (measured in liquid nitrogen Dewar vessel).

The Hamiltonian for a biradical is

$$H = H_{\text{Zeeman}} + H_{\text{hyperfine}} + H_{\text{exchange}} + H_{\text{dipolar}}$$

The anisotropic effect observed in Fig. 1 is due to H_{dipolar}, where $H_{\text{dipolar}}=\mathbf{D}(S_z^2-1/3\cdot S^2)+\mathbf{E}(S_x^2-S_y^2)$. The zero field splitting parameter **D** can be estimated from the rigid glass spectrum as shown in Fig. 1, in which the separation between the outermost of lines in the spectrum is 2**D**.

The frozen MTHF glass spectrum of cyclohexane-1-spiro-2′-(4′-oxoimidazolidine)-5′-spiro-4″-(2″,2″,6″,6″-tetramethylpiperidine)-1′,1″-dioxyl (IV) is given in Fig. 2.

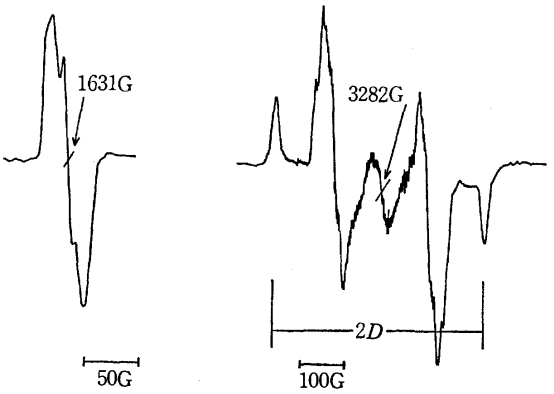

Fig. 2. ESR spectrum of IV in MTHF rigid glass at −196°C.

The spectrum of cyclohexane-1-spiro-2′-(3′-oxoimidazolidine)-5′-spiro-4″-(2″,2″,6″,6″-tetramethylpiperidine)-1′,1″-dioxyl (V) in a rigid glass of MTHF (not shown) exhibited a shape similar to the spectrum of IV.

The parameter **D** for the biradicals IV and V can also be estimated from these spectra. The exact calculations of **E** for the nitroxide biradicals III, IV and V are not possible from our data, but it is clear that $|\mathbf{E}|\ll|\mathbf{D}|$ in each of the biradicals.

In the point dipole approximation, 2**D** is related to the distance r between the >N–O· groups by the equation.[10]

$$2\mathbf{D} = 55600 \times r^{-3} \qquad (1)$$

The zero field splitting parameter **D** and the distance r for the nitroxide biradicals are given in Table 1.

Table 1. The values of zero field parameter **D** and distance between two >N–O· groups r

Biradical	$2\cdot\mathbf{D}$ (gauss)[a]	r (Å)[b]
III	532	4.72
IV	487	4.85
V	530	4.71

a) accuracy ±7 gauss.
b) accuracy ±0.02Å, from calculation by equation (1).

7) P. Ferruti, D. Gill, M. P. Klein, H. H. Wang, G. Entin, and M. Calvin, *J. Amer. Chem. Soc.*, **92**, 3704 (1970).
8) J. F. W. Keana and R. J. Dinerstein, *ibid.*, **93**, 2808 (1971).
9) E. Wasserman, L. C. Snyder, and W. A. Yager, *J. Chem. Phys*, **41**, 1763 (1964).
10) N. Hirota and S. I. Weissman, *J. Amer. Chem. Soc.*, **86**, 2538 (1964).

Measurements on molecular models of III with various conformations for two piperidine rings provide values of 4—6 Å for r which is the distance between each oxygen of two >N–O· groups. It was reported[11] distribution of spin density of unpaired electron is 73% on oxygen atom and 27% on nitrogen atom in the nitroxide radical, 2,2,6,6-tetramethylpiperidine-1-oxyl. When one piperidine ring is in a twisted form[11] and the other in a chair form[12] in III, as shown in Fig. 3, r is about 5 Å, in agreement with the value estimated from its ESR spectrum. When two piperidine rings are in boat forms in III, r is about 6 Å and 2**D** is 257 gauss; in chair forms, 4 Å and 869 gauss.

We reported on the intramolecular hydrogen transfer between the >N–OH and >N–O· groups in 1,9-diaza-(1-^{15}N)-2,2,8,8,10,10-hexamethyl-4-oxo-spiro[5.5]undecane-1-hydroxy-9-oxyl (VIII) corresponding to the precursor of the nitroxide biradical, III.[13] This was found from the ESR spectrum of VIII in toluene solution in which the intensity of the doublet lines resulting from a ^{15}N nucleus increased at high temperatures and decreased at low temperatures.

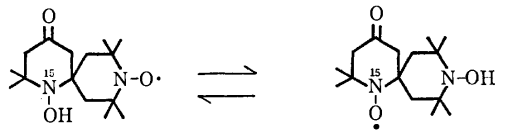

(VIIIa) (VIIIb)

From the intramolecular hydrogen transfer in VIII, it seems that the distance between two radical sites in III is 4.8 Å, because the distance between the hydrogen of >N–OH group and the oxygen of >N–O· group in VIII could approach that of van der Waals radius if the conformation of VIII corresponds to that of III. On the other hand, the values of r obtained for IV and V from these spectra in a MTHF frozen glass are in agreement with those measured from their molecular models in which the conformation of each

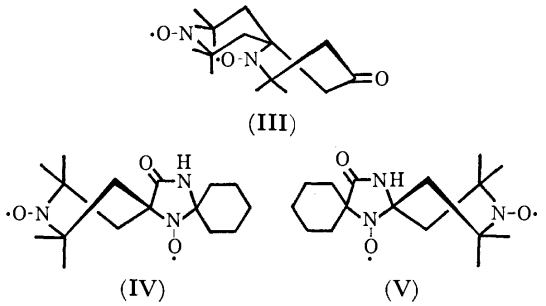

(III)

(IV) (V)

Fig. 3. Conformation of biradicals III, IV, and V.

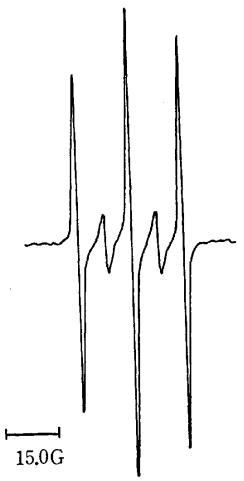

Fig. 4. ESR spectrum of VI in 10^{-3} mol/l toluene solution at room temperature.

piperidine ring is in a twisted form as shown in Fig. 3.

The spectrum of 2,2,6,6-tetramethylpiperidine-4-spiro-2′-(4′-oxoimidazolidine)-5′-spiro-4″-(2″,2″6″6″-tetramethylpiperidine)-1,1″-dioxyl (VI) in toluene solution at room temperature give quintet lines just like the spectrum of the carbonate diester of 4-hydroxy-2,2,6,6-tetramethylpiperidine-1-oxyl[2a] as shown in Fig. 4.

The frozen glass spectrum of VI does not correspond to that of a crystalline triplet. The distance between the two radical sites in VI may be longer than those of the other nitroxide biradicals III—V. The molecular model of VI indicates that two radical sites can approach each other in the molecule when both piperidine rings exist in boat form. However, such a conformation would not be predominant in VI.

Experiments for estimating the values of the triplet-singlet separation **J** in these nitroxide biradicals were not successful since there is no suitable solvent to measure the signal intensity of these solid state spectra at various temperatures.

Experimental

ESR measurements. The spectra were recorded with a Hitachi MES 4001 type X-band spectrometer equipped with the cavity of TE_{011} mode employing 100 kc modulation. The magnetic field was monitored by a Hitachi M 4704 digital gauss meter using a Hall element.

Materials. The nitroxide biradicals were prepared by oxidation of amines with hydrogen peroxide or *m*-chloroperbenzoic acid.[5,6,13]

We would like to thank Dr. Genshun Sunagawa, the director, for his encouragement.

11) E. G. Rozantsev and E. N. Gur'yanova, *Izr. Akad. Nauk SSSR ser. Khim.*, **1966**, 979.
12) C. Y. Chen and R. J. W. LéFevre, *J. Chem. Soc.*, **1965**, 3467.
13) T. Toda, E. Mori, and K. Murayama, This Bulletin, **45**, 1904 (1972).

Effect of Ring Size on the Mass Spectral Fragmentation of Cyclic Sulfoxides

Seizo TAMAGAKI and Shigeru OAE

Department of Applied Chemistry, Faculty of Engineering, Osaka City University, Sumiyoshi-ku, Osaka

(Received February 1, 1971)

Mass spectra of six cyclic sulfoxides were determined in order to study the effects of ring size on the rate of OH-elimination from molecular ions. The ratios of the rates for the OH loss, $[M^+-OH]/[M^+]$, are: trimethylene sulfoxide: 0.23 /tetramethylene sulfoxide: 0.06 /pentamethylene sulfoxide: 0.24 /hexamethylene sulfoxide: 1.21 /9-thiamonoxybicyclo[3.3.1]nonane: 3.14 /7-thiamonoxybicyclo[2.2.1]heptane: 0.02. These findings were explained in terms of the difference in the closest approaching distance between the sulfinyl oxygen and the β- or γ-hydrogen atoms. Geometry of the ionized molecular ions appears to be an important factor in determining these ratios. The loss of HSO was also disucssed.

Although the electron impact fragmentations of open chain alkyl sulfoxides have been scrutinized in detail[1] and their common features can be illustrated as shown below by di-*n*-butyl sulfoxide as an example, no spectrometric study on cyclic sulfoxides has been

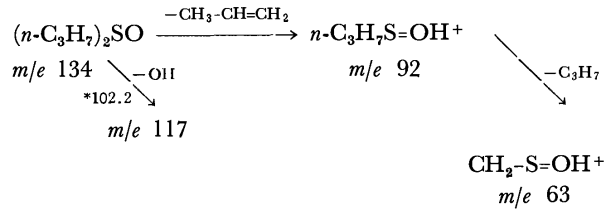

made in connection with the effect of ring size on their fragmentation.

It has been well known that the ejection of simple molecules such as H_2O or HCl from the molecular ion of cyclohexyl alcohol or chloride produced by electron impact does not necessarily take place by way of 1,2-elimination but displays a different behavior from that of the thermal process[2] where usually the elimination occurs exclusively *via* 1,2-elimination process resulting in the concomitant formation of a double bond. While, in the mass spectral fragmentation the extent of the ejection of small molecule or radical has been known to depend on the geometry or structure of molecules. For example, in a series of studies on rigid steroid ketone, Djerassi found that the Mclafferty rearrangement proceeds only if the interatomic distance between the carbonyl oxygen and γ-hydrogen is less than 1.8 Å.[3]

Very recently, Green and his coworkers[4] studies the electron impact induced elimination reactions involving the loss of small molecules, by employing specifically deuterium-labeled cyclohexyl or cycloheptyl chlorides and concluded that the ground-state interatomic distance may be extrapolated to the ionized state and thereby used to predict the position from which the hydrogen arised.

In this work, we have also re-examined the aforementioned Green's posturate in alicyclic sulfoxides from which the OH group is expelled and found that the hydrogen abstraction markedly depends upon the ring-size. For further information concerning the position of hydrogen to be removed, not only the monocyclic but also bicyclic sulfoxides were synthesized and subjected for the study.

Experimental

Synthesis of Alicyclic Sulfoxides. The cyclic sulfoxides were synthesized by the usual methods described in the literatures[5-7] and the sulfides were oxidized to the corresponding sulfoxides with sodium metaperiodate, usually

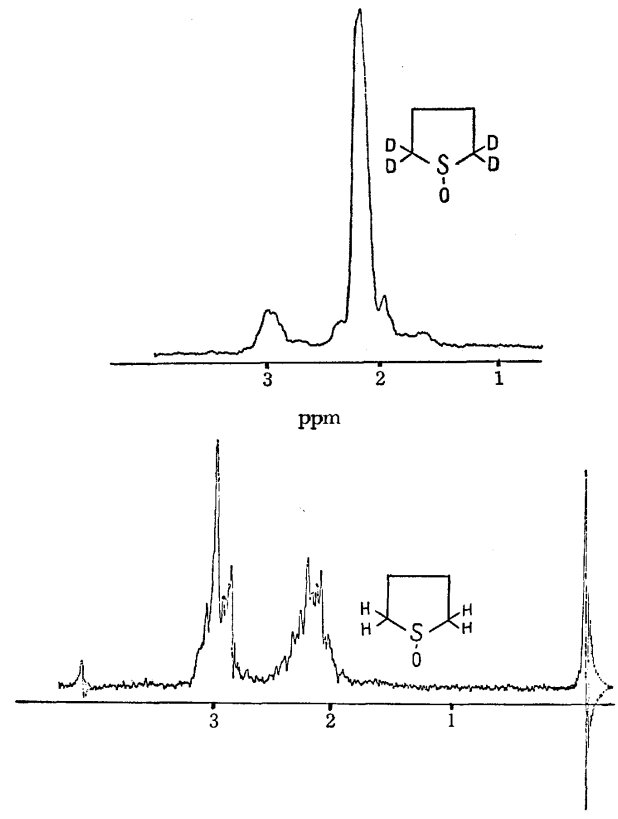

Fig. 1. NMR spectra of Tetramethylene sulfoxide and its deuterated sulfoxide in D_2O.

1) H. Budzikiewicz, C. Djerassi, and D. H. Williams "Mass Spectrometry of Organic Compounds," Holden-Day Inc. (1967), p. 553. J. H. Bowie, D. H. Williams, S. O. Lawesson, J. Madsen, G. Schroll, *Tetrahedron*, **22**, 3515 (1966), R. G. Gillis, and J. L. Occolowitz, *Tetrahedron Lett.*, 1887 (1966). I. D. Entwisle, R. A. W. Johnstone, and B. J. Millard, *J. Chem. Soc.*, C, **1967**, 302.

2) B. Stephenson and O. Banjok, *J. Chem. Soc., B*, **1968**, 805.

3) C. Djerassi *et al.*, "Mass Spectrometry of Organic Compounds", Holden-Day Inc. (1967), p. 157.

4) M. M. Green, R. J. Cook, J. M. Schwak, and R. B. Roy, *J. Amer. Chem. Soc.*, **92**, 3076 (1970).

5) D. S. Tarbell and C. Weaver, *ibid.*, **63**, 2939 (1941).

6) E. V. Whitehead, R. D. Dean, and F. A. Fidle, *ibid.*, **73**, 3632 (1951).

7) G. G. Bennett and A. L. Hoak, *J. Chem. Soc.*, **1927**, 2496.

in ethanol except the oxidation of four-membered cyclic trimethylene sulfide where methanol was found to be the best solvent. The boiling (melting) points are: trimethylene sulfoxide: 91°/14 mmHg; tetramethylene: 113—114°/14 mmHg; pentamethylene: 124—125°/14 mmHg; hexamethylene: 144—145°/14 mmHg; 7-thiamonoxybicyclo [2.2.1]heptane: 205—208°C; 9-thiamonoxybicyclo[3.3.1]-nonane: 140°C/15 mmHg (sublimation temp).

Deuterium Labeling. The deuteration of the α-position to the sulfinyl group was accomplished by heating the corresponding ordinary sulfoxide of 500 mg with deuterium oxide of 5 g dissolving small pieces of sodium metal in a sealed tube at around 100°C for 2 or 3 days. After heating, the solvent was distilled off and the residue was extracted repeatedly with chloroform. The chloroform layer was concentrated and distilled off under reduced nitrogen atmosphere. The typical NMR spectrum of five-membered cyclic sulfoxide is shown in Fig. 1.

Measurement. Hitachi RMU-6E single focus mass spectrometer set at normal (80 eV) ionizing voltages and emission current of 110 mA was used to record the spectra. Samples were introduced into the ionizing chamber through a glass inlet system (141-B) prepared for heating around 200°C.

Results and Discussion

The main decomposition paths are illustrated in Figs. 2—7 and Schemes 1—2, and the main features

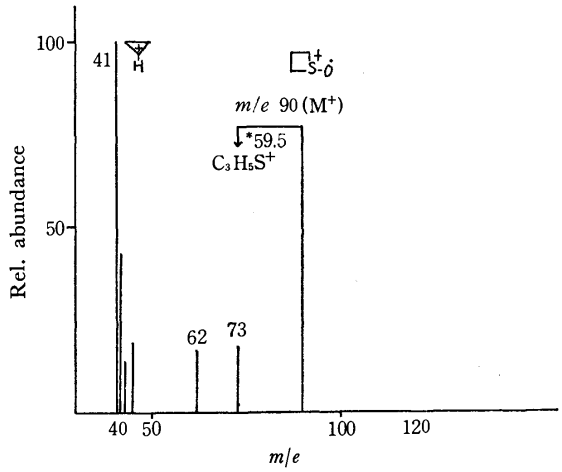

Fig. 2. Mass spectrum of trimethylene sulfoxide.

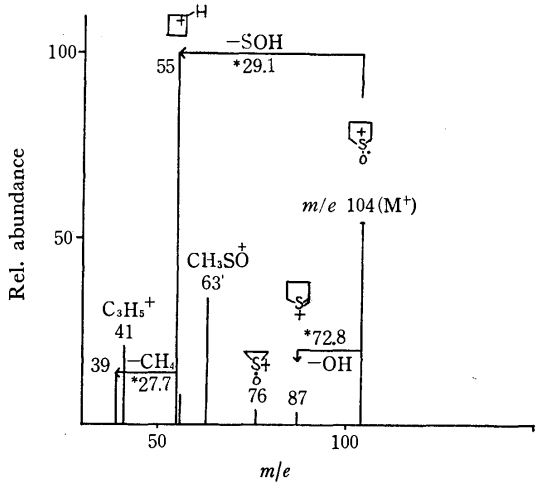

Fig. 3. Mass spectrum of tetramethylene sulfoxide.

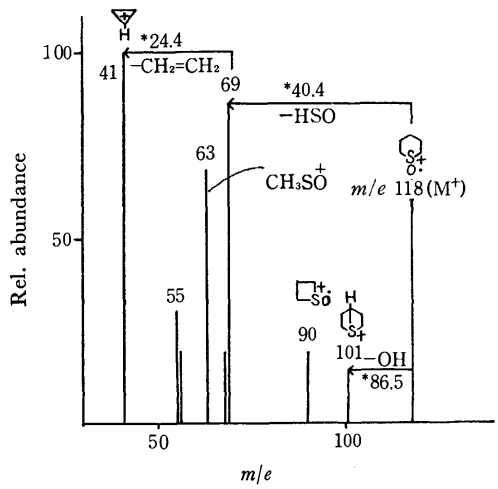

Fig. 4. Mass spectrum of pentamethylene sulfoxide.

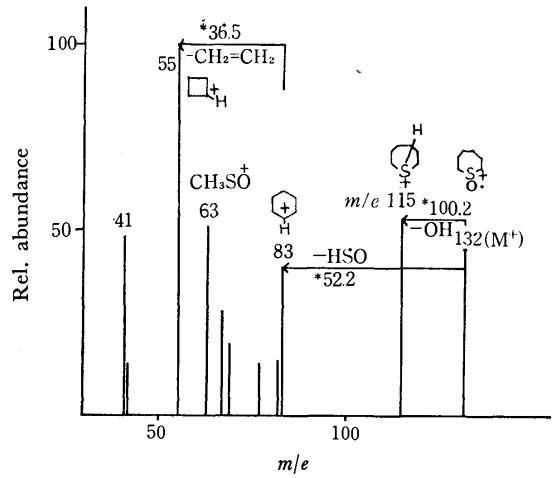

Fig. 5. Mass spectrum of hexamethylene sulfoxide.

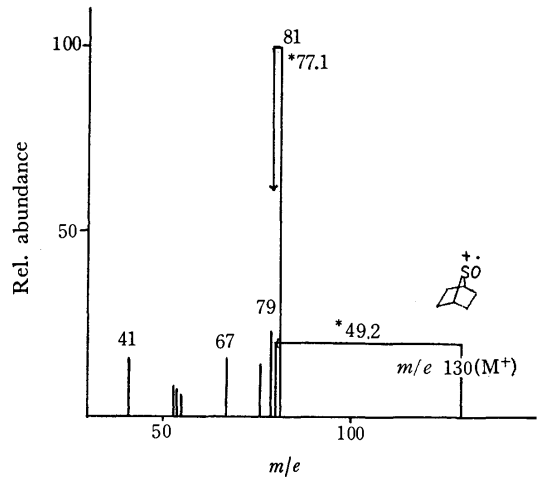

Fig. 6. Mass spectrum of 7-Thiamonoxybicyclo[2.2.1]-heptane at 80 eV.

of the mass spectra of these compounds are summerized as follows: (1) in every case, the molecular ion gives relatively higher peak height. (2) Surprisingly, in contrast to methyl phenyl sulfoxide and pyridine *N*-oxide both bearing similar semipolar linkages, no measurable deoxygenation appears to take place with

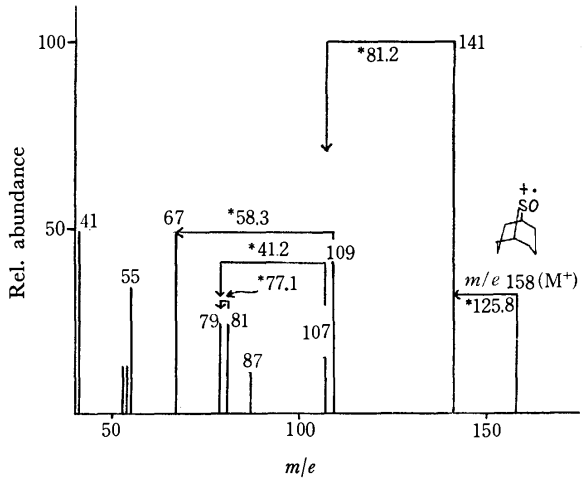

Fig. 7. Mass spectrum of 9-Thiamonoxybicyclo[3.3.1.] nonane at 80 eV.

alicyclic sulfoxides at such high electron ionizing voltage as 80 eV. (3) Instead, the loss of OH and/or SOH takes place with all these sulfoxides although the extent of elimination for these simple molecules depends upon the nature of the sulfoxides. This will be discussed later in detail in connection with the effect of ring size on the dehydroxylation.

The bicyclic sulfoxides such as 7-thiamonoxybicyclo[2.2.1]heptane and 9-thiamonoxybicyclo[3.3.1]-nonane exhibit quite special and interesting behavior along the successive fragmentations.

The decomposition patterns for these compounds are shown as in Schemes 1 and 2, depicted below:

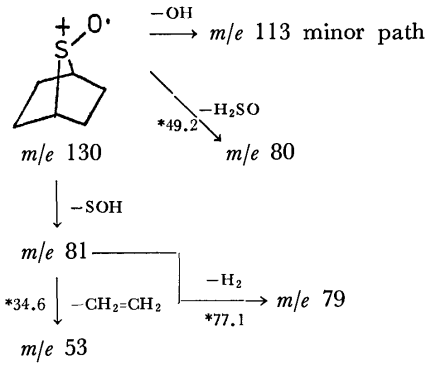

Scheme 1.

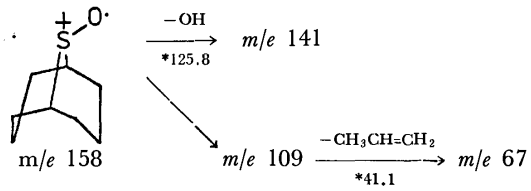

Scheme 2.

From inspection of these spectra, as for the OH loss the appearance of the metastable peaks seems to indicate that the elimination of OH radical proceeds by way of the noticeably similar mechanism for all the compounds investigated except the [2.2.1]bicyclic sulfoxide in which the OH loss is relatively a minor route. While, the elimination of HSO appears to give the corresponding metastable peaks only in the case of the monocyclic compounds with an exception of trimethylene sulfoxide. With the bicyclic derivatives the corresponding metastable peaks are

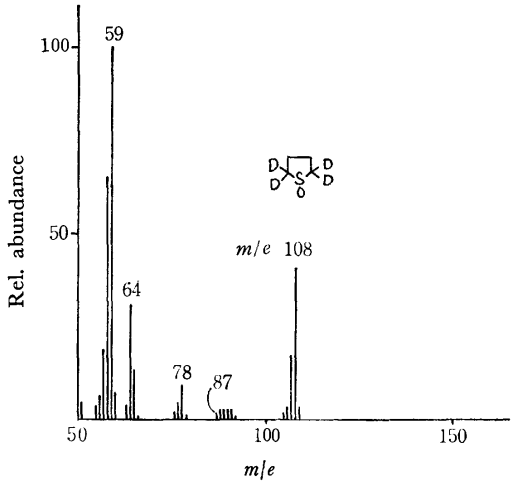

Fig. 8. Mass spectrum of tetramethylene sulfoxide-d_4 at 80 eV.

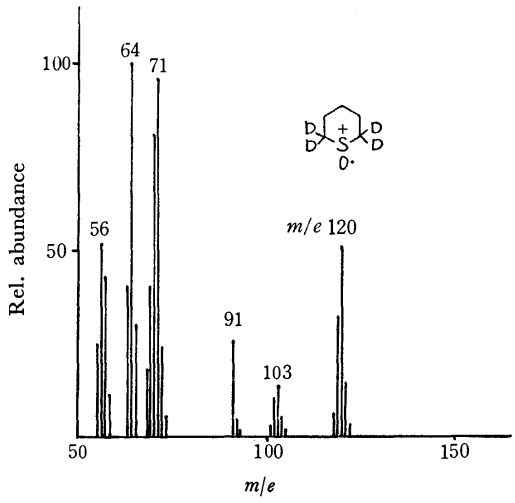

Fig. 9. Mass spectrum of pentamethylene sulfoxide-d_4 at 80 eV.

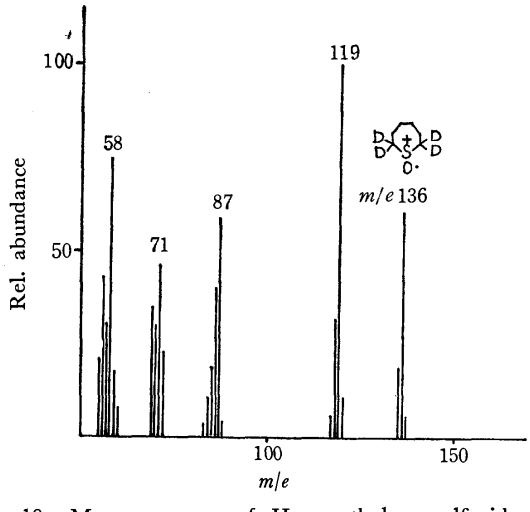

Fig. 10. Mass spectrum of Hexamethylene sulfoxide-d_4 at 80 eV.

not detected at all. At present it is not clear what factors introduce such phenomena.

In order to dislose the origin of hydrogen abstracted in the elimination processes, a few sulfoxides deuterated were subjected to the electron impact analyses and the mass spectra of deuterated sulfoxides are shown in Figs. 8—10.

The deuterium labeling experiments confirm that the six- and seven-membered ring analogs undergo OH elimination reaction predominantly from the site other than the α-positions to the sulfinyl groups (Scheme 3).

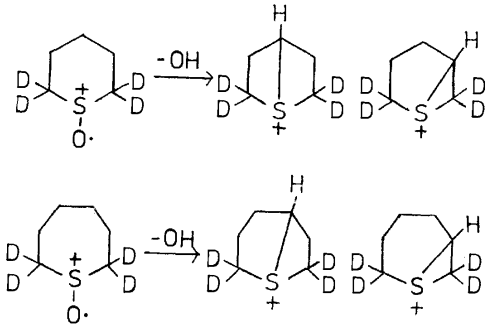

Scheme 3.

Whereas, the behavior of the five-membered ring compound is much different. Abstraction of deuterium or hydrogen from α- and β-positions occurs concomitantly at the ratio of 40 to 60, respectively, resulting in the formation of such ion as:

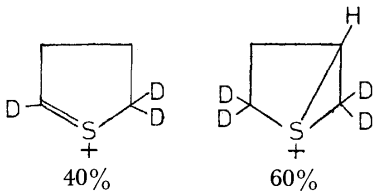

As the deuterium labeling experiments indicate, with all the five-, six-, and seven-membered cyclic sulfoxides, elimination of HSO radical does occur predominantly by abstracting the hydrogen rather than the deuterium. These facts are just consistent with expectation that the OH elimination takes place without destruction of sulfoxide ring, while as for the HSO elimination ring openings prerequisite to ejection of HSO. The deuterium contents in various peaks were calculated and listed in Table 1.

TABLE 1. DEUTERIUM CONTENTS IN VARIOUS PEAKS

Sulfoxide	Peak	Relative Deuterium content,[a] %	Relative Deuterium content, %
Tetramethylene	M^+	87.8	100
	M^+-OH	52.4	59.7
	M^+-HSO	82.5	94.0
Pentamethylene	M^+	42.2	100
	M^+-OH	43.5	100
	M^+-HSO	31.7	75.1[b]
Hexamethylene	M^+	94.7	100
	M^+-OH	91.8	96.9
	M^+-HSO	83.5	88.2

a) Values after corrected for isotope peaks due to ^{13}C and ^{35}S.

b) This low value may be due to uncorrectness for the neighboring peak not attributed to HSO elimination.

Effect of Ring-Size on the Rate of Elimination. When the relative intensity ratios of peak heights of $[M^+ -OH]$ ions to the peak heights of the parent ions, *i.e.*, $[M^+ -OH]/[M^+]$, are plotted against the ring-size as shown in Fig. 11, we can get an upward concave curvature with the value of the five-membered ring sulfoxide being at minimum. The ratio ranges from a low figure of 0.06 for the five-membered sulfoxide to a high one of 1.21 for the seven-membered analog.

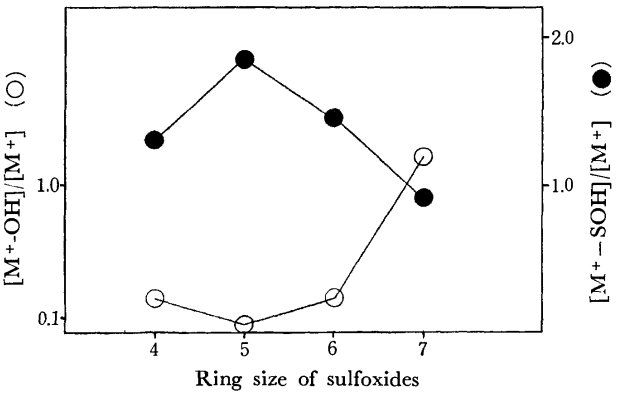

Fig. 11. Plot of intensity of OH- or SOH- eliminated fragment against ring size.

While, the plot of $[M^+ -HSO]$ intensities against those of molecular peaks, $[M^+ -HSO]/[M^+]$, is entirely different in shape from those of the above mentioned, as shown in Fig. 11 where no regularity can be seen in the plot of the $[M^+ -OH]$. Besides, the ratio of the maximum to the minimum values does not exceed only a little more than 2. Different features can be observed in the case of the bicyclic compounds. Even with the [3.3.1] bicyclic sulfoxide, the $[M^+-HSO]/[M^+]$ ratio increased up to 1.31, which is not much different from that of the monocyclic analogs. While, the ratio, $[M^+-OH]/[M^+]$, increased to as much as 3.14. On the other hand, the [2.2.1] bicyclic sulfoxide underwent much more facile HSO elimination, giving rise to the ratio of 8.70. However, $[M^+-OH]/[M^+]$ ratio was found to be negligibly small, *i.e.*, 0.03.

These observations imply that the HSO elimination does not depend so sharply upon the change of the ring size, but the ease of the expulsion of the OH group is markedly dependent on the number of methylene group. The latter finding can be readily rationalized on the basis of the strained structures. Since the five-membered and the [2.2.1] bicyclic sulfoxides are very strained and have only small degrees of freedom, the sulfoxide oxygen atom of these compounds can not easily get close enough to the β-hydrogen for elimination. In fact, on the basis of the molecular models, the closest distance between the center of the oxygen and that of each hydrogen atoms exceeds 3.0

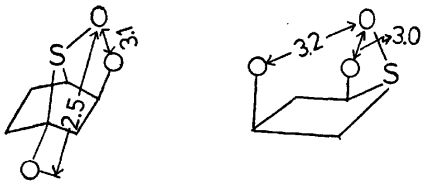

Å with all these ring systems. This explanation may be supported further by the following observation that in the spectra for both compounds taken at 20 eV (Fig. 12) the number of ions attributed to the OH loss is far less than that of the ions arised from loss of oxygen. Namely, the sulfinyl oxygen that cannot find hydrogen atom in close vicinity has to cleave off itself (Scheme 4).

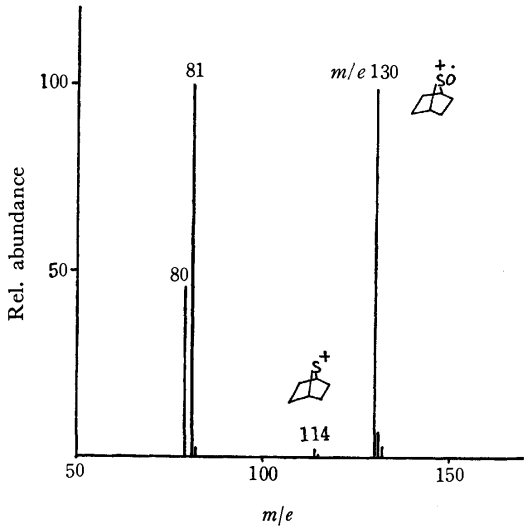

Fig. 12. Mass spectrum of 7-thiamonoxybicyclo[2.2.1]-heptane at 20 eV.

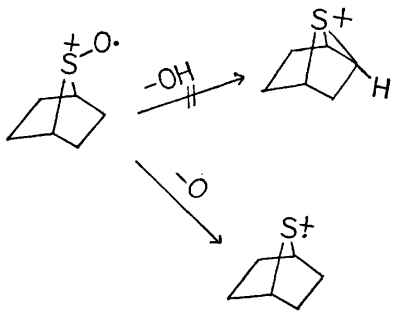

Scheme 4.

As for the more flexible six- and seven-membered cyclic sulfoxides, relative intensities of the dehydroxylated mass peaks against these of the parent ions are considerably higher than those of the strained sulfoxide and loss of OH for the seven-membered analog is more evident than for the six-membered system. All these observations seem to suggest strongly that not only the distances between hydrogen and oxygen in ground state geometry as Green and his coworkers have advocated but also the molecular motions are important for determining the extent of the OH elimination.

This is in keeping with our recent finding in the Ei reactions undergoing via five-membered cyclic transition state.[9] The distances between oxygen and hydrogen for some of possible conformations for the individual compounds studied are shown below:

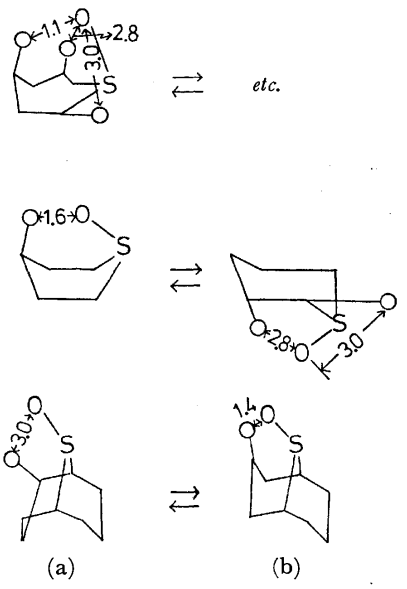

In the first place, the distance between the sulfinyl oxygen and the nearest hydrogen atom in the molecule appears to determine the ease of the loss of OH. In the second place, the factor controlling the OH elimination seems to depend on the statistical stability of the molecular geometry which must satisfy the first condition for the OH elimination.

This latter condition is explicitly exemplified by the comparison of the mass pattern of the seven-membered sulfoxide with that of [3.3.1] bicyclic sulfoxide. The shortest distances between the two atoms calculated from the geometries for these two sulfoxides are 1.0 Å and 1.4 Å, respectively. On the contrary the $[M^+-OH]/[M^+]$ratios increased from 1.18 for the seven membered ring system to 3.12 for the [3.3.1] bicyclic sulfoxide. This is apparently apprehended by the assumption of the geometrical mobility toward the favorable conformation for eliminations under

Table 2. Distance between oxygen and nearest hydrogen atom in various sulfoxides and ratio of $[M^+-OH]/[M^+]$ or $[M^+-HSO]/]M^+]$

Sulfoxide	Å	$[M^+$-OH$]/[M^+]$		$[M^+$-HSO$]/[M^+]$	
4	3.0	0.23		1.30	
5	3.0	0.06	(0.02)	1.85	(0.33)
6	1.6	0.24	(0.15)	1.45	(0.47)
7	1.1	1.21	(0.74)	0.91	(0.20)
221	3.1	0.03[a]	(0.01)	8.70*	(1.01)
331	1.4	3.14	(0.90)	1.31*	(0.10)

a) Indicates the absence of metastable peak
Parentheses indicate the numerals measured at 20 eV.

8) N. J. Leonard and C. R. Johnson, *J. Org. Chem.*, **27**, 282 (1962).

9) K. Tsujihara, N. Furukawa, and S. Oae, *Tetrahedron Lett.*, 2663 (1970).

such a higher temperature as around 200°C in the inlet chamber room. Although the [3.3.1] bicyclic sulfoxide have been said to exist in the conformation (a) in which both six-membered rings are in the chair forms at around the room temperature,[10] at a higher temperature the steric repulsion between two hydrogens on the 3- and 7- positions would force the molecule to assume the conformations of one chair and one boat six-membered rings (b).

Such a conformation, considered to be favorable for the elimination of OH-group, would not be statistically stable in the case of the seven-membered system, because the 7-membered ring is very flexible.

Meanwhile, the behavior of the HSO elimination was found to differ from that of OH elimination. The fact that the OH loss does not depend on the change of the ring-size, *i.e.*, nor even on whether the sulfoxides are mono or bicyclic sulfoxides, may not be accounted for without the hypothesis that the molecular ions of the sulfoxides undergo OH-elimination, keeping the original skeleton, while the HSO loss does not take place without the destruction of the initial structure of the sulfoxide molecules. The C–S bond rupture at the initial step would lead molecular ions to convert to the corresponding open-chain structures.

10) G. A. Russell and R. G. Konlee, *J. Amer. Chem. Soc.*, **91**, 4468 (1969).

BULLETIN OF THE CHEMICAL SOCIETY OF JAPAN, VOL. 45, 1772—1776 (1972)

Liquid Crystalline Properties of Terminally Substituted Benzylideneanilines[1]

Kei MURASE

Ibaraki Electrical Communication Laboratory, Nippon Telegraph and Telephone Public Corporation, Tokai, Naka-gun, Ibaraki

(Received March 25, 1971)

The preparation and mesomorphic characteristics of certain anils (*p*-alkoxybenzylidene-*p'*-alkylanilines and *p*-alkoxybenzylidene-*p'*-alkoxyanilines) are described. Fifteen new compounds were found to exhibit nematic behavior below 100°C. The structural effects of the terminal substituents on nematic temperature range are discussed. It has been found that the anils containing *n*-alkyl substituents in the *p*-position of the aniline moiety exhibit mesophases in a much lower temperature range than those containing *n*-alkoxy substituents. Among *p*-isoalkoxybenzylideneanilines, all compounds except one are non-mesomorphic.

Recently, the electro-optic properties of liquid crystals have attracted considerable attention because of their application for display.[2] The term liquid crystal or mesomorphic state means a unique state of matter intermediate between a crystalline solid and a normal isotropic liquid.[3] A special class of mesomorphic material called nematic liquid crystal changes its transparency when an electric field is applied to its thin film.

Since low temperature nematic materials are desirable for a practical display device, efforts have been made for their preparation.[4–6] With this purpose in view, we prepared and characterized twenty three new anils, three of which were reported[5,6] as low temperature mesomorphic materials.

Results and Discussion

The terminally substituted anils we prepared are given in Table 1 along with their transition temperatures. The compounds are classified into the following three types according to their molecular constitutions.

I: *p-n*-Alkoxybenzylidene-*p'-n*-alkylanilines
II: *p*-Isoalkoxybenzylidene-*p'-n*-alkylanilines
III: *p*-Isoalkoxybenzylidene-*p'-n*-alkoxyanilines

A great number of *p-n*-alkoxybenzylidene-*p'-n*-alkoxyanilines (type IV) are known to exhibit mesomorphisms.[7,8] However, mesomorphic properties of other anils with less polar or branched substituents are scarcely known.

The compounds of type I contain no oxygen atom in the substituent of the aniline moiety. As the atom is polar and considered to contribute to intermolecular terminal cohesion between ordered mesomorphic molecules, it is of great interest to investigate the mesomorphic properties of the compounds. In this study, sixteen new compounds of this type were synthesized. Elemental analyses of most of them are given in Table 2.

Weygand and Gabler[9] studied *p-n*-nonyloxybenzylidene-*p'-n*-alkylanilines, which were found to exhibit smectic mesophases and no nematic mesophase when they have an ethyl or higher alkyl substituent in aniline moiety. Almost all the compounds of type I presented here, however, exhibit enantiotropic mesophases, as shown in Table 1.

It is notable that in homologous series of *p-n*-alkoxy-

1) Presented in part at the 3rd. Symposium on Structural Organic Chemistry, Hiroshima, November, 1970.
2) G. H. Heilmeier, *Sci. Amer.*, **222**, 100 (1970).
3) G. H. Brown and W. G. Shaw, *Chem. Rev.*, **57**, 1049 (1957).
4) J. A. Castellano, J. E. Goldmacher, L. A. Barton, and J. S. Kane, *J. Org. Chem.*, **33**, 3501 (1968).
5) H. Kelker and B. Scheurle, *Angew. Chem.*, **81**, 903 (1969).
6) J. B. Flannery and W. Haas, *J. Phys. Chem.*, **74**, 3611 (1970).
7) C. Weygand and R. Gabler, *J. praket. Chem.*, **151**, 215 (1938).
8) J. S. Dave and P. R. Patel, *Mol. Cryst.*, **2**, 103 (1966).
9) C. Weygand and R. Gabler, *Naturwissenschaften*, **27**, 28 (1938).

TABLE 1. TRANSITION TEMPERATURES OF TERMINALLY SUBSTITUTED ANILS, X-C_6H_4-CH=N-C_6H_4-Y

Compd.	X	Y	Temp. °C of transition to		
			Smectic	Nematic	Isotropic
Ia	*n*-C_3H_7O	C_2H_5			67
Ib	*n*-C_4H_9O	C_2H_5	[39]	51.5[48]	66[62.5]
Ic	*n*-$C_5H_{11}O$	C_2H_5		56	61
Id	*n*-$C_6H_{13}O$	C_2H_5		59	71.5
Ie	*n*-$C_7H_{15}O$	C_2H_5	58	64	70
If	*n*-$C_8H_{17}O$	C_2H_5	65	71	75
Ig	*n*-$C_{16}H_{33}O$	C_2H_5	71		75.5
Ih	CH_3O	*n*-C_3H_7		45.5[42]	60.5[57]
Ii	C_2H_5O	*n*-C_3H_7		75.5[76]	87.5[97]
Ij	*n*-C_3H_7O	*n*-C_3H_7		57.5	68
Ik	*n*-C_4H_9O	*n*-C_3H_7		54	82.5
Il	*n*-$C_5H_{11}O$	*n*-C_3H_7		57	74.5
Im	*n*-$C_6H_{13}O$	*n*-C_3H_7	65	66.5	82.5
In	*n*-$C_7H_{15}O$	*n*-C_3H_7	62.5	71.5	79.5
Io	*n*-$C_8H_{17}O$	*n*-C_3H_7	68	82	85
Ip	*n*-C_3H_7O	*n*-C_4H_9		42	55
IIq	*iso*-C_3H_7O	CH_3			87
IIr	*iso*-$C_5H_{11}O$	C_2H_5			41.5
IIIs	*iso*-C_3H_7O	OCH_3			102
IIIt	*iso*-C_3H_7O	OC_2H_5			104
IIIu	*iso*-$C_5H_{11}O$	OC_2H_5		(89)	112
IIIv	*iso*-C_3H_7O	O*n*-C_4H_9			89
IIIw	*iso*-$C_5H_{11}O$	O*n*-C_4H_9			105

a) Values in parentheses denote monotropic transition.
b) Values in brackets are taken from Refs. 5 and 6.

TABLE 2. ANALYTICAL DATA OF MESOMORPHIC ANILS

Compd.	Formula	Calcd %			Found %		
		C	H	N	C	H	N
Ib	$C_{19}H_{23}NO$	81.10	8.24	4.99	81.02	8.45	4.90
Ic	$C_{20}H_{25}NO$	81.31	8.53	4.74	81.28	8.60	4.65
Id	$C_{21}H_{27}NO$	81.51	8.80	4.53	81.34	8.81	4.47
Ie	$C_{22}H_{29}NO$	81.69	9.04	4.33	81.63	9.18	4.17
If	$C_{23}H_{31}NO$	81.85	9.26	4.15	81.73	9.32	4.06
Ig	$C_{31}H_{47}NO$	82.79	10.53	3.11	83.04	10.69	2.97
Ih	$C_{17}H_{19}NO$	80.20	7.56	5.53	79.77	7.42	5.33
Ii	$C_{18}H_{21}NO$	80.86	7.92	5.24	81.02	8.00	5.14
Ij	$C_{19}H_{23}NO$	81.10	8.24	4.98	81.33	8.48	4.84
Ik	$C_{20}H_{25}NO$	81.31	8.53	4.74	81.47	8.64	4.68
Il	$C_{21}H_{27}NO$	81.51	8.80	4.53	81.77	9.13	4.43
Ip	$C_{20}H_{25}NO$	81.31	8.53	4.74	81.23	8.57	4.56

benzylidene-*p'*-ethylanilines and *p*-*n*-alkoxybenzylidene-*p'*-*n*-propylanilines the smectic phase first appears at C_7-ether[10] and C_6-ether, respectively, while in the series of *p*-*n*-alkoxybenzylidene-*p'*-ethoxyanilines[7] and *p*-*n*-alkoxybenzylidene-*p'*-*n*-propoxyanilines[8] the smectic properties begin at their respective C_9-ethers.

The compounds of type II, which are characterized by their terminal substituents of bulky branched groups as well as less polar *n*-alkyl groups, are non-mesomorphic in two cases.

The compounds of type III have a branched and a *n*-alkoxy substituent. Five compounds of this type were prepared. Only one compound IIIu exhibited monotropic nematic behavior.

Effect of Alkyl Substituents. Various transition temperatures for the homologous series of *p*-*n*-alkoxybenzylidene-*p'*-ethylanilines (type I) and *p*-*n*-alkoxybenzylidene-*p'*-ethoxyanilines (type IV) *vs.* the length of their alkoxy chain (total carbon and oxygen atoms) are plotted in Fig. 1. Those of *p*-*n*-alkoxybenzylidene-*p'*-*n*-propylanilines (type I) and *p*-*n*-alkoxy-

10) Flannery and Haas report the smectic phase of C_4-ether[6].

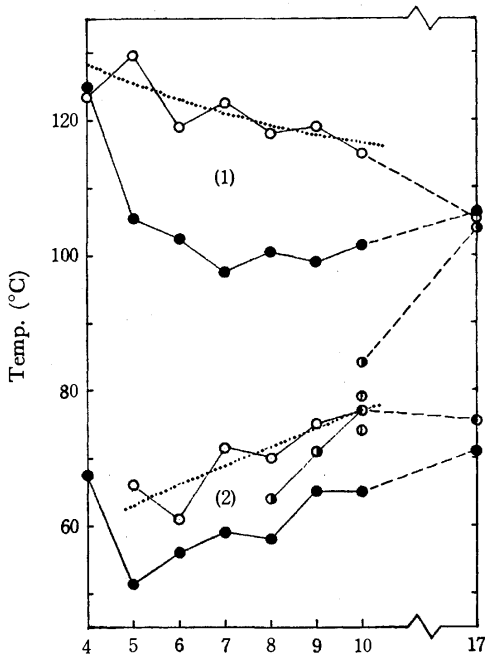

Fig. 1. Transition temperature for the series, (1) *p,p'-n*-$ROC_6H_4CH{=}NC_6H_4OC_2H_5$[7] and (2) *p,p'-n*-$ROC_6H_4CH{=}NC_6H_4C_2H_5$.
●: crystal-mesomorphic or -isotropic, ○: nematic-isotropic, ◐: smectic-isotropic, ◑: smectic-nematic, ⓘ: smectic I-smectic II (Data for nonyloxy derivative from Ref. 9)

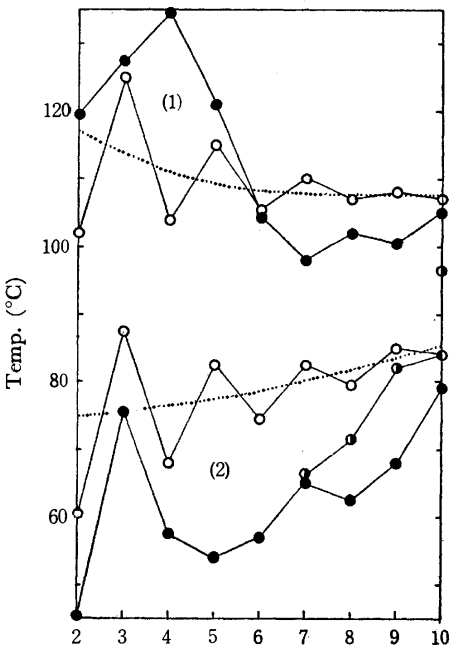

Fig. 2. Transition temperature for the series, (1) *p,p'-n*-$ROC_6H_4CH{=}NC_6H_4OC_3H_7$[8] and (2) *p,p'-n*-$ROC_6H_4CH{=}NC_6H_4C_3H_7$.
●: crystal-mesomorphic or -isotropic, ○: nematic-isotropic, ◐: smectic-isotropic, ◑: smectic-nematic
(Data for nonyloxy derivative in (2) are referred from Ref. 9.)

benzylidene-*p'-n*-propoxyanilines (type IV) are similarly plotted in Fig. 2.

From a comparison of crystal-mesomorphic and nematic-isotropic transition temperatures for the corresponding compounds of type I and type IV, it was found that both transition temperatures for each compound of type I are much lower than those for the corresponding compound of type IV. The features for the compounds of the former type are considered to be due to the decrease of the terminal intermolecular attraction resulting from the lack of a polar oxygen atom in the substituent of aniline moiety. As a matter of fact, smectic phases appear at a shorter alkoxy chain length in these compounds than in the compounds of type IV, because smectic stability increases when terminal attraction decreases and lateral interaction becomes relatively predominant.

It is known that nematic-isotropic transition temperatures for a homologous series lie on two smooth curves, one related to the members with an even-numbered chain and the other to those with an odd-numbered chain. In Figs. 1 and 2, dotted lines are drawn in the middle of the above mentioned two curves. The lines show that the temperatures for the compounds of type I have an unusual rising tendency with the growing chain length, while those for the compounds of type IV have a usual[11,12] falling tendency.

These phenomena can be explained by assuming a

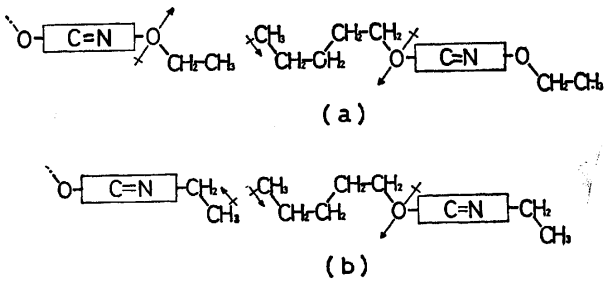

Fig. 3. Head-to-tail arrangement of neighboring molecules (a) compounds of the type IV (b) compounds of the type I.

head-to-tail molecular arrangement in which central C=N bondings of neighboring anils are in the same direction.[13] In the compounds of type IV as shown in Fig. 3(a), the terminal attraction between neighboring molecules is caused mostly by the interaction between dipoles of C–O–C groups. The contribution of other kinds of interactions such as related to the induced dipole moment of terminal methyl group are probably smaller. The nematic-isotropic transition temperatures for these compounds have falling tendency with the growing chain length because of decrease of the interaction between the dipoles. On the other hand, in the compounds of type I as shown in Fig. 3(b), the terminal attraction between

11) C. Weygand and R. Gabler, *Z. physik. Chem.*, **B48**, 148 (1941).
12) G. W. Gray, "Molecular Structure and the Properties of Liquid Crystals," Chap. IX, Academic Press, London and New York (1962), p. 197.

13) The possibility of a head-to-head or tail-to-tail molecular arrangement, where the C=N bondings of neighboring molecules are in opposite direction to each other, cannot be ruled out. However, it will be impossible to explain the phenomena by assuming this arrangement.

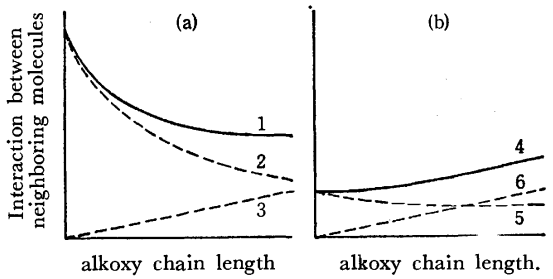

Fig. 4. Terminal interaction *vs.* alkoxy chain length (a) for the compounds of type IV, (b) for the compounds of the type I, curve 1 and 4: total interaction, curve 2: interaction related to two O atoms, curve 3: interaction such as related to polalizability of terminal CH_3 group, curve 5: interaction related to terminal CH_3 group and O atom, curve 6: interaction to two terminal CH_3 group

neighboring molecules is caused by the interaction between the dipole of the C–O–C group in one molecule and the induced dipole of the terminal methyl group in the other molecule and by the interaction between the induced dipoles of the terminal methyl groups in both molecules. The former interaction becomes weaker with the growing alkoxy chain length, but the latter becames stronger because of increase of the induced dipole. The rising tendency is considered to be due to the superiority of the latter interaction. A schematic explanation is given in Fig. 4.

Effect of Odd- and Even-numbered Length of Terminal Chain. In Figs. 1 and 2, the well known change of nematic-isotropic transition temperatures can be seen between homologues containing odd and even numbers of carbon atoms in the terminal substituent of benzylidene moiety. Figure 5 gives the plots of nematic-isotropic transition temperatures for several series of *p*-*n*-alkoxybenzylidene-*p'*-*n*-alkylanilines. Similar changes are found also with regard to the terminal chain length of aniline moiety.

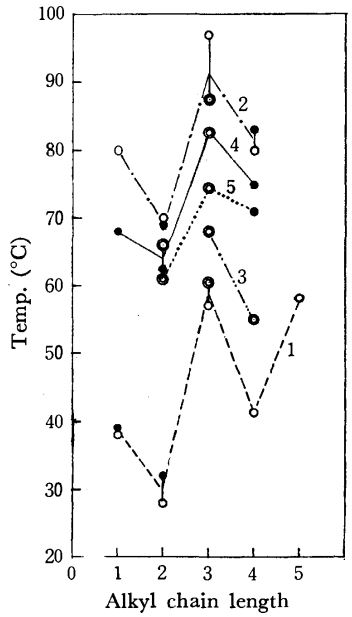

Fig. 5. Nematic-isotropic transition temperature for *p*-alkoxybenzylidene-*p'*-alkylanilines.

(1) CH_3O-⟨○⟩-CH=N-⟨○⟩-R
(2) C_2H_5O-⟨○⟩-CH=N-⟨○⟩-R
(3) C_3H_7O-⟨○⟩-CH=N-⟨○⟩-R
(4) C_4H_9O-⟨○⟩-CH=N-⟨○⟩-R
(5) $C_5H_{11}O$-⟨○⟩-CH=N-⟨○⟩-R

◎: present study, ○: Ref. 5, ●: Ref. 6

When the alkoxy chain length is defined as the number of oxygen plus carbon atoms, and the alkyl chain length as that of carbon atoms, curves of nematic-isotropic transition temperatures related to an odd-numbered chain length lie always above those related to an even-numbered chain length. It is notable that the feature is decided by the altered chain length of one moiety, independent of the chain length of the other moiety.

The behavior can be explained by considering the direction of polarizability of terminal methyl group as suggested by Gray.[12] Using the cog-wheel conformation for the substituted chain, the terminal C–C bond in the odd-numbered chain lies in the direction of the preferred axis of the molecules, but in the even-numbered chain it makes an angle with this axis. Therefore, the terminal intermolecular attraction is considered to be stronger in the molecules containing odd-numbered terminal chain. It is inferred that an oxygen atom in ether bonding makes one unit like a methylene group in this conformation and its polarity has nothing to do with the alternative behavior of the transition temperatures.

Let us consider curves 1 and 2 in Fig. 5. The terminal situations of neighboring molecules are exhibited schematically in Figs. 6 and 7 for the compounds related to curves 1 and 2, respectively. (A), (B) and (C) represent 2, 3, and 4 of alkyl chain length of aniline moiety. It is understood that the terminal intermolecular cohesion of the odd-numbered chain of the aniline moiety should be stronger than that of the even-numbered chain, independent of the chain length of the benzylidene moiety. As the terminal C–C bond of the benzylidene moiety of compounds in Fig. 7 lies in the direction of the preferred axis of the molecule, the terminal cohesion in these compounds should be stronger than that of corresponding compounds in Fig. 6. Thus, a compound with the terminal situation of (A) or (C) has a lower nematic-isotropic transition temperature than a homologous one with

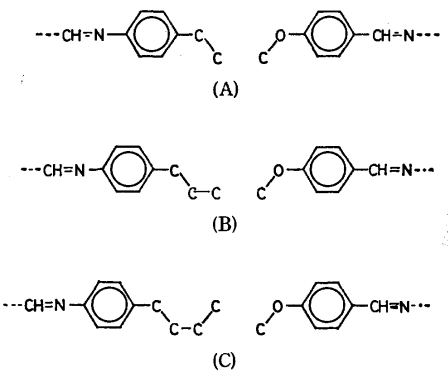

Fig. 6. Terminal situation of neighboring molecules of *p*-methoxybenzylidene-*p*-alkylanilines.

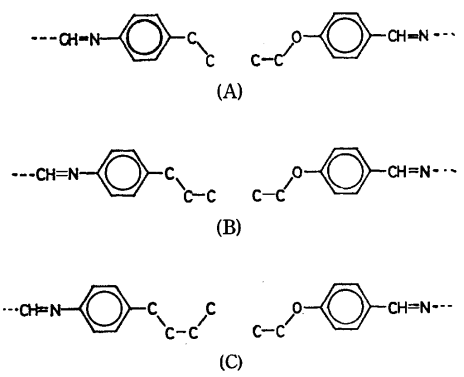

Fig. 7. Terminal situation of neighboring molecules of *p*-ethoxybenzylidene-*p'*-alkylanilines.

terminal situation of (B). The series in Fig. 6 exhibit the transition at a lower temperature than that in Fig. 7.

The consideration is in line with the aspects of curves 1 and 2 of Fig. 5. All the other data on the alternation of nematic-isotropic transition temperatures of anils can be explained as well.

Effect of Branched Chain Substituent. The bulky effect of the branched substituent was expected to weaken the intermolecular cohesion and to make the mesomorphic transition temperatures of type II and III compounds low as was the case with 4'-isoalkoxybenzylidene-1-aminonaphthyl-4-azobenzene.[11] However, all the compounds of these types do not exhibit mesomorphic behavior except for IIIu. The results suggest that the compounds do not possess sufficient intermolecular cohesion for mesomorphic ordering because of too bulky effect.

However, both the nematic-isotropic and the crystal-nematic transition temperatures of the compound IIIu are actually lower than those of the corresponding compound of type IV by about ten degrees. If the melting point of non-mesomorphic materials can be assumed to correspond to the crystal-mesomorphic transition temperature of mesomorphic ones, similar lowering effects are found in a comparison of these temperatures of the compounds of type II or III and the corresponding compounds of type I or IV.[7,8]

Experimental

Materials. p-*Alkoxybenzaldehydes*: *p-n*-Propoxybenzaldehyde (bp 91—92°C/2 mmHg), *p*-isopropoxybenzaldehyde[14], *p-n*-butoxybenzaldehyde (bp 111—112°C/2 mmHg), *p-n*-amyloxybenzaldehyde (bp 114—116°C/2 mmHg), *p*-isoamyloxybenzaldehyde (bp 110—111°C/2 mmHg), *p-n*-hexyloxybenzaldehyde[14], *p-n*-heptyloxybenzaldehyde (bp 136—137°C/2 mmHg), *p-n*-octyloxybenzaldehyde (bp 152—154°C/2 mmHg) and *p-n*-hexadecyloxybenzaldehyde[14] were prepared from *p*-hydroxybenzaldehyde and the corresponding alkylbromide by refluxing in ethanol.[15] The yields were 60—80%. All the aldehydes obtained were identified by IR-spectroscopy, and exhibited the following peaks: ν_{max}^{film} 2925, 2850 (aliphatic C–H), 2730 (aldehyde C=H), 1695 (C=O), 830 cm^{-1} (*p*-substituted).

p-*alkoxyanilines*: *p*-Anisidine and *p*-phenetidine were obtained from commercial sources and distilled. *p-n*-Butoxyaniline was prepared by the reduction of *p-n*-butoxynitrobenzene.[16]

p-*Alkylanilines*: *p*-Toluidine and *p*-ethylaniline were obtained from commercial sources and distilled. *p-n*-Propylaniline and *p-n*-butylaniline were prepared by a method similar to that of Read and Mullin[17] (bp 74—76, 80—86°C/2 mmHg, respectively).

Preparation of Substituted Benzylideneanilines. Equimolar quantities of the appropriate benzaldehyde and aniline were mixed, warmed at about 50°C for a quarter of an hour and then cooled to room temperature until crystalline products appeared. It was necessary to cool the mixture with dry ice-acetone for the synthesis of Ib and Ip.

Since no crystals appeared in the syntnesis of Ih and IIr, the mixture was dissolved in benzene containing a catalytic amount of benzenesulfonic acid, and refluxed for about three hours to remove water azeotropically.[4] After the removal of solvent, the residue was cooled in dry ice-acetane to crystallize.

The products were purified by recrystallization from ethanol. All anils were obtained in 60—85% yield after recrystallization. The absorption band at 1625—1630 cm^{-1} (C=N stretching[18]) in IR-spectra, not belonging to raw materials, confirms the formation of anils.

Determination of Transition Temperature. The melting point and mesomorphic transition temperature were determined with an electrically heated microscope block in conjugation with a projection system. The mesomorphic states of the compounds were readily distinguished by their typical textures.[19]

The author wishes to thank Dr. K. Nakagawa, Dr. H. Toyoda, and Dr. H. Katsuraki for their encouragement, and T. Wachi for his cooperation.

14) Only isolated from extract and not distilled.

15) R. Stoermer and F. Wodarg, *Ber.*, **61**, 2323 (1928).
16) C. Weygand and G. Gabler, *ibid.*, **71B**, 2399 (1938).
17) R. R. Read and D. B. Mullin, *J. Amer. Chem. Soc.*, **50**, 1763 (1928).
18) L. E. Cloupherty, J. A. Sousa, and G. M. Wyman, *J. Org. Chem.*, **22**, 462 (1957).
19) G. W. Gray, "Molecular Structure and the Properties of Liquid Crystals," Chap. II, Academic Press, London and New York (1962) p. 17.

Structure and Reactivity of Small Ring Compounds. IV.[1] Photochemistry of Spirocyclopropyl Ketones[2]

Akio SONODA, Ichiro MORITANI, Jo MIKI, Takashi TSUJI*, and Shinya NISHIDA*

Department of Chemistry, Faculty of Engineering Science, Osaka University, Toyonaka, Osaka

(Received May 10, 1971)

The photochemical transformations of a series of spriocyclopropyl ketones (**1**—**4**) have been investigated in dilute *n*-hexane solutions. Spirocyclopropyl ketones **1** and **2** give mainly the 'Type I' photoproducts of cycloalkanones, *i.e.*, 1-(2'-propenyl)cyclopropanecarboxaldehyde (**5**, 34%) and 1-(3'-butenyl)cyclopropanecarboxaldehyde (**7**, 37%), respectively, in marked contrast to the usual photochemical cleavage of cyclopropyl ketones. Ethylidenecycloalkanones are not detected, but their hydrogenated derivatives, 2-ethylcycloalkanones, are produced in a small amount.

The photoreaction of **1** has been found to be quenched by piperylene, so that it is highly probable that the reaction products are derived from the n–π^* triplet states of the ketones.

The irradiations of nonconjugated spiroketones **3** and **4** afford ring-enlarged 4-methylenecycloalkanones, **9** and **10**, respectively.

The preferential photoisomerization of conjugated cyclopropyl ketones to enones has been extensively studied both in gas and liquid phases.[3] It has been thought that in this characteristic photoisomerization, transfer of the excitation energy absorbed by the carbonyl chromophore to a highly strained cyclopropane ring through a conjugative interaction causes the homolytic ring fission to give the enones.[4]

In order to elucidate this interesting photochemical process on the basis of conformational aspect, we have investigated the photochemistry of some spirocyclopropyl ketones (**1**—**4**). In compounds **1** and **2** bearing a cyclopropane ring in an adjacent position to a carbonyl group, the cyclopropane ring and carbonyl group are fixed to permit the maximum conjugative interaction from their geometry.[5] On the other hand, compounds **3** and **4** are nonconjugated.

In a preliminary paper,[2] we reported the unusual photochemical behaviors of these spiroketones. Recently, Crandall and Seidewand[6], and Turro *et al.*[7] also reported the photoreactions of **1** and **2** in different solvents. In the present paper, we describe the detailed results and discuss the photochemistry of cyclopropyl ketones.

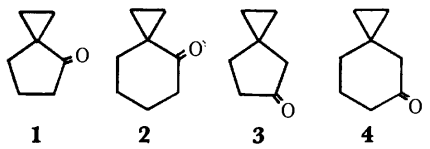

1 **2** **3** **4**

Fig. 1.

Results

Photochemistry of Spiro[2.4]heptan-4-one (1). Irradiation of a *n*-hexane solution of **1** (0.11 mol/*l*) by a high pressure mercury lamp gave 1-(2'-propenyl)-cyclopropanecarboxaldehyde (**5**) and a trace amount of 2-ethylcyclopentanone with a considerable amount of polymeric materials. The prolonged irradiation caused the polymerization. Under optimized reaction conditions (40 hr irradiation) the aldehyde **5** was isolated in 34% yield by means of preparative vpc. The structure of **5** was determined by elemental analysis, IR, and NMR spectra. 2-Ethylcyclopentanone which was obtained in too small a quantity to be isolated was assigned by comparison of its retention times of vpc with an authentic sample.[8]

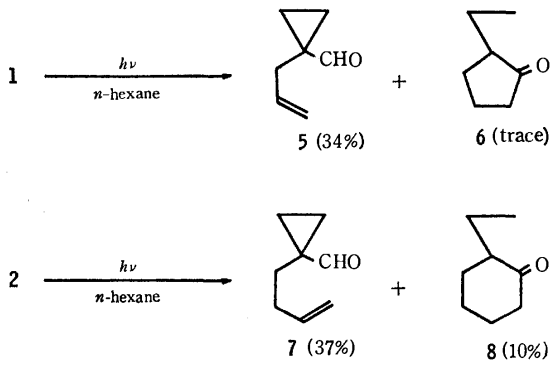

Scheme 1.

Oxygen Effect and Quenching Experiments. On irradiation of ketone **1**, the presence of oxygen caused marked retardation of the photoconversion. In addition, piperylene quenched the photochemical reaction of **1**. These results are shown in Table 1.

* Present adress; Department of Chemistry, Faculty of Science, Hokkaido University, Sapporo.

1) Part III: This bulletin, **40**, 2334 (1967).

2) Presented at the 22nd annual meeting of the Chemical Society of Japan, Tokyo, April, 1969. Preliminary communication has been given; *Tetrahedron Lett.*, **1969**, 3189.

3) a) J. N. Pitts, Jr. and I. Norman, *J. Amer. Chem. Soc.*, **72**, 4815 (1954). b) L. D. Hess and J. N. Pitts, Jr., *ibid.*, **89**, 1973 (1967). c) W. G. Dauben and G. W. Shaffer, *Tetrahedron Lett.*, **1967**, 4415. d) H. E. Zimmerman, K. G. Hancock, and C. C. Licke, *J. Amer. Chem. Soc.*, **90**, 4892 (1968). e) W. G. Dauben L. Schutte, R. E. Wolf, and E. J. Deviny, *J. Org. Chem.*, **34**, 2512 (1969). f) W. G. Dauben, G. W. Shaffer, and E. J. Deviny, *J. Amer. Chem. Soc.*, **92**, 6273 (1970).

4) R. Hoffmann, *Tetrahedron Lett.*, **1965**, 3819; Ref. 3c.

5) E. M. Kosower and M. Ito, *Proc. Chem. Soc.* (London), **1962**, 25.

6) J. K. Crandall and R. J. Seidewand, *J. Org. Chem.*, **35**, 697 (1970).

7) D. R. Morton, E. Lee-Ruff, R. M. Southam, and N. J. Turro, *J. Amer. Chem. Soc.*, **92**, 4349 (1970).

8) F. H. Cose and E. E. Reid, *ibid.*, **50**, 3062 (1928).

9) Prepared by the method reported by G. W. Baily and M. Mandoff, *J. Amer. Chem. Soc.*, **76**, 2707 (1954).

TABLE 1. QUENCHING EXPERIMENTS OF THE PHOTOREACTION OF SPIRO[2.4]HEPTAN-4-ONE (**1**)[a]

Quencher	Irradiarion time (min)	Analytical data[b]	
		1 (recovered)	**5**
None (N_2 bubbling)	60	65%	35%
	120	35	65
O_2 (bubbling)	60	96	4
	120	91	9
Piperylene[c]	60	100	trace
	150	99.5	0.5
	300	99	1
	400	98	2

a) Irradiated by means of 3130 Å using potassium chromate filter solution ($5\times10^{-4}M$, path length 5 cm).
b) Determined by the relative area of vpc.
c) In concentration of 0.16 mole/*l* *n*-hexane.

Photochemistry of Spiro[2.5]octan-4-one (2). Irradiation of ketone **2** in *n*-hexane under the conditions similar to those employed in the photolysis of **1** afforded 1-(3′-butenyl)cyclopropanecarboxyaldehyde (**7**) and 2-ethylcyclohexanone (**8**) in 37% and 10% yields, respectively. The structure of **7** was established by elemental analysis, NMR, and IR spectra. The minor product **8** was identified by comparisons of its IR and NMR spectra with those of an authentic sample.[9]

Irradiation of **2** in diethyl ether for 50 hr also gave **7** and **8** in 23% and 16% yields, respectively. The irradiation through a Pyrex filter did not affect the reaction (after 50 hr, **7** and **8** were produced in 17% and 9% yields, respectively).

Photochemistry of Spiro[2.4]heptane-5-one (3) and Spiro[2.5]octan-5-one (4). Irradiation of a *n*-hexane solution of **3** in a quartz vessel gave only polymeric materials after 20 hr. On irradiation through a Pyrex filter, the ring-enlarged product, 4-methylenecyclohexanone (**9**) was obtained in 39% yield after 3 hr. The structure of **9** was established by the comparison with an authentic sample.[10]

Irradiation of **4** in *n*-hexane produced 4-methylenecycloheptanone (**10**) in 22% yield after 20 hr. The structure of **10** was also confirmed by IR and NMR spectra and elemental analysis. Hydrogenation of **10** gave 4-methylcycloheptanone.[11]

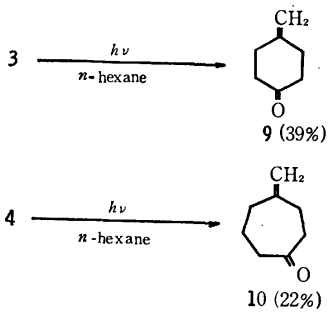

Scheme 2.

10) T. Tsuji, Ph. D. Thesis (1967) Osaka University.

Discussion

The photochemistry of **1** and **2** has been studied by three research groups.[2,6,7] Although their results are slightly different in detail according to the reaction conditions, the most important observation in these studies is that the cyclopropane cleavage (Path A) is not the major path, but the α-cleavage of the bond away from the cyclopropyl group (Path B) is actually the preferred process.[12]

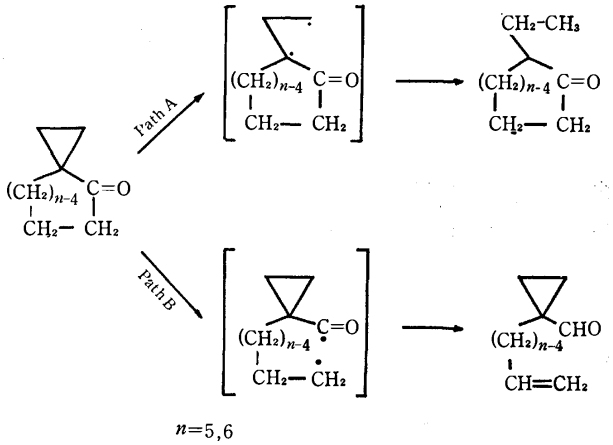

Scheme 3.

Accordingly, it can be concluded that the retention of cyclopropane ring is characteristic for the photoconversions of conjugated spirocyclopropyl ketones. This is a striking contrast to the predominant photocleavage of a cyclopropane ring observed in numbers of cyclopropyl ketones.[3]

The present investigation showed that the irradiation of **1** in *n*-hexane gives 1-(2′-propenyl)cyclopropanecarboxaldehyde (**5**) almost exclusively, whereas the irradiation of **2** in the same solvent produced 1-(3′-butenyl)cyclopropanecarboxaldehyde (**7**, 37%) accompanied by a considerable amount of 2-ethylcyclohexanone (**8**, 10%). The latter compound might be formed *via* a diradical followed by abstraction of hydrogen atoms from the solvent (Scheme 3). This is supported by the fact that the yield of **8** is substantially increased (16%), when **2** is treated in diethyl ether. It becomes apparent that the cyclopropane cleavage is hardly found in the photolysis of **1**, but in **2** it competes with 'Type I'[13] cleavage.

The photochemical cleavage of cyclopropyl ketones to enones is rationalized by the concept that photoexcitation energy is transferred to the cyclopropyl group through conjugative interaction and the strained ring is cleaved by its excess energy.[4] However, this concept would not be able to explain the difference in the photochemical behavior between

11) C. Djerassi, B. F. Burrows, G. G. Overberger, T. Takekoshi, C. D. Gutsche, and C. T. Chang, *J. Amer. Chem. Soc.*, **85**, 949 (1963).
12) In addition to **1** and **2**, Turro *et al.*[7] reported that 1,1-dimethylspiro[2.3]hexan-4-one gives cyclopropane ring-retained acetals as exclusive photoproducts in methanol.
13) J. G. Calvert and J. N. Pitts, Jr., "Photochemistry," John Wiley & Sons, Inc., New York, N. Y. (1966), p. 368—427.

spiroketones and other cyclopropyl ketones. According to Kosower and Ito,[5] the spiroketone **1** has higher degree of conjugation between the cyclopropyl and carbonyl groups than bicyclo[3.1.0]hexan-2-one. This would lead that the spiroketone suffers the cyclopropane cleavage more efficiently than the bicyclic ketone. However, the reverse is true in our case.

We determined the π–π^* absorption maxima of **1** and **2** in ethanol, and compared them with those of corresponding methylene- and dimethyl-cycloalkanones and nonconjugated spiroketones **3** and **4** (Table 2). The result indicates that the spiroketones **1** and **2** have similar conjugative interaction. Again this cannot help to understand the difference in their photochemical transformations.

TABLE 2. UV DATA OF SPIRO[2. *n*]ALKANONES (n=4, 5) AND RELATED KETONES

Compounds	λ_{max} (ethanol) nm	ε_{max}
2-Methylenecyclopentanone[a]	231[a]	7550[a]
1	203	3360
3	<200	—
2,2-Dimethylcyclopentanone[b]	<200	—
2-Methylenecyclohexanone[a]	230[a]	7400[a]
2	205	3440
4	<200	—
2,2-Dimethylcyclohexanone[c]	<200	—

a) Ref. 14
b) Prepared by the known method.[15]
c) Prepared by the known method.[9]

In the photochemistry of bicyclo[4.1.0]heptan-3-ones, Dauben and his coworkers[3c,f] showed that only when a methyl group is substituted at C–3 position, the α-cleavage away from the cyclopropyl group (C-2—C-3) becomes a predominant reaction path. However, this substituent effect to stabilize the radical generated in the photolysis cannot also be the factor controlling the direction of bond fission in these spiroketones. In the bicyclic ketones, the diradical **11**, which is primary–secondary, is proposed to be more stable than diradical **12**.[3c,f] The diradical **13** expected from the cyclopropane cleavage of spiroketone **1** is a primary-tertiary one. The α-cleavage of **1** will give **14**, which may be comparable in its stability with **12**. There will be no reason to expect that the diradical **13** is less stable than **11**, and hence **13** is less stable than **14**.

Crandall and Seidewand[6] have suggested that the apparent resistance of the cyclopropyl group to photochemical ring fission is due to the reversible recombination to the ring. Actually, the cyclopropane ring fission is reversible in several instances,[16] but there

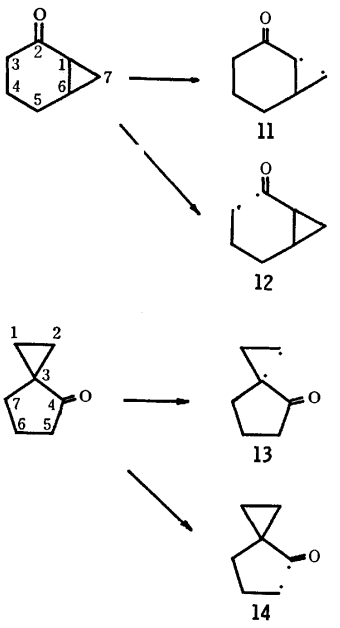

Scheme 4.

may be no reason why such a recombination process is particularly important only in the spiroketones and not so in other cyclopropyl ketones such as bicyclo [n.1.0]alkanones. Therefore, we believe that this explanation is not sufficient enough to account for the present results.

It was demonstrated that the photolysis of **1** using Pyrex-filtered light (>280 nm) proceeds similarly to the direct photolysis, and the photoreaction is quenched by piperylene. These results strongly indicate that the photoreaction of **1** as well as **2** proceeds *via* the n–π^* triplet state.[17] In many cases, the cleavage of cyclopropane ring proceeds through the triplet state.[18]

We would like to propose a hypothesis to rationalize the features of the photochemical behavior of spiroketones of **1** and **2**. Since the present photoreactions are regarded as a triplet reaction, the photoexcitation of these spiroketones leads to their triplet diradical state, where both the carbonyl carbon and the oxygen atoms may behave as a radical-like species.[19] The cyclopropane cleavage would subsequently occur through merely a dark reaction of the cyclopropylcarbinyl radical. Thus, the radical-like carbonyl-carbon would attack the cyclopropyl bond in an intramolecular S_H2 fashion to cleave the cyclopropyl ring giving an enolic diradical which is

14) R. L. Erskin and E. S. Waight, *J. Chem. Soc.*, **1960** 3425.
15) Part I in this series: This Bulletin **40**, 2338 (1967).
16) G. W. Griffin, E. J. O'Connell, and H. A. Hammond, *J. Amer. Chem. Soc.*, **85**, 1001 (1963); G. W. Griffin, J. Covell, R. C. Petterson, R. M. Dodson, and G. Klose, *ibid.*, **87**, 1410 (1965); R. C. Cookson, M. J. Nye, and G. Subrahmanyan, *Proc. Chem. Soc.* (London), **1964**, 144; W. G. Brown and J. F. Neumer, *Tetrahedron*, **22**, 473 (1966); Ref. 3d.
17) Although the measurement of the phosphorescence spectrum of **1** was attempted in M-P-Matrix with an Aminco Bowman Spectrofluorometer, there obtained no well-defined spectrum allowing to calculate the precise E_T value, but a broad peak (350—500 nm, λ_{max} 430 nm) was observed.
18) A. Padwa, Organic "Photochemistry," edited by O. L. Chapman, Marcel Dekker, Inc., New York, N. Y. (1967), Vol. 1, Chapter 2; D. I. Schuster and D. J. Petal, *J. Amer. Chem. Soc.*, **90**, 5145 (1968); Ref. 16a.
19) N. J. Turro, "Energy Transfer and Organic Photochemistry" edited by P. A. Leermakers and A. Weissberger, Interscience Publisher, New York, N. Y. (1969), p. 192.

followed by abstraction or migration of hydrogen atoms. In the S_H2 process[20], the attack would take place from the backside of the dissociating cyclopropyl bond, and hence the relative geometry between the cyclopropyl bond and *p*-orbital at the carbonyl carbon will be important.

The examination of the molecular models of these spiroketones indicates that in ketone **2**, the overlapping of the backside bond of the cyclopropyl bond and *p*-orbital of the carbonyl carbon in a *p*-σ manner might be possible to some extent, whereas in ketone **1**, the two orbitals are so arranged spacially as not to allow significant overlapping because of the rigid conformation of the cyclopentanone structure. The flexibility of the cyclohexane-ring structure in ketone **2** makes this sort of *p*-σ overlapping possible to a certain degree, but not fully as those of acyclic and bicyclic cyclopropyl ketones. Therefore, in the photolysis of **2**, the cyclopropane cleavage would compete with the α-cleavage.

Irradiation of nonconjugated spiroketones, **3** and **4**, afforded the ring-enlarged products, 4-methylenecycloalkanones, **9** and **10**, respectively. The cyclopropane ring was cleaved in these ketones. The reaction could be explained in a following way. The diradical **15** formed by the α-cleavage at C-4—C-5 gives the second diradical **16** *via* the induced ring opening of the cyclopropylcarbinyl radical, and finally the diradical cyclize intramolecularly to afford the reaction product. The ring-opening of the cyclopropylcarbinyl radical to form the second cyclic compound has been demonstrated in the photoreaction of several β-cyclopropyl cyclic ketones[21].

In the reaction of **3** and **4**, the formation of aldehyde **17** expected from the cleavage at C-5—C-6 could not be detected. This fact may suggest that the C-4—C-5 bond fission forming cyclopropylcarbinyl radicals occurs in preference to the C-5—C-6 cleavage.

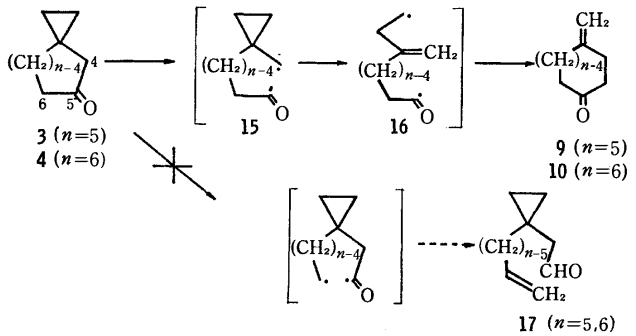

Scheme 5.

Experimental

The IR spectra were recorded on a Hitachi EPI-S2 spectrophotometer. The UV spectra were obtained with a Hitachi EPS-2U spectrophotometer. The NMR spectra were obtained with a JEOLCO JNM-MH-60 or JNM-4H-100 spectrometer at 60 MHz and 100 MHz, respectively, using TMS as an internal standard. The analytic and preparative vpc were carried out using a Yanagimoto GCG-5DH gas chromatograph. All irradiations were conducted with a Eikosha PIH-500 (High pressure mercury lamp, 500 W). All temperatures are uncorrected.

Materials. Spiro[2.4]heptan-4-one (**1**) and spiro[2.5]octan-4-one (**2**) were prepared by sodium dichromate oxidation of the corresponding carbinols[22] as described previously.[1]

Spiro[2.4]heptan-5-one (**3**) was prepared by the known method[23] from spiro[2.4]heptan-5-ol. Bp 58°C/18 mmHg, IR (liquid film): 1743 cm^{-1} (C=O), UV (ethanol): λ_{max} 290 nm (ε=35), NMR (60 MHz, CCl_4): 7.86 τ (2H, s, methylene of cyclopentanone), 7.5—8.3 τ (4H, m, methylenes of cyclopentanone), and 9.43 τ (4H, s, cyclopropane). Found: C, 76.08; H, 9.26%. Calcd for $C_7H_{10}O$: C, 76.32; H, 9.15%.

Spiro[2.5]octane-5-one (**4**) was prepared by the oxidation of spiro[2.5]octan-5-ol which was reported previously.[24] IR (liquid film): 1718 cm^{-1} (C=O). UV (ethanol): λ_{max} 288 nm (ε=35). NMR (60 MHz, CCl_4): 7.91 τ (2H, s, methylene of cyclohexanone), 7.5—8.5 τ (6H, m, methylenes of cyclohexanone), and 9.69 τ (4H, s, cyclopropane).

The spiroketones, starting materials, were purified by either fractional distillation or preparative vpc. Solvent *n*-hexane was purified by treating with fuming sulfuric acid followed by distillation. Diethyl ether and 2-propanol were purified by fractional distillation before use.

Irradiation of **2** *in* n-*hexane.* A solution of 15.0 g of **2** in 450 m*l* of *n*-hexane was irradiated through a quartz vessel under continuous slow bubbling of pure nitrogen. The reaction was monitored periodically by removing aliquots and then analyzing by vpc (Apiezon L at 130°C). When about the half of the starting ketone had been consumed, irradiation was stopped (40 hr). After solvent was evaporated through a short column, the residual oil (14.4 g) was subjected to fractional distillation under reduced pressure. The distillate (11.8 g) was separated by vpc (Apiezon L) into three components. The first compound (2.75 g) was characterized as an aldehyde **7** (37% yield based on consumed **2**) by the analysis, functional tests and the spectral data. IR (liquid film): 2730 cm^{-1} (C–H, aldehyde) 3070, 1025 cm^{-1} (C–H, cyclopropane), 1705 cm^{-1} (C=O), 1635, 900 cm^{-1} (terminal olefin). UV (ethanol): λ_{max} 211 nm (ε=2400), and 280 nm (ε=67). NMR (100 MHz, CCl_4): 1.4 τ (1H, s, aldehyde), 4.25 and 5.05 τ(1H, and 2H, ABC pattern of vinyl), 7.86 τ (2H, q, methylene), 8.35 τ (2H, overlapped d, methylene), and 8.93 and 9.12 τ (2H+2H, AA'BB' pattern of cyclopropane). Found: C, 77.03; H, 9.79%. Calcd for $C_8H_{12}O$: C, 77.37; H, 9.74%. Bp. 60—61°C/7 mmHg. n_D^{20} 1.4612. Olefin test (Br_2, $KMnO_4$) positive. 2,4-Dinitrophenylhydrazone; mp 133—134°C.

20) W. A. Pryor, "Free Radicals," McGraw Hill Book Co., Inc., New York, N. Y., (1966), Chapter 13.

21) L. D. Hess, J. L. Jacobson, K. Schaffner, and J. N. Pitts, Jr., *J. Amer. Chem. Soc.*, **89**, 3684 (1967); D. C. Hechert and P. J. Kropp, *ibid.*, **90**, 4911 (1968); R. H. Eastman, J. E. Starr, R. St. Martin, and M. K. Sakata, *J. Org. Chem.*, **28**, 2162 (1963); J. E. Starr and R. H. Eastman, *ibid.*, **31**, 1393 (1966).

22) Prepared by the procedure reported by W. G. Dauben and G. H. Berezin, *J. Amer. Chem. Soc.*, **85**, 468 (1963).

23) W. G. Dauben and T. L. Chitwood, *ibid.*, **90**, 3835 (1968).

24) S. Nishida, I. Moritani, K. Ito, and K. Sakai, *J. Org. Chem.*, **32**, 959 (1967).

The second product (0.76 g, 10% yield) was identified to be 2-ethylcyclohexanone (**8**) by comparisons of IR, retention times of vpc (Apiezon L and Carbowax 6000) with an authentic sample.[9] IR (liquid film): 1710 cm^{-1} (C=O), and 1382 cm^{-1} (CH_3). NMR (100 MHz, CCl_4): 9.20 τ (3H, t, methyl). Found: C, 75.75; H, 11.03%. Calcd for $C_8H_{14}O$: C, 76.14; H, 11.18%. Bp 51—52°C/8 mmHg. Semicarbazone, mp 157—157.5°C. The mixed mp of the semicarbazone with an authentic sample showed no depression.

The last component was unchanged **2** (7.58 g).

Irradiation of **2** in diethyl ether using a Pyrex reaction vessel for 50 hr afforded a volatile reaction mixture which was composed of **7** (24%), **8** (12%) and **2** (64%).

Irradiation of ***1*** *in* n-*hexane.* A solution of **1** (7.0 g) in *n*-hexane (500 m*l*) was similarly irradiated for 40 hr. The volatile reaction mixture (4.3 g) was separated with a preparative vpc (Apiezon L) into two components. The first eluted product (1.23 g, 34% yield) was characterized as an aldehyde **5**. Bp 34°C/7 mmHg. n_D^{20} 1.4608. UV (ethanol): λ_{max} 211 nm (ε=2700), 260 nm (ε=82). IR (liquid film): 3080, 1030 cm^{-1} (cyclopropane), 2725, 1690 cm^{-1} (aldehyde), 1630, 1410, 995, and 910 cm^{-1} (terminal olefin). NMR (100 MHz, CCl_4): 1.35 τ (1H, s, aldehyde), 4.3 τ (1H, m, vinyl), 4.99 and 5.12 τ (2H, two multiplet peaks, vinyl), 7.68 τ (2H, d, J=6.5 Hz, methylene), and 9.03 τ (4H, AA'BB' pattern, cyclopropane). Found: C, 76.09; H, 9.16%. Calcd for $C_7H_{10}O$: C, 76.32; H, 9.15%. 2,4-Dinitrophenylhydrazone, mp 139—139.5°C. Found: C, 53.96; H, 5.13; N, 19.26%. Calcd for $C_{13}H_{14}O_4N_4$: C, 53.79; H, 4.86; N, 19.26%. The second component was **1** unchanged (3.4 g). The existence of **6** was observed in vpc, but **6** was not isolated. The structure of **6** was confirmed by the identity of retention time (Apiezon L, diglycerol and Carbowax 20 M) with that of authentic 2-ethylcyclopentanone.[8] The yield of **6** was estimated to be less than 0.5%. The photolyses of **1** in diethyl ether, 2-propanol, benzene, and *n*-hexane, respectively, with a Pyrex filter afforded almost the same results as above.

Quenching of photoreaction of **1**. Three *n*-hexane solution of **1**; (A: **1**, 0.16 M), (B: **1**, 0.16 M and piperylene, 0.16 M) and (C: **1**, 0.16 M and piperylene 1.6 M) were degassed by the freeze-thaw method and irradiated in quartz tubes under nitrogen on a round table (5 cm from 500 W mercury lamp) immersed in an aqueous K_2CrO_4 filter solution (5×10^{-4} M). Periodical sampled aliquots of these solutions were subjected to the vpc analysis. While **1** converted to **5** in solution A (16% of **5** formed after 5 hr), in solution B there was observed marked quenching effect as shown in Table 1. In solution C, the photolysis of **1** was found to be completely quenched.

Irradiation of **3** *in* n-*hexane.* A solution of **3** (0.200 g) in *n*-hexane (10 m*l*) was irradiated for 3 hr in a Pyrex tube. After careful removal of the solvent, reaction mixture was subjected to a preparative vpc. Besides unreacted **3** (0.094 g), compound **9** was separated from several minor products. The compound **9** was characterized to be 4-methylenecyclohexanone (0.042 g, 39% yield). IR (liquid film): 1715 cm^{-1} (C=O), 1650, 895 cm^{-1} (olefinic). NMR (60 MHz, CCl_4): 5.15 τ (2H, s, vinyl), 7.55 τ (8H, m, methylene). UV (ethanol): λ_{max} 210 nm (ε=2800) and λ_{max} 283 nm (ε=30). Found: C, 76.44; H, 9.18%. Calcd for $C_7H_{10}O$: C, 76.32; H, 9.15%. The comparisons of **9** with an authentic sample which was prepared by the oxidation of 4-methylenecyclohexanol showed good identity in retention times of vpc (Apiezon L and Carbowax 6000) and in the mixed mp test of the 2,4-dinitrophenylhydrazones (mp 154—155°C).

Irradiation of ***4*** *in* n-*hexane.* A solution of **4** (0.572 g) in *n*-hexane (15 m*l*) was irradiated in a quartz tube for 20 hr. After the reaction mixture was treated as usual, 0.18 g of **4** and 0.086 g of **10** were isolated by vpc (Carbowax 6000). Compound **10** was characterized as 4-methylenecycloheptanone (22% yield). IR (liquid film): 1710 cm^{-1} (C=O), 1640, 890 cm^{-1} (olefinic). UV (ethanol): λ_{max} 286 nm (ε=20). NMR (60 MHz, CCl_4): 5.18 τ (2H, s, vinyl), 7.55 τ (8H, m, methylene) and 8.20 τ (2H, m, methylene). Found: C, 77.01; H, 10.09%. Calcd for $C_8H_{12}O$: C, 77.37; H, 9.74%. The 2,4-dinitrophenylhydrazone, mp 148—149°C.

Compound **10** (0.020 g) was hydrogenated in methanol on Pd-black (0.005 g). The hydrogenated product was identified as 4-methylcycloheptanone by the comparisons of the IR spectra and retention times of vpc (Apiezon L and Carbowax 6000) with an authentic sample.[9]

Studies on the Voges-Proskauer Reaction. II. The Structure of a Pigment from the Diacetyl Reaction of 1-Benzyl-1-methylguanidine[1]

Tamio NISHIMURA, Chiji YAMAZAKI, Tetsuro UENO, Shinichi KITAJIMA, and Koichi ISHIGE

Department of Chemistry, School of Hygienic Sciences, Kitasato University, Shirokane, Minato-ku, Tokyo

(Received July 13, 1971)

A pigment formed in the diacetyl reaction of 1-benzyl-1-methylguanidine was isolated as reddish purple prisms. The reduced pigment was colorless and rapidly converted back to the original pigment on exposure to the air. On the basis of IR, NMR, and mass spectral evidence, the structures of the pigment and the reduced one were established to be 2-(*N*-benzyl-*N*-methylamino)-4-methyl-5-(1-oxo-1,2-dihydro-2-naphthylidenemethyl)-imidazole and 2-(*N*-benzyl-*N*-methylamino)-4-methyl-5-(1-hydroxy-2-naphthylmethyl)imidazole, respectively.

Voges and Proskauer[2] found that glucose peptone cultures of a certain microorganism produced a pink color on addition of aqueous potassium hydroxide solution. It was shown that the coloration occurs as a result of the reaction between acetoin and creatine or certain similar substances, and the former is converted into diacetyl during the course of reaction.[3,4] Barritt[5] modified the reaction by the addition of 1-naphthol, which resulted in a great intensification of the color. This reaction has been called the diacetyl reaction. It has been demonstrated by several investigators that the color reaction is characteristic of 1,1-disubstituted, mono-, and unsubstituted guanidines and the intensity of coloration decreased in the order mentioned.[5-10] It is also obvious from literature[5,11,12] that the ketonic component should be α-diketone having at least one methyl group attached to the carbonyl carbon atom. Although Eggleton *et al.*[6] obtained a crude coloring matter in the diacetyl reaction of creatine, the pigment has not yet been isolated in a pure crystalline form and consequently its structure has remained unknown. The present work deals with the structure determination of a pigment produced in the diacetyl reaction of 1-benzyl-1-methylguanidine as the first step for elucidation of the mechanism of this color reaction.

Results and Discussion

The crude pigment from creatine according to Eggleton's method gave numerous coloring bands on column chromatography, which made it impossible to obtain a pure pigment. Thus we selected 1-benzyl-1-methylguanidine in expectation of ease in isolation of the aimed pigment, because of its expected good solubility in non-polar solvents in addition to good stability of coloration.[10]

Preliminary experiments revealed that the yield of pigment was best, when the guanidine, diacetyl, and 1-naphthol were allowed to react in water in a molar ratio of 1 : 2 : 5. The pigment was formed by the addition of 1-naphthol in 2.5 N sodium hydroxide to a mixture of diacetyl and the guanidine hydrochloride in water, followed by agitation of the mixture at room temperature. The crude pigment was obtained either by adjusting the reaction mixture to pH 10 with hydrochloric acid, or by extracting the sodium chloride-saturated mixture with benzene. The pigment was purified by column chromatography on silica gel with benzene, giving dark reddish purple prisms with mp 149—149.5°C in about 2% yields on the basis of the guanidine employed. It was also obtained in about 5% yields by conducting the reaction in chloroform with an equimolar proportion of reactants. The pigment thus isolated gave a visible spectrum having the same maximum absorption as and a similar shape to that obtained under the conditions of quantitative determination.[10]

Elemental analysis and mass spectrometry of the pigment gave the molecular formula $C_{23}H_{21}ON_3$. NMR data showed the presence of *N*-methyl (3.21

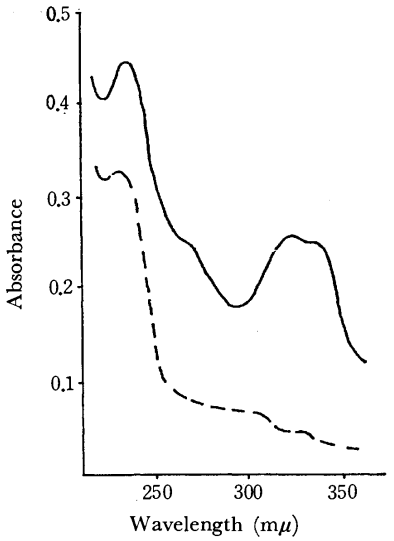

Fig. 1. UV spectra of pigment and reduced pigment (MeOH).
(——): Pigment, (----): Reduced

1) A preliminary communication appeared in *Tetrahedron Lett.*, **1970**, 4815.
2) O. Voges and B. Proskauer, *Z. Hyg. Infektionkrankh.*, **28** 20 (1898).
3) A. Harden, *Proc. Roy. Soc.* (London), **B**, **77**, 424 (1096).
4) A. Harden and D. Norris, *J. Physiol.*, **42**, 332 (1911).
5) M. M. Barritt, *J. Pathol. Bactriol.*, **42**, 441 (1936).
6) P. Eggleton, S. R. Elsden, and N. Gough, *Biochem. J.*, **37**, 526 (1943).
7) A. H. Enorr and L. A. Stocken, *ibid.*, **55**, 310 (1953).
8) J. Roche, N. Thoai, and J. H. Hatt, *Biochim. Biophys. Acta*, **14**, 71 (1954).
9) H. Rosenberg, A. H. Enorr, and J. F. Morrison, *Biochem. J.*, **63**, 153 (1956).
10) T. Nishimura, S. Tanabe, H. Toku, T. Kone, Y. Sakabe, and T. Sakaguchi, *Chem. Pharm. Bull.* (Tokyo), **17**, 639 (1969).
11) K. Lang, *Z. Physiol. Chem.*, **208**, 273 (1932).
12) F. Roos and G. Siest, *Bull. l'Acad. Soc. Lorraines Sci.*, **5**, 24 (1965).

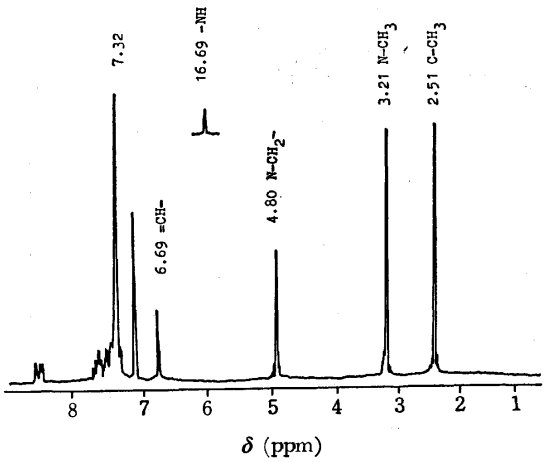

Fig. 2a. NMR spectrum of pigment (CCl_4).

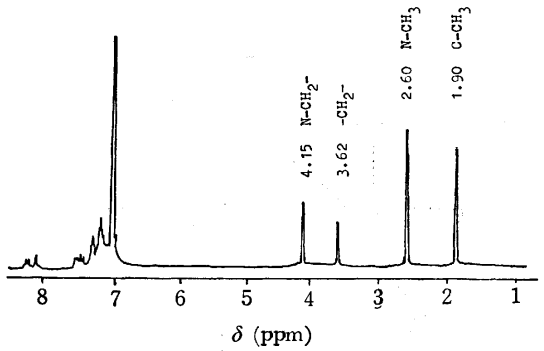

Fig. 2b. NMR spectrum of reduced pigment (CCl_4).

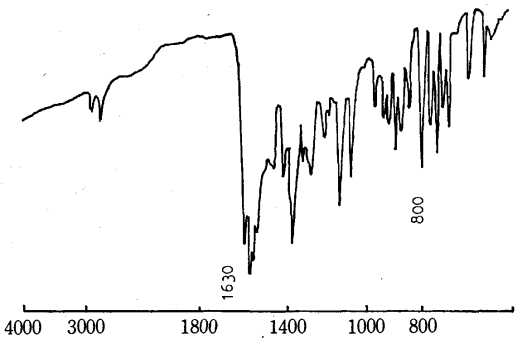

Fig. 3a. IR spectrum of pigment (KBr).

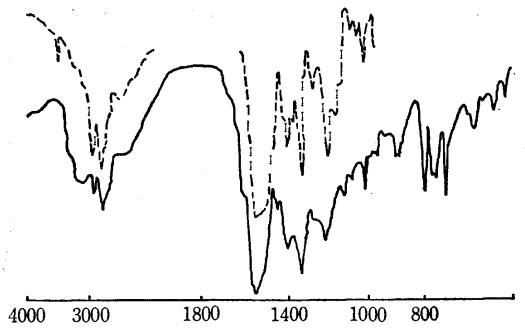

Fig. 3b. IR spectrum of reduced pigment.
(——): KBr, (----): CCl_4

s), *N*-methylene (4.80, s), phenyl (7.32, s), and naphthalene nucleus (7.0—8.4, m) as shown in Fig. 2a.

The IR spectrum of the pigment showed strong peaks at 1630 cm^{-1} (C=O) and 800 cm^{-1} (ring hydrogen out-of-plane vibration) as shown in Fig. 3a. The 800 cm^{-1} band was observed in 1,2-naphthoquinone but not in 1,4-naphthoquinone suggesting the presence of 1,2-naphthoquinoidal system. The pigment absorbed hydrogen on catalytic hydrogenation and yielded a colorless solution, which rapidly restored the original reddish color upon exposure to the air. The recovered pigment gave the same IR spectrum as that of the original pigment. The reduced pigment showed an associated O–H stretching band at 3150—3270 cm^{-1} in KBr disk and a sharp unassociated band at 3460 cm^{-1} in carbon tetrachloride, with simultaneous disappearance of the carbonyl band (Fig. 3b). It also showed a C–O stretching band at 1250 cm^{-1} (in CCl_4) or 1260 cm^{-1} (in KBr). The UV spectrum of the reduced pigment (Fig. 1) was similar to that of 1-naphthol. The hydrogenated pigment should therefore have a naphthol structure. The fact that it has no signal in the neighborhood of 6.7 ppm (Fig. 2b) at which 2-proton of 1-naphthols[13] usually resonates, further suggests that the reduced pigment is 2-substituted 1-naphthol. The absence of this signal in 2-substituted 1-naphthol was confirmed by comparing the NMR spectrum of 2-chloro-1-naphthol with that of 4-chloro-1-naphthol. On the basis of these findings, it was inferred that the pigment has the structure I.

In the NMR spectrum of the reduced pigment (Fig. 2b), the =CH– signal (6.69 ppm) disappeared and a new signal ($-CH_2-$) was observed at 3.62 ppm. In consideration of the presence of an aromatic C-methyl (2.51 ppm, s) and of the highly probable preservation of the guanidine structure in the pigment, it might be reasonable to conclude that the unknown moiety $C_5H_5N_2$ in I is II.

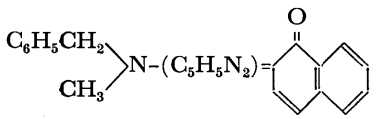

I

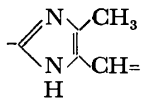

II

An NH chemical shift in imidazole has been reported to be in 11.10—13.50 ppm,[14] whereas the NH signal of the pigment was found in a markedly lower field (16.69 ppm, disappearing on addition of CH_3OD). The exceptional down-field shift and the unusual low frequencies of both N–H (3040—3090 cm^{-1}, independent of concentrations in CCl_4 and the intensity reduced on treatment with CH_3OD) and C=O stretching vibrations in the IR spectrum might be interpreted as the result of intramolecular hydrogen bonding between the NH and carbonyl oxygen atom and might provide an additional evidence supporting the presence of 1,2-quinoid structure. Thus the fol-

13) G. O. Dudek, *Spectrochim. Acta*, **19**, 691 (1963).

14) A. Mannschreck, W. Seitz, and H. Staab, *Ber. Bunsenges. Physik. Chem.*, **67**, 470 (1963).

lowing structures III and IV can be derived for the pigment and the reduced pigment, respectively.

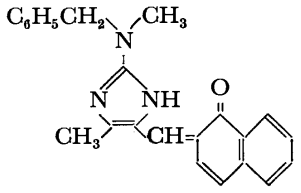

III

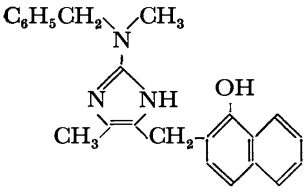

IV

These structures were further confirmed on the basis of mass spectrometric evidence. The molecular and major fragment ions of the pigment and the reduced one are listed in Tables 1 and 2.

TABLE 1. MASS SPECTRUM OF THE PIGMENT

	m/e	Intensity	Composition	Calcd	Found
a	355 (M)	100	$C_{23}H_{21}ON_3$	355.168	355.169
b	340	17	$C_{22}H_{18}ON_3$	340.145	340.142
c	264	8	$C_{16}H_{14}ON_3$	264.114	264.113
d	235	3	$C_{15}H_{11}ON_2$	235.087	235.088
e	223	21	$C_{14}H_{11}ON_2$	223.100	223.097
f	209	6	$C_{14}H_{11}ON$	209.084	209.086
g	194	4	$C_{14}H_{10}O$	194.073	194.068
			$C_{13}H_8ON$	194.065	
h	182	91	$C_{12}H_8ON$	182.059	182.063
i	154	7	$C_{11}H_8N$	154.066	154.072
j	127	31	$C_{10}H_7$	127.055	127.052
k	120	6	$C_8H_{10}N$	120.051	120.053
l	91	38	C_7H_7	91.055	91.057
m	65	11	C_5H_5	65.021	65.039

TABLE 2. MASS SPECTRUM OF THE REDUCED PIGMENT

	m/e	Intensity	Composition	Calcd	Found
n	357 (M)	23	$C_{23}H_{23}ON_3$	357.184	357.184
o	266	9	$C_{16}H_{16}ON_3$	266.129	266.129
p	210	12	$C_{14}H_{12}ON$	210.092	210.092
q	201	74	$C_{12}H_{15}N_3$	201.127	201.125
r	184	5	$C_{12}H_{10}ON$	184.076	184.082
s	156	4	$C_{11}H_8O$	156.058	156.058
t	144	67	$C_{10}H_8O$	144.058	144.058
u	128	6	$C_{10}H_8$	128.063	128.062
v	116	25	C_9H_8	116.063	116.060
w	115	44	C_9H_7	115.055	115.055
x	110	100	$C_5H_8N_3$	110.072	110.072
y	89	7	C_7H_5	89.039	89.040

The mass spectrum of the pigment was consistent with the structure III as shown in the following fragmentation scheme:

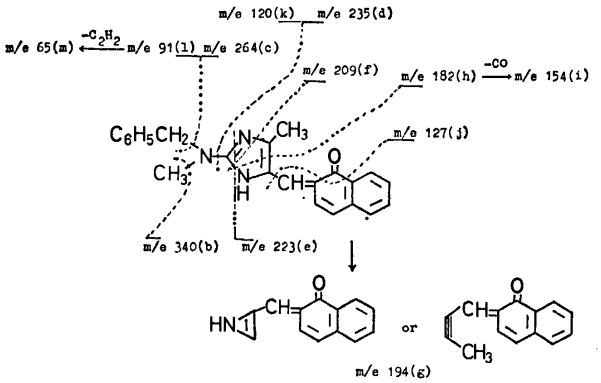

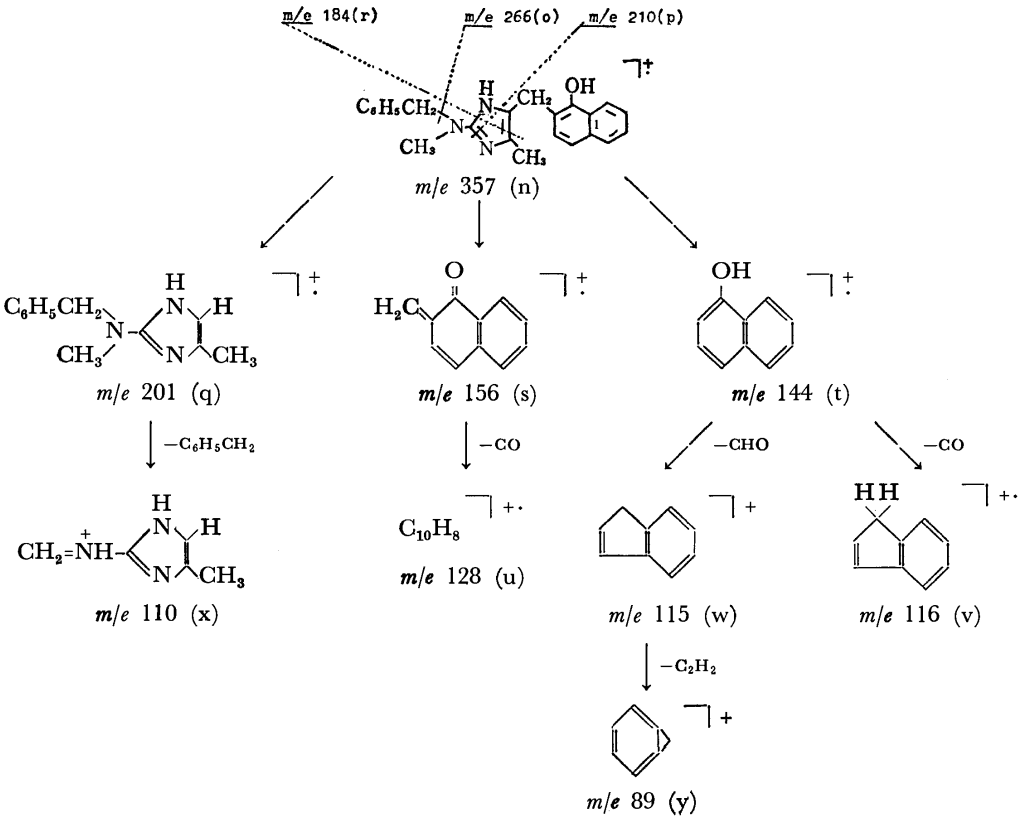

Treatment of the pigment with CH_3OD resulted in the significant increase in M+1 and *m/e* 183 ion peaks, indicating that deuteration occurred at position 1. Thus the methyl group can be located at position 4 in the imidazole ring from the latter peak.

The mass spectrum of the reduced pigment can be explained by the following fragmentation scheme: The ions q, s, and t may arise from the molecular ion n by the hydrogen rearrangement-dissociation reaction by analogy with the fragmentation of diarylmethanes containing *o*-methyl or *o*-hydroxyl substituent,[15] and the presence of the former two ions substantiates the reduced pigment to be 2-substituted-1-naphthol.

From the foregoing discussions it is concluded that the pigment produced in the diacetyl reaction of 1-benzyl-1-methylguanidine is 2-(*N*-benzyl-*N*-methylamino)-4-methyl-5-(1-oxo-1,2-dihydro-2-naphthylidenemethyl)imidazole (III), and the reduced form should be 2-(*N*-benzyl-*N*-methylamino)-4-methyl-5-(1-hydroxy-2-naphthylmethyl)imidazole (IV). Thus it becomes evident that the pigment produced by Barritt's or Eggleton's method differs from that formed by the original Voges-Proskauer reaction carried out in the absence of 1-naphthol.

Recently, Sakaguchi *et al.*[16] reported that the Voges-Proskauer reaction of diacetyl, 1,1-dimethyl guanidine and 1-naphthol by Eggleton's method gives two spots A (reddish purple, R_f 0.76) and B (red, R_f 0.62) on tlc (silica gel, benzene–AcOEt–EtOH (3 : 1 : 1)), and the major product is pigment B. Our pigment corresponds to Sakaguchi's pigment A in view of the color and the R_f value. Isolation of the pigment corresponding to Sakaguchi's pigment B was not successful, because of its instability.

Experimental

Melting points are uncorrected. NMR spectra were obtained on a Japan Electron Optics JNM-100 or Hitachi 3H-60 spectrometer. Chemical shifts are reported as δ values using tetramethylsilane as an internal standard. Abbreviations used in NMR data are: s, singlet; m, complex multiplet. The mass spectra were determined on a Japan Electron Optics JMS-01S high resolution mass spectrometer (Mattauch-Herzog type) operating with an ionizing energy of 70 eV by the direct inlet procedure. The source temperatures were 220°C for the pigment and 170°C for the reduced one. Exact mass measurement was carried out with perfluorokerosene to provide reference masses. Infrared spectra were obtained with a Hitachi recording spectrophotometer EPI G_2. Visible and ultraviolet spectra were obtained with a Hitachi spectrophotometer 101 or EPS-2.

Materials. Commercially available 1-naphthol and 1,4-naphthoquinone were purified by steam distillation and column chromatography on silica gel with benzene, respectively. 2-Chloro-1-naphthol,[17] 4-chloro-1-naphthol,[18] 1,2-naphthoquinone,[19] and 1-benzyl-1-methylguanidine hydrochloride[10] (mp 134—135°C)[20] were prepared according to the known procedures.

Preparation of Pigment. (a) To a solution of 1-benzyl-1-methylguanidine (1.63 g, 0.01 mol) in chloroform (25 m*l*) were added successively diacetyl (0.86 g, 0.01 mol) in chloroform (3 m*l*) and 1-naphthol (1.44 g, 0.01 mol) in chloroform (10 m*l*). The mixture was stirred at 24°C for 6 hr and then allowed to stand at room temperature for 16 hr. The resulting deep red solution was evaporated at about 40°C and the residue, after being dissolved in a small amount of benzene, was charged onto a column (made from 100 g of about 300 mesh Wako-gel, 60 mm diameter and 68 mm depth) and then eluted with benzene. After the first 850 m*l* fraction containing 1-naphthol and unidentified substances had been removed, the main fraction (about 2,800 m*l*) corresponding to a deep reddish purple band of the chromatogram was collected and evaporated at 37°C to give crude pigment (532 mg), which was found to consist of the desired pigment and three other minor components by means of tlc (silica gel, benzene). A reddish purple amorphous product showing a single spot on tlc was obtained by repeated chromatographic purification. The product dissolved in a small amount of benzene gave 182 mg of dark reddish purple prisms, mp 149—149.5°C, on addition of several drops of *n*-hexane and refrigeration. The pigment was readily soluble in ethyl acetate, carbon disulfide, benzene, and carbon tetrachloride; moderately in methanol, ethanol, and dilute aqueous alkali solution; insoluble in water. Found: C, 77.59; H, 6.54; N, 11.62%. Calcd for $C_{23}H_{21}N_3O$: C, 77.72; H, 5.96; N, 11.82%. UV: λ_{max} 535 mμ (ε=37200) in aqueous NaOH+Na_2CO_3.[10]

(b) To a mixture of 1-benzyl-1-methylguanidine hydrochloride (1.50 g, 7.5 mmol) in water (300 m*l*) and diacetyl (1.31 g, 15 mmol) in water (350 m*l*) was added a solution of 1-naphthol (5.41 g, 37.5 mmol) in 2.5 N NaOH (300 m*l*) under stirring at room temperature. The resulting reddish purple solution was stirred at room temperature for 10 min and then saturated with sodium chloride. After 20 min, the solution was separated by decantation from a dark purple gummy precipitate which did not contain the desired pigment. The solution was extracted several times with benzene, and the combined extracts (3500 m*l*) were dried over anhydrous sodium sulfate for 12 hr and then concentrated at 42—45°C to a small volume. The concentrate was purified in the same manner as above to give the pure pigment (131 mg).

Catalytic Hydrogenation of Pigment. A solution of pigment (50 mg) in benzene (50 m*l*) was hydrogenated in the presence of platinic oxide (20 mg) at ambient pressure and temperature. The red color of the pigment disappeared within 100 min, after which the solution was evaporated under reduced pressure to give a glass. Similar results were obtained in combinations of methanol–Pd/C and methanol–PtO_2.

15) S. Meyerson, H. Drews, and E. K. Fields, *J. Amer. Chem. Soc.*, **86**, 4964 (1964).
16) T. Sakaguchi, S. Tanabe, I. Koyahara, and T. Inoue, *Yakugaku Zasshi*, **90**, 1418 (1970).
17) D. Ginsburg, *J. Amer. Chem. Soc.*, **73**, 2723 (1951).
18) H. Kast, *Ber.*, **44**, 1337 (1911).
19) L. F. Fieser, "Organic Syntheses," Coll. Vol. 2, p. 430 (1943).
20) The lower value reported[10] can be ascribed to insufficient drying.

Intramolecular Hydrogen Bonds. XVIII.[1] Intramolecular Hydrogen Bonding in Ethyl α- and β-Alkylamino-alkanoates[2]

Nobuo Mori, Masanori Aihara, Yoshihiro Asabe, and Yojiro Tsuzuki

Department of Chemistry, Science University of Tokyo, Shinjuku-ku, Tokyo

(Received July 28, 1971)

The intramolecular hydrogen bonding in ethyl ω-alkylamino-acetates and -propionates in dilute carbon tetrachloride solutions has been investigated through the measurement of the NH and CO stretching absorption spectra. In the α-esters, the spectral data give no evidence regarding the hydrogen-bond formation. In the β-esters, though, the hydrogen bonding occurs, probably predominantly between the NH and the CO group.

It is known[3] that the hydrogen-donating nature of an amino group is much lower than that of a hydroxyl group, but higher than that of a mercapto group. Infrared spectroscopic investigations indicate that ethyl α- and β-hydroxyalkanoates[4,5] form an intramolecular hydrogen bond, exclusively between the OH and the CO group: thereby, their absorption bands are largely shifted to the lower-frequency side. In the corresponding mercapto-esters,[1] however, there is no spectral evidence for any hydrogen-bond formation between the SH and the ester group, indicating the very poor hydrogen-donating nature of the mercapto group, which is generally recognized.[6] These results have prompted us to investigate the intramolecular hydrogen bonding in the corresponding alkylaminoalkanoates as well.

Experimental

Samples. Ethyl alkylamino- and dialkylamino-acetates were prepared from the corresponding alkylamino-acetonitriles[7] by the usual method.[8] Ethyl β-alkylamino- and β-dialkylamino-propionates were synthesized by the addition of alkylamines to ethyl acrylate in ethanol.[9] The ethyl ethers of ω-ethylaminoalkanols were obtained by the reaction of ω-ethoxyalkyl bromides with ethylamine. They were then purified by several fractional distillations in an atmosphere of nitrogen immediately before the infrared measurement; their purity was checked by means of IR and/or NMR spectroscopy. Some of the samples are unknown compounds, whose analytical data and physical constants are summarized in Table 1. The solvents used were dried over phosphorus pentoxide and distilled.

Infrared Measurements. This was carried out at 20°C, using a grating spectrophotometer of the Japan Spectroscopic Co.[7] The concentrations used were 0.003 mol/*l* (NH spectra; cell-thickness: 5.0 cm) and 0.001 or 0.01 mol/*l* (CO spectra; cell-thickness: 1.1 or 0.1 cm), unless otherwise noted. The calculated spectral slit width was 1.5 cm^{-1} at the wave numbers of 3300 and 1700 cm^{-1}.

Results and Discussion

The analytical data of the unknown compounds are summarized in Table 1.

Table 1. Analytical data of unknown compounds

Compound	R	Bp °C/mmHg	n_D^{20}	Anal. of N, % Found	Calcd
$RNHCH_2$- COOEt	*i*-Pr	71/21	1.4204	9.70	9.65
	t-Bu	75/18	1.4230	9.00	8.80
$RNH(CH_2)_2$- COOEt	*i*-Pr	87/20	1.4232	8.78	8.80
	t-Bu	76/6	1.4254	8.07	8.09

In order to determine the level of concentration below which the intermolecular association is negligible, the concentration dependence has been examined. Figures 1 and 2 show the spectra of two esters in various concentrations in carbon tetrachloride in the NH stretching region. At higher concentrations, three absorptions appear. On dilution, the lowest-frequency band practically disappears, the middle-frequency band increases in its intensity and frequency, and the highest-frequency band remains almost unchanged. Below a certain concentration, the relative intensity of the last two bands remains constant; from their frequencies and intensities, the

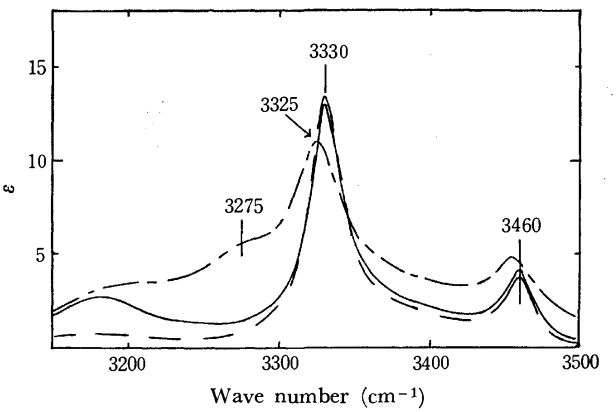

Fig. 1. NH spectra of ethyl *N*-isopropylaminoacetate in various concentrations: neat (———), 0.1 mol/*l* (——), and 0.01 and 0.003 mol/*l* (——).

1) Part XVII: N. Mori, S. Kaido, K. Suzuki, M. Nakamura, and Y. Tsuzuki, This Bulletin, **44**, 1858 (1971).

2) A part of this report was presented at the 21st Annual Meeting of the Chemical Society of Japan, Osaka, 1968, No. 1109.

3) See, for example, G. C. Pimental, and A. L. McClellan, "The Hydrogen Bond," W. H. Freeman and Co., San Francisco (1960), p. 92.

4) N. Mori, S. Ōmura, N. Kobayashi, and Y. Tsuzuki, This Bulletin, **38**, 2149 (1965).

5) N. Mori, Y. Asano, and Y. Tsuzuki, *ibid.*, **41**, 1871 (1968).

6) For example, Ref. 3, p. 201.

7) N. Mori, Y. Asabe, J. Tatsumi, and Y. Tsuzuki, This Bulletin, **43**, 3227 (1970).

8) N. J. Leonard and E. Barthel, *J. Amer. Chem. Soc.*, **72**, 3632 (1950).

9) R. W. Holley and A. D. Holley, *ibid.*, **71**, 2124 (1949); they used methanol as the solvent. We have found that the products obtained in methanol are contaminated with considerable amounts of the corresponding methyl esters.

TABLE 2.[a] APPARENT SPECTRAL DATA OF ETHYL ALKYLAMINOALKANOATES

Compound	In CCl_4						In CH_3CN		
	ν_{NH} cm^{-1}	$\Delta\nu_{1/2}$	ε	ν_{CO} cm^{-1}	$\Delta\nu_{1/2}$	ε	ν_{CO} cm^{-1}	$\Delta\nu_{1/2}$	ε
CH_3NHCH_2COOEt	3348	29	16	1742	17	620	1738	20	450
				(1736)		(100)	(1727)		(80)
$C_2H_5NHCH_2COOEt$	(3348)			1742	17	620	1738	20	450
	3330	40	12	(1736)		(100)	(1728)		(80)
i-$C_3H_7NHCH_2COOEt$	3330	33	13	1742	17	620			
				(1736)		(100)			
t-$C_4H_9NHCH_2COOEt$	3325	30	13	1742.5	17	630			
				(1736)		(100)			
$(CH_3)_2NCH_2COOEt$				1756		250	1746		380
				1738		275	1731		280
$(C_2H_5)_2NCH_2COOEt$				1756		240			
				1740		390			
$CH_3NH(CH_2)_2COOEt$	(3360)			1736	17	500	1730	18	470
	3338	38	13						
$C_2H_5NH(CH_2)_2COOEt$	(3338)			1736	17	520	1730	18	480
	3318	43	10						
i-$C_3H_7NH(CH_2)_2COOEt$	(3341)			1736	17	570			
	3320	46	8						
t-$C_4H_9NH(CH_2)_2COOEt$	(3332)			1736	17	560			
	3314	39	8						
$(C_2H_5)_2N(CH_2)_2COOEt$				1740	17	570	1729	19	480
$C_2H_5NH(CH_2)_2OEt$	3338		3						
	3322		7						
$C_2H_5NH(CH_2)_3OEt$	3330		6						
	3300		3						

a) The numerical values in parentheses are those estimated approximately by band reflection.

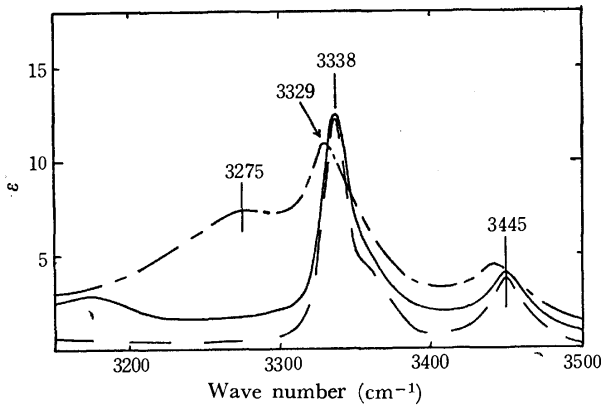

Fig. 2. NH spectra of ethyl *β*-(*N*-methylamino)-propionate in various concentrations: neat (———), 0.1 mol/*l* (——), and 0.01 and 0.003 mol/*l* (——).

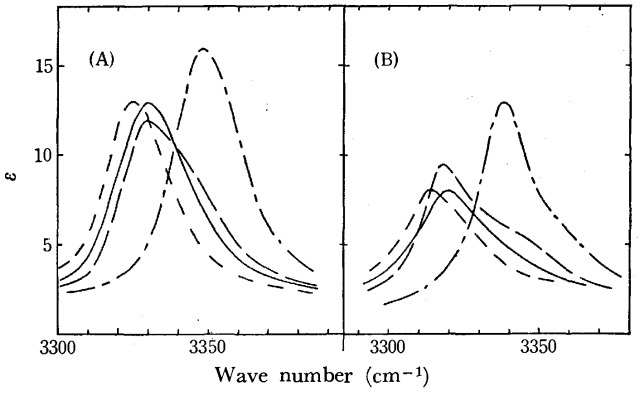

Fig. 3. NH spectra of ethyl *N*-alkylaminoacetates (A) and *β*-*N*-alkylaminopropionates (B); alkyl=methyl (———), ethyl (——), isopropyl (——) and *t*-butyl (———) (concentration 0.003 mol/*l*; cell 5.0 cm).

band near 3350 cm^{-1} can be assigned to the monomeric NH species, and the other, near 3450 cm^{-1}, probably to the carbonyl overtone.[10] Furthermore, these esters are practically monomeric in concentrations of 0.01 mol/*l* or less.

The NH Spectra. As Fig. 3A shows, the bands of ethyl alkylaminoacetates, when the alkyl group is methyl, isopropyl, or *t*-butyl, are very slightly broadened on the higher-frequency side, while the ethyl-

10) L. Joris and P. von R. Schleyer, *ibid.*, **90**, 4599 (1968).

amino-ester shows a highly unsymmetric band. On the other hand, the band of each β-alkylamino-propionate is very much broadened at a frequency higher by *ca.* 20 cm^{-1} than the maximum position (Fig. 3B). The apparent spectral data are summarized in Table 2.

In discussing the data, it may be convenient to examine the molecular model with respect to the rotational isomerism around the N–C bonds. In this examination, the following assumptions were made:[7] (1) the tricovalently-bound nitrogen atom takes a tetrahedron-like structure, (2) the molecule exists in a staggered conformation, but not in an eclipsed one, and (3) the lone electron-pair on the nitrogen atom is practically equal in steric size to the hydrogen atom.

In Fig. 4, the projections, IA and IB, are made along the N–C_α bond of ethyl alkylaminoacetates and along the N–C_β bond of ethyl β-alkylaminopropionates respectively, while the projections, II, III, and IV, are those along the N–C_R bond, where C_R denotes the carbon atom of an alkyl group, R, directly attached to the amino-nitrogen atom; the circle denotes the C_α atom in IA, the C_β atom in IB, or the C_R atom in II, III, and IV.

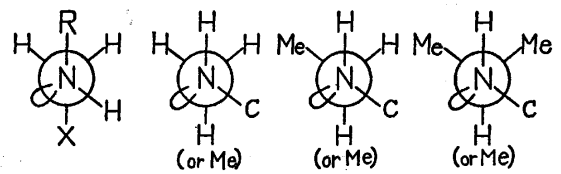

IA: X=COOEt II III IV
IB: X=CH_2COOEt

Fig. 4. Projections along the N–C_α (IA) or the N–C_β bond (IB) and along the N–C_R bond (II, III and IV).

All the acetates may sterically prefer the same conformation, IA, with respect to the C_α–N bond, in which the bulky groups, R and X, are *trans*. The observed differences in peak frequencies may be explained by the steric effect of R, as has previously been done for similar phenomena observed in alkylmethylamines[7] and *N*-alkylanilines.[11] When R is methyl or *t*-butyl, the amino-hydrogen atom always exists in the environment, II or IV respectively, in any rotational position about the N–C_R bond to be favored. In the case of *t*-butyl, thus, the lowering of the NH frequency by 23 cm^{-1} seems attributable to the presence of the two methyl groups *skew* to the NH group. When R is ethyl, there are two steric environments, II and III, around the NH group; the latter may be sterically preferable because of the methyl and the C-group being *trans*. In view of the steric preference, thus, the major component of the unsymmetric band can be assigned to III, and the minor component at the higher frequency can be assigned to II and may correspond to the band of ethyl methylaminoacetate. Finally, when R is isopropyl, two environments, III and IV, are likewise possible; they are practically indiscriminative in steric preference. Thus, the observed, almost symmetric band probably consists of two bands corresponding to these environments, III and IV. The same explanation can apply to the case of the β-esters, because the same steric environments around the NH group are expected.

In addition to the steric stabilization, the conformations, IA and IB, can probably involve a further stabilization resulting from the possible hydrogen bonding between the NH and the COOEt group, as would be expected from a similar situation in the corresponding α- and β-hydroxyalkanoates, which are exclusively internally bonded.[4,5] In the case of the aminoacetates, however, the NH spectral data give no striking evidence for the hydrogen-bond formation. That is, (1) there is no appreciable band-shift from the ν_{NH} values of alkylmethylamines[7] to the lower-frequency side, (2) the half-band widths are very close to those of alkylmethylamines,[7] and (3) the high band-intensites, as compared with those of the latter amines,[7] may also be caused by the electron-attractive nature of the ethoxycarbonyl group. On the other hand, ethyl β-alkylaminopropionates may be internally bonded, as can be evidenced by their lower NH frequencies and high band intensities. A similar result is found in α- and β-alkylaminoalkanonitriles.[7] These findings, particularly the absence of hydrogen bonding in the α-esters, are not expected from the fact that the ethyl ethers of ω-ethylamino-ethanol and -propanol are internally bonded, with similar 5- and 6-membered rings being formed through the bonding.

Recent infrared investigations indicate that an intramolecular hydrogen bonding occurs in *o*-substituted anilines,[12] pyrrolic esters,[13] 2-methylamino-ethanol,[14] acetylureas,[15] and *N*-ω-phenoxyalkyl-anilines.[16] In these cases, the shifts observed in the NH frequencies are very small as compared with those in the corresponding OH bondings, indicating a considerably weaker hydrogen bond, although the frequency shifts of the hydrogen-acceptor groups are larger than those which would be expected from the NH shifts, indicating a considerably strong bond. For example, in methyl *N*-methylanthranilate,[17] the $\Delta\nu_{NH}$ is 81 cm^{-1} from the free ν_{NH} assumed to be equal to the ν_{NH} of 3442 cm^{-1} of *N*-methylaniline, while the $\Delta\nu_{CO}$ is 45 cm^{-1} from the ν_{CO} of 1730 cm^{-1} of methyl *N,N*-dimethylanthranilate (*cf.*, in methyl salicylate, $\Delta\nu_{OH}$: *ca.* 430 cm^{-1}; $\Delta\nu_{CO}$: *ca.* 40 cm^{-1}).[17,18] In the present case, accordingly, an examination of the carbonyl spectra has been carried out.

The Carbonyl Spectra. Ethyl dialkylamino-

11) M. Ōki and K. Mutai, This Bulletin, **33**, 784 (1960).

12) A. N. Hambly and B. V. O'Grady, *Aust. J. Chem.*, **15**, 626 (1963); P. J. Krueger, *Can. J. Chem.*, **41**, 363 (1963); J. D. Scribner and J. A. Miller, *J. Org. Chem.*, **32**, 2348 (1967).

13) R. Grigg, *J. Chem. Soc.*, **1965**, 5149.

14) P. J. Krueger and H. D. Mettee, *Can. J. Chem.*, **43**, 2970 (1965).

15) C. I. Jose and P. R. Pabrai, *Spectrochim. Acta*, **23A**, 736 (1967).

16) M. Ōki and K. Mutai, *ibid.*, **25A**, 1941 (1969).

17) R. S. Rasmussen and R. R. Brattain, *J. Amer. Chem. Soc.*, **71**, 1073 (1949).

18) C. J. W. Brooks, G. Eglinton, and J. F. Morman, *J. Chem. Soc.*, **1961**, 661; N. Mori, Y. Asano, and Y. Tsuzuki, This Bulletin, **42**, 488 (1969).

acetates show, in carbon tetrachloride, two overlapped bands with a spacing of about 15 cm^{-1}, and the intensity of the higher-frequency band increases in acetonitrile relative to that of the lower-frequency band (Fig. 5A). By analogy with the cases of α-halogeno-[19] and α-alkoxy-carbonyl compounds,[5,20] this band splitting can be suitably explained by the rotational isomerism around the C_1–C_2 bond. Thus, the two bands can be assigned to the *cis* and the the *gauche* forms respectively:

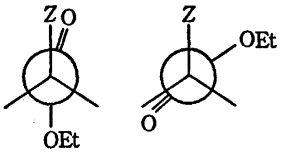

cis-Form with a higher ν_{CO} *gauche*-Form with a lower ν_{CO}

In carbon tetrachloride, the relative intensity (*cis* to *gauche*) increases with the α-substituents in the order: Et_2N (0.6) < Me_2N (0.9). Thus, the diethylamino group is larger in steric size than the dimethyl amino group if the steric size of the α-substituent is the most important factor in determining the *cis-gauche* equilibrium[20]

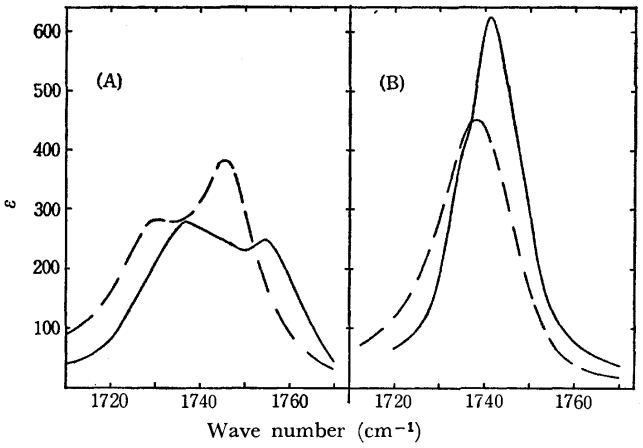

Fig. 5. Carbonyl spectra of ethyl dimethylaminoacetate (A) and of ethyl monomethylaminoacetate (B) in acetonitrile (——) and carbon tetrachloride (——): concentration 0.01 mol/*l*; cell 0.11 cm.

On the other hand, ethyl monoalkylaminoacetates show, in carbon tetrachloride, a strong band at 1742 cm^{-1}, with a very weak shoulder centered near 1736 cm^{-1}. In acetonitrile, a single, somewhat broadened band appears at 1738 cm^{-1}; this band corresponds to the higher-frequency band observed in carbon tetrachloride, since a more polar solvent has the effect of decreasing the ν_{CO}. If no intramolecular hydrogen bonding occurs in carbon tetrachloride, as has been suggested from the NH data, the unsymmetry of the band may again be attributed to the *cis-gauche* isomerism. If this is true, the following two points should be noticed: (1) the band spacing in each

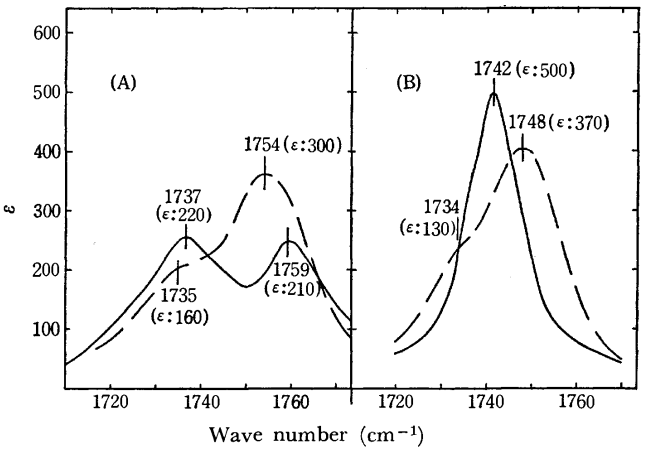

Fig. 6. Carbonyl spectra of ethyl methoxyacetate (A) and of ethyl glycolate (B) in acetonitrile (——) and carbon tetrachloride (——): concentration 0.01 mol/*l*; cell 0.11 cm. The ε values of the band components are given in parentheses.

solvent is smaller than those of the corresponding dialkylaminoacetates, or the peak-frequency in each solvent is lower than those of the *cis* form of the latter esters (the same trend is found in the cases of ethyl glycolate and methoxyacetate), and (2) the intensity ratio (*cis* to *gauche*) of *ca.* 6 is so high as to be not expected, unless an intramolecular hydrogen bonding or attractive interaction occurs to stabilize the *cis* form. The first point can, at least in part, be explained in terms of the lower electron density on the monoalkylamino-nitrogen atom, since the C–N dipole with a lower electron density on the N atom should have the lower field effect of decreasing the double-bond character (or ν_{CO}) of the carbonyl group in the *cis* form.

As for the second point, if the *cis-gauche* equilibrium is determined predominantly by the size of the α-substituent,[20] and if the nonomethylamino group is smaller in size than the dimethylamino group, the former group can be expected to give an intensity ratio higher than the 0.9 of the latter. This expectation agrees with our observation, but the observed ratio of 6 seems too high to be attributed to the decreased steric effect only,[1] since such a high ratio is generally found in internally-bonded carbonyl compounds such as α-hydroxyalkanoates.[5] The high ratio in carbon tetrachloride may be suitably explained by taking account of an attractive interaction which may be operative between the NH and the CO group in the *cis* form in that solvent, but not in acetonitrile, which associates with the NH group to prevent the intramolecular interaction (observed ν_{NH}: 3340 cm^{-1} lower by 8 cm^{-1} than in CCl_4).[21] It is not evident whether the interaction is the usual hydrogen bonding or the electrostatical attraction, but it is probably the latter, because no lowering of the NH frequency is observed. In this connection, it should be mentioned that ethyl glycolate shows, in carbon tetrachloride, an unsymmetric band, because a

19) L. J. Bellamy, "The Infrared Spectra of Complex Molecules," Methuen and Co., London (1958), p. 400.
20) T. L. Brown, *J. Amer. Chem. Soc.*, **80**, 3513 (1958).
21) Aliphatic secondary amines have spectral shifts of at most 10 cm^{-1} in acetone from the free ν_{NH}'s in CCl_4.[22]
22) D. Hagži (Ed.), "Hydrogen Bonding," Pergamon Press, New York (1959), p. 181.

strong hydrogen bond is formed exclusively between the OH and the CO group in the *cis* form (ν_{OH}: 3550 cm^{-1}).[4] In acetonitrile, the bonding to the carbonyl is prevented by the intermolecular association with the solvent (observed ν_{OH}: 3480 cm^{-1}), and two carbonyl bands appear with an intensity ratio of 2.8 (Fig. 6): this ratio is larger than the value of 2 of ethyl methoxyacetate (probably because of the smaller size of the hydroxyl group), but it is only half of the 5.5 of ethyl monomethylaminoacetate, although the hydroxyl group is expected to be smaller in size (hence, to give a higher intensity ratio) than the methylamino group. As one of the reasons for this, there can be considered an electrostatic repulsion between the dipoles in the *cis* form;[23] this repulsion is expected to be less operative between the C–N and the C=O dipole than between the C=O and the C–O dipole, because the C–N, especially the C–N(HCH_3), dipole may have a lower field effect on the C=O dipole, as is suggested by the order in which the band spacing in acetonitrile increases with the α-substituents: $NHCH_3$ (11 cm^{-1}) < $N(CH_3)_2$ (15 cm^{-1}) = OH (14 cm^{-1}) < OCH_3 (19 cm^{-1}). It is, of course, not evident whether this repulsion has such a high effect on the *cis-gauche* equilibrium.

Finally, β-dialkylamino, and also β-monoalkylamino, groups have practically no field effect on the carbonyl group, since ethyl β-diethylaminopropionate shows a single, symmetric CO band at the usual position of 1740 cm^{-1}. Furthermore, the ν_{CO} values, lower by 4 cm^{-1}, of ethyl monoalkylaminopropionates indicate that internal bonding to the carbonyl group occurs.

23) S. Mizushima, T. Shimanouchi, I. Ichishima, T. Miyazawa, I. Nakagawa, and T. Araki, *J. Amer. Chem. Soc.*, **78**, 2038 (1956). The importance of the steric factor in determining the equilibrium was indicated by Brown[20] for highly electronegative groups, such as halogens and alkoxy groups, but the electrostatic factor should be further considered when the electronegativities of the substituents are very different (*cf.*, usually, μ_{C-N}: 0.22; μ_{C-O}: 0.74).

BULLETIN OF THE CHEMICAL SOCIETY OF JAPAN, VOL. 45, 1790—1794 (1972)

Studies on Separation of Amino Acids and Related Compounds. VII. Separation of L-Aspartyl-(α,β)-L-histidine and of L-Glutamyl-(α,γ)-L-histidine[1,2]

Mitsuteru HIRATA,* Kosaku NODA,** and Nobuo IZUMIYA***

Laboratory of Biochemistry, Faculty of Science, Kyushu University, Hakozaki, Fukuoka

(Received July 29, 1971)

As control compounds, the structural α- and ω-isomers of L-aspartyl- and L-glutamyl-L-histidine were synthesized by a conventional manner. The experiments on a column chromatography of Dowex 50 were carried out with a model mixture containing α- and ω-isomer, and the complete separation of the isomers was observed at acidic condition. A mixture of α- and ω-isomers of L-aspartyl- or L-glutamyl-L-histidine prepared through the coupling of benzyloxycarbonyl-L-aspartic or glutamic acid anhydride with L-histidine were separated into each isomer with a large column in moderate yields.

An α-aspartyl or α-glutamyl dipeptide is synthesized without any special difficulty by the coupling of benzyloxycarbonyl-ω-benzyl-aspartic or -glutamic acid with an amino acid benzyl ester and subsequent deprotection from a coupling product.[3] Similarly, benzyloxycarbonyl-α-benzyl-aspartic or -glutamic acid is used for synthesis of a β-aspartyl or γ-glutamyl peptide.[3] An intramolecular anhydride[4] (XIV) is derived from benzyloxycarbonyl-L-aspartic acid by the action of acetic anhydride. Coupling reaction of the anhydride (XIV) with an amino acid ester produces a mixture of α- and β-dipeptide derivative, and the latter can be removed from the reaction mixture by extraction with sodium bicarbonate solution.[3] Similarly, benzyloxycarbonyl-L-glutamic acid anhydride[5] (XVI) is used for synthesis of α- and γ-glutamyl peptide.[3] Although the preparation of the anhydride (XIV or XVI) is much easier than that of benzyloxycarbonyl-α or ω-benzyl-aspartic or glutamic acid, the application of the anhydride for synthesis of α- or ω-peptide is restricted by the low yields and the elaborate preparative efforts.

We attempted to develop a convenient procedure separating α- and ω-structural isomers of L-aspartyl or L-glutamyl dipeptide by a column chromatography. We selected L-aspartyl- and L-glutamyl-L-histidine in this study because some of these dipeptides seemed interesting from the stand point of biochemical materials; β-L-aspartyl-L-histidine (VII) is a normal constituent of human urine,[6] and the VII and α-L-glutamyl-L-histidine (VI) possess tetanus toxic activities.[7]

* Present address: Tokyo Research Laboratories, Kowa Co. Ltd., Higashimurayama, Tokyo.

** Present address: LBS-NICHD, National Institutes of Health, Bethesda, Md., U. S. A.

*** To whom the reprint request should be addressed.

1) Part VI of this series: M. Muraoka and N. Izumiya, *Memoirs Fac. Sci., Kyushu Univ., Series C*, **7**, 133 (1970).

2) Presented at the 24th Annual Meeting of the Chemical Society of Japan, Osaka, April, 1971.

3) J. P. Greenstein and M. Winitz, "Chemistry on the Amino Acids," Vol. 2, John Wiley & Sons New York (1961), p. 1092; E. Schröder and K. Lübke, "The Peptides," Vol. 1, Academic Press, New York (1965), p. 181.

4) W. J. Le Quesne and G. T. Young, *J. Chem. Soc.*, **1952**, 24.

5) W. J. Le Quesne and G. T. Young, *ibid.*, **1950**, 1954.

6) Y. Kakimoto and M. D. Armstrong, *J. Biol. Chem.*, **236** 3280 (1961).

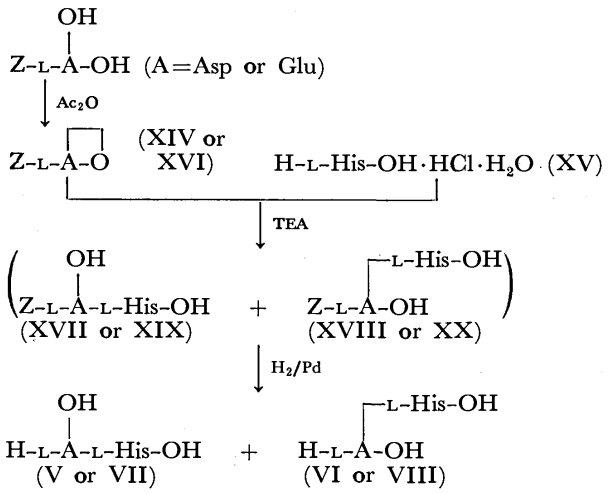

Scheme 1.

The reaction route in this study is shown in Scheme 1.[8] A coupling reaction of the anhydride (XIV or XVI) and L-histidine will produce a mixture of XVII and XVIII or XIX and XX. A whole reaction mixture is subjected to hydrogenolysis and each isomer in a hydrogenated mixture is attempted to separate by the application of a Dowex 50 column.

It should be noted that Kornguth *et al.* reported the separation of a mixture of ε-(α-L-glutamyl)-L-lysine and ε-(γ-L-glutamyl)-L-lysine by an amino acid analyzer.[9] We reported the experimental results to separate the leucyl dipeptide diastereomers by a Dowex column in the analytical and preparative scale,[10] and to separate glycyl tripeptide diastereomers by an amino acid analyzer.[11]

Each isomer of L-aspartyl- and L-glutamyl-L-histidine were prepared in the conventional manner

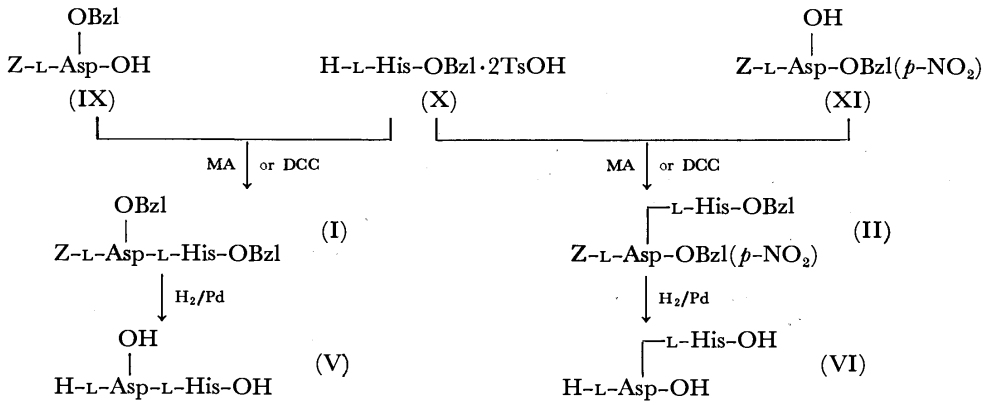

Scheme 2.

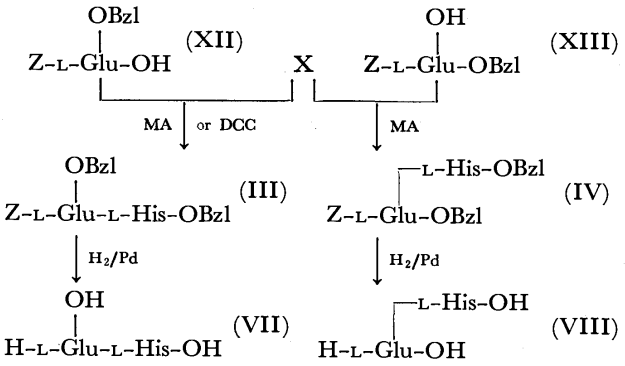

Scheme 3.

shown in Schems 2 and 3. The acid (XI) was used instead of benzyloxycarbonyl-α-benzyl-L-aspartic acid because the preparation[12] of the latter is considerably troublesome compared with that of XI or XIII. It was indicated that a synthetic isomer gave single spot on a paper chromatogram, but the R_f value was different from that of the corresponding isomer (Table 1).

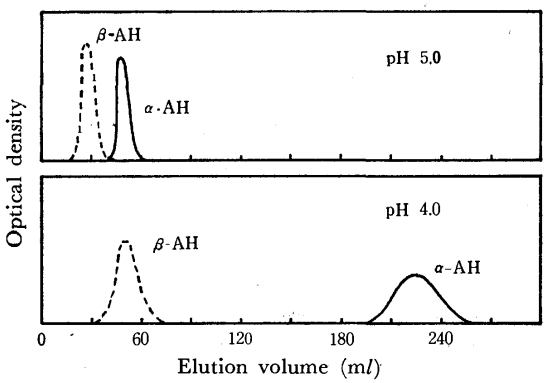

Fig. 1. Effect of pH in buffer system on separation of Asp-His.

7) J. H. Mueller and P. A. Miller, *ibid.*, **223**, 185 (1956).

8) Abbreviations: Z, benzyloxycarbonyl; OBzl, benzyl ester; OBzl(*p*-NO_2), *p*-nitrobenzyl ester; DCC, dicyclohexylcarbodiimide; MA, mixed anhydride; TEA, triethylamine; DMF, dimethylformamide; THF, tetrahydrofuran.

9) M. L. Kornguth, A. Neidle, and H. Waelsch, *Biochemistry*, **2**, 740 (1963).

10) K. Noda, H. Okai, T. Kato, and N. Izumiya, This Bulletin, **41**, 401 (1968).

11) M. Muraoka, N. Yoshida, K. Noda, and N. Izumiya, *ibid.*, **41**, 2134 (1968); N. Izumiya and M. Muraoka, *J. Amer. Chem. Soc.*, **91**, 2391 (1969).

12) M. Bergmann, L. Zervas, and L. Salzmann, *Ber.*, **66**, 1288 (1933); G. L. Miller, O. Behrens, and V. du Vigneaud, *J. Biol. Chem.*, **140**, 411 (1941); P. M. Bryant, R. H. Moore, P. J. Pimlott, and G. T. Young, *J. Chem. Soc.*, **1959**, 3868.

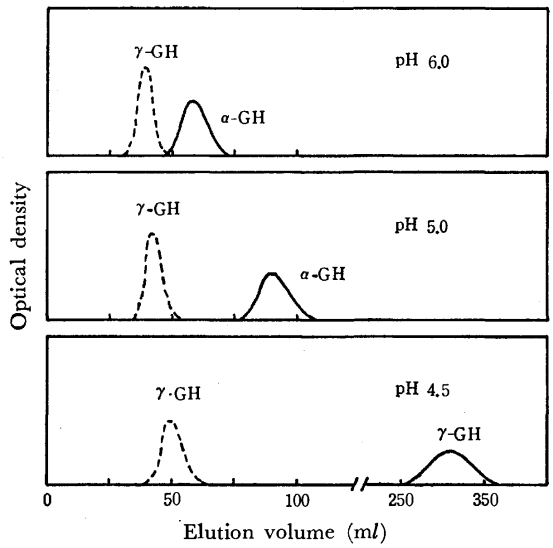

Fig. 2. Effect of pH in buffer system on separation of Glu-His.

Preliminary experiments on a model mixture were performed with a small column (0.9×50 cm) of Dowex 50 using 0.2 N ammonium acetate buffers at different pH, in order to find an optimal condition for the separation. The elution patterns of a model mixture composed of two isomers in the same amount were indicated in Figs. 1 and 2. The α- and γ-isomer of glutamyl-histidine in the mixture were separated each other more efficiently in general than the α- and β-aspartyl-histidine. It was observed that peaks of the free amino acids, aspartic acid and histidine, did not overlap with those of α- and β-aspartyl-histidine when a buffer of pH 4.0 or 5.0 was used. Similarly, peaks of glutamic acid and histidine did not overlap with those of the α- and γ-dipeptide when a buffer of pH 4.5, 5.0 or 6.0 was used.

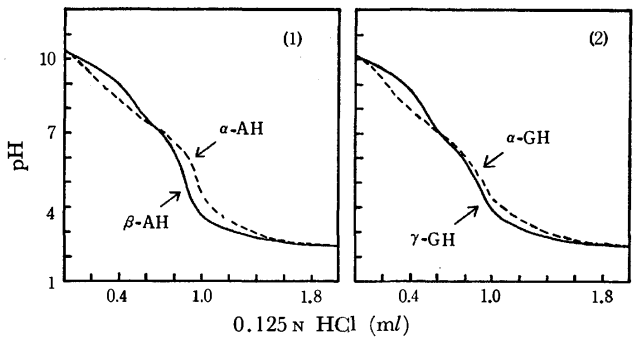

Fig. 3. pH Titration curve of Asp-His (1) and Glu-His (2).

In a previous paper,[10] it was observed that an L-L diastereomer of leucyl-alanine with a solvent of pH 4.5 in a Dowex 50 column was eluted more slowly than the corresponding L-D isomer, whereas the L-L isomer with a solvent of pH 5.5 was eluted rapidly than the L-D. It was also observed that the titration curves for the diastereomers crossed each other around pH 5.0. Then, it was suggested that the positions of peaks were correlated with the pH titration curves. In this study, the titration of α- and ω-isomer or L-aspartyl- or L-glutamyl-L-histidine indicated that the titration curves crossed each other around pH 7 in both cases (Fig. 3). Therefore, separation studies of the model mixture with the small column were performed with solvents of pH 7.0, 8.0 and 9.0; it was found that each of the peptides was eluted very rapidly near to a void volume and not separated each other. Thus, the correlation between the peak positions and the pH titration curves by α- and ω-isomer in this study could not be established.

As the experiments on a preparative scale, two materials which prepared following Scheme 1 were tried to separate into α- and ω-isomer with a large column (1.8×110 cm) of Dowex 50. Each material was composed of four ninhydrin positive components, namely α- and ω-isomer of L-aspartyl or L-glutamyl-L-histidine as majors and aspartic or glutamic acid and histidine as minors. Although a buffer of pH 4.0 or 4.5 might be an efficient solvent for complete separation (see, Figs. 1 and 2), we used a pH 5.0 buffer for an economy of running time. When the material derived from 5 mmol of benzyloxycarbonyl-L-aspartic acid anhydride (XIV) was applied for the column with the pH 5.0 buffer, pure α- and β-L-aspartyl-L-histidine were isolated in 31% and 22% yield respectively. In the similar manner, pure α- and γ-L-glutamyl-L-histidine were isolated in 21% and 28%. Thus, it was indicated that the structural isomers of L-aspartyl- and L-glutamyl-L-histidine can be prepared conveniently by the use of the anhydride and following application of a column chromatography.

Experimental

The R_f(tlc) refers to thin layer chromatography with a solvent of chloroform–methanol (5 : 1, v/v).

α-(Benzyloxycarbonyl-β-benzyl)-L-aspartyl-L-histidine Benzyl Ester (I). *(a) By MA Method*: To a solution of benzyloxycarbonyl-β-benzyl-L-aspartic acid[13] (IX) (3.57 g, 10 mmol) and TEA (1.4 ml, 10 mmol) in THF (20 ml) at −5°C was added isobutyl chloroformate (1.31 ml, 10 mmol). After 15 min, a mixture of L-histidine benzyl ester di-*p*-toluenesulfonate[14] (X) (5.90 g, 10 mmol) and TEA (2.8 ml, 20 mmol) in DMF (20 ml) was added to the solution. The mixture was allowed to stand overnight at room temperature, and then evaporated to dryness *in vacuo*. After the residue was dissolved in ethyl acetate (30 ml), the solution was washed successively with 4% sodium bicarbonate and water, dried over sodium sulfate, and then evaporated. The product was obtained as a semi-solid; yield, 3.1 g (53%); R_f (tlc) 0.59.

(b) By DCC Method: To a solution of IX (0.71 g, 2 mmol) and X (1.18 g, 2 mmol) in DMF (10 ml) were added TEA (0.56 ml, 4 mmol) and DCC (0.41 g, 2 mmol) at 0°C. After the mixture had been stirred overnight at room temperature, it was evaporated and ethyl acetate was added to residue. After dicyclohexylurea was filtered off, the filtrate was washed with 4% sodium bicarbonate and water, dried, and evaporated to give a semi-solid; 0.78 g (67%); R_f(tlc) 0.59.

13) N. Izumiya, H. Uchio, and T. Yamashita, *Nippon Kagaku Zasshi*, **79**, 420 (1958).

14) S. Akabori, S. Sakakibara, and S. Shina, This Bulletin, **31**, 784 (1958).

β-(Benzyloxycarbonyl-α-p-nitrobenzyl)-L-aspartyl-L-histidine Benzyl Ester (II). Benzyloxycarbonyl-α-*p*-nitrobenzyl-L-aspartic acid[15] (XI) (4.02 g, 10 mmol) and X (5.9 g, 10 mmol) were coupled by the MA method as described for the preparation (method a) of I; yield of an oily product, 3.28 g (52%); R_f (tlc) 0.61. The same compound (II) was prepared by the DCC method from XI and X as described for the preparation (method b) of I; yield of an oil, 57%; R_f (tlc) 0.61.

α-(Benzyloxycarbonyl-γ-benzyl)-L-glutamyl-L-histidine Benzyl Ester (III). (a) By MA Method: Benzyloxycarbonyl-γ-benzyl-L-glutamic acid[16] (XII) (3.71 g, 10 mmol) and X (5.9 g, 10 mmol) was coupled as described for the preparation (method a) of I, and the resulting crude product was recrystallized from ethyl acetate–ether–petroleum ether; yield, 2.7 g (45%); mp 92—93°C; $[\alpha]_D^{25}$ −11.0° (*c* 2, ethanol); R_f (tlc) 0.54.

Found: C, 65.70; H, 5.95; N, 9.36%. Calcd for $C_{33}H_{34}O_7N_4$: C, 65.51; H, 5.84; N, 9.55%.

(b) By DCC Method: III was prepared from XII and X; yield, 39%; mp 93—94°C; $[\alpha]_D^{25}$ −11.5° (*c* 2, ethanol); R_f (tlc) 0.54 (Found: C, 65.55; H, 5.91; N, 9.32%).

γ-(Benzyloxycarbonyl-α-benzyl)-L-glutamyl-L-histidine Benzyl Ester (IV). This was obtained from benzyloxycarbonyl-α-benzyl-L-glutamic acid[17] (XIII) (3.71 g, 10 mmol) and X (10 mmol) by the MA method; yield, 2.04 g (34%); mp 130—132°C; $[\alpha]_D^{25}$ −13.2° (*c* 2, ethanol); R_f (tlc) 0.52.

Found: C, 65.82; H, 6.02; N, 9.27%. Calcd for $C_{33}H_{34}O_7N_4$: C, 65.51; H, 5.84; N, 9.55%.

α-L-Aspartyl-L-histidine (α-Asp-His or α-AH) (V). A solution of I (2.92 g, 5 mmol) in 90% acetic acid (25 m*l*) was treated with hydrogen in the presence of palladium black. The filtrate from the catalyst was evaporated to dryness. The residual crystals were recrystallized from water-ethanol; yield, 1.15 g (80%); mp 205—207°C (decomp.); $[\alpha]_D^{25}$ +12.0° (*c* 2, water) (Found as monohydrate: C, 41.45; H, 5.81; N, 19.66%). (lit,[6]; mp 190—194°C; $[\alpha]_D$ +9.7° (water).)

β-L-Aspartyl-L-histidine (β-Asp-His or β-AH) (VI). This was obtained by hydrogenolysis of II (1.89 g, 3 mmol) as described above; yield, 0.354 g (41%); mp 234—238°C (decomp.); $[\alpha]_D^{25}$ +36.8° (*c* 2, water) (Found as monohydrate: C, 41.37; H, 5.66; N, 19.63%). (lit.[18]; mp 235—240°C; $[\alpha]_D$ +38° (water).)

α-L-Glutamyl-L-histidine (α-Glu-His or α-GH) (VII). This was obtained from III (1.8 g, 3 mmol); yield, 0.707 g (78%); mp 199—204°C (decomp.); $[\alpha]_D^{25}$ +18.5° (*c* 2, water) (Found as monohydrate: C, 43.84; H, 6.08; N, 18.26%). (lit,[19]; mp 177—178°C.)

γ-L-Glutamyl-L-histidine (γ-Glu-His or γ-GH) (VIII). This was obtained from IV (1.8 g, 3 mmol); yield, 0.435 g (48%); mp 203—205°C (decomp.); $[\alpha]_D^{25}$ +12.3° (*c* 2, water).

Found: C, 44.01; H, 6.13; N, 18.37%. Calcd for $C_{11}H_{16}O_5N_4 \cdot H_2O$: C, 43.70; H, 6.00; N, 18.54%.

Paper Chromatography of the Dipeptides. The experiments were carried out with ascending technique with Toyo Roshi No. 52 paper, and a peptide on the paper was developed with ninhydrin. It was observed that each (V, VI, VII or VIII) of synthetic dipeptides showed single spot with three different solvents. As recognized from Table 1, the isomers of Asp-His or Glu-His were clearly separated on a chromatogram.

Table 1. R_f values of dipeptides on paper chromatography

Dipeptide	R_f		
	BAPW[a]	BPA[b]	PW[c]
α-Asp-His	0.13	0.17	0.16
β-Asp-His	0.09	0.12	0.11
α-Glu-His	0.19	0.19	0.18
γ-Glu-His	0.12	0.13	0.14

a) *n*-butanol - acetic acid - pyridine - water; 4 : 1 : 1 : 2, v/v.
b) *n*-butanol - acetic acid - water; 3 : 1 : 1, v/v.
c) pyridine - water; 4 : 1, v/v.

Column Chromatography of Model Mixture Composed of Isomeric Dipeptides. A model mixture of Asp-His was made by dissolving each 0.05 mmol of V and VI in water (0.5 m*l*). Similarly, a model mixture of Glu-His (VII and VIII) was prepared. A column (0.9×50 cm) with Dowex 50×8 (200—400 mesh), NH_4^+ form, was equilibrated by washing with 0.2 N ammonium acetate buffer of a definite pH (4.0, 4.5, 5.0 or 6.0), and a model mixture was applied to a column. The column was eluted with the same buffer at room temperature, and two m*l* fractions were collected at a flow rate of about 20 m*l*/hr. Approximately 0.01 m*l* from each tube was spotted on a strip of filter paper. The strip was dried at 100°C for 5 min, immersed in a 0.2% ninhydrin-acetone solution, and again heated. The degrees of coloration developed were determined by a densitometer as described previously.[20] The resulting patterns are shown in Figs. 1 and 2. The nature of a peptide in each peak in Figs. 1 and 2 was identified by means of paper chromatography after the corresponding fractions were concentrated by evaporation.

pH Titration Curve of the Dipeptides. Each isomer (0.05 mmol) of Asp-His and Glu-His was dissolved in 0.1 N sodium hydroxide (1 m*l*), and an automatic titration was carried out with 0.125 N hydrochloric acid with Radiomer pH-stat, model TTT-1, at room temperature. The resulting patterns are shown in Fig. 3.

Preparative Separation of α-Asp-His and β-Asp-His from a Mixture. A solution of benzyloxycarbonyl-L-aspartic acid anhydride[4] (XIV) (1.25 g, 5 mmol) in THF (5 m*l*) was added to a solution of L-histidine monohydrochloride monohydrate (XV) (1.05 g, 5 mmol) and TEA (2.8 m*l*, 20 mmol) in water (10 m*l*) under vigorous stirring at room temperature. After 15 min, the reaction mixture was evaporated to dryness and the residue was dissolved in 90% acetic acid (30 m*l*). The solution was treated with hydrogen in the presence of palladium black. Paper chromatography on the hydrogenated solution showed the presence of α-Asp-His, β-Asp-His, aspartic acid and histidine. The filtrate from the catalyst was evaporated to dryness, and the residue was dissolved in 0.2 N ammonium acetate buffer (1 m*l*) of pH 5.0. The solution was put on a column (1.8×110 cm) of Dowex 50×8 treated previously with the same buffer. The column was eluted with the same buffer (650 m*l*) at a flow rate of 60 m*l*/hr, and each 10 m*l* was fractionated (No. 1—No. 65). Then, the eluting solvent was changed to 2 N ammonium hydroxide. The material in each fraction was identified by means of paper chromatography; it was found

15) E. Schröder and E. Klieger, *Ann. Chem.*, **673**, 208 (1964).
16) W. E. Hanby, S. G. Waley, and J. Watson, *J. Chem. Soc.*, **1950**, 3239.
17) E. Klieger and H. Gibian, *Ann. Chem.*, **655**, 195 (1962).
18) V. du Vigneaud and M. Hunt, *J. Biol. Chem.*, **125**, 269 (1938).
19) F. Schneider, *Z. Physiol. Chem.*, **320**, 82 (1960).
20) H. Aoyagi, H. Okai, M. Ohno, and N. Izumiya, *Nippon Kagaku Zasshi*, **85**, 656 (1964); H. Aoyagi, M. Ohno, N. Izumiya, and B. Witkop, *J. Org. Chem.*, **29**, 1382 (1964).

that the fractions 13—15 contained aspartic acid, the 28—40 β-Asp-His, the 48—61 α-Asp-His and the 70—73 histidine. The fractions from tube number 48 to 61 were evaporated *in vacuo* to dryness. To remove the ammonium acetate contaminated, the residue dissolved in water was treated with a column of Dowex 50×8, H^+ form, and the column was washed with water and eluted with aqueous ammonium hydroxide. The eluate was evaporated, and the residual crystals were recrystallized from water–ethanol; yield of α-Asp-His monohydrate, 440 mg (31% from XIV); mp 205—208°C (decomp.); $[\alpha]_D^{25}$ +12.5° (*c* 2, water) (Found: C, 41.37; H, 5.64; N, 19.70%). A mixture of this product and an authentic sample obtained from I showed a single spot in paper chromatography with different solvent systems.

The fractions from 28 to 40 were treated in the same manner described above to give pure β-Asp-His monohydrate, 308 mg (22% from XIV); mp 234—237°C (decomp.); $[\alpha]_D^{25}$ +37.2° (*c* 2, water) (Found: C, 41.42; H, 5.51; N, 19.66%).

Preparative Separation of α-Glu-His and γ-Glu-His from a Mixture. Benzyloxycarbonyl-L-glutamic acid anhydride[5] (XVI) (1.32 g, 5 mmol) was coupled with XV (5 mmol), and the reaction mixture was treated exactly in the same manner as described above. As only one exception, the eluting solvent was changed from 0.2 N ammonium acetate buffer (pH 5.0) to 2 N ammonium hydroxide at the fraction number 85. It was found that the fractions 10—12 contained glutamic acid, the 16—24 γ-Glu-His, the 59—81 α-Glu-His and the 90—94 histidine. The fractions from 59 to 81 were treated in the same manner as described above to give pure α-Glu-His monohydrate, 314 mg (21% from XVI); mp 202—205°C (decomp.); $[\alpha]_D^{25}$ +18.2° (*c* 2, water) (Found: C, 43.60; H, 6.19; N, 18.75%).

The fractions from 16 to 24 yielded 409 mg (28%) of pure γ-Glu-His monohydrate; mp 205—207°C (decomp.); $[\alpha]_D^{25}$ +11.6° (*c* 2, water) (Found: C, 43.52; H, 6.12; N, 18.66%).

The authors wish to thank Mr. Toshiyasu Matsuo, Morishita Pharmaceutical Co., for his valuable technical assistance.

BULLETIN OF THE CHEMICAL SOCIETY OF JAPAN, VOL. 45, 1794—1797 (1972)

Chemical Constituents of *Alnus sieboldiana* (BETULACEAE). III. The Synthesis and Stereochemistry of Yashabushiketols

Yoshinori ASAKAWA

Department of Chemistry, Faculty of Science, Hiroshima University, Higashisenda-machi, Hiroshima

(Received August 30, 1971)

Dihydroyashabushiketol (**2**), isolated previously from the male flower of *Alnus sieboldiana*, has been synthesized by the condensation of benzaldehyde with acetylacetone, followed by hydrogenation. The absolute configuration at C_5 of yashabushiketol (**1**) and **2** has been identified as S. The geometry between the *trans* double bond and the carbonyl group in **1** was established to be *s-cis*. Eleven more minor components of a known aromatic compound were identified at the same time.

Preceding studies[1,2] of the male flower constituents of *Alnus sieboldiana* belonging to the Betulaceae family have shown the presence of two new ketols, yashabushiketol (**1**) and dihydroyashabushiketol (**2**), with the biosynthetically interesting C_6-C_7-C_6 skeleton and four new flavonoids, together with various phenylpropanoids. The present paper will describe the synthesis of **2**, the stereochemistry of **1** and **2**, and the isolation of other phenylpropanoids from the male flower of *A. sieboldiana*.

Results and Discussion

Synthesis of Dihydroyashabushiketol (2). In connection with the study of the biosynthesis of two new ketols, **1** and **2**, we have examined the synthesis of **2**. The reaction of benzaldehyde with a complex of acetylacetone and boron trioxide in the presence of triisopropyl borate and *n*-butylamine gave dicinnamoylmethane (**3**) in a good yield. The catalytic hydrogenation of **3** over platinum oxide afforded dihydroyashabushiketol (**2**) (the *dl* form of **2**), along with saturated diketone (**4**). The sodium borohydride reduction of the diketone (**4**) easily afforded diol (**5**), which has also been prepared from **2** by the same procedure. The oxidation of **2** with active manganese dioxide gave the diketone (**4**).

Stereochemistry of Yashabushiketol (1) and Dihydroyashabushiketol (2). The absolute configuration at C_5 of **1** and **2** was determined by applying the benzoate rule[3] and Horeau's asymmetric synthesis.[4] The benzoylation of **1** with benzoyl chloride and with 3,5-dinitrobenzoylchloride yielded the corresponding benzoates. The benzoate rule predicts that its benzoates would be more dextrorotatory if the configuration at C_5 had S. Actually, the difference in the molecular rotation ($[M]_{Benzoate}$—$[M]_{Alc.}$) between the benzoates and the ketol (**1**) was positive. It follows that the configuration at C_5 is S. This was corroborated by the asymmetric esterification employing α-phenylbutyric anhydride. The reaction of **1** with an excess of (±)-α-phenylbutyric anhydride resulted in recovery of (−)-α-phenylbutyric acid.

1) a) Y. Asakawa, F. Genjida, S. Hayashi, and T. Matsuura, *Tetrahedron Lett.*, **1969**, 3235. b) Y. Asakawa, This Bulletin, **43**, 575 (1970). c) Y. Asakawa, *ibid.*, **43**, 2223 (1970).

2) a) Y. Asakawa, F. Genjida, and T. Suga, *ibid.*, **44**, 297 (1971). b) Y. Asakawa, *ibid.*, **44**, (1971), in press.

3) J. H. Brewster, *Tetrahedron*, **13**, 106 (1961).

4) A. Horeau and H. B. Kagan, *ibid.*, **20**, 2431 (1964).

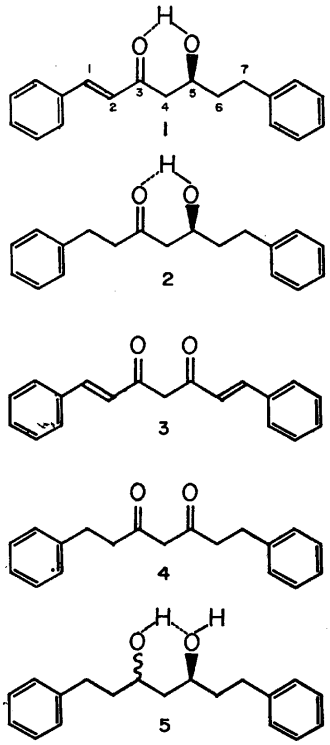

Fig. 1.

Hence, the configuration at C_5 may be deduced to be S. The configuration at C_5 of **2** was also established to be S by the method described above.

Yashabushiketol (**1**) may exist in two geometries, s-*cis* and s-*trans*, with respect to the C_2-C_3 single bond. An inspection of the molecular model predicted that the former form, with a planar zig-zag arrangement of the carbon chain, will be energetically favored over the latter. The infrared spectrum of **1** in nujol mull showed two intense carbonyl bands ($\nu_{C=O}$ 1703 cm^{-1} and $\nu_{C=O}$ 1678 cm^{-1}) and a more intense band of the *trans* ethylenic bond[5] ($\nu_{C=C}$ 1607 cm^{-1}). The arithmetical differences[6] in frequency between $\nu_{C=O}$ and $\nu_{C=C}$ are 96 cm^{-1} and 71 cm^{-1}. These data indicate that **1** is in the *s-cis* form. The infrared spectrum in the hydroxyl strechng region of **1** in carbon tetrachloride showed a concentration-independent band at 3520 cm^{-1} (ε, 32). This surely indicates the existence of an intramolecular hydrogen bonding between the hydroxyl group and the lone-pair electron on the carbonyl oxygen, thus supporting the special arrangement shown in Formula 1.

Previously-known Aromatic Compounds. The isolation of eleven minor components, benzaldehyde, γ-phenylpropyl acetate, cinnamyl acetate, coumarin, cinnamyl cinnamate, β-phenylethyl-β-phenylpropionate, methyl cinnamate, benzoic acid,[7] phenylacetic acid, β-phenylpropionic acid, and eugenol, was performed by a combination of column and preparative thin-layer chromatographies. All the compounds isolated were identified by direct comparisons (mixed mp, UV, IR, NMR and mass spectra) with authentic specimens. It is characteristic that almost all the compounds isolated from the male flower of *A. sieboldiana* carry one or two of the monosubstituted benzene-rings which would arise from shikimic acid. From the viewpoint of biosynthesis it is also interesting that the male flower of *A. sieboldiana* contains only benzaldehyde, whereas that of *A. pendula* contains only cinnamaldehyde.[8]

Experimental

All the melting points are uncorrected. The UV, IR, NMR, and mass spectra and the gas chromatograms were measured in the same manner as reported in the preceding paper.[1c] The optical rotations were measured on a Japan Spectroscopic Co., Ltd., automatically-recording spectropolarimeter, Model ORD/UV-5.

*Dicinnamoylmethane (**3**).* The preparation of dicinnamoylmethane was performed on one-tenth the scale of the Pabon's procedure[9]; 42% yield; mp 141—142°C (lit,[9] 140.5°C); λ_{max}^{EtOH} 235 nm (log ε, 3.41), 310 (3.48), 395 (4.04), 418 (3.87); ν_{max}^{Nujol} 1626 (CO-CH=COH), 1148, 1143, 980 (*trans* CH=CH), 878, 795, 723, 690 cm^{-1}; δ_{ppm} ($CDCl_3$) 5.82 (s, 1H), 6.11 (d, J=16 Hz, 2H), 7.42 (m, 10H), 7.67 (d, J=16 Hz, 2H); *m/e* 276 (M^+), 258 ($M-H_2O$), 248 (M–CO), 199, 171, 157, 145, 144, 131 (base), 117, 115, 103, 91, 77, 69, 51.

Found: C, 82.37; H, 5.81%. Calcd for $C_{19}H_{16}O_2$: C, 82.58; H, 5.84%.

*Hydrogenation of Dicinnamoylmethane (**3**).* Dicinnamoylmethane (**3**) (307 mg) was hydrogenated over a prereduced PtO_2 (68 mg) in methanol for 9 hr under ambient conditions. After the catalyst had been filtered off, the filtrate was evaporated *in vacuo*. The product showed two spots on tlc; it was subjected to preparative thin-layer chromatography, using a 4 : 1 mixture of *n*-hexane and ethyl acetate to give diketone (**4**) (197 mg) as yellow oil and dihydroyashabushiketol (**2**) (90 mg) mp 69—70.5°C (from *n*-hexane); $[\alpha]_D^{25}$ ±0° (*c* 1.6, in $CHCl_3$). The diketone (**4**) showed the following properties: λ_{max}^{EtOH} 272 (4.35), $\lambda_{max}^{n\text{-Hexane}}$ 279 (3.96), $\lambda_{max}^{n\text{-Hexane+NaOH}}$ 297 (4.25); $\nu_{max}^{Liq.}$ 3450, 3026, 1726, 1706, 1626, 1606, 1498, 1455, 751, 704; δ_{ppm} ($CDCl_3$) 2.32—3.08 (m), 3.45 (s, CO–CH$_2$–CO), 5.41 (s, CO–CH=C–), 7.22 (s, 10H); *m/e* 280 (M^+), 262 ($M-H_2O$), 175, 133, 105, 104, 91 (base), 77, 65, 51, 43, 39.

Found: C, 81.58; H, 7.10%. Calcd for $C_{19}H_{20}O_2$: C, 81.39; H, 7.19%.

*Reduction of Diketone **4** to Diol **5**.* Into a solution of **4** (140 mg) in dioxane–water (50 m*l*, 4 : 1 by volume) we stirred sodium borohydride (500 mg) dissolved in dioxane (25 m*l*), and then the mixture was allowed to stand overnight. The mixture was acidified with 1 N hydrochloric acid, and then the solvent was removed *in vacuo*. The residue, after water (10 m*l*) had been added, was extracted with chloroform. The removal of the solvent from the dried extract gave **5** as a colorless oil (130 mg): $[\alpha]_D^{25}$ ±0° (*c* 2.0, in $CHCl_3$); λ_{max}^{EtOH} 247 (2.47), 253 (2.59), 255 (2.59), 259 (2.66), 262 (2.68), 265 (2.56), 269 (2.60); $\nu_{max}^{Liq.}$ 3356, 1601, 1496, 1416, 1336, 1130, 746, 699; δ_{ppm} ($CDCl_3$) 1.30 (m,

5) R. Hirschman, S. C. Snaddy, Jr., C. F. Hiskey, and N. L. Wendler, *J. Amer. Chem. Soc.*, **76**, 4013 (1954); O. Wintersteiner and M. Moore, *ibid.*, **78**, 6193 (1956).

6) E. A. Braude and C. J. Timmons, *J. Chem. Soc.*, **1955**, 3766.

7) Extreme care was taken to avoid airing. However, there is a small possibility that benzoic acid was produced from benzaldehyde during the extraction procedures.

8) T. Suga, Y. Asakawa, and N. Iwata, unpublished data.

9) H. J. J. Pabon, *Rec. Trav. Chim.*, **83**, 379 (1964).

6H), 2.70 (m, 4H), 3.90 (s, 2 OH), 3.85 (quin. 2H, J=6 Hz), 7.23 (s, 10H); *m/e* 284 (M^+), 266 ($M-H_2O$), 248, 149, 91 (base), 77.

Found: C, 80.56; H, 8.59%. Calcd for $C_{19}H_{24}O_2$: C, 80.24; H, 8.51%.

*Reduction of Dihydroyashabushiketol (**2**) to Diol (**5**).* The reduction of **2** (62 mg) with sodium borohydride (250 mg) in the manner described in the preceding paragraph gave a yellow oil (48 mg): $[\alpha]_D^{25}$ +0.66 (*c* 2.6, in $CHCl_3$); $\nu_{max}^{CCl_4(0.0060\ mol)}$ 3665 (ε, 78), 3538 (ε, 20). This oil was identical in all respects to the **5** derived from the diketone (**4**).

*Oxidation of Dihydroyashabushiketol (**2**) to Diketone (**4**).* A solution of **2** (50 mg) in dry chloroform (20 m*l*) was stirred with activated manganese dioxide (0.920 g) at room temperature over a 5-day period. The mixture was filtered, and the precipitate was washed thoroughly with chloroform. The combined filtrate was evaporated *in vacuo* to give a yellow oil (15 mg) which was identical in all respects to **4**.

*The Benzoate of Yashabushiketol (**1**).* Into a solution of **1** (42 mg) in a mixture of dry benzene (1.5 m*l*) and dry pyridine (0.15 m*l*), we stirred benzoyl chloride (0.3 m*l*) at 0°C. The mixture, after having been allowed to stand overnight, was worked up as usual to give the benzoate (30 mg): mp 94—95°C (from *n*-hexane); $[M]_{Benzoate}$ +61.69; $[M]_{Benzoate}-[M]_{Alc.}=+6.42$; λ_{max}^{EtOH} 280 (3.49); ν_{max}^{Nujol} 1715, 1280, 740, 695; M^+ 384 ($C_{26}H_{24}O_3$).

*The 3,5-Dinitrobenzoate of Yashabushiketol (**1**).* The benzoylation was performed using 50 mg of **1**, 92 mg of 3,5-dinitrobenzoyl chloride, 25 m*l* of benzene, and 1.0 m*l* of pyridine in the same manner as above. The crude product was purified on TLC to give the benzoate as a pale yellow oil (77 mg): $[M]_{Benzoate}$+92.20; $[M]_{Benzoate}-[M]_{Alc.}=+36.93$; λ_{max}^{EtOH} 300 (3.98); $\nu_{max}^{Liq.}$ 1725, 1280, 755, 720, 708, M^+ 474 ($C_{26}H_{22}O_7N_2$).

*The Benzoate of Dihydroyashabushiketol (Natural Product) (**2**).* The method described above was employed using 80 mg of **2** and 50 mg of benzoylchloride; it gave the benzoate (105 mg): $[M]_{Benzoate}$+45.93; $[M]_{Benzoate}-[M]_{Alc.}=+38.16$; λ_{max}^{EtOH} 282 (2.08); $\nu_{max}^{Liq.}$ 1725, 1280, 1114, 755, 720, 708; M^+ 386 ($C_{26}H_{26}O_3$).

*The 3,5-Dinitrobenzoate of Dihydroyashabushiketol (**2**).* The benzoylation of **2** (50 mg) with 3,5-dinitrobenzoyl-chloride (92 mg) in dry pyridine gave the benzoate as a yellow oil (72 mg): $[M]_{Benzoate}$+73.56; $[M]_{Benzoate}-[M]_{Alc.}=+65.78$; λ_{max}^{EtOH} 295 (3.38); $\nu_{max}^{Liq.}$ 1730, 1450, 1354, 1285, 1170; M^+ 476 ($C_{26}H_{24}O_7N_2$).

The benzoates and 3,5-dinitrobenzoates of **1** and **2** described above are very unstable compounds. After having been allowed to stand at room temperature for 2 or 3 days, all the benzoates decomposed and showed two spots on tlc. All attempted elemental analyses of these benzoates failed to obtain satisfactory values.

*Reaction of Yashabushiketol (**1**) with α-Phenylbutyric anhydride.* A solution of **1** (2.14×10^{-4} mol) and α-phenylbutyric anhydride (5.83×10^{-4} mol), prepared by refluxing α-phenylbutyric acid with acetic anhydride, in pyridine (2.5 m*l*) was allowed to stand overnight. The excess anhydride was decomposed by adding water, and then the solution was allowed to stand 7 hr at room temperature. The solution was extracted with ether. The ether extract was washed successively with water, 5% sodium bicarbonate (10 m*l*×3), and water (three times). The combined aqueous extract was washed with chloroform and acidified with 1 N sulfuric acid. The acidified solution was extracted with chloroform, after which the chloroform extract was dried and evaporated. α-Phenylbutyric acid (96 mg) was recovered: $[\alpha]_D^{25}$ −3.12° (*c* 1.92, in benzene), theoretical[4] $[\alpha]_D=96.5°/2(2.71)-1=-21.5°$. The optical yield was, therefore, 3.12/21.5=14.5% (−).

The neutral fraction in the ether solution was washed thoroughly with water, 1 N sulfuric acid, and water successively. The removal of the solvent from the ether solution gave the ester (54 mg), which was then purified by tlc to give the pure ester (44 mg): λ_{max}^{EtOH} 300 (3.95); $\nu_{max}^{Liq.}$ 1725, 1168, 750, 701; M^+ 426.

Found: C, 81.20; H, 6.90%. Calcd for $C_{29}H_{30}O_3$: C, 81.66; H, 7.09%.

*Reaction of Dihydroyashabushiketol (**2**) with α-Phenylbutyric anhydride.* The method described above was employed, using **2** (3.3×10^{-4} mol) and α-phenylbutyric anhydride (1.01×10^{-3} mol). The recovered α-phenylbutyric acid weighed 209 mg: $[\alpha]_D^{25}$ −0.34° (*c* 2.90, in benzene); the optical yield was 1.5% (−). On the other hand, the ether extract was worked up as above to obtain the ester (64 mg): λ_{max}^{EtOH} 293 (2.47); $\nu_{max}^{Liq.}$ 1727, 1496, 1170, 746, 709; M^+ 428.

Found: C, 82.78; H, 7.46%. Calcd for $C_{29}H_{32}O_3$: C, 82.27; H, 7.53%.

Extraction and Isolation. The benzene extract (750 g) of the male flower of *A. sieboldiana* was extracted first with a saturated sodium bisulfite solution to isolate the aldehyde fraction (1.24 g), and then it was separated into a neutral fraction (50 g), an acidic fraction (8.0 g), and a phenolic fraction (8.4 g), as has been shown previously.[2b]

Benzaldehyde: The decomposition of the sodium bisulfite solution with 20% sodium hydroxide, followed by extraction with ether, yielded a pale yellow oil (1.24 g); this oil showed one peak on the gas chromatogram and one spot on tlc. The spectral data were completely identical with those of authentic benzaldehyde. The 2,4-dinitrophenylhydrazone derivative melted at 240—241°C.

γ-Phenylpropyl Acetate, β-Phenylethyl β-Phenylpropionate, Coumarin, Cinnamyl Acetate, Cinnamyl Cinnamate, and Methyl Cinnamate: After the isolation of the major components, β-phenylethyl cinnamate, pinostrobin, pinosylvin dimethyl ether and ketols, **1** and **2**, from the neutral fraction, the brown oil (845 mg) remaining unidentified was further chromatographed carefully on silica gel using a mixture of *n*-hexane and ethyl acetate. From the 19 : 1 (by volume) *n*-hexane - ethyl acetate fraction, a colorless oil (80 mg) was obtained. This oil was then subjected to preparative thin-layer chromatography to give γ-phenylpropyl acetate (18 mg) and β-phenylethyl β-phenylpropionate (24 mg). γ-Phenylpropyl acetate: λ_{max}^{EtOH} 260 (3.34); $\nu_{max}^{Liq.}$ 1735, 1240; δ_{ppm} ($CDCl_3$) 2.03 (s, 3H), 1.92 (q, J=8 Hz, 2H), 2.70 (t, J=8 Hz, 2H), 4.08 (t, J=8 Hz, 2H), 7.24 (s, 5H). β-Phenylethyl β-phenylpropionate: $\nu_{max}^{Liq.}$ 1735; δ_{ppm} ($CDCl_3$) 2.49 and 2.85 (t, J=7.5 and 1.5 Hz, A_2B_2, 4H, C_6H_5-C<u>H</u>$_2$-C<u>H</u>$_2$-CO), 2.81 (t, J=7.5 Hz, 2H, C_6H_5–C<u>H</u>$_2$–CH_2–O–), 4.18 (t, J=7.5 Hz, 2H, –CH_2–C<u>H</u>$_2$–O–), 7.11 (s, 10H); *m/e* 254 (M^+), 133, 105, 91 (base).

A pale yellow oil (500 mg) obtained from the 4 : 1 *n*-hexane - ethyl acetate fraction was further subjected to column chromatography on silica gel using a mixture of *n*-hexane, benzene, and ethyl acetate to give coumarin (10 mg), cinnamyl acetate (22 mg), cinnamyl cinnamate (100 mg), and methyl cinnamate (47 mg). Coumarin: mp 70—71°C; δ_{ppm} ($CDCl_3$) 6.42 (d, J=9 Hz, 1H), 7.00 (d, J=9 Hz, 1H), 7.41 (m, 4H). Cinnamyl acetate: λ_{max}^{EtOH} 250 (3.68); $\nu_{max}^{Liq.}$ 1735, 1240; δ_{ppm} ($CDCl_3$) 2.06 (s, 3H), 4.70 (d, J=6 Hz, 2H), 6.17 (d, J_{AB}=16 Hz, t, J_{BX}=6 Hz, 1H), 6.69 (d, J_{AB}=16 Hz, 1H), 7.33 (s, 5H). Cinnamyl cinnamate: mp 40—41°C; λ_{max}^{EtOH} 255 (4.09), 275 (4.13);

$\nu_{max}^{Liq.}$ 1710, 1635, 1450, 1165, 965; δ_{ppm} ($CDCl_3$) 4.84 (d, J_{BX}=6 Hz, 2H), 6.30 (d, J_{AB}=16 Hz, t, J_{BX}=6 Hz, 1H), 6.45 (d, J=16 Hz, 1H), 6.63 (d, J=16 Hz, 1H), 7.43 (m, 10H), 7.74 (d, J=16 Hz, 1H). The hydrolysis of the ester with an alcoholic potassium hydroxide solution gave cinnamic acid and cinnamyl alcohol. Methyl cinnamate: $\nu_{max}^{Liq.}$ 1712, 976; δ_{ppm} ($CDCl_3$) 3.82 (s, 3H), 6.45 (d, J=16 Hz, 1H), 7.49 (m, 5H), 7.78 (d, J=16 Hz, 1H).

Benzoic Acid, Phenylacetic Acid, and β-Phenylpropionic Acid. These acids were identified as their methyl esters. After the isolation of alnustinol (3,5,7-trihydroxy-6-methoxyflavanone) from the acidic fraction by crystallization, the combined filtrate was methylated with diazomethane. The main component of methyl cinnamate was removed by crystallization, and the residual oil (320 mg) was chromatographed on silica gel using a mixture of *n*-hexane, benzene, and ethyl acetate to give methyl benzoate (25 mg), methyl phenylacetate (8 mg), and methyl β-phenylpropionate (80 mg). Methyl benzoate: $\nu_{max}^{Liq.}$ 1740, 1257, 1161; δ_{ppm} ($CDCl_3$) 3.90 (s, 3H), 7.50 (m, 3H), 8.15 (m, 2H). Methyl phenylacetate: $\nu_{max}^{Liq.}$ 1725, 1274, 1109; δ_{ppm} ($CDCl_3$) 3.63 (s, 2H), 3.70 (s, 3H), 7.37 (s, 5H); *m/e* 150 (M^+), 91 (base). Methyl β-phenylpropionate: $\nu_{max}^{Liq.}$ 1740, 1169, 748; δ_{ppm} ($CDCl_3$) 3.77 (s, 3H), 2.82 (m, 4H), 7.28 (s, 5H); *m/e* 164 (M^+), 133, 105, 104 (base), 91.

Eugenol: After the isolation of flavonoids from the phenolic fraction by crystallization, the filtrate (60 mg) was converted into the trimethylsilyl derivative, which was then subjected to gas chromatography and tlc to identify eugenol.

The author wishes to express his hearty gratitude to Professor Kenji Fukui and Dr. Takayuki Suga of Hiroshima University for their guidance and encouragement.

BULLETIN OF THE CHEMICAL SOCIETY OF JAPAN, VOL. 45, 1797—1801 (1972)

Imidothiocarbonates. V.[1] Preparations and Properties of Novel Azomethine Ylides and Thiocarbonyl Ylides from Sulfur-contained Heterocycles

Yoshio Ueno and Makoto Okawara

Research Laboratory of Resources Utilization, Tokyo Institute of Technology, Ookayama, Meguro, Tokyo

(Received September 28, 1971)

Preparations and properties of some novel azomethine ylides and thiocarbonyl ylides containing 1,3-dithiolanium moiety have been studied. Azomethine ylides, **3a**, **b**, and **c**, were prepared by deprotonation of 2-(*N*-methyl-*N*-phenacyl)amino-(**2a**)), 2-(*N*-*p*-nitrobenzyl-*N*-methyl)amino-(**2b**), and 2-(*N*-carbethoxymethyl-*N*-methyl)-amino-1,3-dithiolanium salt (**2c**), respectively. Azomethine ylides **3a**, **b** reacted with benzaldehydes to give 1,3-dipolar cycloadducts which are new class of spiro orthocarbonates, otherwise it is difficult to obtain. Elimination of ethylene sulfide from the spiro orthocarbonates easily occurred to give thiocarbonyl compounds. In the absence of dipolarophiles, **3a** cyclized intramolecularly to give 1,3-oxazoline-2-thione derivative. Formation of the thiocarbonyl ylides by deproptonation of 2-phenacylthio-1,3-oxazolium and 2-*p*-bromophenacylthio-1,3-dithiolanium salts, and their different cyclization to spiro compounds were also studied. Reaction of thiocarbonyl ylides **16** with *p*-nitrobenzaldehyde afforded *p*-nitrochalcone. Mechanisms of these interesting reactions and their synthetic utility were discussed.

In continuation of our studies on iminodithiocarbonates, we have explored the formation of 2-(*N*,*N*-dialkylamino)-1,3-dithiolanium salts (**2**) from 2-methylimino-1,3-dithiolane (**1**) in high yield.[1] We consider here the possibility of the preparation of new azomethine ylides[2] (**3**) by deprotonation of the iminium salts **2**. It is expected that such an azomethine ylide may react with appropriate dipolarophiles (A=B) to yield spiro orthocarbonates. Moreover, such spiro orthocarbonates are expected to give heterocyclic thiocarbonyl compounds with a release of ethylene sulfide, because we have shown that spiro orthocarbonates containing 1,3-dithiolane or 1,3-oxathiolane ring, easily eliminate ethylene sulfide to produce thiocarbonyl or carbonyl compounds.[3,4]

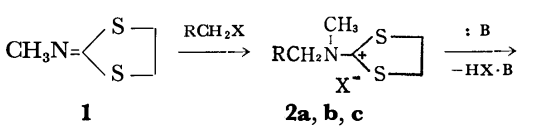

1 **2a, b, c**

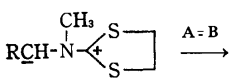

3a R=PhCO
b R=*p*-$NO_2C_6H_4$
c R=EtOCO

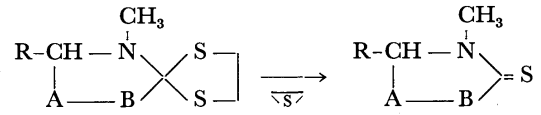

A compound in which the *N*-methyl group of ylide **3** is replaced by sulfur atom is also a new class of compounds named as thiocarbonyl ylide.[5]

1) Part III and Part IV of this series: Y. Ueno, T. Nakai, and M. Okawara, This Bulletin, **44**, 841, 1933 (1971).

2) The terms of azomethine ylide was used for the structure: $\rangle\overset{+}{C}-\overset{|}{\underset{}{N}}-\overset{-}{C}\langle \longleftrightarrow \rangle C=\overset{+}{N}-\overset{-}{C}\langle$ R. Huisgen, *Angew. Chem. Internat. Edit.*, **2**, 565 (1963).

3) Y. Ueno, T. Nakai, and M. Okawara, This Bulletin, **43**, 162 (1970).

4) Y. Ueno, T. Nakai, and M. Okawata, *ibid.*, **43**, 168 (1970).

5) The terms of thiocarbonyl ylide was used for the structure: $\rangle\overset{+}{C}-S-\overset{-}{C}\langle \longleftrightarrow \rangle C=\overset{+}{S}-\overset{-}{C}\langle$ R. M. Kellogg and S. Wassenaar, *Tetrahedron Lett.*, **1970**, 1987.

This paper describes the formation of novel azomethine ylides and thiocarbonyl ylides and their interesting reactions.

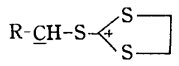

Results and Discussion

Formation of Azomethine Ylides and Their Properties. When 2-(*N*-methyl-*N*-phenacylamino)-1,3-dithiolanium perchlorate (**2a**) was treated with triethylamine in acetonitrile, 3-methyl-5-phenyl-1,3-oxazoline-2-thione (**4**) was obtained in quantitative yield. The infrared spectrum of **4** shows the characteristic bands at 3100 cm^{-1} (–CH=C〈), at 1492, 1462 cm^{-1} (thioamide II), and at 1210, 1195 cm^{-1} (thioamide I). The structure of **4** was further characterized by the formation of the oxazolium salt **5**. Thus methylation of **4** with dimethyl sulfate afforded 2-methylthio-3-methyl-5-phenyl-1,3-oxazolium perchlorate (**5**).

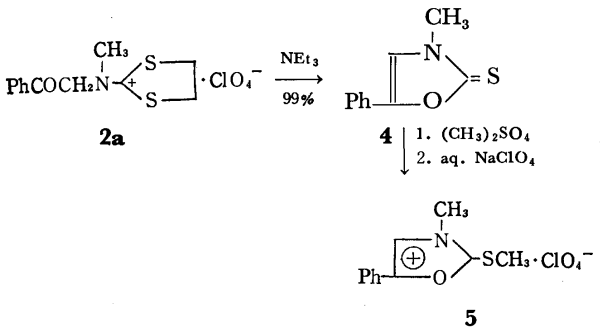

We postulate a mechanism involving prior formation of azomethine ylide **3a**, followed by intramolecular cyclization into spiro orthocarbonate **6**, and then elimination of ethylene sulfide, giving the final product **4** as formulated in Scheme 1.

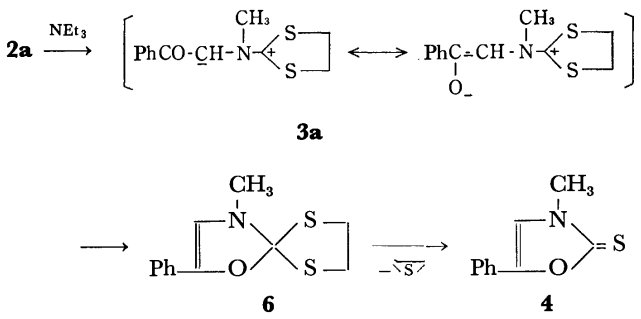

Scheme 1.

Attempts to trap the postulated intermediate, azomethine ylide **3a**, by 1,3-dipolar cycloaddition using phenyl isothiocyanate, carbon disulfide, or diethyl fumarate gave, instead, the intramolecular cyclization product **4** as the only isolated product. On the other hand, when *p*-nitrobenzaldehyde was employed as dipolarophile, 1,3-dipolar cycloaddition to the azomethine ylide **3a** occurred to give spiro orthocarbonate **7a** in 62% yield instead of **4**. Similarly benzaldehyde gave the cycloadduct **7b** in 55% yield.

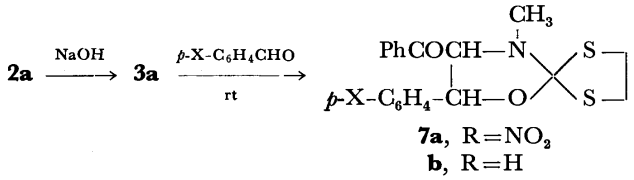

The infrared spectrum of **7a** shows a carbonyl vibrations at 1670 cm^{-1} those of nitro at 1520 and 1350 cm^{-1} and reveals the absence of thiocarbonyl group observed in the compound **4**.

Reactivities of the azomethine ylide **3a** towards dipolarophiles seem to be dependent upon that of the cationic part of **3a**. Thus we have explored that tri(hetero)substituted carbonium ions are greatly stabilized by nitrogen or sulfur atoms and that they have more than two reaction sites.[6] For example, it was shown that 2-(*N*,*N*-dimethylamino)-1,3-dithiolanium salt **8** reacts with various nucleophiles at two sites, A or B, and that whether the reactions take place at A or B, chiefly depends upon the nature of nucleophiles. In general, hard-nucleophiles (HO^-, RO^-) are most powerful to attack at A, whereas soft-nucleophiles (RS^-, $R_2NC(=S)S^-$) at B. Nitrogen-containing nucleophiles are intermediate between the two (aniline at A and triethylamine at B).

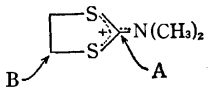

These facts are consistent with the observation that benzaldehydes (hard nucleophile) react with ylide **3a** to give 1,3-dipolar cycloaddition product **7**, and that the other dipolarophiles such as phenyl isothiocyanate, carbon disulfide, and diethyl fumarate (soft-nucleophiles) do not react.

When **2b** was treated with sodium hydride or potassium *t*-butoxide in dimethyl sulfoxide (DMSO) or acetonitrile, the reaction mixture turned to deep violet and returned to colorless by the addition of hydrochloric acid. This deep colored material seems to be the azomethine ylide **3b**. This was confirmed by 1,3-dipolar cycloaddition of *p*-nitrobenzaldehyde to the deep colored material. Thus a mixture of **2b** and *p*-nitrobenzaldehyde in DMSO was treated with sodium hydride at room temperature to produce the spiro orthocarbonate **9** in almost quantitative yield.

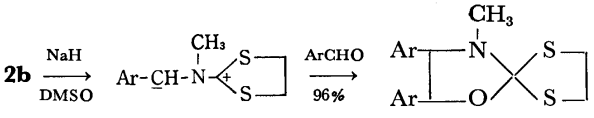

(Ar=*p*-$NO_2C_6H_4$)

The infrared spectrum of **9** reveals the presence of a nitro group (1530, 1350 cm^{-1}) and an etheral group (1062 cm^{-1}). The NMR spectrum in $(CD_3)_2SO$ exibits singlet peak at τ 7.70 (N-CH_3, 3H), triplet peaks at τ 7.60 (CH_2CH_2, 4H), a singlet peak at τ 7.06 (〉CH–

6) T. Nakai, Y. Ueno, and M. Okawara, This Bulletin, **43**, 3175 (1970).

CH〈, 2H), and two multiplet peaks centered at 2.45 and 1.75 (aromatic protons, each 4H). It was found that, as expected, the spiro orthocarbonate **9** afforded 1,3-oxazolidine-2-thione derivative **10** at the temperature above its melting point with a release of ethylene sulfide in quantitative yield.

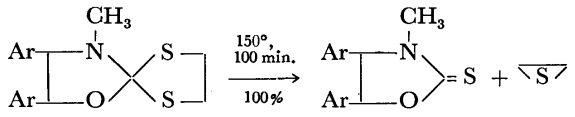

9 **10**

Acylation of the azomethine ylide **3b** with benzoyl chloride gave *C*-benzoylated product **11**, of which infrared spectrum shows the presence of a carbonyl group (1660 cm^{-1}). **11** was stable salt and recovered unchanged on heating at 180°C for 30 min.

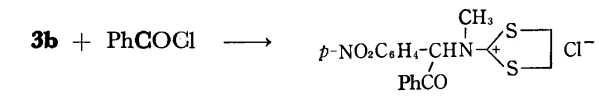

11

An attempt to cyclize the azomethine ylide **3c**, derived from the iminium salt **2c**, into spiro orthocarbonate in a similar manner as in the case of azomethine ylide **3a** failed. It was observed that only the hydrolysis of the salt **2c** by the water added after the reaction,

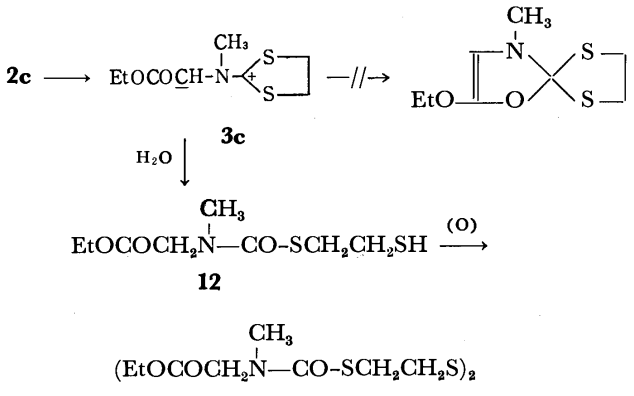

3c **12** **13**

and subsequent air-oxidation of the resulting mercaptan derivative **12** to disulfide **13**. The infrared spectrum of **13** reveals the presence of ester group (1750, 1200 cm^{-1}), and the amide carbonyl (1660 cm^{-1}), and the absence of thiol group. Similar hydrolysis of the iminium salt **8** into mercaptan or disulfide derivative has been reported.[7] No formation of spiro orthocarbonate from **3c** may be explained by the less reactivity of ester carbonyl towards carbonium ion in comparison with ketonic carbonyl of **3a**.

Formation of Thiocarbonyl Ylides and Their Properties. As described above, 1,3-oxazoline-2-thione **4** was easily alkylated to 2-methylthio-1,3-oxazolium salt **5** with deimethyl sulfate. When phenacyl bromide was employed in place of dimethyl sulfate, 2-phenacylthio-1,3-oxazolium salt **14** was obtained in 68% yield. Oxazolium salt **14** was expected to produce a new interesting thiocarbonyl ylide by deprotonation with base. Upon treatment of **14** with sodium hydride in DMSO at room temperature afforded 2-phenacylidene-3-methyl-5-phenyl-1,3-oxazoline **15** in 75% yield.

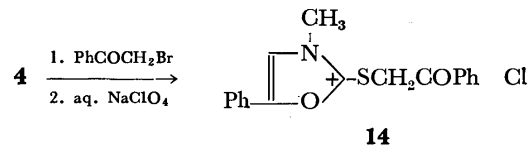

14

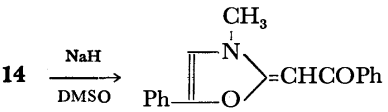

15

A possible reaction sequence for the formation of **15** was indicated in Scheme 2. Thus the thiocarbonyl ylide **16** derived from **14** cyclized into the thiirane derivative[8] **17**, instead to the five-membered ring as observed in azomethine ylide **3a**. The thiirane **17** afforded **15** with liberation of elemental sulfur.

On the other hand, it was found that the thiocarbonyl ylide **19**, derived from 2-(*p*-bromophenacylthio)-1,3-dithiolanium bromide,[9] cyclized into spiro orthocarbonate **20** instead to the thiirane derivative

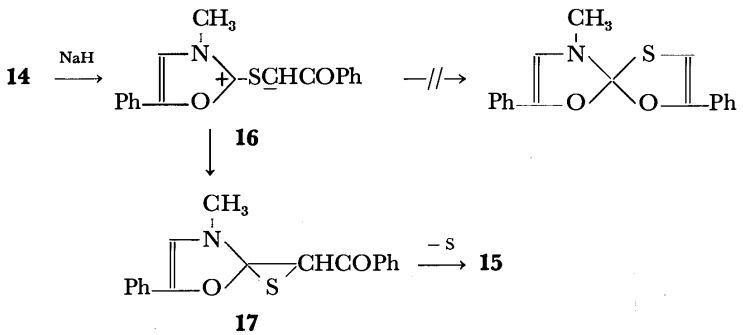

16 **17**

Scheme 2.

7) T. Nakai and M. Okawara, *ibid.*, **43**, 1864 (1970).

8) Takaku *et al.* reported the following reaction, in which thiirane derivative was postulated as intermediate to the isomerized product: $(Me_2N)_2\overset{+}{C}\text{–}SCH_2R\ X^- \xrightarrow{:B} (Me_2N)_2\overset{+}{C}\text{–}S\text{–}\overset{-}{C}HR$ **25** $\longrightarrow (Me_2N)_2C\text{—}CHR \xrightarrow{-O} (Me_2N)_2C{=}C(SH)R$, M. Takaku, S, Mitamura, and H. Nozaki, *Tetrahedron Lett.*, **1969**, 3651.

9) R. Mayer and K. Schafer, *J. Prakt. Chem.*, (4) **26**, 279 (1964).

21. The IR spectrum of **20** shows no absorption bands in carbonyl region. The NMR spectrum in CCl_4 exhibits a singlet peak at τ 6.46 (SCH_2-CH_2S, 4H), a singlet peak at τ 3.97 (CH=, 1H), and multiplet peaks centered at τ 2.65 (aromatic protons, 4H).

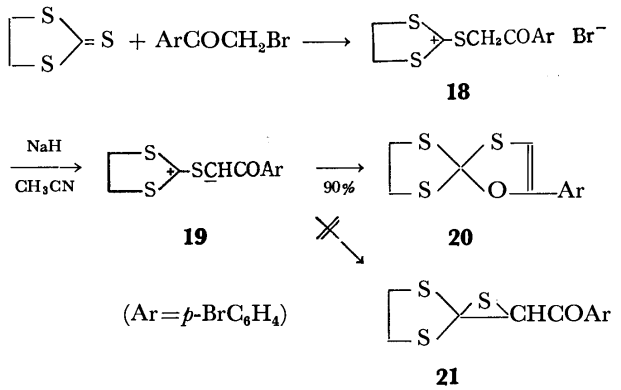

Finally, 1,3-dipolar cycloaddition of thiocarbonyl ylide **16** was undertaken. Thus **14** was treated with sodium hydroxide in the presence of *p*-nitrobenzaldehyde at room temperature to give *p*-nitrochalcone **24** in 85% yield.

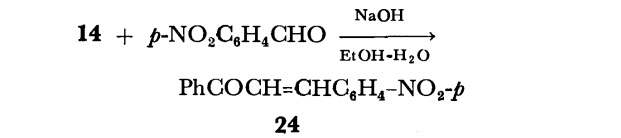

Facile elimination of thiirane from spiro orthocarbonates seems to be a general property of these types of compounds as observed above or as reported previously.[3,4] Moreover, it is well known that some kinds of thiiranes are quite readily decomposed to olefins with liberation of elemental sulfur. On the basis of these facts, a possible reaction mechanism may be illustrated in Scheme 3. Although the fate of the fragmented oxazolone group has not been established, the reaction seems to proceed *via* 1,3-dipolar cycloaddition of *p*-nitrobenzaldehyde to the thiocarbonyl ylide **16**, giving the spiro orthocarbonate **22**, which readily decomposes to the thiirane **23** and, possibly, the oxazolone derivative. The thiirane **23** finally decomposes to *p*-nitrochalcone **24** with liberation of elemental sulfur.

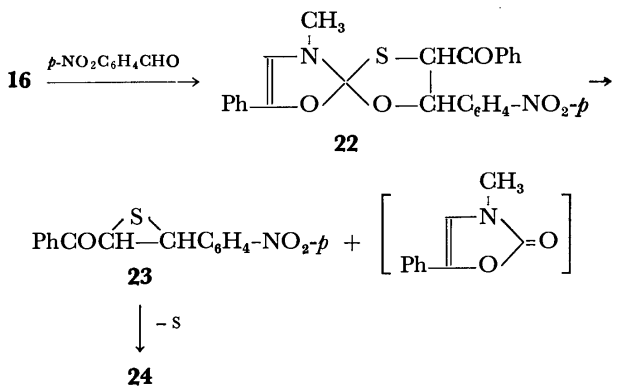

Scheme 3

Differences in the Intramolecular Cyclization Mode between Azomethine Ylides and Thiocarbonyl Ylides. It is quite interesting that two kinds of intramolecular cyclization modes of the azomethine and thiocarbonyl ylides were found. Thus the azomethine ylide **3a** and thiocarbonyl ylide **19** cyclized to five-membered ring at oxygen anion, whereas the thiocarbonyl ylide **16** cyclized to three-membered ring at carbanion as illustrated below.

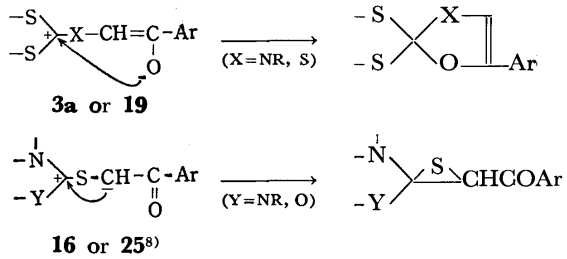

These differences can not be clearly explained at the present stage. However we assume that the formation of thiirane derivatives, which are sterically unfavorable because of their subsequent facile occurrence of elimination or isomerization[8] of sulfur atom, is related to the stabilization or carbanion by sulfur atom in thiocarbonyl ylides. Thus in contrast to the azomethine ylides, the larger contribution of the carbanion-structure is postulated in thiocarbonyl ylides, if in which the carbanion can be stabilized by vacant *d*-orbitals of bivalent sulfur atom. The cyclization at the carbanion to the thiirane derivatives seems to become feasible only in such a case.

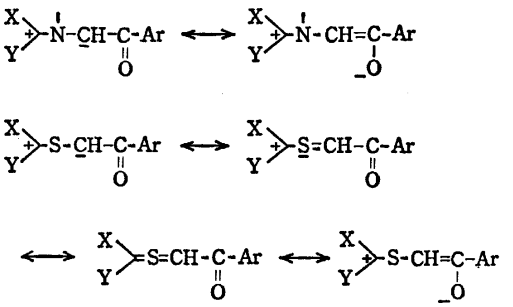

In thiocarbonyl ylide **19**, however, other factors seem to be operative for the cyclization.

Experimental

All the melting points were uncorrected. The IR spectra were recorded on Japan Optics JNL 4H-100 spectrometer using tetramethylsilane (TMS) as an internal standard. All experiments on ylides were carried out under nitrogen atmosphere.

Materials. 2-(*N*-Methyl-*N*-phenacyl)amino-(**2a**), 2-(*N*-*p*-nitrobenzyl-*N*-methyl)amino-(**2b**), and 2-(*N*-carbethoxymethyl-*N*-methyl)amino-1,3-dithiolanium salt (**2c**) were prepared from 2-methylimino-1,3-dithiolane (**1**) and corresponding alkyl bromides, respectively, as previously reported.[1]

Intramolecular Cyclization of Azomethine Ylide ***3a***. A mixture of 1.7 g (4.8 mmol) of 2-(*N*-methyl-*N*-phenacyl)-amino-1,3-dithiolanium perchlorate (**2a**) and 1 m*l* of triethylamine in 20 m*l* of acetonitrile was heated at 60°C for 5 hr. Addition of water, extraction with ether, drying with sodium sulfate, and then concentrating the etheral solution af-

forded 0.9 g (99%) of 3-methyl-5-phenyl-1,3-oxazoline-2-thione (4) : mp 140—141°C (recrystallized from acetonitrile ether)

Found: C, 62.41; H, 4.63; N, 7.32%. Calcd for $C_{10}H_9NOS$: C. 62.82; H, 4.75; N, 7.33%.

The compound **4** was also formed in quantitative yield when the salt **2a** was treated with sodium hydride in dioxane at room temperature for 0.5 hr. Under similar conditions **4** was obtained in almost the same yield even in the presence of the dipolarophiles such as phenyl isothiocyanate, carbon disulfide, or diethyl fumarate.

Methylation of 3-Methyl-5-phenyl-1,3-oxazoline-2-thione ***4***. A mixture of equimolar amount of **4** and dimethyl sulfate was heated at 60°C for 1 hr, followed by treatment with aqueous sodium perchlorate, afforded 2-methylthio-3-methyl-5-phenyl-1,3-oxazolium perchlorate (**5**) in 70% yield: mp 189—190°. IR 1080 cm^{-1} (ClO_4^-).

Found: C, 43.01; H, 3.75; N, 4.47%. Calcd for $C_{11}H_{12}NO_5SCl$: C, 43.22; H, 3.96; N, 4.58%.

Reaction of Azomethine Ylide ***3a*** *with Benzaldehydes.*

A. p-*Nitrobenzaldehyde*: To a mixture of 1.3 g (3.7 mmol) of the 1,3-dithiolanium salt **2a** and 1 g (6.6 mmol) of *p*-nitrobenzaldehyde in 80 m*l* of ethanol and 40 m*l* of water, was added with stirring 0.36 m*l* of 10 N aqueous sodium hydroxide solution. After about 30 min, white solid precipitated out was collected by filtration. Recrystallization from ethanol-acetone solution afforded 0.9 g (62%) of the spiro orthocarbonate **7a** : mp 132—133°C; IR, 1670 cm^{-1} (C=O), 1520, 1350 cm^{-1} (NO_2).

Found: C, 56.44; H, 4.43; N, 6.61%. Calcd for $C_{19}H_{18}N_2O_4S_2$: C, 56.71; H, 4.51; N, 6.96%.

B. Benzaldehyde: Similarly, **3a** reacted with benzaldehyde to give the spiro orthocarbonate **7b** in 54% yield: mp 84—85°C (recrystallized from ether): IR 1690 cm^{-1} (C=O).

Found: N, 3.96%. Calcd for $C_{19}H_{19}NO_2S_2$: N, 3.92%.

Reaction of the Azomethine Ylide ***3b*** *with* p-*Nitrobenzaldehyde.* To a mixture of 0.7 g (2 mmol) of 1,3-dithiolanium bromide **2b** and 0.3 g (2 mmol) of *p*-nitrobenzaldehyde in 10 m*l* of DMSO was added 0.1 g of 50% sodium hydride at room temperature. The reaction mixture turned to deep violet with evolution of hydrogen. The reaction mixture was stirred at room temperature for 2 hr and then poured into 50 m*l* of water to give 0.8 g (96%) of the cycloadduct **9** : mp 142—143°C (recrystallized from ethyl acetate); IR 1530, 1350 cm^{-1} (NO_2).

Found: C, 51.17; H, 3.99; N, 9.64%. Calcd for $C_{16}H_{13}N_3O_5S$: C, 51.15; H, 4.09; N, 10.02%.

Pyrolysis of the Spiro Orthocarbonate ***9***. Pyrolysis of **9** (1 g) at 150—160°C for 15 min. gave 0.85 g (100%) of 3-methyl-4,5-di(*p*-nitrophenyl)-1,3-oxazolidine-2-thione (10): mp 198—199°C (recrystallized from boiling acetone); IR 1505 (thioamide), 1530, 1350 cm^{-1} (NO_2).

Found: C, 53.80; H, 3.48; N, 11.43%. Calcd for $C_{16}H_{13}N_3O_5S$: C, 53.48; H, 3.65; N, 11.70%.

Reaction of the Azomethine Ylide ***3b*** *with Benzoyl Chloride.* *C*-Benzoylated product **11** was isolated in 21% yield in the reaction of the ylide **3b** with benzoyl choride in acetonitrile at room temperature for 3 hr: mp 80—81°C (recrystallized from methanol); IR 1660 cm^{-1} (C=O).

Found: C, 54.94; H, 4.62; N, 6.94; S, 16.59%. Calcd for $C_{18}H_{17}ClN_2O_3S_2$: C, 55.04; H, 4.36; N, 7.13; S, 16.29%.

Hydrolysis of the Azomethine Ylide ***3c***. A solution of 2.8 g (9.9 mmol) of the 1,3-dithiolanium perchlorate **2c** in 10 m*l* of acetonitrile was treated with 4 m*l* of triethylamine at 60°C for 4 hr. Water was added to the reaction mixture and extracted with ether, drying with sodium sulfate and evaporation of the solvent and trituration of the residue with a small amount of ether - *n*-hexane afforded 1 g (43%) of disulfide **13**: mp 75—76°C (recrystallized from ether); IR 1750 (ester C=O), 1660 (amide C=O), and 1200 cm^{-1} (C–O–C).

Found; C, 41.25; H, 6.08; N, 5.87%. Calcd for $C_{16}H_{28}N_2O_6S_4$: C, 40.67; H, 5.95; N, 5.95%.

Alkylation of 3-Methyl-5-phenyl-1,3-oxazoline-2-thione ***4*** *with Phenacyl Bromide.* A mixture of 2.9 g (15 mmol) of **4** and 3 g (15 mmol) of phenacyl bromide in 30 m*l* of tetrahydrofuran (THF) was allowed to stand at room temperature for 2 days. Treatment of the reaction mixture with aqueous sodium perchlorate solution gave 4.26 g (68%) of 2-phenacylthio-3-methyl-5-phenyl-1,3-oxazolium perchlorate **14**: mp 208—209°C (d.) (recrystallized from acetonitrile); IR 1680 cm^{-1} (C=O).

Found; C, 53.39; H, 3.90; N, 3.58%. Calcd for $C_{18}H_{16}ClNO_6S$: C, 52.76; H, 3.94; N, 3.42%.

Formation of 2-Phenacylidene-1,3-oxazoline ***15***. A solution of 1.0 g (2.5 mmol) of oxazolium salt **14** in 10 m*l* of DMSO was treated with 0.12 g of 50% sodium hydride at room temperature. The reaction mixture turned to red with evolution of hydrogen. After standing at room temperature over one night, the mixture was poured into excess water to give 0.5 g (75%) of 2-phenacylidene-3-methyl-5-phenyl-1,3-oxazoline **15**: mp 196—197°C (d). (recrystallized from acetone); IR 1530 cm^{-1} (C=O); NMR ($CDCl_3$) τ 6.65 (s, 3H, *N*-CH_3), τ 4.55 (s, 1H, –CH=), τ 3.21 (s, 1H, –CH=), and τ 2.4 (m, 10H, phenyl protons).

Found: C, 76.95; H, 5.10; N, 4.78%. Calcd for $C_{18}H_{15}NO_2$: C, 77.96; H, 5.45; N, 5.05%.

Intramolecular Cyclization of the Thiocarbonyl Ylide ***19***. To a suspension of 1.24 g (3 mmol) of 2-(*p*-bromophenacylthio)-1,3-dithiolanium bromide (prepared by the method of Mayer[9]) in 40 m*l* of acetonitrile, was added 0.2 g of 50% sodium hydride. The reaction mixture turned to reddish-brown, was stirred at room temperature for 3 hr and then was poured into water (*ca.* 500 m*l*) with stirring to give 0.9 g (90%) of spiro orthocarbonate **20**; mp 85—86°C (d.) (recrystallized from n-hexane–ether).

Found: C, 39.84; H, 2.87%. Calcd for $C_{11}H_9BrOS_3$: C, 39.66; H, 2.72%.

The NMR spectral data of **20** was described in the text.

Reaction of Thiocarbonyl Ylide **16** *with p-Nitrobenzaldehyde.* To a suspension of 0.8 g (2 mmol) of 14 and 0.4 g (2.6 mmol) of *p*-nitrobenzaldehyde in 70 m*l* of water and 50 m*l* of ethanol, was added 0.2 m*l* of aqueous solution of 10 N sodium hydroxide. The reaction mixture turned to orange-brown and deposited the brown precipitates, which were collected by filtration after 2 hr. Recrystallization from ether - ethyl acetate afforded yellowish-brown solid **24** (85): mp 162.0—162.5°C (lit,[10] 162.5°); IR 1655 cm^{-1} (C=O).

Found: C, 70.85; H, 4.14; N, 5.33%. Calcd for $C_{15}H_{11}NO_3$: C, 71.14; H, 4.37; N, 5.53%.

10) H. Wieland, *Ber.*, **37**, 1149 (1904).

Studies on Stable Free Radicals. X.[1] Photolysis of Hindered *N*-Chloroamines

Toshimasa TODA, Eiko MORI, Hideo HORIUCHI, and Keisuke MURAYAMA
Central Research Laboratories, Sankyo Co., Ltd., Shinagawa-ku, Tokyo

(Received October 5, 1971)

Photolysis of the hindered *N*-Chloroamines, 1-chloro-2,2,6,6-tetramethyl-4-oxopiperidine (IIa), 1-chloro-2,2,6,6-tetramethylpiperidine (IIb), and 1-chloro-2,2,5,5-tetramethyl-4-oxoimidazolidine (IIc), in benzene solution were carried out in an ESR spectrometer cavity. The ESR spectra of the corresponding amino radicals IIIa, IIIb, and IIIc were observed in evacuated solutions. In solutions containing oxygen, it was found that amino radicals IIIb and IIIc readily reacted with oxygen to give the corresponding stable nitroxide radicals IVb and IVc, from the shapes of spectra and *g*-values. Amino radical IIIa did not react with oxygen. Although the amino radicals could not be isolated, their formation was confirmed by the isolation of a coupling product with a benzyl radical generated from dibenzylmercury.

Although syntheses and studies of the properties of stable nitroxide radicals have been carried out extensively,[2] stable amino radicals which can be isolated, analyzed and presented for a long time are scarcely known except for the diphenylpicrylhydrazyl and verdazyl radicals,[3] whose stability seems to result from the delocalization of the unpaired electron. The ESR spectra of diaryl amino radicals generated from corresponding hydrazines by pyrolysis in solution can be observed even at high temperatures,[4] but those of dialkyl amino radicals with no conjugated system for the unpaired electron, obtained by photolysis of tetraalkyltetrazenes in solution can be detected only at low temperatures.[5]

It has been reported that dialkyl amino radicals are relatively poor dehydrogenating agents, *e.g.*, dimethylamino radicals give dimethylamine and *N*-methylformaldimine by disproportionation at high temperatures.[6]

$$2\cdot Me_2N\cdot \rightarrow Me_2NH + CH_2 = NMe$$

Thus, a hindered amino radical lacking hydrogen on the α-carbon of the radical group is expected to be more stable than a dimethylamino radical.

Sholle *et al.* succeeded in observing the ESR spectrum of 2,2,6,6-tetramethyl-4-oxo-1-piperidyl radical (IIIa) at room temperature, but it was also unstable.[7]

Although this amino radical has no hydrogen on the α-carbons of the radical group, the hydrogens at the α-positions of the keto group in piperidine ring are easily abstracted.[8]

We have prepared hindered *N*-chloroamines containing no easily abstracted hydrogen and observed the ESR spectra of the corresponding amino radicals generated directly by photolysis of the *N*-chloroamines in a cavity of the ESR spectrometer. The amino radicals thus obtained were sensitive to oxygen and gave the corresponding stable nitroxide radicals.

Results and Discussion

We prepared 1-chloro-2,2,6,6-tetramethyl-4-oxopiperidine (IIa) by the reaction of the corresponding amine (Ia) with sodium hypochlorite,[9] but IIa was unstable. On keeping it to stand 2,2,6,6-tetramethyl-4-oxopiperidine hydrochloride (Ia′) separated as a precipitate.

Formation of Ia′ is plausible, if IIa decomposes into amino radical IIIa and Cl· by homolysis, and both radicals abstract hydrogens from keto α-methylene group in IIa or IIIa to give amine (Ia) hydrogen chloride. The assumption seems reasonable from the consideration that 2,2,6,6-tetramethyl-4-oxopiperidine-1-oxyl (IVa) abstracted hydrogens from keto α-methylene group of IVa to give 1-hydroxy-2,2,6,6-tetramethyl-4-oxopiperidine and phorone under reflux in benzene, while 2,2,6,6-tetramethylpiperidine-1-oxyl (IVb) was recovered unchanged under the same reaction conditions.[8]

We therefore prepared 1-chloro-2,2,6,6-tetramethylpiperidine (IIb) and 1-chloro-2,2,5,5-tetramethyl-4-oxoimidazolidine (IIc) which have no ketonic α-methylene hydrogens, by the reaction of these amines with sodium hypochlorite. Chloroamines IIb and IIc were more stable than IIa.

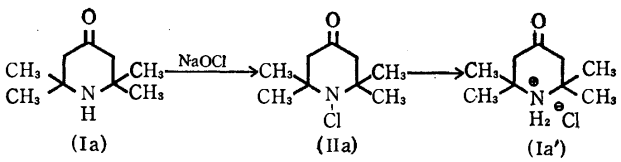

(Ia) (IIa) (Ia′)

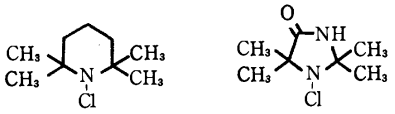

(IIb) (IIc)

1) Part IX: Ref. 16.

2) a) A. R. Forrester, J. M. Hay, and R. H. Thomson, "Organic Chemistry of Stable Free Radicals," Academic Press, New York, N. Y. (1968), pp. 180—238. b) E. G. Rozantsev, "Free Nitroxyl Radicals" Plenum Press, New York, N. Y. (1970), Translated from Russian.

3) R. Kuhn and H. Trischmann, *Angew Chem.*, **75**, 294 (1963).

4) P. H. H. Fischer and F. A. Neugebauer, *Chem. Ber.*, **98**, 844 (1965).

5) W. C. Danen and T. T. Kensler, *J. Amer. Chem. Soc.*, **92**, 5235 (1970).

6) D. Mackay and W. A. Waters, *J. Chem. Soc. C*, **1966**, 813.

7) V. Sholle, E. G. Rozantsev, A. I. Prokof'ev, and S. P. Solodovnikov, *Izv. Akad. Nauk SSSR, Ser. Khim.*, **1967**, 2504.

8) K. Murayama and T. Yoshioka, This Bulletin, **42**, 2307 (1969).

9) G. H. Coleman, *J. Amer. Chem. Soc.*, **55**, 3001 (1933).

The ESR spectra of the radicals generated directly from the chloroamines by photolysis in an ESR spectrometer cavity were recorded at room temperature under two conditions, *viz.*, in the presence and absence of oxygen.

Photolysis of Chloroamine IIa. The radical generated by UV irradiation of IIa in evacuated benzene solution gave the spectrum shown in Fig. 1a. Triplet lines, due to the interaction of a ^{14}N nucleus and supplementary splitting of each component of the triplet caused by the interaction with 12 protons of four methyl substituents in amino radical IIIa, were observed. The radicals generated by UV irradiation of IIa in benzene (containing oxygen) and in toluene (containing or not containing oxygen), gave the same spectrum as that of Fig. 1a. After cessation of UV irradiation, the spectra remained observable for a certain period and then disappeared gradually.

Photolysis of Chloroamine IIb. The radical generated by photolysis of IIb in an evacuated benzene solution gave the spectrum shown in Fig. 1b. Supplementary splittings resulting from 12 protons of four methyl substituents in amino radical IIIb were observed. The spectrum disappeared immediately when UV irradiation was terminated. In an evacuated toluene solution, photolysis of IIb gave no spectrum.

The spectrum of the radical generated by photolysis of IIb in benzene (containing oxygen) is given in Fig. 2. Only triplet lines due to a ^{14}N nucleus were observed. The spectrum remained observable for a long time after cessation of UV irradiation. In toluene (containing oxygen), photolysis of IIb gave a spectrum of triplet lines similar to that in Fig. 2.

Fig. 2. ESR spectrum of Nitroxide Radical IVb generated by the photolysis of IIb in undegassed benzene solution at room temperature.

Photolysis of Chloroamine IIc. The spectrum of the radical obtained from IIc in an evacuated benzene solution is shown in Fig. 1c. Triplet lines due to a ^{14}N nucleus and further splittings caused by the interaction with 12 protons of four methyl substituents in the amino radical IIIc were observed. The interaction with another ^{14}N at the 3-position in IIIc was not observed (Fig. 1c). When UV irradiation was stopped, the spectrum as well as that given in Fig. 1b disappeared immediately. No spectrum was observed in an evacuated toluene solution. The spectra of the radicals generated from IIc in benzene and in toluene (each containing oxygen) gave triplet lines as the spectrum in Fig. 2.

The splitting constants and *g*-values of the radicals obtained in this study were determined from the spectra and are listed in Table 1.

The ESR spectra of the corresponding nitroxide radicals IVa,[10] IVb[10], and IVc[11] were also measured. Each spectrum showed triplet lines as in Fig. 2. Values for their splitting constants and *g*-values are listed in Table 2.

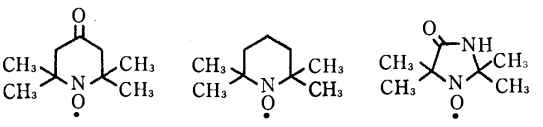

(IVa) (IVb) (IVc)

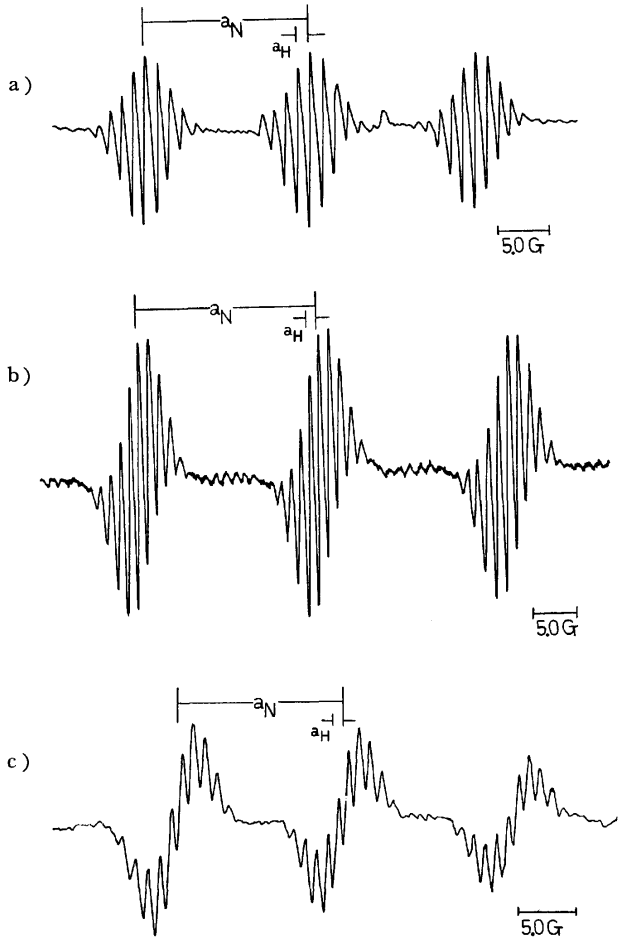

Fig. 1. ESR spectra of Amino Radicals genrated by the photolysis of *N*-chloroamines in degassed benzene solution at room temperature: a) from IIa. b) from IIb. c) from IIc.

10) E. G. Rozantsev and M. B. Neiman, *Tetrahedron*, **20**, 131 (1964).

11) T. Toda, S. Morimura, E. Mori, H. Horiuchi, and K. Murayama, This Bulletin, **44**, 3445 (1971).

Table 1. Values of hyperfine splitting constants and g-values of the radicals generated by photolysis on N-chloroamines[a]

Chloro-amine	Amino radical[b]			Nitroxide radical[c]		
	a_N[d]	a_H[d]	g-value[e]	a_N[d]	a_H[d]	g-value[e]
IIa	15.0	1.2	2.0027	15.0[g]	1.2[g]	2.0043[g]
IIb	14.3	0.78	2.0041	15.0	f)	2.0056
IIc	14.3	1.2	2.0038	14.0	f)	2.0053

a): measured in benzene solution at room temperature. b): in degassed solution. c): in undegassed solution. d): unit in gauss. accuracy ±0.1 gauss. e): accuracy ±0.0001. f): not resolved. g): corresponding amino radical.

Table 2. The values of hyperfine splitting constants and g-values of the nitroxide radicals[a]

Radical	a_N[b]	a_H	g-value[c]
IVa	14.3	d)	2.0055
IVb	15.0	d)	2.0056
IVc	14.0	d)	2.0052

a): measured in benzene at room temperature. The two values obtained in degassed and undegassed solutions were the same. b): unit in gauss. accuracy ±0.1 gauss. c): accuracy ±0.0001. d): not resolved.

The radicals obtained in the absence of oxygen appear to be amino radicals IIIa, IIIb, and IIIc from the following considerations.

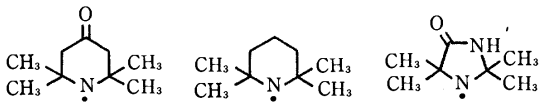

(IIIa) (IIIb) (IIIc)

Supplementary splittings were observed besides the triplet lines in each ESR spectrum as shown in Fig. 1 a-c, while only triplet lines were observed for the corresponding nitroxide radicals. Values for the coupling constants of a ^{14}N nucleus in the amino radicals IIIa and IIIc are larger than those for the corresponding nitroxide radicals (except for radical IIIb). This can be accounted for by the consideration that the density of each unpaired electron is almost entirely localized on the nitrogen atom, while in the corresponding nitroxide radical, each unpaired electron can be delocalized, $>N-O\cdot \leftrightarrow >\overset{\oplus}{N}-\overset{\ominus}{O}$.[12] g-Values for the amino radicals are smaller than those for the corresponding nitroxide radical as shown in Tables 1 and 2. This might be due to the difference in the spin-orbit coupling constants and has been pointed out in the cases of the di-p-tolyl-amino radical[4] and the di-p-tolyl nitroxide radical.[13]

In the presence of oxygen, the radicals obtained from IIb and IIc appear to be nitroxide radicals IVb and IVc, because splittings resulting from protons of the methyl substituents in these compounds were not observed in the ESR spectra, and g-values agreed with those of the corresponding nitroxide radicals. The radicals obtained from IIa in benzene or in toluene (each containing or not containing oxygen) appear to be amino radical IIIa, because their ESR spectra agreed with the spectrum of amino radical IIIa as shown in Fig. 1a.

The following experiments were carried out in order to confirm the formation of the amino radical and the nitroxide radical in photolysis of the chloroamine.

We obtained 1-benzyl-2,2,6,6-tetramethylpiperidine (V) by the photolysis of a mixture of IIb and dibenzylmercury[14] in benzene with bubbling argon gas. The reaction did not proceed in dark. Photodecomposition of IIb in benzene with bubbling oxygen gas gave 2,2,6,6-tetramethylpiperidine-1-oxyl (IVb) and 2,2,6,6-tetramethylpiperidine hydrochloride (Ib').

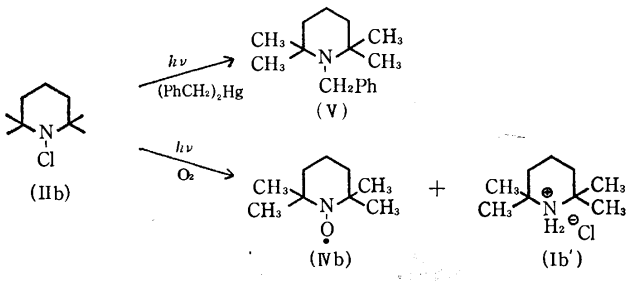

(IIb) (V) (IVb) (Ib')

Thus, the photolysis of the hindered N-chloroamine would proceed as shown in Chart 1.

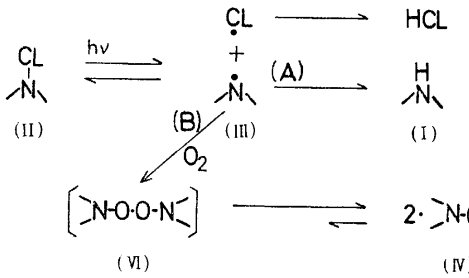

(II) (III) (I) (VI) (IV)

Chart 1

Processes A and B are considered to be competitive reactions for the following reasons. (1) the photodecomposition of IIb in benzene with bubbling oxygen gas gave nitroxide radical IVb and salt Ib'; and (2) no ESR spectra were observed in the photolyses of IIb and IIc in evacuated toluene solutions and the radicals obtained from IIb and IIc in toluene containing oxygen were the corresponding nitroxide radicals IVb and IVc, respectively.

Amino radical IIIa does not react with oxygen and would mainly abstract hydrogens to give corresponding amine Ia, because the radical obtained by photolysis of IIa even in the presence of oxygen was the amino radical IIIa. Salt Ia' was obtained on keeping IIa to stand.

From the fact that amino radicals IIIb and IIIc are converted into nitroxide radicals IVb and IVc in the presence of oxygen, it seems reasonable to assume

12) see Ref. 1b. p. 127.

13) F. A. Neugebauer and P. H. H. Fischer, *Z. Naturforsch.* **19a**, 1514 (1964).

14) W. J. Pope and C. S. Gilson, *J. Chem. Soc.*, **101**, 735 (1912).

the existence of peroxide (VI), precursor of the nitroxide radical as shown in Chart 1. Such a peroxide has been suggested in the photolysis of perfluoro-*N*-fluoropiperidine.[15] We consider that there may be an equilibrium between peroxide VI and nitroxide radical IV in solution[16], but the equilibrium lies far on the side of the radical.

The results suggest that even hindered amino radicals cannot be isolated, because they are sensitive towards oxygen to give the corresponding nitroxide radicals and readily abstract a hydrogen from media or another radical to give the amines, even though these radicals have no hydrogen on the α-carbon in the radical group.

Table 1 shows that the nitrogen coupling constant of IIIb is smaller than that of the corresponding nitroxide radical IVb. This seems to be correlated with the result that amino radical IIIa does not react with oxygen, which would be caused by the effect of 4-oxo group in piperidine ring.

Experimental

Melting points and boiling points are uncorrected. IR spectra were determined by means of Nujol mulls and liquid films. NMR spectra were obtained with a Varian A-60 NMR spectrometer using tetramethylsilane as an internal standard at 32°C. Mass spectra were obtained with a JEOL-JMS-OIS spectrometer at 75 eV.

ESR Measurements. ESR spectra were recorded on a Hitachi MES 4001 type X-band spectrometer employing 100 kHz modulation at room temperature. Degassed samples were prepared in the usual manner. Samples containing *ca.* 5% of dissolved *N*-chloroamine were irradiated with an USIO projector equipped with xenon 2 kw lamp. Splitting constants and *g*-values were measured relative to the aqueous solution of Fremy's salt.

Preparation of N-Chloroamines. The solution of aqueous sodium hypochlorite was prepared by passing chlorine gas (24 g) into a cold solution of sodium hydroxide (36 g) in 300m*l* of water at 0°C.[9]

1-Chloro-2,2,6,6-tetramethyl-4-oxopiperidine (IIa). To a stirred solution of 31.0 g (0.2 mml) of 2,2,6,6-tetramethyl-4-oxopiperidine (Ia)[6,17] and 20 g of aqueous solution of hydrogen chloride (35%) in 200 m*l* of water was added slowly 250 m*l* of aqueous sodium hypochlorite at 0—5°C. After the addition was completed, stirring was continued for 10 min at 0—5°C. The solution was shaken with 300 m*l* of ether. The ether layer was dried over sodium sulfate and evaporated under reduced pressure at room temperature. The residual oil was distilled to give 19.0 g (50.0%) of IIa: bp 63—64°C/0.3 mmHg. Found: C, 56.80; H, 8.61; N, 7.34; Cl, 18.62%. Calcd for $C_9H_{16}ONCl$: C, 56.99; H, 8.50; N, 7.38; Cl, 18.69%. IR(cm^{-1}): $\nu_{C=O}$ 1728. 2,2,6,6-Tetramethyl-4-oxopiperidine hydrochloride (Ia') was precipitated from the distilled oil on standing at room temperature. This was confirmed by comparison of the melting point and IR spectrum with those of the authentic sample prepared by the reaction of Ia with hydrogen chloride in ethanol. Recrystallization from ethanol gave a pure sample: mp 197°C (decomposition). Found: C, 56.41; H, 9.45; N, 7.33; Cl, 18.46%. Calcd for $C_9H_{18}ONCl$: C, 56.39; H, 9.47; N, 7.31; Cl, 18.49%.

1-Chloro-2,2,6,6-tetramethylpiperidine (IIb). In the same way as mentioned above, 34.0 g (96.5%) of IIb was obtained from 28.0 g (0.2 mml) of 2,2,6,6-tetramethylpiperidine (Ib)[10]: bp 65°C/7 mmHg. Found: C, 61.52; H, 10.34; N, 8.23; Cl, 19.69%. Calcd for $C_9H_{18}NCl$: C, 61.52; H, 10.34; N, 8.23; Cl, 19.69%. Calcd for $C_9H_{18}NCl$: C, 61.52; H, 10.32; N, 7.97; Cl, 20.18%. NMR (τ) (in CCl_4): 8.41, broad (6H). 8.80, siglet (12H).

1-Chloro-2,2,5,5-tetramethyl-4-oxoimidazolidine (IIc). To a stirred solution of 1.4 g (10 mmol) of 2,2,5,5-tetramethyl-4-oxoimidazolidine (Ic)[11] in 20 m*l* of water was added slowly 20 m*l* of aquoeus sodium hypochlorite at 0—5°C. The solution was stirred for additional 20 min at 0—5°C, and extracted with 100 m*l* of ether. The ethereal solution was dried over sodium sulfate and evaporated under reduced pressure to give 1.7 g of IIc. Recrystallization from benzene gave an analytically pure sample: mp 153—154°C. Found: C, 48.06; H, 7.66; N, 15.83; Cl, 20.05%. Calcd for $C_7H_{13}ON_2Cl$: C, 47.60; H, 7.42; N, 15.86; Cl, 20.07%. IR(cm^{-1}): $\nu_{C=O}$ 1678 and 1730, ν_{NH} 3150.

Reaction of IIb. a). A solution of 7.75 g (44 mmol) of IIb and 8.45 g (22 mmol) of dibenzylmercury[14] in 170 m*l* of dry benzene with bubbling argon gas was irradiated with a high pressure mercury lamp (Hanovia, 450 W) for 8 hr at 0—5°C. After cessation of UV irradiation, the solution was decanted into a separatory funnel, shaken with 80 m*l* of 10% hydrochloric acid and separated. The aqueous layer was concentrated to half volume under reduced pressure, neutralized with aqueous solution of potassium hydroxide (40%), extracted with 100 m*l* of benzene and dried over potassium carbonate. After evaporating the solvent, the resulting oil was chromatographed on 50 g of aluminum oxide. Eluting with petroleum ether afforded 1.2 g of 1-benzyl-2,2,6,6-tetramethylpiperidine (V). Recrystallization from petroleum ether gave a pure sample: mp 39—40°C. Found: C, 82.91; H, 11.07; N, 5.87%. Calcd for $C_{16}H_{25}N$: C, 83.05; H, 10.89; N, 6.05%. NMR (τ) (in CCl_4): 2.5—3.0 (5H), 6.20 singlet (2H), 8.45 broad (6H), 8.97 singlet (12H). mass spectrum: $M^+=231$ (231). Picrate: mp 170—171°C (from ethanol). Found: C, 57.10; H, 6.14; N, 11.91%. Calcd for $C_{22}H_{28}O_7N_4$: C, 57.38; H, 6.13; N, 12.17%. The benzene layer was concentrated in a vacuum to give 2.5 g of crystallline solids. Recrystallization from ethanol gave dibenzyl melting at 52—53°C (mp 52°C).

b). A solution of 17.6 g (0.1 mol) of IIb in 140 m*l* of dry benzene with bubbling oxygen gas was irradiated with a high pressure mercury lamp (Hanovia, 450 W) for 2 hr at 0—5°C. After cessation of UV irradiation, 5.0 g of 2,2,6,6-tetramethylpiperidine hydrochloride (Ib') was separated from the solution by filtration. This was confirmed by comparison of the melting point and IR spectrum with those of the sample prepared by the reaction of Ib with hydrogen chloride in ethanol. Recrystallization from ethanol gave a pure sample: mp 295°C (decomposition). Found: C, 60.78; H, 11.40; N, 7.85; Cl, 19.91%. Calcd for for $C_9H_{20}NCl$: C, 60.83; H, 11.34; N, 7.88; Cl, 19.95%. The filtrate was concentrated under reduced pressure. The oily residue was chromatographed on a column of aluminum oxide and the column eluted successively with petroleum ether, benzene, and methanol. From petroleum ether eluates, 3.5 g of the starting

15) R. E. Banks, K. Mullen, and G. E. Williamson, *J. Chem. Soc. C*, **1968**, 2608.

16) T. Toda, E. Mori and K. Murayama, This Bulletin, **45**, 1904 (1972).

17) K. Murayama, S. Morimura, O. Amakasu, T. Toda, and E. Yamao, *Nippon Kagaku Zasshi*, **90**, 296 (1969).

material was recovered. This was confirmed by IR and NMR spectra. From benzene eluates, 1.0 g of 2,2,6,6-tetramethylpiperidine-1-oxyl (IVb) was obtained. This was confirmed by comparison of the melting point and IR spectrum with those of an authentic sample.[10] An analytically pure sample was given by sublimation in a vacuum: mp 38—39°C. Found: C, 68.76; H, 11.48; N, 8.96%. Calcd for $C_9H_{18}ON$; C, 69.18; H, 11.61; N, 8.96%. ESR (in benzene): $a_N=15.0$ gauss, g-value$=2.0056$. From methanol eluates, 3.0 g of unknown tarry materials were obtained.

We would like to thank Prof. Makoto Okawara, the Tokyo Institute of Technology, for his valuable comments, Dr. Genshun Sunagawa, the director of these laboratories, for his encouragement and Mr. Susumu Higashida for his technical assistance.

BULLETIN OF THE CHEMICAL SOCIETY OF JAPAN, VOL. 45, 1806—1812 (1972)

On the Configuration of Branched-Chain Derivatives of 1,2 : 5,6-Di-*O*-isopropylidene-*α*-D-*ribo*-hexofuranos-3-ulose

Juji YOSHIMURA, Kazuhiko KOBAYASHI, Ken-ichi SATO, and Masuo FUNABASHI

Laboratory of Chemistry for Natural Products, Faculty of Science, Tokyo Institute of Technology, Ookayama, Meguro-ku, Tokyo

(Received October 7, 1971)

In order to obtain a 3-*C*-hydroxymethyl-D-glucose derivative some nucleophilic reactions of 1,2 : 5,6-di-*O*-isopropylidene-α-D-*ribo*-hexofuranos-3-ulose (**1**) and the configurations of products have been examined. *Gluco*- and *allo*-configurations of known 3-*C*-nitromethyl derivatives of **1** were confirmed by the fact that 3-*C*-acetaminomethyl-1,2-*O*-isopropylidene-α-D-*xylo*- and *ribo*-pentodialdofuranoses, derived by four successive transformations, showed the absence and presence of the aminal-ring formation between the aldehyde and acetamino groups, respectively. A 3-*C*-carbethoxymethyl derivative obtained by the Reformatsky reaction of **1** with ethyl bromoacetate was proved to be of *allo*-configuration by the lactone-formation between C_5-hydroxyl and carboxyl groups. The configuration of 3-*C*-hydroxymethyl derivative (**15**) obtained by treatment of known 3-*C*-methylene derivative of **1** with permanganate was proved to be of *gluco*-type by comparison of the corresponding 3-*C*-aminomethyl derivative (**5**), derived by three-step conversions, with that obtained from 3-*C*-nitromethyl derivatives. **15** was also obtained by epoxidation of **1** with diazomethane followed by ring-opening with alkali. Treatment of **5** and its *allo*-epimer with nitrous acid gave, respectively, a ring-expanded product and the 3′,5-anhydride, the former being also recognized in the epoxidation products. Structures of new compounds were examined by NMR spectra and stereoselectivity of reactions discussed.

Studies are increasingly being made on branched-sugars rarely found in nature[1], and on osuloses as important intermediates for synthesis of deoxy-, amino-, and branched-sugars[2].

In order to obtain a 3-*C*-hydroxymethyl derivative of D-glucose as an intermediate for a total synthesis of tetrodotoxin[3], we examined nitromethane-condensation, the Reformatsky reaction and diazomethane-condensation of 1,2 : 5,6-di-*O*-isopropylidene-α-D-*ribo*-hexofuranos-3-ulose (**1**)[4] and the configurations of the products. The compound was obtained by treatment of 3-*C*-methylene derivative of **1** with permanganate or by diazomethane-condensation of **1**, followed by ring-opening of the resulting epoxide.

Results and Discussion

Nitromethane Condensation and the Reformatsky Reaction. It is known that the nitromethane condensation of **1** afforded 1,2 : 5,6-di-*O*-isopropylidene-3-*C*-nitromethyl-α-D-allofuranose (**2**) or a mixture of **2** and the corresponding 3-epimer (**3**), depending on the conditions[5-7]. The structure of **2** and **3** was confirmed from the fact that 1,2-*O*-isopropylidene-3-*C*-nitromethyl-α-D-pentofuranose derived from **3** by oxidative elimination of atom at position 6 gave the corresponding 3,5-*O*-isopropylidene ring[7] and that a part of **3** was converted into **2** through 3-dehydro-3-deoxy-1,2 : 5,6-di-*O*-isopropylidene-3-*C*-nitromethylene-α-D-*ribo*-hexofuranose[6]. Their structures were confirmed by examining whether the corresponding 3-*C*-acetaminomethyl-1,2-*O*-isopropylidene-α-D-*ribo*-hexofuranose[6]. Their structures were confirmed by examining whether the corresponding 3-*C*-acetaminomethyl-1,2-*O*-isorpopylidene-α-D-pentodialdofuranoses can form an aminal-ring between the aldehyde and

1) F. Shafizadeh, "Advances in Carbohydrate Chemistry," Vol. 11, Academic Press, New York, N. Y. (1956), p. 263.
2) J. S. Brimacombe, *Angew. Chem.*, **81**, 415 (1969).
3) K. Tsuda, C. Tamura, R. Tachikawa, K. Sakai, O. Amakasu M. Kawamura, and S. Ikuma, *Chem. Pharm. Bull.* (Tokyo), **12**, 634, 642 (1964); T. Goto, Y. Kishi, S. Takahashi and Y. Hirata, *Tetrahedron Lett.*, **1964**, 779, 1831; R. B. Woodward, *Pure. Appl. Chem.*, **9**, 49 (1964).
4) P. J. Beynon, P. M. Collins and W. G. Overend, *Proc. Chem. Soc.*, **1964**, 342; K. Onodera, S. Hirano and N. Kashimura, *J. Amer. Chem. Soc.*, **87**, 4651 (1965); K. Onodera, H. Hirano and N. Kashimura, *Carbohyd. Res.*, **6**, 276 (1968); B. T. Lowton, W. A. Szarek and J. K. N. Jones, *ibid.*, **10**, 456 (1969).
5) G. J. Lourens, *Tetrahedron Lett.*, **1969**, 3733.
6) H. P. Albrecht and J. G. Moffat, *ibid.*, **1970**, 1063.
7) A. Rosenthal, K. -S. Ong, and D. Baker, *Carbohyd. Res.*, **13**, 113 (1970).

acetamino groups. Hydrogenation of **2** and **3** in the presence of palladium-charcoal gave the corresponding 3-*C*-aminomethyl derivatives (**4**) and (**5**), respectively. They were then converted into 3-*C*-acetaminomethyl derivatives (**6**) and (**7**) by acetylation in ethanol. The compounds were obtained in crystalline state, and characterized by NMR. The results for **6** and **7** are given in Figs. 1—3.

The first-order analysis of the original spectrum of **6** was hindered by overlapping of proton signals. However, deuteration of the amido and hydroxyl protons and addition of a few drops of benzene to cause a shift in several peaks (Fig. 1) made it easy to assingn $H_{3'a}$ and H_{6b} protons. Other protons were assigned from the intensities and coupling constants. The coupling constant between H_4 and H_5 was also determined by the examination of pseudo-contact

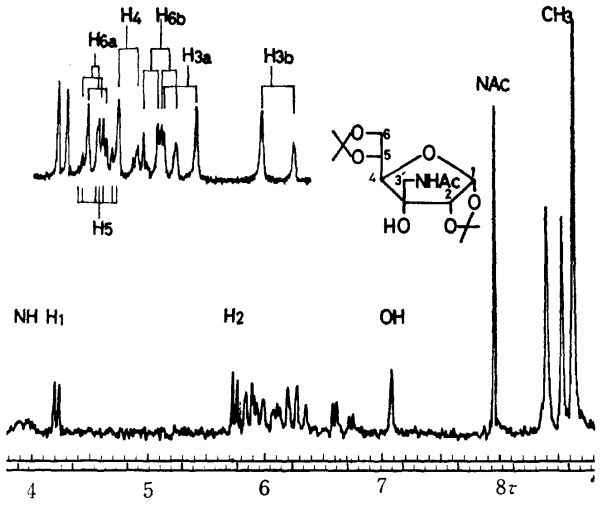

Fig. 1. NMR spectrum of **6** in $CDCl_3$.

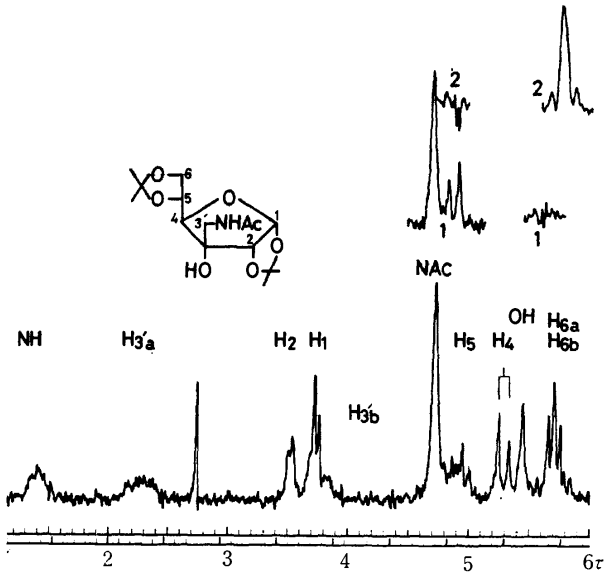

Fig. 2. NMR spectrum of **6** (16 mg) in the presence of $Eu(fod)_3$ (10 mg).

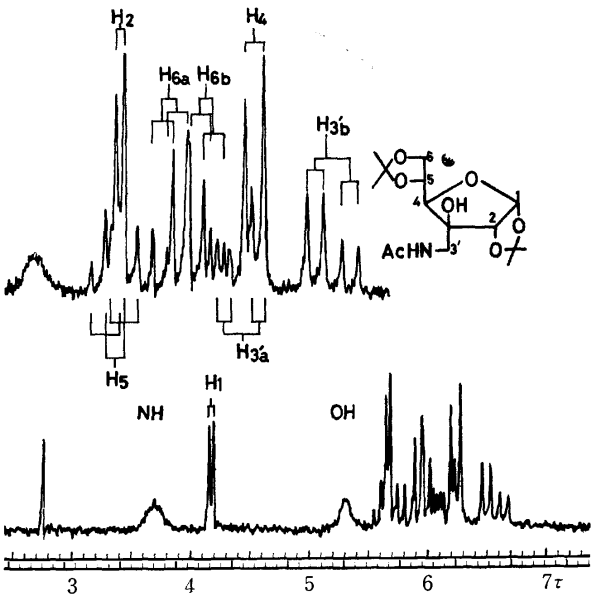

Fig. 3. NMR spectrum of **7** in $CDCl_3$.

shift (Fig. 2) with tris(1,1,1,2,2,3,3-heptafluoro-7,7-dimethyl-4,6-octanedionato)-europium (III)[8] [Eu(fod)$_3$]. Tickling of H_6 protons caused H_5 proton signal to disclose a large coupling corresponding to that of H_4, and irradiation of H_5 changes H_{6a} and H_{6b} signals to a broadened AB quartet from AB part of an ABX system. From a comparison of the magnitude of contact shifts of several kinds of protons, it is concluded that nitrogen atom in **6** is the more predominant ligand than oxygen of *tert*-hydroxyl group.

Signals in the NMR spectrum of **7** (Fig. 3) were assigned only by means of double-resonance technique. Such a difference in D-*allo* and D-*gluco* derivatives was generally observed.

Hydrolyses of 5,6-*O*-isopropylidene groups of **6** and **7** were performed by treatment with 0.01 N sulfuric acid for 2 hr, and the products were directly oxidized with periodate to give 1,2-*O*-isopropylidene-3-*C*-acetaminomethyl-α-D-*xylo*- and and D-*ribo*-pentodialdofuranose (**8**) and (**9**), respectively. **8** showed charac-

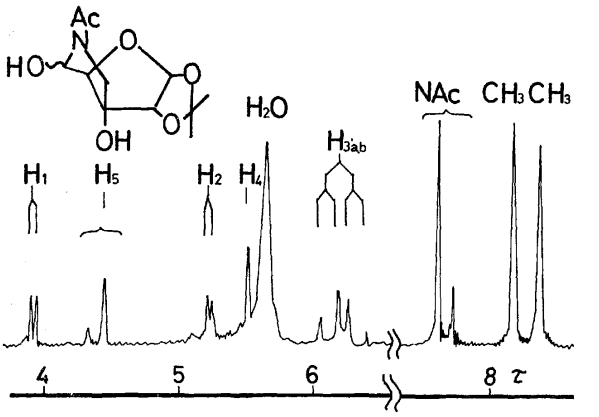

Fig. 4. NMR spectrum of **8** in $CDCl_3$.

8) R. E. Rondeau and R. E. Sievers, *J. Amer. Chem. Soc.*, **93**, 1522 (1971).

teristic absorptions of tertiary amide (1605 and 1615 cm^{-1}) in IR spectrum, and showed no aldehyde proton signal in NMR spectrum (Fig. 4). The existence of two singlets for both *N*-acetyl and H_5 protons which could not collapse at 60°C indicates that **8** exists in aminal structures (**8'**) in which two configurations are possible at C_5. **9** also showed a secondary amide absorption (1640 and 1540 cm^{-1}) and an aldehyde proton signal at τ 0.37 (Fig. 5). The configurations of **2** and **3** were confirmed.

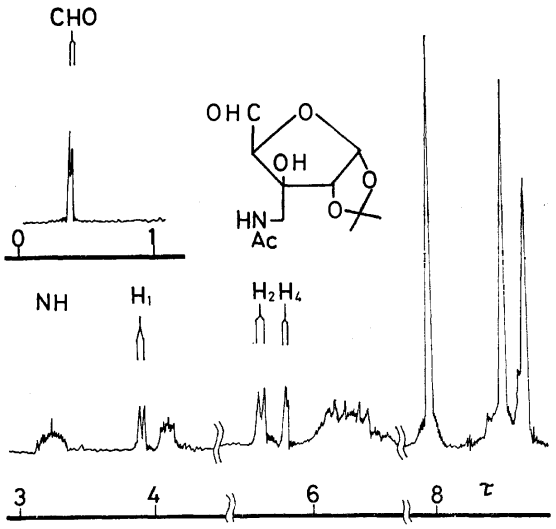

Fig. 5. NMR spectrum of **9** in $CDCl_3$.

Acetylation of **2** with acetic anhydride in the presence of *p*-toluenesulfonic acid gave 3,5,6-tri-*O*-acetyl-1,2-*O*-isopropylidene-3-*C*-nitromethyl-α-D-allofuranose (**10**). However, conversion of **10** into the corresponding 3-*C*-nitromethylene derivative[7] was unsuccessful. Deamination of **4** and **5** was attempted. Treatment of **4** with barium nitrite in acetic acid at 0°C for 12 hr gave 1,2-*O*-isopropylidene-3',5-anhydro-3-*C*-hydroxymethyl-α-D-allofuranose (**11**) in 20% yield. Disappearance of the characteristic absorption of an amino (1580 cm^{-1}) and appearance of that of hydroxyl (3250 and 3410 cm^{-1}) group in IR spectrum, and the presence of H_4 signal as singlet and H_5 as triplet supports the structure (Fig. 6). A similar treatment of **5** gave a sirup. The presence of a six-membered ketone was deduced by IR spectrum (1730 cm^{-1}) and NMR spectrum (two kinds of H_1 signals at τ 4.08 and 4.25, and two quartet at τ 7.1—7.7). The spectral information was also confirmed on a sirup obtained from the mother liquor of **11**. Thus it is concluded that deamination of **4** and **5** induced ring-expansion C_3'-carbonium ion, and a part of carbonium ion cyclized with sterically close C_5-oxygen in the case of **4**.

Treatment of **1** with ethyl bromoacetate in the presence of zinc metal and catalytic amount of iodine, followed by chromatographic separation of the product on a silica gel column gave the corresponding 3-*C*-

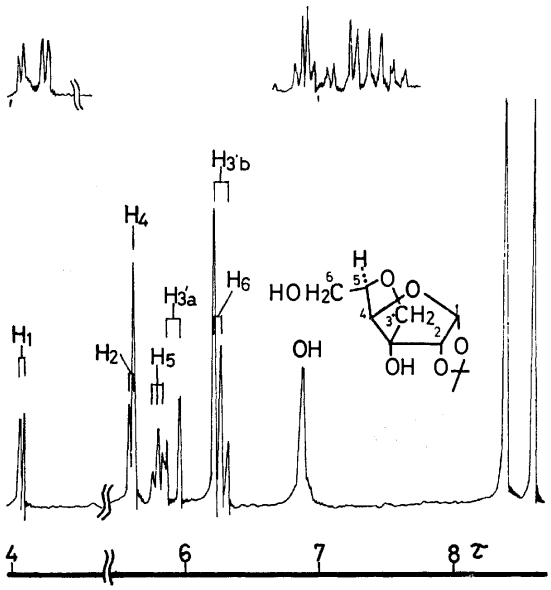

Fig. 6. NMR spectrum of the sirup from the mother liquor.

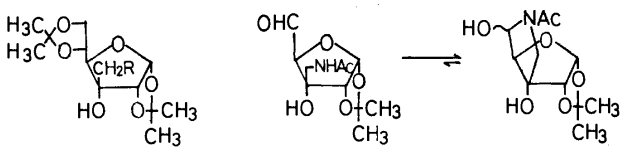

(**2**) R=NO_2
(**4**) R=NH_2
(**6**) R=NHAc
(**12**) R=$CO_2C_2H_5$
(**14**) R=COOH

(**8**) (**8'**)

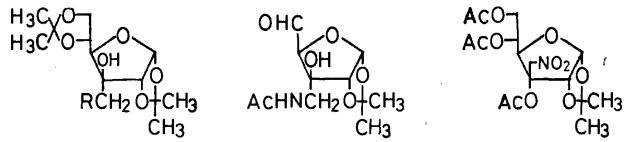

(**3**) R=NO_2
(**5**) R=NH_2
(**7**) R=NHAc
(**15**) R=OH
(**16**) R=OTs

(**9**) (**10**)

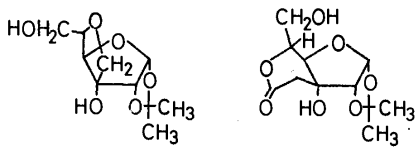

(**11**) (**13**)

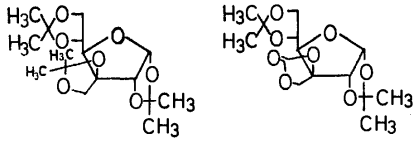

(**17**) (**18**)

carbethoxymethyl derivative (**12**) as a sirup and a small amount of 1,2-*O*-isopropylidene-3-*C*-carboxymethyl-α-D-allofuranose-3′,5-lactone (**13**) as crystals. Treatment of **12** with alkali gave the corresponding 3-*C*-carboxymethyl derivative (**14**). However, application of dehydrative decarboxylation of β-hydroxy-carboxylic acid in quinoline with copper powder[9] to **14** gave unchanged product and again a small amount of **13**. This proves that **12** and **14** have the *allo*-configuration. IR spectrum of **12**, **13** and **14** showed, respectively, characteristic absorption bands of ester (1725 cm^{-1}), lactone (1735 cm^{-1}), and carboxylic acid (1695 cm^{-1}). The presence of much less hindered C_6-methylene signals in the NMR spectrum of **13** also supports the structure (Fig. 7).

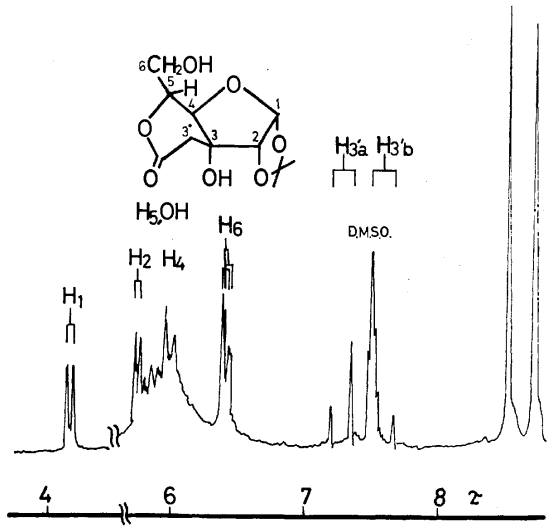

Fig. 7. NMR spectrum of **13** in DMSO.

Synthesis of 3-C-Hydroxymethyl-1,2: 5,6-di-O-isopropylidene-α-D-glucofuranose by means of the Wittig or Diazomethane Reaction. It has been reported that the reaction of **1** with methylenetriphenylphosphorane in dimethyl sulfoxide or in ether gave the corresponding 3-*C*-methylene derivative[10,11]. Treatment of this compound with potassium permanganate gave 3-*C*-hydroxymethyl-1,2 : 5,6-di-*O*-isopropylidene-α-D-glucofuranose (**15**) in 70% yield. The NMR spectrum of **15** gave a pattern close to that of **7**, except for the $C_{3'}$-methylene protons which appeared as a singlet at τ 6.15. The configuration at C_3 was proved chemically as follows. Partial tosylation of **15** gave a monotosylate (**16**) whose tosylated position was deduced to be $C_{3'}$ from the lower shift of $C_{3'}$-methylene signals (at τ 5.05 and 5.80 as AB quartet) in the NMR spectrum. The compound was converted into the corresponding azide, and then hydrogenated to give the corresponding 3-*C*-aminomethyl derivative which was identical with **5** in melting point and spectral data.

As another synthetic method of **15**, direct epoxidation of **1** with diazomethane was tried, followed by ring-opening with alkali and the product was examined by gas liquid chromatography (Fig. 8). When epoxidation was carried out in ether or methanol, the product contained many species, but the products obtained by the reaction in benzene contained the desired compound (peak c) as the main product. In fact, **15** was separated in 25% yield which was identical with the authentic specimen in melting point and spectral data. Three trimethylsilylated species of **1** indicated the occurrence of two kinds of enolization[12] to some extent. The glpc of the sirup obtained from the mother liquor showed nearly complete separation of **15** (peak c) by simple crystallization. Peaks d and b were respectively deduced to be 3-epimer of **15** and a ring expanded product mentioned in the case of the deamination of **4**. However, it could not be isolated.

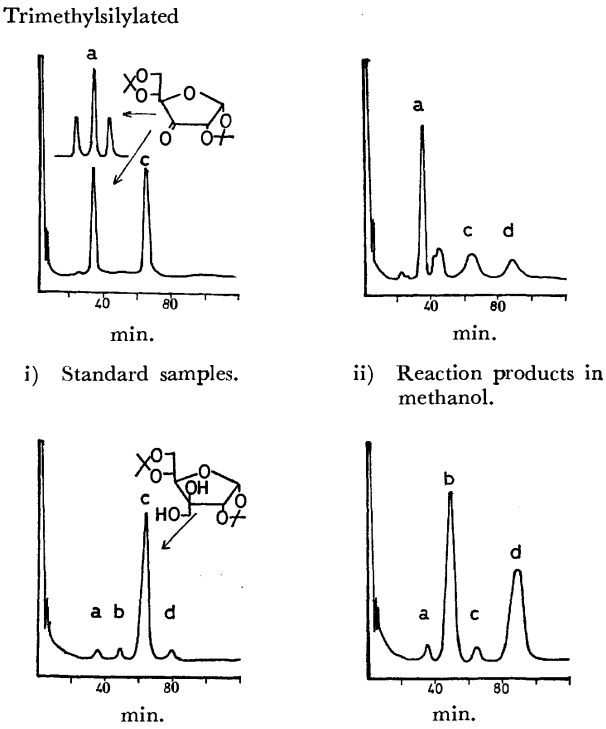

Fig. 8. Gas chromatograms of the reaction products of **1** with diazomethane.
(1.5% OV-17 on Shimalite; 115°C: N_2 flow rate, 60 ml/min.)

The configurations of reaction products obtained can be understood by the attacking of nucleophiles from the outside of the V-shaped fused five-membered ring in **1**, except in the reaction of diazomethane in benzene. Such stereoselectivities have also been recognized in the Grignard reaction of 5-deoxy-1,2-*O*-isopropylidene-β-L-*threo*-pentofuranos-3-ulose[13] and in hydrogenation of **1**[14] or the corresponding

9) M. Vichel and N. A. Abraham, *Bull. Soc. Chim. France*, **1960**, 1196.
10) W. A. Szark, J. S. Jewell, I. Szczerek, and J. K. N. Jones, *Can. J. Chem.*, **47**, 4473 (1969).
11) A. Rosenthal and M. Sprinzl, *ibid.*, **47**, 3951 (1969).
12) W. Meyer zu Reckendorf, *Angew. Chem.*, **79**, 151 (1967).
13) J. R. Dyer, W. E. McGonigal and K. C. Eice, *J. Amer. Chem. Soc.*, **87**, 654 (1965).
14) P. M. Collins, *Tetrahedron*, **21**, 1809 (1965).

cyclohexylidene dreivative[15].

The abnormal stereoselectivity of the reaction of diazomethane in benzene can be explained only by assuming an interaction between oxygen atoms in 1,2-*O*-isopropylidene group of **1** and the polarized structure of diazomethane[16].

Experimenal

All boiling and melting points are uncorrected. The solutions were evaporated under diminished pressure at a bath temperature not exceeding 45°C. Specific rotations were measured in a 0.5-dm tube, with a Carl Zeiss LEP Al Polarimeter. The IR spectra were recorded with a Hitachi Model EPI-GS grating IR spectrophotometer. The NMR spectra were taken in deuteriochloroform unless otherwise stated with a JMN-4H-100 MHz and partly with Varian XL-100 Spectrometer using tetramethylsilane as an internal standard. Chemical shifts and coupling constants were recorded in τ and Hz units, and frequencies in cm^{-1}.

*3-*C*-Aminomethyl-1,2: 5,6-di-*O*-isopropylidene-α-*D*-allofuranose (**4**) and -glucofuranose (**5**).* A solution of 1,2 : 5,6-di-*O*-isopropylidene-3-*C*-nitromethyl-α-D-allofuranose (**2**) or -glucofuranose (**3**) (5 g, 15.6 mmol) in methanol-water (100 ml) was hydrogenated in the presence of palladium-charcoal (5%, 2.5 g). After hydrogenation, the solution was filtered and methanol was evaportaed. The water layer was then extracted with chroloform. The extract was washed with water, dried, and concentrated to give crystals which was recrystallized from methanol-ether. The yield was 4.26 g (94%) in both cases.

Compound **4**: mp 122—123°C; $[\alpha]_D^{23}$ +25.4° (*c* 0.06, ethanol). IR: 3360 and 3290 (NH_2), 1583 (C-N); NMR: 4.26 (H_1; d, $J_{1,2}$=3.81), 5.38 (H_2; d), 5.77—6.20 (H_4, H_5, H_{6a}, H_{6b}), 6.83 and 7.38 ($H_{3'a}$ and $H_{3'b}$; ABq, $J_{a,b}$=13.0), 8.12 (OH and NH_2, s), 8.39, 8.54, and 8.62 (4 C-CH_3).

Found: C, 54.36; H, 8.04; N, 5.18%. Calcd for $C_{13}H_{23}NO_6$: C, 53.96; H, 8.01; N, 4.84%.

Compound **5**: mp 114—115°C; $[\alpha]_D^{23}$ +28.8° (*c* 1.0, ethanol). IR: 3330 and 3280 (NH_2), 1615 (C-N); NMR: 4.13 (H_1; d, $J_{1,2}$=3.5), 5.69 (H_2; d), 6.23 (H_4; d, $J_{4,5}$=7.9), 5.66 (H_5; sex, $J_{5,6a}$=5.6), 5.84 (H_{6a}; q, $J_{5,6b}$=5.7), 5.96 (H_{6b}; q, $J_{6a,6b}$=8.3), 6.90 ($H_{3'a}$; d, $J_{3'a,b}$=13.2), 7.03 ($H_{3'b}$; d), 7.88 (OH and NH, s), 8.49 8.58, 8.65 and 8.68 (4 C-CH_3).

Found: C, 52.58; H, 8.30; N, 4.62%. Calcd for $C_{13}H_{23}NO_6 \cdot 1/2H_2O$; C, 52.40; H, 8.06; N, 4.70%.

*3-*C*-Acetaminomethyl-1,2 : 5,6-di-*O*-isopropylidene-α-*D*-allofuranose (**6**) and -glucofuranose (**7**).* Acetic anhydride (0.5 g, 4.9 mmol) was added to a solution of **4** or **5** (0.3 g, 1.04 mmol) in methanol (3 m*l*) and then kept at room temperature for one day. The solution was treated by the usual procedure to give crystals which were recrystallized from ether-*n*-hexane. Yields were nearly quantitative in both cases.

Compound **6**: mp 156—156.5°C; $[\alpha]_D^{23}$ +56.3° (*c* 1.0, ethanol). IR: 3450 (OH), 3375 (NH), 1645 and 1515 (NHAc); NMR: 4.22 (H_1; d, $J_{1,2}$=4.0), 5.75 (H_2; d), 3.92 (NH), *ca.* 5.88 (H_{6a}; q, $J_{5,6a}$=2.0), *ca.* 5.89 (H_5; sex), 6.01 (H_4; *d*, $J_{4,5}$=8.4), 6.16 (H_{6b}; q, $J_{6a,b}$=8.0, $J_{6b,5}$=6.3), 6.27 ($H_{3'b}$), 6.64 ($H_{3'b}$; q, $J_{a,b}$=13.6, $J_{3'b,NH}$=3.8), 7.08 (OH, s), 7.97 (NAc; s), 8.41, 8.54 and 8.64 (4 C-CH_3).

Found: C, 54.21; H, 7.70; N, 4.08%. Calcd for $C_{15}H_{25}NO_7$: C, 54.37; H, 7.61; N, 4.23%.

The pseudocontact shift was measured in the presence of 5 or 10 mg of Eu(fod)$_3$ to 16 mg of **6**. The extent and order of shift (ppm) of protons in the latter case were as follows; NAc (4.24) > $H_{3'b}$ (3.67) > $H_{3'a}$ (2.84) > NH (2.54) > H_2 (2.23) > OH (1.64) > H_5 (0.09) > H_4 (0.73) > H_1 and H_{6b} (0.47), C-CH_3 (0.30, 0.28, 0.23 and 0.14), H_{6a} (0.18).

Compound **7**: mp 120—121°C, $[\alpha]_D^{23}$ +63.8° (*c* 1.44, ethanol). IR: 1650 and 1542 (NHAc); NMR: 3.55 (NH; broad s), 4.16 (H_1; d, $J_{1,2}$=4.5), 5.29 (OH; s), 5.66 (H_2; d), 5.65 (H_5; q, $J_{5,6b}$=5.8), 5.88 (H_{6a}; q, $J_{5,6a}$=5.9), 6.04 (H_{6b}; q, J_{ab}=8.6), 6.24 (H_4; d, $J_{4,5}$=7.8), 6.22 and 6.55 ($H_{3'ab}$; each q, J_{ab}=14.7, $J_{3'b,NH}$=5 5, $J_{3'b,NH}$= 6.8), 7.96 (NAc; s), 8.50, 8.59, 8.64 and 8.69 (4 C-CH_3).

Found: C, 54.51; H, 7.59; N, 4.20%. Calcd for $C_{15}H_{25}NO_7$: C, 54.37; H, 7.61; N, 4.23%.

*3-*C*-Acetaminomethyl-1,2-*O*-isopropylidene-α-*D*-ribo-pentodialdofuranose-5,*N*-aminal (**8'**).* A solution of **6** (1.5 g, 4.5 mmol) in 0.1 N-sulfuric acid (50 m*l*) was kept at room temperature for 2 hr, neutralized with barium hydroxide and then filtered. The filtrate was extracted with chloroform, and the extract was evaporated to give a sirup (1.10 g). Oxidation of the sirup in water with sodium periodate (0.81 g, 3.78 mmol) gave crystals (0.4 g, 34%) soluble in dimethyl sulfoxide, but insoluble in usual organic solvents. Mp 219.5—220.7°C; $[\alpha]_D^{23}$ +25.4°→+29.7° (after 24 hr, c 1.0, water). IR: 3480 (OH), 1607 and 1625 (=NAc): NMR (DMSO-d_6): 3.92 (H_1; d, $J_{1,2}$=3.1), 4.32 and 4.44 H_5; two kinds of s), 5.23 (H_2; d), 5.52 (H_4; s), 6.12 and 6.33 ($H_{3'ab}$; ABq, $J_{a,b}$=14.0), 7.62 and 7.72 (NAc; two kinds of s), 8.17 and 8.36 (2 C-CH_3).

Found: C, 50.61; H, 6.60; N, 5.37%. Calcd for $C_{11}H_{17}NO_6$: C, 50.96; H, 6.61; N, 5.40%.

*3-*C*-Acetaminomethyl-1,2-*O*-isopropylidene-α-*D*-xylo-pentodialdofuranose (**9**).* A solution of 3-*C*-acetaminomethyl-1,2-*O*-isopropylidene-α-D-glucofuranose (0.5 g, 1.73 mmol) and sodium periodate (0.4 g 1.87 mmol) in water (50 m*l*) was allowed to stand for 5 hr, and the sodium iodate separated by addition of ethanol was filtered off. After evaporation of ethanol from the filtrate, the water layer was extracted with chloroform to give a sirup which could not be crystallized. The amount of sirup was too small for its physical constants to be determined. However, satisfactory spectral information was obtained to deduce the structure without any further purification.

IR: 1725 (CHO), 1640 and 1540 (NHAc); NMR: 0.41 (CHO; d, $J_{4,CHO}$=2.0), 3.81 (H_1; d, $J_{1,2}$=4.0), 5.62 (H_2; d), 5.81 (H_4; d), *ca.* 6.00—6.65 (OH, $H_{3'a}$, $H_{3'b}$), 7.97 (NAc; s), 8.51 and 8.67 (2 C-CH_3).

*3,5,6-Tri-*O*-acetyl-1,2-*O*-isopropylidene-3-*C*-nitromethyl-α-*D*-allofuranose (**10**).* A solution of **2** (6.0 g, 18.8 mmol) and a catalytic amount of *p*-toluenesulfonic acid in acetic anhydride (9.6 g, 95 mmol) was allowed to stand for one day, and poured into excess sodium bicarbonate in water. Extraction of the aqueous solution with chloroform gave crystals which were recrystallized from ethanol. Yield, 3.0 g (39.4%) mp 165—166°C, $[\alpha]_D^{23}$ +77.0° (*c* 1.0, ethanol). IR: 1750, 1730 (OAc), 1560, 1540 (NO_2); NMR: 4.28 (H_1; d, $J_{1,2}$= 4.0), 4.67 (H_2; d), 4.45—4.65 (H_5; m), 4.94 and 5.15 ($H_{3'ab}$; ABq, $J_{a,b}$=11.7), 5.76 (H_4; d, $J_{4,5}$=8.0), 5.05 and 5.83 H_{6ab}; q and q, $J_{5,6a}$=3.0, $J_{5,6b}$=5.5, $J_{a,b}$=12.0), 7.92 and 7.94 (3 OAc), 8.45 and 8.65 (2 C-CH_3).

Found: C, 47.17; H, 5.88; N, 3.30%. Calcd for $C_{16}H_{23}NO_{11}$: C, 47.41; H, 5.72; N, 3.46%.

Treatment of this compound in benzene with sodium bicarbonate at 80°C gave only an intractable sirup.

15) K. James, A. R. Tatchell, and P. K. Ray, *J. Chem. Soc., C*, **1967**, 2681.

16) C. D. Gutsche "Organic Reactions." Vol. 8, John Wiley & Sons. Inc., New York, (1954), p. 364.

*3',5-Anhydro-3-C-hydroxymethyl-1,2-O-isopropylidene-α-D-allofuranose (**11**).* To an ice-cooled solution of **4** (0.6 g, 2.08 mmol) and acetic acid (0.763 m*l*) in water (5 m*l*) was added dropwise barium nitrite monohydrate (0.95 g, 3.84 mmol) in water (5 m*l*) with stirring for 20 min, and the resulting solution was allowed to stand for 12 hr at 10°C. Extraction of the reaction mixture with chloroform gave crystals which were recrystallized from ethanol-*n*-hexane. Yield, 0.1 g (20.6%); mp 115.8—116°C; $[\alpha]_D^{23}$ +73.8° (*c* 1.0, chloroform). IR: 3410 and 3250 (OH); NMR: 4.06 (H_1; d, $J_{1,2}$=4.5), 5.61 (H_2; d), 5.62 (H_4; s), 5.80 (H_5; t, $J_{5,6}$=5.0), 5.92 and 6.27 ($H_{3'ab}$; ABq, $J_{a,b}$=10.5), 6.24 (H_6; d), 6.88 (OH; s), 8.40 and 8.61 (s C-CH_3).

Found: C, 51.63; H, 7.00%. Calcd for $C_{10}H_{16}O_6$: C, 51.72; H, 6.94%.

*Reformatsky Reaction of **1** with Ethyl Bromoacetate.* A suspension of **1** (1.2 g 4.65 mmol), ethyl bromoacetate (3.7 g, 22.2 mmol) and zinc metal (2.1 g, 31.9 mmol) in tetrahydrofuran (11 m*l*) was refluxed for 1.5 hr in the presence of a catalytic amount of iodine and then filtered. The filtrate was poured into ice water containing acetic acid (1.2 m*l*), and extracted with chloroform. The pale yellow sirup 1.2 g) obtained by evaporation of the extracts was fractionated on a silica gel C-100 (20 g) column. The column was succesively eluted with ligroin, ligroin-benzene (1 : 1), benzene, benzene-acetone (5 : 1) and acetone. Concentration of ligroin-benzene and benzene solution gave 3-*C*-carbethoxymethyl-1,2 : 5,6-di-*O*-isopropylidene-α-D-allofuranose (**12**) as a sirup (0.5 g, 29.5%), and 3-*C*-carboxymethyl-1,2-*O*-isopropylidene-α-D-allofuranose 3',5-lactone (**13**) as crystals (0.3 g, 22.4%).

Compound **12**: IR: 1735 (ester); NMR: 4.26 (H_1; d, $J_{1,2}$=3.75), 5.21 (H_2; d), 5.65—6.20 (CH_2, H_4, H_5, H_{6a}, H_{6b}), 7.10 and 7.53 ($H_{3'ab}$; ABq, $J_{a,b}$=15.0), 7.83 (OH; s), 8.41, 8.54 and 8.63 (4 C-CH_3), 8.72 (CH_3 in ethyl; t, J=5.0).

Found: C, 54.95; H, 7.23%. Calcd for $C_{16}H_{26}O_8$: C, 55.48; H, 7.57%.

Compound **13**: mp 195—195.5°C; $[\alpha]_D^{23}$ +136.6° (*c* 1.0, acetone). IR: 1735 (lactone); NMR (DMSO): 4.16 (H_1; d, $J_{1,2}$=4.2), 5.76 (H_2; d), 5.98 (H_4; d, $J_{4,5}$=5.0), 5.78—6.20 (H_4, H_5, OH), 6.40 and 6.42 (H_{6ab}; two d, $J_{5,6}$=5.0), 7.30 and 7.52 ($H_{3'ab}$; ABq, $J_{a,b}$=15.5), 8.51 and 8.20 (2 C-CH_3).

Found: C, 50.62; H, 6.30%. Calcd for $C_{11}H_{16}O_7$: C, 50.77; H, 6.20%.

*3-C-Carboxymethyl-1,2 : 5,6-di-O-isopropylidene-α-D-allofuranose (**14**).* 0.1 N Sodium hydroxide (5 m*l*) was added to a solution of **12** (4.0 g, 10.9 mmol) in water (50 m*l*) which was then allowed to stand for 2 hr. The solution was acidified with acetic acid and extracted with chloroform. Evaporation of the extracts gave crystals which were recrystallized from petroleum ether. Yield, 2.8 g (80%), mp 111.5—112.5°C; $[\alpha]_D^{23}$ +22.7° (*c* 0.54, chloroform). IR: 1695 (COOH); NMR: 4.26 (H_1; d, $J_{1,2}$=4.0), 5.30 (H_2: d), 5.80—6.25 (H_4, H_5, H_{6a}, H_{6b}, OH), 7.04 and 7.52 ($H_{3'ab}$; ABq, $J_{a,b}$=15.0), 8.42, 8.56 and 8.64 (4 C-CH_3).

Found: C, 52.64; H, 6.85%. Calcd for $C_{14}H_{22}O_8$: C, 52.82; H, 6.97%.

An attempted dehydrative decarboxylation of **14** by refluxing in quinoline in the presence of copper powder for 10 hr gave unchanged **14** and a small amount of **13**.

*3-C-Hydroxymethyl-1,2 : 5,6-di-O-isopropylidene-α-D-glucofuranose **15**.* A) To a suspension of 1,2 : 5,6-di-*O*-isopropylidene-3-*C*-methylene-α-D-ribo-hexofuranose (3.4 g, 13.25 mmol) in water (30 m*l*) was added dropwise potassium permanganate (2.6 g, 15.4 mmol) in water (130 m*l*) for 30 min with stirring. After 1 hr, the solution was filtered and the filtrate was extracted with chloroform. The sirup obtained by evaporation of the extracts was crystallized from hexane. Yield, 2.71 g (70.3%); mp 84—86°C; $[\alpha]_D^{23}$ +21.8° (*c* 1.0, chloroform). NMR: 4.12 (H_1; d, $J_{1,2}$=4.0), 5.58 (H_2; d), 5.68 (H_5; m), 5.84 ($H_6{}^a$; q, $J_{5,6a}$=4.8, $J_{6a,6b}$=8.0), 5.96 (H_{6b}; q, $J_{5,6b}$=5.0), 6.15 ($H_{3'ab}$; s), 6.18 (H_4; d, $J_{4,5}$=7.0), 6.45 (OH; s), 8.48, 8.56, 8.63, 8.68 (4 C-CH_3).

Found: C, 54.59; H, 8.22%. Calcd for $C_{13}H_{22}O_7$: C, 53.78; H, 7.64%.

B) Dried diazomethane (0.726 g, 1.2 equivalent calculated from nitrosomethylurea) was added to a solution of **1** (3.42 g, 14.4 mmol) in benzene (40 m*l*), which was then evaporated. A solution of the resulting sirup in acetone-water (100 ml, 1 : 1 v/v) containing potassium hydroxide (0.5 g) was refluxed for 3 hr, and acetone was evaporated. Extraction of the water layer with chloroform gave a sirup which was extracted with hot *n*-hexane to give crystals. Yield, 0.95 g (25%); mp 86.0—86.5°C. It showed no depression of melting point by admixture with an authentic sample. The IR spectral data were found to be identical.

*3-C-Hydroxymethyl-1,2 : 5,6-di-O-isopropylidene-3'-O-(p-toluenesulfonyl)-α-D-glucofuranose (**16**).* To a solution of **15** (0.5 g, 1.72 mmol) was added *p*-toluenesulfonyl chloride (0.36 g, 2.27 mmol) with stirring. After standing overnight, the solution was poured into ice-water and extracted with chloroform. The extract was washed with cold N hydrochloric acid, saturated sodium bicarbonate solution and water. Evaporation of the extracts gave a sirup which was crystallized from ether-*n*-hexane. Yield, 0.66 g (86.4%); mp 116.5—117.5°C; $[\alpha]_D^{23}$ +98.4° (*c* 1.01, chloroform). NMR: 4.18 (H_1; d, $J_{1,2}$=3.5), 5.05 and 5.80 ($H_{3'ab}$; ABq, $J_{a,b}$=10.0), 5.66 (H_2; d), 5.92 (H_{6a}; q, $J_{5,6a}$=6.0, $J_{6a,6b}$=8.0), 6.36 (H_4; d, $J_{4,5}$=8.0), 6.60 (H_{6b}; q, $J_{5,6b}$=6.0), 7.25 (OH; broad s), 8.63, 8.67, 8.70 and 8.77 (4 C-CH_3).

Found: C, 54.52; H, 6.39; S, 7.47%. Calcd for $C_{20}H_{28}O_9S$: C, 54.05; H, 6.35; S, 7.21%.

*Preparation of **5** from **16**.* A solution of **16** (0.5 g, 1.13 mmol) and sodium azide (0.15 g, 2.26 mmol) in dimethylformamide (20 ml) was refluxed for 4 hr at 173°C, then poured into ice-water. The resulting solution was extracted with chloroform. Evaporation of the extracts gave a sirup which could not be completely separated from dimethylformamide. However, it gave a characteristic absorption of azide (2100 cm^{-1}) in IR spectrum. NMR: 4.13 (H_1; d, $J_{1,2}$=3.4), 5.58 (H_2; d), *ca.* 5.71 (H_5; m), 5.88 (H_{6a}; q, $J_{5,6a}$=5.5, $J_{6a,7b}$=7.9), 6.00 (H_{6b}; q, $J_{5,6b}$=4.6), 6.29 and 6.32 ($H_{3'ab}$; ABq, $J_{a,b}$=10.2), *ca.* 6.26 (H_4; d), 8.48, 8.85 and 8.65 (4 C-CH_3).

Hydrogenation of the sirup in ethanol (20 m*l*) in the presence of Raney nickel (0.5 g) at 40°C and 30 atm. gave the corresponding 3-*C*-aminomethyl derivative as crystals. Yield, 0.25 g (61%); mp 113—115°C. The spectral data of the crystals were identical with those of **5**.

*3-C-Hydroxymethyl-1,2 : 3,3' : 5,6-tri-O-isopropylidene-α-D-glucofuranose (**17**).* A suspension of **15** (1 g, 3.45 mmol) and anhydrous copper sulfate (3 g) in acetone (50 m*l*) was refluxed for 72 hr, filtered through active carbon, and the filtrate was evaporated. The sirup crystallized gradually, but it could not be recrystallized because of its small solubility in organic solvents. Yield, 0.8 g (70%); mp 54—56°C; $[\alpha]_D^{23}$ +23.1° (*c* 0.6, ethanol); NMR: 4.18 (H_1; d, $J_{1,2}$=3.5), 5.66 (H_2; d), 6.08 (H_4; d, $J_{4,5}$=13.0), 5.56—6.06 (H_5, H_{6ab} and $H_{3'ab}$), 8.52, 8.58, 8.60, 7.66 and 8.68 (6 C-CH_3).

Found: C, 58.05; H, 7.99%. Calcd for $C_{16}H_{26}O_7$:

C, 58.17; H, 7.93%.

*3-C-Hydroxymethyl-1,2 : 5,6-di-O-isopropylidene-α-D-glucofuranose 3,3'-carbonate (**18**).* To a solution of 15 (1 g, 3.45 mmol) in pyridine (10 ml) was bubbled excess phosgene under cooling. After standing for 1 hr the solution was poured into ice-water and extracted with chloroform. Evaporation of the extracts gave a sirup in 90% (0.98 g) yield. $[\alpha]_D^{23}$ +25.8° (*c* 0.1, chloroform); IR: 1820 (carbonate) NMR: 4.05 (H_1; d, $J_{1,2}$=4.4), 5.41 (H_2; d), 5.32 and 5.45 ($H_{3'ab}$; ABq, $J_{a,b}$=9.0), 5.72 (H_5: m), 5.87 (H_{6a}; q, $J_{5,6a}$=2.9), 5.99 (H_{6b}; q, $J_{6a,6b}$=8.4, $J_{5,6b}$=4.5), 6.10 (H_4; d, $J_{4,5}$=8.4), 8.49, 8.56, 8.65 and 8.66 (4 C-CH_3).

Found: C, 52.55; H, 6.35%. Calcd for $C_{14}H_{20}O_8$: C, 53.16; H, 6.37%.

The authors are grateful to Mr. Masatsune Kainosho and Mr. Katsumi Ajisaka of Ajinomoto Co. for measurement of part of the NMR spectra, to Miss Fumie Hattori for glpc and members of the Laboratory of Organic Analysis for elemental analyses.

BULLETIN OF THE CHEMICAL SOCIETY OF JAPAN, VOL. 45, 1812—1816 (1972)

The Reduction of Stereoisomeric 6-*tert*-Butyl-3-methoxy-3-methylcyclohexenes with Lithium in Ethylamine

Tadashi MASAMUNE, Hajime MATSUE, and Matsuo FUJII

Department of Chemistry, Faculty of Science, Hokkaido University, Sapporo

(Received October 12, 1971)

The synthesis and reduction with lithium in ethylamine of the entitled stereoisomeric allyl ethers **1** and **2** are described. The reaction of both the isomers occurred very readily with concomitant cleavage of the methoxy groups, and gave the same products, 4-*tert*-butyl-1-methylcyclohexene (**13**), and *c*- and *t*-3-*tert*-butyl-6-methylcyclohex-1-enes (**14** and **15**), in the same ratio (87 : 4 : 9), indicating that the respective reactions involved a common intermediate (**16**). Moreover, the reduction of the *cis*-isomer **1** with an axial methoxy group proceeded much more rapidly than that of the *trans*-isomer **2** with an equatorial methoxy.

Although the metal-in-ammonia reduction of aromatic carbocycles or heterocycles has been extensively investigated,[1] comparatively little is known about the corresponding reduction of allyl ethers and, especially, its stereochemistry.[2] In the studies aimed at establishment of C_9-configuration of jervine,[3] we found that "jervine-11β-ol" or 11-deoxojervine produced both Δ^{12}-olefin with 17β-hydrogen[4] and $\Delta^{13(17)}$-olefin with 12α-hydrogen[3] by the Birch reduction, but not any stereoisomers of the olefins. This result led us to have interest in and examine the relevant reaction of simpler, stereoisomeric allyl ethers. In this paper we describe the synthesis and chemical behavior under the Birch conditions of *c*- and *t*-6-*tert*-butyl-*r*-3-methoxy-3-methylcyclohex-1-enes (**1** and **2**).[5]

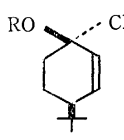

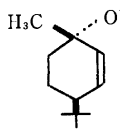

1 R=CH_3, with Δ **2** R=CH_3, with Δ
8 R=H, with Δ **9** R=H, with Δ
11 R=H, without Δ **12** R=H, without Δ

Treatment of 4-*tert*-butylanisole[6] (**3**) with lithium in liquid ammonia[7] followed by distillation afforded a mixture of dihydro compounds (**4**), bp 86—87°C/8 mmHg, in 74% yield. This on acid hydrolysis gave a 4 : 1 mixture (checked by gas chromatography; abbr., vpc) of $\alpha\beta$- and $\beta\gamma$-unsaturated ketones (**5** and **6**) in 91% yield, from which **5**, bp 101—102°C/11 mmHg, and **6**, bp 95—97°C/9 mmHg, were isolated in 42 and 14% yields, respectively, by column chromatography over silicic acid.[8] In accordance with the assigned structures, the former **5** exhibited absorptions at 224 mμ (ε 10500), at 1691 and 1618 cm^{-1}, and at τ 3.99 and 2.98 (two olefinic protons) in the UV, IR and NMR spectra, while the latter **6** those at 1720 cm^{-1} and at τ 4.48 (only one olefinic proton).

$\beta\gamma$-Unsaturated ketone **6** manifested itself to be untenable to oxidation. When allowed to stand in the air at room temperature, **6** spontaneously formed a beautiful crystalline compound (**7**), mp 106—107°C, which was analyzed for $C_{10}H_{16}O_3$, a molecular formula

1) For the recent references concerning the Birch reductions, see: A. J. Birch, E. G. Hutchinson, and G. S. Rao, *J. Chem. Soc., C*, **1971**, 637; W. A. Remers, G. J. Gibs, C. Pidacks, and M. J. Weiss, *J. Org. Chem.*, **36**, 279 (1971); S. Bank and B. Bockrath, *J. Amer. Chem. Soc.*, **93**, 430 (1971); B. C. Newman and E. L. Eliel, *J. Org. Chem.*, **35**, 3641 (1970); E. J. Eisenbraun, R. C. Bansal, D. V. Hertzler, and W. P. Duncan, *ibid.*, **35**, 1265 (1970); P. W. Rabideau and R. G. Harvey, *Tetrahedron Lett.*, **1970**, 4139, and also literatures cited in these papers.

2) A. S. Hallsworth, H. B. Henbest, and T. I. Wrigley, *J. Chem. Soc.*, **1957**, 1969.

3) T. Masamune, K. Kobayashi, M. Takasugi, Y. Mori, and A. Murai, *Tetrahedron*, **24**, 4193 (1969).

4) A. Murai, K. Arita, and T. Masamune, unpublished observations.

5) For nomenclature, see: *J. Org. Chem.*, **35**, 2849 (1970).

6) W. T. Olson, H. F. Hipsher, C. M. Buess, I. A. Goodnan, I. Hart, J. H. Lamneck, Jr., and L. C. Gibbons, *J. Amer. Chem. Soc.*, **69**, 2451 (1947).

7) M. D. Soffer and M. J. Jevnik, *ibid.*, **77**, 1003 (1955).

8) Lewis and Williams recently prepared these ketones **5** and **6** to determine the equilibrium ratio between them. However, the authors reported no physical constants to characterize the compounds and also the ratio in question to be 1 to 1 (vpc). K. G. Lewis and G. J. Williams, *Tetrahedron Lett.* **1965**, 4573.

corresponding to the sum of **6** and an oxygen molecule. In the IR spectrum absorption maxima appeared newly at 3200 and 1660 cm^{-1} instead of that at 1720 cm^{-1} of **6**. Similarly, in the NMR spectrum one-proton singlet and doublet were observed at τ 1.10 and 3.06 instead of the triplet at τ 4.48 of **6**. While compound **7** resisted acetylation under the usual conditions, it was reduced with sodium borohydride to give a mixture, from which a glycol (**7a**), mp 108.5—109.5°C, could be isolated in good yield by preparative tlc. This was readily converted into the acetonide (**7b**), oil, in 60% yield by treatment with acetone and silica gel (Wakogel Q-23). These findings indicated the compound to be formulated by structure **7**.

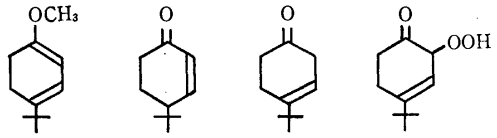

4 **5** **6** **7**

$\alpha\beta$-Unsaturated ketone **5** was treated with methyl lithium in ether[9] to produce a mixture of stereoisomeric tertiary alcohols, which were separated by column chromatography over alumina to give *cis*- and *trans*-alcohols (**8** and **9**), mp 36—37°C and 57—58°C, in 32 and 43% yields, respectively. The same treatment of $\beta\gamma$-unsaturated ketone **6** afforded the corresponding tertiary alcohol (**10**), mp 64—66°C, only in a low yield. The configurations of **8** and **9** were tentatively assigned on the basis of the R_f values on tlc or the elution sequence in column chromatography[10] as well as the predominant axial attack by Grignard reagents on unhindered ketones.[11] This assignment proved to be correct by derivation of these alcohols to the known compounds; hydrogenation of **8** and **9** over platinum yielded quantitatively the corresponding saturated alcohols (**11** and **12**), mp 65.5—67°C and 95—96°C, which were identified as *c*- and *t*-4-*tert*-butyl-1-methyl-*r*-1-cyclohexanols.[12] The olefinic alcohols **8** and **9** were then converted with methyl iodide and sodium hydride into the respective methyl ethers **1** and **2**, bp 76—78°C/25 mmHg and 88—89°C/17 mmHg, in 60 and 70% yields.

The reduction of *cis*-ether **1** with excess of lithium in ethylamine at *ca.* −70°C for 1 hr produced a 87 : 4 : 9 mixture (vpc) of three compounds (**13**, **14** and **15**), which were separated by preparative vpc into the main product **13** and the mixture of minor products **14** and **15** in 72 and 10% yields. Compound **13** was identified as 4-*tert*-butyl-1-methylcyclohexene by comparison of the authentic sample.[13] The mixture in question displayed in the NMR spectrum a broad multiplet and a sharp singlet at τ 4.43 and τ 9.13 due to *two* olefinic and *tert*-butyl protons, indicating that it consisted of stereoisomeric 3-*tert*-butyl-6-methylcyclohex-1-enes. Hydrogenation of the mixture over palladium followed by examination of the resulting saturated hydrocarbons[13] by vpc proved the minor and major components to be *cis*- and *trans*-isomers **14** and **15**, respectively.

The same reaction of *trans*-ether **2** led to the same result; formation of a 87 : 4 : 9 mixture of **13**, **14** and **15**, indicating the products to be formed through a *common* intermediate (**16**) from both the ethers **1** and **2**.

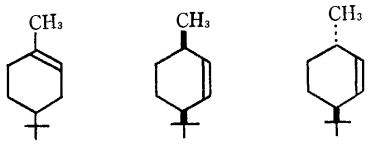

13 **14** with Δ **15** with Δ
21 without Δ **22** without Δ

The reduction was next followed by vpc with time. Thus, excess of lithium was added to a solution of *trans*-ether **2** in ethylamine at *ca.* −70°C, and a small portion of the mixture was picked up and the product components were determined in a short interval of time, after the blue color appeared. It was found that (1) the reduction was extremely fast; while 25% of the starting ether remained unchanged after 30 sec, the reaction had been completed after 50 sec, and (2) the ratio of the reaction products **13**, **14** and **15** was constant (87 : 4 : 9) before and after the starting ether reacted completely. As expected, the compound **13** or the mixture of **14** and **15** itself was recovered unchanged on treatment for 2 hr under the conditions used.

Finally it was attempted to examine the relative rates of *cis*- (**1**, axial methoxy) and *trans*-ether (**2**, equatorial methoxy); that is, equal amounts of **1** and **2** in ethylamine were reacted with excess of lithium. Interestingly, the reduction of *cis*-isomer **1** proceeded much more fast, at least with the rate of 50 times, than that of *trans*-isomer **2**, although the ratio could not be determined quantitatively owing to the extreme rapidness. These results were summarized as shown in Scheme 1.

In this Scheme, the processes of **1** or **2** to allyl radical **19** or allyl anion **16**[14] must involve the rate-determining step and would probably contain some complexes formed between metal or electron and allyl ethers such as **17** or **18**, since the reactions of **1** and **2** proceeded with the different rates and led to the same results. In view of the difficulty of reduction of an isolated double bond and of reductive cleavage of a saturated alkyl ether, it would be very improbable that the processes either consisted of two steps, addition

9) *Cf.*, G. Stork and F. H. Clarke, Jr., *J. Amer. Chem. Soc.*, **83**, 3114 (1961).

10) *Cf.*, D. H. R. Barton and R. C. Cookson, *Quart. Rev.*, **10**, 44 (1956).

11) M. Chérest and H. Felkin, *Tetrahedron Lett.*, **1971**, 383, and literatures cited there; J. C. Richter, *J. Org. Chem.*, **30**, 324 (1965). *Cf.*, E. L. Eliel and Y. Senda, *Tetrahedron*, **26**, 2411 (1970); D. C. Wigfield and D. J. Phelps, *Chem. Commun.*, **1970**, 1152; D. N. Kirk, *Tetrahedron Lett.*, **1969**, 1727.

12) B. Cross and G. H. Whitham, *J. Chem. Soc.*, **1960**, 3895.

13) F. G. Bordwell, P. S. Landis, and G. S. Whitney, *J. Org. Chem.*, **30**, 3764 (1965).

14) The transformation of **19** to **16** would proceed very readily, as the energy level of the highest half-occupied orbital of methylallyl radical corresponding to the anion **20** would be very low ($-0.10\sim-0.20\beta$). We are indebted to Mr. H. Kashiwagi in our Department for calculation as to methylallyl radical.

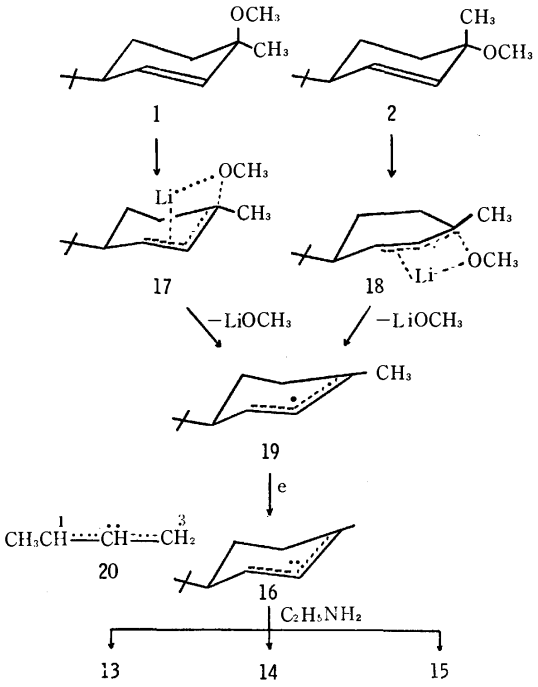

Scheme 1

of an electron to the double bond (the energy of lowest unoccupied molecular orbital,[15] -1.0β) and subsequent removal of the methoxy anion, or direct expulsion of the methoxy group by metal or an electron. The following step, the irreversible protonation of anion **16**, would occur most preferably at the site with the highest total π-electron density.[16] The distribution of π-electron of methylallyl anion **20** was calculated[17] by the Hückel MO orbital method, using more or less standard parameters.[18] The result showed that the site in question was the carbon atom (C_3 of **20**) unsubstituted by the methyl group (the difference in total π-electron density between C_1 and C_3, 0.15—0.25 electron). Thus the predominant formation of compound **13** would be reasonably interpreted by assuming that the afore-mentioned calculation with model **20** could be applied for the present intermediate **16**. On the other hand, the difference in formation of **14** and **15** might be rationalized on the basis of the difference in continued maximum overlap[19] between the axially oriented π-orbitals at C_1, C_2 and C_3 of **16** on approach of the proton of ethylamine, or of that in steric hindrance between the transition states leading to the products **14** and **15** from **16**. Further investigations concerning which factor is generally more or exclusively important are now in progress.

15) *Cf.*, A. Streitwieser, Jr., "Molecular Orbital Theory for Organic Chemistry," John Wiley & Sons, Inc., New York, N. Y. (1962).
16) H. E. Zimmerman, *Tetrahedron*, **16**, 169 (1961).
17) H. Kashiwagi, private communication.
18) T. Yonezawa, C. Nagate, H. Kato, A. Imamura, and K. Morokuma, "Ryoshi Kagaku Nyumon," Kagaku Dozin, Kyoto (1968), p. 56 and 173.
19) *Cf.*, H. E. Zimmerman and A. Mais, *J. Amer. Chem. Soc.*, **81**, 4305 (1959), and their previous papers.
20) *Cf.*, A. J. Birch, *J. Chem. Soc.*, **1946**, 595; *ibid.*, **1944** 430.

Experimental

The melting points were measured in open capillaries and uncorrected. Homogenity of each compound was always checked by tlc on silica gel (Wakogel B-5) and/or alumina (Merck G), and also by vpc (PEG-6000) with Hitachi Gas Chromatograph Model K53. The UV and IR spectra were taken in 99% ethanol and in liquid state, unless otherwise stated. The NMR spectra were measured in deuterochloroform at 60 and/or 100 MHz, TMS being used as an internal standard, unless otherwise stated. The abbreviations "s, d, t, q, br and m" in the NMR spectra denote "singlet, doublet, triplet, quartet, broad and multiplet," respectively.

4-tert-*Butylanisole (3).* 4-*tert*-Butylphenol was converted into **3** in 80% yield by the method of Olson *et al.*,[6] bp 87—88°C/8 mmHg (lit,[6] bp 232.2°C/760 mmHg); IR, ν_{max} 1610, 1247, 1183 and 1039 cm^{-1}; NMR, τ 8.71 (9H, s, *tert*-butyl), 6.23 (3H, s, $OC\underline{H}_3$), and 3.17 and 2.71 (each 1H, ABq J=9 Hz, $\underline{H}$ at C_2 and C_3).

4-tert-*Butyldihydroanisole (4).* Compound **3** was reduced under the conditions similar to those of the Birch reduction of the corresponding isopropyl derivative;[7] small pieces of lithium (6 g) were added under vigorous stirring to a solution of liquid ammonia (300 m*l*) containing **3** (20 g) in dry ether (130 m*l*) cooled with dry ice-acetone. The mixture was stirred for 30 min after the blue color appeared. The color gradually disappeared on addition of ethanol (70 m*l*). After removal of ammonia, the residue was mixed with water and extracted with ether. The ether solution was dried over anhydrous sodium sulfate, evaporated and then distilled to give **4** (14.8 g), which was used for the next reaction without further purification, bp 86—87°C/8 mmHg; IR, ν_{max} 1695, 1658 and 1608 cm^{-1}; NMR, τ 8.94 (9H, s, *tert*-butyl), 7.78 (4H, s, $\underline{H}$ at C_5 and C_6), 6.43 (3H, s, $OC\underline{H}_3$), and 5.08 and 4.37 (each 1H, ABq J=6.5 Hz, $\underline{H}$ at C_2 and C_3). The NMR spectrum indicated that the product (a single peak by vpc) would be the 5,6-dihydro derivative rather than the expected compound, 4-*tert*-butyl-3,6-dihydroanisole.

4-tert-*Butylcyclohex*-2-*en*-1-*one (5) and 4*-tert-*Butylcyclohex*-3-*en*-1-*one (6).* Compound **4** (7.4 g) was refluxed in 5% hydrochloric acid (bath temperature, 140°C) for 10 hr.[8,20] After being cooled, the mixture was treated with ether. The ether solution was washed with 5% sodium carbonate solution and water, dried and evaporated to leave oily residue, which proved to be a 79 : 21 mixture of **5** and **6** by vpc. The residue (6.27 g) was submitted to column chromatography over a mixture of silicic acid (120 g) and celite (35 g), each fraction being checked by vpc. Fractions eluted with benzene, showing a single peak, were collected and purified by distillation to give $\beta\gamma$-unsaturated ketone **6** (1.0 g), bp 95—97°C/9 mmHg; IR, ν_{max} 1720 and 809 cm^{-1}; NMR, τ 8.90 (9H, s, *tert*-butyl), 7.20 (2H, d, J= 3.5 Hz, $\underline{H}$ at C_2), and 4.48 (1H, t, J=3.5 Hz, $\underline{H}$ at C_3).

Found: C, 78.65; H, 10.88%. Calcd for $C_{10}H_{16}O$; C, 78.89; H, 10.59%.

Fractions eluted withb enzene - ether (4 : 1), showing a single peak, were treated in the same manner as mentioned above and afforded $\alpha\beta$-unsaturated ketone **5** (3.0 g), bp 101—102°C/11 mmHg; UV, λ_{max} 224 mμ (ε 10500); IR, ν_{max} 1691 and 1618 cm^{-1}; NMR, τ 9.12 (9H, s, *tert*-butyl), 3.99 (1H, double d, J=10.5 and 2.5 Hz, $\underline{H}$ at C_2), and 2.98 (1H, dobule t, J=10.8, 2.0 and 2.0 Hz, $\underline{H}$ at C_3).

Found: C, 78.77; H, 10.63%. Calcd for $C_{10}H_{16}O$: C, 78.89; H, 10.59%.

The composition ratio of **5** and **6** in the product was about 1 to 1 after 5 hr reflux in 5% hydrochloric acid, and changed

to 4 to 1 after 10 hr reflux. This ratio (4 : 1) was obtained after 3 hr reflux in 7.5% hydrochloric acid.

4-tert-*Butyl-2-hydroperoxycyclohex-3-en-1-one* (**7**). When compound **6** was allowed to stand in the air at room temperature, a crystalline substance gradually separated out. After one month compound **6** became completely crystalline. Recrystallization from carbon tetrachloride afforded hydroperoxide **7**, mp 106—107°C, UV, λ_{max} 216 mμ (ε 12600); IR (Nujol), ν_{max} 3200, 1660 and 871 cm^{-1}; NMR, τ 8.91 (9H, s, *tert*-butyl), 3.78 (1H, d, J=10.5 Hz, H at C_2), 3.06 (1H, d, J=10.5 Hz, H at C_3), and 1.10 (1H, s, OOH).

Found: C, 65.13; H, 8.84%. Calcd for $C_{10}H_{16}O_3$: C, 65.19; H, 8.75%.

A solution of **7** (300 mg) in methanol (20 m*l*) was treated with sodium borohydride (100 mg) under cooling with ice-water and stirring for 1 hr. After addition of acetic acid (0.6 m*l*) and water (50 m*l*), the mixture was extracted with ether. The ether solution was dried and evaporated to leave crystalline substance, which showed two spots on tlc. The main product (**7a**) was obtained by preparative tlc, had mp 108.5—109.5°C, and amounted to 160 mg. Recrystallization from ether afforded an analytical sample, mp 108.5—109.5°C; IR (Nujol), ν_{max} 3250, 1050 and 951 cm^{-1}.

Found: C, 70.21; H, 11.03%. Calcd for $C_{10}H_{18}O_2$: C, 70.54; H, 10.66%.

Compound **7a** (40 mg) dissolved in a small volume of acetone was poured onto a column filled with silica gel (Wako-gel Q-23, 5.0 g) freshly washed with acetone and then with *n*-hexane, and eluted successively with *n*-hexane, and *n*-hexane - acetone (97 : 3, 95 : 5 and 92 : 8). Eluates from the solvent mixtures were purified by preparative tlc (chloroform) to give the acetonide (**7b**, 26 mg), oil; IR, ν_{max} 1060, 1030, 882, and 856 cm^{-1}; NMR, τ 8.90 (9H, s, *tert*-butyl), 8.64 (6H, s, *gem*-CH$_3$), 5.80 and 5.57 (each 1H, br, m, H at C_4 and C_3), and 4.55 (1H, br, d, J=4 Hz, H at C_2).

Found: C, 74.56; H, 10.34%. Calcd for $C_{13}H_{22}O_2$; C, 74.24; H, 10.54%.

c- *and* t-*4*-tert-*Butyl-1-methylcyclohex-2-en*-r-*1-ol* (*8 and 9*). To a cooled, suspended mixture of small pieces of lithium (7.3 g) in dry ether (200 m*l*) was added methyl iodide (30 m*l*) in dry ether (40 m*l*) under stirring and under a stream of nitrogen. The mixture was refluxed for 4 hr and then filtered rapidly through glass-wool.[9] After dropwise addition of $\alpha\beta$-unsaturated ketone **5** (10.1 g) dissolved in ether (50 m*l*) to the filtrate, the whole mixture was stirred at room temperature for 1 hr, then treated with a solution of sodium sulfate (8.0 g) and sodium thiosulfate (0.5 g) in water (100 m*l*) under cooling to decompose excess of the lithium, and extracted with ether. The ether solution was dried and evaporated to leave oily residue (11.8 g), showing two spots on tlc (benzene - ether, 5 : 1 or 4 : 1). This was separated by column chromatography over alumina (standard, active II—III, 130 g). Fractions eluted with *n*-hexane and *n*-hexane - benzene (10 : 1), showing a single spot with higher R_f value were collected and evaporated to give crystalline *cis*-alcohol (**8**, 3.45 g), which on sublimation had mp 36—37°C; IR (CS_2), ν_{max} 3620, 3400, 1100, 902 and 735 cm^{-1}; NMR, τ 9.04 (9H, s, *tert*-butyl), 8.75 (3H, s, CH$_3$ at C_1), and 4.28 (2H, br s, H at C_2 and C_3).

Found: C, 78.29; H, 11.91%. Calcd for $C_{11}H_{20}O$: C, 78.51; H, 11.98%.

Fractions eluted with *n*-hexane - benzene (10 : 1, 8 : 2, 6 : 4 and 1 : 1) showed two spots on tlc. The following fractions eluted with benzene showed a single spot with lower R_f value on tlc and afforded *trans*-alcohol **9** (4.7 g), which on sublimation had mp 57—58°C; IR (CS_2), ν_{max} 3620, 3400, 1120, 918 and 752 cm^{-1}; NMR, τ 9.09 (9H, s, *tert*-butyl), 8.76 (3H, s, CH$_3$ at C_1), and 7.81 (1H, s, OH), and 4.41 (2H, s, H at C_2 and C_3).

Found: C, 78.49; H, 11.97%. Calcd for $C_{11}H_{20}O$: C, 78.51; H, 11.98%.

cis-Alcohol **8** (50 mg) was hydrogenated over rhodium-platinum (30 mg) in ethanol (5 m*l*) for 24 hr. After filtration of the catalysis the solution was evaporated and then extracted with ether. The ether solution was washed with water, dried and evaporated to leave oily residue, which crystallized on trituration with *n*-hexane, had mp 61—63°C and amounted to 48 mg. This was distilled for purification to give *c*-4-*tert*-butyl-1-methyl-*r*-1-cyclohexanol (**11**), mp 65.5—67°C (lit,[12] mp 66—67°C); IR (CS_2), ν_{max} 3600, 1198, 1098, 1026, 990, 925, and 904 cm^{-1} (lit,[12] ν_{max} 1200, 1100, 1031, 995, 923, and 909 cm^{-1}); NMR, τ 9.14 (9H, s, *tert*-butyl) and 8.87 (3H, s, CH$_3$ at C_1).

trans-Alcohol **9** (50 mg) was hydrogenated over platinum (50 mg as PtO_2–H_2O) in methanol (5 m*l*) for 2 hr. The mixture was worked up as usual to give *t*-4-*tert*-butyl-1-methyl-*r*-1-cyclohexanol[12] (**12**, 48 mg), mp 91—93°C, which on recrystallization from aqueous methanol had mp 95—96°C (lit,[12] mp 89—90°C); IR (CS_2), ν_{max} 3600, 3340, 1137, 1100, 977, and 913 cm^{-1} (lit,[12] ν_{max} 1142, 1103, 979, and 914 cm^{-1}); NMR, τ 9.14 (9H, s, *tert*-butyl) and 8.88 (3H, s, CH$_3$ at C_1).

4-tert-*Butyl-1-methylcyclohex-3-en-1-ol* (**10**). To methyl lithium, prepared from methyl iodide (20 g), lithium (2.0 g) and dry ether (60 ml) was dropwise added $\beta\gamma$-unsaturated ketone **6** (1.0 g) in dry ether (20 m*l*). The mixture was refluxed for 25 hr under stirring and then worked up in the same manner as the case of **5** to give oily substance (1.18 g). A part (380 mg) of the oil was purified by preparative tlc (benzene - ether, 4 : 1) to yield crystalline alcohol **10** (137 mg), mp 38—40°C, which on further purification by sublimation had mp 64—66°C and amounted to 82 mg; IR (Nujol), ν_{max} 3320, 1128, 1104, and 884 cm^{-1}; NMR, τ 8.96 (9H, s, *tert*-butyl), 8.82 (3H, s, CH$_3$ at C_1), and 4.66 (1H, m, H at C_3).

Found: C, 78.35; H, 11.85%. Calcd for $C_{11}H_{20}O$: C, 78.51; H, 11.98%.

c- *and* t-*6*-tert-*Butyl*-r-*3-methoxy-3-methylcyclohex-1-enes* (*1 and 2*). A mixture of *cis*-alcohol **8** (2.7 g) and sodium hydride (2.5 g), washed with *n*-hexane repeatedly, was stirred vigorously in dry ether (180 m*l*) at room temperature for 19 hr under a stream of nitrogen. After addition of methyl iodide (50 m*l*), the whole mixture was refluxed overnight under stirring and then filtered. The filtrate was washed with water, dried, evaporated, and then distilled to give the methyl ether (**1**, 1.75 g), showing a single peak by vpc, bp 76—78°C/25 mmHg; IR ($CHCl_3$), ν_{max} 1371, 1110, 1073, 868, and 822 cm^{-1}; NMR, τ 9.10 (9H, s, *tert*-butyl), 8.81 (3H, s, CH$_3$ at C_3), 6.80 (3H, s, OCH$_3$), and 4.34 and 4.08 (each 1H, ABq, J=11 Hz, H at C_1 and C_2 or *vice versa*).

Found: C, 79.35; H, 11.98%. Calcd for $C_{12}H_{22}O$: C, 79.06; H, 12.16%.

trans-Alcohol **9** (3.2 g) was treated in the same manner (sodium hydride 2.6 g, methyl iodide 50 m*l*, and ether 200 ml) as **8**, and afforded the methyl ether (**2**, 2.40 g) after distillation, bp 88—89°C/17 mmHg; IR, ν_{max} 1368, 1110, 1078, 868, and 830 cm^{-1}; NMR, τ 9.11 (9H, s, *tert*-butyl), 8.79 (3H, s, CH$_3$ at C_3), 7.80 (3H, s, OCH$_3$), and 4.43 and 4.18 (each 1H, ABq, J=11 Hz, H at C_3 and C_2).

Found: C, 79.30; H, 11.87%. Calcd for $C_{12}H_{22}O$: C, 79.06; H, 12.16%.

Reduction of cis- *and* trans-*ethers* ***1*** *and* ***2***. To a solution of *cis*-ether **1** (2.2 g) in ethylamine (70 m*l*) cooled with dry ice - acetone (*ca.* −70°C) were added small pieces of lithium (1.0 g) under stirring, and the blue color appeared after 10 min. The mixture was further stirred for 1 hr and the reaction was stopped by addition of ammonium chloride. After removal of the ethylamine, the residue was treated with ether and water, and the ether solution was dried and evaporated carefully to leave oily substance (1.7 g), which was decolorized by passing through alumina column and proved to be a 87 : 4 : 9 mixture of three components by vpc (PEG-6000, 70°C, and nitrogen 0.9 kg/cm^2). A part (1.0 g) of the oily product was separated into the main product (0.59 g) and the mixture of two minor products (84 mg) by preparative vpc with Varian Aerograph Autoprep 700, using DGSP and helium gas (60 m*l*/min) at 60°C. The former was identified as 4-*tert*-butyl-1-methylcyclohex-1-ene (**13**) by comparison (vpc and NMR) with the authentic sample;[13] NMR, τ 9.15 (9H, s, *tert*-butyl), 8.37 (3H, br s, C$\underline{H}_3$ at C_1), and 4.70 (1H, br, $\underline{H}$ at C_2). This compound **13** (290 mg) was hydrogenated over palladium charcoal (12 mg) in ethanol (5 m*l*) according to the known procedure.[13] The vpc analysis showed the product to be a 32 : 68 mixture of *c*- and *t-r*-1-*tert*-butyl-4-methylcyclohexanes (**21** and **22**) (lit,[13] the ratio, 27 : 73).

The latter mixture was supposed to consist of stereoisomeric 3-*tert*-butyl-6-methylcyclohex-1-enes (**14** and **15**) on the basis of the NMR spectrum: τ 9.13 (9H, s, *tert*-butyl), 9.07 (3H, d, J=6 Hz, C$\underline{H}_3$ at C_6), and 4.43 (2H, br m, $\underline{H}$ at C_1 and C_2). This was supported in the following: hydrogenation of the mixture (20 mg) in the same manner as **13** produced a 31 : 69 (*ca.* 4 : 9) mixture (vpc) of the corresponding saturated *cis*- and *trans*-hydrocarbons **21** and **22**.

The reduction of *trans*-ether **2** was carried out in the same manner as that of the *cis*-isomer **1** and gave a 87 : 4 : 9 mixture of **13**, **14**, and **15**. Hydrogenation of the relevant mixture of two minor products afforded a 27 : 73 (*ca.* 4 : 9) mixture (vpc) of **21** and **22**.

To a solution of *trans*-ether **2** (2.2 g) in ethylamine (100 m*l*) cooled at *ca.* −70°C were added small pieces of lithium (0.8 g). A small fraction of the mixture was picked up in a small interval of time (30 and 50 sec, 1, 5, 10, 15, and 20 min, 1 and 1.5 hr) after the blue color appeared, and the composition of each fraction was checked by vpc. The first fraction, picked up after 30 sec, was found to contain **2**, **13**, **14**, and **15** in the ratio of *ca.* 25, 65, 3, and 7. All other fractions consisted only of **13**, **14**, and **15** with the ratio of 87, 4, and 9.

To a solution of equal amounts (150 mg) of *cis*- and *trans*-ethers (**1** and **2**) in ethylamine (30 m*l*) cooled at *ca.* −70°C was added lithium (300 mg) under vigorous stirring. A part of the mixture was taken up as soon as the blue color appeared and the components were determined by vpc, when *cis*-ether **1** practically disappeared and the ratio in area of **2** and **1** was over 50.

BULLETIN OF THE CHEMICAL SOCIETY OF JAPAN, VOL. 45, 1816—1820 (1972)

Methylene Analogs of Cyclobutenedione. III.[1] The Reaction of 2-Bromo- and 2,2-Dibromo-3,4-bis(diphenylmethylene)cyclobutanone with Alcoholic Potassium Hydroxide

Fumio TODA and Yoshikazu TAKEHIRA

Department of Industrial Chemistry, Faculty of Engineering, Ehime University, Matsuyama

(Received October 19, 1971)

The reactions of 2-bromo-3,4-bis(diphenylmethylene)cyclobutanone (III) with methanolic and 2-propanolic potassium hydroxide afforded methyl 4-methoxy-2,3-bis(diphenylmethylene)butyrate (VIII) and 3,4-bis-(diphenylmethylene)-γ-lactone (XXI) respectively. The reaction of the 2,2-dibromo analog of III (XXV) with methanolic potassium hydroxide afforded methyl 4-methoxy-4-bromo-2,3-bis(diphenylmethylene)butyrate (XXVIIIa) and methyl 4,4-diphenyl-3-formyl-2-diphenylmethylenebut-3-enate (XXIIIa) in approximately equal yields. However, the reaction of XXV with 2-propanolic potassium hydroxide afforded XXIIIc exclusively. The reaction mechanism was disclosed to be that the haloester intermediates V and XXVII initially formed from III and XXV respectively, by the addition of alcohol to the carbonyl followed by the ring-opening, react with the alkoxy and hydroxy anions competitively.

It has been reported that the reaction of 2-halo-,[2] 2,4-dihalo,[2] and 2,2-dihalocyclobutanone[3] with a base affords the corresponding cyclopropane carboxylic acid *via* a Favorskii transformation. It has also been reported that the treatment of 2,2-dihalocyclobutanone (I) with a base affords the ring-opened product (II).[3-6]

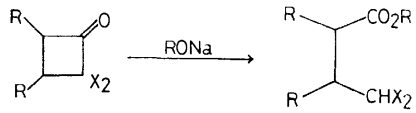

(I) (II)

1) Part II: F. Toda and K. Akagi, *Tetrahedron*, **27**, 2801 (1971). Note the change in the title of the series of publications to "Methylene Analogs of Cyclobutenedione" instead of the previously-used "Methylene Analogs of Cyclobutadienequinone." Since cyclobutadiene is not an aromatic compound, its dicarbonyl derivative is not a real quinone.

2) J. L. Ripoll, *Ann. Chim.* (Paris), **2**, 233 (1967).

3) V. Fletcher and A. Hassner, *Tetrahedron Lett.*, **1970**, 1071.

4) J. M. Conia and J. L. Ripoll, *Bull. Soc. Chim. Fr.*, **1963**, 763.

5) L. Ghosez, R. Montarzine, and P. Mollet, *Tetrahedron Lett.*, **1966**, 135.

6) T. R. Patts and R. E. Harmon, *J. Org. Chem.*, **34**, 2792 (1970).

In connection with these facts, we are interested in the reaction of 2-bromo- (III) and 2,2-dibromo-3,4-bis(diphenylmethylene)cyclobutanone(XXV) with alcoholic potassium hydroxide. The actual products were compounds that were derived by the reaction of both the carbonyl and the bromine of III and XXV with the base. Therefore, of particularly interest to us the determination of the reaction site which the base attacks initially.

The reaction of III[1] with methanolic potassium hydroxide at room temperature for 6 hr afforded VIII in a 93% yield. The structure of VIII was determined by means of the spectral data described in the Experimental section. For the reaction, the two main paths are considerable, as is shown in Scheme 1. One of them proceeds *via* the VI produced by the substitution. The other one proceeds *via* the IV produced by the addition. However, any possibility of the formation of VI in the reaction is neglected, since the reaction of VI, prepared according to a previously-reported method,[1] with methanolic potassium hydroxide afforded IX and XIII in 30 and 43% yields respectively, but no detectable VIII. The structure of IX was identified by means of the spectral data shown in the Experimental section. The UV spectrum of IX in C_2H_5OH, 293 nm (ε, 17600), was comparable to that of the analogous compound, 4-diphenylmethylene-3-diphenylhydroxymethylcyclobut-2-enone in C_2H_5OH, 280 nm (ε, 15400).[1,7] The structure of IX was further identified by the reaction with bromine in chloroform to afford XVI[1] in a 30% yield. The reaction may proceed *via* XIV and XV, as is shown in Scheme 1. The structure of XIII was identified by a comparison of its spectral data with those of an authentic sample prepared by the reaction of XVI with methanol in the presence of a catalytic amount of bromine.[8]

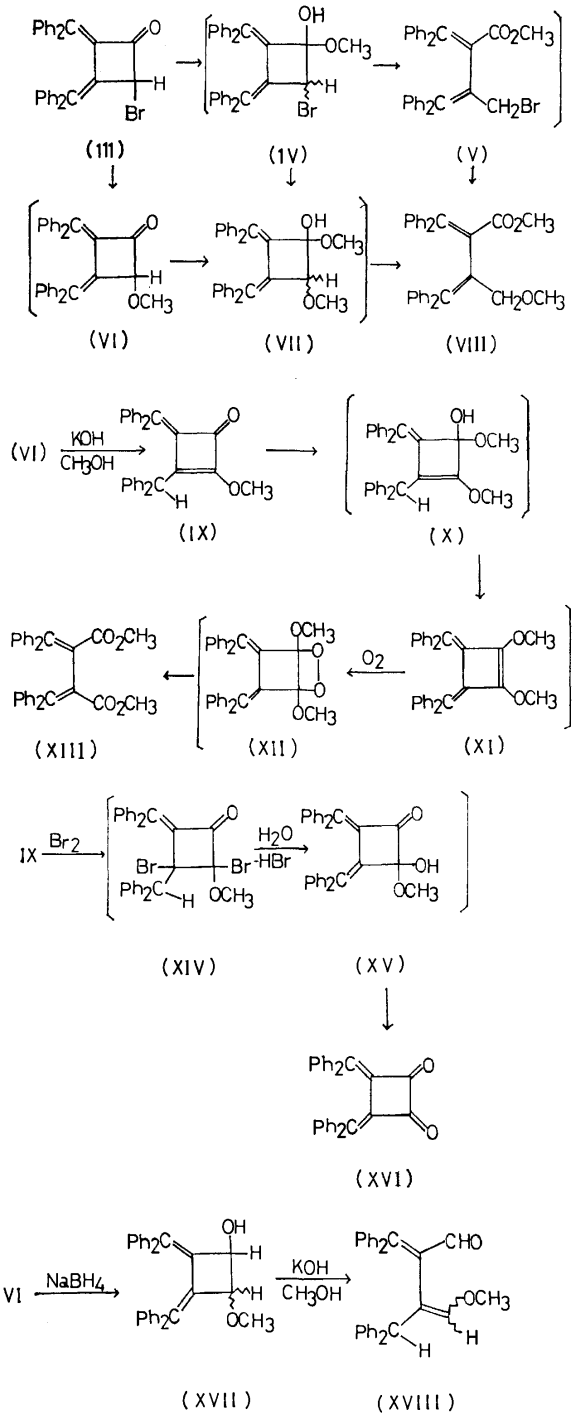

Scheme 1.

It was proven that the IX initially produced by the 1,3-hydrogen shift of VI reacts further with sodium methoxide in the presence of oxygen and finally affords XIII, probably *via* X, XI, and XII. When VI was treated with sodium methoxide under nitrogen, IX was obtained in a 65% yield, besides a small amount of XIII (1%). The treatment of IX with the base under oxygen afforded XIII exclusively. It is probable that XI reacts with oxygen and affords XIII, since it has been established that the analogous compound, 3,4-bis(diphenylmethylene)cyclobutene, reacts with oxygen rapidly even in the course of recrystallization and affords 3,4-bis(diphenylmethylene)butanedial.[9]

On the basis of the results obtained above, the reaction path which proceeds *via* IV was established as reasonable. Nevertheless, there is still the problem to be resolved of whether the conversion of IV into VIII proceeds *via* V or VII. The possibility that VII is an intermediate can, however, be ruled out, since XVII, which is analogous to VII, showed a different type of reaction with the base. The reaction of XVII, prepared by the sodium borohydride reduction of VI, with the base afforded the vinyl ether XVIII, but no compound analogous to VIII.[10]

The reaction of III with 2-propanolic potassium hydroxide to afford XXI exclusively can also be interpreted by assuming XIX as an intermediate. The hydroxy ester, XX, produced by the reaction of XIX with the hydroxy anion undergoes intramolecular cyclization to XXI. The cyclization of XX to XXI is reasonable, since the sodium borohydride reduction of XXIIIa prepared by the reaction of XVI with

7) F. Toda and K. Akagi, *Tetrahedron Lett.*, **1970**, 5289.
8) F. Toda and J. Fujita, This Bulletin, **45**, 1928 (1972).
9) F. Toda, M. Higashi, and K. Akagi, *Chem. Commun.*, **1969**, 1219.
10) F. Toda and N. Ooi, This Bulletin, **45**, 1820 (1972).

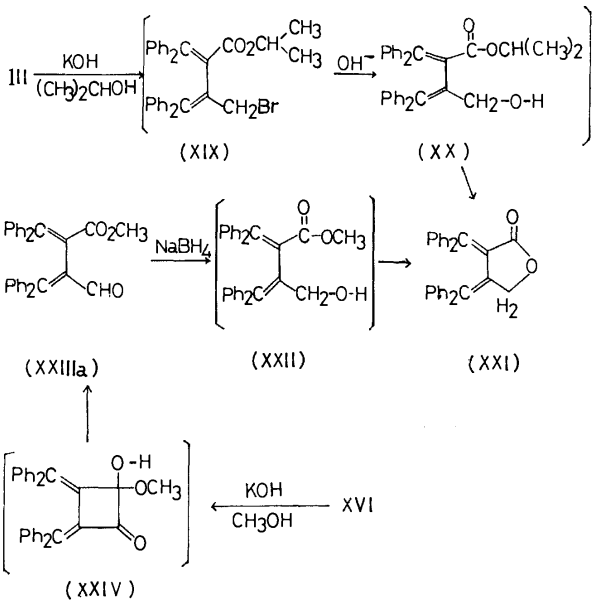

Scheme 2.

methanolic potassium hydroxide afforded XXI quantitatively, probably *via* XXII, which is analogous to XX, and since it has been established that the sodium borohydride reduction of γ-keto ester afford γ-lactones.[11,12]

Finally, the most reasonable path from III to VIII is that which proceeds successively *via* IV and V. Therefore, the reaction type of III with the base is similar to that of I to afford II.[3-6]

The reaction of XXV[1] with methanolic potassium hydroxide at room temperature for 6 hr afforded XXVIIIa and XXIIIa in 48 and 52% yields respectively. The structure of XXVIIIa was identified by means of the spectral data described in the Experimental section.

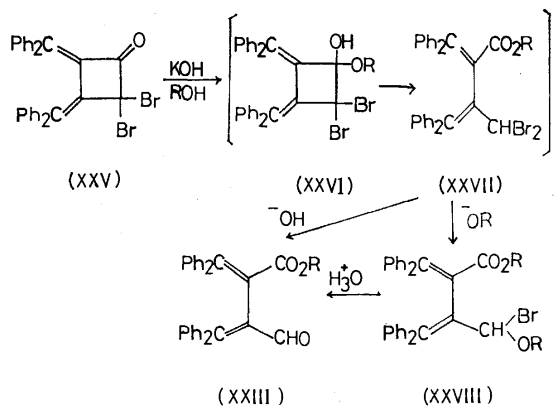

a : $R=CH_3$
b : $R=C_2H_5$
c : $R=CH(CH_3)_2$

Scheme 3.

Under the reaction conditions employed for XXV, XXVIIIa was not converted to XXIIIa, but was recovered unchanged, even though the heating of XXVIIIa with hydrochloric acid in methanol afforded XXIIIa in a 52% yield.

Since XXVIIIa is analogous to the VIII produced by the reaction of III with methanolic potassium hydroxide, a similar reaction mechanism is applicable. As is shown in Scheme 3, the XXVI initially produced by the attack of the methoxy anion on the carbonyl of XXV undergoes ring-opening to afford XXVII. The two competing reactions of XXVII with the methoxy and hydroxy anions afford XXVIII and XXIII respectively. Evidence for the presence of the competing reactions was obtained by the following experiments. When XXV was treated with ethanolic potassium hydroxide. XXVIIIb and XXIIIb were isolated in 15 and 85% yields respectively. However, the same treatment of XXV with 2-propanolic potassium hydroxide afforded XXIIIc exclusively (80% yield). The spectral data of XXVIIIb (Experimental section) were comparable to those of XXVIIIa. The spectral data of XXIIIb and XXIIIc (Experimental section) were also comparable to those of XXIIIa.

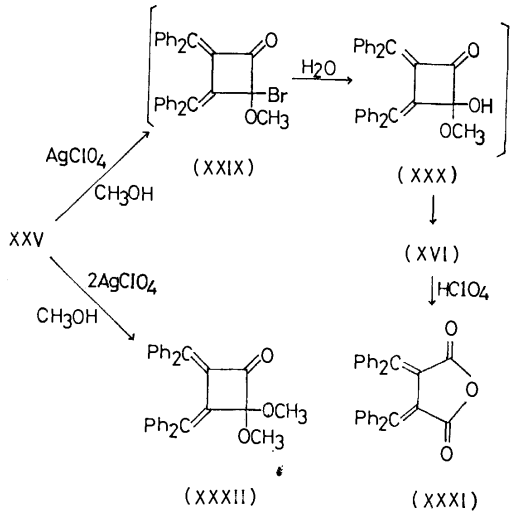

Scheme 4.

The type of the reaction of XXV with the base to afford XXVIII and XXIII *via* XXVII is also similar to that of III and of I. The monomethoxy ketone XXIX, analogous to VI, which was ruled out as a possible intermediate in the reaction of III, is probably not an intermediate for the following reasons. The reaction of XXV with an equimolar amount of silver perchlorate in wet methanol at room temperature afforded XVI and XXXI in 16 and 30% yields respectively. A reasonable reaction path is that shown in Scheme 4, since the reaction of XXV with two molar amounts of silver perchlorate in wet methanol afforded XXXII in a 55% yield, and since the oxidation of XVI into XXXI by perchloric acid has been established.[1] The high reactivity of the bromine of XXIX

11) R. Gelin and M. Chiguac, *C. R. hebd. Séances Acad. Sci.*, **258**, 3313 (1964).

12) P. de Mayo, E. Y. Spencer, and R. W. White, *Can. J. Chem.*, **41**, 2996 (1963).

13) All the IR and NMR spectra were measured in Nujol mull and $CDCl_3$ respectively.

in the acidic media suggests that XXIX in methanolic potassium hydroxide affords a halogen-free product instead of XXVIIIa.

Experimental[13]

The Reaction of III with Methanolic Potassium Hydroxide. A suspension of finely-powdered III[1] (0.35 g) in 5% methanolic potassium hydroxide (30 ml) was stirred at room temperature for 6 hr. The crude product obtained by the addition of water to the reaction mixture was collected by filtration, washed with water, and dried. The crude product was recrystallized from cyclohexane to afford VIII as colorless prisms; 0.25 g (93%); mp 152—153°C. IR, 1710 (C=O), 1435 (ester CH_3), 1265 and 1245 (ester) and 1105 cm^{-1} (C-O-C); UV, ($CHCl_3$), 234 (26400), 260 sh (16200) and 314 nm (ε, 8400); NMR, 2.7—3.2 (m, C_6H_5, 20H), 6.03 (s, CH_2, 2H), 6.53 (s, CO_2CH_3, 3H) and 6.63 τ (s, OCH_3, 3H).

Found: C, 83.38; H, 5.99%. Calcd for $C_{32}H_{28}O_3$: C, 83.48; H, 6.10%.

The Reaction of VI with Methanolic Potassium Hydroxide. A suspension of finely-powdered VI[1] (0.5 g) in 5% methanolic potassium hydroxide (20 ml) was stirred at room temperature for 20 hr. The yellow crystals which separated out were collected by filtration, washed with methanol, and recrystallized from acetone to afford XIII as yellow needles; 0.24 g (43%); mp 233—234°C (lit,[8] 233—234°C). The spectral data were identical with those of an authentic sample prepared by a separate method.[8]

The addition of water to the mother liquor remaining after the separation of the crude crystals of XIII by filtration afforded crude crystals. The recrystallization of the crude crystals from cyclohexane afforded IX as colorless prisms; 0.15 g (30%); mp 126—127°C. IR, 1760 (C=O), 1650 (*exo* C=C), 1590 (*endo* C=C), 1290 (=C-O-) and 1080 and 1060 cm^{-1} (C-O-C); UV (C_2H_5OH), 293 nm (ε, 17600); NMR, 2.6—3.2 (m, C_6H_5, 20H), 5.33 (s, CH, 1H) and 5.95 τ (s, CH_3, 3H).

Found: C, 86.27; H, 5.51%. Calcd for $C_{31}H_{24}O_2$: C, 86.89; H, 5.65%.

When a suspension of VI (0.2 g) in 5% methanolic potassium hydroxide (50 ml) was stirred for 24 hr at room temperature under nitrogen, and when the reaction mixture was then treated as above, 0.13 g (65%) of IX and 2 mg (1%) of XIII were isolated.

The Reaction of IX with Methanolic Potassium Hydroxide under Oxygen. A solution of IX (0.12 g) in 5% methanolic potassium hydroxide (20 ml) was stirred at room temperature under oxygen for 24 hr. The yellow crystals which separated out were collected and recrystallized from acetone to afford XIII as yellow needles; 0.05 g (40%); mp 233—234°C.

The Reaction of IX with Bromide. One drop of bromine was added to a solution of IX (0.05 g) in chloroform (5 ml). The crude product which remained after the evaporation of the solvent was recrystallized from cyclohexane to afford XVI as green needles; 0.015 g (30%); mp 206—207°C (lit,[1] 206—207°C). The spectral data were identical with those reported.[1]

The Preparation of XXIIIa. A suspension of XVI[1] (0.4 g) in 5% methanolic potassium hydroxide (20 ml) was heated under reflux for 10 min. The crude product obtained by the addition of water to the reaction mixture was collected by filtration, washed with water, and dried. The recrystallization of the crude product from cyclohexane afforded XXIIIa as pale yellow prisms; 0.35 g (80%); mp 160—161°C. IR, 2780 (CHO), 1700 (ester C=O), 1660 (aldehyde C=O) and 1265 cm^{-1} (ester); UV (CH_3OH), 236 (20500), 289 (13700) and 335 nm (ε, 7500); NMR, 0.52 (s, CHO, 1H), 2.5—3.1 (m, C_6H_5, 18H), 3.35 (m, C_6H_5, 2H) and 6.50 τ (s, CH_3, 3H).

Found: C, 83.41; H, 5.38%; Mol wt (benzene), 436. Calcd for $C_{31}H_{24}O_3$: C, 83.76; H, 5.44%. Mol wt, 444.

The Preparation of XXI. To a solution of XXIIIa (0.55 g) in tetrahydrofuran (10 ml), we added an excess of sodium borohydride (0.2 g). The reaction mixture was decomposed with water and extracted with benzene. The benzene solution was washed with water and dried over sodium sulfate. The crude product obtained by the evaporation of the solvent was recrystallized from methanol to afford XXI as yellow prisms; 0.32 g (62%); mp 221—222°C. IR, 1750 (C=O), 1580 (C=C) and 1130 cm^{-1} (lactone); UV (C_2H_5OH), 258 (22200) and 388 nm (ε, 9200); NMR, 2.5—3.6 (m, C_6H_5, 20 H) and 5.02 τ (s, CH_2, 2H).

Found: C, 86.37; H, 5.28%; Mol wt (*m/e*), 414. Calcd for $C_{30}H_{22}O_2$: C, 86.93; H, 5.35%; Mol wt, 414.

The Reaction of III with 2-propanolic Potassium Hydroxide. A suspension of finely-powdered III (0.5 g) in 5% 2-propanolic potassium hydroxide (50 ml) was stirred at room temperature for 4 hr. The recrystallization of the crude product obtained by the addition of water to the reaction mixture from cyclohexane afforded XXI as yellow prisms; 0.15 g (35%); mp 221—222°C. Its spectral data were identical with those described above.

The Reaction of XXV with Methanolic Potassium Hydroxide. A suspension of finely-powered XXV (0.58 g) in 5% methanolic potassium hydroxide was stirred at room temperature for 6 hr. The crude product thus formed was collected by filtration, washed with water, and recrystallized from benzene-petroleum ether (bp 70—80°C) to afford XXVIIIa as colorless prisms; 0.28 g (48%); mp 182—183°C. IR, 1720 (C=O), 1240 (ester) and 1090 and 1080 cm^{-1} (C-O-C); UV ($CHCl_3$), 272 nm (ε, 9100); NMR, 2.6—3.0 (m, C_6H_5, 20H), 3.65 (s, CH, 1H), 6.85 (s, CH_3, 3H) and 7.08 τ (s, CH_3, 3H).

Found: C, 71.34; H, 5.36%; Mol wt (benzene), 525. Calcd for $C_{32}H_{27}O_3Br$: C, 71.14; H, 5.04%; Mol wt, 539.

The mother liquor remaining after the separation of the crude XXVIIIa by filtration was diluted with water. The crude crystals which separated out were recrystallized from cyclohexane to afford XXIIIa as pale yellow prisms; 0.28 g (52%); mp 160—161°C. Its spectral data were identical with those recorded for an authentic sample prepared from XVI.

The Reaction of XXV with Ethanolic Potassium Hydroxide. When a suspension of XXV (0.46 g) in 5% ethanolic potassium hydroxide (50 ml) was treated by the same procedure employed for the reaction of XXV with methanolic potassium hydroxide, 0.07 g (15%) of XXVIIIb, mp 175—176°C and 0.35 g (85%) of XXIIIb, mp 165—166°C were obtained.

The structure of XXVIIIb was identified by means of the following spectral and analytical data. IR, 1695 (C=O), 1250 (ester) and 1065 cm^{-1} (C-O-C); UV ($CHCl_3$), 275 nm (ε, 8700); NMR, 2.5—3.2 (m, C_6H_5, 20 H), 3.65 (s, CH, 1H), 6.35 (q, J=7.5 Hz, CH_2, 2H), 7.08 (q, J=7.5 Hz, CH_2, 2H), 8.93 (t, J=7.5 Hz, CH_3, 3H), and 9.25 τ (t, J= 7.5 Hz, CH_3, 3H).

Found: C, 71.24; H, 5.09%; Mol wt (benzene), 549. Calcd for $C_{34}H_{31}O_3Br$: C, 71.86; H, 5.49; Mol wt, 567.

The structure of XXIIIb was identified by means of the following spectral and analytical data. IR, 2720 (CHO), 1690 (ester C=O), 1650 (aldehyde C=O) and 1260 cm^{-1}

(ester); UV (C_2H_5OH), 236 (19300), 289 (12100) and 332 sh nm (ε, 6700); NMR, 0.94 (s, CHO, 1H), 2.85 (m, C_6H_5, 18H), 3.40 (m, C_6H_5, 2H), 6.01 (q, J=7.5 Hz, CH_2, 2H) and 9.15 τ (t, J=7.5 Hz, CH_3, 3H).

Found: C, 84.35; H, 5.62%. Calcd for $C_{32}H_{26}O_3$: C, 83.84; H, 5.68%.

The Reaction of XXV with 2-Propanolic Potassium Hydroxide. A suspension of finely-powdered XXV (0.5 g) in 5% 2-propanolic potassium hydroxide (50 m*l*) was stirred at room temperature for 6 hr. The crude product formed by the addition of water to the reaction mixture was recrystallized from cyclohexane to afford XXIIIc as pale yellow prisms; 0.3 g (80%); mp 115—116°C. IR, 2720 (CHO), 1685 (ester C=O) 1650 (aldehyde C=O) and 1260 cm^{-1} (ester). The IR spectrum was comparable to those of XXIIIa and XXIIIb.

Found: C, 83.65; H, 5.82%. Calcd for $C_{33}H_{28}O_3$: C, 83.87; H, 5.97%.

The Acid-catalyzed Hydrolysis of XXVIII. A solution of XXVIIIa (0.15 g) in methanol (50 m*l*) containing five drops of concentrated hydrochloric acid was heated under reflux for 3 hr. The crude product which remained after the evaporation of the solvent to dryness was recrystallized from cyclohexane to afford XXIIIa; 0.064 g (52%).

The same treatment of XXVIIIb (0.21 g) afforded XXIIIb; 0.1 g (60%).

The Reaction of XXV with Methanol in the Presence of Silver Perchlorate. To a solution of XXV (0.6 g) in methanol (5 m*l*) - tetrahydrofuran (5 m*l*), we added an equimolar amount of silver perchlorate (0.2 g). After the removal of the silver bromide formed by filtration, the filtrate was evaporated to dryness. The residue was taken up in ether (100 m*l*), and the ether solution was washed successively with aqueous sodium chloride and water and dried over sodium sulfate. The evaporation of the solvent afforded a mixture of red and green crystals. After the recrystallization from cyclohexane, this mixture was separated mechanically into components. Each component was further recrystallized from cyclohexane. Red rhombs (0.14 g (30%)) were identified as the anhydride XXXI by a comparison of its spectral data with those recorded for an authentic sample[1]. Green needles (0.07 g (16%)) were found to be the diketone XVI[1] by the same spectroscopic method.

When XXV (0.6 g) was treated with two molar amounts of silver perchlorate (0.4 g) by the same procedure as that employed for the reaction of XXV with an equimolar amount of silver perchlorate, 0.27 g (55%) of XXXII was obtained as the sole product. The structure of XXXII was identified by a comparison of its spectral data with those of an authentic sample prepared according to a previously-reported method.[1]

The authors wish to express their thanks to Mr. Shoichi Kato for the elemental analyses, to Miss Shizuko Konomi for her measurement of the NMR spectra, and to Miss Sayumi Asakawa for her measurement of the UV spectra.

BULLETIN OF THE CHEMICAL SOCIETY OF JAPAN, VOL. 45, 1820—1824 (1972)

Methylene Analogs of Cyclobutenedione. IV.[1] The Reaction of 3,4-Bis(diphenylmethylene)cyclobutanedione Monoacetal and Its Derivatives with Methanolic Potassium Hydroxide

Fumio TODA and Nobuhiro OOI

Department of Industrial Chemistry, Faculty of Engineering, Ehime University, Matsuyama

(Received October 19, 1971)

The reaction of 2,2-dimethoxy-3,4-bis(diphenylmethylene)cyclobutanone (II), 2,2-dimethoxy-3,4-bis(diphenylmethylene)cyclobutanol (III), 2-hydroxy-3,4-bis(diphenylmethylene)cyclobutanone (IV), and 2-methoxy-3,4-bis(diphenylmethylene)cyclobutanol (VIII) with methanolic potassium hydroxide was studied. The three methoxy compounds, II, III, and VIII, afforded the ring-opened products, methyl 4,4-dimethoxy-2-diphenylmethylene-3-diphenylmethylbut-3-enate (X), 4,4-dimethoxy-2-diphenylmethylene-3-diphenylmethylbut-3-enal (XIII), and 4-methoxy-2-diphenylmethylene-3-diphenylmethylbut-3-enal (XVI) respectively. However, the ketoalcohol IV afforded the enolizable cyclobutenedione, 3,4-bis(diphenylmethyl)cyclobutenedione (XXI).

In a previous paper of this series,[1] we have reported the reaction of 2-bromo- (Ia) and 2,2-dibromo-3,4-bis(diphenylmethylene)cyclobutanone (Ib) with alcoholic potassium hydroxide to afford ring-opened products. In the reaction, it has been established that the base attacks the carbonyl initially. In order to certify the generality of the reaction mode, we have studied the reactions of II, III, IV, and VIII with methanolic potassium hydroxide.

Preparation of Compounds II, III, IV, and VIII. The ketoketal II was prepared in a 73% yield according to a previously-reported method,[2] the heating of Ib with methanol. The compound was also prepared in a 91% yield by the heating of a solution of 3,4-bis(diphenylmethylene)cyclobutanedione (VI)[2] in methanol containing a catalytic amount of hydrogen chloride.

The reduction of II in methanol with sodium borohydride afforded the corresponding alcohol III in almost a quantitative yield. The structure of III was identified by means of the spectral data[3] described in the Experimental section. Particularly, the elec-

1) Part III, F. Toda and Y. Takehira, This Bulletin, **45**, 1816 (1972).

2) F. Toda and K. Akagi, *Tetrahedron*, **27**, 2801 (1971).

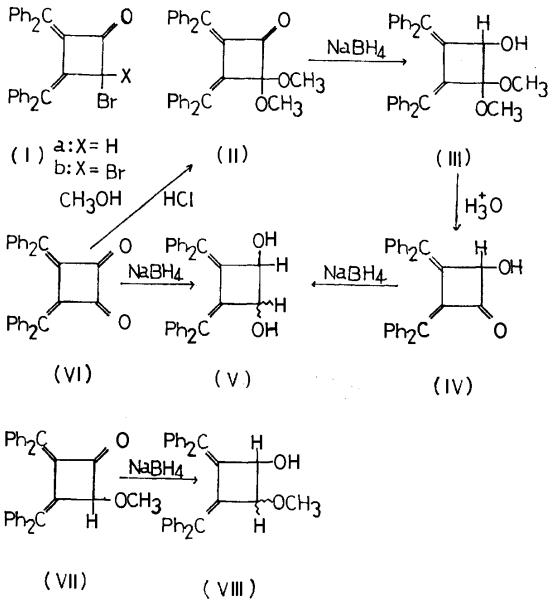

Scheme 1.

tronic absorption band of III, 365 nm (ε, 16800), was comparable to those of various 1,2-bis(diphenylmethylene)cyclobutane derivatives, 357—400 nm (ε, 15000—20000).[2,4]

The acid-catalyzed hydrolysis of III afforded the keto alcohol IV in a quantitative yield. The structure of IV was determined by means of the spectral data (Experimental section).

The structure of IV was further confirmed by the sodium borohydride reduction to the corresponding diol V, the spectral data of which were identical with those recorded for the diol[2,5] prepared by the sodium borohydride reduction of VI. Of the three compounds prepared, II, III, and IV, III differs in stability from the other two. In an atmosphere, III decomposed gradually and was converted finally into IV.

Monomethoxycyclobutanol VIII was obtained in a 46% yield by the sodium borohydride reduction of VII, which had been prepared by the reaction of Ia with methanol in the presence of silver perchlorate according to a previously-reported procedure.[2] The structure of VIII was identified by means of the spectral data (Experimental section), even though the configurational relationship between hydroxy and methoxy was not clear.

The Reaction with Methanolic Potassium Hydroxide. The heating of a solution of II and potassium hydroxide in methanol under reflux for 17 hr afforded X in a 72% yield. The structure of X was determined by means of the spectral data (Experimental section). In the NMR spectrum, X showed two methoxy methyl signals at 6.58 and 7.24 τ. The nonequivalence of the two methoxy methyls agrees with the structure bearing a *gem*-dimethoxy ethylene moiety. The structure of X was further identified by an acid-catalyzed hydrolysis, which afforded dimethyl 2-diphenylmethyl-3-diphenylmethylenesuccinate (XII), probably *via* the intermediate XI (Scheme 2). The structure of XII was identified by means of the spectral data described in the Experimental section. The assignment of the two AB-type doublets, 4.90 and 5.40 τ, was performed with using the monodeutero compound XII-*d*, prepared by the reaction of X with DCl in D_2O. Since XII-*d* showed a singlet at 4.92 τ, the doublet at the lower field (4.90 τ) can be assigned to the benzylic methine proton, H_A.

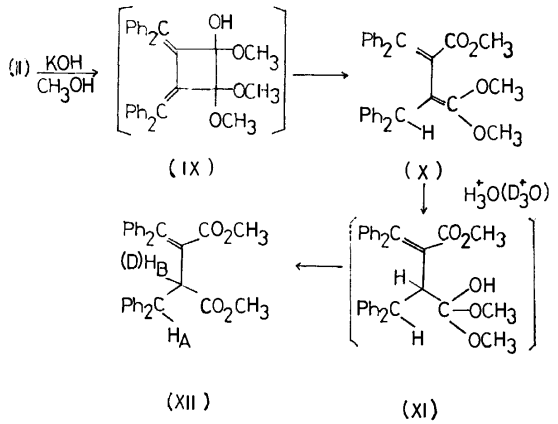

Scheme 2.

The reaction of II with methanolic potassium hydroxide to afford X can be interpreted by assuming the trimethoxy alcohol IX, as an intermediate. Therefore, the alcohol IX, initially produced by the action of methoxy anion on the carbonyl of II can be led to X by ketonization, accompanied by ring-opened, as is shown in Scheme 2. If the assumption is correct, the alcohols III and VIII would react with methanolic potassium hydroxide in the same fashion as that of II.

The reaction of III with methanolic potassium hydroxide under the same conditions as those employed for II was completed in 1 hr and afforded XIII in a quantitative yield. The structure of XIII was identified by means of the spectral data. IR, 2720 (CHO), 1665—1650 (C=O and C=C) and 1240 and 1230 cm^{-1} (C=C–O); UV, 291 (8700) and 356 nm (ε, 3800); NMR, 0.66 (s, CHO, 1H), 2.5—3.5 (m, C_6H_5, 20H), 5.51 (s, CH, 1H), 6.51 (s, OCH_3, 3H) and 7.22 τ (s, OCH_3, 3H). The UV spectrum of XIII was comparable to that of X. Since the two absorption bands of $\nu_{C=O}$ and $\nu_{C=C}$ overlapped and appeared at 1665—1650 cm^{-1} as a broad band, it was impossible to assign each band. The presence of a methoxy-substituted ethylene was certified for the 4,4-dimethoxy-3-diphenylmethyl-2-diphenylmethylene-but-3-enol (XV) obtained quantitatively by the sodium borohydride reduction of XIII. The alcohol XV showed a strong band at 1665 cm^{-1} which was assignable to the methoxy-substituted ethylene.

Further structural proof for XIII was obtained by means of its acid-catalyzed reaction. The treatment of XIII with hydrochloric acid under the same condi-

3) All the IR, UV, and NMR spectra were recorded in Nujol mull, ethanol, and $CDCl_3$ respectively.

4) F. Toda, K. Kumada, N. Ishiguro, and K. Akagi, This Bulletin, **43**, 3535 (1970).

5) F. Toda, H. Ishihara, and K. Akagi, *Tetrahedron Lett.*, **1969**, 2531.

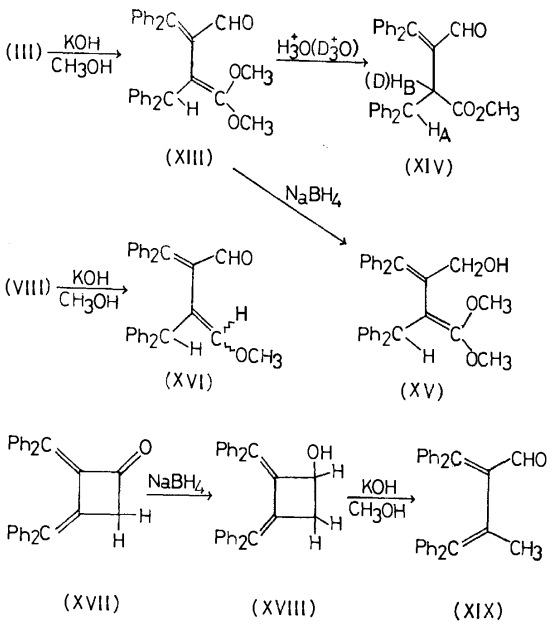

Scheme 3.

tions as those employed for X afforded methyl 2-diphenylmethyl-3-formyl-4,4-diphenylbut-3-enate (XIV) quantitatively. The structure of XIV was determined by means of the spectral data described in the Experimental section. The assignment of the two AB-type doublets of XIV, 4.88 and 5.34 τ, was performed again on the monodeutero derivative, XIV-*d*, prepared by the reaction of XIII with DCl in D_2O. Since XIV-*d* showed a singlet at 4.89 τ, but no other methine proton signal, the signal at 4.88 τ of XIII can be assigned to the benzylic methine proton, H_A.

The same reaction mode as that of II and III was observed in the case of VIII. The heating of VIII with methanolic potassium hydroxide under reflux for 5 hr afforded 4-methoxy-3-diphenylmethyl-2-diphenylmethylenebut-3-enal (XVI) in a 56% yield. The structure of XVI was identified by means of the spectral data. IR, 2720 (CHO), 1670 (C=O) and 1640 cm^{-1} (C=C); UV, 248 (16200), 299 (8600) and 370 sh nm (ε, 3600); NMR, 0.76 (s, CHO, 1H), 2.81 (m, C_6H_5, 18H), 3.34 (m, C_6H_5, 2H), 4.52 (d, J=0.7 Hz, =CH, 1H), 5.41 (d, J=0.7 Hz, CH, 1H) and 6.48 τ (s, CH_3, 3H). The NMR spectral data show the presence of a coupling between the methine proton and the vinyl proton. Since the long-range coupling across one double and three single bonds is well established as an allylic coupling,[6] the NMR spectrum of XVI can be well interpreted by its structure. However, the geometry around the double bond bearing the methoxy group was not determined.

A comparison of the three reactions of II, III, and VIII with methanolic potassium hydroxide makes it clear that the ketone II reacts more slowly than do the alcohols III and VIII. However, it is not clear which, the addition of methanol to the carbonyl of II or the ring-opening of IX, is more retarded.

All the three products, X, XIII, and XVI, have a vinylether structure. It is reasonable to consider that the double bonds of those products are stabilized by one or two methoxy groups, because the reaction of XVIII with methanolic potassium hydroxide afforded 2,3-bis(diphenylmethylene)butan-1-al (XIX). The reaction of XVIII prepared by the sodium borohydride reduction of 2,3-bis(diphenylmethylene)-cyclobutanone (XVII) according to a reported method,[2] with methanolic potassium hydroxide under the same conditions as those employed for VIII, was finished within 10 min and afforded XIX in an 80% yield. The structure of XIX was identified by means of the spectral data (Experimental section).

In order to clarify which, the addition of methanol to the carbonyl of II or the ketonization of IX, occurs more easily, the keto alcohol IV, was reacted with methanolic potassium hydroxide. Contrary to expectations, IV did not give any ring-opened product. Although IV is almost insoluble in methanol, it dissolved in methanolic potassium hydroxide easily. The acidification of the solution afforded 3,4-bis(diphenylmethyl)cyclobutenedione (XXI) in a 62% yield.

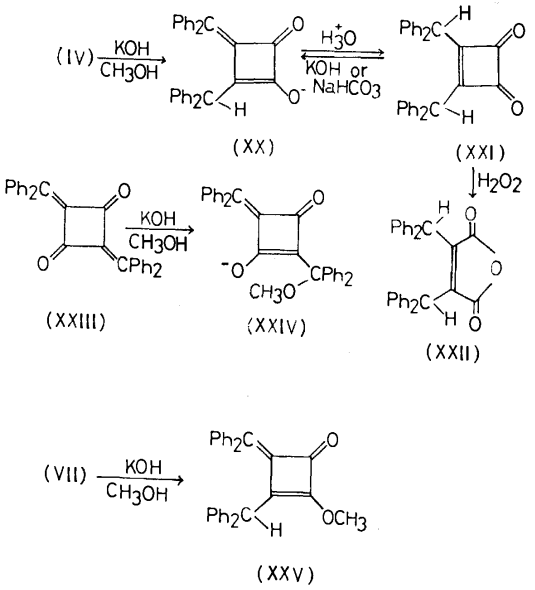

Scheme 4.

The UV spectrum of IV (or of XXI) in 5% methanolic potassium hydroxide, 330 nm (ε, 21700), was comparable to that of the enolate anion (XXIV) obtained by dissolving 2,4-bis(diphenylmethylene)-cyclobutanedione (XXIII) in 5% methanolic potassium hydroxide, 324 nm (ε, 24600).[7] Therefore, IV and XXI must dissolve in the base in the form of the enolate anion, XX. Since the base-catalyzed rearrangement of VII to 4-diphenylmethylene-3-diphenylmethyl-2-methoxycyclobut-2-enone (XXV) has been reported,[1] the base-catalyzed 1,3-hydrogen shift may be characteristic for a system such as IV or VII.

6) L. M. Jackman and S. Sternhell, "Applications of Nuclear Magnetic Resonance Spectroscopy in Organic Chemistry," 2nd ed., Pergamon Press, London (1969), p. 316.

7) G. A. Taylor, *J. Chem. Soc.*, *C*, **1969**, 1755.

All the cyclobutenediones except squaric acid and its derivatives which have been reported to date are sensitive to the base, and all undergo ring-cleavage.[8] The enolization of XXI in the base without ring cleavage differs widely from these facts. The acidity of the benzylic hydrogen of XXI is relatively strong, and XXI dissolves in even methanolic sodium bicarbonate. In connection with the strong acidity[9] of squaric acid, the acidic nature of the hydrogen of XXI is interesting.

Further structural proof for XXI was obtained by oxidation with neutral hydrogen peroxide which afforded bis(diphenylmethyl)maleic anhydride (XXII) in a 24% yield. It is well established that cyclobutenediones undergo a Baeyer-Villiger oxidation with neutral hydrogen peroxide to afford the corresponding maleic anhydrides.[8]

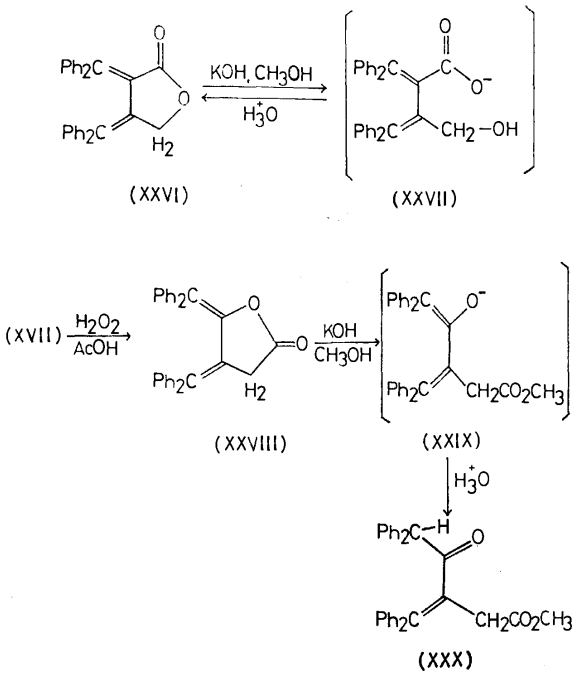

Scheme 5.

Any possibility that the compound derived from IV is a γ-lactone, such as XXVI or XXVIII, is ruled out. 3,4-Bis(diphenylmethylene)-γ-lactone (XXVI) was prepared according to the reported method;[1] it was dissolved in methanolic potassium hydroxide, probably by the formation of a carboxylate anion like XXVII, and XXVI was reformed by acidification. The behavior is similar to that of XXI; however, the spectral data which have been recorded for XXVI differ from those of XXI. 4,5-Bis(diphenylmethylene)-γ-lactone (XXVIII), prepared by the oxidation of XVII according to Corey's procedure,[10] was also dissolved in methanolic potassium hydroxide, probably in the form of an enolate anion like XXIX. However, the ketone XXX was obtained by the acidification of the alkaline solution. Both the spectral data of XXVIII and of XXX are also different from those of XXI (Experimental section).

Experimental[3]

Preparation of III. A suspension of II (5.00 g) in ethanol (100 m*l*) was treated with a large excess of sodium borohydride at 50—60°C for 1 hr. After the reaction mixture had been decomposed with water, the crude product which was separated out was collected by filtration, washed with water, and dried to afford III; 4.71 g (94%). The recrystallization of the product from ethyl acetate gave an analytical pure sample as pale yellow prisms; 4.0 g (80%); mp 131—132°C. IR, 3480 cm^{-1} (OH); UV, 365 nm (ε, 16800); NMR, 2.83 (d, C_6H_5, 10H), 3.18 (d, C_6H_5, 10H), 4.87 (d, J=10 Hz, CH, 1H), 6.53 (s, OCH_3, 3H), 6.83 (s, OCH_3, 3H) and 7.60 τ (d, J=10 Hz, OH, 1H).

Found: C, 83.30; H, 5.97%. Calcd for $C_{32}H_{28}O_3$: C, 83.45; H, 6.13%.

Preparation of IV. To a solution of III (0.60 g) in acetone (10 m*l*), several drops of concentrated hydrochloric acid were added. Crude crystals formed by the addition of water to the reaction mixture were collected by filtration, washed with water, and dried to afford IV; 0.53 g (99%). Recrystallization of the crude crystals from ethyl acetate afforded a pure sample as fine orange needles; 0.425 g (79%); mp 185—186°C. IR, 3420 (OH) and 1775 cm^{-1} (C=O); UV, 271 (15600), 329 (5000) and 422 nm (ε, 9200); NMR, 2.68 (d, C_6H_5, 10H), 3.18 (d, C_6H_5, 10H), 4.44 (s, CH, 1H) and 7.63 τ (s, OH, 1H).

Found: C, 86.74; H, 5.18%. Calcd for $C_{30}H_{22}O_2$; C, 86.93; H, 5.35%.

A suspension of IV (0.25 g) in ethanol (10 m*l*) was treated with a large excess of sodium borohydride at room temperature for 5 min. The crystals formed were collected by filtration, washed with water, and dried to afford V as pale yellow needles; 0.23 g (92%); mp 222—223°C (lit,[2,4] mp 222—223°C). The spectral data were identical with those of an authentic sample prepared according to a previously-reported method.[2,4]

Preparation of VIII. The treatment of VII[2] (0.50 g) in methanol (10 m*l*) with sodium borohydride by the same method as that employed for III afforded VIII as yellow needles; 0.23 g (46%); mp 167—170°C. IR, 3420 cm^{-1} (OH); UV, 365 nm (ε, 17400); NMR, 2.25 (s, C_6H_5, 10H), 3.22 (s, C_6H_5, 10H), 5.18 (d, J=5 Hz, CH, 1H), 5.53 (d, J=5 Hz, CH, 1H), 6.69 (s, CH_3, 3H) and 7.2 τ (broad, OH, 1H).

Found: C, 86.00; H, 5.84%. Calcd for $C_{31}H_{26}O_2$: C, 86.48; H, 6.09%.

Ring-opening Reaction of II. A solution of II (0.30 g) and a large excess of potassium hydroxide (2.5 g) in THF (15 m*l*) - methanol (35 m*l*) was heated under reflux for 17 hr. After decomposition with water, the crude crystals which separated out were collected by filtration, washed with water, and dried to give X; 0.23 g (74%). Recrystallization from cyclohexane gave pure X as colorless prisms; mp 118—119°C. IR, 1710 (C=O), 1655 (C=C), 1240 (ester) and 1250 cm^{-1} (=C–O–); UV, 238 sh (18300) and 315 nm (ε, 6300); NMR, 2.7—3.2 (m, C_6H_5, 20H), 5.45 (s, CH, 1H), 6.58 (s, OCH_3, 3H), 6.68 (s, CO_2CH_3, 3H) and 7.24 τ (s, OCH_3, 3H).

Found: C, 80.97; H, 6.55%; Calcd for $C_{33}H_{30}O_4$; C, 80.79; H, 6.16%.

8) M. P. Cava and M. J. Mitchell, "Cyclobutadiene and Related Compounds," Academic Press, New York and London (1967), pp. 128—156.

9) S. Cohen, J. R. Lacher, and J. D. Park, *J. Amer. Chem. Soc.*, **81**, 3480 (1959).

10) E. J. Corey, Z. Arnold, and J. Hutton, *Tetrahedron Lett.*, **1970**, 307.

Acid-catalyzed Hydrolysis of X. A solution of X (0.09 g) in acetone (5 ml) containing a catalytic amount of hydrochloric acid was heated at 50—60°C for 5 min. The crude crystals formed by the addition of water were filtered, washed with water, and dried to yield XII; 0.08 g (92%). Recrystallization of the crude crystals from methanol gave pure XII as colorless prisms; mp 164—165°C. IR, 1738 (C=O), 1725 (C=O), 1260 (ester) and 1240 cm^{-1} (ester); UV, 264 nm (ε, 7100); NMR, 2.6—3.3 (m, C_6H_5, 20H), 4.90 (d, J=12 Hz, H_A, 1H), 5.40 (d, J=12 Hz, H_B, 1H), 6.45 (s, CO_2CH_3, 3H) and 6.62 τ (s, CO_2CH_3, 3H).

Found: C, 80.22; H, 5.86%. Calcd for $C_{32}H_{28}O_4$: C, 80.64; H, 5.92%.

Ring-opening Reaction of III. A suspension of III (0.50 g) and potassium hydroxide (0.4 g) in methanol (10 ml) was heated under reflux for 1 hr. After decomposition with water, the crude crystals which had formed were filtered, washed with water, and dried to afford XIII; 0.49 g (98%). The recrystallization of the crystals from ethyl acetate yielded pure XIII as yellow prisms; mp 113—114°C.

Found: C, 83.37; H, 5.99%. Calcd for $C_{32}H_{28}O_3$: C, 83.45; H, 6.13%.

The aldehyde XIII (0.09 g) in methanol (5 ml) was treated with an excess of sodium borohydride at 50—60°C for 5 min. Crude crystals (0.09 g (100%)) obtained by the decomposition of the reaction mixture were recrystallized from methanol to afford pure XV as colorless prisms; mp 148—148.5°C. IR, 3520 (OH), 1665 (C=C) and 1240 cm^{-1} (=C–O); UV, 237 sh (9500), 271 sh (4200) and 279 sh nm (ε, 3500); NMR, 2.5—3.5 (m, C_6H_5, 20H), 5.45 (s, CH, 1H), 6.05 (d, J=6 Hz, CH_2, 2H), 6.42 (s, OCH_3, 3H), 7.33 (s, OCH_3, 3H) and 8.87 τ (t, J=6 Hz, OH, 1H).

Found: C, 83.06; H, 6.47%. Calcd for $C_{32}H_{30}O_3$: C, 83.01; H, 6.54%.

Acid-catalyzed Hydrolysis of XIII. To a solution of XIII (0.14 g) in acetone, a few drops of concentrated hydrochloric acid were added, and then the mixture was heated at 50—60°C for 5 min. Crystals (0.13 g (96%)) obtained by the addition of water to the reaction mixture were recrystallized from cyclohexane to afford pure XIV as colorless needles; mp 204—205°C. IR, 2720 (CHO), 1745 (CO_2CH_3), 1660 (CHO) and 1240 cm^{-1} (ester); UV, 238 sh (18300) and 315 nm (ε, 6300); NMR, 0.83 (s, CHO, 1H), 2.4—3.7 (m, C_6H_5, 20H), 4.88 (d, J=11 Hz, H_B, 1H), 5.34 (d, J=11 Hz, H_A, 1H) and 6.36 τ (s, CH_3, 3H).

Found: C, 83.71; H, 5.81%. Calcd for $C_{31}H_{26}O_3$: C, 83.38; H, 5.87%.

To a solution of XIII (0.10 g) in THF (5 ml), was added a few drops of concentrated deuterochloric acid, and then the mixture was heated at 50—60°C for 5 min. The same treatment of the reaction mixture as above afforded XIV-*d* after recrystallization from cyclohexane; 0.08 g (82%).

Ring-opening Reaction of VIII. A solution of VIII (0.32 g) and potassium hydroxide (0.5 g) in methanol (10 ml) was heated under reflux for 5 hr. Crude crystals obtained by the addition of water to the reaction mixture were recrystallized from benzene to afford XVI as yellow prisms; 0.18 g (56%); mp 187°C.

Found: C, 86.25; H, 6.07%. Calcd for $C_{31}H_{26}O_2$: C, 86.48; H, 6.09%.

Ring-opening Reaction of XVIII. A mixture of XVIII (0.40 g), potassium hydroxide (0.5 g), and methanol (20 ml) was heated under reflux for 10 min. Crude crystals obtained by the decomposition of the reaction mixture were recrystallized from petroleum ether (bp 60—70°C) to afford XIX as pale yellow plates; 0.32 g (80%); mp 141—142°C. IR, 2720 (CHO) and 1655 cm^{-1} (C=O); UV, 235 sh (22100), 270 sh (14300) and 305 sh nm (ε, 8600); NMR, 0.55 (s, CHO, 1H), 2.6—3.4 (m, C_6H_5, 20 H) and 7.98 τ (s, CH_3, 3H).

Found: C, 89.60; H, 5.88%. Calcd for $C_{30}H_{24}O$: C, 89.96; H, 6.04%.

Isomerization of IV to XXI. A mixture of IV (1.65 g), potassium hydroxide (1.0 g), and methanol (15 ml) was heated under reflux for 5 min to afford a clear solution. The crude crystals obtained by the acidification of the clear solution with hydrochloric acid were recrystallized from methanol to afford XXI as colorless prisms; 1.02 g (62%); mp 130—131°C. IR, 1790 and 1770 (unsplit doublet, C=O) and 1580 cm^{-1} (C=C); UV, 258 sh (9000), 267 sh (7600) and 276 sh nm (ε, 6200); NMR, 2.5—3.0 (m, C_6H_5, 20H) and 4.73 τ (s, CH, 2H).

Found: C, 86.97; H, 5.15%. Calcd for $C_{30}H_{22}O_2$: C, 86.93; H, 5.35%.

Oxidation of XXI. A mixture of XXI (0.2 g), 30% aqueous hydrogen peroxide (1.5 ml), and acetic acid (60 ml) was stirred at room temperature for 24 hr. The crude crystals formed by the addition of water to the reaction mixture were recrystallized from methanol to afford XXII as colorless prisms; 0.1 g (48%); mp 171—172°C. IR, 1825 and 1770 (C=O) and 1645 cm^{-1} (C=C); UV, 253 sh (6500), 259 sh (5800) and 282 sh nm (ε, 4000); NMR, 2.85 (d, C_6H_5, 20H) and 4.63 τ (s, CH, 2H).

Found: C, 83.85; H, 5.07%. Calcd for $C_{30}H_{22}O_3$: C, 83.70; H, 5.15%.

The same reaction in acetone for 86 hr afforded XXII in a 24% yield.

Preparation of XXVIII. A mixture of XVII (0.66 g), 30% aqueous hydrogen peroxide (1 ml), and acetic acid (60 ml) was stirred at 65°C for 10 hr. The crude crystals formed by the addition of water to the reaction mixture were recrystallized from methanol to afford XXVIII as yellow prisms; 0.07 g (10%); mp 216—217°C. IR, 1795 (C=O) and 1620 cm^{-1} (C=C); UV, 251 (29300) and 345 nm (ε, 11100); NMR, 2.6—3.6 (m, C_6H_5, 20H) and 6.53 τ (s, CH_2, 2H).

Found: C, 86.41; H, 5.11%. Calcd for $C_{30}H_{22}O_2$: C, 86.93; H, 5.35%.

Reaction of XXVIII with Methanolic Potassium Hydroxide. A mixture of XXVIII (0.05 g), potassium hydroxide (0.04 g), and methanol (20 ml) was heated under reflux for 15 min. The crude crystals formed by the decomposition of the reaction mixture were collected by filtration and were then recrystallized from methanol to afford XXX as colorless prisms; 0.025 g (46%); mp 106—107°C. IR, 1740 (C=O) and 1670 cm^{-1} (C=O); 290 nm (ε, 4900); NMR, 2.85 (m, C_6H_5, 20H), 5.15 (s, CH, 1H), 6.62 (s, CH_3, 3H) and 6.75 τ (s, CH_2, 2H).

Found: C, 83.72; H, 5.80%. Calcd for $C_{31}H_{26}O_3$: C, 83.38; H, 5.87%.

The authors wish to express their thanks to Mr. Shoichi Kato for the elemental analyses, to Miss Shizuko Konomi for her measurement of the NMR spectra, and to Miss Sayumi Asakawa for her measurement of the UV spectra.

Layered Compounds. V.[1] Synthesis and Properties of [*m.n*]Paracyclophadiynes

Takahiro MATSUOKA, Taichi NEGI, Tetsuo OTSUBO, Yoshiteru SAKATA, and Soichi MISUMI

The Institute of Scientific and Industrial Research, Osaka University, Suita, Osaka

(Received October 22, 1971)

A series of bisethynyl compounds, IX and XII, were prepared by a modified ethynylation using *N*-methyl-2-pyrrolidone in good yields. Intramolecular oxidative coupling of the bisethynyl compounds has been achieved with high-dilution technique to give relatively good yields of highly strained or strainless [*m.n*]paracyclophadiynes I and cyclic diacetylenes XIII. From the comparison of the electronic spectra of these diacetylenic compounds, it is concluded that abnormal spectra of Ic and Id are attributed to the transannular π-electronic interaction between benzene nucleus and diacetylenic unit rather than the ring strain in the molecules. In addition, a marked down-field shift of aromatic protons in Ic compared with the other paracyclophadiynes is explained in terms of the transannular shielding effect of diacetylenic linkage.

In various types of bridged systems[2], two or more chromophoric groups separated from each other frequently exhibit anomalous behavior when they are forced to bring close together as in the case of [*m.n*]-paracyclophanes. Since an increased proximity of the groups necessarily brings about a severe strain in the molecule owing to a mutual π-orbital repulsion, the resulting strain sometimes makes it difficult to explain the anomalous physical properties of such distorted molecules in terms of a transannular interaction of π-orbitals.

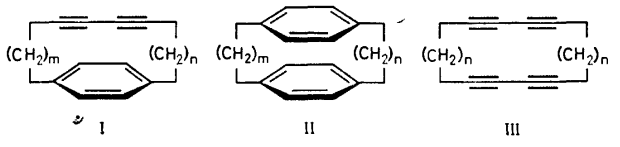

There have been systematic surveys of [*m.n*]paracyclophanes (II),[3] cyclic tetraacetylenes(III),[4] and multilayered cyclophanes[5] in view-points of the transannular interaction and the strain effect. They showed unambiguous evidences supporting the transannular interaction. On the other hand, there are only a few studies on the interaction in bridged compounds containing different chromophoric groups, since a superposition of absorption bands due to both groups often makes a spectral elucidation difficult. Cram and Antar[6] reported two of [*n*]paracyclophyne containing a monoacetylene group in its bridge chain. However, any evidence for transannular electronic interaction could not be observed there.

From examinations of scale models, it has been expected that paracyclophadiynes I are well suitable model compounds for the study of the transannular electronic interaction between a benzene nucleus and a conjugated diacetylene group. It is well known that a variety of highly strained diacetylenic compounds could have been prepared by oxidative coupling reaction of terminal bisethynyl compounds like IX.[7] Thus we have undertaken to investigate a relationship among methylene chain length and the physical properties of paracyclophadiynes I. In this paper we report the synthesis and the spectral properties of I. The name "[*m.n*]paracyclophadiyne" is used here in place of *a,b*-[*n'*]paracyclophadiyne for convenience, in which *m* and *n* are numbers of methylene group, *e.g.* for Ic [3.3]paracyclophadiyne instead of 4,6-[10]paracyclophadiyne.

Results and Discussion

Synthesis. All of the paracyclophadiynes (I) were prepared by the general synthetic sequence outlined in Scheme 1. Cyclic diacetylenes XIII and tetraacetylenes XIV were synthesized as spectral reference compounds (Scheme 2).

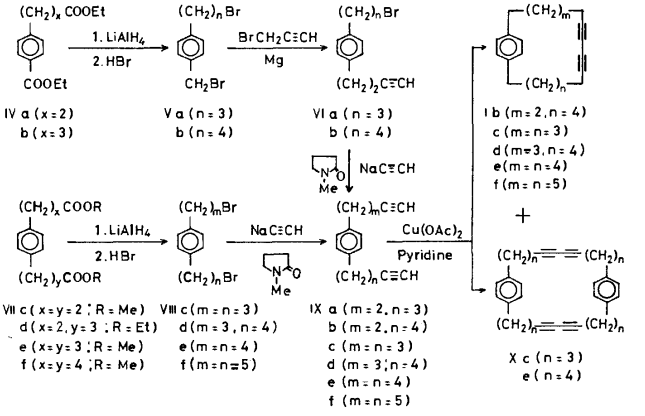

Scheme 1. A synthesis of paracyclophadiynes.

In some preliminary experiments, bisethynyl compounds IX were obtained by bisethynylation of dibromides VIII in ether with liquid ammonia solution of sodium acetylide in autoclave at room temperature in reasonable yields, 79% for $m=n=3$ and

1) The paper by T. Matsuoka, Y. Sakata, and S. Misumi (*Tetrahedron Lett.*, **1970**, 2549) is to be considered Part IV of this series.

2) B. H. Smith, "Bridged Aromatic Compounds," Academic Press, New York, N. Y. (1964).

3) For review; D. J. Cram, *Rec. Chem. Progr.*, **20**, 71 (1959).

4) F. Sondheimer, Y. Amiel, and R. Wolovsky, *J. Amer. Chem. Soc.*, **79**, 6263 (1957).

5) T. Otsubo, S. Mizogami, Y. Sakata, and S. Misumi, *Chem. Commun.*, **1971**, 678; *Tetrahedron Lett.*, **1971**, 4803; S. Mizogami, T. Otsubo, Y. Sakata, and S. Misumi, *ibid.*, **1971**, 2791.

6) D. J. Cram and M. F. Antar, *J. Amer. Chem. Soc.*, **80**, 3109 (1958).

7) O. M. Behr, G. Eglinton, A. R. Galbraith, and A. R. Raphael, *J. Chem. Soc.*, **1960**, 3614; M. Morimoto, S. Akiyama, S. Misumi, and M. Nakagawa, This Bulletin, **35**, 857 (1962); A. J. Hubert and J. Dale, *J. Chem. Soc.*, **1963**, 86; R. Wolovsky and F. Sondheimer, *J. Amer. Chem. Soc.*, **87**, 5720 (1965); R. H. Mitchell and F. Sondheimer, *Tetrahedron*, **24**, 1397 (1968).

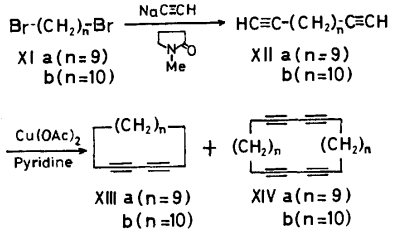

Scheme 2. A synthesis of cyclic acetylenes.

74% for $m=n=4$, accompanied with a small amount of olefinic compounds. After examining several experimental conditions, we observed a more convenient procedure by which the bisethynyl compounds IX were likewise afforded in good yields at atmospheric pressure by the use of *N*-methyl-2-pyrrolidone in place of ether as a co-solvent. This facile procedure was also applied to permit good yields of bisethynyl alkanes XII as shown in Table 1.

On the other hand, bisethynyl compounds, IXa and IXb, each containing a butynyl group were synthesized through stepwise ethynylations as shown in Scheme 1. Thus monoethynyl bromoderivatives VI (a and b) were obtained by the reaction of dibromides V with propargylmagnesium bromide in 80 and 96% yields, respectively. The following ethynylation of VI gave bisethynyl compounds IX (a and b), 77% and 89%, in a same manner stated above. Analytical data and the physical properties of the bisethynyl compounds IX and XII are shown in Table 1.

The paracyclophadiynes I were obtained by Eglinton's oxidative reaction[8] of IX with a high-dilution

TABLE 1. ANALYTICAL DATA AND PHYSICAL PROPERTIES OF IX AND XII

Compound	Mol. Formula	Carbon, %		Hydrogen, %		[Mp] or Bp/mmHg °C	Yield %	ν_{max} (-C≡CH) cm^{-1}
		Calcd	Found	Calcd	Found			
IXa	$C_{15}H_{16}$	91.78	91.67	8.22	8.36	92—94/0.15	76.9	3286, 2119[f]
IXb	$C_{16}H_{18}$	91.37	91.03	8.63	8.49	124—126/2	88.9	3268, 2110[f]
IXc	$C_{16}H_{18}$	91.37	91.10	8.63	8.61	[49.5—50.5][a]	85.7	3247, 3231, 2108[g]
IXd	$C_{17}H_{20}$	91.01	90.94	8.99	9.27	112—114/0.07	77.6	3269, 2110[f]
IXe	$C_{18}H_{22}$	90.70	90.67	9.30	9.34	[18—19][a]	87.7	3266, 2110[f]
IXf	$C_{20}H_{26}$	90.16	90.08	9.84	10.00	[51—52][b]	86.0	3239, 3222, 2104[g]
XIIa	$C_{13}H_{20}$	88.56	88.63	11.44	11.56	81—83/2	87.6 (81)[e]	3275, 2112[f]
XIIb	$C_{14}H_{22}$	88.35	87.89	11.65	11.97	[32.5—33.5][c] [33—34][d]	90.5 (57)[d]	3283, 3257, 2106[g] (3274, 2100)[d]

a) From petroleum ether at −20°C. b) From *n*-pentane at −20°C. c) From ethanol at −20°C. d) From Ref. 8. e) From Ref. 9. f) Liquid film. g) Nujol mull.

TABLE 2. MOLECULAR WEIGHT, ANALYTICAL DATA, AND PHYSICAL PROPERTIES OF I, X, XIII, and XIV

Compound	Mol. Formula	Carbon, %		Hydrogen, %		Mol wt		Mp °C	Yield %	Crystal Form	ν_{max}(-C≡C-) cm^{-1}
		Calcd	Found	Calcd	Found	Calcd	Found				
Ib	$C_{16}H_{16}$	92.26	92.32	7.74	7.58	208	205[a] 208[b]	69.5—70.5	41.1	prisms[g]	2243[k], 2248[l]
Ic	$C_{16}H_{16}$	92.26	92.00	7.74	7.82	208	207[a] 208[b]	134—135	21.3	thick plates[h]	2247, 2153[k]
Id	$C_{17}H_{18}$	91.84	91.99	8.16	8.18	222	214[a] 222[b]	86—87.5	37.2	prisms[h]	2253, 2160[k]
Ie	$C_{18}H_{20}$	91.47	91.32	8.53	8.49	236	214[a] 236[b]	72—73[c] 76—77[e]	46.6	plates[g] thick plates[g]	2248, 2156[k,m] 2257, 2163[l]
If	$C_{20}H_{24}$	90.85	90.64	9.15	9.23	264	260[a] 264[b]	108—109	26.1	plates[h]	2252, 2164[k]
Xc	$C_{32}H_{32}$	92.26	92.14	7.74	7.73	416	417[a] 416[b]	158—159	10.6	plates[i]	2249, 2142[k]
Xe	$C_{36}H_{40}$	91.47	91.31	8.53	8.47	472	469[a] 472[b]	163—164	12.4	needles[i]	2253, 2162[k] 2262, 2167[l]
XIIIa	$C_{13}H_{18}$								55.2	liquid[j]	2246, 2163[n]
XIIIb	$C_{14}H_{20}$	89.29	89.01	10.71	11.14	188	188[b]	d	71.7 (17)[f]	liquid	2250, 2151[n] (2215, 2132)[f]
XIVa	$C_{26}H_{36}$	89.59	89.32	10.41	10.48	348	348[b]	141.5—142 (142)[e]	*ca.* 1	needles[i]	2258, 2162[k]
XIVb	$C_{28}H_{40}$	89.29	89.29	10.71	10.57	376	376[b]	100—101 (101—102)[f]	*ca.* 2	needles[g]	

a) By vapor pressure osmometry. b) By mass spectrometry. c) Dimorphism. d) Evaporative distillation, *ca.* 100°C (bath temp.)/1 mmHg. e) From Ref. 9. f) From Ref. 8. g) From *n*-pentane at −20°C. h) From petroleum ether at −20°C. i) From cyclohexane. j) After chromatography. k) Nujol mull. l) CCl_4 soln. m) For the higher melting point crystals. n) Liquid film.

technique for intramolecular cyclization. The oxidative coupling reaction was achieved with dropwise addition of dilute ether solution of IX for a period of 80—110 hr to anhydrous cupric acetate in pyridine at 85—95°C under nitrogen atmosphere. Chromatography of the coupling products on alumina gave the desired cyclic monomers Ib—f in relatively good yields (47—21%) together with by-product, cyclic dimers X. It is noteworthy that nitrogen atmosphere during the oxidative coupling is presumably necessary to avoid air oxidation of the coupling products, because the coupling reaction of IX in air atmosphere gave a low yield of I, *e.g.* only 8% yield of Ie from IXe. As cyclic diacetylenes, XIIIa and XIIIb, were also afforded by this procedure in 55 and 72% yields, the procedure is excellently applicable to general preparation of cyclic conjugated diacetylenes. The latter compound XIIIb had been previously synthesized under normal Eglinton's condition in a 17% yield.[8] A new compound XIIIa, 1,3-cyclotridecadiyne, is the smallest one of monocyclic conjugated diacetylenes known so far and is highly strained on consideration with a skeletal model. It was observed that this compound is thereby unstable and becomes rapidly orange after isolation, but the dilute solution can be kept for a month at −20°C. All of the paracyclophadiynes I obtained above can be kept without decomposition in diffused light at room temperature.

An attempted synthesis of extremely strained paracyclophadiyne I with $m=2$, $n=3$ failed, but afforded a mixture of cyclic dimer X consisted of two possible isomers.

Analytical data and the physical properties of cyclic di- and tetra-acetylenes I, X, XIII, and XIV are summarized in Table 2.

Geometry of Paracyclophadiynes. An examination of Stuart-Briegleb model for paracyclophadiynes Id—f reveals that in each molecule a benzene nucleus is held parallel to a diacetylene group in the bridge chain and its mutual distance becomes shorter with decreasing number of methylenes in the diacetylene bridge as shown in Fig. 1. [3.3]- and [2.4]-Paracyclophadiynes can not be constructed with this type of model. On the other hand, examination with Dreiding model suggests that two isomeric forms should be present in a highly strained molecule, [3.3]-paracyclophadiyne Ic (Fig. 2). The cyclophadiyne Ic, however, exhibits no evidence for the presence of such isomers on the NMR spectrum even at low temperature as described below. Therefore, it is quite interesting to investigate the mutual arrangement of

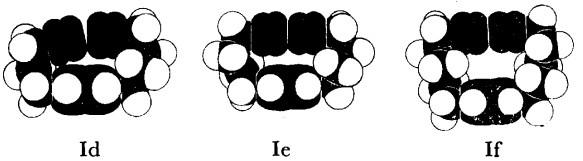

Id Ie If

Fig. 1. The molecular models of I. (Stuart-Briegleb model)

8) G. Eglinton and A. R. Galbraith, *J. Chem. Soc.*, **1959**, 889.
9) J. Dale, A. J. Hubert, and G. S. D. King, *ibid.*, **1963**, 73.

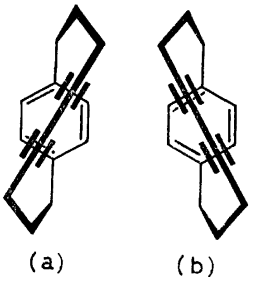

Fig. 2. Two possible isomeric forms of Ic on a consideration of Dreiding Model.

the benzene nucleus and the diacetylene group in the molecule.

Recently the exact molecular structure of [3.3]-paracyclophadiyne was determined with X-ray by Tanaka *et al.*[10] (Fig. 3 and 4). The figures show that the structure of the molecule is characterized as follows: a) atomic group C–C≡C–C≡C–C in Ic is forced to bend by 6—11° from its normal linear arrangement. Both the triple bonds are held with shorter bond lengths than that (1.208 Å)[11] in dimethyldiacetylene, b) the benzene nucleus is less distorted than the benzene nuclei in [3.3]paracyclophane, c) a particular bond angle in the trimethylene chain is unusually greater than the normal, *i.e.* 120.1° or 126.7°, d) the C–C≡C–C≡C–C group is parallel to an axis linked through substituted benzene atoms, C_{11} and C_{14}, as opposed to the examination of Dreiding model (see Fig. 4), e) two shortest distances between

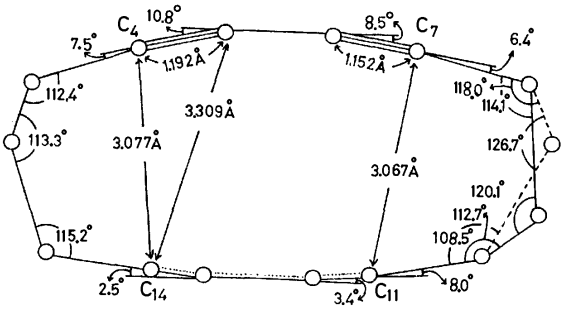

Fig. 3. Profile of crystal structure of [3.3]paracyclophadiyne.

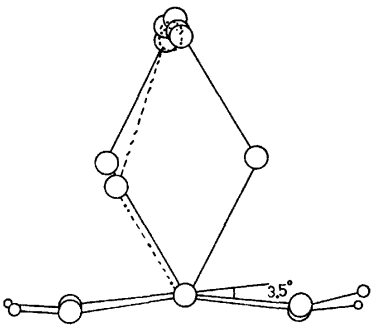

Fig. 4. Profile of crystal structure of [3.3]paracyclophadiyne.

10) T. Aono, C. Katayama, K. Sakabe, T. Sakabe, and J. Tanaka, The 24th Annual Meeting of The Chemical Society of Japan, Summary 13330, Osaka, April, 1971.
11) A. Almenningen, O. Bastriansen, and T. Munthe-Kaas, *Acta Chem. Scand.*, **10**, 261 (1956).

both π-electron systems, 3.067 and 3.077 Å, are much shorter than a minimum distance (3.14 Å)[12] between two benzene nuclei in [3.3]paracyclophane.

The structural features of [3.3]paracyclophadiyne above-stated are most likely interpreted on the basis of a repulsive force arising from enormous π-orbital overlap between the diacetylene group and the benzene nucleus. Of several highly strained cyclic compounds containing a diacetylenic linkage isolated from the other chromophoric groups, [3.3]paracyclophadiyne is the first one of which exact structure was determined.

Nuclear Magnetic Resonance Spectra. The NMR spectra of [*m.n*]paracyclophadiynes I, cyclic dimers X, and open chain compound IX are illustrated in Table 3. It shows that chemical shifts of aromatic protons other than the Ic aromatic protons are about the same as that of the open chain compounds IX. Thus it can be considered that there is no appreciable effect of diacetylenic linkage on the chemical shifts of Id—f because of elongated distances. The aromatic protons of [2.4]homologue Ib appeared also at nearly the same position, indicating that the magnetic effect of diacetylenic linkage is negligible even in such a highly strained molecule. It was observed in a series of [*n*]paracyclophanes[13] that the chemical shift of aromatic protons was little varied even if the benzene ring is highly distorted.

TABLE 3. THE CHEMICAL SHIFTS OF THE AROMATIC PROTONS OF I[a], IXc[a], AND X[b] IN CCl_4 AT ROOM TEMPERATURE

Compound	τ-Value	Pattern	No.
Ib	3.01	s	4
Ic	2.81	s	4
Id	2.97	AA'BB'	4
Ie	2.99	s	4
If	2.99	s	4
IXc	3.01	s	4
Xc	2.88	s	8
Xe	3.01	s	8

Concentration a) 0.14 M, b) 0.06 M.

In the other strained cyclophadiyne Ic, on the other hand, the aromatic protons were found to appear at down-field by *ca.* 0.2 ppm compared with strainless homologues (Table 3). Therefore, this down-field shift should be attributed to the transannular shielding effect from magnetic anisotropy of diacetylenic bond. It remains questionable that the aromatic protons of Id appeared as an expected AA'BB' pattern but those of Ib unexpectedly as a sharp singlet, in same relationship observed for the aromatic protons of [2.4]- and [3.4]-paracyclophanes.[14]

The spectra of methylene protons in I are showed in Fig. 5. The three signals in Ie and If are respectively assigned to benzylic, propargylic, and the rest methylene protons from lower field. The benzylic protons of I appear in a range of 6.9—7.7 τ as complexed multiplets. Unsymmetric paracyclophadiyne Id showed two multiplets at 7.1—7.3 and 7.3—7.6 τ, in which benzylic protons in trimethylene bridge and in tetramethylene bridge respectively were assigned from comparison with [3.3]- and [4.4]-homologues. In the spectrum of Ib a complexed signal at 7.3—7.7 τ is explainable by which the higher field counterpart of A_2B_2 pattern of the dimethylene bridge protons is superimposed with the benzylic protons in the tetramethylene bridge. The propargylic protons in the tetramethylene bridge appeared at 8.1 τ. A remarkable difference between the chemical shifts of two pairs of propargylic protons in Ib seems to be attributed to a difference in shielding effect of benzene ring due to methylene bridge length.

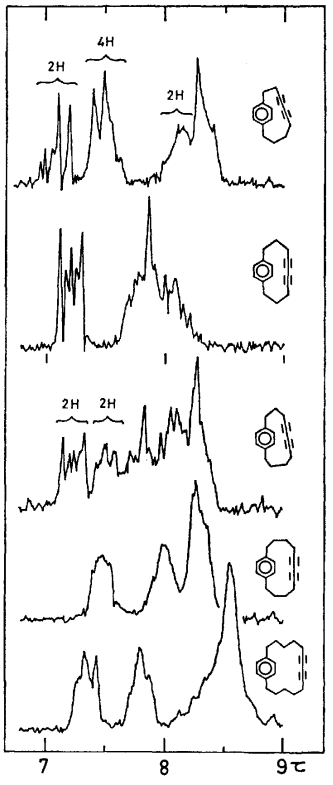

Fig. 5. The NMR spectra of the methylene protons in paracyclophadiynes (60 MHz, in CCl_4, at room temp.).

A long-range shielding effect of diacetylenic linkage is probably responsible to slight down-field shifts of benzylic protons in Ic and in shorter methylene bridges of Ib and Id. In order to confirm this shielding effect, cyclic diacetylenes XIII, in which the majority of protons might be located above the diacetylene linkage, were chosen to examine. Table 4 records the chemical shifts of the propargylic protons and the other methylene protons (τ-values at absorption maxima) in XIII and XIV together with cycloalkanes. Although the propargylic protons of XIII and XIVb

12) P. K. Gantzel, C. L. Coulter, and K. N. Trueblood, *Angew. Chem.*, **72**, 755 (1960); P. K. Gantzel and K. N. Trueblood, *Acta Crystallogr.*, **18**, 958 (1965).

13) D. J. Cram and M. Goldstein, *J. Amer. Chem. Soc.*, **85**, 1063 (1963); H. J. Reich and D. J. Cram, *ibid.*, **91**, 3534 (1969).

14) D. J. Cram and R. C. Helgeson, *ibid.*, **88**, 3515 (1966).

15) J. J. Burke and P. C. Lauterbur, *ibid.*, **86**, 1870 (1964).

Table 4. The NMR spectral data of XIII and XIVb in CCl_4

Compound	Propargylic protons			Other methylene protons		
	τ-Value	Pattern	No.	τ-Value	Pattern	No.
XIIIa	7.80	br t	4	8.48	br s	14
XIIIb	7.80	br t	4	8.48	br s	16
XIVb	7.76	br t	8	8.65	br s	32
Cyclotridecane				8.64 (8.652)[a]		
Cyclotetradecane				8.66 (8.670)[a]		

a) From Ref. 15.

Table 5. The electronic spectral data of Ib—If and Xe in cyclohexane

Compound	λ_{max} in nm and $\varepsilon \times 10^{-2}$ in parentheses									
Ib	199	215[a]	222.5	227[a]	248	261.5	267	276		
	(189)	(61.0)	(56.1)	(47.5)	(4.07)	(4.22)	(4.02)	(3.34)		
Ic	206	233	265	273.5	282					
	(132)	(20.4)	(4.34)	(4.04)	(3.33)					
Id	200	227	245[a]	261	268	276.5				
	(154)	(41.8)	(5.11)	(4.11)	(3.70)	(3.24)				
Ie	214.5	221	225	241[a]	243.5	257.5	259.5	265	267[a]	273.5
	(66.4)	(67.6)	(58.4)	(3.03)	(3.04)	(3.36)	(3.36)	(3.56)	(3.02)	(3.40)
If	214.5	220	225	241	248[a]	257	260	265.5	268	274
	(85.2)	(88.7)	(79.5)	(3.61)	(2.59)	(3.54)	(3.39)	(4.04)	(3.42)	(4.30)
Xe	214	219.5	224	241.5	247[a]	255	259.5	265	267.5	273.5
	(181)	(181)	(153)	(8.58)	(6.14)	(8.28)	(7.89)	(8.85)	(8.26)	(9.34)

a) shoulder

appear at nearly the same position, the other methylene protons (broad singlet) of XIIIa and XIIIb are shifted by 0.17 ppm to down-field from those of XIVb and cycloalkanes. Since XIIIa would considerably be strained and XIIIb be strainless from the examination of model, same chemical shift for the methylene protons of XIIIa and XIIIb provided further evidence that the strain in diacetylenic linkage has little influence on the shielding effect of the linkage. Accordingly, the above-mentioned down-field shift should be mainly attributed to the shielding of diacetylenic linkage. And also the down-field shift (*ca.* 0.2 ppm) of aromatic protons in Ic stated before is possibly ascribed to the same effect.

The spectra of Ic were determined at 70, 35, and −70°C to study the conformational equilibrium (a⇄b in Fig. 2). But the signals of the aromatic protons were kept sharp singlet even at −70°C. This finding is consistent with that the molecule in solution has the same geometry as in crystals (Fig. 4). It is presumed that the relative arrangement of the benzene ring and the diacetylene linkage undergoes no significant change even if an interconversion between a chair form and a boat form arises from the conversion of both trimethylene bridges.

Electronic Spectra. Figure 6 and Table 5 record the electronic spectra of the [*m.n*]paracyclophadiynes I, in which the number of *m* and *n* are varied stepwise. In those spectra, a cyclic dimer Xe, 5,7,23,25-[12.12]paracyclophatetrayne, is a reference compound, in which the interaction between the two chromophores may be unexpected. The spectra show obvious features as follows: a) disappearance of vibrational fine structures with the decrease of

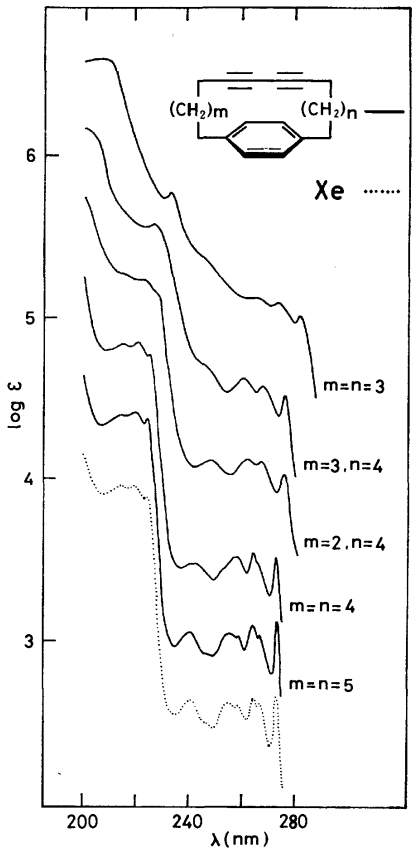

Fig. 6. The electronic spectra of paracyclophadiynes in cyclohexane. The ε-value of the cyclic dimer Xe is reduced to give the value for the unit chromophoric groups, *i.e.*, ε/2. The curves are displaced upward successively by 0.5 log ε unit from the curve immediately below.

methylene number, and then broadening of the curves, b) bathochromic shifts of the longest wavelength absorption bands, and c) appearance of a new peak at 233 nm for Ic and at 227 nm for Id, respectively.

The spectral features are explainable by two plausible elucidations, distortion in the two chromophores and transannular interaction between those. It was reported in the spectra of [*n*]paracyclophanes[16] that the distortion of benzene ring resulted in a disappearance of fine structure and a bathochromic shift of absorption band. However, there has not been investigated the spectral properties of distorted cyclic molecules containing only a conjugated diacetylenic linkage. Figure 7 shows that a strain-free cyclic diacetylene XIIIb exhibits a characteristic fine structure, whereas a strained one XIIIa does a broad absorption maximum, and that there is no significant difference between the positions of absorption bands of both spectra. Upon these facts, a) and b) may be explained by the strain effect of the chromophores, mainly of benzene ring, but c) not by only the strain effect. The reason is that the spectrum of less strained [3.4]paracyclophadiyne Id resembles the spectrum of more strained [3.3]homologue Ic, whereas highly strained one Ib shows an absorption curve similar to the reference compound Xe rather than to [3.3]homologue.

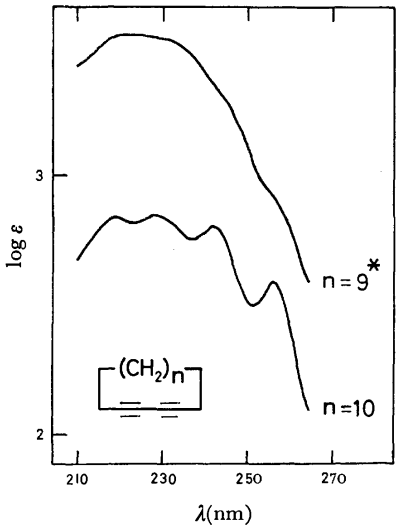

Fig. 7. The electronic spectra of cyclic diacetylenes in cyclohexane. * Qualitative.

Accordingly, it is suggested that new absorption peaks, at 233 nm of Ic and at 227 nm of Id, of the smaller paracyclophadiynes might be ascribed to the transannular interaction between the two chromophores. As is illustrated in Fig. 3, the closest interatomic distances between the two groups, 3.067 Å of C_7—C_{11} and 3.077 Å of C_4—C_{14}, are remarkably small as compared with a minimum interplanar distance of approximately 3.4 Å known for a variety of non-distorted aromatic substances. Thus the overlap of the π-electron orbitals must be particularly significant both at C_7—C_{11} and C_4—C_{14}. On the other hand, [2.4]homologue should be highly strained and less overlapped at the tetramethylene bridge site than in [3.3]homologue from the examination of molecular model. Consequently, it is concluded that the abnormal spectra of [3.3]- and [3.4]-paracyclophadiynes, Ic and Id, are best explained in terms of transannular π-electron interation caused by closely overlapped two chromophores.

[4.4]Paracyclophadiyne Ie shows absorption bands at about same wavelengths as those of the reference compound Xe, but with 0.7—0.8 times of the intensity ($\varepsilon/2$) for each pair of the chromophores as can be seen from Table 5. Such lower intensity was invariably observed on repeated measurements and with various runs of the specimen, indicating noncontamination of impurities. This phenomenon on the intensity has been also observed by Nakagawa and Ando[17] and explained in terms of the dispersion force interaction between excited dipoles by Tinoco[18] and Rhodes.[19] Accordingly, the intensity of the spectrum of Ie seems to be explained in terms of the dispersion force interaction or dipole-dipole interaction rather than the overlap of π-orbitals unlike in the cases of [3.3]- and [3.4]-homologues.

A similarity of the If spectrum to that of Xe is suggestive of the absence of the interaction between the two chromophores. Low intensity bands, occured at 285—295 nm in each spectrum of Ib, Ie, and If, at 285 nm for XIIIb and at 288 nm for XIVa, are considered as an excitation of the diacetylene bond alone.

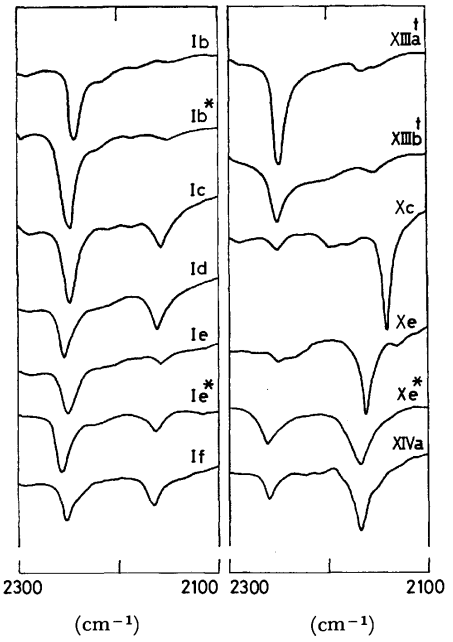

Fig. 8. The infrared spectra of I, X, XIII, and XIV (Nujol mull).
* CCl_4 soln. † Liquid film. The frequencies of the C≡C stretching bands in this figure are summarized in Table 2.

16) D. J. Cram, C. S. Montgomery, and G. R. Knox, *J. Amer. Chem. Soc.*, **88**, 515 (1966).

17) T. Ando and M. Nakagawa, This Bulletin, **40**, 363 (1967).
18) I. Tinoco, Jr., *J. Amer. Chem. Soc.*, **82**, 4785 (1960).
19) W. Rhodes, *ibid.*, **83**, 3609 (1961).

The electronic spectra of paracyclophadiyne-tetracyanoethylene complexes will be reported in near future.

Infrared Spectra. Figure 8 shows the infrared spectra in a range of 2300—2100 cm^{-1} for cyclic acetylenic compounds, I, X, XIII, and XIV. The cyclic monomers I and XIII exhibit stronger higher-frequency band than lower-frequency one, whereas the cyclic dimers X and XIV are *vice versa*. This phenomenon is related probably to the very structure of the molecules and not to intermolecular interaction since the same relationship is observed between spectra of solid state and of solution.

Experimental

Melting points and boiling points are uncorrected. The UV, IR, NMR, and mass spectra were measured with a Hitachi EPS-3T autorecording spectrophotometer, a Hitachi EPI-G2 spectrometer, a Hitachi R-20 spectrometer, and a Hitachi RMU-7 spectrometer, respectively.

Ethyl p-*Ethoxycarbonylhydrocinnamate (IVa).* Acetylation of ethyl hydrocinnamate was accomplished by the procedure of Borshe and Sinn[20] except for using carbon tetrachloride as a solvent, yield 86.0%, bp 144—146°C/3 mmHg (lit,[20] bp 194—197°C/16 mmHg).

To an alkaline solution of sodium hypobromite, prepared from sodium hydroxide (230 g, 5.75 mol) and bromine (310 g, 1.94 mol) in water (1.9 *l*), 65 g (0.30 mol) of ethyl *p*-acetylhydrocinnamate was added over a period of 10 min with stirring keeping the temperature below 0°C. After the addition the mixture was kept at 60°C for 3 hr with stirring. The reaction mixture was cooled and washed well with ether and then acidified with 150 m*l* of conc. sulfuric acid, successively. The acid precipitate was collected, washed well with water and dried in vacuum over calcium chloride to give white crystals (53.7 g, 93%). For analysis a small amount of the sample was recrystallized from acetic acid and then sublimed (bath temp. *ca.* 200°C/3 mmHg) to give white powder, mp 296—297°C (in sealed tube), (Found: C, 61.39; H, 6.05%) (lit,[21] mp 284°C).

p-Carboxyhydrocinnamic acid was converted to diethyl ester *via* acid chloride according to the usual method. From 63.9 g of the dicarboxylic acid was obtained 70.0 g (84.5%) of the diethyl ester IVa as a colorless liquid, bp 148—153°C/4 mmHg. For analysis a sample was distilled under reduced pressure to give a colorless liquid, bp 157—158°C/4 mmHg. Found: C, 67.12; H, 7.26%. Calcd for $C_{14}H_{18}O_4$: C, 67.18; H, 7.25%.

p-*(3-Hydroxypropyl)benzyl Alcohol.* The ester IVa (81.0 g, 0.32 mol) in 200 m*l* of ether was added dropwise over a period of 1.5 hr with stirring to a suspension of 24.4 g (0.64 mol) of lithium aluminum hydride in 800 m*l* of ether. The mixture was kept at reflux with stirring for 4 hr. To the cooled reaction mixture a small amount of water was carefully added dropwise to decompose the excess reducing agent. After addition of 2 N hydrochloric acid (1.8 *l*) and salting out, the mixture was extracted with ether (500 m*l*). The ether solution was washed twice with succesive, 100 m*l* portions of saturated sodium chloride, dilute sodium bicarbonate solution saturated with sodium chloride, and saturated sodium chloride, respectively. The solution was dried over anhydrous sodium sulfate and concentrated under reduced pressure to yield an opaque pale yellow viscous oil (54.0 g).

The bis-*p*-nitrobenzoate of this material was prepared by the usual pyridine-*p*-nitrobenzoyl chloride method, mp 111.5—112.5°C (from ethanol). Found: C, 62.04; H, 4.42; N, 5.90%. Calcd for $C_{24}H_{20}N_2O_8$: C, 62.06; H, 4.34; N, 6.03%.

p-*(3-Bromopropyl)benzyl Bromide (Va).* *p*-(3-Hydroxypropyl)benzyl alcohol (54.0 g) was converted to the dibromide Va (41.5 g, 43.7%) according to the usual method,[22] bp 142—147°C/3 mmHg. For analysis a sample was distilled under reduced pressure to give a colorless liquid, bp 117—119°C/0.08 mmHg; IR (liquid film), 608 and 563 cm^{-1} (C-Br). Found: C, 41.38; H, 4.21%. Calcd for $C_{10}H_{12}Br_2$: C, 41.13; H, 4.14%.

*4-(*p-*(3'-Bromopropyl)phenyl)-1-butyne (VIa).* To a solution of propargylmagnesium bromide,[23] prepared from magnesium (1.3 g, 0.054 mol) and propargyl bromide (6.4 g, 0.054 mol) in ether (15 m*l*) under nitrogen atmosphere, a solution of the dibromide Va (8.7 g, 0.030 mol) in 20 m*l* of ether was quickly added with vigorous stirring. The mixture was stirred for 6 hr at room temperature and then poured into a mixture of crashed ice (100 g) and ether (100 m*l*), and 50 m*l* of 6 N hydrochloric acid was added. The resulting mixture was extracted with ether. The ether solution was washed with a saturated sodium chloride and dried over anhydrous sodium sulfate. The solution was concentrated under reduced pressure to yield an orange liquid (7.38 g). This residue was chromatographed on 30 g of neutral alumina using petroleum ether as an eluent to yield a colorless liquid (6.0 g, 80.0%). For analysis a sample was distilled under reduced pressure to give a colorless liquid, bp 108—110°C/0.08 mmHg; IR (liquid film), 3287, 2120 and 644 (-C≡CH), 573 cm^{-1} (C-Br); NMR (CCl_4), τ: 2.97 (s, 4H), 6.73 (t, J=6 cps, 2H), 7.1—8.1 (m, 8H), 8.19 (t, J=2 cps, 1H). Found: C, 62.22; H, 6.21%. Calcd for $C_{13}H_{15}Br$: C, 62.16; H, 6.02%.

Ethyl p-*(3-Ethoxycarbonylpropyl)benzoate (IVb).* *p*-(3-Ethoxycarbonylpropyl)acetophenone was obtained according to Baddeley and Williamson.[21]

Oxidation of the acetophenone derivative with sodium hypobromite was carried out in the same manner described for the preparation of *p*-carboxyhydrocinnamic acid. From 104 g of the acetophenone derivative was obtained 82.2 g (89.0%) of *p*-(3-carboxypropyl)benzoic acid, mp 184—190°C. A small amount of sample was recrystallized from 50% acetic acid to yield white needles, mp 195.5—196°C (lit,[21] mp 194—195°C).

The dicarboxylic acid was converted to diethyl ester *via* acid chloride according to the usual method. From 65.1 g of the acid was obtained 72.8 g (88.0%) of ethyl *p*-(3-ethoxycarbonylpropyl)benzoate(IVb) as a pale yellow liquid, bp 156—160°C/2 mmHg. For analysis a sample was distilled under reduced pressure to give a colorless liquid, bp 153—155°C/1 mmHg. Found: C, 68.00; H, 7.77%. Calcd for $C_{15}H_{20}O_4$: C, 68.16; H, 7.63%.

p-*(4-Hydroxybutyl)benzyl Alcohol.* Reduction of the ester IVb with lithium aluminum hydride was accomplished in a similar manner described for the preparation of *p*-(3-hydroxypropyl)benzyl alcohol. From 90 g of IVb was obtained 63.7 g of the crude diol as an opaque pale yellow viscous oil. The bis-*p*-nitrobenzoate of this diol was prepared, mp 99—100°C (from ethanol). Found: C, 63.00; H, 4.65; N, 5.75%. Calcd for $C_{25}H_{22}N_2O_8$: C, 62.76; H, 4.64; N, 5.86%.

p-*(4-Bromobutyl)benzyl Bromide (Vb).* *p*-(4-Hydroxybutyl)benzyl alcohol (62.0 g) was converted to the di-

20) W. Borsche and F. Sinn, *Ann. Chem.*, **553**, 260 (1942).
21) G. Baddeley and R. Williamson, *J. Chem. Soc.*, **1956**, 4647.

bromide Vb (63.5 g, 60.5%) according to the usual method,[22] bp 149—153°C/3 mmHg. For analysis a sample was distilled under reduced pressure to give a colorless liquid, bp 126—128°C/0.08 mmHg; IR (liquid film), 608 and 561 cm^{-1} (C–Br). Found: C, 43.34; H, 4.63; Br, 51.91%. Calcd for $C_{11}H_{14}Br_2$: C, 43.17; H, 4.61; Br, 52.22%.

*4-(*p*-(4'-Bromobutyl)phenyl)-1-butyne (VIb).* Propynylation of the dibromide Vb with propargylmagnesium bromide[23] was accomplished in a manner to that described for the propynylation of the dibromide Va. From 20 g of the dibromide Vb was obtained 16.6 g (96.0%) of the monoethynyl compound VIb as a pale yellow liquid after chromatographic treament. For analysis a sample was distilled under reduced pressure to give a colorless liquid, bp 118—120°C/0.09 mmHg; IR (liquid film), 3287, 2120 and 645 (–C≡CH), 563 cm^{-1} (C–Br); NMR (CCl_4), τ: 3.03 (s, 4H), 6.70 (t, J=6 cps, 2H), 7.1—7.8 (m, 6H), 8.1—8.3 (m, 5H). Found: C, 63.24; H, 6.53%. Calcd for $C_{14}H_{17}Br$: C, 63.40; H, 6.46%.

p-Bis(β-methoxycarbonylethyl)benzene (VIIc). A mixture of 36.9 g of dimethyl β,β'-(*p*-phenylene)diacrylate,[24] 360 m*l* of tetrahydrofuran and 3.6 g of 5% palladium-carbon catalyst was shaken in an atmosphere of hydrogen for 3 hr at about 60°C to take up theoretical amount of hydrogen. The hot mixture was filtered through an extraction thimble and the residual material in the thimble was extracted with tetrahydrofuran using a Soxhlet extractor. The combined solution was cooled to 0°C. The precipitated diester VIIc was collected and dried in vacuum, brilliant white scaly crystals (36.6 g, 97.6%), mp 116—118°C (lit,[25] mp 117—118°C).

p-Bis(3-bromopropyl)benzene (VIIIc). Reduction of the dimethyl ester VIIc, which was slightly soluble in ether, with lithium aluminum hydride was carried out by the technique of Nystrom and Brown.[26] From 30 g of VIIc was obtained 20.5 g (88.0%) of *p*-bis(3-hydroxypropyl)-benzene as white crystals, mp 60—61.5°C. A small amount of the sample was recrystallized from benzene to give colorless plates, mp 60.5—61.5°C (lit,[27] mp 61°C).

Bromination of the above diol was accomplished by the method of Ruzicka *et al.*[24] From 20 g of the diol was obtained 24.9 g (75.5%) of the dibromide VIIIc as a colorless liquid, bp 156—160°C/1 mmHg (lit,[24] bp 158—162°C/1 mmHg).

Ethyl p-(3-Ethoxycarbonylpropyl)hydrocinnamate (VIId). 108 g of β-(*p*-(2-carboxyethyl)benzoyl)propionic acid[28] was reduced by the modified Wolff-Kishner method[29] to yield 76.4 g (75.0%) of the *p*-(3-carboxypropyl)hydrocinnamic acid, mp 142—144°C (lit,[28] mp 143—144°C).

This dicarboxylic acid (66.4 g) was converted to the diethyl ester (69.6 g, 85.0%) by the usual acid-ethanol method, bp 165—168°C/2 mmHg. For analysis a sample was distilled under reduced pressure to give a colorless liquid, bp 173—174°C/3 mmHg. Found: C, 69.73; H, 8.51%. Calcd for $C_{17}H_{24}O_4$: C, 69.83; H, 8.27%.

*4-(*p*-(3'-Bromopropyl)phenyl)butyl Bromide (VIIId).* Reduction of VIId with lithium aluminum hydride was accomplished in a similar manner described for the preparation of *p*-(3-hydroxypropyl)benzyl alcohol. From 64.5 g of VIId was obtained 47.9 g of 4-(*p*-3'-hydroxypropyl)-phenyl)butyl alcohol as an opaque pale yellow viscous oil. The bis-*p*-nitrobenzoate of this diol was prepared, mp 100.5—101.5°C (from ethanol). Found: C, 64.07; H, 5.22; N, 5.46%. Calcd for $C_{27}H_{26}N_2O_8$: C, 64.02; H, 5.17; N, 5.53%.

Bromination of the above diol was achieved by the usual dry hydrogen bromide method.[30] From 26.1 g of the diol was obtained 32.9 g (78.7%) of the dibromide VIIId as a colorless liquid, bp 151—155°C/1 mmHg. For analysis a sample was distilled under reduced pressure to give a colorless liquid, bp 174—176°C/3 mmHg. Found: C, 46.78; H, 5.34%. Calcd for $C_{13}H_{18}Br_2$: C, 46.73; H, 5.43%.

p-Bis(4-bromobutyl)benzene (VIIIe). A series of reactions leading to the formation of dibromide VIIIe *via* diethyl ester VIIe was carried out by the method of Cram *et al.*[31]

p-Bis(5-bromopentyl)benzene (VIIIf). Bromination of *p*-bis(5-hydroxypentyl)benzene, which was prepared from dimethyl ester VIIf by the method of Cram and Daeniker,[32] was accomplished by the usual method.[30] From 33.0 g of the diol was obtained 41.5 g (83%) of the dibromide VIIIf as a colorless liquid, bp 188—190°C/3 mmHg. For analysis a sample was chromatographed on alumina using petroleum ether as an eluent and then distilled under reduced pressure to give a colorless liquid, bp 144°C/0.02 mmHg. Found: C, 50.99; H, 6.50; Br, 42.28%. Calcd for $C_{16}H_{24}Br_2$: C, 51.08; H, 6.43; Br, 42.49%.

Ethynylation of VI, VIII, and XI. To a solution of monosodium acetylide, prepared from 3.6 g (0.16 mol) of sodium in liquid ammonia (100 m*l*), a solution of 10 g (0.029 mol) of dibromide VIIIe in 100 m*l* of *N*-methyl-2-pyrrolidone, which was distilled at atmospheric pressure, was added dropwise over a period of 50 min. During this period the bottom of the reaction flask was kept cool on a dry ice-alcohol bath, and vigorous stirring was continued with passage of a slow stream of acetylene. After the addition of VIIIe and the introduction of acetylene were over, stirring was continued overnight at room temperature to allow the evaporation of nearly all the ammonia. To the reaction mixture a small amount of water was carefully added to decompose excess sodium acetylide. After further addition of water (1 *l*) and salting-out, the reaction mixture was extracted with ether. The ether extract was washed well with water, dilute sulfuric acid, dilute sodium bicarbonate solution, and again with water, successively and dried over calcium chloride. The solution was concentrated under reduced pressure to yield 6.4 g of a yellow oil, for which Beilstein's test was negative. This residue was chromatographed on 50 g of alumina using petroleum ether as an eluent to yield 6.0 g (87.7%) of 6-(*p*-(4'-ethynylbutyl)phenyl)-1-hexyne (IXe) as a colorless liquid. For analysis a small amount of the sample was crystallized from petroleum ether at −20°C to give colorless crystals, mp 18—19°C. Bisethynyl compound IXc, IXd, IXf, XIIa, and XIIb were also prepared in good yields from corresponding dibromides by the method described above. VIa and VIb were also ethynylated in a similar method except that two gram atoms of sodium were

22) O. Kamm and C. S. Marvel, "Organic Syntheses," Coll. Vol. I, p. 25 (1947).
23) F. Sondheimer *et al.*, *J. Amer. Chem. Soc.*, **82**, 755 (1960); **83**, 1686 (1961).
24) L. Ruzicka, J. B. Buijs, and M. Stoll, *Helv. Chim. Acta*, **15**, 1220 (1932).
25) H. Hopff and H. Diethelm, *Ann. Chem.*, **691**, 61 (1966).
26) R. F. Nystrom and W. G. Brown, *J. Amer. Chem. Soc.*, **69**, 1197 (1947).
27) K. Murayama, Y. Kato, and S. Morimoto, This Bulletin, **40**, 2645 (1967).
28) M. S. Ahmad and G. Baddeley, *J. Chem. Soc.*, **1961**, 2520.
29) Huang-Minlon, *J. Amer. Chem. Soc.*, **68**, 2487 (1946).
30) W. L. McEwen, "Organic Syntheses," Coll. Vol. III, p. 227 (1955).
31) D. J. Cram, M. L. Allinger, and H. Steinberg, *J. Amer. Chem. Soc.*, **76**, 6132 (1954).
32) D. J. Cram and H. U. Daeniker, *ibid.*, **76**, 2743 (1954).

Table 6. The experimental conditions for I, X, XIII, and XIV

Reaction condition			Condition of chromatography		
Starting material (g)	Bath temp. °C	Dropping period (hr)	Alumina[b] (g)	Cyclic monomer eluent	Cyclic dimer eluent
IXa (3.0)	75	60[a]	200[c]		pet. ether-ether (20 : 1)
IXb (3.0)	85	92	200	pet. ether-ether (20 : 1)	
IXc (3.0)	85	77	200	pet. ether-ether (20 : 1)	pet. ether-benzene (2 : 1)
IXd (2.7)	90	84	200	pet. ether-ether (30 : 1)	
IXe (3.0)	95	110	200	pet. ether-ether (40 : 1)	pet. ether-benzene (2 : 1)
IXf (3.6)	90	114	200	pet. ether-ether (40 : 1)	
XIIa (3.0)	85	90[a]	150	pet. ether	pet. ether-benzene (50 : 3)
XIIb (3.0)	95	74	150	pet. ether	pet. ether-ether (20 : 1)

a) In darkness. b) Sumitomo activated alumina, KCG-30. c) Merck silica gel.

used to 1 mol of the monobromide VI.

Analytical data, yields, and physical properties of these bisethynyl compounds IX and XII were summarized in Table 1.

General Procedure for the Oxidative Coupling of IX and XII. In a 3 *l* separable flask, equipped with a vibromixer, a 1 *l* dropping funnel fitted with a capillary, and a gas inlet tube, are placed 1.3 *l* of pyridine and 20 g (0.11 mol) of anhydrous cupric acetate. The mixture was heated on an oil-bath with vigorous stirring and passage of a slow stream of nitrogen. Keeping the temperature of the bath at about 95°C, the solution of the bisethynyl compound IXe (3.0 g, 0.013 mol) in 2 *l* of ether was added dropwise through the capillary of the dropping funnel into the reaction flask. The addition was completed for 110 hr. During this period vigorous stirring and passage of nitrogen were continued and two 5 g portions of the cupric salt were added at nearly equal intervals. After the addition the reaction mixture was permitted to stand at room temperature for more than 6 hr and poured into a cooled mixture of crashed ice (2.4 kg), conc. sulfuric acid (540 m*l*) and ether (650 m*l*). Then brown insoluble material was filtered, the organic layer was separated and the water layer was extracted with 1 *l* of ether. The combined etherial solution was washed well with dilute sulfuric acid, dilute sodium bicarbonate solution and water, successively and dried over calcium chloride. The solution was concentrated under reduced pressure to yield a red oil (6.8 g) which gave no band at *ca.* 3300 cm^{-1} due to ethynyl group. The residue was dissolved in 10 m*l* of benzene and chromatographed on 200 g of alumina to yield two compounds. The first (1.39 g, 46.6%) was eluted with petroleum ether - ether (40 : 1); it was the cyclic monomer, [4.4]-paracyclophadiyne (Ie). For analysis a small amount of the sample was crystallized from *n*-pentane at −20°C, colorless plates, mp 72—73°C. On the crystallization, however, the alternative colorless thick plates were often obtained, they showed mp 76—77°C. The latter shows identical UV and NMR spectra with those of the former. Once the lower melting point crystals were melted and then solidified, it showed mp 76—77°C. On the other hand, in the case of the higher melting point crystals such phenomenon was not observed in this process. This phenomenon is explainable in terms of a polymorphism. Analytical data and physical properties of the cyclic monomer Ie are shown in Tables 2, 3 and 5 and Figs. 5, 6 and 8. The second substance (0.370 g, 12.4%) was eluted with petroleum ether - benzene (2 : 1); it was the cyclic dimer, 5,7,23,25-[12.12]paracyclophatetrayne (Xe). For analysis a small amount of the sample was recrystallized from cyclohexane, white needles, mp 163—164°C. Analytical data and physical properties of this cyclic dimer are shown in Tables 2, 3 and 5 and Figs. 6 and 8.

In a preliminary experiment, the linear dimer, (HC≡C–$(CH_2)_4$– –$(CH_2)_4$C≡C–)$_2$, was obtained; colorless needles, mp 76—77°C; λ_{max} 219.5 nm (ε 20200), 241.5 (518) and 274 (936) (in cyclohexane); IR 3265, 2320 and 2110 cm^{-1} (KBr disk). Found: C, 91.37; H, 8.83%; mol wt, 457 (osmometry in benzene). Calcd for $C_{36}H_{42}$: C, 91.08; H, 8.92%; mol wt, 475.

The Oxidative Coupling of IXa. The oxidative coupling of IXa (Table 6) resulted in a red oil (7.1 g). Chromatography on silica gel, followed by recrystallization from cyclohexane gave a mixture of two possible cyclic dimers, 3,5,18,20-[9.9]- and 3,5,18,20-[8.10]-paracyclophatetraynes, in poor yield; white needles, mp 159—162°C. Found: C, 92.94; H, 7.35%. Calcd for $C_{30}H_{28}$: C, 92.74; H, 7.26%. Mol wt, Found: 388 (mass spectrometry). Calcd for $C_{30}H_{28}$: 388. UV: (in cyclohexane) λ_{max} 214, 220, 225, 242.5, 256.5, 264, and 273 nm.

Hydrogenation of XIII. 1,3-Cyclotridecadiyne (XIIIa, 704 mg), which was purified by chromatography in *n*-pentane on alumina at *ca.* 5°C, took up 96% of the calculated volume of hydrogen in ethyl acetate (5% Pd-C). The crude product was chromatographed in petroleum ether on alumina, followed by distillation (*ca.* 80°C (bath temp.)/2 mmHg), to give cyclotridecane[33] (430 mg, 60%) as a colorless oil. Found: C, 84.81; H, 14.99% mol wt (mass spectroscopy) 182.

1,3-Cyclotetradecadiyne[8] (XIIIb, 563 mg) similarly gave cyclotetradecane (419 mg, 73%, mp 48—52°C), which was recrystallized from ethanol as colorless needles, mp 56—56.5°C (lit,[33] 53.5—54°C). Found: C, 85.33; H, 14.62%, mol wt (mass spectroscopy) 196.

33) L. Ruzicka, Pl. A. Plattner, and H. Wild, *Helv. Chim. Acta*, **28**, 395 (1945).

Isolation and Structure Proof of Dinitrocyclohexenones Formed in the Nitration of Polyalkylbenzenes with Fuming Nitric Acid[1]

Hitomi SUZUKI,* Mikio SAWAKI,** and Reiji SAKIMOTO**

*Department of Chemistry, Faculty of Science, Kyoto University, Sakyo-ku, Kyoto

**Research Institute, Nihon Soda Co., Ltd., Kohdzu, Odawara

(Received October 22, 1971)

Action of fuming nitric acid upon 1,2,3,5-tetramethylbenzene and 2-ethyl-1,3,5-trimethylbenzene at low temperature was found to yield small amounts of dinitrocyclohexenones in addition to the ring nitration and side-chain nitrooxylation products. Chromatographic separation over silica gel followed by spectral investigation established the structures of these nitro-ketones to be 2,3,4,6-tetramethyl-5,6-dinitro-3-cyclohexen-1-one and 2,4,6-trimethyl-3-ethyl-5,6-dinitro-3-cyclohexen-1-one respectively. The mechanistic interpretation of their formation was briefly discussed.

Treatment of polyalkylbenzenes with fuming nitric acid at low temperature often yields a mixture of ring nitration and side-chain nitrooxylation products.[2] This unusual reaction has an electrophilic feature and is characterized for its peculiar orientation and high positional selectivity.[3] When the samples of the product mixtures from the nitration of polyalkylbenzenes were directly subjected to infrared analyses, it was usually noted that in addition to the major bands due to aromatic nitro compounds and benzyl nitrates, some weak absorptions occur in the regions attributable to carbonyl and aliphatic nitro group stretching vibrations. Carbonyl absorption would at first sight appear to arise from benzaldehydes which could be derived from benzyl nitrates under the influence of acid catalyst,[4] while absorptions owing to aliphatic nitro group would be attributed to phenylnitromethanes, the presence of which was confirmed in some nitration products.[5] However, some of these bands often appear in the regions of too higher frequencies (1370—1380 and 1560—1570 cm^{-1} for nitro group, and 1740—1750 cm^{-1} for carbonyl group) to make such spectral assignment unanimously acceptable. PMR spectra of the crude nitration products from polymethylbenzenes also exhibited weak peaks at quite high field 8.5—9.0 τ, indicating the presence of protons of highly alkane character. These puzzling features of infrared and PMR spectra are now explained by the isolation of alicyclic nitro-ketones, 2,3,4,6-tetraalkyl-5,6-dinitro-3-cyclohexen-1-ones, from the nitration products of isodurene (1,2,3,5-tetramethylbenzene) and ethylmesitylene (2-ethyl-1,3,5-trimethylbenzene), respectively. The structural proof of these unusual products will be the major subject of the present report.

In the preceding paper,[6] we have reported that the chromatographic treatment on silica gel of the nitration product from ethylmesitylene gave from benzene eluates some nitro-carbonyl compounds as a syrupy substance, from which a new nitro-carbonyl compound was obtained as fine colorless needles melting at 140—141°C. The result of elemental analysis and the appearance of a very weak molecular ion at m/e 256 in the mass spectrum indicated that the compound had a molecular formula $C_{11}H_{16}N_2O_5$. Its infrared spectrum revealed the presence of two different nitro groups (1568, 1549, 1379, and 1340 cm^{-1}), a carbonyl group (1737 cm^{-1}), and a double bond (1688 cm^{-1}, weak). The double bond should not be conjugated with carbonyl group nor nitro group, since the ultraviolet spectrum in methanol showed only one weak and broad absorption band at 287—288 nm (ε=265). Nitro groups seem to be attached to the carbon atoms adjacent to the carbonyl group and the double bond, respectively, because the $n\rightarrow\pi^*$ transition at 287—288 nm was appreciably intensified and the carbonyl stretching vibration was substantially shifted to higher wave number. The presence of cyclic structure was confirmed by the examination of the mass spectrum, which exhibited prominent peaks at m/e 210 (M^+-NO_2), 180 ($M^+-NO_2-C_2H_6$), 164 (M^+-2NO_2), 149 ($M^+-2NO_2-CH_3$), 135 ($M^+-2NO_2-CH_3-CH_2$), 121 ($M^+-2NO_2-CH_3-2CH_2$), 107 ($C_7H_6OH^+$), 105 ($C_7H_6CH_3^+$), and 79 ($C_6H_7^+$). The structural detail was obtained from the PMR spectrum, which depicted the presence of one ethyl group (3H 9.12 t, 2H 8.42 q; J=7 Hz. A two-proton quartet was further coupled slightly to the lower-field one proton quartet at 3.91 τ), three methyl groups (3H 8.78 s; 3H 8.15 s; 3H 7.89 d, J=1.7 Hz), and two methine protons (1H 5.01 s; 1H 3.91 q, J=1.6 Hz. A one-proton quartet at 3.91 τ was coupled slightly to the methylene quartet at 8.42 τ). The PMR data offer the partial structures -C(Me)=C(Et)-CH(Me)-, -CH-, and -CMe-, which were compatible with the spectral evidences only when the product was formulated as 2,4,6-trimethyl-3-ethyl-5,6-dinitro-3-cyclohexen-1-one. The appearance of some methyl and methine protons at quite

1) The Reaction of Polysubstituted Aromatics. XXV. Part XXIV: This Bulletin, **45**, 1515 (1972). Preliminary account has been published in *Chem. Commun.*, **1971**, 1509.

2) L. I. Smith and S. A. Harris, *J. Amer. Chem. Soc.*, **57**, 1289 (1935); L. I. Smith and D. Tennenbaum, *ibid.*, **57**, 1293 (1935); L. I. Smith, F. L. Taylor, and I. M. Webster, *ibid.*, **58**, 1082 (1937); L. I. Smith and J. W. Horner, *ibid.*, **62**, 1349 (1940).

3) H. Suzuki, This Bulletin, **43**, 481 (1970); H. Suzuki and K. Nakamura, *ibid.*, **44**, 227 (1971); K. Nakamura, *ibid*,. **44**, 133 (1971); H. Suzuki, K. Nakamura, and M. Takeshima *ibid.*, **44**, 2248 (1971).

4) S. D. Ross, E. R. Coburn, and M. Finkelstein, *J. Org. Chem.*, **33**, 585 (1968); H. Suzuki and K. Nakamura, This Bulletin, **43**, 473 (1970).

5) H. Suzuki, *ibid.*, **43**, 879 (1970).

6) H. Suzuki, M. Sawaki, and R. Sakimoto, *ibid.*, **45**, 1515 (1972).

high field in the PMR spectrum can be understood in terms of anisotropic effect of neighboring nitro groups.

Nitration of isodurene has been reported to yield mononitro or dinitro compounds.[7] However, the products were not as simple as had generally been thought, and besides normal ring nitration products, were obtained appreciable amounts of a non-crystallizable syrupy substance, which could be separated into two major fractions on silica gel chromatography; one containing side-chain nitrooxylated products and the other containing nitrocarbonyl compounds. Further treatment of the latter fraction on silica gel chromatography gave a nitro-ketone with the composition $C_{10}H_{14}N_2O_5$ as the main isolable product. It crystallized from ethanol as fine needles melting at 137—138°C. Its infrared spectrum contained absorption bands at 1738 (C=O), 1680 (C=C, weak), 1573 (NO_2), 1553 (NO_2), 1448, 1380 (NO_2), 1340 (NO_2), 1280, 1038, 1003, and 858 cm^{-1}, and its ultraviolet spectrum (in MeOH) showed a weak band at 285 nm (ε=327), which was characteristic of unconjugated ketones with $n\rightarrow\pi^*$ transition appreciably intensified by the presence of auxiliary chromophores. The PMR spectrum showed three methyl singlets at 8.72, 8.69, and 8.11 τ; one methyl doublet at 7.90 τ coupled to a lower-field methine quartet at 3.92 τ (J=1.5 Hz); and one methine singlet at 5.05 τ. These spectral data and the result of elemental analysis were only consistent with the formulation of the product as 2,3,4,6-tetramethyl-5,6-dinitro-3-cyclohexen-1-one. The assigned structure was further confirmed by the mass spectrum which showed the expected peaks at *m/e* 196 (M^+-NO_2), 166 ($M^+-NO_2-2CH_3$), 150 (M^+-2NO_2), 135 ($M^+-2NO_2-CH_3$), 121 ($M^+-2NO_2-CH_3-CH_2$), 107 ($C_7H_6OH^+$), 105 ($C_7H_6-CH_3^+$), 91 ($C_7H_7^+$), and 79 ($C_6H_7^+$).

The formation of nitrocyclohexenones seems to be general in the nitration of highly alkylated benzenes, although these nitro-carbonyl compounds derived from various hydrocarbons are in most cases a non-crystallizable oil of complicated character, which gradually turned to a dark sticky substance on either repeated attempts to crystallize from solvents or prolonged standing.

The present result is of special interest, not only because it provides a novel mode of abnormal nitration but also because it seems to suggest the possibility of the addition-elimination sequence to be involved partly in the nitration of polyalkylbenzenes, which has generally been accepted to proceed through the S_E2 mechanism. The reaction sequence for the formation of 5,6-dinitro-3-cyclohexen-1-ones may be explained in terms of the addition-elimination mechanism which involves nitronium ion as electrophile and nitrate ion as nucleophile at the initial stage of the reaction. One of the plausible sequences is depicted in Scheme 1. The carbonium ionic intermediate (I) may be stabilized by the favorable orientation of alkyl substituents to such an extent that the addition process in which the nucleophile is captured can compete well with the ordinary substitution process. The process is supported by the recent observation[8] that the nitration of 1,2,3-trimethylbenzene and 4-bromo-*o*-xylene with acetic anhydride-nitric acid, a system containing a strong nucleophile, can lead to the extensive formation of 1-nitro-4-acetoxycyclohexa-2,5-dienes.

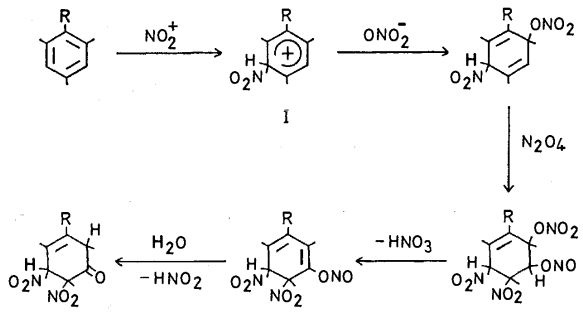

Scheme 1

Experimental

Infrared spectra were run as KBr disc on a Jasco DS-402G spectrophotometer and only prominent peaks are recorded. PMR measurements were carried out on a Varian A-60A and HA-100 spectrometer with deuteriochloroform as solvent and TMS as internal standard. Ultraviolet spectra were determined in methanol solutions on a Shimadzu QV-50 spectrophotometer. Mass spectra were obtained by Dr. A. Ohno of Sagami Chemical Research Center.

Isolation of Dinitrocyclohexenones. General procedures for the nitration of polyalkylbenzenes were described in the preceding paper. Although alumina chromatography was an efficient tool for the separation of side-chain substitution products from ordinary ring nitro compounds, it proved to be unsatisfactory for the isolation of dinitrocyclohexenones in crystallizable state from the crude nitration product mixtures. The oily nitration product was passed through a column of silica gel using light petroleum as eluant to give a mixture of nitro compounds and benzyl nitrates. Further elution with a mixture of benzene and light petroleum gave a fraction containing nitro-carbonyl compound as a yellow syrupy substance, which on trituration with ethanol gave a white powder in the crude yield of 2—4%. It was recrystallized several times from ethanol to give the nitro-ketone as colorless fine needles.

2,3,4,6-tetramethyl-5,6-dinitro-3-cyclohexen-1-one: mp 137—138°C.

Found: C, 49.75; H, 5.79%. Calcd for $C_{10}H_{14}N_2O_5$: C, 49.59; H, 5.79%.

2,4,6-trimethyl-3-ethyl-5,6-dinitro-3-cyclohexen-1-one: mp 140—141°C.

Found: C, 51.71; H, 6.40; N, 11.03%. Calcd for $C_{11}H_{16}N_2O_5$: C, 51.56; H, 6.25; N, 10.93%.

7) P. Jannasch and M. Weiler, *Ber.*, **27**, 3441 (1894); G. Illuminati and G. Marino, *J. Amer. Chem. Soc.*, **75**, 4593 (1953).

8) D. J. Blackstock, M. P. Hartshorn, A. J. Lewis, K. E. Richards, J. Vaughan, and G. J. Wright, *J. Chem. Soc., B*, **1971**, 1212.

The Photo-Beckmann Rearrangement of 3α,5-Cyclo-5α-cholestan-6-one Oxime[1,2]

Hiroshi SUGINOME, Hajime TAKAHASHI, and Tadashi MASAMUNE

Department of Chemistry, Faculty of Science, Hokkaido University, Sapporo

(Received October 23, 1972)

Photolysis of 3α,5-cyclo-5α-cholestan-6-one oxime affords two isomeric lactams with cyclopropane rings arising from photo-Beckmann rearrangement although the yields are poor. The result gives further support to our view on the C→N migration process in photo-Beckmann rearrangement. The major part of the products of the reaction consisted of the parent ketone and several products probably derived from it. The results are compared with those obtained in our photolysis of 5α-cholestan-6-one oxime and the isomeric 5β-cholestan-6-one oximes. The poor yields of the lactams is probably ascribable to the presence of the cyclopropane ring in this conjugated cyclopropyl ketone oxime.

Since the first paper[3] on the photochemical Beckmann rearrangement on arylaldoximes, additional results on aliphatic ketone oximes,[4] alicyclic ketone oximes[4,5,6,9] and α,β-unsaturated ketone oximes[7,8] have been reported. Mechanistic aspects of the reaction have been extensively investigated[8,9,10] and the intermediacy of oxaziridine in this reaction has been confirmed.[8,10]

We have shown[9] that in the photo-Beckmann rearrangement of 5α-cholestan-6-one oxime and the isomeric 5β-cholestan-6-one oximes the bond migration from the intermediary oxaziridines to amides proceeds in a stereospecific manner, the migration of C-5 occurring with retention of the configuration.

With regard to the effect of substituents on the migrating carbon it has been shown[11] that mono-, di-, or tri-substituted α-carbon atom migrates to yield the corresponding lactams and that the migration of the more alkyl-substituted α-carbon atom occurs predominantly, although the irradiation of a certain strained oxime with bridge-head tri-substituted α-carbon leads to the photo-Beckmann fission.[12]

In this paper, we report on the photolysis of 3α,5-cyclo-5α-cholestan-6-one oxime (II). Although the distinct difference in the mode of photolysis between conjugated cyclopropyl ketones and alkyl ketones has been clarified,[13] no investigation has so far been carried out on the photolysis of the conjugated cyclopropyl ketone oxime. Results of the photolysis of II may afford additional information on the bond migration process and also on the synthetic utility of this photochemical reaction.

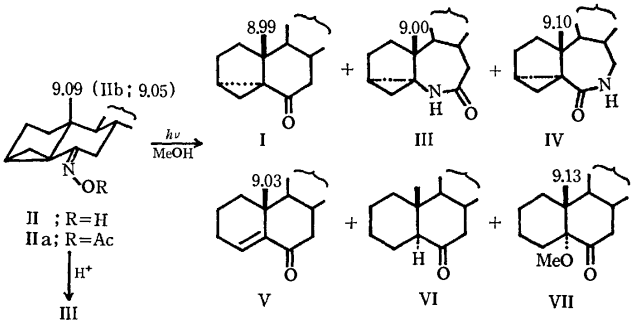

Arabic numerals denote chemical shifts (τ) of 19-methyl protons.

Results

Oxime[14] of 3α,5-cyclo-5α-cholestan-6-one (I) was described by Wallis *et al.* and repetition of this work was found to give the corresponding *single* oxime (II). This revealed the $\pi\rightarrow\pi^*$ band[15] at λ_{max} 197—200 nm (*n*-hexane, ε; 9440).[16] In order to confirm the configuration of the oximino group, II was submitted to the ground state Beckmann rearrangement with polyphosphoric acid.[17] This led to an amorphous single lactam III in 65% yield.[18] The structure of III should be either (III) or (IV). Compound III exhibited one-proton singlet at τ 4.18 which is exchangeable with deuterium and a single-proton quartet centered at τ 9.56. The former is ascribable to lactam NH and the chemical shift of the latter corresponds to proton attached to cyclopropane ring.[19]

On the basis of this NMR spectrum, structure III, 6-aza-3α,5-cyclo-*B*-homo-5α-cholestan-7-one, is found to be correct. The configuration of the oximino group of II is, therefore, safely assigned as an anti-

1) Photo-induced Transformations, XVIII. Part of a paper read before The 23rd Annual Meeting of the Chemical Society of Japan, Tokyo, April (1970). Abstracts of papers No. 3, p. 1291; Previous paper in this series, H. Suginome, T. Mizuguchi, and T. Masamune, *Chem. Commun.*, **1972**, 376.

2) In this paper, the prefix photo- is used in accordance with the usage recommended by Pitts *et al.* (J. N. Pitts, Jr., F. Wilkinson, and G. S. Hammond, "Advances in Photochemistry," ed. by W. A. Noyes, Jr., G. S. Hammond, and J. N. Pitts, Jr., Wiley-Interscience, New York, (1963), vol. 1, p. 20).

3) J. H. Amin and P. de Mayo, *Tetrahedron Lett.*, **1963**, 1585.

4) R. T. Taylor, M. Douek, and G. Just, *ibid.*, **1966**, 4143.

5) T. Sasaki, S. Eguchi, and T. Toru, *Chem. Commun.*, **1970**, 1239.

6) B. L. Fox and H. M. Rosenberg, *ibid.*, **1969**, 1115.

7) G. Just and C. Pace-Asciak, *Tetrahedron*, **22**, 1069 (1966).

8) T. Oine and T. Mukai, *Tetrahedron Lett.*, **1969**, 157.

9) H. Suginome and H. Takahashi, *ibid.*, **1970**, 5119.

10) H. Izawa, P. de Mayo, and T. Tabata, *Can. J. Chem.*, **47**, 51 (1969).

11) G. Just and L. S. Ng, *Can. J. Chem.*, **46**, 3381 (1968).

12) T. Sato and H. Obase, *Tetrahedron Lett.*, **1967**, 1633.

13) For leading reference see W. G. Dauben, G. W. Shaffer, and E. J. Deviny, *J. Amer. Chem. Soc.*, **92**, 6273 (1970).

14) E. S. Wallis, E. Fernholz, and F. T. Gephart, *ibid.*, **59**, 137 (1937).

15) P. J. Orenski and W. D. Closson, *Tetrahedron Lett.*, **1967**, 3629.

16) We are grateful to Professor H. Baba and Mr. I. Yamazaki, of the Research Institute of Applied Electricity, Hokkaido University, for the measurement of UV spectra.

17) E. C. Horning, V. L. Stromberg, and H. A. Lloyed, *J. Amer. Chem. Soc.*, **74**, 5153 (1952).

18) Subsequent to the completion of this work, the ground state Beckmann rearrangement of II was reported by Ahmad *et al.* (M. S. Ahmad, Shafiullah, and M. Mushfiq, *Tetrahedron Lett.*, **1970**, 2739).

19) F. A. Bovey, "NMR Data Tables for Organic Compounds," Interscience, New York, (1967) Vol. 1, p. 102.

C_5C_6 bond. This assignment is conclusive since it is extremely unlikely that in the ground state Beckmann rearrangement of II, a complete isomerization from *syn* to *anti* takes place before the rearrangement. Hydrogen atoms attached to carbon α to oximino group are known to appear downfield[20] in the NMR spectrum of saturated oximes. 100 MHz NMR spectrum of II revealed a double doublet at τ 6.70 with J=12.2 Hz and 2.3 Hz and the coupling constant requires that the singnal should be assignable to 7α-equatorial hydrogen deshielded by OH of the oximino group. The acetyl derivative IIa (mp 99—101°C) of II showed only a doublet due to 7α-hydrogen at τ 6.76 with J=10.9 Hz.

Compound II (5g) in dry methanol (300 m*l*) was irradiated for 31 hr with a 150-W low pressure mercury arc lamp. Since further irradiation caused transformation of the initial products, it was stopped at this stage. Extensive column chromatography and the preparative tlc of a complex mixture of the products led to the isolation of six products, besides recovery of the starting oxime (31%).[21] They were 3α,5-cyclo-5α-cholestan-6-one (I)[22] (8%), amorphous III (3%), amorphous IV (2%), cholest-4-en-6-one (V)[23] (1%), 5α-cholestan-6-one (VI)[24] (1%), and compound (VII), mp 134—138°C (2%).

Compound III proved to be identical with lactam III obtained by the ground state Beckmann rearrangement of II. The mass spectrum of IV (the molecular ion at 399) and elemental analysis disclosed that it was isomeric with II having the molecular formula $C_{27}H_{45}ON$. The infrared spectrum of IV demonstrated typical lactam carbonyl bands at 1635 cm^{-1}. While the NMR spectrum of III revealed a signal due to lactam as a singlet, that of IV showed the corresponding signal as a triplet at τ 3.93 (J=5.9 Hz). Moreover, two single-proton double doublets appeared at τ 6.4 (J=5.9 Hz and 14.9 Hz) and at τ 7.06 (J=5.9 Hz and 14.9 Hz). These two protons are ascribable to CH_2 protons α to the lactam nitrogen. On addition of D_2O, the two double doublets coalesced into two doublets centered at the same position (J=14.9 Hz) and the NH signal vanished. It is therefore, evident that the smaller splitting is due to a coupling between CH_2 protons and a proton attached to nitrogen. Thus, structure IV, 7-aza-3α,5-cyclo-*B*-homo-5α-cholestan-6-one is assigned to the compound. The observed two doublets are ascribable to geminal protons attached to C-7 and the magnitude of splitting (J_{AB}= 14.9 Hz) is in agreement with geminal coupling. Although these geminal protons may appear as AB part of ABX system in which X is the C-8 proton, the observed doublet signal shows $J_{AX}=J_{BX}\simeq 0$ Hz, and suggests that dihedral angles between C-7α and C-7β protons and C-8β proton are about 60° and the C-8 proton approximately bisects the angle between the C-7-methylene protons. Protons attached to the cyclopropane ring were not observable since they would be hidden in the methylene envelope.[25]

The mass spectrum (molecular ion 416) and elemental analysis of VII were in agreement with $C_{28}H_{48}O_2$. The presence of a methoxyl group in VII was proved by the NMR spectrum which showed a three-proton singlet at τ 6.64. The infrared spectrum of VII revealed a 6-membered ring ketone at 1714 cm^{-1} but no hydroxyl group. It is clear that the carbonyl group was generated from the oximino group since generation of the parent carbonyl group from the oximino group was found to be usual.[4,8,11] Thus VII might be 3-, 4- or 5-methoxycholestan-6-one formed by the addition of methanol[26] to either I or V. Since in the NMR spectrum of VII we could find no signal attributable to a proton attached to a carbon atom with a OCH_3 group, the methoxyl group should be located at the carbon bearing no hydrogen. Therefore, VII is 5-methoxycholestan-6-one. Since a comparison of chemical shifts of 19-methyl protons of VI (τ 9.25) and VII (τ 9.31) reveals no deshielding of 19-methyl protons in VII by the newly introduced methoxyl group, the structure of VII should be 5α-methoxycholestan-6-one (VII). The mass spectrum of VII showed the base peak at *m/e* 401 and a prominent peak at *m/e* 385 (79%). It seems somewhat unusual that the expulsion of methyl group from aliphatic methyl ether gives a base peak. However, $M-CH_3$ base peak perhaps originates from the cleavage of acyl-carbon bond[27] followed by the loss of methyl unit to afford the following fragment ion A.

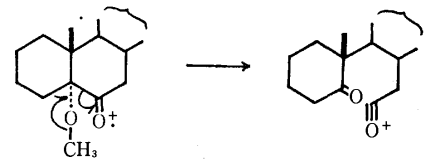

A: *m/e* 401 (100%)

Fragment ion 385 corresponds to fragment B.

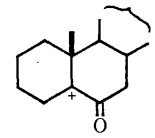

B: *m/e* 385 (79%)

Discussion

The results we obtained demonstrate that the photo-Beckmann rearrangment can be achieved even in the conjugated cyclopropanone oxime and affords the corresponding lactams with cyclopropane ring. However, the yields of lactams were poor and the major portion of the products was the parent ketone arising

20) W. D. Phillips, *Ann. N. Y. Acad. Sci.*, **70**, 817 (1958); H. Saito, K. Nukada, and M. Ohno, *Tetrahedron Lett.*, **1964**, 2124; W. F. Trager and A. C. Huitric, *ibid.*, **1966**, 825.

21) The isomeric *syn*-oxime was neither observed on tlc nor isolated.

22) A. Windaus and E. K. Dalmer, *Ber.*, **52**, 162 (1919). J. R. Bull, Sir E. R. H. Jones, and G. D. Meakins, *J. Chem. Soc.*, **1965**, 2601.

23) H. Reich, F. E. Walker, and R. W. Collins, *J. Org. Chem.*, **16**, 1753 (1951).

24) W. G. Dauben and E. J. Deviny, *ibid.*, **31**, 3794 (1966).

25) T. Shono, T. Morikawa, A. Oku, and R. Oda, *Tetrahedron Lett.*, **1964**, 791.

26) W. G. Dauben and W. T. Wipke, *Pure Appl. Chem.*, **9**, 539 (1964).

27) P. E. Butler, *J. Org. Chem.*, **29**, 3024 (1964).

from the elimination of the nitrogen moiety of the intermediary oxaziridine. Thus, compared with the results of the photo-Beckmann rearrangements of 5α-cholestan-6-one oxime and the isomeric 5β-cholestan-6-one oximes[9] the effects of the presence of cyclopropane ring and those of steric origin are evident.

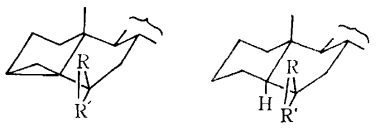

VIII IX

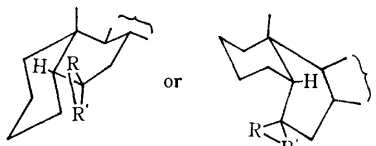

X

R=O, R'=NH or R=NH, R'=O

This would imply that in the intermediate oxaziridine VIII the rearrangement into lactam becomes less easy, owing to the presence of cyclopropane ring, than in the case of oxaziridine IX, and the elimination of nitrogen as N_2, hydrazine[8] or ammonia[11] becomes dominant in the present case. Compared with the isomeric 5β-cholestan-6-one oximes (plausible conformation of the intermediate oxaziridine is depicted as is X) less easy formation of lactams from 5α-isomer is mainly attributable to the conformational factors. Formation of two lactams with cyclopropane ring gives additional support to our view[9] on the C→N migration process in the photo-Beckmann rearrangement.

With regard to the mode of formation of three ketones V, VI and VII obtained as the minor products, it is almost certain that V was derived from I since the formation of α,β-unsaturated ketone from the conjugated cyclopropyl ketone was recognized as general[13,28] and the mode of reaction was recently investigated in detail.[13,29] The other two ketones VI and VII can be derived either directly from I or through the formation of V by photo-reduction as well as photo-addition. Several investigators encountered the photo-reduction of double bond of α,β-unsaturated ketons. Addition of methanol to α,β-unsaturated carbonyl compound generally gives β-methoxy-carbonyl compound[30] and therefore the formation of VII is better understandable by the direct addition of methanol to cyclopropyl ketone (I).

Experimental

All mps were determined by a Yanagimoto type hot-stage and uncorrected. Unless otherwise stated, IR was determined in Nujol using a Jasco model IR-E spectrophotometer. Except for compound VII, all NMR spectra were determined on a Japan Electron Optics PS-100 high resolution NMR spectrometer in $CDCl_3$ solution using TMS as an internal reference. NMR spectrum of compound VII was taken with a Hitachi H-60 high resolution NMR spectrometer. Mallinckrodt silicic acid (100 mesh) was used for column chromatography and Wakogel B-5 for preparative tlc. The progress of the reactions was followed by tlc.

3α,5-Cyclo-5α-cholestan-6-one Oxime.[14] *(II).* Oximation of I by the usual procedure was found to give a single oxime, mp 125—126°C. Literature mp 143—144°C.[14] (from EtOH), $[\alpha]_D^{25}$ ($CHCl_3$) +83.3°. Mass M^+ 399. NMR: τ 9.31 (18-CH_3), τ 9.09 (19-CH_3). Acetate (IIa): *O*-acetate was prepared by the usual method. mp 99—101°C. NMR: τ 6.76 (d, J=10.9 Hz) (7αH), τ9.31 (s, 18-CH_3) τ 9.05 (s, 19-CH_3) τ 7.84 (s, O-Ac).

Beckmann Rearrangement of 3α-5-Cyclo-5α-cholestan-6-one Oxime. II (200 mg) was added to polyphosphoric acid (2 g) which was kept at *ca.* 100°C. The mixture was stirred for 10 min. After cooling the mixture was poured into 10% aqueous sodium carbonate solution. The mixture was extracted with ether. After the usual work up, tlc of the residue (200 mg) showed two spots and the major and more polar compound was purified by preparative tlc ($CHCl_3$ - ether 1 : 1). III (130 mg, 65%) was obtained in an amorphous form. (Found: C, 81.04; H, 11.60; N, 3.63%. Calcd for $C_{27}H_{45}ON$: C, 81.14; H, 11.35; N, 3.51%). IR ($CHCl_3$): 1656 cm^{-1} (CONH). NMR: τ 4.18 (s, NH), τ 9.00 (s, 19-methyl), τ 9.31 (s, 18-methyl). (τ 9.56 quartet J=8.2 and 4.8 Hz) C-4α or C-4βH (τ 7.71, broad s) C-7 methylene. Mass. M^+ 399.

Photolysis of 3α,5-Cyclo-5α-cholestan-6-one Oxime. II (5 g) in dry methanol (300 m*l*) was photolyzed for 31 hours by a 150 W low pressure Hg arc lamp under a nitrogen atmosphere. After removal of the solvent the residue was dissolved in ether (150 m*l*). The ethereal solution was washed with water, dried and evaporated. The residue was subjected to column chromatography by using 100 g of adsorbent. Elution was first made with *n*-hexane and then with a mixture of *n*-hexane and benzene with an increasing amount of benzene (*n*-hexane, 300 m*l*, hexane - benzene 9:1, 300 m*l* hexane - benzene 8:2, 300 m*l*, hexane - benzene 7 : 3, 700 m*l*, hexane - benzene 6 : 4, 600 m*l*, hexane - benzene 5 : 5, 400 m*l*), affording fraction A (1.4 g). Elution was then continued with *n*-hexane - benzene (3 : 7) (300 m*l*), pure benzene (200 m*l*) and finally benzene - $CHCl_3$ (8 : 2) (400 m*l*) to afford fraction B (1.6 g). Elution was continued with benzene - $CHCl_3$ (6 : 4) (200 m*l*), benzene - $CHCl_3$ (4 : 6) (200 m*l*) and benzene - $CHCl_3$ (2 : 8) (300 m*l*) to afford fraction C (0.24 g).

Elution was further carried out with $CHCl_3$ (200 m*l*), $CHCl_3$ - ether (8 : 2) (200 m*l*) and $CHCl_3$ - ether (6 : 4) (200 m*l*) to afford fraction D (1.3 g). Finally, elution was carried out with $CHCl_3$ - ether (4 : 6) (200 m*l*), $CHCl_3$ - ether (2 : 8) (100 m*l*), $CHCl_3$ - ether (1 : 1) (100 m*l*) and ether (200 m*l*) to give fraction E (0.9 g). Fractions A, B, C, and D were subjected to further separation as follows. Fraction A: This was again chromatographed with 26 g of adsorbent, some fractions obtained being further purified by preparative tlc to afford four products. The least polar compound was recrystallized from ethanol to afford 5α-cholestan-6-one (VI), mp 95—97°C,[31] identical with authentic specimen. (30 mg, 0.6%). The second least polar fraction (620 mg) was recrystallized from ethanol to yield 3α,5-cyclo-5α-cholestan-6-

28) C. H. Robinson, O. Gnoj, and E. E. Carlon, *Tetrahedron*, **21**, 2509 (1965). R. Beugelmans, *Bull. Soc. Chim. Fr.*, **1967**, 244.

29) B. Nann, D. Gravel, R. Schorta, H. Wehrli, K. Schaffner, and O. Jeger, *Helv. Chim. Acta*, **46**, 2473 (1963). I. A. Williams and P. Bladon, *Tetrahedron Lett.*, **1964**, 257.

30) R. Stoermer and H. Stockmann, *Ber.*, **48**, 1786 (1914).

31) The literature mps for 5α-cholestan-6-one are mp 98.5—99.5°C[22] and mp 96°C (D. N. Jones, J. R. Lewis, C. W. Shoppee, and G. H. R. Summers, *J. Chem. Soc.*, **1955**, 2876.

one (I) (392 mg, 8%). The third least polar fraction (130 mg) yielded 62 mg (1.3%) of crystals mp 104—106°C, NMR: τ 3.65 (C-4H) (t, J=3.0 Hz), τ 9.30 (s, 18-CH_3) and τ 9.03 (s, 19-CH_3) which were identical with cholest-4-en-6-one.[23] The most polar fraction (200 mg) afforded crystals of the starting oxime (130 mg). Fraction B: This was recrystallized from ethanol to yield the starting oxime (1.4 g) which was then combined with oxime from fraction A. Total yield of pure recovered oxime was thus 31%. Fraction C: This was purified by preparative tlc ($CHCl_3$ containing a small amount of ether). Oily material obtained was recrystallized from ethanol to yield 5α-methoxycholestan-6-one, mp 134—138°C (110 mg, 2%). (Found: C, 80.70; H, 11.64%; Calcd for $C_{28}H_{48}O_2$: C, 80.71; H, 11.61%). IR: 1714 cm^{-1} (6-membered cyclic ketone) 1090 cm^{-1} (C-O). NMR: τ 6.65 (s, OCH_3), τ 9.31 (s, 19-CH_3) τ 9.36 (s, 18-CH_3). Mass: M^+ 416. Fraction D: This was purified by column chromatography (adsorbent 26 g; solvent, benzene - chloroform). Preparative tlc of the eluates with chloroform containing a small amount of ether then afforded 300 mg of crude material which was subjected again to preparative tlc (ethyl acetate - ether - benzene 3 : 2 : 1) to afford two amorphous compounds. Less polar compound IV (100 mg; 2%) (Found: C, 81.11; H, 11.29; N, 3.55%. Calcd for $C_{27}H_{45}ON$: C, 81.14; H, 11.35; N, 3.51%). IR ($CHCl_3$): 1635 cm^{-1} (NHCO), 3420 cm^{-1} (NH). More polar compound III (160 mg; 3%) was identical with the lactam obtained by the ground-state Beckmann rearrangement.

We are grateful to Mrs. S. Araki in this department for the measurements of NMR spectra, also to the staffs of the laboratories for mass spectrometric analysis and elemental analysis of the Faculty of Pharmaceutical Sciences of this University, for the mass spectral determinations and the elemental analyses.

BULLETIN OF THE CHEMICAL SOCIETY OF JAPAN, VOL. 45, 1839—1843 (1972)

The Structure of κ-Carrageenan from *Gigartina Tenella*

Susumu HIRASE and Kyoko WATANABE

Department of Chemistry, Faculty of Industrial Arts, Kyoto Technical University, Matsugasaki, Kyoto

(Received October 25, 1971)

An alkaline treatment of κ-carrageenan from *Gigartina tenella* resulted in the change of the proportions of galactose, 3,6-anhydro-galactose and sulfate from 100 : 91 : 124 to 95 : 96 : 119. Fragmentation of the methylated polysaccharide gave 2,4,6-tri-*O*-, 2,6-di-*O*-, and mono-*O*-methyl-D-galactose in the molar proportions of 1 : 18 : 0.8 together with 3,6-anhydro-D-galactose and its 2-*O*-methyl-derivative in the molar proportion of 1 : 4. From these and other data, it is concluded that the polysaccharide is composed of the residues of 1,3-linked β-D-galactose 4-sulfate (95 mol), 1,4-linked α-D-galactose 6-sulfate (5 mol), and 1,4-linked 3,6-anhydro-α-D-galactose (67 mol) and its 2-sulfate (24 mol), and that the 1,3- and 1,4-linked residues are repeated alternatingly to form a chain macro-molecule.

The chemical structure of κ-carrageenan obtainable from several species of red seaweeds of the *Chondrus and Gigartina* families has been extensively investigated by many workers.[1)]

Our previous studies on the κ-carrageenan from *G. tenella*[2)] showed the presence of D-galactose, 3,6-anhydro-D-galactose and ester sulfate in the molar proportions of 100 : 98 : 117, together with very small amounts of L-galactose and D-xylose. Partial methanolysis provided evidence that carrabiose (3,6-anhydro-4-*O*-β-D-galactopyranosyl-D-galactose) represented the repeating units of the backbone structure of the sulfated polysaccharide. In the present paper, further details of the structure have been investigated by means of alkali-treatment, methylation and IR spectroscopic measurement.

The κ-carrageenan used in this work has been prepared in the same manner as that described in the preceding paper.[2)] On analysis it contained galactose, 3,6-anhydro-galactose and sulfate in the molar proportions of 100 : 91 : 124, the proportions being in approximate agreement with those of the previous preparations. When this polysaccharide sample was treated with alkaline borohydride according to the method of Rees,[3)] the molar proportions of the components changed from those described above to 95 : 96 : 119. It is apparent that both galactose and sulfate decreased by 5 mol with concurrent increase of an equimolar amount of the anhydro-sugar. This could be explained by the presence of 2-linked galactose 3-or 6- sulfate or 4-linked galactose 3- or 6-sulfate residues, any of which could be convertible into 3,6-anhydro-galactose residues by the alkali treatment. However, from the general concept[4)] of chemical structures, based on extensive investigations of a variety of sulfated polysaccharides of red seaweed origin, it is most probable that 5 mol of 4-linked galactose 6-sulfate residues exist in the sulfated polysaccharide under investigation.

The sulfated polysaccharide was then methylated ten times with dimethyl sulfate and sodium hydroxide solution. The product contained 17.3% of methoxyl groups and 16.7% of sulfate groups. If the methylation was complete for the alkali-modified polysaccharide, 4-linked galactose 6-sulfate residues should have been converted into 3,6-anhydro-galactose re-

1) E. Percival and R. H. Mcdowell, "Chemistry and Enzymology of Marine Algal Polysaccharides," Academic Press, London and New York (1967).

2) S. Hirase and K. Watanabe, This Bulletin, **40**, 1442 (1967).

3) D. A. Rees, *J. Chem. Soc.*, **1961**, 5168.

4) N. S. Anderson, T. C. S. Dolan, and D. A. Rees, *Nature* **205**, 1060 (1965); D. A. Rees, *Adv. Carbohyd. Chem. Biochem.*, **24**, 267 (1969).

sidues, and consequently, the product would contain 17.2% of methoxyl groups and 20.6% of sulfate groups. That the observed sulfate content was lower than the expected one suggested that additional desulfation had occurred during the methylation.

TABLE 1. FRAGMENTATION OF METHYLATED κ-CARRAGEENAN

Methylated sugar	Molar ratio
2,4,6-Tri-*O*-methyl-D-galactose	1.0
2,6-Di-*O*-methyl-D-galactose	18.0
Mono-*O*-methyl-D-galactose	0.8
2-*O*-Methyl-3,6-anhydro-D-galactose	4.0
3,6-Anhydro-D-galactose	1.0

The complete degradation of the methylated polysaccharide gave the products shown in Table 1. 2,4,6-Tri-*O*-methyl-D-galactose and 2,6-di-*O*-methyl-D-galactose were identified by the isolation of crystalline reducing sugars. Mono-*O*-methylgalactoses were shown to be mainly 2-*O*-methyl- and 6-*O*-methyl derivatives by paper chromatography, gas liquid chromatography and paper electrophoresis. 3,6-Anhydro-D-galactose was obtained as a syrupy dimethylacetal, and was then converted into crystalline diphenylhydrazone. 2-*O*-Methyl-3,6-anhydro-D-galactose was identified by the isolation of its crystalline methyl β-glycoside. In addition, a trace amount of 2,4-di-*O*-methyl-D-galactose was also shown to be present.

Among the partially methylated D-galactoses obtained above, 2,6-di-*O*-methyl-D-galactose was the major product in accordance with the cases of κ-carrageenans of other origin.[5] This product is derived either from 3-linked D-galactose 4-sulfate or 4-linked D-galactose 3-sulfate residues. But the latter possibility is completely excluded, because the 3-sulfate residues would have been converted into 3,6-anhydro-D-galactose residues by the action of alkali during methylation. The formation of 2,4,6-tri-*O*-methylgalactose appears to indicate the presence of non-sulfated, 3-linked D-galactose residues. However, on the basis that the yield was as small as one eighteenth of that of 2,6-di-*O*-methyl-D-galactose, and also that some desulfation occurred during methylation as discussed above, it seems more probable that this tri-*O*-methylgalactose has been derived by desulfation followed by methylation from 3-linked D-galactose 4-sulfate residues. The yield of the tri-*O*-methylgalactose relative to that of the di-*O*-methylgalactose indicated that 5% of the 4-sulfate residues were desulfated during methylation. The formation of small amounts of 2-*O*-, and 6-*O*-methylgalactose could be accounted for by incomplete methylation of 3-linked D-galactose 4-sulfate residues. 2,4-Di-*O*-methyl-D-galactose was formed in so small an amount that it had no structural significance. After all, all the D-galactose residues seem to be joined 1,3 with sulfate groups on C_4 in the native polysaccharide.

On the other hand, the formation of 2-*O*-methyl-3,6-anhydro-D-galactose and non-methylated 3,6-anhydro-D-galactose as the cleavage fragments from the methylated polysaccharide indicates that all the anhydro-sugar residues are joined 1,4 as has been proved by the isolation of carrabiose derivatives in high yield[2], and also that some of the anhydro-sugar residues are 2-sulfated. The proportion of the 2-sulfated residues to the non-sulfated residues may not be directly evaluated from the relative yields of the anhydro-sugar fragments from the methylated polysaccharide, because a part of the 2-sulfate groups might have possibly been released during methylation. This possibility is supported by the fact[6] that the treatment of methyl 2-*O*-p-toluensulfonyl-3,6-anhydro-D-galactoside with strong alkali resulted in complete desulfonation without configurational inversion.

Now the problems to be solved are concerned with the proportion of 2-sulfation on anhydro-sugar residues in the native polysaccharide and also with the proportion of desulfation of these sulfate groups during methylation. These problems have been tentatively solved as shown in Table 2, which includes the summary of discussion as well. As has been already mentioned, the native polysaccharide contains galactose, anhydrogalactose and sulfate in the molar proportions of 100 : 91 : 124. Since, on the basis of the results of alkali treatment, 5 mol per 100 mol of galactose residues are joined 1,4 with 6-sulfate groups, as has been mentioned above, the residual 95 mol are joined 1,3 with 4-sulfate groups. These two residues account for 100 mol per 124 mol of total sulfate groups so that

TABLE 2. STRUCTURAL FEATURES OF THE κ-CARRAGEENAN

κ-Carrageenan	Residues in relative moles					
	3-Linked galactose		4-Linked galactose			Total
	non-S	4-S	6-S	A, non-S	A, 2-S	sulfate
Native	nil	95	5	67	24	124
		100		91		
Alkali-modified	nil	95	nil	67+5[a]	24	124−5[a]
Methylated	5[b]	95−5[b]	nil	67+5[a]+5[b]	24−5[b]	124−5[a]−10[b]

S: sulfate, A: 3,6-anhydride.
a) due to desulfation with concurrent formation of 3,6-anhydro sugar.
b) due to desulfation during methylation.

5) N. S. Anderson, T. C. S. Dolan, and D. A. Rees, *J. Chem. Soc., C*, **1968**, 596.

6) P. A. Rao and F. Smith, *ibid.*, **1944**, 229.

24 mol of sulfate groups could exist on C_2 of anhydro-sugar residues. Then the non-sulfated anhydro-sugar residues exist by 67 mol, the proportion of 2-sulfation to non-sulfation being approximately 1 : 3. When the polysaccharide was methylated, 5 mol per 95 mol of galactose 4-sulfate residues seems to have been desulfated, as was discussed above. Similarly, if it is presumed that 5 mol per 24 mol of anhydro-sugar 2-sulfate residues were desulfated during methylation, fragmentation of the methylated polysaccharide would produce 3,6-anhydro-D-galactose and its 2-methyl ether in the molar proportion of 77 : 19, which agrees with the experimental result (4 : 1), Furthermore, when such desulfation as discussed above are taken into consideration, the molar proportion of methoxyl groups to sulfate groups should be 2.48 for the completely methylated polysaccharide. This value is again reasonable for the experimental result (2.67).

In conclusion, the κ-carrageenan under investigation is a hybrid consisting of three structural units a (70%), b (25%), and c (5%) shown in Fig. 1, the α-linkages being presumed from the positive value of optical rotation of the native polysaccharide.[2] Although the indicated proportions between the units are based on the discussion about Table 2, the κ-carrageenan seems to contain a family of related polysaccharide molecules, which differ more or less in the proportions of a, b, and c, as has been pointed out by Anderson and his co-workers[7]. The structure proposed above is similar in outline to that reported for the κ-carrageenan from *Gigartina stellata* as well as from *Chondrus crisps*.[5]

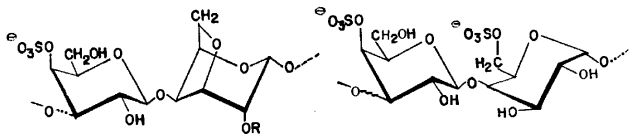

(a) R=H
(b) R=$SO_3^{\ominus}$ (c)

Fig. 1. The possible structure of the κ-carrgeenan from *G. tenella*

The proposed structure is also supported by infrared spectrum, which showed absorption bands at 850 cm^{-1} and 805 cm^{-1}. The former band is attributed to the sulfate groups attached to secondary axial hydroxyl groups[8] (C_4 of D-galactose residues), while the latter band is characteristic to the 2-sulfate groups on anhydro-sugar residues.[7] The band (820 cm^{-1}) due to the sulfate groups on primary hydroxyl groups (C_6 of galactose residues) was not observed. The 6-sulfated residues exist in so small amounts that the band may be masked in the broadening region of neighboring bands.

Experimental

General Method. Solutions were concentrated under reduced pressure at 40°C in a rotary evaporator. Melting points were measured on Yanagimoto apparatus Model MP-S2. Paper electrophoresis was performed on Toyo filter paper No. 51 with 0.1 M sodium borate buffer (pH 10) and a potential gradient of 17 volts/cm. Infrared spectra were recorded with Hitachi Infrared Spectrophotometer Model 215 (sample as a potassium bromide disk).

Paper Chromatography (pc) and Thin Layer Chromatography (tlc). Pc was performed on Toyo-filter paper No. 51, and the solvents (in v/v) used were as follows: A) 1-butanol - acetic acid - water (4 : 1 : 2); B) 1-butanol - ethanol-water (5 : 1 : 4, upper layer); C) butanone - 28% ammonium hydroxide - water (20 : 0.1 : 1.7); D) cyclohexanol saturated with water; E) 1-butanol - pyridine - water (10 : 3 : 3); F) benzene - ethanol (5 : 1) saturated with water; G) ethyl acetate - pyridine - water saturated with ammonium borate (12 : 4.5 : 3); and H) 1-butanol-water saturated with ammonium borate (4 : 1 : 2). In the case of the solvents G and H, filter paper was dipped into ammonium borate solution and dried before use. Spray reagents used were a) aniline hydrogen phthalate,[9] b) *p*-anisidine hydrochloride,[10] and c) *o*-aminophenol phosphate.[11] Tlc was carried out on glass plates (20 cm in length) coated with silica gel G containing calcium sulfate as binder, using the solvents J ethyl acetate-pyridine-water (30 : 2 : 1), and K benzene-ethanol-water (40 : 15 : 1). Chromatograms were sprayed with 2N-methanolic sulfuric acid and heated at 110°C.

Gas Liquid Chromatography (glc). The apparatus used was a Hitachi Gas Chromatograph Model K53 equipped with a hydrogen flame ionization detecter, using nitrogen as a carrier gas. Analyses were carried out by the following methods depending upon the purpose: Method A: For the general purpose, methyl glycosides and dimethyl acetals of methylated sugars were analysed on a column (3 mm × 1 m) packed with 2.5% neopentylglycol succinate on chromosorb W (100—200 mesh) at 160°C. This method has the disadvantage that some of the peaks are overlapped each other especially in the analysis of a complicated mixture. Method B: For the purpose of identifying anhydro-sugar derivatives, a mixture (10 mg) of methyl glycosides and dimethyl acetals of methylated sugars was dissolved in concentrated hydrochloric acid (0.2 m*l*) at 0°C, ethanethiol (0.1 m*l*) added, and the mixture was vigorously stirred at 0°C for 15 min. By this treatment, anhydro-sugar derivatives were converted into diethyl dithioacetals, while methylated methyl galactosides were mostly unchanged. The reaction mixture was neutralized with saturated sodium bicarbonate solution, evaporated to dryness, and the trimethylsilylated with pyridine (0.5 m*l*), trimethylchlorosilane (0.1 m*l*), and hexamethyldisilazane (0.2 m*l*). The products in chloroform (3 m*l*) were washed three times with cold water (1 m*l*), dried with anhydrous magnesium sulfate, evaporated, and then analysed on a column (1 m) packed with 5% neopentyl glycol succinate on chromosorb W (100—200 mesh) at 160°C. Retention times of trimethylsilylated diethyl dithioacetals were much higher than those of trimethylsililated methyl galactosides. Method C: For the purpose of identifying galactose derivatives, the sample to be analysed was hydrolysed with 1 N-sulfuric acid at 100°C for 5 hr. During this treatment, anhydro-sugar derivatives are, if present, completely degraded. The remaining methylated galactoses were converted into alditol acetates, which were then analysed on a column (2 m)

7) N. S. Anderson, T. C. S. Dolan, A. Penman, D. A. Rees, G. P. Mueller, D. J. Stancioff, and N. F. Stanley, *ibid.*, **1968**, 602.
8) J. R. Turvey and T. P. Williams, ibid., **1962**, 2119.
9) S. M. Partridge, *Nature*, **164**, 443 (1949).
10) J. B. Pridham, *Anal. Chem.*, **28**, 1967 (1956).
11) S. Hirase, C. Araki, and S. Nakanishi, This Bulletin, **26**, 183 (1953).

packed with 3% ECNSS-M on chromosorb W.[12,13]

Column Chromatography. Effluents were collected in an automatic fraction collector, and examined for their contents by pc, tlc, and/or coloration with an anthrone-sulfuric acid reagent and a resorcinol-hydrochloric acid reagent.[14] Fractions containing the same contents were combined, evaporated and again examined by pc, tlc and/or glc.

Alkali Treatment of Polysaccharide. According to the method of Rees,[3] the polysaccharide (0.42 g) dissolved in water (250 m*l*) was treated with sodium borohydride (0.1 g) at room temperature for 24 hr. Sodium hydroxide (10 g) and sodium borohydride (1.5 g) were then added, and the mixture was heated at 80°C for 3 hr. The solution was neutralized with acetic acid, dialysed against running tap water for 2 days, concentrated, precipitated with ethanol, and finally dried *in vacuo*; yield, 0.33 g (78.5%).

The product, as well as the sample before alkali treatment, was analysed for sugars by the colorimetric method with a resorcinol reagent and an anthrone reagent after Yaphe,[14] and for sulfate by the volumetric method[15] modified as follows: the sample (2—5 mg) to be analysed was dissolved in water (3—10 m*l*), and about 0.005 N glycol chitosan solution (2 m*l*) was added in excess to precipitate the polysaccharide sulfate in a stoichiometric reaction. To this mixture, 1 N-hydrochloric acid (0.5 m*l*) and one or two drops of 0.2% toluidine blue indicator solution were added. The excess of the glycol chitosan was titrated with a standard 0.0025 N potassium polyvinyl alcohol sulfate solution (equivalent 162) until the indicator changed from blue to reddish purple. The sulfate content of the sample was calculated from the difference between the titration value and the blank value. The results were as follows: the molar proportions of galactose, 3,6-anhydro-galactose and sulfate were 1 : 0.91 : 1.24 in the native polysaccharide, and 0.95 : 0.96 : 1.19 (1 : 1.01 : 1.25) in the alkali-treated sample.

Methylation of Polysaccharide. To a solution of polysaccharide (12.4 g) in water (150 m*l*) treated with sodium borohydride (0.5 g) overnight at room temperature was added dimethyl sulfate (50 g) and 30% sodium hydroxide (80 m*l*) dropwise with vigorous stirring during 6 hr at 60°C under at atmosphere of nitrogen. The reaction mixture was left overnight. Dimethyl sulfate (50 g) and 30% alkali (80 m*l*) were again added in the same manner. The reaction mixture was left overnight, then heated at 80°C for 1 hr to decompose the excess of dimethyl sulfate, neutralized with 2 N-sulfuric acid, dialysed against running tap water for 50 hr, and concentrated. The resulting solution was treated four more times with dimethyl sulfate and alkali in the same manner as above-mentioned. Finally, the methylated polysaccharide was precipitated with 99% ethanol and dried *in vacuo*; yield, 10 g; $[\alpha]_D^{10}$ +57.3° (*c* 0.79, water), (Found: OCH_3, 17.3; SO_3, 16.7%).

Methanolysis of Methylated Polysaccharide. The methylated polysaccharide (8.1 g) was treated with 3% methanolic hydrogen chloride at 80°C for 20 hr. The reaction mixture was then neutralized with silver carbonate, filtered and evaporated. The resulting syrup was treated with 0.2 N-barium hydroxide solution (100 m*l*) at 60°C for 2 hr, neutralized with carbon dioxide, and filtered. The filtrate was passed through Amberlite IR-120 (200 m*l*) and IR-45 (300 m*l*) in succession, and the deionized solution was evaporated to a syrup; yield, 4.82 g.

Analysis of the Methanolysis Products. Examination of the methanolysis products obtained above by pc (solvent D, spray reagent c) indicated the presence of 3,6-anhydro-galactose dimethyl acetal (**1**), its 2-methyl ether (**2**), and the methyl β-glycopyranoside (**3**) corresponding to **2**. Analysis by glc (method B) showed two peaks of diethyl dithioacetals, one of which was derived from **1**, and the other from **2**. and **3**. From the peak areas measured and the molar response factor determined for authentic samples, it was shown that 3,6-anhydrogalactose and its 2-methyl ether existed in the molar proportion 1 : 4.

On the other hand, when a portion of the methanolysis products was hydrolysed and examined by pc (solvent A, B and C; spray reagent a and b), there were detected 2,6-di-*O*-methylgalactose (**4**) together with small amounts of 2,4,6-tri-*O*-methylgalactose (**5**) and mono-*O*-methylgalactose (**6**). Analysis by glc (method C) showed that **4**, **5** and **6** existed in the molar proportions of 1 : 18 : 0.8, the figure being based on the peak areas and molar response factors.

Separation of the Methanolysis Products. Methanolysis products (1.3 g) obtained above were applied to a Dowex 1×4 column (OH form, 5×36 cm) and eluted first with distilled water to give fractions I, II, and III. The column was then eluted with 0.2 M-ammonium carbonate aqueous solution, and the effluent was deionized with Amberlite IR-120 and IR-45 resins, and evaporated to give fraction IV. All the fractions were obtained in syrups.

Fraction I: Yield, 0.61 g. This fraction should be a mixture of methyl glycosides of partially methylated galactoses, as it showed color reaction with an anthrone reagent and no color reaction with a resorcinol reagent. It was combined with a similar fraction obtained by the same procedure as that mentioned above, and the resulting mixture (1.4 g) was hydrolysed with 1 N-sulfuric acid (20 m*l*) at 100°C for 30 hr. The resulting mixture of reducing sugars (1.08 g) was separated on a cellulose powder column (5×40 cm), which was eluted first with a benzene-ethanol (5 : 1) mixture saturated with water, to give fractions I-1 (0.24 g), and I-2 (0.88 g) in syrups. The proportion of the solvent mixture was then changed to 3 : 1 to give fraction I-3 (0.04 g) in a syrup.

Examination of the fraction I-1 by pc (solvent F, spray reagent b) showed two spots, one (R_f 0.73, pink brown) corresponding to 2,4,6-tri-*O*-methylgalactose, and the other (R_f 0.63, pale brown) corresponding to an unidentified compound. In tlc (solvent J and K), the former component gave a darker spot with slightly higher R_f value than the latter component. The mixture was separated to the components on an Avicel column (3×92 cm) with a benzene-ethanol (5 : 1) mixture saturated with water. The faster moving component (0.077 g) was identified as 2,4,6-tri-*O*-methyl-D-galactose, which was crystallized from ether; mp and mmp 102—103.5°C,[16] $[\alpha]_D^{10}$ +116.9°→+79.8°[16,19] (*c* 0.46, water), (Found: C, 48.66; H, 8.19%). The slower-moving component (0.07 g) was not examined further.

Fraction I-2 (0.88 g) gave a single spot corresponding to 2,6-di-*O*-methylgalactose both in pc (solvent B and C, spray reagent b) and tlc (solvent K). It crystallized readily and was recrystallized from ethanol - petroleum ether, 2,6-di-*O*-

12) J. S. Sawardeker, J. H. Sloneker, and A. Jeanes, *Anal. Chem.*, **37**, 1602 (1965).
13) H. Björndal, B. Lindberg, and S. Svensson, *Acta. Chem. Scand.*, **21**, 1801 (1967).
14) W. Yaphe, *Anal. Chem.*, **32**, 1327 (1960).
15) S. Okimasu, *Nippon Nogei Kagaku Zasshi*, **22**, 63 (1958).
16) C. Araki, *Nippon Kwagaku Kwaishi*, **58**, 1362 (1937).
17) E. T. Dewar and E. G. V. Percival, *J. Chem. Soc.* **1947**, 1622.
18) P. Andrews, L. Hough, and J. K. N. Jones, *ibid.*, **1954**, 806.
19) C. Araki and S. Hirase, This Bulletin, **33**, 291 (1960).

methyl-D-galactose was obtained as plates; mp and mmp 118—119.5°C,[17,18] $[\alpha]_D^{10}$ +47.7°→+90.7°[17,18] (*c* 0.73, water), (Found: C, 46.16; H, 7.91%).

Fraction I-3 (0.04 g) was shown by pc (solvent C and F, spray reagent b) to be a mixture of 2,6-di-*O*-methylgalactose, 2,4-di-*O*-methylgalactose and mono-*O*-methylgalactose. The mixture was separated to the components on an Avicel column (2×30 cm), which was first eluted with benzene-ethanol (5 : 1) saturated with water to give two fractions. The proportion of the solvent mixture was then changed to 3 : 1 to give an additional fraction. The first fraction (0.11 g) on crystallisation gave 2,6-di-*O*-methyl-D-galactose; mp and mmp 118—119.5°C, $[\alpha]_D^{12}$ +45.3°→+88.5° (*c* 0.46, water). The second fraction (0.005 g), $[\alpha]_D^{28}$ +76.7° (*c* 0.45, water),[18] was obtained as a syrup, which showed exactly the same behavior as that of an authentic sample of 2,4-di-*O*-methyl-D-galactose both in pc[18] (solvent C and F, spray reagent b) and glc (method C). This fraction was obtained in too small an amount to be crystallized. The last fraction (0.025 g) was obtained as a syrup, which was shown to be a mixture of 2-*O*-, 3-*O*-, 4-*O*-, and 6-*O*-methylgalactoses both by paper electrophoresis and glc (method C), the first and last components being predominant. Isolation of the components was not attempted.

Fraction II. Yield, 0.48 g; $[\alpha]_D^{23}$ −21.6° (*c* 0.85, water). Examination of the fraction II by pc and tlc with any solvent system, detected a single spot, respectively. But examination by glc (method A) revealed the presence of three components, one of which had exactly the same retention time as that of an authentic sample of 2-*O*-methyl-3,6-anhydro-galactose dimethyl acetal. The other two seemed to be methyl 2,6-di-*O*-methyl-α- and -β-galactofuranosides. The negative value of optical rotation of this fraction II supported the above view. As the mobilities of these three were identical both on a filter paper and a thin layer chromatogram with any solvent system, the separation on a column was not attempted. Instead, the fraction was treated with methanolic hydrogen chloride to give an equilibrium mixture in the following manner. The fraction was combined with a similar fraction (1.2 g) obtained from the methanolysis products of the methylated polysaccharide, and the resulting mixture (1.68 g) was heated with 1.5% methanolic hydrogen chloride (20 m*l*) at 80°C for 23 hr, at which time optical rotation of the reaction solution reached a constant value (α_D −2.5→+0.8°). The reaction solution was treated in the usual manner, and the products were chromatographed on a Dowex 1×4 column (OH form, 3×46 cm) with distilled water as a eluting solvent, three fractions being obtained. The first fraction (0.41 g), $[\alpha]_D^{15}$ +120.2° (*c* 0.88, water) was identified as methyl 2,6-di-*O*-methyl-α- and -β-D-galactopyranosides, which on hydrolysis with N-sulfuric acid at 100°C for 5 hr gave 2,6-di-*O*-methyl-D-galactose; mp and mmp 118—119°C, $[\alpha]_D^{10}$ +47°→+86° (*c* 0.52, water). The second fraction (0.75 g), $[\alpha]_D^{15}$ −18.2° (*c* 0.61, water) was a mixture of the same components as those of the fraction II itself. The last fraction (0.29 g) was identified as methyl 2-*O*-methyl-3,6-anhydro-β-D-galactopyranoside, which was crystallized from ether; mp 65.5°C, $[\alpha]_D^{10}$ −65.1° (*c* 0.87, water).

Fraction III. Yield, 0.126 g; $[\alpha]_D^{23}$ −44.0° (*c* 1.45, water). In pc (solvent D, spray reagent c) the fraction III showed a single spot. It crystallized on standing. Recrystallization from ether gave methyl 2-*O*-methyl-3,6-anhydro-β-D-galactopyranoside. This is the first information of this compound, although its enantiomorph was reported before;[19] mp 65—65.5°C, $[\alpha]_D^{10}$ −66.3° (*c* 0.79, water), (Found: C, 50.52; H, 7.5%).

Fraction IV. Yield, 0.061 g; $[\alpha]_D^{23}$ +24.0° (*c* 1.1, water). This fraction was identified as 3,6-anhydro-D-galactose dimethyl acetal[2,20,21] by the optical rotation, pc (solvent A, B, and D, spray reagent c) and also by the hydrolysis with 0.1 N-sulfuric acid at 100°C for 2 hr to the reducing sugar, which was then converted into the diphenylhydrazone;[20] mp and mmp 156—157.5°C, $[\alpha]_D^{10}$ +40.0°→+31.9° (*c* 0.26, methanol), (Found: C, 66.07; H, 5.75; N, 7.94%).

The authors are grateful to the Ministry of Education for a Grant in Aid for Scientific Research.

20) C. Araki and S. Hirase, *ibid.*, **29**, 770 (1956).
21) S. Hirase, C. Araki, and K. Watanabe, *ibid.*, **40**, 1445 (1967).

The Synthesis of 3,6-Anhydro-5-*O*-methyl-D-galactose

Susumu HIRASE and Kyoko WATANABE

Department of Chemistry, Faculty of Industrial Arts, Kyoto Technical University, Matsugasaki, Kyoto

(Received November 6, 1971)

3,6-Anhydro-5-*O*-methyl-D-galactose has been synthesized for the first time through a series of reactions composed of blocking the hydroxyl groups at C_2 and C_4 of methyl 3,6-anhydro-α-D-galactopyranoside with the phenylcarbamoyl groups, converting the resulting derivative of the methyl glycoside into the corresponding dimethyl acetal, methylating the newly formed hydroxyl group at C_5, removing the blocking substituents, and finally hydrolysing the dimethyl acetal. The partially methylated anhydro-sugar obtained was uncrystallizable, and was characterized by its crystalline dimethyl acetal and crystalline aldonamide.

3,6-Anhydro-D- and -L-galactoses occur in a variety of red seaweed polysaccharides as their component sugars.[1] In a course of our structural investigation on some of these polysaccharides, 3,6-anhydro-5-*O*-methyl-D-galactose has been needed as a reference compound. This partially methylated anhydro-sugar has never appeared in literatures, although its isomeric 2-*O*-methyl[2,3] and 4-*O*-methyl[4] derivatives have been described. Its synthesis has been carried out for the first time through the route described below.

Methyl 3,6-anhydro-α-D-galactopyranoside(I) has been used as a starting compound. Its hydroxyl groups at C_2 and C_4 were blocked with the phenylcarbamoyl groups. The resulting phenylcarbamoylated methyl glycoside(II) was converted into the corresponding dimethyl acetal(III) with the open chain structure by an action of boiling methanolic hydrogen chloride. This opening of the pyranose ring has been reported to be an unusual property of 3,6-anhydro-galactosides.[5,6] The newly formed hydroxyl group at C_5 was then methylated(III→IV). Reductive removal of the blocking substituents[7] from IV gave crystalline 3,6-anhydro-5-*O*-methyl-D-galactose dimethyl acetal(V), which was further characterized by its crystalline *p*-nitrobenzoate. Three isomers are possible for 3,6-anhydro-mono-*O*-methyl-D-galactose dimethyl acetal in respect to the position of the *O*-methyl group. As the dimethyl acetal obtained above was distinguished in properties from the 2-*O*-methyl and 4-*O*-methyl isomers, the *O*-methyl group of the dimethyl acetal should exist on C_5 as expected. Mild hydrolysis of the dimethyl acetal(V) afforded 3,6-anhydro-5-*O*-methyl-D-galactose, which was uncrystallizable. Any other reducing derivatives of the anhydro-sugar as well as the anhydro-sugar itself have never been crystallized.

The partially methylated anhydro-sugar obtained above showed a ketose reaction, reduced a Fehling's solution at room temperature, and restored the color to a Schiff's reagent. These properties are in agreement with those of the parent anhydro-sugar.[5] When oxidized with bromine, the partially methylated anhydro-sugar gave 3,6-anhydro-5-*O*-methyl-D-galactonic acid, which was characterized by its crystalline amide. This amide was again distinguishable from the 2-*O*-methyl and 4-*O*-methyl isomers.

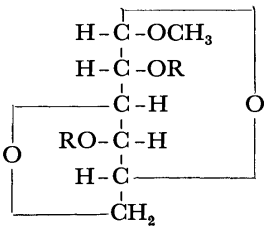

(I) R=H

(II) R=CONHC$_6$H$_5$

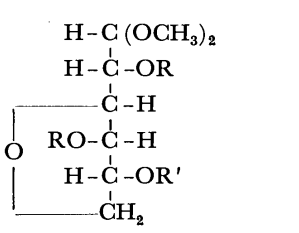

(III) R=CONHC$_6$H$_5$, R'=H

(IV) R=CON(CH$_3$)C$_6$H$_5$, R'=CH$_3$

(V) R=H, R'=CH$_3$

Experimental

General Methods. Solutions were concentrated under reduced pressure below 40°C with a rotary evaporator. Melting points were determined on a micro hot stage with Yanagimoto apparatus Model MP-S2. Paper chromatography was carried out on Toyo filter paper No. 51 with, unless otherwise stated, 1-butanol - acetic acid - water(4 : 1 : 2 v/v) as a solvent. Spots were located with an *o*-aminophenol reagent.[8]

Methyl 3,6-Anhydro-2,4-di-O-phenylcarbamoyl-α-D-galactopyranoside(II). To a solution of methyl 3,6-anhydro-α-D-galactopyranoside(I)[9] (2.0 g) in dry pyridine(20 m*l*) was added phenylisocyanate(3.5 g) and the mixture was heated at 100°C for 2 hr. A small amount of methanol was added to destroy the excess of the reagent, the mixture concentrated, and the residual syrup was dissolved in methanol(20 m*l*). Diphenylurea, which crystallized on standing, was removed by filtration and the filtrate was concentrated to a glass (4.7 g); $[\alpha]_D^{25}$ +50.8° (*c* 1.24 in methanol), $[\alpha]_D^{25}$ +44.6° (*c* 1.04 in chloroform), (Found: N, 6.95; OCH_3, 7.18%. Calcd for $C_{21}H_{22}O_7N_2$: N, 6.76; OCH_3, 7.49%).

3,6-Anhydro-2,4-di-O-phenylcarbamoyl-D-galactose Dimethyl Acetal(III). A solution of II(4.7 g) in 1% methanolic hydrogen chloride(50 m*l*) was refluxed for 1.5 hr, when the optical rotation of the solution reached a constant value

1) E. Percival and R. H. McDowell, "Chemistry and Enzymology of Marine Algal Polysaccharides," Academic Press., New York, (1967).
2) C. Araki and S. Hirase, This Bulletin, **33**, 291 (1960).
3) S. Hirase and K. Watanabe, *ibid.*, **45**, 1839 (1972).
4) C. Araki and K. Arai, *Nippon Kagaku Kaishi*, **63**, 1720 (1942).
5) W. N. Haworth, J. Jackson, and F. Smith, *J. Chem. Soc.*, **1940**, 620.
6) C. Araki and K. Arai, *Nippon Kagaku Kaishi*, **61**, 503 (1940).
7) H. O. Bouveng, *Acta Chem. Scand.*, **15**, 87 (1961).
8) S. Hirase, C. Araki, and S. Nakanishi, This Bulletin, **26**, 183 (1953).
9) P. A. Rao and F. Smith, *J. Chem. Soc.*, **1944**, 229.

TABLE 1. PROPERTIES OF THE DERIVATIVES OF 3,6-ANHYDRO-MONO-*O*-METHYL-D-GALACTOSES

Derivative	Properties	2-*O*-Methyl[a]	4-*O*-Methyl[4]	5-*O*-Methyl
Dimethyl acetal	Mp (°C)	liquid	liquid	53—54
	$[\alpha]_D$ (°) (H_2O)	−31.1	+33.9	+45.3 (*c* 0.93, 25°C)
	R_f[b]	0.61	0.68	0.53
	Retention time (min)[c]	5.5	3.0	4.4
Aldonamide	Mp (°C)	171—172	111	47—48 (monohydrate)
	$[\alpha]_D$ (°) (H_2O)	−75.4	+82.66	+65.5 (*c* 1.80, 25°C)

a) The values reported for L-compounds[2] are cited herein, as the corresponding D-compounds have not been reported so far.
b) Paper chromatograms were irrigated with cyclohexanol saturated with water.[2]
c) Gas liquid chromatography was carried out on a column (1 m) packed with 3% ECNSS-M on Chromosorb-W at 160 °C. Xylitol pentaacetate, added as an internal marker, showed the retention time 9.2 min.

($[\alpha]_D$ +51°→39°). The solution was neutralized with silver carbonate, filtered, and concentrated to a colorless thick syrup(4.7 g); $[\alpha]_D^{25}$ +30.0° (*c* 0.40 in methanol), $[\alpha]_D^{25}$ +53.4° (*c* 0.88 in chloroform). The slightly lower value of the methoxyl content indicated that the product was contaminated with a small amount of II and its β-isomer, which had been in equilibrium with III during the reaction. (Found: N, 6.40; OCH_3, 13.10%. Calcd for $C_{22}H_{26}O_8N_2$: N, 6.28; OCH_3, 13.90%).

3,6-Anhydro-5-O-methyl-2,4-di-O-(N-methylphenylcarbamoyl)-D-galactose Dimethyl Acetal (IV). The syrup (4.6 g) obtained above, was methylated twice with iodomethane (10 m*l*) and silver oxide(10 g) in *N,N*-dimethylformamide (40 m*l*) according to the method of Kuhn and his coworkers.[10] The product(IV) was obtained as a slightly colored syrup (5.0 g); $[\alpha]_D^{25}$ +34.5° (*c* 1.51 in methanol), $[\alpha]_D^{25}$ +28.4° (*c* 0.81 in chloroform). (Found: OCH_3, 18.51%. Calcd for $C_{25}H_{32}O_8N_2$: OCH_3 19.06%).

3,6-Anhydro-5-O-methyl-D-galactose Dimethyl Acetal(V). Accroding to the procedure of Bouveng,[7] IV(5.0 g) was treated with lithium aluminum hydride (2.0 g) in boiling tetrahydrofuran(100 m*l*) for 3 hr. The crude product obtained was purified by dissolution in water(20 m*l*) and extraction with hexane to remove an oily by-product. Evaporation of the aqueous solution gave a colorless syrup(1.8 g). Paper chromatographic examination of this syrup showed the presence of a small amount of methyl 3,6-anhydro-galactosides (R_f 0.68) in addition to V(R_f 0.75). The mixture was separated on a charcoal-Celite column(4.6×33 cm), which was eluted first with 2% ethanol(4.7 *l*) and then 5% ethanol (15 *l*). The methyl glycosides together with a small amount of V were eluted with the former eluant. Concentration of the effluent containing V gave a syrup, which was further purified by solution in acetone, filtration and re-concentration. V was obtained as a colorless syrup, which crystallized on standing for several months; yield 1.2 g (48% based on I). It was recrystallized twice from ethyl acetate-benzene-hexane(1 : 1 : 2). Its mp, specific optical rotation, R_f value in paper chromatography, and retention time in gas liquid chromatography are recorded in Table 1. These properties are distinguishable from those of 2-*O*-methyl and 4-*O*-methyl isomers, as compared in the same table.

Found: C, 48.46; H, 8.17; OCH_3, 41.60%. Calcd for $C_9H_{18}O_6$: C, 48.64; H, 8.16; OCH_3, 41.90%.

3,6-Anhydro-5-O-methyl-D-galactose Dimethyl Acetal 2,4-Di-p-nitrobenzoate. A mixture of V(0.10 g), *p*-nitrobenzoyl chloride(0.50 g), and dry pyridine(5 m*l*) was allowed to stand at room temperature for 24 hr. Water (0.5 m*l*) was added to hydrolyse the excess of the reagent, and a saturated sodium bicarbonate solution(50 m*l*) was then added with strirring. The *p*-nitrobenzoate(0.24 g), which was precipitated, was recrystallized twice from ethanol; mp 145—146°C, $[\alpha]_D^{27}$ +69.7° (*c* 0.76 in chloroform).

Found: C, 52.89; H, 4.61; N, 5.31%. Calcd for $C_{23}H_{24}O_{12}N_2$: C, 53.08; H, 4.65; N, 5.38%.

3,6-Anhydro-5-O-methyl-D-galactose. The dimethyl acetal(V) (0.80 g) was hydrolysed with 0.02 N sulfuric acid (30 m*l*) at 100°C for 1.5 hr. The product, isolated in the usual manner, was further purified by dissolution in methanol, filtration and concentration to give the reducing sugar as a colorless syrup(0.60 g). It showed a Seliwanoff's ketose reaction, reduced a Fehling's solution at room temperature and restored the color to a Schiff's reagent; $[\alpha]_D^{28}$ +23.2°→+26.8° (*c* 0.56 in water). (Found: OCH_3, 17.26%. Calcd for $C_7H_{12}O_5$: OCH_3, 17.61%).

3,6-Anhydro-5-O-methyl-D-galactonamide. The reducing sugar (0.58 g) obtained above was oxidized with bromine (0.40 m*l*) in water(10 m*l*) in the dark at room temperature for 24 hr. The excess of the oxidant was removed by aeration, and the solution was neutralized with silver carbonate and filtered. The filtrate was passed through a column of Amberlite IR-120(H^+ form)(10 m*l*), and then neutralized with a barium hydroxide solution. Concentration of the solution gave the barium salt, which was purified by dissolution in ethanol, filtration, and precipitation with acetone. The salt was then dissolved in water and treated with Amberlite IR-120(H^+ form) (10 m*l*). Evaporation of the solution gave 3,6-anhydro-5-*O*-methyl-D-galactonic acid as a colorless syrup (0.50 g); $[\alpha]_D^{25}$ +25.4° (*c* 0.63 in water). Crystallization was unsuccessful. This acid was converted into the methyl ester by reaction with boiling 3% methanolic hydrogen chloride(5 m*l*) for 4 hr. The product was purified by dissolution in ethyl acetate, filtration, and concentration. The ester was obtained as a colorless syrup(0.40 g); $[\alpha]_D^{25}$ +22.7° (*c* 0.66 in water). Crystallization was again unsuccessful.

The methyl ester obtained above was dissolved in cold methanol(8 m*l*) saturated with dry ammonia, and the mixture was left to stand in a refrigerator for 24 hr. Concentration of the reaction solution gave a syrup, which crystallized on addition of a drop of water. Solids were collected on a porous plate, and recrystallized twice by dissolving in 2-propanol(0.5 m*l*) and adding ethyl acetate saturated with water(2.0 m*l*). The amide was obtained as tetragonal monohydrate. The physical constants are recorded in Table 1, and compared with those of 2-*O*-methyl and 4-*O*-methyl isomers.

Found: C, 40.05; H, 7.49; N, 6.82%. Calcd for $C_7H_{13}O_5N\cdot H_2O$: C, 40.19; H, 7.23; N, 6.70%.

We are grateful to the Ministry of Education for a Grant in Aid for Scientific Research.

10) R. Kuhn, H. Trischmann, and I. Löw, *Angew. Chem.*, **67**, 32 (1955).

Propiolamidines I. Syntheses of *N,N'*-Disubstituted Phenylpropiolamidines and New Routes to 5-*N*-Substituted Amino-3-phenylisoxazoles and 5-*N*-Substituted Amino-1,3-diphenylpyrazoles

Hiroshi FUJITA, Rokuro ENDO, Akira AOYAMA, and Takeshi ICHII

Central Research Laboratories, Sankyo Co., Ltd., Hiromachi, Shinagawa-ku, Tokyo

(Received November 9, 1971)

N,N'-Disubstituted phenylpropiolamidines were synthesized from phenylacetylene and carbodiimides. They were inert toward nucleophiles in a neutral or basic medium, but reactive in an acidic one. They reacted in the presence of hydrogen chloride with hydroxylamine, hydrazine, and arylhydrazines to give 5-*N*-substituted amino-3-phenylisoxazoles, 5-*N*-substituted amino-3-phenylpyrazole and 5-*N*-substituted amino-1-aryl-3-phenylpyrazoles, respectively, by nucleophilic addition followed by cyclization. The reaction mechanism is discussed on the basis of the structures of these heterocyclic compounds.

Although syntheses and reactions of amidines have been investigated in detail,[1] amidines conjugated with a carbon-carbon triple bond have not yet been reported. Even in the category of imidic acid derivatives, only two examples are known, namely substituted propiolimidates[2] and phenylpropiolamidoxime.[3]

In the present paper, syntheses and reactions of *N,N'*-disubstituted phenylpropiolamidines are described. Reaction of these amidines with hydroxylamine and hydrazines constitutes a new route to 5-*N*-substituted amino-isoxazoles and -pyrazoles, respectively.

Results and Discussion

Syntheses of N,N'-*Disubstituted Phenylpropiolamidines.* Preparation of the propiolamidines was accomplished as shown in Scheme 1. In general, sodium phenylacetylide (Ia) reacted satisfactorily with carbodiimides to give amidines (Method A), but in a few cases, the Grignard reagent (Ib) was preferred (Method B).

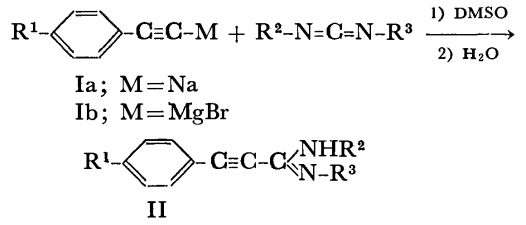

Scheme 1.

Phenylacetylene was added to metallic sodium dispersed in xylene to afford sodium phenylacetylide. The presence of tertiary amines, *e. g.*, triethylamine, *N,N*-dimethylaniline or *N,N,N',N'*-tetramethylethylenediamine, exerted a remarkable effect on the smooth formation of the acetylide at a moderate temperature in hydrocarbon solvents. The tertiary amines may stabilize the acetylide by coordination in non-polar solvents.

When dimethylsulfoxide (DMSO) was added to the sodium phenylacetylide dispersion, complex formation took place as suggested by Kriz *et al*,[4] and nucleophilic attack of the acetylide anion on carbodiimides was accelerated. No significant reaction seems to take place if no DMSO is present.

The phenylpropiolamidines were obtained as crystals, which showed infrared absorption maxima in the 2200 cm^{-1} region for acetylenic bond and near 3200 cm^{-1} attributable to N-H stretching vibration.

N,N'-Bis(*p*-nitrophenyl)phenylpropiolamidine (IIf) was not obtained from the sodium acetylide, probably because of the susceptibility of *N,N'*-bis(*p*-nitrophenyl)carbodiimide to base, but was synthesized by a reaction with the Grignard reagent of phenylacetylene.

Reactions with Hydroxylamine. Amidines are known to react with hydroxylamine in the presence

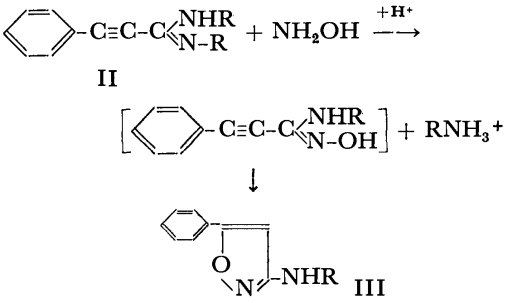

Scheme 2.

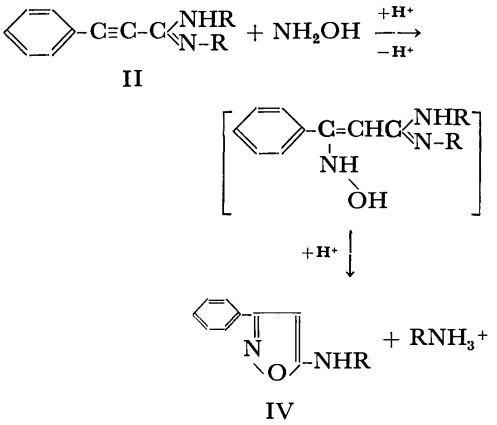

Scheme 3.

1) R. L. Shriner and F. W. Neuman, *Chem. Rev.*, **35**, 351 (1944); P. A. Smith, "Open Chain Nitrogen Compounds," Vol. 1, W. A. Benjamin Inc., New York, (1966); p. 177; S. Tanimoto, *Yuki Gosei Kagaku Kyokai Shi*, **27**, 551 (1969).

2) B. Fisher and C. A. Grob, *Helv. Chim. Acta*, **39**, 417 (1956).

3) L. Lopez, *C. R. Acad. Sci., Paris, Ser. C*, **263**, 557 (1966).

4) J. Kriz, M. J. Benes, and J. Peska, *Collect. Czech. Chem. Commun.*, **32**, 398 (1967).

TABLE 1. *N,N'*-DISUBSTITUTED PHENYLPROPIOLAMIDINES

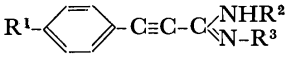

No.	R^1	R^2	R^3	Method	Mp °C	Yield %
IIa	H	H	H	A	187—188[a]	99[c]
IIb	H			A	122—123.5	50
IIc	H	CH_3-	CH_3-	A	140.5—141	49
IId	H	CH_3O-	CH_3O-	A	122—123	65
IIe	H	Cl-	Cl-	A	153—154	31
IIf	H	NO_2-	NO_2-	B	264—265	30
IIg	H	-CH_2-	-CH_2-	A	190—191[a]	89[c]
IIh	CH_3	H	H	A	141—142[b]	88[c]
IIi	H	H		A	113—114	44
IIj	H	*n*-Bu		A	55—56	26
IIk	H	-CH_2-		A	94—95	36

a) Picrate. b) Benzoate. c) Crude viscous oil.

of acid to form amidoximes[1] and phenylpropiolamidoxime readily cyclizes to give 3-amino-5-phenylisoxazole.[3] A reaction of the propiolamidine (II) with hydroxylamine would, therefore, be presumed to proceed according to Scheme 2 to give III; but the reaction afforded a 5-*N*-substituted amino-3-phenylisoxazole (IV) and released an amine hydrochloride.

Consequently, the nucleophilic addition of hydroxylamine to the triple bond followed by cyclization might occur according to Scheme 3.

The structures of these isoxazoles (IV) were characterized on the basis of their mass and NMR spectra. The isoxazole, thus derived from IIa, was concluded to be 5-cyclohexylamino-3-phenylisoxazole (IVa), by comparison of the fragmentation pattern in the mass spectrum (Fig. 1) and the chemical shift of the C-4 proton in the NMR spectrum with those of 3-amino-5-phenyl- and 5-amino-3-phenylisoxazole.[5] As shown in Fig. 1, IVa readily released cyclohexene to give an aminoisoxazole which gave the same fragmentation pattern as that of 5-amino-3-phenylisoxazole and which was inconsistent with that of 3-amino-5-phenylisoxazole.

The NMR spectral data of IVa also supported the 5-aminoisoxazole structure. The signal at 5.26 ppm, assigned to C-4 proton of IVa, was comparable to 5-amino-3-phenylisoxazole.

The signals due to C-4 protons of 5-arylamino-3-phenylisoxazoles appeared at a reasonably lower field on account of the anisotropic effect of the phenyl ring. The chemical shift of the C-4 proton of several 5-*N*-substituted amino-3-phenylisoxazoles is given in Table 2.

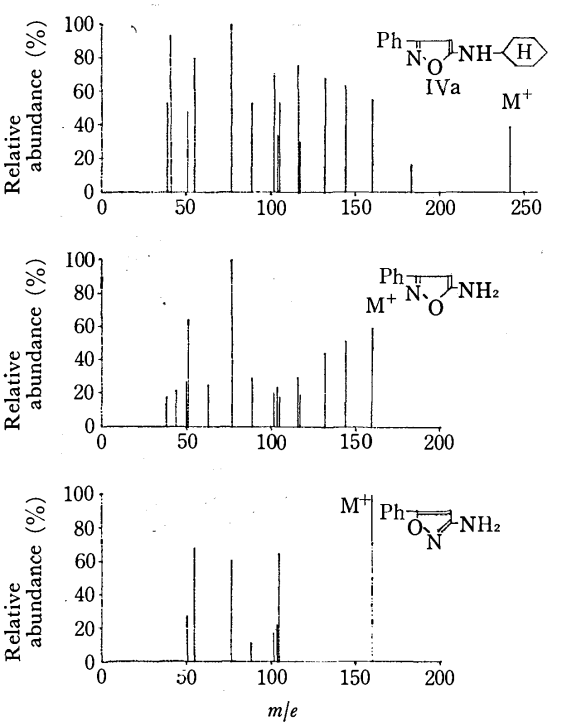

Fig. 1. Mass fragmentation patterns of 5-cyclohexylamino-3-phenylisoxazole (IVa), 5-amino-3-phenylisoxazole and 3-amino-5-phenylisoxazole.

5) I. Iwai and N. Nakamura, *Chem. Pharm. Bull.* (Tokyo), **14**, 1277 (1966).

Table 2. 5-*N*-Substituted amino-3-phenylisoxazoles

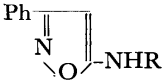

No.	R	Mp, °C	Yield %	Chemical shift of C-4 proton[a,b]
IVa		128—129.5	37	5.26
IVb		136—137[c]	55	5.85
IVc	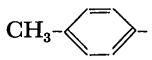	145—146	38	5.76
IVd	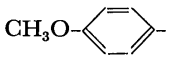	150—151	53	5.65

a) δ ppm in $CDCl_3$, internal standard, TMS.
b) 3-Amino-5-phenylisoxazole: $\delta=6.09$ ppm.
5-Amino-3-phenylisoxazole: $\delta=5.40$ ppm.
c) Lit, mp. 137°C (Ref. 14).

Reactions with Hydrazines. It is well-known that some acetylenic compounds readily undergo addition-cyclization reactions with hydrazines to give pyrazole derivatives such as pyrazolones[6,7] and aminopyrazoles.[8]

Reactions of the propiolamidines with hydrazines were therefore carried out in a similar manner to that for the isoxazole synthesis. In the presence of sodium ethoxide, as well as under neutral conditions, phenylpropiolamidine (IIb) was chiefly recovered in a reaction of IIb with phenylhydrazine; but in the reaction with phenylhydrazine hydrochloride, the expected product, a pyrazole, was obtained together with eliminated aniline. The reaction of IIb with phenylhydrazine hydrochloride afforded predominantly a single isomer (VIIIc) of an anilinodiphenylpyrazole; namely 3-anilino-1,5-diphenyl-[9] or 5-anilino-1,3-diphenylpyrazole.[10] Both structures were assigned to the pyrazole derived from benzoylthioacetanilide and phenylhydrazine,[9,10] and exhibited the same melting point as that of VIIIc. Pocar and his co-workers[10] reported some intermediate hydrazones but presented no spectral data regarding their structures. It was supposed that these intermediates could be another structure such as VIIb in Scheme 4, whose formation was attributable to the nucleophilic attack of the α-nitrogen in phenylhydrazine at the β-acetylenic carbon and was postulated under acidic conditions[7] as in Pocar's case. We therefore confirmed the structure of an intermediate (VIIa) obtained from benzoylthioacetanilide (VI) and *o*-nitrophenylhydrazine, and compared the pyrazole cyclized from VIIa with the one derived from the amidine IIb as shown in Scheme 4.

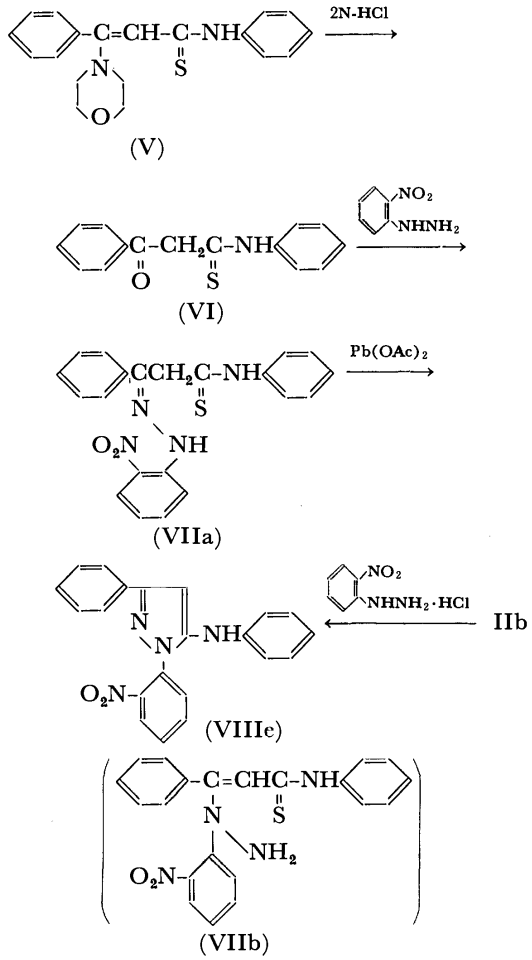

Scheme 4.

As indicated in Table 3, the structure of the intermediate is undoubtedly the hydrazone VIIa. Consequently, the cyclization of VIIa should give 5-anilino-1-(*o*-nitrophenyl)-3-phenylpyrazole, which is completely consistent with the product from IIb and *o*-nitrophenylhydrazine hydrochloride in terms of the IR, mass and NMR spectra and melting point.

Table 3. NMR data of V, VI, and VIIa.[a]

No.	$-CH_2-$	=CH-	Enolic OH or =N-NH-	Solvent
V	—	5.91	—	$CDCl_3$
VI	4.62	6.25[b]	14.80[b]	$CDCl_3$
VIIa	4.55	—	11.05	$(CD_3)_2CO$

a) δ value from TMS.
b) Due to the presence of the enolic tautomer.

The pyrazoles homologous to 5-anilino-1,3-diphenylpyrazole were also presumed to be produced predominantly in reactions of the propiolamidines with arylhydrazines. An exception was the two isomeric pyrazoles found in the case of the reaction of *N,N'*-bis(*p*-tolyl)phenylpropiolamidine (IIc) with phenylhydrazine hydrochloride. The main product was assigned as VIIIg, by analogy with the other pyrazoles (VIII) in the reaction scheme and in spectral data, so the minor product was assumed to be 1,5-diphenyl-

6) R. v. Rosenburg, *Chem. Ber.*, **27**, 783 (1894).
7) F. G. Baddar, M. F. El-Newaihy, and M. R. Salem, *J. Chem. Soc., C*, **1969**, 836.
8) D. E. Worrall, *J. Amer. Chem. Soc.*, **59**, 933 (1937).
9) S. Hünig and K. Hübner, *Chem. Ber.*, **95**, 937 (1962).
10) D. Pocar, G. Bianchetti, and S. Maiorana, *Gazz. Chim. Ital.*, **93**, 100 (1963).

Table 4. Aminopyrazoles

No.	R	Ar	Mp, °C	Yield, %	Chemical shift of C-4 proton[a]
VIIIa		H	153.5—155[b]	49	6.32[f]
VIIIb	H		67—68.5	50	5.87
VIIIc			153.5—154.5[c]	50	6.46
VIIId		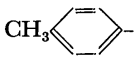	141—142.5	38	6.34[e]
VIIIe		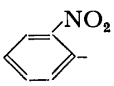	165—166[d]	69	6.64[f]
VIIIf	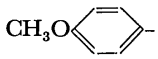		103—104	54	6.30
VIIIg	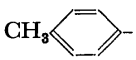		94—95	40	6.43
VIIIh	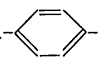		100—101	34	6.45
IXg	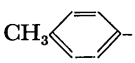		180—181.5	7	6.24

a) δ value from TMS in $CDCl_3$. b) Lit, mp 152.5—153.5°C (Ref. 9). c) Lit, mp 153°C (Ref. 10). d) Lit, mp 164—165°C (Ref. 10). e) in CCl_4. f) in acetone-d_6.

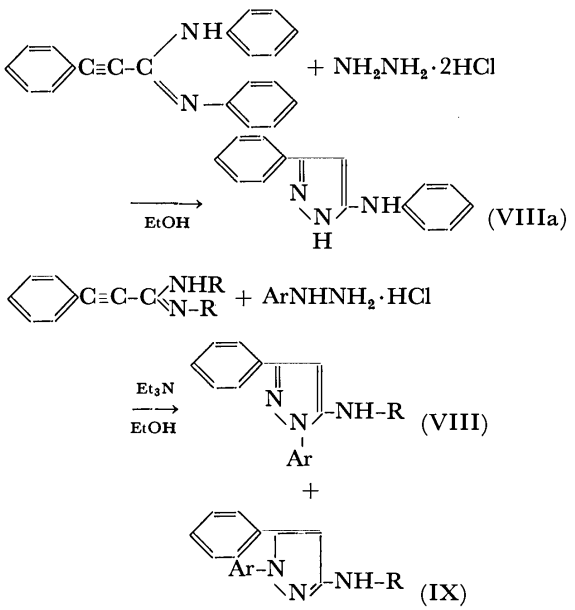

Scheme 5.

3-(*p*-toluidino)pyrazole (IXg).

Reaction Mechanism. As described above, the reactions of the propiolamidines with nucleophiles took place under acidic conditions and the acetylenic β-carbon rather than the amidino carbon was preferentially attacked. This situation was confirmed by the reaction of IIb with morpholine in the presence of hydrogen chloride resulting in addition to the triple bond giving *N,N'*-diphenyl-β-morpholinocinnamamidine (X) in preference to the addition-elimination to the amidino carbon (Scheme 6).

Consequently, as shown in Scheme 3, the propiolamidine would be activated by the protonation at the amidine nitrogen to form the diaminoallene cation, and readily attacked by a nucleophile, such as hydroxylamine, to give the adduct. The central carbon atom of allene in the adduct corresponds to β-carbon of enamines, so that the prototropic change to the enamino amidine intermediate might take place smoothly. The cyclization process would also be prompted by protonation, and an protonated amino group in the cyclic product would be released to give the amine hydrochloride together with an isoxazole, since the more basic amine, cyclohexylamine, was recovered predominantly in the reaction of *N*-cyclohexyl-*N'*-phenylphenylpropiolamidine (IIi) with hydroxylamine hydrochloride.

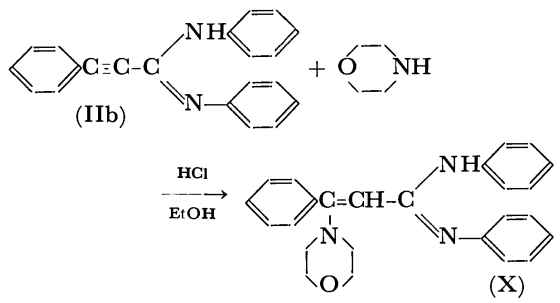

Scheme 6.

Experimental

All melting points are uncorrected. The NMR spectra were measured with a Varian A-60 NMR spectrometer, using tetramethylsilane as an internal standard. The mass spectra were obtained using a JEOL-JMS-OIS Mass spectrometer. The IR spectra were determined by means of nujol mulls or liquid films.

Materials. *N,N'*-Dicyclohexylcarbodiimide was obtained commercially, *N,N'*-bis(*p*-methoxyphenyl)carbodiimide was derived from *N,N'*-bis(*p*-methoxyphenyl)chloroformamidiniumchloride,[11] *N,N'*-bis(*p*-nitrophenyl)carbodiimide was synthesized from *p*-nitrophenylisocyanate using 3-methyl-1-phenyl-1-phospha-3-cyclopenten-1-oxide as a catalyst.[12] The other carbodiimides were prepared from the corresponding thioureas employing yellow mercuric oxide.

Preparation of N,N'-*Disubstituted Phenylpropiolamidines (II). Method A: General Procedure*: Metallic sodium (1.15 g, 50 mg-atom) was dispersed in 50 m*l* dry xylene by means of a Sodium Dispersator (Taneda Co., Ltd., Toyama city) at about 110°C in the presence of one drop of oleic acid under dry nitrogen. After cooling to 60°C, triethylamine (5.0 g, 50 mmol) was added, followed by dropwise addition of phenylacetylene (5.2 g, 51 mmol) in 10 m*l* of xylene at a rate so that the reaction temperature was kept at about 60°C. Acetylide formation took place immediately. After the exothermic reaction ceased, the mixture was warmed at the same temperature for 30 min. The corresponding carbodiimide (50 mmol) in 10 m*l* xylene was introduced dropwise at room temperature for 10 min, but no significant change was observed. When dimethylsulfoxide (3.9 g, 50 mmol) in 10 m*l* xylene was added with cooling in a cold water bath, the reaction mixture almost dissolved and turned dark brown.[13] After 30 min, the mixture was poured into ice water, the organic layer was separated and the aqueous layer was extracted twice with ethyl acetate. The combined organic layers were washed with saturated aqueous sodium chloride, dried over anhydrous sodium sulfate and concentrated *in vacuo*. The concentrate was purified by silica gel column chromatography and/or recrystallization.

N,N'-*Dicyclohexylphenylpropiolamidine (IIa)*. A yellow viscous oil. IR: 3400 (NH), 2200 (C≡C) cm^{-1}. Further purification on a silica gel column (benzene - ethanol 50 : 1) was not successful. Picrate: mp 187—188°C (decomp., from ethanol). Found: C, 60.55; H, 5.95; N, 12.84%. Calcd for $C_{27}H_{31}N_5O_7$: C, 60.32; H, 5.81; N, 13.03%. IR: 2190 (C≡C) cm^{-1}.

N,N'-*Diphenylphenylpropiolamidine (IIb)*. Yellow needles (from *n*-hexane); mp 122—123.5°C. Found: C, 84.89; H, 5.43; N, 9.41%. Calcd for $C_{21}H_{16}N_2$: C, 85.11; H, 5.44; N, 9.45%. IR: 3200 (NH), 2200 (C≡C) cm^{-1}. Picrate: mp 198—200°C (decomp., from methanol). Found: C, 61.52; H, 3.77; N, 13.24%. Calcd for $C_{27}H_{19}N_5O_7$: C, 61.71; H, 3.64; N, 13.33%. IR: 2200 (C≡C) cm^{-1}.

N,N'-*Bis(*p-*tolyl)phenylpropiolamidine (IIc)*. Yellow needles (from ethanol); mp 140.5—141°C. Found: C, 84.93; H, 6.20; N, 8.58%. Calcd for $C_{23}H_{20}N_2$: C, 85.15; H, 6.21; N, 8.64%. IR: 3230 (NH), 2220 (C≡C) cm^{-1}. NMR (δ in CCl_4): 2.30 (6H, s, CH_3), 6.85—7.3 (phenyl protons).

N,N'-*Bis(*p-*methoxyphenyl)phenylpropiolamidine (IId)*. Yellow needles (from ethanol); mp 122—123°C. Found: C, 77.44; H, 5.75; N, 7.82%. Calcd for $C_{23}H_{20}N_2O_2$: C, 77.50; H, 5.66; N, 7.86%. IR: 3350 (NH), 2210 (C≡C) cm^{-1}. NMR (δ in $CDCl_3$): 3.97 (6H, s, OCH_3).

N,N'-*Bis(*p-*chlorophenyl)phenylpropiolamidine (IIe)*. Colorless needles (from ethanol-*n*-hexane); mp 153—154°C. Found: C, 69.40; H, 3.86; N, 7.50; Cl, 19.41%. Calcd for $C_{21}H_{14}N_2Cl_2$: C, 69.05; H, 3.86; N, 7.67; Cl, 19.41%. IR: 3240, 3160 (NH), 2260 (C≡C) cm^{-1}. NMR (δ in CCl_4): 7.26 (s, phenyl protons).

N,N'-*Dibenzylphenylpropiolamidine (IIg)*. Viscous oil. IR: 2200 (C≡C) cm^{-1}. Further purification of this material was not successful, so it was converted into the picrate and characterized. Picrate: mp 190—191°C (decomp., from ethanol). Found: C, 62.71; H, 4.12; N, 12.39%. Calcd for $C_{29}H_{23}N_5O_7$: C, 62.92; H, 4.19; N, 12.65%. IR: 2230 (C≡C) cm^{-1}. NMR (δ in DMSO-d_6): 4.74, 4.88 (4H, benzyl protons).

N,N'-*Dicyclohexyl*-p-*tolylpropiolamidine (IIh)*. *p*-Tolylacetylene, instead of phenylacetylene, was converted into sodium acetylide and reacted with *N,N'*-dicyclohexylcarbodiimide in a similar way. A oily crude amidine was crystallized as the benzoate. Benzoate: Colorless crystals (from 50% ethanol); mp 141—142°C. Found: C, 78.08; H, 8.32; N, 6.60%. Calcd for $C_{29}H_{36}N_2O_2$: C, 78.34; H, 8.16; N, 6.30%. IR: 2190 (C≡C) cm^{-1}. NMR (δ in $CDCl_3$): 2.43 (3H, s, CH_3), 3.66 (2H, broad bands,).

N-*Cyclohexyl*-N'-*phenylphenylpropiolamidine (IIi)*. White needles (from *n*-hexane); mp 113—114°C. Found: C, 83.52; H, 7.28; N, 9.14%. Calcd for $C_{21}H_{22}N_2$: C, 83.40; H, 7.33; N, 9.26%. IR: 3190, 3090 (NH), 2190 (C≡C) cm^{-1}. Benzoate: White crystals (from 50% ethanol); mp 115—116°C. Found: C, 79.11; H, 6.57; N, 6.38%. Calcd. for $C_{28}H_{28}N_2O_2$: C, 79.21; H, 6.65; N, 6.60%. IR: 2220 (C≡C) cm^{-1}.

N-n-*Butyl*-N'-*phenylphenylpropiolamidine (IIj)*. Yellow needles (from *n*-hexane); mp 55—56°C. Found: C, 82.50; H, 7.31; N, 10.05%. Calcd for $C_{19}H_{20}N_2$: C, 82.57; H, 7.29; N, 10.14%. IR: 3200 (NH), 2200 (C≡C) cm^{-1}. Picrate: mp 169—170°C (decomp., from ethanol). Found: C, 59.24; H, 4.63; N, 13.67%. Calcd for $C_{25}H_{23}N_5O_7$: C, 59.40; H, 4.59; N, 13.86%. IR: 2190 (C≡C) cm^{-1}.

N-*Benzyl*-N'-*phenylphenylpropiolamidine (IIk)*. Yellow needles (from *n*-hexane); mp 94—95°C. Found: C, 85.17; H, 5.78; N, 9.18%. Calcd for $C_{22}H_{18}N_2$: C, 85.13; H, 5.85; N, 9.03%. IR: 3200 (NH), 2200 (C≡C) cm^{-1}. NMR (δ in $CDCl_3$): 4.95 (2H, s, CH_2).

Method B: N,N'-*Bis(*p-*nitrophenyl)phenylpropiolamidine (IIf)*. Phenylethynylmagnesium bromide was prepared from ethylmagnesium bromide and phenylacetylene in ether in the usual way. One equimolar of *N,N'*-bis(*p*-nitrophenyl)-carbodiimide in tetrahydrofuran and then DMSO (two equimolar) were introduced subsequently at room temperature. The mixture was stirred for 45 min and poured into ice water. After the precipitate was filtered off, the filtrate was extracted with ether. The precipitate and extract were crystallized from ethyl acetate to afford crude amidine. Recrystallization from dimethylformamide gave yellow crystals. Mp 264—265°C (decomp.). Found: C, 65.45; H, 3.88; N, 14.71%. Calcd for $C_{21}H_{14}N_4O_4$: C, 65.28; H, 3.65; N, 14.50%. IR: 3350 (NH), 2210 (C≡C) cm^{-1}.

*Syntheses of 5-*N-*Substituted Amino-3-phenylisoxazoles. General Procedure*: A mixture of the phenylpropiolamidine (II) and a slight excess of hydroxylamine hydrochloride in ethanol was refluxed for several hours. After removal of the solvent under reduced pressure, the residue was treated as usual with hot benzene to recover the eliminated amine hydrochloride and the benzene soluble materials were subjected to silica gel column chromatography using a suitable solvent system or purified by recrystallization.

11) H. Eilingsfeld, G. Neubauer, M. Seefelder, and H. Weidinger, *Chem. Ber.*, **97**, 1237 (1964).

12) T. W. Campbell, J. J. Monagle, and V. S. Fordi, *J. Amer. Chem. Soc.*, **84**, 3673 (1962).

13) In some cases, DMSO was added to the sodium acetylide suspension before addition of a carbodiimide solution. In this case, the sodium phenylacetylide-DMSO complex was observed.[4] However, the order of addition does not seem to affect the yield of amidines.

5-Cyclohexylamino-3-phenylisoxazole (IVa). Colorless needles (from *n*-hexane); mp 128—129.5°C. Found: C, 74.42; H, 7.64; N, 11.78%. Calcd for $C_{15}H_{18}N_2O$: C, 74.35; H, 7.49; N, 11.56%. IR: 3370 (NH), 1622, 1501 cm^{-1}. NMR (δ in $CDCl_3$): 5.26 (1H, s, C-4 proton), 4.46 (1H, broad band, NH), 3.25 (1H, broad band, 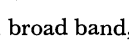). Mass (*m/e*): 242 (M^+), 160 (M− 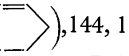),144, 132, 116, 89, 77.

5-Anilino-3-phenylisoxazole (IVb).[14] Pale yellow plates (from ethanol); mp 136—137°C. Found: C, 76.13; H, 5.28; N, 11.76%. Calcd for $C_{15}H_{12}N_2O$: C, 76.25; H, 5.12; N, 11.86%. IR: 3290, 3210 (NH), 1650, 1497, 1473 cm^{-1}. NMR (δ in $CDCl_3$): 5.85 (1H, s, C-4 proton). Mass (*m/e*): 236 (M^+). Aniline hydrochloride, characterized by the IR spectrum, was recovered in 82% yield.

3-Phenyl-5-p-toluidinoisoxazole (IVc). Colorless crystals (from ethanol); mp 145—146°C. Found: C, 76.67; H, 5.63; N, 11.05%. Calcd for $C_{16}H_{14}N_2O$: C, 76.78; H, 5.64; N, 11.19%. IR: 3280, 3200 (NH), 1645, 1510, 1485, 1475 cm^{-1}. NMR (δ in $CDCl_3$): 5.76 (1H, s, C-4 proton), 2.33 (3H, s, CH_3).

5-p-Anisidino-3-phenylisoxazole (IVd). Colorless needles (from ethanol); mp 150—151°C. Found: C, 72.01; H, 5.24; N, 10.72%. Calcd for $C_{16}H_{14}N_2O_2$: C, 72.16; H, 5.30; N, 10.52%. IR: 3330, 3260 (NH), 1658, 1518, 1502, 1483, 1464 cm^{-1}. NMR (δ in $CDCl_3$): 5.65 (1H, s, C-4 proton), 3.80 (3H, s, OCH_3).

Reaction of IIi with Hydroxylamine hydrochloride. An ethanolic solution of IIi and excess hydroxylamine hydrochloride was refluxed for 5 hr. After removal of the solvent, the concentrate was treated with benzene to separate the released amine hydrochloride, which was characterized by IR spectrum as cyclohexylamine hydrochloride (IR spectrum showed no absorption maximum attributable to the phenyl ring). The soluble material was chromatographed on a silica gel column (benzene - ethanol 50 : 1). The eluted isoxazole was recrystallized from ethanol. Mp 136—137°C. The IR spectrum was identical with that of IVb.

Synthesis of 5-Anilino-1-o-nitrophenyl-3-phenylpyrazole (VIIIe) from β-Morpholinothiocinnamanilide (V).[10] *β-Morpholinothiocinnamanilide (V):*[15] The reaction of 1-morpholino-1-phenylethylene (9.5 g) with phenylisothiocyanate (6.75 g) in ethyl acetate afforded yellow needles of V (12.8 g, 79%), followed by recrystallization from the same solvent to give an analytically pure sample having mp 154.5—156.5°C (decomp.). Found: C, 70.36; H, 6.31; N, 8.77; S, 9.88%. Calcd for $C_{19}H_{20}N_2OS$: C, 70.34; H, 6.21; N, 8.63; S, 9.88%. NMR (δ in $CDCl_3$): 5.91 (1H, s, =CH).

Benzoylthioacetanilide (VI):[15] V (9.72 g) in 60 m*l* hot ethanol was treated with 16 m*l* of 2N-HCl and left overnight in a refrigerator. The precipitate was collected and recrystallized from 50% ethanol repeatedly. Yield: 63%. Colorless powder. Mp 78—79.5°C. Found: C, 70.84; H, 5.17; N, 5.59; S, 12.60%. Calcd for $C_{15}H_{13}NOS$: C, 70.56; H, 5.13; N, 5.49; S, 12.56%. NMR (δ in $CDCl_3$): 4.62 (s, CH_2), 6.25 (s, =CH), 14.80 (s, enolic OH).

o-Nitrophenylhydrazone of VI (VIIa):[10] To an ethanolic solution of VI (1.72 g), *o*-nitrophenylhydrazine (1.03 g) dissolved in 50% aqueous acetic acid was added and the mixture was heated at 95°C for 5 min. The resulting deposit was filtered off and triturated with ethyl acetate - petroleum ether to give an orange solid (2.1 g, 80%). Recrystallization from ethyl acetate three times afforded orange needles. Mp 169.5—172.5°C (decomp.). Found: C, 64.84; H, 4.70; N, 14.55; S, 8.30%. Calcd for $C_{21}H_{18}N_4O_2S$: C, 64.60; H, 4.65; N, 14.35; S, 8.20%. NMR (δ in acetone-d_6): 4.55 (2H, s, CH_2), 11.05 (1H, broad band, NH).

5-Anilino-1-o-nitrophenyl-3-phenylpyrazole (VIIIe) from VIIa:[10] VIIa (0.78 g) was cyclized by lead diacetate trihydrate (0.76 g) in a gently refluxing aqueous acetic acid. After 30 min, the mixture was filtered, the filtrate poured into ice water, and the yellow precipitate of VIIIe was collected and washed with water. Yield: 46%. Repeated recrystallization from ethanol afforded yellow needles. Mp 164—165°C. Mixed mp with one derived from IIb; 165—166°C. The respective IR, NMR, and mass spectra of both samples were also superimposable.

Syntheses of 5-N-Substituted amino-3-phenylpyrazoles. 5-Anilino-3-phenylpyrazole (VIIIa):[9] IIb (1.0 g) reacted with hydrazine dihydrochloride in the presence of an equimolar amount of triethylamine in boiling ethanol for 3 hr. A benzene soluble red oil was triturated with benzene - *n*-hexane to yield a yellow solid, followed by recrystallization from dilute ethanol to give crystalline powders of VIIIa (278 mg, 35%). Mp 153.5—155°C. Found: C, 76.25; H, 5.56; N, 17.60%. Calcd for $C_{15}H_{13}N_3$: C, 76.57; H, 5.57; N, 17.86%. NMR (δ in acetone-d_6): 6.32 (1H, s, C-4 proton).

General Procedure for Syntheses of 1-Aryl-3-phenyl-5-N-substituted Aminopyrazoles. Phenylpropiolamidine (II) and a slight excess of arylhydrazine hydrochloride were refluxed in ethanol for several hours. After the solvent was distilled off, the residual material was treated with hot benzene in order to recover the eliminated amine hydrochloride. Benzene soluble materials were purified by silica gel column chromatography and/or recrystallization using suitable solvents.

5-Cyclohexylamino-1,3-diphenylpyrazole (VIIIb): Cyclohexylamine hydrochloride (61%) was recovered. After being separated by silica gel column (benzene - ethanol 50 : 1), crude VIIIb was recrystallized from petroleum ether (bp 30—70°C) to afford colorless prisms having mp 67—68.5°C. Yield: 50%. Found: C, 79.75; H, 7.41; N, 13.14%. Calcd for $C_{21}H_{23}N_3$: C, 79.46; H, 7.30; N, 13.24%. NMR (δ in $CDCl_3$): 5.87 (1H, s, C-4 proton).

5-Anilino-1,3-diphenylpyrazole (VIIIc):[10] After separation of aniline hydrochloride [73%, mp 197.5—199°C (decomp.) Lit, mp 198°C. Found: C, 55.36; H, 6.28; N, 10.92; Cl, 27.08%], VIIIc was solidified with *n*-hexane and recrystallization from ethanol to give colorless prisms. Mp 153.5—154.5°C. Found: C, 80.92; H, 5.55; N, 13.55%. Calcd for $C_{21}H_{17}N_3$: C, 81.00; H, 5.50; N, 13.50%. NMR (δ in $CDCl_3$): 6.46 (1H, s, C-4 proton).

5-Anilino-3-phenyl-1-p-tolylpyrazole (VIIId): Colorless crystals (from ethanol); mp 141—142.5°C. Found: C, 80.82; H, 5.86; N, 12.66%. Calcd for $C_{22}H_{19}N_3$: C, 81,20; H, 5.89; N, 12.91%. NMR (δ in CCl_4): 6.34 (1H, s, C-4 proton), 2.25 (3H, s, CH_3).

5-Anilino-1-o-nitrophenyl-3-phenylpyrazole (VIIIe):[10] Yellow needles (from ethanol); mp 165—166°C. Found: C, 70.42; H, 4.65; N, 15.74%. Calcd for $C_{21}H_{16}N_4O_2$: C, 70.77; H, 4.53; N, 15.72%. NMR (δ in acetone-d_6): 6.64 (1H, s, C-4 proton). Mass (*m/e*): 356 (M^+), 310, 207, 102, 77. Aniline hydrochloride was also recovered (73%).

5-Anisidino-1,3-diphenylpyrazole (VIIIf): Colorless prisms (from benzene - *n*-hexane); mp 103—104°C. Found: C, 77.28; H, 5.62; N, 12.41%. Calcd for $C_{22}H_{19}N_3O$: C, 77.39; H, 5.61; N, 12.31%. NMR (δ in $CDCl_3$): 6.30 (1H, s, C-4 proton), 3.76 (3H, s, OCH_3).

14) A. Umani-Ronchi, M. Acampora, G. Gaudiano, and A. Selva, *Chim. Ind.* (Milan), **1967**, 388.

15) S. Hünig, K. Hübner, and E. Benzing, *Chem. Ber.*, **95**, 926 (1962).

5-p-*Toluidino-1,3-diphenylpyrazole (VIIIg) and 3*-p-*Toluidino-1,5-diphenylpyrazole (IXg)*: After removal of *p*-toluidine hydrochloride (82%), benzene soluble materials were chromatographed on a silica gel column. VIIIg was first eluted with benzene and then IXg with the same solvent. Both were recrystallized from *n*-hexane - benzene to afford analytical samples. VIIIg: Colorless needles. Yield: 40%. Mp 94—95°C. Found: C, 80.95; H, 5.82; N, 13.19%. Calcd for $C_{22}H_{19}N_3$: C, 81.20; H, 5.89; N, 12.91%. NMR (δ in $CDCl_3$): 6.43 (1H, s, C-4 proton), 2.29 (3H, s, CH_3). IXg: Colorless crystals. Yield: 7%. Mp 180—181.5°C. Found: 81.49; H, 6.05; N, 12.88%. NMR (δ in $CDCl_3$): 6.24 (1H, s, C-4 proton), 2.29 (3H, s, CH_3).

5-p-*Chloroanilino-1,3-diphenylpyrazole (VIIIh)*: Colorless prisms (from ethanol); mp 100—101°C. Found: C, 73.25; H, 4.57; N, 12.03; Cl, 10.18%. Calcd for $C_{21}H_{16}N_3Cl$: C, 72.93; H, 4.66; N, 12.15; Cl, 10.25%. NMR (δ in $CDCl_3$): 6.45 (1H, s, C-4 proton).

A Reaction of IIb with Morpholine. A mixture of IIb (7.4 g) and morpholine (2.18 g) in 60 m*l* ethanol was heated for 5.5 hr in the presence of one equivalent of hydrogen chloride. After distilling off the solvent, the residue was suspended in benzene and shaken with aqueous potassium carbonate solution. The resulting benzene solution was washed with water, dried over anhydrous sodium sulfate and concentrated. Recrystallization of the residual solid from ethanol afforded yellow prisms of *N,N'*-diphenyl-*β*-morpholinocinnamamidine (X, 5.0 g, 52%). Mp 137—138°C. Found: C, 78.10; H, 6.58; N, 10.98%. Calcd for $C_{25}H_{25}N_3O$: C, 78.30; H, 6.57; N, 10.96%. NMR (δ in $CDCl_3$): 2.80 and 3.64 (8H, CH_2 in morpholine), 5.04 (1H, s, =CH), 6.9—7.5 (phenyl protons).

The authors are grateful to Prof. Makoto Okawara, Tokyo Institute of Technology, for his valuable comments.

BULLETIN OF THE CHEMICAL SOCIETY OF JAPAN, VOL. 45, 1852—1854 (1972)

Studies on Stable Free Radicals. XII.[1] ESR Spectra of 2-*t*-Butylaminotropone *N*-Oxyl Radicals

Toshimasa TODA, Eiko MORI, and Keisuke MURAYAMA
Central Research Laboratories, Sankyo Co., Ltd., Shinagawa-ku, Tokyo

(Received November 15, 1971)

We observed a well resolved ESR spectrum of 2-*t*-butylaminotropone *N*-oxyl radical generated by the oxidation of the corresponding amine with perbenzoic acid, and assigned the values of hyperfine coupling constants of protons in the tropone ring by a comparison with the ESR spectra of deuterium substituted 2-*t*-butylaminotropone *N*-oxyl radicals: $a_N = 12.7$ gauss, $a_H{}^3 = a_H{}^5 = a_H{}^7 = 1.86$ gauss and $a_H{}^4 = a_H{}^6 = 0.93$ gauss for protons on tropone ring.

ESR spectra of arylnitroxide radicals, such as diphenylnitroxide radical[2] or *t*-butylphenylnitroxide radical[3] have been reported. However, the ESR spectrum of the nitroxide radical having aromatic seven-membered ring has not yet been reported. We observed the ESR spectrum of 2-*t*-butylaminotropone *N*-oxyl radical (IIa) and assigned the values of hyperfine splitting constants of protons on the tropone ring in IIa by a comparison with the ESR spectra of deuterium substituted 2-*t*-butylaminotropone *N*-oxyl radicals.

Results

We prepared 2-*t*-butylaminotropone (Ia) by the reaction[4] of 2-methoxytropone[5] with *t*-butylamine and obtained the corresponding nitroxide radical (IIa) by the oxidation of Ia with perbenzoic acid.[6]

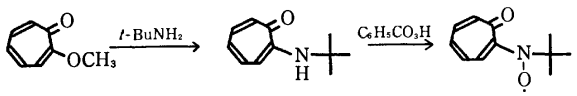

(Ia) (IIa)

Since the nitroxide radical IIa is unstable and unisolable, we measured the ESR spectrum of IIa obtained by mixing a solution of Ia in benzene and perbenzoic acid in the ESR sample tube directly at room temperature.

The ESR spectrum of IIa is presented in Fig. 1-a. Triplet lines due to the interaction of a ^{14}N (12.7 gauss) and nine lines (0.93 gauss, the intensity ratio is 1 : 2 : 4 : 6 : 6 : 6 : 4 : 2 : 1) of each component of the triplet were observed. Further splittings in each component of the triplet would be caused by the interaction with protons on the tropone ring, because no interaction with protons of *t*-butyl group in *t*-butylphenylnitroxide radical have been observed in the ESR spectrum.[3]

1) Part XI: T. Toda, E. Mori, and K. Murayama, This Bulletin, **45**, 1764 (1972).

2) a) J. C. Baird and J. R. Thomas, *J. Chem. Phys.*, **35**, 1507 (1961). b) Y. Deguchi, This Bulletin, **35**, 260 (1962).

3) H. Lamaire, Y. Marechal, R. Ramasseul, and A. Rassat, *Bull. Soc. Chim. Fr.*, **1965**, 372.

4) N. Soma, J. Nakazawa, T. Watanabe, Y. Sato, and G. Sunagawa, *Chem. Pharm. Bull.* (Tokyo), **13**, 819 (1965).

5) T. Nozoe, S. Seto, T. Ikemi, and T. Arai, *Proc. Jcpan Acad.*, **27**, 102 (1959).

6) a) K. Tokumaru, H. Sakuragi, and O. Simamura, *Tetrahedron Lett.*, **1964**, 3945. b) T. Toda, E. Mori, and K. Murayama, This Bulletin, **45**, 1904 (1972).

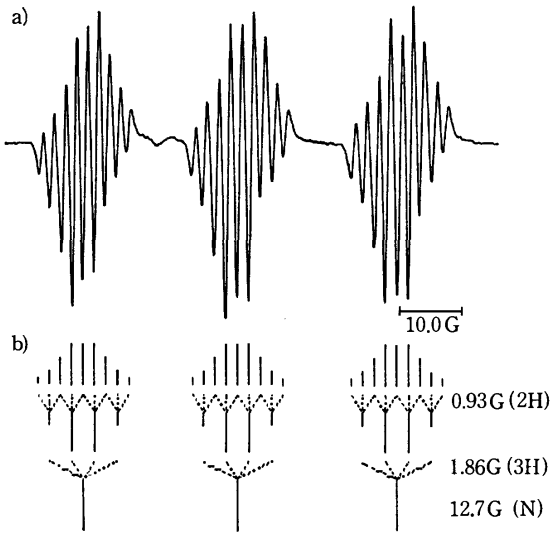

Fig. 1. ESR spectra of 2-*t*-butylaminotropone *N*-oxyl radicals (IIa).
a): Spectrum observed in benzene at room temperature.
b): Stick spectrum consisting of the values of the assigned splitting constants.

To assign the values of coupling constants of protons on the tropone ring in IIa, we prepared deuterium substituted 2-*t*-butylaminotropones (Ib, Ic, and Id) as shown in Chart 1 and measured the ESR spectra of the corresponding nitroxide radicals (IIb, IIc, and IId).

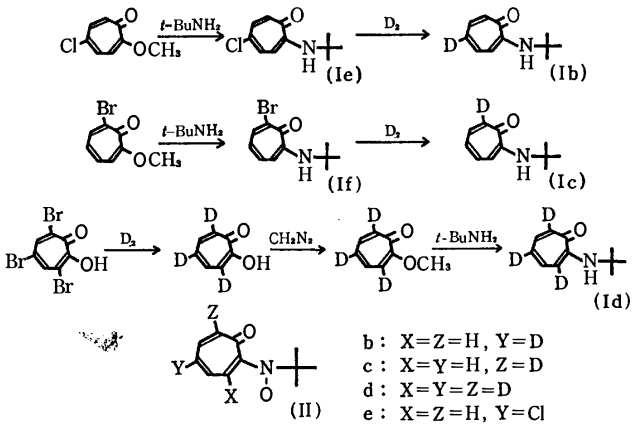

Chart 1

The nitroxide radical IIb gave the spectrum shown in Fig. 2, in which seven lines (splitting at 0.93 gauss, 1 : 3 : 3 : 4 : 3 : 3 : 1) were observed in each component of the triplet. Radical IIc also showed a spectrum (each component of the triplet was split into seven lines at 0.93 gauss) similar to that of IIb. Similarity of both spectra of IIb and IIc suggests that each value for the coupling constants of protons at the 5- and 7-positions on the ring in IIa is the same.

We observed slightly broadened triplet lines (a_N= 12.7 gauss) in the spectrum of IId as shown in Fig. 3. Each component of the triplet lines would not be resolved in the ESR spectrum because of small coupling constant values of the protons at the 4- and 6-positions and of deuterium at the 3-, 5- and 7-positions on the ring in IId.

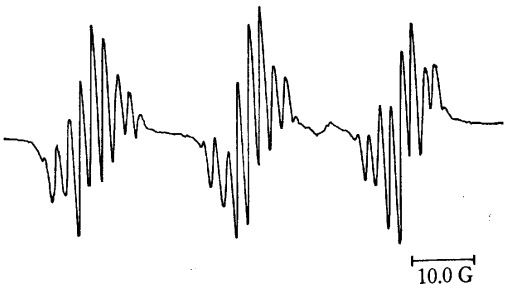

Fig. 2. ESR spectrum of 2-*t*-butylamino-5-*d*-tropone *N*-oxyl radical (IIb).

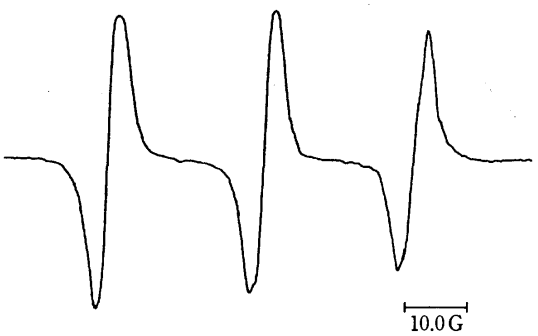

Fig. 3. ESR spectrum of 2-*t*-butylamino-3,5,7-tri-*d*-tropne *N*-oxyl radical (IId).

From the results, we assigned the values of the coupling constants of protons on the tropone ring and of nitrogen in IIa as follows: $a_H^3=a_H^5=a_H^7=$ 1.86 gauss, $a_H^4=a_H^6=0.93$ gauss and $a_N=12.7$ gauss. The stick spectrum consisting of these values is shown in Fig. 1-b and agrees with the observed spectrum of IIa.

The results obtained for IIa are comparable with those for *t*-butylphenylnitroxide radical ($a_H^4=a_H^2=a_H^6=2\cdot a_H^3=2\cdot a_H^5=1.9$ gauss and $a_N=13.4$ gauss).[3]

We obtained the following values for the coupling constants of nitrogen and the protons in 2-*t*-butylamino-5-chlorotropone *N*-oxyl radical, IIe : $a_N=12.4$ gauss and $a_H^3=a_H^7=2\cdot a_H^4=2\cdot a_H^6=1.98$ gauss. The spectrum is given in Fig. 4. The values are also comparable to those of the *t*-butyl-*p*-chlorophenylnitroxide radical ($a_N=13$ gauss and $a_H^2=a_H^6=2\cdot a_H^3=2\cdot a_H^5=2.01$ gauss).[3]

Fig. 4. ESR spectrum of 2-*t*-butylamino-5-chlorotropone *N*-oxyl radical (IIe).

The results indicate that the distribution of an unpaired electron at the 3—7 positions on the tropone

ring in IIa is similar to that at the 2—6 positions on the phenyl ring in the *t*-butylphenylnitroxide radical.

Experimental

Melting points and boiling points are uncorrected.

ESR Measurements. ESR spectra were obtained with a Hitachi MES 4001 type X-band spectrometer employing 100 kHz modulation. The samples prepared by mixing the solution of the amines (*ca.* 3%) in benzene and perbenzoic acid (*ca.* 5 mg) in an ESR sample tube were fully degassed and sealed. The splitting constants were measured relative to the aqueous solution of Fremy's salt.

2-t-Butylaminotropone (Ia). A solution of 13.6 g (0.1 mol) of 2-methoxytropone[5] and 14.6 g (0.2 mol) of *t*-butylamine in 100 m*l* of ethanol was heated under reflux for 24 hr. After removal of ethanol, the resulting oil was distilled: bp 122—133°C/2 mmHg. Yield, 12.7 g (68.3%). The distilled oil solidified on standing. Recrystallization from cyclohexane gave an analytically pure sample: mp 61—62°C. Found: C, 74.28; H, 8.56; N, 7.78%. Calcd for $C_{11}H_{15}ON$: C, 74.54; H, 8.53; N, 7.90%. IR (cm^{-1}) (Nujol): 3250, 1604 and 1597. UV (mμ): λ_{max}^{EtOH} 248, 338 and 407. NMR (τ) (in CCl_4): 2.95—3.50(5H) and 8.50 (9H).

2-t-Butylamino-5-chlorotropone (Ie). A solution of 8.0 g (45 mmol) of 2-methoxy-5-chlorotropone[7] and 6.6 g (90 mmol) of *t*-butylamine in 100 m*l* of ethanol was heated under reflux for 24 hr. After removal of ethanol, the redidue was chromatographed on an alumina column. Eluting with ethanol afforded 6.2 g (65.0%) of Ie. Recrystallization from petroleum ether gave a pure sample: mp 81.5—83°C. Found: C, 62.42; H, 6.68; N, 6.67; Cl, 16.75%. Calcd for $C_{11}H_{14}ONCl$: C, 62.40; H, 6.66; N, 6.64; Cl, 16.74%.

2-t-Butylamino-7-bromotropone (If). A solution of 8.6 g (40 mmol) of 2-methoxy-7-bromotropone[5] and 6.0 g (83 mmol) of *t*-butylamine in 100 m*l* of ethanol was refluxed for 27 hr. After ethanol was removed under reduced pressure, the resulting crystalline solid was recrystallized from methanol to give 6.1 g (59.5%) of If: mp 138.5—140°C. Found: C, 51.35; H, 5.52; N, 5.41; Br, 30.90%. Calcd for $C_{11}H_{14}ONBr$: C, 51.57; H, 5.51; N, 5.49; Br, 31.19%.

2-t-Butylamino-5-d-tropone (Ib). A solution of 4.3 g (20 mmol) of Ie and 3.0 g of triethylamine in dry dioxane was shaken with 1.0 g of anhydrous palladium chloride and 6 m*l* of deuterium oxide in an atmosphere of deuterium. After about 130 m*l* of deuterium was absorbed, the reaction mixture was filtered to separated a precipitate. The filtrate was concentrated under reduced pressure and the residue was distilled: bp 126—130°C/2 mmHg. The distilled oil solidified on standing. Recrystallization from cyclohexane furnished a pure sample: mp 61.0—62.5°C. Yield, 2.1 g (59.0%). Found: C, 74.20; H(D), 9.19; N, 7.85%. Calcd for $C_{11}H_{14}DON$: C, 74.12; H(D), 9.07; N, 7.89%.

2-t-Butylamino-7-d-tropone (Ic). By a method similar to the above, 2.6 g (73.0%) of Ic was obtained from 5.1 g (20 mmol) of If: mp 61.5—62.5°C. Found: C, 73.91; H(D), 9.05; N, 7.81%. Calcd for $C_{11}H_{14}DON$: C, 74.12; H(D), 9.07; N, 7.89%.

2-t-Butylamino-3,5,7-tri-d-tropone (Id). A solution of 35.8 g (0.1 mol) of 3,5,7-tribromotropolone[8] and 40.0 g of triethylamine in 300 m*l* of dry dioxane was shaken with 5.0 g of anhydrous palladium chloride and 30 m*l* of deuterium oxide in an atmosphere of deuterium. After about 7 *l* of deuterium was absorbed during 4 hr, the reaction mixture was filtered to separate a precipitate. The precipitate was dissolved in 60 m*l* of aqueous sodium hydroxide (50%) and extracted with 200 m*l* of chloroform. The filtrate and the chloroform layer were combined, dried over sodium carbonate and concentrated under reduced pressure. The residue was distilled to give 6.5 g of 3,5,7-tri-*d*-tropolone: bp 106—110°C/12 mmHg. The oil solidified on standing. Recrystallization from benzene gave a pure sample: mp 51.5—53°C. Found: C, 66.99; H(D), 7.75%. Calcd for $C_7H_3D_3O_2$: 67.19; H(D), 7.25%. NMR (τ) (in CCl_4): 1.50(1H) and 2.78(2H). To a solution of 2.9 g (23 mmol) of 3,5,7-tri-*d*-tropolone in 50 m*l* of ether was added a solution of diazomethane (3 g) in 100 m*l* of ether dropwise with ice bath cooling. The solution was allowed to stand overnight at room temperature. After removal of ether, the resulting oil was distilled to give 2.0 g (57.5%) of 2-methoxy-3,5,7-tri-*d*-tropone: bp 138—142°C/5 mmHg. By a similar procedure used for Ia, 1.6 g (61.4%) of Id was obtained from 2.0 g (14 mmol) of 2-methoxy-3,5,7-tri-*d*-tropone: mp 60.0—62°C. Found: C, 73.07; H(D), 10.36; N, 7.59%. Calcd for $C_{11}H_{12}D_3ON$: C, 73.28; H(D), 10.05; N, 7.78%.

Perbenzoic Acid. Perbenzoic acid was prepared by the usual way[9] and purified by sublimation under reduced pressure: 35—40°C/4 mmHg.

The authors are grateful to Dr. Nobuo Soma for his helpful suggestions in the preparation of the amines, and to Dr. Genshun Sunagawa, the director, for his encouragement.

7) T. Sato, *Nippon Kagaku Zasshi*, **80**, 1171 (1959).

8) T. Nozoe, Y. Kitahara, K. Yamane, and A. Yoshikoshi, *Proc. Japan Acad.*, **27**, 18 (1959).

9) G. Braun, "Organic Syntheses", Coll. Vol. I, p. 431 (1956).

Studies on Stable Free Radicals. XIII.[1] Synthesis and ESR Spectral Properties of Hindered Piperazine *N*-Oxyls

Takao YOSHIOKA, Eiko MORI, and Keisuke MURAYAMA

Central Research Laboratories, Sankyo Co., Ltd., Shinagawa-ku, Tokyo

(Received November 15, 1971)

New hindered 3,5-dioxopiperazines (VII, IX), hindered piperazines (VIII, X), and the corresponding *N*-oxyls (XI, XIII, XII, and XIV) were synthesized. The substituent and solvent effects of the nitrogen coupling constants (a_N) in the *N*-oxyls were measured and compared with each other; the introduction of carbonyl groups at the *C*-3 and *C*-5 ring positions decreased these values, which increased in a protic polar solvent.

Many papers have recently reported synthetic methods for and the properties of extremely stable free radicals.[2] Especially, the introduction of *N*-oxyl into such heterocyclic rings as pyrrolines (I), pyrrolidines (II), piperidines (III), oxazolines (IV),[3] imidazolines (V),[4] and imidazolidines (VI)[5] were synthesized in number (Chart 1), and some of them were found useful as a radical scavenger,[5] and oxidizing agent,[5] and a spin labeling compound.[6]

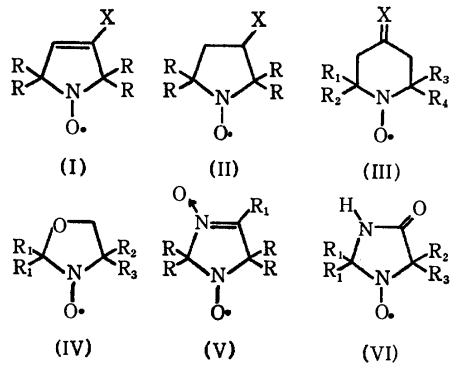

Chart 1.

However, piperazine *N*-oxyls have not as yet been reported, although some hindered piperazines are known;[7] this may be because of the difficulties in the direct oxidation of such hindered piperazines, as will be discussed later.

This paper will describe the synthesis of new hindered piperazine *N*-oxyls, their chemical properties, and their ESR coupling constants (a_N). The substituent and solvent effects on the coupling constant in the *N*-oxyls are of interest in connection with those of the piperidine *N*-oxyls (III).[8] Chart 2 summarizes starting hindered amines and the corresponding *N*-oxyls.

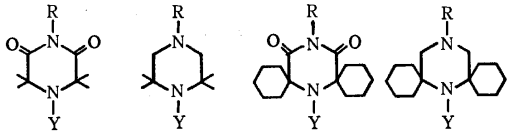

Y=H	$VII_{H,B,C}$	$VIII_{H,B}$	$IX_{H,B,C}$	$X_{H,B}$
Y=O·	$XI_{H,B,C}$	XII_B	$XIII_{H,B,C}$	XIV_B

H : R=H, B : R=$CH_2C_6H_5$, C : R=COOEt

Chart 2.

Results and Discussion

I. The Synthesis of 3,5-Dioxopiperazines, VII and IX. The starting amine, IX_H (R=H), was synthesized from bis(1-cyanocyclohexyl)amine (XV), itself derived from an aminonitrile of cyclohexanone, in a concentrated sulfuric acid solution according to a literature procedure.[7] Although the application of this method to the synthesis of VII_H met with failure, the following method, using basic conditions, successfully led to the formation of VII_H (Chart 3): the treatment of an aminonitrile of acetone with potassium hydroxide in refluxing methanol gave VII_H, plus 2,2,5,5-tetramethyl-4-oxoimidazolidine (XVI).[5] The alkylation or acylation of VII_H or IX_H gave the corresponding 4-substituted derivatives; after VII_H or IX_H was treated with sodium hydride in *N*,*N*-dimethylformamide (DMF), benzylation or carbethoxylation of the resulting Na-salts gave VII_B, IX_B (R=$CH_2C_6H_5$), VII_C, IX_C (R=COOEt) (Chart 4).

Piperazines $VIII_{H,B}$ and $X_{H,B}$ were synthesized by

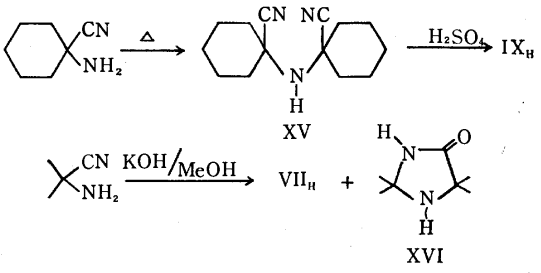

Chart 3.

1) Part XII: T. Toda, E. Mori, and K. Murayama, This Bulletin, **45**, 1852 (1972).

2) a) E. G. Rozantzev, "Free Nitroxyl Radicals", Plenum Press, New York, N. Y. (1970), p. 1. b) K. Murayama, *Yuki Gosei Kagaku Kyokaishi*, **29**, 366 (1971). c) A. R. Forrester, J. M. Hay, and R. H. Thomson, "Organic Chemistry of Stable Free Radicals," Academic Press, London (1968), p. 180.

3) a) J. F. W. Keana, S. B. Keana, and D. Beetham, *J. Amer. Chem. Soc.*, **89**, 3055 (1967). b) J. F. W. Keana and R. J. Dinerstein, *ibid.*, **93**, 2808 (1971).

4) L. B. Volodarsky, G. A. Kutikova, R. Z. Sagdeev, and Yu, N. Molin, *Tetrahedron Lett.*, **1968**, 1065.

5) K. Murayama, S. Morimura, and T. Yoshioka, This Bulletin, **42**, 1640 (1969).

6) a) T. L. Stone, T. Buckman, P. L. Nordio, and H. M. McConnell, *Proc. Nat. Acad. Sci. U. S.*, **54**, 1010 (1965). b) H. M. McConnell and B. G. McFarland, *Quart. Rev. Biophys.*, **3**, 91 (1970).

7) a) R. Sudo and S. Ichihara, This Bulletin, **36**, 34 (1963). b) E. F. J. Duynstee, M. E. A. F. Mevis, H. K. Ostendorf, and D. J. D. Kock, *Rec. Trav. Chim. Pays-Bas*, **87**, 945 (1968).

8) a) Ref. 1-c), p. 194. b) R. Briere, H. Lemaire, and A. Rassat, *Bull. Soc. Chim. Fr.*, **1965**, 3273.

the reduction of the coresponding dioxopiperazines, $VII_{H,B}$ and $IX_{H,B}$ respectively, with lithium aluminum hydride (LAH). (Chart IV)

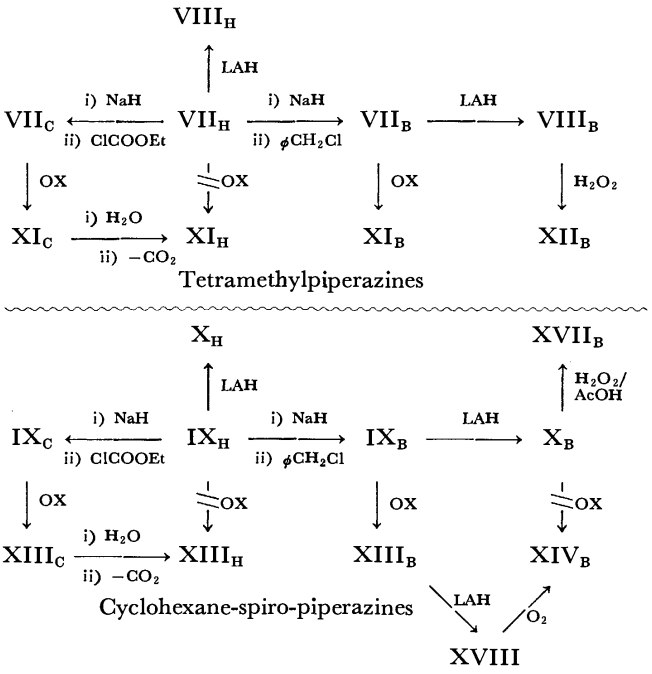

B: $C_6H_5CH_2$, OX: oxidiation

Chart 4.

II. Oxidation of the Dioxopiperazines VII and IX to the Corresponding N-*Oxyls, XI and XIII.* The direct oxidation of the 4-unsubstituted dioxopiperazines, VII_H and IX_H, to XI_H and $XIII_H$ respectively was unsuccessful (Chart 4.); when *m*-chloroperbenzoic acid (CPBA) was used as an oxidizing agent, a rapid decomposition of VII_H and IX_H occurred with blue coloration, and none of the desired *N*-oxyls XI_H and $XIII_H$ were formed. Using 30% aqueous hydrogen peroxide in the presence of EDTA and sodium tungstate did not afford the desired products. However, the 4-substituted dioxopiperazines, $VII_{B,C}$ and $IX_{B,C}$, were oxidized with CPBA or 30% aqueous hydrogen peroxide to give the desired *N*-oxyls, $XI_{B,C}$ and $XIII_{B,C}$ respectively. The relative ease of the formation of the cyclohexane-spiro-piperazine-*N*-oxyl, $XIII_B$, was observed by comparing the degree of orange coloration; it was smaller than that of the tetramethyl-*N*-oxyl XI_B upon the oxidation of the corresponding amines with 30% aqueous hydrogen peroxide in methanol in the presence of the catalysts.

The 4-unsubstituted derivatives, VII_H and IX_H, were synthesized by the hydrolysis of XI_C and $XIII_C$, respectively, followed by spontaneous decarboxylation.

III. Oxidation of the VIII and X Piperazines to the XII and XIV N-*Oxyls.* The direct oxidation of the VIII and X piperazines should require controlled reaction conditions because of the presence of the *tert*-amine group. In fact, the oxidation of $XIII_B$ and X_B with CPBA met with failure; a rapid decomposition occurred, with a green coloration, and one of the the desrifed *N*-oxyls XII or XIV were obtained. On the other hand, the oxidation of $VIII_B$ (the tetramethylpiperazine derivative) with 30% aqueous hydrogen peroxide in the presence of the catalyst *in methanol* was successful in producing the desired *N*-oxyl, XII_B. The application of this procedure to the oxidation of X_B (cyclohexane-spiro-piperazine derivative) was, however, unsuccessful; X_B was recovered quantitatively under the same reaction conditions.

The difference in the reactivity between $VIII_B$ and X_B, or that between VII_B and IX_B, described above, may be explained by the steric effect at *C*-2 and *C*-6 in the ring. The same relationship has been observed in the imidazolidine series[5] and in the piperidine series.[9]

The oxidation of X_B with 30% aqueous hydrogen peroxide in the presence of the catalyst gave an undesirable product, N^1-oxyl-N^4-oxide ($XVII_B$) *in acetic acid.*

Since the direct oxidation of X_B failed to produce XIV_B, another route was attempted; we reduced[10] the 3,5-dioxo derivative, $XIII_B$, with LAH to give the corresponding hydroxylamine (XVIII), which was then oxidized with air[11], thus affording the dseired *N*-oxyl, XIV_B.

IV. Coupling Constants (a_N) in the ESR Spectra. The ESR spectra of the piperazine *N*-oxyls were measured in a 10^{-3} M solution, using Fremy's salt as the reference. Table 1 summarizes the substituent effects on the nitrogen-coupling constant (a_N) in the piperazine *N*-oxyls, and shows that carbonyl groups at *C*-3 and *C*-5 or a nitroxide group at *N*-4 decrease the value by about 1.0 gauss, *e.g.*, XI_B, XII_B, and $XVII_B$. This suggests that the unpaired electron distribution is altered to a small extent by a dipolar field effect. A similar trend has been observed with the ipperidine *N*-oxyl series.[8] Anomalously, the *N*-oxyl $XIII_C$

Table 1. Substituent effects in ESR spectra of the piperazines (10^{-3} M in CH_2Cl_2)

Compound	a_N gauss ±0.1	Compound	a_N gauss ±0.1
XI_C	14.5	$XIII_C$	13.7
XI_B	14.5	$XIII_B$	14.2
XI_H	14.7	$XIII_H$	14.5
—	—	$XVII_B$	14.7
XII_B	15.8	XIV_B	15.5

Table 2. Solvent effects in ESR spectra of the piperazines (10^{-3} M)

Compound	CH_2Cl_2	C_6H_6	CH_3OH
XI_C	14.5	14.5	15.0
XI_B	14.5	14.5	14.9
XI_H	14.7	14.8	15.0
XII_B	15.8	15.8	16.4

9) T. Yoshioka, S. Higashida, and K. Murayama, This Bulletin, **45**, 636. (1972).

10) V. A. Golubev, E. G. Rozantzev, and M. B. Neiman, *Izv. Akad. Nauk SSSR, Ser. Khim.*, **1965**, 1927.

11) E. G. Rozantzev and V. A. Golubev, *ibid.*, **1966**, 891.

exhibited a relative low value (13.7); no reasonable explanation of this has been proposed because of the uncertainty of the conformation.

Table 2 shows solvent effects which are attributable to the hydrogen bonding between the *N*-oxyl and solvent (HS), altering the unpaired electron distirbution in favor of the (B) form, *i.e.*, the form with the more nucleophilic oxygen atom,[8] as is shown in Chart 5.

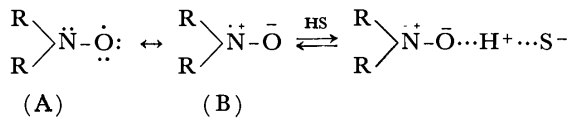

Chart 5.

Experimental

All the melting points are uncorrected.

Unless otherwise stated, the IR spectra were taken with a Hitachi EPI-S2 spectrometer (Nujol mull); the NMR spectra, with a Varian A-60 using tetramethylsilane as the internal standard; the Mass spectra, with a JEOL-JMS-OIS app aratus, and the ESR spectra, with a Hitachi MES 4001 type X-band spectrometer employing 100 kc modulation. Table 3 shows the formula molecular ion peak, mp, bp, yield, and result of elemental analysis of all the prdoucts; the IR spectra are shown in Table 4, and the NMR in Table 5.

2,2,6,6-Tetramethyl-3,5-dioxopiperazine (VII_H). A solution of 100 g (1.19 mol) of an aminonitrile of acetone and 26.6 g (474 mmol) of potassium hydroxide in 1000 m*l* of methanol was refluxed for 7 hr. Then 49.2 g (479 mmol) of a 35% aqueous hydrochloric acid solution was added into the reaction mixture to neutralize the used potassium hydroxide with stirring at 20°C. After 1 hr, the potassium chloride thus produced was removed by filtration; the filtrate was evaporated *in vacuo* to give a semi-solid, which was then washed at room temperature with 1000 m*l* of benzene in order to separate the oxoimidazolidine, XVI. The treatment of the obtained insoluble solid with a solution of 90.1 g of 35% aqueous hydrochloric acid in 180 m*l* of methanol gave 40.2 g of the monohydrochloride of VII_H. Recrystallization from water gave pure prisms. The hydrochloride was dissolved in water on heating and was neutarlized with potassium carbonate. The extract with chloroform from the mixture was dried over anhydrous magnesium sulfate and evaporated *in vacuo* to give the free base, VII_H, which was subsequently recrystallized from DMF to give colorless needles.

2,2,6,6-Tetramethyl-3,5-dioxo-4-benzylpiperazine (VII_B). Into a solution of 28.5 g (168 mmol) of VII_H in 500 m*l* of dry DMF, were added thirteen 0.5 g-portions (9.65 g, 201 mmol) of 50% sodium hydride (Nujol dispersion) with stirring at 40°C. After the vigorous evolution of hydrogen had ceased, the reaction mixture was stirred for 1 hr at 40°C. Into the mixture we then added a solution of 28.4 g (224 mmol) of benzyl chloride in 50 m*l* of dry DMF at 45—50°C. After stirring overnight at room temperature, the DMF was evaporated *in vacuo* to give a residue, which was dissolved in benzene (200 m*l*) and water (200 m*l*). The separated benzene layer was washed with water, dried over anhydrous magnesium sulfate, and treated with active charcoal. The evaporation of the benzene *in cacuo* left an oil, which was then dissolved in petroleum benzine and cooled

Table 3. Piperazines and piperazine-*N*-oxyles

Compound	Formula	M$^+$ (*m/e*)	Mp or bp °C	Yield (%)	Elemental analysis (Found/Calcd)			
					C	H	N	Cl
VII_H	$C_8H_{14}N_2O_2$	170	236—238 (DMF)	89.5[a]	56.71/56.47	8.48/8.29	16.68/16.47	
VII_H·HCl	$C_8H_{15}N_2O_2Cl$	—	>250 (H_2O)	32.8	46.41/46.49	7.60/7.31	13.52/13.56	17.12/17.19
VII_B	$C_{15}H_{20}N_2O_2$	260	79—80 (petr. benzine)	62.7	69.02/69.23	7.78/7.76	10.89/10.77	
VII_C	$C_{11}H_{18}N_2O_4$	242	104—105 (ethanol)	56.5	54.66/54.53	7.52/7.49	11.77/11.56	
$VIII_H$	$C_8H_{18}N_2$	142	74—75 (petr. ether)	61.5	65.63/65.93[b]	12.59/12.64	19.02/19.23	
$VIII_H$·2HCl	$C_8H_{20}N_2Cl_2$	—	>200 (ethanol)	>95	44.48/44.73	9.39/9.38	12.81/13.04	32.89/33.01
$VIII_B$	$C_{15}H_{24}N_2$	232	104—105/1 mmHg	75.5	77.47/77.53	10.30/10.41	11.77/12.06	
IX_B	$C_{21}H_{28}N_2O_2$	340	92—93 (petr. benzine)	75.8	73.96/74.08	8.55/8.29	8.34/8.23	
IX_B·HCl	$C_{21}H_{29}N_2O_2Cl$	—	250 (ethanol)	>95	66.62/66.84	7.80/7.75	7.76/7.43	9.44/9.39
IX_C	$C_{17}H_{26}N_2O_4$	322	102—105 (*n*-hexane)	62.4	63.50/63.33	8.11/8.13	8.97/8.69	
X_H	$C_{14}H_{26}N_2$	222	88—89 (*n*-hexane)	74.4	75.38/75.68	11.77/11.80	12.79/12.61	
X_B	$C_{21}H_{32}N_2$	312	91—93 (petr. benzine)	78.6	80.83/80.71	10.36/10.32	8.95/8.97	
XI_H	$C_8H_{13}N_2O_3$	185	150—160 (ether)[c]	60.7	51.91/51.89	7.07/7.08	15.17/15.14	
XI_B	$C_{15}H_{19}N_2O_3$	275	71.5—72.5 (detr. ether)	47.4	65.70/65.45	7.02/6.98	10.04/10.18	
XI_C	$C_{11}H_{17}N_2O_5$	257	99—101 (ether)	66.2	51.36/51.36	6.96/6.68	10.83/10.89	
XII_B	$C_{15}H_{23}N_2O$	247	61.5—62.5 (petr. ether)	29.4	72.64/72.87	9.42/9.39	11.32/11.34	
$XIII_H$	$C_{14}H_{21}N_2O_3$	265	174—175 (99.5% ethanol)	67.2	63.41/63.40	8.01/8.00	10.79/10.57	
$XIII_B$	$C_{21}H_{27}N_2O_3$	355	50—51 (*n*-hexane)	61.0	70.75/70.99	7.52/7.61	8.05/7.89	
$XIII_C$	$C_{17}H_{25}N_2O_5$	337	73—74 (*n*-hexane)	62.5	60.38/60.51	7.52/7.47	8.13/8.31	
XIV_B	$C_{21}H_{31}N_2O$	327	143—144 (*n*-hexane)	95.0	76.92/77.06	9.53/9.57	8.54/8.56	
$XVII_B$	$C_{21}H_{31}N_2O_2$	343	163—164 (methanol)	68.0	73.50/73.46	9.31/9.13	8.23/8.16	

a) from VII_H·HCl. b) sublimes under reduced pressure; calcd for $C_8H_{18}N_2 \cdot 1/5\,H_2O$. c) on a hot plate.

12) F. Johnson, N. A. Starkovsky, A. C. Paton, and A. A. Carlson, *J. Amer. Chem. Soc.*, **88**, 149, 157 (1966).

Table 4. IR Spectra of the products (cm^{-1})

VII_H	3300(w)	3170(m)	3050(m)	1725		1700		1290		
IX_H	3310(w)	3170(m)	3045(m)	1727		1675(br)		1285		
XI_H	3220	3115(m)		1735		1710	1420	1315		
$XIII_H$	3220	3095		1724		1695(br)	1400	1322		
VII_B	3350(m)			1715		1660			755	700
IX_B	3320(w)			1720		1670			745	695
XI_B				1738		1675	1425		750	695
$XIII_B$				1736(m)		1690	1420(sh)		740	695
VII_C	3360		1788[a]	1730		1690	1380(m)			
IX_C	3350		1783[a]	1737		1700	1375(m)			
XI_C			1785[a]	1740	1720(sh)	1700	1380	1305		
$XIII_C$			1785[a]	1736		1700	1384(m)	1315		
$VIII_B^l$	—								740	700
X_B	—								730	695
XII_B							1400(m)		750	700
XIV_B							1405(w)		745	695
$VIII_H$	3250									
X_H	3250									

br = broad, l = liquid film, a) Ref. 12

Table 5. NMR Spectra of the piperazines

Compound	Solvent	Chemical shift at τ, (Coupling constant J (Hz))			
VII_H	d_6-DMF				8.60(12H, s)
$VIII_H$	CCl_4			7.58(4H, s)	8.94(12H, s)
X_H	$CDCl_3$			7.35(4H, s)	8.1—9.0(20H, broad)
VII_B	$CDCl_3$	2.70(5H, s)	5.04(2H, s)		8.60(12H, s)
$VIII_B$	CCl_4	2.75(5H, m)	6.58(2H, s)	7.96(4H, s)	8.90(12H, s)
IX_B	CCl_4	2.5—3.0(5H, m)	5.17(2H, s)		7.8—9.0(20H, broad)
X_B	CCl_4	2.76(5H, m)	6.61(2H, s)	7.88(4H, s)	8.1—9.0(20H, broad)
VII_C	CCl_4		5.50(2H, q, J=7.0)	8.59(12H, s)	8.61(3H, t, J=7)

at 5°C to give 27.4 g of colorless prisms of VII_B.

2,2,6,6-Tetramethyl-3,5-dioxo-4-carbethoxypiperazine (VII_C). This was prepared from VII_H and ethyl chlorocarbonate in a manner similar to that described above; the extract with benzene from the reaction mixture was washed with ice-water (7—10°C).

2,2,6,6-Tetramethylpiperazine ($VIII_H$). To a suspension of 9.1 g (240 mmol) of LAH in 1000 m*l* of dry ether, we added twenty 0.5-g portions (58.8 mmol) of VII_H at 5—8°C. The resulting solution was stirred for 30 min at 5°C and then refluxed for 1 hr. On cooling to room temperature, a solution of 34.3 g of ethyl acetate in 60 m*l* of ether was added to the resulting mixture in order to decompose the excess LAH. After the reaction mixture had been kept at room temperature for 1 hr, a solution of 2.3 g of sodium hydroxide in 45 m*l* of water was added at 5°C into the mixture, and then the mixture was stirred for 1 hr at room temperature. The ether layer was separated and dried over anhydrous magnesium sulfate. The evaporation of the ether give 5.1 g of crude crystals, which readily sublimed *in vacuo*. The amine, $VIII_H$, turned yellow on exposure to air.

2,2,6,6-Tetramethyl-4-benzylpiperazine ($VIII_B$) was synthesized from VII_B in a manner similar to that described above (in tetrahydrofuran (THF), at 15—20°C).

Cyclohexane-1-spiro-2'-(3',5'-dioxopiperazine)-6'-spiro-1''-cyclohexane (IX_H) was synthesized by the literature procedure.[7]

Cyclohexane-1-spiro-2'-(3',5'-dioxo-4'-benzylpiperazine)-6'-spiro-1''-cyclohexane (IX_B) was prepared from IX_H at 65°C as colorless prisms by a procedure similar to that used in the synthesis of VII_B.

Cyclohexane-1-spiro-2'-piperazine-6'-spiro-1''-cyclohexane (X_H) was prepared from IX_H in ether at 5—8°C in a manner similar to that used in the synthesis of $VIII_H$.

Cyclohexane-1-spiro-2'-(4'-benzylpiperazine)-6'-spiro-1''-cyclohexane (X_B) was similarly prepared from IX_B in ether at 5—8°C.

Oxidation of the Piperazines. 2,2,6,6-Tetramethyl-3,5-dioxopiperazine-1-oxyl (XI_H). By the Direct Oxidation of VII_H. i) With 30% Aqueous Hydrogen Peroxide in the Presence of EDTA and Sodium Tungstate (HPO) in Methanol: Into a suspension of 0.1 g (0.589 mmol) of VII_H in 3.0 g of methanol, was slowly added 1.5 g (13.2 mmol) of HPO. The solution was allowed to stand for 5 days at room temperature. No desired reddish-orange solution, which would indicate the formation of *N*-oxyls, was obtained; the mixture merely turned pale yellow. The methanol was evaporated *in vacuo*, and 15 m*l* of benzene and 0.5 g of potassium carbonate were added to the mixture in order to decompose the excess hydrogen peroxide. The resulting mixture was stirred at room temperature overnight. When the benzene layer, separated from the reaction mixture, was evaporated *in vacuo*, it gave none of the desired prroduct, XI_H.

ii) With HPO in Acetic Acid: None of the desired product ws obtained.

iii) With CPBA in Dichloromethane: Into a solution of 0.1 g (0.589 mmol) of VII_H in 10 m*l* of dichloromethane, was slowly added 0.3 g (1.74 mmol) of CPBA at room temperature. The solution gradually turned blue and then discolored; none of the desired reddish-orange solution was observed. When the dichloromethane was evaporated *in vacuo* after washing with a 10% aqueous solution of potassium carbonate, it gave no *N*-oxyl.

By Hydrolysis Followed by the Decarboxylation of VII_C. Into 2.5 g of a 9.15×10^{-3}% solution (0.264 μmol) of potassium hydroxide in methanol, was added 67.7 mg (0.264 μmol) of VII_C at room temperature. The mixture was allowed to stand for 1 hr at room temperature; then the methanol was evaporated *in vacuo* below room temperature to leave a residue, which was washed with ether three times to remove the VII_C. The residue was then dissolved in methanol and treated with a solution of an equimolar hydrogen chloride in methanol at 10°C. The methanol was removed *in vacuo*, and the resuting residue was extracted with ether. The concentration of the extract gave yellow prisms. A small piece of the prisms gradually sublimed at 150—160°C (on the hot plate of a micro melting-point apparatus).

2,2,6,6-Tetramethyl-3,5-dioxo-4-benzylpiperazine-1-oxyl (XI_B). To a solution of 3.0 g (11.5 mmol) of VII_B in 10 m*l* of acetic acid, was added dropwise 5.25 g (46.2 mmol) of HPO at 20°C. The solution was then allowed to stand at room temperature. After 3 days the solution began to turn reddish. After standing for additional 4 days, 100 m*l* of benzene and 23.7 g potassium carbonate were added to the reaction mixture below 15°C in order to neutralize the acetic acid employed as a solvent and in order to decompose the excess hydrogen peroxide. The suspension was stirred for 2 hr at room temperature. Separation, drying over potassium carbonate, and the evaporation of the benzene gave 4.1 g of a reddish oil, which was then chromatographed on 100 g Brockmann aluminum oxide, using petroleum benzine as the eluent. The subsequent evaporation of the elute *in vacuo* left a reddish oil, which crystallized on standing overnight (1.5 g). Recrystallization gave reddish-orange neeldes. As a by-product along with XI_B, *2,2,6,6-tetramethyl-3,5-dioxo-4-benzyl-1-hydroxypiperazine* was obtained from an ether-elute; mp 97—98°C (from petroleum ether); (1.2 g, 44%). Found: C, 64.95, H; 7.29, N; 9.96%. Calcd for $C_{15}H_{20}N_2O_3$: C, 65.22, H; 7.32, N; 10.14%. IR(cm^{-1}): 3450, 1735, 1675, 735, and 700.

2,2,6,6-Tetramethyl-3,5-dioxo-4-carbethoxypiperazine-1-oxyl (XI_C) was prepared by the oxidation of VII_C with CPBA in a procedure similar to that described above; the extract was washed with water below 10°C.

2,2,6,6-Tetramethyl-4-benzylpiperazine-1-oxyl (XII_B). i) Oxidation of $VIII_B$ with CPBA: As soon as a solution of 0.6 g (3.48 mmol) of CPBA in 10 m*l* of dichloromethane was added dropwise to a solution of 0.25 g (1.08 mmol) of $VIII_B$ in 10 m*l* of dichloromethane at 15°C, a rapid decomposition of $VIII_B$ occurred with green coloration; none of the desired *N*-oxyl was obtained.

ii) Oxidation of $VIII_B$ with HPO in Methanol: To a solution of 1.92 g (8.28 mmol) of $VIII_B$ in 5 m*l* of methanol, was added dropwise 3.0 g (26.5 mmol) of HPO at room temperature. After the reaction mixture had been allowed to stand for 20 hr at room temperature, 10 more grams of HPO were added to the mixture. After standing overnight, a reddish oil separated spontaneously. To the mixture was then added 50 ml of benzene and 5 g of potassium carbonate. Vigorous stirring was continued for 3 hr, and then the benzene layer was separated, washed with water saturated with sodium chloride, and dried over anhydrous magnesium sulfate. The subsequent removal of the benzene left 1.7 g of a reddish oil, which was chromatographed on 100 g of a silica gel (M. WOELM for Dry-Column Chromatography) using petroleum benzine as the eluent. The evaporation of the elute *in vacuo* gave 0.6 g of reddish crystals.

Cyclohexane-1-spiro-2'-(3',5'-dioxopiperazine-1'-oxyl)-6'-spiro-1''-cyclohexane ($XIII_H$). The direct oxidation of IX_H with HPO or CPBA failed to produce $XIII_H$ in a manner similar to that used for the oxidation of VII_H. However, hydrolysis, followed by decarboxylation of $XIII_C$, gave $XIII_H$ in a procedure similar to that used for VII_C.

Cyclohexane-1-spiro-2'-(3',5'-dioxo-4'-benzylpiperazine-1'-oxyl)-6'-spiro-1''-cyclohexane ($XIII_B$). i) To a suspension of 0.1 g (0.294 mmol) of IX_B in 0.7 m*l* of acetic acid, was added dropwise 0.35 g (3.08 mmol) of HPO. The suspension was then stirred at room temperature. After 2 days, a reddish oil separated spontaneously from the acetic acid. To the mixture, after 4 days, were addde 5 m*l* of benzene and 0.2 g of potassium carbonate at room temperature in order to neutralize the acetic acid and in order to decompose the excess hydrogen peroxide. The resulting suspension was stirred at room temperature for 2 hr. The benzene was then evaporated *in vacuo* to give 0.109 g of a reddish oil. The oil was dissolved in a small amount of *n*-hexane and cooled at −5—0°C overnight to give reddish crystals.

ii) To a solution of 4.0 g (11.7 mmol) of IX_B in 800 m*l* of dichloromethane, was gradually added 8.0 g (46.6 mmol) of crystals of CPBA at room temperature. The reaction mixture immediately turned red, and was then kept for 5 days at room temperature. The resulting solution was washed with 200 m*l* of a 10% aqueous potassium carbonate solution three times and with water. After the solution had then been dried over potassium carbonate, the removal of the solvent left a reddish oil, which was chromatographed on 100 g of Brockmann aluminum oxide using petroleum benzine as the eluent. The evaporation of the elute gave 2.5 g of crude crystals, which were recrystallized to give pure reddish crystals. The physical data completely accorded with those of the sample obtained by *Method i)* above.

Cyclohexane-1-spiro-2'-(3',5'-dioxo-4'-carbethoxypiperazine-1'-oxyl)-6'-spiro-1''-cyclohexane ($XIII_C$) was synthesized from IX_C in a manner similar to that used in the synthesis of XI_C; a reddish oil obtained by the evaporation of the extract solidified during 3 days' storage at −10—0°C. The solid was washed with cold (−50°C) *n*-hexane and chromatographed on silica gel using *n*-hexane–ether (9 : 1) to give reddish-orange prisms.

Cyclohexane-1-spiro-2'-(4'-benzylpiperazine-1'-oxyl)-6'-spiro-1''-cyclohexane (XIV_B). i) Oxidation of X_B with CPBA: An attempt to do this in a manner similar to that used in the oxidation of $VIII_B$ met with failure.

ii) Oxidation of X_B with HPO in Methanol: A mixture of 0.2 g (0.641 mmol) of X_B, 0.5 g (4.42 mmol) of HPO and 2 m*l* of methanol was stirred at room temperature. After 6 days, the starting amine was quantitatively revovered.

iii) Oxidation of X_B with HPO in Acetic Acid: This gave none of the desired product, but another product, *cyclohexane-1-spiro-2'-(4'-benzylpiperazine-1'-oxyl-4'-oxide)-6'-spiro-1''-cyclohexane ($XVII_B$)*, when conducted in a manner similar to that used in the preparation of $XIII_B$.

iv) Reduction of $XIII_B$ with LAH Followed by the Air-Oxidation of the Resulting Hydroxyl Amine (XVIII): Into a suspension of 0.248 g (6.5 mmol) of LAH in 6 ml of dry ether, was gradually added 0.5 g (1.41 mmol) of $XIII_B$ at room temperature. The ether was refluxed for 30 min and then allowed to stand at room temperature. After 12 hr, the

reddish solution gradually became colorless. The discolored solution was poured into ice-water, and the mixture was stirred at room temperature for 3 days while being exposed to air. The ether layer gradually turned red again and was separated, washed with water three times, dried over anhydrous magnesium sulfate, treated with active charcoal, and evaporated *in vacuo* to give 0.437 g of crude crystals, which gave reddish crystals upon recrystallization.

We wish to thank Dr. Genshun Sunagawa, the Director of these laboratories, for his encouragement and Mr. Tsutomu Kanai for his technical assistance during the course of this work.

BULLETIN OF THE CHEMICAL SOCIETY OF JAPAN, VOL. 45, 1860—1863 (1972)

Steric Effect in the Nucleophilic Attack of Bromide Anion on Diaryl- and Aryl-2-thienyliodonium Ions

Yorinobu YAMADA and Makoto OKAWARA

Research Laboratory of Resources Utilization, Tokyo Institute of Technology, Ookayama, Meguro-ku, Tokyo

(Received November 15, 1971)

Duryl-, mesityl-, and *o*-tolyl-phenyl- and 2-thienyliodonium bromides have been synthesized. When these substances were allowed to decompose in molten (235°C) and solution (100°C) states, the nucleophile (bromide anion) preferentially attacked the substituted phenyl ring. Steric and electronic effects of phenomena have been discussed.

The nucleophilic substitution reaction on the aryl ring of diaryliodonium salts is usually influenced by the inductive and resonance effects of the substituent group.[1] Generally, the nucleophile preferentially attacks the phenyl ring containing the electron-withdrawing group. The site of the nucleophilic attack, however, is influenced by the steric hindrance of the substituent group.

Le Count and Reid reported on the steric effect by the *ortho*-methyl group in the reaction of diaryliodonium salts.[2] Hydrolysis of *p*-tolylmesityliodonium bisulfate which contains two methyl groups *ortho* to the iodine atom, gives 90% of iodomesitylene and 10% iodotoluene.

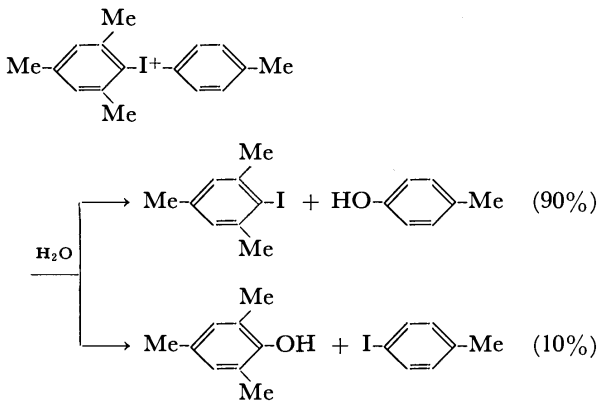

We showed that the nucleophile (bromide and chloride ions) attacks the aryl ring rather than the thienyl ring in the reaction of aryl-2-thienyliodonium halides.[3] The reaction seems to be an aromatic bimolecular substitution reaction and to proceed *via* the π-p orbital interaction of the aryl ring and halide ion in the trigonal-bipyramidal structure of iodonium salt. However, if the methyl group is introduced into the *ortho*-position on the phenyl ring of phenyl-2-thienyliodonium salt, it can be expected that the nucleophile attacks the thienyl ring predominantly. The same situation can be expected in the case of diaryliodonium salt. The present paper describes the steric effect in the reaction of substituted diphenyl- and substituted phenyl-2-thienyliodonium bromides containing the *ortho*-methyl substituent on the phenyl ring.

Results and Discussion

Substituted phenyl-2-thienyl- (I) and substituted diphenyl-iodonium bromides (II) were synthesized from substituted phenyliodoso acetate and thiophene or benzene in a mixture of acetic anhydride and concentrated sulfuric acid, respectively. The products are summarized in Table 1.

The thermal decomposition of the iodonium salts I and II was carried out in the molten state (23±55°C) for 5 min and the reaction products aryl halides and 2-thienyl halides were confirmed by gas chromatography in comparison with their authentic samples. The reaction of I and II proceeds along the following paths, the bromide ion competitively attacking the aryl ring or the thienyl ring (or phenyl ring.) The results are given in Table 2. The results in the solution state (100°C) of the iodonium bromides in *N*,*N*-dimethylformamide (DMF) and DMF-dioxane

1) F. M. Beringef, M. Drexler, E. M. Gindler, and C. C. Lumpkin, *J. Amer. Chem. Soc.*, **75**, 2708 (1953).

2) D. J. Le Count and J. A. W. Reid, *J. Chem. Soc., C*, **1967**, 1298.

3) Y. Yamada and M. Okawara, This Bulletin, in press.

Table 1. Preparation of I and II

Iodonium bromide		Mp (°C)	Yield (%)	Elemental analysis (%) Found C	Found H	Calcd C	Calcd H
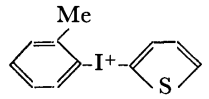	(Ia)	210—215	68.8	34.67	2.55	34.64	2.65
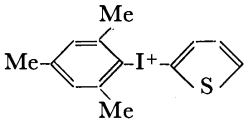	(Ib)	153—156	26.3	37.90	3.39	38.17	3.45
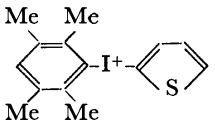	(Ic)	140—144	46.0	39.04	3.68	39.55	3.79
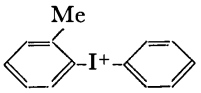	(IIa)	205—210	47.1	41.45	3.26	41.63	3.23
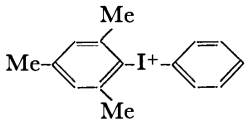	(IIb)	170—172	68.7	44.64	4.15	44.69	4.00
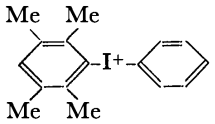	(IIc)	150—152	90.1	44.83	4.54	44.74	4.53

Table 2. Cleavage tendency of I and II in molten

Aryl group	Ar-I⁺-Th (I) mode-A	Ar-I⁺-Th (I) mode-T	Ar-I⁺-Ph (II) mode-A	Ar-I⁺-Ph (II) mode-B
o-Tolyl (a)	92.3	7.7	86.7	13.3
Mesityl (b)	100	0	96.5	3.5
Duryl (c)	100	0	97.7	2.3

Th-: Thienyl ring; Ph-: Phenyl ring

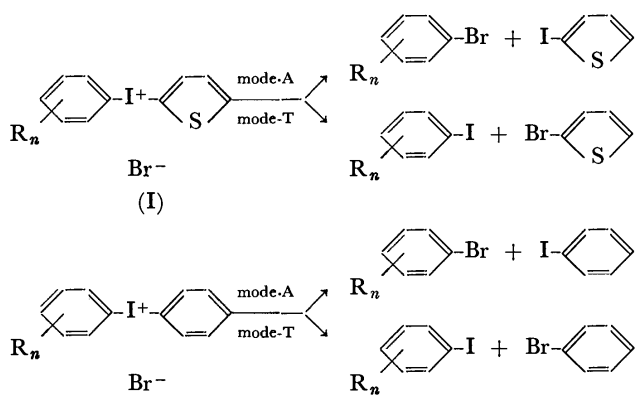

R=Methyl group, $n=1, 3, 4$

are summarized in Table 3. They are similar to those in the molten state. In every case the reaction proceeded without side reaction.

We see from Table 2 that the mode-A reaction, in which the nucleophile attacks the aryl ring, takes place completely for Ib and Ic and it is accompanied by the mode-T reaction, in which the nucleophile attacks the thienyl ring, only in the case of Ia. Similarly, for II the mode-A reaction takes place more predominantly than mode-B, in which the nucleophile attacks the phenyl ring. The reaction of II, however, does not proceed so selectively as that of I. The results are in contrast to those in the hydrolysis of *p*-tolylmesityliodonium salt reported by Le Count and Reid.

An aromatic bimolecular substitution mechanism has been proposed for *m*- or *p*-substituted phenyl-2-thienyl- and *p*-tolyliodonium salts.[5] If an aromatic bimolecular substitution mechanism is operative in the present case, the reaction of II should give unsubstituted phenyl bromide rather than methyl substituted phenyl bromide, but the result is the opposite. Thus, the *ortho*-methyl group is effective in the intramolecular strain to facilitate the dissociation of the bond between substituted phenyl 1-carbon and iodine. The substituted phenyl cation produced seems to be

4) F. M. Beringer, M. Drexler, E. M. Gindler, and C. C. Lumpkin, *J. Amer. Chem. Soc.*, **75**, 2705 (1953); F. M. Beringer, H. E. Bachofner, R. A. Fakl, and M. Lett, *ibid.*, **80**, 4279 (1958).

5) Y. Yamada, K. Kashimk, and M. Okawara, Presented at the 25th Annual Meeting of the Chemical Society of Japan, Tokyo, October, 1971.

TABLE 3. CLEAVAGE TENDENCY OF I AND II IN SOLUTION STATE

Aryl group	Solvent	Ar-I⁺-Th (I) mode-A : mode-T	Ar-I⁺-Ph mode-A : mode-B
o-Tolyl (a)	DMF	100 : 0	86.8 : 13.2
Mesityl (b)	DMF	100 : 0	96.0 : 4.0
Duryl (c)	DMF	100 : 0	100 : 0
o-Tolyl (a)	Dioxane-DMF (1 : 1)	100 : 0	92.3 : **7.7**
Mesityl (b)	Dioxane-DMF (1 : 1)	100 : 0	*ca.* 100 : trace
Duryl (c)	Dioxane-DMF (1 : 1)	100 : 0	100 : 0

Th-: Thienyl ring; Ph-: Phenyl ring

stabilized by some methyl groups, and an analogous mechanism to an aromatic S_N1 is plausible. Similar results have been observed in the case of *m*- or *p*-substituted phenyl-2-thienyliodonium salts. However, there is a slight difference in the reaction tendency between I and II, *viz.*, the mode-T reaction takes place unfavorably compared to mode-B. Thus, it is very difficult for the thienyl ring to be attacked by the halide ion regardless of the position of the substituent group in the phenyl nucleus. A remarkable distinction between the reactions of the iodonium bromides containing one *ortho*-methyl group (Ia and IIa) and two *ortho*-methyl groups (Ib, c and IIb,c) was not observed either in the molten or solution states. This suggests that even the one *ortho*-methyl group affords a considerable steric strain enough to break the substituted phenyl 1-carbon-iodine bond.

Wiegand and McEwen reported on the steric effect in the pyrolysis reaction of triarylsulfonium bromides.[6] The reaction of phenyl-*p*-tolyl-2,5-dimethylphenylsulfonium bromide gives aryl bromides in the order of preference of 2,5-dimethylbromobenzene > bromobenzene > *p*-bromotoluene. This is explained by the

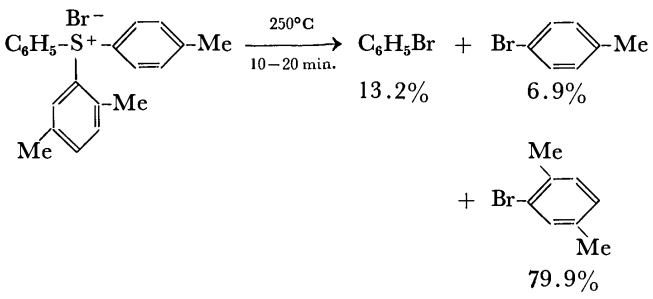

fact that the sulfonium bromide decomposes preferentially in such a manner as to give maximum relief of steric strain.

Thus, it is reasonable to assume that the reaction of the iodonium bromides containing *ortho*-methyl groups proceeds by an analogous mechanism to an aromatic S_N1.

When the substituted phenyl-2-thienyliodonium bromide (I) was allowed to react in the solvent, only the mode-A reaction took place. DMF and dioxane act to stabilize the substituted phenyl cation and help the dissociation of the substituted phenyl 1-carbon-iodine bond. In the case of substituted diphenyliodonium bromide (II), the mode-A reaction increases to some extent in DMF and dioxane, but the remarkable solvent effect was not observed compared to the reactions of Ia and II is attributed to the greater reactivity of phenyl ring than that of thienyl ring.

Experimental

Substituted Phenyl Iodide. Subsittuted phenyl iodides were prepared from substituted benzene by the usual method.[7]

Subsitituted Phenyliodoso Acetate. Iodosobenzene diacetate was prepared by the oxidation of iodobenzene in a mixture of hydroge nperoxide and acetic anhydride.[8] Other subsitituted phenyliodoso acetates were prepared by a procedure like that given for mesityliodoso acetate.[9] To 24.6 g (0.1 mol) of iodomesitylene in 50 m*l* of ethyl acetate was added dropwise with stirring 95 g (0.25 mol) of 20% peracteic acid in acetic acid and ethyl acetate. The flask was chilled with an ice-water bath during the course of addition (30 min). The solution was then stirred for two hours below 10°C and allowed to stand overnight at room temperature. The solvent was removed under reduced pressure. The white crystals were washed with ether and dried overnight, giving 27.8 g of mesityliodoso acetate (yield, 78.5%), mp 110—125°C. (See Table 4 for melting points and yield data).

TABLE 4. ARYLIODOSO ACETATE

Aryl group	Mp (°C)	Yield (%)
o-Tolyl	145—148	69.2
Mesityl	110—120	78.5
Duryl	130—137	77.9

o-*Tolylphenyliodonium Bromide.* To a suspension of 3.4 g (10 mmol) of *o*-tolyliodoso acetate and 5 m*l* of benzene in 100 ml of acetic anhydride was added 5 m*l* of concd. sulfuric acid with stirring below 10°C. After stirring for one hour, the reaction mixture was allowed to stand for 5 hr at room temperature. The mixture was poured into 200 m*l* of ice water and extracted with two 50 m*l* portions of ether. The aqueous layer was treated with activated carbon and 30 g of sodium bromide in 100 m*l* of water. The precipitate was washed with water and with methanol and then dried to give 1.8 g of *o*-tolylphenyliodonium bromide. Recrystal-

6) G. H. Wiegand and W. E. McEwen, *J. Org. Chem.*, **33**, 2671 (1968).

7) H. O. Wirth, O. Konigstein, and W. Kern, *Ann. Chem.*, **634**, 84 (1960).

8) M. Okawara and K. Mizuta, *Kogyo Kagaku Zasshi*, **64**, 232 (1961).

9) J. E. Leffler and L. J. Story, *J. Amer. Chem. Soc.*, **89**, 2333 (1967).

lization from methanol gave a pure product.

Mesitylphenyliodonium Bromide. To a well-stirred mixture of 11 g (34 mmol) of phenyliodoso acetate, 3.6 g (30 mmol) of mesitylene and 150 m*l* of acetic anhydride kept below 10°C was added 10 m*l* of concd. sulfuric acid over 30 min. After the mixture had been stirred for 6 hr at room temperature, 200 m*l* of ice-water was added, and the mixture was extracted with two 50 m*l* portions of ether. The aqueous layer was treated with activated carbon and then with 30 g of sodium bromide in 100 m*l* of water. The precipitate was recrystallized from methanol to give 8.3 g of mesitylphenyliodonium bromide.

Durylphenyliodonium Bromide. In a similar way the reaction of phenyliodoso acetate (9 g, 28 mmol) with durene (3 g, 22 mmol) gave 8.3 g of durylphenyliodonium bromide.

o-*Tolyl-2-thienyliodonium Bromide.* To a well-stirred mixture of 100 m*l* of acetic anhydride, 6.7 g (20 mmol) of *o*-tolyliodoso acetate and 5.0 g (60 mmol) of thiophene, 5 m*l* of concd. sulfuric acid was added dropwise below 10°C. After 4 hr, 200 m*l* of ice-water was added. Extraction twice with 50 m*l* portions of ether followed by treatment with activated carbon produced an almost colorless solution, which was treated with 20 g of sodium bromide in 100 m*l* of water. The precipitates were collected and crystallized from methanol to give 2.6 g of *o*-tolyl-2-thienyliodonium bromide.

Mesityl-2-thienyliodonium Bromide. To a vigorously stirred solution of 8.2 g (22 mmol) of mesityliodoso acetate, 2.8 g (33 mmol) of thiophene and 200 m*l* of acetic anhydride, was added 5 m*l* of concd. sulfuric acid below 10°C. Subsequent treatments were carried out in the same way to give 8.8 g of mesityl-2-thienyliodonium bromide.

Duryl-2-thienyliodonium Bromide. In a similar way 2.3 g of duryl-2-thienyliodonium bromide was obtained from 4.5 g (12 mmol) of duryliodoso acetate and 2.5 g (30 mmol) of thiophene.

Pyrolysis Reaction of Iodonium Bromides (I and II). 0.25 g of substituted phenyl-2-thienyliodonium bromide (I) was enclosed in a pyrex ampoule. The ampoule was then placed in an oil bath kept at 235°C for 5 min. After the end of the pyrolysis the pyrolysate was dissolved in a small quantity of ether, and the amounts of 2-iodothiophene and 2-bromothiophene were determined by a Hitachi Gas Chromatograph 025—5051 on a 1 m column packed with Silicone SE-30 at 100°C. Chlorobenzene was used as an internal standard.

The pyrolysis reaction of substituted diphenyliodonium bromide (II) was also carried out in a similar way. Amounts of iodobenzene and bromobenzene were determined in the same way.

Reaction of Iodonium Bromides (I and II) in DMF and DMF-Dioxane. The reaction of iodonium bromides was carried out by a procedure similar to that given for *o*-tolylphenyliodonium bromide. *o*-Tolylphenyliodonium bromide (0.469 g, 1.25 mmol) dissolved in 100 m*l* of DMF was held at 100°C for 5 hr. At the end of the reaction the mixture was poured into cold water, extracted twice with ether and the extract was dried over anhydrous magnesium sulfate. After removing the solvent by distillation, the residue was redissolved in a small quantity of ether and the amounts of iodobenzene and bromobenzene were determined by means of gas chromatography. Subseuqent treatment was carried out in a similar way to that for the pyrolysis reaction. In every case the concentration was kept at 0.125 mmol/*l*.

BULLETIN OF THE CHEMICAL SOCIETY OF JAPAN, VOL. 45, 1863—1866 (1972)

The Photolysis and Thermolysis of Ethyl Azidoformate in the Presence of Ketones

Tamejiro HIYAMA, Hiroaki TAGUCHI, Shinsaku FUJITA, and Hitosi NOZAKI

Department of Industrial Chemistry, Kyoto University, Yosida, Kyoto

(Received November 29, 1971)

The photochemical decomposition of ethyl azidoformate (I) in an acetone solution gives the nitrene adduct, oxazirane II, whereas the thermolysis of the solution gives a C–H insertion product, III. The photolysis of I in cyclohexanone gives an α-insertion product, IX, while the thermolysis affords a β-insertion product, X, and an oxazole, XIII, in addition to IX. The multiplicity of the reactive species is examined in terms of the heavy-atom effect.

In contrast with carbene chemistry, few examples have been reported of the reactions of nitrenes with *n*-bases.[1,2] An arylnitrene has been observed to react intramolecularly with a carbonyl group to produce anthranil,[3] but the attempted intermolecular reaction of benzenesulfonylnitrene with cyclohexanone failed to afford any products arising from nitrene-addition.[4] We wish now to report that ethoxycarbonylnitrene generated by photolysis or thermolysis has been incorporated into acetone and cyclohexanone.

Table 1 lists the reaction conditions and product distributions in the reaction of ethyl azidoformate (I) with acetone. The irradiation[5] of an acetone solution of I gave 2-ethoxycarbonyl-3,3-dimethyloxazirane (II), hexane-2,5-dione (IV), and ethyl carbamate (V). The thermally labile oxazirane II polymerized upon slight heating and gave no satisfactory analyses, but the exact mass was compatible with the molecular formula of $C_6H_{11}NO_3$. The hydrolysis of II gave an

1) "Nitrenes," ed. by W. Lwowski, John Wiley & Sons, New York (1970).

2) H. Nozaki, S. Fujita, H. Takaya, and R. Noyori, *Tetrahedron*, **23**, 45 (1967).

3) P. A. S. Smith, B. B. Brown, R. K. Putney, and R. F. Reinisch, *J. Amer. Chem. Soc.*, **75**, 6335 (1953).

4) G. P. Balabanov, Y. I. Dergunov, and V. A. Gal'perin, *J. Org. Chem. USSR*, **2**, 1797 (1966); see also Ref. 1, p. 280.

5) Since the solution of I in acetone showed none of the UV absorptions which are absent in those of the components, the possibility of the formation of a CT-complex under the photolysis may be excluded.

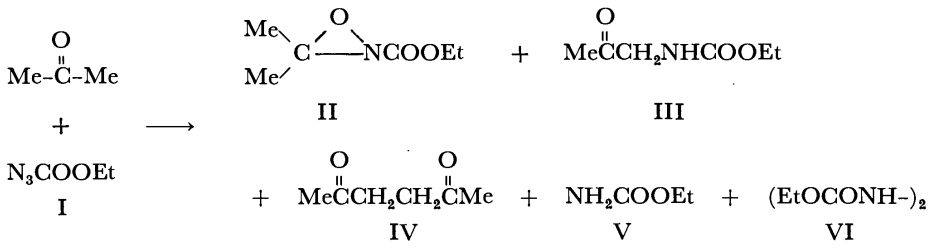

Table 1. Photolysis and thermolysis of I in acetone

Condition	Solvent	Reaction time (hr)	Products (%)[a]				
			II	III	IV	V	VI
$h\nu$[b]	none	40	60	0	4	23	0
$h\nu$[b]	CH_2Cl_2[c]	45	0	27	0	15	0
Δ[d]	none	4	0	26	0	5	4
Δ[d]	CH_2Cl_2[c]	3	0	45	0	11	0

a) All products were isolated by column chromatography, and the isolation yields are given.
b) An 0.4 M acetone solution of I was irradiated by means of a 200-W high-pressure mercury lamp externally at room temperature.
c) An 0.4 M acetone solution of I was diluted with an equi-volume of dichloromethane.
d) Thermolysis was performed in an autoclave at 180°C.

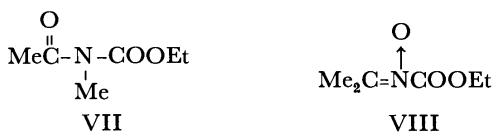

acetone identified as the 2,4-dinitrophenylhydrazone. The NMR spectrum (see Experimental section) may also be explained by two alternative structures, VII and VIII, but both are unlikely.[6]

When the photolysis was carried out in dichloromethane, ethyl acetonylcarbamate (III)[9] and V were obtained, but no trace of II was isolated (Table 1). The solvent effect[2,10] observed in the formation of II probably indicates that the formation of oxazirane II is to be ascribed to attack of the singlet nitrene on acetone. On the other hand, triplet nitrene is involved in the formation of III. The formation of IV and V can be understood in terms of the hydrogen-abstraction reaction of the triplet nitrene.

The thermal decomposition of I in acetone yielded III, V, and *N,N'*-diethoxycarbonylhydrazide (VI), while the reaction under dilution with dichloromethane resulted in increased yield of III and V (Table 1). This indicates that the carbamates are possibly derived from the triplet nitrene. As is shown in Scheme 1, we may assume that the reaction of the singlet nitrene yields oxazirane II, while the triplet nitrene gives carbamate III. The possible formation of III *via* II was excluded, as the heating of the crude II at 180°C gave no carbamate III, but only polymeric products.

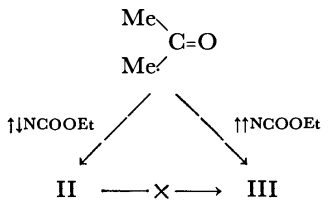

Scheme 1

The reactions in a cyclohexanone solution are summarized in Table 2. Photolysis gave 2-ethoxycarbonylaminocyclohexanone (IX),[11] bicyclohexyl-2,2'-dione (XI),[12] and V, while the photoreaction in a dichloromethane solution gave 3-ethoxycarbonylaminocyclohexanone (X)[13] in addition to IX, V, and 2-(1-cyclohexenyl)cyclohexanone (XII).

The thermolysis of I in cyclohexanone yielded another novel compound, 2-ethoxy-4,5-tetramethyleneoxazole (XIII), which exhibited an IR band at 1597 cm^{-1} and a UV absorption at 265 nm (log ε 1.48), both characteristic of oxazoles.

6) An authentic sample of VII prepared from *N*-methylurethane[7] was not identical with II. Another possibility, VIII, may be rejected because a strong absorption between 1050—1200 cm^{-1} due to nitrones[8] is absent in the IR spectrum of II and because the photochemistry of nitrones is known to give rise to oxaziranes. Further, the structure of VIII implies a positive charge on the nitrogen atom bearing an electronegative ethoxycarbonyl group; this is not possible.

7) D. Ben-Ishai and E. Katchalski, *J. Org. Chem.*, **16**, 1025 (1951).

8) R. Bonnett, V. M. Clark, and S. R. Todd, *J. Chem. Soc.*, **1959**, 2102; E. Schmitz, "Advances in Heterocyclic Chemistry," Vol. 2, ed. by A. R. Katritzky and A. J. Boulton, Academic Press, New York (1963), p. 89.

9) J. F. W. Keana, S. B. Keana, and D. Beetham, *J. Org. Chem.*, **32**, 3057 (1967).

10) J. M. Simson and W. Lwowski, *J. Amer. Chem. Soc.*, **91**, 5107 (1969); W. Lwowski and T. J. Maricich, *ibid.*, **87**, 3630 (1965); A. J. L. Beckwith and J. W. Redmond, *Chem. Commun.*, **1967**, 165.

11) S. Fujita, T. Hiyama, and H. Nozaki, *Tetrahedron*, **26**, 4347 (1970).

12) M. S. Kharasch, H. C. McBay, and W. H. Urry, *J. Amer. Chem. Soc.*, **70**, 1269 (1948).

13) The authentic sample was obtained in an independent study by the ethoxycarbonylation of *m*-aminophenol, followed by hydrogenation and oxidation. In a similar manner, 4-ethoxycarbonylaminocyclohexanone was prepared. Details of the syntheses will be given elsewhere in the near future.

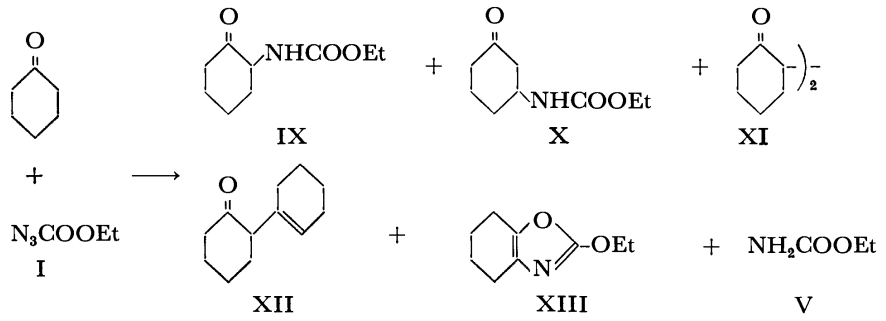

Table 2. Photolysis and thermolysis of I in cyclohexanone

Condition	Solvent	Reaction time (hr)	Products (%)[a]					
			IX	X	XI	XII	XIII	V
$h\nu$[b]	none	40	8	0	5	0	0	22
$h\nu$[b]	CH_2Cl_2[c]	45	15	8	0	24	0	7
Δ[d]	none	2	29	11	2	0	17	4
Δ[e]	CH_2Cl_2[c]	3	18	7	2	0	13	4

a) All products were isolated by column chromatography, and the isolation yields are given.
b) A 0.4 M solution of I in cyclohexanone was irradiated by means of a 200-W high-pressure mercury lamp externally at room temperature.
c) A 0.4 M cyclohexanone solution of I was diluted with an equi-volume of dichloromethane.
d) Thermolysis was performed by adding I to cyclohexanone at 156°C.
e) Thermolysis was performed in an autoclave at 150°C.

A possible account of the products is given in Scheme 2. The formation of XIII should involve the attack of I or the nitrene on the *enol* form, XIV, of cyclohexanone,[14] since IX could not be converted to XIII under thermolytic conditions. The precursor of XIII may be a 1,3-dipolar adduct, hydroxyaziridine XV, and/or a triazoline, but no conclusive data are yet available.

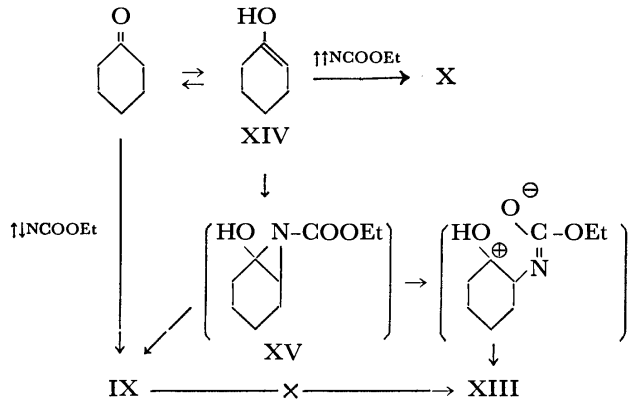

Scheme 2.

The observed heavy-atom effect implies that X is derived from the triplet nitrene. The absence of 4-ethoxycarbonylaminocyclohexanone in the products suggests that the allylic insertion of triplet nitrene into the enolized cyclohexanone led to X. The reactive species in the formation of IX is either singlet nitrene or hydroxyaziridine, XV.[15]

14) Cyclohexanone involves several percentages of the enol form at room temperature; this form is often the reactive species.
15) The photolysis of ethyl azidoformate in 1-cyclohexenyl acetate gives the acetate of the hydroxyaziridine XV, which is transformed to IX on hydrolysis.[9]

Experimental

All the melting points are uncorrected. The infrared spectra were recorded on a Shimadzu spectrophotometer IR-27-G, the ultraviolet spectra, on a Hitachi EPS-2 spectrometer, the nuclear magnetic resonance spectra on a JEOL C-60-H spectrometer, and the mass spectra, on a Hitachi RMU-6L spectrometer.

Photolysis of Ethyl Azidoformate in Acetone. A mixture of acetone (20 ml) and ethyl azidoformate (1.00 g, 8.7 mmol) was placed in a quartz tube, degassed by bubbling nitrogen and irradiated externally at room temperature with a 200-W high-pressure mercury lamp until nitrogen evolution had ceased and the characteristic IR bands at 2185 and 2137 cm^{-1} due to the azide group had disappeared (*ca.* 40 hr). After the removal of the excess acetone under reduced pressure, the yellow oily residue (1.5 g) was separated by column chromatography on silica gel. Elution with *n*-hexane, benzene, and finally with ether gave 2-ethoxycarbonyl-3,3-dimethyloxazirane (II) (0.76 g, 60%); bp 100°C (bath temperature) at 2 mmHg. IR (neat): 1715, 1400, 1375, 1327, 1212, 1004 cm^{-1}; NMR (CCl_4): δ 1.35 (t, 3H, $\underline{CH_3}CH_2$-), 1.45 (s, 3H, $C\underline{H_3}$-), 1.52 (s, 3H, $C\underline{H_3}$-), 4.12 (q,2 H, $CH_3\underline{CH_2}$); MS: *m/e* 145 (19%), 73 (100), 59 (73), 58 (72).

Found: *m/e* 145.075 (M^+). Calcd for $C_6H_{11}NO_3$: *m/e* 145.074.

Further elution gave hexane-2,5-dione (IV) (0.04 g, 4%) and ethyl carbamate (V) (0.18 g, 23%). Both IV and V were identified by a comparison of their infrared spectra and retention times on gas chromatography with those of authentic samples.

Photolysis of Ethyl Azidoformate in an Acetone-dichloromethane Mixture. A solution of ethyl azidoformate (0.50 g, 4.4 mmol) in acetone (10 ml) and dichloromethane (10 ml) was irradiated as has been described above. After concentration, the residual mixture was separated by column chro-

matography on alumina. Successive elution with *n*-hexane, benzene, and ether gave ethyl acetonylcarbamate (III) (0.11 g, 27%). IR (neat): 3350, 1705, 1525, 1330, 1065 cm^{-1}; NMR (CCl_4): δ 1.26 (t, 3H, $\underline{CH_3}CH_2$-), 2.17 (s, 3H, CH_3-), 3.9—4.3 (m, 4H, doublet at δ 4.00, -CH_2-, quartet at δ 4.10, $CH_3\underline{CH_2}$-), 5.59 (broad s, 1H, NH); MS: *m/e* 145 (M^+, 3%), 102 (39), 78 (19), 74 (18), 62 (58), 44 (100). Ethyl carbamate (V) (0.07 g, 15%) was obtained as a by-product.

Hydrolysis of Oxazirane II. A mixture of 2,4-dinitrophenylhydrazine (0.70 g), concentrated sulfuric acid (3 m*l*), water (3 m*l*), and ethanol (10 m*l*) was added, drop by drop, to a solution of oxazirane (0.45 g, 3.1 mmol) in ethanol (5 m*l*). The reaction mixture was then allowed to stand at 50°C overnight, and the red crystals thus precipitated were filtered; mp 119—120°C. The mixed melting point with acetone 2,4-dinitrophenylhydrazone was 119—120°C.

Thermolysis of Ethyl Azidoformate in Acetone. Ethyl azidoformate (2.00 g, 17.4 mmol) dissolved in acetone (40 m*l*) was heated under a nitrogen atmosphere in an autoclave at 180°C for 4 hr. The removal of the excess acetone *in vacuo* gave a dark-colored residue (2.38 g), which then was subjected to chromatography on an alumina column. Elution with benzene and ether gave ethyl acetonylcarbamate (III) (0.67 g, 26%), *N,N'*-diethoxycarbonylhydrazide (VI) (0.12 g, 4%), and ethyl carbamate (V) (0.07 g, 5%).

Thermolysis of Ethyl Azidoformate in Acetone-dichloromethane. A solution of ethyl azidoformate (1.00 g, 8.7 mmol) in acetone (20 m*l*) and dichloromethane (20 m*l*) was placed in an autoclave and heated at 160—180°C for 3 hr. The subsequent separation of the crude mixture by chromatography on a column of silica gel afforded III (0.51 g, 45%), and V (0.08 g, 11%).

Photolysis of Ethyl Azidoformate in Cyclohexanone. Ethyl azidoformate (1.00 g, 8.7 mmol) in cyclohexanone (20 m*l*) was irradiated in a manner similar to that described above (*ca.* 40 hr). The subsequent removal of the excess cyclohexanone *in vacuo* afforded a yellow oil, which was separated by chromatography on an alumina column. Elution with benzene and ether gave bicyclohexyl-2,2'-dione (XI) (0.08 g, 5%); mp 70—71°C (*n*-hexane) (lit,[12] 70—71°C). IR (neat): 1705, 1220, 1125 cm^{-1}; NMR (CCl_4): δ 1.2—2.1 (m, 12H, methylene), 2.2—2.6 (m, 4H, methylene), 2.6—3.1 (m, 2H, methine); MS: *m/e* 194 (M^+, 17%), 98 (100). Further elution with ether afforded 2-ethoxycarbonylaminocyclohexanone (IX)[11] (0.14 g, 8%), IR (neat): 3330, 1710, 1510, 1257, 1052 cm^{-1}; NMR (CCl_4): δ 1.20 (t, 3H, $\underline{CH_3}CH_2$-), 1.5—2.8 (m, 8H, methylene), 4.02 (q, 2H, $CH_3\underline{CH_2}$-), 4.0—4.4 (m, 1H, methine), 5.73 (broad d, 1H, NH); MS: *m/e* 185 (M^+, 8%), 157 (8), 141 (10), 128 (51), 62 (34), 56 (49), 44 (100), and ethyl carbamate (V) (0.15 g, 22%).

Photolysis of Ethyl Azidoformate in Cyclohexanone-dichloromethane. A solution of ethyl azidoformate (0.50 g, 4.4 mmol) in cyclohexanone (10 m*l*) and dichloromethane (10 m*l*) was irradiated much as has been described above. Work-up and chromatography on alumina gave 2-(1-cyclohexenyl)cyclohexanone (XII) (0.18 g, 24%), IR (neat): 3050, 1717, 1120, 678 cm^{-1}; NMR (CCl_4): δ 0.7—3.0 (m, 17H, methylene and methine), 5.4—5.5 (m, 1H, olefinic); MS: *m/e* 178 (M^+, 57%), 149 (100), 81 (70), 79 (69), 67 (67). Subsequent elution with ether gave 2-ethoxycarbonylaminocyclohexanone (IX) (0.12 g, 15%), 3-ethoxycarbonylaminocyclohexanone (X) (0.06 g, 8%), IR (neat): 3370, 1700, 1535, 1268, 1244, 1217, 1046 cm^{-1}; NMR (CCl_4): δ 1.22 (t, 3H, $\underline{CH_3}CH_2$-), 1.6—2.9 (m, 8H, methylene), 3.5—4.2 (m, 1H, methine), 4.04 (q, 2H, $CH_2\underline{CH_3}$-), 5.8—5.9 (broad s, 1H, NH); MS: *m/e* 185 (M^+, 9%), 156 (57), 128 (79), 96 (84), 43 (100), and ethyl carbamate (V) (0.02 g, 7%).

Thermolysis of Ethyl Azidoformate in Cyclohexanone. A mixture of ethyl azidoformate (1.00 g, 8.7 mmol) and cyclohexanone (5 m*l*) was added, drop by drop, to refluxing cyclohexanone (*ca.* 1 hr) After an additional hour of refluxing, the excess cyclohexanone was removed *in vacuo*. The subsequent work-up of the residual mixture and chromatography on an alumina column afforded 2-ethoxy-4,5-tetramethylene oxazole (XIII) (0.25 g, 17%). IR (neat): 1712, 1597, 1450, 1387, 1315, 1210 cm^{-1}; NMR (CCl_4): δ 1.40 (t, 3H, $\underline{CH_3}CH_2$–), 1.5—2.1 (m, 4H, methylene), 2.1—2.7 (m, 4H, methylene), 4.36 (q, 2H, $CH_3\underline{CH_2}$–); MS: *m/e* 167 (M^+, 44%), 139 (97), 111 (100), 66 (85), 55 (60); UV: λ_{max} (EtOH) 265 nm (log ε 1.48), $<$220 nm (log $\varepsilon$$>$2.54).

Found: C, 64.5; H, 8.1; N, 8.2%. Calcd for $C_9H_{13}NO_2$: C, 64.7; H, 7.8; N, 8.4%.

The subsequent eluants were 2-ethoxycarbonylaminocyclohexanone (IX) (0.47 g, 29%), 3-ethoxycarbonylaminocyclohexanone (X) (0.18 g, 11%), bicyclohexyl-2,2'-dione (XI) (0.04 g, 2%), and ethyl carbamate (V) (0.04 g, 4%).

Thermolysis of Ethyl Azidoformate in Cyclohexanone-dichloromethane. A mixture of ethyl azidoformate (1.00 g, 8.7 mmol), cyclohexanone (20 m*l*), and dichloromethane (20 m*l*) was heated at 150°C in an autoclave for 3 hr. A subsequent work-up gave the oxazole XIII (0.18 g, 13%), XI (0.03 g, 2%), IX (0.29 g, 18%), X (0.11 g, 7%), and V (0.03 g, 4%).

The authors are grateful to Professor Keiiti Sisido for his generous help. Financial support from the Ministry of Education, the Japanese Government, and from the Toray Science Foundation is acknowledged with pleasure.

Chemistry of Nitrosoimines. II.[1] Photolysis of 2-Nitrosoimino-2,3-dihydrothiazoles

Kin-ya AKIBA, Isaburo FUKAWA, Noboru NOMURA, and Naoki INAMOTO

Department of Chemistry, Faculty of Science, The University of Tokyo, Hongo, Tokyo

(Received November 30, 1971)

Irradiation of 3-substituted 2-nitrosoimino-2,3-dihydrobenzothiazoles (I) with a medium pressure mercury lamp gave bis[*o*-(*N*-substituted cyanamino)phenyl] disulfides (III) in high yields. Irradiation of 4,5-diphenyl-2-nitrosoimino-2,3-dihydrothiazole (VI) gave bis[(2-phenyl-2-*N*-phenylcyanamino)vinyl] disulfide (VIII).

The photolysis was shown to be due to the π-π^* excitation from the results of specific irradiation to π-π^* and n-π^* bands. The relative rates of photolysis of 2-nitrosoimino-3-phenyl-2,3-dihydrobenzothiazole (Ia) were measured in several solvents. The mechanism has been discussed in connection with that in alkyl nitrites and nitrosamines.

Simple *N*-nitrosoimines were not known until recently since they are unstable and decompose into the corresponding carbonyl compounds and nitrogen. In 1968, Thoman and Hunsberger prepared sterically hindered *N*-nitrosoketimines.[2] However, a few heterocyclic compounds carrying the nitrosoimino group stabilized by conjugation have been known to be stable at room temperature. They also decompose into the corresponding carbonyl compounds and nitrogen in refluxing toluene.[3]

We wish to report that the photolysis of 2-nitrosoimino-2,3-dihydrothiazoles gives the corresponding disulfides through π-π^* excitation accompanied by the C-S bond cleavage and nitric oxide formation.

Results and Discussion

Reaction Products. 2-Nitrosoimino-3-phenyl-2,3-dihydrobenzothiazole (Ia) in benzene-dichloromethane was irradiated with a medium-pressure mercury lamp (100W) through a pyrex filter under nitrogen for 5 hr at about 10°C. Evolution of nitric oxide was observed during the irradiation. Bis[*o*-(*N*-phenylcyanamino)phenyl] disulfide (IIIa) was obtained in 74% yield.

In the cases of 3-methyl- (Ib) and 3-ethyl-2-nitrosoimino-2,3-dihydrobenzothiazoles (Ic), the photolyses proceeded considerably more slowly than that of Ia. In order to suppress further decomposition of the resulting disulfides (IIIb and IIIc), irradiation was discontinued after 13—15 hr, during which time 50—60% of the starting nitrosoimines was consumed. The products were IIIb (48%) and IIIc (45%) together with 2-imino-2,3-dihydrobenzothiazoles (IVb, 17%, IVc, 5%). Irradiation of Ib for a longer period (20—25 hr) gave IVb (15%) and the corresponding immonium chloride (Vb, 37%), the formation of which showed formation of hydrogen chloride due to the decomposition of dichloromethane.

Photolysis of nitrosoimines (I) gave no 3-substituted 2,3-dihydro-2-benzothiazolones (II), showing that the photochemical reaction differs completely from that of a thermal one.

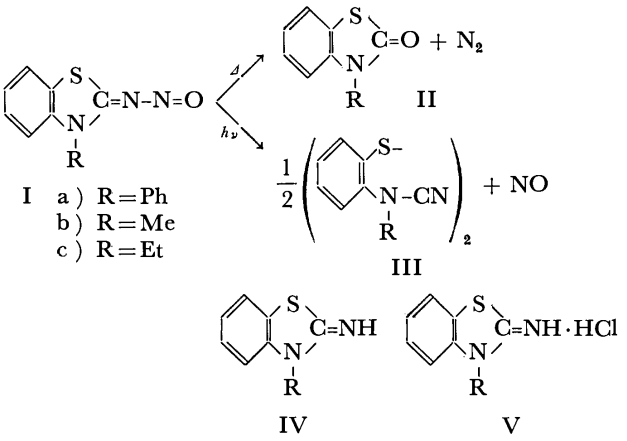

3,4-Diphenyl-2-nitrosoimino-2,3-dihydrothiazole (VI) was also irradiated in acetonitrile for 30 min, 51% of VI being decomposed. Bis[(2-phenyl-2-*N*-phenylcyanamino)vinyl] disulfide (VIII) was obtained in 50% yield based on photolyzed VI. When it was irradiated for 50 min for completion, several compounds were detected by thin layer chromatography. Thiazolone (VII), the product in thermal decomposition of VI, was not produced at all during the photolysis.

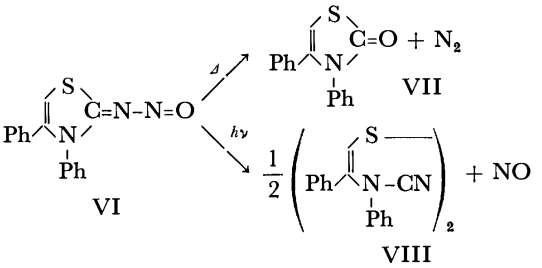

Irradiation of nitrosoimine (Ia) in benzene-dichloromethane in the presence of cyclohexane (ten times of Ia in mol) gave the nitrate of 2-imino-3-phenyl-2,3-dihydrobenzothiazole in 20% yield, the structure of which was determined by elemental analysis and quantitative nitrosation to Ia with sodium nitrite and acetic acid. Formation of nitric acid may be due to the reaction of nitric oxide with hydrogen donor, cyclohexene, as shown in the following.

$$NO + C_6H_{10} \rightarrow HNO + C_6H_9\cdot$$

1) For Part I: K. Akiba, I. Fukawa, K. Mashita, and N. Inamoto, *Tetrahedron Lett.*, **1968**, 2859.

2) C. J. Thoman, S. J., and I. M. Hunsberger, *J. Org. Chem.*, **33**, 2852 (1968).

3) a) H. Passing, *J. Parkt. Chem.*, **153**, I (1939). b) E. Besthorn, *Ber.*, **43**, 1523 (1910). c) W. Gebhart, *ibid.*, **17**, 2088 (1884). d) J. Goerdeler, A. Huppertz, and K. Wember, *Chem. Ber.*, **87**, 68 (1954).

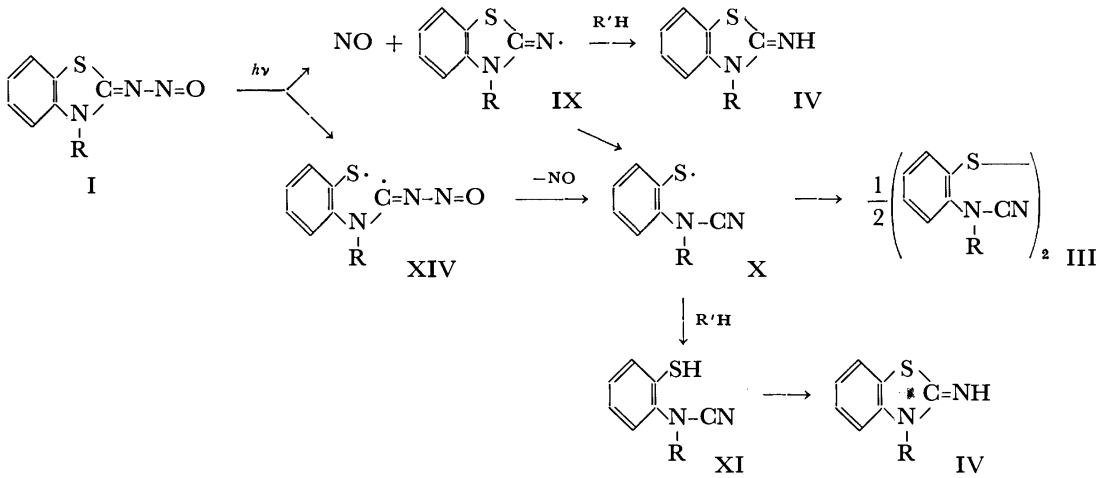

$$HNO + 2\,NO \rightarrow HNO_3 + N_2$$

The second reaction seems to be analogous to the formation of benzenediazonium nitrate from nitrosobenzene and nitric oxide.[4] Only black tar was obtained when oxygen was passed through the solution during the photolysis.

We propose a general scheme as given above.

The presence of thiyl radical (X) is quite clear because of the formation of disulfide (III). Whether imino radical (IX) exists as a primary intermediate to give thiyl radical (X) or not cannot be determined in spite of isolation of imines (IV), because *o*-cyanaminothiophenol (XI) tends to cyclize to imine (IV) rapidly as shown below.

When IIIa was reduced with lithium aluminum hydride in tetrahydrofuran (THF) and benzoylated soon after with benzoyl chloride and triethylamine, 2-benzoylimino-3-phenyl-2,3-dihydrobenzothiazole (XII) was obtained in 68% yield. This shows that the intermediate thiophenol (XI) forms 2,3-dihydrothiazole ring (IVa) before it undergoes benzoylation.[5]

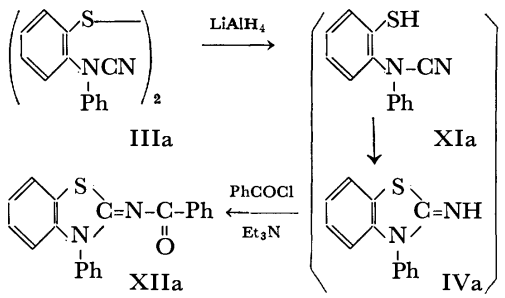

The results of oxidation of imines with lead tetraacetate are worth mentioning, although direct correlation between the oxidation and the proposed mechanism is not clear.

Oxidation of 3,4-diphenyl-2-imino-2,3-dihydrothiazole (VI') with lead tetraacetate in benzene gave 2-acetylimino-3,4-diphenyl-2,3-dihydrothiazole in 35% yield with some unidentified products. In the case of the hydrochloride of imine VI', the 2-acetylimino compound was obtained in 19% yield.

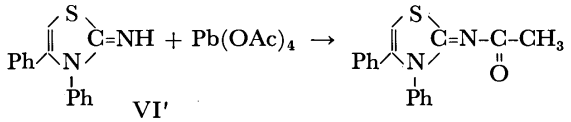

A similar oxidation of 2-imino-3-phenyl-2,3-dihydrobenzothiazole hydrobromide gave 2-*N*-bromoimino compound (XIII) and disulfide (IIIa) in 50% and 6.7% yields, respectively.

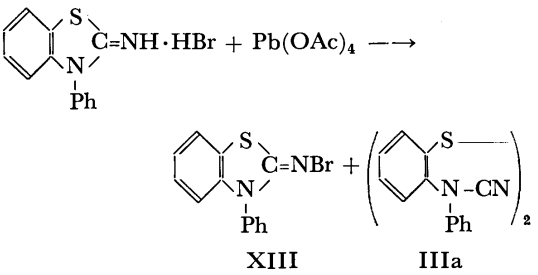

Kinetic Study. Ultraviolet and visible absorptions of 2-nitrosoimino-2,3-dihydrothiazoles (I and VI) are summarized in Table 1. Other absorptions of Ia in chloroform at 265 (ε 6.43×10^3), 273 (6.55×10^3) and 289 nm (4.21×10^3) are common to those of other compounds listed in Table 1 and attributed to excitation of the 2,3-dihydrothiazole ring.

Table 1. Ultraviolet and visible absorptions of 2-nitrosoimino-2,3-dihydrothiazoles

Compound	Solvent	λ_{max} (nm)	ε	λ_{max} (nm)	ε
Ia	$CHCl_3$	354	1.18×10^4	506	62.2
Ib	$CHCl_3$	350	1.45×10^4	496	68.2
Ic	$CHCl_3$	350	1.28×10^4	496	65.0
VI	CH_3CN	350	1.08×10^4	454	111.0

Visible absorptions (450—520 nm) of the nitrosoimines shift toward the shorter wavelength (blue shift) by changing solvents from non-polar to polar ones (see Table 3), and are assigned to the n-π^* transition of the nitrosoimino group. The most intense absorptions at about 350 nm, which are not affected by

4) E. Bamberger, *Ber.*, **30**, 506 (1897).

5) E. H. Rodd, "Chemistry of Carbon Compounds", Vol. IVa, Elsevier Publishing Co., Amsterdam (1957) p 425.

the polarity of the solvent (see Table 3), were assigned to the π-π^* transition of the nitrosoimino group, which is conjugated to the 2,3-dihydrothiazole ring. These assignments were supported by the fact that such absorptions were absent in the spectra of the corresponding 2-imino compounds. As an example, 2-imino-3-phenyl-2,3-dihydrobenzothiazole (IVa) showed the following absorption in chloroform: 281 (ε 5.3×10^3) and 288 nm (5.9×10^3).

2-Nitrosoimino-3-phenyl-2,3-dihydrobenzothiazole (Ia) was chosen as the substrate for most of the kinetic study, since its photolysis in various solvents produced disulfide (IIIa) in high yield (72—79%) and the π-π^* and n-π^* absorption bands were completely separate from one another.

Specific irradiation of the π-π^* and n-π^* bands of Ia was carried out in order to decide which excitation initiated the reaction (see Experimental). Irradiation of the π-π^* absorption region at 365 nm showed the same relative decomposition rates as those by a pyrex filter as shown in Table 2.

Table 2. Relative rates of photolysis of Ia with filters

Solvent	Filter		
	Pyrex	365 nm[a]	546 nm[b]
C_6H_6	2.3	2.3	—
CH_2Cl_2	1.0	1.0	—
CH_3CN	1.0	1.0	—

a) Aqueous solution of cobaltous sulfate and cupric sulfate.
b) Aqueous solution of calcium chloride and cupric chloride.

On the other hand, irradiation of the n-π^* absorption region at 546 nm for 5 hr did not initiate photoreaction at all, and led to complete recovery of the starting nitrosoimine (Ia), both in benzene and dichloromethane. Thus, the photoreaction of nitrosoimine (Ia) is completely due to the π-π^* excitation.

Quantum yield (0.38) was measured in acetonitrile by irradiation with 365 nm light.

The photolysis rates of I were then measured in various solvents with a pyrex filter. We chose the rate of Ia in acetonitrile (4.3×10^{-2} mmol/min) to be the standard value 1.0.

As shown in Fig. 1, plots of the nitrosoimine concentration against time showed a straight line. The linearity indicates that the amount of nitrosoimine (I) decomposed per unit time was constant. Because of intense π-π^* absorption, the solution of I absorbs 100% effective incident radiation at 365 nm.

As shown in Table 3, a greater decomposition rate of Ia was observed in aromatic solvents such as benzene, toluene and anisole, and the rates in non-aromatic solvents were almost constant in spite of the wide change of dielectric constants of the solvents. The decomposition rates of Ib and Ic were considerably less than that of Ia, and the rate of Ic was scarcely accelerated at all in benzene.

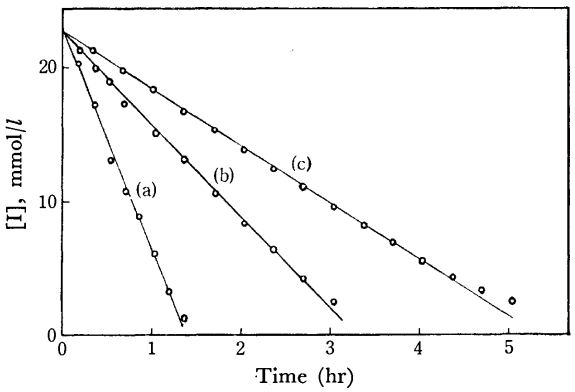

Fig. 1. Photolysis of the nitrosoimines (I).
(a) Ia in C_6H_6; (b) Ia in CH_3CN; (c) Ic in CH_3CN

Aromatic solvents might not act as a photosensitizer for Ia, because the rate in a mixture of benzene and acetonitrile is equal to that in acetonitrile. Benzene is completely transparent and not photochemically

Table 3. Relative photolysis rates and electronic spectra of 3-substituted 2-nitrosoimino-2,3-dihydrobenzothiazole(I) in various solvents (λ_{max} by nm)

I (7.8 mmol)	Solvent (350ml)	Relative rate	n-π^*		π-π^*	
			λ	ε	λ	ε
Ia	C_6H_6	2.3	521	57.8	353	1.40×10^4
Ia	$C_6H_5CH_3$	2.3	522	53.9	353	1.26×10^4
Ia	$C_6H_5OCH_3$	1.4	519	60.0	354	1.32×10^4
Ia	C_6H_6-CH_3CN (2 : 5)[a]	1.0	508	57.9	351	1.41×10^4
Ia	CH_3CN	1.0[b]	508	57.9	351	1.41×10^4
Ia	CH_2Cl_2	1.0	508	61.3	353	1.27×10^4
Ia	$CHCl_3$	1.1	506	62.5	354	1.18×10^4
Ia	C_2H_5OH-CH_2Cl_2 (5 : 2)[a]	1.2	491	63.4	351	1.20×10^4
Ia	CH_3OH-CH_2Cl_2 (5 : 2)[a]	1.2	484	64.9	351	1.39×10^4
Ib	C_6H_6	0.5	513	56.9	349	1.59×10^4
Ic	C_6H_6	0.7	512	58.3	349	1.55×10^4
Ic	CH_3CN	0.6	501	60.4	349	1.36×10^4

a) Volume ratio of the solvents.
b) Rate, 4.3×10^{-2} mmol/min, was taken to be the standard rate 1.0.

Table 4. Absorption spectra of unsaturated compounds of nitrogen

Compound	Solvent	n-π^*	π-π^*	Ref.
Ib	$CHCl_3$	496 (68.2)	350 (14500)	a
VI	CH_3CN	454 (111)	350 (10800)	a
$(Ph_2N)_2C=N-N=O$	$CHCl_3$	519 (183)	330 (9550)	b
$(p\text{-}ClC_6H_4)_2C=N-N=O$	CCl_4	596 (107), 522 (107)	306 (8770)	2
$p\text{-}MeC_6H_4$, $o\text{-}MeC_6H_4$ >C=N-N=O	EtOH	520 (33), 494 (24)	312 (8414)	2
Ph-N=N-Ph(*trans*)	EtOH	443 (510)	320 (21300)	7
$Ph_2C=NH$	$CHCl_3$	340 (125)		7
t-Bu-N=O	EtOEt	665 (20), 300 (100)		7
$Me_2N-N=O$	C_5H_{12}	361 (125)	232 (5900)	7
t-Bu-O-N=O	C_5H_{12}	356 (87)	222 (1700)	7
$Ph-NO_2$	C_6H_{14}	330 (125)	280 (1000)	7

a) The present work. b) Unpublished result.

excited at all by irradiation with 365 nm.

Since an interaction of *N*-nitrosamines with the solvent benzene was observed by NMR,[6] the solvent effect on the decomposition rate of Ia might also be ascribed to an interaction of nitrosoimine with the aromatic solvents. However, this explanation is not consistent with the fact that the rate of Ic is scarcely accelerated at all in benzene. The reason for the specific acceleration of photolysis rate of Ia in aromatic solvents is not yet clear.

From the results, we propose that the photolysis of the nitrosoimines is due to π-π^* excitation, and some radical intermediate (X) is produced according to the ring opening followed by loss of nitric oxide from the resulting biradical (XIV).

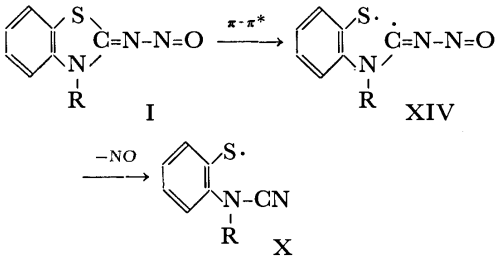

General Discussion. Compounds containing the double-bonded nitrogen group, such as nitroso, azo, and imino compounds, have weak absorptions in the longer wavelengths due to the n-π^* excitation of the non-bonding nitrogen electrons, as shown in Table 4.

Thoman and Hunsberger reported that the absorption spectra of di(*p*-chlorophenyl)-nitrosoiminomethane showed two visible absorptions at 596 and 522 nm, probably due to the n-π^* excitations of nitrogens of the nitroso and imino parts of the nitrosoimino group, respectively.[2] On the other hand, heterocyclic nitrosoimino compounds show apparently only one n-π^* absorption at a shorter wavelength than di(*p*-chlorophenyl)-nitrosoiminomethane.

In the case of the heterocyclic nitrosoimino compounds such as I, the two lone pairs of N-atoms might be nearly equivalent with respect to their electronic energy and the two n-π^* bands might overlap each other. As a result, only one apparent n-π^* excitation was observed as with the azo compound, indicating that the resonance structure (I′) appears to be predominant.

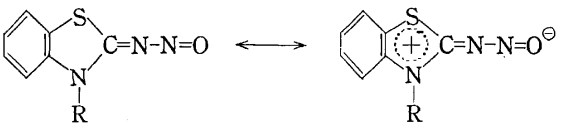

A large contribution of I′ is supported by the fact that 2,3-dihydrothiazoles are one of the "π-electron excess aromatic compounds". The thermal stability of I is consistent with resonance stabilization. The nitrosoimino group of I shows the π-π^* absorption at a longer wavelength (*ca.* 350 nm) than that of di(*p*-chlorophenyl)-nitrosoiminomethane (*ca.* 306 nm), indicating a high degree of conjugation with the 2,3-dihydrothiazole ring. The fact that absorption bands of di(diphenylamino)-nitrosoiminomethane lie between those of the above two cases shows resonance contribution of nitrogens in the diphenylamino group.

Thus, the photoreaction of I is due to π-π^* excitation, but does not occur by the irradiation of n-π^* absorption. This result is in significant contrast to photoreactions of nitrites[8] or nitrosoalkanes[9] which lead to the cleavage of RO-NO bond or C-NO bond with high quantum yield even by the irradiation of their n-π^* bands to give alkoxyl or alkyl radical together with nitric oxide, respectively.

The different behavior of nitrosoimine is ascribable to the fact that its N-N bond has a strong double bond character with a larger bond energy than O-N and C-N bond of the nitrites and the nitrosoalkanes, respectively.

N-Nitrosamines are inert for photolysis in neutral

6) C. J. Karabatos and R. A. Taller, *J. Amer. Chem. Soc.*, **86**, 4373 (1964).

7) S. F. Mason, *Quart. Rev.*, **15**, 314 (1961).

8) M. Akhtor and D. H. R. Barton, *J. Amer. Chem. Soc.*, **86**, 1528 (1964); M. Akhtor, "Advances in Photochemistry", **2**, 263 (1964).

9) K. D. Anderson, C. J. Crumpler, and D. L. Hammick, *J. Chem. Soc.*, **1935**, 1679.

and in strong acidic media.[10] This is explained by a similar double bond character of the N-N bond both in the photoexcited state and in strong acidic media as shown below.

$$\begin{matrix}R\\R\end{matrix}\!\!>\!N\text{-}N\!=\!O \longleftrightarrow \begin{matrix}R\\R\end{matrix}\!\!>\!\overset{+}{N}\!=\!N\text{-}\overset{-}{O}$$

These considerations support the idea that the π-π^* irradiation of nitrosoimine induces a cleavage of the C-S bond of the 2,3-dihydrothiazole ring followed by that of N-N bond of the nitrosoimino group to give directly thiyl radical (X) and nitric oxide. However, there is no definite evidence at present to exclude the mechanism involving the photochemical cleavage of the N-N bond of the nitrosoimino group to give nitric oxide and the vibrationally excited imino radical (IX), which isomerizes into more stable thiyl radical (X).

Experimental

Materials. 2-Imino-3-phenyl-2,3-dihydrobenzothiazole (IVa) was prepared by the method of Passing,[3a] mp 73—74°C (lit, 74—75°C). 2-Nitrosoimino-3-phenyl-2,3-dihydrobenzothiazole (Ia) was prepared by nitrosation of IVa in acetic acid with a concentrated aqueous solution of sodium nitrite, and then reprecipitated twice from dichloromethane solution by adding petroleum ether, mp 138°C (decomp.) (lit,[3a] mp 141°C). 2-Imino-3-methyl- (IVb) and 3-ethyl-2-imino-2,3-dihydrobenzothiazole (IVc), 3-methyl-2-nitrosoimino- (Ib) and 3-ethyl-2-nitrosoimino-2,3-dihydrobenzothiazole (Ic) were prepared according to reported procedures.[3b,3c] IVb: mp 122—123°C (lit, 123°C), IVc: mp 86—87°C (lit, 86°C), Ib: 104—105°C (decomp.) (lit, 103—104°C), and Ic: mp 108—109°C (decomp.) (lit, 110°C).

3,4-Diphenyl-2-imino-2,3-dihydrothiazole hydrochloride and the corresponding free imine (mp 107°C, lit, 111°C) were prepared according to the method of Beyer and Ruling.[11] 3,4-Diphenyl-2-nitrosoimino-2,3-dihydrothiazole (VI) was prepared by nitrosation of hydrochloride in 42% yield, mp 152—153°C (decomp.).

Found: C, 63.74; H, 4.20; N, 14.67%. Calcd for $C_{15}H_{11}N_3SO$: C, 64.04; H, 3.93; N, 14.94%.

General Procedure of Photolysis. The nitrosoimines were irradiated through a pyrex filter with a 100W medium-pressure mercury lamp immersed in the reaction solution. The temperature of the solution was kept at *ca.* 10°C with a water-cooled jacket around a lamp and an external ice bath. Nitrogen was passed through the solution during irradiation.

Photolysis of 2-Nitrosoimino-3-phenyl-2,3-dihydrobenzothiazole (Ia). a) Nitrosoimine (Ia, 4.0 g, 15.7 mmol) in a mixture of benzene (50 m*l*)-dichloromethane (100 m*l*) was irradiated. Irradiation was stopped when the absorption at 350—360 nm region disappeared completely. The crystalline product obtained after evaporation of the solvent was recrystallized from ethanol to give bis[*o*-(*N*-phenylcyanamino)phenyl] disulfide (IIIa, 2.2 g, 5.8 mmol, 74%); mp 151.5—152.0°C and IR: 2200 cm^{-1} (C≡N).

Found: C, 69.15; H, 4.16; N, 12.64; S, 14.23%. mol wt (Rast), 410. Calcd for $C_{26}H_{18}N_4S_2$: C, 69.31; H, 4.03; N, 12.44; S, 14.23%; mol wt, 450.

b) Nitrosoimine (Ia, 4.0 g, 15.7 mmol) in a mixture of benzene (50 m*l*)-dichloromethane (100 m*l*) was irradiated in the presence of cyclohexene (157 mmol). Removal of volatile materials gave the immonium nitrate of 2-imino-3-phenyl-2,3-dihydrobenzothiazole (3.1 mmol, 20%), mp 198°C (decomp.), after washing with benzene.

Found: C, 53.77; H, 3.54; N, 14.89%. Calcd for $C_{13}H_{11}N_3SO_3$: C, 53.97; H, 3.83; N, 14.51%.

Nitrosation of the immonium nitrate with sodium nitrite and acetic acid gave Ia quantitatively. The benzene washings were evaporated and the brown residual oil was chromatographed on alumina. No crystalline product was obtained. The infrared spectrum of the oil showed a strong absorption at 2200 cm^{-1} (C≡N) indicating the presence of IIIa.

Reduction of Disulfide (IIIa) with $LiAlH_4$. A solution of lithium aluminum hydride (0.5 g, 33.3 mmol) in THF (50 m*l*) was added in small portions to the disulfide (IIIa, 1.5 g, 3.3 mmol) in THF (50 m*l*) cooled with an ice bath. After the addition had been completed, the reaction mixture was stirred for 1 hr. The remaining lithium aluminum hydride was decomposed by adding aqueous solution of sodium hydroxide (20%, 1 m*l*) and then water (15 m*l*). After filtration, the precipitates were extracted with dichloromethane (150 m*l*) and the combined solution was dried over anhydrous sodium sulfate. The concentrated solution (50 m*l*) was refluxed with triethylamine (1.5 g, 16.4 mmol) and benzoyl chloride (1.5 g, 10.7 mmol) for 1 hr, and 100 m*l* of dichloromethane was then added. After shaking several times with 1 N aqueous solution of sodium hydroxide (40 m*l*) to remove excess benzoyl chloride, the dichloromethane layer was washed with water and dried over anhydrous sodium sulfate. The pale yellow solid obtained after evaporation of the solvent was recrystallized from ethanol to give 2-benzoylimino-3-phenyl-2,3-dihydrobenzothiazole (XIIa, 1.5 g, 4.5 mmol, 68%), mp 205.5—206.5°C. IR: 1620 cm^{-1} (C=O).

Found: C, 72.72; H, 3.99; N, 8.50%. Calcd for $C_{20}H_{14}N_2SO$: C, 72.70; H, 4.28; N, 8.48%. XIIa was identified by comparison with the melting point and IR spectrum of an authentic sample, prepared by a similar benzoylation of 2-imino-3-phenyl-2,3-dihydrobenzothiazole (IVa).

Photolysis of 3-Methyl-2-nitrosoimino-2,3-dihydrobenzothiazole (Ib). Nitrosoimine (Ib, 6.0 g, 30.9 mmol) in a mixture of benzene (50 m*l*) and dichloromethane (100 m*l*) was irradiated for 17 hr, during which time 60% of Ib was consumed. After evaporation of the solvent, the residue was extracted with petroleum ether (200 m*l*). The extract was concentrated *in vacuo* at room temperature and the resulting precipitates were recrystallized from petroleum ether to give 2-imino-3-methyl-2,3-dihydrobezothiazole (IVb, 0.6 g, 3.1 mmol, 17%), mp 122—123°C. The remaining crystalline residue was refluxed in ethanol for 8 hr to decompose the remaining nitrosoimine (Ib) into 3-methyl-2,3-dihydro-2-benzothiazolone (IIb). After evaporation of the solvent, the residue was extracted repeatedly with petroleum ether to remove IIb. The remaining white solid was recrystallized from ethanol to give bis[*o*-(*N*-methylcyanamino)-phenyl] disulfide (IIIb, 1.4 g, 4.3 mmol, 48%), mp 140.0—141.0°C. IR: 2200 cm^{-1} (C≡N).

Found: C, 58.90; H, 4.34; N, 17.27; S, 19.52%; mol wt (Rast), 376. Calcd for $C_{16}H_{14}N_4S_2$: C, 58.87; H, 4.32; N, 17.17; S, 19.64%; mol wt, 326.

Photolysis of 3-Ethyl-2-nitrosoimino-2,3-dihydrobenzothiazole (Ic). Ic (6.0 g, 29.2 mmol) was irradiated in a mixture of benzene (50 m*l*) and dichloromethane (100 m*l*) for 13 hr, 60% of Ic being consumed. A treatment similar to that

10) E. M. Burgess and J. M. Lavanish, *Tetrahedron Lett.*, **1964**, 1221; Y. L. Chow, *idid.*, **1964**, 2333; **1965**, 2473; *Can. J. Chem.*, **43**, 2711 (1965); L. P. Kuhn, G. G. Kleinspehn, and A. C. Duckworth, *J. Amer. Chem. Soc.*, **89**, 3858 (1967).

11) H. Beyer and G. Ruling, *Chem. Ber.*, **89**, 107 (1956).

for Ib gave 3-ethyl-2-imino-2,3-dihydrobenzothiazole (IVc, 0.2 g, 0.9 mmol, 5%), mp 86—87°C, and bis[*o*-(*N*-ethylcyanamino)phenyl] disulfide (IIIc, 1.4 g, 4.0 mmol, 45%), mp 83.0—84.0°C, and IR: 2200 cm^{-1} (C≡N).

Found: C, 60.97; H, 5.17; N, 15.67; S, 17.83%; mol wt (Rast), 364. Calcd for $C_{18}H_{18}N_4S_2$: C, 60.81; H, 5.39; N, 15.76; S, 18.04%; mol wt 354.

Photolysis of 3,4-Diphenyl-2-nitrosoimino-2,3-dihydrothiazole (VI). A solution of nitrosoimine (VI, 1.165 g, 4.15 mmol) in acetonitrile (250 m*l*) was irradiated for 30 min, 51% of the starting material being photolyzed. Photolysis on the same scale was repeated four times. Solutions from two runs were combined and treated as follows.

The solvent (500 m*l*) was evaporated with a rotary evaporator to 50 m*l*. The resulting yellow precipitates (0.728 g, VI) were filtered and the filtrate was condensed to almost dryness. A mixture of petroleum ether (110 m*l*) and ethanol (10 m*l*) was added to the residue and the resulting precipitates (0.484 g, VI) were filtered. White crystalline product (0.643 g, almost pure VIII) and brown tar (0.6 g) were obtained from the filtrate by condesation. In order to purify the crystalline product, the main fractions of R_f 0.6—0.7 (with chloroform) were collected on silica gel thin layer chromatograms and extracted with methanol (30 m*l*). The extract was condensed to 10 m*l* to give bis[(2-phenyl-2-phenylcyanamino)vinyl] disulfide (VIII, 0.510 g), mp 141.0—142.0°C. IR: 2210 cm^{-1} (C≡N), UV: $\lambda_{max}^{CHCl_3}$ 280 nm (ε 3.47×10^4) and MS: 476 (5.5%, M^+-CN), 251 (62, 1/2 M^+), 180 (99, $PhC{\equiv}\overset{+}{N}Ph$), 134 (26, $PhCHCS^+$), 91 (10.5, PhN^+), 77 (100, Ph^+), and 26 (50, CN^+).

The parent peak (M^+, 502) could not be detected in spite of some change in the ionization voltage. The yield of VIII was 50% based on the photolyzed material.

Thermal Decomposition of 3,4-Diphenyl-2-nitrosoimino-2,3-dihydrothiazole (VI). Nitrosoimine (VI, 1.02 g, 3.63 mmol) was refluxed in xylene (50 m*l*) until the orange-red color of VI disappeared. Removal of the solvent gave 0.67 g (2.65 mmol, 73%) of the corresponding thiazolone (VII) as colorless crystals, mp 121.5—123°C. IR (nujol): 1640 cm^{-1} (C=O). Found: C, 71.00; H, 4.35; N, 5.28; S, 12.70%. Calcd for $C_{15}H_{11}NOS$: C, 71.12; H, 4.38; N, 5.53; S, 12.66%.

Oxidation of 3,4-Diphenyl-2-imino-2,3-dihydrothiazole (VI') with Lead Tetraacetate. To a benzene solution (40 m*l*) of the imine (VI', 4.0 g, 16.0 mmol), lead tetraacetate (5.5 g, 12.4 mmol) was added portionwise at 0°C with stirring which was continued overnight at room temperature. After filtration of yellow crystals (lead acetate, 3.5 g), the filtrate was condensed with a rotary evaporator. The condensate was chromatographed on silica gel to give 2-acetylimino-3,4-diphenyl-2,3-dihydrothiazole (1.66 g, 4.34 mmol), mp 200°C, in 35% yield, which was eluted with dichloromethane-ether (4 : 1). An authentic sample of 2-acetylimino compound (mp 200°C) was prepared according to the method of Beyer and Ruling.[11] There were some unidentified products.

The hydrochloride of imine (VI') was oxidized with lead tetraacetate in a similar way to that above. The 2-acetylimino compound was obtained in 19.0% yield with some unidentified products.

Oxidation of 2-Imino-3-phenyl-2,3-dihydrobenzothiazole Hydrobromide with Lead Tetraacetate. To a suspension of the imine hydrobromide (4.0 g, 13.0 mmol) in benzene (30 m*l*), lead tetraacetate (4.0 g, 18.2 mmol) was added portionwise at room temperature with stirring, which was continued overnight. Lead tetraacetate was consumed completely as confirmed by iodometry. After the yellow precipitates, lead acetate (3.64 g), were filtered, the filtrate was condensed and the condensate was chromatographed on silica gel. *N*-Bromoimino-3-phenyl-2,3-dihydrobenzothiazole (XIII, 2.0 g, 6.5 mmol, 50% yield) was eluted with benzene and the disulfide (IIIc, 0.20 g, 2.1 mmol, 6.7%) was eluted with benzene-dichloromethane. XIII: mp 139°C (decomp.), UV: $\lambda_{max}^{CH_3CN}$ 263 nm (ε 1.48×10^4) and MS: 306 (M^+), 304 (M^+) and 225 (M^+-Br, 100).

Found: C, 51.10; H, 2.78; N, 9.41; S, 10.13%. Calcd for $C_{13}H_9N_2SBr$: C, 51.16; H, 2.77; N, 9.18; S, 10.50%.

Kinetic Studies. The photolysis rates of the nitrosoimines (I, 7.8 mmol) were measured in several solvents (350 m*l*) with the same apparatus. The concentration of the remaining nitrosoimines (I) was measured by UV absorption at *ca.* 350 nm at appropriate intervals. Because of the poor solubility of I in alcohols, the mixed solvents of ethanol (250 m*l*)-dichloromethane (100 m*l*) were used. The electronic spectra of nitrosoimine (Ia) in alcohols were not affected by the addition of dichloromethane. 3.9 mmol of Ia was used in the case of toluene (350 m*l*).

The decomposition rate of Ia in acetonitrile (4.31×10^{-2} mmol/min) was chosen to be the standard relative rate 1.0. Two filter solutions were used for the specific irradiation of π-π^* and n-π^* absorption bands. They were cooled with an ice bath and circulated through a cooling jacket (path length 1 cm) around the lamp, instead of with water. An aqueous solution of cobaltous sulfate and cupric sulfate (a mixture of 490 g of $CoSO_4\cdot7H_2O$, 100 g of $CuSO_4\cdot5H_2O$ and 900 m*l* of H_2O)[12] was used as one filter solution for isolation of 365 nm radiation from a medium-pressure mercury lamp.

The decomposition rates of Ia in benzene solution with unfiltered light and filtered light (π-π^* irradiation) were 9.3×10^{-2} and 8.5×10^{-2} mmol/min, respectively. The reduced rate of the latter corresponds to the transmittance of the filter solution (Fig. 2).

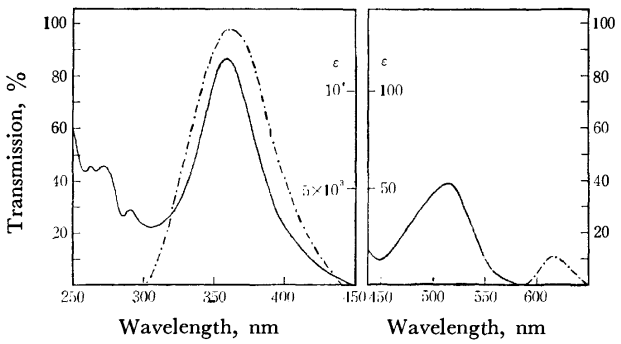

Fig. 2. Electronic spectrum of Ia in $CHCl_3$ (solid line) and transmission of the filter solution (dotted line; $CoSO_4$-$CuSO_4$)

An aqueous solution of cupric chloride and calcium chloride (100 g of $CuCl_2$, 300 g of $CaCl_2$ in 1 *l* of aqueous solution, slightly acidified with HCl) was used as the other filter solution for the isolation of the n-π^* absorption band at 546 nm. This filter solution transmitted 60% at 546 nm and 25% at 577 nm and no light was transmitted at either a wavelength shorter than 500 nm or one longer than 600 nm. No photodecomposition of Ia was observed with the use of this filter solution both in benzene and in dichloromethane. The transmission of both filters remained unchanged with time.

Quantum Yield Measurement. The isolation of 365 nm radiation from a medium-pressure mercury lamp (100 W) was accomplished by a combination of the filter solution

12) J. G. Calvert and J. N. Pitts, "Photochemistry," Chapter 7, John Wiley & Sons, Inc., New York (1967).

(120 g of $Cu(NO_3)_2$ in 100 m*l* of H_2O, path length 1 cm) and a Corning glass filter(No. CS-7-607). The transmission was 0% below 355 nm, 57% at 365 nm, and 0% above 400 nm. The light intensity was measured by potassium ferrioxalate actinometry[13] and was 2×10^7 Einstein l^{-1} sec^{-1}. The quantum yields of photolysis of Ia in acetonitrile were 0.384 and 0.372 by repeated determinations.

13) C. A. Parker, *Proc. Roy. Soc., Ser. A*, **220**, 104 (1953); C. G. Hatchard and C. A. Parker, *ibid., Ser. A*, **235**, 518 (1956).

BULLETIN OF THE CHEMICAL SOCIETY OF JAPAN, VOL. 45, 1873—1876 (1972)

The Oxidation of (+)-3-Carene and the Related Compounds with *t*-Butyl Chromate[1,2]

Takayuki SUGA, Tsuyoshi SHISHIBORI, and Tamon MATSUURA

Department of Chemistry, Faculty of Science, Hiroshima University, Higashisenda-machi, Hiroshima

(Received October 11, 1971)

The oxidation of (+)-3-carene with *t*-butyl chromate was found to afford 3,α-dimethylstyrene (**2**), eucarvone (**3**), 1,1,4-trimethylcyclohepta-2,4-dien-6-one (**4**), 3-methylacetophenone (**5**), 8-hydroxy-*m*-cymene (**6**), car-3-en-2-one (**7**), (−)-car-3-en-5-one (**8**), and (−)-car-3-ene-2,5-dione (**9**). The aromatized compound (**6**) was a major product in the oxidation in an acidic medium, whereas the oxidation in the neutral and the basic media gave the enedione (**9**) and the enone (**8**) as major products. It was, furthermore, proved that methylenes adjacent to the cyclopropane ring of (−)-*cis*-carane (**10**) and (+)-caran-3β-ol (**11**) were scarcely attacked by *t*-butyl chromate.

Recently the oxidation of (+)-3-carene (**1**) with permanganate[3] or with chromium trioxide[4] has been reported. The *t*-butyl chromate oxidation of a compound with a cyclopropane ring has not yet been examined, although the endocyclic mono-[5] and di-unsaturated[6,7] compounds have been subjected to this oxidation. We have now examined the oxidation of (+)-3-carene (**1**), (−)-*cis*-carane (**10**), and (+)-caran-3β-ol (**11**) in order to establish further details of the oxidative behavior of *t*-butyl chromate in relation to compounds with both a cyclopropane ring

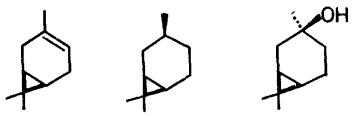

(**1**) (**10**) (**11**)

and an ethylenic bond. While we were preparing the manuscript of this report on our results, there appeared a brief paper[8] reporting the oxidation of **1** with *t*-butyl chromate. This prompted us to publish our paper involving the results of a more detailed examination of the reaction conditions which control the yield of products in the oxidation of (+)-3-carene (**1**) with *t*-butyl chromate.

Results and Discussion

(+)-3-Carene (**1**) was oxidized at 50°C for 48 hr under the reaction conditions shown in Table 1, with an equimolar or with three molar equivalents of the oxidant in various solvents, such as benzene, a mixture of benzene, glacial acetic acid and acetic anhydride, benzene admixed with pyridine. After the usual treatment[9] or the reaction mixture, the gas-liquid chromatographic analysis of a neutral product showed the presence of at least eight components, in a different ratio of the components in every oxidation. The neutral fraction was subjected to separation, purification, and identification as based on a combination of fractional distillation, column chromatography, analytical and preparative glc, spectroscopic analyses, comparisons of its physical data with those of known specimens, and the preparation of the crystalline derivatives. The procedure indicated neutral products to be composed of such compounds as 3,α-dimethylstyrene (**2**), eucarvone (**3**), 1,1,4-trimethylcyclohepta-2,4-dien-6-one (**4**), 3-methylacetophenone (**5**), 8-hydroxy-*m*-cymene (**6**), car-3-en-2-one (**7**), (−)-car-3-en-5-one (**8**), and (−)-car-3-ene-2,5-dione (**9**). The results are shown in Table 1. In addition to the formation of compounds **2**, **6**, **7**, **8**, and **9**, which have recently been reported by another group,[8] compounds **3**, **4**, and **5** were newly identified in this study.

8-Hydroxy-*m*-cymene (**6**) was the main reaction product in Experiments 1 and 2, in which the oxidation was carried out in an acidic medium. The yield

1) This paper has been read at the 23rd Annual Meeting of the Chemical Society of Japan, Tokyo, April 3, 1970. It forms Part X[2] in the Hiroshima University series on "Oxidation of Terpene Compounds with *t*-Butyl Chromate."

2) Part IX, T. Suga, M. Sugimoto, K. Fujita, and T. Matsuura, This Bulletin, **39**, 2546 (1966).

3) W. D. P. Burns, M. S. Carson, W. Cocker, and P. V. R. Shannon, *J. Chem. Soc., C*, **1968**, 3073.

4) M. S. Carson, W. Cocker, D. H. Grayson, and P. V. R. Shannon, *ibid., C*, **1969**, 2220.

5) Reference 2, its preceding reports, and references cited therein.

6) T. Matsuura and T. Suga, *J. Org. Chem.*, **30**, 518 (1965).

7) N. B. Haynes, D. Redmore, and C. J. Timmons, *J. Chem. Soc.*, **1963**, 2420.

8) P. H. Boyle, W. Cocker, D. H. Grayson, and P. V. R. Shannon, *J. Chem. Soc., C*, **1971**, 1073.

9) T. Suga, This Bulletin, **31**, 569 (1958).

Table 1. The oxidation of (+)-3-carene with *t*-butyl chromate

Exp.	Type of oxidant[a]	Sample to oxidant (mol ratio)	Yield of a neutral product (%)[b]	Products (%)[c]								I/II[d]
				2	**3**	**4**	**5**	**6**	**7**	**8**	**9**	
1	B	1 : 1	11.8	24.8	2.5	8.6	10.9	34.2	3.2	9.5	6.3	0.36
2	B	1 : 3	68.8	11.8	1.2	3.3	8.8	43.6	1.2	4.1	26.0	0.54
3	A	1 : 1	29.2	16.8	3.4	6.3	9.2	27.1	1.0	6.5	29.7	0.88
4	A	1 : 3	21.0	18.7	0.8	10.1	7.1	14.3	0.4	14.6	34.0	1.49
5	C	1 : 1	28.4	2.4	1.1	5.3	9.5	9.3	0.6	28.9	42.9	3.72
6	C	1 : 3	71.1	1.9	0.6	2.1	7.1	6.7	0.3	27.1	54.2	5.37

a) A denotes *t*-butyl chromate dissolved in benzene, B does the chromate dissolved in a mixture of benzene, glacial acetic acid and acetic anhydride, and C does the chromate dissolved in benzene containing pyridine.
b) The yield is based on the sample, (+)-3-carene, taken.
c) The yield of products is based on the peak area on the glc of the neutral product.
d) 'I/II' denotes the ratio of the sum of percentages of **3**, **4**, **7**, **8**, and **9** to the sum of these of **2**, **5**, and **6**.

of **6** is, however, reduced to nearly a half in Experiments 3 and 4, and to nearly a quarter in Experiments 5 and 6, which employed a mixture of benzene and pyridine as the solvent. The same incident as above was also observed for the formation of 3,α-dimethylstyrene (**2**). This seems to suggest the initial opening of the cyclopropane ring, followed by the formation of the aromatized compounds. The formation of increased amounts of car-3-en-5-one (**8**) was observed upon oxidation in a rather basic medium. This indicates that the oxidation in the basic status is favorable for the allylic oxidation at the C-5 position of 3-carene (**1**). The same tendency was observed in the formation of car-3-ene-2,5-dione (**9**). The oxidation using three molar equivalents of the oxidant in the presence of pyridine afforded a neutral product in the highest yield, which was almost entirely composed of the dione (**9**). The seven-membered ring compounds, (**3**) and (**4**), might have resulted from the isomerization of the bicyclic ketones, (**7**) and (**8**), as in the case of the oxidation of **1** with permanganate[3] or with chromium trioxide.[4] In all the experiments, **7** and **3** were produced in lower yields than **8** and **4** respectively.

The oxidation of (−)-*cis*-carane (**10**) and (+)-caran-3β-ol (**11**) was carried out with three molar equivalents of the oxidant containing glacial acetic acid and acetic anhydride respectively over a 48-hr period. However, scarcely no oxidation products were produced, rather the starting material was recovered almost unchanged. It has been shown that *t*-butyl chromate does not attack methylenes adjacent to only the cyclopropane ring.

The following conclusions may be drawn from the results. The oxidation of 3-carene with *t*-butyl chromate involves two pathways, (I) and (II). Route I is mainly concerned with the oxidation of an allylic methylene to a carbonyl group, while Route II involves the aromatization of carene, followed by the subsequent oxidation of the benzillic position. As is shown in Scheme 1, the unsaturated ketones, (**7**), (**8**), and (**9**), may be given from **1** through Route I. The aromatized compounds, (**6**), (**2**), and (**5**), seem to be formed through Route II, such as has been observed previously in the oxidation of α-terpinene.[6] The ratio (I/II) of the respective total sum of the yields of compounds produced by the two routes was larger

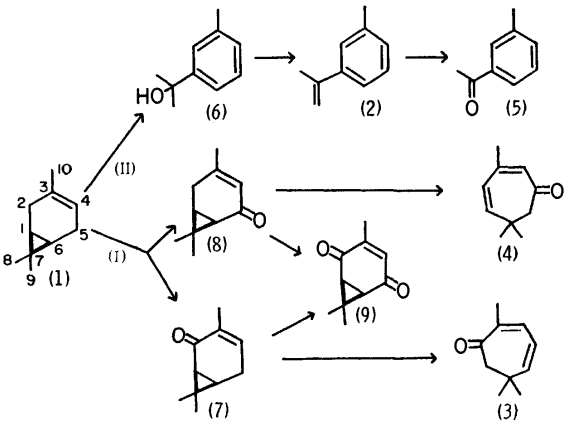

Scheme 1.

in a basic medium than in an acidic one (Table 1). By considering the results of the oxidation of *cis*-carane (**10**) and caran-3β-ol (**11**), as well as endocyclic monounsaturated compounds,[5] it seems that the double bond would contribute more than the cyclopropane ring to the formation of the α,β-unsaturated ketones, (**7**) and (**8**), and of the diketone, (**9**), by the preferential attack of the methylene situated between an ethylenic bond and a cyclopropane ring.

Experimental

Measurements. The melting points are uncorrected. The IR spectra were measured on a Hitachi, EPI-S, Infrared Spectrophotometer. The UV spectra were obtained on a JASCO, ORD/UV-5, Spectrophotometer. The NMR spectra were recorded on a Hitachi Perkin-Elmer, R-20, High-resolution Spectrometer at 60 MHz, using tetramethylsilane as the internal standard. Analytical glc was carried out on a Hitachi Perkin-Elmer, F6-D, Gas Chromatograph equipped with a flame-ionization detector at 160°, with a flow rate of nitrogen of 50 ml/min and using a 10% Carbowax column (3 mm × 2 m). Preparative glc was performed on a Shimadzu, GC-1A, Gas Chromatograph, using a 10% Carbowax column (10 mm × 2 m). The silica gel used was Kieselgel (Merck) (less than 0.08 mm).

Oxidation and Treatment of the Reaction Mixture.
Exp. 1: A *t*-butyl chromate solution was prepared from chromium trioxide (10.0 g, 0.1 mol), *t*-butyl alcohol (22.2 g, 0.3 mol), benzene (60 ml), acetic anhydride (10.2 g, 0.1 mol), and glacial acetic acid (6.0 g, 0.1 mol) in the same

manner as in the previous report.[5,9] The oxidant solution was added, drop by drop, to (+)-3-carene (**1**) (13.6 g, 0.1 mol) (bp 168.0—168.5°C, d_4^{25} 0.8601, $[\alpha]_D^{25}$ +13.9°, neat) over a period of 4 hr, with agitation at 50°C, and then the mixture was maintained at the same temperature for 44 hr while being stirred in an atmosphere of dry nitrogen. The treatment of the mixture in the same manner as in our previous reports[9,10] afforded a neutral oily product (3.5 g); the reaction products were then identified.

Exp. 2: A solution of three molar equivalents of the oxidant with the same concentration as in Exp. 1 was added to **1** (50 g) in the same manner as in Exp. 1. The subsequent treatment of the reaction mixture in the same manner as above gave a neutral product (35.5 g).

Exp. 3: A benzene solution, not containing acetic anhydride and glacial acetic acid, of the equimolar oxidant was added to **1** (13.6 g) in the same manner as in Exp. 1. A neutral oily product (11.5 g) was then obtained from the reaction mixture by the same treatment as above.

Exp. 4: The oxidation was carried out using a benzene solution of three molar equivalents of the oxidant and 8.0 g of **1** in the same manner as above. Thus, 2.83 g of a neutral product was obtained.

Exp. 5: A benzene solution of *t*-butyl chromate was prepared by adding chromium trioxide (2.21 g) to *t*-butyl alcohol (4.90 g), after which the solution was diluted with benzene (24 m*l*) as above. The solution, after having been dried over anhydrous sodium sulfate, was concentrated to 20 m*l*, and then pyridine (0.5 g) was added. To the oxidant solution, 3.0 g of **1** dissolved in 25 m*l* of benzene was added, drop by drop, over a 4-hr period at 50°C. The mixture was maintained at the same temperature for a further 44 hr with stirring. The subsequent treatment of the reaction mixture in a manner similar to that used in Exp. 1 gave 2.75 g of a neutral product.

Exp. 6: To an oxidant solution prepared in the same manner as in Exp. 5, 1.0 g of **1** dissolved in 25 m*l* of benzene was added. After 48 hr, the similar treatment of the reaction mixture gave a neutral product (0.87 g).

In each experiment, the glc of the neutral product showed the presence of at least eight components, **2** (retention time, 2.5 min), **3** (4.4), **4** (6.8), **5** (7.8), **6** (9.0), **7** (11.0), **8** (13.9), and **9** (16.9). The retention times of the peaks on the glc were the same in every experiment.

Identification of Reaction Products. The identification of the products is exemplified by Exp. 2, shown below. The distillation of a neutral product (25 g) gave 14.6 g of a distillate with a boiling point of 50—115°C/10 mmHg and 3.5 g of a residue which was almost entirely composed of yellow crystals (mp 100—102°C). The distillate was chromatographed on a silica-gel column with mixtures of *n*-hexane and increasing amounts of ethyl acetate; we thus separated it into eight eluates.

*3,α-Dimethylstyrene (**2**)*: This hydrocarbon was obtained as the first eluate of the column chromatography. Its IR spectrum was identical with that of 3,α-dimethylstyrene reported[11] and derived from 8-hydroxy-*m*-cymene (see below) by dehydration with phosphorous oxychloride. Ozonization of **2** afforded 3-methylacetophenone (the 2,4-dinitrophenylhydrazone, mp and mixed mp 207—208°C) and formaldehyde (the same phenylhydrazone derivative, mp and mixed mp 165—166°C).

*Eucarvone (**3**)*: The second eluate was identical in respects of the retention time on the glc and the IR spectrum with a specimen of eucarvone.[12] The 2,4-dinitrophenylhydrazone (mp 151—152°C) showed no depression of the melting point on admixed with the known specimen.

*1,1,4-Trimethylcyclohepta-2,4-dien-6-one (**4**)*: This compound was isolated as the third eluate. This eluate, after purified further by the preparative glc, gave a pale yellow oil: λ_{max}^{EtOH} 294 nm (log ε 3.31). The IR (1631 and 1575 cm^{-1}) and the NMR (1.10, 2.02, 2.51, 5.63, 5.91, and 6.03 ppm) spectra were identical with those of **4** reported.[3] The 2,4-dinitrophenylhydrazone melted at 176.5—177.5°C (lit,[3] mp 175—176°C).

*3-Methylacetophenone (**5**)*: The fourth eluate afforded an oil: ν_{max}^{liq} 1682 cm^{-1} (C=O); δ ($CDCl_3$) 2.36 (s, 3H, Ar–CH_3), 2.54 (s, 3H, $COCH_3$), and 7.0—7.8 ppm (m, 4H, Ar–H). The oil gave a 2,4-dinitrophenylhydrazone derivative (mp 207—208°C), which was identified as that[13] of 3-methylacetophenone by a mixed-melting-point determination.

*8-Hydroxy-*m*-cymene (**6**)*: The fifth eluate was the main component of the neutral part and gave an oil: mass *m/e* 150 (M^+); ν_{max}^{liq} 3381 (OH), 3027, 1618, and 1598 (benzene ring), 824, 789, and 710 cm^{-1} (1,3-disubst. benzene); δ ($CDCl_3$) 1.53 (s, 6H, $(CH_3)_2C$), 1.75 (s, 1H, OH exchanged with D_2O), 2.31 (s, 3H, Ar–CH_3), and *ca.* 7.1 ppm (m, 4H, Ar–H). These spectral data coincided with those[3,13] reported for **6**. The 3,5-dinitrobenzoate derivative showed a mp of 93—94°C (lit,[3] mp 93—94°C): (Found: C, 59.31; H, 4.59; N, 8.23%. Calcd for $C_{17}H_{16}N_2O_6$: C, 59.30; H, 4.68; N, 8.14%).

*Car-3-en-2-one (**7**)*: The sixth eluate showed a certainly different retention time from that of eucarvone upon glc. However, in the course of performing the preparative glc, the compound changed to eucarvone (**3**). It was, therefore, judged that the compound obtained from the sixth eluate was probably car-3-en-2-one (**7**).

*(−)-Car-3-en-5-one (**8**)*: The seventh eluate gave an oil showing $[\alpha]_D^{25}$ −265° (*c* 0.5, EtOH) and λ_{max}^{EtOH} 227 nm (log ε 3.55). Its IR and NMR spectral data were identical with those of car-3-en-5-one (**8**) previously reported.[3]

*(−)-Car-3-ene-2,5-dione (**9**)*: This was isolated, both from the residue in the distillation of the neutral product and from the last eluate in the column chromatography, as yellow crystals: mp 102—102.5°C, $[\alpha]_D^{25}$ −15.1° (*c* 0.3, EtOH); mass 164 (M^+); λ_{max}^{EtOH} 241 nm (log ε 4.11), 226 (sh. 4.03). The melting point and the IR and NMR spectra were identical with those reported for **9**.[3]

Found: C, 72.88; H, 7.56%. Calcd for $C_{10}H_{12}O_2$; C, 73.17; H, 7.32%.

*Oxidation of (−)-*cis*-Carane (**10**).* (−)-*cis*-Carane (bp 99—101°C/130 mmHg, n_D^{25} 1.4558, $[\alpha]_D^{25}$ −35.1° (*c* 1.1, *n*-hexane)) was prepared from (+)-3-carene (**1**) following the literature method.[14] The oxidation of **10** (1.0 g) was performed in the same manner as in Exp. 2. The molar ratio of **10** to the oxidant was 1 to 3. The same treatment of the reaction mixture as in Exp. 1 gave an oil (0.61 g). Glc and tlc analyses showed the presence of only a little oxygenated compound, but the sample was recovered.

*Oxidation of (+)-Caran-3β-ol (**11**).* (+)-3-Carene (**1**) was hydrated by the oxymercuration-demercuration.[15]

10) T. Matsuura, K. Saito, and Y. Shimakawa, *ibid.*, **33**, 1151 (1960).

11) K. Gollnick, G. Schade, and S. Schroeter, *Tetrahedron*, **22**, 139 (1966).

12) T. Suga, K. Mori, and T. Matsuura, *J. Org. Chem.*, **30**, 669 (1965).

13) O. L. Brady and J. N. E. Day, *J. Chem. Soc.*, **1934**, 114.

14) W. Cocker, P. V. R. Shannon, and P. A. Staniland, *J. Chem. Soc., C*, **1966**, 946.

15) H. C. Brown and P. Geoghegan, Jr., *J. Amer. Chem. Soc.*, **89**, 1522 (1967).

After the chromatographic purification, 0.8 g of **11** was obtained: mp 70.5—71.5°C (lit,[16] mp 71.5—72.5°C), $[\alpha]_D^{25}$ +10.2° (*c* 1.5, EtOH). The caranol (**11**) (0.8 g) was oxidized with three molar equivalents of the oxidant in the same manner as in Exp. 2. The product (0.6 g) was composed of unchanged **11** (over 95% by glc) and traces of other materials. The latter were impossible to subject to further investigations because of the very small quantities.

16) H. Kuczinski and Z. Chabudzinski, *Roczniki Chem.*, **34**, 177 (1960).

We wish to thank Miss S. Fujita, who assisted us in a part of this research.

BULLETIN OF THE CHEMICAL SOCIETY OF JAPAN, VOL. 45, 1876—1880 (1972)

Mass-spectral Fragmentation of 3-(5-Nitro-2-furyl)-1,2,4-triazoles[1]

Yasuhiko KATO and Ichiro HIRAO

Laboratory of Organic Synthesis, Department of Chemical Engineering, Kyushu Institute of Technology, Tobata-ku, Kita-Kyushu

(Received October 23, 1971)

The mass spectra of 3-(5-nitro-2-furyl)- (I), 5-methyl-3-(5-nitro-2-furyl)- (II), 5-ethyl-3-(5-nitro-2-furyl)- (III), and 5-trideuteriomethyl-3-(5-nitro-2-furyl)-1,2,4-triazole (IV) and their 1-acetyl, 1-trideuterioacetyl, and 1-propionyl derivatives were examined. The mother compounds, I–IV, gave the most prominent molecular ions and showed the same fragmentation pattern. The molecular ions undergo two modes of cleavages; one is the elimination of NO (1) and CO (2), followed by the loss of C_2H_2 (3), thus giving the M−84 ions which include the 5-substituents of the triazole ring, while the other is the loss of NO_2-CO, which directly gives rise to the fragment M−74 ions. The 1-acyl derivatives gave extremely weak molecular ion peaks. In the first step of the fission of the molecular ions, the elimination of an acyl group occurred, with the rearrangement of a hydrogen atom, thus giving rise to prominent ions. These ions correspond to the molecular ions of the mother compounds, I–IV, and are expected to show a similar fragmentation pathway. The fragmentation of these compounds was also considered to occur in view of the existence of meta-stable ion peaks. The meta-stable peaks appearing at the transition of the loss of NO are flat-topped, releasing kinetic energy of 0.78±0.04 eV.

The mass spectra of simple furans were investigated, and the fragmentation has been established,[2-5] but no systematic mass-spectral investigation concerning more complex nitrofuran derivatives has yet been reported.

3-(5-Nitro-2-furyl)- and 5-alkyl-3-(5-nitro-2-furyl)-1,2,4-triazoles and their 1-acyl derivatives are easily prepared by the reactions of 5-nitro-2-furimidoylhydrazine derivatives with acid anhydrides (or ethyl orthoformate).[6,7] We have prepared nine derivatives of of 3-(5-nitro-2-furyl)-1,2,4-triazole and its seven deuterium-labeled compounds by the reported methods[6,7] and have examined their mass spectra in order to describe the fragmentation schemes of the compounds.

Experimental

Mass-spectral Measurement. The mass spectra were obtained on a Hitachi mass spectrometer, Model RMU-6L, except for two compounds, Ia and Ic, for which a Japan Electron Optics Co., JEOL-OlSG mass spectrometer with a direct inlet was used. The operating conditions were as follows:

	RMU-6L	JEOL-01SG
Ionizing energy (eV)	70	70
Accelerating voltage (kV)	3.20	1.75
Total electron current (μA)	80	80
Temperature of ionization chamber (°C)	220	210
Temperature for vaporization (°C)	110—150	100
Vapor pressure (mmHg)	2.0×10^{-6}	5.0×10^{-7}

Samples. The samples employed in this experiment were prepared by the methods previously reported.[6,7] All the deuterium-labeled compounds except for the 1-deuterated compound (V) were also obtained in a similar manner, by the use of hexadeuterioacetic anhydride. V was obtained by refluxing II or by the hydrolysis of acetyl-II with D_2O for 2—3 hr, and then crystallized from D_2O. The compounds thus obtained were found by mass-spectrometric analysis to be 99% deuterated for Ib-IIIb, IV, IVa, and IVc, and 85% deuterated for V. The mps of the unpublished compounds are shown in Table 1.

1) Presented at the 25th Annual Meeting of the Chemical Society of Japan, Tokyo, October, 1971.

2) a) S. Meyerson and P. N. Rylander, *J. Chem. Phys.*, **27**, 901 (1957). b) P. N. Rylander, S. Meyerson, and H. M. Grubb, *J. Amer. Chem. Soc.*, **79**, 842 (1957). c) S. Meyerson and P. N. Rylander, *J. Phys. Chem.*, **62**, 2 (1958).

3) J. Collin, *Bull. Soc. Chim. Belges*, **69**, 449 (1960); **69**, 575 (1960).

4) R. I. Reed and W. K. Reid, *J. Chem. Soc.*, **1963**, 5933.

5) G. Spiteller, "Mass Spectrometry of Heterocyclic Compounds," in "Advances in Heterocyclic Chemistry," ed. by A. R. Katritzky, Academic Press, New York and London, (1966), Vol. 7, p. 305.

6) I. Hirao, Y. Kato, T. Hayakawa, and H. Tateishi, This Bulletin, **44**, 780 (1971).

7) I. Hirao, Y. Kato, and H. Tateishi, *ibid.*, **45**, 208 (1972).

Table 1. The melting points of unpublished compounds

Compound	Mp (°C)	Solvent for recrystallization
1-Acetyl-3-(5-nitro-2-furyl)-1,2,4-triazole (Ia)	167—168	Benzene
1-Trideuterioacetyl- (Ib)	245—246	Benzene
1-Propionyl- (Ic)	167—169	Benzene
5-Methyl-1-trideuterioacetyl- (IIb)	196—197	Ether-ligroin[a)]
5-Ethyl-1-trideuterioacetyl- (IIIb)	112—113	Ether-ligroin[a)]
5-Methyl-1-deuterio- (V)	251—252	Deuterium oxide
5-Trideuteriomethyl- (IV)	246—247	Water
5-Trideuteriomethyl-1-methyl- (IVa)	201—202	Acetone
5-Trideuteriomethyl-1-propionyl- (IVc)	139—140	Ligroin

a) Washed with ether-ligroin (1 : 3).

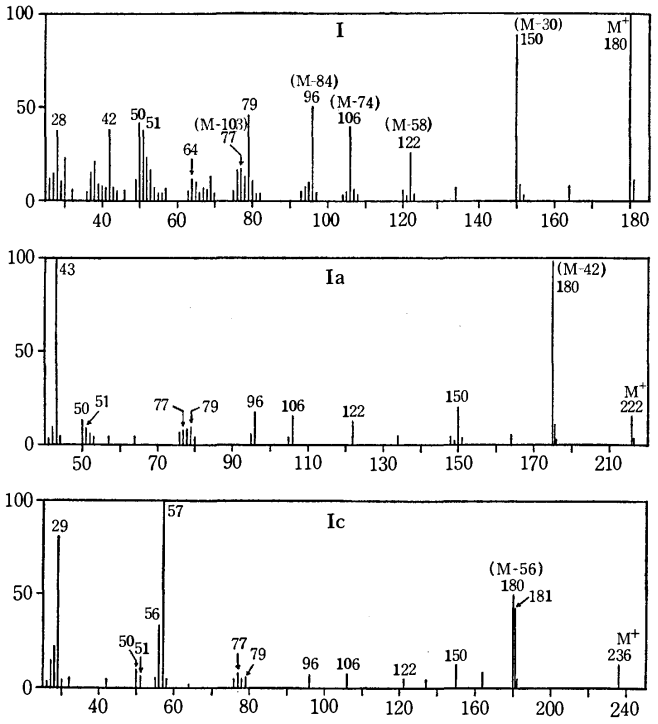

Fig. 1. Mass spectra of I, Ia, and Ic.

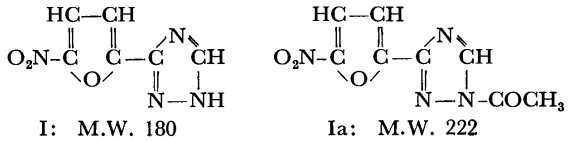

I: M.W. 180 Ia: M.W. 222

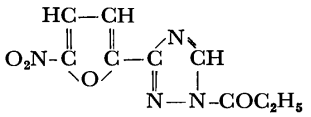

Ic: M.W. 236

Results and Discussion

3-(5-Nitro-2-furyl)-1,2,4-triazoles. The mass spectra of 3-(5-nitro-2-furyl)- (I), 5-methyl-3-(5-nitro-2-furyl)- (II), and 5-ethyl-3-(5-nitro-2-furyl)-1,2,4-triazole (III) are shown in Fig. 1 and Table 2. The compounds give the most prominent molecular ions (M^+) (the base peaks) with masses of 180, 194, and 208 respectively, as would be predicted from the presence of the stabilized heteroaromatic nucleus. The distinct fragment ions (M−30) of the masses at 150, 164, and 178 are formed by the elimination of NO from the molecular ions; this differs somewhat from nitrobenzene in that the M−46 (NO_2) fragment is weak, and is similar to the behavior of 5-nitro-2-bromofuran.[8] The M−30 ions may lose carbon monoxide[9] to give ion peaks (M−58) with masses of 122, 136, and 150 respectively. The subsequent loss of an acetylene molecule would lead to M−84 ion peaks (*m/e* I: 96, II: 110, and III: 124). There is a three-step process concerned with the fission of the furan ring in the molecular ions. The M−84 ions undergo two modes of cleavage of the triazole ring to give two distinct ions, RCN_2H^+ (*m/e* 42, 56, and 70) and $RCNH^+$ (*m/e* 28, 42, and 56) respectively.

The occurrence of another process of cleavage of the furan ring in the molecular ions is confirmed on the basis of the appearance of the meta-stable ion peaks. The molecular ions lose NO_2 and CO fragments by a one-step process to give M−74 ions at the masses of 106, 120, and 134 respectively. The M−74 ions show four modes of cleavage and give *m/e* 79 (common to all spectra), 65, 64, and M−103 (77, 91, and 105) ions by, respectively, the loss of RCN, $(R-H)CN_2H$, RCN_2H, and N_2H fragments. The common ion (79) gives two fragment ions at the masses of 51 and 50 from its two modes of cleavage, and the M−103 ions lose RCN to give the *m/e* 50 ion.

To define more precisely the mechanism and ions involved, the 5-trideuteriomethyl compound was synthesized and the hydrogen atom on the triazole nucleus on II was exchanged by equilibration with D_2O. In the mass spectra of 5-trideuteriomethyl-3-(5-nitro-2-furyl)-1,2,4-triazole (IV) and 5-methyl-3-

8) R. Grigg, M. V. Sargent, D. H. Williams, and J. A. Knight, *Tetrahedron*, **21**, 3441 (1965).

9) The possibility of the loss of N_2 in this pathway was eliminated because the mass spectra of 5-nitro-2-bromofuran (Ref. 8) and 5-nitro-2-furonitrile (measured under the same experimental conditions) showed a fragmentation step which corresponds to the loss of 28 amu. The mass-spectral fragmentation of 5-nitro-2-furonitrile may be shown as follows:

$$m/e\ 138\ (M^+) \xrightarrow{-30} m/e\ 108 \xrightarrow{-28} m/e\ 80 \xrightarrow{-26} m/e\ 54 \xrightarrow{-27} m/e\ 27$$

(m*: meta-stable ion observed)

TABLE 2. MASS-SPECTRAL DATA OF 5-ALKYL-3-(5-NITRO-2-FURYL)-1,2,4-TRIAZOLES

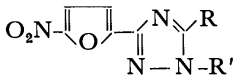

II R=CH_3, R'=H		V R=CH_3, R'=D		IV R=CD_3, R'=H		III R=C_2H_5, R'=H	
m/e	Rel. Int. (%)	*m/e*	Rel. Int. (%)	*m/e*	Rel. Int. (%)	*m/e*	Rel. Int. (%)
194	100	195	100	197	100	208	100
164	53	165	51	167	50	178	36
136	16	137	15	139	16	150	15
120	44	121	30	123	44	134	31
110	46	111	43	113	45	124	33
91	16	91	11	94	16	105	11
80	14	81	12	80	12	80	13
79	67	80	84	79	70	79	57
65	26	65	11	66	20	70	28
64	29	64	15	64	19	65	18
56	73	57	62	59	66	64	27
53	19	54	14	53	18	56	53
52	31	53	17	52	25	55	18
51	54	52	50	51	49	52	27
50	46	51	16	50	48	51	46
42	84	43	68	45	76	50	34

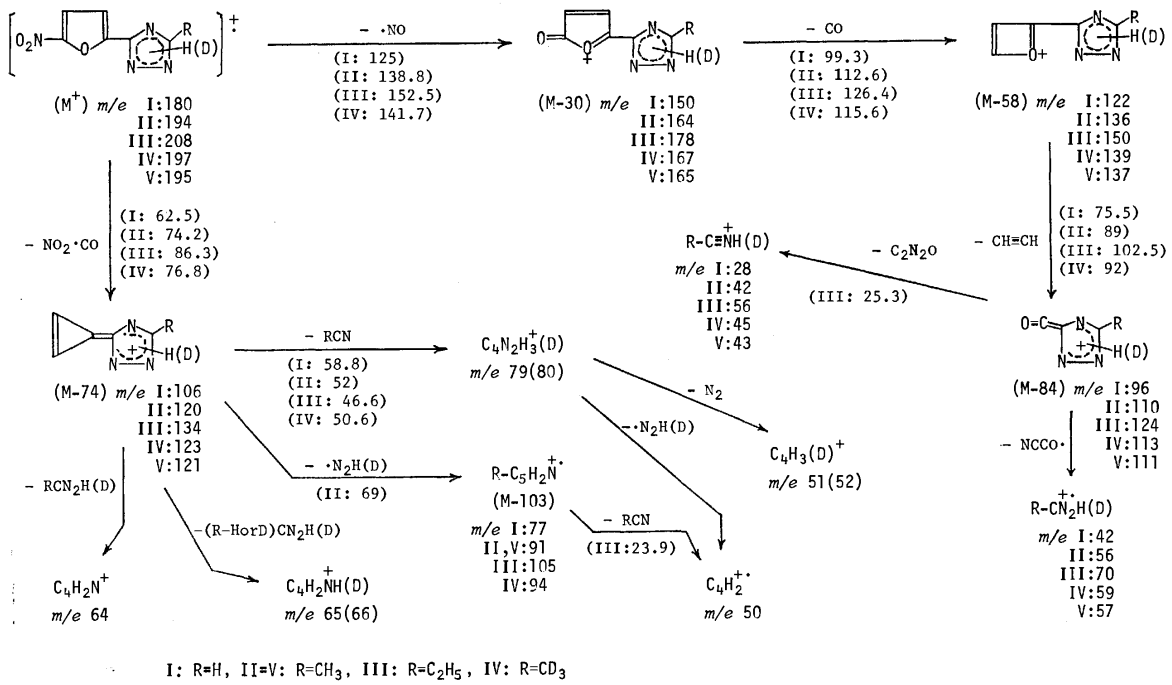

Scheme 1. Fragmentation of I, II, III, IV, and V.

(5-nitro-2-furyl)-1-deuterio-1,2,4-triazole (V) (Table 2), *m/e* 194, 164, 136, 110, 56, and 42 are shifted completely to *m/e* 197, 167, 139, 113, 59, and 45, and to *m/e* 195, 165, 137, 111, 57, and 43, respectively. Moreover, the two peaks at *m/e* 79 and 51 in the spectrum of II are shifted to, respectively, *m/e* 80 and 52 in that of V, while *m/e* 91 and 64 remain without being shifted. We may conclude, therefore, that the fragmentation pathways in the foregoing occur for I, II, III, and IV.

The major fragmentation, common to I–V, is postulated in Scheme 1. Some of the pathways of the fragmentation were confirmed by the presence of meta-stable ion pekas.

1-Acetyl and 1-Trideuterioacetyl Derivatives of I, II, and III. The mass-spectral data of 1-acetyl- (Ia), 1-trideuterioacetyl- (Ib), 5-methyl-1-acetyl- (IIa), 5-methyl-1-trideuterioacetyl- (IIb), 5-ethyl-1-acetyl- (IIIa), 5-ethyl-1-trideuterioacetyl- (IIIb), and 5-trideuteriomethyl-1-acetyl-3-(5-nitro-2-furyl)-

TABLE 3. MASS-SPECTRAL DATA OF 1-ACETYL- AND 1-TRIDEUTERIOACETYL-3-(5-NITRO-2-FURYL)-1,2,4-TRIAZOLES

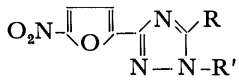

Ib R=H, R'=COCD$_3$		IIa R=CH$_3$, R'=COCH$_3$		IIb R=CH$_3$, R'=CO$_3$CD$_3$		IVa R=CD$_3$, R'=COCH$_3$		IIIa R=C$_2$H$_5$, R'=COCH$_3$		IIIb R=C$_2$H$_5$, R'=COCD$_3$	
m/e	Rel. Int. (%)	*m/e*	Rel. Int. (%)	*m/e*	Rel. Int. (%)	*m/e*	Rel. Int. (%)	*m/e*	Rel. Int. (%)	*m/e*	Rel. Int. (%)
225	6	236	14	239	5	239	12	250	10	253	5
181	43	194	100	195	47	197	100	208	100	209	63
151	10	164	17	165	13	167	24	178	24	179	14
123	5	136	11	137	6	139	12	150	10	151	4
107	8	120	12	121	8	123	13	134	13	135	7
97	10	110	12	111	7	113	12	124	11	125	6
80	6	91	8	91	7	94	9	105	9	105	4
77	5	79	10	80	8	79	13	79	14	80	9
64	3	65	8	65	8	66	8	70	7	71	4
52	7	64	7	64	6	64	4	65	10	65	7
50	11	56	9	57	6	59	9	64	10	64	8
46	100	51	7	52	9	51	7	56	11	57	7
43	6	50	8	50	10	50	10	51	10	52	8
30	6	43	53	46	100	45	11	50	9	50	6
29	4	42	11	43	8	43	89	43	83	46	100
18	9	15	16	18	8	15	10	15	14	18	11

1,2,4-triazole (IVa) are summerized in Table 3 (Ia, in Fig. 1). The 1-acetyl compounds, Ia–IVa, give weak molecular-ion peaks (10—15% of the base peak). The elimination of an acetyl group from the molecular ion occurs in the following processes. One process, by the rearrangement of a hydrogen atom, produces base peaks at M—42, which are consistent with the masses of the molecular ion of I, II, III, or IV, by the loss of a ketene (CH_2=C=O). The other process, without any rearrangement, produces a strong peak with a mass of 43 due to $CH_3C{\equiv}O^+$ and a distinct peak of the CH_3^+ ion at mass 15. The M—42 ions of the masses at 180, 194, and 208 may undergo the same fragmentation as the corresponding mother compound (I, II, III, or IV), as has been described above. On the other hand, in the mass spectra of 1-trideuterioacetyl compounds, Ib–IIIb, the molecular ions are extremely weak (5—6% of the base peak). The

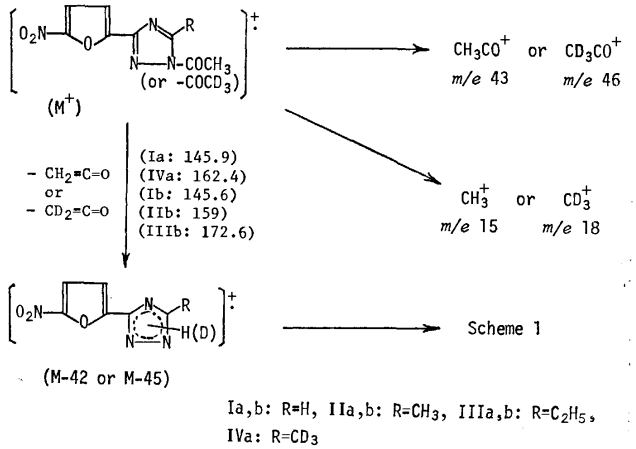

Scheme 2. Fragmentation of 1-acetyl (Ia-IVa) and 1-trideuterioacetyl (Ib-IIIb) compounds.

peaks corresponding to M—42 in Ia-IIIa are shifted completely to one atomic mass unit (amu); those corresponding to *m/e* 43 and 15 are consistent with a mass shift of 3 amu. This suggests that a similar mode of the cleavage of the trideuterioacetyl group also occurs, with or without the rearrangement of a deuterium atom, giving the prominent peaks (M—44) by the loss of CD_2=C=O, the base peak at mass 46 ($CD_3C{\equiv}O^+$), and a fragment ion peak with mass 18 (CD_3^+) by N^1-CO and α-bond cleavages (Scheme 2). It might, therefore, be expected that a mode of fragmentation similar to that of V would occur for the M—44 ions with the masses of 181, 195, and 209.

1-Propionyl Derivatives of I, II, III, and IV. The mass-spectral data of 1-propionyl- (Ic), 5-methyl-1-propionyl- (IIc), 5-ethyl-1-propionyl- (IIIc), and 5-trideuteriomethyl-1-propionyl-3-(5-nitro-2-furyl)-1,2,4-triazole (IVc) are shown in Table 4. The molecular ions here are also weak (10—15% of the base peak). In the first step of the fission of the molecular ions, as is shown in Scheme 3, there are four modes of the elimination of the propionyl group. With the rearrangement of one or two atoms of hydrogen, strong peaks (the base peak of IIIc) at M—56 result from the eliminations of (1) the CH_3CH=C=O (or CH_2=CHCHO) molecule and (2) the CH_2=CHC=O radical, successively a hydrogen atom. On the other hand, cleavage occurs without any rearrangment, giving (3) the base peaks (except for IIIc) at the mass 57 ($C_2H_5C{\equiv}O^+$) and (4) a prominent ion ($C_2H_5^+$) at mass 29, which also might come somewhat from the cleavage of the ion *m/e* 57. The M—56 ions correspond to the molecular ions of I—IV and may be expected to show the same fragmentation as that of the corresponding compounds, as is indicated in Shceme 1.

TABLE 4. MASS-SPECTRAL DATA OF 1-PROPIONYL-3-(5-NITRO-2-FURYL)-1,2,4-TRIAZOLES.

IIc, R=CH_3		IVc, R=CD_3		IIIc, R=C_2H_5	
m/e	Rel. Int. (%)	*m/e*	Rel. Int. (%)	*m/e*	Rel. Int. (%)
250	15	253	10	264	12
195	57	198	43	209	52
194	81	197	66	208	100
164	25	167	22	178	25
136	8	139	6	150	6
120	9	123	8	134	8
110	8	113	7	124	6
91	13	94	10	105	7
79	9	79	7	79	8
65	10	66	8	70	5
64	7	64	4	65	8
57	100	59	4	64	7
56	23	57	100	57	95
51	7	56	18	56	22
50	9	51	6	51	7
42	12	50	8	50	8
41	6	45	10	41	9
29	82	29	85	29	76
28	24	28	8	28	16
27	19	27	14	27	16

The molecular ions in the spectra of I–IV and the ions of $[M-(R'CO-H \text{ or } D)]^+$ in the spectra of the acyl compounds decompose to yield meta-stable ion peaks corresponding to the following transitions:

$$M^+ \rightarrow (M\text{-}30)^+ + NO$$

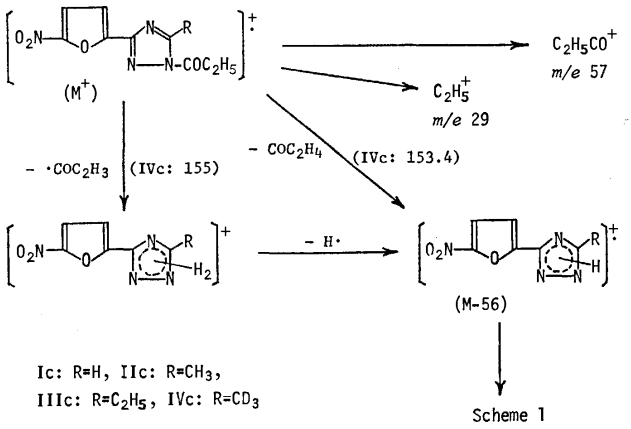

Scheme 3. Fragmentation of 1-propionyl compounds (Ic-IVc).

$$[M-(R'CO-H \text{ or } D)]^+ \rightarrow [M-(R'CO-H \text{ or } D)-30]^+ + NO$$

The meta-stable peaks in these transitions are flat-topped, indicating a formation with a release of kinetic energy.[10] As is shown in Table 5, the energy values found for these compounds correspond approximately to that of *o*-nitrophenol[10a] and are 2.5 times that of 5-nitro-2-furonitrile.

The authors wish to thank Massrs. Y. Takigawa, K. Umeno, and Y. Ohotani, staff members of the Research and Development Department of Mitsubishi Industrial Co., Ltd., for the mass spectral measurements and useful discussions. Thanks are due to the Ministry of Education for its financial aid.

TABLE 5. THE KINETIC ENERGY RELEASED IN THE FLAT-TOPPED META-STABLE TRANSITION

Compound	Molecular weight	Precursor ion	Transition	Kinetic energy (eV)
I	180	M^+	180→150	0.81
II	194	M^+	194→164	0.77
III	208	M^+	208→178	0.75
IV	197	M^+	197→167	0.79
Ib	225	$(M\text{-}COCD_2)^+$	181→151	0.77
IIb	239	$(M\text{-}COCD_2)^+$	195→165	0.77
IIIb	253	$(M\text{-}COCD_2)^+$	209→179	0.77
IVa	239	$(M\text{-}COCH_2)^+$	197→167	0.79
IVc	253	$(M\text{-}COC_2H_4)^+$	197→167	0.78
o-Nitrophenol[11a]	139	M^+	139→109	0.75
5-Nitro-2-furonitrile	138	M^+	138→108	0.29

10) a) J. H. Beynon, R. A. Saunders, and A. E. Williams, *Z. Naturforsch.*, **20A**, 180 (1965). b) T. W. Shannon, F. W. McLafferty, and C. R. McKinney, *Chem. Comm.*, **1966**, 478. Many applications of meta-stable peak study were attempted by F. W. McLafferty *et al.*, *cf.*, for example, *J. Amer. Chem. Soc.*, **88**, 5021 (1966), and related papers.

The 1-Methylene Derivatives of [7](2,6)Pyridinophane. Preparative and Conformational Studies

Shinsaku FUJITA, Kazuo IMAMURA, and Hitosi NOZAKI

Department of Industrial Chemistry, Kyoto University, Yoshida, Sakyo-ku, Kyoto

(Received December 1, 1971)

The 1-*exo*-methylene derivatives (IV, V and VII) of [7](2,6)pyridinophane (I) are synthesized by Wittig's reaction of [7](2,6)pyridinophan-1-one (III) or by the dehydration of the corresponding carbinol (VI). The C-4 protons are all shielded magnetically to varying extents, depending on their respective 1-substituents. The shielding effect is ascribed to the anisotropy of the pyridine ring. The signals of the C-4 protons are temperature-dependent, and the energy barriers for the conformational changes are estimated to be 8.7 for III, 9.1 for IV, 9.1 for V and 9.8 kcal/mol for VII.

Dynamic NMR spectrometry has revealed the conformational details of [7](2,6)pyridinophane (I), particularly the flipping of the heptamethylene chain.[1,2] The present report will describe the synthesis of several 1-π derivatives (IV, V, and VII) of I and the conformational changes induced by the incorporation of a trigonal (sp^2) carbon on C-1.

The Synthesis of 1-Methylene[7](2,6)pyridinophanes. The treatment of [7](2,6)pyridinophane (I) with *n*-butyllithium gave an orange-red solution of 1-lithio-[7](2,6)pyridinophane (II), which afforded [7](2,6)-pyridinophan-1-one (III) upon quenching with oxygen and subsequent Cornforth oxidation.[1] The reaction of III with methylenetriphenylphosphorane yielded 1-methylene[7](2,6)pyridinophane (IV), which exhibited IR bands characteristic of an *exo*-methylene double bond at 1633 and 894 cm^{-1}. A similar Wittig reaction of III with isopropylidenetriphenylphosphorane gave 1-isopropylidene[7](2,6)pyridinophane (V). The IR absorptions characteristic of an isopropylidene group appeared at 1642, 1373, and 1365 cm^{-1}. The reaction of the 1-lithio derivative (II) with benzophenone afforded 1-(α-hydroxybenzhydryl)[7](2,6)pyridinophane (VI). 1-Diphenylmethylene[7](2,6)pyridinophane (VII) was obtained by the dehydration of VI with thionyl chloride in pyridine. All the new compounds gave elemental analyses and spectral data consistent with the assigned structures.

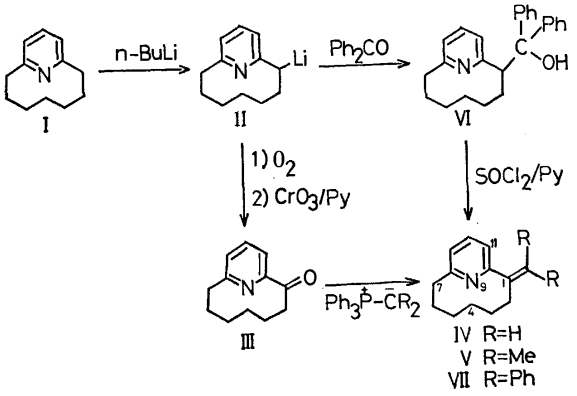

Dynamic NMR Spectrometry and Conformational Changes of 1-Oxo- and 1-exo-Methylene[7](2,6)pyridinophanes. The NMR spectra of IV, V, and VII at room temperature are shown in Fig. 1. The C-4 protons are magnetically shielded to various extents, depending on their 1-substituents (Table 1).[3] The chemical shift of the C-4 protons of IV (δ 0.92 ppm) is comparable to the value of 1-ketone III (δ 1.07 ppm),[1] and the stereochemical requirements of the oxo and methylene groups are similar to each other. The conjugation of the pyridine ring of IV with the 1-*exo*-methylene group should favor such an extreme conformer as VIII, in which one of the C-4 protons, H_x, is above, but slightly out of the center of the pyridine ring as

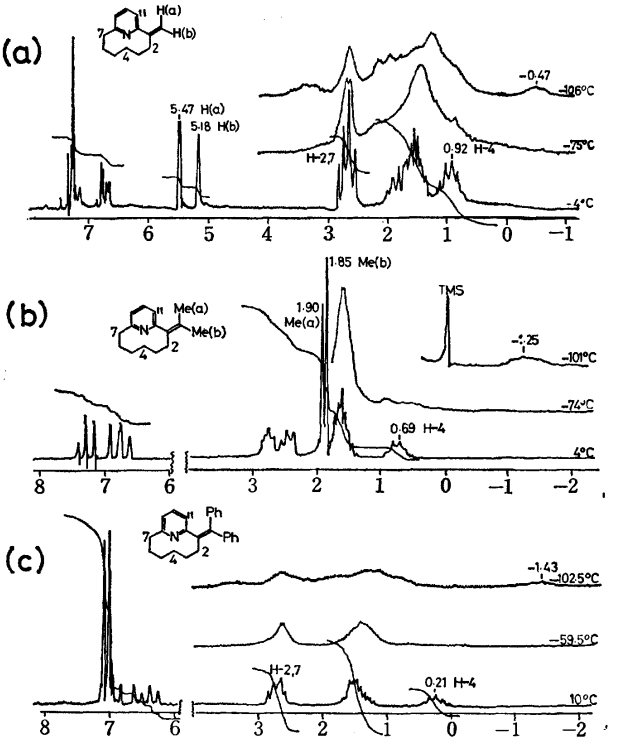

Fig. 1. Dynamic NMR spectra of IV (a), V (b) and VII (c); 60 MHz in $CFCl_3$, TMS as an internal standard.

1) a) S. Fujita and H. Nozaki, This Bulletin, **44**, 2827 (1971). b) H. Nozaki, S. Fujita, and T. Mori, *ibid.*, **42**, 1163 (1969).

2) a) H. Nozaki, T. Koyama, T. Mori, and R. Noyori, *Tetrahedron Lett.*, **1968**, 2181; *Tetrahedron*, **25**, 5357 (1969). b) S. Fujita, T. Kawaguti, and H. Nozaki, This Bulletin, **43**, 2596 (1970). c) S. Fujita, T. Kawaguti, and H. Nozaki, *Tetrahedron Lett.*, **1971**, 1119.

3) The shielding effect may be ascribed to the diamagnetic ring current of the pyridine ring and/or to the anisotropy of the nitrogen atom (See Ref. 1).

TABLE 1. ENERGY BARRIERS OF THE FLIPPING OF THE HEPTAMETHYLENE BRIDGES OF 1-π-[7](2,6)-PYRIDINOPHANES[a)]

Compound	Observed chemical shift of C-4 proton(s) (temperature)		$\Delta\nu$	T_c	k_c[b)]	$\Delta G^{\neq}_c$[c)]
	Average δ ppm (°C)	Fixed δ ppm (°C)	(Hz)	(°C)	sec^{-1}	kcal/mol
III	1.07(0)	−0.15(−109)	146	−84.0	324	8.7
IV	0.92(−4)	−0.47(−106)	167	−75.0	371	9.1
V	0.69(4)	−1.25(−101)	233	−74.0	510	9.1
VII	0.21(10)	−1.43(−102)	197	−59.5	437	9.8
I[d)]	0.22(−10)	−1.40(−111)	194	−75.5	432	9.0

a) Determined in $CFCl_3$ at 60 MHz. See Fig. 1.
b) $k_c=\pi\Delta\nu/\sqrt{2}$ (Ref. 5)
c) $\Delta G^{\neq}_c=2.303RT_c$ $(10.319-\log k_c+\log T_c)$ (Ref. 5)
d) Reported in Ref. 1.

compared with the corresponding proton of I.[4)] However, the C-4 protons of VII are more shielded than those of III and IV, and the chemical shift (δ 0.21 ppm) is comparable to that (δ 0.22 ppm) of unsubstituted [7](2,6)pyridinophane (I) itself. In the case of VII, steric hindrance arising from the H-11 of the pyridine ring and the phenyl group should influence the coplanarity of the pyridine and the *exo*-methylene group and consequently, the conformation of the heptamethylene bridge. The chemical shift (δ 0.69 ppm) of V is intermediate between those of IV and VII.

The NMR signals of the heptamethylene chain of IV are temperature-dependent as is illustrated in Fig. 1a. At room temperature, the heptamethylene bridge flips up and down (VIII⇄VIII') and its protons show an average chemical shift. At low temperatures, one of the C-4 protons (δ −0.47 at −106°C) of IV is more shielded than at room temperature. This fact indicates the fixation of the heptamethylene bridge to an extreme conformation such as VIII. The bridges of the other 1-π derivatives exhibited similar dynamic NMR spectra (Figs. 1b and 1c).

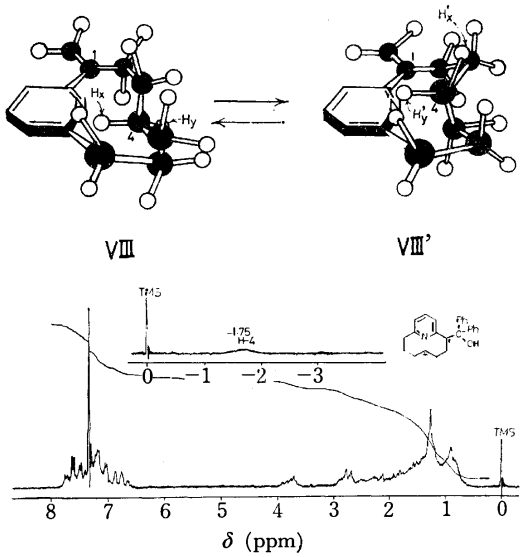

Fig. 2. The NMR spectrum of VI (24°C, 60 MHz in $CDCl_3$).

The estimated energy barriers for the conformational changes of 1-π-[7](2,6)pyridinophanes are shown in Table 1 as well as that of the mother compound (I). The introduction of π-bonds on C-1 reduces the energy barriers for the flipping of the heptamethylene chains, as is exemplified in III. In the *exo*-methylene derivatives, the steric crowding between H-11 and the 1-substituents compensates the above-mentioned reduction by the incorporation of π-bonds on C-1. Thus, the coalescence temperature (T_c) and the $\Delta G^{\neq}_c$ values of IV and V are comparable to those of the unsubstituted pyridinophane (I) itself. Moreover, those of VII are much higher and indicate that the steric hindrance becomes dominant. In conclusion, the chemical shifts of the C-4 protons, the coalescence temperature, and the $\Delta G^{\neq}_c$ values may be regarded as adequate measures of the relative steric bulkiness of 1-substituents.

The NMR spectrum of the carbinol VI (Fig. 2) is an extreme case as compared with those of other 1-monosubstituted [7](2,6)pyridinophanes.[1)] The one proton on C-4 is highly shielded (δ −1.75 ppm in $CDCl_3$) even at room temperature. In contrast, the two C-4 protons of [7](2,6)pyridinophan-1-ol have been reported to show an average signal at δ −0.08 ppm ($CDCl_3$) at room temperature.[1)] Probably, the bulky 1-substituent ($Ph_2(HO)C$-) prevents the flipping of the heptamethylene chain of VI.

Experimental

The dynamic NMR spectra were determined on a JEOL C-60-H spectrometer at 60 MHz, using fluorotrichloromethane ($CFCl_3$) as the solvent and tetramethylsilane (TMS) as the internal standard unless otherwise stated. The mass spectra were obtained on a Hitachi RMU-6L spectrometer.

1-Methylene[7](2,6)pyridinophane (IV). A solution (1.0 N, 4.0 *ml*) of *n*-butyllithium in *n*-hexane was added at room temperature under a nitrogen atmosphere to a suspension of triphenylmethylphosphonium bromide[6)] (1.29 g,

4) The anisotropy of the pyridine rings should be dependent upon the electron densities of the respective pyridine rings conjugated by π bonds.

5) a) G. Binsch, "Topics in Stereochemistry," Vol. 3, ed. by E. L. Eliel and N. L. Allinger, Interscience Publishers, New York (1968), p. 97—192. b) I. C. Calder and P. J. Garratt, *J. Chem. Soc., B*, **1967**, 660.

3.6 mmol) in tetrahydrofuran (15 ml). After stirring under nitrogen for 2 hr, the resulting red solution was added to a solution of III[1] (0.57 g, 3.0 mmol) in tetrahydrofuran (25 ml), after which stirring was continued for 24 hr. The reaction mixture was then poured into water and extracted with ether (200 ml). The combined extracts were dried over sodium sulfate and concentrated *in vacuo*. The oily residue was separated by preparative-scale thin layer chromatography (TLC) on silica gel, using *n*-hexane-benzene (1 : 3) as the solvent. The crude product was distilled to give IV (0.15 g, 26%); bp 70°C (bath temperature)/2 mmHg. IR (neat): 3055, 2924, 2840, 1633, 1580, 1461, 894, 838, 821, 799, 745, and 725 cm^{-1}. MS *m/e* (relative abundance): 187 (88), 186 (43), 172 (78), 159 (100), 158 (79), 146 (21), 144 (35), 133 (65), 130 (22), 117 (23), 77 (22), 65 (22), 39 (29). UV $\lambda_{max}^{n\text{-hexane}}$ (log ε): 246 nm (3.94), 277 nm (3.74). The NMR spectrum is shown in Fig. 1a.

Found: C, 83.6; H, 9.4; N, 7.4%. Calcd for $C_{13}H_{17}N$: C, 83.4; H, 9.2; N, 7.5%.

1-Isopropylidene[7](2,6)pyridinophane (V). A red solution of phosphorane, prepared from triphenylisopropylphosphonium bromide[7] (1.39 g, 3.6 mmol) and *n*-butyllithim (1.0 N, 4.5 ml), was added to a solution of III (0.57 g, 3.0 mmol) in tetrahydrofuran (25 ml). After stirring for 24 hr under nitrogen, the white precipitates were filtered off and the filtrate was concentrated. The residual oil was separated by preparative TLC (silica gel, *n*-hexane-benzene (1 : 3)) and distilled to give V (0.21 g, 33%); bp 117—118°C/0.5 mmHg. IR (neat): 3055, 2924, 2840, 1642, 1579, 1455, 1373, 1365, 1190, 1160, 853, 826, 801, 787, 753, and 731 cm^{-1}. MS *m/e* (relative abundance): 215 (100), 214 (63), 200 (62), 187 (85), 186 (88), 174 (20), 172 (48), 161 (34), 158 (27), 144 (30), 131 (24), 130 (21), UV $\lambda_{max}^{n\text{ hexane}}$ (log ε): 250.5 nm (3.92), 274 nm (3.80). The NMR spectrum is shown in Fig. 1b.

Found: C, 83.8; H, 9.9; N, 6.4%. Calcd for $C_{15}H_{21}N$: C, 83.7; H, 9.8; N, 6.5%.

1-(α-Hydroxybenzhydryl)[7](2,6)pyridinophane (VI). A solution (0.90 N, 4.4 ml) of *n*-butyllithium in *n*-hexane was added to solution of I[1] (0.70 g, 4.0 mmol) in tetrahydrofuran (75 ml) at room temperature. After stirring under a nitrogen atmosphere for 30 min, a solution of benzophenone (0.73 g, 4.0 mmol) in tetrahydrofuran (25 ml) was added to the resulting orange-red solution of II. The reaction mixture was stirred for 2 hr and then treated with aqueous ammonium chloride (100 ml), extracted with ether, and dried over sodium sulfate. Concentration and recrystallization gave VI (1.42 g, quantitative); mp 162—163°C (benzene). IR (KBr disk): 3300, 3050, 2960, 2940, 2885, 2810, 1593, 1570, 1495, 1463, 1450, 1412, 1350, 1279, 1174, 1049, 1031, 999, 960, 943, 930, 908, 889, 864, 853, 845, 810, 784, 775, 765, 757, 746, 728, 700, 689, 671, 640, 601 cm^{-1}. The NMR may be found in Fig. 2.

Found: C, 83.9; H, 7.5; N, 4.0%. Calcd for $C_{25}H_{27}NO$: C, 84.0; H, 7.6; N, 3.9%.

1-Diphenylmethylene[7](2,6)pyridinophane (VII). Thionyl chloride (1.0 ml) was added in one portion under nitrogen to a solution of VI (0.17 g, 0.5 mmol) in pyridine (10 ml), and then the solution was heated at 50°C for 5 hr. The reaction mixture was subsequently poured onto ice, extracted with ether, and dried over sodium sulfate. After the removal of the ether, the residual solid was recrystallized from *n*-hexane to afford VI as white crystals (0.14 g, 85%); mp 116—118°C. IR (KBr disk); 3075, 3050, 3015, 2960, 2950, 2910, 2840, 1597, 1582, 1567, 1494, 1454, 1444, 1203, 870, 838, 815, 794, 769, 760, 754, 736, 827, 714, 702, 674, 630, and 602 cm^{-1}. MS *m/e* (relative abundance): 339 (100), 338 (98), 311 (47), 310 (76), 182 (37), 105 (100), 77 (76), 57 (20), 51 (35). UV $\lambda_{max}^{n\text{-hexane}}$ (log ε): 236 nm (4.21), 309.5 nm (4.16). The NMR spectrum is shown in Fig. 1c.

Found: C, 88.3; H, 7.4; N, 4.3%. Calcd for $C_{25}H_{25}N$: C, 88.5; H, 7.4; N, 4.1%.

The financial support of the Ministry of Education, the Japanese Govermnent, and of the Toray Science Foundation is acknowledged with pleasure.

6) G. Wittig and U. Schoelkopf, "Organic Synthesis," Vol. 40, p. 66 (1960); N. A. Milas, L. Chiang, C. P. Priesing, A. A. Hyatt, and J. Peter, *J. Amer. Chem. Soc.*, **77**, 4180 (1955).

7) U. H. M. Fagerlund and D. R. Idler, *ibid.*, **79**, 6473 (1957).

Synthetic Reactions by Complex Catalysts. XXVI.[1] The Copper-catalyzed Reaction of α,β-Unsaturated Isocyanide with Active Methylene Compounds

Takeo SAEGUSA, Ichiki MURASE, and Yoshihiko ITO

Department of Synthetic Chemistry, Faculty of Engineering, Kyoto University, Sakyo-ku, Kyoto

(Received December 13, 1971)

The Cu_2O-catalyzed reaction of α,β-unsaturated isonitrile with active methylene compound is described. Vinyl isocyanide (VIC) and propenyl isocyanide (PPIC) were employed as the isocyanide components. In addition, allyl isocyanide (AIC), which has been known to be rearranged readily to PPIC by Cu_2O, was also used as a precursor of PPIC. Five types of products were isolated and identified. These products were explained by a scheme starting with an intermediate of the organocopper-isonitrile complex (**9**) derived from the active methylene compound.

In a previous communication,[2] we have described a new formimidation of active methylene compounds with isonitrile in the presence of a *catalytic amount* of Cu_2O. In the formimidation, isonitrile is inserted between the C–H bond of active methylene compounds (**1**), thus leading to the transient species (**2**), which then rearranges readily to the tautomeric isomer (**3**) (Eq. (1)).

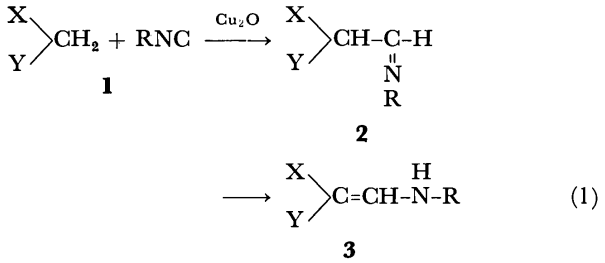

(1)

The formimidation was possible only with aryl and α,β-alkenyl isocyanides. Saturated alkyl isocyanide did not react with active methylene compounds under the conditions of our study.

When the amount of Cu_2O catalyst was increased in the reaction of alkenyl isocyanide with the active methylene compound, some other reactions occurred and the selectivity of the formimidation was lowered. The present paper will describe this reaction as a whole. As the α,β-unsaturated alkenyl isocyanides, vinyl isocyanide (VIP), and propenyl isocyanide (PPIC) were employed. In addition, allyl isocyanide (AIC) was used as a convenient precursor of PPIC, because it was known to be rearranged very readily to PPIC by the Cu_2O catalyst.[3]

$$CH_2{=}CHCH_2NC \rightarrow CH_3{-}CH{=}CHNC \qquad (2)$$

The types of products are **3**, **5**, **6** (or **7**), and **8**. The relative amounts of these products are dependent upon the nature of the active methylene compound.

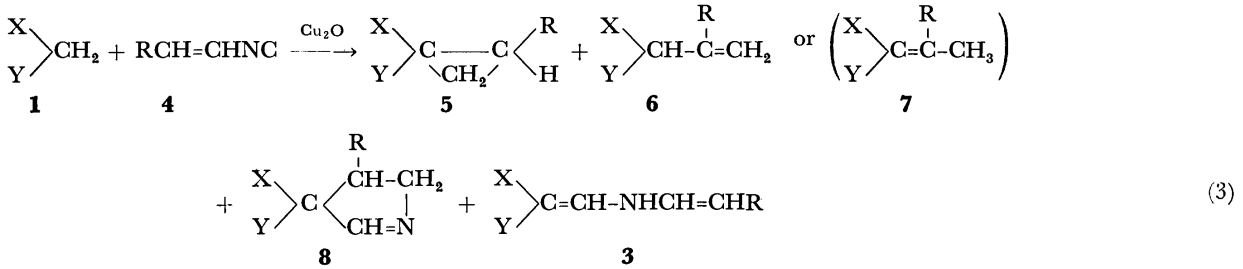

(3)

a. X=Y=CO_2Et, R=H b. X=Y=CO_2Et, R=CH_3 c. X=COMe, Y=CO_2Me, R=H
d. X=COMe, Y=CO_2Et, R=H e. X=Y=COMe, R=H
f. X=C_6H_5, Y=CO_2Me, R=H g. X=C_6H_5, Y=CO_2Me, R=Me

Results and Discussion

In the reactions of alkenyl isocyanides (VIC, PPIC and AIC) with diethyl malonate in the presence of increasing amounts of the Cu_2O catalyst, cyclopropane derivatives of **5a** and **5b** were obtained in significant yields. Both PPIC and AIC gave the same product of **5b**. This fact can be well explained by the rapid isomerization of AIC to PPIC by Cu_2O (Eq. (2),) which takes place prior to the reaction with diethyl malonate. The amounts of olefinic products, **7a** and **6b**, were small. Presumbaly, **7a** was formed by the double-bond isomerization of **6a**.[4] Under the present reaction conditions, saturated alkyl isocyanide does not react with the active methylene compound.[1] The reactions of VIC with some other active methylene compounds (*i.e.*, methyl acetoacetate, ethyl acetoacetate and acetylacetone) were also examined. The results are shown in Table 1.

The relative ratios of **5** to the combined yield of the four products decrease as the acid strength of the active methylene compound is increased; *i.e.*, $CH_3COCH_2COCH_3$ — $CH_3COCH_2CO_2C_2H_5$ — $C_2H_5O_2C$-

1) Part XXV. T. Saegusa, I. Murase, and Y. Ito, This Bulletin, **45**, 830 (1972).

2) T. Saegusa, I. Murase, and Y. Ito, *Synthetic Commun.*, **1** (3), 145 (1971).

3) T. Saegusa, I. Murase, and Y. Ito, *Tetrahedron*, **27**, 3795 (1971).

4) T. Saegusa, Y. Ito, S. Tomita, and H. Kinoshita, *J. Org. Chem.*, **35**, 670 (1970).

TABLE 1. Cu_2O-CATALYZED REACTION OF ISOCYANIDE WITH ACTIVE METHYLENE COMPOUNDS

Active methylene[a] compd.	Isocyanide (mmol)	Cu_2O (mmol)	Benzene (ml)	Time (hr)	Temp. (°C)	Yields[b] (%) 5	6 (or 7)	8	3
$CH_2(CO_2Et)_2$	VIC (12)	0.5	3	12	80	6	—	—	—
	AIC (12)	0.35	3	12	80	4.5	—	—	—
	VIC (15)	15	20	7	80	17	5[d]	—	—
	AIC (12)	12	20	7	80	47	3	—	5
	PPIC (12)	12	20	7	80	31	14	—	—
$MeCOCH_2CO_2Me$	VIC (15)	7.7	10	24	90	29	trace	14	14
$MeCOCH_2CO_2Et$	VIC (15)	7.7	10	3	80	17	trace	5	21
$MeCOCH_2COMe$	VIC (24)	12	20	48	r. t.	—	—	12	22
$PhCH_2CO_2Me$	VIC (15)	7.7	10[c]	12	80	14	—	18	—
	AIC (12)	6	10	8	80	—	3	—	—
							15b ≈ 27		

a) An equimolecular mixture of active methylene compounds and isonitrile was employed. VIC=vinyl isocyanide, AIC=allyl isocyanide, PPIC=propenyl isocyanide
b) The yield was based upon the amount of the product isolated by distillation.
c) The reaction was carried out in *N,N*-dimethylformamide.
d) The type of product was **7a**.

$CH_2CO_2C_2H_5$. Probably, active methylene compounds with more acidic hydrogen undergo formimidation more readily.

These products may be explained by the following reaction scheme.

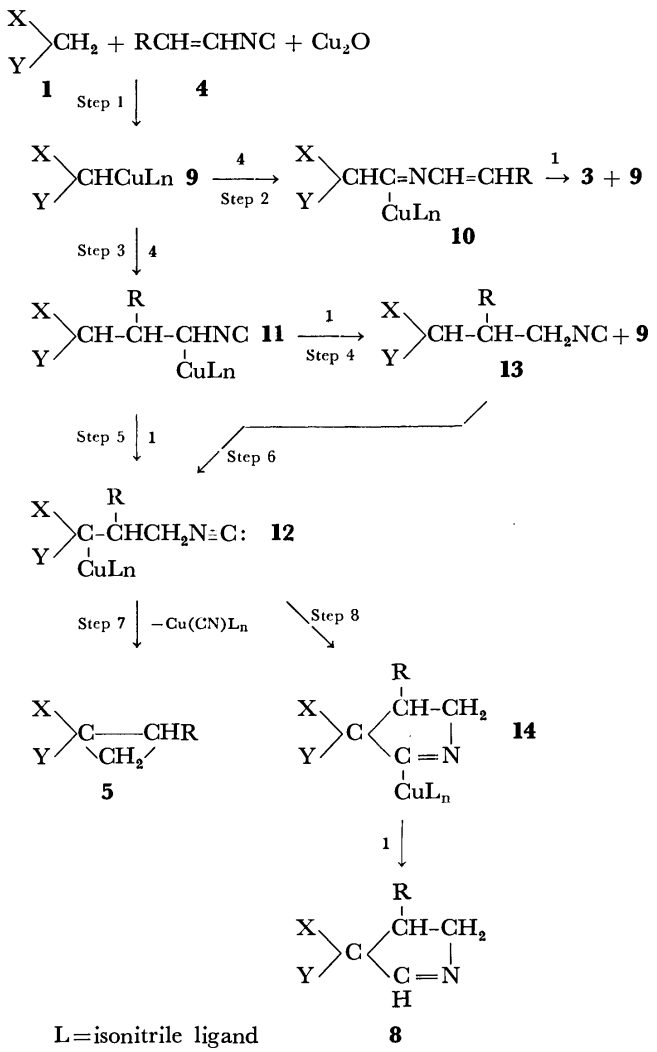

L=isonitrile ligand

The first step is the formation of an organocopper complex (**9**)[5], which possibly has the ligand of isonitrile (Step 1). The hydrogen abstraction from the active methylene compound (**1**) by Cu_2O-isonitrile has been proposed and well supported in the Michael-type addition reaction induced by the Cu_2O-isonitrile system.[5,6] The α,α-addition of organocopper of **9** to the terminal carbon atom of the isonitrile group gives **10**, which then abstracts a hydrogen atom from another molecule of **1** to produce the formimidation product, **3**, and the key intermediate of organocopper (**9**)[2] (Step 2).

The α,β-addition of organocopper of **9** to the olefinic double bond of alkenyl isocyanide affords **11** (Step 3), and the subsequent step of the hydrogen abstraction by **11** (Step 5) gives rise to the adduct, **13**, and the intermediate, **9**. The combination of Steps 3 and 4 corresponds to the addition of the active methylene compound to α,β-unsaturated isonitrile, which may interestingly be compared with the corresponding Michael addition to α,β-unsaturated nitrile[6] (Eq. (4)):

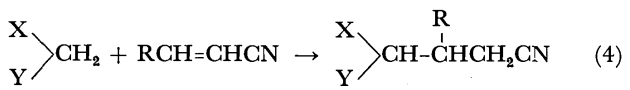

It has been reported[7] that the terminal carbon atom of the vinyl group of VIC has an increased electron density due to a canonical form of $^-CH_2-CH=\overset{+}{N}=C:$. The polarization character of VIC is opposite to that of acrylonitrile. Consequently, the nucleophilic addition to VIC may not be a favorable reaction. The addition of diethyl malonate to VIC was not observed in the presence of the *tert*-BuOK catalyst under the

5) T. Saegusa, Y. Ito, and S. Tomita, *J. Amer. Chem. Soc.*, **93**, 5656 (1971).
6) T. Saegusa, Y. Ito, S. Tomita, and G. Kinoshita, This Bulletin, **45**, 496 (1972).
7) a) D. S. Matteson and R. A. Baiely, *Chem. Ind.* (London), 191 (1967); b) D. S. Matteson and R. A. Bailey, *J. Amer. Chem. Soc.*, **90**, 3762 (1968).

Table 2. Identification data of products

Compd.	Mass (*m/e*)	IR spectrum, neat (cm^{-1})	NMR absorption (τ)	Anal.
		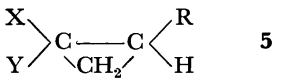 **5**		
5a bp. 65°C(6)	186(M^+), 159, 158, 141, 130, 114, 113, 112	3098, *ca.* 1730 1030	Ethyl proton, 8.56(s, 4H)	Authentic.[12]
5b bp. 63°C(4)	200(M^+), 172, 155, 144, 127, 126, 125	3098, *ca.* 1730 1034	Ethyl proton, *ca.* 8.10 (m, 1H), *ca.* 8.63(5H)	Found: C, 60.28; H, 8.25. Calcd for $C_{10}H_{16}O_4$: C, 59.98; H, 8.05.
5c bp. 60°C(5)	142(M^+), 127, 110, 111, 95, 82, 69, 59	3095, 1720, 1040	6.21(s, 3H), 7.52(s, 3H), 8.56(4H)	Found: C, 59.29; H, 7.07. Calcd for $C_7H_{10}O_3$: C, 59.14; H, 7.07.
5d bp. 82°C(7)	156(M^+), 141, 128, 113, 111, 110, 86, 69	3098, 1720, 1030	Ethyl protons, 7.51(s, 3H), 8.48(4H)	Found: C, 60.91; H, 7.69. Calcd for $C_8H_{12}O_3$: C, 61.51; H, 7.75.
5f	176(M^+), 144, 117, 116, 115, 91	1715, 1603, 1300	Phenyl protons, 6.35(s, 3H), 8.35(m, 2H), 8.76(m, 2H)	
		Olefins		
7a	186(M^+), 171, 141, 140, 113, 95, 85	1729, 1650, 1450, 1059, 1030	2.90(q, 1H), 8.02(d, 3H), Ethyl protons	
6b	200(M^+), 155, 154, 149, 127, 108	1732, 1650, 1460, 1062, 1038, 925	3.02(t, 1H), 7.72(m, 2H), Ethyl protons, 8.82(q, 3H)	Found: C, 59.72; H, 8.17. Calcd for $C_{10}H_{16}O_4$: C, 59.98; H, 8.05.
6g	190(M^+), 158, 131, 130, 129, 115, 91	1722, 1638, 1050	Phenyl protons, 2.85(t, 1H), 6.24(s, 3H), 7.85(m, 2H), 8.92(q, 3H)	Found: C, 75.58; H, 7.47. Calcd for $C_{12}H_{14}O_2$: C, 75.76; H, 7.42.
		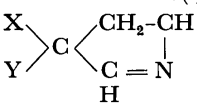		
8c	169(M^+), 138, 137, 110, 109, 96, 95	1738, 1643, 1518, 935	3.25(s, 1H), 6.33(s, 3H), 7.29(4H), 7.73(s, 3H)	Found: C, 56.47; H, 6.79; N, 8.08 Calcd for $C_8H_{11}NO_3$: C, 56.76; H, 6.55; N, 8.28.
8d	183(M^+), 138, 110, 109, 96	1738, 1640, 1515, 1120, 935	2.35(s, 1H), Ethyl protons, 7.25(4H), 7.70(s, 3H)	Found: C, 58.86; H, 7.30; N, 7.74. Calcd for $C_9H_{13}NO_3$: C, 59.00; H, 7.15; N, 7.65.
8e	153(M^+), 126, 111, 110, 96, 69	1715, 1670, 1610, 1512, 1125, 940	2.30(s, 1H), 7.21(4H), 7.70(s, 3H), 7.83(s, 3H)	Found: C, 62.25, H, 7.44; N, 9.30. Calcd for $C_8H_{11}NO$: C, 62.72; H, 7.24; N, 9.14
8f	203(M^+), 176, 144, 117, 116, 115, 103	1738, 1621, 1500, 1492, 1249, 700	2.18(s, 1H), Phenyl protons, 6.02(t, 2H), 7.2(m, 1H), 7.8(m, 1H), 6.28(s, 3H)	Found: C, 70.72; H, 6.36; N, 7.70. Calcd for $C_{12}H_{13}NO_2$: C, 70.91; H, 6.45; N, 6.89.
		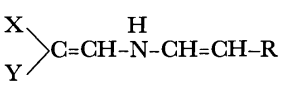		
3b		1730, 1678, 1635, 1595, 1245, 1153, 1103, 1070, 912	−0.8(1H), 2.0(d, 1H, J=13.1 Hz), 3.81(t, 1H), 5.07(m, 1H), Ethyl protons, 8.30(3H)	

TABLE 2. (continued)

Compd.	Mass (*m/e*)	IR spectrum, neat (cm^{-1})	NMR absorption (τ)	Anal.
3c bp. 88°C(3)		3180, 1708, 1640, 1589, 1250, 1179, 1080, 980	−2.2(1H), 1.98(d, 1H, J=12.5 Hz), *ca.* 3.6, 5.2 (vinyl protons, 3H), 6.25 (s, 3H), 7.55 s, 3H)	
3d bp. 114°C(2)		3180, 1705, 1635, 1589, 1245, 1178, 1071, 980	−2.2(1H), 2.01(d, 1H, J=12.5 Hz), *ca.* 3.6, 5.4 (vinyl proton, 3H), ethyl protons, 7.50 (s, 3H)	Found: C, 59.24; H, 7.38; N, 7.43. Calcd for $C_9H_{13}NO_3$: C, 59.00; H,7.15; N, 7.65.
3e bp. 113—115°C(2)		1665, 1640, 1610, 1200, 1120, 1025, 971, 921	−2.25(1H), 2.12(d, 1H, J=12.5 Hz), vinyl proton, 7.50(s, 3H), 7.72(s, 3H)	Found: C, 62.51; H, 7.48; N, 9.12. Calcd for $C_8H_{11}NO_2$: C, 62.72; H, 7.24; N, 9.14.
		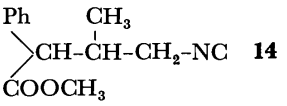 **14**		
15g	217(M^+), 202, 190, 158	2148, 1735, 1610	2.61(5H, phenyl protons), 6.22(d, 1H), 6.35(s, 3H), 6.5—6.6(2H), 7.5(m, 1H), 8.8—9.4(3H)	Found: C, 71.99; H, 7.18; N, 6.36. Calcd for $C_{13}H_{15}NO_2$: C, 71.86; H, 6.96; N, 6.45.

conditions shown in Table 1. The polarization character of VIC, however, may be much changed by its coordination through the termical carbon atom of the isocyano group to copper. In each of the reaction mixtures of VIC and AIC with methyl phenylacetate with the Cu_2O catalyst, the Michael addition products, **15f** and **15g**, were actually isolated.

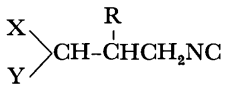

15

f. X=C_6H_5, Y=CO_2Me, R=H
f. X=C_6H_5, Y=CO_2Me, R=Me

When the reaction of VIC with methyl phenylacetate was carried out in dimethylformamide, **15f** was not formed, but **5f** and **8f** were produced (see Table 1). Complex **12** is formed by the 1,3-rearrangement of **11** (Step 5) or from **13** (Step 6), which has an active hydrogen at the γ-carbon. The elimination of CuCN from **12** gives rise to the formation of **5** (Step 7). Step 7 is closely related to the following reaction of CuCN elimination:[8]

$$EtO_2CCH_2CH_2NC + \frac{1}{2}Cu_2O \rightarrow EtO_2CCH{=}CH_2 + CuCN + \frac{1}{2}H_2O$$

$$EtO_2CCH_2\underset{\displaystyle CH_3}{\underset{|}{C}}HNC + \frac{1}{2}Cu_2O \rightarrow EtO_2CCH{=}CHCH_3 + CuCN + \frac{1}{2}H_2O$$

On the other hand, the insertion of the isocyano group into the carbon-copper band in **12** is a cyclization process[9] (Step 8) which produces **14**, which in turn abstracts hydrogen from another molecule of **1** to give **8** and **9**. The olefinic compound, **6**, is a minor product, whose formation has not yet been elucidated.

The production of olefin suggests another possibility for the formation of the cyclopropane derivative.

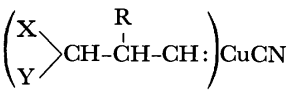

16

It seems likely that a carbene intermediate (**16**) is formed by the α,α-elimination from α-isocyanoorganocopper (**11**), which may be regarded as a kind of copper carbenoid. Kirmse and Wächtershäuser[10] reported that cyclopropane and olefin were obtained in the reaction of 1,1-diiodoneoalkanes with copper. This reaction has been explained in terms of a process involving a copper carbenoid (**17**).

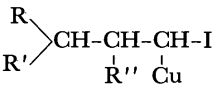

17

Experimental

Reagent. VIC was prepared according to Matteson's procedure.[7] AIC was prepared according to Ugi's procedure,[11] while PPIC was prepared by the isomerization of

8) T. Saegusa, Y. Ito, S. Tomita, and K. Goda, unpublished work.

9) T. Saegusa, Y. Ito, S. Tomita, and H. Kinoshita, *J. Org. Chem.*, **36**, 3316 (1971).

10) W. Kirmse and G. Wächtershäuser, *Tetrahedron*, **22**, 73 (1966).

11) I. Ugi, *Angew. Chem.*, **77**, 492 (1965).

AIC with a Cu_2O catalyst.[4] The active methylene compounds were all commercial reagents and were purified by distillation under nitrogen. The Cu_2O was a commercial reagent of an analytical reagent grade and was dried under nitrogen prior to use.

Reactions of Isonitriles with Active Methylene Compounds. A mixture of equimolecular amounts of isonitrile and an active methylene compound, together with Cu_2O in benzene, was heated under nitrogen. Then, the excess solid Cu_2O was removed by filtration and wahed with CH_2Cl_2. The filtrate and washings were combined and treated with a 4 N KCN aqueous solution. The organic layer was subjected to distillation under reduced pressure. The products were purified by preparative glpc. The product structures were determined by studying the IR, NMR, and Mass spectra and by elemental analysis. The identification data of the products are summarized in Table 2.

12) W. H. Perkin, *J. Chem. Soc.*, **47**, 807 (1885).

BULLETIN OF THE CHEMICAL SOCIETY OF JAPAN, VOL. 45, 1888—1892 (1972)

The Synthesis of an Etiojervane Analog of Corticosterone.[1]

Tadashi MASAMUNE and Takako ORITO

Department of Chemistry, Faculty of Science, Hokkaido University, Sapporo

(Received December 20, 1971)

The synthesis of C-nor-D-homo-17-epicorticosterone 21-acetate (**1**) from jervine (**3**), which possesses the corticosterone configuration at each of the ring junctions, is described. Etiojerv-5-ene-3β,11β-diol-17-one (**4**), obtained by a seven-step process from **3**, was subjected to the Darzens reaction and afforded glycidic ester (**7**), which was converted by treatment with boron trifluoride into olefin (**9**). Catalytic hydrogenation followed by reduction with lithium aluminum hydride gave rise to tetraol (**15**), which was isolated as the acetonide (**16**). After Oppenauer oxidation of **16**, acid hydrolysis and subsequent partial acetylation, the resulting monoacetate (**19**) was oxidized with dicyclohexylcarbodiimide in dimethylsulfoxide to give compound **1**. Spectral and chemical evidence are presented for configurational assignment to both the compound and the synthetic intermediates.

Interest continues in the search for analogs with enhanced or more specific pharmacological properties in the synthesis of modified steroid hormones. During the last few years etiojervane analogs of cortisone,[2] progesterone,[3,4a] testosterone,[4b,5,6] estrone,[4c,5,7] and others[8-11] have been prepared. We describe herewith the synthesis of C-nor-D-homo-17-epicorticosterone 21-acetate (**1**), which possesses the corticosterone configuration at each ring junction and differs from the corresponding aldosterone (**2**) only in the function at C_{18} and the configuration at C_{17}.

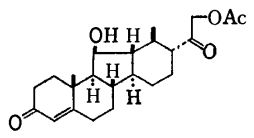

1

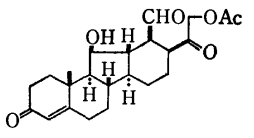

2

The readily available veratrum alkaloid jervine (**3**) was converted by a seven-step process into etiojerv-5-ene-3β,11β-diol-17-one[2] (**4**) *via* trienone[4b,12] (**5**) in an over-all yield of 13.5%. Compound **4** was selected as the starting material for the following reasons. (1) A synthetic route[3,13] *via* hydration of the 17,20-double bond of **5** followed by selective oxidation at C_{20} to the *17-acetyl group* would be impractical, in view of the instability of a closely related compound, 17α-acetyletiojerva-5,12-dien-3β-ol[14] (**6**), owing to the facile oxidative cleavage. (2) Dihydrojervine derivatives with *trans*-fused C/D linkage and open ring E, obtained by the double Birch reductions of **3**[3,15,16] or by acetolysis of 12,13-dihydrojervine and subsequent hydrogenation,[16,17] led to formation of the corresponding 17α-*acetyl* (*not* 17β) derivatives by the fragmentation of ring E.[18,19] However, selective introduction of a hydroxyl or an acetoxyl group

1) Part XIX of "C-Nor-D-homosteroids and Related Alkaloids"; Part XVIII, T. Masamune, I. Yamazaki, K. Orito, and M. Takasugi, *Tetrahedron*, **27**, 3387 (1971).

2) T. Masamune, A. Murai, and S. Numata, *ibid.*, **25**, 3145 (1969).

3) T. Masamune, K. Orito, and A. Murai, This Bulletin, **39**, 2503 (1966).

4) a) S. M. Kupchan and M. J. Abu El-Haj, *J. Org. Chem.*, **33**, 647 (1968). b) S. M. Kupchan and S. D. Levine, *J. Amer. Chem. Soc.*, **86**, 701 (1964). c) S. M. Kupchan, A. W. By, and M. S. Flom, *J. Org. Chem.*, **33**, 911 (1968).

5) T. Masamune and K. Orito, *Tetrahedron*, **25**, 4551 (1969).

6) W. F. Johns, *J. Org. Chem.*, **36**, 711 (1971), and previous papers.

7) M. J. Green, N. A. Abraham, E. B. Fleischer, J. Case, and J. Fried, *Chem. Commun.*, 234 (1970), and references cited.

8) H. Mitsuhashi and K. Kawahara, *Tetrahedron*, **21**, 1215 (1965), and previous papers.

9) A. Chatterjee and S. Banerjee, *ibid.*, **26**, 2599 (1970), and reference cited.

10) G. Lukacs, P. Longevialle, and X. Lusinchi, *ibid.*, **26**, 583 (1970), and references cited.

11) J. M. Coxon and M. P. Hartshorn, D. N. Kirk, and M. A. Wilson, *ibid.*, **25**, 3107 (1969), and previous papers.

12) J. Fried and A. Klingsberg, *J. Amer. Chem. Soc.*, **75**, 4029 (1953); S. Okuda, K. Tsuda, and H. Kataoka, *Chem. & Ind.*, **1951**, 512.

13) *Cf.*, S. M. Kupchan, T. Masamune, and G. W. A. Milne, *J. Org. Chem.*, **29**, 755 (1964).

14) A. Murai, K. Arita, and T. Masamune, to be published.

15) T. Masamune, M. Takasugi, M. Gohda, H. Suzuki, S. Kawahara, and T. Irie, *J. Org. Chem.*, **29**, 2282 (1964).

16) T. Masamune, A. Murai, K. Orito, H. Ono, S. Numata, and H. Suginome, *Tetrahedron*, **25**, 4853 (1969).

17) O. Wintersteiner and M. Moore, *ibid.*, **20**, 1947 (1964); **21**, 779 (1965).

into C_{21} in a final stage of the synthesis would be difficult.

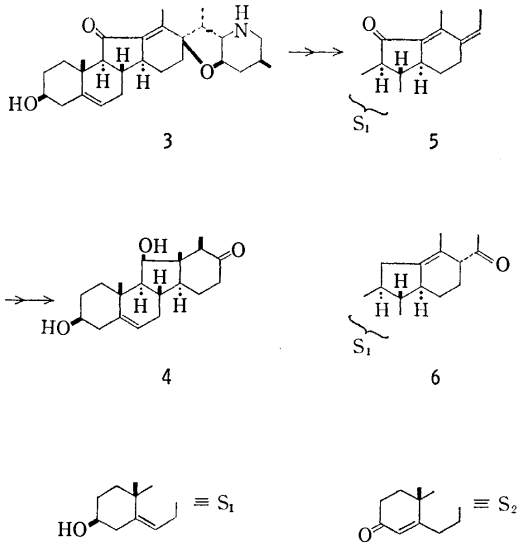

Alkylation at C_{17}, the most important step, was carried out under various conditions. The Wittig reaction of **4** with carbethoxymethylenetriphenylphosphorane[2] and the Darzens reaction under the conditions used for steroidal 3-ketones[20] were attempted for preparing compounds with 17-substituents convertible to the side chain of corticosterone, but proved to be unsuccessful, most of the starting compound **4** being recovered unchanged. However, treatment of **4** by a modified procedure of the latter reaction, using ethyl chloroacetate (8 mol) and sodium ethoxide (5 mol) in dimethyl sulfoxide (DMSO) at room temperature, resulted in formation of glycidic ester (**7**), mp 176—178°C, in 36% yield after chromatographic separation, along with an almost equal amount of the unreacted compound **4**. Compound **7** displayed a peak at *m/e* 390 due to the molecular ion and absorptions at 1747 cm^{-1} and at τ 8.84 (triplet) and 5.75 (quartet) due to the carbethoxy group in the mass, IR, and NMR spectra, respectively, which were consistent with the structure. The configuration of the side chain at C_{17} was assigned β (α-epoxide) on the analogy of the Grignard reactions in unhindered ketones[21] and, especially, of the ethynylation of C-nor-D-homocortisone synthesis (17β-ethynyl 40% and 17α-ethynyl 5%).[2]

Glycidic ester **7**, on treatment with boron trifluoride etherate in a refluxing solution of tetrahydrofuran (THF) and DMSO, afforded a 1 : 2 mixture of two allyl alcohols. The mixture was subjected to separation by preparative thin layer chromatography (tlc) to give **8**, mp 150—151°C, and **9**, mp 152—153°C, in 23 and 40% yields, respectively. The former showed a signal (singlet) due to the methyl protons attached to the 13,17-double bond at τ 8.07, and the latter one (W_H=12 Hz) due to the new olefinic proton at τ 4.11 in the NMR spectrum. The presence of a double bond at C_{12}–C_{13} of **8** was excluded, because the 18-methyl protons of etiojerv-12-en-11β-ol derivatives appeared at a higher field over τ 8.20.[14]

Kupchan and El-Haj[4a] obtained etiojerva-4,16-dien-20-ol-3,11-dione (**10**) as the only isolable product by treatment of a compound with an epoxy function at C_{17} and C_{20} (**11**) under almost the same conditions. They assigned the β-configuration to the relevant epoxy group on the basis of this reaction result, which was rationalized by a concerted cleavage of the diaxially oriented C_{17}–O and C_{16}–H bonds.[22] In view of the stereochemical peculiarity in C and D rings of etiojervanes, the rationalization leading to the preferential elimination of proton from the less hindered carbon C_{16} would not be unreasonable. Contrary to expectation, the present result differed from theirs in the formation of two olefins **8** and **9**. This would be explicable on the premise of a two-step elimination mechanism; cleavage of the presumed α-epoxy group at C_{17} followed by removal of one of the protons on two adjacent carbons C_{13} and C_{16}. It would be improbable that the reaction proceeded with a concerted mechanism, whereby compounds with two *trans*-fused five-membered rings should result from contraction of the D ring.[23] It is to be noted that compound **8** is the first etiojervane derivative with both the 13,17-double bond and *trans*-fused C/D linkage (12βH, 14αH).

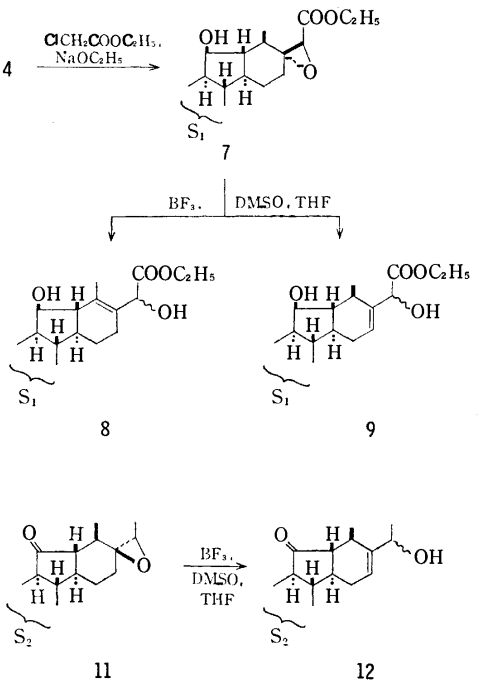

18) R. W. Franck, G. P. Rizzi, and W. S. Johnson, *Steroids*, **4**, 463 (1964).
19) H. Suginome, M. Murakami, and T. Masamune, This Bulletin, **41**, 468 (1968); H. Suginome, H. Umeda, and T. Masamune, *Tetrahedron Lett.*, **1970**, 4571.
20) W. A. Yarnall and E. S. Wallis, *J. Org. Chem.*, **4**, 270 (1939).
21) M. Chérest and H. Felkin, *Tetrahedron Lett.*, **1971**, 383 and references cited; J. C. Richter, *J. Org. Chem.*, **30**, 324 (1965).
22) H. B. Henbest and T. I. Wrigley, *J. Chem. Soc.*, **1957**, 4596.
23) D. N. Kirk and M. P. Hartshorn, "Steroid Reaction Mechanisms," Elsevier Publishing Company, New York, N. Y. (1968), p. 354.

Hydrogenation of olefin **9** over platinum in ethanol took place selectively, giving the 16,17-dihydro derivative (**12**), mp 177—179°C, in 81% yield. A signal at τ 4.11 due to the proton at C_{16} of **9** disappeared in the NMR spectrum of **12**. On the other hand, compound **8** with the tetra-substituted double bond remained unchanged by the same treatment. The side chain configuration at C_{17} of **12** was tentatively assigned to α on the basis that (1) hydrogenation of an imino-jervane derivative (**13**) with the double bond at C_{16} and C_{17} as well as the *trans*-fused C/D linkage produced a compound (**14**) with the 17α-side chain, resulting from attack of hydrogen from the upper (β) side,[16] and (2) adsorption of the double bond in question on the catalyst would possibly occur at the same side as the fixed 11-hydroxy group rather than the rotatable 20-hydroxyl.[24]

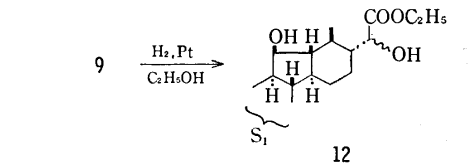

12

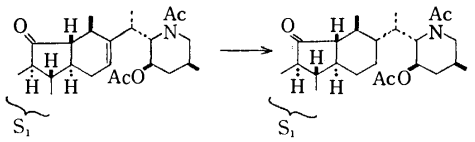

13 3-Acetate 14 3-Acetate

Reduction of ester **12** with lithium aluminum hydride (LAH) gave rise to etiojerv-5-ene-3β,11β,20ξ,-21-tetrol (**15**) as crystalline state, which was scarcely soluble in the usual organic solvents, and without further purification, converted by treatment with acetone and *p*-toluenesulfonic acid (PTS) into the acetonide (**16**), mp 217—220°C in 47% yield from **12**. The mass (*m/e* 390, M$^+$), IR (ν_{max} 1068 and 1052 cm^{-1}) and NMR spectra (τ 8.62, 6H, singlet) were in good accord with the structure. The Oppenauer oxidation[13] of acetonide **16** proceeded without any change of the 11β-hydroxy group and afforded an $\alpha\beta$-unsaturated ketone (**17**), mp 160—162°C, in 85% yield, which showed strong absorption maxima at 1650 and 1610 cm^{-1} in the IR spectrum.

Acetonide **17** was then subjected to hydrolysis with acid to give triol (**18**), which was also hardly soluble in the usual organic solvents and used for the next reaction without further purification. Treatment of **18** with acetic anhydride (1.3 mol) in dioxane effected partial acetylation at C_{21}, giving monoacetate (**19**), oil, after separation by preparative tlc. Selective oxidation of the 20-hydroxyl to the oxo function by the usual procedures, using anhydrous chromic acid in acetic acid or in pyridine or Jones' reagent,[25] failed owing to the susceptibility of the 11β-hydroxyl group to oxidation. However, oxidation was achieved by treatment of **19** with dicyclohexylcarbodiimide (DCC), trifluoroacetic acid and pyridine in DMSO at room temperature.[26] The resulting product (**1**) mp 209—211°C, isolated in 30% yield from **17** by preparative tlc, was analyzed for $C_{23}H_{32}O_5$, which was supported by the mass spectrum (*m/e* 388, M$^+$). In accordance with the assigned structure, the compound exhibited absorption maxima at 3420, 1748, 1728, 1665, and 1610 cm^{-1} due to the hydroxyl and carbonyl functions in the IR spectrum, and two singlets at τ 8.60 and 7.88 (19-CH_3 and $OCOCH_3$), a doublet with J of 6 Hz at τ 9.05 (18-CH_3), a multiplet and a singlet at τ 5.35 and 4.38 (H at C_{11} and C_4) in the NMR spectrum. The CD and ORD curves of **1** clearly exhibited a positive Cotton effect, as compared with those of acetonide **17** (Fig. 1). Analogous with the fact that two epimeric, well established etiojervanes (**20** and **21**) with the 17β- and 17α-acetyl group displayed negative and positive Cotton effects (a=−91° and +61°), respectively.[14] The positive Cotton effect due to the 20-oxo function of **1** indicated the 17-substituent to be α-oriented, supporting the hydrogenation result of **9**. Accordingly, compound **1** is regarded as C-nor-D-homo-17-epicorticosterone 21-acetate. Since functionalization of the 18-methyl group of related compounds has been achieved,[27] compound **1** or the synthetic intermediates would be useful for the synthesis of etiojervane analogs of aldosterone. The present synthesis involves 16 steps and the over-all yield from jervine **3** is 0.3%. Improved syntheses of **1** and **2** are now in progress.

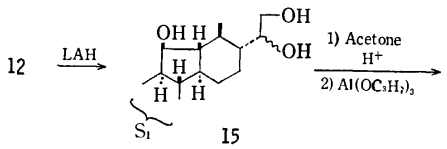

15

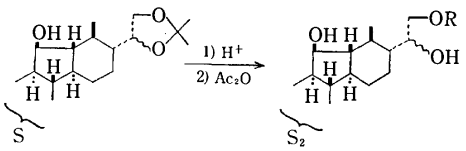

16 S=S_1 18 R=H

17 S=S_2 19 R=Ac

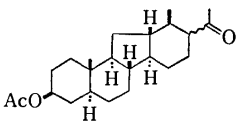

20 17αH

21 17βH

24) S. Nishimura, *Kagaku no Ryoiki*, **23**, 746 (1969).

25) A. Bowers, T. G. Halsall, E. R. H. Jones, and A. J. Lemin, *J. Chem. Soc.*, **1953**, 2548.

26) K. E. Pfitzer and J. G. Moffatt, *J. Amer. Chem. Soc.*, **87**, 5661 (1965).

27) H. Suginome, T. Kojima, K. Orito, and T. Masamune, *Tetrahedron*,, **27**, 291 (1971); H. Suginome, N. Sato, and T. Masamune, *Tetrahedron Lett.*, **1969**, 2671.

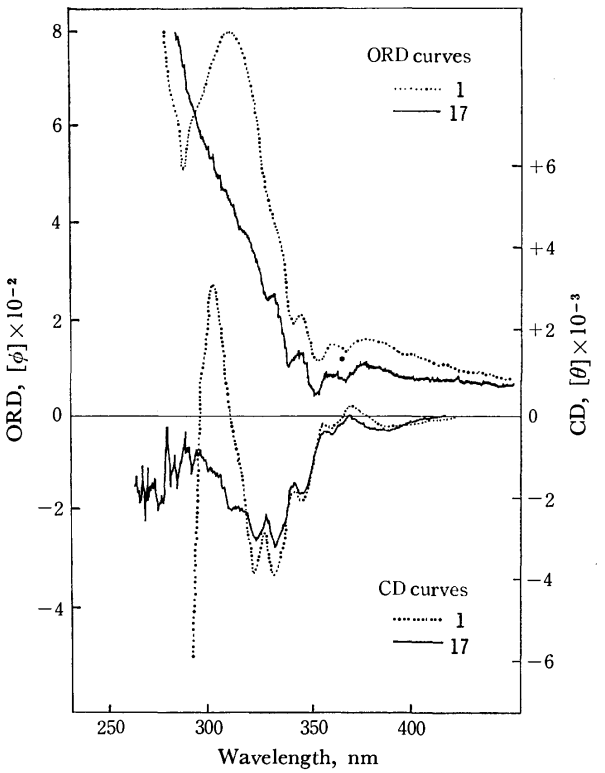

Fig. 1. The ORD and CD curves of 20-oxo and 20-hyoxy-ethiojervanes **1** and **17**.

Experimental

The melting points were measured in open capillaries and uncorrected. Homogeneity of each compound was always checked by TLC on silica gel (Wakogel B-5) and/or alumina (Merck G). The optical rotations and IR spectra were taken in methanol and in Nujol unless otherwise stated. The NMR spectra were measured in deuterochloroform at 60 and/or 100 MHz, tetramethylsilane being used as an internal reference, unless otherwise sated. The abbreviations s, d, t, q, br, and m in the NMR spectra denote singlet, doublet, tripelt, quartet, broad, and multiplet, respectively.

17β-Carbethoxymethylen-17α,20ξ-expoxyetiojerv 5-ene-3β,11β-diol-(7). To a solution of etiojerv-5-ene-3β,11β-diol-17-one[2] (**4**, 9.14 g), 194—195°C, in DMSO (400 m*l*), freshly distilled at bp 95°C/35 mmHg over sodium hydride, were added ethyl chloroacetate (13.5 m*l*) and sodium ethoxide (11.7 g) under cooling, and the mixture was stirred at room temperature for 48 hr in a sealed tube. The mixture was shaken with water (400 m*l*) and chloroform (200 m*l*). After separation of the chloroform layer, the aqueous solution was extracted with chloroform (3×100 m*l*). All the chloroform solutions were combined, washed with an aqueous sodium chloride solution and water, dried over anhydrous sodium sulfate, and evaporated to leave brown oil. The oil (14.35 g) was chromatographed over alumina (Merck, neutral 250 g), using benzene, benzene-ether, ether, and acetone as eluents. Fractions eluted with benzene-ether and ether amounted to 9.66 g after removal of the solvents and, on trituration with acetone-ether, yielded crystalline material (**7**, 3.07 g), which was collected by filtration and showed a single spot. The filtrate was evaporated off to leave amorphous residue (4.68 g), which was again chromatographed over silica gel (Merck, 70—325 mesh, 181 g), using the same solvents as mentioned above. Eluates with benzene-ether contained **7** (checked by tlc) and crystallized partially on trituration with ether or ether-acetone. The crystalline substance (**7**, 1.11 g), collected by filtration, was combined with the afore-mentioned and recrystallized from ether-acetone for analysis to give **7** (3.80 g), mp 176—178°C; $[\alpha]_D$ −58.9°; mass, *m/e* 390 (M^+); IR, ν_{max} 3470 and 1747 cm^{-1}; NMR, τ 9.11 (3H, d, J=7 Hz, 18-CH_3), 8.84 (3H, t, J=7 Hz, $COOCH_2CH_3$), 8.76 (3H, s, 19-CH_3), 6.50 (1H, m, *H* at C_3), 5.75 (2H, q, J=7 Hz, $COOCH_2CH_3$), 5.70 (1H, m, *H* at C_{11}), 4.77 (1H, br s, *H* at C_6), and 4.43 (1H, s, *H* at C_{20}).

Found: C, 70.45; H, 8.73%. Calcd for $C_{23}H_{34}O_5$: C, 70.45; H, 8.78%.

Examination of the mother liquors obtained on removal of **7** by tlc indicated the presence of an almost equal amount of **4**.

17-Carbethoxymethylenetiojerva-5,13(17)-diene-3β,11β,20-ξ-triol (8) and 17-carbethoxymethylenetiojerva-5,16-diene-3β,11β,20ξ-triol (9). A solution of **7** (500 mg) in dry THF (25 m*l*) and DMSO (25 m*l*) was refluxed with boron trifluoride etherate (0.5 m*l*) for 5 hr and for another 3 hr after addition of the same fluoride (0.5 m*l*). After being cooled, the solution was mixed with water (150 m*l*) and then extracted with chloroform (50, 25, and 25 m*l*). The chloroform solutions were dried and evaporated under reduced pressure to leave amorphous residue (506 mg). This was separated into 2 parts by preparative tlc using ether and 18 plates; each plate was made of silica gel (Wakogel B-5, 10 g) with an area 20×20 cm^2. A less mobile fraction showing a single spot was extracted with acetone-methanol and gave amorphous substance (140 mg) after removal of the solvent, which crystallized on trituration with acetone-ether to yield **8** (115 mg), mp 149—150°C. This was recrystallized from the same solvent for analysis; mp 150—151°C; $[\alpha]_D$ −146.9°; IR, ν_{max} 3370, 3270 (shoulder), 1749 and 1295 cm^{-1}; NMR, τ 8.65 (3H, s, 19-CH_3), 8.65 (3H, t, J=7 Hz, $COOCH_2CH_3$), 8.07 (3H, s, 18-CH_3), 6.50 (1H, m, *H* at C_3), 5.75 (2H, q, J=7 Hz, $COOCH_2CH_3$), 5.70 (1H, m, *H* at C_{11}), 4.94 (1H, s, *H* at C_{20}), and 4.72 (1H, br s, *H* at C_6).

Found: C, 70.54; H, 8.72%. Calcd for $C_{23}H_{34}O_5$: C, 70.74; H, 8.78%.

The more mobile fraction (288 mg) showing a single spot crystallized on trituration with acetone-ether to give **9** (199 mg), mp 147—149°C. This was recrystallized from the same solvent for analysis; mp 152—153°C; $[\alpha]_D$ −145.3°; IR, ν_{max} 3520, 3390, 3210, 1723, and 1285 cm^{-1}; NMR, τ 8.82 (3H, d, J=6 Hz, 18-CH_3), 8.72 (3H, s, 19-CH_3), 8.72 (3H, t J=7 Hz, $COOCH_2CH_3$), 6.50 (1H, m, *H* at C_3), 5.75 (2H, q, J=7 Hz, $COOCH_2CH_3$), 5.70 (1H, m, *H* at C_{11}), 5.36 (1H, s, *H* at C_{20}), 4.75 (1H, br s, *H* at C_6), and 4.11 (1H, br s W_H=12 Hz, *H* at C_{16}).

Found: C, 70.66; H, 9.07%. Calcd for $C_{23}H_{34}O_5$: C, 70.74; H, 8.78%.

17α-Carbethoxymethylenetiojerv-5-ene-3β,11β,20ξ-triol (12). Compound **9** (1.70 g) was hydrogenated over prereduced Adams platinum (800 mg as $PtO \cdot H_2O$) in ethanol (125 m*l*) at room temperature for 2 days, when 100 m*l* of hydrogen (1 mol) had been absorbed. The reaction was continued for 3.5 days. After removal of the catalyst and the solvent, the residue was dissolved in chloroform. The solution was washed with an aqueous sodium chloride solution and water, dried and evaporated to leave amorphous residue (1.97 g), which crystallized on trituration with acetone-ether to give **12** (1.49 g), mp 167—170°C, showing a single spot. This was recrystallized from the same solvent for analysis; mp 177—179°C; $[\alpha]_D$ −53.5°; IR, ν_{max} 3470, 1717 and 1240 cm^{-1}; NMR, τ 8.98 (3H, d, J=6Hz, 18-CH_3), 8.77 (3H, s, 19-CH_3), 8.72 (3H, t, J=7 Hz, $COOCH_2CH_3$), 6.50 (1H,

m, *H* at C_3), 5.76 (2H, q, J=7 Hz, $COOCH_2CH_3$), 5.72 (2H, m, *H* at C_{11} and C_{20}), and 4.75 (1H, br s, H at C_6).

Found: C, 70.21; H. 9.43%. Calcd for $C_{23}H_{36}O_5$: C, 70.37; H, 9.24%.

*17α-Ethyletiojerv-5-ene-3β,11β,20ξ,21-tetrol 20,21-Acetonide (**16**).* To a suspension of LAH (500 mg) in dry THF (40 m*l*) was added compound **12** (500 mg) in dry THF (35 m*l*) under stirring during 50 min, and the mixture was stirred at room temperature for 1 hr. To the cooled mixture were added dropwise methanol (2 m*l*) and water (20 m*l*) under stirring to decompose excess of the LAH, and then 1 N hydrochloric acid to dissolve the resulting aluminum hydroxide. The mixture was extracted with ethyl acetate (3×20 m*l*), and the solution was washed with water. The aqueous washings were again extracted with ethyl acetate (20 m*l*). All the acetate solutions were combined, evaporated and dried over phosphorus pentoxide under reduced pressure to leave crystalline material (crude tetrol **15**, 427 mg), which was used for the next reaction without further purification.

A solution of the crude tetrol **15** in acetone (40 m*l*), freshly distilled over potassium carbonate after reflux with potassium permanganate, was stirred with PTS (400 mg) at room temperature for 10 min, when the spot of **15** had disappeared. After 40 min, the solution was mixed with an aqueous, saturated sodium bicarbonate solution and extracted with chloroform (3×40 m*l*). The chloroform solution was washed with water, dried and evaporated to leave amorphous residue (513 mg), which showed 2 spots on tlc and was separated by preparative tlc (ether and 13 plates). The more mobile, main fraction gave amorphous substance which was crystallized and recrystallized from acetone-ether to give **16** (237 mg), mp 217—220°C; $[\alpha]_D$ −49.2°; mass, *m/e* 390 (M^+); IR, ν_{max} 3430, 1068, and 1052 cm^{-1}; NMR, τ 8.85 (3H, d, J=5 Hz, 18-CH_3), 8.75 (3H, s, 19-CH_3). 8.62 (6H, s, CH_3CCH_3), 6.50 (1H, m, *H* at C_3), 6.00 (3H, m, *H* at C_{20} and C_{21}), 5.70 (1H, m, *H* at C_{11}), and 4.75 (1*H*, br s, *H* at C_6).

Found: C, 73.87; H, 9.74%. Calcd for $C_{24}H_{38}O_4$: C, 73.80; H, 9.81.

*17α-Ethyletiojerv-4-ene-11β,20ξ,21-triol-3-one 20,21-Acetonide (**17**).* A solution of compound **16** (200 mg) in toluene (55 m*l*) containing cyclohexanone (5 m*l*) was heated under stirring until 28 m*l* of the toluene was removed. After addition of aluminum isopropoxide (480 mg), the whole mixture was refluxed for 3.7 hr and cooled. After addition of acetone (8 m*l*) and water (8 m*l*), the mixture was stirred at room temperature overnight and filtered. The filtrate was subjected to steam distillation to give oily residue which was extracted with chloroform repeatedly. The extracts yielded amorphous substance (225 mg) which crystallized on trituration with ether to give **17** (168 mg), mp 156—158°C. This was recrystallized from acetone-ether for analysis; mp 160—162°C; $[\alpha]_D$ +100.0°; IR, ν_{max} 3410, 1650, 1610, 1075, and 1060 cm^{-1}; NMR, τ 8.87 (3H, d, J=5 Hz, 18-CH_3), 8.64 (6H, s, CH_3CCH_3), 8.59 (3H, s, 19-CH_3), 6.05 (4H, m, *H* at C_{11}, C_{20}, and C_{21}), and 4.28 (1H, s, *H* at C_4).

Found: C, 74.10; H, 9.26%. Calcd for $C_{24}H_{36}O_4$: C, 74.19; H, 9.34%.

*17α-Ethyletiojerv-4-ene-11β,21-diol-20-one 21-Acetate (C-Nor-D-homo-17-epicorticosterone 21-Acetate, **1**).* A solution of compound **17** (100 mg) in methanol (8 ml) containing concentrated hydrochloric acid (4 drops) was stirred at room temperature for 1.5 hr. After removal of the methanol below 40°C, the residue was extracted with chloroform, and the chloroform solution was evaporated and dried over phosphorus pentoxide under reduced pressure to leave resinous substance (crude **18**, 93 mg).

The resin was dissolved in pyridine (0.2 m*l*) and treated with acetic anhydride (36 m*l*) in dioxane (0.4 m*l*) at room temperature for 15 hr. The mixture was poured into ice-water (70 m*l*) and extracted with chloroform repeatedly. The chloroform solution was washed with 1 N hydrochloric acid and water, dried and evaporated to leave oily residue (126 mg) which was separated by preparative tlc (ether and 3 plates). The main fraction afforded oil (crude **19**, 60 mg) which was used for the next reaction without further purification.

A solution of the oil (50 mg) in a 1 : 3 mixture of dry DMSO and benzene (0.64 m*l*) was treated with DCC (80 mg, 3 equiv) and 0.5 M trifluoroacetic acid and 1 M pyridine in DMSO (0.13 m*l*) at room temperature for 3.5 hr in a sealed tube. On addition of ether, precipitates separated out and were removed by filtration. The ether filtrate was washed with water, dried and evpaorated to leave amorphous residue (66 mg) which was separated into 3 parts by preparative TLC (ether and 1 plate). The main fraction gave crystalline material (**1**, 20 mg), mp 208—211°C, on removal of the solvent. This was recrystallized from acetone-ether for analysis; mp 209—211°C; CD and ORD (Fig. 1); mass, *m/e* 388 (M^+); IR, ν_{max} 3420, 1748, 1728, 1665, and 1610 cm^{-1}; NMR, τ 9.05 (3H, d, J=6 Hz, 18-CH_3), 8.60 (3H, s, 19-CH_3), 7.88 (3H, s, $OCOCH_3$), 5.80 (1H, m, *H* at C_{11}), 5.35 (2H, s, *H* at C_{21}), and 4.38 (1H, s, *H* at C_4).

Found: C, 70.88; H, 8.43%. Calcd for $C_{23}H_{32}O_5$: C, 71.10; H, 8.30%.

The authors are grateful to Mr. Shigezo Shimokawa for the measurement of NMR, to Mr. Naofumi Hanabusa for that of CD and ORD curves, to Miss Masako Takahashi for that of mass spectra, and also to Misses Hiroko Kakizaki and Motoko Sato for the microanalysis.

The Synthesis of the 1,2,4-Thiadiazine-1,1-dioxides[1]

Kiyoshi HASEGAWA and Syuzi HIROOKA

Department of Industrial Chemistry, Faculty of Engineering, Toyama University, Takaoka-shi

(Received January 5, 1972)

N-(2-Phenylethene-1-sulfonyl)-*N'*-monoalkyl *S*-methylisothioureas, **2**, were ring-closed to yield Michael cycloadducts, 3-methylthio-4-alkyl-5-phenyl-1,1-dioxo-5,6-dihydro-1,2,4-thiadiazines, **3**. Bulky *N'*-alkyl groups hindered the cycloaddition. The base-catalyzed hydrolysis of **3** and 3-chloro-derivatives **4** gave 4-methyl-5-phenyl-2,3,5,6-tetrahydro-1,1,3-trioxo-1,2,4-thiadiazines, **5**, which in turn underwent *N*-alkylation to give **6**. The reaction of **4** with amines or with sodium methoxide yielded 3-amino-, **7**, or 3-methoxy-thiadiazine derivatives, **9**.

Recently we have reported[2,3] the synthesis of a new heterocyclic system, 5,6-dihydro-1,4,2-dithiazine-1,1-dioxide, by the intramolecular Michael cycloaddition of *N*-(2-phenylethene-1-sulfonyl)-*N'*-alkylthioureas, dithiocarbamates, and *O*-alkyl thiocarbamates. This paper will describe a new route to the little-known 1,2,4-thiadiazine-1,1-dioxide derivatives,[4] starting from the substituted isothioureas. The process is outlined below.

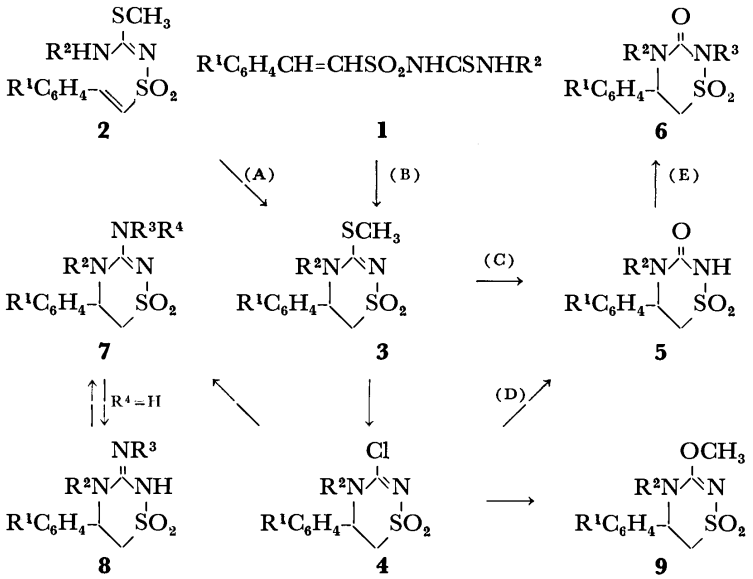

Results and Discussion

The reaction of *N*-(2-phenylethene-1-sulfonyl)-*N'*-monoalkylthioureas (**1**) with dimethyl sulfate in DMF afforded *N*-(2-phenylethene-1-sulfonyl)-*N'*-alkyl *S*-methylisothioureas (**2**) (Table 1). They were ring-closed in ethanol containing catalytic amounts of sodium hydroxide to yield intramolecular cycloadducts, 3-methylthio-4-alkyl-5-phenyl-1,1-dioxo-1,2,4-thiadiazines (**3**) (Table 2, Method (A)). The IR spectrum of **3a** displayed a strong band at 1530 cm^{-1} due to the N=C bond, but no absorption due to the NH bond was observed. In the NMR pattern of **3a**, ring protons, $H_AH_CH_B$, showed an ABX pattern consisting of three quartets of H_A centered at δ 3.36, H_C 3.53, and H_B 5.03 (J_{AC}=13.5 Hz, J_{AB}=10.5 Hz, J_{BC}=6.0 Hz) (Fig. 1). The peak at *m/e* 118.066 in the mass spectrum was in complete agreement with the fragment ion, $C_6H_5CN^+CH_3$, derived from only the six-membered heterocycle, **3**. The structures of **3b**—**3h** were inferred because they were analogous with **3a** in their preparations and spectral data.

Cycloaddition is subject to steric hindrance, and it was unsuccessful here when the alkyl group, R^2, in **2** was bulky or branched, like the cyclohexyl, isopropyl, *s*-, and *t*-butyl groups. The amounts of a base required to complete the cycloaddition of **2**'s in 6 hr at 25—30°C were determined. Table 2 shows that only from a sixth to a third equivalent of the base was sufficient to effect the cycloaddition of **2** when R^2 was the methyl group, while more bases were required when R^2 became bulky. The *N'*-dialkylisothiourea could not be ring-closed, presumably because of the lack of a hydrogen atom at the *N'*-position. The reaction of **1** with dimethyl sulfate and sodium hydroxide in ethanol afforded **3** directly (Table 2, Method (B)). The C–N bond in **3** could not be cleaved by a strong base at elevated temperatures, but hydrolytic products, 4-methyl-5-phenyl-2,3,5,6-tetrahydro-1,1,3-trioxo-1,2,4-thiadiazines (**5**) resulted (Table 4, Method (C)). They were identified by

1) Presented in part at the 25th Annual Meeting of the Chemical Society of Japan, Tokyo, October, 1971.

2) K. Hasegawa and S. Hirooka, This Bulletin, **45**, 525 (1972).

3) K. Hasegawa and S. Hirooka, *ibid.*, **45**, 1567 (1972).

4) A. Lawson and R. B. Tinkler, *Chem. Rev.*, **70**, 593 (1970).

Table 1. $R^1C_6H_4CH_B{=}CH_ASO_2N{=}C(NHR^2)(SCH_3)$ **2**

Compd.	R^1	R^2	Yield (%)	Mp (°C)	Found (%)				Calcd (%)			
					C	H	N	S	C	H	N	S
2a	H	CH_3	89	80— 81	49.04	5.33	10.30	23.49	48.89	5.22	10.37	23.68
2b	H	C_2H_5	89	107—108	50.66	5.78	9.63	21.04	50.70	5.67	9.86	22.51
2c	H	n-C_3H_7	84	99—100	52.07	5.93	9.41	21.31	52.34	6.08	9.39	21.45
2d	H	i-C_3H_7	79	135—136	52.16	5.78	9.48	21.38	52.34	6.08	9.39	21.45
2e	H	n-C_4H_9	90	148—149	53.87	6.19	9.07	21.20	53.84	6.45	8.97	20.51
2f	H	i-C_4H_9	87	141—142	53.61	5.86	9.07		53.84	6.45	8.97	20.51
2g	H	s-C_4H_9	95	112—113	53.47	6.26	9.05	20.37	53.84	6.45	8.97	20.51
2h	H	t-C_4H_9	83	139—140	54.02	6.44	9.28	19.92	53.84	6.45	8.97	20.51
2i	H	n-C_6H_{13}	67	40— 41	56.37	7.12	8.15		56.46	7.11	8.23	
2j	H		87	152—153	56.36	6.48	8.33	18.65	56.79	6.45	8.28	18.91
2k	p-Cl	CH_3	84	168—169	43.30	4.25	9.35	21.35	43.34	4.30	9.19	21.04
2l	p-Cl	C_2H_5	91	130—131	45.13	4.67	8.60	20.02	45.21	4.74	8.79	20.11
2m	p-Br	CH_3	80	167—168	38.05	3.84	7.95	18.06	37.82	3.75	8.02	18.36
2n	p-Br	C_2H_5	81	138—140	39.86	4.44	7.66	17.28	39.67	4.16	7.71	17.65
2o	p-CH_3	CH_3	90	152—153	51.00	5.64	10.12	22.50	50.70	5.67	9.86	22.51
2p	p-CH_3	C_2H_5	89	103—104	52.07	6.14	9.43	21.39	52.34	6.08	9.39	21.45

Table 2. 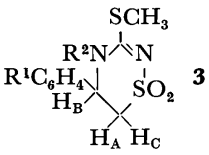 **3**

Compd.	R^1	R^2	Moles of base[a] mol of **2**	Yield (%) Method (A)	Yield (%) Method (B)	Mp (°C)	Found (%) C	H	N	S	Calcd (%) C	H	N	S
3a	H	CH_3	1/6	82	69	140—141	48.53	5.58	10.28	23.50	48.89	5.22	10.37	23.68
3b	H	C_2H_5	1/2	82	76	196—197	50.33	5.75	9.79	22.11	50.68	5.67	9.85	22.55
3c	H	n-C_3H_7	1.0	83		144—145	52.24	5.98	9.38	21.14	52.34	6.08	9.39	21.45
3d	H	n-C_4H_9	2.0	89		93— 95	53.62	6.63	9.20	20.27	53.84	6.45	8.97	20.51
3e	H	i-C_4H_9	2.0	81		141—142	53.48	6.36	9.00	20.16	53.84	6.45	8.97	20.51
3f	H	n-C_6H_{13}	2.0	71		85— 86	57.14	7.31	8.34		56.46	7.11	8.23	
3g	p-Cl	CH_3	1/3	90		210—211	43.29	4.14	9.24	20.75	43.34	4.30	9.19	21.04
3h	p-CH_3	CH_3	1/3	78		171—172	50.56	5.75	9.79	22.11	50.68	5.67	9.85	22.55

a) 1 N NaOH solution was used.

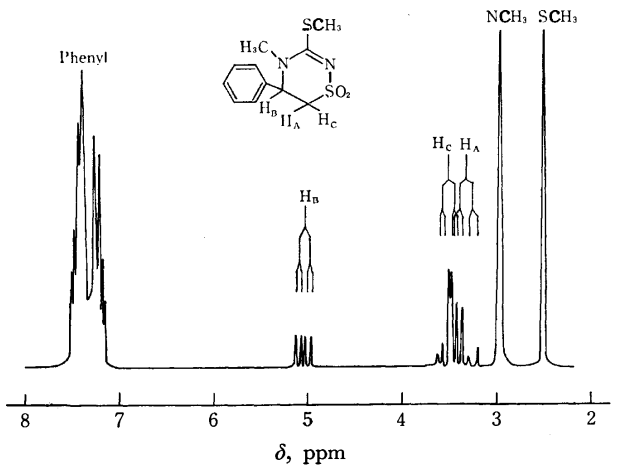

Fig. 1. NMR spectrum of **3a** in $CDCl_3$.

means of the IR (1650 cm^{-1} for C=O, 2960 cm^{-1} for NH), NMR (δ 3.30 for NH) and mass spectra, and also by means of the results of elemental analyses. The methylthio group in **3** was replaced by a chlorine atom to give 3-chloro-derivatives (**4**) (Table 3). The base-catalyzed hydrolysis of **4** gave **5** (Table 4, Method (D)), and **5** was readily methylated to afford 2,4-dimethyl-5-phenyl-2,3,5,6-tetrahydro-1,1,3-trioxo-1,2,4-thiadiazine (**6**) (Table 4, Method (E)). The reaction of **4** with various amines or with sodium methoxide yielded 3-alkylamino- or -hydrazino- (**7**), or 3-methoxy-derivatives (**9**) (Table 3). When the R^4 in **7** is a hydrogen atom, the tautomerism between **7** and **8** can be expected. The possibility that the solid product is an alternative isomer, **8**, was discounted by its insolubility in alkali, thereby demonstrating the absence of the SO_2NH group. The IR

TABLE 3.

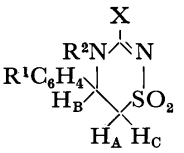

Compd.	R^1	R^2	X	Yield (%)	Mp (°C)	Found (%)				Calcd (%)			
						C	H	N	S	C	H	N	S
4a	H	CH_3	Cl	92	156—157	46.65	4.22	11.06	12.35	46.80	4.25	10.83	12.39
4b	H	C_2H_5	Cl	86	155—156	48.37	4.79	10.46	11.73	48.44	4.80	10.27	11.76
4c	*p*-Cl	CH_3	Cl	81	196—197	40.78	3.38	9.36	10.95	40.97	3.44	9.56	10.94
4d	*p*-CH_3	CH_3	Cl	83	148—149	48.22	4.87	10.00	12.38	48.44	4.80	10.27	11.76
7a	H	CH_3	$NHCH_3$	81	202—203	51.90	5.91	16.40	12.62	52.17	5.97	16.59	12.64
7b	H	CH_3	NHC_2H_5	95	168—169	53.86	6.45	15.79	12.01	53.92	6.41	15.72	11.97
7c	H	CH_3	$N(CH_3)_2$	99	228—229	53.72	6.40	15.66	12.16	53.92	6.41	15.72	11.97
7d	H	CH_3	$N(C_2H_5)_2$	87	170—171	56.93	7.18	14.09	10.98	56.93	7.17	14.23	10.84
7e	H	CH_3	$NHNH_2$	61	212—213	46.98	5.54	21.77	12.26	47.24	5.55	22.04	12.59
7f	H	C_2H_5	NH-⟨H⟩	98	160—161	57.53	7.56	11.92	9.12	57.77	7.70	11.89	9.06
7g	*p*-Cl	CH_3	$NHCH_3$	98	280—282	45.66	4.83	14.33	11.28	45.91	4.90	14.60	11.14
7h	*p*-Cl	CH_3	$NHNH_2$	91	218—220	41.84	4.52	19.26	11.03	41.59	4.54	19.40	11.10
7i	*p*-CH_3	CH_3	$NHCH_3$	87	218—219	54.17	6.51	15.86	12.08	53.92	6.41	15.72	11.97
7j	*p*-CH_3	CH_3	$N(CH_3)_2$	90	196—197	55.78	6.71	15.19	11.63	55.50	6.81	14.94	11.38
9a	H	CH_3	OCH_3	37	155—156	51.96	5.46	10.84	12.51	51.96	5.55	11.02	12.59

TABLE 4.

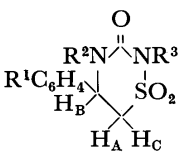

Compd.	R^1	R^2	R^3	Yield (%) Method (C) (E)	Yield (%) Method (D)	Mp (°C)	Found (%)				Calcd (%)			
							C	H	N	S	C	H	N	S
5a	H	CH_3	H	82	96	227—229	49.96	5.00	11.78	13.37	50.00	5.04	11.66	13.32
5b	*p*-Cl	CH_3	H	72	78	236—238	43.55	3.95	10.28	11.65	43.72	4.04	10.20	11.67
5c	*p*-CH_3	CH_3	H	77	81	247—249	51.79	5.61	10.81	12.67	51.95	5.55	11.02	12.60
6a	H	CH_3	CH_3	52		123—124	51.68	5.50	11.06	12.63	51.95	5.55	11.02	12.60
6b	*p*-Cl	CH_3	CH_3	58		142—143	45.61	4.36	9.54		45.75	4.54	9.70	

spectra of **7a** and **7b** in KBr tablets displayed absorption peaks in the same region as the N=C group in **7c** and **7d**. However, NMR studies of **7a**, **7g**, and **7i** dissolved in DMSO-d_6 offered evidence for the presence of the **8** isomer in a tautomeric mixture in the solution. In the $NHCH_3$ group in **7a**, methyl protons showed a doublet at δ 2.71 (J=4.0 Hz), and a NH proton, a broad quartet at δ 6.94 (J=4.0 Hz), with a peak area of 0.52H. In addition, there was a sharp singlet at δ 2.70, assignable to the $=NCH_3$ protons in **8** between a doublet methyl signal. However, a sulfonamide NH proton of **8** could not be observed because of overlapping with a signal of water contained in DMSO-d_6 at 3.34. After the treatment with D_2O, the NH proton signal (δ 6.94) was eliminated and only a sharp singlet due to the $=NCH_3$ protons appeared. The relative peak areas of the methyl and NH peaks assignable to the structures of **7** and **8** indicated that **7a** consisted of about a 50 : 50 mixture of **7** and **8** in DMSO-d_6.

Experimental

The melting points were determined on a Yanagimoto micro-melting-point measuring apparatus, MP-S2, and are uncorrected. The IR spectra were recored on a JASCO IRA-1 spectrometer. The NMR spectra were determined with a Varian HA-100 spectrometer, with TMS as the internal standard, and the mass spectra, with a JMS-OlSG spectrometer.

*N-(2-Phenylethene-1-sulfonyl)-N'-methyl S-Methylisothiourea (**2a**).* To a stirred solution of *N*-(2-phenylethene-1-sulfonyl)-*N'*-methylthiourea (1.20 g, 0.0040 mol) in DMF (10 m*l*), we added a 1 N NaOH solution (9.6 m*l*, 0.0096 mol) and dimethyl sulfate (0.61 g, 0.0048 mol), drop by drop, at 0—10°C. After being stirred for 3 hr at room temperature, the reaction mixture was poured into ice water (100 m*l*) and kept overnight. The precipitated white solid was filtered to give 0.96 g (89%) of **2a**. Recrystallization from benzene-petroleum ether gave colorless crystals. IR (KBr): 3330 (NH), 3040 (=CH), 1610 (C=C), 1560 (N=C),

1335, and 1115 (SO_2) cm^{-1}. NMR ($CDCl_3$): δ 2.44 (s, 1H, SCH_3), 2.99 (d, J_{NHCH_3}=5.0 Hz, 3H, $NHCH_3$), 6.93 (d, J_{AB}=15.5 Hz, 1H, H_A), 7.54 (d, J_{AB}=15.5 Hz, 1H, H_B), 7.45±0.02 (m, 5H, phenyl), 8.10 (broad, 1H, NH). Mass spectrum *m/e*: 270 (M^+).

*3-Methylthio-4-methyl-5-phenyl-1,1-dioxo-5,6-dihydro-1,2,4-thiadiazine (**3a**).* *Method (A)*: To a solution of **2a** (0.54 g, 0.0020 mol) in ethanol (20 m*l*), we added a 1 N NaOH solution (0.34 m*l*, 0.00033 mol), after which the mixture was stirred for 6 hr at 25—30°C. An ethanol solution containing white precipitates was concentrated *in vacuo*, water (5 m*l*) was added, and the precipitates were collected to obtain 0.44 g (82%) of **3a**. Recrystallization from ethanol gave colorless crystals. IR (KBr): 1530 (N=C), 1300, and 1140 (SO_2) cm^{-1}. NMR ($CDCl_3$): δ 2.47 (s, 3H, SCH_3), 2.86 (s, 3H, NCH_3), 3.36 (q, J_{AC}=13.5 Hz, J_{AB}=10.5 Hz, 1H, H_A), 3.53 (q, J_{AC}=13.5 Hz, J_{BC}=6.0 Hz, 1H, H_C), 5.03 (q, J_{AB}=10.5 Hz, J_{BC}=6.0 Hz, 1H, H_B), 7.34±0.12 (m, 5H, phenyl). Mass spectrum (75 eV) *m/e* (rel intensity): 77 (17), 78 (13), 91 (10), 104 (100), 105 (10), 118.066 (12), 119 (6), 132 (6), 159 (6), 173 (3), 191 (4), 206 (5), 207 (10), 270.105 (calculated molecular weight, 270.106, 10).

Method (B): Into a solution of *N*-(2-phenylethene-1-sulfonyl)-*N'*-methylthiourea (10.25 g, 0.0400 mol) in a 1 N NaOH solution (80 m*l*, 0.0800 mol) and ethanol (80 m*l*), we stirred, drop by drop, dimethyl sulfate (6.40 g, 0.050 mol) at 0—10°C. Stirring was continued for a further 4 hr at room temperature. An ethanol solution containing white precipitates was concentrated *in vacuo*, and the precipitates were collected to afford 7.50 g (69%) of **3a**. The aqueous filtrate was acidified with concentrated hydrochloric acid to give 2.20 g of **5a**.

*3-Chloro-4-methyl-5-phenyl-1,1-dioxo-5,6-dihydro-1,2,4-thiadiazine (**4a**).* Into a solution of **3a** (2.70 g, 0.0100 mol) in chloroform (20 m*l*) we bubbled excess chlorine at 30—40°C until the colorless solution turned orange. The evaporation of the chloroform left white precipitates, which were recrystallized from methanol to obtain 2.40 g (92%) of colorless crystals. IR (KBr): 1590 and 1575 (N=C), 1330 and 1150 (SO_2) cm^{-1}. NMR ($CDCl_3$): δ 3.04 (s, 3H, CH_3), 3.48 (q, J_{AC}=14.0 Hz, J_{AB}=9.5 Hz, 1H, H_A), 3.63 (q, J_{AC}=14.0 Hz, J_{BC}=7.0 Hz, 1H, H_C), 5.18 (q, J_{AB}=9.5 Hz, J_{BC}=7.0 Hz, 1H, H_B), 7.44 (s, 5H, phenyl). Mass spectrum *m/e*: 258.088 (calculated molecular weight, 258.082).

*4-Methyl-5-phenyl-2,3,5,6-tetrahydro-1,1,3-trioxo-1,2,4-thiadiazine (**5a**).* *Method (C)*: To a solution of **3a** (0.54 g, 0.0020 mol) in acetone (10 m*l*), we added a 1 N NaOH solution (4.0 m*l*, 0.0040 mol), after which the reaction mixture was refluxed for 2 hr. The acetone was evaporated *in vacuo*, and the solution was acidified with concentrated hydrochloric acid to afford 0.44 g (82%) of **5a**. Recrystallization from ethanol gave colorless crystals. IR (KBr): 2960 (NH), 1650 (C=O), 1340, 1320, and 1140 (SO_2) cm^{-1}. NMR (DMSO-d_6): δ 2.59 (s, 3H, NCH_3), 3.30 (broad, 1H, NH), 3.73 (q, J_{AC}=13.7 Hz, J_{AB}=9.8 Hz, 1H, H_A), 3.94 (q, J_{AC}=13.7 Hz, J_{BC}=5.6 Hz, 1H, H_C), 4.89 (q, J_{AB}=9.8 Hz, J_{BC}=5.6 Hz, 1H, H_B), 7.38 (s, 5H, phenyl). Mass spectrum *m/e*: 240.083 (calculated molecular weight, 240.085).

Method (D): To a solution of **4a** (0.52 g, 0.0020 mol) in acetone (20 m*l*), we added a 1 N NaOH solution (4.0 m*l*, 0.0040 mol), after which the reaction mixture was stirred for 1 hr at room temperature. The acetone was evaporated *in vacuo*, and water (10 m*l*) was added to the residue. The solution was then acidified with concentrated hydrochloric acid to afford 0.46 g (96%) of **5a**.

*2,4-Dimethyl-5-phenyl-2,3,5,6-tetrahydro-1,1,3-trioxo-1,2,4-thiadiazine (**6a**).* Into a solution of **5a** (0.64 g, 0.0027 mol) in a 1 N NaOH solution (5.5 m*l*, 0.0054 mol) and ethanol (5.5 m*l*), we stirred, drop by drop, dimethyl sulfate (0.40 g, 0.0032 mol) over a 4-hr period at room temperature. The alkaline solution containing white precipitates was concentrated and collected to obtain 0.35 g (52%) of **6a**. Recrystallization from aqueous methanol gave colorless crystals. IR (KBr): 1650 (C=O), 1350, 1340, and 1145 (SO_2) cm^{-1}. NMR ($CDCl_3$): δ 2.77 (s, 3H, $C_6H_5\underset{|}{C}HN(\underline{CH_3})$-), 3.24 (s, 3H, $-N(CH_3)SO_2-$), 3.43 (q, J_{AC}=13.2 Hz, J_{AB}=12.0 Hz, 1H, H_A), 3.65 (q, J_{AC}=13.2 Hz, J_{BC}=6.0 Hz, 1H, H_C), 4.81 (q, J_{AB}=12.0 Hz, J_{BC}=6.0 Hz, 1H, H_B), 7.37±0.1 (m, 5H, phenyl). Mass spectrum *m/e*: 254.075 (calculated molecular weight, 254.073).

*3-Methylamino-4-methyl-5-phenyl-1,1-dioxo-5,6-dihydro-1,2,4-thiadiazine (**7a**).* To a stirred solution of **4a** (1.03 g, 0.0040 mol) in chloroform (10 m*l*), we added a 30% aqueous methylamine solution (0.83 g, 0.0080 mol) at room temperature, and then the mixture was stirred for 1 hr. The chloroform was evaporated *in vacuo*, and water (10 m*l*) was added to the residue. The cooled precipitates were collected to obtain 0.82 g (81%) of **7a**. Recrystallization from chloroform–petroleum ether gave colorless crystals. IR (KBr): 3350 (NH), 1560—1530 (N=C), 1340 and 1115 (SO_2) cm^{-1}. NMR (DMSO-d_6): δ 2.65 (s, 3H, NCH_3), 2.71 (d, J_{NHCH_3}=4.0 Hz, $NHCH_3$), 2.70 (s, $=NCH_3$), 3.20 (q, J_{AC}=13.5 Hz, J_{AB}=10.0 Hz, 1H, H_A), 3.45 (q, J_{AC}=13.5 Hz, J_{BC}=6.0 Hz, 1H, H_C), 4.89 (q, J_{AB}=10.0 Hz, J_{BC}=6.0 Hz, 1H, H_B), 6.94 (q, J_{NHCH_3}=4.0 Hz, 0.52H,NH), 3.34 (SO_2NH), 7.34 (s, 5H, phenyl). Mass spectrum *m/e*: 253.116 (calculated molecular weight, 253.118).

*3-Methoxy-4-methyl-5-phenyl-1,1-dioxo-5,6-dihydro-1,2,4-thiadiazine (**9a**).* To a solution containing sodium metal (0.3 g) dissolved in methanol (4 m*l*), we added **4a** (0.78 g, 0.0030 mol) in portions over a 30-min period at room temperature. The mixture was then allowed to stand for 2 hr, water (10 m*l*) was added, and the precipitates (0.27 g (37%) of **9a**) were collected. The filtrate was acidified with concentrated hydrochloric acid to afford 0.28 g of a hydrolytic product of **4a**. Recrystallization of **9a** from methanol gave colorless crystals. IR (KBr): 1570 (N=C), 1300, and 1130 (SO_2) cm^{-1}. NMR ($CDCl_3$): δ 2.73 (s, 3H, NCH_3), 3.90 (s, 3H, OCH_3), 3.25 (q, J_{AC}=15.0 Hz, J_{AB}=10.4 Hz, 1H, H_A), 3.54 (q, J_{AC}=15.0 Hz, J_{BC}=6.0 Hz, 1H, H_C), 4.97 (q, J_{AB}=10.4 Hz, J_{BC}=6.0 Hz, 1H, H_B), 7.38±0.05 (m, 5H, phenyl). Mass spectrum *m/e*: 254 (M^+).

Automatic Problem Solving Applied to Synthetic Chemistry

Malcolm BERSOHN
Department of Chemistry, University of Toronto, Toronto 181, Ontario, Canada
(Received September 24, 1970)

The first computer program that plans multi-step organic syntheses has been written. In the course of its operation the program generates partially complete synthetic pathways and ranks them as to efficiency. At each stage the program develops that partially complete route which it judges to be the most efficient, and extends it by one step. Partially complete routes which lose too much material are discarded. After each tolerably efficient pathway from available starting materials to the goal molecule is completed, the entire pathway is printed, together with the yield of each step and the overall yield.

The Information Structure of a Synthesis Problem

The various alternative methods of synthesizing a substance can be represented by a diagram like that of Fig. 1. Note that the figure is by no means a complete statement of all of the possible ways of making benzene from cheaper or simpler substances. For clarity, small molecules like CO_2, O_2, H_2, H_2O etc. are omitted from the diagram.

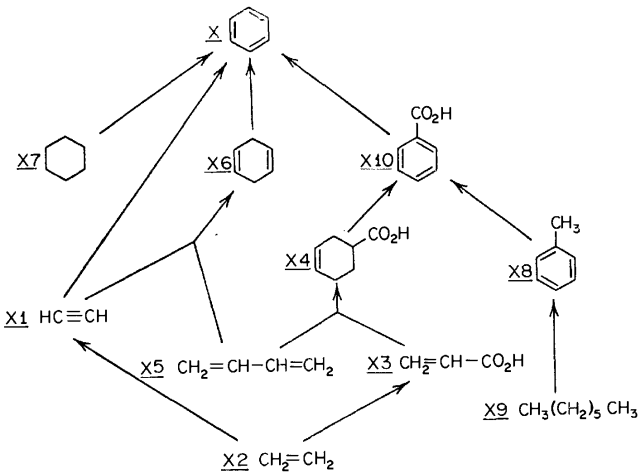

Fig. 1.

Such a two dimensional diagram can become very difficult to decipher because the more pathways that are included the more intersecting lines are possible. In addition, we will have more and more cases like X2, which is both four steps and two steps removed from the goal molecule. Hence there is no well defined level structure or generation structure. Also, evidently, we cannot describe the structure as a tree since there are cycles in it, such as X, X1, X2, X3, X4, and X10. A tree in a forest has no such rings and the tree of graph theory is also acyclic. Nonetheless, despite the unsuitability of two dimensional diagrams for representing it and the absence of a familiar name, the structure does have definite properties, as follows:

(1) Every molecule except the goal molecule has at least one successor molecule.
(2) Every molecule except the starting molecules has at least one parent molecule.
(3) Some molecules have coreactants with which they react to form their common successor molecule. For example, acetylene is the coreactant of butadiene and butadiene is the coreactant of acetylene in the problem of Fig. 1.

These three kinds of relationships link all the molecules of the problem together and these links must be suitably represented in the memory of a computer.

The Strategy Used by Chemists for Finding Good Synthetic Routes

Suppose that we wish to synthesize a molecule named M, starting from readily available molecules. The usual way of attacking this problem is to consider all possible synthetic reactions which could directly produce M. Suppose, for example that L1 and L2 react to form M, L3 can be rearranged to give M, L4 and L5 also react to produce M, all with satisfactory yield. Then we must next consider ways to make the set of molecules {L1, L2, L3, L4, L5}. For example, L1 can be made from K1 and K2; it can also be prepared by isomerization of K3 or K4 etc. We keep on moving backwards in this fashion until available substances are reached, *e.g.* the set {C1, C2, C3, B1, B3, A1, ···, A12}. Some of the pathways found from available substances to M have higher yield and consequently are cheaper to execute than others; we select the most efficient synthetic route(s) for experimental trial.

There are two major difficulties in the carrying out of the above method for planning a synthesis. The first difficulty is that our memory may fail us when considering how to make an intermediate substance, *e.g.* K3; we may not recall a particularly good reaction that could produce K3 from, let us say, J27.

The second difficulty is much greater. Even when and if we remember all relevant synthetic reactions, the complete set of possible pathways is too enormous for human consideration. Suppose, for example, that we have a molecule as complicated as the anti-biotic aureomycin, and assume there exists at least "some" possible synthetic routes which can produce aureomycin in 20 steps. If we assume that at each step there are five possible ways to produce a given intermediate in one step, then there are not only "some" possible routes but actually there are something like 5^{20} possible routes capable of being carried out experimentally. Some of these routes are grossly inefficient; neglecting then is no loss. But some that we do not consider may be much more efficient than the route that we choose to test experimentally.

Elimination of Bad Pathways

We can improve our performance with the following trick. Let us decide on a cutoff overall yield, *i.e.* an overall yield such that if a given incomplete pathway has a lower overall yield than this cutoff value, then we are no longer interested in further developing this pathway. For example, if the series of reactions that convert K3 to M has an overall yield less than the cutoff overall yield, then we will not concern ourselves with the problem of how to synthesize K3. In other words, we will neglect all pathways through K3. A realistic value for the cutoff overall value yield depends on the difficulty of synthesizing the molecule M, and the selection of this value must utilize the experience of the pharmaceutical companies. 0.2% is perhaps the right order of magnitude for a difficult molecule.

This one trick will eliminate most of the possible pathways. But considering that we are dealing with numbers like 5^{20}, we must neglect still more of the pathways. Let us reluctantly decide that we have only time to consider the most promising pathways. Those incomplete pathways have the maximum promise which have demonstrated the greatest simplification in the molecule at lowest cost in some monetary unit. The units of simplification depend on the increase, in going from the given intermediate to M, in the number of rings, number of functional groups and number of non-hydrogenic atoms. Based on this criterion, simplification/cost, we give each intermediate molecule a score. Using this score, at any given time we can confine our efforts to the intermediate substance which at the moment has the highest score. If K3 has the highest score, *i.e.* the route from K3 to M is more efficient than any other route from an intermediate substance to M so far discovered, then we will obtain all possible parents of K3. Suppose the possible parents of K3 are called J1, J2, J3, and J4, and suppose also that J1, J2, J3, and J4 are all less promising (have a lower score) than K6, which is now the most promising of all the intermediate molecules for which we do not have parent molecules. In this case the next thing to do is to look for all possible parents of K6. In this scheme some molecules will be generated and then never considered again because the routes through them never look as promising as other routes. Finally one must terminate the synthesis planning when a pre-decided number of apparently useful synthetic routes have been produced and/or a pre-decided number of man days have been consumed in the search.

Implementation of the Strategy by a Computer Program

The essence of the foregoing scheme has been programmed and run for a number of cases on a computer. For convenience the program was written in the LISP language. A sample problem solved by the program is shown in Fig. 2.

Cost. The cost of doing the problem of Fig. 2 on an IBM 360/65 Computer in 1971 is the equivalent of about 1800 yen. The actual computer time is about six seconds. This relatively high cost suggests that in the future the program must be translated into the most economical type of computer language, assembly language.

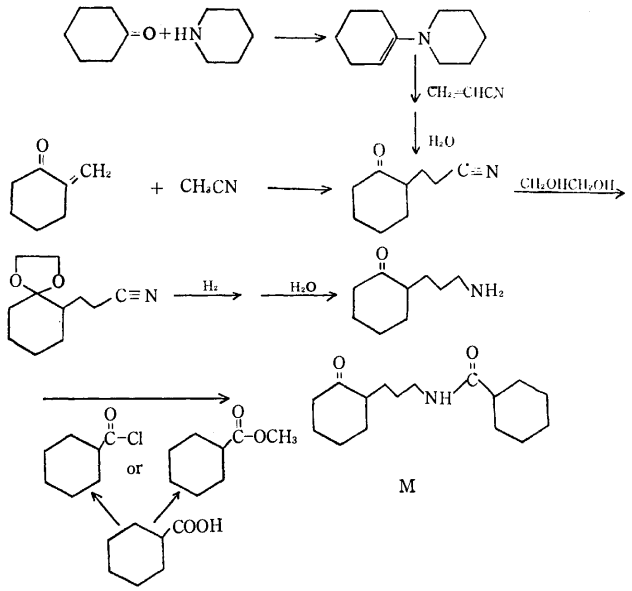

Fig. 2. A sample problem solved by a computer.

Representation of Molecular Structure in a Computer

Three dimensional molecular structures can be represented in the one dimensional memories of computers in a variety of ways. In this section I describe the representation used in this program. Each non-hydrogenic atom is given a name. The name given makes no difference whatsoever provided that no two atoms have the same name. For example, the non-hydrogenic atoms of 1-propanal could be named as follows:

$$\underset{\text{C1}}{CH_3}—\underset{\text{C2}}{CH_2}—\underset{\text{C3}}{CH}=\underset{\text{C4}}{O}$$

The structure of a molecule is representable as a list of sublists. To take the case of 1-propanal, the list is:

```
(C 1 carbon 3 ((C 2 1)       ))
(C 2 carbon 2 ((C 3 1)(C 1 1)))
(C 3 carbon 1 ((C 2 1)(O 4 2)))
(O 4 oxygen 0 ((C 3 2)       ))
```

We use parentheses here to mark the beginning and end of lists and sublists. A program in assembly language does not need this parenthesis notation.

Let us consider the first sublist: (C1 carbon 3 ((C2 1))). The first symbol, C1, is the name of an atom. It is convenient, but certainly not necessary to refer to carbon atoms with a name that begins with C. The second symbol, carbon, is the name of the element of which the atom C1 is an example. The third symbol, 3, is the number of hydrogen atoms bonded to C1. The last item in the sublist is a list of pairs. In this case there is only one such pair, (C2 1). This means that C2 is singly bonded to C1. The pair (C2 3) would mean that C2 is triply bonded to C1. An aro-

matic bond between C1 and C2 would be shown as (C2 0).

The reader will note various redundancies in this representation. It is obvious that since C1 is bonded to only one non-hydrogenic atom, and by a single bond, then C1 must have three attached hydrogen atoms. Hence, if we neglect stable radicals, the number of hydrogen atoms need not be entered. The program could compute this number when needed. I have temporarily taken the view that time is more important than space so the present program stores this redundant number for quick retrieval. Another redundancy may be noted: the sublist for C1 contains the pair (C1 1) which tells us that C2 is singly bonded to C1. The sublist for C2 contains the pair (C1 1), which conveys the same information. In fact all such bonding information is stored in two places. For another example, (O4 2) in the C3 sublist conveys the same information as (C3 2) in the O4 list. Here again, speed of retrieval has been the dominant consideration. Similarly, in a machine or assembly language program it would be simple to recognize the C in C2 and infer that it is a carbon atom. In a higher level language such as LISP, breaking off the alphabetic part of a name from the numerical part consumes computer time.

Let us call this kind of list of sublists a molecular structure list. Since each sublist refers to a particular non-hydrogenic atom, we can call the sublists atomic property lists. We mention in passing that *cis-trans*, chirality, and isotopic labelling information can be added to an atomic property list when necessary.

The reader will find it instructive to write down the Kekule structure, with appropriate labels, corresponding to the following molecular structure list:

```
((C 1 carbon 0 ((C 2 0)(C 6 0)(C 7 1)))
 (C 2 carbon 1 ((C 1 0)(C 3 0)      ))
 (C 3 carbon 1 ((C 2 0)(C 4 0)      ))
 (C 4 carbon 1 ((C 3 0)(C 5 0)      ))
 (C 5 carbon 1 ((C 4 0)(C 6 0)      ))
 (C 6 carbon 1 ((C 5 0)(C 1 0)      ))
 (C 7 carbon 0 ((C 1 1)(O 8 2)(O 9 1)))
 (O 8 oxygen 0 ((C 7 2)             ))
 (O 9 oxygen 1 ((C 7 1)             )))
```

Representation of Chemical Reactions in a Computer

From the above discussion it is apparent that a molecular structure list, which is conveniently one dimensional, can be put into a computer to represent molecular structure unambiguously. Chemical reactions can then be represented in a computer as transformations of these molecular structure lists. The four basic transformations of the program are called ADDH (add a hydrogen atom), REMOVEH (remove a hydrogen atom), MAKEBOND, and BREAKBOND. In addition, changes of chirality or of *cis-trans* arrangement of allylic atoms or of ring junctions are made on the atomic property lists of the parent molecules whenever the reaction concerned requires this.

We define the programming term *subroutine*. A subroutine is a set of instructions inside a program which form a unit and carry out a particular function. The subroutine is given one or more symbols, numbers or structures as input. It produces one or more symbols, numbers or structures as results. These results are then used by the section of the program which called upon the subroutine for answer(s). Typically a subroutine is called upon to produce an answer at several places in a program; hence, it is executed several or many times in the course of running the program, each time with different input. An example from this program is a subroutine called RINGCOUNT which, given the structure list of a molecule as input, returns an integer as answer, telling how many rings the molecule has. Another example is a subroutine CARBON which given the name of an atom as input, states as output (after searching the atomic property list for the second item, the element name) whether it is true or false that the given atom is a carbon atom.

Subroutines that represent chemical reactions always have as one of their inputs the name of a molecule. These subroutines usually begin by making a copy of the molecular structure list of the input molecule. The transformations are then performed on this copy. In this way the structure of the input molecule is always preserved in memory.

The subroutine HYDROGENATE is supplied with the names of two non-hydrogenic atoms as well as the name of the molecule to which the two atoms belong. For each of the two atoms the subroutine calls upon ADDH to increase the number of bonded hydrogens by one. It also changes the number 2 in the atomic property lists into the number 1, unless the two atoms are triply bonded to each other in which case it changes the number 3 to 2 in both of the atomic property lists. (Complete hydrogenation of a triple bond requires the use of this subroutine twice). If the two atoms are aromatically bonded to each other the subroutine HYDROGENATE makes them singly bonded to each other and changes the bonding of the other atoms in the same ring, which are not part of another aromatic ring, from aromatic to double bonding. If the two atoms are not bonded to each other the subroutine sends an error message.

Suppose the program's internal name for 1-propanal is X51. Then the command "HYDROGENATE C3 O4 X51" results in the following new molecular structure list:

```
(C 1 carbon 3 ((C 2 1)      ))
(C 2 carbon 2 ((C 3 1)(C 1 1)))
(C 3 carbon 2 ((C 2 1)(O 4 1)))
(O 4 oxygen 1 ((C 3 1)      ))
```

The program gives this new structure a unique but arbitrary name. DEHYDROGENATE is also given the names of two non-hydrogenic atoms and the name of the molecule to which they belong as input. Thus, if X51 is 1-propanal as before, then the command "DEHYDROGENATE C1 C2 X51" results in the acrolein molecular structure list:

```
(C 1 carbon 2 ((C 2 2)      ))
(C 2 carbon 1 ((C 3 1)(C 1 2)))
(C 3 carbon 1 ((C 2 1)(O 4 2)))
(O 4 oxygen 0 ((C 3 2)      ))
```

This new substance is similarly given some temporary internal name by the program, not any chemical name.

To illustrate the operations MAKEBOND and BREAKBOND, let us consider the case of benzoic acid, whose molecular structure list was given above. We examine the reaction

$$C_6H_5Br \xrightarrow[\substack{2\ CO_2\\3\ H_2O}]{1\ Mg\ or\ Li} C_6H_5CO_2H$$

The program allows this type of reaction only when the product is a monocarboxylic acid. Let us call benzoic acid B1. Let us further introduce a variable Q, which will exist only inside of this subroutine. *Initially* we will set Q equal to B1, that is Q will initially have the same structure as benzoic acid. The structure list of Q will be successively modified by four commands of the subroutine for this type of carboxylation. The end result will be to re-organize the final structure list of Q into the structure lists of the parents of B1.

The first of the four commands is "BREAKBOND C1 C7 Q." The reslut of this first operation is to produce the following modified structure list for Q:

(C 1 carbon 0 ((C 2 0)(C 6 0)))
(C 2 carbon 1 ((C 1 0)(C 3 0)))
(C 3 carbon 1 ((C 2 0)(C 4 0)))
(C 4 carbon 1 ((C 3 0)(C 5 0)))
(C 5 carbon 1 ((C 4 0)(C 6 0)))
(C 6 carbon 1 ((C 5 0)(C 1 0)))
(C 7 carbon 0 ((O 8 2)(O 9 1)))
(O 8 oxygen 0 ((C 7 2)))
(O 9 oxygen 1 ((C 7 1)))

In the atomic property list of C7 the subroutine has removed any reference to C1; in the atomic property list of C1 the reference to C7 has also been removed. In the structure list of Q the bond has now been broken. At the next command in the subroutine "MAKEBOND C1 BR10 Q" the structure list of Q is modified again. The name BR10 is chosen by the program for convenience. After execution of this MAKEBOND command the structure list of Q is:

(C 1 carbon 0 ((BR10 1)(C 2 0)(C 6 0)))
(C 2 carbon 1 ((C 1 0)(C 3 0)))
(C 3 carbon 1 ((C 2 0)(C 4 0)))
(C 4 carbon 1 ((C 3 0)(C 5 0)))
(C 5 carbon 1 ((C 4 0)(C 6 0)))
(C 6 carbon 1 ((C 5 0)(C 1 0)))
(C 7 carbon 0 ((O 8 2)(O 9 1)))
(O 8 oxygen 0 ((C 7 2)))
(O 9 oxygen 1 ((C 7 1)))
(BR10 bromine 0 ((C 7 1)))

We remark in passing that the input to the BREAKBOND subroutine is the names of two atoms followed by the name of the molecule to which they belong; the arguments of the MAKEBOND subroutine, however, are the names of two atoms followed by the name of the molecule to which the *first* mentioned atom belongs. Thus, in the command just discussed, MAKEBOND C1 BR10 Q is correct but MAKEBOND BR10 C1 Q is syntactically incorrect.

For the third command we introduce the variable K which refers to the hydroxyl oxygen of the carboxyl group in question, namely O9, in this case. The execution of the command MAKEBOND C7 K Q results in the following structure list for Q:

(C 1 carbon 0 ((BR10 1)(C 2 0)(C 6 0)))
(C 2 carbon 1 ((C 1 0)(C 3 0)))
(C 3 carbon 1 ((C 2 0)(C 4 0)))
(C 4 carbon 1 ((C 3 0)(C 5 0)))
(C 5 carbon 1 ((C 4 0)(C 6 0)))
(C 6 carbon 1 ((C 5 0)(C 1 0)))
(C 7 carbon 0 ((O 8 2)(O 9 2)))
(O 8 oxygen 0 ((C 7 2)))
(O 9 oxygen 1 ((C 7 2)))
(BR10 bromine 0 ((C 1 1)))

If the inputs to MAKEBOND are atoms which are singly bonded to each other, MAKEBOND adds one more bond, making then doubly bonded.

The last command is "REMOVEH K." This command results in the final structure list for Q:

(C 1 carbon 0 ((BR10 1)(C 2 0)(C 6 0)))
(C 2 carbon 1 ((C 1 0)(C 3 0)))
(C 3 carbon 1 ((C 2 0)(C 4 0)))
(C 4 carbon 1 ((C 3 0)(C 5 0)))
(C 5 carbon 1 ((C 4 0)(C 6 0)))
(C 6 carbon 1 ((C 5 0)(C 1 0)))
(C 7 carbon 0 ((O 8 2)(O 9 2)))
(O 8 carbon 0 ((C 7 2)))
(O 9 carbon 0 ((C 7 2)))
(BR10 bromine 0 ((C 1 1)))

The generation is now complete. After each generation is complete, a subroutine called REORGANIZE is called in to form, out of the changed copy of the original structure list (*i.e.* out of the final structure list for Q), one or more parent structure lists consisting of connected atoms. (In some reactions, like the esterification of a dicarboxylic acid, there are more than two "parent" molecules.) Here the subroutine REORGANIZE finds one group of three connected atoms and another group of seven connected atoms. REORGANIZE then forms two new structure lists, as follows:

I (C 7 carbon 0 ((O 8 2)(O 9 2)))
(O 8 oxygen 0 ((C 7 2)))
(O 9 oxygen 0 ((C 7 2)))

The program does not know that this molecule is called carbon dioxide; it gives it an arbitrary name such as B2. The program does know, as we shall see, that a molecule this small can be considered to be available.

II (C 1 carbon 0 ((BR10 1)(C 2 0)(C 6 0)))
(C 2 carbon 1 ((C 1 0)(C 3 0)))
(C 3 carbon 1 ((C 2 0)(C 4 0)))
(C 4 carbon 1 ((C 3 0)(C 5 0)))
(C 5 carbon 1 ((C 4 0)(C 6 0)))
(C 6 carbon 1 ((C 5 0)(C 1 0)))
(BR10 bromine 1 ((C 1 1)))

This parent, bromobenzene, is given an arbitrary name, such as B3. The names Q and K and L and their associated information are discarded as we exit from the reaction subroutine. REORGANIZE also attaches to the name B3 the names B1 as successor and B2 as coreactant. To the name B1 is attached the name B3 as parent. B2 is formally also a parent but it is not

marked as such by the program, because it is the smaller parent. B2 has attached to it the name B3 as coreactant. To the largest parent, B3, is also attached the name of the reaction, BROMIDECARBOXYLATION, which causes the relationships. Yield information is also inserted at this point. In the present program all the yields supplied by the reaction subroutines are average values from the literature. In future versions of the program subroutines like STERICHINDRANCE (which calculates degree of branching near a site) will be called in to calculate the estimated deviation of the yield from the average yield, so that chemical experience can be fully utilized.

A Generalized Form for Writing the Chemical Transformations of a Reaction Subroutine

In the previous discussion of the reaction BROMIDECARBOXYLATION, the first command given was BREAKBOND C1 C7 Q. Actually this is the content of the command at a comparatively low level. The initial, *i.e.* the highest level version of this command merely says something like BREAKBOND CARBON-NEXT-TO CARBOXYL-CARBON CARBOXYL-CARBON Q. It is left to the detailed operation of the subroutine as it calls in other subroutines to find that C7 is a carboxyl carbon and that C1 is its neighbouring carbon atom. Similarly "MAKEBOND C1 BR10 Q" is originally something equivalent to "MAKEBOND CARBON-NEXT-TO-CARBOXYL-CARBON INVENTED-NAME-FOR-BROMINE-ATOM Q." The command MAKEBOND C7 O9 Q is at the higher level also essentially MAKEBOND CARBOXYL-CARBON HYDROXYL-OXYGEN-NEXT-TO-CARBOXYL-CARBON Q. It is apparent from this that if we just provide a subroutine with the simple $-C-CO_2H$ structure and give directions for converting it to $-C-Br$ and CO_2 then the reaction subroutine can be made more compact. The useful procedure GENREACTION takes as its arguments (inputs) a general "structure," such as $-C-CO_2H$ Br, in the form of a structure list, a list of pairs of atoms in the general structure between which we should break a bond, a list of pairs of atoms of the general structure between which we should make a bond, a list of the atoms of the general structure to which we should add a hydrogen atom and a list of atoms of the general structure from which we should remove a hydrogen atom. Some of these lists may be empty. The output of GENREACTION will be the required predecessor(s).

Thus in the latest version of the program, inside of the BROMIDECARBOXYLATION subroutine is the command

```
GENREACTION (E1 C 0 ((E2.1)))
            (E2 C 0 ((E1.1)(E3.2)(E4.1)))
            (E3 O 0 ((E2.2)))
            (E4 O 1 ((E2.1)))
            (E5 Br 0 nil))
     ((E1.E2)) ((E2.E4) (E1.E5)) nil (E4).
```

In the future the program will be modified to "learn" synthetic reactions at a rapid rate. All this means is that the program will accept input data in the form of: *name of the reaction, model structure list, lists of atom pairs from the model structure list* for BREAKBOND and MAKEBOND, *lists of atoms of the model structure* for ADDH and REMOVEH, *yield, structural conditions* which decrease the yield, *presence of acid, base, oxidizers or reducing agents* among reagents of the reaction. The program will then convert this input data into appropriately named subroutines and add the subroutines to itself permanently. (The new expanded program will be written onto a disk file or punched out onto cards.) The program must also insert the name of the new subroutine into the proper list, *e.g.* carbonyl reactions, so that it will be called when appropriate. It is evident that compact procedures like GENREACTION will be required for this "learning" of chemistry by the program.

Minimizing of Repetition

Hydrogenation and dehydrogenation subroutines are available in the program. In order to prevent a long series consisting of useless alternate addition and removal of hydrogen the dehydrogenation subroutine is defined so that it cannot be used to cancel the effect of an immediately adjacent hydrogenation. At least one other chemical reaction must intervene between a hydrogenation and a dehydrogenation. Similarly hydrolysis may not immediately follow or precede ketal formation or esterification. Also, wherever possible, the temporary attachment and subsequent removal of a blocking, protective, activating or solubilizing group is treated together with the reaction that requires this as a single reaction.

The program indeed performs much useless hydrogenation and dehydrogenation but pathways along which this occurs automatically get a lower score than otherwise identical pathways along which the useless reactions did not occur.

The Operation of the Program

The general operation of the program can be summarized in the following three steps.

1. Put goal molecule on NEWLIST. Examine goal molecule.
2. GENERATEPREDECESSORS of the first molecule on NEWLIST.
3. If NEWLIST is empty then STOP. Otherwise go to Step 2.

Newlist and Oldlist. A list named NEWLIST is maintained which consists of the names of all of the molecules whose predecessors we do not know. There is a corresponding list called OLDLIST which consists of the names of all of the molecules which are not available but for which we have found all possible immediate predecessors.

Beginning of the Program. The program begins by establishing NEWLIST, with a single item on it, *i.e.* the name of the goal molecule M. It then calls in the subroutine EXAMINE to survey the goal molecule,

noting all structural features and combinations of structural feature, *i.e.* relations of functional groups to one another and to rings, etc. A list of these features is attached to the name of the molecule.

Main Part of the Program. In the next step of the program the first item on NEWLIST is subjected to the action of a subroutine called GENERATEPREDECESSORS. This subroutine will be repeatedly called and does the main work of the program. Initially, of course, the first item on NEWLIST is the only item on NEWLIST, *i.e.* the name of the goal molecule. For generality let us call the input molecule to GENERATEPREDECESSORS by the name X. GENERATEPREDECESSORS first decides whether or not it has previously seen this molecule in the solution of this problem. It searches for an isomer of X on OLDLIST. If there are no such isomers we proceed to the next phase. All isomers of X on OLDLIST are subjected to a detailed examination to see if they have exactly the same structure as X. If there is a molecule, *e.g.* by the name of Y, which is on OLDLIST but which has the same structure as X then there must exist two separate pathways from this structure to the goal molecule. The pathway of higher score, *i.e.* greater efficiency, is chosen. The other one is erased from memory. If X is erased we go back to get the first item on NEWLIST and subject it in turn to GENERATEPREDECESSORS etc. If Y is erased we continue with the next phase of GENERATEPREDECESSORS.

Generation Stage. GENERATEPREDECESSORS now collects the list of reactions associated with each structural feature of X. (For example if X has the amide functional group, there are associated with this functional group the list of two reactions: aminolysis of methyl ester and aminolysis of acyl chloride.) For each reaction there is a reaction subroutine which is immediately used to generate the appropriate predecessor(s). An example is the generation of bromobenzene as a predecessor of benzoic acid by the reaction subroutine BROMIDECARBOXYLATION. To take another example, if a certain diene and a dienophile can react in a Diels-Alder reaction to give X then the DIELSALDER reaction subroutine generates the diene and a dienophile structures in response to the input of X. For this to happen the procedure EXAMINE must have found a cyclohexenyl group in X with a -M group just outside of the ring, three atoms away from the nearer of the two vinyl carbons in the ring.

Case Where the Program is Baffled. If no predecessor of X can be generated, *i.e.* the EXAMINE subroutine has failed to detect a feature familiar to it and the program is therefore unable to find an applicable reaction subroutine, then the structure and the arbitrary name of X are printed out together with the question, "How do you make this?"

Disposition of the Predecessors. As soon as each predecessor is generated it is disposed of in some way. Let us call the predecessor Z. There are four cases.

A. If the overall yield from Z to the goal molecule is less than the cutoff value discussed previously then the pathway and yield are printed out together with the comment that the overall yield is inadequate to justify further development of this pathway. Then the pathway is removed from the computer memory, "erased," an absolutely necessary step to preserve unfilled memory space.

B. If Z is available *and* all necessary coreactants on the path to the goal molecule are also either available or can be synthesized by a method now known to the program, then the entire pathway from the available predecessor to the goal molecule is printed out together with the yield of each step, the name of each reaction and the overall yield. The program recognizes as available any molecule which satisfies any one of the following three criteria:

1. It has no more than eight non-hydrogenic atoms.
2. It is an ester or a carboxylic acid, or it has only one heteroatom, and it has nine non-hydrogenic atoms.
3. A molecule with identical structure appears on a list called AVAILABLELIST.

The last criterion is important in practice because very often we have a large number of byproducts of other processes available to us. If the program knows about them much computer time will be saved.

C. If Z is available but on the pathway to the goal molecule there are necessary coreactants which are neither available nor does the program yet have a synthesis for them, then no action is taken in regard to Z. The information that Z is a predecessor of X is permanently attached to the name of X. In this way information about Z can be easily retrieved when and if the entire synthetic route has been generated.

D. If Z is not available and the yield from Z to M is not less than the cutoff value, then Z is put onto NEWLIST. This is the most usual case.

Scoring. Just before being put on NEWLIST the predecessor Z must be scored. In the program at present the cost part of the scoring procedure has not yet been reduced to specific monetary units. It is assumed for the present that cost depends on the overall yield, the number of steps required and the amount of material carried through the route. To illustrate the last point we note that a reaction with a 50% yield followed by a reaction with a 100% yield is cheaper, other things being equal, than a two step sequence consisting of a reaction with a 100% yield followed by a reaction with a 50% yield. The overall yield is the same in both cases but in the first case there is less material carried into the second reaction.

A procedure called SCORE considers all these aspects in calculating a somewhat arbitrary cost. The program knows a yield for each reaction; in some cases this yield depends on the structure of the molecules involved. A monetary cost could also be easily inserted if the necessary chemical engineering data were available.

When there are two or more coreactants generated as predecessors SCORE gives all of them the same score which is that calculated for the largest of the molecules. SCORE calculates the cost expended for the amount of simplification achieved in the largest of the coreactants. The cost is the cost of going from Z to M and the "simplification" is really the number of atoms and

functional groups added in going from Z to M.

Hierarchy of NEWLIST. Each predecessor of X is placed on NEWLIST in a definite position which depends upon its score. All molecules closer to the front of the list than Z must have a score greater or equal to that of Z. All molecules which follow Z on NEWLIST must have a lower score than Z or the same score that Z has. In this way when the program takes the first molecule on NEWLIST for processing by GENERATEPREDECESSORS it is really considering the most promising incomplete pathway.

End of GENERATEPREDECESSORS. When, within the limits of the repertory of reactions of the program, all possible predecessors of X have been generated and suitably placed, the name of X is taken off NEWLIST and placed on OLDLIST.

Table 1.

Cycle[a]	NEWLIST	OLDLIST	Available Molecules Generated
0	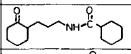		
1	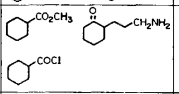	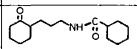	
2	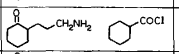	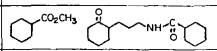	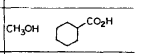
3	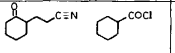	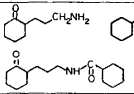	
4	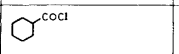	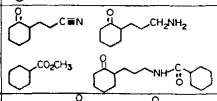	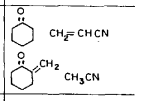
5		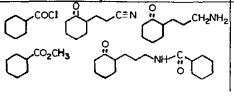	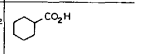

a) cycle: the number of times the subroutine has been called

Example of the Operation of the Program

In the example of Fig. 2 GENERATEPREDECESSORS was called five times. The result of each application of this subroutine is shown in Table 1. In this case EXAMINE found that M is an amide and hence GENERATEPREDECESSORS calls in the subroutines for acylating an amine with a methyl ester and with an acyl chloride and generates the corresponding amine and methyl ester and acyl chloride. In the next cycle the methyl ester stands at the head of NEWLIST. EXAMINE has found out that it is an ester, hence the reaction subroutine for esterification is called in, and it generates the carboxylic acid and methanol. The carboxylic acid is available hence it is not put on OLDLIST. The CH_2NH_2 functional group is related to the reaction subroutine called HYDROGENATENITRILE. This latter subroutine generates the corresponding nitrile, but recognizes the simultaneous presence of an active carbonyl group that needs to be protected, the ketone group, and a note is included for the final printout that the ketone group must be protected from hydrogenation by a ketal before the reaction is done and that this ketal is to be removed after the reaction is finished. EXAMINE has seen that in the nitrile there are exactly three saturated carbons between two -M groups and hence an alpha-beta addition is suggested. The corresponding subroutine is quite complicated since it generates cyclohexanone and acrylonitrile which can react *via* the Stork enamine reaction[1] to obtain the nitrile. The subroutine also generates acetonitrile and α-methylenecyclohexanone. In one case a ketone adds across the double bond of an unsaturated nitrile; in the other case a nitrile adds across the double bond of an unsaturated ketone. A note is added in the case of the enamine reaction that the enamine must be prepared first. The yield is also different in the two similar reactions. Since all of the predecessors are available the synthesis of M can be effected in an overall yield of 58%, or 51% depending on the pathway. The successful pathways are printed out.

In the fifth and final cycle of GENERATEPREDECESSORS, cyclohexane carboxylic acid is generated, as the predecessor of the corresponding acyl chloride.

The reader will note that there was no attempt to generate a secondary alcohol, *i.e.* to synthesize the ketone from a secondary alcohol. The reason is that since we do not wish to oxidize alcohols indiscriminately, the exact conditions under which we want to do this should be specified in the routine. At the time of running of this example I had not yet thought out the matter to completion, hence the alcohol oxidation reaction subroutine had not yet been written. (The conclusion now reached is that it is perfectly satisfactory to oxidize any alcohol to the corresponding aldehyde or ketone, provided that the next reaction step is not hydrogenation of the aldehyde or ketone.)

Conslusion

Computing synthetic pathways is now possible without human intervention at any intermediate stage. The process is expensive, however, and only when it is made cheap will a computer program become indispensable to the synthetic chemist.

The author gratefully acknowledges support of this work by the John Simon Guggenheim Memorial Foundation and by the National Research Council of Canada.

1) G. Stork, *J. Amer. Chem. Soc.*, **85**, 207 (1963).

Studies on Stable Free Radicals. IX.[1] Peroxy Acid Oxidation of Hindered Secondary Amines to Nitroxide Radicals

Toshimasa TODA, Eiko MORI, and Keisuke MURAYAMA

Central Research Laboratories, Sankyo Co., Ltd., Shinagawa-ku, Tokyo

(Received August 21, 1971)

The hindered secondary amines, 2,2,6,6-tetramethyl-4-oxopiperidine (II) and 1,9-diaza-2,2,8,8,10,10-hexamethyl-4-oxo-spiro[5.5]undecane (VI), were oxidized with *m*-chloroperbenzoic acid, and the corresponding hydroxylamine (III) and *N*-oxyl-hydroxylamine (VIII), respectively, were isolated. The further oxidation of III and VIII with the peracid afforded the corresponding nitroxide radical IV and IX, in good yields respectively. The stoichiometry of the oxidation reaction of the hydroxylamine III to the nitroxide radical IV was elucidated on the basis of the ESR signal intensities of oxidation products at various molar ratios with the peracid and III. An ESR study of the 1-^{15}N-labelled *N*-oxyl-hydroxylamine (XII) indicated that there was an intramolecular hydrogen transfer between >N–OH and >N–O· groups in the *N*-oxyl-hydroxylamines VIII and XII.

The peracid oxidation of organic molecules in a solution are known to proceed *via* heterolytic[2] or homolytic[3] processes. Organic peracids have been found to be good reagents for the oxidation of hindered secondary amines to the corresponding nitroxide radicals.[4,5] Recently, Duynstee and his co-workers[6] studied the oxidation of a hindered secondary amine (I) with perbenzoic acid to the corresponding nitroxide radical and suggested that the reaction proceeds through the corresponding hydroxylamine, although no hydroxylamine intermediate was isolated.

(I)

In the present work, we isolated the intermediate hydroxyl-amine (III) and *N*-oxyl-hydroxylamine (VIII) in the oxidation of 2,2,6,6-tetramethyl-4-oxopiperidine (triacetonamine) (II) and 1,9-diaza-2,2,8,8,10,10-hexamethyl-4-oxo-spiro[5.5]undecane (pentacetonediamine) (VI)[7] with *m*-chloroperbenzoic acid respectively, and found that when the *N*-oxyl-hydroxylamine VIII resulted, there was an intramolecular hydrogen transfer between the >N–OH and >N–O· groups.

Results and Discussion

Oxidation of Triacetonamine (II). The reaction of the amine II with 1 mol-equivalent of *m*-chloroperbenzoic acid in chloroform at room temperature afforded 1-hydroxy-2,2,6,6-tetramethyl-4-oxopiperidine (III) (40.7%), the corresponding nitroxide radical (IV) (30.3%), and some unchanged amine II (16.0%).

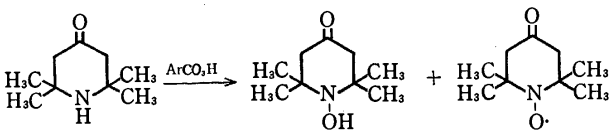

(II) (III) (IV)

Using 2 mol-equivalents of the peracid under the same reaction conditions, the amine II formed the nitroxide radical IV in good yield (91.0%). The formation of the hydroxylamine III must be due to a nucleophilic attack of the amine II on a hydroxy group of the peracid, by analogy to the oxidation of aniline with the peracid to phenylhydroxylamine.[8]

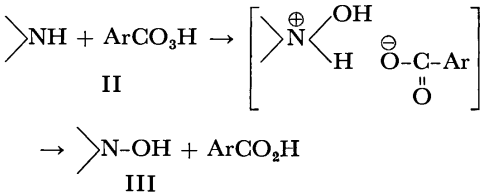

The further oxidation of the hydroxylamine III with 1 mol-equivalent of the peracid gave the nitroxide radical IV quantitatively. We attempted to follow this peracid oxidation process of the hydroxylamine III to the nitroxide radical IV in detail. Attempts to titrate the remaining peracid in the reaction mixture by means of iodometry were unsuccessful, since the nitroxide radical formed also liberated iodine from potassium iodide. Therefore, we estimated the yield of the nitroxide radical IV by comparing its ESR signal intensities with those of a standard sample IV. Table 1 summarizes the results of this estimation and proves the stoichiometry of this oxidation reaction to be as follows:

$$2\,\rangle\text{N–OH} + \text{ArCO}_3\text{H} \rightarrow 2\,\rangle\text{N–O}\cdot + \text{ArCO}_2\text{H} + \text{H}_2\text{O}.$$

This shows that the yield of the nitroxide radical IV is not affected by the addition of an efficient radical scavenger, 1,3,5-trinitrobenzene.[9] Moreover, in the oxidation reaction, the coupled product[10] of the

1) Part VIII: T. Yoshioka, S. Higashida, and K. Murayama, This Bulletin, **45**, 636 (1972).

2) H. O. House, "Modern Synthetic Reactions," W. A. Benjamin, Inc., New York, N. Y. (1965), p. 105.

3) K. Tokumaru and O. Simamura, This Bulletin, **35**, 1678, 1955 (1962).

4) K. Tokumaru, H. Sakuragi, and O. Simamura, *Tetrahedron Lett.*, **1964**, 3945.

5) G. Chapelet-Letourneux, H. Lamaire, and A Rassat, *Bull. Chim. Soc. Fr.*, **1966**, 3283.

6) E. F. J. Duynstee, M. E. A. Mevis, H. K. Ostendorf, and R. J. De Kock, *Rec. Trav. Chim. Pays-Bas*, **87**, 945 (1968).

7) K. Murayama, S. Morimura, O. Amakasu, T. Toda, and E. Yamao, *Nippon Kagaku Zasshi*, **90**, 296 (1969).

8) K. M. Ibne-Rasa and J. O. Edward, *J. Amer. Chem. Soc.*, **84**, 763 (1962).

9) C. G. Swain, W. H. Stockmayer, and J. T. Clarke, *ibid*, **72**, 5426 (1950).

10) E. G. Rozantzev and V. A. Golubev, *Izv. Akad. Nauk SSSR, Ser. Khim.*, **1966**, 891.

Table 1. Stoichiometry of the reaction of the hydroxylamine III with the peracid in benzene

Molar concentration × 10^3		
Solution[a]		Nitroxide radical (IV)[b,c]
Hydroxylamine	Peracid	
3	4	3
3	3	3
3[d]	3	3
3	1.5	3
3[d]	1.5	3
3	1	2[e]

a) A solution of the hydroxylamine III (5 m*l*, 6×10^{-3} M) and a solution of the peracid were combined to 10 m*l* total volume.
b) Measurements were carried out in the same sample tube under the same conditions after 100 sec reaction time at room temperature.
c) The ESR signal intensities were compared with those of the pure nitroxide radical IV in the same sample tube under the same conditions.
d) 1,3,5-Trinitrobenzene (50 mg) was added. The ESR signal intensity of the pure nitroxide radical IV itself in solution was not influenced by an addition of 1,3,5-trinitrobenzene.
e) The ESR signal intensity did not increased after an additional 1 hr reaction time.

free radical IV with a phenyl radical arising from the peracid was not found, and no evolution of carbon dioxide was observed. From these results, this oxidation reaction is presumed to proceed through an ionic process[11], but we have no conclusive proof for this reaction mechanism.

Oxidation of Pentacetonediamine (VI). The similar treatment of pentacetonediamine (VI) with *m*-chloroperbenzoic acid in chloroform afforded two products melting at 113°C (A) and at 145°C (B). The product A was identified as 1,9-diaza-2,2,8,8,-10,10-hexamethyl-4-oxo-spiro[5.5]undecane-1,9-dioxyl

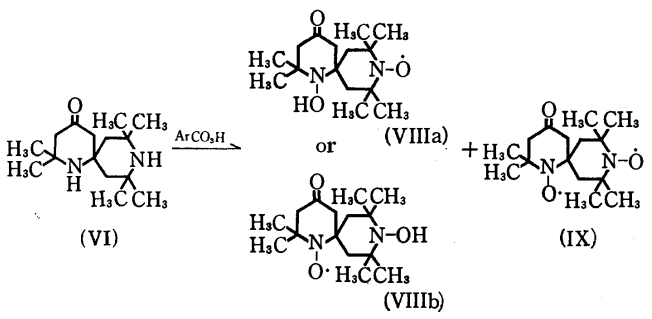

(IX) by elementary analysis and by an IR spectral comparison with an authentic sample.[7] The product B was formulated as $C_{15}H_{27}O_3N_2$ and shown to be a *N*-oxyl-hydroxylamine (VIIIa) or (VIIIb) by its spectral data (mass, IR, and ESR). No other possible intermediary products including dihydroxylamine (VII) were obtained under the present reaction conditions. As in the case of the hydroxylamine III, the further peracid oxidation of VIII gave the nitroxide biradical IX in a good yield.

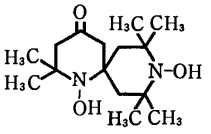

(VII)

In order to determine the structure of VIII, the following isotope-labelling experiments were carried out.

The 1-^{15}N-labelled pentacetonediamine (XI) was prepared by the reaction of 4-amino(^{15}N)-4-methyl-pentan-2-one (X) with II and then, submitted to peracid oxidation to give a biradical (XIII) and a *N*-oxyl-hydroxylamine compound (XIIa or XIIb).

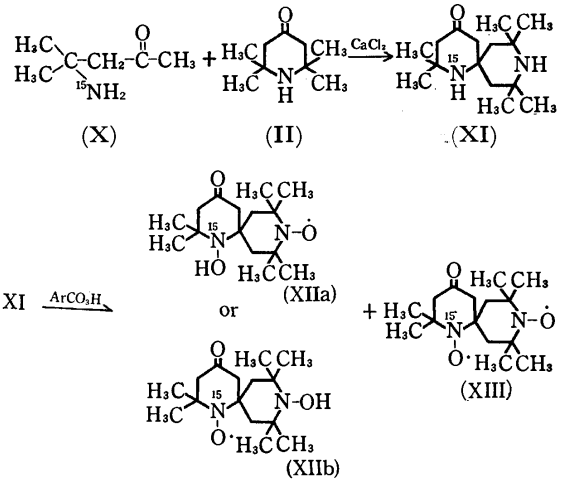

The structure of *N*-oxyl-hydroxylamine XII may be determined by the ESR measurements, since triplet lines due to the interaction with the ^{14}N-nucleus can be expected for the structure XIIa, while doublet lines due to the interaction of the ^{15}N-nucleus can be expected for the structure XIIb. The ESR spectrum of the product XII (Fig. 1) showed five lines, suggesting the existence of mixture of these isomers XIIa and XIIb, but the intensity of the doublet lines (due to ^{15}N-nucleus) increased at higher temperatures and decreased at lower temperatures reversibly. This suggests the existence of an equilibrium between XIIa and XIIb in solution; such as equilibrium may result from an intramolecular hydrogen exchange between >N–OH and >N–O· groups in a solution of a 10^{-4} M concentration. The equilibrium constants were obtained from the ratio of the area of triplet lines to that of doublet lines at various temperatures; they are plotted to determine the equilibrium enthalpy and entropy in Fig. 2.

Since the difference in the structures of the two isomers is very small, the small enthalpy and entropy values seem to be reasonable. The molecular model of VIII indicates that the >N–OH and >N–O· groups can approach each other closely when one

11) Blackly and Reinhard [*J. Amer. Chem. Soc.*, **87**, 802 (1965)] have reported that bis(trifluoromethyl)nitroxide radicals exist in equilibrium wtith its dimer in $CFCl_3$:
$2(CF_3)_2N\text{-}O\cdot \rightleftarrows (CF_3)_2N\text{-}O\text{-}O\text{-}N(CF_3)_2$.
In this oxidation process, homolysis of the peroxide (V) might be involved: >N-O-O-N< (V) ⟶ 2 >N-O· (IV).

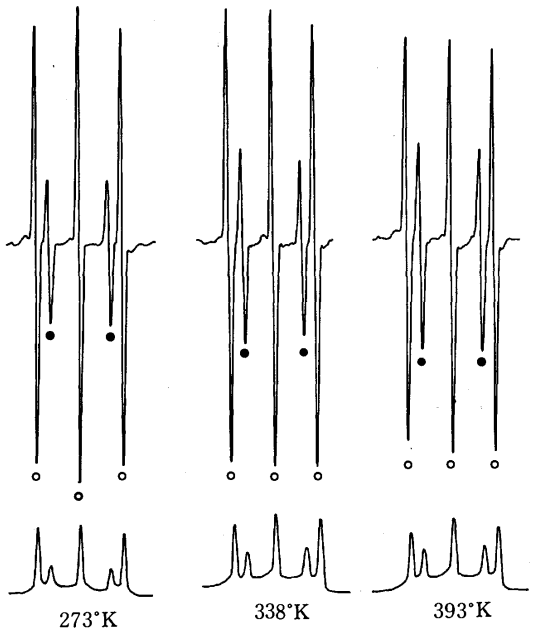

Fig. 1. ESR spectra of XII in toluene at 10^{-4} M concentration.
In the bottom half of the figure are given the integrated spectra: ○ triplet lines due to ^{14}N nucleus ($a_{^{14}N}=15.2$ G).
● doublet lines due to ^{15}N nucleus ($a_{^{15}N}=23.3$ G).

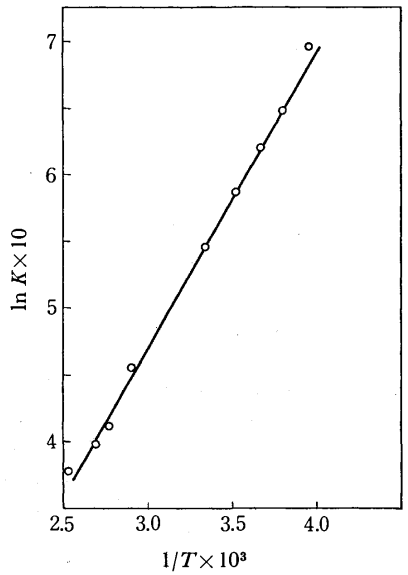

Fig. 2. Plot of ln K against $1/T$.
$\Delta H_0=-1.09$ kcal/mol
$\Delta S=0.253$ e.u.

piperidine ring is twisted[12] and the other piperidine ring is in a chair form,[13] and *vice versa*. Therefore, it may be considered that such an intramolecular transfer of a hydrogen between >N–OH and >N–O· groups in VIII is possible and that the structure VIIIa is a predominant isomer at ordinary temperatures; these conclusions are based on the results of the ESR measurement of XII at various temperatures.

Recently, Poindexter and Glazer[14] have suggested, on the basis of studies of dynamic nuclear polarizability, that a nitroxide radical III and dimethyl phosphite form a transient hydrogen bond between P–H and ·O–N<. Our results concerned the intramolecular hydrogen exchange also suggest the formation of a transient hydrogen bond between >N–OH and >N–O· groups in the transition state.

It has been reported[6,15] that the mass spectra of stable nitroxide radicals exhibit a characteristic peak corresponding to $(M+1)^+$ in addition to the molecular ion peak; the $(M+1)^+$ peak was assigned to hydroxylamine formed by the hydrogen abstraction of the nitroxide radical from water or the free radical compound. In VIII, a prominent $(M+1)^+$ peak was observed, as is shown in Fig. 3, but the mass spectrum

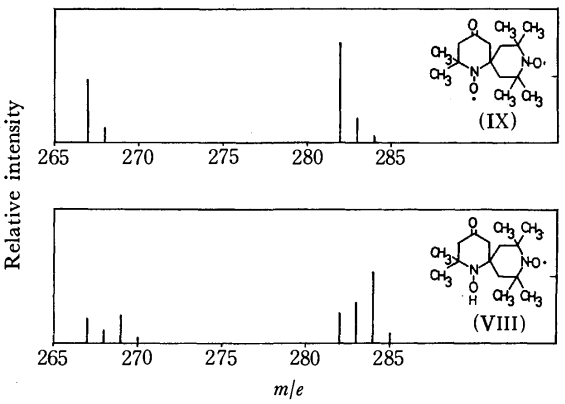

Fig. 3. Mass spectra of VIIIa and IX.

of the biradical IX did not show such a characteristic $(M+1)^+$ peak. This suggests that a hydrogen of the hydroxy group in VIII may be easily abstracted to give the dihydroxylamine VII and the biradical IX in a mass spectrometer.

Experimental

The melting points are uncorrected. The IR spectra were determined by means of Nujol mulls or liquid films. The mass spectra were obtained using a JEOL-JMS-OIS mass spectrometer at 75 eV. The ESR spectra were recorded using a Hitachi MES 4001 spectrometer employing 100 kc modulation at X-band in conjunction with a Hitachi MES 4701 thermo controller, the sample temperature being measured with a copper-constantan thermocouple. The integrated curves were obtained using a Hitachi 4703 integrator. The splitting constants and g-values were measured relative to the aqueous solution of Fremy's salt.

m-Chloroperbenzoic Acid. The commercially-available *m*-chloroperbenzoic acid (PBA) used here had a purity of 85.5%, as determined by iodometric analysis.

Oxidation of 2,2,6,6-Tetramethyl-4-oxopiperidine (II). a): A solution of 8.1 g (40 mmol) of PBA in 60 m*l* of chloroform was slowly stirred into a solution of 6.2 g (40 mmol) of 2,2,6,6-tetramethyl-4-oxopiperidine (II) in 50 m*l* of chloroform at ice-water-bath temperature. The solu-

12) E. G. Rozantzev and E. N. Gur'yanova, *Izv. Akad. Nauk SSSR, Ser. Khim.*, **1966**, 979.
13) C. Y. Chen and R. J. W. LéFevre, *J. Chem. Soc.*, **1965**, 3467.
14) E. H. Poindexter and R. L. Glazer, *J. Amer. Chem. Soc.*, **92**, 4784 (1970).
15) A. Morrison and A. P. Davies, *Org. Mass. Spect.*, **3**, 353 (1970).

tion was allowed to stand for an additional 24 hr at room temperature. Then, the solution was washed with 100 ml of aqueous sodium hydroxide (40%), dried over potassium carbonate, and freed of the solvent by evaporation under reduced pressure. The oily residue (6.0 g) was chromatographed on a column of aluminum oxide, and the column was eluted successively with petroleum ether, benzene, and methanol.

1). From petroleum ether eluates, 1.0 g (16.0%) of II was recovered. Confirmation was done by means of an IR spectral comparison with the starting material.

2). From benzene eluates, 2.1 g (30.3%) of 2,2,6,6-tetramethyl-4-oxopiperidine-1-oxyl (IV) was obtained. It was identified by a comparison of the melting point (36°C) and the IR and ESR spectra with those of an authentic sample.[7]

3). From methanol eluates, 2.8 g (40.7%) of 1-hydroxy-2,2,6,6-tetramethyl-4-oxopiperidine (III) was isolated; it was identified by comparing its melting point (mp 90—91°C) and IR spectrum with those of an authentic sample.[10] Found: C, 63.06; H, 10.01; N, 8.18%. Calcd for $C_9H_{17}O_2N$: C, 63.13; H, 10.00; N, 8.18%.

b): In a way similar to that described above, the reaction of 6.2 g (40 mmol) of II with 16.2 g (80 mmol) of PBA in chloroform gave 6.3 g of an oily residue. By column chromatography on aluminum oxide, 6.2 g (91.0%) of IV was obtained. It was identified by means of its melting point (mp 36°C), and IR and ESR spectra.

Oxidation of 1-Hydroxy-2,2,6,6-tetramethyl-4-oxopiperidine (III). The reactions described below were carried out under a nitrogen atmosphere, leading to a trap filled with an aqueous barium hydroxide solution.

a): A solution of 1.0 g (5 mmol) of PBA in 60 ml of chloroform was stirred into a solution of 1.7 g (10 mmol) of III in 40 ml of chloroform at room temperature. The solution was then stirred for an additional 3 hr at room temperature.

At this point, the yield of IV was 67%, as was determined by comparing the ESR signal intensity of the reaction mixture with that of the standard sample IV in chloroform. Then, the solution was washed with 40 ml of aqueous sodium hydroxide (40%), dried over potassium carbonate, and evaporated under vacuum. The resulting oil was chromatographed on a column of aluminum oxide. The benzene eluates afforded 1.1 g (64.6%) of IV, and the methanol eluates gave 0.2 g (11.7%) of the unchanged starting hydroxylamine III. These compounds were identified by a comparison of the IR spectra and the melting points with those of the respective authentic samples.

b): A solution of 1.0 g (5 mmol) of PBA in 60 ml of benzene was stirred into a solution of 1.7 g (10 mmol) of III in 40 ml of benzene at room temperature. The solution was then stirred for an additional 1.5 hr at room temperature. At this point, the yield of IV was 100%, as was determined by comparing the ESR signal intensity of the reaction mixture with that of the standard sample IV in benzene. The column chromatography of the oily material obtained in a a way similar to that described above gave 1.3 g (75.0%) of IV. In these reactions a) and b), no detectable precipitates of barium carbonate were observed in the trap.

Oxidation of 1,9-Diaza-2,2,8,8,10,10-hexamethyl-4-oxo-spiro[5.5]undecane (VI).[7] A solution of 6.1 g (30 mmol) of PBA in 60 ml of chloroform was added to a stirred solution of 2.5 g (10 mmol) of VI in 50 ml of chloroform under ice-water cooling and the solution was stirred for an additional 15 min under ice-water cooling. The solution was washed with 70 ml of aqueous sodium hydroxide (40%), dried over potassium carbonate, and evaporated under vacuum. The resulting oil solidified upon the addition of petroleum ether and 1.6 g of the crystalline solid was separated by filtration. This crude material was dissolved in 5 ml of benzene and placed onto a column of aluminum oxide. The column was eluted successively with petroleum ether, benzene, and methanol. The benzene eluates afforded 0.8 g (28.4%) of 1,9-diaza-2,2,8,8,10,10-hexamethyl-4-oxo-spiro[5.5]-undecane-1,9-dioxyl (IX). Recrystallization from petroleum benzine gave a pure sample; mp 112—113°C. Found: C, 63.81; H, 9.35; N, 10.04%. Calcd for $C_{15}H_{26}O_3N_2$: C, 63.80; H, 9.28; N, 9.92%. IR (cm^{-1}): $\nu_{C=O}$ 1728. From the methanol eluates, 0.6 g (21.2%) of 1,9-diaza-1-hydroxy-2,2,8,8,10,10-hexamethyl-4-oxo-spiro[5.5]undecane-9-oxyl (VIIIa) was obtained. By the recrystallization of the crude material from cyclohexane, an analytically pure sample was obtained; mp 145—146°C. Found: C, 63.58; H, 9.60; N, 9.76%. Calcd for $C_{15}H_{27}O_3N_2$: C, 63.57; H, 9.60; N, 9.88%. IR (cm^{-1}): $\nu_{C=O}$ 1728, ν_{OH} 3400. ESR (in toluene): $a_N=15.0\pm0.1$ gauss. $g=2.0060\pm0.0001$.

Oxidation of 1,9-Diaza-1-hydroxy-2,2,8,8,10,10-hexamethyl-4-oxo-spiro[5.5]undecane-9-oxyl (VIIIa). A solution of 1.2 g (6 mmol) of PBA in 20 ml of benzene was stirred into a solution of 1.7 g (6 mmol) of VIIIa in 20 ml of benzene at room temperature, after which the solution was stirred for an additional 3 hr at room temperature. The solution was then treated by a procedure similar to that described above, and the resulting oil was chromatographed on a column of aluminum oxide. The benzene eluates afforded 1.3 g (71.5%) of IX, which was identified by comparing its melting point (mp 112—113°C) and IR spectrum with those of an authentic sample.

Oxidation of 1,9-Diaza(1-^{15}N)-2,2,8,8,10,10-hexamethyl-4-oxo-spiro[5.5]undecane (XI). Similarly as described above, 1.0 g of the crystalline solid was obtained from 2.5 g (10 mmol) of XI. By means of column chromatography, from 1.0 g of the crystalline solid, 0.35 g (12.7%) of XIII and 0.65 g (23.0%) of XIIa were obtained. Pure samples were obtained by recrystallization. XIII : mp 112—113°C (from petroleum benzine). XIIa : mp 145—146°C (from cyclohexane), ESR (in toluene): $a_{^{14}N}=15.2\pm0.1$ gauss. $a_{^{15}N}=23.3\pm0.1$ gauss. $g=2.0056\pm0.0001$.

Synthesis of 2-Amino-^{15}N-2-methylpentan-4-one (X). To a stirred solution of 14.1 g (0.26 mol) of ammonium chloride-^{15}N (90% ^{15}N contents)[16] and 14.6 g (0.26 mmol) of potassium hydroxide in 50 ml of water at room temperature was added 14.7 g (0.15 mol) of mesityl oxide. The solution was then stirred continuously for 18 hr at room temperature, after which 10.0 g of potassium carbonate was added into the stirred solution at 0—5°C. An oil separated and was extracted into 100 ml of ether, dried over potassium carbonate, and evaporated under reduced pressure. The resulting oil was distilled to give X; bp 55—58°C/15 mmHg; yield, 10.8 g (62.1%). IR (cm^{-1}): $\nu_{C=O}$ 1760, ν_{NH} 3550, 3360 and 3280.

Synthesis of 1,9-Diaza(1-^{15}N)-2,2,8,8,10,10-hexamethyl-4-oxo-spiro[5.5]undecane (XI). By the reaction of 10.8 g (94 mmol) of X and 8.3 g (54 mmol) of II with calcium chloride (0.3 g), 4.6 g (50.0%) of XI was obtained in the same way as has been reported previously.[7] The recrystallization from cyclohexane gave an analytically pure sample; mp 91—95°C (This mp corresponds to that of the monohydrate of XI). Found: C, 66.31; H, 11.12; N, 10.85%.

16) Available from The Institute of Physical and Chemical Research, Wako-shi, Saitama, Japan.

Calcd for $C_{15}H_{30}O_2N^{15}N$: C, 66.39; H, 11.14; N, 10.69%. IR(cm^{-1}): $\nu_{C=O}$ 1708, ν_{NH} 3150 and 3330. Mass spectrum: $M^+=253$.

The authors wish to thank Prof. Makoto Okawara of the Tokyo Institute of Technology for his valuable comments and Dr. Genshun Sunagawa, the director of these laboratories, for his encouragement.

BULLETIN OF THE CHEMICAL SOCIETY OF JAPAN, VOL. 45, 1908—1912 (1972)

The Preparation and General Properties of Ion-exchange Carbon Fiber

Sugio OTANI, Masao TAMURA, Yatsuo YOSHIDA, and Yoshio TSUJI

Faculty of Technology, Gunma University, Kiryu, Gunma

(Received November 17, 1971)

Cation-exchange carbon fibers were prepared from pitch-based carbon fiber by oxidizing treatment with a mixture of $K_2Cr_2O_7$, HNO_3, and water. Their most characteristic properties were a large electric conductivity, a large thermal stability, and their shape. Their exchanging properties varied with the composition of the mixture and the treating conditions. The following composition and the conditions were adopted as standard.

Composition of the mixture: $K_2Cr_2O_7$, 10 g; HNO_3, 20 m*l*; H_2O, 80 m*l*

Condition of the treatment: temperature, 104°C; period, 2.5 hr

Amount of carbon fiber: carbon fiber prepared at 1000°C 1 g

The cation-exchange capacity obtained by the standard procedure was 2.0 ± 0.1 mequiv/g. Carbon fiber prepared at 1000°C was a better material than that prepared at 2000°C. Even after the exchangers were heated at 220°C in air, no change was observed in the capacity measured at room temperature. The electric resistivity increased from 7×10^{-3} ohm-cm to 8×10^{-2} ohm-cm with an increase in the capacity, and no difference was obserbed between exchangers of the acidic form and the sodium form. The tensile strength of the filament(1.9 mequiv/g in the capacity) was 6.7×10^{6} g/cm^2, and the breaking load of the spinning yarn of 1300 den. (2.0 mequiv./g) was 3.0 kg.

A number of investigations have been carried out on the preparation of high-modulus or high-strength carbon fibers and their applications. On the other hand, it seems that little attention has been paid to improving the application of low-modulus carbon fibers. However, we thought that the application of the low-modulus carbon fibers should also be developed as fully as possible. The present paper will, then, deal with ion-exchange carbon fibers prepared from low-modulus carbon fibers.

As compared with other ion-exchangers, the ion-exchange carbon fibers are characterized by their electric conductivity, their thermal stability, and their flexibility. Ion-exchange carbon fibers were prepared by oxidation. For the purpose of the surface treatment of high-modulus carbon fibers, the oxidation of carbon fibers has been attempted by various manners.[1] However, the ion-exchange capacity of the resulting carbon fibers is only less than 0.02 milliequivalents per gram. Therefore, the previous manners are not very good for preparing ion-exchangers.

On the other hand, some attempts have been reported to prepare the ion-exchangers by sulfonation from such carbonaceous materials as coal or char.[2,3] Sulfonation is effective for carbonaceous materials which contain same hydrogen atoms, but it does not give satisfactory results for carbon fibers practically composed only of carbon atoms.

After several preliminary examinations, it has been found that oxidizing treatment with a mixture of $K_2Cr_2O_7$, HNO_3 and water is a promising method for the preparation of ion-exchange carbon fiber without any intensive deterioration of its mechanical properties.

Experimental and Results

Preparation. The present ion-exchangers were prepared by the procedure shown in Fig. 1. This procedure is characterized by the use of a mixture of nitric acid, potassium dichromate, and water, and

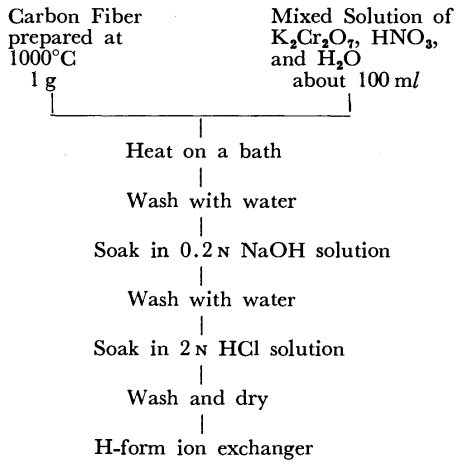

Fig. 1. Procedure of preparation.

1) D. W. McKee and V. J. Mimeault, General Electric Technical Information Series ICMT JUSE No 1/4, Nov., 6, 1970.
2) M. Roy, *J. Appl. Chem.*, **6**, 335 (1956).
3) K. Araki and H. Yanai, *Kogyo Kagaku Zasshi*, **69**, 28 (1966).

by the use of carbon fibers prepared at 1000°C from pitch material. The cation-exchange capacity of the resulting exchangers was affected by several conditions, for example, the composition of the mixed solution, the oxidizing temperature, and the period. In this work, most of the cation-exchange capacities have been measured with sodium ions. Therefore, the cation-exchange capacity will be represented by the exchange capacity with sodium ions. Unless otherwise stated, the measurement of the capacity was carried out as follows: about 1 g of the exchangers, weighed exactly, was allowed to stand in a 0.2 N NaOH solution for 24 hours, and then the decrease in alkali was determined by titration with hydrochloric acid. Figure 2 shows the relationship between the composition of the mixed solution and the exchange

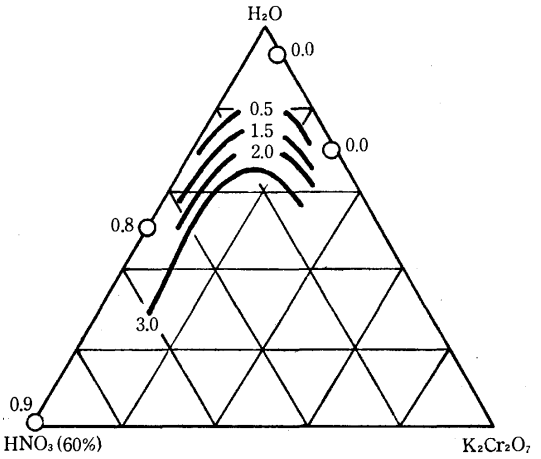

Fig. 2. Relationship between the composition of the mixed solution and the exchange capacity of the resulting fibers.

capacity of the fibers finally obtained. The numbers in Fig. 2 represent the capacity. In this experiment, the weight of the original carbon fibers used was about 1 g, the oxidizing temperature was 104°C, and the oxidizing period was 2.5 hr. By the use of mixtures having compositions lower than the line denoted by 3.0, capacities larger than 3.0 mequiv/g were obtained. However, those fibers were remarkably weak in tensile strength, and some soluble matters were formes in an alkaline solution. Therefore, the composition and the conditions shown in Table 1 were adopted as standard. This standard procedure gave the exchange capacity of 2.0±0.1 mequiv/g.

Table 1. Standard composition and conditions

Composition of the treating mixture	HNO_3	20 m*l*
	$K_2Cr_2O_7$	10 g
	H_2O	80 m*l*
Oxidizing conditions		
temperature	104°C	
period	2.5 hr	
Amount of carbon fiber		
Carbon fiber prepared at 1000°C		1 g

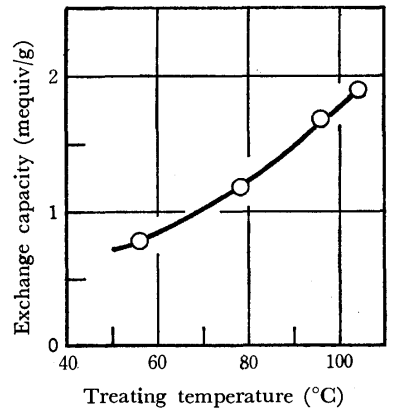

Fig. 3. Effect of the treating temperature. (Other treating conditions and composition of the mixture were the same as those of the standard procedure shown in Table 1.)

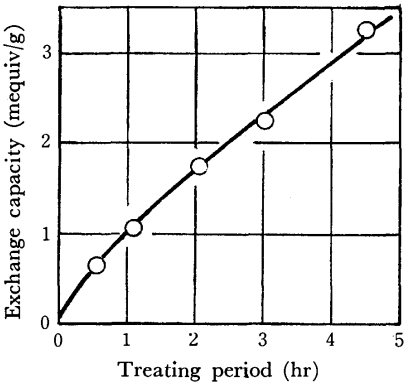

Fig. 4. Effect of the treating period. (Other treating conditions and composition of the mixture were the same as those of the standard procedure shown in Table 1.

Figures 3 and 4 show the effects of the oxidizing temperature and the oxidizing period respectively. These results indicate that it was possible to control the capacity of the fibrous exchangers by selecting well the composition of the mixed solution, the oxidizing temperature, and the oxidizing period.

Chemical Composition and Structure. The chemical composition and infrared spectrum of a typical ion-exchanger having a capacity of 2.0 mequiv/g are shown in Table 2 and Fig. 5 respectively.

The original carbon fiber had, before treatment, a carbon content of 99.2 wt%, and it had no characteristic absorption band in its infrared spectrum. By

Table 2. Chemical composition of ion exchange carbon fiber
(2.0 mequiv/g)

Element	Content	
	wt%	atom%
C	87.4	82.3
H	0.8	9.3
N	1.3	1.1
O(diff.)	10.5	7.3
Cr[a)]	trace	trace

a) by emission spectroscopoy

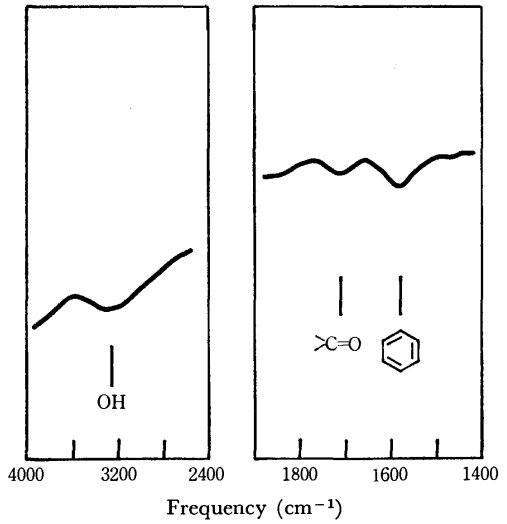

Fig. 5. Infrared spectrum of the ion exchange carbon fiber having 2 mequiv/g in the capacity.

TABLE 3. CHANGES OF d_{002} AND L_c BY THE OXIDIZING TREATMENT

State	Original	Exchanger	
		H-form	Na-form
Inter-layer distance	3.7_7	3.6_7	3.6_3
Crystalline thickness	17	19	18

the oxidizing treatment, the weight of the fiber increased by about 10% in the case of preparing a fibrous exchanger with a capacity of 2.0 mequiv/g. The resulting ion-exchange carbon fiber was very hydroscopic and was found to take up water of about 10 wt% upon exposure to the atmosphere. Its infrared spectrum indicates that some carbonyl and hydroxyl groups were introduced by the treatment.

In order to get some information on the structural changes upon treatment, the powdered samples were used for X-ray diffraction analysis. X-ray diffraction profiles of the original and the treated carbon fibers were composed of (002) and (10) diffraction bands. The two bands were very broad in all cases. The structural parameters of the original one, calculated from the (002) diffraction band, were 3.7_7 Å in inter-layer distance, d_{002}, and 17 Å in the crystalline thickness, L_c. By the oxidizing treatment, the (10) band was weakened to some extent, and the inter-layer distance was decreased slightly, as is shown in Table 3. On the basis of these data, it seems that the structure was not affected very much by the oxidizing treatment.

Exchanging Properties. The first examination of the exchanging properties consisted of measuring the variation in the exchange capacity upon a repetition of the cycle of exchanging and regenerating. The H-form carbon fiber was allowed to stand in a 0.2 N NaOH solution for one day to measure the exchange capacity, and then the resulting carbon fiber-(Na-form fiber) was regenerated with the 0.2 N HCl

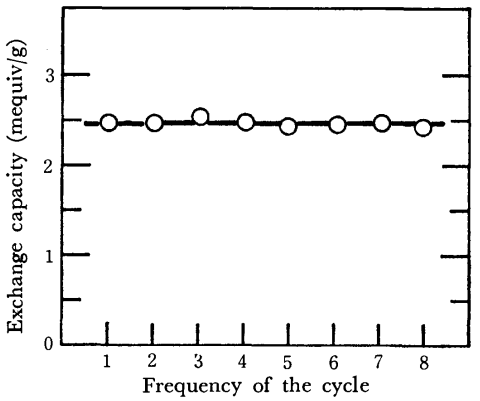

Fig. 6. Variation of the capacity by repeating the cycle of exchanging and regenerating.

solution over a one-day period. The exchange capacity of the regenerated H-form fiber was again measured by the above method, and then the cycles of the exchanging and regenerating were repeated. As is shown in Fig. 6, even after the cycles had been repeated 8 times, the exchange capacity remained at the same value as that of the original exchanger.

In order to determine the exchanging rate, a 50-m*l* portion of the 0.2 N NaOH solution was placed in each of 7 flasks, and one gram of the H-form exchanger was taken into each alkaline solutions, then the decreases in alkali after 5, 10, 15, 20, 30, 40, and 50 min were determined by titration with the 0.2 N HCl solution. The results are shown in Fig. 7. Two curves, (1) and (2), were obtained for the present ion exchangers, while curve (3) was that of a weakly acidic exchange resin obtained commercially. The value of 100% exchange was considered to be reached at the end of 2 days.

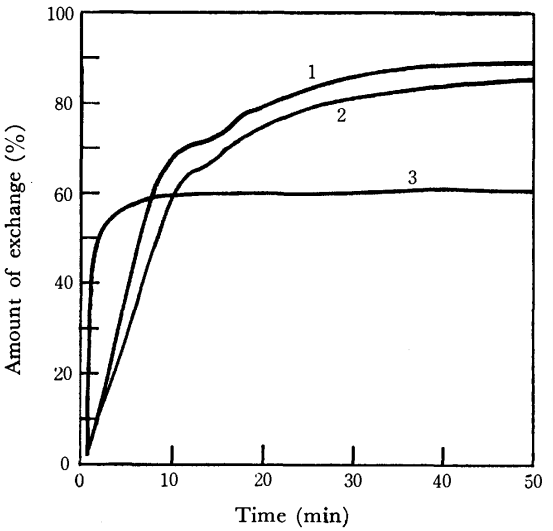

Fig. 7. Rate of ion exchange
1) exchange carbon fiber, 2.1 mequiv/g in the capacity
2) exchange carbon fiber, 1.9 mequiv/g in the capacity
3) weakly acidic exchange resin (as control)

When one gram of the exchange carbon fiber in 100 m*l* of distilled water was titrated with the 0.2 N NaOH solution, the pH of the solution varied as is shown in Fig. 8. The curve (a) is the result of a blank

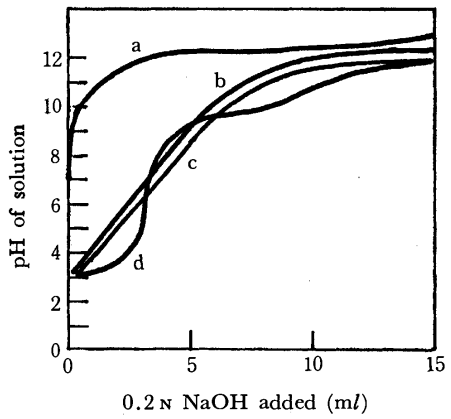

Fig. 8. Titration curves with NaOH solution.
a) pure water (blank test)
b) exchange carbon fiber, 2.1 mequiv/g in the capacity
c) exchange carbon fiber, 3.5 mequiv/g in the capacity
d) mixture of strongly acidic and weakly acidic exchange resins (as control)

test with distilled water alone, while curve (d) is that on a mixture of strongly acidic and weakly acidic exchangers obtained commercially. The titration curves of the present carbon fibers gradually rose from 3 to 12 in pH value.

Figure 9 shows the thermal stability of the present ion-exchange carbon fiber. After heating in air for one hour, the ion-exchange capacity was measured at room temperature. Until the heating temperature was over 220°C, no change was observed in the capacity, at 320°C, the capacity decreased by 20%.

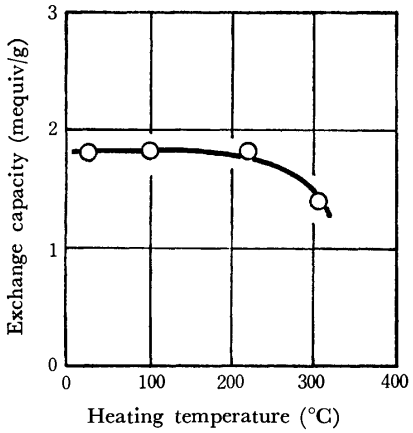

Fig. 9. Change of the exchange capacity after heating in air for one hour.

The effect of the exchanging temperature is shown in Fig. 10. Since the experimental error was about ±0.1 mequiv/g, it seems that an increase in the exchanging temperature up to 100°C caused scarcely no change in the capacity.

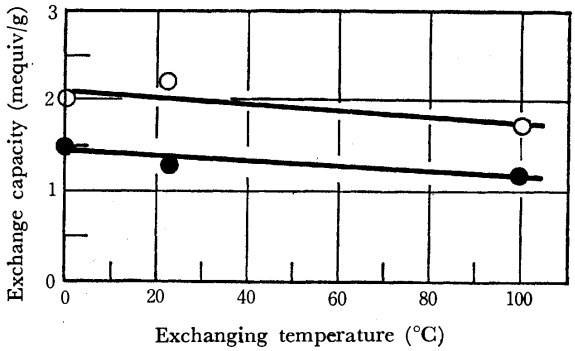

Fig. 10. Effect of the exchanging temperature.

Electric and Mechanical properties. The electric resistivity of the present exchangers is shown in Fig. 11. The measurement was carried out at room temperature by the use of the Universal Bridge TF 1313A made by Marconi Instrument, Ltd. As is shown in Fig. 11, the electric resistivity increased with the increase in the capacity, and no difference was observed between the H-form and the Na-form.

The mechanical properties of a typical ion-exchanger

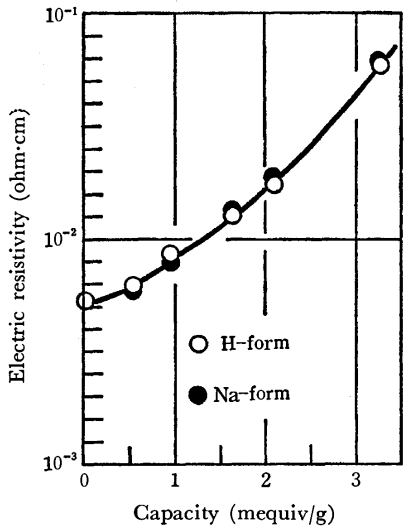

Fig. 11. Relationship between elecctric resistivity and the ion exchange capacity.

Table 4. Mechanical properties of the original and the ion exchange carbon fiber

Sample	Tensile strength ($\times 10^6$ g/cm^2)	Breaking load (Kg)	Elongation (%)	Young's modulus ($\times 10^6$ g/cm^2)
Filament				
original	8.7	—	2.1	420
ion exchanger (1.9 mequiv/g)	6.7	—	2.5	260
Spinning yarn (1300 den.)				
original	—	4.0	—	—
ion exchanger (2.0 mequiv/g)	—	3.0	—	—

are shown in Table 4. The tensile strength decreased by 20% as compared with that of the original carbon fiber, and Young's modulus decreased by 33%. When the graphite fiber prepared at 2000°C was used as the original fiber in the standard procedure, the resulting fibrous exchanger had a tensile strength of only one half of these values and an exchange capacity of less than one third. Carbon fiber heated at 1000°C was a much better material for the exchanger than that prepared at 2000°C.

Discussion

From the results presented above, it has been found that the new ion-exchangers can easily be prepared from carbon fiber. The resulting fibrous exchangers have a satisfactory tensile strength for common use and several other characteristic properties. The most interesting properties other than their shape and mechanical properties are their large electric conductivity and their large thermal stability.

The exchanging properties shown in Fig. 8 resemble those of amorphous zirconium phosphate[4] rather than a commercial strongly or weakly acidic resin exchanger which has a single functional group. From this result, it seems that the ion-exchange carbon fibers have many kinds of functional groups and/or exchanging mechanisms. It is a well known fact that graphite oxide is formed from graphite crystallites or graphitized carbon materials by oxidizing treatment with various agents, such as a mixed solution of phosphoric acid and sulfuric acid.[5,6] Graphite oxide, however, is a very complicating material, and its chemical composition and structure are not known definitely. According to Hofmann *et al.*,[7,8] the chemical composition can be represented by $C_8O_2(OH)_2$ and oxygen atoms exist in both the *keto*-type and the *enol*-type. The inter-layer distance, d_{002}, of the graphite oxide was expanded to 7.96 Å even in a dry state. However, on the basis of the results obtained in the present work, it is doubtful that the previous considerations of the graphite oxide are applicable to the present investigation. In the present work, use was made of a new oxidizing agent and the carbon material not graphitized. Carbon fiber prepared at 1000°C had a larger exchange capacity than that produced from carbon fiber prepared at 2000°C. The inter-layer distance of the exchanger, in spite of the large amount of oxygen introduced, kept almost the same value as that of the original fiber. The exchangers have acidic functional groups, and their infrared spectra indicate the presence of carbonyl and hydroxyl groups. Moreover, it is also well known that mellitic acid is formed from carbon materials by oxidation with some oxidizing agents, such as nitric acid. From these results, it seems most reasonable to assume that the ion-exchange properties are due mainly to the carboxyl groups substituted at various positions of the carbon structure.

4) C. B. Amphlet, L. A. McDonald, and M. J. Redman, *J. Inorg. Nucl. Chem.*, **6**, 220 (1958).
5) L. Standenmaire, *Ber. Deutsch Chem., Ges.* **31**, 1481 (1898).
6) W. S. Hummers and R. E. Offeman, *J. Amer. Chem. Soc.* **80**, 1339 (1958).
7) A. Clauss, R. Plass, H. P. Boehm, and U. Hofmann, *Z. Anorg. Allgem. Chem.*, **291**, 205 (1957).
8) W. Rudorff and U. Hofmann, *ibid.*, **238**, 1 (1938).

NOTES

BULLETIN OF THE CHEMICAL SOCIETY OF JAPAN, VOL. 45, 1913—1914 (1972)

The Allylic Oxidation of Thujopsene

Masaaki Ito, Kazuo Abe, and Hitoshi Takeshita*

Department of Industrial Chemistry, Kitami Institute of Technology, Kitami, Hokkaido

** Department of Chemistry, Faculty of Science, Tohoku University, Sendai*

(Received June 30, 1971)

The allylic oxidation[1] of olefins to their acetate by mercuric acetate in acetic acid or other solvents occurs by means of an electrophilic addition. Brown[2] has shown that the oxymercuration-demercuration of olefins is an excellent method of obtaining alcohols. The procedure achieves the Markovnikov hydration of carbon-carbon double bonds without rearrangement, and it results in the preferential formation of *exo* hydroxyl derivatives.

Although several attempts to prepare a saturated alcohol by Brown's procedure have been unsuccessful with regard to thujopsene (**1**), we have obtained some findings on the reaction of thujopsene **1**, with mercuric acetate in acetic acid. Thus, it may be seen that, besides a skeletal conversion to give a bicyclic acetate (**4**), an allylic oxidation occurs at the methyl group, while these are no Markovnikov addition to **1**. Thus, **1** was first mercurated by heating it with mercuric acetate in acetic acid at 70°C for 3 hr; it was then demercurated by heating at 100—120°C for 3—4 hr. Glpc and tlc analyses of the reaction mixture showed two major products, (**2**) and (**3**), and a minor product, **4**. Samples of the three products were readily isolated from the mixture by means of preparative tlc.

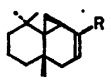

1 : R=CH_3
2 : R=CH_2OAc
3 : R=CH_2OH

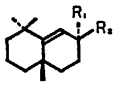

4 : R_1=CH_2OAc, R_2=CH_3
6 : R_1=CH_3, R_2=CH_2Br

The **2** product was a colorless liquid; its IR spectrum showed a presence of an acetoxyl group, while the NMR spectrum indicated the cyclopropane ring intact and the replacement of a methyl group by an acetoxymethyl group. The structure assigned to this product, **2**, was verified when the hydrolysis of **2** afforded thujopsenol (**5**).[3]

The **3** product, pale yellow crystals, was identified as thujopsenal by a direct comparison of its melting point and IR and NMR spectra with those of an authentic sample.

The minor product, **4**, a colorless liquid, was analyzed to be $C_{17}H_{28}O_2$. The NMR spectrum revealed the absence of any cyclopropane ring and the presence of an acetoxymethyl group. Because of the close resemblance of the NMR data to the related compound (**6**),[4] the structure of **4** was deduced to be as depicted.

Whenever the reaction carried out in an atmosphere of nitrogen or oxygen, the ratio of the yield of **3** to **2** was not affected. Although the reaction was attempted in various solvents (*e.g.*, in acetic acid-acetic anhydride, tetrahydrofuran-water, and acetic acid, acetone-water) the reaction products were almost always the same. The reaction in the presence of silver acetate[5] or hydroquinone does not seem to improve the yield.

Experimental

Materials and Methods. The thujopsene was obtained from Hiba (*Thujopsis dolabrata* Sieb. et Zucc.) oil. Thin-layer chromatography (tlc) and preparative tlc were performed on silica gel Merck G. The equipment used in this study was a Varian A-60 NMR spectrometer, a Shimadzu IR-27G grating IR spectrometer, a Shimadzu MPS-50 multipurpose UV spectrometer, and a Shimadzu UM-2 elemental-analyses apparatus.

Allylic Oxidation of Thujopsene. A solution of 5.8 g (28 mmol) of thujopsene in 10 m*l* of acetic acid was treated with a solution of 9.6 g (30 mmol) of mercuric acetate in 40 m*l* of acetic acid. The mixture was heated at 70°C for 3 hr. After the mercuration, the reaction temperature was elevated to 120°C, and then the solution was maintained at that temperature for 4 hr. The reaction mixture was cooled, treated with water, and extracted with ether. The ether solution was dried and evaporated, and the residue was distilled. After the removal of the unchanged hydrocarbon, these products, **2**, **3**, and **4**, were isolated by preparative tlc using a mixed solvent of *n*-hexane and ethyl acetate (9 : 1, by volume).

The sample of **2** (0.53 g, 14.4%) was a colorless liquid and showed the following spectral data: UV λ_{max}^{EtOH} 222 (ε 4509), λ_{max}^{Hexane} 221.5 mμ(ε 4488); IR (CCl_4) 1728 (C=O), 1227 (CH_3CO), 3011 cm^{-1} (cyclopropyl); NMR (CCl_4) 0.63 (s, 3, CH_3), 1.12 (s, 3, CH_3), 1.15 (s, 3, CH_3), 2.01 (s, 3,$OC-OCH_3$), 4.50 (s, 2 CH_3OAc), 5.25 ppm (m, 1, olefinic proton).

Found C, 77.68; H, 9.89%. Calcd for $C_{17}H_{26}O_2$: C, 77.82; H, 9.99%.

The sample of **3** (0.34 g, 11.1%) consisted of pale yellow crystals; mp 75°C; IR (CCl_4) 1692 (C=O), 1649 cm^{-1} (C=C).

The sample of **4** (0.2 g, 5.4%) was a colorless liquid and showed the following spectral data: UV λ_{max}^{EtOH} 208 mμ. IR (CCl_4) 1730 (C=O), 1237 cm^{-1} (CH_3CO–), and NMR (CCl_4) 1.06 (d, 6, $2CH_3$), 1.14 (s, 3, CH_3), 1.20 (s, 3, CH_3),

1) J. Chatt, *Chem. Rev.*, **48**, 7 (1951); N. S. Zefirove, *Russ. Chem. Rev.*, **34**, 527 (1965); W. Kitchins, *Organometal. Chem. Rev.*, **3**, 61 (1968).

2) H. C. Brown and P. Geoghegen, Jr., *J. Amer. Chem. Soc.*, **89**, 1522 (1967).

3) O. Okuda, *Yakugaku Zasshi*, **73**, 1, 4, 6, and 9 (1953).

4) M. Ito, K. Abe, H. Takeshita, and M. Yatagai, This Bulletin, **44**, 2168 (1971).

5) S. Moon and B. H. Waxman, *J. Org. Chem.*, **34**, 1157 (1969).

2.05 (s, 3, $OCOCH_3$), 3.53 (1H, d, J=12 Hz), 3.95 (1H, d, J=12 Hz), 5.7 ppm (1H, singlet).

Found: C, 77.02; H, 10.48%. Calcd for $C_{17}H_{28}O_2$: C, 77.22; H, 10.67%.

Hydrolysis of Thujopsenyl Acetoate. The saponification of **2** with alcoholic potassium hydroxide for 20 min at 60°C led to the thujopsenol, **5**: mp 107—108°C; UV λ_{max}^{EtOH} 213 mμ(ε 4732), IR (KBr) 3350 (-OH), 3011 (cyclopropyl), 1674 cm^{-1} (C=C), and NMR (CCl_4) 0.65 (s, 3, CH_3), 1.15 (s, 6, $2CH_3$), 4.0 (m, 2, $-CH_2OH$), 5.41 ppm (m, 1, olefinic).

Found: C, 81.52; H, 10.81%. Calcd for $C_{15}H_{24}O$: C, 81.76; H, 10.98%.

BULLETIN OF THE CHEMICAL SOCIETY OF JAPAN, VOL. 45, 1914—1915 (1972)

The Autocatalytic Oxidation of Thujopsene. A Facile Synthesis of Mayurone

Masaaki Ito, Terumi Nishimura, and Kazuo Abe

Department of Industrial Chemistry, Kitami Institute of Technology, Kitami, Hokkaido

(Received June 30, 1971)

The autoxidation of cyclic terpenes, including an allyl methyl moiety, is known to give a small amount of a preferential product, accompanied by minor products. For example, the autoxidation of limonene[1] produces carveol, carvone, 8-*p*-menthene-1,2-diol, and limonene 1,2-oxide. Our interest in the autocatalytic oxidation and in the chemistry of thujopsene has led us to seek favorable catalysts for the autocatalytic oxidation of thujopsene to mayurone.

In the course of our investigations utilizing metal chelate catalysts for synthetic purposes, it has been found that the oxidation of thujopsene (**1**) with molecular oxygen in dioxane gives mayurone (**2**) and an unidentified product (**4**) in poor yields, but the oxidation was accelerated in the presence of metal chelate catalysts, as is shown in Table 1. $CoCl_2$–dioxane[2] was most effective in giving **2**, **3**, and **4**. In this system, however, the products were not obtained in good yields in the absence of the catalysts and the solvent. From this observation, it seems that the chelate complex formed from $CoCl_2$ and dioxane has a remarkably catalytic effect. Also, catalysts composed of a metallic salt, and a synthetic organic adsorbent showed a catalytic effect, affording the same products. This study promised to be of interest because of the possibility of effecting a new type of chelate-catalyzed reactions. New types of catalysts were realized. The results are summarized in Table 1.

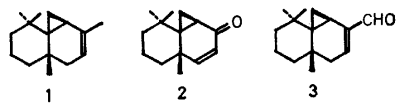

1 2 3

The IR and NMR spectra of **2** were all consistent with those of an authentic sample, which has been prepared by the potassium permanganate and sodium perchromate oxidation[3] and the photosensitized oxidation[4] of thujopsene, and which has also been isolated from several conifers.[5,6,7] Compound **3** was identified by glpc analysis with thujopsenal which had been prepared by the selenium dioxide oxidation

Table 1. Autocatalytic oxidation of thujopsene at 70°C

Entry No.	Catalysts, g	Dioxane, m*l*	Distribution of products		
			Mayurone (**2**)	Thujopsenal (**3**)	Unidentified prodt. (**4**)
1	$CuCl_2$-N-GHP, 0.2	10	44	trace	5
2	$CuCl_2$-GHP, 0.2	10	23	trace	8
3	$RuCl_3$-N-GHP, 0.2	10	86	trace	16
4	$RuCl_3$-GHP, 0.2	10	67	3	19
5	$CoCl_2$-GHP, 0.2	10	31	2	6
6	$CoCl_2 \cdot 6H_2O$, 0.015	10	221	45	57
7	——	10	7	none	4
8	$CoCl_2 \cdot 6H_2O$, 0.015	—	39	2	6
9	$CoCl_2$-GHP, 0.2	—	35	4	2
10	$CoCl_2 \cdot 6H_2O$, 0.015	THF, 10 ml	153	14	23

1) E. Gildemeister und Fr. Hoffman, "Die Ätherischen Ole", Akademie-Verlag, Berlin (1960), IIIa, s 69.

2) Yu. I. Rozenberg, *Fiz. Tverd. Tela*, **1968**, 3017; M. Perrier E. Giesbrecht and G. Vicentini, *An. Ass. Brazil. Quim.*, **25**, 39 (1966).

3) S. Akiyoshi and S. Nagahama, This Bulletin, **30**, 886 (1957); S. Nagahama, H. Kobayashi, and S. Akiyoshi, *ibid.*, **35**, 1140 (1962); H. Kobayashi, S. Nagahama, and S. Akiyoshi, *ibid.*, **34**, 1123 (1961).

4) H. Takeshita, T. Sato, T. Muroi, and S. Ito, *Tetrahedron Lett.*, **1969**, 3095.

5) S. Ito, K. Endo, H. Homma, and K. Ota, *ibid.*, **1965**, 3777.

6) G. L. Chetty and S. Dev, *ibid.*, **1965**, 3773.

7) B. Tomita, Y. Hirose, and T. Nakatsuka, *ibid.*, **1968**, 843.

of thujopsene Compound **4** was not identified.

Experimental

The melting point was determined on a Büchi melting-point apparatus. The NMR spectrum was recorded on a Hitachi R-20A spectrometer at 60 MHz, using tetramethylsilane as the internal standard. The IR spectrum was determined on a Shimadzu IR-27G spectrophotometer. The UV spectrum was recorded on a Shimadzu MPS-50 spectrophotometer. Glpc analyses were performed on a Shimadzu GC-1C gas chromatograph with a 1.1-m stainless-steel column packed with 15% OV-17, at 180°C.

Materials. The thujopsene used was purified by the careful distillation of Cedar H oil (Takasago Perfumery Co., Ltd.) through a concentric column and had a boiling point of 119°C/10 mmHg, showing no trace of an impurity upon glpc analysis. The inorganic salts used for preparing the catalysts were commercial, extra-pure reagents.

Preparation of the Chelate Catalysts. Some of the catalysts shown in Table 1 were prepared according to the reported method for preparing kieselguhr using synthetic organic absorbents, GHP[8] or N-GHP[9]. For example, a 1.5-g portion of N-GHP dissolved in 6 m*l* of water was added to a solution of 0.158 g of $RuCl_3$-xH_2O in 2 m*l* of ethyl alcohol, after which the mixture was kneaded in a mortar. The slurry was washed with water and dried at 100°C.

General Procedure for Autocatalytic Oxidation. Into a stirred mixture of 3.0 g of thujopsene and 0.2 or 0.015 g of the catalyst in 10 m*l* of dioxane or without the solvent, we passed a stream of dry oxygen at a rate of 62 m*l*/min for 21 hr. The mixture was then chilled, filtered, and evaporated. The components of the reaction mixture were analyzed by means of glpc. Thier yields were accounted on the basis of the area ratio of peaks on a chromatogram, regarding the peak area of hydrocarbons in the reaction mixtures as 100. The yield of mayurone was found to be 20% by glpc, using naphthalene as the internal standard; the retention times were 18 min for mayurone (**2**), 15 min for thujopsenal (**3**), and 11 min for the unidentified product (**4**).

*Isolation of Mayurone (**2**).* Into a stirred mixture of 20.4 g (0.1 mol) of thujopsene and 1.0 g of the $RuCl_3$-N-GHP catalyst in 300 m*l* of dioxane, we passed a stream of dry oxygen at a rate of 408 m*l*/min at 70°C for 29 hr. The mixture was then chilled and filtered. After the removal of the solvent, the reaction mixture thus obtained was distilled through a concentric column to collect the distillate with a bp of 150°C/7.5 mmHg, which deposited a crystalline matter on chilling. Two recrystallizations of the crystals from petroleum ether (bp 30—40°C) gave 1.45 g of **2** as colorless crystals; mp 70.0—71.0°C; $[\alpha]_D^{27}$ +221.0 (*c* 10.0 CCl_4); MW 201.86 (benzene) (calcd 204.16); NMR (CCl_4) 0.66 (CH_3), 1.11 (CH_3), 1.30 (CH_3), 1.30 (CH_3), 5.44 (1H, J=11.9 Hz), 6.00 (1H, J=11.0 Hz); IR (CCl_4) 3010 (cyclopropyl), 1661 (conj. C=O). 1619 cm^{-1} (conj. C=C); UV $\lambda_{max}^{cyclohexane}$ 226 mμ(ε 6646).

8) M. Ito, K. Abe, T. Tsuchiya, M. Umehara, and S. Yamashiro, *Mem. Kitami Inst. Tech.*, **3**, 131 (1971).

9) M. Ito, T. Tsuchiya, and K. Abe, *ibid.*, to be published.

BULLETIN OF THE CHEMICAL SOCIETY OF JAPAN, VOL. 45, 1915—1917 (1972)

Reaction of Urea with Ethylene in the Presence of Oxygen and a Nitrile-Sodium Tetrachloropalladate-Cupric Chloride Catalyst System

Tadashi INOUE, Hiroshi HARADA, and Shingo MIYAJIMA

The Central Research Laboratories, Chisso Corporation, Kamariya, Kanazawa-ku, Yokohama

(Received August 12, 1971)

The reactions of amines and amides with olefins in the presence of palladium chloride are generally complicated because of the fact that both the nucleophiles and the products form complexes with palladium chloride.[1-3] By hydrogenation of the resulting complexes Stern and Spector demonstrated the addition of nitrogen functions to olefins.[1] Hirai and Sawai reported the formation of *N*-vinylamides along with their complexes with palladium chloride by the reaction of ethylene-palladium(II) chloride complex with some cyclic amides in tetrahydrofuran.[3]

We found that urea in an acidic aqueous solution reacts with ethylene at room temperature to yield acetylurea in the presence of oxygen and a nitrile-sodium tetrachloropalladate-cupric chloride catalyst system. Sodium tetrachloropalladate was stirred in acetonitrile or benzonitrile for 1 to 3 hr. Most of the palladate dissolved to form a reddish-orange solution of the nitrile-palladium(II) chloride complex[4] leaving precipitates of sodium chloride. Toluene and an aqueous hydrochloric acid solution of urea and cupric chloride were added, and the mixture was stirred while ethylene and oxygen were bubbled through.[5] Crystals of crude acetylurea separated. The results are summarized in Table 1. In the absence of nitrile, Pd(II) readily combined with urea to form precipitates of bis(urea)dichloropalladium(II), which could not catalyze the reaction.

When the reaction temperature was above 30°C, formation of 6-methyl-2-oxo-4-hexahydropyrimidinylurea became predominant. There is hardly any doubt that this compound results from the condensation of urea with acetaldehyde formed by the oxidation of ethylene with Pd(II), since it is known that the

1) E. W. Stern and M. L. Spector, *Proc. Chem. Soc.*, **1961**, 370.
2) H. Hirai, H. Sawai, and S. Makishima, This Bulletin, **43**, 1148 (1970).
3) H. Hirai and H. Sawai, *ibid.*, **43**, 2208 (1970).
4) R. A. Walton, *Spectrochim. Acta*, **21**, 1795 (1965).
5) Cupric chloride and oxygen obviously function to regenerate Pd(II) by the redox cycle [J. Smidt, W. Hafner, R. Jira, J. Sedlmeier, R. Sieber, R. Ruttinger, and H. Kojer, *Angew. Chem.*, **71**, 176 (1959)].

Table 1. Reaction of urea with ethylene in the presence of oxygen and a nitrile-sodium tetrachloropalladate-cupric chloride catalyst system[a)]

Expt. No.	Nitrile, m*l*	Na_2PdCl_4 g	$PhCH_3$ m*l*	H_2O m*l*	$CuCl_2$ g	Urea g	pH	Time hr	Yield of acetylurea[b)] %
1	CH_3CN, 50	1.34	50	100	2.5	15	0.9[c)]	18	1810
2	CH_3CN, 50	1.34	50	200	2.5	15	1.4[c)]	18	3150
3[e)]	CH_3CN, 50	3.4	—	50	5.5	15	1.5[d)]	13	f)
4	PhCN, 50	1.34	50	100	2.5	15	0.9[c)]	7	860
5	PhCN, 50	1.34	50	100	2.5	15	1.3[c)]	13	1510
6	PhCN, 50	1.34	50	100	2.5	15	3.2[c)]	13	770
7[e,g)]	PhCN, 50	1.34	50	50	2.5	7.5	1.4[c)]	14	340

a) Reactions were carried out at room temperature and at flow rates of ethylene and oxygen, 0.25 and 0.5 mol/hr, respectively, unless otherwise stated.
b) The yields are given based on Pd(II), assuming the stoichiometry of 1 mole of acetylurea per 2 moles of Pd(II).
c) The value indicates the pH of the aqueous phase containing $CuCl_2$ and urea.
d) The value indicates the pH of aqueous hydrochloric acid, in which $CuCl_2$ and urea were dissolved.
e) Flow rate was 0.3 mol/hr for both ethylene and oxygen.
f) 10.7 g of a mixture of acetylurea and 6-methyl-2-oxo-4-hexahydropyrimidinylurea was obtained.
g) Reaction was carried out at 0—5°C.

condesnation leads to the cyclic product in an acidic aqueous solution and at an elevated temperature.[6)]

N-vinylation (Eq. 1) rather than ethylolation of urea (Eq. 2) might be involved in acetylurea formation:[3)] Acetaldehyde in place of ethylene gives no acetylurea under otherwise similar reaction conditions.

$$CH_2{=}CH_2 + H_2NCONH_2 \xrightarrow{Pd^{++}} [CH_2{=}CHNHCONH_2] + 2H^+ + Pd^0$$
$$[CH_2{=}CHNHCONH_2] \xrightarrow[H_2O]{Pd^{++}} CH_3CONHCONH_2 + 2H^+ + Pd^0 \quad (1)$$

$$CH_3CHO + H_2NCONH_2 \longrightarrow [CH_3CH(OH)NHCONH_2]$$
$$[CH_3CH(OH)NHCONH_2] \xrightarrow[or\ Pd^0]{Pd^{++}} CH_3CONHCONH_2 \quad (2)$$

Experimental

Melting points are uncorrected. The infrared spectra were obtained with a Nihon Bunko Model IR-S spectrophotometer using KBr disks.

Typical Procedure. Acetylurea (Expt. 2): Sodium tetrachloropalladate (1.34 g, 4.55 mmol) was stirred in acetonitrile (50 m*l*) for 1 hr at room temperature. Toluene (50 m*l*) and an aqueous solution (200 ml) containing cupric chloride (anhydrous, 2.5 g) and urea (15 g, 0.25 mol) and adjusted at pH 1.4 with hydrochloric acid were added. The mixture was stirred at room temperature while ethylene and oxygen were bubbled through the mixture. After 18 hr, the crude crystals of acetylurea were filtered, washed successively with cold water, methanol and ether, and dried. The yield was 7.3 g. Recrystallization from ethanol gave needles, mp 215—216°C (lit,[7)] 216—217°C, corrected).

Found: C, 35.32; H, 5.99; N, 27.31%. Calcd for $C_3H_6N_2O_2$: C, 35.29; H, 5.92; N, 27.44%.

The IR spectrum was identical with that of acetylurea reported.[8)] A mixture melting point with the authentic sample showed no depression.

The yield was calculated on the basis of the crude product, which amounted to 29% based on starting urea, corresponding to 3150% based on Pd(II) charged; the crude product was proved to be pure by its IR spectrum.

6-Methyl-2-oxo-4-hexahydropyrimidinylurea: Sodium tetrachloropalladat e(3.4 g, 0.0116 mol) was stirred with benzonitrile (130 m*l*) for 3 hr and ethylene was bubbled for about 30 min. The temperature was raised to 50—60°C and a solution of cupric chloride (5.5 g) and urea (15 g, 0.25 mol) in aqueous hydrochloric acid (25 m*l*; pH, 1.5) was added. The mixture was stirred at 50—60°C, while ethylene and oxygen were bubbled through the mixture each at a flow rate of 0.3 mol/hr. After 6.5 hr, the crude crystals of 6-methyl-2-oxo-4-hexahydropyrimidinylurea were collected, washed with cold water, methanol and ether, and dried (8.4 g). Analytical sample was obtained by recrystallization from water, mp 238°C (lit,[6)] 245°C).

Found: C, 41.86; H, 7.14; N, 32.39%. Calcd for $C_6H_{12}N_4O_2$: C, 41.85; H, 7.03; N, 32.54%.

The IR spectrum was identical with that of the authentic sample prepared from crotonaldehyde and urea.[9)] A mixture melting point determination showed no depression.

The yield of the crude product, the IR spectrum of which was apparently the same as that of the pure one, was 39% based on starting urea, corresponding to 840% based on Pd(II).

Attempted Reaction Using Acetaldehyde in Place of Ethylene. Pd(II) Catalyst: Sodium tetrachloropalladate (1.3 g) was treated with acetonitrile (50 m*l*). Toluene (100 m*l*) and a solution of cupric chloride (2.5 g) and acetaldehyde (5.5 g) in aqueous hydrochloric acid (30 m*l*; pH, 1.3) were added. With the mixture kept at 0—6°C, oxygen was introduced and a solution of urea (7 g) in aqueous hydrochloric acid (20 m*l*; pH, 1.3) was gradually added under stirring. After 13 hr at 0—6°C and additional 2 hr at 15°C, the reaction was stopped. No crystals separated. On standing at room temperature overnight, some crystals deposited from the reaction mixture (1.1 g). The IR spectrum revealed

6) G. Zigeuner, E. A. Gardziella, and G. Bach, *Monatsh. Chem.*, **92**, 31 (1961).
7) R. W. Stoughton, *J. Org. Chem.*, **2**, 518 (1938).
8) "Sadler Infrared Prism Spectra," No. 36705, Sadler Research Laboratories Inc., Philadelphia, Pa. (1969); T. Uno, K. Machida, K. Hanai, and Y. Saito, This Bulletin, **42**, 619 (1969).
9) A. M. Paquin, *Kunststoffe*, **37**, 165 (1947).

that the product was hexahydro-6-methyl-2-oxo-4-pyrimidinylurea free from acetylurea.

Metallic Palladium Catalyst: Sodium tetrachloropalladate (3.4 g) was treated with benzonitrile (75 m*l*) and ethylene was bubbled through to form ethylene-palladium(II) chloride complex. Metallic palladium was formed when a solution of acetaldehyde (22 g) in aqueous hydrochloric acid (50 m*l*; pH, 1.5) was added and the mixture was stirred for some time. A solution of urea (15 g) in aqueous hydrochloric acid (50 m*l*; pH, 1.5) was gradually added, while oxygen was bubbled through at 0—5°C. The supply of oxygen was continued for 13 hr at 0—5°C under stirring. The precipitate was filtered, which proved to be only metallic palladium.

BULLETIN OF THE CHEMICAL SOCIETY OF JAPAN, VOL. 45, 1917—1918 (1972)

The Synthetic Intermediate of Pyridoxine. III.[1] The Simple Synthesis of Ethyl *N*-Ethoxalylalaninate and Ethyl *N*-Formylalaninate

Itsutoshi MAEDA, Soichiro ASAI, Hideshi MIYAYASHIKI, and Ryonosuke YOSHIDA

Central Research Laboratories, Ajinomoto Co., Inc. Suzuki-cho, Kawasaki

(Received August 18, 1971)

Ethyl *N*-ethoxalylalaninate (I), which is an important intermediate on the synthesis of pyridoxine, had been obtained from alanine through two steps. That is compound I had been prepared by the treatment of ethyl alaninate hydrochloride with ethoxalyl chloride[2] or with diethyloxalate in the presence of triethylamine, as was in our previous paper.[3] Our further investigation was undertaken to determine a simple method. Compound I and ethyl *N*-formylalaninate (II) could be obtained by heating a mixture of alanine, oxalic acid, and ethanol at various temperatures, as is shown in Fig. 1.

The yield of Compound I increased when the mixture was heated in the range from 110 to 140°C, while at temperatures above 150°C the yield of Compound I decreased and that of Compound II increased remarkably. After the water formed and the unreacted ethanol had been distilled off from the reaction mixture, ethanol was added again to the residue and the

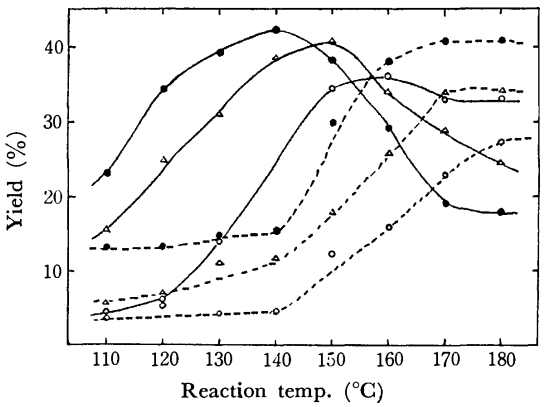

Fig. 1. One-step method of synthesizing ethyl *N*-ethoxalylalaninate.

The yield of ethyl *N*-ethoxalylalaninate ——
The yield of ethyl *N*-formylalaninate ……
Reaction time: ○—○, 1 hr; △—△, 3 hr; ●—●, 5 hr.

TABLE 1. SIMPLE METHOD OF THE SYNTHESIS OF *N*-ALKOXALYLAMINO ACID ESTERS

RCHCOOR′ NHCOCOOR′		Reaction conditions			Yield (%)	
R	R′	Temp. (°C)	Time (hr)	Repeat (times)	FAE[a]	OXE[b]
H	C_2H_5	120	3	3	3.6	80.9
		180	3	1	31.9	29.8
CH_3	C_2H_5	120	3	3	10.6	58.0
		120	3	3	trace	70.1[c]
		150	3	3	15.9	65.3
		150	3	3	trace	70.5[c]
$(CH_3)_2CHCH_2$	C_2H_5	120	3	3	5.5	78.4
		140	3	3	4.3	74.8
		180	5	1	37.2	24.3
$C_6H_5CH_2$	C_2H_5	180	5	1	28.5	12.9

a) *N*-Formylamino acid ester.
b) *N*-Alkoxalylamino acid ester.
c) Alanine (0.15 mol), oxalic acid (0.15 mol), diethyl oxalate (0.75 mol), and ethanol (138 g) were used.

1) Part II of this series: I. Maeda, M. Takehara and R. Yoshida, This Bulletin, **44**, 1407 (1971).
2) W. Kerp and K. Unger, *Ber.*, **30**, 579 (1897).
3) I. Maeda, M. Takehara, K. Togo, S. Asai, and R. Yoshida, This Bulletin, **42**, 1435 (1969).

mixture was heated again. When the mixture was heated at 120°C and the above treatment was repeated three times, the yield of Compound I amounted to 58.0%, while the yield of Compound II was 10.6%. A mixture of alanine (0.15 mol), oxalic acid (0.15 mol), diethyl oxalate (0.75 mol), and ethanol was heated at 120°C, and the treatment described above was repeated three times. The yield of Compound I was 70.1%, while the amount of Compound II was a trace. The results of these methods preparing *N*-alkoxalylamino acid esters are shown in Table 1.

Compound II, which is also an important intermediate for the synthesis of pyridoxine, can be obtained by heating a mixture of alanine, formic acid, and ethanol. *N*-Formylamino acid esters have been prepared from amino acids in two steps. In general, they are prepared by the esterification of *N*-formylamino acids with diazomethane[4] or by the formylation of amino acid esters with formic acid and acetic anhydride.[5]

By a similar simple method, these various *N*-formylamino acid esters could be synthesized from amino acid, formic acid, and alcohol in one step. The results are shown in Table 2.

Table 2. Simple method of the synthesis of *N*-formylamino acid esters

RCHCOOR' NHCHO		Reaction conditions		
R	R'	Temp. (°C)	Time (hr)	Yield[a] (%)
CH_3	CH_3	160	5	71.0
CH_3	C_2H_5	160	8	70.0
CH_3	C_4H_9	170	5	50.2
$(CH_3)_2CHCH_2$	C_2H_5	170	5	56.4
H	CH_3	160	5	62.8
H	C_2H_5	170	5	56.4
$C_6H_5CH_2$	C_2H_5	170	3	52.7
CH_3SCH_2	CH_3	160	5	35.5

a) Based on amino acid.

Experimental[6]

Ethyl N-ethoxalylalaninate. A mixture of DL-alanine (13.35 g, 0.15 mol), oxalic acid (39.5 g, 0.45 mol), and ethanol (138 g) was put into a 300-m*l* autoclave. The autoclave was kept at 120°C by electrical heating for 3 hr, and then it was chilled. The ethanol and water formed in the reaction mixture were distilled off under reduced pressure. Then ethanol (138 g) was added to the residue, and the mixture was again treated in a manner similar to that used in the experiment described above. This treatment was repeated three times. After the unreacted ethanol and diethyl oxalate, which was one of the by-products, had been removed, the residue was distilled under reduced pressure to afford ethyl *N*-formylalaninate (bp 115—120°C/4 mmHg; yield, 2.3 g; 10.6%) and ethyl *N*-ethoxaylalaninate (bp 140—145°C/4 mmHg; yield, 18.9 g; 58.0%). The following *N*-alkoxylalamino acid esters were prepared by the same method. Ethyl *N*-ethoxalylglycinate (bp 135—138°C/5 mmHg; yield, 24.6 g; 80.9%). Found: C, 47.31; H, 6.65; N, 7.04%. Calcd for $C_8H_{13}NO_5$: C, 47.29; H, 6.45; N, 6.89%. Ethyl *N*-ethoxalylleucinate (bp 150—154°C/4 mmHg; yield, 29.1 g; 74.8%). Found: C, 55.89; H, 8.40; N, 5.69%. Calcd for $C_{12}H_{21}NO_5$: C, 55.58; H, 8.16; N, 5.40%. Ethyl *N*-ethoxalylphenylalaninate (bp 180—185°C/1 mmHg; yield, 5.7 g; 12.9%). The results are summarized in Table 1.

The investigation of the reaction temperature and time shown in Fig. 1 was carried out as follows. A mixture of DL-alanine (4.45 g, 0.05 mol), oxalic acid (13.5 g, 0.15 mol), and ethanol (46.0 g, 1 mol) was put into a 100-ml autoclave. The reaction was then carried out at 110—180°C at intervals of 10°C for 1, 3, or 5 hr respectively. The reaction mixtures were diluted with ethanol to 100 m*l* after which the amounts of ethyl *N*-formylalaninate and ethyl *N*-ethoxalylalaninate were analyzed by gas chromatography, which was carried out with 4% Versamid 900 on Chromosorb T (4 mmϕ × 1 m; column temperature, 190°C; flow rate of He, 60 m*l*/min; internal standard, benzophenone).

N-Formylamino Acid Esters. A mixture of amino acid (0.2 mol), 98.5% formic acid (0.6 mol), and ethanol (4 mol) was put into a 300-m*l* autoclave. The autoclave was then kept under the conditions listed in Table 2. After the removal of the solvent from the reaction mixture, the product was obtained as a syrup; the *N*-formylamino acid ester was then distilled at reduced pressure, as will be described below.

Methyl *N*-formylalaninate (bp 102—105°C/2 mmHg. Found: C, 45.79; H, 7.18; N, 10.82%). Ethyl *N*-formylalaninate (bp 110°C/2 mmHg. Found: C, 49.84; H, 7.91; N, 9.61%). Butyl *N*-formylalaninate (bp 131—133°C/2 mmHg. Found: C, 55.51; H, 9.02; N, 8.29%. Calcd for $C_8H_{15}O_3N$: C, 55.47; H, 8.73; N, 8.09%). Ethyl *N*-formylleucinate (bp 143°C/8 mmHg. Found: C, 58.09; H, 9.45; N, 7.60%). Methyl *N*-formylglycinate (bp 137°C/28 mmHg. Found: C, 41.26; H, 6.43; N, 11.76%). Ethyl *N*-formylglycinate (bp 136°C/5 mmHg. Found: C, 45.61; H, 7.22; N, 10.87%). Ethyl *N*-formylphenylalaninate (bp 158—159°C/1 mmHg. Found: C, 65.29; H, 7.07; N, 6.50%). Methyl *N*-formylmethionate (bp 152—153°C/1 mmHg. Found: C, 44.05; H, 7.02; N, 7.22%).

The authors wish to thank Professor Dr. Masanao Matsui of The University of Tokyo for his many helpful discussions and suggestions.

4) D. S. Tarbell, H. P. Hirschler, and R. B. Carlin, *J. Am. Chem. Soc.*, **72**, 3138 (1950).
5) R. G. Jones, *J. Am. Chem. Soc.*, **71**, 644 (1949).
6) All the boiling points are uncorrected.

BULLETIN OF THE CHEMICAL SOCIETY OF JAPAN, VOL. 45, 1919—1921 (1972)

Electronic Spectra and Structures of 3-Substituted 1,2-Diphenylcyclopropenyl Cations

Zen-ichi Yoshida and Hideki Miyahara

Department of Synthetic Chemistry, Kyoto University, Yoshida, Kyoto, 606

(Received September 2, 1971)

The simplest and most strained non-benzenoid aromatic, cyclopropenyl cation($2\pi 3c$) system is expected to have unique electronic properties. Thus, the electron donating σ-inductive effect of an attached *n*-propyl group is more significant for the stabilization of this carbonium ion than the electron donating π-conjugative effect of an attached phenyl group,[1] in contrast to most other carbonium ions. The ^{13}C–H coupling constant of parent cyclopropenyl cation indicates that the orbital used for bonding with the hydrogens is *sp* hybrid.[2]

Only a few papers[3] have appeared on the electronic spectra and structures of the cyclopropenyl system. This paper deals with the electronic spectra and structures of 3-substituted 1,2-diphenylcyclopropenyl system (Fig. 1) obtained by using the variable integrals method I (VI/I)[4] devised to contain only one arbitrary molecular parameter.

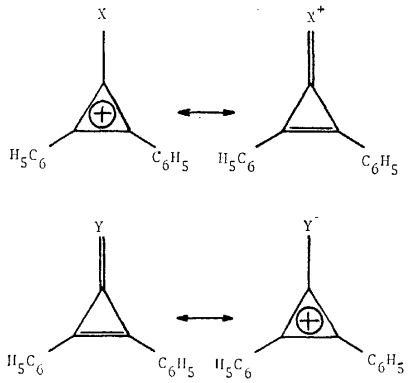

Fig. 1. 3-Substituted-1,2-diphenylcyclopropenyl system taken up in this study.
X: OC_2H_5 (**2**), SC_2H_5 (**4**), $N(CH_3)_2$ (**5**)
Y: O (**1**), S(**3**)

Experimental

Materials. 1,2-Diphenylcyclopropenone[5] (**1**), 1,2-diphenyl-3-ethoxycyclopropenyl tetrafluoroborate[5] (**2**), 1,2-diphenylcyclopropenethione[6] (**3**), and 1,2-diphenyl-3-dimethylaminocyclopropenyl tetrafluoroborate[5] (**5**) were prepared according to literature. 1,2-Diphenyl-3-ethylthiocyclopropenyl tetrafluoroborate (**4**), mp 149—150°C (decomp.) (Anal. Found: C, 60.20; H, 4.54%; Calcd for $C_{17}H_{15}BF_4$: C, 60.37; H, 4.47%) was prepared from **3** and triethyloxonium tetrafluoroborate in 70% yield in a similar manner to that for **2**.

Measurements of Spectra. Ultraviolet spectra were taken on a Hitachi Model ESP-3T spectrometer. Solvents used were of spectrograde from E. Merck & Co.

Method of Calculation

Details of the VI/I method have been described.[4] In order to assume reasonable geometries of the molecules the linear bond order(p) - bond length(l) relationships are used in each iteration step of the SCF procedure.[7] For the three membered ring the reference of the double bond length was taken to be equal to that of cyclopropene[8]:

$$l_{C-C} = 1.477 - 0.177p \quad (1)$$

The procedure is known to give satisfactory bond lengths for fulvenes *etc.*[7] The molecules were assumed to be planar. Numbering of atoms in the molecules are giving in Fig. 2. The CI calculations were made on the singly excited configurations for which inner orbitals of five occupied and five unoccupied levels are responsible.

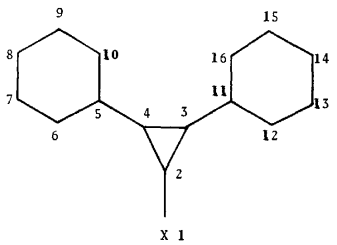

Fig. 2. Numberings of the atoms.

Results and Discussion

The observed electronic spectra of **1** and **3** in cyclohexane and **2**, **4**, and **5** in methylene chloride solutions are given in Table 1 with calculated transition energies. For **1** and **3** the weak least energy bands were obviously assigned to the n-π^* bands which shifted toward higher energy in ethanol.[3a,9] This is not included in our calculation.

We see that the agreement between calculated and observed values is relatively satisfactory and the reasonable assignments of the bands could be made

1) R. Breslow, H. Höver, and H. W. Chang, *J. Amer. Chem. Soc.*, **84**, 3168 (1962).
2) R. Breslow and J. T. Groves, *ibid.*, **92**, 984 (1970).
3) a) G. Laban, J. Fabian, and R. Mayer, *Z. Chem.*, **8**, 411 (1968). b) A. Watanabe, H. Yamaguchi, Y. Amako, and H. Azumi, This Bulletin, **41**, 2196 (1968).
4) Z. Yoshida and T. Kobayashi, *Theor. Chem. Acta*, **19**, 377 (1970).
6) Y. Kitahara and M. Funamizu, This Bulletin, **37**, 1897 (1964).
7) Z. Yoshida and T. Kobayashi, *ibid.*, **45**, 316 (1972).
8) P. H. Kasai, R. J. Meyers, D. F. Eggers, Jr., and K. B. Wiberg, *J. Chem. Phys.*, **30**, 512 (1959).
9) E. Osawa, K. Kitamura, and Z. Yoshida, *J. Amer. Chem. Soc.*, **89**, 3814 (1967).

TABLE 1. CALCULATED SINGLET-SINGLET TRANSITION ENERGIES E (eV) AND OSCILLATOR STRENGTH f[a)]

Compound		E calcd, eV	f	Dominating configurations	E exp., eV[b)] (log ε)
1	E_0				4.13 (3.30) n-π^*
	E_1	4.299	0.570	8—9, 0.953	4.20 (4.35)
	E_2	4.743	0.005	7—9, 0.596	
	E_3	4.744	0.007	8—11, 0.597	4.68 (4.00) sh
	E_4	5.507	0.076	5—9, 0.792	
	E_5	5.570	0.062	6—12, 0.701	5.64 (4.25)
2	E_0				
	E_1	4.307	0.831	8—9, 0.907	4.13 (4.52)
	E_2	4·510	0.040	7—9, 0.779	
	E_3	4.531	0.140	6—9, 0.766	
	E_4	5.240	0.212	5—9, 0.674	5.38 (4.20)
				8—10, 0.541	
3	E_0				2.69 (2.36) n-π^*
	E_1	3.455	0.245	8—9, 0.996	3.44 (3.98)
	E_2	4.348	0.697	8—10, 0.813	4.34 (4.28)
				8—13, 0.517	
	E_3	4.787	0.015	5—9, 0.632	
	E_4	4.790	0.020	6—9, 0.630	
	E_5	5.184	0.422	7—9, 0.880	5.06 (4.52)
	E_6	5.751	0.011	4—9, 0.608	5.25 (4.32)
				5—11, 0.672	
4	E_0				
	E_1	4.395	0.626	8—9, 0.842	3.96 (4.40)
	E_2	4.506	0.020	7—9, 0.689	
	E_3	4.516	0.282	6—9, 0.667	
	E_4	4.840	0.577	5—9, 0.311	4.40 (4.30)
				4—10, −0.452	
				8—10, 0.793	
	E_5	5.719	0.081	5—9, 0.678	
5	E_0				
	E_1	4.323	0.776	8—9, 0.887	3.96 (4.30)
	E_2	4.516	0.097	7—9, 0.760	
	E_3	4.521	0.124	6—9, 0.755	
	E_4	5.064	0.346	5—9, −0.564	4.85 (4.50)
				8—10, 0.764	
	E_5	5.790	0.075	5—9, 0.653	

a) E_j denotes the energy of the state Φ_j relative to the energy $E_0=0$ of the ground state Φ_0. The number beside the dominating configuration $i-k(\Phi_i{}^{-1}\Phi_k)$ is the CI coefficient in the linear combination Φ_j. The assumed geometries of the compounds are shown.

b) The solvent is cyclohexane for **1** and **3** and methylene dichloride for **2**, **4**, and **5** (room temperature).

TABLE 2. CALCULATED FORMAL π-CHARGES AND π-DIPOLE MOMENTS, μ

Atoms	Compounds				
	1	**2**	**3**	**4**	**5**
1	−0.667	0.096	−0.636	0.131	0.176
2	0.339	0.235	0.261	0.235	0.230
3, 4	0.140	0.221	0.151	0.213	0.196
5, 11	−0.050	−0.133	−0.060	−0.125	−0.123
6, 10, 12, 16	0.034	0.037	0.038	0.031	0.027
7, 9, 13, 15	0.012	0.035	0.013	0.035	0.034
8, 14	0.027	0.098	0.033	0.092	0.092
μ_{Debye}	6.63	6.55	8.27	5.67	5.35

using the forms of the CI wave functions. The least energy $^1\pi$-$^1\pi^*$ bands for **1**—**4** have a characteristic of the stilbene chromophore[10] with fine structurs due to vibrational levels, though the corresponding band for **5** appears broad. The second allowed lower energy $^1\pi$-$^1\pi^*$ bands in **3**, **4** and **5** are interesting. The strong band in **3** observed near 4.3 eV might be due to the intramolecular charge-transfer transition from ring to sulfur. The 4.40 eV band observed in **4** and 4.85 eV band observed in **5** could also be assigned to the intramolecular charge-transfer transition from heteroatom to ring. In **1** and **2**, however, no intramolecular charge-transfer transitions as above were observed being in line with the prediction from calculations that the bands in question would be shifted toward relatively higher energy. This trend of the substituents at 3-position in these systems for the interaction with the diphenylcyclopropenyl ring is similar to that found in monosubstituted benzenes, in which thiol and amino groups interact strongly with the benzene ring, in contrast to weakly interacting hydroxyl group.[11] The observed $^1\pi$-$^1\pi^*$ bands of **1** show essentially no solvent shift, in ethanol. However, those of ethanol solution of **3** are noticeably shifted to higher energy, and those of **2**, **4**, and **5** in ethanol containing sulfuric acid exhibited slight blue shifts. The spectral features toward solvent polarity can be explained by large polarization in the ground state of these molecules. This can be understood by the calculated formal charges and dipole moments shown in Table 2. It seems that the geometries of these molecules are nearly planar in their dominant conformation in solution.[12]

Financial support (in part) of the present work by a Grant for Scientific Research from the Ministry of Education is gratefully acknowledged.

10) D. L. Beverige and H. H. Jaffé, *ibid.*, **87**, 5340 (1965).

11) S. Nagagura and K. Kimura, *Nippon Kagaku Zasshi*, **86**, 1 (1965).

12) For general discussions of this problem see R. Hoffmann, R. Bissell, and D. G. Farnum, *J. Phys. Chem.*, **73**, 1789 (1969).

BULLETIN OF THE CHEMICAL SOCIETY OF JAPAN, VOL. 45, 1921—1922 (1972)

Photosensitive Ionomer. IV. Preparation of Mercurous Copoly(vinyl alcohol-methacrylate) and Properties of the Plate

Kazuyuki SUGITA, Masahide HASE*, and Shin SUZUKI

Department of Graphic Engineering, Faculty of Engineering, Chiba University, 1-33, Yayoi-cho, Chiba

(Received September 13, 1971)

Mercurous copoly(vinyl alcohol-acrylate) was studied in order to produce a new type of photosensitive system by applying the disproportionation reaction of mercurous acetate to an ionically crosslinked polymer.[1,2] It was found that the plate prepared thereform was sensitive to ultraviolet light, and that a dark brown relief image was formed by a printing-out process. The latent image could be amplified by reducing development; visible image formation was due to metallic mercury which was isolated as a product of the disproportionation and reduction of mercurous ion. The latent image was also intensified by oxidizing development; relief image formation was ascribed to the ionic crosslinking by mercuric ion formed in the disproportionation and oxidation of mercurous ion. We have studied mercurous copoly(vinyl alcohol-methacrylate), comparing its image-forming characteristics with those of copoly(vinyl alcohol-acrylate).

Experimental

Preparation of Mercurous Copoly(vinyl alcohol-methacrylate) and Photosensitive Plates. Various copolymers of methacrylic acid with vinyl alcohol were prepared from methacrylic acid, vinyl acetate and xylene in the quantities given in Table 1, in the same way as copolymers of acrylic acid.[1] One g of copolymer of methacrylic acid with vinyl alcohol was dissolved in 50 m*l* of water and exactly neutralized with 0.5 N sodium hydroxide. Under vigorous agitation in the dark, the mercurous nitrate solution was added to the sodium copoly(vinyl alcohol-methacrylate) solution. The solution turned into a milky white emulsion. The mercurous salt of the copolymer was separated by centrifugation at 10000 rpm. The mercurous salt precipitated was again uniformly dispersed in a small quantity of water, spread over glass plates, and left to dry.

Results and Discussion

Film Formation and Spectral Sensitivity. In preparing the emulsion, the volume of the mercurous nitrate solution was at first so controlled that an equimolar amount of nitrate and sodium ions was sustained in the copolymer solution. However, the emulsion did not dry up to a smooth, transparent layer and could not be used as a photosensitive layer. The volume of the mercurous nitrate solution was therefore determined in order to obtain a good photosensitive layer, taking into consideration the fact that too much mercurous methacrylate decreased the film-forming ability of the copolymer and too small an amount of it did not bring about the fixing ability. The wedge spec-

* Present address; Odawara Factory, Fuji Photo Film Co., 220, Isaida, Odawara-shi, Kanagawa.

1) K. Sugita and S. Suzuki, *Polym. J.*, **2**, 283 (1971).
2) S. Suzuki and K. Sugita, *Photogr. Sci. Eng.*, **15**, 464 (1971).

Table 1. Preparation and properties of photosensitive layer

Copolymer number	Raw materials[a]			Polymeric acid		Emulsion	Image-forming characteristics			
	Methacrylic acid, g	Vinyl acetate, g	Xylene, g	Yield, wt%	η_{sp}/C[b]	Hg methacrylate in copolymer[c]	Film formation	Photosensitivity	Development	Fixation
501	0.5	9.5	1.0	21.5	8.6	8.3	0	0	0	×
502	0.5	9.5	2.0	12.9	6.3	10.9	0	0	0	×
505	0.5	9.5	5.0	14.1	4.8	16.2	0	0	0	×
510	0.5	9.5	10.0	22.4	3.4	14.8	0	0	0	△
1001	1.0	9.0	1.0	31.0	6.7	17.3	0	0	0	×
1002	1.0	9.0	2.0	32.0	5.6	14.6	0	0	0	△
1005	1.0	9.0	5.0	34.6	4.6	15.0	0	0	0	0
1010	1.0	9.0	10.0	32.5	4.1	13.2	0	0	0	△

a) 0.1 g of benzoyl peroxide was used as an initiator in each case.
b) A reduced viscosity, η_{sp}/C, was measured at 30°C on an aqueous solution of the copolymer (0.25 g/100 m*l*).
c) Calculated value (in wt%) by assuming that the quantity of mercurous ions in the nitrate solution was quantitatively fixed to side chains of each copolymer.

trogram showed that the layer turned dark brown on exposure to light ranging from 250 to 315 nm. Irradiation was performed with a low-pressure mercury lamp.

Photosensitivity and Reducing Development. Each photosensitive plate was divided into three parts, the first part being irradiated for 50 min, the second for 1—2 min, and the third not at all. The first turned dark brown, and a photographic image was formed on the plate by a printing-out process. The second remained transparent and could not be distinguished from the third. The plate was immersed in a hydroquinone solution (1 g in 20 m*l* of water and 80 m*l* of alcohol). In a few minutes, the second part became dark grey, but not the third. Development was completed in 10—15 min. This means that irradiation for 1—2 min formed a latent image which could be developed into a visible image on the plate.

Fixation and Oxidizing Development. The plate made from Copolymer 1005 (see Table 1) was stepwise irradiated for 50, 5, and 0 min, respectively, and placed in a mixed solvent of acetic acid (15 m*l*), water (15 m*l*), and alcohol (70 m*l*). In 10—15 min the photosensitive layer of the second and third parts swelled and became detached from the plate, but that of the first part was unchanged. The polymer remaining on the plate formed a relief image. In the case of the plates from Copolymer 510, 1002, and 1010, the layer of the first part was swollen and partly dissolved away. The exposed layers which were made from Copolymer 501, 502, 505, and 1001 and irradiated for 50 min, were dissolved away and the image could not be fixed.

The plate which was irradiated stepwise by changing exposing duration was immersed in a potassium permanganate solution (0.05 g in 30 m*l* of acetic acid and 70 m*l* of water). The layer in the exposed area for 50 min exposure remained on the plate. Though the surface of the layer for 5 min exposure turned insoluble, the inner part of the layer remained soluble, and the latent image could not be intesnified to a relief image by oxidizing development.

Comparison with Acrylate Plates. When the image-forming characteristics of mercurous copoly(vinyl alcohol-methacrylate) are compared with those of mercurous copoly(vinyl alcohol-acrylate), smaller photosensitivity, imperfect fixation, and failure of oxidizing development are notable. Irradiation for 30—50 min gave the methacrylate plate a print-out image and that for 1—2 min a latent image. On the other hand, irradiations for 20—30 min and for 0.5—1 min were sufficient to form a print-out image and a latent image, respectively, on the acrylate plate under the same exposing conditions. A relief image was fixed on the methacrylate plate made from Copolymer 1005, but the areas of the plate from which the photosensitive layers had become detached were not perfectly transparent, some residual layers being left. The selective swelling of unexposed layer was deduced to be due to the difference in bond strength of ionic crosslinkages.[1] The methyl substituent of methacrylate group may decrease the difference in bond strength.

Failure of oxidizing development can be explained by the intrinsic optical property of copoly(vinyl alcohol-methacrylic acid); this copolymer partly absorbed ultraviolet light ranging from 250 to 350 nm. It might be difficult for disproportionation to occur in the inner part of the photosensitive layer on exposure.

The authors wish to thank Prof. Takahiro Tsunoda, Chiba University, for allowing the use of the monochromator.

BULLETIN OF THE CHEMICAL SOCIETY OF JAPAN, VOL. 45, 1923—1924 (1972)

Iron Compounds Formed by the Aerial Oxidation of Ferrous Salt Solutions

Masao KIYAMA and Toshio TAKADA

Institute for Chemical Research, Kyoto University, Uji, Kyoto

(Received September 23, 1971)

Many reports have been published on the formation of iron compounds, α-FeOOH, γ-FeOOH, and Fe_3O_4, by the oxidation of aqueous suspensions of ferrous precipitates, such as hydroxide, carbonate, and basic sulfate.[1-5] Accroding to these reports, their formation depends on the oxidation rate, the temperature, the pH, *etc.* However, no detailed report has yet been presented on the formation of iron compounds by the oxidation of ferrous salt solutions in which no ferrous precipitate is present. In this note experimental results will be reported on the formation of iron compounds by the aerial oxidation of such ferrous salt solutions.

Experimental

Procedure. Aqueous solutions of ferrous salts were prepared by dissolving ferrous salt of an analytical grade in water. Three liters of each solution were poured into a round flask with a capacity of about 4 *l*. This flask had four inlet necks, into which a thermometer, a reflux condenser, a temperature regulator, and an air-introducing tube (0.7 cm in internal diameter) were inserted. The flask was quickly heated up to a given temperature. Compressed air was then blown into it at the rate of 200 *l*/hr so as to oxidize and stir the solution. During oxidation the temperature was kept constant. Each iron compound precipitated was filtered, washed with water, and then dried at about 105°C.

Identification. Each iron compound obtained was examined by a usual chemical analysis and by the X-ray diffraction method using Mn filtered Fe-K_α radiation.

Results and Discussion

Table 1 shows the kind of iron compounds formed by the oxidation of ferrous salt solutions at 70°C for 30 hr. In connection with the starting solution, in a $FeSO_4$ solution only α-FeOOH is obtained; in the other solutions, mixtures of α-FeOOH and the other compounds are obtained, depending on the kinds and concentrations of the anions present. It is expected that the content of each compound in the mixture depends on the oxidation time by which the composition of the solution is determined. In order to verify this, the following experiments were conducted by use of a fractional precipitation method.

Table 1. Iron compounds formed by the aerial oxidation of ferrous salt solutions with 0.72 M in the ferrous ion at 70°C for 30 hr

Starting solution	pH value	Iron compounds formed
$FeSO_4$	1.9	α-FeOOH
$FeSO_4(NH_4)_2SO_4$	1.8	α-FeOOH≈(NH_4)-$Fe_3(OH)_6(SO_4)_2$
$FeCl_2$	1.7	β-FeOOH≈α-FeOOH
$FeCl_2(NH_4Cl)_2$	1.2	β-FeOOH>α-FeOOH
$FeBr_2$	1.6	α-FeOOH>γ-FeOOH>α-Fe_2O_3

0.72 M-$FeCl_2$ and 0.72 M-$FeSO_4$ solutions were oxidized at 70°C. After 20 hr, the precipitates formed were sufficiently separated from the solutions by filtration, after which the whole filtrates were further oxidized at 70°C for 20 hr. This treatment was repeated several times every 20 hr. With repeated oxidation, the concentration of the free acid in each filtrate, HCl or H_2SO_4, and its Fe^{3+}/Fe^{2+} ratio increased. Table 2 shows the iron compounds fractionally precipitated for different oxidation times. After the first 60 hr of the total oxidation time has passed, only a basic sulfate is formed in the $FeSO_4$ solution, whereas in the $FeCl_2$ solution β-FeOOH is formed with a slight amount of α-FeOOH even after 100 hr. The X-ray diffraction pattern of the basic sulfate obtained (Fig. 1) shows that it differs sharply from a jarosite-type basic sulfate, as will be described later. Its composition was $(Fe_2O_3)_2SO_3(H_2O)_5$ (Found: Fe_2O_3, 65.3; SO_3, 16.8; H_2O, 17.9 wt%).

Table 2. Iron compounds fractionally precipitated by the oxidation of 0.72 M-$FeCl_2$ and 0.72 M-$FeSO_4$ solutions for different times at 70°C

Time (hr)	$FeCl_2$ solution	$FeSO_4$ solution
to 20	α-FeOOH≈β-FeOOH	α-FeOOH
20 to 40	β-FeOOH>α-FeOOH	α-FeOOH>basic sulphate[a]
40 to 60	β-FeOOH>α-FeOOH	basic sulphate[a]>α-FeOOH
60 to 80	β-FeOOH>α-FeOOH	only basic sulphate[a]
80 to 100	β-FeOOH≫α-FeOOH	
100 to 120	β-FeOOH≫α-FeOOH	

a) Its chemical composition was $(Fe_2O_3)_2SO_3(H_2O)_5$.

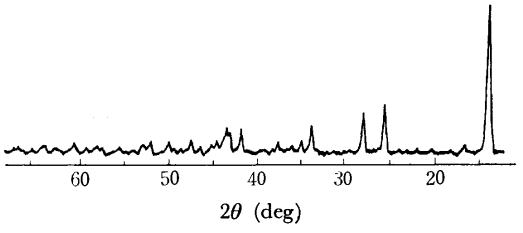

Fig. 1. X-Ray diffraction pattern of the $(Fe_2O_3)_2SO_3(H_2O)_5$ by using Fe-Kα radiation.

1) W. H. Albrecht, *Ber.*, **62** 1475 (1729).
2) G. Schikorr, *Z. Anorg. Allg. Chem.*, **191** 322 (1930).
3) U. Schwertmann, *ibid.*, **298**, 337 (1959).
4) W. Feitknecht, *Z. Electrochem.*, **63** (1) 34 (1959).
5) J. D. Bernal, E. R. Dusgputa, and A. L. Mackay, *Clay. Min. Bull.*, **4** (21) 15 (1959).

The addition of NH_4Cl to the $FeCl_2$ solution and that of a sulfate to the $FeSO_4$ solution favorably affected the formation of β-FeOOH and a basic sulfate respectively. Only β-FeOOH began to be formed at 70°C in the filtrate obtained by oxidizing a mixture of 0.72 M-$FeCl_2$ and 1.44 M-NH_4Cl solutions at 70°C for 20 hr. Also, only a basic sulfate began to be formed at 70°C in the filtrate obtained from a mixture of a 0.72 M-$FeSO_4$ solution and one of 0.72 M-K_2SO_4, Na_2SO_4 or $(NH_4)_2SO_4$ solution at 70°C for 20 hr. Its composition was $RFe_3(SO_4)_2(OH)_5$(R= K, Na, or NH_4), and its crystal structure was of the jarosite type.[6]

By blowing the air into the chloride or the sulfate solution, some of the ferrous ions in it are oxidized to ferric ions, which are then hydrolyzed to form both the acid, HCl or H_2SO_4, and α-FeOOH as the first precipitate. As oxidation progresses, the concentration of the ferric chloride or ferric sulfate increases with an increase in that of HCl or H_2SO_4, and β-FeOOH or the basic sulfate begins to be formed as the second precipitate. This may indicate that their formation is closely connected with the kinds and concentrations of the ferric complex ions in such solutions.

The kinds of the iron compounds formed in the chloride or the sulfate solutions did not depend strongly on the temperature, but that of the iron compounds formed in a ferrous bromide solution did. When the temperature was decreased, an amorphous compound was formed instead of α-FeOOH in the former solutions. Table 3 shows the iron compounds which were formed by the oxidation of a 0.33 M-$FeBr_2$ solution at various temperatures for 20 hr. It was also found that γ-FeOOH, α-FeOOH, β-FeOOH, and α-Fe_2O_3 were all formed by oxidizing a mixture of $FeCl_2$ and excess NaI solutions under conditions similar to the above.

Table 3. Iron compounds formed by the aerial oxidation of a 0.33 M-$FeBr_2$ solution at various temperatures for 20 hr

Temp. (°C)	Iron compounds obtained
10	β-FeOOH
20	β-FeOOH$>\alpha$-FeOOH
40	γ-FeOOH$\approx\alpha$-FeOOH
65	α-FeOOH$>\gamma$-FeOOH$>\alpha$-Fe_2O_3
80	α-$Fe_2O_3\approx\alpha$-FeOOH$>\gamma$-FeOOH

It is known that, on the slow oxidation of $Fe(OH)_2$ in a ferrous salt solution with a pH of about 7, γ-FeOOH can be obtained by selecting the proper oxidizing conditions. In this case a dark green compound, called a green rust, I or II, is always formed before the formation of γ-FeOOH. Accordingly, the presence of the green rust has so far been considered to be indispensable for the formation of γ-FeOOH. Since the solutions of $FeBr_2$ and the mixture of $FeCl_2$ and NaI were acidic (pH<3), no iron compound containing ferrous ions was formed as the intermediate one. In conclusion, γ-FeOOH can be formed not only by the slow oxidation of the green rust in the solution, but also by that of the ferrous salt solution by selecting the proper conditions.

6) "Dana's System of Mineralogy, Vol. 2," J. Wiley and Sons, New York (1951) p. 560.

BULLETIN OF THE CHEMICAL SOCIETY OF JAPAN, VOL. 45, 1924—1926 (1972)

Synthesis of (4-Pyridyl)-1,2-ethanediol and α-Acetoxy-4-vinylpyridine

Toshiyuki FURUYAMA, Koichi MORI, and Ryoichi WAKASA

Technical Research Laboratory, Asahi Chemical Industry Co. Ltd., Nakadai, Itabashi-ku, Tokyo

(Received October 5, 1971)

Aaron *et al.*[1] synthesized (4-pyridyl)-1,2-ethanediol as an intermeidate compound in the process of obtaining 3-quinuclidiol using 4-vinylpyridine and potassium permanganate. Haas *et al.*[2] similarly carried out the synthesis and obtained (4-pyridyl)-1,2-ethanediol as a pasty mass which could not be readily purified. They produced α-acetoxy-4-vinylpyridine by the reaction of (4-pyridyl)-1,2-ethanediol with acetic anhydride[2] and polymerized it with azobisisobutyronitrile as an initiator. Both the above procedures gave a low yield of the compound.

The present authors investigated the synthetic process of (4-pyridyl)-1,2-ethanediol and α-acetoxy-4-vinylpyridine, and found a very much improved route in comparison with the above synthetic methods[1,2]. By our process the polymeriaztion grade of α-acetoxy-4-vinylpyridine is easily obtained. The α-acetoxy-4-vinylpyridine was polymerized with γ-rays, and its physical properties were studied. Results of the polymerization have been presented elsewhere[3].

Results and Discussion

It is known that glycol synthesis from a C=C double bond with permanganates proceeeds favorably in an alkaline condition[4]. If the synthesis is carried out in

1) H. S. Aaron, O. O. Owens, P. D. Rosenstock, S. Leonard, S. Elkin, and J. I. Miller, *J. Org. Chem.*, **30**, 1331 (1965).

2) H. C. Haas, H. S. Kolesinski, and N. W. Schuler, *J. Polym. Sci., Part B*, **3**, 879 (1965).

3) T. Furuyama, K. Mori, and R. Wakasa, *J. Polym. Sci., Part A*, **9**, 3411 (1971).

4) Y. Ogata, "Oxidation and Reduction", Nankodo, Tokyo (1963), pp. 348—403.

either acidic or neutral conditions, the main product turns out to be an oxidized material which could be produced by cleavage of the C=C[4].

In the initial experiments we carried out glycol synthesis with a potassium hydroxide solution (alkaline condition), and, contrary to expectation, obtained isonicotinic acid as the main product. When we used water as a solvent (neutral condition), potassium hydroxide formed from the consumed potassium permanganate facilitated the formation of isonicotinic acid. It can be concluded that the methods of Aaron *et al.* and Haas *et al.* give an appreciable amount of isonicotinic acid together with (4-pyridyl)-1,2-ethanediol.

We used magnesium sulfate as a scavenger of the potassium hydroxide formed, as shown in reaction scheme (1), and obtained (4-pyridyl)-1,2-ethanediol in an exceptionally high yield, 84% or quantitatively.

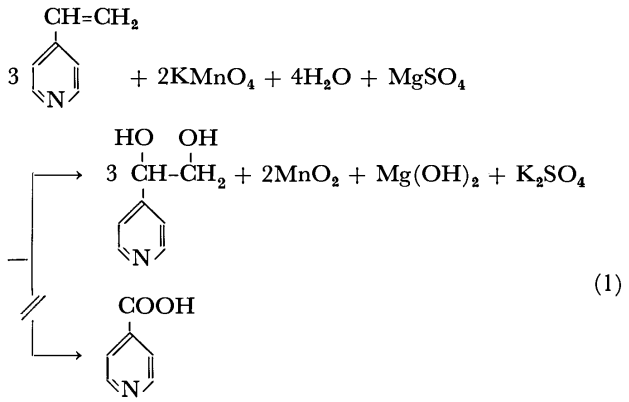

(1)

As regards the mechanism of the reaction of potassium permanganate with a C=C, Wiberg and Saegabarth[5] discussed a mechanism based upon the formation of a cyclic ester between the permanganate ion and the C=C[6], as shown in (I).

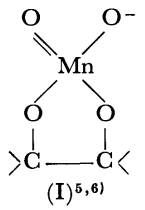

(I)[5,6]

In 4-vinylpyridine, the proton abstraction reaction may easily take place with the attack of the hydroxyl ion on a similar cyclic ester, which may lead to the formation of isonicotinic acid, the cleavage product.

The solubility of (4-pyridyl)-1,2-ethanediol is summarized in Table 1 against Hildebrand's solubility parameter. (4-Pyridyl)-1,2-ethanediol seems to dissolve in solvents with a solubility parameter greater than 12.7. Our results make us doubtful of those given by Aaron *et al.*[1] with respect to the solubility and melting point of (4-pyridyl)-1,2-ethanediol. Haas *et al.*[2] also indicated a similar doubt.

With respect to the synthesis of α-acetoxy-4-vinylpyridine (II), we carried out a method similar to that of Haas *et al.*[2] except for one difference, removal of

Table 1. Solubility of (4-pyridyl)-1,2-ethanediol

Solvents		Hildebrand's solubility parameters
Diethyl ether	insoluble	7.4
Carbon tetrachloride	insoluble	8.6
Benzene	insoluble	9.2
Chloroform	insoluble	9.3
Acetone	insoluble	9.9
Acetonitrile	insoluble	11.9
Ethanol	soluble	12.7
Methanol	soluble	14.5
Water	soluble	23.4

contaminated water. This water seems to facilitate the formation of the by-product 4-acetylpyridine (III) according to reaction scheme (2):

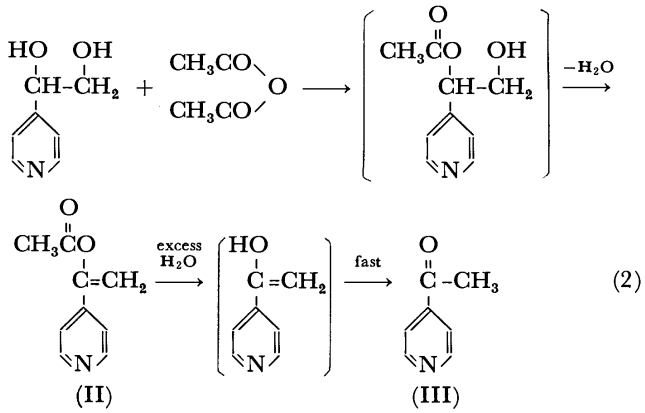

(II) (III)

(2)

Repetition of azeotropic removal of water elevates the yield of α-acetoxy-4-vinylpyridine to a great extent. In the NMR spectrum of α-acetoxy-4-vinylpyridine, the coupling constant of the vinyl protons indicates that the acetoxy group is on α-carbon.

Experimental

(4-Pyridyl)-1,2-ethanediol. 25.2 g (0.24 mol) of 4-vinylpyridine was dissolved in 300 m*l* of acetone. The resulting solution was maintained at 2—5°C under strong magnetic stirring. 25.3 g of potassium permanganate (0.16 mol) and 9.6 g of anhydrous magnesium sulfate (0.08 mol) were dissolved in 500 m*l* of water. The solution was added dropwise from a dropping funnel onto the above acetone solution over a period of 20 min. Mechanical agitation was continued for an additional 10 min and the temperature of the reaction system was raised to room temperature. After addition of a very small amount of hydroquinone, the mixture was filtered with a glass filter. The solid material, manganese dioxide and magnesium hydroxide, was discarded. The clear pale yellow filtrate was concentrated under nitrogen atmosphere with a bath temperature of 50°C under reduced pressure. When the amount of the concentrate became approximately 50 m*l*, 200 m*l* of ethanol was added to the precipitate potassium sulfate, and the solution was kept in a refrigerator overnight. After filtration of the resulting potassium sulfate, (4-pyridyl)-1,2-ethanediol was condensed from the ethanol solution as a pale yellow viscous liquid. Yield, 84% or quantitative. NMR (60 MHz, DSS reference, in D_2O at 80°C): $H_{(a)}$, δ3.83; $H_{(b)}$, 4.40; $H_{(c)}$, 4.90; $H_{(d)}=H_{(d')}$, 7.50; $H_{(e)}=H_{(e')}$, 8.57.

5) K. B. Wiberg and K. A. Saegebarth, *J. Amer. Chem. Soc.*, **79**, 2822 (1957).

6) G. Wagner, *J. Russ. Phys. Chem. Soc.*, **27**, 219 (1895).

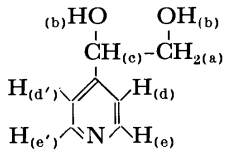

α-Acetoxy-4-vinylpyridine. 100 g of (4-pyridyl)-1,2-ethanediol was dissolved in 300 m*l* of ethanol and 100 m*l* of benzene was added. The ethanol and benzene were removed under reduced pressure. The azeotropic procedure was repeated three times. 500 g of acetic anhydride was added to the dried (4-pyridyl)-1,2-ethanediol and the mixture was subjected to gentle boiling overnight. Acetylation was exothermic and no external heating was required at the initial stage of the reaction. Excess acetic anhydride was removed under reduced pressure. The following high vacuum distillation gave α-acetoxy-4-vinylpyridine. In order to obtain the polymerization grade of α-acetoxy-4-vinylpyridine, high vacuum distillation was repeated twice. The yield of polymerization grade material was 50%. Bp 80°C/0.58 mmHg. Found: C, 66.3; H, 5.6; N, 8.4%. Calcd for $C_9H_9O_2N$: C, 66.2; H, 5.6; N, 8.6%. NMR (60 MHz, TMS reference, in $CDCl_3$ at room temperature): $H_{(a)}$, δ2.25; $H_{(b)}$, 5.28; $H_{(c)}$, 5.80; $H_{(d)}=H_{(d')}$, 7.42; $H_{(e)}=H_{(e')}$, 8.70; $|J_{(b)(c)}|$, 2.5 Hz.

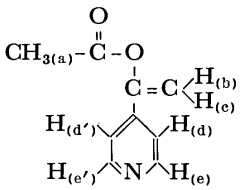

BULLETIN OF THE CHEMICAL SOCIETY OF JAPAN, VOL. 45, 1926—1927 (1972)

Catalytic Hydrogenolysis of 7-Chloro-7-fluorobicyclo[4.1.0]heptane in the Presence of Ethylenediamine

Hideki KANO, Kazuo KOBAYASHI, and Koji ISOGAI
Faculty of Engineering, Niigata University, Gakko-cho, Nagaoka, Niigata

(Received October 22, 1971)

During the course of an investigation on the catalytic hydrogenolysis of *gem*-dichlorocyclopropanes to monochlorocyclopropanes,[1] it became desirable to confirm the stereochemical behavior of the substrates in the formation of *endo* and *exo* isomers of monochlorocyclopropanes. Ando *et al.*[2] reported that cyclopropyl radical is formed and partly inverted in the reduction of some *gem*-chlorofluorocyclopropanes with tri-*n*-butyltin hydride. The behavior of *gem*-halofluorocyclopropanes in their catalytic hydrogenolyses seemed of interest to investigate. This paper deals with the catalytic hydrogenolysis of 7-chloro-6-fluorobicyclo-[4.1.0]heptane (**1**) with Raney nickel catalyst (R–Ni) in the presence of various basic additives.

7-*exo*-Chloro-7-*endo*-fluorobicyclo[4.1.0]heptane (*exo*-Cl-**1**), 7-*endo*-chloro-7-*exo*-fluorobicyclo[4.1.0]heptane (*endo*-Cl-**1**), and a mixture of isomers (*mixture*-**1**, *exo*-Cl-**1**/*endo*-Cl-**1**=43/57) were catalytically hydrogenolyzed with R-Ni in a methanol solution in the presence of sodium hydroxide, potassium hydroxide, lithium hydroxide, ethylamine, diethylamine, triethylamine, piperidine, ethylenediamine, trimethylenediamine, hexamethylenediamine, benzylamine, and monoethanolamine under ordinary conditions. 7-Fluorobicyclo[4.1.0]heptane (**2**) was obtained predominantly without monochlorocyclopropane only in the presence of ethylenediamine as an additive, with considerable evolution of hydrogen. No reaction occurred in the presence of other basic additives.

The results of catalytic hydrogenolyses of *exo*-Cl-**1** and *endo*-Cl-**1** are shown in Table 1. Hydrogenolyses proceeded stereospecifically with retention of configuration and gave 7-*endo*-fluorobicyclo[4.1.0]heptane (*endo*-F-**2**) and 7-*exo*-fluorobicyclo[4.1.0]heptane (*exo*-F-**2**) from *exo*-Cl-**1** and *endo*-Cl-**1** respectively. *Exo*-Cl-**1** was hydrogenolyzed more easily than *endo*-Cl-**1**. The difference seems to be attributable to the effect of hindrance of condensed ring.

TABLE 1. CATALYTIC HYDROGENOLYSIS OF *exo*-Cl-**1** AND *endo*-Cl-**1**

Substrate: 0.005 mol, Catalyst: 2.5 g as Ni, Additive: $NH_2(CH_2)_2NH_2$ 0.03 mol, Reaction time: 24 hr

	Composition of product			
	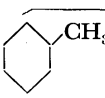			
		endo-F	*exo*-F	
Substrate	%	%	%	%
exo-Cl-**1**	6	39	—	55
endo-Cl-**1**	5	—	17	78

Hydrogenolysis of *mixture*-**1** with various amount of R-Ni and ethylenediamine is shown in Table 2. Increase in the amounts of R-Ni and ethylenediamine gave rise to the increase of hydrogenolyzed products.

It is of interest that *gem*-dichlorocyclopropanes are hydrogenolyzed readily in the presence of common amines and alkali hydroxides[1], whereas **1** is hydrogenolyzed gradually only in the presence of ethylenediamine. Poor reactivity of **1** may be caused by the

1) K. Isogai, S. Kondo, K. Katsura, S. Sato, N. Yoshihara, Y. Kawamura, and T. Kazama, *Nippon Kagaku Zasshi*, **91**, 561 (1970).

2) T. Ando, F. Namigata, H. Yamanaka, and W. Funasaka, *J. Amer. Chem. Soc.*, **89**, 5719 (1967), *J. Org. Chem.*, **35**, 33 (1970).

Table 2. The influence of quantities of R-Ni and ethylenediamine
Substrate: *mixture*-**1** 0.005 mol, Reaction time: 24 hr

R-Ni g as Ni	$NH_2(CH_2)_2NH_2$ mol	Composition of product: 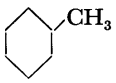 %	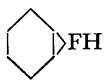 %	(*endo*-F : *exo*-F)		%	(*exo*-Cl : *endo*-Cl)	
2.5	10 μl	—	—			100	(43	57)
2.5	0.015	4	20	(79	21)	76	(30	70)
2.5	0.03	4	28	(75	25)	68	(21	79)
2.5	0.10	6	39	(74	26)	55	(15	85)
2.5	0.30	3	55	(63	37)	42	(—	100)
5.0	0.03	9	35	(71	29)	56	(14	86)
7.5	0.03	12	48	(67	33)	40	(—	100)

polarizability of C-F bond and the weak affinity to the catalyst surface. By stirring the methanol solution of ethylenediamine with R–Ni, a colored complex was formed which dissolved into the solution with the evolution of hydrogen. The catalytic hydrogenolysis of **1** was retarded when ethylenediamine and R–Ni were stirred in the reaction medium for several hours before addition of **1**. The behavior of ethylenediamine is not clear, but it might be explained as follows: chlorine atom adsorbed on the catalyst is extracted by the complex formed from ethylenediamine and R-Ni, and concerted reduction takes place simultaneously by the transfer of electron to the substrate in the transition from Ni(0) to Ni(II).

Experimental[3]

*Preparation of 7-Chloro-7-fluorobicyclo[4.1.0]heptane (**1**).* The compound was prepared by the method of Ando *et al.*[4] To a mixture of cyclohexene, sodium hydride and methyl dichlorofluoroacetate, methanol was added gradually at 0°C. A mixture of *endo*-chloro and *exo*-chloro isomers of **1** (*mixture*-**1**; *exo*-Cl/*endo*-Cl=43/57) was obtained in 30% yield, bp 23.5—25°C/4 mmHg. Found: C, 57.02; H, 6.87%; Calcd for $C_7H_{10}ClF$: C, 56.98; H, 6.83%. Isomer ratio of **1** was identified by NMR and vpc. ^{19}F NMR of isomers; *exo*-Cl-**1** (R_t: 6.4 min): δ 80.0 (J=5 Hz); *endo*-Cl-**1** (R_t: 7.3 min): δ 45.1 (J=19 Hz). Isolation of two isomers of **1** was carried out by preparative vpc.

*7-Fluorobicyclo[4.1.0]heptane (**2**).* A mixture of *endo*- and *exo*-fluoro isomers of **2** isolated from hydrogenolyzed products of *mixture*-**1** by preparative vpc gave satisfactory ^1H NMR and data of elemental analysis. NMR; *exo*-F-**2** (R_t: 3.6 min); δ 4.12 (J=2 Hz); *endo*-F-2 (R_t: 4.0 min): δ 4.38 (J=7 Hz). Found: C, 73.58; H, 9.76%. Calcd for $C_7H_{11}F$: C, 73.65; H, 9.71%.

General Procedure of Catalytic Hydrogenation. A mixture of chlorofluorocyclopropane (0.005 mol), R–Ni (2.5 g as Ni), methanol (50 m*l*) and commercial amine or alkali hydroxide (0.03 mol) was stirred under ordinary pressure of hydrogen at 18—22°C for 24 hr. The solution was separated from catalyst, poured into 500 m*l* of water and extracted with ether. Ether solution was washed with dilute HCl and water, and then dried (Na_2SO_4). After removal of ether, the residue was identified and determined by vpc.

The authors wish to thank Prof. Ichiro Murata, Osaka University, for the elemental analysis.

3) ^1H NMR spectrum was obtained with a JEOLCO JNM-4H-100 spectrometer in CCl_4 with TMS as an internal reference. ^{19}F NMR spectrum was obtained with a JEOLCO JNM-4H-100 spectrometer (94 MHz) in CCl_4 with trifluoroacetic acid as an external reference. Vpc analyses and separations were performed with an OHKURA MODEL 6000 or an OHKURA MODEL 1200 gas chromatograph. For analytical purposes, a 3 mm×2 m column with 15% TCP on 60—80 Celite 545 or a 3 mm×3 m column with 15% HV grease on 60—80 Celite 545 was used. As carrier gas, hydrogen was used at a rate of 60 ml/min. For preparative purposes, a 8 mm×5 m column was used with 30% HV grease or 30% TCP on 40—60 Celite 545.

4) T. Ando, H. Yamanaka, S. Terabe, A. Horike, and W. Funasaka, *Tetrahedron Lett.*, **1967**, 1123.

BULLETIN OF THE CHEMICAL SOCIETY OF JAPAN, VOL. 45, 1928—1929 (1972)

Methylene Analogs of Cyclobutenedione. V.[1] The Reactions of 3,4-Bis(diphenylmethylene)cyclobutanedione with Water, Alcohol, and Amine in the Presence of Bromine. The Approach to a Bisketene

Fumio TODA and Junji FUJITA

Department of Industrial Chemistry, Faculty of Engineering, Ehime University, Matsuyama

(Received November 10, 1971)

The approach to the bisketene (I) is an interesting subject. Evidence for the formation of I as an intermediate has been reported by several investigators. Both the ethanolysis of diphenylcyclobutenedione[2] and the photolysis of phenylcyclobutenedione[3] in methanol to afford diethyl 2,3-diphenylsuccinate and dimethyl 2-phenylsuccinate respecitvely have been interpreted as proceeding *via* the corresponding bisketene intermediate (I). A similar photochemical transformation of benzocyclobutenedione to a bisketene intermediate has also been reported.[4,5]

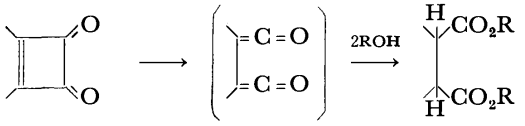

(I)

On the contrary, 3,4-bis(diphenylmethylene)-cyclobutanedione (II)[6] was stable in methanol for 24 hr, whereas under the same conditions diphenyl cyclobutenedione was completely destroyed within 12 hr[2]. The stability of II is probably the result of the impossibility of its transformation into a bisketene intermediate. If this assumption is correct, a reagent which localizes the π-electrons of the diene system of II will promote the transformation of II into a bisketene intermediate. This expectation was confirmed using bromine, and II was converted, probably *via* a bisketene intermediate into various products depending on the nucleophiles added.

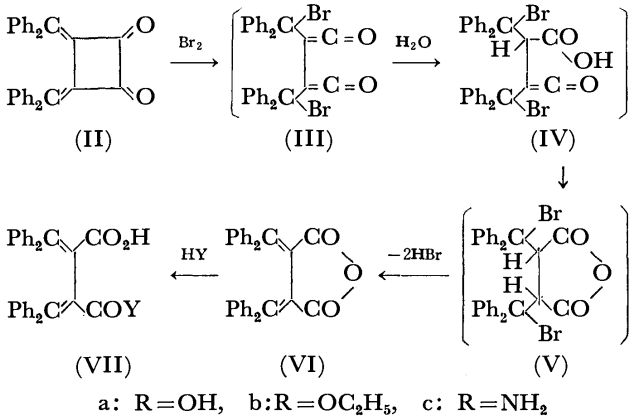

a: R=OH, b: R=OC_2H_5, c: R=NH_2

Scheme 1

The heating of a solution of II in wet carbon tetrachloride containing about 2.5 molar amounts of bromine under reflux for 30 min afforded VI. VI was identified by a comparison of its IR spectrum with that of an authentic sample prepared accroding to a previously-reported method[6]. The structure of VI was further confirmed by its hydrolysis, ethanolysis, and ammonolysis, which afforded VIIa, VIIb, and VIIc respectively.

The formation of VI can be well interpreted by assuming the bisketene (III) as an intermediate, even though it is not clear whether or not the C–Br bond of III is a real σ-bond. A possible reaction mechanism of the formation of VI from III is an intramolecular cyclization of the IV initially produced by the addition of water to III, accompanied by dehydrobromination, as is shown in Scheme 1, even though it is again not clear whether or not the intramolecular cyclization of IV into V precedes the dehydrobromination of IV.

The reactions of II with alcohol and amine in the presence of bromine to afford the diester IX and the succinimide X respectively can also be interpreted by assuming the bisketen III as an intermediate. The heating of a solution of II in dry carbon tetrachloride containing methanol and bromine under reflux for 30 min afforded IXa in a 68% yield. By a similar procedure, IXb was obtained in a 71% yield. IX was identified by means of the spectral data described in the Experimental section. The reaction of II with *n*-propyl-, isopropyl-, and *n*-butylamine in dry carbon tetrachloride containing a small amount of bromine at room temperature for 30 min afforded three succinimides, Xc, Xd, and Xe, in 63, 58, and 59% yields respectively. X was identified by means of the spectral data described in the Experimental section.

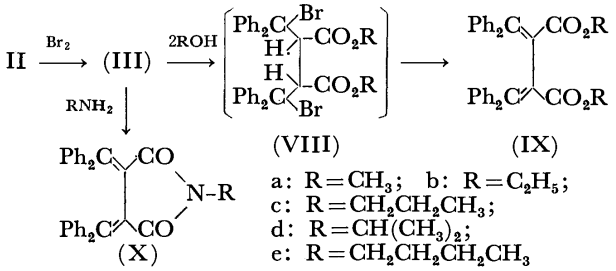

a: R=CH_3; b: R=C_2H_5;
c: R=$CH_2CH_2CH_3$;
d: R=$CH(CH_3)_2$;
e: R=$CH_2CH_2CH_2CH_3$

Scheme 2

1) Part IV: F. Toda and N. Ooi, This Bulletin, **45**, 1820 (1972).
2) A. T. Blomquist and E. A. LaLancette, *J. Amer. Chem. Soc.*, **83**, 1387 (1961).
3) J. D. Roberts and F. B. Mallory, *ibid.*, **83**, 393 (1961).
4) R. F. C. Brown and R. K. Solly, *Tetrahedron Lett.*, **1966**, 169.
5) H. A. Staab and J. Ipaktaschi, *Chem. Ber.*, **101**, 1457 (1968).
6) F. Toda and K. Akagi, *Tetrahedron*, **27**, 2801 (1971).

Experimental

The Reaction of II with Water. A solution of II (0.5 g) and bromine (0.3 g) in wet carbon tetrachloride (50 m*l*) was refluxed for 30 min. The crude crystals obtained by the subsequent evaporation of the solvent were recrystallized from acetonitrile to afford VI as red rhombs; 0.385 g (74%); mp 230—231°C (lit,[6] mp 230°C). IR (Nujol), 1795 and 1755 (C=O) and 1545 cm^{-1} (C=C). The IR spectrum was identical with that of an authentic sample prepared according to a previously-reported method.[6]

The Hydrolysis, Ethanolysis, and Ammonolysis of VI. A mixture of VI (0.25 g), KOH (0.04 g), and acetone (25 m*l*)-water (5 m*l*) was refluxed for 2 hr. The reaction mixture was concentrated to *ca.* 10 m*l* and was acidified with hydrochloric acid. The solid thus formed was collected by filtration, washed with water, and recrystallized from ethanol to leave VIIa as pale yellow needles; 0.165 g (63%); mp 233—234°C. IR (Nujol), 1695 and 1670 cm^{-1} (C=O); UV (EtOH), 228 (20300), 266 (11700), and 320 sh nm (ε, 6800).

Found: C, 80.40; H, 4.76%. Calcd for $C_{30}H_{22}O_4$: C, 80.70; H, 4.97%.

A mixture of VI (0.15 g), KOH (0.05 g), and ethanol (3 m*l*) was refluxed. The solid obtained by the same treatment of tlie reaction mixture as that employed for the hydrolysis of VI was recrystallized from cyclohexane to afford VIIb as colorless needles; 0.12 g (68%); mp 188—189°C. IR (Nujol), 1735 and 1665 (C=O) and 1230 cm^{-1} (ester); UV (EtOH), 232 (22300), 267 (13300) and 320 nm (ε, 7600).

Found: C, 81.10; H, 5.65%. Calcd for $C_{32}H_{26}O_4$: C, 80.99; H, 5.52%.

Through a solution of VI (0.1 g) in chloroform (30 m*l*), ammonia was bubbled for 30 min. The crude product which remained after the evaporation of the solvent was recrystallized from acetone to afford VIIc as colorless needles; 0.07 g (67%); mp 243—244°C. IR (Nujol), 3320 and 3200 (NH) and 1675 cm^{-1} (C=O); UV (EtOH), 232 (11600), 265 (6500) and 320 sh nm (ε, 4100).

Found: C, 80.65; H, 5.31%. Calcd for $C_{30}H_{23}O_3N$: C, 80.88; H, 5.20%.

The Reaction of II with Alcohol. A solution of II (0.5 g) and bromine (0.3 g) in carbon tetrachloride (dried over P_2O_5) (50 m*l*)-methanol (5 m*l*) was heated under reflux for 30 min. The crude product obtained by the evaporation of the solvent was recrystallized from acetone to yield IXa as yellow needles; 0.39 g (68%); mp 233—234°C. IR (Nujol), 1700 (C=O), and 1240 and 1270 cm^{-1} (ester); UV ($CHCl_3$), 246 (22700), 272 (14500), and 330 nm (ε, 8600).

Found: C, 81.22; H, 5.56%. Calcd for $C_{32}H_{26}O_4$: C, 80.99; H, 5.52%.

The heating of a solution of II (0.25 g) and bromine (0.2 g) in carbon tetrachloride (dried over P_2O_5) (30 m*l*)-ethanol (5 m*l*) under reflux for 30 min afforded IXb as pale yellow prisms; 0.22 g (71%); mp 210—211°C. IR (Nujol), 1690 (C=O), and 1245 and 1270 cm^{-1} (ester); UV ($CHCl_3$), 245 245 (21400), 270 (14400), and 326 nm (ε, 7400); NMR ($CDCl_3$), 2.8—3.2 (m, Ph, 20H), 6.13 (q, CH_2, 4H), and 9.18 τ (t, CH_3, 6H).

Found: C, 81.37; H, 5.99%. Calcd for $C_{34}H_{30}O_4$: C, 81.24; H, 6.02%.

The Reaction of II with Amine. A mixture of II (0.3 g), bromine (0.2 g), carbon tetrachloride (dried over P_2O_5) (30 m*l*) and *n*-propylamine (1 g) was stirred at room temperature for 30 min. After the removal of the amine salt by filtration, the mother liquor was concentrated to dryness. The crude product which remained was recrystallized from acetone to afford Xa as yellow needles; 0.215 g (63%); mp 249—250°C. IR (Nujol), 1740 and 1685 cm^{-1} (C=O); UV ($CHCl_3$), 258 (20800), 310 (14600), and 400 nm (ε, 8700).

Found: C, 84.14; H, 5.57%. Calcd for $C_{33}H_{27}O_2N$: C, 84.40; H, 5.80%.

By the same treatment of II with isopropylamine as above, Xb was obtained as yellow needles in a 58% yield; mp 256—257°C. IR (Nujol), 1747 and 1685 cm^{-1} (C=O); UV ($CHCl_3$); 258 (22100), 310 (15600), and 400 nm (ε 9500).

Found: C, 84.12; H, 5.58%. Calcd for $C_{33}H_{27}O_2N$: C, 84.40; H, 5.80%.

By the same treatment of II with *n*-butylamine as above. Xc was obtained as yellow needles in a 59% yield; mp 234—235°C. IR (Nujol), 1750 and 1690 cm^{-1} (C=O); UV ($CHCl_3$); 258 (21600), 310 (15200) and 400 nm (ε, 9000).

Found: C, 84.36; H, 5.81%. Calcd for $C_{34}H_{29}O_2N$: C, 84.44; H, 6.04%.

BULLETIN OF THE CHEMICAL SOCIETY OF JAPAN, VOL. 45, 1930—1931 (1972)

Kinetic Studies of Copper(II) Chloroacetate Complex Formation Reaction in Aqueous Solutions

Shoji HARADA, Yoshikuni TSUJI, and Tatsuya YASUNAGA

Department of Chemistry, Faculty of Science, Hiroshima University, Higashi-sendamachi, Hiroshima

(Received November 15, 1971)

Rate constant of the complex formation reaction depends on the nature of the metal ion, *e.g.*, on the charge, the electronic configuration, the ionic radius, and the coordination structure.[1] The development of the relaxation methods has made it possible to study kinetically on many complex formation reactions which proceed too fast to be studied by the conventional method. On copper(II) complex formation reaction, however, relatively few kinetic studies have been carried out.[2,3] This is presumably because of the fast rate of the reaction and ease of the formation of hydroxy species even at relatively low pH's. The purpose of the present investigation is to study on the copper(II) chloroacetate complex formation reaction, which can be studied at low pH's, with the help of the ultrasonic absorption method.

Experimental

Reagent-grade copper nitrate, chloroacetic acid, sodium hydroxide, and sodium perchlorate were used. The ionic strength of the solutions was adjusted to 1.0 by an addition of sodium perchlorate. Ultrasonic absorption measurements were carried out at 25°C by the pulse method over the frequency range from 5.5 to 220 MHz. Details of the apparatus have been described elsewhere.[4]

Theoretical

The metal ion and the ligand are hydrated in an aqueous solution. In the case of the complex formation, therefore, two or three-step mechanisms, the rate-determining step of which is the release of a water molecule from the metal ion, have been proposed;[5]

$$\underset{\text{(I)}}{M^{m+}_{aq} + L^{n-}_{aq}} \underset{k_{21}}{\overset{k_{12}}{\rightleftharpoons}} \underset{\text{(II)}}{\left[M^{m+}O\langle^{H}_{H}L^{n-}\right]_{aq}} \underset{k_{32}}{\overset{k_{23}}{\rightleftharpoons}} \underset{\text{(III)}}{[ML]^{m-n}_{aq}} \quad (1)$$

where M is the metal ion, L is the ligand, state I is free ions, state II is the ion-pair, and state III is the complex, and the subscript means that the ions are hydrated. Step I—II represents the diffusion of the ions to form the ion-pair and the rate constants, k_{12}, k_{21}, seem to be very fast. Step II—III is the rate-determining process of the inner-sphere complex formation. With the assumption that k_{12}, $k_{21} \gg k_{23}$, k_{32}, the relaxation frequency, f_r, for the step II—III is related to the rate constants and the ionic concentrations by the following form;

$$2\pi f_r = k_{32} + k_{23}\{1 + k_{21}/k_{12}(C_M + C_L)\}^{-1} \quad (2)$$

where C_M and C_L are the concentrations of M and L respectively. The relaxation absorption is expressed by the single relaxation equation;

$$\alpha/f^2 = A\{1 + (f/f_r)^2\}^{-1} + B \quad (3)$$

where α is the absorption coefficient, f is the frequency, and A and B are constants.

Results and Discussion

The concentrations of the species, which were calculated by the use of the formation constants of copper(II) chloroacetate[6] are summarized in Table 1. Representative absorption curves are shown in Fig. 1. The relaxation frequencies obtained are also listed in

TABLE 1. EXPERIMENTAL CONDITIONS AND THE RELAXATION FREQUENCY OF THE SOLUTION

Sample number	$\sum$Cu (10^{-1} M)	$\sum$L (10^{-1} M)	Ionic concentrations (10^{-3} M)					f_r (MHz)
			L	Cu	CuL	CuL_2	CuL_3	
1	1	1	61	65	32	3	—	37
2	1	2	130	43	45	9	3	40
3	1	3	200	30	49	14	7	44
4	2	2	92	107	80	11	2	49
5	2	3	145	79	93	21	7	45
6	3	1	32	236	61	3	—	56
7	3	2	70	183	104	11	2	53
8	3	3	110	144	129	22	5	53
9	3	5	73	300	178	19	3	58
10	3	7	54	475	208	15	2	65

1) M. Eigen, *Pure Appl. Chem.*, **6**, 97 (1963).
2) M. Eigen and R. G. Wilkins, *Advan. Chem. Ser.*, **49**, 55 (1964).
3) A. F. Pearlmutter and J. Stuehr, *J. Amer. Chem. Soc.*, **90**, 858 (1968).
4) N. Tatsumoto, *J. Chem. Phys.*, **47**, 4561 (1967).
5) M. Eigen and G. Maass, *Z. Physik. Chem., N. F.*, **49**, 163 (1966).

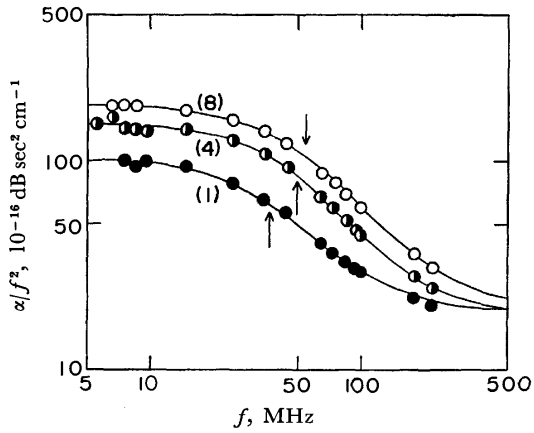

Fig. 1. Ultrasonic absorption in copper(II) chloroacetate solutions. The arrows indicate the relaxation frequencies. Numeral shows the sample number.

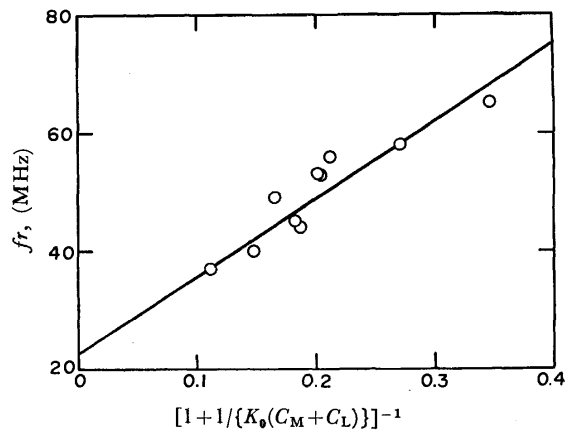

Fig. 2. Plot of relaxation frequency (f_r) *vs.* $[1+1/\{K_0(C_M+C_L)\}]^{-1}$.

Table 1. To ensure that the observed relaxation absorption is due to the complex formation reaction of copper(II) chloroacetate, blank experiments were carried out with solutions containing copper(II) nitrate or chloroacetic acid in the same conditions. In no case was a relaxation absorption observed.

The principal equilibria between copper and chloroacetate ions at low concentrations are;

$$Cu^{2+} + ClAc^- \rightleftharpoons Cu(ClAc)^+ \quad (4)$$

$$Cu(ClAc)^+ + ClAc^- \rightleftharpoons Cu(ClAc)_2 \quad (5)$$

where $ClAc^-$ means the chloroacetate ion. $Cu(ClAc)_3^-$ and higher-order complexes may exist, but the concentrations are very low. Both of the equations have been investigated in trying to correlate the experimental data. In applying Eq. (2) to Eq. (4), the ratio k_{12}/k_{21}, which is the ion-pair constant K_0, can be estimated using the Fuoss equation.[7,8] At ionic strength 1.0, K_0 is calculated to be about 1 for the 2—1 electrolytes. With the data in Table 1 and K_0, f_r is plotted against $[1+1/\{K_0(C_{Cu^{2+}}+C_{ClAc^-})\}]^{-1}$ in Fig. 2. From the slope and the intercept of the line in Fig. 2, k_{23} and k_{32} were obtained; $k_{23}=8.5\times10^8$ sec^{-1}, and $k_{32}=1.4\times10^8$ sec^{-1}. Over-all formation constant, K, can be approximately given by $K_0(1+k_{23}/k_{32})$ and is calculated to be; 7.1 M^{-1}. Taking into account the uncertainty of K_0, this value is in good agreement with the value reported in Ref. 6, 8.1 M^{-1}, which had been previously used in the calculation of the ionic concentrations. On the other hand, the same plots for Eq. (5) do not show a linear relation. These results suggest that Eq. (4) is responsible for the present absorption.

By the ultransonic absorption measurements in the aqueous solution of copper(II) acetate, the rate constant of water substitution of Cu^{2+} ion is reported[9]; $k_{H_2O}=(1—2)\times10^9$ sec^{-1}.

The rate constant k_{23} of copper(II) chloroacetate complex formation reaction obtained above is very close to the value in the case where the ligand is acetate. Moreover the rate constant k_{23} is also close to the water substitution rate studied by the NMR; $k_{ex}\gtrsim3\times10^9$ sec^{-1}. These facts show that the rate-determining step of the complex formation reaction is the loss of a water molecule from the inner-sphere of the metal ion.

As is well known, the d^9 copper(II) ion is subject to Jahn-Teller distortion, and the axial water molecules are in a great lability. Consequently, the fast water substitution rate of copper(II) obtained above may be mainly caused by its peculiar electronic configuration.

6) S. Fronaeus, *Doct. Diss. Lund.*, (1948).
7) R. M. Fuoss, *J. Amer. Chem. Soc.*, **80**, 5059 (1958).
8) G. G. Hammes and J. I. Steinfeld, *ibid.*, **84**, 4639 (1962).
9) G. Maass, quoted in Ref. 3.
10) C. W. Meredith, Ph. D. Dissertation. University of California at Berkeley, (1965).

BULLETIN OF THE CHEMICAL SOCIETY OF JAPAN, VOL. 45, 1932—1933 (1972)

An Electrochemical Study of the Photosensitivity of Poly-*N*-vinylcarbazole

Hiroshi YONEYAMA, Masatoshi HIRAI, and Hideo TAMURA

Department of Applied Chemistry, Faculty of Engineering, Osaka University, Yamadakami, Suita, Osaka

(Received December 6, 1971)

Recently, the photosensitization of ZnO by dyes was studied by means of an electrochemical method, in which dyes were dissolved into a solution and the ZnO crystal was used as a test electrode; it was found that the photosensitization of ZnO by dyes is due to direct electron transfer from excited dyes to ZnO.[1-6] These studies also showed the usefulness of the electrochemical method for the investigation of the photosensitivity of a semiconductor material. In this communication, the application of the electrochemical method to the study of the photosensitivity of poly-*N*-vinylcarbazole (PVCz) will be reported. As is well known, PVCz has a high electronic resistivity, which causes various difficulties in the electrochemical measurements. However, the usefulness of this method will be demonstrated in this paper. The improvement of the photosensitivity of PVCz by the addition of dyes has already been reported[7-9] for a mixed solid system of PVCz and dyes.

Experimental

The PVCz film was prepared by the method described by Okamote *et al.*,[7] using commercial PVCz (Lubican M 170). Evaporated gold or silver paste was used as the electrical contact. No remarkable difference due to the contact material was found. The assembly of the PVCz electrode is shown in Fig. 1, in which a cell assembly is also shown. The PVCz electrode was dipped in a 2 N H_2SO_4 aqueous solution for at least 2 hr before being set in a cell which contained a 0.1 N H_2SO_4 aqueous solution. A freshly-prepared electrode was used for each measurement.

The current was measured by means of a pico-ammeter equipped with a current compensator for the residual current. Measurements were made at 25°C by means of the circuit schematically shown in Fig. 1. No reference electrode was used in this study, and the potential differemce between the PVCz electrode and the counter electrode was recorded. As will be described below, the current was so small that the polarization of the counter electrode was almost negligible. In this case, the platinized platinum counter electrode probably acts as an oxygen electrode[10] or as a hydrogen peroxide electrode.[11]

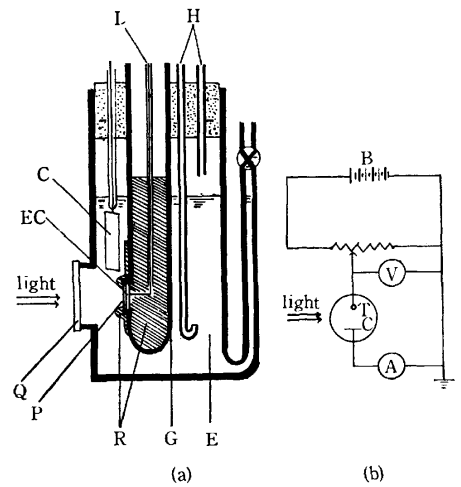

Fig. 1. Schematic illustration of a cell assembly (a) and a circuit for measurements (b). P: PVCz, EC: electrical contact, R: epoxy resin, G: glass tube, C: counter electrode (platinized platinum), E: electrolyte, L: lead wire, Q: quartz plate, H: nitrogen inlet and outlet, B: dry battery, V: voltmeter (input resistance 10^{11} Ω), A: pico-ammeter

A 500 W xenon arc lamp was used as the light source. Various color glass filters, different by 50—60 nm in cut-off wavelength, were chosen for the measurements of the spectral sensitization of PVCz by Rhodamine B.

Result

Figure 2 shows the *I-V* curves of the PVCz electrode in 0.1N H_2SO_4. The photocurrent in this figure was measured under the illumination of a xenon lamp without any filters. It may be observed in this figure that the anodic current was larger than the cathodic current for the same polarization voltage. Figure 3

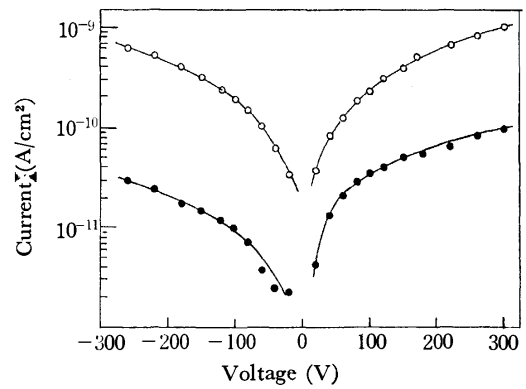

Fig. 2. *I-V* curves of the PVCz in 0.1 N H_2SO_4.
-●- dark current, -○- photocurrent

1) H. Gerischer, and H. Tributsch, *Ber. Bunsenges. Phys. Chem.*, **72**, 437 (1968).
2) H. Tributsch and H. Gerischer, *ibid.*, **73**, 850 (1969).
3) H. Tributsch and H. Gerischer, *ibid.*, **73**, 251 (1969).
4) K. Hauffe, H. Pusch, and J. Range, *Z. Physik. Chem. N. F.*, **64**, 122 (1969).
5) K. Hauffe, H. J. Danzmann, H. Pusch, J. Range, and H. Volts, *J. Electrochem. Soc.*, **117**, 993 (1970).
6) H. Tributsch, *Ber. Bunsenges. Phys. Chem.*, **73**, 582 (1969).
7) K. Okamoto, Y. Hasegawa, S. Kusabayashi, and H. Mikawa, This Bulletin, **41**, 2563 (1968).
8) Y. Hayashi, M. Kuroda, and A. Inami, *ibid.*, **39**, 1660 (1966).
9) L. Hoegel, *J. Phys. Chem.*, **69**, 755 (1965).
10) T. P. Hoar, *Proc. Roy. Soc., Ser., A* **142**, 628 (1933).
11) J. O'M. Bockris and A. K. M. S. Huq, *ibid., Ser., A*, **237**, 277 (1956).

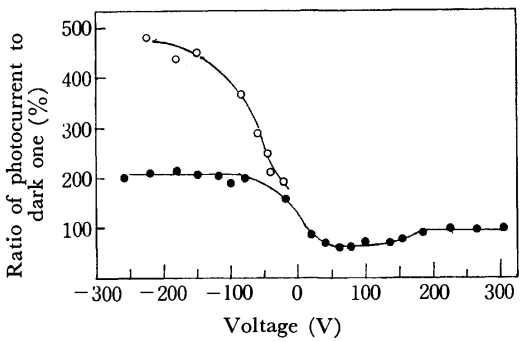

Fig. 3. A ratio of photocurrent to the dark one under illumination of xenon lamp.
-●- PVCz, -○- PVCz+1 mol% TCNE

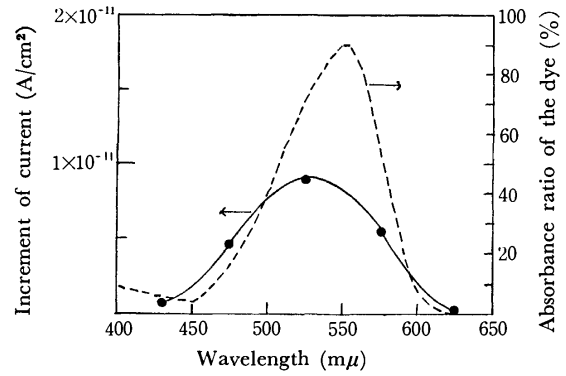

Fig. 4. Spectral sensitization of PVCz by addition of 10^{-5} M Rhodamine B to 0.1N H_2SO_4.
Solid line: increment of the cathodic current
Dotted line: absorption spectrum of the dye

shows the ratio of the photocurrent to the dark one, which was estimated on the basis of Fig. 2. This figure clearly shows that the ratio was by far larger for the cathodic than for the anodic polarization. The current ratio obtained on the PVCz electrode containing 1 mol% tetracyanoethylene (TCNE) as an electron acceptor[12] is also shown in the figure.

12) H. Meier, W. Albrecht, and U. Tschirwitz, *Ber. Bunsenges. Phys. Chem.*, **73**, 795 (1969).

A noticeable spectral sensitization, one which accords with the absorption spectrum of the dye, was observed in the electrolyte containing 10^{-5} M Rhodamine B when the electrode was polarized cathodically. Figure 4 shows the increment of the cathodic photocurrent at −250V by the addition of the dye. No increase of the anodic current by the addition of the dye was observed.

Discussion

When the PVCz electrode was polarized cathodically, the electron energy in the surface region of the electrode becomes lower than that in the bulk of the electrode. Therefore, there must exist an electric field which drifts free electrons from the bulk to the surface and positive holes from the surface to the bulk. In this case, the free electrons, which move from the bulk to the surface and then transfer to a species in the electrolyte, will increase in number upon illumination if the illumination produces the large number of electrons as well as positive holes. On the other hand, if no excited species is produced in the electrolyte by the illumination, the cathodic current due to positive holes will not be influenced by the illumination. Similarly, free holes produced by the illumination will increase the anodic current, while this current will not be increased by photogenerated free electrons if the illumination does not produce any excited species in the electrolyte. Hence, it can be said, from the *I-V* curves in the electrolyte without dyes (Fig. 2), that the cathodic current and the anodic current are carried by electrons and holes respectively. The high current gain upon the illumination which was observed on the cathodic polarization is ascribed to the fact that the electrons are the minority carriers.

On the basis of such considerations, the increase of the cathodic current caused by the excited dye indicates that the injection of a positive hole from Rhodamine B into the PVCz electrode occurred, while the injection of an electron from the dye to the electrode probably did not occur.

BULLETIN OF THE CHEMICAL SOCIETY OF JAPAN, VOL. 45, 1934—1935 (1972)

ESR Study of γ-Irradiated Isobutylene-Silica Gel System

Siro NAGAI, Shun-ichi OHNISHI, and Isamu NITTA

Osaka Laboratory for Radiation Chemistry, Japan Atomic Energy Research Institute, 508 Mii, Neyagawa-shi, Osaka

(Received December 14, 1971)

In a previous paper,[1] we reported that monomer and dimer cations of some methylbenzenes are produced in the adsorbed states upon γ-irradiation. Isobutylene is known to be a vinyl monomer polymerizing through a cationic mechanism. The present study was undertaken to examine the possibility of observing isobutylene radical cation. A detailed study of the nature of the adsorbed radicals seems to be of importance.

We describe our ESR study of free radicals produced in the γ-irradiated isobutylene-silica gel system. It is seen that the well-resolved spectra observed under certain conditions not only make the identification of radicals possible but also show the phenomena of asymmetric linewidth variation of the hf lines.

Experimental

Silica gel was the same as that reported.[1] Isobutylene (99.0%) was obtained from Takachiho Trading Co. Ltd., and was used without further purification. All experimental procedures were the same as described.[2] The isobutylene contents in the adsorbed samples were in the range 1—20% of the monolayer value.

Results and Discussion

A typical spectrum of adsorbed isobutylene observed at −196°C consists of 10 lines with 22.4 gauss splitting and of several weak lines as shown in Fig. 1a. The 10-line spectrum was assigned to *t*-butyl radical $\dot{C}(CH_3)_3$ from the hyperfine splitting constant.

It should be noted that the linewidths of individual hf lines differ from each other. The $M_I=-1/2$ line is the narrowest of the 10 lines throughout the whole temperature range investigated, and gives the partially resolved second-order structure even at −196°C. At higher temperatures, the structures of the other two lines, $M_I=1/2$ and $-3/2$ become observable (Fig. 1b). The spacings of the second-order components of the $M_I=-1/2$ line at −60°C are 0.70, 0.50, 0.39, and 0.25 gauss which agree with the data in liquid phase.[3] The asymmetric linewidth variation can be explained in terms of a modulation of the anisotropic hyperfine and g-tensor interactions.[4]

The ESR spectrum becomes well-resolved at higher temperatures. The main part of the spectrum (±70 gauss) is shown in Fig. 2a. In this region 6 lines of the 10-line spectrum of the *t*-butyl radical appeared.

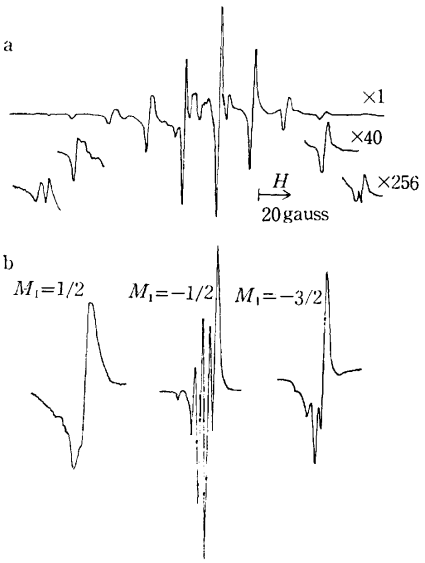

Fig. 1. a; ESR spectrum of γ-irradiated isobutylene-silica gel at −196°C. b; Second-order structures of the central three lines of the *t*-butyl radical spectrum observed at −80°C.

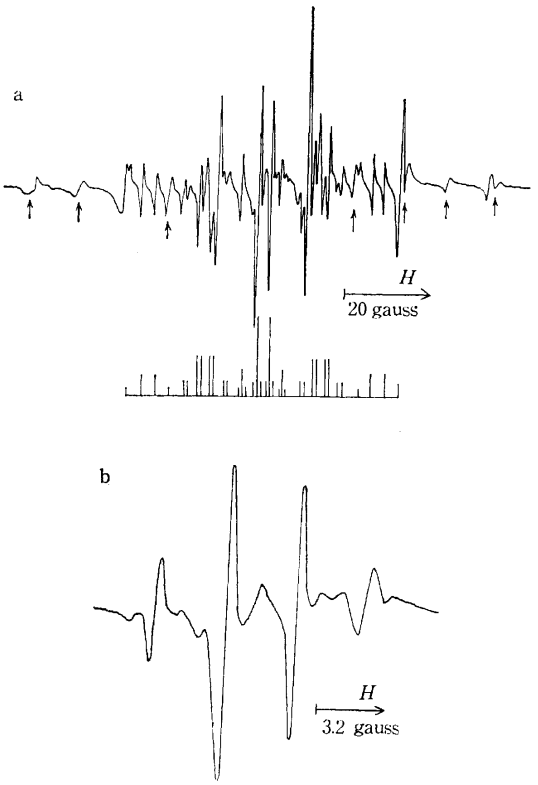

Fig. 2. a; ESR spectrum of γ-irradiated isobutylene-silica gel at −80°C in the ±70 gauss range. b; Central part of the 2-methylallyl radical spectrum.

1) S. Nagai, S. Ohnishi, and I. Nitta, This Bulletin, **44**, 1230 (1971).
2) S. Nagai, S. Ohnishi, and I. Nitta, *Chem. Phys. Lett.*, **13**, 379 (1972).
3) R. W. Fessenden and R. H. Schuler, *J. Chem. Phys.*, **39**, 2147 (1963).
4) J. H. Freed and G. K. Fraenkel, *ibid.*, **39**, 326 (1963).

The weak signals at −196°C (Fig. 1a) are well-resolved and the 36 lines (3×3×4) drawn by sticks were assigned to 2-methylallyl radical $CH_2{=}C(CH_3){-}CH_2$. The hf splitting constants measured at −80°C were $a(CH_2)=13.8$ gauss, $a'(CH_2)=14.6$ gauss and $a(CH_3)=3.2$ gauss. The splitting values of methylenic protons show a good correspondence with $a(CH_2)=13.93$ gauss and $a'(CH_2)=14.83$ gauss of the unsubstituted allyl radical.[3]

The asymmetric linewidth variation is appreciable in the spectrum due to the 2-methylallyl radical (Fig. 2b). Qualitative examination of the spectrum shows that the methyl proton lines are broader on the high-field side of the spectrum than on the low-field side. The behavior may be explained on the basis of the theory of ESR linewidth developed by Freed and Fraenkel,[4] provided that the theory is applicable to the spectra of adsorbed radicals. Detailed analyses, however, have not been made because of overlapping of the hf lines with those of two other radicals.

In addition to the 36-line spectrum, we note other lines indicated by arrows in Fig. 2a. The widths of the lines are broader than those of the other two radicals. They may be regarded as a part of the spectrum of the propagating radical $\dot{C}(CH_3)_2{-}CH_2{-}R$ on the basis of the approximate hf splitting values of 22 gauss for methyl protons and 12 gauss for methylene protons. A similar propagating radical on silica gel was found from adsorbed ethylene.[5] From the fact that the signal intensity decreases with the rise of temperature, the propagating radicals are considered to be formed at −196°C during irradiation. It is reasonable to assume that the condensation of isobutylene molecules occurs inhomogeneously on the surface of silica gel before irradiation. The related phenomena were observed in the formation of benzene dimer cations from adsorbed benzene,[1,6] and also in that of benzene monomer cations from adsorbed acetylene.[2]

ESR spectra from the samples with amounts of adsorption less than 2.0 cc STP/g are mainly due to positive holes in irradiated silica gel.[7] With the rise of temperature, the intensity of the spectrum of the *t*-butyl radical is found to increase slightly at the expense of the silica gel signal, suggesting the formation of the *t*-butyl radical partly through a cationic mechanism.

5) P. O. Kinell, A. Shimizu, O. Edlund, and A. Lund, *J. Polym. Sci.*, Part B, **6**, 133 (1968).
6) O. Edlund, P. O. Kinell, A. Lund, and A. Shimizu, *J. Chem. Phys.*, **46**, 3678 (1967).
7) N. F. Shamonia, A. G. Kotov, and S. Ya. Pshezhetskii, *Khimiya Vysokikh Energii*, **4**, 43 (1970).

BULLETIN OF THE CHEMICAL SOCIETY OF JAPAN, VOL. 45, 1935—1936 (1972)

6β-Acetoxyfuranoeremophilan-3α-yl Angelate and 6β-Hydroxyfuranoeremophilan-3α-yl Angelate.[1] New Furanoeremophilane Derivatives from *Farfugium hiberniflorum* Kitamura

Hajime NAGANO and Takeyoshi TAKAHASHI

Department of Chemistry, Faculty of Science, The University of Tokyo, Bunkyo-ku, Tokyo

(Received December 18, 1971)

In connection with the structural studies of farfugin A and farfugin B isolated from *Farfugium japonicum* Kitamura (=*Ligularia tussilaginea* Makino; Tsuwabuki in Japanese),[2] we have examined the constituents of *Farfugium hiberniflorum* Kitamura (=*Liguralia hiberniflora* Makino; Kan-tsuwabuki in Japanese) and isolated 6β-acetoxyfuranoeremophilan-3α-yl angelate (I) and 6β-hydroxyfuranoeremophilan-3α-yl angelate (II),[1] which constitute two new furanoeremophilane derivatives related to furanofukinol (III).[3]

Compound I, $C_{22}H_{30}O_5$ (M^+ at m/e 374), a viscous oil, was positive to the Ehrlich test. IR, UV, PMR, and mass spectra (see Experimental) suggest the presence of a furan, a secondary and a tertiary methyl, and also that of partial structures: $CH_3COO-\underset{|}{C}H$

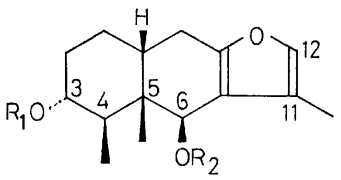

	R_1	R_2
(I)	-OC(CH$_3$)=CH-CH$_3$	Ac
(II)	-OC(CH$_3$)=CH-CH$_3$	H
(III)	H	H
(IV)	H	-OC(CH$_3$)=CH-CH$_3$

1) The structures refer to those of relative configurations.

2) H. Nagano, Y. Moriyama, Y. Tanahashi, T. Takahashi, M. Fukuyama, and K. Sato, *Chem. Lett.*, **1972**, 13.

3) K. Naya, M. Nakagawa, M. Hayashi, K. Tsuji and M. Naito, *Tetrahedron Lett.*, **1971**, 2961.

and $CH_3CH{=}C(CH_3)COO{-}\underset{|}{C}H$. The latter moiety was determined as angelyl group by benzene induced solvent shift[4] ($\delta^{CDCl_3} - \delta^{C_6D_6} = 0.44$ ppm) of the olefinic proton found to be *trans* to the ester group. Reduction of I with lithium aluminum hydride gave a diol $C_{15}H_{22}O_3$ identical (IR, PMR, and tlc) with furanofukinol (III)[3] (3α,6β-dihydroxyfuranoeremcphilane) isolated by Naya *et al.* from *Petasites japonicus* Maxim. Thus, compound I is either 6β-acetoxyfuranoeremophilan-3α-yl angelate (I) or 3α-acetoxyfuranoeremophilan-6β-yl angelate.[1]

Acetylation of II, $C_{20}H_{28}O_4$, an oil, with acetic anhydride and pyridine afforded a monoacetate identical (IR, vpc and tlc) with I. On reduction with lithium aluminum hydride, II gave III. However, spectral data of II differ from those of 6-angelylfuranofukinol (IV)[3] (3α-hydroxyfuranoeremophilan-6β-yl angelate).

Thus substances I and II should be represented by 6β-acetoxyfuranoeremophilan-3α-yl angelate and 6β-hydroxyfuranoeremophilan-3α-yl angelate,[1,5] respectively.

Experimental

Isolation. The dried roots of *Farfugium hiberniflorum* Kitamura (100 g) were extracted three times with boiling benzene (each 400 m*l*). The roots were then powdered and further extracted with boiling benzene. The combined extracts (1.6 g) were chromatographed on silica gel (Wako-gel, C-200; 120 g) with light petroleum-ether (5 : 1) as eluent to give a pale yellow oil containing I. Successive elution with light petroleum-ether (3 : 1) afforded crude II. Pure I (60 mg) and II (100 mg) were obtained by repeated chromatography of each crude oil on silica gel.

6β-Acetoxyfuranoeremophilan-3α-yl Angelate (I). Spectral data of I, $C_{22}H_{30}O_5$, an oil, are as follows; UV: λ_{max}^{EtOH} 215 nm (ε 17000); IR: $\nu_{max}^{CHCl_3}$ 1730, 1710, 1640, 1560, 1235, and 1160 cm^{-1}; PMR ($CDCl_3$): δ 0.97 (d, J=7 Hz, $C_{(4)}$-CH_3), 1.03 (s, $C_{(5)}$-CH_3), 1.87 (d, J=1.5 Hz, $C_{(11)}$-CH_3), 1.87 [s, $CH_3CH{=}C(CH_3)COO$-], 1.97[d,[6] J=7 Hz, $CH_3CH{=}C(CH_3)COO$-], 2.12 (s, CH_3CO-), 5.37 (m, $C_{(3)}$-H), 6.01[q,[6] J=7 Hz, $CH_3CH{=}C(CH_3)COO$-], 6.37 (br. s, $C_{(6)}$-H), and 7.05 ppm (m, $C_{(12)}$-H); PMR (C_6D_6): δ 0.90 (d, J=7 Hz, $C_{(4)}$-CH_3), 0.95 (s, $C_{(5)}$-CH_3), 1.76 (s, CH_3-CO-), 1.8—2.2[$C_{(11)}$-CH_3, $CH_3CH{=}C(CH_3)COO$- and $CH_3CH{=}C(CH_3)COO$-], 5.57[m, $C_{(3)}$-H and $CH_3CH{=}C(CH_3)COO$-], 6.51 (br. s, $C_{(6)}$-H) and 6.95 ppm (m, $C_{(12)}$-H); MS: *m/e* 374 (relative intensity 2%, M^+), *m/e* 124 (100%, *retro*-Diels-Alder fragment), *m/e* 83 (82%, $[CH_3CH{=}C(CH_3)CO]^+$), *m/e* 55 (70%, $[CH_3CH{=}CCH_3]^+$) and *m/e* 43 (80%, $[CH_3CO]^+$).

6β-Hydroxyfuranoeremophilan-3α-yl Angelate (II). Characterization of II, $C_{20}H_{28}O_4$, an oil, is as follows; IR: $\nu_{max}^{CHCl_3}$ 3450, 1700, 1640, 1560, 1240 and 1160 cm^{-1}; PMR ($CDCl_3$): 0.95 (s, $C_{(5)}$-CH_3), 1.00 (d, J=7 Hz, $C_{(4)}$-CH_3), 1.8—2.1 [$C_{(11)}$-CH_3, $CH_3CH{=}C(CH_3)COO$- and $CH_3CH{=}C(CH_3)COO$-], 5.07 (br. s, $C_{(6)}$-H), 5.30 (m, $C_{(3)}$-H), 6.05 [m, $CH_3CH{=}C(CH_3)COO$-] and 7.04 ppm (m, $C_{(12)}$-H).

Reduction of 6β-Acetoxyfuranoeremophilan-3α-yl Angelate (I) with Lithium Aluminum Hydride. A solution of I (43 mg) in dry ether was added to a suspension of lithium aluminum hydride (50 mg) in dry ether and the reaction mixture was refluxed for 1.5 hr under nitrogen atmosphere. The usual treatment gave a crystalline material (34 mg), which was purified by chromatography on silica gel to afford furanofukinol (III), UV: λ_{max}^{EtOH} 219 nm (ε 6200); IR: ν_{max}^{Nujol} 3375 and 3320 cm^{-1}; PMR (DMSO-d_6): 0.77 (s, $C_{(5)}$-CH_3), 0.84 (d, J=7 Hz, $C_{(4)}$-CH_3), 1.98 (d, J=*ca.* 1 Hz, $C_{(11)}$-CH_3), and 7.14 ppm (m, $C_{(12)}$-H); MS: *m/e* 250 (3%, M^+) and *m/e* 124 (100%, *retro*-Diels-Alder fragment).

6β-Hydroxyfuranoeremophilan-3α-yl angelate (II) was reduced with lithium aluminum hydride to give furanofukinol (III) by the same procedure as abave.

The authors wish to thank Prof. K. Naya, Kwansei Gakuin University, for the gift of the authentic sample of furanofukinol, and also for the PMR and IR spectra of furanofukinol and its derivatives.

4) J. Ronayne and D. H. Williams, *J. Chem. Soc., C*, **1967**, 2642.

5) Since no optical rotation data were described for furanofukinol (III),[2] absolute configurations of compounds I and II are left undetermined. From biogenetic considerations, absolute configurations of I and II are plausible for compounds I and II.

6) Further long-range couplings are observed for these signals.

BULLETIN OF THE CHEMICAL SOCIETY OF JAPAN, VOL. 45, 1937—1938 (1972)

The Temperature Dependence of the Fluorescence and Polarization Spectra of 1-Naphthol

Satoshi SUZUKI, Tsuneo FUJII, and Kohei SATO

Department of Industrial Chemistry, Faculty of Engineering, Shinshu University, Wakasato, Nagano

(Received January 10, 1972)

In general, the fluorescence of an organic compound in a condensed medium originates from the lowest excited singlet state, because the internal conversion between excited singlet states is fast compared with the fluorescence emission. If two excited singlet levels are closely situated in the region of the lowest absorption band, a dual emission is expected to be observed.[1-5] On the other hand, it is well accepted that a molecule in a fluid solution is first excited to the Franck-Condon excited state, and that it then passes into the equilibrium excited state from which the fluorescence emission occurs. At sufficiently low temperatures, such a relaxation process cannot take place during the fluorescence lifetime because of the high viscosity of a solvent. As a result of this phenomenon, the fluorescence emission originates from the Franck-Condon excited state and, hence, shifts to the blue. This note will report the inversion of the fluorescent state in 1-naphthol caused by a lowering of the temperature.

Experimental

1-Naphthol was recrystallized three times from water and then sublimed *in vacuo*. Glycerin (Wako Pure Chemical Industiries, Inc., JIS S grade) was used without further purification.

The absorption spectra were recorded on a Hitachi EPS-2 recording spectrophotometer. The fluorescence and excitation spectra were obtained by means of a Hitachi MPF-2A fluorescence spectrophotometer. The temperatures of the solutions were controlled by using a cryostat (Torisha Laboratory, Ltd.) with an accuracy of about ±1 K. The degree of polarization, P, was measured by the method of photoselection.[6-8]

Results and Discussion

The temperature dependence of the fluorescence spectra for 1-naphthol in a glycerin solution is shown in Fig. 1, together with the absorption and polarization spectra.

1-Naphthol has four absorption bands in the near-ultraviolet region. The lowest frequency band with a sharp fine structure is assigned to the ^1L_b transition, the broad band near 3.4 kK which overlaps the ^1L_b, to the ^1L_a transition, and the other two strong bands at higher frequencies than 4 kK, to the ^1B_b transition.[9-11] The moments of the ^1L_b and ^1B_b transitions lie nearly along the direction of the long axis of the molecule, while the moment of the ^1L_a transition is nearly along the short axis.[11-13]

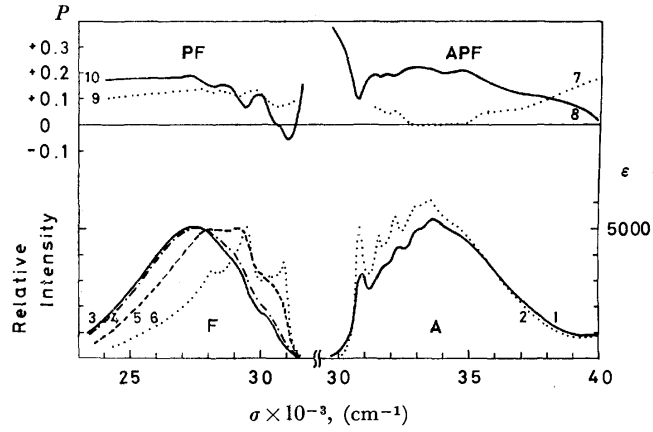

Fig. 1. Temperature dependence of the absorption, fluorescence, and polarization spectra of 1-naphthol in glycerin. a) Absorption spectra(A) 1: 299 K; 2: 135 K. b) Fluorescence spectra(F) Excitation wavelength: 297 nm; 3: 329 K; 4: 261 K; 5: 242 K; 6: 168 K. c) Fluorescence excitation polarizarion spectra(APF) 7: 200 K, observed at 325 nm; 8: 200 K, observed at 360 nm. d) Fluorescence polarization spectra (PF) Excitation wavelength: 297 nm; 9: 283 K; 10: 195 K.

At room temperatures, 1-naphthol has a broad, structureless fluorescence band. In the excitation polarization spectrum at 200 K, obtained by monitoring the fluorescence at the wavelength of 360 nm, which corresponds to the maximum of the broad fluorescence band, the peaks of the ^1L_b-absorption band correspond to the polarization minima, whereas the polarization spectrum has large positive P values in the ^1L_a-band region. Further, the degree of polarization is negative in the region of the ^1B_b transition. Such behavior in the excitation polarization spectrum is very similar to that observed in the system of 1-naphthol and triethylamine.[4] The fluorescence polarization curve obtained with excitation at the ^1L_a band has nearly the same positive P values over the whole region of the fluorescence band. These observations indicate that the polari-

1) E. Lippert, W. Lüder, F. Moll, W. Nägele, H. Boos, H. Prigge, and I. Seibold-Blankenstein, *Angew. Chem.*, **73**, 695 (1961).
2) N. Mataga, This Bulletin, **36**, 654 (1963).
3) N. Mataga, Y. Torihashi, and K. Ezumi, *Theor. Chem. Acta*, **2**, 158 (1964).
4) S. Suzuki and H. Baba, This Bulletin, **40**, 2199 (1967).
5) P. S. Song and W. E. Kurtin, *J. Amer. Chem. Soc.*, **91**, 4892 (1969).
6) A. C. Albrecht, *J. Mol. Spectrosc.*, **6**, 84 (1961).
7) A. K. Kalantar and A. C. Albrecht, *Ber. Bunsenges. Phys. Chem.*, **68**, 361 (1964).
8) F. Dörr, *Angew. Chem.*, **78**, 457 (1966).
9) H. Baba and S. Suzuki, This Bulletin, **34**, 82 (1961).
10) H. Baba and S. Suzuki, *J. Chem. Phys.*, **35**, 1118 (1961).
11) S. Suzuki, T. Fujii, and H. Baba, *J. Mol. Spectrosc.*, to be published.
12) K. Nishinoto, *J. Phys. Chem.*, **67**, 1443 (1963).
13) L. S. Forster and K. Nishimoto, *J. Amer. Chem. Soc.*, **87**, 1459 (1965).

zation of the broad fluorescence transition is parallel to that of the ^1L_a and that, hence, the fluorescent state is the ^1L_a state.

As the temperature is lowered, the fluorescence spectrum shifts to the blue and changes to a structured band, the peaks of which lie in mirror-symmetry positions with respect to the ^1L_b absorption peaks.

At a low temperature, the excitation polarization spectrum obtained by monitoring the highest-frequency peak of the fluorescence band exhibits minima at the wavelengths corresponding to the region of the ^1L_a-absorption band. The degree of polarization is positive in the region of the ^1B_b-absorption band. The degree of polarization of the fluorescence emission obtained with an excitation wavelength of 297 nm shows a considerable decrease in the short-wavelength region. The wavelengths at which the minima of the polarization curve occur coincide with the peaks of the fluorescence band. The behavior of the polarization spectra confirms that the fluorescence emission from 1-naphthol in glycerin at sufficiently low temperatures is predominantly from the ^1L_b state. The same temperature dependence of fluorescence and polarization spectra was observed in both propylene glycol and ethanol solvents.

The results may be interpreted as follows. In the equilibrium excited state, the interaction of a solute molecule with solvent molecules lowers the ^1L_a energy below the ^1L_b, so that the broad ^1L_a fluorescence is observed. At a sufficiently low temperature, where the solute and solvent molecules do not have enough time to relax to the equilibrium configuration, the ^1L_a state lie above the ^1L_b, therefore, the blue-shifted ^1L_b fluorescence is observed. This interpretation is consistent with the finding of the theoretical calculation that the π-moment of the ^1L_a state is larger than that of the ^1L_b.[12]

The degree of polarization in glycerin increases to a maximum value at 10°C. This means that 1-naphthol cannot re-orient itself during its fluorescence lifetime at a temperature below 10°C. It should be noted that the temperature at which the fluorescence from the ^1L_b state becomes appreciable is lower by about 30 degrees than that at which the re-orientation of the solute ceases. The effects of molecular motions on the fluorescent state will be discussed later.

BULLETIN OF THE CHEMICAL SOCIETY OF JAPAN, VOL. 45, 1938—1939 (1972)

The Syntheses and Properties of Chloro(acrylonitrile) Complexes of Platinum(0)

Keinosuke SUZUKI and Hideshi OKUDA

Inorganic Chemistry Laboratory, Faculty of Science, Nagoya University, Chikusa-ku, Nagoya

(Received January 10, 1972)

In the reaction of $Pt(PPh_3)_4$ with haloolefins, the formation of two kinds of complexes, *i.e.*, the olefin complex and the vinyl complex, has been reported.[1)]

Olefin complex Vinyl complex

This paper will deal with the reaction of $Pt(PPh_3)_4$ and $Pt(AsPh_3)_4$ with chloroacrylonitrile, CH_2=CClCN, and with the structures of the complexes formed; the discussion will be based on the spectroscopic data.

The treatment of the benzene solution of $Pt(PPh_3)_4$ with chloroacrylonitrile resulted in a pale yellow solution, from which $Pt(PPh_3)_2(CH_2CClCN)$ (I) was subsequently isolated. A similar treatment of $Pt(AsPh_3)_4$ with the same ligand gave a pale yellow substance formulated as $Pt(AsPh_3)_2(CH_2CClCN)$ (II). Both complexes, (I) and (II), are stable in air; they decompose at 160—170 and 160—165°C respectively. The infrared and proton magnetic resonance spectra data of the two complexes are summarized in Table 1. As is clear from the table, the stretching frequency, $\nu_{C=C}$ disappeared upon the complex formation, while ν_{C-Cl} was still present. Since Bland and Kemmitt[1)] proposed the coordination of the double bond, *i.e.* the formation of the olefin complex on the basis of the disappearance of $\nu_{C=C}$, it may be reasonable to assume the formation of olefin complexes for both the complexes studied here. The far-infrared spectral data also indirectly support the above assumption, because the stretching frequency, ν_{Pt-Cl}, expected for the product of the oxidative addition was not observed. For the complex II this was not clear due to the strong ligand absorption in the region 320—350 cm^{-1}.

The proton magnetic resonance spectra of methylene protons in the complexes I and II are shown in Fig. 1. For these complexes, it was difficult to obtain well-resolved spectra because of their low solubility in common organic solvents.

Furthermore, the non-equivalence of the methylene protons caused another difficulty in interpreting the spectra. The CH_2 protons of the coordinated ligand showed a high-field shift in both complexes, indicating the formation of olefin complexes, and the satellite due to the coupling with ^{195}Pt was also observed. In the complex I, the central peak of the CH_2 proton appeared as a complicated multiplet centered at around $\tau = \sim 7.6$ ppm. This complex signal may be

1) W. J. Bland and R. D. W. Kemmitt, *J. Chem. Soc., A*, **1969**, 2062.

Table 1. Infrared and proton magnetic resonance data of the complexes I and II

Compound	Infrared		Proton magnetic resonance	
	$\nu_{C=C}$	ν_{C-Cl}	τ	J(Pt-H)
CH_2=CClCN	1608[2]	660[2] cm^{-1}	H_a=3.78 ppm H_b=3.86	3.0[b] Hz
(I)	—	667, 652[a]	~7.7	~50
(II)	—	672, 658[a]	~7.5	~55 (~7[b])

a) Tow strong absorptions were observed. One of them may probably be due to ν_{C-Cl}.
b) $J(H_a-H_b)$.

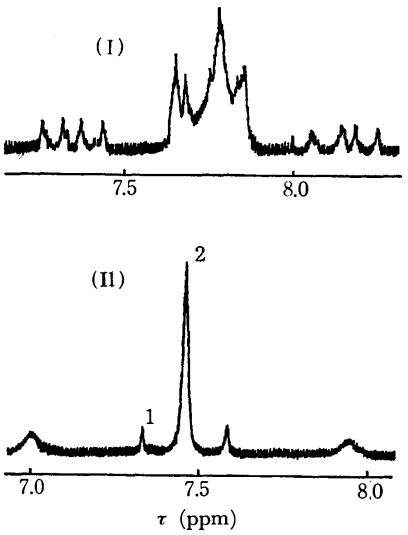

Fig. 1. PMR spectra of the CH_2 protons of the complexes I and II.
I: $Pt(PPh_3)_2(CH_2$=CClCN)
II: $Pt(AsPh_3)_2(CH_2$=CClCN)

due to the existence of an AB pattern, which is, in turn, able to couple with two non-equivalent phosphorus atoms. Since the CH_2 protons do not couple with an arsenic atom, the signal of the complex II can be expected to be much simpler than that of the complex I. However, as is shown in Fig. 1, the central peak of the CH_2 signal appeared as a triplet with the intensity ratio of 1 : 28 : 1. We interpret this triplet as being the case when the inside peakes of an AB quartet come very close to one another and as being a quartet changed into a triplet. To obtain accurate values of the coupling constant and chemical shift, the use of an AB quartet pattern is required, but the signal obtained could not be further resolved. Consequently, the $J(H_a-H_b)$ value was approximated to the difference in the values of the two signals, 1 and 2, and τ, to the value of the signal 2 in Fig. 1.

The electronic spectra of the complexes were measured in the 220—360 nm, region. They are quite similar to each other; there are three absorption maxima at 36.5, 39.7, and 43.2×10^3 cm^{-1} ($\varepsilon=1.8\times10^4$ sh, 2.6×10^4, and 3.8×10^4) far the complex I and at 35.8, 39.7, and 44.4×10^3 cm^{-1} ($\varepsilon=1.1\times10^4$ sh, 2.6×10^4, and 4.7×10^4) for the complex II. From these results, the formation of the olefin complexes is concluded for both cases. We further tried to prepare a vinyl complex by refluxing the complex I in ethanol but without success.

2) S. B. Lie and P. Klaboe, *Spectrochem. Acta*, **26A**, 1191 (1970).

Experimental

Materials. The $Pt(PPh_3)_4$ and $Pt(AsPh_3)_4$ were prepared by a method previously reported by other authors.[3,4]

Chloroacrylonitrilebis(triphenylphosphine)platinum(O)=(I). 2-Chloroacrylonitrile (0.2 m*l*, 2 mmol) was added to a solution of tetrakis(triphenylphosphine)platinum (12. g, 1 mmol) in benzene (100 m*l*) under nitrogen. The reddish-brown color of the original solution turned to a pale yellow, and a white substance was obtained on concentrating the solution. It was reprecipitated from a mixture of chloroform and ethyl ether as a white powder; mp 160—170°C (decomp.). Found: C, 57.86; H, 3.61: N, 1.35%. Calcd for $C_{39}H_{32}NClP_2Pt$≡$Pt(PPh_3)_2(CH_2CClCN)$: C, 58.03; H, 4.00; N, 1.74%.

Chloroacrylonitrilebis(triphenylarsine)platinum(O)=(II). To a suspension of tetrakis(triphenylarsine)platinum (1.4 g, 1 mmol) we added 0.2 m*l* (2 mmol) of 2-chloroacrylintirile. The suspension changed to a pale yellow solution in about 30 min. After the solution had then been stirred for 2 hr, it was filtered and the filtrate was concentrated under reduced pressure to give a pale yellow compound. It was precipitated from a mixture of dichloromethane and ethyl ether as a pale yellow powder; mp 160—165°C (decomp.). Found: C, 51.49; H, 3.48; N, 1.37%. Calcd for $C_{39}H_{32}NClAs_2Pt$≡$Pt(PPh_3)_2(CH_2CClCN)$: C, 52.33; H, 3.60; N, 1.57%.

Measurements. The infrared spectra were recorded with JASCO-DS-402G and HITACHI EPI-L2 spectrophotometers. The electronic spectra in the CH_3CN solution were obtained with a HITACHI 323 spectrometer. The proton magnetic resonance spectra were obtained with a JEOL C-60H spectrometer, using $CDCl_3$ as the solvent and TMS as the internal standard.

3) W. L. Jolly, "Inorganic Syntheses," Vol. 11, McGraw-Hill, New York (1968), p. 105.
4) L. Malatesta and C. Cariello, *J. Chem. Soc.*, **1958**, 2323.

SHORT COMMUNICATIONS

Crystal Structures of 1-(2-Thiazolylazo)-6-bromo-2-naphthol and Bis(1-(2-thiazolylazo)-2-naphthol)iron(II)

Masayasu KURAHASHI, Akira KAWASE, Ken HIROTSU,* Makoto FUKUYO,* and Akira SHIMADA*

Metal Chemistry Division, National Research Institute for Metals, Meguro-ku, Tokyo

** Department of Chemistry, Faculty of Science, Osaka City University, Sumiyoshi-ku, Osaka*

(Received December 13, 1971)

The crystal structures of 1-(2-thiazolylazo)-6-bromo-2-naphthol(TAN-Br) and bis(1-(2-thiazolylazo)-2-naphthol)iron(II) ([Fe[TAN)$_2$]) have been determined by X-ray diffraction. Our main interest lies in the reactions of thiazolylazo-naphthol(TAN) with various metal ions as an analytical reagent. 6-Bromo-derivative of TAN was chosen for the elucidation of structure by the heavy atom method.

The crystals of TAN-Br were grown by sublimation of crude materials. Crystal data are: $C_{13}H_8N_3OSBr$, M.W. 334.2, mp 189°C, orthorhombic, $a=19.07\pm0.03$, $b=32.08\pm0.05$, $c=4.22\pm0.01$ Å. $Dm=1.72$g·cm^{-3}, $Z=8$, $Dx=1.72$ g·cm^{-3}; space group $P2_12_12_1$. Intensities of the three-dimensional reflections were measured visually from equi-inclination Weissenberg photographs for 0—3 layers around the c-axis and 0th layer around the a-axis. In total, 2074 independent reflections were collected and converted into $|F|$ values in the usual way. The structure was solved by the heavy atom method. Parameters were refined by the least-squares method and the R value was reduced to 0.12.

Crystal data of [Fe(TAN)$_2$] are: $[Fe(C_{13}H_8N_3OS)_2]\cdot CHCl_3\cdot C_2H_5OH\cdot H_2O$, F.W. 784.0, triclinic, $a=12.63$, $b=11.97$, $c=10.52$ Å, $\alpha=87°12'$, $\beta=99°36'$, $\gamma=104°46'$. $Dm=1.63$ g.cm^{-3}, $Z=2$, $Dx=1.64$ g.cm^{-3}; space group $P\bar{1}$. Using Cu$K\alpha$ radiation, 3318 intensity data were collected by photographic method for 0—8 layers around the c-axis and 0—2 layers around the a-axis. The structure was solved by the heavy atom method and refined by the block-diagonal least-squares method. R factor was found to be 0.18.

The two crystallographically independent TAN-Br molecules are similar in shape and size. They are planar within a deviation of ±0.03 and ±0.15 Å. Both molecules conform to the chemical formula presented in Fig. 1a. The N···O distance of 2.50 Å suggests an intramolecular hydrogen bonding between N and O atoms as indicated in Fig. 1a.

The structure of [Fe(TAN)$_2$] is shown in Figs. 1b and 2. The TAN acts as a terdentate ligand. One Fe(II) ion is bonded octahedrally to two phenolic

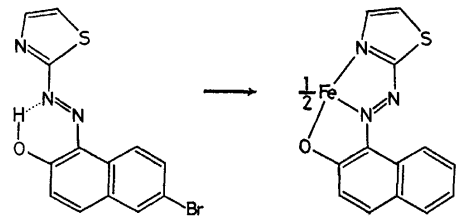

a TAN-Br b [Fe(TAN)$_2$]

Fig. 1. Comparison between TAN-Br and [Fe(TAN)$_2$].

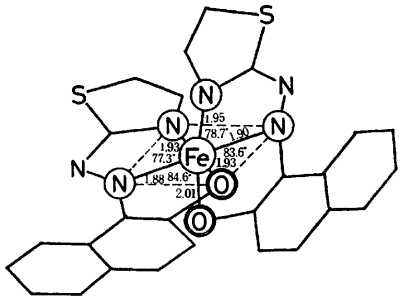

Fig. 2. The Structure of Fe(II) chelate [Fe(TAN)$_2$].

oxygens, two azo nitrogens adjacent to the naphthol ring and two thiazole nitrogens to form four five-membered chelate rings. The ligand molecules are very nearly planar and the mean planes of the ligands are perpendicular to each other. The two ligands are in *mer* coordination. Thus the structure determined from the measurement of stability constant and absorption spectra has been verified. Since the structure of TAN-Br and probably also of TAN is as shown in Fig. 1a, 180° rotation around the two N–C bonds should occur in chelate ring formation and turn the structure into that shown in Fig. 1b.

The general feature of coordination of TAN to Fe(II) is very similar to that of 1-(2-pyridylazo)-2-naphthol(PAN) observed in crystals of [Cu(PAN)-H_2O]·ClO_4.[1]

1) S. Ooi, D. Carter, and Q. Fernand, *Chem. Commun.*, **1967**, 1301.

The Complex of Poly-α,L-glutamic Acid with Acridine Orange in the Neutral and Alkaline pH Region

Yukio SATO, Michio YONEYAMA, and Masahiro HATANO
The Chemical Research Institute of Non-aqueous Solutions, Tohoku University, Sendai
(Received December 10, 1971)

It is well known that an extrinsic optical activity is induced in the region corresponding to the absorption bands of acridine orange (AO) only when the dye combines with helical form of poly-α,-L-glutamic acid (PLGA).[1-3] Myhr and Foss,[4] and Eyring and Yang[5] reported that the Cotton effect could be induced for the complex even at pH 8.0, where the structure of PLGA is regarded to be a random coil form. The cause of the induced circular dichroism (CD) of the PLGA-AO complexes and their structures are, however, not yet completely clarified.

In this communication, we present preliminary results on the optical activities and structures of the complexes in the PLGA-AO system for R/D values smaller than 10. It was found that, in the cases of R/D of around unity, complexes with ordered structures can be formed in the neutral and alkaline pH region.

The complexes were prepared by adding an aqueous solution of AO to that of PLGA with pH of 4.5. The pH of the complex solutions was brought to the desired value by addition of NaOH. The total molarity of AO was fixed at 2×10^{-5} M. The CD curves of these complexes were recorded at several R/D values for various pH. When R/D exceeds 4, the intensity of the induced CD was found to diminish in the neutral and alkaline pH regions. However, the induced CD spectra were observed even in the neutral and alkaline pH regions for R/D of around unity (Fig. 1).

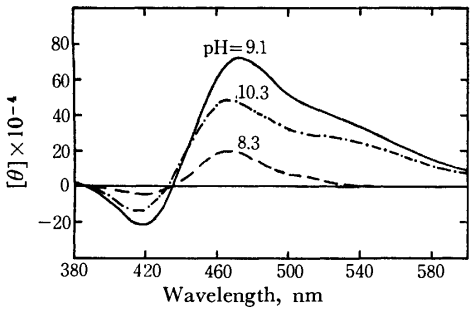

Fig. 1. pH dependence of CD spectra of PLGA-AO system at $R/D=1$.

As shown in Fig. 1, the induced CD which starts to develop at pH of about 6 reaches a maximum intensity at pH of about 9 and diminishes at pH of about 12. It is likely that the induced CD spectra developed in the neutral and alkaline pH regions for the case of R/D of around unity are due to the ordered structures of the complexes.

For the sake of confirmation, we also measured the specific viscosity η_{sp} of PLGA with various degrees of polymerization (DP) at pH of 4.5 and those of PLGA-AO complexes of R/D of unity at pH of 9.0. By means of the following Simha equation, J values were calculated from specific viscosity.

$$\frac{\eta_{sp}}{\Phi} = \frac{J^2}{15(\ln 2J-1.5)} + \frac{J^2}{5(\ln 2J-0.5)} + \frac{14}{15} \qquad (1)$$

where J is the axial ratio of a postulated ellipsoid of the polymer and Φ is the volume fraction of the polymer in the solution. As shown in Fig. 2, J values of PLGA-AO complexes are proportional to the DP of PLGA. These results indicate that PLGA-AO complexes with R/D of unity at pH 9.0 have rigid rod-like structures, *e.g.*, helical structures.

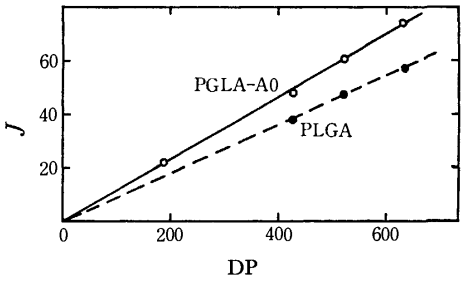

Fig. 2. Simha's J values as a function of degree of polymerization (DP) for PLGA in H_2O (pH 4.5) and PLGA-AO complex of $R/D=1$ in MeOH:H_2O (5:3) (pH 9.0).

In the case of R/D of unity, almost all available AO molecules can be bound to PLGA by ionic bonds between the cationic ring nitrogen atoms of AO molecules and ionized carboxyl groups of the side chains of PLGA in the neutral and alkaline pH regions. As a result of neutralization of the side chains of PLGA by the AO cations, PLGA can be compelled to form a helical structure with AO molecules around it. In the strong alkaline region above the pK_a value of AO,[6] the molecules are deprotonated to be neutral. It seems to be difficult for AO molecules to be bound to PLGA and to stabilize the helical structure of PLGA. Ballard *et al.*[2] inferred, in the case of R/D larger than 20 at pH of 4.5, the presence of a left-handed super-helix of AO molecules around the right-handed helix of PLGA on the basis of a negative CD band polarized parallel to the helix axis at 470 nm. In comparing our results with theirs, we tentatively conclude that AO molecules bound to the carboxylate groups of the side chains of PLGA are arranged to form a right-handed super-helix surrounding the core of the right-handed helix of PLGA, since in this case a positive CD band at about 470 nm is observed.

1) E. R. Blout and L. Stryer, *Proc. Natl. Acad. Sci. U.S.*, **45**, 1591 (1959); E. R. Blout and L. Stryer, *J. Am. Chem. Soc.*, **85**, 1141 (1961).
2) R. E. Ballard, A. J. McCaffery, and S. F. Mason, *Biopolymers*, **4**, 97 (1966).
3) K. Yamaoka and R. A. Resnik, *J. Phys. Chem.*, **70**, 4051 (1966).
4) B. C. Myhr and J. G. Foss, *Biopolymers*, **4**, 949 (1966).
5) E. J. Eyring and J. T. Yang, *ibid.*, **6**, 703 (1968).
6) The pK_a value of ring nitrogen in AO was estimated to be 10.45. (V. Zanker, *Z. Phys. Chem.*, **199**, 225 (1952).)

The Flexibility of the Tribenzylamine Molecule in Both Solution and the Solid State as Revealed by NMR Measurements

Ariyuki AIHARA and Masatoki YOKOI*

Department of Materials Science, Denki-Tsushin University, Chofu, Tokyo

** Department of Chemistry, Faculty of Science, Shinshu University, Matsumoto*

(Received January 7, 1972)

The molecule of tribenzylamine has a possibility of taking a number of conformations due to the intramolecular rotation of the moieties of the molecule about various axes of rotation; there is also the possibility of the molecular inversion of the pyramidal structure of N–$(CH_2)_3$ bonds.[1,2] We have performed NMR measurements of tribenzylamine in the crystalline state as well as in solution in order to get some knowledge about the flexibility of this molecule.

A JNM-4H-100 spectrometer (100 MHz)[3] has been used to measure the high-resolution NMR absorption in the CCl_4 solution, while the measurement of the broad-line NMR was done with a conventional autodyne spectrometer constructed in our laboratory,[4] operating at a frequency of 19.8 MHz (proton) and with a modulating field of 35 Hz superimposed on the main magnetic field.

Despite a presumed complication of the molecular conformation, the NMR spectrum of tribenzylamine dissolved in CCl_4 exhibits only a single sharp absorption signal of methylene protons (δ=3.52 ppm, ref. TMS). This fact suggests that the molecule must be undergoing some flexing motions in such a way that all the protons of methylene groups become magnetically equivalent on the average. In Table 1, the δ values of methylene protons as well as those of phenyl protons are compared with the chemical shift data of mono- and dibenzylamine, and also of dibenzylmethylamine, observed in CCl_4 solutions. The values are all corrected for possible intermolecular interactions by extrapolating the measured δ's at several concentrations to an infinite dilution.

It is interesting to see that the signal of the C_6H_5 protons in tribenzylamine shows somewhat complicated features, with three main peaks at δ=7.16, 7.22, and 7.28 ppm, while those of mono- and dibenzylamine are rather simple. Dibenzylmethylamine seems to behave much like tribenzylamine so far as the chemical shift is concerned.

TABLE 1. THE CHEMICAL SHIFT DATA OF MONO-, DI-, AND TRIBENZYLAMINE, AND ALSO OF DIBENZYLMETHYLAMINE
(in CCl_4 solutions at 25°C; δ in ppm, and the reference is TMS)

Compounds	δ (NH,NH_2,CH_3)	$\delta(CH_2)$	$\delta(C_6H_5)$
$NH_2(CH_2C_6H_5)$	1.21(NH_2)	3.76	7.18
$NH(CH_2C_6H_5)_2$	1.37(NH)	3.74	7.22
$N(CH_2C_6H_5)_3$	—	3.52	7.16, 7.22, 7.28
$N(CH_2C_6H_5)_2CH_3$	2.13(CH_3)	3.47	7.16, 7.22, 7.27

The results of the broad-line NMR measurements add further evidence that this molecule is flexible even in the crystalline state: the magnitude of the second moment at 29°C, 6.23±0.10 Gauss^2 (corrected for modulation broadening after Andrew[5]), is smaller than the theoretical value of the intramolecular contribution to the second moment, 7.38 Gauss^2, which is calculated with the molecular structure data obtained by Drs. Fujiko and Hitoshi Iwasaki from the three-dimensional X-ray crystal structure analysis,[6] assuming the molecule to be rigid in the crystal. It is almost certain, without calculating further the intermolecular contribution to the second moment, that the molecule has some degrees of freedom of motion in the crystal even at room temperature. The width of the absorption spectrum shows a tendency to decrease gradually with the rise in the temperature up to ~70°C.

In view of the bulky molecular structure in a rather loose-packed crystal lattice of tribenzylamine,[6] a tentative calculation has been made of the reduction in the intramolecular contribution to the second moment due to the rotational movement of the phenyl groups about axes joining them to methylene carbons to each other; this rotational motion does not cause any translational shift of the molecule as a whole.

Following the equation introduced by Gutowsky and Pake[7] to correlate the reduction of the second moment due to the rotation of a pair of protons with the angle, γ_{jk}, between the line joining the j and k protons and the axis of rotation;

$$F(\gamma_{jk}) = (3\cos^2\gamma_{jk} - 1)^2/4,$$

we get 5.97 Gauss^2 as the reduced intramolecular contribution to the second moment due to the phenyl-group rotation. This value is slightly less than the observed value of the second moment, 6.23 Gauss^2, the difference being due to the intermolecular contribution to the second moment in a non-rigid lattice. Any intramolecular movements other than that postulated above are improbable, for they would cause a shift of the center of mass of the molecule in the crystal lattice. The details will be published later in this Bulletin.

1) M. J. S. Dewar and W. B. Jennings, *J. Amer. Chem. Soc.*, **93**, 401 (1971).
2) C. H. Bushweller, J. W. O'Neil, and H. S. Bilofsky, *ibid.*, **93**, 542 (1971).
3) Japan Electron Optics Laboratory, Ltd.
4) K. Hayashi and A. Aihara, *Denki-Tsushin Daigaku Gakuho* (Reports of the University of Electro-Communications), **22**, No. 2, 59 (1971).
5) E. R. Andrew, *Phys. Rev.*, **91**, 425 (1953).
6) F. Iwasaki and H. Iwasaki, Papers read at the 25th Annual Meeting of the Chemical Society of Japan, Tokyo (October, 1971).
7) H. S. Gutowsky and G. E. Pake, *J. Chem. Phys.*, **18**, 162 (1950).

A Cation-dependent Conformational Change of the 2,2′:6′,2″-Terpyridine Anion Radical

Kazuo NAKAMURA

Department of Chemistry, Nagoya Institute of Technology, Gokiso-cho, Showa-ku, Nagoya

(Received January 20, 1972)

Although the structure of the ion pair between the aromatic anion radical and the alkali metal cation in solution has been extensively studied by means of ESR and optical spectra, the case in which the conformation of the anion radical varied with the species of the counter cation has not yet been reported. In the present work, the visible spectra of the 2,2′ : 6′,2″-terpyridine anion radical revealed the presence of two species of ion pairs. The solvent and cationic dependence of the equilibrium between the two species indicated that the species can be distinguished by means of the conformation of the anion.

The visible spectrum of the anion radical produced with lithium in tetrahydrofuran (THF) exhibited an absorption maximum in the 610-mμ range, together with a slight shoulder in the 560-mμ range. With the change in the alkali metal in the order of increasing cationic radius, the shoulder was developed at the expense of the peak in the 610-mμ range. In the spectrum of the cesium-produced radical, the intensity in the 560-mμ range exceeded that in the 610-mμ range. The relative intensity of two peaks also depended on the solvent. The use of 2-methyl tetrahydrofuran (MTHF) enhanced the intensity of the peak in the 610-mμ range, while the use of dimethoxyethane (DME) weaken the intensity of the same peak. The maximum in the 610-mμ range almost disappeared in the spectrum of the cesium-produced radical in DME. The spectrum of the radical in dimethylformamide showed a single maximum, at 573-mμ, which was independent of the metal used. This absoprtion certainly arises from the free terpyridine anion. ESR studies of the nitrogen-hetrocyclic anion radicals have proved that those anions existed as ion pairs in an ethereal solvent.[1-5] Each of the two separated bands in the ranges of 560 mμ and 610 mμ should be assigned to one of the structurally-different ion pair. Examples of the spectra are presented in Fig. 1.

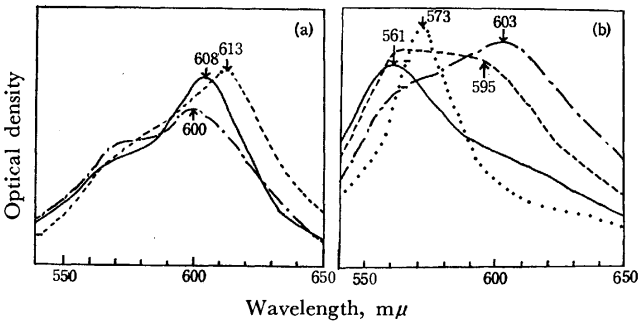

Fig. 1. Visible spectra of the terpyridine anion.
(a): Cationic dependence of the spectra in THF.
----, Li; ——, Na; – – –, Rb.
(b): Solvent dependence of the spectra of the cesium-produced radical.
——, DME; ----, THF; – – –, MTHF; ·····, DMF.
Concentration of the radical, $(1-5)\times10^{-3}$ mol/l.

The repulsions among the nonbonding and antibonding electrons on the three nitrogen atoms of the terpyridine anion keep those atoms far from each other. This situation holds with regard to the conformation of the free terpyridine anion. Three nitrogen atoms are able to coordinate to a cation only when the interaction of the cation with nitrogen atoms is strong enough to compensate for the above repulsions. The interaction of a cation with an anion, especially with the nonbonding electrons on the anion, is intensified by a decrease in the cationic size, while an increase in the solvation of the cation in the order of MTHF<THF<DME[6] weakens such interactions. Both the solvent dependence and the cationic dependence of the relative intensities of the two peaks, therefore, strongly suggested that, in the species exhibiting the peak of the 610-mμ range, the cation is enclosed by three nitrogen atoms and several solvent molecules. When an additional solvent molecule participates this first layer surrounding the cation, one of the nitrogen atoms will become free from coordination to the cation, as is schematically shown in Fig. 2. In such a case, an appreciable change in the spectrum can be expected. The shift of the absorption maximum from the 610-mμ range to the 560-mμ range is due to this conformational change.

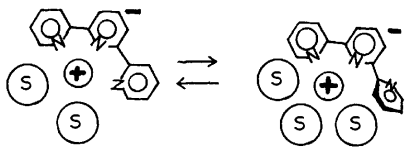

(A) (B)

Fig. 2. Possible structures of the ion pair.
The species with absorption maximum in 610 mμ range (A) and in 560 mμ range (B).

Contrary to the case observed thus far, the increase in the cationic field, which resulted from the decrease in the cationic size or in the solvation of the cation, caused a red shift of the absorption maximum in the 610-mμ range.

1) N. M. Atherton and A. E. Goggins, *Trans. Faraday Soc.*, **61**, 1399 (1965).
2) C. A. McDowell and K. F. G. Paulus, *Can. J. Chem.*, **43**, 225 (1967).
3) J. Dos Santos Veiga and A. F. Neiva Correia, *Mol. Phys.*, **9**, 394 (1965).
4) J. Dos Santos Veiga, W. L. Reynolde, and J. R. Bolton, *J. Chem. Phys.*, **44**, 2214 (1966).
5) Y. Torii, T. Yazaki, Y. Kaizu, and S. Murasato, This Bulletin, **42**, 2264 (1969).
6) T. H. Hogen-Esch and S. Smid, *J. Amer. Chem. Soc.*, **88**, 307 (1966).

Promoting Effect of Zirconium Compound on Catalytic Activity for Oxychlorination of Butadiene

Hiroyuki HAGIWARA and Naoyuki TODO

Government Chemical Industrial Research Institute, Tokyo, Mita, Meguro-ku, Tokyo

(Received January 28, 1972)

It is generally accepted that certain carriers not only display a large exposed surface of active constituent but also modify the catalytic activity or the selectivity of the active agent. It has been suggested that the surface compound can be formed between the carrier and the supported material giving a complex which has better catalytic properties.[1-2] During the course of studies on the catalyst for the oxychlorination of butadiene to get 1,2- or 3,4-dichlorobutene, a material of chloroprene monomer, it was found that the activities of the catalysts we developed, $CuCl_2$-LiCl-H_3PO_4 supported on sintered commercial alumina-silica carriers, depend considerably on the amount of contaminant zirconium compound on the carriers.

This communication reports on some characteristic effects of the zirconium compound on activity. The carriers used were sintered alumina-silica ($S<1 m^2/g$) of low surface area, obtained from Fujimi Kenmazai Kogyo Co. (SNO3) and Tokai Konetsu Kogyo Ltd. (TA124). Their approximate chemical compositions were Al_2O_3-10 wt% SiO_2 containing zirconium to some extent or practically none. The catalysts were prepared by the usual coimpregnation method. The amounts of $CuCl_2$, LiCl, and H_3PO_4 supported were 1.81 wt%, 0.21 wt%, and 0.08 wt%, respectively. The activity was measured by a conventional flow type apparatus at a space velocity of 210 per hour at temperatures 160—250°C. A stoichiometric reactant mixture was used. Prior to the activity measurement, the catalysts were preactivated at 300°C for 3 hours under the atmosphere of nitrogen. It is shown in Table 1 that the conversion of butadiene depends obviously on the zirconium content in the carriers: the catalyst prepared from SNO3 revealed a much higher conversion than that prepared from TA124. Its ability was modified by treating the carrier with a concentrated hydrochloric acid to reduce the zirconium content. The amount of zirconium is optimum when the activity of the catalyst is maximum. Thus, in order to get the quantitative relationship between activity and zirconium content, we measured the activity of a series of catalysts prepared from a carrier impregnated with various amounts of zirconium oxychloride by calcination at 700°C prior to supporting the active components.

TABLE 1. ACTIVITIES OF THE CATALYST PREPARED BY USING VARIOUS CARRIERS

Carrier	Conversion of butadiene (%)	Selectivity to 1,2- and 3,4-dichlorobutene (%)
SNO3	52.1	94.4
SNO3 treated with HCl	73.0	96.2
TA124	15.8	94.8

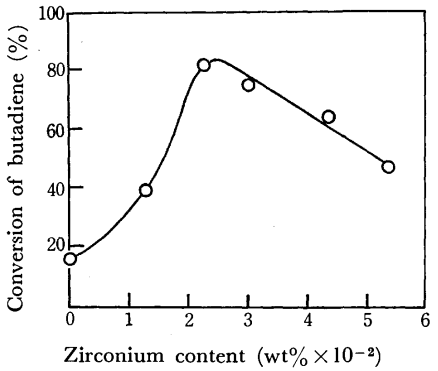

Fig. 1. Effect of zirconium content on the catalytic activity.

We see from Fig. 1 that the addition of an optimum amount of zirconium gave rise to an increase in conversion about five times as high as that obtained without addition of zirconium salts. In contrast, the activity of the catalyst prepared by using silicon carbide as a carrier was not improved by the addition of zirconium salts. The alumina-silica surface might play an important role in cooperation with the zirconium ion for the formation of an active compound composed of $CuCl_2$, LiCl, and H_3PO_4, although neither the structure nor the promoting mechanism of zirconium have been made clear as yet.

1) S. Ogasawara, Y. Nakata, Y. Iwata, and Y. Sato, *Kogyo Kagaku Zasshi*, **73**, 509 (1970).

2) T. Sukeno, M. Mimura and H. Nomura, *ibid.*, **68**, 1838 (1965).

3*H*-2,1-Benzoxathiole-1,1-dioxide, an Unusual By-Product from the Jacobsen Reaction[1]

Hitomi Suzuki and Kiyoshi Kawamura

Department of Chemistry, Faculty of Science, Kyoto University, Sakyo-ku, Kyoto

(Received March 13, 1972)

Since the discovery of the non-conventional chlorination of hexamethylbenzene,[2] substitution on the alkyl side-chain of polyalkyl aromatics under ionic conditions has been a problem of interest. However, the character and scope of the unusual reaction have not yet fully been understood because of the paucity of relevant findings.[3] We would like to report on an example of anomalous substitution product, 3*H*-2,1-*benzoxathiole*-1,1-*dioxide*, which has been obtained from the Jacobsen reaction of some dichloroxylenes and monochlorotrimethylbenzenes.

2,5-Dichloro-*p*-xylene was dissolved in 20%-fuming sulfuric acid and the dark mixture was kept at 65—70°C for 14 hr to complete isomerization. Quenching with water, extraction of the insoluble part with ether and the subsequent removal of the solvent gave a light brown crystalline solid which was recrystallized from ethanol to yield white needles (*ca.* 1—2%), mp 170—171°C. The elemental analysis was in good agreement with the composition $C_8H_6Cl_2O_3S$ (M= 253; Found: C, 37.98; H, 2.30; O, 19.24; S, 12.34%. Calcd for $C_8H_6Cl_2O_3S$: C, 37.94; H, 2.37; O, 18.97; S, 12.65%); its mass spectrum showed revealing fragment ion peaks at *m/e* 252, 187, 176, 159, 141, and 125. Its infrared spectrum (KBr disk) contained absorptions at 755, 870, 896, 975, 1120 (CH_2–O), 1191 (SO_2), 1242, 1278, 1358 (SO_2), and 1453 cm^{-1}. Its ^1H NMR spectrum (100 MHz, $CDCl_3$) exhibited three singlet peaks at 7.51 (CH_3), 4.60 (CH_2), and 2.45 τ (aromatic H) of relative intensities 3 : 2 : 1. The elemental analysis and spectral data were compatible only with the structure of dichloro-methyl-3*H*-2,1-benzoxathiole-1,1-dioxide, and ^1H NMR spectral comparison with the reference compounds allowed for the ring substituents to be arranged as shown in formula I (R=R′ ′=Cl, R′=CH_3). Similar products were obtained from 4,5-dichloro-*o*-xylene and 4,6-dichloro-*m*-xylene in a smaller amount.

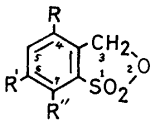

(I)

Ease of the formation of the cyclic ester seems to depend on the orientation of substituents. Thus, 5-chloropseudocumene gave a mixture of three isomeric sultones, of which 4-chloro-6,7-dimethyl-3H-2,1-benzoxathiole-1,1-dioxide (I, R=Cl, R′=R″ =CH_3) was the major component, while chloromesitylene and 5-chlorohemimellitene did not afford any detectable amount of ester but were mostly converted into intractable polymeric substance. Some physical properties of these cyclic esters are summarized in the Table. A noteworthy feature of these products is the preferential sulfo-oxylation on the methyl group attached to the more positively polarized ring carbon ortho to chlorine atom. Similar trends have been observed in the diarylmethane formation,[4] as well as the side-chain nitro-oxylation of polyalkylbenzene derivatives.[5] The sultones were usually formed in a small amount and their separation from the accompanying polymeric by-product was often troublesome. The cyclic ester may share the intermediate with diarylmethane,[6] but the mode of its formation is not clear at present.

Table 1. Physical properties of some 3*H*-2,1-benzoxathiole-1,1-dioxides formed in the Jacobsen reaction of dichloroxylenes and monochlorotrimethylbenzenes[a]

3*H*-2,1-Benzoxathiole-1,1-dioxide (I)			Mp (°C)	^1H NMR spectra ($CDCl_3$, τ)		
R	R′	R″		Aromatic H	CH_2	CH_3
CH_3	Cl	Cl	205—211	2.45	4.65	7.73
Cl	Cl	CH_3	213—214	2.36	4.64	7.40
Cl	CH_3	CH_3	172—173	2.53	4.60	7.75 7.40
CH_3	Cl	CH_3		2.53	4.60	7.60 7.47
CH_3	CH_3	Cl		2.63	4.67	7.57 7.57

a) The orientation of substituent groups has been assigned on the basis of ^1H NMR spectral comparison with reference compounds.

1) The Reaction of Polysubstituted Aromatics. Part XXVIII. Part XXVII: This Bulletin, **45**, in press (1972).

2) E. Baciocchi, A. Ciana, G. Illuminati, and C. Pasini, *J. Amer. Chem. Soc.*, **87**, 3953 (1965).

3) Formation of the side-chain substituted products has so far been reported in the nitration, chlorination, bromination, sulfonation and positive hydroxylation of certain polyalkylbenzenes and their derivatives.

4) H. Suzuki, This Bulletin, **42**, 2618 (1969).

5) H. Suzuki and K. Nakamura, *ibid.*, **44**, 227 (1971); H. Suzuki, K. Nakamura, and M. Takeshima, *ibid.*, **44**, 2248 (1971).

6) H. Suzuki and Y. Tamura, *Chem. Commun.*, **1969**, 244.

A Free Radical Mechanism for the Formation of Zinc-Carbenoid Reagent from Diethylzinc and Chloroiodomethane

Sotaro MIYANO, Junzo YAMASHITA, and Harukichi HASHIMOTO
Department of Applied Chemistry, Faculty of Engineering, Tohoku University, Aramaki, Sendai

(Received February 28, 1972)

Chloroiodomethane is useful as a methylene source for the cyclopropanation of olefins by the oxygen catalyzed zinc-carbenoid reaction.[1] Cyclohexene (99%), cyclooctene (99%), 1-heptene (79%), 2-heptene (94%), and 1-octene (88%) gave the corresponding cyclopropane in the yields given in parentheses.

We wish to present the possibility of a radical mechanism for the formation of the zinc-carbenoid reagent from diethylzinc and chloroiodomethane. Chloroiodomethane (38 mmol) was allowed to react with diethylzinc (25 mmol) in the presence of styrene (25 mmol) in benzene (20 m*l*) at 50°C under nitrogen atmosphere. The starting materials were recovered unchanged after 3 hr indicating that no reaction took place. By passing oxygen into the space above the reaction mixture at a rate of 10 m*l*/min, chloroiodomethane completely reacted within 1.5 hr giving phenylcyclopropane in 66% yield. When oxygen was introduced just after the addition of chloroiodomethane, the reaction was also completed within 1.5 hr giving phenylcyclopropane in 70% yield. AIBN and UV light also catalyzed the cyclopropanation of styrene (Table 1). Without diethylzinc, chloroiodomethane did not cyclopropanate styrene in the presence of AIBN or UV light, though peroxides[2] or UV light[3] catalyzed the cyclopropanation of olefins with diiodomethane.

TABLE 1. CYCLOPROPANATION OF STYRENE[a]

Catalyst	Reaction		Phenylcyclopropane
	Time (h)	Temp (°C)	Yield (%)
—[b]	3	50	0
—	4	70	0
—	7	70	3.7
Oxygen[b]	1.5	50	70
AIBN[c,d]	2	70	46
AIBN[c]	4.5	70	22
UV light[e]	1.5	23	73

a) Reactions were carried out under nitrogen atmosphere. Styrene 50 mmol; CH_2ClI 60 mmol; Et_2Zn 50 mmol; benzene 50 m*l*.
b) Styrene 25 mmol; CH_2ClI 38 mmol; Et_2Zn 25 mmol; benzene 20 m*l*.
c) AIBN 2.5 mmol.
d) CH_2ClI 94 mmol.
e) In 150 m*l* of benzene. High pressure mercury lamp (100 W) was used.

When a mixture of styrene, chloroiodomethane and diethylzinc in *n*-hexane was irradiated with a UV light at −70°C, chloroiodomethane reacted with diethylzinc with the formation of ethyl iodide in equivalent amount to the reacted chloroiodomethane, while styrene remained unchanged. When the light was turned off and the reaction mixture was allowed to stand at room temperature, an exothermic reaction took place, and phenylcyclopropane was obtained in 50% yield within 1 hr. This indicates the following reaction sequences (R=Et or CH_2Cl);[4]

$$ClCH_2I + Et_2Zn \xrightarrow{\text{Initiator or } h\nu} \underset{\text{(I)}}{ClCH_2ZnEt} + EtI$$

$$CH_2ClI + \text{(I)} \xrightarrow{\text{Initiator or } h\nu} \underset{\text{(II)}}{(ClCH_2)_2Zn} + EtI$$

$$\text{(I) or (II)} + PhCH{=}CH_2 \rightarrow Ph\text{-}\triangleleft + ClZnR$$

There are evidences that ethyl radical is formed by the reaction of diethylzinc with oxygen[6] or by the decomposition of AIBN in the presence of diethylzinc.[7]

This suggests that the zinc-carbenoid reagent is formed via free radical processes from diethylzinc and chloroiodomethane. The methylene transfer step from the zinc-carbenoid reagent to olefins seems to be a conventional, one-step and three-centered carbenoid reaction if we consider the stereospecific methylene addition to 2-heptenes, the absence of C–H insertion products, and the fact that the formed zinc-carbenoid reagent can cyclopropanate styrene without any free radical catalyst.

1) S. Miyano and H. Hashimoto, *Chem. Commun.*, **1971**, 1418.
2) L. Kaplan, *J. Amer. Chem. Soc.*, **89**, 4566 (1967).
3) D. C. Blomstrom, K. Hering, and H. E. Simmons, *J. Org. Chem.*, **30**, 959 (1965).
4) ICH_2ZnEt and $(ICH_2)_2Zn$ are said methylene transferring reagent for the zinc-carbenoid reaction with diethylzinc and diiodomethane.[5]
5) J. Furukawa, N. Kawabata, S. Taniguchi, and J. Nishimura, *Kogyo Kagaku Zasshi*, **72**, 1674 (1969).
6) A. G. Davies and B. P. Roberts, *J. Chem. Soc., B*, **1968**, 1074.
7) T. Hirano, T. Miki, and T. Tsuruta, *Makromol. Chem.*, **104**, 230 (1967).

Dimerization and Electronic Absorption Spectra of Tetracyanoethylene Anion in Solution and in Solid

Michiya Itoh

Faculty of Pharmaceutical Sciences, The University of Tokyo, Bunkyo-ku, Tokyo 113

(Received May 6, 1971)

The 2-methyltetrahydrofuran solutions of several alkali tetracyanoethylenides (M^+, $TCNE^-$, where M=Na, K, Rb, and Cs) show strong visible absorption spectra at low temperature which might be considered to be charge-transfer bands between two TCNE anions. Temperature dependence of the electronic absorption and ESR spectra of $TCNE^-$ in solution yields the monomer-dimer equilibrium of the TCNE anion. The heat of dimer formation of the anion was found to decrease in the order $Na^+ > K^+ > Rb^+ > Cs^+$ with the size of the counter ions. The heat of dimer formation in $Na^+(TCNE)^-$ also depends considerably on the solvent system. The absorption spectra of the solid TCNE anions were found to resemble the spectrum of the TCNE anion dimer $(TCNE^-)_2$ in solution to a great extent. A comparison of the electronic absorption and ESR spectra of $M^+(TCNE)^-$ in solution and in solid demonstrates that the solid $TCNE^-$ is almost diamagnetic, and the anion dimer can be the unit of structure in the solid salts.

Numerous studies were carried out on the electronic and magnetic properties of radical dimer $(TCNQ^-)_2$ and dimer radical $(TCNQ)_2^-$ of 7,7,8,8-tetracyanoquinodimethane anion $(TCNQ)^-$ in solution[1] and in solid[2-4]. However, few spectroscopic studies of the TCNE anion dimer have been reported since the first preparation of the solid TCNE anion by Webster *et al.*[5] Phillips and Powell[6] suggested complex formation taking place between the TCNE anion and its parent molecule $(TCNE)_2^-$ on the basis of the reversible color change of the THF solution with decreasing temperature. In a previous paper,[7] the present author erroneously proposed the formation of the dimer radical in the MTHF solution at low temperature by means of electronic absorption spectroscopy for which a MTHF solution of TCNE anion containing neutral TCNE was used. Subsequently, the author came to observe the electronic absorption spectra of the solid TCNE anion, ($M^+(TCNE)^-$, M=Na, K, Rb, and Cs), which were very similar to the low temperature spectra of the MTHF solution of $TCNE^-$. Recently, Chang[8] has proposed the formation of the TCNE anion dimer in MTHF by ESR spectroscopy.

The author investigated the solid TCNE anion, and reinvestigated the anion in solution by both optical and ESR spectroscopies. The results indicate the formation of the radical dimer in solution at a low temperature, and suggest that the dimer of $TCNE^-$ can be the unit of structure in solid $M^+(TCNE)^-$. The heat of dimer formation of $TCNE^-$ depends largely on the counter cation (Na^+, K^+, Rb^+, and Cs^+) and also on the solvent composition. The electronic absorption spectra of $TCNE^-$ and $(TCNE^-)_2$ were discussed.

1) R. H. Boyd and W. D. Phillips, *J. Chem. Phys.*, **43**, 2927 (1965).
2) D. B. Chesnut, H. Foster, and W. D. Phillips, *ibid.*, **34**, 684 (1961).
3) D. B. Chesnut and W. D. Phillips, *ibid.*, **35**, 1002 (1961).
4) R. G. Kepler, *ibid.*, **39**, 3528 (1963).
5) O. W. Webster, W. Mahler, and R. E. Benson, *J. Amer. Chem. Soc.*, **84**, 3678 (1962); *J. Org. Chem.*, **25**, 1470 (1960).
6) W. D. Phillips and J. C. Powell, *J. Chem. Phys.*, **33**, 626 (1960).
7) M. Itoh, *J. Amer. Chem. Soc.*, **92**, 886 (1970).
8) R. Chang, *J. Phys. Chem.*, **74**, 2029 (1970).

Experimental

Preparation and Materials. To a degassed acetonitrile solution (~8 ml) of TCNE (~0.3 g) was added NaCN or KCN (~1.5 g) in a sealed vessel. The dark brown reaction solution was stirred on a magnetic stirrer at 5°C for 3—4 days. The reaction mixture was filtered through a glass filter, and the solvent (CH_3CN) was removed by vacuum evaporation. The solid residue was washed two or three times with THF (~5 ml). Dark brown or black solid $Na^+(TCNE)^-$ or $K^+(TCNE)^-$ was obtained. Each procedure was performed in a sealed glass vessel in a vacuum.

$Rb^+(TCNE)^-$ and $Cs^+(TCNE)^-$ were prepared by the same procedures as for $Na^+(TCNE)^-$ from RbI and CsI, respectively. The compositions of the solid salts were confirmed by the elementary analysis of carbon and nitrogen.

$M^+(TCNE)^-$ film was prepared in a quartz optical cell (1 mm or 1 cm) by vacuum evaporation of the solvent from the CH_3CN solution of the salt. Reddish blue or purple film was obtained.

Purification of the solvent was carried out in the same manner as described previously.[7]

Measurements. Electronic absorption spectra were determined with a Cary recording spectrophotometer Model 11. However, spectroscopic study of the monomer-dimer equilibrium was made on a Beckman DK-2U spectrophotometer.[7] All the ESR measurements were made on a JEOLCO P-10 ESR spectrometer (100 kc modulation) with a variable temperature equipment.

Results and Discussion

Electronic Absorption Spectra and ESR in Solid TCNE Anion. Since Webster *et al.*[5] reported the solid formation of metal tetracyanoethylenides from an acetonitrile solution of TCNE and metal iodide or cyanide, few spectroscopic studies of the solid TCNE anion have been reported. This seems to be due to the fact that the preparation of solid $M^+(TCNE)^-$ is more difficult than that of the 7,7,8,8-tetracyanoquinodimethane anion or Würster's salt. In this work, electronic absorption spectra of the pure samples of $M^+(TCNE)^-$ were determined in film and in KBr pellet. The spectra of the solid salts in KBr pellets, shown in Fig. 1, are almost unaltered by changing

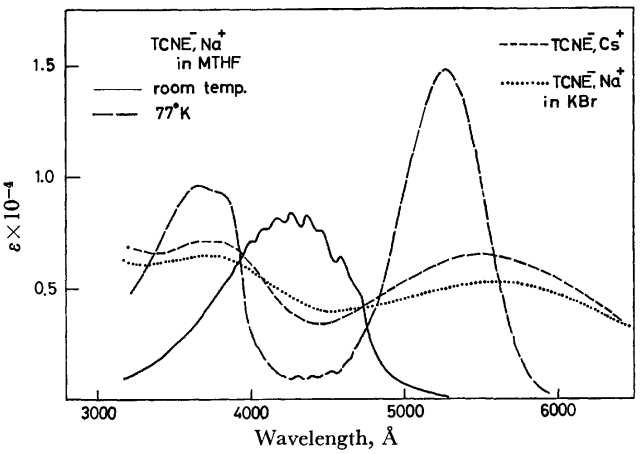

Fig. 1. Electronic absorption spectra of the solid TCNE anions in KBr pellets, and of the MTHF solution of $Na^+(TCNE)^-$ at room temperature and at liquid nitrogen temperature. The ordinate for the spectra of the solid salts is in an arbitary scale.

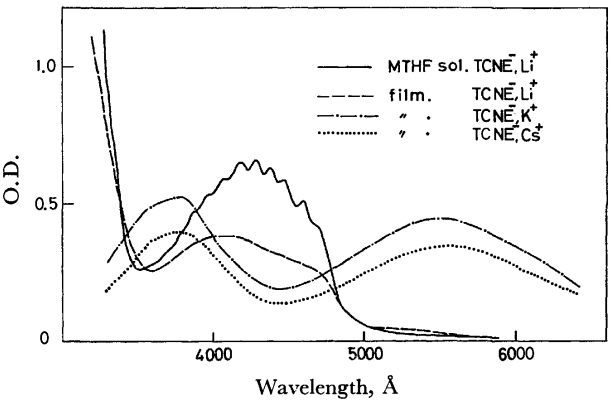

Fig. 2. Electronic absorption spectra of $M^+(TCNE)^-$ (M= Li, K, and Cs) in films at room temperature, and of the MTHF solution of $Li^+(TCNE)^-$ at room temperature.

M^+. It is noteworthy that these spectra of solid $M^+(TCNE)^-$ are differ remarkably from those in solution at room temperature, but are similar to the low temperature spectra (77°K) of the anion in MTHF.

Chesnut and Phillips[3] explained the temperature dependence of ESR intensity of the solid $Na^+(TCNE)^-$ by a singlet-triplet model with $J=0.26$ eV. The apparent relative concentration of paramagnetic species in the solid $M^+(TCNE)^-$ (Na^+, K^+, Rb^+, and Cs^+) were determined to be only 0.1—0.01 mol%. In powdered sample of the solid $M^+(TCNE)^-$, apparent relative concentration of paramagnetic species showed a slight change with temperature (123—380°K). It seems that this paramagnetic species in the salt is impurity or one with defect in solid.

The absorption spectrum of $Li^+(TCNE)^-$ in film, shown in Fig. 2, was determined to be similar to that in solution at room temperature. No significant temperature dependences were observed with the ESR and absorption spectra in the MTHF solution of $Li^+(TCNE)^-$. Thus $Li^+(TCNE)^-$ is considered to be monomeric both in solid and in solution even at a low temperature. Repeated attempts of preparation and isolation of the solid $Li^+(TCNE)^-$ failed.

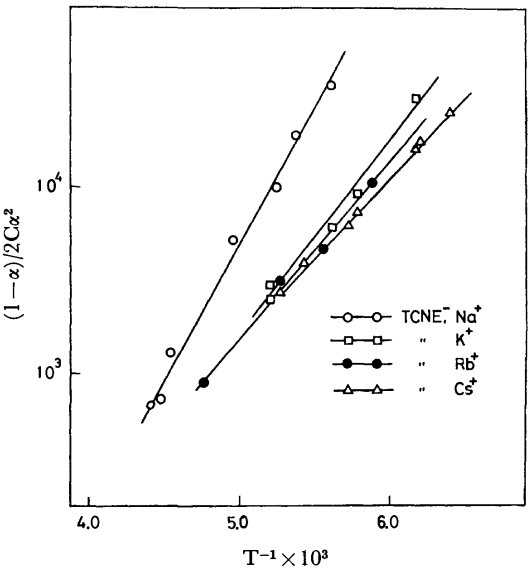

Fig. 3. Plots of log $(1-\alpha)/2C\alpha^2$ against 1/T in the MTHF solutions of $M^+(TCNE)^-$.

Monomer-Dimer Equilibrium Determined by ESR. A procedure similar to that for the investigation of the dimerization of Würster's cation by Kawamori *et al.*[9] was applied to the temperature dependence of ESR signal strength in the MTHF solution of $M^+(TCNE)^-$. Monomer-dimer equilibrium constant $K=K_0\exp(-\Delta H/RT)=(1-\alpha)/2C\alpha^2$, where C is the concentration of the TCNE anion and α is the fractional concentration of the monomer at a certain temperature, which is given by IT/C; I is the relative ESR intensity. Figure 3 shows the plots of log $(1-\alpha)/2C\alpha^2$ against $1/T$ in the MTHF solutions of the Na, K, Rb, and Cs salts. The slope of the straight line which suggests the dimerization of $TCNE^-$ gave the heat of dimer formation. The results are summarized in Table 1.

Table 1. Heat of dimer formation of $M^+(TCNE)^-$

M^+	Na^+	K^+	Rb^+	Cs^+
$-\Delta H$, kcal	7.1	4.8	4.3	4.0

Values of $-\Delta H$ (*l*/mol) depend considerably on the counter ion in the order $Na^+>K^+>Rb^+>Cs^+$. The value of $-\Delta H$ obtained in $Na^+(TCNE)^-$ (7.1 kcal) agrees well with that obtained by Chang (8 kcal), and is comparable to the value (10 kcal) obtained by Boyd and Phillips for the dimerization of $TCNQ^-$ in an aqueous solution. If the difference of solvent system in the formation of $(TCNE^-)_2$ and $(TCNQ^-)_2$ is taken into account, $-\Delta H$ might be smaller in the former.

Reinvestigation of the Monomer-Dimer Equilibrium by Electronic Absorption Spectra. The absorption spectra of the MTHF solution of $Na^+(TCNE)^-$ (analytically pure) were determined at room temperature and at 77°K, as shown in Fig. 1. A strong absorption band at 5400 Å region was tentatively assigned to be a charge-transfer band between two TCNE anions. This

9) A. Kawamori, A. Honda, K. Suzuki, and Y. Ooshika, *J. Chem. Phys.* **44**, 4363 (1966).

absorption at low temperature was confirmed to be independent of the neutral TCNE by the addition of TCNE to the solution of anion. The previous results[7] were reinvestigated by assuming the monomer-dimer equilibrium of $TCNE^-$ at low temperature. Itoh and Nagakura[10] demonstrated the dimerization of the substituted pyridinyl radicals by means of the equation $\log K = \log \varepsilon \cdot \varepsilon_d / 2a(\varepsilon_d - \varepsilon)^2$, where K is equilibrium constant of dimerization and a is stoichiometric concentration of the monomer; a was determined from optical absorbance at 4500 Å of the MTHF solution of $M^+(TCNE)^-$ at room temperature, assuming the TCNE anion to be entirely monomer at room temperature. The values, ε and ε_d are apparent absorption coefficient and molar absorption coefficient of the absorption maxima at 5400 Å at various temperatures, respectively. The absorption of monomer at 5400 Å region was neglected. If $TCNE^-$ in a considerably concentrated solution of MTHF is assumed to be in the dimer form $(TCNE^-)_2$ at 77°K (see Fig. 1), ε_d is evaluated to be 15,000 at 77°K. However, while the oscillator strength (f-value) of the absorption band of the dimer was assumed to be independent of temperature, ε_d at absorption maxima gradually increased but a half-width decreased with decreasing temperature, as shown in Fig. 4.

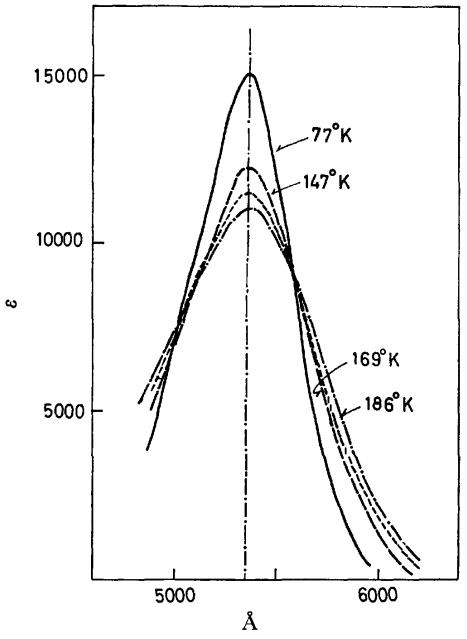

Fig. 4. Temperature dependence of the molar absorption coefficient, ε_d, of the charge-transfer band in $(TCNE^-)_2$, determination of which was made as follows. The molar absorption coefficient ($\varepsilon_{d_{77}}$) and intensity (I_{77}) at 77°K were evaluated by assuming that Na^+ $(TCNE)^-$ in a highly concentrated solution (MTHF) was entirely dimeric at 77°K. The absorption spectra of the MTHF solution of the salts were measured at several temperatures. Apparent absorbance (ε_d') and intensity (I') of the charge-transfer band were determined at a certain temperature. The molar absorption coefficient (ε_d) at a certain temperature was obtained by the equation $\varepsilon_d = \varepsilon_d' \cdot I_{77}/I'$, where the integrated intensity ($I \propto f$-value) of charge-transfer band was assumed to be independent of temperature.

10) M. Itoh and S. Nagakura, *J. Amer. Chem. Soc.*, **89**, 3959 (1967).

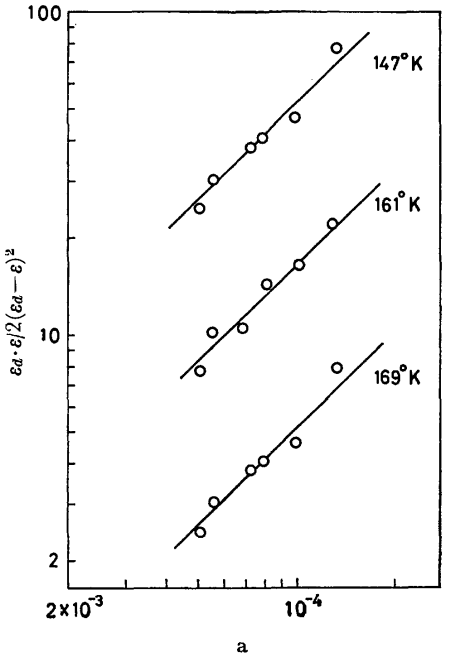

Fig. 5. Plots of $\log \varepsilon \cdot \varepsilon_d/2\ (\varepsilon_d-\varepsilon)^2$ against $1/T$ in the MTHF solution of Na^+ $(TCNE)^-$ at various temperatures.

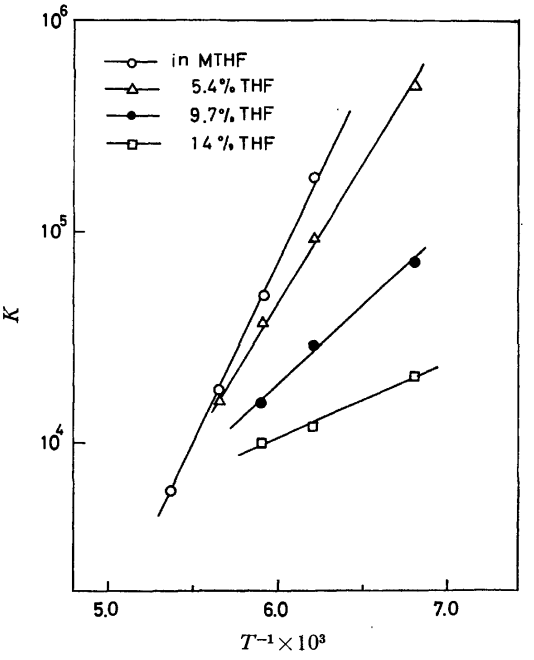

Fig. 6. Temperature dependence of the monomer-dimer equilibrium constant K in MTHF and THF-MTHF mixed systems.

Using ε_d obtained at several temperatures, straight lines close to a slope were obtained in the plots, $\log \varepsilon \cdot \varepsilon_d/2(\varepsilon_d-\varepsilon)^2$ against $\log a$, as shown in Fig. 5. The slope=1 suggests the monomer-dimer equilibrium of $TCNE^-$ at various temperatures. Equilibrium constant K (l/mol) at several temperatures was obtained by a least-squares fit. Figure 6 shows temperature dependence of K in the MTHF and MTHF-THF mixed systems. Heats of dimer formation for $Na^+(TCNE)^-$ were obtained from slopes of the straight lines of each solvent system. The results are sum-

Table 2. Thermodynamic data for the formation of $(Na^+)_2$ $(TCNE^-)_2$ by means of electronic absorption spectroscopy

Solvent	MTHF	5.4% THF	9.6% THF	14.5% THF
K, mol^{-1} (169°K)	5.0×10^4	3.6×10^4	1.5×10^4	1.0×10^4
$-\Delta H$, kcal	7.6	5.7	3.4	1.8
ΔS, eu	−11.8	−6.5	−0.5	3.7

marized in Table 2. As for $Na^+(TCNE)^-$ in MTHF, the value of $-\Delta H$ obtained by absorption spectroscopy was in good agreement with that obtained by ESR, as shown in Tables 1 and 2. However, the values of K corresponding to log $(1-\alpha)/2C\alpha^2$ in Fig. 3 show considerable deviation from those of absorption spectra. Although $-\Delta H$ obtained by ESR might be fairly accurate, the values of K by ESR seem to be much less accurate than those by absorption spectra. The value, $-\Delta H$ in $Na^+(TCNE)^-$ is largely dependent upon the solvent system (Table 2). When MTHF was mixed with a small amount of THF which is more polar than MTHF, $-\Delta H$ decreased remarkably while the entropy change increased. The decrease in $-\Delta H$ and the increase in ΔS (from large minus to plus) with increasing solvent polarity were observed in the dimer formation of the ketyl radicals reported by Hirota and Weissman.[11] These results seem to be attributed to the greater solvation in monomer than in dimer.

Electronic Absorption Spectra of Monomer and Dimer of TCNE$^-$. The MTHF solution of $TCNE^-$ shows a broad absorption spectrum with a vibrational structure at 3600—4700 Å region. From the shape of absorption, it seems that the absorption spectrum of $TCNE^-$ at 3600—4700 Å region consists of two electronic transitions. This is supported by an open shell SCF MO calculation of $TCNE^-$. The observed and calculated data are summarized in Table 3.

From the experimental results of $TCNE^-$ both in solution and in solid, it is clearly seen that the strong absorption spectrum at 5300—5500 Å region and another absorption at 3500—4000 Å region are attributed to the dimer. From the standpoint of charge-transfer interaction in the radical dimer, the visible absorption at ~5400 Å observed for the TCNE anion dimer can be interpreted to be the charge-transfer band between two $TCNE^-$ and the shorter wavelength absorption with two maxima is ascribed to the shifted local excitations.

Table 3. Observed and calculated electronic transition energies and oscillator strengths (f-values)

Obsd		Calcd	
E(eV)	f	E(eV)	f
2.7, 2.8	0.21	2.2	0.11
		2.4	0.08
—	—	3.4	0.42

The electronic absorption spectra of the solid $M^+(TCNE)^-$ were found to greatly resemble the spectra of the dimer in solution. The magnetic and optical properties of the solid salt suggest that the TCNE radical dimer is the unit of structure in the solid state where the spin exchange interaction in the dimer is extremely great in a considerably wide range of temperature (123—380°K) in comparison with those of Würster's salt,[12-14] ethylphenazyl[15] and other radical salts.[3,4,16]

The author wishes to express his sincere thanks to Professor R. S. Mulliken for giving him the opportunity to work at the University of Chicago where a part of this work was done. He wishes to thank Professor S. Nagakura for reading the manuscript. Thanks are also due to Dr. S. Iwata, the Institute of Physical and Chemical Research, for computation of the open shell SCF MO of TCNE anion.

11) N. Hirota and S. I. Weissman, *J. Amer. Chem. Soc.* **89**, 2538 (1964).

12) D. D. Thomas, H. Keller, and H. M. McConnell, *J. Chem. Phys.*, **39**, 2321 (1963).

13) T. Sakata and S. Nagakura, This Bulletin, **43**, 2414 (1970).

14) See references cited in 12.

15) T. Sakata and S. Nagakura, This Bulletin, **42**, 1497 (1969).

16) Y. Sato, M. Kinoshita, M. Sano, and H. Akamatu, *ibid.*, **42**, 3051 (1969); *ibid.*, **42**, 548 (1969).

Photo-decoloration Process of the Reverse Photochromic Spirans

Eiichi INOUE, Hiroshi KOKADO, Isamu SHIMIZU, Hajime KOBAYASHI, and Yohnosuke TAKAHASHI

Imaging Science and Engineering Laboratory, Tokyo Institute of Technology, Ookayama, Meguro-ku, Tokyo

(Received July 30, 1971)

The unstable colorless form (A′) of the reverse photochromic spiran (SP-3) (1,3,3-trimethyl-5-methoxyspiro[indoline-2,2′-benzopyran]-8′-carboxylic acid) was obtained in a stable state by vacuum evaporation (10^{-5} Torr) on a KBr substrate. It was confirmed by IR spectral analysis that reverse photochromism occurred between the colored (B′; merocyanine-like structure) and the colorless forms (A′; spiropyran). A colorless transient intermediate (X) was observed in the photo-decoloration process of the (SP-3). X was transformed into both A′ and B′. Thus the photo-decoloration efficiency ($\phi_{B'\to A'}$) depends on the ratio of the conversion from X to A′. State (B′) is stabilized in a polar or proton donative solvent. The life time of X is greatly influenced by the solvent as well as the stability of B′. The photo-decoloration efficiency ($\phi_{B'\to A'}$) of the spirans is effectively improved by substituting SP-2 with (methoxyl group) at 5-position. Whether X is observable or not depends on the substituent and its position. The reversibility of photochromic cycle of the spirans was restricted by the photobleaching of B′ by UV irradiation. It was observed that the photo-bleaching of B′ is accelerated in a degassed solution.

Derivatives of 1,3,3-trimethylspiro[indoline-2,2′-benzopyran] (SP-1) are well-known photochromic materials.[1]

The mechanism and kinetics of photo-coloration of spirans have been studied,[2] but detailed discussions on photo-decoloration process do not seem to have been made. This might be due to the unstability of the colored species of the photochromic spirans. It has been found that a compound substituted with –COOH at 8′-position (SP-2) exhibited reverse photochromism.[3] The colored form is more stable than the spiran form. The photo-induced bleaching of SP-2 and its derivatives were studied by means of flash photolysis.

The structure of the colored species of the reverse photochromic spirans is like that of a merocyanine dye, the colored form of the normal photochromic spirans. The color changes corresponding to the intramolecular transformation as follows.

(a) normal photochromism

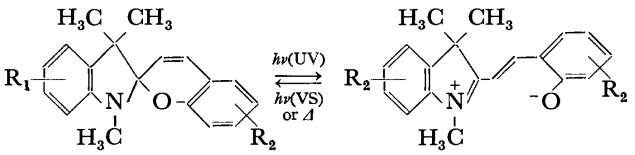

(A′) (B′)

Stable, colorless Unstable, colored

(b) reverse photochromism

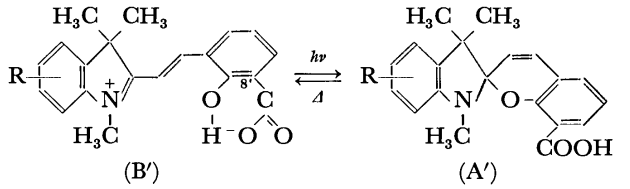

(B′) (A′)

Stable, colored Unstable, colorless

Symbols A′ and B′ denote the colorless and the colored forms, respectively.

The existence of a colorless transient intermediate (X) was observed during the photo-decoloration of a reverse photochromic spiran (SP-3). In this paper, we propose a reaction scheme for the photo-decoloration process of the spirans.

We also describe the influence of both solvents and substituents on the photo-transformation and the effect of oxygen on the reversibility of the reverse photochromic process.

Experimental

Experiments were carried out with a set of flash spectrographic instrument (USHIO UFP-1). The half width of flash was 18 μsec with a power of 200 Joule/pulse. A quartz cell, 7 mmφ and 100 mm thick, was used at room temperature. The temperature of the solution during the measurement was kept constant in a range 5—60°C by using a doubly sealed quartz tube, in which water at constant temperature is circulated from a thermoregulated bath (Fig. 1).

The spirans are listed in Table 1. The photo-decoloration efficiency ($\phi_{B'\to A'}$) was obtained at a sufficiently low temperature (−40°C) to avoid thermal recoloration during measurements.

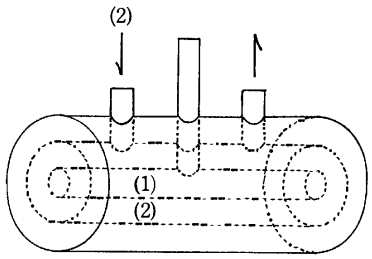

Fig. 1. Doubly sealed tube cell for measurement of flash photolysis at constant temperature.
1) sample solution, 2) circulated water

Results and Discussion

Molecular Structures of Colored and Colorless Forms of Reverse Photochromic Spirans. Reversible color change (photochromism) of spiropyrans has been confirmed to

1) Y. Hirshberg and E. Fischer, *J. Chem. Soc.*, **1954**, 297; R. Heiligman-Rim, Y. Hirshberg, and E. Fischer, *ibid.*, **1961**, 156.

2) N. W. Tyer, Jr. and R. S. Becker, *J. Amer. Chem. Soc.*, **92**, 1289 (1970).

3) I. Shimizu, H. Kokado, and E. Inoue, This Bulletin, **42**, 1730 (1969).

TABLE 1. REVERSE PHOTOCHROMIC SPIRANS

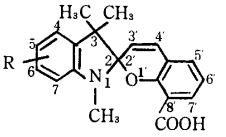

No	Substituent, R
SP-2	H
SP-3	5-CH_3O
SP-4	4-CH_3O
SP-5	6-CH_3O
SP-6	5-Br
SP-7	5-CH_3CONH
SP-8	β-naphtho
SP-9	7-CH_3O
SP-10	5-Cl

be induced from intramolecular transformation between colorless spiropyran (A′) and colored merocyanine (B′) by irradiation of light. The colored form was formed on the rupture of C_{spiro}–O bond.

The photo-generated colored form (B′) was unstable, and the color diminished spontaneously when illumination was stopped. SP-1 substituted by –COOH at 8′-position (SP-2) and its derivatives are known to be "reverse photochromic" spirans. The colored form (B′) was more stable than the colorless one (A′) and was converted into A′ by irradiation with visible light. The color reappeared gradually when illumination was stopped.

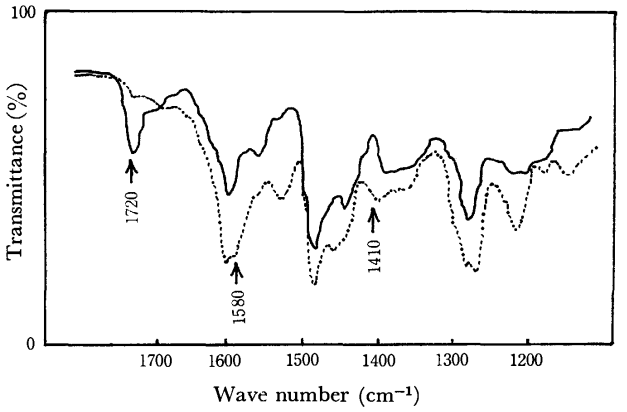

Fig. 2. I.R. spectra of the evaporated film of (SP-3) in the colorless and colored species on KBr.
(a): ——colorless (b): ·····colored

When a layer of SP-3 (1,3,3-trimethyl-5-methoxy spiro[indoline-2,2′-benzopyran]-8′-carboxylic acid) was formed on a KBr crystal surface by vacuum evaporation, its (A′) state was preserved for a long time at room temperature. The IR spectra of A′ and B′ forms of SP-3 are shown in Fig. 2. The spectrum (a) almost coincided with that of the colorless form of SP-1 except for the bands at 1720 cm^{-1} and 3000—4000 cm^{-1} which are assigned to –COOH group. The colorless film on KBr crystal became gradually colored in the dark, and the IR spectrum was also transformed from (a) to (b) in the colored form. The band at 1720 cm^{-1} in (b) diminished and new bands due to CO_2^- appeared at 1580 cm^{-1} and 1410 cm^{-1}. The others were almost the same as the spectrum of colored form of SP-1. The structures of the colorless and colored forms (SP-3) were estimated as follows.

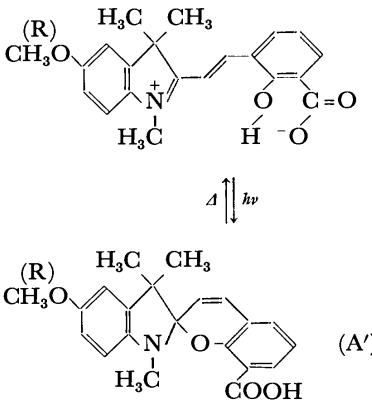

The stable colored form may be stabilized by a six membered ring between $-CO_2^-$ and –OH groups. The stable colored form was observed in all derivatives (presented in Eq. (2′)) having –COOH group at 8′-position. Thus the reverse photochromism of (SP-2) and its derivatives are given by Eq. (2′).

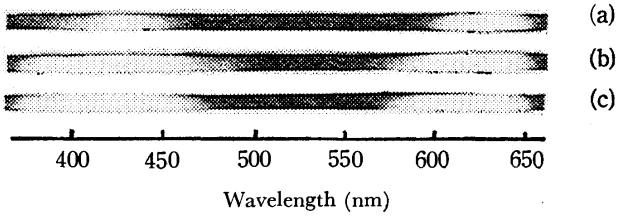

Fig. 3. Spectrographies of (SP-3) in acetone at each delay time (t) after illumination with flash light.
(a) before illumination.
(b) t=30 μsec.
(c) t=30 msec.

Photo-decoloration Process of SP-3. The color of the solution (ethanol, acetone, *etc.*) of SP-3 disappeared by irradiation with visible or ultraviolet light. Spectrograms of SP-3 in acetone at each delay time after illumination with flash light are shown in Fig. 3. Absorption band at visible range (near 550 nm) decreased just after illumination (delay time 30 μsec). The color reappeared partly within 30 msec after the illumination.

By photochemical analysis in the steady state, the coloration rate (A′→B′) k has been obtained at the same temperature in several solvents as shown in Table 2. Thus, there are fast and slow processes in the

TABLE 2. SPECIFIC RATE CONSTANTS ($k_{A'\to B'}$) OF SP-3 IN VARIOUS SOLVENTS (at room temperature)

Solvent	$k_{A'\to B'}$ (sec^{-1})
Methanol	1.82×10^{-3}
Ethanol	7.91×10^{-4}
2-Propanol	8.81×10^{-3}
Acetone	3.59×10^{-3}
Acetonitrile	5.45×10^{-3}

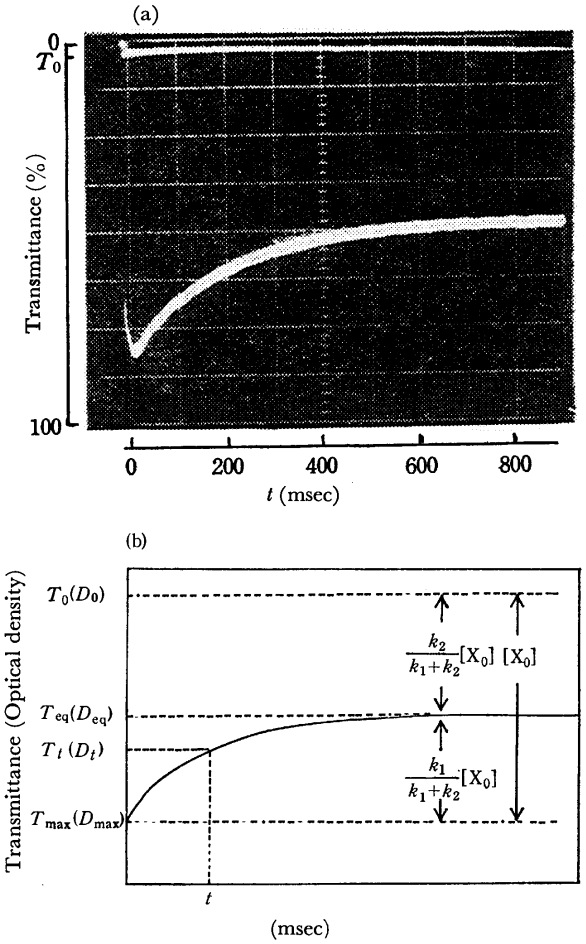

Fig. 4. Typical curve tracing the change in transmittance at λ_{max}(475 mμ) on the synchroscope and its diagram for the analysis.
(a): curve of SP-3 ethanol solution.
(b): diagram for analyzing of the curve.

recoloration of SP-3 solution. From the results, we assumed the existence of an intermediate state (X) during the course of photo-decoloration. Since no new band except for A''s and B''s could be observed, the absorption spectrum of X should resemble that of the colorless form.

When the change of B′ after illumination was traced at the absorption maximum (470 nm) by a synchroscope, a typical recoloration curve was obtained as shown in Fig. 4 (a).

The photo-decoloration process can be assumed as follows.

$$B' + h\nu \longrightarrow B^* \quad (3)$$

$$B^* \xrightarrow{\text{fast}} X \quad (4)$$

$$X \xrightarrow{k_1} B' \quad (5)$$

$$X \xrightarrow{k_2} A' \quad (6)$$

where $h\nu$, $k_1(k_2)$, and B* represent light quantum, specific rate of X→B′ (X→A′) process and the excited species of B′, respectively. The specific rates (k_1 and k_2) were obtained by the analysis of the recoloration curves as follows.

The rate equation for the reaction is

$$-\frac{d[X]}{dt} = (k_1+k_2)[X] \quad (7)$$

By integrating, we have

$$\frac{[X]}{[X]_0} = e^{-(k_1+k_2)t} \quad (8)$$

where [X] and [X_0] denote the concentration of X at t(sec) and initial state just after flash. The values of [X_0] and [X] are converted into the optical density (D) at λ_{max} of B′ by means of the following equations.

$$[X_0] = \frac{1}{\varepsilon_{B'} l}(D_{eq} - D_{max})\frac{k_1+k_2}{k_1} \quad (9)$$

$$[X] = \frac{1}{\varepsilon_{B'} l}(D_{eq} - D_t)\frac{k_1+k_2}{k_1} \quad (10)$$

where $\varepsilon_{B'}$ and l denote the absorption coefficient of B′ at λ_{max} and cell length, respectively. D_0, D_{eq}, D_{max}, and D_t give optical density as shown in Fig. 4(b).

From Eqs. (8), (9), and (10), we get

$$\ln\left(\frac{D_{eq} - D_t}{D_{eq} - D_{max}}\right) = -(k_1+k_2)t \quad (11)$$

A plot of $\ln(D_{eq}-D_t/D_{eq}-D_{max})$ against time t was linear for the photo-decoloration of SP-3 in ethanol as shown in Fig. 5. The slope gives the specific rate (k_1+k_2) 2.9 sec^{-1} at room temperature.

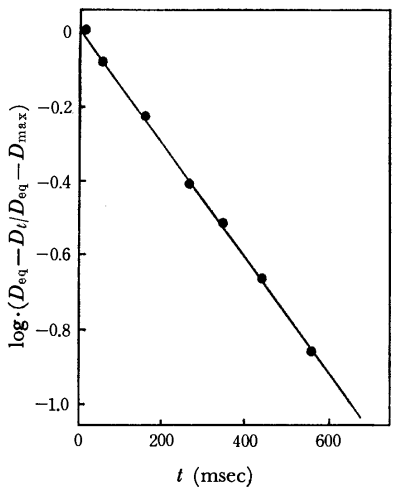

Fig. 5. A plot of log ($D_{eq}-D_t/D_{eq}-D_{max}$) against time ($t$) for SP-3 in ethanol at room temperature.

The ratio of the specific rates k_2/k_1 is given by

$$\frac{k_2}{k_1} = \frac{D_0 - D_{eq}}{D_{eq} - D_{max}} \quad (12)$$

The values obtained for the photo-decoloration of SP-3 in ethanol are summarized in Table 3.

Arrhenius' plots for the specific rates k_1 and k_2 (Fig. 6) showed good linearity. Activation energy ΔE^* and

Table 3. Kinetic data obtained in the photo-decoloration of SP-3 in ethanol
(at room temperature)

k_1+k_2 (sec^{-1})	k_1 (sec^{-1})	k_2 (sec^{-1})	k_2/k_1+k_2	ΔE^* (kcal/mol) X→A′	ΔE^* (kcal/mol) X→B′
2.9	0.38	2.5	0.87	20.3	18.6

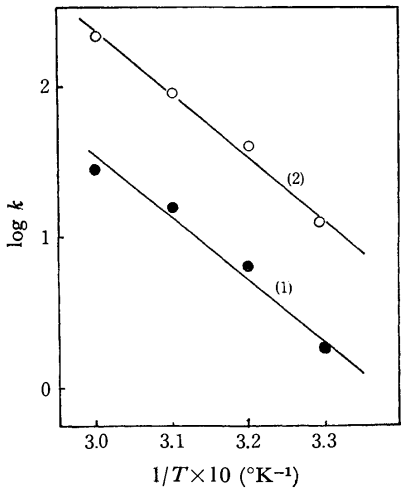

Fig. 6. The Arrhenius plots of SP-3 in ethanol.
(1): log k_1 *vs.* $1/T$
(2): log k_2 *vs.* $1/T$

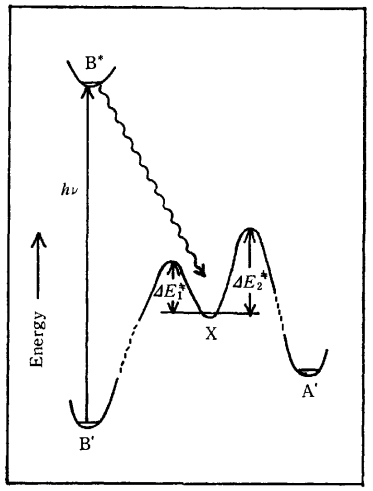

Fig. 7. Energy diagram showing the photo-decoloration process of reverse-photochromic spiran.

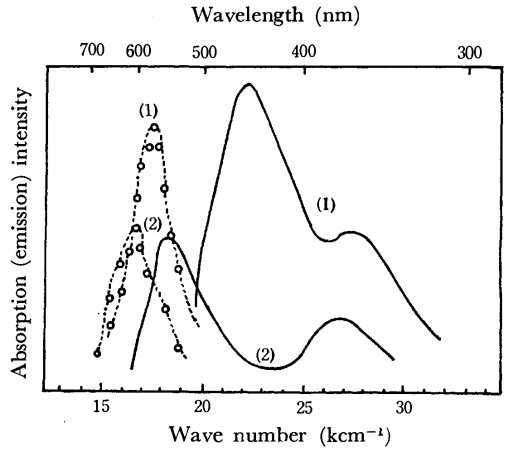

Fig. 8. Absorption and emission spectra of SP-2 in acetone and methanol.
(1): in acetone (2): in methanol

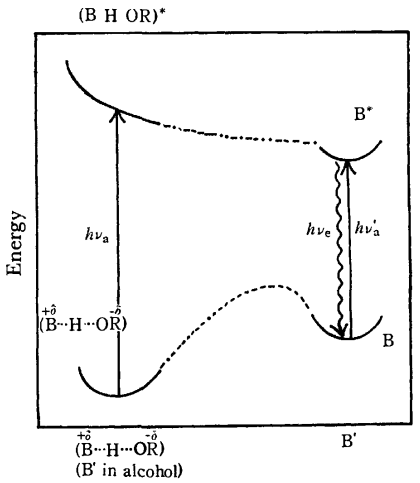

Fig. 9. Energy diagram illustrating large Stokes' shift of B in alcohol.
B': colored species
(B···H···OR): hydrogen bonded from with alconol (HO-R)
$h\nu_a$, $h\nu_a'$: absorbed photon
$h\nu_e$: emitted photon

the pre-exponential factor A were calculated (Table 3) from these slopes and Arrhenius' law

$$k = Ae^{-\Delta E^*/RT} \qquad (13)$$

An energy scheme for the photo-decoloration of SP-3 was assumed as given in Fig. 7. Colorless intermediate species (X) can be formed from the photo-excited state of B'. According to this assumption, X is transformed into the unstable colorless one A' in the ratio (k_2/k_1+k_2). Therefore, the photo-decoloration efficiency of B' seems to be determined by the product of the transition probability from B* to X and the conversion ratio (k_2/k_1+k_2) from X to A'.

Solvent Effect. The absorption band of B' in the visible region shifted towards longer wavelength in polar solvents, especially in proton donative solvents such as alcohol. Stokes' shift was observed in the fluorescence spectrum of an alcohol solution of B'. Typical curves of absorption and fluorescence spectra of B' are shown in Fig. 8. The ground state of B' which was supposed to be of Zwitter-ionic structure can be stabilized by interaction with polar solvents. The largest stability of B' was observed in an alcohol solution. This implies that the hydrogen bond would be formed between B' and alcohol. Stabilization of B' by solvent was supposed to cause the blue shift of the absorption band. Stokes' shift in alcohol was uncommonly large compared with that in acetone. This implies that some structural change of the system occurred in the equilibrium state of the excited species. Since the stabilized ground state of B' is supposed to be a hydrogen-bonded form ($B^{+\delta}\cdots H\cdots OR^{-\delta}$), it is considered that the rupture of the hydrogen bond (B' HOR) might occur in the excited equilibrium state. A schematic diagram is shown in Fig. 9 to illustrate the large Stokes' shift.

When the Brønsted acid such as hydrochloric acid was added, the colored species (B') was transformed into a yellow salt-type species (C; $B^+H\cdots X^-$).[4] C was photochemically converted into A' with a quantum yield of nearly 1. On the other hand, the quantum yield of photo-conversion from B' to A' was higher in proton donative solvents such as alcohol than in

Table 4. Life time of the transient intermediate (X) and the conversion ratio of the reaction (X→A′) of (SP-3) in various solvents (at room temperature)

Solvent	$k(1/\tau)$, sec^{-1}	$\eta_2(k_2/k_1+k_2)$
Methanol	0.57	0.85
Ethanol	2.9	0.87
2-Propanol	4.3	0.80
n-Butanol	8.2	0.84
Acetone	9.6×10^2	0.78
Acetonitrile	7.0×10	0.34

other solvents. The results also supported the view that the structure of ($B^{+\delta}\cdots H\cdots OR^{-\delta}$) was described as a hydrogen-bonded form in the alcohol solution of B′.

It is to be noticed that the life time (τsec) of X observed during the photo-decoloration of the reverse photochromic spirans was also influenced by solvents. Table 4 shows the specific rate constants ($k_1+k_2=k$ (sec^{-1})) and the conversion ratios ($\eta_2=k_2/(k_1+k_2)$) of the reaction to A′ from X of the SP-3 in various solvents. The value (k) was much smaller in alcoholic solvents compared with that in solvents such as acetone. X was stabilized with both the acidity as proton donor and the polarity of solvents. The value (η_2) was almost constant in alcohols and decreased in acetone and acetonitrile. The solvent effect on η_2 was less distinct than that on (k).

Table 5. Kinetic data on the reactions (X→A′, X→B′) of (SP-3) in various solvents.

Solvent	$\Delta E^{\ddagger}$ (kcal/mol)		A (sec^{-1})		$\Delta G^{\ddagger}$ (kcal/mol)	
	$\Delta E^{\ddagger}_{X\to A'}$	$\Delta E^{\ddagger}_{X\to B'}$	$A_{X\to B'}$	$A_{X\to B'}$	$\Delta G^{\ddagger}_{X\to A'}$	$\Delta G^{\ddagger}_{X\to B'}$
Ethanol	20.3	18.6	$10^{15.2}$	$10^{13.2}$	17.3	18.4
2-Propanol	19.8	22.5	$10^{15.5}$	$10^{16.6}$	16.3	17.3
Acetone	18.9	18.9	$10^{16.6}$	$10^{16.1}$	13.8	14.6

Kinetic data on the temperature dependence on the specific rate constants (k_1, k_2) in various solvents are summarized in Table 5. The large pre-exponential factor (A) and the high activation energy ($\Delta E^{\ddagger}$) were the inherent characteristics of the thermal transformations of the spirans (*e.g.* A′→B′, X→A′, and X→B′). The activated free energy ($\Delta G^{\ddagger}$) of the reactions increased in ethanol owing to the effect of the stabilization of X by the proton donative solvent.

The photo-decoloration efficiency ($\phi_{B'\to A'}$) of the reverse photochromic spirans should be determined by the product of η_1 and η_2 which are the ratios of the interconversions B*→X and X→A′ under the hypothetical reaction scheme for photo-decoloration. Because of the difficulty to determine the absolute value of η_1, we measured the relative value (η_{1rel}) for (SP-3) in various solvents. The results are given in Table 6. The relative efficiencies (ϕ_{rel}) obtained with the steady light coincided qualitatively with the relative values ($S_{rel}=\eta_{rel}/(\eta_{rel})_{ethanol}$) as shown in Table 6. The deviation between ϕ_{rel} and S_{rel} might be

4) I. Shimizu, H. Kokado, and E. Inoue, This Bulletin **42**, 1726 (1969).

Table 6. Photo-decoloration efficiency of SP-3 in various solvents

Solvent	$\eta_{x,rel}$	η_2	S_{rel} [a)]	$\phi_{(B'\to A')rel}$
Methanol	0.69	0.85	0.68	0.53
Ethanol	1.00	0.87	1.00	1.00
Acetone	0.59	0.78	0.53	0.31
Acetonitrile	0.31	0.34	0.12	0.14

a) S_{rel} were obtained at room temperature. $\phi_{(B'\to A')rel}\to -40°C$.

caused by the neglect of the temperature effect on η_2.

Effect of Substituents. Photo-decoloration efficiency was influenced by the substituent in the indoline part of the reverse photochromic spiran (SP-2). Existence of X also depended on the substituent.

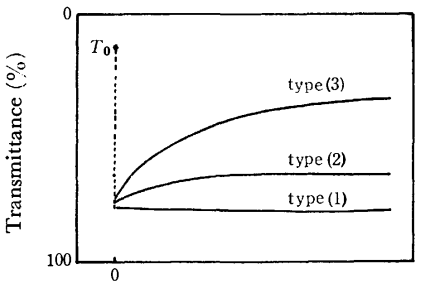

Fig. 10. Typical curves showing the changes of trasmittance at λ_{max}, against time after flash illumination. T; transmittance before illumination.

Typical curves of transmittance at the absorption maximum after the flash illumination are shown in Fig. 10. They can be classified into three groups. SP-2, 9, and 10 are of type 1, in which X could not be observed. It seemed that the photo-decoloration occurred in the process from B* to A′, or the energy barrier between X and A′ or B′ could be neglected. X was observed in SP-3, 4, 5, and 6 which are of type 3. SP-7 and 8 are of type 2, in which X was hardly detected at all by analysis. No explanation has been given on the influence of the substituents on the process.

Kinetic data on X of the spirans belonging to the type 3 are shown in Table 7. The longer the life time of X, the higher the interconversion ratio (η_2).

It was found that the photo-decoloration efficiency ($\phi_{B'\to A'}$) of the spiran substituted with an electron-

Table 7. Life time and conversion ratio (η_2) of the reverse photochromic spirans

Spiran	Solvent	$k(sec)^{-1}$	$\eta_2(k_2/k_1+k_2)$
SP-3	Ethanol	2.9	0.87
	n-Butanol	8.2	0.84
	Acetonitrile	9.6×10^2	0.78
SP-4	Ethanol	7.6×10	0.49
	n-Butanol	1.0×10^2	0.65
	Acetonitrile	4.1×10^3	0.37
SP-5	Ethanol	4.8×10	0.77
	n-Butanol	1.9×10^2	0.72
SP-6	Ethanol	5.4×10^2	0.50
	n-Butanol	1.5×10^3	0.56

releasing group ($-OCH_3$) was higher than that with an electron attractive substituent (–Br). These substituent effects were similar to those on stability of the colored form of the spirans of type 3 as given in Table 7.

Effect of the Dissolved O_2 on the Photo-bleaching of Spirans. Reversibility of spirans gradually decreased during repetition of the photo-interconversion between A′ and B′. The term "fatigue" of the photochromism was given to such a phenomenon. The fatigue process of reverse photochromic spirans depended largely on the dissolved oxygen and the photon energy of the light.

When a degassed ethanol solution of SP-3 was irradiated with a flash pulse with no filter, the existence of X was recognized during the decoloration process, but coloration was not completely restored. After the illumination of 4 pulses, no photo-decoloration occurred. The fatigue phenomenon was scarcely noticeable in a solution saturated with air.

No fatigue was observed even in the degassed sample when visible light (with a UV cut off filter) was passed on the solution. It was supposed that the fatigue from the irradiation of UV light, *viz.*, irreversible bleaching of the color was induced from the higher excited state. Deactivation from the higher excited state to the lower state may be accelerated by the dissolved oxygen in high efficiency.

BULLETIN OF THE CHEMICAL SOCIETY OF JAPAN, VOL. 45, 1956—1960(1972)

Mechanism of Hydrogen Exchange Reactions on 1:2 Electron Donor-Acceptor Complexes of Anthracene with Sodium

Masaru ICHIKAWA,* Sadao TANAKA,** Shuichi NAITO,* Takahiro NAKAMURA, Mitsuyuki SOMA, Takaharu ONISHI, and Kenzi TAMARU

Department of Chemistry, The University of Tokyo, Hongo, Bunkyo-ku, Tokyo

(Received August 25, 1971)

The mechanisms of the H_2–D_2 and D_2–HZ exchange reactions over 1:2 Electron Donor-Acceptor (EDA) complexes of anthracene with sodium, where HZ denotes the EDA complexes, were studied kinetically and spectroscopically in the temperature range 20—90°C. It was found that molecular hydrogen exchanges directly with the hydrogen of the complexes ($An^{2-}2Na^+$ or An^-Na^+) and also with the monohydroanion complex (AnH^-Na^+), which is formed by the dissociative adsorption of hydrogen. The H_2–D_2 exchange reaction proceeded *via* not only the σ-bonded hydrogen of the complexes, but also homolytically dissociated "mobile" hydrogen.

The reactions of hydrogen over various electron donor-acceptor (EDA) complexes of various aromatic compounds, such as aromatic hydrocarbons, their substituted compounds[1a] and phthalocyanines,[1b] with alkali metals were studied previously. It was found that H_2–D_2 and D_2–HZ exchange reactions (HZ denotes the EDA complexes) took place at room temperature at considerable rates, hydrogen being dissociatively adsorbed. It is of interest to elucidate the reasons for this reactivity which appears on the formation of the EDA complexes.

The composition of the complexes studied so far[1a] was not always well defined. In this study, however, stoichiometric complex films were employed, and the role of the chemisorbed hydrogen on the EDA complexes was studied. The active intermediates for the hydrogen exchange reactions were determined by NMR and UV spectroscopic techniques.

Experimental

Stoichiometric complex films of anthracene with sodium ($An^{2-}Na^+$ and An^-Na^+: An=anthracene) were prepared from their stoichiometric tetrahydrofuran (THF) solutions by evaporating the solvent.[2,3]

The formation and composition of the complexes as films or in solution[4] were confirmed by their characteristic absorption spectra. The complex films were evacuated at about 100°C for one day, prior to the experiments. Anthracene was purified by repeated recrystallization and the zone-melting method. Sodium was purified by distillation. In the hydrogen exchange reactions the isotopic hydrogen mixtures were analyzed by gas chromatography using an activated alumina column.

The reactions were carried out in a closed circulating system, which included a U-type reaction vessel.

Results and Discussion

Hydrogen Exchange Reaction between D_2 and the Hydrogen of 1:2 Anthracene-sodium Complex Film (D_2–HZ Exchange

* Present address: Sagami Chemical Research Center, Ohnuma, Sagamihara-shi.

** Present address: Faculty of Engineering, Hokkaido University, Sapporo.

1a) M. Ichikawa, M. Soma, T. Onishi, and K. Tamaru, *Trans. Faraday Soc.*, **63**, 997, 2015 (1967); *J. Catal.*, **6**, 336 (1966), **9**, 418 (1968); This Bulletin, **40**, 1050, 1294 (1967).

1b) M. Ichikawa, M. Soma, T. Onishi, and K. Tamaru; *Trans. Faraday Soc.*, **63**, 1215 (1967); This Bulletin, **41**, 1739 (1968).

2) S. Tanaka, M. Ichikawa, S. Naito, M. Soma, T. Onishi, and K. Tamaru, This Bulletin, **41**, 1278 (1968).

3) S. Tanaka, S. Naito, M. Ichikawa, M. Soma, T. Onishi, and K. Tamaru, *Trans. Faraday Soc.*, **66**, 976 (1970).

4) M. Ichikawa, M. Soma, T. Onishi, and K. Tamaru, *J. Amer. Chem. Soc.*, **91**, 6505 (1969).

Reaction). When D_2 (40 cmHg) was introduced onto the film of $An^{2-}2Na^+$, 5.6×10^{-3} mol, at temperatures between 20 and 90°C, a considerable amount of D_2 was adsorbed, and at the same time the gaseous deuterium was diluted by hydrogen from the complex forming HD in the gas phase, as shown in Fig. 1.

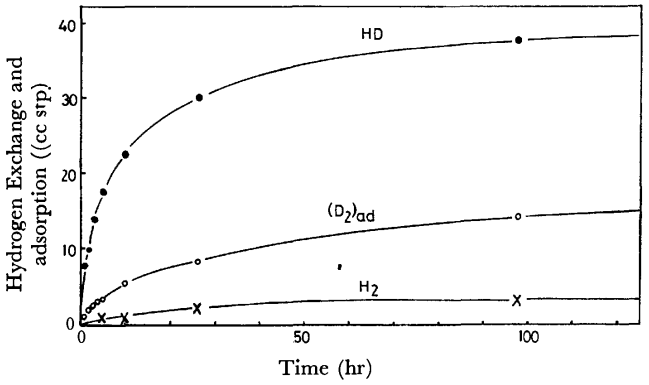

Fig. 1. The kinetics of the D_2-HZ exchange reaction and the hydrogen adsorption $(D_2)_{ads}$ over $An^{2-}2Na^+$ complex film at 80°C, $P_{D_2}=40$ cmHg.

The hydrogen adsorbed over the $An^{2-}2Na^+$ film could be completely removed by evacuating the system at 100°C for 20 hr. Reproducible results were obtained for the D_2–HZ reaction and the hydrogen adsorption.

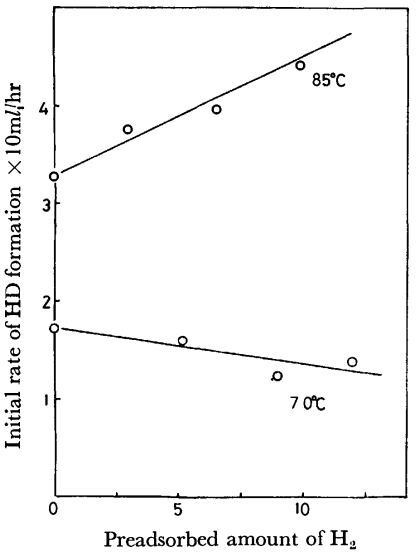

Fig. 2. Intial rates of HD formation *versus* the amount of preadsorbed hydrogen, $(H_2)_{abs}$ over an An^{2-} $2Na^+$ film (5×10^{-3} mol). $P_{D_2}=20$ cmHg.

The behaviour of the hydrogen adsorbed on the $An^{2-}2Na^+$ film in the hydrogen exchange reaction was examined at temperatures between 25 and 85°C, and by admitting D_2 (20 cmHg) onto a film (5×10^{-3} mol) deposited on silica wool on which various amounts of H_2 (from 2 to 42 m*l* stp) had been preadsorbed. The desorption of hydrogen was very slow at lower temperatures. We see from the results given in Fig. 2 that at lower temperatures (25 to 70°C) the rate of HD formation decreased slightly with increasing amounts of preadsorbed hydrogen. On the other hand, at higher temperatures such as 85°C, the rates increased slightly with increasing amount of the preadsorbed hydrogen. The initial rates of HD formation for all temperatures extrapolated to zero H_2 adsorption are not zero, but correspond to those observed over the fresh $An^{2-}2Na^+$ films. These results suggest that at least in the initial stage of the reaction the D_2–HZ exchange reaction takes place directly between the gas phase D_2 and the hydrogen of the $An^{2-}2Na^+$ complex, not through the hydrogen chemisorbed on the complex. This is also supported by the fact that the rate of HD formation was faster than that of D_2 adsorption (Fig. 1).

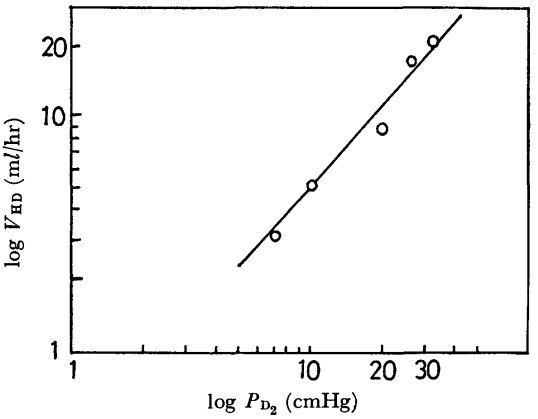

Fig. 3a. Dependence of the D_2-$(H_2)_{ads}$ exchange reaction rate upon the deuterium pressure over An^{2-} $2Na^+$ which had been adsorbed with H_2 (42 cc stp) at 62°C.

The exchange reaction between D_2 (20 cm) and an almost saturated adsorbed hydrogen layer, $[(H_2)_{ads}/(An^{2-}2Na^+)_0=0.9]$ was studied at temperatures between 20 and 90°C. Near saturation the kinetics of the HD formation were represented by the following equation (Fig. 3a).

$$-d(HD)/dt = kP_{D_2}(H_2)_{ads}$$

To determine the position of the hydrogen taking part in the D_2–HZ exchange, the complex film was decomposed by oxygen after exchange with D_2, and the resulting anthracene was analyzed by mass and NMR spectrometry. The results suggested that the mono-deuterated (9-position of the anthracene) product was obtained in the initial exchange ($d_0=80$, $d_1=18$, $d_2=2$, $d_3=0\%$).

As was suggested previously,[2,3] 9-monohydroanthracenium sodium (AnH^-Na^+) and sodium hydride were produced by hydrogen adsorption over the $An^{2-}2Na^+$ film.

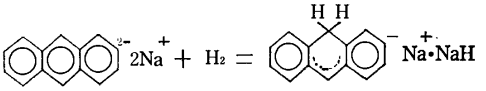

AnH^-Na^+ was also separately prepared by reacting $An^{2-}2Na^+$ and 9,10-dihydroanthracene (AnH_2) in THF at 25°C;[3]

$$An^{2-}2Na^+ + AnH_2 = 2AnH^-Na^+$$

The AnH^-Na^+ thus prepared (identified by its charac-

5) M. Ichikawa, M. Soma, T. Onishi, and K. Tamaru, This Bulletin, **43**, 3672 (1970).

teristic electronic absorption band at 432 mμ) was deposited on the wall of the reaction vessel (270 ml) by evaporating the solvent at 25°C. The film of AnH^-Na^+ was stable at temperatures below 80°C, but when strongly evacuated for several hours above 80°C it slowly changed to the monoanion anthracene complex by giving off hydrogen;

$$2AnH^-Na^+ = 2An^-Na^+ + H_2$$

When 20 cmHg of D_2 was introduced onto the AnH^-Na^+ film at temperatures between 20 and 80°C, the reversible HD formation proceeded following first-order kinetics, and attained an equilibrium value. The apparent activation energy for the hydrogen exchange between D_2 and the AnH^-Na^+ film was determined to be 10 kcal/mol. It was also found that at 65°C the rate of HD formation in the D_2–AnH^-Na^+ exchange reaction was proportional to the pressure of D_2 (6.5 to 45 cmHg) and to the amount of exchangeable AnH^-Na^+ (Fig. 3b).

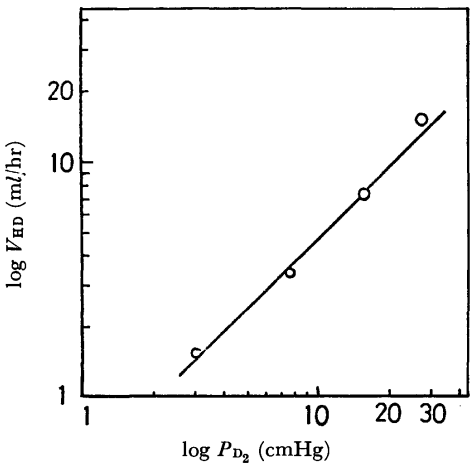

Fig. 3b. Depencence of the D_2-AnH^-Na^+ exchange reaction rate upon the deuterium pressure at 65°C.
AnH^-Na^+ (7×10^{-3} mol)

AnH^-Na^+ dissolved in d_8-tetrahydrofuran (from Merck Co., 98% pure) was completely exchanged with D_2 at 65°C, and the complex solution was analyzed by NMR spectrometry. It was found that the deuterium exchange took place selectively at the 10-position of the 9-monohydroanthracenium sodium, and a small amount of monodeuterated 9,10-dihydroanthracene was formed in the resulting solution. Interpretation of the spectra was carried out using the results obtained by Schneider.[6] The deuterium exchanged monohydroanthracene was evacuated ($AnH^-Na^+ = An^-Na^+ + 1/2\ H_2$), decomposed by oxygen, collected by sublimation and analyzed by mass and NMR spectrometry. It was shown that monodeuterio(9-position) anthracene was the major product.

d_0-anthracene = 10, d_1 = 88, d_2 = 2, and d_3 = 0%

The results seem to indicate that the monohydroanthracenium complex participates in the hydrogen exchange reaction at the carbon atom opposite to the one where hydrogen was added, and during the course of the hydrogen exchange reaction desorption of the added hydrogen takes place rather slowly. Thus, only the d_1 species is produced to any extent by the deuteration, and no marked mixing at two equivalent carbon atoms (9- and 10-positions) was observed. From these results it is suggested that the D_2–AnH^-Na^+ exchange reaction proceeds as follows.

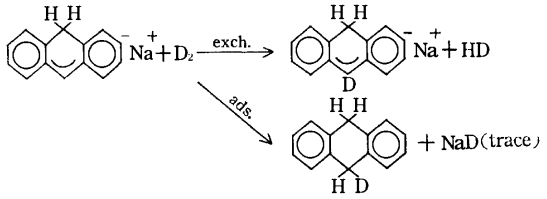

To clarify the role of the NaH in the hydrogen exchange reaction, a slight excess sodium hydride (or NaD) (75 mg, 3×10^{-3} mol) was added to the AnH^-Na^+ (2.8×10^{-3} mol) in THF, and a mixed film of AnH^-Na^+ and NaH was thus deposited on silica wool (The hydrogen exchange reaction did not proceed over the NaH alone under these reaction conditions).

The hydrogen exchange reaction was carried out in the three different systems as follows:

$$(AnH^-Na^+, NaH) + D_2 \longrightarrow HD \quad d(HD)/dt = r_1$$

$$(AnH^-Na^+, NaD) + D_2 \longrightarrow HD \quad r_2$$

$$(AnH^-Na^+, NaD) + H_2 \longrightarrow HD \quad r_3$$

where AnH^-Na^+ (3×10^{-3} mol) and AnH or NaD (*ca.* 1 g, 4×10^{-2} mol) were employed to make the mixed films. The rates, r_1 and r_2, were found to be almost equal (*ca.* 4 ml/hr), whereas r_3 was negligibly small at 65°C under the same reaction conditions.

When an adduct film of AnH^-Na^+ (3×10^{-3} mol) and NaD (*ca.* 4×10^{-2} mol) was heated at 85°C for several hours *in vacuo*, a small amount of hydrogen gas was collected. Gas chromatographic analysis gave its composition as H_2=2%, HD=87%, and D_2=11%. From UV-spectroscopic measurements it was found that $An^{2-}2Na^+$ was regenerated and AnH^-Na^+ decreased by eliminating hydrogen:

$$AnH^-Na^+ + NaD \longrightarrow An^{2-}2Na^+ + HD$$

The results suggest that it is the hydrogen in the AnH^-Na^+ which participates in the exchange with molecular hydrogen, the hydrogen of NaH being unreactive for the exchange reaction at the temperatures studied.

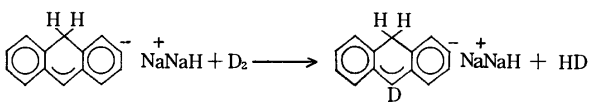

It was therefore concluded that the overall process for the D_2–HZ exchange reaction occurred simultaneously with D_2 adsorption on the $An^{2-}2Na^+$ film as follows.

i) Direct hydrogen exchange between $An^{2-}2Na^+$ and D_2 accompanied by dissociative chemisorption:

6) W. G. Schneider, Nucl. Magnetic Resonance Chem. Proc. Symp., (Cagliari, Italy, 1964).

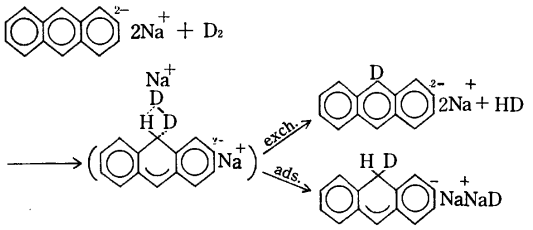

ii) Direct hydrogen exchange of D_2 with AnD^-Na^+ which was formed by the D_2 adsorption:

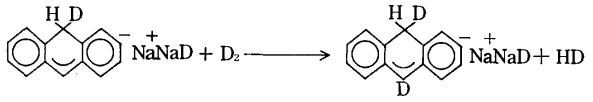

iii) At temperatures above 85°C the desorption process also contributes to the hydrogen exchange reaction, *viz.*,

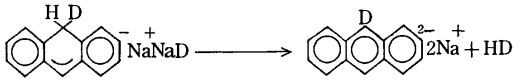

The H_2–D_2 Exchange Reaction over the 1:2 Anthracene-sodium Complex Film. When a 1:1 mixture of H_2 and D_2 (total pressure 20 cmHg) was admitted onto a fresh $An^{2-}2Na^+$ film (5.2×10^{-3} mol) deposited on silica wool, HD was produced and total deuterium content in the gas phase decreased as shown in Fig. 4.

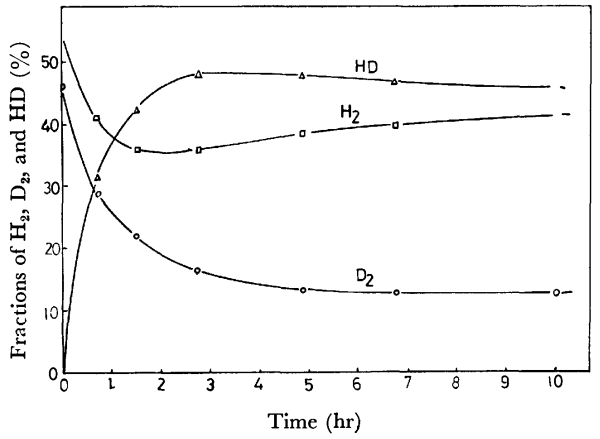

Fig. 4. The kinetics of the H_2-D_2 exchange reaction over an An^{2-} $2Na^+$ film (5.2×10^{-3} mol) at 82°C.
$p_{H_2+D_2}$=20 cmHg.

The initial rate of HD formation in the H_2–D_2 exchange reaction was studied after the complete evacuation of the residual adsorbed hydrogen and was compared with that of the D_2–HZ reaction, which lead to the following conclusions: Above 82°C the temperature dependence and the initial rate of HD formation from a H_2–D_2 mixture were similar to those of the D_2–HZ exchange reaction (P_{D_2}=20 cmHg) as shown in Fig. 5. The HD formation in the H_2–D_2 exchange reaction thus results mainly from the following two exchange reactions which involve the bonded hydrogen of the $An^{2-}2Na^+$ complex.

$$D_2 + HZ = HD + DZ$$

$$H_2 + DZ = HD + HZ$$

HZ: $An^{2-}2Na^+$ or AnH^-Na^+

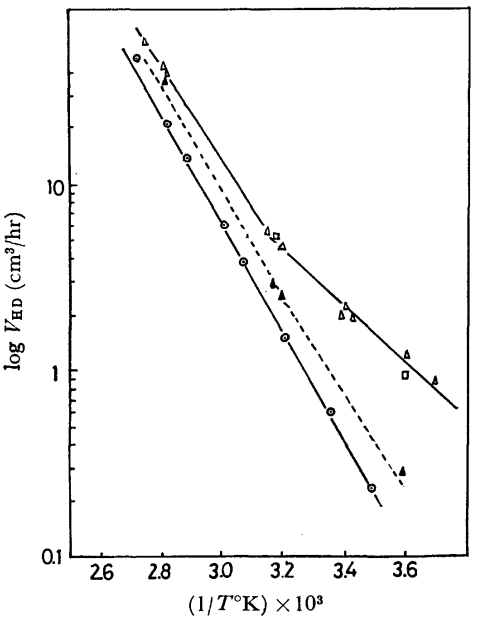

Fig. 5. Arrhenius' plot for the initial HD formation in the H_2-D_2 exchange reaction over $An^{2-}2Na^+$ films (-△-△-), and in the D_2HZ (HZ=$An^{2-}2Na^+$) exchange reaction (-○-○-). The rates of HD formation in the H_2-D_2 exchange reaction after the preadsorption of CO (*ca.* 4.5 cc) (-▲-▲-), and after evacuation of the preadsorbed CO from the complex film (-□-□-).

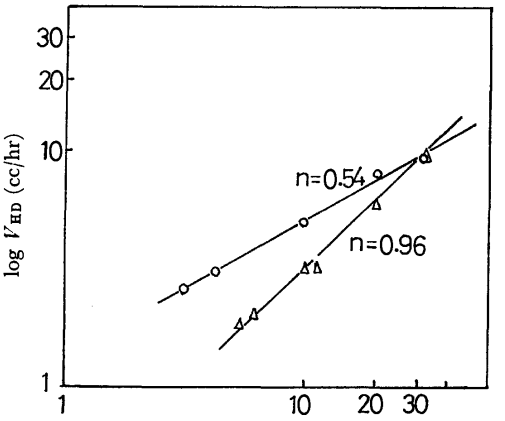

Fig. 6. Dependence of the H_2-D_2 exchange reaction rate upon the total pressure of H_2+D_2 (1:1) mixture and the deuterium pressure (P_{H_2}=10 cmHg) over $An^{2-}2Na^+$ (5.2×10^{-3} mol) film at 45°C.
-○- log P_{D_2} (cmHg) -△- log $P_{H_2+D_2}$ (cmHg)

On the other hand, at lower temperatures, *e.g.* 42°C, the HD formation from a H_2–D_2 mixture was faster than in the D_2–HZ exchange reaction (Fig. 5). The initial rate of HD formation could not be explained by the above mentioned bonded mechanism alone and the H_2–D_2 exchange reaction almost reached thermal equilibrium in the gas phase. The pressure dependence of the rates of the H_2–D_2 exchange reaction at 45°C was found to be proportional to the total pressure of the H_2–D_2 mixture (1 : 1), and to the square root of each of the H_2 and D_2 pressures as shown in Fig. 6.

$$d(HD)/dt = kP_{H_2}^{1/2}P_{D_2}^{1/2}$$

It is thus suggested that at lower temperatures the

H_2–D_2 exchange reaction takes place mainly *via* the recombination of "mobile" hydrogen chemisorbed on the complex film:

$$\left.\begin{array}{l} D_2 \rightleftarrows 2D(a) \\ H_2 \rightleftarrows 2H(a) \end{array}\right\} \rightleftarrows 2HD$$

It should be noted that when the $An^{2-}2Na^{+}$ film adsorbed carbon monoxide (4.5 and 16 m*l* stp) at 40°C, the HD formation from the H_2–D_2 exchange reaction decreased markedly, and the initial rates of HD formation became almost equal to those obtained at similar temperatures for the D_2–HZ exchange reaction. After evacuation of the complex film at 85—100°C for 20 hr, the activity of the film for the H_2–D_2 exchange reaction was completely restored as shown in Fig. 5. It is suggested that CO effectively inhibited the "weakly chemisorbed hydrogen" mechanism, but had negligible effect on the exchange between D_2 and the hydrogen of the complex molecule.

BULLETIN OF THE CHEMICAL SOCIETY OF JAPAN, VOL. 45, 1960—1972(1972)

Calorimetric Study of the Glassy State. VII. Phase Changes between the Crystalline Phases of Cycloheptanol with Various Degrees of Stability

Keiichiro ADACHI, Hiroshi SUGA, and Syûzô SEKI
Department of Chemistry, Faculty of Science, Osaka University, Toyonaka, Osaka, Japan
(Received November 8, 1971)

The heat capacities of 8 kinds of stable and meta-stable crystalline phases including the glassy crystal of cycloheptanol were measured at temperatures from 13 to 300 K. The crystalline phases have been named crystals I, II, II′, III, III′, III″, I_β, and glassy crystal. Transition temperatures between crystals II and I, III and II, II′ and II, III′ and III, III″ and III were determined to be 258.45, 227.26, 172.23, 152.30, and 128.2 K, respectively. The melting point and glass transition point of the glassy crystal were determined to be 280.30 and 140 K, respectively. The heats of transition between crystals II and I, III and II, III′ and III and the heat of melting were determined to be 876, 554, 58.1, and 1604 $Jmol^{-1}$, respectively. The residual entropy of the glassy crystal was found to be 0.7 $JK^{-1}mol^{-1}$ assuming that of crystal III′ to be zero. The stabilization phenomenon in the glassy crystalline state was also studied from the measurements of enthalpy relaxation. The stability of the various phases was determined by calculating their free energies. The degree of freedom which is frozen in the glassy crystalline state was discussed from molecular viewpoints. Classification of various phase transitions found in this material was also made from the viewpoint of thermodynamical stability.

In general the glassy state results from an elongation of a relaxation time by cooling a material which is in a supercooled metastable state. Thus, the glassy state is looked upon as a non-equilibrium state in a thermodynamic sense.[1] We measured the heat capacities of the quenched high-temperature crystalline phases of cyclohexanol and 2,3-dimethylbutane and concluded that these crystalline phases have definite residual entropies at 0 K and exhibit glass transition phenomena characteristic of non-equilibrium glassy states.[2,3,4] We proposed the term "*glassy crystal*" for defining the glassy crystalline state as the non-equilibrium frozen-in state of crystals which have glass transition points. The present paper describes the results of measurements of heat capacity for cycloheptanol expected to form the glassy crystal from a preliminary study of the differential thermal analyses (DTA).

In previous studies,[2,3] we attempted to explain the residual entropies in terms of the degrees of freedom frozen-in below the glass transition points and proposed two possible explanations, the orientational degree of freedom of the molecules and the conformational one. However, the residual entropies were so small that they were accounted for only by taking into consideration the conformational degree of freedom frozen below the glass transition point. An important feature of the present investigation may be found in the fact that the molecule of cycloheptanol can be expected to have more kinds of possible conformations than that of cyclohexanol or 2,3-dimethylbutane. We can expect 42 kinds of distinguishable conformations for this molecule. Although we do not know much about the energy difference between these conformers, we can expect the conformational degree of freedom to contribute greatly to the residual entropy of the glassy crystal of this material, if the conformational degree of freedom is frozen at or below the glass transition point.

The influence of the complicated molecular structure on the behaviors of phase transitions is also of interest. Various metastable phases were found and some thermodynamic functions were determined for them.[2,3,4] In the present study we have also found the occurrence of 8 kinds of stable and metastable crystalline phases from DTA measurement and clarified the relation of

1) W. Kauzmann, *Chem. Revs.*, **43**, 219 (1948).
2) K. Adachi, H. Suga, and S. Seki, This Bulletin, **41**, 1073 (1968).
3) *Idem, ibid.*, **43**, 1916 (1970).
4) *Idem, ibid.*, **44**, 77 (1971).

the instability by measuring their heat capacities.

It is well-known that the glassy state is not a completely frozen-in state but is stabilized very gradually into an equilibrium state. In this respect we measured the enthalpy relaxation time of the stabilization process.

We also measured the Raman and IR spectra in order to analyze the magnitude of the heat capacities. From the results the magnitude of heat capacity due to internal vibrations was calculated and that due to the change of the configuration of molecules was estimated. Variation in the magnitude of heat capacity caused by annealing in the glassy crystalline state was also examined.

Experimental

Material. The sample employed was synthesized by reducing cycloheptanone prepared by the reaction of cyclohexanone with diazomethane. The equations of the chemical reactions are as follows.

$$C_6H_{10}O + CH_2N_2 \longrightarrow C_7H_{12}O$$
$$C_7H_{12}O + LiAlH_4 \longrightarrow C_7H_{13}OH.$$

Cycloheptanone was synthesized by adding 550 g of nitrosomethylurethane little by little with violent stirring into a mixture of 400 g of cyclohexanone, 2 *l* of ethylether and 1200 g of 50% KOH aqueous solution. The temperature of the reacting system was regulated to 10±5°C. It took about 6 hr to complete the reaction. Fractional distillation of the reaction product yielded about 200 m*l* of pure cycloheptanone. Hydrogenation of the cycloheptanone was carried out with the aid of $LiAlH_4$ in an ethylether solution by the usual method. The reaction product was then purified by repeating fractional distillation. About 50 m*l* of the purified cycloheptanol was obtained. In order to remove the trace of water, vacuum distillation was craried out over baked CaO. The absolute purity of the sample was finally determined to be 99.932% from the equilibrium temperatures in the melting process.

Apparatus. The measurement of the heat capacity was made with an adiabatic calorimeter.[5] The cryostat was reconstructed in such a way that liquid nitrogen could be introduced into the inside of the inner jacket when the sample was required to be quenched. The platinum resistance thermometer was calibrated after the completion of investigation by comparison with the laboratory standard thermometer which had been calibrated at the US National Bureau of Standards. The deviation of the temperature scale was, however, too small to cause any error in spite of severe thermal treatment. The sample cell contained 26.774 g of the sample as well as a small amount of helium gas for heat exchange medium (1 atm at room temperature).

The Raman spectra were obtained with a Nihon Bunko Co. Raman spectrometer model R 1000 and the IR spectra with a Nihon Bunko Co. Double beam spectrometer model DS 402 G. The apparatus for DTA was reported previously.[6]

Results

DTA. Thermal behaviors were studied preliminarily by means of DTA before the precise measurements of heat capacity. The results are shown in Fig.

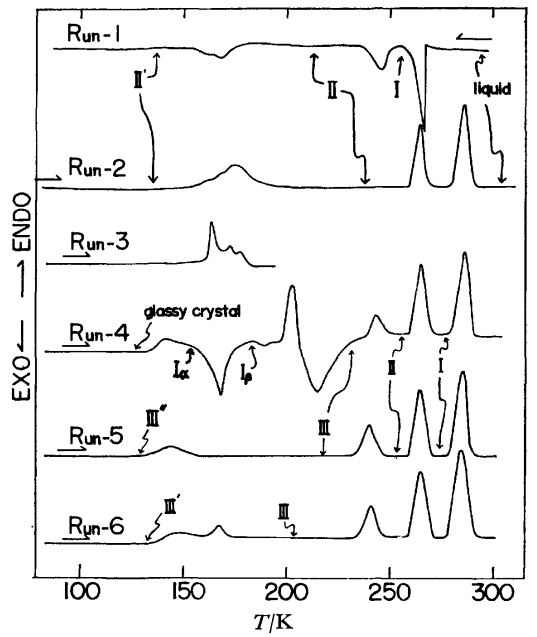

Fig. 1. DTA curves of cycloheptanol.

1. Run 1 is the cooling curve measured at a rate of about −1.5 K/min. A sharp exothermic peak due to abrupt crystallization was observed at 267 K followed by a phase transition at about 245 K. A small exothermic anomaly was observed at about 165 K on further cooling. Run 2 is the heating curve measured after the specimen had been slowly cooled down to 80 K from 280 K. The heating rate was about 2 K/min. A small and broad anomaly with two shoulders was observed at about 170 K and peaks due to a phase transition and melting followed at 259 and 278 K, respectively. We named the phases as follows, table between 259 and 278 K, Crystal I; between 170 and 259 K, Crystal II; below 170 K, Crystal II′. The heating curve taken after crystal II had been rapidly chilled at a rate of about 4 K/sec by steeping the DTA sample container in liquid nitrogen is shown in Run 3. The DTA curve taken after crystal I had been chilled rapidly by the same procedure is shown in Run 4. When the specimen in the liquid state was chilled at the same cooling rate, nearly the same DTA diagram as for Run 3 was obtained. In Run 4 an anomaly resembling that for glass transition was observed at 140 K. This is considered to be the glass transition. We thus called the phase below 140 K the glassy crystal. On further heating, an exothermic transition followed around 167 K. We named the phase between 140 and 160 K Crystal I_α and that established by the transition around 167 K Crystal I_β. A phase change took place from crystal I_β to another unknown phase at 197 K. A small exothermic anomaly was recognized around 190 K. The phase to which crystal I_β was transformed at 197 K was unstable and irreversibly transformed into the more stable one at about 210 K. A new peak appeared at 239 K which was not observed in Run 2. Above 250 K, nearly the same thermogram as in Run 2 was obtained. We named the phase with transition point at about 239 K Crystal III. In order to obtain crystal III as a pure

5) H. Suga and S. Seki, This Bulletin, **38**, 1000 (1965).

6) H. Suga, H. Chihara, and S. Seki, *Nippon Kagaku Zasshi* (*J. Chem. Soc. Japan, Pure Chem. Sect.*), **82**, 24 (1961).

phase, crystal II was annealed at dry ice temperature for 3 days. Run 5 is a heating curve taken after the annealing. A small and broad anomaly was observed around 130 K. The peak at about 240 K is slightly larger than the one in Run 4. Since no peak due to the transition from crystal II′ to crystal II appeared at 170 K, it was concluded that crystal III had been established in pure state by the annealing. By annealing at 140±3 K for 5 days, crystal III changed to another phase, the DTA thermogram for which is represented by Run 6. However, when crystal III was annealed at 115—125 K for 5 days, nearly the same thermogram as in Run 5 was obtained. The phases appearing at the lowest temperature in Runs 5 and 6 were named Crystals III′ and III″, respectively.

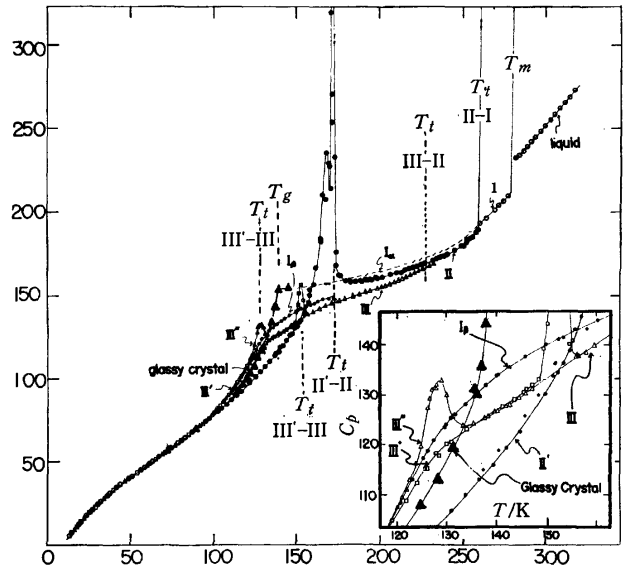

Fig. 2. Heat capacities of cycloheptanol

▲: crystals I, I_α, and glassy crystal
●: crystals II and II
△: crystals III and III″
□: crystal III′
○: crystal I_β

Heat Capacity Measurements. Selected values of the heat capacity data are listed in Table 1; a complete set of the heat capacity data is preserved by the Chemical Society of Japan.[7] These heat capacity data are plotted against temperature in Fig. 2. In Series 1, the heat capacities were measured after the liquid specimen at room temperature had been chilled at a rate of about −50 K/min (Series 1). Under these conditions, it was expected from DTA that crystal I would be supercooled and the glassy crystalline state established below 140 K. The data listed in Series 2 and 2′ were taken before measurement of the enthalpy relaxation in annealing treatment, *i.e.* determination of the points D and E shown in Fig. 8. In Series 1, 2, and 2′, the heat evolution or absorption due to a stabilization effect near T_g was subtracted by correction of temperature drift. In the II′—II transition temperature region (Series 3′, 3″) the heat capacity changed slightly with thermal history. Measurements were carried out after the following thermal histories. In Series 3′ crystal II was cooled down to 100 K at the rate of −6 K/min and then annealed for 18 hr at 138 K. In Series 3″ the specimen was annealed for 12 hr at 156 K after cooling. Measurements for the supercooled crystal II in the temperature region 200—215 K were somewhat difficult on account of the exo-thermic transition from this phase to crystal III. Crystal III (Series 4) was prepared under the same conditions as for DTA (Run 5, Fig. 1). When it was annealed at 140 K for 3 days, it was transformed irreversibly into another phase which showed a phase transition to crystal III at 152.3 K. We named this phase crystal III′ (Run 6, Fig. 1). At the ordinary cooling rate (−1 K/min), crystal III was supercooled easily with no III′—III transition. The heat capacity curve of the supercooled crystal III showed a small anomaly at about 128 K. We named the supercooled phase below 128 K crystal III″ (Run 6 Fig. 1). The results for crystal III′ and crystal III″ are listed in Series 5 and 6, respectively. Crystl I (Series 9) was prepared from the results of DTA (Run 4, Fig. 1). The results for crystal III′ and crystal III″ are listed in Series 5 and 6 respectively. Crystal I_β (Series 9) was prepared from the results of DTA (Run 4, Fig. 1). Measurements for I_β were carried out after the phase had been annealed at 123 K for 15 hr (Series 9′). The aim of these measurements was to check a possible relaxation phenomenon of I_β having different thermal histories. However, no such effect was observed.

Determination of the Transition Points and the Heats and Entropies of Transition. *(1) II—I Transition*: The transition point was determined to be 258.45 K from the heat capacity measurement. Determination of the heat of transition was carried out for three series of independent measurement. As is shown in Table 2, the values obtained in experiments 1 and 3 were smaller than those of experiment 2. The deviation is beyond experimental error. This might have been caused by the thermal history of crystal II. In Expts. 1 and 3, measurements were carried out for crystal II (fresh sample produced by cooling crystal I to about 245 K), whereas in Expt. 2 crystal II prepared from crystal III was employed. It was expected that a small amount of crystal I was included in crystal II in Expts. 1 and 3 and caused a decrease in the magnitude of the heat of transition. Accordingly the values from Expts. 1 and 3 were abandoned and those from Expt. 2 were taken for calculation of the thermodynamic variables.

(2) II′—II Transition: Figure 2 indicates that, the heat capacity curve in this transition region has two maxima at 167.88 and 172.33 K, respectively, of which the latter is taken as the true transition point. Since the transition takes place over a wide temperature range, it is difficult to determine the exact heat of transition owing to the difficulty in estimation of the

7) The complete data of the heat capacity are kept as Document No. 7207 at the office of the Bulletin of the Chemical Society of Japan. A copy may be secured by citing the document number and by remitting, in advance ¥700 for photoprints. Pay by check or money order payable to: Chemical Society of Japan.

TABLE 1. THE MOLAR HEAT CAPACITIES OF CYCLOHEPTANOL
Mol. wt. = 114.189 0°C = 273.15K

$T_{av.}$/K	$\Delta H/\Delta T$/JK^{-1} mol^{-1}	ΔT/K	$T_{av.}$/K	$\Delta H/\Delta T$/JK^{-1} mol^{-1}	ΔT/K	$T_{av.}$/K	$\Delta H/\Delta T$/JK^{-1} mol^{-1}	ΔT/K
Series 1 (Quenched glassy crystal)			Series 2[a] (Annealed glassy crystal)			Series 3 (Crystals II′ and II)		
13.955	6.964	1.82	13.804	6.561	1.43	13.993	6.722	2.54
17.920	11.156	2.47	16.473	9.589	1.94	18.393	11.304	2.25
21.725	15.520	2.43	19.782	13.902	2.41	22.181	15.628	2.03
14.161	6.902	2.20	14.405	7.285	1.72	25.784	19.562	1.90
18.146	11.418	1.79	17.815	11.088	1.61	29.783	25.739	1.89
22.375	16.209	2.62	20.590	14.165	1.52	33.481	26.903	1.77
26.786	20.659	1.96	23.201	17.150	1.24	37.468	30.712	2.01
31.082	25.001	2.10	26.062	20.207	1.54	41.408	31.876	2.15
35.066	28.831	2.28	29.352	23.414	1.65	45.444	37.045	1.94
39.279	32.537	1.99	32.574	26.579	1.87	49.334	39.941	2.16
43.322	35.326	2.39	36.029	29.709	1.64	53.467	43.054	2.00
47.819	39.028	2.15	39.926	32.951	1.99	57.628	46.095	2.49
52.104	42.133	2.36	44.344	36.405	1.91	60.456	48.065	2.39
56.622	45.396	2.19	49.075	39.941	2.30	65.056	51.426	2.24
61.054	48.624	2.04	53.815	43.429	2.34	69.398	54.352	2.12
65.213	51.665	2.34	58.307	46.696	2.17	73.541	57.120	2.03
98.889	76.866	2.07	63.322	50.398	2.06	78.469	60.916	1.92
102.982	80.317	2.01	67.022	52.906	1.77	83.631	64.929	2.66
119.422	97.747	2.39	70.634	55.358	2.03	88.812	68.946	2.55
134.369	131.393	1.94	74.602	58.114	1.94	93.792	72.691	2.47
138.134	144.337	1.81	78.770	61.223	2.10	98.604	76.355	2.39
141.602	153.050	1.73	82.886	64.490	2.03	104.600	81.263	3.15
145.058	155.541	1.71	87.175	67.893	2.15	110.764	87.179	2.99
			91.577	71.126	2.42	116.612	92.936	2.85
124.930	109.693	1.67						
128.302	117.025	1.59	Series 2′[b]			112.794	88.724	3.27
132.553	126.825	2.02	(Annealed glassy crystal)			121.472	97.295	4.59
						128.199	103.872	2.91
78.727	61.197	1.44	13.977	6.557	2.28	133.991	109.825	2.79
82.136	63.931	1.78	21.621	15.295	2.93	139.515	115.720	2.69
86.726	67.509	2.18	26.815	20.766	2.75	144.802	122.556	2.58
91.008	71.211	2.09	31.604	25.444	2.16	149.934	130.092	2.47
95.135	73.757	2.03	35.627	29.244	1.85	154.803	138.720	2.35
			39.359	32.507	2.18			
59.132	44.538	1.84	43.506	34.861	2.03	140.423	118.897	2.73
63.328	50.322	2.15	48.274	38.994	2.43	145.768	125.729	2.61
67.995	53.537	2.02	53.145	42.922	2.21	151.398	133.713	3.40
74.748	58.224	2.33	57.714	46.266	2.67			
79.209	61.508	2.18	62.849	50.027	2.49	191.381	159.247	2.94
101.084	78.687	1.72	70.948	55.606	2.24	197.986	159.985	4.39
104.958	81.950	2.65	76.133	59.188	1.63	206.737	162.305	3.34
108.888	87.384	2.57	91.867	71.313	1.65			
115.177	92.864	2.43	97.496	75.711	3.15	244.267	176.695	4.03
119.954	99.854	2.30	109.590	86.445	2.85	252.206	182.516	3.94
124.470	107.493	2.19	114.266	91.444	2.74			
128.758	116.602	2.06	119.879	98.784	3.11	189.474	157.396	2.97
131.821	125.482	1.97				195.379	158.650	2.94
136.903	143.753	2.17	119.428	97.589	3.14	201.251	160.531	2.91
139.869	152.402	1.25	125.474	108.047	2.92			
			131.512	119.451	3.52	214.743	164.966	2.29
			143.235	152.074	1.71	219.667	166.574	2.27

TABLE 1 (Continued)
Mol. wt. = 114.189 0°C = 273.15K

$T_{av.}$/K	$\Delta H/\Delta T$/JK^{-1} mol^{-1}	ΔT/K
224.195	167.721	2.26
231.237	169.769	2.19
235.576	171.765	2.16
239.868	174.072	2.14
	Series 3′	
	(II′-II transition)	
157.396	149.979	3.12
164.762	181.075	2.35
169.729	226.453	2.27
171.854	269.793	1.97
172.974	167.713	4.28
179.510	158.343	2.96
185.474	157.993	2.96
	Series 3″	
	(II′-II transition region)	
155.758	135.833	2.38
160.330	156.398	2.15
164.405	183.045	1.91
167.882	234.778	1.60
170.610	213.245	0.65
171.702	318.968	0.45
172.976	232.292	0.88
175.240	161.960	1.86
	Series 4	
	(Crystal III)	
208.655	157.686	2.33
213.282	159.759	2.30
218.546	162.028	2.29
223.089	164.374	2.26
227.587	166.463	2.24
232.038	168.711	2.22
178.713	147.267	4.85
187.570	149.796	4.78
195.473	152.389	4.71
202.488	154.918	3.10
210.570	158.479	3.04
	Series 5	
	(Crystal III′)	
13.881	6.643	2.24
17.551	10.771	1.92
20.757	14.490	1.73
24.595	18.621	2.45
28.884	23.069	2.30
33.158	27.133	2.23
37.453	31.061	2.35
41.809	34.597	2.08
45.890	37.727	2.19
50.054	40.832	2.00
54.826	44.381	2.45
59.529	47.818	2.28
62.345	49.857	2.18
66.558	52.872	2.06
71.080	55.955	2.32
75.558	59.048	2.18
80.208	62.604	2.08
85.387	67.087	3.21
93.140	73.604	2.99
98.977	79.280	2.83
103.525	84.671	2.79
108.780	91.107	2.55
113.749	97.892	2.42
119.046	105.040	3.45
124.101	112.205	2.19
128.398	117.750	2.11
133.799	123.047	2.86
138.796	129.615	2.31
143.433	129.235	2.31
125.516	115.144	2.19
129.804	120.057	2.11
134.482	123.767	3.08
140.888	127.555	3.66
125.230	113.604	2.18
129.506	119.033	2.10
	Series 5′	
	(II′-III transition region)	
145.354	130.395	1.72
148.326	132.881	0.85
150.359	144.183	1.07
152.426	155.933	1.01
154.522	140.477	1.08
157.762	138.801	1.80
15.859	8.773	2.53
19.700	13.133	1.71
23.660	17.572	2.20
27.508	21.538	2.14
31.545	25.517	2.30
35.722	29.432	1.96
39.924	33.023	2.09
43.862	36.094	1.89
47.876	39.152	2.00
52.012	42.359	2.46
57.753	45.255	2.33
59.361	47.652	2.28
63.754	50.893	2.14
68.020	53.874	2.22
72.360	56.911	2.12
76.742	60.067	2.35
81.668	64.178	3.52
86.440	72.328	1.99
91.062	71.817	2.38
96.301	76.401	3.40
102.918	83.110	3.19
108.629	89.815	2.01
105.933	86.633	2.78
112.660	94.992	2.60
120.149	107.599	2.38
124.785	119.622	2.20
128.014	131.790	2.06
133.243	123.767	2.14
137.515	125.362	2.12
141.736	127.559	2.09
146.919	131.167	2.04
138.181	125.576	1.94
142.352	127.892	2.51
121.078	109.612	2.15
126.233	127.218	1.93
109.648	90.928	1.98
115.693	99.470	2.39
122.022	110.772	3.32
127.828	131.244	1.96
132.438	132.344	2.91
	Series 6	
	(Crystal III″)	
	Series 7	
	(Crystal-I)	
259.534	192.462	1.40
265.674	197.908	2.68

Table 1 (Continued)
Mol. wt. = 114.189 0°C = 273.15K

$T_{av.}$/K	$\Delta H/\Delta T$/JK^{-1} mol^{-1}	ΔT/K	$T_{av.}$/K	$\Delta H/\Delta T$/JK^{-1} mol^{-1}	ΔT/K	$T_{av.}$/K	$\Delta H/\Delta T$/JK^{-1} mol^{-1}	ΔT/K
270.958	203.218	2.62	17.559	10.763	1.83	120.837	107.787	2.74
276.139	208.788	2.57	21.080	14.800	2.19	125.482	117.306	2.15
			25.181	19.255	2.06	129.784	123.575	2.13
276.689	210.545	1.74	28.910	22.971	1.92	133.977	128.190	2.07
			33.211	27.065	2.19	138.066	132.058	2.02
			37.318	30.801	2.21			
	Series 8		41.693	34.362	2.55	153.570	141.625	2.32
	(Liquid)		46.477	37.962	2.28	158.202	143.639	2.29
			52.009	42.235	2.45	162.799	145.715	2.26
283.167	233.064	2.44	56.698	45.575	2.27	169.097	147.156	3.37
285.471	235.589	2.39	59.029	47.328	2.71			
290.211	241.035	2.36	64.836	51.494	2.05			
295.444	247.142	3.46	68.817	54.211	1.95		Series 9′	
			72.619	57.307	1.87			
298.265	250.256	3.05	76.862	59.901	2.18	114.059	94.050	1.82
304.377	257.417	3.18	81.109	63.270	2.08	117.624	100.067	1.74
310.344	264.176	2.91	85.183	66.456	2.00	121.023	107.032	1.67
316.075	271.098	2.85	89.424	69.812	1.87	124.057	113.788	1.19
			93.601	73.066	2.14	126.379	118.637	1.15
			97.807	76.504	2.07	136.207	130.305	6.02
	Series 9		101.872	80.300	1.99	142.739	135.453	2.34
	(Crystal I_β)		107.227	85.115	2.84	150.160	140.012	2.27
			111.912	91.627	2.04	152.432	141.202	2.26
14.001	6.871	1.82	116.596	99.206	1.93			

a) Annealed at 130.7 K for 75 hr
b) Annealed at 133.2 K for 68 hr

'normal' heat capacity. We thus calculated only the difference of enthalpy between crystal II′ at 162.5 K and crystal II at 176.5 K as given in Table 2.

(3) III—II Transition: The transition point could not be determined on account of the superheating effect of crystal III above the transition point. Thus the determination was carried out by measuring the magnitude of the temperature drift which was brought about by a spontaneous heat evolution or absorption due to the transition between crystals II and III. For this purpose a mixture of crystals II and III in the ratio about 1 : 1 was used since the rate of transition is expected to be maximum at this ratio where the best sensitivity is expected for the measurement. The temperature dependence of the drift for this specimen was measured at the temperature region 215—240 K and the transition point was determined as shown in

Table 2. Transition points, heats of transition, and transition entropies

II—I Transition T_t=258.45K

Enthalpy of transition

		T_i/K	T_f/K	$\Delta_t H$/Jmol^{-1}
Expt	1	252.606	261.592	827.3
Expt	2	252.103	260.307	875.5
Expt	3	249.892	260.228	849.3

$\Delta_t S$=3.39 JK^{-1}mol^{-1}

III—II Transition T_t=227.26K

Enthalpy of transition

		T_i/K	T_f/K	$\Delta_t H$/Jmol^{-1}
Expt	1	230.127	239.667	551.3
Expt	2	226.236	239.911	555.8
			mean	554±2

$\Delta_t S$=2.44 JK^{-1}mol^{-1}

III′—III Transition T_t=152.30K

Enthalpy of transition=58.07 Jmol^{-1}

$\Delta_t S$=0.381 JK^{-1}mol^{-1}

II′—II Transition T_t=172.23K

Enthalpy difference between 162.500 and 176.500K

Expt	1	2919 Jmol^{-1}
Expt	2	2930 Jmol^{-1}
	mean	2925 Jmol^{-1}

Melting T_m=280.30K

Heat of melting

		T_i/K	T_f/K	ΔH_m/Jmol^{-1}
Expt	1	276.622	281.958	1606.9
Expt	2	276.571	282.239	1598.5
Expt	3	275.829	282.276	1606.4
			mean	1604±3

$\Delta_m S$=5.72 JK^{-1}mol^{-1}

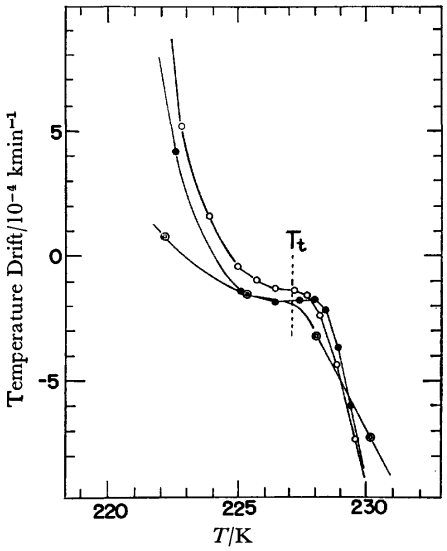

Fig. 3. Determination of the transition point between the crystal-II and III.

Fig. 3. The heat of transition was measured twice and the results are shown in Table 2. The values from Expt. 1 were determined by measuring the enthalpy difference between superheated crystal III (at 230.1 K) and crystal II at 239.7 K, since we did not know the superheating effect at that stage. The measurement in Expt. 2 was carried out between 226 and 240 K.

(4) III′—III Transition: The transition point was determined to be the temperature at which the heat capacity curve reaches a maximum value. Although this curve has a shape similar to that of second order phase transition, it took more than one hour to attain equilibrium after heating was over. The heat and entropy of transition are given in Table 2.

(5) III″—III Transition: The transition is considered to be that of higher order judging from the shape of the heat capacity curve. In contrast to the III′—III transition, equilibrium temperature was attained in a few minutes. As in the case of the II—II′ transition, estimation of contribution from the lattice part was difficult and no accurate determination

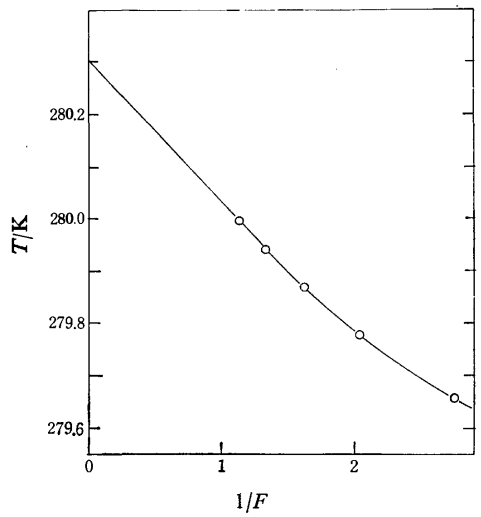

Fig. 4. Melting curve for cycloheptaol

of the entropy of transition could be made. The transition point was determined to be 128.2 K from the heat capacity curve.

(6) Melting Process: The data of fractional melting are plotted in Fig. 4. The melting point and the content of impurities which do not form solid solution with crystal I were determined from the curve. The melting point is the value obtained under the pressure of about 1 atm since the calorimeter cell contained helium gas. The difference between this and the triple point cannot be calculated since the data of the volume change at the melting is not available. The purity of the specimen was found to be 99.932%. The value of the enthalpy of melting is given in Table 2.

Estimation of the Heat Capacity of Crystal I_α Between 140 and 258 K. The heat capacity of crystal I_α (supercooled crystal I) between the temperature region 145—258 K could not be measured on account of its instability. Thus it was estimated in such a way that the difference of the enthalpy between 145 and 258 K agrees with that determined experimentally. The result is given in Fig. 2 by dashed line. Between 228 and 258 K, the heat capacity curve of crystal I is estimated to be parallel to that of crystal II and represented as follows.

$$C_p(\mathrm{I}) = C_p(\mathrm{II}) + 4.30. \quad (1)$$

Between 145 and 288 K, the interpolation equation is estimated to be;

$$C_p(\mathrm{I}_\alpha) = 180.35 - 0.45888T + 1.8769 \times 10^{-3}T^2. \quad (2)$$

By these equations the enthalpy of crystal I_α at 144.097 K is calculated to be 9036 J mol^{-1}. Here the enthalpy of crystal III′ at 0 K was taken as the reference point of enthalpy. The value obtained by direct measurement was 9010 J mol^{-1} which is in good agreement with that calculated by Eqs. 1 and 2. The procedure of the direct measurement was reported previously.[3]

Estimation of the Heat of Transition Between Crystal I and the Unidentified Phase. From DTA, it was found that crystal I_α is transformed into an unidentified phase at 197 K. We attempted to calculate the heat of transition for this phase change assuming that the unidentified phase was either crystal I or crystal II. For this purpose it is necessary to determine the enthalpies for crystals I_α, I_β, and II at 197 K. The values for crystals I_α and II were calculated to be 17.35 and 16.71 kJ mol^{-1}, respectively, from the above data. The value for crystal I_β was determined directly[3] at 163.9 K to be 11.48 kJ mol^{-1}. The value at 197 K was then calculated to be 16.49 kJ mol^{-1} by means of the following equation which was estimated to be between 165 and 197 K as

$$C_p = 0.291T + 99. \quad (3)$$

The heat of transition is thus determined to be either 0.86 ± 0.05 or 0.22 ± 0.05 kJ mol^{-1} by assuming that the unidentified phase is either crystal I_α or crystal II. It is reasonable, however, to consider the value of transition between I_β and the unidentified phase to be close to that of the II—I transition (0.875 kJ mol^{-1}) from a comparison of the peak areas of DTA thermogram (Run 4, Fig. 1). Accordingly, we estimated that the phase into which crystal I_β is transformed would be

TABLE 3. CALCULATION OF THIRD LAW ENTROPIES.

1) The third law entropy of crystal I at 258.45 K *via* III′—III, III—II, and II—I transition

Temperature	Contribution	ΔS / $JK^{-1}mol^{-1}$
0 — 12.5	Debye extrapolation θ_D=112.9	1.73
12.5—152.30	$\int C_p(III')\, d\ln T$	114.04
152.30	Transition $\left(\frac{58.07}{152.30}\right)$	0.38
	$\sum$ =	116.15
152.30—227.26	$\int C_p(III)\, d\ln T$	60.08
227.26	Transition $\left(\frac{554}{227.3}\right)$	2.44
	$\sum$ =	178.67
227.26—258.45	$\int C_p(II)\, d\ln T$	22.70
258.45	Transition $\left(\frac{875.5}{258.45}\right)$	3.39
	$\sum$ =	204.76

2) The third law entropy of crystal I_α at 258.45K *via* crystal I.

0 — 13.5	Debye extrapolation θ_D=112.7	2.17
13.5 — 145.5	$\int C_p$(Glassy cryst.) $d\ln T$	107.07
145.5 —258.45	$\int C_p(I_\alpha)\, d\ln T$	94.82
	$\sum$ =	204.06

a) Equations 18 and 19 were used for the calculation.

3) The third law entropy of crystal II at 227.26K *via* crystal II′

Temperature	Contribution	ΔS
0 — 13.5	Debye extrapolation θ_D=114.2	2.09
13.5 — 162.5	$\int C_p(II')\, d\ln T$	118.65
162.5 — 177.5	Transition region	18.15
177.5 —227.26	$\int C_p(II)\, d\ln T$	39.97
	$\sum$ =	178.86

4) The third law entropy of crystal III at 152.30K

Temperature	Contribution	ΔS
0 — 13.5	Debye extrapolation	2.31
13.5 —152.30	$\int C_p(III'')\, d\ln T$	114.41
	$\sum$ =	116.41

5) Zero-point entropy calculated by assuming that of crystal III′ to be zero.

Glassy crystal	0.70
Crystal II′	—0.19
Crystal III″	—0.26

crystal I_α and the heat of transition between the phases 860±50 J mol^{-1}.

Residual Entropies of Various Phases. Assuming the entropy of crystal III′ at 0 K to be zero, we calculated the zero-point entropies for various other phases. The calculation for glassy crystal and crystal I_β are based on the above estimations. The results are given in Table 3. Below 13 K, the entropy changes were calculated with use of the Debye equation assuming

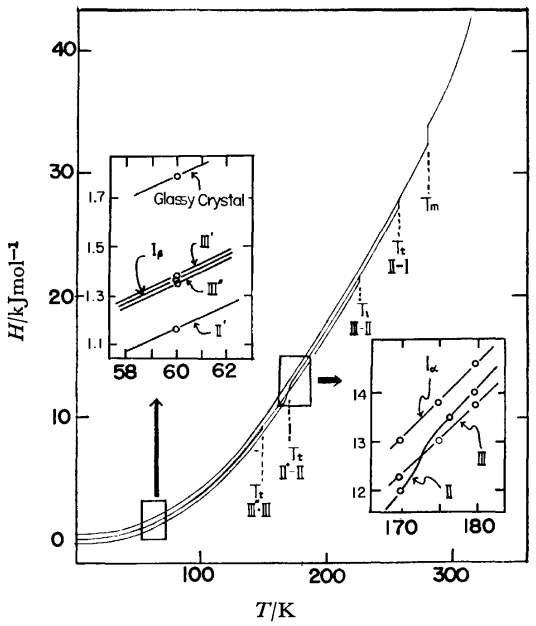

Fig. 5. Enthalpy curves of cycloheptanol.

6 degrees of freedom. The Debye temperatures are given in Table 3. The residual entropy determined for glassy crystalline state amounts to 0.70 $JK^{-1}mol^{-1}$, whereas the zero point entropies of other phases can be considered to be zero within experimental error.

Thermodynamic Functions of Various Phases. The thermodynamic functions derived from the data are given in Table 4 and the enthalpies in Fig. 5. The enthalpy curves are close to each other on account of small heats of transition. The entropy curves behave in a similar way. The relative Gibbs energies as well as the relative enthalpies of each phase with reference to crystals III′ and III are plotted in Figs. 6 and 7 for comparison of the stabilities of various phases. We see in Fig. 6, that crystal II′ is more stable than crystal III′ below 150 K. Thus the phase transformation from crystal III′ or III″ to crystal II′ should take place by annealing crystal III′ or III″ below 150 K. However, annealing of crystal III′ for 6 days at 140 K gave no such an effect by DTA study. The enthalpies of crystals II and III become equal at about 170 K

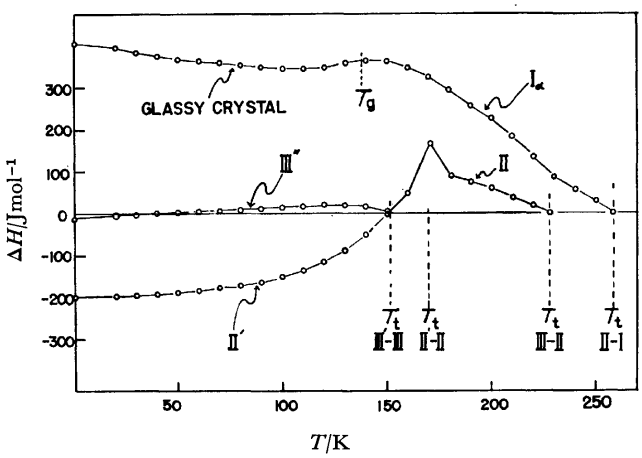

Fig. 6. Difference in Gibbs energy between the crystal-III′ and the other various phases.

TABLE 4. THERMODYNAMIC FUNCTIONS OF CYCLOHEPTANOL

T/K	$C_p°$ JK^{-1}mol^{-1}	$S°-S_0°$ JK^{-1}mol^{-1}	$[H°-H_0°]/T$ JK^{-1}mol^{-1}	$-[G°-H_0°]/T$ JK^{-1}mol^{-1}
		(Crystal III')		
10	(2.67)	(0.898)	(0.6730)	(0.2250)
20	13.66	5.951	4.304	1.647
30	24.18	13.524	9.213	4.310
40	33.04	21.74	14.105	7.635
50	40.80	29.96	18.676	11.284
60	48.22	38.06	22.985	15.075
70	55.23	46.02	27.09	18.93
80	62.60	53.86	31.06	22.80
90	70.82	61.70	35.01	26.69
100	80.39	69.64	39.05	30.59
110	92.65	77.86	43.35	34.51
120	106.38	86.50	48.03	38.48
130	119.58	95.56	53.05	42.52
140	127.18	104.73	58.09	46.64
150	141.41	113.73	62.91	50.82
		Transition 152.30K		
		(Crystal III)		
160	139.97	122.94	67.90	55.04
170	144.63	131.58	72.29	59.29
180	147.60	139.93	76.39	63.53
190	150.57	147.99	80.22	67.77
200	154.08	155.80	83.82	71.98
210	158.23	163.42	87.26	76.16
220	162.82	170.88	90.59	80.29
		Transition 227.26K		
		(Crystal II)		
230	169.71	180.69	96.27	84.42
240	174.05	188.00	99.41	88.59
250	180.60	195.23	102.52	92.71
		Transition 258.45K		
		(Crystal I)		
260	192.83	205.88	109.07	96.82
270	202.20	213.33	112.34	100.99
280	213.13	220.87	115.78	105.10
		Fusion 280.30K		
290	240.83	234.83	125.37	109.46
300	252.35	243.18	129.41	113.77
310	264.02	251.65	133.56	118.09

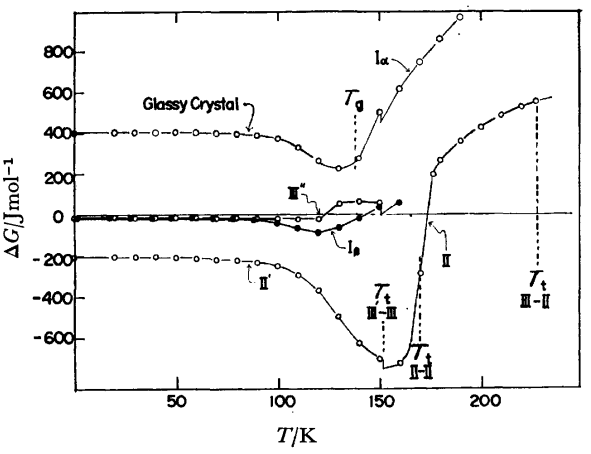

Fig. 7. Difference in enthalpy between the crystal-III' and the other various phases.

as shown in Fig. 7. The irreversible phase change might take place at this temperature, with neither heat evolution nor heat absorption. It was found, however, that the annealing of crystal II at about 170 K (II'—II transition region) for several days caused no phase change in crystal III. The Gibbs energy of crystal III'' is slightly smaller than that of crystal III'. This might be due to experimental error.

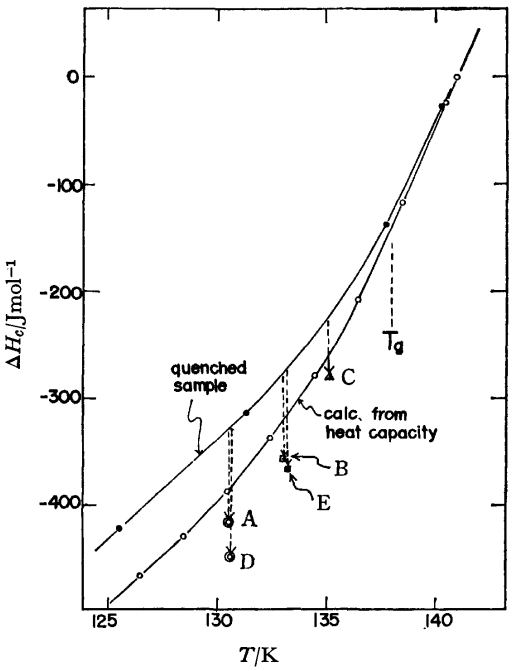

Fig. 8. Decrease of the configurational enthalpy of the glassy crystal by annealing treatment.

Relaxation Phenomenon of Enthalpy. The relaxation of the enthalpy of the glassy crystalline state was investigated by annealing for 20 hr at 130.6, 133.0, and 135.2 K. The values of the enthalpy decrease during the treatments are given by points A, B, and C in Fig. 8 where the ordinate indicates the configurational enthalpy for the sake of convenience. The method of calculation of the configurational enthalpy has been given.[2,3] For the calculation it was necessary to estimate the heat capacity due to lattice and internal vibrations. This is difficult on account of the gradual increase of the heat capacity curve below T_g (Fig. 2), but it was estimated by the equation

$$C(\text{vib}) = 0.7197T + 4.62. \quad (4)$$

Point D represents the value of the enthalpy after annealing for 75 hr at 130.7±0.5 K and point E stands for the value after the annealing for 68 hr at 133.3 K. From the results, the conventional relaxation times were calculated to be 24 hr at 130.7 K on the assumption that the enthalpy decreased exponentially. This might not be correct since it was found that the relaxation in the glassy crystalline state of 2,3-dimethylbutane is not the genuine exponential type.[3] Thus the present data of the relaxation time give only approximate values of the time constant.

Measurements of Raman and IR Spectra. In order to estimate the contribution of internal vibrations to heat capacities, the Raman and IR spectra were

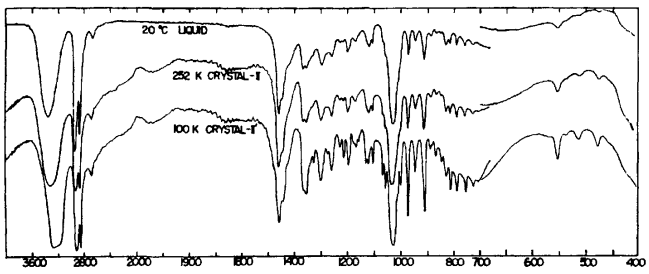

Wave number (cm^{-1})

Fig. 9. Infrared spectra of cycloheptanol.

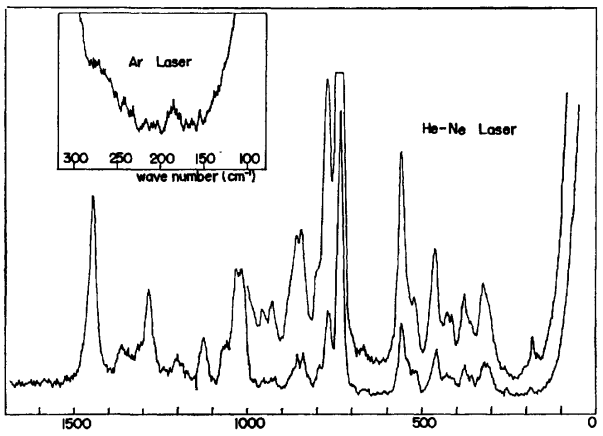

Wave number (cm^{-1})

Fig. 10. Raman spectra of cycloheptanol.

measured in liquid state. The observed Raman and IR spectra are shown in Figs. 9 and 10, respectively. The frequencies of bands are as follows;

Raman: 179, 255, 295, 319, 355, 372, 410, 420, 456, 516, 553, 661, 725, 764, 790, 835, 853, 922,

IR: 455, 474, 512, 535, 552, 570, 725, 730, 760, 790, 816, 813, 850, cm^{-1}.

Since the band at 179 cm^{-1} was observed by using both a He–Ne laser and an Ar laser as a light source, it was not a noise accompanied by a He–Ne laser. The weak infrared bands at 474, 535, and 570 cm^{-1} were assigned to combination bands, *i.e.* 179+295=474, 179+355=534, and 255+319=574. From the results, the frequencies of the normal modes were estimated. Among the possible 60 modes, the following 37 modes are assigned empirically (Table 5). The remaining 23 modes are assigned to the CH_2 rocking ($\times 6$) and skeletal modes ($\times 17$). Since the molecule of cycloheptane belongs to a symmetry group of C_s or C_2,[8] it is expected that it has at most only a mirror plane for a symmetry element and that all of the modes are not degenerate and active both in the IR and Raman spectra. We therefore adopted the following 15 bands; 179, 255, 295, 319, 355, 372, 410, 421, 456, 516, 553, 661, 725, 764, and 790 cm^{-1} as the normal modes which are not degenerate. There still remain 8 modes. Since it is known empirically that the CH_2 rocking modes have frequency below 1100 cm^{-1}, we assumed 4 modes with an average frequency of 900 cm^{-1} and other 4 modes with one of 1100 cm^{-1}. Since the heat capacity due to the mode whose frequency is greater than 800 cm^{-1} is small below 200 K, ambiguity in the estimation causes no trouble.

8) J. B. Hendrickson, *J. Amer. Chem. Soc.*, **83**, 4537, (1961).

Table 5.

Assignment	Wave number	Number of modes
OH stretching	3500	×1
OH bending	1300	×1
OH bending	725	×1
CH stretching	3000	×13
CH_2 scissors	1450	×6
CH_2 wagging	1300	×6
CH_2 twist	1300	×6
CH bending	1300	×2
CO stretching	1030	×1

Discussion

Residual Entropy. We have used a term "glassy crystal" for the phase which was established below 140 K by rapid cooling of crystal I. The residual entropy of this crystalline phase amounted to 0.7 $Jmol^{-1}K^{-1}$. This is too small to claim that the phase has a residual entropy because its magnitude is the same order as that of the experimental error. However, we can give several reasons for assuming that the phase should be in a glassy crystalline state. First, it is possible that the value we obtained for the residual entropy is not correct, since it was determined on the assumption that crystal III′ has no residual entropy. It is necessary to determine the absolute value of the entropy from a comparison of the entropy in the gaseous state determined by thermal method with that determined from spectroscopic data. Second, the stabilization phenomenon characteristic of glassy state was actually observed in this phase. Thus it can be concluded that the phase is in a non-equilibrium state. Third, if crystal II′ is taken as the reference state with no residual entropy (Table 3 and Fig. 6), the value of the residual entropy increases to 0.9 $Jmol^{-1}K^{-1}$. This value is slightly larger than the limit of experimental error (0.6 J $mol^{-1}K^{-1}$) and might indicate the presence of the residual entropy. Fourth, the shapes of the heat capacity curve and the DTA diagram closely resemble those of known glassy crystals.[2,3,4] The empirical rule for the glassy crystals states that the ratio of T_g and T_2 is nearly constant (1.15—1.20).[3] Here T_2 is the temperature defined by Gibbs and DiMarzio,[9] at wihch the configurational entropy of supercooled liquid vanishes. By means of the rule we attempted to estimate the true value of the residual entropy of the glassy crystalline state. The value of a ratio between T_g and T_2 is related to a residual entropy S_0 by the following equation.

$$\Delta C_p \ln (T_g/T_2) = S_0. \quad (5)$$

Here ΔC_p is the jump of the heat capacity at the glass

9) J. H. Gibbs and E. A. DiMarzio, *J. Chem. Phys.*, **28**, 373 (1958).

transition point. Since the value of T_g/T_2 is known to be 1.15—1.20 for the glassy crystals and the ΔC_p for the present glassy crystal amounts to about 30 $JK^{-1}mol^{-1}$, the value of S_0 is determined to be 5.0 $JK^{-1}mol^{-1}$ from the equation. If this is correct, all the other phases also have a residual entropy of about 5 $JK^{-1}mol^{-1}$. We therefore consider that the residual entropy of glassy crystal is not so large as compared with 5 $JK^{-1}mol^{-1}$. The order of magnitude seems to be too small since this molecule has the following conformations.

If one assumes a chair form, there are seven distinguishable conformations with respect to the carbon atom on which a hydroxyl group is bonded. Furthermore, there are two positions to locate the hydroxyl group on the carbon atom *i.e.* an equatorial position and an axial one. Thus we can anticipate at least 14 conformations. If the position of a hydrogen atom of the hydroxyl group is considered with respect to its internal rotation, the number of conformations may increase further by a factor of three *i.e.* 42 kinds of conformations. The value of $R\ln(14)$ and/or $R\ln(42)$ amount to 22 and/or 31 $JK^{-1}mol^{-1}$ respectively. Here R reprensents the gas constant. Although we do not know the energy difference between the conformations, we can expect that the configurational degree of freedom will contribute greatly if they are frozen at the glass transition point. Thus it seems to be reasonable to consider that not all of these conformational degrees of freedom are frozen at the T_g. It is suggested that some motional degrees of freedom exist even below T_g. This might be explained in terms of interconversions between the molecules with various conformations in the glassy crystalline state.

The Plastic Crystalline State. Since the value of the entropy of melting is 5.72 $JK^{-1}mol^{-1}$, crystal I is considered to be plastic. The sum of the values of the entropy of melting and those of I—II transition amounts to 11.6 $JK^{-1}mol^{-1}$. Since this is still smaller than that of the Timmermans criterion,[9] crystals II and III might also be considered to be plastic. This is supported further by the motional narrowing phenomenon of the NMR spectra for these phases and the magnitude of the heat capacities. We see in Fig. 2 that the supercooled states of crystals II and III show no anomaly similar to that in glass transition in their heat capacity curves. In contrast to the glassy crystal, the high degree of configurational degrees of freedom for crystals II and III give rise to the λ-type phase transitions as shown in Fig. 2. We suggested that crystals II and III have residual entropy and these phases are also looked upon as frozen-in states at low temperatures. However, since no glass transition phenomenon could be observed for the crystals down to the lowest temperature, we are not convinced that we can call them glassy crystals. We might say that plastic crystals such as II or III do not always show the glass transition when they are cooled down without irreversible transformation into other more stable phases. In order to solve the so-called Kauzmann paradox,[1] Gibbs and DiMarzio postulated that a supercooled liquid will show the second order phase transition with infinitely slow cooling rate.[9,11] If we adopt this point of view for crystal I and cool it down very slowly below T_g, this phase might also have a second order phase transition similar to that of crystal II or III as far as the internal equilibrium is maintained below 140 K.

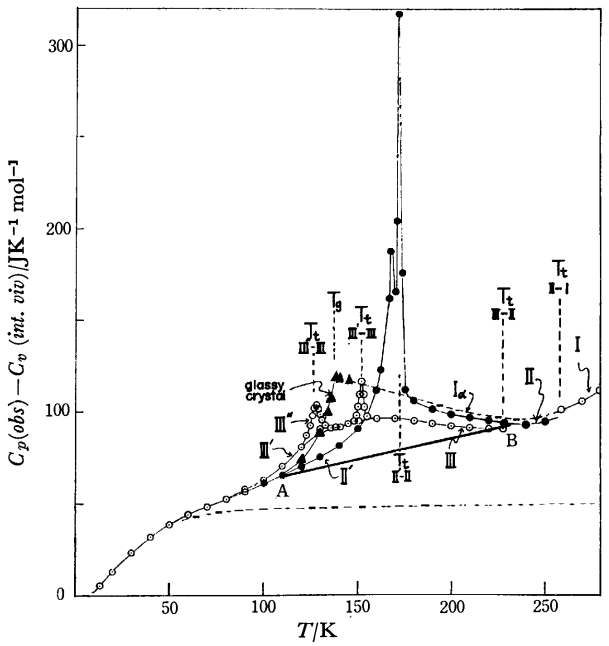

Fig. 11. Plot of C_p(obs)–C_v(internal vib.).

Analysis of Heat Capacities. From the data of Raman and IR spectra, the magnitude of contribution of internal vibrations to the heat capacity was calculated. The value was then subtracted from the observed total heat capacities. The result is shown in Fig. 11. The dashed line represents the heat capacity due to the lattice vibration calculated by using the Debye model with 6 degrees of freedom. The difference between the plotted value of (C_p(obs)—C_v(int)) and the value of the dashed line is explained as the sum of anomalous heat capacity C(an) and (C_p—C_v). The C(an) becomes noticeable above around 70 K and amounts to about 50 $JK^{-1}mol^{-1}$ around 200 K for all the phases. This is considered to be another evidence for these phases to be plastic crystals which are generally known to have a large heat capacity whose magnitude can not be explained in terms of only a contribution of vibrations and (C_p—C_v). It is known that the material belonging to the plastic crystals has first order phase transition point in its crystalline state and that the entropy of transition is much larger than that of melting. On the contrary, the entropy of transition of cycloheptanol does not amount to such a large value and the magnitude of the heat capacity of the low temperature form (crystal III) is too large to be explained only from vibrational contribution. This should indicate the evidence of continuous ordering of the molecular orientation and conformations with decreasing temperature. Although the magnitude of

10) J. Timmermans, *J. Phys. Chem. Solids*, **18**, 1 (1961).

11) G. Adam and J. H. Gibbs, *J. Chem. Phys.*, **43**, 139 (1965).

the C(an) is not explained from the molecular motions, we might expect that the changes of configurations and conformations cause this effect.

II—II′ Transition. The difficulty of determining the entropy change for II—II′ transition has been already pointed out. As is shown in Fig. 11, the heat capacity due to the change of configuration does not vanish at temperatures far above the transition point. We calculated the entropy of transition assuming that the "normal" heat capacity is given by the straight line A—B. The procedure is based on an assumption that the configurational heat capacity can be separated into two parts *i.e.* the configurational heat capacity accompanied by the phase transition and that independent of the transition. The entropy of transition thus determined amounted to 17.2 $Jmol^{-1}K^{-1}$ (Rln 7.9).

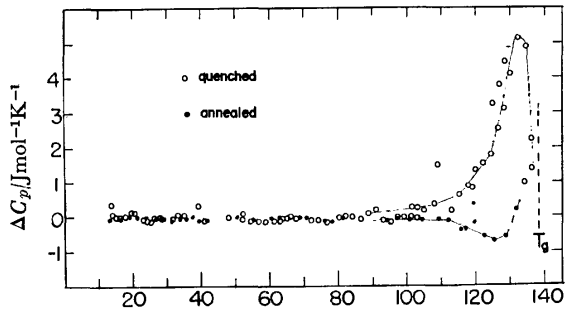

Fig. 12. The deviation of the heat capacities of the quenched glassy crystal and annealed one from the smoothed values.

Difference Between the Heat Capacity of Annealed Glassy Crystal and the Quenched One. The heat capacity of the glassy crystalline state was measured with the specimens which was annealed below T_g and then quenched. The aim of this measurement is to detect the difference in heat capacities of specimens. The difference is shown in Fig. 12. Hardly any difference can be seen below 100 K. However above this temperature it becomes noticeable with a maximum value of 5 $JK^{-1}mol^{-1}$ around 130 K. As a possible explanation, an experimental error might be considered at first since the heat evolution or absorption due to the stablilization effect disturbed the measurements of the heat capacity around 130 K. However, the observed temperature drift due to this effect was not so large as to account for the actual difference at least below 130 K. Thus the fact can be ascribed to the variation of the configurational heat capacity caused by annealing since the anomalous heat capacity was recognized in the glassy crystalline state above 70 K as is seen in Fig. 11. Existence of the degree of freedom not frozen below the glass transition point was confirmed in the glassy crystalline state of cyclohexanol and 2,3-dimethylbutane in the study of broad line NMR and dielectric loss. The decrement of the anomalous heat capacity in the glassy crystalline state caused by annealing can be explained in terms of the variation of the shape and size of the potential energy curves for various conformations caused by annealing.

Crystal I_β. Run-4 in Fig. 1 shows that crystal I_α is transformed into a meta-stable phase around 170 K. Similar phenomena of the supercooled plastic crystals transformed into other meta-stable phases just above their glass transition points were also observed for cyclohexanol[2] and 2,3-dimethylbutane.[3] The heat capacity curve of crystal I_β showed an anomalous increase around 130 K. However, this is not as steep as in the case of glass transition (Fig. 2). The heat capacity curve of the meta-stable phase of 2,3-dimethylbutane also shows a similar hump. The residual entropy of crystal I_β was calculated to be -1.0 ± 1 $JK^{-1}mol^{-1}$ based on the above assumption. On the other hand, the residual entropy of the meta-stable phase of 2,3-dimethylbutane was found to be 2.7 $JK^{-1}mol^{-1}$. In order to see whether this meta-stable phase can be considered as a glassy crystal or not below the temperature at which the anomaly was observed, we measured the heat capacity of crystal I_β in two series subjected to different thermal histories. No change was detected in the magnitude of the heat capacity due to the difference in thermal history. Thus the anomalous increase of the heat capacity can not be attributed to the relaxation phenomenon. It would be noted that this phase does not show any phase transition as in the case of crystal II or III. We may regard this phase as a plastic crystal above 140 K from the magnitude of its heat capacity.

Phase Transition Between Phases with Various Degrees of Stability. In general the degree of stability of a material system can be classified into three steps, *i.e.* stable, meta-stable, and non-equilibrium states. A stable state is the state in which free energy is at its absolute minimum. The meta-stable state is the state in which free energy is at the minimum, but not absolute minimum. The two states are, however, classified as thermodynamically equilibrium states. On the other hand, non-equilibrium state is the state at which free energy is not in its minimum. From this point of view, the phase changes which occur in cycloheptanol can be classified into five groups as shown in Table 6.

Table 6. Classification of phase transitions from the standpoint of thermodynamical stabilities

Type	Stability relation	Example
	Irreversible Transitions	
(1)	non-equilibrium→metastable	Glassy crystal → I_α
(2)	metastable→metastable or stable	$I_\alpha \rightarrow I_\beta$ $I_\alpha \rightarrow$ II II→III
	Reversible Transitions	
(3)	metastable⇌metastable	III″⇌III III′⇌III $I_\beta \rightleftharpoons I_\alpha$
(4)	stable⇌metastable	II′⇌II
(5)	stable⇌stable	III⇌II II⇌I I⇌liquid

(1) includes phase changes between non-equilibrium and meta-stable states. A typical example might be the so-called glass transition, although this is a kind of relaxation phenomenon and not a "phase transition" in a strict sense. In cycloheptanol, the glass transition

between glassy crystal and crystal I_α corresponds to this group. Since the state of glassy crystal changes gradually and continuously with time, the transition is regarded to be irreversible.

(2) includes irreversible transitions between a meta-stable and a stable state or between one meta-stable and another meta-stable phase. These phase transitions are considered to be exo-thermic peaks of the thermogram of DTA (Run 4, Fig. 1).

(3), (4), and (5) include various kinds of reversible phase changes. An example of group (3) can, however, be classified into group (1), since crystals III′, III″, and I_β can be in a non-equilibrium state with residual entropy. At the present stage of investigation, however these phases may be regarded as meta-stable since no thermal histories were detected. The example in (4) might be peculiar in the sense that we can follow the phase transition from each side of the starting phase. Usually we know only the examples from right to left with exothermic effect.

In the previous papers,[2,3,4] we have reported that various kinds of supercooled plastic crystals are transformed stepwise into more stable states. The phenomenon is known as "Ostwald's law of stage" (or step rule). Transitions of this type are those between the discrete states in the phase space and the transitions proceed at the boundary of the phases. There also exists a transition which occurs continuously between the different states in the phase space. This phase change takes place homogeneously. When it happens to occur irreversibly, then one of two phases between which the transition proceeds should be invariably in a non-equilibrium state. Cycloheptanol shows both these trends depending on the thermal histories, and provides good examples for a study of phase changes from thermodynamic or statistical-mechanical as well as kinetic aspects.

Summary

(1) The heat capacities of cycloheptanol were measured from 13 to 300 K. It was found that there exist 8 crystalline phases *i.e.* Crystals I, II, II′, III, III′, III″, I_β, and glassy crystal.

(2) The transition points for transitions II—I, III—II, II′—II, III′—III, and III″—III were determined to be 258.45, 227.26, 127.23, 152.30, and 128.2 K, respectively. Melting point and the glass transition point of glassy crystal were also determined to be 280.30 and 240 K, respectively.

(3) Heats of transition for transitions II—I, III—II, and III′—III and the heat of melting were determined to be 876, 554, 58.1, and 1604 $Jmol^{-1}$, respectively. The entropies of transition corresponding to these phase changes were calculated to be 3.39, 2.44, 0.38, and 5.72 $JK^{-1}mol^{-1}$, respectively.

(4) The residual entropies were also determined for glassy crystal, crystals II and III″ to be 0.70, −0.19, and −0.26 $JK^{-1}mol^{-1}$, respectively, assuming that crystal III′ has no residual entropy.

(5) The free energies and enthalpies of the various crystalline phases were calculated, the instability being determined by comparison of their free energies. It was concluded that crystal II′ was most stable in the temperature region below 170 K, III between 170 and 227.26 K, II between 227.26 and 258.45 K and I between 258.45 and 280.30 K.

(6) Relaxation of the enthalpy in the glassy crystalline state was studied and the relaxation time was determined to be about 24 hr at 133.3 K.

(7) The degree of freedom frozen in the glassy crystalline state was discussed from the viewpoint of conformations of the molecule.

(8) The heat capacities due to internal vibrations were calculated from the data of IR and Raman spectra and the magnitude of heat capacities in the various phases were discussed.

(9) Various kinds of phase transitions found in cycloheptanol were classified from the viewpoint of thermodynamical stabilities.

The authors wish to thank Mr. Shinichi Ishikawa and Mr. Mitsuo Ohama for the measurements of infrared and Raman spectra.

Exciton-Exciton Interaction and Exciton Migration in Anthracene, Pyrene, and Perylene Crystals

Akinori INOUE, Keitaro YOSHIHARA,* and Saburo NAGAKURA

The Institute for Solid State Physics, The University of Tokyo, Roppongi, Minato, Tokyo

**The Institute of Physical and Chemical Research, Wako, Saitama*

(Received November 17, 1971)

The bimolecular annihilation of singlet excitons in pyrene, perylene, and anthracene crystals was studied by the aid of a nitrogen gas laser. The rate constant, γ, for bimolecular annihilation was estimated at 293°K to be 9×10^{-15} and 8×10^{-14} $cm^3\,sec^{-1}$ for pyrene and perylene, respectively. The temperature dependence of γ was measured with the result that it increases with the increasing temperature for the pyrene and perylene crystals, while it is almost independent of temperature for anthracene between 77°K and 293°K. The difference in the temperature dependence of γ was attributed to the difference in the mechanism of the exciton migration of the crystals. The method developed by the present authors for studying the exciton migration based on the exciton bimolecular annihilation was compared with that obtained previously by the use of mixed crystals.

In the last decade, a number of studies have been made of the singlet-exciton migration in aromatic hydrocarbon crystals;[1-5] most of them have been concerned with the fluorescence from host or guest molecules in mixed crystals. However, in the study of the exciton migration, it is desirable to use pure crystals to avoid specific host-guest interaction, the reflection of excitons by guest molecules, and the reabsorption of host fluorescence by guest molecules.[5] The exciton-exciton collision annihilation first sutdied by Bergman, Levine, and Jortner[6] may be useful for this purpose. They studied this phenomenon by observing the radiative decay of the fluorescence from a densely-excited anthracene crystal. Bimolecular collision annihilation was also observed for the pyrene crystal.[7]

The mechanism of the bimolecular exciton annihilation involves the exciton-transfer process followed by a collision ionization of an exciton pair through the autoionization level.[8] Since the former process may be rate-determining,[9,10] the exciton transfer in molecular crystals may be studied by measuring the rate constant, γ, for the bimolecular annihilation. In the present work, the γ value was estimated by measuring the fluorescence decay of densely-excited pyrene and perylene crystals. Furthermore, its temperature dependence was studied for anthracene, pyrene, and perylene crystals in order to clarify the mechanism of the exciton migration.

Experimental

Pyrene and anthracene were purified by vacuum sublimation and zone refining. Pure perylene was obtained by recrystallization of the synthetic material from a toluene solution.[11] Single crystals and polycrystalline samples of these materials were used for the experiment. The samples were excited by pulse radiations with half-widths of about 4 nsec at 3371 Å from a coaxial nitrogen laser.[12,13] The laser power of ~20 kW was measured by the chemical actinometry[14] in each experiment, in order to evaluate the exciton density. The laser beam was focused on a spot about 0.8 mm of diameter on the crystal surface. Filters were used in order to attenuate the intensity of the laser beam. The fluorescence from the samples was passed through a Bausch and Lomb monochromator and was detected by an RCA 1P28 photomultiplier, a Toshiba UV-39 filter being set in front of the entrance slit of the monochromator to eliminate the scattered laser light. By the use of neutral density filters, the photomultiplier pulse current was adjusted to be of the order of magnitude of a few mA, far below its saturation current. The decay curves were displayed on a Tektronix 585 oscilloscope and were photographed. The bimolecular rate constant was estimated by the least-squares method.

Results and Discussion

Estimation of γ Values. Some typical oscilloscope tracings of the fluorescence decays at the low- and high-density excitations are shown in Fig. 1, taking the perylene at 293°K as an example. Semilogarithmic plots of the decay curves are shown in Fig. 2. The decay curve deviates pronouncedly from an exponential decay at the high-density excitation, while it is regarded as exponential at the low-density excitation. The results can be interpreted in terms of the exciton-exciton annihilation. When the bimolecular annihilation of excitons takes place, the singlet-exciton density, n, after the termination of the laser may be represented by Eq. (1):

$$dn/dt = -\alpha n - \gamma n^2 \quad (1)$$

1) D. C. Northrop and O. Simpson, *Proc. Roy. Soc., Ser. A*, **234**, 136 (1956).
2) K. Geschwendtner and H. C. Wolf, *Naturwiss.*, **48**, 42 (1961).
3) H. C. Wolf, "Advance in Atomic and Molecular Physics," Vol. 3, Academic Press, New York (1967).
4) W. Klöpffer and H. Bauser, *Chem. Phys. Lett.*, **6**, 279 (1970).
5) K. Kawaoka and D. R. Kearns, *J. Chem. Phys.*, **45**, 147 (1966).
6) A. Bergman, M. Levine, and J. Jortner, *Phys. Rev. Lett.*, **18**, 593 (1967).
7) C. R. Goldschmidt, Y. Tomkiewicz, and I. B. Berlman, *Chem. Phys. Lett.*, **2**, 520 (1968).
8) S. Choi and S. A. Rice, *J. Chem. Phys.*, **38**, 366 (1963).
9) J. Jortner, *Phys. Rev. Lett.*, **20**, 244 (1968).
10) T. Kobayashi, K. Yoshihara, and S. Nagakura, Sym. Molecular Structure, Kyoto (1971).
11) The pure pyrene and perylene were provided by Professor S. Iwashima, Meisei University and Professor H. Inokuchi, The University of Tokyo.
12) M. Geller, D. E. Altman, and T. A. DeTemple, *J. Appl. Phys.*, **37**, 3639 (1966).
13) A. Inoue, K. Yoshihara, S. Nagakura, T. Kasuya, A. Minoh, S. Kobayashi, and K. Shimoda, *Reports I.P.C.R.*, **47**, 40 (1971).
14) C. G. Hatchard and C. A. Parker, *Proc. Roy. Soc., Ser. A*, **235**, 518 (1956).

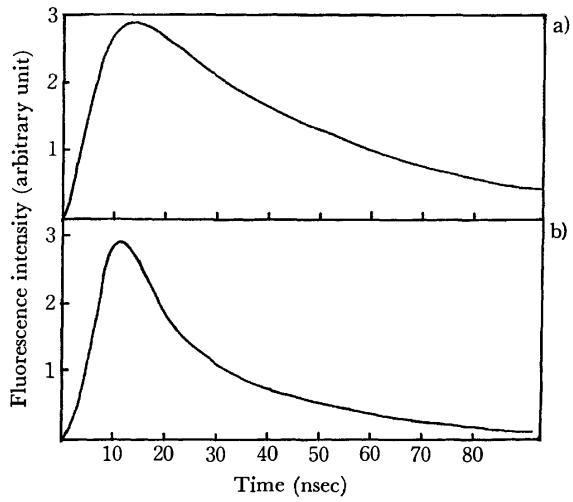

Fig. 1. The fluorescence decay of singlet excitons of perylene crystal at low (a) and high (b) density excitations at 293°K.

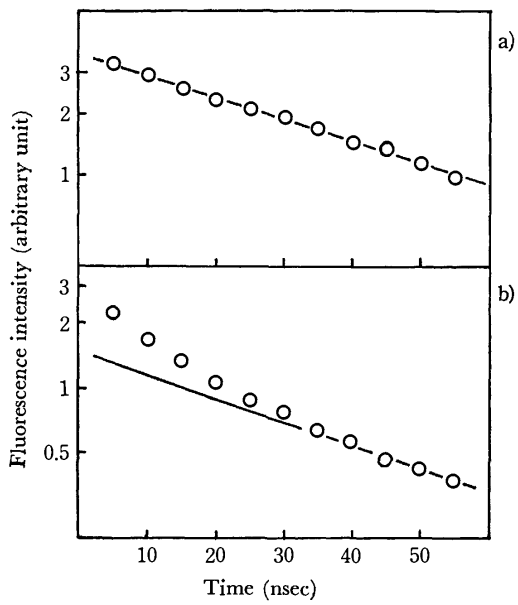

Fig. 2. Semilogarithmic plots of perylene fluorescence intensity *versus* time at low (a) and high (b) exciton density at 293°K.

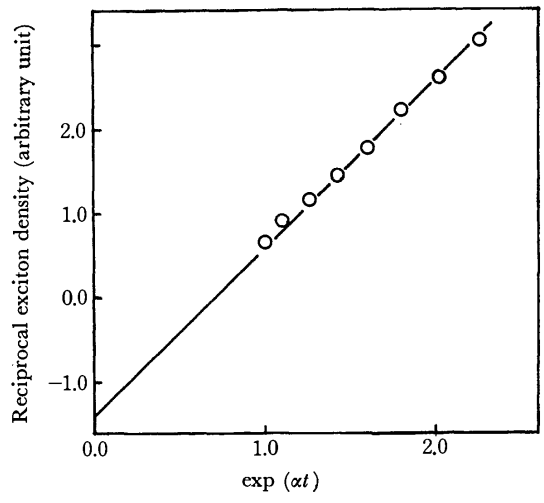

Fig. 3. A plot of the reciprocal exciton density *versus* $\exp(\alpha t)$ of perylene crystal at 293°K.

Integration of Eq. (1) gives the following equation:

$$1/n = (1/n_0 + \gamma/\alpha)\exp(\alpha t) - \gamma/\alpha \qquad (2)$$

where n_0 is the initial exciton density. A linear relationship is expected to be satisfied between $1/n$ and $\exp(\alpha t)$. This relationship was found to be satisfied for the perylene and pyrene crystals at 293°K. The result for the perylene crystal taken as an example is shown in Fig. 3. The γ value was obtained from γ/α corresponding to the intercept of the straight line with the ordinate and from the monomolecular decay constant, α, obtained by the low-density excitation.

The initial exciton densities, n_0's, were estimated for the pyrene and perylene crystals on the following three assumptions. (1) Since the life-times of singlet excitons in the crystal are much longer than the pulse duration of the nitrogen laser, the time dependence of the excitation pulse may be represented by a delta function. (2) The crystals absorb the laser-pulse photons following the Lambert-Beer law. The initial exciton density (cm^{-3}) can be written:

$$n_0 = (N_0/S)(1 - 1/10^{\varepsilon cl})/l \qquad (3)$$

Here, N_0, S, and ε are the number of photons in a laser pulse, the area of the crystal surface illuminated by the laser beam, and the molar extinction coefficient of the crystal, respectively. Furthermore, c is the molar concentration of the crystal, as determined from the crystal data.[15] By determining the penetration depth, l, in such a way that $10^{\varepsilon cl}$ equals e, the mean exciton density in a volume of Sl was calculated. (3) Since the unpolarized laser beam was irradiated perpendicular to the *ab* plane of the perylene single crystal, the molar extinction coefficient was estimated by averaging the polarized values in this plane observed by Hochstrasser.[16] For pyrene, the molar extinction coefficient of the solution[17] was used, since the fluorescence decay was observed for a multicrystalline sample. In the case of anthracene, the exciton may not stay within the irradiated volume during the measurement time, since its migration rate is considered to be very fast. This makes it difficult to determine the accurate value of n_0 and prevents us from determining the γ value for anthracene.

The γ values at 293°K were estimated to be 9×10^{-15} and 8×10^{-14} cm^3sec^{-1} for the pyrene and perylene crystals, respectively.

Mechanism of Exciton Transfer. It is a central question whether the band model or the hopping model is applicable to the energy transfer in molecular crystals. The applicability of these two models is dependent upon the strength of the molecular interaction in the crystals.[18] Under the framework of the band model, the efficienty of energy transfer may be expected to decrease with the increasing temperature since the phonon scatters the coherent diffusion of the

15) For perylene crystal; D. M. Donaldson, J. M. Robertson, and J.G. White, *Proc. Roy. Soc., Ser. A*, **220**, 311 (1953). For pyrene crystal; J. M. Robertson and J. G. White, *J. Chem. Soc.*, **1947**, 358.
16) R. M. Hochstrasser, *J. Chem. Phys.*, **40**, 2559 (1964).
17) R. A. Friedel and M. Orchin, "Ultraviolet Spectra of Aromatic Compounds," John Wiley & Sons, New York (1951).
18) Th. Förster, "Modern Quantum Chemistry," Part III, ed. by O. Sinanoglu, Academic Press, New York (1965).

exciton and limits the mean free path of the exciton.[19] This has actually been found by Hammer and Wolf[20] for naphthalene in the temperature range from 100°K to 6°K. In careful experiments adopting the host-guest systems, no indication of a thermally activated energy transfer process was found in such monomeric molecular crystals as anthracene and naphthalene.[3]

The magnitude of the molecular interaction in the crystal is related with that of the jump time. The time for pyrene was determined to be 2×10^{-11} sec at room temperature from an impurity-quenching experiment.[4] This value is larger by two orders of magnitude than that of anthracene (2×10^{-13} sec) which was obtained from the Davydov-splitting or impurity-quenching experiment.[3] This means that the exciton diffusion is slower by two orders of magnitude for pyrene than for anthracene.

When the free path approaches the distance between neighboring molecules, the hopping model may be a good approximation for the energy transfer. In such dimeric crystals as pyrene and perylene, the lowest excited singlet state is an excited dimer state.[21] Since the electronic interaction between an excited dimer and a ground state dimer is weak,[22] the hopping model may be applicable to this case. Hence, the transfer of the dimer exciton will be assisted by the thermal activation through the lattice phonon.

We measured the temperature dependence of γ; the results are shown in Figs. 4 and 5, which give the plots of log γ *versus* $1/T$ for the pyrene and perylene crystals, respectively. From the slopes of the straight lines, we determined the apparent activation energies to be 330 and 290 cm^{-1} for the pyrene and perylene crystals, respectively.

These results are consistent with the recent studies by Klöpffer and Bauser.[4] They measured the fluorescence

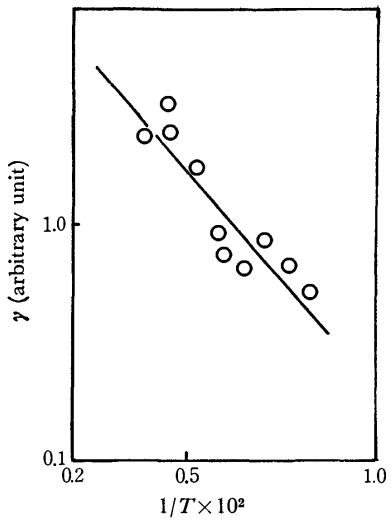

Fig. 4. A plot of log γ *versus* $1/T$ of pyrene multicrystalline sample.

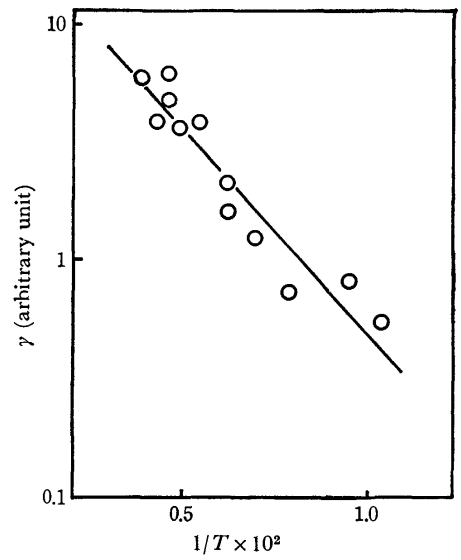

Fig. 5. A plot of log γ *versus* $1/T$ of perylene single crystal.

spectra of the mixed crystal of 10^{-3} mol/mol coronene in pyrene and observed structured coronene fluorescence spectra at 298°K, while at 77°K the only broad fluorescence spectrum of pyrene was observed. This result shows that the energy transfer in the pyrene crystal is completely frozen-in at low temperature.

The anthracene crystal takes the monomeric structure and no excited dimer is formed in the crystal. The electronic interaction between the excited singlet state and the ground state is very strong. The energy transfer is accomplished by the diffusion of monomer excitons due to the dipole-dipole and exchange interactions, and it requires no thermal activation energy. The band model may be applicable to this case. As is seen in Fig. 6, the γ value is almost independent of temperature in the range of 77—293°K. This result is also consistent with the study of energy transfer in a mixed crystal done by Geschwendtner and Wolf.[2] The fluorescence intensity of the guest tetracene molecule in the host anthracene crystal was temperature-independent between 45—80°K, indicating a small coupling of phonon for the energy-transfer process in the anthracene crystal.

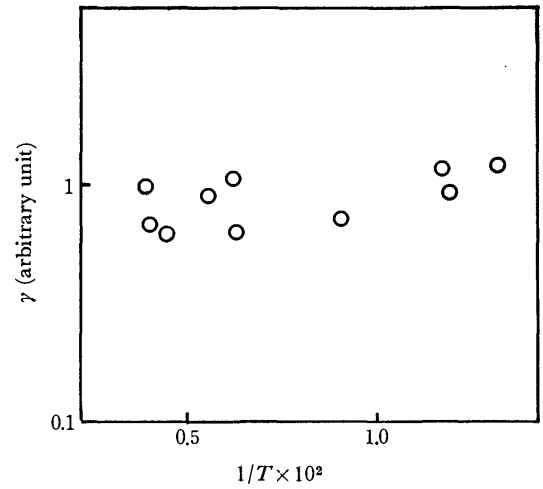

Fig. 6. A plot of log γ *versus* $1/T$ of anthracene single crystal.

19) V. M. Agranovich and Yu. V. Konobeev, *Soviet Phys. Solid State*, **5**, 999 (1963).
20) A. Hammer and H. C. Wolf, Symp. Org. Scintillator, Chicago (1966).
21) B. Stevens, *Spectrochim. Acta*, **18**, 439 (1962).
22) J. Tanaka and J. N. Murrell, *Mol. Phys.*, **7**, 363 (1964).

The present study of the exciton interaction based on the exciton-transfer process gives the results consistent with those obtained by previous studies using guest molecules in host crystals. In our opinion, however, the present method may be superior to the host-guest systems since it deals with pure crystals. This avoids specific host-guest interactions, the reflection of the excitons by guest molecules, and the reabsorption of the host fluorescence by guest molecules.[5] It is also in favor of the present method that there is no difficulty in choosing the proper guest substances; therefore, we can remove the limitation that the energy-transfer experiment have been made for only a few molecular crystals.

The authors wish to express their thanks to Professor Satoru Iwashima, Meisei University, and Professor Hiroo Inokuchi, The University of Tokyo, for their kind offer of pure materials. Their thanks are also due to Mr. Takayoshi Kobayashi for his helpful discussion.

BULLETIN OF THE CHEMICAL SOCIETY OF JAPAN, VOL. 45, 1976—1978(1972)

An Electron Spin Resonance Study of the Tropone Anion Radical

Yusaku IKEGAMI, Hidetoshi WATANABE, and Shuichi SETO

Chemical Research Institute of Non-Aqueous Solutions, Tohoku University, Katahira-2-chome, Sendai

(Received December 14, 1971)

The ESR spectrum of the tropone anion radical has been examined. The radical was generated from the neutral species by the electrolytic reduction in *N,N*-dimethylformamide. Splitting constants are satisfactorily explained in terms of the calculated spin densities by the McLachlan procedure, confirming that the unpaired spin orbital belongs to an a_2 symmetrical species. The complete delocalization of the π-electrons was assumed for the anion radical.

The physico-chemical properties of tropone (I) have been studied by means of various techniques such as dipole moment,[1] vapor-phase electron diffraction,[2] ionization potential,[3] and infrared and Raman spectra.[4] Theoretical treatments of the electronic spectrum have also been discussed by some investigators.[5-6] It has been clarified from the above results and the chemical properties of troponoid compounds[7] that tropone has a planar C_{2v} symmetrical structure possessing both the unsaturated character as a conjugate ketone (Ia) and the aromatic character of a 6π-electron ring system (Ib) caused by the polarization of the carbonyl group. The magentic resonance of tropone, however, has been little studied until recently.[8] The measurement and analysis of the nuclear magnetic resonance of tropone were reported in detail by Bertelli *et al.*,[9] proposing a reevaluation of the question of aromatic character of tropone as well as its derivatives.

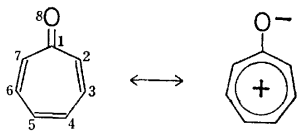

Ia Ib

The ESR study is interesting from two points of view. One is related to the stability of the radical in which an extra electron is added to a seven-membered ring. Since the instable character is known for some seven-membered aromatic radicals such as cycloheptatrienyl,[10] tropolonyl,[11] and cycloheptatriene anion,[12] the stability would be related to whether the radical has a ketyl structure as seen in the stable benzophenone radical anions. The other point is the expectation that the splitting constants, if observed, might be related to the calculated spin densities at the carbon atoms of the radical. This would be a good approach to getting the relationship between the experiments and the molecular orbital calculations.

We have measured the ESR spectrum of the tropone

1) Y. Kurita, S. Seto, T. Nozoe, and M. Kubo, This Bulletin, **26**, 272 (1953); A. Di Giacomo and C. P. Smyth, *J. Amer. Chem. Soc.*, **74**, 4411 (1952); D. J. Bertelli and T. G. Andrews, Jr., *Tetrahedron Lett.*, No. 45, 4467 (1967).

2) K. Kimura, S. Suzuki, M. Kimura, and M. Kubo, This Bulletin, **31**, 1051 (1958).

3) K. Higashi, T. Nozoe, and I. Omura, *ibid.*, **30**, 408 (1957).

4) Y. Ikegami, *ibid.*, **35**, 967, 972 (1962).

5) R. D. Brown, *J. Chem. Soc.*, **1951**, 2670; H. Hosoya, J. Tanaka, and S. Nagakura, *Tetrahedron*, **18**, 859 (1962); E. Weltin, H. Heilbronner, et H. Labhart, *Helv. Chim. Acta*, **46**, 2041 (1963); A. Julg und M. Bonnet, *Tetrahedron*, **20**, 2243 (1964); K. Inuzuka and T. Yokota, *J. Chem. Phys.*, **44**, 911 (1966).

6) H. Yamaguchi, Y. Amako, and H. Azumi, *Tetrahedron*, **24**, 267 (1968).

7) D. M. G. Lloyd, "Carbocyclic Non-Benzenoid Aromatic Compounds," Elsevier, New York (1966), p. 117.

8) D. J. Bertelli, C. Golino, and D. L. Dreyer, *J. Amer. Chem. Soc.*, **86**, 3329 (1964); M. J. Cook and E. J. Forbes, *Tetrahedron*, **24**, 4501 (1968).

9) D. J. Bertelli, T. G. Andrews, Jr., and P. O. Crews, *J. Amer. Chem. Soc.*, **91**, 5286 (1969); D. J. Bertelli and T. G. Andrews, Jr., *ibid.*, **91**, 5280 (1969).

10) J. D. Santos-Veiga, *Mol. Phys.*, **5**, 639 (1962); A. Carrington and I. C. P. Smith, *ibid.*, **7**, 99 (1964); G. Vincow, M. Lee Morrell, W. V. Volland, H. J. Dauben, Jr., and F. R. Hunter, *J. Amer. Chem. Soc.*, **87**, 3527 (1965).

11) G. A. Russell and J. Lokensgard, *ibid.*, **89**, 5059 (1967).

12) D. H. Levy and R. J. Myers, *J. Chem. Phys.*, **43**, 3063 (1965).

anion radical.[13] Details of the study will be reported.

Results and Discussion

Generation and ESR Spectrum of Tropone Anion Radical. Treatment of tropone with lithium, sodium, or potassium metal in degassed tetrahydrofuran or 1,2-dimethoxyethane caused immediate change in color to reddish violet at temperatures above −40°C. However, no ESR signal was observed at temperatures above −75°C. On the other hand, the electrolytic reduction of tropone solution in degassed *N,N*-dimethylformamide (DMF) at room temperature gave the spectrum shown in Fig. 1. The radical was not stable so that the signal intensity decreased to one half during 15 minutes at room temperature after the current was turned off. The color of the solution changed gradually to a reddish brown during the electrolysis. The use of acetonitrile as the solvent did not favor the generation of the radical.

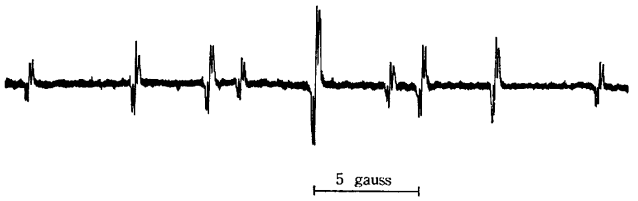

Fig. 1. ESR spectrum of tropone anion radical generated by electrolytic reduction of tropone in DMF at room temperature.

Hyperfine structure of the spectrum is readily analyzed with three splitting constants as expected for the symmetrical structure of I. Assignments for the constants are reasonably made by comparison with calculated spin densities. The observed splitting constants and the experimental spin densities calculated by the relation, $a_i^H = Q_{CH}^H \rho_i$,[14] where $|Q_{HC}^H| = 23.7$ gauss, are given in Table 1.

Table 1. Observed splitting constants (a_i) and calculated spin densities (ρ_i) for tropone anion radical

Position	a_i gauss	Spin density, ρ_i Exptl[a]	Calcd Hückel	Calcd McLachlan[b] (1)	Calcd McLachlan[b] (2)
1			0	−0.0562	−0.0571
2, 7 (2H)	8.578	0.3619	0.2716	0.3741	0.3726
3, 6 (2H)	0.10	0.004	0.0538	−0.0186	−0.0200
4, 5 (2H)	5.050	0.2131	0.1746	0.1861	0.1849
8			0	−0.0270	−0.0179

a) Spin densities using the McConnell relation.[14]

b) The Coulomb and resonance integral parameters for the carbonyl group of tropone were chosen as:
(1) $\beta_{1,8} = 1\beta$ and $\alpha_8 = \alpha + \beta$,
(2) $\beta_{1,8} = 1.4\beta$ and $\alpha_8 = \alpha + 2\beta$.
The λ-parameter in McLachlan procedure was fixed at the value $\lambda = 1.2$.

13) Briefly communicated in This Bulletin, **41**, 2225 (1968).
14) H. M. McConnell, *J. Chem. Phys.*, **24**, 632, 764 (1956).

Calculation of Spin Densities. Calculation of unpaired spin densities (ρ_i) for the anion radical was carried out by employing the Hückel MO theory and the approximate configuration interaction treatment proposed by McLachlan.[15] The bond alternation parameter k was introduced in order to represent the aromaticity of the tropone molecule. It is defined by $k = \beta_s/\beta_d$, where β denotes the resonance integral parameter, and the subscripts s and d the single and double bond in Ia, respectively. $k = 1$ means complete delocalization and $k = 0$ complete localization of π-electrons. The Coulomb and resonance integral parameters for the carbonyl group were chosen.

It was shown from the calculations that, if $k = 1$, the calculated spin densities by the Hückel MO theory are independent of the Coulomb and resonance integral parameters for the carbonyl group, because the unpaired spin orbital for the radical belongs to an a_2 symmetrical species of C_{2v} symmetrical structure. The effects of the carbonyl parameters appear slightly at second hand in the McLachlan spin densities. Two calculations using different parameters for the carbonyl group are included in Table 1 togehter with the Hückel spin densities. The McLachlan procedure showed better values than by Hückel MO calculation.

Dependence of the orbital energies of tropone on k-parameter is shown in Figs. 2a and 3a for the cases of two different Coulomb integral parameters. It is assumed that $\beta_{C=O} = \beta_{C=C}$. These figures disclose that the reduction of k-parameter replaces the unpaired spin orbital by the b_2 symmetrical one. The replacement of the orbitals is unavoidable unless one adopts the unusually small parameter α_8 for the carbonyl oxygen. The spin density at the carbonyl group in the b_2 orbital is so large that the total extent of the ESR spectrum can not be rationalized. It is thus concluded that the k-parameter must be close to 1, which means the complete delocalization of π-electrons in the tropone anion radical.

Total Binding Energy. The above conclusion for the anion radical is inconsistent with the considerations

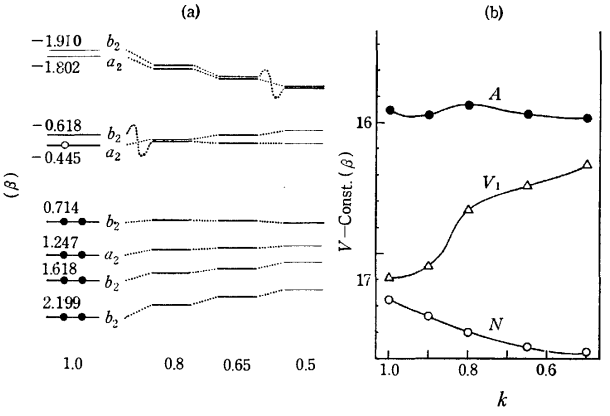

Fig. 2. Dependence of the Hückel molecular orbitals and total binding energy (V) on the bond alternation parameter k. $\beta_{1,8} = 1\beta$, $\alpha_8 = \alpha + 1\beta$.
(a): Orbital energy. (b): V-k Curves for tropone (N), the lowest excited state (V_1), and tropone anion radical (A). All the energies are in terms of β.

15) A. D. McLachlan, *Mol. Phys.*, **3**, 233 (1960).

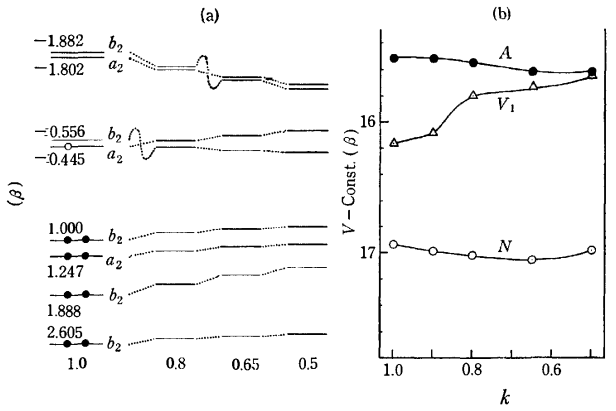

Fig. 3. Dependence of the Hückel molecular orbitals and total binding energy on the bond alternation parameter. $\beta_{1,8}=1\beta$, $\alpha_8=\alpha+2\beta$. Representation is the same as for Fig. 2.

for the neutral molecule by Yamaguchi *et al.*[6] and Bertelli *et al.*[9] who emphasized the reduced delocalization of the π-electrons in tropone. It is considered that a comparison between the *V-k* curves for tropone and the anion radical might provide information on the difference in the bond alternations. The *V-k* curve depicts the dependence of the total binding energy on *k*-parameter. We thus examined the curves for both species. The total binding energies (V) were calculated by the procedure by Longuet-Higgins and Salem,[16] adapted to non-benzenoid aromatic compounds by Nakajima and Katagiri.[17] The procedure is as follows.

Bond lengths r are given by

$$r(\text{in Å}) = 1.520 - ap$$

$$a = 0.186$$

where p designates the bond orders. Resonance integral $\beta(r)$ is given as an exponential function of the form

$$\beta(r) = \beta \exp[b(1.397-r)]$$

with

$$b = 4.599\,\text{Å}^{-1}.$$

The total binding energy of the molecule is given by

$$V = E_\pi + E_\sigma = (2/ab)\sum_{i<j}\beta_{ij} + \sum_i q_i\alpha_i + \text{const}$$

with

$$\alpha_i = \alpha + \omega(1-q_i)\beta$$

in which α designates the Coulomb integral parameter, q_i the electron density, and ω a proportionality coefficient here taken to be unity. β_{ij} corresponds to the $\beta(r)$ calculated for the bond between the i- and j-atoms. Calculations using the above equation afforded the *V-k* curves shown in Figs. 2b and 3b for the ground states of the neutral molecule (N) and the anion radical (A). For comparison, the curves for the lowest excited states (V_1) are included in the figures.

16) H. C. Longuet-Higgins and L. Salem, *Proc. Roy. Soc.*, (London), *Ser. A*, **251**, 172 (1959).

It is to be noticed in that the total binding energy of the anion radical is little affected by the bond alternation parameter k, while the other two states, N and V_1, show a distinct dependency like that for some non-benzenoid aromatic molecules.[17] Since the variation of the energy with *k*-parameter for the anion radical is estimated to be few kilocalories which can be covered by thermal energy at normal temperature, the calculations do not permit assumption of the stable electronical configuration for the anion radical. This implies that the electronical configuration of the radical is largely affected by the counter-ion and the supporting electrolyte.

Conclusion. It is clear that the unpaired spin orbital belongs to an a_2 species and the spin is located mainly on the seven-membered ring. Thus the structure IIc is predominant over the ketyl forms IIa and IIb for the radical. As the radical was generated at room temperature, it is more stable than the cycloheptatriene anion radical,[12] which could only be generated at low temperature and was assumed to have a nonplanar boat conformation. The considerable stability of the tropone anion radical might be attributed to the environmental factors besides the complete delocalization of π-electrons in a planar tropone structure.

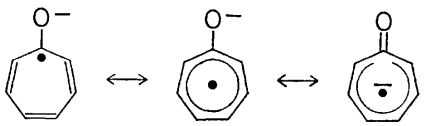

IIa IIb IIc

Experimental

Tropone was carefully purified by distillation in a high vacuum. *N,N*-Dimethylformamide was degassed by at least five freezing-pumping cycles after being purified and distilled on to a Molecular Sieve 4A which had been flame-dried in a vacuum.

The technique employed in the electrolytic generation of the free radical is similar to that used by Hirayama.[18] A cell with platinum electrodes was constructed so that electrolysis could be performed within a cavity for the preparation of radical unstable at room temperature. Electrolysis was performed with a concentration less than 0.7% in DMF, using tetra-*n*-propylammonium perchlorate as a supporting electrolyte.

The ESR spectrum was measured with a Hitachi X-band ESR spectrometer Model MPU-3B using a field modulation of 100 kHz.

The authors wish to express their appreciation to Professor T. Isobe and Dr. H. Yokoi for helpful discussions.

17) T. Nakajima and S. Katagiri, *Mol. Phys.*, **7**, 149 (1964); T. Nakajima, "Molecular Orbitals in Chemistry, Physics, and Biology," ed. by Per-Olov Löwdin and B. Pullman, Academic press, New York (1964), p. 451.

18) M. Hirayama, This Bulletin, **40**, 1822 (1967).

Electronic Absorption Spectra and Geometry of Molecule Ions Generated from Stilbene and Related Compounds. I. Dianions

Hiroshi SUZUKI, Kinko KOYANO,

Department of Chemistry, College of General Education, The University of Tokyo, Komaba, Meguro-ku, Tokyo

and Tosiyasu L. KUNII

Information Science Laboratory, Faculty of Science, and Computer Centre, The University of Tokyo, Hongo, Bunkyo-ku, Tokyo

(Received December 27, 1971)

Stilbene and some of its alkyl-substituted derivatives were reduced with alkali metals to dianions in 1,2-dimethoxyethane. From comparison of the electronic absorption spectra of these dianions with one another and with the results of semiempirical SCF-MO-CI calculation of the π-electronic state, the geometries of the dianions were inferred to be as follows: (a) the preferred geometry of a sterically unhindered dianion, such as the dianion of stilbene, is probably planar or nearly planar; (b) when alkyl substituents are introduced into the central ethylenic carbon atoms, the steric interference caused by the substituents is relieved chiefly by the rotation about the central ethylenic bond; (c) the steric interference caused by *ortho* methyl substituents seems to be comparatively small or to be relieved by the rotation about the bonds connecting benzene rings to the ethylenic carbon atoms as well as the ethylenic bond. From the influence of alkali-metal cations on the spectra of the dianions, it was inferred that the dianions exist mainly as contact ion aggregates in which the counter-ions are located near the central ethylenic bond, one probably almost above an ethylenic carbon atom and the other almost below the other ethylenic carbon atom.

Aromatic hydrocarbons are reduced with alkali metals in ethereal solvents to mononegative ion radicals (anion radicals) and, further, in some cases, to dinegative ions (dianions). Geometries of these ions are probably not always similar to those of the parent molecules. The question of how the molecular geometry changes with charge state is of interest, but information on the geometry of the ions is scarce. As regards the ions generated from stilbene, a planar geometry has been proposed for the anion radical,[1] and a nonplanar geometry in which the two benzylidene moieties are rotated about the central ethylenic bond (the α—α' bond) to make an angle of about 90° has been proposed for the dianion.[2] However, direct evidence does not seem to have been given.

One of us (H. S.) studied the relation between the electronic absorption spectrum and the molecular geometry of the neutral molecules of stilbene and related compounds.[3-8] The purpose of the present study is to disclose the corresponding relation for the negative and positive ions generated from stilbene and related compounds and to answer partly the above question. We have studied the geometries and spectra of the dianions by means of semiempirical SCF–MO–CI calculation.

Experimental

A deaerated solution of *trans*-stilbene in 1,2-dimethoxyethane (DME) cooled in ice was contacted with a potassium mirror in a vacuum line system, essentially similar to the one described by Ishitani *et al.*[9] After a while, the solution turned yellowish brown, and exhibited a distinct ESR signal with fine structure; its electronic absorption spectrum has main bands at about 701 and 494 nm, as shown in Fig. 1 (1) (curve b), and closely resembles the spectrum of the anion radical produced by γ-ray irradiation of a glassy solution of *trans*-stilbene in 2-methyltetrahydrofuran (MTHF) at 77°K.[10] The yellowish brown solution is considered to contain the stilbene anion radical and the neutral stilbene as main components. After the solution had been kept cool and in contact with a potassium mirror for a sufficiently long time (about one day), the color turned a beautiful red. This red solution exhibited substantially no ESR signal. Its electronic absorption spectrum has a broad intense band with a peak at about 503 nm and no intense bands in the near ultraviolet region, as shown by curve c in Fig. 1 (1). The solution decolored when it was brought into contact with air. The electronic absorption and NMR spectra of the decolored solution were essentially the same as those of the solution of neutral *trans*-stilbene. When anthracene was dissolved into the red solution, the color of the solution changed to blue, and the solution showed electronic absorption and ESR spectra characteristic of the anthracene anion radical. It is evident that the red solution contains the stilbene dianion as the main component and does not contain the neutral molecule and anion radical of stilbene in any significant amounts.

Some alkyl-substituted derivatives of stilbene were reduced by procedures similar to the one described above. The electronic absorption spectra of stilbene and its derivatives in various reduction stages, measured by the use of cells of path length 10 mm at room temperature, are shown in Figs. 1 (1)—(8). In each figure, curve a is the spectrum of the neutral molecule (S) in *n*-heptane, curve b that of a DME

1) R. Chang and C. S. Johnson, Jr., *J. Chem. Phys.*, **41**, 3272 (1964); *ibid.*, **46**, 2314 (1967).

2) J. F. Garst, J. G. Pacifici, and E. R. Zabolotny, *J. Amer. Chem. Soc.*, **88**, 3872 (1966).

3) H. Suzuki, This Bulletin, **25**, 145 (1952).

4) H. Suzuki, *ibid.*, **33**, 379 (1960).

5) H. Suzuki, *ibid.*, **33**, 396 (1960).

6) H. Suzuki, *ibid.*, **33**, 406 (1960).

7) H. Suzuki, *ibid.*, **35**, 1715 (1962).

8) H. Suzuki, "Electronic Absorption Spectra and Geometry of Organic Molecules," Academic Press Inc., New York, N.Y. (1967), Chapter 14.

9) A. Ishitani, K. Kuwata, H. Tsubomura, and S. Nagakura, This Bulletin, **36**, 1357 (1963); A. Ishitani and S. Nagakura, *Theor. Chim. Acta*, **4**, 236 (1966).

10) The spectra of the anion radicals produced by γ-ray irradiation were measured by Dr. Tadamasa Shida of the Institute of Physical and Chemical Research, Yamato-machi, Saitama, to whom the authors are greatly indebted.

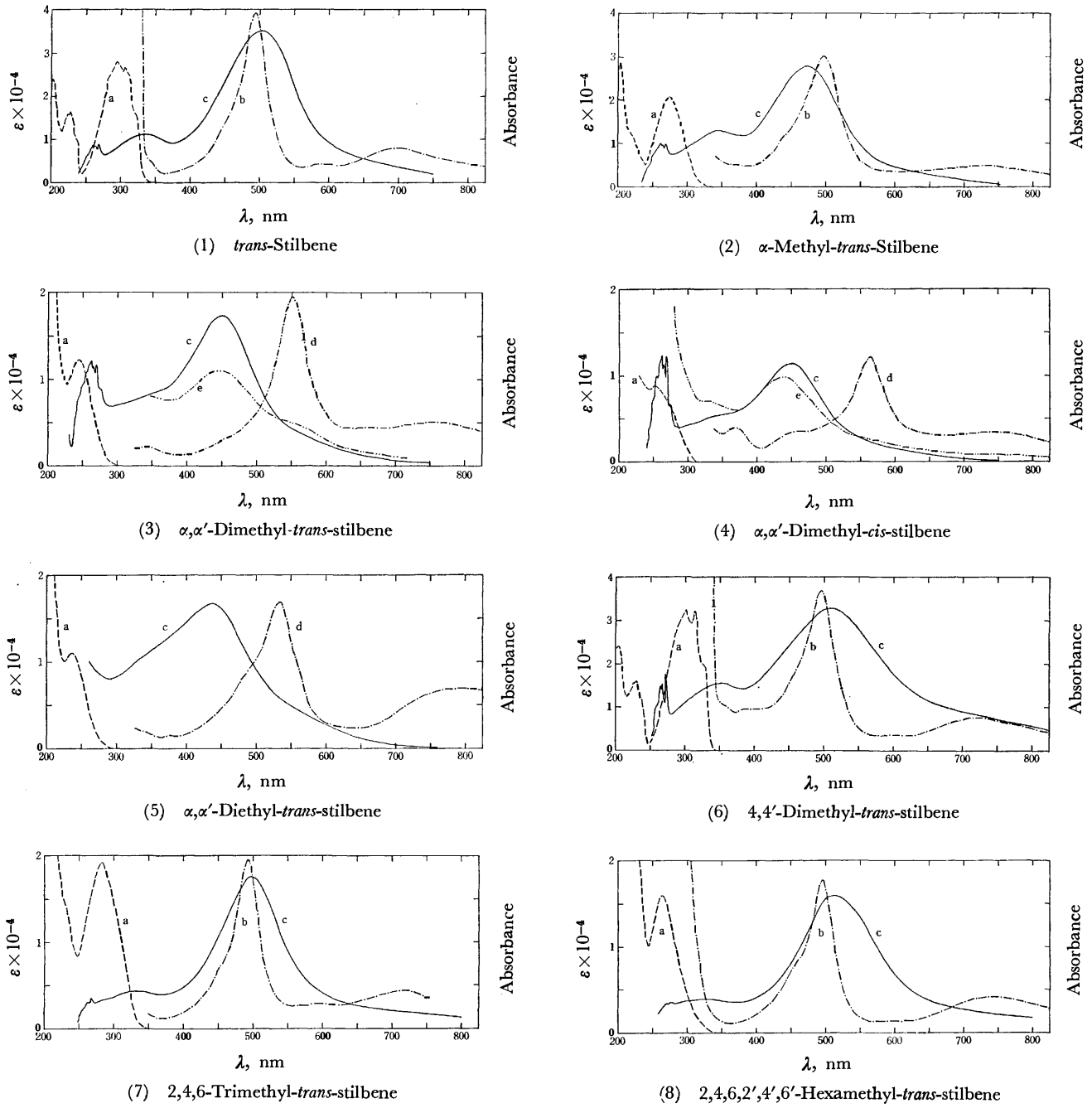

Fig. 1. Electronic absorption spectra of stilbenes (S) and their anion radicals (S^-) and dianions (S^{2-}). Curve a is the spectrum of S dissolved in *n*-heptane. Curve c is the spectrum of a DME solution in which S has been reduced with K to S^{2-}. For explanation of other cruves, see text. For curve a the intensity is represented with the molar absorptivity (ε); for other curves it is represented with the absorbance on arbitrary scale.

solution which is considered to contain the anion radical (S^-) and the neutral parent compound S as main solutes, and curve c that of a DME solution containing the dianion (S^{2-}) as the most important solute and not S^- and S in any significant amounts. Intensity is represented by the molar absorptivity for curve a, and by absorbance in a different arbitrary scale for all other curves. Each spectrum represented by curve b closely resembles that of the anion radical produced by γ-ray irradiation,[10] except that the former is slightly broader. The wavelengths of the main absorption maxima (λ_{max}) and some relevant data are given in Table 1.

In the case of α,α'-dialkylstilbenes the spectra of the anion radicals could not be obtained by means of alkali-metal reduction. In Figs. 1 (3)—(5), the spectra of the anion radicals produced by γ-ray irradiation[10] are shown by curve d, and those of DME solutions in which reduction with potassium has not sufficiently occurred exhibiting weak and broad ESR signals by curve e. These spectra indicate that each solution corresponding to curve e contains the neutral molecule of the stilbene derivative in a large amount, the dianion in a fair amount and the anion radical in a very small amount. This means that the equilibrium constant (K_{disp}) of the disproportionation

$$2S^- \rightleftarrows S + S^{2-}$$

Table 1. The main absorption bands of molecules, anion radicals, and dianions of stilbenes

Stilbene	Molecule[a] λ_{max}[c]	Anion radical[b] λ_{max}[c]	Color[d]	Dianion[b] λ_{max}[c]	Color[d]
Unsubstituted *trans*-	294	701; 494	YB	503	R
α-Methyl-*trans*-	274	*ca.* 725; 497	YB	472	BR
α,α′-Dimethyl-*trans*-	243	—	—	450	BY
α,α′-Dimethyl-*cis*-	252	—	—	450	BY
α,α′-Diethyl-*trans*-	237	—	—	437	BY
4,4′-Dimethyl-*trans*-	301	*ca.* 725; 496	DB	509	R
2,4,6-Trimethyl-*trans*-	283	*ca.* 715; 493	B	497	R
2,4,6,2′,4′,6′-Hexamethyl-*trans*-	263	740; 494	DB	510	R

a) Dissolved in *n*-heptane.
b) Generated from stilbene by reduction with potassium in DME.
c) The wavelength of the absorption maximum in units of nm.
d) Color of solution: YB, yellowish brown; DB, dark brown; B, brown; R, red; BR, brownish red; BY, brownish yellow.

is much greater for these derivatives than for *trans*-stilbene and other derivatives. It has been found that even the K_{disp} value for α-methylstilbene is greater than that for stilbene.[2] It is noteworthy that the spectra of the dianions generated from *trans*- and *cis*-α,α′-dimethylstilbene are essentially the same as each other, while the spectra of the anion radicals produced from these isomers by γ-ray irradiation distinctly differ from each other.

Reductions with sodium and with cesium were also carried out for most of the compounds. As a whole, the spectra of the dianions produced by the use of these alkali metals are closely similar to those obtained by the use of potassium, except for comparatively small differences in the position of the absorption maximum.

In contrast to the α,α′-dialkyl derivatives, it was difficult to reduce the derivatives bearing methyl substituents on the benzene nuclei to dianions, but not to anion radicals. With the 4,4′-dimethyl and 2,4,6-trimethyl derivatives, when the spectra of the anion radicals were measured a broad absorption band having a peak at about 790 or 800 nm often developed and the color of the solutions changed from yellowish brown to deep blue. The species responsible for this band could not be identified; it is certain that it is neither the anion radical nor the dianion. The 2,4,6,2′,4′,6′-hexamethyl derivative was also readily reduced to the anion radical by the use of any alkali metal, but all attempts to reduce it to the dianion with sodium and with cesium were unsuccessful. The spectra of the solutions kept in contact with the alkali metal for a sufficiently long time were those of the anion radical. There were no signs of bands due to the dianion or to the neutral molecule. A spectrum considered to be due to the dianion was obtained by the use of potassium. However, it changed its shape in a comparatively short time. It is therefore questionable whether the spectrum shown as curve c in Fig. 1 (8) can be regarded as that of the pure dianion. The corresponding λ_{max} value in Table 1 is also questionable. With these nuclear-methylated derivatives the values of K_{disp} appear to be very small. According to qualitative observations, the value for 4,4′-dimethylstilbene appears to become larger to some extent as the temperature is lowered. This tendency, if true, is quite the opposite of that reported for reduction of tetraphenylethylene with sodium in tetrahydrofuran.[11-16]

MO Calculation

It is assumed that all the tervalent carbon atoms in the dianions have sp^2 hybrid orbitals and the π-electron approximation is applicable. This seems to be reasonable, although the possibility of rehybridization should be taken into consideration in the case of smaller systems such as ethylene,[17] and in cases where the reductant is, for example, lithium and where on association of the dianion with the alkali-metal cations the ethylenic carbon atoms might be linked to the alkali-metal atoms with bonds having partially covalent character. Semiempirical SCF–MO–CI calculation of the π-electronic states of the dianions was carried out on many geometrical models designed to represent rotations about the central CC "double" bond (the α—α′ bond) and the two CC "single" bonds (the α—1 and the α′—1′ bond). The carbon skeleton of the stilbene π-system is illustrated in Fig. 2, together with the numbering of the carbon atoms and the coordinate system.

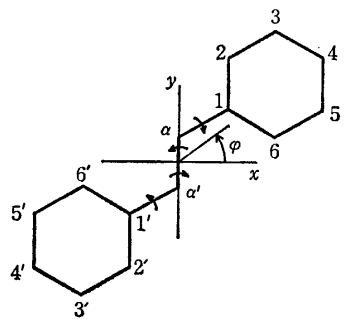

Fig. 2. The skeleton of the stilbene π-system. The planar *trans* form, that is, geometry (0,0,0), is shown.

The length of CC bond p—q is denoted by R_{pq} (Å), and the angle of twist of this bond, *viz.*, the dihedral angle between the σ-skeleton planes of carbon atoms p and q, is denoted by θ_{pq}. The value of $\theta_{aa'}$ is taken to be 0° for the *trans* form, and 180° for the *cis* form. For the sake of convenience, essentially the same assumptions as those made for the treatment of neutral stilbenes are made on the geometry.[3,4,8] Thus, the following relations are assumed:[18]

$$R_{a1} = 1.517 - 0.067 \times |\cos\theta_{a1}|$$
$$R_{a'1'} = 1.517 - 0.067 \times |\cos\theta_{a'1'}|$$
$$R_{aa'} = 1.517 - 0.177 \times |\cos\theta_{aa'}|$$

All bond angles are assumed to be 120°, and all CC bond lengths in the benzene rings 1.397 Å. Thus the geometry of the π-system can be described as a function

11) A. G. Evans and B. J. Tabner, *J. Chem. Soc.*, **1963**, 4613.
12) A. G. Evans, J. C. Evans, and C. L. James, *ibid.*, **B 1967**, 652.
13) J. F. Garst and E. R. Zabolotny, *J. Amer. Chem. Soc.*, **87**, 495 (1965).
14) R. C. Roberts and M. Szwarc, *ibid.*, **87**, 5542 (1965).
15) A. Cserhegyi, J. Jagur-Grodzinski, and M. Szwarc, *ibid.*, **91**, 1892 (1969).
16) M. Szwarc, *Accounts Chem. Res.*, **2**, 87 (1969).
17) See, for example, C. D. Cook, and K. Y. Wan, *J. Amer. Chem. Soc.*, **92**, 2595 (1970).
18) For the foundation of these assumptions, see Ref. 8, pp. 183—186.

of angles of twist θ_{a1}, $\theta_{a'1'}$, and $\theta_{aa'}$. Hereafter geometries are represented as $(\theta_{a1}, \theta_{a'1'}, \theta_{aa'})$. As an example, geometry (0,0,0) represents the geometry in which $\theta_{a1}=\theta_{a'1'}=\theta_{aa'}=0°$. The calculations were carried out for geometries in which $\theta_{a1}=\theta_{a'1'}$ and which belong to symmetry group C_2, with the exception of geometries (0,0,0) and (0,0,180), which belong to symmetry groups C_{2h} and C_{2v}, respectively.[19]

Calculation was carried out by means of the Pariser-Parr-Pople method, using an HITAC 5020E at the computer Centre, the University of Tokyo. The parameter values were taken as proposed by Nishimoto and Forster.[20] Thus, for all the carbon π-centers, the values of the one-center core integral (α_p) and one-center repulsion integral (γ_{pp}) were taken to be -11.16 and 11.13 eV, respectively. The two-center core integral (β_{pq}) was taken to be zero for nonneighboring π-centers, and was estimated for neighboring π-centers by the use of a modification of the Nishimoto-Forster equation,[20]

$$\beta_{pq}(\text{in eV}) = -(2.04+0.51P_{pq})\times|\cos\theta_{pq}|,$$

where P_{pq} represents the π-bond order of the p—q bond calculated from the starting set of MO's. The two-center repulsion integral (γ_{pq}) was estimated by the use of the following Nishimoto-Mataga type equation[21] for all the pairs of π-centers:

$$\gamma_{pq}(\text{in eV}) = 14.397/(1.294+R_{pq})$$

Satisfactory self-consistency was attained after 10 iterations in SCF–MO calculation. In the iterations the geometry and all the values of β_{pq} and γ_{pq} were kept fixed, and no interaction between the π-electron distribution and the σ-electron distribution was taken into consideration.

The values of the resonance integral (β^0_{pq}) for neighboring π-centers were determined by the use of the equation

$$\beta^0_{pq} = k_{pq}\beta^0,$$

where

$$k_{pq} = [S(R_{pq}, 0°)/S(1.397\text{Å}, 0°)]\times|\cos\theta_{pq}|.$$

$S(R,0°)$ represents the π–π overlap integral for a CC bond whose length is R and whose angle of twist is 0°. For the values of S the values calculated by Mulliken and others[22] for Slater atomic orbitals were used.

19) Calculation was also carried out for geometries (a, $-a$, 0) and (a, $-a$, 180), which belong to symmetry groups S_2 and C_s, respectively. The calculated values of energies and oscillator strengths of electronic transitions and of the ground-state energy of the π-electronic system coincide almost completely with those for the corresponding C_2 geometries, (a, a, 0) and (a, a, 180). The S_2 geometries (a, $-a$, 0) seem to be almost as probable as the corresponding C_2 geometries (a, a, 0). The C_s geometries (a, $-a$, 180), however, seem to be much less probable than the corresponding C_2 geometries (a, a, 180), since the steric repulsion between the two phenyl groups must be much stronger in the former than in the latter. Geometries (a, $-a$, b) with b different from 0 and 180 have no symmetry elements. The probability of these geometries also seems to be small.

20) K. Nishimoto and L. S. Forster, *Theor. Chim. Acta*, **3**, 407 (1965); *ibid.*, **4**, 155 (1966).

21) K. Nishimoto and N. Mataga, *Z. Phys. Chem.* (Frankfurt), **12**, 335 (1957); N. Mataga and K. Nishimoto, *ibid.*, **13**, 140 (1957).

22) R. S. Mulliken, C. A. Rieke, D. Orloff, and H. Orloff, *J. Chem. Phys.*, **17**, 1248 (1949).

Table 2. Calculated results for the lowest singlet excited states (having an energy lower than 6 eV) of the stilbene dianion of geometry (0,0,0)

State	Symmetry	Coef.[a]	Conf.[b]	E[c]	f[d]	φ[e]
S_1	A_g	0.9891	(8—10)	1.6364	0	—
S_2	B_u	0.9624	(8—9)	1.6444	0.0306	−67°36′
S_3	B_u	0.9678	(8—11)	2.6840	1.9545	+36°57′
S_4	A_g	0.9281	(8—12)	3.7101	0	—
S_5	A_g	0.9050	(7—9)	4.5412	0	—
S_6	B_u	0.9454	(7—10)	4.5627	0.2101	−60°45′
S_7	A_g	0.8495	(7—11)	4.7912	0	—
S_8	B_u	0.9475	(8—13)	4.8381	0.0347	+35°21′
S_9	A_g	0.9483	(8—14)	5.5512	0	—

a) Coefficient with which the electron configuration appears in the state function.

b) Electron configuration that makes the most important contribution to the state. (i—j) denotes the singlet electron configuration arising from the ground configuration by promotion of an electron from π orbital ψ_i to ψ_j. The orbital index i takes the increasing integer from 1 for the lowest orbital to 14 for the highest orbital in the order of increasing energy.

c) Energy of the excited state relative to the ground state (S_0) in eV.

d) Oscillator strength of the transition from the ground state to the excited state.

e) Direction of the transition moment: φ represents the angle that the transition moment makes with the x axis in the xy plane (see Fig. 2).

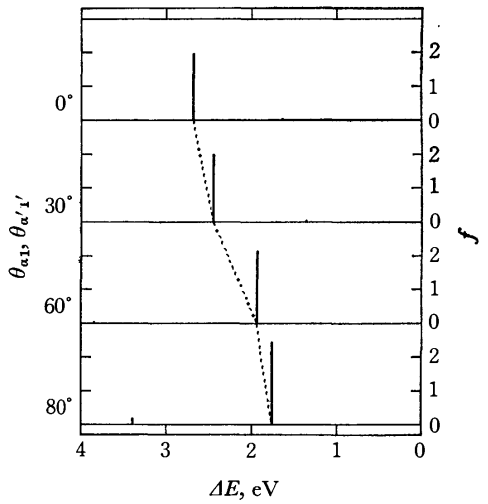

Fig. 3. The calculated energies (ΔE) and oscillator strengths (f) of transitions from the ground state to singlet excited states in the stilbene dianion for various values of θ_{a1} and $\theta_{a'1'}$ when $\theta_{aa'}$ is fixed at 0°.

In the CI calculation 30 singlet and 30 triplet lowest-energy singly excited electron configurations were taken into account.

Some results of the calculation are shown in Table 2 and Figs. 3 and 4. In Table 2 are listed the energies and some other data of the lowest singlet excited states of the dianion of geometry (0,0,0). Figures 3 and 4 illustrate the variations in the energies (ΔE) and oscillator strengths (f) of the transitions from the ground state to the lowest singlet excited states associated with the variations in geometry.

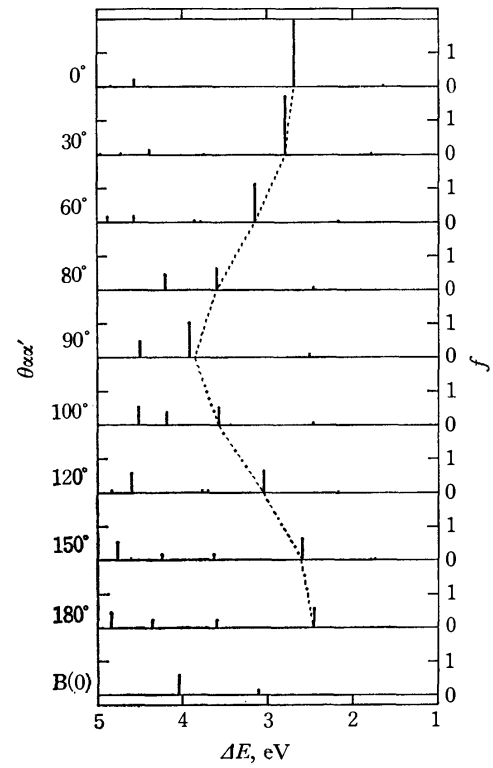

Fig. 4. The calculated energies (ΔE) and oscillator strengths (f) of transitions from the ground state to singlet excited states in the stilbene dianion for various values of $\theta_{\alpha\alpha'}$ when $\theta_{\alpha 1}$ and $\theta_{c'1'}$ are fixed at 0°. For comparison, the corresponding quantities in the benzyl anion of a planar geometry are also shown, being indicated by B(0). In every case there is no singlet excited state having energy lower than 1 eV.

Discussion

Band A. As shown in Fig. 1 and Table 1, each dianion has an intense absorption band with its maximum in the region of about 420—520 nm (according to Zabolotny and Garst,[23] for the dianion generated from *trans*-stilbene, $\lambda_{max}=504$ nm, and $\varepsilon_{max}=ca.\ 3.8\times10^4$). Hereafter, attention is focused on this band, which is referred to as band *A*. It should be noted that in every case this band is structureless and very wide.

Besides this band, most of the "dianion spectra" (curve c, Fig. 1) show a very broad band in the region of 330—350 nm and a comparatively weak band with fine structure in the region of 260—270 nm. It is somewhat questionable whether all these weak absorptions are due to the dianions.

Regarding the position of band *A*, the following facts should be noted: (1) band *A* of the 4,4'-dimethylstilbene dianion is at slightly longer wavelength than that of the stilbene dianion; (2) the position of band *A* of the 2,4,6-trimethyl- and 2,4,6,2',4',6'-hexamethylstilbene dianions does not differ much from that of the stilbene dianion, in spite of the presence of a number of methyl substituents; (3) band *A* shifts progressively to shorter wavelengths as alkyl substituents are introduced to the α and α' positions, in the order stilbene, α-methylstilbene, α,α'-dimethylstilbene, and α,α'-diethylstilbene.

Band *A* can undoubtedly be attributed to the transition from the ground state (S_0) to the singlet excited state to which the singlet electron configuration arising from one-electron transition from the 8th orbital (the highest occupied orbital) to the 11th orbital, (8—11), makes the most important contribution (see Table 2). In geometries (0,0,0) and (0,0,180), this excited state is the 3rd singlet excited state S_3 belonging to symmetry species B_u and B_2, respectively. In other geometries of symmetry C_2 this state belongs to symmetry species B. Hereafter, this state is called the *A* state, and the transition from the ground state to this state is called the *A* transition.

There seem to be at least three factors influencing the position of band *A*: (1) the geometry of the dianion, (2) the electronic effect of alkyl substituents, and (3) the effect of the counter-ion. The purpose of the present paper is to infer the geometry of the dianions from the position of their *A* bands, but before proceeding to such a discussion, it seems necessary to examine other factors.

The Electronic Effect of Alkyl Substituents. Band *A* of the 4,4'-dimethylstilbene dianion is at longer wavelength than that of the stilbene dianion by about 6 nm. If additivity is assumed, the bathochromic shift due to one methyl substituent at the *para* position is about 120 cm^{-1}.

The electronic effect of a methyl substituent on the energy of a π-electronic transition is usually ascribed to the inductive and the hyperconjugative effect, and can be approximately treated by perturbation theory.[24] Roughly speaking, the change in wavenumber at the absorption maximum caused by introduction of one methyl substituent $\Delta\nu$ depends on the change in the π-electron density at the substitution position (p) upon the electronic transition ΔP_{pp} in the following way. When the value of ΔP_{pp} is negative, the value of $\Delta\nu$ is also negative (the shift is bathochromic); the larger the absolute value of ΔP_{pp}, the larger the absolute value of $\Delta\nu$; when the value of ΔP_{pp} is zero, or positive (if small amount) the value of $\Delta\nu$ can be negative owing to the hyperconjugative effect; when the value of ΔP_{pp} is positive and very large, the value of $\Delta\nu$ can be positive (the shift can be hypsochromic).

Table 3. The calculated π-electron densities in the ground and *A* states of the stilbene dianion of geometry (0,0,0)

Position (p)	$P_{pp(G)}$	$P_{pp(A)}$	$\Delta P_{pp(GA)}$
α; α'	1.2444	1.1759	−0.0685
1; 1'	1.0687	1.1505	+0.0818
2; 2'	1.1531	1.0747	−0.0784
3; 3'	1.0674	1.1409	+0.0735
4; 4'	1.2756	1.3321	+0.0565
5; 5'	1.0687	1.0532	−0.0155
6; 6'	1.1221	1.0727	−0.0494

23) R. Zabolotny and J. F. Garst, *J. Amer. Chem. Soc.*, **86**, 1645 (1964).

24) See, for example, H. Suzuki, the book cited in Ref. 8, pp. 408—410; A. Streitwieser, Jr., "Molecular Orbital Theory for Organic Chemists," John Wiley & Sons, Inc., New York, N.Y. (1961), pp. 131—134.

In Table 3 are shown the values of the π-electron densities (P_{pp}) in the ground and A states, together with the values of the π-electron density changes (ΔP_{pp}) associated with the A transition, calculated for geometry (0,0,0). It should be noted that the value of ΔP_{pp} is negative at the α and *ortho* positions and positive at the *para* positions. Essentially the same tendency is found in other geometries such as (0,0,30) and (30,30,0). Since the electronic effect of a methyl substituent on band A is bathochromic even at the *para* position, it must be bathochromic to much greater extent at the α and *ortho* positions. Accordingly, if it were not for the electronic effect of the methyl (or ethyl) substituents, the hypsochromic shift of band A associated with progressive introduction of alkyl substituents into the α and α' positions should be greater than observed. Even in the series of stilbene, 2,4,6-trimethyl-, and 2,4,6,2′,4′,6′-hexamethylstilbene, band A would shift hypsochromically, though the extent of the shift might be comparatively small, with increasing introduction of methyl substituents.

Table 4. Dependence of the position of the A band maximum on the counter-ion

trans-Stilbene	λ_{max}, nm (in DME)		
	Na^+	K^+	Cs^+
Unsubstituted	500	503	513
α,α′-Dimethyl-	436	450	457.5
α,α′-Diethyl-	427	437	440

Effect of the Counter-ion. The spectra of the dianion generated from the same compound by reduction with different alkali metals are similar to one another in shape, but the position of band A differs for different alkali metals. Table 4 shows that in every case the A band maximum shifts to longer wavelengths as the alkali metal becomes larger, in the order Na, K, and Cs.

If the dianions existed as unassociated ions or as so-called solvent-separated ion aggregates, the spectra would be substantially independent of the kind of the counter-ion.[25,26] The fact that the position of the absorption maximum varies depending on the kind of the alkali metal indicates that the dianions S^{2-} exist at least for a great part as contact ion aggregates (S^{2-}, $2M^+$) (called triple ions or diassociates), being associated with the alkali-metal ions M^+, although DME, the solvent used, is said to be a powerful solvating agent for alkali-metal ions and hence a very suitable solvent for making solvent-separated ion aggregates[25,26] or unassociated ions.[27]

In addition to the contact diassociates, possibly some other species, such as solvent-separated diassociates, contact and solvent-separated monoassociates (S^{2-},M^+), and unassociated dianions, may exist, though probably in much smaller amounts. The contact ion aggregates may assume various geometries around the equilibrium geometry. These might be responsible at least partly for the broadness of band A.

The fact that the band shifts to longer wavelengths with increasing size of the counter-ion suggests that band A of the unassociated dianion is located at a still longer wavelength than that of the same dianion associated with cesium ions. As is seen in Table 4, for every alkali metal the band shifts to shorter wavelengths with increasing alkyl substitution, in the order stilbene, α,α′-dimethyl-, and α,α′-diethylstilbene. It is plausible that the order will also be maintained in the spectra of the unassociated dianions.

Geometry of the Dianions. It might be said that, if it were not for the electronic effect of alkyl substituents and the effect of the counter-ions, band A would behave as follows: (1) it shifts comparatively rapidly to shorter wavelengths as the α and α' positions are increasingly substituted with alkyl groups; (2) it shifts comparatively slowly to shorter wavelengths as the *ortho* positions are increasingly substituted with methyl groups. These behaviors should be related to the geometry of the dianions.

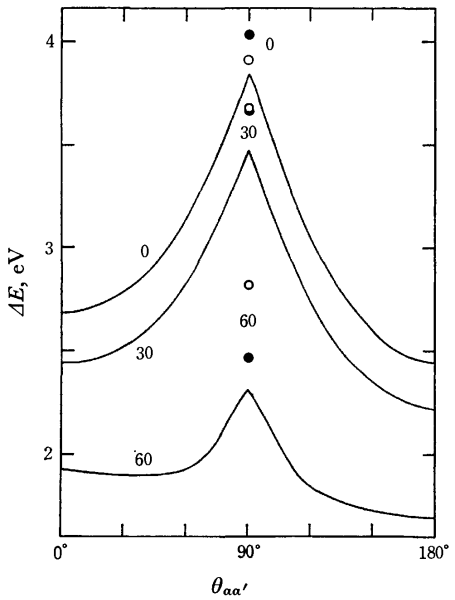

Fig. 5. The relationship of the calculated energy of the A transition of the stilbene dianion (ΔE) to angles of twist $\theta_{\alpha 1}$, $\theta_{\alpha' 1'}$, and $\theta_{\alpha\alpha'}$. The numerals written near curves and circles indicate the values of $\theta_{\alpha 1}$ ($=\theta_{\alpha' 1'}$) in units of degree. For geometries with $\theta_{\alpha\alpha'}=90°$, the A transition being forbidden, the energies of the main allowed transition are also shown with open circles. These are to be compared with the energies of the main allowed transition of the benzyl anion of the corresponding geometries, which are shown with black spots.

As is seen in Figs. 3 and 4, the results of calculation show that the energy of the A transition decreases with increasing deviation of $\theta_{\alpha 1}$ and $\theta_{\alpha' 1'}$ from 0° and increases with increasing deviation of $\theta_{\alpha\alpha'}$ from 0° or from 180°. These tendencies can be seen more clearly in Fig. 5, in which the energy of the A transition is plotted against $\theta_{\alpha\alpha'}$ for various values of $\theta_{\alpha 1}$ and $\theta_{\alpha' 1'}$. The π-electronic state of the stilbene dianion having a geometry in which $\theta_{\alpha\alpha'}=90°$ is considered to resemble that of two mutually independent benzyl anions. For the sake of comparison,

25) T. E. Hogen-Esch and J. Smid, *J. Amer. Chem. Soc.*, **88**, 307 (1966).
26) L. L. Chan and J. Smid, *ibid.*, **90**, 4654 (1968).
27) K. H. J. Buschow, J. Dieleman, and G. J. Hoijtink, *J. Chem. Phys.*, **42**, 1993 (1965).

Table 5. The main absorption band maximum of the benzyl anion in tetrahydrofuran

Counter-ion	λ_{max}, nm	ε_{max}	Ref.
Li^+	330	9.6×10^3	23)
Na^+	354.6	1.2×10^4	22)
Na^+	350	3.5×10^3	24)
Cs^+	356	—	24)

results of a similar calculation for the benzyl anion are also given in Figs. 4 and 5.

The benzyl anion has been reported to have its first intense absorption band at about 350 nm,[28-30] as shown in Table 5. This position is of much shorter wavelength than that of band *A* of the stilbene dianion. The stilbene dianion is iso-π-electronic with hydrazobenzene, and the benzyl anion with aniline. The spectral resemblance of hydrazobenzene and aniline suggests that the most preferred geometry of hydrazobenzene is probably a nonplanar conformation in which the central NN bond is twisted.[31] The situation is quite different in the case of the stilbene dianion and the benzyl anion.

We thus conclude as follows. The most preferred geometry of a sterically unhindered dianion such as the dianions of stilbene and 4,4′-dimethylstilbene is probably planar or nearly planar. It is probably the *trans* form, in view of the result of calculation of the total energy.

When alkyl substituents are introduced into the α and α' positions, the steric interference caused by the substitution are probably relieved chiefly by partial rotation about the α—α' bond. From examination of the electronic absorption spectra of α-methyl- and *cis*-β-methylstyrene and *cis*- and *trans*-α-methylstilbene it has been concluded that a phenyl group in such a system sterically interacts more strongly with a methyl group at the *cis*-β position than with a methyl group at the α position.[32,33] This leads to the inference that in the planar *trans* form of the α,α'-dimethylstilbene dianion the steric interference of the α-phenyl group with the α'-methyl group is probably stronger than that with the α-methyl group. The former can be relieved by comparatively small rotation about the α—α' bond. This means that major part of the steric interference in the dianion can be relieved by rotation about the α—α' bond. The rotation about the α—α' bond is, of course, not the only possible mode of geometry change relieving the steric interference. Rotation about the α—1 and the α'—1′ bonds and some other modes of geometry change probably take place to smaller extents. The possibility also cannot entirely be excluded that a small change in hybridization of the valence orbitals of the α and α' carbon atoms, resulting in a small deviation of the geometry about these atoms from planarity, may contribute to the relief of the steric interference.

The fact that the dianion spectra of *cis*- and *trans*-α,α'-dimethylstilbene are essentially the same indicates that the same dianion, probably of a *trans*-like geometry, is produced from either isomer.

The steric effect of introduction of methyl groups into the *ortho* positions is apparently smaller than that of introduction of methyl groups into the α and α' positions. This is rather surprising, in view of the fact that in the case of neutral molecules the steric effect of the *ortho* substitution is almost comparable to that of the α and α' substitution.[6] This is considered to indicate one of the following two possible causes: (1) in the dianions the steric interference caused by the *ortho* substitution is much smaller than that caused by the α and α' substitution; (2) the former cannot be relieved by rotation about the α—α' bond as effectively as the latter, and can be relieved more effectively by rotation about the α—1 and α'—1′ bonds; consequently, the values of $\theta_{\alpha 1}$ and $\theta_{\alpha' 1'}$ in the 2,4,6,2′,4′,6′-hexamethylstilbene dianion, for example, are larger than those in the α,α'-dimethylstilbene dianion and the value of $\theta_{\alpha\alpha'}$ in the former is smaller than that in the latter. The second possibility seems to be more plausible.

In the dianion the increase in the total energy associated with deviation of $\theta_{\alpha 1}$ and $\theta_{\alpha' 1'}$ from 0° is considered to be much larger than that associated with deviation of the same extent of $\theta_{\alpha\alpha'}$ from 0°. The fact that the formation of the dianion is difficult with the nuclear-substituted stilbenes but easy with the α,α'-substituted stilbenes may have some connection with the possible difference in the extent of the steric interference involved or that in the manner in which the steric interference is relieved, in addition to the possible difference in the magnitude of the electron-donating effect of the substituents at different positions. The relative difficulty of the dianion formation is due to many factors, such as the energy of formation of the aggregates of the dianion and anion radical with the counter-ion and of external and internal solvation of the ion aggregates, besides that of formation of the unassociated dianion from the unassociated anion radical, and deserves further investigation.

Total Energy and π-Bond Order. The phenomenon that the main absorption band shifts to shorter wavelengths with increasing steric interference is very similar to that observed with the neutral molecules of stilbenes.[3-8] However, while in the neutral molecules the steric interference is relieved chiefly by rotation about the α—1 and α'—1′ "single" bonds, in the corresponding dianions it is inferred as above to be relieved chiefly by rotation about the α—α' "double" bond. The difference is understandable in terms of calculated values of the total energy as well as the π-bond order.

Table 6. The calculated total energies of the stilbene molecule and dianion of various geometries in the ground state

Geometry	Total Energy, eV	
	Molecule	Dianion
(0,0,0)	−179.8883	−180.5341
(0,0,180)	−179.9029	−180.2377
(30,30,180)	−179.5502	−179.3771

28) R. Asami, M. Levy, and M. Szwarc, *J. Chem. Soc.*, **1962**, 361.
29) R. Waack and M. A. Doran, *J. Amer. Chem. Soc.*, **85**, 1651 (1963).
30) F. J. Hopton and N. S. Hush, *Mol. Phys.*, **6**, 209 (1963).
31) H. Suzuki, the book cited in Ref. 8, p. 518.
32) H. Suzuki, This Bulletin, **33**, 619 (1960).
33) G. Favini and M. Simonetta, *Theor. Chim. Acta*, **1**, 294 (1963).

Table 7. The π-bond orders of some bonds of the stilbene molecule and molecule ions of geometry (0,0,0)

Bond	Calculated by SCF-MO method		Calculated by Hückel method		
	Molecule	Dianion	Molecule	Anion radical Cation radical	Dianion Dication
α—α'	0.8859	0.4477	0.8577	0.6760	0.4942
α—1; α'—1′	0.3413	0.7109	0.3825	0.4867	0.5908

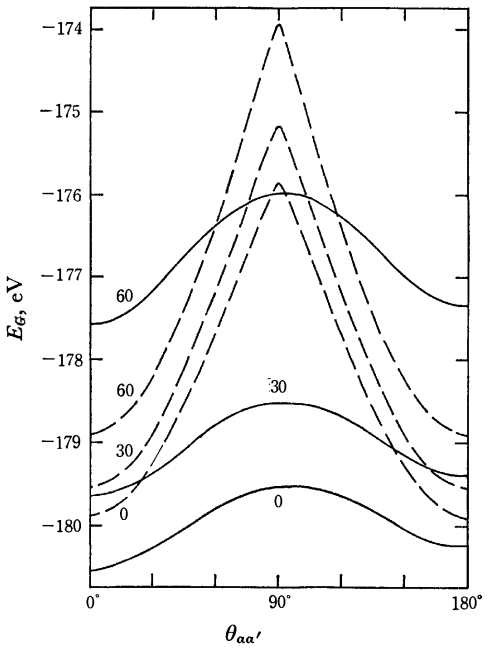

Fig. 6. The relationship of the calculated total energies (E_G) of the stilbene molecule (— — —) and dianion (———) in the ground state to angles of twist $\theta_{\alpha 1}$, $\theta_{\alpha' 1'}$, and $\theta_{\alpha\alpha'}$. The numerals written near curves indicate the values of $\theta_{\alpha 1}$ ($=\theta_{\alpha' 1'}$) in terms of degree.

In Fig. 6 and Table 6 are shown results of the SCF calculation of the total energy of the ground state, as the sum of the π-electron energy and the energy of core-core interaction, for the stilbene dianion and molecule of various geometries. In the calculation the energy of core-core interaction was assumed to be given by

$$\sum_p \sum_{q \neq p} \gamma_{pq},$$

where γ_{pq} is the two-center repulsion integral for the $2p\pi$ atomic orbitals centered at carbon atoms p and q.

From the results, both for the dianion and the molecule, geometries (0,0,0) and (0,0,180) correspond to the energy minima. In addition, the results show that in the case of the dianion the α—α' bond is twisted with a smaller energy increase than the α—1 and α'—1′ bonds, while in the case of the molecule the reverse is true. These tendencies agree with those expected from correlation diagrams[34] connecting the HMO levels of the planar stilbene π-system with those of two non-interacting benzyl groups and those of non-interacting two benzene rings and one ethylenic bond.

In Table 7 are shown the π-bond orders calculated for geometry (0,0,0). In the dianion the π-bond order of the α—α' bond is smaller than that of the α—1 as well as the α'—1′ bond, while in the molecule the reverse is true. The π-bond orders of bonds of the anion radical (as well as the cation radical) must be intermediate between those of the corresponding bonds of the molecule and the dianion (as well as the dication). Therefore, it is of interest to examine how steric interferences affect the geometry and the spectrum in the case of these ion radicals.

It is noteworthy that in the case of the dianion the calculated ground-state energy of geometry (0,0,0) is lower by as much as about 0.3 eV than that of geometry (0,0,180), while in the case of the molecule the energy of geometry (0,0,0) is slightly higher than that of geometry (0,0,180). Even in the case of the molecule, *trans*-stilbene is more stable than its *cis* isomer by about 3[35,36] or 6[37] kcal/mol. In the *cis*-stilbene molecule the two phenyl groups cannot be simultaneously coplanar with the central ethylenic bond plane, owing to steric interference, and the most preferred geometry of this molecule is considered to be close to geometry (30,30,180).[3,4,8,38] According to the results of calculation, the energy of this geometry is higher by about 0.3 eV than that of geometry (0,0,0). Thus, it may be said that the present calculation gives quite adequate results. It seems reasonable to infer that the most preferred geometry of the dianion is the *trans* form, at least if steric interference is absent or small.

Location of the Alkali-Metal Cations in the Contact Ion Aggregates. The geometry of the contact ion aggregates (S^{2-},$2M^+$), the location of M^+'s with respect to S^{2-} in (S^{2-},$2M^+$), is examined.

Schlenk and Bergmann found that addition of carbon dioxide to products resulting from the reduction of *trans*-stilbene with alkali metals, followed by hydrolysis, gave α,α'-diphenylsuccinic acid, which was the racemic mixture when the alkali metal was lithium and the *meso* isomer when the alkali metal was sodium or potassium.[39] These stereochemical findings suggest that, in the reduction with lithium, two lithium atoms undergo *cis* addition to the α and α' carbon atoms of stilbene with bonds possessing covalent character to a large extent, and that in the reduction with sodium or potassium the product exists for a great part as ion aggregates (S^{2-},$2M^+$) which are in equilibrium with the unassociated ions. The thermodynamically most stable geome-

34) A. Imamura and R. Hoffmann, *J. Amer. Chem. Soc.*, **90**, 5379 (1969).

35) G. B. Kistiakowsky and W. R. Smith, *ibid.*, **56**, 638 (1934).

36) T. W. J. Taylor and A. R. Murray, *J. Chem. Soc.*, **1938**, 2078.

37) P. Borrell and H. H. Greenwood, *Proc. Roy. Soc., Ser. A*, **298**, 453 (1967).

38) D. L. Beveridge and H. H. Jaffé, *J. Amer. Chem. Soc.*, **87**, 5340 (1965).

39) W. Schlenk and E. Bergmann, *Ann.*, **463**, 1 (1928).

try of the ion aggregate is probably a geometry in which one of the two cations is located on one side of the dianion plane and the other on the opposite side.

The energy of interaction between the ions in the contact aggregate of the dianion in the ground state with the cations ΔE_G and the change in the energy of the A transition of the dianion caused by the ion aggregation $\Delta\Delta E_{GA}$ were tentatively calculated for various locations of the cations in the following approximate manner. In the calculation solvent effects were not considered.

It is assumed that two alkali-metal cations are located symmetrically with respect to the origin of the coordinate system assigned to the dianion (see Fig. 2). That is, if the coordinate of one of the two cations is denoted by (x_M, y_M, z_M), that of the other is assumed to be $(-x_M, -y_M, -z_M)$. The energy of interaction between the ions in the aggregate of the two cations with the dianion in the ith π-electronic state ΔE_i is given by

$$\Delta E_i = 2(E_{\text{core,M}} - E_{\pi(i),M}) + E_{MM'},$$

where $E_{\text{core,M}}$ is the energy of repulsive interaction between the cores of the dianion and one of the cations, $E_{\pi(i),M}$ is that of attractive interaction between the π-electronic cloud of the dianion and one of the cations, and $E_{MM'}$ is that of repulsive interaction between the two cations. These quantities are assumed to be given by the following equations:[40]

$$E_{\text{core,M}} = e^2 \sum_p (1/R_{pM})$$

$$E_{\pi(i),M} = e^2 \sum_p (P_{pp(i)}/R_{pM})$$

$$E_{MM'} = e^2/R_{MM'},$$

where e is the quantum of electricity, R_{pM} the distance between the pth carbon π-center of the dianion and one of the cations, $P_{pp(i)}$ the π-electron density at the pth carbon π-center of the dianion in the ith π-electronic state, $R_{MM'}$ the distance between the two cations, and the summations are carried out over all the π-centers. The change in the energy of transition from the ith to the jth π-electronic state associated with the aggregation $\Delta\Delta E_{ij}$ is given by

$$\Delta\Delta E_{ij} = 2(E_{\pi(i),M} - E_{\pi(j),M}).$$

The calculation was carried out for the dianion of geometry (0,0,0), by the use of the values of π-electron densities $P_{pp(G)}$ and $P_{pp(A)}$ shown in Table 3. After Hush and Rowlands,[41] the perpendicular distance of a cation from the plane of the dianion z_M was assumed to be given by

$$z_M = r_{M^+} + 2.5(\text{Å}),$$

where r_{M^+}, the Goldschmidt ionic radius of the alkali-metal cation, was taken to be 0.97, 1.33, and 1.70 Å for Na^+, K^+, and Cs^+, respectively. The results of the calculation for various locations of the cations are shown in Fig. 7.

The A band maximum shifts to shorter wavelengths as the alkali metal is changed from Cs to K, and further to Na. From comparison of this fact with the result of the calculation of $\Delta\Delta E_{GA}$ shown in Fig. 7(2) and inspection of the result of the calculation of ΔE_G shown in Fig. 7(1), the possibility of geometries in which the alkali-metal cations are located near the benzene rings is excluded. It is inferred that the cations are located near the ethylenic bond. The results show that geometries a and b have large and nearly equal probabilities.

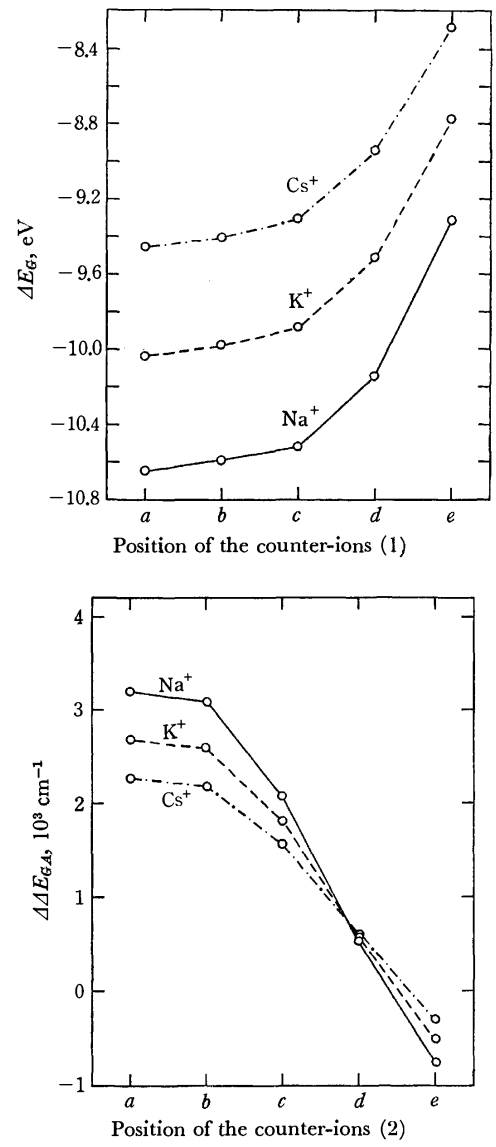

Fig. 7. The relationship of (1) ΔE_G and (2) $\Delta\Delta E_{GA}$ of the stilbene dianion of geometry (0,0,0) to the location of the counter-ions. The positions of the counter-ions are represented by the projection of one of them on the plane of the dianion as follows: (*a*) the center of the α-α' bond; (*b*) the position of carbon atom α; (*c*) the position of carbon atom 1; (*d*) the center of a benzene ring; (*e*) the position of carbon atom 4. The perpendicular distances of the counter-ions from the dianion plane are taken as described in text.

In addition to the electrostatic interaction between the ions, charge transfer from the dianion to the alkali-metal cations seems to make a minor contribution to the stability of the ion aggregate. The most important component of the charge-transfer interaction is probably the interaction between the highest occupied orbital (the 8th π orbital) of the dianion and the lowest vacant orbital (an s orbital) of each cation. Since the former

40) For justification of adopting the point-charge approximation, see Ref. 41.

41) N. S. Hush and J. R. Rowlands, *Mol. Phys.*, **6**, 201 (1963).

has a nodal plane bisecting the α—α′ bond perpendicularly and the latter is centrosymmetric, if the cations were located near the center of the α—α′ bond (geometry *a*), the charge-transfer interaction would make substantially no contribution to the stability. It is therefore concluded that the most preferred or equilibrium geometry of the ion aggregate is probably close to geometry *b*, that is, the geometry in which one of the cations is located above carbon atom α and the other below carbon atom α′.

BULLETIN OF THE CHEMICAL SOCIETY OF JAPAN, VOL. 45, 1988—1992(1972)

The Effect of the Wavelength of an Exciting Light on Four-center-type Photopolymerization in the Crystalline State

Takashi TAMAKI, Yasuzo SUZUKI, and Masaki HASEGAWA
Research Institute for Polymers and Textiles, Kanagawa-ku, Yokohama
(Received March 12, 1971)

The effect of the wavelength of an exciting light on four-center-type photopolymerization in the crystalline state has been investigated. 2,5-Distyrylpyrazine (DSP), 1,4-bis[β-pyridyl-(2)vinyl]benzene (P2VB), *p*-phenylenediacrylic acid (*p*-PDA) dimethyl ester were converted quantitatively into highly crystalline oligomers (pentamers on the average) on irradiation at the long-wavelength edge of the absorption of the monomer. On subsequent exposure to the light which is absorbed by each oligomer, the oligomer crystals *as*-polymerized were converted quantitatively into high polymer crystals. The polymer thus obtained was found to be identical with the polymer produced by the light of a xenon or a high-pressure mercury lamp. The quantum yields for the oligomerization and polymerization reactions of DSP and the *p*-PDA dimethyl ester were found to be between 1 and 2 on the basis of the number of olefinic double bonds consumed to form the cyclobutane ring. These results confirmed that the four-center-type photopolymerization in the crystalline state consists of two kinds of separable, step-by-step addition mechanisms: an oligomerization of the diolefinic compound and a growth reaction of the terminal group in the growing chain. From the crystallographic information on the DSP oligomer, the oligomerization as well as the polymerization process of DSP were concluded to proceed by a monomer lattice-controlled mechanism.

The method of investigating four-center-type photopolymerization in the crystalline state of diolefinic compounds, such as 2,5-distyrylpyrazine (DSP), its related compounds, *p*-phenylenediacrylic acid (*p*-PDA) derivatives, and *p*-benzene (α-cyano)diacrylic acid (*p*-BCA) derivatives, has recently been developed in this laboratory.[1-8]

Many diolefinic compounds which are photopolymerizable in the crystalline state have been synthesized.[1-4] They can be roughly classified into high and low photopolymerizable compounds according to their reaction times. For example, DSP and the *p*-PDA dimethyl ester belong to the former type, and 1,4-bis[β-pyridyl-(2) vinyl]benzene (P2VB) belongs to the latter.

A previously-reported kinetic study[5] of the photopolymerization of DSP in the crystalline state has shown that the reduced viscosity of the polymer increases with the reaction time, that it continues to rise on irradiation even after the conversion is completed, and that the molecular weight of the polymer at a low conversion is widely distributed. From these facts, it has been concluded that the polymerization follows a step-by-step mechanism.

Recently in a X-ray crystallographic study of DSP the photopolymerization of DSP in the crystalline state was concluded to be a topochemical reaction which is lattice-controlled and which is strictly governed by the spatial arrangement of monomer molecules in a crystal.

In this paper the effects of the wavelength of an irradiating light on four-center-type photopolymerization and the quantum yields are described. The mechanism of the polymerization is discussed in terms of the oligomerization process and the growth process producing a high polymer.

Experimental

Preparation of the Monomers. DSP, P2VB, and the *p*-PDA dimethyl ester were prepared and recrystallized as has been described in earlier papers.[2,3]

Optical Measurements. To examine the effect of the wavelength of an exciting light on the polymerization of each monomer in the crystalline state, UV and IR spectral changes were measured during polymerization upon irradiation with monochromatic light. For the UV measurements the monomer crystals were deposited on a quartz plate in

1) M. Hasegawa and Y. Suzuki, *J. Polym. Sci., Part B*, **5**, 815 (1967).
2) M. Hasegawa, Y. Suzuki, F. Suzuki, and H. Nakanishi, *ibid., Part A-1*, **7**, 743 (1969).
3) F. Suzuki, Y. Suzuki, H. Nakanishi, and M. Hasegawa, *ibid., Part A-1*, **7**, 2319 (1969).
4) F. Nakanishi and M. Hasegawa, *ibid., Part A-1*, **8**, 251 (1970).
5) H. Nakanishi, Y. Suzuki, F. Suzuki, and M. Hasegawa, *ibid., Part A-1*, **7**, 753 (1969).
6) Y. Sasada, H. Shimanouchi, H. Nakanishi, and M. Hasegawa, This Bulletin, **44**, 1262 (1971).
7) S. Fujishige and M. Hasegawa, *J. Polym. Sci., Part A-1*, **7**, 2037 (1969).
8) M. Hasegawa, Y. Suzuki, and T. Tamaki, This Bulletin, **43**, 3020 (1970).

the form of a thin layer by slow evaporation from a concentrated solution, while for the IR measurements KBr pellets containing the monomer crystals were prepared.

The exciting light was furnished by a spectroirradiator (Jasco) composed of a 2000-W xenon lamp as the light source and a grating monochromator.

To attenuate the scattered light, the UV measurements were performed by the method of an integrating sphere attached to a spectrophotometer.

The disappearing rate of the olefinic double bonds during the oligomerization and the polymerization was followed by IR analysis. In the case of the oligomerization, KBr pellets (150 mg) containing 1.5 mg of monomer crystals were prepared by pressing in an evacuated die at 9 kbars for 4 min. In the case of the polymerization of the oligomer, KBr pellets containing 6—7 mg of monomer crystals were prepared in the same way, before the measurement they were exposed to the light at the long-wavelength edge of the absorption of the monomer until the monomer was completely converted into the oligomer.

The excitation light for the measurement of the quantum yields was furnished by a grating monochromator (Shimadzu Bausch and Lomb), to which a 450 W high-pressure mercury lamp was attached as a light source. The light intensity was measured by potassium ferrioxalate actinometry.[9] The actinometric estimates were checked with a thermopile (Eppley).

Preparation of the Oligomer and the Polymer. Fine crystals of the monomer (200 mg) were dispersed in 50 m*l* of water-methanol (4: 6) in a Pyrex flask; they were then irradiated for one hour at room temperature by means of a 450-W high-pressure mercury lamp with a suitable cut-off filter—for example, Corning 3-73 for DSP and P2VB, and Corning 0-52 for the *p*-PDA dimethyl ester.

In order to check the photopolymerizability of the oligomer molecules in the crystalline state, they were exposed to the light of a high-pressure mercury lamp without any color filter.

The oligomer and the polymer thus obtained were identified by means of their melting points, IR and NMR spectra, and reduced viscosities (360 mg in 100 m*l* of CF_3COOH).

Results and Discussion

Wavelength Effect on the Photopolymerization. The crystalline UV absorption of DSP, as measured in a thin layer deposited on a quartz plate, is shown in Fig. 1a (Curve 1). DSP molecules in the crystal (*orthorhombic*, P_{bca}) are piled up plane-to-plane along the *c*-axis, to which the long axis of the molecules makes an angle of about 30°; the distance between olefinic double bonds of the nearest neighbouring molecules in 3.94 Å.[6] From these facts, a dipole-dipole interaction may be supposed to exist among DSP molecules in the crystal, as in the case of *trans*-cinnamic acid.[10]

It was found that, on the irradiation of crystalline DSP at a wavelength longer than 400 mμ, the UV absorption spectrum was changed into one with peaks at 350 mμ and 290 mμ, as may be seen in Fig. 1a (Curve 2), in which the band at 430 mμ was excited. Under those conditions, an IR absorption band at 970 cm^{-1} corresponding to the ν_{CH} of the *trans* HC=CH bond

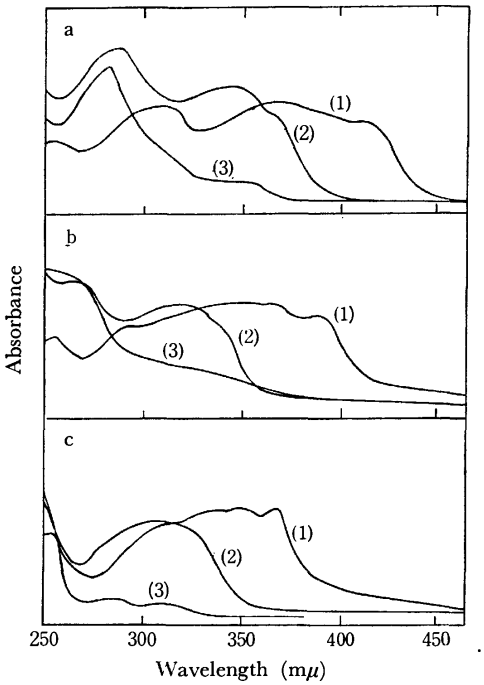

Fig. 1. The crystalline UV spectra of DSP (a): (1) non-irradiated, (2) irradiated at 430 mμ and (3) successively irradiated at 350 mμ, of P2VB (b): (1) non-irradiated, (2) irradiated at 410 mμ and (3) successively irradiated at 350 mμ, and of the *p*-PDA dimethyl ester (c): (1) non-irradiated, (2) irradiated at 360 mμ and (3) successively irradiated at 310 mμ.

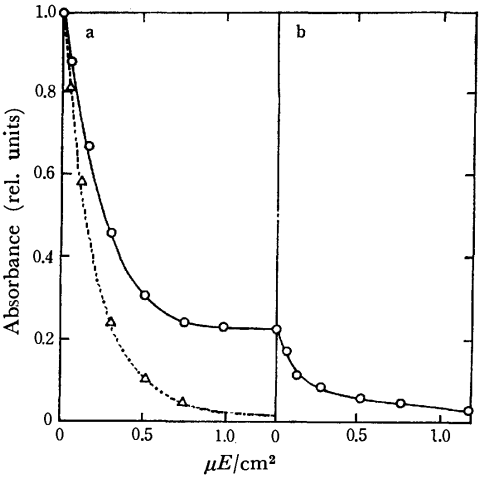

Fig. 2. Kinetics of polymerization of DSP in KBr irradiated (a) at 430 mμ and (b) at 350 mμ: the figure (—○—) corresponds to IR absorbance measurement at 970 cm^{-1}, and the one (---△---) to UV absorbance measurement at 384 mμ taken after dissolution of irradiated pellets in 95% EtOH.

gradually decreased, and then reached a constant level about one-fifth of the initial value, while the monomer in KBr pellets, as measured by UV analysis at 384 mμ after dissolving each pellet in 95% ethanol, decreased and finally almost disappeared, as is shown in Fig. 2a.

These facts imply that crystalline DSP is converted into the oligomer on irradiation at a wavelength longer than 400 mμ. To confirm this, the preparative experiment described in the Experimental section was performed, and the characteristics of the product were examined.

9) C. G. Hatchard and C. A. Parker, *Proc. Roy. Soc., Ser. A*, **235**, 518 (1956).

10) J. Tanaka, This Bulletin, **36**, 833 (1963).

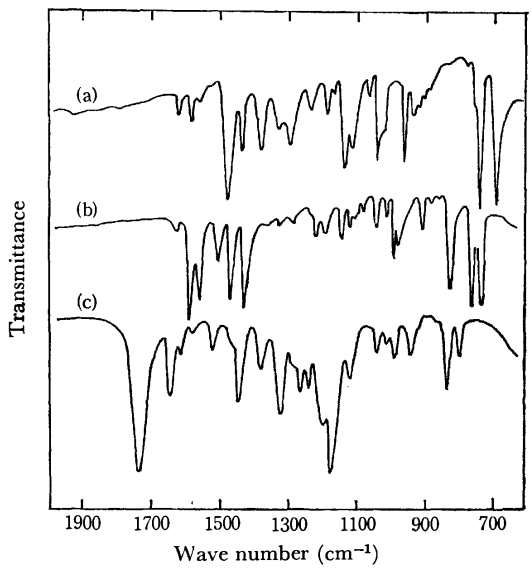

Fig. 3. IR spectra of (a) the DSP oligomer, (b) the P2VB oligomer and (c) the *p*-PDA dimethyl ester oligomer.

The product was quantitatively obtained from DSP, and it melted at 285—290°C. In the IR absorption spectrum, shown in Fig. 3(a), bands attributable to the olefinic double bond are recognized both at 970 cm^{-1} and 1630 cm^{-1}; they completely disappear in that of poly-DSP, as was demonstrated previously.[2] Assuming that the absorption coefficient of the product at 970 cm^{-1} is the same as that of the monomer, the product can be said to correspond to a pentamer, on the average, because the absorbance remains at one-fifth of the initial level (Fig. 2a).

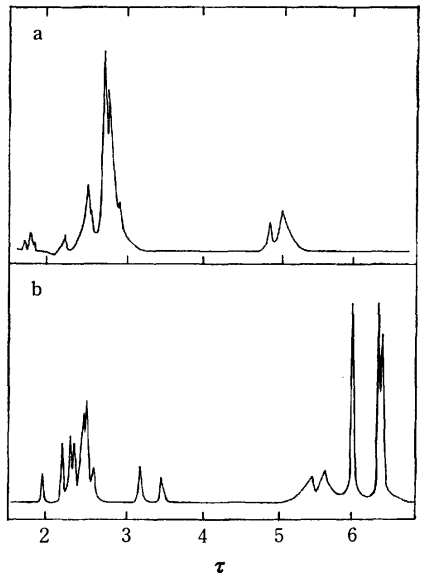

Fig. 4. NMR spectra of (a) the DSP oligomer and (b) the *p*-PDA dimethyl ester oligomer.

The NMR spectrum in Fig. 4a shows the peaks of protons attached to the cyclobutane ring near 5 τ, and those attached to aromatic rings at 2—3 τ. The degree of polymerization, as calculated from the ratio of the number of cyclobutane-ring protons *vs.* that of the other, was equal to about one-fifth. This value corresponds to a pentamer, in good agreement with that estimated by the IR measurements.

Upon the further irradiation of the DSP oligomer at a wavelength longer than 400 mμ, no change was any longer observed. This is reasonable because the oligomer is transparent in that wavelength region. However, the oligomer was found to be converted into a high polymer by exposure to the light at a wavelength shorter than 400 mμ. For example, the excitation at 350 mμ induced a decrease in an UV absorption band at 350 mμ, while leaving the one at 290 mμ unchanged, as may be seen in Fig. 1a (Curve 3). At the same time, the IR absorbance at 970 cm^{-1} decreased, and then completely disappeared (Fig. 2b). The product preparatively obtained was identical with the poly-DSP described previously.[2]

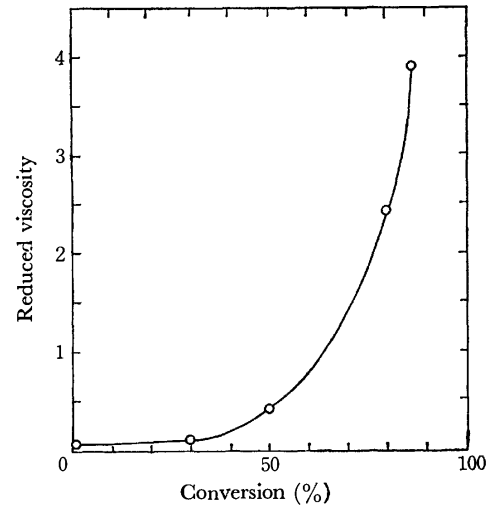

Fig. 5. The reduced viscosity as a function of conversion of olefinic double bonds (measured by IR analysis) during polymerization of the DSP oligomer.

Figure 5 shows the plot of the reduced viscosity *vs.* the conversion during the polymerization of the DSP oligomer. The reduced viscosity increased with an increase in the conversion, as in the case previously reported.[5] This demonstrates that the polymerization of the DSP oligomer proceeds by the step-by-step addition of the terminal group.

When DSP monomer crystals were irradiated at 350 mμ from the beginning, the UV and IR absorption spectra were gradually changed into those of the polymer, without apparently showing those of the oligomer on the way.

It may be concluded that, on irradiation at a wavelength longer than 400 mμ, crystalline DSP was not converted into a high polymer, but quantitatively into the oligomer (a pentamer, on the average), and that a wavelength shorter than 400 mμ was required for the further growth of the terminal group in the oligomer.

It was found that P2VB and the *p*-PDA dimethyl ester, which are photopolymerizable,[2,3] also oligomerized in the crystalline state on irradiation at the long-wavelength edge of the absorption (Fig. 1b, c, 3b, c, and 4b), and that each oligomer polymerized to give a high polymer on irradiation, as may be seen in Fig. 1b and

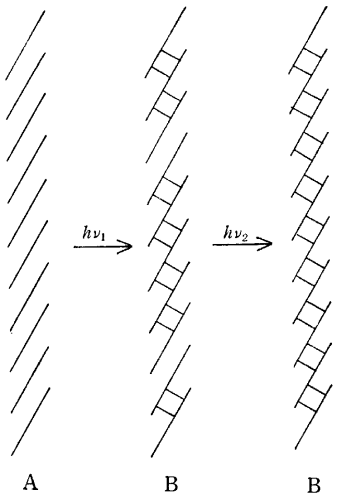

Fig. 6. The scheme of four-center-type photopolymerization in the crystalline state (see text for details).

c. The NMR spectrum of the P2VB oligomer thus obtained was almost the same as that of the poly-P2VB shown in the previous paper.[2]

The effect of the wavelength of an exciting light on the four-center-type photopolymerization confirms the step-by-step mechanism in the polymerization suggested in a previously-reported kinetic study.[5] The polymerization reaction in the crystalline state is schematically illustrated in Fig. 6, where A and B represent the monomer molecule and the molecule larger than the dimer with a cyclobutane ring in the main chain respectively.

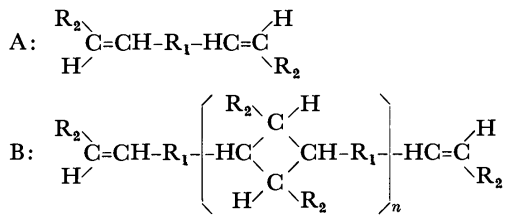

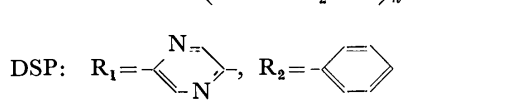

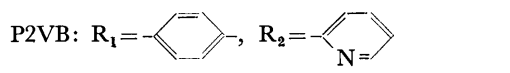

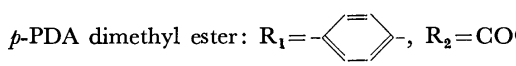

The reaction scheme is as follows:

$$A + h\nu_1 \longrightarrow A^* \quad (1)$$

$$A + A^* \xrightarrow{k_1} B \quad (2)$$

$$A^* + B \xrightarrow{k_2} B \quad (3)$$

$$B + h\nu_2 \longrightarrow B^* \quad (4)$$

$$B + B^* \xrightarrow{k_3} B \quad (5)$$

where A* and B* represent A and B in the excited state respectively. Equation (2) represents a dimerization reaction, while Eqs. (3) and (5) represent growth reactions.

Since the π-electron conjugation of A is interrupted by the formation of the cyclobutane ring to produce B, the π–π^* electronic transition energy of B can be expected to be higher than that of A (Fig. 1). Therefore, it is possible to excite A alone on irradiation at the long-wavelength edge of the absorption of A ($h\nu_1$), leaving B in the ground state.

Under those conditions, A is converted into B through Eqs. (2) and (3). This first reaction stage is designated as an oligomerization process, because the B produced in this stage is equivalent to a pentamer.

On successive irradiation with the light ($h\nu_2$) which excites B, a high polymer is produced through Eq. (5), a growth reaction of the terminal group in the growing chain. The second reaction stage is designated as a higher polymerization process.

Exposure to the light which excites both A and B from the beginning can induce the oligomerization and the polymerization reaction through Eqs. (1) to (5) successively to give a high polymer. At this time, a A+B*→B reaction may also proceed.

The rate constants, k_1 and k_2, of these elemental reactions in the oligomerization of DSP can be estimated from the kinetic data shown in Fig. 2a. From Eqs. (2) and (3), Eq. (6) is given:

$$-\mathrm{d[A]}/\mathrm{d}t = 2k_1[\mathrm{A}][\mathrm{A}^*] + k_2[\mathrm{A}^*][\mathrm{B}] \quad (6)$$

Since these reactions proceed in the crystalline state, Eq. (6) does not strictly hold good in this system. However, it may be sufficient to evaluate the ratio of k_1 and k_2. It is supposed that [A*] is proportional to the absorbed light intensity, *i.e.*, $[\mathrm{A}^*] \propto 1-\exp(-\kappa[\mathrm{A}])$, in which κ is the constant related to the absorption coefficient and the light-path length. By replacing A* with $1-\exp(-\kappa[\mathrm{A}])$, Eq. (6) can be integrated to give Eq. (7):

$$[\mathrm{A}_0] - [\mathrm{A}] = (2k_1 - k_2)\int_0^t [\mathrm{A}]\mathrm{d}t + k_2\int_0^t [\mathrm{C}]\mathrm{d}t \quad (7)$$

where $[\mathrm{A}_0]$ is the initial concentration of A in a pellet, [C] is the sum of [A] and [B], and $\exp(\kappa[\mathrm{A}]) > 1$ is assumed. The conversion of [A] was followed by UV measurements, and that of [C], by IR measurements, as is shown in Fig. 2a.

The result that $k_2/k_1 \simeq 10$ was obtained. This result is reasonable considering that the B produced in the oligomerization process corresponds to a pentamer. The reason why k_2 is larger than k_1 could not be thoroughly explained. One possible explanation for this acceleration is that the distance between the olefinic double bonds of A and B becomes shorter than that between A and A as a result of the molecular rearrangement from A to B. However, other alternatives may be acceptable.

Quantum Yields. The quantum yields for the oligomerization and the polymerization of DSP, P2VB, and the *p*-PDA dimethyl ester were measured. The quantum yield, (ϕ), is defined by the equation:

$$\phi = -(\mathrm{d[double\ bonds]}/\mathrm{d}t)/I_{abs} \quad (8)$$

where $-(\mathrm{d[double\ bonds]}/\mathrm{d}t)$ is the disappearing rate of the olefinic double bond per unit of volume, and where I_{abs} is the rate at which the incident light is absorbed per unit of volume of a pellet containing the sample.

There are two IR absorption bands, at 970 cm^{-1} and

at 1630 cm^{-1}, attributable to the olefinic double bond. The former can be used for the measurement in DSP and P2VB, and the latter, in the *p*-PDA dimethyl ester, because they are more intense than the others.

ε_A, an IR absorption coefficient of A, was exactly determined from the calibration curve of the IR absorbance *vs.* the monomer concentration in a pellet. However, ε_B, that of B, could not be determined since B was not a homogeneous species, but an oligomer mixture with various degrees of polymerization. Hence, we assumed that $\varepsilon_B=\varepsilon_A$. This may be approximately correct because the substitutions of the olefinic double bonds in A and B are similar.

I_{abs} could not be precisely evaluated because of the ambiguity in the amount of scattered light. I_{abs} should be equal to the intermediate value between two extreme ones calculated on the assumption that the scattered light is either all lost or not lost at all.[11] The extreme values are calculated as the difference between the intensity of the radiation transmitted through a pure KBr pellet (I_{KBr}) and a pellet containing the sample (I_{sam}) in the former case, and between the incident light intensity (I_0) and I_{sam} in the latter case. I_{KBr} was about 70% of I_0 at 365 mμ under these experimental conditions.

The substitution of the upper limit of I_{abs}, I_0-I_{sam}, in the denominator of Eq. (8) gives the quantum yield at the lower limit, and *vice versa*.

The initial quantum yields for the oligomerization and the polymerization of DSP, P2VB, and the *p*-PDA dimethyl ester are summarized in Table 1. These are the values at the lower limit.

TABLE 1. QUANTUM YIELDS OF OLIGOMERIZATION AND POLYMERIZATION OF DSP, P2VB, AND THE *p*-PDA DIMETHYL ESTER

	Oligomerization		Polymerization	
	Excitation (mμ)	ϕ	Excitation (mμ)	ϕ
DSP	436	1.2	365	1.6
P2VB	405	0.04	—	—
p-PDA dimethyl ester	365	1.2	313	0.7

The quantum yields of DSP and the *p*-PDA dimethyl ester were all between 1 and 2 except for that of the polymerization of the latter. This indicates that these photoreactions all belong to one type of reaction in which, theoretically, the maximum value is equal to 2, and that they proceed very efficiently compared with the model compounds photodimerizable in the crystalline state, such as stilbazole[12] and *trans*-cinnamic acid.[13]

The true value of the quantum yield may be expected to be larger than those listed in Table 1. One of the quantum yields calculated at the upper limit was beyond 2, but the other was not. At least mechanistically, the quantum yield which is beyond 2 cannot be visualized for this kind of photopolymerization.

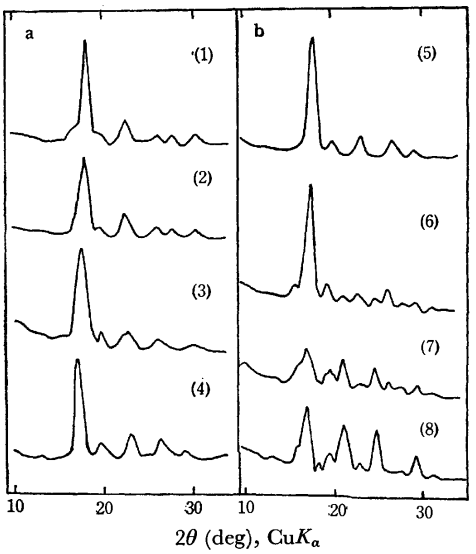

Fig. 7. The changes of X-ray diffraction diagram (a) during oligomerization of DSP: (1) monomer crystals, (2) 35% of conversion, (3) 65% and (4) 100% (*as*-oligomerized), and (b) during polymerization of the oligomer: (5) oligomer crystals, (6) 46% (7) 83% and (8) 100% (*as*-polymerized). Conversion was followed by measuring an IR absorbance at 970 cm^{-1}.

The quantum yield for the oligomerization of P2VB was 0.04. That for the polymerization could not be measured because several bands near 970 cm^{-1} overlap each other and the absorption coefficient at 1630 cm^{-1} is too low in the IR absorption spectrum of the oligomer.

The reason for the difference between the quantum yields in DSP and P2VB cannot be explained until more detailed studies of the crystal structure and the photochemical behavior of these compounds are made.

Structure of the DSP Oligomer. Figure 7 shows the changes in the X-ray diffraction diagram of DSP during the oligomerization and the polymerization. The diffraction diagram of the oligomer is clearly different from those of the monomer and the polymer.

It is noteworthy that the crystallinity of the oligomer (*as*-polymerized) is very high. Once the oligomer is dissolved in a solution, the same crystal structure cannot be reproduced by reprecipitation. In contrast to the DSP oligomer crystal (*as*-polymerized), the recrystallized oligomer could not be photopolymerized. This observation suggests that the thermodynamically quasi-stable oligomer crystals are produced, as in the case of the high polymer crystals *as*-polymerized.[7]

From these facts it is evident that both the oligomerization and the polymerization proceed through a direct rearrangement from the monomer crystals to the polymer crystals by means of a three-dimensional, monomer-lattice-controlled mechanism.

11) W. Fuchtbauer and P. Matur, *Photochem. Photobiol.*, **5**, 323 (1966).
12) J. L. R. Williams, *J. Org. Chem.*, **25**, 1839 (1960).
13) M. D. Cohen, G. M. J. Schmidt, and F. I. Sonntag, *J. Chem. Soc.*, **1964**, 2000.

Conformations of the Esters. VI.[1] The Conformations of Monothiocarbonates

Michinori Ōki and Hiroshi Nakanishi

Department of Chemistry, Faculty of Science, The University of Tokyo, Hongo, Tokyo

(Received September 3, 1971)

The presence of two or three conformational isomers in monothiocarbonates has been confirmed by nuclear magnetic resonance and infrared spectroscopies and by dipole moment techniques. The data can best be interpreted by assuming that the conformations involving the *s-cis* conformation are more stable than that of *s-trans, s-trans*.

It has been confirmed recently that some formates[2] and carbonates[1] exist as both *s-cis* and *s-trans* conformers with respect to the ester group, and the stability of the two conformational isomers has been discussed. As a natural extension of the study of the conformational analysis of carbonates, the conformations of monothiocarbonates have now been studied.

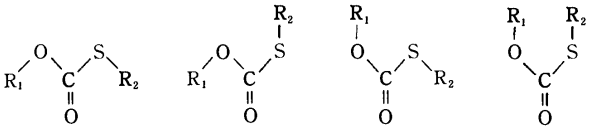

Fig. 1. Conformations of monothiocarbonate.

The following conformational isomers of monothiocarbonates may be considered: *s-trans,s-trans* (A), *s-trans, s-cis* (B), *s-cis,s-trans* (C), and *s-cis,s-cis* (D) (Fig. 1). The conformer D is unstable because of the steric repulsion between R_1 and R_2 groups, although the repulsion should be somewhat smaller in monothiocarbonates than in ordinary carbonates because the C–S bond distance is greater than that of C–O, (C–S, 1.82 Å; C–O, 1.42 Å).[3] Therefore, the conformer D can be neglected.

The chief factors governing the conformations of the ester and the carbonate have been described in previous papers.[1,2] The same factors may be considered for the monothiocarbonates, although there are some points which are different in the monothiocarbonates from the carbonates: 1) the bond moment[4] of the C–S (0.9 D) is a little larger than that of the C–O (0.85 D); 2) the sulfur atom has a larger van der Waals radius (1.85 Å) than oxygen (1.4 Å);[5] 3) the distance of the C–S bond (1.82 Å) is larger than that of the C–O (1.42 Å).

Regarding the first factor, the dipole-dipole interaction between the C=O and the C–S bonds or the C–O and the C–S bonds will be somewhat larger in the monothiocarbonates than in ordinary carbonates (Fig. 2(1)). The second factor necessarily increases the repulsion between sulfur and oxygen in monothiocarbonates, although a part of the repulsion may be released by the third factor. Therefore, the coformer C may be a little more stable than the conformers A and B (Fig. 2(2)). Regarding the third factor, it may be postulated that, in determining the preference of the conformations, the contributions of the steric repulsion between C=O and the R_2 group in the conformers A and C, that between O_{ether} and the R_2 group in the conformer B, and that between the R_1 group and S in the conformer C are smaller in monothiocarbonates than in the carbonates (Fig. 2(3)).

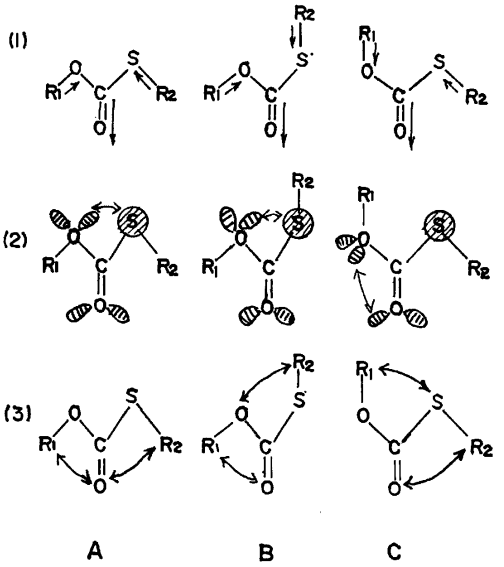

Fig. 2. Factors governing the conformations of monothiocarbonate.

In addition to the above considerations, the sulfur atom may influence the stability of these conformers because its polarizability is larger than that of oxygen.

The purpose of this paper is to present the results of nuclear magnetic resonance and infrared spectral studies and dipole moment measurements undertaken to confirm the existence of conformational isomers in monothiocarbonates.

Experimental

Materials. General Procedure: The sodium thiolate, which was prepared by refluxing sodium in thiol and dry ether for several days, was poured into methyl chloroformate in dry ether with ice cooling. The solution was freed from the precipitate, and the monothiocarbonate was distilled.

1) Part V: M. Ōki and H. Nakanishi, This Bulletin, **44**, 3419 (1971).

2) M. Ōki and H. Nakanishi, This Bulletin, **43**, 2558 (1970).

3) L. E. Sutton, "Tables of Interatomic Distances and Configurations in Molecules and Ions," Chemical Society, London (1958).

4) T. Shimozawa, "Yudenritsu no Kaishaku (Interpretation of Dielectric Constants)," Kyoritsu Shuppan Co., Tokyo (1967).

5) L. Pauling, "The Nature of the Chemical Bond," Cornell Univ. Press, Ithaca (1967).

Dimethyl Monothiocarbonate: bp 63°C/93 mmHg. NMR (τ): OCH_3, 6.13; SCH_3, 6.34.

S-*Ethyl Methyl Monothiocarbonate*: bp 66—67°C/81 mmHg. NMR (τ): OCH_3, 6.12; $C\underline{H}_2CH_3$, 7.07; $CH_2C\underline{H}_3$, 8.62.

S-*Isopropyl Methyl Monothiocarbonate*: bp 50.5°C/20 mmHg. NMR (τ): OCH_3, 6.20; $C\underline{H}(CH_3)_2$, 6.53; $CH(C\underline{H}_3)_2$, 8.64.

S-t-*Butyl Methyl Monothiocarbonate*: bp 86—87°C/72 mmHg. NMR (τ): OCH_3, 6.25; $C(C\underline{H}_3)_3$, 8.53.

S-*Phenyl Methyl Monothiocarbonate*: bp 125.5°C/20 mmHg. NMR (τ): OCH_3, 6.25; aromatic H, 2.60.

Found: C, 57.36; H, 4.66%. Calcd for $C_8H_8O_2S$: C, 57.14; H, 4.80%.

The purities of these compounds were checked by gas chromatography and by studying the infrared spectra and the NMR spectra. The infrared and NMR spectra were measured with the spectrometers previously described.[1] The dipole moment was measured in a benzene solution by the heterodyne beat method.

Results and Discussion

Nuclear Magnetic Resonance Spectra. The NMR spectra of several methyl monothiocarbonates were measured in a carbon tetrachloride solution at room temperature. The results are shown in Table 1. The chemical shifts of the methoxy methyl protons of alkyl methyl monothiocarbonates from TMS change from compound to compound. Since it is difficult to consider that this large shift is due merely to the difference in electronic effects of the alkylthio group, the authors should like to claim that the change is attributable to the change in the population of conformational isomers by the steric effect.

Table 1. NMR spectral data of monothiocarbonates MeOCOSR in CCl_4 ($c=15\%$)

	R	$OC\underline{H}_3$
I	Me	6.10(τ)
II	Et	6.12
III	*i*-Pr	6.20
IV	*t*-Bu	6.25
V	Ph	6.25

In order to obtain further information on the existence of conformational isomers, the NMR spectra of *S*-*t*-butyl methyl monothiocarbonate were measured at low temperatures in CS_2–CH_2Cl_2. The results are shown in Table 2 and Fig. 3. The peak heights of the methoxy and *t*-butyl protons decrease as the temperature is lowered: the peak height of the methoxy proton at −110°C is 57% of that at 34°C, while that of the *t*-butyl

Table 2. The intensity change of NMR spectra peaks of *S*-*t*-butyl methyl carbonate in $CS_2+CH_2Cl_2+$toluene

(The peak area of the methyl signal of toluene added as an internal standard is taken as unity.)

T°C	34	−70	−90	−100	−110	Chemical shift
arom-$\underline{H}$	1.32	1.38	1.37	1.41	1.68	2.77(τ)
arom-$C\underline{H}_3$	1.00	1.00	1.00	1.00	1.00	7.54
$OC\underline{H}_3$	1.60	1.36	1.21	1.00	0.91	6.23
$C(C\underline{H}_3)_3$	4.55	3.42	2.21	1.94	0.95	8.43

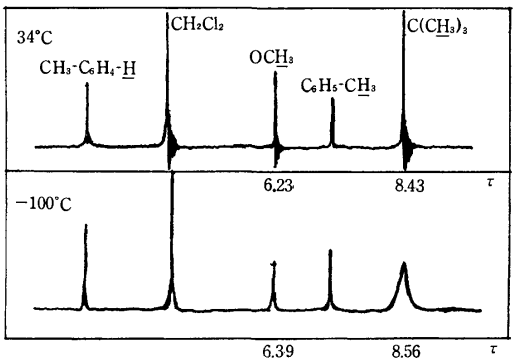

Fig. 3. NMR spectra of MeOCOS-*t*-Bu in $CS_2+CH_2Cl_2+CH_3C_6H_5$.

is merely 21% (Fig. 3). These results may best be interpreted by assuming the presence of two or three conformers in this compound and by assuming that the exchange rate among the conformers is slow on the NMR time scale at this low temperature. The broadening both in the peaks of methoxy and *t*-butyl groups may mean the coexistence of three conformers, A, B, and C, or two conformers, B and C, because the chemical shift of the methoxy protons in the conformer A can be considered to be almost the same as that of the conformer B and the same would be true for the chemical shifts of *t*-butyl protons in the conformers A and C, provided that the anisotropic effect of the carbonyl group is the most important in determining the chemical shifts.

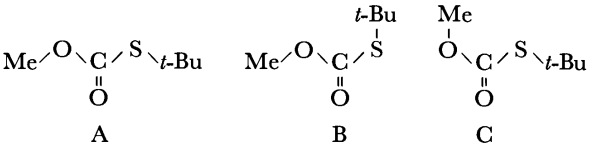

Infrared Spectra. Only a few infrared spectra of carbonyl absorptions of monothiocarbonates have been reported so far;[6,7] only one carbonyl absorption has been reported. However, as was pointed out earlier,[1,2,8] by using an infrared spectrophotometer with a high resolution, we may find two or three carbonyl absorptions for the monothiocarbonates, especially because of the NMR behavior described above. Thus, infrared spectra of carbonyl stretching vibration absorptions of monothiocarbonates were measured in hexane, carbon tetrachloride, and acetonitrile.

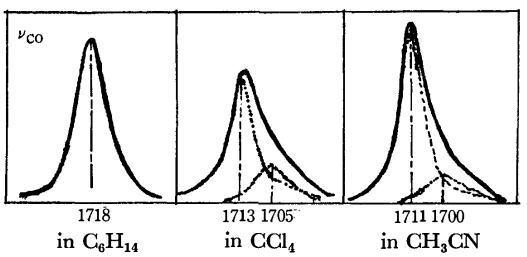

Fig. 4. Carbonyl absorption shapes of *S*-*t*-butyl methyl monothiocarbonate in three solvents.

6) R. N. Nyquist and W. J. Patts, *Spectrochim. Acta*, **17**, 679 (1961).

7) A. W. Barker and G. H. Harris, *J. Amer. Chem. Soc.*, **82**, 1923 (1960).

8) M. Ōki and H. Nakanishi, This Bulletin, **44**, 3148 (1971).

Table 3. Carbonyl absorptions of monothiocarbonates CH_3OCOSR

	R	Solvent: C_6H_{14} $C=0.02$ mol/l cm^{-1} (ε)	CCl_4 $C=0.0004$ mol/l cm^{-1} (ε)	CH_3CN $C=0.02$ mol/l cm^{-1} (ε)
II	Et	1713 (106)	1707 (41)	1701 (91)
		1720 (1712)	1715 (600)	1713 (1065)
III	*i*-Pr	1712 (174)	1705 (92)	1698 (114)
		1718 (2000)	1714 (787)	1712 (1050)
IV	*t*-Bu	—	1705 (74)	1700 (114)
			1713 (739)	1711 (928)
V	Ph	1718 (330)	1711 (112)	1702 (148)
		1728 (64)	1722 (46)	1715 (86)
		1736 (1711)	1730 (715)	1728 (918)

The results confirmed our expectations: monothiocarbonates show unsymmetrical carbonyl absorptions, although the shape of the absorption is not that of the multiple peaks, as is shown in Fig. 4. These unsymmetrical absorptions were graphically separated into two symmetrical peaks.[9] The results are shown in Table 3. With compounds II, III, and IV, the band at a higher frequency is stronger than the lower one in both polar and nonpolar solvents. Apparently in these solvents, the effect of the bulkiness of alkyl groups does not play an important role in determining the conformation of the ester group in contrast to the case of carbonates. From the NMR data, the existing conformers are considered to be B and C or A, B, and C. The directions of the bond dipoles of C=O and C–O or C–S in various conformations suggest that the wave number of the carbonyl absorption of the conformer A is the lowest among the three conformations. However, at the present time, it is not known which of the two conformers, B and C, gives the carbonyl absorption at a higher frequency. Therefore, the most stable conformation cannot be known from the infrared spectral data, although the conformation A is clearly the most unstable.

Compound V has three absorptions in these three solvents, probably indicating that three conformations, A, B, and C, are present. However, since there is a possibility that the third band arises because of the enhancement due to the Fermi resonance, it is necessary to obtain further information. Thus, the infrared spectra of the carbonyl overtone absorptions of *S*-alkyl methyl monothiocarbonate were measured. The results are given in Fig. 5 and Table 4.

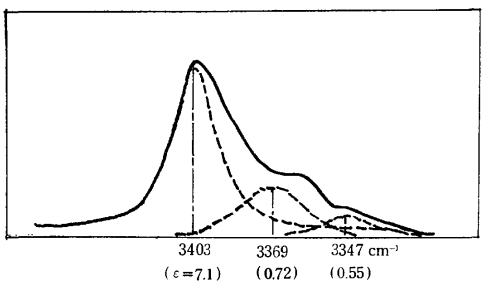

Fig. 5. Carbonyl overtone spectra of MeOCOS-*t*-Bu in CCl_4 C=0.0097 mol/*l*.

Table 4. Carbonyl overtone absorptions of monothiocarbonates MeOCOSR in CCl_4 $C=0.01$ mol/*l*

	R	cm^{-1}	(ε)
I	Me	3388	(0.41)
		3397	(0.34)
		3416	(3.81)
II	Et	3362	(0.20)
		3380	(0.36)
		3409	(4.51)
III	*i*-Pr	3368	(0.66)
		3389	(1.28)
		3406	(4.73)
IV	*t*-Bu	3347	(0.55)
		3369	(0.72)
		3403	(7.10)

The shapes of the absorption curves of compounds I—V are unsymmetrical, and the curves fit best when three rather than two overlapping absorptions are considered.[10] These results strongly suggest that these compounds really show three carbonyl absorptions.

Dipole Moment. The temperature dependency of the dipole moment of *S*-*t*-butyl methyl thiocarbonate (IV) was measured in order to obtain information about the stability of these conformers. The results are given in Table 5.

Table 5. Dipole moment of *t*-BuSCOMe in benzene

T°C	16	32	53
(D)	1.01	0.95	0.83

The calculated dipole moment values of *S*-*t*-butyl methyl monothiocarbonate are 0.1 D for the *s-trans, s-trans* conformer (A), 2.1 D for the *s-trans,s-cis* conformer (B), and 2.0 D for the *s-cis,s-trans* conformer (C).[11] The dipole moment of compound IV decreases as the temperature of the measurement is raised. Since the calculated dipole moment of the conformer B is not very different from that of the conformer C, the results may mean that the *s-trans,s-trans* conformer (A) is present, that A is the most unstable, and that the *s-cis* conformers, B and/or C, are the main conformers.

In conclusion, all the data presented above suggest that, among the three possible conformations, the conformation A is the least stable. Thus, although it has not been possible to determine which of the conformations, B and C, is the most stable, it is apparent that the conformations involving the *s-cis* part are more stable than the *s-trans,s-trans* conformation. It may be pointed out, as a difference between carbonates and thiocarbonates, that even the simplest example of the latter, dimethyl monothiocarbonate, shows signs of the presence of the three conformers, while the simplest example of the former, ethyl methyl carbonate, gives no such sign.

9) The possibility of an absorption including three bands cannot be ruled out. This is especially so when the intensity of the second band is very small and its wave number is close to that of the strong band.

10) The decomposition of the absorption curves into the component bands is more easily performed in the overtone region because the separation of the components becomes larger.

11) The calculation was made using the bond moments of 2.4 D for C–O and 0.4 D for C–H. The values for C–O and C–S were cited earlier (See Ref. 4).

Ligand Effects in the Cooligomerization of Butadiene and Ethylene by a Nickel-based Catalyst System[1]

Yoshio INOUE, Teruhiko KAGAWA, Yasuzo UCHIDA, and Harukichi HASHIMOTO*

Department of Industrial Chemistry, Faculty of Engineering, The University of Tokyo, Tokyo
**Department of Applied Chemistry, Faculty of Engineering, Tohoku University, Sendai*

(Received October 12, 1971)

The cooligomerization of butadiene and ethylene catalyzed by a $NiCl_2$–$AlEt_3$–phosphine system was investigated. The cooligomerization product was 1,*cis*-4-hexadiene or/and 1,*trans*-4,9-decatriene. Bidentate ditertiary phosphines had remarkable effects on the reaction. The effects of ditertiary phosphines are also described.

Several complex catalyst systems for the cooligomerization of a conjugated diene and a monoolefin have been reported. Iwamoto reported the codimerization of butadiene and ethylene to give 1,*cis*-4-hexadiene by means of a catalyst system composed of cobalt chloride, ditertiary phosphine, and triethylaluminum.[2] An iron-based catalyst system for the synthesis of 1,*cis*-hexadiene has also been reported.[3] Müller and his coworkers found the reaction of butadiene and ethylene to give 1,5,9-decatriene.[4] Wilke reported a cotrimerization of butadiene and ethylene giving *trans*-1,*cis*-5-cyclodecadiene and 1,*trans*-4,9-decatriene by means of a nickel acetylacetonate-diethylaluminum ethoxide catalyst system.[5] The addition of α-olefins to conjugated dienes was accomplished by means of a catalyst derived from the interaction of bis(tri-*n*-butylphosphine) nickel chloride, and diisobutylaluminum chloride.[6] Linear 1,4-dienes were the primary products. The synthesis of 1,*trans*-4-hexadiene with rhodium trichloride was reported by Alderson.[7] A detailed study of the reaction of butadiene and ethylene catalyzed by a nickel hydride complex, $HNi(P(OEt)_3)_4^+$, was also reported.[8]

In a previous paper, the present authors reported briefly on the cooligomerization of butadiene and ethylene by means of a nickel-based catalyst system;[9] in this paper, they will describe the effects of ditertiary phosphine in the catalyst system.

Experimental

Reagents. The toluene was purified by washing it with sulfuric acid and by then distilling it over sodium under a nitrogen atmosphere. The triethylaluminum and ethylene were used without further purification. The butadiene was dried by passing it through columns of calcium chloride and of silica gel. The nickel chloride and triphenylphosphine were commercial reagents. The ditertiary phosphines were prepared according to the method described by Hewertson and Watson.[10] Nickel complexes of the phosphines were prepared by adding nickel chloride to an alcoholic solution of the phosphines.

Ditertiary phosphine	Mp (°C)
$Ph_2P(CH_2)_nPPh_2$	
$n=1$	119.9—120.9(120.5—121.5)[10]
$n=2$	139.6—140.9(143—144)[10]
$n=3$	63.3—65.3(61—62)[2,11]
$n=4$	133.8—133.9(137—139)[12]
$n=5$	43.1—46.1(liquid)[12]
$n=6$	125.2—126.0
$Ph_2PCH_2OCH_2PPh_2$	90.3—95.3
$Ph_2PCH_2CH_2OCH_2CH_2PPh_2$	liquid (liquid)[12]

Procedure. A 100 m*l* stainless-steel autoclave equipped with a magnetic stirrer was charged with nickel chloride, ditertiary phosphine (or its nickel complex), toluene (with or without), butadiene, and triethylaluminum in a glass ampoule under a nitrogen atmosphere. At room temperature, ethylene was introduced until a pressure of *ca.* 20 kg/cm² was reached, after which the ampoule of triethylaluminum was broken with agitation. Then the autoclave was heated to 110°C, where the reaction pressure reached approximately 50 kg/cm²; this pressure was maintained during the reaction by introducing ethylene. After 3 hr, the autoclave was cooled to room temperature and the catalyst was quenched by adding a small amount of methanol. The reaction mixture was washed with water and dried with anhydrous sodium sulfate. The products were analyzed by gas chromatography.

*Product Analysis. 1,*trans*-4,9-Decatriene*: 1,*trans*-4,9-Decatriene was distilled from the reaction mixture at 83°C/52 mmHg. The IR spectrum of the compound exhibited absorption bands at 3065, 1637, 987, 965, and 910 cm^{-1}, showing the existence of terminal vinyl and *trans* double-bond groups. No peak attributable to conjugated diene was observed. NMR spectrum showed a very complicated pattern. The signals at τ=3.7—4.6(4H), 4.7—5.2(4H), 7.1—7.5(2H), 7.6—8.2(4H), and 8.3—8.9(2H) were attributable to $-C=CH-$, $-C=CH_2$, $=C-CH_2-C=$, $-C-CH_2-C=$, and $-C-CH_2-C-$ respectively. Hydrogenation was carried out in methanol at 50°C by means of a palladium black catalyst under an atmospheric hydrogen pressure. Three moles of hydrogen were absorbed, and *n*-decane was obtained.

1) Ligand effects. II.
2) M. Iwamoto and S. Yuguchi, *Kogyo Kagaku Zasshi*, **70**, 1505 (1967); This Bulletin, **41**, 150 (1968).
3) M. Iwamoto and S. Yuguchi, *J. Org. Chem.*, **31**, 4290 (1966); G. Hata and A. Miyake, This Bulletin, **41**, 2762 (1968).
4) H. Müller, D. Wittenberg, H. Seibt, and E. Scharf, *Angew. Chem. Internat. Edit.*, **4**, 327 (1965).
5) P. Heimbach and G. Wilke, *Ann. Chem.*, **727**, 183 (1969).
6) R. G. Miller, T. J. Kealy, and A. L. Barney, *J. Amer. Chem. Soc.*, **89**, 3756 (1967).
7) T. Alderson, E. L. Jenner, and R. V. Lindsey, Jr., *ibid.*, **87**, 5638 (1965).
8) C. A. Tolman, *ibid.*, **92**, 6777 (1970).
9) Y. Inoue, T. Hagawa, and H. Hashimoto, *Tetrahedron Lett.*, **1970**, 1099.
10) W. Hewertson and H. R. Watson, *J. Chem. Soc.*, **1962**, 1490.
11) G. R. Van Hecke and W. D. Horrocks, Jr., *Inorg. Chem.*, **5**, 1960 (1966).
12) L. Sacconi and J. Gelsomini, *Inorg. Chem.*, **7**, 291 (1968).

The gas chromatogram of the reaction mixture showed a shoulder peak on that of 1,4,9-decatriene, the fraction of which was separated by preparative gas chromatography. The IR spectrum of the compound exhibited a pattern fairly similar to that of 1,4,9-decatriene. The peaks at 3075, 1634, 1374, 989, 965, and 912 cm^{-1} showed the existence of terminal vinyl, *trans* double-bond, and methyl groups. No peak attributable to conjugated diene was observed. The peaks at 989 and 912 cm^{-1}, attributable to the terminal vinyl group, were weaker than those of 1,4,9-decatriene. On the hydrogenation of a mixture of the compound and 1,4,9-decatriene, only *n*-decane was formed. The compound is presumed to be 1,4,8-decatriene.

*1,*cis*-4-Hexadiene*: 1,*cis*-4-Hexadiene was distilled from a reaction mixture at 66.5—67.0°C. Its IR and NMR spectra were identical with those of an authentic sample of the *cis* isomer.

4-Vinylcyclohexene, 1,5-cyclooctadiene, and 1,5,9-cyclododecatriene were identified by gas chromatography, and by IR and NMR spectroscopy.

Results and Discussion

1. $NiCl_2$–$AlEt_3$ System. In the reaction of butadiene and ethylene with this catalyst system, the main products were higher oligomers. 4-Vinylcyclohexene(VCH), 1,5-cyclooctadiene(COD), 1,4,9-decatriene(DT), and 1,5,9-cyclododecatriene(CDT) were also produced. The selectivity of the DT(DT(g)/products (g)) was about 25 wt%. The yield of 1,4-hexadiene (HD) was negligible.

2. PPh_3–$NiCl_2$–$AlEt_3$ System. In this catalyst system, the main products were also higher oligomers. The increase in triphenylphosphine suppressed the formation of DT and CDT.

3. $Ph_2PCH_2PPh_2$(DPM)–$NiCl_2$–$AlEt_3$ System. The main cooligomerization product was 1,4,9-decatriene, plus some 1,4,8-decatriene. The yield of 1,4-hexadiene was also negligible.

When the molar ratio of DPM to $NiCl_2$ reached 3, the reaction stopped almost completely.

4. $Ph_2PCH_2CH_2PPh_2$(DPE)–$NiCl_2$–$AlEt_3$ System. The main cooligomerization product was 1,4,9-decatriene when the molar ratio of DPE to $NiCl_2$ was less than unity. However, when the ratio exceeded unity, the sole cooligomerization product was 1,4-hexadiene. When the molar ratio of DPE to $NiCl_2$ reached 3, the reaction stopped almost completely at 110°C. If the reaction temperature was elevated to 130°C, the catalytic activity was observed even though the molar ratio of DPE to $NiCl_2$ was 4.

Table 1. Effects of PPh_3
$NiCl_2=6.02\times10^{-4}$ mol, 110°C, 3 hr, 50 kg/cm, toluene 5 m*l* as solvent

PPh_3/Ni (mol/mol)	Al/Ni (mol/mol)	BD[a] (g)	Yield (g)	Products (wt%) VCH	COD	DT	CDT
0	19	33	27	3.7	4.3	26	18
2[b]	18	25	21.5	1.4	4.7	23	4.7
5	18	33	22.2	1.4	15	17	trace

a) BD=butadiene
b) $Ni(PPh_3)_2Cl_2$ complex 5.61×10^{-4} mol

Table 2. Effects of DPM
$NiCl_2=6.02\times10^{-4}$ mol, 110°C, 3 hr, 50 kg/cm^2 toluene 5 m*l* as solvent

DPM/Ni (mol/mol)	Al/Ni (mol/mol)	BD (g)	Yield (g)	Products (wt%) VCH	COD	DT[b]	CDT
0	19	33	27	3.7	4.3	26	18
1	19	32	29	7.9	8.6	38	13
2	18	33	28	9.4	10	33	5.5
2[a]	25	31	17	5.9	5.9	70	7.6
2.25	19	31	6.5	23	12	46	15
3	18	40	1.0	+	+	+	+

a) $Ni(DPM)_2Cl_2$ complex 4.55×10^{-4} mol
b) DT=1,4,9-+1,4,8-decatriene

Table 3. Effects of DPE
$NiCl_2=6.02\times10^{-4}$ mol, $AlEt_3=1.14\times10^{-2}$ mol, 110°C, 3 hr, 50 kg/cm^2, toluene 5 m*l* as solvent

DPE/Ni (mol/mol)	BD (g)	Yield (g)	Products (wt%) HD[a]	VCH	COD	DT	CDT	Higher oligomers
0	33	27	trace	3.7	4.3	26	18	+
0.5	34	35	trace	4.3	4.0	51	17	+
1.0	30	27	trace	5.5	10	54	23	+
1.05	31	25	87	trace	—	trace	—	—
1.25	32	26	88	trace	—	trace	—	—
1.5	33	28	96	trace	—	—	—	—
2.0	32	26	95	trace	—	—	—	—
2.5	34	19	89	trace	—	trace	—	—
3.0	32	1	+	+	—	—	—	—
4.0[b]	25	20	95	trace	—	—	—	—

a) HD=1,4-hexadiene b) 130°C, 1 hr

It was expected that triethylaluminum took an important role in the cooligomerization reaction of butadiene and ethylene. To ascertain the effect of triethylaluminum, the molar ratio of triethylaluminum to nickel chloride was gradually changed at DPE/$NiCl_2$=0.5 and the distribution of the products was examined.

Table 4. Effects of $AlEt_3$
$NiCl_2=6.02\times10^{-4}$ mol, DPE/Ni=0.5, 110°C, 3 hr, 50 kg/cm^2

Al/Ni (mol/mol)	BD (g)	Yield (g)	Products (wt%) HD	VCH	COD	DT	CDT	Higher oligomers
3.1	28	24	41	2.6	4.6	18	8.4	+
4.2	25	19	24	2.9	5.8	27	8.3	+
8.3	27	27	0.4	3.1	4.2	27	9.3	+
19.6	34	35	trace	4.4	4.0	51	17	+

When the molar ratio of triethylaluminum to nickel chloride was 19.5, 1,4-hexadiene was not produced; 1,4,9-decatriene was obtained as the main cooligomerization product. However, the molar ratio of triethyl aluminum to nickel chloride became 3.1, 1, 4-hexadiene and 1,4,9-decatriene were obtained together. There was a tendency for the yield of 1,4-hexadiene to increase as the molar ratio of triethylaluminum to nickel chloride became smaller.

As was suggested in discussing the reaction of buta-

diene with ethylene catalyzed by the $HCo(Ph_2PCH_2CH_2PPh_2)_2$–triethylaluminum system,[13] it seems that triethylaluminum can interact with the coordinated phosphorus atom, release it from the metal atom, and make a coordinatively unsaturated state. This interaction should be more effective at a higher concentration of triethylaluminum. The coordinatively unsaturated state would promote the reaction of butadiene with ethylene. It would depend on the degree of unsaturation whether 1,4,9-decatriene or 1,4-hexadiene was produced. Clearly, the formation of 1,4,9-decatriene requires a higher unsaturated state around the nickel atom than that of 1,4-hexadiene, and so it is always accompanied by other products, such as VCH, COD, and CDT.

It is very interesting to note that the $Ni(DPE)Cl_2$–$AlEt_3$ system showed no catalytic activity for the cooligomerization of butadiene and ethylene. However, the addition of $NiCl_2$ to the catalyst system caused the catalytic activity for the butadiene-ethylene reaction to recover and 1,4,9-decatriene was yielded. A Lewis acid such as $AlCl_3$ or $FeCl_3$ was ineffective, unlike $NiCl_2$. On the other hand, the addition of DEP to the $Ni(DPE)Cl_2$–$AlEt_3$ system did not cause any catalytic activity. The effect of the added $NiCl_2$ is shown in Table 5.

Table 5. Effects of $NiCl_2$ added to $Ni(DPE)Cl_2$–$AlEt_3$ system
$Ni(DPE)Cl_2=5.68\times10^{-4}$ mol, Al/Ni(DPE)Cl_2=18.5—20.2, 110°C, 3 hr, 50 kg/cm²

$NiCl_2$/Ni(DPE)Cl_2 (mol/mol)	BD (g)	Yield (g)	DT (g)
3.1	36	0.5	trace
6.8	32	9.0	5.1
13.5	40	27.0	12.0
27.0	34	27.5	15.0

5. $Ph_2P(CH_2)_3PPh_2$(DPP)–$NiCl_2$–$AlEt_3$ System.
The DPP ligand showed almost the same catalytic effect as DPE; *i.e.*, when the molar ratio of DPP to $NiCl_2$ was less than unity, the main cooligomerization product was 1,4,9-decatriene and 1,4-hexadiene was produced. When it was more than unity, 1,4,9-decatriene was not produced and 1,4-hexadiene was the sole cooligomerization product. In contrast with the catalyst system containing DPE, the reaction did not stop even at DPP/$NiCl_2$=5 at 110°C.

Table 7. Effects of DPB
$NiCl_2=6.02\times10^{-4}$ mol, 110°C, 3 hr, 50 kg/cm²

DPB/Ni (mol/mol)	Al/Ni (mol/mol)	BD (g)	Yield (g)	Products (wt%) VCH	COD	DT	CDT	Higher oligomers
0	19	33	27	3.7	4.3	26	18	+
1.0[a]	22	33	23	+	+	62	+	+
1.5	19	33	11	29	15	16	7.2	+
2.0	18	37	11	25	9.4	5.7	3.8	+

a) Ni(DPB)Cl_2 complex 5.58×10^{-4} mol

6. $Ph_2P(CH_2)_4PPh_2$(DPB)–$NiCl_2$–$AlEt_3$ System.
In this reaction system, the main products were higher oligomers, and no formation of 1,4-hexadiene was observed.

7. Other Bidentate Ligands–$NiCl_2$–$AlEt_3$ Systems.
In the reaction of the complexes coordinated with $Ph_2P(CH_2)_nPPh_2$ (n=5,6), $Ph_2PCH_2OCH_2PPh_2$, and $Ph_2PCH_2CH_2OCH_2CH_2PPh_2$, no ligand effects were observed distinctly. The distribution of products resembled that of the $NiCl_2$–$AlEt_3$ system.

In the present study, the added or coordinated ditertiary phosphine had a great influence on the distribution of products. When the molar ratio of DPE or DPP to $NiCl_2$ became unity, a great change in the distribution of products was observed.

Table 8. Effects of the other bidentate ligands
110°C, 3 hr, 50 kg/cm², toluene 5 ml as solvent

Complex (g)	Al/Ni (mol/mol)	BD (g)	Yield (g)	DT (g)
Ni(DPPE)Cl_2 0.310	23	33	26	10
Ni(DPH)Cl_2 0.320	18	34	28	7.1
Ni(DPMO)Cl_2 0.315	22	33	29	9.6
Ni(DPEO)Cl_2 0.310	25	39	37	20

DPPE=$Ph_2P(CH_2)_5PPh_2$, DPH=$Ph_2P(CH_2)_6PPh_2$, DPMO=$Ph_2PCH_2OCH_2PPh_2$, DPEO=$Ph_2PCH_2CH_2OCH_2CH_2PPh_2$

Table 6. Effects of DPP
$NiCl_2=6.02\times10^{-1}$ mol, 110°C, 3 hr, 50 kg/cm²

DPP/Ni (mol/mol)	Al/Ni (mol/mol)	BD (g)	Yield (g)	Products (wt%) HD	VCH	COD	DT	CDT	Higher oligomers
0	19	33	27	trace	3.7	4.3	26	18	+
0.5	17	29	26	trace	5.9	10.8	37	20	+
1.0[a]	20	33	9.5	trace	+	+	73	+	+
1.5	17	33	15	96	trace	—	—	—	—
3.0	17	31	27	97	trace	—	trace	—	—
5.0	18	29	29	98	trace	—	—	—	—

a) Ni(DPP)Cl_2 complex 5.62×10^{-4} mol

13) M. Iwamoto and S. Yuguchi, *Kogyo Kagaku Zasshi*, **71**, 237 (1968).

Generally, a phosphine ligand coordinates to a low-valent nickel atom which is produced by reduction with an organoaluminum compound, and stabilizes it. This function of a phosphorus atom is stronger with bidentate ditertiary phosphine than with monodentate phosphine because of its chelating effect. Especially, the chelation of the ditertiary phosphines, $Ph_2P(CH_2)_nPPh_2$ (n=2,3), is stronger than those of the other ditertiary phosphines because of the easy formation of a five- or six-membered chelate ring. The high coordinating ability of DPE and DPP is supposed to be the promoting power for the selective formation of 1,4-hexadiene.

BULLETIN OF THE CHEMICAL SOCIETY OF JAPAN, VOL. 45, 1999—2003(1972)

Generation and Cycloaddition of 8,8-Dimethylisobenzofulvene[1]

Hiroshi TANIDA,* Tadashi IRIE, and Kazuo TORI
Shionogi Research Laboratory, Shionogi & Co., Ltd., Fukushima-ku, Osaka

(Received December 3, 1971)

Transient 8,8-dimethylisobenzofulvene (**5**) was generated by thermal decomposition of two materials; one is formally an adduct of cyclopentadienone with 9-isopropylidenebenzonorbornadiene (**6**), and the other an adduct of 3,6-di(2′-pyridyl)-*S*-tetrazine with **6**. The former was prepared by cycloaddition of **6** to tetrachlorodimethoxycyclopentadiene followed by dechlorination giving a ketal, then hydrolysis of the ketal function. Generation without any trapping reagent instantaneously yielded one kind of dimer of a stereospecific structure. In the presence of dimethyl maleate, dimethyl 9-isopropylidenebenzonorbornene-*exo,cis*-2,3-dicarboxylate and its *endo-cis* isomer were formed. In the presence of dimethyl fumarate, the *trans* isomer was obtained. Trapping with tropone led to a 1 : 1 adduct resulting from participation of the exocyclic C_2–C_8 double bond in **5**. All attempts to isolate **5** or prepare a stable metal complex of **5** by conventional means were unsuccessful.

The preparation and properties of non-planar valence bond isomers of benzene and its derivatives such as the Dewar benzenes (bicyclo[2.2.0]hexa-2,5-dienes), benzvalenes (tricyclo[3.1.0.0^{2,6}]hex-3-enes) and prismanes (tetracyclo[2.2.0.0^{2,6}.0^{3,5}]hexanes) have received considerable attention in recent years.[2-4] The planar fulvene is the most classical valence isomer and has been known for more than seventy years.[5] Benzo derivatives of these compounds can be considered as valence bond isomers of naphthalene, of which benzobenzvalene (or naphthvalene)[4] and benzofulvene (**1**)[6] are known. The isoconjugate isomer of **1**, benzoisofulvene (**2**), is of considerable interest, being isoelectronic with both the recently prepared isobenzofuran (**4a**)[7], and isobenzothiophene (**4b**)[8] known for some

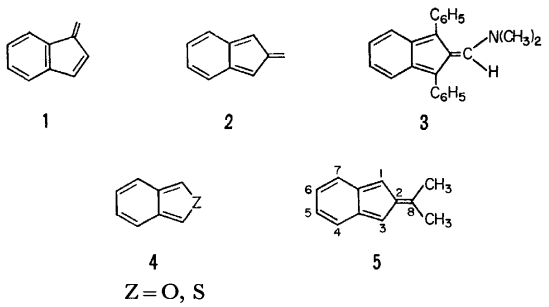

1 2 3

4 5

Z = O, S

years. Hafner[9] was the first to succeed in the isolation of a derivative of this ring system. He isolated *N,N*-dimethyl-*N*-(1,3-diphenyl-2-indenylidenemethyl)amine (**3**) and reported on the observation of transient *N,N*-dimethyl-*N*-(2-indenylidenemethyl)amine. In connection with this, we are interested in the preparation and reactivity of 8,8-dimethylisobenzofulvene **5**.

Results

The preparation of **5** was tried through two independent sequences starting from 9-isopropylidenebenzonorbornadiene (**6**), obtained by the addition of benzyne to 6,6-dimethylfulvene.[10] The first was modelled after the method of Mackenjie.[11] Heating **6** with 1,2,3,4-tetrachloro-5,5-dimethoxycyclopentadiene (**7**) at 165°C for 5 hr yielded the 1 : 1 adduct (**8**)

1) Presented in part at the 4th Symposium on Chemistry of Nonbenzenoid Aromatic Compounds, Sendai, Japan, October 8th, 1971. Numberings used in the paper are those given in Charts.

* To whom inquiries should be addressed.

2) As reviews, H. G. Viehe, *Angew. Chem. Int. Ed. Engl.*, **4**, 746 (1965); W. Schäfer and H. Hellman, *ibid.*, **6**, 518 (1967).

3) H. R. Ward and J. S. Wishnok, *J. Amer. Chem. Soc.*, **90**, 1085 (1968); L. Kaplan and K. E. Wilzbach, *ibid.*, **90**, 3291 (1968); L. Kaplan, L. A. Wendling, K. E. Wilzbach, *ibid.*, **93**, 3821 (1971); M. G. Barlow, R. N. Haszeldine, and R. Hubbard, *J. Chem. Soc., C*, **1970**, 1232.

4) T. J. Katz, E. J. Wang, and N. Acton, *J. Amer. Chem. Soc.*, **93**, 3782 (1971).

5) a) J. Thiele, *Ber.*, **33**, 666 (1900); b) E. D. Bergmann, "Progress in Organic Chemistry," Vol. 3, ed. by J. W. Cook, Butterworths Publications Ltd., London, (1955), p. 81—171.

6) R. F. C. Brown, G. E. Gream, D. E. Peters, and R. K. Solly, *Aust. J. Chem.*, **21**, 2223 (1968), and reference 25 therein.

7) a) R. N. Warrener, *J. Amer. Chem. Soc.*, **93**, 2346 (1971); b) D. Wege, *Tetrahedron Lett.*, **1971**, 2337.

8) R. Mayer, H. Kleinert, S. Richter, and K. Gewald, *J. Prakt. Chem.*, **20**, 244 (1963); M. P. Cava and N. M. Pollack, *J. Amer. Chem. Soc.*, **88**, 4112 (1966).

9) K. Hafner and W. Bauer, *Angew. Chem. Int. Ed. Engl.*, **7**, 298 (1968); *Angew. Chem.*, **80**, 312 (1968).

10) R. Muneyuki and H. Tanida, *J. Org. Chem.*, **31**, 1988 (1966).

11) a) K. Mackenjie, *J. Chem. Soc.*, **1960**, 473; K. Mackenjie and W. P. Lay, *Tetrahedron Lett.*, **1970**, 3241; W. P. Lay and K, Mackenjie, *Chem. Commun.*, **1970**, 398; b) R. McCulloch, A. R. Rye, and D. Wege, *Tetrahedron Lett.*, **1969**, 5163; c) **1969**, 5231; also Ref. 7b.

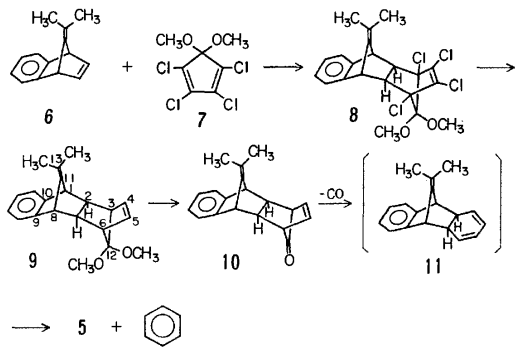

in 87% yield. Dechlorination of **8** with sodium in *t*-butyl alcohol-tetrahydrofuran gave ketal **9**, hydrolysis of which with 70% aqueous acetic acid provided ketone **10**. Stereochemistry of these compounds was determined from their PMR spectra as indicated in the chart, principally following the assignments[11b] presented for closely related compounds; the addition compounds of norbornene or benzonorbornadiene to **7**, and their derivatives. In the stereochemistry, it is of importance that the signal assigned to H_2 (H_7) in the adduct **8** appears as a singlet at δ 2.59 ppm indicating the absence of significant spin-coupling to H_1 (H_8), and that the signal at δ 2.30 ppm due to H_2 (H_7) in the dechlorinated ketal **9** is a multiplet indicative of spin-coupling to H_3 (H_6). These observations led to the configuration in which H_2 and H_7 are *endo* to the benzonorbornene ring and *exo* to the norbornene ketal ring.

Decarbonylation of **10** in a dioxane solution proceeded at 100°C at a fair rate. Attempts to isolate the diene **11** by conventional methods were unsuccessful due to the subsequent reverse cycloaddition liberating benzene and **5**, but its formation was confirmed by the addition of maleic anhydride which rapidly forms the adduct **12**. Evidence for the indicated structure **12**

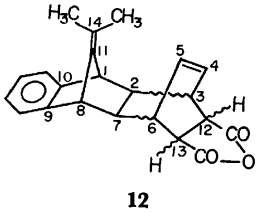

12

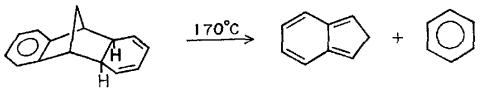

13

was provided by the PMR spectrum (see Experimental). A related compound **13** prepared through the same reaction sequence starting from benzonorbornadiene instead of **6**, has been reported to require a temperature of 170°C for thermal decomposition leading to indene (presumably *via* isoindene) and benzene.[11c] The large difference in reactivity between **11** and **13** clearly demonstrates a significant participation of the isopropylidene group in **11** in the transition state of thermal decomposition.

The second route for **5** began with the reaction of a suspension of 3,6-di(2′-pyridyl)-*S*-tetrazine[12] with **6** in dioxane solution at room temperature (exothermic, N_2 elimination). In the dioxane solution the adduct **14** decomposed rapidly at about 50°C and slowly in the solid state on storage.

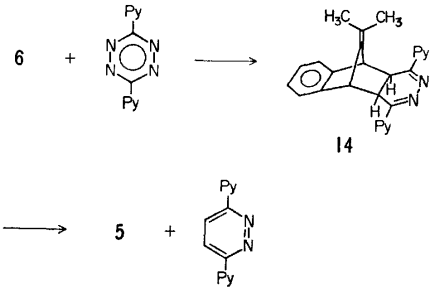

The thermal decomposition of both **10** and **14** in the absence of any trapping reagent instantaneously and quantitatively yielded only one kind of dimer (**15**, Fig. 1) displaying a remarkable stereochemical preference in dimerization. The parent peaks in the mass spectrum and elementary analysis are consistent with the formula $(C_{12}H_{14})_2$. Although the catalytic reduction of **15** resulted in no up-take of hydrogen, the Raman spectrum in chloroform revealed three kinds of unsaturated bonds at 1582(m),[13] 1616(s), and 1708(m) cm^{-1}, assignable to unsaturation due, respectively, to a benzene ring, a cyclopentenyl double bond, and an isopropylidene double bond.[14] The UV spectrum

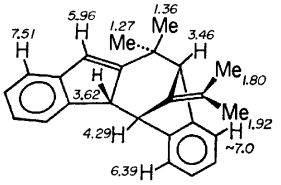

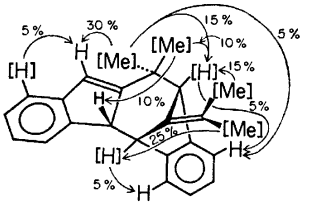

15

Fig. 1. Chemical shifts (δ in ppm downfield from TMS) and nuclear Overhauser effects (indicalted by arrows) in the PMR spectrum of dimer **15** in $CDCl_3$.

(λ_{max}^{ether} 262 mμ (ε 12810), 268 (12490), and 274 (10750)) is compatible with the existence of a double bond conjugated with a benzene ring. Confirmatory evidence for the structure was obtained by a detailed analysis of the 100 MHz PMR spectrum in $CDCl_3$. The signal assignments were made on the basis of spin-decoupling

12) J. F. Geldard and F. Lions, *J. Org. Chem.*, **30**, 318 (1965),
13) m=medium, s=strong, and w=weak.
14) Raman $\nu_{C=C}$ in chloroform appear, for 7-isopropylidenebenzonorbornene,[9] at 1725 (w) cm^{-1} (isopropylidene) and, for benzonorbornadiene, at 1620 (w) (C=C), 1607 (w) (C=C and/or benzene), and 1578 (m) (benzene). Infrared spectrum of **15** shows no absorption at 1708 cm^{-1}.

and nuclear Overhauser effect (NOE).[15,16] Chemical shifts and the positive NOE value observed are shown in Fig. 1.[17] When the signals marked by brackets were saturated with double irradiation, the positive enhancement of intensities was observed at the signals marked by arrows. It is considered that the anisotropy effect of the benzene ring of the indene moiety is responsible for the shift of the proton on the other benzene being at such a high field (δ 6.39 ppm); likewise the anisotropy effect of this latter benzene ring causes a high value for the shift of the vinyl proton (δ 5.96 ppm). Furthermore, orientation of the methine proton at position 3 of the indene moiety was established as β by the NOE results. Some coupling constants are given in Experimental. All our attempts to isolate **5** or to prepare a stable metal complex of **5** were unsuccessful. Experiments carried out are thermal decomposition of **10** and **14** under reduced pressure (1×10^{-3} mm) using a cold finger, thermal decomposition of **10** and **14** in the presence of iron pentacarbonyl, and photochemical decomposition of **10** and **14** in the absence and presence of iron pentacarbonyl. The only product characterized on these treatments was **15**.

Trapping of 5 with Dienophiles. Generation of **5** was carried out by warming dioxane solutions of **10** at 100°C (method A, Table 1) and of **14** at 50°C (method B, Table 1) in the presence of dimethyl maleate. The products were *exo-cis* adduct (**16**), *endo-cis* adduct (**17**), and dimer **15**. No detectable amount of *trans* adduct (**18**) was found by vpc. Structures of the adducts were established by their PMR spectra (Experimental). The yields of the three products varied with the amount of dimethyl maleate added (Table 1). Although the yield of **15** decreased on increasing the mole ratio of dimethyl maleate to **10** or **14**, the relative yield ratio of **16** to **17** was nearly independent of the amount of dimethyl maleate and the methods of generation. The constancy of ratio indicates the existence of an identical intermediate **5** in the decompositions of **10** and **14**. The formation of **18** but no other adduct was observed in the reaction of **10** or **14** with dimethyl fumarate.

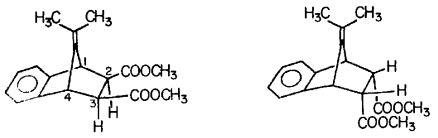

16

17

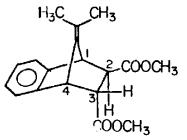

18

Table 1. Products of 5 with dimethyl maleate

Method[a]	Maleate mol ratio[b]	Product, %[c] *exo-cis* **16**	*endo-cis* **17**	Dimer **15**	*exo/endo* ratio
A	1	10.8	5.2	42.4	2.1
	5	32.8	15.2	25.7	2.2
	10	41.9	19.8	13.9	2.1
	30	55.1	26.3	3.3	2.2
	100	56.5	26.8	0	2.1
B	30	29.1	12.3	24.1	2.4
	100	34.8	16.0	7.5	2.2

a) A: Decomposition of **10** in dioxane at 100°C. B: Decomposition of **14** in dioxane at 50°C.
b) Relative to **10** or **14**.
c) Theoretical percentage determined by vpc with an internal standard.

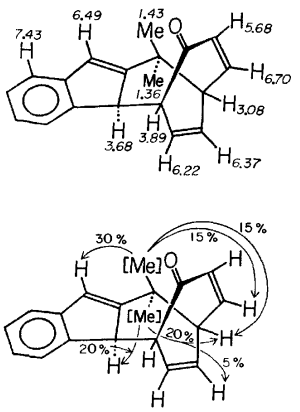

Fig. 2. Chemical shifts (δ in ppm downfield from TMS) and nuclear Overhauser effects (indicated by arrows) in the PMR spectrum of the tropone adduct **19** in $CDCl_3$.

Trapping with Tropone. Decomposition of **10** was carried out at 120°C in the presence of ten equivalents of tropone. Distillation of excess of tropone under reduced pressure left a crystalline 1 : 1 adduct in an almost quantitative yield. The IR carbonyl absorption at 1657 cm^{-1} is compatible with the presence of cyclohepta-2,5-diene but not a cyclohepta-3,5-dienone moiety. The 100-MHz PMR spectrum in $CDCl_3$ included singlet methyl signals at δ 1.36 and 1.43 ppm and five olefinic proton resonances, as well as all other signals in agreement with structure **19**, given in Fig. 2 with chemical shifts and positive NOE values observed. Appearance of the vinyl proton α to the carbonyl at such a high field as δ 5.68 ppm is thought to be due to the anisotropy effects of benzene and the ethylene bridge. Orientation of the methine proton at position 3 of the indene moiety was established as α by the NOE experiments. The proton readily underwent a base-catalyzed 1,3-shift to give **20**.

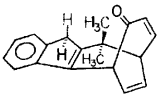

20

Thus we see that **5** acts as a 6π electron addend due to participation of the exocyclic π bond in both dimerization and the tropone reaction though the mode of addition of **5** toward the 4π reactants (**5** and tropone) is just the reverse. The orbital-symmetry rule of

15) F. A. L. Anet and A. J. R. Bourn, *J. Amer. Chem. Soc.*, **85**, 5250 (1965).
16) For experimental procedure, see K. Tori, M. Ohtsuru, I. Horibe, and K. Takeda, *Chem. Commun.*, **1968**, 943.
17) The indicated structure was consistent with the results from X-ray analysis.

Woodward and Hoffmann[18] suggests that the concerted [6+4] cycloaddition reaction has a preference for *exo* addition as far as symmetry factors are dominant. Some evidences have been reported. The tropone adduct **19** bearing the α hydrogen at position 3 might be an additional evidence, but not the dimer **15** having β hydrogen. However, the mechanism of neither reaction, whether concerted or stepwise *via* diradicals, has yet been established.

During the course of this investigation, Houk *et al.*[19] reported a cycloaddition reaction between dimethylfulvene and tropone analogous to the present reaction with tropone.[19] However, the initial adduct (**21**) is very labile because of the fact that the resulting cyclopentadiene system undergoes further addition to tropone. Thus the main product finally obtained in a stable form is a 1:2 adduct of dimethylfulvene and tropone (**22**). Their overall results are therefore very complicated. Nevertheless, their mechanistic interpretation is compatible with ours. It is suggested that the first addition of dimethylfulvene to tropone to form **21**, though not yet proven, takes place from *exo* direction.

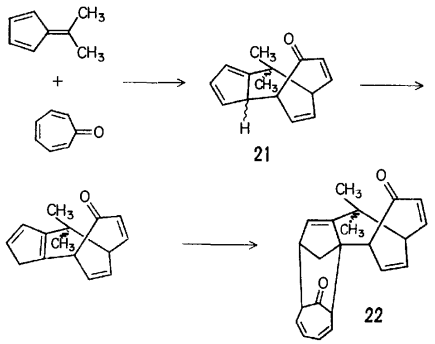

Experimental

Melting points were taken by capillary and are corrected. Boiling points are uncorrected. Infrared spectra were determined with a Nippon Bunko IR-S spectrometer, ultraviolet spectra with a Hitachi EPS-3T spectrometer, PMR spectra with Varian A-60A and HA-100 spectrometers, and mass spectra with a Hitachi RMU-6 mass spectrometer. VPC analysis was carried out on a Hitachi gas chromatograph K-53 equipped with a hydrogen flame ionization detector and a 15 m capillary column coated with butanediol succinate or a 2 m×4 mm glass column packed with 3% diethylene glycol succinate on Chromosorb W.

Addition of 9-Isopropylidenebenzonorbornadiene (6) to 1,2,3,4-Tetrachloro-5,5-dimethoxycyclopentadiene (7). A mixture of 3.65 g (0.02 mol) of **6** and 13.2 g (0.05 mol) of **7** was heated at 165°C under nitrogen with stirring for 5 hr. After removal of excess of **7** under reduced pressure, the residue was recrystallized from pentane giving the 1:1 adduct (**8**) in 87% yield, mp 176.5—177.5°C; PMR (CCl_4) δ: ~7.00 (4, aromatic), 3.71 (s, 2, C_1,C_8–H), 3.48 (s, 6, CH_3O), 2.59 (s, 2, C_2, C_7–H), and 1.65 ppm (s, 6, CH_3).

Found: C, 56.80; H, 4.58; Cl, 31.72%. Calcd for $C_{21}H_{20}Cl_4O_2$: C, 56.52; H, 4.52; Cl, 31.79%.

Ketal 9 from 8. To a solution of 4.46 g (0.01 mol) of **8** in 10 ml of anhydrous tetrahydrofuran was added 2.76 g (0.12 g-atom) of sodium metal and 8.90 g (0.12 mol) of *t*-butyl alcohol, and the mixture was refluxed for 6 hr with stirring. After destruction of the remaining sodium by addition of methanol, the reaction mixture was concentrated by distillation of the solvent and extracted with ether. The ether solution was washed with a saturated sodium chloride solution and water, dried over sodium sulfate and evaporated. Recrystallization of the residue (2.99 g, 97% yield) from *n*-hexane yielded a pure sample of **9**, mp 155—160°C (decomp.); PMR ($CDCl_3$) δ: ~7.01 (4, aromatic), 5.88 (t, 2, CH=CH), 3.45 (2, s, C_1,C_8–H), 3.09 (s, 6, CH_3O), 2.91 (2, m, C_3,C_6–H), 2.30 (2, qua, C_2,C_7–H), and 1.44 ppm (s, 6, CH_3).

Found: C, 81.80; H, 8.01%. Calcd for $C_{21}H_{24}O_2$: C, 81.78; H, 7.84%.

Ketone 10. A suspension of 1.5 g of ketal (**9**) in 50 ml of 70% aqueous acetic acid was warmed at 80°C for 30 min. After dissolution of the crystals, new crystals gradually separated, which were then extracted with ether. The ether extract was washed with saturated sodium chloride solution and with water, dried and evaporated. Recrystallization of the residue (1.3 g) from a mixture of hexane and methylene chloride gave 1.07 g of **10** (83.6%), mp 140—141°C (decomp.); UV max (95% C_2H_5OH): 264 mμ (ε 1840), 270 (2700), and 276 (2810); IR (CCl_4) cm^{-1}: 1775 and 1800 (C=O); PMR ($CDCl_3$) δ: ~7.05 (4, aromatic), 6.20 (t, 2, CH=CH), 3.66 (2, s, C_1,C_8–H), 3.10 (qui, 2, C_3,C_6–H), 2.29 (qua, 2, C_2,C_7–H), and 1.45 (s, 6, CH_3).

Found: C, 86.77; H, 6.92%. Calcd for $C_{19}H_{18}O$: C, 86.98; H, 6.91%.

Thermal Decomposition of 10 in the Presence of Maleic Anhydride. A solution of **10** (525 mg, 0.002 mol) and maleic anhydride (1.96 g, 0.02 mol) in 50 ml of dioxane was heated under reflux for 16 hr. Evaporation of the solvent followed by washing with ether to remove excess maleic anhydride yielded 478 mg of the adduct **12**. Recrystallization from a mixed solvent of methylene chloride and ether gave a pure sample, mp>230°C; IR ($CHCl_3$) cm^{-1}: 1756 and 1776 (acid anhydride); PMR ($CDCl_3$) δ: 6.10 (qua, 2, CH=CH), 3.52 (s, 2, C_1,C_8–H), 3.35 (broad m, 2, C_3,C_6–H), 3.00 (t, 2, COCH–CHCO), 1.90 (broad s, 2, C_2,C_7–H), 1.45 (s, 6, CH_3).

Found: C, 79.22; H, 6.18%. Calcd for $C_{22}H_{20}O_3$: C, 79.49; H, 6.06%.

Generation of Dimethylisobenzofulvene (5) and its Dimer (15). Method A. A solution of 510 mg of ketone **10** in 50 ml of dioxane was heated under reflux for 16 hr. Evaporation of the solvent yielded 333 mg of **15**, mp 155—156°C (ether-petroleum ether); mass spectrum (70 eV) *m/e* 312 (parent peak); molecular weight by osmometry 321; UV max (ether): 262 mμ (ε 12800), 268 (12500), and 274 (10800); PMR ($CDCl_3$) for δ, see Fig. 1; $J_{1.29,3.62}$=3.5 Hz[20] and positive allylic coupling $J_{3.62,5.96}$ and metabenzylic coupling $J_{7.51,3.62}$.

Found: C, 92.54; H, 8.04%. Calcd for $C_{21}H_{21}$: C, 92.26; H, 7.74%.

The decomposition of **10** was completed within 2 hr in boiling *o*-dichlorobenzene.

Method B. To a solution of 182 mg of 9-isopropylidenebenzonorbornadiene (**6**) in 5 ml of dioxane were added portionwise crystals of 236 mg of 3,6-di(2'-pyridyl)-*S*-tetrazine which dissolved gradually. The reaction proceeded with evolution of nitrogen to give the adduct **14**. Heating the

18) R. B. Woodward and R. Hoffmann, "The Conservation of Orbital Symmetry," Verlag Chemie-GmbH—Academic press. (1970), p. 145—151.

19) K. N. Houk, L. J. Luskus, and N. S. Bhacca, *J. Amer. Chem. Soc.*, **92**, 6392 (1970); b) N. S. Bhacca, L. J. Luskus, and K. N. Houk, *Chem. Commun.*, **1971**, 109.

20) Coupling constant, *J*, between signals at δ A and δ B is expressed as $J_{A,B}$.

dioxane solution at 50°C caused decomposition of **14**, giving **15** and 3,6-di(2′-pyridyl)pyridazine, mp 176—177°C in the absence of a trapping reagent.

Reaction of **5** *with Dimethyl Maleate.* Generation of **5** was conducted in the presence of dimethyl maleate by heating a dioxane solution of **10** at 100°C or one of **14** at 50°C. The results obtained are given in Table 1. The product was isolated by preparative vpc performed on a Yanagimoto gas chromatograph GCG-3 equipped with a 1 m × 14 mm stainless steel column packed with 5% diethylene glycol succinate on Chromosorb W.

The *exo-cis* adduct **16**, mp 157—158°C; UV max (95% C_2H_5OH): 262 mμ (ε 1340), 268 (2010), and 274 (2080); IR (CCl_4) cm^{-1}: 1749 (COOMe); PMR ($CDCl_3$) δ: ~7.13 (4, aromatic), 4.08 (2, s, C_1,C_4–H), 2.79 (s, 2, C_2,C_3–H), and 1.71 ppm (s, 6, $C\underline{H}_3$).

Found: C, 71.83; H, 6.56%. Calcd for $C_{18}H_{20}O_4$: C, 71.98; H, 6.71%.

The *endo-cis* adduct **17**, mp 145.5—146°C; UV max (95% C_2H_5OH): 261 mμ (ε 995), 267 (1510), and 274 (1510); IR (CCl_4) cm^{-1}: 1749 and 1731 (COOMe); PMR ($CDCl_3$) δ: 7.18 (4, aromatic), 4.05 (split t, 2, C_1,C_4–H), 3.40 (overlapped with $COOC\underline{H}_3$, 2, C_2,C_3–H), and 1.61 ppm (s, 6, $C\underline{H}_3$).

Found: C, 72.04; H, 6.76%.

The presence of dimethyl fumarate yielded the *trans* adduct **18**, mp 89—90°C; UV max (95% C_2H_5OH): 261 mμ (ε 1120), 267 (1680), and 274 (1720); IR (CCl_4) cm^{-1}: 1740 (COOMe); PMR ($CDCl_3$) δ: 7.20 (4, aromatic), 4.19 (s, 1, C_1–H), 4.15 (X part of AMX type, 1, C_4–H), 3.55 (M of AMX, 1, C_3–H), 2.95 (A of AMX (doublet), 1, C_2–H), 1.68 (s, 3, $C\underline{H}_3$), and 1.60 (s, 3, $C\underline{H}_3$).

Found: C, 72.08; H, 6.64%.

Reaction of **5** *with Tropone.* A mixture of 1 g (0.382 mmol) of **10** and 4.05 g (3.82 mmol) of tropone was heated at 120°C in the dark under argon atmosphere for 30 min. Removal of excess of tropone under reduced pressure left 1.02 g of crystals which were recrystallized from ether to yield a pure sample of **19**, mp 120.5—121.5°C; UV max (95% C_2H_5OH): 224 mμ (ε 21400) and 259 (11100); IR (CCl_4) cm^{-1}: 1657 (C=O); PMR ($CDCl_3$) for δ, see Fig. 2; $J_{5.68,6.70}$=12.0 Hz, $J_{6.70,3.08}$=8.7, $J_{5.68,3.08}$≈0.2, $J_{3.89,5.68}$=1.7, $J_{6.22,6.37}$=11.5, $J_{6.22,3.89}$≈8, $J_{3.08,6.37}$≈8, $J_{3.08,6.22}$=1.7, $J_{3.89,6.37}$=1.7, and positive allylic coupling $J_{6.49,3.68}$.

Found: C, 86.75; H, 6.89%. Calcd for $C_{19}H_{18}O$: C, 86.98; H, 6.91%.

Passing **19** through an alumina column gave the double bond isomer **20**; mp 107—108.5°C; UV max (95% C_2H_5OH): 238 mμ (ε 10100) and 261 (8950); IR (CCl_4) cm^{-1}: 1680 and 1662 (one split absorption, C=O); PMR ($CDCl_3$) δ: ~6.75 (m, 1, vinyl β to CO), ~6.2 (m, 2, $C\underline{H}$=$C\underline{H}$), 5.85 (d of d, 1, vinyl α to CO), 4.37 (d of m, 1, bridgehead α to CO in cycloheptadienone moiety), 3.37 (s, 2, benzyl), and 3.19 ppm (m, 1, bridgehead γ to CO in cycloheptadienone moiety).

BULLETIN OF THE CHEMICAL SOCIETY OF JAPAN, VOL. 45, 2003—2006(1972)

Oxidation by Transition Metal Complexes. V. Oxidation of Vinyl Esters Catalyzed by Rhodium Complex.

Kiyotomi TAKAO, Hiromichi AZUMA, Yuzo FUJIWARA, Toshinobu IMANAKA, and Shiichiro TERANISHI

Department of Chemical Engineering, Faculty of Engineering Science, Osaka University, Machikaneyama, Toyonaka, Osaka

(Received December 15, 1971)

The oxidation of styryl acetate, vinyl acetate, vinyl propionate, methyl acrylate, and methyl cinnamate with $RhCl(PPh_3)_3$ catalyst has been studied. The reaction is remarkably affected by the substituent on an olefinic carbon atom. The oxidation mechanism was discussed in connection with decarbonylation.

Recently we reported on the oxidation of olefins catalyzed by rhodium complexes to give carbonyl compounds.[1] Oxidation products could be classified into two types, the carbon-carbon double bond cleavage products and the noncleavage products. The carbonyl compounds formed by olefin oxidation underwent decarbonylation.

We investigated rhodium complex catalyzed oxidation of some vinyl esters bearing a carbonyl group in connection with decarbonylation reaction. It was found that the formation of two type oxidation products is greatly affected by the site of the carbonyl group on olefins.

In this paper the oxidation of vinyl esters is described and discussed in relation to the substituent effect of olefins.

Results and Discussion

The olefin oxidation catalyzed by rhodium complex was carried out by heating mixtures of the reactant vinyl ester and the rhodium complex in toluene or ethanol for 8 hr under a constant bubbling of oxygen. The results are summarized in Table 1, showing that $RhCl(PPh_3)_3$ complex is a good catalyst.

Oxidation of Styryl Acetate. Heating of styryl ace-

1) a) K. Takao, Y. Fujiwara, T. Imanaka, and S. Teranishi, This Bulletin, **43**, 1153 (1970); b) K. Takao, M. Wayaku, Y. Fujiwara, T. Imanaka, and S. Teranishi, *ibid.*, **43**, 3898 (1970); c) K. Takao, M. Wayaku, Y. Fujiwara, T. Imanaka, and S. Teranishi, *ibid.*, **45**, 1505 (1972).

Table 1. Oxidation of vinyl esters by $RhCl(PPh_3)_3$

Olefin	Solvent	Oxidation products: C=C bond cleavage	Oxidation products: Noncleavage	Decarbonylation products
Styryl acetate[b]	Toluene	Benzaldehyde (403%)[a]	Benzyl acetate (10%)	
		Acetic acid (240)	Methyl phenylacetate	
		Methyl formate (157)	(trace)	
	Ethanol	Benzaldehyde (trace)	Benzyl acetate (56)	Benzyl methyl ketone (29%)
			Methyl phenylacetate (trace)	
Vinyl acetate[c]	Toluene		Methyl acetate (24)	Acetone (93)
				Propionaldehyde (15)
				Methyl vinyl ether (trace)
	Ethanol		Methyl acetate (238)	Acetone (110)
				Propionaldehyde (trace)
				Methyl vinylether (trace)
Vinyl propionate[c]	Toluene		Ethyl acetate (91)	Methyl ethyl ketone (83)
			Methyl propionate (trace)	Ethyl vinyl ether (10)
				Butyraldehyde (5)
Methyl cinnamate[b]	Toluene	Benzaldehyde (125)	Methyl phenylacetate (20)	
		Methyl formate (110)		
	Ethanol	Benzaldehyde (5)	Methyl phenylacetate (93)	
		Methyl formate (trace)		
Methyl acrylate[c]	Toluene		Methyl acetate (315)	
	Ethanol		Methyl acetate (837)	

a) Yields are based on the catalyst utilized.
b) Olefin (30 mmol), $RhCl(PPh_3)_3$ (1.3 mmol), Reaction temp. 80°C, Reaction time 8 hr.
c) Olefin (60 mmol), $RhCl(PPh_3)_3$ (1. 3mmol),Reaction temp. 70°C, Reaction time 8 hr.

tate (*cis* and *trans* mixture) in toluene gave benzaldehyde (403%),[2] acetic acid (240%), and methyl formate (157%) as the main product with benzyl acetate (10%), and methyl phenylacetate (trace).

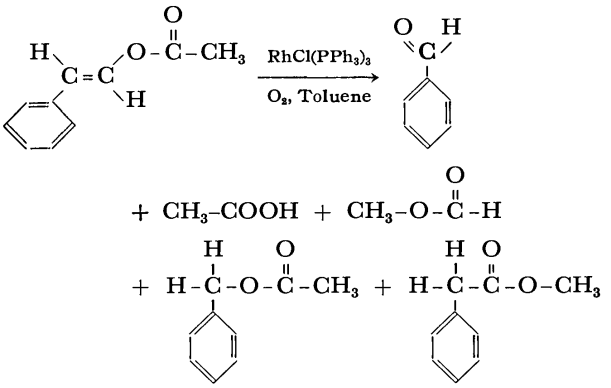

The formation of these oxidation products might be explained in the following way: The main products such as benzaldehyde, acetic acid and methyl formate are derived from the double bond cleavage of styryl acetate. Presumably a four-center intermediate in which both oxygen molecule and olefin coordinate to rhodium(I) is formed as shown in scheme 1.

The cleavage of C=C and O=O bonds of the intermediate would give benzaldehyde and acid anhydride of formic and acetic acids. This four-center type intermediate has been proposed in the reaction of singlet oxygen molecule and indene.[3] The acid anhydride of

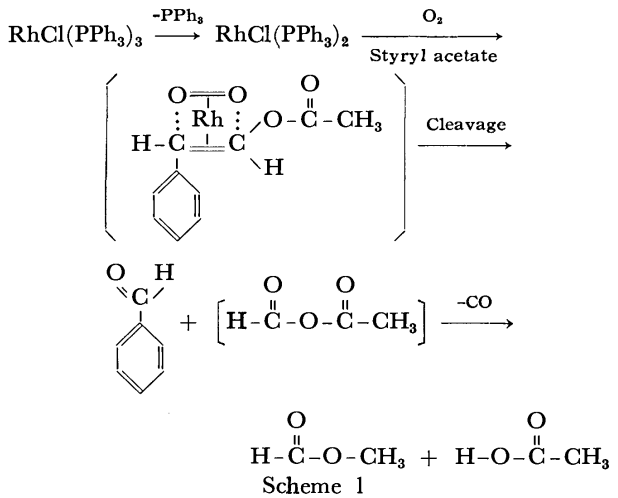

Scheme 1

formic and acetic acids formed would undergo decarbonylation by the rhodium complex to give acetic acid and methyl formate. From the solid phase of the reaction mixture, $RhCl(CO)(PPh_3)_2$ and unidentified complexes (ν_{CO}: 2055 cm^{-1}) were obtained. We confirmed that acid anhydrides, such as acetic anhydride could be easily decarbonylated to give ester compounds by $RhCl(PPh_3)_3$.[4]

The formation of a small amount of benzyl acetate and methyl phenylacetate classified as the noncleavage oxidation products might take place in the following way: the addition of oxygen to bond of styryl acetate followed by a hydrogen shift would give an anhydride of acetic and phenylacetic acids. The anhydride would be further decarbonylated to benzyl ace-

2) Yields of the oxidation products which appear hereafter in this paper are all based on the amount of the complexes used.

3) W. Fenical, D. R. Kearns, and P. Radlick, *J. Amer. Chem. Soc.*, **91**, 3396 (1969).

4) J. Blum and Z. Lipshes, *J. Org. Chem.*, **34**, 3076 (1969).

tate and methyl phenylacetate as shown below.

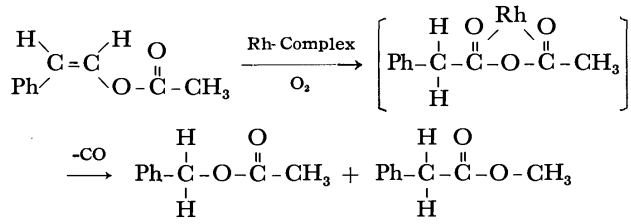

Scheme 2

Table 1 also shows that the oxidation of styryl acetate undergoes a similar remarkable solvent effect as styrene.[1b] In ethanol solvent, the double bond cleavage hardly takes place at all.

Oxydation of Vinyl Acetate and Propionate. In the oxidation of vinyl acetate and propionate in toluene, no double bond cleavage products were obtained. However, acetone (93%) and methyl ethyl ketone (83%) were obtained in marked contrast to the case of styryl acetate.

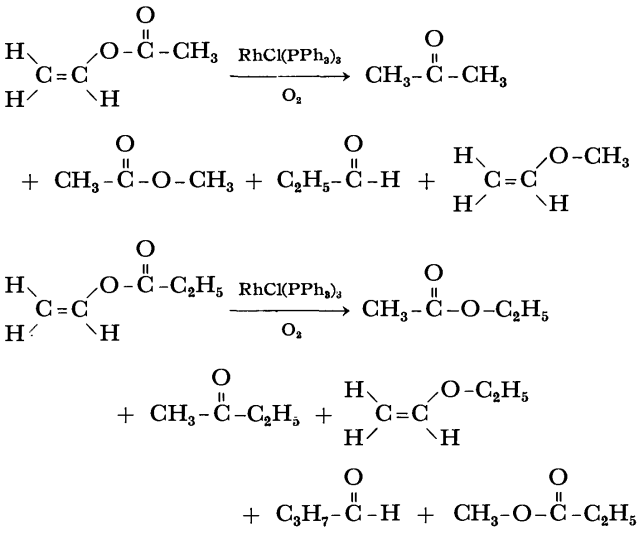

The products acetone, propionaldehyde and methyl vinyl ether from vinyl acetate, and methyl ethyl ketone, butyraldehyde and ethyl vinyl ether from vinyl propionate might be explained in terms of decarbonylation of the starting vinyl carboxylates as shown in scheme 3.

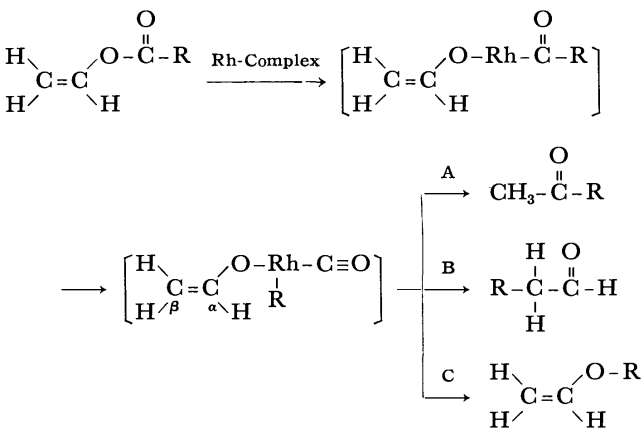

Scheme 3

Presumably vinyl propionate is added oxidatively to the rhodium complex $RhCl(PPh_3)_2$ forming a vinyloxy acyl-rhodium complex. The acyl complex would then be converted into an alkyl carbonyl complex through acyl-alkyl rearrangement.[5] The decomposition of the complex followed by the recombination of the ligands would give the products.[6]

Ethyl acetate and methyl propionate may be derived from the noncleavage oxidation of vinyl propionate. Similarly methyl acetate from vinyl acetate as in the case of styryl acetate oxidation.

It should be noted that styryl acetate undergoes oxidation with the C=C bond cleavage, but not vinyl acetate or vinyl propionate. It might be that styryl acetate having an electron withdrawing phenyl group can form more easily the four-center intermediate described above than vinyl carboxylates.[7]

Oxydation of Methyl Cinnamate and Acrylate. Methyl cinnamate and acrylate were chosen as the reactant in order to investigate the conjugation effect between the C=C and C=O groups on oxidation and decarbonylation.

Oxidation of methyl cinnamate in toluene gave benzaldehyde (125%), methyl formate (110%) and methyl phenylacetate (20%). In contrast to the oxidation of vinyl esters bearing no carbonyl group on an olefinic atom, no decarbonylation products was obtained. No C=C bond cleavage oxidation was observed in the case of methyl acrylate which has no phenyl group on the olefinic carbon atom.

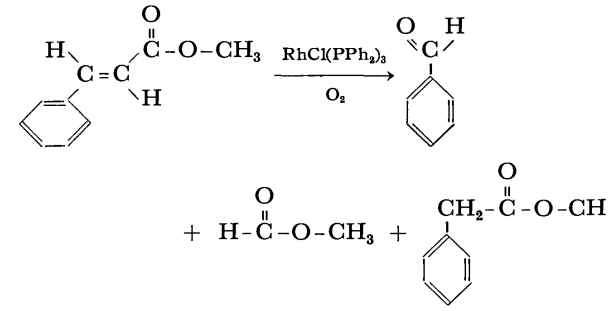

The result suggests that the conjugation of the carbonyl group with the C=C bond prevents decarbonylation reaction.

In conclusion, vinyl esters undergo oxidation smoothly by the rhodium triphenylphosphine complex, and the product distribution is influenced by the substituent on olefins.

Experimental

Materials and Analysis. All the temperatures were uncorrected. The IR spectra were recorded on a JASCO IR-E spectrometer. The NMR spectra were measured on a Japan Electron Optics JNM-4H-100 spectrometer. Chemical shifts are given in τ units together with splitting patterns

5) R. J. Mawby, F. Basolo, and R. G. Peason, *J. Amer. Chem. Soc.*, **86**, 5043 (1964).

6) No reaction occurring in argon atmosphere in place of O_2 suggests that O_2 plays an important role. Details of the behavior, however, are not apparent yet.

7) M. S. Kharash, R. C. Seyler, and F. R. Mayo, *J. Amer. Chem. Soc.*, **60**, 882 (1938).

and relative integrated area. Vpc analysis was carried out with a Yanagimoto G-8 gas chromatograph using Apiezon-L, Silicone OV-17, diethyl phthalate columms. $PhCl(PPh_3)_3$ was prepared by the method of Osborn *et al.*[8] Styryl acetate (*cis* and *trans* mixture) was prepared according to the method of Semmler.[9] Vinyl acetate, vinyl propionate, methyl cinnamate, and methyl acrylate were of commercial grade and dried over anhydrous magnesium sulfate and distilled before use. Toluene and ethanol were purified as mentioned previously.[1]

Oxidation of Styryl Acetate. In a flask described previously,[1] was charged a mixture of 1.21 g (1.3 mmol) of $RhCl(PPh_3)_3$, 4.96 g (30 mmol) of styryl acetate (*cis* and *trans* mixture) and 75 m*l* of toluene. The mixture was heated at 80°C with a constant bubbling of oxygen for 8 hr. The resulting mixture was concentrated and the liquid phase was analyzed and isolated by vpc to give 0.555 g (403%) of benzaldehyde (I), 0.187 g (240%) of acetic acid (II), 0.122 g (157%) of methyl formate (III), 0.020 g (10%) of benzyl acetate (IV) and a trace of methyl phenylacetate (V). These compounds were identified by comparison with authentic samples. Compound I: IR (neat): 685, 744, 1200, and 1675 cm^{-1}; NMR (CCl_4): 0.15 (s, 1) and 2.10—2.70 (m, 5). Compound II: NMR (CCl_4): —1.35 (s, 1) and 7.90 (s, 3). Compound III: NMR (CCl_4): 1.92 (s, 1) and 6.23 (s, 3). Compound IV: IR (neat): 710, 765, 1240, 1380, and 1740 cm^{-1}; NMR (CCl_4): 2.73 (s, 5), 4.99 (s, 2), 7.99 (s, 3).

The residual solid material was chromatographed on a silica gel column (50 g). Elution with benzene (300 m*l*) gave dark brown carbonyl complexes. Separation of the complexes by column chromatography (silica gel, 15 g) gave $RhCl(CO)(PPh_3)_2$ (0.1 g) and unidentified complexes (ν_{CO}: 2055 cm^{-1}) (0.5 g). Further elution with ether (300 m*l*) gave triphenylphosphine oxide.

Oxidation of Vinyl Acetate. The same procedure was used as for styryl acetate. Reaction products were methyl acetate (VI), acetone (VII), propionaldehyde (VIII), and methyl vinyl ether (IX). These compounds were assigned by comparison of NMR spectra and retention times with those of authentic samples. Compound VI: NMR (CCl_4): 6.35 (s, 3) and 7.99 (s, 3). Compound VII: NMR (CCl_4): 7.94 (s).

Oxidation of Vinyl Propionate. The same procedure was used as above. Reaction products were ethyl acetate (X), methyl ethyl ketone (XI), ethyl vinyl ether (XII), butyraldehyde (XIII), and methyl propionate (XIV). The compounds were identified by a comparison of NMR and retention time with those of authentic samples. Compound X: NMR (CCl_4): 5.94 (q, 2), 8.05 (s, 3), and 8.77 (t, 3). Compound XI: NMR (CCl_4): 7.53 (q, 2), 7.87 (s, 3), and 8.95 (t, 3).

Reaction of Acetic Anhydride with Rhodium Complex. In a flask as described above was placed a mixture containing 0.61 g (0.65 mmol) of $RhCl(PPh_3)_3$, 6.12 g (60 mmol) of acetic anhydride and 50 m*l* of toluene. The reaction was carried out at 80°C with a constant bubbling of oxygen for 8 hr. The resulting reaction mixture was treated as usual and the liquid phase was analyzed and separated by vpc to give 3.76 g (2.550%) of methyl acetate. The solid phase was chromatographed on silica gel (25 g) to give triphenylphosphine oxide and $RhCl(CO)(PPh_3)_2$ (0.40 g).

8) J. A. Osborn, F. H. Jardine, J. F. Young, and G. Wilkinson, *J. Chem. Soc., A*, **1966**, 1711.

9) F. W. Semmler, *Ber. Dtsch. Chem. Ges.*, **42**, 584 (1909).

The Additive Effect of Triphenylphosphine on the Polymerization of Vinyl Monomers by Copper(II) Chelates

Toshiyuki SHONO, Yuko YAMASHOJI, and Koichiro SHINRA

Department of Applied Chemistry, Faculty of Engineering, Osaka University, Yamada-Kami, Suita, Osaka

(Received November 1, 1971)

Various copper(II) chelates were found to be effective initiators in the polymerization reaction of the methyl methacrylate in the presence of triphenylphosphine. The conversion increases with an increase in the concentration of triphenylphosphine, reaching a constant level at the ratio of 1 : 2 between copper chelates and triphenylphosphine. Di-μ-methoxo-bis(ethylacetoacetato)dicopper(II) was the most effective initiator. The dependence of the rate of the polymerization on the square root of the concentration of the complexes suggests that the polymerization by this initiation system proceeds *via* a radical mechanism. It can be assumed that the copper chelate coordinated the triphenylphosphine and that homolytic fission occurred to give a free ligand radical, accompanied by the reduction of the central copper atom. Stable copper(I) mixed chelates were obtained under conditions similar to those of the polymerization.

The radical polymerization of vinyl monomers by using copper acetylacetonate [$Cu(acac)_2$] and its derivatives as catalysts has been reported.[1-3] The solvent effects and effects resulting from the additives, as well as a high order with respect to the monomer, are characteristic of these polymerization reactions. These characteristics indicate the participation of monomers and additives in the initiation step. Recently, Bamford and Ferrar[4] showed by radiochemical investigations that donor additives enhance the rates of the initiation of free radical polymerization by transition-metal acetylacetonate and that the propagating chain carries one acetylacetonate residue, but that the fragments derived from the additives are incorporated in the polymer to only a minor extent.

In the present study, various copper(II) chelates were found to be effective initiators in the polymerization reaction of the vinyl monomer in the presence of triphenylphosphine.

During the initiating step, a ligand displacement is supposed to occur, with the simultaneous reduction of Cu(II)→Cu(I). Various Cu(I) triphenylphosphine mixed chelates were separated.

Experimental

Materials. The monomer was purified by the usual method and was distilled under reduced pressure before use. The triphenylphosphine was recrystallized several times from ether. The methoxo-copper(II) chelates were synthesized according to the method of Bertrand[5]; that is, the copper chelate, CuL_2, was allowed to react with potassium hydroxide in methanol to produce the methoxo complexes,

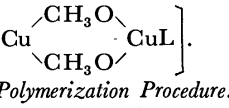

Polymerization Procedure. A copper chelate, the monomer, and the solvent were placed in a glass tube. After the tube had been degassed by repeated freezing, evacuating, and thawing, it was sealed off. Polymerization was carried out under shaking in a thermostat maintained at a given temperature. The resulting polymers were precipitated in methanol containing hydrochloric acid, filtered, and dried *in vacuo* to a constant weight.

Measurements. The NMR spectra were measured in order to determine the tacticities of the poly(methyl methacrylates) according to the method of Kato.[6]

Polarographic measurements were carried out in acetonitrile with a Yanagimoto potential-controlled Polarograph at 25°C. Tetrabutylammonium perchlorate was used as the supporting electrolyte, and Triton X was added to each solution in order to diminish the maximum wave.

Result and Discussion

Additive Effect of Triphenylphosphine. Copper(II) acetylacetonate and di-μ-methoxo-bis(acetylacetonato)-dicopper(II) $[Cu(acac)OCH_3]_2$ each has its own accelerative effect on the polymerization of various vinyl monomers in organic solvents. Tables 1 and 2 show the remarkable accelerative effects of triphenylphosphine on the polymerization of methyl methacrylate (MMA) by copper(II) chelates. The accelerative effects of μ-methoxo copper(II) complexes were superior to those of the original copper(II) chelates. The methoxo ethyl acetoacetate chelate was the most effective.

The stereoregularity of the resulting polymer was calculated from the NMR spectra. The syndiotacticities were slightly higher than those of ordinary polymers

TABLE 1. ADDITIVE EFFECT OF THE TRIPHENYLPHOSPHINE ON THE POLYMERIZATION OF MMA

Chelate	Chelate concentration (mol/l)	Triphenylphosphine concentration (mol/l)	Conversion (%/hr)
$Cu(acac)_2$	0.01	0	2.18
$Cu(acac)_2$	0.01	0.04	5.00
$[Cu(acac)OCH_3]_2$	0.01	0	5.40
$[Cu(acac)OCH_3]_2$	0.01	0.04	12.05

Solvent: acetonitrile, [MMA]: 5 mol/l, Temp: 70°C, 4 hr.

1) Y. Nishikawa and T. Otsu, *Kogyo Kagaku Zasshi*, **72**, 1836 (1969) and references therein.
2) K. Uehara, Y. Kataoka, M. Tanaka, and N. Murata, *ibid.*, **73**, 1053 (1970) and references therein.
3) K. Kaeriyama, This Bulletin, **43**, 1511 (1970).
4) C. H. Bamford and A. N. Ferrar, *Chem. Commun.* **1970**, 315 *Proc. Roy. Soc.* (London), **A321**, 425 (1971).
5) J. A. Bertrand, R. I. Kaplan, *Inorg. Chem.*, **4**, 1657 (1965).
6) Y. Kato, H. Watanabe, and A. Nishioka, This Bulletin, **37**, 1762 (1964).

TABLE 2. ADDITIVE EFFECT OF THE TRIPHENYLPHOSPHINE ON THE POLYMERIZATION OF MMA BY VARIOUS CHELATES

Chelate	Chelate concentration (mol/l)	Triphenylphosphine concentration (mol/l)	Rate of polymerization (mol/l/sec)
$Cu(acac)_2$	0.001	0.004	1.83×10^{-5}
$[Cu(acac)OCH_3]_2$	0.001	0.004	2.86×10^{-5}
$Cu(eacac)_2$	0.001	0.004	7.55×10^{-5}
$[Cu(eacac)OCH_3]_2$	0.001	0.004	8.70×10^{-5}
$Cu(dpm)_2$	0.001	0.004	0.43×10^{-5}
$[Cu(dpm)OCH_3]_2$	0.001	0.004	1.21×10^{-5}
$Cu(SA)_2$	0.001	0.004	0.97×10^{-5}
$[Cu(SA)OCH_3]_2$	0.001	0.004	1.32×10^{-5}
$Cu(3\text{-foc})_2$	0.001	0.004	2.51×10^{-5}

Polymerization condition; solvent: acetonitrile, [MMA]: 5 mol/l, Temp: 70°C, 4 hr.
eacac=ethylacetoacetato, dpm=dipivaloylmethanato, SA=salicylaldehydato, 3-foc=3-formyl camphor.

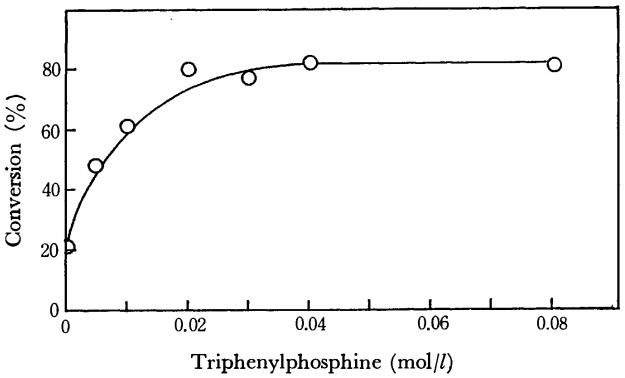

Fig. 1. The dependence of the concentration of triphenylphosphine. Solvent: acetonitrile, $[Cu(acac)OCH_3]_2$: 0.01 mol/l, [MMA]: 5 mol/l, at 70°C, 4 hr.

obtained by radical polymerization. (74.0%, polymerized by $[Cu(eacac)OCH_3]_2$ at 20°C; 68.8%, polymerized by $Cu(acac)_2$ at 50°C; 65.6%, at 70°C.)

Figure 1 shows the dependence of the conversion on the concentration of triphenylphosphine. The conversion increases with an increase in the concentration of triphenylphosphine, reaching a constant level at the ratio of 1:2 of the copper chelate and triphenylphosphine. Above this ratio, the polymerizing mixture loses its blue color at the end of the polymerization. In the absence of copper(II) chelates, traces of the polymer were obtained in the presence of 0.1 mol/l of triphenylphosphine ([MMA]: 5 mol/l).

TABLE 3. SOLVENT EFFECTS ON THE POLYMERIZATION RATE IN $[Cu(acac)OCH_3]_2$–PPh_3 SYSTEM

Solvent	Rate of polymerization (mol/l/sec)
Acetonitrile	7.09×10^{-5}
Chloroform	2.88×10^{-5}
Dimethylformamide	3.24×10^{-5}
Pyridine	2.29×10^{-5}
Tetrahydrofuran	4.03×10^{-5}

$[Cu(acac)OCH_3]_2$: 0.005 mol/l, $[PPh_3]$: 0.02 mol/l, [MMA]: 5 mol/l, at 70°C, 4 hr.

Table 3 shows the solvent effects on the reactivity of the Cu(II)-chelate-triphenylphosphine system. The rates of polymerization are in the following order: $CH_3CN>THF>DMF>CHCl_3>Py$. The effectiveness of the solvent might be due to the stabilization of the univalent copper. The univalent copper is known to

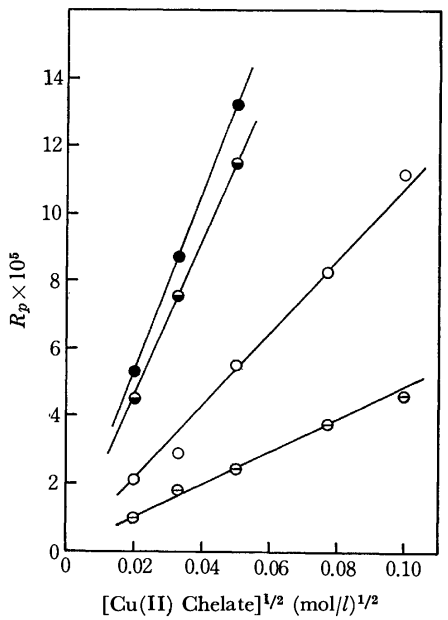

Fig. 2. The dependence of the polymerization rate on the square root of the concentration of the copper(II) chelates. [MMA]: 5 mol/l, Solvent: acetonitrile, at 70°C, 2 hr. [Chelate]/$[PPh_3]$=1/4
●: $[Cu(eacac)OCH_3]_2$, ◒: $Cu(eacac)_2$, ○: $[Cu(acac)OCH_3]_2$, ⊖: $Cu(acac)_2$.

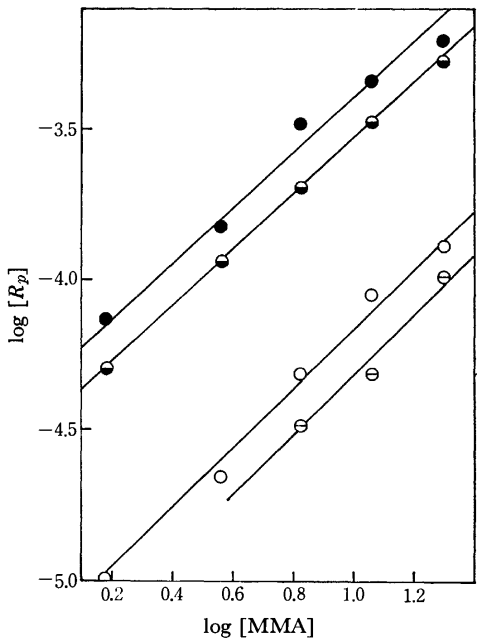

Fig. 3. The dependence of the polymerization rate on the MMA concentration.
[Chelate]: 0.005 mol/l, $[PPh_3]$: 0.02 mol/l, Solvent: acetonitrile, at 60°C, 1 hr.
●: $[Cu(eacac)OCH_3]_2$, ◒: $Cu(eacac)_2$, ○: $[Cu(acac)OCH_3]_2$, ⊖: $Cu(acac)_2$.

Table 4. Polymerization rate of various monomers

Monomer	Chelate	Chelate concentration (mol/l)	PPh_3 concentration (mol/l)	Solvent	Temp. (°C)	Time (hr)	Conversion (%/hr)
Ethyl acrylate	$Cu(acac)_2$	0.05	0.2	bulk	50	5	2.4
	$[Cu(acac)OCH_3]_2$	0.05	0.2	bulk	50	3	30.7
Acrylonitrile	$Cu(acac)_2$	0.05	0.2	bulk	50	5	1.6
	$[Cu(acac)OCH_3]_2$	0.05	0.2	bulk	50	3	9.3
Styrene	$Cu(acac)_2$	0.005	0.02	benzene	70	10	0.4
	$[Cu(acac)OCH_3]_2$	0.005	0.02	benzene	70	10	0.4
	$[Cu(eacac)OCH_3]_2$	0.005	0.02	benzene	70	10	2.6
	$Cu(3\text{-foc})_2$	0.005	0.02	benzene	70	10	2.2

[Styrene]: 5 mol/l, 3-foc=3-formylcamphor.

be stabilized by acetonitrile.[7]

Kinetics. From the straight line in the time-conversion plots, the rates of polymerization were evaluated by graphically determining a tangent at a given time. The dependences of the rate of polymerization on the square root of the concentrations of the four complexes are shown in Fig. 2. Figure 3 shows the rate of polymerization as a function of the monomer concentration at a constant concentration of copper chelates and additives. From the slopes of these straight lines, the order with respect to the monomer was found to be 1.0. Judging from this order, the coordination of the monomer to the copper chelate cannot be considered at the initiation step. It can be assumed that the Cu(II) chelate coordinated the triphenylphosphine and that homolytic fission occurred to give a free-ligand radical or an alkoxy radical, accompanied by the reduction of the central copper atom.

The reduction potentials of the copper(II) chelates were measured and plotted against the rate of polymerization. A good linearity was obtained (see Fig. 4).

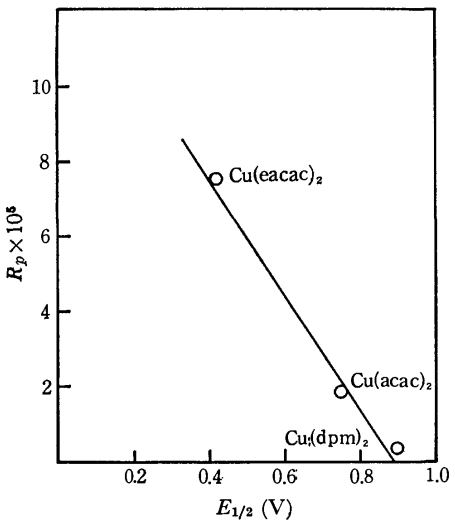

Fig. 4. The relationship between the reduction potentials of the copper(II) chelates and the rate of polymerization (Table 2).
Solvent: acetonitrile, [Chelate]: 0.001 mol/l, $[(C_4H_9)_4NClO_4]$: 0.1 mol/l, [Triton X]: 0.1%.

7) C. Sigwart, P. Kroneck, and P. Hemmerich, *Helv. Chim. Acta*, **53**, 177 (1970).

Table 5. The isolated Cu(I) chelates

Cu(I) Chelate	Color	Mp (°C)
$Cu(acac)(PPh_3)_2$	colorless	177—179
$Cu(SA)(PPh_3)_2$	yellow	175
$Cu(3\text{-foc})(PPh_3)_2$	colorless	105—107

(3-foc=3-formylcamphor)

Reactivity of Other Monomers. As is shown in Table 4, these initiation systems were effective with styrene, acrylonitrile, and ethyl acrylate.

Reaction of Triphenylphosphine with Cu(II) Chelates. As is shown in Table 5, stable Cu(I) mixed chelates were obtained under conditions similar to those of the polymerization. The details of the preparations and the properties of the copper(I) mixed chelates will be reported in a separate paper.[8] The initiation reactions can be summarized schematically as follows:

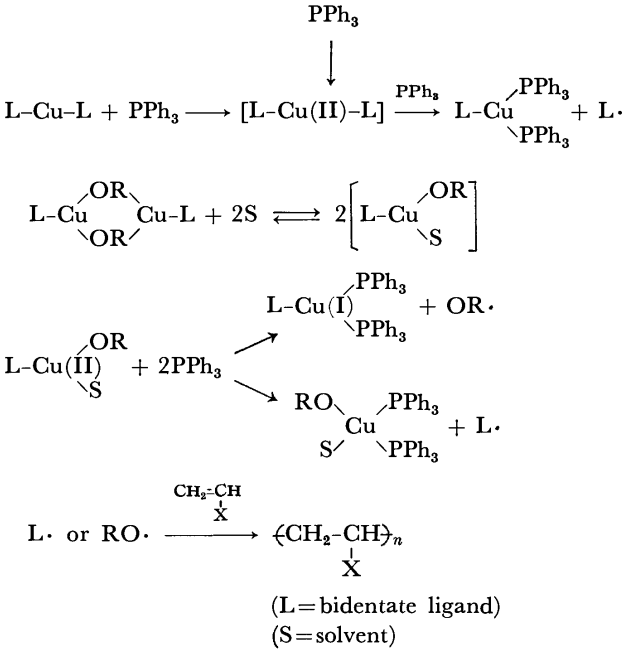

8) T. Shono, Y. Fujii, and K. Shinra, *Chem. Lett.*, **1**, 163 (1972).

The Reaction Mechanism of 2-Dimethoxymethyl-3-methoxypropionitrile with Acetamidine. II.[1] A Novel Reaction Pathway[2]

Takenori NISHINO, Masumi KIYOKAWA, Yoshiyuki MIICHI, and Kanji TOKUYAMA

Shionogi Research Laboratory, Shionogi & Co., Ltd., Fukushima-ku, Osaka

(Received December 18, 1971)

The reaction of 2-dimethoxymethyl-3-methoxypropionitrile (**1**) with acetamidine produces pyrimidopyrimidine (**8**) *via* the consecutive process of **1**→an intermediate→**8**. The intermediate was not isolated, but two structures have been proposed for it. We have now succeeded in the isolation of the intermediate and determined it to be 2-methyl-4-amino-5-dimethoxymethyl-5,6-dihydropyrimidine (**4**). Several key intermediates were also successfully isolated. The novel reaction pathway for the title reaction was concluded to be as follows: the elimination of methanol from **1**, followed by the addition of acetamidine affords 3-acetamidinopropionitrile (**3**), the subsequent quick cyclization of which produces the intermediate, **4**; the further elimination of methanol from **4**, followed by a replacement reaction with acetamidine, gives an acetamidinomethylene compound (**6**), which is converted into the final product, **8**, *via* an intermediate (**7**). Some minor pathways will also be presented.

Although it has been known that enol ether and acetal derivatives of α-formylnitriles react with amidines to give the same final products,[3-5] Takamizawa and his co-workers have reported an unusual result on 2-formyl-3-alkoxypropionitriles.[6] When treated with acetamidine, 2-methoxymethylene-3-methoxypropionitrile (**12**) of an enol ether-type affords 2-methyl-4-amino-5-methoxymethylpyrimidine (**13**) of the usual type,[7] but 2-dimethoxymethyl-3-methoxypropionitrile (**1**) of an acetal type yields 2,7-dimethyl-5,6-dihydropyrimido-[4,5-*d*]pyrimidine (**8**) *via* an intermediate showing the absorption maximum at 262 mμ in methanol in the UV spectrum. An unusual product, **8**, is also obtained from 2-dimethoxymethylacrylonitrile (**2**); this reaction can be explained in terms of the fast conversion of **2** into **1** at the initial stage. As the hydrolyses of **8** give 2-methyl-4-amino-5-acetamidomethyl- (**9**) and 2-methyl-4-amino-5-aminomethylpyrimidine (**10**) quantitatively,[8] the reaction of **1** (or **2**) is very important for thiamine production. However, the reaction mechanism is not unequivocally established because of the unsuccessful isolation of the intermediate. For the structure of the intermediate, 2-acetamidinomethylene-3-methoxypropionitrile (**14**) has been proposed on the basis of a comparison with the reaction of 2-aminomethylene-3-alkoxypropionitrile with methyl acetimidate.[6] On the other hand, in view of the behavior of **1** under basic conditions we have proposed a revised structure, 2-methyl-4-amino-5-dimethoxymethyl-5,6-dihydropyrimidine (**4**), which would be formed *via* the pathway of **1**→**2**→2-dimethoxymethyl-3-acetamidinopropionitrile (**3**)→**4**.[1] The present investigation was carried out in order to establish the exclusive reaction pathway by isolating the intermediate.

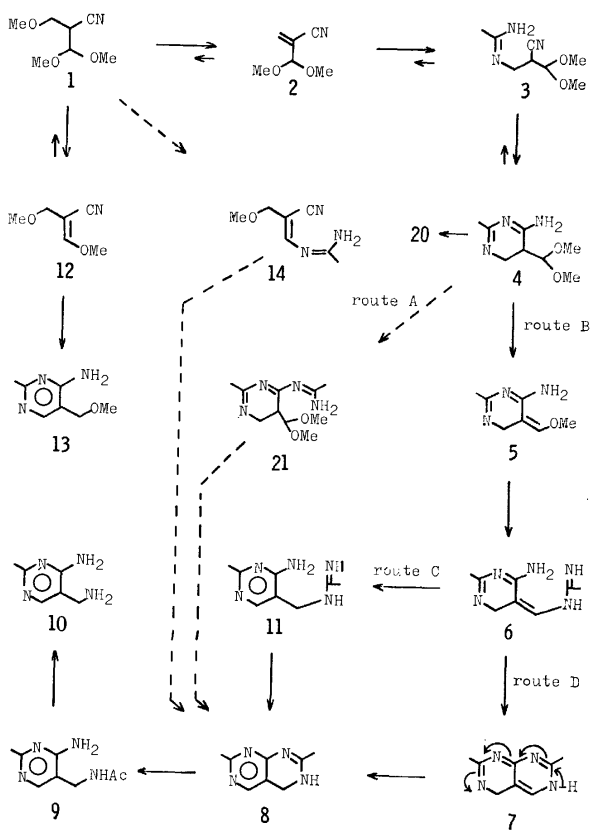

Chart 1

The reaction of **1** with acetamidine in methanol can be generalized into the equation of **1**→the intermediate →**8**.[6] Although the first step of this consecutive process proceeds even at room temperature to some extent, a reflux temperature and another one mole of acetamidine are required to conclude the second step. For the iso-

1) For part 1, see T. Nishino, M. Kiyokawa, Y. Miichi, and K. Tokuyama, This Bulletin, **45**, 1127 (1972). A part of this paper was reported in a preliminary form; T. Nishino, M. Kiyokawa, and K. Tokuyama, *Tetrahedron Lett.*, **1969**, 3553.

2) Pyrimidines, 10. For part 9, see F. Takami, S. Wakahara, and T. Maeda, *Chem. Lett.*, **1972**, 409.

3) D. J. Brown, "The Pyrimidines," Interscience, New York (1962), p. 59.

4) M. Hoffer, E. Gruberg, M. Mitrovic, and A. Brossi, *J. Med. Chem.*, **14**, 462 (1971).

5) R. M. Cresowell, J. W. Mentha, R. L. Seaman, and D. A. Yeowell, Abstracts of The Third International Congress of Heterocyclic Chemistry, Sendai, 1971, C-26-1.

6) A. Takamizawa, K. Tokuyama, and K. Tori, This Bulletin, **32**, 188 (1959), and earlier papers in this series.

7) H. Andersag and K. Westphal, *Ber.*, **70**, 2035 (1937); R. Grewe, *Z. Physiol. Chem.*, **242**, 89 (1936).

8) A. Takamizawa, K. Ikawa, and M. Narisada, *Yakugaku Zasshi*, **78**, 637 (1958); A. Takamizawa, *ibid.*, **74**, 748 (1954).

9) Y. Okamoto, T. Tsuji, and T. Ueda, *Chem. Pharm. Bull.* (Tokyo,) **17**, 2273 (1969).

lation of the intermediate, the retardation of the rate of second step is naturally necessary, so it seemed to be desirable to use a relatively low reaction temperature and to deactivate the remaining acetamidine by neutralizing it when the formation of the intermediate to a considerable amount was observed.

The lack of success in the isolation of the intermediate has long been attributed to its instability. If the intermediate is **4**, it is conventionally isolated as a hydrochloride, since 4-amino-5,6-dihydropyrimidines are stable as hydrochlorides.[9] On the preparation of hydrochloride of **4**, however, the presence of moisture and an excess of hydrogen chloride should be avoided, because 4-amino- and 5-dimethoxymethyl (acetal) groups of **4** can easily be hydrolyzed under acidic conditions.[1]

When a solution of **1** and acetamidine in anhydrous methanol was kept at 55°C for 1 hr, the characteristic band due to the intermediate appeared strongly in the UV spectrum. To the solution, methanolic hydrogen chloride was added in amounts strictly equimolar with the acetamidine used, and then the solution was concentrated. The repeated recrystallization of the crystals which appeared gave a hydrochloride whose analytical data corresponded to those of the hydrochloride of **4**. The yield was about 44%. Its UV spectrum in methanol showed an absorption maximum at 278 mμ which was shifted to 262 mμ on neutralization. The reaction of the hydrochloride with acetamidine showed a consecutive increase in the absorbancy due to **8** at 305 mμ, and from the reaction mixture **8** was isolated. Therefore, the hydrochloride was identified as the hydrochloride of the intermediate.

The spectral data suggested that the intermediate was **4**. It showed a behavior similar to that of 2-methyl-4-amino-5,6-dihydropyrimidine (**18**)[1] in the UV spectrum, as has been described above, signals due to an acetal group (two singlets due to methyls at 3.32 δ and 3.37 δ and one doublet (J=7.5 Hz) due to the methine proton (H_Y) at 4.48 δ) in the NMR (DMSO-d_6), but no characteristic band due to a nitrile group in the IR. The signals of the remaining protons in the NMR also consisted of **4**. The H_6 signals constitute the AB portion (3.75 δ and 3.63 δ) of an ABXY system, whose X and Y portions are H_5 (3.10—3.40 δ) and H_Y respectively. The 2-methyl signal appears at 2.33 δ as a broad singlet due to homoallylic coupling with H_6.[1]

The treatment of the intermediate with p-quinone in benzene gave 2-methyl-4-amino-5-dimethoxymethylpyrimidine (**15**).[10] Therefore, the structure of the intermediate was established as **4**. Much as in the acid-catalyzed hydrolysis of **18** to 2-methyl-3*H*-4-oxo-5,6-dihydropyrimidine (**19**),[1] **4** was easily hydrolyzed to a 4-oxo-compound (**16**), whose structure was confirmed by the UV spectrum in methanol to show behavior similar to that of **19** and by the NMR spectrum to show a pattern quite similar to that of **4**. The reaction of **4** with methylamine gave a transaminated compound (**17**). The presence of an *N*-methyl signal[11] in the NMR supported this structure. Further, the treatment of **4** with sodium methoxide gave **13**. Therefore, the structure of the intermediate was unequivocally established as **4**.

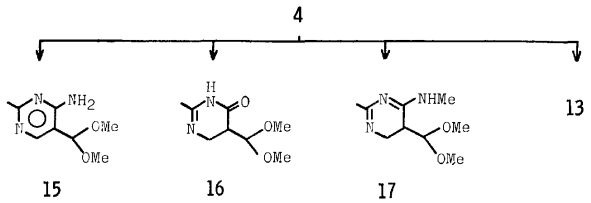

Chart 2

The establishment of the structure of the intermediate clearly supported our idea that the first step in the reaction of **1** with acetamidine proceeds *via* the pathway of **1**→**2**→**3**→**4**.[1]

The treatment of **2** with acetamidine at 0°C in the absence of methanol, followed by neutralization with hydrogen chloride, gave another hydrochloride, whose elementary analytical data agreed with those of the hydrochloride of **4**. This hydrochloride showed the characteristic band due to a non-conjugate nitrile group in the IR spectrum and was quickly converted into **4** upon neutralization. Therefore, it was identified as the hydrochloride of **3**. The UV spectrum, showing an absorption maximum similar to that of acetamidine hydrochloride, and the NMR, showing the presence of an acetal group, a CH_2–$\underset{|}{\overset{|}{C}}$–H moiety, and a C-methyl group, also supported the structure. The fast reactions of **2**→**3** and **3**→**4** suggested that the step, **1**→**2**, was rate-determining in the first step. The fact that **2** was hardly detected in the tlc of the reaction of **1** with acetamidine also supported this idea.

The heating of **4** in the absence of acetamidine, followed by hydrolysis, gave **9** in a 25% yield. This means the existence of the reverse reaction of **4**, that is **4**→**3**→**2**+acetamidine, which reacted with **4**. Therefore, the first step, **1**→**4**, should be expressed as follows: **1**⇌**2**⇌**3**⇌**4**.

A minor product (**20**) was isolated from the above reaction. The analytical data and mass spectrum determined that it was a dimeric substance, $C_{14}H_{22}N_6O_2 \cdot HCl$, which was thought to be formed from the dimerization of **4** by the elimination of two moles of methanol. The compound **20** was also detected in the reaction of **1** or **4** with acetamidine to a limited extent. Studies of the structure of **20** will be reported separately.

A small amount of **13** was newly obtained from the reaction of **1** with acetamidine. However, it was not isolated from the reaction of **4**. This fact suggested that **13** was formed *via* the pathway of **1**→**12**→**13**. Consequently, the existence of an equilibrium **1**⇌**12** under basic conditions due to the presence of an acetamidine base was confirmed.

On the basis of above facts, the reaction process of **1** with acetamidine should be **1**⇌**2**⇌**3**⇌**4**→**8**, in which

$$\begin{array}{ccc} \mathbf{1} & \rightleftarrows & \mathbf{2} \\ \Downarrow & & \\ \mathbf{12} & \rightarrow & \mathbf{13} \end{array} \qquad \begin{array}{ccc} \rightleftarrows & \mathbf{3} & \rightleftarrows & \mathbf{4} & \rightarrow & \mathbf{8}, \\ & & & \downarrow & & \\ & & & \mathbf{20} & & \end{array}$$

1→**2**→**3**→**4**→**8** is most important.

10) S. Mizukami and E. Hirai, *ibid.*, **14**, 1321 (1966).

11) R. H. Bible, "Interpretation of NMR Spectra," Plenum Press, New York (1965), p. 16.

The second step, **4**→**8**, presented further interesting problems. For this step, two pathways route A (**4**→**21**→**8**) and route B (**4**→**5**→**6**→**8**), are possible (see Chart 1). If the reaction proceeds *via* route A, the reaction of **4** with methyl acetimidate can be expected to give **8** in a yield similar to that in the reaction with acetamidine.[8,12] However, the yield of **8** in the reaction with acetimidate was only 17%, which was similar to that from the reverse reaction of **4**. Further, the starting materials were recovered from the reaction of **18** or its phenyl analog **22**[13] with acetamidine. No transaminated compounds, such as **23** and **24**, were obtained from either reaction. Therefore, the possibility of the reaction pathway *via* route A was excluded.

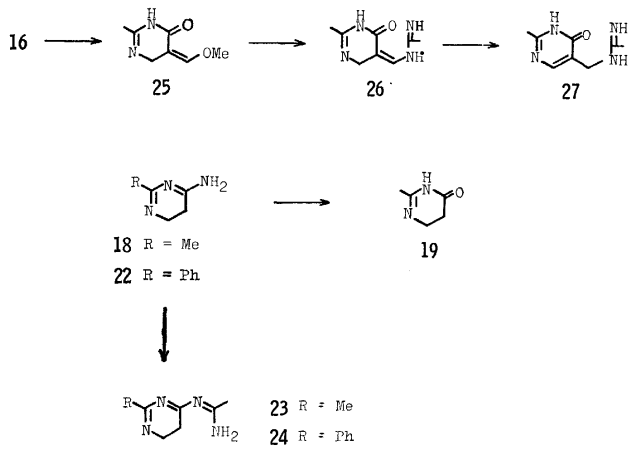

Chart 3

To examine the possibility of the pathway *via* route B, the reaction of a deaminated compound, **16**, was attempted. When treated with acetamidine in methanol at reflux temperature, **16** gave **27**, which was then purified as its dihydrochloride, $C_8H_{12}N_4O \cdot 2HCl$. The spectral data suggested that it was 2-methyl-3*H*-4-oxo-5-acetamidinomethylpyrimidine. The UV spectrum showed the characteristic band due to 2-methyl-4-hydroxypyrimidines in acidic or in alkaline media,[14,15] while the NMR spectrum showed signals due to methyl groups at C_2 position, and at the acetamidino moiety, the 5-methylene group and the pyrimidine-ring proton. It is quite natural to consider that the reaction of **16** proceeds *via* the pathway of **16**→**25**→**26**→**27**. Consequently, route B can be proposed as a reliable pathway. If this idea is probable, **16** and **4** can be said to react with acetamidine at comparable rates. By heating a mixture of one mole each of **4**, **16**, and acetamidine in methanol, **8** and **27** were formed in a 1 : 1 ratio, as expected. Therefore, the second step was confirmed to proceed *via* route B.

Two more pathways can be proposed for the final step of route B. One is route C (**6**→**11**→**8**), and the other is route D (**6**→**7**→**8**) (see Chart 1). For the determination of the predominant pathway, the reaction of **4** with propioamidine was carried out, in

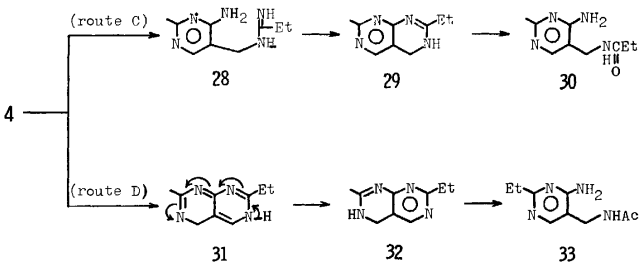

Chart 4

which the reaction product **29** should be formed when the reaction proceeds *via* route C, and **32**, when it proceeds *via* route D (see Chart 4). Both products, **29** and **32**, were easily identified by hydrolysis to 5-propioamidomethylpyrimidine (**30**) and 5-acetamidomethylpyrimidine (**33**) respectively. The heating of **4** and propioamidine in methanol, followed by hydrolysis, gave a mixture of the two pyrimidines in high yields. The major pyrimidine was isolated in a pure state. As the NMR spectrum showed a 3-proton singlet due to an acetyl methyl group, the major one was identified as **33**. The remaining signals also supported the structure; signals due to the ethyl group and singlets due to the methylene group and the pyrimidine-ring proton were observed. The attempt to isolate the minor pyrimidine was unsuccessful because of its low yield and because its solubilities are similar to those of **33**. However, it was identified as **30** by a comparison of the retention times in the gas chromatograms. The authentic sample of **30** was prepared by the propionylation of **10**. The relative ratio of **30** and **33** was about 8 : 92, as determined by gas chromatography. This result clearly revealed that route D is predominant. The existence of a minor route, C, was also supported by the isolation of **11** from a reaction mixture of **1** and acetamidine, though its yield was very poor. Proof of the structure of **11** was provided by a comparison of the IR and mass spectra of an authentic sample, which was prepared by the reaction of **10**[7] with methyl acetimidate.

The presence of an acid, usually acetamidine hydrochloride, was desirable for the accelation of the second step **4**→**8**. This fact seemed to suggest that the elimination of methanol, **4**→**5**, was the rate-determining step. A detailed discussion on the reaction mechanism will be presented kinetically in a following paper.

In conclusion, the reaction of **1** with acetamidine has been established to proceed *via* the major pathway of **1**⇌**2**⇌**3**⇌**4**→**5**→**6**→**7**→**8**, along with the minor one of **6**→**11**→**8** and two side pathways of **1**→**12**→**13** and **4**→**20**.

Experimental

All the melting points were recorded on a Kofler block and have been uncorrected. The NMR spectra were taken with a Varian A-60-A spectrometer, using tetramethylsilane as the internal reference; the chemical shifts were expressed in δ unit (s: singlet, d: doublet, t: triplet, q: quartet, m: multiplet, bs: broad singlet). The UV spectra were observed in methanol. The solvents used were removed under a reduced pressure. The percentages of methanolic sodium methoxide and hydrogen chloride are shown in w/w and the ratios of solvent systems used for the purification, in v/v.

12) T. Matsukawa, *Yakugaku Zasshi*, **62**, 417 (1942).
13) S. Pietra, *Boll. Sci. Fac. Chim. Ind. Bologna*, **11**, 78 (1953).
14) Ref. 3, p. 492.
15) A. Takamizawa, *Yakugaku Zasshi*, **74**, 756 (1954).

2-Methyl-4-amino-5-dimethoxymethyl-5,6-dihydropyrimidine (4). *(1) Isolation as Its Hydrochloride (4·HCl)*: 2-Dimethoxymethyl-3-methoxypropionitrile (**1**; 147 g) was added to an acetamidine solution, prepared from acetamidine hydrochloride (256 g) and 22% methanolic sodium methoxide (697 g), after which the solution was kept at 55°C. After 1 hr, 30% methanolic hydrogen chloride (220 g) was added to the solution below 10°C. After the concentration of the solution to 450 g, crystals appeared; they were collected by filtration. The repeated recrystallization of the crystals from methanol-ether (9: 1) gave cubics of **4·HCl** (89.7 g), mp 155—160°C (decomp.). UV: 278 (ε 11500); (+NaOH) 262 mμ (ε 7500). Found: C, 43.32; H, 7.45; N, 18.78%. Calcd for $C_8H_{15}N_3O_2\cdot HCl$: C, 43.34; H, 7.28; N, 18.95%.

(2) Reaction with Acetamidine: *(i) Isolation of the Product*: To a solution of sodium (517 mg) in methanol (20 m*l*), we added hydrochlorides of acetamidine (2.125 g) and **4** (1.662 g). The solution was refluxed for 4 hr, filtered from precipitated sodium chloride, and then evaporated to dryness. A solution of the residue in water (5 m*l*) was heated on a boiling-water bath for 1 hr and then evaporated to dryness. The recrystallization of the residue from water gave 2-methyl-4-amino-5-acetamidomethylpyrimidine (**9**; 652 mg); mp 208—209°C.[6]

(ii) Effect of the Presence of Acetamidine Hydrochloride: (a) Hydrochlorides of acetamidine (283 mg) and **4** (321 mg) were added to 6 m*l* of methanolic sodium methoxide [a methanol solution (20 m*l*) containing sodium (431 mg)]. The solution was diluted to 20 m*l* with methanol and then refluxed for 1.5 hr. The yield of **8** was 35%, which was determined using the absorption maximum of **8** at 310 mμ in the UV spectrum. (b) Hydrochlorides of acetamidine (425 mg) and **4** (329 mg) were dissolved in 10 m*l* of methanolic sodium methoxide [a methanol solution (50 m*l*) containing sodium (517 mg)] and then diluted to 20 m*l* with methanol. The solution was refluxed for 1.5 hr, after which the yield of **8** was determined. The yield was 76%.

(3) Dehydrogenation with p-Quinone: The hydrochloride (**4·HCl**, 4.42 g) was neutralized with methanolic sodium methoxide, which had been prepared from sodium (460 mg) and methanol (10 m*l*). The methanol solution was shaken for a few minutes, and quickly filtered from the precipitated sodium chloride, and the methanol was removed. To a benzene solution (250 m*l*) of the residue, we then added *p*-quinone (2.5 g) dissolved in benzene (20 m*l*), after which the solution was refluxed for 3 hr. After cooling, the insoluble materials were eliminated by decantation. The benzene layer was washed with 1N sodium hydroxide (10 m*l*×2) and water (10 m*l*×1), and dried, and the solvent was removed. The subsequent recrystallization of the residue from benzene and *n*-hexane gave 2-methyl-4-amino-5-dimethoxymethylpyrimidine (**15**, 53 mg), mp 107—108°C.[10]

(4) Hydrolysis: 21% Methanolic hydrogen chloride (890 mg) was added to a solution of **4·HCl** (1.1 g) in methanol (20 m*l*) containing water (90 mg) at −30°C. The solution was kept at 0°C for 2 hr, and then the solvent was removed. The recrystallization of the residue gave the hydrochloride of 2-methyl-3*H*-4-oxo-5-dimethoxymethyl-5,6-dihydropyrimidine (**16**) as needles; mp 212—213°C (decomp.). The yield was 816 mg. UV: 228 (ε 6500); (+NaOH) 220 mμ. NMR (DMSO-d_6): 4.75 (d, 1H, C$\underline{H}$(OMe)$_2$, J=4 Hz), 3.37 (s, 6H, OMe), 3.1—3.4 (m, 1H, H_5), 3.6—3.8 (m, 2H, H_6), 2.23 (bs, 3H, –C(–)–Me). Found: C, 43.38; H, 6.34; N, 12.48%. Calcd for $C_8H_{14}N_2O_3\cdot HCl$: C, 43.15; H, 6.74; N, 12.58%.

(5) Reaction with Methylamine: The hydrochloride of **4** (395 mg) was neutralized with methanolic sodium methoxide, which had been prepared from sodium (41 mg) and methanol (17 m*l*). To the solution we then added methylamine (4.6 g) in methanol (30 m*l*). The mixture was kept at room temperature for 2 days, neutralized with 1% methanolic hydrogen chloride (3.5 g), and filtered from the precipitates, and the solvent was removed. The residue was extracted with chloroform. The subsequent removal of the chloroform gave the syrup of 2-methyl-4-methylamino-5-dimethoxymethyl-5,6-dihydropyrimidine hydrochloride (**17·HCl**; 318 mg). No satisfactory elementary analysis was obtained for **17·HCl** because of its hydroscopicities, but the UV and NMR data supported the structure. UV: 280; (+NaOH) 260 mμ. NMR (methanol-d_4): 4.55 (d, 1H, –C$\underline{H}$(OMe)$_2$, J=7 Hz), 3.7—3.5 (m, 2H, H_6), 3.40 (s, 6H, OMe), 3.08 (s, 3H, N–Me), 2.25 (t, 3H, C–Me, $J\fallingdotseq$1 Hz).

(6) Treatment with Sodium Methoxide: The hydrochloride of **4** (1.88 g) was neutralzed with methanolic sodium methoxide, which had been prepared from sodium (1.67 g) and methanol (26 m*l*), and then the solution was refluxed. After 8 hr, the solution was neutralized with methanolic hydrogen chloride, filtered from precipitated sodium chloride, and evaporated to dryness. The residue was chromatographed on silica gel (Wakogel Q-23, 100—200 mesh, 40 g). Elution with acetone (100 m*l*) and, subsequently, with acetone-methanol (20: 1, 400 m*l*) gave 2-methyl-4-amino-5-methoxymethylpyrimidine (**13**, 913 mg), mp 118—120°C.[16]

(7) Reverse Reaction (The Formation of 8 and 20): A solution of **4·HCl** (590 mg) was added to a sodium methoxide solution, which had been prepared from sodium (46 mg) and methanol (6 m*l*), and then the mixture was warmed at 60°C for 7 hr. After cooling, the solution was filtered from precipitated sodium chloride and the solvent was removed. The yellow residue was chromatographed over alumina (Wako activated alumina, 300 mesh, 9.2 g). Elution with ethyl acetate-benzene-methanol (2: 1: 1) gave **8** (144 mg) as the first fraction (500 m*l*), a mixture of **8** and **20** (285 mg) as the second one (300 m*l*), and **8** (133 mg) as the third one (30 m*l*). The second crop was further chromatographed over the alumina (10 g). Elution with benzene-methanol (50: 1, 100 m*l*) gave **8** (54 mg), while subsequent elution with benzene-methanol (25: 1, 100 m*l*) gave **20** (153 mg). This **20** was purified by recrystallization from methanol and ethyl acetate. Mp 208—210°C (decomp.). MS 306 (M^+). Found: C, 49.04; H, 6.65; N, 24.36; Cl, 10.63%. Calcd for $C_{14}H_{22}N_6O_2\cdot HCl$: C, 49.13; H, 6.78; N, 24.58; Cl, 10.37%.

(8) Reaction with Methyl Acetimidate: i) Hydrochlorides of methyl acetimidate (3.28 g) and **4** (2.217 g) were added to methanolic sodium methoxide, which had been prepared from sodium (690 mg) and methanol (20 g). After the removal of the precipitated sodium chloride by filtration, the total weight of the filtrate was made to 21 g by adding methanol, and then the solution was refluxed. The reaction mixture was quenched with acetic acid, and the yield of **8** was determined by gas chromatography (30% Apiezon grease L; column temperature, 236.5°C; flow rate, 90 m*l*/min; carrier gas, He; retention time of **8**, 2.2 min) as follows: 13.1% (after 0.5 hr), 13.1% (after 2 hr), and 13.1% (after 3 hr). ii) Hydrochlorides of methyl acetimidate (1.64 g) and **4** (1.11 g) were neutralized with a sodium methoxide solution, which had been prepared from sodium (450 mg) and methanol (15 m*l*). The mixture was worked up in a way similar to the above. The yield of **8** was 16.7% (after 1 hr) and 13.3% (after 2 hr).

(9) Reaction with Propioamidine: A solution of sodium methoxide in methanol, which had been prepared from

16) A. Takamizawa and R. Maeda, *ibid.*, **74**, 746 (1954).

sodium (138 mg) and methanol (6 ml), was added to a mixture of hydrochlorides of propioamidine (651 mg) and **4** (443 mg) and then quickly filtered from the precipitated sodium chloride. The filtrate was refluxed for 5 hr and then evaporated to dryness. To the residue we added water (8 ml), after which the aqueous solution was heated on a boiling-water bath for 1 hr. The removal of the water gave syrupy crystals (1.01 g) of a mixture of 2-methyl-4-amino-5-propioamidomethyl- (**30**) and 2-ethyl-4-amino-5-acetamidomethylpyrimidine (**33**). The relative ratio of **30** and **33** was 8:92, which was determined by means of the peak height in the gas chromatogram (4% polyethyleneglycol 20M; column temperature, 240°C; flow rate, 100 ml/min; carrier gas, He; retention time, **30**: 13 min and **33**: 11 min). After a part of the syrupy crystals (120 mg) had been used for gas-chromatographic analysis, the crystals were collected by filtration. The subsequent recrystallization of the crystals from acetone gave leaflets of **33** (111 mg); mp 206.5—207.5°C. UV: 236 (ε 8900), 275 (ε 5400); (+HCl) 251 mμ. NMR (methanol-d_4): 7.93 (s, 1H, H_6), 4.28 (s, 2H, $-CH_2-$), 2.69 (q, 2H), 1.23 (t, 3H) (C_2H_5, J=7 Hz), 1.93 (s, 3H, CH_3CO). Found: C, 55.87; H, 7.07; N, 28.68%. Calcd for $C_9H_{14}N_4O$: C, 55.65; H, 7.27; N, 28.85%.

The mother liquors of the filtration of the syrupy crystals and the recrystallization of **33** were combined, and the combined solution was evaporated to dryness. The residue was chromatographed over the alumina (12 g). Elution with benzene-methanol (50:3, 100 ml) gave **33** (180 mg), while further elution with the same solvent-system gave a syrup (170 mg) which contained **30** and/or **33** (46.5 mg), as determined by studying UV spectrum.

*2-Methyl-4-amino-5-propionylamidomethylpyrimidine (**30**).* Freshly-distilled propionyl chloride (750 mg) was added to a solution of 2-methyl-4-amino-5-aminomethylpyrimidine (**10**; 850 mg)[7] in pyridine under cooling, and the mixture was kept in a refrigerator overnight. The solvent was then removed. The residue was neutralized with N sodium hydroxide and then evaporated to dryness. The recrystallization of the residue from acetone gave needles of **30** (320 mg); mp 181°C. UV: 236 (ε 11400), 275 (ε 7100); (+HCl) 250 mμ. NMR (chloroform-d): 7.80 (s, 1H, H_6); 4.30 (s, 1H), 5.82 (s, 1H) ($-CH_2-$); 2.25 (q, 2H, J=7.3 Hz), 1.25 (t, 3H) (C_2H_5-). Found: C, 55.66; H, 7.29; N, 28.67%. Calcd for $C_9H_{14}N_4O$: C, 55.65; H, 7.25; N, 28.85%.

*2-Dimethoxymethyl-3-acetamidinopropionitrile (**3**).* *(1) Isolation*: Acetamidine hydrochloride (4.2 g) was added to a solution of sodium (0.95 g) in methanol (20 ml); the mixture was shaken and quickly filtered from the precipitated sodium chloride, and then the methanol was removed. Under stirring, 2-dimethoxymethylacrylonitrile (**2**; 3 g) was added drop by drop, to a solution of the residue in 1,2-dimethoxyethane (17 ml) at 0°C. After 3 hrs' stirring, the solution was kept in a refrigerator for 2 days and then neutralized with 30% methanolic hydrogen chloride (4.5 g). The crystals which appeared (5.4 g) were collected by filtration and recrystallized from ethanol. Cubics of the hydrochloride of **3** (2.97 g) were obtained; mp 144—146°C. UV: 206 mμ (ε 6170). IR_{KBr}: 2256 cm^{-1} (non-conjugate nitrile). NMR (methanol-d_4): 2.32 (s, 3H, C–CH_3), 3.8—3.14 (m, 3H, CH_2–CH), 4.70 [d, 1H, CH(OMe)$_2$, J=5 Hz], 3.51 (s, 6H, C(OMe)$_2$]. Found: C, 43.16; H, 7.08; N, 19.00%. Calcd for $C_8H_{15}N_3O_2\cdot HCl$: C, 43.34; H, 7.28; N, 18.95%.

*(2) Cyclization to **4***: The hydrochloride of **3** (350 mg) was neutralized with methanolic sodium methoxide, prepared from sodium (46 mg) and methanol (5 g), and kept at room temperature for 2 hr. The solution was neutralized with 36% methanolic hydrogen chloride (300 mg) and filtered from the precipitated sodium chloride, and then the methanol was removed. The recrystallization of the residue (511 mg) from ether and methanol gave **4**·**HCl** (200 mg).

*2-Methyl-4-amino-5-acetamidinomethylpyrimidine (**11**).* *(1) Isolation*: Acetamidine hydrochloride (20 g) and **1** (26 g) were added to methanolic sodium methoxide, which had been prepared from sodium (3.68 g) and methanol (58 ml), and the mixture was stirred at 43°C for 3 hr. After cooling, 43% methanolic hydrogen chloride (9.2 g) was added to the solution. The yellow crystals which appeared were collected by filtration and washed with ethyl acetate (100 ml). The residue was dissolved with hot methanol, and the methanol solution was cooled to 0°C. The precipitates (the monohydrochloride of **11**) were collected by filtration and washed with a small portion of methanol. The yield was 134 mg; mp 246—250°C (decomp.). UV: 233 (ε 10900), 273 (ε 4930); (+HCl) 246 mμ. MS: 179 (M^+), 162 (M^+-NH_3), 122 ($M^+-NH-\overset{NH}{\overset{\|}{C}}-Me$). Found: C, 44.26; H, 6.68; N, 31.75%. Calcd for $C_8H_{13}N_5\cdot HCl$: C, 44.55; H, 6.54; N, 32.47%.

(2) Synthesis: A solution of 2-methyl-4-amino-5-aminomethylpyrimidine (**10**, 13.8 g)[7] in methanol (30 ml) was added, drop by drop and over a 20-min period, to a solution of methyl acetimidate hydrochloride (11 g) in methanol (5 ml) at 15°C. After stirring at 15°C for 1 hr, precipitates which appeared (the monohydrochloride of **11**) were collected by filtration and washed with a mixture of methanol (9 ml) and pyridine (5 ml). The yield was 870 mg; mp 246—250°C (decomp.).

*Reaction of 2-Methyl-4-amino-5,6-dihydropyrimidine (**18**) with Acetamidine.* (1) Acetamidine hydrochloride (473 mg) and **18** (556 mg)[1] were added to a solution of sodium methoxide, prepared from sodium (115 mg) and methanol (14 g), and then filtered from the precipitated sodium chloride. The solution was refluxed for 4 hr and then evaporated to dryness. The residue was extracted with acetonitrile (100 ml), and the acetonitrile was removed. The recrystallization of the residue from acetonitrile gave **18** (113 mg).

(2) A solution of acetamidine hydrochloride (945 g) and **18** (555 mg) in methanol (5 ml) was refluxed for 4 hr. The UV spectrum of the reaction mixture showed only the characteristic band due to the hydrochloride of **18**.

*Reaction of 2-Phenyl-4-amino-5,6-dihydropyrimidine (**22**) with Acetamidine.* A solution of acetamidine hydrochloride (510 mg) and **22** (467 mg)[13] in methanol (5 g) was refluxed for 5 hr. The UV spectrum of the reaction mixture showed only the characteristic band due to the hydrochloride of **22**.

*Reaction of 2-Methyl-3H-4-oxo-5-dimethoxymethyl-5,6-dihydropyrimidine (**16**) with Acetamidine.* Hydrochlorides of **16** (550 mg) and acetamidine (630 mg) were added to methanolic sodium methoxide, prepared from sodium (204 mg) and methanol (20 ml), and then filtered from the sodium chloride thus precipitated. The solution was refluxed for 2 hr and then evaporated to dryness. The recrystallization of the residue from ethanol gave needles of 2-methyl-4-hydroxy-5-acetamidinomethylpyrimidine (**27**; 250 mg), (mp 218—238°C (decomp.)), which was subsequently purified as its dihydrochloride (mp 197—202°C (decomp.)). UV: 207 (ε 9000), 220 (shoulder), 278 (ε 5540); (+HCl) 224, 262; (+NaOH) 232, 262 mμ. NMR (methanol-d_4): 8.13 (s, 1H, H_6), 4.39 (s, 2H, $-CH_2-$), 2.28 (s, 3H, >C–Me), 2.68 (s, 3H, 2-Me). Found: C, 38.01; H, 5.67; N, 22.26; Cl, 28.70%. Calcd for $C_8H_{12}N_4O\cdot 2HCl$: C, 37.95; H, 5.53; N, 22.13; Cl, 28.01%.

*Reaction of 2-Methyl-4-amino-5-dimethoxymethyl- (**4**) and 2-Methyl-3H-4-oxo-5-dimethoxymethyl-5,6-dihydropyrimidine (**16**) with Acetamidine.* Hydrochlorides of **4** (372 mg), **16**

(372 mg) and acetamidine were added to a solution of sodium methoxide, which had been prepared from sodium (157 mg) and methanol (10 m*l*) and the mixture was refluxed for 5 hr. After cooling, the solution was filtered from the precipitated sodium chloride and then evaporated to dryness. A mixture of **8** and **27** was obtained as a yellow powder (708 mg). The relative ratio of **8** and **27** was about 1: 1, as determined from the NMR spectrum of the mixture in methanol-d_4. Singlets due to the methylene group of **8** at 4.95 and to that of **27** at 4.18 δ were used for the determination.

*Isolation of 2-Methyl-4-amino-5-methoxymethylpyrimidine (**13**) from the Reaction of 2-Dimethoxymethyl-3-methoxypropionitrile (**1**) with Acetamidine.* To methanolic sodium methoxide, prepared from sodium (0.64 g) and methanol (7 m*l*), we added **1** (1.6 g). The solution was refluxed for 4 hr, filtered from the precipitated sodium chloride, and then evaporated to dryness. The aqueous solution (6 m*l*) of the residue was warmed at 100°C for 1 hr and then evaporated to dryness. 48% Sodium hydroxide (3 g) was added to the residue, and the crystals which appeared were collected by filtration and washed with water and then with ethyl acetate. The evaporation of the ethyl acetate gave syrupy crystals, from which **13** was isolated by preparative tlc (a silica gel plate, chloroform-ethyl acetate, 1: 1). The recrystallization of crude **13** from benzene gave a pure product 141 mg); mp 118—120°C.[16]

The authors wish to express their deep gratitude to Professor Toshihiko Okamoto, the University of Tokyo, for his interest.

BULLETIN OF THE CHEMICAL SOCIETY OF JAPAN, VOL. 45, 2015—2018(1972)

The Reaction of Aspartyl Dipeptide Esters with Ketones

Yasuo ARIYOSHI and Naotake SATO

Central Research Laboratories, Ajinomoto Co., Inc., Suzuki-cho, Kawasaki, Kanagawa

(Received December 18, 1971)

The methyl and ethyl esters of α-L-aspartyl-L-phenylalanine (I and II), -L-tyrosine (III and IV), -L-(β-cyclohexyl)alanine (V and VI), and -L-[β-(4-hydroxycyclohexyl)]alanine (VII and VIII) have been found to react with ketones (acetone, methyl ethyl ketone, and cyclohexanone), in the absence of any catalysts, to give the corresponding 4-imidazolidinone derivatives (XVII—XXX). The NMR spectra of the imidazolidinones with an aromatic side chain (XVII—XXVIII) have indicated that these compounds exist in the folded conformation (in which the aromatic ring faces the imidazolidinone ring) in the solution. The imidazolidinones (XVII—XXX) were hydrolyzed with hot water to give the peptide esters (I—VIII), all in their original optical purity. On the other hand, the β-isomers of the peptide esters (IX—XVI) did not react with these ketones under the same conditions. These characteristics were used successfully in the separation of the two structural isomers of these peptide esters.

The methyl and ethyl esters of α-L-aspartyl-L-phenylalanine (I and II), -L-tyrosine (III and IV), -L-(β-cyclohexyl)alanine (V and VI), and -L-[β-(4-hydroxycyclohexyl)]alanine (VII and VIII) all have a sweet taste very similar to that of sucrose, and they have recently become well known as sweetening agents.[1,2]

In the course of studies of these sweet peptides, it was found that the dipeptide esters (I—IV) readily reacted with ketones, such as acetone, methyl ethyl ketone, and cyclohexanone, in the absence of any catalysts, to give crystalline 4-imidazolidinone derivatives (XVII—XXVIII) (Fig. 1 and Table 2). However, most of the reactions of the hexahydroderivatives (V—VIII), obtained by the hydrogenation of the aromatic rings of the corresponding dipeptide esters (I—IV) with hydrogen and platinum catalyst, with these ketones gave oily products. Among them, only the reactions of V and VI with acetone gave analytically pure crystalline products (XXIX and XXX). Similar reactions have been observed in the cases of carbobenzoxyamino acid amides,[3] ampicillin,[4] and oxytocin.[5]

The structures of the reaction products (XVII—XXX) were determined on the basis of their analytical and spectral data and their chemical behavior. The results of the elemental analyses of the reaction products were in agreement with the values calculated for the imidazolidinones (XVII—XXX) (Table 2). The IR spectra of the imidazolidinones containing the phenylalanyl or the β-cyclohexylalanyl residue (XVII—XXII, XXIX, and XXX) showed two carbonyl absorptions at 1740—1750 cm^{-1} (ester) and at 1700—1703 cm^{-1} (a composite band of the amide and carboxyl groups), whereas the imidazolidinones containing the tyrosyl residue (XXIII—XXVIII) showed two carbonyl absorptions at 1720—1725 cm^{-1} (a composite band of the ester and carboxyl groups) and 1695 cm^{-1} (amide). All of these imidazolidinones (XVII—XXX) lacked amide-II absorptions of the starting materials in the region of 1500—1600 cm^{-1}.

1) R. H. Mazur, J. M. Schlatter, and A. H. Goldkamp, *J. Amer. Chem. Soc.*, **91**, 2684 (1969).
2) J. M. Schlatter, German Pat., 1936159 (1970).
3) U. Zehavi and D. Ben-Ishai, *J. Org. Chem.*, **26**, 1097 (1961).
4) G. A. Hardcastle, Jr., D. A. Johnson, and C. A. Panetta, *ibid.*, **31**, 897 (1966).
5) V. J. Hruby, D. Yamashiro, and V. du Vigneaud, *J. Amer. Chem. Soc.*, **90**, 7106 (1968).

Table 1. Dipeptide esters used in this experiment

Compound	Mp °C	$[\alpha]_D$ (water)	Found %			Calcd %				Lit	
			C	H	N	Formula	C	H	N	Mp °C	$[\alpha]_D$ (water)
I	235—236	+32.0[a]	55.47	6.21	9.35	$C_{14}H_{18}O_5N_2 \cdot 1/2H_2O$	55.44	6.31	9.24	246—247[1),b)]	0[1),b)]
II	236—237	+25.0[a]	56.73	6.89	8.62	$C_{15}H_{20}O_5N_2 \cdot 1/2H_2O$	56.77	6.67	8.83	244—246[1)]	−6[1),c)]
III	173—174	+5.5	54.40	6.14	8.91	$C_{14}H_{18}O_6N_2$	54.19	5.85	9.03	180—185[1)]	+4[1)]
IV	174—175	+5.0	55.93	6.43	8.47	$C_{15}H_{20}O_6N_2$	55.55	6.22	8.64	189—190[1)]	+20[1),d)]
V	119—120	−10.5	51.49	8.58	8.41	$C_{14}H_{24}O_5N_2 \cdot 3/2H_2O$	51.36	8.31	8.56	130—137[2)]	−13.5[2)]
VI	117—118	−17.0	55.54	8.64	8.49	$C_{15}H_{26}O_5N_2 \cdot 1/2H_2O$	55.71	8.42	8.66		
VII	149—150	−11.5	53.48	7.84	8.69	$C_{14}H_{24}O_6N_2$	53.15	7.65	8.86	101—135[2)]	−12.5[2)]
VIII	102—105	−15.5	54.77	7.96	8.42	$C_{15}H_{26}O_6N_2$	54.53	7.93	8.48		
IX	198—199	+40.5[a]	55.37	6.43	9.31	$C_{14}H_{18}O_5N_2 \cdot 1/2H_2O$	55.44	6.31	9.24	196—197[1)]	+4[1)]
X	182—183	+1.0	55.12	6.99	8.74	$C_{15}H_{20}O_5N_2 \cdot H_2O$	55.20	6.80	8.58		
XI	197—198	+14.5	54.37	5.93	9.13	$C_{14}H_{18}O_6N_2$	54.19	5.85	9.03	202—204[1)]	+13[1)]
XII	200—205	+10.5	52.62	6.34	7.90	$C_{15}H_{20}O_6N_2 \cdot H_2O$	52.62	6.48	8.18		
XIII	164—165	−30.0	55.54	8.61	8.08	$C_{14}H_{24}O_5N_2 \cdot C_2H_5OH$	55.47	8.78	8.09		
XIV	188—189	−26.5	55.49	8.17	8.74	$C_{15}H_{26}O_5N_2 \cdot 1/2H_2O$	55.71	8.42	8.66		
XV	75— 85	−25.5	53.60	7.59	8.89	$C_{14}H_{24}O_6N_2$	53.15	7.65	8.86		
XVI	127—130	−28.5	54.64	8.11	8.24	$C_{15}H_{26}O_6N_2 \cdot 1/2C_2H_5OH$	54.37	8.27	7.93		

a) Measured in acetic acid. b) Ref. 10, mp 246—247°, $[\alpha]_D$ −2.3 (nHCl). c) Methanol. d) 75% Acetic acid.

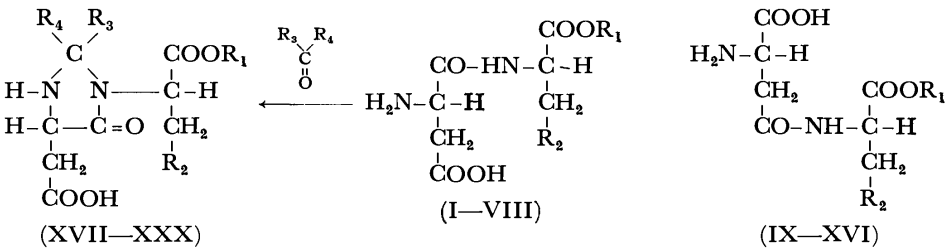

(XVII—XXX) (I—VIII) (IX—XVI)

Dipeptide	R_1	R_2	Dipeptide	R_1	R_2
I	CH_3	C_6H_5	IX	CH_3	C_6H_5
II	C_2H_5	C_6H_5	X	C_2H_5	C_6H_5
III	CH_3	C_6H_5O	XI	CH_3	C_6H_5O
IV	C_2H_5	C_6H_5O	XII	C_2H_5	C_6H_5O
V	CH_3	C_6H_{11}	XIII	CH_3	C_6H_{11}
VI	C_2H_5	C_6H_{11}	XIV	C_2H_5	C_6H_{11}
VII	CH_3	$C_6H_{11}O$	XV	CH_3	$C_6H_{11}O$
VIII	C_2H_5	$C_6H_{11}O$	XVI	C_2H_5	$C_6H_{11}O$

Imidazolidinone	R_1	R_2	R_3	R_4
XVII	CH_3	C_6H_5	CH_3	CH_3
XVIII	CH_3	C_6H_5	CH_3	C_2H_5
XIX	CH_3	C_6H_5	$(CH_2)_5$	
XX	C_2H_5	C_6H_5	CH_3	CH_3
XXI	C_2H_5	C_6H_5	CH_3	C_2H_5
XXII	C_2H_5	C_6H_5	$(CH_2)_5$	
XXIII	CH_3	C_6H_5O	CH_3	CH_3
XXIV	CH_3	C_6H_5O	CH_3	C_2H_5
XXV	CH_3	C_6H_5O	$(CH_2)_5$	
XXVI	C_2H_5	C_6H_5O	CH_3	CH_3
XXVII	C_2H_5	C_6H_5O	CH_3	C_2H_5
XXVIII	C_2H_5	C_6H_5O	$(CH_2)_5$	
XXIX	CH_3	C_6H_{11}	CH_3	CH_3
XXX	C_2H_5	C_6H_{11}	CH_3	CH_3

Fig. 1. Dipeptides and 4-imidazolidinones

When the NMR spectra of the compounds with an aromatic side chain (XVII—XXVIII) were measured in acetone-d_6 or dimethyl sulfoxide-d_6, the protons of one of the two alkyl groups on the C-2 carbon were found to be shifted to a higher field (appearing at δ 0.4—0.6 ppm) by the magnetic shielding effect of the aromatic ring; for example, the H_a and H_b protons of the 2,2-dimethyl group of XVII appeared at δ 0.57 ppm (3H, singlet) and δ 1.33 ppm (3H, singlet) respectively in acetone-d_6, whereas the corresponding six protons of the hexahydroderivative (XXIX) were found at δ 1.45 ppm as a singlet. The two protons on the β-carbon atom of the aspartyl residue of XVII were almost unaffected (Fig. 2). Therefore, this shift suggests that

Table 2. 4-Imidazolidinones

Compound	Yield %	Mp °C	Found %			Calcd %			
			C	H	N	Formula	C	H	N
XVII	61	145[a)]	60.91	6.80	8.24	$C_{17}H_{22}O_5N_2$	61.06	6.63	8.38
XVIII	67	140[a)]	62.17	7.18	8.05	$C_{18}H_{24}O_5N_2$	62.05	6.94	8.04
XIX	81	207—208[b)]	64.08	7.18	7.50	$C_{20}H_{26}O_5N_2$	64.15	7.00	7.48
XX	34	142[a,b)]	62.06	6.98	8.13	$C_{18}H_{24}O_5N_2$	62.05	6.94	8.04
XXI	22	138—139[a)]	62.88	7.33	7.78	$C_{19}H_{26}O_5N_2$	62.96	7.23	7.73
XXII	54	171—172[b)]	64.95	7.49	7.25	$C_{21}H_{28}O_5N_2$	64.93	7.27	7.21
XXIII	95	139.5—140[b)]	58.30	6.64	7.70	$C_{17}H_{22}O_6N_2$	58.27	6.33	8.00
XXIV	54	169[b)]	59.45	6.67	7.72	$C_{18}H_{24}O_6N_2$	59.33	6.64	7.69
XXV	84	191.5[b)]	61.23	6.95	7.10	$C_{20}H_{26}O_6N_2$	61.52	6.71	7.18
XXVI	67	151[b)]	59.45	6.78	7.53	$C_{18}H_{24}O_6N_2$	59.33	6.64	7.69
XXVII	41	151.5—152.5[b)]	60.28	7.17	7.46	$C_{19}H_{26}O_6N_2$	60.30	6.93	7.40
XXVIII	35	178[b)]	62.39	7.13	6.83	$C_{21}H_{28}O_6N_2$	62.36	6.98	6.93
XXIX	54	114—115	59.96	8.47	8.34	$C_{17}H_{28}O_5N_2$	59.98	8.29	8.23
XXX	45	125—126	60.91	8.35	7.62	$C_{18}H_{30}O_5N_2$	60.99	8.53	7.90

a) Raised rapidly. b) Decomposition.

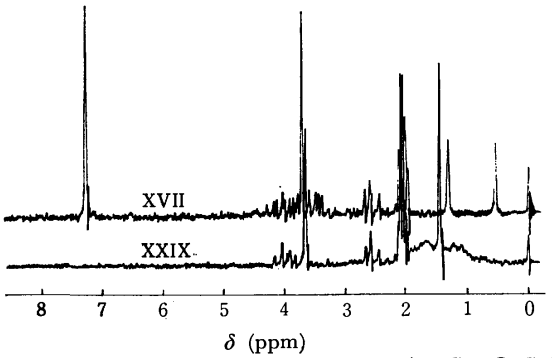

Fig. 2. NMR spectra of XVII and XXIX (in CD_3COCD_3).

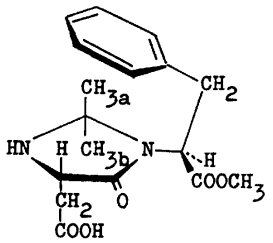

Fig. 3. Preferred conformation of XVII

compound XVII takes the folded conformation, in which the aromatic ring faces the imidazolidinone ring, as is shown in Fig. 3.

In boiling water, all the imidazolidinones except for the spiroderivatives were completely hydrolyzed within twenty minutes to give the corresponding peptide esters in their original optical purity. The spiroderivatives (XIX, XXII, XXV, and XXVIII) were much more stable to hydrolysis. Under the same conditions, they were only partly hydrolyzed to the corresponding peptide esters. Some two hours were required for their complete hydrolysis.

The reactions of the peptide esters (I—VIII) with aldehydes, such as acetaldehyde, propionaldehyde, or isobutylaldehyde, failed to give crystalline products.

The corresponding β-isomers of the peptide esters (IX—XVI), which have a bitter taste, did not react with these ketones under the same conditions. These characteristics were used successfully in the separation of the two structural isomers of these sweet peptide esters. When these peptides were conveniently prepared by the condensation of such *N*-protected aspartic anhydrides as carbobenzoxy-L-aspartic anhydride with the appropriate amino acid esters, followed by deprotection, they were always mixtures of α- and β-aspartyl peptides. Several methods of separating α- and β-aspartyl peptides have been reported, including techniques of fractional extraction,[6] column chromatography,[7] and selective precipitation.[8]

When a mixture of the α- and β-aspartyl peptide esters (I and IX, II and X, III and XI, IV and XII, V and XIII, or VIII and XVI) was treated in acetone, the α-isomer changed to the corresponding soluble imidazolidinone, whereas the unchanged β-isomer remained insoluble. The β-isomer was filtered and recrystallized from water to give the pure β-isomer. The filtrate from the β-isomer was concentrated to dryness to give the imidazolidinone, which was then hydrolyzed with hot water to afford the pure α-isomer. The results are summarized in Table 3.

Experimental

All the melting points are uncorrected. The IR spectra were recorded in Nujol mull with a Jasco IR-S spectrometer. The NMR spectra were obtained with a Varian T-60 spectrometer at 60 MHz, and the chemical shifts are given from tetramethylsilane as the internal reference. The structural isomers were determined by a method described previously.[8]

Preparation of the Starting Materials. The α-L-aspartyl-L-phenylalanine methyl and ethyl esters (I and II), and the α-L-aspartyl-L-tyrosine methyl and ethyl esters (III and IV) were prepared by the condensation of β-benzyl *N*-carbobenzoxy-L-aspartate[9] and the appropriate amino acid esters

6) W. J. Le Quesne and G. T. Young, *J. Chem. Soc.*, **1952**, 24.
7) D. L. Buchanan, E. E. Haley, and R. T. Markiw, *Biochemistry*, **1**, 612 (1962); D. L. Buchanan, E. E. Haley, F. E. Dorer, and B. J. Corcoran, *ibid.*, **5**, 3240 (1966).
8) Y. Ariyoshi and N. Sato, This Bulletin, **45**, 942 (1972).
9) L. Benoiton, *Can. J. Chem.*, **40**, 570 (1962).

Table 3. Separation of the α- and β-aspartyl peptide esters

Run No.	Mixture of α- and β-isomers				Reaction conditions			Recovery of pure isomers			
	α-isomer,	g	β-isomer,	g	acetone ml	temp.	time hr	α-isomer,	g (%)	β-isomer,	g (%)
1	I	4	IX	4	200	r.t.	15	I	3.3 (83)	IX	3.3 (83)
2	II	1	X	1	100	reflux	1	II	0.8 (80)	X	0.6 (60)
3	III	1	XI	1	100	reflux	2.5	III	0.7 (70)	XI	0.7 (70)
4	IV	1	XII	1	100	reflux	2.5	IV	0.7 (70)	XII	0.6 (60)
5	V	0.5	XIII	0.5	25	r.t.	0.5	V	0.2 (40)	XIII	0.4 (80)
6	VIII	0.5	XVI	0.5	25	r.t.	0.5	VIII	0.2 (40)	XVI	0.4 (80)

with ethyl chloroformate, followed by deprotection. A typical run (I in Table 1) was as follows: To a chilled solution of β-benzyl *N*-carbobenzoxy-L-aspartate (17.9 g) and triethylamine (5.1 g) in chloroform (120 ml) was added ethyl chloroformate (5.5 g) at −5——10°C with stirring. After the solution had been stirred for 20 min at this temperature, a chilled mixture of methyl L-phenylalaninate hydrochloride (11.9 g) and triethylamine (6.5 g) in chloroform (150 ml) was stirred into the mixed anhydride solution at −5——10°C. Stirring was continued for 3 hr at room temperature. The reaction mixture was washed with N hydrochloric acid and then water, and dried over sodium sulfate. The solvent was removed by distillation *in vacuo*, and the residue was recrystallized from ethyl acetate-petroleum ether to give β-benzyl *N*-carbobenzoxy-L-aspartyl-L-phenylalanine methyl ester as needles; yield, 21 g (81%); mp 114.5—115.5°C. (Found: C, 67.16; H, 6.13; N, 5.43%). lit, 116—117°C,[10] 118.5—119.5°C.[1] A solution of the dipeptide ester (8.3 g) in 75% aqueous acetic acid (150 ml) was hydrogenated in the presence of 5% palladium on charcoal (1.0 g) for 6 hr. The filtrate from the catalyst was then concentrated *in vacuo*, and the residual crystals were recrystallized from water to give I as needles; yield, 4.0 g (83%). The data are given in Table 1.

The β-L-aspartyl-L-phenylalanine methyl and ethyl esters (IX and X), and the β-L-aspartyl-L-tyrosine methyl and ethyl esters (XI and XII) were prepared from α-benzyl *N*-carbobenzoxy-L-aspartate[11] and the appropriate amino acid esters according to the method used in the preparation of the α-isomers. A typical run (IX in Table 1) was as follows: α-Benzyl *N*-carbobenzoxy-L-aspartate (7.2 g) was condensed with methyl L-phenylalaninate hydrochloride (5.2 g) by the method described in the preparation of the α-isomers; this gave 7.8 g (75%) of α-benzyl *N*-carbobenzoxy-L-aspartyl-L-phenylalanine methyl ester; mp 121—122°C. lit,[1] mp 131—133°C. (Found: C, 67.37; H, 6.05; N, 5.45%). The hydrogenolysis of 10 g of the dipeptide ester gave 3.8 g of IX. All of the compounds (IX—XII) were hygroscopic. The data are given in Table 1.

The α-L-aspartyl-L-(β-cyclohexyl)alanine methyl and ethyl esters (V and VI), the α-L-aspartyl-L-[β-(4-hydroxycyclohexyl)]alanine methyl and ethyl esters (VII and VIII), the β-L-aspartyl-L-(β-cyclohexyl)alanine methyl and ethyl esters (XIII and XIV), and the β-L-aspartyl-L-[β-(4-hydroxycyclohexyl)]alanine methyl and ethyl esters (XV and XVI) were obtained by the hydrogenation of the aromatic ring of the corresponding dipeptides (I—IV and IX—XII). A typical run (V in Table 1) was as follows: A solution of I (5.0 g) in 0.1 M aqueous acetic acid (250 ml) was hydrogenated in the presence of platinum oxide (1.0 g) at atmospheric pressure and room temperature. The filtrate from the catalyst was then concentrated to dryness *in vacuo*. The residue was triturated with ether to give V as a crystalline powder, which was then recrystallized from water to give platelets; 4.8 g (94%).

VIII, XIV, XV, and XVI were hygroscopic. The data are given in Table 1.

4-Imidazolidinones (XVII—XXX). The imidazolidinones (XVII—XXX) were prepared by the condensation of the dipeptides (I—VIII) with acetone, methyl ethyl ketone, or cyclohexanone at 25—100°C for 0.5—12 hr. A typical run (XVII in Table 2) was as follows: A suspension of I (6.0 g) in acetone (100 ml) was heated under reflux for 30 min. The insoluble crystals (1.5 g) were then filtered off. The crystals were identified with I by studying the IR spectrum. After the filtrate had been kept in a refrigerator overnight, the crystals thus formed were collected by filtration; yield, 3.0 g. The second crop (1.0 g) was recovered from the mother liquor; total yield, 4.0 g (61%); mp 145°C (raised rapidly); $[\alpha]_D^{25}$ −157.5° (*c* 1, acetone); IR: 3310 (NH), 1750 (ester), and 1703 (amide-I and carboxyl group) cm^{-1}; NMR (CD_3COCD_3): δ 0.57 (s, 3H, $-CH_3$), 1.33 (s, 3H, $-CH_3$), 2.57 (m, 2H, $-CH_2COO$), 3.50 (m, 2H, $-CH_2C_6H_5$), 3.73 (s, 3H, $-COOCH_3$), 3.50—4.20 (m, 2H, 2 $-CH\langle$), 4.37 (broad s, NH), and 7.30 (s, 5H, $-C_6H_5$) ppm. For the NMR spectrum, see also Fig. 2. For anal. and mp, see Table 2.

Separation of the α- and β-Isomers with Acetone. A typical run (No. 1 in Table 3) was as follows: A suspension mixture of I (4 g) and IX (4 g) in acetone (200 ml) was stirred for 15 hr at room temperature. An insoluble, amorphous material was then collected by filtration. The compound was identified as anhydrous IX by studying the IR spectrum, which failed to absorb the water of crystallization of the starting material. The compound was recrystallized from water (40 ml) to give 3.3 g (83%) of IX as needles, which were found by paper electrophoresis to be free from the α-isomer; mp 198—199°C (decomp.); $[\alpha]_D^{22}$ +40.5° (*c* 1, acetic acid).

On the other hand, the filtrate from the β-isomer was concentrated to dryness *in vacuo*. The residual crystals were dissolved in hot water, concentrated to dryness *in vacuo*, and then recrystallized from water (40 ml) to give 3.3 g (83%) of I as needles; mp 235—236°C (decomp.); $[\alpha]_D^{25}$ +32.0° (*c* 1, acetic acid). These results showed that no racemization occurred during the reaction. The crystals were found by paper electrophoresis to be free from the β-isomer. The results are summarized in Table 3.

10) J. M. Davey, A. H. Laird, and J. S. Morley, *J. Chem. Soc.*, *C*, **1966**, 555.

11) M. Bergamnn, L. Zervas, and L. Salzmann, *Ber.*, **66**, 1288 (1933).

The Reaction of Sulfilimine with Phenyl Grignard Reagent*,[1]

Shigeru OAE, Toshiaki YOSHIMURA, and Naomichi FURUKAWA

Department of Applied Chemistry, Faculty of Engineering, Osaka City University, Sugimotocho, Sumiyoshi-ku, Osaka

(Received December 27, 1971)

The reactions of diphenyl (I), phenyl benzyl (II), and phenyl methyl *N*-*p*-tosylsulfilimines (III) with phenylmagnesium bromide were carried out. (I) gave biphenyl and diphenyl sulfide in high yields. A tracer experiment with diphenyl sulfilimine-1-^{14}C revealed that the reaction proceeds *via* the initial formation of triphenylsulfonium salt upon which the attack of phenylmagnesium bromide affords the products. "Benzyne" mechanism is ruled out. (II) and (III) gave various compounds, the major products being α-phenylated sulfides which are presumed to be formed by the Pummerer type rearrangement initiated by the abstraction of α-proton by the Grignard reagent.

N-*p*-Tosylsulfilimines can generally be prepared by allowing the corresponding sulfides to react with chloramine-T[2] (sodium salt of *N*-chloro *p*-toluenesulfonamide). Spectroscopic analysis indicates that the sulfilimine has a semipolar S–N bond similar to the S–O bond in sulfoxides.[3] In contrast to the massive works on sulfoxides,[4] the chemical properties of sulfilimines have not been explored. Recently Cram *et al.*[5] and Johnson *et al.*[6] studied the stereochemistry of nucleophilic substitution reactions of sulfilimines while Petranek and Vecera investigated the sigmatropic rearrangement of allylic *N*-*p*-tosylsulfilimines.[7] We have also studied the substitution,[8] elimination,[9] E*i* reaction[10], and pyrolysis reactions of sulfilimines.[10] Since sulfilimines have a labile S–N bond they are as reactive as the corresponding sulfoxides, and are, therefore, good substrates for examining the possible reactions which occur on the trivalent sulfur atom. This paper describes a detailed account of the reaction of *N*-*p*-tosylsulfilimines with phenyl Grignard reagent.

Reaction of Diphenyl Sulfilimine with Phenylmagnesium Bromide. Diphenyl *N*-*p*-tosylsulfilimine was dissolved in anhydrous THF. Into the resulting solution was added 5 mol excess of phenylmagnesium bromide. When the mixture was allowed to stand at room temperature, no reaction occurred and the sulfilimine was recovered almost quantitatively. The mixture was therefore refluxed in an oil bath for several hours. The reaction mixture was then decomposed with water, and the products were isolated and identified as shown in Table 1.

TABLE 1. PRODUCTS AND YIELDS OF THE REACTION OF $PhS\overset{+}{\underset{-}{\underset{|}{N}}}TsPh$ WITH PhMgBr

Products	Yield (%)	
	A	B
PhSPh	trace	73
Ph–Ph		59
$TsNH_2$	trace	73
Recovered	quantitatively	20
$(Ph)_3S^+X^-$	not identified	not identified

A; Carried out at room temperature.
B; Carried out by refluxing in THF.

Contrary to expectation, the major products are biphenyl and diphenyl sulfide, no sulfonium salt being isolated. Both biphenyl and diphenyl sulfide are known to be obtained by the attack of phenyl anion on triphenylsulfonium salt[12] incipiently formed during the reaction. The mechanism of the reaction was investigated. In a previous paper, it was shown that sulfilimine has two attacking sites, *i.e.* S and N for nucleophiles.[13] If the attack of the Grignard reagent takes place on the sulfur (IV) atom (Path (A), Fig. 1), triphenylsulfonium salt might be formed as an incipient intermediate which is then attacked by another molecule of the Grignard reagent either at the *ortho* proton to form benzyne and diphenyl sulfide (Path (A)-(a)) or at the phenyl carbon attached to the sulfur atom to form directly biphenyl and diphenyl sulfide (Path (A)-(b)). If the attacking site is the sulfilimino nitrogen (Path (B)), diphenyl sulfide would be obtained directly while biphenyl would result from the reaction between *N*-phenyltosylamide and phenylmagnesium bromide. Another alternative path (Path (C)), would be the one which involves the initial attack of the Grignard reagent on the α-hydrogen atom of the sulfilimine giving

* Recently, Manya *et al.* reported the same sort of reaction. They obtained nearly the same results as ours but they could isolate the triphenylsulfonium salt. P. Manya, S. Sekera, and P. Rumpf, *Bull. Soc. Chim. Fr.*, **1971**, 286.

1) Sulfilimine and sulfoximine Part X. Part IX. K. Tsujihara, N. Furukawa, and S. Oae, *Tetrahedron*, in press (1971).

2) B. H. Nicolet and J. Willard, *Science*, **53**, 217 (1921).

3) a) K. Tsujihara, N. Furukawa, and S. Oae, This Bulletin, **43**, 2153 (1970). The related references are cited therein. b) C. C. Price and S. Oae, "Sulfur Bonding" Ronald Press. N. Y. (1962).

4) C.R. Johnson, "Quart. Reports of Sulfur Chem.," Vol. 1, (1969), p. 1.

5) J. Day and D. J. Cram, *J. Amer. Chem. Soc.*, **87**, 4398 (1965). D. J. Cram, J. Day, D. R. Reyner, D. M. von Schritz, D. U. Buchamp, and D. C. Garwood, *ibid.*, **92**, 7369 (1970).

6) C. R. Johnson and J. J. Rigau, *J. Org. Chem.*, **33**, 4340 (1968). C. R. Johnson, J. J. Rigau, M. Haake, D. MacCants. Jr., E. Keiser, and A. Gertseman, *Tetrahedron Lett.*, **1968**, 3791.

7) J. Petranek, M. Vecera, *Collect. Czech. Chem. Commun.*, 24, 2191 (1959).

8) S. Oae, T. Aida, K. Tsujihara, and N. Furukawa, *Tetrahedron Lett.*, **1971**, 1145.

9) S. Oae, K. Tsujihara, and N. Furukawa, *ibid.*, **1970**, 2663.

10) H. Kobayashi, N. Furukawa, T. Aida, and S. Oae, *ibid.*, **1971**, 3109.

11) K. Tsujihara, A. Aida, N. Furukawa, and S. Oae, *ibid.*, **1970**, 3415.

12) K. K. Andersen and N. E. Papanikolaou, *ibid.*, **1966**, 5445.

13) B. S. Wildi, S. W. Taylor, and H. A. Potratz, *J. Amer. Chem. Soc.*, **73**, 1965 (1951).

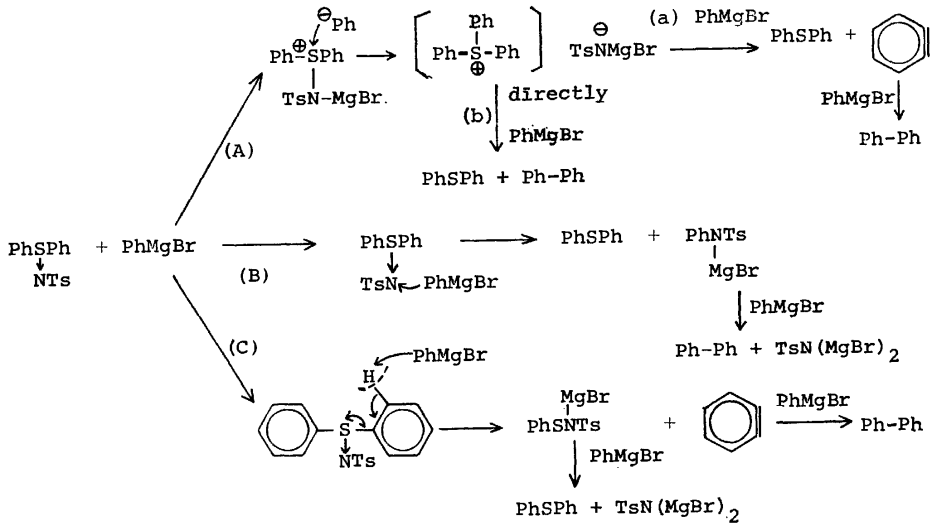

Fig. 1. The mechanism of the reaction.

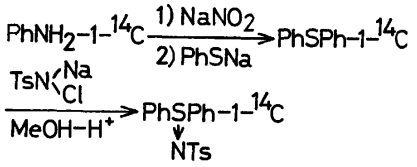

Fig. 2. The synthetic method of sulfilimine-1-^{14}C.

benzyne and *N*-phenylmercaptotosylamide upon which the attack of the Grignard reagent[14] produces diphenyl sulfide. The above four mechanistic schemes are shown in Fig. 1. In order to make a choice from the four mechanisms, the sulfilimine labeled with ^{14}C at 1-position was synthesized and allowed to react with phenylmagnesium bromide. The synthetic procedure to prepare the *N*-*p*-tosylsulfilimine-1-^{14}C is shown in Fig. 2. If the reaction proceeds *via* the formation of triphenylsulfonium ion (Path (A), either (a) or (b)), the original ^{14}C activity of the sulfilimine should be distributed between diphenyl sulfide and biphenyl, 2/3 (66.7%) for the sulfide and 1/3 (33.3%) for biphenyl, if the ^{14}C isotope effect is neglected. The reaction that proceeds *via* path (B) will require all the ^{14}C activity to be found in the diphenyl sulfide alone, that *via* path (C) 50% each in both diphenyl sulfide and biphenyl. A choice between paths (a) and (b) can be made by tracing the ^{14}C activity within the molecule of biphenyl by means of degradation. Thus, diphenyl sulfilimine-1-^{14}C was treated with phenylmagnesium bromide. The ^{14}C analytical data obtained from the above experiment are shown in Table 2.

The distribution of ^{14}C activity among the products indicates that *ca.* 70% is in diphenyl sulfide the rest in biphenyl. These data rule out (B) and (C), leaving the first two plausible mechanisms that involve the initial formation of triphenylsulfonium salt. (A) is consistent with the mechanism proposed by Andersen[15] for the reaction between diphenyl sulfoxide with phenyllithium.

14) T. Mukaiyama, S. Kobayashi, and T. Kumamoto, *Tetrahedron Lett.*, **1970**, 5115.

15) K. K. Andersen and S. A. Yeager, *J. Org. Chem.*, **28**, 865 (1963).

TABLE 2. ^{14}C DISTRIBUTION IN THE PRODUCTS

Compound	^{14}C Activities dpm/mM	(%)
Ph–Ph	4.80×10^{6}	30.0
Ph–S–Ph[a]	1.11×10^{6}	69.2
Ph–S–Ph	1.60×10^{6}	(100)
↓ NTs		
(original)		
(recovered)[b]	1.57×10^{6}	98.2
Ph–S–Ph[c]		
(original)	1.65×10^{6}	(100)
(recovered)	1.61×10^{6}	97.6

a) The activity of diphenyl sulfide was measured, after its oxidation to diphenyl sulfone with H_2O_2.
b) The reaction was interrupted and the activity of the recovered sulfilimine measured.
c) Diphenyl sulfide-1-^{14}C was treated with phenylmagnesium bromide in order to check a possible ^{14}C exchange reaction between the diphenyl sulfide formed and phenyl Grignard reagent.

The fact that the ^{14}C activity of the recovered sulfilimine is practically the same as that of the original one, seems to indicate that the decomposition of the intermediate triphenylsulfonium salt to diphenyl sulfide is faster than the possible reverse reaction to the sulfilimine. Under the same conditions, diphenyl sulfide does not undergo phenyl exchange with phenyl Grignard reagent. Thus, the ^{14}C activity of diphenyl sulfide should come from the sulfilimine alone. All these data support the mechanism involving the initial formation of triphenylsulfonium ion. However, the question still remains through which of the paths (a) and (b) the reaction proceeds.

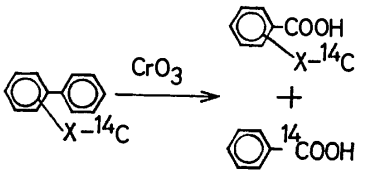

Fig. 3. The degradation of biphenyl.

In order to ascertain this, biphenyl-X-^{14}C obtained from the above experiment was allowed to degrade by the following method.

As shown in Fig. 1, if the reaction proceeds by the nucleophilic attack of phenyl anion at the sulfonium salt (Path (b)), the ^{14}C activity found in biphenyl-X-^{14}C should be the same as that found in benzoic acid-X-^{14}C, since no ^{14}C migration occurs at all during the reaction. On the other hand, the benzyne route (a) requires the ^{14}C activity of benzoic acid to be 3/4 of that of biphenyl. The results obtained from the degradation are shown in Table 3, and indicate that the reaction proceeds *via* path (A)-(b).

Table 3. Degradation data of biphenyl-X-^{14}C

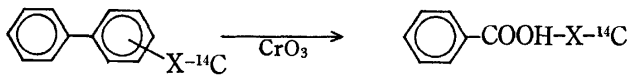

Theor. (%)		
For (Aa)	(100)	(75)
For (Ab)		(100)
Found		
Activities (dmp/mM)		
1.53×10^4		1.58×10^4
	(100)	(103)

The result seems to contradict our earlier observation[16] and also that of Franzen's[17] on the reaction of triarylsulfonium salt with phenyllithium where benzyne route is confirmed. The difference between the above two reactions might be due to the less basic nature of the Grignard reagent than phenyllithium. Namely, phenyllithium is so strong a base that it can attack a proton *ortho* to the sulfonio group to form "benzyne", while the Grignard reagent is not a powerful base but a good nucleophile to attack the phenyl carbon.

Reactions of Phenyl Methyl and Phenyl Benzyl N-*Tosylsulfilimines with Phenylmagnesium Bromide.* These two reactions were carried out in a similar way to that of diphenyl *N*-tosylsulfilimine and phenylmagnesium bromide. After the reaction, the products were separated through a column packed with silica gel. The products and their yields obtained from the above sulfilimines are shown in Table 4.

We see that no sulfonium salt was isolated, however, the products are rather complicated. The results are in a marked contrast to those of diphenyl *N*-*p*-tosylsulfilimine. The pattern of distribution of the products is very close to that for the reaction of the corresponding sulfoxide with phenylmagnesium bromide.[18]

In the case of phenyl benzyl *N*-*p*-tosylsulfilimine, the major product is *N*-benzhydryl-*p*-toluenesulfonamide which was identified by comparing the IR, NMR, and mass spectra with those of the authentic sample prepared from benzhydrylamine and *p*-tosyl chloride. In addition to the *N*-benzhydryl-*p*-toluenesulfonamide, diphenyl sulfide and phenyl benzyl sulfide were isolated, identified and their yields were determined. With the present data only, it is difficult to postulate any plausible mechanism for the reaction. However, as in the case of the sulfoxides α-hydrogen abstraction by phenyl anion (or radical) might be the initial step followed by either the Pummerer or Stevens-type rearrangement as shown

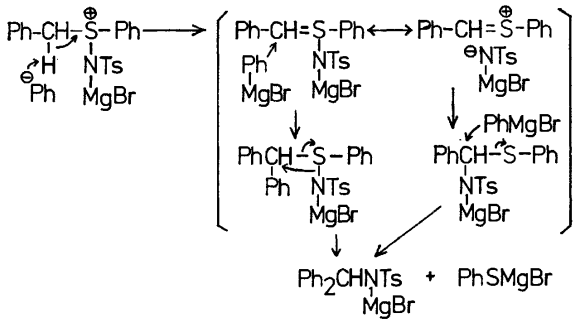

Fig. 4. The mechansim of the reaction.

below. A large excess of the Grignard reagent and a prolonged reaction time gave diphenyl sulfide in an increasing yield and diphenyl disulfide in a smaller amount. Diphenyl sulfide is probably obtained from diphenyl disulfide and not from the direct attack by phenylmagnesium bromide on sulfinyl sulfur. This was

Table 4. Products and yields in the reaction of phenyl benzyl and phenyl methyl *N*-tosylsulfilimines and phenylmagnesium bromide

Sulfilimine	Condition		Products and yields (%)
Ph–S(+)–CH_2–Ph | –NTs (1 mol)	PhMgBr (2 mol)	room temp. 3 hr	Ph–Ph, PhS–Ph(7), PhCHSPh (25) PhSSPh(10), $Ph_2CHNHTs$(17) $TsNH_2$, Recovered (48)
	PhMgBr (5 mol)	room temp. 24 hr	Ph–Ph, PhSPh(38), $PhCH_2SPh$(20) PhSSPh(1.7), $Ph_2CHNHTs$ (40) $TsNH_2$, Recovered (16)
Ph–S(+)–CH_3 | –NTs (1 mol)	PhMgBr (5 mol)	reflux 1 hr	Ph–Ph, $PhSCH_3$(5), PhSPh(16) $PhCH_2SPh$(21), $TsNH_2$(56), PhSH $PhCHCH_2CH_2CH_2OH$, $Ph_2CCH_2CH_2CH_2OH$ OH (16) OH (2.4)

16) Y. H. Khim and S. Oae, This Bulletin, **42**, 1968 (1969).
17) V. Franzen and C. Mertz, *Angew. Chem.*, **72**, 416 (1960).
18) P. Manya, A. Sekera, and P. Rumpf, *Tetrahedron*, **26**, 467 (1970).

found to be the case for the reaction with the diphenyl sulfilimine. In the case of phenyl methyl *N-p*-tosylsulfilimine, the major product is phenyl benzyl sulfide which might be formed by a Pummerer type rearrangement.

Experimental

Preparation of N-p-*Tosylsulfilimines.* The sulfilimines used in the study were prepared according to the known method.[19]

Reaction of Diphenyl N-p-*Tosylsulfilimine with Phenylmagnesium Bromide.* Diphenyl *N-p*-tosylsulfilimine (1 g) was dissolved in 30 m*l* anhydrous THF. To this was added 20 m*l* solution of phenylmagnesium bromide prepared from bromobenzene (1.6 g) and magnesium (0.25 g) in 20 m*l* anhydrous THF. The solution was then refluxed for 12 hr. After the reaction, the solution was decomposed with water and then with dilute hydrochloric acid. The aqueous solution was then extracted with chloroform. The chloroform extract was separated, washed with water, extracted again with 10% of aqueous sodium hydroxide, washed with water and then dried over anhydrous sodium sulfate. After removing the solvent, the residue was chromatographed through a column packed with silica gel.

The chromatogram indicated two spots, each of which was nicely separated; diphenyl sulfide and biphenyl were identified by glc from the first layer and the sulfilimine from the second layer. *p*-Tosylamide was isolated from the aqueous layer after acidifying the solution with hydrochloric acid. All the products were identified by comparing their IR, NMR, and glc with those of the authentic samples. The yields are shown in Table 1.

^{14}C Tracer Study with Diphenyl N-p-*Tosylsulfilimine-1-^{14}C with Phenylmagnesium Bromide.* N-p-*Tosylsulfilimine-1-^{14}C*: Diphenyl sulfide-1-^{14}C (3 g) prepared from diazotizing of aniline-1-^{14}C and thiophenol[20] was dissolved in 10 m*l* methanol containing a drop of acetic acid. To the solution was added 4.6 g of chloramine-T in 5 m*l* methanol. After being kept standing for 1 hr, the solution was poured into ice water. To this was added 10% of aqueous sodium hydroxide. The precipitates were separated. The crude sulfilimine was recrystallized from ethanol, yield 5 g, mp 111—112°C.

Exchange Reaction of Diphenyl Sulfide-1-^{14}C with Phenylmagnesium Bromide. In order to confirm the possibility of phenyl group interchange between the sulfide and phenyl Grignard reagent, a mixture of 0.6 g of diphenyl sulfide-1-^{14}C and phenylmagnesium bromide prepared from bromobenzene (1.6 g) and magnesium (0.24 g) in 10 m*l* of anhydrous THF was treated under the same conditions applied for the above reaction. After the reaction, diphenyl sulfide was recovered and oxidized to diphenyl sulfone by hydrogen peroxide for treatment such as degradation and ^{14}C activity determination.

Degradation of Diphenyl Sulfide-1-^{14}C.[21] In order to locate the specific position of ^{14}C activity of diphenyl sulfide-1-^{14}C the sulfide was oxidized first to the diphenyl sulfone which was then irradiated with 150 W UV lamp in benzene solution for 42 hr to afford biphenyl. After biphenyl was isolated and purified by sublimation, biphenyl (0.55 g) was oxidized by anhydrous chromic acid to benzoic acid, yield 0.16 g (37%). During those reactions no ^{14}C migration was observed. By the above method the labeled position and amount of ^{14}C activity in the diphenyl sulfide were found.

Degradation of Biphenyl-x-^{14}C. Biphenyl-x-^{14}C prepared from the sulfilimine and phenylmagnesium bromide was degraded similarly. After oxidation of biphenyl, benzoic acid-x-^{14}C was obtained in 58% yield. Both biphenyl and benzoic acid were purified by sublimation.

Measurement of ^{14}C Activity. The ^{14}C activity of the products obtained from the above reactions was measured by means of a Packard Tri Carb liquid scintillation counter by dissolving aliquot amounts of the samples in toluene. POP and POPOP were used as scintillators.

Reaction of Phenyl Benzyl N-p-*Tosylsulfilimine with Phenylmagnesium Bromide.* A typical experiment is as follows. Phenyl benzyl *N-p*-tosylsulfilimine (1 g prepared from the sulfide and chloramine-T) was dissolved in 20 m*l* anhydrous THF. To this solution was added phenylmagnesium bromide (2: 1 mol of sulfilimine) in anhydrous THF, and the solution was stirred overnight at room temperature. The solution was then decomposed with aqueous hydrochloric acid solution. The aqueous solution was extracted with chloroform. The chloroform solution was extracted again with an aqueous alkaline solution. The chloroform extract was condensed and the residue was chromatographed through a column packed with silica gel. From the chloroform eluent, a mixture of the sulfide and biphenyl was separated and the sulfilimine was recovered. The mixture was separated by means of glc (diethylene glycol succinate polyester on Neosorb). Their yields were determined by glc. After eluting the above mixture, chloroform was used to separate the polar compounds from which *N*-benzhydryl-*p*-tosylamide was obtained together with the recovered sulfilimine. *N*-Benzhydryl-*p*-tosylamide: mp 152°C; IR νSO_2 1165, 1320 cm^{-1}, νNH 3260 cm^{-1}; NMR methyl proton 7.57, methine C–H and N–H protons 4.30, phenyl protons 2.1—3.0 τ.

Found: C, 70.83; H, 5.81; N, 4.04%. Calcd for $C_{20}H_{19}SNO_2$: C, 71.20; H, 5.67; N, 4.15%.

From the alkaline extract only *p*-tosylamide was isolated.

Reaction of Phenyl Methyl N-p-*Tosylsulfilimine with Phenylmagnesium Bromide.* The reaction was carried out by the same method as for phenyl benzyl sulfilimine and after the usual work up the products given in Table IV were isolated.

19) K. Tsujihara, N. Furukawa, K. Oae, and S. Oae, This Bulletin, **42**, 2631 (1969).

20) S. Oae and N. Furukawa, *ibid.*, **39**, 2260 (1966).

21) S. Oae, M. Nakai, N. Furukawa, and T. Nakabayashi, *ibid.*, **45**, 1268 (1972).

Reaction of α-Chloro Sulfoxides with Carbonyl and Thiocarbonyl Compounds

Gen-ichi TSUCHIHASHI and Katsuyuki OGURA

Sagami Chemical Research Center, Ohnuma, Sagamihara, Kanagawa 229

(Received January 18, 1972)

Chloromethyl methyl sulfoxide undergoes a Darzens-type reaction with carbonyl compounds in the presence of potassium *t*-butoxide in *t*-butanol to afford methylsulfinyloxirane derivatives. The stereochemistry of this reaction has been studied. The reaction with a symmetrical ketone appeared to proceed stereospecifically to give only one isomer. On the other hand, the reaction with unsymmetrical ketones such as pinacolone or acetophenone produced a mixture of two diastereoisomers, in which a thermodynamically unstable isomer was predominant. The reaction with thiobenzophenone gave 1,1-diphenyl-2-methylsulfinylethylene which seems to have been formed from the intermediacy of 2,2-diphenyl-3-methylsulfinylthiirane. Mechanisms of these reactions are also discussed.

Preparation of α-chlorosulfoxides can be readily accomplished by the reaction of sulfoxides with ordinary chlorinating agents such as chlorine,[1] sulfuryl chloride,[2] *t*-butyl hypochlorite,[3] or *N*-chlorosuccinimide.[4] We have examined the synthetic utility of these α-chlorosulfoxides, particularly chloromethyl methyl sulfoxide, in order to find a way to obtain sulfoxide derivatives of a new type. Application of Darzens-type condensation to α-chlorosulfoxide, *i.e.*, the reaction with carbonyl compounds in the presence of a base, is of considerable interest.

In 1969, Durst reported that the metallation of chloromethyl phenyl sulfoxide followed by the addition to ketones, hydrolysis and successive dehydrochlorination with a base gave phenylsulfinyloxiranes as shown in the following.[5]

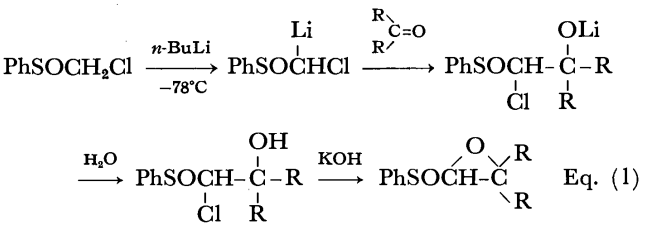

Eq. (1)

When alkyl chloromethyl sulfoxide is subjected to reaction with carbonyl compounds, two reactions as shown in Eq. 2 should be taken into consideration, a Darzens-

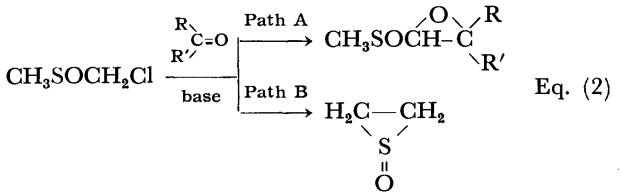

Eq. (2)

type (Path A) and a Ramberg-Bäcklund-type (Path B). We studied the reaction of chloromethyl methyl sulfoxide with carbonyl compounds in the presence of a base in order to see which reaction this sulfoxide favors.

During the course of our investigation, Tavares and his co-workers reported that chloromethyl *p*-tolyl sulfoxide is directly converted into *p*-tolylsulfinyloxiranes by treatment with carbonyl compounds and potassium *t*-butoxide in *t*-butanol–ether.[6] However, Durst and Tin pointed out that Tavares' procedure might be restricted to the sulfoxides which cannot undergo the Ramberg-Bäcklund-type reaction and they prepared methylsulfinyloxiranes by a procedure similar to that shown in Eq. (1).[7]

We found that the reaction of chloromethyl methyl sulfoxide with carbonyl compounds in the presence of potassium *t*-butoxide resulted in the formation of methylsulfinyloxiranes. The application of this reaction to unsymmetrical ketones was investigated. Two diastereomeric isomers of methylsulfinyloxiranes were obtained, and the stereochemistry of these isomers was studied in order to elucidate the steric course of the reaction. In the present paper, we describe the results as well as a study on the reaction with thiobenzophenone.

Results and Discussion

Potassium *t*-butoxide was added to a solution of *t*-butanol containing chloromethyl methyl sulfoxide and benzophenone, and the solution was kept at room temperature with stirring. After the usual work-up, colorless crystals, mp 109—110°C, were obtained in a 62% yield. The IR spectrum of the product showed an absorption at 1034 cm^{-1}, characteristic of a sulfinyl group, and no absorption around 4000—3000 cm^{-1} and 1800—1600 cm^{-1}, indicating that the product has neither hydroxyl nor carbonyl group. In its NMR spectrum, four singlets appeared at δ 7.37 (5H), 7.35 (5H), 4.58 (1H), and 2.57 (3H, CH_3SO).[8] These data as well as the following facts show the structure of this material to be 2,2-diphenyl-3-methylsulfinyloxirane (**1**). The reduction of **1** with lithium aluminum hydride gave 1,1-diphenyl-2-methylthioethanol, which was independently synthesized by the reduction of 1,1-diphenyl-2-

1) G. Tsuchihashi and S. Iriuchijima, This Bulletin, **43**, 2271 (1970).

2) G. Tsuchihashi, K. Ogura, S. Iriuchijima, and S. Tomisawa, *Synthesis*, **1971**, 89.

3) S. Iriuchijima and G. Tsuchihashi, *Tetrahedron Lett.*, **1969**, 5259.

4) G. Tsuchihashi and K. Ogura, This Bulletin, **44**, 1726 (1971).

5) T. Durst, *J. Amer. Chem. Soc.*, **91**, 1034 (1969).

6) D. F. Tavares, R. E. Estep, and M. Blezard, *Tetrahedron Lett.*, **1970**, 2373.

7) T. Durst and K.-C. Tin, *ibid.*, **1970**, 2369.

8) The protons of a normal methylsulfinyl group showed an NMR signal near δ 2.6. For example, dimethyl sulfoxide: δ 2.62; methyl methylthiomethyl sulfoxide: δ 2.59.

methylsulfinylethanol.[9]

Similarly, acetone reacted with chloromethyl methyl sulfoxide in the presence of potassium *t*-butoxide to afford a methylsulfinyloxirane in a 95% yield, its structure being assigned to 2,2-dimethyl-3-methylsulfinyloxirane (**2**) from its physical properties [IR (KBr): 1039 cm^{-1}, NMR (in CCl_4): δ 3.80 (s, 1H), 2.66 (s, 3H), 1.48 (s, 3H), and 1.45 (s, 3H)]. Oxidation of **2** gave the corresponding sulfone **3**.[10]

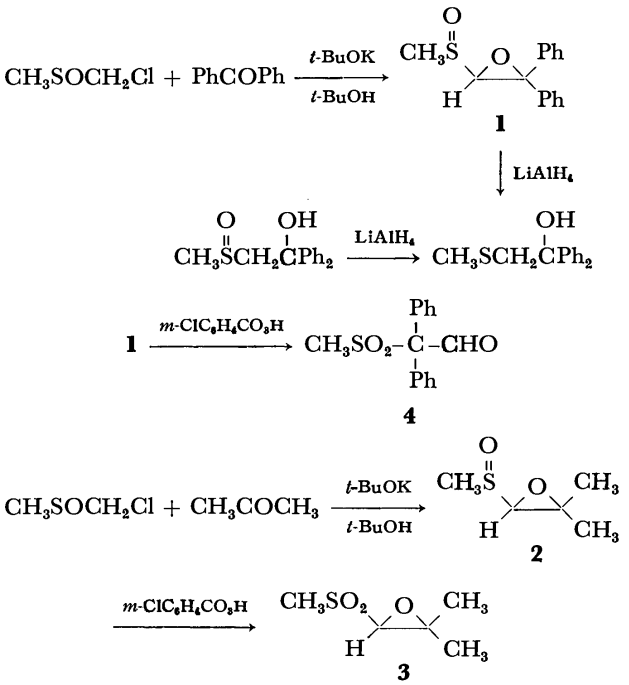

Scheme 1

When pinacolone was subjected to this Darzens-type reaction of chloromethyl methyl sulfoxide, a mixture shown by NMR analysis to consist of two isomeric methylsulfinyloxiranes **5** and **6** (3: 1) was formed in a 66% yield. One isomer (the major component) could be isolated, showing four singlets at δ 3.78 (1H), 2.58 (3H), 1.48 (3H), and 1.00 (9H) in its NMR spectrum and an absorption at 1034 cm^{-1} in its IR spectrum. In the NMR spectrum of the other isomer, four singlets also appeared at δ 3.44 (1H), 2.88 (3H), 1.40 (3H), and 1.08 (9H). These data are consistent with the structures given in formulas **5** and **6**. The stereochemical structure of the major component was unambiguously determined on the basis of the result of an intramolecular nuclear Overhauser effect. It was found that irradiation of the methyl signal in the NMR spectrum of the major component caused a significant increase (15%) in the intensity of the methine proton which was not effected by irradiation of the *t*-butyl signal, as shown in Fig. 1. This indicates that the methyl group and the

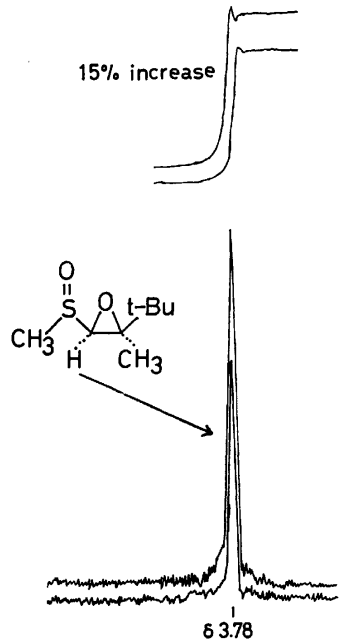

Fig. 1. Intramolecular Overhauser Effect of **5**. irradiation of the methyl signal (δ 1.41)

methine proton of the major component are close together in space. Thus its stereochemical structure was assigned to be **5** in which hydrogen atom and methyl group are in *cis* position.

Acetophenone reacted with chloromethyl methyl sulfoxide by an action of potassium *t*-butoxide to afford a mixture of two diastereoisomers, **7** and **8** (3: 2) in a 60% yield. We tentatively assigned the stereochemical formulas **7** and **8** to the structures of the major and the minor products, respectively, by considering a similar stereochemical course to that of the reaction of pinacolone with chloromethyl methyl sulfoxide.

The reaction of thiobenzophenone with chloromethyl methyl sulfoxide in the presence of potassium *t*-butoxide did not give the expected product, 2,2-diphenyl-3-methylsulfinylthiirane **9**, but an α,β-unsaturated sulfoxide (**10**) in a 38% yield.

The structure of **10** was determined from its IR (1021 cm^{-1}) and NMR (δ 7.28 (s, 10H), 6.88 (s, 1H), and 2.59 (s, 3H)) spectra. The structure was further confirmed by an independent synthesis. The treatment of the methyl ether (**11**) derived from 1,1-diphenyl-2-methylsulfinylethanol with potassium *t*-butoxide af-

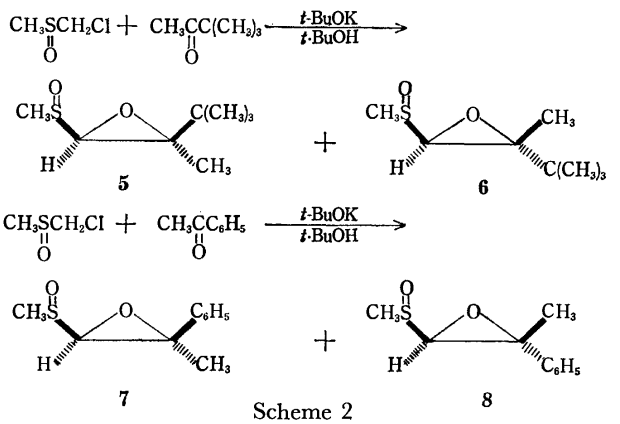

Scheme 2

9) E. J. Corey and M. Chaykovsky, *J. Amer. Chem. Soc.*, **87**, 1345 (1965).

10) The oxidation of **1** with *m*-chloroperbenzoic acid, accompanied by a rearrangement, yielded diphenyl(methylsulfonyl)-acetaldehyde(**4**), of which the structure was assigned by its physical properties (see Experimental Section). The analogous rearrangements of α-epoxy sulfoxides and α-epoxy sulfones to the corresponding aldehydes were already reported.[6,7]

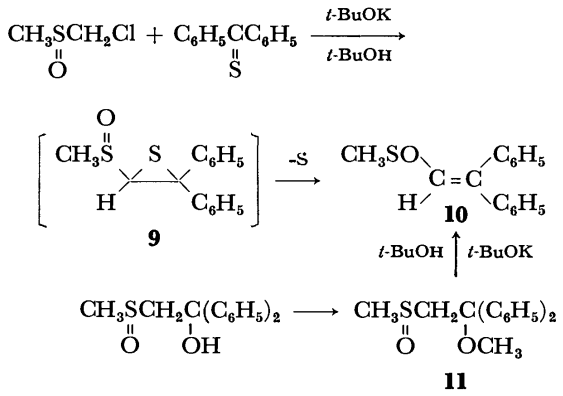

Scheme 3

forded **10**. It is reasonable to assume that **10** was formed by the desulfurization of the expected product **9**.

It should be noted that only one isomer was given in the reaction of chloromethyl methyl sulfoxide with symmetrical ketones such as benzophenone or acetone. This is in line with the result reported by Durst who found a high stereoselectivity in the Darzens-type reaction of chloromethyl phenyl sulfoxide with cyclohexanone, acetone or benzophenone.[5] On the other hand, when an unsymmetrical ketone such as pinacolone or acetophenone was used as a carbonyl component, two diastereoisomers were produced. It is of interest that a thermodynamically unstable isomer, **5** or **7**, was predominantly formed as described above. This tendency was also reported by Tavares and his co-workers. They stated that chloromethyl *p*-tolyl sulfoxide reacted with benzaldehyde to yield mainly *cis*-2-phenyl-3-(*p*-tolylsulfinyl)oxirane whose structure was assigned tentatively from the NMR coupling constant between the methine protons in the oxirane ring. They explained that their result can be attributed to precipitation of a less soluble *cis* isomer. This does not hold in our observation because the reaction condition is homogeneous. We would like to propose a plausible mechanism for the formation of a thermodynamically unstable isomer in the Darzens-type reaction of chloromethyl methyl sulfoxide with an unsymmetrical ketone. The carbanion (**12**) derived from chloromethyl methyl sulfoxide attacks a carbonyl compound to form an intermediate (**13**) in the first step of the reaction. We assume that this step is not reversible. The formation of **13a** proceeds through a less hindered transition state than the formation of **13b**, owing to the difference in bulkiness between M and L (M<L). If the oxy anion in **13a** attacks the carbon atom bearing chlorine atom from behind, as in the usual ring-closure reaction of chlorohydrins, the thermodynamically unstable isomer (**14a**) will be formed from the kinetically preferred intermediate (**13a**).

It is interesting to compare this result with that of Darzens-type condensation of α-halosulfones studied by Vogt and Tavares.[11] According to their report, a thermodynamically stable isomer, *i.e. trans* isomer, was produced exclusively. They assume that the initial nucleophilic attack upon a carbonyl compound is

11) P. F. Vogt and D. F. Tavares, *Can. J. Chem.*, **47**, 2875 (1969).

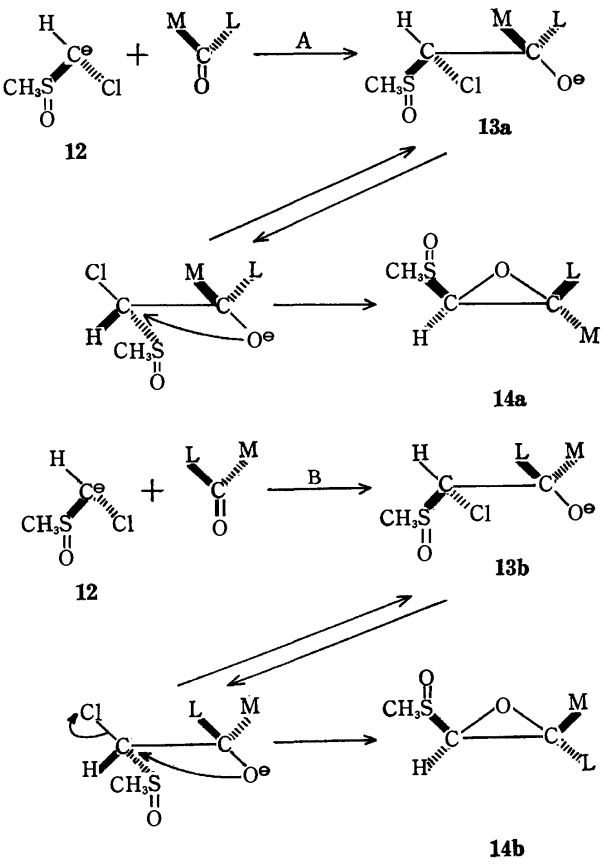

Scheme 4

rapidly reversible and the product determining step is the ring closure (**16**→**17**). The thermodynamically stable isomer was formed predominantly, passing through the preferred transition state, from the dynamic equilibrium between two diastereoisomers of **16**.

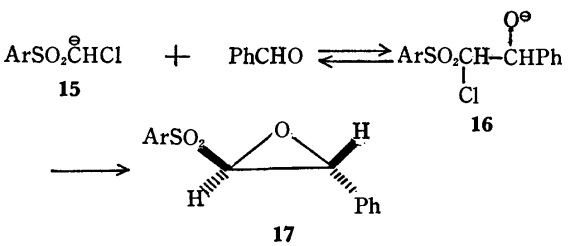

We believe that the conflicting behaviors in α-halosulfoxides and α-halosulfones can be ascribed to the difference of stability in anions **12** and **15**. Anion **15** is much more stable than anion **12**.

Experimental

Reaction of Chloromethyl Methyl Sulfoxide with Benzophenone. To a solution containing 550 mg of chloromethyl methyl sulfoxide and 970 mg of benzophenone in 5 m*l* of *t*-butanol, 10 m*l* of potassium *t*-butoxide solution (0.77N) in *t*-butanol was added and the resulting solution was stirred for 6 hr at room temperature. The solid deposited by the addition of methylene chloride (50 m*l*) was filtered off and the filtrate was evaporated under reduced pressure. The residue was crystallized from carbon tetrachloride to give 780 mg of 2,2-diphenyl-3-methylsulfinyloxirane **1** as colorless crystals.

An analytical sample was obtained by recrystallization from methylene chloride-carbon tetrachloride (mp 109—110°C); IR (neat): 1034 cm^{-1}, NMR ($CDCl_3$): δ 7.37 (s, 5H), 7.35 (s, 5H), 4.58 (s, 1H), and 2.57 (s, 3H).

Found: C, 69.61; H, 5.43; S, 12.45%. Calcd for $C_{15}H_{14}O_2S$: C, 69.74; H, 5.46; S, 12.39%.

Reduction of **1** *with Lithium Aluminum Hydride.* To a solution containing 200 mg of **1** in 10 m*l* of ether, 150 mg of lithium aluminum hydride was added and the reaction mixture was stirred for 40 hr at room temperature. After the addition of 3N sulfuric acid (3 m*l*), the mixture was extracted with methylene chloride. The organic layer was dried over anhydrous sodium sulfate and evaporated under reduced pressure. The residue was purified by column-chromatography (on silica gel, elution with benzene) to afford 96 mg of a colorless oil. This oil was identical with the product obtained by the reduction of 1,1-diphenyl-2-methylsulfinylethanol[9] with lithium aluminum hydride; bp 120°C/0.2 mmHg, NMR (CCl_4): δ 7.5—7.0 (m, 10H), 3.54 (s, 1H, OH), 3.29 (s, 2H), and 1.98 (s, 3H).

Found: C, 73.97; H, 6.47; S, 13.15%. Calcd for $C_{15}H_{16}OS$: C, 73.73; H, 6.60; S, 13.12%.

Oxidation of **1** *with* m-*Chloroperbenzoic Acid.* *m*-Chloroperbenzoic acid (175 mg) was added to a solution containing 208 mg of **1** in 15 m*l* of methylene chloride and the mixture was stirred for 1 hr under cooling with ice water. After the addition of sodium carbonate (200 mg) to the mixture and stirring for 1 hr at room temperature, insoluble material was filtered off and the filtrate was evaporated under reduced pressure. The residual crystals were recrystallized from carbon tetrachloride-*n*-hexane to yield 100 mg of the aldehyde **4** as colorless crystals; mp 125—126°C, IR (KBr): 1715, 1303, and 1136 cm^{-1}, NMR (CCl_4): δ 9.94 (s, 1H), 7.7—7.2 (m, 10H), and 2.74 (s, 3H), MS (70 eV): *m/e* 274 (M^+), 195 (base peak), 167 (69%), 166 (20%), 165 (51%), and 152 (18%).

Found: C, 65.39; H, 5.17; S, 11.67%. Calcd for $C_{15}H_{14}O_3S$: C, 65.67; H, 5.14; S, 11.69%.

Reaction of Chloromethyl Methyl Sulfoxide with Acetone. To a solution containing 815 mg of chloromethyl methyl sulfoxide in 2.5 m*l* of acetone, 12 m*l* of potassium *t*-butoxide (0.77N) in *t*-butanol was added and the solution was stirred for 11 hr at room temperature. After the addition of methylene chloride (50 m*l*), the deposited solid was filtered off and the filtrate was evaporated under reduced pressure. The residue was chromatographed on silica gel (elution with methylene chloride and methanol-ethyl acetate (1: 5)) to afford 924 mg (95%) of pale yellow crystals which were recrystallized from carbon tetrachloride to give **2** as colorless crystals; mp 88—89°C, IR (KBr): 1039 cm^{-1}, NMR (CCl_4): δ 3.80 (s, 1H), 2.66 (s, 3H), 1.48 (s, 3H), and 1.45 (s, 3H).

Found: C, 44.82; H, 7.50; S, 23.77%. Calcd for $C_5H_{10}O_2S$: C, 44.75; H, 7.51; S, 23.89%.

Oxidation of **2** by *m*-chloroperbenzoic acid was carried out in methylene chloride to yield the corresponding sulfone **3** as a colorless oil; IR (neat): 1317 and 1150 cm^{-1}, NMR ($CDCl_3$): δ 3.85 (s, 1H), 3.00 (s, 3H), 1.72 (s, 3H) and 1.46 (s, 3H).

Found: C, 39.38; H, 6.74; S, 21.10%. Calcd for $C_5H_{10}O_3S$: C, 39.98; H, 6.71; S, 21.35%.

Reaction of Chloromethyl Methyl Sulfoxide with Pinacolone. To a mixture containing 580 mg of chloromethyl methyl sulfoxide and 1.65 g of pinacolone, 10 m*l* of 0.77N potassium *t*-butoxide solution in *t*-butanol was added and the solution was stirred for 11 hr at room temperature. After the addition of 100 m*l* of methylene chloride and 1 m*l* of water, the mixture was dried over anhydrous sodium sulfate. After filtration, the filtrate was evaporated under reduced pressure. The residue was shown by NMR analysis to contain **5** and **6** in a ratio of 74: 26, and was chromatographed on Florisil to give 244 mg of a mixture consisting of **5** and **6** (5: 3), and 247 mg of **5**. An analytical sample of **5** was obtained by recrystallization from methylene chloride-*n*-hexane as colorless crystals; mp 79—81°C, IR (KBr): 1034 cm^{-1}, NMR (CCl_4): δ 3.78 (s, 1H), 2.58 (s, 3H), 1.48 (s, 3H), and 1.00 (s, 9H).

Found: C, 54.60; H, 9.09; S, 18.16%. Calcd for $C_8H_{16}O_2S$: C, 54.51; H, 9.15; S, 18.19%.

Although **6** was not isolated, a compound whose NMR signals (CCl_4) appeared at δ 3.44 (s, 1H), 2.88 (s, 3H), 1.40 (s, 3H), and 1.08 (s, 9H) was assigned to be **6**.

Reaction of Chloromethyl Methyl Sulfoxide with Acetophenone. To a solution containing 365 mg of chloromethyl methyl sulfoxide and 412 mg of acetophenone in 5 m*l* of *t*-butanol, 6 m*l* of 0.77N potassium *t*-butoxide in *t*-butanol was added and the reaction mixture was stirred for 1 hr at room temperature. After the addition of 90 m*l* of methylene chloride and a small amount of activated charcoal, the insoluble solid was filtered off. The filtrate was evaporated under reduced pressure, and the residue was crystallized from carbon tetrachloride - *n*-hexane to give 383 mg (60%) of pale yellow crystals which were shown by NMR analysis to consist of **7** and **8** (3: 2). An analytical sample was obtained by successive recrystallization from carbon tetrachloride and water as a colorless solid; mp 124—128°C, IR (KBr): 1036 cm^{-1}. The NMR signals ($CDCl_3$) of **7** appeared at δ 7.36 (s, 5H), 3.92 (s, 1H), 2.71 (s, 3H), and 1.87 (s, 3H). The NMR of **8** showed the absorption ($CDCl_3$) at δ 7.36 (s, 5H), 4.16 (s, 1H), 2.40 (s, 3H), and 1.80 (s, 3H).

Found: C, 61.04; H, 6.41; S, 16.37%. Calcd for $C_{10}H_{12}O_2S$: C, 61.19; H, 6.16; S, 16.34%.

Reaction of Chloromethyl Methyl Sulfoxide with Thiobenzophenone. To 3.5 m*l* of potassium *t*-butoxide solution (0.77N) in *t*-butanol, 245 mg of chloromethyl methyl sulfoxide and 310 mg of thiobenzophenone were added and the reaction mixture was stirred for 15 min at room temperature. The solid deposited by the addition of 50 m*l* of methylene chloride was filtered off and the filtrate was evaporated under reduced pressure. Crystallization of the residue from *n*-hexane gave 165 mg of colorless crystals. These crystals were dissolved in methanol-methylene chloride. After separation of insoluble crystals, the mother liquor was evaporated under reduced pressure to give 145 mg (38%) of colorless crystals. An analytical sample was obtained by recrystallization from methylene chloride - *n*-hexane; mp 106—107°C, IR (KBr): 1021 cm^{-1}, NMR (CCl_4): δ 7.28 (broad s, 10H), 6.88 (s, 1H), and 2.59 (s, 3H).

Found: C, 74.53; H, 5.91; S, 13.23%. Calcd for $C_{15}H_{14}OS$: C, 74.34; H, 5.82; S, 13.23%.

Independent Synthesis of 1,1-Diphenyl-2-methylsulfinylethylene. Sodium hydride (185 mg) was added to a solution of 1,1-diphenyl-2-methylsulfinylethanol[9] (1.04 g) in 15 m*l* of tetrahydrofuran and the mixture was stirred for 20 min at room temperature. Methyl iodide (3 m*l*) was added and the solution was kept for 30 min at room temperature with stirring. After the addition of water (10 m*l*), the reaction mixture was extracted with methylene chloride. The organic layer was dried over anhydrous sodium sulfate and evaporated under reduced pressure to give colorless crystals which were recrystallized from *n*-hexane to give the corresponding methyl ether (**11**), mp 130.5—132.5°C.

A mixture containing 150 mg of **11** and 2 m*l* of 0.77N potassium *t*-butoxide in *t*-butanol was refluxed for 3.5 hr. After removal of the solvent under reduced pressure, the

residue was chromatographed on silica gel (elution with methylene chloride and ethyl acetate) to afford 39 mg of **9** as colorless crystals, mp 107—107.5°C. These crystals were identical with those obtained by the reaction of chloromethyl methyl sulfoxide with thiobenzophenone (by IR and mixture mp).

We thank Mr. K. Sato and Dr. M. Fukuyama for measurement of the intramolecular nuclear Overhauser effect.

We are grateful for financial support from the Kawakami Memorial Foundation.

BULLETIN OF THE CHEMICAL SOCIETY OF JAPAN, VOL. 45, 2027—2032(1972)

Aminosugars. XX. Synthesis of Some Derivatives of 2-Acetamido-2-deoxy-D-mannose[1]

Juji YOSHIMURA, Hideo SAKAI, Nobuteru ODA, and Hironobu HASHIMOTO

Laboratory of Chemistry for Natural Products, Faculty of Science, Tokyo Institute of Technology, Ookayama, Meguro-ku, Tokyo

(Received January 11, 1972)

Preparation of 2-acetamido-2-deoxy-D-mannose (**2**) by epimerization of the corresponding D-glucose was improved by addition of Ni^{2+} ion to the equilibration system, and several derivatives of **2** were synthesized. *N*-glycosides were obtained by using ammonium chloride as a catalyst, and *p*-nitrophenyl glycoside by a fusion method. The composition of four isomers in benzylglycosidation of **2** was determined to be 66% α-pyranoside (**6**), 11% β-pyranoside, 16% α-furanoside (**5**) and 7% β-furanoside. Benzylidenation of **6** gave the corresponding 4,6-*O*-benzylidene derivative which was converted into the 3-*O*-acetate (**8**) by acetylation, and to the corresponding 2-amino-2-deoxy derivative by treatment with ethanolic potassium hydroxide. Oxidation of **6** with oxygen in the presence of platinum-charcoal and following esterification gave the corresponding methyl uronate which was derived to the di-*O*-acetate (**11**). Periodate oxidation and the following hydrogenation of **5** gave benzyl 2-acetamido-2-deoxy-α-D-lyxofuranoside which was then derived to di-*O*-acetate (**13**). Nitromethane condensation of **2** in barium hydroxide solution gave one isomeric 1-*C*-nitro-1-deoxy-D-heptitol which was converted into methyl 3-acetamido-3-deoxy-D-*glycero*-D-*galacto*-α-heptopyranoside (**18**). First-order analyses of NMR spectra of **8**, **11**, **13**, and tetra-*O*-acetate of **18** are described.

Of the 2-aminosugars found in nature 2-amino-2-deoxy-D-glucose and -D-galactose derivatives have been extensively studied.[2] However, the corresponding D-mannose derivatives have been scarcely investigated at all due to difficulty of availability from both natural and synthetic resources. In addition, 2-acetamido-2-deoxy-D-mannose (**2**) is known to be a component of *N*-acetyl-neuraminic acid,[3] and the corresponding uronic acid was recently found in polysaccharides of bacterial cell walls.[4-6] The authors studied an improved preparation of **2** by the epimerization of 2-acetamido-2-deoxy-D-glucose (**1**), and have synthesized several derivatives.

Results and Discussion

The epimerization of **1** in alkaline mediums such as sodium or ammonium hydroxide solution has been examined,[7-9] but, the formation of **2** at the pseudo-equilibrium did not exceed *ca.* 15%. Considering the yield would increase if the equilibrium was shifted toward **2** by a complex formation with metallic ions, we examined their effect on the epimerization of **1** in ammonium hydroxide solution by PPC. Ions such as Mg^{2+}, Cu^{2+}, $Cr_2O_7^{2-}$, Ca^{2+}, Zn^{2+}, or Ba^{2+} decreased and MoO_4^{2-}, Ni^{2+}, Mn^{2+}, Fe^{3+}, Co^{2+}, or Pb^{2+} ion increased the formation of **2**. Effects of the latter were studied in detail by glc. The results given in Fig. 1 indicate that the addition of nickel ion increased markedly the yield of **2** up to 25%. Though the mechanism is not yet clear, it is obvious that the coexistence of metallic ion change more or less the equilibration between **1** and **2**. From the equilibration mixture, **2** was isolated by an improved method of Carlo *et al.*[10]

As derivatives of **2**, some *N*-glycosides were first prepared in the usual way.[11] When ethanol solution of **2** and aromatic amines (aniline, *o*-toluidine, *m*- and *p*-nitroaniline, and α- and β-naphthylamine) were refluxed

1) Part XIX: This Bulletin, **45**, 1227 (1972).
2) A. B. Fostor and M. Stacey, "Advances in Carbohydrate Chemistry", Vol. 7, ed. by C. S. Hudson, M. L. Wolfrom, and S.M. Cantor, Academic Press Inc., New York, N.Y. (1952), p. 247.
3) D. J. Comb and S. Roseman, *J. Amer. Chem. Soc.*, **80**, 497 (1958).
4) H. R. Perkins, *Biochem. J.*, **83**, 5 (1962).
5) H. Mayer, *European J. Biochem.*, **8**, 139 (1969).
6) T. Miyazaki and T. Yadomae, *Chem. Pharm. Bull.* (Tokyo), **18**, 1249 (1970).
7) S. Roseman and C. T. Spivak, *J. Amer. Chem. Soc.*, **81**, 2403 (1959).
8) P. M. Carroll and J. W. Cornforth, *Biochem. Biophys. Acta*, **39**, 161 (1960).
9) R. Kuhn and G. Baschang, *Ann. Chem.*, **636**, 164 (1960).
10) M. J. Carlo, A. Cosmatos, and H. K. Zimmerman Jr., *ibid.*, **650**, 187 (1961).
11) A. Bertho and D. Koziollek, *Chem. Ber.*, **87**, 934 (1954).

Table 1. Physical constants of *N*-aryl 2-acetamido-2-deoxy-β-D-mannopyranosides (**3**).

	R	Mp (°C)	Yield (%)	$[\alpha]_D^{23}$ (*c* methanol)	Formula	Analysis (%) Calcd C	H	N	Found C	H	N
3a	Phenyl	154—155	62	−163 (1.05)	$C_{14}H_{20}N_2O_5$	56.74	6.80	9.45	55.98	6.57	9.52
3b	*o*-Tolyl	172—173	56.6	−182 (1.10)	$C_{15}H_{22}N_2O_5$	58.05	7.15	9.03	57.93	7.30	9.05
3c	*m*-Nitrophenyl	161—162	28.4	−196 (0.84)	$C_{14}H_{19}N_3O_7H_2O$	46.79	5.91	11.69	47.10	5.72	11.51
3d	*p*-Nitrophenyl	188—189	38.2	−220 (1.04)	$C_{14}H_{19}N_3O_7 1/3H_2O$	48.41	5.71	12.10	48.56	5.61	11.76
3e	β-Naphthyl	146—147	2.6	−179 (0.95)	$C_{18}H_{22}N_2O_5 1/2H_2O$	60.82	6.83	7.88	60.81	6.57	7.78
3f	α-Naphthyl	164—165	8	−154 (0.74)	$C_{18}H_{22}N_2O_5 1/3H_2O$	61.35	6.58	7.95	61.52	6.41	7.93

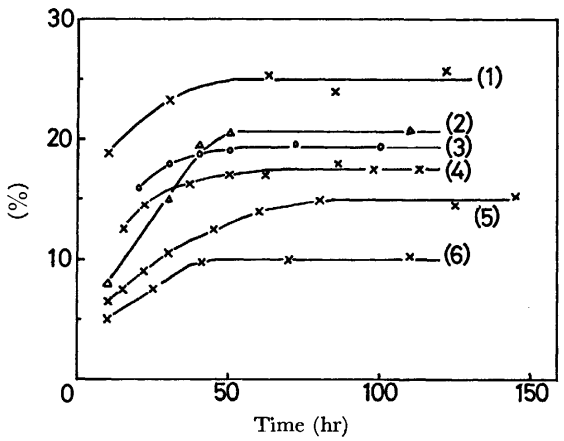

Fig. 1. Effect of metallic salt on the formation of **2** by epimerization of **1**.
(1): $NiCO_3 \cdot Ni(OH)_2$, (2): $Fe_2(SO_4)_3$, (3): $Co(OAc)_2$, (4): $(NH_4)_2MoO_4$, (5): Without metallic salt. (6): $MnSO_4$

in the presence of ammonium chloride as a catalyst, the corresponding *N*-glycosides (**3a**—**f**) were obtained as crystals. However, in the cases of *o*-nitroaniline, 2,4-dinitroaniline and diphenylamine, the starting materials were recovered. Anomeric configuration of **3a**—**f** was deduced to be β from their negative optical rotations. Their physical constants are summarized in Table 1. *p*-Nitrophenyl glycoside (**4**) of **2** was newly prepared from the corresponding *N,O*-pentaacetate by a fusion method[12] in 20.8% yield.

On the other hand, in the benzylglycosidation of **2** in the presence of boron trifluoride and hydrogen chloride carried out by Plimmer *et al.*,[13] only the corresponding α-furanoside (**5**) was isolated as the tri-*O*-acetate in a low yield after acetylation of the products. We repeated the experiment and proved the composition of the corresponding α-pyranoside, β-pyranoside, α-furanoside, and β-furanoside in the product to be 66%, 11%, 16%, and 7%, respectively. After benzylglycosidation, the reaction mixture was poured into water and extracted with ether. Concentration of the aqueous solution gave crystalline benzyl 2-acetamido-2-deoxy-α-D-mannopyranoside (**6**) in 31.7% yield, which was identical with that derived *via* 4,5-(3,4,6-tri-*O*-acetyl-2-deoxy-D-mannopyrano)-2-methyl-Δ^2-oxazoline.[14] The ether extracts were re-extracted with water. Evaporation of the resulting solution gave **5** in 0.5% yield. In order to elucidate the ratio of the four isomers, sirups A and B obtained from the mother liquors of **6** and **5**, respectively, were examined by glc. Sirups A and B showed four and three peaks, respectively, in the ratio given in Fig. 2, and peaks a and d were identified with **6** and **5**, respectively. The other two peaks b and c were deduced to be β-pyranoside and β-furanoside, respectively, from their retention times. The ratio of the four isomers of benzyl glycoside mentioned above was calculated from the yields of **5** and **6**, the area ratio of each peak and the amount of sirup A and B. The results are consistent with the fact that Gross *et al.*[15] isolated ethyl 2-acetamido-2-deoxy-α-D-mannopyranoside from the glycosidation mixture by column chromatography in 62% yield.

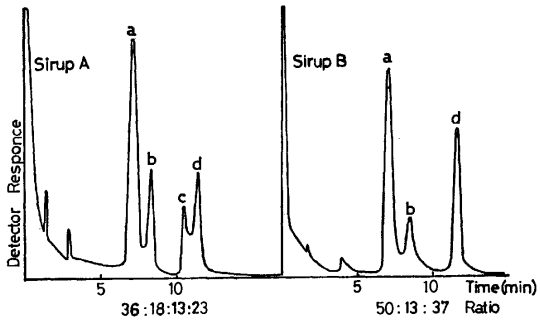

Fig. 2. Gas chromatogram of sirup A and sirup B.
(Column: 1.5% OV-17 on Chromosorb G, 2m×4 mm; carrier gas: N_2, 60 ml/min; temperature: 235°C).

Benzylidenation of **6** gave benzyl 2-acetamido-4,6-*O*-benzylidene-2-deoxy-α-D-mannopyranoside (**7**), whose structure was ascertained by the NMR spectrum of its 3-*O*-acetyl derivative (**8**). *N*-Deacetylation of **7** with potassium hydroxide in ethanol gave benzyl 2-amino-4,6-*O*-benzylidene-2-deoxy-α-D-mannopyranoside (**9**). Catalytic oxidation of **6** with oxygen in the presence of platinum-charcoal gave benzyl 2-acetamido-2-deoxy-α-D-mannopyranosiduronic acid (**10**), whose structure was ascertained by the NMR spectrum of the corresponding methyl 3,4-di-*O*-acetyl-uronate (**11**). In addition, **5** was converted into benzyl 2-acetamido-2-

12) M. L. Wolfrom, P. Chakravarty, and D. Horton, *J. Org. Chem.*, **30**, 2728 (1965).
13) J. R. Plimmer, N. Pravdic, and H. G. Fletcher Jr., *ibid.*, **32**, 1982 (1967).
14) N. Pravdic, T. D. Inch, and H. G. Fletcher Jr., *ibid.*, **32**, 1815 (1967).
15) P. H. Gross, K. Brendel, and H. K. Zimmerman Jr., *Ann. Chem.*, **691**, 198 (1966).

deoxy-α-D-lyxofuranoside (**12**) by periodate oxidation and the succeeding reduction with sodium borohydride. The NMR spectrum of its 3,5-di-*O*-acetyl derivative (**13**) was completely in line with its structure.

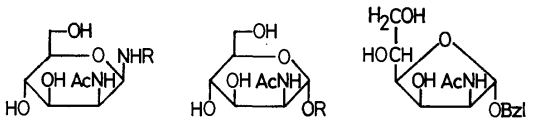

3a: R=phenyl **4** R=*p*-nitrophenyl **5**
b: R=*o*-tolyl **6** R=benzyl
c: R=*m*-nitrophenyl
d: R=*p*-nitrophenyl
e: R=α-naphthyl
f: R=β-naphthyl

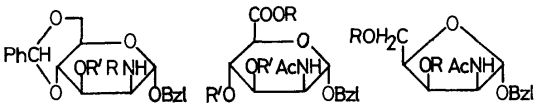

7 R=H, R'=Ac **10** R=R'=H **12** R=H
8 R=R'=Ac **11** R=CH_3 **13** R=Ac
9 R=R'=H R'=Ac

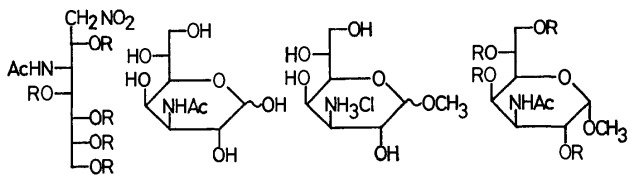

14 R=H **16** **17** **18** R=H
15 R=Ac **19** R=Ac

In a previous paper, one of the authors (J. Y.) reported that nitromethane condensation of D-glucose was accomplished only in water in the presence of barium hydroxide as a catalyst, but not that of **1**.[16] However, 1-*C*-nitro-1-deoxy derivative (**14**) from **2** was easily obtained under the same conditions, which gave the corresponding tetra-*O*-acetate (**15**). The configuration at *C*-2 of **14** was determined by conversion into the corresponding 3-acetamido-3-deoxy-D-heptose (**16**) by the Nef reaction, which was nearly the same as 3-acetamido-3-deoxy-D-*glycero*-D-*galacto*-heptose synthesized by the cyanohydrin method.[9] Methyl-glycosidation of **16** with 3% methanolic hydrogen chloride was accompanied by de-*N*-acetylation to give the corresponding methyl α,β-glycoside hydrochloride (**17**). *N*-Acetylation and per-acetylation of **17** gave pure *N*-acetate (**18**)[9] and *N*,*O*-pentaacetate (**19**) of the corresponding methyl α-D-glycoside, respectively. The configuration of **19** was proved to be methyl 3-acetamido-3-deoxy-D-*glycero*-D-*galacto*-α-heptopyranoside by the analysis of NMR spectrum (Fig. 3). The irradiation of NH or H_4 caused H_3 proton signals to change from an octet to a quartet. However, no change of H_5 proton signals indicates that $J_{4,5}$ is nearly zero. Moreover, irradiation of H_7 caused $H_{7'}$ proton signals to collapse to a doublet and changed the appearance of H_2 and H_6 proton signals. Assignments of H_2 and H_6 protons were also supported by the fact that their tickling caused H_7 and $H_{7'}$ proton signals to collapse to a doublet, and H_5 to a singlet. It would be rational that proton signals attached to carbons having secondary acetoxyl groups appear in lower magnetic field than that of others. NMR parameters of **8**, **11**, **13**, and **19** are summarized in Table 2. We see that coupling constants of ring protons in **8** and **11** present the characteristics of the configuration of α-D-mannopyranoside. The same value for $J_{2,3}$ and $J_{3,4}$ in **13** indicates that it exists in a twist conformation in which C_2 and C_3 atoms are displaced in the opposite sense to the plane of the other ring atoms.[17,18] Similarly, the value for $J_{2,3}$ of **19** is consistent with the di-axial relationship of the D-*glycero*-D-*galacto*-heptopyranoside configuration. It should be noted that distortion of the pyranoside-ring in **19** is suggested by the values for $J_{4,5}$ and $J_{1,2}$.

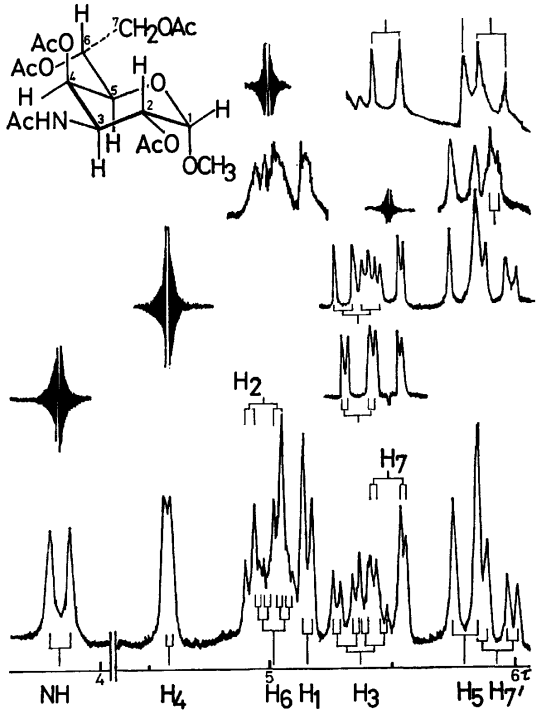

Fig. 3. NMR spectrum of methyl 3-acetamido-3-deoxy-2,4,6,7-tetra-*O*-acetyl-D-*glycero*-D-*galacto*-α-heptopyranoside (100 MHz, $CDCl_3$).

Experimental

The melting points were determined on a sulfuric acid bath and uncorrected. Optical rotations were measured in 0.5 or 0.2-dm tubes with a Carl Zeiss Photoelectric Polarimeter. NMR spectra were recorded at 100 MHz with a JNM 4H-100 Spectrometer, with tetramethylsilane as an internal standard. Glc was carried out with a Shimadzu 4-A Chromatograph using a flame ionization detector. IR spectra were recorded with a Hitachi Model EPI-GS Spectrophotometer. Chemical shifts and coupling constants were recorded in τ and Hz scales, and IR frequencies in cm^{-1}.

Examination of the Effect of Metallic Ions on the Epimerization of 2-Acetamido-2-deoxy-D-glucose (1). *(i) Paper Chromatography*: An aqueous solution of **1** (10 mg) and one of the metallic salts (5 mg) described below was adjusted with

16) J. Yoshimura and H. Ando, *Nippon Kagaku Zasshi*, **85**, 138 (1964).

17) L. D. Hall, *Chem. Ind.* (London), **1963**, 950.

18) H. Ando and J, Yoshimura, This Bulletin, **43**, 2966 (1970).

Table 2. Chemical shifts and coupling constants of ring protons of compounds **8**, **11**, **13**, and **19**[a]

Compound	H_1	H_2	H_3	H_4	H_5	H_6	Other protons
8	4.86(d)	4.62(oct)	4.10(q)	5.55(t)	5.69(sex)	6.43(t)	1.07(NH: d, $J_{NH,H_2}=9.5$), 2.65(Ph), 4.35
	$J_{1,2}=1.0$	$J_{2,3}=6.5$	$J_{3,4}=10$	$J_{4,5}=10$	$J_{5,6'}=11$	5.72(q)	(methine), 5.23 and 5.43 (CH_2: ABq, $J=12$),
					$J_{5,6}=4.5$	$J_{6,6'}=11$	7.85(OAc), 7.98(NAc)
11	5.07(d)	5.30(m)	4.60(q)	4.75(q)	5.67(d)	—	2.66(Ph), 3.64(NH: d, $J_{NH,H_2}=8.8$), 5.26
	$J_{1,2}=2.0$	$J_{2,3}=4.5$	$J_{3,4}=10$	$J_{4,5}=10$	—	—	and 5.44 (CH_2: ABq, $J=12$), 6.27(OCH_3),
							7.99(OAc), 8.03(NAc)
13	4.96(d)	5.27(sep)	4.41(t)	5.54(q)[b]	5.78[b]	—	2.70(Ph), 3.61(NH: d, $J_{NH,H_2}=8.8$), 5.29
	$J_{1,2}=2.5$	$J_{2,3}=5.5$	$J_{3,4}=5.5$	$J_{4,5}=4.4$	—	—	and 5.49 (CH_3: ABq, $J=12$), 7.92 and 7.94
				$J_{4,5'}=6.1$			(OAc), 8.03(NAc)
19	5.15(d)	4.98(q)	5.37(sep)	4.58(d)	5.80(d)	5.01(oct)	3.83(NH: d, $J_{NH,H2}=8.1$), 5.48 and 5.93
	$J_{1,2}=3.5$	$J_{2,3}=11$	$J_{3,4}=2.9$	$J_{4,5}=0.5$	$J_{5,6}=9.4$	$J_{6,7'}=3.9$	($H_{7,7'}$: $J_{7,7'}=12.2$), 6.60(OMe), 7.85,
						$J_{6,7}=2.1$	7.88, 8.02,and 8.13 (NAc and 4×OAc)

a) Compound **8** was measured in pyridine-d_5 and the others in chloroform-d_1.
b) The peaks of H_4, H_5, and H_5 were analyzed as an AB_2 system.

ammonia (*ca.* 1 m*l*) to pH 11, allowed to stand at room temperature for 24 hr, and examined by ppc with a borated paper of Tokyo Filter Paper No. 50A and 1-butanol-pyridine-water (6:4:3, v/v) as a developing solvent. R_f values of **1** and 2-acetamido-2-deoxy-D-mannose were 0.58 and 0.16, respectively, and the amounts of both compounds were roughly estimated by visual comparison of both spots developed with aniline hydrogen phthalate. Metallic salts such as nickel carbonate, ferric sulfate, lead acetate, manganese sulfate, cobalt sulfate, and ammonium molybdate (Group A) increased, and barium hydroxide, magnesium acetate, cupric acetate, calcium acetate, zinc chloride, and potassium dichromate (Group B) decreased the formation of **2**.

(ii) Gas-Liquid Chromatography: A solution of a metallic salt (0.5 g) of group A, **1** (5.0 g), and concentrated aqueous ammonia (0.4 m*l*) in water (15 m*l*) was allowed to stand at room temperature. An aliquot (0.2 m*l*) of the reaction mixture was evaporated to dryness at suitable intervals, and the residue was subjected to gas-liquid chromatography after trimethylsilylation. The yield of **2** was calculated from the ratio of peak areas of **1** and **2**. The retention times of **1** and **2** were 9.2 and 5 min, respectively, under the following conditions. Column: 1.5% OV-17 on Chromosorb G, 3 m×3 mm. Carrier gas: N_2, 1.12 kg/cm^2. Temp.: 165°C.

Preparation of 2-Acetamido-2-deoxy-D-mannose (2). A solution of **1** (500 g) and nickel carbonate (25 g) in water (1.5 *l*) was adjusted to pH 11 with concentrated ammonia (*ca.* 15 m*l*), allowed to stand at room temperature for 3 days under nitrogen atmosphere, and then neutralized by addition of dry ice. Nickel ions were removed from the reaction mixture as sulfide, and the aqueous solution was evaporated. Unchanged **1** deposited during the course of the concentration was recovered by filtration. The sirup remained was dried on phosphorus pentoxide, extracted several times with hot ethanol (each 150 m*l*), and the combined extracts were evaporated after filtration of **1** precipitated. The residual sirup was crystallized from aqueous ethanol (50%)-acetone, and recrystallized from water-acetone. Yield, 100 g (20%); mp 124—126°C (lit,[10] mp 127—128°C).

N-Aryl 2-Acetamido-2-deoxy-β-D-mannopyranosyl Amines (3a—f). A solution of **2** (200 mg), an amine (4 molar equivalent), and ammonium chloride (4 mg) in absolute ethanol (6 m*l*) was refluxed for 1 hr. Partial evaporation of ethanol (4 or 5 m*l*) and addition of ether gave crystals. *N*-Glycosides were recrystallized from ethanol–ether. The results are shown in Table 1. The compounds show characteristic IR absorptions of an amide and aromatics, respectively.

p-Nitrophenyl 2-Acetamido-2-deoxy-α-D-mannopyranoside (4). Acetylation of **2** with a mixture of acetic anhydride and pyridine gave 2-acetamido-2-deoxy-1,3,4,6-tetra-*O*-acetyl-β-D-mannopyranose[12] in 53% yield. To a fused mixture of this acetate (200 mg, 0.51 mmol) and *p*-nitrophenol (287 mg, 2.1 mmol) was added a mixture of acetic acid and acetic anhydride (1 m*l*; 19: 1 v/v) containing *p*-toluenesulfonic acid (4 mg), and heated for 75 min at 120—125°C, with continuous evacuation by a water pump to remove acetic acid. A chloroform solution of the reaction mixture was then washed with water, N-sodium hydroxide, and again water, and concentrated to a sirup. To a solution of the dried sirup in absolute methanol was added metallic sodium (10 mg) under cooling and the reaction mixture was allowed to stand for 2 hr at room temperature, neutralized with Amberlite IR-120 (H^+), and concentrated to a sirup crystallized from ethyl acetate. Yield, 40 mg (20.8%); mp 101—102.5°C; $[\alpha]_D^{23}$ +65.4° (*c* 1.0, methanol). IR: 1640 and 1540 (NHAc), 1590 and 1505 (phenyl), and 1500 (NO_2).

Found: C, 48.26; H, 5.53; N, 7.92%. Calcd for $C_{14}H_{18}N_2O_8 \cdot 1/3H_2O$: C, 48.28; H, 5.40; N, 8.04%.

Benzylglycosidation of 2-Acetamido-2-deoxy-α-D-mannose. An admixture of **2** (100 g, 0.42 mol), distilled benzyl alcohol (920 m*l*) and boron trifluoride etherate (10 m*l*) was heated at 100—105°C for 1 hr under stirring and the reaction was continued for 1 hr after the addition of hydrochloric acid (5 g). The reaction mixture was evaporated *in vacuo* to give a sirup, which was dissolved in water and extracted with ether to remove benzyl alcohol. The water layer was passed through a column of Amberlite IRA-410 (OH^-), decolorized and concentrated to a loose sirup from which benzyl 2-acetamido-2-deoxy-α-D-mannopyranoside (**6**) was deposited. **6** was recrystallized from water; yield, 40.3 g (31%); mp 76—79°C; $[\alpha]_D^{23}$+97.5° (*c* 0.6, chloroform), (lit,[14] mp 73—78°C; $[\alpha]_D^{20}$+97.3°). IR: 1630 and 1560 (NHAc).

Found: C, 57.99; H, 7.10; N, 4.50%. Calcd for $C_{15}H_{21}NO_6$: C, 57.86; H, 6.80; N, 4.50%.

When **6** could not be obtained as crystals, benzylidenation of a part of the dried sirup easily gave benzyl 2-acetamido-4,6-*O*-benzylidene-2-deoxy-α-D-mannopyranoside (**7**) as crys-

tals in *ca.* 30% yield, and hydrolysis of **7** with 60—70% aqueous acetic acid gave **6** as crystals available for seeding.

The ether extract was re-extracted with water, and the water solution was neutralized with Amberlite IRA-410 and concentrated to a sirup, which was crystallized from methanol–*n*-hexane to give benzyl 2-acetamido-2-deoxy-α-D-mannofuranoside (**5**) as crystals. Yield, 0.65 g (0.5%); mp 167—168°C; $[\alpha]_D^{23}$+134.7° (*c* 0.5, methanol), (lit,[13] mp 172—173°C, $[\alpha]_D^{20}$+132°). IR: 1620 and 1560 (NHAc).

Found: C, 58.07; H, 6.91; N, 4.46%. Calcd for $C_{15}H_{21}NO_6$: C, 57.86; H, 6.80; N, 4.50%.

A pure sample of **5** also could be obtained by the purification of crude products *via* 5,6-*O*-isopropylidenation and de-5,6-*O*-isopropylidenation, but the isopropylidene derivative could not be crystallized.

The results of the analysis of sirup obtained from the mother liquor of **5** and **6** by glc are given in Fig. 2.

*Benzyl 2-Acetamido-4,6-*O*-benzylidene-2-deoxy-α-D-mannopyranoside (**7**).* A mixture of **6** (10 g, 32 mmol), benzaldehyde (100 m*l*) and zinc chloride (21 g) was shaken for one day at room temperature, and then poured into ice-water (200 m*l*). The resulting mixture was allowed to stand for 2 hr under occasional stirring, and the water layer was decanted off. An oily liquid which remained was triturated three times with petroleum ether to give a powder, which was washed with ether and crystallized from methanol. Yield, 9.0 g (70%); mp 210—211.5°C; $[\alpha]_D^{23}$+45.6° (*c* 0.8, methanol). IR: 3350 (NH), 1640 and 1520 (NHAc).

Found: C, 66.34; H, 6.42; N, 3.65%. Calcd for $C_{22}H_{25}NO_6$: C, 66.15; H, 6.31; N, 3.51%.

*Benzyl 2-Acetamido-3-*O*-acetyl-4,6-*O*-benzylidene-2-deoxy-α-D-mannopyranoside (**8**).* A sample of **7** (200 mg, 0.5 mmol) was acetylated with acetic anhydride (2 m*l*, 20 mmol) and pyridine (2 m*l*) in the usual way to give **8** quantitatively; mp 221—222°C; $[\alpha]_D^{23}$+61.4° (*c* 1.0, methanol). IR: 3375 (NH), 1715 (OAc), 1670 and 1515 (NHAc).

Found: C, 65.17; H, 6.03; N, 3.26%. Calcd for $C_{24}H_{27}NO_7$: C, 65.29; H, 6.16; N, 3.17%.

*Benzyl 2-Amino-4,6-*O*-benzylidene-2-deoxy-α-D-mannopyranoside (**9**).* A solution of **7** (14.6 g) and potassium hydroxide (39 g) in ethanol (150 m*l*) was refluxed for 16 hr, and then poured into ice-water. The resulting precipitate was filtered, washed with water and recrystallized from ethanol-petroleum ether to give crystals in 78% (10.1 g) yield. Mp 133—134°C; $[\alpha]_D^{23}$+64.7° (*c* 0.6, methanol). IR: 3375, 3310, 1570 (NH_2); NMR ($CDCl_3$): 2.69 (phenyl), 4.52 (methine), 5.24 (H_1; s), 5.35 and 5.56 (–CH_2–; ABq, J=11.8), 6.78 (H_2; d, $J_{2,3}$=4.9), 5.48 (H_3; q, $J_{3,4}$=8.5), 7.78 (OH and NH_2).

Found: C, 67.21; H, 6.84; N, 4.12%. Calcd for $C_{20}H_{23}NO_5$: C, 67.21; H, 6.49; N, 3.92%.

*Benzyl 2-Acetamido-2-deoxy-α-D-mannopyranosiduronic Acid (**10**).* A suspension of **6** (30 g, 96 mmol) and platinum-charcoal (10%, 20 g) in water (600 m*l*) was stirred on a bath at 89—93°C with bubbling of oxygen gas. The pH of the reaction mixture was occasionally adjusted to 7.0—7.8 by the addition of sodium bicarbonate solution, and over oxidation was controlled by the addition of *sec*-butanol. The reaction was followed by tlch wit 1-butanol–water–acetic acid (4:5:1, upper phase), and stopped when a spot of the starting material disappeared. The undissolved materials were then filtered off, and the filtrate was treated with Amberlite IR-120 (H^+) to remove sodium ions, decolorized and concentrated to give a solid which was crystallized from water; yield, 16.0 g (51%), mp 197°C (decomp.), $[\alpha]_D^{23}$+52.6° (*c* 0.5, water). IR: 1705 (COOH), 1615 and 1540 (NHAc).

Found: C, 55.67; H, 5.85; N, 4.25%. Calcd for $C_{15}H_{19}NO_7$: C, 55.38; H, 5.89; N, 4.31%.

*Methyl (Benzyl 2-Acetamido-3,4-di-*O*-acetyl-α-D-mannopyranoside)uronate (**11**).* To a solution of **10** (1.0 g, 3.1 mmol) in methanol (70 m*l*) was added diazomethane (*ca.* 1.1 g, 26 mmol) in ether (15 m*l*) under ice-cooling, and the reaction mixture was allowed to stand for 1 hr at room temperature, and then evaporated to give a sirup which showed two spots on a tlc. An aqueous solution of the sirup was extracted with ether to remove impurities, and concentrated. The resulting sirup was dried and acetylated by the usual method to give **11** as a sirup. Yield, 0.85 g (65%); $[\alpha]_D^{22}$+77.3° (*c* 0.8, methanol). IR: 3280 (NH), 1750 (OAc), 1650 and 1540 (NHAc).

Found: C, 57.20; H, 6.49; N, 3.02%. Calcd for $C_{20}H_{25}NO_9$: C, 56.73; H, 5.95; N, 3.31%.

*Benzyl 2-Acetamido-2-deoxy-α-D-lyxofuranoside (**12**).* To a solution of **5** (1.0 g, 3.2 mmol) in water (16 m*l*) was added sodium metaperiodate (0.76 g, 3.5 mmol) in water (10 m*l*), and the reaction mixture was allowed to stand for 1 hr at room temperature and then sodium borohydride (0.21 g, 5.5 mmol) in water (5 m*l*) was added dropwise under stirring. The resulting solution was deionized with Amberlite IR-120B and IRA-410 and concentrated. The sirup obtained was decolorized in methanol. Evaporation of methanol gave crystals which was recrystallized from methanol–petroleum ether. Yield, 0.8 g (90%); mp 127—128°C; $[\alpha]_D^{23}$+76.7° (*c* 0.26, methanol); IR: 1635 and 1540 (NHAc).

Found: C, 59.39; H, 6.74; N, 4.94%. Calcd for $C_{14}H_{19}NO_5$: C, 59.77; H, 6.81; N, 4.98%.

*Benzyl 2-Acetamido-3,5-di-*O*-acetyl-2-deoxy-α-D-lyxofuranoside (**13**).* Acetylation of **12** (99 mg, 0.35 mmol) with acetic anhydride (1 m*l*, 10 mmol) and pyridine (1 m*l*) gave **13** in 78.6% (102 mg) yield. The substance was recrystallized from ether; mp 122—124°C; $[\alpha]_D^{21}$+99.8° (*c* 0.6, methanol); IR: 3280 (NH), 1750 (OAc), 1650 and 1540 (NHAc).

Found: C, 59.39; H, 6.35; N, 3.79%. Calcd for $C_{18}H_{23}NO_7$: C, 59.18; H, 6.33; N, 3.83%.

*3-Acetamido-1,3-dideoxy-1-*C*-nitro-*D*-glycero-*D*-galacto-heptitol (**14**).* To a mixed solution of **2** (40 g, 167 mmol) in water (80 m*l*) and nitromethane (100 m*l*, 1.85 mol) was added barium hydroxide octahydrate (112 g, 356 mmol) under cooling and stirring. The reaction mixture was stirred for 1 hr at 40—45°C. Ethanol (120 m*l*) was then added to precipitate barium salts. The mixture was allowed to stand overnight in a refrigerator, and the supernatant layer was decanted off, from which **2** was recovered (11.6 g, 29%). The precipitate was dissolved in 2N-acetic acid, and barium ions were immediately removed by addition of 2N-sulfuric acid and filtration. The filtrate was concentrated to give **15** as crystals. When **15** could not be obtained as crystals, the sirup was dissolved in water (50 m*l*) and impurities were extracted with ethyl acetate. The solution was then concentrated again to give **15** as crystals. The product was recrystallized from water-ethanol; yield, 8.4 g (26%); mp 213—214°C (decomp.); $[\alpha]_D^{23}$−50.1° (*c* 1.2, water). IR: 1620 and 1550 (NHAc), 1520 (NO_2).

Found: C, 38.02; H, 6.24; N, 10.20%. Calcd for $C_9H_{18}N_2O_8$: C, 38.30; H, 6.43; N, 9.93%.

*3-Acetamido-2,4,6,7-tetra-*O*-acetyl-1-*C*-nitro-1,3-dideoxy-*D*-glycero-*D*-galacto-heptitol (**12**).* To a suspension of **14** (100 mg, 0.36 mmol) in acetic anhydride (2 m*l*, 19 mmol) was added one drop of concentrated sulfuric acid. The mixture was allowed to stand overnight at room temperature, poured into ice-water (30 m*l*) and extracted with chloroform. The extract was washed with water thorougly and concentrated to give crystals quantitatively, which were recrystallized from

ethanol-ether; mp 131—132°C; $[\alpha]_D^{23}$ −13.7° (*c* 1.04, methanol). IR: 1745 (OAc), 1650 and 1550 (NHAc), 1520 and 1365 (NO_2).

Found: C, 45.98; H, 5.80; N, 5.68%. Calcd for $C_{19}H_{28}N_2O_{13}$: C, 46.35; H, 5.73; N, 5.69%.

3-Acetamido-3-deoxy-D-glycero-D-galacto-*heptose (**16**)*. A solution of **14** (4.0 g, 14.2 mmol) in 2N-sodium hydroxide (50 m*l*) was added dropwise to 14.4N-sulfuric acid (100 m*l*) at a temperature controlled under 2°C. Ice-water (250 m*l*) was poured into the reaction mixture in order to prevent temperature rise. Barium carbonate (284 g) was added to remove sulfate ions, and the mixture was stirred for 6 hr. After the precipitate was filtered off, the filtrate was treated with Amberlite IR-120 (H^+), concentrated to give a residue which was crystallized and recrystallized from water-ethanol. Yield, 3.07 g (86%); mp 215—216°C (decomp.); $[\alpha]_D^{23}$ +162° (5 min), +116° (24 hr), (*c* 0.48, water), (lit,[9] mp 223—225°C, $[\alpha]_D$ +150°→+110°). IR: 1605 and 1555 (NHAc).

Found: C, 42.74; H, 6.81; N, 5.53%. Calcd for $C_9H_{17}NO_7$: C, 43.02; H, 6.82; N, 5.58%.

Methyl 3-Amino-3-deoxy-D-glycero-D-galacto-*α,β-heptopyranoside Hydrochloride (**17**)*. A suspension of dried **16** (1.5 g, 48 mmol) and Drierite (1 g) in methanol (46 m*l*) containing hydrochloric acid (3%) was refluxed for 50 hr, and filtered and the filtrate was evaporated. Hydrochloric acid was completely removed by evaporation three times of a methanol solution of the residue and the residue was crystallized from methanol-ethyl acetate. Yield, 0.90 g (55.8%); mp 212°C (decomp.); $[\alpha]_D^{22}$ +126° (*c* 0.5, water). IR: 1605 and 1520 (NH_3^+).

Found: C, 36.71; H, 7.01; N, 5.62%. Calcd for $C_8H_{17}NO_6 \cdot HCl$: C, 37.00; H, 6.99; N, 5.39%.

Methyl 3-Acetamido-3-deoxy-D-glycero-D-galacto-*α-heptopyranoside (**18**)*. To a solution of **17** (330 mg, 1.27 mmol) in methanol (30 m*l*) containing 31 mg (1.35 mmol) of sodium metal was added acetic anhydride (0.14 m*l*) under stirring. After standing for 1 hr at room temperature, the reaction mixture was treated with silver carbonate (0.3 g) and filtered. The filtrate was deionized with Amberlite IR-120B (H^+), and evaporated to give crystals (326 mg, 97%), which were recrystallized from methanol-ethyl acetate-petroleum ether. Yield, 200 mg (60%): mp 224°C (decomp.); $[\alpha]_D^{22}$ +203° (*c* 0.5, water), (lit,[9] mp 233—236°C, $[\alpha]_D^{23}$ +207°). IR: 3300 (NH), 1640 and 1550 (NHAc).

Found: C, 45.55; H, 7.33; N, 5.56%. Calcd for $C_{10}H_{19}NO_7$: C, 45.28; H, 7.22; N, 5.28%.

Methyl 3-Acetamido-3-deoxy-2,4,6,7-tetra-O-*acetyl*-D-glycero-D-galacto-*α-heptopyranoside (**19**)*. Acetylation of **17** by the usual method gave the corresponding tetraacetate which was recrystallized from ether, in 53.8% yield. Mp 184—186°C; $[\alpha]_D^{21}$ +172° (*c* 1.01, methanol). IR: 3350 (NH), 1740 (OAc), 1660 and 1535 (NHAc).

Found: C, 49.61; H, 6.34; N, 3.00%. Calcd for $C_{18}H_{27}NO_{11}$: C, 49.88; H, 6.28; N, 3.23%.

The authors are indebted to Messrs. K. Fukukawa and H. Matsumoto for NMR measurements, and members of the Laboratory of Organic Analysis for the microanalyses.

BULLETIN OF THE CHEMICAL SOCIETY OF JAPAN, VOL. 45, 2032—2035(1972)

Kinetic Study on Homolysis of Aryl Arylazo Sulfones[1)]

Minoru KOJIMA, Hiroshi MINATO, and Michio KOBAYASHI*

Department of Chemistry, Tokyo Metropolitan University, Fukazawa, Setagaya-ku, Tokyo

(Received December 7, 1971)

Aryl arylazo sulfones were prepared, and the rates of homolyses in chlorobenzene were determined in the presence of a base for suppression of acid catalysis at 80—118°C. An isokinetic relationship was found to hold between $\Delta H^{\ddagger}$ and $\Delta S^{\ddagger}$ (β=101.0°C). The substituents on the benzenesulfonyl group influenced the rates very little, whereas the substituents on the phenylazo group decreased the rates (especially the electron-releasing substituents).

Phenylazo *p*-tolyl sulfone was found to undergo homolysis when such bases as pyridine, quinoline, and magnesium oxide were present for suppression of heterolysis catalyzed by acidic products.[2)]

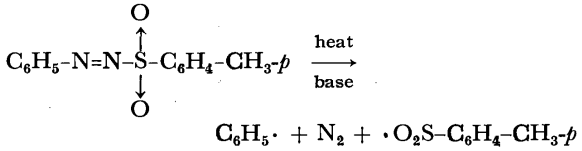

$$C_6H_5\text{-}N{=}N\text{-}\overset{\overset{O}{\uparrow}}{\underset{\underset{O}{\downarrow}}{S}}\text{-}C_6H_4\text{-}CH_3\text{-}p \xrightarrow[\text{base}]{\text{heat}} C_6H_5\cdot + N_2 + \cdot O_2S\text{-}C_6H_4\text{-}CH_3\text{-}p$$

Rates of homolyses of substituted phenylazotriphenylmethanes[3)] and aryl arylazo sulfides[4)] were reported. In contrast to the case of substituted benzoyl peroxides, the rates of decomposition of these azo compounds containing electron-releasing and electron-withdrawing substituents (except that with *p*-methyl) were smaller than that of the non-substituted azo compounds. The effect of the substituents of aryl arylazo sulfones on the rates of decomposition appears to be of great interest, and kinetic studies have been carried out in chlorobenzene. The results will be described in the present paper.

* To whom correspondence should be sent.

1) Organic Sulfur Compounds, Part XXVIII.

2) M. Kobayashi, H. Minato, M. Kojima, and N. Kamigata, This Bulletin, **44**, 2501, (1971).

3) T. Yamamoto, *Nippon Kagaku Zasshi*, **83**, 844, (1962).

4) H. van Zwet and E. C. Kooyman, *Rec. Trav. Chim. Pays-Bas*, **86**, 1143, (1967).

TABLE 1. PHYSICAL PROPERTIES OF ARYL ARYLAZO SULFONES

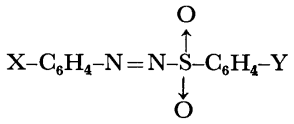

	Substituents		Mp (°C)	Color	Elemental analysis (%)				Ref.
					Found		Calcd		
	X	Y	(decomp.)		C	H	C	H	
a	*p*-$(CH_3)_2N$	*p*-CH_3	130—131	reddish purple	59.45	5.91	59.40	5.65	
b	*p*-CH_3O	*p*-CH_3	110—111	yellow	58.20	4.60	57.92	4.86	(9)
c	*p*-CH_3	*p*-CH_3	96— 97	orange					(7)
d	*p*-Cl	*p*-CH_3	118—119	yellow					(7)
e	*p*-NO_2	*p*-CH_3	135—136	orange	51.03	3.42	51.14	3.63	
f	*m*-CH_3O	*p*-CH_3	84— 85	yellow	58.06	4.66	57.92	4.86	
g	*m*-CH_3	*p*-CH_3	69— 70	yellow					(7)
h	*m*-NO_2	*p*-CH_3	113—114	yellow	51.21	3.70	51.14	3.63	
i	H	*p*-CH_3	90— 91	yellow					(7)
j	H	H	76— 77	orange					(8)
k	H	*p*-Cl	94— 95	yellow	51.13	3.30	51.33	3.23	
l	H	*m*-NO_2	89— 90	yellow	49.38	3.03	49.48	3.11	

Experimental

Materials. Aryl arylazo sulfones except the *p*-dimethylamino derivative were prepared from substituted benzenediazonium chlorides and sodium salts of substituted benzenesulfinic acids according to the method of Hantzsch.[5]

p-Dimethylaminophenylazo *p*-tolyl sulfone was prepared by isolating *p*-dimethylaminobenzenediazonium fluoroborate[6] and letting it react with sodium *p*-toluenesulfinate in water.

Kinetic Measurements. Since the thermal homolyses of aryl arylazo sulfones are complicated because of the occurrence of the heterolyses catalysed by the acidic products (sulfonic acids, sulfinic acids),[2] the rates of decomposition were determined in the presence of pyridine (3 mol per mol of an azosulfone) except the *p*-dimethylamino azosulfone. The rates of decomposition of *p*-dimethylaminophenylazo *p*-tolyl sulfone were determined in the presence of triethylamine (3 mol per mol of the azosulfone), since the azosulfone itself possesses a basicity comparable to that of pyridine.

An azosulfone (3 mmol) was dissolved in a mixture of chlorobenzene (60 m*l*) and pyridine (or triethylamine) in a flask placed in a constant-temperature bath. Decomposition was followed by determining the amount of nitrogen gas evolved by use of a gas buret. The evolution of nitrogen was almost quantitative (more than 90%) with all the azosulfones.

Results and Discussion

Aryl arylazo sulfones prepared are summarized in Table 1. The rates of decomposition of these azosulfones followed first-order equations when a base was present. Some examples are shown in Fig. 1. From

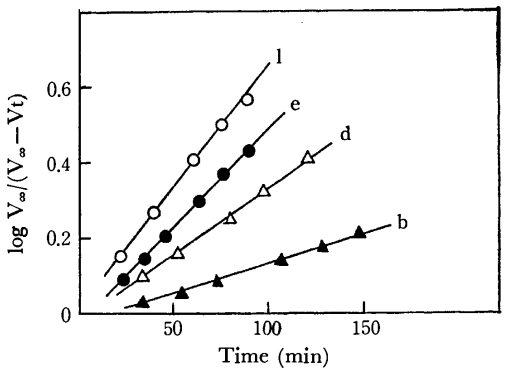

Fig. 1. Typical plots for the rates of decomposition of aryl arylazo sulfones in chlorobenzene at 90.6°C. (Letters in the figure correspond to the compounds described in Table 1. V_∞ and V_t are the volumes of the nitrogen evolved at time ∞ and time t, respectively.)

the rate constants at four or five different temperatures, activation parameters were obtained. Tables 2 and 3 show the rate constants and activation parameters. Figure 2 shows that an isokinetic relationship holds

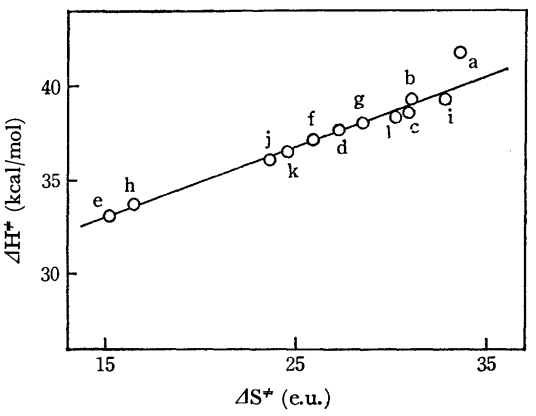

Fig. 2. Isokinetic relationship of aryl arylazo sulfones. (Letters in the figure correspond to the compounds described in Table 1.)

5) A. Hantzsch and M. Singer, *Ber.*, **30**, 312 (1897), **31**, 636, (1898).
6) G. Shiemann and W. Winkelmuller, *ibid.*, **66**, 727, (1933).
7) P. K. Dutt, H. R. Whitehead, and A. Wormall, *J. Chem. Soc.*, **119**, 2088, (1921); *ibid.*, **125**, 1463, (1924).
8) C. G. Overberger and A. J. Rosenthal, *J. Amer. Chem. Soc.*, **82**, 108, (1960).
9) R. L. Schlessinger, U. S. 2588885 (1952).

Table 2. Results of decomposition of substituted phenylazo *p*-tolyl sulfones in chlorobenzene

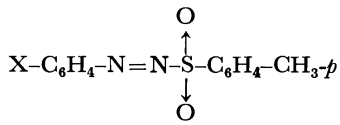

	Substituents	$10^4 \times k(\mathrm{sec}^{-1})$[a]						$\Delta H^{\ddagger}$	$\Delta S^{\ddagger}$
	X	80.0°C	85.4°C	90.6°C	95.6°C	99.4°C	102.7°C	(kcal/mol)	(e.u.)
b	*p*-CH_3O			0.697	1.38	2.24	4.21	39.4	30.0
c	*p*-CH_3		0.638	1.41	2.85	4.07		38.7	29.9
d	*p*-Cl		0.696	1.39	2.09	5.06		37.7	27.2
e	*p*-NO_2		1.16	2.08	4.06	6.81		33.1	15.2
f	*m*-CH_3O		0.797	1.51	2.84	6.13		37.1	25.9
g	*m*-CH_3		0.961	1.66	3.45	6.72	10.8	38.1	28.5
h	*m*-NO_2		0.897	1.58	3.12	5.48		33.7	16.5
i	H	0.494	1.08	2.52	5.38			39.4	32.8
		$10^4 \times k(\mathrm{sec}^{-1})$							
			105.0°C	109.0°C	115.0°C	118.0°C			
a	*p*-$(CH_3)_2N$		1.13	2.17	5.36	7.23		41.8	33.5

a) Rate constants are reproducible within ± 3%.

Table 3. Results of decomposition of aryl phenylazo sulfones in chlorobenzene

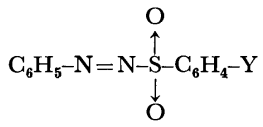

	Substituents	$10^4 \times k$ (sec^{-1})						$\Delta H^{\ddagger}$	$\Delta S^{\ddagger}$
	Y	80.0°C	85.4°C	90.6°C	95.6°C	99.4°C	102.7°C	(kcal/mol)	(e.u.)
j	H	0.536	1.16	2.68	4.63			36.0	23.5
i	*p*-CH_3	0.494	1.08	2.52	5.38			39.4	32.8
k	*p*-Cl			2.07	4.14	6.93	10.86	36.5	24.5
l	*m*-NO_2		1.35	2.46	4.73	9.38		38.4	30.2

between the $\Delta H^{\ddagger}$ and $\Delta S^{\ddagger}$ values, and β is equal to 101.0°C. This fact suggests that all the azosulfones decompose by the same mechanism.

Figure 3 is the plots of log k_X/k_H *versus* the Hammett σ values for substituted phenylazo *p*-tolyl sulfones at 90.6°C. It is remarkable that the rates of all the substituted azosulfones are smaller than that of phenylazo *p*-tolyl sulfone itself, and the rates of the azosulfones with electron-releasing substituents are especially small. A

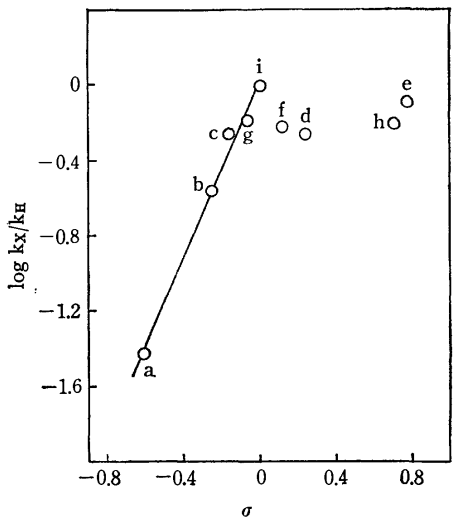

Fig. 3. Relationship between σ values and log k_X/k_H (90.6°C) (Letters in the figure correpond to the compounds described in Table 1. The value for a was calculated from those at higher temperatures.)

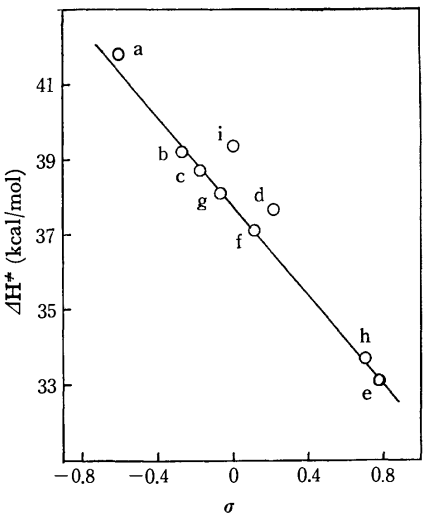

Fig. 4. Relationship between $\Delta H^{\ddagger}$ and σ values. (Letters in the figure correspond to the compounds described in Table 1.)

linear relationship seems to hold for azosulfones containing electron-releasing substituents, but not for those with electron-withdrawing substituents. These findings are in contrast with the results with substituted phenylazotriphenylmethanes and aryl arylazo sulfides; in the latter cases, the rates of the azo compounds containing electron-withdrawing substituents were especially small.

Figure 4 shows that a fair linear relationship holds between $\Delta H^{\ddagger}$ and the Hammett σ values.

The $\Delta S^{\ddagger}$ values for these azosulfones are much greater than those of other azo compounds. It is likely that in the ground states, these azosulfones are greatly polarized and strongly solvated, whereas in their transition states the C–N and S–N bonds are stretched and the extent

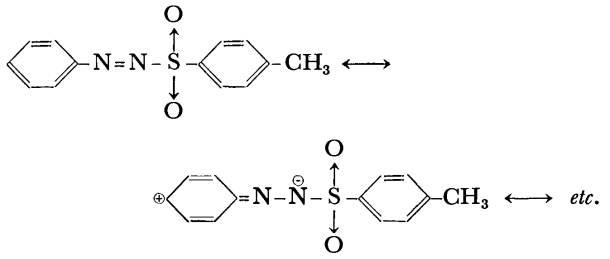

of solvation is much smaller, and therefore the $\Delta S^{\ddagger}$ values are very large.

Table 3 summarizes the rate constants of aryl phenylazo sulfones. The rate constants do not vary greatly with the substituents. These results are in contrast with those of p-MeC_6H_4–N=N–S–C_6H_4–Y (for example, $k_H/k_{p\text{-}NO_2}$ is equal to about 20).[4]

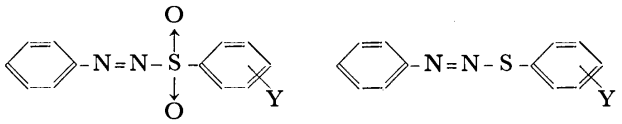

It is reasonable that the strength of the N–S bond of the azosulfide is greatly influenced by the resonance involving the S lone pair and the electrophilic substituents on the benzene ring, whereas the strength of the N–S bond of the azosulfone is very little affected by the substituents across the sulfonyl group.

Aryl arylazo sulfones can be synthesized very easily and are fairly stable (no decomposition for several months at 0°C). Therefore, they are very useful as a source of substituted phenyl free radicals.

BULLETIN OF THE CHEMICAL SOCIETY OF JAPAN, VOL. 45, 2035—2039(1972)

Aroyl Arenesulfonyl Peroxides. V. Mechanisms of the Reactions of Benzoyl *p*-Toluenesulfonyl Peroxide with Several Nucleophiles[1)]

Ryuki HISADA, Michio KOBAYASHI, and Hiroshi MINATO

Department of Chemistry, Faculty of Science, Tokyo Metropolitan University, Fukazawa, Setagaya, Tokyo

(Received January 14, 1972)

Reactions of benzoyl *p*-toluenesulfonyl peroxide (BTP) with several nucleophiles were investigated. The reaction with triphenylphosphine gave benzoyl *p*-toluenesulfonate and triphenylphosphine oxide, that with diphenyl sulfide gave benzoyl *p*-toluenesulfonate and diphenyl sulfoxide, and that with *p*-tolylmagnesium bromide gave *p*-tolyl *p*-toluenesulfonate and benzoic acid. In the reaction of BTP[carbonyl-^{18}O] with triphenylphosphine, 88% of carbonyl oxygen-18 was retained as the carbonyl oxygen of the benzoyl *p*-toluenesulfonate formed, whereas in the reaction of BTP[carbonyl-^{18}O] with diphenyl sulfide only 58% of the label in the starting peroxide was found in the carbonyl oxygen of the benzoyl *p*-toluenesulfonate formed. In the reaction of BTP[sulfonyl-^{18}O] with *p*-tolylmagnesium bromide, it was found that the two sulfonyl oxygens of BTP were completely retained in the two sulfonyl oxygens of the *p*-tolyl *p*-toluenesulfonate formed. Possible mechanisms of these reactions are discussed.

Benzoyl *p*-toluenesulfonyl peroxide (BTP) has been synthesized in our laboratories. Investigation on its decomposition under various conditions has revealed that the O–O bond of BTP tends to undergo heterolytic cleavage, and that the heterolysis is the main reaction unless some base is present in the medium for suppression of autocatalysis.[2)]

Diacyl and diaroyl peroxides are known to react with such nucleophiles as triphenylphosphine.[3)] The reactions of BTP with various nucleophiles seem to be of great interest. Detailed investigation was carried out in order to determine which of the two peroxidic oxygen atoms is attacked and what products are formed from this unsymmetrical peroxide. The results are given in this paper.

Results and Discussion

When a carbon tetrachloride solution of triphenylphosphine or diphenyl sulfide was stirred into a carbon tetrachloride solution of benzoyl *p*-toluenesulfonyl peroxide (BTP) at 10°C, the mixture became turbid in five minutes, and fine needles precipitated. When such a mixture was heated at 30°C for 30 min, it became transparent again. The completion of the reaction was

1) Organic Sulfur Compounds. XXXI.

2) R. Hisada, H. Minato, and M. Kobayashi, This Bulletin, **44**, 2541 (1971).

3) a) L. Horner and W. Jurgeleit, *Ann. Chem.*, **591**, 138 (1955). b) M. A. Greenbaum, D. B. Denney, and A. K. Hoffmann, *J. Amer. Chem. Soc.*, **78**, 2563 (1956). c) D. B. Denney and M. A. Greenbaum, *ibid.*, **79**, 979 (1957).

Table 1. Reaction products of BTP with triphenylphosphine and diphenyl sulfide (mol/100 mol of BTP)

Products	Nucleophiles	
	Ph_3P	Ph_2S
Ph_3PO	96	—
Ph_2SO	—	81
$PhCO_2Ts$[a]	86[b] 98[c]	98[e] 96[c]
$PhCO_2H$	11[d]	

a) Determined by conversion into BzNHPh and TsOH or BzOH and TsOH on account of its instability.
b) Determined as BzNHPh.
c) Determined as TsOH.
d) Probably formed by hydrolysis during the reaction with aniline.
e) Determined as BzOH.

shown by disappearance of the infrared absorption of the peroxidic carbonyl group of BTP. The reaction was completed in about one hour with triphenylphosphine, but it took about 6 hr with diphenyl sulfide. The main product was identified to be benzoic *p*-toluenesulfonic anhydride, on the basis of a comparison of its infrared spectrum with that of an authentic sample prepared by the method of Karger and Mazur.[4] Since the anhydride is unstable toward hydrolysis, it was determined by converting it into BzNHPh and TsOH or BzOH and TsOH. The results are shown in Table 1. The reactions can be expressed as follows.

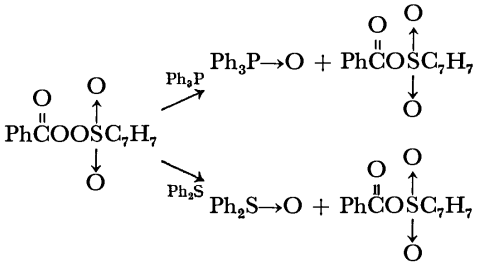

In order to investigate the detailed mechanism of these reactions, BTP [carbonyl-^{18}O] was synthesized

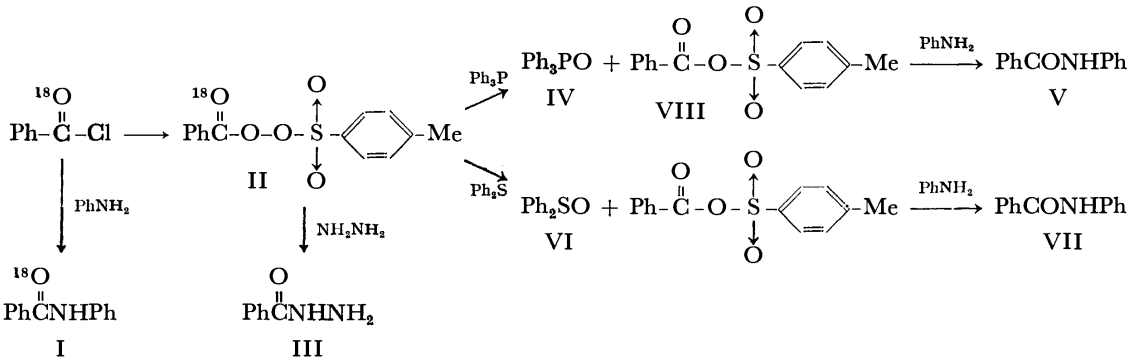

Table 2. Excess oxygen-18 atom % in various compounds related to the reactions with triphenylphosphine and with diphenyl sulfide[a]

	Nucleophile							
	Ph_3P				Ph_2S			
	Run 1		Run 2		Run 1		Run 2	
	Found	Calcd[b]	Found	Calcd[b]	Found	Calcd[b]	Found	Calcd[b]
$PhC(^{18}O)NHPh$ (I)	1.28	(1.28)	1.20	(1.20)	1.28	(1.28)	1.20	(1.20)
$PhC(^{18}O)OOTs$ (II)	0.27	0.26	0.24	0.24	0.27	0.26	0.24	0.24
$PhC(O)NHNH_2$ (III)	1.27	1.28	1.00	1.20	1.27	1.28	1.00	1.20
$PhC(O)NHPh$ (V or VII)	1.14	1.28	1.06	1.20	0.66	1.28	0.62	1.20
Ph_3PO (IV)	0.14	0	0.17	0	—	—	—	—
Ph_2SO (VI)	—	—	—	—	0.47	0	0.46	0
TsOH formed from $PhCOTs$	(c)	0	0.01	0	(c)	0	0.04	0

a) Experimental error in two experiments for the same sample was within ±0.02 excess atom %.
b) Calculated on the assumption that the carbonyl oxygen of BTP becomes the carbonyl oxygen of the anhydride without scrambling.
c) Not determined.

4) M. H. Karger and Y. Mazur, *J. Org. Chem.*, **36**, 528 (1971).

and the products of its reaction with triphenylphosphine and diphenyl sulfide were analyzed. The oxygen-18 contents of compounds (I)—(VIII) shown in the above scheme were determined. The results are shown in Table 2.

Benzanilide (V) formed from the anhydride obtained by the reaction with triphenylphosphine contains 88% of the excess oxygen-18 in the original BTP, whereas benzanilide (VII) formed from the anhydride obtained by the reaction with diphenyl sulfide contains only 58% of the excess oxygen-18 in the original BTP. This means that during the reaction with triphenylphosphine the carbonyl oxygen of the original BTP is retained as the carbonyl oxygen of the anhydride to a considerable extent, whereas the carbonyl oxygen of BTP is almost completely scrambled during the reaction with diphenyl sulfide.

These reactions can be expressed as follows.

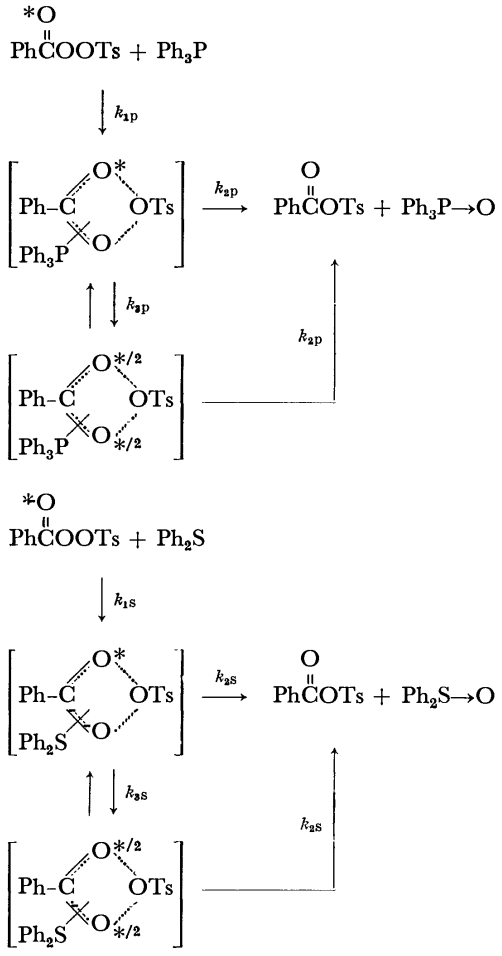

In this scheme, k_{1p} (or k_{1s}) is the rate of the complex formation between BTP and the nucleophile, k_{3p} (or k_{3s}) that of the oxygen scrambling in the complex, and k_{2p} (or k_{2s}) the rate of the formation of the final products from the complex. The exact nature of the complex has not been clarified as yet.

The results of ^{18}O analyses indicate that k_{2p} is greater than k_{3p} whereas k_{2s} is smaller than k_{3s}.

The fact that both triphenylphosphine oxide and diphenyl sulfoxide contain some excess oxygen-18 can be explained by the assumption that (a) the nucleophiles attack both the carbonyl and peroxidic oxygen atoms, or (b) the nucleophiles attack the peroxidic oxygen atom and then some scrambling takes place before the anhydride is formed. Although the possibility (a) cannot be strictly excluded, it is less likely since both benzoyl peroxide[3b] and *m*-nitrobenzenesulfonyl peroxide[5] react with triphenylphosphine at their peroxidic oxygen atoms.

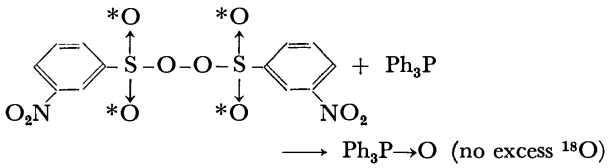

It is interesting to note that in the reactions of BTP with triphenylphosphine and diphenyl sulfide the peroxidic oxygen atom attacked is the one adjacent to the benzoyl group, and not the one adjacent to the more electron-withdrawing tosyl group. Denney and Greenbaum[3c] studied the reaction of *p*-nitrobenzoyl *p'*-methoxy-benzoyl peroxide with tri-*t*-butylphosphine, and showed that the peroxidic oxygen atom adjacent to the more electron-withdrawing *p*-nitrobenzoyl group was attacked by tri-*t*-butylphosphine.

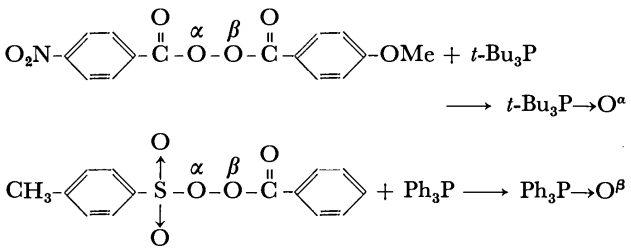

p-Tolylmagnesium bromide was chosen as another nucleophile and its reaction with BTP was investigated. When an ethereal solution of *p*-tolylmagnesium bromide was stirred into an ethereal solution of BTP under a nitrogen atmosphere at 3°C, white precipitates were formed immediately. The products were analyzed after stirring for 3 hr. Results: benzoic acid (91%), *p*-tolyl *p*-toluenesulfonate (41%) and *p*-toluenesulfonic acid (46%).

In order to study the mechanism of this reaction in detail, BTP [sulfonyl-^{18}O] was synthesized and its reaction with *p*-tolylmagnesium bromide investigated. The distribution of the excess oxygen-18 in *p*-tolyl *p*-toluenesulfonate formed was determined by converting it into *p*-cresol and *p*-toluenesulfonic acid, according to the scheme (next page). The results are summarized in Table 3.

The data in Table 3 show that the sulfonyl oxygen of BTP is completely retained as the sulfonyl oxygen of *p*-tolyl *p*-toluenesulfonate within experimental error. This indicates that the following mechanism (next page) is plausible.

The reaction with the Grignard reagent is in contrast to the reactions with triphenylphosphine and diphenyl sulfide; and coordination between the basic carbonyl oxygen atom and the electrophilic magnesium atom takes place first, probably determining the course of the reaction. It is known that carbonyl oxygen atoms are much more basic than sulfonyl oxygen atoms.

5) Y. Yokoyama, H. Wada, M. Kobayashi, and H. Minato, This Bulletin, **44**, 2479 (1971).

Table 3. Excess oxygen-18 atom % in various compounds related to the reaction of BTP[sulfonyl-^{18}O] with *p*-tolylmagnesium bromide[a)]

Compound	Run 1		Run 2	
	Found	Calcd[b)]	Found	Calcd[b)]
H_3C-C$_6$H$_4$-$S^{18}O_2Cl$ (VIII)	0.46	(0.46)	0.91	(0.91)
H_3C-C$_6$H$_4$-S(^{18}O)OOBz (IX)	0.20	0.18	0.37	0.36
H_3C-C$_6$H$_4$-SO(=O)-C$_6$H$_4$-CH_3 (X)	0.29	0.31	0.55	0.61
H_3C-C$_6$H$_4$-SO_3H (XI)	0.32	0.31	0.60	0.61
$CH_3C_6H_2Br_2OH$ (XII)	0.01	0	0.03	0

a) Experimental error in two experiments for the same sample was within ±0.02 excess atom %.
b) Calculated on the assumption that the sulfonyl oxygen-18 is not equilibrated with the peroxidic oxygen.

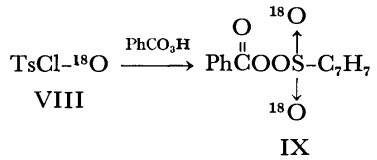

VIII IX

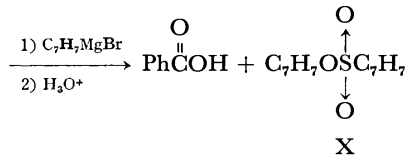

X

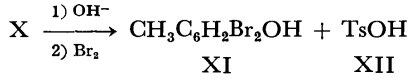

XI XII

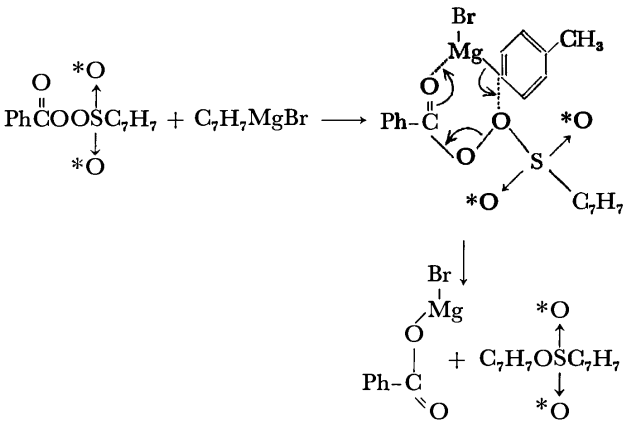

Ōkubo, Maruyama, and Ōsugi[6)] studied the reactions of substituted benzoyl peroxides with Grignard reagents, and found that even *p*-fluorobenzoyl *p'*-methoxybenzoyl peroxide is attacked at both the peroxidic oxygens yielding two esters.

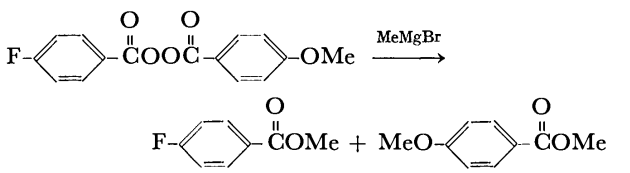

6) M. Ōkubo, K. Maruyama, and J. Ōsugi, This Bulletin **44**, 125 (1971).

When BTP is mixed with excess anhydrous hydrazine, its carbonyl carbon atom is attacked by the nucleophile, benzhydrazide being formed in 67% yield. Sodium methoxide reacts with BTP in a similar manner, producing methyl benzoate.

Thus, benzoyl *p*-toluenesulfonyl peroxide is attacked by nucleophiles at three different positions, *viz.*, a) the peroxidic oxygen atom adjacent to the benzoyl group (Ph_3P and Ph_2S), b) the peroxidic oxygen atom adjacent to the sulfonyl group (RMgBr) and c) the carbonyl carbon atom (N_2H_4 and NaOMe).

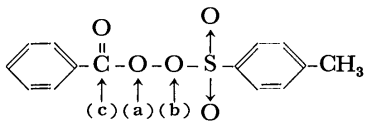

Experimental

Materials. Triphenylphosphine, extra pure grade of Wako Chemicals, was used without further purification. Diphenyl sulfide was prepared according to the procedure of Hartman, Smith and Dickey[7)] and distilled under reduced pressure; the fraction boiling at 162—163°C/18 mmHg was collected and used. The preparation of BTP[carbonyl-^{18}O] and BTP[sulfonyl-^{18}O] was described in a previous paper.[8)] *p*-Tolylmagnesium bromide was prepared according to the procedure of Lawesson and Yang.[9)]

Reaction of BTP[carbonyl-^{18}O] with Triphenylphosphine. To 1.46 g (5 mmol) of BTP[carbonyl-^{18}O] dissolved in 200 m*l* of carbon tetrachloride was added 1.44 g (5.5 mmol) of triphenylphosphine in 50 m*l* of carbon tetrachloride with stirring at 10°C. The reaction mixture was then warmed up to 30°C and allowed to stand for 15 hr. After 1.12 g (12 mmol) of freshly distilled aniline was added to the reaction mixture, it was refluxed for 30 min, washed successively with water, dilute hydrochloric acid and water, and then dried over anhydrous magnesium sulfate. Carbon tetrachloride

7) W. W. Hartman, L. A. Smith, and J. B. Dickey, "Organic Syntheses," Coll. Vol. II, p. 242.
8) R. Hisada, H. Minato, and M. Kobayashi, submitted to This Bulletin.
9) S. O. Lawesson and N. C. Yang, *J. Amer. Chem. Soc.*, **81**, 4230 (1959).

was evaporated under reduced pressure. The residue was chromatographed on active alumina (300 mesh).

Benzanilide (86% yield), mp 162—163°C (lit,[10] 160—161°C) and triphenylphosphine oxide (96% yield), mp 153°C (lit,[11] 153.5°C) were obtained and recrystallized three times from a mixture of benzene and ether. They were subjected to the determination of ^{18}O-contents, according to the method described previously.[5] From the aqueous layer, benzoic acid was isolated and weighed (11% yield) and *p*-toluenesulfonic acid was weighed as its *S*-benzylisothiuronium salt (98% yield).

Reaction of BTP[carbonyl-^{18}O] with Diphenyl Sulfide. To 1.46 g (5 mmol) of BTP[carbonyl-^{18}O] dissolved in 200 m*l* of carbon tetrachloride was added 1.02 g (5.5 mmol) of diphenyl sulfide in 50 m*l* of carbon tetrachloride with stirring at 10°C. The mixture was treated in a manner similar to that for the reaction with triphenylphosphine.

Benzanilide and diphenyl sulfoxide obtained from the reaction mixture of BTP[carbonyl-^{18}O]-diphenyl sulfide-aniline could not be completely separated from each other by elution chromatography. They were purified by repeated recrystallizations from a mixture of benzene and *n*-hexane; BzNHPh, mp 162°C, and Ph_2SO, mp 70°C (lit,[12] 70—71°C).

Since the yields could not be determined by this technique, unlabeled BTP was allowed to react with diphenyl sulfide, and benzoic *p*-toluenesulfonic anhydride produced was hydrolyzed to benzoic acid and *p*-toluenesulfonic acid; the former was weighed (98% yield), and the latter was converted into its *S*-benzylisothiuronium salt and weighed (96% yield). Diphenyl sulfoxide and unreacted diphenyl sulfide were determined by gas chromatography (column: silicone oil SE 30, 1 m; 190°C; internal standard, *p*-tolyl benzoate), yield, 81% and 13%, respectively.

Reaction of BTP[sulfonyl-^{18}O] and p-*Tolylmagnesium Bromide.* To 2.64 g (9 mmol) of BTP[sulfonyl-^{18}O] in 100 m*l* of anhydrous ether was added 9 mmol of *p*-tolylmagnesium bromide in 50 m*l* of ether under a nitrogen atmosphere at 3°C with stirring. After the reaction mixture was allowed to stand at 3—5°C for 3 hr with stirring, water was added. The ethereal layer was separated from the aqueous layer, washed successively with a 10% sodium hydrogen carbonate solution and water, and dried over anhydrous magnesium sulfate. After the ether was removed under reduced pressure, the residue was chromatographed on silica gel (Wako Gel Q 22). *p*-Tolyl *p*-toluenesulfonate isolated (41% yield) was recrystallized three times from *n*-hexane, mp 69—69.5°C (lit,[13] 69—70°C). The aqueous layer was acidified with hydrochloric acid and extracted with ether. After the combined extracts were dried over anhydrous magnesium sulfate, the solvent was evaporated and the benzoic acid isolated was weighed (91% yield). *p*-Toluenesulfonic acid was determined as its *S*-benzylisothiuronium salt (46% yield).

p-Tolyl *p*-toluenesulfonate was hydrolyzed to *p*-cresol and *p*-toluenesulfonic acid. *p*-Cresol was converted by bromine water into 2,6-dibromo-*p*-cresol, which was purified twice by sublimation, mp 48—49°C (lit,[14] 49°C). *p*-Toluenesulfonic acid was obtained as *S*-benzylisothiuronium salt, and recrystallized three times from water, mp 180—181°C.

10) C. N. Webb, "Organic Syntheses," Coll. Vol. I, p. 82.
11) A. Michaelis and W. La Coste, *Ber.*, **18**, 2118 (1885).
12) O. Hinsberg, *ibid.*, **43**, 289 (1910).
13) F. Reverdin and P. Crépieux, *ibid.*, **35**, 1439 (1902).
14) C. Schall and C. Dralle, *ibid.*, **17**, 2528 (1884).

BULLETIN OF THE CHEMICAL SOCIETY OF JAPAN, VOL. 45, 2039—2042(1972)

Photolysis of Phenylazo *p*-Tolyl Sulfones[1)]

Michio KOBAYASHI, Sadao FUJII, and Hiroshi MINATO

Department of Chemistry, Tokyo Metropolitan University, Fukazawa, Setagaya-ku, Tokyo

(Received January 14, 1972)

Photolysis of phenylazo *p*-tolyl sulfone and *p*-chlorophenylazo *p'*-tolyl sulfone in aromatic solvents at room temperature was investigated. The products were analyzed, and the isomer distribution and partial rate factors in arylation of mono-substituted benzenes were determined. The results indicate that the photolysis involves formation of aryl radicals and *p*-tolylsulfonyl radicals.

Arylazo aryl sulfones are interesting compounds; they undergo both heterolysis and homolysis. As an example, when phenylazo *p*-tolyl sulfone (I) is placed in an acidic medium, phenyl cation is formed,[2)] whereas I yields phenyl radical when it is heated in a medium containing magnesium oxide, pyridine, or quinoline which captures *p*-toluene sulfonic acid.[3)]

Thermal decomposition of I in a non-acidic medium is not so fast, and the half-life at 60°C is about 20 hr

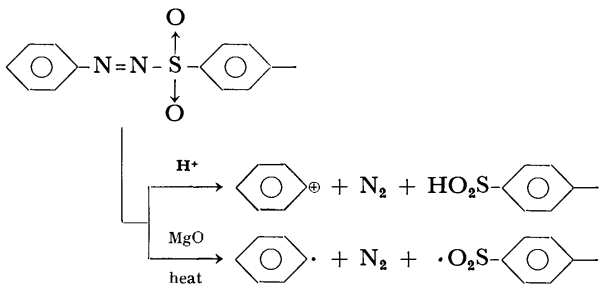

($\Delta H^{\ddagger}$=30.8 kcal/mol, $\Delta S^{\ddagger}$=10.7 e.u./mol)[3)] in ethylbenzene.

Since azosulfones absorb at wavelength over 400 nm owing to the n-π^* transition of the azo group, they are

1) Organic Sulfur Compounds. Part XXXII.

2) M. Kobayashi, H. Minato, and N. Kobori, This Bulletin, **43**, 219 (1970).

3) M. Kobayashi, H. Minato, M. Kojima, and N. Kobori, *ibid.*, **44**, 2501 (1971).

expected to undergo photolysis. The photolyses of I and *p*-chlorophenylazo *p'*-tolyl sulfone (II) have been investigated in aromatic solvents, and the results are described in this paper.

Results and Discussion

Solutions of I in equimolar mixtures of benzene and a monosubstituted benzene were degassed and irradiated with a high pressure mercury lamp at room temperature. Considerable amounts of biaryls were isolated when reaction mixtures were washed with water and the organic layers were subjected to column chromatographic separation on Florisil or alumina. Quantitative determination of biphenyl and substituted biphenyl isomers were carried out by gas chromatography, and the partial rate factors were calculated. As regards anisole or nitrobenzene, photolysis was performed in a mixture with chlorobenzene instead of benzene, and the amounts of substituted biphenyls formed were determined. The partial rate factors in these solvents were calculated by using the partial rate factors in chlorobenzene. The results are summarized in Table 1.

TABLE 1. ISOMER DISTRIBUTIONS AND PARTIAL RATE FACTORS IN PHENYLATION WITH I

Substrate	Isomer distribution (%)			Partial rate factors		
	o	*m*	*p*	*o*	*m*	*p*
Anisole	72.6	13.5	13.9	4.99	0.94	1.92
Ethylbenzene	54.8	29.6	15.6	2.41	1.30	1.37
Chlorobenzene	62.5	22.5	15.0	2.95	1.06	1.42
Benzonitrile	50.0	20.0	30.0	3.64	1.46	4.37
Nitrobenzene	61.7	13.2	25.1	5.34	1.14	4.37

When the values of log (partial rate factors at para positions) were plotted *versus* the Hammett σ-values, a V-shaped line was obtained as shown in Fig. 1. The ρ value for the right half was +0.90 (γ, 0.988), which is comparable to the ρ value (1.21) obtained by the thermal homolysis of I.[3] The isomer distributions and partial rate factors shown in Table 1 are similar to those obtained with phenyl radical (Table 2 (a)), but quite different from those with phenyl cation (Table 2 (b)).[2]

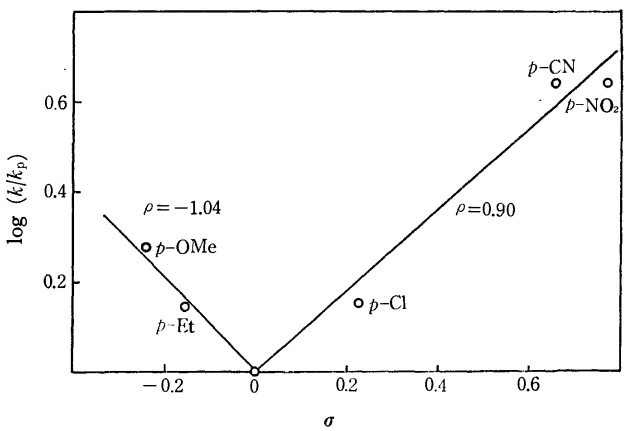

Fig. 1. The Hammett plots for phenylation of substituted benzenes by phenylazo *p*-tolyl sulfone

These data indicate that the biphenyls shown in Table 1 arose from the attack of phenyl radical on aromatic solvents. The free-radical nature of the substitution is exemplified by the values in benzonitrile and nitrobenzene; –CN and $-NO_2$ are *o*,*p*-directors and the partial rate factors are greater than unity.

TABLE 2. ISOMER DISTRIBUTIONS AND PARTIAL RATE FACTORS IN PHENYLATION WITH (a) PHENYL RADICAL AND (b) PHENYL CATION

(a) Phenyl Radical (from I in a non-acidic medium)[3]

Substrate	Isomer distribution (%)			Partial rate factors		
	o	*m*	*p*	*o*	*m*	*p*
Anisole	65.8	21.4	12.8	4.79	1.56	1.89
Ethylbenzene	53.5	30.1	16.4	2.02	1.14	1.24
Chlorobenzene	60.6	22.8	16.6	3.63	1.36	1.99
Benzonitrile	49.4	15.6	35.0	5.20	1.66	7.38
Nitrobenzene	65.7	8.3	26.0	11.07	1.42	8.72

(b) Phenyl Cation (from I in an acidic medium)[2]

Substrate	Isomer distribution (%)			Partial rate factors		
	o	*m*	*p*	*o*	*m*	*p*
Anisole	74.7	5.0	20.3	2.66	0.18	1.45
Ethylbenzene	53.8	21.7	24.5	1.32	0.56	1.20
Chlorobenzene	71.6	8.0	20.4	0.59	0.08	0.34
Nitrobenzene	26.0	68.9	5.1	0.08	0.20	0.03

In order to determine the mechanism of photolysis of phenylazo sulfones, photochemical and thermal decompositions of *p*-chlorophenylazo *p'*-tolyl sulfone (II) in benzene were investigated. The products are shown in Table 3. Although II absorbs at 226 (ε=29000), 305 (ε=15000) and 430 nm (ε=190), the results of photo-

TABLE 3. PRODUCTS OF DECOMPOSITION OF *p*-CHLOROPHENYLAZO *p'*-TOLYL SULFONE

Product	Yield (mol/100 mol-II)		
	Photolysis		Thermolysis (in the presence of CaO)
	Run 1	Run 2	
p-$CH_3C_6H_4SO_3H$	25.1		12.6
p-$CH_3C_6H_4SO_2SC_6H_4CH_3$-*p*	3.3	3.6	3.6
p-$CH_3C_6H_4$–S(=O)–C_6H_4Cl-*p*	15.6	15.0	1.6
p-$CH_3C_6H_4SO_2OC_6H_4Cl$-*p*	2.1	4.4	4.7—12.3
p-$ClC_6H_4C_6H_5$	34.2	38.1	47.6
p-ClC_6H_4–N=N–C_6H_4Cl-*p*	0.04		6.2
p-$CH_3C_6H_4$–S(=O)–C_6H_5	less than 1.0(glc)		
Polymer sulfone	(10.8 wt%)	(6.1 wt%)	(13.0 wt%)
p-$CH_3C_6H_4SSC_6H_4CH_3$-*p*	trace		
p-$ClC_6H_4C_6H_4C_6H_4Cl$-*p*	0.2	0.3	
A hydrazine derivative	0	0	(19.4 wt%)

lyses in a quartz vessel and in a pyrex vessel were similar. Thus, the absorption at 430 nm is mainly responsible for the photolysis.

Formation of the products of the photolysis of II can be explained by the following scheme.

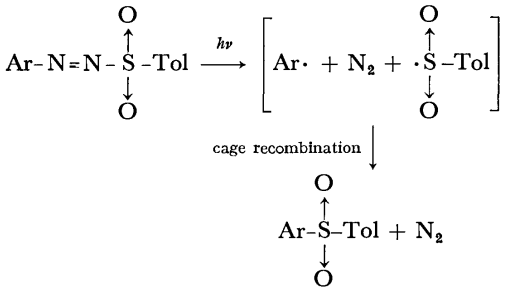

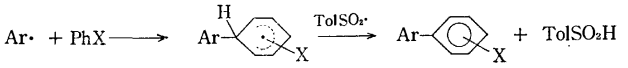

Yields of phenyl *p*-chlorophenyl sulfone were very small both in photolysis and thermolysis (less than 1 mol % by glc). This indicates that *p*-toluenesulfonyl radical functions only as a hydrogen abstractor. However, it is possible that the sulfonyl radical adds to benzene, forming a sulfonylcyclohexadienyl radical in the following equilibrium.

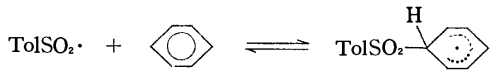

Such a possibility is not rejected by the experimental results. It is likely that the life of the sulfonyl radical is prolonged by existence of such equilibrium.

When a sulfonyl radical abstracts hydrogen, a sulfinic acid should be produced. However, a sulfinic acid was not detected in the reaction mixture, though a sulfonic acid and a thiolsulfonate were found. It is known that a sulfinic acid disproportionates easily, forming such products.[4]

$$3\ p\text{-TolSO}_2\text{H} \longrightarrow p\text{-TolSO}_3\text{H} + p\text{-TolSO}_2\text{S-Tol-}p$$

Isomer distributions and partial rate factors in phenylation of substituted benzenes, shown in Table 1, are in general similar to those of thermal homolysis shown in Table 2(a), and are characteristic of free radical reactions. However, the values are somewhat different and the differences in partial rate factors being fairly large in the case of benzonitrile and nitrobenzene.

It is known that sulfones undergo photolysis in aromatic solvents, yielding biphenyls,[5] and occurrence of such photolysis could be the cause for the difference in partial rate factors. However, when a benzene solution of phenyl *p*-tolyl sulfone was degassed and irradiated for 45 hr, the yield of biphenyl was only 9%. Since the yield of *p*-chlorophenyl *p'*-tolyl sulfone in the photolysis of II was only 15%, photolysis of the sulfone so produced cannot influence the partial rate factors greatly.

Photolysis was carried out at room temperature (20°C), and thermolysis at 80°C. However, it was established by a previous investigation that isomer distribution and partial rate factors in phenylation by phenyl radical do not vary much with the reaction temperature.[3] Thus, the cause for the difference in phenylations by photolysis and thermal homolysis cannot be the difference in reaction temperature.

A most probable explanation for the difference is as follows. In photolysis, the azosulfone is photolyzed by the n-π^* transition, yielding free phenyl radical and free *p*-toluenesulfonyl radical; the free phenyl radical adds to a substituted benzene, yielding phenylcyclohexadienyl radical. In thermal homolysis, a π-complex between the azosulfone and the solvent is formed prior to the cleavage of the C–N and S–N bonds, and the bond between phenyl radical and the solvent molecule is formed concertedly with the cleavage of the C–N and S–N bonds.

The yield of *p*-chlorophenyl *p'*-tolyl sulfone in photolysis was very much greater than that in thermolysis as shown in Table 3. The difference can also be explained in terms of the free phenyl radical in the photolysis and the solvated free phenyl radical in the thermolysis. In photolysis, free *p*-chlorophenyl radical and free *p*-toluenesulfonyl radical recombine in a solvent cage and form the sulfone in a fair yield.

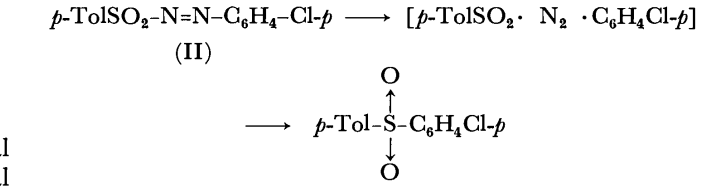

In the thermolysis, cleavages of the C–N and S–N bonds are aided by formation of weak bonds between solvent molecules and the radicals being produced, and therefore the yield of the sulfone is much smaller.

Formation of *p*-chlorophenyl *p'*-toluenesulfonate cannot be easily explained. A plausible route is disproportionation of *p*-chlorophenyl *p'*-toluenesulfinate formed in the following way.

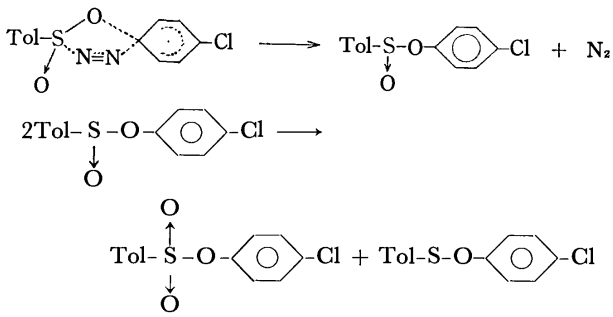

Formation of 4,4'-dichloroazobenzene can be explained in terms of the addition of *p*-chlorophenyl radical to the starting azosulfone.

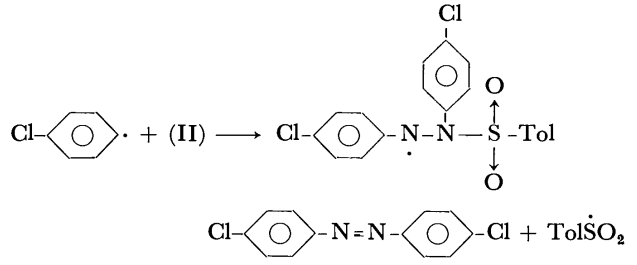

4) J. L. Kice and K. W. Bowers, *J. Amer. Chem. Soc.*, **84**, 605 (1962).

5) N. Kharasch and A. I. A. Khodair, *Chem. Commun.*, **1967**, 98.

The reaction is analogous to the attack of phenyl radical to phenylazotriphenylmethane. In both cases, a less stable radical adds to the azo bond, and a more stable radical is released.

$$Ph\cdot + Ph\text{-}N{=}N\text{-}CPh_3 \longrightarrow Ph\text{-}\underset{\cdot}{N}\text{-}\underset{\displaystyle Ph}{N}\text{-}CPh_3 \longrightarrow Ph\text{-}N{=}N\text{-}Ph + Ph_3C\cdot$$

Experimental

Materials. Phenylazo *p*-tolyl sulfone was synthesized by the method described previously.[3] UV, λ_{max} (hexane) 221 nm (ε, 19000), 287 nm (ε, 16000), 432 nm (ε, 150). *p*-Chlorophenylazo *p'*-tolyl sulfone (II) was synthesized by the reaction between *p*-chlorobenzenediazonium chloride and sodium *p*-toluenesulfinate in water, and recrystallized from methanol; mp 118.5—119.0°C (decomp.). UV, λ_{max} (hexane) 226 nm (ε, 29000), 305 nm (ε, 15000), 430 nm (ε, 190).

Determinations of Biaryls Formed by Photolysis of I. About 3 mmol of I was dissolved in a mixture of 1/8 mol each of benzene (or chlorobenzene) and a substituted benzene, and the solution was degassed by the freezing-evacuation technique. The solution was irradiated with a high-pressure mercury lamp for 15—60 hr (irradiation was continued for 5 hr after the evolution of nitrogen ceased). An internal standard (bibenzyl) was added, and the reaction mixture was washed with water, a 5% sodium carbonate solution and then concentrated by evaporation of the solvent. When azobenzene formed in a small yield interfered glc determinations, it was removed by reduction with zinc and hydrochloric acid in methanol. The amounts of biaryl isomers were determined with a Hitachi K-53 Flame Ionization Gas Chromatograph (Apiezon L column, 4 m).

Products of Photolysis of p-*Chlorophenylazo* p'-*Tolyl Sulfone (II) in Benzene.* A solution of II (35.4 mmol) in benzene (450 m*l*) was photolyzed with a high-pressure mercury lamp for 25.5 hr at 20°C under nitrogen. A considerable amount of *p*-toluenesulfonic acid precipitated. After the reaction mixture was washed with a 5% sodium carbonate solution and then concentrated, the products in the residue were separated by elution chromatography on alumina or Florisil. Products separated were rechromatographed when necessary. Each product was identified by its mp, IR and/or NMR spectra.

The sodium carbonate extracts were concentrated under reduced pressure, made weakly acidic by addition of hydrochloric acid, and the *p*-toluenesulfonic acid in the solution was precipitated as its *S*-benzylisothiuronium salt. No *p*-toluenesulfinic acid was detected.

4,4'-Dichloroazobenzene was determined by use of its absorption at 444 nm (ε, 880) after column-chromatographic separation.

Products of Thermal Decomposition of II in Benzene. A solution of II (35.4 mmol) in benzene (600 m*l*) containing CaO powder (5.4 g) was kept at 70°C for 82 hr under nitrogen. The products of decomposition were analyzed by the procedure described for photolysis.

By a separate experiment, the rate of decomposition of II was determined (II, 3.260 mmol; benzene, 60 m*l*; CaO, 0.54 g). The rate of evolution of nitrogen showed that rate constant k is equal to 2.1×10^{-5} sec^{-1} at 70.0°C.

BULLETIN OF THE CHEMICAL SOCIETY OF JAPAN, VOL. 45, 2042—2046(1972)

Aromatic Arylation with Aryl Radicals. IV. The Kinetic Hydrogen Isotope Effect in the Aromatic Phenylation with Phenyl Radical

Nobumasa KAMIGATA, Hiroshi MINATO, and Michio KOBAYASHI

Department of Chemistry, Faculty of Science, Tokyo Metropolitan University, Fukazawa, Setagaya, Tokyo

(Received March 21, 1972)

Anisole-4*d*, chlorobenzene-4*d*, chlorobenzene-d_5, nitrobenzene-d_5, *m*-dinitrobenzene-d_4, and 1,3,5-tri-*t*-butylbenzene-d_3 were phenylated with phenyl radical generated from PhN_2BF_4–$NaNO_2$, *N*-nitrosoacetanilide or phenylazotriphenylmethane(PAT), and the isotope effect in these phenylations was determined. The values of k_H/k_D in the phenylations of chlorobenzene and 1,3,5-tri-*t*-butylbenzene are not so larger than unity, whereas that in the phenylation at the 2-position of *m*-dinitrobenzene with PAT was very large ($\sim$11).

Large isotope effect was observed in the phenylation of arenes with the phenyl radical generated from benzoyl peroxide (BPO) in highly diluted solutions (k_H/k_D=6.6),[1] whereas no isotope effect was observed in the phenylations with *N*-nitrosoacetanilide (NNA) or phenylazotriphenylmethane.[2] It has been proposed that in highly diluted solutions of BPO the hydrogen-abstraction from the cyclohexadienyl radicals produced proceeds slowly by disproportionation between the cyclohexadienyl radicals themselves since benzoyloxy radical is ineffective due to its low concentration,[1] whereas in the phenylations with NNA or PAT no isotope effect is observed since the hydrogen-abstraction from the cyclohexadienyl radicals proceeds quickly by the presence of efficient hydrogen abstractors in rather high concentrations.[2]

1) E. L. Eliel, Z. Welvart, and S. H. Wilen, *J. Org. Chem.*, **23**, 1821 (1958); E. L. Eliel, S. Meyerson, Z. Welvart, and S. H. Wilen, *J. Amer. Chem. Soc.*, **82**, 2936 (1960).

2) E. L. Eliel, M. Eberhardt, O. Simamura, and S. Meyerson, *Tetrahedron Lett.*, **1962**, 749; E. L. Eliel, J. G. Saha, and S. Meyerson, *J. Org. Chem.*, **30**, 2451 (1965).

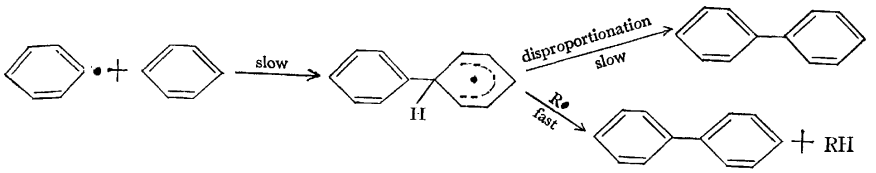

A previous paper from our laboratories described the generation of phenyl radical from PhN_2BF_4–$NaNO_2$ in DMSO according to the following scheme, and an isotope effect was observed in the phenylation of arenes with this system.[3]

$$PhN_2BF_4 + NaNO_2 \longrightarrow PhN{=}N{-}O{-}N{=}O + NaBF_4$$
$$PhN{=}N{-}O{-}N{=}O \longrightarrow Ph\cdot + N_2 + NO_2$$
or
$$2PhN{=}N{-}O{-}N{=}O \longrightarrow PhN{=}N{-}O{-}N{=}NPh + N_2O_3$$
$$PhN{=}N{-}O{-}N{=}NPh \longrightarrow Ph\cdot + N_2 + \cdot ON{=}NPh$$

In this system, abstraction of the hydrogen atom from the cyclohexadienyl radicals is efficiently carried out either by NO_2 or PhN=NO·, the latter radical being the hydrogen abstractor in the phenylation with NNA.[4] Existence of isotope effect in the phenylation in the presence of an efficient hydrogen-abstractor contradicts with the interpretation proposed by Eliel *et al.*[2] In an attempt to gain further understanding in this problem, various deuterated arenes have been phenylated with phenyl radicals produced from PhN_2BF_4–$NaNO_2$, BPO, NNA and PAT, and the results will be described in this paper.

Table 1. Isomer distributions and partial rate factors in the phenylation of PhX and deuterated PhX with PhN_2BF_4–$NaNO_2$ in DMSO at 20°C[a]

Substrate	Isomer distributions (%)			Partial rate factors		
	o-,	*m*-,	*p*-,	k_o/k	k_m/k	k_p/k
$PhOCH_3$	72.4	14.2	13.4			
$PhOCH_3$-4*d*	71.6	14.3	14.1			
PhCl	56.5	23.5	20.0	3.45	1.44	2.44
PhCl-4*d*	55.3	24.2	20.5			
PhCl-d_5	58.2	23.4	18.4	3.13	1.26	1.98
$PhNO_2$	77.4	5.9	16.7	19.8	1.51	8.55
$PhNO_2$-d_5	73.4	6.8	19.8	12.3	1.14	6.62

a) The average values of two experiments.

Results and Discussion

Table 1 shows the isomer distributions and partial rate factors in the phenylation of arenes and deuterated arenes. The isomer distributions in phenylated $PhOCH_3$-4*d* and PhCl-4*d* are not too much different from those in the corresponding methyldiphenyls and chlorodiphenyls. From the partial rate factors in the phenylations of PhCl-d_5, PhCl, $PhNO_2$-d_5, and $PhNO_2$, the values of k_H/k_D at the *ortho*, *meta* and *para* positions were calculated. The results are shown in Table 2.

Table 2. Kinetic isotope effect in the phenylation with phenyl radical

Substrate	k_H/k_D in the formation of substituted diphenyls[a]		
	2-,	3-,	4-,
PhCl-d_5	1.10	1.14	1.23
$PhNO_2$-d_5	1.61	1.32	1.29

a) These values were calculated from the partial rate factors listed in Table 1. Experimental errors were ±0.10

Isotope effect is fairly small in the case of chlorobenzene (k_H/k_D=1.10~1.23), whereas it is considerably large in the case of nitrobenzene (k_H/k_D=1.29~1.61). It is interesting that the k_H/k_D values are different at different positions of these arenes.

The fact that isotope effect was observed in the presence of an efficient hydrogen-abstractor (PhN=NO· or NO_2) contradicts with the explanation proposed by Eliel *et al.*[2] In order to determine isotope effect more directly and in greater details, competitive phenylations of an arene and the corresponding deuterated arene were carried out by use of the phenyl radicals generated from PhN_2BF_4–$NaNO_2$, *N*-nitrosoacetanilide and phenylazotriphenylmethane. The results are shown in Table 3.

In the phenylation of $C_6D_5NO_2$–$C_6H_5NO_2$, the k_H/k_D values at *para* position were nearly unity regardless of the phenyl radical source, whereas those at *ortho* position were fairly large in the cases of PhN_2BF_4–$NaNO_2$ and NNA (k_H/k_D=2.36 and 2.02). It appears strange that no isotope effect was observed at *ortho* position of nitrobenzene when PAT was used as the radical source.

In the phenylation of *m*-$C_6D_4(NO_2)_2$–*m*-$C_6H_4(NO_2)_2$, isotope effects were observed both at 4 and 2 positions with the phenyl radicals generated from all the sources. In the case of the phenylation with PAT, the k_H/k_D value at the more crowded 2 position was greater than that expected from the zero-point energies of the C–H and C–D bonds ($k_H/k_D \fallingdotseq 11$).

Bromberg, Muszkat, and Fischer observed an unusually large isotope effect (k_H/k_D=95) in the initiation step of the reaction of 4a,4b-dihydrophenanthrene with oxygen.[5] They stated that the large kinetic isotope effect is due to both a considerable loss of zero-point energy of stretching and bending vibration in the transition state and a large contribution from quantum-mechanical tunnelling.

Shih, Hey, and Williams reported absence of isotope effect in the phenylation of tritiated benzene with benzoyl peroxide,[6] and Price and Convery also reported absence of isotope effect in the phenylation of 2,4-

3) M. Kobayashi, H. Minato, N. Kobori, and E. Yamada, This Bulletin, **43**, 1131 (1970).

4) C. Rüchardt and B. Freudenberg, *Tetrahedron Lett.*, **1964**, 3623.

5) A. Bromberg, K. A. Muszkat, and E. Fischer, *Chem. Commun.*, **1968**, 1352.

6) C. Shih, D. H. Hey, and G. H. Williams, *J. Chem. Soc.*, **1959**, 1871.

TABLE 3. KINETIC HYDROGEN ISOTOPE EFFECT IN THE COMPETITIVE PHENYLATION OF ARENES WITH PHENYL RADICAL

Substrate	Radical source	Temperature (°C)	k_H/k_D in the formation of substituted diphenyls[a]		
			2-,	3-,	4-,
$C_6D_5NO_2+C_6H_5NO_2$	PhN_2BF_4–$NaNO_2$	20±3	2.36	b	1.06
$C_6D_5NO_2+C_6H_5NO_2$	$PhN(NO)COCH_3$	20±0.1	2.02	b	1.03
$C_6D_5NO_2+C_6H_5NO_2$	$PhN{=}NCPh_3$	55±0.1	1.01	b	1.00
				2, 4, 6-	
1,3,5-C_6D_3t-Bu_3+1,3,5-C_6H_3t-Bu_3	$PhN(NO)COCH_3$	20±0.1		1.06	
1,3,5-C_6D_3t-Bu_3+1,3,5-C_6H_3t-Bu_3	$PhN{=}NCPh_3$	55±0.1		1.01	
			2,4-,		2,6-,
m-$C_6D_4(NO_2)_2$+m-$C_6H_4(NO_2)_2$	PhN_2BF_4–$NaNO_2$	20±3	1.54		1.55
m-$C_6D_4(NO_2)_2$+m-$C_6H_4(NO_2)_2$	$PhN(NO)COCH_3$	20±0.1	1.45		1.77
m-$C_6D_4(NO_2)_2$+m-$C_6H_4(NO_2)_2$	$PhN{=}NCPh_3$	55±0.1	1.76		~11
m-$C_6D_4(NO_2)_2$+m-$C_6H_4(NO_2)_2$	BPO[c]	90—100	2.03		e
m-$C_6D_4(NO_2)_2$+m-$C_6H_5(NO_2)_2$	BPO[d]	80±0.1	2.53		e

a) The average values of two experiments; experimental errors were ±0.10.
b) Yields of the meta isomer were low, and isolation was not possible.
c) Without solvent. d) In acetonitrile. e) Yields of 2,6-isomers were low, and they were not isolated.

dinitrotritiobenzene with benzoyl peroxide.[7] Both of these groups used benzoyl peroxide in rather large concentrations, and it is conceivable that many benzoyloxy radicals (a highly active hydrogen-abstractor) are present in the media and effectively abstract hydrogens of the intermediate cyclohexadienyl radicals. In an attempt to establish whether or not isotope effect exists under such conditions, the experiment of Price and Convery was repeated with benzoyl peroxide in a m-$C_6H_4(NO_2)_2$–m-$C_6D_4(NO_2)_2$ mixture. As shown in Table 3, k_H/k_D was found to be 2.03. Since the conditions of this experiment are somewhat drastic (a solid mixture of benzoyl peroxide and m-dinitrobenzene is heated up over 90°C for melting and decomposition), a similar mixture was dissolved in acetonitrile and the homogeneous solution was let to decompose at 80°C. Again, isotope effect was observed (k_H/k_D=2.53). In the experiment with a solid mixture of BPO and m-dinitrobenzene, some decomposition of BPO must have taken place in solid phase before melting, and therefore the result is somewhat ambiguous. In the experiment with an acetonitrile solution, however, the result clearly shows that isotope effect exists in phenylation of m-dinitrobenzene with BPO.

It has been said that there is no isotope effect in nitration of arenes. However, recently Myhre, Beug, and James have observed kinetic isotope effects in nitrodeprotonation of a series of 1-X-2,4,6-tri-t-butylbenzenes and reported that the k_H/k_D values changed from 1.0 to 3.8 as X is varied from H to CH_3.[8] Such a correlation between isotope effect and the size of the substituent may exist in our systems too, since 1) almost no isotope effect at the *para* positions and greater isotope effect was observed at *ortho* positions, and 2) a very large isotope effect (~11) was observed with the phenylation of m-dinitrobenzene at its 2-position with the phenyl radical produced from PAT (the hydrogen abstractor is bulky trityl radical).

In order to clarify the relationship between isotope effect and the size of the substituents, 1,3,5-tri-t-butylbenzene and 1,3,5-tri-t-butylbenzene-2,4,6-d_3 were competitively phenylated with the phenyl radicals generated from NNA and PAT. However, the k_H/k_D values obtained were 1.06 and 1.01, and thus there is no definite correlation between isotope effect and the size of the substituents in free-radical phenylation of arenes.

TABLE 4. ISOMER DISTRIBUTIONS IN THE PHENYLATION OF m-DINITROBENZENE AND m-DINITROBENZENE-d_4

Substrate	Radical source	Temperature (°C)	Yields of dinitrodiphenyls (%)	
			2,6-	2,4-
m-$C_6H_4(NO_2)_2$	PhN_2BF_4–$NaNO_2$	20±3	67.1	32.9
m-$C_6H_4(NO_2)_2$	$PhN{=}NCPh_3$	60±0.1	36.5	63.5
m-$C_6D_4(NO_2)_2$	$PhN{=}NCPh_3$	60±0.1	14.5	85.5

In an attempt to gain further understanding on this problem, m-dinitrobenzene and m-dinitrobenzene-d_4 were phenylated with the phenyl radicals produced from PhN_2BF_4–$NaNO_2$ and PAT, and the isomer distributions of the dinitrodiphenyls were determined. The results are shown in Table 4. In the case of m-$C_6H_4(NO_2)_2$–PhN_2BF_4–$NaNO_2$, the amount of 2,6-dinitrodiphenyl produced was 67%, whereas in the case of m-$C_6H_4(NO_2)_2$–PAT it decreased to 36.5%. This finding can be rationalized by assuming that very bulky trityl radical abstracts the hydrogen at the crowded 2 position of the 1,3-dinitro-2-phenylcyclohexadienyl radical much more slowly than that at the less crowded 4 position of the 1,3-dinitro-4-phenylcyclo-

7) C. C. Price and R. J. Convery, *J. Amer. Chem. Soc.*, **79**, 2941 (1957); **80**, 4101 (1958).
8) P. C. Myhre, M. Beug, and L. L. James, *ibid.*, **90**, 2105 (1968).

hexadienyl radical. The amount of 2,6-dinitrodiphenyl produced further decreased to 14.5% in the case of m-$C_6D_4(NO_2)_2$–PAT. These data are consistent with the abnormally large k_H/k_D value (~11) observed in the case of m-$C_6H_4(NO_2)_2$–m-$C_6D_4(NO_2)_2$–PAT (Table 3).

Thus, a very large isotope effect was observed in free-radical phenylation at the crowded 2-position of m-dinitrobenzene, and not at the crowded 2-position of 1,3,5-tri-t-butylbenzene. Resonance stabilization of the intermediate cyclohexadienyl radical must be taken into consideration in addition to the bulkiness of the substituents. The more resonance-stabilized is the cyclohexadienyl radical, the more slowly proceeds the following hydrogen-abstraction step. If this is so, it is reasonable that no isotope effect was shown by t-butyl group which is bulky but possesses no ability of resonance-stabilization.

The k_H/k_D value observed for phenylation at the 2-position of m-dinitrobenzene (~11) was greater than the value expected from the zero-point energy of the C–H bond (6~7). This finding can be rationalized only by assuming a large contribution from quantum-mechanical tunnelling effect or assuming that in the free-radical substitution at such an overcrowded position the activation entropy factor varies with isotopes.

Experimental

Materials. Benzenediazonium tetrafluoroborate was prepared according to the directions described previously.[9] *N*-Nitrosoacetanilide was prepared by the method reported in the literature[10] and dried in a desiccator which was kept in a refrigerator; mp 75°C (decomp.). Phenylazotriphenylmethane (PAT) was prepared by the bromine-water oxidation of phenylhydrazotriphenylmethane,[11] which was synthesized from phenylhydrazine and triphenylmethyl chloride in ether.[12] Crude PAT was recrystallized from benzene-ethanol; mp 111—112°C (decomp.). Dimethyl sulfoxide was dried with calcium hydride and distilled; bp 86°C/25 mmHg. Benzene and chlorobenzene were washed with concentrated sulfuric acid and water successively, dried over calcium chloride, and distilled; bp 80 and 131°C, respectively. Anisole was washed with an aqueous sodium hydroxide solution and water, dried over calcium chloride, and distilled; bp 153°C. Nitrobenzene was washed repeatedly with a potassium dichromate solution, dried over calcium chloride, and distilled; bp 95.5°C/18 mmHg.

Authentic samples of substituted diphenyls were prepared by the methods described previously.[13] Anisole-4*d* was prepared by the hydrolysis of p-methoxyphenylmagnesium bromide in D_2O (isotopic purity, 99.75%, E. Merck AG, Darmstadt); bp 58°C/15 mmHg. Its isotopic purity was determined to be 92% by mass spectrometry. Chlorobenzene-4*d* was prepared in a similar manner from p-bromochlorobenzene; bp 131°C. Its isotopic purity was 90%. Chlorobenzene-d_5 and nitrobenzene-d_5 of CIBA Limited were used without further purification. Isotopic purity was 98.5% and 99%, respectively. m-Dinitrobenzene-d_4 was prepared by the nitration of benzene-d_6 (isotopic purity>99 atom % D, E. Merck AG, Darmstadt) with anhydrous potassium nitrate and sulfuric acid-d_2, which was produced from sulfuric anhydride and deuterium oxide-d_2 (isotopic purity, 99.75%, E. Merck AG, Darmstadt). Crude m-dinitrobenzene-d_4 was recrystallized from ethanol; mp 89°C. Its isotopic purity was determined to be 97.5% by mass spectrometry. 1,3,5-tri-t-butylbenzene was prepared by the method described in the literature;[14] mp 72—73°C (from methanol). 1,3,5-tri-t-butylbenzene-2,4,6-d_3 was obtained by hydrogen-deuterium exchange (six times was needed) from 1,3,5-tri-t-butylbenzene and trifluoroacetic acid-d_1 which was prepared from trifluoroacetic anhydride (Aldrich Chemical Co., Inc.) and deuterium oxide-d_2 (E. Merck AG, Darmstadt, isotopic purity: 99.75%) in carbon tetrachloride according to the method described in the literature.[8] After the exchange reaction was repeated for six times, exchange was shown to be 98% complete by its NMR spectrum (comparison of its integrated signal with that of the known amount of ferrocene as an internal standard).

*Phenylation of Anisole, Anisole-4*d, *Chlorobenzene or Chlorobenzene-4*d *with Benzenediazonium Tetrafluoroborate-Sodium Nitrite.* Under a nitrogen atmosphere a solution of 0.25 g (1.3 mmol) of benzenediazonium tetrafluoroborate dissolved in DMSO (2.0 g) was added drop by drop at 20°C into a vigorously stirred solution of sodium nitrite (3 mol/mol of PhN_2BF_4) and an aromatic substrate (anisole, anisole-4*d*, chlorobenzene or chlorobenzene-4*d*; 50 mol/mol of PhN_2BF_4) in 10 g of DMSO. Evolution of nitrogen was instantaneous upon addition of each drop of the diazonium salt solution, and the addition was completed in about five minutes. Treatment of the reaction mixtures and the quantitative determination of the diphenyl isomers produced were made according to the method reported previously.[3]

Competitive Phenylation of Chlorobenzene–Benzene and Chlorobenzene-d_5*–Benzene.* Under a nitrogen atmosphere a solution of 0.2 g of benzenediazonium tetrafluoroborate in DMSO (2.0 g) was added drop by drop at 20°C into a vigorously stirred solution of sodium nitrite (3 mol/mol of PhN_2BF_4) in 6.0 g of DMSO and an equimolar mixture of benzene and chlorobenzene (or benzene and chlorobenzene-d_5; 50 mol/mol of PhN_2BF_4). The reaction mixture was treated according to the method described previously.[3]

Competitive Phenylation of Nitrobenzene–Chlorobenzene and Nitrobenzene-d_5*–Chlorobenzene.* Competitive phenylation of nitrobenzene-chlorobenzene (or nitrobenzene-d_5–chlorobenzene) with benzenediazonium tetrafluoroborate-sodium nitrite were carried out in a manner similar to that described above, and the diphenyl isomers produced were determined by glc.

Partial rate factors in the phenylation at each position of an arene were calculated by using the following equation.

$$k_x/k = (k_x/k_{o\text{-}Cl}) \times (k_{o\text{-}Cl}/k)$$

where,

k_x/k: the partial rate factor in the phenylation of PhX at the x (o-, m-, or p-) position

k_x/k_{o-Cl}: the ratio of the phenylation rate at the x position of PhX *versus* that at the *ortho* position of chlorobenzene

k_{o-Cl}/k: the partial rate factor in the phenylation at the *ortho* position of chlorobenzene

9) E. B. Starkey, "Organic Syntheses," Coll. Vol. 2, p. 225, Wiley, New York, N. Y. (1943).

10) H. France, I. M. Heilbron, and D. H. Hey, *J. Chem. Soc.*, **1940**, 369.

11) M. Gomberg and H. W. Berger, *Ber.*, **36**, 1088 (1903).

12) C. R. Hauser and B. E. Hudson, Jr., "Organic Syntheses," Coll. Vol. 3, p. 842, Wiley, New York, N. Y. (1955).

13) M. Kobayashi, H. Minato, E. Yamada, and N. Kobori, This Bulletin, **43**, 215 (1970).

14) J. M. A. Baas, H. V. Bekkum, M. A. Hoefnagel, and B. M. Wepster, *Rec. Trav. Chim. Pays-Bas*, **88**, 1110 (1969).

Competitive Phenylation of Nitrobenzene–Nitrobenzene-d_5. An equimolar mixture of nitrobenzene (40 mmol) and nitrobenzene-d_5 (40 mmol) was phenylated by using 8 mmol of a phenylating agent (PhN_2BF_4–$NaNO_2$–DMSO (150 g) or *N*-Nitrosoacetanilide or PAT) under a nitrogen atmosphere. The reaction mixture was dissolved in ether and washed with water. The solvent was removed under reduced pressure, and elution chromatography of the residue on alumina yielded an *o*-nitrodiphenyl–*o*-nitrodiphenyl-d_4 mixture and a *p*-nitrodiphenyl–*p*-nitrodiphenyl-d_4 mixture. The *m*-isomer mixture could not be isolated because of its low yield. The kinetic isotope effect was calculated from the parent peak ratio (I_{199}/I_{203}) of the mass spectrum of each mixture (Hitachi Mass Spectrometer RM-60).

$$\frac{\text{yield of } PhC_6H_4NO_2}{\text{yield of } PhC_6D_4NO_2} = \frac{k_H}{k_D} \times \frac{[C_6H_5NO_2]}{[C_6D_5NO_2]}$$

Competitive Phenylation of m-*Dinitrobenzene–*m-*Dinitrobenzene-*d_4. *m*-Dinitrobenzene (25 mmol) and *m*-dinitrobenzene-d_4 (25 mmol) were phenylated by using 5 mmol of a phenylating agent (PhN_2BF_4–$NaNO_2$, *N*-nitrosoacetanilide or PAT) in DMSO (150 g) under a nitrogen atmosphere. The reaction mixture was dissolved in chloroform and washed with water to remove DMSO. Evaporation under reduced pressure removed chloroform and then unreacted *m*-dinitrobenzene and *m*-dinitrobenzene-d_4. Elution chromatography of the residue on alumina gave a 2,4-dinitrodiphenyl–2,4-dinitrodiphenyl-d_3 mixture and a 2,6-dinitrodiphenyl–2,6-dinitrodiphenyl-d_3 mixture. The kinetic isotope effect was calculated from the parent peak ratio (I_{244}/I_{247}). It was ascertained that the parent peak ratio did not change when ionization potential was changed from 15 to 70 eV.

*Competitive Phenylation of 1,3,5-tri-*t*-butylbenzene–1,3,5-tri-*t*-butylbenzene-2,4,6-*d_3. 1,3,5-tri-*t*-butylbenzene (7.0 mmol) and 1,3,5-tri-*t*-butylbenzene-2,4,6-d_3 (7.0 mmol) were phenylated under nitrogen either by NNA (2 mmol) in acetonitrile (20 g) or by PAT (2 mmol) in benzene (18 g). The reaction mixture was dissolved in ether and washed with water. After the ether was removed, most of the unreacted 1,3,5-tri-*t*-butylbenzene and 1,3,5-tri-*t*-butylbenzene-2,4,6-d_3 was removed by chromatography on alumina. The substituted diphenyl fraction was subjected to a Hitachi glc K-53 (column: Apiezon L, 1 m) which is connected with a Hitachi Mass Spectrometer RM-60. The k_H/k_D value was calculated from the parent peak ratio (I_{322}/I_{324}) of 2,4,6-tri-*t*-butyldiphenyl and 2,4,6-tri-*t*-butyldiphenyl-3,5-d_2.

Phenylation of m-*Dinitrobenzene and* m-*Dinitrobenzene-*d_4 *with PAT or* PhN_2BF_4–$NaNO_2$. Ten mmol of *m*-dinitrobenzene (or *m*-dinitrobenzene-d_4) was phenylated with 1 mmol of PAT (or PhN_2BF_4–$NaNO_2$) in 50 g of DMSO under a nitrogen atmosphere. The reaction mixture was diluted with ether, washed with water, and dried over anhydrous magnesium sulfate. The ether and about 70% of the unreacted *m*-dinitrobenzene (or *m*-dinitrobenzene-d_4) was distilled off under reduced pressure. The residual *m*-dinitrodiphenyl isomers were analyzed by a Hitachi glc K-53 (column: Apiezon L, 10%, 1 m on Chromosorb W).

Phenylation of m-$C_6H_4(NO_2)_2$–m-$C_6D_4(NO_2)_2$ *with BPO.*
1) A solid mixture of BPO (3 mmol), *m*-$C_6H_4(NO_2)_2$ (17 mmol) and *m*-$C_6D_4(NO_2)_2$ (17 mmol) was placed in an oil bath at 90°C, and then heated up to and kept at 100°C for one day.

2) An acetonitrile solution (60 g) of BPO (2 mmol), *m*-$C_6H_4(NO_2)_2$ (26 mmol) and *m*-$C_6D_4(NO_2)_2$ (26 mmol) was let to decompose at 80 ± 0.1°C under nitrogen for one day.

The two reaction mixtures were subjected to distillation under reduced pressure for removal of *m*-dinitrobenzenes (and acetonitrile). Elution chromatography of the residue gave a mixture of 2,4-dinitrodiphenyl and 2,4-dinitrodiphenyl-d_3. Isotope effect was calculated from the ratio of the parent peaks (I_{244}/I_{247}).

The authors are indebted to Messrs. Kisaburo Yamazaki and Takamichi Ichimura at the Central Research Laboratories of Yamanouchi Pharmacy Co., Limited for mass spectrometric measurements.

Cationic Arylation. V. Reaction of Substituted Benzenes with *p*-Nitrophenyl Cation

Nobumasa KAMIGATA, Michio KOBAYASHI, and Hiroshi MINATO

Department of Chemistry, Faculty of Science, Tokyo Metropolitan University, Fukazawa, Setagaya, Tokyo

(Received March 24, 1972)

The cationic arylation of substituted benzenes was investigated with *p*-nitrophenyl cation generated from *p*-nitrobenzenediazonium tetrafluoroborate in acetonitrile and from *p*-nitrophenylazo *p'*-tolyl sulfone in the presence of trifluoroacetic acid. The isomer distribution of substituted nitrobiphenyls produced and the partial rate factors indicated electrophilic character of the *p*-nitrophenyl cation. Selectivity of *p*-nitrophenyl cation is low compared with those of nitronium or sulfonyl cation, and similar to that of phenyl cation. These facts suggest that the *p*-nitrophenyl cation functions as a cation diradical with concerted uncoupling of a pair of π-electrons, one of which falls into the vacant sp^2 σ-orbital.

Benzenediazonium tetrafluoroborate undergoes heterolysis in aprotic polar solvents, and substituted diphenyls are produced when some substituted benzene was present. The partial rate factors in this phenylation are of electrophilic nature, and hence the reactive intermediate produced is considered to be phenyl cation.[1] However, the positional selectivity of phenyl cation is considerably different from those of nitro, sulfonyl, alkyl, or acyl cations in ordinary electrophilic substitutions on arenes.[2] Abramovitch *et al.*[3] modified a proposal originally made by Taft[4] concerning the stabilization of the *m*-methoxyphenyl cation, and suggested that aryl cation (I) initially formed in the thermal decomposition of diazonium salts may isomerize to a diradical cation (II) with concerted uncoupling of a pair of π-electrons, one of which falls into the vacant sp^2 σ-orbital, and that the resulting species would be expected to behave like a highly electrophilic free radical in aromatic substitution reactions. Canonical structures (II) would have the properties of a triplet carbene. If a second π-electron fell into the σ-orbital, the species (III) resulted might behave as a singlet carbene.

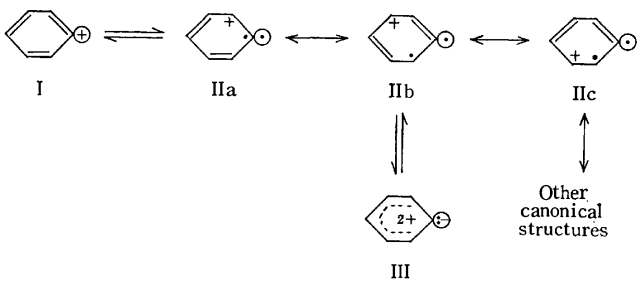

Preliminary molecular-orbital calculations made by Absar and McEwen[5] indicate the order of stabilization (II)>(III)>(I) for the phenyl cation itself, the triplet diradical cation (II) being the ground state.

In an attempt to study further the electronic state of phenyl cation, the isomer distributions and partial rate factors in substitutions of arenes with *p*-nitrophenyl cation have been investigated. The results will be described in this paper.

Results and Discussion

p-Nitrophenyl cation was generated from *p*-nitrobenzenediazonium tetrafluoroborate in acetonitrile or from *p*-nitrophenylazo *p'*-tolyl sulfone and trifluoroacetic acid. A substituted benzene was mixed with the *p*-nitrophenyl cation source, and the isomer distributions and partial rate factors in the *p*-nitrophenylation were determined. Table 1 and 2 show the results, together with the data on phenyl cation[1b,6] and *p*-nitrophenyl radical[7] for comparison.

The data in Table 1 show that *p*-nitrophenyl cation, not *p*-nitrophenyl radical, is produced, since with nitrobenzene as the substrate the *meta* position of the nitrobenzene is substituted extensively and the partial rate factors are much smaller than unity and quite different from those with *p*-nitrophenyl radical.

Zollinger reported that when *p*-nitrobenzenediazonium tetrafluoroborate was decomposed in a mixture of nitrobenzene and DMSO, the isomer distribution of the 4,X'-dinitrodiphenyls produced was *ortho* 65.3, *meta* 9.5 and *para* 25.2%.[8] Since this isomer distribution is similar to that with *p*-nitrophenyl radical produced from *p*-nitrobenzoyl peroxide, he proposed that *p*-nitrobenzenediazonium cation combines with DMSO, forming an intermediate, which then decomposes to *p*-nitrophenyl radical, nitrogen and DMSO cation radical. Our results are quite different from Zollinger's, and the difference can be ascribed to the solvents; all the data are in agreement with the interpretation that in acetonitrile *p*-nitrobenzenediazonium ion forms *p*-nitrophenyl cation whereas it forms *p*-nitrophenyl radical in DMSO.

When the partial rate factors with phenyl cation and

1) a) R. A. Abramovitch and F. F. Gadallah, *J. Chem. Soc., B*, **1968**, 497. b) M. Kobayashi, H. Minato, E. Yamada, and N. Kobori, This Bulletin, **43**, 215 (1970).

2) R. O. C. Norman and R. Taylor, "Electrophilic Substitution in Benzenoid Compounds," Elsevier Publishing Company, New York, (1965).

3) R. A. Abramovitch and G. Tertzakian, *Can. J. Chem.*, **43**, 940 (1965); R. A. Abramovitch and J. G. Saha, *ibid.*, **43**, 3269 (1965); R. A. Abramovitch and J. G. Saha, *Tetrahedron*, **21**, 3297 (1965).

4) R. W. Taft, *J. Amer. Chem. Soc.*, **83**, 3350 (1961).

5) G. H. Williams, "Advances in Free-Radical Chemistry," Vol. 2, Academic Press, London (1967), p. 116.

6) M. Kobayashi, H. Minato, and N. Kobori, This Bulletin, **43**, 219 (1970).

7) R. Ito, T. Migita, N. Morikawa, and O. Simamura, *Tetrahedron*, **21**, 955 (1965).

8) H. Zollinger, The abstract of Post ISNA Symposium held in Tokyo, Aug. 30, 1970.

TABLE 1. ISOMER DISTRIBUTIONS AND PARTIAL RATE FACTORS IN THE ARYLATION OF AROMATIC SUBSTRATES WITH $XC_6H_4N_2BF_4$ IN ACETONITRILE AT 60°C

Substrate	Arylating reagent	Isomer distributions			*m*/*p*	Partial rate factors		
		o-	*m*-	*p*-		f_o	f_m	f_p
$C_6H_5OCH_3$	$C_6H_5N_2BF_4$ (I)[a]	64.7	8.4	26.9	0.31	1.77	0.23	1.47
	p-$NO_2C_6H_4N_2BF_4$ (II)[b]	55.0	13.1	31.9	0.41	2.55	0.61	2.96
	p-$NO_2C_6H_4N(NO)COCH_3$ (III)[c]	72	12	16	0.75	5.17	0.84	2.30
C_6H_5Cl	(I)[a]	59.8	15.2	25.0	0.61	0.67	0.17	0.56
	(II)[b]	55.6	23.4	21.0	1.11	1.01	0.43	0.77
	(III)[c]	57	24	19	1.26	1.53	0.65	1.01
$C_6H_5NO_2$	(I)[a]	32.3	48.4	19.3	2.53	0.10	0.15	0.12
	(II)[b]	50.0	46.9	3.1	15.1	0.16	0.15	0.02
	(III)[c]	46	17	37	0.46	0.93	0.35	1.53

a) Ref. 1b b) This work c) Ref. 7

TABLE 2. ISOMER DISTRIBUTIONS AND PARTIAL RATE FACTORS IN THE ARYLATION OF AROMATIC SUBSTRATES WITH $XC_6H_4N_2Ts$ IN THE PRESENCE OF CF_3CO_2H AT 60°C

Substrate	Arylating reagent	Isomer distributions			*m*/*p*	Partial rate factors		
		o-	*m*-	*p*-		f_o	f_m	f_p
$C_6H_5OCH_3$	$C_6H_5N_2Ts$ (I)[a]	76.0	4.8	19.2	0.25	2.66	0.17	1.34
	p-$NO_2C_6H_4Ts$ (II)[b]	77.7	9.9	12.4	0.88	3.97	0.51	1.27
	p-$NO_2C_6H_4N(NO)COCH_3$ (III)[c]	72	12	16	0.75	5.17	0.84	2.30
C_6H_5Cl	(I)[a]	70.3	9.4	20.3	0.46	0.56	0.08	0.33
	(II)[b]	63.6	23.3	13.1	1.78	1.46	0.53	0.60
	(III)[c]	57	24	19	1.26	1.53	0.65	1.01
$C_6H_5NO_2$	(I)[a]	27.2	67.8	5.0	13.6	0.08	0.19	0.03
	(II)[b]	82.8	11.0	6.2	1.77	0.88	0.12	0.13
	(III)[c]	46	17	37	0.46	0.93	0.35	1.53

a) Ref. 6 b) This work c) Ref. 7

those with *p*-nitrophenyl cation are compared, the latter are greater with all the substrates (except f_p with nitrobenzene). *p*-Nitrophenyl cation is more selective than phenyl cation, and according to Brown's selectivity rule *p*-nitrophenyl cation is considered to be less reactive than phenyl cation.

When the *m*/*p* ratios are compared in order to examine the selectivity within a molecule, they are always greater with *p*-nitrophenyl cation than with phenyl cation. This finding also shows that *p*-nitrophenyl cation is less reactive than phenyl cation. This intramolecular selectivity is greater with the substrate with an electron-withdrawing substituent and hence less prone to make a bond with an aryl cation. This is reasonable since the activation energy is greater with less reactive substrates, the transition state is at a later stage on the reaction coordinate and hence the intramolecular selectivity is greater.

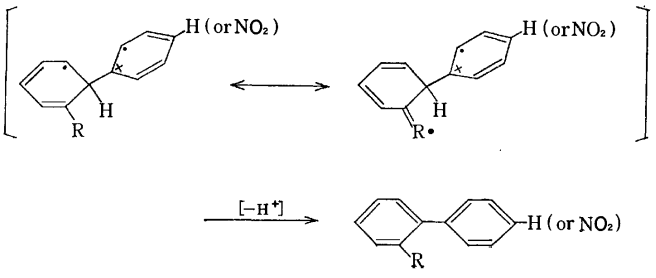

The yields of *ortho* isomers are always great, and this shows the radical nature of aryl cations. An intermediate σ-complex can be expressed as shown in the above structural formula and it roughly approximates the transition state. The more stable structure is that possessing the substituent R at the end of the resonance system of the cyclohexadienyl radical, and it gives rise to the *ortho* isomer.

The data shown in Table 2 also indicate that both the intermolecular (the partial rate factors) and intramolecular (the *m*/*p* ratios) selectivities of *p*-nitrophenyl cation are in general greater than those of phenyl cation. Hence, *p*-nitrophenyl cation is less reactive than phenyl cation.

The comparison of the data in Table 1 and 2 reveals that the isomer distributions and partial rate factors somewhat differ when the source and the medium are different. Such differences could be ascribed to the following reasons. 1) Difference of the counter anions: The counter anion is BF_4^- in the case of the diazonium salts and $CF_3CO_2^-$ (or $ArSO_2^-$) in the case of the azosulfones. The tightness of the ion pairs naturally differs. 2) Difference in the rates of abstraction of proton from the σ-complex: Since the basicities of the counter anions differ, the rates of proton abstraction may be different. However, no isotope effect was observed as reported in a previous paper,[1b] and hence the rate-determining step must be the forma-

tion of the σ-complex. 3) Difference in the solvents: The diazonium salts are decomposed in acetonitrile which is fairly basic, and therefore fairly extensive solvation is expected at the transition state although smaller than that at the ground state. The medium in which azosulfones are decomposed contains about 20% trifluoroacetic acid, and the solvation is expected to be very little. The fact that f_m and f_p are smaller with azosulfones could be ascribed to lack of stabilization by solvation at the transition state.

The reactivities at the *ortho* positions are somewhat greater in azosulfones than those in diazonium salts, and especially the values with *p*-nitrophenyl cation toward the *ortho* position of nitrobenzene are unusually great. At present, it is not possible to give an adequate explanation to this finding.

The fact that *p*-nitrophenyl cation is more selective and less reactive than phenyl cation in reactions with arenes could be explained as follows. If phenyl cation and *p*-nitrophenyl cation do not possess diradical cation nature, certainly *p*-nitrophenyl cation would be less stable and more reactive than phenyl cation. However, *p*-nitrophenyl cation is stabilized considerably by resonance with the nitro group as shown below. Thus, because of the diradical cation nature of the aryl cations, *p*-nitrophenyl cation is more stable and less reactive than phenyl cation.

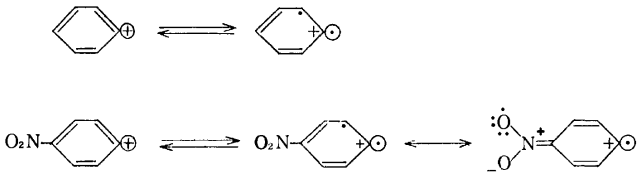

Experimental

Materials. Acetonitrile was purified according to the method in the literature[9] and distilled; bp 81.5°C. Trifluoroacetic acid of Wako Pure Chemical Industries Limited was used without further purification. Benzene and chlorobenzene were washed with concentrated sulfuric acid and water successively, dried over calcium chloride and distilled. Boiling points were 80 and 131°C, respectively. Anisole was washed with an aqueous sodium hydroxide solution and water, dried over calcium chloride, and distilled; bp 153°C. Nitrobenzene was washed repeatedly with a potassium dichromate solution, dried over calcium chloride, and distilled; bp 95.5°C/18 mmHg.

p-Nitrobenzenediazonium tetrafluoroborate was prepared according to the method described in the literature.[10]

p-Nitrophenylazo *p'*-tolyl sulfone was prepared according to the method described previously.[11]

4-Nitrodiphenyl was prepared by nitration of diphenyl according to the method of Maki and Obayashi,[12] mp 112.8—113°C (from methanol).

2-Methoxy-4'-nitrodiphenyl was prepared from *N*-nitroso-*p*-nitroacetanilide[13] and anisole, and was purified by elution chromatography and recrystallized from methanol, mp 63—64°C.

3-Methoxy-4'-nitrodiphenyl was prepared from diazotized *m*-anisidine and nitrobenzene by the Gomberg reaction. After removal of the solvent from the reaction mixture, the residue was distilled with superheated steam. The crystals obtained were then fractionated by chromatography on alumina in *n*-hexane–benzene (1: 1), mp 90—91°C (from methanol).

4-Methoxy-4'-nitrodiphenyl was prepared from *N*-nitroso-*p*-acetanisidide[12] and nitrobenzene, and was purified by elution chromatography on alumina in *n*-hexane–benzene and recrystallized from methanol, mp 110°C.

2-Chloro-4'-nitrodiphenyl was prepared by reaction of *N*-nitroso-*p*-nitroacetanilide[13] with chlorobenzene. After removal of chlorobenzene under reduced pressure, distillation with superheated steam and then elution chromatography on alumina (*n*-hexane–benzene, 4:1), yielded the product, mp 79—80°C (from methanol).

3-Chlorodiphenyl and 4-chlorodiphenyl were prepared by the method reported previously.[14]

3-Chloro-4'-nitrodiphenyl was prepared by the nitration of 3-chlorodiphenyl with fuming nitric acid in acetic anhydride. The crude oily product was fractionally distilled under reduced pressure (bp 157—160°C/1 mmHg) and purified by elution chromatography on alumina in *n*-hexane–benzene (4: 1); mp 93—94°C (from methanol).

4-Chloro-4'-nitrodiphenyl was prepared by the nitration[15] of 4-chlorodiphenyl, and was then purified by elution chromatography on alumina in *n*-hexane–benzene and recrystallized from ethanol; mp 145.5°C.

2,4'- and 4,4'-Dinitrodiphenyl were prepared by the nitration of 4-nitrodiphenyl according to the method of Maki and Obayashi.[12] The 2,4'-isomer was recrystallized from ethanol (mp 93.5—94°C), and the 4,4'-isomer from acetone (mp 237°C).

3-Nitrodiphenyl was prepared by the method described in the literature.[16]

3,4'-Dinitrodiphenyl was prepared by the nitration of 3-nitrodiphenyl according to the method reported in the literature,[17] mp 188.5°C (from ethanol).

General Procedure for p-*Nitrophenylation with* p-*Nitrobenzenediazonium Tetrafluoroborate.* In acetonitrile (70.0 g) *p*-nitrobenzenediazonium tetrafluoroborate (2.1 g) was dissolved, and the solution was diluted with an equimolar mixture of benzene and monosubstituted benzene (50 mol of the total substrate/mol of p-$NO_2C_6H_4N_2BF_4$). The homogeneous solution was placed in a bath at 60±0.1°C, and the decomposition was followed by measuring the evolution of nitrogen. After the evolution of nitrogen ceased, the mixture was diluted with ether and triphenylmethane was added as an internal standard for the glc analyses. The ethereal solution was washed with water to remove the acetonitrile,

9) R. A. Riddick and E. E. Toops, Jr., "Weissberger, Technique of Organic Chemistry," Vol. 7, "Organic Solvent," Interscience Publishers, Inc. (1955), p. 435.

10) E. S. Lewis and W. H. Hinds, *J. Amer. Chem. Soc.*, **74**, 304 (1952); D. T. Flood, "Organic Syntheses," Coll. Vol. 2, p. 295 (1943).

11) M. Kobayashi, H. Minato, and M. Kojima, This Bulletin, **45**, 2032 (1972).

12) T. Maki and K. Obayashi, *Kogyo Kagaku Zasshi*, **54**, 375 (1951).

13) H. France, I. M. Heilbron, and D. H. Hey, *J. Chem. Soc.*, **1940**, 361.

14) M. Kobayashi, E. Yamada, M. Matsui, and N. Kobori, *Org. Preparations and Procedures*, **1**, 221 (1969).

15) C. K. Bradsher and L. J. Wissow, *J. Amer. Chem. Soc.*, **68**, 404 (1946).

16) Bachmann and Hoffman, "Organic Reactions," Vol. 2, John Wiley & Sons, New York (1944), p. 249.

17) R. Ito, T. Migita, N. Morikawa, M. Okuni, and O. Simamura, This Bulletin, **36**, 985 (1963).

washed with a 5% sodium hydroxide solution to remove acidic products, and water successively, and dried over anhydrous magnesium sulfate.

General Procedure for p-*Nitrophenylation with* p-*Nitrophenylazo* p'-*Tolyl Sulfone in the Presence of Trifluoroacetic Acid.* *p*-Nitrophenylazo *p'*-tolyl sulfone (2.0 g, 6.6 mmol) was dissolved in a mixture of benzene (0.250 mol) and a substituted benzene (0.250 mol), and then trifluoroacetic acid (6.0 g, 52.6 mmol) was added to this homogeneous solution. The mixture was decomposed in a constant temperature bath at 60 ± 0.1°C. After the decomposition was over, the reaction mixture was treated in a manner similar to that described for the reaction with *p*-nitrobenzenediazonium tetrafluoroborate.

Quantitative Analyses. The substituted nitrodiphenyl isomers produced in the *p*-nitrophenylation were separated by gas chromatography. The compounds corresponding to the individual peaks were identified by comparing their retention times with those of the authentic specimens and their amounts were determined by use of calibration curves. The columns used were packed with Apiezon L (10%) on Chromosorb W, 1 m.

BULLETIN OF THE CHEMICAL SOCIETY OF JAPAN, VOL. 45, 2050—2052(1972)

The Migratory Aptitudes in the 1,3-Dipolar Cycloadducts of Substitiuted 1-Benzoyliminopyridinium Ylides with Dimethyl Acetylenedicarboxylate[1]

Tadashi SASAKI, Ken KANEMATSU, Akikazu KAKEHI, and Gin-ichi ITO

Institute of Applied Organic Chemistry, Faculty of Engineering, Nagoya University, Chikusa, Nagoya, 464

(Received November 4, 1971)

The 1,3-dipolar cycloaddition of substituted 1-benzoyliminopyridinium ylides (**1**, **6**, and **9**) with dimethyl acetylenedicarboxylate (DAC) produced the corresponding rearrangement compounds (**3**, **4**, **7**, **8**, and **10**). On the other hand, the similar reaction of **11** with DAC in acetonitrile gave **12**, accompanied with a Sommelet-type rearrangement compound, **13**. The structural elucidation of these products was accomplished by spectral inspections.

In continuation of our previous work,[2] we wish to report here on a comparative study of the cycloaddition reactions of 1-benzoyliminopyridinium ylides[3] with DAC.

Results and Discussion

In the reaction of 2-methyl-1-benzoyliminopyridinium ylide (**1**) with DAC in benzene at room temperature, the products were characterized as 1-benzoyl-2,3-bis(methoxycarbonyl)-3a-methyl-1,3a-dihydropyrazolo[1,5-*a*]pyridine (**2**) (5%) and a mixture of two rearranged isomers, dimethyl α-(2-methyl-3-pyridyl)-α'-benzoylaminomaleate (**3**) and dimethyl α-(2-methyl-5-pyridyl)-α'-benzoylaminomaleate (**4**) (9%) in a ratio of 7: 2.[4] An unstable compound (**2**) was spontaneously transformed, after 3 days at room temperature, into a mixture of **3** and **4**, and the reaction of **2** with tetracyanoethylene in benzene afforded a crystalline Diels-Alder adduct, **5**.

Thus, the isomeric products, **3** and **4**, may be assumed to be formed through Path **a** *via* 1,2-migration (intermediates **A**→**B**) in competition with Path **b** *via* 1,4-migration (intermediates **C**→**D**) by the rearrangement of **2**.

The 2,4-dimethyl compound, **6**, did not react with DAC in benzene under the above conditions. The present reactions were carried out in refluxing benzene, they gave an isomeric mixture of the rearranged products, **7** and **8** (51%) in a ratio of 1: 1.2 (as determined by nmr analyses).

A similar reaction of **9** with DAC in benzene or acetonitrile at 60—65°C afforded the expected rearranged product, **10** (28%).

These results are summarized in Scheme 1.

The reaction of 2,6-dimethyl-1-benzoyliminopyridinium ylide (**11**) with DAC in benzene at room temperature afforded the rearranged product, **12**, in a 74% yield. The NMR spectrum showed signals at τ 7.65 (s, 3H, Me), 7.44 (s, 3H, Me), 6.01 (s, 3H, COOMe), 6.30 (s, 3H, COOMe), 2.92 (d, 1H, C_5-H), 2.3—2.8 (m, 6H, Ph and C_4-H), and 2.32 (br s, 1H, NH, exchanged by D_2O), suggesting the intermediacy of dihydropyrazolopyridine, which might then rapidly rearrange into a stable compound, **12**. However, in acetonitrile, two products, **12** and **13**, were produced in 44 and 10% yields respectively. The NMR spectrum of **13** showed signals of one methyl proton at τ 7.63 (s, 3H), of pyridine ring protons at τ 3.00 (dd, 2H, overlapped with each proton at C_3- and C_5-H), of methylene

1) Studies of Heteroaromaticity. Part LVI. Part LV of this series: T. Sasaki, K. Kanematsu, and M. Murata, *Tetrahedron*, **27**, 5359 (1971).

2) T. Sasaki, K. Kanematsu, and A. Kakehi, *J. Org. Chem.*, **36**, 2978 (1971).

3) Several ring-substituted 1-benzoyliminopyridinium ylides have been prepared by a modification of the Gösl method; see T. Okamoto, M. Hirobe, C. Mizushima, and A. Osawa, *Yakugaku Zasshi*, **83**, 308 (1963).

4) These products were assigned on the basis of the foregoing data; see Ref. 2.

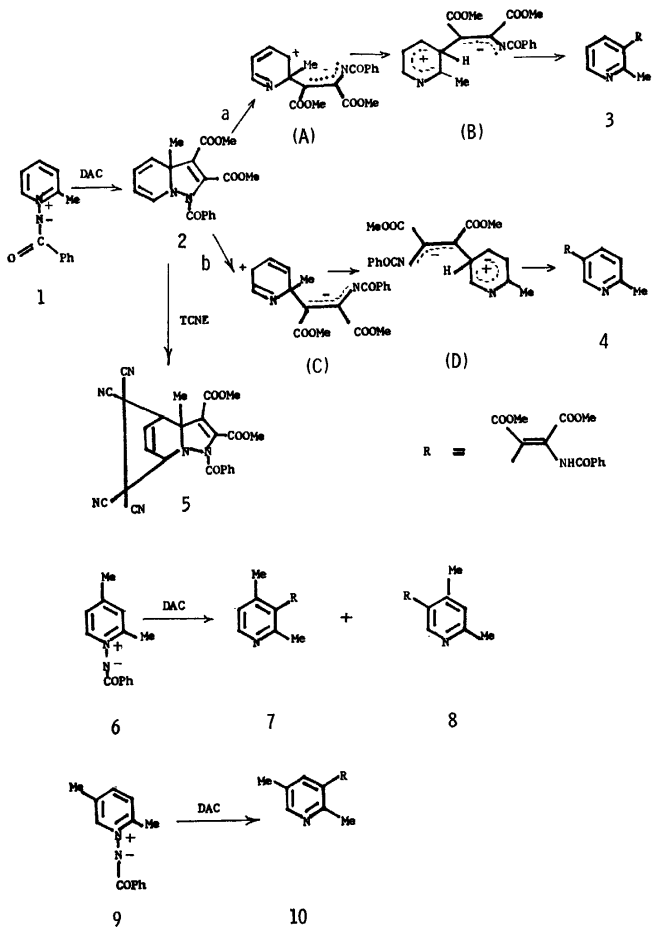

Scheme 1.

protons at τ 6.08 (s, 2H), of phenyl protons and C_4-H at τ 1.75—2.80 (m, 6H), of two methoxycarbonyl protons at τ 6.12 (s, 3H) and 6.20 (s, 3H), and of NH proton at τ −2.02 (br s, 1H, exchanged by D_2O). In particular, the singlet signal at τ 6.08 clearly arises from the methylene group at the 2-position in the pyridine moiety, suggesting that a Sommelet-type rearrangement has occurred. Moreover, a signal at τ −2.02 indicates the presence of a hydrogen-bonding amido group, showing that *cis-trans* isomerization has occurred. The heating of **12** in xylene at reflux for 5 hr afforded **14**, suggesting the presence of a hydrogen-bonding amido group at τ −2.09 (br s, exchanged by D_2O) by NMR. These results are summarized in Scheme 2.

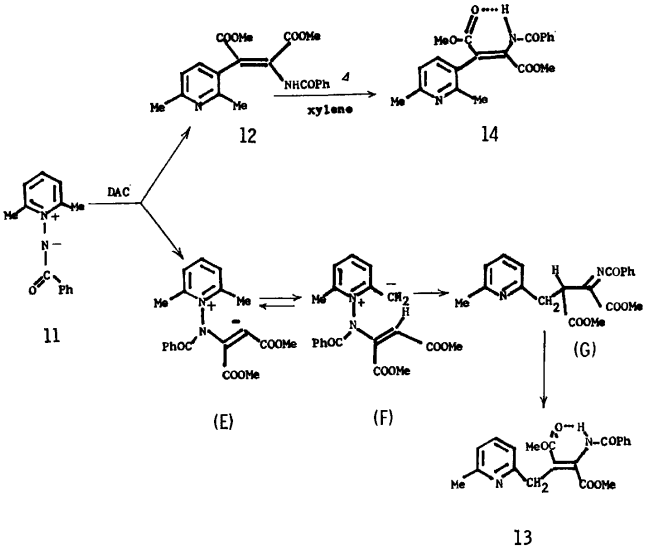

Scheme 2.

Finally, an additional discussion may be made of these studies. The mechanisms of the formations of the several rearranged products were discussed in our previous report.[2] However, the rearrangement behaviour is different from that of the substituents between the alkoxycarbonyl and benzoyl groups attached to the iminopyridinium moiety. The former undergoes rearrangement in the 1,4-fashion, but the latter proceeds competitively in the 1,2- and 1,4-fashions.

In addition, a Sommelet-type rearrangement product, **13**, was obtained by the reaction of **11** with DAC; this reaction might be initiated by a prototropic shift *via* intermediates, **E**→**F**→**G**, followed by a rearrangement to **13**, as is illustrated in Scheme 2. A similar rearrangement has been observed in the case of 2,6-dimethyl-1-phenyliminopyridinium ylide (**14**) as is shown in Scheme 3.[5]

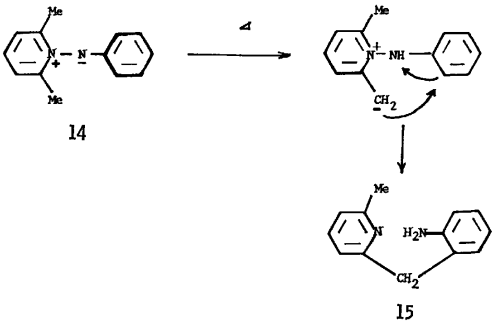

Scheme 3.

Experimental[6]

The 1,3-Dipolar Cycloaddition Reactions of the Ylides with DAC. General Method: Into a benzene or acetonitrile solution of DAC, an equimolar amount of the ylide was stirred at room temperature or at the reflux temperature. After the disappearance of the deep color of the solution, the solvent was removed *in vacuo* and the oily mixture was separated by column chromatography (silica gel), using benzene as the eluent.

Reaction of 1 with DAC. From 0.64 g of **1** and 0.43 g of DAC, we obtained **2** (0.055 g, 5%) as a pale yellow oil; ν_{max}^{neat} 1663, 1715, 1742 cm^{-1}, τ (CCl_4) 2.00—2.25 (m, 2H, 2,6-protons of C_6H_5), 2.40—2.80 (m, 3H, 3,4,5-protons of C_6H_5 and 1H, H_7), 4.30 (m, 2H, H_4 and H_5), 5.06 (m, 1H, H_6), 6.16 (s, 3H, OCH_3), 6.28 (s, 3H, OCH_3), 8.44 (s, 3H,

5) K. Dimroth, G. L. Buchanan, A. S. von Eichen, and G. Schiffler, *Ann. Chem.*, **604**, 221 (1947).

6) The melting points were measured with a Yanagimoto micromelting point apparatus and are uncorrected. Microanalyses were performed on a Perkin-Elmer 240 Elemental Analyser. The UV spectra were determined with a JASCO Model ORD/UV-5 recorder. The NMR spectra were taken with a Japan Electric Optics Lab. Co., Ltd., Model C-60-XL NMR spectrometer and with a Varian A-60 recording spectrometer, with tetramethylsilane as the internal standard. The chemical shifts are expressed in τ values. The IR spectra were taken with a JASCO Model IR-S spectrophotometer.

CH_3), and a mixture of **3** and **4** (mp 163—169°C, 0.096 g, 9%), which was identified as a 7:2 mixture because the integrated areas for the ring-substituted methyl protons and the C_2–H of the pyridine ring appeared at τ 7.57 (s) and 1.46 (br d) in **3** and at 7.45 (s) and 1.71 (br s) in **4**. The isomers could not be separated either by column chromatography or by repeated recrystallization.

Found: C, 64.46; H, 5.13; N, 7.84%. Calcd for $C_{19}H_{18}O_5N_2$: C, 64.40; H, 5.12; N, 7.91%.

Preparation of the Adduct, 5. A solution of 0.05 g of **2** and 0.02 g of tetracyanoethylene in 20 m*l* of benzene was stirred at room temperature for 3 hr. The precipitated solid was collected by filtration and recrystallized from methanol to give **5** (0.02 g, 29%); mp 182—184°C; τ ($CDCl_3$) 8.43 (s, 3H, CH_3), 6.23 (s, 3H, $COOCH_3$), 6.26 (s, 3H, $COOCH_3$), 5.78 (dd, $J_{4,5}$ 7.5 Hz, $J_{4,6}$ 1.5 Hz, 1H, H_4), 5.54 (dd, $J_{7,6}$ 7.0 Hz, $J_{7,5}$ 1.5 Hz, 1H, H_7), 3.48 (br t, $J_{5,6}$ 7.5 Hz, $J_{6,7}$ 7.0 Hz, 1H, H_6), 3.18 (br t, $J_{5,4}$ 7.5 Hz, $J_{5,6}$ 7.5 Hz, 1H, H_5), 2.10—2.80 (m, 5H, C_6H_5).

Found: C, 62.24; H, 3.85; N, 17.52%. Calcd for $C_{25}H_{18}N_6O_5$: C, 62.24; H, 3.76; N, 17.42%.

Reaction of 6 with DAC. From 0.68 g of **6** and 0.43 g of DAC (in benzene at 80°C), we obtained a mixture of **7** and **8** (mp 169—171°C, 0.56 g, 51%), which was identified as a 1:1.2 mixture because the integrated areas for the methyl protons and the C_2 proton of the pyridine ring appeared at τ 7.63 (s, CH_3 at C_2) and 1.77 (d, $J_{5,6}$ 7.5 Hz, H_6) in **7**, and at τ 7.52 (s, CH_3 at C_2) and 1.83 (s, H_6) in **8**. The mixture could not be separated either by column chromatography or by repeated recrystallization, but it gave a satisfactory analytical value.

Found: C, 65.41; H, 5.46; N, 7.42%. Calcd for $C_{20}H_{20}O_5N_2$: C, 65.21; H, 5.47; N, 7.61%.

Reaction of 9 with DAC. From 1.2 g of **9** and 0.7 g of DAC (in benzene or acetonitrile at 65°C), we obtained **10** (mp 186—188°C, 0.51 g 28%); ν_{max}^{KBr} (C=O) 1671, 1719, 1739 cm^{-1}, τ ($CDCl_3$) 7.68 (s, 3H, CH_3), 7.58 (s, 3H, CH_3), 6.02 (s, 3H, $COOCH_3$), 6.30 (s, 3H, $COOCH_3$), 2.4—2.9 (m, 7H, 5H of C_6H_5, 1H of ring proton of C_4 and 1H of NH).

Found: C, 65.30; H, 5.50; N, 7.48%. Calcd for $C_{20}H_{20}O_5N_2$: C, 65.21; H, 5.47; N, 7.61%.

Reaction of 11 with DAC. 1) From 0.68 g of **11** and 0.43 g of DAC (in benzene at room temperature for 1.5 hr), we obtained **12** (mp 208—211°C, 0.83 g, 74%); ν_{max}^{KBr} (C=O) 1677, 1708, 1731 cm^{-1}, τ ($CDCl_3$) 7.65 (s, 3H, CH_3), 7.44 (s, 3H, CH_3), 6.01 (s, 3H, $COOCH_3$), 6.30 (s, 3H, $COOCH_3$), 2.92 (d, $J_{4,5}$ 8.0 Hz, 1H, H_5), 2.30—2.80 (m, 6H, 5H of C_6H_5 and 1H or H_4), 2.32 (br s, 1H, NH).

Found: C, 65.10; H, 5.52; N, 7.40%. Calcd for $C_{20}H_{20}O_5N_2$: C, 65.21; H, 5.47; N, 7.61%. 2) From 0.68 g of **11** and 0.43 g of DAC (in acetonitrile at room temperature for 1.6 hr), we obtained **12** (0.26 g, 44%) and **13** (mp 172—176°C, 0.06 g, 10%); ν_{max}^{KBr} (C=O) 1680, 1706, 1730 cm^{-1}, τ ($CDCl_3$) 7.63 (s, 3H, CH_3), 6.20 (s, 3H, $COOCH_3$), 6.12 (s, 3H, $COOCH_3$), 6.08 (s, 2H, CH_2), 3.00 (dd, $J_{3,4}=J_{4,5}$ 7.5 Hz, 2H, H_3 and H_5), 1.75—2.00 and 2.30—2.80 (br m, 6H, 5H of C_6H_5 and 1H of H_4), −2.02 (br s, 1H, NH).

Thermal Isomerization of 12. A solution of 0.33 g of **12** in 20 m*l* of xylene was heated in an oil bath at 140—145°C for 5 hr. The solvent was then removed under reduced pressure, and the residue was purified by silica-gel chromatography, with benzene as the eluent, to give colorless crystals; **14** (0.20 g, 65%); mp 152—153°C; τ ($CDCl_3$) 7.56 (s, 3H, CH_3), 7.46 (s, 3H, CH_3), 6.45 (s, 3H, $COOCH_3$), 6.27 (s, 3H, $COOCH_3$), 3.07 (d, $J_{4,5}$ 8.0 Hz, 1H, H_5), 1.91—2.19 and 2.33—2.76 (br m, 6H, 5H of C_6H_5 and 1H of H_4), −2.09 (br s, 1H, NH, exchanged by D_2O .

Found: C, 65.41; H, 5.45; N, 7.57%. Calcd for $C_{20}H_{20}O_5N_2$: C, 65.21; H, 5.47; N, 7.61%.

BULLETIN OF THE CHEMICAL SOCIETY OF JAPAN, VOL. 45, 2052—2055(1972)

Reactive Species Produced by Laser Irradiation. The Reaction of CN Radicals with Hydrocarbons

Ko Taki, Pil Hyon Kim, and Susumu Namba
The Institute of Physical and Chemical Research, Wako-shi, Saitama
(Received January 17, 1972)

The reactive species, CN radicals, were produced by the irradiation of the focused laser beam on the metal cyanide target. The reaction of CN radicals with low-molecular-weight hydrocarbons gave fragmented hydrocarbons and CN (and NC) compounds, while that with hydrogen gave hydrogen cyanide. From the experimental results, it seems that the products may be formed mainly by the reaction of the reactive species with fragment hydrocarbon radicals which are produced by the collision of the high-temperature reactive species (CN*) with the parent hydrocarbons.

When the intense laser beam is focused upon a suitable target, its surface material is rapidly heated and then vaporized or decomposed.[1] It is of interest to study the chemical reaction of an organic compound with decomposed reactive species produced by laser irradiation. As has previously been shown,[2] in a binary system, such as metal compounds and hydrocarbons, the laser beam decomposes metal compounds selectively, because it is absorbed by the metal compounds only. The reaction of decomposed reactive

1) W. T. Ristau and N. E. Vanderborgh, *Anal. Chem.*, **43**, 702 (1971).

2) K. Taki, P. H. Kim, and S. Namba, This Bulletin, **43**, 1450 (1970).

species with some substrates present may then be observed.

In this experiment, copper cyanide and some other metal cyanides were decomposed by laser heating to form CN radicals, and the reaction of the CN radicals thus obtained with hydrocarbons was investigated.

Free CN radicals in the gaseous state have been formed from cyanogen by electric discharge,[3] thermal decomposition,[4] photodissociation,[5] and reaction with nitrogen.[6] It has also been found that carbon atoms produced by laser irradiation on carbon target[7] react with nitrogen to produce CN, as in the case of the carbon arc.[8] However, little work has been reported on the reaction[9,10] of CN with hydrocarbons in the gaseous state.

Experimental

1) Preparation of Copper Cyanide.[11] A potassium cyanide solution was added to a copper sulphate solution at 60°C in order to precipitate CuCN. The elemental analysis of this copper cyanide showed C, 13.70% and N, 15.73%. It has the empirical formula of CuCN (Calcd: C, 13.41; N, 15.61%). The freshly-prepared CuCN was used for decomposition. AgCN (prepared from $AgNO_3$ and KCN) powder was also used.

2) Laser Irradiation. Copper cyanide powder or other metal cyanides in a 7-cc cell filled with substrate gas (700—760 Torr) was irradiated by a ruby laser beam focused by a lens 10 cm in focal length. The ruby laser used was a normal laser, the output energy and pulse duration of which were 3 J and 0.5 msec respectively. The temperature of the irradiated region on metal cyanide is estimated to be above 1000°C, and the heated region of the target surface is about 10^{-2} cm^2.

3) Analysis. The volatile products were collected and analysed by gas chromatography using dioctyl phthalate, dinonyl phthalate, silica gel, and squalane columns. The reliable value in detection was about 10^{-8} mol.

Results

1) Decomposition of Copper Cyanide. The noncondensable products at −196°C (one-fifth of all the products) were analysed mass spectrometrically; they were found to be nitrogen and small amounts of oxygen and carbon monoxide. The condensable gas was almost pure cyanogen, like that produced by the conventional heating.[12] Therefore, the decomposition may show the formation of CN, which then gives cyanogen by the combination of two CN radicals. (AgCN was also decomposed. The products were almost the same as those from copper cyanide.)

The presence of the N_2 and CO[13] gases in the products suggested that the decomposition of copper cyanide might produce N and C atoms. However, their yields are small and N and O atoms do not play any significant role in the reaction with hydrocarbons.[7,14]

Table 1. Product yield in the reaction of CN with low molecular weight hydrocarbons for 6 pulse laser irradiations

Substrate	Product	Yield (10^{-6}mol)
Methane	C_2N_2	0.20
	CH_3CN	0.007
	CH_3NC	0.03
	C_2H_6	trace
Ethane	C_2N_2	0.20
	CH_3CN	0.03
	CH_3NC	0.03
	C_2H_5CN	0.003
	C_2H_5NC	0.006
	C_2H_3CN	0.02
	CH_4	0.10
	C_2H_4	0.40
	C_2H_2	0.20
Ethylene	C_2N_2	0.20
	C_2H_3CN	0.05
	CH_4	0.02
	C_2H_6	0.03
	C_2H_2	0.60
	Vinylacetylene	trace
	Diacetylene	trace

2) Reaction of CN with Low-molecular-weight Hydrocarbons. In the presence of methane, the products were acetonitrile, methyl isocyanide, and some other hydrocarbons (small amounts of ethane). In ethane, the products were methyl isocyanide,[15] acetonitrile, propionitrile, ethyl isocyanide, and other hydrocarbons. In ethylene, acrylonitrile and propionitrile were produced. The results are summarized in Table 1. In the table, the data of the noncondensable products (N_2, O_2, H_2, and CO) and HCN (see Appendix) are excluded. In the reaction with acetylene, small amounts of ethyl isocyanide, propionitrile, acrylonitrile, and black polymeric products were observed, but cyanoacetylene and dicyanoacetylene were not detected.

3) Reaction of CN with Other Substrates. In the reaction of propylene and cyclohexane, the low-molecular-weight cyanides and isocyanides (CH_3CN, CH_3NC,

3) J. U. White, *J. Chem. Phys.*, **8**, 79 (1940).
4) J. U. White, *ibid.*, **8**, 459 (1940).
5) A. Mele and H. Okabe, *ibid.*, **51**, 4798 (1969).
6) D. R. Safrany and W. Jaster, *J. Phys. Chem.*, **72**, 3318 (1968).
7) K. Taki, P. H. Kim, and S. Namba, This Bulletin, **42**, 823 (1969). *Sci. Papers, I. P. C. R.*, **63**, 41 (1969).
8) G. Herzberg, F. R. S., "Molecular Spectra and Molecular Structure," I. Spectra of Diatomic Molecules, Second Edition, D. Van Nostrand Co., Inc., New York 1950, p. 31.
9) C. A. Goy, D. H. Shaw, and H. O. Pritchard, *J. Phys. Chem.*, **69**, 1504 (1965).
10) D. E. McElcheran, M. H. J. Wijnen, and E. W. R. Steacie, *Can. J. Chem.*, **36**, 321 (1958).
11) M. C. Sneed, J. L. Magnard, and R. C. Brasted, "Comprehensive Inorganic Chemistry," Vol. II, D. Van Nostrand Co., Inc., New York 1954, p. 81.
12) S. Nakamura, *I & EC Product Research and Development*, **7**, 159 (1968); *Yukigosei Kyokaishi*, **26**, 23 (1968).
13) CO may be produced by the decomposition of an impurity of CuCN (for example, $CuCO_3$).
14) Y. Titani and N. N. Lichtin, *J. Phys. Chem.*, **72**, 526 (1968).
15) Authentic methyl and ethyl isocyanide were prepared by the method of Ref. 16; in the reaction with HgO, they changed to isocyanate.
16) H. L. Jackson and B. C. McKusick, "Organic Syntheses," Coll. Vol. IV, p. 438, (1963).

C_2H_5CN, C_2H_5NC), hydrocarbons, and C_2N_2 were produced, but the cyanides or isocyanides of the parent molecules were not obtained. The reaction with benzene produced benzonitrile and phenyl isocyanide[17] in an almost equivalent yield ($0.7-2\times10^{-8}$ mol for 7 pulses), hydrocarbons (mainly C_2H_2), and C_2N_2. In the reaction with toluene, benzyl cyanide was not obtained, but benzonitrile, phenyl isocyanide, hydrocarbons, and C_2N_2 were obtained.

Discussion

From the reaction products, it may be considered that the formation process of nitrile and isonitrile is the combination of alkyl radicals with CN. The formation of alkyl radicals may be brought about either by hydrogen abstraction by CN, resulting in the formation of hydrogen cyanide,[9] or by the decomposition of the hydrocarbons mentioned below.

It seems that the CN radicals produced by laser irradiation are probably in the high-temperature state at the moment of production, and that they collide with the hydrocarbons and decompose them thermally into fragments. The CN radicals may react with the fragments thus produced near the target surface, because the mean free path of CN vapor is about 10^{-5} cm at 1 atm; subsequently, low-molecular-weight CN (and NC) compounds and hydrocarbons may be formed. The formation of benzonitrile may be due to the stability of the benzene ring.

The thermal decomposition at the target surface may be negligible for the following reasons; the hydrocarbon may not decompose at the heated surface during the time of CN vaporization because the hydrocarbon can not collide with the heated surface because of the vapor pressure of the CN species, and the reaction of the CN species with the fragmented hydrocarbon produced before the vaporization of CN may also be negligible because the life-time of a fragmented hydrocarbon (such as CH, CH_2,$\cdots$) is much shorter than the vaporization time ($\sim10^{-4}$ sec).

The collisional and thermal decomposition may be supported by the fact that the laser irradiation on nickel plate in ethane gives the products of hydrocarbon listed in Table 2.

Table 2. Product yield in the reaction of Ni vapor with ethane (about 700 torr) for 7 pulse irradiations

Substrate	Product	Yield (10^{-6}mol)
Ethane	CH_4	0.32
	C_2H_4	0.77
	C_2H_2	0.37
	C_3H_8	0.10

From the above considerations, the formation of CN products may follow the thermal (collisional) decomposition caused by the high-temperature CN radicals or the hydrogen abstraction caused by CN radicals, as follows:

[1] $CuCN \xrightarrow{\text{laser heating}} CN^*$ species and others[19]

[2] $2CN^* \longrightarrow C_2N_2$

[3] $CN^* + RH \longrightarrow [RHCN]^*$

[4] $[RHCN]^* \xrightarrow{\text{fragmentation}}$ CN; H_2, C_2N_2; HCN, CN(or NC) compounds; hydrocarbon products

[5] $RH + CN \longrightarrow R\cdot + HCN$; CN(or NC) compounds

CN*; CN at the high-temperature state

The authors wish to acknowledge the enthusiastic assistance of Miss K. Motegi in carrying out this work; they wish also to express their appreciation to Mr. S. Satooka for his mass-spectroscopic analysis.

Appendix

Reaction of CN with Hydrogen. The laser irradiation on freshly-prepared copper cyanide in the presence of hydrogen shows the formation of hydrogen cyanide, as in the reaction of hydrocarbons with the CN radicals formed by the photolysis of ICN.[5] However, when the copper cyanide was aged the yield of hydrogen cyanide decreased with the time; at last no hydrogen cyanide was given after about a week. The above copper cyanide, when heated at 100—200°C under a vacuum, gave hydrogen cyanide again. Moreover, the yield of cyanogen was not changed by the time of the ageing of copper cyanide. The copper cyanide obtained from $Cu[Cu(CN)_2]_2$ and $Cu[Cu(CN)_3]$ by thermal decomposition also gave hydrogen cyanide, and when the decomposition temperature was at about 150°C, the ratio of hydrogen cyanide to cyanogen showed the highest value, as is shown in Fig. 1. No differences in these samples were found in the X-ray diffraction pattern or in emission spectrum excited by the laser irradiation.

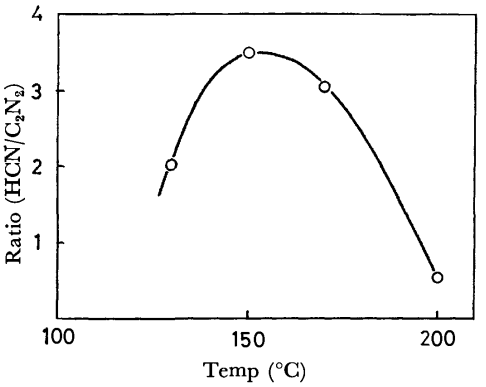

Fig. 1. The ratio of HCN to C_2N_2 in the reaction of hydrogen with CN produced by the laser irradiation on CuCN prepared from $Cu[Cu(CN)_2]_2$ and $Cu[Cu(CN)_3]$ at various temperatures. The yield of C_2N_2 is about 0.2×10^{-6} mol for 6 pulses.

17) The phenyl isocyanide was prepared by the method of Ref. 18.

18) J. U. Nef, *Liebig's Ann. Chem.*, **270**, 275 (1892).

19) All the high-temperature species (CuO, Cu, $\cdots$) except CN radicals may also decompose the substrate.

In order to examine the formation of hydrogen cyanide, several experiments were performed. The laser irradiation on a carbon target[20] in a mixture of hydrogen and nitrogen gave the hydrogen cyanide. The addition of a small amount of oxygen in this case caused a decrease in the yields of hydrogen cyanide and cyanogen. Oxygen molecules react with CN radicals quickly, resulting in a decrease in the yields of hydrogen cyanide and cyanogen. Moreover, it was found that hydrogen cyanide does not react with copper oxide, but that it does react with copper hydroxide quickly and disappears. It seems that the failure to detect hydrogen cyanide when ageing copper cyanide is used may be caused by the presence of copper hydroxide formed in the air. This consideration is supported by the fact that the copper cyanide prepared by an excess of a potassium cyanide solution with a copper sulfate solution did not give hydrogen cyanide, because a small amount of copper hydroxide may be formed in the alkali solution.

By using copper cyanide containing a trace of copper hydroxide on its surface in the reaction with various substrates, the yield of hydrogen cyanide is affected, but the yield of the other CN products may not be affected, because these CN products are not reactive with copper hydroxide.

20) The laser irradiation of a carbon target in nitrogen gives CN radicals.[7]

BULLETIN OF THE CHEMICAL SOCIETY OF JAPAN, VOL. 45, 2055—2057(1972)

Studies of the Synthesis of Furan Compounds. XXVII.[1] Derivatives of 3-(5-Nitro-2-furyl)acrylonitrile

Ichiro HIRAO and Yasuhiko KATO

Laboratory of Organic Synthesis, Department of Chemical Engineering, Kyushu Institute of Technology, Tobata-ku, Kita-Kyushu

(Received January 17, 1972)

In a continuation of our previous papers[2,3] concerning the syntheses with 5-nitro-2-furonitrile, 2-(5-nitro-2-furyl)vinyl-1,2,4-oxadiazoles and -1,2,3-triazoles were prepared from 3-(5-nitro-2-furyl)acrylonitrile (I). When I was treated with diazomethane in ether, 4-[2-(5-nitro-2-furyl)vinyl]-1,2,3-triazole (II) was obtained. II gave *N*-acetyl (IIa) and *N*-morpholinomethyl (IIb) compounds when treated with acetic anhydride and when the Mannich reaction was utilized respectively. 3-(5-Nitro-2-furyl)acrylamide oxime (III) was prepared by the usual method from I and hydroxylamine. The treatment of III with benzaldehyde and acid anhydrides or chlorides afforded 3-[2-(5-nitro-2-furyl)vinyl]-5-phenyl-4,5-dihydro-1,2,4-oxadiazoline (IV) and *O*-acyl-3-(5-nitro-2-furyl)acrylamide oximes (IIIa—IIIe) respectively. The *O*-acyl-amide oximes were found to cyclize to 3-[2-(5-nitro-2-furyl)vinyl]-5-alkyl-1,2,4-oxadiazole (V—VII) in their thermal analyses.

3-(5-Nitro-2-furyl)acrylonitrile (I) has been prepared from 3-(5-nitro-2-furyl)acrolein oxime acetate and pyridine,[4] by the dehydration of the corresponding acid amide with *p*-toluenesulfonyl chloride,[5] and by the Wittig reaction of 5-nitrofurfural with cyanomethylenetriphenylphosphorane.[6] However, the above procedures may be supposed to be unsuitable for supplying I as a synthetic raw material from the following points of view: 1) the low yields of the product, 2) the lack in the economy, and 3) the complicated procedure necessary because of the isomerization of the product. Therefore, a better procedure for the preparation of I and the synthesis of its derivatives shall be described in this paper.

Results and Discussion

3-(5-Nitro-2-furyl)acrylonitrile (I) was prepared in a good yield by the reaction of 3-(5-nitro-2-furyl)acrylamide with phosphoryl chloride. When treated with diazomethane in ether, I cyclized to 4-[2-(5-nitro-2-furyl)vinyl]-1,2,3-triazole (II). The structure of this compound was confirmed on the basis of its analytical and IR spectral data. By heating II with acetic anhydride or with 37% formaldehyde and morpholine, *N*-acetyl (IIa) and *N*-morpholinomethyl (IIb) compounds were obtained respectively, though the position of the substituents on the triazole ring was uncertain. 3-(5-Nitro-2-furyl)acrylamide oxime (III) was readily obtained from I and hydroxylamine in the usual way.[2,7,8] The IR spectrum of III exhibited two N–H stretching bands, one at 3448 and the other at 3405 cm^{-1}, besides a broad absorption at 2807 cm^{-1} which might be assumed to be a intramolecular chelated[9] O–H stretching frequency.

3-(5-Nitro-2-furyl)acrylamide was prepared from *trans*-3-(5-nitro-2-furyl)acrylic acid[10] by the usual method. In comparing the NMR spectrum of the acrylamide with that of the *trans*-acrylic acid, the *trans*

1) Part XXVI of this series: I. Hirao, Y. Kato, and H. Tateishi, This Bulletin, **45**, 208 (1972).
2) Y. Kato and I. Hirao, *Bull. Kyushu Inst. Technol.*, No. **15**, 57 (1965).
3) I. Hirao, Y. Kato, T. Hayakawa, and H. Tateishi, This Bulletin, **44**, 780 (1971).
4) M. Ikeda, *Ann. Rept. Fac. Pharm. Kanazawa Univ.*, No. **3**, 25 (1953).
5) A. Sugihara, *Yakugaku Zasshi*, **86**, 525 (1966).
6) H. Saikachi and S. Nakamura, *ibid.*, **88**, 110 (1968).
7) W. R. Sherman and A. M. von Esch, *J. Med. Chem.*, **8**, 25 (1965).
8) I. Saikawa and A. Takai, *Yakugaku Zasshi*, **85**, 948 (1965).
9) L. J. Bellamy, "The Infrared Spectra of Complex Molecules," John Willey & Sons, New York 1958, p. 104.
10) H. Saikachi and A. Tanaka, *Yakugaku Zasshi*, **83**, 240 (1963).

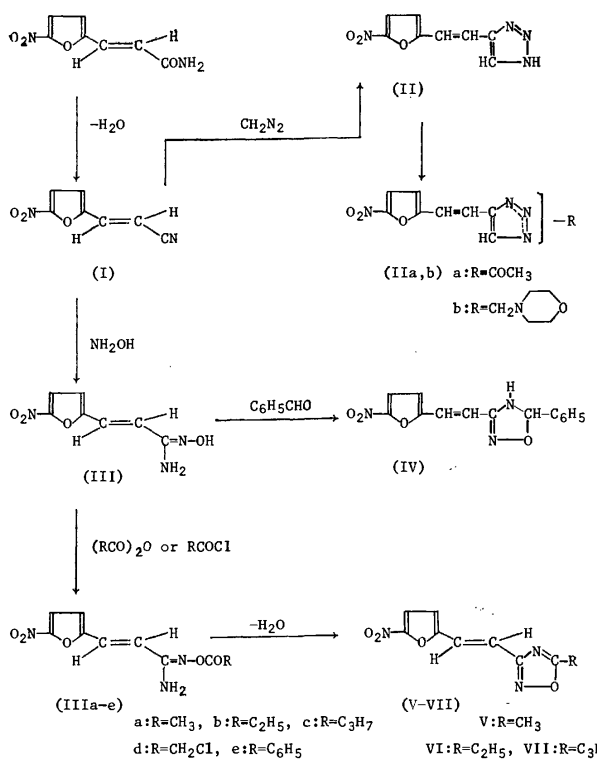

configuration of the acrylamide can be deduced from a coupling constant ($J_{\alpha\beta}$) of the ethylene-bonding α- and β-protons similar to that of the *trans*-acrylic acid ($J_{\alpha\beta}$=15.8 Hz). In the NMR spectra of I and III, the observed $J_{\alpha\beta}$ values were approximately the same as that of the starting acrylamide. Therefore, the geometrical configuration was confirmed to be retained during the process of acrylamide→I→III.

When amide oximes are heated with aldehydes, they are converted to 4,5-dihydro-1,2,4-oxadiazolines.[11] Thus, III reacted with benzaldehyde to afford 3-[2-(5-nitro-2-furyl)vinyl]-5-phenyl-4,5-dihydro-1,2,4-oxadiazoline (IV). On the treatment of III with acid anhydrides or chlorides in the usual manner, *O*-acyl-3-(5-nitro-2-furyl)acrylamide oximes (IIIa—IIIe) were produced. The assignment of the *O*-acyl structures to IIIa—IIIe is based on their IR spectra. As in the case of the *N*-acylamide oxime, only one sharp band is observed in the 3400 cm^{-1} region.[12] On the other hand, in the IR spectra of IIIa—IIIe these compounds showed two absorptions, at about 3460 and 3350 cm^{-1}, presumably due to the N–H stretching of the primary amino group, and a C=O absorption at about 1750 cm^{-1}. Furthermore, the characteristic O–H absorption at 2807 cm^{-1} in the mother compound, III, disappeared.

The results of differential thermal analysis (DTA) and thermogravimetric analysis (TGA) indicated that IIIa—IIIc underwent a cyclization reaction, with the release of a molecule of water; this was supported by the absence of the C=O and NH_2 absorptions in the IR spectra of the heating residues of IIIa—IIIc. The DTA curves show an endothermic peak at 173°C for IIIa, at 161°C for IIIb, and at 156°C for IIIc. These peaks coincide with the melting points of each of the corresponding compounds, and are in agreement with a stage in the reduction of the weight at 172—190°C for IIIa, at 160—187°C for IIIb, and at 155—184°C for IIIc, as shown by the TGA curves. About 8.0, 7.4, and 7.1% losses of the weight were observed for IIIa, IIIb, and IIIc respectively at this stage; these losses correspond to the loss of a molecule of water (theoretical: IIIa 7.5, IIIb 7.1, and IIIc 6.7%). Thus, the cyclization reaction was successfully carried out when IIIa—IIIc were heated at the corresponding melting point in a nitrogen stream to give 5-methyl (V), 5-ethyl (VI), and 5-propyl-3-[2-(5-nitro-2-furyl)vinyl]-1,2,4-oxadiazole (VII) respectively.

The geometrical configurations of the compounds, IIIa—IIIe and V—VII, were concluded to be *trans* by a comparison of the $J_{\alpha\beta}$ values of IIId and VI with that of I or III.

Experimental

All the melting points are uncorrected. The elemental analyses were carried out with a Yanagimoto CHN Corder, MT-2 type. The infrared absorption spectra (IR) were performed on a JASCO Model IRA-2 grating infrared spectrophotometer. The nuclear magnetic resonance spectra (NMR) were determined by means of a Japan Electron Optics NMR spectrometer, JNM-C-60HL (60 MHz). All the spectra were measured in DMSO-d_6 (concentration, 7—8 wt%), with tetramethylsilane as the internal reference; the peak positions were expressed in δ-values. The thermal analyses were carried out with a Chyo Balance and with Rigaku Denki Thermoflex in a nitrogen stream.

trans-*3-(5-Nitro-2-furyl)acrylonitrile (I).* A mixture of 18.2 g (0.1 mol) of *trans*-3-(5-nitro-2-furyl)acrylamide, 35 m*l* of phosphoryl chloride, and 2—3 drops of *N,N*-dimethylaniline was heated at 65—70°C for 1.5 hr. After cooling, the reaction mixture was poured onto crushed ice, and the precipitates were collected by filtration, washed with cold water, and dried. They were then recrystallized from ethanol to afford 14 g (84.7%) of the pure nitrile (I) as yellow needles; mp 110°C. IR (KBr) cm^{-1}: 2218 (C≡N). NMR (DMSO-d_6) δ: 6.41 (d, 1H, J=16.3 Hz, ethylene bond C_α–H), 7.18 (d, 1H, J=4.0 Hz, furan ring C_3–H), 7.57 (d, 1H, J=16.3 Hz, ethylene bond C_β–H), and 7.67 (d, 1H, J=4.0 Hz, furan ring C_4–H).

Found: 51.49; H, 2.01; N, 17.05%. Calcd for $C_7H_4N_2O_3$: C, 51.22; H, 2.44; N, 17.07%.

The NMR data of the ethylenic protons of the *trans*-acrylic acid and acrylamide were obtained as follows:

trans-acrylic acid: α-H 6.53, β-H 7.42, J=15.8 Hz. acrylamide: α-H 6.68, β-H 7.23, J=15.8 Hz.

4-[2-(5-Nitro-2-furyl)vinyl]-1,2,3-triazole (II). To a stirred suspension of I (5 g, 30 mmol) in 100 m*l* of ether, we added an ethereal solution containing 32 mmol of diazomethane. The mixture was refluxed for 4 hr, and then the insoluble material was filtered off. The filtrate was taken to dryness *in vacuo*, and the residue was washed with boiling ligroin. Recrystallization from benzene gave 1 g (16.2%) of II as ochreous granules which melted at 133—134°C. IR (KBr) cm^{-1}: 3500 (N–H).

Found: C, 46.61; H, 2.86; N, 27.38%. Calcd for $C_8H_6N_4O_3$: C, 46.60; H, 2.91; N, 27.18%.

4-[2-(5-Nitro-2-furyl)vinyl]-N-acetyl-1,2,3-triazole (IIa). A mixture of II (0.3 g, 1.5 mmol) and acetic anhydride (0.5 g)

11) F. Tiemann, *Ber.*, **22**, 2412 (1889).

12) F. Floy, R. Lenears, and C. Moussebois, *Helv. Chim. Acta*, **45**, 437 (1962).

in 10 ml of dioxane was refluxed for 2 hr. The resulting solution was taken to dryness *in vacuo*, and the residue was washed with water and then dried. Crystallization from benzene gave 0.28 g (76%) of IIa as yellow needles; mp 146—148°C. IR (KBr) cm^{-1}: 1670 (C=O).

Found: C, 48.14; H, 3.43; N, 22.69%. Calcd for $C_{10}H_8N_4O_4$: C, 48.38; H, 3.22; N, 22.58%.

4-[2-(5-Nitro-2-furyl)vinyl]-N-morpholinomethyl-1,2,3-triazole (IIb). A mixture of II (0.3 g, 1.5 mmol), 37% formaldehyde (0.15 g), morpholine (0.15 g), *N,N*-dimethylformamide (0.15 g), and dioxane (10 ml) was stirred at 10—12°C for 1 hr. The resulting mixture was poured onto ice water, and the precipitates were collected on a filter. Recrystallization from methanol afforded pale yellow granules (IIb) which melted at 62—63°C and which weighed 0.2 g (43.7%).

Found: C, 51.52; H, 5.07; N, 23.30%. Calcd for $C_{13}H_{15}N_5O_4$: C, 51.15; H, 4.92; N, 22.95%.

trans-*3-(5-Nitro-2-furyl)acrylamide oxime (III).* To a stirred, warmed (50—55°C) mixture of I (1.64 g, 10 mmol), *N,N*-dimethylaniline (2 drops), and ethanol (50 ml) was added a solution of hydroxylamine hydrochloride (2.1 g, 30 mmol) and sodium hydroxide (0.96 g, 24 mmol) in 10 ml of water over a period of 15—20 min. After the addition, the mixture was stirred at 60°C for an additional hour. On cooling, the precipitated product was filtered and dried. Recrystallization from ethanol afforded 1.58 g (80.2%) of III as orange needles; mp 217—218°C. IR (KBr) cm^{-1}: 3448, 3405 (NH_2), and 2807 (O–H···NH_2). NMR (DMSO-d_6) δ: 5.78 (s, 2H, NH_2 proton), 6.61 (d, 1H, J=16.3 Hz, ethylene bond C_α–H), 7.00 (d, 1H, J=4.0 Hz, furan ring C_3–H), 7.05 (d, 1H, J=16.3 Hz, ethylene bond C_β–H), and 7.68 (d, 1H, J=4.0 Hz, furan ring C_4–H).

Found: C, 42.77; H, 3.37; N, 21.49%. Calcd for $C_7H_7N_3O_4$: C, 42.64; H, 3.55; N, 21.32%.

3-[2-(5-Nitro-2-furyl)vinyl]-5-phenyl-4,5-dihydro-1,2,4-oxadiazoline (IV). A 10-mmol (1.97 g) portion of III was heated with benzaldehyde (50 ml) at 100°C for 4 hr. The resulting solution was taken to dryness *in vacuo*, and the residue was washed with ether and then dried. Recrystallization from methanol gave 1.6 g (56.1%) of IV as ochre-colored needles; mp 158—159°C.

Found: C, 59.09; H, 3.77; N, 14.73%. Calcd for $C_{14}H_{12}N_3O_4$: C, 58.94; H, 2.86; N, 14.73%.

trans-O-*Acetyl-3-(5-nitro-2-furyl)acrylamide oxime (IIIa).* A mixture of acetic anhydride (20 ml) and III (0.99 g, 5 mmol) was heated at 60—65°C for 0.5—1 hr. After cooling, water was added to decompose the surplus acid anhydride, and the precipitated product was filtered, washed with water, and dried. It was then recrystallized from dioxane to give 0.88 g (73.4%) of IIIa as yellow leaflets; mp 171—172°C. IR (KBr) cm^{-1}: 3457, 3350 (NH_2), and 1745 (C=O). Thermal analysis: 173°C (DTA; endothermic), 172—190°C (TGA; weight loss 8.0%).

Found: C, 45.03; H, 3.80; N, 17.26%. Calcd for $C_9H_9N_3O_5$: C, 45.19; H, 3.76; N, 17.57%.

trans-O-*Propionyl-3-(5-nitro-2-furyl)acrylamide oxime (IIIb).* This was prepared by the method used for IIIa, using 20 ml of propionic anhydride. Work up as above afforded 0.91 g (72%) of pure IIIb as yellow leaflets; mp 157—158°C (from dioxane). IR (KBr) cm^{-1}: 3455, 3350 (NH_2), and 1745 (C=O). Thermal analysis: 161°C (DTA; endothermic), 160—187°C (TGA; weight loss 7.4%).

Found: C, 47.09; H, 4.32; N, 16.15%. Calcd for $C_{10}H_{11}N_3O_5$: C, 47.43; H, 4.37; N, 16.60%.

trans-O-*Butyryl-3-(5-nitro-2-furyl)acrylamide oxime (IIIc).* The procedure described above for IIIa was employed using butyric anhydride (35 ml). The resulting solution was kept standing at room temperature until the product was isolated. The product was obtained as yellow leaflets; mp 153—154°C (from dioxane); weight, 1.1 g (78.7%). IR (KBr) cm^{-1}: 3455, 3350 (NH_2), 2970, 2885 (CH_2, CH_3), and 1745 (C=O). Thermal analysis: 156°C (DTA; endothermic), 155—184°C (TGA; weight loss 7.1%).

Found: C, 49.39; H, 4.95; N, 15.43%. Calcd for $C_{11}H_{13}N_3O_5$: C, 49.44; H, 4.86; N, 15.73%.

trans-O-*Chloraocetyl-3-(5-nitro-2-furyl)acrylamide oxime (IIId).* To a stirred, warmed (50—60°C) mixture of III (0.99 g, 5 mmol), sodium bicarbonate (1.05 g, 12.4 mmol), and dioxane (20 ml), we added, drop by drop, a solution of chloroacetyl chloride (0.57 g, 5.1 mmol) in 10 ml of dioxane. The resulting mixture was stirred for an additional hour, and then it was poured into ice water. The precipitates were collected, washed with water, and dried. Crystallization from ethanol afforded 1.1 g (80.4%) of IIId as yellow-ochre needles; mp 147—148°C. IR (KBr) cm^{-1}: 3465, 3345 (NH_2), 1767 (C=O), and 1285 (CH_2Cl). NMR (DMSO-d_6) δ: 4.46 (s, 2H, $COCH_2Cl$ proton), 6.57 (d, 1H, J=16.3 Hz, ethylene bond C_α–H), 6.86 (broad s, 2H, NH_2 proton), 7.12 (d, 1H, J=4.0 Hz, furan ring C_3–H), 7.28 (d, 1H, J=16.3 Hz, ethylene bond C_β–H), and 7.68 (d, 1H, J=4.0 Hz, furan ring C_4–H).

Found: C, 39.62; H, 3.15; N, 15.09%. Calcd for $C_9H_8N_3O_5Cl$: C, 39.41; H, 2.92; N, 15.32%.

trans-O-*Benzoyl-3-(5-nitro-2-furyl)acrylamide oxime (IIIe).* This was prepared in the same way as IIId, but using benzoyl chloride (1.4 g). In this way, 1.1 g (73.4%) of IIIe were obtained; mp 197°C. Recrystallization from dioxane gave a yellow powder; mp 200—201°C. Yield: 1.8 g (59.2%). IR (KBr) cm^{-1}: 3470, 3345 (NH_2), and 1726 (C=O).

Found: C, 55.97; H, 3.69; N, 13.46%. Calcd for $C_{14}H_{11}N_3O_5$: C, 55.81; H, 3.65; N, 13.95%.

trans-*3-[2-(5-Nitro-2-furyl)vinyl]-5-methyl-1,2,4-oxadiazole (V).* Compound IIIa (0.55 g, 2.3 mmol) was heated at 173—175°C under a nitrogen stream for 5 min, by which time the evolution of water had ceased. The residue was then recrystallized from ethanol to give 0.23 g (45.6%) of V as yellow-ochre granules; mp 189—190°C.

Found: C, 48.48; H, 3.19; N, 18.73%. Calcd for $C_9H_7N_3O_4$: C, 48.87; H, 3.16; N, 19.00%.

trans-*3-[2-(5-Nitro-2-furyl)vinyl]-5-ethyl-1,2,4-oxadiazole (VI).* The method used here was virtually identical with that described for V; 0.75 g (2.9 mmol) of IIIb was heated at 162—164°C. Work-up as above afforded 0.4 g (58.6%) of VI as yellow needles; mp 123—125°C (from ethanol). NMR (DMSO-d_6) δ: 1.30 (t, 3H, J=7.2 Hz, $-CH_2-C\underline{H}_3$ proton), 2.91 (q, 2H, J=7.2 Hz, $-C\underline{H}_2-CH_3$ proton), 7.12 (d, 1H, J=16.9 Hz, ethylene bond C_α–H), 7.18 (d, 1H, J=4.0 Hz, furan ring C_3–H), 7.43 (d, 1H, J=16.9 Hz, ethylene bond C_β–H), and 7.66 (d, 1H, J=4.0 Hz, furan ring C_4–H).

Found: C, 50.62; H, 3.73; N, 17.67%. Calcd for $C_{10}H_9N_3O_4$: C, 51.06; H, 3.83; N, 17.87%.

trans-*3-[2-(5-Nitro-2-furyl)vinyl]-5-propyl-1,2,4-oxadiazole (VII).* The method used here was virtually identical with that used for V; a 2.1-g (7.9 mmol) portion of IIIc was heated at 155—156°C. Ochre-colored leaflets; mp 67—68°C (from ethanol). Yield: 0.65 g (43.3%). IR (KBr) cm^{-1}: 2971, 2940, and 2880 (CH_2, CH_3).

Found: C, 53.14; H, 4.56; N, 16.71%. Calcd for $C_{11}H_{11}N_3O_4$: C, 53.01; H, 4.41; N, 16.88%.

The authors are indebted to Mr. S. Iwasaki and Mr. Y. Hanada for their technical assistance, to Mr. T. Uchida for the infrared spectral measurements, and to Mr. Y. Uemura for the elemental analysis.

Chemical Constituents of the Male Flower of *Alnus pendula* (BETULACEAE)

Takayuki SUGA, Nobuo IWATA, and Yoshinori ASAKAWA

Department of Chemistry, Faculty of Science, Hiroshima University, Higashisenda-machi, Hiroshima

(Received January 26, 1972)

The structure of alnustone (**1**) isolated from the male flower of *Alnus pendula* Matsum. has been established to be 1,7-diphenyl-1,3-heptadien-5-one. Previously-known compounds, β-phenylethyl cinnamate (**6**), cinnamaldehyde, benzylacetone, β-phenylethyl alcohol, pinocembrin (**7**), pinostrobin (**8**), alpinetin (**9**), galangin (**11**), pinosylvin (**13**), and its monomethyl ether (**14**), eugenol, chavicol, cinnamic acid, β-phenylpropionic acid, and benzoic acid, were identified along with the above new ketone.

Alnus pendula Matsum. (*A. multinervis* Call.)[1] belongs to Betulaceae and can be used as a water-erosion-control plant. Previous studies[2-6] of the chemical constituents of the male flower of *Alnus sieboldiana* (Betulaceae) have shown the presence of two new ketols, yashabushiketol (**4**) and dihydroyashabushiketol (**5**), with a biosynthetically interesting skeleton, four new flavonoids, together with twenty-five aromatic compounds, and small amounts of aliphatic and isoprenoid compounds. The present paper will describe the isolation and structure elucidation of a new ketone, named alnustone (**1**),[7] with the same Ph–C_7–Ph skeleton as that of the ketols (**4**) and (**5**) and the identification of fifteen aromatic compounds from the male flower of *A. pendula*. From the viewpoint of biosynthesis and chemotaxonomy, the chemical constituents of the male flower of *A. pendula* will also be compared with those of *A. sieboldiana*.

Results and Discussion

The benzene extraction of a viscous material secreted on the fresh male flower (catkin) of *A. pendula* Matsum. gave a brown viscous oil. After the removal of the acidic and phenolic constituents, a neutral fraction was separated into three fractions by silica gel column chromatography, using *n*-hexane, benzene, and ethyl acetate successively as eluents.

Alnustone (**1**). The chromatography of the benzene-elution fraction over silica gel yielded alnustone (**1**) in fairly considerable amounts as pale yellow needles (mp 61.0—62.5°C). Its formula, $C_{19}H_{18}O$, was based on the high-resolution mass spectral analysis of the molecular ion. The spectral properties indicated that alnustone possessed a *trans, trans*-dienone group (ν_{max} 1665 and 990 cm^{-1}; λ_{max} 325 nm (log ε 4.40) and two monosubstituted benzene-rings (ν_{max} 750 and 700 cm^{-1}; δ 7.11 (s, 5H) and 7.20 ppm (m, 5H)). The base peak (*m/e* 157) and the signals at δ 6.11 (d, 1H, –CH=CH–CO–), 6.77 (m, 2H, =CH–CH=), and 7.18 ppm (m, 1H, overlapped with the signals of benzene-ring protons, Ph–CH=CH–) indicated the presence of the Ph–CH=CH–CH=CH–CO– group. The presence of the Ph–CH_2–CH_2–CO– group was confirmed by the NMR signals at δ 2.82 ppm (m, 4H). The hydrogenation of **1** over the platinum oxide catalyst readily gave the tetrahydroderivative (**2**), $C_{19}H_{22}O$, which was established on the bases of the disappearance of absorption bands due to the *trans, trans*-dienone moiety and the newly-appearing absorption bands of an isolated carbonyl group. On the other hand, the reduction of **1** by sodium borohydride afforded a secondary alcohol (**3**) with a conjugated diene group adjacent to the benzene ring, judging from its spectral data. Thus, alnustone has been confirmed to be *trans, trans*-1,7-diphenyl-1,3-heptadien-5-one (**1**).

Known Aromatic Compounds. *a) Neutral Components*: The isolation of β-phenylethyl cinnamate (**6**), cinnamaldehyde, benzylacetone, and β-phenylethyl alcohol was performed by a combination of the silica gel column chromatography and the preparative thin-layer chromatography of the neutral fractions. All the compounds isolated were identified by a direct comparison of their physical and spectral data with those of the authentic samples or with those reported in our previous papers.[2-6]

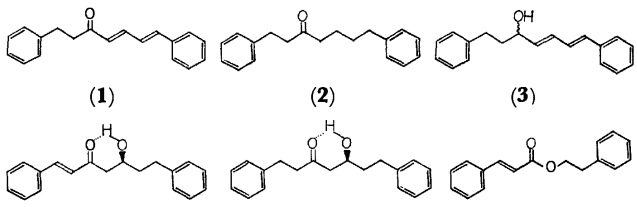

Fig. 1.

b) Phenolic and Acidic Components: Four flavonoids, pinocembrin (**7**), pinostrobin (**8**), alpinetin (**9**), and galangin (**11**), two stilbenes, pinosylvin (**13**) and pinosylvin monomethyl ether (**14**), and two phenols, eugenol and chavicol, were isolated from the phenolic fraction and subsequently identified by the above method. As acidic components, cinnamic acid, β-phenylpropionic acid, and benzoic acid were identified by a direct comparison of their retention times in gas chromatography and of the spectra of the methyl esters of authentic specimens.

A Comparison between the Constituents of the Male Flower of A. pendula and A. sieboldiana. The first object of this study was to compare the occurrence and distribution of the Ph–C_3 compounds in *A. pendula* with those

1) Japanese name is Hime-yashabushi.
2) Y. Asakawa, F. Genjida, S. Hayashi, and T. Matsuura, *Tetrahedron Lett.*, **1969**, 3235.
3) Y. Asakawa, This Bulletin, **43**, 575 (1970).
4) Y. Asakawa, *ibid.*, **43**, 2223 (1970).
5) Y. Asakawa, F. Genjida, and T. Suga, *ibid.*, **44**, 297 (1971).
6) Y. Asakawa, *ibid.*, **44**, 2761 (1971).
7) We have reported a part of the structural elucidation of alnustone (**1**) in the form of a preliminary communication on *Chem. Ind.* (London), **1971**, 766.

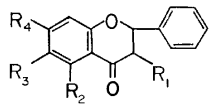

(**7**) $R_1=R_3=H$, $R_2=R_4=OH$
(**8**) $R_1=R_3=H$, $R_2=OH$, $R_4=OMe$
(**9**) $R_1=R_3=H$, $R_2=OMe$, $R_4=OH$
(**10**) $R_1=R_2=R_4=OH$, $R_3=OMe$

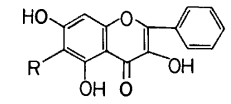

(**11**) R=H
(**12**) R=OMe

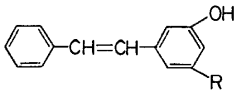

(**13**) R=OH
(**14**) R=OMe
Fig. 2.

of the compounds in *A. sieboldiana* from the points of view of biosynthesis and chemotaxonomy. β-Phenylethyl cinnamate (**6**) was most abundant in the male flower of both plants. Alnustone (**1**) was found in *A. pendula*, but not in *A. sieboldiana*. On the other hand, yashabushiketol (**4**) and dihydroyashabushiketol (**5**) appeared only in *A. sieboldiana*. These facts are very interesting with respect to the biosynthesis of these three components. The co-occurrence of flavonoids and stilbenes was found in both plants. Four flavonoids with the $C_{(6)}$–OMe group, such as alnustinol (**10**) and alnusin (**12**), have been found in *A. sieboldiana*, in contrast with the case of *A. pendula*. One of the most significant discoveries of the present survey is that the great majority of components isolated from *A. pendula* are composed of simple aromatic compounds with one or two Ph–C_3 skeletons, in the same manner as in *A. sieboldiana*, with the exception of eugenol and chavicol. In addition to the above aromatic constituents, small amounts of *n*-paraffins, α-olefins, triterpenes (taraxerone, β-amyrenone, and a triterpenic acid), unsaturated aliphatic ketones, and fatty acids are commonly present in both plants. Thus, it is clear that the two plants belong to closely related species from the viewpoint of chemotaxonomy.

Experimental

All the melting points are uncorrected. The UV spectra were measured by means of a Japan Spectroscopic Co., Ltd., ORD/UV-5 Spectropolarimeter in ethanol. The mass spectra were recorded on a Hitachi, RMS-4, Mass Spectrometer. The high-resolution mass spectra were obtained by means of a Hitachi, RMU-TL, Mass Spectrometer. The NMR spectra (100 MHz) were recorded on a JEOL, JNM-4H-100, High-Resolution Spectrometer in a carbon tetrachloride solution, using tetramethylsilane as the internal standard. The measurements of the IR and NMR (60 MHz) spectra and the glc were performed in the same manner as was reported in our preceding paper.[4]

Extraction and Isolation. Male flowers (6.59 kg) of *A. pendula* grown in the suburbs of Hiroshima were collected in March in 1970 and were, after having been minched mechanically, extracted with benzene over a two-month period. The evaporation of the solvent gave a brown viscous oil (3.6%). This viscous oil was successively extracted with a 5% sodium bicarbonate solution (Acid), a 5% sodium carbonate solution (Phenol I), a 0.4% sodium hydroxide solution (Phenol II), and a 5% sodium hydroxide solution (Phenol III); the subsequent acidification of each fraction with 5% hydrochloric acid gave an acidic fraction (2.3 g) and three phenolic fractions, Phenol I (2.5 g), Phenol II (38.2 g), and Phenol III (7.7 g). After the removal of the acidic and phenolic constituents, the neutral fraction (184 g) was obtained. A part (13 g) of it was fractionated into two fractions by silica gel column chromatography using *n*-hexane (Fraction 1) and benzene (Fraction 2). The Fraction 2 was further subjected to silica gel column chromatography to separate it into three fractions (i), (ii), and (iii), using benzene as the eluting agent.

Alnustone (1). From the fraction (i), a conjugated ketone (**1**) was isolated as pale yellow needles (236 mg): mp 61.0—62.5°C (from ethanol); *m/e* 262.1360 (calcd for $C_{19}H_{18}O$: 262.1357), 171 (Ph–CH=CH–CH=CH–CO–CH_2)$^+$, 157 (base, Ph–CH=CH–CH=CH–CO)$^+$, 129 (Ph–CH=CH–CH=CH)$^+$, 105 (Ph–CH_2–CH_2)$^+$, 103 (Ph–CH=CH)$^+$, 91 (C_7H_7)$^+$, 77 (C_6H_5)$^+$. These fragment ions were identified on the basis of a high-resolution mass-spectral analysis.

Found: C, 86.60; H, 7.19%. Calcd for $C_{19}H_{18}O$: C, 86.98; H, 6.91%.

The Catalytic Hydrogenation of Alnustone (1). Alnustone (**1**) (42 mg) was hydrogenated over a prereduced PtO_2 catalyst (10 mg) in ethanol for 1 hr under ambient conditions. After the catalyst had then been filtered off, the removal of the solvent from the filtrate gave the tetrahydroderivative (**2**) (34 mg): λ_{max}^{EtOH} 288 nm (log ε 1.99); $\nu_{max}^{liq.}$ 1710 cm^{-1}; δ ($CDCl_3$) 1.4—1.9 (m, 4H, Ph–CH_2–C$\underline{H}_2$–C$\underline{H}_2$–CH_2–CO–), 2.2—3.0 (m, 8H, 2×Ph–C$\underline{H}_2$– and –C$\underline{H}_2$–CO–C$\underline{H}_2$–), 7.21 ppm (s, 10H); *m/e* 266 (M$^+$), 175 (Ph–CH_2–CH_2–CH_2–CH_2–CO–CH_2)$^+$ or (Ph–CH_2–CH_2–CO–CH_2–CH_2–CH_2)$^+$, 161 (Ph–CH_2–CH_2–CH_2–CH_2–CO)$^+$, 133 (Ph–CH_2–CH_2–CO)$^+$, 105 (Ph–CH_2–CH_2)$^+$, 91 (base, C_7H_7)$^+$, 77 (C_6H_5)$^+$.

The Reduction of Alnustone (1) with Sodium Borohydride. Into a solution of **1** (140 mg) in methanol (20 m*l*), we stirred sodium borohydride (60 mg) dissolved in methanol (10 m*l*) at 0°C. The mixture was then stirred for 1 hr. The reaction mixture was acidified with 1N hydrochloric acid, and then the solvent was removed *in vacuo*. The product, after water (10 m*l*) had been added, was extracted with ether. The removal of the solvent from the dried extract gave a secondary alcohol (**3**) (134 mg): λ_{max}^{EtOH} 222 (log ε 4.06), 228 (4.06), 235 (3.94), 288 nm (4.50); $\nu_{max}^{liq.}$ 3400, 1100 (OH), 1640, 990 (*trans*-CH=CH–CH=CH–), 750, 690 cm^{-1} (monosubst. benzene-ring); δ ($CDCl_3$) *ca.* 1.9 (m, 2H, –CH(OH)–C$\underline{H}_2$–CH_2–Ph), 2.08 (bs, 1H, O$\underline{H}$, disappeared upon the addition of D_2O), *ca.* 2.7 (m, 2H, Ph–C$\underline{H}_2$–), 4.10 (q, *J*=7 Hz, 1H, =CH–C$\underline{H}$(OH)–CH_2–), 5.80 (dd, *J*=15 Hz and 7 Hz, 1H, –CH=C$\underline{H}$–CH(OH)–), 6.1—6.8 (m, 3H, Ph–C$\underline{H}$=C$\underline{H}$–C$\underline{H}$=), 7.24 (s, 5H, $C_6\underline{H}_5$–CH_2–), 7.33 ppm (m, 5H, $C_6\underline{H}_5$–CH=); *m/e* 264 (M$^+$), 246 (M−H_2O), 173 (Ph–CH=CH–CH=CH–CHOH–CH_2)$^+$, 159 (Ph–CH=CH–CH=CH–CHOH)$^+$, 155 (Ph–CH=CH–CH=CH–CH=CH)$^+$, 129 (Ph–CH=CH–CH=CH)$^+$, 117 (Ph–CH_2–CH=CH)$^+$, 105 (Ph–CH_2–CH_2)$^+$, 91 (C_7H_7)$^+$, 77 (C_6H_5)$^+$, 65 (C_5H_5)$^+$.

n-Paraffins, α-Olefins, Unsaturated Aliphatic Ketones, and Triterpenes (Taraxerone and β-Amyrenone). The Fraction 1, when eluted with *n*-hexane, gave a mixture of *n*-paraffins and α-olefins, (1.5 g). The *n*-paraffins (C_{21}–C_{31}: C_{27} main) and α-olefins, (C_{23}–C_{29}) were identified by a comparison

with the retention times in gas chromatography of authentic samples and by the hydrogenation of the mixture. After the isolation of alnustone (**1**) from the fraction (i), the filtrate which showed three spots on tlc was purified by preparative thin-layer chromatography to give a mixture of unsaturated aliphatic ketones (10 mg), mp 71—74°C, β-amyrenone (44 mg), and taraxerone (127 mg).

β-Amyrenone: mp 178—179°C (lit,[8] mp 178—179°C); ν_{max}^{Nujol} 1710 cm^{-1}; *m/e* 424 (M^+) 409, 218 (base), 203, 189. All the spectral and physical data of this compound agreed with those of β-amyrenone derived from β-amyrin.

Taraxerone: mp 233—235°C (lit,[9] mp 237—238°C); ν_{max}^{Nujol} 1705 cm^{-1}; *m/e* 424 (M^+), 409, 300, 285, 204 (base), 218, 189, 133.[9]

*Pinostrobin (**8**), β-Phenylethyl Cinnamate (**6**), β-Phenylethyl Alcohol, Benzylacetone, and Cinnamaldehyde.* The fraction (ii) afforded a colorless viscous oil, which was then further chromatographed on a silica gel column, using a mixture of *n*-hexane and ethyl acetate, to give β-phenylethyl cinnamate (2.170 g), mp 51—52°C, pinostrobin (96 mg), mp 91—92.5°C, and β-phenylethyl alcohol (220 mg). The fraction (iii) gave a pale yellow oil (30 mg) which showed two spots on tlc and two peaks (1 : 1) on the gas chromatogram (R_t=4.0 and 7.1, 10% PEG 6000 on Diasolid L (60—80 mesh) at 180°C). The chromatographic separation of the oil by tlc gave cinnamaldehyde (R_t=7.1) and benzylacetone (R_t=4.0). All of the spectral data of the compounds were identical with those of the authentic samples.

*Pinocembrin (**7**) and Galangin (**11**).* The Phenol I (2.5 g) was chromatographed on a silica gel column, using ethyl acetate as the eluting agent, to give pinocembrin (340 mg), mp 201—202.5°C (lit,[6] mp 200—201°C) and galangin (460 mg), mp 220—222°C (lit,[10] 214—215°C). The 3,7-dimethylether derivative: mp 145—147°C (lit,[11] 145—146°C). The spectral data of these compounds coincided completely with those of the known specimens.

*Pinosylvin (**13**), Pinosylvin Monomethyl Ether (**14**), Alpinetin (**9**), Eugenol, Chavicol, a Triterpenic Acid, and Benzoic Acid.* The chromatography of the Phenol II (15.5 g) on a silica gel column using a mixture of *n*-hexane and ethyl acetate gave pinosylvin (250 mg), mp 158—159°C (lit,[6] 156—158°C), pinosylvin monomethyl ether (3.5 g), mp 122—122.5°C (lit,[6] 119—120°C), alpinetin (1.18 g), mp 224—225.5°C (lit,[4] mp 224.5—225.0°C), eugenol (140 mg), n_D^{25} 1.5410, chavicol (60 mg), n_D^{25} 1.5405, benzoic acid (1.93 g), mp and mixed mp 122—123°C, and an unidentified triterpenic acid (50 mg), mp 195—196°C, M^+ 470. The identities were established by a comparison of their spectral data.

Pinosylvin monomethyl ether (1.54 g) and benzoic acid (840 mg) were also isolated from the Phenol III (7.7 g).

β-Phenylpropionic Acid, Cinnamic Acid, and Fatty Acids. The acidic fraction (2.3 g) was methylated with diazomethane. The methyl ester was then chromatographed on silica gel to give methyl cinnamate (50 mg), minute amounts of methyl β-phenylpropionate and methyl benzoate, and a trace amount of a mixture of methyl myristate, methyl palmitate, and methyl stearate. These compounds were identified by a direct comparison of their retention times in glc (10% SE-30 and 10% DEGS on Diasolid L (60—80 mesh) at 100°C) and their IR spectra with those of authentic samples.

8) T. G. Halsall and R. T. Aplin, *Fortschr. Chem. Org. Naturst.*, **22**, 174 (1964).

9) T. Takemoto and T. Ishiguro, *Yakugaku Zasshi*, **86**, 530 (1966).

10) T. Heap and R. Robinson, *J. Chem. Soc.*, **1926**, 2336.

11) K. V. Rao and T. R. Seshadri, *Proc. Indian Acad. Sci. Sect. A*, **22**, 383 (1945).

BULLETIN OF THE CHEMICAL SOCIETY OF JAPAN, VOL. 45, 2060—2064(1972)

Stereochemical Studies of Monoterpene Compounds. XVIII.[1] A Conformational Study of Monoterpene α,β-Unsaturated Ketones by Means of the Temperature-dependent Circular Dichroism

Takayuki SUGA and Kiyoshi IMAMURA

Department of Chemistry, Faculty of Science, Hiroshima University, Higashisenda-machi, Hiroshima

(Received January 31, 1972)

The conformations of flexible, cyclic α,β-unsaturated ketones, (−)-*p*-menth-3-en-5-one (**1**), (+)-carvone (**2**), (−)-piperitone (**3**), (−)-carvenone (**4**), and (+)-pulegone (**5**), were examined by means of the temperature-dependent circular dichroism (CD) in the region of the n-π^* transition. In polar solvents, the simultaneous occurrence of the conformational equilibrium and the asymmetric solvation was observed markedly for the compound **1** of these compounds, along with a change in the large rotational strength at lower temperatures.

In the region of the ultraviolet absorption, α,β-unsaturated ketones generally exhibit three optically-active, absorption bands:[2] the first band (320—350 nm) is ascribed to the n-π^* transition, and the others (240 nm and 210 nm), to the π-π^* transition. The sign of a Cotton effect of the third band has been correlated[3] with the chirality contribution of the α′-pseudo-axial bond. On the other hand, the sign of a

1) Part XVII of this series: T. Hirata, *J. Sci. Hiroshima Univ. Ser. A*, **35**, 239 (1971).

2) L. Velluz and M. Legrand, *Angew. Chem.*, **77**, 842 (1965).

3) A. W. Burgstahler and R. C. Barkhurst, *J. Amer. Chem. Soc.*, **92**, 7601 (1970).

Cotton effect of the second band has been interpreted[4] on the basis of the chirality, or sense of twist, of the enone system, compared with the diene system, while the other one has been related[5] to a normal octant rule for the cisoid enone system and to a reverse octant rule for the transoid one. However, it has recently been shown[6-8] that the sign of a Cotton effect of the last two bands varies irregularly in dependence on the α-axial and the γ-axial substituents, regardless of the alteration in the conformation.

We have now examined the conformations of five *s-trans* and *s-cis* α,β-unsaturated ketones, (−)-*p*-menth-3-en-5-one (**1**), (+)-carvone (**2**), (−)-piperitone (**3**), (−)-carvenone (**4**), and (+)-pulegone (**5**), by means of the temperature-dependent CD in the region of the *n*-π* transition; we chose this region because of the availability and the facility of the band in it.

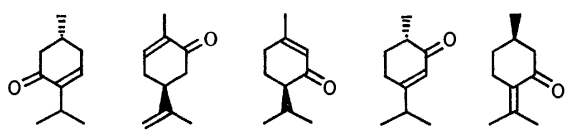

1 **2** **3** **4** **5**

Results and Discussion

The predictions of the sign of a Cotton effect for each conformer have been based on the rule[5] of the correlation between the chirality of an enone system and its sign of a Cotton effect for the *n*-π* transition. The alteration of the magnitude of a Cotton effect in the optical rotatory dispersion (ORD) and the CD curves of α,β-unsaturated ketones with a change in the temperature results from the following factors: (i) the conformational alteration, *i.e.*, the increase or the decrease in the population of a conformation with the opposite sign of a Cotton effect, as in the cases of *trans*-2-chloro-5-methylcyclohexane,[9] (−)-menthone, and 1-hydroxymenthone,[10] (ii) the asymmetric solvation,[11] *i.e.*, the association of a solvent molecule, which is more strengthened at lower temperatures, in the asymmetric manner, and (iii) the vibronic effect.[12] The contribution of the last factor is negligible, however, because the compounds used here showed a remarkable increase in the rotational strength at the lower temperature rather than an enhancement of a fine structure.

A half-chair form of four possible conformations of a cyclohexenone ring has been suggested[13] as being stable on the basis of the conformational analysis of the cyclohexene ring. Therefore, (−)-*p*-menth-3-en-5-one (**1**) and (+)-carvone (**2**), 2,5-disubstituted cyclohexenone, may exist in two interconvertible half-chair conformations, **1a** and **1b**, and **2a** and **2b**, respectively (Fig. 1). A positive Cotton effect may be predicted for the **1a** and **2b** conformers, whereas the opposite one may be predicted for the **1b** and **2a** conformers. The CD curves of the compounds **1** and **2** showed the double-humped

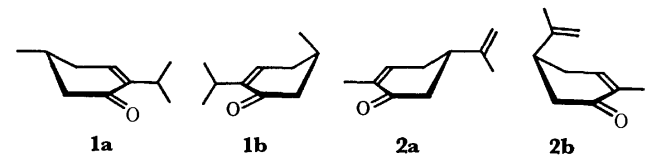

1a **1b** **2a** **2b**

Fig. 1. Preferred conformation of (−)-*p*-menth-3-en-5-one (**1**) and (+)-carvone (**2**).

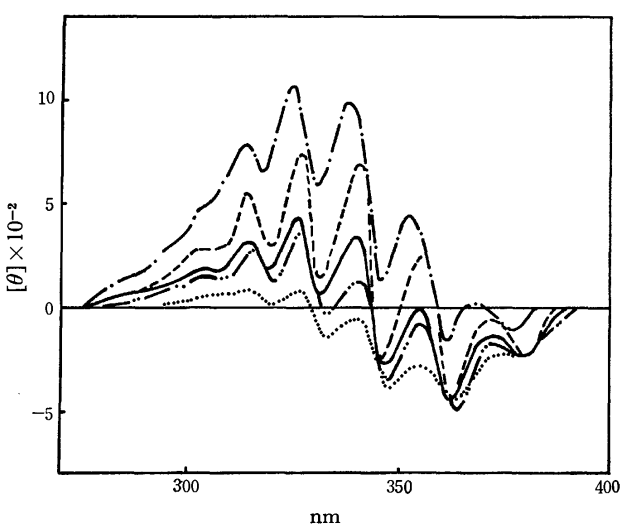

Fig. 2. CD curves of (−)-*p*-menth-3-en-5-one (**1**):—, at 25°C, ----, at −92°C, and —·—, at −186°C in the MI solvent, and —··—, at 25°C and ·····, at 147°C in decalin.

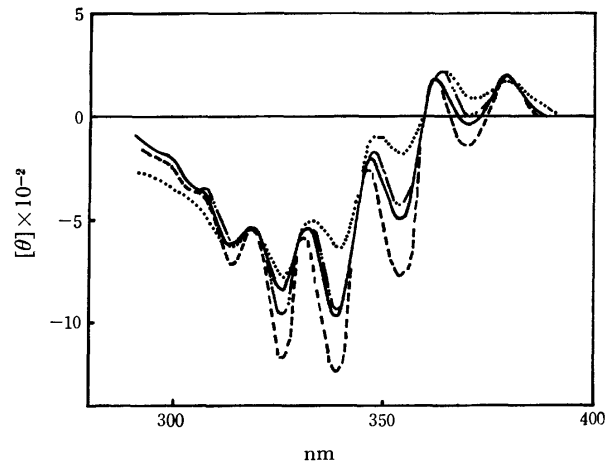

Fig. 3. CD curves of (+)-carvone (**2**): —, at 25°C and ----, at −92°C in the MI solvent, and —··—, at 25°C and ·····, at 146°C in decalin.

4) C. Djerassi, R. Records, E. Bunnenberg, K. Mislow, and A. Moscowitz, *J. Amer. Chem. Soc.*, **84**, 870 (1962).
5) G. Snatzke, *Tetrahedron*, **21**, 413, 421, and 439 (1965).
6) K. Kuriyama, M. Moriyama, T. Iwata, and K. Tori, *Tetrahedron Lett.*, **1968**, 1661.
7) W. L. Duax, Y. Osawa, A. Cooper, and D. A. Norton, *Tetrahedron*, **27**, 331 (1971).
8) R. T. Torry and J. Hudec, *Chem. Commun.*, **1971**, 785.
9) K. M. Wellman, E. Bunnenberg, and C. Djerassi, *J. Amer. Chem. Soc.*, **85**, 1870 (1963).
10) K. M. Wellman, P. H. A. Laur, W. S. Briggs, A. Moscowitz, and C. Djerassi, *ibid.*, **87**, 66, 73 (1965).
11) G. Snatzke, "Optical Rotatory Dispersion and Circular Dichroism in Organic Chemistry," Heyden & Son, London (1967), pp. 314, 329.
12) O. E. Weigang, Jr., *J. Chem. Phys.*, **43**, 3609 (1965).
13) N. L. Allinger and E. L. Eliel, "Topics in Stereochemistry," Vol. 2, John Wiley & Sons, New York (1967), p. 160.

Cotton effect with an increase in the positive rotational strength for the compound **1** and the negative one for the compound **2** in the shorter-wavelength region with a lowering of the temperature in both the MI solvent and decalin (Figs. 2 and 3). These observations indicate a conformational alteration, but not an asymmetric solvation and, accordingly, the predominance of the **1a** conformer with an *eq*-methyl group and the **2a** conformer with an *eq*-isopropenyl group in the conformational equilibrium, as is shown in Fig. 1.

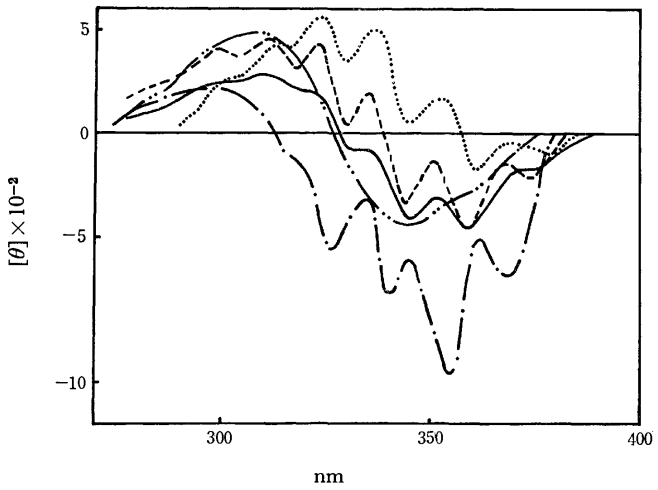

Fig. 4. CD curves of (−)-*p*-menth-3-en-5-one (**1**): ·····, at 25°C in isooctane, —··—, at 25°C in ethanol, and —, at 25°C, ----, at −92°C, and —·—, at −186°C in the EPA solvent.

However, the compound **1** showed unexpected temperature-dependent CD curves in the EPA solvent (Fig. 4); the positive rotational strength in the shorter-wavelength region increased with a change in the temperature from 25 to −92°C, while the negative one in the longer-wavelength region increased at the expense of the positive one with the hypsochromic shift of the band when the temperature was further lowered from −92 to −186°C. Considering the conformational equilibrium between the **1a** and **1b** conformers, this phenomenon may be explained as follows: a lowering of the temperature to −92°C increases the population of the unsolvated conformer **1a** with a positive Cotton effect, rather than resulting in an increase in the solvated species, but a further lowering of the temperature to −186°C favors the solvated form **1b** with a negative Cotton effect, as has been shown for pulegone oxide.[14] With changing a solvent from a nonpolar solvent to a polar one, the magnitude of a negative Cotton effect of the compound **1** in the longer-wavelength region remarkably increased with the hypsochromic shift of the band; this suggests an asymmetric solvation, but not a conformational change (Fig. 4). These observations of the temperature-dependent CD curves seem to indicate that the asymmetric solvation principally contributes to the preference of the conformation of *p*-menth-3-en-5-one in the polar solvents. For the compound **2**, such a phenomenon was also observed, but it was very small in magnitude in a comparison with that of the compound **1**.

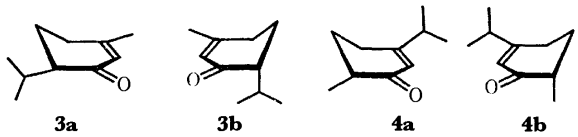

3a **3b** **4a** **4b**

Fig. 5. Preferred conformation of (−)-piperitone (**3**) and (−)-carvenone (**4**).

(−)-Piperitone (**3**) and (−)-carvenone (**4**), 3,6-disubstituted cyclohexenone, may also exist in two interconvertible half-chair conformations, **3a** and **3b**, and **4a** and **4b**, respectively (Fig. 5). The predicted Cotton effect is positive for the **3a** and **4a** conformers and negative for the **3b** and **4b** conformers.

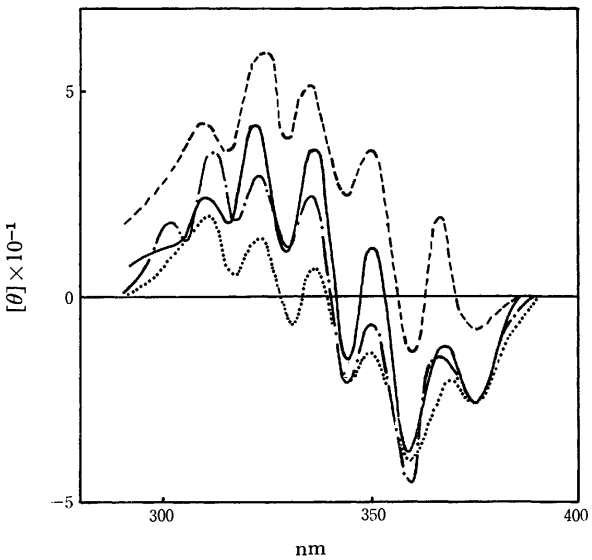

Fig. 6. CD curves of (−)-piperitone (**3**): —, at 25°C and ----, at −92°C in the MI solvent, and —·—, at 25°C and ·····, at 146°C in decalin.

The CD curves of the compound **3** showed a double-humped Cotton effect at 25°C in both the MI solvent and decalin. The positive rotational strength of the Cotton effect in the shorter-wavelength region increased at the expense of the negative one in the longer-wavelength region with a lowering of the temperature in both the solvents (Fig. 6). This indicates the preference of the **3a** conformer with an *eq*-isopropyl group in the conformational equilibrium between **3a** and **3b**.

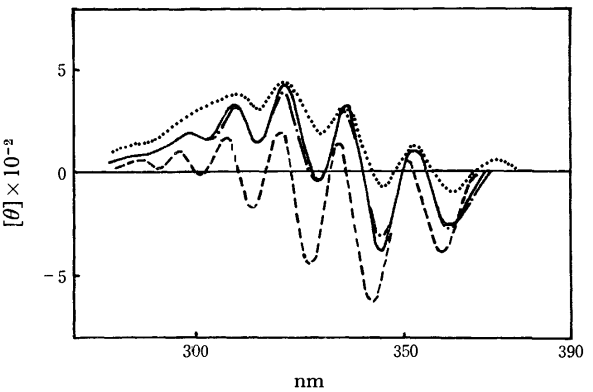

Fig. 7. CD curves of (−)-carvenone (**4**): —, at 25°C and ----, at −127°C in the MI solvent, and —·—, at 25°C and ·····, at 149°C in decalin.

On the other hand, the compound **4** also showed a double-humped Cotton effect, but a less amplified one, on its CD curves (Fig. 7) in the MI solvent at room temperature. The curves exhibited an increase in the negative rotational strength in the longer-wavelength region with a lowering of the temperature in both the MI solvent and decalin. These facts seem to imply the preference of the **4b** conformer with an *ax*-methyl group in the conformational equilibrium between **4a** and **4b**. However, a small shift ($\delta^{CDCl_3}-\delta^{C_6H_6}=0.00$ ppm and $\delta^{CCl_4}-\delta^{C_5H_5N}=-0.09$ ppm) of the α-methyl signal of the compound **4** was observed in the examination of the NMR solvent effects.[15,16] This fact favors the conformer with an *eq*-methyl group, which has been recognized to be more stable energetically.[17] These observations may be successfully explained in terms of a conformational equilibrium between the two envelope forms,[18] **4c** and **4d**, where the planes of the C=C and C=O double bonds are coplanar. From the energetic point of view, the conformational energy between the envelope form and the half-chair one of a cyclohexenone system is small. The reverse octant rule can be applied[5] to the envelope forms; it predicts a negative Cotton effect for the **4c** conformer and a positive one for the **4d** conformer (Fig. 8). Thus, the CD and NMR spectral data indicate the predominance of the **4c** conformer with the *eq*-methyl group in the conformational equilibrium between **4c** and **4d**. This is also supported by the rotational strength, which is smaller than that of the other compounds at lower temperatures.

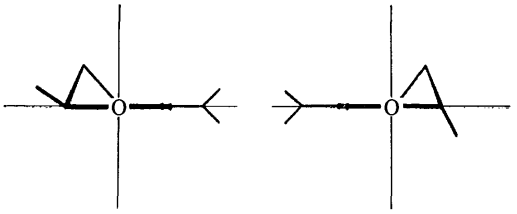

4c **4d**

Fig. 8. The octant projection diagrams of the envelope forms, (**4c**) and (**4d**), of (−)-carvenone (**4**).

(+)-Pulegone (**5**), a *s-cis*, α,β-unsaturated ketone, may exist in two interconvertible half-chair conformations, (**5a**) and (**5b**), as is shown in Fig. 9. A positive Cotton effect is predicted for the **5a** conformer, and a negative one, for the **5b** conformer. The CD curves of

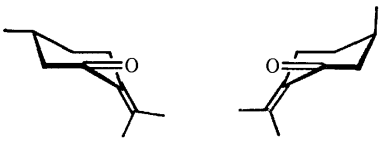

5a **5b**

Fig. 9. Preferred conformation of (+)-pulegone (**5**).

the compound **5** exhibited a positive Cotton effect without the double hump and a fine structure in both the MI solvent and decalin at various temperatures (Fig. 10). The increase in the positive rotational strength with a lowering of the temperature indicates the predominance of the **5a** conformer with an *eq*-methyl group in the conformational equilibrium between **5a** and **5b**. We have recently estimated[19] the conformational energy in this equilibrium to be 1.1 kcal/mol; we also estimated the rotational strengths of the **5a** and **5b** conformers.

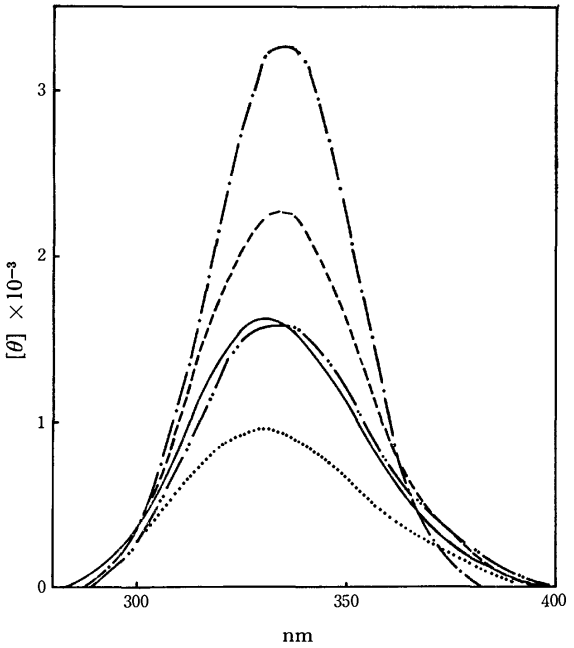

Fig. 10. CD curves of (+)-pulegone (**5**): —, at 25°C and – – –, at −67°C, and —·—, at −186°C in the MI solvent, and —··—, at 25°C and ·····, at 152°C in decalin.

The temperature-dependent CD curves of the compounds **3**, **4**, and **5** in the EPA solvent acted the same as in both the MI solvent and decalin at various temperatures. Thus, it may be said that temperature-dependent CD measurements offer useful information about the conformational alteration of the optically-active, flexible α,β-unsaturated ketones. However, it should be noted that there is a possibility of the occurrence of such unexpected behavior as in cases of (−)-*p*-menth-3-en-5-one (**1**) and (+)-carvone (**2**), on the CD curves of the α,β-unsaturated ketones in the polar solvent because of the asymmetric solvation.

Experimental

Measurements. The temperature-dependent CD curves were measured by means of a Japan Spectroscopic Co. Ltd., ORD/UV-5, automatically-recording spectrometer equipped with a CD attachment in the MI solvent (methylcyclohexane-isopentane, 1 : 3 by volume), the EPA solvent (ether–isopentane–ethyl alcohol, 5:5:2 by volume), and decalin, using a variable-temperature CD cell. The NMR spectra were recorded on a Hitachi Perkin-Elmer, R-20, high-resolution spectrometer at 60 MHz, using tetramethylsilane as the

14) W. Reusch and P. M. Mottison, *Tetrahedron*, **24**, 4933 (1968).
15) D. H. Williams and N. S. Bhacca, *ibid.*, **21**, 2021 (1965).
16) D. H. Williams, *Tetrahedron Lett.*, **1965**, 2305.
17) E. L. Eliel, N. L. Allinger, S. J. Angyal, and G. A. Morrison, "Conformational Analysis," John Wiley & Sons, New York (1965), p. 36.
18) R. R. Sobti, J. Bordner, and S. G. Levine, *J. Amer. Chem. Soc.*, **93**, 5598 (1971).
19) T. Suga, K. Imamura, and T. Shishibori, *Chem. Commun.*, **1971**, 126.

internal standard. Gas chromatography was carried out on a Hitachi Perkin-Elmer, F-6D, apparatus attached with a column packed with 20% DEGS on Diasolid L (60—80 mesh) and with 20% PEG 6000 on Celite (60—80 mesh) at 120°C.

Materials. *(−)-p-Menth-3-en-5-one (1)*: Into a pyridine (45 ml) solution of 4-hydroxy-menthone (1.0 g) prepared from 3-*p*-menthene following the method reported in the literature,[20] we dropped phosphorus oxychloride (23 ml) at 0°C. The reaction mixture was left at room temperature for 36 hr and then treated in the usual manner. The refinement of the product by column chromatography on silica gel gave the compound **1** (0.23 g) in a 100% purity (as determined on the basis of analytical glc) and with the following properties: bp 55.0°C/2 mmHg, $[\alpha]_D^{25}-72.4°$ (*c* 2.78, ethanol) (lit,[21] $[\alpha]_D^{20}-78.0°$, neat).

(+)-Carvone (2): A commercial sample was purified by converting it to the sodium bisulfite adduct and by also rectifying the regenerated oil. The compound **2** thus obtained was 100% pure (as determined on the basis of analytical glc) and showed the following properties: bp 74.0—77.0°C/4 mmHg, n_D^{25} 1.4967, d_4^{25} 0.9567, $[\alpha]_D^{25}+61.7°$ (neat) (lit,[22] $[\alpha]_D^{20}+62.3°$, neat).

(−)-Piperitone (3): A commercial sample was purified by rectification under a reduced pressure to give the compound **3** (95.0% pure by analytical glc), with the following properties: bp 94.0°C/8 mmHg, n_D^{25} 1.4808, d_4^{25} 0.9280, $[\alpha]_D^{25}$ −5.20° (neat) (lit,[23] $[\alpha]_D^{20}-51.5°$, neat).

(−)-Carvenone (4): (−)-Dihydrocarvone (2.0 g; bp 105.0—106.5°C/18 mmHg, n_D^{25} 1.4685, d_4^{25} 0.9227, $[\alpha]_D^{25}-18.6°$ (neat), prepared[24] by the reduction of (+)-carvone, was treated with a mixture of acetic acid (25.6 ml) and hydrobromic acid (25.6 ml) for 30 min at room temperature. The reaction mixture was then poured into water and extracted with ether. The oil (1.97 g) obtained after the removal of the solvent was refined by column chromatography on silica gel. The compound **4** (100% pure by analytical glc) showed the following properties: bp 70.0—72.0°C/4.5 mmHg, n_D^{25} 1.4799, d_4^{25} 0.9231, $[\alpha]_D^{25}-41.0°$ (neat) (lit,[25] $[\alpha]_D^{25}+45.4°$ (neat) for the enantiomer of **4**).

The NMR spectra of the methyl proton signal at the 1-position appeared at δ 1.13 in both deuterochloroform and benzene, at 1.06 in carbon tetrachloride, and at 1.15 ppm in pyridine.

(+)-Pulegone (5): The purification of pennyroyal oil by means of the formation of the sodium bisulfite adduct, followed by regeneration and then distillation, gave the compound **5**, with the following properties: bp 65.5°C/2.5 mmHg, n_D^{25} 1.4845, d_4^{25} 0.9352, $[\alpha]_D^{25}+22.7°$ (neat) (lit,[26] $[\alpha]_D^{20}+23.4°$, neat).

The authors are indebted to the Takasago Perfumery Co., Ltd., Tokyo, for the gift of samples of carvone, piperitone, and pulegone.

20) T. Suga, T. Shishibori, and T. Matsuura, *J. Org. Chem.*, **32**, 965 (1967).
21) O. Wallach, *Ann. Chem.*, **305**, 272 (1899).
22) J. L. Simonsen, "The Terpenes," Vol. 1, Cambridge Univ. Press, London (1947), p. 396.
23) J. Reat and H. G. Smith, *J. Chem. Soc.*, **123**, 2268 (1923).
24) O. Wallach and H. Schrader, *Ann. Chem.*, **279**, 377 (1894).
25) K. Fujita, This Bulletin, **34**, 968 (1961).
26) J. Doeuvre and H. Perret, *Bull. Soc. Chim. Fr.*, **2**, 298 (1935).

A Negative Ion-molecule Reaction in Nitroethylene

Tetsuo SHIGA and Hitoshi YAMAOKA*
Department of Polymer Chemistry, Kyoto University, Kyoto
Kazuo ARAKAWA and Toshio SUGIURA
Takasaki Radiation Chemistry Research Establishment, Japan Atomic Energy Research Institute, Takasaki, Gunma
(Received November 4, 1970)

The formation of negative ions and the negative ion-molecule reaction in nitroethylene by electron impact have been studied. The nondissociative resonance electron capture of the nitroethylene molecule led to the formation of the molecular negative ion. The ionization efficiency curves and the appearance potentials of several fragment negative ions and the molecular negative ion were measured. The dimer negative ion of nitroethylene was found to be formed by the ion-molecule reaction between the molecular negative ion and a neutral nitroethylene molecule, and the rate constant of this ion-molecule reaction was estimated to be approximately 3.2×10^{-13} cc molecule^{-1}sec^{-1}.

A number of studies of ion-molecule reactions for positive ions done by the use of a mass spectrometer have been reported in recent years. Such investigations have provided useful information on those radiation-induced chemical reactions where more than one-half of the product formation usually results from the reactions of intermediate ions. For negative ion-molecule reactions, however, detailed studies have been limited to reactions which occur in oxygen and other gases of ionospheric interest,[1-6] although negative ions have also been considered to play an important role as active species in radiation-induced reactions.

In the course of investigations of radiation-induced polymerizations, it has been elucidated on the basis of the results of kinetic experiments[7] that the polymerization of nitroethylene proceeds by a free anionic mechanism through negative intermediates. An ESR study[8] and preliminary mass spectrometric observations[9] of nitroethylene have indicated that the polymerization was initiated by anion radicals of nitroethylene formed by the capture of electrons.

In the present study done by the use of a mass spectrometer, the formation of negative ions from nitroethylene and the dimer-negative-ion formation of nitroethylene by the ion-molecule reaction were investigated in order to obtain some information on the initial process of the radiation-induced polymerization of nitroethylene.

Experimental

The apparatus used for this study was a 90° single-focusing Hitachi RMU-6D mass spectrometer which had been modified to measure negative ions as described in a previous paper.[10] A conventional-type electron gun was used without paying any attention to the energy spread of the impact electrons. A 10-stage Ag–Mg electron multiplier combined with a DC amplifier was used as the ion detector, and the output current was recorded by means of a Rikadenki B-34 three-pen recorder. The minimum detectable ion current was 5×10^{-19}A. During the experiments, except when studying the effect of the ion-accelerating potential, the ion-acceleration voltage and the voltage supplied to the conversion dynode of the electron multiplier were kept at —3.5 and —1.5 kV respectively. The electron-trap voltage was maintained at the same potential as the ionization chamber. The repeller potential was always adjusted to 0 V in order to obtain the molecular negative ions of nitroethylene with thermal velocity. A source magnet, which had a flux intensity of 150 gausses, was also used for the collimation of the electron beam. The total emission was maintained at 100 μA throughout the energy range of the electron impact, and then the 40% trap current was obtained above 10 eV electron energies. The electron-accelerating potentials were read at each 1/50 V by means of a 10-turn precision Helipot variable resister in the range from 0 to 20 V; the resister had previously been well calibrated by means of a Yokokawa DC Voltage Standard GOS-11.

Sulfur hexafluoride and oxygen were used to calibrate the electron-energy scale. The appearance potentials of the SF_6^- ion from sulfur hexafluoride and the O^- ion from oxygen were taken as 0.03 eV[11] and 4.53 eV[12] respectively. The appearance potentials of the negative ions formed by the resonance-capture process were determined by the linear extraporation method.

The pressure in the ionization chamber was determined indirectly from the pressure in the sample reservoir, which was measured by means of a manometer, a McLeod gauge, and a CEC 23-105 Micro-Manometer. The ratio of the

* Present address: Research Reactor Institute, Kyoto University, Kumatori-cho, Sennan-gun, Osaka.

1) B. P. Burtt and J. Henis, *J. Chem. Phys.*, **41**, 1510 (1964).
2) J. F. Paulson, in "Ion-molecule Reactions in the Gas Phase" (Advan. Chem. Ser. 58), American Chemical Society, Washington, D. C., 1966, p. 28.
3) J. M. Warman and R. W. Fessenden, *J. Chem. Phys.*, **49**, 4718 (1968).
4) J. L. Moruzzi and J. T. Dakin, *ibid.*, **49**, 5000 (1968).
5) P. J. Chantry, *ibid.*, **51**, 3380 (1969).
6) E. E. Ferguson, *Can. J. Chem.*, **47**, 1815 (1969); and references cited therein.
7) a) H. Yamaoka, R. Uchida, K. Hayashi, and S. Okamura, *Kobunshi Kagaku*, **24**, 79 (1967); b) H. Yamaoka, F. Williams, and K. Hayashi, *Trans. Faraday Soc.*, **63**, 376 (1967); c) H. Yamaoka, H. Mori, K. Hayashi, and S. Okamura, *J. Polymer Sci. B*, **7**, 371 (1969); d) H. Yamaoka, I. Obama, K. Hayashi, and S. Okamura, *J. Polymer Sci. A-1*, **8**, 495 (1970).
8) a) K. Tsuji, H. Yamaoka, K. Hayashi, H. Kamiyama, and H. Yoshida, *J. Polymer Sci. B*, **4**, 629 (1966); b) K. Tsuji, H. Yoshida, K. Hayashi, and S. Okamura, *Kobunshi Kagaku*, **25**, 31 (1968).
9) H. Yamaoka, T. Shiga, K. Hayashi, S. Okamura, and T. Sugiura, *J. Polymer Sci. B*, **5**, 329 (1967).
10) T. Sugiura, K, Arakawa, and A. Matsumoto, *Mass Spectroscopy*, **14**, 187 (1966).
11) W. M. Hickam and R. E. Fox, *J. Chem. Phys.*, **25**, 642 (1956).
12) D. C. Frost and C. A. McDowell, *J. Amer. Chem. Soc.*, **80**, 6183 (1958).

sample pressure of the steady state in the ionization chamber to that in the reservoir was determined by the static operation of the inert gases (He, Ne, and Ar[13]) in the energy range in which the ion intensity of the resonance-electron capture was linearly proportional to the pressure.

Nitroethylene was prepared by the dehydration of 2-nitroethanol and purified as has been described previously.[7b] Sulfur hexafluoride (Allied Chemical Co.) was purified by trap-to-trap distillation in a vacuum. Oxygen and methane (Takachiho Chemical Ind.) were used without further purification.

Results

Formation of Negative Ions. A large number of negative ions were observed to be formed from nitroethylene by an electron impact of 100 eV. The relative abundance of the main negative ions, which were normalized to the intensity of NO_2^-, is shown in Table 1.

TABLE 1. RELATIVE ABUNDANCE OF THE MAIN NEGATIVE IONS PRODUCED FROM NITROETHYLENE BY ELECTRON IMPACT OF 100 eV

m/e	Ion	Source pressure (mmHg) 2.6×10^{-6}	Source pressure (mmHg) 9×10^{-3}
16	O^-	7.4	6.8
17	OH^-	6.8	9.1
25	C_2H^-	19	22
30	NO^-	0.93	0.96
42	CNO^-	3.4	7.3
46	NO_2^-	100	100
55	C_2HNO^-	0.62	0.85
72	$C_2H_2NO_2^-$	0.03	5.8
73	$C_2H_3NO_2^-$	0.27	88
98	$C_2H_3NO_2C_2H^-$	—	0.2
99	$C_2H_3NO_2C_2H_2^-$	—	0.6
146	$(C_2H_3NO_2)_2^-$	—	0.1
219	$(C_2H_3NO_2)_3^-$	—	2×10^{-4}

The molecular negative ion of nitroethylene, $C_2H_3NO_2^-$, was found at a pressure of 2.6×10^{-6} mmHg, and the relative abundance of $C_2H_3NO_2^-$ increased remarkably with the increase in the source pressure. At a pressure of 9×10^{-3} mmHg, the dimer negative ion of nitroethylene, $(C_2H_3NO_2)_2^-$, and the trimer negative ion, $(C_2H_3NO_2)_3^-$, were also observed, although the intensity of the trimer ion was very low.

The ionization efficiency curves of the main negative ions from nitroethylene, such as O^-, C_2H^-, NO_2^-, and $C_2H_3NO_2^-$, and that of SF_6^- from sulfur hexafluoride are shown in Fig. 1. The intensity of these negative ions in the electron-energy region less than 10 eV was proportional to the pressure of nitroethylene in the ionization chamber. From these curves, the appearance potentials and the apparent energy widths of the resonance-electron-capture processes from the molecular and fragment ions were obtained. The main results are summarized in Table 2. The appearance potential

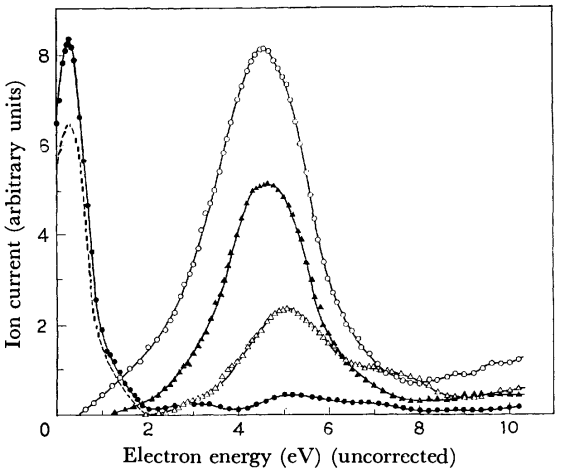

Fig. 1. Ionization efficiency curves of the main negative ions from nitroethylene.
-△-: O^- (×10), -▲-: C_2H^- (×2), -○-: NO_2^- (×1), -●-: $C_2H_3NO_2^-$ (×4), ----: SF_6^-.

TABLE 2. APPEARANCE POTENTIALS AND APPARENT ENERGY WIDTHS OF THE MAIN NEGATIVE IONS FORMED BY THE RESONANCE ELECTRON CAPTURE PROCESSES FROM NITROETHYLENE

m/e	Ion	1st Appearance potential (eV)	Half width (eV)
16	O^-	2.5±0.2	1.5
17	OH^-	2.8±0.2	1.6
25	C_2H^-	2.2±0.2	1.4
26	$C_2H_2^-$	2.8±0.2	1.5
30	NO^-	2.8±0.2	1.4
46	NO_2^-	1.5±0.2	1.8
55	C_2HNO^-	2.5±0.2	1.3
72	$C_2H_2NO_2^-$	2.1±0.2	1.5
73	$C_2H_3NO_2^-$	0	0.7

of NO_2^- in this study is higher than that of the NO_2^- from nitroalkanes (below 1 eV[14]).

From the ionization efficiency curve of $C_2H_3NO_2^-$ shown in Fig. 1, it is clear that the appearance potential is about 0 eV and that the width of the resonance capture is very narrow; both of those properties are also exhibited in the molecular negative ion of sulfur hexafluoride. These facts indicate that the nitroethylene molecule has the ability to capture thermal electrons easily by means of nondissociative process. Similar results in the cases of nitrocompounds of benzene derivatives have been reported by Christophorou *et al.*[15] and Jäger and Henglein.[16] The width of the nondissociative resonance capture of nitroethylene seems to be due to the energy spread of the impact electrons used, since the energy spread of the resonance-electron-capture process of SF_6 has been considered to be narrower than 0.05 eV.[11]

13) T. Sugiura, Y. Inoue, O. Toyama, T. Hayakawa, J. Okamoto, and T. Noda, *Mass Spectroscopy*, **11**, 141 (1964).

14) S. Tsuda, A. Yokohata, and M. Kawai, This Bulletin, **42**, 614 (1969).

15) L. G. Christophorou, R. N. Compton, G. S. Hurst, and P. W. Reinhardt, *J. Chem. Phys.*, **45**, 536 (1966).

16) K. Jäger and A. Henglein, *Z. Naturforsch.*, **22A**, 700 (1967).

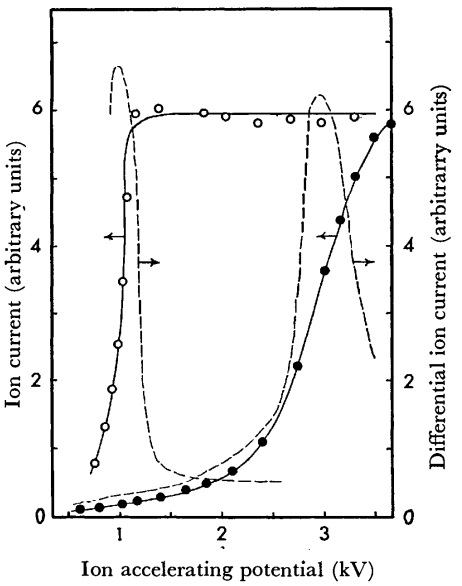

Fig. 2. Dependences of the ion accelerating potential on the ion intensity for $C_2H_3NO_2^-$ and SF_6^-.
-●-: $C_2H_3NO_2^-$. -○-: SF_6^-.

Compton *et al.*[17] measured the lifetimes of the molecular negative ions for SF_6, $C_6H_5NO_2$ and $(CH_3CO)_2$ by the use of a time-of-flight mass spectrometer. For the molecular negative ion of nitroethylene, an attempt to estimate the mean lifetime was made using the following procedures. The ion intensity of $C_2H_3NO_2^-$ was remarkably dependent upon the ion-accelerating potential. As is shown in Fig. 2, the dependence of the ion-accelerating potential on the ion intensity was measured for $C_2H_3NO_2^-$ and SF_6^- by using a Faraday cage as the ion detector. The dotted lines in Fig. 2 are the first differential curves obtained from the relations between the ion intensity and the ion-accelerating potential. Neglecting the change in the ion-collection efficiency with the variation in the accelerating potential, the sum of the residence time of the ions in the ionization chamber and the flight time of the ions at the peak of the first differential curve can be approximately considered as the mean lifetime of the ions. From the results of Fig. 2 and the estimated residence times in the ionization chamber to be described in the next section, the mean lifetimes for $C_2H_3NO_2^-$ and SF_6^- were calculated to be 14 μ sec and 28 μ sec respectively. The value for SF_6^- shows a close agreement with the result obtained by Compton *et al.* (25 μ sec[17]).

Dimer-negative-ion Formation by Ion-molecule Reaction. In the case of an electron impact of 100 eV, many secondary products of ion-molecule reactions were observed. However, at an electron energy of less than 1 eV, the secondary ions were the only products obtained by the reaction with $C_2H_3NO_2^-$; the mass numbers of the main secondary ions were 99, 119, and 146.

From the viewpoint of studying the initial process of the polymerization, special attention was paid to the formation process of the dimer negative ion. The ionization efficiency curves of $C_2H_3NO_2^-$ and $(C_2H_3NO_2)_2^-$ are shown in Fig. 3. The close agreement of the shapes of the two peaks indicates that the precursor of $(C_2H_3NO_2)_2^-$ is $C_2H_3NO_2^-$. The intensity of $(C_2H_3NO_2)_2^-$ at the peak in Fig. 3 was proportional to the square of the pressure of nitroethylene, whereas that of $C_2H_3NO_2^-$ was linear to the pressure, as is shown in Fig. 4. The plots of the $(C_2H_3NO_2)_2^-/C_2H_3NO_2^-$ ratio *vs.* the pressure of nitroethylene give a linear relation, as is shown in Fig. 5. From these results, it is evident that $(C_2H_3$-

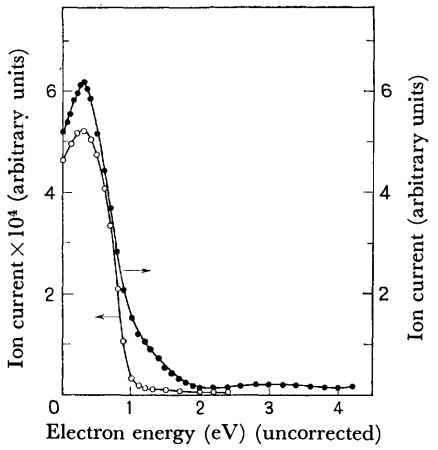

Fig. 3. Ionization efficiency curves of $C_2H_3NO_2^-$ and $(C_2H_3NO_2)_2^-$. Source pressure: 4.4×10^{-4} mmHg.
-●-: $C_2H_3NO_2^-$, -○-: $(C_2H_3NO_2)_2^-$.

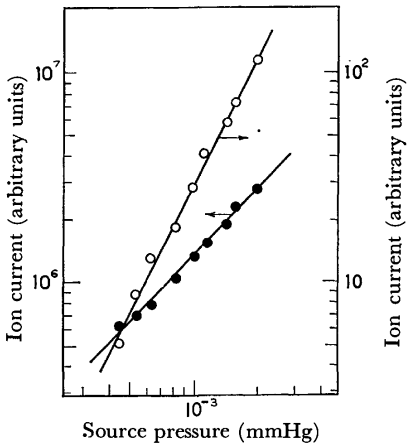

Fig. 4. Dependences of the pressure in the ionization chamber on the ion intensity for $C_2H_3NO_2^-$ and $(C_2H_3NO_2)_2^-$.
-●-: $C_2H_3NO_2^-$, -○-: $(C_2H_3NO_2)_2^-$.

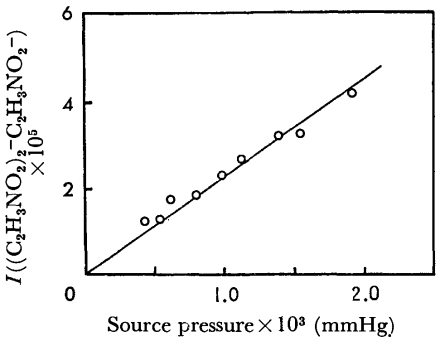

Fig. 5. Relation between the intensity ratio $(C_2H_3NO_2)_2^-/C_2H_3NO_2^-$ and the pressure in the ionization chamber.

17) R. N. Compton, L. G. Christophorou, G. S. Hurst, and P. W. Reinhardt, *J. Chem. Phys.*, **45**, 4634 (1966).

$NO_2)_2^-$ is produced by the ion-molecule reaction of the molecular ion with a neutral nitroethylene molecule, which can be demonstrated as follows:

$$C_2H_3NO_2^- + C_2H_3NO_2 \xrightarrow{k} (C_2H_3NO_2)_2^- \quad (a)$$

The rate constant of the (a) reaction was estimated by the following procedures. Assuming that the source pressure is low and that the fraction of the molecular ion which reacts is very small, Eq. (1) is obtained by introducing a treatment similar to that developed by Koyano *et al.*[18] for a reaction cross section:

$$g\left(\frac{I_D}{I_P}\right) = k[C_2H_3NO_2]\tau_N \quad (1)$$

where I_D/I_P is the ratio of the intensities of the dimer ion and the molecular ion, $[C_2H_3NO_2]$ is the concentration of nitroethylene, τ_N is the residence time of the molecular ion in the ionization chamber, and g is the ratio of the electron-multiplier gain of I_D to that of I_P. g was experimentally obtained as $1/\sqrt{2}$. For the estimation of τ_N, the ion-molecule reaction of the methane positive ions, represented by the (b) formula, was taken as a standard:

$$CH_4^+ + CH_4 \longrightarrow CH_5^+ + CH_3 \quad (b)$$

Using the published value of the rate constant for this reaction (1.1×10^{-9} cc mol^{-1}sec^{-1} [19]), the residence time of CH_4^+ in this apparatus ($\tau_{CH_4^+}$) was determined to be 2.1 μ sec from the slope of the linear relation between $I_{CH_5^+}/I_{CH_4^+}$ and the pressure of methane in the ionization chamber. It is generally known that the residence time of ions in the ionization chamber is a function of the mass of ions, the field strength in the chamber, and the distance from the electron beam to the exit slit of the chamber. In both the (a) and (b) reactions, the distance from the electron beam to the exit slit is the same, and the field strength is considered to be equal for positive and negative ions, although the signs of the gradients are the opposite. Consequently, the residence time of ions in this study is only a function of the mass of ions. By multiplying $\tau_{CH_4^+}$ by the square root of the mass ratio of $C_2H_3NO_2^-$ and CH_4^+, τ_N was estimated as 4.6 μ sec. Since $k\tau_N$ in Eq. (1) was obtained from the slope of Fig. 5, the rate constant of Reaction (a) was determined to be 3.2×10^{-13} cc mol^{-1}sec^{-1}.

Discussion

The results presented in Table 2 clearly show that many of the fragment ions from nitroethylene have appearance potentials which are almost identical. It might be expected that some of them result from ion-molecule reactions. However, the experimental evidence that the intensities of the ions increase linearly with the increase in the pressure in the ionization chamber indicates that these fragment ions are not produced by ion-molecule reactions, but are formed by the dissociative-resonance-capture processes.

It is interesting that the molecular negative ion of nitroethylene is observed at a lower pressure in the ionization chamber. The formation of molecular negative ions is generally classified into two different processes as has been pointed out by Compton *et al.*[17]: (i) metastable molecular negative ion formation, and (ii) molecular negative ion formation, in which the ion is stabilized by collision or radiation.

In the present study, the intensity of the molecular negative ion of nitroethylene is also proportional to the pressure by an electron impact of less than 1 eV. This fact indicates that the molecular negative ion is predominantly formed by the (i) process, in which the molecule is able to capture thermal electrons while maintaining its interatomic distances. The exact cross section of the electron capture can not be determined by the apparatus used. However, the relative intensity of the molecular ion of nitroethylene in the energy range of the resonance capture was about 1/200 of that for SF_6^- at a normalized pressure. Several values for the cross section of SF_6^- formation by nondissociative electron attachment have been reported.[11,17,20-24] Among them, the value of 2.6×10^{-14} cm^2 determined by Mahan and Young[24] was chosen as the most reliable one. Consequently the cross section of the nondissociative resonance capture of nitroethylene was estimated to be approximately 1.3×10^{-16} cm^2.

Now, the technique used in the present study for determining the ion lifetime should be discussed, since it has not been clearly established. As is well known, there is a strong tendency toward defocusing as the ion accelerating potential is reduced, and, of course, the beam will tend to spread as the retention time in the analyzer tube is increased. It is, therefore, necessary to obtain some information on the effect of the ion-accelerating voltage upon the collected current of several positive ions. In an attempt to correct some uncertain effects, the dependence of the accelerating voltage on the ion intensities of Ar^+ and SF_6^- was measured by changing the sign of the supplied voltage. The ion-intensity ratio of SF_6^-/Ar^+ changed in almost the same manner as is shown in Fig. 2 with the variation in the accelerating voltage. This fact, and the close agreement of the lifetime for SF_6^- between the values obtained by Compton[17] and by ourselves seem to imply that the method in the present study is still valid despite the limitations imposed by the obvious oversimplification.

The lifetime of the molecular negative ion thus formed is closely related to the electron affinity of the molecule.[17] Kamiyama *et al.*[25] calculated the electronic configurations, matrix elements, and energy levels for the molecular negative ion of nitroethylene by a semi-empirical MO method; they also gave the value of

18) I. Koyano, I. Omura, and I. Tanaka, *J. Chem. Phys.*, **44**, 3850 (1966).

19) a) V. I. Tal'roze and E. L. Frankevich, *Izv. Akad. Nauk SSSR, Otd. Khim. Nauk*, 1351 (1959); b) C. W. Hand and H. von Weyssenhoff, *Can. J. Chem.*, **42**, 195 (1964).

20) I. S. Bucelh'nikova, *Zh. Eksperim. i. Teor. Fiz.*, **35**, 1119 (1958); *Soviet Phys. JETP*, **8**, 783 (1959).

21) R. K. Asundi and J. D. Craggs, *Proc. Phys. Soc.* (London), **83**, 611 (1964).

22) D. Rapp and D. D. Briglia, *J. Chem. Phys.*, **43**, 1480 (1965).

23) J. B. Hasted and S. Beg, *Brit. J. Appl. Phys.*, **16**, 1779 (1965).

24) B. H. Mahan and C. E. Young, *J. Chem. Phys.*, **44**, 2192 (1966).

25) H. Kamiyama, K. Hayashi, and S. Okamura, *Ann. Rept. Japan Assoc. Rad. Res. Polymers*, **7**, 145 (1965/1966).

1.53 eV as the electron affinity of nitroethylene. The observed long lifetime of the molecular negative ion of nitroethylene may be given by this positive electron affinity and the stable molecular configuration in the electron attachment.[25] The nature of the nitroethylene molecule as a strong electron acceptor shown in this study is in reasonable agreement with those suggested by the ESR[8] and the optical investigations.[25] On the other hand, in the case of the electron impact with 100 eV, the remarkable increase in the molecular negative ion at higher pressures shown in Table 1 seems to be caused by the (ii) process or by other processes.

It is clear from the results shown in Figs. 2 and 3 that the precursor of the dimer negative ion is the molecular negative ion of nitroethylene, and that the dimer negative ion is formed by the ion-molecule reaction of the molecular ion with a neutral nitroethylene molecule. The theoretical kinetic equation of ion-molecule reactions was first derived by Gioumousis and Stevenson[26] on the basis of an ion-induced-dipole model. Moran and Hamill[27] have considered the interaction of an ion with a molecule possessing a permanent dipole. Using a similar model, Harridon *et al.*[28] have proposed a modified collision theory including the effect of ion-dipole interaction. They have shown that the mean rate constant for collisions where both an ion and a neutral molecule have thermal velocities is given by the following equation:

$$\bar{k}_{\text{therm}} = 2\pi e\left(\frac{\alpha}{\mu}\right)^{1/2} + \frac{2\pi e\mu_D}{\mu}\left(\frac{2\mu}{\pi kT}\right)^{1/2}$$

where e is the electron charge, μ is the reduced mass of the colliding pair, α is the polarizability of the molecule, μ_D is the dipole moment of the molecule, and kT is the thermal kinetic energy.

According to this theory, the rate constant for the dimerization reaction of nitroethylene was calculated. Although the polarizability and the dipole moment of the nitroethylene molecule are unknown, it can be assumed that they are in the same order as those of nitroethane. The calculated values are 6.2×10^{-9} and 5.9×10^{-9} cc mol^{-1}sec^{-1} at 323°K and 373°K respectively. The rate constant measured experimentally (3.2×10^{-13} cc mol^{-1}sec^{-1}) is several orders of magnitude smaller than that predicted by the theory. This may indicate that a great portion of collisions do not give rise to dimerization reactions. The reasons for the apparent low rate constant of the dimerization reaction are not clear. One possible explanation is that the collisions lead to other ion-molecule reactions. However, the secondary ions observed at an electron energy of less than 1 eV are not abundant, as has already been mentioned. It would appear, therefore, that the contribution of other ion-molecule reactions is not very large. Alternatively, the apparent low rate constant could be explained by the occurrence of a charge transfer or a collision-induced electron detachment from the molecular negative ion which was not detected in the present study. A more likely explanation is that the model used does not adequately describe the ion-molecule collision since it contains no consideration of the electronic structures of the interacting species. Recently, Schaefer and Henis[29] have presented a qualitative description of low-energy ion-molecule reactions based on the assumption that the probability of reaction can be described by the change in the electron density around the nulcear centers involved. For the dimerization reaction of nitroethylene, however, this description cannot be applied because of the difficulty in calculating the detailed electron density distribution in complicated reaction systems.

In general, the mass-discrimination effect must be considered in determining the rate constants of ion-molecule reactions. However, this effect, caused by the repeller potential, was not present in the present study, where the repeller potential was always kept at 0 V. Other factors in the mass-discrimination effect, such as the space charge, the surface potential, and the source magnet in the ionization chamber, were not taken into consideration.

No experiment on the polymerization in the gas phase has yet been carried out, since the vapor pressure of nitroethylene is extremely low at room temperature. The rate constant of the polymerization in the liquid phase was determined from the kinetic experiments to be 6.7×10^{-14} cc mol^{-1}sec^{-1} at 20°C.[7b]

For the trimer negative ion, the measurements of the ionization efficiency curve and the dependence of the source pressure were difficult because of the low intensity of the trimer ion. In the positive-ion mass spectra, however, neither dimer nor trimer positive ions were observed in the pressure range examined. This fact also indicates that neither the dimer nor the trimer negative ions are produced by a direct electron capture process of a neutral nitroethylene dimer or trimer; rather, both are formed as secondary products. Consequently, the formation process of the trimer negative ion can involve only a consecutive reaction:

$$(C_2H_3NO_2)_2^- + C_2H_3NO_2 \longrightarrow (C_2H_3NO_2)_3^- \qquad (c)$$

Although only a limited range of the pressure was examined, the mass spectrometric observation mentioned above supports the concept that the precursor of the radiation-induced polymerization of nitroethylene is the molecular negative ion.

The authors wish to express their appreciation to Professor Koichiro Hayashi for his valuable advice and helpful discussions. They are also indebted to Professor Seizo Okamura and Dr. Hirobumi Danno for their continous encouragement during the course of this work.

26) G. Gioumousis and D. P. Stevenson, *J. Chem. Phys.*, **29**, 294 (1958).
27) T. F. Moran and W. H. Hamill, *ibid.*, **39**, 1413 (1963).
28) S. K. Gupta, E. G. Jones, A. G. Harrison, and J. J. Myher, *Can. J. Chem.*, **45**, 3107 (1967).
29) J. Schaefer and J. M. S. Henis, *J. Chem. Phys.*, **49**, 5377 (1968).

The Solid Complex of Aminomalonic Acid with β-Alanine and Its Thermal Decomposition[1]

Juziro NISHIJO, Isamu IMANISHI, and Genzo HASHIZUME*
Kobe Womens College of Pharmacy, Higashinada-ku, Kobe
(Received June 25, 1971)

For the crystallization of aminomalonic acid with several amino acids from an aqueous solution, solid complex formation was studied by means of an X-ray diffractometer. No complex formation of aminomalonic acid with α-alanine, *dl*-α-amino-*n*-butyric acid, *l*-isoleucine, *l*-leucine, *dl*-serine, *dl*-norleucine, α-amino-iso-butyric acid, *dl*-valine, *dl*-threonine, or *dl*-norvaline was observed. However, with β-alanine, the formation of a solid complex with a molar ratio of 1:1 was ascertained. When this solid complex was analyzed by the differential thermogravimetric method in air at a heating rate of 1.4°C/min, a decarboxylation reaction, accompanied by endothermic and exothermic peaks, was observed at 115—133°C. On the other hand, the decarboxylation of aminomalonic acid alone occurred in the temperature range of 112—138°C. The areas of the endothermic peak, which was attributed to the decarboxylation, and the endothermic peak, which was attributed to the crystallization energies of γ-glycine and β-alanine, were, respectively, about 3 and 3/2 times those of the peaks observed in the case of aminomalonic acid. It was also observed that the exothermic process proceeded in two steps. The X-ray analysis of the products of the decarboxylation process suggested that the complex first melted to become amorphous to X-rays, and that it was then decarboxylated to amorphous glycine and amorphous β-alanine with these subsequent crystallization. The two-step exothermic process was explained in terms of a somewhat earlier crystallization of amorphous glycine than in terms of that of the amorphous β-alanine. The activation energy of the solid complex was estimated to 119.2 kcal/mol from the thermogravimetric curve. This large value of the apparent activation energy may be considered to result because the solid complex turns to an amorphous phase much more sensitive to decarboxylation prior to decomposition, and the steep slope of the thermogravimetric curve which results from the rapid decarboxylation of the amorphous gives the large apparent activation energy.

The present authors have previously reported[2] that aminomalonic acid reacted with glycine to form a solid complex with a 1:1 molar ratio when they were crystallized from an aqueous solution, and that the complex was thermally more stable than aminomalonic aicd alone. This paper will describe the solid-complex formation of aminomalonic acid with several other amino acid, and the thermal characteristics of the complex, if formed, will be compared with those of aminomalonic acid.

Experimental

Materials. Aminomalonic acid purified by recrystallization and various amino acids (special grade chemicals) were dissolved (in a molar ratio of 1:1) into water. By then evaporating the solvent at 25°C under a pressure of 3—5 mmHg, and easily crystallizable or a highly viscous residue was obtained. When the highly viscous residue was allowed to stand in air, a crystalline powder was obtained. This crystalline powder was pulverized in an agate mortar and was then used as the sample.

Analysis. The X-ray analysis was carried out with an X-ray diffractometer, Rigaku Denki Geigerflex, using Ni filter-CuK_α radiation. The infrared absorption spectra were measured with a Nihon Bunko Grating Infrared Spectrophotometer, type DS-402G. The Nujol-mull method was adopted in the measurements. DTA-TGA was carried out by an apparatus previously reported.[3] Measurements were carried out in air, because no significant difference had been observed in air as in a nitrogen stream. Samples of 200—500 meshes were used for the measurements.

Determination of Aminomalonic Acid and β-Alanine by the X-ray Diffraction Technique. Aminomalonic acid was mixed with a solid complex, AM_1-β-AL_1 (AM: aminomalonic acid, AL: β-alanine, the subscripts refer to the molar ratio), in order to obtain samples with various weight ratios of aminomalonic acid to AM_1-β-AL_1. The mixture was triturated well in a mortar to diminish the orientation of the crystals. Then, the sample was set in a sample holder (the same sample holder was used throughout this work). The intensity [(half width) × (height)] of the diffraction peak due to aminomalonic acid at 24.1° (2θ) in these samples was measured in order to obtain a calibration curve, which was then used for the determination of the aminomalonic acid content (Fig. 3). The measuring conditions were as follows: 40 kV—1.5 mA;[4] full scale, 400 count/sec; time constant, 4: scanning speed, 0.5°(2θ)/min, and chart speed, 20 mm/min. The determination of β-alanine was carried out by the same method as that used for aminomalonic acid and under analogous condition, except for 40 kV—3 mA[4] and a chart speed of 40 mm. In this case, the height of the diffraction peak of β-alanine at 24.1° (2θ) was adopted as its intensity (Fig. 4).

Results and Discussion

Solid Complex-formation Ability. The solid complex-formation abilities of aminomalonic acid with several amino acids, studied by X-ray analysis, are shown in Table 1. The absence of any solid-complex formation is shown by the sign ×. In these cases, only the diffraction patterns of aminomalonic acid were observed. In the cases shown with the sign ○, a new diffraction pattern, different from those of the component amino acids, was observed, indicating a complex

1) Presented at the 91st Annual meeting of the Pharmaceutical Society of Japan, April, 1971.

* Present address: Industrial Research Institute of Hyogo Prefecture, Suma-ku, Kobe.

2) T. Kinugasa, J. Nishijo, and G. Hashizume, and I. Imanishi, This Bulletin, **44**, 2035 (1971).

3) T. Kinugasa, J. Nishijo, and G. Hashizume, *Nippon Kagaku Zasshi*, **90**, 584 (1969).

4) Each constant X-ray intensity was ascertained by measuring the height of the diffraction peak of γ-glycine at 21.8° (2θ).

Table 1. Solid complex-formation ability of aminomalonic acid with amino acids

α-Alanine	△
dl-α-Amino-*n*-butyric acid	△
l-Isoleucine	△
l-Leucine	×
dl-Serine	×
dl-Norleucine	×
α-Aminoisobutyric acid	△
dl-Valine	△
dl-Threonine	△
dl-Norvaline	×
β-Alanine	○
Glycine	○

formation. In the cases shown with the sign △, diffraction pattern consisted of the peaks due to unknown species and those of the component amino acid, (aminomalonic acid or added amino acid). The former were found to correspond to the diffraction peaks of the hydrate of aminomalonic acid or the added amino acid. Thus, we concluded that no complex is formed in these cases.

The fact that aminomalonic acid can form solid complexes with β-alanine and glycine, but not with α-substituted amino acids, seems to suggest that steric factors in the neighborhood of amino and carboxyl groups of amino acids have a bearing on the complex-formation ability of aminomalonic acid with other amino acids.

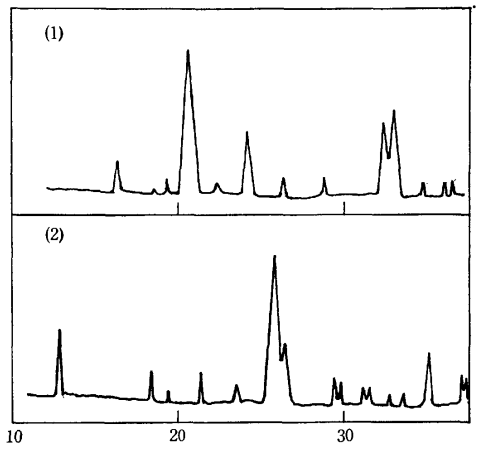

Fig. 1. X-ray diffraction patterns of aminomalonic acid (1) and β-alanine (2).

Solid Complex of Aminomalonic Acid with β-Alanine. The X-ray diffraction patterns of aminomalonic acid and β-alanine are shown in Fig. 1, while those of the samples, whose molar ratios of aminomalonic acid to β-alanines are 1 : 1, 2 : 1, and 1 : 2, are shown in Fig. 2. In the case of AM_1-β-AL_1, a new diffraction pattern, different from those of the components, aminomalonic acid and β-alanine, was obtained, while in the cases of AM_2-β-AL_1 and AM_1-β-AL_2, diffraction patterns of AM_1-β-AL_1 with those of aminomalonic acid or β-alanine respectively were observed. Also, AM_3-β-AL_2 and AM_4-β-AL_3 gave patterns of AM_1-β-AL_1 and

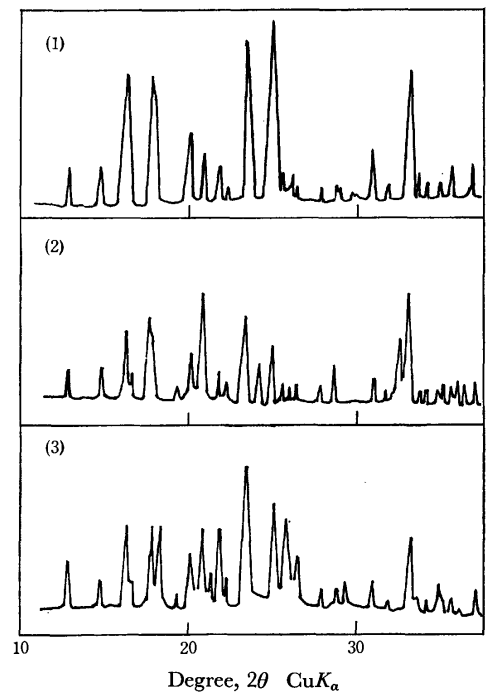

Fig. 2. X-ray diffraction patterns of AM_1-β-AL_1 (1), AM_2-β-AL_1 (2) and AM_1-β-AL_2 (3).

aminomalonic acid, while AM_2-β-AL_3 and AM_3-β-AL_4 gave patterns of AM_1-β-AL_1 and β-alanine. To determine the molar ratio of aminomalonic acid to β-alanine in the complex, the content of aminomalonic acid in AM_2-β-AL_1, AM_3-β-AL_2, and AM_4-β-AL_3, and that of β-alanine in AM_1-β-AL_2, AM_2-β-AL_3, AM_3-β-AL_4, were estimated by using the calibration curves (Figs. 3, 4). The contents of aminomalonic acid and β-alanine, which exist excessively in these samples, were calculated by assuming that the crystals corresponding to the diffraction pattern of AM_1-β-AL_1 were composed of aminomalonic acid and β-alanine in a molar ratio of 1 : 1. These calculated values agreed fairly well with the found values, as shown in Table 2. It was concluded

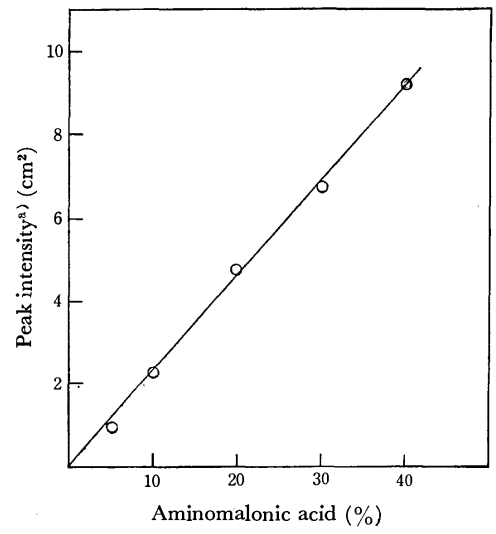

Fig. 3. Calibration Curve for Aminomalonic Acid in AM_x-β-AL_y($x>y$)
a) [(half width) × (height)] of diffraction peak

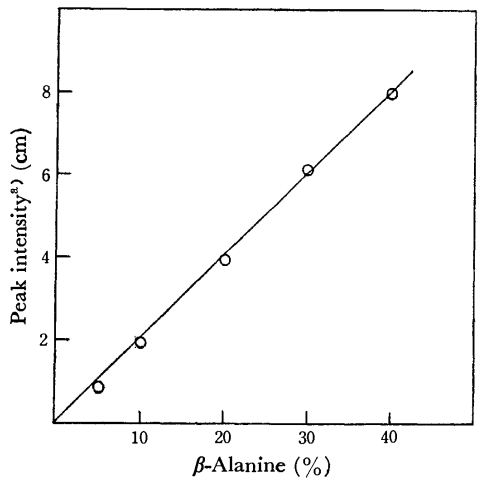

Fig. 4. Calibration Curve for β-Alanine in AM_x-β-AL_y ($x<y$)
[a] height of diffraction peak

TABLE 2. QUANTITATIVE DETERMINATION OF EXCESS AMINOMALONIC AICD IN AM_2-β-AL_1, AM_3-β-AL_2 AND AM_4-β-AL_3 AND EXCESS β-ALANINE IN AM_1-β-AL_2, AM_2-β-AL_3 AND AM_3-β-AL_4 BY X-RAY ANALYSIS

	Calcd (%)		Found (%)	
	AM	β-AL	AM	β-AL
AM_2-β-AL_1	36.4		34.8	
AM_3-β-AL_2	22.2		19.0	
AM_4-β-AL_3	16.0		16.5	
AM_1-β-AL_2		30.0		33.5
AM_2-β-AL_3		17.6		16.8
AM_3-β-AL_4		12.5		13.1

that aminomalonic acid reacts with β-alanine in a 1:1 molar ratio to produce a solid complex which gives the diffraction pattern of AM_1-β-AL_1.

The infrared absorption spectra of aminomalonic acid, β-alanine, and AM_1-β-AL_1 are shown in Fig. 5. In the spectrum of AM_1-β-AL_1, absorption bands observed in the neighborhood of 820, 910, and 1100 cm^{-1} were especially different from those of aminomalonic acid or β-alanine. In addition, the band at 1710 cm^{-1},

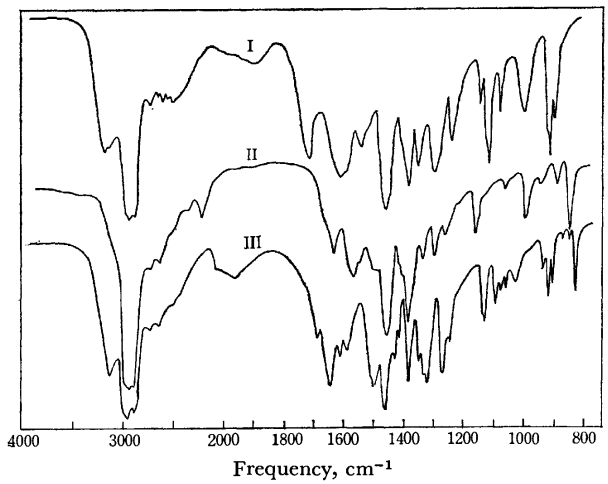

Fig. 5. Infrared absorption spectra of aminomalonic acid (I), β-alanine (II) and AM_1-β-AL_1 (III) in Nujol

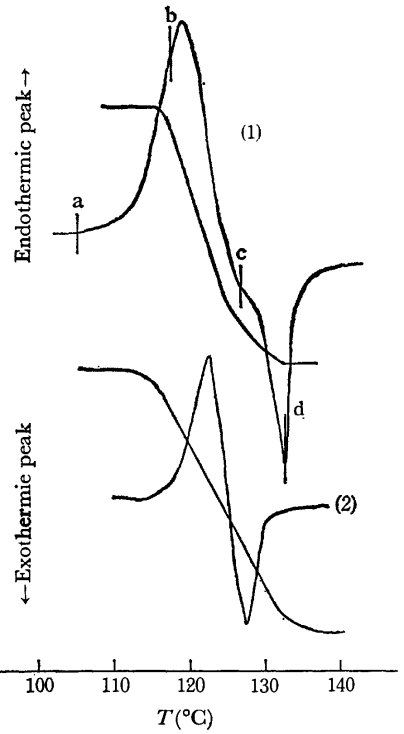

Fig. 6. DTA-TGA curves of AM_1-β-AL_1(1) and aminomalonic acid (2), in air. heating rate: 1,4/min.
Sensibility: ± 50 μv reference: silica powder

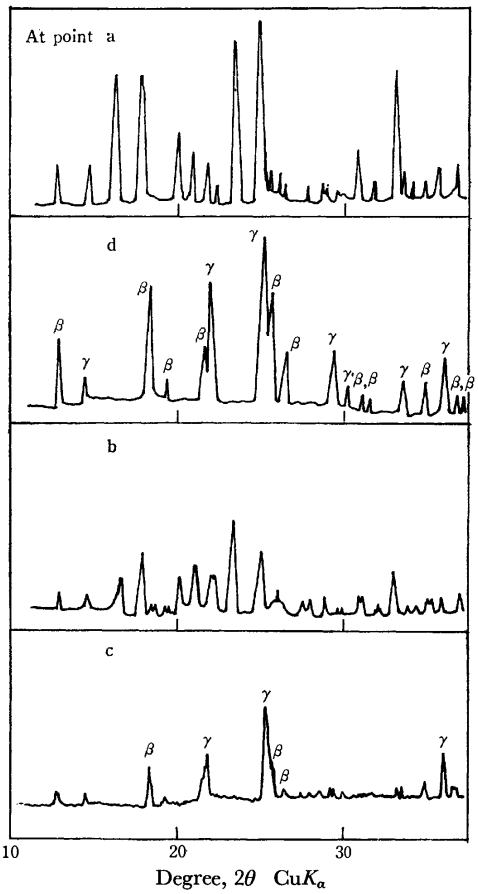

Fig. 7. X-ray diffraction patterns of samples taken out rapidly at point a, d, b and c in DTA curve in Fig. 4.
γ: γ-glycine β: β-alanine

attributed to the carboxyl group of aminomalonic acid, was shifted to about 1685 cm^{-1}. On the contrary,when no complex was formed, only superimposed absorption bands of aminomalonic acid were observed.

Differential Thermal Analysis and Thermogravimetric Analysis. The DTA–TGA curve of AM_1-β-AL_1 in air, using 87.4 mg of the sample at a heating rate of 1.4°C/min, is shown in Fig. 6, together with the corresponding curve of aminomalonic acid. These curves show that the beginning temperature of the decarboxylation of AM_1-β-AL_1 is slightly higher than that of aminomalonic acid, while the completion temperature of the former was about 5°C lower than that of the latter and that, consequently, the rate of decomposition of the former was larger than that of the latter. On the other hand, it is confirmed that, in the case of AM_1-β-AL_1, the endothermic process slightly precedes a decrease in weight, and the peak area is about 3 times that of aminomalonic acid. It is also found that the exothermic process proceeds in two steps. The peak area was about 3/2 times that of aminomalonic acid. To study the decarboxylation process of AM_1-β-AL_1, the samples were taken out rapidly at the a, b, c, and d points in the DTA curve shown in Fig. 6 and these samples were subjected to X-ray analysis. The results are shown in Fig. 7. Figure 7 shows that, at the a point, diffraction pattern is identical with that of AM_1-β-AL_1. This means that no change in AM_1-β-AL_1 occurs untill the decarboxylation begins. The diffraction patterns of the sample at the d point, where the decarboxylation is almost completed, were identical with those of γ-glycine and β-alanine. The sample rapidly taken out at the b point, where the decarboxylation proceeds about 15%, gives only a diffraction pattern identical with that of AM_1-β-AL_1. The sample at the c point, where the differencial thermal curve tends to a large second exothermic peak and where the decomposition fraction is about 70%, gives diffraction patterns of γ-glycine and β-alanine. These samples were allowed to stand in air in the sample holder for an X-ray diffractometer, and an X-ray analysis of the samples was carried out under the same conditions. The results are shown in Fig. 8. With the sample at the b point, the intensity of the diffraction pattern of AM_1-β-AL_1 increases and the diffraction peaks of γ-glycine and β-alanine appear. With the sample at the c point, the intensities of the diffraction peaks due to γ-glycine and β-alanine increase, but the increasing rate of intensity in β-alanine is larger than that in γ-glycine. Moreover, the diffraction peaks of AM_1-β-AL_1 appear, they can not be observed in the sample rapidly taken out. As it takes 7—10 min to transfer the sample from the DTA-TGA apparatus to the sample holder for X-ray analysis and to measure its diffraction pattern, the following decarboxylation process may be suggested. At first, AM_1-β-AL_1 may melt as a complex amorphous to X-ray analysis, and the amorphous complex may decarboxylate to amorphous glycine and amorphous β-alanine, which then soon crystallize to γ-glycine and β-alanine. The crystallization of amorphous glycine to γ-glycine may take place slightly earlier than that of β-alanine. Therefore, it can be considered that the endothermic peak corresponds to the heat required for the decarboxylation with melting, while the exothermic peak corresponds to the energy of crystallization to γ-glycine and β-alanine from their amorphous forms. The two-step change from the endothermic to the exothermic process can be interpreted in terms of a slight difference in crystallization velocity between the two compounds.

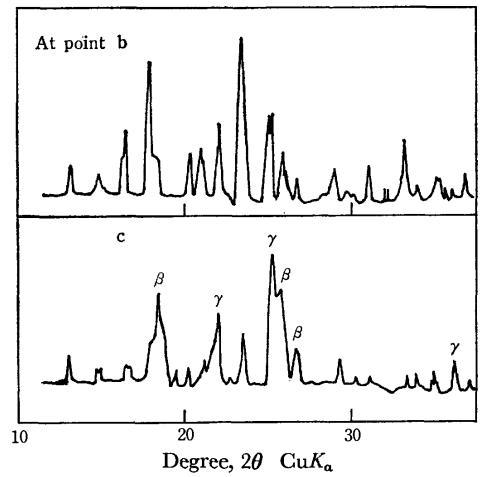

Fig. 8. X-ray diffraction patterns of samples at point b, c, left overngiht at room temperature.
γ:γ-glycine β:β-alanine

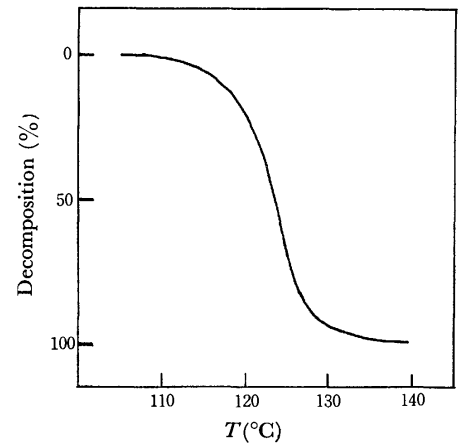

Fig. 9. Thermogravimetric curve of AM_1-β-AL_1 in air. heating rate: 1.0°C/min. sample amount: 50 mg.

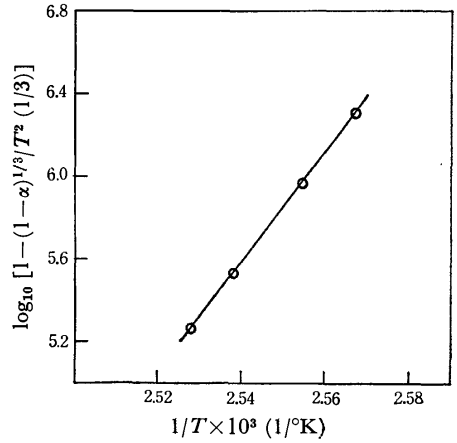

Fig. 10. Decarboxylation from AM_1-β-AL_1. n=2/3

5) A. W. Coats and J. P. Redfern, *Nature*, **201**, 68 (1968).

Activated Energy. By applying the equation previously proposed by Coats and Redfern[5] for the determination of the activation energy of a solid state reaction accompanied by a weight decrease, the activation energies of the decarboxylation of aminomalonic acid and AM_1-G_1 were calculated as 69.4 kcal/mol and 20.3 kcal/mol respectively. The determination of the activation energy of the decarboxylation of AM_1-β-AL_1 from its thermogravimetric curve with a heating rate of 1°C/min (Fig. 9) was attempted using the same equation. In the decomposition range from 10 to 63%.

$$\log_{10}\{1-(1-\alpha)^{1-n}/T^2(1-n)\} \text{ or } \log_{10}\{-\log(1-\alpha)/T^2\}$$

was plotted against $1/T$, assuming $n=0$, 1/2, 2/3, or 1. The best linearity was found with $n=2/3$ (Fig. 10). From the slope, the activation energy was calculated as 119.2 kcal/mol. This very large value may be explained as follows, amorphous AM_1-β-AL_1, to which the complex has melted prior to its decomposition, is so active in the decarboxylation that the reaction proceeds very rapidly; consequently, the slope of the thermogravimetric curve may be so steep that a very large apparent activation energy can be obtained.

It was concluded from these experimental results that a solid complex of aminomalonic acid with β-alanine was formed, but unlike the complex of aminomalonic acid with glycine, thermal stabilization can be obtained in this complex.

BULLETIN OF THE CHEMICAL SOCIETY OF JAPAN, VOL. 45, 2074—2078(1972)

The Diffusion of Gases at High Pressures. IV. The Diffusion of CTH_3 in the CH_4-CO_2 System

Shinji TAKAHASHI

The Chemical Research Institute of Non-Aqueous Solutions, Tohoku University, Katahira, Sendai

(Received June 24, 1971)

The diffusion coefficients of radioactive methane (CTH_3) in normal methane, in carbon dioxide, and in a mixture of normal methane with carbon dioxide (0.522 mol fraction of methane) were measured at the temperatures of 25, 50, and 75°C in the 15—250 atm pressure range. The measurements were made through a plug of porous bronze in the diffusion cell, using the radioactive tracer technique. The diffusion coefficient-density products, $D\rho$, for the CTH_3–normal methane system and the CTH_3– the binary mixture system increased slightly with an increase in the density in the lower-density region at 25 and 50°C, but they were nearly constant at 75°C. The $D\rho$ for the CTH_3–carbon dioxide system decreased with an increase in the density at each temperature. The $D\rho$-values at 1 atm, obtained by extrapolation, agreed fairly well with those reported in the literature. The density dependence of the $D\rho$ values at high densities could not be predicted by Enskog-Thorne's theory.

Although the diffusion coefficients of gases at high pressures have been reported by several investigators since 1950,[1] the relative scarcity of high-pressure diffusion data suggests a need for additional measurements in order to evaluate the various theoretical relations[2] and the generalized chart[3] available for the prediction of the transport properties of dense gases. In the present investigation, the diffusion coefficients of radioactive methane (CTH_3) in methane, in carbon dioxide, and in a mixture of normal methane with carbon dioxide (0.522 mole fraction of methane) were measured at the temperatures of 25, 50, and 75°C in the 15—250 atm pressure range, and the depencence on the pressure, the temperature, and the composition was studied.

Experimental

The apparatus and the experimental procedure were the same as those described previously.[4] The diffusion path in the cell was a porous bronze plug with a grain size of 60—70 μ. Radioactive methane, obtained from New England Nuclear Corp., was diluted with non-radioactive methane to a specific activity of about 20 μCi per m*l* at NTP. The purities of the carbon dioxide and non-radioactive methane used in this investigation were 99.9 and 99.6% respectively. The mixture of carbon dioxide with non-radioactive methane was prepared in a storage cylinder. The exact composition (0.522 mol fraction of methane) was determined by absorbing carbon dioxide from the sample into a potassium hydroxide solution. Under the conditions studied, the mixture is not in a liquid state.[5]

The proportionality betweeen the concentration of radioactive methane and the ionization current, essential for a quantitative treatment of the diffusion data, was confirmed experimentally for pure methane, carbon dioxide, and the mixture at a constant temperature and pressure. As examples, the results at 50°C are shown in Fig. 1.

Results and Discussion

The experimental results are given in Table 1. D is

1) Z. Balenovic, M. N. Myers, and J. C. Giddings, *J. Chem. Phys.*, **52**, 915 (1970).

2) J. O. Hirschfelder, C. F. Curtiss, and R. B. Bird, "Molecular Theory of Gases and Liquids," John Wiley & Sons, Inc., New York (1954), Chap. 9.

3) J. C. Slattery and R. B. Bird, *A. I. Ch. E. Journal*, **4**, 137 (1958), A. N. Berezhnoi and A. G. Usmanov, *Teor. Osn. Khim. Tekhnol.*, **2**, 820 (1968).

4) S. Takahashi and H. Iwasaki, This Bulletin, **39**, 2105 (1966), S. Takahashi, *ibid.*, **41**, 1573 (1968).

5) G. Kaminishi and T. Toriumi, *Rev. Phys. Chem. Jap.*, **38**, 79 (1968).

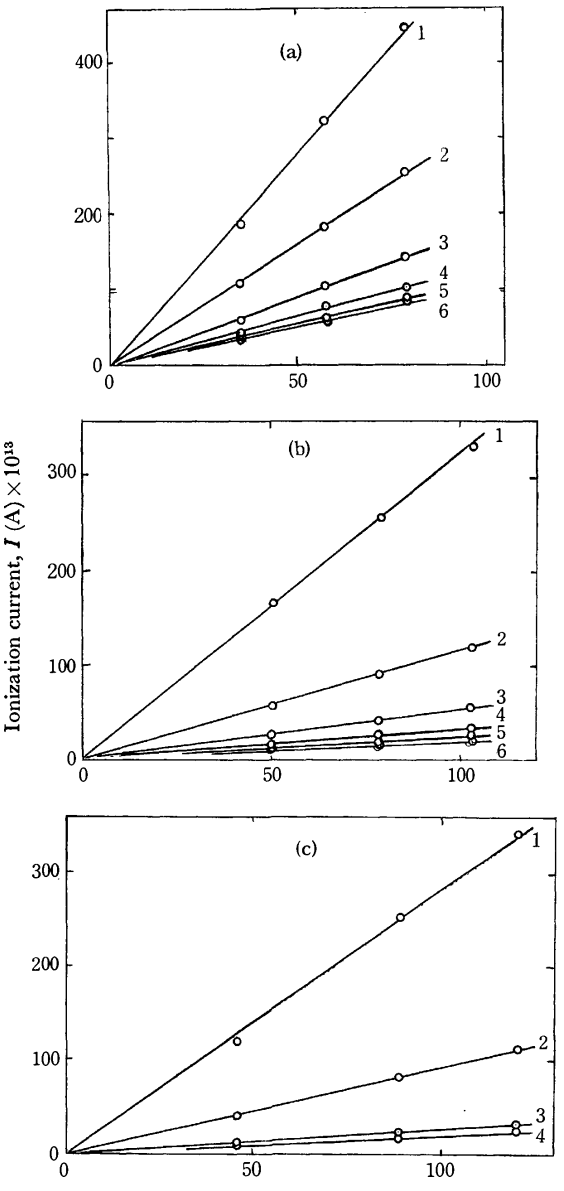

Fig. 1. Relations between the amount of radioactive methane and the ionization current at 50°C.
Composition, (a): $x_3=1.000$, (b): $x_3=0.522$, (c): $x_3=0.000$. Pressure, 1: 14.55 atm, 2: 49.4 atm, 3: 97.8 atm, 4: 146.2 atm, 5: 194.6 atm, 6: 243.0 atm

the diffusion coefficient of radioactive methane in the CH_4–CO_2 system. The densities of the gases, ρ (mol/l), were calculated from the compressibility data given by Kvalnes and Gaddy for methane,[6] by Michels and Michels for carbon dioxide,[7] and by Reamer *et al.* for the mixture.[8]

The diffusion coefficient-density products, $D\rho$, are plotted against the density in Fig. 2. The open circles refer to the values obtained in the present experiment. Curves have been drawn through the experimental points for the three systems where the mole fractions of methane, x_3, are 1.000, 0.522, and 0.000. The D at $x_3=1.000$ is the diffusion coefficient of radioactive methane with normal methane, D_{13}, where the 1 and 3 subscripts denote radioactive methane and normal methane respectively. The $D_{13}\rho$ increases slightly with an increase in the density in the lower-density regions to 5 mol/l, and decreases slightly in the higher-density regions. Extrapolations of $D_{13}\rho$ *vs.* ρ curves to 1 atm provide a basis for comparison with published low-pressure experimental results. Applying the mass correction[9] to the self-diffusion coefficient of normal methane, D_{33}, reported by Winn,[10] the diffusion coefficient of radioactive methane with mormal methane, D_{13}, was obtained; the values of $D_{13}\rho$ thus calculated are denoted by darkened triangles in Fig. 2. As can be seen from Fig. 2, the values reported by Winn yield values which are in agreement with those extrapolated in this investigation. The D at $x_3=0.000$ is the diffusion coefficient of radioactive methane with carbon dioxide, D_{12}, where the 2 subscript denotes carbon dioxide. The $D_{12}\rho$ decreases with an increase in the density at each temperature. Applying the mass correction to the diffusion coefficient of normal methane with carbon dioxide, D_{23}, calculated by the empirical formula,[11] the diffusion coefficient of radioactive methane with carbon dioxide, D_{12}, at 1 atm was obtained; the values of $D_{12}\rho$ at 1 atm are denoted by darkened circles in Fig. 2. The empirical formula yields values which agree with those extrapolated. The $D\rho$ at $x_3=0.522$ increases slightly with an increase in the density in the lower-density regions to 5 mol/l, decreases in the higher-density regions at 25 and 50°C, and is nearly constant at 75°C. The diffusion coefficient of the trace of radioactive methane in the mixture, D, at 1 atm may be calculated using the following equation:

$$1/D=x_2/D_{12}+x_3/D_{13} \qquad (1)$$

where x_2 and x_3 are the mole fractions of carbon dioxide and non-radioactive methane respectively, and where $x_2+x_3\fallingdotseq1$. The calculated values of $D\rho$ at 1 atm are shown by darkened squares in Fig. 2. As Fig. 2 shows, Eq. (1) yields values which are about 7% lower than those extrapolated at 25 and 50°C, and 4% lower at 75°C.

The D_{23}(CH_4 trace) and the D_{23}(CO_2 trace) were obtained by applying the mass correction to the diffusion coefficient of the trace of radioactive methane with normal carbon dioxide measured in the present investigation, and to the diffusion coefficient of the trace of radioactive carbon dioxide with normal methane reported in the previous paper, respectively. They are shown by open circles and open triangles in Fig. 3. The extrapolation of the $D_{23}\rho$(CH_4 trace) *vs.* ρ curves to 1 atm yields values which agree with those obtained by the extrapolation of the D_{23}(CO_2 trace) *vs.* ρ curves to 1 atm. This means that the values of D_{23} in such

6) H. M. Kvalnes and V. L. Gaddy, *J. Amer. Chem. Soc.*, **53**, 394 (1931).
7) A. Michels and C. Michels, *Proc. Roy. Soc.* (London), **153A**, 201, 214 (1935).
8) H. H. Reamer, R. H. Olds, B. H. Sage, and W. N. Lacey, *Ind. Eng. Chem.*, **36**, 88 (1944).
9) F. Hutchinson, *J. Chem. Phys.*, **17**, 1081 (1949).
10) E. B. Winn, *Phys. Rev.*, **80**, 1024 (1950).
11) "International Critical Tables," Vol. V, McGraw-Hill Book Comp., Inc., New York (1929), p. 29.
12) C. R. Wilke, *Chem. Eng. Progress*, **46**, 95 (1950).

TABLE 1. EXPERIMENTAL RESULTS

P atm	ρ mol/l	$D\times10^3$ cm^2/sec	$D\rho\times10^3$ cm^2·mol/sec·l
	25°C		
	$x_3=1.000$		
14.41	0.6035	16.5	9.96
24.7	1.0528	9.41	9.91
50.2	2.2330	4.58	10.23
66.0	2.9633	3.46	10.25
103.2	4.9583	2.03	10.07
151.5	7.5404	1.39	10.48
175.9	8.7597	1.12	9.81
211.7	10.3564	0.970	10.01
	$x_3=0.522$		
14.41	0.6095	14.7	8.96
14.41	0.6095	14.2	8.65
14.41	0.6095	14.4	8.78
45.5	2.1477	4.32	9.28
49.9	2.3921	3.77	9.02
99.0	5.7532	1.56	8.97
101.1	5.9300	1.58	9.37
149.3	10.065	0.833	8.38
149.3	10.065	0.843	8.48
149.3	10.065	0.878	8.83
153.1	10.355	0.814	8.42
	$x_3=0.000$		
14.41	0.6342	11.3	7.17
36.5	1.8957	3.69	6.99
36.6	1.9031	3.61	6.87
46.7	2.7235	2.41	6.56
49.3	2.9824	2.26	6.74
	50°C		
	$x_3=1.000$		
14.38	0.5513	18.2	10.04
14.44	0.5635	18.8	10.41
51.1	2.0485	4.95	10.14
51.3	2.0571	5.05	10.39
103.3	4.4615	2.40	10.71
151.2	6.5020	1.66	10.79
201.5	8.6069	1.26	10.84
252.3	10.4255	1.01	10.53
	$x_3=0.522$		
14.41	0.5619	16.5	9.27
49.0	2.0743	4.45	9.23
81.2	3.7225	2.44	9.08
104.1	5.0581	1.85	9.36
124.2	6.2859	1.42	8.93
161.2	8.5234	1.03	8.78
199.4	10.6192	0.813	8.63
	$x_3=0.000$		
14.33	0.5698	12.5	7.12
14.41	0.5731	12.4	7.11
50.0	2.4112	3.06	7.38
50.3	2.4332	2.99	7.28
60.0	3.1127	2.25	7.00
76.2	4.6343	1.50	6.95
82.5	5.4483	1.26	6.86
92.9	7.2333	0.935	6.76
102.2	9.6988	0.620	6.50
	75°C		
	$x_3=1.000$		
14.41	0.5101	21.3	10.87
50.1	1.8285	5.97	10.92
103.0	3.8844	2.85	11.07
105.0	3.9636	2.73	10.82
153.1	5.8456	1.93	11.28
202.3	7.6886	1.44	11.07
243.5	9.0358	1.21	10.93
250.0	9.2394	1.17	10.81
	$x_3=0.522$		
15.30	0.5499	17.0	9.35
15.38	0.5528	17.1	9.45
50.4	1.9241	5.09	9.79
50.5	1.9283	5.04	9.72
69.2	2.7299	3.53	9.64
100.9	4.1901	2.23	9.34
133.8	5.7908	1.65	9.55
173.9	7.7407	1.24	9.60
233.8	10.3740	0.892	9.25
	$x_3=0.000$		
14.41	0.5249	14.9	7.82
14.41	0.5249	14.6	7.66
50.0	2.0675	3.65	7.55
51.0	2.1279	3.63	7.72
72.3	3.3323	2.22	7.40
72.5	3.3460	2.19	7.33
104.8	5.8402	1.28	7.48
123.3	7.7370	0.910	7.04
129.2	8.4064	0.837	7.04
155.3	11.1898	0.633	7.08

limiting cases as when $x_2\rightarrow0$ and $x_3\rightarrow0$ are identical at 1 atm. Similar results were reported by Walker and Westenberg.[13] for the CO_2—N_2 system. Although the $D_{23}\rho(CH_4$ trace) decreases with an increase in the density at each temperature, the $D_{23}\rho(CO_2$ trace) is nearly constant, and the difference between them become larger with an increase in the density. This means that the D_{23} is dependent on the composition at high densities.

According to Enskog-Thorne's theory, which is the only theoretical treatment offering any practical application, the binary diffusion coefficient is given by the following equation:

$$D_{ij}\rho=(D_{ij})^0\rho/\chi_{ij} \tag{2}$$

where $(D_{ij})^0$ is the binary diffusion coefficient calculated on the basis of the low-density kinetic theory as follows:

$$(D_{ij})^0=\frac{3}{16n\sigma_{ij}^2\,\Omega_{ij}^{(1,1)*}}\left(\frac{2kT}{\pi\mu}\right)^{\frac{1}{2}} \tag{3}$$

where n is the number density of the molecules (cm^{-3}); σ_{ij}, the collision diameter (cm); $\Omega_{ij}^{(1,1)*}$ the reduced

13) R. E. Walker and A. A. Westenberg, *J. Chem. Phys.*, **29**, 1139 (1958).

collision integral; k, the Boltzmann constant; T, the absolute temperature (°K), and μ, the reduced mass. χ_{ij} is a correction factor which is given for a two-component gas by the following series:

$$\chi_{ij}=1+0.2618n_i\sigma_i^3(8-3\sigma_i/\sigma_{ij}) +0.2618n_j\sigma_j^3(8-3\sigma_j/\sigma_{ij})+\cdots \quad (4)$$

where n_i and n_j are the number densities of the i and j species (cm^{-3}); σ_i and σ_j, the collision diameters of the i and j species between like molecules (cm), and σ_{ij} is that between unlike molecules, which may be obtained from the empirical combining law: $\sigma_{ij}=(\sigma_i+\sigma_j)/2$, and hence $\sigma_1=(\sigma_1+\sigma_j)/2\fallingdotseq(\sigma_3+\sigma_j)/2$, $(j=2,3)$. The collision diameters, $\sigma_2=3.996$ Å and $\sigma_3=3.882$ Å, were taken from Ref. 2. They are those determined from the viscosity measurement for the Lennard-Jones model. Since the 1 species is present only as a trace in this investigation, the second term on the right hand of Eq. (4) may be neglected. As the $(D_{1j})^0\rho$ quantity is constant at a constant temperature and is independent

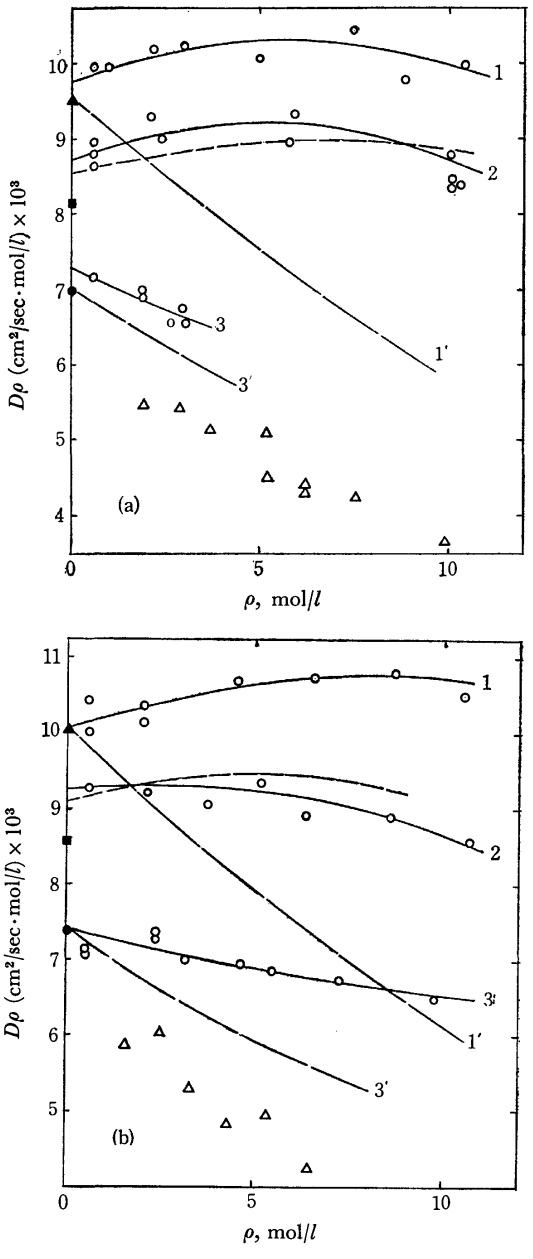

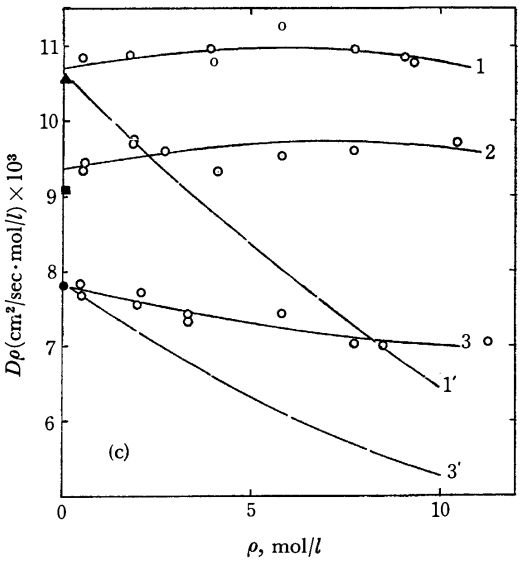

Fig. 2. Variation of $D\rho$ with density.
Temperature, a: 25°C, b: 50°C, c: 75°C
○: Present work, ▲: $D_{13}\rho$ obtained from D_{33} reported by Winn, ●: $D_{12}\rho$ obtained from D_{23} calculated by the empirical formula, ■: $D\rho$ calculated by Eq. (1) for the mixture, Δ: $D_{13}\rho$ reported by Jeffries and Drickamer. Solid lines are the smoothed curves for the experimental values obtained in the present work, 1: $x_3=1.000$, 2: $x_3=0.522$, 3: $x_3=0.000$. Long-dashed lines are the theroretical curves, 1′: $D_{13}\rho$, 3′: $D_{12}\rho$. Dashed lines are the smoothed curves for $D_{13}\rho$ obtained from $D_{33}\rho$ reported by Dawson *et al.*

of the density, the extrapolated values of the $D_{1j}\rho$ to 1 atm were used in place of the $(D_{1j})^0\rho$. As is shown in Fig. 2, the theoretical values of both the $D_{12}\rho$ and the $D_{13}\rho$ decrease with an imcrease in the density and are about 20—26% lower than those obtained in the present work at $\rho=5$ mol/l.

The diffusion coefficient of a trace amount of CTH_3 in methane, D_{13}, measured at high pressures using a

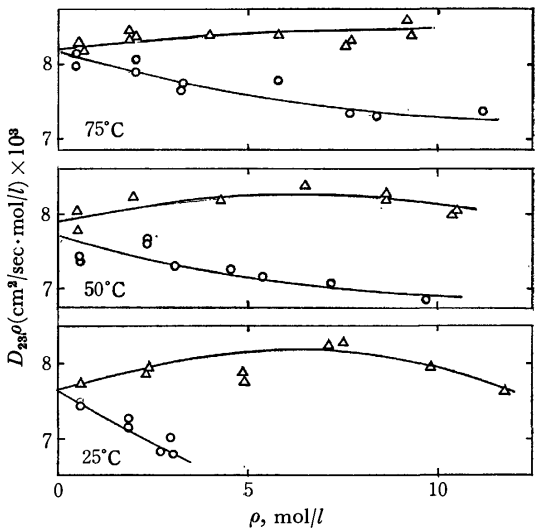

Fig. 3. Comparison of $D_{23}\rho$ (CH_4 trace) with $D_{23}\rho$ (CO_2 trace).
○: $D_{23}\rho$ (CH_4 trace), △: $D_{23}\rho$ (CO_2 trace)

14) S. Chapman and T. G. Cowling, "The Mathematical Theory of Non-uniform Gases," Cambridge Univ. Press, London (1960), p. 292.

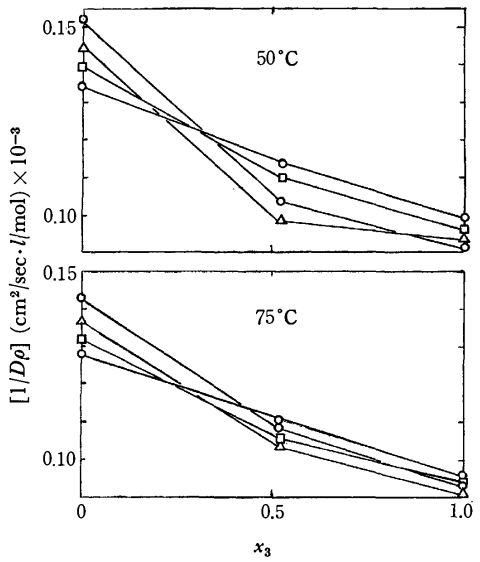

Fig. 4. Variation of $1/D\rho$ with composition.
○: 1 atm, □, △, and ●: 2,5, and 10 mol/l

modified Loschmidt-type diffusion cell was reported by Jeffries and Drickamer.[15] As is shown in Fig. 2, their values of the $D_{13}\rho$ decrease monotonously with an increase in the density and much lower than those obtained in the present work.

15) Q. R. Jeffries and H. G. Drickamer, *J. Chem. Phys.*, **21**, 1358 (1953).

The self-diffusion coefficient of CH_4, as measured by the use of a pulsed NMR spectrometer, were reported by Trappeniers and Oosting[16] and Dawson *et al.*[17] The values of the $D_{13}\rho$ obtained by applying the mass correction to the results of Dawson *et al.* are shown by dashed lines in Fig. 2. These are 10% lower than those obtained in this investigation, but the shapes of the $D\rho$ *vs.* ρ curves are similar. It may be noted that the values obtained by the extrapolation of their curves to 1 atm agree well with those calculated by Eq. (3). The experimental values obtained by Trappeniers and Oosting agree very well with those calculated by Eq. (3); hence, the $D\rho$ is independent of the density.

The data may be cross-plotted to show the composition dependence of the diffusion coefficient at a constant density. If Eq. (5) derived from Eq. (1) is valid, the $1/D\rho$ *vs.* x_3 plots should be linear:

$$1/D\rho = x_2/D_{12}\rho + x_3/D_{13}\rho \qquad (5)$$

Fig. 4 shows that such cross-plots made at 2, 5, and 10 mol/l are concave lines and that Eq. (5) is not valid in this system.

The author wishes to express his deep gratitude to Professor Hiroji Iwasaki for his kind direction and encouragement throughout this work.

16) N. J. Trappeniers and P. H. Oosting, *Phys. Lett.*, **23**, 445 (1966).
17) R. Dawson, F. Khoury, and R. Kobayashi, *A. I. Ch. E. Journal*, **16**, 725 (1970).

Catalytic Properties of BF_3-treated Aluminas. IV. The Effect of BF_3 Adsorption on the Acidic Properties of Aluminum Oxides

Kanjiro MATSUURA, Akira SUZUKI, and Mitsuomi ITOH
Department of Chemical Process Engineering, Hokkaido University, Sapporo
(Received October 19, 1971)

An account was given of the surface acidic properties of a series of BF_3-treated aluminum oxides, ranging in their precalcination temperature up to 1000°C. It was concluded that all aluminum oxides dehydrated over 300°C were converted to solid acids with new strong acid centers of $H_0 \leqq -8.2$ by adsorption with BF_3. This new acid centers would be certainly of the Brönsted type. Their catalytic activities in some carbonium ion type reactions are well correlated with the *n*-butylamine acidity in the presence of Hammett's indicators, and the maximum number of acid centers was observed in catalyst samples precalcined at 450 and 800°C respectively. The present study also suggests that the acid centers developed on the surface of aluminum oxides are somewhat different in nature depending upon their precalcination temperatures. Since there was a good correlation between the amount of the remaining hydroxyl groups and that of the absorbed BF_3, the surface hydroxyl groups, in addition to the aluminum atoms serving as the Lewis centers, which are not fully coordinated, were discussed as the most important factors in the formation of such acid centers.

It is well known that BF_3-treated acidic oxides are effective for catalysis in some hydrocarbon conversion reactions. Some studies of catalysts activated with BF_3 have been published in the literature;[1-5] however, little work has been done to clarify the effect of BF_3 adsorption on the nature of the acid centers responsible for catalytic activity. Recent results reported by Antipina and Vinokurora[5] have indicated that the treatment of aluminum oxide with HF or BF_3 does not greatly increase the strength of the acid centers on the surface, but is accompanied by the formation of a certain number of new, relatively weak centers. Since BF_3 is believed to react with the surface hydroxyl groups, it can be accepted that the activity and stability of activated aluminum oxide depend substantially upon the surface properties of the initial alumina.

Pure aluminum oxide has intrinsic acidic properties and thus has been widely employed as a catalyst or as a catalyst support. It is now well established that the acid center of pure alumina can generally be characterized as a Lewis type. On the other hand, there are very little consideration of the presence or absence of Brönsted acid centers on the surface. When aluminum hydroxide is calcined at various temperatures up to 1000°C, it may be expected that the alumina formed will have a great variety of acidity and activities corresponding to the respective surface properties. For example, Peri[6] has demonstrated that several acidic types of hydroxyl groups exist on the surface of dehydrated alumina; it is considered that such surface properties are strongly affected by BF_3 treatment.

Accordingly, we have attempted to clarify the nature of the acid centers developed by such a treatment, and to find whether these centers are of the Brönsted and/or the Lewis type. In this study, we selected a series of aluminum oxides ranging in precalcination temperature from 130°C to 1000°C as adsorbents and investigated the effect of BF_3 treatment on the acidic properties after modification.

Experimental

Materials. The alumina (A-) used in this work was obtained by the thermal decomposition of bayerite. The aluminum hydroxide was prepared by the hydrolysis of aluminum isopropoxide with water. The product was washed with distilled water, kept standing overnight at 130°C, and finally calcined at various temperatures for 3 hr a stream of dry nitrogen. The boron trifluoride was a commercial product of the Hashimoto Kasei Co. (Osaka), with a purity of 99.5%. All the chemicals, cumene, toluene, *o*-xylene, and benzene, were the reagent-grade commercial products. They were dried over metallic sodium and then distilled. The propylene was used after purification by distillation. The ethylmagnesium bromide used for the determination of the hydroxyl content was prepared by mixing ethyl bromide with a magnesium ribbon in di-*n*-butyl ether at 30°C. The Hammett's and arylmethanol indicators for the determination of the acidity distribution are

Table 1. Hammett and arylmethanol indicators

Indicator	pK	H_2SO_4 Concn (wt%)
Hammett indicators:		
p-Dimethylaminoazobenzene	+3.3	3×10^{-4}
4-Phenylazodiphenylamine	+1.5	2×10^{-2}
Dicinnamalacetone	−3.0	48
Benzalacetophenone	−5.6	71
Anthraquinone	−8.2	90
Arylmethanol indicators:		
4,4′,4″-Trimethyltriphenylmethanol	−4.0	36
Triphenylmethanol	−6.6	50
Diphenylmethaonl	−13.3	77

1) C. J. Plank, U. S. 2428741 (1947).
2) Y. M. Paushkin and Y. U. Lipatov, *Dokl. Akad. Nauk SSSR*, **76**, 547 (1951).
3) a) T. V. Antipina and E. H. Avdonika, *Zh. Fiz. Khim.*, **33**, 192 (1959); b) T. V. Antipina and E. M. Cherednik, *ibid.*, **35**, 836 (1961); c) V. A. Chernov and T. V. Antipina, *Kinet. Katal.*, **4**, 595 (1963).
4) G. L. Herbert and C. B. Linn, U. S. 3114785 (1963).
5) T. V. Antipina and E. B. Vinokurora, *Kinet. Katal.*, **9**, 199 (1968).
6) J. B. Peri, *J. Phys. Chem.*, **69**, 220 (1965).

listed in Table 1, together with the pK_a and pK_r values.

Apparatus and Procedure. The adsorption of BF_3 was carried out at room temperature under atomospheric pressure by exposing the dehydrated aluminum oxides for 5 min or less; then immediate evacuation was done to remove any residual vapors. Differential thermal analysis was carried out under atomospheric pressure. The water loss of alumina with heating was determined gravimetrically on a silica spring balance, as has been reported elsewhere.[7] The X-ray data were obtained using nickel-filtered Cu-$K\alpha$ radiation, a Geiger-counter X-ray spectrometer of the Toshiba Electric Co. The specific surface area (BET) was measured with nitrogen as the adsorbate. The micropore volume was determined by a method proposed by Benesi.[8] The surface hydroxyl content was determined by the technique of Satoh *et al.*[9] The butylamine acidity was determined in the way described by Benesi.[10] All the catalyst sample, screened to 100—200 mesh particles, were evacuated by a high vacuum technique at 300°C for 3 hr before the measurement of their acidity. The catalytic activity for cumene cracking, *o*-xylene isomerization, and toluene disproportionation were studied using an all-glass, fixed-bed-flow reactor system. Each reactant mixture was fed in continuously by means of a gas-syringe drive. The reaction products were analyzed by glpc using a column packed with 5% silicon DC-550. Propylene polymerization was carried out in a closed apparatus, as has been described by Tamele.[11]

Results

Aluminum Oxides as Adsorbents. The characteristics of the various aluminum oxides used in this work are summarized in Table 2. Thermograms of a starting hydroxide are shown in Fig. 1. The main residual water is shown to have a sharp endothermic peak at around 350°C, which is believed to be characteristic of bayerite or gibbsite. The water loss of hydrous alumina at several dehydration temperatures is shown in Fig. 2. It is shown that a rapid decline in the water content occurred between 200 and 400°C, while above 600°C only a little loss of weight was detectable. These results are in good agreement with those of the endothermic heat change shown in Fig. 1.

TABLE 2. SURFACE PROPERTIES OF ALUMINUM OXIDES

Calctn. temp. (°C)	Surf.[a] area (m^2/g)	Pore[b] volume (ml/g)	Av. pore dia (Å)	Hydroxyl content ($OH/g \times 10^{-20}$)	X-Ray diffraction pattern
A-130					bayerite
A-300	256	0.34	27	—	some *eta*
A-400	250	0.39	31	11.4	some *eta*
A-450	238	0.42	34	10.2	essentially *eta*
A-500	233	0.43	37	7.7	essentially *eta*
A-600	213	0.41	39	6.5	*eta*
A-700	183	—	—	5.8	*eta*, some *theta*
A-800	166	0.43	52	4.5	*eta* and *theta*
A-900	124	—	—	2.8	*theta*
A-1000	78	0.30	77	1.8	*theta* and *alpha*

a) by nitrogen adsorption (BET)
b) by a method described by Benesi[9]

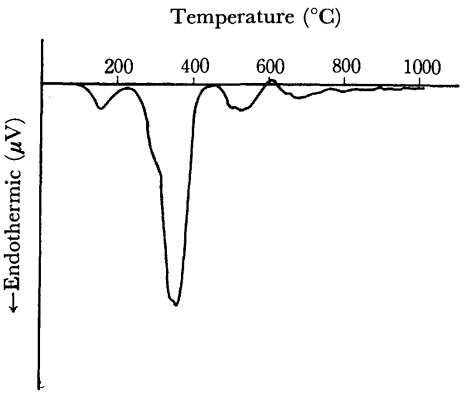

Fig. 1. Differential thermal analysis.
(Heating rate: 10°C/min)

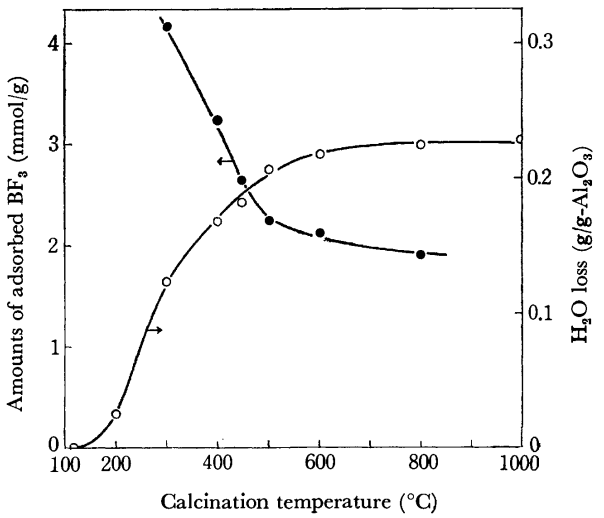

Fig. 2. Water loss with calcination temperature *vs.* amount of adsorbed BF_3 on aluminum oxides.

The specific surface area gradually decreases with the increase in calcination temperature. This diminution is appreciable after the elimination of the residual water shown in the endothermic peaks. The total pore volume of aluminum oxides increases as the heating temperature is raised, and they become simultaneous in pores of 18 to 77 Å. The maximum volume in the micropore is exhibited at around 500°C, indicating that the materials are obviously highly porous at this temperature.

The X-ray diffraction pattern of the original hydrate indicated a well-crystallized bayerite containing a trace of boehmite. As far as was determined by X-ray diffraction, no major phase transformations took place between 300° to 600°C, and the usual transformation to *theta* and *alpha* alumina was found above 600°C. It was indicated that when this material was heated at 400° to 500°C, it became a highly porous solid showing an X-ray pattern characteristic of relatively poorly crystallized *eta* alumina. This is possibly of great interest from the point of view of their catalytic action.

The acidic properties of a series of aluminum oxides

7) D. S. MacIver, H. H. Tobin, and R. T. Barth, *J. Catal.*, **2**, 485 (1963).
8) H. A. Benesi, R. U. Bonnar, and C. F. Lee, *Anal. Chem.*, **27**, 1963 (1955).
9) M. Satoh, T. Kanbayashi, K. Kobayashi, and Y. Shima, *J. Catal.*, **7**, 342 (1967).
10) H. A. Benesi, *J. Phys. Chem.*, **61**, 970 (1957).
11) M. W. Tamele, *Discuss. Faraday Soc.*, **8**, 270 (1950).

Table 3. *n*-Butylamine acidity of aluminum oxides

Catalyst[a)]	Acidity within intervals of pK_a (meq/g)				
	-8.2	-8.2 ≀ -5.6	-5.6 ≀ -3.0	-3.0 ≀ $+1.5$	$+1.5$ ≀ $+3.3$
A(B)-300	0.25	0.06	0.09	00.0	0.01
A(B)-400	0.49	0.04	0.01	0.01	0.07
A(B)-500	0.56	0.01	0.02	0.01	0.03
A(B)-600	0.47	0.01	0.08	0.03	0.05
A(B)-700	0.44	0.03	0.02	0.03	0.03
A(B)-800	0.36	0.05	0.05	0.02	0.01
A(B)-900	0.19	0.02	0.05	0.02	0.03
A(B)-1000	0.06	0.01	0.16	0.00	0.00
A(G)-500	0.37	0.00	0.11	0.01	0.01
A(G)-800	0.06	0.03	0.14	0.00	0.00

a) A(B)=bayerite as a starting material.
A(G)=gibbsite as a starting material.

were determined by *n*-butylamine titration using Hammett's indicators. The concentrations and strengths of the surface acid centers are demonstrated in Table 3. It is shown that some aluminas had a certain number of acid centers (~0.56 meq/g at $H_0 \leq -8.2$). It was also observed that the acidity at any acid strength varied remarkably with the increase in the dehydration temperature, which had its maximum at 500°C. Since these dehydrated aluminum oxides have such different surface properties, the appearance of an interesting surface behavior both for acidity and activity possibly resulted from their modification with BF_3.

Surface Properties of Aluminum Oxides after BF_3 Adsorption. The characteristics of a series of BF_3-treated aluminum oxides are summarized in Table 4. The adsorption of BF_3 was studied on various aluminum oxides, ranging in precalcination temperature from 300 to 1000°C. It was found that the amount of BF_3 adsorbed on the adsorbents dehydrated below 500°C decreases markedly with the increase in preheating temperature. However, the difference in the amount was negligibly small above approximately 600°C. When the results in Table 2 are compared with those in Table 4, it is clear that there is a good correlation between the remaining hydroxyl content and the amount of adsorbed BF_3.

The acidity of the BF_3-treated aluminum oxides was also determined by butylamine titration using two types of indicators, Hammett's and arylmethanol indicators. The distribution of the acid centers at different strengths is shown in Table 5 and Fig. 3. The following conclusions were obtained:

Table 4. Surface properties of BF_3-treated aluminas

Catalyst and precalcination temperature (°C)	Surf. area (m^2/g)	Pore volume (ml/g)	Av. pore dia. (Å)	Amount of adsorbed BF_3 (wt%)	Amount of adsorbed BF_3 (mmol/g)
BA-300	200	0.22	25	21.9	4.1
BA-400	192	0.23	22	17.6	3.2
BA-450	190	0.30	31	15.2	2.6
BA-500	158	0.29	35	12.8	2.2
BA-600	134	0.29	43	12.5	2.1
BA-700	130	—	—	—	—
BA-800	119	0.25	41	11.7	1.9
BA-900	111	—	—	—	—
BA-1000	67	0.17	51	6.0	1.0

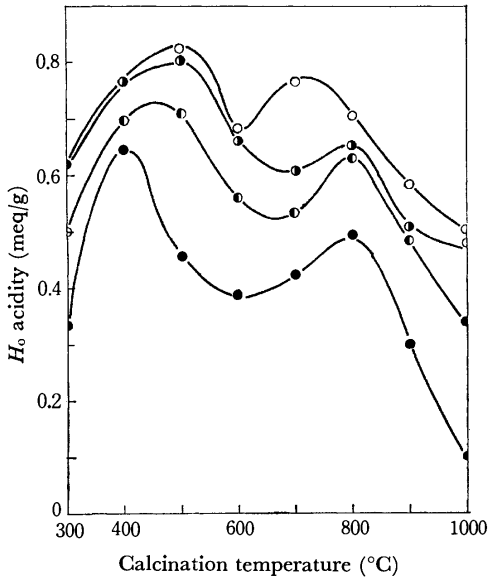

Fig. 3. *n*-Butylamine acidity of BF_3-treated aluminas at various temperatures.
-○-: $pK_a \leq +3.3$, -◑-: $pK_a \leq -3.0$, -◐-: $pK_a \leq -5.6$, -●-: $pK_a \leq -8.2$

Table 5. *n*-Butylamine acidity of BF_3-treated aluminas

Catalyst	Total acidity within intervals of pK (meq/g)							
	pK_a					pK_r		
	-8.2	-8.2 ≀ -5.6	-5.6 ≀ -3.0	-3.0 ≀ $+1.5$	$+1.5$ ≀ $+3.3$	-13.3	-13.3 ≀ -6.6	-6.6 ~ -4.0
BA-300	0.33	0.16	0.12	0.00	0.00	0.41	0.04	0.02
BA-400	0.64	0.05	0.06	0.00	0.01	0.70	0.14	0.02
BA-500	0.45	0.25	0.09	0.01	0.00	0.66	0.11	0.03
BA-600	0.38	0.17	0.11	0.00	0.01	0.61	0.09	0.04
BA-700	0.42	0.12	0.06	0.06	0.10	0.58	0.06	0.07
BA-800	0.49	0.14	0.02	0.05	0.00	0.61	0.07	0.03
BA-900	0.30	0.18	0.02	0.01	0.07	0.53	0.01	0.01
BA-1000	0.10	0.24	0.14	0.00	0.02	0.25	0.05	0.01

a) BF_3-treated aluminas had an appreciable number of acid centers at a strength of $H_0 \leq -8.2$ ($\sim$0.64 meq/g), but none or little acidity was observed in relatively weak centers ($H_0 > -3.0$). This does not coincide with the results of Antipina and Vinokurora.[5]

b) As the precalcination temperature is raised from 300 to 1000°C, there is a remarkable difference in overall acidity; namely, the number of strong acid centers at $H_0 \leq -8.2$ reaches a maximum in the catalysts dehydrated at about 400 and 800°C. The catalyst obtained at 600°C indicated a considerably low acid number as is shown in Fig. 3.

c) All of the aluminum oxides, after treatment with BF_3, convert some arylmethanol indicators to the corresponding acid forms. On the other hand, initial pure aluminas do not change any H_r indicators to the acid form. This is evidently due to the difference in the nature of the surface acid centers.

As will be shown in the later part of this paper, such differences in acid number among several aluminum oxides are related to the results on the catalytic activity of various carbonium ion type reactions. The results for acidities shown in Table 5 enable us to differentiate the H_0 from the H_r acidity. BA-300 to BA-500 in Table 5 have large number of acid centers in both indicators. BA-800 to BA-1000, on the other hand, have relatively small H_r acidities but, more overall acidity exists.

TABLE 6. ACTIVITY FOR VARIOUS MODEL REACTIONS

Catalyst	Cumene[a] cracking 365°C (mol%)	*o*-Xylene[a] isomerzn. 350°C (mol%)	Toluene[b] disproptn. 500°C (mol%)	Propylene[c] polymerzn. 200°C *k*
BA-300	56.0	41.0	6.6	4.57
BA-400	77.3	77.0	13.5	7.13
BA-450	—	—	—	8.44
BA-500	74.9	67.0	12.9	6.54
BA-600	65.5	58.0	11.7	4.38
BA-700	76.1	57.1	—	5.38
BA-800	83.5	69.0	13.6	8.15
BA-1000	73.2	37.0	9.4	2.04
A-600	0.0	0.0	0.0	0.00
SA-500	85.8	49.5	18.5	—
SPA-350	19.6	—	0.0	—

a) SV=2.16 hr^{-1}, b) SV=0.4 hr^{-1}, c) P_0=360 mmHg; k= $min^{-1} \times g^{-1}$

Catalytic Activity. The comparative catalytic activities for some acid-catalyzed reactions are examined. The results are shown in Table 6. It was generally concluded that all of the catalytic activities of BF_3-treated alumina were much higher than those of non-treated alumina; the latter indicated no activity for any conversion reactions examined under the present experimental conditions. The BF_3-treated samples of BA-450 and BA-800 indicated a maximum conversion for all reactions, and BA-600 showed a quite low conversion. This activity profile shows a good fit the acid-site distribution shown in Fig. 3. The activity for *o*-xylene isomerization in Table 6 is plotted against the number of relatively strong acid centers. The plots with $H_0 \leq -5.6$ lie on a comparatively good straight line, as is shown in Fig. 4. Therefore, it seems likely that the acid centers having a strength of $H_0 \leq -5.6$ are responsible for the reactions studied in this paper.

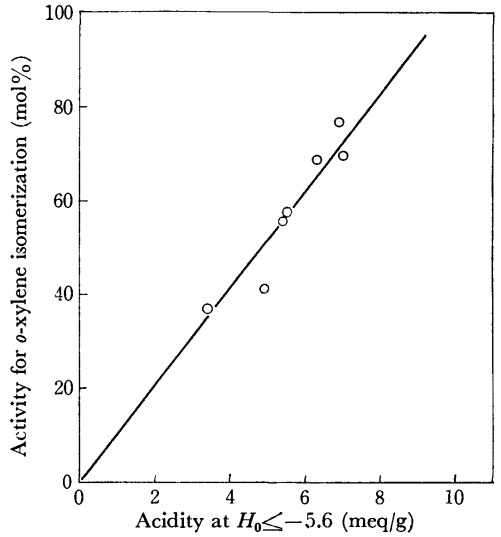

Fig. 4. Acidity at $H_0 \leq -5.6$ *vs.* activity for *o*-xylene isomerization at 350°C.

Discussion

Mainly in view of the acidic behavior of aluminum oxides before and after BF_3-treatment, the difference in surface properties due to the variation of their dehydration temperatures was studied, and it was demonstrated that the surface acidity of the activated catalysts depended, at least in part, on the initial properties, such as the hydroxyl content and the crystallinity.

Table 6 shows the catalytic activities with some other solid acids. It was found that the BF_3-treated aluminas, especially those precalcinated at around 450 and 800°C, indicated nearly the same high activity as the silica-alumina catalyst. However, non-treated pure alumina showed no activity for any of the reactions in this work. The catalytic action of BF_3-treated aluminas is assumed to be due to the formation of new Brönsted centers. As may be seen in Tables 2 and 4, it has already been described that the concentration of the surface hydroxyl groups of aluminum oxides decreases gradually as the dehydration temperature is raised to 1000°C, and there is a proportional relationship between the hydroxyl content and the amount of BF_3 adsorbed. Since all of the BF_3-treated aluminum oxides converted the arylmethanol indicators to their respective acid forms, it has generally been suggested that the appearance of Brönsted acid centers in the case of alumina activated with BF_3 is associated with the hydroxyl groups of the initial alumina. Accordingly, it may be considered that the hydroxyl concentration has an effective influence upon the catalytic action after the treatment with BF_3. According to Rhee and Basila,[12] hydrogen-bonding interactions similar to those in the BF_3-aliphatic alcohol complexes[13] may occur on the surface

12) K. H. Rhee and M. R. Basila, *J. Catal.*, **10**, 243 (1968).
13) K. Nakamoto and M. Margoshes, *J. Phys. Chem.*, **77**, 6480 (1955).

of alumina. A similar interaction between adjacent surface hydroxyl groups, which is promoted by the BF_3 complex formation, seems to be strongly affected at higher concentrations. Thus, it is possible that the most effective sites for all reactions in the present work result from the coordination of BF_3 with the remaining hydroxyl group, which varies gradually in its concentration and acidic property with the heating temperature of the initial aluminum oxide.

On the other hand, other higher conversions were observed with the catalyst samples of BA-800 or BA-900, although relatively small hydroxyl contents were found at such higher precalcination temperatures (Table 2). Though either of the O atoms in the Al-O-Al, Al-O^- or surface OH group on the dehydrated aluminas was regarded as the adsorption site of BF_3, it was demonstrated that a greater part of the BF_3 adsorbed on the surface OH group to form Brönsted acid centers. However, it can also be assumed from the results shown in Table 5 that BF_3 generally coordinates with the O atoms in Al-O^- or Al-O-Al to strengthen the Lewis acidity on the surface, especially on the alumina dehydrated over 700°C. It is believed that Brönsted centers on alumina, if present at all, are of a very low acid strength. The Lewis acid centers of the dehydrated alumina can be best explained by not-fully-coordinated aluminum atoms, and their formation during calcination can be pictured by the model suggested by Hindin and Weller:[14]

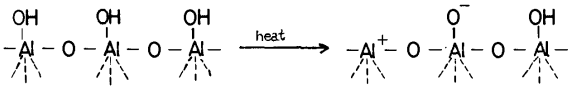

As to the effect of the surface properties of alumina, such factors as the number of Lewis acid centers, besides the concentration and acidic behavior of each remaining surface hydroxyl group, must be causes of the difference in the catalytic activities with the aluminum oxides promoted by BF_3 complex formation, as is shown in Table 6.

As has been mentioned above, in the effective sites of a series of BF_3-treated aluminum oxides there are a considerable number of Brönsted centers and a small number of Lewis centers, and these acid centers are responsible for the acid-catalyzed reactions in this work. These catalytic activities correspond well to the *n*-butylamine acidity in the presence of a Hammett indicator rather than an arylmethanol indicator. Although some arylmethanol indicators are believed to be converted to their respective acid forms on Brönsted acid centers, as has been discussed by Hirschler,[15] it is an open question whether their butylamine titers are equal to the number of Brönsted centers; the Lewis center, if present, should also be taken into consideration, as should other adsorption sites of the amine. It is also demonstrated that the activity and product selectivity in the isomerization of 1-butene differ considerably depending upon their respective precalcination temperatures. This is largely due to the difference in the nature of active centers, as was described in a recent work.[16]

14) S.G. Hindin and S.W. Weller, *J. Phys. Chem.*, **60**, 1506 (1956).
15) A.E. Hirschler, *J. Catal.*, **2**, 428 (1963).
16) K. Matsuura, A. Suzuki, and M. Itoh, *ibid.*, in press.

BULLETIN OF THE CHEMICAL SOCIETY OF JAPAN, VOL. 45, 2083—2087(1972)

Ultrasonic Absorption in Solutions of Propionic Acid

Nobuhide TATSUMOTO, Takayuki SANO, Norihiko MATSUNAGA,
Eiso TOCHIGI, and Tatsuya YASUNAGA

Department of Chemistry, Faculty of Science, Hiroshima University, Higashisenda-machi, Hiroshima

(Received October 20, 1971)

The effect of a solvent on the ultrasonic relaxation of propionic acid has been studied. The relaxation frequency is affected a little in hydrophilic solvents, while in non-hydrophilic solvents it shifts to a higher-frequency side. The activation enthalpy in a reaction from open to cyclic dimers decreases with dilution in the non-hydrophilic solvents; the magnitude of the change in the hydrophilic solvents is less than in the non-hydrophilic solvents. This means that the open dimer is destabilized by non-hydrophilic solvents. The sequence of the magnitude of the solvent effect on the relaxation frequency is consistent not with that estimated from the magnitude of the dielectric constant of the solvent, but with that estimated from the magnitude of the non-hydrophilic strength of the solvent. The stability of an open dimer in a hydrophilic or polar solvent is attributed to the interaction of the free OH group on the open dimer with the solvent.

The present authors have previously reported that the mechanism of ultrasonic relaxation in solutions of propionic acid[1] and other carboxylic acids[2] is associated with the perturbation of the equilibrium between the cyclic and open dimers formed by intermolecular hydrogen bonding between carboxyl groups. It was reported there[1] that the relaxation frequency increased with the dilution for various solvents. A similar result has also been observed for acetic acid

1) N. Tatsumoto, *J. Chem. Phys.*, **47**, 4561 (1967).
2) T. Sano, N. Tatsumoto, T. Niwa, and T. Yasunaga, This Bulletin, in press.

by Piercy and Lamb.[3] One purpose of this paper is to study in more detail the effect of solvents on the relaxation in solutions of propionic acid. The solvents used are dioxane, methyl propionate, benzene, chlorobenzene, cyclohexane, and xylene.

Experimental

The measurements of ultrasonic absorption in various solutions were made over the frequency range from 2.5 to 95 MHz, at various temperatures from 15 to 35°C, by the pulse method. The apparatus and experimental techniques have been fully described in a previous paper.[1] The velocity of sound at 1.92 MHz was measured with a sing-around system produced by Cho Onpa Kogyo Kaisha (Tachikawa, Tokyo, Japan), model UVM-2-1, and that at 3.00 MHz, with an ultrasonic interferometer. The experimental procedures have also been described in previous papers.[4] The dielectric constant was measured with the bridge method at 200 kHz. The chemical shift of the acid proton of propionic acid in NMR was measured at 34°C in various solvents, where tetramethylsilane was used as the reference. The chemicals used were all guaranteed reagents and were used without further purification except in the case of propionic acid. Propionic acid was purified by fractional distillation under reduced pressure.

Results and Discussion

As is shown in Fig. 1, the ultrasonic absorption in solutions of propionic acid in various solvents can be represented by a single relaxation equation:

$$\alpha/f^2 = \frac{A}{1+(f/f_m)^2} + B \qquad (1)$$

where α is the ultrasonic absorption coefficient; f, the frequency of sound; f_m, the relaxation frequency, and

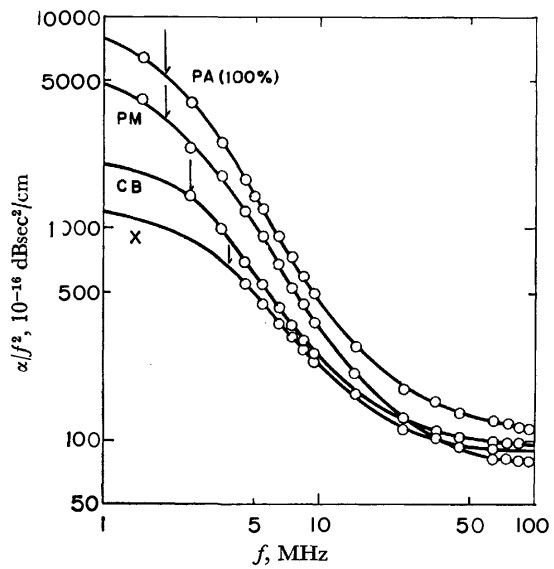

Fig. 1a. Ultrasonic absorption spectra in various solvents at 20°C: PA (100%), 100% propionic acid; PM, in methyl propionate; CB, 10M in chlorobenzene; X, 10M in xylene.

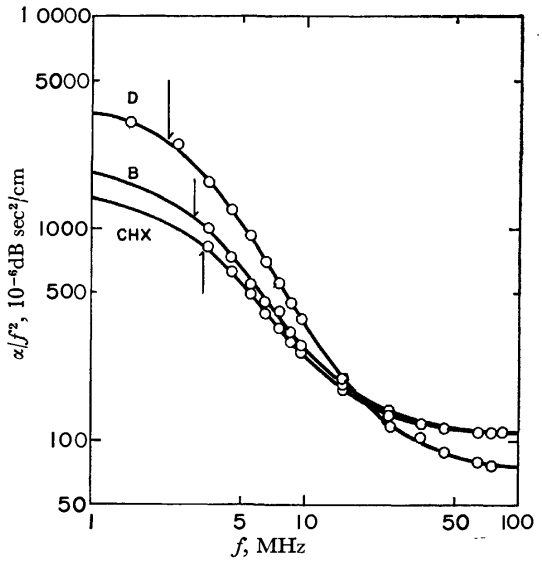

Fig. 1b. Ultrasonic absorption spectra at 20°C: D, 10M in dioxane; B, 10M in benzene; CHX, 10M in cyclohexane.

A, and B, the chemical and classical absorptions respectively. The values of f_m calculated from the experimental data are listed in the table. In Fig. 2, the relaxation frequencies are plotted against the concentrations. As can be seen in Fig. 2, the relaxation frequency, f_m, does not change with the concentration in methyl propionate, but it decreases in dioxane, chlorobenzene, benzene, cyclohexane, and xylene. The magnitude of its change with the concentration increases in the order noted. Since the relaxation frequency changes monotonously with the concentration, it is highly probable that the relaxation mechanism in those solutions is identical with that in liquid propionic acid itself. The relaxation mechanism may, therefore, be associated with an equilibrium:

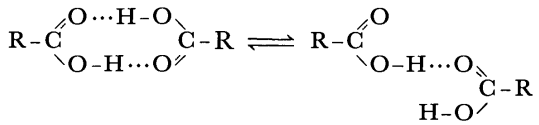

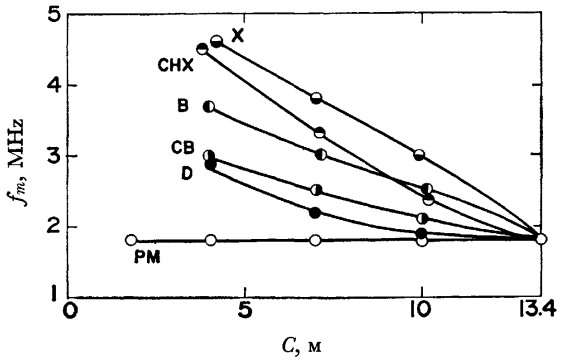

Fig. 2. Changes in relaxation frequencies at 20°C with concentration of propionic acid in various solvents:
○ PM, methyl propionate;
● D, dioxane;
◑ CB, chlorobenzene;
◐ B, benzene;
◓ CHX, cyclohexane;
◒ X, xylene.

3) J. E. Piercy and J. Lamb, *Trans. Faraday Soc.*, **52**, 930 (1956).
4) T. Yasunaga, N. Tatsumoto, and M. Miura, This Bulletin, **37**, 1655 (1964). T. Yasunaga, M. Tanoura, and M. Miura, *J. Chem. Phys.*, **43**, 3512 (1965).

TABLE. THE RELAXATION FREQUENCY AND KINETIC VALUES FOR THE REACTION BETWEEN CYCLIC AND OPEN DIMERS OF PROPIONIC ACID

t (°C)	f_m (MHz)	K (10^{-2})	H (kcal/mol)	k_f (10^5 sec^{-1})	k_b (10^7 sec^{-1})	H_f^* (kcal/mol)	H_b^* (kcal/mol)
	100% propionic acid						
15	—	—		—	—		
20	1.8	2.5		2.6	1.06		
25	2.2	2.8	4.3	3.6	1.29	~11	6.8
30	2.8	3.2		5.2	1.62		
35	3.8	3.6		7.0	1.96		
	10.0M in methyl propionate						
15	—	—		—	—		
20	1.8	2.7		2.9	1.06		
25	2.2	3.1	4.4	4.0	1.29	~11	6.8
30	2.8	3.5		5.7	1.63		
35	3.8	3.9		7.7	1.97		
	7.6M in methyl propionate						
15	—	—		—	—		
20	1.8	2.8		3.0	1.07		
25	2.2	3.1	4.3	4.0	1.30	~11	6.8
30	2.8	3.5		5.8	1.65		
35	3.8	3.9		7.7	1.99		
	4.1M in methyl propionate						
15	—	—		—	—		
20	1.8	3.7		4.0	1.07		
25	2.2	4.2	3.7	5.5	1.31	~11	6.8
30	2.8	4.6		7.6	1.65		
35	3.8	5.1		10.2	1.99		
	10.0M in dioxane						
15	—	—		—	—		
20	1.9	3.3		3.6	1.08		
25	2.4	3.7	4.1	5.1	1.37	~11	6.8
30	2.9	4.2		7.1	1.68		
35	3.6	4.6		9.4	2.03		
	7.2M in dioxane						
15	—	—		—	—		
20	2.2	3.8		4.9	1.29		
25	2.7	4.3	3.4	6.8	1.59	~11	6.8
30	3.3	4.7		9.1	1.94		
35	4.1	5.2		12.4	2.38		
	4.1M in dioxane						
15	—	—		—	—		
20	2.9	2.9		5.0	1.72		
25	3.6	3.2	3.7	7.0	2.19	~11	6.6
30	4.5	3.6		9.6	2.68		
35	5.5	4.0		13.0	3.25		
	10.0M in chlorobenzene						
15	1.7	1.0		1.0	1.04		
20	2.1	1.2		1.5	1.28		
25	2.6	1.4	5.1	2.2	1.57	~12	6.6
30	3.2	1.6		3.1	1.92		
35	3.9	1.8		4.2	2.33		
	7.0M in chlorobenzene						
15	2.0	0.52		0.64	1.24		
20	2.5	0.62		0.96	1.54		
25	3.0	0.73	5.8	1.3	1.85	~12	6.5
30	3.7	0.86		2.0	2.27		
35	4.5	1.0		2.8	2.75		
	4.0M in chlorobenzene						
15	2.5	0.30		0.47	1.56		
20	3.0	0.36		0.67	1.87		
25	3.7	0.43	5.8	0.99	2.30	~12	5.8
30	4.3	0.51		1.36	2.67		
35	5.2	0.58		1.87	3.23		
	10.1M in benzene						
15	2.0	1.1		1.3	1.22		
20	2.5	1.3		2.0	1.52		
25	3.0	1.5	4.8	2.7	1.81	~11	6.2
30	3.7	1.7		3.8	2.23		
35	4.4	1.9		5.0	2.64		
	7.1M in benzene						
15	2.5	0.48		0.74	1.55		
20	3.0	0.57		1.1	1.85		
25	3.5	0.67	5.8	1.4	2.16	~11	5.4
30	4.3	0.79		2.1	2.64		
35	5.0	0.92		2.8	3.06		
	4.1M in benzene						
15	3.1	0.30		0.58	1.93		
20	3.7	0.35		0.81	2.31		
25	4.3	0.42	5.7	1.1	2.68	~11	5.1
30	5.0	0.48		1.5	3.11		
35	5.9	0.56		2.1	3.66		
	10.1M in cyclohexane						
15	2.0	1.1		1.3	1.22		
20	2.4	1.2		1.8	1.46		
25	3.0	1.4	4.7	2.5	1.82	~11	5.4
30	3.6	1.6		3.5	2.17		
35	4.4	1.8		4.8	2.64		
	7.0M in cyclohexane						
15	2.7	0.55		0.92	1.67		
20	3.3	0.64		1.3	2.04		
25	4.0	0.73	4.7	1.8	2.47	~10	5.5
30	4.7	0.83		2.4	2.90		
35	5.5	0.94		3.2	3.39		
	3.9M in cyclohexane						
15	3.8	0.22		0.52	2.37		
20	4.5	0.26		0.73	2.81		
25	5.0	0.30	5.7	0.94	3.12	~10	4.1
30	5.7	0.36		1.3	3.55		
35	6.5	0.41		1.7	4.05		
	9.9M in xylene						
15	2.5	0.58		0.87	1.54		
20	3.0	0.68		1.3	1.84		
25	3.5	0.80	5.7	1.7	2.14	~11	5.4
30	4.2	0.94		2.4	2.56		
35	5.0	1.1		3.3	3.03		
	7.0M in xylene						
15	3.3	0.41		0.84	2.05		
20	3.8	0.48		1.1	2.36		
25	4.2	0.57	5.5	1.5	2.60	~9	3.9
30	4.9	0.66		2.0	3.03		
35	5.5	0.77		2.6	3.39		
	4.2M in xylene						
15	4.2	0.29		0.76	2.62		
20	4.6	0.34		0.98	2.87		
25	5.1	0.40	5.5	1.3	3.18	~8	2.5
30	5.5	0.46		1.6	3.42		
35	6.0	0.54		2.0	3.73		

The relaxation time, τ, in this reaction is represented by this equation:

$$\tau^{-1}=2\pi f_{inf}\ (C_V^{\infty}/C_V^0)=k_f+k_b\simeq 2\pi f_m \qquad (2)$$

where f_{inf} is the frequency of the inflection point in the curve of the dispersion of the sound velocity; C_V^0, the heat capacity at a constant volume and at zero frequency; C_V^{∞}, the heat capacity at an infinite frequency, and k_f and k_b, the forward and backward rate constants respectively.

When the reaction in this solution is principally one involving enthalpy rather than volume change, the temperature change in the heat capacity resulting from the chemical reaction at a constant pressure, C_p^r, is expressed as:

$$C_p^r=\frac{H^2}{RT^2}\cdot\frac{K}{(1+K)^2} \qquad (3)$$

$$K=k_f/k_b \qquad (4)$$

The equilibrium constants, K_1 and K_2, at the temperatures of T_1 and T_2 respectively are represented as:

$$K_1/K_2=exp\left\{\frac{H}{R}\left(\frac{1}{T_2}-\frac{1}{T_1}\right)\right\} \qquad (5)$$

where H is the enthalpy of reaction. Equations (3)—(5) are used to calculate H and K from the change in C_p^r with the temperature ascertained by using experimental data for the velocity of sound, density, thermal expansion coefficient, and heat capacity at a constant pressure and zero frequency, C_p^0. The C_p^0 values for the solutions at various concentrations are determined by the interpolation using those values found in the literature and our experimental data for the solute and solvents.[1,5] The reaction rate constants, k_f and k_b, are calculated by means of Eq. (2). As can be seen in the table, k_b is much greater than k_f, and the tendencies of the changes in k_b with the concentration are similar to those in f_m, as can be seen in Fig. 3. The enthalpy of activation is given by the temperature dependence of the rate constant:

$$k/T=C\exp(-H^*/RT)\exp(S^*/R) \qquad (6)$$

where C is a constant and where H^* and S^* are the enthalpy and the entropy of activation respectively. As can be seen in Figs. 2, 3, and 5, f_m and k_b increase with the concentration, while H_b^* decreases with it. This shows that H_b^* is one of the factors changing f_m and k_b. The magnitude of the change in f_m with the concentration stands in the order of the non-hydrophilic strength rather than in that of the dielectric constants of the solvents. This means that the open dimer is stabilized by the hydrophilic solvent; this increase in the stability is probably to be ascribed to the interaction of hydrophilic groups in the solvent with the free OH groups in the open dimer. In xylene, the change in f_m with the concentration is greater than that in other non-hydrophilic and non-polar solvents, benzene and cyclohexane. This seems to be attributable to the interaction of hydrophobic groups in propionic acid with two methyl groups in the benzene ring.

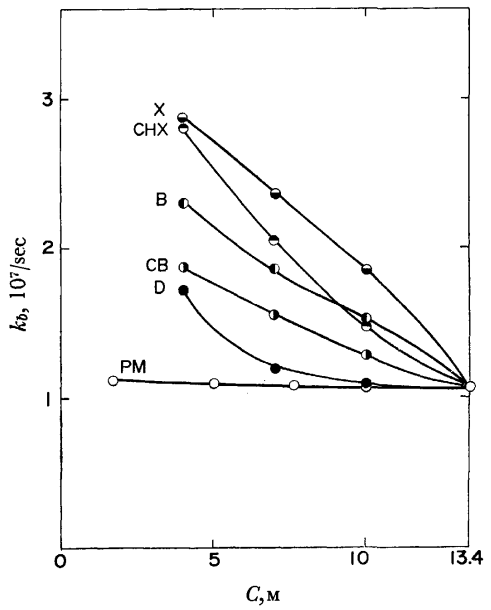

Fig. 3. Changes in backward reaction rates at 20°C with concentration of propionic acid in various solvents:
○ PM, methyl propionate;
● D, dioxane;
◑ CB, chlorobenzene;
◐ B, benzene;
◓ CHX, cyclohexane;
◒ X, xylene.

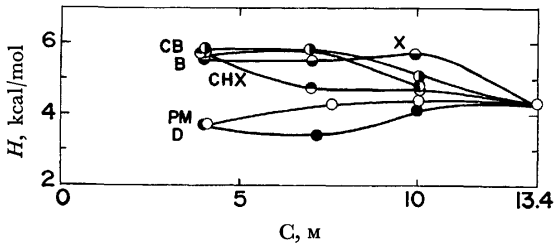

Fig. 4. Changes in reaction enthalpies with concentration of propionic acid in various solvents:
○ PM, methyl propionate; ● D, dioxane; ◑ CB, chlorobenzene; ◐ B, benzene; ◓ CHX, cyclohexane; ◒ X, xylene.

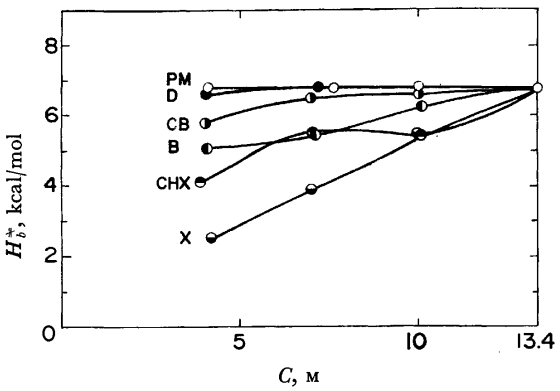

Fig. 5. Changes in activation enthalpies for backward reaction with concentration of propionic acid in various solvents
○ PM, methyl propionate; ● D, dioxane; ◑ CB, chlorobenzene; ◐ B, benzene; ◓ CHX, cyclohexane; ◒ X, xylene.

5) H. H. Landolt and R. Börnstein, Physikalische Chemische Tabellen (Springer-Verlag, Berlin, 1931) part 2, p. 1203. International Critical Tables, **5**, 108.

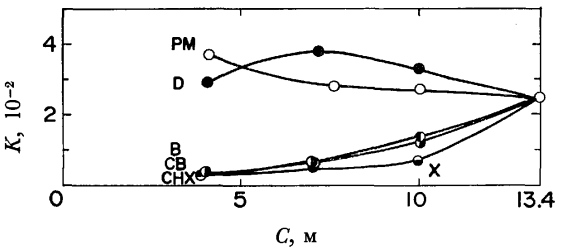

Fig. 6. Changes in equilibrium constants at 20°C with concentration of propionic acid in various solvents:
○ PM, methyl propionate; ● D, dioxane; ◑ CB, chlorobenzene; ◐ B, benzene; ◓ CHX, cyclohexane; ◒ X, xylene.

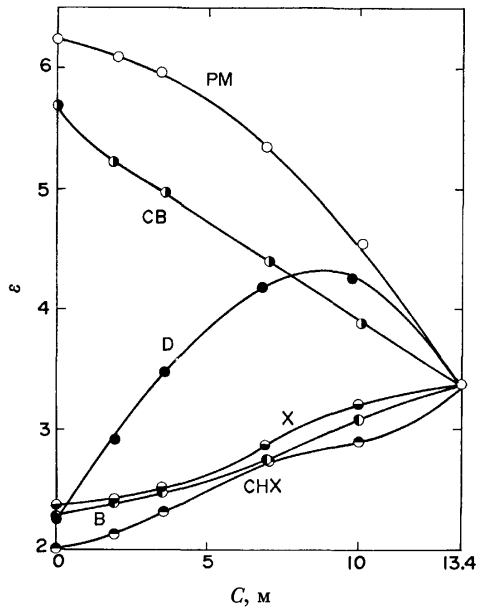

Fig. 7. Changes in dielectric constants at 20°C with concentration of propionic acid in various solvents:
○ PM, methyl propionate; ● D, dioxane; ◑ CB, chlorobenzene; ◐ B, benzene; ◓ CHX, cyclohexane; ◒ X, xylene.

Since the accuracy in H_f^* is rather poor, the change in it with the concentration will not be fully discussed here.

The energy and equilibrium constant of the reaction are listed in the table, while the changes in H and K with the concentration are shown in Figs.4 and 6. With dilution, the enthalpy of reaction, H, decreases in dioxane and methyl propionate and increases in the other solvents. From the changes in H and K with the concentration, it can be concluded that H can be regarded as a measure of the destabilization of the open dimer and K, as a measure of the stabilization. Figure 7 shows the changes in the dielectric constant with the concentration. As can be seen in the figure, they are concavo or complex curves, deviating little from the corresponding ideal straight line, for the benzene, cyclohexane, xylene, and chlorobenzene solutions, and clearly convex curves for the dioxane and methyl propionate solutions. The changes in the dielectric constants of hydrophilic solvents with the concentration, therefore, seem to be different from those of the other solvents. This is probably due to the fact that the open dimer, the dipole moment of which is greater than that of the cyclic dimer, is more abundant in the hydrophilic solvents than in the other solvents, as may be found from the changes in H and K with the concentration, as shown in Figs. 5 and 6. This conclusion is also confirmed by the NMR spectra. As can be seen in Fig. 8, the absorption of NMR shifts with dilution to the side of a higher magnetic field in the hydrophilic solvents and to the lower-side field in the non-hydrophilic solvents.

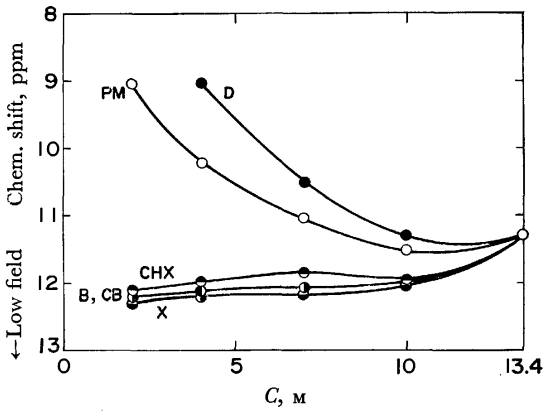

Fig. 8. Chemical shift of carboxylic acid proton in propionic acid in various solvents:
○ PM, methyl propionate; ● D, dioxane; ◑ CB, chlorobenzene; ◐ B, benzene; ◓ CHX, cyclohexane; ◒ X, xylene.

As was stated above, H increases with dilution in the non-hydrophilic solvent. This shows that the solvent effect on the open dimer decreases, until finally the value of H reaches that of the standard energy of the breakage of one hydrogen bond. The open dimer does not exist in an extremely dilute solution because of the decreases in H_b^* and K with dilution. In an extremely dilute solution, the equilibrium between the dimer and the monomer is similar to that in the gas state of propionic acid.[6] Further studies are in progress in a dilute solution of propionic acid; they will be reported in due course.

6) R. C. Herman and R. Hofstadter, *J. Chem. Phys.*, **7**, 460 (1939).

Ion-Solvent Interaction of Tetraalkylammonium Ions in Solvents of High Dielectric Constant. II. Conductance and Walden Product of Tetraalkylammonium Ions in *N*-Methylformamide and *N*-Methylpropionamide at Different Temperatures

Raj Deo SINGH and Ram GOPAL

Department of Chemistry, Lucknow University, Lucknow, India

(Received January 25, 1971)

Ion-solvent interaction of the tetraalkylammonium ions (R_4N^+) in *N*-methylformamide and *N*-methylpropionamide has been investigated from the electrical conductance point of view. It appears that the R_4N^+ ions act as net structure breakers in these solvents as in *N*-methylacetamide. The appreciable negative deviation of the experimental slope of the Λ *vs.* $\sqrt{c}$ curves from the theoretical slope suggests some kind of obstruction to the movement of the R_4N^+ ions, probably due to their unwieldy size or to some kind of cation-anion association, although the usual kind of association is ruled out in view of the high dielectric constant of these solvents. The cation-anion interaction may be the penetration of the cations by the anions which has been suggested as a possible reason for the negative slope in the apparent molal volume *vs.* $\sqrt{c}$ curves, obtained at higher concentrations, to which apparent molal volume measurements usually have to be confined on account of difficulties in accurate density measurements at low concentrations. The smaller alkali metal ions appear to be more solvated than the R_4N^+ ions, so much so that the λ_0^+-values of Na^+ and K^+ ions are lower than the corresponding values of the Me_4N^+ and Et_4N^+ ions.

Earlier studies[1,2] on the conductance of the tetraalkylammonium ions (R_4N^+) in *N*-methylacetamide (NMA) suggest that these ions are net structure breakers in this solvent. It seems desirable to extend the study to other similar solvents, such as *N*-methylformamide (NMF), *N*-methylpropionamide (NMP) which have high dielectric constant and strong hydrogen bonding. The study should give us a more general idea about the behaviour of these ions in highly polar nonaqueous solvents of high dielectric constant and strong hydrogen bonding. The study should give us a more general idea about the behaviour of these ions in highly polar nonaqueous solvents of high dielectric constant. The present communication deals with the results on the study of conductance of some R_4NI salts ($R=CH_3-$ to $R=C_7H_{15}-$) in NMF and NMP.

Experimental

R_4NI salts, obtained from M/S Distillation Products Industries, U.S.A., were purified by fractional crystallisation from suitable solvents or their mixtures.

Solvents (NMF and NMP) were purified by repeated drying over freshly ignited quicklime and vacuum distillation as for NMA. The conductivity of the samples of the solvents thus obtained was around 10^{-6} mho. Solvents were stored in dark amber-coloured bottles in a dry nitrogen box and were used, as far as possible, the day after distillation. While NMP appeared to be stable, NMF was found to be slightly unstable. Solvent correction was applied in determining the conductances of solutions. The rest of the experimental procedure and the degree of reliability of the apparatus were the same as those given in the previous communication on NMA[1].

Results and Discussion

The equivalent conductance Λ was plotted against Λ *vs.* $\sqrt{c}$ curves were found to be almost straight lines for all the R_4NI salts in NMF and NMP, within the concentration and temperature ranges studied. The Λ *vs.* $\sqrt{c}$ curves for different salts are given in Figs. 1 and 2 at one temperature only (25°C in NMF and 40°C in NMP); the curves at other temperatures are similar and hence have been omitted. Extrapolation of Λ *vs.* $\sqrt{c}$ curves to infinite dilution leads to Λ_0-values given in Tables 1 and 2. From these Λ_0-values, the ionic conductances, λ_0^+, of the R_4N^+ ions at different temperatures, were obtained, using the appropriate transport number data given in literature;[3,4] these λ_0^+-values are given in Tables 1 and 2.

The applicability of the Debye-Hückel-Onsager conductance equation to solutions under study was examined.

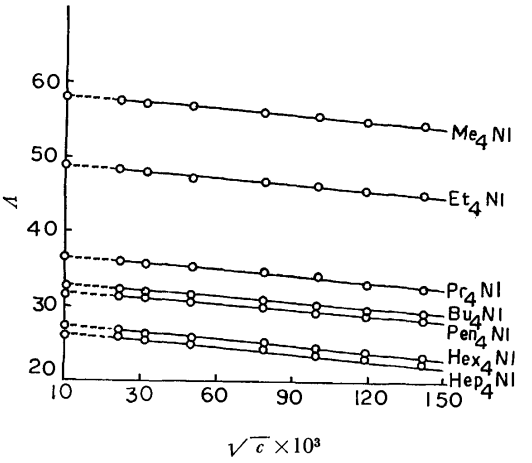

Fig. 1. Λ *vs.* $\sqrt{c}$ curves for R_4NI salts in NMF at 25°C.

1) R. D. Singh, P. P. Rastogi, and R. Gopal, *Can. J. Chem.*, **46**, 3525 (1968).

2) C. M. French and K. H. Glover, *Trans. Faraday Soc.*, **51**, 1428 (1955).

3) R. Gopal and O. N. Bhatnagar, *J. Phys. Chem.* **70**, 3007 (1966).

4) R. Gopal and O. N. Bhatnagar, *ibid.*, **70**, 4070 (1966).

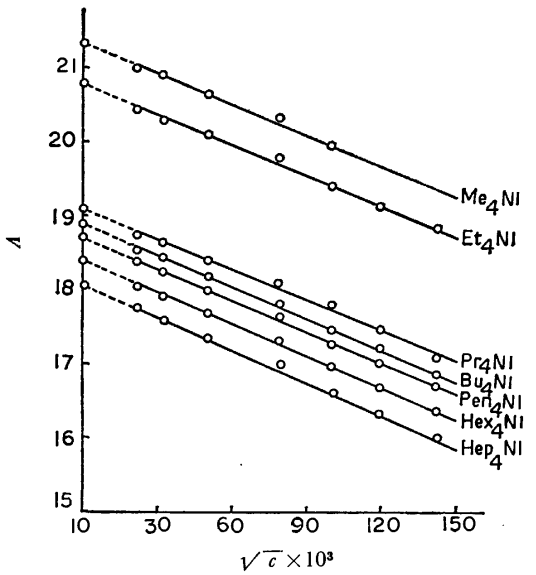

Fig. 2. Λ *vs.* $\sqrt{c}$ curves for R_4NI salts in NMP at 40°C.

Table 1. Limiting equivalent conductance of R_4NI salts and R_4N^+ ions at different temperatures in NMF

R_4NI salt and R_4N^+ ion	Limiting equivalent conductances at				
	15°C	20°C	25°C	30°C	35°C
Me_4NI	50.10	54.12	58.22	61.72	66.41
Me_4N^+	30.90	33.13	35.46	37.15	40.06
Et_4NI	42.32	45.10	48.95	51.55	55.14
Et_4N^+	23.12	24.11	26.19	26.98	28.79
Pr_4NI	31.81	34.25	36.70	39.18	42.10
Pr_4N^+	12.61	13.26	13.94	14.61	15.75
Bu_4NI	28.35	30.90	33.06	35.29	37.68
Bu_4N^+	9.15	9.91	10.30	10.72	11.33
Pen_4NI	27.74	29.75	32.29	34.55	36.70
Pen_4N^+	8.54	9.76	9.53	9.98	10.35
Hex_4NI	23.47	25.35	27.30	29.20	31.10
Hex_4N^+	4.27	4.36	4.54	4.63	4.75
Hep_4NI	22.97	24.84	26.71	28.60	30.61
Hep_4N^+	3.77	3.85	3.95	4.03	4.26

From Λ_0-values and other appropriate data on dielectric constant[5,6] and on viscosity η_0 (determined in this laboratary[7]), the theoretical slopes S of the Λ *vs.* $\sqrt{c}$ curves have been obtained and compared with the experimental slopes S_E in Table 3, in which the data for solutions in NMA have also been included for the sake of comparison.

5) G. R. Leader and J. F. Gormley, *J. Amer. Chem. Soc.*, **73**, 5731 (1951).
6) T. B. Hoover, *J. Phys. Chem.*, **68**, 876 (1964).
7) Viscosity of NMF

15°C	20°C	25°C	30°C	35°C	
0.0199	0.0182	0.0165	0.0154	0.0141	poise

Viscosity of NMP

30°C	35°C	40°C	45°C	50°C	
0.04568	0.04004	0.03541	0.03173	0.02825	poise

Table 2. Limiting equivalent conductances of R_4NI salts and R_4N^+ ions at different temperatures in NMP

R_4NI salt and R_4N^+ ion	Limiting equivalent conductances at				
	30°C	35°C	40°C	45°C	50°C
Me_4NI	17.00	19.10	21.35	23.60	26.30
Me_4N^+	8.66	9.75	10.90	12.05	13.36
Et_4NI	16.55	18.60	20.80	23.00	25.71
Et_4N^+	8.21	9.25	10.35	11.45	12.77
Pr_4NI	15.19	17.07	19.10	21.15	23.70
Pr_4N^+	6.85	7.72	8.65	9.60	10.76
Bu_4NI	15.04	16.90	18.92	20.98	23.48
Bu_4N^+	6.70	7.55	8.47	9.43	10.54
Pen_4NI	14.89	16.75	18.72	20.75	23.24
Pen_4N^+	6.55	7.40	8.27	9.20	10.30
Hex_4NI	14.64	16.48	18.41	20.40	22.85
Hex_4N^+	6.30	7.13	7.96	8.85	9.91
Hep_4NI	14.38	16.14	18.08	20.03	22.43
Hep_4N^+	6.04	6.79	7.63	8.48	9.49

Table 3. Onsager slopes in NMF, NMP, and NMA

Salt	Theoretical slope (S_T)	Experimental slope (S_E)	% deviation $\frac{S_E-S_T}{S_T}\times 100$
	NMF (temp.=25°C)		
Me_4NI	58.22	−25.2	−26.9	7
Et_4NI	48.95	−24.6	−27.1	10
Pr_4NI	38.70	−23.8	−27.4	16
Bu_4NI	33.06	−23.6	−27.6	17
Pen_4NI	32.29	−23.5	−27.8	18
Hex_4NI	27.30	−23.2	−28.1	21
Hep_4NI	26.71	−23.2	−28.3	22
	NMP (temp.=40°C)		
Me_4NI	21.35	−12.3	−14.2	16
Et_4NI	20.30	−12.3	−13.8	12
Pr_4NI	19.10	−12.1	−13.8	14
Bu_4NI	18.92	−12.1	−14.2	17
Pen_4NI	18.72	−12.1	−14.4	19
Hex_4NI	18.41	−12.1	−14.4	19
Hep_4NI	18.08	−12.1	−14.6	21
	NMA (temp.=40°C)		
Me_4NI	26.75	−13.8	−16.6	20
Et_4NI	26.25	−13.8	−16.0	16
Pr_4NI	23.80	−13.6	−15.4	13
Bu_4NI	22.50	−13.6	−15.5	14
Pen_4NI	22.00	−13.5	−15.7	16
Hex_4NI	21.80	−13.5	−16.1	19
Hep_4NI	21.47	−13.5	−16.5	20

It is to be noted from Table 3 that there is a significant negative deviation from the theoretical slope S_T for the R_4NI salts in all the three solvents. The percentage deviation, in general, increases with the increase in the radius of the R_4N^+ ion. In view of the high dielectric constant of these solvents, incomplete dissociation of the salts in the usual sense is un-

thinkable, although Dawson and coworkers[8,9] have tried to explain their conductance results in NMA on this ground. Does this behaviour (appreciable negative deviation) indicate penetration of R_4N^+ ions by anions causing a sort of association,[10] or does it simply indicate that the solvent molecules offer a greater resistance to the movement of the R_4N^+ ions, than that caused by viscosity of the solvent medium, so that the movement of these ions is more sluggish than expected from theory? There is, apparently, no way to decide which factor is actually responsible. Since the larger the ion, the larger the deviation, one feels that the geometry and size of the ions have something to do with their sluggish movement; their tetrahedral, open structure and their large volume will favour their penetration by anions and will also cause obstruction in their movements. It should be mentioned that penetration has been ascribed as one of the factors responsible for the reported abnormal negative slope in the apparent molar volume *vs.* $\sqrt{c}$ curves of these salts in aqueous and nonaqueous solvents.[11,17] The conductance data of these salts at higher concentrations in a variety of solvents can be expected to throw further light on their behaviour.

The cationic Walden products of different R_4N^+ ions at different temperatures have been calculated from the appropriate λ_0^+-values (given in Tables 1 and 2) and viscosity data given earlier. From the Walden product data, thus obtained, $\lambda_0^+\eta_0$ *vs.* temperature curves have been drawn and are given in Figs. 3 and 4.

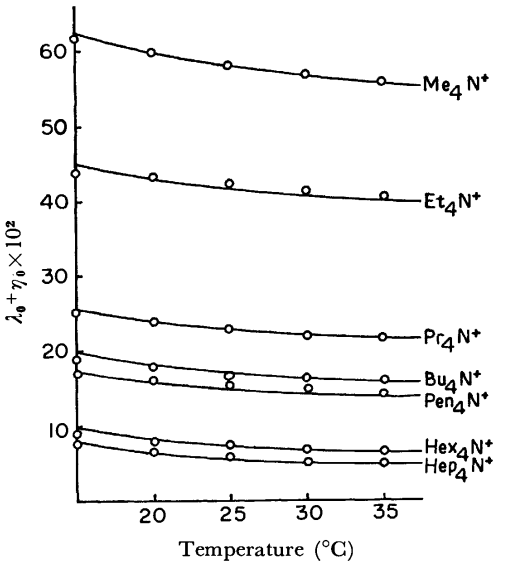

Fig. 3. Plot of $\lambda_0^+\eta_0$ *vs.* t°C in NMF.

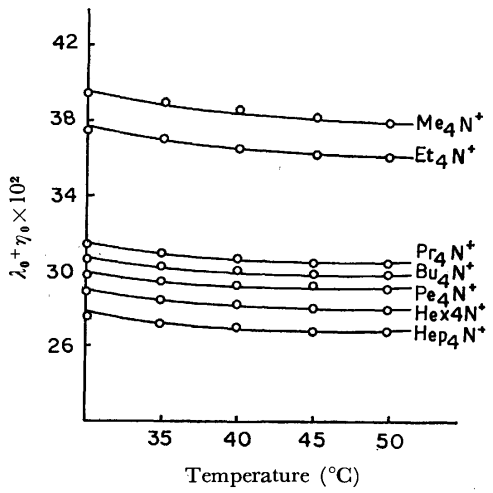

Fig. 4. Plot of $\lambda_0^+\eta_0$ *vs.* t°C in NMP.

It is obvious that the Walden product decreases with the rise in temperature in both solvents, as in NMA,[1] indicating a net structure breaking role of the R_4N^+ ions in these amides. It should be pointed out that in aqueous solutions, the dependence of Walden product on temperature indicates that Me_4N^+ ion (perhaps Et_4N^+ ion also) is a net structure breaker whereas the larger R_4N^+ ions are net structure promoters.[18]

A comparison of λ_0^+-values of R_4N^+ ions in the three solvents with those in water brings out some points of interest. Both Λ_0 and λ_0^+-values are comparatively lower in these solvents than the corresponding values in water, probably on account of the highly viscous nature of these solvents and, perhaps, due to a possible stronger ion-solvent interaction.[1,19,20] It may be noted that λ_0^+ of the smaller R_4N^+ ions are actually larger than those of the alkali metal ions, *e.g.*, in NMF at 25°, $\lambda_0(Me_4N^+)=35.45$ and $\lambda_0(Et_4N^+)=26.19$, whereas $\lambda_0(Na^+)=21.64$ and $\lambda_0(K^+)=22.20$ and in NMP at 30°, $\lambda_0(Me_4N^+)=8.66$ and $\lambda_0(Et_4N^+)=8.21$, whereas $\lambda_0(Na^+)=5.06$ and $\lambda_0(K^+)=5.36$, in spite of the much larger radii of the R_4N^+ ions. This obviously indicates a stronger solvation of alkali metal ions in NMF and NMP as compared to R_4N^+–NMF and R_4N^+–NMP interactions, as one would expect from the much higher electrical charge density on the smaller alkali metal ions. This also indicates a net structure breaking role of R_4N^+ ions and a possible structure promotion by the smaller alkali metal ions.

The authors wish to acknowledge the financial assistance given by the Society of the Sigma *Xi* of U.S.A. and the State's Council of Scientific and Industrial Research (U.P.), India. The junior author (R.D.S.) is also obliged to the C.S.I.R., New Delhi, India, for the grant of a fellowship during the course of this investigation.

8) L. R. Dawson, P. G. Sears, and R. H. Graves, *J. Amer. Chem. Soc.*, **77**, 1986 (1955).
9) L. R. Dawson, E. G. Wilhoit, and P. G. Sears, *ibid.*, **78**, 1569 (1956).
10) S. R. Hughes and D. H. Price, *J. Chem. Soc., A*, **1967**, 1093.
11) W. Y. Wen and S. Saito, *J. Phys. Chem.*, **68**, 2639 (1964).
12) B. E. Conway, R. E. Verrall, and J. E. Desnoyers, *Trans. Faraday Soc.*, **62**, 2738 (1966).
13) R. Gopal and M. A. Siddiqi, *J. Phys. Chem.*, **72**, 1814 (1968).
14) R. Gopal and A. K. Rastogi, *J. Indian Chem. Soc.*, **43**, 269 (1966).
15) R. Gopal and M. A. Siddiqi, *J. Phys. Chem.*, **73**, 3390 (1969).
16) R. Gopal and M. A. Siddiqi, *Z. Physik. Chem.*, **67**, 122 (1969).
17) R. Gopal and K. Singh, *ibid.*, **69**, 81 (1970).
18) R. L. Kay and D. F. Evans, *J. Phys. Chem.*, **70**, 2325 (1966).
19) J. M. Notley and M. Spiro, *ibid.*, **70**, 1502 (1966).
20) W. A. Adams and K. J. Laidler, *Can. J. Chem.*, **46**, 1989 (1969).

The Crystal and Molecular Structure of Averufin

Yukiteru KATSUBE, Tomitake TSUKIHARA, Nobuo TANAKA,* Kazuto ANDO,**
Takashi HAMASAKI,*** and Yuichi HATSUDA***
Faculty of Engineering, Tottori University, Koyama-cho, Tottori
(Received November 12, 1971)

The crystal structure of averufin has been determined by means of the X-ray diffraction method. The space group is $P2_1/a$, with $a=23.70$ Å, $b=7.24$ Å, $c=9.48$ Å, and $\beta=105.5°$. The structure was solved by the interpretation of the three-dimensional Patterson function and was refined by the least-squares method. The molecular structure is in agreement with that proposed by Roffey and Grandjean. In the crystal, the molecules are linked to form a molecular pair by a OH----O hydrogen bond across the center of symmetry.

Aspergillus versicolor (Vuillemin) Tiraboschi produces a number of xanthones and anthraquinones. The fact that all these metabolites are produced by the same mold leads to the postulate that some of them may be biogenetic precursors of the carsinogenic sterigmatocystin. In a previous paper, the crystal structure of *p*-bromobenzoate of sterigmatocystin was reported by Tanaka *et al.*[1]

Averufin was isolated as the metabolite of this mold by Pusey *et al.*,[2] and its chemical structure was proposed by Holker *et al.*[3] and Roffey and Sargent.[4]

The present paper will describe the crystal and molecular structure of averufin, as analyzed by means of the X-ray diffraction method, as one of a series of studies of the crystal structures of some metabolites from this mold. After this study was completed, it was discovered that the structure of averufin had been elucidated by Grandjean by means of NMR spectroscopy.[5] The molecular structure determined by us is in agreement with that proposed by Roffey and Sargent[4] and Grandjean.[5]

Experimental

The crystal grown from an acetone solution was in the form of a reddish, flat, rectangular plate elongated in the *a*-axis direction. The unit cell dimensions are shown in Table 1.

TABLE 1. CRYSTAL DATA OF AVERUFIN

Molecular formula;	$C_{20}H_{16}O_7$
	$M=368.328$
Monoclinic; space group	$P2_1/a$
	$a=23.704$Å
	$b=7.239$Å
	$c=9.483$Å
	$\beta=105.46°$
	$V=1568.3$Å^3
	d(obs)$=1.562$ g/cm^3
	d(cal)$=1.558$ g/cm^3
	$Z=4$

Mo-K_α radiation filtered by means of a zirconium foil was used to collect all the reflections in the $0<\sin\theta/\lambda<0.651$ range, within the (hkl) and $(hk\bar{l})$ octants. All the intensities were measured on a Rigaku Denki computer-controlled four-circle diffractometer (AFC-II). A scintillation counter with a pulse-height discriminator was used. Altogether, 2909 independent reflections were collected. A crystal of the approximate dimensions of $0.23\times0.22\times0.13$ mm^3 ($0.964<e^{-\mu r}<0.968$) was mounted with the *b*-axis parallel to the ϕ-axis of the diffractometer. The ω-2θ scan technique was employed, with a scan speed of 1°/min by ω, backgrounds were measured for 10 seconds at each start and end points of the scan range. The scan range for each reflection was calculated by means of the formula indicated by Alexander *et al.*[6]: ω scan range$=0.70°+0.40°\tan\theta$. Attenuators were automatically inserted when the maximum counting rate exceeded 5000 cps. The intensities were corrected only for Lorentz and polarization factors. Measurements of three reference reflections, (14 0 0), (0 0 8), and (0 4 0), were repeated every fifty reflections; for 62 repetitions of the measurements, $|F_0(14\ 0\ 0)|=144.26\pm0.33$, $|F_0(0\ 0\ 8)|=42.78\pm0.11$, and $|F_0(0\ 4\ 0)|=56.37\pm0.10$.

Determination of the Structure

The angular coordinates defining the orientation of the planar anthraquinone group in the molecule were readily established by means of the vector-set-seeking method;[7] the vector set of the anthraquinone skeleton was superposed on the three-dimensional Patterson function and rotated until the best fit was obtained. The location of this planar group in the unit cell was determined from the Patterson function, in which a large non-Harker peak is expected corresponding to the anthraquinone-anthraquinone vector from molecules related by a center of symmetry. Of several possible peaks, the one which satisfied a reasonable packing condition in the crystal and which gave the best match with the Patterson function was selected. This interpretation was proved to be correct. The 780 largest structure factors were calculated by the use of the atomic positions of the anthraquinone group only, and the *R* value defined by $R=\sum||F_o|-|F_c||/\sum|F_o|$ was 0.69. The Fourier synthesis phased by the anthraquinone group was computed. The peaks corresponding to some additional atoms were clearly visible, their peak-heights were approximately

* Present address: Institute for Protein Research, Osaka University.
** Present address: Japan Electron Optics Laboratory, Co., Ltd.
*** Faculty of Agriculture, Tottori University.

1) N. Tanaka, Y. Katsube, Y. Hatsuda, T. Hamasaki, and M. Ishida, This Bulletin, **43**, 3635 (1970).
2) D. F. G. Pusey and J. C. Roberts, *J. Chem. Soc.*, **1963**, 3542.
3) J. S. E. Holker, S. A. Kagal, L. J. Mulheirin, and P. M. White, *Chem. Commun.*, **1966**, 911.
4) P. Roffey and M. V. Sargent, *ibid.*, **1966**, 913.
5) J. Grandjean, *ibid.*, **1971**, 1060.
6) T. C. Furnas, "Single Crystal Orienter Instruction Manual" Milwaukee, General Electric Co. (1957).
7) Y. Katsube, Y. Sasada, and M. Kakudo, This Bulletin, **39**, 6108 (1966).

TABLE 2. FINAL PARAMETERS OF CARBON AND OXYGEN ATOMS

The anisotropic temperature factors are of the form

$\exp[-(\beta_{11}h^2+\beta_{22}k^2+\beta_{33}l^2+2\beta_{12}hk+2\beta_{13}hl+2\beta_{23}kl)]$

	x	y	z	$\beta_{ij}\times 10^4$					
				β_{11}	β_{22}	β_{33}	β_{12}	β_{13}	β_{23}
C (1)	−0.1346	0.0387	−0.0667	13	120	65	0	10	−1
C (2)	−0.1123	−0.1356	−0.0806	13	123	62	−7	17	−17
C (3)	−0.0610	−0.1911	0.0203	14	118	70	9	19	−5
C (4)	−0.0320	−0.0741	0.1348	12	121	59	6	13	−9
C (5)	0.0199	−0.1364	0.2438	12	122	80	−2	17	−23
C (6)	0.0468	−0.0149	0.3653	11	133	75	−3	17	1
C (7)	0.0953	−0.0737	0.4775	11	160	86	2	14	−12
C (8)	0.1202	0.0404	0.5952	12	180	71	0	4	−6
C (9)	0.0978	0.2156	0.6008	14	153	72	−21	15	−26
C (10)	0.0507	0.2794	0.4908	13	127	85	−9	10	−19
C (11)	0.0248	0.1635	0.3747	11	129	68	−2	11	8
C (12)	−0.0280	0.2293	0.2655	14	116	77	−1	18	2
C (13)	−0.0559	0.1022	0.1443	13	109	67	0	11	−14
C (14)	−0.1061	0.1587	0.0441	15	101	86	13	9	−4
C (15)	−0.2183	−0.0273	−0.2706	14	138	73	−7	7	−13
C (16)	−0.1461	−0.2590	−0.2015	17	129	77	5	8	−49
C (17)	−0.1867	−0.3891	−0.1489	20	120	120	−16	−8	21
C (18)	−0.2312	−0.2773	−0.0949	19	212	110	−24	18	87
C (19)	−0.2606	−0.1351	−0.2086	14	174	85	−12	4	−4
C (20)	−0.2480	0.0933	−0.3976	18	206	87	0	−13	53
O (1)	−0.1850	0.1001	−0.1588	15	123	91	12	−11	−11
O (2)	−0.1789	−0.1426	−0.3168	16	171	59	1	7	−7
O (3)	−0.0410	−0.3615	0.0034	18	132	108	25	2	−84
O (4)	0.0404	−0.2946	0.2355	16	138	111	27	−3	−41
O (5)	0.1184	−0.2443	0.4770	16	184	114	35	−10	−31
O (6)	0.1228	0.3207	0.7189	15	210	90	−9	−5	−83
O (7)	−0.0491	0.3800	0.2774	21	131	105	16	−3	−55

TABLE 3. ATOMIC PARAMETERS OF HYDROGEN ATOMS

Atom	x	y	z	B	Atom	x	y	z	B
H (1)	−0.124	0.279	0.050	1.3Å²	H (9)	−0.208	−0.464	−0.228	3.5Å²
H (2)	0.032	0.411	0.488	1.9	H (10)	−0.212	−0.208	−0.002	2.2
H (3)	0.099	0.421	0.717	5.1	H (11)	−0.260	−0.350	−0.068	2.8
H (4)	0.155	−0.002	0.674	2.9	H (12)	−0.284	−0.046	−0.170	3.5
H (5)	0.096	−0.300	0.400	5.3	H (13)	−0.285	−0.194	−0.288	2.2
H (6)	−0.008	−0.390	0.085	5.2	H (14)	−0.273	0.181	−0.355	3.4
H (7)	−0.115	−0.330	−0.242	3.0	H (15)	−0.275	0.025	−0.461	3.9
H (8)	−0.162	−0.458	−0.067	3.1	H (16)	−0.216	0.154	−0.444	4.9

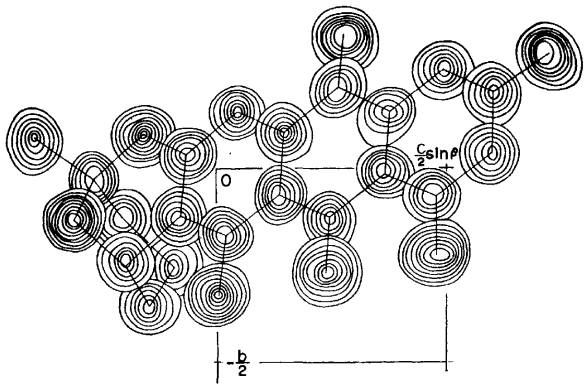

Fig. 1. The electron density map.
The contours are at equally spaced intervals on an arbitrary scale.

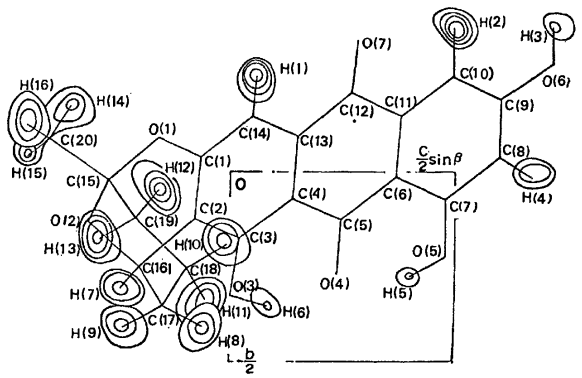

Fig. 2. The difference electron density map, for which the contributions of hydrogen atoms were excluded from the calculated structure factors.

TABLE 4. INTERATOMIC DISTANCES AND ANGLES

Bond	Length (Å)	Bond	Length (Å)	Bond	Length (Å)
C(1)–C(2)	1.387(5)	C(1)–C(14)	1.392(5)	C(1)–O(1)	1.354(4)
C(2)–C(3)	1.393(5)	C(2)–C(16)	1.504(5)	C(3)–C(4)	1.406(5)
C(3)–O(3)	1.344(4)	C(4)–C(5)	1.456(5)	C(4)–C(13)	1.404(5)
C(5)–C(6)	1.455(5)	C(5)–O(4)	1.252(4)	C(6)–C(7)	1.410(5)
C(6)–C(11)	1.407(5)	C(7)–C(8)	1.385(5)	C(7)–O(5)	1.353(5)
C(8)–C(9)	1.382(5)	C(9)–O(6)	1.353(4)	C(9)–C(10)	1.388(5)
C(10)–C(11)	1.386(5)	C(11)–C(12)	1.474(5)	C(12)–C(13)	1.485(5)
C(12)–O(7)	1.219(4)	C(13)–C(14)	1.375(5)	C(15)–C(19)	1.510(5)
C(15)–C(20)	1.505(5)	C(15)–O(1)	1.467(4)	C(15)–O(2)	1.403(4)
C(16)–C(17)	1.521(5)	C(16)–O(2)	1.435(4)	C(17)–C(18)	1.523(6)
C(18)–C(19)	1.518(6)	C(14)–H(1)	1.00 (4)	C(10)–H(2)	1.11 (4)
O(6)–H(3)	0.96 (5)	C(8)–H(4)	1.04 (4)	O(5)–H(5)	0.92 (5)
O(3)–H(6)	0.96 (5)	C(16)–H(7)	1.08 (5)	C(17)–H(8)	0.97 (5)
C(17)–H(9)	0.96 (5)	C(18)–H(10)	1.00 (4)	C(18)–H(11)	0.98 (4)
C(19)–H(12)	1.02 (5)	C(19)–H(13)	0.97 (4)	C(20)–H(14)	1.01 (5)
C(20)–H(15)	0.85 (5)	C(20)–H(16)	1.03 (5)		

	Angle(°)		Angle(°)
C(2)–C(1)–C(14)	121.4(3)	C(2)–C(1)–O(1)	122.0(3)
C(14)–C(1)–O(1)	116.6(3)	C(1)–C(2)–C(3)	118.9(3)
C(1)–C(2)–C(16)	118.3(3)	C(3)–C(2)–C(16)	122.8(3)
C(2)–C(3)–C(4)	120.8(3)	C(2)–C(3)–O(3)	117.1(3)
C(4)–C(3)–O(3)	122.2(3)	C(3)–C(4)–C(5)	120.4(3)
C(3)–C(4)–C(13)	118.5(3)	C(5)–C(4)–C(13)	121.0(3)
C(4)–C(5)–C(6)	118.9(3)	C(4)–C(5)–O(4)	120.7(3)
C(6)–C(5)–O(4)	120.4(3)	C(5)–C(6)–C(7)	120.9(3)
C(5)–C(6)–C(11)	121.1(3)	C(7)–C(6)–C(11)	118.0(3)
C(6)–C(7)–C(8)	121.1(3)	C(6)–C(7)–O(5)	121.4(3)
C(8)–C(7)–O(5)	117.5(3)	C(7)–C(8)–C(9)	119.4(3)
C(8)–C(9)–C(10)	121.1(3)	C(8)–C(9)–O(6)	117.3(3)
C(10)–C(9)–O(6)	121.6(3)	C(9)–C(10)–C(11)	119.7(3)
C(6)–C(11)–C(10)	120.7(3)	C(6)–C(11)–C(12)	120.6(3)
C(10)–C(11)–C(12)	118.6(3)	C(11)–C(12)–C(13)	117.7(3)
C(11)–C(12)–O(7)	121.0(3)	C(13)–C(12)–O(7)	121.3(3)
C(4)–C(13)–C(12)	120.6(3)	C(4)–C(13)–C(14)	121.1(3)
C(12)–C(13)–C(14)	118.3(3)	C(1)–C(14)–C(13)	119.4(3)
C(19)–C(15)–C(20)	113.4(3)	C(19)–C(15)–O(1)	109.0(3)
C(19)–C(15)–O(2)	112.5(3)	C(20)–C(15)–O(1)	104.9(3)
C(20)–C(15)–O(2)	107.7(3)	O(1)–C(15)–O(2)	109.0(3)
C(2)–C(16)–C(17)	112.0(3)	C(2)–C(16)–O(2)	107.6(3)
C(17)–C(16)–O(2)	110.6(3)	C(16)–C(17)–C(18)	109.7(3)
C(17)–C(18)–C(19)	110.6(3)	C(15)–C(19)–C(18)	113.6(3)
C(1)–O(1)–C(15)	118.1(3)	C(15)–O(2)–C(16)	112.4(3)
C(1)–C(14)–H(1)	118 (2)	C(13)–C(14)–H(1)	122 (2)
C(9)–C(10)–H(2)	123 (2)	C(11)–C(10)–H(2)	116 (2)
C(9)–O(6)–H(3)	106 (3)	C(7)–C(8)–H(4)	118 (3)
C(9)–C(8)–H(4)	122 (3)	C(7)–O(5)–H(5)	104 (3)
C(3)–O(3)–H(6)	109 (3)	C(2)–C(16)–H(7)	108 (3)
C(17)–C(16)–H(7)	109 (3)	O(2)–C(16)–H(7)	108 (3)
C(16)–C(17)–H(8)	106 (3)	C(18)–C(17)–H(8)	108 (3)
H(9)–C(17)–H(8)	116 (4)	C(16)–C(17)–H(9)	110 (3)
C(18)–C(17)–H(9)	104 (3)	C(17)–C(18)–H(10)	109 (3)
C(19)–C(18)–H(10)	105 (3)	H(11)–C(18)–H(10)	105 (4)
C(17)–C(18)–H(11)	112 (3)	C(19)–C(18)–H(11)	112 (3)
C(15)–C(19)–H(12)	111 (3)	C(18)–C(19)–H(12)	109 (3)
H(13)–C(19)–H(12)	108 (4)	C(15)–C(19)–H(13)	104 (3)
C(18)–C(19)–H(13)	110 (3)	C(15)–C(20)–H(14)	104 (3)
H(15)–C(20)–H(14)	102 (4)	H(16)–C(20)–H(14)	118 (4)
C(15)–C(20)–H(15)	108 (3)	H(16)–C(20)–H(15)	115 (4)
C(15)–C(20)–H(16)	109 (3)		

Intramolecular hydrogen bond:

O(3)·····O(4) 2.561(4)Å O(4)·····O(5) 2.554(4)Å O(4)·····H(6) 1.72 (6)Å
O(4)·····H(5) 1.70 (5)Å O(3)–H(6)···O(4) 151 (6)°Å O(5)–H(5)···O(4) 151 (5)°Å

Estimated standard deviations shown in parentheses refer to the last decimal positions.

half of those of the atoms of the anthraquinone group. The whole structure of the molecule except for the hydrogen atoms was revealed after three successive Fourier synthesis. At this stage, the R value was 0.46. The structure was refined by a diagonal-matrix least-squares procedure with the isotropic temperature factors, until the R value of 0.15 was reached. Further refinement was carried out by the least-squares of block-diagonal matrix approximations with anisotropic temperature factors, using all the reflections. The R value was thus reduced to 0.12. At this stage, the difference Fourier synthesis showed all the hydrogen atoms. The final refinement was made by including the positional parameters and the isotropic temperature factors of the hydrogen atoms, where upon the R value decreased to 0.083. The final atomic parameters are listed in Tables 2 and 3. The final electron density map is shown in Fig. 1. The difference electron density map, for which the contributions of the hydrogen atoms were excluded from the calculated structure factors, is shown in Fig. 2.

A list of the observed and calculated structure factors is available from the authors on request.

Most of the calculations were done on the TOSBAC-3400 by the use of the programs written by the authors. The block-diagonal least-squares refinement was performed on the HITAC 5020E of the university of Tokyo using a program written by T. Ashida, the weighting scheme in the calculation was $w=1.0$ for reflections with $|F_o|\geq 1.5$ and $w=0.5$ for the others. The atomic scattering factors were taken from Ref. 8.

Description of the Structure and Discussion

The bond lengths and bond angles are given in Table 4. The mean bond length of the carbon-carbon bonds in the benzenoid rings is 1.393 Å, which is the same as the length, 1.397 Å, formed in the benzene ring[9] within the limits of error. However, the lengths of C–C bonds adjacent to the quinonoid carbonyl bonds, C(4)–C(5), C(5)–C(6), C(11)–C(12), and C(12)–C(13), are considerably longer than those in the benzenoid rings. The lenghts of the C(12)–O(7) and C(5)–O(4) of the quinonoid carbonyl bonds are 1.219 Å and 1.252 Å respectively. The former agrees well with the C–O bond length in acetaldehyde (1.215)[9] and may be a normal double bond. The latter is longer than the former, the elongation of the latter bond may be due to the influence of the adjacent hydroxyl groups. The lengths of the C–O bonds attached to the anthraquinone skeleton, C(1)–O(1), C(3)–O(3), C(7)–O(5), and C(9)–O(6), are almost constant and have a mean of 1.351 Å. All are in agreement with the length of a single bond between an oxygen and an sp^2-hybridized carbon atom.

The dimensions of the quinonoid group in the averufin show features similar to those in other related molecules whose structures have been studied: *p*-benzoquinone,[10] anthraquinone,[11] 1,5-dihydroxyanthraquinone,[12] 1:2,5:6-dibenzanthraquinone,[13] and some derivatives of anthraquinone.[14]

There are no significant differences among the five bond lenghts of C(sp^3)–C(sp^3), and the mean value (1.515 Å) is shorter than that of a pure single C–C bond. The lengths of the C–O bonds involving C(sp^3) have a mean of 1.435 Å and agree with the C–O single bond distance.

The least-squares plane for the aromatic condensed ring including O(3) to O(7) can be represented by the equation:

$$Z=1.3981X+0.6983Y+3.2390$$

where $X=ax+cz\cos\beta$, $Y=by$, and $Z=cz\sin\beta$. The perpendicular displacements of the atoms from the plane are given in Table 5. As may be seen in Table 5, these atoms are coplanar.

Table 5. Deviations from the least-squares plane

Atom	Deviation	Atom	Deviation
Atoms included in plane			
C(1)	−0.098Å	C(2)	−0.079Å
C(3)	−0.005	C(4)	0.051
C(5)	0.065	C(6)	0.045
C(7)	−0.014	C(8)	−0.062
C(9)	−0.023	C(10)	0.061
C(11)	0.076	C(12)	0.056
C(13)	0.039	C(14)	−0.020
O(3)	0.004	O(4)	0.058
O(5)	−0.063	O(6)	−0.098
O(7)	0.009		
Atoms not included in plane			
O(1)	−0.202	C(16)	−0.194
H(1)	−0.05	H(2)	−0.10
H(3)	−0.24	H(4)	−0.10
H(5)	−0.09	H(6)	−0.04

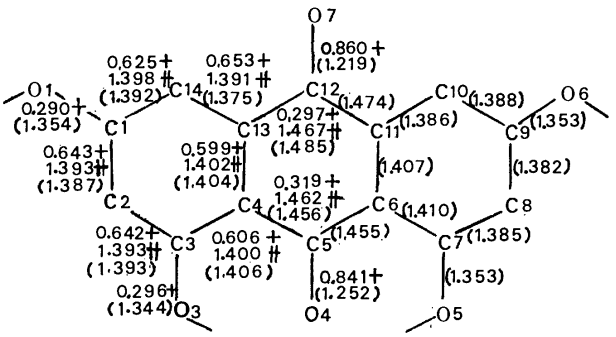

Fig. 3. The π-bond orders and the bond lenghts (Å).
+ the π-bond orders
# the bond lenghts calculated from Coulson's equation
The values in the parentheses are the observed lengths (Å).

8) "International Tables for X-ray Crystallography", Vol. III, Kynoch Press, Birmingham (1962), p. 202.
9) L. E. Sutton, "Tables of Interatomic Distance (Suppl.)" The Chemical Society, London (1965).
10) J. Trotter, *Acta Crystallogr.*, **13**, 86 (1960).
11) B. V. R. Murty, *Z. Kristallogr.*, **113**, 445 (1960).
12) D. Hall and C. L. Nobbs, *Acta Crystallogr.*, **21**, 927 (1966).
13) R. F. Entwistle, J. Iball, W. D. S. Motherwell, and B. P. Thompson, *ibid.*, **B25**, 770 (1969).
14) J. Gaultier and C. Hauw, *ibid.*, **B25**, 419 (1969).

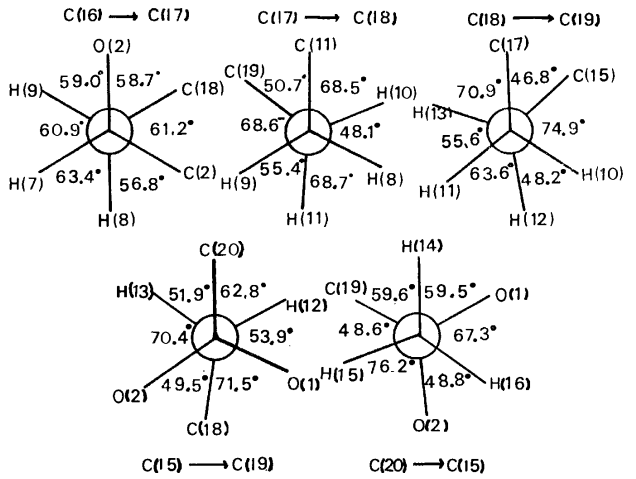

Fig. 4. Internal rotation angles.

The π-bond orders were obtained from a simple LCAO molecular orbital treatment (simple Hückel's method) for the π-electron system alone. The set of Coulomb and exchange integral values suggested by Pullman[15] were used. There are:

$$\alpha(\mathrm{C})=\alpha_0,\ \alpha(=\mathrm{O})=\alpha_0+1.2\beta_0,\ \alpha(-\mathrm{O}-)=\alpha_0+2.0\beta_0,$$
$$\beta(\mathrm{C}-\mathrm{C})=\beta_0,\ \beta(\mathrm{C}=\mathrm{O})=2.0\beta_0,\ \beta(\mathrm{C}-\mathrm{O})=0.9\beta_0$$

where α_0 is the Coulomb integral of the carbon atom in the benzene and whose β_0 is the exchange integral of the C–C bond in the benzene. The lengths of the C–C bonds were estimated from the existing bond order-bond length curve.[16] In the C–C bonds, the agreement between the calculated and observed bond lengths is within 0.02 Å. The lengths of the C–O bonds were not predicated in the present work, because the C–O bond order–bond length data generally have a much wider range of values than the corre sponding curve for the C–C bond. The results of the MO calculation are given in Fig. 3.

The conformation of the six-membered ring, C(16)–C(17)–C(18)–C(19)–C(15)–O(2), is a chair form. The internal rotation angles around the C(sp^3)–C(sp^3) bonds are illustrated in Fig. 4. They show a stable, staggered conformation. The average bond angle at the C(sp^3) is 109.8°, and that at the C(sp^2) is 119.9°. The C(15)–O(2)–C(16) angle in the six-membered ring of the chair form is 112.4°; this agrees well with the corresponding angles in sugars.[17] There are two

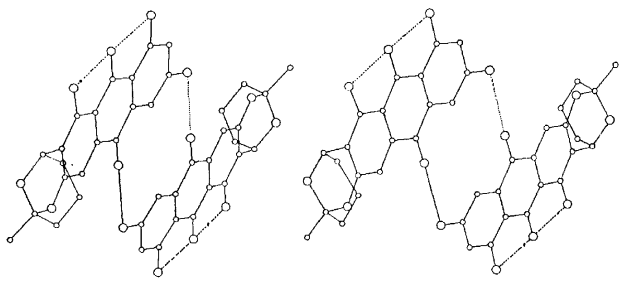
Fig. 5. Stereoscopic drawing of a pair of molecules.

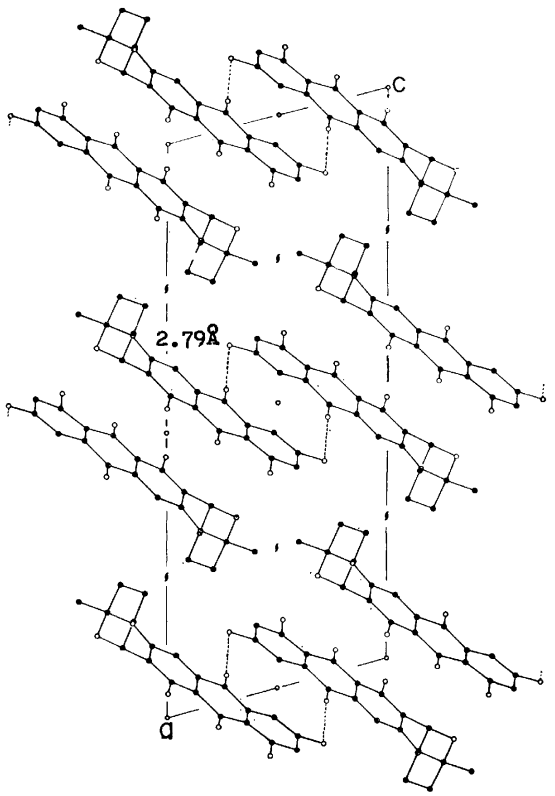

Fig. 6. The crystal structure projected along the *b*-axis.

intramolecular hydrogen bonds of the OH···O type: O(3)···O(4)=2.56 Å and O(4)···O(5)=2.55 Å. The molecule has, therefore, the conformation which might be expected to have the lowest energy. A stereoscopic drawing of the molecule is given in Fig. 5.

The crystal structure projected along the *b*-axis is shown in Fig. 6. The closest intermolecular distances are listed in Table 6. The reference molecule at (x, y, z) is connected by the intermolecular hydrogen bond of OH···O of 2.79 Å with the molecule at ($-x$, $1-y$, $1-z$), thus forming a pair of molecules across the center of symmetry. Although the molecule itself has two asymmetric centers, the crystal of averufin is racemized by the molecules related by the centers of symmetry. The intermolecular approach distance between O(3) and O(3) in the "*b*-molecule" is 2.81 Å. Although this distance corresponds to the sum of the van der Waals radii, it is less than the intermolecular O···O distances found in common compounds and compares with the rather long intermolecular hydrogen bonds. Such a close distance has been found in 1,5-dihydroxyanthraquinone: according to Hall *et al.*,[12] this intermolecular interaction is due to the proton of the hydrogen atom in the hydroxyl group, which may participate in the interactions among the closest oxygen atoms. However, in averufin, it appears that the approach of these oxygen atoms may correspond to the van der Waals interaction, because the hydrogen atom attached to the O(3) atom may participate only in the formation of the intramolecular hydrogen bond.

The other intermolecular distances require no special comment; all correspond to the normal van der Waals interaction.

15) B. Pullman and A. Pullman, "Quantum Biochemistry," Interscience Publishers, N. Y., (1963), pp. 108, 356.
16) C. A. Coulson, *Proc. Roy. Soc.*, **A169**, 413 (1939).
17) C. A. Beevers and H. N. Hansen, *Acta Crystallogr.*, **B27**, 1323 (1971).

TABLE 6. INTERMOLECULAR CONTACTS

Atom	Neighbour atom	Distance	Atom	Neighbour atom	Distance
C(1)	C(5) a	3.63 Å	C(7)	C(12) c	3.44Å
C(2)	C(5) a	3.59	C(8)	C(12) c	3.45
C(2)	C(6) a	3.62	C(8)	C(13) c	3.39
C(3)	C(4) a	3.53	C(9)	C(13) c	3.66
C(3)	C(13) a	3.59	C(11)	C(16) a	3.74
C(4)	C(4) a	3.47	C(11)	C(11) c	3.76
C(4)	C(9) c	3.44	O(6)	C(3) c	3.33
C(4)	C(13) a	3.79	O(6)	C(4) c	3.37
C(5)	C(9) c	3.53	O(7)	C(10) d	3.31
C(5)	C(10) c	3.53	O(2)	C(7) a	3.21
C(6)	C(16) a	3.72	O(2)	C(8) a	3.38
C(6)	C(10) c	3.54	O(2)	C(20) e	3.39
C(6)	C(11) c	3.51	O(3)	O(3) b	2.81
C(7)	C(11) c	3.56	O(7)	O(6) d	2.79

Key for position of molecules
a $(-x \quad -y \quad -z)$
b $(-x \quad -1.0-y \quad -z)$
c $(-x \quad -y \quad 1.0-z)$
d $(-x \quad 1.0-y \quad 1.0-z)$
e $(-0.5-x \quad -0.5+y \quad -1.0-z)$

The authors wish to express their thanks to Dr. Tamaichi Ashida for permission to use his program and to the staff of the Institute for Protein Research of Osaka University for the use of the four-circle diffractometer. The authors are also gratful to the Computer Center of the University of Tokyo for the use of HITAC 5020E.

BULLETIN OF THE CHEMICAL SOCIETY OF JAPAN, VOL. 45, 2096—2100(1972)

The Electrical Properties of Iodine Complexes of *N*-Methyl- and *N*-Ethyl-phenothiazines and Their Mixtures

Kazuo KAN* and Yoshio MATSUNAGA**

Department of Chemistry, Faculty of Science, Hokkaido University, Sapporo

(Received January 7, 1972)

The electrical resistivities and Seebeck coefficients of 2: 3 iodine complexes of *N*-methyl- and *N*-ethyl-phenothiazines were measured. The former complex exhibits a resistivity of 2.0 ohm cm and an activation energy for semiconduction of 0.20 eV at 20°C. Applying the equation of Johnson and Lark-Horowitz for the Seebeck coefficient of an intrinsic semiconductor, the ratio of the electron mobility to the hole mobility in the *N*-methyl-phenothiazine complex was found to be 2.08 and the electron mobility was estimated as 0.23 $cm^2/Vsec$. The resistivity of the *N*-ethylphenothiazine complex is 74 ohm cm, and the activation energy 0.15 eV at 20°C. In this complex, the hole appears to be more mobile by a factor of five than the electron. Lichtenecker's logarithmic rule is observed neither by the resistivity nor by the activation energy of the mixtures of these two complexes.

N-Methyl-phenothiazine has been found by one of the present authors to form a 2: 3 iodine complex exhibiting an electrical resistivity as low as 1.4 ohm cm at room temperature.[1] As this value is only about one-tenth of the resistivity shown by the iodine complex of the unsubstituted donor, it seemed that a further examination of the size effect of the alkyl group on the electrical properties would be interesting. A preliminary study of this problem indicated an increase in the resistivity upon the introduction of larger alkyl groups.[2] However, the comparison made in that study was merely qualitative because no complexes with a definite composition were isolated. Here, we wish to report a comparison of the resistivities and Seebeck coefficients of 2: 3 iodine complexes of *N*-methyl- and *N*-ethyl-phenothiazines in order to see how the introduction of a larger group modifies the properties.

According to Lichtenecker, a logarithmic rule ap-

* Present address: Sumitomo Bayer Urethane Co., Ltd., Amagasaki, Hyogo.

** To whom inquiries may be addressed.

1) Y. Matsunaga, *Helv. Phys. Acta*, **36**, 800 (1963).

2) Y. Matsunaga, *Nippon Kagaku Zasshi*, **89**, 905 (1968).

plies for the resistivity value when two non-interacting materials are mechanically mixed.[3] The essential expression derived by him is:

$$\rho_m = \rho_1^{1-x}\rho_2^{x} \quad (1)$$

where ρ_m is the resistivity of the mixture; ρ_1 and ρ_2 are the resistivities of the respective components, and x is the volume fraction of the second component. If the materials are semiconductors, we obtain:

$$\rho_m = \rho_{01}^{1-x}\rho_{02}^{x} \exp\{[(1-x)E_1 + xE_2]/kT\} \quad (2)$$

where ρ_{01} and ρ_{02} are preexponential factors of the components and where E_1 and E_2 are the respective activation energies for semiconduction. Recently, Ulbert has studied the electrical properties of mechanical mixtures of two chemically-stable organic semiconductors, 4,4′-bis(dimethylamino)-diphenylamine iodide and the iodine complex of *N*,*N*′-bis(aminophenyl)-*p*-phenylenediamine.[4] The generalized logarithmic rule, Eq. (2), has been well observed not only by the resistivity but also by the activation energy of the mixtures. Therefore, we examined the properties of the mixtures to see whether or not the same rule applies to the present iodine complexes.

Experimental

Materials. The *N*-alkyl-phenothiazines were prepared by the reaction of the corresponding alkyl iodide on phenothiazine following the procedure given by Bernthsen.[5] The complexes were precipitated by mixing the components dissolved in ether. As was described in our earlier paper, the complexes dissociate into their components when dissolved in benzene, so the compositions were determined by iodometric titration.[1] For the examination of the (*N*-methyl- and *N*-ethyl-phenothiazines)-iodine, the weighed complexes were thoroughly mixed by grinding in an agate mortar. Samples with the following volume percents of the *N*-ethyl-phenothiazine complex were prepared: 13.5, 27.1, 44.7, 49.4, 58.2, and 72.6.

Measurements. The resistivities of compressed polycrystalline samples were measured by a potential probe method in the range from −90°C to room temperature. Below the lower limit, the contact between the pellet and the probe became too sluggish for any reliable measurements to be made. The pellet and its holder were accommodated in a thick copper cylinder and cooled with liquid nitrogen. When the temperature of the sample had been lowered enough, the whole was transferred into an empty Dewar and allowed to warm up slowly to room temperature. During this process, the temperature of the holder was recorded on the X axis of a Yokogawa X–Y recorder, Type 3078, and the potential drop between the probes and that in the standard resistance, on the Y_1 and Y_2 axes respectively.

The Seebeck voltage measurements were carried out on the same pellets as those employed for the resistivity measurements. In this mounting, the faces painted with colloidal graphite were clamped between copper electrodes. The temperatures on the upper and lower faces of the pellet were measured by means of copper-constantan thermocouples attached to the electrodes. The Seebeck coefficient observed with a dried colloidal graphite block was 1—3 μV/deg over the entire temperature range; therefore, no correction was made for the following data. The temperature difference between the two faces was not controlled except near room temperature; it ranged from 10 to 30°C. The limit of the measurable low temperature, the mean value of those temperatures at the two faces, was about −130°C. The measurements were made by recording the Seebeck voltage on the X axis and the thermocouple potentials on the Y_1 and Y_2 axes.

The densities of the complexes were determined from the pellets.

Results and Discussion

The complexes of *N*-methyl- and *N*-ethyl-phenothiazines consist of two molecules of thiazine and three of iodine. The former complex is black, and the latter dark green. They melt at 72° and 74.5°C respectively. In Fig. 1 the logarithm of the resistivity is plotted

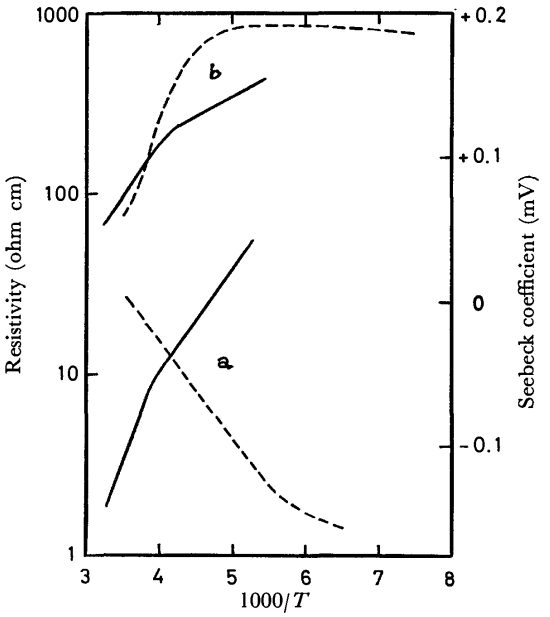

Fig. 1. Electrical resistivities (——) and Seebeck coefficients (----) of (a) *N*-methyl-phenothiazine-iodine and (b) *N*-ethylphenothiazine-iodine complexes.

against the reciprocal temperature. The plot gives two straight lines, with a break around −70°C in both cases. The activation energy for semiconduction, calculated on a basis of:

$$\rho = \rho_0 \exp(E/kT) \quad (3)$$

is 0.20 eV in the higher temperature region and 0.11 eV in the lower temperature region of the curve for the *N*-methyl-phenothiazine-iodine complex. In our earlier work, the activation energy was estimated as 0.14 eV by measurements over a rather narrow temperature range (from 0 to 40°C). This value must be compared with that of 0.20 eV obtained in the present work. The resistivity value at 20°C is 2.0 ohm cm; it is in reasonable agreement with the previously-reported one, 1.4 ohm cm. Similarly, 0.15 and 0.045 eV can be estimated for the *N*-ethyl-phenothiazine-iodine complex. The resistivities at 20°C and the activation energies at this temperature are summarized in Table

3) K. Lichtenecker, *Z. Elektrochem.*, **40**, 11 (1934).
4) K. Ulbert, *Aust. J. Chem.*, **23**, 1347 (1970).
5) A. Bernthsen, *Ann.*, **230**, 73 (1885).

TABLE 1. ELECTRICAL PROPERTIES OF THE IODINE COMPLEXES OF PHENOTHIAZINE AND ITS *N*-ALKYL DERIVATIVES IN THE HIGHER TEMPERATURE REGION

Substituent	ρ at 20°C (ohm cm)	E(eV)	μ_e/μ_h	m_e/m_h	Ref.
None	20	0.17	—	—	1
None	13	0.19	—	—	6
Methyl	1.4	0.14	—	—	1
Methyl	2.0	0.20	2.08	1/130	This work
Ethyl	74	0.15	1/5.0	530[a]	This work

a) By extrapolation of the Seebeck coefficient curve in the higher temperature region.

1. The values for the phenothiazine-iodine complex, taken from our previous papers are included for the sake of comparison.[1,6] The results clearly indicate that the methyl substitution makes the arrangement of thiazine molecules in the iodine complex the optimum for electrical conduction. When the size of the group on the nitrogen atom is either smaller or larger, the overlapping of the thiazine molecules appears to decrease, resulting in an increase in the resistivity. Effects of such a size have been noted in several works on anion-radical salts derived from tetracyanoquinodimethane and also those derived from tetrahalo-*p*-diphenoquinones.[7-10] It is interesting to note that, contrary to the iodine complexes, the 2,3-dichloro-5,6-dicyano-*p*-benzoquinone complex of *N*-methyl-phenothiazine was found to have a resistivity about ten times higher than that of unsubstituted phenothiazine.[2,11] A compensating relation between the activation energy and the logarithm of resistivity has been frequently pointed out when a series of compounds, such as a series of derivatives of a given compound, is examined.[12-14] From this standpoint, the present complexes are rather anomalous. The most conducting *N*-methylphenothiazine complex is found to exhibit the highest activation energy for semiconduction.

The temperature dependence of the Seebeck coefficient, Q, is also presented in Fig. 1. First of all, the change in the sign by the kind of alkyl group must be noted; that is, the coefficient of the *N*-methyl-phenothiazine complex is negative except near and above room temperature, while that of the *N*-ethyl-phenothiazine complex is positive over the whole measurable range. A further observation of the alternation of the sign by the substituent is provided by the experiment on the phenothiazine-iodine complex, the Seebeck coefficient of which is positive (about 0.15 mV/deg in the vicinity of room temperature).[15] It must be added that the sign of the Seebeck coefficient in the phenothiazine-iodine system has been reported by Bhat and Rao to vary with the donor-acceptor ratio.[16] The following values, measured at 30°C, have been presented by them: +0.132 mV/deg at a composition of 1:3, −0.150 mV/deg at 1:1, and +0.300 mV/deg at 3:1. Unfortunately, none of the compositions mentioned here corresponds to the 2:3 stoichiometry reported by us and also by Gutmann and Keyzer.[1,6,17]

The higher-temperature region of the curve is practically straight and seems to fit in with the expression for the thermoelectric motive force of an intrinsic semiconductor:[18,19]

$$Q=-\frac{k}{e}\left[\frac{b-1}{b+1}\left(\frac{E_G}{2kT}+2\right)+\frac{3}{4}\ln\frac{m_e}{m_h}\right] \quad (4)$$

where E_G is the width of the forbidden band and where m_e and m_h are the effective masses of the electron and the hole respectively. In this equation, b denotes the ratio of the electron mobility, μ_e, to the hole mobility, μ_h; it is given by:

$$b=\frac{\mu_e}{\mu_h}=\left[\frac{E_G}{2}-\frac{\Delta Q}{\Delta(10^3/T)}\right]\left[\frac{E_G}{2}+\frac{\Delta Q}{\Delta(10^3/T)}\right]^{-1} \quad (5)$$

provided that Q is measured in mV. The application of these two equations implies that we should accept the band model as a basic work hypothesis. In the case of the *N*-methyl-phenothiazine complex, b is evaluated as 2.08, assuming that $E_G/2=0.20$ eV. As is shown in Fig. 1, the change of the sign is observed at $10^3/T=3.60$. Therefore, m_e/m_h can be estimated to be about 130 by means of Eq. (4). The values obtained for the *N*-ethyl-phenothiazine complex are listed in Table 1. The conductivity, σ, is given by:

$$\sigma=\frac{1}{\rho}=e(\mu_e+\mu_h)N\exp(-E/kT)=e\mu_e\left(\frac{b+1}{b}\right)N\exp(-E/kT) \quad (6)$$

where $N=2.53\times10^{22}$ *N*-methyl-phenothiazine molecules or 2.30×10^{22} *N*-ethyl-phenothiazine molecules per cm^3 of the complex. With the values given in Table 1, the electron mobility in the *N*-methyl-phenothiazine complex is estimated as 0.23 cm^2/Vsec. This value falls right on the borderline between the band and hopping conduction and is of the same order as the only known Hall mobility observed with iodine complexes.[20] On the other hand, the hole mobility in the *N*-ethyl-phenothiazine complex is estimated to be smaller by a factor of hundreds. The width of a forbidden band is expected to reflect the strength of the interactions amongst the molecular orbitals; this strength, in turn, depends upon the degree of overlap of the orbitals. When the overlap is poor, the band is narrow

6) Y. Matsunaga and K. Shono, This Bulletin, **43**, 2007 (1970).
7) L. R. Melby, R. J. Harder, W. R. Hertler, W. Mahler, R. E. Benson, and W. E. Mochel, *J. Amer. Chem. Soc.*, **84**, 3374 (1962).
8) L. R. Melby, *Can. J. Chem.*, **43**, 1448 (1965).
9) H. Kusakawa and K. Akashi, This Bulletin, **42**, 263 (1969).
10) Y. Matsunaga and Y. Narita, *ibid.*, **45**, 408 (1972).
11) Y. Matsunaga, *Nature*, **205**, 72 (1965).
12) M. S. Frant and R. Eiss, *J. Electrochem. Soc.*, **110**, 769 (1963).
13) F. Beck, *Ber. Bunsenges. Physik. Chem.*, **68**, 558 (1964).
14) K. Ulbert, *J. Polymer Sci.*, Part C, No. 22, 881 (1969).
15) Y. Suzuki and Y. Matsunaga, Paper presented at the 24th Annual Meeting of the Chemical Society of Japan, Suita, April 1971.
16) S. N. Bhat and C. N. R. Rao, *Can. J. Chem.*, **47**, 3899 (1969).
17) F. Gutmann and H. Keyzer, *J. Chem. Phys.*, **46**, 1969 (1967).
18) V. A. Johnson and K. Lark-Horowitz, *Phys. Rev.*, **92**, 226 (1953).
19) J. Tauc, *ibid.*, **95**, 1394 (1954).
20) A. M. Hermann and A. Rembaum, *J. Appl. Phys.*, **37**, 3642 (1966).

and the carrier mobility is low. Consequently, both the small activation energy and the high resistivity observed in the *N*-ethyl-phenothiazine complex may be attributed to the poor overlapping of the thiazine molecules.

The slope of the Seebeck coefficient curve of the *N*-methylphenothiazine complex gradually becomes smaller in the temperature region which is markedly lower than the break observed in the resistivity curve. In the lower temperature region, the complex may be considered as an extrinsic semiconductor. The Seebeck coefficient may be expressed by:

$$Q=\pm\frac{k}{e}\left\{2+\ln\left[2\left(\frac{2\pi m^{*}kT}{h^{2}}\right)^{3/2}\right]-\ln c\right\} \quad (7)$$

where c is the concentration of the free electron or the hole, depending upon which is the major carrier and where m^{*} is the effective mass of the carrier. If kT is relatively small compared with the energy difference, ΔE, between an impurity level and the edge of the conduction or valence band, Q can be approximated by:

$$Q=\pm\frac{k}{e}\left[C+\frac{3}{2}\ln(kT)+\Delta E/2kT\right] \quad (8)$$

where C represents all the terms independent of the temperature. This expression is for a semiconductor with a partially-ionized impurity level. The (3/2) $\ln(kT)$ and $\Delta E/2kT$ terms vary in the opposite direction with respect to the temperature. As was pointed out by Hadek and Ulbert, a relatively good compensation between these two terms can be expected when the activation energy, $\Delta E/2$, is about 0.02 eV.[21] If we assume that the activation energy estimated by the resistivity measurement in the lower temperature region is valid even in the lower temperature region of the Seebeck coefficient curve, the change due to the former term can be expected to be overbalanced by that due to the latter, in accordance with the observations. However, the agreement is only qualitative. For example, the slope in the unit of $\Delta Q/\Delta(10^{3}/T)$ is calculated by Eq. (8) to be about 0.08 mV if $\Delta E/2=0.11$ eV. This value cannot be differentiated from the slope found in the higher temperature region. Unless the change in the activation energy occurs below the lower limit of the resistivity measurement, the observed slope is in serious disagreement with the calculated one. In the case of the *N*-ethyl-phenothiazine complex, the changes in the slope of the Seebeck coefficient curve are found around -15 and -50°C ($10^{3}/T=3.9$ and 4.5). None of them is located close to the break in the resistivity curve. The observed slope in the intermediate temperature region, 0.18 mV, is appreciably higher than that given by Eq. (8) with $\Delta E/2=0.045$ eV. Thus, it appears to be difficult to explain the Seebeck coefficient in the lower temperature region by the band model. This conclusion is not surprising if we consider the values of the carrier mobilities estimated above.

The resistivity-composition isotherms at $10^{3}/T=3.5$ and 4.5, where the component complexes may be supposed to behave as intrinsic and extrinsic semiconductors

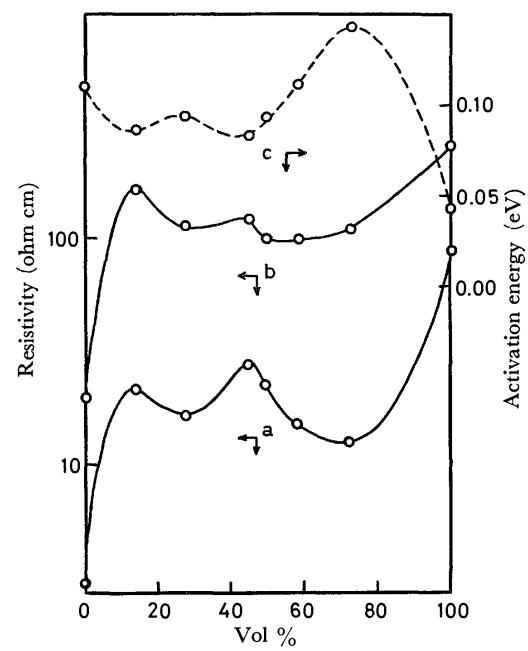

Fig. 2. Resistivities at (a) $10^{3}/T=3.5$ and (b) $10^{3}/T=4.5$ and (c) activation energies for semiconduction in the lower temperature region determined for the mixtures of iodine complexes of *N*-methyl- and *N*-ethyl-phenothiazines.

respectively, are presented in Fig. 2. Clearly, the present system does not obey Lichtenecker's logarithmic rule. The resistivity of the mixture at room temperature is much higher than that given by Eq. (1) when the volume percent of the *N*-ethyl-phenothiazine complex is less than 50%, and much lower when the percent is higher than 50%. In other words, the resistivity of the component complex is much more sensitive to the addition of a small amount of the other one than one would expect from Eq. (1). The resistivity exhibits a rather complicated temperature-dependence near room temperature; therefore, the relationship between the activation energy and the composition cannot be obtained.

When the temperature is lowered below -20°C ($10^{3}/T=4.0$), straight lines are obtained in the resistivity curve of all the mixtures. The isotherm at $10^{3}/T=4.5$ bears some resemblance to that observed in the higher temperature region. The deviation from Eq. (1) is small when the percent of the *N*-ethyl-phenothiazine complex is high; however, such a coincidence is accidental. As is plotted in Fig. 2, the activation energy does not obey Eq. (2), but depends, in a complicated way, on the composition. A marked maximum in the activation energy is found around 75% (see Curve *c* in Fig. 2); therefore, the resistivity-composition isotherm gives a large positive deviation from Eq. (1) in the entire composition if measured below -70°C ($10^{3}/T=5.0$). As a result, an increase in the resistivity of the *N*-ethyl-phenothiazine complex by the addition of a small amount of the *N*-methyl-phenothiazine complex is observed in such a temperature range. In addition, it must be noted that the shallow minimum around 30% in the resistivity-composition isotherm becomes less pronounced upon cooling. This change arises partially from the shift of the minimum at a

21) V. Hadek and K. Ulbert, *Coll. Czech. Chem. Commun.*, **32**, 1118 (1967).

higher content of the *N*-ethylphenothiazine complex to about 50%. The remarkable difference in the electrical properties between Ulbert's mixed system and ours must be attributed to the interaction of the two complexes in the latter system. As the room temperature is as high as 0.85 T_m, where T_m is the melting point given in °K, it is very likely that mixing results in the mutual, possibly partial, dissolution of the complexes.

The present work was supported by a grant-in-aid from the Ministry of Education, to which the authors' thanks are due.

BULLETIN OF THE CHEMICAL SOCIETY OF JAPAN, VOL. 45, 2100—2107(1972)

Light-scattering Studies of the Interaction between Bovine Serum Albumin and Guanidine Hydrochloride in Aqueous Solutions[1)]

Masayuki NAKAGAKI and Yoh SANO
Faculty of Pharmaceutical Sciences, Kyoto University, Sakyo-ku, Kyoto

(Received January 25, 1972)

The denaturation of bovine serum albumin (BSA) by guanidine hydrochloride (GuHCl) was studied by means of the light-scattering method. The Zimm plots were curved so that apparently imaginary values of the radius of gyration were obtained, but the modified Zimm plots, drawn by applying the correction factor for the optical anisotropy of segments, gave reasonable values of the weight-average molecular weight, the radius of gyration, and the second virial coefficient. The correction factor was calculated by using the experimental values of the scattering ratio at 90° of the scattering angle. The analysis of the intrinsic viscosity showed that the BSA molecules were elongated. According to these results, it has been concluded that the BSA molecules are streched by the denaturation the more as the GuHCl concentration is higher, and that the denatured BSA molecules, at first, form dimers by the side-by-side aggregation of two molecules, but that the intermolecular bindings, too, are broken with the further addition of GuHCl. The length reached at 5M GuHCl was about 1/5 of the fully stretched length. This suggests the possibility that the denatured BSA molecules can keep their local natural conformations.

It has been well established that proteins form complexes with various kinds of molecules and ions. The interaction between bovine serum albumin and sulfamines has also been studied by many investigators, including one of the present authors.[2)] As a continuation of these studies, the present authors intend to discuss the denaturation of bovine serum albumin (BSA) by guanidine hydrochloride (GuHCl) on the basis of a physico-chemical interpretation of the results from light-scattering measurements.

Bovine serum albumin is one of the well-studied proteins; its molecular weight is said to be about 70000, and its isoelectric is 6.4. Guanidine hydrochloride is a typical denaturating agent extensively used for various proteins. The mechanism of the denaturation is considered to involve the breaking-down of the secondary intramolecular bonds, such as ionic bonds, hydrogen bonds and hydrophobic bonds, as a result of the selective combination of GuHCl on the proteins, the conformation of the latter being changed according to the complex formation. The mechanism of the denaturation, however, has not yet been made very clear, particularly in relatively low concentrations of the denaturating agent or in the earlier stages of the denaturation process.

In the present investigation, the denaturation of BSA by GuHCl in aqueous solutions has been studied, including the low concentration range of the latter. The experimental method mainly used was light-scattering measurements, which were undertaken with particular attention paid to the following two points: (1) the variation in the refractive index increment, $(\partial n/\partial c)$, due to the complex formation, and (2) the deformation of the so-called Zimm plots due to the optical anisotropy of segments of the macromolecules.

Experimental

Materials. The guanidine hydrochloride used was a guaranteed reagent supplied by Nakarai Chemicals, Ltd. A solution of 6M was prepared gravimetrically, and from it solutions of various concentrations were prepared volumetrically.

The bovine serum albumin used was Fraction V from Armour Co. Ltd. (No. G5717, D. 1029), the same as that used in the previous paper.[3)] The concentration of BSA was determined by measuring the optical density at 278 mμ by means of a Shimadzu photoelectric spectrometer QR-50 with quartz cells 1 cm thick.

Water was distilled, refined by ion-exchange resin, and distilled again with an all-glass still.

Scattered Light Intensity. The method of the light-scattering measurements was the same as in the previous paper.[3)] A Shimadzu electrophotometric light-scattering photometer, PG-21, was used at 436 mμ and at 25°C. The

1) Presented at the 90th Annual Meeting of the Pharmaceutical Society of Japan held in Fukuoka in April, 1970.

2) M. Nakagaki *et al.*, *Yakugaku Zasshi*, **83**, 586 (1963); **84**, 516 (1964); **86**, 447 (1966); **87**, 817, 980, 1089 (1967).

3) M. Nakagaki and Y. Sano, This Bulletin, **45**, 1077 (1972).

reduced scattering intensity for unpolarized incident light, $R_u(\theta)$, was obtained and examined by the Zimm plot method, where θ is the scattering angle. The solutions and the solvent for the light-scattering measurements were made optically clear by ultrafiltration with Membrane Filter No. 15 from Sartorius Co., Ltd. It has been ascertained that the concentration of BSA does not change upon the ultrafiltration.

Scattering Ratio. The measurements were made by using the light-scattering photometer described above. The photometer was, for this experiment, equipped with a polarizer but not with an analyzer. The direction of the vibration of the electric vector of the light which passed through the polarizer was determined by using a reflecting glass plate set perpendicular to the plane of observation, for the intensity of the reflected light is greatest when the light vibrates perpendicularly to the plane of observation. The scattering ratio, $S(\theta)$, defined by the following equation:

$$S(\theta)=J_{//}(\theta)/J_{\perp}(\theta) \quad (1)$$

was determined, rotating the polarizer by 90°, where $J_{//}(\theta)$ and $J_{\perp}(\theta)$ are the Rayleigh ratios for incident beams vibrating, respectively, parallel to and perpendicular to the plane of observation, the latter being the plane containing the incident and scattered beams.

Refractive Index Increment. The measurements were made by means of a Shimadzu photoelectric differential refractometer, DR-3 type (Brice type) at 436 mμ and at 25°C, according to the method described in the previous paper.[3]

Two kinds of refractive index increment, ϕ_c and ϕ_μ, are defined as follows:

$$\phi_c=(\partial n/\partial c_2)_{T,P,c_3} \quad (2a)$$

$$\phi_\mu=(\partial n/\partial c_2)_{T,P,\mu_3} \quad (2b)$$

where n is the refractive index of the solution, T is the temperature, P is the pressure, and c_2 and c_3 are the concentrations in g/ml of BSA and GuHCl respectively. The ϕ_c quantity is measured by diluting a mixed solution of BSA and GuHCl with a GuHCl solution whose concentration is the same as in the mixed solution. The ϕ_μ quantity, on the other hand, is measured by diluting it with a GuHCl solution which has been in membrane equilibrium with the mixed solution.

In the latter case, the membrane equilibrium was achieved by using a size-18/32 cellotube (diameter, 1.5 cm) of the Visking Co. It was swollen in pure water, soaked in a 0.05M EDTA solution for 30 min treated with hot water of 90°C for 30 min, washed sufficiently with pure water, and then used for the membrane equilibrium. The cellotube containing a mixed solution of BSA (about 0.5%) and GuHCl was shaken for 3 days at 25°C in an "outer" solution which contained GuHCl of the same concentration as the "inner" solution, the volume of the former being twice the latter. The concentration of GuHCl was determined by two methods: (1) by the measurement of the refractive index of the solution by means of the differential refractometer mentioned above, and (2) by the Mohr method of titrating the chloride ion with an $AgNO_3$ solution. The results of these two methods agreed well with each other. The concentration of BSA was determined spectrophotometrically, and it was ascertained that no BSA was present in the outer solution after the equilibrium.

Intrinsic Viscosity. The viscosity of the BSA solution containing GuHCl was measured by means of an Ostwald Viscometer in a thermostat at 25°C. It took about 120 sec for pure water to flow down. The intrinsic viscosity, $[\eta]$, of BSA was calculated according to the Huggins equation:

$$\eta_{sp}/(100c_2)=[\eta]+k[\eta]^2\cdot(100c_2) \quad (3)$$

where η_{sp} is the specific viscosity of the solution calculated by considering the GuHCl solution as the solvent. Here, c_2 is the concentration of BSA in g/ml, and k is the Huggins constant.

Density. A picnometer (about 35 ml) was used a 25°C. The methods of the measurements and of the analysis of the results were the same as those described in the previous paper.[3]

Results

Viscosity and Density. The viscosity, η, of the BSA solution containing GuHCl has been measured at various BSA concentrations, c_2(g/ml), by diluting the original solution with the solvent that contains GuHCl at the same concentration, [GuHCl] (M), as in the original solution. The relation between the reduced viscosity, $10^{-2}\cdot\eta_{sp}/c_2$, and the concentration of BSA, $100c_2$, is shown in Fig. 1 for various GuHCl

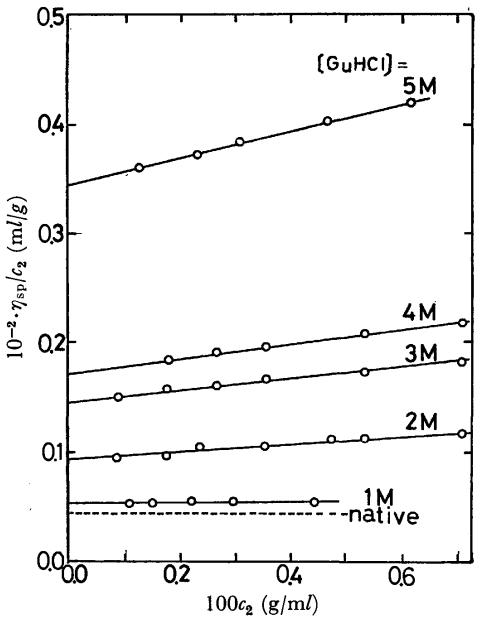

Fig. 1. Relations between the reduced viscosity and concentration of BSA for various GuHCl concentration.

concentrations. A linear relationship was seen for each case, with a good reproducibility. The dotted line in Fig. 1 is for native BSA, that is, for [GuHCl]=0. The intrinsic viscosity, $[\eta]$, the slope of the straight lines, $k[\eta]^2$, and the Huggins constant, k, obtained from these data according to Eq. (3) are shown in Table 1. The intrinsic viscosity of the denatured BSA increases

Table 1. Intrinsic viscosity and specific volume of denatured BSA

[GuHCl] (M)	$[\eta]$ (100 ml/g)	$k[\eta]^2$ (100 ml/g)^2	k	$\bar{v}_2$ (ml/g)
0	0.045	0	0	0.7265
1	0.054	0	0	—
2	0.093	0.033	3.4	—
3	0.145	0.054	2.1	0.7265
4	0.172	0.066	2.2	—
5	0.345	0.120	1.0	0.7265

with the GuHCl concentration, particularly in the range between 4M and 5M.

The partial specific volume of BSA, $\bar{v}_2$, in GuHCl solutions did not vary with the concentration of the latter; the average value was 0.7265 ml/g, as is shown in Table 1. This is in accord with the fact that the partial specific volume of BSA does not change upon the addition of urea, as has been reported in the literature.[4]

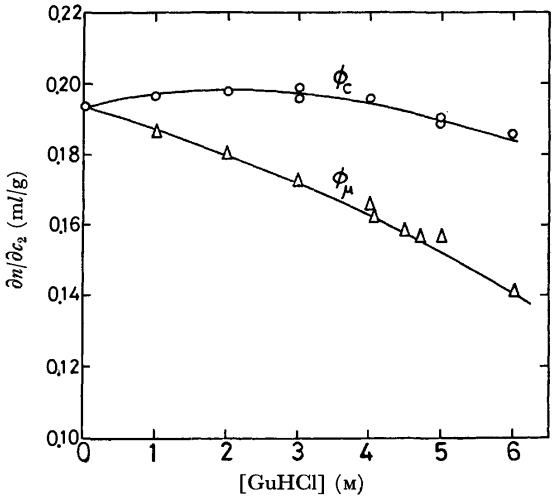

Fig. 2. Refractive index increments, ϕ_c(○) and ϕ_μ(△), of BSA in GuHCl solutions.

Refractive Index Increment. The refractive index of the solution, n, was found to be linear to the BSA concentration, c_2 (g/ml). Two kinds of refractive index increment, ϕ_c and ϕ_μ, as defined by Eqs. (2a) and (2b) respectively, were obtained at various GuHCl concentrations, [GuHCl] (M). The results are shown in Fig. 2. The concentration of GuHCl in the outer solution at the membrane equilibrium was the same as that in the inner solution, at least within the limits of accuracy of the chemical analysis, since the concentration used here was relatively high. In spite of this, the values of these two refractive index increaments, ϕ_c and ϕ_μ, were definitely different from each other, as is shown in Fig. 2. This means that GuHCl is bound to BSA, as will be quantitatively discussed later on.

Light Scattering. The reduced scattering intensity for unpolarized incident light, $R_u(\theta)$, was measured as a function of the scattering angle, θ, at various BSA concentrations, c_2(g/ml), using GuHCl solutions of the respective concentrations. [GuHCl] (M), as the solvents. According to the usual Zimm-plot method, the apparent values of the weight-average molecular weight, M*, the radius of gyration, R_g*, and the second virial coefficient, A_2, are expected to be obtained on the basis of the following well-known equation:

$$\frac{K'\phi_\mu^2 c_2}{R_u(\theta)}=\frac{1}{M^*}\left(1+\frac{16\pi^2}{3\lambda^2}R_g^{*2}\sin^2\frac{\theta}{2}\right)+2A_2c_2 \quad (4)$$

where:

$$K'=2\pi^2 n_1^2/N_0\lambda_0^4 \quad (5)$$

4) S. Katz and T. G. Ferris, *Biochemistry*, **5**, 3246 (1966).

It has been established[5] that ϕ_μ, instead of ϕ_c, must be used in Eq. (4) for multi-solute systems.

In the case of [GuHCl]=0, it has been reported[3] that the Zimm plot of native BSA in a 0.01M sodium chloride solution (pH=5.40) is in accord with Eq. (4), that the value of the molecular weight (M^* in Eq. (4)) is 71900, which is in good agreement with the value reported in the literature,[6] and that the value of the second virial coefficient, A_2, is nearly equal to zero. On the other hand, the Zimm plot of the BSA denatured by the addition of GuHCl could not completely be analyzed according to Eq. (4).

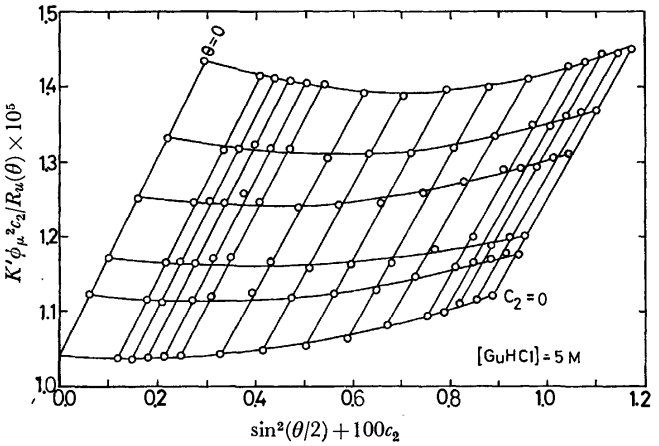

Fig. 3. Zimm plot of BSA at [GuHCl]=5M.

Table 2. Results of light scattering measurements

GuHCl (M)	$M^*\times10^{-4}$	$A_2\times10^4$ (mol·ml/g^2)	$M\times10^{-4}$	M/M_0	R_g (Å)
0	7.09	0	6.84	1.00	45
1	9.34	1.23	8.97	1.26	58
2	13.70	1.20	13.23	1.85	77
3	13.70	0.83	13.33	1.88	92
4	12.05	3.00	11.61	1.64	113
5	9.61	6.75	9.24	1.30	147

It can be seen from Fig. 3, which shows the case of [GuHCl]=5M as an example, that the plots obtained by the extrapolation to zero of θ are linear against c_2, and that the intersection and the inclination of the straight line give the apparent molecular weight, M^*, and the second virial coefficient, A_2, according to Eq. (4). The values of M^* and A_2 thus obtained are given in Table 2. However, the plots obtained by the extrapolation to zero of c_2 are not linear against $\sin^2(\theta/2)$, so Eq. (4) cannot be used to obtain the apparent value of R_g*. The initial slope (the slope at the limit of $\theta\to0$) cannot be used, either, because the slope is negative in the case of Fig. 3 and because R_g* cannot take an imaginary value. This anomalous behavior may be supposed to be due to the optical anisotropy of segments. The correction factor for this can be calculated, according to the theory presented previously,[7] by using the

5) J. G. Kirkwood and R. J. Goldberg, *J. Chem. Phys.*, **18**, 54 (1950); W. H. Stockmayer, *J. Chem. Phys.*, **18**, 58 (1950).

6) J. T. Edsall, H. Edelhoch, R. Lontie, and P. R. Morrison, *J. Amer. Chem. Soc.*, **72**, 464 (1950).

7) M. Nakagaki, This Bulletin, **34**, 834 (1961).

value of the scattering ratio at $\theta=90°$.

Scattering Ratio. If the segments of a macromolecule are completely isotropic and are sufficiently small compared to the wavelength of light, the light scattered at $\theta=90°$ must be completely polarized and vibrating perpendicularly to the plane of observation, even when unpolarized light is used as the incident light. If the incident light is linearly polarized, the intensity of the scattered light at $\theta=90°$ must be zero when the incident light is vibrating parallel to the plane of observation, as long as the segments are isotropic and sufficiently small.

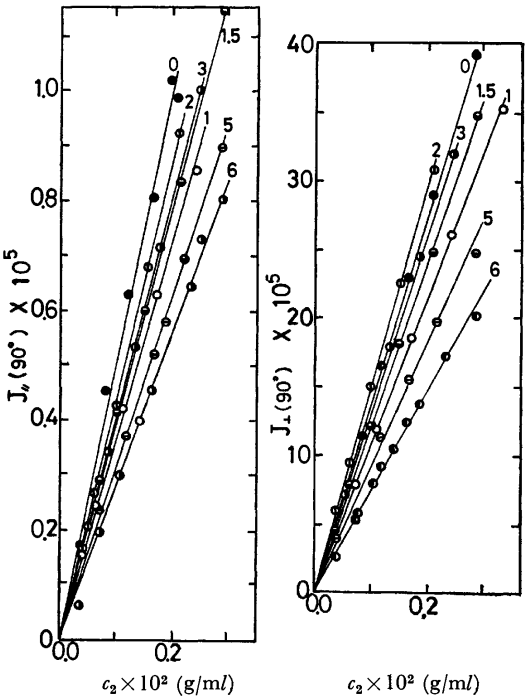

Fig. 4. The proportionality of the Rayleigh ratios, $J_\perp$ (90) and $J_{//}(90)$, to BSA concentration, at various GuHCl concentrations.

On the other hand, if the segments are optically anisotropic, the scattered light is depolarized even at $\theta=90°$, or the scattered light has some intensity even when the linearly-polarized incident light is vibrating parallel to the plane of observation. The Rayleigh ratio, that is, the scattered light intensity per unit of solid angle from a unit of the volume of the solution per unit of the intensity of the incident light, was measured at $\theta=90°$ for the incident light vibrating perpendicular to and parallel to the plane of observation; the results, $J_\perp$ (90°) and $J_{//}$ (90°) respectively, are shown in Fig. 4 as functions of the BSA concentration, c_2 (g/ml). The parameter values in Fig. 4 show the GuHCl concentration, [GuHCl] (M). In each case, the scattered light intensity is proportional to the BSA concentration.

The values of the scattering ratio at $\theta=90°$, Q, defined by the following equation:

$$Q=S(90°)=J_{//}(90°)/J_\perp(90°) \tag{6}$$

are given in Table 3 for various GuHCl concentrations. The scattering ratio is of the same numerical value as the depolarization ratio for unpolarized incident light, but the latter has an experimental disadvantage because perfectly unpolarized incident light is rather difficult to obtain. The scattering ratio is, therefore, used in the present paper. As is shown in Table 3, the scattering ratio is slightly dependent on the GuHCl concentration, although it is nearly independent of the BSA concentration.

Table 3. Scattering ratio and anisotropy of BSA segments

[GuHCl] (M)	$Q\times10^2$	p_a	m
0	3.70	1.65	1.199
1	3.40	1.62	1.199
2	2.96	1.57	1.198
3	3.08	1.59	1.194
4	3.15	1.59	1.194
5	3.33	1.62	1.182

Discussion

Variation in the Refractive Index Increment due to the Complex Formation. In a ternary system, water (1)-protein (2)-low-molecular-weight substance (3), the analysis of the refractive index increment and, therefore, of the light-scattering data is simple if one can treat the aqueous solution of the third component as a solvent (1+3) and the ternary system as a solution of the protein (2) in the solvent (1+3). According to this conventional method, the refractive index increment, ϕ_c, defined by Eq. (2a) is measured by diluting the ternary system with a "solvent" (1+3) whose concentration is c_3 (g/ml).

If, however, a special interaction such as complex formation exists between the protein (2) and the third component (3), the "free" concentration or the chemical potential of the third component decreases with the complex formation. This results in a change in the composition of the solvent (1+3). In order to obtain the refractive index increment, ϕ_μ, defined by Eq. (2b), the solvent composition must be kept constant by diluting the ternary system with a solution which is in a membrane equilibrium with the ternary system.

Several theoretical papers discussing the relation between the ϕ_c and ϕ_μ are found in the literature.[5,8] In most cases reported so far, the difference between ϕ_c and ϕ_μ is small enough, particularly when the concentration of the third component is smaller than about 0.5M. If, however, the c_3 concentration is higher than this, or if the third component has a particularly strong affinity to the protein, the difference between these two quantities becomes important. In this case, the following equation is used at a constant temperature and pressure:

$$\left(\frac{\partial n}{\partial c_2}\right)_{\mu_3}=\left(\frac{\partial n}{\partial c_2}\right)_{c_3}+\left(\frac{\partial n}{\partial c_3}\right)_{c_2}\cdot\left(\frac{\partial c_3}{\partial c_2}\right)_{\mu_3} \tag{7}$$

Here, the quantity $(\partial n/\partial c_3)_{c_2}$ is the refractive index increment of the third component at a constant protein

8) R. H. Ewart, C. P. Roe, P. Debye, and J. R. McCartney, *J. Chem. Phys.*, **14**, 687 (1946); H. C. Brinkman and J. J. Hermans, *ibid.*, **17**, 574 (1949); J. Ooi, *J. Polymer Sci.*, **28**, 459 (1958); B. E. Read, *Trans. Faraday Soc.*, **56**, 382 (1960).

concentration, c_2. Since the value does not change very much, the value in water, ϕ_3, may be used for it as long as the protein concentration is not high. The quantity;

$$\delta' = \left(\frac{\partial c_3}{\partial c_2}\right)_{\mu_3} \tag{8}$$

is the amount of the third component bound to the protein (g/g), if c_2 and c_3 are expressed in g/m*l*. Therefore, Eq. (7) may be rewritten as follows:

$$\phi_\mu = \phi_c + \phi_3 \cdot \delta' \tag{9}$$

The apparent binding ratio, δ', can thus be calculated from the data shown in Fig. 2 and the experimental value for GuHCl: $\phi_3 = 0.1938$ m*l*/g. The value of δ' is negative, however, as is shown in Table 4, because ϕ_μ is smaller than ϕ_c. The negative value of the apparent binding ratio, δ', is due to the effect of the volume excluded by BSA molecules. The actual value of the binding ratio, δ (g/g), is obtained by means of:

$$\delta = \delta' + c_3\bar{v}_2 \tag{10}$$

Here, $\bar{v}_2$ is the specific volume of BSA, 0.7265 (m*l*/g), and is independent of the GuHCl concentration, c_3, as is shown in Table 1.

The molar binding ratio of GuHCl per amino-acid residue of BSA, δ_m (mol/mol), may be calculated on the basis of the average molecular weight per amino-acid residue, $\bar{M}_a = 112.8$, which is obtained by means of the data on amino-acid composition of BSA reported in the literature.[9] As may be seen in Table 4, the value of δ_m increases with the GuHCl concentration, but it is less than 1 even at concentrations as high as 6M GuHCl.

TABLE 4. BINDING RATIOS OF GuHCl TO BSA

[GuHCl] (M)	δ' (g/g)	δ (g/g)	δ_m (mol/mol)
1	−0.0465	0.1159	0.1369
2	−0.0929	0.2318	0.2738
3	−0.1280	0.3363	0.3972
4	−0.1662	0.4439	0.5243
5	−0.1863	0.5334	0.6299
6	−0.2338	0.6503	0.7679

Optical Anisotropy of BSA Segments and of Benzene. It has already been discussed theoretically in a previous paper[7] that the angular variation in the scattered light intensity from macromolecules depends on the optical anisotropy of the segments, and that the degree of the anisotropy could be estimated by means of measurements using polarized incident light.

In the case of isotropic segments which can be treated as Rayleigh spheres, the Rayleigh ratio for unpolarized incident light, $J_u(\theta)$, is proportional to the $(1+\cos^2\theta)$ factor. According to this fact, the reduced scattering intensity, $R_u(\theta)$, used in Eq. (4) may be defined by the following equation:

$$R_u(\theta) = J_u(\theta)/(1+\cos^2\theta) \tag{11}$$

If the segments are Rayleigh scatterers, the value of $R_u(\theta)$ is independent of the scattering angle, θ, except the anglar dependency due to the interference factor which contains the term of the radius of gyration.

In the case of anisotropic segments, however, $R_u(\theta)$ is dependent on the scattering angle, θ. If the segments are considered to be Rayleigh-Gans scatterers, as in the previous paper,[7] the Rayleigh ratios are given as follows, since $R_u(90°) = J_u(90°)$:

$$\frac{J_{/\!/}(\theta)}{R_u(90°)} = \frac{2Q}{1+Q} + 2\left(\frac{1-Q}{1+Q}\right)\cos^2\theta \tag{12a}$$

$$\frac{J_\perp(\theta)}{R_u(90°)} = \frac{2}{1+Q} \tag{12b}$$

$$\frac{J_u(\theta)}{R_u(90°)} = 1 + \left(\frac{1-Q}{1+Q}\right)\cos^2\theta \tag{12c}$$

Before going further, these relations were examined experimentally by using benzene, a standard liquid commonly used to determine the cell constants of the light-scattering apparatus. The values of $R_u(90°)$ and Q for benzene are known from the literature[10] to be $R_u(90°) = 4.85 \times 10^{-5}$ and $Q = 0.41$, the latter being equal to the depolarization ratio, ρ_u. Eqs. (12a—c) for benzene are, therefore:

$$\left.\begin{aligned} J_{/\!/}(\theta) \times 10^5 &= 2.82 + 4.06\cos^2\theta \\ J_\perp(\theta) \times 10^5 &= 6.89 \\ J_u(\theta) \times 10^5 &= 4.85 + 2.03\cos^2\theta \end{aligned}\right\} \tag{13}$$

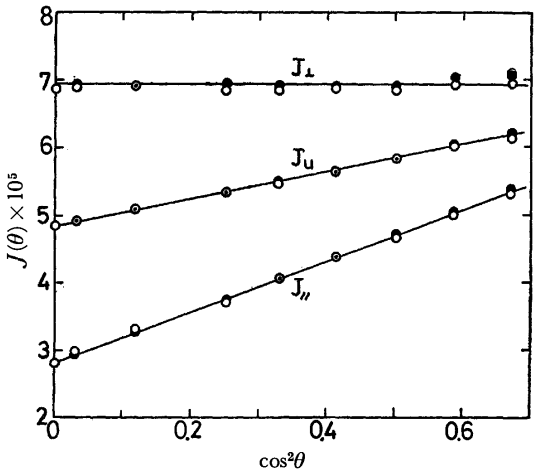

Fig. 5. The relation between the Rayleigh ratios, $J(\theta)$ and $\cos^2\theta$, for benzene. (○) $\theta < 90°$, (●) $\theta > 90°$.

The experimental values obtained for benzene purified by the method described in the previous paper[3] are shown in Fig. 5, with open circles for $\theta < 90°$ and closed circles for $\theta > 90°$, together with the straight lines drawn according to Eq. (13). The agreements between the experiment and the theory are satisfactory.

Since Eqs. (12a—c) have been justified experimentally, the treatment may be extended to explain the anomalous behaviour of the Zimm plots of BSA, an example of which has been shown in Fig. 3. For this purpose, the following equation, which can be derived easily from Eq. (12c), may be used:

$$P_u(\theta) = \frac{R_u(\theta)}{R_u(0)} = 1 + Q\frac{1-\cos^2\theta}{1+\cos^2\theta} \tag{14}$$

9) W. H. Stein and S. Moore, *J. Biol. Chem.*, **178**, 79 (1949).

10) C. L. Carr and B. H. Zimm, *J. Chem. Phys.*, **18**, 1616 (1950).

Before doing this, the Q-values of BSA given in Table 3 will be discussed further. The Q quantity is related to the excess-polarizability ratio, p_α, defined by:

$$p_\alpha = \alpha_a/\alpha_b \tag{15}$$

where α_a and α_b are the principal values of the excess polarizability (in excess of that of the solvent) of the segments parallel to and perpendicular to, respectively, the axis of the rotation of the spheroidal segments. The relation is given by the following equation:[11]

$$Q = \frac{(2/15)(p_\alpha-1)^2}{1+(2/3)(p_\alpha-1)+(1/15)(p_\alpha-1)^2} \tag{16}$$

It is obvious that $Q=0$ for optically-isotropic segments ($p_\alpha=1$). The p_α-values of BSA obtained by Eq. (16) are given in Table 3. It may be seen that the value of p_α changes only a little with the GuHCl concentration and shows its minimum point at about 2—3M of the latter. This is related to the side-by-side dimerization of BSA molecules, as will be discussed later on.

As for the magnitude of the p_α value, it has already been concluded in a previous paper[7] that the value should be within the following range, if the anisotropy is due to the anisometry, that is, the segments are considered to be non-spherical particles of an isotropic material. If the value of p_α is outside the range, the segments must have intrinsic anisotropy:

$$(m^2+1)/2 > p_\alpha > 1/m^2 \tag{17}$$

where m is the relative refractive index of the segments.

The value of m may be estimated according to the following equation:[7]

$$\phi_\mu = (m-1)n_1\bar{v}_2 \tag{18}$$

Here, $\bar{v}_2$ is the specific volume of BSA, as is given in Table 1, and n_1 is the refractive index of the solvent, that is, the GuHCl solution of the corresponding concentration. As is shown in Table 3, the value of m is about 1.2, which is the value usually obtained for various organic substances in water.

The range given by Eq. (17) for this m-value is:

$$1.21 > p_\alpha > 0.70 \tag{19}$$

The p_α value of BSA shown in Table 3 is definitely outside this range. The optical anisotropy of BSA may, therefore, be concluded to be intrinsic.

Modified Zimm Plot of Denatured BSA. For the macromolecules of anisotropic segments, it has already been stated[7] that the light-scattering equation must be modified by replacing M^* of Eq. (4) with $M\cdot P_u(\theta)/F$, where $P_u(\theta)$ is the function already given by Eq. (14), and where the factor, F, is given by the following equation:[12]

$$F = 1-(7/6)Q \tag{20}$$

Equation (4) can, therefore, be rewritten as follows, since $P_u(0)=1$:

$$[P_u(\theta)/F]\cdot[K'\phi_\mu^2 c_2/R_u(\theta)] = \frac{1}{M}\left(1+\frac{16\pi^2}{3\lambda^2}R_g^2\sin^2\frac{\theta}{2}\right)+2\frac{A_2}{F}c_2 \tag{21}$$

11) The quantity, p_α, defined here is the reciprocal of that used in Ref. 7. Equation (16) may be derived readily from Eqs. (21) and (29) of the same paper.

12) The equation $F=1+Q/2$, derived from Eqs. (29) and (37) of Ref. 7, is in error. This point will be discussed in a separate paper.

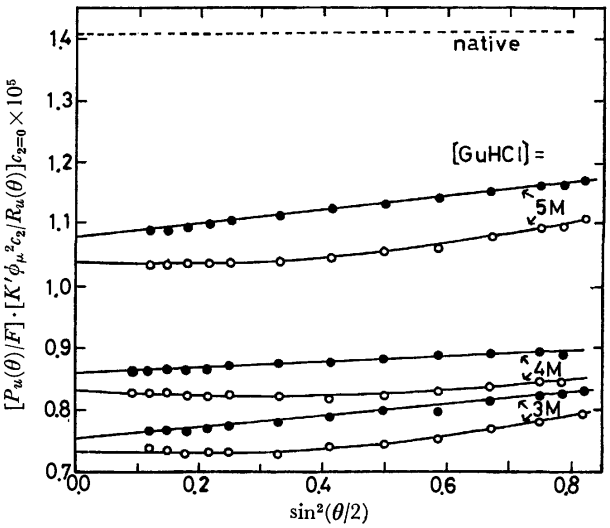

Fig. 6. Usual (open circles) and modified (closed circles) Zimm plots of BSA at $c_2\to 0$, for various GuHCl concentrations.

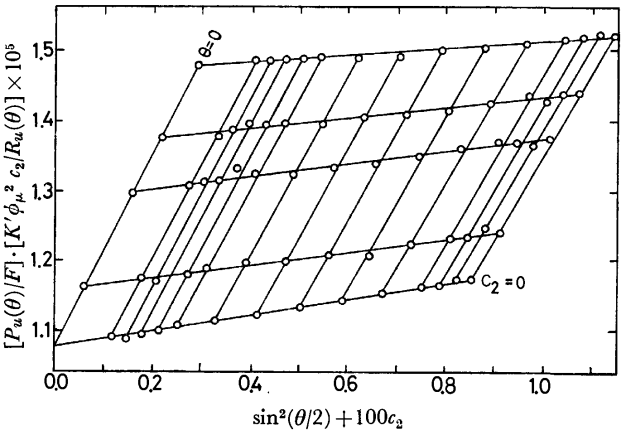

Fig. 7. Modified Zimm plot of BSA at [GuHCl]=5M.

The left side of Eq. (21) can be plotted on the ordinate to draw the modified Zimm plot, because $P_u(\theta)$ and F can be calculated by using the value of Q obtained experimentally, as is shown in Table 3.

It can be seen from Fig. 6 that the plots for $c_2\to 0$ are curved in the usual Zimm plots, as is shown by the open circles, but that the plots are on straight lines in the modified Zimm plots, as is shown by the closed circles. As an example, the modified Zimm plot of BSA in 5M GuHCl is given in Fig. 7; it is composed of straight lines only, in contradistinction to the usual Zimm plot of the same system shown in Fig. 3. It may, therefore, be concluded that the curved feature of the usual Zimm plot, and also the apparently imaginary value of the radius of gyration, R_g^*, are due to the optical anisotropy of BSA. The correct values of the molecular weight, M, and the radius of gyration, R_g, as obtained from the modified Zimm plot, are given in Table 2.

Molecular Weight of Denatured BSA. The weight-average molecular weight, M, of BSA, obtained from the modified Zimm plot, increases with the GuHCl concentration at first and then reaches a maximum point at about 3M GuHCl, as is shown in Table 2. The ratio (M/M_0) of the molecular weight to that of

native BSA is nearly equal to 2 at the maximum point. This means that dimers are formed by the intermolecular binding of two denatured BSA molecules. With a further increase in the GuHCl concentration, however, the intermolecular binding seems to be broken, because the molecular weight decreases to as low as $M/M_0=$ 1.30 at 5M GuHCl.

The following conclusions may, therefore, be drawn: (1) GuHCl, at first, breaks the intramolecular binding of BSA and changes the shape of the molecules, as will be discussed in the next section. (2) The broken bonds, which have been brought to the outer surface of the molecule by the change in the molecular shape, combine with those of another denatures BSA molecule to form a dimer. (3) These intermolecular bonds, too, are broken with a further increase in the GuHCl concentration.

Molecular Shape and Intrinsic Viscosity of Denatures BSA. As has been described above, the following three quantities, the intrinsic viscosity, $[\eta]$; the molecular volume, V_m (which is equal to $M\bar{v}_2/N_0$, where N_0 is the Avogadro number), and the radius of gyration, R_g, of BSA at various GuHCl concentrations have been determined. On the basis of these results, the shape and size of BSA molecules may be discussed if the molecular shape is approximated by a suitable model, as has already been shown in a previous paper[13] on chondroitin sulfate.

If the denatured BSA molecule is approximated by a random coil;[14]

$$[\eta]=6^{3/2}\Phi R_g^3/M \tag{22}$$

where $\Phi=2.87\times10^{21}$.

In the case of a cylindrical rod or a sheroid,

$$[\eta]=0.025\bar{v}_2\cdot\nu(p) \tag{23}$$

where $\nu(p)$ is the shape factor as a function of the axial ratio, p.

$$p=L/D=a/b \tag{24}$$

where L and D are the length and diameter respectively of the cylindrical rod, and where a and b are the radii of the sheroid in the direction parallel to and parpendicular to respectively, the axis of rotation. The shape factor is given by one of the following equations.[15]

$$\nu(p)=0.373+0.08p^2\left\{\frac{1}{3(\ln 2p-1.8)}+\frac{1}{(\ln 2p-0.8)}\right\} \tag{25a}$$

For a prolate sheroid ($p>1$),

$$\nu(p<15)=1+0.163(p-1)^{1.508} \tag{25b}$$

$$\nu(p>15)=0.64+0.08p^2\left\{\frac{1}{3(\ln 2p-1.5)}+\frac{1}{(\ln 2p-0.5)}\right\}$$

For a oblate spheroid ($p<1$),

$$\nu(p)=1+0.272\frac{1-p}{p}-0.251\left\{\frac{1-p}{1-0.075p}\right\} \tag{25c}$$

The value of $[\eta]$ may, therefore, be calculated if the value of the axial ratio, p, is known.

The molecular volume, V_m, is given by the equation:

$$V_m=\frac{\pi}{4}L^3/p^2=\frac{4}{3}\pi a^3/p^2 \tag{26}$$

The radius of gyration, R_g, is given as follows. For a cylindrical rod,

$$R_g^2=\frac{L^2}{12}(1+3/2p^2) \tag{27a}$$

For a sheroid,

$$R_g^2=\frac{a^2}{5}(1+2/p^2) \tag{27b}$$

According to these equations, the molecular dimensions, L and D or a and b, and the axial ratio, p, can be calculated.

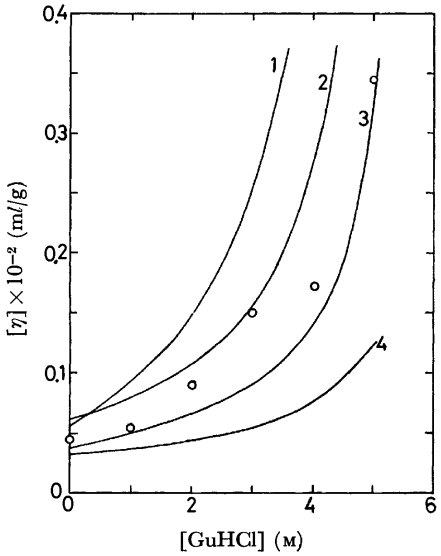

Fig. 8. Intrinsic viscosity of BSA in GuHCl solutions.
(1) Random coil, (2) cylindrical rod, (3) prolate spheroid and (4) oblate spheroid.

The value of the intrinsic viscosity, $[\eta]$, obtained experimentally and theoretically are compared in Fig. 8. The experimental values, already given in Table 1 and shown in Fig. 8 by open circles, are close to the theoretical curve of the prolate spheroid, except at a GuHCl concentration of about 3M, where the experimental plot is close to the theoretical curve of the cylindrical rod, probably because the dimer formation is the most complete at this GuHCl concentration. At any rate, the experimental plots are located between the theoretical curve of the prolate spheroid and that of the cylindrical rod. It may, therefore, be concluded that the denatured BSA molecules are shape in elongated.

TABLE 5. DIMENSIONS OF DENATURED BSA MOLECULES AS PROLATE SPHEROIDS

[GuHCl] (M)	a (Å)	b (Å)	p	b_1 (Å)	p_1
0	71.2	16.8	4.23	16.8	4.23
1	91.7	17.0	5.40	14.8	6.20
2	122.4	17.8	6.87	12.8	9.56
3	145.5	16.1	9.02	11.8	12.3
4	179.3	13.8	13.0	10.6	16.9
5	231.9	10.6	21.9	9.31	24.9

13) M. Nakagaki and K. Ikeda, This Bulletin, **41**, 553 (1968).
14) P. J. Flory, "The Principles of Polymer Chemistry," Cornell University Press (1953), p. 611.
15) R. Simha, *J. Phys. Chem.*, **44**, 25 (1940); *J. Chem. Phys.*, **13**, 188 (1945); W. Kuhn and H. Kuhn, *Helv. Chim. Acta*, **28**, 97 (1945); H. A. Scheraga, *J. Chem. Phys.*, **23**, 1526 (1955).

The dimensions and the axial ratio of BSA molecules as prolate spheroids are shown in Table 5. These values were calculated on the basis of the radius of gyration determined by the light-scattering measurements and on the basis of the molecular volume determined by the density measurements.

It may be mentioned here that the axial ratio, p, increases from 4.23 to 21.9 with the GuHCl concentration, in contradistinction to the excess-polarizability ratio, p_α, which scarcely changes with the GuHCl concentration, as shown in Table 3. This is because p_α expresses the optical anisotropy of each segment, while p expresses the anisometry of the molecule as a whole, and the molecule is composed of many segments.

According to Table 5, the length, $2a$, of BSA molecules increases monotonously with the GuHCl concentration, but the diameter, $2b$, has a maximum point at about 2M GuHCl. This maximum may be supposed to be due to the maximum of the dimerization of BSA at about this GuHCl concentration, suggesting that the dimerization is realized by a side-by-side combination of two denatured BSA molecules. If this is so, then the radius, b_1, and the corresponding axial ratio, p_1, of one BSA molecule in the aggregate may be calculated by means of the following equations:

$$b_1 = b/\sqrt{M/M_0}$$
$$p_1 = a/b_1 \tag{28}$$

As is shown also in Table 5, the value of b_1 monotonously decreases, and that of p_1 monotonously increases, with the GuHCl concentration. It may, therefore, be concluded that the denaturating agent, GuHCl, breaks the intramolecular bonds of BSA to make the molecular shape the longer as the GuHCl concentration is higher, and that two molecules of denatured BSA aggregate side-by-side to form a dimer.

The largest length of a BSA molecule observed here is $2a=464$ Å at 5M GuHCl. This is about 1/5 of the length of a fully-stretched BSA molecule, that is estimated to be about 2200 Å for BSA containing 602 amino-acid residues.[9] This is in contrast to sodium chondroitin sulfate C whose length is between 1/2 ($J=\infty$) and 2/3 ($J=0.01$M) of the fully-stretched length,[13] where J is the ionic strength. The relatively small stretching of the BSA molecule by denaturation suggests that denatured BSA molecules keep their natural local conformation even in a GuHCl solution as concentrated as 5M.

BULLETIN OF THE CHEMICAL SOCIETY OF JAPAN, VOL. 45, 2107—2110(1972)

An Isothermal Displacement Calorimeter for Measuring Enthalpies of Mixing

Reiji TANAKA, Sachio MURAKAMI, and Ryoichi FUJISHIRO

Department of Chemistry, Faculty of Science, Osaka City University, Sumiyoshi-ku, Osaka

(Received January 21, 1972)

An isothermal displacement calorimeter of the Van Ness type has been constructed. The calorimeter was tested on three systems, benzene+cyclohexane, cyclohexane+*n*-hexane, and benzene+dichloromethane, at 25°C, and the performance of the calorimeter was discussed in connection with the literature values. The precision of the new calorimeter was within 0.5%; this was equal to, or better than, that of calorimeters of a similar type which have been constructed by several investigators.

After the pioneering work of Van Ness and his co-workers[1-3] in isothermal dilution calorimetry, several calorimeters based upon a similar principle have been constructed and relatively precise enthalpies of mixing have been measured for various kinds of binary systems.

We have great interest in the measurements of enthalpies of mixing for non-ideal solutions at a high dilution, and this type of calorimeter seems to be most suitable for our purpose. The calorimeter was designed with the following features. (a) It is capable of measuring both exothermic and endothermic heats of mixing without any external calibration.[3] (b) The wall inside the mixing vessel is kept free from any dampness from the bath water by employing a vessel of fixed dimensions, the type of calorimeter designed by Stockes and his co-workers.[4,5] (c) By adopting a flange-type lid for sealing the vessel, the calorimeter is simple and can easily be washed after a run. Furthermore, the use of a flange-type lid makes a precision bore tube unnecessary.

The principle and the operation of this type of calorimeter have been fully described by Van Ness and his co-workers, so only a brief outline describing some improvements in our instrument will be given in the next section.

Apparatus and Procedure

A schematic drowing of the apparatus is shown in

1) R. V. Mrazek and H. C. Van Ness, *Amer. Inst. Chem. Engrs. J.*, **7**, 190 (1961).

2) C. G. Savini, D. R. Winterhalter, L. H. Kovach, and H. C. Van Ness, *J. Chem. Eng. Data*, **11**, 40 (1966).

3) D. R. Winterhalter and H. C. Van Ness, *ibid.*, **11**, 189 (1966).

4) R. H. Stokes, K. N. Marsh, and R. P. Tomlins, *J. Chem. Thermodynamics*, **1**, 211 (1969).

5) M. B. Ewing, K. N. Marsh, R. H. Stokes, and C. W. Tuxford, *ibid.*, **2**, 751 (1970).

Fig. 1, accompanied by enlarged sections of the mixing vessel. The vessel, A, is a 130 m*l* Dewar flask which is silvered and which has a strip window. The upper face of the vessel is polished flat, and on it lid, B, is fitted with two O-rings, C, held by six bolts, to provide a tight seal. The lid contains six main parts: the stirrer, the feed tube to introduce the second component, the air vent to introduce the first component, the thermistor, the heater, and the cooling assembly.

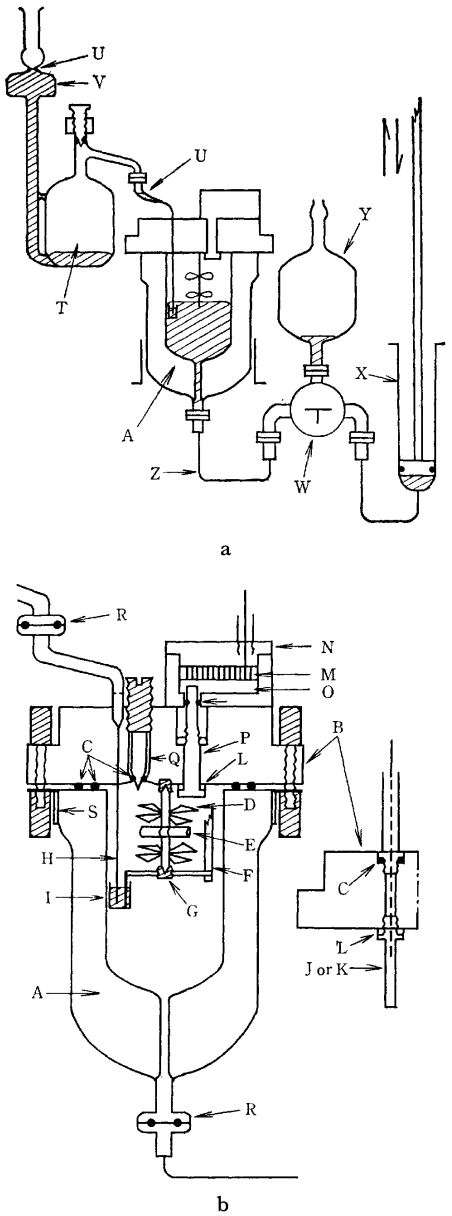

Fig. 1. Diagram of isothermal displacement calorimeter. A, silvered Dewar flask with strip window, capacity 130 ml; B, lid of Teflon impregnated with molybdenum disulphide and carbon; C, Viton O-ring; D, 4-blade propl lar (stainless steel), 19 mm diameter; E, magnet coated with Teflon attached to stirrer axle; F, stainless steel frame for stirrer; G, stainless teel screw to support stirrer; H, feed tube (needle of hypodermic syringe); I, mercury cup of stainless steel, capacity 1 m*l*; J, 37 KΩ thermistor in blass tube; K, 50Ω manganin wire heater in brass tube; L, Teflon washer; M, cooling module; N, stainless steel heat sink; O, copper cooling plate; P, copper cooling rod, 6 mm diameter; Q, air vent, sealed with bakelite screw and Teflon needle; R, glass or Teflon connector; S, brass collar, cemented to Dewar. T, feed bulb for second component, capacity 70 m*l*; U, meniscuss; V, mercury reservior, capacity 15 m*l*; W, three way tap, Teflon-glass; X, precision piston burette; Y, mercuty reservior; Z, stainless steel tube, 0.8 mm internal diameter.

The stirrer, D, is supported between the bottom of the lid and the stainless steel frame, F. It is rotated at 430 min^{-1}, activated by an external magnet by means of a constant-speed motor. The feed tube, H, is inserted through the lid into the cup, I, located on the stirrer frame. The cup is filled with mercury in order to separate the second component from the first.

The thermistor, J, about 37KΩ at 25°C, is used as the temperature-sensing element in the calorimeter vessel; it is mounted in a thin-walled brass tube containing a drop of oil in order to improve the thermal contact. The thermistor is balanced against a D.C. bridge, and its output signal is amplified and taken to a recorder. The thermistor is calibrated against the bath temperature each time before a run begins.

The wire heater, K, with a resistance of about 50Ω, consists of manganin wire wound on a small glass capillary and mounted in a thin-walled brass tube. The brass tube contains grease to make a good thermal contact and is sealed on the top with a small Teflon plug to prevent heat leakage from the top of the tube. The heater is connected in series with a 5V D.C. power supply, a rheostat, and a standard 1Ω resistance. A volt box, which contains two standard resistances of 30KΩ and 100Ω connected in series, is connected in parallel with the heater in order to reduce the potential drop across the heater by a factor of 301 for measurring the voltage of the heater. Before switching over to the calorimeter heater, the D.C. power supply is discharged into a dummy heater for 1 hr to stabilize the voltage output. The heater control switch turns the current from a dummy heater load to the heater and simultaneously activates an electronic timer. The heater power is calculated by measuring the voltages across the standard 1Ω resistance and reduced voltages across the 100Ω standard resistance in the volt box.

The cooling assembly consists of a 1500 mA cooling module (Cambion Thermoionic Corp. Model 3952-1), M, sandwiched between a stainless steel heat sink, N, and a copper cooling plate, O. The 6-mm-diameter copper rod, P, is connected to the copper plate, O, and penetrates through the lid into the mixing vessel. The thermal contact between the components is promoted by a thin film of silicon grease. The upper face of the stainless-steel heat sink is exposed to the water in a thermostatted bath.

The stabilized D.C. power supply, connected in series with a rheostat and with the cooling module, is used to activate the cooling module. The current through the cooling module is fed into a standard resistance in the by-passed circuit and the potential drop across the standard resistance is amplified by a D.C. amplifier in order to get the same sensitivity as the measurement of the heater power, and is monitored on a recorder.

After the calorimeter has been placed over 2 hr in a thermostatted bath controlled to within ±0.001°C, the temperature in the vessel is controlled by means of cooling module to the set temperature of the surroundings

within ± 0.0002°C. The stirring energy causes the steady temperature in the vessel to be higher than that of the thermostat by $\Delta T \approx 0.01$°C, so for the endothermic systems the current of the cooling module needs to compensate for only the energy dissipated by the stirrer. On the other hand, for the exothermic systems it needs to remove the energy supplied previously to the calorimeter heater. As soon as the temperature control is obtained, the run begins.

When the run is endothermic, the heater is switched on and the second component is introduced into the calorimeter vessel at such a rate that the contents of the vessel are kept at the set temperature within ± 0.003°C. At the end of each injection, the mercury level in the feed tube and in the mercury reservoir is restored before the final addition of energy is made. The equilibrium temperature is restored within 0.0002°C by the manipulation of the burette drive and heater switches.

When the run is exothermic, the heater is turned off so that the thermal energy of mixing is removed from the mixing vessel at a net rate equal to the rate of energy added previously by the heater before mixing. The other procedures in the exothermic run are the same as that in the endothermic run.

Test on Standard Systems

Materials. The systems used for testing the new calorimeter were benzene+cyclohexane, and cyclohexane+*n*-hexane at 25°C as endothermic systems and dichloromethane+benzene at 25°C as an exothermic system. The materials used in the cyclohexane+*n*-hexane system were Phillips Petroleum Company "Research Grade." The specified purity of the two hydrocarbon reagents has 99.98 mol per cent; these materials were used without further purification. The benzene was shaken with sulphuric acid about 10 hr and then washed with water. After drying over calcium chloride about 6 months, the benzene was distilled through a 1.5-meter column over P_2O_5 at a reflux rate of 80: 1. The boiling range was 79.9 to 80.2°C. The cyclohexane used in the cyclohexane+benzene system was shaken with a 10: 50 nitric acid+sulphuric acid mixture about 40 hr and then washed with water. After having been dried over calcium chloride about 6 months, the cyclohexane was distilled through the same column over P_2O_5 at a reflux rate of 80: 1. The boiling range was 80.5 to 80.7°C. The dichloromethane was a commercially-available "special-grade" reagent; it was distilled through the same column at a reflux rate of 80: 1. The boiling range was from 39.6 to 39.8°C. The distilled dichloromethane did not react with mercury. The chromatographic analysis of all the materials showed no impurities.

Results and Discussion. The benzene+carbon tetrachloride system has been used in evaluating the calorimeter performance. This system is suitable for testing the efficiency of stirring because of the large density difference between components, but the study of this system is not well established as a standard. Therefore, we adopted the cyclohexane+*n*-hexane

Table 1. Experimental results for the excess enthalpies of mixing

$C_6H_6+C_6H_{12}$ (25°C) $H^E/J\ mol^{-1}$			$C_6H_{12}+n\text{-}C_6H_{14}$ (25°C) $H^E/J\ mol^{-1}$			$C_6H_6+CH_2Cl_2$ (25°C) $H^E/J\ mol^{-1}$		
X_1	(Expt.)	(calc.)	X_1	(Expt.)	(calc.)	X_1	(Expt.)	(calc.)
0.0429	127.5	126.7	0.0287	19.3	19.4	0.0350	−3.2	−3.2
0.1003	280.5	279.9	0.0691	45.4	45.2	0.0703	−8.0	−8.0
0.1747	448.9	449.4	0.1197	75.3	75.4	0.1176	−15.9	−16.1
0.2418	573.5	574.0	0.1738	104.9	104.9	0.1786	−28.2	−28.4
0.2986	658.0	658.2	0.2263	130.7	130.8	0.2369	−41.0	−41.0
0.3594	726.8	727.0	0.2760	152.7	152.7	0.2881	−51.9	−51.7
0.4113	767.8	768.0	0.3352	175.5	175.3	0.3349	−61.0	−60.8
0.4603	791.3	791.7	0.3906	192.9	192.7	0.3794	−68.9	−68.3
0.5053	800.7	800.5	0.4396	204.8	204.9	0.4527	−77.3	−77.8
0.5159	801.6	800.7	0.4930	214.3	214.4	0.4899	−80.5	−81.0
0.5236	801.4	800.5	0.5342	218.4	218.8	0.5315	−82.8	−83.0
0.5289	799.8	800.2	0.5595	220.4	220.2	0.5796	−83.3	−83.3
0.5521	797.1	796.4	0.6064	219.8	219.8	0.6397	−80.6	−80.4
0.5973	779.7	779.5	0.6551	214.8	214.9	0.7171	−71.5	−71.4
0.6511	741.8	742.3	0.6977	206.7	206.6	0.7866	−58.9	−58.8
0.6948	697.3	698.2	0.7446	192.6	192.6	0.8597	−41.6	−41.3
0.7454	630.2	631.0	0.7957	171.0	170.9	0.9197	−24.3	−24.6
0.7949	547.7	547.8	0.8385	147.0	147.0	0.9639	−10.8	−11.3
0.8414	454.0	453.5	0.8778	119.9	120.0			
0.8947	325.5	324.8	0.9194	85.8	85.6			
0.9369	206.5	206.2	0.9547	51.1	51.4			
0.9750	85.8	86.0	0.9814	21.9	22.2			

Table 2. Values of coefficients for Eq. (1) by method of least squares

System (25°C)	c_1	c_2	c_3	c_4	$\sigma/J\ mol^{-1}$
$C_6H_6+C_6H_{12}$	3200.51	−180.95	117.97	−59.61	0.53
$C_6H_6+n\text{-}C_6H_{14}$	861.32	−257.76	98.20	−14.82	0.18
$C_6H_6+CH_2Cl_2$	−326.46	116.94	135.62	6.18	0.29

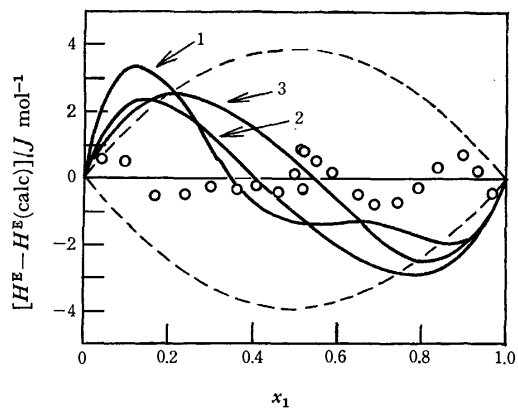

Fig. 2. Deviations of experimental and literature values of excess enthalpies for system benzene+cyclohexane at 25°C where x_1 is the mole fraction of benzene. ○, deviations of our experimental points; 1, data of Lundberg (8); 2, data of Stokes, Marsh and Tomlins (4); 3, data of Murakami and Benson (7); dashed curves represent ±0.5 per cent deviations.

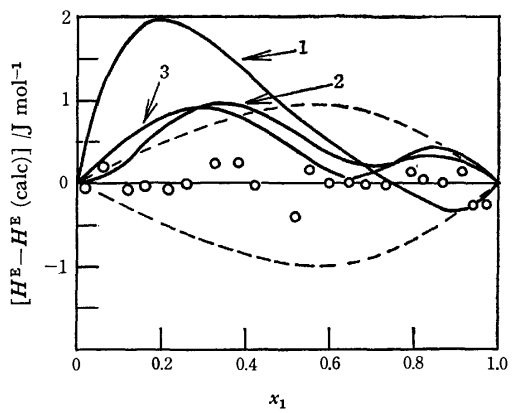

Fig. 3. Deviations of experimental and literature values of excess enthalpies for system cyclohexane+n-hexane system at 25°C where x_1 is the mole fraction of cyclohexane. ○, deviations of our experimental points; 1, data of McGlashan and Stoeckli (9); 2, Marsh and Stokes (10); 3, data of Murakami and Benson (7); dashed curves represent ±0.5 per cent deviations.

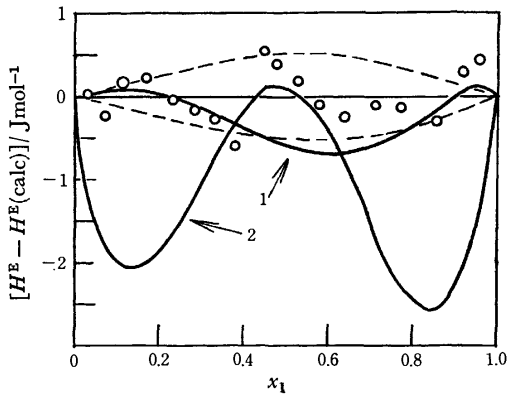

Fig. 4. Deviations of experimental and literature values of excess enthalpies for system benzene+dichloromethane at 25°C where x_1 is the mole fraction of benzene. ○, divations of our experimental points; 1, data of Murakami and Benson (7); 2, Otterstedt and Missen (11); dashed curves represent ±0.5 per cent deviations.

system, which had been suggested as a possible standard by McGlashan.[6]

All three systems used for testing our new calorimeter were measured at 25°C. The results are summarized in Table 1. The experimental points were fitted with the form[12]

$$H^E(\text{calc})/J\,\text{mol}^{-1}=x_1(1-x_1)\sum c_p(1-2x_1)^{p-1} \quad (1)$$

by the least-squares method, where x_1 is the mole fraction of the (1) component. The coefficients, c_p, adopted are listed in Table 2, along with the corresponding standard deviations. The values of the standard deviations were estimated by means of the following equation:

$$\sigma=[\sum\{H^E-H^E(\text{calc})\}^2/n]^{1/2} \quad (2)$$

where n is the number of observed points. The deviations of our experimental points from the smoothed function calculated from Eq. (2), $H^E-H^E_{\text{calc}}$, are shown in Figs. 2—4, together with those of other investigators, which are cited so that they can be compared with our results. Our results for the benzene+cyclohexane and cyclohexane+n-hexane systems are in close agreement with those of other investigators,[4,7-10] since the deviations of all sets fall almost entirely within about 0.5 per cent. However, it may be noted that our results appear to be slightly high at a low x_1 value and slightly low at a high x_1 value when compared with the results of other investigators.

At present, there is no suitable exothermic system for the test of a calorimeter. We used the benzene+dichloromethane system as an exothermic system, since the enthalpy of mixing for this system has been measured by several authors and since reliable data seem to have been obtained by using a similar type of calorimeter.[7] In the low-mole fraction of benzene, we observed an endothermic reaction which had too small a heat to be estimated. Our results agree well with those of Murakami and Benson,[7] but the results of Otterstedt and Missen[11] deviate fairly much at $x_1=0.15$ and 0.85 from ours.

The results obtained with our calorimeter seem to be internally consistent to better than 0.5 per cent, and the accuracy for the measurement of the enthalpy of mixing is believed to be equal to, or better than, that of the calorimeter described previously.

Results have been obtained by using this calorimeter for a number of systems containing polar materials; they will be reported in the near future.

This investigation was supported in part by a grant from the Ministry of Education. The authors wish to thank Dr. G. C. Benson, National Research Council of Canada, for his continuous interest during the design of the calorimeter.

6) M. L. McGlashan, "Experimental Thermochemistry," Vol. 2, ed. by H. A. Skinner, Interscience, New York (1962), Chap. 15.
7) S. Murakami and G. C. Benson, *J. Thermodynamics*, **1**, 559 (1969).
8) G. W. Lundberg, *J. Chem. Eng. Data*, **9**, 193 (1964).
9) M. L. McGlashan and H. F. Stoeckli, *J. Chem. Thermodynamics*, **1**, 589 (1969).
10) K. N. Marsh and R. H. Stokes, *ibid.*, **1**, 223 (1969).
11) J-E. A. Otterstedt and R. W. Missen, *J. Chem. Eng. Data*, **11**, 360 (1966).
12) G. Scatchard and W. J. Hamer, *J. Amer. Chem. Soc.*, **57**, 1805 (1935).

The Reaction of Mono-, Di-, and Trisodium Orthophosphate in a Mixed Solution of Acetic Acid and Acetic Anhydride

Makoto WATANABE and Tetsushi SENDA

Department of Industrial Chemistry, Chubu Institute of Technology, Matsumoto-cho, Kasugai-shi, Aichi

(Received May 31, 1971)

Mono-, di-, or trisodium orthophosphate was heated at 100°C in an equivolume mixture of acetic acid and its anhydride. By X-ray diffractometry and paper chromatography, the products from these three sodium salts of orthophosphate were found to be sodium trimetaphosphate. At the end of the 30-hr reaction period, the purity of the trimetaphosphate was higher than 90%. The ease of formation of the trimetaphosphate ring under various conditions was shown, and the stability of the ring was discussed on the basis of the strain of the bonding angle.

Some condensed phosphates are synthesized by the dehydration of orthophosphate at a high temperature. Thilo and his co-workers made potassium trimetaphosphate by treating monopotassium dihydrogen orthophosphate with a mixture (1: 1) of acetic acid and its anhydride at 90°C.[1] Kasparek reported the dehydration of alkalimetal salts of dihydrogen orthophosphates with acetic anhydride.[2] In the present work, we succeeded in synthesizing trimetaphosphate not only from monosodium orthophosphate, but also from di- and trisodium orthophosphate, which had been treated in an equivolume mixture of acetic acid and its anhydride at 100°C. The reactivity of these three sodium salts of orthophosphate in the mixed solution was examined.

Experimental

Materials and Instruments. All the materials used were of a commercial grade. The water of crystallization of the orthophosphates was removed by heating them at 120°C in an air bath. The instruments used for the analysis of phosphates were a Toshiba X-ray diffractometer, ADG-102, and a Shimadzu photoelectric photometer, Spectronic-20.

Reaction of the Orthophosphates in a Mixture (1: 1) of Acetic Acid and Its Anhydride. After 50-m*l* portions of acetic acid and of acetic anhydride had been taken in a 300-m*l*, four-necked, round-bottom flask, 5 g of the orthophosphate was added to the solution and then the mixture was heated at 100°C with a mantle-heater, while being stirred and refluxed at the same time, for 5, 10, 15, 20, 25, or 30 hr. At first, these sodium salts of orthophosphates were completely dissolved in the mixed solution at 100°C, the solution gradually became turbid, with a white deposit. The quantity of the white deposit increased with the increase in the reaction time. The reaction mixture at each reaction time was cooled; the deposit was filtered off and then washed with ethyl alcohol. The compositions of the deposit and of the filtrate were estimated from the data obtained by X-ray diffractometry and paper chromatography.

X-ray Diffractometry. The samples were ground with an agate mortar until they could pass through a 150-mesh screen. Their X-ray diffraction patterns were taken by means of the powder method.

Paper Chromatography. About 1 g of the white deposit was dissolved in 50 m*l* of water, and then 3 μl of the solution or the filtrate obtained by the filtration of the reaction mixture were placed on a filter paper (Toyo No. 51A of 2 by 40 cm) and developed at room temperature for 20 hr by using an acidic and a basic solvent. The acidic solvent was prepared by mixing 73.5 m*l* of isopropyl alcohol, 5.0 g of trichloroacetic acid, 0.25 m*l* of concentrated aqueous ammonia, and 26.5 m*l* of water; it was used for the separation of ortho-, pyro-, tripoly-, and long-chain phosphates. The basic solvent was prepared by mixing 38.7 m*l* of isopropyl alcohol, 20.0 m*l* of isobutyl alcohol, 0.5 m*l* of concentrated aqueous ammonia, and 40.8 m*l* of water and was used for the separation of trimeta- and tetrametaphosphates. After the solutions of phosphate had been developed for 20 hr, the filter paper was dried at 75°C for more than 30 minutes in an air bath. The paper was sprayed with a perchloric acid-molybdate solution. After it had dried again, the paper was exposed to ultraviolet rays in order to reduce the molybdophosphates to blue complexes. Each band of the phosphates on the filter paper was identified by the same treatment as in the case of a reference solution of a known mixture of phosphates.

Colorimetric Determination of Phosphorus. The separated phosphates on the paper chromatograms were determined as follows. Filter paper containing each separated phosphates was cut at the demarcation line, and each part was immersed in 10 m*l* of a 0.1N aqueous solution of ammonia in a 50-m*l* Erlenmeyer flask for 1 hr. The resulting solution was transferred to a 25-m*l* volumetric flask, and then 10 m*l* of water and 2 m*l* of Lucena-Conde and Prat's reagent[3] were added. The flask was placed in boiling water for 1 hr, then cooled in a bath of cold water, and diluted to the mark with water. The absorbance of the solution was measured at 800 mμ. The compositions of the phosphates were calculated from the absorbance data.

Results and Discussion

The chemical compositions of the phosphates contained in the white deposit are shown in Tables 1, 2, and 3. The data indicate that the main product from these three sodium salts of orthophosphate is trimetaphosphate and that its purity increases with an increase in the reaction time and is higher than 90% at a reaction time of 30 hr. The compositions of the filtrate at the reaction time of 30 hr were as follows: for monosodium orthophosphate, 45.8% of orthophosphate, 16.7% of pyrophosphate, and 37.5% of an unknown substance; for disodium orthophosphate, 53.7% of orthophosphate, 19.2% of pyrophosphate, and 27.1% of an unknown substance; for trisodium orthophosphate,

1) I. Grunze, K. Dostal, and E. Thilo, *Z. Anorg. Allg. Chem.*, **302**, 221 (1959).

2) F. Kasparek, *Monatsch.*, **92**, 1023 (1961).

3) F. Lucena-Conde and L. Prat, *Anal. Chim. Acta*, **16**, 473 (1957).

TABLE 1. DISTRIBUTION OF PHOSPHATES OF THE PRODUCTS FROM THE NaH_2PO_4–$(CH_3CO)_2O$–CH_3COOH SYSTEM (P%) (R. T.: reaction time)

R. T. (hr)	Ortho	Pyro	Tri	Tri-meta	Tetra-meta	Higher
5	2.3	2.9	9.4	70.2	—	15.2
10	2.2	2.5	8.6	73.0	—	13.7
15	2.0	2.2	6.3	86.4	—	3.1
20	1.7	2.0	5.2	89.2	—	1.9
25	1.3	1.8	5.4	89.7	—	1.8
30	1.0	1.0	5.0	91.5	—	1.5

TABLE 2. DISTRIBUTION OF PHOSPHATES OF THE PRODUCTS FROM THE Na_2HPO_4–$(CH_3CO)_2O$–CH_3COOH SYSTEM (P%) (R. T.: reaction time)

R. T. (hr)	Ortho	Pyro	Tri	Tri-meta	Tetra-meta	Higher
5	3.2	5.4	7.7	69.0	—	14.7
10	2.2	3.0	9.3	75.4	—	10.1
15	2.7	3.4	9.4	76.7	—	7.8
20	2.7	2.8	5.5	86.0	—	3.0
25	1.4	1.5	4.8	88.9	—	3.4
30	1.4	1.0	4.2	91.0	—	2.4

TABLE 3. DISTRIBUTION OF PHOSPHATES OF THE PRODUCTS FROM THE Na_3PO_4–$(CH_3CO)_2O$–CH_3COOH SYSTEM (P%) (R. T.: reaction time)

R. T. (hr)	Ortho	Pyro	Tri	Tri-meta	Tetra-meta	Higher
5	1.9	2.1	8.6	76.0	—	11.4
10	1.4	1.9	3.1	82.0	—	11.0
15	1.8	1.5	4.0	89.3	—	3.4
20	1.0	1.0	4.2	91.3	—	2.5
25	1.3	1.5	2.8	92.4	—	2.0
30	0.5	1.4	2.7	93.7	—	1.7

86.8% of orthophosphate, and 13.2% of pyrophosphate, while the quantity of the unknown substance was so small that it could not be determined. The unknown substances contained in these filtrate, are all the same substance, which has an R_f value of 0.60 for the acidic solvent employed in this chromatography. The unknown substance may be an orthophosphate the hydrogen atoms of which are replaced by acetyl groups.

The X-ray diffraction patterns of the white deposits are given in Fig. 1. From the results, it is clear that the white deposits are sodium trimetaphosphate. The sodium trimetaphosphate was identified by comparing the X-ray patterns of the white deposits with those of the "A.S.T.M. Diffraction Data File." According to the above results, the following reactions were considered for the formation of trimetaphosphate:

$$3NaH_2PO_4 + 3(CH_3CO)_2O = (NaPO_3)_3 + 6CH_3COOH$$

$$\begin{pmatrix} 3Na_2HPO_4 + 3CH_3COOH = 3NaH_2PO_4 + 3CH_3COONa \\ 3NaH_2PO_4 + 3(CH_3CO)_2O = (NaPO_3)_3 + 6CH_3COOH \end{pmatrix}$$

$$\begin{pmatrix} 3Na_3PO_4 + 6CH_3COOH = 3NaH_2PO_4 + 6CH_3COONa \\ 3NaH_2PO_4 + 3(CH_3CO)_2O = (NaPO_3)_3 + 6CH_3COOH \end{pmatrix}$$

By using the above equations, the theoretical amounts of sodium trimetaphosphate to be obtained per 100 g of each orthophosphate were calculated. The theoretical values, the experimental values, and the yields of sodium trimetaphosphate are given in Table 4.

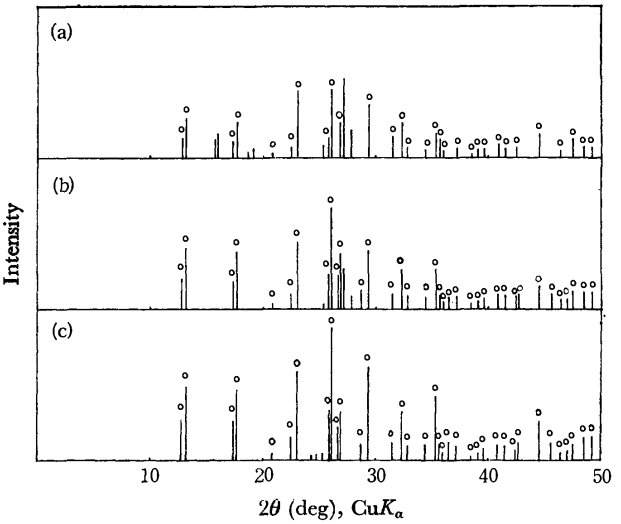

Fig. 1. X-Ray diffraction patterns of white deposites.
(a): NaH_2PO_4–$(CH_3CO)_2O$–CH_3COOH system
(b): Na_2HPO_4–$(CH_3CO)_2O$–CH_3COOH system
(c): Na_3PO_4–$(CH_3CO)_2O$–CH_3COOH system
○: Lines due to sodium trimetaphosphate

TABLE 4. THE YIELDS OF SODIUM TRIMETAPHOSPHATE

	NaH_2PO_4	Na_2HPO_4	Na_3PO_4
EV	80.6	67.1	57.5
CV	85.0	71.8	62.2
Yield	94.8	93.4	92.4

EV: Gram quantities of sodium trimetaphosphate obtained by the experiment per 100 g of each orthosphate.
CV: Gram quantities of sodium trimetaphosphate obtained by calculation per 100 g of each orthophosphate.
Yield: The yields (%) of sodium trimetaphosphate.

It is well known that sodium trimetaphosphate is usually made by heating monosodium orthophosphate to temperatures between 500 and 600°C. The sodium trimetaphosphate is formed very readily as a well-crystallized salt. It can also be prepared by cooling a sodium metaphosphate melt to the right temperature or by heating various mixtures of sodium phosphates exhibiting an over-all composition corresponding to the metaphosphate. It is very difficult, on the other hand, to prepare tetrametaphosphates by heating monomer phosphates; they are prepared by slowly adding phosphorus pentoxide to ice water. Anhydrous sodium tetrametaphosphate is irreversibly transormed to sodium trimetaphosphate at temperatures around 400°C; it cannot be restored by any known subsequent treatment of the sodium trimetaphosphate. Sodium salts of pyro- and tripolyphosphate are made by heating sodium phosphates which have a composition corresponding to these phosphates. It is difficult to prepare tetrapolyphosphates by heating phosphates, however, they are made by the alkaline hydrolysis of tetrametaphosphate. Usually, it is very difficult to prepare condensed phosphates, which are larger than tetra. Condensed phosphates hydrolyze to the uncondensed form in an aqueous solution. It is also well known that small

rings (mainly trimeta and a little tetrameta) are formed as the long chains are hydrolyzed. In view of the above facts, sodium trimetaphosphate may have a very stable structure and the trimetaring may be made readily. Phosphorus exhibits sp^3-bonding in the phosphates. The usual hybridization of the oxygen atom lies between p^2 and sp, so the bond angle of P–O–P lies between 90° and 180°. If the P–O–P angle is near the average value of 135° and if the O–P–O angle is 109°28′, the total bond angle of the trimetaring is very close to that of the six membered-ring, which is planar. The trimetaphosphate ion is considered to have a D_{3h} symmetry in an aqueous solution.[4]

4) W. P. Griffith and K. J. Rutt, *J. Chem. Soc. A*, 2331 (1968).

BULLETIN OF THE CHEMICAL SOCIETY OF JAPAN, VOL. 45, 2113—2120(1972)

The Syntheses of 3-(Carboxyalkyl)salicylaldehyde Derivatives and Their Copper Chelates[1)]

Tsuguo TANAKA

Department of Science and Technology, Saga University, Saga

(Received March 26, 1971)

In order to study the influence of the side-chain carboxylic acid groups on the formation of the metal chelates, 5-bromo-3-carboxymethyl-, 5-methyl-3-β-carboxyethyl-, and 5-chloro-3-β-carboxyethyl-salicylaldehyde (**2a, b c**) were synthesized. The green binuclear copper chelates of these aldehydes, di-μ-aquo-bis-(5-bromo-3-carboxymethylsalicylaldehyde)-, di-μ-aquo-bis-(5-methyl-3-β-carboxyethylsalicylaldehyde)-, and di-μ-aquo-bis-(5-chloro-3-β-carboxyethylsalicylaldehyde)-dicopper (**11a, b, c**) yielded the green binuclear bis-ethylenediimine chelates (**12a, b, c**), while bis-(5-bromo-3-carboxymethylsalicylaldehyde)-, bis-(5-methyl-3-β-carboxyethylsalicylaldehyde)-, and bis-(5-chloro-3-β-carboxyethylsalicylaldehyde)-ethylenediimine (**14a, b, c**) gave a brown (**13a**) and gray-purple (**13b, c**) mononuclear copper chelates. The reduction of **14a, b, c** with sodium borohydride yielded the hexadentate ligands *N,N'*-bis-(5-bromo-2-hydroxy-3-carboxymethylbenzyl)-, *N,N'*-bis-(5-methyl-2-hydroxy-3-β-carboxyethylbenzyl)-, and *N,N'*-bis-(5-chloro-2-hydroxy-3-β-carboxyethylbenzyl)-ethylenediamine (**15a, b, c**), which proved useful for the spectrophotometric determination of the copper (II) ion from solutions containing copper (II) and nickel (II) ions, and the iron (II) ion from solutions containing iron (II) and nickel (II) ions.

Since the isolation of purple penta-coordinate addition compounds of bis-salicylaldehyde-ethylenediiminecopper with the carboxylic acids and the phenols,[2)] many penta-coordinate copper chelates have been reported.[3)] In view of the role of carboxylic acid groups in the penta-coordination as well as in the formation of the ethylenediamine conjugates,[4)] the aldehydes **2a,b,c**, their ethylenediimine derivatives **14a,b,c**, and their copper chelates were synthesized for a study of the physical properties and chemical behaviors of the ligands as well as their chelates.

A binuclear structure of the copper chelate of **2a** was deduced from the analyses, IR spectrum and mass spectrum of the copper chelate. The mass spectrum[5)] of **11a** is illustrated in Fig. 2. Ions having values of *M/e* 474 ($-CO_2$, $-2Br$, $+2H$), 429 ($-2CO_2$, $-2Br$, $+H$) and others with values of *M/e* higher than 337 of the ion of monomeric form (**20**) were observed in the spectrum. The ions are considered to originate from the dimeric chelate **11a**. Four sets of twin peaks (240, 242), (228, 230), (200, 202), and (184, 186) represent those of the bromine containing fragments.

The carboxylate, the coordinated aldehyde and the phenoxide structures of **11a** were assigned on the basis of the 1580 and 1400 cm^{-1} IR peaks due to the antisymmetric and the symmetric vibration of the carboxylate ions,[6,4)] the 1611 cm^{-1} IR peak due to the shifted C=O stretching vibration of the aldehyde groups and the 1535 cm^{-1} absorption, respectively (Table 2 (B)).

Lower magnetic moments of binuclear copper chelates were summarized.[7)] The magnetic moments of the penta-coordinate copper chelates were normal.[8)] The

1) Part X of "Some addition compounds of bis-salicylaldehyde-ethylenediimine-copper". Preliminary communication: T. Tanaka, This Bulletin, **41**, 1277 (1968).

2) a) T. Tanaka, *ibid.*, **29**, 93 (1956). b) T. Tanaka, Proceedings of IX I.C.C. C., St. Moritz-Bad, Switzerland, 1966, p. 71.

3) Reviews are available: E. L. Muetterties and R. A. Schun, *Quart. Revs.*, **20**, 245 (1966). L. Sacconi, Coordination chemistry (plenary lectures of X I. C. C. C., Butterworth, London, 1968, p. 95.

4) T. Tanaka, This Bulletin, **39**, 2558 (1966).

5) H. Budzikiewicz, C. Djerassi, and D. H. Williams, "Interpretation of mass spectra of organic compounds." Holden-Day, San Francisco, 1964, p. 162. M. Tsutsui, "Characterization of organometallic compounds." Part I, Interscience publishers, New York, 1969, p. 137—203.

6) L. J. Bellamy, "The infrared spectra of complex molecules," Methuen, London, 1964, p. 140. K. Nakamoto and P. J. McCarthy, "Spectroscopy and structure of metal chelate compounds," John-Wiley and Sons, New York 1968, p. 269—281.

7) M. Kato and H. B. Jonassen, *Chem. Rev.*, **64**, 104 (1964).

8) The measured magnetic moments of the penta-coordinate addition compounds were 1.74 Bohr magneton (at 256.2°K, $\Delta = -1°$) for the addition compound of bis-(5-methylsalicylaldehyde)-ethylenediimine-copper with propionic acid and 1.68 Bohr magneton (at 219°K, $\Delta = 0°$) for the addition compound of the same chelate with hydroquinone of the composition $(C_{18}H_{18}N_2O_2Cu)_2$-$C_6H_4(OH)_2$. The magnetic moments were measured by K. Hirakawa and his collaborators on their instrument. K. Hirakawa, K. Hirakawa, and S. Yoneyama, *Japan J. Appl. Phys.*, **2**, 816 (1963).

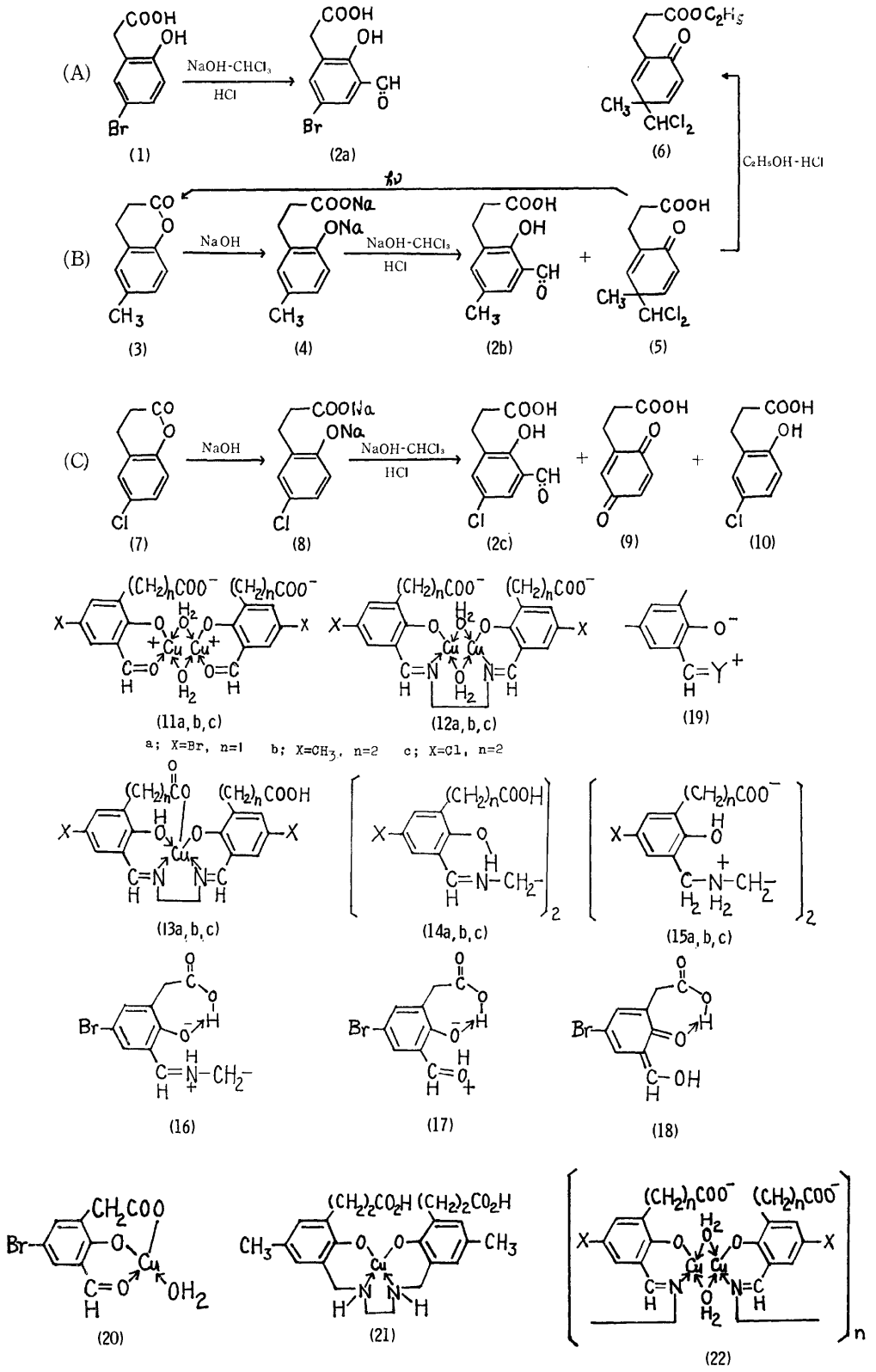

Fig. 1.

magnetic moments of **11a**,**b**,**c** were 1.90 Bohr magneton (273°K,$\Delta = -70°$), 1.77 Bohr magneton (272°K,$\Delta = -52°$), and 1.73 Bohr magneton (273°K,$\Delta = -77°$), respectively, and a deviation from the Curie-Weiss law was observed for **11c** at low temperatures (Fig. 3).

In the mass spectrum of **11b**, 345 (-2 $CH_2CH_2CO_2$, -2 CH_3, -2 CO, $+$H) and 317 were observed for M/e indicating a dimeric structure. The structure of **11c** was deduced from the similarity of results of its analysis, IR and UV spectra to those of **11a**,**b**.

The reaction of **11a**,**b**,**c** with ethylenediamine gave deep green ethylenediimine chelates which were considered to be either **12a**,**b**,**c** or the polymer **22a**,**b**,**c**. On the other hand, the Schiff base **14a**,**b**,**c** yielded

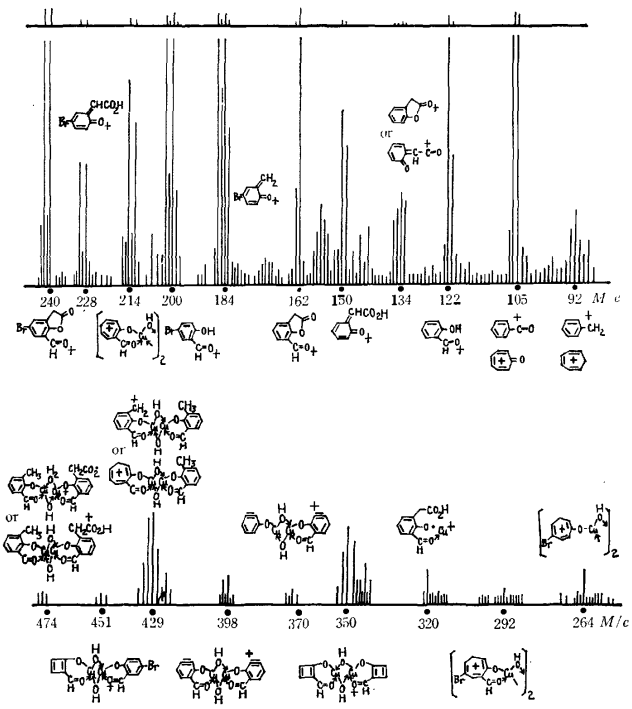

Fig. 2. Mass spectrum of **11a**. Ionizing voltage, 75 eV; ionizing current, 200 μA; sample temperature, 240°C; chamber temperature, 280°C. The formulae are possible ionic species.

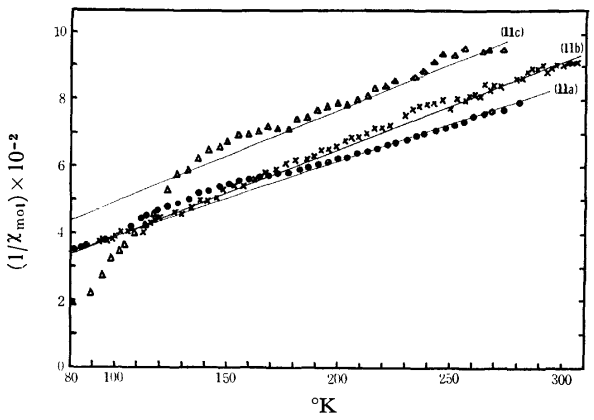

Fig. 3. Magnetic susceptibilities of **11a**, **b**, **c**.

mononuclear chelates **13a,b,c** respectively. The pentacoordinated structure of the mononuclear chelates is discussed with reference to absorption spectra.

The ligand **15a** formed a colorless stable chelate with Ni(II) ion in aqueous buffer solution of pH 10, and revealed the purple color of murexide on addition to a solution of nickel-murexide complex. Thus, the quantitative determination of nickel(II) ion was attained by chelatometric titration by use of M/100 aqueous solution of the disodium salt of **15a** and murexide in a buffer solution of pH 10.[9] Ligands **15b,c**, which, were colorless, formed no stable chelate with Ni(II), but formed green copper(II) and red iron(II) chelates in buffer solutions of pH 10 and pH 7, respectively. Spectrophotometric determinations were achieved for the copper(II) ion from the solutions containing Cu(II) and Ni(II) ions, and for the iron(II) ion from those containing Fe(II) and Ni(II)[10] as illustrated in Fig. 8. Of the Mg, Ca, Sr, Ba, Hg, Zn, Cd, Pb, Sn, Ni, Fe(II), Co(III) and Cu(II) ions, Co(III) (green), Cu(II) (green), and Fe(II) (red) ions formed colored chelates with **15a,b,c** in the aqueous solutions of pH 10 and 7.

Structure of the Abnormal Product of the Reimer-Tiemann Reaction[11]

Formation of dienone (**5**) as the main product of reaction B (Fig. 1), was deduced from the following experiments. 1. In the NMR spectrum of the product **Q** (see Experimental), a singlet CH_3 proton peak of 8.60 τ[12] and a singlet $HCCl_2$ proton peak of 4.40 τ were observed. 2. In the IR spectrum of **Q**, clear doublet dienone peaks of 1663 and 1640 cm^{-1} were observed together with the 1705 cm^{-1} peak of the carboxylic acid group. 3. In the mass spectrum, the ions with *M/e* values of 262, 244, 227, 216, 208,[13] 190, 180 and others with the value 262 corresponding to the molecular weight of **5** were observed. 4. Esterification of **Q** with ethanol and hydrogen chloride gave a fairly good yield of **6**. The semicarbazone of **6** was also obtained. 5. Distillation of **Q** after irradiation with sunlight for 20 hrs gave 69% of the lactone **3**,[14] while ditillation without irradiation resulted in polymerization into a resinous substance.

Structure of 6. Comparison of the UV absorption maxima of **6**, 202 mμ (log ε 3.58), 233 mμ (log ε 3.99), 267 mμ (shoulder, log ε 3.47), and 332 mμ (log ε 2.82) with those of its semicarbazone, 201 mμ (log ε 3.62), 251 mμ (log ε 3.84), and 301 mμ (log ε 4.25) suggested the cyclohexadienone structure of **6**, because on the formation of the semicarbazone, the 233 mμ absorption band of **6** disappeared and a 301 mμ band appeared as is usually the case with a dienone.[15] In the NMR spectrum of **6**, the singlet methyl protons

9) Buffer solution: H. A. Flaschka, EDTA titration, Pergamon, Oxford, 1964, p. 72. Titration: *ibid.*, p. 83. The results of titration were reported in the preliminary communication. It should be added that the reagent solution separated white precipitate when stored for more than four or five days.

10) Spectrophotometric determination of iron: W. Nielsch and G. Böltz, *Microdhim. Acta*, 481 (1954); *Z. Anal. Chem.*, **144**, 401 (1954). P. Schneider and J. Janko, *Chem. Listy*, **50**, 899 (1956). Of copper: W. Nielsch and G. Böltz, *Z. Anal. Chem.*, **142**, 406 (1954); *ibid.*, **143**, 1 (1954). Reviews are available: K. Ueno and B. Sakaguchi, The metal chelates (Japanese) Vol. II, Nankodo, Tokyo, 1966, p. 208—228.

11) H. Wynberg, *Chem. Rev.*, **60**, 169 (1960).

12) L. M. Jackmann, "Application of nuclear magnetic resonance spectroscopy in organic chemistry," Pergamon, New York 1959, pp. 53, 58.

13) Since the *M/e* value 208, corresponding to the molecular weight of **2b**, was observed in the mass spectrum of **Q**, part of it was treated with an aqueous alcoholic solution of potassium acetate and semicarbazide hydrochloride. Semicarbazone of mp 207°C was obtained in 8.83% yield. The yield of **2a** in the reaction B preliminary reported should be revised to 9.48%.

14) H. E. Zimmermann, *J. Amer. Chem. Soc.*, **84**, 4527 (1962); *ibid.*, **88**, 4895 (1966). J. S. Swenton, E. Sauerborn, R. Srinivasan, and F. I. Sonntag, *ibid.*, **90**, 2990 (1968). D. I. Schuster, and D. J. Patel, *ibid.*, **87**, 2516 (1965).

15) A. I. Scott, "Interpretation of the ultraviolet spectra of natural products." Pergamon, Oxford, 1964, p. 78.

of 8.55 τ, the triplet methylene protons adjascent to the double bond (4H) of 7.5 τ (J=7.7 cps), a singlet $HCCl_2$ proton (1H) of 4.20 τ, a doublet vinyl proton (1H) of 3.72 τ (J_1=9.4 cps), a quartet vinyl proton (1H) of 3.17 τ (J_1=9.4 cps, J_2=2.6 cps), and a doublet vinyl proton (1H) of 3.32 τ (J_2=2.6 cps) were observed corresponding to **6**, as illustrated in Fig. 4. The 1735 cm^{-1} IR peak of the ester carbonyl group together with the clear doublet peaks 1663 and 1640 cm^{-1} of the dienone indicated the structure **6**. Of the mass spectrum (Fig. 5), the triplet sets of ions with M/e values such as 290, 292, 294, and 240, 242, 244 whose intensity ratio was approximately 1.0: 0.65: 0.15, seemed to be those of the dichloro fragments, while the doublet sets (254, 256), (181, 183), and (155, 157), whose intensity ratio was approximately 1.0: 0.4, seemed to be the monochloro fragments. Structures of **6** and **5** were confirmed by these physical measurements and chemical transformations.

Absorption Spectra

The O–H stretching IR peak of 3400 cm^{-1} of **2a** was considered from its similarity to those of hydroxyacids **1a** and **9** to be due to the hydrogen bond between the carboxyl and the hydroxyl groups and not to that between the hydroxyl and the aldehyde groups.

The UV spectra of **2a,b,c** in the ethanolic solutions as well as in the 0.5% aqueous sodium hydroxide solutions were nearly the same. However, in the hexane solutions in which acid exerts strong action, the 344 mμ n-π^* transition band[16] of **2a** disappeared while those of **2b,c** remained (Table 1).

TABLE 1. ABSORPTION MAXIMA OF **2a,b,c** MEASURED IN HEXANE SOLUTIONS AND THEIR RELATIVE INTENSITIES[a]

2a		**2b**		**2c**	
mμ	(intensity)	mμ	(intensity)	mμ	(intensity)
217.5	(2.50)				
219	(2.41)	218.5	(0.58)	219	(1.26)
229	(0.60)			229	sh. (0.58)
234	(0.80)				
239	(1.21)			239	(0.42)
245	(1.41)			244	(0.59)
				248	sh. (0.49)
251	(1.55)			250	(0.63)
255	sh. (1.51)			254	sh. (0.57)
258	sh. (1.39)			256	(0.64)
261	(1.30)	260	(1.70)	260	sh. (0.54)
		265	(1.88)	262	(0.61)
269	(0.73)			269	(0.20)
342	(0.01)	345	(0.57)	347	(0.08)

a) Absorbance of their saturated solutions. sh. Shoulder.

The results suggest a dipolar ion such as **17**, with the following structure: — phenoxide and the protonated + carbonyl groups. A shoulder of 248 mμ ascribed to the phenoxide ion, was observed in the spectrum of **14a** but not in those of **14b,c** in the ethanolic solutions and the intensity of 347 mμ n-π^* band of the former decreased. A strong absorption peak of 1543 cm^{-1} was observed in the IR spectrum of the ligand **14a** but not in those of **14b,c**.

The absorption peak 1540 cm^{-1} of the salicylaldehyde Schiff base chelates was discussed and its assignment based on three different views. 1. the C=N stretching vibration.[17] 2. the C–O$^-$ stretching vibtation of the phenoxide ion endowed with a double bond character.[18] 3. the skeletal vibration of the aromatic ring loosened by ctoss resonance between the aromatic and the chelate ring.[19] It was recognized that the IR as well as the UV spectra of **14a** were closely related to those of the Schiff base chelates. It was thus considered that the proton shifted from the phenol oxygen atom toward the nitrogen atom to form a dipolar structure such as **19**. The structure **16** was introduced in place of **14a** on this basis.

In contrast to those of **11a,b,c**, and **12 a,b,c,** the IR absorption peaks of the carboxylic acid groups of **13a,b,c**, were observed between 1703 and 1710 cm^{-1} together with the shoulders appearing between 1725 and 1730 cm^{-1} as illustrated in Fig. 6 and in Table 2 (B). The shoulders were ascribed to the C=O stretching vibration

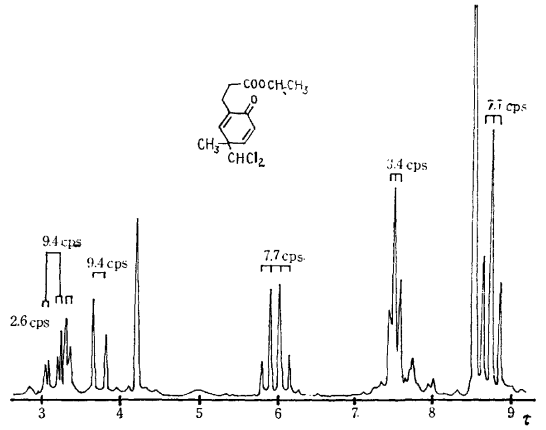

Fig. 4. NMR spectrum of **6** ($CDCl_3$).

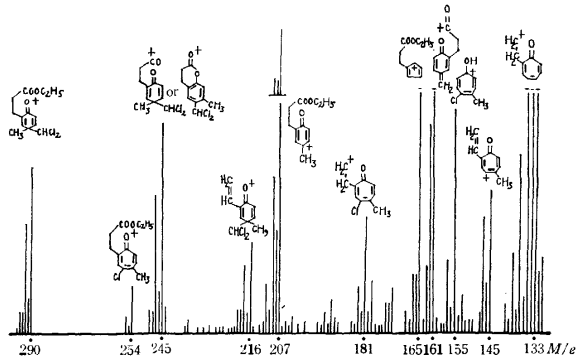

Fig. 5. Mass spectrum of **6**. Ionizing voltage, 75 eV; ionizing current, 200 μA; Sample temperature, 75°C; chamber temperature, 80°C. The formulae are possible ionic species.

16) Ref. 15, p. 103.

17) K. Ueno and A. E. Martell, *J. Phys. Chem.*, **59**, 998 (1955); *ibid.*, **60**, 1270 (1956).

18) P. L. Teyssie and J. J. Charette, *Spectrochim. Acta*, **19**, 1403 (1963). G. E. Batley and D. P. Graddon, *Aust. J. Chem.*, **20**, 877 (1967).

19) R. C. Burrows and J. C. Bailar. Jr., *J. Amer. Chem. Soc.*, **88**, 4150 (1966).

of the COO–Cu/2 bond,[20] in analogy with those of the penta-coordinate addition compounds of bissalicylaldehyde-ethylenediimine-copper derivatives with propionic acid. The broad first bands of binuclear chelates **11a,b,c** and **12a,b,c** were observed between 690 and 750 mμ and between 624 and 700 mμ (blue shift), respectively, while the distinct first bands of **13a,b,c** were observed between 553 and 560 mμ as shown in Fig. 7 and Table 2 (A). The wave lengths of the absorption maxima of **13a,b,c** were nearly the same as those of the addition compounds of bis-salicylaldehyde-ethylene-diimine-copper derivatives with propionic acid. This indicates that one of the side chain carboxylic acid groups form the addition compound of the chelate itself to make the pentacoordinate structure such as **13a,b,c**.

The absorption peaks of 1610—1645 cm^{-1} due to the carboxylate ions of the ligands **15a,b,c** and the $-\overset{+}{N}H_2-$ peaks of 1550—1565 cm^{-1} indicate their dipolar structure.

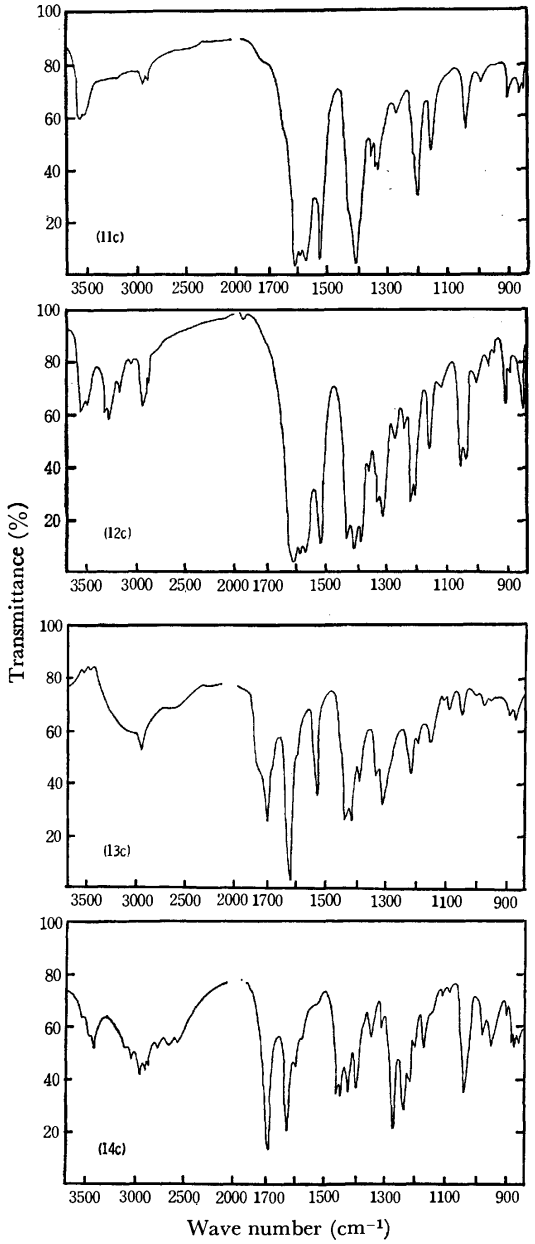

Fig. 6. Infrared spectra of **11c**, **12c**, **13c**, and **14c**. (KBr disc)

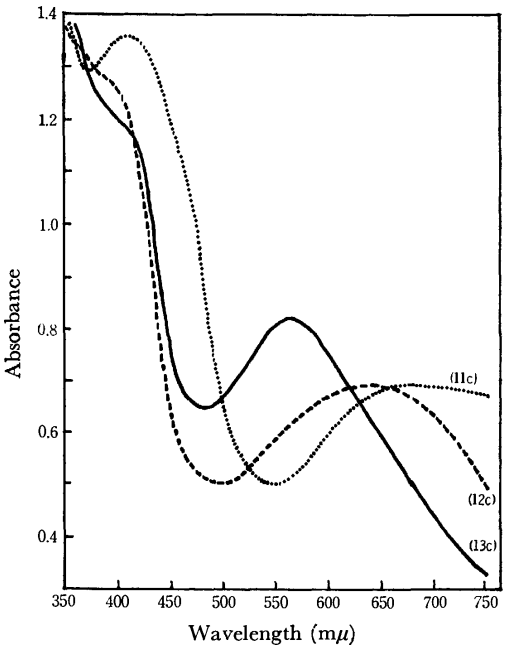

Fig. 7. Reflectance spectra of **11c**, **12c**, and **13c**.

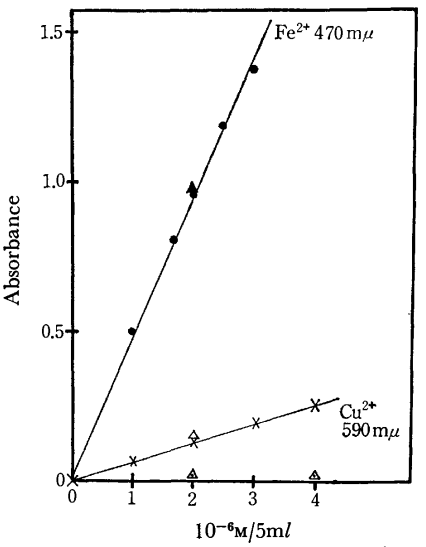

Fig. 8. Spectrophotometric determination of Cu(II) and Fe(II). Measurements were made of 5 m*l* of aqueous solutions containing 0.5 m*l* of 1/100 M solution of disodium salt of (15c), 0.1 m*l* of pH 10 and 7 buffer solutions respectively and; ×, moles of copper acetate; ●, moles of ferrous chloride; ◬, moles of nickel acetate; △, ▲, mixtures of each moles of Cu(II)-Ni (II) and Fe (II)-Ni (II) respectively. Cell depth 1 cm and pure water as reference.

20) Most of the copper carboxylates are of the symmetric carboxylate ion coordination type (ref. 5) and references are not available for the asymmetric copper carboxylate of this structure. Assignment of the structure, nevertheless, was based on the steric hindrance studies: T. Tanaka, *Nippon Kagaku Zasshi*, **79**, 942 (1958) and the IR spectra: T. Tanaka, *ibid.*, **81**, 1013 (1960).

TABLE 2. (A). UV AND VISIBLE ABSORPTION SPECTRA

Compound	Solvent	mμ (log ε)			
2a	Ethanol	200.5 (4.10),	223 (4.30),	260.5 (3.86),	344 (3.48)
2b	Ethanol	200 (4.09),	218 (4.25),	264 (4.06),	348 (3.49)
2c	Ethanol	198 (4.09),	222 (4.36),	260.5 (4.00),	345 (3.68)
2a	0.5% aq. NaOH		237 (4.23),	275 sh(3.65),	399 (3.75)
2b	0.5% aq. NaOH		231 (4.20),	276 (3.83),	400 (3.82)
2c	0.5% aq. NaOH		237 (4.30),	275 sh(3.72),	398 (3.84)
14a	Etahnol	200.5 (3.79),	226 (3.93),	248 sh(3.67),	264sh(3.47),
		347 (3.08),	430 (ref)		
14b	Ethanol	200.5 (5.07),	220 (4.89),	267 (4.61),	336 (4.16),
		424 (2.60)			
14c	Ethanol	198.5 (4.58),	224 (4.68),	260 (4.22),	334 (3.77),
		412 (2.66)			
11a	Ethanol	200.5 (*),	224 (*),	256 (*),	420 (ref),
		750 (ref)			
11b	Ethanol	200.5 (3.55),	228sh(3.51),	269sh(3.13),	285sh(3.08),
		432 (2.83),	412 (ref),	710 (ref)	
11c	Ethanol	200 (3.54),	228 (3.72),	248sh(3.50),	277sh(3.28),
		406 (2.92),	410 (ref),	690 (ref)	
12a	Pyridine	305 (3.15),	386 (3.23),	496 (2.67),	406 (ref),
		700 (ref)			
12b	Ethanol	200.5 (3.38),	228sh(3.32),	256sh(2.98),	388 (ref),
		624 (ref)			
12c	Ethanol	200.5 (*),	231sh(*),	256sh(*),	426 (*),
		370 sh(ref),	400sh(ref),	640 (ref)	
13a	Pyridine	280 sh(3.39),	302 (3.53),	380 (3.83),	416sh(ref),
		553 (ref)			
13b	Ethanol	202 (4.41),	235 (4.42),	280 (4.21),	377 (3.81),
		416 sh(ref),	560 (ref)		
13c	Ethanol	200.5 (3.70),	232 (3.61),	282sh(3.39),	378 (3.18),
		415 sh(ref),	560 (ref)		
15b	Ethanol	202.5 (3.97),	223sh(3.22),	287 (2.63)	
21b	Ethanol	203 (4.85),	241 (4.04),	285 (3.88),	340sh(2.98),
		410 (3.01),	600 (2.35)		

Abbreviations: sh···shoulder, *···saturated solution, ref···reflective measurement.

TABLE 2 (B). INFRARED SPECTRA (BETWEEN 1500 AND 1800 cm^{-1})

Compound/Group	Wave number cm^{-1}					
	COO-Cu/2	COOH	HC=O	HC=N	aromatic ring	COO^- structure **19**
2a		1701s	1660s		1605m	
2b		1710s	1645s		(1620sh) 1600m	
2c		1705s	1650s		1606m	
14a		1703m		1625s	1593w	1543s
14b	(1722sh)	1705s		1632s	1605m	
14c		1703s		1635s	1603sh	
11a			1611vs			1580s 1535m
11b		(1640sh)	1603s			1580s 1535s
11c			1612s		1595m	1578s 1530s
12a			(1645sh)	1610vs		1580vs 1535s
12b			(1630s)	1610vs		1575s 1530s
12c				1620vs	1595s	1578s 1528s
13a	1725sh	1710m		1630vs	1595w	1540m
13b	1725s	1705s		1620s		1542s
13c	1730sh	1703s		1625vs	1600sh	1540s

Abbreviations: s ··· strong, m ··· medium, w ··· weak, v ··· very, ( ) ··· not assigned.

Experimental

The melting points were uncorrected. The spectra were taken on a Hitachi EPS-3T ultraviolet and visible spectrophotometer, Hitachi EPI-G2 infrared spectrophotometer, Hitachi H-60 NMR spectrometer and Nihon-Densi JMS-O1S-G mass spectrometer. The infrared spectra were measured over 400—4000 cm^{-1} in Nujol mull and a potassium

bromide disk. The wave numbers of the observed absorption bands were calibrated with polystyrene. The samples for magnetic measurements were purified by washing twice with hot ethanol, three times with hot water and four times with 70% (v/v) aqueous ethanol in an amount from which **11a**, **b**, **c** could be recrystallized.

*5-Methyl-3-β-carboxyethylsalicylaldehyde (**2b**).* Forty grams of 6-methyldihydrocoumarin[21] was dissolved in an aqueous sodium hydroxide solution (110 g of sodium hydroxide in 650 m*l* of water) at 65—70°C. To the solution was added 90 g of chloroform for an hour at the same temperature under thorough stirring which was continued for 7 hr and a half. The reaction mixture was cooled, acidified with hydrochloric acid and extracted twice with ether. The combined ether solution was washed with water and extracted twice with a saturated aqueous solution of sodium bisulfite (30 g of sodium bisulfite was used). The ether layer (A) and the sodium bisulfite solution were separated. The combined sodium bisulfite solution was acidified with hydrochloric acid and extracted with ether (B). The ethereal extract (B) was washed with water, dried over sodium sulfate. A grease-like residue obtained after the evaporation of ether was extracted with hot petroleum ether. Crystals obtained from the petroleum ether solution were recrystallized from the same solvent. Pale yellow crystal, mp 93°C. Yield 332 mg.[22] In another run, extraction with an aqueous solution of 50 g of sodium bisulfite yielded 956 mg of the aldehyde.

*4-Methyl-4-dichloromethyl-2-β-carboxyethyl-cyclohexa-2,5-dien-1-one (**5**).* The ether layer (A) obtained as above was washed with water and dried over sodium sulfate. Evaporation of ether in a vacuum at room temperature yielded 31 g of residual dark red oil **Q**. Examination of the mass spectrum and thin layer chromatogram of **Q** indicated that it consisted of **5** (main fraction), **2b** (minor fraction) and a small amount of other compounds.

*Separation of **2b** in **Q** as Semicarbazone.* Three grams of semicarbazide hydrochloride and 3 g of potassium acetate were dissolved in 9 m*l* of water. To the solution was added 5.9 g of **Q** dissolved in 8 m*l* of ethanol. The semicarbazone of **2b** separated immediately after the addition was recrystallized from ethanol. Mp 207°C. Yield 1.1 g. This was identified by both the mixed melting point and a comparison of the IR spectra with those of the authentic sample.

Found: C, 53.40; H, 5.75; N, 15.39%. Calcd for $C_{12}H_{15}O_4N_3$: C, 54.33; H, 5.70; N, 15.84%.

*Conversion of **5** into 6-Methyldihydrocoumarin (**3**).* Thirty grams of **Q** dissolved in 100 m*l* of dioxane was irradiated with sunlight for twenty hours. The solution was dried over sodium sulfate and distilled. A distillate of bp 120—150°C/4 mmHg was obtained and solidified by the seeding. Recrystallization of the distillate from aqueous alcohol (alcohol 7: water 3) gave 12.68 g of 6-methyldihydrocoumarin. Distillation without any irradiation gave a resinous polymerizate.

*The Ethyl Ester **6**.* Fifteen grams of **Q** was dissolved in 100 m*l* of ethanol (in which 3 g of dry hydrogen chloride was contained), warmed in a water bath at 60°C for 3 hr and left to stand overnight. The solution was treated with 50 m*l* of benzene, washed with water, dried over sodium sulfate and distilled. Fraction I. bp —153°C/6 mmHg, 1.4 g; Fraction II. bp 135—155°C/5 mmHg, 1.8 g; Fraction III. bp 155—168°C/5 mmHg, 9.1 g. Redistillation of Fraction III gave slightly yellow colored distillate of bp 158—162°C/5 mmHg (tlc, R_f=0.58, silica gel; benzene 8: ethyl acetate 2) which was proved to be the ester **6** as discussed above. Fractions I and II contained a compound of R_f=0.72 as the major component and *6* as a minor component.

Found: C, 53.98; H, 5.53; Cl, 22.60%. Calcd for $C_{13}H_{16}O_3Cl_2$: C, 53.62; H, 5.54; Cl, 24.35%.

*The Semicarbazone of **6**.* To a solution of 600 mg of semicarbazide hydrochloride and 600 mg of potassium acetate in 1.8 m*l* of water was added 920 mg of ***6*** and a small amount of ethanol. The solution was left to stand for 4 days at room temperature. The crystals separated were recrystallized from ethanol. Mp 153°C. Yield 586 mg.

Found: C, 48.34; H, 5.49; N, 12.07; Cl, 20.21%. Calcd for $C_{14}H_{20}O_3N_3Cl_2$: C, 48.14; H, 5.77; N, 12.03; Cl, 20.29%.

*5-Chloro-3-β-carboxyethylsalicylaldehyde (**2c**) and 2-β-carboxyethyl-1,4-benzoquinone (**9**).* The same procedure as for the Reimer-Tiemann reaction by use of 30 g of 6-chlorodihydrocoumarin,[21] 72.6 g of sodium hydroxide in 220 m*l* of water and 62 g of chloroform followed by bisulfite extraction yielded a mixture of compounds. On recrystallization of the mixture from benzene, a compound with very small solubility 2-β-carboxyethyl-1,4-benzoquinone, mp 160°C, separated out. Yield 232 mg (after recrystallization from benzene). IR spectrum, 1703 cm^{-1} (COOH), 1650, 1586 cm^{-1} (quinonoid enone). NMR spectrum ($(CD_3)_2SO$), 1H (COOH) 0.25 τ; 3H (quinone ring) 1H doublet 3.06 τ (J_1=9 cps), 1H doublet 2.38 τ (J_2=2 cps), 1H quartet 2.41 τ (J_1=9 cps, J_2=2 cps).

Found: C, 60.64; H, 5.25%. Calcd for $C_9H_8O_3$: C, 60.00, H, 4.48%.

From the mother liquor of recrystallization, **2c** of mp 118°C was obtained. Yield 2.15 g (after recrystallization from benzene).[22]

As a non-carbonyl fraction (not removed by bisulfite extraction) 19.5 g of crystal was obtained which after recrystallization from benzene melted at 136°C and was identified to be **10** by melting point, analysis and the superimposable IR spectra.

*5-Bromo-2-hydroxyphenylacetic acid (**1**).* To a vigorously stirred mixture of 30.2 g of 2-hydroxyphenylacetic acid[23] in 200 m*l* of carbon disulfide cooled in an ice-salt bath, was added a solution of 32 g of bromine in 80 m*l* of carbon disulfide for two hours. Stirring was continued for 2 hr, and left to stand overnight at room temperature. The precipitate separated was filtered and recrystallized from benzene. Mp 151°C, yield 23.7 g.[22]

*5-Bromo-3-carboxymethylsalicylaldehyde (**2a**).* 1.60 g of **2a** was obtained by the same Reimer-Tiemann procedure, starting with 11.6 g of 5-bromo-2-hydroxyphenylacetic acid, 22 g of sodium hydroxide in 120 m*l* of water and 18 g of chloroform. Recrystallized from benzene. Pale yellow crystal. Mp 204°C.[22]

*Bis-(5-bromo-3-carboxymethylsalicylaldehyde)-ethylenediimine (**14a**).* To a solution of 1.036 g of **2a** in 50 m*l* of ethanol heated on a water bath was added a solution of 0.156 g of ethylenediamine in 10 m*l* of ethanol and the mixture was heated for 30 min on the water bath. The precipitate with a small solubility in ethanol separated immediately, and was filtered (1.1 g) and recrystallized from a large amount of ethanol. Yellow crystal. Mp 242°C.[22]

*Bis-(5-methyl-3-β-carboxyethylsalicylaldehyde)-ethylenediimine (**14b**).* To a hot solution of 51 mg of ethylenediamine in 4 m*l* of ethanol were added crystals of 312 mg of **2b** and the mixture was heated on a water bath for 30 min. On

21) K. Sato, T. Amakasu, and S. Abe, *J. Org. Chem.*, **29**, 2971 (1964).

22) Analytical values were given in a preliminary report. This Bulletin, **41**, 1277 (1968).

23) J. Levine, T. E. Eble, and H. Fischbach, *J. Amer. Chem. Soc.*, **60**, 1930 (1948).

cooling and scratching the wall of the flask with a glass rod, yellow crystals separated; readily soluble in ethanol and recrystallized from ethanol, mp 195°C, yield 276 mg.[22]

Bis-(5-chloro-3-β-carboxyethylsalicylaldehyde)-ethylenediimine (14c). Prepared in the same way as **14b**, from 457 mg of **2c** and 65 mg of ethylenediamine in 6 m*l* of ethanol. Yellow crystal. Mp 204°C. Yield 226 mg.[22]

N,N'-*bis-(5-chloro-2-hydroxy-3-β-carboxyethylbenzyl)-ethylenediamine (15c).* To a suspension of 150 mg of the Schiff base **14c** in 18 m*l* of absolute methanol heated to 48—50°C in an oil bath, was gradually added 100 mg of crystals of sodium borohydride after the frothing subsided.[24] When the addition was over, the temperature of the reaction mixture was gradually raised to 90°C, and then cooled and filtered. To the filtrate was added 15 m*l* of water and then a dilute aqueous acetic acid solution until turbidity appeared. In a few minutes white crystals separated out and which were filtered and dried. For further purification, the product was dissolved in 15 m*l* of a dilute aqueous sodium hydroxide solution (*ca.* 1/10 N), to which was added 18 m*l* of methanol and a dilute aqueous acetic acid solution until turbidity ensued. Crystals which separated out in a few minutes were filtered, washed with water and dried. Colorless crystals. Mp (dec.) 280—300°C, yield 128 mg.

Found: C, 53.55; H, 5.70; N, 5.19%. Calcd for $C_{22}H_{26}O_6N_2Cl_2$: C, 54.43; H, 5.40; N, 5.79%.

N,N'-*bis-(5-bromo-2-hydroxy-3-carboxymethylbenzyl)-ethylenediamine (15a).* Prepared in the same way as **15c**, starting with 437 mg of **14a** and 322 mg of sodium borohydride. Colorless crystal. Mp (dec.) 300°C, yield 287 mg.[22]

N,N'-*bis-(5-methyl-2-hydroxy-3-β-carboxyethylbenzyl)-ethylenediamine (15b).* Prepared in the same way as **15c**, starting with 700 mg of **14b** and 500 mg sodium borohydride in 56 m*l* of absolute methanol. Colorless crystal. Mp (dec.) 285°C, yield 559 mg.[22]

Di-μ-aquo-bis-(5-bromo-3-carboxymethylsalicylaldehyde)-dicopper (11a). To a hot solution of 518 mg (1/1000 mol) of **2a** in ethanol was added an aqueous solution of 399 mg (1/1000 mol) of copper acetate and the mixture was heated on a water bath for 20 min. The precipitate separated out immediately was filtered while hot and purified by washing several times with hot ethanol and water; bright green crystal, yield 587 mg. The yield and composition of the chelate were not altered even when twice as much aldehyde was used.

Found: C, 31.70; H, 1.58; Cu, 18.77%. Calcd for $C_{18}H_{14}O_{10}Br_2Cu_2$: C, 31.92; H, 2.08; Cu, 18.77%.

Di-μ-aquo-bis-(5-methyl-3-β-carboxyethylsalicylaldehyde)-dicopper (11b). Prepared in the same way as **11a**, starting with 412 mg of **2b** and 400 mg of copper acetate. Bright green powder. Yield 496 mg.

Found: C, 46.18; H, 4.57; Cu, 21.02%. Calcd for $C_{22}H_{24}O_{10}Cu_2$: C, 45.91; H, 4.20; Cu, 22.08%.

Di-μ-aquo-bis-(5-chloro-3-β-carboxyethylsalicylaldehyde)-dicopper (11c). Prepared in the same way as **11a**, starting with 115 mg of **2c** and 98 mg of copper acetate; bright green powder. Yield 140 mg.

Found: C, 38.51; H, 3.02; Cu, 21.01%. Calcd for $C_{20}H_{18}O_{10}Cl_2Cu_2$: C, 38.97; H, 2.94; Cu, 20.62%.

Di-μ-aquo-bis-(5-chloro-3-β-carboxyethylsalicylaldehyde)-ethylenediimine-dicopper (12c). To a suspension of 100 mg of **11c** in 5 m*l* ethanol was added a solution of 10 mg of ethylenediamine in 3 m*l* of water and the mixture was heated on a water bath for 20 min. Green crystals precipitated which were purified by washing repeatedly with ethanol and water. Yield 91 mg.

Found: C, 41.55; H, 3.64; N, 4.92; Cu, 20.53%. Calcd for $C_{22}H_{22}O_8N_2Cl_2Cu_2$: C, 41.26; H, 3.46; N, 4.37; Cu, 19.84%.

Di-μ-aquo-bis-(5-bromo-3-carboxymethylsalicylaldehyde)-ethylenediimine-dicopper (12a). Prepared by the reaction of 102 mg of **11a** and 10.2 mg of ethylenediamine; green powder, yield 89 mg.

Found: C, 33.63; H, 2.22; N, 4.85; Cu, 18.60%. Calcd for $C_{20}H_{18}O_8N_2Br_2Cu_2$: C, 34.25; H, 2.59; N, 4.01; Cu, 18.12%.

Di-μ-aquo-bis-(5-methyl-3-β-carboxyethylsalicylaldehyde)-ethylenediimine-dicopper (12b). Prepared by the reaction of 87 mg of **11b** in 3 m*l* of ethanol with 10 mg of ethylenediamine in 1 m*l* of water; green powder, yield 85 mg.

Found: C, 47.35; H, 5.13; N, 4.64; Cu, 20.38%. Calcd for $C_{24}H_{28}O_8N_2Cu_2$: C, 48.08; H, 4.70; N, 4.67; Cu, 21.20%.

Bis-(5-chloro-3-β-carboxyethylsalicylaldehyde)-ethylenediimine-copper (13c). To a hot solution of 240 mg of **14c** in 20 m*l* of ethanol was added a solution of 100 mg of copper acetate in 10 m*l* of water. The reaction mixture was heated on a water bath for 30 min and the precipitate was filtered hot. The gray purple product was recrystallized from a large amount of ethanol, yield 239 mg.

Found: C, 47.94; H, 3.73; N, 5.13; Cu, 12.03%. Calcd for $C_{22}H_{20}O_6N_2Cl_2Cu$: C, 48.67; H, 3.71; N, 5.16; Cu, 11.70%.

Bis-(5-methyl-3-β-carboxyethylsalicylaldehyde)-ethylenediimine-copper (13b). Prepared in the same way as **13c** by the reaction of 220 mg of **14b** in 20 m*l* of ethanol with 100 mg of copper acetate in 10 m*l* of water. Gray purple crystal, yield 208 mg.

Found: C, 56.10; H, 5.32; N, 5.59; Cu, 13.12%. Calcd for $C_{24}H_{26}O_6N_2Cu$: C, 57.42; H, 5.22; N, 5.58; Cu, 12.66%.

Bis-(5-bromo-3-carboxymethylsalicylaldehyde)-ethylenediimine-copper (13a). The reaction of 108 mg of **14a** and 40 mg of copper acetate yielded 103 mg of a brown copper chelate. The chelate could not be obtained in a pure state owing to the low solubility of **14a** and the copper chelate; purplish brown powder.

Found: C, 39.13; H, 3.02; N, 5.63; Cu, 9.50%. Calcd for $C_{20}H_{16}O_6N_2Br_2Cu$: C, 39.79; H, 2.67; N, 4.64; Cu, 10.53%.

N,N'-*bis-(5-methyl-2-hydroxy-3-β-carboxyethylbenzyl)-ethylenediamine-copper (21).* A solution of 40.8 mg of copper acetate in 3 m*l* of water was added to a solution of 89.38 mg of **15b** in 5.4 m*l* of 1/10 N aqueous sodium hydroxide (f= 0.744) at room temperature with stirring. Yellow green crystals separated immediately. After stirring for one and a half hour, the precipitate was filtered, washed thoroughly with water and ethanol and recrystalized from 70% aqueous ethanol. Green crystal, yield 88.08 mg.

Found: C, 51.88; H, 6.40; N, 5.01; Cu, 10.91%. Calcd for $C_{24}H_{30}O_6N_2Cu$–$3H_2O$: C, 51.46; H, 6.48; N, 5.01; Cu, 11.34%.

The author wishes to thank Dr. M. Nakanishi and Mr. T. Kuriyama, Yoshitomi Pharmaceutical Company, for the mass spectral measurements, Profs. M. Kikutani and T. Kuraishi and the staff of NMR center, Nagasaki University, for the NMR measurements, and Prof. K. Hirakawa, Tokyo University, Prof. K. Hirakawa and their co-workers, Kyushu University, for the magnetic measurements.

24) I. L. Finar and K. Utling, *J. Chem. Soc.*, **1959**, 4015.

Kinetics of the Acid Hydrolysis of Carboxylatopentammineruthenium(III) Complexes

Akira OHYOSHI, Akinori JYO, and Noriaki SHIN

Department of Industrial Chemistry, Faculty of Engineering, Kumamoto University, Kurokami-machi, Kumamoto

(Received April 23, 1971)

The kinetics of the hydrolysis of pentammineruthenium(III) complexes containing carboxylates and α-substituted acetates (glycolate and glycinate) have been studied. The experiments were carried out in a solution of $[H^+]=0.025$—0.1 M, at 40—70°C. For each complex, the rate law was found to be: rate$=[\text{complex}](k_{H_2O}+k_H[H^+])$. The k_{H_2O} and k_H values for the formato, acetato, propionato, isobutyrato, glycolato, and glycinato complexes are, respectively (at $\mu=0.10$, 59—61°C): k_{H_2O}, 5.37×10^{-5}, 11.8×10^{-5}, 14×10^{-5}, 13.7×10^{-5}, 5.7×10^{-5}, and 6.75×10^{-5} sec^{-1}; k_H, 3.3×10^{-3}, 2.3×10^{-3}, 2.5×10^{-3}, 1.7×10^{-3}, 0.75×10^{-3}, and 3.1×10^{-3} $M^{-1}sec^{-1}$. The mechanisms of acid hydrolysis are discussed for the two reaction paths.

Recently, the kinetic studies of the hydrolysis of halogenopentammineruthenium(III)[1,2] and related complexes[2] have been reported. The kinetics of aquation have also been studied with some carboxylatopentammine complexes $[M(NH_3)_5OOCR]^{2+}$ (where M= Co(III), Rh(III), and Ir(III)) by Basolo *et al.*,[3,4] Kuroda,[5,6] and Saito *et al.*[7,8] These metal ions have six *d*-electrons, but Ru(III) has five. Therefore, it is of interest to study the aquation of a similar type of Ru(III) complexes and to compare them with d^6-metal complexes. In this paper, we will report on the kinetics of the aquation of several alkyl-, hydroxyl-, or amino-substituted-carboxylatopentammineruthenium-(III) complexes.

Experimental

Reagents. All the chemicals used were of a reagent grade. Twice-distilled water was used in all the kinetic runs. The ionic strength and the acidity of the reaction solution were adjusted with *p*-toluenesulfonic acid and its sodium salt. The sodium salt was prepared by the neutralization of *p*-toluenesulfonic acid with sodium hydroxide.

Preparation of Complexes. *Chloropentammineruthenium(III) chloride* was prepared by the method of Allen *et al.*[9,10] from ruthenium trichloride and hydrazine hydrate.

Found: H, 5.08; N, 23.75%. Calcd for $[RuCl(NH_3)_5]Cl_2$: H, 5.19; N, 23.98%.

Aquopentammineruthenium perchlorate was prepared by the method of Endiccot and Taube.[11]

Found: H, 3.20; N, 13.74%. Calcd for $[Ru(H_2O)(NH_3)_5](ClO_4)_3$: H, 3.42; N, 13.94%.

Formatopentammineruthenium and other carboxylatopentammineruthenium perchlorates were prepared by the method of Stritar and Taube[12] from chloropentammineruthenium chloride, a carboxylate buffer solution, and a zinc amalgam.

Found: C, 3.00; H, 3.62; N, 16.39%. Calcd for $[Ru(NH_3)_5OOCH](ClO_4)_2$: C, 2.79; H, 3.75; N, 16.28%.

Found: C, 5.37; H, 3.86; N, 15.61%. Calcd for $[Ru(NH_3)_5OOCCH_3](ClO_4)_2$: C, 5.41; H, 4.08; N, 15.77%.

Found: C, 7.90; H, 4.29; N, 15.15%. Calcd for $[Ru(NH_3)_5OOCC_2H_5](ClO_4)_2$: C, 7.86; H, 4.41; N, 15.28%.

Found: C, 10.44; H, 4.32; N, 14.70%. Calcd for $[Ru(NH_3)_5OOCCH(CH_3)_2](ClO_4)_2$: C, 10.17; H, 4.70; N, 14.83%.

Found: C, 5.47; H, 3.75; N, 14.97%. Calcd for $[Ru(NH_3)_5OOCCH_2OH](ClO_4)_2$: C, 5.22; H, 3.94; N, 15.22%.

Found: C, 4.37; H, 3.80; N, 14.84%. Calcd for $[Ru(NH_3)_5OOCCH_2NH_3](ClO_4)_3$: C, 4.28; H, 3.60; N, 14.99%.

These complexes were also characterized by their electronic and IR spectra.

Kinetic Runs. The rates of the reactions were followed spectrophotometrically. It was found that the usual inorganic acids were unsuitable for the study of acid hydrolysis. In perchloric and nitric acid solutions, the aquation and decomposition of the complex occurred simultaneously. Several hours later, the appearance of the reaction mixture changed from a transparent pale yellow to a turbid dark brown. These phenomena are probably due to the oxidation of ruthenium(III) by acid anions. In hydrochloric and sulfuric acid, ligand replacements were spectrophotometrically identified. *p*-Toluenesulfonic acid is the best for studying the kinetics of aquation. Since *p*-toluenesulfonate has a strong $\pi\leftrightarrow\pi^*$ absorption below 280 mμ, the rates of hydrolysis were followed by measuring the changes in the absorbances of the respective complex ion in the wavelength region of 290—300 mμ.

All the kinetic experiments were performed in a stoppered quartz cell placed in a cell compartment of HITACHI 124 spectrophotometer. The reaction mixture in the cell was kept at a constant temperature, ±0.2°C, by circulating water from a thermostated bath. After thermal equilibrium has been achieved, a weighed amount of the complex (about 1 mg) was rapidly dissolved in an aqueous solution of a given ionic strength and acid concentration. The absorbances of the complexes in the reaction mixtures were measured at appropriate intervals.

Identification of the Reaction Product. Since aquopentammineruthenium(III), which has an absorption maximum at 268 mμ,[5] can not be directly detected, as was mentioned above, it was separated and identified. About six half-lives

1) J. A. Broomhead, F. Basolo, and R. G. Pearson, *Inorg. Chem.*, **3**, 826 (1964).
2) J. A. Broomhead and C. Sutton, *ibid.*, **8**, 1544 (1969).
3) F. Basolo, J. G. Bergmann, and R. G. Pearson, *J. Phys. Chem.*, **56**, 22 (1952).
4) F. Monacelli, F. Basolo, and R. G. Pearson, *J. Inorg. Nucl. Chem.*, **24**, 1241 (1962).
5) K. Kuroda, *Nippon Kagaku Zasshi*, **82**, 572 (1961).
6) K. Kuroda, *ibid.*, **82**, 1481 (1961).
7) K. Ogino, T. Murakami, and K. Saito, This Bulletin, **41**, 1615 (1968).
8) T. Murakami, K. Ogino, H. Kobayashi, H. Yamazaki, and K. Saito, *ibid.*, **44**, 120 (1971).
9) A. D. Allen, F. Bottomley, R. O. Harris, V. P. Reinsalu, and C. V. Senoff, *J. Amer. Chem. Soc.*, **89**, 5595 (1967).
10) A. D. Allen and C. V. Senoff, *Can. J. Chem.*, **45**, 1337 (1967).
11) J. F. Endicott and H. Taube, *J. Amer. Chem. Soc.*, **84**, 4984 (1962).
12) J. A. Stritar and H. Taube, *Inorg. Chem.*, **8**, 2281 (1969).

later, the reaction mixture was passed through a column of ion-exchange resin (Dowex 50X-8, 100—200 mesh). The column was washed several times with water until no *p*-toluenesulfonate ion was detected in the washings, and then a 3M sodium perchlorate solution (pH 1.0 with perchloric acid) was passed through the column. The electronic spectrum of this eluate was measured and compared with that of the authentic aquopentammine complex.

Results

The electronic spectrum of the reaction product coincided with that of the aquopentammineruthenium(III) ion prepared from chloropentammineruthenium(III) and ammonia water (Fig. 1). The extent of the absorbance of the reaction product contributing to that of the reactant was smaller than 3% at one half-life of the reaction. The changes in the spectrum during the acid hydrolysis of the acetatopentammine complex are exemplified in Fig. 2. The acid hydrolysis reaction is an irreversible one, for the plot of log C_t *vs.* the reaction time is linear over a period of approximately one half-life, as is shown in Fig. 3, where C_t denotes the concentration of the complex at the reaction time, t. As is shown in Fig. 3, the slopes of the first-order plots are independent of the initial concentration of the reactant complex at the same hydrogen-ion concentration, ionic strength, and reaction temperature.

The pseudo first-order rate constants, k_{obs}, for the acid hydrolysis of carboxylatopentammines as a function of the hygrogen-ion concentration are listed in Table 1. The values of k_{obs} have a precision of $\pm 5\%$ or better. As is shown in Fig. 4, the plots of k_{obs} *vs.* the hydrogen-ion concentration are linear for the formatopentammine complex, and similar relationships were obtained for the other five complexes. From these results, it is possible to estimate an acid-independent rate constant, k_{H_2O}, and an acid-dependent rate constant k_H. The observed rate constant, k_{obs}, can be expressed by Eq. (1):

$$k_{obs} = k_{H_2O} + k_H[H^+] \quad (1)$$

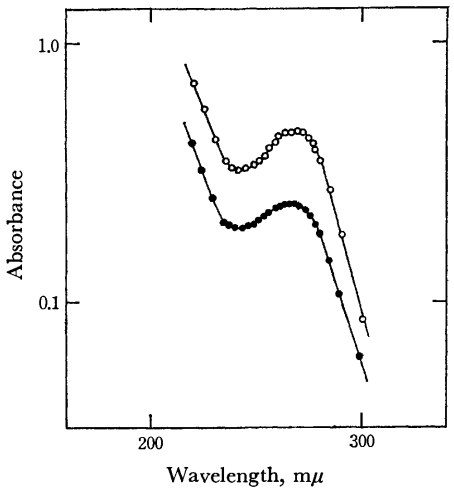

Fig. 1. Identification of the reaction product.
A: Spectrum of $[Ru(H_2O)(NH_3)_5]^{3+}$ prepared from $[RuCl(NH_3)_5]^{2+}$ in 0.1M $HClO_4$.
B: Spectrum of the reaction product eluted from cation exchange resin.
Reactant complex=$[Ru(NH_3)_5OOCH]^{2+}$

The calculated k_{H_2O} and k_H values are listed in Table 2, together with the pK_a values of the carboxylic acids.

The influence of the ionic strength on the rate of the hydrolysis was also investigated, the results are given in Table 3. The rates of hydrolysis increase with an increase in the ionic strength. This fact indicates that there is a positive kinetic salt effect.

The activation parameters for the reactions were evaluated from the kinetic data at 40—70°C and at an ionic strength of 0.1. The results are listed in Table 4.

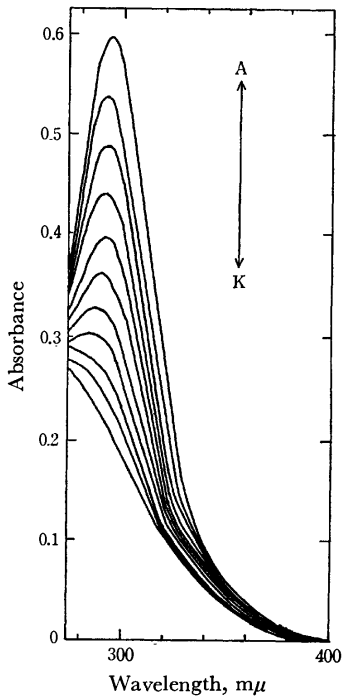

Fig. 2. Spectral changes during the acid hydrolysis of $[Ru(NH_3)_5OOCCH_3]^{2+}$. $[H^+]=0.1$M, $\mu=0.1$, Temp=60.2°C. A=4 min, B=9 min, C=14 min, D=19 min, E=20 min, F=29 min, G=34 min, H=39 min, I=43 min, J=49 min, K=54 min.

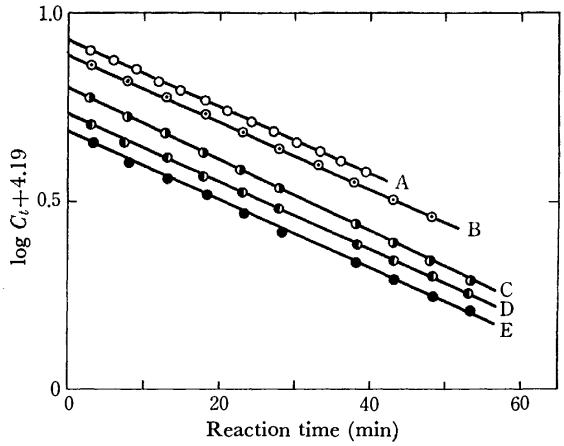

Fig. 3. The rates of hydrolyses of $[Ru(NH_3)_5OOCCH_3]^{2+}$ Temp=60.2°C, 0.1M *p*-toluenesulfonic acid, $\mu=0.1$.
Initial concentrations: A=5.36×10^{-4}M, B=5.05×10^{-4}M, C=4.05×10^{-4}M, D=3.40×10^{-4}M, E=3.08×10^{-4}M.

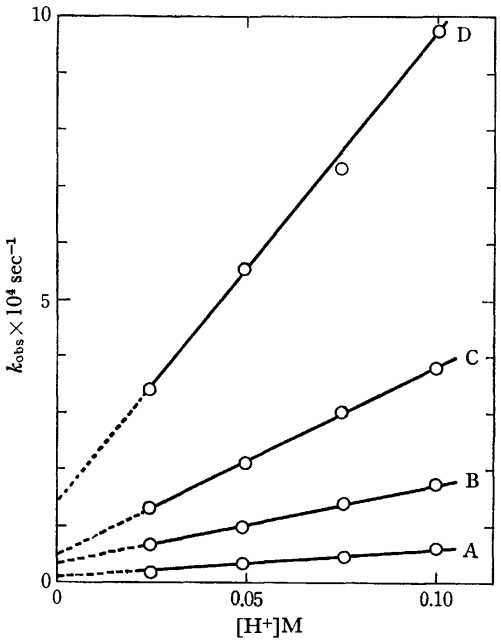

Fig. 4. The rate constant of hydrolysis *vs.* [H$^+$] Complex; $[Ru(NH_3)_5OOCH]^{2+}$, μ=0.1. Temp=A; 40.0°C, B; 51.0°C, C; 61.0°C, D; 71.0°C.

Table 1. The rates of hydrolysis of carboxylatopentammineruthenium(III) at various hydrogen ion concentrations and μ=0.10

Complexes	Temp °C	[H$^+$]M	$k_{obs} \times 10^4$sec^{-1}
Formato-	61.0	0.0244	1.36
		0.0499	2.13
		0.0745	3.03
		0.0996	3.80
Acetato-	60.2	0.0260	1.78
		0.0511	2.35
		0.0767	2.92
		0.1020	3.53
Propionato-	60.0	0.0244	1.98
		0.0500	2.76
		0.0756	3.24
		0.0998	3.88
iso-Butyrato-	61.0	0.0252	1.80
		0.0487	2.20
		0.0748	2.60
		0.0995	3.07
Glycolato-	61.0	0.0200	0.70
		0.0400	0.90
		0.0800	1.15
		0.0995	1.32
Glycinato-	59.0	0.0247	0.68
		0.0494	0.69
		0.0741	0.70
		0.0988	0.71

Discussion

Equation (1) shows that the rate of hydrolysis of the complex is dependent on the hydrogen-ion concentration and that the two reaction paths are involved in the reaction mechanism of the hydrolysis. This can be expressed by Eq. (2) for one path and by Eqs. (3) and

Table 2. Rate constant of acid-catalyzed and uncatalyzed path of the hydrolysis of carboxylatopentammineruthenium(III) at μ=0.10

Complexes	Temp °C	pK_a	$k_{H_2O} \times 10^5$sec^{-1}	$k_H \times 10^4$M^{-1}sec^{-1}
Formato-	40.0	3.75	0.38±0.08	5.7±0.1
	51.0		3.19±0.04	14 ±1
	61.0	3.81	5.37±0.04	33 ±1
	71.0		13.8 ±1.9	83 ±3
Acetato-	40.0	4.76	0.99±0.07	3.5±0.1
	51.0		4.1 ±0.1	9.6±0.2
	60.2	4.81	11.8 ±0.1	22.9±0.2
	68.0		25 ±2	46 ±3
Propionato-	40.0	4.89	0.7 ±0.2	3.6±0.2
	50.0		4.2 ±0.5	11 ±1
	60.0	4.94	14 ±1	25 ±1
	70.0		40 ±4	61 ±4
iso-Butyrato-	40.6	4.92	1.0 ±0.8	2 ±1
	51.0		4.4 ±0.4	7.5±0.5
	61.0	4.99	13.7 ±0.2	16.9±0.5
	71.5		42.3 ±0.5	35 ±1
Glycolato-	50.0	4.85	2.1 ±0.1	2.0±0.2
	61.0		5.7 ±0.2	7.5±0.5
	65.0		9.6 ±0.2	10.1±0.3
	70.0		16.7 ±0.5	15.4±0.8
Glycinato-	59.0	2.32	6.75±0.01	0.31±0.02
	66.0		15.2±0.1	1.4 ±0.2
	70.0		22.6 ±0.1	1.5 ±0.9

Table 3. Influence of ionic strength (μ) on the rate of hydrolysis of carboxylatopentammineruthenium-(III) at [H$^+$]=0.1M and Temp=60.0±0.2°C

Complexes	μ	$k_{obs} \times 10^4$sec^{-1}
Formato-	0.10	3.80
	0.28	5.76
	0.55	6.91
	0.88	8.56
	1.01	8.90
Acetato-	0.10	3.53
	0.33	4.76
	0.55	5.87
	0.77	6.71
	1.00	7.56
Propionato-	0.10	3.88
	0.28	5.03
	0.55	6.37
	0.82	6.99
	1.00	8.06
iso-Butyrato-	0.10	2.36
	0.33	3.30
	0.55	3.95
	0.78	4.51
	1.00	5.15
Glycolato-	0.10	0.90
	0.24	1.13
	0.50	1.33
	1.00	1.49
Glycinato-	0.10	0.71
	0.50	0.64
	1.00	0.62

Table 4. Activation parameters for carboxylatopentammine complexes $\mu=0.1$

Complexes	k_{H_2O}		k_H	
	E_a kcal/mol	ΔS^* e.u.	E_a kcal/mol	ΔS^* e.u.
$[Ru(NH_3)_5OOCH]^{2+}$	24	−9	19	−16
$[Ru(NH_3)_5OOCCH_3]^{2+}$	24	−7	20	−15
$[Ru(NH_3)_5OOCC_2H_5]^{2+}$	25	−5	20	−15
$[Ru(NH_3)_5OOCCH(CH_3)_2]^{2+}$	25	−4	16	−26
$[Ru(NH_3)_5OOCCH_2OH]^{2+}$	22	−11	22	−6
$[Ru(NH_3)_5OOCCH_2NH_3]^{3+}$	26	−2	—	—
$[Co(NH_3)_5OOCH]^{2+}$ [a]	—	—	25.2	—
$[Co(NH_3)_5OOCCH_3]^{2+}$ [b]	25.3	−8	25	+2
$[Rh(NH_3)_5OOCCH_3]^{2+}$ [b]	26.3	—	23	−4
$[Ir(NH_3)_5OOCCH_3]^{2+}$ [b]	—	—	25	−8
$[Co(NH_3)_5OOCC_2H_5]^{2+}$ [a]	—	—	25.4	—
$[Co(NH_3)_5OOCCH_2NH_3]^{3+}$ [c]	22.6	−20	29.6	+3

a) Results from Ref. 6. b) Results from Ref. 4.
c) Resluts from Kef. 7.

(4) for the other path:

$$[(NH_3)_5Ru\text{-}O\overset{O}{\overset{\|}{C}}R]^{2+} + H_2O \xrightarrow{k_2} [(NH_3)_5RuOH_2]^{3+} + RCOO^- \quad (2)$$

$$[(NH_3)_5Ru\text{-}O\overset{O}{\overset{\|}{C}}R]^{2+} + H^+ \overset{K_3}{=} [(NH_3)_5Ru\text{-}O\overset{OH}{\overset{|}{C}}R]^{3+} \quad (3)$$

$$[(NH_3)_5Ru\text{-}O\overset{OH}{\overset{|}{C}}R]^{3+} + H_2O \xrightarrow{k_4} [(NH_3)_5RuOH_2]^{3+} + RCOO^- + H^+ \quad (4)$$

The rate constant of an uncatalysed path [Eq. (2)], k_2, corresponds to k_{H_2O}. Equations (3) and (4) indicate an acid-catalysed path, the rate constant, k_H, of which can be expressed by Eq. (5):

$$k_H = k_4K_3 \quad (5)$$

these relationships for the hydrolyses of similar complexes of Co(III), Rh(III), and Ir(III) have previously reported.[4-8] However, it should be noted that the values of k_{H_2O} and k_H for ruthenium(III) complexes are greater than those of the Co(III), Rh(III), and Ir(III) complexes. In view of the electrostatic attraction between the metal and the ligand ion, the aquation of the d^5-metal complex should proceed faster than that of the d^6-metal complex if the break of the metal-ligand bond is the rate-determining step.

As is shown in Table 2, the k_{H_2O} values in a solution of $\mu=0.1$ at 59—61°C decrease in the order of isobutyrato-, (≃propionato-), acetato-, glycinato-, glycolato-, and formatocomplex. This suggests that the rate becomes faster, the greater the size of the leaving group, and that the reactions proceed through a dissociation-type mechanism.

The rates of the aquation of some carboxylatopentammineruthenium(II) complexes have been reported by Stritar and Taube.[12] In the acid-independent path, the values of the rate constants are 1.28 sec^{-1} and <5 sec^{-1} for the formato- and acetatocomplexes at 25°C and an ionic strength of 0.1. The values for the corresponding ruthenium(III) complexes which are obtained from the present experiments and extrapolated to the same experimental conditions are 1×10^{-5} and 7×10^{-6} sec^{-1} respectively. The ratios of the rate constants of the Ru(II) complexes to those of the Ru(III) complexes are 10^5 and 10^6. The effect of the positive charge of the complex on the rate could be interpreted as follows. The separation of a negative charge in the form of the carboxylate ion is more difficult as the remaining charge on the complex increases. These facts may indicate that the bond break is important and that we are dealing with an S_N1 mechanism in the present reactions.

The rate constant of hydrolysis, k_{obs}, increases with the increase in the ionic strength of the acidic solution (Table 3). This indicates that both of the reactants have same kinds of charge. When $[H^+]=0.1$ M, we can assume k_{H_2O} to be much smaller than k_H; thus, k_{obs} is nearly equal to k_4K_3. As may be seen from Eqs. (3) and (4), a positive kinetic salt effect can be expected in Eq. (3), the equilibrium constant of which is K_3. Therefore, it can be concluded that K_3 is the more effective fraction in the acid-dependent path.

Basolo *et al.*[4] reported that the k_{H_2O} values of carboxylatopentamminecobalt(III) complexes tend to decrease with an increase in the pK_a values of the ligand acids. The results in Table 2 do not indicate that such a relation fits the ruthenium(III) complexes. On the contrary, the k_H values for the ruthenium(III) complexes decrease with the increase in the pK_a values. The pK_a values affect the equilibrium constant, K_3, of Eq. (3), and hence the k_H values. The k_H values of the glycolato- and glicinatocomplexes are smaller than those of the other complexes. Concerning the glicinatocomplex of cobalt(III), Saito *et al.*[8] described the small k_H value as being due to the difficulty with which the protonated species are formed. For the similar complex of ruthenium(III), the same effect seems to be exhibited. The influence of the substituting hydroxyl group in the glycolatocomplex is not very clear, but it may be considered that there are some interactions between the hydroxyl and the carboxylate groups such as those in the aminoacid complex.

With regard to the hydrolysis of acetatopentamminecobalt(III), Monacelli *et al.*[4] reported that the acid-independent path proceeds by means of metal-oxygen bond fission and that the acid-dependent path takes place through the breaking of the acyl-oxygen bond. Bunton and Llewllyn[13] found that the aquation of this complex proceeds by means of metal-oxygen bond cleavage on the basis of a tracer study with oxygen-18.

The k_{H_2O} values for Co(III)[4] and Ru(III) acetatopentammine are, respectively, $8.0\times10^{-1}sec^{-1}$ and $2.9\times10^{-4}sec^{-1}$ at 70°C and an ionic strength of 0.1. Thus, the ratio of the rate constants, k_{H_2O}, for these complexes is 1 : 36, while the ratio of k_H is 1 : 5 under the same experimental conditions.

These facts suggest that the influence of the central metal ion on the rate of aquation is larger for the acid-independent path than for the acid-dependent path. Therefore, it may be supposed that the bond fission occurs at a position farther from the central metal ion

13) C. A. Bunton and D. R. Llewellyn, *J. Chem. Soc.*, **1953**, 1692.

in the acid-dependent path than that in the acid-independent path. Thus, we believe that the acid-dependent path proceeds *via* acyl-oxygen bond fission and that the acid-independent reaction takes place through the breaking of the ruthenium-oxygen bond. These reaction mechanism are shown in Eq. (8) and (9):

$$[(NH_3)_5Ru\text{-}\overset{O}{\overset{\|}{O}}CR]^{2+} \longrightarrow [(NH_3)_5Ru\cdots\overset{O}{\overset{\|}{O}}CR]^{2+} \xrightarrow{H_2O} [(NH_3)_5RuOH_2]^{3+} + RCOO^- \quad (8)$$

$$[(NH_3)_5Ru\text{-}\overset{O}{\overset{\|}{O}}CR]^{2+} + H^+ \overset{K_3}{\rightleftharpoons} [(NH_3)_5Ru\text{-}\overset{OH}{\overset{|}{O}}CR]^{3+}$$

$$[(NH_3)_5Ru\text{-}\overset{OH}{\overset{|}{O}}CR]^{3+} \longrightarrow [(NH_3)_5Ru\text{-}O\cdots\overset{OH}{\overset{|}{C}}R]^{3+} \xrightarrow{H_2O} [(NH_3)_5RuOH_2]^{3+} + RCOO^- + H^+ \quad (9)$$

As another possibility, the attack of the water molecule on the carboxyl group may be considered; this would also lead to the acyl-oxygen bond cleavage.[13] We have, however, not yet obtained any experimental evidence to confirm this mechanism.

As is shown in Table 4, the activation energies for the acid-independent paths are generally larger than those for the acid-dependent paths. These values are independent of the substituting group in carboxylic acids except for the acid-dependent path of isobutyrato-complex. The activation energies for the k_{H_2O} values of d^5-(Ru^{III}) metal complexes are nearly the same as those of the d^6-(Co^{III}, Rh^{III}, and Ir^{III}) metal complexes. However, it was found that the activation energies for the k_H values of d^5-metal complexes are less than those of the d^6-metal complexes. The difference between the values of the formatocomplexes amounted to 6.2 kcal/mol.

The entropies of activation for k_H are more negative than those for k_{H_2O}. This suggests that the difference in the extent of hydration between the transition state and the ground state is larger in the acid-dependent path than in the acid-independent path. As is shown in Eqs. (8) and (9), there is an increase of +1 unit charge in the acid-dependent path, while no variation of the charge arises in the acid-independent path.

In the acid-dependent path, the entropy of activation, $\Delta S^{\ddagger}$, obtained may be expressed as follows:

$$\Delta S^{\ddagger} = \Delta S_{K_3} + \Delta S^{\ddagger}_{K_4}$$

where ΔS_{K_3} is the change of entropy for the process of protonation to the complex cation with the equilibrium constant K_3, and where $\Delta S^{\ddagger}_{K_4}$ is the entropy of activation with respect to the rate constant, K_4, described in Eq. (9). When reactions take place between two ions, an important contribution to the entropy of activation arises from the electrostatic force. For a reaction between two ions, A (Z_A charge) and B (Z_B charge), in a dilute aqueous solution, the entropy of activation is approximately $-10\ Z_AZ_B$ e.u./mol.[14] Considering that Z_AZ_B is +2 in the process of protonation, the value of −20 e.u./mol can be calculated for ΔS_{K_3}. This is comparatively close to the observed values of activation entropies, and they are nearly the same for the cases of the formato-, acetato-, and propionatocomplexes. Therefore, it may be considered that a large part of $\Delta S^{\ddagger}$ consists of ΔS_{K_3} in these cases. The values of the activation entropies for k_H are considerably different in the case of the isobutyrato- and glycinatocomplexes. This indicates that the extent of the contribution of ΔS_{K_3} to $\Delta S^{\ddagger}$ may not be the same as in the other cases.

14) S. Glasstone, K. J. Laidler, and H. Eyring, "The Theory of Rate Processes" McGraw-hill book company, Inc., New York and London (1941), p. 433.

Study of Hydration and Association of Ions in Solution. II.[1] Complete Resolution of Tris(ethylenediamine)Cobalt(III), Chromium(III), and Rhodium(III) Complexes by Means of Paper Electrophoresis

Hayami YONEDA* and Takao MIURA

Chemistry Department A, The Technical University of Denmark, Lyngby, Denmark
Department of Chemistry, Wakayama University, Masagocho, Wakayama, Japan

(Received August 21, 1971)

Complete resolution of racemic $[M\ en_3]^{3+}$ ($M=Co^{III}$, Cr^{III}, and Rh^{III}) by means of electrophoresis was achieved in a background solution of sodium *d*-tartrate and aluminum chloride. Electrophoretic data obtained under various conditions (various compositions, concentrations, and pH values of supporting electrolyte solutions) indicated that the separation of the enantiomers of $[M\ en_3]^{3+}$ complexes was accomplished not by the *d*-tartrate anion but by some aluminum *d*-tartrate complex anion.

Racemic mixtures of complex ions can be resolved by combining them with some optically-active counterions to form diastereoisomers which can be separated by the use of solubility differences. For example, $\Lambda(+)_{589}$-$[Co\ en_3]Cl\cdot d\text{-tart}\cdot H_2O$ is easily separated as crystals, while $\Delta(-)_{589}$-$[Co\ en_3]^{3+}$ remains in solution. This suggests that the tendency of the Λ and Δ forms of the $[Co\ en_3]^{3+}$ complex cation towards association with the *d*-tartrate anion is different. In fact, Ogino and Saito[2] showed that the association constant of the $\Lambda(+)_{589}$-$[Co\ en_3]^{3+}$-*d*-tartrate^{2-} system differs from that of the $\Delta(-)_{589}$-$[Co\ en_3]^{3+}$-*d*-tartrate^{2-} system by analyzing the increase in the optical density of the charge-transfer absorption band.

On the other hand, the studies[3] of the electrophoretic behavior of complex salts revealed that the mobility of the complex depends largely on the type and concentration of the supporting electrolyte. This can be attributed to the different degrees of association between the complex ion and the counterion in a supporting electrolyte solution.

This leads to a possible method for resolution of the racemate into optically-active enantiomers by electrophoresis. That is, when the Λ and Δ forms of the complex ion have quite large difference in association tendency to some optically-active counterion, the Λ and Δ cations should have different mobilities. Therefore, under suitable conditions, complete resolution can be expected. With this idea in mind, Mazzei and Lederer[4] attempted to resolve racemic complex salts by electrophoresis in a chiral supporting electrolyte solution. However, they did not succeed in resolution. We also attempted the electrophoretic resolution and tried to resolve the racemic $[Co\ en_3]^{3+}$ complex by running it in sodium *d*-tartrate solutions. This also proved to be unsuccessful. However, we achieved complete resolution just by adding aluminum chloride to the sodium *d*-tartrate background solution.[5] Further, we achieved resolution of the racemic $[Co\ en_3]^{3+}$ by means of thin-layer chromatography[6] using a solution of a similar composition to that used in electrophoretic resolution.

In order to obtain a deeper insight into the mechanism of resolution, we carried out electrophoresis in various background solutions having various compositions, concentrations, and pH values. We also tried three other trisethylenediamine complexes and obtained similar resolution in the cases of $[Cr\ en_3]^{3+}$ and $[Rh\ en_3]^{3+}$, but not in the case of $[Pt\ en_3]^{4+}$.

Experimental

A migration apparatus with multicompartment cells was used, so that ten samples could be run at the same time. A paper strip was dipped uniformly in the background solution, and then the excess of the solution was removed by hanging the strip. After that about 5 μl of a sample solution was placed on the paper (Toyoroshi No. 51A, 2×40 cm).

Samples were run for 2—3 hr under a potential gradient 250 V/34 cm, keeping the temperature of the migrating box at 25°C (The box is filled with carbon tetrachloride in which the strips are immersed). In the case of the $[Cr\ en_3]^{3+}$ complex, the whole apparatus was covered with black cloth to prevent the photodecomposition.

The spot of cobalt, rhodium, and platinum complexes was detected by spraying with sodium sulfide solution, while in the case of the chromium complex, it could be easily detected by the red color which was developed after by exposure to daylight.

Results and Discussion

Table 1 shows the mobilities of four kinds of trisethylenediamine complexes in background solutions of stepwise concentrations which contain only sodium *d*-tartrate as a supporting electrolyte. In this study, the mobility of a complex is defined as a migration distance relative to that of the $[Co\ en_3]^{3+}$ complex in 0.1 M NaCl solution. The data clearly indicate the effect of ionic association, because the mobility of these complexes goes down with the increase in the background tartrate concentration. However, the migrat-

1) Part I: This Bulletin, **44**, 689 (1971).
* Present address: Department of Chemistry, Hiroshima University, Hiroshima, Japan.
2) K. Ogino and U. Saito, This Bulletin, **40**, 826 (1967).
3) H. Yoneda, M. Muto, T. Baba, and T. Miura, *ibid.*, **44**, 689 (1971).
4) M. Mazzei and M. Lederer, *J. Chromatog.*, **31**, 196 (1967).
5) H. Yoneda and T. Miura, This Bulletin, **43**, 574 (1970).
6) H. Yoneda and T. Baba, *J. Chromatog.*, **53**, 610 (1970).

Table 1. The mobilities of four kinds of racemic trisethylenediamine complexes in sodium *d*-tartrate solutions. (250 V, 2.5 hr., 25°C)

Na_2*d*-tart	pH	[Co en_3]Cl_3	[Cr en_3]Cl_3	[Rh en_3]Cl_3	[Pt en_3]Cl_4
0.72M	7.90	0.34	0.30	0.31	0.43
0.36M	7.60	0.40	0.35	0.35	0.49
0.18M	7.52	0.42	0.39	0.40	0.62
0.12M	7.50	0.44	0.46	0.45	0.69
0.09M	7.30	0.48	0.51	0.48	0.73
0.06M	7.20	0.55	0.63	0.54	0.83
0.03M	7.10	0.73	0.80	0.76	0.98

ing racemic species appeared always in one spot, irrespective of the concentration of sodium *d*-tartrate. This means that the difference in the degree of ionic association between the *Λ*-complex-*d*-tartrate and the *Δ*-complex-*d*-tartrate combinations is too small to be observed in electrophoresis.

However, the addition of the aluminum salt caused a marvellous effect as reported in the earlier communication.[5] In this paper, the extended work is presented in Table 2. Here the mole ratio between Al^{3+} and *d*-tartrate was fixed at 2: 3, and the concentration of the tartrate was increased stepwise just as in Table 1.

To facilitate the understanding of general features, the data concerning the [Co en_3]$^{3+}$ complex are shown in Fig. 1. As is clearly seen in this figure, the addition of Al^{3+} causes the separation of two spots in a wide concentration range of the background solution (from 0.06M up to 0.36M *d*-tartrate).

Table 2. The mobilities of four kinds of racemic trisethylenediamine complexes in sodium *d*-tartrate–aluminum chloride mixed solutions. (250 V, 2.5 hr., 25°C)

Na_2*d*-tart / $AlCl_3$	pH	[Co en_3]$^{3+}$	[Cr en_3]$^{3+}$	[Rh en_3]$^{3+}$	[Pt en_3]$^{4+}$
0.72M / 0.48M	1.65	0.29	0.22	0.25	0.29
0.36M / 0.24M	2.00	0.14—0.31 / 0.45	0.11—0.29 / 0.39	0.09—0.23 / 0.40	0.45
0.18M / 0.12M	2.23	0.14—0.32 / 0.60	0.12—0.32 / 0.59	0.11—0.32 / 0.61	0.61
0.12M / 0.08M	2.50	0.11—0.32 / 0.63	0.15—0.28 / 0.61	0.18—0.38 / 0.63	0.64
0.09M / 0.06M	2.60	0.14—0.33 / 0.69	0.15—0.31 / 0.64	0.18—0.38 / 0.65	0.70
0.06M / 0.04M	2.71	0.16—0.35 / 0.69	0.12—0.35 / 0.68	0.41—0.62 / 0.68	0.85
0.03M / 0.02M	2.79	1.03	1.03	1.03	1.12

This can be regarded as resolution, because the *Λ* or *Δ* form of the complex showed only either one of these two spots in the background solution having the same composition (The *Λ* form corresponds to the spot of longer migration, the *Δ* form to that of shorter migration).

Here it must be noted that the background solutions are fairly acidic due to the presence of aluminum chloride. To see the effect of pH variation upon

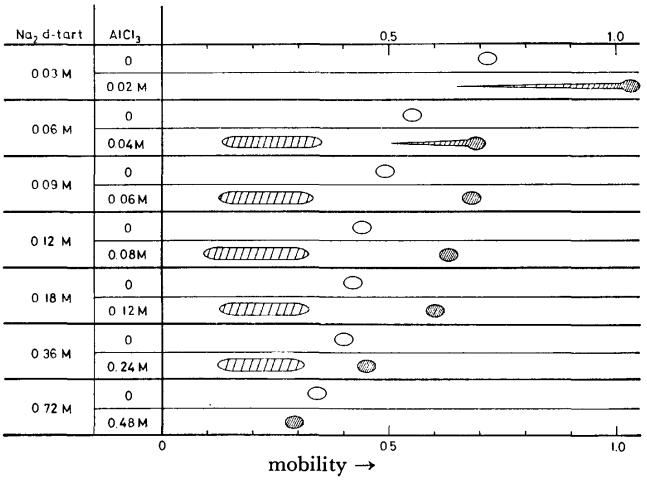

Fig. 1. Electrophoresis pattern of the racemic [Co en_3]$^{3+}$ complex in sodium *d*-tartrate solution with and without aluminum chloride.

resolution, a sample was migrated in several background solutions of different pH values which were prepared by adding a small amount of HCl or NaOH to the original solution containing 0.18M Na_2 *d*-tartrate and 0.12M $AlCl_3$. The result is shown in Fig. 2. It is easily understood that no resolution was achieved in the solution of pH 1. In such a solution, the tartrate is protonated and becomes a neutral molecule. However, it was a surprise to find that resolution was successful only within a limited acidic pH range of the solution. Even in a neutral background (pH 7), it was worth noting that resolution is incomplete.

If the resolution were due to the different degrees of association of the *d*-tartrate to the *Λ* and *Δ* forms of the complex cation, resolution should take place in neutral and alkaline solutions. However, this is not the case, which implies that the mechanism is more complicated than considered before.[6] In connection with this discussion, one thing must be pointed out. That is, the addition of aluminum chloride effects the migration of the *Λ* and *Δ* forms of the complex in opposite directions. As is seen in Fig. 1, the one component of the separated two spots in the presence of aluminum ions appears

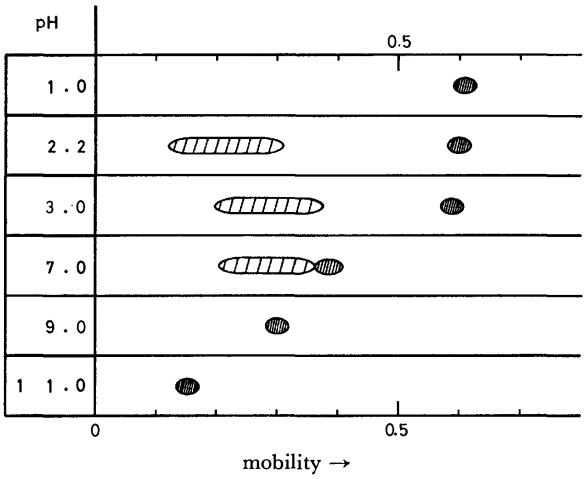

Fig. 2. Effect of pH upon the electrophoretic resolution of the racemic [Co en_3]$^{3+}$ complex.
(The background solution contains 0.18M Na_2*d*-tratrate and 0.12M $AlCl_3$ in all cases).

Table 3. The mobilities of the $[Coen_3]^{3+}$ ion in *d*-tartrate, *meso*-tartrate, and *l*-malate solutions with and without aluminum chloride.
(The *meso*-trartrate and malate solutions were prepared by neutralizing the free acids with sodium carbonate)

	Conc.	pH	Mobility	$AlCl_3$ conc.	pH	Mobility
Na_2*d*-tart	0.36M	7.60	0.42	0.24M	2.00	0.14—0.31, 0.45
	0.18M	7.52	0.44	0.12M	2.23	0.14—0.32, 0.60
	0.09M	7.30	0.50	0.06M	2.50	0.14—0.33, 0.69
Na_2*meso*-trartrate	0.36M	6.70	0.37	0.24M	2.10	0.44
	0.18M	6.60	0.41	0.12M	2.50	0.60
	0.09M	5.59	0.51	0.06M	2.90	0.65
Na_2*l*-malate	0.36M	6.00	0.44	0.24M	2.40	0.64
	0.18M	5.95	0.56	0.12M	2.50	0.67
	0.09M	6.00	0.62	0.06M	2.90	0.76

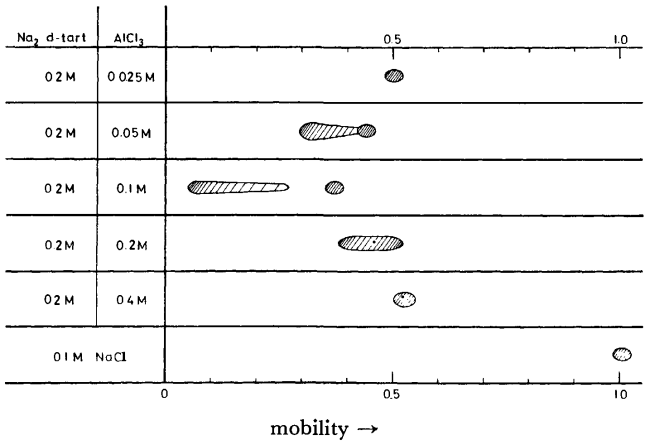

Fig. 3. Effect of the addition of aluminum chloride upon the electrophoretic resolution of the racemic $[Co\ en_3]^{3+}$ complex.

behind and the other component ahead of the original spot observed in the absence of aluminum ions. If the role of aluminum ions is simply dehydration of the complex ion, the split two spots should be both behind of the original spot due to increased ionic association. Therefore it is more reasonable to assume that the aluminum ion forms the *d*-tartrate complex anion which can select the Λ and Δ form of the $[Co\ en_3]^{3+}$ complex.

To find the favorable concentration of aluminum chloride for resolution, five supporting electrolyte solutions, each of which contains 0.2M sodium *d*-tartrate and various concentrations of aluminum chloride, were tested as shown in Fig. 3.

Thus it was revealed that the mole ratio between the aluminum ion and the tartrate for successful resolution was also confined to a certain limited range.

As shown in Table 2, the resolution of $[Cr\ en_3]^{3+}$ and $[Rh\ en_3]^{3+}$ was achieved in the same way as the resolution of $[Co\ en_3]^{3+}$. The small difference in their ionic weight did not cause any practical difference in migration distance. However, the quadrivalent $[Pt\ en_3]^{4+}$ ion could not be resolved in the same way. This is probably because the complex is more highly hydrated than the tervalent complex, and the situation of ionic association concerning this complex may be quite different from that in the case of tervalent complexes.

With regard to the mechanism of resolution, we can obtain information from the data obtained using the *meso*-tartrate and *l*-malate as a supporting electrolyte. Since the *meso*-tartrate is not optically-active, no resolution is expected even in the presence of aluminum ions. Nevertheless, it is worthwhile to see whether the spot appears near the longer migrating component or near the shorter migrating component in the case of the aluminum-*d*-tartrate system. Actually, the mobility in the aluminum-*meso*-tartrate system is almost the same as that of the longer migrating component in the corresponding aluminum-*d*-tartrate system (See Table 3). Although the *l*-malate is optically active, no resolution was achieved in the aluminum-*l*-malate system, and the mobility of the complex is even higher than those in the corresponding aluminum-*d*-tartrate and aluminum-*meso*-tartrate systems.

These findings can be interpreted in the following way. While the *d*- and *l*-tartrates are constructed with two *d* and two *l* moieties, respectively, the *meso*-tartrate consists of one *d* and one *l* moiety. Suppose two or three *d*-tartrate anions are coordinated to the aluminum ion to form a complex, they use their *d* moiety for coordination and leave the other *d* moiety free. When two or three optically active ligands are coordinated in the metal ion, the complex produced takes as a whole one type of enantiomeric form, say D or L. Thus if we represent the *d*-tartrate as *d-d*, we may represent the aluminum *d*-tartrate complex with D-*d-d*. Usually there is no L-*d-d*. On the other hand, the aluminum-*meso*-tartrate complex can exist in two enantiomeric forms D-*d-l* and L-*l-d*. Although there are four possible combinations between the aluminum-*meso*-tartrate complex (D-*d-l* and L-*l-d*) and the racemic $[Co\ en_3]^{3+}$ complex (*d* and *l*) ion, we obtained only one spot corresponding to the spot of longer migration distance in the case of the aluminum-*d*-tartrate (D-*d-d*) system.

Thus, it was revealed that among these three aluminum-tartrate systems D-*d-d*, D-*d-l*, and L-*l-d*, only D-*d-d* shows a strong interaction with the $\Delta(-)_{589}$-$[Co\ en_3]^{3+}$ complex. This interaction is therefore stereospecific.

In addition, the aluminum-*l*-malate system gives even longer migration than the component of longer migration in the D-*d-d* system. Therefore, it is presumed that cooperation of the OH and COO^- groups is necessary for such a stereospecific interaction.

Finally, we wish to go further to the discussion of the

probable structure of D-*d*-*d*. Since it attracts the complex cation, it must be an anion. Thus, we have two possible aluminum tartrate complex anions, $[Al(d\text{-tart})_3]^{3-}$ and $[Al(H_2O)_2(d\text{-tart})_2]^-$. The possibility of $[Al(d\text{-tart})_3]^{3-}$ can be excluded, because this should also give resolution in neutral and alkaline solution, contrary to the observations. Therefore, we may presume that the most probable D-*d*-*d* is $[Al(H_2O)_2(d\text{-tart})_2]^-$.

Our sincere appreciation is due to Professor Flemming Woldbye for his keen interest in and his stimulating discussion on this subject.

BULLETIN OF THE CHEMICAL SOCIETY OF JAPAN, VOL. 45, 2129—2137(1972)

Metal Complexes Containing Six-Membered Chelate Rings. II. Preparation and Structure of 2,4-Pentanediamine Complexes of Cobalt(III)

Fujio MIZUKAMI, Haruko ITO, Junnosuke FUJITA, and Kazuo SAITO
Department of Chemistry, Faculty of Science, Tohoku University, Sendai

(Received September 13, 1971)

New cobalt(III) complexes containing optically active (*RR* and *SS*) and *meso*(*RS*) 2,4-pentanediamine (2,4-ptn) have been synthesized. $[Co(RR\text{-}2,4\text{-ptn})_3]^{3+}$ gives two diastereoisomers, prismatic crystals with $(-)_{546}$ rotation and needle-like crystals with $(+)_{546}$ rotation. The former is produced much more than the latter. The conformations of the *RR*- (or *SS*-) and *RS*-2,4-pentanediamine chelate of the complexes were assigned to λ- (or δ-) twist and chair form, respectively, from comparison of their PMR spectra with those of the corresponding tetraacetato complexes. $[Co(RS\text{-}2,4\text{-ptn})_3]^{3+}$ seems to have *fac* structure with respect to the coordination of the amino groups adjacent to the *R*- and *S*-carbon atoms. The circular dichroism spectra of mono and *trans*-bis-(*RR*-2,4-ptn) complexes in the first band region are essentially the same as those of the corresponding *R*-propylenediamine complexes. The circular dichroism spectra of $(+)_{546}$- and $(-)_{546}$-$[Co(RR\text{-}2,4\text{-ptn})_3]^{3+}$ and $(-)_{546}$-$[Co(RS\text{-}2,4\text{-ptn})_3]^{3+}$ are very different from those of the triscobalt(III) complexes of *R*-propylenediamine and trimethylenediamine. Such differences have been discussed with reference to the stereochemistry of six-membered chelate complexes.

The stereospecificity of complex formation from metal ions and ligands has been elucidated mostly in terms of a specific conformation of the ligand and the repulsive interaction between non-bonded atoms of the coordinated ligands. Most of such studies, however, have been made on metal complexes containing five-membered chelates such as α-diamines or α-aminoacids. It is, therefore, of great interest to investigate whether a similar specificity is seen in metal complexes containing six-membered chelates. In the previous paper,[1] we reported that the formation of cobalt(III) complexes of *RR*- (or *SS*-) and *RS*-2,4-pentanediaminetetraacetate was stereospecific to give a sexadentate Δ-type (or Λ-type) and a quinquedentate complex, respectively. The tendency of the methyl groups on the carbon atoms to take equatorial orientation was thus demonstrated to be very strong in these puckered six-membered rings as well as in the five-membered rings. This paper deals with preparation and stereochemistry of cobalt(III) complexes containing six-membered β-diamines, optically active and *meso*-2,4-pentanediamine (2,4-ptn), which are expected to have a preferred, non-convertible conformation upon coordination.

Circular dichroism (CD) study provides useful information on the absolute configuration of metal complex and the conformation of chelated ligands. However, the work on metal complexes of β-diamines is limited to those of trimethylenediamine(tn),[2-6] in contrast to the extensive work on α-diamine complexes. Furthermore, these trimethylenediamine complexes are known to exhibit CD curves considerably different from those of the corresponding α-diamine complexes in the region of the first absorption band. Thus, the CD data reported in this paper on 2,4-pentanediamine complexes of cobalt(III) will give valuable information for elucidating the origin of optical activity of metal complexes as well as the conformation of six-membered chelate rings.

Experimental

RR-, SS-, *and* RS-*2,4-pentanediamine.* These isomers of 2,4-pentanediamine were obtained by the method reported previouly.[1]

trans-Dinitro- and -dichloro-bis(2,4-pentanediamine)cobalt(III) complexes were prepared by modifying the method of

1) F. Mizukami, H. Ito, J. Fujita, and K. Saito, This Bulletin, **44**, 3051 (1971).

2) F. Woldbye, *Record of Chemical Progress*, **24**, 197 (1963).

3) P. G. Beddoe and S. F. Mason, *Inorg. Nucl. Chem. Lett.*, **4**, 433 (1968).

4) J. R. Gollogly and C. J. Hawkins, *Chem. Commun.*, **1968**, 689.

5) R. R. Judkins and D. J. Royer, *Inorg. Nucl. Chem. Lett.*, **6**, 305 (1970).

6) H. Kawaguchi and S. Kawaguchi, This Bulletin, **43**, 2103 (1970).

Dippel.[7]

trans-[*Co(NO$_2$)$_2$(RR- or SS-ptn)$_2$]ClO$_4$*. An aqueous solution containing 11.5 g of $Na_3[Co(NO_2)_6]$[8] and 5.8 g of *RR*- or *SS*-2,4-pentanediamine in 40 m*l* of water was heated at 60—70°C for 5 hr, and filtered. To the filtrate was added a large excess of sodium perchlorate. Yellow flakes were precipitated, filtered off, washed with a small amount of cold water and dried over phosphorus pentoxide under reduced pressure.

Found: C, 26.55; H, 6.26; N, 18.58%. Calcd for $C_{10}H_{28}N_6O_8CoCl$: C, 26.41; H, 6.21; N, 18.48%.

trans-[*CoCl$_2$(RR- or SS-2,4-ptn)$_2$]ClO$_4$*. Twelve grams of *trans*-$[Co(NO_2)_2$(*RR*- or *SS*-ptn)$_2]ClO_4$ was dissolved in 100 m*l* of 6N hydrochloric acid by heating at 65—70°C for 10 hr with occasional stirring. To the resultant green solution was added 100 m*l* of 60% perchloric acid. Upon cooling at 5°C, green crystals were precipitated, filtered off, washed with a small amount of cold water and dried over phosphorus pentoxide under reduced pressure.

Found: C, 27.70; H, 6.56; N, 13.24%. Calcd for $C_{10}H_{28}N_4O_4CoCl_3$: C, 27.70; H, 6.51; N, 12.92%.

trans-[*CoCl$_2$(RS-2,4-ptn)$_2$]Cl*. This complex was prepared from cobalt(II) chloride-hexahydrate and *RS*-2,4-pentanediamine by air oxidation according to Dippel's method.[7]

Found: C, 32.16; H, 7.70; N, 14.97%. Calcd for $C_{10}H_{28}N_4CoCl_3$: C, 32.49; H, 7.64; N, 15.16%.

trans-[*CoBr$_2$(RR- or SS-2,4-ptn)$_2$]ClO$_4$*. To an aqueous solution of 1 g of *trans*-$[CoCl_2$(*RR*- or *SS*-2,4-ptn)$_2]ClO_4$ in 25 m*l* of water was added 1 g of silver perchlorate. The solution was stirred for 3 hr at room temperature, and then filtered to remove the silver chloride. The filtrate was treated with 10 m*l* of 47% hydrobromic acid and evaporated to about 8 m*l* in a vacuum desiccator over potassium hydroxide. Yellowish green crystals were filtered off, washed with cold ethanol and recrystallized from hot ethanol.

Found: C, 23.48; H, 5.56; N, 10.78%. Calcd for $C_{10}H_{28}N_4O_4Br_2CoCl$: C, 22.98; H, 5.40; N, 10.72%.

trans*(Br-Br)-[CoBr$_2$(NH$_3$)$_2$(RR- or SS-2,4-ptn)]Br·H$_2$O*. A suspension of $NH_4[Co(SO_3)_2(NH_3)_4]$[9] in 10% aqueous solution of *RR*- or *SS*-2,4-pentanediamine (1 : 1 mole ratio) was heated at 80°C for 2 hr with stirring and cooled to room temperature. To the dark brown solution was added a large amount of methanol. After a while, the solution was filtered. An oily product was precipitated by adding ether to the filtrate and separated from the supernatant. A yellow complex was obtained as powder by treating the oily product with an appropriate amount of ethanol, filtering off, washing with ethanol and air-drying. This complex which was believed to be crude $NH_4[Co(SO_3)_2(NH_3)_2$(*RR*- or *SS*-2,4-ptn)], was dissolved in a small amount of 47% hydrobromic acid and the solution was warmed at 35—40°C for 2 hr to give yellowish green crystals. After a while, the crystals were filtered off, washed with ethanol and recrystallized from methanol by adding ether.

Found: C, 12.86; H, 4.74; N, 12.47%. Calcd for $C_5H_{22}N_4OCoBr_3$: C, 13.26; H, 4.90; N, 12.37%.

[Co(NH$_3$)$_4$(RR- or SS-2,4-ptn)](ClO$_4$)$_3$. This complex was synthesized according to a similar method to that for the corresponding *R*-propylenediamine complex by Hawkins *et al.*[10]

Liquid ammonia was poured onto *trans*(Br-Br)-$[CoBr_2$-$(NH_3)_2$(*RR*- or *SS*-ptn)]Br·H_2O to give an orange solution. Orange powder which remained after the ammonia had evaporated, was dissolved in a minimum amount of hot water, and the solution was cooled to room temperature and filtered. To the filtrate was added an appropriate amount of 60% perchloric acid. Upon cooling at 0°C, orange crystals were precipitated and filtered off. The crystals were dissolved in a minimum amount of water and concentrated in a vacuum desiccator over sodium hydroxide. Deposited orange crystals were filtered off, washed with ethanol and air-dried.

Found: C, 11.11; H, 5.20; N, 15.72%. Calcd for $C_5H_{26}N_6O_{12}CoCl_3$: C, 11.38; H, 4.97; N, 15.93%.

[Co(NH$_3$)$_4$(RS-2,4-ptn)](ClO$_4$)$_3$·H$_2$O, [Co(NH$_3$)$_4$(tn)]Br·H$_2$O and [Co(NH$_3$)$_4$(d,l-1,3-btn)]Br$_3$.[11]

These complexes were prepared from $NH_4[Co(SO_3)_2(NH_3)_4]$ and *RS*-2,4-ptn, tn, or *d,l*-1,3-btn by a similar method to that for the corresponding *RR*- or *SS*-2,4-ptn complex described above. The complexes of tn and *d,l*-1,3-btn were obtained as bromide by use of 47% hydrobromic acid instead of 60% perchloric acid.

Found: C, 11.10; H, 5.01; N, 15.36%. Calcd for $C_5H_{28}N_6O_{13}CoCl_3$: C, 11.01; H, 5.17; N, 15.40%.

Found: C, 7.80; H, 4.86; N, 17.89%. Calcd for $C_3H_{24}N_6O_{13}Br_3Co$: C, 7.85; H, 5.27; N, 18.31%.

Found: C, 10.84; H, 5.44; N, 18.17%. Calcd for $C_4H_{24}N_6Br_3Co$: C, 10.56; H, 5.32; N, 18.47%.

(−)$_{546}$-[Co(RR-2,4-ptn)$_3$](ClO$_4$)$_3$·H$_2$O. An aqueous solution containing 1 g of *trans*-$[CoCl_2$(*RR*-2,4-ptn)$_2]ClO_4$, 0.5 g of *RR*-2,4-pentanediamine and 1 g of activated charcoal in 20 m*l* of water was warmed at 60°C. After about 2 hr, prismatic crystals began to appear. CD study showed that each of these single crystals was composed of about 90% $(-)_{546}$-isomer and 10% $(+)_{546}$-isomer of tris-diamine complex. Without separating these crystals, the reaction was still caused to proceed for 8—10 hr, and then the reaction mixture was cooled to room temperature. The precipitate containing activated charcoal was filtered off and washed with 60 m*l* of hot water (70°C). To the filtrate was added 34 m*l* of 60% perchloric acid. Upon cooling at 0°C for half an hour, first fraction of orange needle crystals was precipitated. They were filtered off, washed with a small amount of cold water, and recrystallized by evaporating the aqueous solution in a vacuum desiccator over potassium hydroxide. All the filtrates and washings were combined, concentrated to 30 m*l* at 50°C under reduced pressure and cooled to room temperature. The second fraction was obtained and recrystallized from water according to the method described above. The species remained in the final fraction on the above procedure seemed to be mostly bis-diamine complexes, since the filtrate changed its color to green on warming with hydrochloric acid and green dichloro complex was precipitated. Yield: Total 0.78 g.

Found: 26.35; H, 6.51; N, 12.07%. Calcd for $C_{15}H_{44}N_6O_{13}Cl_3Co$: C, 26.42; H, 6.50; N, 12.33%.

(+)$_{546}$-[Co(RR-2,4-ptn)$_3$]Cl$_3$·2H$_2$O. Two grams of *trans*-$[CoCl_2$(*RR*-2,4-ptn)$_2]ClO_4$ was converted into chloride by use of the anion exchanger Dowex 1-X4. This chloride was dissolved in 60 m*l* of 50% aqueous ethanol, and 0.5 g of *RR*-2,4-pentanediamine was added. The solution was warmed at 55—60°C for 8—10 hr. Deposited orange needle crystals were filtered off in hot, and recrystallized from water in a similar way as for $(-)_{546}$-isomer. Yield: 0.09 g.

Found: C, 35.74; H, 9.40; N, 16.61%. Calcd for $C_{15}H_{46}N_6Cl_3CoO_2$: C, 35.47; H, 9.13; N, 16.55%.

Orange prismatic crystals were obtained by evaporating

7) C. J. Dippel, *Rec. Trav. Chim.*, **50**, 525 (1931).
8) E. Billman, *Z. Anal. Chem.*, **39**, 284 (1900).
9) A. Werner and H. Gruger, *ibid.*, **16**, 398 (1898).
10) C. J. Hawkins, E. Larsen, and I. Olsen, *Acta Chem. Scand.*, **19**, 1915 (1965).
11) 1,3-btn. 1,3-diaminobutane. Details on 1,3-btn complexes will be published later.

the filtrate to almost dryness in a vacuum desiccator. The crystals recrystallized from water in a similar way gave the chemical composition $[Co(RR\text{-}2,4\text{-ptn})_3]Cl_3 \cdot 2H_2O$. Yield: 0.48 g.

Found: C, 35.32; H, 9.34; N, 16.55%. Calcd for $C_{15}H_{46}N_6Cl_3CoO_2$: C, 35.47; H, 9.13; N, 16.55%.

However, the CD spectra of each of these single crystals in water coincided with that of a mixed sample consisting of 93% $(-)_{546}$-isomer and 7% $(+)_{546}$-isomer.

Racemic-*[Co(RS-2,4-ptn)$_3$](ClO$_4$)$_3 \cdot 3H_2O$.* An aqueous solution containing 5 g of *trans*-$[CoCl_2(RS\text{-}2,4\text{-ptn})_2]Cl$ and 2 g of *RS*-2,4-pentanediamine and 1.5 g of activated charcoal was warmed at 60°C for a day, and filtered. Orange crystals were precipitated by the addition of sodium perchlorate to the filtrate, filtered off and recrystallized by evaporating an aqueous solution in a desiccator over phosphorus pentoxide under reduced pressure. Yield: 5 g.

Found: C, 25.49; H, 6.34; N, 11.29%. Calcd for $C_{15}H_{48}N_6O_{15}CoCl_3$: C, 25.10; H, 6.34; N, 11.29%.

$(-)_{546}$-[Co(RS-2,4-ptn)$_3$](ClO$_4$)$_3 \cdot 3H_2O$. Five grams of *racemic*-$[Co(RS\text{-}2,4\text{-ptn})_3](ClO_4)_3 \cdot 3H_2O$ was converted into chloride by use of the anion exchanger Dowex 1-X4. To the aqueous chloride solution was added 4 g of silver tartrate with stirring. After half an hour, silver chloride was filtered off and the filtrate was concentrated to about 15 m*l* in a desiccator over phosphorus pentoxide under reduced pressure. Reddish orange powder (0.5 g) was obtained by filtration, and recrystallized by concentrating its aqueous solution in a similar way. This procedure was repeated to give a constant CD curve. Pure sample was dissolved in a small amount of water and sodium perchlorate was added. The perchlorate salt was recrystallized from water.

Found: C, 25.31; H, 6.30; N, 11.72%. Calcd for $C_{15}H_{48}N_6O_{15}CoCl_3$: C, 25.10; H, 6.74; N, 11.71%.

Measurements. Visible and ultraviolet absorption spectra were recorded with a Hitachi 124 recording spectrophotometer. The CD curves were recorded with a Model ORD/UV-5 spectrophotometer of Japan Spectroscopic Co. with its CD attachment. PMR spectra were obtained with a Varian T-60 spectrometer using HOD signal as an internal standard. The complexes prepared here were hardly soluble in deuterium oxide containing Na-TMS. All the measurements were made at room temperature.

Results and Discussion

Conformation of Chelate Rings and Geometrical Isomerism. As shown in Part I, four conformations, chair, boat, and a pair of twist (skew boat) forms are possible in β-diamine chelate rings. The boat form is generally unstable and not formed in octahedral complexes such as those of cobalt(III), because big steric hindrance is involved between apical ligands and the central methylene group of the equatorial ligand. Hence chair and a pair of twist forms are the more probable conformations. A pair of twist forms are mirror images to each other, and they are designated as δ and λ, as shown in Part I.

It is generally understood that substituting groups on carbon atoms in puckered chelate rings always tend to take equatorial positions. Therefore, *RR*-, *SS*-, and *RS*-2,4-pentanediamine are expected to give λ- and δ-twist and chair conformation, respectively in six-membered chelate rings (Figs. 1 and 2). Such conformations of 2,4-pentanediaminetetraacetato-(2,4-ptnta)cobalt(III) complexes in Part 1.

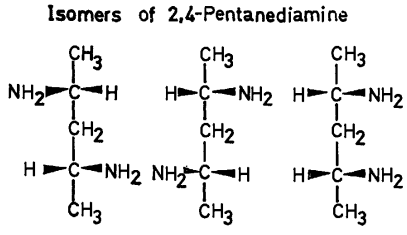

Ligand	Conformation		
	chair	δ-twist	λ-twist
R,R-2,4-ptn	a,e	a,a	e,e
S,S-2,4-ptn	a.e	e,e	a,a
R.S-2,4-ptn	a,a e,e	a,e	a,e

e:methyl equatorial a:methyl axial

Fig. 1. Isomers of 2,4-pentanediamine and their conformations in the chelate.

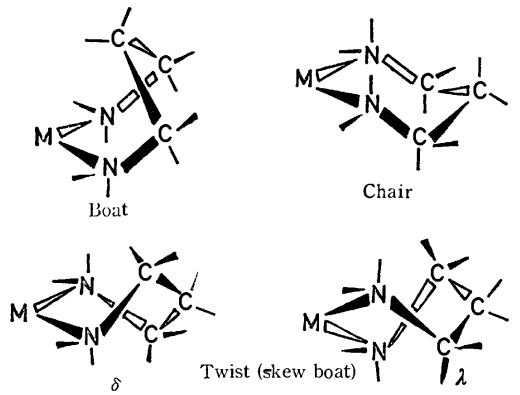

Fig. 2. Possible conformations of six-membered 1,3-diamine chelate.

The interconversion between δ- and λ-twist and between twist and chair form is not likely because of the steric hindrance among the chelate rings and the preference of equatorial orientation of the methyl groups. Appleton and Hall[12] studied the PMR spectra of a number of complexes of platinum(II) and palladium(II) with trimethylenediamine and its methyl-substituted derivatives including 2,4-pentanediamine. They suggested that the 2,4-pentanediamine chelates in these complexes might take stable conformations with equatorial orientation of the methyl groups.

As Fig. 3 shows, the PMR spectrum of $[Co(NH_3)_4(RR\text{-}2,4\text{-ptn})]^{3+}$ in deuterium oxide gives a sharp doublet of the methyl signal and a sharp triplet of the central methylene signal. The pattern of these multiplets is very similar to that of the diamine part of $[Co(RR\text{-}2,4\text{-ptnta})]^-$.[1] Since the diamine part of the tetraacetato complex should have fixed λ-twist form, the *RR*-2,4-pentanediamine chelate of the tetrammine complex should take λ-twist form, and the interconversion among conformers would not take place in an aqueous solution at room temperature. The PMR spectrum of $[Co(NH_3)_4(RS\text{-}2,4\text{-ptn})]^{3+}$ in deuterium oxide gives a sharp doublet and a broad triplet corre-

12) T. G. Appleton and J. R. Hall, *Inorg. Chem.*, **9**, 1807 (1970).

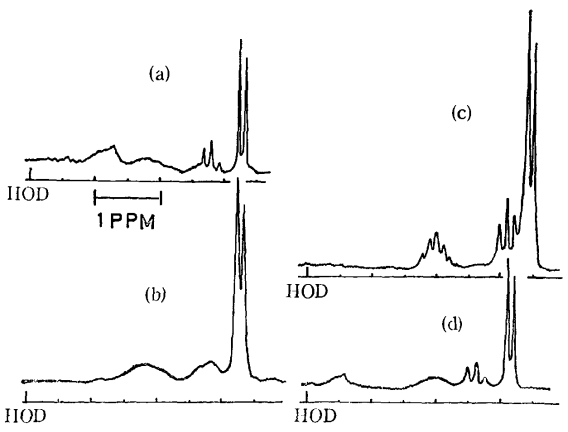

Fig. 3. PMR spectra of a) $[Co(NH_3)_4(RR\text{-}2,4\text{-ptn})]^{3+}$, b) $[Co(RR\text{-}2,4\text{-ptn})_3]^{3+}$, c) *trans*-$[Co(NO_2)_2(SS\text{-}2,4\text{-ptn})_2]^{+}$, d) $(-)_{546}$-$[Co(RR\text{-}2,4\text{-ptn})_3]^{3+}$ in D_2O. (Relative shifts in ppm from the HOD signal.)

sponding to the signals of the methyl and the central methylene protons, respectively. Such a signal of methyl protons indicates that the two methyl groups are equivalent in the chelate. Therefore, the conformation of the *RS*-2,4-pentanediamine of $[Co(NH_3)_4(RS\text{-}2,4\text{-ptn})]^{3+}$ was assigned to chair form with equatorial methyl groups.

The spectral pattern in a lower field region is complicated because of the overlapping of the signals of -CH, $-NH_2$, and -NHD, and depends sensitively on the other ligands. Hence it is not useful for discussing the conformation of 2,4-pentanediamine chelates.

Figure 3 shows also the PMR spectra of $[Co(NO_2)_2(SS\text{-}2,4\text{-ptn})_2]^{+}$ and $(-)_{546}$-$[Co(RR\text{-}2,4\text{-ptn})_3]^{3+}$. These spectra are also similar to that of $[Co(NH_3)_4(RR\text{-}2,4\text{-ptn})]^{3+}$ in the region of the methyl and the central methylene signals, indicating that the chelate rings have also twist form. Furthermore, each spectrum of these complexes seems to consist of the signals due to one kind of chelate ring. These facts suggest that the dinitro complex is in trans form and the tris complex has D_3 symmetry. The diastereoisomer, $(+)_{546}$-$[Co(RR\text{-}2,4\text{-ptn})_3]^{3+}$ gives the same PMR spectrum as that of $(-)_{546}$-$[Co(RR\text{-}2,4\text{-ptn})_3]^{3+}$ at 60 MHz. The *trans* structure of the dinitro complex may also be supported from comparison of *cis* and *trans* isomers of the corresponding trimethylenediamine complex, $[Co(NO_2)_2(tn)_2]^{+}$. Kawaguchi and Kawaguchi[6] obtained the *cis* isomer by treating the *trans* isomer with a warm aqueous nitrite solution, and found that the former gives the first absorption band at a lower wavelength than does the latter. When the present dinitro complex was treated similarly with an aqueous nitrite solution, the resultant solution gave the first absorption band at lower wavelength by 11 nm as compared with that of the original complex. The CD spectrum also changed substantially. An attempt to isolate the product was unsuccessful because of its high solubility in water.

As Fig. 3 shows, the PMR spectrum of $[Co(RS\text{-}2,4\text{-ptn})_3]^{3+}$ exhibits a broader methyl signal than that of $[Co(RR\text{-}2,4\text{-ptn})_3]^{3+}$. This complex can have two geometrical isomers with respect to *mer* and *fac* coordination of the amino groups adjacent to the *R*- and *S*-carbon atoms. However, studies with molecular models disclose that only the *fac* isomer is formed without big steric hindrance among the chelate rings. Therefore, the broad methyl signal may not be due to the presence of two geometrical isomers, but will be due to C_3 symmetry of the *fac* isomer. The two methyl groups on *R*- and *S*-carbon atom are in a different environment from each other in this complex.

The dichloro and dibromo complexes prepared here were assigned to *trans* (Cl-Cl, or Br-Br) structure from their characteristic green color.

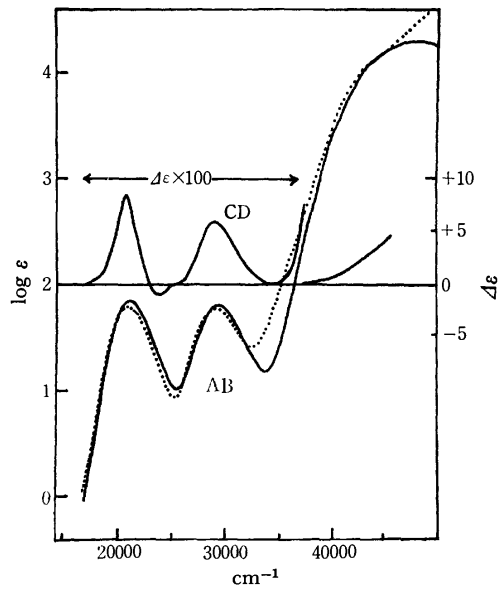

Fig. 4. Absorption (AB) and CD sepectra of (——) $[Co(NH_3)_4(RR\text{-}2,4\text{-ptn})]^{3+}$, (·····) $[Co(NH_3)_4(tn)]^{3+}$ in water.

Absorption Spectra. Table 1 and Fig. 4 compare the absorption spectra of four tetrammine-β-diamine cobalt(III) complexes. The absorption bands including the first, the second and the charge transfer band are shifted from longer to shorter wavelength with increase in the number of methyl group, *i.e.* in the order $[Co(NH_3)_4tn]^{3+}$, $[Co(NH_3)_4(1,3\text{-btn})]^{3+}$, and $[Co(NH_3)_4(2,4\text{-ptn})]^{3+}$. The absorption spectra of $[Co(NH_3)_4(RR\text{-}2,4\text{-ptn})]^{3+}$ and $[Co(NH_3)_4(RS\text{-}2,4\text{-ptn})]^{3+}$ are almost identical with each other, regardless of the different conformation of the chelate rings. A similar relationship also holds between *trans*-$[CoCl_2(RR\text{-}2,4\text{-ptn})_2]^{+}$ and *trans*-$[CoCl_2(RS\text{-}2,4\text{-ptn})_2]^{+}$ as shown in Fig. 5. On the other hand, the absorption bands of the four tris complexes are shifted to shorter wavelength in the sequence $[Co(RS\text{-}2,4\text{-ptn})_3]^{3+}$, $[Co(tn)_3]^{3+}$, $(+)_{546}$-$[Co(RR\text{-}2,4\text{-ptn})_3]^{3+}$, and $(-)_{546}$-$[Co(RR\text{-}2,4\text{-ptn})_3]^{3+}$, as shown in Fig. 6 and Table 1. Such a sequence is not in accord with that of tetrammine complexes given above. The differences in the absorption maxima of the first bands amount to 380 cm^{-1} between $[Co(RS\text{-}2,4\text{-ptn})_3]^{3+}$ and $(-)_{546}$-$[Co(RR\text{-}2,4\text{-ptn})_3]^{3+}$ and 220 cm^{-1} between $(+)_{546}$-$[Co(RR\text{-}2,4\text{-ptn})_3]^{3+}$ and $(-)_{546}$-$[Co(RR\text{-}2,4\text{-ptn})_3]^{3+}$. It is not possible to discuss these results in detail at present. However, they seem to be related to the steric interaction among chelate rings. Such an inter-

Table 1. Numerical data of absorption (AB) and circular dichroism (CD) $\tilde{\nu}$ in $10^3\,cm^{-1}$, ($\log\varepsilon$) and ($\varepsilon_l-\varepsilon_r$)

Complex	AB	CD
$[Co(NH_3)_4tn]Br_3\cdot H_2O$	20.90 (1.79)	
	29.20 (1.78)	
$[Co(NH_3)_4(1,3\text{-btn})]Br_3$	20.94 (1.82)	
	29.24 (1.79)	
$[Co(NH_3)_4(RS\text{-}2,4\text{-ptn})](ClO_4)_3\cdot H_2O$	20.96 (1.83)	
	29.24 (1.78)	
	47.62 (4.30)	
$[Co(NH_3)_4(RR\text{-}2,4\text{-ptn})](ClO_4)_3$	20.96 (1.84)	20.62 (+0.085)
		23.53 (−0.010)
	29.24 (1.80)	28.82 (+0.059)
	47.62 (4.29)	
trans-$[Co(NO_2)_2(RR\text{-}2,4\text{-ptn})_2]ClO_4$	22.37 (2.23)	21.51 (−0.695)
		24.27 (+0.245)
	28.90 (3.44)	28.57 (+0.325)
		34.25 (−1.300)
	39.84 (4.34)	42.74 (+6.250)
trans-$[CoCl_2(RS\text{-}2,4\text{-ptn})_2]Cl$	15.75 (1.59)	
	21.37 (1.48)	
	25.32 (1.85)	
	38.76 (4.35)	
	45.05 (4.02)	
trans-$[CoCl_2(RR\text{-}2,4\text{-ptn})_2]ClO_4$	15.75 (1.63)	16.00 (+0.475)
	21.37 (1.57)	20.92 (−0.575)
	25.32 (1.81)	26.46 (+0.470)
	ca. 32.0 (3.14)	34.01 (−2.000)
	38.76 (4.37)	38.76 (+10.625)
	46.08 (4.06)	
trans-$[CoBr_2(NH_3)_2(SS\text{-}2,4\text{-ptn})]Br\cdot H_2O$	14.90 (1.76)	15.15 (−0.162)
		20.62 (+0.202)
	ca. 27.8 (3.22)	25.32 (−0.550)
trans-$[CoBr_2(SS\text{-}2,4\text{-ptn})_2]ClO_4$	14.79 (1.78)	15.11 (−0.275)
		20.70 (+0.424)
	27.79 (3.28)	25.97 (−0.369)
$(-)_D$-$[Co(tn)_3]Br_3\cdot H_2O$	20.49 (1.90)	18.80 (+0.067)
		21.10 (−0.140)
	28.57 (1.88)	27.80 (−0.015)
$(-)_{546}$-$[Co(RR\text{-}2,4\text{-ptn})_3](ClO_4)_3\cdot H_2O$	20.75 (1.88)	19.61 (−0.586)
	28.82 (1.87)	28.57 (+0.066)
	43.48 (4.43)	43.48 (+18.337)
$(+)_{546}$-$[Co(RR\text{-}2,4\text{-ptn})_3]Cl_3\cdot 2H_2O$	20.53 (1.99)	20.83 (+2.690)
	28.65 (1.96)	28.41 (−0.283)
	42.92 (4.43)	43.86 (+7.164)
$(-)_{546}$-$[Co(RS\text{-}2,4\text{-ptn})_3](ClO_4)_3\cdot 3H_2O$	20.37 (1.96)	19.69 (−0.548)
	28.41 (1.95)	28.17 (−0.013)
	42.37 (4.40)	39.37 (+6.543)
		44.64 (−9.347)
$[Co(NH_3)_6]Cl_3$	21.10 (1.76)	
	29.50 (1.67)	

action may affect more or less the strength of coordination bonds, when a large and bulky ligand such as 2,4-pentanediamine forms a tris type complex. Molecular models indicate that the steric interaction among twist chelate rings in the tris complexes is much smaller than that among chair chelate rings, and that $\Delta(\lambda\lambda\lambda)$ form involves less congestion of ligand atoms than $\Lambda(\lambda\lambda\lambda)$ form. As shown later, the $(-)_{546}$- and $(+)_{546}$-isomer of $[Co(RR\text{-}2,4\text{-ptn})_3]^{3+}$ have $\Delta(\lambda\lambda\lambda)$ and $\Lambda(\lambda\lambda\lambda)$ absolute configuration, respectively. The diamine chelate rings in $[Co(tn)_3]^{3+}$ can take both twist and chair form in solution without involving big mutual interaction, although they have chair form in crystals.[13] The fact that the absorption bands of $[Co(tn)_3]^{3+}$ are at shorter wavelengths than those of $[Co(RS\text{-}2,4\text{-ptn})_3]^{3+}$ may be caused by conformational interconversion of the trimethylenediamine chelate rings in solution. Thus, it seems that the complexes involving less steric

13) T. Nomura, F. Marumo, and Y. Saito, This Bulletin, **42**, 1016 (1969).

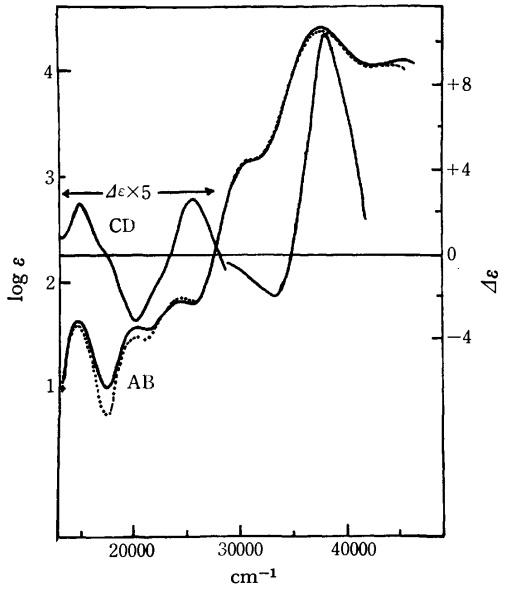

Fig. 5. Absorption (AB) and CD spectra of
(——) *trans*-[$CoCl_2$(*RR*-2,4-ptn)$_2$]$^+$,
(·····) *trans*-[$CoCl_2$(*RS*-2,4-ptn)$_2$]$^+$ in ethanol.

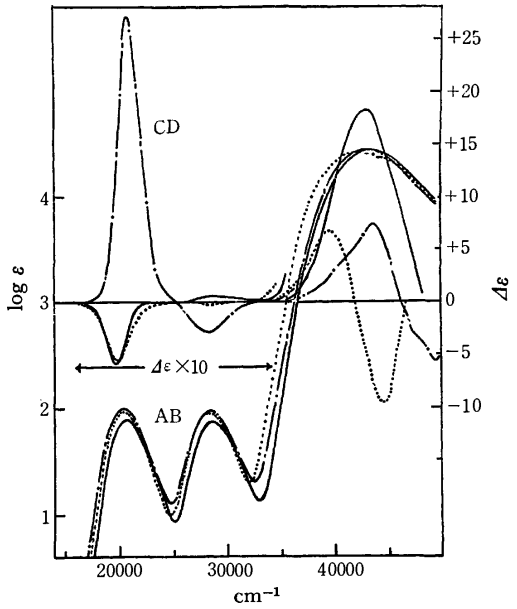

Fig. 6. Absorption (AB) and CD spectra of
(——) $(-)_{546}$-[Co(*RR*-2,4-tpn)]$^{3+}$,
(-·-·) $(+)_{546}$-[Co(*RR*-2,4-ptn)$_3$]$^{3+}$,
(·····) $(-)_{546}$-[Co(*RS*-2,4-ptn)$_3$]$^{3+}$ in water.

interaction cause the absorption peaks to shift to shorter wavelength. It is worth noticing that such a shift has not been observed clearly for the complexes with five-membered chelates. For example, the absorption peaks of two diastereoisomers, $\Lambda(\lambda\lambda\lambda)(lel)$- and $\Lambda(\lambda\lambda\lambda)$-$(ob)$-[Co(*R*-pn)$_3$]$^{3+}$(*R*-pn=*R*-propylenediamine) are at almost identical wavelengths with each other.[14] The mono and *trans*-bis diamine complexes studied here should involve smaller steric interactions among ligands, and in fact give their absorption peaks at the wavelengths expected from the spectrochemical series.

14) K. Ogino, K. Murano, and J. Fujita, *Inorg. Nucl. Chem. Lett.*, **4**, 351 (1968).

Circular Dichroism and Absolute Configuration. So far as the methyl group on the carbon atoms tends to take equatorial orientation to the chelate ring, *RR*-2,4-pentanediamine and *R*-propylenediamine should give λ-twist and λ-gauche conformation, respectively. Since these two belong to the chirality λ, it seems interesting to compare the CD spectra of their cobalt(III) complexes with one another.

(1) Mono- and bis-2,4-Pentanediamine Cobalt(III) Complexes: As shown in Figs. 7 and 8, the CD pattern of *trans*-[$Co(NO_2)_2$(*RR*-2,4-ptn)$_2$]$^+$ is very similar to that

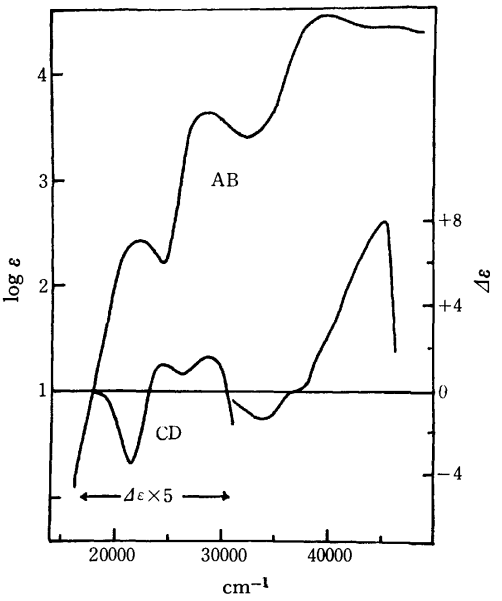

Fig. 7. Absorption (AB) and CD spectra of *trans*-[$Co(NO_2)_2$-(*RR*-2,4-ptn)$_2$]$^+$ in water.

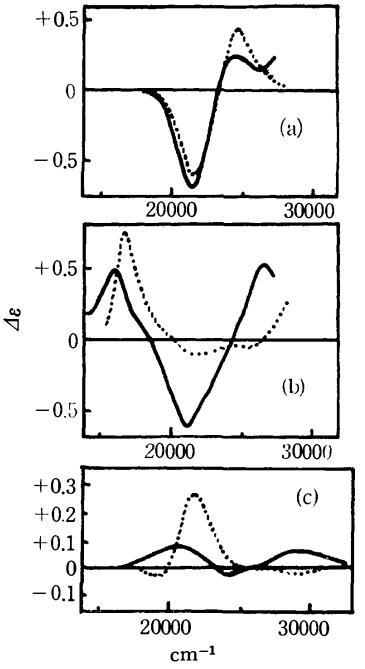

Fig. 8. Comparison of the CD spectra of *RR*-2,4-pentanediamine (——) and *R*-propylenediamine (·····) complexes. a) *trans*-dinitro complexes, b) *trans*-dichloro complexes, c) tetrammine complexes.

of *trans*-$[Co(NO_2)_2(R\text{-pn})_2]^+$.[15] The CD curve of *trans*-$[CoCl_2(RR\text{-2,4-ptn})_2]^+$ shown in Figs. 5 and 8 is also similar to that of *trans*-$[CoCl_2(R\text{-pn})_2]^+$[16] essentially, but the CD band with minus sign of the former in the Ib band region (A_2) is much stronger than that of the latter. The CD curves of the tetrammine complexes of *RR*-2,4-pentanediamine and *R*-propylenediamine are different from each other. In the first band region, the former gives a plus and a small minus peak at 20620 and 23530 cm^{-1}, respectively, whereas the latter a small minus and a plus peak at 19300 and 21580 cm^{-1}, respectively.[10] (Fig. 8)

Such a difference could be explained if the location for propylenediamine and 2,4-pentanediamine in the spectrochemical series were taken into consideration. The first absorption bands of $[Co(NH_3)_4(R\text{-pn})]^{3+}$, $[Co(NH_3)_6]^{3+}$ and $[Co(NH_3)_4(RR\text{-2,4-ptn})]^{3+}$ are at 21500,[10] 21100, and 20960 cm^{-1}, respectively. Thus, the order of these ligands in the spectrochemical series may be determined as *R*-pn>NH_3>*RR*-2,4-ptn. Since the complex, $[Co(NH_3)_4AA]^{3+}$ (AA=diamine) can be approximated as C_{2v} symmetry, the first absorption band would consist of two components, Ia(B_1) and Ib(A_2, B_2; accidentaly degenerate) as predicted by Yamatera's theory.[17] These components may be arranged in the order Ia and Ib, and Ib and Ia from longer to shorter wave length in $[Co(NH_3)_4(R\text{-pn})]^{3+}$ and $[Co(NH_3)_4(RR\text{-2,4-ptn})]^{3+}$, respectively, on the basis of the spectrochemical series of the ligands given above. Hence the CD patterns of the tetrammine complexes of *R*-propylenediamine and *RR*-2,4-pentanediamine are understood as due to such a different arrangement of the two components, Ia and Ib.

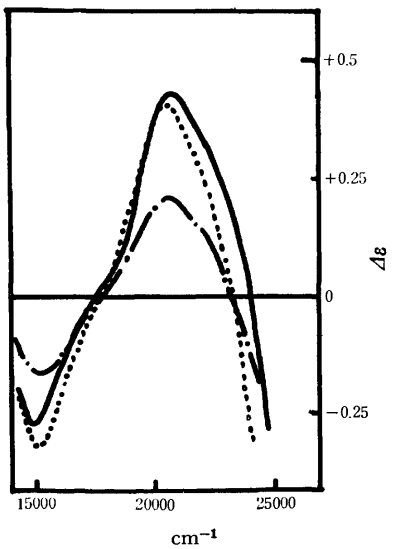

Fig. 9. CD spectra in the first absorption band region.
(——) *trans*-$[CoBr_2(SS\text{-2,4-ptn})_2]^+$
(-·-·) *trans*(Br-Br)-$[CoBr_2(NH_3)_2(SS\text{-2,4-ptn})]^+$
(·····) *trans*(Br-Br)-$[CoBr_2(NH_3)_2(SS\text{-2,4-ptn})]^+$ with doubled $\Delta\varepsilon$ value, in a mixture of methanol and 47% hydrobromic acid (9:1, v/v).

15) R. A. D. Wentworth and T. S. Piper, *Inorg. Chem.*, **4**, 202 (1965).
16) H. Ito, J. Fujita, and K. Saito, This Bulletin, **42**, 1286 (1969).
17) H. Yamatera, *ibid.*, **31**, 95 (1958).

The CD of $[Co(NH_3)_4(RR\text{-2,4-ptn})]^{3+}$ in the region of the second absorption band is entirely different from that of $[Co(NH_3)_4(R\text{-pn})]^{3+}$; the sign is reversed, and the magnitude is almost the same as in the region of the first absorption band. However, the reasons are unknown.

Figure 9 shows the absorption and CD spectra of *trans*(Br-Br)$[CoBr_2(NH_3)_2(SS\text{-2,4-ptn})]^+$ and *trans*-$[CoBr_2(SS\text{-2,4-ptn})_2]^+$ in a mixture of methanol and 47% hydrobromic acid (9: 1, v/v). The absorption spectra are essentially equal, and the CD curves have the same pattern. The dotted line in Fig. 9 shows the CD curve of the former complex with doubled $\Delta\varepsilon$ value. This curve coincides well with the CD curve of the latter complex. Thus the magnitude of CD due to the vicinal effect is proportional to the number of optically active ligand. The same relation was observed between *trans*(Cl-Cl)-$[CoCl_2(NH_3)_2(R\text{-pn})]^+$ and *trans*-$[CoCl_2(R\text{-pn})_2]^+$ by Hawkins *et al.*[10] It is, thus, suggested that the six-membered chelate rings in the two dibromo complexes have almost the same state in the given solution and there seems to be no substantial interaction between the chelate rings in the *trans*-bis-complex.

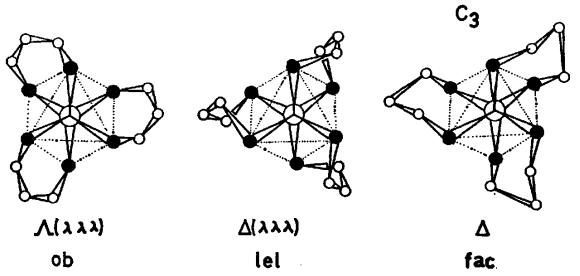

Fig. 10. Schematic structures of tris(1,3-diamine) complexes.

(2) Tris-RR-*2,4-pentanediamine Complexes*: Tris-*RR*-2,4-pentanediamine cobalt(III) complex gives two diastereoisomers, prismatic crystals with $(-)_{546}$ rotation and needle-like crystals with $(+)_{546}$ rotation. The CD and absorption spectra are shown in Fig. 6. We tentatively assigned that the former and the latter have *Δ* and *Λ* configuration, respectively, on the basis of the sign of CD bands in the region of the first absorption band.[18] Lately two of us, together with colaborators, examined the absolute configuration of $(+)_{546}$-isomer by X-ray diffraction method and found that it has *Λ* configuration and the three chelate rings have *λ*-twist conformation.[19] The line connecting two asymmetric carbon atoms of *RR*-2,4-pentanediamine chelate is oblique to the C_3 axis of the complex ion. Hence this isomer is written as *Λ*(*λλλ*)(*ob*). Thus, the other $(-)_{546}$-isomer should have unequivocally *Δ*(*λλλ*)(*lel*) form. (Fig. 10) Therefore, the empirical rule that the diastereoisomer with plus main CD sign in the region of the first absorption band has *Λ* configuration, seems to hold in the two diastereoisomers, $(+)_{546}$- and$(-)_{546}$-$[Co(RR\text{-2,4-ptn})_3]^{3+}$. However, the magnitudes of the CD are very different from each other, even if the vicinal

18) F. Mizukami, H. Ito, J. Fujita, and K. Saito, *ibid.*, **43**, 3973 (1970).
19) A. Kobayashi, F. Marumo, Y. Saito, J. Fujita, and F. Mizukami, *Inorg. Nucl. Chem. Lett.*, **7**, 777 (1971).

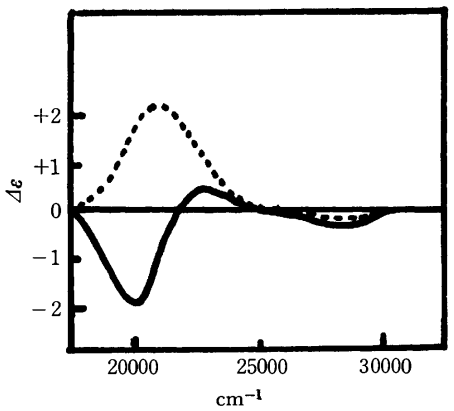

Fig. 11. CD spectra of (——) Δ ($\lambda\lambda\lambda$)(*lel*)-[Co(*R*-pn)$_3$]$^{3+}$, (·····) Λ($\lambda\lambda\lambda$)(*ob*)-[Co(*R*-pn)$_3$]$^{3+}$. (Ref. 13)

contribution of the *RR*-2,4-pentanediamine is taken into account.

In general, the optical activity of a metal complex is understood as a superposition of configurational and conformational (vicinal effect of optically active ligand) chirality. In other words, both chiralities contribute to the CD of a metal complex additively. The CD spectra of Δ($\lambda\lambda\lambda$)(*lel*)- and Λ($\lambda\lambda\lambda$)(*ob*)-[Co(*R*-pn)$_3$]$^{3+}$ shown in Fig. 11 was interpreted satisfactorily by such an additive law.[14,20] However, this law does not hold in the present two diastereoisomers as stated above. There should be some kinds of factors affecting the optical activity of these complexes. Although the factors are not clear at present, they seem to be characteristic of the six-membered tris-complexes, since the CD spectra of mono and *trans*-bis-(*RR*-2,4-ptn) complexes given before are rather normal as compared with those of the corresponding *R*-propylenediamine complexes.

It was stated previously that the Λ($\lambda\lambda\lambda$)(*ob*) isomer might involve larger steric interaction among chelate rings than the Δ($\lambda\lambda\lambda$)(*lel*) isomer, and such an interaction seemed to correlate with the frequency difference of absorption bands between the two diastereoisomers. The same interpretation may be useful for the CD spectra. The interaction among chelate rings may produce a somewhat different field from that expected from a superposition of configurational and conformational chirality. A large interaction of such kind may also induce delicate change in conformation or configuration of the complex. These factors may be reflected sensitively on the CD spectra, although the PMR spectra of the two diastereoisomers are almost identical with each other at 60 MHz. The CD of Λ($\lambda\lambda\lambda$)(*ob*) isomer which involves larger steric interaction seems to be exceptionally strong as compared with those of other tris-β-diamine complexes shown in Figs. 6 and 13. However, further studies on such anomalous CD will be needed.

Both $(+)_{546}$ and $(-)_{546}$ isomers of [Co(*RR*-2,4-ptn)$_3$]$^{3+}$ give plus CD bands in the charge transfer region. This fact may be attributed to the vicinal contribution of the optically active ligand, *RR*-2,4-pentanediamine.[14] Details on the CD in the charge transfer region will be discussed later.

The Δ($\lambda\lambda\lambda$)(*lel*) isomer may be more stable thermodynamically than the Λ($\lambda\lambda\lambda$)(*ob*) isomer because of smaller steric interaction. The yield of diastereoisomers is governed by various factors including kinetics and solubility, and does not necessarily reflect the relative stability of the isomers. However, it should be pointed out that the Δ($\lambda\lambda\lambda$)(*lel*) isomer was produced much more than the Λ($\lambda\lambda\lambda$)(*ob*) isomer as stated in the Experimental part.

As also stated in the Experimental part, [Co(*RR*-2,4-ptn)$_3$]$^{3+}$ gives large single crystals of pseudo-racemate with different moles of the two diastereoisomers. The CD spectrum of the single crystal dissolved in water indicates the composition, 93% Δ($\lambda\lambda\lambda$)(*lel*) and 7% Λ($\lambda\lambda\lambda$)(*ob*) (Fig. 12).

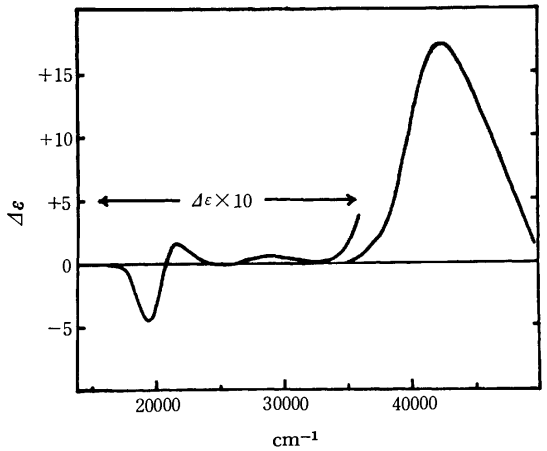

Fig. 12. CD spectra of pseudo-racemate, (Δ(93)+Λ(7))-[Co(*RR*-2,4-ptn)]$^{3+}$ in water.

*(3) Tris-*RS*-2,4-pentanediamine Complex*: Figure 6 shows the CD spectrum of $(-)_{546}$-[Co(*RS*-2,4-ptn)$_3$]$^{3+}$ in water. As stated before, [Co(*RS*-2,4-ptn)$_3$]$^{3+}$ can give two geometrical isomers. We assigned the $(-)_{546}$-isomer as *fac*, and the conformation of the chelated ligands as chair form, on the basis of the PMR spectrum. The absolute configuration of this isomer, however, can be assigned with difficulty from the CD spectrum. When the empirical rule that the main CD of Δ-isomer in the region of the first absorption band has minus sign, is applied, the $(-)_{546}$-isomer seems to have Δ configuration. This assignment seems to be in good harmony with the CD sign of $(+)_{546}$- and $(-)_{546}$-[Co(*RR*-2,4-ptn)$_3$]$^{3+}$ given before, but contradicts the fact that the major CD peak of Λ-$(-)_D$-[Co(tn)$_3$]$^{3+}$ has minus sign[3] (Fig. 13). The trimethylenediamine chelates in this complex have chair conformation in crystals.[12] Gollogly and Hawkins[4] reported that the major CD component (A_2) of Δ-$(+)_D$-[Co(tn)$_3$]$^{3+}$ was increased while the minor CD component (E) decreased in 0.05M-selenite or 0.05M-phosphate solution. The resultant CD pattern seems to be enantiomeric with that of $(-)_{546}$-[Co(*RS*-2,4-ptn)$_3$]$^{3+}$ as shown in Fig. 14. A similar CD change was also observed by Beddoe and Mason[3] with Λ-$(-)_D$-[Co(tn)$_3$]$^{3+}$ in 0.01M sodium selenite. Very recently Beddoe *et al.*[21] observed that

20) B. E. Douglas, *Inorg. Chem.*, **4**, 1813 (1965).

21) P. G. Beddoe, M. J. Harding, S. F. Mason, and B. J. Peart, Private communication.

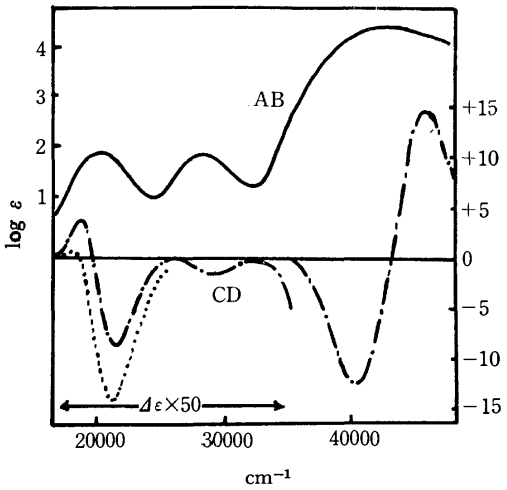

Fig. 13. Absorption (AB) and CD spectra of Λ-(−)$_D$-]Co(tn)$_3$]$^{3+}$. (——) AB in water, (-·-·) CD in water, (·····) CD in 0.01M sodium selenite. (Ref. 3)

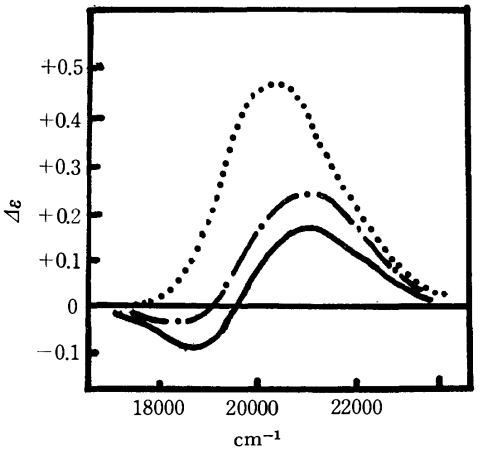

Fig. 14. CD spectra of Λ-(+)$_D$-[Co(tn)$_3$]$^{3+}$. (——) in water, (-·-·) in 0.01M-sulfate, (·····) in 0.05M-selenite. (Ref. 4)

the CD spectrum of Λ-(+)$_D$-[Co(tn)$_3$]$^{3+}$ in 0.05M oxy-anion solutions are almost identical with that in the solid state. They suggested that the [Co(tn)$_3$]$^{3+}$ in water exists in an equilibrium between a tris-chair and a tris-skew boat form, and that the CD change on the addition of oxy-anions can be attributed to the stabilization of the tris-chair form by ion-association. The solid-state CD spectrum of Λ-(+)$_D$-[Co(tn)$_3$]Br$_3$·H$_2$O (tris-chair form[13]) are almost enantiomeric with the solution CD spectrum of (−)$_{546}$-[Co(*RS*-2,4-ptn)$_3$]$^{3+}$ which is constrained to the tris-chair conformation by the equatorial preference of the methyl groups in the chelate rings. Thus, these experiments seem to support strongly that the (−)$_{546}$-[Co(*RS*-2,4-ptn)$_3$]$^{3+}$ has Λ configuration.

On the other hand, the CD pattern of (−)$_{546}$-[Co(*RS*-2,4-ptn)]$^{3+}$ in the charge transfer region is enantiomeric with that of Λ-(−)$_D$-[Co(tn)$_3$]$^{3+}$ as shown in Fig. 13. Previously, one of the authors[14] suggested that the sign of the CD bands of a tris(diamine)cobalt(III) complex in the charge transfer region seemed to depend on the absolute configuration of the complex; Λ-isomer gives a CD band with minus sign at longer wavelength side. The CD pattern of Λ-(−)$_D$-[Co(tn)$_3$]$^{3+}$ in the charge transfer region is in good accord with this rule. When this rule is applied, the (−)$_{546}$-[Co(*RS*-2,4-ptn)$_3$]$^{3+}$ seems to have Λ configuration.

These conflicting results discourage us to give any plausible assignment of the absolute configuration of this complex on the basis of the CD spectrum. Further studies including an X-ray analysis will be needed.

We thank Professor S. F. Mason for information in advance of publication. We also thank the Ministry of Education for Grant-in-aid.

Synthesis and Properties of Metal Complexes with a New Multidentate Schiff Base Containing Ethereal Oxygen Atoms[1)]

Ichiro MURASE, Kuniko YAMANOUCHI,* and Shoichiro YAMADA*

Laboratory of Chemistry, College of General Education, Kyushu University, Ropponmatsu, Fukuoka
**Institute of Chemistry, College of General Education, Osaka University, Toyonaka, Osaka*

(Received October 6, 1971)

A new multidentate Schiff base, 1,4-bis(*o*-salicylideneaminophenyl)-1,4-dioxabutane having six atoms which may be available for bonding with a metal ion was prepared. With this ligand several metal complexes have been synthesized. From their magnetic properties, electronic absorption spectra and X-ray powder diagrams, it has been concluded that the cobalt(II), nickel(II), and zinc(II) complexes are isomorphous, having a five-coordinated configuration, in which one of the ethereal oxygen atoms of the ligand is bound with the metal ion. The copper(II) complex with a similar composition has a different configuration.

It is well known that the ability of the ethereal oxygen atom to be coordinated with a transition metal ion is significantly lower than that of the alcoholic oxygen atom, and only a small number of complexes which involve the linkage between the ethereal oxygen atom and the metal ion have so far been reported.[2)] It is expected, however, that the oxygen atom, when incorporated into a multidentate ligand, may be bound with a metal ion more readily than that in a unidentate ligand.

In the present work, we have synthesized a new multidentate ligand (I), which contains six atoms capable of coordination with a metal ion and may function as a sexa-, a quinqui-, or a quadridentate ligand, depending upon the nature of the metal ion involved.

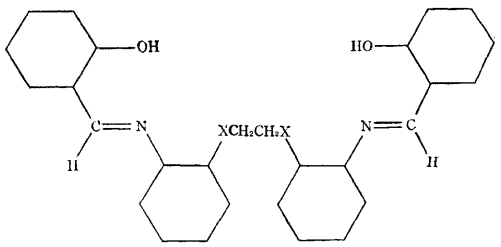

I: X=O (abbreviated as H_2L)
II: X=S (abbreviated as H_2Ls)

Furthermore, complexes of several transition metal ions with this ligand have been synthesized, and their stereochemistry has been investigated, in order to examine the effect of the metal ions upon the behaviour of the ligand.

Experimental

Materials. 1,4-Bis(*o*-salicylideneaminophenyl)-1,4-dioxabutane. A mixture of ethyleneglycol-bis(2-aminophenyl-ether)[3)] (0.0044 mol) and salicylaldehyde (0.016 mol) in 20 m*l* of ethanol was refluxed on a water bath for 2 hr. On cooling, the resulting crystals were collected and recrystallized from a large amount of ethanol; mp 178°C. The yield was almost quantitative. Yellow crystals. Found: C, 73.61; H, 5.33; N, 6.19%. Calcd for $C_{28}H_{24}N_2O_4$: C, 74.32; H, 5.35; N, 6.19%.

[*NiL*]: To a hot solution of the Schiff base H_2L (0.0022 mol) in 50 m*l* of dimethylformamide (DMF) was added nickel(II) acetate (0.0024 mol) in 50% DMF-water, and the mixture was heated on a water bath. The formation of the metal chelate was completed in 10 min. The crystals were filtered and washed with hot ethanol and dried over phosphoric oxide under vacuum at 110°C. Yellow-brown crystals. Found: C, 65.25; H, 4.38; N, 5.6%. Calcd for $C_{28}H_{22}N_2O_4Ni$: C, 66.04; H, 4.36; N, 5.50%.

[*CoL*]: The procedure was the same as described above, except that cobalt(II) acetate was used in place of nickel(II) acetate. Red-violet crystals. Found: C, 65.15; H, 4.31; N, 5.66%. Calcd for $C_{28}H_{22}N_2O_4Co$: C, 65.42; H, 4.32; N, 5.45%.

[*CuL*]: A mixture of the Schiff base (0.0022 mol) and copper(II) acetate (0.0024 mol) in 15 m*l* of DMF was heated on a water bath and the resulting solution was filtered. Methanol was added to the hot filtrate until the solution began to become turbid, and the solution was allowed to cool to room temperature. Brown plates were filtered and washed with hot methanol and dried over phosphoric oxide under vacuum at 110°C. Found: C, 64.66; H, 4.36; N, 5.49%. Calcd for $C_{28}H_{22}N_2O_4Cu$: C, 65.42; H, 4.32; N, 5.45%.

[*ZnL*]: The procedure was the same as described above, except that zinc(II) acetate was used instead of nickel(II) acetate. The product was recrystallized from chloroform to yield yellow-orange crystals. Found: C, 65.17; H, 4.38; N, 5.50%. Calcd for $C_{28}H_{22}N_2O_4Zn$: C, 65.19; H, 4.30; N, 5.43%. The zinc(II) complex is soluble in methanol, ethanol, and chloroform, but insoluble in acetone and benzene.

The other metal complexes, [CoL], [NiL], and [CuL], are almost insoluble in organic solvents, but they were found to be pure and crystalline without recrystallization.

Measurements. Electronic absorption spectra of the ligand and its metal complexes were determined with a Shimadzu MPS-50L spectrophotometer.

Powder diffraction diagrams were obtained with a Toshiba ADX-103 X-ray diffractometer.

Magnetic measurements were carried out by the Gouy method at room temperature.

Infrared spectra of the compounds were determined in the rock-salt region with a Hitachi EPU-2A infrared spectrophotometer using the potassium bromide disc method.

Results and Discussion

It was confirmed by the X-ray powder diagrams that the metal complexes prepared in the present work

1) Presented, in part, at the 24th Annual Meeting of the Chemical Society of Japan, Osaka, April 1971.

2) F. Dwyer, N. S. Gill, E. C. Gyarfasand, and F. Lions, *J. Amer. Chem. Soc.*, **75**, 1526 (1953); *ibid.*, **78**, 4905 (1956).

3) E. Wagner, *J. Prakt. Chem.*, [2] **27**, 201 (1883).

were not polymeric but crystalline.

The ligand, 1,4-bis(*o*-salicylideneaminophenyl)-1,4-dioxabutane, contains an N_2O_4 ligand set consisting of six atoms capable of combining with a metal ion. Judging from the low ability of the ethereal oxygen atom to be bound with a metal ion, however, coordination numbers lower than six may also be possible.

It is presumed that the cobalt(II) complex, [CoL], is not a six-coordinated one, since it is paramagnetic with a magnetic moment of 4.33 B.M. This value is considered to be in the range of magnitude so far observed for a tetrahedral or a five-coordinated cobalt(II) complex, but far below the moment for a six-coordinated one.[4,5] The electronic absorption spectrum of [CoL], as shown in Fig. 1, is quite different from those of octahedral cobalt(II) complexes and tetrahedral ones, but has the main characteristics of the spectrum for the five-coordinated cobalt(II) complex.[6] It is thus concluded that the cobalt(II) ion in [CoL] is five-coordinated, with one of the ethereal oxygen atom bound to the cobalt(II) ion. Any attempt to isolate the cobalt(III) complex with L as a ligand by oxidizing [CoL] has so far been unsuccessful. With 1,4-bis(*o*-salicylideneaminophenyl)-1,4-dithiabutanate (Ls), however, six-coordinated cobalt(III) complexes only were previously reported.[7] This result probably indicates that the ligand field produced by L may be weaker than that produced by Ls, showing significant difference between sulfur and oxygen as a coordinating atom.

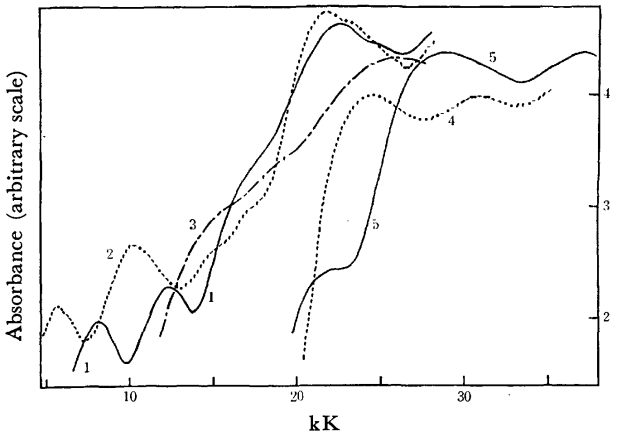

Fig. 1. Electronic absorption spectra of 1,4-bis(*o*-salicylideneaminophenyl)-1,4-dioxabutane (H_2L) and its metal complexes: 1, [CoL], solid; 2, [NiL], solid; 3, [CuL], solid; 4, [ZnL], in chloroform; 5, H_2L, in chloroform. The solid spectra are shown in aribitrary scale.

For the nickel(II) ion in [NiL], the planar four-coordination is excluded, since the nickel(II) complex is paramagnetic with a magnetic moment of 2.86 B.M. at room temperature. The moment observed is much smaller than those reported for tetrahedral nickel(II) complexes.[5] Moreover, the electronic absorption spectrum of [NiL], which is shown in Fig. 1, is similar to that of the typical five-coordinated nickel(II) complex, but is different from that of the octahedral complex.[6] It is concluded that the nickel(II) ion in [NiL] is five-coordinated.

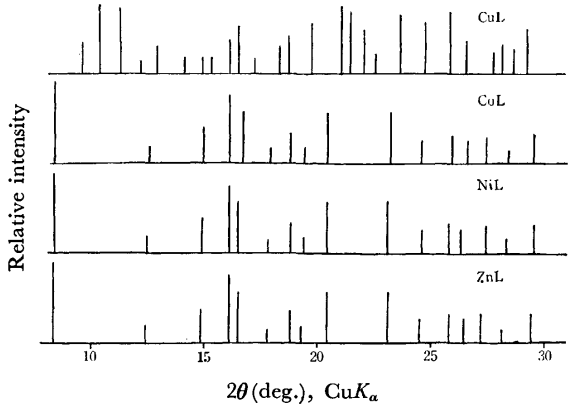

Fig. 2. X-Ray diffraction diagrams of [CuL], [CoL], [NiL], and [ZnL]

The X-ray powder diffraction diagram of [NiL], as shown in Fig. 2 is similar to that of [CoL], indicating that the cobalt(II) and the nickel(II) complexes have a similar configuration, namely the configuration containing the metal ion in five-coordination. Moreover, the infrared spectrum in the rock-salt region of [NiL] is also virtually identical with that of [CoL], in agreement with the conclusion derived above about their structure.

Since the zinc(II) complex, [ZnL], also shows an X-ray powder diagram and an infrared spectrum similar to those of [CoL] and [NiL], it is concluded that the three complexes [CoL], [NiL], and [ZnL] have a similar configuration, in which the metal ion assumes the five-coordination.

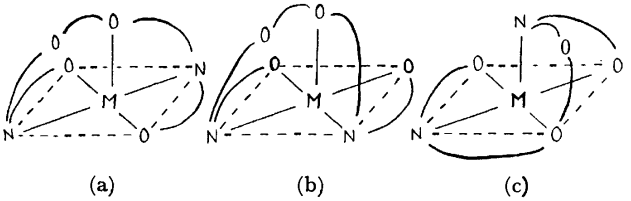

Fig. 3. Some possible configurations for the five-coordinated complexes of the [ML] type.

Some possible configurations for the five-coordinated complexes are shown in Fig. 3. The configuration (a) seems to be more favorable than the other configurations from the steric condition alone, but the definitive conclusion about the precise configuration must await the more detailed X-ray studies. It should be noted, in any case, that the ligand in these complexes is not sexadentate but quinquedentate, with only one of the two ethereal oxygen atoms bound to the metal ion.

The absorption spectrum of [ZnL], which is shown in Fig. 1, may be interpreted on the basis of previous results about *N*-substituted-salicylideneiminato-metal(II) complexes.[8] It is thus considered that the absorp-

4) L. Sacconi, M. Ciampolini, and G. P. Speroni, *Inorg. Chem.*, **4**, 116 (1965).
5) B. N. Figgis and J. Lewis, *Progr. Inorg. Chem.*, **6**, 37 (1964).
6) L. Sacconi, *Coordin. Chem. Rev.*, **1**, 192 (1966).
7) F. Dwyer, N. S. Gill, E. C. Gyarfas, and F. Lions, *J. Amer. Chem. Soc.*, **76**, 383 (1954).
8) B. Bosnich, *ibid.*, **90**, 627 (1968).

tion bands at about 24.4 kK (log ε, 4.0) and 30.5 kK (log ε, 4.0) of [ZnL] are originated mainly from excitations involving both the metal ion and the ligand and π-π^* transitions within the ligand, respectively.

The X-ray diffraction diagram of [CuL] is different from those of the other three metal complexes. The infrared spectrum of [CuL] in the region from 1200 to 1275 cm^{-1}, where compounds having an ethereal structure similar to that in the ligand, L, is known to absorb,[9] is very different from that of [ZnL] but similar to that of HL.

The electronic absorption spectrum of [CuL] may be interpreted on the basis of the model having a four-coordinated configuration, scarcely distorted from a planar one. As shown in Fig. 1, [CuL] shows *d-d* absorption bands at frequencies nearly identical with, or even higher than, those of bis(*N*-aryl-salicyliden-iminato)copper(II) and related complexes;[10,11] their *d-d* bands in the lowest frequency region appear at about 15 kK.

From these data combined, a four-coordinated, essentially planar configuration seems to be likely for [CuL], but any definitive conclusion about its structure may not safely be drawn, except that [CuL] has a different configuration from that of [CoL], [NiL], or [ZnL].

The present authors are grateful to Professor Mitsue Koizumi and Dr. Satoru Ueda of Osaka University for the determination of the X-ray powder diffraction diagrams. Thanks are also due to the Ministry of Education for financial support.

9) L. J. Bellamy, "The Infrared Absorption Spectra of Complex Molecules," Methuen, London (1958), p. 117.

10) S. Yamada, A. Takeuchi, K. Yamanouchi, and K. Iwasaki, This Bulletin, **42**, 131 (1969).

11) S. Yamada, H. Nishikawa, and E. Yoshida, *ibid.*, **39**, 994 (1966).

BULLETIN OF THE CHEMICAL SOCIETY OF JAPAN, VOL. 45, 2140—2143(1972)

Six-coordinate Chromium(III) Complexes with *N,N'*-Ethylene-bis(acetylacetoneiminate) as a Ligand[1]

Katsumoto YAMANOUCHI (Formerly IWASAKI) and Shoichiro YAMADA
Institute of Chemistry, College of General Education, Osaka University, Toyonaka, Osaka

(Received January 13, 1972)

Numerous six-coordinate chromium(III) complexes with *N,N'*-ethylene-bis(acetylacetoneiminate) (abbreviated as Acen) have been synthesized. The complexes obtained are of the type $[Cr(Acen)X_2]Y$, where $X=H_2O$, NH_3, CH_3NH_2, n-$C_3H_7NH_2$, and n-$C_4H_9NH_2$ for Y=Cl and X=CN, NCS, and NO_2 for Y=K. The complex $[Cr(Acen)(H_2O)_2]Cl$ has been obtained by a reaction of anhydrous chromium(III) chloride with *N,N'*-ethylene-bis(acetylacetoneimine) in tetrahydrofuran. The other complexes have been derived from the diaquo-complex. Infrared spectra show that the nitrite ions in $[Cr(NO_2)_2(Acen)]^-$ and the thiocyanate ions in $[Cr(NCS)_2(Acen)]^-$ are bound with the chromium(III) ion through oxygen and nitrogen atoms, respectively. Electronic absorption bands of all these complexes, which arise from internal transitions within the ligand Acen, differ greatly from those of the free ligand, suggesting that the electronic states of the ligand in the complexes differ from those of the free ligand.

A number of papers have been published on metal complexes with Schiff bases.[2,3] However, not many chromium(III) complexes have so far been reported.[4-7] Chromium(III) complexes with Schiff bases obtained from salicylaldehyde derivatives and various amines have recently been synthesized.[4,5] As an extension of the previous study on six-coordinate chromium(III) complexes with *N,N'*-ethylenebis(salicylideneiminate) (abbreviated as Salen),[6] this paper deals with six-coordinate chromium(III) complexes with *N,N'*-ethylenebis(acetylacetoneiminate)[8] as a quadridentate ligand (I, abbreviated as Acen). These complexes have not been reported, although tris(*N*-arylacetylacetoneiminato)chromium(III) complexes have been known for some years.[7]

Experimental

Materials. Chromium(III) complexes with *N,N'*-ethylene-bis(acetylacetoneiminate) as a ligand are shown in Table 1, together with analytical data.

$[Cr(Acen)(H_2O)_2]Cl$. *N,N'*-ethylene-bis(acetylacetoneimine) (0.1 mol) and potassium ethoxide (0.2 mol) in ethanol

1) Presented at the 21st Symposium on Coordination Chemistry, Nagoya, October, 1971.

2) R. H. Holm, G. W. Everett, Jr., and Chakravorty, "Progress in Inorganic Chemistry," Vol. VII, ed. by F. A. Cotton, Interscience, New York (1966), p. 83.

3) S. Yamada, *Coordin. Chem. Rev.*, **1**, 415 (1966).

4) M. J. O'Connor and B. O. West, *Austral. J. Chem.*, **21**, 369 (1968).

5) S. Yamada and K. Iwasaki, This Bulletin, **41**, 1972 (1968).

6) S. Yamada and K. Iwasaki, *Inorg. Chim. Acta*, **5**, 3 (1971); This Bulletin, **42**, 1463 (1969).

7) J. P. Collman and E. T. Kittleman, *Inorg. Chem.*, **1**, 499 (1962).

8) For the sake of convenience, this ligand is referred to as *N,N'*-ethylene-bis(acetylacetoneiminate) in the present paper.

Table 1. Analytical data of complexes of the type $[Cr(Acen)X_2]Y \cdot nH_2O$

X	Y	n	found, %			calcd, %		
			C	H	N	C	H	N
H_2O	Cl	1	41.68	6.20	8.02	41.30	6.41	8.10
NH_3	Cl	1.5	38.90	7.24	15.24	38.86	7.34	15.11
CH_3NH_2	Cl	2	40.09	7.71	13.89	41.22	7.90	13.74
$C_2H_5NH_2$	Cl	1.5	45.04	8.33	13.09	45.01	8.26	13.12
n-$C_3H_7NH_2$	Cl	1	48.87	8.60	12.74	48.47	8.59	12.56
n-$C_4H_9NH_2$	Cl	1	50.17	8.99	11.99	50.67	8.93	11.82
$C_6H_5NH_2$	Cl	2.5	52.95	6.62	10.58	53.28	6.89	10.36
CN	K	2	42.07	5.57	14.45	41.88	5.52	13.96
NO_2	K	0	35.75	4.45	13.91	35.55	4.47	13.82
NCS	K	1	37.35	4.50	12.60	37.57	4.50	12.52

(50 m*l*) were added to 300 m*l* of tetrahydrofuran in a flask attached to a Soxhlet apparatus. Anhydrous chromium(III) chloride (0.1 mol) and zinc dust (1 g) were placed in the thimble of the apparatus, and the tetrahydrofuran solution was allowed to reflux for about 4 hr until the recycling liquid became colorless. The reaction mixture was allowed to cool down to room temperature. Potassium chloride which precipitated in the solution was filtered, and a reddish brown filtrate obtained was concentrated nearly to dryness on a rotary evaporator. The residue was dissolved again in ethanol (150 m*l*), and the resulting solution was filtered, diluted with 200 m*l* of benzene and concentrated to about 50 m*l*. The procedure with the residue was repeated several times. Brown crystals which separated out in the solution were collected by filtration and dried *in vacuo* for 24 hr.

$[Cr(Acen)(NH_3)_2]Cl \cdot 1.5H_2O$. $[Cr(Acen)(H_2O)_2]Cl$ (0.01 mol) was dissolved in a mixture of methanol (50 m*l*) and 30% aqueous ammonia (50 m*l*) at about 50°C. The resulting solution was heated at this temperature for 15 min, filtered and allowed to stand overnight. Reddish orange needle-like crystals which separated out in the solution were collected.

$[Cr(Acen)(RNH_2)_2]Cl \cdot nH_2O$. ($R=CH_3$, C_2H_5, n-C_3H_7, and n-C_4H_9; n=2, 1.5, 1, and 1, respectively). $[Cr(Acen)(H_2O)_2]Cl$ (0.01 mol) was added to a solution of an appropriate alkyl amine (0.2—0.3 mol) in methanol (20—30 m*l*) and the solution was stirred for 15 min at about 50°C. Diethyl ether or benzene was added to the solution until the solution became turbid. It was then allowed to stand overnight to give orange needle-like crystals.

$[Cr(Acen)(C_6H_5NH_2)_2]Cl \cdot 2H_2O$. Aniline (0.1 mol) and $[Cr(Acen)(H_2O)_2]Cl$ (0.01 mol) were added to acetone (50 m*l*), stirred at about 50°C for 15 min, then filtered and allowed to stand overnight. Yellow-brown crystals were collected.

$K[Cr(CN)_2(Acen)] \cdot 2H_2O$. An aqueous solution of potassium cyanide (0.04 mol) was added to a solution of $[Cr(Acen)(H_2O)_2]Cl$ (0.01 mol) in methanol (30 m*l*). The resulting solution was heated at about 50°C for 15 min and allowed to stand overnight to give reddish orange crystals.

The chromium(III) complexes described so far were pure enough without recrystallization. However, purification was carried out whenever necessary by recrystallization from methanol or ethanol. The complexes are soluble in methanol, ethanol, water, tetrahydrofuran and acetonitrile, but insoluble in diethyl ether and benzene.

$K[Cr(NCS)_2(Acen)] \cdot H_2O$. A suspension of $[Cr(Acen)(H_2O)_2]Cl$ (0.01 mol) and potassium thiocyanate (0.04 mol) in acetone (50 m*l*) was heated at about 50°C for 1 hr. The potassium chloride which separated out in the solution was removed by filtration. The filtrate was concentrated to yield the crude product of the desired complex which was recrystallized from acetone. Dark red crystals were obtained. The compound is soluble in acetone.

$K[Cr(ONO)_2(Acen)]$. A suspension of $[Cr(Acen)(H_2O)_2]Cl$ (0.01 mol) and potassium nitrite (0.045 mol) in methanol (50 m*l*) was heated under stirring at about 50°C for 1 hr, and the resulting potassium chloride was filtered. On concentrating the filtrate, the desired complex was obtained as yellowish brown crystals. Purification was carried out by filtration from methanol or ethanol.

All the complexes except for the dicyano-complex are gradually decomposed by water. The diisothiocyanato-complex undergoes decomposition even in methanol or ethanol.

Measurements. The electronic absorption spectra of the chromium(III) complexes were determined with a Shimadzu MPS-50L spectrophotometer. The infrared absorption spectra were measured in the region 600—4000 cm^{-1} with a Hitachi EPI-G31 infrared spectrophotometer using Nujol mull and potassium bromide disc methods.

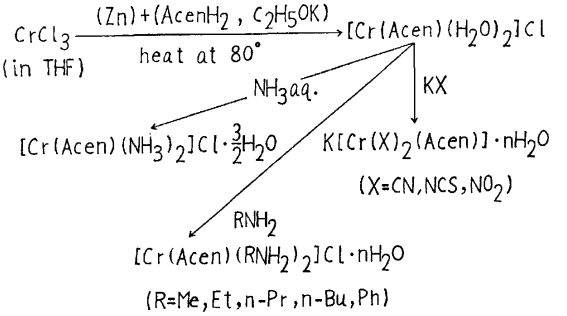

Fig. 1. Synthetic routes of the complexed of the type $[Cr(Acen)X_2]Y$

Results and Discussion

The synthetic routes of the chromium(III) complexes are summarized in Fig. 1. A method which involves reactions in ethyleneglycol at a higher temperature and which was successful for preparing $[Cr(Salen)(H_2O)_2]Cl$,[5,6] did not yield $[Cr(Acen)(H_2O)_2]Cl$, but gave instead tris(acetylacetoneiminato)chromium(III). The method for preparing $[Cr(Acen)(H_2O)_2]Cl$ proved to be more appropriate for the synthesis of $[Cr(Salen)(H_2O)_2]Cl$ than the previously one.

Since the quadridentate ligand Acen usually requires, but not necessarily a square-planar coordination, it most likely that the chromium(III) complexes prepared have a six-coordinate, *trans*-configuration.

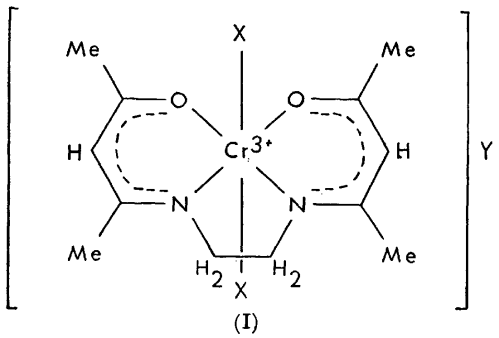

(I)

The main infrared bands of $[Cr(ONO)_2(Acen)]^-$ and $[Cr(NCS)_2(Acen)]^-$ are shown in Table 2. From the table and with the aid of the criteria previously established,[9,10] it is concluded that the nitrite ions in $[Cr(ONO)_2(Acen)]^-$ are coordinated through their oxygen atoms to the chromium(III) ion. This is in agreement with the results for other chromium(III) complexes.[11]

TABLE 2. INFRARED ABSORPTION MAXIMA OF THIOCYANATO-ISOTHIOCYANATO AND NITRO-NITRITO ISOMERS

Nitro-nitrito isomers	ν_{as}	ν_s	δ	reference
free NO_2^- (in $NaNO_2$)	1328	1261	828	a
$K[Cr(ONO)_2(Acen)]$	1450	1075	847	this work
		1063	835	
$[Cr(ONO)(NH_3)_5]Cl_2$	1460	1048	839	b
$[Co(ONO)(NH_3)_5]Cl_2$	1468	1065	825	b
$[Co(NO)_2(NH_3)_5]Cl_2$	1428	1310	824	b
thiocyanato-isothiocyanato isomers	ν(CN)	ν(CS)		
free NCS^- (in KNCS)	2053	748		c
$K[Cr(NCS)_2(Acen)]\cdot H_2O$	2085	785		this work
$NH_4[Cr(NCS)_4(NH_3)_2]$	2120	823		c
$[Co(NCS)(NH_3)_5](ClO_4)_2$	2125	806		d
$[Co(SCN)(NH_3)_5](ClO_4)_2$	2100	710		d
$(Et_4N)_2[Pd(SCN)_4]$	2109	694		e
	2112	698		

ν : cm^{-1}

(a) R.E. Weston and T.F. Broodasky, *J. Chem. Phys.*, **27**, 683 (1957).
(b) K. Nakamoto, J. Fujita, and H. Murata, *J. Amer. Chem. Soc.*, **80**, 4817 (1958).
(c) J. Lewis, R.S. Nyholm, and P.W. Smith, *J. Chem. Soc.*, **1961**, 4590.
(d) D.A. Buckingham, I. I. Creaser, and A. M. Sargeson, *Inorg. Chem.*, **9**, 635 (1970).
(e) A. Sabatini and I. Bertini, *Inorg. Chem.*, **4**, 959(1965).

In a similar way, we see that the thiocyanate ions are bound through their nitrogen atoms to the chromium(III) in $[Cr(NCS)_2(Acen)]^-$. It seems to be generally accepted that the ν (CS), which appears at about 690 to 860 cm^{-1}, is useful for the diagnostic purposes, the band being observed at 780 to 860 cm^{-1} for the M–NCS complex and at 690 to 730 cm^{-1} for the M–SCN complex.

The electronic absorption spectra of some of the chromium(III) complexes are shown in Fig. 2, the maxima of the bands being given in Table 3. It should be noted that, as far as the main peaks are concerned, the absorption spectra of the complexes are similar, regardless of the position of a ligand X in the spectrochemical series. As an example, the maxima of these bands for $[Cr(CN)_2(Acen)]^-$ are nearly the same as those for $[Cr(Acen)(H_2O)_2]^+$, in spite of the fact that the cyanide ion is far apart from H_2O in the spectrochemical series. Consequently, it is concluded that the bands at about 22—23, 27—28, and 36—37 kK observed for all the chromium(III) complexes may not be assigned to *d-d* bands. It is more likely that they correspond to internal transitions within the coordinated Acen and/or transitions, in which the ligand Acen is mainly involved. This situation seems to be similar to that with complexes of the type $[Cr(Salen)L_2]$.[6]

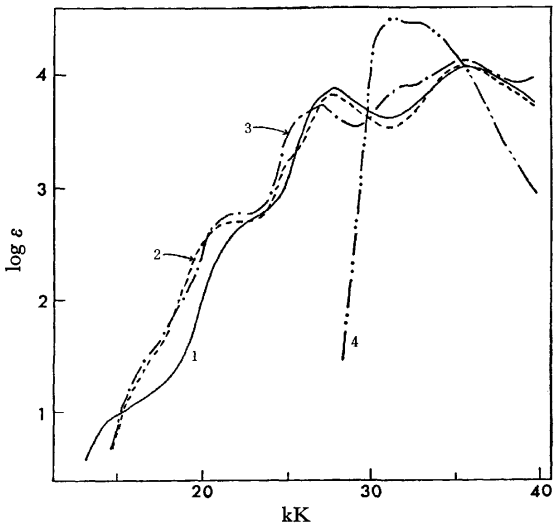

Fig. 2. Electronic absorption spectra of complexes of the type $[Cr(Acen)X_2]Y$ in solution: 1, X=H_2O, in methanol: 2, X=CN, in methanol; 3, X=NCS, in acetonitrile; 4, *N,N'*-ethylene-bis(acetylacetoneimine), in methanol

Their ligand field bands are probably hidden under more intense bands of other origins, except for some complexes which show a small shoulder in the lower frequency side of the absorption curves, possibly arising from *d-d* transitions.

The inflation at about 32 kK in the spectrum of $[Cr(NCS)_2(Acen)]^-$ indicates the presence of a band, which may be assigned to a "specific absorption band" due to the isothiocyanate group linked with the chromium(III) ion. A band of a similar nature has also been reported to appear in the neighbourhood of this frequency region for chromium(III) ammine complexes.[12] A specific absorption band due to the coordinated nitrite ion is known to be generally weaker and may be considered to be hidden under more

9) J. L. Burmeister, *Coordin. Chem. Rev.*, **3**, 225 (1968).
10) D. M. L. Goodgame and M. A. Hitchman, *Inorg. Chem.*, **4**, 721 (1965); A. Takeuchi, K. Sato, K. Sone, S. Yamada, and K. Yamasaki, *Inorg. Chim. Acta*, **1**, 399 (1967).
11) W. W. Fee, C. S. Garmer, and J. N. M. Harrowfield, *Inorg. Chem.*, **6**, 87 (1967).
12) R. Tsuchida and M. Kobayashi, This Bulletin, **13**, 471 (1938).

Table 3. Main absorption maxima of complexes of the type $[Cr(Acen)X_2]Y$ in solution[a)]

X	ν (logε)[b)]			
H_2O	15.7 (1.05),	23.0 (2.68),	27.7 (3.88),	36.1 (4.08)
NH_3	22.6 (2.59),	27.7 (3.80),	36.2 (4.06)	
CH_3NH_2	22.5 (2.68),	27.5 (3.78),	36.2 (4.08)	
n-$C_3H_7NH_2$	22.6 (2.58),	27.5 (3.78),	36.2 (4.05)	
$C_6H_5NH_2$	22.8 (2.68),	27.8 (3.84),	35.9 (4.12)	
CN	22.0 (2.68),	27.8 (3.84),	36.0 (4.06)	
NCS[c)]	22.0 (2.78),	27.0 (3.74),	32.0 (3.90),	36.0 (4.14)
NO_2[d)]	16.3 (1.24),	22.6 (2.60),	27.7 (3.83),	36.2 (4.04)
free ligand $AcenH_2$	31.0 (4.48),	33.0 (4.45)		

a) Unless otherwise indicated, the values in the table refer to those of the methanolic solutions.
b) ν: 10^3 cm^{-1}
c) in acetonitrile
d) in methanol containing sodium nitrite

intense bands of other origins.

We see from Fig. 2 and Table 3 that the bands of $[Cr(Acen)X_2]$, due to internal transitions within the ligands, differ remarkably from those of the free ligand itself. This is also found to be the case with the corresponding cobalt(III) complexes,[13)] which show spectra with main features similar to those of the chromium(III) complexes. This indicates that the electronic state of the ligand in the chromium(III) complexes, as well as in the cobalt(III) complexes, differ from that in the free ligand. Comparison also shows that the spectra of tris(*N*-arylacetylacetoneiminato)chromium(III) complexes[7)] have features similar to those of complexes of the type $[Cr(Acen)X_2]Y$.

Since it is known that these free ligands exist in the form of β-ketoamines rather than β-ketoimines,[14)] the above result seems to show that their electronic state in the chromium(III) complexes differs considerably from that of the β-ketoamines.

The present authors are grateful to the Ministry of Education for financial support.

13) G. Costa, G. Mestroni, G. Tauzher, and L. Stefani, *J. Organometal. Chem.*, **6**, 181 (1966).

14) G. O. Dudek and R. H. Holm, *J. Amer. Chem. Soc.*, **83**, 2099 (1966).

BULLETIN OF THE CHEMICAL SOCIETY OF JAPAN, VOL. 45, 2143—2147(1972)

Syntheses of Formato-, Acetato-, Benzoato-, and Chlorosubstituted Acetatoruthenium Complexes, and Their Properties

Masao MUKAIDA, Terunosuke NOMURA, and Tatsujiro ISHIMORI*

Department of Chemistry, Sophia University, Chiyoda, Tokyo

**Department of Chemistry, Rikkyo (St. Paul's) University, Ikebukuro, Tokyo*

(Received October 29, 1971)

Complexes with the general formula of $[Ru_2(RCOO)_4X]$, where R=H, X=Cl, or Br; R=Me, X=Cl, Br, I, SCN, NO_3, or MeCOO; R=ph, X=Cl, or Br, were prepared. The magnetic properties, conductivities, polarographic behavior, and infrared spectra of these complexes were investigated. All the complexes show magnetic moments of 2.84—2.96 B.M., and their susceptibilities, at from about 300 to 100°K, can be fitted to the Curie-Weiss law with negative values of the Weiss constant (θ=−30—−60°K). These complexes seem to be isostructural. Monochloroacetato-, and trichloroacetatoruthenium complexes ($[Ru_2(CH_2ClCOO)_4Cl]\cdot 2H_2O$ and $[Ru(OH)(CCl_3COO)_2(H_2O)]$) were also prepared.

Carboxylatoruthenium complexes of the $[Ru_2(RCOO)_4Cl]$ (R=Me, Et, *n*-Pr) type have been prepared by the reaction of hydrated ruthenium trichloride with carboxylic acid-acid anhydride mixtures, and the complexes have been formulated as containing Ru(II) and Ru(III).[1] $[Ru_2(RCOO)_4Cl]$ (R=H, Me) complexes have also been obtained by the reaction of ruthenium(III and IV) chlorides with acetic or formic acid in a sealed tube.[2] An X-ray investigation of the analogue butyrato complex has recently been accomplished.[3] In this study, formato-, acetato-, and benzoatoruthenium complexes were

1) T. A. Stephenson and G. Wilkinson, *J. Inorg. Nucl. Chem.*, **28**, 2285 (1966).

2) M. Mukaida, T. Nomura, and T. Ishimori, This Bulletin, **40**, 2462 (1967).

3) M. J. Bennett, K. G. Caulton, and F. A. Cotton, *Inorg. Chem.*, **8**, 1 (1969).

prepared and their properties were investigated. Monochloroacetato- and trichloroacetatoruthenium complexes, $[Ru_2(CH_2ClCOO)_4Cl]\cdot 2H_2O$ and $[Ru(OH)(CCl_3COO)_2(H_2O)]$, were also prepared.

Experimental

Syntheses. $[Ru_2(MeCOO)_4Cl]$ (Complex [1]). A ruthenium(III, IV)-hydrochloric acid solution (Ru, 250 mg) was evaporated to dryness on a water bath. The residue was dissolved in 12N acetic acid (30 m*l*) and then gently heated for about 100 min at 110°C in a sealed, stainless-steel (SUS 32) tube. The solution thus obtained was concentrated on a water bath to prepare crystals. The crude crystals were recrystallized from a 3N acetic acid solution. Brown crystals were thus obtained; they were filtered and washed several times with ethanol and ether, and then dried *in vacuo*, to yield about 300 mg. The complex is poorly soluble both in water and in methanol.

Found: Ru, 42.23; C, 20.3; H, 2.40; Cl, 7.17%. Calcd for $Ru_2(MeCOO)_4Cl$: Ru, 42.66; C, 20.27; H, 2.53; Cl, 7.49%.

$[Ru_2(MeCOO)_4Br]$ (Complex [2]), $[Ru_2(MeCOO)_4I]$ (Complex [3]), and $[Ru_2(MeCOO)_4SCN]$ (Complex [4]) were prepared by adding large amounts of sodium bromide, sodium iodide, and potassium thiocyanate respectively to an acetic acid solution of Complex [1]. Complex [2] is poorly soluble both in water and in methanol, and Complexes [3] and [4] are insoluble in these solvents.

Complex [2]. Found: Ru, 38.54; C, 18.7; H, 2.44; Br, 15.08%. Calcd for $Ru_2(MeCOO)_4Br$: Ru, 39.00; C, 18.54; H, 2.32; Br, 15.43%.

Complex [3]. Found: Ru, 35.34; C, 17.3; H, 2.05; I, 21.30%. Calcd for $Ru_2(MeCOO)_4I$: Ru, 35.76; C, 16.99; H, 2.12; I, 22.45%.

Complex [4]. Found: C, 21.86; H, 2.12; N, 2.82%. Calcd for $Ru_2(MeCOO)_4SCN$: C, 21.77; H, 2.44; N, 2.82%.

$[Ru_2(MeCOO)_4NO_3]$ (Complex [5]). An 1N acetic acid solution containing 500 mg of Complex [1] was passed through an anion exchange column of Dowex 1-X4 (30 m*l* of the NO_3^- form). To the effluent, a 200-mg portion of potassium nitrate was then added, and the solution was concentrated on a water bath. The brown crystals thus obtained were filtered, washed with water, methanol, and ether, and dried *in vacuo*, to yield about 350 mg. The complex is poorly soluble both in water and in methanol.

Found: C, 18.90; H, 2.48; N, 2.91%. Calcd for $Ru_2(MeCOO)_4NO_3$: C, 19.21; H, 2.42; N, 2.80%.

$[Ru_2(MeCOO)_4OCOMe]$ (Complex [6]). An 1N acetic acid solution containing 400 mg of Complex [1] was passed through an anion exchange column of Dowex 1-X4 (30 m*l* of the SO_4^{2-} form). The effluent was concentrated on a water bath. The brown crystals thus obtained were filtered, washed with water, methanol, and ether, and dried *in vacuo*, to yield about 200 mg. The complex is poorly soluble both in water and in methanol.

Found: C, 23.58; H, 3.62%. Calcd for $Ru_2(MeCOO)_4OCOMe$: C, 24.15; H, 3.04%.

$[Ru_2(HCOO)_4Cl]$ (Complex [7]). This complex was prepared by the same procedure as was Complex [1], but using formic acid, as was reported previously.[2]

$[Ru_2(HCOO)_4Br]$ (Complex [8]). The bromo-formato complex was prepared by adding a large amount of sodium bromide to a solution of Complex [7]. The complex is poorly soluble both in water and in methanol.

Found: Ru, 43.35; C, 10.5; Br, 16.82%. Calcd for $Ru_2(HCOO)_4Br$: Ru, 43.73; C, 10.39; Br, 17.30%.

$[Ru_2(phCOO)_4Cl]$ (Complex [9]). The chloro-formato complex [7] (100 mg) was dissolved in a mixture of methanol and water (30 m*l*+30 m*l*), and then a methanol solution of benzoic acid (100 mg/10 m*l*) was added to that solution. The mixture thus obtained was kept at room temperature for a week. The brown, crystalline material thus obtained was filtered, washed with water, methanol, and ether, and dried *in vacuo*, to yield about 150 mg. The complex is insoluble in most organic solvents and in water.

Found: Ru, 28.04; C, 46.4; H, 2.61; Cl, 4.90%. Calcd for $Ru_2(phCOO)_4Cl$: Ru, 27.98; C, 46.54; H, 2.77; Cl, 4.91%.

$[Ru_2(phCOO)_4Br]$ (Complex [10]). The bromo-benzoato complex was prepared in the same way as was the chloro-benzoato complex, using the bromo-formato complex [8] as the starting material. (Yield, about 150 mg). The complex is insoluble in most organic solvents and in water.

Found: Ru, 26.51; C, 43.9; H, 2.60; Br, 9.64%. Calcd for $Ru_2(phCOO)_4Br$: Ru, 26.36; C, 43.85; H, 2.61; Br, 10.43%.

$[Ru_2(CH_2ClCOO)_4Cl]\cdot 2H_2O$ (Complex [11]). To Complex [1] (200 mg) in a mixture of methanol (50 m*l*) and water (50 m*l*), a monochloroacetic acid solution (500 mg/10 m*l* H_2O) was added. The solution was then kept at room temperature for one or two weeks. The brown crystals thus obtained were filtered, washed with methanol, and ether, and dried *in vacuo*, to give 200 mg. Recrystallization was made from a 2M monochloroacetic acid solution. The complex is slightly soluble in methanol.

Found: Ru, 31.14; C, 15.52; H, 2.40; H_2O, 5.85%. Calcd for $Ru_2(CH_2ClCOO)_4Cl\cdot 2H_2O$: Ru, 31.20; C, 14.83; H, 1.85; H_2O, 5.55%.

$[Ru(OH)(CCl_3COO)_2(H_2O)]$ (Complex [12]). To a solution of Complex [1] (500 mg) in a mixture of methanol (100 m*l*) and water (100 m*l*), trichloroacetic acid (8 g) was added. The solution was then heated about 10 min. A flaky, brown crystalline material was thus obtained; and it was filtered, washed with water, and dried in a vacuum line (10^{-3} mmHg), to give 200 mg. The complex is soluble in most organic solvents.

Found: Ru, 22.02; C, 10.58; H, 0.61%. Calcd for $Ru(OH)(CCl_3COO)_2(H_2O)$: Ru, 21.87; C, 10.39; H, 0.87%.

Apparatus and Reagents. The molar conductivity was measured with a Metrohm Konduktoskope E365, the IR spectra, with Leitz 221, JASCO DS-301, and Hitachi EPI-L IR spectrometers, and the molecular weight, with a Mecrolab Osmometer 302. The magnetic susceptibility was measured by the Gouy method.

Ruthenium (III, IV) in a hydrochloric acid solution was prepared from a distillate of ruthenium(VIII) tetroxide passed into an alcoholic acid solution. All the other reagents used were of an analytical grade.

Results and Discussion

The complexes obtained are summarized in Table 1, along with the magnetic data, the conductivity data, the molecular weights, and the absorption maxima in their visible spectra.

The chloro-acetato complex [1] and chloro-formato complex [7] were prepared by the reaction of ruthenium(III and IV) chloride with acetic and formic acid respectively in a sealed tube. Complex [1] was confirmed by X-ray fluorometry to be free from contamination by the components of the sealed, stainless-steel

Table 1. The carboxylatoruthenium complexes and their properties

Complex No.	Chemical formula	$\chi_g \cdot 10^6$ (c.g.s.)	μ_{eff}(°C) (B.M.)[a]	Visible absorption spectra[d] mμ(ε in parentheses)	Molar conductivities[c] (mho cm^{-1})	Molecular weight[d]
1	$Ru_2(MeCOO)_4Cl$	14.89	2.90 (20)	428 (793)	80	460[e]
2	$Ru_2(MeCOO)_4Br$	13.39	2.89 (23)	426—430 (787)		608[e]
3	$Ru_2(MeCOO)_4I$	12.11	2.85 (18)			
4	$Ru_2(MeCOO)_4SCN$	13.73	2.85 (19)			
5	$Ru_2(MeCOO)_4NO_3$	13.74	2.87 (19)	426—430 (798)	93	
6	$Ru_2(MeCOO)_4OCOMe$	13.54	2.84 (20)	424—428 (830)	69	
7	$Ru_2(HCOO)_4Cl$	16.96	2.92 (24)	428—430 (774)	70	423[e]
8	$Ru_2(HCOO)_4Br$	15.77	2.94 (20)	428—430 (1160)		
9	$Ru_2(phCOO)_4Cl$	10.08	2.96 (19)			
10	$Ru_2(phCOO)_4Br$	9.13	2.91 (20)			
11	$Ru_2(CH_2ClCOO)_4Cl \cdot 2H_2O$[b]	11.28	2.99 (20)	435 (816)	79	648[e]
12	$Ru(OH)(CCl_3COO)_2(H_2O)$	3.54	2.10 (20)	460 (217)	3	461[e]

a) Corrections for diamagnetism were made and effective magnetic moments in Bohr magnetons, μ_{eff}, were calculated according to the formula, $\mu_{eff}=8T\chi_{corr}^{1/2}$, where χ_{corr} is the molar susceptibility corrected for diamagnetism and T is the absolute temperature.
b) The hydrated water was determined by the weight loss at 140°C.
c) in MeOH (30°C), 10^{-3} mol/*l*.
d) in MeOH. e) The values in Table are twice the observed ones for 1:1 electrolytes.

tube.[4] The chloro-benzoato complex [9] was obtained from a mixture of the chloro-formato complex [7] and benzoic acid. The other acetato complexes [2]—[6] were obtained from solutions of the chloro-acetato complex [1] in acetic acid containing an excess of the anions. A similar derivation can also be expected for the chloro-formato complex [7]. The conversion from the chloro-acetato complex [1] to the chloro-formato complex [7], and *vice versa*, are possible. The monochloroacetato and trichloro-acetato complexes, [11] and [12], $[Ru_2(CH_2ClCOO)_4Cl]\cdot 2H_2O$ and $[Ru(OH)(CCl_3COO)_2(H_2O)]$, were obtained as reaction products of Complex [1] and the corresponding monocarboxylic acid. In Fig. 1, these conversion procedures are shown schematically.

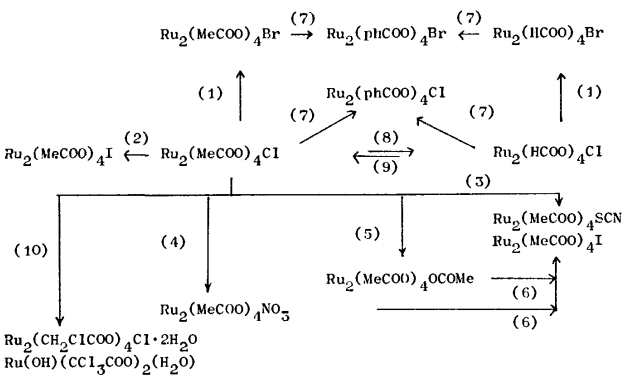

Fig. 1. Preparative conversion procedure of carboxylatoruthenium complexes.
1—3), 6): addition of the anions.
4,5): addition of the anions (after complex [1], chloroacetato complex, was passed through an anion exchanger column).
7): crystallized from a mixture solution of complex [1], $[Ru_2(MeCOO)_4Cl]$, or complex [7], $[Ru_2(HCOO)_4Cl]$, and benzoic acid.
8,9): interconversion of acetato and formato complexes.
10): crystallized from a mixture solution of complex [1], $[Ru_2(MeCOO)_4Cl]$, and monochloroacetic acid or trichloroacetic acid.

As has been described above, several monocarboxylatoruthenium complexes, $[Ru_2(RCOO)_4Cl]$ (R= Me, Et, *n*-Pr), have been reported.[1] An X-ray diffraction study of the analogous butyratoruthenium complex has indicated that the complex contains binuclear units consisting of two ruthenium atoms bridged by four *n*-butyrato groups, and that these binuclear units are linked by bridging chlorine atoms into infinite zigzag chains.[3] The complexes of the $[Ru_2(RCOO)_4X]$ type prepared in this study are thought to be analogous to those reported in Refs. 1 and 3.

Conductivities and Molecular Weight. The molar conductivities for Complexes [1], [5], [6], [7], and [11] are within 70 to 90 mho cm^{-1}, indicating that these complexes are 1:1-type electrolytes. The small conductivity for Complex [12] suggests that the complex is non-electrolyte. The chloride ion of Complex [1] in an acetic acid solution was adsorbed quantitatively by the NO_3^--form ion exchanger (Dowex 1-X4). These facts suggest that the formato and acetato complexes can dissociate into $Ru_2(RCOO)_4(solvent)^+$ and X^-, and that the cation formed is present without decomposition.

The molecular weights measured for Complexes [1], [2], [7], [11], and [12] support the formulae expected for these complexes.

Polarographic Measurement. The polarographic behavior of the $[Ru_2(OAc)_4]^+$ cation has very recently been described.[5] The acetato complex [1] gave two polarographic waves when acetic acid was used as the supporting electrolyte (Fig. 2). One of them is the oxidation wave of mercury in the presence of the chloride ion; this supports the idea that the complex

4) The authors wish to thank Mr. Tadao Ooizumi of the Rigaku Denki Co., Ltd., for this data.

5) F. A. Cotton, J. G. Norman, A. Spencer, and G. Wilkinson, *Chem. Commun.*, **1971**, 967.

Table 2. The magnetic susceptibility and effective magnetic moment per ruthenium atom of the carboxylatoruthenium complexes at various temperatures

$[Ru_2(MeCOO)_4Cl]$ M.W: 473.5; Diamagnetic correction: 135×10^{-6};								
Temp. (K)···	277.6	262.5	227.9	227.6	202.8	168.2	129.8	98.6
$10^6\chi_a$ ·····	3496.5	3666.9	4152.9	4147.0	4578.5	5440.2	6484.6	7991.3
μ_{eff} ·····	2.79	2.77	2.75	2.75	2.73	2.71	2.59	2.51
$[Ru_2(HCOO)_4Cl]$ M.W.: 417.5; Diamagnetic correction: 88×10^{-6};								
Temp. (K)···	268.6	257.6	232.8	220.1	198.1	174.3	150.5	129.0	89.0
$10^6\chi_a$ ·····	3616.7	3705.5	4016.5	4187.3	4554.4	5040.7	5583.3	6195.9	7683.2
μ_{eff} ·····	2.79	2.76	2.74	2.72	2.69	2.65	2.59	2.53	2.34
$[Ru_2(C_6H_5COO)_4Cl]$ M.W: 721.9; Diamagnetic correction: 244×10^{-6};								
Temp. (K)···	269.8	256.8	235.1	211.9	173.6	149.7	125.8	103.8
$10_6\chi_a$ ·····	3815.7	3996.9	4295.7	4669.1	5490.9	6044.6	6831.1	7714.4
μ_{eff} ·····	2.87	2.87	2.84	2.81	2.76	2.69	2.62	2.53

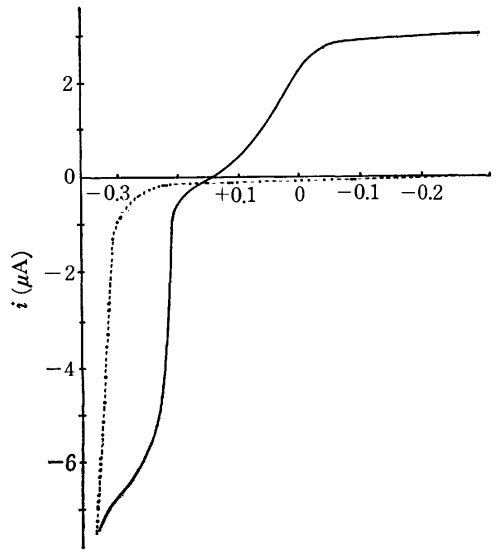

Fig. 2. D.C. polarogram of $[Ru_2(MeCOO)_4Cl]$, [1].
concentration=1 mM complex [1]. supporting electrolyte= 0.5M acetato buffer+0.5M KNO_3+0.005% gelatin.
pH=5.0, 25°C.
Dotted line indicates the curve for the supporting electrolyte only.

in an aqueous solution dissociates to give the chloride ion. The other wave ($E_{1/2}=+0.06$ V *vs* S.C.E.) results from the reduction of the complex. The nitrato-acetato complex [5] also gave the same polarographic wave as that of Complex [1] except for the oxidation wave due to the chloride ion. The reversibilities of the second step were confirmed by the measurement of the A. C. polarogram. The log-plot analysis of the reduction wave gave linear relations, with a reciprocal slope following into 63 mV. These facts indicate that the electrode reduction of the complex solutions proceeds reversibly in the usual polarographic sense; the reduction is thought to be a one-electron one on the basis of the diffusion current.

Magnetic Property and Visible Absorption Spectra. As is shown in Table 1, Complexes [1]—[10] have effective magnetic moments of 2.84—2.96 B.M. at room temperature. The values are significantly higher than the spin-only moment for a binuclear ruthenium-(II, III) complex with a single unpaired electron. The temperature variation in the experimental atomic susceptibilities and effective magnetic moments of Complexes [1]—[3] and [7]—[10] were also examined. The data for Complexes [1], [7], and [9] are given in Table 2. The reciprocal susceptibilities varied linearly with the temperature and obeyed the Curie-Weiss law with θ over the range of −30——60°K. These results are similar to those obtained by Stephenson *et al.*[1] Bennett, Caulton, and Cotton have explained the effective magnetic moments of $[Ru_2(RCOO)_4Cl]$ complexes by saying that the paramagnetism indicates three unpaired electrons per pair of metal atoms. They also suggested that the two ruthenium atoms in the complexes exist in the same nonintegral oxidation state of +2.5.[3]

Table 3. Infrared absorption bands (cm^{-1}) in carboxyl stretching frequency region of $[Ru_2(HCOO)_4Cl]$, [7], $[Ru_2(MeCOO)_4Cl]$, [1], $[Ru_2(CH_2ClCOO)_4Cl]$, [11],[a] and $[Ru(OH)(CCl_3COO)_2(H_2O)]$,[12]. (KBr disk).

Complex [1]	Complex [11][a]	Complex [7]	Complex [12]	Tentative assignments
1643 w	1618 m	1580 vw	1670 sh	ν_{antt}COO (?)
		1498 sh	1608 s	ν_{antt}COO
		1480 s	1598 sp	
1470 sh	1488 sh			
1444 s	1427 s			ν_{antt}COO and
1420 sh	1397 sh			ν_{sym}COO
1402 sp	1350 sh			
		1336 vs	1380 s	ν_{sym}COO

a) dehydrated complex.

The monochloroacetato complex [11], $[Ru_2(CH_2ClCOO)_4Cl]\cdot 2H_2O$, shows a magnetic moment close to that of the acetato complex, suggesting a similar dimeric structure. On the other hand, the magnetic moment of the trichloroacetato complex [12], $[Ru(OH)(CCl_3COO)_2(H_2O)]$, is reasonable compared with the values reported for Ru(III) complexes.[6]

The visible absorption spectra of the complexes of the $[Ru_2(RCOO)_4X]$ type in a methanolic solution were almost the same. Such data for analogous complexes have also been reported.[1] The band has been assigned to the $b_{2g}-a_{1g}$ and/or $b_{2g}-a_{2u}$ transitions using a molecular orbital diagram for an M_2X_8 species.[3] The absorption spectra of the trichloroacetato complex [12], $[Ru(OH)(CCl_3COO)_2(H_2O)]$, was quite different from those of other monocarboxylato complexes, indicating that Complex [12] is different from the other monocarboxylato complexes.

Infrared Spectra. The infrared spectra of the complexes were measured over the range of 4000—200 cm^{-1}. The general features of the spectra of the chloro-monocarboxylato complexes were very similar to those of the corresponding bromo- and iodo-monocarboxylato complexes. No absorption bands due to OH and H_2O groups were found in Complexes [1]—[10]. The infrared absorption bands in the carboxyl stretching frequency region are shown in Table 3, along with their tentative assignments.

The chloro-formato complex [7] displays two strong absorption bands at 1480 and 1336 cm^{-1} in the carboxyl-stretching frequency region. These bands can be assigned to the antisymmetric and the symmetric COO-stretching vibrations respectively. The separation ($\Delta=144$ cm^{-1}) between the two absorption bands may indicate the symmetrical coordination of the carboxyl groups.[7]

The chloro-acetato complex [1], however, shows a strong band with several shoulders near 1444 cm^{-1} in this region; the band is very different in shape from that in the chloro-formato complex. This carboxyl band has been explained by assuming an overlapping of the antisymmetric and symmetric COO-stretching vibrations of a bridged carboxyl group.[1] Since the antisymmetric COO-stretching frequency is known to be sensitive to the electronic environment of a carboxylato ion,[8] the observed different features in the carboxyl region between the formato and the acetato complexes are probably due to the difference in the character of the coordinating carboxyl bands.

The monochloroacetato complex [11], $[Ru_2(CH_2ClCOO)_4Cl]\cdot 2H_2O$, showed a carboxyl band similar to that of the acetato complex. On the other hand, the trichloroacetato complex [12], $[Ru(OH)(CCl_3COO)_2(H_2O)]$, exhibited two characteristic peaks in this region. These bands are thought to be due to the antisymmetric and symmetric stretching vibrations of the bidentate carboxyl groups respectively. The separation between the two absorption bands for the trichloroacetato complex [12], $[Ru(OH)(CCl_3COO)_2(H_2O)]$, is appreciably larger than those of known binuclear acetato metal complexes.[9] The increase in the separation may reflect the considerable influence of the halogens on the carboxyl vibrations of trichloroacetato groups.[10]

It is possible to distinguish the complex type between $[Ru_2(MeCOO)_4X]$ and $[Ru_2(MeCOO)_4]X$ on the basis of the infrared spectra of the nitrato-caetato complex [5]. Complex [5] shows N–O stretching bands of the nitrato group at 1388, 1288, and 809 cm^{-1}. The observation of three absorption bands indicates that the nitrato group in Complex [5] is present as a coordinate ligand, according to the Gatehouse *et al.* interpretation.[11]

With respect to the properties observed, a series of complexes of the $[Ru_2(RCOO)_4X]$ type were very similar. No remarkable substitution effect of R groups or X groups was observed. This might be understood on the basis of the structure for the butyrato complex.[3]

The trichloroacetato complex [12], $[Ru(OH)(CCl_3COO)_2(H_2O)]$, was thought to be monomeric. Since the ruthenium(III) complexes prefer a six-coordinated structure, the octahedral arrangement appears probable.

The authors wish to express their appreciation to Professor Gen P. Sato and Mr. Kunio Shimizu of Sophia University for their helpful discussions and for the measurement of the polarogram, and to Dr. Eiichi Miki of St. Paul's (Rikkyo) University for the measurement of the IR spectra. Thanks are also due to Mr. Norihiko Iida, Mr. Tsuguo Takaku, Mr. Kenji Ogisu, Mr. Masahiko Hayashi, Mr. Hiroshi Ogata, and Mr. Yujiro Saito for their technical assistance.

6) B. N. Figgis and J. Lewis, "Modern Coordination Chemistry," ed. by J. Lewis, R. G. Wilkins, Interscience Publ., New York (1960), p. 448.

7) N. F. Curtis, *J. Chem. Soc., A*, **1968**, 1579.

8) R. E. Kagarise, *J. Phys. Chem.*, **59**, 271 (1955); K. Kuroda and M. Kubo, *ibid.*, **64**, 759 (1960).

9) K. Nakamoto, Y. Morimoto, and A. E. Martell, *J. Amer. Chem. Soc.*, **83**, 4528 (1961).

10) C. A. Agambar and K. G. Orrell, *J. Chem. Soc., A*, **1969**, 897.

11) B. M. Gatehouse, S. E. Livingston, and R. S. Nyholm, *J. Chem. Soc.*, **1957**, 4222.

Cobalt(I) Tetraphenylporphin

Hiroshi KOBAYASHI, Tetsuo HARA, and Youkoh KAIZU

Department of Chemistry, Tokyo Institute of Technology, Ookayama, Meguro-ku, Tokyo

(Received October 14, 1971)

Cobalt(I) tetraphenylporphin was prepared by reduction of tetraphenylporphinatocobalt(II) with sodium benzophenone ketyl in tetrahydrofuran (THF) and was purely isolated. The compound was identified as Na-[Co(I)TPP]·5THF (tetraphenylporphin is abbreviated to TPP). On the basis of electronic absorption spectrum, magnetic circular dichroism, magnetic susceptibility and NMR spectrum, the complex formed was concluded to be a complex of cobalt(I). Although some part of cobalt electron is migrated into the conjugated system of porphin, an electron furnished by the reducing reagent is mainly trapped by the central cobalt. The compound should be named sodium tetraphenylporphinatocobaltate(I).

When a metalloporphyrin is reduced, an electron given by the reducing reagent is trapped by either porphyrin π^* orbital or metal d orbital depending upon the electronic structure of the central metal. Metalloporphyrins with vacancies in $d\pi$ orbitals can capture electrons into the central metal ion, whereas metalloporphyrins with a d^8, d^9, or d^{10} dipositive metal cation accept electrons into the porphyrin conjugated system. By one-electron reduction, tetraphenylporphinatozinc(II), for example, traps an electron in the porphyrin conjugated system.[1] Thus it shows an electronic absorption spectrum of the mononegative ion of tetraphenylporphin and also an ESR signal with a g-value of almost free-spin.

If the lowest antibonding π molecular orbital of the coordinating conjugated systems is lower than the ligand field antibonding orbitals, z^2 and x^2-y^2, an electron from the reducing reagents will be trapped in the conjugated system. This gives rise to a mononegative ion of the coordinating ligand. The present authors have isolated a complex coordinated by bipyridine negative ion, $[Cr(0)(CO)_4(bipy^-)]^-$ (bipy denotes bipyridine), which was prepared by reduction of $[Cr(0)(CO)_4bipy]$.[2] Similarly $[Fe(bipy)_3]$ was a complex coordinated by bipyridine negative ions.[3] On the contrary, however, the isoelectronic $[Co(bipy)_3]^+$ was not a complex of bipyridine negative ions but a complex of Co(I) in the triplet ground state.[4] In this particular case, the lowest vacant π molecular orbital of the coordinating bipyridine must be higher than the ligand field antibonding orbitals. This arises from a rather high electron affinity of Co(II) ion. Co(I) in an octahedral ligand field should be in a triplet state with electronic configuration of $(d\pi)^6(z^2)(x^2-y^2)$, while in a planar environment it should be either in a singlet state of $(d\pi)^6(z^2)^2$ or in a triplet state of $(d\pi)^6(z^2)(x^2-y^2)$ depending upon an energy gap of z^2 and x^2-y^2 orbitals. Since z^2 and x^2-y^2 orbitals are the antibonding orbitals of the coordination binding, an electron occupation in these orbitals results in a dissociation of the coordination binding unless an electrostatic attraction between the metal ion and the ligands is present as in $[Co(bipy)_3]^+$. Although $[Co(bipy)_3]^+$ shows a trend to form $[Co(bipy)_2]^+$, it keeps two electrons with parallel spin in z^2 and x^2-y^2 orbitals, which are predominantly localized on the central metal, rather than in the lowest antibonding π molecular orbital of bipyridine. A planar cobalt(II) complex, tetraphenylporphinatocobalt(II), for example, traps an electron furnished upon reduction into a molecular orbital predominantly localized on cobalt ion. Since a gap of z^2 and x^2-y^2 orbitals in a strong planar ligand field of metalloporphyrin is appreciably large, the ground configuration of cobalt(I) at almost center of the planar ligand field turns out to be diamagnetic $(d\pi)^6(z^2)^2$. The formations of other planar diamagnetic cobalt(I) species have been established.[5]

Whitlock and Bower[6] first presumed the reduction product of tetraphenylporphinatocobalt(II) as the spin-paired cobalt(I) porphin on the basis of gram-equivalents of sodium amalgam to complete the reduction, NMR spectrum and Gouy balance experiments of the reduced species in tetrahydrofuran, and activity of catalyzing the sodium borohydride reduction of nitrobenzene.[7,8] Recently we succeeded in isolation of the cobalt(I) tetraphenylporphin. In this paper, we will present an identification of the porphin on the basis of electronic absorption spectrum, magnetic circular dichroism, magnetic susceptibility and NMR spectrum.

Experimental

Materials. $\alpha, \beta, \gamma, \delta$-Tetraphenylporphin (abbreviated to TPP) was synthesized from pyrrole and benzaldehyde by the method of Adler, *et al.*[9] Chromatographic purification was repeated on activated alumina columns using chloroform

1) G. L. Closs and L. E. Closs, *J. Amer. Chem. Soc.*, **85**, 818 (1963).

2) Y. Kaizu and H. Kobayashi, This Bulletin, **43**, 2492 (1970).

3) Y. Kaizu, T. Yazaki, Y. Torii, and H. Kobayashi, *ibid.*, **43**, 2068 (1970).

4) Y. Kaizu, Y. Torii, and H. Kobayashi, *ibid.*, **43**, 3296 (1970).

5) a) O. Müller and G. Müller, *Biochem. Z.*, **336**, 299 (1962); S. L. Tackett, J. W. Collatt, and J. C. Abott, *Biochemistry*, **2**, 919 (1963); P. K. Das, H. A. O. Hill, J. M. Pratt, and R. J. P. Williams, *Biochim. Biophys. Acta*, **141**, 644 (1967). b) R. Taube, M. Zach, K. A. Stauske, and S. Heidrich, *Z. Chem.*, **3**, 392 (1963); D. H. Bush, J. H. Weber, D. H. Williams, and N. J. Rose, *J. Amer. Chem. Soc.*, **86**, 5161 (1964); P. Day, H. A. O. Hill, and M. G. Price, *J. Chem. Soc., A*, **1968**, 90; L. D. Rollman and R. T. Iwamoto, *J. Amer. Chem. Soc.*, **90**, 1455 (1968). c) G. N. Schrauzer and J. Kohnle, *Chem. Ber.*, **97**, 3056 (1964); G. N. Schrauzer and E. Deutsch, *J. Amer. Chem. Soc.*, **91**, 3341 (1969).

6) H. W. Whitlock, Jr. and B. K. Bower, *Tetrahedron Lett.*, **1965**, 4827.

7) A. A. Vlček and A. Rusina, *Proc. Chem. Soc.*, **1961**, 161.

8) R. D. Gillard and G. Wilkinson, *J. Chem. Soc.*, **1963**, 3594.

9) A. D. Adler, F. R. Longo, J. D. Finarelli, J. Goldmacher, J. Assour, and L. Korsakoff, *J. Org. Chem.*, **32**, 476 (1967).

as solvent and also eluent. Cobalt(II) complex, TPPCo(II), was prepared from the metal-free base and cobalt(II) acetate by the method of Rothemund and Menotti.[10] The complex was purified by sublimation at 250—300°C under reduced pressure. Lustrous violet crystals thus obtained was identified by elemental analysis.

Found: C, 78.8; H, 3.9; N, 8.4; Co, 8.6%. Calcd for $C_{44}H_{28}N_4Co$: C, 78.7; H, 4.2; N, 8.3; Co, 8.8%.

Cobalt(III) complex, TPPCo(III)Cl·Py·C_2H_5OH, where Py denotes pyridine, was prepared from TPPCo(II) in benzene being refluxed with a mixture of pyridine, ethanol, and hydrochloric acid by the method of Yamamoto and Tonomura.[11]

Found: C, 73.4; H, 4.3; N, 8.6%. Calcd for $C_{51}H_{39}N_5$-CoCl: C, 73.6; H, 4.7; N, 8.4%.

All other reagents and solvents were commercially available. Tetrahydrofuran (THF) used for solvent was purified by careful distillation over cuprous chloride and a trace of water was removed by adding $LiAlH_4$.

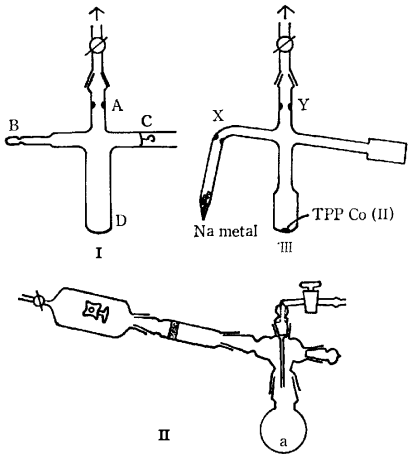

Fig. 1. Apparatus for reduction.
Benzophenone ketyl was prepared in I. The reduction of TPPCo (II) with benzophenone ketyl was carried out in II. The vessel III was used to measure absorption spectrum during the reduction process of TPPCo(II) with sodium metal in THF.

Preparation of Co(I) Complexes. Benzophenone (0.2 g) and sodium metal (0.2 g) were placed in D of the apparatus I shown in Fig. 1. The apparatus was connected to a vacuum system. After deaerated dry THF (20 m*l*) was transferred into D by distillation, the apparatus was sealed off at A and shaken for 2 hr. Thus sodium benzophenone ketyl was obtained with deep reddish violet color. TPPCo(II) (0.35 g) was placed at a under dry nitrogen in the apparatus II shown in Fig. 1. Being connected with a dry nitrogen atmosphere, the break-seal C of the apparatus I was broken, and then the tube B was cut at the top. In the nitrogen atmosphere sodium benzophenone ketyl was transferred from B onto TPPCo(II) in the apparatus II. After the mixture was stirred for 3 hr, solvent THF was removed by vacuum distillation into a trap cooled in liquid nitrogen. Then the residue was added with a mixture of deaerated dry ether (10 m*l*) and petroleum ether (10 m*l*) and then filtered. The product was dried *in vacuo*.

Found: Co, 5.4%. Calcd for $C_{64}H_{68}N_4O_5CoNa$ (Na[TPP-Co]·5THF): Co, 5.6%.

Reduction of TPPCo(II) with sodium metal in THF was also followed using the apparatus III shown in Fig. 1. After the apparatus was evacuated being connected with a vacuum system, sodium mirror was formed on the wall of the branch X and then the branch was sealed off at X. Deaerated dry THF was transferred by distillation into the container of TPPCo(II) and the apparatus was sealed off at Y. The solution was shaken being contacted with the mirror. The absorption spectrum of the solution was recorded after a period of the shaking.

Electronic Absorption Spectra and Magnetic Circular Dichroism. Measurements of the electronic absorption spectra of the air-sensitive compounds were described in a previous paper.[12] Spectra were taken on a Shimadzu automatic recording spectrophotometer Model MPS-50. Circular dichroism under an external magnetic field of 10,000 gauss was measured by a JASCO automatic recording spectropolarimeter Model ORD/UV-5 with CD attachment.[13]

Magnetic Susceptibility. Magnetic susceptibility of the complexes was measured by means of Gouy method. The measurements were carried out at room temperature. After it was calibrated for the diamagnetic term by the usual method,[14] magnetic moment of the complex was calculated.

Nuclear Magnetic Resonance. NMR spectra were recorded at room temperature on a 100 MHz Japan Electron Optics Laboratory spectrometer Model JNM 4H-100. Solvents were THF and pyridine. In the case of Co(III) complex, THF and $CDCl_3$ were used as solvent. Tetramethylsilane was used as an external reference.

Results and Discussion

Spectral change during the reduction process of TPPCo(II) with sodium metal in THF is shown in Fig. 2. The change takes place stepwise. During the first step of the reduction, remarkable isosbestic points are observed at 18.7, 19.2, 23.4, and 25.7 kK. Further reduction proceeds rather successively, therefore isosbestic points are shifted during the reaction. The complex, which has been isolated successfully in the present study, is first step product of the reduction. Absorption spectrum of the isolated complex (Fig. 3) is in good agreement with the one observed in the first step of the reduction shown in Fig. 2. The absorption maxima also coincide with those given by Whitlock and Bower.[6]

The reduced complex is extremely soluble in THF and pyridine. The spectra of the complex in benzene, THF and pyridine are actually the same in shape (Fig. 3). However the results indicate that there occurs no such axial coordination as to give a drastic change in the electronic structure, since the axial coordination by pyridine or THF may give rise to a change in the ligand field electronic structure as has been observed in Fe(II)tetraphenylporphin.[15]

10) P. Rothemund and A. R. Menotti, *J. Amer. Chem. Soc.*, **70**, 1808 (1948).

11) K. Yamamoto and S. Tonomura, *Sci. Papers Inst. Phys. Chem. Res.*, **58**, 122 (1964).

12) Y. Torii, T. Yazaki, Y. Kaizu, S. Murasato, and H. Kobayashi, This Bulletin, **42**, 2264 (1969).

13) H. Kobayashi, M. Shimizu, and I. Fujita, *ibid.*, **43**, 2335 (1970).

14) See for example, B. N. Figgis, and J. Lewis, "Modern Coordination Chemistry" ed. by J. Lewis and R. G. Wilkins, Interscience Publishers, New York, (1960), p. 415.

15) H. Kobayashi and Y. Yanagawa, This Bulletin, **45**, 450 (1972).

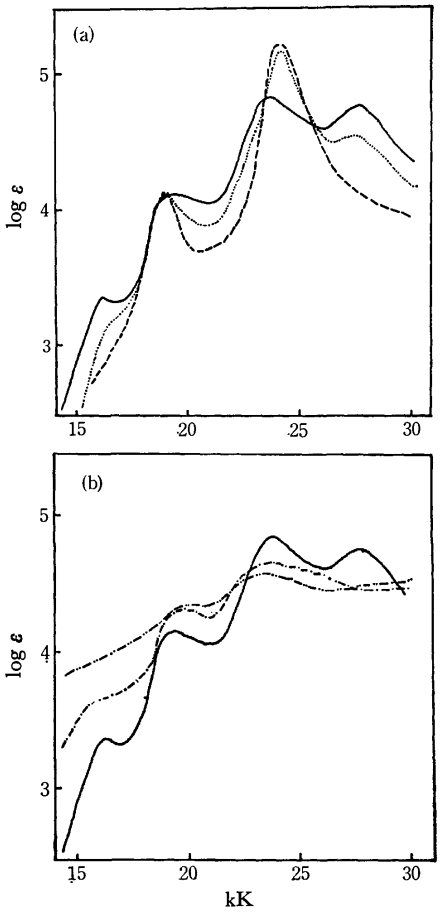

Fig. 2. Spectral change of the reduction process of TPPCo(II) with sodium metal in THF.
(a) The first step of the reduction.
-·-·-: TPPCo(II); ·····: after 1/2 hr;
——: after 1 hr
(b) Further step of the reduction.
——: after 2 hr; -·-·-: after 3 hr:
-·-·-·-: after 5 hr

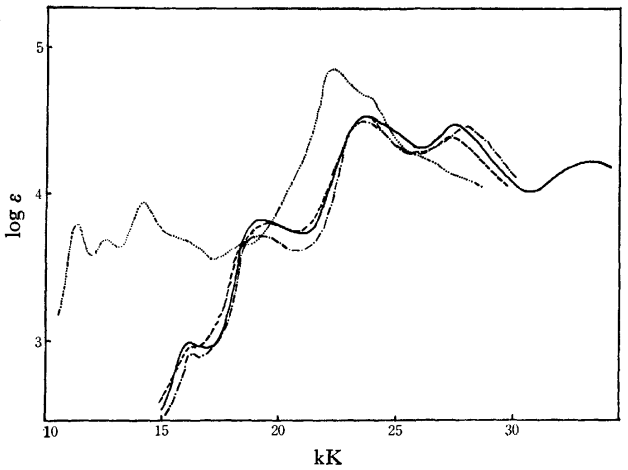

Fig. 3. Absorption spectra of Na[Co(I)TPP]·5THF.
-·-·-: in benzene
——: in THF ·····: Na[ZnTPP⁻] in THF[1,16,17]
-·-·-·-: in pyridine

The reduced complex in solution is very sensitive to oxygen and moisture and opening the solution to air leads to the immediate oxidation to TPPCo(II) and/or

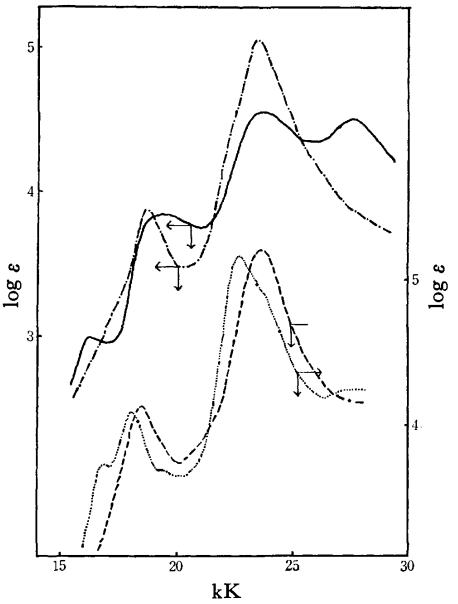

Fig. 4. Spectral change upon air-oxidation of Na[Co(I)TPP]–5THF in THF.
——: Na[Co(I)TPP]·5THF
-·-·-: after it was exposed to air
-·-·-·-: TPPCo(II) in THF
·····: TPPCo(III)Cl·Py·C_2H_5OH in THF
(Arrows indicate scales for the respective curves.)

TPPCo(III)X (Fig. 4). As is seen in Fig. 3, the absorption spectrum of reduced complex lacks the near-infrared bands at 11.3, 12.5, and 14.2 kK characteristic of the mononegative ion of tetraphenylporphin, which have been observed with a mononegative ion complex coordinated to Zn(II),[1,16,17] and therefore an electron furnished by the reducing reagent is much likely to localize on the central metal ion.

The first step product of the reduction was isolated in the solid state. The complex was identified by elemental analysis as Na[Co(I)TPP]·5THF. The crystal-containing THF was detected by NMR as described later. Measurements of the magnetic susceptibility reveal that the isolated first step product is diamagnetic in the solid state. Cobalt(II) ion in TPPCo(II) has an unpaired electron in the configuration $(d\pi)^6(z^2)$, whereas the observed value of the magnetic moment is larger than that expected for $S=1/2$ because of a mixing of the excited states by spin-orbit coupling perturbation.[18] Since there is no appreciable overlap between z^2 orbital and the lowest vacant π orbitals of porphin and thus there is no strong interaction between them, the ground state of the reduced complex must be triplet, $(d\pi)^6(z^2)(\pi^*)$, when an electron is trapped in one of the lowest vacant π orbitals of porphin, π^*. The observed diamagnetism of the complex prepared by one-electron reduction of TPPCo(II) should be interpreted in terms of the configuration $(d\pi)^6(z^2)^2$, where the central cobalt is

16) J. W. Dodd and N. S. Hush, *J. Chem. Soc.*, **1964**, 4607.
17) H. Kobayashi, Y. Kato, and Y. Kaizu, unpublished.
18) J. S. Griffith, "The Theory of Transition-Metal Ions" Cambridge Univ. Press, (1961), p. 370.

trapping an electron given by the reducing reagent. Whitlock and Bower have observed a diamagnetic behavior of the reduced complex present in THF solution.[6] However the fact that NMR spectrum of the complex in THF could be measured is regarded for first-order approximation as an evidence of diamagnetism of the complex in THF. As a matter of fact, opening the solution to air leads to immediate disappearance of the porphin signal and broadening of the solvent peaks.

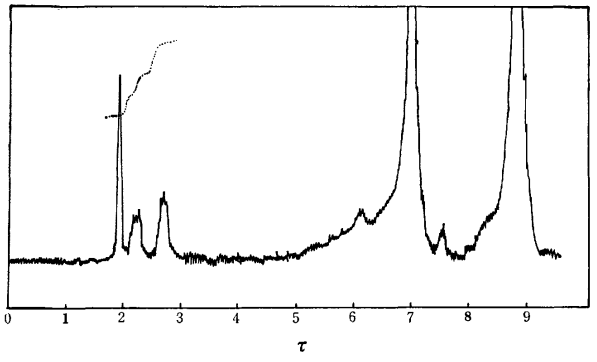

Fig. 5. NMR spectrum of Na[Co(I)TPP]·5THF in THF.

Table 1.

	a(τ)	b(τ)	c(τ)	Solvent	
TPP	1.05	1.70	2.20	$CDCl_3$	19)
TPPMg·2Py	1.05	1.70	2.20	$CDCl_3$	19)
TPPCo(III)Cl	1.03	1.98	2.35	$CDCl_3$	This work
	1.03	1.98	2.35	THF	This work
Na[Co(I)TPP]·5THF	1.95	2.10	2.55	THF	This work

TPP: tetraphenylporphin
Py: pyridine
THF: tetrahydrofuran

NMR spectrum of the complex was measured in THF and pyridine. In THF, a singlet was observed at 1.95 τ, a multiplet, at 2.10 τ and another multiplet, at 2.55 τ (Fig. 5). The singlet at 1.95 τ (band a in Table 1) is assigned to pyrrole ring protons. The multiplet at 2.10 τ (band b) is assigned to *o*-protons of phenyl groups and the one at 2.55 τ (band c), to *m*- and *p*-protons. The chemical shift values are summarized in Table 1. As is seen in the case of TPP-Co(III)Cl, the chemical shift of pyrrole protons are not influenced with the central metal ion which is less $d\pi$-donating and solvent effect of the NMR spectrum is not so appreciable. However NMR signal of the pyrrole ring protons in $[Co(I)TPP]^-$ is shifted toward higher field. This high-field shift is attributed to an increase of electron density at the pyrrole ring protons which arises from a back-donation of $d\pi$ electron to the lowest vacant π molecular orbitals of porphin.

NMR spectrum of a pyridine solution of the isolated solid sample is shown in Fig. 6. Multiplets were observed at 6.25 τ and 8.15 τ. These multiplets are very close to the ones observed with free THF. THF included in Na[Co(I)TPP]·5THF is set free in pyridine

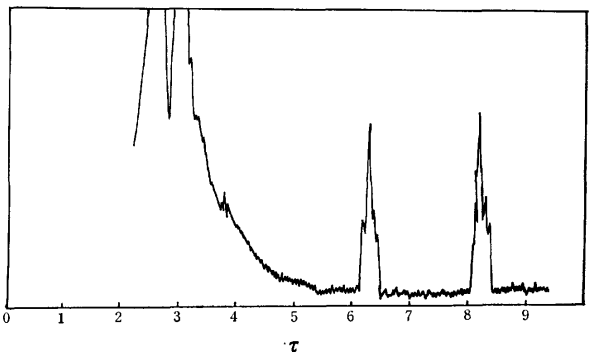

Fig. 6. NMR spectrum of Na[Co(I)TPP]·5THF in pyridine.

solution. The THF molecules are much likely to coordinate toward sodium ion in the crystal. Further studies are required concerning with the location of sodium ion in pyridine solution of the complex. However the THF molecules in the solution are present in considerably distant locations from the porphin moiety, since the THF multiplets are free from the ring current of porphin. This type of the crystal-containing THF has been found in various similar reduced metal phthalocyanines.[20]

Molecular orbital calculations on porphin yield two top filled orbitals a_{2u} and a_{1u}, and the lowest degenerate empty orbital pair e_g.[21-24] Thus the lowest excited states arise from the electronic configurations $(a_{2u})^2a_{1u}e_g$ and $(a_{1u})^2a_{2u}e_g$, whereas the ground state is $(a_{2u})^2(a_{1u})^2$. A circular box is described by a radial coordinate r and an angular coordinate θ. Orbitals are written $|\pm k)=f(r)\exp(\pm ik\theta)$, where k denotes orbital angular momentum.[25] Gouterman has pointed out that the top filled orbitals are accidentally degenerate and the orbital pair $(a_{2u}\pm ia_{1u})/\sqrt{2}$ can be identified with the degenerate pair of circular box orbitals $|\pm 4)=f(r)\exp(\pm 4i\theta)$, while the lowest empty e_g orbitals, $|\pm 5)=f(r)\exp(\pm 5i\theta)$.[26,26a]

In the ground state, the orbital pair which has z components of angular momentum $\lambda_z=\pm 4$ and angular momentum $\lambda=4$ are filled with four electrons; the configuration is denoted $(4)^4$ and has zero angular momentum $\lambda_z=0$. The first excited configurations arise by exciting a $\lambda=4$ electron to an orbital with $\lambda=5$, and are denoted $(4)^35$. This configuration gives rise to degenerate pairs of states with $\Lambda_z=\pm 1$ and with $\Lambda_z=\pm 9$. A selection rule allows a pair of transitions $\Delta\Lambda_z=\pm 1$. The allowed transition pair, $\Delta\Lambda_z=\pm 1$, is assigned to the intense Soret band of porphin

19) C. B. Storm and A. H. Corwin, *J. Org. Chem.*, **29**, 3700 (1964).

20) R. Taube, *Z. Chem.*, **6**, 8 (1966); S. Herzog and M. Schmidt, *ibid.*, **3**, 392 (1963).

21) H. C. Longuet-Higgins, C. W. Rector, and J. R. Platt, *J. Chem. Phys.*, **18**, 1174 (1950); G. R. Seely, *ibid.*, **27**, 125 (1957); H. Kobayashi, *Nippon Kagaku Zasshi*, **81**, 519 (1960).

22) H. Kobayashi, *J. Chem. Phys.*, **30**, 1373 (1959).

23) C. Weiss, H. Kobayashi, and M. Gouterman, *J. Mol. Spectrosc.*, **16**, 415 (1965).

24) M. Zerner and M. Gouterman, *Theoret. Chim. Acta*, **4**, 44 (1966).

25) $|a)$ denotes the molecular orbital a, whereas $|k^\circ>$, Slater determinantal wave function of the configuration k°. The state $|j>$ is described as a linear combination of $|k^\circ>$'s.

26) M. Gouterman, *J. Chem. Phys.*, **33**, 1523 (1960).

26a) M. Gouterman, *ibid.*, **30**, 1139 (1959).

in the near-ultraviolet denoted B band, whereas the forbidden pair, $\Delta A_z = \pm 9$, the vibronically-allowed weak visible band denoted Q band.

The measurements of magnetic circular dichroism (MCD) will give an evidence of the orbital angular momentum in the excited state.[27] As a matter of fact, an A-type dispersion of MCD observed at each of the Q and B bands of TPPZn(II) reveals an orbital angular momentum arising in the respective excited state.[13] The lowest excited states of TPPCo(II) and TPPCo(III)X can be described by pure (π, π^*) excitations. As are shown in Figs. 7 and 8, MCD spectra of these complexes preserve such a characteristics as observed with TPPZn(II).

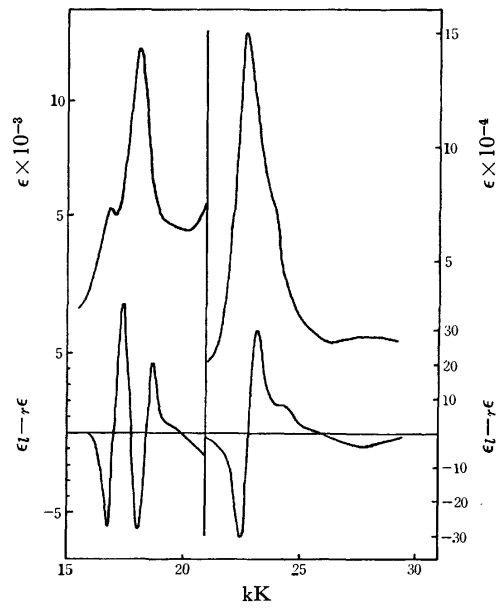

Fig. 7. Absorption spectrum and magnetic circular dichroism of TPPCo(III)Cl·Py·C_2H_5OH in THF.

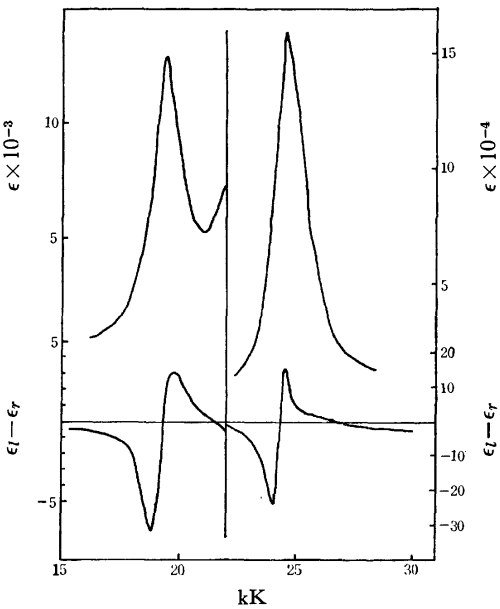

Fig. 8. Absorption spectrum and magnetic circular dichroism of TPPCo(II) in THF.

27) P. J. Stephens, W. Suëtaka, and P. N. Schatz, *J. Chem. Phys.*, **44**, 4592 (1966).

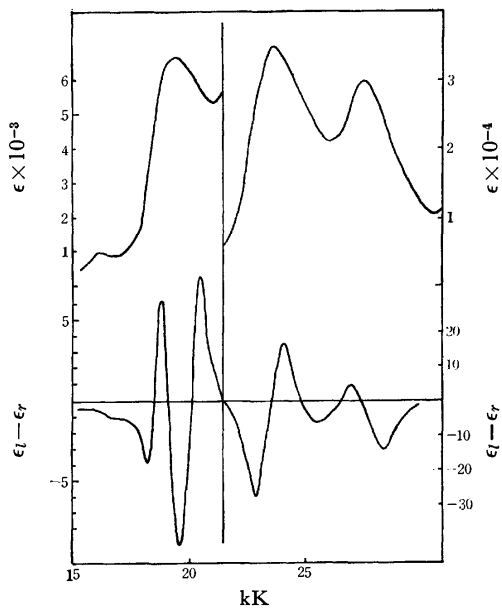

Fig. 9. Absorption spectrum and magnetic circular dichroism of Na[Co(I)TPP]·5THF in THF.

In the case of $[TPPCo(I)]^-$, back-donation of the cobalt $d\pi$ electron toward the porphin conjugated system should be appreciable in the ground state and the excited states, since an electron furnished by the reducing reagent is trapped in the cobalt z^2 orbital. Therefore the lowest excited states of $[TPPCo(I)]^-$ should be described in terms of a configuration-interaction admixture of the porphin (π, π^*) excitations and the "metal to porphin" charge-transfer excitations. Even so, as shown in Fig. 9, MCD spectrum of $[TPPCo(I)]^-$ still preserves a characteristics of the porphin Q and B bands and gives rise to A-type dispersions at 18.5, 20.0, and 23.5 kK corresponding to 0-0 and 0-1 components of Q band and B band, respectively, which are typically shown with TPPCo(III) and TPPCo(II) in Figs. 7 and 8. Two other bands were observed at 17.0 and 27.5 kK. No remarkable A-type MCD could be observed at the 17.0 kK weak band under a magnetic field of 10000 gauss. On the other hand, however, a reverse A-type dispersion was observed at 27.5 kK.

The molecular orbitals of $[TPPCo(I)]^-$ responsible to

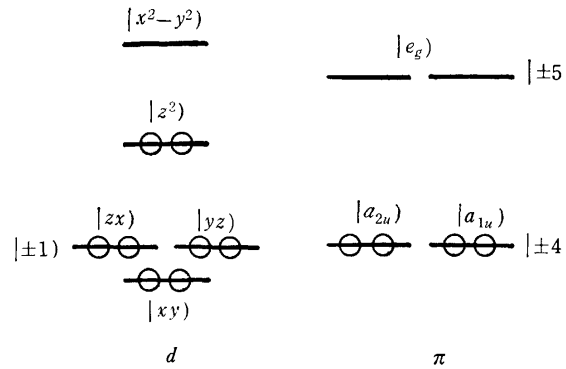

Fig. 10. The highest occupied and the lowest vacant molecular orbitals of $[TPPCo(I)]^-$.

the outer electronic configuration are schematically shown in Fig. 10. A degenerate $d\pi$ orbital pair, zx and yz, makes charge-transfer interactions with the porphin π molecular orbitals of e_g symmetry. The degenerate $d\pi$ orbital pair can be rewritten by $|\pm1)=(zx\pm iyz)/\sqrt{2}$, where ±1 denote z components of angular momentum $\lambda=1$. A one-electron term connecting the orbitals $|\pm1)$ and $|\pm5)$, $(\pm1|\hat{h}^{\text{eff}}|\pm5)\equiv\beta$, gives rise to a delocalization of the cobalt $d\pi$ electrons toward the lowest vacant porphin π orbital.

The electrons in the orbitals with $\lambda=1$, $\lambda=4$, or $\lambda=5$ (*i.e.*, the top eight electrons) are assumed to move in a one-electron effective potential set up by the nuclei and the remaining electrons. These electrons are assumed to interact with one another by two-electron term e^2/r_{ij}. There is no interaction between states with different Λ_z except the states which are connected with $(\pm1|\hat{h}^{\text{eff}}|\pm5)$. Wave functions are taken as Slater determinants which are eigenfunctions of total spin singlet.

E^0 is defined as the ground state energy, except for the electron interaction of the top eight electrons. I_1, I_4, and I_5 denote one-electron core energy of the orbitals with $\lambda=1$, $\lambda=4$, and $\lambda=5$. The Coulomb and exchange integrals over molecular orbitals are defined as

$$J_{ab}=e^2\int\frac{\phi_a^*(1)\phi_b^*(2)\phi_a(1)\phi_b(2)}{r_{12}}d\tau_1d\tau_2$$

$$K_{ab}=e^2\int\frac{\phi_a^*(1)\phi_b^*(2)\phi_b(1)\phi_a(2)}{r_{12}}d\tau_1d\tau_2$$

where 1 and 2 refer to the position of electrons 1 and 2, ϕ_a and ϕ_b, two molecular orbitals, and the star, complex conjugate. The numbers a and b refer of the λ_z value of the orbitals.

Table 2 shows the singlet states arising from the configurations $(1)^4(4)^4$, $(1)^3(4)^4(5)$, $(1)^4(4)^3(5)$, and $(1)^3(4)^3(5)^2$. Two singlets appear from a configuration of four electrons in four different orbitals. Slater determinants were then taken as follows:

$$|+5a\rangle\equiv[|1\bar{1}4\bar{4}-1-45-\bar{5}|-|1\bar{1}4\bar{4}-1-\bar{4}\bar{5}-5|+|1\bar{1}4\bar{4}-\bar{1}-\bar{4}5-5|-|1\bar{1}4\bar{4}-\bar{1}-45-\bar{5}|]/2,$$

TABLE 2. EXCITED SINGLET STATES AND ENERGIES OF THE COBALT(I) PORPHIN (CIRCULAR BOX MODEL)

Configuration	Orbitals occupied	Λ_z	Wave function	Diagonal energy	Approximate diagonal energy cm^{-1}	
$(1)^4(4)^4$	$(1)^2(-1)^2(4)^2(-4)^2$	0	$\|0°\rangle$	W_0	0	0
$(1)^3(4)^4(5)$	$(1)(-1)^2(4)^2(-4)^2(5)$ $(1)^2(-1)(4)^2(-4)^2(-5)$	± 4	$\|\pm 4°\rangle$	W_2+2K_{15}	Δ_{CT}	4000
	$(1)^2(-1)(4)^2(-4)^2(5)$ $(1)(-1)^2(4)^2(-4)^2(-5)$	± 6	$\|\pm 6°\rangle$	W_2+2K_{1-5}	Δ_{CT}	4000
$(1)^4(4)^3(5)$	$(1)^2(-1)^2(4)^2(-4)(5)$ $(1)^2(-1)^2(4)(-4)^2(-5)$	± 9	$\|\pm 9°\rangle$	W_1+2K_{4-5}	$\Delta+2K$	15900
$(1)^3(4)^3(5)^2$	$(1)^2(-1)(4)^2(-4)(5)^2$ $(1)(-1)^2(4)(-4)^2(-5)^2$	±15	$\|\pm 15°\rangle$	$W_1+W_2-W_0+(J_{55}-J_{45})+(J_{14}-J_{15})+K_{14}+K_{1-5}+K_{4-5}$	$\Delta+\Delta_{CT}+K$	19100
	$(1)(-1)^2(4)^2(-4)(5)^2$ $(1)^2(-1)(4)(-4)^2(-5)^2$	±13	$\|\pm 13°\rangle$	$W_1+W_2-W_0+(J_{55}-J_{45})+(J_{14}-J_{15})+K_{1-4}+K_{15}+K_{4-5}$	$\Delta+\Delta_{CT}+K$	19100
	$(1)^2(-1)(4)^2(-4)(5)(-5)$ $(1)(-1)^2(4)(-4)^2(5)(-5)$	± 5	$\|\pm 5a°\rangle$	$W_1+W_2-W_0+(J_{55}-J_{45})+(J_{14}-J_{15})+1/2(-K_{14}+K_{15}+4K_{1-5}+4K_{45}+K_{4-5}-K_{5-5})$	$\Delta+\Delta_{CT}+2K_1$	27700
			$\|\pm 5b°\rangle$	$W_1+W_2-W_0+(J_{55}-J_{45})+(J_{14}-J_{15})+1/2(K_{14}+3K_{15}+3K_{4-5}+K_{5-5})$	$\Delta+\Delta_{CT}+2K$	20900
$(1)^4(4)^3(5)$	$(1)^2(-1)^2(4)(-4)^2(5)$ $(1)^2(-1)^2(4)^2(-4)(-5)$	± 1	$\|\pm 1°\rangle$	W_1+2K_{45}	$\Delta+2K_1$	23700
$(1)^3(4)^3(5)^2$	$(1)^2(-1)(4)(-4)^2(5)^2$ $(1)(-1)^2(4)^2(-4)(5)^2$	± 7	$\|\pm 7°\rangle$	$W_1+W_2-W_0+(J_{55}-J_{45})+(J_{14}-J_{15})+K_{1-4}+K_{1-5}+K_{45}$	$\Delta+\Delta_{CT}+K_1$	22500
	$(1)(-1)^2(4)(-4)^2(5)^2$ $(1)^2(-1)(4)^2(-4)(5)^2$	± 5	$\|\pm 5°\rangle$	$W_1+W_2-W_0+(J_{55}-J_{45})+(J_{14}-J_{15})+K_{14}+K_{15}+K_{45}$	$\Delta+\Delta_{CT}+K_1$	22500
	$(1)^2(-1)(4)(-4)^2(5)(-5)$ $(1)(-1)^2(4)^2(-4)(5)(-5)$	∓ 3	$\|\mp 3a°\rangle$	$W_1+W_2-W_0+(J_{55}-J_{45})+(J_{14}-J_{15})+1/2(-K_{1-4}+4K_{15}+K_{1-5}+4K_{45}+K_{4-5}-K_{5-5})$	$\Delta+\Delta_{CT}+2K_1$	27700
			$\|\mp 3b°\rangle$	$W_1+W_2-W_0+(J_{55}-J_{45})+(J_{14}-J_{15})+1/2(K_{1-4}+3K_{1-5}+3K_{4-5}+K_{5-5})$	$\Delta+\Delta_{CT}+2K$	20900

$W_0\equiv E^0+4I_1+4I_4+6J_{11}+16J_{14}+6J_{44}-2K_{1-1}-4K_{14}-4K_{1-4}-2K_{4-4}$
$W_1\equiv E^0+4I_1+3I_4+I_5+6J_{11}+12J_{14}+4J_{15}+3J_{44}+3J_{45}-2K_{1-1}-3K_{14}-3K_{1-4}-K_{15}-K_{1-5}-K_{4-4}-K_{45}-K_{4-5}$
$W_2\equiv E_0+3I_1+4I_4+I_5+3J_{11}+12J_{14}+3J_{15}+6J_{44}+4J_{45}-K_{1-1}-3K_{14}-3K_{1-4}-K_{15}-K_{1-5}-2K_{4-4}-K_{45}-K_{4-5}$

Mixing term	Energy	Approximate energy cm^{-1}		Mixing term	Energy	Approximate energy cm^{-1}	
$\langle 0°\|\boldsymbol{H}\|\pm 4°\rangle$	$\sqrt{2}\,\beta$	$\sqrt{2}\,\beta$	−5660				
$\langle\pm 9°\|\boldsymbol{H}\|\pm 13°\rangle$	$-\beta$	$-\beta$	4000	$\langle\pm 1°\|\boldsymbol{H}\|\pm 5°\rangle$	$-\beta$	$-\beta$	4000
$\langle\pm 9°\|\boldsymbol{H}\|\pm 5a°\rangle$	$\sqrt{2}\,/2\beta$	$\sqrt{2}\,/2\beta$	−2830	$\langle\pm 1°\|\boldsymbol{H}\|\mp 3a°\rangle$	$\sqrt{2}\,\beta$	$\sqrt{2}\,\beta$	−5660
$\langle\pm 9°\|\boldsymbol{H}\|\pm 5b°\rangle$	$-\sqrt{6}\,/2\beta$	$-\sqrt{6}\,/2\beta$	4900	$\langle\pm 1°\|\boldsymbol{H}\|\mp 3b°\rangle$	0	0	0
$\langle\pm 5a°\|\boldsymbol{H}\|\pm 5b°\rangle$	$\sqrt{3}\,/2(K_{14}-K_{15}+K_{5-5}-K_{4-5})$	0	0	$\langle\mp 3a°\|\boldsymbol{H}\|\mp 3b°\rangle$	$\sqrt{3}\,/2(K_{1-4}-K_{1-5}+K_{5-5}-K_{4-5})$	0	0

$$|+5b\rangle \equiv [\{|1\bar{1}4\bar{4}-\bar{1}-4\bar{5}-5|+|1\bar{1}4\bar{4}-1-\bar{4}5-\bar{5}|\}$$
$$-\frac{1}{2}\{|1\bar{1}4\bar{4}-1-4\bar{5}-\bar{5}|+|1\bar{1}4\bar{4}-1-\bar{4}\bar{5}-5|$$
$$+|1\bar{1}4\bar{4}-\bar{1}-\bar{4}5-5|+|1\bar{1}4\bar{4}-\bar{1}-45-\bar{5}|\}]/\sqrt{3};$$
$$|-3a\rangle \equiv [|1\bar{1}-4-\bar{4}-14\bar{5}-\bar{5}|-|1\bar{1}-4-\bar{4}-1\bar{4}5-\bar{5}|$$
$$+|1\bar{1}-4-\bar{4}-\bar{1}45-5|-|1\bar{1}-4-\bar{4}-\bar{1}4\bar{5}-5|]/2,$$
$$|-3b\rangle \equiv [\{|1\bar{1}-4-\bar{4}-\bar{1}45-\bar{5}|+|1\bar{1}-4-\bar{4}-1\bar{4}\bar{5}-5|\}$$
$$-\frac{1}{2}\{|1\bar{1}-4-\bar{4}-14\bar{5}-\bar{5}|+|1\bar{1}-4-\bar{4}-1\bar{4}5-\bar{5}|$$
$$+|1\bar{1}-4-\bar{4}-\bar{1}\bar{4}5-5|$$
$$+|1\bar{1}-4-\bar{4}-\bar{1}4\bar{5}-5|\}]/\sqrt{3},$$

where no bar implies spin α, a bar implies spin β and the molecular orbitals are denoted by their λ_z values. In the circular box model, $\phi_a^* \cdot \phi_a$ are identical for all the porphin molecular orbitals. It then follows that,

$$J_{44} = J_{45} = J_{55} = e^2 \int \frac{f^2(r_1) f^2(r_2)}{r_{12}} d\tau_1 d\tau_2 \equiv J$$

and

$$J_{14} = J_{15} = e^2 \int \frac{f_1^2(r_1) f^2(r_2)}{r_{12}} d\tau_1 d\tau_2 \equiv J'$$

For the K values, we set

$$K_{4-4} = K_{4-5} = K_{5-5} \equiv K$$
$$K_{45} \equiv K_1$$

as Gouterman assumed.[26] The orbitals $|\pm 1\rangle$ and $|\pm 5\rangle$ are overlapping. Therefore $(\pm 1|\hat{h}^{\text{eff}}|\pm 5)$ could be non-zero. However K_{15} and also K_{1-5} are assumed very small and are neglected. We define

$$\Delta_{CT} \equiv W_2 - W_0$$
$$\Delta \equiv W_1 - W_0.$$

For TPPZn(II), the Soret band $(\Delta + 2K_1)$ appears at 23700 cm^{-1} and the visible band $(\Delta + 2K)$, at 16900 cm^{-1}.[13] The phosphorescence of TPPCu(II) (Δ) occurs at 13300 cm^{-1}.[28] We then find

$$\Delta = 13300\ cm^{-1},\ K = 1800\ cm^{-1},\ K_1 = 5200\ cm^{-1},$$

for the tetraphenylporphins. The last column of Table 2 shows the values of the state energies in terms of Δ, Δ_{CT}, K_1, and K using the empirical values. For a variety of the values of Δ_{CT} and β, the transition energies of the cobalt(I) porphin were calculated. The singlet energy levels of the cobalt(I) porphin are shown in Fig. 11 as a function of β, assuming $\Delta_{CT} = 4000\ cm^{-1}$. The excited states of $[TPPCo(I)]^-$ can be reproduced for $\Delta_{CT} = 4000\ cm^{-1}$, $\beta = -4000\ cm^{-1}$. This β value is close to the value estimated from molecular orbital coefficient of the central nitrogens[23] and a similar resonance integral value as used by Hanazaki and Nagakura for a calculation of $[Fe(bipy)_3]^{2+}$ [29].

The calculation shows that the visible band of $[TPPCo(I)]^-$ arises mainly from $|\pm 9\rangle \leftarrow |0\rangle$ and the near-ultraviolet band, $|\pm 1\rangle \leftarrow |0\rangle$. A-type dispersions observed at 18.5, 20.0, and 23.5 kK reveal the orbital angular momentum expected for these porphin (π, π^*) excited states. The 17.0 kK weak band,

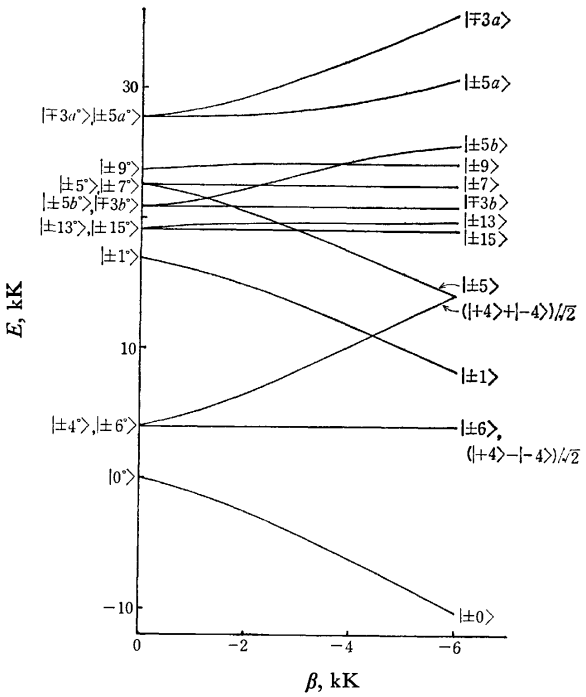

Fig. 11. The singlet energy levels of the cobalt(I) porphin as a function of β. (Δ_{CT} is assumed 4000 cm^{-1}).

however, is assigned to a "cobalt to porphin" charge-transfer transition, $(|+4\rangle + |-4\rangle)/\sqrt{2} \leftarrow |0\rangle$, which gives no orbital angular momentum in the excited state. In fact no remarkable A-type MCD could be observed at the 17.0 kK band. A reverse A-type dispersion observed at 27.5 kK may be assigned as arising from a transition mainly consisting of $|\mp 3b\rangle \leftarrow |0\rangle$. However spectral intensity of the transition $|\mp 3b\rangle \leftarrow |0\rangle$ is formally zero based on an assumption of the accidental degeneracy of a_{2u} and a_{1u} orbitals. From the same reason, the visible Q bands, $|\pm 9\rangle \leftarrow |0\rangle$, are formally prohibited. As shown in Figs. 7 and 8, intensity of the visible Q bands is appreciably high, although it is forbidden in character. Since the highest occupied a_{2u} and a_{1u} are not exactly degenerate, a term equal to half their energy difference,

$$(-4|\hat{p}|4) = 1/2[(a_{2u}|\hat{h}^{\text{eff}}|a_{2u}) - (a_{1u}|\hat{h}^{\text{eff}}|a_{1u})] \equiv \varepsilon,$$

connects two wave functions that differ by a single orbital, which is the one is $|+4\rangle$ and in the other $|-4\rangle$. This carries an spectral intensity from the allowed transition pair $|\pm 1\rangle \leftarrow |0\rangle$ to the forbidden transition apir $|\pm 9\rangle \leftarrow |0\rangle$. To reproduce the transition energies and the ratio of Q and B bands of TPPCo(II), we redetermined

$$\Delta = 14810\ cm^{-1},\ K = 2530\ cm^{-1},\ K_1 = 4600\ cm^{-1}$$
and $\varepsilon = \pm 1480\ cm^{-1}$.

As was pointed out by Gouterman on the empirical basis, the a_{1u} orbital is slightly higher than the a_{2u} orbital which is reverse to the ordering predicted by the conventional molecular orbital calculations.[26a]

From these parameters with $\Delta_{CT} = 4{,}000\ cm^{-1}$ and $\beta = -4{,}000\ cm^{-1}$, we can well reproduce the excited states of $[TPPCo(I)]^-$ as shown in Fig. 12. To get a better fit of the spectral intensity of Q and B bands,

28) M. Gouterman, R. A. Mathles, and B. E. Smith, *J. Chem. Phys.*, **52**, 3795 (1970).

29) I. Hanazaki and S. Nagakura, *Inorg. Chem.*, **8**, 648 (1969); see also, I. Hanazaki, F. Hanazaki, and S. Nagakura, *J. Chem. Phys.*, **50**, 265 (1969).

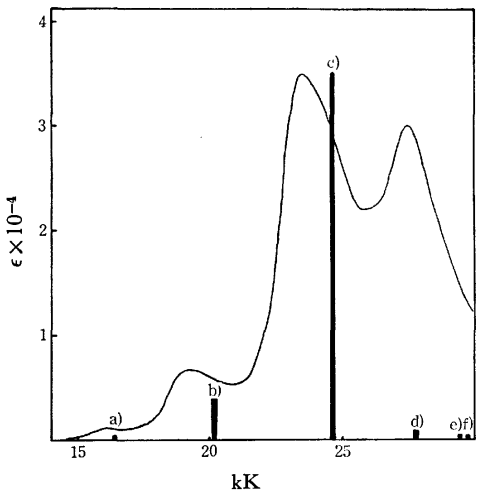

Fig. 12. Absorption spectrum of $[Co(I)TPP]^-$.
Curve: observed spectrum Vertical lines: calculated spectrum
a): $(|+4\rangle+|-4\rangle)/\sqrt{2} \leftarrow |0\rangle$, b): $|\pm 9\rangle \leftarrow |0\rangle$,
c): $|\pm 1\rangle \leftarrow |0\rangle$, d): $|\pm 13\rangle \leftarrow |0\rangle$, e): $|\mp 3b\rangle \leftarrow |0\rangle$,
f): $|\pm 15\rangle \leftarrow |0\rangle$

the parameters for $[TPPCo(I)]^-$ may be replaced by $\Delta = 14310\ cm^{-1}$ and $\varepsilon = \pm 2560\ cm^{-1}$. However the theory could not get an intensity of the band at 27.5 kK, although it could predict a reverse A-type dispersion. The (π, π^*) excited states of porphin in the ultraviolet region can not be well described without being mixed with higher energy configurations. In this context, a self-consistent molecular orbital calculation including cobalt electrons will be reported elsewhere. In a recent paper, Gouterman and his coworkers obtained $(\pm 4|\hat{\mu}_z|\pm 4) = \mp 2.27\ \beta$ and $(\pm 5|\hat{\mu}_z|\pm 5) = \mp 2.09\ \beta$ by a molecular orbital calculation.[30] If this is the case, some D_{4h} porphin should show a reverse A-type dispersion at the Soret band.[31] The circular box model predicts

$$(\pm 4|\hat{\mu}_z|\pm 4) = -\beta/\hbar(\pm 4|\hat{l}_z|\pm 4) = \mp 4\beta$$

and

$$(\pm 5|\hat{\mu}_z|\pm 5) = -\beta/\hbar(\pm 5|\hat{l}_z|\pm 5) = \mp 5\beta.$$

In a more exact treatment such as molecular orbital calculations based on a linear combination of atomic orbitals, these values are reduced. However magnetic circular dichroism of the cobalt porphin in the oxidation states, (I), (II), and (III), presented in this paper does not show any reverse A-type dispersion at B band. This indicates that $|(\pm 5|\hat{\mu}_z|\pm 5)| > |(\pm 4|\hat{\mu}_z|\pm 4)|$ even if it is treated with extensive configuration interactions.

Absorption spectrum and also magnetic circular dichroism spectrum of the cobalt(I) porphin were reproduced taking back-donation effect of the cobalt $d\pi$ electrons to porphin. To get the best fit, we assumed $\Delta_{CT} = 4000\ cm^{-1}$. However the experimental energy levels of $[TPPCo(I)]^-$ are qualitatively reproduced for $2000\ cm^{-1} < \Delta_{CT} < 8000\ cm^{-1}$. Such a positive charge-transfer energy, even if it is small, indicates an energy necessary to carry an electron from the cobalt to the porphin. Since an electron furnished by the reducing reagent is being trapped in d_{z^2} orbital of the central cobalt, a back-donation tendency of the cobalt $d\pi$ electrons to the porphin antibonding π orbital is sufficiently enhanced. The calculation predicts a transfer of the net charge 0.38 e from the cobalt $d\pi$ orbitals. Felton and Linschitz have made measurements of polarographic halfwave potentials on a number of TPP complexes in dimethyl sulfoxide.[32] A gap between the first and second waves is almost constant for various systems except Co(II). Halfwave potential of the first step reduction of TPPCo(II) is appreciably lower than those of the other complexes, whereas that of the second step is rather close to those of the others. The second step reduction is assigned to an electron trapping in the porphin conjugated system, while the first step is an electron trapping in the central cobalt ion which arises from a higher electron affinity of the cobalt(II) ion in a strong planar ligand field. On the contrary, however, TPP metal free base and the metal complexes of divalent ion such as Mg(II), Ni(II), Cu(II), or Zn(II) capture an electron into the porphin conjugated system during the first step reduction process. This trend has been reproduced by an extended Hückel molecular orbital calculation.[24]

We should like to express our appreciation to Dr. M. Uyemura of the Research Laboratory of Resources Utilization, Tokyo Institute of Technology, for numerical calculation. One of the authors (H. K.) should appreciate Professor S. Nagakura and Dr. I. Hanazaki and also Professor M. Gouterman for helpful discussions. This work was supported by a grant from the Ministry of Education.

30) A. J. McHugh, M. Gouterman, and C. Weiss, Jr., *Theoret. Chim. Acta*, **24**, 346 (1972).

31) Molecular constant A of the A-term magnetic circular dichroism at the porphin degenerate transition $|j\rangle \leftarrow |0\rangle$ is defined as follows,

$$A = 3\sum_j \langle j|\mu_z|j\rangle \cdot Im\{\langle 0|\hat{m}_x|j\rangle\langle j|\hat{m}_y|0\rangle\},$$

where $\hat{\mu}$ and $\hat{m}$ are the magnetic and electric dipole operators, respectively, $\langle j|\hat{\mu}_z|j\rangle = -\beta/\hbar\langle j|\hat{l}_z|j\rangle$. Magnetic circular dichroism spectrum shows a normal dispersion when $A/D<0$, where $D=3\sum_j\{|\langle 0|\hat{m}_x|j\rangle|^2+|\langle 0|\hat{m}_y|j\rangle|^2\}$. For $A/D>0$, the spectrum shows an anomalous dispersion. "A-type dispersion" in this paper denotes the normal dispersion ($A/D<0$), whereas "reverse A-type dispersion", the anomalous dispersion ($A/D>0$).

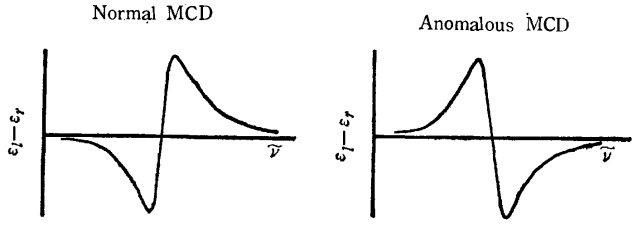

32) R. H. Felton and H. Linschitz, *J. Amer. Chem. Soc.*, **88**, 1113 (1966).

Electronic Absorption Spectra of Tris(2,2′-bipyridine)- and Tris(1,10-phenanthroline) Complexes of Vanadium(II) and Chromium(II)

Ichiro FUJITA, Takanori YAZAKI, Yasuo TORII,* and Hiroshi KOBAYASHI
Department of Chemistry, Tokyo Institute of Technology, Ookayama, Meguro-ku, Tokyo
(Received November 11, 1971)

Electronic absorption spectra of tris(2,2′-bipyridine) complexes of vanadium(II) and chromium(II) were measured. When methyl groups are introduced into the coordinating bipyridine, (d, d^*) transitions in the central metal, (π, π^*) transitions in the coordinating ligand, and "metal to ligand" charge-transfer transitions show their respective characteristic shifts. Thus the visible and near-infrared bands of tris(2,2′-bipyridine) complexes of vanadium(II) and chromium(II) are assigned to "metal to ligand" charge-transfer transitions as well as the visible bands of tris(2,2′-bipyridine)iron(II). A comparison between the corresponding bands of tris(2,2′-bipyridine) complexes and tris(1,10-phenathroline) complexes also verifies the assignment.

Transition metal complexes of 2,2′-bipyridine, 1,10-phenanthroline and their derivatives are one of the best studied group of metal complexes.[1] The complexes of a divalent cation of the first transition-metals such as manganese(II), cobalt(II), nickel(II), copper(II), or zinc(II) give rise to feeble colors in the solid state and in solutions.[2-6] Formation of the tris complexes of divalent iron, however, gives intense red coloration which permits an effective amplification of iron signal in the colorimetry.[7] The electronic absorption spectra of the divalent complexes have been established on the basis of considerable experimental and theoretical work. Strong absorption bands in the ultraviolet region are assigend to (π, π^*) transitions of the coordinating ligands.[2-6,8,9] The absorption bands of the coordinating ligand are slightly shifted in position and also changed in intensityf or a possible conformational change upon chelation and for inductive and/or mesomeric perturbation by the central metal ion. The feebly colored complexes of manganese(II), cobalt(II), nickel(II), or copper(II) show weak absorption bands arising from (d, d^*) transitions in the visible and near-infrared regions.[2-6] On the other hand, the deeply colored iron complexes show intense absorption bands in the visible region. The intense absorption bands are assigned to "metal to ligand" charge-transfer transitions. An electron in a molecular orbital primarily localized on a $d\pi$ orbital of the central iron is promoted to one of the antibonding π molecular orbitals distributed over the coordinating ligands.[9,10] Similar visible bands observed in the corresponding ruthenium(II) complexes were also assigned to "metal to ligand" charge-transfer transitions.[6,11]

Tris(bipyridine)- and tris(phenanthroline) complexes of divalent vanadium and chromium are known to be deeply colored. Some of their intense absorption bands were observed in the visible and near-infrared region.[12] The observed absorption bands were as intense as those of the iron(II) complexes. So far, however, assignment of the electronic absorption spectra of these complexes has never been established on the basis of sufficient experimental evidences. In this paper, we present the electronic absorption spectra of tris(2,2′-bipyridine), tris(4,4′-dimethyl-2,2′-bipyridine) and tris(5,5′-dimethyl-2,2′-bipyridine), and also tris(1,10-phenanthroline) complexes of vanadium(II) and chromium(II). On the basis of the observed evidences, the visible and near-infrared bands of the vanadium(II) and chromium(II) complexes will be assigned to "metal to ligand" charge-transfer transitions.

Experimental

Materials. By means of Sasse's method, 2,2′-bipyridine and its 4,4′-dimethyl- and 5,5′-dimethyl derivatives were prepared (Fig. 1).[13,14] Commercially available 1,10-phenanthroline of analytical reagent grade made by Tokyo Kasei Co., Ltd. was used without further purification. 2,2′-Bipyridine and its 4,4′-dimethyl- and 5,5′-dimethyl derivatives and 1,10-phenanthroline are abbreviated to bipy, 4dmbip, 5dmbip, and phen, respectively.

Tris(2,2′-bipyridine)vanadium(II), -chromium(II), -iron(II), and -nickel(II) perchlorates, and tris(1,10-phenanthroline)chromium(II), -iron(II), and -nickel(II) perchlorates were prepared by the methods given in the literature.[15-20]

Since vanadium(II) and chromium(II) ions are very sensitive to oxygen in the air, all the preparations were carried out in an oxygen-free dry nitrogen atmosphere. The

* Present Address: Laboratory of Chemistry, Yokohama National University, Minami-ku, Yokohama.

1) W. R. McWhinnie and J. D. Miller, "Advances in Inorganic Chemistry and Radiochemistry," Vol. 12, ed. by H. J. Emeléus and A. G. Sharpe, Academic Press, New York (1969), p. 135.
2) K. Yamazaki, H. Yokoi, and K. Sone, *Nippon Kagaku Zasshi*, **69**, 137 (1948).
3) C. K. Jǿrgensen, *Acta Chem. Scand.*, **9**, 1362 (1955).
4) H. Ito, *Nippon Kagaku Zasshi*, **77**, 1399 (1956).
5) A. Kiss and J. Császár, *Acta Chim. Acad. Sci. Hung.*, **38**, 405, 421 (1963).
6) R. A. Palmer and T. S. Piper, *Inorg. Chem.*, **5**, 865 (1966).
7) E. B. Sandell, "Colorimetric Determination of Traces of Metals," Interscience Publishers, New York (1959), p. 537.
8) H. L. Schläfer, *Z. Phys. Chem. (N. F.)*, **8**, 373 (1956).
9) I. Hanazaki and S. Nagakura, *Inorg. Chem.*, **8**, 648 (1969).
10) C. K. Jǿrgensen, *Acta Chem. Scand.*, **11**, 166 (1957).
11) W. W. Brandt and G. F. Smith, *Anal. Chem.*, **21**, 1313 (1949).
12) E. König and S. Herzog, *J. Inorg. Nucl. Chem.*, **32**, 585, 601 (1970).
13) W. H. F. Sasse, *J. Chem. Soc.*, **1956**, 618.
14) W. H. F. Sasse and C. P. Whittle, *ibid.*, **1961**, 1347.
15) S. Herzog, *Z. Anorg. Allgem. Chem.*, **294**, 155 (1958).
16) G. Brauer, "Handbuch der Präparativen Anorganischen Chemie," Ferdinand Enke Verlag, Stuttgart (1954), p. 1021.
17) F. H. Burstall and R. S. Nyholm, *J. Chem. Soc.*, **1952**, 3570.
18) G. T. Morgan and F. H. Burstall, *J. Chem. Soc.*, **1931**, 2213; F. M. Jaeger and J. A. van Dÿk, *Z. Anorg. Chem.*, **227**, 273 (1936).
19) S. Herzog, *Chem. Tech.*, **8**, 544 (1956).
20) F. Blau, *Monatsh. Chem.*, **19**, 669 (1898); P. Pfeiffer and Fr. Tappermann, *Z. Anorg. Chem.*, **215**, 273 (1938).

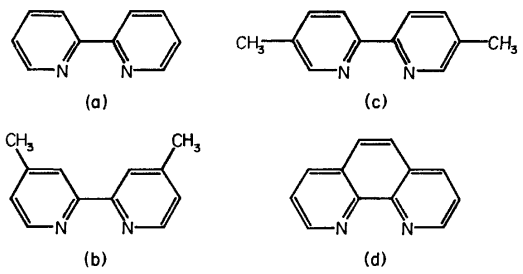

Fig. 1. Ligands.
(a) 2,2′-bipyridine (bipy)
(b) 4,4′-dimethyl-2,2′-bipyridine (4dmbip)
(c) 5,5′-dimethyl-2,2′-bipyridine (5dmbip)
(d) 1,10-phenanthroline (phen)

solvent used for the preparation should be thoroughly freed from oxygen.

Tris(4,4′-dimethyl-2,2′-bipyridine)vanadium(II) diperchlorate, $[V(4dmbip)_3](ClO_4)_2$. One gram of 4,4′-dimethyl-2,2′-bipyridine was dissolved in a mixture of 25 m*l* of methanol, 3 m*l* of 2N hydrochloric acid and 50 m*l* of water. To this solution was added 2 m*l* of 1M solution of vanadium(II) sulfate prepared by electrolytic reduction of oxovanadium(IV) sulfate.[22] When the complex was formed, the solution turned dark blue-green. It was stirred for several hours, and then mixed with a solution of 0.5 g of ammonium perchlorate in 20 m*l* of water. After standing for 3 hr, dark blue-green crystals were collected by filtration, washed twice with water and once with methanol, and dried over calcium chloride *in vacuo*.

Found: V, 6.1%. Calcd for $[V(4dmbip)_3](ClO_4)_2$: V, 6.35%.

Tris(5,5′-dimethyl-2,2′-bipyridine)vanadium(II) diperchlorate, $[V(5dmbip)_3](ClO_4)_2$. In a mixture of 25 m*l* of methanol and 20 m*l* of water, 2.7 g of 5,5′-dimethyl-2,2′-bipyridine was dissolved and then 6.0 m*l* of 1M solution of vanadium(II) sulfate was added. The solution turned dark blue-green. After it was stirred for several hours, a solution of 1.5 g of ammonium perchlorate in 15 m*l* of water was added to the colored solution. After standing for 24 hr, the dark blue-green precipitate was collected by filtration, washed with water and dried over calcium chloride *in vacuo*.

Found: V, 6.0%. Calcd for $[V(5dmbip)_3](ClO_4)_2$: V, 6.35%.

Tris(1,10-phenanthroline)vanadium(II) diperchlorate, $[V(phen)_3](ClO_4)_2$. 0.6 g of vanadium(II) sulfate hydrate was dissolved in 50 m*l* of water, and then 1.3 g of 1,10-phenanthroline previously dissolved in a small amount of methanol was added.[22] The solution turned dark blue. After it was stirred for several hours, the solution was added a mixture of 0.5 g sodium perchlorate hydrate and 0.3 m*l* of 70% perchloric acid in a small amount of water. The dark blue fine crystal thus formed was collected, washed several times with water and dried *in vacuo*.

Found: V, 6.4%. Calcd for $[V(phen)_3](ClO_4)_2$: V, 6.46%.

Tris(4,4′-dimethyl-2,2′-bipyridine) chromium(II) diperchlorate, $[Cr(4dmbip)_3](ClO_4)_2$. 0.5 g of chromium(II) acetate was dissolved in a mixture of 1.0 m*l* of 6N hydrochloric acid and 50 m*l* of water. To this was added 1.2 g of 4,4′-dimethyl-2,2′-bipyridine dissolved in a mixture of 0.1 m*l* of 6N hydrochloric acid and 100 m*l* of water. The dark brown solution was then thoroughly stirred, and to this was added 1 g of sodium perchlorate dissolved in a small amount of water. Black precipitate thus obtained was collected by filtration, washed several times with water and dried *in vacuo*.

Found: Cr, 6.3%. Calcd for $[Cr(4dmbip)_3](ClO_4)_2$: Cr, 6.47%.

Tris(5,5′-dimethyl-2,2′-bipyridine)chromium(II) diperchlorate, $[Cr(5dmbip)_3](ClO_4)_2$. The procedure was the same as that for tris(4,4′-dimethyl-2,2′-bipyridine)chromium(II) diperchlorate.

Found: Cr, 6.3%. Calcd for $[Cr(5dmbip)_3](ClO_4)_2$: Cr, 6.47%.

Measurements of Electronic Absorption Spectra. Electronic absorption spectra were taken on a Beckman spectrophotometer Model DU and a Shimadzu automatic recording spectrophotometer Model MPS-50. Quartz cuvettes of 1 and 10 mm optical path were used. Cylindrical cells of 100 mm path with quartz windows were used for measurements of weak (*d*, *d**) bands.

Since the vanadium(II) and chromium(II) complexes in the solid state are fairly stable against oxidation, the samples were weighed in the usual way in a dried atmosphere. The sample thus weighed was sealed in a vessel with a branch attached to an optical cuvette previously saturated with dry nitrogen. The vessel was connected through a ground joint to a vacuum line and evacuated. The procedure was carried out as quickly as possible.

Methanol was used as a solvent. The methanol was thoroughly degassed by successive freeze-thaw pumping cycles and transferred by distillation into the vessel. After the vessel was sealed off from the vacuum line, the sample was allowed to dissolve in methanol. Both procedure and apparatus were described in detail in a previous paper.[23]

Results and Discussion

Electronic absorption spectra of vanadium(II), chromium(II), iron(II), and nickel(II) complexes of 2,2′-bipyridine and its 4,4′-dimethyl- and 5,5′-dimethyl derivatives and of 1,10-phenanthroline are shown in Figs. 2—6.

Two intense absorption bands were observed in the ultraviolet region. They are assigned to (π, π^*) transitions within the molecular orbitals of the coordinating ligand. The lowest transitions of free bipyri-

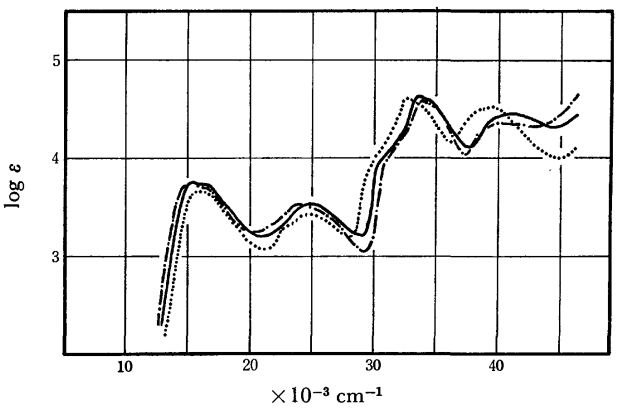

Fig. 2. Electronic absorption spectra of tris(bipyridine)-vanadium(II) in methanol.
——: $[V(bipy)_3]^{2+}$
-·-·-: $[V(4dmbip)_3]^{2+}$
----: $[V(5dmbip)_3]^{2+}$

21) G. B. Kauffman and L. T. Takahashi, "Inorganic Syntheses," Vol. 8, (1966), p. 227.
22) M. Kranz, "Inorganic Syntheses," Vol. 7 (1963), p. 94.
23) Y. Torii, T. Yazaki, Y. Kaizu, S. Murasato, and H. Kobayashi, This Bulletin, **42**, 2264 (1969).

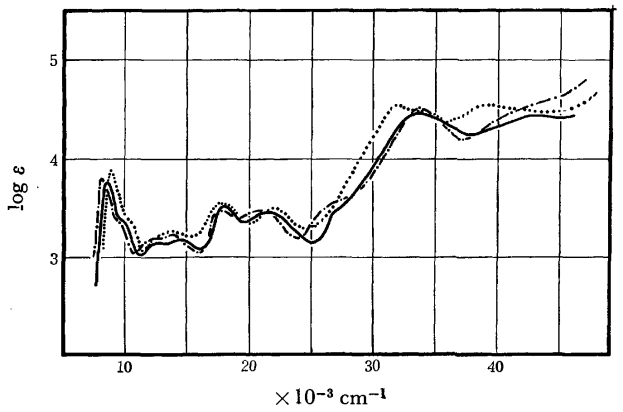

Fig. 3. Electronic absorption spectra of tris(bipyridine)-chromium(II) in methanol.
——: $[Cr(bipy)_3]^{2+}$
-·-·-: $[Cr(4dmbip)_3]^{2+}$
------: $[Cr(5dmbip)_3]^{2+}$

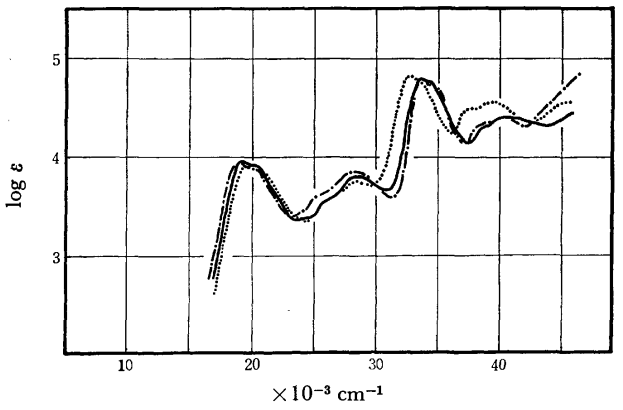

Fig. 4. Electronic absorption spectra of tris(bipyridine)-iron(II) in methanol.
——: $[Fe(bipy)_3]^{2+}$
-·-·-: $[Fe(4dmbip)_3]^{2+}$
------: $[Fe(5dmbip)_3]^{2+}$

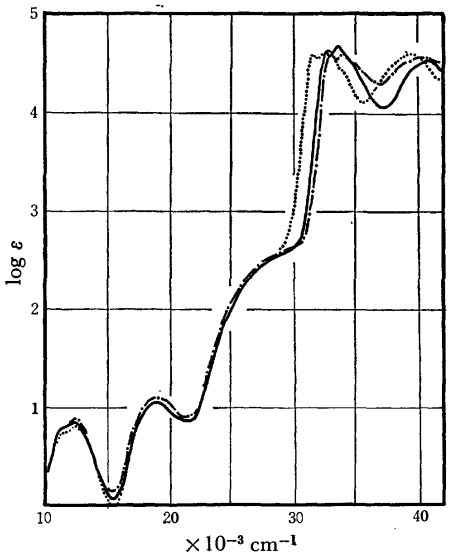

Fig. 5. Electronic absorption spectra of tris(bipyridine)-nickel(II) in methanol.
——: $[Ni(bipy)_3]^{2+}$
-·-·-: $[Ni(4dmbip)_3]^{2+}$
------: $[Ni(5dmbip)_3]^{2+}$

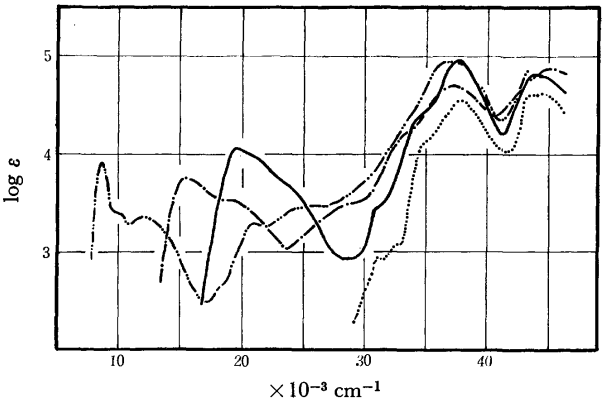

Fig. 6. Electronic absorption spectra of tris(phenanthroline) complexes of vanadium(II), chromium(II), and iron(II) in methanol.
-·-·-: $[V(phen)_3]^{2+}$
-·-·-: $[Cr(phen)_3]^{2+}$
——: $[Fe(phen)_3]^{2+}$
------: phenanthroline

dine which are assigned to (π, π^*) transitions are shifted by such a weak perturbation as methyl substitutions (Fig. 7). The lowest wave number band of the bipyridine is shifted to higher wave number in the order 5dmbip < bipy < 4dmbip. The ordering is preserved in the lowest (π, π^*) transition of the coordinating bipyridines. A conformational change of two pyridine rings in bipyridine on the chelate formation is expected to change the (π, π^*) transition. However, such an effect, at least to the lowest excited states, was estimated to be negligibly small by theoretical calculation. The lowest (π, π^*) transition of the bipyridines coordinating to Mn(II), Fe(II), Co(II), Ni(II), Cu(II), and Zn(II) was observed around 33000 cm^{-1}, whereas the corresponding band of free bipyridine was observed at 35000 cm^{-1}. This shift might be attributed to a spectral shift arising from an excitation coupling between three bipyridines in a tris complex. However, the exciton interaction predicts another direction of the spectral shift. The coordinat-

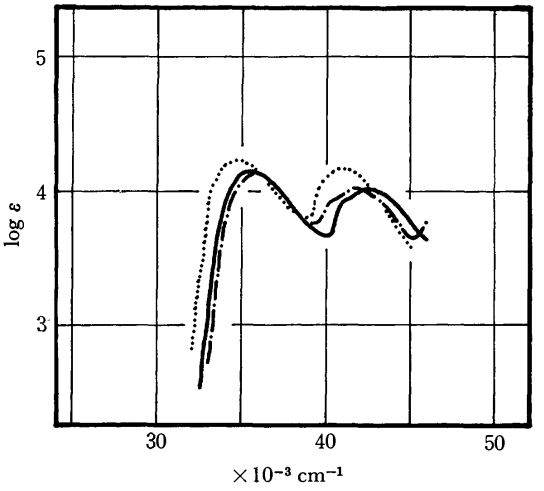

Fig. 7. Electronic absorption spectra of bipyridine.
——: 2,2′-bipyridine
-·-·-: 4,4′-dimethyl-2-2′-bipyridine
------: 5,5′-dimethyl-2,2′-bipyridine

ing bipyridine is polarized partially by an electrostatic interaction due to the residual positive charge on the central metal ion and partially by σ donation of the coordinating nitrogens. Such a polarization, however, gives rise to a slight red-shift. The lowest wave number band is shifted to lower wave number in the order Fe(II) $<$ Mn(II) $\sim$ Zn(II) $<$ Co(II) $\sim$ Ni(II) $<$ Cu(II). Although the observed shift is within several hundred wave numbers, it is almost parallel to the natural order of complex stability except for Fe(II).[24]

Since iron(II) in the diamagnetic state is highly π-donating, π electronic system of the bipyridine coordinating to the iron can not be described in terms of a simple electronic polarization as in the complexes of less π-donating metal ions such as Mn(II), Co(II), Ni(II), Cu(II), and Zn(II). The vanadium(II) and chromium(II) complexes show absorption bands corresponding to those of the coordinating bipyridine at almost the same position as in the iron(II) complexes. Since V(II), Cr(II) as well as Fe(II) are less π electron-attractive, the coordinating ligand should accept migration of π electron into the vacant molecular orbitals. The lowest excited states of the coordinating bipyridine in such a complex should be described in terms of a configuration admixture of "metal to ligand" charge-transfer excited states and coupled (π, π^*) excited states of three coordinating bipyridines.

When such a high π-donating power is attained as in V(II), Cr(II), or Fe(II), some "metal to ligand" charge-transfer excited states should be lower than (π, π^*) excited states. These charge-transfer transitions, however, should be very weak unless they can borrow their intensities from the allowed (π, π^*) transitions by a mixing due to the configuration interaction mentioned above. In fact, the vanadium(II) and chromium(II) complexes give rise to a series of superposing intense and diffuse absorption bands over the visible and near-infrared region (Figs. 2—3). These bands are assigned to charge-transfer transitions as well as those observed in the iron(II) complexes (Fig. 4). The fact that the charge-transfer transitions were observed indicates that mixing due to the configuration interaction takes place. The vanadium(II) complexes show a remarkable extra shoulder at 31600 cm^{-1} besides the corresponding band of the iron(II) complexes, while the chromium(II) complexes show a rather diffuse composite system of bands. In the case of the open-shell ions such as V(II) and Cr(II), not only singlet-singlet (π, π^*) excited states but also singlet-triplet (π, π^*) excited states can appreciably participate in the lowest excited states of the coordinating bipyridine.

As is shown in Fig. 2, the visible absorption spectrum of the vanadium(II) complexes indicates a characteristic of the allowed transition very similar both in shape and intensity to that of the iron(II) complexes except for the position which is shifted by about 4000 cm^{-1} to lower wave number. The visible absorption spectrum of the chromium complexes is rather complicated, but also shows a characteristic of the allowed transition as well (Fig. 3). The lowest wave number bands at *ca.* 20000 cm^{-1} of the iron(II) complexes are charge-transfer bands and are shifted to the higher wave number upon methyl substitutions in the order 4dmbip $<$ bipy $<$ 5dmbip. The ordering is the reverse of that observed in the lowest (π, π^*) transitions of the coordinating bipyridine. The band at 16000 cm^{-1} of the vanadium(II) complexes and that at 8500 cm^{-1} of the chromium(II) complexes show a similar spectral shift as observed in the charge-transfer band at 20000 cm^{-1} of the iron complexes. On the other hand, the band at 25000 cm^{-1} of the vanadium(II) complexes, that at 28000 cm^{-1} of the iron(II) complexes and that at 18000 cm^{-1} of the chromium(II) complexes are observed in the order 4dmbip $<$ 5dmbip $<$ bipy. This does not coincide with the ordering observed for either the lowest wave number charge-transfer transition or for the lowest (π, π^*) transition. The bands are assigned to charge-transfer transitions from a $d\pi$ orbital to a second antibonding π molecular orbital of the ligand. The band at 21500 cm^{-1} of the chromium complexes, however, contrary to the band at 18000 cm^{-1} shows a similar behavior upon methyl substitutions to that observed for the band at 8500 cm^{-1}. The molecular orbitals involved in both transitions are very similar.

Nickel(II) complexes give rise to two weak (d, d^*) bands of Laporte forbidden character in the visible region (Fig. 5). When the coordinating bipyridine is introduced methyl groups, "metal to ligand" charge-transfer bands in the vanadium(II), chromium(II), and iron(II) complexes are shifted, but not much the (d, d^*) transitions in the nickel(II) complexes. Energy of the first (d, d^*) transition, $^3T_2 \rightarrow {}^3A_2$, of an octahedral nickel(II) complex corresponds to the ligand-field splitting parameter, 10 Dq.[25] The fact that no shifts of the first band of the nickel(II) complexes were observed upon methyl substitutions indicates that σ donation of the ligand, hence the ligand-field splitting of the d orbitals, is not influenced by such a weak perturbation as introduced by methyl substitutions. This must be true in the (d, d^*) transitions of other metal ions.

The spectral shifts arising from dimethyl substitutions of tris(bipyridine) complexes are summarized in Fig. 8.

The coordinating phenanthroline gives rise to (π, π^*) transitions in the ultraviolet region. Absorption spectrum of the coordinating ligand preserves the band shape of free ligand and is slightly shifted to lower wave number in the order Fe(II) $<$ V(II) $<$ Cr(II) (Fig. 6).

The visible absorption bands of $[Fe(phen)_2]^{2+}$ are assigned to "metal to ligand" charge-transfer transitions as well as the visible bands of $[Fe(bipy)_3]^{2+}$.[26] The band at 16000 cm^{-1} of $[V(phen)_3]^{2+}$ corresponds to that at almost the same position as $[V(bipy)_3]^{2+}$. As was observed in $[Cr(bipy)_3]^{2+}$, the visible and near-infrared spectrum of $[Cr(phen)_3]^{2+}$ is much more complicated than those of $[V(phen)_3]^{2+}$ and $[Fe(phen)_3]^{2+}$. However, a similar spectral corre-

24) H. Irving and R. J. P. Williams, *J. Chem. Soc.*, **1953**, 3192.

25) J. S. Griffith, "The Theory of Transition-Metal Ions," Cambridge University Press (1961), p. 286.

26) T. Ito, N. Tanaka, I. Hanazaki, and S. Nagakura, This Bulletin, **42**, 702 (1969).

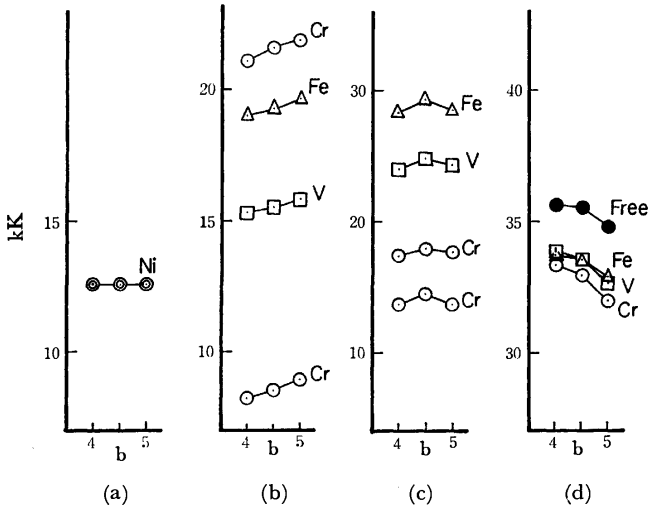

Fig. 8. Dimethyl substitution effects of the absorption spectra of tris(bipyridine) complexes.
(a) (d,d^*) transition
(b) the lowest charge-transfer transition (A charge-transfer band of the chromium(II) complexes at 21500 cm^{-1} shows a similar dimethyl substitution effect to that of the lowest charge-transfer transition.)
(c) the second charge-transfer transition
(d) (π,π^*) transition of the free and coordinating bipyridines
□: vanadium(II) complexes
○: chromium(II) complexes
△: iron(II) complexes
4: 4dmbip; b: bipy; 5: 5dmbip

spondence is observed between $[V(phen)_3]^{2+}$ and $[V(bipy)_3]^{2+}$, and also $[Cr(phen)_3]^{2+}$ and $[Cr(bipy)_3]^{2+}$. The absorption spectra of $[V(phen)_3]^{2+}$ and $[Cr(phen)_3]^{2+}$ in the visible and near-infrared region are assigned to "metal to ligand" charge-transfer transitions.

Transition energy of the lowest charge-transfer excitation should be proportional to a difference of the ionization potential of the metal $d\pi$ orbitals in complex and the electron affinity of the lowest vacant antibonding π orbitals in the coordinating ligand.

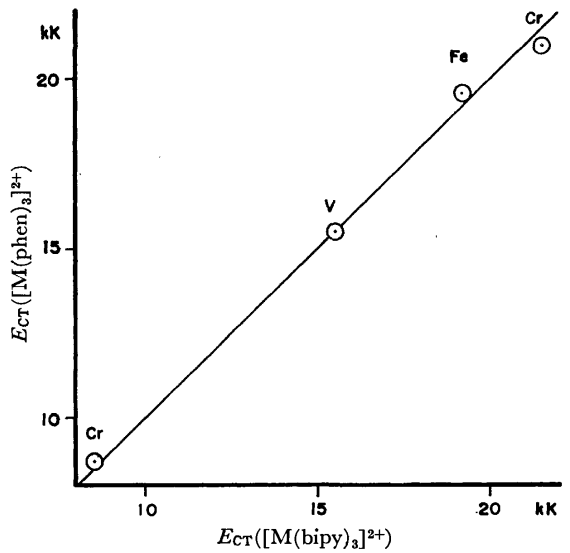

Fig. 9. Plots of the charge-transfer excitation energies of tris(1,10-phenanthroline) complexes, $E_{CT}([M(phen)_3]^{2+})$ *vs.* tris(2,2′-bipyridine) complexes, $E_{CT}([M(bipy)_3]^{2+})$.

Excitation energy of the charge-transfer band of tris(bipyridine) complexes, for example, varies primarily depending upon the $d\pi$ ionization potential of the central metals. Since the same argument holds for tris(phenanthroline) complexes as well, a linear relationship is expected between transition energies of the corresponding charge-transfer bands of tris(bipyridine) complexes and tris(phenanthroline) complexes. In fact, plots of the transition energies show an excellent linearity as seen in Fig. 9. This will very likely verify an assignment of "metal to ligand" charge-transfer transitions to the visible and near-infrared bands observed in the vanadium(II) and chromium(II) complexes.

Figure 9 reveals that the $d\pi$ ionization potential of the central metals is decreased in the order Cr < V < Fe. The ionization potential of M(II) in the ground state was experimentally estimated to be 29.31 eV for V(II), 30.95 eV for Cr(II) and 30.64 eV for Fe(II). When the ionization potential is estimated for the valence state, the values are obtained as follows: 29.5 eV for V(II)$(d\pi)^3$, 28.8 eV for Cr(II)$(d\pi)^4$, and 35.3 eV for Fe(II)$(d\pi)^6$.[27] The observed ordering of π-donating power of the central metals can be reproduced. However, a divalent cation in such a complex must be electroneutralized by σ-donation of the coordinating nitrogens and the values should be corrected for the electroneutrality. The ionization potentials were evaluated for the neutral species with the configuration $d^n s^2$,[28] where s^2 is assumed to be furnished by σ-donation of the coordinating nitrogens. The values thus obtained seem to be a rather realistic approximation and are, in fact, linear to the lowest charge-transfer transition energy of the respective complexes.

	$d\pi$ ionization potential	$E_{CT}([M(bipy)_3]^{2+})$	$E_{CT}([M(phen)_3]^{2+})$
$V(II)\sigma^2(d\pi)^3s^2$	11.27 eV	1.92 eV	1.93 eV
$Cr(II)\sigma^2(d\pi)^4s^2$	10.25 eV	1.05 eV	1.06 eV
$Fe(II)\sigma^2(d\pi)^6s^2$	12.61 eV	2.38 eV	2.43 eV

In the case of Cr(II), however, there are two types of the lowest $d\pi$ ionization as follows:

$$\text{I}\quad (d\pi_1)^2(d\pi_2)(d\pi_3) \longrightarrow (d\pi_1)(d\pi_2)(d\pi_3) + e$$

$$\text{II}\quad (d\pi_1)^2(d\pi_2)(d\pi_3) \longrightarrow (\overline{d\pi_1})(d\pi_2)(d\pi_3) + e$$

In the process I an electron with β spin pairing in a $d\pi$ orbital is detached, while in the process II an electron with α spin is transferred. The difference in the inter-electronic electrostatic repulsion energy between the processes I and II is given in terms of Racah's parameters and estimated at 13000—15000 cm^{-1} by the empirical values of the central metal ion. There must be two types of the charge-transfer transition from chromium(II) to the lowest antibonding π orbitals of the coordinating ligands. In fact, as was shown in

27) J. S. Griffith, "The Theory of Transition-Metal Ions," Cambridge University Press, (1961), p. 100.
28) C.E. Moore, "Atomic Energy Levels," Vol. 1 and 2, National Bureau of Standards, Washington (1949, 1952).

Fig. 8, $[Cr(bipy)_3]^{2+}$ gives rise to a charge-transfer band at 21500 cm^{-1}, which shows a similar dimethyl substitution effect to that of the lowest charge-transfer band at 8500 cm^{-1}. The energy difference is 13000 cm^{-1}. For the other ligands, the observed energy differences are 12850 cm^{-1} for 4dmbip, 12800 cm^{-1} for 5dmbip and 12400 cm^{-1} for phen. These values indicate a reduction of Racah's parameters in the complexes due to the delocalization of $d\pi$ electrons over the ligands.

BULLETIN OF THE CHEMICAL SOCIETY OF JAPAN, VOL. 45, 2161—2165(1972)

Platinum(II)-Olefin Complexes Containing Amino Acids. III.[1] Optical Inversion and Substitution of Coordinated Olefins in Optically Active *trans(N)*-Chloro-L-prolinato-olefin-platinum(II) Complexes in Organic Solvents

Kazuo KONYA,[2] Junnosuke FUJITA, Hiroaki KIDO, and Kazuo SAITO

Department of Chemistry, Faculty of Science, Tohoku University, Sendai

(Received December 6, 1971)

Optical inversion of coordinated 2-methyl-2-butene and *trans*-2-butene in *trans(N)*-chloro-L-prolinato-olefin-platinum(II),[1] *trans(N)*-[PtCl(L-prol)(olefin)] (nitrogen of L-prolinate ion is *trans* to the olefin), *i.e.* the interconversion between diastereoisomers (Fig. 1), has been kinetically studied in acetone by measuring the decrease in the intensity of circular dichroism (CD) in near ultraviolet region. The rate was measurable only in the presence of olefin, and can be expressed by the relation, Rate=k[complex][olefin]. The E_a and the $\Delta S^{\neq}$ values for the two complexes are 7.8 ± 1.0 and 9.0 ± 1.0 kcal/mol, and -44 and -39 entropy unit, respectively. The coordinated *trans*-2-butene is replaced by other olefins, 2,3-dimethyl-2-butene, 2-methyl-2-butene, *trans*-2-butene (optical inversion), and styrene, under similar conditions to give the same rate formula. The second order rate constant increases in the given order. The inversion seems to take place *via* bimolecular mechanism with excessive olefin as nucleophile. The corresponding complexes containing styrene and its *para* derivatives give such an inversion much faster in the absence of excess of olefin. With change of *para* substituents, the rate increases in the order, methoxy<methyl<hydrogen<chloro<nitro. This seems to be related with their electrondrawing ability.

Kinetics of substitution of coordinated olefins in Zeise type complexes have been studied by several authors. Cramer found that the rate of exchange between free and coordinated ethylene is greater than 70 sec^{-1} at 75°C on the basis of nuclear magnetic resonance spectroscopy.[3] Paiaro and Panunzi examined the mutarotation of diastereoisomers of olefin complexes of platinum(II) and suggested that the exchange takes place through S_N2 Smechanism.[4] Joy and Orchin[5] and Shupack and Orchin[6] measured the equilibrium constants between some platinum(II) complexes of 1-dodecene and various substituted styrenes, and discussed the relative affinity of the olefins toward the platinum(II) ion. Recently, Venanzi and his co-workers studied the formation constants of Zeise type complexes systematically in aqueous solutions containing halo complexes of platinum(II) and various olefins.[7-10]

In previous papers we reported on the preparation and characterization of platinum(II)-olefin complexes containing amino acids,[11] and also on the preparation and circular dichroism (CD) of optically active *trans(N)*-chloro-L-prolinato-olefinplatinum(II), *trans(N)*-[PtCl(L-prol)(olefin)] (nitrogen of L-prolinate ion is *trans* to the olefin).[1] These optically active olefin-platinum(II) complexes seem particularly suitable for the kinetic study of the exchange reaction of coordinated olefins, by following the change in CD spectra, due to the asymmetric coordination of olefins to platinum(II). In this paper we report on the kinetics of optical inversion and substitution of coordinated olefins in such complexes.

The inversion reaction of coordinated olefins, shown in Fig. 1, is an interconversion between (a) and (b) and involves the cleavage of both the so-called σ- and

1) Part II of this series, K. Konya, J. Fujita, and K. Nakamoto, *Inorg. Chem.*, **10**, 1699 (1971).
2) Present address, Department of Chemistry, Marquette University, Milwaukee, Wisconsin, U.S.A.
3) R. Cramer, *Inorg. Chem.*, **4**, 445 (1965).
4) G. Paiaro and A. Panunzi, *Ric. Sci. Rend. Sez., A*, **4**, 601 (1964).
5) J. R. Joy and M. Orchin, *J. Amer. Chem. Soc.*, **81**, 805 (1959).
6) S. I. Shupack and M. Orchin, *ibid.*, **86**, 586 (1964).
7) R. G. Denning, F. R. Hartley, and L. M. Venanzi, *J. Chem. Soc. A*, **1967**, 324, 328.
8) F. R. Hartley and L. M. Venanzi, *ibid.*, **1967**, 330.
9) R. G. Denning and L. M. Venanzi, *ibid.*, **1967**, 336.
10) R. M. Milburn and L. M. Venanzi, *Inorg. Chim. Acta*, **2**, 97 (1968).
11) J. Fujita, K. Konya, and K. Nakamoto, *Inorg. Chem.*, **9**, 2794 (1970).

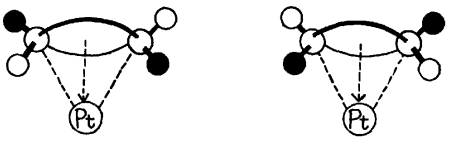

(a) (b)

Fig. 1. Enantiomeric coordination of an olefin ligand, *e.g.* *trans*-2-butene.

π-bond between the metal ion and the olefin.

The complexes of such olefins as 2-methyl-2-butene and *trans*-2-butene show no change in absorption and CD spectra in the absence of free olefin in organic solvents such as ethanol, chloroform, and acetone. When the same kind of olefin as in the complex is added, the CD spectrum changes with time and approaches a constant pattern, but the ultraviolet absorption spectrum remains unchanged. This fact indicates that only inversion reaction of the coordinated olefin takes place without involving any other reaction. When another kind of olefin is added to the solution, both ultraviolet absorption and CD spectrum change with time. The absorption pattern of the final solution suggests that an exchange of the coordinated olefin takes place with the added olefins. We have followed the change in peak height of CD spectra in near ultraviolet region of optically active $(+)^{\Delta\varepsilon}_{380}$-*trans*(*N*)-[PtCl(L-prol)(*trans*-2-butene)] and $(+)^{\Delta\varepsilon}_{380}$-*trans*(*N*)-[PtCl(L-prol)(2-methyl-2-butene)] on the addition of various olefins, and found that the rate depends on the kind of added olefin. The reaction mechanism has been discussed on the basis of the rate constants and other kinetic parameters.

The corresponding complexes containing styrene and its derivatives *trans*(*N*)-[PtCl(L-prol)(styrene)], on the other hand, show a significant change in ultraviolet absorption and CD spectrum in the absence of free olefin in organic solvents. The change is fast even at 0°C. The rate has been qualitatively examined at temperatures 0—15°C, and the influence of the substituting groups on styrene is discussed.

Results and Discussion

Optical Inversion of Coordinated Olefins in Optically Active $(+)^{\Delta\varepsilon}_{380}$-trans(N)-[*PtCl(L-prol)(2-methyl-2-butene)*] *and* $(+)^{\Delta\varepsilon}_{380}$-trans(N)-[*PtCl(L-prol)*(trans-*2-butene)*].

The inversion reaction of olefins in both complexes was studied in acetone. Decrease in the peak height of the CD spectrum was measured on addition of the same olefin as the ligand. No change in the absorption spectrum was observed. Only the inversion reaction of coordinated olefins seemed to take place in the solution. No stereoselective coordination of the olefins was observed, when 2-methyl-2-butene and *trans*-2-butene were added to the *trans*(*N*)-[PtCl(L-prol)-(ethylene)]. Thus, we can presume that neither stereoselective reaction would take place on the addition of these olefins to the solution of their complexes.

The change in CD peak height ($\Delta\varepsilon$) at 380 nm with time, when 2-methyl-2-butene (0.50M) is added to $(+)^{\Delta\varepsilon}_{380}$-*trans*(*N*)-[PtCl(L-prol)(2-methyl-2-butene)]

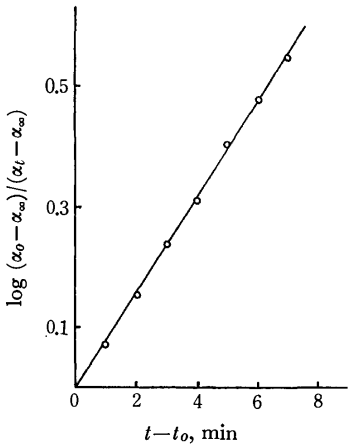

Fig. 2. CD change at 380 nm of *trans*(*N*)-[PtCl(L-prol)(2-methyl-2-butene)] with time in acetone. (23.6±0.3°C, complex (2×10^{-3}M), 2-methyl-2-butene (0.5M)).

(0.0020M) in acetone, is shown in Fig. 2. The rate of change in CD follows the first order rate law, and the apparent rate constant is given by

$$k_{obs}=\ln[(\alpha_0-\alpha_\infty)/(\alpha_t-\alpha_\infty)]/(t-t_0) \quad (1)$$

where α_o, α_t, and α_∞ denote the $\Delta\varepsilon$ values at time t_o, t, and infinite time, respectively. k_{obs} is related to the rate constant of inversion reaction, k_{inv}, by the relation $k_{obs}=2k_{inv}$. However, the k_{obs} values are used in the following discussion for a comparison with the rate constants of substitution reactions.

The relationship between k_{obs} and the amount of added 2-methyl-2-butene at three temperatures is shown in Fig. 3, the concentration of the complex being kept constant at 1.9×10^{-3}M. In a given con-

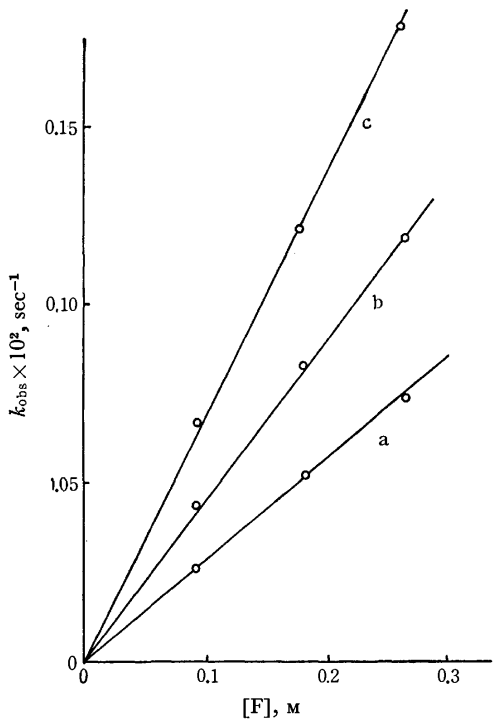

Fig. 3. Relationship between k_{obs} and the concentration of added 2-methyl-2-butene. (*trans*(*N*)-[PtCl(L-prol)(2-methyl-2-butene)] (1.90×10^{-3}M)). a, 3.7±0.3°C; b, 13.2±0.3°C; c, 21.6±0.3°C.

centration range, k_{obs} is proportional to the amount of added olefin. The lines showing the proportionality pass the origin. This coincides with the observation that the CD spectrum does not change in the absence of excessive olefin. Thus the apparent rate is given by

$$\text{Rate} = k_{obs}[\text{complex}] = k[\text{F}][\text{complex}] \quad (2)$$

where [F] is the concentration of added olefin.

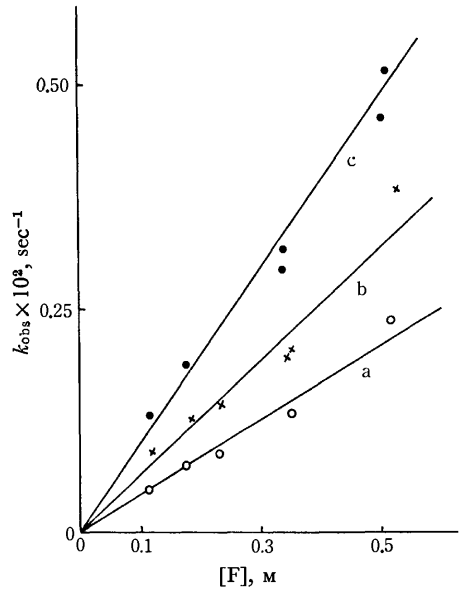

Fig. 4. Relationship between k_{obs} and the concentration of added *trans*-2-butene. (*trans*(*N*)-[PtCl(L-prol)(*trans*-2-butene)] (1.50×10^{-3}M)). a, 8.1±0.3°C; b, 17.0±0.3°C; c, 23.6±0.3°C.

The CD strength of the corresponding *trans*-2-butene complex also decreases in a similar way. In the relationship between k_{obs} and the amount of added *trans*-2-butene complex shown in Fig. 4, the fluctuation in individual plots is slightly greater than that in Fig. 3. This is due to the inaccuracies involved on the addition of the olefin to the sample solution, since *trans*-2-butene is a gas at room temperature (bp +0.88°C).

The Arrhenius plots of the results for the two complexes are given in Fig. 5, and the kinetic parameters summarized in Table 1.

In general, substitution reactions of square planar complexes obey the formula

$$\text{Rate} = -\text{d[substrate]}/\text{d}t = [\text{substrate}](k_1 + k_2[\text{Y}]) \quad (3)$$

where [Y] stands for the concentration of the nucleophile substituting for the ligand. The k_1 and k_2 term represent the solvent path and the reagent path, respectively. Both paths are believed to proceed *via*

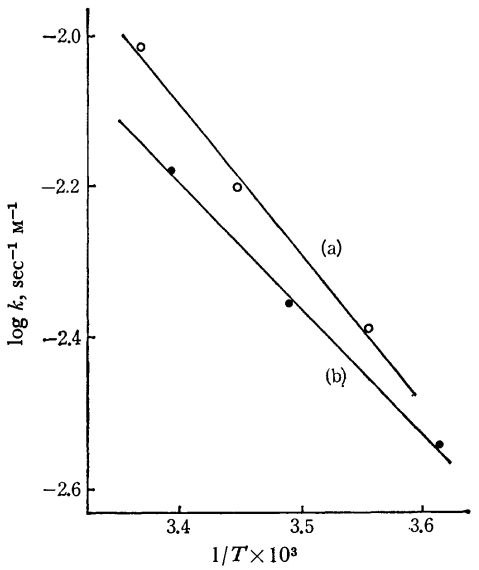

Fig. 5. Arrhenius plots for the interconversion reaction of *trans*-2-butene(a) and 2-methyl-2-butene(b) complex.

S_N2 reaction mechanism. Our rate formula (Eq. (2)) corresponds to Eq. 3 where k_1 is equal to zero.

The small E_a and the big absolute value of ΔS^* given in Table 1 indicate that the inversion of coordinated olefins would take place through S_N 2reaction mechanism. A probable intermediate state is shown in Fig. 6. Since proline has a large pyrolidine ring, the olefin could approach the complex only from one side of the complex plane. The very big negative values of ΔS^* seem to reflect this limited possibility in the formation of the intermediate state with coordination number five.

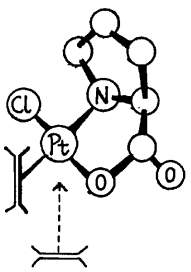

Fig. 6. Probable intermediate state.

Negligible contribution of the solvent path to the inversion reaction could be understood by considering the fact that acetone is a very weak nucleophile towards platinum(II).[12]

Substitution Reaction of Optically Active $(+)^{Ae}_{360}$-trans(N)-[*PtCl(L-prol)(*trans-*2-butene)*]. In order to examine the steric effect of the nucleophile, we have examined

Table 1. Activation parameters for the inversion reaction of olefins in *trans*(*N*)-[PtCl(L-prol)(2-methyl-2butene)] and *trans*(*N*)-[PtCl(L-prol)(*trans*-2-butene)] in acetone

Complex	T, °C	$k \times 10^3$(sec^{-1}M^{-1})	E_a,kcal/mol	ΔS^*, e.u.
trans(*N*)-[PtCl(L-prol)(2-methyl-2-butene)]	13.2	4.44±0.02	7.8	−44
trans(*N*)-[PtCl(L-prol)(*trans*-2-butene)]	17.0	6.3 ±0.1	9.0	−39

12) R. G. Pearson, H. B. Gray, and F. Basolo, *J. Amer. Chem. Soc.*, **82**, 787 (1960).

the replacement of coordinated *trans*-2-butene in $(+)^{\Delta\varepsilon}_{380}$-*trans*(*N*)-[PtCl(L-prol)(*trans*-2-butene)] by various olefins including styrene, 2-methyl-2-butene, and 2,3-dimethyl-2-butene. Although the reaction products were not isolated crystalline, change in absorption spectra indicated that substitution reaction took place as follows.

$$trans(N)\text{-}[PtCl(L\text{-}prol)(trans\text{-}2\text{-}butene)] + \text{olefin} \rightleftharpoons trans(N)\text{-}[PtCl(L\text{-}prol)(\text{olefin})] + trans\text{-}2\text{-}butene \quad (4)$$

The substitution reactions were best followed by measuring the change in CD, since it is much more marked than the change in absorption spectra on the substitution reaction.

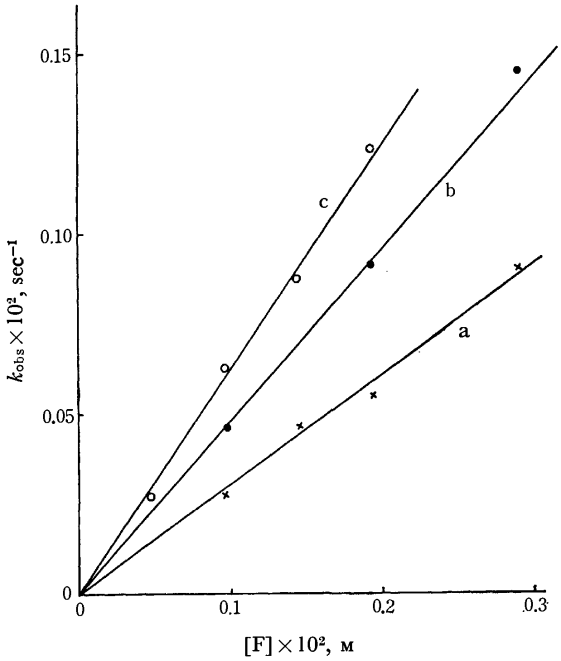

Fig. 7. Relationship between k_{obs} and the concentration of added styrene. (*trans*(*N*)-[PtCl(L-prol)(*trans*-2-butene)] (1.50×10^{-3}M)). a, 8.1±0.3°C; b, 17.0±0.3°C; c, 23.6±0.3°C.

All the reactions obeyed the second order rate expression with regard to both the concentration of the complex and that of added olefin (Eq. (2)). The relationship between the k_{obs} and the concentration of styrene at three temperatures is shown in Fig. 7. 2-Methyl-2-butene and 2,3-dimethyl-2-butene give similar diagrams on the substitution reaction. All the straight lines have zero intercepts. The rate constants and the activation parameters are given in Table 2.

The rate constants increase in the order 2,3-dimethyl-2-butene < 2-methyl-2-butene < *trans*-2-butene(optical inversion) < styrene.

We also see that the activation energies are almost equal to one another in the given substitution reactions, and the order of increase in the rate constant is the same as the order of decrease in $-\Delta S^*$ values. The order of increase in nucleophilicity of the olefins seems to be the reverse of that for the increase in the rate constant, since methyl is more electron pushing than phenyl, and the increase in number of methyl group will certainly result in the increase in electron density on the C=C bond of the olefins. Thus, a steric effect seems to be more responsible for determining the rate of the substitution reaction of such prolinato olefin complexes. A decrease in the number of substituting groups on the carbon atoms of C=C double bond would make it easier for the olefin to approach the complex as shown in Fig. 6.

Observation on the Change in CD of trans*(*N*)-*L*-Prolinatoplatinum(II) Complexes Containing Styrene and Its Derivatives.* The CD strength of the optically active complexes *trans*(*N*)-[PtCl(L-prol)(*p*-X-styrene)] (X=methoxy, methyl, chloro, nitro, and hydrogen) decreases with time in acetone, and becomes constant within 5 to 10 min at room temperature in the absence of excessive styrenes as shown in Fig. 8. The rate increases with the progress of reaction. The absorp-

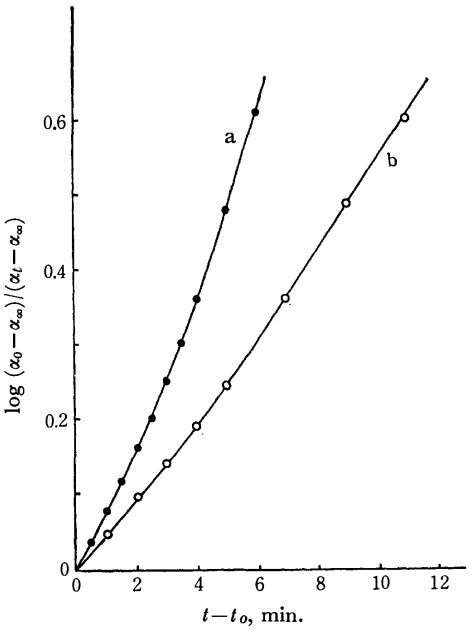

Fig. 8. CD change at 380 nm with time of *trans*(*N*)-[PtCl(L-prol)(styrene)] (1.326×10^{-3}M)(a) and *trans*(*N*)-[PtCl(L-prol)(*p*-methoxystyrene)] (1.455×10^{-3}M) (b) in acetone. (17.1±0.3°C).

TABLE 2 RATE CONSTANTS AND ACTIVATION PARAMETERS FOR THE SUBSTITUTION REACTIONS OF *trans*(*N*)-[PtCl(L-prol)(*trans*-2-butene)] WITH VARIOUS OLEFINS IN ACETONE

Olefin	$k\times10^3$(sec^{-1}M^{-1})						E_a, kcal/mol	ΔS^*, e.u.
	T, °C 8.1	17.0	23.6	31.5	39.5	Error		
Styrene	303	480	621	—	—	±20	8.2	−34
trans-2-Butene	4.1	6.3	9.7	—	—	±1.0	9.0	−39
2-Methyl-2-butene	3.41	5.35	7.29	—	—	±0.20	8.6	−41
2,3-Dimethyl-2-butene	—	—	0.220	0.325	0.463	±0.020	8.6	−46

Table 3. Results of microanalysis

	C(%) Found	C(%) Calcd	H(%) Found	H(%) Calcd	N(%) Found	N(%) Calcd
trans(*N*)-[PtCl(L-prol)(*p*-methoxystyrene)]	35.02	35.19	3.85	3.59	2.98	2.93
trans(*N*)-[PtCl(L-prol)(*p*-methylstyrene)]	35.96	36.41	3.92	3.71	2.95	3.03
trans(*N*)-[PtCl(L-prol)(*p*-chlorostyrene)]	32.67	32.37	3.22	2.93	2.81	2.90
trans(*N*)-[PtCl(L-prol)(*p*-ntrostyrene)]	31.56	31.68	3.07	2.87	5.51	5.68

tion spectra of these complexes change simultaneously and seem to approach a constant pattern in a few hours at room temperature. Thus the following solvolytic equilibrium might be involved.

$$\textit{trans}(N)\text{-[PtCl(L-prol)}(p\text{-X-styrene)}] + \text{solvent} \rightleftharpoons \textit{trans}(N)\text{-[PtCl(L-prol)(solvent)]} + p\text{-X-styrene} \quad (5)$$

The decrease in CD strength can be presumed to proceed *via* two routes, the solvent path and the reagent path, as in most square planar complexes. If the inversion reaction were accompanied by the solvolysis, the styrene liberated on solvolysis would operate as nucleophile and bring about an increase in the rate of CD change with the progress of reaction. Preliminary experiments showed that the CD strength of optically active styrene complexes decreased rapidly when a very small amount (*e.g.* 1% to the complex in molar ratio) of styrene was added to the complex solution.

The final pattern of the absorption spectrum should correspond to that of the equilibrated state of Eq. (5). However, the absorption spectrum of the product is unknown. Thus, we analyzed the initial part of the curves in Fig. 8 by use of Eq. (1), as in other olefin complexes in order to find the effect of substituents on styrene. The k_{obs} values increase almost linearly with the increase in the initial concentration of the complex, and are too great to enable kinetic treatment. It is seen, however, that the apparent rate constant k_{obs} increases in the sequence

p-methoxystyrene$<$*p*-methylstyrene$<$styrene$<$*p*-chlorostyrene$<$*p*-nitrostyrene

The order of such an increase is in accord with that of electrondrawing ability of the substituents on the *para* position. The stronger the attraction of electrons by substituent, the smaller the electron density on the C=C double bond in the side chain. The smaller electron density on the C=C double bond may result in a decrease in the σ-donating ability and an increase in the π-accepting ability of the olefin ligand.[5,6] The rate for the present reactions should have both non-zero k_1 and k_2 term (Eq. 3), although their values were not obtained separately. Thus the true mechanism of the reaction remains uncertain. However, the above sequence of the styrene derivatives suggests that the racemization is closely related to the strength of the metal-olefin σ-bond.

Experimental

Material. (+)-$^{\Delta\varepsilon}_{380}$*trans*(*N*)-[PtCl (L-prol) (2-methyl-2-butene)] and (+)$^{\Delta\varepsilon}_{380}$-*trans*(*N*)-[PtCl(L-prol)(*trans*-2-butene)] were prepared as described previously.[1] 2-Methyl-2-butene, *trans*-2-butene, styrene, and 2,3-dimethyl-2-butene are of extra-pure grade (Tokyo Kasei Co.) and used without further purification. Derivatives of styrene (*p*-methoxy, *p*-methyl, *p*-chloro, and *p*-nitrostyrene) were prepared by the method of Walling and Wolfstirn.[13] The complexes were synthesized as in the case of styrene.[1] Commercial acetone of spectro-grade was used as solvent without purification. The results of microanalysis are shown in Table 3.

Equipments. Circular dichroism was measured with a JASCO Model ORD/UV-5 Spectrometer with CD attachment and a cell jacket to keep the temperature constant within ±0.3°C (Komatsu-Yamato Coolnics). A Takara Thermister Type SPD-1D thermometer was calibrated with Toa's standard thermometer and the unit was placed inside the CD cell. Absorption spectra were recorded with a Hitachi 124 Spectrometer.

Procedure. Inversion reaction of coordinated olefins in (+)$^{\Delta\varepsilon}_{380}$-*trans*(*N*)-[PtCl(L-prol)(olefin)] (olefin = 2-methyl-2-butene, *trans*-2-butene). To a thermostated acetone solution of the complex ($\simeq 10^{-3}$M) was added a certain amount ($\simeq 10^{-1}$M) of olefin with a micro syringe. The solution was kept in the cell box of the spectrometer which had also been thermostated. The $\Delta\varepsilon$ value at 380 nm was continuously recorded.

The complexes of styrene and its derivatives were dissolved in acetone and the decrease in CD was measured at 380 nm, the temperature being controlled within ±0.3°C.

We are grateful to the Ministry of Education for a Grant-in-aid for our studies on optically active complexes.

13) C. Walling and K. B. Wolfstirn, *J. Amer. Chem. Soc.*, **69**, 852 (1947).

Thermal Decomposition Reactions of Metal Oxalato Complexes in the Solid State. I. Thermographic Studies of Metal Oxalato Complexes

Kenzo NAGASE

Department of Chemistry, Tohoku University, Kawauchi, Sendai

(Received December 24, 1971)

The thermal decomposition reactions of metal oxalato complexes in the solid state were studied by the TG and DSC methods. The results from TG indicated that the thermal stability of the anhydrous complex decreases approximately with the increase in the electron affinity of the central metal ion. From DSC, the complexes can be divided into two groups, giving endothermic and exothermic peaks on the decomposition of their anhydrous complexes respectively. The two enthalpy changes, ΔH, corresponding to the dehydration and to the decomposition of the anhydrous complexes, are also presented.

Although the thermal properties of metal oxalates have been extensively studied, few studies have been made of metal oxalato-type complexes. Wendlandt and George[1] carried out the thermogravimetry (TG) of $K_3[Cr(ox)_3]3H_2O$, $K_3[Fe(ox)_3]3H_2O$, $K_3[Co(ox)_3]$-$3H_2O$, and $K_3[Rh(ox)_3]2.5H_2O$.

Tanaka and Nanjo[2] have followed the change in the valence state of the central metal ions on the thermal decomposition reactions of $K_3[Fe(ox)_3]$ and $K_3[Co(ox)_3]$; they have suggested that the decomposition of these complexes is initiated by the electron transfer from the coordianted oxalate ion to the central metal ion.

Information on the intermediates and kinetic data on the thermal decomposition reactions of $K_3[Mn(ox)_3]$-$3H_2O$,[3] $K_3[Fe(ox)_3]3H_2O$,[4-7] and $K_3[Co(ox)_3]$-$3H_2O$,[8,9] have been presented by several workers.

In this study, the TG and DSC curves of a number of metal oxalato complexes will be presented, and the relations between the thermal property of the complex and the nature of the central metal ion will be examined.

Experimental

TG and DSC. Thermogavimetric (TG) and Differential scanning calorimetric (DSC) curves were obtained with a Rigaku 2008 CS thermobalance equipped with a standard differential scanning calorimeter in a dynamic nitrogen atmosphere. About ten milligrams of a powdered sample in an aluminum crucible were used in each measurement. The heating rate was exactly linear with the time at about 4°C per min.

Materials. The complexes of Al(III),[10] V(III),[11] Cr(III),[12] Mn(III),[13] Fe(III),[14] Co(III),[15] Rh(III),[16] Cu(II),[17], Pd(II),[18] and Pt(II),[19] were prepared according to the litterature. The $K_2[Zn(ox)_2]2H_2O$ was prepared by boiling $Zn(OH)_2$ with a stoichiometric amount of aqueous $H_2C_2O_4 \cdot 2H_2O$ and $K_2C_2O_4 \cdot H_2O$ until the solution was neutral. The analytical results on the complexes were as follows: $K_3[Al(ox)_3]3H_2O$; C, found, 15.45, calcd, 15.85; H, found, 0.90, calcd, 1.30; $K_3[V(ox)_3]3H_2O$; C, found, 14.76, calcd, 14.79; H, found, 1.19, calcd, 1.23; $K_3[Cr(ox)_3]3H_2O$; C, found, 14.77, calcd, 14.78; H, found, 0.86, calcd, 1.23; $K_3[Fe(ox)_3]3H_2O$; C, found, 14.49, calcd, 14.65; H, found, 0.81, calcd, 1.22; $K_3[Co(ox)_3]3H_2O$; C, found, 14.41; calcd, 14.57; H, found, 1.21, calcd, 1.21; $K_3[Rh(ox)_3]4.5H_2O$; C, found, 12.43, calcd, 12.74; H, found, 1.25, calcd, 1.25; $K_2[Cu(ox)_2]2H_2O$; C, found, 13.48, calcd, 13.56; H, found, 0.93, calcd, 1.13; $K_2[Zn(ox)_2]2H_2O$; C, found, 13.39, calcd, 13.48; H, found, 0.83, calcd, 1.12; $K_2[Pd(ox)_2]3H_2O$; C, found, 11.54, calcd, 11.56; H, found, 1.43, calcd, 1.45; $K_2[Pt(ox)_2]2H_2O$; C, found, 9.55, calcd, 9.89; H, found, 0.66, calcd, 0.83.

Results and Discussion

TG Study. The thermogravimetric curves of the metal oxalato complexes obtained in this work are given in Figs. 1 and 2. The TG curves of Al(III), V(III), Cu(II), Zn(II), Pd(II), and Pt(II) complexes seem to be the first to appear. Although the TG curves of the remaining metals have been presented by several workers, these curves were reproduced under the experimental conditions employed in the present work. The temperature range and the percentage of mass loss are summarized in Table 1. Except for $K_3[Mn(ox)_3]3H_2O$, all the complexes evolved hydrated water at about 100°C to form the corresponding anhydrous complexes. The dehydration of K_3-$[Mn(ox)_3]3H_2O$ took place, along with the decomposition of the anhydrous complex. Except for

1) W. W. Wendlandt and T. D. George, *J. Inorg. Nucl. Chem.*, **21**, 69 (1961).
2) N. Tanaka and M. Nanjo, This Bulletin, **40**, 330 (1967).
3) E. L. Simmons and W. W. Wendlandt, *J. Inorg. Nucl. Chem.*, **27**, 2325 (1965).
4) G. M. Bancroft, K. G. Dharmawardena, and A. G. Maddock, *Inorg. Nucl. Chem. Lett.*, **6**, 403 (1970).
5) D. B. D. Dollimore and J. Dollimore, *J. Chem. Soc., A*, **1967**, 1451.
6) N. Tanaka and K. Sato, This Bulletin, **43**, 789 (1970).
7) J. D. Danforth and J. Dix, *Inorg. Chem.*, **10**, 1623 (1971).
8) W. W. Wendlandt and E. L. Simmons, *J. Inorg. Nucl. Chem.*, **27**, 2317 (1965).
9) N. Tanaka, K. Nagase, and S. Nagakura, This Bulletin, **41**, 1143 (1968).
10) H. S. Booth, "Inorganic Syntheses," Vol. 1, McGraw-Hill, New York (1936), p. 36.
11) A. Picoini and N. Brxxi, *Z. Anorg. Chem.*, **19**, 394 (1899).
12) A. Rosenheim, *ibid.*, **11**, 196 (1892).
13) G. H. Cartledge and W. P. Ericks, *J. Amer. Chem. Soc.*, **56**, 2061 (1936).
14) F. M. Jager, *Rec. Trav. Chim.*, **38**, 242 (1919).
15) S. P. L. Sörensen, *Z. Anorg. Chem.*, **11**, 2 (1896).
16) M. Del epine, *An Espan.*, **27**, 490 (1929).
17) H. L. Riley, *J. Chem. Soc.*, **1929**, 1307.
18) M. Vezes, *Bull. Soc. Chim. Fr.*, **21**, 172 (1899).
19) M. Vezes, *ibid.*, **19**, 875 (1898).

Table 1. Temperature range and mass loss of metal oxalato complexes

Complex	Dehydration			Decomposition of anhydrous complex		
	Tamperature range, °C	Mass loss, %		Temperature range, °C	Mass loss, %	
		Obsd.	Calcd.		Obsd.	Calcd.
$K_3[Al(ox)_3]3H_2O$	55—100	9.2	11.7 for $3H_2O$	335—426	28.8	31.2 for $2CO+2CO_2$
$K_3[V(ox)_3]3H_2O$	35—124	10.2	11.1 for $3H_2O$	331—414	23.9	23.9 for $CO+2CO_2$
$K_3[Cr(ox)_3]3H_2O$	32—162	10.5	11.1 for $3H_2O$	325—450	18.8	—
$K_3[Mn(ox)_3]3H_2O$	45—225	16.7	20.0 for $3H_2O+CO_2$			
$K_3[Fe(ox)_3]3H_2O$	30—122	9.1	11.1 for $3H_2O$	230—265	8.7	8.8 for CO_2
$K_3[Co(ox)_3]3H_2O$	48—115	9.5	10.9 for $3H_2O$	115—231	8.7	8.8 for CO_2
$K_3[Rh(ox)_2]4.5H_2O$	25—150	14.6	14.3 for $4.5H_2O$	225—260	23.4	23.4 for $3CO_2$
$K_2[Cu(ox)_2]2H_2O$	85—117	9.8	10.2 for $2H_2O$	247—285	24.4	24.9 for $2CO_2$
$K_2[Zn(ox)_2]2H_2O$	80—130	5.8	10.1 for $2H_2O$	360—430	11.0	11.0 for $1/2CO+1/2CO_2$
$K_2[Pd(ox)_2]3H_2O$	28—110	13.7	13.0 for $3H_2O$	116—190	21.2	21.2 for $2CO_2$
$K_2[Pt(ox)_2]2H_2O$	75—110	6.7	7.4 for $2H_2O$	207—223	18.7	18.1 for $2CO_2$

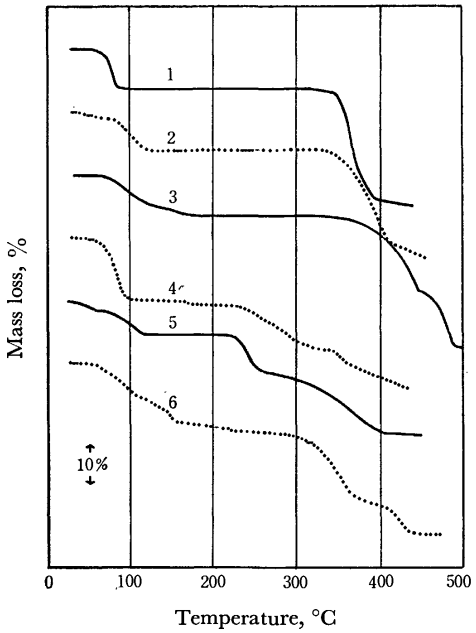

Fig 1. TG curves of (1) $K_3[Al(ox)_3]3H_2O$, (2) $K_3[V(ox)_3]$-$3H_2O$, (3) $K_3[Cr(ox)_3]3H_2O$, (4) $K_3[Mn(ox)_3]3H_2O$, (5) K_3-$[Fe(ox)_3]3H_2O$ and $K_3[Co(ox)_3]3H_2O$ in a nitrogen atmosphere.

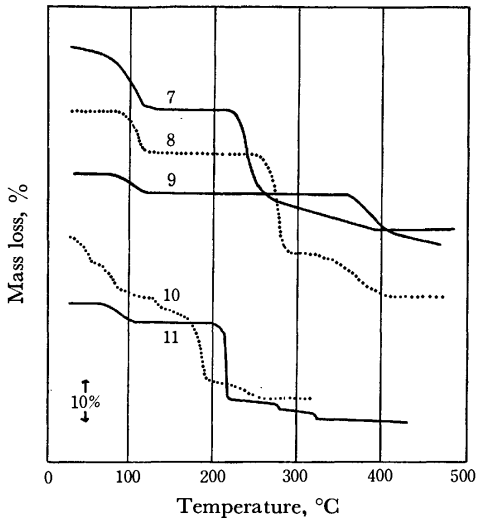

Fig. 2. TG curves of (7) $K_3[Rh(ox)_3]4.5H_2O$, (8) $K_2[Cu(ox)_2$-$]2H_2O$, (9) $K_2[Zn(ox)_2]2H_2O$, (10) $K_2[Pd(ox)_2]3H_2O$ and (11) $K_2[Pt(ox)_2]2H_2O$ in a nitrogen atmosphere.

$K_3[Rh(ox)_3]4.5H_2O$ and $K_2[Pd(ox)_2]3H_2O$, the observed values of mass loss corresponding to the dehydration were somewhat lower than the calculated values for the formula described. This difference may be due to the partial evolution of the hydrated water before measurement. In a previous paper,[1] it has been reported that the rhodium(III) complex evolved 2.5 mol of water in two steps; however, it evolved 4.5 mol of water in one step in the present work.

The order of the decomposition temperatures of the anhydrous complexes is as follows:

$K_3[Mn(ox)_3]<K_3[Co(ox)_3]<K_2[Pd(ox)_2]<$
$K_2[Pt(ox)_2]<K_3[Rh(ox)_3]<K_3[Fe(ox)_3]<$
$K_2[Cu(ox)_2]<K_3[Cr(ox)_3]<K_3[V(ox)_3]<$
$K_3[Al(ox)_3]<K_2[Zn(ox)_2]$

This order has no relation to the strength of the metal-oxygen bond as obtained by the infrared spectroscopic

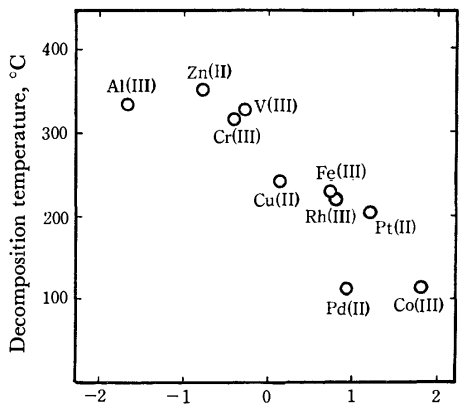

Fig. 3. Correlation of decomposition temperatures of metal oxalato complexes with oxidation-reduction potentials of central metal ions in aqueous solution. The redox potentials adopted correspond to the couples M(II)/M(III) for V, Cr, Fe, and Co, M(0)/M(III) for Al and Rh, and M(0)/M(II) for Cu, Zn, Pd, and Pt, respectively.

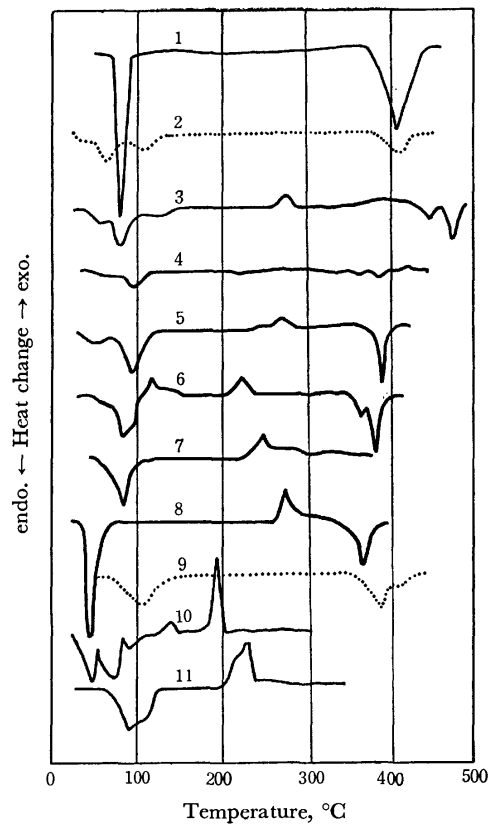

Fig. 4. DSC cruves of (1) $K_3[Al(ox)_3]3H_2O$, (2) $K_3[V(ox)_3]$-$3H_2O$, (3) $K_3[Cr(ox)_3]3H_2O$, (4) $K_3[Mn(ox)_3]3H_2O$, (5) $K_3[Fe(ox)_3]3H_2O$, (6) $K_3[Co(ox)_3]3H_2O$, (7) $K_3[Rh$-$(ox)_3]4.5H_2O$, (8) $K_2[Cu(ox)_2]2H_2O$, (9) $K_2[Zn(ox)_2]$-$2H_2O$, (10) $K_2[Pd(ox)_2]3H_2O$ and $K_2[Pt(ox)_2]2H_2O$ in a nitrogen atmosphere.

study.[20] In Fig. 3, the plots of the decomposition temperatures of the anhydrous complexes *versus* the oxidation-reduction potentials[21] of the central metal ions forming an aquo complex are given. These potentials are considered to measure the relative electron affinities of the central metal ions forming an oxalato complex, since Dq value of H_2O is near to that of $C_2O_4^{2-}$. The results in Fig. 3, therefore, indicate that the thermal stability of the anhydrous complex decreases approximately with the increase in the electron affinity of the central metal ion.

DSC Study. The differential calorimetric curves of the complexes obtained in the present work are given in Fig. 4. The values of the enthalpy change, ΔH, corresponding to the dehydration and to the decomposition of the anhydrous complexes are both summarized in Table 2.

Table 2. Enthalpy change of dehydration and decomposition of metal oxalato complexes

Complex	Dehydration (kcal/mol)	Decomposition of anhydrous complex (kcal/mol)
$K_3[Al(ox)_3]3H_2O$	13.9	15.3
$K_3[V(ox)_3]3H_2O$	8.2	4.1
$K_3[Cr(ox)_3]3H_2O$	9.7	−1.9
$K_3[Fe(ox)_3]3H_2O$	12.8	−2.4
$K_3[Co(ox)_3]3H_2O$	13.6	−2.5
$K_3[Rh(ox)_3]4.5H_2O$	12.4	−6.6
$K_2[Cu(ox)_2]2H_2O$	12.1	−3.4
$K_2[Zn(ox)_2]2H_2O$	9.3	2.8
$K_2[Pd(ox)_2]3HO$	9.3	−2.4
$K_2[Pt(ox)_2]2H_2O$	11.3	−6.5

In connection with the enthalpy change corresponding to the dehydration, it should be noticed that there is some difference between the amount of hydrated water from TG and the theoretical value for the formula described. The values calibrated, therefore, are given in Table 2. The values of ΔH corresponding to the dehydration are about 10 kcal/mol for all of the complexes.

From the values of ΔH corresponding to the decomposition of the anhydrous complexes, the anhydrous complexes can be divided into two groups: the complexes of Cr(III), Fe(III), Co(III), Rh(III), Cu(II), Pd(II), and Pt(II), all decomposing with a negative value of ΔH, belong to the first group, while the complexes of Al(III), V(III), and Zn(II), which decompose with a positive value, belong to the second group.

From the analyses of the gaseous products, this division for metal oxalato complexes seems to be suitable; *i.e.*, all the complexes in the first group except for $K_3[Cr(ox)_3]$ evolved only CO_2 upon their decomposition, suggesting an electron transfer from the coordinated oxalate ion to the central metal ion, while the complexes in the second group evolved both CO and CO_2, suggesting the formation of the metal oxide. The details of the gaseous and solid products will be reported later.

The DSC curve of the chromium(III) complex shows a small exothermic peak without any mass loss in the 265—290°C temperature range. This may be due to the transition of the anhydrous complex from the amorphous state (after water removal) to the crystalline state. The ΔH value of this transition was 1.4 kcal/mol. The details of the transition will be reported later.

The author wishes to thank Dr. N. Tanaka, Professor of Tohoku University, for his advice.

20) K. Nakamoto, "Infrared Spectra of Inorganic and Coordination Compounds," John Wiley & Sons, New York (1963).

21) W. M. Latimer, "The Oxidation State of the Elements and Their Potentials in Aqueous Solution," Prentice-Hall, New York (1952).

Polarographic Study of the Rates of the Dissociation Reactions of the Nickel(II)-, Zinc(II)-, and Cadmium(II)-2,2′-Ethylenedioxybis[ethyliminodi(acetate)] (GEDTA) Complexes

Mutsuo KODAMA and Noboru OYAMA*

Department of Chemistry, Ibaraki University, Bunkyo, Mito, Ibaraki

**Chemistry Department, Faculty of Engineering, Ibaraki University, Narisawa, Hitachi, Ibaraki*

(Received January 27, 1972)

In GEDTA solutions with pH's lower than 7.0_0, the nickel(II), zinc(II), and cadmium(II) ions were found to yield the one-step, two-step, and three-step polarographic waves respectively. The polarographic wave of the nickel(II) ion, the first step of the zinc(II) ion, and the first and second steps of the cadmium(II) ion showed a kinetic-controlled nature. In this study, the polarographic wave of the nickel(II) ion, the first step of the zinc(II) ion, and the second step of cadmium(II) ion were studied systematically. From an experimental examination of the nature of the kinetic currents of these complexes, the mechanisms for the above polarographic steps were determined as:

i) $NiHY^- \rightleftharpoons Ni^{2+} + HY^{3-}$ rate-determining step
$\downarrow\uparrow$ rapid
pH<5.70 NiY^{2-}
$Ni^{2+} + 2e^- + Hg = Ni(Hg)$
$NiY^{2-} \rightleftharpoons Ni^{2+} + Y^{4-}$ rate-determining step
$\downarrow\uparrow$ rapid
pH>5.70 $NiHY^-$
$Ni^{2+} + 2e^- + Hg = Ni(Hg)$

ii) $ZnHY^- + H^+ = Zn^{2+} + H_2Y^{2-}$ rate-determining step
$\downarrow\uparrow$ rapid
ZnY^{2-}
$Zn^{2+} + 2e^- + Hg = Zn(Hg)$

iii) $Cd(HY)_2^{4-}$
$\downarrow\uparrow$ rapid
$CdHY^- = CdHY^{-*}$ rate-determining step
$\downarrow\uparrow$ rapid
CdY^{2-}
$CdHY^{-*} + 2e^- + Hg = Cd(Hg) + HY^{3-}$

where $CdHY^{-*}$ is the electroactive cadmium(II)-GEDTA complex. By comparing the dissociation rate constant of the nickel(II)-GEDTA complex with that of the nickel(II)-aspartate complex, the detailed dissociation mechanism was determined. The rates and mechanisms of the dissociations of zinc(II) and cadmium(II)-GEDTA complexes were also discussed in detail.

In a previous paper,[1] we studied the polarographic behavior of the copper(II)-2,2′-ethylenedioxybis[ethyliminodi(acetate)] (GEDTA) complex systematically. In contrast with the copper(II)-ethylenediaminetetraacetate and *N*-(2-hydroxyethyl)-ethylenediamine-*N*,*N*′,*N*′-triacetate (EDTA-OH) complexes, it has been found to give two polarographic waves, both of which are diffusion-controlled in nature. From the GEDTA concentration dependence of the half-wave potential, it was concluded that the hexadentate GEDTA anion can form a complex with a 1:2 composition with the copper(II) ion. The GEDTA complex of the zinc(II) ion also gives the two-step polarographic wave in GEDTA solutions of pH's lower than 7.00. The second polarographic step of the zinc(II)-GEDTA complex was diffusion-controlled in nature. However, the first step showed a kinetic-controlled nature. The nickel(II) and cadmium(II) ions in GEDTA solutions were also found to give kinetic waves. In this paper, we will investigate the polarographic behaviors of nickel(II), zinc(II)-, and cadmium(II)-GEDTA complexes systematically, and will determine the rate constants and the electrode reaction mechanisms by analyzing the experimental data with the aid of theoretical relations derived previously.[2] The structure of the reaction intermediate and the reaction mechanism will also be discussed in detail on the basis of a comparison of the observed rate constant with that calculated from the reaction intermediate proposed.

Experimental

Reagents. The way of preparing the standard nickel(II) nitrate solution was given previously.[2] Standard zinc(II) and cadmium(II) solutions were prepared by dissolving known amounts of pure cadmium(II) and zinc(II) sulfates in redistilled water. GEDTA (2,2′-ethylenedioxybis[ethyliminodi(acetic acid)]) was recrystallized from its aqueous solution by adding pure ethanol and hydrochloric acid. All the other chemicals used were of an analytical-reagent grade and were used without further purification.

Apparatus and Experimental Procedures. All the DC current-voltage curves were measured by using a manual polarograph similar to that of Kolthoff and Lingane or a

1) M. Kodama and Y. Tominaga, This Bulletin, **42**, 394 (1969).

2) M. Kodama, H. Nunokawa, and N. Oyama, *ibid.*, **44**, 2387 (1971).

Yanagimoto pen-recording polarograph, PA-102. The characteristic features of the dropping mercury electrode (DME) used in this study were given previously.[2] All the other apparatuses used and the experimental procedures were also described in that previous paper.[2] The ionic strength of the solution was adjusted to 0.30 by adding an appropriate amount of pure sodium perchlorate. To keep the solution's pH constant, a sodium acetate–acetic acid mixture or a potassium dihydrogen phosphate–disodium hydrogen phosphate mixture was used.

Results and Discussion

Polarographic Behavior of the Nickel(II) Ion in the GEDTA Solution. From the thermodynamic point of view,[3] all the nickel(II) ions in a 10.0 mM GEDTA solution with a pH higher than 5.0 are considered to exist as GEDTA complex. Even under these experimental conditions, the nickel(II)-GEDTA complex gives the polarographic step at the potentials where the nickel(II) aquo ions give a polarographic wave

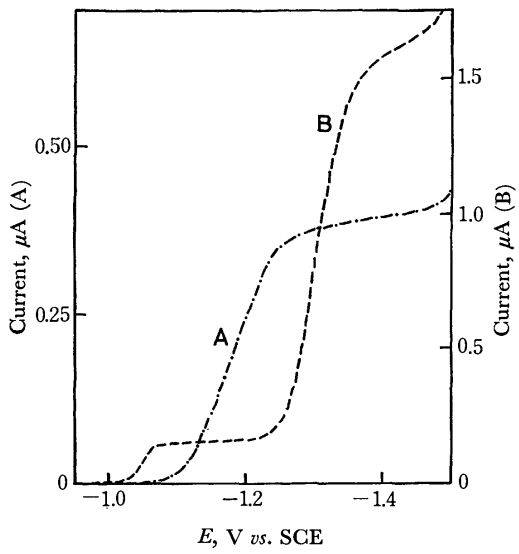

Fig. 1. Polarograms of metal(II)-GEDTA complexes.
A) Ni(II)-GEDTA system
The concentration of uncomplexed GEDTA=20.0 mM
The concentration of nickel(II) ion=1.00 mM
The total concentration of phosphate=0.12 M
pH=6.11, μ=0.30, 25°C
B) Zn(II)-GEDTA system
The concentration of uncomplexed GEDTA=10.0 mM
The concentration of zinc(II) ion=0.50$_0$ mM
The concentration of uncomplexed acetate ion=20.0 mM
pH=5.24, μ=0.30, 25°C

(Fig. 1). Although the results are not shown, its limiting current was almost independent of the effective pressure of the mercury column within the limits of experimental error. This fact clearly implies that the polarographic step of the nickel(II)-GEDTA complex is kinetic-controlled in nature. In order to maintain the solution's pH constant, an acetic acid–acetate buffer mixture (5.00<pH<5.70) or a potassium dihydrogen phosphate–disodium hydrogen phosphate mixture

3) A. Ringbom, "Complexation in Analytical Chemistry," John Wiley & Sons, New York (1963).

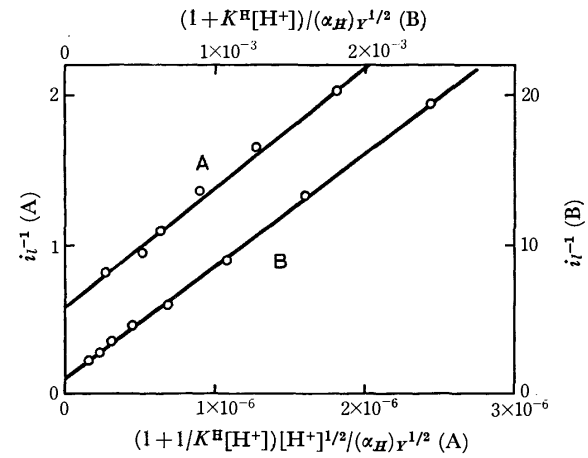

Fig. 2. The plot of i_l^{-1} against $(1+1/K^H[H^+])[H^+]^{1/2}/(\alpha_H)_Y^{1/2}$ or $(1+K^H[H^+])/(\alpha_H)_Y^{1/2}$.
The concentration of uncomplexed GEDTA=20.0 mM
The concentration of nickel(II) ion=1.00 mM
μ=0.30, 25°C
A) The plot of i_l^{-1} *vs.* $(1+1/K^H[H^+])[H^+]^{1/2}/(\alpha_H)_Y^{1/2}$ 5.00<pH<5.70, The total concentration of acetate=0.05M
B) The plot of i_l^{-1} *vs.* $(1+K^H[H^+])/(\alpha_H)_Y^{1/2}$ 5.70<pH<7.00, The total concentration of phospate=0.12M

(5.70<pH<7.00) was used in this study. However, these buffer mixtures had no effect on the wave-height and the half-wave potential of the reduction wave of the nickel(II)-GEDTA complex. In the pH range from 5.00 to 5.70, the plot of a reciprocal of the wave-height, i_l^{-1}, against the $(1+1/K^H\cdot[H^+])\cdot[H^+]^{1/2}/(\alpha_H)_Y^{1/2}$ or the $[Y]_f^{1/2}$ gave a straight line with an intercept nearly identical to the reciprocal of i_d (Fig. 2). Here, i_d is the limiting current when it is completely diffusion-controlled and is represented by the well-known Ilkoviç equation. K^H is the protonation constant of the nickel(II)-GEDTA complex (defined as $K^H=[NiHY^-]/[NiY^{2-}]\cdot[H^+]$); $(\alpha_H)_Y$, the (α_H) value of GEDTA, and $[Y]_f$, the concentration of uncomplexed GEDTA On the other hand, in solutions with pH

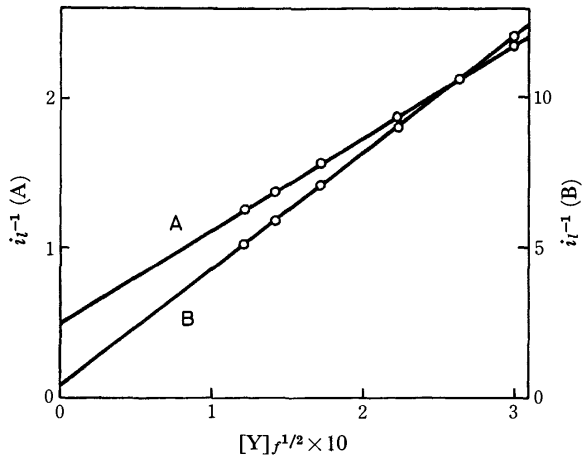

Fig. 3. The plot of i_l^{-1} against $[Y]_f^{1/2}$.
μ=0.30, 25°C
The concentration of nickel(II) ion=1.00 mM
A) pH=5.37
The total concentration of acetate=0.05M
B) pH=6.69
The total concentration of phosphate=0.12M

values from 5.70 to 7.00, the plot of i_l^{-1} *vs.* the $(1+K^{H}\cdot[H^+])/(\alpha_H)_Y^{1/2}$ or $[Y]_f^{1/2}$ gave a straight line (Fig. 3). As was discussed in connection with polarography of the nickel(II)-aspartate and glutamate complexes,[2] these facts evidently show that the reaction mechanism for the polarographic wave of the nickel(II)-GEDTA complex can be expressed as:

$5.00<pH<5.70$

$$NiHY^- \overset{(k_d)_{NIHY}}{\rightleftharpoons} Ni^{2+}+HY^{3-} \text{ r.d.s.}$$
$$\downarrow \text{ rapid}$$
$$NiY^{2-} \qquad \text{I}$$
$$Ni^{2+}+2e^-+Hg=Ni(Hg)$$

$5.70<pH<7.00$

$$NiY^{2-} \overset{(k_d)_{NIY}}{\rightleftharpoons} Ni^{2+}+Y^{4-} \text{ r.d.s.}$$
$$\downarrow \text{ rapid}$$
$$NiHY^- \qquad \text{II}$$
$$Ni^{2+}+2e^-+Hg\rightleftharpoons Ni(Hg)$$

where Y^{4-} denotes the completely-deprotonated GEDTA anion. In consideration of the chemical equilibria in solution, the following two equations can be derived for the above reaction mechanisms, I and II respectively:

$$\frac{1}{i_l}=\frac{K_{NIHY}^{1/2}\left(1+\dfrac{1}{K^{H}[H^+]}\right)\cdot[Y]_f^{1/2}}{2AF\cdot D^{1/2}(k_d)_{NIHY}^{1/2}\cdot(\alpha_H)_Y^{1/2}}+\frac{1}{i_d} \qquad (1)$$

$$\frac{1}{i_l}=\frac{K_{NIY}^{1/2}\,(1+K^{H}\cdot[H^+])\cdot[Y]_f^{1/2}}{2AF\cdot D^{1/2}\cdot(k_d)_{NIY}^{1/2}\cdot(\alpha_H)_Y^{1/2}}+\frac{1}{i_d} \qquad (2)$$

All the symbols used in Eqs. (1) and (2) have their usual meanings.[2]

Table 1. Rate constants (μ=0.30, 25°C)

Elementary reaction	Rate constant
$NiHY^-=Ni^{2+}+HY^{3-}$	9.3×10^{-4} sec^{-1}
$NiY^{2-}=Ni^{2+}+Y^{4-}$	$2.5_3\times10^{-3}$ sec^{-1}
$ZnHY^-+H^+=Zn^{2+}+H_2Y^{2-}$	14.9 M^{-1} sec^{-1}

From the slopes of the linear relations in Figs. 2. and 3, the $(k_d)_{NIHY}$ and $(k_d)_{NIY}$ values were determined; they are listed in Table 1 together with other numerical values. If the electrode reaction mechanisms for the polarographic step of the nickel(II)-GEDTA complex at pH's lower than 5.70 and that at pH's higher than 5.70 are given by I and II respectively, the half-wave potentials should be given by (3) and (4) respectively:

$$E_{1/2}=\text{constant}_1+\frac{0.0591}{4\alpha}\cdot\log\frac{[Y]_f[H^+]}{(\alpha_H)_Y} \qquad (3)$$

$$E_{1/2}=\text{constant}_2+\frac{0.0591}{4\alpha}\cdot\log\frac{[Y]_f}{(\alpha_H)_Y} \qquad (4)$$

These relations were examined by using some typical experimental data. Typical results obtained at pH's lower than 5.70 are shown in Tables 2 and 3. The agreement between the shift of the half-wave potential obtained experimentally, $(\Delta E_{1/2})_{ob}$, and that calculated with the aid of Eq. (3), using the α value of 0.50, can be regarded as satisfactory. In solutions of pH's higher than 7.00, the nickel(II)-GEDTA complex give no polarographic wave.

Polarographic Behavior of Zinc(II) Ions in a GEDTA Solution. Reported equilibrium constants for the formation of the zinc(II)-GEDTA complex[3] show that all the zinc(II) ions in the 10.0 mM GEDTA solutions with pH's higher than 4.60 invariably exist as GEDTA complex. As is illustrated by the polarogram in Fig. 1, in the pH range from 5.0 to 6.0, the zinc(II) ions in 10.0 mM GEDTA solutions yielded two polarographic steps. Under the present experimental conditions, the total wave-height was almost constant, but was exactly proportional to the square-root of the effective pressure on the DME and zinc(II) ion concentrations. However, the wave-height of the first reduction step was

Table 2. The dependence of $E_{1/2}$ on the pH
The concentration of uncomplexed GEDTA=20.0 mM
The concentration of nickel(II) ion=1.0 mM
The total concentration of acetate=0.05 M
μ=0.30, 25°C

pH	$E_{1/2}$ V *vs.* SCE	$\Delta E_{1/2}$, mV Obsd	Calcd
5.04	−1.082	0	0
5.17	−1.087	− 5.0	− 7.8
5.35	−1.102	−20.0	−18.6
5.51	−1.107	−25.0	−28.2
5.65	−1.112	−30.0	−31.6

Table 3. The dependence of $E_{1/2}$ on the concentration of uncomplexed GEDTA
The concentration of nickel(II) ion=1.0 mM
The total concentration of acetate=0.05 M
μ=0.30, 25°C, pH=5.35

Concentration of GEDTA, mM	$E_{1/2}$ V *vs.* SCE	$\Delta E_{1/2}$, mV Obsd	Calcd
15.0	−1.094	0	0
20.0	−1.102	− 8.0	− 7.5
30.0	−1.109	−15.0	−18.0
60.0	−1.133	−39.0	−36.1
90.0	−1.139	−45.0	−46.6

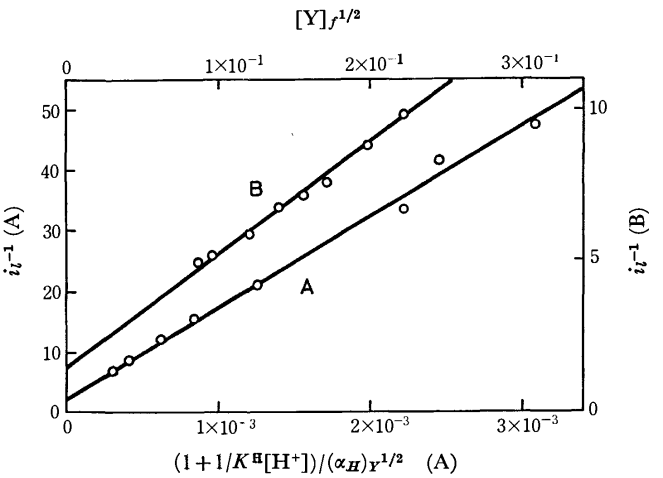

Fig. 4. The plot of i_l^{-1} against $(1+1/K^{H}[H^+])/(\alpha_H)_Y^{1/2}$ or $[Y]_f^{1/2}$.
The concentration of zinc(II) ion=0.50 mM
The concentration of uncomplexed acetate ion=20.0 mM
μ=0.30, 25°C
A) The plot of i_l^{-1} *vs.* $(1+1/K^{H}[H^+])/(\alpha_H)_Y^{1/2}$
The concentration of uncomplexed GEDTA=10.0 mM
B) The plot of i_l^{-1} *vs.* $[Y]_f^{1/2}$
pH=5.04

almost independent of the effective mercury pressure, suggesting its kinetic nature (the results are not shown here). As in the case of the polarography of the nickel(II)-GEDTA complex, the nature of the first polarographic wave of the zinc(II)-GEDTA complex was investigated thoroughly. Provided that the other experimental conditions are kept constant, the plot of the reciprocal of the limiting current, i_l^{-1}, against $[Y]_f^{1/2}$ or $(1+1/K^H\cdot[H^+])/(\alpha_H)_Y^{1/2}$ invariably gives a linear relation (Fig. 4). Considering that the first wave is located at the potentials where the zinc(II)-aquo ions will give the reduction wave, it seems that the electrode-reaction mechanism for the first step of the zinc(II)-GEDTA complex can be depicted as:

$$\begin{array}{l} ZnY^{2-} \\ \quad \downarrow\uparrow \text{ rapid } (k_d)^H_{ZnHY} \\ ZnHY^- + H^+ \rightleftharpoons Zn^{2+} + H_2Y^{2-} \quad \text{r.d.s} \\ Zn^{2+} + 2e^- + Hg = Zn(Hg) \end{array} \qquad \text{III}$$

Although, in the polarographic study of the zinc(II)-GEDTA complex, an acetate buffer mixture was used to keep the solution pH constant, it has practically no effect on the polarographic behavior of the zinc(II)-GEDTA complex provided that the acetate ion concentration was lower than 0.025M. Therefore, all the kinetic measurements were carried out by using an acetate buffer mixture where the acetate-ion concentration was lower than 0.025M. If the above reaction mechanism is correct, the half-wave potential of the first wave should shift linearly to the negative potentials with an increase in the log $[Y]_f\cdot[H^+]^2/(\alpha_H)_Y$ value, giving the slope of $0.0591/4\alpha$ V. Although the experimental data are not shown here, the above linear relation could be examined successfully. From the slope of the linear relation between i_l^{-1} and $[Y]_f^{1/2}$ or $(1+1/K^H\cdot[H^+])/(\alpha_H)_Y^{1/2}$, the proton-assisted dissociation rate constant of $ZnHY^-$, $(k_d)^H_{ZnHY}$, was determined. The $(k_d)^H_{ZnHY}$ value obtained is also given in Table 1.

Polarographic Behavior of Cadmium(II) Ions in GEDTA Solutions. Previously,[4] the polarographic behavior of the cadmium(II)-GEDTA complex in acetate buffer solutions containing a large excess of calcium(II) ions, was studied by Fujisawa and Tanaka. In the presence of an excess of calcium(II) ions, the cadmium(II)-GEDTA complex gives two polarographic steps. By investigating the nature of the first reduction step systematically, they concluded that the first step can be ascribed to the reduction of the free cadmium(II) ion liberated by the dissociation of the normal cadmium-(II)-GEDTA complex at the electrode surface (Reaction mechanism IV).

$$\begin{array}{l} CdY^{2-} + jH^+ \rightleftharpoons Cd^{2+} + H_jY^{j-4} \\ Cd^{2+} + 2e^- + Hg \rightleftharpoons Cd(Hg) \end{array} \qquad \text{IV}$$

On the other hand, the cadmium(II) ions in GEDTA solutions not containing calcium(II) ions give three polarographic steps at pH's lower than 3.50. With an increase in the solution's pH, the first wave-height decreased, and it disappeared completely at pH's higher than 3.50. Thus, the cadmium(II)-GEDTA complex

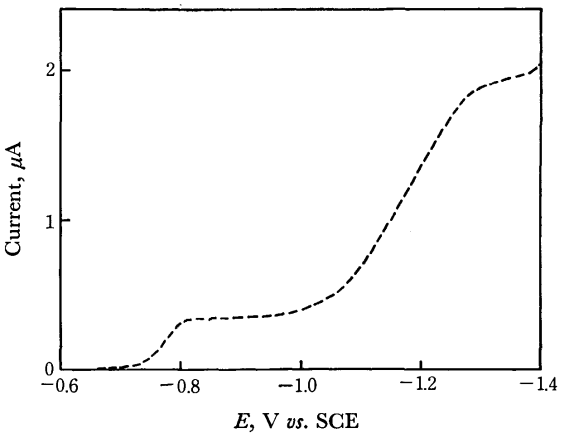

Fig. 5. Polarogram of cadmium(II)-GEDTA complex.
The concentration of cadmium(II) ion=1.00 mM
The concentration of uncomplexed GEDTA=14.0 mM
The total concentration of acetate=0.05 M
μ=0.30, 25°C, pH=4.00

in GEDTA solutions of pH's higher than 3.50 yields the two-step polarographic wave (Fig. 5). In view of the reduction potential of the first wave at pH's lower than 3.50, and in view of the effect of the GEDTA concentration on the limiting current, the first polarographic step of the cadmium(II)-GEDTA complex at pH's lower than 3.50 may be considered to correspond to the first polarographic wave reported by Fujisawa and Tanaka. In this investigation, we studied the polarographic behavior of the cadmium(II)-GEDTA complex in GEDTA solutions not containing calcium-(II) ions at pH's higher than 3.50. The positive polarographic step observed in solutions containing an excess of GEDTA salt showed the characteristic kinetic-controlled nature (its limiting current is independent of the effective mercury pressure on the DME). The limiting current was decreased remarkably by increasing the solution's pH. However, the GEDTA concentration had little effect on it. By rearranging Eq. (5_a) in Ref. 2, one can easily derive the following relation:

$$\frac{i_l}{i_d - i_l} = \text{constant}_3 \times \frac{t^{1/2} k_2^{1/2}}{K_{1a}^{-1} K_{2a}^{-1/2}} \qquad (5)$$

This relation is the same as that derived by Koryta[5] for the kinetic current. With the aid of this relation, we analyzed the experimental data. Provided that the other experimental conditions are kept constant, the plot of $(i_d-i_l)/i_l$ against the reciprocal of the hydrogen-ion concentration or the GEDTA concentration, $[Y]_f$, invariably gives a linear relation. The results are reproduced in Figs. 6 and 7.

Under the present experimental conditions, the total wave-height of the cadmium(II)-GEDTA complex was exactly proportional to the square-root of the effective mercury pressure on the DME. However, it decreased appreciably with an increase in the concentration of uncomplexed GEDTA. If this can be ascribed to the formation of the cadmium(II)-GEDTA complex with a 1:2 composition, one can determine the second successive formation constant by examining the effect

4) T. Fujisawa and N. Tanaka, *Nippon Kagaku Zasshi*, **89**, 1206 (1968).

5) J. Koryta, *Collect. Czech. Chem. Commun.*, **23**, 1408 (1958).

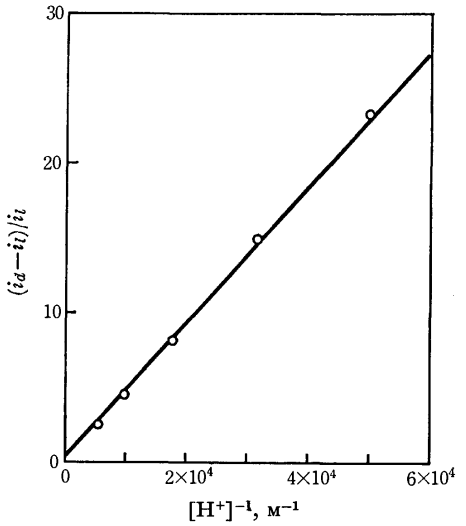

Fig. 6. The plot of $(i_d-i_l)/i_l$ against the reciprocal of hydrogen ion concentration.
The concentration of cadmium(II) ion=1.00 mM
The concentration of uncomplexed GEDTA=14.0 mM
The total concentration of acetate=0.05M
μ=0.30, 25°C

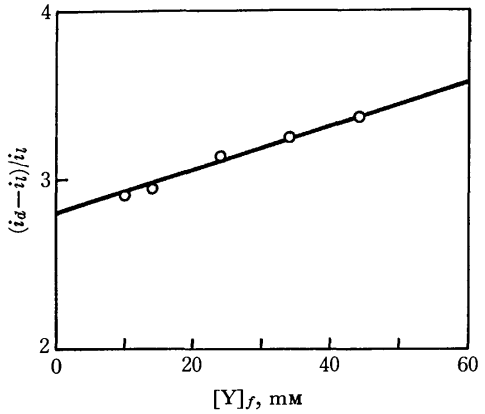

Fig. 7. The plot of $(i_d-i_l)/i_l$ against the concentration of uncomplexed GEDTA.
The concentration of cadmium(II) ion=1.00 mM
The total concentration of acetate=0.05 M
pH=4.00, μ=0.30, 25°C

of the GEDTA concentration on the limiting current with the aid of the following well-known relation (6):

$$D_{ob}=\frac{D_1+D_2\cdot K'_2[Y]_f}{1+K'_2\cdot[Y]_f} \quad (6)$$

If the composition of a 1:2 ratio complex is given by $Cd(HY)_2^{4-}$, K'_2 in Eq. (6) should be given by $K_2^{HY}\cdot[H^+]/(1+K^{H-1}\cdot[H^+]^{-1})\cdot K_4\cdot(\alpha_H)_Y$. On the other hand, if the composition of the 1:2 ratio complex is given by CdY_2^{6-}, K_2 will be given by $K_2^Y/(1+K^H\cdot[H^+])\cdot(\alpha_H)_Y$. Here, $K_2^{HY}=[Cd(HY)_2^{4-}]/[CdHY^-]\cdot[HY^{3-}]$, $K_2^Y=[CdY_2^{6-}]/[CdY^{2-}][Y^{4-}]$, and K_4 is the fourth dissociation constant of GEDTA. By introducing the Ilkoviç equation into Eq. (6) and by rearranging the resulted equation, we can obtain the following relation:

$$(i_d)_{ob}^2=\frac{(i_d)_0^2-(i_d)_{ob}^2}{[Y]_f}\times\frac{1}{K_2}+(i_d)_l^2 \quad (7)$$

where $(i_d)_{ob}$ is the diffusion current of the cadmium(II)-

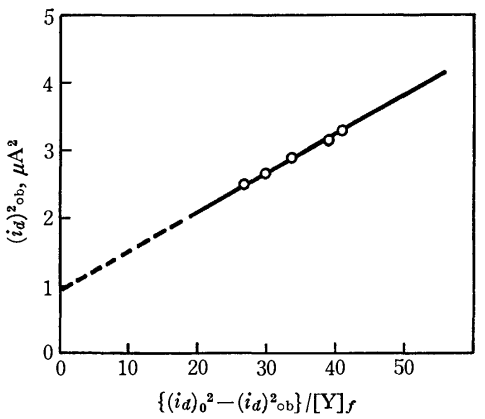

Fig. 8. The plot of $(i_d)^2_{ob}$ against $[(i_d)_0^2-(i_d)^2_{ob}]/[Y]_f$.
The concentration of cadmium(II) ion=1.00 mM
The total concentration of acetate=0.05M
μ=0.30, 25°C, pH=4.00
The concentration of uncomplexed GEDTA ranged from 10.0 to 44.0 mM

GEDTA complex in a solution where 1:1 and 1:2 complexes coexist; $(i_d)_0$, the diffusion current in a solution where all the complex ions have the 1:1 composition, and $(i_d)_l$, the diffusion current in a solution where all the complex ions have the 1:2 composition. The above relation was examined by using some typical experimental data. A typical result is shown in Fig. 8. From the slope of the straight line in Fig. 8, the K_2^{HY} or K_2^Y value was determined to be $10^{6.34}$ or $10^{11.34}$. The latter value is too large to be understood, disproving the formation of CdY_2^{6-}. It was also found that the solution's pH and the concentration of free GEDTA had practically no effect on the half-wave potential. All the above findings evidently indicate that the electrode reaction mechanism for the second step of the cadmium(II)-GEDTA complex can be expressed as:

$$\begin{array}{l} CdY^{2-} \\ \quad\downarrow \text{ rapid} \\ CdHY^- \underset{K}{\overset{k_f}{\rightleftharpoons}} CdHY^{-*} \quad \text{r.d.s.} \\ \quad\downarrow \text{ rapid} \\ Cd(HY)_2^{4-} \end{array} \quad \text{V}$$

$$CdHY^{-*}+2e^-+Hg=Cd(Hg)+HY^{3-}$$

Here, $CdHY^{-*}$ means the electroactive protonated-cadmium(II)-GEDTA complex. For the above reaction mechanism, the (5) relation can be rewritten as:

$$\frac{i_l}{i_d-i_l}=\text{constant}_4\times\frac{t^{1/2}\cdot k_f^{1/2}}{\left(1+\frac{1}{K^H\cdot[H^+]}+\frac{K_2^{HY}\cdot K_3\cdot[H_2Y^{2-}]}{[H^+]}\right)} \quad (8)$$

where K_3 is the third dissociation constant of GEDTA and K, $[CdHY^{-*}]/[CdHY^-]$. We can mention here that, under the present experimental conditions, $[H_2Y^{2-}]$ is practically equal to the $[Y]_f$ value. Equation (8) evidently indicates that, from the slope of linear relations shown in Figs. 6 and 7, the k_f value can be estimated. However, the lack of data on the K value prevents us from calculating the k_f value from

the slope of linear relations shown in Figs. 6 and 7.

The formation constant of the protonated nickel(II)-GEDTA complex, $NiHY^-$, $K_{NiHY}=[NiHY^-]/[Ni^{2+}]\cdot[HY^{3-}]$, can be calculated to be $10^{7.94}$ ($\mu=0.30$) from the relation $K_{NiHY}=K_{NiY}\cdot K^H K_4$. This value is in good agreement with the formation constant of the 1 : 1 ratio nickel(II)-iminodiacetate complex. This agreement suggests that the tervalent GEDTA anion in the protonated nickel(II)-GEDTA complex is coordinated to the nickel(II) ion through an iminodiacetate chelate ring. Therefore, it is reasonable to believe that the protonated nickel(II)-GEDTA complex can be depicted by (A) in Fig. 9. If the structure proposed above is reasonable, the reaction intermediate in the dissociation reaction of $NiHY^-$ must be given by (B) in Fig. 9.

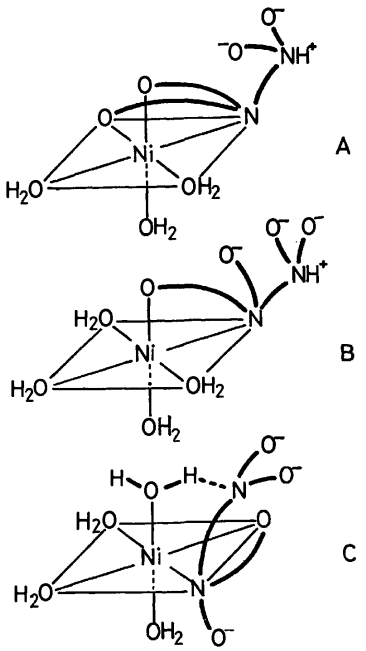

Fig. 9. Reaction intermediates.

As has been reported previously,[2] the nickel(II)-aspartate complex dissociates through the glycinate reaction intermediate, in which the leaving aspartate anion is bonded to the nickel(II) ion through a glycinate chelate ring. When the structure of the reaction intermediate in the dissociation of $NiHY^-$ is depicted by (B), and when the dissociations of aspartate and GEDTA anions from the glycinate reaction intermediates are rate-determining steps, the dissociation-rate-constant ratio between the aspartate and GEDTA systems should be given by $K_{NiHY}/K_{Ni(II)-Asp}\times 2=7.0$. Here, 2 is the statistical factor for the reaction intermediate (B). The observed ratio was 13.0. The agreement between the observed ratio and that calculated on the basis of the glycinate reaction intermediates can be regarded as satisfactory. Furthermore, the rate constant for the formation of the protonated nickel(II)-EDTA complex has been reported to be $10^{5.30}$ by Margerum and Zabin.[6] This corresponds to the dissociation constant of $2.4\times10^{-6}\,sec^{-1}$. The dissociation rate constant ratio between the protonated GEDTA and EDTA complexes, calculated by using the above rate constant, was found to be nearly equal to the ratio of the reciprocals of the K_{NiHY} value between the GEDTA and EDTA complexes of the nickel(II) ion. This suggests that the protonated nickel(II)-EDTA complex also dissociates through the reaction intermidiate in which the leaving tervalent EDTA anion is bonded to the nickel(II) ion through the glycinate chelate ring. The formation rate constant of the protonated nickel(II)-GEDTA complex, k_f, from Ni^{2+} and HY^{3-} was claculated to be $8.1\times10^4\,M^{-1}sec^{-1}$ from the relation $K_{NiHY}=k_f/k_d$. This value is slightly larger than the reported rate constant for the water loss from the aquated nickel(II) ion.[7] Considering that the association constant of the outer-sphere complex between the nickel(II) ion and the HY^{3-} anion is expected to be larger than unity from the Fuoss equation,[8] the k_f value thus estimated suggests that the rate-determining step in the formation of $NiHY^-$ is the water loss from the nickel(II)-aquo ion. As is shown in Table 1, the k_d value for the dissociation of the normal nickel(II)-GEDTA complex, NiY^{2-}, was $2.5_3\times10^{-3}\,sec^{-1}$. As has been discussed in the dissociation of $NiHY^-$ with reference to the dissociation of the nickel(II)-aspartate complex, if the normal complex, NiY^{2-}, also dissociates through the glycinate reaction intermediate, the dissociation-rate-constant ratio between the protonated and normal nickel(II)-GEDTA complexes should be approximately 1.4×10^2. Here, the electrostatic contribution to the stability of the reaction intermediate and the statistical factor are also taken into account. The observed ratio was 0.36. This is approximately 360 times smaller than that calculated on the basis of the simple glycinate reaction intermediate. The larger discrepancy between the observed and calculated ratios evidently implies that the stability of the reaction intermediate in the dissociation of NiY^{2-} is much greater than that of the simple glycinate reaction intermediate. Here, we can mention that the second protonation constant of the GEDTA anion ($pK_{a_3}=8.74$) is nearly identical to the protonation constants of $Ni(OH_2)_5(OH)^+$ ($\log K^{Ni-H}=9.0$).[9] This similarity in the two protonation constants strongly suggests the possibility of a hydrogen-bond formation between the water molecule coordinated to the nickel(II) ion and the free nitrogen donor atom of the GEDTA anion in the reaction intermediate. This internal hydrogen-bond formation within the reaction intermediate will effectively increase its stability and, thus, will give an enhanced rate constant. Therefore, it is reasonable to assume the following reaction intermediate (C) for the dissociation of NiY^{2-}. On the other hand, the tervalent GEDTA anion in the reaction intermediate of the dissociation of $NiHY^-$ has no such nitrogen donor atom available for the formation of a hydrogen bond with the coordinated water molecule. For this reason, the observed dissociation rate constant of $NiHY^-$ agrees well with

6) D. W. Margerum and B. A. Zabin, *J. Phys. Chem.*, **66**, 2214 (1962).

7) M. Eigen, *Ber. Bunsenges. Phys. Chem.*, **67**, 753 (1963).

8) R. M. Fuoss, *J. Amer. Chem. Soc.*, **80**, 5059 (1958).

9) D. B. Rorabacher, *Inorg. Chem.*, **5**, 1891 (1966).

that calculated on the basis of a simple glycinate reaction intermediate.

The rate constant, $(k_d)^{H}_{ZnHY}$, for the proton-assisted dissociation of the protonated zinc(II)-GEDTA complex was determined to be 13.0 sec^{-1} from the slope of the linear relation between i_l^{-1} and $(1+1/K^{H}\cdot[H^+])/(\alpha_H)_Y^{1/2}$. By using the $(k_d)^{H}_{ZnHY}$ value thus determined, the rate constant for the formation of $ZnHY^-$ from Zn^{2+} and H_2Y^{2-}, $(k_f)_{ZnHY}$, was calculated to be 2.5$M^{-1}sec^{-1}$ with the aid of the relation $(k_f)_{ZnHY}=(k_d)_{ZnHY}\cdot K_{ZnY}\cdot K^{H}_{ZnY}\cdot K_3\cdot K_4$. The estimated $(k_f)_{ZnHY}$ value is very small as compared with the reported water exchange rate of the zinc(II) aquo complex, $k_{Zn}^{-H_2O}$, 5×10^7 sec^{-1}.[10] Genearlly, it is assumed that, in the formation of a metal complex in an aqueous solution, the metal ion and the ligand first diffuse together to form an outer-sphere complex, and that then a water molecule dissociates from the aquated metal ion and a donor group of the ligand coordinates with the metal ion. If the dissociation of the proton from the ligand is rapid enough, and if the water loss from the aquated metal ion is the rate-determining step, the formation-rate constant should be given by $K_{as}k_M^{-H_2O}$. Here, K_{as} means the association constant for the formation of an outer-sphere complex. Since the K_{as} value for the formation of the outer-sphere complex between Zn^{2+} and H_2Y^{2-} is considered to be larger than unity, if the formation of $ZnHY^-$ from Zn^{2+} and H_2Y^{2-} has a water-loss mechanism, the $(k_f)_{ZnHY}$ value should be larger than $5\times10^7M^{-1}sec^{-1}$. Sudmeier and Reilley have reported in their NMR study of the protonation of the GEDTA anion in an aqueous solution[11] that two nitrogen atoms of the divalent GEDTA anion, H_2Y^{2-}, are completely protonated. Although the small $(k_f)_{ZnHY}$ value obtained may be explained by assuming an alternative mechanism, it is also possible to interpret it by assuming that the reactive species in the complex formation of the divalent GEDTA anion with the zinc(II) ion is not the nitrogen-protonated GEDTA due to the blocking of the nitrogen atoms by the proton, but is the carboxylate-protonated H_2Y^{2-} isomer with a small equilibrium concentration, in which at least one of the two nitrogen atoms is deprotonated. Similar reactive species has been proposed for the reaction of the diprotonated EDTA anion with the nickel(II) ion.[12] As was suggested by Rabenstein,[10] the relative amount of the carboxylate-protonated H_2Y^{2-} species is calculated from the relative basicity of the nitrogen atom and that of the carboxylate oxygen group of GEDTA. Since the K_4 and K_1 values approximate the basicity of the nitrogen and carboxylate oxygen groups of the GEDTA anion, the relative amount of carboxylate-protonated species is approximated as 1×10^{-7}. This estimated value will explain satisfactorily the discrepancy between the observed $(k_f)_{ZnHY}$ value and the value calculated on the basis of the simple water-loss mechanism.

Equation (8) indicates that, at a constant pH, the slope and the intercept of the linear relation between the $(i_d-i_l)/i_l$ value and the concentration of uncomplexed GEDTA $[Y]_f$, should be $K_2^{HY}\cdot K_3/K^{1/2}\cdot t^{1/2}\cdot k_f^{1/2}\cdot[H^+]$ constant$_4$ and $1/K^{1/2}\cdot t^{1/2}\cdot k_f^{1/2}\cdot K^{H}_{CdY}\cdot[H^+]$ constant$_4$ respectively. By using the $1/K^{1/2}\cdot t^{1/2}\cdot k_f^{1/2}$ constant$_4$ value determined from the slope of the linear relation between the $(i_d-i_l)/i_l$ value and $1/[H^+]$, the slope and intercept were calculated as 9.6 and 4.0 respectively. The observed slope and intercept were 12.6 and 3.0. The agreement between the observed value and the calculated one can be regarded as satisfactory. This agreement also gives strong support to the reaction mechanism (V) proposed by the present authors. The formation constant of $CdHY^-$, K_{CdHY}, was estimated to be $10^{10.23}$ from the relation $K_{CdHY}(=[CdHY^-]/[Cd^{2+}][HY^{3-}])=K_{CdY}K^{H}_{CdY}K_4$. In sharp contrast to the finding observed in the nickel(II)-GEDTA system, this value is much greater than the first successive formation constant of the cadmium(II)-iminodiacetate ($10^{5.35}$) or -*N*-2-hydroxyethyliminodiacetate complex ($10^{7.21}$). This fact suggests that two iminodiacetate groups of the GEDTA anion are involved in the complex formation of $CdHY^-$. Therefore, it is reasonable to believe that the electroactive form, $CdHY^{-}$*, proposed in the dissociation reaction of the cadmium(II)-GEDTA complex is that resulting from the partial rupture of the cadmium(II)-GEDTA bonds in the $CdHY^-$. To describe the detailed structure of $CdHY^{-}$* precisely, further systematic investigations will be necessary.

10) D. L. Rabenstein, *J. Amer. Chem. Soc.*, **91**, 2501 (1969).
11) J. L. Sudmeier and C. N. Reilley, *Anal. Chem.*, **36**, 1698 (1964).
12) J. C. Cassatt and R. G. Wilkins, *J. Amer. Chem. Soc.*, **90**, 6045 (1968).

Studies of Ethylenediamine-*N,N'*-diacetatocobalt(III) Complexes. III.[1] The Preparation and Identification of Ethylenediamine-*N,N'*-diacetatocobalt(III) Complexes with Ammonia, Pyridine, or Alkylamines as the Additional Ligand

Kashiro KURODA

Department of Chemistry, Faculty of Science, Ehime University, Matsuyama, Ehime

(Received January 5, 1972)

A group of cobalt(III) complexes containing the tetradentate ethylenediamine-*N,N*-diacetate anion (EDDA) and ammonia, pyridine, or alkylamines have been derived from ethylenediamine-*N,N'*-diacetato(diaquo)cobalt-(III) perchlorate. Three different series among the complexes—(1) the aquo(amine) series, $[Co(EDDA)(H_2O)(am)]ClO_4$, (2) the *α-cis*-bis(amine) series, *α-cis*-$[Co(EDDA)(am)_2]ClO_4$, and (3) *β-cis*-$[Co(EDDA)(NH_3)_2]ClO_4$ as well as *β-cis*-$[Co(EDDA)(en)]ClO_4$, have been obtained, depending on the conditions of the reaction between the starting diaquo complex and the amines. Some properties of the complexes have been examined, and the geometrical configuration of each complex has been identified on the basis of the electronic absorption spectra and the proton NMR spectra. The coordination tendency of EDDA and the amines have also been discussed.

In contrast to the great many cobalt(III)-ammine and cobalt(III)-polyamine complexes which have been synthesized, the number of complexes in which monoamines coordinate to the metal ion is extremely small. Only a few types of complexes, such as $[Co(Cl)(amine)(en)_2]^{2+}$ and $[Co(amine)_2(en)_2]^{3+}$, have been prepared,[2] and in such complexes the amine is mostly a primary amine. The weaker tendency of the coordination of monoamines has been attributed to its basic character being larger than ammonia, although the character itself should promote the coordination. That is, in the substitution reaction of a starting complex, *e.g.*, $[Co(Cl)_2(en)_2]^+$, with an amine, a hydroxo-complex, *e.g.*, $[Co(Cl)(OH)(en)_2]^+$, is formed instead of the desired amine-complex (especially in the cases of the secondary and tertiary amines). Furthermore, cobalt-(III) complexes in general are relatively unstable in a basic solution and decomposition may occur during the substitution.

In the preceding report of this study,[3] it has been shown that ethylenediamine-*N,N'*-diacetato(diaquo)-cobalt(III) perchlorate, $[Co(EDDA)(H_2O)_2]ClO_4$, is a suitable starting complex for the preparation of various species of the Co(III)-EDDA series. Since EDDA is a strong chelating agent to the metal, and since the Co(III)-EDDA entity is stable enough in a basic solution, it has been considered to be worth examining the reaction between the diaquo-complex and various amines. Thus, the resulting complexes will be dealt with in this report. It will be shown that aquo(amine)-complexes or *α-cis* isomers of bis(amine)-complexes were obtained, depending on the reaction conditions, and that the *β-cis* isomer of the diammine complex was obtained by the reaction at 100°C. The *β-cis* diammine complex is the first example of a *β-cis* isomer in which two unidentates occupy the residual coordination sites of the Co(III)-EDDA complex.

Experimental

Materials, Analysis, Apparatus, and Measurements. Ethylenediamine-*N,N'*-diacetic acid (Dotite Reagents), alkylamines, and pyridine (Nakarai Chemicals), and all the other reagent-grade chemicals were used without further purification. The apparatus used and the procedures for the analysis and the measurements have been described in a preceding report.[3]

Preparations. *(1) Ethylenediamine-*N,N'*-diacetatoaquoamminecobalt(III) Perchlorate, $[Co(EDDA)(H_2O)(NH_3)]ClO_4$*: Into 5 m*l* of water, 0.5 g of ethylenediamine-*N,N'*-diacetato-(diaquo)cobalt(III) perchlorate[3] was dissolved, and then 1 m*l* of 6N ammonia was added. The mixture was stirred at 45°C until the first-formed blue precipitate disappeared, and then for a further 10 min. After one milliliter of 6N $HClO_4$ had been added, the mixture was cooled at 0°C. A violet precipitate thus formed was recrystallized from about 3 m*l* of warm water by the addition of a few drops of 6N $HClO_4$. Yield, 0.2 g.

Found: C, 19.22; H, 4.17; N, 11.11%. Calcd for $[Co(EDDA)(H_2O)(NH_3)]ClO_4 = CoC_6H_{15}O_9N_3Cl$ (367.59): C, 19.61; H, 4.11; N, 11.43%.

All the filtrates of the above procedure were combined and mixed with 1 m*l* of 6N ammonia and 0.1 g of active charcoal. Then the mixture was evaporated to dryness at ~45°C with the aid of an air stream. The residue was extracted with cold water and then with hot water. From the latter extract, bright reddish violet crystals appeared upon cooling. A few drops of 6N $HClO_4$ were added for complete precipitation. This is *α-cis*-$[Co(EDDA)(NH_3)_2]ClO_4 \cdot H_2O$. (A different procedure for the preparation of this complex has been described elsewhere.[3,4]) Yield, 0.2 g.

*(2) β-*cis*-Ethylenediamine-*N,N'*-diacetato(diammine)cobalt-(III) Perchlorate Monohydrate, β-*cis*-$[Co(EDDA)(NH_3)_2]ClO_4 \cdot H_2O$:*[5] One milliliter of 6N ammonia was added to a solution of the diaquo complex (0.5 g) in 3 m*l* of water. The blue solution, which contained a precipitate, was immersed in boiling water and then concentrated to nearly dryness with stirring. During this process, the precipitate soon disappeared and the solution turned red. After cooling, when the tarry product was stirred with a glass rod, crystals

1) Part II of this series, K. Kuroda and K. Watanabe, This Bulletin, **44**, 2550 (1971).

2) a) J. Meisenheimer and E. Kiderlen, *Ann.*, **438**, 240 (1924); b) J. C. Bailar and L. B. Clapp, *J. Amer. Chem. Soc.*, **67**, 177 (1945); c) S. C. Chan and F. Leh, *J. Chem. Soc., A*, **1966**, 129; d) T. Yasui and Y. Shimura, This Bulletin, **36**, 1286 (1963).

3) K. Kuroda and K. Watanabe, This Bulletin, **44**, 1034 (1971).

4) J. I. Legg and D. W. Cooke, *Inorg. Chem.*, **4**, 1576 (1965).

5) This complex has been reported briefly in the following paper: K. Kuroda, *Chem. Lett.*, **1972**, 197.

deposited suddenly and the whole solidified. The product, after washing with methanol, was dissolved in 3 m*l* of warm (~50°C) water, and then the solution was filtered and cooled. A few drops of 6N $HClO_4$ were added for precipitation. Bright red crystals came out after a while. The product was washed with methanol and ether. Yield, 0.3 g.

Found: C, 18.75; H, 4.60; N, 14.67%. Calcd for $[Co(EDDA)(NH_3)_2]ClO_4 \cdot H_2O = CoC_6H_{18}O_9N_4Cl$ (384.62): C, 18.74; H, 4.72; N, 14.57%.

(3) Ethylenediamine-N,N'-*diacetatoaquopyridinecobalt(III) Perchlorate*, $[Co(EDDA)(H_2O)(py)]ClO_4$: In 10 m*l* of water, 0.2 g of the diaquo complex and 0.1 g of pyridine were dissolved, and then the mixture was evaporated at 45°C. During the evaporation red-violet crystals appeared. After the evaporation was complete, the residue was washed with methanol and then recrystallized from 10 m*l* of warm water with the addition of a few drops of 6N $HClO_4$. Yield, 0.2 g.

Found: C, 30.89; H, 3.91; N, 9.96%. Calcd for $[Co(EDDA)(H_2O)(py)]ClO_4 = CoC_{11}H_{17}O_9N_3Cl$ (429.66): C, 30.75; H, 3.99; N, 9.78%.

(4) α-cis-*Ethylenediamine*-N,N'-*diacetato(dipyridine)cobalt(III) Perchlorate Hemihydrate*, α-cis-$[Co(EDDA)(py)_2]ClO_4 \cdot 0.5H_2O$: In 10 m*l* of water, the diaquo complex (0.3 g), pyridine (0.3 g), and active charcoal (0.1 g) were mixed; the mixture was heated at ~50°C for 1 hr and then evaporated to ~2 m*l* with continuous stirring. The excess of pyridine was removed by mixing the product with ether several times. The resulting product, which contained crystals, was extracted with 15 m*l* of warm water, and a few drops of 6N $HClO_4$ were added to the extract. After standing for 1 hr, the red crystals were collected and washed with ethanol and ether. The product was recrystallized once more. Yield, 0.2 g.

Found: C, 38.30; H, 4.13; N, 11.33%. Calcd for $[Co(EDDA)(py)_2]ClO_4 \cdot 0.5H_2O = CoC_{16}H_{21}O_{8.5}N_4Cl$ (499.75): C, 38.45; H, 4.24; N, 11.21%.

(5) Ethylenediamine-N,N'-*diacetatoaquo(methylamine)cobalt(III) Perchlorate Monohydrate*, $[Co(EDDA)(H_2O)(mam)]ClO_4 \cdot H_2O$: To a solution of the diaquo complex (0.3 g) in 10 m*l* of water, 0.2 g of an aqueous solution of monomethylamine (30%) was added. The mixture turned from red-violet to blue, and then it gradually returned to red-violet. After the mixture had evaporated to dryness at 45°C, the residue was recrystallized from a small amount (~3 m*l*) of water with the addition of a few drops of 6N $HClO_4$. The product was washed with methanol and ether. Yield, 0.3 g.

Found: C, 20.93; H, 4.76; N, 10.80%. Calcd for $[Co(EDDA)(H_2O)(mam)]ClO_4 \cdot H_2O = CoC_7H_{19}O_{10}N_3Cl$ (399.63): C, 21.04; H, 4.79; N, 10.51%.

(6) α-cis-*Ethylenediamine*-N,N'-*diacetatobis(methylamine)cobalt(III) Perchlorate Monohydrate*, α-cis-$[Co(EDDA)(mam)_2]ClO_4 \cdot H_2O$: In 10 m*l* of water, 0.3 g of the diaquo complex, 1 g of aqueous methylamine (30%), and 0.1 g of charcoal were mixed, after which the mixture was evaporated to dryness at ~50°C. The residue was extracted with cold water (~3 m*l*), and then with warm (~60°C) water amounting about 30 m*l*. Bright violet-pink crystals appeared upon cooling. A few drops of 6N $HClO_4$ were added to complete the precipitation. The crystals were washed with methanol and ether. Yield, 0.3 g.

Found: C, 23.18; H, 5.15; N, 13.22%. Calcd for $[Co(EDDA)(mam)_2]ClO_4 \cdot H_2O = CoC_8H_{22}O_9N_4Cl$ (412.67): C, 23.28; H, 5.37; N, 13.58%.

(7) Ethylenediamine-N,N'-*diacetatoaquo(ethylamine)cobalt(III) Perchlorate Monohydrate*, $[Co(EDDA)(H_2O)(eam)]ClO_4 \cdot H_2O$: This complex was prepared in a manner analogous to that used for the aquo(methylamine)-complex (5), using an equivalent amount of ethylamine instead of methylamine. Violet crystals. Yield, 0.3 g.

Found: C, 22.60; H, 4.94; N, 9.91%. Calcd for $[Co(EDDA)(H_2O)(eam)]ClO_4 \cdot H_2O = CoC_8H_{21}O_{10}N_3Cl$ (413.66): C, 23.23; H, 5.11; N, 10.16%.

(8) α-cis-*Ethylenediamine*-N,N'-*diacetatobis(ethylamine)cobalt(III) Perchlorate*, α-cis-$[Co(EDDA)(eam)_2]ClO_4$: This complex was prepared in a way similar to that used for the bis(methylamine)-complex (6). Bright pink-violet crystals. Yield, 0.3 g.

Found: C, 27.65; H, 5.62; N, 13.25%. Calcd for $[Co(EDDA)(eam)_2]ClO_4 = CoC_{10}H_{24}O_8N_4Cl$ (422.71): C, 28.41; H, 5.72; N, 13.25%.

(9) Ethylenediamine-N,N'-*diacetatoaquo(*n*-propylamine)cobalt(III) Perchlorate Monohydrate*, $[Co(EDDA)(H_2O)(n\text{-}pam)]ClO_4 \cdot H_2O$: This complex was prepared in a way similar to that used for the aquo(methylamine)-complex (5). Since methanol dissolved the complex to some extent, ethanol was used for washing. Reddish-violet crystals. Yield, 0.3 g.

Found: C, 25.26; H, 5.39; N, 9.91%. Calcd for $[Co(EDDA)(H_2O)(n\text{-}pam)]ClO_4 \cdot H_2O = CoC_9H_{23}O_{10}N_3Cl$ (427.68): C, 25.28; H, 5.42; N, 9.83%.

(10) α-cis-*Ethylenediamine*-N,N'-*diacetatobis(*n*-propylamine)cobalt(III) Perchlorate*, α-cis-$[Co(EDDA)(n\text{-}pam)_2]ClO_4$: This complex was prepared in a way analogous to that used for the bis(methylamine)-complex (6). Pink-violet crystals. Yield, 0.3 g.

Found: C, 31.70; H, 6.15; N, 12.38%. Calcd for $[Co(EDDA)(n\text{-}pam)_2]ClO_4 = CoC_{12}H_{28}O_8N_4Cl$ (450.76): C, 31.98; H, 6.26; N, 12.43%.

(11) Ethylenediamine-N,N'-*diacetatoaquo(isopropylamine)cobalt(III) Perchlorate*, $[Co(EDDA)(H_2O)(i\text{-}pam)]ClO_4$: This complex was prepared from 0.5 g of the diaquo complex and 0.2 g of isopropylamine by a procedure similar to that used for the aquo(methylamine)-complex (5). The use of an exess of the amine made an unknown insoluble product, while in the preparations of the other aquo(amine)-complexes the quantity of amines was not so decisive as this case. Violet crystals. Yield, 0.2 g.

Found: C, 25.92; H, 5.06; N, 10.25%. Calcd for $[Co(EDDA)(H_2O)(i\text{-}pam)]ClO_4 = CoC_9H_{21}O_9N_3Cl$ (409.67): C, 26.39; H, 5.15; N, 10.26%.

(12) Ethylenediamine-N,N'-*diacetato(ethanolamine)cobalt(III) Perchlorate*, $[Co(EDDA)(elam)]ClO_4$: A mixture of the diaquo complex (0.5 g) and ethanolamine (0.2 g) in 10 m*l* of water was evaporated to nearly dryness at 50°C. The mixture turned from blue to a dark reddish-violet during the process. The tarry residue was dissolved in 4 m*l* of water; after filtration, 6N $HClO_4$ was added till the mixture became more reddish. Crystals appeared gradually when the wall of the vessel was rubbed. After about 5 hr, the violet crystals were recrystallized from a small amount of water by the addition of a few drops of 6N $HClO_4$. Yield, 0.4 g.

Found: C, 24.47; H, 4.32; N, 10.71%. Calcd for $[Co(EDDA)(elam)]ClO_4 = CoC_8H_{17}O_9N_3Cl$ (393.63): C, 24.41; H, 4.35; N, 10.68%.

(13) β-cis-*Ethylenediamine*-N,N'-*diacetato(ethylenediamine)cobalt(III) Perchlorate*, β-cis-$[Co(EDDA)(en)]ClO_4$: This complex was first prepared by Legg and Cooke.[4] They separated this isomer from the α-*cis* isomer by means of ion-exchange chromatography; this took a long time, and the yield was very low. The following procedure, which is similar to that used for the β-*cis* isomer of the diammine complex (2), is very simple and gives a higher yield. A vessel containing a mixture of the diaquo complex (0.5 g) and ethylenediamine hydrate (0.1 g) in 3 m*l* of water was immersed in boiling water, and the solution was concentrated to nearly dryness. The tarry evaporation product was extracted by 5 m*l* of

TABLE 1. PREPARATION SCHEME OF Co(III)-EDDA-AMINE COMPLEXES
(The water of crystallization is omitted.)

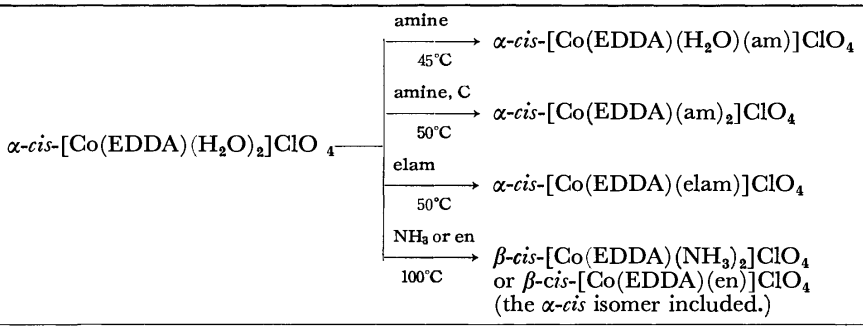

water, and the orange extract, after the addition of a few drops of 6N $HClO_4$, was placed in a refrigerator overnight. The deposit thus formed was recrystallized from 3 m*l* of water, and then washed with methanol and ether. Yield, 0.2 g. The less soluble red residue of the extraction consisted of the *α-cis* isomer. Upon recrystallization from 20 m*l* of warm water, it was purified easily. Yield of the *α-cis* isomer, 0.2 g.

Results and Discussion

Preparation Procedures. The general scheme of the preparations in this study is shown in Table 1. The diaquo complex, $[Co(EDDA)(H_2O)_2]ClO_4$, was used as the starting complex, and all of the complexes were derived by the substitution of the coordinated water with various amines under different conditions. The merit of this preparation procedure has been discussed previously.[3]

As has been described in the preceding section and the Table, the aquo(amine) complexes occurred at relatively low temperatures (~45°C) without charcoal, the *α-cis* isomers of the bis(amine) complexes at low temperatures with charcoal, and the *β-cis* isomers, although the only two species were isolated, at high temperatures (~100°C). It was presumed at the beginning of this study that the coordination mode of EDDA depended on the temperature and that the *α-cis* mode was more stable than the *β-cis* and *trans*; therefore, the occurrence of the *β-cis* isomers needed a heat of rearrangement and, hence, a higher temperature.[3] The preparations were attempted on these assumptions; they were verified to some extent by the isolation of the *β-cis* isomers of the diammine and the ethylenediamine complexes.

The preparation of the complexes containing a secondary amine or a tertiary amine was also attempted in a similar way. The red-violet color of the starting diaquo complex changed to blue and then returned to reddish, as in the cases of the preparation of the primary amine complexes. However, no desired complex has been isolated so far. Since the color change suggests the coordination of the amines in solution, attempts at isolation are still being continued.

Electronic Absorption Spectra. Table 2 and Figs. 1—4 show the electronic absorption spectra of the complexes studied. In the case of the bis(amine) complexes, the *α-cis* isomers are of the *trans(O)*-$[CoN_4O_2]$-type, whereas the *β-cis* and *trans* isomers belong to the *cis(O)*-$[CoN_4O_2]$-type. It has been well-established, both experimentally and theoretically, that the *trans(O)* isomers exhibit a largely split first band, while the *cis(O)* isomers show a more intense, nearly symmetrical first band.[6] As may be seen in Figs. 1 and 2, all the

TABLE 2. ABSORPTION MAXIMA OF THE ELECTRONIC SPECTRA OF Co(III)-EDDA-AMINE COMPLEXES

	I $\bar{\nu}$ (kK) (ε) Ia	Ib	II $\bar{\nu}$ (kK) (ε)
$[Co(EDDA)(H_2O)(NH_3)]ClO_4$	18.90 (101.6)		26.74 (87.0)
$[Co(EDDA)(H_2O)(mam)]ClO_4$	18.87 (105.1)		26.88 (100.5)
$[Co(EDDA)(H_2O)(eam)]ClO_4$	18.87 (117.1)		26.70 (105.6)
$[Co(EDDA)(H_2O)(n\text{-pam})]ClO_4$	18.90 (125.9)		26.63 (108.4)
$[Co(EDDA)(H_2O)(i\text{-pam})]ClO_4$	18.80 (133.6)		26.45 (111.2)
$[Co(EDDA)(H_2O)(py)]ClO_4$	19.12 (133.4)		26.60 (98.0)
α-cis-$[Co(EDDA)(NH_3)_2]ClO_4$	18.59 (92.0)	~22 (sh)	27.55 (118.2)
α-cis-$[Co(EDDA)(mam)_2]ClO_4$	18.55 (99.3)	~22 (sh)	27.28 (129.7)
α-cis-$[Co(EDDA)(eam)_2]ClO_4$	18.48 (104.4)	~22 (sh)	27.21 (138.8)
α-cis-$[Co(EDDA)(n\text{-pam})_2]ClO_4$	18.45 (111.0)	~22 (sh)	27.17 (150.0)
α-cis-$[Co(EDDA)(py)_2]ClO_4$	19.05 (121.3)	~22	27.32 (130.1)
β-cis-$[Co(EDDA)(NH_3)_2]ClO_4$	20.04 (153.2)		27.93 (159.4)
β-cis-$[Co(EDDA)(en)]ClO_4$	20.24 (150.4)		27.93 (150.6)
$[Co(EDDA)(elam)]ClO_4$	18.69 (90.3)		26.50 (85.1)

6) M. Linhard and M. Weigel, *Z. Anorg. Allg. Chem.*, **264**, 321 (1951) and many other literatures.

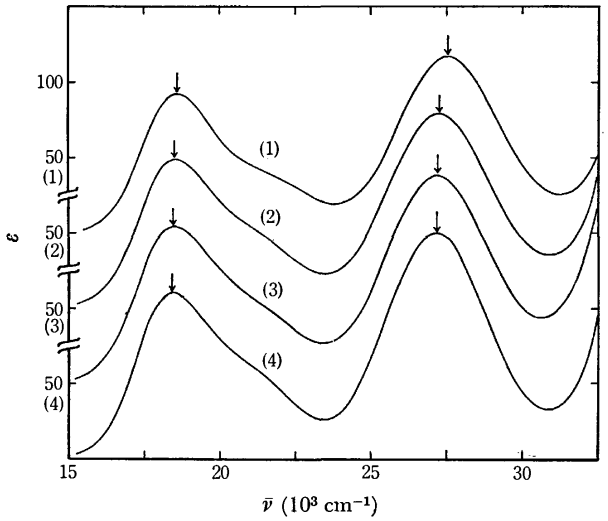

Fig. 1. Absorption Spectra of α-*cis*-[Co(EDDA)(amine)$_2$]-ClO_4.
(1): α-*cis*-[Co(EDDA)$(NH_3)_2$]ClO_4,
(2): α-*cis*-[Co(EDDA)(mam)$_2$]ClO_4,
(3): α-*cis*-[Co(EDDA)(eam)$_2$]ClO_4,
(4): α-*cis*-[Co(EDDA)(*n*-pam)$_2$]ClO_4

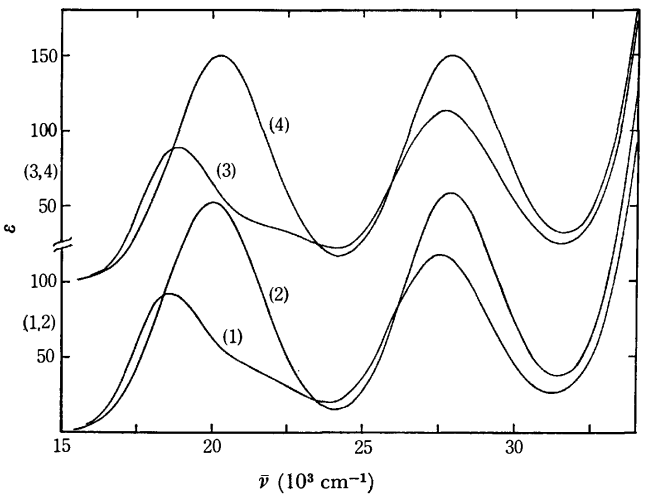

Fig. 2. Absorption Spectra of [Co(EDDA)$(NH_3)_2$]ClO_4 and [Co(EDDA)(en)]ClO_4.
(1): α-*cis*-[Co(EDDA)$(NH_3)_2$]ClO_4,
(2): β-*cis*-[Co(EDDA)$(NH_3)_2$]ClO_4,
(3): α-*cis*-[Co(EDDA)(en)]ClO_4,
(4): β-*cis*-[Co(EDDA)(en)]ClO_4

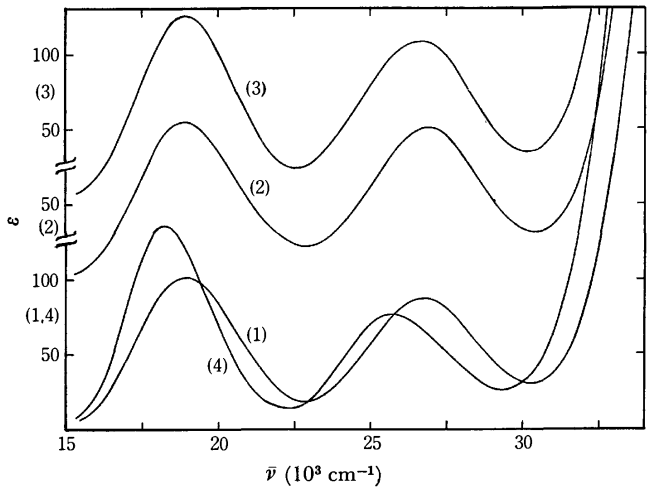

Fig. 3. Absorption Spectra of Some [Co(EDDA)(H_2O)-(amine)]ClO_4.
(1): [Co(EDDA)$(H_2O)(NH_3)$]ClO_4,
(2): [Co(EDDA)(H_2O)(mam)]ClO_4,
(3): [Co(EDDA)(H_2O)(*n*-pam)]ClO_4,
(4): [Co(EDDA)$(H_2O)_2$]ClO_4

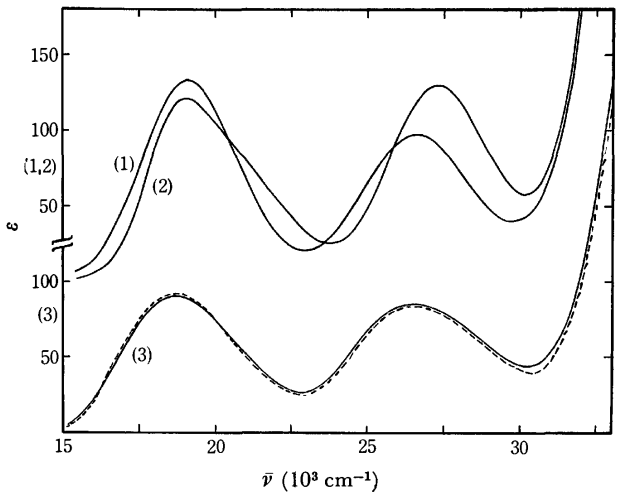

Fig. 4. Absorption Spectra of Pyridine and Ethanolamine Complexes.
(1): [Co(EDDA)(H_2O)(py)]ClO_4,
(2): α-*cis*-[Co(EDDA)(py)$_2$]ClO_4,
(3): [Co(EDDA)(elam)]ClO_4
——: in water, ----: in dilute $HClO_4$

bis(amine) complexes show a first band which is apparently composed of two components, and the spectra closely resemble those of such well-known complexes as *trans*-[Co$(CH_3CO_2)_2(NH_3)_4]^+$,[7] *trans*-[Co$(CH_3CO_2)_2$(en)$_2]^+$,[7] α-*cis*-[Co(EDDA)$(NH_3)_2]^+$, and α-*cis*-[Co(EDDA)(en)]$^+$.[3,4] Therefore, the configuration of the bis(amine) complexes is α-*cis*, without any question. Some trends are observable in the spectra of the isomers; the maxima of both the first and the second bands shift slightly to a lower wave number, and the intensities of the bands increase with the increase in the methylene number in the amines. It may be estimated that the ligand field strength of amines decreases with the enlargement of the amines, and that the enlargement decreases the symmetry of the complexes and, hence, makes the intensity larger.

The spectra of the aquo(amine) complexes are similar to one another. Again, with the increase in methylene in the amines, the maxima of the first and the second bands shift to a lower wave number and the absorption intensity increases, although a few cases of the reverse are included.

The spectrum of the β-*cis* isomer of the ethylenediamine complex has already been reported by Legg and Cooke.[4] The spectrum of the isomer which was prepared by the present procedure agreed with their spectrum except for slight differences in the ε values. The spectrum of the red isomer of the diammine complex closely resembles that of the β-*cis* ethylenediamine

7) K. Kuroda and P. S. Gentile, This Bulletin, **38**, 1368 (1965).

complex, as may be seen in Fig. 2. The ethylenediamine complex can exist only as the α-*cis* or the β-*cis* isomer; therefore, the similarity indicates that the configuration of the diammine complex is the β-*cis* and not the *trans*.

Infrared Spectra. The infrared spectra were supplementally used to confirm the structure of the complexes prepared. All of the complexes showed a strong fairly broad absorption around 1650 cm^{-1}, the CO-stretching region. The lack of absorption between 1700—1800 cm^{-1} indicates that the carboxyl groups of EDDA certainly coordinate to the central cobalt and are not present as free-acid.[8] Another strong absorption was observed around 1080 cm^{-1}, the absorption of the perchlorate ion. It is, thus, certain that the aquo(amine) complexes are cationic and not the hydroxo(amine) species. (This is natural, since the complexes were precipitated in an acid medium with perchloric acid.)

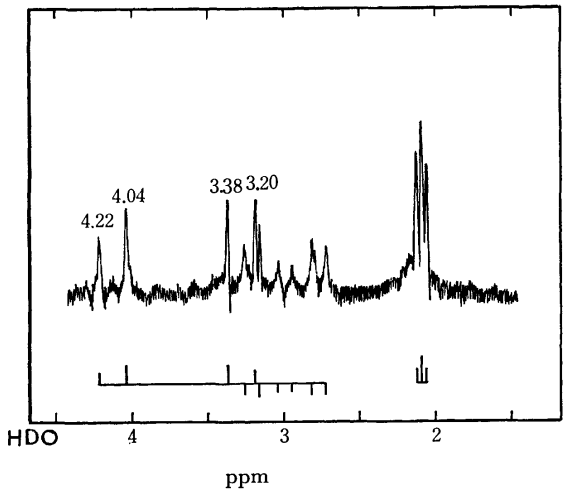

Fig. 5. PMR Spectrum of α-*cis*-$[Co(EDDA)(mam)_2]ClO_4$ in D_2O.

Proton Nuclear Magnetic Resonance Spectra. In the α-*cis* isomer of a bis(amine) complex, the two glycinate rings of EDDA are equivalent and only one AB quartet pattern due to the glycinate ring protons can be expected. In fact, such simple absorptions have been previously observed in several α-*cis* isomers of the Co(III)-EDDA system, *e.g.*, $[Co(EDDA)(NH_3)_2]^+$,[4] $[Co(EDDA)(H_2O)_2]^+$,[3] $[Co(EDDA)(ox)]^-$,[9] and $[Co(EDDA)(N_3)_2]^-$.[1] Figure 5 illustrates the PMR spectrum of α-*cis*-$[Co(EDDA)(mam)_2]ClO_4$ in D_2O as an example. As may be seen in the figure, the absorptions can be divided into three groups—one AB quartet due to the glycinates, a symmetrical absorption from the ethylene backborn protons, and a sharp triplet due to the methyl groups in the coordinated amines. The appearance of the triplet can be attributed to the spin-spin coupling with the amino protons which had not completely exchanged with deuterium at the time of the measurement. Thus, the assignment of the α-*cis* isomers is supported by the PMR spectra.

In the cases of the β-*cis* isomers, the two glycinates are not equivalent and a more complicated absorption pattern can be expected. Legg and Cooke[4] first measured the PMR spectrum of β-*cis*-$[Co(EDDA)(en)]^+$ and observed a single strong absorption due to the protons of glycinate coplanar with the ethylene ring. Legg and his co-workers[10] extended such an observation to the other β-*cis* isomers, such as those of $[Co(EDDA)(ox)]^-$ and $[Co(EDDA)(mal)]^-$; in order to explain the singlet absorption, they indicated that the two protons in the in-plane glycinate are located at magnetically very similar situations. Thus, the appearance of the strong singlet is a remarkable characteristic of the β-*cis* isomers. In Fig. 6, the PMR spectra of the α-*cis* and the β-*cis* isomers of the diammine complex are shown. In contrast to the relatively simple pattern of the α-*cis* isomer, the β-*cis* isomer exhibits an intense absorption as well as the AB quartet of the out-of-plane glycinate protons and the absorptions of the ethylene backborn protons with an unsymmetrical feature.

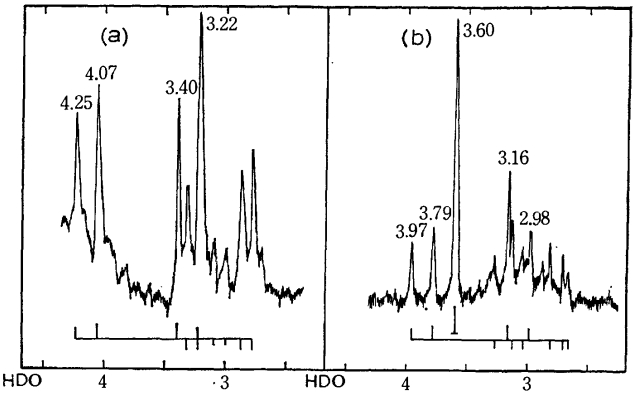

Fig. 6. PMR Spectra of $[Co(EDDA)(NH_3)_2]ClO_4$ in D_2O.
(a) α-*cis* isomer, (b) β-*cis* isomer

The aquo(amine) complexes are considered to have the α-*cis* configuration, since one of the coordinated water molecules of the starting α-*cis* diaquo complex was replaced at a relatively low temperature and since further substitution at that same temperature gave the α-*cis* bis(amine) complexes, as has been discussed above. Even in the α-*cis* configuration, however, the two glycinate rings are not equivalent in these complexes because of the coordination of the two different molecules as the additional ligands. Thus, as may be seen in Fig. 7, two sets of an AB quartet are observable; this is in accordance wih the expected configuration. From a comparison of the spectrum with those of the α-*cis* diammine and diaquo complexes, the quartet of the lower field can be assigned to the glycinate protons near the coordinated ammonia.

In all the AB quartets of the out-of-plane glycinate protons, the differences in the chemical shifts, δ_{AB}, are in the range of 0.80—0.87 ppm and the coupling constants, J_{AB}, are 18 Hz; these values are in good

8) D. H. Busch and J. C. Bailar, *J. Amer. Chem. Soc.*, **75**, 4574 (1953) and many other literatures.

9) C. W. Van Saun and B. E. Douglas, *Inorg. Chem.*, **8**, 115 (1969).

10) P. F. Coleman, J. I. Legg, and J. Steele, *ibid.*, **9**, 937 (1970).

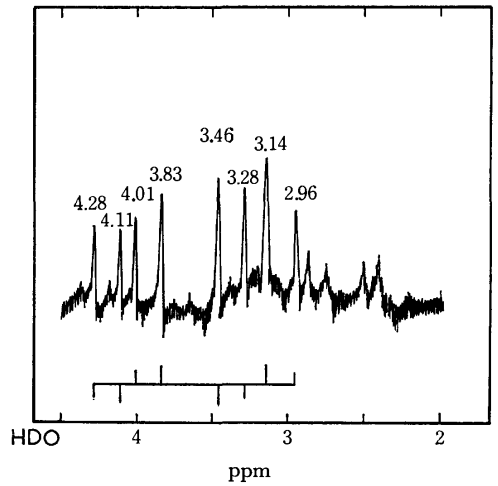

Fig. 7. PMR Spectrum of $[Co(EDDA)(H_2O)(NH_3)]ClO_4$ in D_2O.

accordance with those previously obtained in the other Co(III)-EDDA complexes.

Ethanolamine Complex. Ethanolamine may be a unidentate or a bidentate, and as a bidentate it may be a neutral (as NH_2–CH_2–CH_2–OH) or an uninegative (as NH_2–CH_2–CH_2–O^-) ligand.[11] Therefore, the coordination of the ligand in the ethanolamine complex (12) is worth considering. Although the complex was prepared by a procedure similar to those used for the aquo(amine) complexes, it is certain that the complex is not the aquo(ethanolamine) complex, because the calculated composition for the aquo(ethanolamine) complex disagrees more than the limits of experimental error with the analytical results. (For example, C is 23.34% for the aquo(ethanolamine) complex against the experimental value of 24.47%.) The coordination of ethanolamine as a bidentate is supported further by its absorption spectrum, which is considerably different from those of the aquo(amine) complexes, as may be seen in Figs. 3 and 4. That is, both the first and the second bands are broad and the intensities are considerably lower than those of the aquo(amine) complexes. These characteristics may indicate that the central cobalt ion is surrounded by a different field from that of the aquo(amine) complexes.

As is indicated in Fig. 4, however, the spectrum of the ethanolamine complex changed slightly upon the addition of perchloric acid, while there was no change in those of the aquo(amine) complexes. In the basic solution, both the aquo(amine) and the ethanolamine complexes, as well as the diaquo complex, exhibited different spectra from those in neutral water. These facts indicate that the hydroxy proton in the ethanolamine complex is more dissociative than that of the coordinated water, and that the complex exists partly in the form of $[Co(EDDA)(NH_2–CH_2–CH_2–O)]$ in water. This conclusion is consistent with the low pH value of the aqueous solution which contains nothing but the complex (3.94 in a 0.0025 molar solution).

Finally, the coordination of EDDA in this complex is considered to be of the *α-cis* mode. The complex was prepared from the *α-cis* diaquo complex at low temperatures (~50°C), as were the *α-cis*-aquo(amine) and *α-cis*-bis(amine) complexes; no sign of the rearrangement of the coordinated EDDA was observed during the reaction. The assignment is supported by the relatively low intensities of its absorption maxima. (The ε_1's of the *β-cis* isomers prepared so far are all over 150, possibly because of the highly unsymmetric structure of the isomers.) The PMR spectrum also showed no characteristic indicating that the complex had the *β-cis* configuration.

11) H. Yoneda and S. Kida, *J. Amer. Chem. Soc.*, **82**, 2139 (1960).

ESR of Hot Ions: Zn(I), Cd(I), and Hg(I) in γ-Irradiated Potassium Tetracyano Zincate(II), Cadmate(II), and Mercurate(II)

Jun-Ichi Isoya and Shizuo Fujiwara

Department of Chemistry, Faculty of Science, The University of Tokyo, Hongo, Tokyo

(Received July 6, 1971)

It is known that X-ray or γ-ray irradiation of inorganic complexes produces hot ions which have lower valence states than the original ones and yet are sited in the regular crystalline array of the undamaged mother complexes. ESR study reveals that the hot ions of paramagnetic Zn(I), Cd(I), and Hg(I) complexes are formed by γ-irradiation of $K_2[Zn(CN)_4]$, $K_2[Cd(CN)_4]$, and $K_2[Hg(CN)_4]$, respectively. Hyperfine structures of the ESR signals shows that the Zn(I) and Cd(I) complexes have C_{3v} symmetry instead of T_d symmetry of the original complex, and Hg(I) complex has a slightly distorted C_{3v} symmetry. In Zn(I) complex, one of the four symmetry axes along Zn(II)–CN bondings is stretched. This occurs evenly with respect to each axis, resulting in the formation of four sites of the electron spins. For Cd(I) complexes, four species are produced as an irradiation product, where each species has four sites which are axially symmetric with respect to any one of the four Cd(II)–CN bondings. In Hg(I) complex, there exist twenty-four sites and the symmetry axis of each site lies along a direction slightly deviated from the original Hg(II)–CN bonding. From the behavior of the decay of ESR signal intensity at liquid nitrogen temperature, it is concluded that the stability is in the order Hg(I)>Cd(I)>Zn(I).

X-ray or γ-ray irradiation of diamagnetic substances results in the production of ESR active paramagnetic centers. It has been found that the central metal ions are reduced to the lower valence state in the case of X-ray or γ-ray irradiated Co(III) or Pd(II) complexes.[1-5] These metastable paramagnetic centers have been referred to as hot ions[5] because they are hot (unstable) in the sense that the valence state differs from that of the original complex and yet they are sited in the host lattices of the original complex.

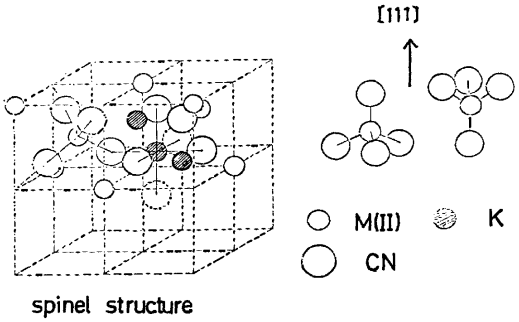

Fig. 1. Crystal structure of $K_2[Zn(CN)_4]$, $K_2[Cd(CN)_4]$, and $K_2[Hg(CN)_4]$.
$M(II)(CN)_4$ forms a regular tetrahedron with four M(II)-CN bondings aong [111], [1$\bar{1}\bar{1}$], [$\bar{1}$1$\bar{1}$], and [$\bar{1}\bar{1}$1].
The figure of spinel structure is quoted from E.W. Gorter *Philips Res. Repts.* **9**, 295, (1954).

Since Zn(II), Cd(II), and Hg(II) ions are formed of closed *d*-shell, the reduced ions Zn(I), Cd(I), and Hg(I) are expected to have an unpaired electron of large *s*-character. No report has so far been found with regard to the presence of stable complex of Zn(I). The only example reported is of $Cd_2[AlCl_4]_2$. However, as it is a diamagnetic diatomic ion,[6] no ESR signal is expected. The situation is the same with all stable Hg(I) salts such as Hg_2Cl_2. The existence of paramagnetic Zn(I) and Cd(I) ions was evidenced in the γ-ray irradiated frozen solutions of Zn(II) or Cd(II) salts.[7,8] ESR was observed with Cd(I) ion which was isolated in the matrix of rare gas.[9] All the systems referred to in literature are amorphous with respect to the host lattices, and not crystalline. We carried out ESR investigation with single crystals of Zn(II), Cd(II), and Hg(II) complexes. Formation of hot ions of paramagnetic Zn(I), Cd(I), and Hg(I) by γ-ray irradiation was evidenced. The total dose of γ-rays was made to not exceed the magnitude with which the host lattices are destroyed. It is expected that the metastable M(I) complexes are formed in the mother compounds, where M(I) refers to either one of Zn(I), Cd(I), or Hg(I). It will be shown that the crystal fields of the M(I) ions still keep the symmetry properties of the mother compounds fairly well. The location of the electron spins and the bonding nature of Zn(I), Cd(I), and Hg(I) ions are elucidated. It should be noted that the hot ions can be used for making possible ESR investigation of diamagnetic inorganic complexes which are normally ESR insensitive.

Experimental

Compounds investigated were potassium tetracyanozincate(II) $K_2[Zn(CN)_4]$, potassium tetracyanocadmate(II) $K_2[Cd(CN)_4]$, and potassium tetracyanomercurate(II) $K_2[Hg(CN)_4]$. Single crystals of $5\times10\times10$ mm^3 are easily obtained by slow evaporation of aqueous solution. They exihibit the faces of the octahedron (111), generally tabular in habit. Dickinson[10] confirmed that $K_2[Zn(CN)_4]$, $K_2[Cd(CN)_4]$, and $K_2[Hg(CN)_4]$ have a spinel structure with the tetrahedral

1) W. C. Lin, C. A. McDowell, and D. J. Ward, *J. Chem. Phys.*, **49**, 2883 (1968).
2) J. Danon, R. P. A. Muniz, A. O. Caride, and I. Wolfson, *J. Mol. Structure*, **1**, 127 (1968).
3) S. Fujiwara and M. Nakamura, *J. Chem. Phys.*, **52**, 6299 (1970).
4) S. Fujiwara and M. Nakamura, *J. Coord. Chem.*, in press.
5) S. Fujiwara, T. Watanabe, and H. Tadano, *ibid.*, in press.
6) J. D. Corbett, *Inorg. Chem.*, **1**, 700 (1962).
7) P. N. Moorthy and J. J. Weiss, *Nature*, **201**, 1318 (1964).
8) R. S. Eachus and M. C. R. Symons, *J. Chem. Soc. A*, **1970**, 3080.
9) P. H. Kasai, *Phys. Rev. Lett.*, **21**, 67 (1968).
10) R. G. Dickinson, *J. Amer. Chem. Soc.*, **44**, 774 (1922).

complex ion $[M(II)(CN)_4]^{2-}$. The direction of the four M(II)–CN bondings in the tetrahedral complex ion are parallel to the crystallographic axes [111], [1$\bar{1}\bar{1}$], [$\bar{1}$1$\bar{1}$], and [$\bar{1}\bar{1}$1]. The neutron diffraction study by Sequeira and Chidambaram[11] confirmed that $[Zn(CN)_4]^{2-}$ forms a regular tetrahedron.

The crystals and powder samples were exposed to γ-rays from a ^{60}Co source in a vacuum ($\sim$1 mmHg) or nitrogen atmosphere with a dose rate of 5×10^4 R/hr for 20 hr at 77°K. After irradiation, ESR spectra were recorded at 77°K by a JEOL 3BS X-band spectrometer and a JEOL SK-1 K-band spectrometer using 100 kHz field modulation. On irradiation, the color of the crystals turned reddish orange (Zn), yellow (Cd), and orange (Hg). When the crystals were taken out of the liquid nitrogen Dewar vessel into the air, the color diminished rapidly and the ESR signals of M(I) complexes disappeared. Single crystals were attached to a glass or Teflon rod, and irradiated by γ-rays in a liquid nitrogen Dewar vessel. After irradiation they were transferred immediately to another Dewar vessel for ESR measurements. Powders were sealed in one end of a quartz tube and subjected to irradiation. After irradiation, the tube was quickly turned upside down, the sample being transferred to the other end which had been protected from irradiation. ESR measurements were performed twice, first with the sample in the γ-ray irradiated end and then in the other non-irradiated end. In the first measurement, the doublet signal of H atom observed beside the signal of hot ions was used as the reference for the field sweep caliblation. The H atom is assumed to have been produced by irradiation in the quartz tube. Inversion of the sample tube was carried out as quickly as possible to make the decrease of the signal intensity negligible.

Results and Discussion

The spectra of γ-irradiated powder $K_2[Zn(CN)_4]$, $K_2[Cd(CN)_4]$, and $K_2[Hg(CN)_4]$ are shown in Figs. 2—5, where signals of radicals (central sharp line) and metal complexes can be seen. The latter was mainly examined. All the spectra show hyperfine structures of fairly large splitting constants, g value of about 2 and isotropic and small linewidth. The results can be interpreted in terms of the electronic configuration of $nd^{10}(n+1)s^1$ (n=3, 4, and 5 for Zn, Cd, and Hg, respectively). Thus the products of γ-irradiation are the cyano complex of Zn(I), Cd(I), and Hg(I). The location of the electron spin in the outer shell was investigated. Two locations are possible, spherical isotropic distribution in the outermost s shell and that confined in any one of the four metal-cyano bondings. The crystal structure of the mother compounds is of the spinel type. If the structure of tetrahedron symmetry of the mother compound is maintained and the electronic distribution is completely spherical in $[M(I)(CN)_4]^{3-}$, a simple spectrum of a single line or of hyperfine structure is expected. No angular de-

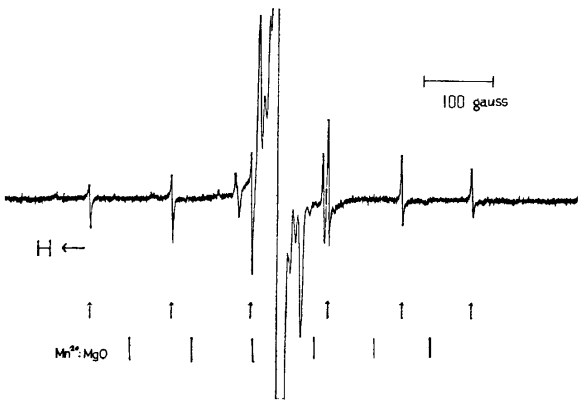

Fig. 2. The powder spectrum of γ-irradiated $K_2[Zn(CN)_4]$ (X-band, 100 kHz modulation, at 77°K)
The strong absorption in the center is the signal of Zn(I) with no nuclear spin. Six arrows indicate ^{67}Zn(I) hyperfine structure. Other signals near the center are those of radicals.

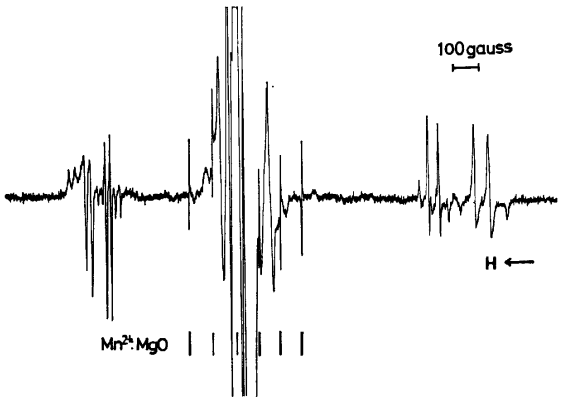

Fig. 3(a). The powder spectrum of γ-irradiated $K_2[Cd(CN)_4]$. (X-band, 100 kHz field modulation, at 77°K)
The spectrum indicates that four species are produced.

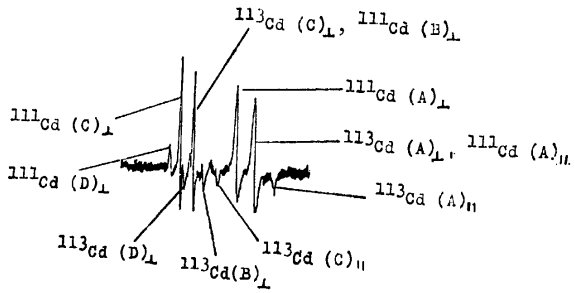

Fig. 3(b). Assignment of Cd(I) species in the low field.

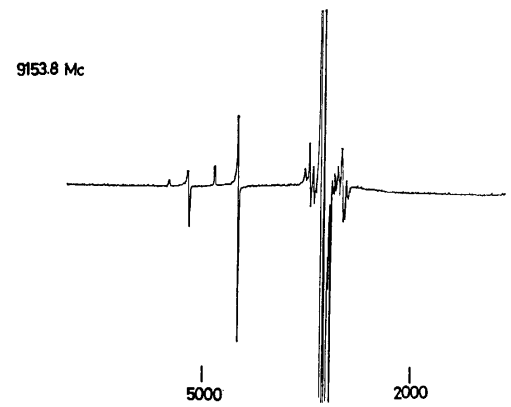

Fig. 4. The powder spectrum of γ-irradiated $K_2[Hg(CN)_4]$. (X-band, 100 kHz modulation, at 77°K)
The signal in 5400 gauss is the fourth line of ^{201}Hg hyperfine structure. The signal in 4600 gauss is the second line of ^{199}Hg hyperfine structure.

11) A. Sequeira and R. Chidambaram, *Acta Crystallogr.*, **20**, 910 (1966).

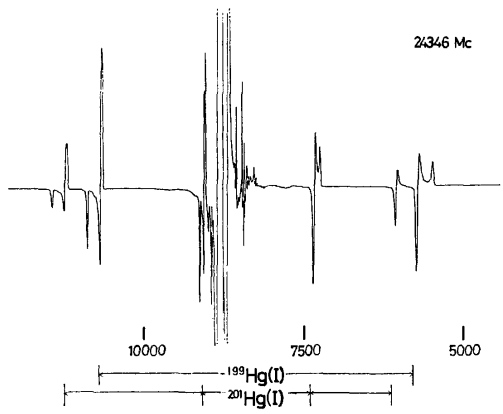

Fig. 5. The powder spectrum of γ-irradiated $K_2[Hg(CN)_4]$. (K-band, 100 kHz field modulation, at 77°K)
Full hyperfine structure can be observed at this frequency. The large hyperfine structure constants shift the apparent g-value far away from the position of $g=2$. The shoulder in the perpendicular line in the high field shows a slight deviation from axial symmetry.

pendence is expected with respect to the spectrum of single crystal samples. The results show angular dependence eliminating the spherical distribution of spins, and suggest that M(I) ions are in C_{3v} field. Namely, the electron spins in $[M(I)(CN)_4]^{3-}$ occupy the outermost s orbital but are confined in one of the four bondings. Detailed results will be given in the following.

(1) γ-Irradiated $K_2[Zn(CN)_4]$. The spectrum consists of a single strong line ($g=2$) and six satellite lines (the spectrum of this structure will be referred to as a set). The satellites are attributed to the isotope of ^{67}Zn ($I=5/2$) with a natural abundance of 4.11%. The intensity ratio of satellites to the central signal agrees with the abundance ratio of isotopes.

The single crystal shows a spectrum of four sets which suggests the coexistence of four sites for the distribution of electron spin. Angular variation cannot be seen distinctly with respect to the g value, but clearly with A values. Hence, the symmetry of Zn(I) complexes is fairly accurately determined by an examination of the angular dependence of hyperfine structure. An example of a γ-irradiated single crystal of $K_2[Zn(CN)_4]$ being rotated around [111] axis which is perpendicular to the static magnetic field is shown in Fig. 6. During the rotation, the crystallographic face [111] preserved the direction parallel to the magnetic field, in which one site is invariant and the relation of the remaining three sites displays threefold rotational

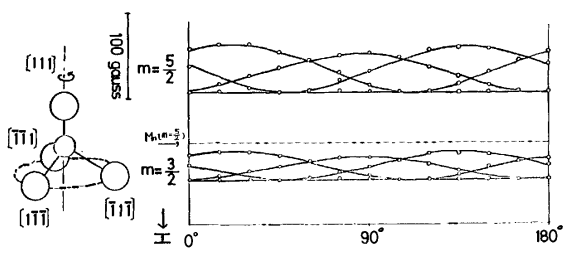

Fig. 6. Anglular dependence of the hyperfine structure lines of γ-irradiated single crystal of $K_2[Zn(CN)_4]$ with respect to the rotation of the crystal around $[111]\perp H$.
(X-band, 100 kHz field modulation, at 77°K)

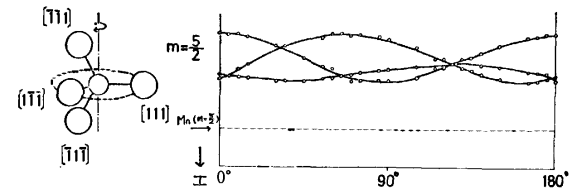

Fig. 7. Anglar dependence of hyperfine structure lines of γ-irradiated single crystal of $K_2[Zn(CN)_4]$ with $[0\bar{1}1]\perp H$. In this rotation, [111] and $[1\bar{1}\bar{1}]$ varies from 0° to 90° against H. The largest splitting occurs where one of these two axis is parallel to H. The samllest splitting occurs where H becomes perpendicular to Zn(II)-CN direction.

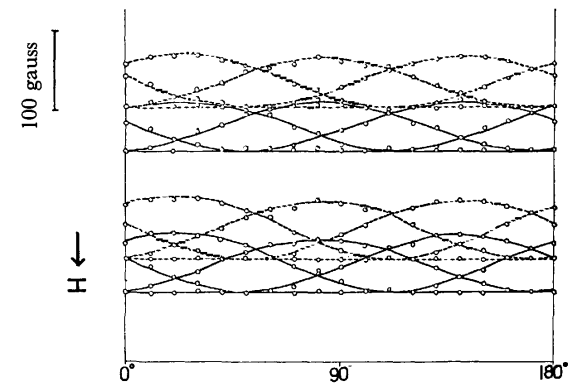

Fig. 8(a). Angluar dependence of hyperfine structure lines of γ-irradiated single crystal of $K_2[Cd(CN)_4]$ with the rotation with $[111]\perp H$ (the lines in the low field).
——^{113}Cd, ------^{111}Cd
The sets of lines appearing on the outer side are of species A and those on in the inside species C.

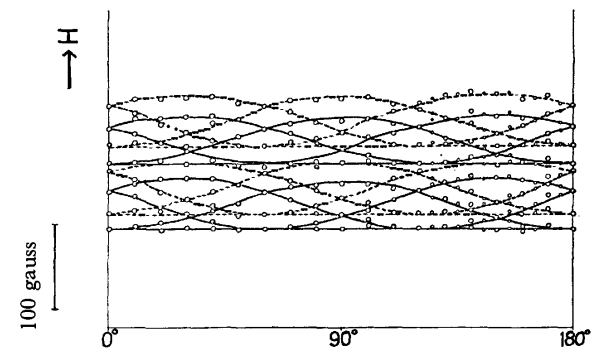

Fig. 8(b). Angular dependence of hyperfine structure lines of γ-irradiated single crystal of $K_2[Cd(CN)_4]$ with rotation with $[111]\perp H$ (the lines in the higher field).

symmetry with respect to the [111] axis. The results of the rotation $[0\bar{1}1]$ axis perpendicular to the static field are given in Fig. 7. The crystal rotates with the [111] face parallel to the rotational axis. Two sites show the same variation with an interval of the tetrahedral angle and the other two are found to be equivalent. At the positions of the crystal where the static field bisects the tetrahedral angles, four sites of lines collapse into one.

It is to be noted that if g-tensor and A-tensor of Zn(I) are (within experimental error) axially symmetric along the Zn–CN bond of the original complex ion $[Zn(CN)_4]^{2-}$, the angular dependence of its ESR spectrum can be readily inferred. When one of the four Zn(II)–CN directions in the host crystal, [111], $[1\bar{1}\bar{1}]$,

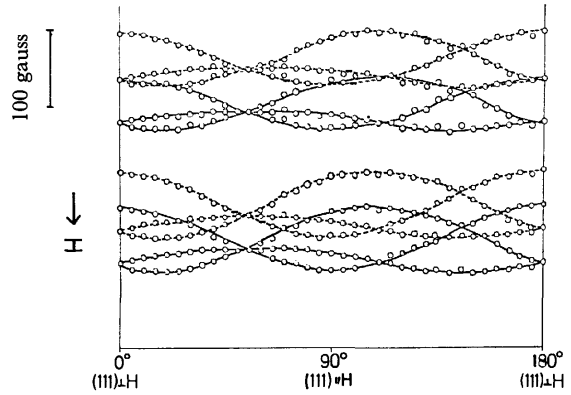

Fig. 9(a). Angluar dependence of hyperfine structure lines of γ-irradiated single crystal of $K_2[Cd(CN)_4]$ with rotation with $[0\bar{1}1]\perp H$ (the lines in the low field).

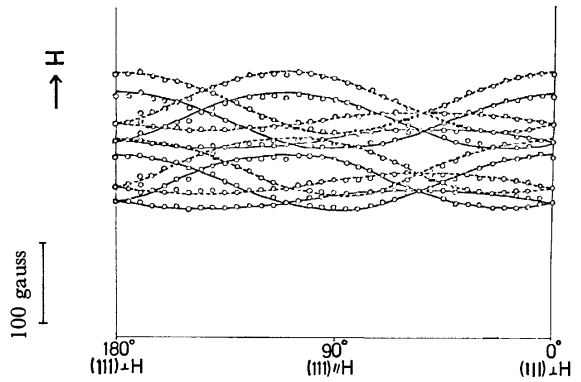

Fig. 9(b). Angular dependence of hyperfine structure lines of γ-irradiated single crystal of $K_2[Cd(CN)_4]$ with rotation with $[0\bar{1}1]\perp H$ (the lines in the higher field).

$[\bar{1}\bar{1}1]$, and $[\bar{1}1\bar{1}]$, is parallel to the static field, the corresponding site shows the largest splitting. The smallest splitting occurs when one of the axes is perpendicular to the static field. It is thus concluded that the paramagnetic Zn(I) complex is axially symmetric with respect to the symmetry axis along Zn(II)–CN bonding of the host lattice. Since each Zn(II)–CN bonding coincides with the threefold symmetry axis in the original complex $[Zn(CN)_4]^{2-}$, it is probable that the Zn(I) complex has C_{3v} symmetry instead of T_d symmetry. As the four Zn(II)–CN bondings are equivalent in the original complex $[Zn(CN)_4]^{2-}$, the location of the spin is assumed to be of equal probability with respect to all four bondings. Hence, in the Zn(I) complex produced by γ-ray irradiation, one of the Zn(II)–CN directions becomes the unique axis, and such a distortion is assumed to occur evenly with respect to the four bondings. Thus the symmetry is lowered from T_d to C_{3v}. The signal intensities indicate that four sites are produced in an equal quantity.

ESR parameters are calculated by the following spin Hamiltonian:

$$\mathcal{H}=\beta\mathbf{S}\cdot\mathbf{G}\cdot\mathbf{H}+\mathbf{S}\cdot\mathbf{A}\cdot\mathbf{I} \qquad (1)$$

In the case of $[Zn(I)(CN)_4]^{3-}$, the high field approximation is adopted satisfactorily. Under conditions where the g-tensor and A-tensor are axially symmetric about the same axis, the solution of the spin Hamiltonian has been given by Abragam and Bleany.[12]

$$h\nu=g\beta H+Km+\frac{B^2}{4g\beta H}\left(\frac{A^2+B^2}{K^2}\right)\{I(I+1)-m^2\}+\frac{1}{2g\beta H}\left(\frac{A^2-B^2}{K}\right)\left(\frac{g_{//}-g_\perp}{g^2}\right)\sin^2\theta\cos^2\theta m^2 \qquad (2)$$

$$K^2g^2=A^2g_{//}^2\cos^2\theta+B^2g_\perp^2\sin^2\theta \qquad (3)$$

($S=1/2$, $I=5/2$, quadrupole term is not taken into account.)

Using Eq. (2), we obtain for $[^{67}Zn(I)(CN)_4]^{3-}$:

$g_{//}=2.000\pm0.005$ $\quad g_\perp=1.999\pm0.005$
$A=131\pm1$ gauss $\quad B=110\pm1$ gauss

For $[Zn(I)(CN)_4]^{3-}$ of zinc isotopes with no nuclear spin we get:

$g_{//}=2.001\pm0.005$ $\quad g_\perp=1.999\pm0.005$

(2) γ-Irradiated $K_2[Cd(CN)_4]$. Of the stable isotopes of cadmium, two isotopes, ^{111}Cd ($I=1/2$, natural abundance 12.86%) and ^{113}Cd ($I=1/2$ natural abundance 12.34%), possess nuclear spins. In accordance with the constitution of isotopes, the ESR spectrum of the irradiated compound shows two sets of hyperfine lines. One set with larger splitting refers to that of ^{113}Cd which has a larger absolute value of magnetic moment. The signals of the isotopes of zero nuclear spin cannot clearly be distinguished from those of radicals.

We see from the spectrum of powdered sample (Fig. 3) that four different species of the Cd(I) complexes are produced for each isotope. These species are denoted by A, B, C, and D in decreasing order of magnitude of hyperfine splitting. Each species differs with regard to the value of hyperfine splitting, signal intensity, behavior of the decay at 77°K and linewidth.

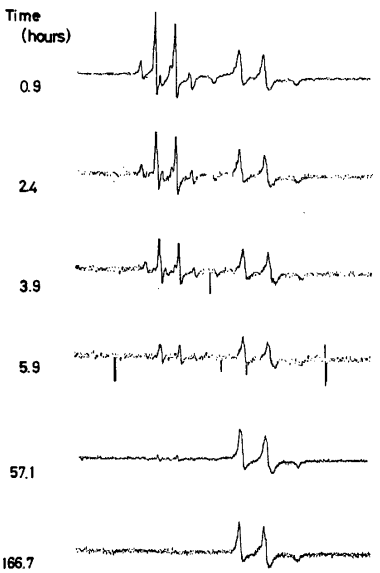

Fig. 10. Decay behaviour of Cd(I) complex (powder, non-degassed, at 77°K)
Intensities are almost normalized by Mn^{2+} signal present in the sample. Species A is sable at this temperature. Other species decay into nothing.

12) A. Abragam and B. Bleany, "Electron Paramagnetic Resonance of Transition Ions.," Clarendon Press, Oxford (1970), p. 173.

Immediately after irradiation, the signal intensity of each species is in the order C>A≫B~D. The intensity of B and D is very small. At 77°K, B, C, and D decay with the half-life of about 1/2 day. A which shows the largest hyperfine splitting is stable at this temperature in non-degassed sample. The decay behavior is shown in Fig. 10.

The number of sites and the symmetry of the Cd(I) complexes were determined by single crystal spectra. The results of experiments where γ-irradiated single crystal of $K_2[Cd(CN)_4]$ was rotated around the [111] axis and the [0$\bar{1}$1] axis perpendicular to the static magnetic field are given in Figs. 8 and 9, respectively. Measurements of the ESR spectra of B and D could not be carried out owing to the weakness of intensity. The angular dependence of these species is assumed to be similar to that of A and C in the whole range of rotation. This is confirmed by the fact that at the direction where the four sites of A and C merge in one, four sites of B and D also collapse in one. We thus assume that the number of sites and the angular variation of each species are the same except for the magnitude of the splitting. The same is assumed to hold for Zn(I) complex. Thus the hyperfine spectrum of Cd(I) consists of 2 (isotopes) $\times$4 (species) $\times$4 (sites). Each species has four sites axially symmetric with respect to the Cd(II)–CN direction in the host lattice, [111], [1$\bar{1}\bar{1}$], [$\bar{1}$1$\bar{1}$], and [$\bar{1}\bar{1}$1]. The paramagnetic Cd(I) complex is stretched along the symmetry axis (z-axis) which is parallel to any one of the four Cd(II)–CN directions in the host lattice. It was thought that the reduction of Cd(II) to Cd(I) might accompany the distortion of the mother complex, particularly that along the Cd(II)–CN bonding. As in the case of $K_2[Zn(CN)_4]$, γ-irradiation produced Zn(I) ion with C_{3v} symmetry. We assume that this holds with Cd(I), but in this case four species are produced. We take it for granted that the distortion occurs along Cd(II)–CN bonding with four different magnitudes in each Cd(II)–CN direction, resulting in the formation of the four species.

The parameters of ESR hyperfine spectrum are calculated for A and C by Eq. (1). For both isotopes ^{111}Cd(I) and ^{113}Cd(I), $S=1/2$ and $I=1/2$. In this case, the hyperfine splitting is too large for application of high field approximation. If the principal axes of the g- and A-tensors are taken to be parallel and the static magnetic field parallel to one of the principal axes, Eq. (1) can be exactly solved. With axial symmetry, the Hamiltonian becomes simpler. The method for $S=1/2$ and $I=1/2$ has been developed.[13]

The strongly allowed transitions under the experimental conditions are as follows. For the case of H parallel to the z-axis (symmetry axis), we have

$$\begin{aligned} h\nu &= \frac{1}{2}g_{//}\beta H_1 + \frac{1}{2}A + \frac{1}{2}[(g_{//}\beta H_1)^2 + B^2]^{1/2} \\ h\nu &= \frac{1}{2}g_{//}\beta H_2 - \frac{1}{2}A + \frac{1}{2}[(g_{//}\beta H_2)^2 + B^2]^{1/2} \end{aligned} \quad (4)$$

For the case of H perpendicular to the z-axis, we have

$$\begin{aligned} h\nu &= \frac{1}{2}\left[(g_{\perp}\beta H_1)^2 + \left(\frac{A-B}{2}\right)^2\right]^{1/2} + \frac{1}{2}B + \frac{1}{2}\left[(g_{\perp}\beta H_1)^2 + \left(\frac{A+B}{2}\right)^2\right]^{1/2} \\ h\nu &= \frac{1}{2}\left[(g_{\perp}\beta H_2)^2 + \left(\frac{A-B}{2}\right)^2\right]^{1/2} - \frac{1}{2}B + \frac{1}{2}\left[(g_{\perp}\beta H_2)^2 + \left(\frac{A+B}{2}\right)^2\right]^{1/2} \end{aligned} \quad (5)$$

Taking the difference in each two equations of Eqs. (4) and (5), the hyperfine splitting constants A and B are connected to the observed magnetic field values H_1 and H_2. The difference between the observed separation H_2-H_1 and the true hyperfine splitting constants A and B becomes smaller at higher microwave frequency. First, with the use of an approximate value of B for the observed separation in the K-band powder spectrum, Eq. (4) and the single crystal data with z-axis parallel to H give an approximate value of A. Due to the nearly isotropic nature of g-value, calculation is easy. With the use of the A value thus obtained and the observed value of the magnetic field for the single crystal spectrum with z-axis perpendicular to H as well as Eq. (5), a more appropriate value of B is obtained. This process is repeated until the values of A and B become consistent within experimental error. Next, $g_{//}$ and $g_{\perp}$ are calculated with the use of A and B thus obtained. The results are as follows.

Species A for ^{113}Cd (I)
$g_{//}=1.99\pm0.01$ $g_{\perp}=1.998\pm0.005$
$A=(1.58\pm0.01)\times10^3$ gauss
$B=(1.47\pm0.01)\times10^3$ gauss
for ^{111}Cd (I)
$g_{//}=1.99\pm0.01$ $g_{\perp}=1.998\pm0.005$
$A=(1.52\pm0.01)\times10^3$ gauss
$B=(1.40\pm0.01)\times10^3$ gauss
Species C for ^{113}Cd (I)
$g_{//}=2.00\pm0.01$ $g_{\perp}=1.986\pm0.005$
$A=(1.37\pm0.01)\times10^3$ gauss
$B=(1.23\pm0.02)\times10^3$ gauss
for ^{111}Cd (I)
$g_{//}=2.00\pm0.01$ $g_{\perp}=1.986\pm0.005$
$A=(1.31\pm0.01)\times10^3$ gauss
$B=(1.18\pm0.01)\times10^3$ gauss

(3) γ-Irradiated $K_2[Hg(CN)_4]$. The ESR spectrum of the γ-irradiated powder sample of $K_2[Hg(CN)_4]$ consists of the signals of the radicals and those of mercury isotopes of $I=0$, 1/2, and 3/2. The signal of $I=0$ spin mercury appears in the field very close to the free spin. Due to the very large magnitude of A, the hyperfine constant and the limited range of the field sweep of the ESR spectrometer used, all the components of the hyperfine lines have not been recorded at X-band frequency as seen in Fig. 4, but they are measurable at K-band frequency as shown in Fig. 5. The center of the hyperfine lines does not refer to the true g-value for Hg(I) because the quantization axis of the electron spin differs from the applied magnetic field.

The K-band spectrum of powder gives the whole hyperfine spectrum and allows calculation of all prin-

13) P. W. Atkins and M. C. R. Symons, "The Structure of Inorganic Radicals.," Elsevier Publishing Co., Amsterdam (1967), p. 236.

cipal values. With respect to the hyperfine spectrum of Hg(I), due to its large hyperfine splitting the difference in intensity of the hyperfine lines is distinctly observed. This is interpreted by the fact that the transition moment is a function of the magnetic field at which the signal appears. From the whole structure of the spectrum of the powdered sample and the number of isotopes it is concluded that the number of species of the hot ion of Hg(I) is one and the structure of its crystal field is slightly deviated from axial symmetry.

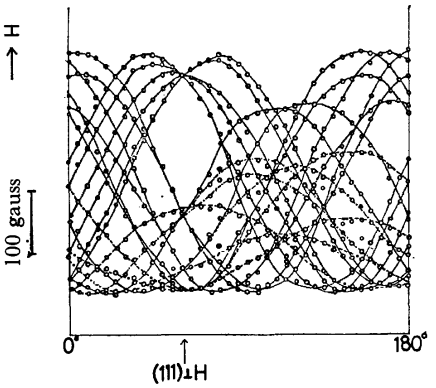

Fig. 11. Angular dependence of hyperfine structure line of γ-irradiated single crystal of $K_2[Hg(CN)_4]$ with the rotation with $[0\bar{1}1]\perp H$.
The second line of ^{199}Hg hyperfine structure is shown. (X-band)

The number of sites and the orientation of Hg(I) complex have been determined from X-band single crystal spectra. For examination of the spectrum, the lines of ^{199}Hg are chosen as an example. The result of the rotation of the γ-irradiated single crystal of $K_2[Hg(CN)_4]$ with the $[0\bar{1}1]$ axis perpendicular to the static magnetic field is shown in Fig. 11. When the [111] axis is parallel to the static magnetic field, the spectrum is the simplest consisting of four lines. The one in the highest field is assumed to refer to Hg(I) in the site of Hg(II)–CN along the [111] axis. With the variation of the angle, the line begins to be separated into six lines. The largest splitting does not occur at the angle where Hg(II)–CN of the host lattice is parallel to the magnetic field, but occurs at the angle about 20° deviated from the direction of Hg(II)–CN. At an interval of the tetrahedral angle, six lines similarly appear in the higher field which are assumed to refer to the sites corresponding to Hg(II)–CN along $[1\bar{1}\bar{1}]$. The other nine lines are assigned to those resulting from the sites corresponding to the remaining two Hg(II)–CN directions $[\bar{1}\bar{1}1]$ and $[\bar{1}1\bar{1}]$. With this rotation, $[\bar{1}\bar{1}1]$ and $[\bar{1}1\bar{1}]$ are equivalent, which makes the number of lines smaller than twelve (6×2).

From the results we reach the following conclusion. The reduction is accompanied by the distortion of the mother lattice of the complex to some extent. The symmetry of Hg(I) complex is not far from the axial symmetry of the diamagnetic compound with a structure slightly distorted from C_{3v}. The distortion occurs nearly parallel to the Hg(II)–CN bonding and the deviation is estimated to be about 20°. Six directions of the distortion are distributed around each Hg(II)–CN direction, probably with the distribution determined by the arrangement of the neighboring atoms. The number of sites is twenty-four (6×4). The Hg(I) complex is orientated to a direction slightly deviated from Hg(II)–CN bonding in the host lattice.

The parameters of ESR hyperfine spectrum are calculated from the K-band powder spectrum by Eq. (1). For the sake of simplification, approximation by means of the equation for the strong allowed transition under the conditions of axial symmetry was adopted. Equations for ^{199}Hg ($I=1/2$) are (4) and (5). The equations for $S=1/2$ and $I=3/2$ are found in literature[14] and quoted for ^{201}Hg ($I=3/2$):
For the symmetry axis parallel to H, we have

$$\begin{aligned}
h\nu &= \frac{1}{2}g_{//}\beta H_1 + A + \frac{1}{2}[(g_{//}\beta H_1 + A)^2 + 3B^2]^{1/2} \\
h\nu &= \frac{1}{2}[(g_{//}\beta H_2 + A)^2 + 3B^2]^{1/2} + \frac{1}{2}[(g_{//}\beta H_2)^2 + 4B^2]^{1/2} \\
h\nu &= \frac{1}{2}[(g_{//}\beta H_3 - A)^2 + 3B^2]^{1/2} + \frac{1}{2}[(g_{//}\beta H_3) + 4B^2]^{1/2} \\
h\nu &= \frac{1}{2}g_{//}\beta H_4 - A + \frac{1}{2}[(g_{//}\beta H_4 - A)^2 + 3B^2]^{1/2}
\end{aligned} \tag{6}$$

For the symmetry axis perpendicular to H, we have

$$\begin{aligned}
h\nu &= \frac{1}{2}g_{\perp}\beta H_1 + B + \frac{1}{2}\left[(g_{\perp}\beta H_1 + B)^2 + 3\left(\frac{A+B}{2}\right)^2\right]^{1/2} \\
h\nu &= \frac{1}{2}\left[(g_{\perp}\beta H_2 + B)^2 + 3\left(\frac{A+B}{2}\right)^2\right]^{1/2} + \\
&\qquad \frac{1}{2}\left[(g_{\perp}\beta H_2)^2 + 4\left(\frac{A+B}{2}\right)^2\right]^{1/2} \\
h\nu &= \frac{1}{2}\left[(g_{\perp}\beta H_3 - B)^2 + 3\left(\frac{A+B}{2}\right)^2\right]^{1/2} + \\
&\qquad \frac{1}{2}\left[(g_{\perp}\beta H_3)^2 + 4\left(\frac{A+B}{2}\right)^2\right]^{1/2} \\
h\nu &= \frac{1}{2}g_{\perp}\beta H_4 - B + \frac{1}{2}\left[(g_{\perp}\beta H_4 - B)^2 + 3\left(\frac{A+B}{2}\right)^2\right]^{1/2}
\end{aligned} \tag{7}$$

Calculations were repeated following the method adopted for Cd(I) from the observed separation of members. First, from the observed magnetic field values for z-direction and x-direction in the powder spectrum, principal values for z-direction and x-direction were calculated under the assumption of the axial symmetry. The principal values for y-direction were calculated next. The results are:

For ^{199}Hg ($I=1/2$)

$g_{zz}=1.97\pm0.05$	$A_{zz}=(5.02\pm0.05)\times10^3$ gauss
$g_{yy}=1.96\pm0.05$	$A_{yy}=(4.58\pm0.00)\times10^3$ gauss
$g_{xx}=1.96\pm0.05$	$A_{xx}=(4.56\pm0.05)\times10^3$ gauss

and for ^{201}Hg ($I=3/2$)

$g_{zz}=1.97\pm0.05$	$A_{zz}=(1.85\pm0.01)\times10^3$ gauss
$g_{yy}=1.96\pm0.05$	$A_{yy}=(1.68\pm0.02)\times10^3$ gauss
$g_{xx}=1.96\pm0.05$	$A_{xx}=(1.66\pm0.02)\times10^3$ gauss

(4) Comparison of the Results for M(I) Complexes. The analysis of ESR spectrum shows that hot ion of paramagnetic M(I) is produced by γ-ray irradiation of M(II) complex compounds, where M(I) ion is trapped in the host lattice of M(II) compound with a small distortion. The concentration of M(I) ion is

14) W. C. Lin and C. A. McDowell, *Mol. Phys.*, **7**, 223 (1964).

evaluated to be less than about 10^{-1} % by measurement of the intensity of the ESR signal of M(I).

When M(II) is reduced to M(I) by γ-rays, the symmetry of M(II) is also reduced from T_d to C_{3v}. In the case of cyanomercurate(I) in cyanomercurate(II), the symmetry is more distorted than C_{3v}. However, even in this case, the deviation from C_{3v} is small. The symmetry around M(I) is not C_∞ but C_{3v}. We assume the product to be assigned to $[M(I)(CN)_4]^{3-}$ and not to $[M(I)(CN)_3]^{2-}$, because we consider it difficult to eliminate one cyano radical from the sphere of complex.

Details of the characteristic difference of Zn(I), Cd(I), and Hg(I) are as follows. In Zn(I), one of the four Zn–CN bondings is stretched with equal probability of stretching for four bondings. Hence, the irradiation product Zn(I) is one species with four equivalent sites of electron. In the case of Cd(I), stretching similar to that in Zn(I) occurs along four Cd–CN bondings equivalently. However, in the former, four different kinds of stretching occur along one bonding, which results in possible 16 sites (4 species $\times$ 4 bondings) of electron, all with C_{3v} symmetry. In Hg(I), electron is not sited along any one of Hg(II)–CN bondings, but at a place slightly apart from the bonding. Six different sites are referred to for one Hg(II)–CN direction from the pattern of the spectra. The number of possible sites of the electron is 24.

The electronic structure of the product is also of interest. The values of $|\Psi(0)|^2$ and $\langle r^{-3}\rangle$ for the M(I) ions have not been determined qualitatively. We can evaluate the hyperfine splitting constants for $(n+1)s$ orbital electron with the use of the data of isoelectronic Cu, Ag, and Au atoms using Goudsmit's relation $z_i z_o^2 \propto |\Psi(0)|^2$ [15] and the value of the nuclear gyromagnetic ratio. In the case of Cd(I), the reported data of the Cd(I) ions isolated in argon matrix at 4.2°K is available.[9] It gives the isotropic hyperfine splitting constants, $A=(5137\pm1)$ gauss for ^{111}Cd(I) and $A=(5347\pm1)$ gauss for ^{113}Cd(I). In our experiment, Cd(I) complex has axial symmetry and the hyperfine splitting is divided into the isotropic and anisotropic parts. The ratio of the hyperfine splitting constants of the two nuclei ^{111}Cd and ^{113}Cd agrees with the ratio of the nuclear gyromagnetic ratio within experimental error. The isotropic parts of the observed hyperfine splitting constants leads to the spin population of $5s$ orbital of 0.24 for species C and 0.28 for species A. Taking the anisotropic part of the hyperfine splitting constant into consideration, the hybridization for the unpaired electron orbital is taken to be between sp^2 and sp^3. The same statement might hold for the electronic structure of Hg(I) complex from the estimated hyperfine splitting constants. This supports the assumed symmetry of C_{3v}. We assume further that the complexes of Cd(I) and Hg(I) do not differ so much from each other with respect to the electron densities. This agrees with the observed result after normalization by nuclear gyromagnetic ratio. In contrast to the case of Cd(I) and Hg(I), the observed hyperfine splitting of Zn(I) complex is considerably small, suggesting that the unpaired electron density on zinc nucleus is small and the electron is delocalized considerably to the ligand atoms.

The remarkable difference between the M(I) complexes lies in the stability of the oxidation number, (I). First, the sequence of the signal intensity under the same γ-ray dose is Hg(I)>Cd(I)>Zn(I). Second, Zn(I) and three species of Cd(I) decay at 77°K and species A of Cd(I) and Hg(I) are stable at this temperature. It should be noted that of the Cd(I) species those which decay at 77°K have smaller hyperfine splitting constant than the stable one.

We wish to thank Dr. Yoji Arata, Dr. Tokuko Watanabe, Mr. Michihiro Nakamura, and Dr. Yoshio Umezawa for valuable discussions. We are also indebted to Mr. Shingo Katsura of γ-ray irradiation station for his experimental assistance.

Note Added in Proof. We have recently noticed that M. C. R. Symons and J. K. Yardell have measured the ESR of Hg(I) (*J. Chem. Soc.*, *A*, **1971**, 761). However, they only report the production of Hg(I) in the γ-irradiated frozen solutions.

15) S. Goudsmit, *Phys. Rev.*, **43**, 636 (1933).

ESR Studies of the Copper(II) Complexes of Amino Acids

Hiroshi Yokoi, Mitsuru Sai, Taro Isobe, and Shigeru Ohsawa*

Chemical Research Institute of Non-aqueous Solutions, Tohoku University, Katahira, Sendai

**Department of Chemistry, Faculty of Science, Tohoku University, Katahira, Sendai*

(Received February 2, 1972)

The X-band and K-band ESR spectra of the *trans*-planar copper(II) complexes of amino acids, whose crystal structures are now known, were measured in a polycrystalline state at room temperature and in frozen aqueous-methanolic solutions at the temperature of liquid nitrogen. The polycrystalline samples showed a variety of ESR line shapes, most of which had three different principal g values; $g_1=2.04$—2.07, $g_2=2.08$—2.12, and $g_3=2.16$—2.29. On the other hand, all the ESR line shapes observed for the frozen solutions were quite similar, and they indicate a normal tetragonal copper(II)-ion environment. There was, moreover, a remarkable difference in the g values between the complexes in the two states. The correlation among the g values, the *d-d* band energies, the bonding parameters (a measure of the degree of covalency of the copper-ligand bondings), and the geometrical configurations of the coordinating atoms for the complexes in a crystal is discussed in some detail.

ESR studies of metal complexes present much useful information about coordination bonding.[1-11] It is very important to see how the ESR data correlate practically with various structural factors for the metal complexes with complicated structures. Recently, some works along this line have been reported; the optical absorption and ESR studies of various ammine and ethylenediamine complexes of copper(II) whose crystal structures are known were carried out in the form of single crystals or of polycrystals, and rhombic g tensors have been discussed in terms of a ground-state of the form: $\varphi=a|x^2-y^2\rangle-b|z^2\rangle$.[6,12-14]

The metal complexes of amino acids have structures likely to participate in hydrogen-bonding with their surroundings, and any of their crystal structures is unpredictably unique because of their characteristic hydrogen-bonding behavior.[15,16] The purpose of this paper is to present the ESR spectra of the copper(II) complexes of amino acids, whose crystal structures are known, in the form of polycrystals and in frozen aqueous-methanolic solutions, and to investigate the ESR and optical absorption data in connection with the structures. This kind of investigation seems to be fundamentally important for the structural estimation of various other metal complexes and the metal-binding sites of various metalloenzymes.[17]

Experimental

Materials. The samples employed here are listed in Table 1, together with their abbreviations. The amino acids used were all commercial products except for cyclopentane-1-amino-1-carboxylic acid, which was prepared and purified according to the method of Henze and Speer.[18] The copper(II) complexes of these amino acids were prepared by the usual method,[19,20] and were recrystallized from water. The results of the chemical analyses are also listed in Table 1.

Measurements. The X-band and K-band first-derivative ESR spectra were measured for the powdered samples at room temperature and for the frozen solutions at the temperature of liquid nitrogen with a Hitachi ESR spectrometer, Model MES-4001. The sample solutions were in concentrations of 10^{-3}—10^{-4}M of the complexes, with an equivolume mixture of water and methanol used as the solvent. The field was calibrated with an Oki magneto-field scope, Model WX-601, using the NMR signals of proton and lithium, and then with a benzene solution of vanadyl acetylacetonate. The visible absorption spectra were measured for the powdered samples at room temperature with a Cary model 14 spectrometer, using the so-called opal-glass method, where a suspension of finely-powdered samples in

1) A. Abragam and M. H. L. Pryce, *Proc. Roy. Soc., Ser. A*, **205**, 135 (1951).
2) K. W. H. Stevens, *ibid., Ser. A*, **219**, 542 (1953); J. Owen, *ibid., Ser. A*, **227**, 183 (1955).
3) A. Abragam and B. Bleaney, "Electron Paramagnetic Resonance of Transition Ions," Clarendon Press, Oxford (1970).
4) B. R. McGarvey, "Transition Metal Chemistry," Vol. 3, ed. by R. L. Carlin, Marcel Dekker, New York (1967), p. 89.
5) S. Fujiwara, "Spectroscopy and Structure of Metal Chelate Compounds," ed. by K. Nakamoto and P. J. McCarthy, John Wiley & Sons, New York (1968), p. 286.
6) J. Hathaway and D. E. Billing, *Coordin. Chem. Rev.*, **5**, 143 (1970).
7) B. G. Malmstrom and T. Vånngård, *J. Mol. Biol.*, **2**, 118 (1960).
8) A. H. Maki and B. R. McGravey, *J. Chem. Phys.*, **29**, 31, 35 (1958).
9) D. Kivelson and R. Neiman, *ibid.*, **35**, 149 (1961).
10) H. Yokoi and T. Isobe, This Bulletin, **41**, 2835 (1968); *ibid.*, **42**, 2187 (1969).
11) H. Yokoi, M. Sai, and T. Isobe, *ibid.*, **42**, 2232 (1969); *ibid.*, **43**, 1078 (1970).
12) I. M. Procter, B. J. Hathaway, and P. Nicholls, *J. Chem. Soc., A*, **1968**, 1678.
13) A. A. G. Tomlinson, B. J. Hathaway, D. E. Billing, and P. Nicholls, *ibid.*, **1969**, 65; B. J. Hathaway, D. E. Billing, P. Nicholls, and I. M. Procter, *ibid.*, **1969**, 312, 319.
14) M. A. Hitchman, C. D. Olson, and R. L. Belford, *J. Chem. Phys.*, **50**, 1195 (1969); M. H. Hitchman, *J. Chem. Soc. A*, **1970**, 4.
15) H. C. Freeman, "The Biochemistry of Copper," ed. by J. Peisach, P. Aisen, and W. E. Blumberg, Academic Press, New York (1966), p. 77.
16) W. E. Hatfield and R. Whyman, "Transition Metal Chemistry," ed. by R. L. Carlin, Vol. 5, Marcel Dekker, New York (1969), p. 47.
17) J. Peisach and W. E. Blumberg, "Electron Spin Resonance of Metal Complexes," ed. by T. F. Yen, Plenum Press, New York (1969), p. 71, and the references therein.
18) H. R. Henze and R. J. Speer, *J. Amer. Chem. Soc.*, **64**, 522 (1942).
19) E. Abderhalden and E. Schnitzler, *Z. Physiol. Chem.*, **163**, 94 (1927).
20) D. P. Graddon and L. Munday, *J. Inorg. Nucl. Chem.*, **23**, 231 (1961).

Table 1. Sample complexes and chemical analyses

Ligand (Abbreviation of the anion of ligand)	Copper(II) complex	C, %		H, %		N, %	
		Found	Calcd	Found	Calcd	Found	Calcd
L-Alanine (L-Ala)	$[Cu(L\text{-}Ala)_2]$	30.34	30.06	4.91	5.05	11.85	11.68
DL-α-Amino-*n*-butyric acid (DL-α-NH_2but)	$[Cu(DL\text{-}\alpha\text{-}NH_2but_2)]$	35.97	35.88	5.73	6.02	10.50	10.46
DL-Methionine (DL-Met)	$[Cu(DL\text{-}Met)_2]$	33.45	33.37	5.39	5.60	7.90	7.78
DL-Valine (DL-Val)	$[Cu(DL\text{-}Val)_2]$	40.73	40.60	6.52	6.82	9.56	9.47
DL-Serine (DL-Ser)	$[Cu(DL\text{-}Ser)_2]$	26.80	26.52	4.40	4.45	10.52	10.31
Cyclopentane-1-amino-1-carboxylic acid (Pen)	$[Cu(Pen)_2]$	44.98	45.06	6.05	6.30	8.86	8.76
DL-Proline (DL-Pro)	$[Cu(DL\text{-}Pro)_2]\cdot 2H_2O$	36.76	36.64	6.42	6.16	8.69	8.55
L-Proline (L-Pro)	$[Cu(L\text{-}Pro)_2]\cdot 2H_2O$	36.35	36.64	5.98	6.16	8.37	8.55
β-Alanine (β-Ala)	$[Cu(\beta\text{-}Ala)_2]\cdot 6H_2O$	21.13	20.72	6.65	6.96	8.31	8.06
β-Amino-*n*-butyric acid (β-NH_2but)	$[Cu(\beta\text{-}NH_2but)_2]\cdot 2H_2O$	31.42	31.63	6.62	6.64	9.41	9.22
L-Glutamic acid (L-Glu)	$Cu(L\text{-}Glu)\cdot 2H_2O$	24.13	24.54	4.49	4.53	5.67	5.72

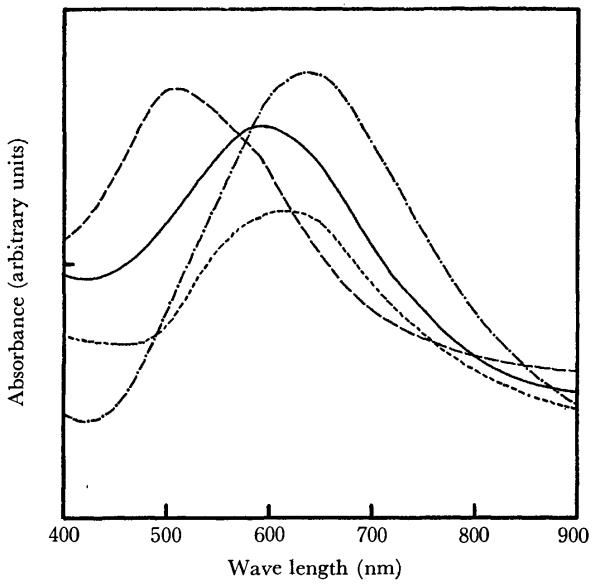

Fig. 1. Visible absorption spectra in a polycrystalline state.
——: $[Cu(L\text{-}Ala)_2]$, – – –: $[Cu(Pen)_2]$,
·····: $[Cu(DL\text{-}Pro)_2]\cdot 2H_2O$, —·—: $[Cu(\beta\text{-}Ala)_2]\cdot 6H_2O$.

liquid paraffin is dealt with;[21] several of the observed spectra are shown in Fig. 1.

Results and Discussion

Principal Values of g. The observed powder ESR spectra, which are shown in Figs. 2—5, were analyzed by the use of the approximation of Kneubühl;[22] the results are shown in Table 2.

The principal values of g for the copper(II) ion in a rhombic field, for which the ground-state may be written as in Eq. (1),

$$\varphi=\cos\delta(d_{x^2-y^2})-\sin\delta\,(d_{z^2}) \qquad (1)$$

can generally be given by the following expressions;[6,14,23,24]

$$g_x=2-\frac{2k_x^2\lambda}{\Delta E_{xz}}(\sqrt{3}\,\sin\delta-\cos\delta)^2$$
$$g_y=2-\frac{2k_y^2\lambda}{\Delta E_{yz}}(\sqrt{3}\,\sin\delta+\cos\delta)^2 \qquad (2)$$

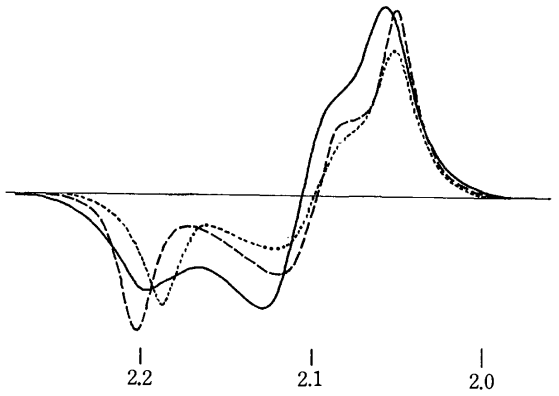

Fig. 2. Powder K-band ESR spectra at room temperature (the numbers represent g values).
——:$[Cu(L\text{-}Ala)_2]$, – – –:$[Cu(DL\text{-}\alpha\text{-}NH_2but)_2]$,
·····:$[Cu(DL\text{-}Met)_2]$.

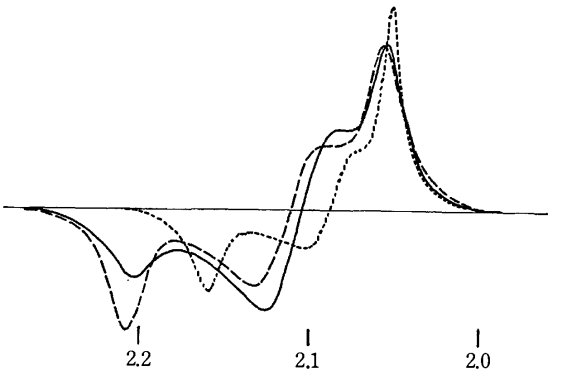

Fig. 3. Powder K-band ESR spectra at room temperature (the numbers represnt g values).
——:$[Cu(DL\text{-}Val)_2]$, – – –:$[Cu(DL\text{-}Ser)_2]$,
——:$[Cu(Pen)_2]$.

21) K. Shibata, "Jikken Kagaku Koza," Vol. 11, ed. by Chem. Soc. Japan, Maruzen, Tokyo (1965), p. 192; "Methods of Biochemical Analysis," Vol. 7, ed. by D. Glick, Interscience Publ., New York (1959), p. 77; *ibid.*, Vol. 9 (1962), p. 217.
22) F. K. Kneubühl, *J. Chem. Phys.*, **33**, 1074 (1960).
23) B. Bleaney, K. D. Bowers, and M. H. L. Pryce, *Proc. Roy. Soc. Ser. A*, **228**, 166 (1955).
24) G. F. Kokoszka, H. C. Allen, and G. Gordon, *J. Chem. Phys.*, **42**, 3693 (1965).

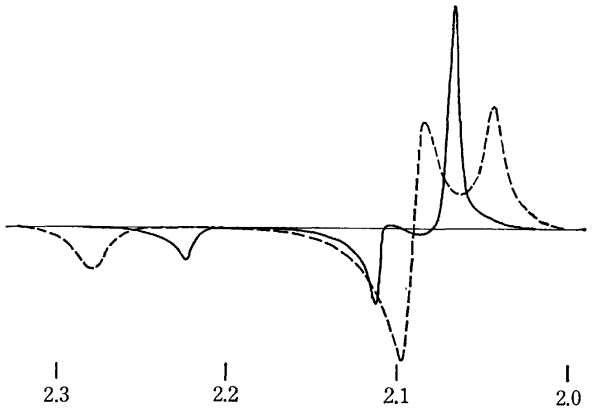

Fig. 4. Powder K-band ESR spectra at room temperature (the numbers represent g values).
——:[Cu(β-Ala)$_2$]·6H$_2$O, – – –:[Cu(β-NH$_2$but)$_2$]·2H$_2$O.

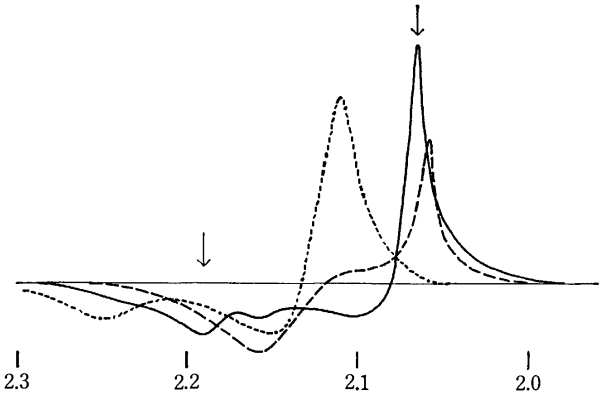

Fig. 5. Powder K-band ESR spectra at room temperature (the numbers represent g values).
——:[Cu(DL-Pro)$_2$]·2H$_2$O, – – –:[Cu(L-Pro)$_2$]·2H$_2$O,
·····:Cu(L-Glu)·2H$_2$O.

TABLE 2. g VALUES AND VISIBLE ABSORPTIONS IN A POLYCRYSTALLINE STATE

Copper(II) complex	g_1	g_2	g_3	λ_{max} (nm)
[Cu(L-Ala)$_2$]	2.059	2.107	2.197	590
[Cu(DL-α-NH$_2$but)$_2$]	2.052	2.098	2.204	585
[Cu(DL-Met)$_2$]	2.053	2.100	2.190	580
[Cu(DL-Val)$_2$]	2.057	2.105	2.202	605
[Cu(DL-Ser)$_2$]	2.058	2.112	2.208	615
[Cu(Pen)$_2$]	2.053	2.089	2.160	490, 590[a]
[Cu(DL-Pro)$_2$]·2H$_2$O[b]	(2.065)[c]		(2.190)	605
[Cu(L-Pro)$_2$]·2H$_2$O	2.058	2.158[c]		610
[Cu(β-Ala)$_2$]·6H$_2$O	2.068	2.109	2.223	635
[Cu(β-NH$_2$but)$_2$]·2H$_2$O	2.044	2.090	2.280	655
Cu(L-Glu)·2H$_2$O	2.111[c]		2.250	720

a) These values were roughly estimated by a Gaussian analysis.
b) The g values were tentatively determied from the positions shown by arrows in Fig. 5.
c) The numbers written between the neighboring g columns express the same g values in both of the columns.

$$g_z = 2 - \frac{8k_z^2\lambda}{\Delta E_{xy}}(\cos\delta)^2$$

where k^2s are the orbital reduction factors, which are regarded as an approximate measure of the degree of covalency for the coordinate bonds of planar copper(II) complexes,[2,5,25] and where the other symbols have their usual meanings. In Eqs. (1) and (2), the normal tetragonal copper(II)-ion environment with which we have most often met means $\cos\delta=1$. It is clear from Eq. (2) that the inclusion of a small amount of a d_z^2 character in the ground-state is sufficient to account for the fairly large difference between the g_x and g_y values. On the assumption of a square-planar configuration to start with, none of the small distortions except for a rhombic or rectangular one is important in affecting the g values and the d-d band energies.[26] g_x, g_y, and g_z can now be assumed to correspond to g_1, g_2, and g_3 respectively in Table 2.

Before discussing the g values directly determined from the powder ESR spectra, it is necessary to check whether these g values reflect the local copper(II)-ion environment. If a large spin-exchange interaction is present between crystallographically non-equivalent molecules, the determined g values will not be equal to the principal g values of the local copper(II) ions. Hathaway *et al.* defined the value of $(g_{//}-2)/(g_{\perp}-2)$ as G and used this G value as a criterion for examining whether there is such a strong spin-exchange interaction in a crystal; when $G<4$, such a strong interaction is considered to be present.[5,12] Much reliance, however, can not always be placed on this criterion, since many planar copper(II) complexes have been known to have $G<4$ even in the magnetically-diluted state,[9,27] and since there is always a possibility that $G<4$ can be established for certain planar copper(II) complexes because of the unusual order of the d-orbital levels or of the bonding parameters.

The results of the X-ray analysis of all the copper(II) complexes of amino acids whose crystal structures are known are listed in Table 3. A spin-exchange interaction between crystallographically-equivalent molecules makes the ESR absorption line widths decrease, but does not change the g values; in such a case, the determined g values directly reflect the local copper(II)-ion environment. The three different g values clearly observed for [Cu(β-NH$_2$but)$_2$]·2H$_2$O are, accordingly, just its true principal g values, since this complex has one molecule per unit cell.[34] Similarly, all the other complexes in Table 3 except [Cu(DL-Pro)$_2$]·2H$_2$O and Cu(L-Glu)·2H$_2$O have three different g values in spite of their having two molecules per unit cell. Evidently the first four complexes in Table 3, which have no water molecules in the crystal, are significantly different in the relative configurations of the two crystallographically non-equivalent molecules in an unit cell. Nevertheless, these four complexes are quite similar in ESR line shape, as is shown in Figs. 2 and 3. This suggests that there may be no such strong spin-exchange interactions as has been mentioned above in most crystals of the copper(II) complexes of amino acids. This is also

25) M. Gerloch and J. R. Miller, *Progr. Inorg. Chem.*, **10**, 1 (1968).
26) W. E. Blumberg, "The Biochemistry of Copper," ed. by J. Peisach, P. Aisen, and W. E. Blumberg, Academic Press, New York (1966), p. 49.
27) A. K. Wiersema and J. J. Windle, *J. Phys. Chem.*, **68**, 3216 (1964); S. E. Harrison and J. M. Assour, *J. Chem. Phys.*, **40**, 365 (1964); T. Chiang, *ibid.*, **48**, 1814 (1968).

Table 3. X-ray crystallographic data

Copper(II) complex	Space group	Z	L_N Cu–N distance (Å)	L_O Cu–O distance (Å)	L_A[a] Cu–O(apical) distance (Å)	θ ∠N–Cu–O (deg.)	Ref.
$[Cu(L\text{-}Ala)_2]$	$P2_1$	2	2.01—2.02	1.96—1.97	2.70 (carboxyl) 2.90 (carboxyl)	87	28
$[Cu(DL\text{-}\alpha\text{-}NH_2but)_2]$	$P2_1/c$	2	2.02	1.98			29
$[Cu(DL\text{-}Met)_2]$	$P2_1/a$	2	1.98	1.95	2.71 (carboxyl)	84	30
$[Cu(Pen)_2]$	$P2_1/a$	2	1.98	1.91	3.17 (carboxyl)	85	31
$[Cu(DL\text{-}Pro)_2]\cdot 2H_2O$	$P2_1/n$	2	1.99	2.03	2.52 (water)	82	32
$[Cu(\beta\text{-}Ala)_2]\cdot 6H_2O$	$P2_1/c$	2	2.04	2.01	2.53 (water)	91	33
$[Cu(\beta\text{-}NH_2but)_2]\cdot 2H_2O$	P_1	1	1.99	2.00	2.45 (waer)	92	34
$Cu(L\text{-}Glu)\cdot 2H_2O$[b]	$P2_12_12_1$	4	2.00	1.97	2.3 (carboxyl) 2.6	84	35

a) The apical oxygen atoms belong to the groups shown in parentheses.
b) The square planar coordination of this complex is due to two oxygen atoms and a nitrogen atom of glutamates and one oxygen atom of a water molecule.

supported by other ESR experiments concerning the aggregation and dimerization of the complexes in frozen aqueous media.[36] Therefore, it may be concluded that almost all the g values determined here are correct as principal g values.

Correlation Between g *Values and Crystal Structures.* The *trans*-planar copper(II) complexes of amino acids are mainly dealt with in this work. The coordination about the copper atom is schematically represented in Fig. 6, where O_{A1} and O_{A2} are the double-bonded oxygen atoms of adjacent molecules for some complexes, or the oxygen atoms of water molecules for other complexes.

$[Cu(L\text{-}Ala)_2]$ showed a typical powder ESR spectrum, with relatively broad absorption lines and three different g values. Many other copper(II) complexes of amino acids, such as $[Cu(DL\text{-}\alpha\text{-}NH_2but)_2]$, $[Cu(DL\text{-}Met)_2]$, $[Cu(DL\text{-}Val)_2]$, $[Cu(DL\text{-}Ser)_2]$, and $[Cu(Pen)_2]$, showed similar powder ESR line shapes, as may be seen in Figs. 2 and 3. $[Cu(Pen)_2]$ is characterized by the smallest g_3 value. On the other hand, $[Cu(\beta\text{-}Ala)_2]\cdot 6H_2O$ and $[Cu(\beta\text{-}NH_2but)_2]\cdot 2H_2O$ showed comparatively sharp absorption lines, as Fig. 4 shows, and they had large g_3 values compared with all the other complexes. $Cu(L\text{-}Glu)\cdot 2H_2O$ also had large g values. It has been a generally-accepted rule that the g values decrease as the planar ligand field becomes stronger, or as the axial ligand field becomes weaker,[4,11,37] and that this behavior of the ligand field is accompanied by a blue-shift of the *d-d* absorption bands.[38] The above-mentioned characteristics of the g values for $[Cu(Pen)_2]$, *etc.* can be understood from their structures and observed visible absorptions according to this general rule. $[Cu(Pen)_2]$ has an especially large L_A value and relatively small L_N and L_O values, and its visible absorption appears at shorter wavelengths, as Tables 2 and 3 show. $[Cu(\beta\text{-}Ala)_2]\cdot 6H_2O$ and $[Cu(\beta\text{-}NH_2but)_2]\cdot 2H_2O$ have comparatively large L_N and L_O values and small L_A values, and their visible absorptions appear at longer wavelengths. $Cu(L\text{-}Glu)\cdot 2H_2O$, which showed a visible absorption at the longest wavelength, has an especially small L_A value.

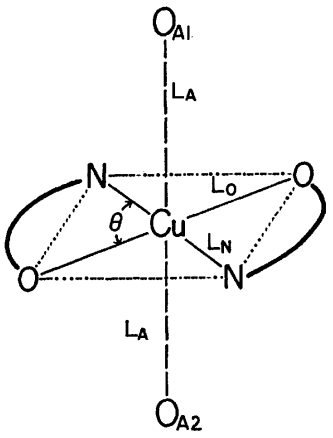

Fig. 6. The schematically represented structure of the *trans*-planar copper(II) complexes of amino acids.

It has generally been believed that the g_3 (or g_z) is oriented along the axis normal to the molecular plane and that the g_1 and g_2 (or g_x and g_y) axes lie on the plane;[34,39] moreover, in view of the crystal-field theory, it is a most probable assumption that the g_1 and g_2 axes are nearly oriented along the different respective coordinate bond directions. All the complexes employed here except three have three different principal values of g. This fact indicates that the copper(II) ions of these complexes are present in rhombically-distorted ligand fields. However, the differences between the g_1 and g_2 values were almost constant for

28) A. Dijkstra, *Acta Crystallogr.*, **20**, 588 (1966).
29) A. J. Stosick, *J. Amer. Chem. Soc.*, **67**, 362 (1945).
30) M. V. Veidis and G. J. Palenik, *Chem. Commun.*, **1969**, 1277.
31) C. A. Barclay and F. S. Stephens, *J. Chem. Soc.*, **1963**, 2027.
32) A. McL. Mathieson and H. K. Welsh, *Acta Crystallogr.*, **5**, 599 (1952).
33) K. Tomita, This Bulletin, **34**, 297 (1961).
34) R. F. Bryan, R. J. Poljak, and K. Tomita, *Acta Crystallogr.*, **14**, 1125 (1961).
35) C. M. Gramaccioli and R. E. Maesh, *ibid.*, **21**, 594 (1966).
36) H. Yokoi and T. Isobe, *Chem. Lett.*, **1972**, 95.
37) H. Yokoi and T. Isobe, This Bulletin, **39**, 2054 (1966); S. Antosik, N. M. D. Brown, A. A. McConnel, and A. L. Porte, *J. Chem. Soc.*, *A*, **1969**, 545.
38) R. L. Belford, M. Calvin, and G. Belford, *J. Chem. Phys.*, **26**, 1165 (1957).
39) C. J. Ballhausen, "Introduction to Ligand Field Theory," McGraw-Hill, New York (1962).

all of them, regardless of the fact that their values of L_N, L_O, L_A, and Θ vary over considerably wide ranges, as may be seen in Tables 2 and 3. It may, accordingly, be suggested that there are certain factors which lead to almost constant differences between the g_1 and g_2 values in their crystals. The data of the X-ray analysis listed in Table 3 indicate that L_O is somewhat smaller than L_N for most of the complexes. In spite of this fact, however, the Cu–N bonding is considered to be a little more covalent than the Cu–O bonding, since the overlap integrals for the bond lengths given in Table 3 can be calculated to be larger for the Cu–N bond than for the Cu–O bond using the table of overlap integrals (we can regard the overlap integral as a measure of the degree of covalency).[40] This small difference between the two bondings in the degree of covalency, accordingly, seems to be responsible for a rhombically-distorted field around the copper atom and, therefore, for a rhombic g tensor. (Just for information, the mixing parameter, δ, in Eq. (1) could be calculated to be about 5° on the rough assumption that $\Delta E_{xy}=\Delta E_{yz}$ and $k_x^2=k_y^2$ in Eq. (2)).

$[Cu(DL\text{-}Pro)_2]\cdot 2H_2O$ showed a complicated powder ESR line shape which was quite different from all the others, as is shown in Fig. 5; its g values also can naturally be expected to be different from the others. It can, however, be suggested from its powder ESR line shape that the powder sample of this complex may be contaminated by a significant amount of an impurity, which could not be removed by repeated recrystallizations from water. Since this sample in a frozen solution showed a typical ESR line shape due to a single complex species, as will be described below, the impurity may be considered as either a geometrical isomer of the *cis*-form or another hydrate. Interestingly, this complex has a characteristic structure of $L_N<L_O$ (contrary to the other complexes) and has the smallest θ value. The abnormal properties of the complex are also demonstrated by the powder ESR spectrum of its isomer, $[Cu(L\text{-}Pro)_2]\cdot 2H_2O$, whose crystal structure is yet unknown; the ESR line shape of $[Cu(L\text{-}Pro)_2]\cdot 2H_2O$ is a so-called reverse one ($g_{//}<g_{\perp}$, $\sin\delta=1$ in Eq. (1)), as is shown in Fig. 5. It is also an interesting fact that the ESR line shape of Cu(L-Glu)$\cdot 2H_2O$ showed a normal tetragonal copper(II)-ion environment, in spite of the fact that four different coordinating groups form a planar coordination about the copper atom.[35]

Visible Absorption and Bonding Parameters. Any of the complexes employed here in both the polycrystal state and an aqueous solution showed only a single broad band in the visible region. It has been a generally accepted rule for the copper(II) complexes that the visible absorptions shift to shorter wavelengths and the g values become smaller as the copper-ligand bondings in the molecular plane become more covalent.[4,11,37,38] The mean, g_0, of the g_1, g_2, and g_3 values was plotted against the energies at the visible absorption peak, ΔE_{max}, for all the complexes under discussion; it is shown in Fig. 7. It is clear from this figure that the g_0 value decreases uniformly as the value of ΔE_{max} increases.

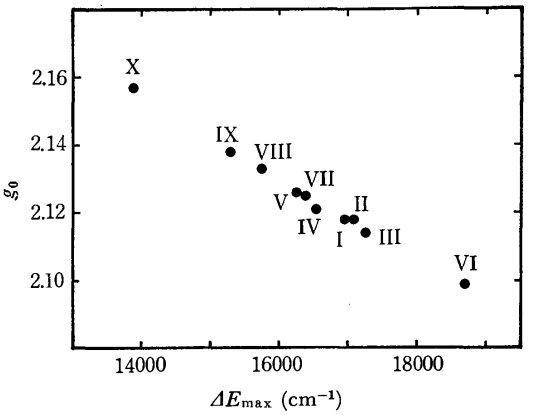

Fig. 7. A plot of g_0 against ΔE_{max} (the numbers are referred to in Table 4).

The following equation can be derived from Eq. (2):

$$k_0^2=-\frac{\Delta E_0}{4\lambda}(g_0-2)-\frac{\Delta E_0}{12\lambda}\{(e_{xz}-h_x)(g_x-2)+(e_{yz}-h_y)(g_y-2)+(e_{xy}-h_z)(g_z-2)\}+\frac{\Delta E_0}{12\lambda}\{e_{xz}h_x(g_x-2)+e_{yz}h_y(g_y-2)+e_{xy}h_z(g_z-2)\} \quad (3)$$

where $k_0^2=(1/3)(k_x^2+k_y^2+k_z^2)$ and $\Delta E_0=(1/3)(\Delta E_{xy}+\Delta E_{xz}+\Delta E_{yz})$, and where $k_s^2=k_0^2(1+h_s)$ for $s=x$, y, or z and $\Delta E_t=\Delta E_0(1+e_t)$ for $t=xy$, yz, or xz. The second and third terms on the right-hand side of Eq. (3) are much smaller than the first term. Roughly speaking, the value of (g_0-2) is inversely proportional to ΔE_0. The k_0^2 values can be regarded as a measure of the degree of covalency for the copper-ligand bondings. The approximate values of k_0^2 were calculated only from the first term, using the value of ΔE_{max} as an approximate value of ΔE_0. The k_0^2 values thus obtained, together with the values of (g_0-2) and $-4\lambda/\Delta E_{max}$, are listed in Table 4. It is shown by this table that the k_0^2 values can be arranged in the same order as that obtained in Fig. 7; the complexes become

Table 4. The values of g_0, ΔE_{max}, and k_0^2 in a polycrystalline state[a]

No.	Copper(II) complex	g_0-2	$-4\lambda/\Delta E_{max}$[b]	k_0^2
I	$[Cu(L\text{-}Ala)_2]$	0.118	0.195	0.59
II	$[Cu(DL\text{-}\alpha\text{-}NH_2but)_2]$	0.118	0.194	0.60
III	$[Cu(DL\text{-}Met)_2]$	0.114	0.192	0.58
IV	$[Cu(DL\text{-}Val)_2]$	0.121	0.200	0.60
V	$[Cu(DL\text{-}Ser)_2]$	0.126	0.204	0.61
VI	$[Cu(Pen)_2]$	0.099	0.178[c]	0.55
VII	$[Cu(L\text{-}Pro)_2]\cdot 2H_2O$	0.125	0.202	0.61
VIII	$[Cu(\beta\text{-}Ala)_2]\cdot 6H_2O$	0.133	0.210	0.62
IX	$[Cu(\beta\text{-}NH_2but)_2]\cdot 2H_2O$	0.138	0.217	0.63
X	$Cu(L\text{-}Glu)\cdot 2H_2O$	0.157	0.238	0.65

a) The meanings of these parameters are described in Eq. (3).
b) $\lambda=-825$ cm^{-1}.
c) The mean of the two absorption band energies listed in Table 2 was adopted as ΔE_{max}.

40) H. H. Jaffé and G. O. Doak, *J. Chem. Phys.*, **21**, 196 (1953).

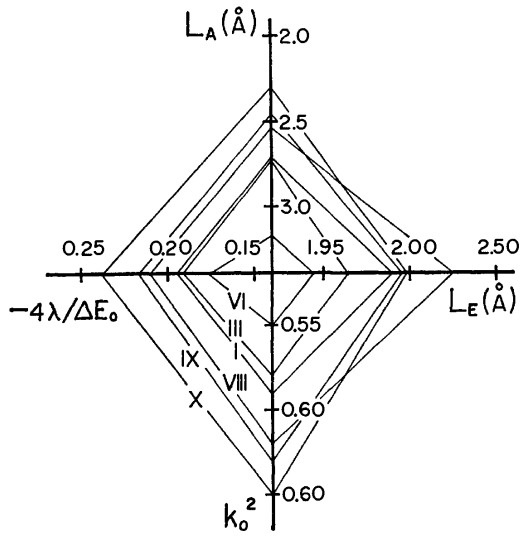

Fig. 8. A graph of L_E, L_A, k_0^2 and $-4\lambda/\Delta E_{max}$ (the numbers are referred to in Table 4).

more covalent in the copper-ligand bondings as they go to the right in Fig. 7.

It is interesting to see once more how the k_0^2 and ΔE_{max} values correlate with the actual geometry of the coordinating atoms. A plot of the values of k_0^2 and $-4\lambda/\Delta E_{max}$ and the bond lengths of L_E and L_A on the different axes is shown in Fig. 8, where $L_E=(1/2)(L_N+L_O)$, and where, for the complexes with two different L_A values, the smaller one was adopted. The meaning of this figure is as follows: as a complex has a smaller circle on this figure, the complex becomes more covalent in the coordinate bond, and there is a smaller L_E value and a larger L_A value. It is clearly shown in this figure that many circles become concentric, although there is one exception to this tendency, and the facts that the coordinate bond becomes more covalent as L_E value is smaller and the L_A value is larger may be established for this kind of complex in a crystal.

Table 5. Magnetic parameters and visible absorptions in solution[a)]

Copper (II) complex	$g_{//}$[b)]	$g_\perp$[c)]	$\lvert A_{//}\rvert$[b)] $\times 10^4 cm^{-1}$	λ_{max} (nm)
Cu(L-Ala)$_2$	2.264	2.056	178	617
Cu(DL-α-NH$_2$but)$_2$	2.265	2.056	176	614
Cu(DL-Val)$_2$	2.270	2.055	175	618
Cu(DL-Ser)$_2$	2.265	2.057	179	624
Cu(Pen)$_2$	2.258	2.057	186	612
Cu(DL-Pro)$_2$	2.266	2.058	179	610
Cu(L-Pro)$_2$	2.261	2.058	188	610
Cu(β-Ala)$_2$	2.285	2.067	139	635
Cu(β-NH$_2$but)$_2$	2.280	2.058	148	630

a) The ESR spectra were measured in aqueous–methanolic (1:1 volume ratio) solutions at 77°K, while the visible absorption spectra were measured in aqueous solution at room temperature.
b) The values were determined from the X-band ESR spectra.
c) The $g_\perp$ values were determined from the K-band ESR spectra (see Fig. 10).

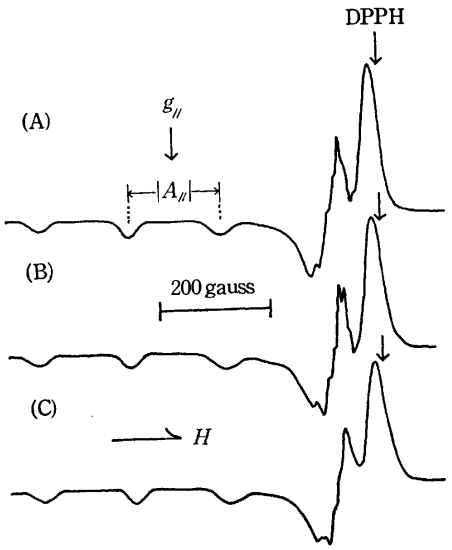

Fig. 9. X-band ESR spectra in frozen solution (at 77°K, Solvent: an equivolume mixture of water and methanol). (A):[Cu(L–Ala)$_2$], (B):[Cu(Pen)$_2$], (C):[Cu(L-Pro)$_2$]·2H$_2$O.

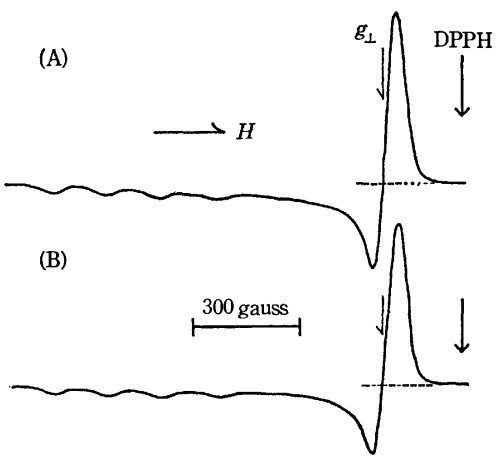

Fig. 10. K-band ESR spectra in frozen solution (at 77°K, Solvent: an equivolume mixture of water and methanol). (A):[Cu(L–Ala)$_2$], (B):[Cu(Pen)$_2$].

The Complexes in Frozen Solution. Several of the X-band and K-band ESR spectra of the complexes employed here in frozen aqueous-methanolic solutions at 77°K are shown in Figs. 9 and 10; the results are listed in Table 5. The magnetic parameters of the first seven complexes in this table were found to be almost equal to each other; $g_{//}=2.264\pm0.006$, $g_\perp=2.057\pm0.002$, and $|A_{//}|=(181\pm7)\times10^{-4}$ cm^{-1}. On the other hand, the last two complexes have somewhat larger g values and much smaller values of $|A_{//}|$ than the others.

It is characteristic of all the complexes in the solution that the observed ESR line shapes are quite similar to each other and indicate a normal elongated-tetragonal copper(II)-ion environment ($g_1\fallingdotseq g_2<g_3$), as is shown in Figs. 9 and 10; this tetragonality is clearly demonstrated, especially by the K-band ESR line shapes. This is a very interesting fact and is in contrast with the fact that the powder samples of the same com-

plexes showed a variety of ESR line shapes, with three different principal g values, as has been mentioned above. It seems, therefore, that it is a general property for the copper(II) complexes of amino acids in solution to keep the symmetry of the ligand field in a higher degree. Furthermore, this property is consistent with a previously-obtained result concerning the mixed-ligand complexes of copper(II), which also keep a high symmetry of ligand field in solution in spite of the asymmetrical coordination about the copper atom due to all the different coordinating groups.[41]

$[Cu(Pen)_2]$, whose crystals are purple, turns blue in an aqueous solution; the visible absorption spectrum of this complex shifts to a longer wavelength in the solution and resembles that of $[Cu(L\text{-}Ala)_2]$. $[Cu(Pen)_2]$ has the smallest g_3 value in a crystal, but its g_3 value becomes as large as that of $[Cu(L\text{-}Ala)_2]$ in a solution. These facts indicate that the water molecules can come close to the cupric ions in an aqueous solution for $[Cu(Pen)_2]$ as well as for $[Cu(L\text{-}Ala)_2]$, and that there is an accompanying strengthening of the axial-ligand field. Judging from the data on g and the visible absorptions, a tendency for the axial-ligand field to be strengthened in an aqueous solution can be seen in a greater or lesser degree for the anhydrous complexes. The properties of $[Cu(\beta\text{-}Ala)_2]\cdot 6H_2O$ and $[Cu(\beta\text{-}NH_2but)_2]\cdot 2H_2O$ were similar in a solution; their g values are larger than the others', and their visible absorptions appear at somewhat longer wavelengths. These two complexes, therefore, are less covalent in the coordinate bond than the others; this fact seems to be consistent with a general accepted theory that the complexes with six-membered chelate rings are less stable than those with five-membered ones.

All the facts mentioned above indicate that the copper(II) complexes of amino acids change their structures according to the molecular surroundings, and that their structures resemble each other in an aqueous solution, a normal tetragonal copper(II)-ion environment being kept.

41) H. Yokoi, M. Otagiri, and T. Isobe, This Bulletin, **44**, 2395 (1971); *ibid.*, to be published.

NOTES

BULLETIN OF THE CHEMICAL SOCIETY OF JAPAN, VOL. 45, 2196—2197(1972)

CNDO/2 Calculations of Hydrogen Bonding; Phenol- and *p*-Nitrophenol-Ammonia Systems

Akio MATSUYAMA and Akira IMAMURA

Biophysics Division, National Cancer Center Research Institute, Tokyo 104

(Received July 24, 1971)

Detailed information on the double minimum potential curve for the proton of a hydrogen-bonded complex is especially useful for understanding the nature of hydrogen bonding and of great interest in connection with many biological problems. Baba, Matsuyama, and Kokubun showed[1] that in the *p*-nitrophenol–triethylamine system the second potential minimum which corresponds to an ion pair becomes stable upon excitation, while unstable in the ground state. On the other hand, recent development of the semi-empirical MO method which can treat all valence electrons has made it possible to calculate directly the potential energy curve of a rather complicated hydrogen-bonding system. Along this line, the CNDO/2 method[2,3] has been applied recently to some simple hydrogen-bonding systems[4] and guanine–cytosine base pair.[5] The main purpose of the present study was to see whether the CNDO/2 method can explain successfully the previous experimental results or not. Owing to the limited capacity of the computer used, ammonia was used as a proton acceptor instead of triethylamine throughout the calculations. However, this does not seem to have caused any essential effects.

Method of Calculation

The method of calculation was the same as described previously.[6] Molecular constants of phenolic compounds were taken from the results of X-ray diffraction analysis,[7] ammonia being assumed to be tetrahedral. Proton-donor and -acceptor molecules were arranged as shown in Fig. 1. In order to obtain the hydrogen-bonding energies and potential energy curves for the hydroxyl proton, the total energies of the hydrogen-bonded complexes were calculated at intervals of 0.1 or 0.2 Å of the O···N and O–H distances, respectively.

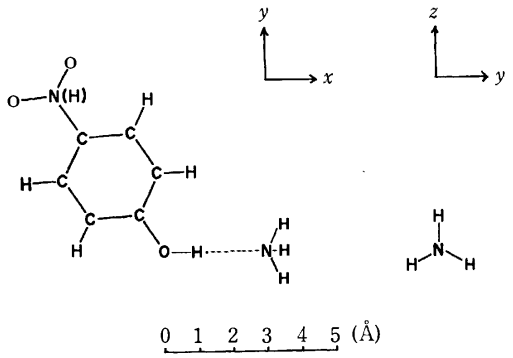

Fig. 1. Molecular arrangement of *p*-nitrophenol or phenol and ammonia.

Results and Discussion

First the total energies of the two hydrogen-bonded complexes, phenol–ammonia and *p*-nitrophenol–ammonia, were calculated as a function of the O···N distance. Distinct minima of the energies were obtained at 2.6 Å for both complexes. The hydrogen-bonding energies were found to be 10.2 and 11.1 kcal for phenol- and *p*-nitrophenol–ammonia complexes, respectively. These values seem to be slightly larger than those reported as the usual hydrogen-bonding energy.[8] However, the stronger proton-donating power of *p*-nitrophenol can be reasonably predicted by the present calculations.

Next, the potential energy curves for the hydroxyl proton in both the ground and excited states were calculated by varying the coordinate of the proton, keeping the O···N distance constant. The O···N distance of 3.0 Å was used instead of the calculated value (2.6 Å), since the latter seems to be short for the hydrogen-bonding distance related to a weak base such as ammonia.[8] The potential energy curves in the excited states were obtained using the ground state wave functions in the virtual orbital approximation. Although the CNDO/2 method is recognized as unreliable for the interpretation of electronic spectra, it should be noted that the energy concerned is not an absolute value but a relative one on varying the coordinate of the proton. Kroto and Santry[9] have shown that this virtual orbital approximation can predict successfully conformations of molecules in the excited state. These facts will permit us to adopt this procedure as a first approximation. The total energies in the ground and excited states are plotted against the coordinate of the proton in the phenol–ammonia system in Fig. 2. With regard to the excited states, only the lowest states of a (π,π^*) type are shown. In addition to potential minima at 1.0 Å, distinct shoulders

1) H. Baba, A. Matsuyama, and H. Kokubun, *Sepctrochim. Acta*, **25A**, 1709 (1969).
2) J. A. Pople, D. P. Santry, and G. A. Segal, *J. Chem. Phys.*, **43**, S129 (1965); J. A. Pople and G. A. Segal, *ibid.*, S136 (1965).
3) J. A. Pople and G. A. Segal, *ibid.*, **44**, 3289 (1966).
4) A. S. N. Murthy, R. E. Davis, and C. N. R. Rao, *Theoret. Chim. Acta*, **13**, 81 (1969).
5) A. C. Blizzard and D. P. Santry, *J. Theoret. Biol.*, **25**, 461 (1969).
6) A. Imamura, H. Fujita, and C. Nagata, This Bulletin, **42**, 3118 (1969).
7) P. Coppens and G. M. J. Schmidt, *Acta Crystallogr.*, **18**, 654 (1965).
8) G. C. Pimentel and A. L. McClellan, "The Hydrogen Bond", W. H. Freeman and Co., San Francisco, Calif., (1960).
9) H. W. Kroto and D. P. Santry, *J. Chem. Phys.*, **47**, 792 (1967).

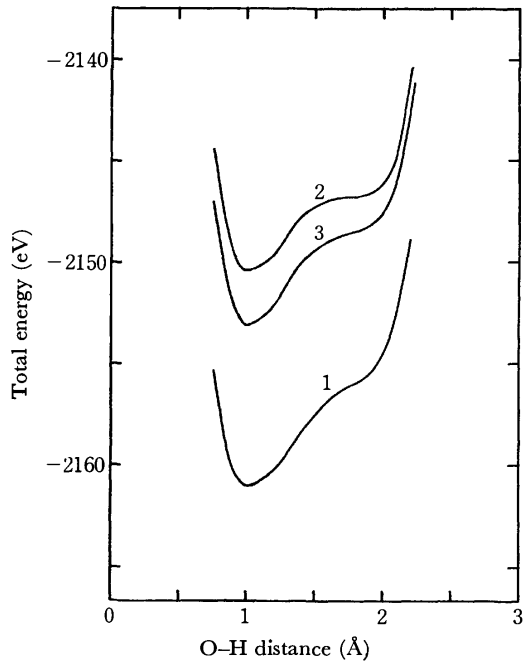

Fig. 2. Variations of the total energies in the ground and excited states of a phenol–ammonia complex as a function of the coordinate of the hydroxyl proton. 1; ground state, 2; the lowest singlet-excited state, 3; the lowest triplet-excited state.

or minima are found at 1.8 Å in all curves, which correspond to a proton-transferred species or an ion pair. The ion pair is unstable in both the ground and excited states, apparently due to the use of ammonia instead of more basic triethylamine as proton acceptor. It is evident, however, that the ion pair becomes less unstable upon excitation. Similar curves were obtained also for the *p*-nitrophenol–ammonia system. This finding is in qualitative agreement with the experimental evidence that the ion pair is more stable than the hydrogen-bonded complex in the singlet-excited state of *p*-nitrophenol–triethylamine system, but less stable in the ground state.[1)]

Table 1. The energy differences between the hydrogen-bonded complex and ion pair

State	Energy difference (eV)	
	Phenol–Ammonia	*p*-Nitrophenol–Ammonia
Ground state	5.082	4.686
Singlet-excited state	3.574	3.697
Triplet-excited state	4.001	4.417

The energy differences between the hydrogen-bonded complex and ion pair in the ground and excited states are summarized in Table 1. The values indicate the differences between the total energies at the O–H distances of 1.8 and 1.0 Å. In the ground state, the energy differences are 5.082 and 4.686 eV for phenol and *p*-nitrophenol complexes, respectively. Greater lowering of the second potential minimum in the *p*-nitrophenol system can be reasonably interpreted in terms of the stronger acidity of the molecule. In both systems the energy differences in the singlet-excited state are smaller than those in the triplet-excited state, *viz.*, the ion pair is more stable in the singlet state than in the triplet state. This is consistent with the fact that the acidity of a phenolic compound is in general weaker in the triplet-excited state than in the singlet-excited state.[10)]

In conclusion, it can be said that the present calculations could explain at least qualitatively the following experimental results: Existence of the second potential minimum, lowering of the minimum in the excited state, greater lowering in the singlet-excited state than in the triplet-excited state and a stronger proton-donating power of *p*-nitrophenol.

The authors wish to thank Dr. Chikayoshi Nagata of our Laboratory and Professor Hiroaki Baba of Hokkaido University for their helpful discussions and encouragement.

10) G. Jackson and G. Porter, *Proc. Roy. Soc., Ser. A*, **260**, 13 (1961).

BULLETIN OF THE CHEMICAL SOCIETY OF JAPAN, VOL. 45, 2198—2199(1972)

The Structure of a New Pteridine Compound Produced by *Pseudomonas ovalis*

Akira SUZUKI, Toshiaki MIYAGAWA, and Miki GOTO
Department of Chemistry, Gakushuin University, Toshima-ku, Tokyo

(Received September 28, 1971)

The following ribityllumazines were hitherto isolated from microorganisms: 6,7-dimethyl-8-(1-D-ribityl)-2,4-dioxohexahydropteridine (Masuda's G-compound),[1] 6-methyl-8-(1-D-ribityl)-2,4,7-trioxohexahydropteridine (Masuda's V-compound)(II),[2] 6-(3-indolyl)-8-(1-D-ribityl)-2,4,7-trioxohexahydropteridine,[3] 6-(*p*-hydroxyphenyl)-8-(1-D-ribityl)-2,4,7-trioxohexahydropteridine and 6-(2-carboxyethyl)-8-(1-D-ribityl)-2,4,7-trioxohexahydropteridine (Putidolumazine)(III).[4,5]

This paper describes the isolation of D-*erythro*-neopterin and three ribityllumazine compounds from cultures of *Pseudomonas ovalis*. Two of them have been identified as compounds II and III, but the last compound (I) has not been isolated from natural sources. The structure of this compound was deduced to be 8-(1-D-ribityl)-2,4,7-trioxohexahydropteridine from UV-spectra and chemical degradation. The compound was synthesized by condensation of 2,6-dihydroxy-5-amino-4-D-ribitylaminopyrimidine and glyoxylic acid, and its identity with the natural compound I was confirmed.

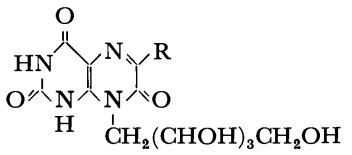

(I) R: -H (II) R: $-CH_3$
(III) R: $-CH_2CH_2COOH$

Experimental

Isolation of Compound I. *Pseudomonas ovalis* (IAM 1506) was cultivated for 10 days in six fermentation jars (total quantity: 60 liters) at 30°C with aeration. The medium for cultivation was as follows: sodium glutamate 200 g, glucose 50 g, $Na_2HPO_4 \cdot 12H_2O$ 56 g, KH_2PO_4 2.5 g, $MgSO_4 \cdot 7H_2O$ 1.0 g, $FeSO_4 \cdot 7H_2O$ 50 μg, $Ca(NO_3)_2 \cdot 4H_2O$ 14.4 mg and water 10 liters. The pH was adjusted to 7.6. After cells were removed by centrifuging at 13000 rpm, fluorescent compounds were adsorbed on charcoal (240 g), eluted with 50% ethanol–4% ammonia (1:1) solution and the concentrated eluate was subjected to chromatography as shown in Fig. 1.

Characterization of Compound I. The aqueous solution of this compound shows strong purple fluorescence. R_f-values and UV-spectra are given in Table 1 and Fig. 2.

Periodate Oxidation: One milliliter of aqueous solution of I (4.56×10^{-5}M) was treated with 2 m*l* of aqueous potassium metaperiodate solution (11.1×10^{-5}M, pH 3.5) at room temperature. At intervals the amount of undestroyed periodate was estimated from UV-absorption (222 mμ) by the method of Dixon and Lipkin.[6] The compound (M, 314) consumed 2.77 mol of periodate per mole.

$NaBH_4$ Reduction of the Periodate Oxidation Product: I (*ca.* 0.3 mg) was dissolved in 0.3 m*l* of water and 0.4 mg of potassium metaperiodate was added. After 1 hr, the oxidation product was purified by paper chromatography using 1-butanol–acetic acid–water (4:1:1) and 2-propanol–water

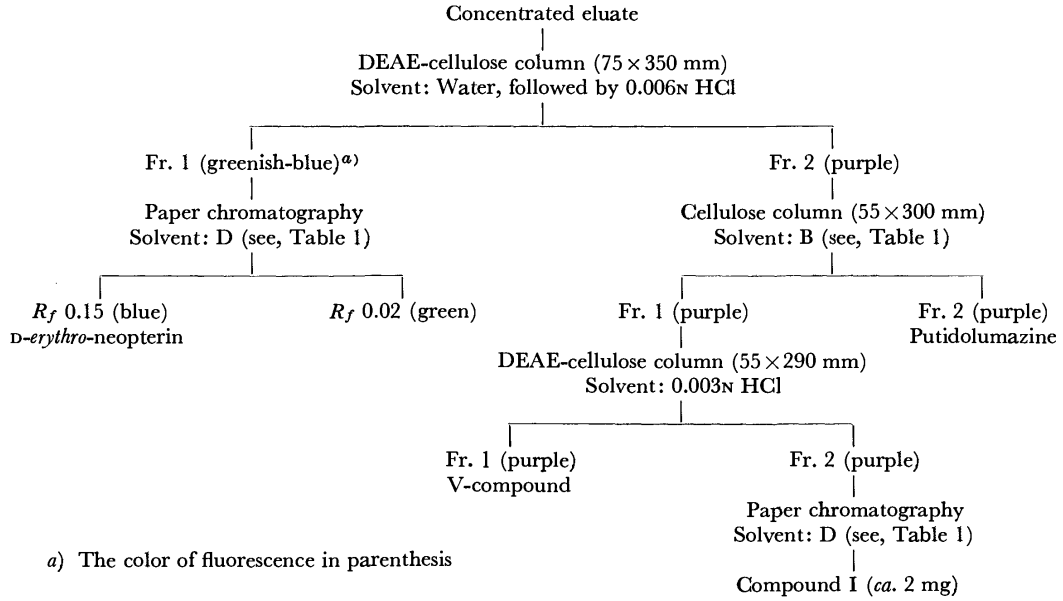

a) The color of fluorescence in parenthesis

Fig. 1. Isolation of compound I

1) T. Masuda, *Chem. Pham. Bull. Japan*, **5**, 375 (1957).
2) T. Masuda, T. Kishi, and M. Asai, *ibid.*, **6**, 291 (1958).
3) I. Takeda and S. Hayakawa, *Agr. Biol. Chem.*, **32**, 873 (1968).
4) A. Suzuki and M. Goto, *Nippon Kagaku Zasshi*, **91**, 404 (1970).
5) A. Suzuki and M. Goto, This Bulletin, **44**, 1869 (1971).

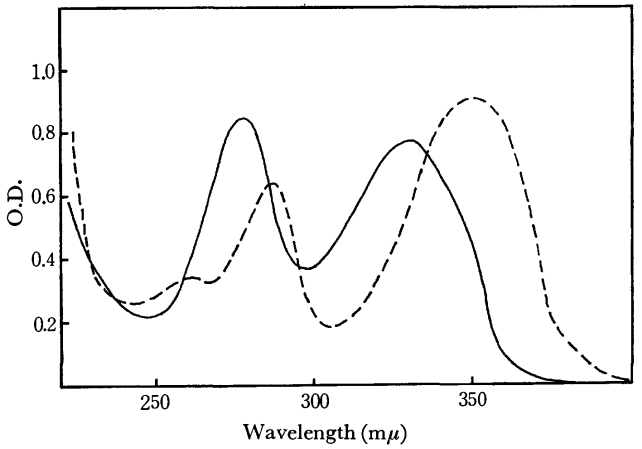

Fig. 2. Ultraviolet spectra of compound I.
——: in 0.1N HCl, ------: in Water

(2: 1) as solvents. The oxidation product was then reduced with a small amount of sodium borohydride in 0.2 m*l* of water. The solution was kept standing at room temperature for 30 min, then adjusted to pH 1 with hydrochloric acid. The product was again purified by paper chromatography using a solvent of 2-propanol–1% ammonia (2: 1). The final product was identified as 8-(2-hydroxyethyl)-2,4,7-trioxohexahydropteridine (IV)[7] by comparison with synthetic material. (Table 1)

Table 1. Paper chromatography and electrophoresis of pteridines

Substance	R_f values[a]				Electrophoresis[b]
	A	B	C	D	
Compound I	0.49	0.52	0.64	0.08	22
After KIO_4 oxidation and $NABH_4$ reduction	0.55	0.60	0.62	0.19	29
Synthetic material (I)	0.49	0.52	0.64	0.08	22
Synthetic material (IV)	0.55	0.60	0.62	0.19	29
V-compound	0.55	0.56	0.64	0.13	18
Putidolumazine	0.42	0.50	0.72	0.11	28
D-*erthro*-neopterin	0.52	0.47	0.63	0.15	—8

a) Solvents: A. 2-propanol:2% ammonium acetate (1:1)
B. 2-propanol:1% ammonia (2:1)
C. 3% aqueous ammonium chloride
D. 1-butanol:acetic acid:water (4:1:1)
b) Distance (in mm) to anode after paper electrophoresis at pH 4.65 (sodium acetate buffer) for 60 min at 25V/cm.

6) J. S. Dixon and D. Lipkin, *Anal. Chem.*, **26**, 1092 (1954).
7) T. Rowan and H. C. S. Wood, *J. Chem. Soc.*, **1960**, 452.

Synthesis of 8-(1-D-Ribityl)-2,4,7-trioxohexahydropteridine (I). 2,6-Dihydroxy-5-nitro-4-D-ribitylaminopyrimidine[8] (625 mg) in water (80 m*l*) was hydrogenated over a platinum oxide catalyst (300 mg). After the theoretical amount of hydrogen was taken up, the catalyst was removed by filtration. The solution was acidified with acetic acid (3 m*l*). Glyoxylic acid (400 mg) was added and the mixture was heated for 5 hr on a water bath. The solution was neutralized with aqueous ammonia and concentrated *in vacuo* to about 30 m*l* below 40°C. The product was purified by chromatography using a DEAE–cellulose column (5.5×32 cm; elution: 0.005N HCl) and a cellulose column (7.5×30 cm; elution: 2-propanol–1% ammonia (2: 1)). The eluate was concentrated to dryness *in vacuo* below 40°C. The residue was recrystallized from water, yield, 76 mg, mp 262—263°C (decomp.).

Found: C, 40.65; H, 4.52; N, 16.79%. Calcd for $C_{11}H_{14}O_7N_4 \cdot 1/2H_2O$: C, 40.86; H, 4.64; N, 17.33%.

The UV-absorption spectrum of the substance in 0.1N HCl was as follows: $\varepsilon_{mln}^{250m\mu}$ 3410, $\varepsilon_{max}^{278m\mu}$ 12800, $\varepsilon_{min}^{298m\mu}$ 5520, $\varepsilon_{max}^{332m\mu}$ 11800; in H_2O: $\varepsilon_{mln}^{243m\mu}$ 3930, $\varepsilon_{max}^{261m\mu}$ 5190, $\varepsilon_{mln}^{267m\mu}$ 4940, $\varepsilon_{max}^{287m\mu}$ 9680, $\varepsilon_{mln}^{305m\mu}$ 2860, $\varepsilon_{max}^{350m\mu}$ 13700.

Discussion

Four pteridines have been isolated from the culture of *Pseudomonas ovalis*. Three of them were characterized as D-*erythro*-neopterin, 6-methyl-8-(1-D-ribityl)-2,4,7-trioxohexahydropteridine (II) and 6-(2-carboxyethyl)-8-(1-D-ribityl)-2,4,7-trioxohexahydropteridine (III).

The fourth compound (I) was a new pteridine. UV-spectra of this compound suggests that it is a 2,4,7 (1H,3H,8H) pteridinetrion with alkyl side chains at N-8 and C-6 position (Fig. 2). I is stable against Al–Hg reduction suggesting that it has –H or $-CH_2-$ bound to carbon-6.[9] It is stable against esterification, suggesting that it has no carboxyl group. One mole of compound I consumed 3 mol of KIO_4 and reduction of the product with $NaBH_4$ yielded a substance identical with 8-(2-hydroxyethyl)-2,4,7-trioxohexahydropteridine (IV);[7] this was identified by cochromatography with the synthetic material (Table 1). From these results the structure of 8-(1-D-ribityl)-2,4,7-trioxohexahydropteridine (I) was postulated for I. The compound was synthesized by condensation of 2,6-dihydroxy-5-amino-4-D-ribitylaminopyrimidine and glyoxylic acid and its identity with the natural product was confirmed.

8) R. M. Cresswell and H. C. S. Wood, *ibid.*, **1960**, 4768.
9) S. Matsuura, S. Nawa, M. Goto, and Y. Hirata, *J. Biochem.*, **42**, 413 (1955).

BULLETIN OF THE CHEMICAL SOCIETY OF JAPAN, VOL. 45, 2200—2201 (1972)

A NMR Study of the Thioacetic Acid-Acetone Mixture

Toyokazu Horii, Shunichi Kawamura, and Jitsuo Tsurugi
Radiation Center of Osaka Prefecture, Shinke-cho, Sakai, Osaka

(Received November 10, 1971)

It is well known that thiols add readily and reversibly to the carbonyl group of aldehydes and ketones to form hemimercaptals and hemimercaptols as intermediates to mercaptals and mercaptols respectively. Hemimercaptals and hemimercaptols have been isolated only for aldehydes and ketones which contain electron-withdrawing groups.[1] Although it was demonstrated that thioacetic acid adds to simple aldehydes to form vacuum-distillable hemimercaptals,[2] the isolation of hemimercaptol has never been reported.

In the present study, we measured the NMR spectra of mixtures of acetone and thioacetic acid (**1a**), α-chlorothioacetic acid (**1b**), or α-dichlorothioacetic acid (**1c**). These mixtures were considered to be in equilibrium, as is shown below:

$$RCOSH + CH_3COCH_3 \rightleftharpoons (CH_3)_2C(OH)SCOR \quad (1)$$

1a: R = CH_3 **2**a: R = CH_3
b: R = CH_2Cl b: R = CH_2Cl
c: R = $CHCl_2$ c: R = $CHCl_2$

Therefore, we can expect at the lower temperatures to detect the spectra of α-hydroxyisopropyl thioacetate (**2a**), α-chlorothioacetate (**2b**), and α-dichlorothioacetate (**2c**). We determined each equilibrium constant in a large excess of acetone-d_6. Such substituents as α-chloro- and α-dichlorothioacetate were chosen for the sake of the simplicity of the NMR spectra.

Experimental

Acetone was dried over anhydrous calcium sulfate and distilled. Thioacetic,[3] chlorothioacetic[4], and dichlorothioacetic acid[4] were prepared and purified by the method described in the literature. The NMR spectra were measured on a JNM 3H-60 spectrometer, with tetramethylsilane as the internal standard. The probe temperature was determined immediately after each spectral measurement, using a thermocouple in a sample tube containing 0.5 m*l* of acetone. The accuracy of the temperature thus obtained should be within 1°.

Measurements of Equilibrium Constants. The NMR spectra of thioacetic acid solutions (3—7%) in a large excess of acetone-d_6 were taken, and the areas of the resonances of the R-group protons of RCOSH (**1**) and $(CD_3)_2C(OH)SCOR$ (**2**) were measured at various temperatures. The equilibrium constants were determined from:

$$K = [\text{Area of } (CD_3)_2C(OH)SCO\underline{R}]/[\text{Area of } \underline{R}COSH]$$

In 6.8, 4.2, and 3.0% solutions of thioacetic acid, all the plots of $\log K$ against $1/T$ gave only a straight line, with a correlation coefficient of 0.993 (Fig. 2). Therefore, at concentrations below 7% the molar fraction of acetone can safely be anticipated to be 1. Each measurement was initiated about 10 min after the solution in an NMR tube and the NMR probe had been temperature-equilibrated.

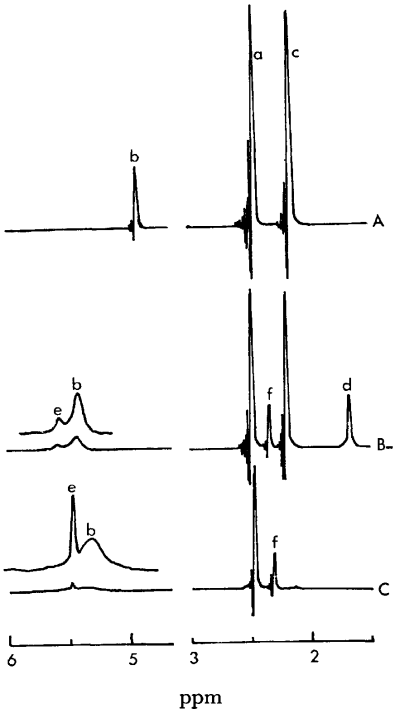

Fig. 1. The NMR spectra of thioacetic acid. A: 70 w/w% acetone solution at 25°C, B: at −56°C, C: 40 w/w% acetone-d_6 solution at −36°C.

$$\underset{a}{C\underline{H}_3}COS\underset{b}{\underline{H}} + (\underset{c}{C\underline{H}_3})_2CO \rightleftharpoons (\underset{d}{C\underline{H}_3})_2C(\underset{e}{O\underline{H}})SCO\underset{f}{C\underline{H}_3}$$

Results and Discussion

The NMR spectrum of the mixture of acetone and thioacetic acid at room temperature showned only resonances of acetone and thioacetic acid (Fig. 1A). However, in the spectrum at a low temperature, two additional peaks appeared reversibly at δ=1.7 (d) and δ=2.3 (f) (Fig. 1B). The intensities of these spectra increased as the temperature was lowered, and integral ratios of these peaks were always 2: 1. When acetone was replaced with acetone-d_6, only the peak of δ=2.3 remained (Fig. 1C). Therefore, these peaks (d and f) may be considered to be responsible for the methyl groups of the 1: 1 adduct of thioacetic acid and acetone, which was concluded to be hemimercaptol (**2a**). As another possible adduct of thioacetic acid and acetone,

1) E. E. Reid, "Organic Chemistry of Bivalent Sulfur," Vol. 2, Chemical Publishing Co., Inc., New York, N. Y. (1960), p. 205, and Vol. 3, p. 320; E. Campaigne, "Organic Sulfur Compounds," Vol. 1, ed. by N. Kharasch, Pergamon Press Inc., New York, N. Y. (1961), p. 134.

2) H. Böhme, H. Bezzenberger, M. Clement, A. Dick, E. Nurnberg, and W. Schlephack, *Ann.*, **623**, 92 (1959).

3) E. K. Ellingboe, "Organic Syntheses," Vol. 31, (1950), p. 105.

4) J. I. Cunneen, *J. Chem. Soc.*, **1947**, 134.

we may consider α-hydroxyisopropyl thionacetate $(CH_3)_2C(OH)OCSCH_3$, which is produced by the addition of tautomeric thionacetic acid to acetone. This possibility could not be excluded experimentally.[5] However, thioacetic acid reacted with aldehyde to produce hemimercaptal,[6] and also no example has been reported of thionesters being prepared from thioacetic acid.[7] Therefore, the authors prefer the first conclusion. In the spectrum of the lower field, the sharp former peak of the hydroxy proton (e) of **2a** can be interpreted as partly overlapped on the broad peak of the sulfhydryl proton (b) of thioacetic acid by comparing their strengths.

Mercaptol (**2a**) is expected to have the following intra-molecular hydrogen bond.[8] The most striking

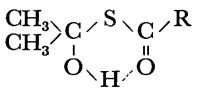

characteristic of an intra-molecular hydrogen bond is the absence of any shift upon dilution with an inert solvent.[9] Therefore, we tried to obtain the spectra in a dilute solution of an inert solvent. However, in a large excess of carbon disulfide Eq. (1) lies so far to the left, even at a low temperature, and the concentration of **2a** is so small that the peak of the hydroxyl proton can not be detected. Therefore, the following experiment was carried out. A mixture of **1a** (20 mg) and acetone (0.5 m*l*) in an NMR tube was cooled slowly to −78°C. Fortunately, we found that, at such a low temperature, the rates of both the formation and decomposition of **2** in Eq. (1) become very slow. (See the bending of the straight line at lower temperatures in Fig. 2.) The NMR tube maintained at this temperature was attached to a vaccum line; in this way the acetone was almost evaporated, whereupon about 0.5 m*l* of carbon disulfide was added. The NMR spectrum of this solution was measured at −78°C. The spectrum indicated the presence of a large amount of hemimercaptol (**2a**) ([**2a**]/[acetone]=1.5). The peaks of the sulfhydryl and hydroxyl protons were detected separately at δ=4.72 and δ=5.38 respectively in such an inert solvent. The chemical shift of the latter peak did not move when the solvent was changed from acetone to carbon disulfide. This fact supports the above chelating structure.

The proton resonances of the methylene and methine groups in **2b** and **2c** appeared at δ=4.68 and at δ=6.84 respectively at −35°C; they were in a field lower by 0.22 and 0.14 ppm than those of the corresponding thioacetic acids, **1b** and **1c**. However, the peak of the hydroxyl proton seemed to be superposed on, and was indistinguishable from, that of the sulfhydryl proton.

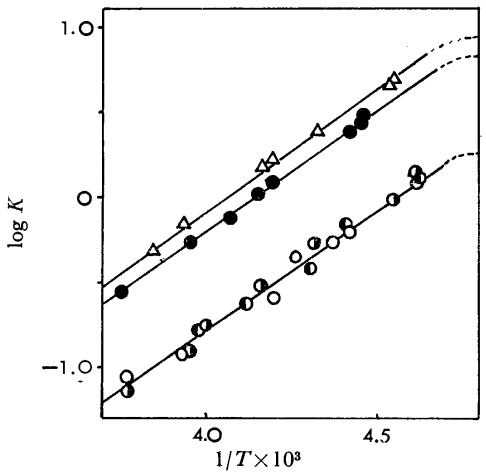

Fig. 2. Plots of log K *vs.* $1/T$ in acetone-d_6.
○: **2a** (3%), ◑: **2a** (4.2%), ◐: **2a** (6.8%), ●: **2b** (5.0 %), △: **2c** (6.8%).
Full lines were drawn by the method of least-squares and dashed lines indicated that experimental points were not on the full lines below *ca.* −60°C.

Table 1. Thermodynamic quantities for the formation of **2** in a large excess of acetone-d_6

Thioacetic acid	ΔH (kcal/mol)	ΔS (e.u.)	Correlation coefficient
CH_3COSH	−6.5±0.2	−30±1	0.993
$ClCH_2COSH$	−6.6±0.1	−27.4±0.6	0.999
$Cl_2CHCOSH$	−6.5±0.1	−26±0.5	0.999

The equilibrium constants were determined in the presence of a large excess of acetone-d_6 between −5 and −50°C. Figure 2 shows a plot of these data employed to determine the thermodynamic quantities (Table 1). The substitution of the electronegative group for the proton of thioacetic acid influences the entropy term more than enthalpy term in the equilibrium. Thus, the value of $-\Delta S$ in the formation of **2b** and **2c** is smaller than that of **2a**. These results can be explained by the view that the substitution of groups which weaken the six-membered chelation increases the degree of freedom of hemimercaptol.

5) In IR spectra, either C=O or C=S stretching absorption of the adduct could not be detected because of being concealed behind the very large absorptions of a large amount of acetone and thioacetic acid.

6) We prepared the adducts of thioacetic acid and aldehyde, RCHO (R: H, CH_3, and CH_3CH_2), described in Ref. 2, and in IR spectra detected the C=O stretching absorptions, respectively in 1680, 1670, and 1675 cm^{-1}.

7) E. E. Reid, "Organic Chemistry of Bivalent Sulfur," Vol. 4, Chemical Publishing Co., Onc., New York, N. Y. (1962), p. 12.

8) Böhme claimed the presence of six-membered chelation of hemimercaptal in Ref. 2.

9) "Jikken Kagaku Koza, Zoku," Vol. 12, ed. by K. Kotake, Maruzen Co., Tokyo, (1967), p. 371.

BULLETIN OF THE CHEMICAL SOCIETY OF JAPAN, VOL. 45, 2202—2203(1972)

Synthetic Studies of the Flavone Derivatives. XXIV.[1] The Synthesis of 5-Hydroxy-7,8,3′,4′-tetramethoxyflavone, A Pigment from Bergamott Oil

Mitsuru NAKAYAMA, Shûichi HAYASHI, Kenji FUKUI, Tokunaru HORIE,* and Mitsuo MASUMURA*

Department of Chemistry, Faculty of Science, Hiroshima University, Higashisenda-machi, Hiroshima
**Department of Applied Chemistry, Faculty of Engineering, University of Tokushima, Tokushima*

(Received December 17, 1971)

In 1968, 5-hydroxy-7,8,3′,4′-tetramethoxyflavone (I) was isolated from Bergamott oil by Farid.[2] In previous papers,[3,4] the present authors reported the syntheses of 5,7-dihydroxy-8-methoxyflavone derivatives from 4,6-dibenzyloxy-2-hydroxy-3-methoxyacetophenone (II). The present paper will describe the synthesis of I in a manner similar to that previously described.[3,4]

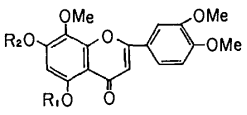

I R_1=H, R_2=Me,
IV R_1=R_2=$C_6H_5CH_2$,
V R_1=R_2=H,
VI R_1=R_2=Ac,
VII R_1=H, R_2=Et,
VIII R_1=Ac, R_2=Me,

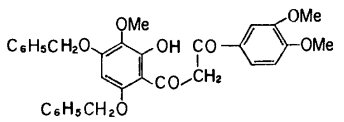

III

By the Baker-Venkataraman transformation, 4,6-dibenzyloxy-2-hydroxy-3-methoxy-ω-(3,4-dimethoxybenzoyl)acetophenone (III) was obtained from II and 3,4-dimethoxybenzoyl chloride *via* the corresponding ester. The cyclodehydration of III with sodium acetate afforded 5,7-dibenzyloxy-8,3′,4′-trimethoxyflavone (IV). The catalytic hydrogenolysis of IV gave 5,7-dihydroxy-8,3′,4′-trimethoxyflavone (V). The flavone (V) was easily converted into a diacetate (VI) and a monoethyl ether (VII). The partial methylation of V yielded the desired flavone, I, which was then easily converted into an acetate (VIII). The properties of the flavone, I, and of VIII were found to be almost the same as those recorded in the literature.[2]

Experimental[5]

4,6-Dibenzyloxy-2-hydroxy-3-methoxy-ω-(3,4-dimethoxybenzoyl)-acetophenone (III). A mixture of II[3] (510 mg) and 3,4-dimethoxybenzoyl chloride (700 mg) in anhydrous pyridine (5 m*l*) was heated at 120°C for 2 hr. The cooled reaction mixture was then poured into diluted hydrochloric acid. The mixture was extracted with ether, and the ether layer was washed with a sodium carbonate solution and then water. The solvent was removed, and the resulting semi-solid was dried in a desiccator.

A mixture of the above crude ester, powdered potassium hydroxide (1.5 g), and anhydrous pyridine (12 m*l*) was heated at 60°C for 4 hr with stirring. The reaction mixture was acidified with diluted hydrochloric acid, and then extracted with ether. The ether layer was allowed to stand overnight in a refrigerator. The separated crystals were recrystallized from ethyl acetate to give III; mp 169.5—170.5°C (yellow needles); yield, 457 mg (60%). It gave a green color with ferric chloride in ethanol.

Found: C, 70.84; H, 5.62%. Calcd for $C_{32}H_{30}O_8$: C, 70.83; H, 5.57%.

5,7-Dibenzyloxy-8,3′,4′-trimethoxyflavone (IV). A mixture of III (400 mg), sodium acetate (1 g), and acetic acid (10 m*l*) was heated at 140°C for 1 hr. The reaction mixture was diluted with water, and then extracted with ether. The product was recrystallized from ethyl acetate-methanol (1:1) to give IV; mp 157—158.5°C (colorless needles); yield, 350 mg (91%). UV: λ_{max}^{EtOH} nm (log ε); 249 (4.35), 273.5 (4.36), 343 (4.37). NMR:[5] ($CDCl_3$) 6.51_s (H-3); 6.62_s (H-6).

Found: C, 73.43; H, 5.41%. Calcd for $C_{32}H_{28}O_7$: C, 73.27; H, 5.38%.

5,7-Dihydroxy-8,3′,4′-trimethoxyflavone (V). A mixture of IV (300 mg) and palladium-charcoal (Pd: 10%; 90 mg) in a mixed solvent of ethyl acetate and methanol was shaken in an atmosphere of hydrogen for 4 hr. The product was recrystallized from ethyl acetate to give V; mp 217—218°C (yellow prisms); yield, 170 mg (86%). It gave a green color with ferric chloride in ethanol. UV: λ_{max} nm (log ε); (EtOH) 252.5_{sh} (4.20),[5] 278.5 (4.32), 336 (4.26); (EtOH–AcONa) 286.5 (4.46), 315 (4.24), 383 (4.05); (EtOH–$AlCl_3$) 286 (4.28), 349 (4.30), 400_{sh} (3.92). NMR: (DMSO) 3.79_s (3×MeO); 6.28_s (H-6); 6.95_s (H-3); 7.05_d (J=9) (H-5′); 7.46_{bs} (H-2′); 7.59_q (J=2.5, 9) (H-6′); 10.7_{bs}, 12.63_s (2×OH).

Found: C, 63.04; H, 4.52%. Calcd for $C_{18}H_{16}O_7$: C, 62.79; H, 4.68%.

Diacetate (VI): mp 163—164°C (colorless needles from aqueous methanol). UV: λ_{max}^{EtOH} nm (log ε); 247 (4.39), 262_{sh} (4.21), 341 (4.39). NMR: ($CDCl_3$) 6.59_s (H-3); 6.79_s (H-6).

Found: C, 61.84; H, 4.66%. Calcd for $C_{22}H_{20}O_9$: C, 61.68; H, 4.71%.

Monoethyl ether (VII): mp 184.5—185.5°C (yellow needles from ethanol). UV: λ_{max} nm (log ε); (EtOH) 256.5 (4.18), 292 (4.27), 359 (4.42); (EtOH–$AlCl_3$) 262.5 (4.17), 286.5 (4.31), 353 (4.30), 406 (4.09). NMR: ($CDCl_3$) 6.42_s (H-3); 6.60_s (H-6).

Found: C, 64.21; H, 5.40%. Calcd for $C_{20}H_{20}O_7$: C, 64.51; H, 5.41%.

1) Part XXIII: T. Horie, M. Tsukayama, M. Masumura, K. Fukui, and M. Nakayama, This Bulletin, **44**, 3198 (1971).
2) S. Farid, *Tetrahedron*, **24**, 2121 (1968).
3) K. Fukui, M. Nakayama, and T. Horie, This Bulletin, **42**, 2327 (1969).
4) M. Nakayama, K. Fukui, T. Horie, Y. Shimizu, and M. Masumura, *Nippon Kagaku Zasshi*, **91**, 1174 (1970).
5) All the melting points are uncorrected. The NMR spectra were measured with a Hitachi R-20 spectrometer (60 MHz), using tetramethylsilane as the internal standard (δ, ppm): s, singlet; d, doublet; q, quartet; b, broad. sh=shoulder.

5-Hydroxy-7,8,3′,4′-tetramethoxyflavone (I). V (36 mg) was methylated with diazomethane, and the product was recrystallized from ethyl acetate to give I; mp 209—210°C (lit,[2] mp 210—212°C) (yellow needles); yield, 30 mg (81%). It gave a green color with ferric chloride in ethanol. UV: λ_{max} nm (log ε); (EtOH) 254.5 (4.27), 276 (4.31), 294.5_{sh} (4.14), 343 (4.30); (EtOH–$AlCl_3$) 263 (4.16), 285.5 (4.28), 350 (4.31), 405 (4.04). NMR: ($CDCl_3$) 3.97_s (6H), 4.00_s (6H) (4×MeO); 6.47_s (H-6); 6.62_s (H-3); 7.04_d (J=9) (H-5′); 7.49_d (J=2.5) (H-2′); 7.56_q (J=2.5, 9) (H-6′); 12.6_{bs} (OH).

Found: C, 63.65; H, 5.06%. Calcd for $C_{19}H_{18}O_7$: C, 63.68; H, 5.06%.

Acetate (VIII): mp 178—180°C (lit,[2] mp 178—180°C) (colorless needles from methanol). UV: λ_{max}^{EtOH} nm (log ε); 245 (4.36), 262_{sh} (4.23), 338 (4.37). NMR: ($CDCl_3$) 6.57_s (H-3), 6.71_s (H-6).

Found: C, 62.83; H, 5.05%. Calcd for $C_{21}H_{20}O_8$: C, 62.99; H, 5.04%.

BULLETIN OF THE CHEMICAL SOCIETY OF JAPAN, VOL. 45, 2203—2204(1972)

A Convenient Synthesis of Methyl Methylthiomethyl Sulfoxide

Katsuyuki OGURA and Gen-ichi TSUCHIHASHI

Sagami Chemical Research Center, Ohnuma, Sagamihara, Kanagawa 229

(Received December 27, 1971)

Recently we have developed a new method for synthesizing labile aldehydes by using methyl methylthiomethyl sulfoxide (**1**); the method is shown by the following scheme:[1]

$$RX + \underset{\textbf{1}}{CH_2(SOCH_3)(SCH_3)} \xrightarrow[THF]{NaH} RCH(SOCH_3)(SCH_3) \xrightarrow{H^+} RCHO + CH_3SSCH_3$$

The synthetic utility of this method seems to be widely recognized, and we have received many inquiries about the details of the method for the preparation of this new reagent (**1**). In this note we will describe a convenient way to synthesize **1** and the related compounds.

Although **1** can be obtained by the substitution reaction of chloromethyl methyl sulfoxide[2] with the methyl mercaptide anion, as has previously been reported by us,[3] this method does not appear to be suitable for the large-scale preparation of **1**, because chloromethyl methyl sulfoxide is relatively unstable. Therefore, we searched for a way to obtain **1** on a large scale and developed the improved method for the synthesis of **1** which will be described below.

Formaldehyde dimethyl mercaptal, which had easily been obtained by the acid-catalyzed condensation of formaldehyde with methyl mercaptan, was oxidized by one mole-equivalent of hydrogen peroxide in acetic acid to afford **1** in a 78% yield. In a similar manner, ethyl ethylthiomethyl sulfoxide (**2**), isopropyl isopropylthiomethyl sulfoxide (**3**), and phenyl phenylthiomethyl sulfoxide (**4**) were formed in yields of 83, 76, and 96% respectively. The oxidation with other oxidizing reagents did not give satisfactory results. For example, *m*-chloroperbenzoic acid and sodium metaperiodate converted formaldehyde diethyl mercaptal into **2** in yields of 56% and 9% respectively.

It should be noted that the oxidation of acetaldehyde

$$RSCH_2SR \xrightarrow[AcOH]{H_2O_2} RSOCH_2SR$$

1, R=Me
2, R=Et
3, R=*i*-Pr
4, R=Ph

dimethyl mercaptal with hydrogen peroxide in acetic acid gave a mixture of two diastereoisomeric methyl 1-methylthioethyl sulfoxides (**5**, 66% yield, in a ratio of 66: 34).[4]

$$\underset{}{CH_3CH(SCH_3)(SCH_3)} \xrightarrow[AcOH]{H_2O_2} \underset{\textbf{5}}{CH_3CH(SOCH_3)(SCH_3)}$$

Experimental

Oxidation of Formaldehyde Dimethyl Mercaptal. To a solution containing 25.09 g of formaldehyde dimethyl mercaptal in 50 m*l* of acetic acid, 26.5 m*l* of an aqueous solution of hydrogen peroxide (concentration: 30%) was added under cooling with ice, and then the resulting mixture was stirred for 30 min at room temperature. After 300 m*l* of methylene chloride had been added, the acetic acid was neutralized with 60 g of potassium carbonate. The mixture was filtered, and the filtrate was dried with anhydrous sodium sulfate. Upon the removal of the solvent, the residue was subjected to fractional distillation to yield 22.41 g of methyl methylthiomethyl sulfoxide (**1**) as a colorless liquid; bp 92—93°C/2.5 mmHg, IR (neat): 1040 cm^{-1}, NMR (in $CDCl_3$): δ 3.63 (s, 2H), 2.59 (s, 3H), and 2.32 (s, 3H).

Found: C, 28.97; H, 6.78%. Calcd for $C_3H_8OS_2$: C, 29.00; H, 6.49%.

The oxidation of this sulfoxide (**1**) with excess hydrogen peroxide in acetic acid yielded bis(methylsulfonyl)methane; mp 148—149°C (lit,[5] mp 145°C).

1) K. Ogura and G. Tsuchihashi, *Tetrahedron Lett.*, **1971**, 3151.
2) G. Tsuchihashi and K. Ogura, This Bulletin, **44**, 1726 (1971).
3) K. Ogura and G. Tsuchihashi, *Chem. Commun.*, **1970**, 1689.
4) There are a number of examples of the asymmetric oxidation of a sulfide to a sulfoxide in which one of a pair of diastereoisomers is produced predominantly. For example, J. D. Morrison and H. S. Mosher, "Asymmetric Organic Reactions," Prentice-Hall, Englewood Cliffs, N. J. (1971), p. 351.
5) H. Böhme, R. Frand, and W. Kause, *Chem. Ber.*, **82**, 433 (1949).

Oxidation of Formaldehyde Diethyl Mercaptal. (a) To a solution containing 2.486 g of formaldehyde diethyl mercaptal in 15 m*l* of acetic acid, 2.07 m*l* of an aqueous solution of hydrogen peroxide (concentration: 30%) was added while cooling with ice, and then the resulting mixture was stirred for 2 hr at room temperature. The same work-up as above and the fractional distillation of the leavings afforded 2.305 g of ethyl ethylthiomethyl sulfoxide (**2**) as a colorless liquid; bp 95—97°C/2.5 mmHg, IR: 1042 cm^{-1}, NMR (in $CDCl_3$): δ 1.32 (t, 3H, J=7.4 Hz), 1.36 (t, 3H, J=7.4 Hz), 2.5—3.3 (m, 4H), and 3.72 (s, 2H).

Found: C, 39.22; H, 8.00; S, 42.04%. Calcd for $C_5H_{12}OS_2$: C, 39.43; H, 7.94; S, 42.12%.

(b) To a solution containing 871 mg of formaldehyde diethyl mercaptal in 10 m*l* of methylene chloride, a 1.382-g portion of *m*-chloroperbenzoic acid (80% active) was added while the mixture was being cooled with ice. After continuous stirring for 1.5 hr, the mixture was neutralized with 500 mg of potassium carbonate and then subjected to filtration. The subsequent concentration of the filtrate under reduced pressure and the purification of the residue by column chromatography (Florisil, methylene chloride) gave 543 mg of ethyl ethylthiomethyl sulfoxide (**2**). (c) To a solution containing 2.652 g of formaldehyde diethyl mercaptal in 14 m*l* of water and 7 m*l* of methanol, a 4.11-g portion of sodium metaperiodate was added under cooling with ice. After 1 hr of stirring, the mixture was subjected to filtration, and then the filtrate was extracted with methylene chloride. The extract was dried with anhydrous sodium sulfate and concentrated under reduced pressure. The residue was separated by column chromatography (silica gel, methylene chloride, and ethyl acetate) to afford 260 mg of ethyl ethylthiomethyl sulfoxide (**2**).

Oxidation of Formaldehyde Diisopropyl Mercaptal. To a solution containing 4.324 g of formaldehyde diisoproply mercaptal in 15 m*l* of acetic acid, a 3.00-m*l* portion of an aqueous solution of hydrogen peroxide (concentration: 30%) was added while cooling with ice, and then the resulting mixture was stirred for 4.5 hr at room temperature. The same work-up as above, followed by the distillation of the residue under reduced pressure, gave 3.606 g of isopropyl isopropylthiomethyl sulfoxide (**3**) as colorless crystals; mp 39—40°C (bp 87—88°C/1 mmHg), IR: 1048 cm^{-1}, NMR (in $CDCl_3$): δ 1.28 (d, 3H, J=6.8 Hz), 1.32 (d, 3H, J=6.8 Hz), 1.34 (d, 6H, J=6.8 Hz), 2.7—3.6 (m, 2H), and 3.68 (s, 2H).

Found: C, 46.51; H, 9.00; S, 35.76%. Calcd for $C_7H_{16}OS_2$: C, 46.62; H, 8.92; S, 35.56%.

Oxidation of Formaldehyde Diphenyl Mercaptal. To a solution containing 1.538 g of formaldehyde diphenyl mercaptal in 5 m*l* of acetic acid, 0.75 m*l* of an aqueous solution of hydrogen peroxide (concentration: 30%) was added, and then the mixture was stirred for 1 hr at room temperature. After 100 m*l* of methylene chloride, 6 g of potassium carbonate, and a small amount of water had then been added, the resulting mixture was dried with anhydrous sodium sulfate and filtered. The filtrate was concentrated under reduced pressure, and the residue was separated by column chromatography (silica gel, methylene chloride) to afford 1.585 g of phenyl phenylthiomethyl sulfoxide (**4**) as a colorless liquid; IR: 1049 cm^{-1}, NMR (in CCl_4): δ 3.98 (d, 1H, J=13.5 Hz), 4.03 (d, 1H, J=13.5 Hz), and 7.1—7.8 (m, 10H).

Found: C, 62.78; H, 4.85; S, 25.87%. Calcd for $C_{13}H_{12}OS_2$: C, 62.87; H, 4.87; S, 25.82%.

Oxidation of Acetaldehyde Dimethyl Mercaptal. To a solution containing 4.72 g of acetaldehyde dimethyl mercaptal in 10 m*l* of acetic acid, 4.05 m*l* of an aqueous solution of hydrogen peroxide (concentration: 30%) was added, drop by drop, while the mixture was being cooled with ice. After the addition of methylene chloride, the mixture was neutralized with potassium carbonate and filtered. The filtrate was dried with anhydrous sodium sulfate, and, on distilling under reduced pressure, a 3.62-g portion of methyl 1-methylthioethyl sulfoxide (**5**, bp 84°C/2 mmHg) was obtained as a colorless liquid. This liquid was shown by its NMR analysis to consist of two diastereoisomers in a ratio of 66: 34. NMR (in $CDCl_3$): the major component; δ 1.62 (d, 3H, J=7.2 Hz), 2.23 (s, 3H), 2.69 (s, 3H), and 3.64 (q, 1H, J=7.2 Hz), the minor component; δ 1.57 (d, 3H, J=7.2 Hz), 2.31 (s, 3H), 2.55 (s, 3H), and 3.73 (q, 1H, J=7.2 Hz).

Found: C, 34.36; H, 7.44%. Calcd for $C_4H_{10}OS_2$: C, 34.75; H, 7.29%.

BULLETIN OF THE CHEMICAL SOCIETY OF JAPAN, VOL. 45, 2205(1972)

The ESR Spectrum of 2-Dimethylaminoazulene Anion Radical

Yusaku IKEGAMI, Hidetoshi WATANABE, and Shuichi SETO

Chemical Research Institute of Non-Aqueous Solutions, Tohoku University, Katahira-2-chome, Sendai

(Received January 12, 1972)

ESR studies of the anion radicals of biazulenyls[1] and methoxyazulenes[2] were reported in previous papers. A similar study has been carried out on the anion radical of 2-dimethylaminoazulene obtained in a relatively stable form.

Experimental

2-Dimethylaminoazulene, mp 99°C,[3] was purified by recrystallization. The solvent *N,N*-dimethylformamide (DMF) and acetonitrile (AN) were distilled onto Molecular Sieve after being purified and degassed. Electrolytic reduction was carried out using DMF and AN as the solvent and tetra-*n*-propylammonium perchlorate as a supporting electrolyte.

The ESR spectra were measured at room temperature with a Hitachi X-band ESR spectrometer, Model 771. A JEOL spectrum computer, JEC-5, was used for spectral simulation.

Results and Discussion

The anion radical of 2-dimethylaminoazulene was prepared by the electrolytic technique which was found useful for the generation of radical ions, particularly of azulene anion radicals.[1,2,4] The electrochemical reduction of the compound in degassed AN gives the ESR spectrum shown in Fig. 1. A similar spectrum was also presented by the electrolysis in DMF.

Hyperfine structure of the spectrum was analyzed with six splitting constants listed in Table 1. The analysis was confirmed by a spectral simulation with the constants and a half-width of 200 milligauss. The assignments for the constants were given according to the type of splitting and by a comparison of the constants with the calculated spin densities.

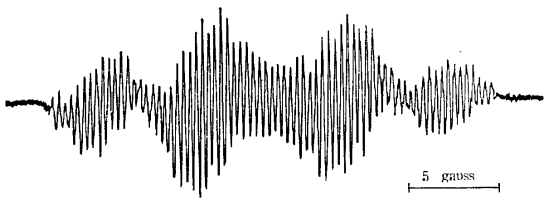

Fig. 1. ESR spectrum of 2-dimethylaminoazulene anion radical generated by the electrolytic reduction in acetonitrile (g=2.0017).

Table 1. Splitting constants (a_i) and spin densities for 2-dimethylaminoazulene anion radical

Position	a_i, gauss		Calcd spin density[a] ρ_i		$\lvert Q^H_{CH}\rvert$[b]
	in AN	in DMF	Hückel	McLachlan	
1,3	0.1	0.1	0.0000	−0.0402	2.5
2			0.1033	0.1060	
4,8	5.62	5.58	0.1937	0.2794	20.0
5,7	1.40	1.40	0.0132	−0.0670	20.9
6	8.01	7.94	0.2435	0.3653	21.8
9,10			0.1020	0.0946	
11 (N)	1.05	1.02	0.0310	−0.0032	
12,14	0.35	0.35	0.0000	−0.0006	
13,15			0.0022	−0.0003	

a) The following parameters were used for the calculation:

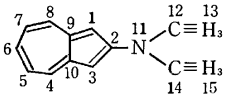

$\alpha_{11}=\alpha+1\beta$, $\alpha_{13}=\alpha_{15}=\alpha-0.5\beta$, $\beta_{9,10}=0.9\beta$, $\beta_{2,11}=\beta_{11,12}=\beta_{11,14}=0.8\beta$, $\beta_{12,13}=\beta_{14,15}=3\beta$, and $\lambda=1.2$.
All other bond length variations were neglected.

b) $\lvert Q^H_{CH}\rvert$ value in the relation of $a_i=Q^H_{CH}\rho_i$, in which the average a_i observed and the McLachlan spin density were used.

Calculations of unpaired spin densities (ρ_i) for the anion radical were carried out by means of the Hückel MO theory and the approximate configuration interaction treatment proposed by McLachlan.[5] The Coulomb and resonance integral parameters for the dimethylamino group were chosen by referring to a conjugation model for the methyl group.[6] The values are given in the footnote of Table 1. The calculated spin densities are shown in the table. The McLachlan procedure gives a much more satisfactory result than the Hückel MO calculation. The Q^H_{CH} values obtained by the McConnell relation are reasonable for the seven-membered ring and close to those for azulene anion radicals.[2,4] The low Q^H_{CH} value for the 1- and 3-positions arises mainly from the inaccuracies of both the spin density and the splitting constant for these positions. The splitting constant is less than the halfwidth of a spectral line. Such a calculation might be applied for the analogous anion radicals.

1) Y. Ikegami and S. Seto, *Mol. Phys.*, **16**, 101 (1969); This Bulletin, **43**, 2409 (1970).
2) Y. Ikegami and S. Seto, *ibid.*, **44**, 1905 (1971).
3) T. Nozoe and T. Asao, "Daiyuki-Kagaku", Vol. 13, Asakura-shoten, Tokyo (1960), p. 496.
4) I. Bernal, P. H. Rieger, and G. K. Fraenkel, *J. Chem. Phys.*, **37**, 1489 (1962).
5) A. D. McLachlan, *Mol. Phys.*, **3**, 233 (1960).
6) A. Streitwieser, Jr., "*Molecular Orbital Theory for Organic Chemists*", John Wiley & Sons, New York (1962), p. 132.

BULLETIN OF THE CHEMICAL SOCIETY OF JAPAN, VOL. 45, 2206—2207(1972)

A Fluorescence Study of a Random Coil-to-α-Helix Transition of a 1-Dimethylaminonaphthalene-5-sulfonyl Poly-L-lysine Conjugate

Takayoshi Iio, Yoshihiro Iwashita, and Hideharu Watanabe
Department of Physics, Faculty of Science, Nagoya University, Chikusa-ku, Nagoya

(Received February 7, 1972)

In this communication, we wish to report on our studies of a 1-demethylamino-naphthalene-5-sulfonyl poly-L-lysine (DNS-PLy) conjugate by the fluorescence method.

Poly-L-lysine is reversibly transformed in its conformation from a random coil to an α-helix at room temperature when the pH value of the solution is changed from 8 to 11.[1] We intended to obtain information on the state of the L-lysyl residue in each conformation. For this purpose, we bound a fluorescent molecule, DNS, to the ε-N atom of the lysyl residue and observed the polarization of the fluorescence under various conditions.

We found that the L-lysyl residue got some flexibility in the random coiled conformation, while the flexibility of the L-lysyl residue was almost completely suppressed in the α-helical conformation.

Experimental

PLy was obtained according to the usual *N*-carboxyanhydride method.[2] The molecular weight of PLy was determined to be 30000 by the Archibald method;[3] the degree of polymerization was 230.

DNS was coupled to the L-lysyl residue according to the method reported by Weber.[4] The molar ratio of the bound DNS to the L-lysyl residue was 1 : 48.5.

All the fluorescence measurements were performed in polymer concentrations ranging from 0.75×10^{-7} to 3.7×10^{-7} mol residue/*ml*. In these concentrations, the relative fluorescence intensity was proportional to the polymer concentration.

The fluorescence spectra and the relative fluorescence intensity were measured with a Hitachi Fluorescence Spectrometer, MPF-2A.

The polarization of the fluorescence was measured with an improved apparatus which had originally been made for light scattering experiments by Shimadzu Seisakujo, Kyoto. The apparatus was improved in the same manner as is shown in Fig. 5 of ref. 5. A monochromatic filter for excitation light with a maximum of transmittance at 350 mμ, and a cut off filter for emitted light which transformed light only above 420 mμ, were used in this experiment. The size of a fused quartz cell was $6.5\times1.0\times1.0$ cm. The value of polarization (P) was calculated according to Eq. (1);

$$p=\frac{I_v-I_h}{I_v+I_h} \tag{1}$$

where I_v and I_h are the fluorescence intensity of vertically polarized light and that of horizontally polarized light when the solution is excited with vertically polarized light.

The optical rotatory dispersion curves were measured with a JASCO ORD/UV 5 apparatus.

Results and Discussion

The conformational change in PLy with the pH value is shown in Fig. 1, curve a.

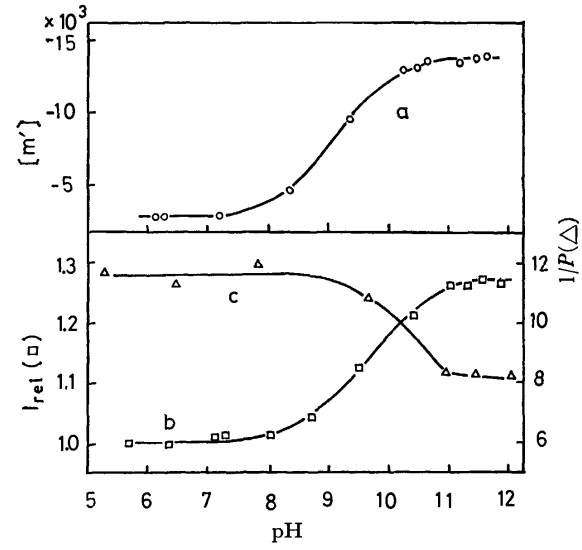

Fig. 1. pH Dependences of mean residue rotation [m'] at 233 mμ of PLy solution (curve a), relative fluorescence intensity (I_{rel}) of DNS-PLy conjugate (curve b), and of inverses value of polarization of the conjugate (curve c). These experiments were performed at room temperature (18—20°C)

DNS bound to PLy had a fluorescence maximum at 495 mμ when it was excited with a light of 350 mμ. The relative fluorescence intensity increased when the pH value of the solution was increased from 8 to 11, as shown in Fig. 1, curve b. In the following discussion, we will make use of the curve b for the purpose of estimating the lifetime of the DNS bound to α-helical PLy.

The inverse value of polarization indicates the degree of flexibility of the L-lysyl residue to which DNS is bound.[6] The pH dependence of this value is shown in curve c (Fig. 1). From an inspection of the curve

1) J. Applequist and P. Doty, "Polyamino acids, Polypeptides and Proteins" ed. by M. Stahmann, University of Wisconsin Press, (1962), p. 161.

2) J. Noguchi, "Poly condensation and Polyaddition Reaction" (in Japanese), Kyoritsu Shuppan, Tokyo (1952), p. 301.

3) K. Kakiuchi, *Seibutsubutsuri*, **7**, 38, (1967).

4) G. Weber, *Biochem. J.*, **51**, 155, (1952).

5) T. Takagi, "Atarashii Seibutsu Butsuri Kagaku Kenkyu-hou" ed. by T. Isemura, J. Tanaka, H. Noda, and T. Miyazawa, Kagakudojin, Kyoto (1967), p. 155.

6) G. Weber, Adv. in Protein Chem. VIII, 415 (1953).

c, we can conclude that the flexibility of the L-lysyl residue decreased as the conformation of PLy changed from the random coil to the α-helix.

Further information can be obtained from the Perrin plots for the DNS-PLy conjugate. In Fig. 2, we show the effects of the temperature and the viscosity on the polarization of the fluorescence. The data allow the conclusion that Perrin's law of depolarization (Eq. (2)) is closely followed in the cases of both the random coiled and the α-helical PLy.

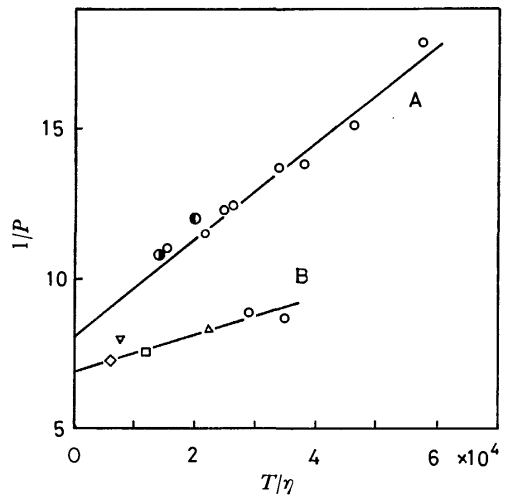

Fig. 2. Effects of temperature and viscosity on the polarization of the fluorescence of the conjugate. Plot A for random coiled conformation was obtained in pH 5.5—6.0 and plot B for α-helix was obtained in pH 11.3—11.9. Open circules were from aqueous solutions at various temperatures and the others were from conjugate-water-glycerine systems at 20°C; glycerine content were 15% (◐), 25% (◑), 10% (△), 30% (□), 40% (▽), and 50% (◇).

From the linear plots in Fig. 2, we can calculate the mean rotational relaxation time (ρ_h) of the DNS molecule bound to PLy according to Eq. (2);[6]

$$\left(\frac{1}{p}-\frac{1}{3}\right)=\left(\frac{1}{p_0}-\frac{1}{3}\right)\left(1+\frac{3\tau_0}{\rho_h}\right) \qquad (2)$$

where P_0 is an intrinsic polarization and where τ_0 is the lifetime of the excited state of the fluorescent molecule. The τ_0 value is proportional to the relative fluorescesce intensity.[7] In the neutral pH region, the τ_0 value has been reported as 1.2×10^{-8} sec,[4] so the τ_0 value in the high pH region (above 11.0) was estimated as 1.5×10^{-8} sec.

The ρ_h value was obtained as 5.6×10^{-8} sec at 20°C in the case of the random coil, and as 16.2×10^{-8} sec at 20°C in the case of the α-helix. The former value is equivalent to a rotational relaxation time of a sphere with a radius of 26 Å; this means that the DNS bound to the L-lysyl residue rotates with a few lysyl residues in the polypeptide chain. The latter value is approximately equal to a harmonic mean rotational relaxation time of an α-helical PLy molecule with a degree of polymerization of 230; that is, the flexibility of the L-lysyl residue is completely suppressed and the rotational motion of the DNS molecule coincide with that of one rigid α-helical PLy molecule.

These results are reasonable because the following situation may occur in the PLy molecule: in low-pH regions, where PLy takes the random coil, the main chain of PLy assumes a locally-extended form because of repulsive interaction between charged side chains, and both the main chain and the side chain get some flexibility. On the other hand, in the case of the α-helix, the main chain is regularly folded and the flexibility of the side chain may be completely suppressed.

Other evidence on this suppression of the flexibility of the L-lysyl residue in the α-helical conformation was obtained by a nuclear magnetic resonance study in D_2O solutions.[8]

As the temperature of an α-helical PLy solution (pH>11.0) is increased to 30°C or more, PLy is transformed in its conformation from the α-helix to the β-form.[9] An intermolecular β-form was also assumed in this case. The hydrophobic bonding between side chains is one of the main factors in stabilizing the β-form.[9] Therefore, we expected the $1/P$ value to decrease when PLy took the β-form. In fact, when the temperature of the PLy solution in pH 11.5 was raised to 34°C from 20°C, the $1/P$ value decreased to 6.0 from 8.7. The details of the fluorescence studies of the β-form will be published elsewhere.

The authors wish to thank to Dr. Sho Takahashi of the Institute for Chemical Research, Kyoto University, for his valuable discussions.

7) J. R. Laurence, "Physical Methods in Macromolecular Chemistry", ed. by B. Carroll, Marcel Dekker, New York (1969), p. 275.

8) E. M. Bradbury, C. C. Robinson, H. Goldman, and H. W. E. Rattle, *Biopolymers*, **6**, 851, (1968).

9) B. Davidson and G. D. Fasman, *Biochemistry*, **6**, 1616, (1967).

BULLETIN OF THE CHEMICAL SOCIETY OF JAPAN, VOL. 45, 2208—2209(1972)

The Convenient Preparation of L-Aspartic Anhydride Hydrochloride and Hydrobromide

Yasuo ARIYOSHI, Tetsuo YAMATANI, Noboru UCHIYAMA, and Naotake SATO

Central Research Laboratories, Ajinomoto Co., Inc., Suzuki-cho, Kawasaki, Kanagawa

(Received January 26, 1972)

L-Aspartic anhydride hydrochloride (I) and hydrobromide (II) are useful intermediates for the preparation of aspartyl peptides,[1] aspartic acid α-esters,[1] and polyaspartic acid.[2] II has been prepared thus far by the deprotection of carbobenzoxy-L-aspartic anhydride with hydrogen bromide in acetic acid[1] or by the direct dehydration of L-aspartic acid with an excess of thionyl chloride in chlorosulfonic acid or trifluoroacetic acid, followed by the removal of the strong acid used as the solvent and treatment with hydrogen bromide in acetic anhydride.[3] The strongly acidic solvent has played a role in protecting the amino group from undesirable reactions during the dehydration reaction. However, it seems that these methods are somewhat inconvenient because of the need to protect the amino group or the use of the strongly acidic solvent. Furthermore, the properties of I have not been reported in the literature.

We wish to report a more convenient method for preparing I and II. The synthesis was conducted as a heterogeneous reaction in a more convenient solvent, tetrahydrofuran, in which the dehydrating reagent is dissolved. The reaction proceeds smoothly according to the equation (Fig. 1). L-Aspartic acid was readily

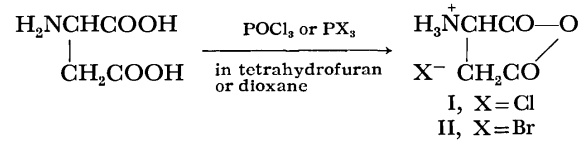

Fig. 1. L-Aspartic anhydride hydrochloride (I) and hydrobromide (II)

dehydrated with phosphorous oxychloride or phosphorous trichloride in tetrahydrofuran at room temperature to give, after filtration, an analytically pure I in a fairly good yield (Table 1). Because of the salt formation at the amino nitrogen, the further condensation of the product to polyaspartic acid does not occur under these conditions. In order to confirm its optical purity, the I obtained here was converted to L-aspartic acid and its optical rotation was measured. The value of the optical rotation of an aqueous solution

Table 1. Summarized data of reactions

No	1	2	3	4
L-Aspartic acid g	13.3	20	13.3	4
Reagent g	$POCl_3$ 15.3	PCl_3 11	$POCl_3$ 15.3	PBr_3 4
Solvent ml	Tetrahydrofuran 200	Tetrahydrofuran 100	Dioxane 150	Tetrahydrofuran 20
Reaction temp °C	25—5	25	25	5
Reaction period hr	5.5	4	6	3.5
Product	I	I	I	II
Yield g (%)	8.0 (53)	21.9 (96)	10.6 (70)	3.2 (54)
Mp °C (decomp.)	139—140	139—140	128—130	157—158[a]
$[\alpha]_D^{25}$	+23.2[b]	+23.3[b]	+24.0[c]	+26.9[d]
IR cm^{-1}	1875, 1815, 1790	1875, 1815, 1790	1885, 1795	1875, 1805, 1785
Anal. Found %	C, 31.41; H, 4.21; N, 9.07; Cl, 23.22[e]	C, 31.70; H, 4.27; N, 9.25; Cl, 23.10[e]	C, 36.26; H, 5.44; N, 7.19; Cl, 18.27[f]	C, 24.22; H, 3.27; N, 6.98; Br, 40.98[g]

a) mp 166—169°C (decomp.).[1]
Specific rotations of L-aspartic acid in various solutions (b—d);
b) $[\alpha]_D^{25}$ +24.5° (*c* 2, 6N HCl).
c) $[\alpha]_D^{25}$ +25.0° (*c* 2, 6N HCl with 0.5 molecular equivalent of dioxane).
d) $[\alpha]_D^{25}$ +25.1° (*c* 2, 6N HBr).
e) Calcd for $C_4H_6O_3NCl$: C, 31.70; 3.99; N, 9.24; Cl, 23.40%.
f) Calcd for $C_4H_6O_3NCl \cdot 1/2C_4H_8O_2$: C, 36.84; H, 5.15; N, 7.16; Cl, 18.13%. NMR (D_2O, DSS) of the product: δ 3.80 ppm (4H, singlet, dioxane).
g) Calcd for $C_4H_6O_3$ NBr: C, 24.51; H, 3.09; N, 7.15; Br, 40.77%.

1) J. Kovacs, H. N. Kovacs, and R. Ballina, *J. Amer. Chem. Soc.*, **85**, 1839 (1963).
2) J. Kovacs, H. N. Kovacs, I. Könyves, J. Császár, T. Vajda, and H. Mix, *J. Org. Chem.*, **26**, 1084 (1961).
3) J. Kollonitsch and A. Rosegay, *Chem. Ind.*, **1964**, 1867; *Chem. Abstr.*, **64**, 9820f (1966).

of hydrochloric acid in which a given amount of I had been dissolved agreed with that of an aqueous solution of hydrochloric acid containing the corresponding amount of L-aspartic acid (Table 1). These results show that no racemization occurred during the dehydration reaction. Attempts to measure the optical rotation of the anhydride itself in *N,N*-dimethylformamide, dimethyl sulfoxide, or pyridine did not give reproducible results. The anhydride hydrochloride decomposed slightly in such a solvent, even under anhydrous conditions.

When dioxane was used as the solvent for the dehydration reaction, the anhydride (I) contained half a mole of dioxane as the solvent of crystallization; this was confirmed by the elemental analysis and by the NMR spectrum of I (Fig. 1 and Table 1).

A similar treatment of L-aspartic acid with phosphorous tribromide in tetrahydrofuran gave pure L-aspartic anhydride hydrobromide (II) (Fig. 1 and Table 1). The anhydrides (I and II) decomposed slowly on exposure to atmospheric moisture, but they were found to be stable for more than two weeks when stored *in vacuo* over phosphorous pentoxide. Their use for peptide synthesis will be described elsewhere.

Experimental

All the melting points are uncorrected. The IR spectra were obtained in Nujol mull with a Jasco IR-S spectrometer. The optical rotations were measured in 6N hydrochloric acid or 6N hydrobromic acid with a visual polarimeter.

L-Aspartic Anhydride Hydrochloride (I). A typical run (No. 1 in Table 1) was as follows. To a stirred suspension of L-aspartic acid (13.3 g) in tetrahydrofuran (200 m*l*) was added phosphorous oxychloride (15.3 g) at 25°C over a period of 5 min. The mixture was stirred for 1.5 hr at the same temperature. After being stirred for an additional 4 hr at 5—10°C, the crystals thus formed were collected by filtration and washed with tetrahydrofuran. The anhydride hydrochloride so obtained was analytically pure without further purification. Purification by recrystallization is ineffective because the anhydride slightly decomposes in a solution, as has been described in connection with the attempted measurements of its optical rotation.

In the case of phosphorous trichloride (No. 2 in Table 1), the crystals obtained were accompanied with a disagreeable odor but the odor could be removed by adding acetic acid (20 m*l*) to the reaction mixture before filtration.

The results are summarized in Table 1.

L-Aspartic Anhydride Hydrobromide (II). This compound was prepared by the direct dehydration of L-aspartic acid with phosphorous tribromide in tetrahydrofuran according to the procedure described in connection with the preparation of I. The results are shown in Table 1.

As moisture may cause the anhydrides (I and II) to undergo decomposition, dried solvents should be empolyed in order to obtain satisfactory results in their preparation.

BULLETIN OF THE CHEMICAL SOCIETY OF JAPAN, VOL. 45, 2209—2211(1972)

Préparations des Sels de Diiodobis(éthylènediamine)cobalt(III)

Masayoshi NAKAHARA et Motoko MITSUYA

Laboratoire de Chimie Minérale, Faculté des Sciences, Rikkio Université, Ikebukuro, Tokio

(Reçu, le 9, Mars 1972)

La littérature abonde en nombreux exemples rélatifs à la détermination des bandes d'absorption du transfert de charge entre les atomes d'halogènes et l'atome cobaltique ou l'atome chromique. Linhard et son collaborateur,[1] ont tout particulièrement effectués des études sur des complexes du cobalt(III) avec la pentammine et le bis(éthylènediamine). Cependant, il n'y a pas de résultat concernant les bandes d'absorption du complexe diiodobis(éthylènediamine)cobalt(III), ceci s'explique par le fait, qu'il est difficile d'obtenir le sel de diiodo-complexe approrié. Seul le triiodure de ce complexe, $[CoI_2(en)_2]I_3$, a été déjà préparé par G. Spacu et P. Spacu,[2] mais on ne peut pas mesurer les bandes d'absorption du champ des coordinats et du transfert de charge à cause de la présence des bandes d'absorption de I_3^-. Nous nous sommes intéressés aux bandes d'absorption du champ des coordinats et du transfert de charge du diiodocomplexe et nous avons comparés les valeurs observées avec les valeurs déterminées par Linhard et son collaborateur pour le difluoro-, dichloro- et dibromo-complexe.

Partie Expérimentale

Préparations. 1) L'iodure de carbonatobis(éthylènediamine)cobalt(III), $[CoCO_3(en)_2]I$, a été préparé selon le procédé de Werner.[3] L'acide iodhydrique utilisé a été purifié selon la méthode usuelle[4] et a été employé fraîchement distillé. 2) Iodure de diiodobis(éthylènediamine)cobalt(III), $[CoI_2(en)_2]I$. Environ 10 g de poudre de $[CoCO_3(en)_2]I$ sont ajoutés, petit à petit, à 15 m*l* d'acide iodhydrique concentré en isolant de l'air par une couche d'éther de pétrole. Le sel de complexe obtenu est un solide brun-rouge. On l'a purifié par recristallisation dans l'alcool méthylique et ensuite séche à l'air. Rendement 10 g.

Trouvé: Co, 10.34; I, 66.94; C, 8.40; H, 2.94; N, 9.73%. Calculé: Co, 10.53; I, 68.00; C, 8.58; H, 2.88; N, 10.01%.

Ce composé est soluble dans l'alcool méthylique, l'alcool éthylique, l'acétone et le dioxane en donnant une solution brun-rouge, par contre il est insoluble dans l'hexane et le

1) M. Linhard et M. Weigel, *Z. Anorg. Allg. Chem.*, **266**, 49 (1951), 271, 101 (1952).

2) G. Spacu et P. Spacu, *Bl. Soc. Stiinte Cluj*, **7**, 369 (1933).

3) A. Werner et J. Papipart, *Lieb. Ann.*, **386**, 74 (1912).

4) "Inorganic Syntheses." Vol. 1. p. 158.

dichlorométhane. 3) Perchlorate de diiodobis(éthylènediamine)cobalt(III), $[CoI_2(en)_2]ClO_4$. A une solution d'iodure de diiodobis(éthylènediamine)cobalt(III) dans l'alcool méthylique on ajoute du perchlorate de sodium en solution dans l'alcool méthylique et en léger excés par rapport à l'iodure. On obtient un précipité brun-rouge. On filtre et lave à l'alcool méthylique, puis on séche à l'air.

Trouvé: Co, 11.00; I, 49.63; C, 9.25; H, 3.19; N, 10.81%. Calculé: Co, 11.07; I, 47.67; C, 9.02; H, 3.03; N, 10.52%.

La composé obtenu est une poudre brun-rouge, insoluble dans l'alcool méthylique et l'éther. 4) Nitrate de diiodobis(éthylènediamine)cobalt(III), $[CoI_2(en)_2]NO_3$. L'iodure de diiodobis(éthylènediamine)cobalt(III) a été dissous dans l'alcool méthylique; sur la solution ainsi obtenue on verse du nitrate d'ammonium en solution dans CH_3OH et en léger excés par rapport à l'iodure. On filtre et lave le précipité avec de l'alcool méthylique, puis on séche à l'air.

Trouvé: Co, 11.55; I, 50.94; C, 9.40; H, 3.15; N, 13.58%. Calculé: Co, 11.10; I, 51.28; C, 9.71; H, 3.25; N, 14.15%.

Poudre brun-rouge, insoluble dans l'alcool méthylique et l'éther.

Analyse. *1) Cobalt*: On a dosé le cobalt sous forme de sulfate par l'α-nitroso-β-naphthol. Le sulfate de cobalt est obtenu en fondant un mélange constitué par le complexe lui-même et l'hydrogénosulfate de potassium.

2) Iode: On aquotise le complexe en procédant à sa dissolution à chaud dans une solution de NH_3 diluée. On ajoute de l'acide sulfurique et on oxyde par le nitrite de sodium. On extrait l'iode par le tétrachlorure de carbone et on fait alors l'analyse colorimétrique.

Les Spectres d'Absorption. Nous avons enregistré les spectres d'absorption dans l'ultraviolet et dans le visible des différents complexes en solution dans l'alcool méthylique ou à l'état solide avec un spectrophotomètre du type HITACHI EPS2A et un appareil annexe pour mesurer la réflexion diffuse. Les cuves de quartz ont une épaisseur de 1 cm. Les échantillons solides que nous avons utilisés ont été, tout d'abord, pulvérisés et nous en avons déterminé le pourvoir réflecteur diffuse (R_d) en prenant la magnésie comme étalon. Les valeurs de $f(R_d)$ qui sont en rapport direct avec ε peuvent être calculées par l'expression de Kubelka-Munk pour obtenir la courbe $\log f(R_d)$.[5] Nous avons également déterminé les spectres d'absorption infrarouge avec un appareil JASCO (Japan Spectroscopic Co., Ltd) DS 402 G en adoptant la méthode Nujol-Mull.

Résultats et Discussion

Dans les spectres d'absorption visible du $[CoI_2(en)_2]I$ en solution dans l'alcool méthylique, les positions et les configurations des bandes du champ des coordinats coïncident presque parfaitement dans la région comprise entre 12000 cm^{-1} et 20000 cm^{-1} avec les spectres d'absorption à l'état solide des composés $[CoI_2(en)_2]I$, $[CoI_2(en)_2]ClO_4$ et $[CoI_2(en)_2]NO_3$. Nous avons donc réussi à observer en solution le spectre d'absorption du complexe sans décomposition. Dans la figure 1, nous avons representé pour la région comprise entre 12000 cm^{-1} et 22000 cm^{-1} les spectres d'absorption du complexe $[CoI_2(en)_2]^+$ en solution et également ceux des composés *trans*-$[CoX_2(en)_2]ClO_4$ (avec X=F, Cl, Br)[1] afin de pouvoir les comparer. Les données ainsi obtenues sont rassemblées dans le tableau 1.

En ce qui concerne les spectres d'absorption de

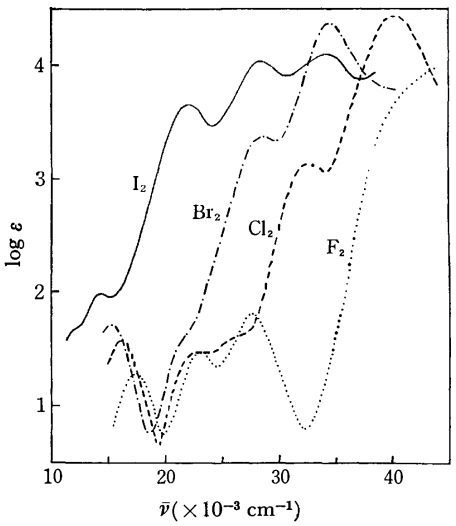

Fig. 1. Spectres d'absorption de $[CoX_2(en)_2]^+$ (X=F,Cl,Br,I)

TABLEAU 1. MAXIMA DES BANDES D'ABSORPTION (cm^{-1}) ET COEFFICIENT D'EXTINCTION MOLAIRE (log ε)

trans-$[CoX_2(en)_2]^+$	Ia	Ib	II	III	IV	V
X=F	17200	22620	27600			
	(1.35)	(1.49)	(1.67)			
X=Cl	16120	22490	25920	32500	40270	
	(1.61)	(1.46)	(1.49)	(3.12)	(4.43)	
X=Br	15210	21680		28100	34600	
	(1.73)	(1.49)		(3.35)	(4.34)	
X=I	14000			21700	28600	33900
	(2.01)			(3.68)	(4.02)	(4.17)

$[CoI_2(en)_2]^+$ nous avons trouvé une bande interdite par spin, une bande permise par spin et trois bandes de transfert de charges. Les bandes de champ de coordinat Ib et II ont été couvertes par les bandes de transfert de charges III et IV. Nous n'avons pas pu aboutir à un résultat précis du fait que la bande d'absorption III empiéte sur la bande d'absorption Ia; le maximum de la bande Ia s'est déplacé vers les plus fortes longueurs d'ondes et son coefficient d'éxtinction molaire augmente; ces résultats sont à comparer avec ceux obtenus dans les cas du dibromo, dichloro et difluoro-complexe. Le déplacement de la bande Ia vers les longueurs d'ondes élevées et l'augmentation de l'extinction molaire se font suivant l'ordre F, Cl, Br, I. Les positions du maximum de la bande d'absorption III, du dichloro, dibromo et diiodocomplexe sont déplacées vers les plus fortes longuers d'ondes; les coefficients d'extinctions molaires augment suivant l'ordre précédent. La bande d'absorption IV se déplace dans le même sens que les bandes précédents, mais par contre son coefficient d'extinction molaire évolue en sens inverse. Nous avons observé une bande d'absorption V uniquement dans le cas du diiodocomplexe.

Les spectres d'absorption du *cis*-$[CoX_2(en)_2]^+$ (où X=Cl, Br) mesurés par Linhard et son collaborateur[1] montrent que les bandes d'absorption correspondantes à III et IV sont très plates et tout à fait différentes avec des bandes III et IV observées dans le complexe *trans*-

5) P. Kubelka et F. Munk, *Z. Tech. Physik.*, **12**, 593 (1931).

Tableau 2. Maxima des bandes d'absorption infrarouge (cm^{-1}) de *trans*-$[CoX_2(en)_2]X$

X=Cl	585	555	513	473
X=Br	580, 575	554	507	470
X=I	570	544	497	460

$[CoX_2(en)_2]^+$ (où X=Cl, Br).

De ces faits nous avons conclu que les composés que nous avons préparés sont du type *trans*.

Nous avons étudié également le spectre d'absorption infrarouge dans la région comprise entre 4000 cm^{-1} et 400 cm^{-1}. Nous avons remarqué entre 4000 cm^{-1} et 600 cm^{-1} les diverses bandes d'absorption à haut coefficient d'extinction molaire qui correspondent aux bandes d'absorption de l'éthylènediamine dans le complexe *trans*-$[CoX_2(en)_2]X$ (où X=Cl, Br).[6] Nous avons trouvé les bandes d'absorption des liaisons Co–N et de la déformation de l'anneau du chélate entre 600 cm^{-1} et 400 cm^{-1} (le tableau 2). Les position des bandes ainsi que leur déplacement vers les longueurs d'ondes élevées sont en bon accord avec les résultats de Hughes et collaborateurs.[6]

6) M. N. Hughes et W. R. McWhinnie, *J. Inorg. Nucl. Chem.*, **28**, 1659 (1960).

BULLETIN OF THE CHEMICAL SOCIETY OF JAPAN, VOL. 45, 2211—2212(1972)

The Prins Reaction of Styrene in the Presence of Cation-exchange Resin

Yasuhiko KURUSU

Department of Chemistry, Faculty of Science and Technology, Sophia University, 7 Kioicho, Chiyoda-ku, Tokyo

(Received August 24, 1971)

The application of ion-exchange resin to the Prins reaction has been investigated by several workers. The reactions of styrene, methyl styrene[1] and propyrene[2] were carried out with KU-2 cation-exchange resin, which gave the corresponding 1,3-dioxanes in good yields. However, in any case, no detailed study from the viewpoint of a solid acid catalyst has been reported on a Prins reaction in the presence of ion-exchange resin. Because the active site of a solid catalyst is the surface of the resin, the reactivity of the ion-exchange resin is largely dependent upon a crosslinkage which is determined by the content of divinylbenzene(DVB), and the crosslinkage makes a micropore in the state of swelling. The ion-exchange resin with a higher DVB content has smaller micropores. Besides the micropores, the ion-exchange resin polymerized with a macroreticular reagent has macropores. Thus, the reaction of styrene with formaldehyde in the presence of various types of ion-exchange resins was carried out, and the relation of the reactivity and the crosslinkage was investigated. The ion-exchange resins used were Diaion SK 1B, SK 104, the Diaion PK series, and Amberlite XE 284, all of which are strongly acidic cation-exchange resins and WK 10, and WK 11, which are weakly acidic cation-exchange resins.

When the SK series was used, the crosslinkage was dependent upon the yield of 4-phenyl-1,3-dioxane. The crosslinkage of SK 104 is 4%, and that of SK 1B is 8%. The crosslinkage in the PK series varies from 4%(PK 208) to 14%(PK 228). It is interesting that the yield of 4-phenyl-1,3-dioxane is highest with the crosslinkage of 10% among the other PK series. It may be found from this result that the size of the micropores is related to the reactivity. As the size of the pores of the resins becomes larger, the yield of 4-phenyl-1,3-dioxane increases. However, the micropore sizes of No. 8, 9, and 10 in Table 1 are so large that swelling occurs and it is difficult to separate the product because of its adsorption by resin. Also, the macropore has an important effect upon the yield; the porous type of 10% crosslinkage is most effective. However, the highly porous types (HPK, XE 284) prepared from higher contents of DVB are not so excellent as the PK series. The highly porous ion-exchange resin adsorbs the start-

TABLE 1. PRINS REACTION OF STYRENE WITH ION EXCHANGE RESIN

No	Ion exchange resin	Reaction condition		Yield	
		Temp (°C)	Time (hr)	g	%
1	SK 104	50—53	27	20.2	41.2
2	SK 104	50—53	10	11.0	22.4
3	SK 104	50—53	10	11.0	22.4
4	SK 104	50—53	10	12.5	25.5
5	SK 104	25	10	3.0	6.1
6	SK 1B	50—53	18	9.0	18.0
7	SK 1B	25	10	2.3	4.6
8	PK 208	55	10	5.2	10.6
9	PK 212	55	10	25.0	51.0
10	PK 216	55	10	20.0	40.8
11	PK 220	55	10	34.5	70.4
12	PK 220	30	10	3.5	6.4
13	PK 224	55	10	19.0	38.8
14	PK 228	55	10	11.2	22.9
15	HPK	55	10	11.0	22.4
16	XE 284	55	3	12.0	24.5
17	WK 10	50—53	13	trace	
18	WK 11	50—53	13	trace	

1) V. I. Isagnlyants and M. G. Safarov, *Zh. Prikl. Khim.*, **39**, 1148 (1966); *Chem. Abstr.*, **65**, 5455; V. I. Isagnlyants, M. G. Safarov and D. I. Rakahncakulov, *Zh. Prikl. Khim.*, **40**, 1160 (1967); *Chem. Abstr.*, **67**, 108609.

2) B. N. Bolylev, E. P. Tepenitsya, and M. I. Farberov, *Neftekhimia*, **9**, 71 (1969); *Chem. Abstr.*, **70**, 115083.

ing materials and products, so filtration is troublesome. It may safely said that the highly porous ion-exchange resin is a good adsorbent, but is unsuitable for the catalyst of the Prins reaction. That is, XE 284 gave a considerable yield in 3 hr, but this resin was gradually wrecked by the reaction. Therefore, it is difficult to carry out the reaction further, and a repeated reaction with XE 284 is impossible.

In No. 2, 3, and 4 in Table 1, reactions with the same catalyst were repeated. The results show that this catalyst was sufficiently used without regeneration.

To examine the effect of the temperature, the reaction was carried out with PK 220 at 30°C. In the case of PK 220, the yield was 6.4%. When SK 1B and SK 104 were used as the catalysts, the same results were obtained. These results show that the reaction is dependent upon the temperature.

Swelling is a very important factor in a porous-type ion-exchange resin. Therefore the reactions were investigated in various solvents. As the solvents, dimethylsulfoxide, methylene chloride, dioxane, and methanol were used, and paraformaldehyde was employed instead of formalin. In dimethylsulfoxide, a small amount of 4-phenyl-1,3-dioxane was obtained. However, in the other solvent, 4-phenyl-1,3-dioxane was not obtained but an unidentified product was obtained besides recovered styrene. A further investigation of the reaction in nonaqueous solvents is now in progress.

When the reaction is carried out with ion-exchange resin as the solid acid catalyst insted of sulfulic acid, phospholic acid, acetic acid or Lewis acid, it is easy to separate the product and the catalyst, and styrene and formalin are made to flow from the top of the column, packed with resin, and 4-phenyl-1,3-dioxane is obtained at the bottom of the column. It is possible to recycle the unreacted material after the separation in order to raise the yield and the efficiency.

Experimental

The ion-exchange resin (100 m*l*) was immersed into 250 m*l* of 50% H_2SO_4 for 8 hr at room temperature, and then filtered and washed with water until the washings were found by litumus paper to be no longer acid.[3] The treated ion-exchange resin, 35 g of styrene, and 100 m*l* of formalin (37%) were mixed in a 300 m*l*, three-necked, round-bottom flask for a given time at an appropriate temperature. After the reaction, the mixture was poured into 300 m*l* of water and the resin was filtered off. The filtrate was extracted with ether. The ether solution was distilled, and the unreacted styrene was obtained at 42°C and 20 Torr. The product was distilled at 90—95°C and 3 Torr. This compound was identified as 4-phenyl-1,3-dioxane by comparison with the IR spectrum of an authentic sample. The results are shown in Table 1. In these reactions, the unreacted styrene was recovered quantitatively.

The SK series are the strongly acidic sulfonic-acid-type cation-exchange resins, and the WK series are the weakly acidic carboxylictype cation-exchange resins. The PK series are the porous ion-exchange resins, which are of the sulfonic-acid type. The HPK and XE 284 are highly porous ion-exchange resins.

The author wishes to thank Mr. Moriyama, Mitsubishi Chemical Industries, Ltd., for his supply of ion-exchange resins.

3) "Diaion Ion-exchange Resin Manual (I)" revised ed., Mitsubishi Chemical Industries, Ltd. (1970).

BULLETIN OF THE CHEMICAL SOCIETY OF JAPAN, VOL. 45, 2212—2213(1972)

Synthesis of Dimethyl 4-(Alkyliminomethyl)-4-methylheptanedioates

Kuniyuki TAKAHASHI, Akihisa MIYAKE, and Go HATA

Basic Research Laboratories, Toray Industries, Inc., Tebiro, Kamakura, Kanagawa-ken

(Received November 11, 1971)

We wish to report the synthesis of dicarboxylic acid esters having an alkylimino group by a Michael type addition of aldimines with methyl acrylate.

N-Propylideneisopropylamine reacted with methyl

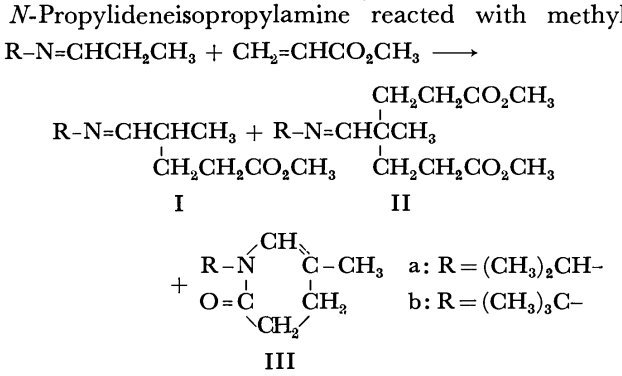

I II

III a: R = $(CH_3)_2CH$- b: R = $(CH_3)_3C$-

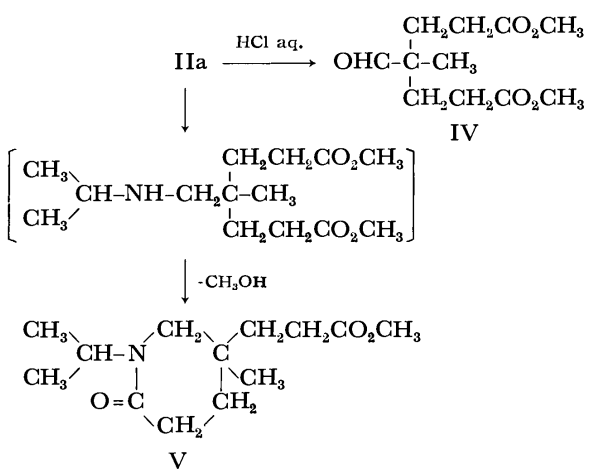

IV V

Table 1. Physical and analytical data of products

Product	bp °C/mmHg	n_{20}^{D}	C%		H%		N%	
			Found	Calcd	Found	Calcd	Found	Calcd
Ia	57—57.5/2	1.4438	64.83	64.58	10.34	10.26	7.56	7.53
IIa	128—132/3	1.4539	61.97	62.24	9.29	9.29	5.16	5.16
IIIa	62—63/1.5	1.4892	70.55	69.96	9.87	9.85	9.14	9.05
Ib	65/2	1.4357	66.29	65.88	10.62	10.61	7.03	7.09
IIb	130—131/2	1.4540	63.13	63.13	9.54	9.48	4.91	4.82
IV	135—137/2	1.4545	57.37	57.60	7.88	7.84		
V	165—168/2	1.4756	64.70	64.24	9.41	9.44	5.80	5.62

acrylate (a molar ratio 1 : 2) in pyridine at 110—120°C to afford a dicarboxylic acid ester IIa in a 66% yield with small amounts of Ia and IIIa.

Products Ia and IIa are normal Michel addition products. The cyclic product IIIa would be formed through the cyclization of Ia, since heating of Ia in pyridine afforded IIIa.

Product IIa was hydrolyzed by hydrochloric acid to give an aldehyde IV and hydrogenated with PtO_2 to form a saturated cyclic product V.

N-Propylidene-*t*-butylamine reacted in the same way to give IIb and Ib in 74 and 11% yields, respectively.

Experimental

The reaction products were identified by means of elemental analysis, molecular-weight measurement, and IR, NMR spectral measurements. The physical and analytical data of the products, which are all new compounds, are given in Table 1.

Reaction of N-*Propylideneisopropylamine*[1] *with Methyl Acrylate.* A mixture of 20 m*l* of pyridine, 9.9 g (0.1 mol) of *N*-Propylideneisopropylamine, 17.2 g (0.2 mol) of methyl acrylate, and a small amount of hydroquinone was heated at 110—120°C for 16 hr. The reaction mixture was fractionally distilled to afford 0.8 g (4%) of methyl 5-isopropylimino-4-methylvaleate (Ia), 17.9 g (66%) of dimethyl 4-(isopropylimino)methyl-4-methylheptanedioate (IIa) and 1.1 g (7%) of 1-isopropyl-3-methyl-6-oxopyperidine-2-ene (IIIa).

Hydrolysis of IIa. A mixture of 5.4 g (0.02 mol) of IIa and 10 m*l* of 1N HCl aqueous was refluxed for 30 min. The usual work-up of the resultant solution afforded 3.0 g (63%) of dimethyl 4-formyl-4-methylheptanedioate (IV).

Hydrogenation of II. A mixture of 26 g (0.1 mol) of IIa, 0.15 g of PtO_2 and 25 m*l* of absolute ethanol was stirred at a room temperature under a hydrogen pressure of 20 kg/cm^2 for 2 hr in a 100 m*l* autoclave to give 19.3 g (80%) of methyl 3-(1-isopropyl-3-methyl-6-*oxo*-3-piperidyl) propionate (V).

1) K. N. Campbell, A. H. Sommers, and B. K. Campbell, *J. Amer. Chem. Soc.*, **66**, 82 (1944).

BULLETIN OF THE CHEMICAL SOCIETY OF JAPAN, VOL. 45, 2213—2214(1972)

On the Catalytic Addition of Alcohols to 1,3-Butadiene with Rhodium Trichloride Hydrates

Hiroshi KAWAZURA and Toshio OHMORI

Research Laboratory, Japan Synthetic Rubber Co., Mochi-izaka, Ikuta, Kawasaki

(Received November 20, 1971)

Recently, it was disclosed by Dewhirst[1] that ethanol added to 1,3-dienes in the presence of $RhCl_3 \cdot 3H_2O$ to give allylic ethers, but the mechanism of formation of the ethers was left uncertain.

We wish to report some facts which may shed light on the mechanisms of this new addition reaction.

Table 1 summarizes the results of the addition reactions of various alcohols to 1,3-butadiene. The reaction proceeds at room temperature under nitrogen in the presence of catalytic amount of $RhCl_3 \cdot nH_2O$ (n=2 or 3) to give an addition product which is found to be a single component from glc analysis. The addition product of EtOH separated by preparative glc, a colorless liquid of bp 76°C, was confirmed to be 3-ethoxybut-1-ene by comparison of the IR and NMR spectra with those of an authentic sample.[2] Similarly, the addition products of the other alcohols were identified as 3-alkoxybut-1-ene.

$$CH_2{=}CH{-}CH{=}CH_2 + ROH \longrightarrow CH_3{-}\underset{\displaystyle OR}{\underset{|}{CH}}{-}CH{=}CH_2$$

The known binuclear rhodium complex (I)[3] was

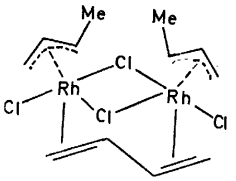

(I)

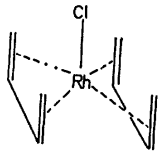

(II)

1) K. C. Dewhirst, *J. Org. Chem.*, **32**, 1297 (1967).

2) J. D. Roberts, Wm. G. Young, and S. Winstein, *J. Amer. Chem. Soc.*, **61**, 2157 (1942).

3) J. Powell and B. L. Shaw, *J. Chem. Soc., A*, **1968**, 597.

Table 1. Addition reaction of alcohols to 1,3-butadiene

Alcohol) (100 m*l*	Butadiene (mmol)	$RhCl_2 \cdot 3H_2O$ (mmol)	Time (hr)	Addition (mmol)	Product %[c]	Intensity of ν_{OH}[d] (*l*. mol^{-1} cm^{-1}) 10^{-4}
Me-	240	0.95	63	12.4	5.2	0.53
Et-[a]	600	3.05[b]	20	33.0	5.5	0.62
Pr^n-	144	2.05	60	15.8	11.0	—
Bu^n-	180	0.95	96	32.8	18.2	0.72
Bu^i-	180	0.95	96	21.1	11.8	—
Bu^s-	180	0.95	96	21.1	11.8	0.58
Bu^t-	180	0.95	96	6.3	3.5	0.42
Allyl-	240	0.95	48	9.8	4.1	—

a) EtOH 30 m*l*.
b) Dihydrate was used.
c) On the basis of butadiene fed.
d) Cited from Ref. 7).

isolated from the reaction mixture as brown crystals, and this was found to be able to catalyze the selective addition of *n*-PrOH to butadiene to give 3-*n*-propoxybut-1-ene. Therefore it is likely that I is an intermediate of the reaction, although other nascent π-allylic complex which might be convertible to I is not necessarily excluded.

The mononuclear rhodium complex (II)[3,4] which may be formed at lower temperature in the reaction mixture would not be a true intermediate, since the yield of 3-*n*-propoxybut-1-ene decreased drastically at lower temperature as shown in the Table 2.

Table 2. Temperature dependence of the addition reaction of *n*-PrOH to 1,3-butadiene[a]

Reaction Temp (°C)	Time (hr)	Yield of 3-*n*-propoxybut-1-ene (mmol)	% [b]
70	40	1.9	0.5
50	40	24.3	6.1
20	42	7.8	2.0
10	42	1.1	0.3

a) $RhCl_3 \cdot 3H_2O$ 1 mmol, *n*-PrOH 800 mmol, and 1,3-Butadiene 400 mmol.
b) On the basis of butadiene fed.

It should be noted that the Pd complex catalyzes dimerization of butadiene in alcohols[5,6] producing predominantly 1-alkoxy derivatives of butadiene dimer in contrast to the present rhodium catalyst.

The yields of the addition products seem to have linear correlations with intensities of the OH stretching vibrations of the alcohols which are considered to be a measure of ionization degree of the OH bonds.[7] This indicates a predominant contribution of the ionic nature of the alcohols to the addition reaction, while the steric influence of the alkyl group should not be overlooked since the butanol family shows somewhat different correlation.

4) L. Porri, A. Lionetti, G. Allegra, and A. Immirzi, *Chem. Commun.*, **1965**, 336.
5) S. Takahashi, H. Yamazaki, and N. Hagihara, This Bulletin, **41**, 254 (1968).
6) E. J. Smutny, *J. Amer. Chem. Soc.*, **89**, 6793 (1967).
7) G. M. Barrow, *J. Phys. Chem.*, **59**, 1129 (1955).

BULLETIN OF THE CHEMICAL SOCIETY OF JAPAN, VOL. 45, 2214—2215(1972)

Charge-Transfer Absorption in the Solid Aromatic Diamine Complexes with Picrates

Gunzi SAITO and Yoshio MATSUNAGA

Department of Chemistry, Faculty of Science, Hokkaido University, Sapporo

(Received December 3, 1971)

Molecular complexes have received considerable attention for many years. Nonetheless, most of those described in the literature are derived from neutral donor and acceptor molecules; relatively little is known about complexes made from neutral molecules and salts. Recently, we reported on the vibrational and electronic spectra of Kofler's ternary complex, α-naphthylamine-pyridine-picric acid (1 : 1 : 1), and postulated that the interaction between the amine molecule and the picrate ion is of the charge-transfer type.[1] Our interest in the acceptor strength of the picrate ion has led to a further study of the molecular complexes with picrates. As it seemed highly desirable to have simple counter ions, we chose sodium, potassium, and ammonium picrates. Their electron-acceptor strengths are expected to be comparable with that of *s*-trinitrobenzene; therefore, strong electron-donors must be combined with the picrates if one is to observe the charge-transfer absorption separated from the spectrum of the yellow-colored component. Benzidine, *o*-tolidine, and *o*-dianisidine were thought to be best suited to our purpose. These donors have low enough ionization potentials and were extensively used in the related work to be described in forthcoming papers.

The picrates were prepared by the addition of an aqueous solution of an appropriate carbonate or nitrate to picric acid dissolved in alcohol. The diffuse reflection spectra were recorded on a Beckman DK 2A spectroreflectometer and were plotted using the Kubelka-Munk function, as has been described in a

1) Y. Matsunaga and G. Saito, This Bulletin, **45**, 963 (1972).

previous paper.[2] Our attempts to prepare the solid complexes with sodium picrate from a solution failed except in the case of *o*-dianisidine. With this combination, dark brown-colored crystals were obtained from hot acetone. As is shown in Fig. 1, comparison with the spectrum of sodium picrate clearly indicates the appearance of a weak low-energy absorption upon the complex formation. When an equimolecular mixture of *o*-dianisidine and sodium picrate was thoroughly ground and heated to the melting point of the diamine, the same spectrum could be observed with the product. Therefore, all the other combinations were examined by the latter technique. The spectra of the *o*-dianisidine complexes with potassium and ammonium picrates

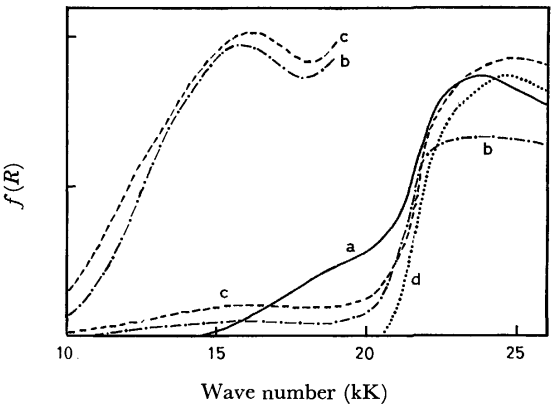

Fig. 1. Diffuse reflection spectra of the *o*-dianisidine complexes with (a) sodium picrate, (b) potassium picrate, (c) ammonium picrate, and (d) sodium picrate alone.

are also presented in Fig. 1. The strong absorptions around 24 kK common to all three complexes should be assigned to the picrate ion. In the complexes with potassium and ammonium picrates, the maxima of the low-energy absorptions are located at 15.8 and 16.1 kK respectively; see the spectra, the ordinates for which are expanded. The results with all the donors are summarized in Table 1. An examination of the data for each picrate shows a hypsochromic shift going from *o*-dianisidine→*o*-tolidine→benzidine. This shift is nearly parallel to that of the charge-transfer absorption observed in the *s*-trinitrobenzene complexes. These pieces of spectroscopic evidence lead to the conclusion that the weak absorptions are due to a charge-transfer interaction between the diamine and the picrate. The weakness of the charge-transfer absorptions was noted also in Kofler's ternary complex and in a related one;[1] it now appear to be characteristic of the complexes with picrates.

Table 1. The energies of the charge-transfer absorptions appeared in the solid diamine complexes with picrates (in kK)

Donor	Acceptor			
	Na picrate	K picrate	NH_4 picrate	*s*-Trinitrobenzene
None	24.8	23.7	24.2	—
Benzidine	*ca.* 20	16.6	17.0	19.0
o-Tolidine	*ca.* 19	15.8	16.7	17.6
o-Dianisidine	*ca.* 19	15.8	16.1	17.3[a]

a) The composition is known to be 1:2, see Ref. 3.

Although the charge-transfer absorption in the present solid complex is close to that in the corresponding *s*-trinitrobenzene complex, the location is somewhat affected by the kind of cation in the picrate. In Fig. 1, we see that the absorption maximum in the complex with sodium picrate appears at an energy higher by a few kK than that in the complex with potassium or ammonium picrate. This displacement may be, at least qualitatively, interpreted in terms of the polarization theory. The polarizing power of alkali ions is in the order of decreasing ionic radius: $K^+ > Na^+$. Consequently, the sodium ion in the crystal brings about an enhanced partial localization of the electron cloud of the picrate ion. Besides, the constancy of the absorption maximum in the three picrates implies that the lowest vacant orbital, with which the charge-transfer from the diamine is associated, becomes as unstable as the occupied orbital. Thus, the polarization of the picrate ion may account for the shift of the charge-transfer absorption toward the high-energy side. The ammonium ion is known to be a little larger when it rotates freely than the potassium ion. However, the present results suggest that the anion in the ammonium salt is slightly more polarized than that in the potassium salt.

Our finding is unique in the sense that the complex has an anion acting as an electron-acceptor. As early as 1910 Sudborough and Beard reported that potassium *o*-, *m*-, and *p*-aminobenzoates form deeply-colored molecular complexes with *s*-trinitrobenzene.[4] In addition, a black potassium α-anthranolate-*s*-trinitrobenzene complex with a 1:2 composition was isolated by Cadre and Sudborough.[5] More recently, several complexes containing the phenazinium ion and related ions were prepared.[6,7] Furthermore, there are some hydrocarbon complexes with tropylium bromide acting as an acceptor.[8] In the cases which have appeared so far in the literature, the complexes are of anionic donors and neutral acceptors or of neutral donors and cationic acceptors.

2) K. Abe, Y. Matsunaga, and G. Saito, This Bulletin, **41**, 2852 (1968).
3) J. J. Sudborough, *J. Chem. Soc.*, **109**, 1339 (1916).
4) J. J. Sudborough and S. H. Beard, *ibid.*, **97**, 773 (1910).
5) S. T. Cadre and J. J. Sudborough, *ibid.*, **109**, 1349 (1916).
6) H. Inoue, S. Hayashi, and E. Imoto, This Bulletin, **37**, 336 (1964).
7) A. Ray, A. V. Guzzo, and G. Tollin, *Biochim. Biophys. Acta*, **94**, 258 (1965).
8) S. N. Bhat and C. N. R. Rao, *J. Chem. Phys.*, **47**, 1863 (1967).

BULLETIN OF THE CHEMICAL SOCIETY OF JAPAN, VOL. 45, 2216—2217(1972)

The Formation of Benzoyl Chlorides from 1,2-Dibenzoylhydrazines or Dibenzoyldiimides

Tsuneo IMAMOTO

The Institute of Scientific and Industrial Research, Osaka University, Yamadakami, Suita, Osaka

(Received December 13, 1971)

The reaction of acid hydrazide with chlorine was reported by Carpino.[1,2] He obtained acid chlorides in good yields from the corresponding hydrazides by successive treatments with hydrogen chloride and chlorine. Later, Kissinger and Ungnade showed that the prior conversion of acid hydrazide to the hydrochloride was not necessary.[3]

The pathway of the reaction was proposed by Carpino to be as in Scheme (1).[2] This mechanism appears to be

$$\text{R-CONHNH}_2 \xrightarrow{\text{HCl}} \text{R-CONH}\overset{+}{\text{N}}\text{H}_3\text{Cl}^- \xrightarrow{\text{Cl}_2} [\text{R-CO-N=N-Cl}] \xrightarrow{-\text{N}_2} \text{R-COCl} \qquad (1)$$

reasonable for his reaction conditions. However, in the cases of no concomitant addition of hydrogen chloride (Kissinger's conditions), the reaction seems to proceed not solely through the above pathway (1).

In order to clarify the reaction pathways, we first isolated the intermediates under Kissinger's conditions, using benzoylhydrazine as a representative acid hydrazide.

When benzoylhydrazine was treated with chlorine in nitromethane without prior conversion to the hydrochloride, large amounts of white precipitates appeared at the initial stage of the reaction. These precipitates completely disappeared upon the further introduction of chlorine to give benzoyl chloride in a good yield (78%). The precipitates were identified as a mixture of benzoylhydrazine hydrochloride and1,2-dibenzoylhydrazine (mol ratio: *ca.* 4: 1).

On the other hand, no 1,2-dibenzoylhydrazine was detected at any stage of the reaction under Carpino's conditions.

These results indicate that benzoylhydrazine hydrochloride and 1,2-dibenzoylhydrazine may both be precursors of benzoyl chloride under Kissinger's conditions. This was supported by the results of the reaction of pure 1,2-dibenzoylhydrazine with excess chlorine in nitromethane or dichloromethane; benzoyl chloride was obtained in yields of 76 and 82% in the respective solvents.

Further, several 1,2-bis(substituted benzoyl)hydrazines were allowed to react with chlorine. Table 1 shows the yields of the corresponding chlorides obtained. In the cases of *m*-chloro and *p*-chloro derivatives, the reaction rates were fairly slow, and the chlorides were scarcely obtained.

It is well known that 1,2-diaroylhydrazine is oxidized by halogen to afford diaroyldiimide.[4,5] This suggests that dibenzoyldiimide is also the precursor of benzoyl chloride. Thus, we treated dibenzoyldiimide with chlorine in the same solvents as in the cases of the preceding dibenzoylhydrazines. The reaction proceeded quite smoothly at room temperature. The yields of benzoyl chloride are also shown in Table 1, along with those of other chlorides.

Table 1. Yields of benzoyl chlorides

X	X-C_6H_4-CONH-NHCO-C_6H_4-X		X-C_6H_4-CON=NCO-C_6H_4-X	
Solvent	CH_3NO_2	CH_2Cl_2	CH_3NO_2	CH_2Cl_2
H	76%	82%[a]	79%	89%
p-CH_3O	87[c]	49[b]+44[c]	11[b]+81[c]	93[b]
p-CH_3	82	87[a]	86	91
o-CH_3	81	90	81	90
o-Cl	79	88	—	—

a) The reaction time was 10—30 hr at room temperature.
b) *p*-Anisoyl chloride.
c) 3-Chloro-4-methoxybenzoyl chloride.

These results lead to the conclusion that acid chloride is formed through both the pathways, (1) and (2), under Kissinger's conditions.[6]

$$2\ \text{R-CONHNH}_2 \xrightarrow{\text{Cl}_2} \text{R-CONHNHCO-R} \xrightarrow{\text{Cl}_2} \text{R-CO-N=N-CO-R} \xrightarrow{\text{Cl}_2} 2\ \text{R-COCl} \qquad (2)$$

Experimental

Isolation of Intermediates. Into a solution of 3.91 g of benzoylhydrazine in 120 m*l* of anhydrous nitromethane, dry chlorine gas was passed at about 0.5 m*l*/sec, while stirring was continued for 5 min. The white precipitates thus formed were collected, washed with nitromethane, and dried. This material (1.99 g) was then triturated with 40 m*l* of water; a subsequent filtration left a colorless powder I (0.43 g; mp 238—240°C). The filtrate was evaporated to afford colorless crystals, II (1.50 g, mp 192—194°C (decomp.)).

1) L. A. Carpino, *Chem. Ind.* (London), 123 (1956).
2) L. A. Carpino, *J. Amer. Chem. Soc.*, **79**, 96 (1957).
3) L. W. Kissinger and H. E. Ungnade, *J. Org. Chem.*, **24**, 1244 (1959).
4) P. A. S. Smith, "Open-Chain Nitrogen Compounds," Vol. II, W. B. Benjamin, Inc., New York (1966), p. 119.
5) a) R. Stollé and A. Benrath, *Ber.*, **33**, 1770 (1900); b) R. Stollé and A. Benrath, *J. Prakt. Chem.*, [ii], **70**, 263 (1900); c) E. Mohr, *ibid.*, [ii], **70**, 281 (1904); d) R. Stollé, *Ber.*, **45**, 245 (1912); e) L. Horner and W. Naumann, *Ann. Chem.*, **587**, 93 (1954).
6) Dibenzoyldiimide could not be isolated under these reaction conditions. However, we observed that reddish orange color, which was perhaps due to dibenzoyldiimide being formed, appeared in the course of the reaction, and that this color faded just when the reaction was completed.

Table 2. 1,2-Bis(substituted benzoyl)hydrazines

Subst	Mp °C	Analysis (Calcd)			
		C%	H%	N%	Cl%
o-CH_3	219—220	71.82	6.00	10.44	
		(71.62)	(6.01)	(10.44)	
o-Cl	219—221	54.27	3.27	8.79	22.98
		(54.39)	(3.26)	(9.06)	(22.94)
m-Cl	272—274	54.47	3.20	9.23	23.22
		(54.39)	(3.26)	(9.06)	(22.94)

The substances (I and II) separated above were identified as 1,2-dibenzoylhydrazine and benzoylhydrazine hydrochloride respectively by comparing their infrared spectra with those of authentic samples.

1,2-Dibenzoylhydrazines. These were prepared by the usual method.[7] The melting points and analytical data for the new hydrazines are listed in Table 2.

Dibenzoyldiimides. The general procedures were as follows. 1,2-Dibenzoylhydrazine (0.20 mol) was saturated in dimethylformamide. Bromine (48 g, 0.30 mol) was added dropwise into this solution with vigorous stirring for 15 min. After the addition of bromine, stirring was continued for 2 hr, and then the reaction mixture was poured into *ca.* 3 *l* of ice water. The precipitated solid was collected, washed with water, and dried *in vacuo* at 50—60°C. The yield of the crude product was 87—94%. This crude diimide was recrystallized from *n*-hexane-benzene (2: 1).

The melting points and analytical data for bis(substituted benzoyl)diimides are shown in Table 3.

The Reaction of 1,2-Dibenzoylhydrazine with Chlorine. 1,2-Dibenzoylhydrazine (6—8 g) was suspended in 50 m*l* of nitromethane or dichloromethane. Chlorine gas was passed slowly into this suspension at room temperature until the dibenzoylhydrazine had been completely dissolved. This required 1—5 hr. The solvent was then removed by rotary evaporation, and the liquid was distilled under reduced pressure.

The benzoyl chlorides obtained were identified by comparing their infrared spectra with those of authentic samples.

The Reaction of Dibenzoyldiimides with Chlorine. Dibenzoyldiimides were treated with chlorine under the same conditions as in the cases of the preceding dibenzoylhydrazine. The reactions were completed within 30 min.

Table 3. Bis(substituted benzoyl)diimides

Subst	Mp °C (lit)	Analysis (Calcd)		
		C%	H%	N%
o-CH_3	106—107	72.16	5.19	10.57
		(72.17)	(5.30)	(10.52)
p-CH_3O	136—137	64.62	4.72	9.40
	(131.5—132.0)[b]	(64.42)	(4.73)	(9.39)
p-CH_3	120—121	71.93	5.19	10.65
	(118)[a]	(72.17)	(5.30)	(10.52)
H	119—121	70.36	4.02	11.78
	(119.5—121.5)[b]	(70.53)	(4.23)	(11.81)

a) Ref. 5e
b) Ref. 8

The author wishes to express his sincere appreciation to Professor Yasuhide Yukawa and Professor Yuho Tsuno for their kind advice. Thanks are due to Mr. Yoshio Takai for his assistance.

7) H. H. Hatt, "Organic Syntheses," Coll. Vol. II, p. 208 (1966).

8) J. E. Leffler and W. B. Bond, *J. Amer. Chem. Soc.*, **78**, 335 (1956).

BULLETIN OF THE CHEMICAL SOCIETY OF JAPAN, VOL. 45, 2217—2219(1972)

Halogen Migration of 2,2-Dihaloadamantane Induced by Aluminum Halides

Kwan Her YANG, Koichi KIMOTO, and Mituyosi KAWANISI

Department of Industrial Chemistry, Faculty of Engineering Kyoto University, Yoshida, Kyoto

(Received February 4, 1972)

We reported on the halogen migration in the reaction of organic dihalides with aluminum halide.[1] McKervey and coworkers have shown the formation of 1,3-dichloroadamantane (IVa) from 2,2-dichloroadamantane (Ia) when Ia was treated with aluminum chloride in carbon tetrachloride.[2] When the reaction of Ia was effected in nitromethane, they could identify a mixture of *trans*- and *cis*-1,4-dichloroadamantanes (Va) (VIa) from the reaction mixture. However, no experimental details were given. As an effective means for the synthesis of new haloadamantane,[3] we have reinvestigated the reaction in more detail under slightly different conditions.

When a solution of 2,2-dichloroadamantane[2] (Ia) was treated with anhydrous aluminum chloride at a low temperature, six compounds IIa—VIIa (conversion 100%) could be separated by a combination of column chromatography and preparative glc (Scheme 1; % ratio in brackets). Compounds IIa, IIIa, and IVa were identified by comparison with the corresponding authentic samples. The structure of stereoisomers (Va) and (VIa) were assigned to *trans*- and *cis*-1,4-dichloroadamantanes, respectively, mainly by spectroscopic

1) H. Nozaki, M. Kawanisi, M. Okazaki, M. Yamae, Y. Nisikawa, T. Hisida, and K. Sisido, *J. Org. Chem.*, **30**, 1303 (1965).

2) M. A. McKervey, D. Grant, and H. Hamill, *Tetrahedron Lett.*, 1975 (1970).

3) *Cf.* R. Keese and E.-P. Krebs, *Angew. Chem.*, **83**, 254 (1971).

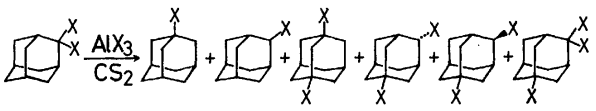

	I	II	III	IV	V	VI	VII
a	X=Cl	a(0.3)	a(6.4)	a(1.8)	a(22.9)	a(62.7)	a(5.9)
b	X=Br	b(3.9)	b(16.0)	b(0.3)	b(22.9)	b(40.1)	b(16.8)

Scheme 1

methods. The fragmentation patterns of mass spectra of Va and VIa were very similar. NMR spectrum of Va showed the existence of one proton due to CH–Cl at δ 4.26, and that of VIa at δ 4.19. When these shift values were compared with those of a mixture of Va and VIa derived from 1,4-dihydroxyadamantane[4] a very good coincidence was observed (Table 1). The

Table 1. Chemical shift values (δ) of the secondary protons in 1,4-dichloroadamantanes

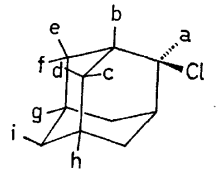

Proton	Calcd for[a] 1,4-*ax.* (h=Cl)	Found for[b] VIa (h=Cl)	Calcd for[a] 1,4-*eq.* (g=Cl)	Found for[b] Va (g=Cl)
a	4.31	4.19 (4.23)[c]	4.31	4.26 (4.33)[c]
c	2.60	2.67 (2.66)	2.19	
d	1.90		1.49	1.50 (1.50)
e,f	1.78	1.84 (1.82)	2.19	
i	2.09	2.13 (3.13)	2.09	2.17 (2.13)

a) Values calculated by using the substituent shift data of 1- and 2-chloroadamantanes.[4]
b) Observed values.
c) Values estimated from the mixture of 1,4-dichloroadamantanes.[4]

product (VIIa) was assigned to 1,4,4-trichloroadamantane, since VIIa was identical with the compound obtained by the reaction of 1-hydroxyadamantan-4-one[4] with a mixture of phosphorus trichloride and phosphorus pentachloride. 2,2-Dibromoadamantane (Ib)[5] being more reactive than Ia, its reaction with aluminum bromide was carried out at lower concentration and temperature. Six products (IIb—VIIb) were obtained (conversion 100%; % ratio in brackets in Scheme 1) and each was identified similarly, Vb, VIb, and VIIb being new compounds.

The reactions of VIa and IIIa were also investigated. A solution of VIa was treated with aluminum chloride

$$\text{VIa} \xrightarrow[CS_2]{AlCl_3} \text{IIa}(1.2) + \text{IIIa}(5.6) + \text{IVa}(18.5) + \text{Va}(74.4)$$

$$\text{IIIa} \xrightarrow[CS_2]{AlCl_3} \text{Adamantane}(21.9) + \text{IIa}(71.1) + \text{Va}(1.0) + \text{VIa}(5.4)$$

Scheme 2

at −15——20°C. The formation of IIa—Va was confirmed by glc method (conversion 38.3%) (Scheme 2). A similar reaction of IIIa was conducted at −35——40°C, and adamantane, IIa, Va, and VIa were produced (conversion 61.6%).

Experimental

All mp are uncorrected. IR spectra were obtained in nujol mull on a Shimadzu IR-27 spectrophotometer. MS spectra were taken using a Hitachi RMS-4 mass spectrometer. NMR spectra were obtained on a JEOL C-60H spectrometer in CCl_4 solution, TMS being chosen as an internal standard.

Authentic Samples. 1-Chloroadamantane (IIa),[6] 2-chloroadamantane (IIIa),[7] 1,3-dichloroadamantane (IVa),[8] 1-bromoadamantane (IIb),[6] 2-bromoadamantane (IIIb),[7] and 1,3-dibromoadamantane (IVb)[9] were prepared according to the reported methods.

Reaction of Ia with aluminum chloride. To a solution of Ia (3.83 g) in 80 m*l* of carbon disulfide, 4 g of aluminum chloride was added at −40°C. The solution was stirred at −35——40°C for 3.5 hr. It was then poured onto ice and extracted three times with ether. The extract was washed with dil. aqueous NaOH and dried ($CaCl_2$). Evaporation of the solvent yielded 3.7 g (96%) of a white solid which was separated into six compounds (IIa—VIIa) by silica gel column chromatography with *n*-hexane as an eluent followed by preparative glc (15% HVSG on chromosorb W AW, 3 m, 150°C, 40 m*l* N_2/min). Va: mp 131.5—133.5°C, MS: 204 (M^+), 159 (100%), 133, 91, NMR: δ 4.26 (1H, bs), 1.20—2.95 (13H, adamantyl), IR: 1347 (m), 1231 (m), 1102 (m), 1030 (s), 946 (m), 923 (m), 823 (s), 783 (m), 764 (s) cm^{-1}, Found: C, 58.50; H, 6.85%. Calcd for $C_{10}H_{14}Cl_2$: C, 58.55; H, 6.88%. VIa: mp 157—159°C, MS: 204 (M^+), 169 (100%), 133, 91, NMR: δ 4.19 (1H, bs), 1.43—3.00 (13H, adamantyl), IR: 1350 (m), 1099 (m), 1025 (s), 923 (m), 833 (s), 786 (m), 763 (m) cm^{-1}, Found: C, 58.48; H, 7.01%. Calcd for $C_{10}H_{14}Cl_2$: C, 58.55; H, 6.88%. VIIa: MS: 238 (M^+), 203 (100%), 167, 131, 91, NMR: δ 1.45—3.05 (13H), IR: 1348 (m), 1028 (s), 946 (m), 926 (m), 800 (s) cm^{-1}, mp 152/153°C with no depression when admixed with the authentic specimen described below. Found: C, 50.13; H, 5.53%. Calcd for $C_{10}H_{13}Cl_3$: C, 50.12; H, 5.47%.

Reaction of Ib with Aluminum Bromide. To a solution of Ib (3 g) in 100 m*l* of carbon disulfide, 3 g of aluminum bromide was added at −78°C. The mixture was stirred at −73——78°C for 2.5 hr. The same treatment as above yielded 2.98 g (98%) of a white solid. This mixture was separated into six compounds (IIb—VIIb) by the same procedure as described above (column temp: 175°C). Vb: mp 143—146°C, MS: 292 (M^+), 213 (100%), 133, 91, NMR: δ 4.55 (1H, bs, CH–Br), 1.40—2.75 (13H, adamantyl), IR: 1342 (m), 1196 (m), 1019 (s), 937 (m), 918 (m), 806 (s), 738 (s) cm^{-1}, Found: C, 40.80; H, 4.85%. Calcd for $C_{10}H_{14}Br_2$: C, 40.85; H, 4.80%. VIb: mp 109/110°C, MS: 292 (M^+), 213 (100%), 133, 91, NMR: δ 4.50 (1H, bs, CH–Br), 1.57—3.31 (13H, adamantyl), IR: 1348 (m), 1258 (m), 1191 (m), 1100 (m), 1018 (s), 939 (m), 918 (m), 817 (m), 808 (m), 773 (m), 738 (s) cm^{-1}, Found: C, 40.76;

4) H. W. Geluk and J. L. M. A. Schlatmann, *Tetrahedron*, **24**, 5369 (1968).
5) H. W. Geluk, *Synthesis*, **1970**, 652.
6) H. Stetter, M. Schwarz, and A. Hirschhorn, *Chem. Ber.*, **92**, 1629 (1959).
7) J. Strating and H. Wynberg, *Rec. Trav. Chim.*, **85**, 1045 (1966).
8) H. Stetter, M. Krause, and W.-D. Last, *Chem. Ber.*, **102**, 3357 (1969).
9) G. L. Bughman, *J. Org. Chem.*, **29**, 238 (1964).

H, 4.92%. Calcd for $C_{10}H_{14}Br_2$: C, 40.85; H, 4.80%. VIIb: mp 120—122°C, MS: 291 (M^+–Br), 211, 131, 91, NMR: δ 1.50—3.50 (13H), IR: 1342 (m), 1290 (m), 1248 (m), 1096 (m), 1023 (s), 936 (m), 914 (s), 812 (s), 757 (s) cm^{-1}, Found: C, 32.26; H, 3.62%. Calcd for $C_{10}H_{13}Br_3$: C, 32.21; H, 3.51%.

Reaction of VIa with Aluminum Chloride. To a solution of VIa (62 mg) in 1 m*l* of carbon disulfide, 134 mg of aluminum chloride was added at −20°C. The mixture was stirred at −15——20°C for 3 hr. The usual work-up yielded 60 mg (96%) of a white solid which was analyzed by glc (column temp: 120°C).

Reaction of IIIa with Aluminum Chloride. To a solution of IIIa (51 mg) in 1 m*l* of carbon disulfide, 134 mg of aluminum chloride was added at −40°C. The mixture was stirred at −35——40°C for 3 hr. The usual work-up gave 49 mg (96%) of a white solid which was subjected to glc analysis (column temp: 120°C).

Preparation of a Mixture of Va and VIa. To 1,4-dihydroxyadamantane (100 mg; a mixture of *trans*- and *cis*-isomers),[4] 3 m*l* of PCl_3 and 2 g of PCl_5 were added. The mixture was stirred for 26 hr at 70°C. Hydrolysis followed by extraction (Et_2O) gave 155 mg (95%) of a mixture of Va and VIa, mp 146—149°C (lit.[4] mp 148—151°C).

Preparation of a Mixture of Vb and VIb. This was obtained in 98% yield with a mixture of PBr_3 and PBr_5 by a similar procedure to that mentioned above, mp 99—101°C.

Preparation of VIIa. The authentic sample was obtained in 88% yield by treating 1-hydroxyadamantan-4-one[4] (150 mg) with a mixture of PCl_3 (3 m*l*) and PCl_5 (2 g) and gave correct analysis, mp 151—153°C.

Preparation of VIIb. The authentic specimen was obtained in 88% yield with a mixture of PBr_3 and PBr_5 by a similar procedure to the mentioned above and gave correct analysis, mp 120.5—122.5°C.

The authors wish to thank Prof. Hitosi Nozaki for help and encouragement.

BULLETIN OF THE CHEMICAL SOCIETY OF JAPAN, VOL. 45, 2219—2220(1972)

Chlorine-35 NQR of Hexachlorodisilazane and the Si-Cl Bond of $SiCl_3$-Groups

Keinosuke HAMADA and E. A. ROBINSON*

Faculty of Education, Nagasaki University, Nagasaki

**Department of Chemistry, University of Toronto, Toronto, Canada*

(Received February 14, 1972)

Chlorine-35 NQR of hexachlorodisiloxane ($Cl_3SiOSiCl_3$), hexachlorodisilazane ($Cl_3SiN(H)SiCl_3$), and hexachlorodisilane ($Cl_3SiSiCl_3$) are measured with a superregenerative spectrometer. All samples exhibit complex chlorine NQR spectra: the average frequencies for $Cl_3SiOSiCl_3$, $Cl_3SiN(H)SiCl_3$, and $Cl_3SiSiCl_3$ are 19.89, 19.66, and 19.29 MHz respectively. The very small difference among the averages of the NQR frequency values of the three compounds may be due to the difference in the ionic character of the Si–Cl bond, and it may be due to an increase in the double-bond character of the $F^{\ominus}\overset{|}{Si}{=}Cl^{\oplus}$ type that the NQR frequency of $FSiCl_3$ is less than that of $SiCl_4$.

Experimental

The hexachlorodisilane and hexachlorodisiloxane were obtained from commercial sources. The hexachlorodisilazane was synthesized as follows: an ammonia gas diluted with a nitrogen gas was passed through ether containing silicon tetrachloride at −75°C.[1,2] The product was purified by distillation. All the compounds were measured at −196°C with a superregenerative spectrometer, the details of which have been given elsewhere.[3]

Results and Discussion

The present authors asked Professor Whitehead[4] to measure the NQR of $Cl_3SiN(H)SiCl_3$. The frequencies he obtained were 19.723, 19.704, 19.699, 19.663, 19.635, and 19.551±0.001 MHz, the mean value being 19.66 MHz. The NQR frequencies of $Cl_3SiSiCl_3$ and $Cl_3SiOSiCl_3$ we measured were in good accordance with those reported in the literature;[5] the mean values are 19.29 MHz for $Cl_3SiSiCl_3$ and 19.89 MHz for $Cl_3SiOSiCl_3$.

The increasing nuclear quadrupole resonance frequencies in the sequence from $Cl_3SiSiCl_3$, $Cl_3SiN(H)SiCl_3$, $Cl_3SiOSiCl_3$ to $SiCl_4$[6] may reflect a decrease in the ionic character of the Si–Cl bond. This is consistent with the view that replacing a chlorine of $SiCl_4$ with the groups whose electronegativity decreases in the order $Cl > Cl_3SiO > Cl_3SiN(H) > Cl_3Si$ produces progressively less competition for silicon electrons and, hence, an increased ionic character in the Si–Cl bond.

When chlorine is replaced by fluorine, a still larger increase in the NQR frequency can be expected, since fluorine is much more electronegative than chlorine. However, the NQR frequency of $FSiCl_3$, 19.753 MHz[7]

1) W. H. Schumb, *J. Amer. Chem. Soc.*, **75**, 6085 (1935).
2) H. Bürger, M. Schultze, and U. Wannagat, *Inorg. Nucl. Chem. Lett.*, **3**, 43 (1967).
3) K. E. Weber and J. E. Todd, *Rev. Sci. Instr.*, **33**, 390 (1962).
4) M. A. Whitehead, Private Communication.
5) I. P. Biryukov, M. G. Voronkov, and I. A. Safin, "Tables of Nuclear Quadrupole Resonance Frequencies", Israel, IPST Press (1969).
6) R. Livingston, *J. Phys. Chem.*, **57**, 496 (1953).
7) K. Hamada, G. A. Ozin, and E. A. Robinson, This Bulletin, **44**, 2555 (1971).

is less than the average frequency of $SiCl_4$, 20.390 MHz.[6] It has been proposed,[8] in order to explain such an unexpected consequence, that there is an increase in the double-bond character due to the contributions of resonant structures of the $F^{\ominus}\overset{|}{\underset{|}{Si}}=Cl^{\oplus}$ type. Since a double-bond character is in the direction of decreasing NQR frequencies, this effect could explain the decrease in the NQR frequency when chlorine is replaced by fluorine. The increase in the double-bond character due to a fluorine substitution may be clarified by the shortening of the Si–Cl distance. That is, the Si–Cl distance of $SiCl_4$ is 2.01 Å, but that of $SiClF_3$ is only 1.99Å.[8]

The increase in the NQR frequencies in the sequence from CF_3Cl, CF_2Cl_2, $CFCl_3$ to CCl_4 has been reported,[6] but the NQR frequencies of $SiCl_mF_{4-m}$ have not been previously reported, except for that of $SiFCl_3$.[7] Therefore, it would be of interest to obtain the NQR frequencies of SiF_2Cl_2 and SiF_3Cl; thus far, however, attempted NQR measurements of them have been unsuccessful.[7]

The authors are indebted to Professor M. A. Whitehead and his collaborators of McGill University for their NQR measurements.

8) L. Pauling, "The Nature of the Chemical Bond", 2nd Ed. Cornell University Press, Ithaca, N. Y. (1944).

BULLETIN OF THE CHEMICAL SOCIETY OF JAPAN, VOL. 45, 2220—2221 (1972)

Reactions of Thiobenzophenones with Benzenediazonium-*o*-carboxylate, and Salicyloyl and *o*-Mercaptobenzoyl Chlorides as 1,4-Dipolar Reagents

Hirokazu TOKUNAGA, Takayuki KAWASHIMA, and Naoki INAMOTO

Department of Chemistry, Faculty of Science, The University of Tokyo, Hongo, Bunkyo-ku, Tokyo

(Received January 18, 1972)

Recently cycloaddition of *o*-carboxybenzenediazonium chloride to thiobenzophenone has been reported.[1] It has been known that salicyloyl chloride reacts with ketones as a 1,4-dipolar reagent.[2]

In order to obtain heterocycles containing sulfur atom by 1,4-cycloaddition, we carried out reactions of substituted thiobenzophenones (I) with benzenediazonium-*o*-carboxylate (II), and salicyloyl (III) and *o*-mercaptobenzoyl chlorides (IV).

Reactions of II and III with I gave 2,2-diarylbenzo[*d*][1,3]oxathian-6-one (V) and 2,2-diarylbenzo[*e*][1,3]oxathian-4-one (VI), respectively (see Table).

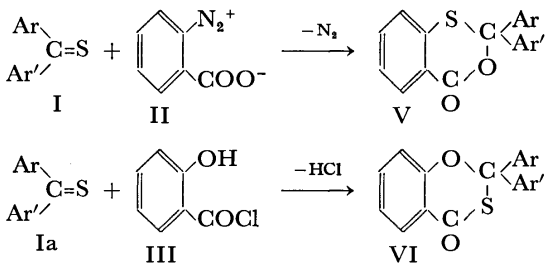

a: Ar=Ar′=Ph; b: Ar=Ph, Ar′=*p*-MeC_6H_4;
c: Ar=Ph, Ar′=*p*-ClC_6H_4; d: Ar=Ar′=*p*-MeC_6H_4;
e: Ar=Ar′=*p*-ClC_6H_4

The structures of V and VI were confirmed on the basis of the elemental analyses, and the MS and IR spectra.

Table. 2,2-Diaryl-benzoxathian-6- and 4-ones (V and VI)

	Yield (%)	Mp (°C)		Elemental analyses C(%)	H(%)	S(%)
Va	40	182.3—182.8 (lit[1], 185)	Found	75.75	4.66	10.06
Vb	32	136.3—138.3	Found	75.95	5.18	9.54
			Calcd	75.88	4.85	9.65
Vc	31	88—90	Found	68.29	3.73	9.14
			Calcd	68.08	3.71	9.09
Vd	30	101—102	Found	76.24	5.21	9.41
			Calcd	76.27	5.24	9.26
Ve	10	119.5—120.0	Found	61.79	2.99	8.09
			Calcd	62.03	3.12	8.28
VIa	80	119.5—121.0	Found	75.21	4.59	10.13
			Calcd	75.45	4.43	10.07
VIb	55	128.3—129.7	Found	75.84	4.65	9.95
			Calcd	75.88	4.85	9.65
VIc	57	113.2—114.3	Found	68.26	3.56	8.93
			Calcd	68.08	3.71	9.09
VId	60	120.0—121.5	Found	76.07	5.13	8.98
			Calcd	76.27	5.24	9.26

On the contrary, treatment of IV with Ia did not evolve hydrogen chloride, but gave oily products (A). Treatment of A with aniline gave bis[*o*-(phenylcarbamoyl)phenyl] disulfide (VII) (65%), diphenylmethyleneaniline (VIII) (40%) and aniline hydrochloride (99%). Similar treatment with pyridine gave Ia (70%) and pyridine hydrochloride (94%). On heating A afforded benzo[*d*][1,2]dithiolan-3-one (IX) (60%) and diphenylmethyl chloride (X) (80%). Moreover,

1) D. C. Dittmer and E. S. Whitman, *J. Org. Chem.*, **34**, 2004 (1969).

2) E. Ziegler and H. D. Hanus, *Monatsh. Chem.*, **95**, 1053 (1964).

A exhibited no absorptions due to thioester and SH groups in the IR spectrum. Therefore, A was assigned as the structure of *o*-(diphenylmethyldithio)benzoyl chloride (XI), although it was unsuccessful to obtain pure XI.

Benzophenone did not react with II and IV.

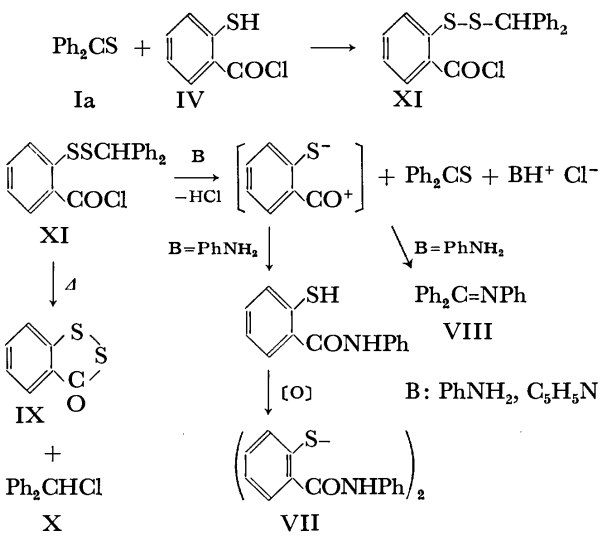

Experimental

Materials. Substituted thiobenzophenones were prepared by the method previously reported.[3] Benzenediazonium-*o*-carboxylate,[4] salicyloyl[5] (bp 57—58°C/0.5 mmHg) and *o*-mercaptobenzoyl chlorides[6] (bp 110—111°C/0.45 mmHg, mp 56—58°C) were prepared by the methods described in the literature.

Reactions with Benzenediazonium-o-carboxylate (II). A typical procedure is described for a reaction of *p,p'*-dimethylthiobenzophenone (Id).

To Id (3.3 g, 14.5 mmol) in dichloromethane (200 m*l*) was added II (5.4 g, 36 mmol), and the mixture was refluxed for 3 hr with stirring under nitrogen atmosphere. After removal of the solvent, the residual oil was chromatographed on silica gel. Elution with benzene gave 1.5 g (30%) of Vd, mp 101—102°C (from ethanol-petroleum ether). IR (KBr disk): 1727 cm^{-1} (-COO-); *m/e*: 346 (M^+, 11%), 136 ([M−Tol_2CO]$^+$, 100), 120 ([M−Tol_2CS]$^+$, 11), 108 ([M−Tol_2COCO]$^+$, 20), and 105 ($PhCO^+$, 6), where Tol represents *p*-MeC_6H_4.

Other results were summarized in Table.

Reactions with Salicyloyl Chloride (III). A typical procedure is described for a reaction of thiobenzophenone (Ia).

A mixture of Ia (8.7 g, 44 mmol) and III (7.0 g, 45 mmol) was heated for 6 hr at 100—120°C under nitrogen atmosphere, until evolution of hydrogen chloride ceased. The cooled solution was extracted with 1 *l* of petroleum ether. Removal of the solvent from the extract gave 11.2 g (80%) of VIa, mp 119.5—121°C (from petroleum ether). IR (KBr disk): 1660 cm^{-1} (-COS-); *m/e*: 318 (M^+, 62%), 258 ([M−COS]$^+$, 33), 198 (Ph_2CS^+, 100), 165 (($C_6H_4)_2CH^+$, 84.5), 121 ([M−Ph_2CS+H]$^+$, 67), and 77 (Ph^+, 61).

Other results were summarized in Table.

Reaction with o-Mercaptobenzoyl Chloride (IV). a) A mixture of Ia (5.55 g, 28 mmol) and IV (4.86 g, 28 mmol) in benzene (200 m*l*) was stirred for 10 hr at room temperature, until the blue color of the mixture disappeared. After removal of the solvent, the residual oil, which could not be purified, was heated for 3 hr at 180—190°C, and then distilled *in vacuo* (bp 112—116°C/0.2 mmHg). After cooling, 2.8 g (60%) of yellow crystals (IX) thus obtained were recrystallized from petroleum ether, mp 76—78°C (lit,[7] 77°C). After removal of IX, diphenylmethyl chloride (4.5 g, 80%) was detected in the distillate by gas chromatography.

b) To a similar reaction mixture from Ia (5.55 g, 28 mmol) and IV (4.86 g, 28 mmol) in benzene (200 m*l*) was added aniline (8.0 g, 86 mmol), and the mixture was stirred for 3 hr at room temperature. Hydrogen sulfide evolved and white precipitates appeared. The precipitates were washed with water and recrystallized from pyridine-petroleum ether to afford 4.2 g (65%) of disulfide (VII), mp 236—240°C (lit,[8] 243°C). Concentration of the filtrate and the above aqueous washings gave 2.9 g (40%) of VIII, mp 104—110°C (from petroleum ether) (lit,[9] 109°C) and aniline hydrochloride (3.6 g, 99%), respectively.

In the addition of pyridine instead of aniline, pyridine hydrochloride (1.5 g, 94%) and Ia (70%, by UV spectroscopy) were produced.

3) H. Tokunaga, K. Akiba, and N. Inamoto, This Bulletin, **45**, 506 (1972).

4) F. M. Logullo, A. H. Seitz, and L. Friedeman, "Organic Syntheses", Vol. 48, 12 (1968).

5) E. H. Wilson, U. S. 2899458 (1959).

6) E. Ziegler and H. D. Hanus, *Monatsh. Chem.*, **96**, 411 (1965).

7) M. McKibben and E. W. McClelland, *J. Chem. Soc.*, **123**, 170 (1923).

8) A. Reissert and E. Manns, *Ber.*, **61**, 1308 (1928).

9) G. Reddelien, *ibid.*, **46**, 2718 (1913).

BULLETIN OF THE CHEMICAL SOCIETY OF JAPAN, VOL. 45, 2222—2223(1972)

The Reactions of 4-Aminothiazolium Salts with Amines

Akiko CHINONE, Mineo MARUYAMA, and Masaki OHTA

Department of Chemistry, Faculty of Science, Tokyo Institute of Technology, Ookayama, Meguro-ku, Tokyo

(Received February 25, 1972)

In our previous papaer,[1] we reported that 4-amino-2,3-diphenylthiazolium chloride (**1**) reacted to give 4-anilino-2-phenylthiazole (**2**) in the presence of aniline. In this report, we wish to describe the further detail of the reactions of 4-amino-2,3-diarylthiazolium chlorides with amines.

A benzene solution of **1** was heated with excess amount of *p*-chloroaniline at 50°C for 6 hr and neutralized with hydrochloric acid to give **2** and 4-*p*-chloroanilino-2-phenylthiazole (**3**). The structure of **3** was determined by elementary analysis and spectral data. The IR spectrum of **3** showed absorption peaks at 3330 cm^{-1} due to an NH stretching vibration and at 1530 cm^{-1} due to a thiazole ring. As in the UV spectrum of **2**, **3** showed characteristic absorption peaks at 278 mμ (ε 34000) and 360 mμ (ε 4600), which are suggestive of an aromatic heterocyclic system. In the NMR spectrum, **3** showed a peak at τ 3.64 which was attributed to 5-proton. When a toluene solution of **1** was heated with excess amount of *p*-chloroaniline at 100°C for 3 hr, **3** was obtained exclusively. In the presence of excess amount of aniline and *p*-chloroaniline (1 : 1) or aniline and *p*-anisidine (1 : 1) at room temperature, **1** afforded **2**. Expecting that the reaction of 4-amino-3-*p*-chlorophenylthiazolium chloride (**4**) with aniline may proceed *via* the same intermediate as that of the reaction of **1** with *p*-chloronailine, we examined the reaction of **4** with aniline. Treatment of **4** with aniline followed by neutralization with hydrochloric acid afforded **3** at room temperature. The products from the reaction of **4** with aniline were dependent on reaction temperature as in the case of the reaction of **1** with *p*-chloroaniline. The reaction of **4** with aniline was carried out at 50°C to give **2** and **3**, and at 100°C **2** was obtained exclusively. Treatment of **4** with *p*-chloroaniline at 50°C gave **3**, which was not obtained by treating *S*-cyanomethylisothiobenz-*p*-chloroanilide with *p*-chloroaniline in benzene at 50°C. The consideration that the substituent at 2-phenyl group may effect the course of the reaction led us to examine the reaction of 2-*p*-methoxy derivative **5** with amines. Compound **5** was treated with aniline at room temperature to give **2**, and treatment of **5** with *p*-chloroaniline, *p*-anisidine or *o*-toluidine afforded intractable oil. Treatment of 2-*o*-tolyl derivative **6** with aniline afforded **2**, and with *o*-toluidine, the corresponding thiazole **7** was obtained only as the picrate. Compound **6** was treated with *p*-chloroaniline at 50°C to give **3**. Compound **3** was not converted to **2** in the presence of amine at 100°C, and *vice versa*.

These results indicated that the reaction mechanism previously postulated,[1] in which amine used was not involved in a final product, required revision for the reaction of **5** and **6** even at room temperature. But we could not show the reasonable reaction mechanism and intermediate conclusively which was commonly involved. In the presence of equimolar amount of *p*-chloroaniline in toluene, DMSO or pyridine at 100°C, **1** afforded **2** instead of **3**. The reaction may probably proceed as shown below. It seems plausible that amine interchange occurs at the step **8**→**9** preferentially at 100°C, and consequently, the reaction may be controlled by the concentration of the amine.

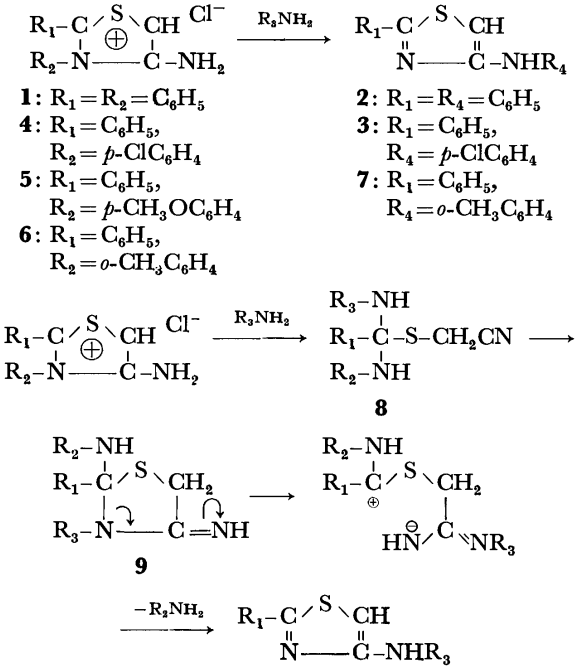

1: $R_1=R_2=C_6H_5$
4: $R_1=C_6H_5$, $R_2=p\text{-}ClC_6H_4$
5: $R_1=C_6H_5$, $R_2=p\text{-}CH_3OC_6H_4$
6: $R_1=C_6H_5$, $R_2=o\text{-}CH_3C_6H_4$

2: $R_1=R_4=C_6H_5$
3: $R_1=C_6H_5$, $R_4=p\text{-}ClC_6H_4$
7: $R_1=C_6H_5$, $R_4=o\text{-}CH_3C_6H_4$

8

9

Experimental

The Reaction of 4 with Aniline. Compound **4** (0.6 g) was dissolved in 6 g of aniline and heated at 50°C for 6 hr. After cooling, the reaction mixture was neutralized with 10% hydrochloric acid under cooling with ice-water. Precipitates were collected by filtration and filtrate was treated as shown below. Precipitates were recrystallized from ethanol to give **2**; yield 0.4 g (80%). From the filtrate, **3** was precipitated out on standing for 3 days, which was recrystallized from ethanol to give needles with a mp of 104—105°C; yield 0.1 g (20%).

Found: C, 62.55; H, 3.95; N, 9.93; S, 11.19%. Calcd for $C_{15}H_{11}N_2SCl$: C, 62.83; H, 3.84; N, 9.81; S, 11.17%. IR: 3330, 1595, 1530, 820, 770, and 695 cm^{-1}. λ_{max}^{EtOH} mμ (ε) 278 (34000) and 360 (4600). NMR: τ ($CDCl_3$) 3.64 (1H) and 2.0—2.9 (10H).

The Reaction of 4 with p-*Chloroaniline.* A mixture of **4** (1 g), *p*-chloroaniline (10 g) and benzene (15 m*l*) was heated at 50°C for 14 hr. After cooling the reaction mixture was neutralized with 10% hydrochloric acid and extracted

1) S. Sato and M. Ohta, This Bulletin, **41**, 2801 (1968).

with ether. Ether layer was washed with water, dried over sodium sulfate and concentrated to give **3**, which was treated as shown above.

The Reaction of ***6*** *with* o-*Toluidine.* In 10 g of *o*-toluidine **6** (1 g) was heated at 50°C for 12 hr. The reaction mixture was treated as mentioned above to give **7**, which was converted to the picrate. The picrate was recrystallized from ethanol to give prisms with a mp of 105—106°C; yield 0.2 g (10%).

Found: C, 53.47; H, 3.36; N, 14.40; S, 6.51%. Calcd for $C_{22}H_{17}O_7N_5S$: C, 53.33; H, 3.46; N, 14.14; S, 6.47%. IR: 3350, 1600, 1570, and 1535 cm^{-1}.

BULLETIN OF THE CHEMICAL SOCIETY OF JAPAN, VOL. 45, 2223—2224 (1972)

Kinetics of the Autoxidation of Dialkyl Phenylphosphonites*

Yoshiro OGATA, Mitsuji YAMASHITA, and Toshinao UKAI

Department of Applied Chemistry, Faculty of Engineering, Nagoya University, Chikusa-ku, Nagoya

(Received April 17, 1972)

The kinetics and mechanism for the autoxidation of trialkylphosphine and trialkyl phosphite have been reported,[1,2] but little is known about the autoxidation of phosphonite and phosphinite. The present note reports our kinetic study on the radical-initiated autoxidation of dialkyl phenylphosphonite in *o*-dichlorobenzene to discuss the mechanism.

Results and Discussion

The autoxidation of dimethyl phenylphosphonite (I) at 60—80°C with 2,2′-azobisisobutyronitrile (AIBN) gave quantitatively dimethyl phenylphosphonate. The observed stoichiometry is shown in Table 1, and expressed as Eq. (1). No reaction of I with AIBN or *o*-dichlorobenzene was observed.

$$PhP(OR)_2 + \frac{1}{2}O_2 \longrightarrow PhP(O)(OR)_2 \qquad (1)$$

(I) R=Me
(II) R=Et
(III) R=*i*-Pr

Table 1. The stoichiometry in autoxidation of dimethyl phenylphosphonite in *o*-dichlorobenzene at 60°C[a]

$PhP(OMe)_2$ (10^{-4} mol)	O_2 absorption (10^{-4} mol)	$O/PhP(OMe)_2$[b]
5.55	2.68	0.97
6.61	3.24	0.98

a) 5×10^{-6} mol of AIBN was used.
b) The ratio of consumed amount of atomic oxygen to phosphonite.

The autoxidation of dimethyl phenylphosphonite (I) in *o*-dichlorobenzene with AIBN at 60°C was followed by measuring the consumption of O_2 in the apparatus previously reported by us.[4] The effects of concentration of I, partial pressure of O_2 (p) and concentration of AIBN are shown in Table 2, which shows that the rate law of autoxidation of dimethyl phenylphosphonite (I) in *o*-dichlorobenzene is expressed as Eq. (2) up to 70—85% conversion.

Table 2. Autoxidation of dimethyl phenylphosphonite in *o*-dichlorobenzene at 60.0°C

Partial pressure of O_2 (mmHg)	$[PhP(OMe)_2]_0$[a] (10^{-2} M)	$[AIBN]_0$[a] (10^{-3} M)	$10^4 k_a$[b] (sec^{-1})
200	1.31	5.39	5.00
200	3.92	5.39	4.02
200	6.54	5.39	4.84
200	5.94	9.25	10.4
200	5.94	4.62	4.50
200	5.94	2.31	3.22
200	5.94	0.00	0.0
420	5.55	4.42	6.17
200	5.55	4.42	6.17
100	5.55	4.42	6.15

a) [ ]$_0$ means initial concentration.
b) Pseudo-first-order rate constant.

$$v = -\frac{d[O_2]}{dt} = k[PhP(OMe)_2][AIBN] \qquad (2)$$

The value of k was calculated to be $0.105 M^{-1}sec^{-1}$ at 60.0°C.

The autoxidation of dialkyl phenylphosphonite was found to involve radical intermediates, since no autoxidation occurs without AIBN. The zero-order dependence of rate on oxygen pressure (p) was observed. The same phenomenon has been observed in the autoxidation of tributyl phosphite.[1b] This suggests a mechanistic similarity of the autoxidation of phosphonite to that of phosphite. The first-order dependence on AIBN concentration suggests that the autoxidation may involve a unimolecular termination.[5] The autoxidation product of dialkyl phenylphosphonites was the corresponding phosphonates. These results suggest the following mechanism.

$$AIBN \xrightarrow{k_i} 2R'\cdot + N_2 \qquad (3)$$

* Contribution No. 178.

1) a) S. A. Buckler, *J. Amer. Chem. Soc.*, **84**, 3093 (1962); b) M. B. Floyd and C. B. Boozer, *ibid.*, **85**, 984 (1963).
2) a) W. G. Bentrude, *Tetrahedron Lett.*, 3543 (1965); b) J. I. G. Cadogan, M. C. Wood, and W. R. Foster, *J. Chem. Soc.*, **1963**, 2549.
3) J. I. G. Cadogan, *Quart. Rev.*, **16**, 208 (1962).
4) Y. Ogata and Y. Kosugi, *Tetrahedron*, **24**, 4057 (1968).
5) D. J. Carlsson, J. A. Howard, and K. U. Ingold, *J. Amer. Chem. Soc.*, **88**, 4725 (1966); D. J. Carlsson, J. A. Howard, and K. U. Ingold, *ibid.*, **88**, 4726 (1966).

$$R'\cdot + O_2 \xrightarrow{k_1} R'O_2\cdot \quad (4)$$

$$R'O_2\cdot + PhP(OR)_2 \xrightarrow{k_2} PhP(O)(OR)_2 + R'O\cdot \quad (5)$$

$$R'O\cdot + PhP(OR)_2 \xrightarrow{k_3} PhP(O)(OR)_2 + R'\cdot \quad (6)$$

$$R'O_2\cdot \xrightarrow{k_t} \text{inactive product} \quad (7a)$$

$$R'O\cdot \xrightarrow{k'_t} \text{inactive product} \quad (7b)$$

Here, R is Me, Et, and *i*-Pr, and R'· is $Me_2\dot{C}CN$. Even if O_2 may be produced from steps 7a and 7b, the amount of formed O_2 is negligible when the radical chain length is long enough. Thus the rate of absorption of O_2 is expressed as:

$$v = -d[O_2]/dt = k_i[R'\cdot][O_2] \quad (8)$$

If the termination occurs *via* step 7a alone, the application of steady state method assuming approximate constant concentrations of $R'O_2\cdot$, R'O·, and R'· as probable carriers leads to Eq. (9).

$$v = 2k_i[AIBN] + \frac{2k_ik_2}{k_t}[AIBN][PhP(OR)_2] \quad (9)$$

Since $k_t \ll k_2$, Eq. (9) is reduced to Eq. (10).

$$v = k[AIBN][PhP(OR)_2] \quad (10)$$

Here, $k = 2k_ik_2/k_t$

If the termination is effected by step 7b alone, the analogous derivation gives Eq. (11).

$$v = k'[AIBN][PhP(OR)_2] \quad (11)$$

Here, $k' = 2k_ik_3/k'_t$

In general, R'O· seems to be more reactive than $R'O_2\cdot$ with dialkyl phenylphosphonites.[6] Therefore, the unimolecular termination of $R'O_2\cdot$ is more probable than that of R'O·. The other termination mechanisms (*e.g.*, R'· → inactive product or simultaneous reactions of Eqs. (7a) and (7b)) lead rate equations conflicted with the observed rate law.

The effect of substituent R of $PhP(OR)_2$ on the autoxidation rate was estimated in *o*-dichlorobenzene at 60.0°C. The rate law for $PhP(OR)_2$ [R=Et (II) and R=*i*-Pr (III)] was the same as that of $PhP(OMe)_2$. The second-order rate constants (*k*) for R at 60.0°C were Me, 0.105; Et, 0.110; *i*-Pr, 0.112 $M^{-1}sec^{-1}$. The Taft plot for $PhP(OR)_2$ gives a ρ^* value of −0.058 (correlation coefficient, *r*, −0.95). Hence, the substituents in dialkyl phenylphosphonites affects the autoxidation rate much more than that of the radical intermediate.

The radical chain length (*CL*) was calculated to be 200—2000 by means of Eq. (12), using values of $a = 0.6$ and $k_i = 3.2 \times 10^{-6}$ sec^{-1}.[1b]

$$CL = (k_2[R'O_2\cdot] + k_3[R'O\cdot])[PhP(OR)_2]_0/2ak_i[AIBN]_0 = k_a[PhP(OR)_2]_0/2ak_i[AIBN]_0 \quad (12)$$

Here, *a* is the efficiency of initiation and k_i is the decomposition rate of radical initiator (AIBN), and k_a is an apparent first-order rate constant.[1b]

Experimental

Materials. Phenylphosphonous dichloride was prepared by the Friedel-Crafts reaction of benzene with PCl_3,[8] bp 101—104°C/17 mmHg (lit,[8] bp 68—70°C/1 mmHg), yield 68%. Dimethyl phenylphsophonite was prepared by the esterification of phenylphosphonous dichloride,[9] bp 101—102°C/23 mmHg (lit,[9] bp 98°C/17 mmHg), yield 30%. Diethyl and diisopropyl phenylphosphonites were also prepared by the similar procedure; bp and yield were 78—79°C/8 mmHg (lit,[10] bp 110—111°C/10—13 mmHg), 27% and 82—85°C/8 mmHg (lit,[11] bp 121—122°C/10 mmHg), 11%, respectively. Dimethyl phenylphosphonate was prepared by the Ullmann reaction of trimethyl phosphite with iodobenzene,[12] bp 122—125°C/7 mmHg (lit,[12] bp 115°C/0.9 mmHg), yield 35%. Diisopropyl phenylphosphonate was prepared by the esterification of phenylphosphonic dichloride, bp 116—117°C/3 mmHg (lit,[12] bp 94°C/0.1 mmHg), yield 33%. All phosphonates were identified by IR (a Perkin-Elmer Model 337 spectrophotometer) and NMR (a JNM-C-60HL spectrometer). Commercial solvents, AIBN, O_2, and N_2 were purified by ordinary methods and used.

Product Analysis. The autoxidation product of dialkyl phenylphosphonite was confirmed to be the corresponding phosphonate alone by means of glc (a Yanagimoto GCG 550F gas chromatograph with a flame ion detector) with 3% Apiezone Grease L on Cellite 545 using programming attachment.

Kinetic Procedure. The autoxidation apparatus has been reported previously.[4] A typical kinetic run was as follows: O_2 gas at 200 mmHg and N_2 gas at 350 mmHg were mixed in the apparatus and introduced into the reaction vessel at 60.0°C containing 6.54×10^{-2}M dimethyl phenylphosphonite in *o*-dichlorobenzene (10 ml), then 5.39×10^{-3}M AIBN in *o*-dichlorobenzene (1 ml) was added into it. The reaction was started with vigorous stirring. The partial pressure difference between the reaction mixture and the reference solution was measured at appropriate intervals of time. The observed pseudo-first-order rate constant was calculated by means of Eq. (13).

$$\log(a - 2x) = -\frac{2}{2.303}k_at + \log a \quad (13)$$

Here, *a* and *a*-2*x* are the concentrations of substrate at the start and at time *t*, respectively.

The authors are thankful to Dr. Y. Sawaki for his helpful suggestion and discussion, and also to Nissan Chemical Co., Ltd. for their kind supply of diethyl phenylphosphonate and phenylphosphonic dichloride.

6) C. Walling and R. Rabinowitz, *J. Amer. Chem. Soc.*, **81**, 1243 (1959).

7) R. E. Hudson, "Structure and Mechanism in Organo-Phosphorus Chemistry," Academic Press, London (1965), p. 11.

8) B. Buchner and L. B. Lockhart, Jr., *Org. Syn.*, Coll. Vol., IV, 784 (1963).

9) H. J. Harwood and D. W. Grisley, Jr., *J. Amer. Chem. Soc.*, **82**, 423 (1960).

10) G. Kamai, *J. Gen. Chem. USSR*, **18**, 443 (1948); *Chem. Abstr.*, **42**, 7723c (1948).

11) A. E. Arbuzov, G. Kh. Kamai, and O. N. Belorossova, *J. Gen. Chem. USSR*, **15**, 766 (1945); *Chem. Abstr.*, **41**, 105f (1947).

12) D. Tava and F. Korte, *Tetrahedron*, **23**, 4677 (1967).

BULLETIN OF THE CHEMICAL SOCIETY OF JAPAN, VOL. 45, 2225—2226(1972)

Infrared Intensities of Crystalline NH_3 and ND_3

Masakatsu UYEMURA and Shiro MAEDA

Research Laboratory of Resources Utilization, Tokyo Institute of Technology Meguro-ku, Tokyo

(Received November 11, 1971)

The infrared spectra of crystalline ammonia were investigated by Reding and Hornig,[1] by Anderson and Walmsley,[2] and by Wolf, Rollar, and Wolf[3] for films deposited on a cold window, and interpreted on the basis of the cubic structure of the space group T^4, as given by X-ray diffraction.[4] However, Mauer and McMurdie[5] have reported that the X-ray pattern of such a deposited film can not be solely attributed to the cubic structure; they have suggested the intermixing of one or two non-cubic phases. Staats and Morgan[6] observed rather remarkable changes in the infrared spectra when they annealed the film or deposited it at a higher temperature, but they came to no definite conclusion concerning the structure of the film. The spectral changes mentioned above are so spectacular that the investigation of its origin is of great interest in connection with the role of hydrogen bonding in this crystal. In the present paper, the absolute infrared intensities of crystalline NH_3 and ND_3 films will be reported, and then the intensity behavior in the course of annealing will be described.

Experimental

Commercial NH_3 gas of a reagent grade was used without purification. The ND_3 was obtained by the reaction of Mg_3N_2 with D_2O; it was distilled several times to remove all traces of water. In both samples, no evidence of the impurities was observed in the infrared spectra except for a small amount of H-species remaining in the ND_3 sample, whose deuterium concentration was determined from the intensity of a remaining NH_3 band to be 95—97%. The measurement of the absolute intensity was made using a conventional vacuum cell with a KRS-5 window for depositing the sample. Another metal cell equipped with a wire heater and an extra chamber sealed with Ge and KRS-5 windows was used in observing the spectral changes by annealing. The sample films were formed on the inside surface of the Ge window, and the chamber was filled with helium gas (20—30 Torr) to suppress the dissipation of the film.

Results

The spectral features of the films deposited at 77°K were, in general the same, as those reported by Reding and Hornig,[1] as is shown in Fig. 1 (i). In evaluating the intensity, the density was assumed to be equal to the cubic value (NH_3; 0.861 gr cm^{-3} at 77°K) calculated from the X-ray data.[7] The refractive index at the wavelength of 1 micron, where the interference

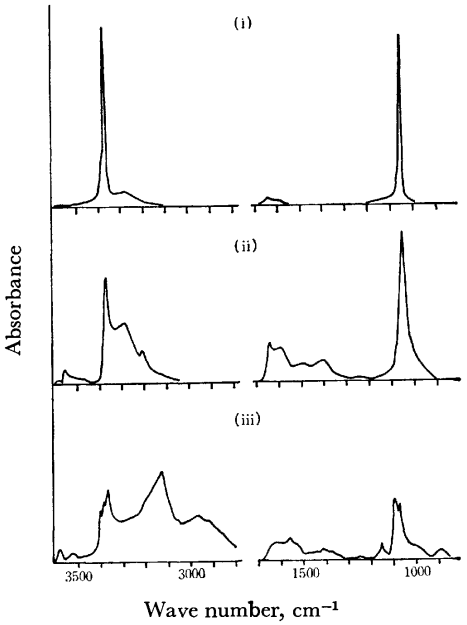

Fig. 1. Spectra of crystalline NH_3.
(i): Deposited at 77°K.
(ii): Deposited at 77°K and annealed to 180°K with suppressive gas.
(iii): Annealed up to a temperature higher than 180°K without suppressive gas.

TABLE 1.

	Cryst. (77°K)			Gas (Ref. 8)		
	Freq. cm^{-1}	A_i[a] $\times 10^4$ darks	$\lvert\partial\mu/\partial Q_i\rvert$ $\times 10^2$ cm$^{3/2}$sec^{-1}	Freq. cm^{-1}	A_i $\times 10^4$ darks	$\lvert\partial\mu/\partial Q_i\rvert$ $\times 10^2$ cm$^{3/2}$sec^{-1}
NH_3						
$\nu 1$	3223	1.92	1.65[b]	3337	0.045	0.31[b]
$\nu 3$	3378			3444	0.029	
$\nu 2$	1060	0.83	1.09	950	1.24	1.39
$\nu 4$	1646	0.12	0.29	1627	0.15	0.42
ND_3						
$\nu 1$	2318	1.08	1.24[b]			
$\nu 3$	2500					
$\nu 2$	815	0.53	0.87			
$\nu 4$	1196	0.097	0.26			

a) Values corrected for effective field by Polo-Wilson's equation with $n=1.47$ (Ref. 15).
b) Given as a quantity $\{(\partial\mu/\partial Q_1)^2+2(\partial\mu/\partial Q_3)^2\}^{1/2}$.

1) F. P. Reding and D. F. Hornig, *J. Chem. Phys.*, **19**, 594 (1951); *ibid.*, **23**, 1053 (1955).
2) A. Anderson and S. H. Walmsley, *Mol. Phys.*, **9**, 1 (1965).
3) H. Wolf, H.-G. Rollar, and E. Wolf, *J. Chem. Phys.*, **55**, 1373 (1971).
4) H. Mark and H. F. Pohland, *Z. Krist.*, **61**, 532 (1925).
5) F. A. Mauer and H. F. McMurdie, reported at the 1958 meeting of the American Crystallographical Association, Milwaukee, Wisconsin.
6) P. A. Staats and H. W. Morgan, *J. Chem. Phys.*, **31**, 553 (1959).
7) I. Olovsson and D. H. Templeton, *Acta Crystallogr.*, **12**, 823 (1959).
8) D. C. McKean and P. N. Schatz, *J. Chem. Phys.*, **24**, 316 (1956).

Table 2.

	$\lvert\partial\mu_{(NH)}/\partial r_{NH}\rvert$	$\lvert\partial\mu/\partial S_2\rvert$	$\lvert\partial\mu/\partial S_4\rvert$
Gas (Ref. 8)			
NH_3	0.24	1.53	0.34
Cryst. (77°K)			
NH_3	1.20	1.38	(+) 0.29[c] (−) 0.24
ND_3	1.24	1.45	(+) 0.37 (−) 0.28
Average	1.22	1.42	0.26
	D/Å	D/rad	D/rad

c) Two possihle choices of relative sign in $\lvert\partial\mu/\partial Q_3\rvert$ and $\lvert\partial\mu/\partial Q_4\rvert$ are denoted by (+) and (−), where (−) combination gives better agreement in NH_3 and ND_3.

fringes were recorded for measuring the film thicknesses,[9] was estimated to be 1.47, on the basis of the data in the visible region. Linear Beer's law plots were obtained; the resulting intensities and dipole-moment derivatives are given in Tables 1 and 2. Since the two stretching absorptions were not well separated, the results were interpreted by assuming the vector addition of NH(ND) bond moment derivatives.[10] It is equivalent to assume that:[11]

$$\lvert\partial\mu_{(NH)}/\partial r\rvert = (3L_{11}^2)^{-1/2}\{(\partial\mu/\partial Q_1)^2+2(\partial\mu/\partial Q_3)^2\}^{1/2}.$$

The derivatives with respect to the bending coordinate, *i.e.*, $(\partial\mu/\partial S_2)$ and $(\partial\mu/\partial S_4)$, are given by the following equations:

$$\lvert\partial\mu/\partial S_2\rvert = L_{22}^{-1}\lvert\partial\mu/\partial Q_2\rvert \pm L_{12}^{-1}\lvert\partial\mu/\partial Q_1\rvert$$
$$\lvert\partial\mu/\partial S_4\rvert = L_{34}^{-1}\lvert\partial\mu/\partial Q_3\rvert \pm L_{44}^{-1}\lvert\partial\mu/\partial Q_4\rvert.$$

In these expressions the contributions from stretching modes are relatively small and $\lvert\partial\mu/\partial Q_1\rvert$ is estimaed to be by far smaller than $\lvert\partial\mu/\partial Q_3\rvert$, so that the $\lvert\partial\mu/\partial S\rvert$'s were evaluated by ignoring $\lvert\partial\mu/\partial Q_1\rvert$ and assuming that the stretching intensities are to be attributed solely to $\lvert\partial\mu/\partial Q_3\rvert$. In general, the observed intensity change from gas to crystal shows the characteristic features of hydrogen-bonded systems.

When the films were annealed up to about 180°K,[12] the spectra showed rather striking changes, as was also found by Staats and Morgan[6] mentioned above, although the present observations were not quite consistent with theirs. Figure 1 (ii) shows the spectra of NH_3 when the film deposited at 77°K[12] was annealed to 180°K[12] with the suppressive gas in the chamber, while (iii) shows the spectra when the film was annealed to a somewhat higher temperature than (ii) without suppressive gas.[13] Similar behavior was observed for ND_3 too. Although Staats and Morgan attributed the (iii) to the cubic phase, the preliminary results on the Raman spectra[14] seem to suggest that the (ii) is more likely to be cubic.

As the sample dissipation on annealing was considerable, no measurement of the absolute intensity was possible for (ii) and (iii). It may be pointed out, however, that the relative intensities in the various phases are appreciably different; the enhancement of the stretching band in the (iii) is particularly notable, suggesting still stronger hydrogen bonding in this phase than in the others.

9) J. L. Hollenberg and D. A. Dows, *J. Chem. Phys.*, **34**, 1061 (1961); *ibid.*, **37**, 1300 (1962).
10) S. Ikawa and S. Maeda, *Spectrochim. Acta*, **24A**, 655 (1968).
11) Symbols and subscrips are the same in Ref. 8.
12) Temperature of the copper block holding the window.
13) When the vacuum seal of the sample chamber was poor.
14) Will be published shortly.
15) S. R. Polo and M. K. Wilson, *J. Chem. Phys.*, **23**, 2376 (1955).

BULLETIN OF THE CHEMICAL SOCIETY OF JAPAN, VOL. 45, 2226—2228(1972)

Effect of Acetic acid on the Polarographic Behavior of Copper(II) Acetate in Acetonitrile

Eiki ITABASHI*

Department of Chemistry, Faculty of Science, Osaka University, Toyonaka, Osaka

(Received November 18, 1971)

Dimeric copper(II) acetate in acetonitrile solution is reduced at the dropping mercury electrode and gives a two-step reduction wave. The reduction wave is distorted in dilute $LiClO_4$ and $NaClO_4$ solutions.[1] This distortion results from the interaction of alkali metal ions with acetate ions which are liberated from the monovalent copper species.

Acetic acid in acetonitrile solution keeps the liberated acetate ions from precipitating as an insoluble film of alkali metal acetates on the surface of the electrode. The present investigation deals with the polarographic behavior of copper(II) acetate in acetonitrile in the presence of acetic acid.

The experimental details were the same as previously described.[2,3]

Results and Discussion

The effect of acetic acid on the polarograms o copper(II) acetate in $NaClO_4$ solution is shown in Fig. 1. With small amounts of acetic acid present,

* Present address: Department of Chemistry, Miyagi University of Education, Aoba, Sendai.

1) E. Itabashi, *J. Electroanal. Chem.*, **36**, 179 (1972).

2) E. Itabashi and S. Ikeda, This Bulletin, **42**, 1901 (1969).

3) E. Itabashi and S. Ikeda, *J. Electroanal. Chem.*, **26**, 97 (1970).

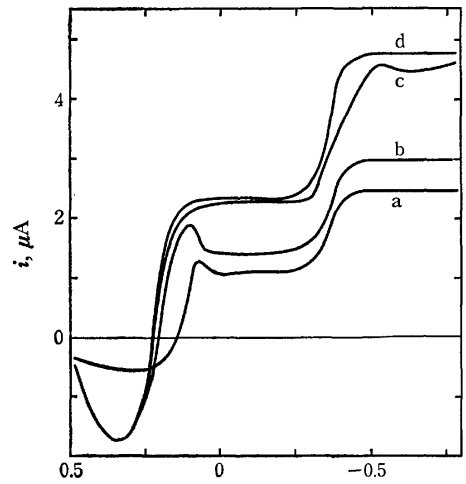

Fig. 1. Effect of the acetic acid concentration on the polarograms of 0.5 mM copper(II) acetate in 0.05M $NaClO_4$. [CH_3COOH]: (a), 0; (b), 0.032%; (c), 0.064%; (d), 0.096%.

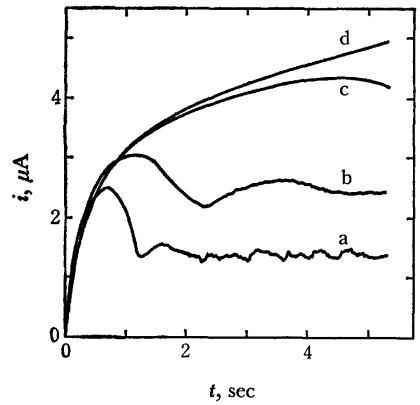

Fig. 2. Effect of the acetic acid concentration on the *i-t* curves for the reduction wave of 0.5 mM copper(II) acetate in 0.05M $NaClO_4$. The electrode potential is set up at −0.55 V *vs.* SCE. [CH_3COOH]: (a), 0; (b), 0.032%; (c), 0.064%; (d), 0.096%.

the limiting current of the wave was enhanced, and a peak current was observed in the anodic part. When the concentration of acetic acid exceeded 0.1% in volume, there was no apparent change in the shape of the developed wave. The zero current potential is a mixed potential where the cathodic current caused by the one-electron reduction of copper(II) acetate to monovalent copper species is equal to the anodic current caused by the oxidation of mercury to mercuric acetate. In the absence of acetic acid, the current-time (*i-t*) curves of individual drops at the constant potential exhibited remarkable irregularities at the whole potential region examined. Figure 2 presents the typical *i-t* curves in $NaClO_4$ solution in the presence and the absence of acetic acid. This irregularity is due to the formation of the insoluble film of sodium acetate on the surface of the electrode. On addition of small amounts of acetic acid, the irregularities of the *i-t* curves disappeared when the acetic acid concentration reached a critical value. The *i-t* curves for the reduction wave in 0.05M $NaClO_4$ solution containing 0.1% acetic acid had the characteristics of normal diffusion control. This result suggests that acetic acid keeps the liberated acetate ions from precipitating as an insoluble film of sodium acetate on the electrode surface. The solubility of sodium acetate in $NaClO_4$ acetonitrile solution was found to increase as the acetic acid concentration increased.

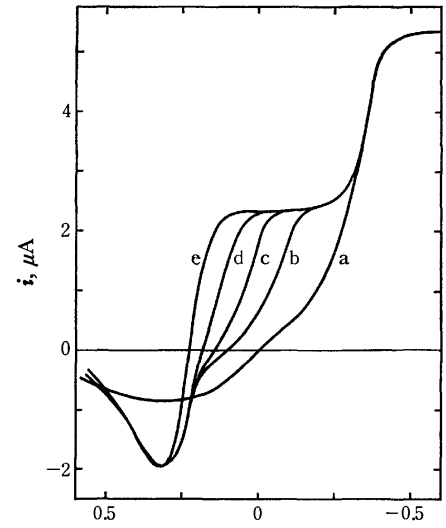

Fig. 3. Effect of the acetic acid concentration on the polarograms of 0.5 mM copper(II) acetate in 0.05M *n*-Bu_4NClO_4. [CH_3COOH]: (a), 0; (b), 0.032%; (c), 0.096%; (d), 0.24%; (e), 0.64%.

In the presence of acetic acid, the one-electron reduction wave of copper(II) acetate to monovalent copper species shifts towards more positive potentials. This is due to the shift of the potential of mercury dissolution and not to the involvement of any chemical reaction prior to the electron transfer of copper(II), because there was no apparent change on the absorption spectrum of copper(II) acetate in acetonitrile with and without acetic acid. A similar displacement of the one-electron reduction wave was also observed in tetra-*n*-buthylammonium perchlorate (*n*-Bu_4NClO_4) solution in the presence of acetic acid, as shown in Fig. 3. In *n*-Bu_4NClO_4 solution in the absence of acetic acid, no well-defined one-electron reduction wave was observed. The value of the limiting current at −0.65 V *vs.* SCE corresponds to a two-electron reduction, that is, Cu(II)→Cu(O). With acetic acid present, the one-electron reduction wave began to appear and shifted towards more positive potentials as the acetic acid concentration increased. The half-wave potentials of the anodic wave caused by the oxidation of mercury to mercuric acetate in 1.0 mM *n*-Bu_4NOAc and 0.05M *n*-Bu_4NClO_4 solutions in the presence and the absence of 0.64% acetic acid were found to be +0.24 V and −0.02 V *vs.* SCE, respectively. Therefore, the appearance of the one-electron reduction wave of Cu(II) to Cu(I) results from the displacement of the anodic wave caused by the oxidation of mercury to mercuric acetate.

The anodic part of the composite anodic-cathodic waves in the presence of acetic acid exhibits a peak

current rather than a limiting plateau. This peaking could be the result of the difference in the electron numbers involved in the anodic and cathodic prosesses. It was predicted by Vlček[4] that the anodic part of the composite wave exhibits a peak current when the electron number involved in the anodic process caused by the electrooxidation of the reduction products is larger than that in the cathodic process. The reaction mechanism of the composite anodic-cathodic waves of copper(II) acetate at the dropping mercury electrode may be written as follows.

$$1/2Cu_2(OAc)_4 + e \longrightarrow 1/2Cu_2(OAc)_4^{2-} \quad (1)$$

$$1/2Cu_2(OAc)_4^{2-} \xrightarrow{k} Cu(I) + 2OAc^- \quad (2)$$

$$2OAc^- + Hg \longrightarrow Hg(OAc)_2 + 2e \quad (3)$$

where the coordinated molecules were omitted for convenience, and k is the rate constant for the dissociation reaction of monovalent copper species. The peak current of the anodic part has the characteristics of kinetically control. The exponent of the i-t curves for the peak current of the anodic wave in 0.05M n-Bu_4NClO_4 solution containing acetic acid had a value of 0.52 ± 0.02. This value is well beyond the value of 0.17 expected for a diffusion controlled electrode mechanism. This could indicate that the rate of the reaction (2) is finite in order that the limiting current is attained.

The author would like to express his hearty thanks to Professor Shigero Ikeda.

4) A. A. Vlček, "Progress in Inorganic Chemistry," Vol. 5, ed. by F. A. Cotton, Interscience Publishers, New York, N. Y. (1963), p. 321.

BULLETIN OF THE CHEMICAL SOCIETY OF JAPAN, VOL. 45, 2228—2229(1972)

A Chlorine NQR Study of *anti*-Perchloro-(3,4,7,8-tetramethylenetricyclo [4.2.0.0^{2,5}] octane), $C_{12}Cl_{12}$

Masao HASHIMOTO, Kenshô SAGISAWA, and Koichi MANO*

Department of Chemistry, Faculty of Science, Kobe University, Nada-ku, Kobe

**Research Institute for Atomic Energy, Osaka City University, Sumiyoshi-ku, Osaka*

(Received March 1, 1972)

In our previous work, we investigated the correlations between the molecular structures and the NQR frequencies of perchloro-compounds, using seven perchloro-compounds for which the crystal or molecular structures have been well established.[1)]

In the present paper, in connection with the previous work, we wish to report on the NQR study of *anti*-perchloro-(3,4,7,8-tetramethylenetricyclo[4.2.0.0^{2,5}]-octane) (I), for which the crystal and molecular structures have been determined.[2)] The details of the experimental procedures have also been reported previously.[1,3)]

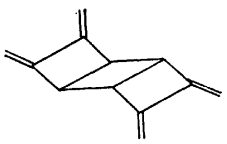

I

The NQR frequencies were measured at temperatures in the range from 77 to 360°K. The experimental results at 77°K are given in Table 1. The intensities of these resonance lines were rather weak, and the half-widths were about 6.0±0.5 KHz at 77°K. The temperature dependence of these lines is shown in Fig. 1. Two lines, ν_2 and ν_3, were found to disappear at about 273 and 225°K respectively (fade-out). Figure 1 shows that the resonance frequencies of the other four lines decrease monotonously with an increase in the temperature. This suggests that I undergoes no phase transition between 77°K and room temperature. Therefore, six crystallographically-nonequivalent chlorine atoms exist in the unit cell of the crystal of I at room temperature, although only four resonance lines were observable at room temperature. Furusaki, in his X-ray study of I at room temperature, assumed that the space group was $P\bar{1}$.[2)] Our NQR results are consistent with his assumption.

From a structural point of view, I is related to perchloro-(3,4-dimethylenecyclobutene) (II) and perchloro-(1,2-dimethylenecyclobutane) (III). Their

Table 1. The nuclear quadrupole resonance frequencies of ^{35}Cl of I and the relative intensities of the resonance lines at liquid nitrogen temperature

No.	Resonance frequency (MHz)	Relative intensity
ν_1	38.070 (30.003)[a)]	9
ν_2	37.862 (29.839)	7
ν_3	37.784 (29.779)	10
ν_4	37.555 (29.598)	10
ν_5	37.541 (29.587)	9
ν_6	37.101 (29.239)	8

a) The value in ( ) is the frequency of ^{37}Cl.

1) M. Hashimoto and K. Mano, This Bulletin, **45**, 706, (1972).
2) A. Furusaki, *ibid.*, **40**, 758 (1967).
3) K. Mano, K. Kusuda, A. Fujino, and T. Sakan, *Tetrahedron Lett.*, **1966**, 489.

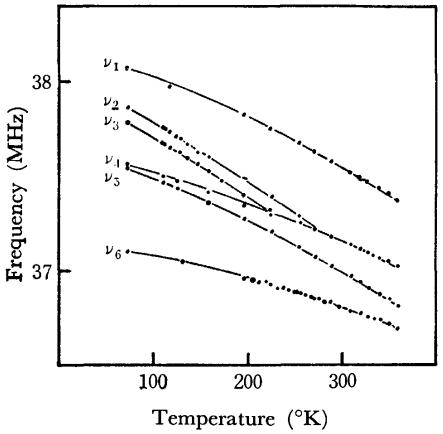

Fig. 1. Temperature dependence of the NQR frequencies of I.

NQR spectra, discussed in the previous paper, are of assistance in assigning the resonance lines of I.

II III

The NQR frequencies of ^{35}Cl in the dichloromethylene groups of II and III lie in a frequency region from about 37.8 to 38.1 MHz at 77°K.[1] Among the six lines of I, therefore, the five lines besides ν_6 are assignable to the chlorine atoms in the dichloromethylene groups on the basis of a comparison with the data for II and III.

The chlorine atoms corresponding to ν_2 and ν_3 may have large temperature factors, because the fade-out found for the two lines may be due to the reorientation of the chlorine atoms. In fact, according to the X-ray study of I,[2] two of the chlorine atoms, Cl(4) and Cl(5)

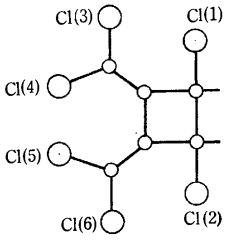

Fig. 2. One half of the molecule of I.

in Fig. 2, have unusually large temperature factors. Therefore, ν_2 and ν_3 are assignable to Cl(4) and Cl(5). For several other compounds, a correlation between the fade-out and the large temperature factor has also been found.[1,4]

Although the symmetry of I is C_i, the molecular geometry shows that Cl(1) is nearly equivalent to Cl(2).[2] Consequently, the characteristics of the torsional vibrations may be almost the same for these two chlorine atoms. This means that the temperature coefficient of the resonance frequency of Cl(1) is also similar to that of Cl(2).[5] For a similar reason, the temperature coefficients of the resonance frequencies of Cl(3) and Cl(6), and those of Cl(4) and Cl(5), may be almost the same. Figure 1 shows, on the basis of a comparison of the temperature dependence of the resonance frequency, that the six lines of I can be divided into three pairs of lines, ν_1 and ν_5, ν_2 and ν_3, and ν_4 and ν_6. As has been described above, the second pair, ν_2 and ν_3, are assignable to Cl(4) and Cl(5). The first pair, ν_1 and ν_5, may be assigned to Cl(3) and Cl(6), and the third, to Cl(1) and Cl(2).

4) M. T. Rogers and J. A. Ryan, *J. Phys. Chem.*, **72**, 1340 (1968).

5) H. Bayer, *Z. Phys.*, **130**, 227 (1951).

BULLETIN OF THE CHEMICAL SOCIETY OF JAPAN, VOL. 45, 2230—2231(1972)

Transition Metal Ions on Molecular Sieves. I. Complexes of Copper(II) on Y Molecular Sieves and Their Catalytic Activities

Isao MOCHIDA, Akio KATO, and Tetsuro SEIYAMA

Department of Applied Chemistry, Faculty of Engineering, Kyushu University, Fukuoka

(Received October 30, 1971)

An isolated metal ion attached to a molecular sieve would be expected to behave quite differently from a metal ion or atom in an ordinary metal oxide. In the latter case, the metal atoms are located that their interaction is possible, while on a molecular sieve the metal ions or atoms are more isolated and tend to behave as their homogeneous analogues even though they are located on a solid surface. Catalytic activities of transition metal ions bound to molecular sieves have been reported for the oxidation of propylene.[1,2]

Molecular sieve-bound metal ions have been extensively studied.[3] However, the interactions of a metal ion with polydentate chelating agents have scarcely been investigated in spite of the fact that such a system can be compared with that of an analogous homogeneous case. Burwell *et al.*[4] studied the exchange of complex metal ions with the hydroxide group of silica gel.

We have investigated the adsorption of bidentate chelating reagents such as ethylenediamine on isolated cupric ions by visible and infrared spectroscopy and also the heterogeneous catalytic activities of these compounds for the decomposition of hydrogen peroxide.

Experimental

Chemicals. Ethylenediamine(en) was obtained from Tokyo Kasei Co, ethanedithiol and dimethylglyoxime from Nakarai Chemicals Co. They were used without further purification.

The Cu(II)-form of the Y molecular sieves (Linde) was obtained by the exchange of sodium ion with aqueous cupprammonium ion. This treatment was followed by a thorough washing with deionized water and calcined at 400°C in the atmosphere. Details have been reported.[1] Cu(II)-Y, saturated with atmospheric water vapor, was found to contain 5.2% copper by weight.

Adsorption of Chelating Reagents. Cu(II)-Y was stirred for 2 days with aqueous diamine or ethanedithiol solution and washed with dry ethanol to yield the chelate-impregnated material. The dimethylglyoxime complex was similarly prepared using ethanol as a solvent.

Spectroscopic Analysis. Electronic spectra were obtained by the decalin mull method in a quartz cell on a Hitachi Type 124 Double Beam Spectrophotometer. The original Y sieve in decalin was used as a reference. Infrared spectra were measured in KBr on a IR-G double beam spectrophotometer of the Nippon Bunko Co.

Decomposition of Hydrogen Peroxide. The rates of decomposition of hydrogen peroxide were determined by the manometric measurement of oxygen evolved. After the reaction flask (containg 50 cc of aqueous NaOH solution of pH 11.8 and the catalyst) was immersed in a constant temperature bath for 2 hr, 1 cc of 30% aqueous hydrogen peroxide was added. After the reaction, the pH of the reaction media was found to be 9.8 for each catalyst.

Results and Discussion

Adsorption of Chelating Agents on Cu(II)-Y. Impregnation of Cu(II)-Y with ethylenediamine turned the sieve deep blue with heat evolution. The complex of the sieve Y-Cu(II)-en kept its color (visible absorption maximum, 660 mμ) in dry air, but turned purple (visible absorption maximum, 550 mμ) in contact with moisture. Similar values were reported for bisethylenediaminecopper(II) complexes.[4,5,6]

Y-Cu(II)-en had an infrared absorption band at 1048 cm^{-1} in addition to those at 1573, 1475, and 1318 cm^{-1} due to the adsorption of ethylenediamine on Cu(II)–Y. The absorption at 1048 cm^{-1} was overlapped by a strong band due to the molecular sieve, but was resolved by using a molecular sieve-containing KBr reference plate. Formation of chelates is indicated by the presence of this band which was assigned to the ring skeletal vibration by Powell and Sheppard.[7]

Ethanedithiol and dimethylglyoxime formed light green complexes on the sieve. These colors coincide with those of the corresponding sulfate complexes. In the case of ethenedithiol, the conformation of the coordinating ethanedithiol rings was determined by inspection of the infrared spectrum. This solid showed a weak absorption band at 1280 cm^{-1} (lit, 1275 cm^{-1})[8] which suggests that the rings are in a gauche form.

Thus, all the results indicate that cupric ions on molecular sieves have an affinity for chelating agents. The affinity suggests a new type of catalytically active sites which are expected to behave much like the usual coordination compound, but kept on the rigid surface.

Decomposition of Hydrogen Peroxide. Various copper compounds have been investigated as models for the

1) I. Mochida, S. Hayata, A. Kato, and T. Seiyama, *J. Catal.*, **15**, 314 (1969), **19**, 405 (1970), **23**, 31 (1971), This Bulletin, **44**, 2282, 2595 (1971).

2) J. Rouchaud and J. Mawaka, *J. Catal.*, **19**, 172 (1970).

3) R. F. Gould, ed., "Molecular Sieve, Zeolites" (Advances in Chemistry Series 101 and 102), American Chemical Society, Washington (1971).

4) R. L. Burwell, Jr., R. G. Pearson, G. L. Haller, P. B. Tjok, and S. P. Chock, *Inorg. Chem.*, **4**, 1123 (1965), D. Cornet and R. L. Burwell, Jr., *J. Amer. Chem. Soc.*, **90**, 2489 (1968).

5) G. Gordon and R. K. Birdwhistell, *ibid.*, **81**, 3567 (1959).

6) M. E. Baldwin, *Spectrochim. Acta*, **19**, 35 (1963).

7) D. B. Powell and N. Sheppard, *ibid.*, **17**, 68 (1961).

8) D. M. Sweeny, S. Mizushima, and J. V. Quagiliano, *J. Amer. Chem. Soc.*, **77**, 6521 (1955), S. Mizushima, I. Ichikawa, I. Nakagawa, and J. V. Quagliano, *J. Phys. Chem.*, **59**, 293 (1955), I. Nakagawa, "Infrared Absorption Spectra of Metal Complexes, (Infared Absorption Spectra: Kagaku no Ryoiki, Supplement Issue)", **15**, 37 (1963), M. Hayashi and Y. Jyo, Vibrational Spectra of Mercaptans and Sulfides (*ibid.*), **17**, 31 (1965).

enzyme by testing their ability to decompose hydrogen peroxide in basic aqueous solution.[9] The catalytic activity of ethylenediaminecopper(II) complex for this reaction was reported.[10] Jacobson and Smith[11] reported on the catalytic activities of ammine and diamine complexes of metal ions on silica gel.

The catalytic activities of Cu(II)–Y, Y–Cu(II)-en, and Y–Cu(II)-dimethylglyoxime toward the decomposition of hydrogen peroxide were observed in aqueous sodium hydroxide. In this pH region, no measurable decomposition of hydrogen peroxide could be observed without catalyst in the sodium hydroxide solution. For Y–Cu(II)-en, the decomposition rate was proportional to the weight of the catalyst. It was found that one molecule of the complex on the surface decomposed more than four hundred molecules of hydrogen peroxide. The reaction seemed to proceed in the first order with 90% decomposition.

Y–Cu(II)-en had a five times larger catalytic activity than Cu(II)–Y at the same pH region as shown in Fig. 1. The fact that catalytic activity of the dimethylglyoximato-complex is significantly less than that of Y–Cu(II)-en (Fig. 1) shows that the catalysis strongly depends on the type of chelating ligand employed. Such catalytic activity enhanced by chelation is of interest as an example of a complex catalyst on the rigid surface.

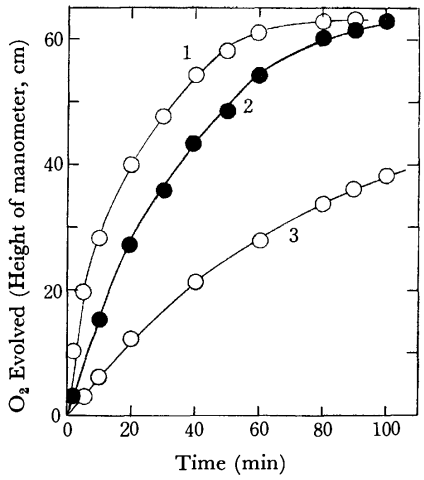

Fig. 1. Decomposition of hydrogen peroxide catalyzed by cupric ions on the molecular sieve at 26°C. The relative activities are calculated 4.6 (Y–Cu(II)-en), 1.0 (Cu(II)–Y), and 0.93 (Y–Cu(II)-dimethylglioxime).
1: Y–Cu(II)-en, 82 mg. 2: Cu(II)–Y, 132 mg.
3: Y–Cu(II)-dimethylglyoxime, 52.5 mg.

Our thanks are due to Mr. E. Sakamoto, Kinki University, for his fluorescent X-ray analysis of copper.

9) N. Uri, *Chem. Rev.*, **50**, 375 (1952), J. H. Baxendale, *Advan. in Catalysis and Related Subjects*, **4**, 31 (1952), J. Peisavh, P. Aisen, and W. E. Blumberg, "The Biochemistry of Copper" Academic Press, New York, 1966; V. S. Sharma and J. Schubert, *J. Amer. Chem. Soc.*, **91**, 6291 (1969); H. Sigel, *Angew. Chem.*, (International Edition in English), **8**, 1667 (1969).

10) H. Sigel and T. Kaden, *Helv. Chim. Acta*, **51**, 947 (1968); V. S. Sharma and J. Schubert, *Inorg. Chem.*, **10**, 252 (1971).

11) H. W. Jacobson and G. W. Smith, *J. Amer. Chem. Soc.*, **76**, 4494 (1954).

BULLETIN OF THE CHEMICAL SOCIETY OF JAPAN, VOL. 45, 2231—2233(1972)

The Nature of Acid Sites on the Surface of Silica-alumina. III. The Mechanism of the Photo-ionization of Perylene and Anthracene Adsorbed on the Surface of Silica-alumina

Kazuto TAKIMOTO and Masaji MIURA

Department of Chemistry, Faculty of Science, Hiroshima University, Higashisenda-machi, Hiroshima

(Received August 13, 1971)

The photo-ionization of various aromatic compounds has been extensively studied in solid matrices and solutions.[1-3] However, hardly no work on the dynamic behavior or the mechanism for the photo-ionization on solid surfaces has been done, although the identification and structure of the radicals generated on the surfaces by UV irradiation have been widely investigated.[4] The purpose of this work is to reveal the mechanism of the photo-ionization of polyacenes adsorbed on the surface of silica-alumina with Lewis-acid sites of various strengths.

Experimental

Anthracene, perylene, and 40% silica-alumina were used; they were the same as those used in our preceding work.[5] The polyacenes were adsorbed from their vapor phase on a silica-alumina surface pretreated at 500°C for 3 hr in a vacuum of 5×10^{-5} mmHg. The increase in the amount of the cation radical under irradiation of UV light was continuously measured by fixing the magnetic field at one of the peaks of the ESR spectrum. UV light was supplied from a 1-kW high-pressure mercury lamp or a 1-kW, point-source, superhigh-pressure mercury arc. The light intensity was controlled by means of nets of various meshes. The filters used were Toshiba UVD-25, UV-39, VY-42, and VY-46, while a Shimadzu-Bausch-Lomb Model 33-86-01 Mono-

1) H. Tsubomura, *Nippon Kagaku Zasshi*, **89**, 1 (1967).
2) W. A. Gibbons and G. Porter, *Nature*, **206**, 1355 (1965).
3) G. E. Johnson and A. C. Albrecht, *J. Chem. Phys.*, **44**, 3179 (1966).
4) A. Terenin, *Advan. Catal.*, **15**, 227 (1964).
5) M. Miura, Y. Kubota, T. Iwaki, K. Takimoto, and Y. Muraoka, This Bulletin, **42**, 1476 (1969).

chromator was also used. The ESR spectra and diffuse reflection spectra were obtained by using, respectively, the spectrometer and spectrophotometer described previously.[6]

Results and Discussion

When perylene was adsorbed on the surface of silica-alumina from the vapor phase, an ESR spectrum with nine well-resolved peaks was observed. On the other hand, the diffuse reflection spectrum showed the absorption maxima at 540, 600, and 700 mμ.[4,6] These spectra are due to the cation radical of perylene. The increment of the cation radical with the irradiation time is shown in Fig. 1. The initial rate of the radical formation was approximately proportional to the intensity of the exciting light which includes wavelengths longer than 320 mμ, as may be seen in Fig. 2. In the case of anthracene, the situation was the same. These phenomena suggest that the photo-ionization of these two polyacenes proceeds through a single-photonic process on the silica-alumina surface.

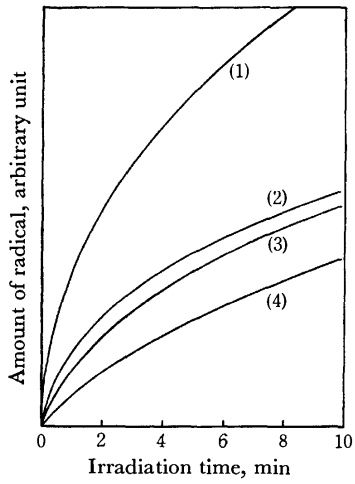

Fig. 1. Rates of the radical formation of perylene adsorbed on the 40% silica-alumina. Transmittancy of net (%): (1) 100, (2) 42.2, (3) 37.0, and (4) 14.0.

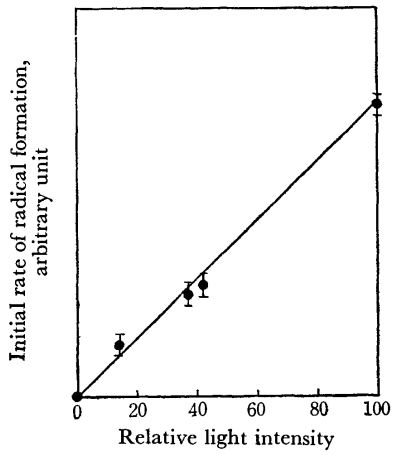

Fig. 2. Relation between the initial rate of the radical formation of perylene adsorbed on the silica-alumina and the intensity of exciting light.

6) K. Takimoto and M. Miura, This Bulletin, **44**, 1534 (1971).

Silica-alumina has Lewis-acid sites with various strengths; the strong acid sites exist in the range of $-3.0>H_0>-8.0$, while the weak ones exist in the range of $H_0>+3.0$.[5] The cation radical and the trapped electron are formed on the strong Lewis-acid sites even in the absence of UV irradiation and are stabilized on the surface.[6] A sort of charge-transfer complex with polyacene is formed on the weak Lewis-acid site even in the ground state.[6] Physically-adsorbed perylene which possesses absorption maxima at 410 and 430 mμ is present on much weaker Lewis-acid sites.[4,6]

The cation radicals of polyacenes were not formed in a sulfuric acid solution of 48 weight-percent, which corresponds to $H_0=-3.0$; the cation radicals are formed only in the range of $H_0<-3.0$ in the absence of UV irradiation. In addition, the amount of the cation radicals decreased markedly with an increase in the value of the ionization potential in the absence of UV light.[6] It may be considered, therefore, that the critical acid strength of the Lewis-acid sites required for the ionization of these polyacenes is situated in the range of $-3.0>H_0>-8.0$. The charge-transfer complexes and the physically-adsorbed polyacenes are presumably generated on the Lewis-acid site with an acid strength weaker than the critical value.

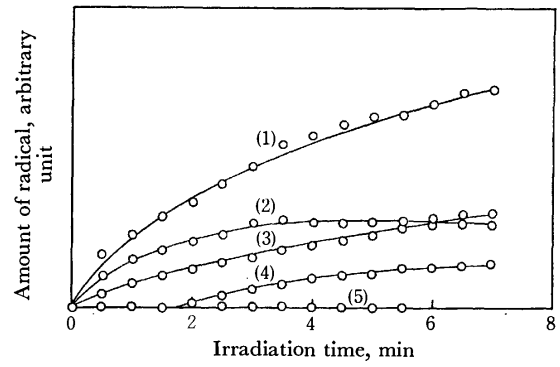

Fig. 3. Filter effect on the radical formation of perylene adsorbed on the silica-alumina: (1) full line, (2) UV-39, (3) UVD-25, (4) VY-42, and (5) VY-46.

The effect of the energy of the photon on the photo-ionization of the perylene adsorbed on the silica-alumina surface is shown in Fig. 3. The increment of the cation radical by using the VY-42 ($\lambda>420$ mμ) filter and a high-pressure mercury lamp was smaller than those caused by the use of the UV-39 ($\lambda>390$ mμ) and UVD-25 ($250<\lambda<400$ mμ) filters. When the VY-46 ($\lambda>460$ mμ) filter was employed during the irradiation of UV light from the same light source, no increase was observed. However, an increase was observed when the 1-kW, point-source, superhigh-pressure mercury lamp and the VY-46 filter were used. The VY-42 and VY-46 filters transmit the light of wavelengths longer than those absorbed by the physically-adsorbed perylene. The charge-transfer bands ($\lambda>480$ mμ) which are situated at wavelengths longer than those ($400<\lambda<450$ mμ) of the perylene physically adsorbed on much weaker Lewis-acid sites may exist even in the ground state, although they can not usually be observed because of the band-broadening

due to the broad distribution of the acid strength of the Lewis-acid sites on the silica-alumina surface.[6] These phenomena may indicate that the photo-ionization is caused by the absorption of photons with an energy corresponding to $h\nu_{CT}$. On the other hand, the light of wavelengths absorbed only by the physically-adsorbed perylene was separated by the use of a monochromator. An increase in the amount of the cation radical was also observed here, though it was appreciable only with difficulty because of the low transmittancy of the monochromator. The cation radical was formed on the surface even by exciting the physically-adsorbed perylene which may be present on much weaker Lewis-acid sites.

The photo-ionization of polyacenes can possibly occur through the following two processes.[1] In the case of the single-photonic process, the amount of the cation radical generated is proportional to the intensity of the exciting light, I, while in the case of the two-photonic process it is proportional to I^2. When a charge-transfer complex has been formed on the surface, the photo-ionization is accomplished through a single-photonic process. For the photo-ionization of these physically-adsorbed polyacenes, the following two processes may be considered: one through the triplet state as an intermediate (two-photonic process), and the other through the formation of a charge-transfer complex *via* a first excited singlet state of these polyacenes, resulting in the formation of the cation radical and the trapped electron (single-photonic process). The photo-ionization of these physically-adsorbed polyacenes probably takes place through the latter process, since the amount of the cation radical formed is approximately proportional to I.

BULLETIN OF THE CHEMICAL SOCIETY OF JAPAN, VOL. 45, 2233—2234(1972)

On Inhibition of Polarographic Reduction of the Dioxalatocuprate(II) Ion by the One-Electron Reduction Product of Phenylmercury Hydroxide

Teisuke MURAYAMA and Akio TAKAYANAGI

Department of Industrial Chemistry, Faculty of Engineering, Shizuoka University, Hamamatsu

(Received March 29, 1972)

Organomercury salts are reduced at a dropping mercury electrode in double one-electron steps. Benesch and Benesch observed that the first wave of phenylmercury hydroxide has severe irregularities on the diffusion current plateau.[1] They considered that this is due to the coating of the electrode caused by an insoluble product. They also showed that the polarographic reduction of Cd^{2+} and Pb^{2+} ions is inhibited in the range of potentials between the end of the first and the beginning of the second waves of phenylmercury hydroxide. We studied inhibition of the polarographic reduction of the dioxalatocuprate(II) ion in oxalate buffer solutions.

Experimental

The phenylmercury hydroxide was made from phenylmercury acetate (Shudzui, Tokyo) and sodium hydroxide,[2] and recrystallized from water: mp with decomposition 226—230°C (lit.[3] 226—233°C). The stock solution of phenylmercury hydroxide was prepared by dissolving a weighed amount.

The concentration of the copper sulfate was determined by means of complexometric titration.[4]

The oxalate buffer solution of pH 4.08 was prepared from guaranteed reagents.

The test solution was prepared by mixing stock solutions of phenylmercury hydroxide, oxalate buffer, copper sulfate, and sodium nitrate, and diluting it to the desired volume. Sodium nitrate was added to control the ionic strength of the test solution to 0.35. Five one-thousandths of 1% gelatin was also added as a maximun suppressor.

All solutions were prepared with redistilled water.

Test solutions were degassed with nitrogen and thermostated at 25.0 ± 0.1°C.

The dropping mercury electrode had the following characteristics (in 0.3M KNO_3 at zero applied potential *vs.* SCE). Rate of flow of mercury, 1.978 mg/sec; drop time, 4.13 sec. The cell and the salt bridge were described elsewhere.[5] Polarograms were recorded with a Yanagimoto PA-102 polarograph. Current-time curves were recorded by a Mini Writer-H (Watanabe Instruments Co.) in terms of a potential drop across a resistor inserted in series with the cell circuit.

Results and Discussion

Polarograms of the dioxalatocuprate(II) ion (I) are shown in Fig. 1. They are corrected for the current due to the reduction of phenylmercury hydroxide (II) and for the residual current. In the presence of II the single step reduction of I splits into two waves.

1) R. Benesch and R. E. Benesch, *J. Amer. Chem. Soc.*, **73**, 3391 (1951); R. E. Benesch and R. Benesch, *J. Phys. Chem.*, **56**, 648 (1952).

2) L. G. Makarova and A. N. Nesmeyanov, "Methods of Elemento-Organic Chemistry," Vol. IV, North-Holland Publishing Co., Amsterdam (1967), p. 420.

3) L. R. Barlow and J. M. Davidson, *J. Chem. Soc., A*, **1968**, 1613.

4) G. Schwarzenbach, "Complexometric Titrations," Methuen & Co., London (1957), p. 82.

5) T. Murayama, T. Sawaki, and S. Sakuraba, This Bulletin, **43**, 2820 (1970).

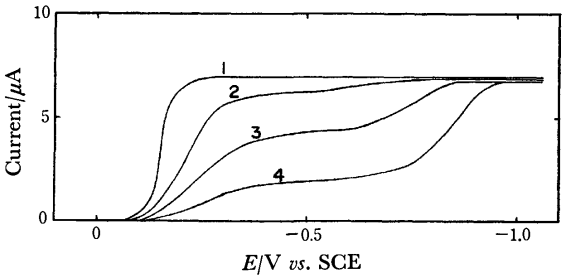

Fig. 1. Polarograms of I in the presence of II. Concentration of I, 0.934 mM. Concentration of II: 1, 0 mM; 2, 0.123 mM; 3, 0.198 mM; 4, 0.297 mM.

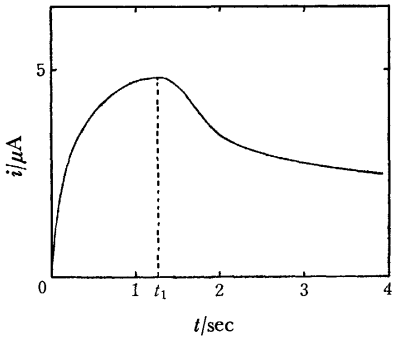

Fig. 2. Current-time curve for the reduction of I in the presence of II at a potential of −0.50 V *vs.* SCE. Concentration of I, 0.934 mM; concentration of II, 0.198 mM.

The potential of the second wave coincides with that of the second step of II, which shifts to negative potentials with increasing concentration of II. Current-time curves were recorded at a potential of −0.50 V *vs.* SCE, which lies in the limiting current region of the first wave of I. A current-time curve is shown in Fig. 2, where the current is corrected for that due to the reduction of II and the residual current. The current reaches a maximum at t_1 and then decreases. This is caused by the reduction product of II, adsorbed as soon as it was formed. If Q is the quantity of electricity consumed for the reduction of II until t_1, the quantity $Q/t_1^{2/3}$ is proportional to the fraction of the electrode surface covered by the reduction product of II. Figure 3 shows the relation between $Q/t_1^{2/3}$ and $\log t_1$. Since t_1 increases tenfold, it is surprising that there is a linear relationship between these two quantities.

This relationship may be explained as follows. The current which flows at the electrode surface is a function of the concentration gradient of I and the surface area of the electrode. At around t_1 the fraction θ of the electrode surface covered by the reduction product of II increases so rapidly that the concentration gradient decreases very slowly. Thus the change of the surface area gives rise to a larger effect on the current than the change of the concentration gradient does. Under these circumstances one may assume that the concentration gradient is constant at around t_1. Hence, the increase of θ is equal to the increase of the electrode surface divided by the total surface area of the electrode dq/q at t_1, where $di/dt=0$. Thus

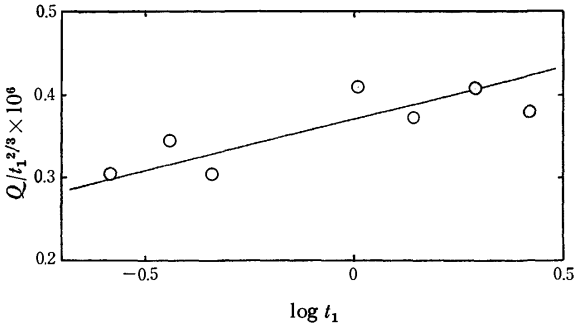

Fig. 3. Relation of $Q/t_1^{2/3}$ *vs.* $\log t_1$.

$$d\theta = \frac{dq}{q} \tag{1}$$

at t_1. Integrating Eq. (1), one has

$$\theta = \ln q + b \tag{2}$$

where b is a constant. The surface fraction θ is related to Q by the following equations.

$$\theta = \frac{\Gamma}{\Gamma_m} \tag{3}$$

$$\Gamma = \frac{Q/F}{q} \tag{4}$$

where Γ is the surface concentration of the reduction product of II at t_1, Γ_m the maximum surface concentration in a monolayer of the product, and F Faraday. By introducing Eqs. (3) and (4) and the relation $q=0.00852(mt_1)^{2/3}$ into Eq. (2), and rearranging, one obtains

$$Q/t_1^{2/3} = 0.0131F\Gamma_m m^{2/3}\log t_1 + b' \tag{5}$$

where m is the rate of flow of mercury in mg/sec, and b' a constant. Equation (5) shows that $Q/t_1^{2/3}$ is a linear function of $\log t_1$, in agreement with results given in Fig. 3.

From the slope of the straight line in Fig. 3 and Eq. (5), $1/\Gamma_m$ was calculated to be 291 Å^2/molecule. It seems to be too large compared with a value of 60 Å^2/molecule which was estimated from a molecular model. This is not the case, however. Inhibition occurs not only at the surface covered by adsorbed molecules, but also at narrow strips which encircle islets of adsorbed molecules with a width equal to the radius of the ion of I. In addition, hydration increases the apparent ionic size of I. If these facts are taken into consideration, $1/\Gamma_m$ might be several times as large as the area of cross section of the molecule. Thus Γ_m should be redefined as the minimum surface concentration to inhibit the electrode reaction completely.

BULLETIN OF THE CHEMICAL SOCIETY OF JAPAN, VOL. 45, 2235—2236 (1972)

Preparation of Orthoesters Having Functional Group

Javad AZIZIAN*
Department of Chemistry, A.A.C. Jundi-Chapour University, Ahwaz, Iran
(Received March 1, 1971)

During the course of studies on the selective protection of hydroxyl group of nucleosides reported in our previous communication,[1] it became necessary to prepare orthoesters in which alcohol residue is substituted by functional group. Among various orthoesters, methyl and ethyl orthoformate are most commonly used in organic synthesis but their applications as a protecting reagent is rather limited.

Most of the orthoesters already known are those in which the alcohol residue is alkyl, aryl, aralkyl, or alkylene[2] and only a few orthoesters are prepared hitherto in which alcohol residue has a functional group. Hence the author attempted the synthesis of orthoesters having functional group in alcohol residue.

One of the most convenient and practical method of preparation of orthoesters is the ester interchange between methyl or ethyl orthoformate and alcohol and in this note the ester interchange between ethyl orthoformate or orthoacetate with alcohols having functional group are described. As substituted alcohols, ethylene chlorohydrin, 3-chloro-1-propanol, 1,3-dichloro-2-propanol, 2,2,2-trichloroethanol, 2-aminoethanol, 2-dimethylaminoethanol, and ethylene cyanohydrin were used.

The ester interchange reactions were carried out in the usual manner by heating the mixture of alcohol and ethyl orthoformate in the presence or absence of catalyst, ethanol being continuously removed through fractionating column. After nearly the theoretical amount of ethanol was removed, the residual reaction mixture was fractionated.

The interchange reaction proceeds partially or completely depending on the structure of substituted alcohol and the reaction conditions such as the molar ratio of the reactants. The orthoesters which were obtained in this study are listed in Table 1.

The ester interchange between ethyl orthoacetate and ethylene chlorohydrin was also attempted and 2-chloroethyl orthoacetate was obtained.

In our detailed examination on the reaction conditions of the ester interchange between ethyl orthoformate and ethylene chlorohydrin, it was found that the presence of catalyst such as zinc chloride, *p*-toluenesulfonic acid, or sulfosalicyclic acid reduced the reaction time but not affected the yield and increasing amount of catalyst decreased the yield due to the decomposition of ethyl orthoformate to form ethyl formate.

The reaction of ethyl orthoformate with 2-aminoethanol was failed to give interchanged orthoester. Thus, when 1 mol of orthoformate was heated with 4 mol of 2-aminoethanol in the presence of *p*-toluenesulfonic acid, 3 mol of ethanol distilled over, but on distilling the reaction mixture, 2 mol of 2-aminoethanol

Table 1. Reaction of ethyl orthoformate with substituted alcohol (ROH)

R	$CH(OC_2H_5)_3$/ROH g/g	$CH(OC_2H_5)_3$/ROH mol/mol	Catalyst	$CH(OR)_3$ (g)	$CH(OR)_2OC_2H_5$ (g)	$CH(OR)(OC_2H_5)_2$ (g)
$ClCH_2CH_2$	30/48	1/3	—	11[a]	23[b]	—
$ClCH_2CH_2$	30/65	1/4	$ZnCl_2$	35	—	—
$ClCH_2CH_2CH_2$	30/75	1/4	$ZnCl_2$	31[c]	—	—
$(ClCH_2)_2CH$	15/52	1/4	$ZnCl_2$	10[d]	11[e]	—
Cl_3CCH_2	13/50	1/4	—	—	16[f]	6[g]
$(CH_3)_2NCH_2CH_2$	30/71	1/4	TsOH	9[h]	10[i]	—
$NCCH_2CH_2$	18/21	1/3	—	—	residue[j]	—

Bp (°C/mmHg) and elemental analysis [Found (Calcd), %] of the products.
a) 125—130/4. C, 33.52 (33.39); H, 5.44 (5.16); Cl, 42.76 (42.34).
b) 95—100/4. Cl, 32.24 (32.74). c) 155—156/3. C, 41.03 (40.88); H, 6.45 (6.47).
d) 184—185/3. Cl, 52.07 (53.65). e) 132—134/3. C, 34.65 (34.39); H, 5.11 (5.09); Cl, 46.02 (45.22).
f) 150—152/12. C, 23.99 (23.65); H, 3.00 (2.81). g) 105—110/12. C, 32.92 (33.39); H, 5.13 (5.13).
h) 125/2. C, 56.90 (56.31); H, 11.00 (10.87); N, 15.48 (15.70).
i) 133—135/17. N, 11.44 (11.11). j) C, 54.41 (54.53); H, 7.07 (7.12); N, 14.20 (14.13).

* Present Address: Department of Chemistry, Faculty of Science, Tokyo Institute of Technology, Ookayama, Meguro-ku, Tokyo.

1) T. Hata and J. Azizian, *Tetrahedron Lett.* **1969**, 4443.
2) A. W. Williamson and G. Kay, *Ann.*, **92**, 346 (1854); P. P. T. Sah and T. S. Ma, *J. Amer. Chem. Soc.*, **54**, 2965 (1932); F. Tieman, *Ber.* **15**, 2686 (1882); H, Baines and J. E. Driver, *J. Chem. Soc.*, **125**, 907 (1924); E. R. Alexander and H. M. Buch, *J. Amer. Chem. Soc.*, **74**, 554 (1952); F. F. Beilstein and E. Wiegand, *Ber.*, **18**, 482 (1885).

was recovered and on further distillation caused decomposition and the distillate was found to be 2-aminoethanol.

Experimental

In all cases the ethyl orthoformate and the alcohols employed were redistilled before use. Unless otherwise stated, the experiments summarized in Table 1 were carried out according to the following procedure using the same apparatus. It is illustrated here with the preparation of 2-chloroethyl orthoformate. All boiling points are uncorrected.

2-Chloroethyl Orthoformate. In a 100 m*l* flask was added 30 g (0.2 mol) of ethyl orthoformate, 65 g (0.8 mol) of ethylene chlorohydrin and 0.1 g of anhydrous zinc chloride. In order to remove the ethanol as it was formed, a 25 cm column packed with glass helices was used and adjusted so that a maximum temperature of the condensing vapor was 79°C by controlling the heating of the flask. After 2—3 hr, nearly theoretical amount of ethanol (27 g) was removed. The residual reaction mixture was distilled under vacuum and the fraction boiling at 125—130°C/4 mmHg was collected.

Reaction of Ethylene Chlorohydrin with Ethyl Orthoacetate. The reaction was carried out using 32 g (0.2 mol) of ethyl orthoacetate and 65 g (0.8 mol) of ethylene chlorohydrin. After 3.5 hr, 27 g of ethanol was removed. The residual mixture was distilled under vacuum and 19.5 g of unreacted ethylene chlorohydrin and 30 g (56%) of 2-chloroethyl orthoacetate (bp 135°C/4 mmHg) was obtained.
Found: C, 36.98; H, 5.98; Cl, 38.92%. Calcd for $C_8H_{15}O_3Cl_3$: C, 36.15; H, 5.90; Cl, 40.10%.

The author wishes to express his hearty thanks to Professor Masaki Ohta for his encouragement.

BULLETIN OF THE CHEMICAL SOCIETY OF JAPAN, VOL. 45, 2236—2237 (1972)

Electron Spin Resonance of Manganese Ions on Magnesium Oxide

A. J. TENCH
Chemistry Division, A.E.R.E., Harwell, England

(Received June 8, 1971)

The study of surface properties of oxides using transition metal ions as a probe to investigate the environment of surface ions is potentially a very valuable technique; however, the interpretation of the results can present some difficulties since the location of the paramagetic ions observed is often not known. The reactivity of MgO doped with manganese[1] has been studied previously both by ESR and chemisorption; the results indicate that the Mn^{2+} ion is present in a variety of environments. A recent paper by Yamamura *et al.*[2] reports an ESR study of the behaviour of the Mn^{2+} ion on the surface of MgO. In this note, we wish to suggest an alternative interpretation of the data which indicates that not all the Mn^{2+} is on the surface.

In the latter paper,[2] it is assumed that Mn^{2+} ions initially adsorbed on the surface remain on the surface throughout the various treatments *in vacuo* and in oxygen *etc.*, even when the treatments are carried out at 1000°C. A variation in the A and D values (the hyperfine splitting and zero field splitting values of the Hamiltonian for Mn^{2+}) is attributed to changes of environment at the surface. We suggest that the observed changes in A and D could arise from a changing environment of the Mn^{2+} due to the onset of ionic diffusion processes above 500°C which allow the diffusion of some of the Mn^{2+} ions into substitutional sites in the bulk oxide, where the environment is more nearly octahedral and is characterised by lower D values. The existence of this ionic diffusion phenomena at 600°C has been well characterised,[1] and would be expected, since the ionic sizes of Mg^{2+} and Mn^{2+}, and Mn^{3+} are similar (0.65, 0.80, and 0.66 Å respectively[3]).

Up to 300°C, *in vacuo*, the MgO surface is covered with close to a monolayer of hydroxyl groups[4] and the environment of the manganese ions will not be characteristic of the oxide surface. Heating to 500—600°C reduces the OH^- coverage to less than 10% of a monolayer with the desorption of water. In the paper the authors do not indicate how the ESR spectral intensity was measured but the loss of Mn^{2+} intensity between 300—600°C could arise from the oxidation of Mn^{2+} ions to Mn^{3+} by the water vapour although this appears unlikely, and it seems more probable that Mn^{2+} ions on the bare surface experience a considerable crystal field effect giving rise to large D terms and an apparent loss in Mn^{2+} concentration. Heating the samples at higher temperatures permits the diffusion of manganese ions into the bulk where the environment is more nearly octahedral and the D values will be progressively smaller away from the surface thus giving an apparent increase in concentration of Mn^{2+}. The extremely broad spectrum shown in Fig. 1(b)[2] after treatment at 1000°C for 4 hr *in vacuo* can be interpreted by assuming the broad wings arise from surface Mn^{2+} ions which have a D value of >100 gauss whilst the sharper lines are more characteristic of ions incorporated into the bulk.

1) D. Cordischi, R. L. Nelson, and A. J. Tench, *Trans. Faraday Soc.*, **65**, 2740 (1969).
2) T. Yamumura, A. Hasegawa, Y. Yamata, and M. Miura, This Bulletin, **43**, 3377 (1970).
3) J. E. Wertz and P. Auzins, *Phys. Rev.*, **106**, 484 (1957).
4) P. J. Anderson, R. F. Horlock, and J. F. Oliver, *Trans. Faraday Soc.*, **61**, 2754 (1965).

The influence of added gases on the Mn^{2+} spectrum can be explained in a similar manner. For example, previous work[1] has shown that Mn^{2+} ions on a surface can be oxidised very easily with oxygen at comparatively low temperatures and if all the Mn^{2+} was present on the surface as isolated ions, we would expect the intensity to drop to zero after treatment at 300°C. This apparently does not occur and the observed change in D values (Fig. 7)[2] can be explained by a progressive oxidation of the Mn^{2+} ions inwards from the surface and the remaining ions have progressively lower D values. At the same time, some line narrowing would occur due to the reduction in the Van Vleck dipole-dipole interaction[5] as the Mn^{2+} ions are converted to Mn^{3+}. The effect on the hyperfine A values is not so clear, but it seems likely that those Mn^{2+} ions remote from the surface will have an A value close to that reported for single crystals, whereas, those ions near the surface may have a slightly higher value, similar perhaps, to that observed in CaO where the ionic spacing is a little higher. However, this is not regarded as being very significant.

The results reported for Mn^{2+} on silica gel suggest that in this case the Mn^{2+} ion is not incorporated into the silica gel and remains on the surface. When the surrounding hydroxyl groups are removed by thermal treatment *in vacuo* no detailed ESR structure of the Mn^{2+} ion can be resolved and only a broad line is observed due to either the high D values from the surface field or the formation of aggregates of ions. This latter alternative certainly influences the susceptibility studies on MgO, which were carried out using a doping level of 3% manganese ion,[2] and makes any comparison with the ESR studies difficult. It is possible that ion pair formation (with very high D values[6]) also influences the results observed in the ESR study reported by Yamamura[2] where levels of 3000 ppm were used but it is regarded as very unlikely to occur in the earlier studies[1] where doping concentrations of <250 ppm were used.

We think that ESR studies of the Mn^{2+} can be used as a valuable probe of surface properties but the possible diffusion of the ion needs to be considered, and in addition, the concentration of the dopant must be kept low if the formation of ions pairs is to be ignored.

5) C. Kittel and E. Abrahams, *Phys. Rev.*, **90**, 238 (1953).

6) B. A. Coles, J. W. Orton, and J. Owen, *Phys. Rev. Lett.*, **4**, 116 (1960).

BULLETIN OF THE CHEMICAL SOCIETY OF JAPAN, VOL. 45, 2237—2239 (1972)

Remarks on the Crystallization and Dehydration of Copper Sulfate Pentahydrate

K. HEINZINGER and B. MAIWALD

Max - Planck - Institut für Chemie (Otto-Hahn-Institut), Mainz, Germany

(Received July 20, 1971)

Isotope effects have been used in studying crystallization and dehydration processes in hydrated crystals.[1-3] In drawing conclusions it has to be taken into consideration that there may exist different kinds of water molecules distinguished by their binding in the crystal. In copper sulfate pentahydrate there occur two kinds of bonding as shown by the neutron diffraction study of Bacon and Curry.[4] Four water molecules are bonded as ligands by a metal-oxygen bond and two hydrogen bonds and one water molecule by four hydrogen bonds. This grouping of the water molecules into two main classes is a general feature of hydrated crystals (see *e. g.* Hamilton and Ibers[5]). Another property of relevance for this discussion is, that the unit cell consists of two molecules $CuSO_4 \cdot 5H_2O$. To each of the copper ions four water molecules are coordinated. They form together with two sulfate oxygens two octahedra, slightly different in geometry.

The available hydrogen and oxygen isotope fractionation factors between the different kinds of water in the crystal, and between crystal water and the saturated solution which are relevant in respect to crystallization and dehydration processes are listed in Table 1. The reported oxygen isotope fractionation factors are still preliminary; exact numbers cannot be given yet but the direction of the enrichment alone is significant for this discussion.

Crystallization

In studying the crystallization process with the help of isotope effects, it would be an unjustified simplification to consider only the overall fractionation factor between saturated solution and total crystal water, α_{S-G}. In the case of the hydrogen isotopes, the two kinds of water in $CuSO_4 \cdot 5H_2O$ show different preferences for the isotopes.[3] This follows from the fact that the D/H ratios of four water molecules are equal in the limits of error while the D/H ratio of the fifth water molecule is bigger by 5.7%.

It has been shown that the enrichment of deuterium in the fifth molecule is not a result of a Rayleigh dis-

1) H. Tanaka and H. Negita, This Bulletin, **43**, 3079 (1970).
2) H. Oki, E. Kyuno, and R. Tsuchiya, *ibid.*, **43**, 3263 (1970).
3) K. Heinzinger, *Z. Naturforsch.*, **24a**, 1502 (1969).
4) G. E. Bacon and N. A. Curry, *Proc. Roy. Soc.* (London), **A266**, 95 (1962).
5) W. C. Hamilton and J. A. Ibers, "Hydrogen Bonding in Solids," W. A. Benjamin Inc., New York (1968).

TABLE 1. HYDROGEN AND OXYGEN ISOTOPE FRACTIONATION FACTORS BETWEEN DIFFERENT KINDS OF WATER MOLECULES IN COPPER SULFATE PENTAHYDRATE AND BETWEEN CRYSTAL WATER AND THE SATURATED SOLUTION

α_{x-y}	α_{K_1-G}	α_{K_2-G}	α_{L-G}	α_{S-G}	Ref.
$(D/H)_x/(D/H)_y$	—	—	—	1.022	6
	0.988	0.988	1.045	1.023	3
$(T/H)_x/(T/H)_y$	—	—	—	1.044	1
$(^{18}O/^{16}O)_x/(^{18}O/^{16}O)_y$	α_{K_1-G} >	α_{K_2-G}	—	<1	7

K_1 refers to the first two moles of water per mol of $CuSO_4 \cdot 5H_2O$ liberated on dehydration, K_2 to the third and fourth and L to the fifth mol. G means total crystal water and S stands for saturated solution.

tillation. Therefore, the fractionation can only be caused by a difference in bonding. Then it can be concluded from the crystal structure together with α_{S-G} that in the water coordinated with the copper ion the light isotope is enriched, in the fifth water molecule bonded by four hydrogen bonds, the heavy isotope is enriched compared with the saturated solution, as can be seen from Table 1:

$$\alpha_{K_1-S} = \frac{\alpha_{K_1-G}}{\alpha_{S-G}} < 1, \quad \alpha_{L-S} = \frac{\alpha_{L-G}}{\alpha_{S-G}} > 1$$

This difference shows that the fractionation of the hydrogen isotopes is not a consequence of a diffusion isotope effect during crystallization, as has been suggested by Tanaka and Negita.[1] This conclusion is supported by the result of the oxygen isotope effect measurement: $\alpha_{S-G}<1$; for the overall enrichment of ^{18}O in the crystal water cannot be explained by the diffusion of the water molecules.

Therefore, it has to be concluded that during crystallization either the water on the surface of the crystal is in isotopic equilibrium with the water in the solution or that four water molecules are carried into the crystal with the cation and the fifth is taken from the bulk water. Both possibilities are reasonable, as it has been shown that in the solution a remarkable isotope fractionation between hydration water and bulk water exists. In the solution the hydration water of the cations is by a few percent enriched in the light hydrogen isotope and in ^{18}O compared with the bulk water (see *e.g.* Heinzinger and Weston,[8] and Taube[9]).

The similarity of the fractionation factors between hydration water and bulk water in the solution to those between the two kinds of water in $CuSO_4 \cdot 5H_2O$ can be understood by considering that the bonding of the hydration water in the solution is similar to the bonding of the four water molecules to the copper ion in the crystal, while the bonding of the water molecules in the bulk water of the solution is similar to the bonding of the fifth water molecule in the crystal. The vibrational spectra of concentrated solutions and hydrated crystals are similar (see *e.g.* Leung and Safford[10]).

Dehydration

From the hydrogen isotope effect measurements it has been concluded that the fifth water molecule bonded in the pentahydrate by four hydrogen bonds becomes quantitatively the water molecule of the monohydrate at dehydration temperatures below 50°C.[3] This conclusion is independent of a possible change of structure, because at these low temperatures the water molecules are not mixed up and the isotope ratios of the different kinds of water in the crystal are not changed during dehydration.

As there exists a slight difference in geometry between the two octahedra in the unit cell, it is not unreasonable to expect that at room temperature first one octahedron breaks up and looses its four waters and then the other, in agreement with the existence of a stable trihydrate. While the hydrogen isotope fractionation data do not allow a conclusion, because $\alpha_{K_1-G} = \alpha_{K_2-G}$ (Table 1), the oxygen isotope measurements support this assumption, for $\alpha_{K_1-G} > \alpha_{K_2-G}$. The enrichment of ^{18}O in the first water fraction relative to the second is necessarily a consequence of differences in the binding of the water molecules in the crystal. An isotope shift during dehydration could only be caused by some kind of a Rayleigh distillation, which would mean that the first fraction would have to be enriched in ^{16}O.

While it can be concluded from the oxygen isotope measurements that one octahedron breaks up after the other, the information from these measurements is still insufficient to decide which one of the two octahedra breaks up first. Analysis of vibrational spectra would be helpful for this decision.

Concluding this short discussion, it should be mentioned that the possibility to attribute the water molecules, collected on stepwise dehydration, to certain bonding situations in the crystal does not provide, by reversing the process, a possibility to produce a $CuSO_4 \cdot 5H_2O$ crystal with the water molecules of a given isotopic composition at given positions. The following simple experiment has been performed: $CuSO_4 \cdot 5H_2O$ was dehydrated to the monohydrate and then exposed to D_2O vapor. After the pentahydrate had formed again (checked by the amount of water taken up), dehydration in vacuum at room temperature was started. After 80% of the water was again collected, the isotopic composition was determined and it was found that deuterium and hydrogen were mixed up. This implies that the water of the monohydrate

6) R. M. Barrer and A. F. Denny, *J. Chem. Soc.*, **1964**, 4677; M. Johansson and K. E. Holmberg, *Acta Chem. Scand.*, **23**, 765 (1969).
7) B. Maiwald and K. Heinzinger, to be published
8) K. Heinzinger and R. E. Weston, Jr., *J. Phys. Chem.*, **68**, 744 (1964).
9) H. Taube, *ibid.*, **58**, 523 (1954).
10) P. S. Leung and G. J. Safford, *ibid.*, **74**, 3696 (1970).

does not become quantitatively the fifth water molecule of the pentahydrate because of rearrangement during hydration.

Thanks are due to Prof. Dr. A. Klemm for helpful discussions.

BULLETIN OF THE CHEMICAL SOCIETY OF JAPAN, VOL. 45, 2239—2241 (1972)

Fractionation of Oxygen and Carbon Isotopes during Floatation of Calcite

T. SHARMA, A. K. BISWAS,* and N. V. PILLAI

Department of Chemistry, Indian Institute of Technology, Kanpur, India

** Department of Metallurgical Engineering, Indian Institute of Technology, Kanpur, India*

(Received September 17, 1971)

Fractionation of oxygen and carbon isotopes in systems containing CO_2, HCO_3^-, CO_3^{2-}, and H_2O has been investigated by many workers due to its importance in explaining the isotope variations in natural calcium carbonate deposits.[1-4] In addition to various factors like temperature, source deposition, and equilibrium conditions, the isotopic composition will be affected also by postdepositional exchanges and recrystallisation. If calcium carbonate from a particular site is transported by water to a different location through a process of floatation, the isotopic composition of calcium carbonate at the new site will depend on fractionations involved in the floatation process as well. In the present work oxygen and carbon isotopic compositions of calcium carbonate (calcite) obtained from floatation concentrates and tailings have been determined to see whether any isotopic fractionation occurs during the floatation of calcium carbonate.

Basic principles underlying floatation have been discussed by various authors.[5-7] During floatation, concentration of finely divided material occurs on the variations in their ability to keep themselves on a phase interface. Processess occuring in floatation are based on specific chemical and physical interactions between the various components involved in the system. Froth-floatation has been used to beneficiate the lime content of limestone as well as for removing it out as one of the gangue constituents of other ores. Role of oleic acid as a collector for calcite has been investigated by Lee[8] and Breewood and Miller.[9] Klassen and Kokrousov[6] have given the collecting properties of oleic acid and oleate ions under different conditions. Recently the role of sodium oleate on the floatation of calcite using different collector concentrations and different activators was investigated by Biswas and coworkers.[10,11] They have shown that the recovery of calcite increases with collector concentration, and by using carbon dioxide as the lifting agent instead of air. The nature of acids used to adjust the pH of the pulp before floatation was also found to affect the floatation yield considerably. In the present investigations, calcite from the floatation concentrates and tailings obtained in the presence of hydrochloric, benzoic, citric, and oxalic acids have been used for isotopic studies.

Experimental

Floatation. About 100 g of powdered calcite (−100+200 mesh ASTM) was mixed with about one litre of distilled water. The pH of the solution was adjusted to about 5.7 by the addition of hydrochloric, benzoic, citric, or oxalic acid. Calculated amount of sodium oleate was added so that the concentration was about $2.5—3\times10^{-6}$ mol/l in the solution. About 5 ml of 5% Dowfroth-250 was added and the pulp was conditioned for about 3 min at an impeller speed of 900 rpm. The pH after conditioning was 6.1 to 6.4. Air was introduced by opening the suction valve and and impeller speed was set to 2100 rpm. Froth was collected and the floatation was over within 3 min. Calcite was collected from the froth (floatation concentrate) and from the solution (tailing), washed, dried, and weighed. Calcite slurry bubbled with carbon dioxide and calcite slurry kept under distilled water also were sampled for isotopic analysis. the experiments were carried out at 27°C. Floatation concentrates and tailings used for isotopic analysis are listed in Table 1.

Isotope Analysis. Samples were decomposed using 100% phosphoric acid according to the procedure of McCrea[1] and the liberated carbon dioxide collected and the yield measured. The isotopic analysis of the carbon dioxide was done on a 6''-60°-RMS-19 double collecting isotope ratio mass spectrometer. The values were corrected as described by Craig.[12] The $^{18}O/^{16}O$ ratio of the carbonate was calculated using the isotope fractionation factor given by Sharma

1) J. M. McCrea, *J. Chem. Phys.*, **18**, 849 (1950).
2) H. C. Urey and R. J. Greiff, *J. Amer. Chem. Soc.*, **57**, 321 (1935).
3) P. M. Jefferey, W. Compston, D. Greenhalgh, and J. Delater, *Geochim. Cosmochim. Acta*, **7**, 255 (1955).
4) H. G. Thode, M. Shima, C. E. Rees, and K. V. Krishnamurthy, *Can. J. Res.*, **43**, 582 (1965).
5) V. L. Klassen and V. A. Kokrousov, "An Introduction to Theory of Floatation," Butterworths, London (1963).
6) A. M. Gaudin, "Floatation," McGraw Hill Book Co., New York (1957).
7) V. A. Glemboltskii, V. I. Klassen, and I. N. Plasksin, "Floatation," Primary Sources, New York (1969).
8) O. Lee, *U. S. Bur. Mines, Rep. of Invest.*, No. 2744(1969).
9) C. H. Breerwood and B. L. Miller, *Am. Inst. Minging Met. Engrs. Tech. Pub.*, 606 (1935).
10) A. K. Biswas, *Ind. J. Tech.*, **5**, 187 (1968).
11) A. K. Biswas and V. K. Sampath Kumar, *Nature*, **217**, 1255 (1969).
12) H. Craig, *Geochim. Cosmochim. Acta*, **12**, 133 (1957).

Table 1. Description of samples and percentage recovery

Sample No	Description of the sample	% Recovery
R_1	Floatation concentrate, calcite slurry brought to pH 5.7 by the addition of HCl and floated with sodium oleate.	93.5
R_2	Floatation tailings from R_1	
R_3	Floatation concentrate, calcite slurry brought to pH 5.7 by addition of benzoic acid.	95.0
R_4	Floatation tailings of R_3	
R_5	Floatation concentrate, calcite slurry brought to pH 5.7 by the addition of citric acid.	43.4
R_6	Floatation tailings of R_5	
R_7	Floatation concentrate, calcite slurry brought to pH 5.7 by the addition of oxalic acid.	19.0
R_8	Floatation tailings of R_7	
R_9	Calcite slurry kept under distilled water.	—
R_{10}	Calcite slurry bubbled with 3.75 *l* of CO_2 for 2.5 min.	—

Table 2. Isotopic composition of floatation concentrates and tailings

Sample No	$\delta\ ^{18}O$ (‰) SMOW	$\delta\ ^{13}C$ (‰) PDB	$\delta\ ^{18}O$[a] (‰) SMOW	$\delta\ ^{13}C$[a] (‰) PDB
R_1	11.50	−2.83	11.53	−2.81
R_2	12.00	−2.48		
R_3	11.70	−2.57	11.69	−2.55
R_4	11.50	−2.20		
R_5	10.80	−2.65	11.20	−2.52
R_6	11.50	−2.40		
R_7	11.30	−2.80	11.54	−2.95
R_8	11.60	−2.80		
R_9	11.32	−2.70	—	—
R_{10}	11.60	−2.60	—	—

a) Calculated from the following material balance calculation

$$\delta = \frac{\left[\begin{matrix}\%\text{ yield of}\\ \text{concentrate}\end{matrix}\right] \times \delta_{\text{concentrate}} + \left[\begin{matrix}\%\text{ yield}\\ \text{of tailing}\end{matrix}\right] \times \delta_{\text{tailing}}}{100}$$

and Clayton.[13] The isotopic ratios are reported in the delta terminology defined as:

$$\delta = \left[\frac{R_{\text{sample}}}{R_{\text{standard}}} - 1\right] \times 1000 \qquad (1)$$

where $R = {}^{18}O/{}^{16}O$ or $^{13}C/^{12}C$ ratio. The oxygen and carbon isotope values are reported with respect to SMOW (standard mean ocean water) and Chicago PDB carbonate standards respectively. The results of isotopic analyses are presented in Table 2.

Discussion

Factors that can affect the distribution of oxygen and carbon isotopic composition of calcite in the floatation concentrate and tailings are (1) various chemical equilibria involved when calcite dissolves in water, (2) isotope exchange reactions occurring in the solution, (3) solubility of calcium carbonate, (4) relative affiinity of various isotopic molecules towards collector anions, (5) pH of the floatation pulp, and (6) temperature. Isotopic fractionation will accompany the several reactions that take place in the system. The various reactions that occur when calcite is placed in water are the following:

$$CO_3^{2-}\ (\text{solid}) \rightleftarrows CO_3^{2-}\ (\text{aq}) \qquad (2)$$

$$CO_3^{2-} + H_2O \rightleftarrows HCO_3^- + OH^- \qquad (3)$$

$$HCO_3^- + H_2O \rightleftarrows H_2CO_3 + OH^- \qquad (4)$$

$$H_2CO_3 \rightleftarrows H_2O + CO_2 \qquad (5)$$

In a closed system at equilibrium each component will possess characteristic carbon and oxygen isotopic ratios.[3] This is the result of isotopic fractionation occurring between the various components and existence of several exchange reactions of the type:

$$H_2{}^{12}CO_3 + H^{13}CO_3^- \rightleftarrows H_2{}^{13}CO_3 + H^{12}CO^{3-} \qquad (6)$$

$$1/3\ C^{18}O_3^{2-} + H_2{}^{16}O \rightleftarrows 1/3\ C^{16}O_3^{2-} + H_2{}^{18}O \qquad (7)$$

Relative solubility of calcium carbonate in the solution in presence of different ionic species will change the isotopic composition of solid calcite in the floatation pulp and hence will affect the isotopic composition of calcite in the floatation conecntrate and tailing. Experimental investigations of calcium carbonate solubility have shown that solubility varies with temperature, pressure, added salts, pH, and the total amount of CO_2 in the solution.[14] An increased solubility of calcium carbonate will make the remaining calcite isotopically heavier. The affinity of the collector anions towards the various isotopic molecules will also affect the relative isotopic composition in the floatation concentrate and tailing.

The results in Table 2 show that except in the case when benzoic acid was used to adjust the pH, the floatation concentrate is found to be richer in the lighter isotope. This enrichment of lighter isotopes in the floatation concentrate may be due to the greater affinity of the collector anions towards the lighter isotopic molecules and consequent increase in the lighter calcite particles in the froth. Other factors like differences in the solubility of the light and heavy isotopes and partial dissolution of calcite when it is in contact with water will make the tailings enriched in heavy isotopes due to preferential dissolution of lighter isotopic molecules. Oxygen and carbon isotopic fractions between the solid and the dissolved species also might have caused the observed enrichment in the tailings.

Although we do observe differences in the ^{13}C and ^{18}O contents of the floatation concentrates and tailings, the differences are found to be very small, compared to the equilibrium fractionations in other systems. This is owing to nonattainment of isotopic equilibrium conditions due to short period of time. Since all

13) T. Sharma and R. N. Clayton, *Geochim. Cosmochim. Acta*, **29**, 1347 (1965).

14) R. M. Garrels and R. M. Dreyer, *Bull. Geol. Soc. Amer.*, **63**, 325 (1952).

the floatation experiments are over within ten minutes much fractionation cannot be expected. Moreover, since the relative amount of bicarbonate and carbonate ion concentration in the solution is much less compared to the total amount of calcite present in the system, change in isotopic composition due to isotopic exchange and solubility differences will be small. The total $\delta^{18}O$ and $\delta^{13}C$ values calculated from material balance of floatation concentrates and tailings are very close to that of calcite kept under distilled water.

Calcite slurry bubbled with CO_2 is found to be heavier than calcite kept under distilled water. When carbon dioxide is bubbled through the slurry, more calcium carbonate will dissolve to form calcium bicarbonate.

$$CaCO_3 + CO_2 + H_2O \rightleftarrows Ca(HCO_3)_2 \quad (8)$$

As explained earlier, the lighter $CaCO_3$ particles will undergo preferential dissolution making the remining calcite heavier. The observed enrichment in $\delta^{18}O$ and $\delta^{13}C$ are in agreement with this view.

The foregoing results show that there is isotopic fractionation during the floatation of calcium carbonate. The floatation experiments carried out here were in presence of floatation reagents and may be far from conditions under which floatation occurs in nature. Still, it might be one of the factors which determine the distribution of oxygen and carbon isotopes in natural calcium carbonate deposits.

BULLETIN OF THE CHEMICAL SOCIETY OF JAPAN, VOL. 45, 2241—2242 (1972)

Nouvelle Synthèse Totale de la Cétone Sabinique (*dl*)

Christian ALEXANDRE et Francis ROUESSAC

Laboratoire de Synthèse Organique, Centre Universitaire du Mans, Route de Laval 72, Le Mans France

(Reçu le 5 Octobre, 1971)

En dehors de l'oxydation du sabinene en cétone sabinique **1**,[1,2] on ne trouve en faisant l'examen de la littérature, que deux voies de synthèse totale conduisant à cette cétone.

Dans ces deux méthodes, les auteurs créent le cycle cyclopropanique soit par réaction de Simmons-Smith sur le cyclopenténol **2**[3] soit par addition intramoléculaire d'un α-cétocarbène sur une double liaison éthylénique[4] (Composé **3**).

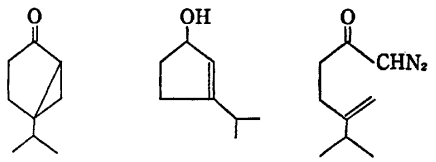

1 **2** **3**

Nous décrivons ici une nouvelle synthèse de la cétone sabinique racémique dans laquelle l'α-cyclopropylcétone est créée par deshydratation intramoléculaire du γ-cétol **4**, en présence de dicyclohexylcarbodiimide (DCC), selon la méthode que nous avons développée au laboratoire.[5,6]

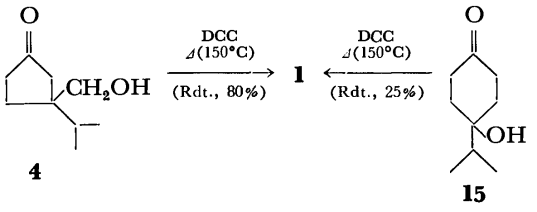

4 **1** **15**

L'acide isopropyl-1 cyclohexène-3 carboxylique **6**, obtenu (Rdt.: 80%) par réaction de Diels et Alder entre l'acide α-isopropylacrylique **5**[4] et le butadiene est transformé en ester méthylique **7** avec une solution éthérée de diazométhane (Rdt : 90%). Par oxydation permanganique **7** conduit à **8** (Rdt: 77%) qui est alors estérifié de façon classique (EtOH, Rdt : 75%) en triester **9**. Ce dernier est converti par une cyclisation de type Dieckmann en un mélange des deux cétoesters isomères **10** et **11** (Rdt : 62%) dont l'hydrolyse ménagée conduit dans l'un et l'autre cas au cétoester **12** (Rdt : 79%): Après le blocage préalable de la fonction cétone en dioxolanne **13** (Rdt.: 90%), la réduction de ce composé par $LiAlH_4$ donne l'alcool **14** (Rdt : 84%) puis l'alcool **4** par traitement acide aqueux (HCl) (Rdt : 92%).

4 réagit avec un équivalent de DCC pour donner un carbamidate dont le chauffage à 150°C pendant 2 heures suffit pour obtenir (Rdt : 80%) la cétone sabinique (*dl*) dont la pureté (CPV) est supérieure à 98%.

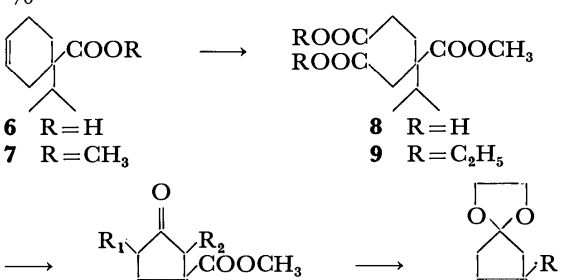

6 R=H
7 R=CH_3
8 R=H
9 R=C_2H_5
10 R_1=H R_2=COOEt
11 R_1=COOEt R_2=H
12 R_1=R_2=H
13 R=$COOCH_3$
14 R=CH_2OH

Nous rappelons que le rendement en cétone **1** à partir de l'hydroxy-4 isopropyl-4 cyclohexanone **15**

1) A. G. Short et J. Read, *J. Chem. Soc.*, **1939**, 1415.
2) P. A. Stadler, *Helv. Chim. Acta*, **43**, 1601, (1960).
3) W. I. Fanta et W. F. Erman, *J. Org. Chem.*, **33**, 1656 (1968).
4) K. Mori, M. Ohki, et M. Matsui, *Tetrahedron*, **26**, 2821 (1970).
5) C. Alexandre et F. Rouessac, *Tetrahedron Lett.*, **1970**, 1011.
6) C. Alexandre et F. Rouessac, *Bull. Soc. Chim. Fr.*, **1971**, 1837.

est seulement de 25%,[6] la réaction d'élimination étant beaucoup moins rapide dans ce cas, que pour le composé **4**.

Partie Experimentale

Acide Isopropyl-1 Cyclohexène-3 Carboxylique ***6***. 60 g d'acide isopropyl-2 acrylique,[4] 100 m*l* de butadiène et 1 g d'hydroquinone sont maintenus à 170°C pendant 20 hr. Après distillation, on obtient 73 g d'acide **6**. $Eb_{0,03}$: 98—100°C. F : 61°C. Rdt.=84%.

Isopropyl-1 cyclohexène-3 Carboxylate de Méthyle ***7***. Une solution éthérée de diazométhane est ajoutée à une solution de 50 g de **6** dans l'éther, le tout refroidi à 0°C. Aprés concentration, le résidu distillé donne 48 g de **7**. Eb_{12} : 86—87°C. Rdt,=90%.

Isopropyl-1 Oxo-3 Cyclopentanecarboxylate de Méthyle ***12***. Préparé selon le mode opératoire de Toki.[7] On ajoute par petites portions, 148 g de $KMnO_4$ a 57,5 g d'ester **7** dans 600 m*l* d'eau. Après filtration, concentration et extraction à l'ether, on obtient 60 g (77%) de diacide **8** que l'on estérifie directement en triester **9** (54 g) $Eb_{0.2}$: 125—127°C (Rdt.= 75%). **9** (54 g) est ajouté goutte a goutte à une suspension de 4,2 g de sodium dans 200 ml de benzene puis porté à reflux une nuit; apres isolation, on obtient 28 g du mélange **10** et **11**. $Eb_{0,07}$: 114—115°C. Rdt.=62%. Ce mélange traité 3 hr à reflux dans 250 m*l* d'H_2SO_4 à 8% donne 15 g d'ester **12**. Eb_{15} : 132—133°C. Rdt.=75%.

Isopropyl-7 Dioxa-1,4 Spiro[4.4]nonanecarboxylate-7 de Méthyle ***13***. Préparé selon la technique habituelle avec un rendement de 90%. Eb_{15} : 142—143°C.

Isopropyl-7 Hydroxyméthyl-7 Dioxia-1,4 Spiro[4,4]nonane ***14***. A partir de 13.5 g de cétone et 4 g de $LiAlH_4$ dans 300 m*l* d'éther, on isole 10 g d'alcool ***14***. $Eb_{0.01}$: 100—102°C. Rdt.=94%.

Hydroxyméthyl-3 Isopropyl-3 Cyclopentanone ***4***. **14** (9 g) est débloqué à 0°C par une solution d'HCl concentré dans l'acétone pendant 1/2 hr. On obtient 5,9 g de **4**. $Eb_{0,01}$: 93—94°C. Rdt.=92%.

Cetone Sabinique ***1***. Le carbamidate (4 g) (préparé en agitant 12 hr à température ambiante, 1,7 g de cétol **4**, 2,5 g de DCC et 50 mg de chlorure cuivreux), est chauffé à 150°C pendant 2 hr, la cetone sabinique étant distillée sous vide au fur et à mesure de sa formation. On obtient 1,25 g de cétone **1** (Rdt.=80%). Constantes en accord avec la littérature.[1,4]

7) K. Toki, Ce Bulletin, **32**, 233 (1959).

8) Des analyses et des spectres IR et de RMN corrects ont été obtenus pour les composés nouveaux décrits dans cet article.

SHORT COMMUNICATIONS

Studies on Chrysanthemate Derivatives. II.[1] Pyrolysis of Pyrethrin-I

Yasuo NAKADA, Yasuo YURA, and Keisuke MURAYAMA
Central Research Laboratories, Sankyo Co., Ltd., Hiromachi, Shinagawa-ku, Tokyo

(Received May 8, 1972)

Five compounds were obtained by the pyrolysis of allethrin.[2] In this communication we wish to report a new product obtained by the pyrolysis of pyrethrin-I.

Pyrethrin-I, cinerin-I, and jasmolin-I were advantageously separated from the mixtures extracted from pyrethrum flowers,[3] using a special column chromatography on silica gel impregnated with silver nitrate. Pyrolysis of pyrethrin-I was carried out at 400°C as reported previously.[2] The reaction products were separated into an acidic and a neutral fraction by alkaline extraction.

The acidic fraction gave chrysanthemic acid (I) as the only product.

The neutral fraction consisted of pyrocin (II) and a new compound (III) separated by column chromatography on silica gel. Compound III revealed the following spectral data; *m/e* 160 (M^+) and 145 (M-15); IR, ν_{max} cm^{-1}: 1680 and 1640; UV, $\lambda_{max}^{EtOH}m\mu$ ($\log \varepsilon$): 230 (3.50) and 319 (3.64); NMR,[4] a doublet methyl at 9.39 (3H; J=7.1 Hz), a singlet methyl at 8.87 (3H), a multiplet proton on a tertiary carbon at 7.73 (1H), and five olefinic protons at 3.70—3.90 (m, 3H), 3.41 (ddd, 1H; J=1.0, 2.1, and 5.0 Hz), and 2.55 (dd, 1H; J=1.0 and 6.0 Hz). Heating compound III with concentrated hydrochloric acid afforded a white crystalline substance, mp 84—86°C, which was designated as 4,5-dimethyl-1-indanone(IV) on the basis of the following mass, IR, UV, and NMR spectral data and by comparison with those of the independent synthetic product prepared from *o*-xylene using the method of Hart and Teble;[5] *m/e* 160 (M^+), 145 (M-15), and 132 (M-28); IR, ν_{max} cm^{-1}: 1709 and 818 (1,2,3,4-tetrasubstituted phenyl); UV, $\lambda_{max}^{EtOH}m\mu$ ($\log \varepsilon$): 258 (4.19) and 292 (3.46); NMR,[6] two singlet methyls at 7.80 (3H) and 7.67 (3H), two multiplet methylenes at 7.48 (2H) and 7.09 (2H), and two aromatic protons centered at 2.95 (d, 1H; J=4.0 Hz) and 2.65 (d, 1H; J=4.0 Hz).

From these results compound III is presumed to be 4,5-dimethyl-bicyclo[4.3.0]nona-2,6,8-triene.

We propose that the reaction mechanisms for the pyrolysis of pyrethrin-I and for the acid catalyzed rearrangement of compound III to compound IV take place as shown in Scheme 1 and 2, respectively.

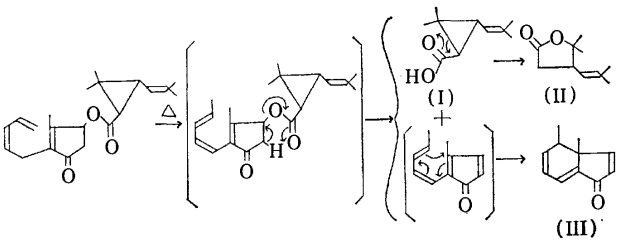

Scheme 1

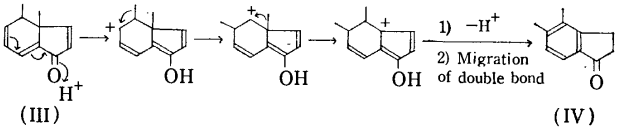

Scheme 2

1) The previous paper[2] is regarded as Part I of this series.

2) Y. Nakada, Y. Yura, and K. Murayama, This Bulletin, **44**, 1724 (1971).

3) R. M. Sawicki and E. M. Thain, *J. Sci. Food Agr.*, **12**, 137 (1961).

4) NMR spectra were determined at 60 MHz in CCl_4 and chemical shift is expressed in τ from internal TMS.

5) R. T. Hart and R. F. Teble, *J. Amer. Chem. Soc.*, **72**, 3286 (1950).

6) NMR spectra were determined at 100 MHz in CCl_4.

The Reaction of Trialkylboron and α-Lithiobenzyl-2-pyridyl or Phenylsulfide. A Convenient Method for the Preparation of Alkylbenzenes

Teruaki MUKAIYAMA, Shoji YAMAMOTO, and Manzo SHIONO

Laboratory of Organic Chemistry, Tokyo Institute of Technology, Ookayama, Meguro-ku, Tokyo

(Received May 6, 1972)

Recently it was shown[1] that benzyl-2-pyridylsulfide is easily metalated at −75°C in tetrahydrofuran by *n*-butyllithium or phenyllithium to give α-lithiobenzyl-2-pyridylsulfide, which in turn successfully reacts with various carbonyl compounds and halides.

Now we wish to report a new synthetic method for the preparation of alkylbenzenes by the use of the α-lithio derivatives of sulfides and trialkylborons.

It is well known[2] that trialkylboron reacts with the carbanion (I) to form the quaternary salt (II), in which subsequently one alkyl group migrates to a carbon atom from a boron atom to produce a new trialkylboron (III) accompanied with the elimination of ML as shown in Scheme 1.

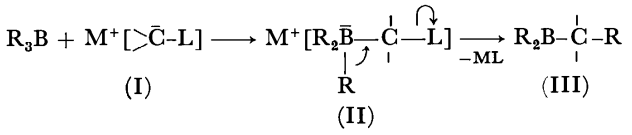

(I) (II) (III)

M: metal L: leaving group

Scheme 1

When the α-lithio derivative of benzyl-2-pyridylsufide or benzylphenylsulfide was treated at −75°C in tetrahydrofuran under argon atmosphere with tri-*n*-butylboron, the formation of the quaternary salt was observed. The salt was converted into two alkylbenzenes, *n*-amylbenzene and 1,2-diphenylhexane in 63% and 24% yields, respectively, after refluxing for 3 hr and alkaline hydrolysis. The products were identified on the basis of NMR spectra and gas chromatographical data.

In a similar way, various trialkylborons reacted with the α-lithio derivatives to give the corresponding alkylbenzenes. But tricyclohexyl and tricyclopentylboron failed to react with α-lithiobenzylphenylsulfide. The results are summarized in Table 1.

An undesirable by-product, diphenylethane derivative is considered to be formed by the further reaction of the new trialkylboron (III) and the α-lithio derivative.

Table 1. YIELDS OF TWO ALKYLBENZENES

R_3B	Isolated yield %			
	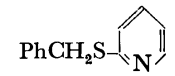		$PhCH_2SPh$	
	$PhCH_2R$	$PhCH_2$-CHPhR	$PhCH_2R$	$PhCH_2$-CHPhR
$(n\text{-}C_4H_9)_3B$	63	24	71	16
$(n\text{-}C_6H_{13})_3B$	70	23	75	20
$(n\text{-}C_8H_{17})_3B$	73	trace	61	12
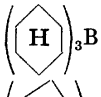	85	0	0	0
	83	0	0	0

In order to minimize the formation of the by-products, the reactions were tried in the presence of the additives which would facilitate the elimination of the mercapto group from the quaternary salt.

It was found that the addition of cuprous iodide at −75°C or dimethylsulfate at room temperature was effective for the prevention of the formation of the by-products in the reaction between trialkylboron and α-lithiobenzylphenylsulfide. In each case, the desired alkylbenzene was obtained in good yield without accompanying the formation of the by-product. The results are summarized in Table 2. The reaction is considered to proceed involving cuprous quaternary salt (IV) or sulfonium betaine (V) as shown in Scheme 2.

Table 2. YIELDS OF ALKYLBENZENES

R_3B	Isolated Yield % $PhCH_2R$	
	CuI	$(CH_3)_2SO_4$
$(n\text{-}C_4H_9)_3B$	92	78
$(n\text{-}C_6H_{13})_3B$	80	75
$(n\text{-}C_8H_{17})_3B$	69	63

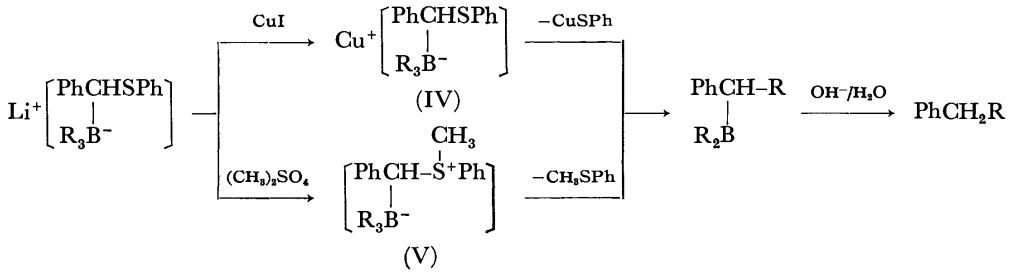

Scheme 2

1) T. Mukaiyama, K. Narasaka, K. Maekawa, and M. Furusato, This Bulletin, **44**, 2285 (1971).

2) J. J. Tufariello and L. T. Lee, *J. Amer. Chem. Soc.*, **88**, 4757 (1966); W. K. Musker and R. R. Stevens, *Tetrahedron Lett.*, **1967**, 995; J. Hooz and S. Linke, *J. Amer. Chem. Soc.*, **90**, 5936 (1968); H. C. Brown, M. M. Rogić, and M. W. Rathke, *ibid.*, **90**, 6218 (1968).

The Bromine Nuclear Quadrupole Resonance of the Molecular Complex of Aluminum Tribromide with Benzene

Tsutomu OKUDA, Yoshihiro FURUKAWA, and Hisao NEGITA
Department of Chemistry, Faculty of Science, Hiroshima University, Hiroshima
(Received January 26, 1972)

The bromine nuclear quadrupole resonance (NQR) and its Zeeman effect have been observed in the molecular complex of aluminum tribromide with benzene at room temperature. The resonance frequencies are 79.99, 90.10, and 91.18 MHz for ^{81}Br at 301°K. The asymmetry parameters of the field gradient are 28.9±1.1, 8.6±1.0, and 6.0±0.9% for the bromine atoms in the order of increasing resonance frequency. Aluminum tribromide forms the dimer in the complex crystal as well as in the pure state. The bond angle between a pair of terminal bromine atoms and the interbond angle at the bridging bromine atom are found to be 117.3±0.5° and 95.5±0.2° respectively; these values correspond to those of 122±2° and 87±2° obtained from the X-ray analysis. Furthermore, the charge-transfer from the benzene ring to the bromine atom is discussed on the basis of the NQR parameters.

It has been established that aluminum tribromide forms molecular complexes with many organic compounds, and they have been studied extensively by various methods. These complexes with organic compounds belong mostly to the type of $AlBr_3 \cdot D$,[1] where the aluminum atom coordinates the oxygen or nitrogen atom of the donor, D. There is also another type of complex, such as $Al_2Br_6 \cdot D$,[2] where the bromine atom may combine with the aromatic ring of a donor, D, such as benzene or toluene.

The NQR frequency depends on the electric-field gradient at the site of the resonant nucleus. As the bromine atom seems to be involved in the binding between the component molecules in the complex of $Al_2Br_6 \cdot D$, the Br NQR will clarify the extent and direction of the charge-transfer as well as the molecular structure of Al_2Br_6. In this respect, it will be interesting to examine the Br NQR of the $Al_2Br_6 \cdot C_6H_6$ complex and to observe the Zeeman effect on the NQR, using the single crystal of the complex.

Concerning aluminum tribromide itself, both the Al[3] and Br NQR frequencies[4] as well as the Br Zeeman effect[5] have been measured. The ^{81}Br NQR spectrum is composed of the singlet of 81.82 MHz and the doublet of 95.01 and 96.43 MHz at 77°K. The singlet was attributed to the bridging bromine atom, and the doublet, to the two different sites of the terminal bromine atoms in the dimer. NQR studies of the bromine atoms in some complexes of $AlBr_3 \cdot D$ have been reported,[6] but none on the complex of $Al_2Br_6 \cdot D$ are known to us.

According to the crystal structure of $Al_2Br_6 \cdot C_6H_6$ established by X-ray analysis,[7] the space group is C_i, with one species, $Al_2Br_6 \cdot C_6H_6$, in a unit cell of the dimensions of $a=6.85$ Å, $b=6.91$ Å, $c=9.00$ Å, $\alpha=104.6°$, $\beta=103.1°$, and $\gamma=90.0°$. The aluminum tribromide molecule in the complex was confirmed to form the dimer as in its pure crystal, and the centers of both the Al_2Br_6 and C_6H_6 components are centrosymmetric. Figure 1 shows the crystal structure projected along the b axis. The shortest distance between the layer of the bromine atoms and the plane of the benzene ring is 3.2 Å.

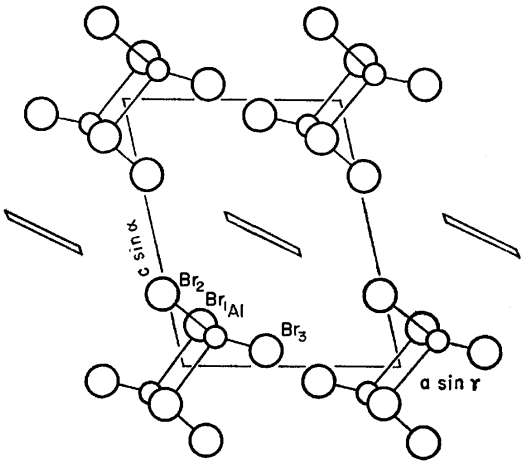

Fig. 1. Crystal structure of $Al_2Br_6 \cdot C_6H_6$ projected along b axis.

Experimental

Aluminum tribromide was prepared by dropping liquid bromine into aluminum metal and was purified by distillation several times. The purification of benzene and the synthesis of the complex were performed with reference to the literature.[7] The single crystal of the complex was obtained by lowering an ampoule of the saturated benzene solution of aluminum tribromide slowly through an electric furnace at about 40°C.

The NQR spectrometer employed was a superregenerative oscillator with frequency modulation, and the absorption lines were displayed on an oscilloscope. The resonance frequencies, ν, were measured with a standard frequency generator whose frequency was determined by means of a universal counter, TR-5578, of the Takeda Riken Industry

1) M. J. Sienko, R. A. Plane, and R. E. Hester, "Inorganic Chemistry," Benjamin, Inc. New York (1965), Part 2, p. 91.

2) H. C. Brown and W. J. Wallace, *J. Amer. Chem. Soc.*, **75**, 6265 (1953).

3) P. A. Cassabella, P. J. Bray, and R. G. Barnes, *J. Chem. Phys.*, **30**, 1393 (1959).

4) R. G. Barnes and S. L. Segel, *ibid.*, **25**, 180 (1956).

5) T. Okuda, H. Terao, O. Ege, and H. Negita, *ibid.*, **52**, 5489 (1970).

6) Yu. K. Maksyutin, E. V. Bryukhova, G. K. Semin, and E. N. Cur'yanova, *Izv. Akad. Nauk SSSR. Ser. Khim.*, **1968**, 2658.

7) D. D. Eley, J. H. Taylor, and S. C. Wallwork, *J. Chem. Soc.*, **1961**, 3869.

Co., Ltd. The Zeeman effect was measured by means of the zero-splitting cone method in the low-magnetic field. The magnetic field of about 300 gauss was supplied by a Helmholtz coil, and the patterns of the zero-splitting loci were observed at room temperature.

Results and Discussion

The observed NQR frequencies for the bromine atoms in the complex at 301°K are listed in Table 1.

TABLE 1. ^{81}Br NQR PARAMETERS OF $Al_2Br_6 \cdot C_6H_6$ AND Al_2Br_6 AT 301°K

Compound	ν (MHz)	e^2Qq (MHz)	η (%)	ρ
$Al_2Br_6 \cdot C_6H_6$	79.99	157.8	28.9±1.1	0.45
	90.10	180.0	8.6±1.0	0.67
	91.18	182.3	6.0±0.9	0.67
Al_2Br_6	79.85	158.1	24.8[a]	0.45
	92.36	184.6	7.3[a]	0.66
	93.47	186.6	10.6[a]	0.66

a) Ref. 5

The spectrum of each bromine isotope consists of three resonance lines; in the case of ^{81}Br, the singlet is about 10 MHz below the doublet in the 90 MHz region, and three lines have almost the same intensity. This feature of the spectrum and the asymmetry parameters calculated from the Zeeman effect are quite similar to those in pure aluminum tribromide and other trihalides of the IIIb group.[4,8] Therefore, the two resonance lines in the 90 MHz region may be ascribed to two kinds of terminal bromine atoms, and the remaining one, to the bridging bromine atom.

Bond Angle. The zero-splitting patterns observed are shown in Fig. 2, where Br_1, Br_2, and Br_3 are the directions of the z axes of the field gradient on the bromine atoms contributing to the resonance frequency, in order from the lower to the higher. The asymmetry parameter, η, and the quadrupole coupling constant, e^2Qq, may be determined from the following relation:[9]

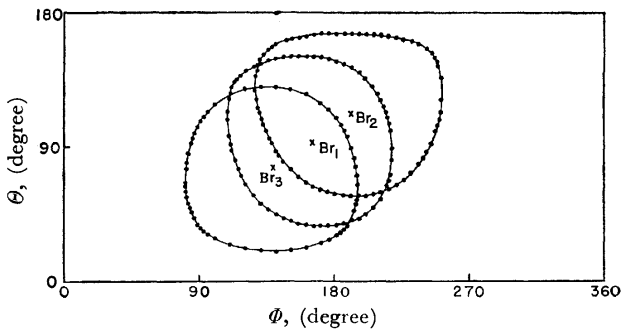

Fig. 2. Zero-splitting patterns of Zeeman lines of $Al_2Br_6 \cdot C_6H_6$. The axis of $\Theta=0$ is taken as the rotational axis of the sample tube. The plane of $\Phi=0$ is arbitrarily chosen.

$$\eta = 3(\sin^2\theta_{max} - \sin^2\theta_{min})/(\sin^2\theta_{max} + \sin^2\theta_{min}) \quad (1)$$

$$\nu = \tfrac{1}{2} e^2Qq(1+\eta^2/3)^{1/2} \quad (2)$$

where θ_{max} and θ_{min} are the maximum and minimum zero-splitting angles corresponding to the directions of the x and y axes of the field gradient respectively. The values of η and e^2Qq are listed in Table 1, along with those of pure aluminum tribromide. The z axes on the monovalent bromine atoms, Br_2 and Br_3, are usually parallel to the relevant bond directions. The bond angle, α, and the asymmetry parameter, η, at Br_1 are related by the following equation[3] under the coordinate system of the field gradients, as is shown in Fig. 3:

$$\eta = -3\cos\alpha. \quad (3)$$

The molecular shape of aluminum tribromide in the complex thus obtained is shown in Fig. 3; it is similar

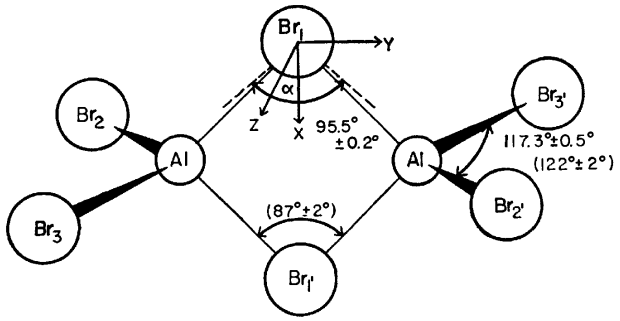

Fig. 3. The coordinate system of the principal field gradient on the bridging bromine atom and the molecular shape of Al_2Br_6 in $Al_2Br_6 \cdot C_6H_6$. Values in parenthsis are cited from the X-ray analysis.

to that in the pure state.[5] The agreement of the results of the NQR with those of the X-ray analysis is fairly good for the $\angle Br_2$–Al–Br_3 angle, but not good for the $\angle$Al–Br_1–Al angle. This discrepancy is probably caused by the bent bond, as is the case in pure Al_2Br_6[5] and Ga_2Cl_6.[10]

The z axis of Br_1 is parallel to the plane including the z axes of Br_2 and Br_3, as may be seen in Fig. 2. The angles which the z axis of Br_1 makes with those of Br_2 and Br_3 are 30.5° and 32.2° respectively.

Intramolecular and Intermolecular Bonds. The asymmetry parameter depends on the unbalance of the π-electrons of the atom and on the intermolecular interaction, as is seen in the case of solid iodine.[11] Fairly large values of η for the terminal bromine atoms are observed, so the intermolecular interaction can not be ignored in the solid state. In this complex, two kinds of intermolecular interaction are possible. One would be that between a given terminal bromine atom and the nearest bromine of the neighboring Al_2Br_6 molecule. There are short interatomic distances, 3.7Å and 3.9Å for $Br_3 \cdots Br''_3$ and $Br_2 \cdots Br'_1$ whereas the sum of the van der Waals radii of the

8) S. L. Segel and R. G. Barnes, *J. Chem. Phys.*, **25**, 578 (1956); R. G. Barnes, S. L. Segel, P. J. Bray, and P. A. Cassabella, *ibid.*, **26**, 1345 (1957).

9) T. P. Das and E. L. Hahn, "Nuclear Quadrupole Resonance Spectroscopy," Solid State Physics, Suppl. 1, Academic Press, New York (1958).

10) G. E. Peterson and P. M. Bridenbaugh, *J. Chem. Phys.*, **51**, 238 (1969).

11) Ref. 9, p. 173.

bromine atoms is 3.90Å. The shorter distance for $Br_3\cdots Br''_3$ is evidently ascribable to the intermolecular bonding. The $\angle Al\text{–}Br_3\cdots Br''_3$ angle is about 140°, whereas the $\angle Al\text{-}Br_2\cdots Br'_1$ angle is 90°. Accordingly the η of Br_2 can be expected to be larger than that of Br_3. This is really the case.

The other intermolecular interaction may be seen between the bridging bromine atom and benzene. The interatomic distance for $Br_1\cdots C$ is 3.7Å, which is comparable to the sum of the van der Waals radii, 3.65Å. The interaction seems to be smaller than the $Br_3\cdots Br''_3$ bonding. All the other distances between bromine and carbon atoms are not less than 4Å.

The quadrupole coupling constant of the bromine atom depends primarily on its own bonding electron population. If the charge transfers from the benzene to the bromine atom, the e^2Qq value of the atom may be expected to decrease due to an increase in its electronic charge. As can be seen from Table 1, the e^2Qq values of the terminal bromine atoms are lower by about 4 MHz than those of pure aluminum tribromide. On the other hand, the shift of the e^2Qq of the bridging bromine atom is only 0.3 MHz. According to Townes and Dailey, the field gradient can be ascribed to $4p$ electrons of the bromine atom, and one may calculate the number of the electrons, ρ, which the bromine atom gains from its own molecule and neighboring ones. The equations used here are

$$\rho = 1 - Up/0.85 \tag{4}$$

for the terminal bromine atom, and

$$\rho = (1+2\,Up)/(1-2\,\varepsilon\,Up) \tag{5}$$

for the bridging bromine atom,[3] where Up is the number of unbalanced p electrons and where ε, which is estimated to be 0.25, is a known factor. These values of ρ are listed in Table 1. Those at the terminal Br_2 and Br_3 of the complex are increased by only 0.01, and that of the bridging Br_1 remains almost unchanged in comparison with those of pure aluminum tribromide. Therefore, taking account of the asymmetry parameters and the quadrupole coupling constants at the bromine atoms in the complex, it may be suggested that the charge transfer if any, takes place from the benzene to the terminal bromine atoms.

BULLETIN OF THE CHEMICAL SOCIETY OF JAPAN, VOL. 45, 2247—2250 (1972)

The Photo-induced Electron Transfer Reactions between Crystals of Aromatic Hydrocarbons and Quinones

Mitsuyuki SOMA

Department of Chemistry, Faculty of Science, The University of Tokyo, Hongo, Tokyo

(Received December 6, 1971)

The photo-induced electron transfer reactions between crystals of aromatic hydrocarbons and several quinones were studied by measuring the increase of the photocurrent in the crystals due to the carrier injection from the ethanol electrode containing the quinones. The reaction rates were shown to be independent of sorts of quinones used when its concentration was sufficiently high. The excitation limited mechanism of the reaction was proposed to be consistent with this behavior and the observed concentration dependence of the reaction.

It has been reported previously[1,2] that the photo-induced electron transfer reaction occurs with high efficiency between a crystal of aromatic hydrocarbon and a π-electron acceptor dissolved in the liquid electrode contracted with the crystal. The rate of the electron transfer reaction is proportional to the saturation value of the photo-hole-current in the crystal which is attained by applying sufficiently high voltages.

In such cases as the photo-hole injection from tetrachloro-phthalonitrile into anthracene crystals, the saturation photocurrent depends linearly upon the concentration of added electron acceptor. On the other hand when *p*-benzoquinone is used as an acceptor, the saturation photocurrent begins to deviate from the linear dependence as the concentration increases and reaches a limiting value. This behavior was attributed tentatively to the electron transfer including *p*-benzoquinone adsorbed on the surface of the crystal.

It is reported in this paper that this feature is found generally in the photo-induced electron transfer reactions between the crystals of aromatic hydrocarbons and quinones with fairly high electron affinities, and the evidences which suggest another explanation for this behavior are presented

Experimental

The measuring procedures for the photocurrent in the crystals due to the photo-induced hole injection from the liquid ethanol electrode were the same as previously described[1] where the simplified type of Kallmann- and Popes' cell[3] was used. Thin platelets of single crystals of the aromatic hydrocarbons, anthracene, naphthacene, perylene, and *p*-terphenyl were prepared following the method previously reported.[2] All the quinones except *o*-chloranil were of com-

1) M. Soma, *J. Amer. Chem. Soc.*, **92**, 3289 (1970).
2) A. Yamagishi and M. Soma, This Bulletin, **43**, 3741 (1970).
3) H. Kallmann and M. Pope, *Rev. Sci. Instr.*, **30**, 44 (1959).

mercial source, purified by recrystallization and by sublimation if possible. *o*-Chloranil was synthesized according to Brook,[4] purified by recrystallization from carbon tetrachloride and by sublimation.

Results

Figure 1 shows changes in the saturation photo-hole-current in an anthracene single crystal with the

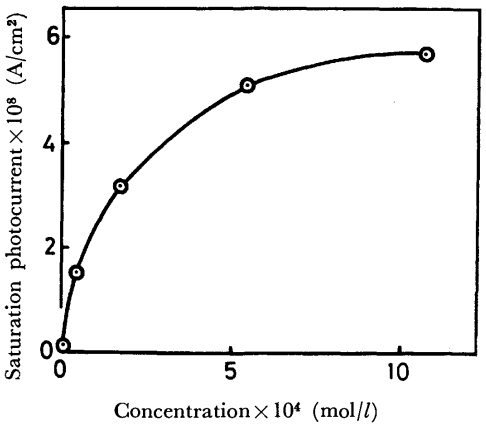

Fig. 1. Changes in the saturation photocurrent in anthracene crystal with the concentration of added *p*-chloranil.
Electrode arrangement, water|crystal|ethanol+*p*-chloranil, water electrode illuminated by 4010 Å light, ethanol electrode biased positive.

concentration of *p*-chloranil added to the dark side (back face concerning to the direction of illumination) electrode. The crystal was excited by the light of wavelength at 4010 Å. As the back face electrode was positively biased, the observed photocurrent was attributed to the hole injection from the electrode, *i.e.* to the photo-induced electron transfer reaction between the excited anthracene crystal and *p*-chloranil. The saturation photocurrent reached to the certain limiting value as the concentration of *p*-chloranil increased. This behavior of concentration dependence of the photocurrent was already reported for the anthracene crystal/*p*-benzoquinone system,[1] and now, was found to be a general feature of the photo-induced electron transfer between excited aromatic hydrocarbons and various quinones. Figures 2a and 2b exemplify this behavior in the perylene crystal/*p*-benzoquinone, and the naphthacene crystal/*o*-chloranil systems. In these cases the crystals were illuminated at 5025 Å. Perylene and naphthacene have considerably lower ionization potentials than holes from the electrode to the crystal. The electron transfer reaction from the aromatic crystals to the quinones occurred without photo-excitation. In Figs. 2a and 2b, the concentration dependence of the dark injection was shown for comparison. They are quite different from those of the photo-injection. The dark currents were almost proportional to the concentration of the added electron acceptors in the concentration range studied.

This fact suggests that there might be specific

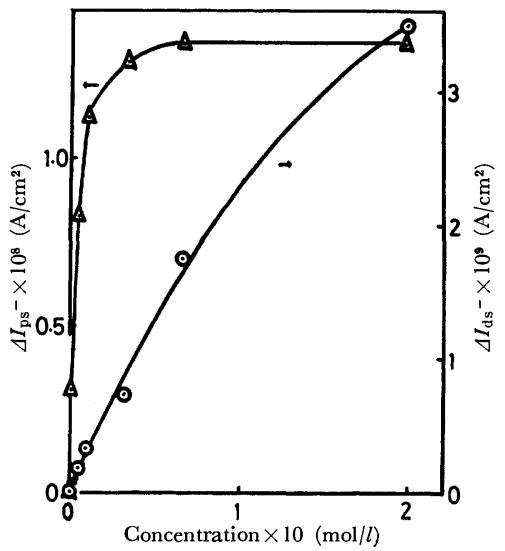

a) perylene crystal/*p*-benzoquinone system excited by 5020 Å

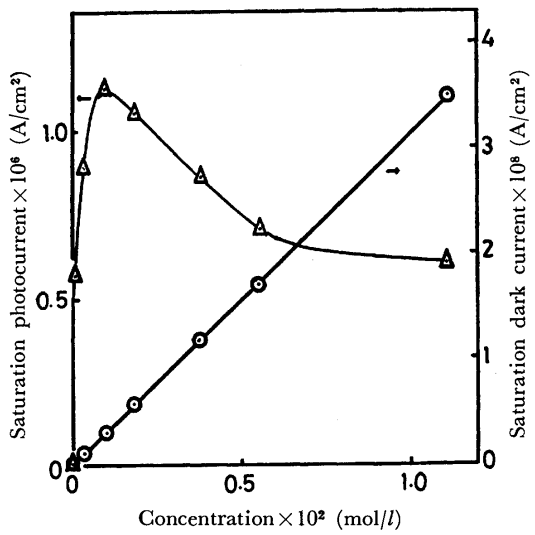

b) tetracene crystal/*o*-chloranil system excited by 5020 Å

Fig. 2. Changes in the saturation photo-(ΔI_{ps}^-) and dark (ΔI_{ps}^-) current in the aromatic hydrocarbons with the concentration of the added acceptors.
Electrode arrangements were the same with Fig. 1.

circumstances causing the appearance of the limiting values in the photocurrents but not in the dark current. To get more information about the phenomena, the photo-induced electron transfer reactions with various quinones as electron acceptor were compared. Two types of comparison were made.

The relative limiting values of the saturation photo-hole current in an anthracene crystal with four quinones as electron acceptor are shown in Table 1. In the last column are the reduction potentials of the quinones[5] which are the measure of their electron affinities in the polar organic solvents. The limiting values were attained at the lower concentrations of the acceptor, the larger the electron affinity (smaller the reduction potential) of the acceptor was. Although the electron affinity varies in fairly wide range

4) A. G. Brook, *J. Chem. Soc.*, **1952**, 5040.

5) Data sited in G. Briegleb, *Angew. Chem.*, **76**, 326 (1964).

TABLE 1. RELATIVE LIMITING VALUES OF THE INCREASE IN THE PHOTO-HOLE-CURRENT (ΔI_{ps}) FOR THE ANTHRACENE CRYSTAL/QUINONE SYSTEMS[a)]

Acceptor	Concentration mol/l	Relative limiting value of ΔI_{ps}	Reduction potential[5)] $E_{1/2}^{red}$ (volts)
p-chloranil	1.62×10^{-3}	1	−0.01
2,6-dichloro-p-benzoquinone	6.02×10^{-3}	0.93—1.04	0.18
p-benzoquinone	1.56×10^{-2}	0.86—0.91	0.51
1,4-naphtoquinone	2.28×10^{-2}	0.77—0.78	0.71

a) Electrode arrangement, water|crystal|ethanol+quinone, water electrode illuminated by 4010Å light, ethanol electrode biased positive.

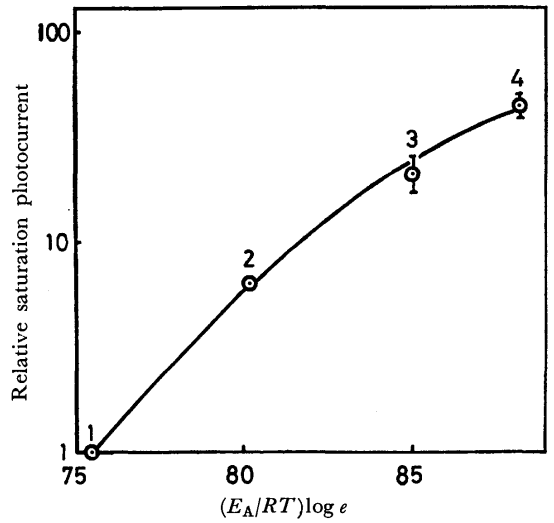

a) anthracene crystal/quinone systems excited by 4010 Å light.

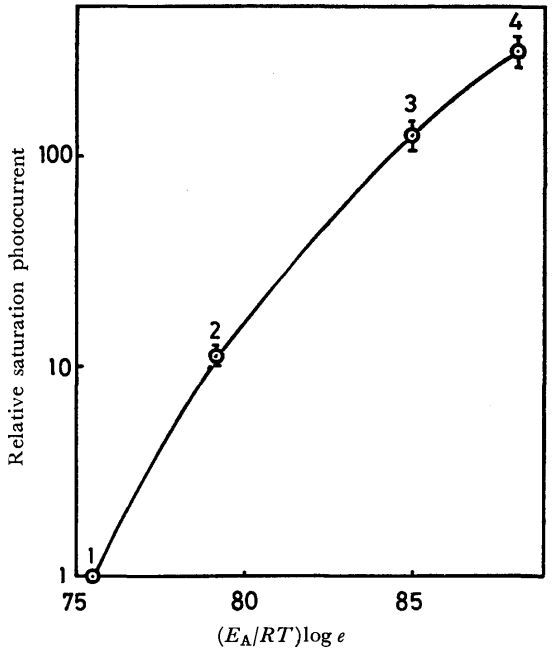

b) tetracene crystal/quinone systems excited by 5020 Å light.

Fig. 3. Dependence of the saturation photocurrent upon the electron affinity(E_A) of the quinones. The photocurrent was normalized per unit concentration. Electrode arrangements were the same with Fig. 1.

among the quinones used, the differences in the limiting values of the photocurrents were small. The limiting values of the photocurrents in the naphthacene crystal with p-chloranil and 2,6-dichloro-p-benzoquinone as acceptors were also roughly the same, while with p-benzoquinone it gave substantially smaller limiting value (one third or one fourth of the former). The latter might be attributed, at least partly, to the presence of another concentration effect which caused the photocurrent to decrease below the limiting value with further increasing the concentration as was the case in the naphthacene crystal/o-chloranil system shown in Fig. 2b.

The second comparison was made in the small concentration region where the photocurrent was almost proportional to the concentration of the electron acceptor. In Fig. 3, the relative saturation photocurrents normalized per unit concentration in anthracene and naphthacene crystals are plotted aginst the electron affinities of the various quinones.

Discussion

The saturation photocurrent I_{ps} attained by applying sufficiently high voltage can be related to the number of holes, n, injected per unit time by the following equation.

$$n = \frac{F}{q} I_{ps} \tag{1}$$

where F is Faraday constant and q is the charge of an electron. Accordingly, changes in the saturation photo-hole-current upon the addition of the electron acceptor are the direct measure of the rate of the electron transfer reactions between the excited crystal and the electron acceptor. The rate of the photo-induced electron transfer reaction was shown to have a different concentration dependence from that of the electron transfer reaction in the dark. It reached a limiting value.

In the case of the anthracene crystals the limiting value was almost independent of the acceptor as demonstrated in Table 1. The steady state for the concentration of the excited molecule M* in the lowest singlet excited state in the surface molecular layer of the crystal might be expressed as follows

$$p - \{k_f + k_d + k_e[A]\}[M^*] = 0, \tag{2}$$

where k_f is the fluorescence life time of M*, k_d nonradiative decay constant of M*, k_e rate constant of the electron transfer reaction between M* and the acceptor molecule A, [A] the concentration of the acceptor molecule, and p is the rate of the production of the excited molecule M* at the surface, including those produced by direct excitation and by excitation migration. The rate of electron transfer reaction, $R=k_e\cdot[A][M^*]$, therefore, using Eq. (2) is expressed by

$$R = \frac{k_e p[A]}{k_f + k_d + k_e[A]} \quad (3)$$

If the concentration of the acceptor is sufficiently high, so that $k_e[A] \gg k_f + k_d$, R reaches to the limiting value as was experimentally observed. In these cases, the rate is limited by the rate of the production of the excited molecules, p. Equation (3) can also be expressed in the following form

$$\frac{[A]}{R} = c_1 + c_2[A], \quad (4)$$

where c_1, c_2 are constants. This type of concentration dependence of R,*i.e.* concentration dependence of the saturation photo-hole-current was reported previously in the case of the anthracene crystal/*p*-quinone system[1] and now proved to be generally the case as exemplified by the anthracene/*p*-chloranil system (Fig. 1). It was attributed tentatively to the formation of the adsorbed layer of the acceptor molecule. However, the present with the acceptor-independent limiting value of the saturation photo-current is preference of the excitation limited mechanism.

The electron transfer reaction from excited anthracene crystal to organic electron acceptors were shown to be a very efficient process.[1,2] In fact, the limiting values of the saturation photocurrent in the anthracene and naphthacene crystal were at least several times as large as the photocurrent due to the photo-induced hole injection from the aqueous electrode, whereas the quantum efficiencies for the hole injection were reported to be 0.033 (at 3650Å)[6] and 0.075 (at 5050Å)[7] respectively.

The relative photo-currents in the smaller concentration region are the direct measure of the rate constant, k_e, of the electron transfer reaction between the excited aromatic molecule at the surface and the quinones, if the reaction is assumed to occur *via* direct collision of the excited molecule and the electron acceptors. In this case the rate constant may be expressed in the conventional equation.

$$k_e = Z \exp(-\Delta F^{\ddagger}/RT) \quad (5)$$

where Z is the collision number and $\Delta F^{\ddagger}$ is the free energy of activation. On the other hand, the standard free energy of the reaction ΔF° is expressed as follows

$$\Delta F^{\circ} = I_c - E_a - E_x \quad (6)$$

where I_c is the ionization potential of the crystal, E_a is electron affinity of the quinone including the solvation energy, and E_x is the energy supplied by light. For the same crystal only E_a is changed in Eq. (6) from one acceptor to another. The collision number Z in Eq. (5) can be reasonably assumed to be the same for all the quinones used. In such circumstances, Figs. 3a and 3b represent the relation between the rate constant or the free energy of activation and the changes in the standard free energy of reaction. The observed increase in the rate constant with the increasing electron affinity of the acceptor is in accordance with trend of the efficiency of acceptors in quenching the fluolescence of aromatic hydrocarbons in solution *via* the electron transfer reaction.[8]

The larger the reaction rate constant, the limiting value was attained at the lower concentration of the acceptor, which is again consistent with Eq. (3).

The author wishes to express his gratitude to Professor Kenzi Tamaru for his constant encouragements through the work.

6) H. Kallmann and M. Pope, *Nature*, **185**, 753 (1960).

7) N. Geacintov, M. Pope, and H. Kallmann, *J. Chem. Phys.*, **45**, 2639 (1966).

8) A. Nakajima and H. Akamatu, This Bulletin, **41**, 1961 (1968).

BULLETIN OF THE CHEMICAL SOCIETY OF JAPAN, VOL. 45, 2250—2254 (1972)

Ternary Lamellar Compounds of Graphite with Aluminum Bromide and Bromine

Tadashi SASA, Yoichi TAKAHASHI, and Takashi MUKAIBO

Department of Nuclear Engineering, The University of Tokyo, Hongo, Bunkyo-ku, Tokyo

(Received December 7, 1971)

Graphite was allowed to react with binary reactants of aluminum bromide and bromine. The formation of ternary lamellar compounds was observed. A change in the activity of the reactants in the system gave three compounds I, II, and III with different contents of aluminum bromide and bromine. Compound I, obtained as the reaction product of graphite with the solution of bromine saturated with aluminum bromide, has a composition of $C_9AlBr_3 \cdot Br_2$, and a lamellar structure of the first stage with I_c of 10.24 Å. Compound II, which has the lowest bromine content, has a composition of $C_{24}AlBr_3 \cdot Br_{0.3}$ and a lamellar structure of the second stage with I_c of 13.35 Å. Compound III, obtained at a bromine activity higher than that for compound I, has a non-stoichiometric composition of about $C_{5-6}Br(AlBr_3)_{0.2}$, and a structure of the second stage with I_c from 13.58 to 13.72 Å. The phase diagram of the ternary system was derived. Compounds I and III have higher bromine contents than C_8Br, which is the saturation compound of graphite-bromine system. This is supposed to be due to the stabilization of bromine by the coexistence of aluminum bromide.

There are a large number of chemical substances which react with graphite to form lamellar compounds. In some cases, two different chemical species are intercalated together in the graphite crystal. They are called ternary lamellar compounds. Halogens and alkali metals form a type such as $C_8Br_xCl_{1-x}$[1] or

1) G. Furdin, B. Bach, and A. Herold, *C. R. Acad. Sci. Paris, Ser. C*, **271**, 683 (1970).

$C_8Cs_xRb_{1-x}$.[2] These compounds are considered to be a solid solution of two kinds of binary lamellar compounds. Most ternary lamellar compounds known, such as $C_nCl(AlCl_3)_3$,[3] are defined to be compounds containing three components. It is peculiar that the mole ratio of the two reactants takes a fixed value in the ternary lamellar compound of this type. In many cases, the reactant does not react with graphite by itself and requires another component for the lamellar reaction to occur. Hennig[3] studied the lamellar compounds of this type extensively, especially on the ternary system of graphite–metal chloride–chlorine.[3,4] Alkali or alkaline-earth metals[5] are also known to form this type of graphite compound with ammonia. Other graphite compounds of the ternary system containing alkali metals have recently come to be known.[6,7] However, most of them are studied under limited conditions and what the phases with respect to the compositions and structures in each ternary system are not known.

The authors[8] reported that aluminum bromide ($AlBr_3$) forms a ternary compound of graphite in the presence of bromine. In the present study, the compositions and structures of the ternary lamellar compounds of graphite–$AlBr_3$–Br_2 were investigated in detail under the conditions of various activities of bromine and aluminum bromide.

Experimental

Materials. The following two types of graphite were used.

(1) Natural graphite with pitch-binder, heat-treated at 3000°C, $c_0=6.708\pm0.002$ Å.

(2) Pyrolytic graphite deposited at 1700°C and heat-treated at 3000°C, $c_0=6.712\pm0.002$ Å.

GR-grade bromine was distilled and passed through concentrated sulfuric acid before use. Aluminum bromide was prepared by the reaction between aluminum chips of high purity and bromine vapor and the following distillation to remove excess free bromine and aluminum.

Formation of the Ternary Compounds and X-ray Structural Analysis. The ternary compounds of graphite–$AlBr_3$–Br_2 were prepared by the direct reaction of graphite and a liquid mixture of $AlBr_3$ and Br_2. Pyrolytic graphite, about 0.5 mm in thickness, was placed in an evacuated glass bulb, which was connected by a constriction to another bulb containing the mixture of the reactants. In some cases bromine was doped directly to the graphite sample into the form of a residue compound. The graphite sample was exposed to the reactant liquid at 120°C for 24 hr. The whole system was then cooled gradually for 24 hr to attain equilibrium at room temperature (25°C). The excess reactant condensed on the surface of the sample was removed carefully by evaporation during the course of cooling.

The changes in weight and macroscopic thickness of the sample were measured after the reaction. The sample was taken out of the glass tube in an atmosphere of dry argon and mounted on a sample holder for X-ray diffraction. The front surface of the sample was then covered with a Teflon sheet 0.05 mm thick to prevent decomposition in the air. X-ray diffraction measurements were carried out by means of a G. M. counter with a strip-chart recorder.

Chemical Analyses of the Compounds. The sample of the ternary compound prepared from natural graphite was heated in vacuum at 500°C for the decomposition. The released $AlBr_3$ and Br_2 were collected separately, and their amounts were determined by both weight measurements and chemical analyses. After decomposition, a few per cent of the reactants was found to remain persistently in the graphite sample. The residue compound was burnt at 1200°C in a stream of air for the determination of Al in the form of Al_2O_3, from which the amounts of $AlBr_3$ and Br_2 contained in the compound were estimated. The total content of each reactant was determined as the sum of the amounts of released and residual reactants. The original weight of the graphite sample was used as the amount of carbon in the ternary compound.

The samples prepared from pyrolytic graphite were found to be inadequate for chemical analyses, as their decomposition was much more difficult than that of the samples prepared from natural graphite. It was confirmed that the samples prepared from the two different types of graphite had nearly the same contents of reactants under the same conditions of reaction.

Results

(1) Formation of Ternary Compounds. The change of composition of the ternary compound with the increase of activity of bromine with activity of $AlBr_3$ fixed at unity is shown in Fig. 1. As the solubility of $AlBr_3$ in Br_2 liquid is known to be about 40 mol% at 25°C,[9] the activity of $AlBr_3$ remains at unity until Br_2 content exceeds 60 mol% in the binary reactant.

We investigated the relation between the content of $AlBr_3$ and that of Br in the ternary compound over relatively low range in bromine content, where the

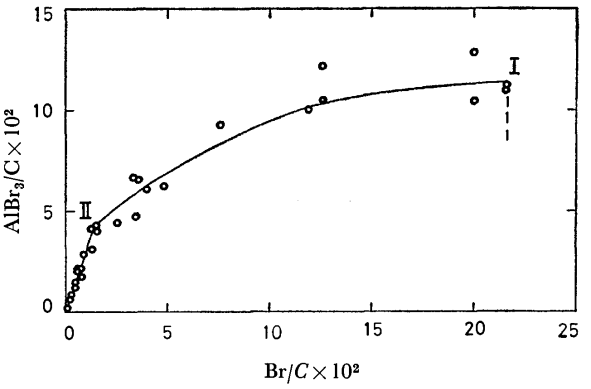

Fig. 1. Compositions of ternary lamellar compounds of graphite with $AlBr_3$ and bromine, while the activity of $AlBr_3$ is unity.

2) D. Billaud and A. Herold, *ibid.*, **269**, 490 (1969).

3) M. L. Dzurus and G. R. Hennig, *J. Amer. Chem. Soc.*, **79**, 1051 (1957).

4) W. Rüdorff, E. Stumpp, W. Spriessler, and F. W. Siecke, *Angew. Chem.*, **75**, 130 (1963).

5) W. Rüdorff, S. Schulze, and O. Rubisch, *Z. Anorg. Allgem. Chem.*, **282**, 232 (1955).

6) M. Nomine and L. Bonnetain, *J. Chim. Phys.*, **66**, 1731 (1969).

7) D. Ginderow and R. Setton, *Carbon*, **6**, 81 (1968).

8) T. Sasa, Y. Takahashi, and T. Mukaibo, This Bulletin, **45**, 937 (1972).

9) J. J. Burbage and A. B. Garrett, *J. Phys. Chem.*, **56**, 730 (1952).

ratio of $AlBr_3$ to Br was found to be nearly three up to the bromine content of Br/C=0.14[8] (Fig. 1). Beyond this bromine content, the ratio of $AlBr_3$ to Br decreased so that a distinct break of the curve was observed. This break point (II, Fig. 1) corresponds to an approximate atomic composition of $C_{24}AlBr_3 \cdot Br_{0.3}$. Beyond point II, the composition changes along a line extending to point I. The compound corresponding to I was obtained when the sample was kept in equilibrium with the solution of bromine saturated with $AlBr_3$ at room temperature. The contents of the reactants in compound I were determined by chemical analysis to be $AlBr_3$/C=0.11±0.02 and Br/C=0.22± 0.02 in mole ratio, which lead to an approximate composition of $C_9AlBr_3 \cdot Br_2$.

(2) Compounds I and II. It is remarkable that compound I ($C_9AlBr_3 \cdot Br_2$) had a bromine content far higher than C_8Br, which is the saturation compound of the binary system of graphite–bromine. The formation of compound I was accompanied by a considerable dimensional change and a distinct color change of the graphite. The samples prepared from the pyrolytic graphite gave a thickness about three times as large as the original samples and a dark green color with metallic luster. Compound I was hygroscopic and unstable in the air, and easily released bromine vapor. It decomposed to compound II in a vacuum at room temperature.

Compound II had the same black color as that of the original pyrolytic graphite, and its macroscopic thickness was about twice as large as that of the original one. Although compound II was comparatively stable, a gradual decomposition was observed in moist air.

The results of X-ray study of compounds I and II prepared from pyrolytic graphite sample are shown in Tables 1 and 2. The lattice constant I_c indicates the distance from one reactant layer to the next along the direction of *c*-axis, neglecting the AB stacking of carbon layers or reactant layers. The results shown in Table 1, together with the observations of the macroscopic dimensional change of the sample along the direction of *c*-axis, lead to the conclusion that compound I has a structure of the first stage, where every layer spacing of graphite is intercalated by reactants and expands from 3.35 Å to 10.24 Å. It is concluded also, from the results shown in Table 2, that compound II has a structure of the second stage with an expansion of every other carbon layer spacing from 3.35 Å to 10.00 Å.

TABLE 1. X-RAY DIFFRACTION PATTERNS OF COMPOUND I
$C_9AlBr_3 \cdot Br_2$, I_c=10.24Å, Cu$K\alpha$

0 0 *l*	$2\theta^\circ_{obs}$	$2\theta^\circ_{calc}$	Intensity (obs)
0 0 1	8.7	8.6	59
0 0 2	17.3	17.3	50
0 0 3	26.2	26.1	1000
0 0 4	34.9	35.0	66
0 0 5	44.2	44.2	8
0 0 6	53.6	53.7	385
0 0 7	63.5	63.6	22
0 0 8	—	74.0	—
0 0 9	85.3	85.3	88
0 0 10	97.6	97.6	9
0 0 11	—	111.7	—
0 0 12	128.9	128.9	34

TABLE 2. X-RAY DIFFRACTION PATTERNS OF COMPOUND II
$C_{24}AlBr_3 \cdot Br_{0.3}$, I_c=13.35Å, Cu$K\alpha$

0 0 *l*	$2\theta^\circ_{obs}$	$2\theta^\circ_{calc}$	Intensity (obs)
0 0 1	6.7	6.6	6
0 0 2	13.3	13.3	29
0 0 3	20.0	19.9	45
0 0 4	26.7	26.7	1000
0 0 5	33.6	33.6	24
0 0 6	40.5	40.5	19
0 0 7	47.8	47.7	9
0 0 8	55.0	55.0	297
0 0 9	62.6	62.6	9
0 0 10	70.6	70.5	4
0 0 11	—	78.8	—
0 0 12	87.7	87.7	79
0 0 13	97.5	97.3	6
0 0 14	—	107.8	—
0 0 15	—	119.9	—
0 0 16	134.7	134.7	30

The X-ray study on the sample with an intermediate composition between the compounds I and II showed the coexistence of these two phases, no other intermediate phase being observed. The X-ray diffraction pattern of the sample with the reactant contents below that of compound II showed a mixture of patterns of original graphite and compound II.

(3) Intermediate Phase between Compound I and C_8Br. The reaction of graphite with the binary solution of $AlBr_3$ and Br_2 was carried out, in which the activity of $AlBr_3$ was changed from zero to unity. The change of the composition of the compound with the change of activity of $AlBr_3$ is shown in Fig. 2. The diversity of the results of chemical analyses might be attributed to the possible errors caused by the condensation of excess reactants or decomposition of the compounds during the course of removing excess reactants. The curve in Fig. 2, which extends from C_8Br to compound

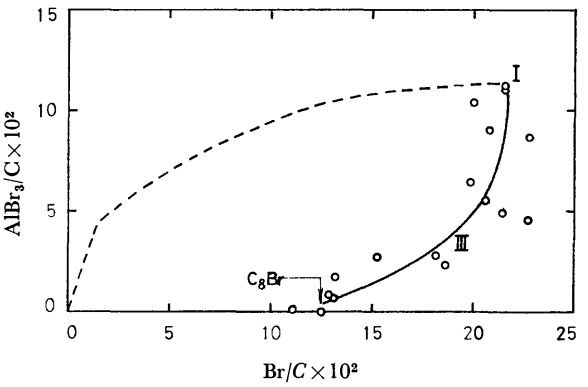

Fig. 2. Compositions of the ternary compounds with the change of the activity of $AlBr_3$.
Dashed line, from Fig. 1.

Table 3. X-ray diffraction patterns of compound III $C_6Br(AlBr_3)_{0.2}$, I_c=13.59Å, Cu$K\alpha$

0 0 l	$2\theta^\circ_{obs}$	$2\theta^\circ_{calc}$	Intensity (obs)
0 0 1	—	6.5	—
0 0 2	—	13.0	—
0 0 3	19.5	19.6	41
0 0 4	26.0	26.2	1000
0 0 5	32.7	33.0	123
0 0 6	39.6	39.8	106
0 0 7	46.4	46.8	48
0 0 8	53.8	54.0	747
0 0 9	61.2	61.4	62
0 0 10	69.0	69.1	41
0 0 11	—	77.2	—
0 0 12	85.7	85.8	232
0 0 13	94.9	95.0	21
0 0 14	—	105.2	—
0 0 15	—	116.6	—
0 0 16	130.4	130.4	186

I, shows a bend in its midst (III in Fig. 2). X-ray diffraction confirmed the existence of the third new phase around point III. The results of structural analysis of compound III (Table 3) and the macroscopic dimensional change of the sample lead to the conclusion that compound III has a structure of the second stage similar to compound II. Its composition was observed to change from $C_{6.2}Br(AlBr_3)_{0.2}$ to $C_{5.1}Br(AlBr_3)_{0.2}$, and its lattice constant I_c varied also from 13.72 to 13.58 Å. It is considered that compound III is non-stoichiometric. It was black like the original graphite or compound II, not being so stable in the air. Decomposition of compound III was observed in a vacuum to produce compound II finally. No new phase other than compound III was found in the composition range from C_8Br to compound I.

The composition, stage and spacing of carbon layers which contain a reactant layer between them are summarized in Table 4 for each compound together with the data for C_8Br.

Table 4. Ternary lamellar compounds of graphite with aluminum bromide and bromine

Compound	Composition	Stage	Carbon layer spacing (Å)
I	$C_9AlBr_3 \cdot Br_2$	1	10.24
II	$C_{24}AlBr_3 \cdot Br_{0.3}$	2	10.00
III	$C_{5-6}Br(AlBr_3)_{0.2}$	2	10.22 ~ 10.37
C-Br	C_8Br	2	7.03

Discussion

(1) Ternary System, Graphite–$AlBr_3$–Br_2. The phase diagram of the present ternary system at 25°C is derived from Figs. 1 and 2, and illustrated in Fig. 3. The region surrounded by the dashed curve represents the extent of the composition of the graphite lamellar compounds. Points I, II, and III in Fig. 3 correspond to compounds I, II, and III. The non-stoichiometric compound III is not represented by a single point, but has a certain range of composition. Along line O–A, the existence of several graphite bromine lamellar compounds having the structures of 5th stage to 2nd stage are known.[10] On line O–II, no phase other than compound II and original graphite was observed. Along line I–II, the coexistence of I and II with a varying ratio was observed. The situations are similar on lines I—III and A-III.

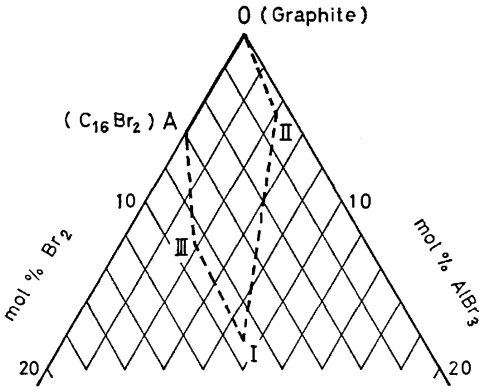

Fig. 3. Phase diagram of the ternary system of graphite $AlBr_3$–Br_2 (25°C).

(2) Formation and Stability of the Ternary Compounds. It is well-known[3,11] that aluminum chloride ($AlCl_3$) and chlorine form ternary lamellar compounds with graphite. Hennig[3] interpreted the role of the third component chlorine as follows. In the system, graphite–$AlCl_3$, $AlCl_3$ can not raise the charge-transfer with the carbon layers by itself, which is necessary for the formation of lamellar compounds with graphite. When chlorine is added to the system, it forms an ionic bonding with the carbon layers and stabilizes the neutral $AlCl_3$ molecules in the interstices of the carbon layers. The ratio of $AlCl_3$ to Cl in the compound was found to remain nearly three up to the saturation compound of the first stage.

The ternary compound in the present study, graphite–$AlBr_3$–Br_2, is very similar system to that of graphite–$AlCl_3$–Cl_2. $AlBr_3$ does not react with graphite by itself and requires bromine for the occurrence of lamellar reaction. The mole ratio of $AlBr_3$ to Br was also found to be nearly three up to the compound of the second stage (compound II). The situation is, however, different for the compound of the first stage. The atomic composition of the lamellar compound with $AlCl_3$–Cl_2 was reported to be approximately $C_9AlCl_3 \cdot Cl_{0.3}$,[3] whereas that with $AlBr_3$–Br_2 is $C_9AlBr_3 \cdot Br_2$. The ratio of $AlBr_3$ to Br does not remain three for the first stage, decreasing to nearly 1/2, which means that the mole ratio of $AlBr_3$ to Br_2 is unity. The difference in composition of both

10) T. Sasa, Y. Takahashi, and T. Mukaibo, *Carbon*, **9**, 407 (1971).

11) W. Rüdorff and R. Zeller, *Z. Anorg. Allgem. Chem.*, **279**, 182 (1955).

compounds of the first stage may be attributed to the fact that chlorine is scarcely absorbed by graphite at room temperature by itself,[12] while bromine is easily absorbed in the same condition.

The bromine content of the first stage compound of graphite–$AlBr_3$–Br_2 is far higher than that of C_8Br. Figure 2 shows that the bromine content of the ternary compound increases with the increase of $AlBr_3$ content from the value corresponding to C_8Br to that of compound I *via* compound III. It is obvious that the coexistence of $AlBr_3$ molecules stabilizes the bromine molecules in the graphite crystal, in the same way as bromide stabilizes $AlBr_3$. $AlBr_3$ and Br_2 are considered to be complementary with each other in the lamellar reaction with graphite. It is also remarkable that although the activity of bromine in the system decreases when the composition changes from C_8Br to compound I, the bromine content in the lamellar compound increases due to the stabilizing effect of $AlBr_3$ on Br_2 molecules. It should be noted that in the case of the ternary compound, graphite–bromine–chlorine $C_8Br_xCl_{1-x}$,[1] the bromine content of the compound is known to decrease as the activity of bromine in the system decreases.

In the system, graphite–$AlCl_3$–Cl_2, the stabilization of chlorine by $AlCl_3$ is also observed. Although chlorine is hardly intercalated in graphite above room temperature, a considerable amount of chlorine is found to be intercalated in graphite in the presence of $AlCl_3$. The energy of stabilization by the coexistence of aluminum halide in both cases may be attributed to a kind of solvation energy between halogen molecules and aluminum halide molecules.

(3) Arrangements of Reactant Molecules in an Interstice of Graphite Layers. Table 4 shows that the carbon layer spacings containing reactant molecules have similar values in the three compounds in spite of different molecular compositions. It is considered that the skeleton of $AlBr_3$ determines the layer spacing in all the three cases, because Br_2 molecules are too small to maintain such a large layer spacing as 10 Å.

The arrangements of reactant molecules in an interstice of graphite layers are investigated in several graphite lamellar compounds,[13–15] and found to be analogous to that of pure reactant solid. The structural analysis was carried out on the assumption that the skeleton of $AlBr_3$ in an interstice of graphite layers is analogous to that of pure solid of $AlBr_3$. It is known that in the crystal of $AlBr_3$,[16] Br atoms form trigonal layer planes and Al atoms are distributed in the interstices of Br layers. The experimental value of the spacing of carbon layers of compound I, 10.24 Å, was found to coincide with the calculated value, if it is assumed that two Br layers of $AlBr_3$ are included in an interstice. The structure factors calculated based on the assumed stacking sequence of the reactant molecules gave qualitative agreement with the experimental values (Table 1). The quantitative agreements, however, were not satisfactory.

The composition of $C_9AlBr_3 \cdot Br_2$ and the interlayer spacing of 10.24 Å give a density of 4.4 g/cc for the reactants in the interstices of graphite layers. This is much higher than the density of solid $AlBr_3$, 3.01, or liquid Br_2, 3.10. The arrangements of the molecules in an interstice of graphite layers should be deformed considerably from those in pure reactant solids to give dense packings corresponding to 4.4 g/cc.

Conclusion

Aluminum bromide and bromine were found to form ternary lamellar compounds with graphite. Three phases of the ternary system were found to exist with the changes of activity of $AlBr_3$ and Br_2 in the system at 25°C. The first phase (compound I), which has the highest reactant contents among the three, has the approximate composition $C_9AlBr_3 \cdot Br_2$, and a lamellar structure of the first stage where every interstice of graphite layers is intercalated with reactants and expands from 3.35 Å to 10.24 Å. The second phase (compound II) formed at a lower activity of bromine than that for compound I, has the composition of $C_{24}AlBr_3 \cdot Br_{0.3}$, and the structure of second stage with I_c of 13.35 Å. The third phase (compound III) formed at the activity of bromine between compound I and C_8Br, has a non-stoichiometric composition of $C_{5-6}Br(AlBr_3)_{0.2}$, and a structure of the second stage similar to compound II. The bromine content of the ternary compounds was found to increase with the increase of $AlBr_3$ content from C_8Br to compound I through compound III. It is concluded that $AlBr_3$ and Br_2 stabilize with each other complementarily in graphite crystal.

The authors are grateful to Mr. M. Iwakura for his collaboration in the experimental work.

12) A. Herold, *Bull. Soc. Chim. Fr.*, **1955**, 999.
13) J. M. Cowley and J. A. Ibers, *Acta. Crystallogr.*, **9**, 421 (1956).
14) W. T. Eeles and J. A. Turnbull, *Proc. Roy. Soc.* **A 283**, 179 (1965).
15) A. W. S. Johnson, *Acta. Crystallogr.*, **23**, 770 (1967).
16) R. W. G. Wyckoff, "Crystal structures", Vol.2, 7 g, Interscience Publishers, New York, N. Y. (1960).

Dimerization of Ethylene Catalyzed by σ-Aryl Nickel Compound in the Presence of Trifluoro Boron Etherate

Ken-ichi MARUYA, Tsutomu MIZOROKI, and Atsumu OZAKI

Research Laboratory of Resources Utilization, Tokyo Institute of Technology, Ohokayama, Meguro-ku, Tokyo

(Received January 13, 1972)

It was found that σ-aryl nickel(II) complex catalyzes the dimerization of ethylene rapidly and selectively when trifluoro boron etherate is added. The rate of dimerization increases in order Br≪mesityl<naphthyl<*o*-tolyl. The aryl ligands remain in the nickel complexes during the course of dimerization, since vinyl naphthalene, butenyl-naphthalene, *etc.*, which are expected to be the reaction products of ethylene with the σ-aryl lingands, were not detected. The isotopic exchange between ethylene and deuteroethylene and the dimerization of deuteroethylene were studied to confirm the active species of this catalyst system. The isotopic exchange is faster than both the dimerization and isomerization of 1-butene formed. No increase in the atomic fraction of hydrogen of deuteroethylene was observed after treatment with the catalyst system. Thus it is concluded that the nickel hydride formed by the dissociative addition of ethylene is the active species of the catalyst system. The role of trifluoroboron etherate was also elucidated by a comparison of its effect on the rate of ethylene dimerization with that of sodium tetraphenyl borate.

Much interest has been shown in the use of transition metal catalysts for the dimerization of monoolefins and has extended recently to homogeneous catalysis. Of the catalysts, complex nickel catalysts are considered to greatest interest.

In solid catalyst systems such as $NiO–SiO_2$ and $NiCl_2$ for ethylene dimerization, the active species was proposed by one of the authors to consist of an exposed nickel ion possibly of low valence and an acid site of the catalyst; the former catalyzes the isotopic exchange of $C_2H_4–C_2D_4$, but has no activity for the dimerization in the absence of the acid site. In homogeneous catalysis, a wide range of nickel compounds are known to show excellent catalytic activity for olefin dimerization in an organic solvent, when they coexist with certain Lewis acids such as aluminium alkyl halide.[3-6] This indicates that the coexistence of the Lewis acid with the nickel compound is essential for olefin dimerization in heterogeneous as well as homogeneous catalysis. Several mechanisms for olefin dimerization have been proposed, but the real configuration of active species is still obscure.

In a previous paper it was reported that bis(triphenylphosphine)nickel(II) dihalide in organic solvent catalyzes the isotopic exchange of $C_2H_4–C_2D_4$ in the presence of molecular hydrogen, and that a nickel hydride formed by the heterolytic splitting of molecular hydrogen is responsible for the exchange.[7] However, no dimerization of ethylene was observed. From the characteristics of the catalyst for dimerization the nickel compound is expected to have catalytic activity for ethylene dimerization, in the presence of some Lewis acid. This was realized by using trifluoroboron etherate as the Lewis acid. Dimerization into butenes was observed. The catalytic activity, however, was considerably smaller than that of the catalyst system composed of nickel(II) halide compound and alkyl aluminium halide. In the coexistence of nickel(II) halide with alkyl aluminium halide, it has been proposed that a σ-alkyl nickel complex is formed by the substitution of a halide coordinated to nickel with an alkyl ligand of alkyl aluminium halide, and the σ-alkyl nickel complex thus formed promotes the dimerization of olefin not isolated probably because of its unstability.[4,5] This suggests the use of the well-known stable σ-aryl nickel(II) halide in place of bis(triphenylphosphine)nickel(II) dihalide as a component of the catalyst, leading to the result that both the activity and selectivity are effectively enhanced for ethylene dimerization.[8] This work was undertaken to investigate the active species of the catalyst system composed of bis(triphenylphosphine)σ-arylnickel(II) bromide and trifluoroboron etherate by examining the effect of the amounts of trifluoroboron etherate and σ-aryl ligand of the nickel compound on the catalytic activity for ethylene dimerization and also by using deuteroethylene.

Experimental

Materials. Bis(triphenylphosphine)nickel(II) dibromide (Found: C, 58.2%; H, 4.0%, Calcd C, 58.2%; H, 4.1%) was prepared according to the method of Venanzi.[9] Bis(triphenylphosphine)1-naphthylnickel(II) bromide (Found: C, 69.9%; H, 4.5%. Calcd: C, 69.9%; H, 4.7%), bis(triphenylphosphine)*o*-tolylnickel(II) bromide (Found: C, 67.9%; H, 4.6%. Calcd: C, 68.5%; H, 4.9%) and bis(triphenylphosphine)mesityl nickel(II) bromide (Found: C, 69.1%; H, 4.7%. Calcd: C, 69.1%; H, 5.3%) were prepared by almost the same method as that of Chatt and Shaw.[10] Organic solvents were dried with sodium, magnesium, or molecular sieve before they were distilled under dry nitrogen. Trifluoroboron etherate

1) K. Kimura, H. A-i, and A. Ozaki, *J. Catal.*, **18**, 271 (1970).
2) K. Maruya, N. Ando, and A. Ozaki, *Nippon Kagaku Zasshi*, **91**, 1125 (1970),
3) G. Wilke, B. Bogdanovic, P. Hardt, P. Heimbach, W. Keim, M. Kröner, W. Oberkirch, K. Tanaka, E. Steinrücke, D. Walter, and H. Zimmermann, *Angew. Chem.*, **78**, 157 (1966).
4) M. Uchino, Y. Chauvin, and G. Lefebvre, *Compt. Rend.*, 1967, **C265**, 103.
5) O. T. Onsager, H. Wang, and U. Blindheim, *Helv. Chim. Acta*, **52**, 187, 196, 215, 224, 230 (1969).
6) J. R. Jones, *J. Chem. Soc., C*, **1971**, 1117.
7) N. Ando, K. Maruya, T. Mizoroki, and A. Ozaki, *J. Catal.*, **20**, 299 (1971).
8) K. Maruya, T. Mizoroki, and A. Ozaki, **43**, 3630 (1970).
9) L. M. Venanzi, *J. Chem. Soc.*, **1958**, 719,
10) J. Chatt, and B. L. Shaw, *ibid.*, **1960**, 1718.

TABLE 1. DIMERIZATION OF C_2H_4 CATALYZED BY $NiBrL(P\phi_3)_2$-BF_3OEt_2

No	L[a]-Ni (mmol)	$BF_3 \cdot OEt_2$ / Ni complex (mole ratio)	Solvent[b] (ml)	C_2' introduced (ml, STP)	React time (hr)	React temp (°C)	Conv of C_2' (%)	Select into C_4 (%)	aryl-H[c] (%)	$(aryl)_2$[c] (%)
1	Br-Ni(1.0)	1	Bz(50)	98	5	30	11	51		
2	n-Ni(0.1)	10	Mc(5)	107	1/5	0	83	92		
3	t-Ni(0.1)	10	Mc(5)	99.1	1/12	0	94	95		
4	m-Ni(0.1)	10	Mc(5)	105	1/2	0	93	99		
5	n-Ni(0.25)	1	Bz(50)	68.6	1	35	92	82	tr.	0
6	n-Ni(0.25)	1	Bz(50)	68.7	20	35	93	95	11	4.0
7	n-Ni(1.0)	1	Mc(5)	69.2	1	0	94	100	1.3	0
8	t-Ni(2.0)	10	Mc(20)	120.8	1/2	0	100	78	0.7	0

a) Br=Br; n=1-naphthyl; t=*o*-tolyl; m=mesityl.
b) Bz=C_6H_6; MC=CH_2Cl_2
c) Based on the amount of σ-aryl-nickel complex used.

obtained from commercial sources was also distilled under dry nitrogen and its benzene solution (10 vol %) was prepared. Moisture in ethylene was trapped by dry ice methanol. Deuteroethylene (C_2D_4 93.3%, C_2D_3H 6.7%) obtained from partial deuteration of deuteroacetylene was purified by means of a gas chromatographic column of silica gel. Deuteroacethylene was obtained from the reaction of heavy water with calcium carbied preevacuated at 800°C for 3 hr.

Procedure, All the experiments were carried out under nitrogen atmosphere. One of nickel compounds placed in a flask (50 or 100 ml) was dried in a vacuum at 50°C before organic solvents were added in order to dissolve the compound completely. The benzene solution of trifluoro boron etherate was then poured into the flask with stirring. Before ethylene was introduced into the flask at the reaction temperature, the nitrogen gas in the flask was evacuated with the solution cooled to liquid nitrogen temperature. The rate of ethylene absorption was measured with a mercury manometor or a gas burette. After the dimerization had been carried out for a given period of time with vigorous stirring, it was stopped by cooling the flask with liquid nitrogen. All volatile materials (butenes, ethylene, and solvent) were transferred to another flask by means of liquid nitrogen and the amounts of olefins were quantitatively determined by gas chromatography. Non-volatile materials were extracted with *n*-hexane, when necessary.

Isotopic exchange of C_2H_4–C_2D_4 and dimerization of C_2D_4 were also carried out according to the same procedure as described above, where a part of the butenes formed and the residual ethylene were separated from the solvent by gas chromatographic column and subjected to mass spectrometry with an ionization potential of 12 eV.

Results

Dimerization Catalyzed by Bis(triphenylphosphine)-Nickel(II) Dibromide and Trifluoroboron Etherate. When isotopic exchange of C_2H_4–C_2D_4 was catalyzed by bis(triphenylphosphine)nickel(II) dibromide in benzene solution in the presence of molecular hydrogen, no dimerization was observed.[7] In the presence of trifluoroboron etherate, however, a small amount of ethylene was dimerized into butenes even in the absence of hydrogen as shown in Table 1 (Run 1). The effect of the amount of trifluoroboron etherate on the rate of ethylene absorption was examined. The result is plotted against the mole ratio of trifluoroboron etherate to nickel compound ($BF_3 \cdot OEt_2/Ni(P\phi_3)_2Br_2$) in Fig. 1, where the rate was determined by the decrease in ethylene pressure during initial 10 min. It shows that the rate increases with the added amount of trifluoroboron etherate.

Dimerization Catalyzed by Bis(triphenylphosphine)σ-Arylnickel(II) Bromide–Trifluoroboron Etherate. Bis(triphenylphosphine)σ-arylnickel(II) bromide was used in place of the corresponding nickel(II) dibromide. Ethylene dimerization with this catalyst system selectively took place without any induction period at room temperature under atmospheric pressure. The result is also given in Fig. 1. It is seen that the rate of ethylene absorption is considerably faster than that by bis(triphenylphosphine)nickel(II) dibromide catalyst and that the rate increases in the order Br≪mesityl<1-naphthyl<*o*-tolyl. The products of these runs are shown in Table 1 (Run 2, 3, and 4). More than 97% of the consumed ethylene is converted into butenes accompanied only by a small

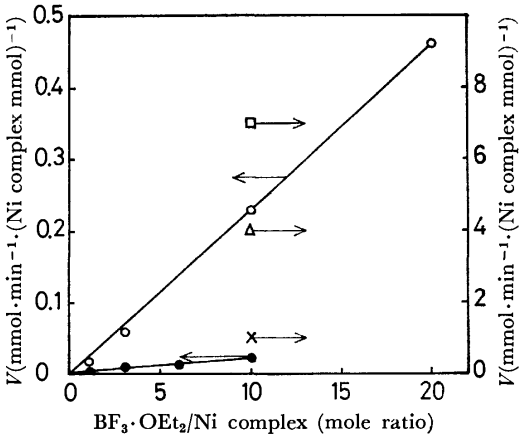

Fig. 1. Rate of ethylene absorption as a function of mole ratio $BF_3 \cdot OEt_2$/Ni-complex.
○: NiBr(1-naphthyl)$(P\phi_3)_2$(1 mmol) in benzene (50 ml) soln., react. temp. 35°C, $P_{C_2H_4}$ 45 cmHg.
●: $NiBr_2(P\phi_3)_2$(2 mmol) in benzene (50 ml) soln., react. temp. 42°C, $P_{C_2H_4}$ 50 cmHg.
□: NiBr(*o*-tolyl)$(P\phi_3)_2$, △: NiBr(1-naphthyl)$(P\phi_3)_2$, ×: NiBr(mesityl)$(P\phi_3)_2$ in dichloromethane (5 ml) soln., react. temp. 0°C, $P_{C_2H_4}$ 60 cmHg.

amount of hexene. Propylene seems to be less reactive than ethylene. When an equimolar amount of triphenylphosphine was added to the solution of bis(triphenylphosphine)-1-naphthylnickel(II) bromide ($BF_3 \cdot OEt_2$/1-$C_{10}H_7Ni(P\phi_3)_2Br$=1), the rate of ethylene absorption under the same reaction conditions as shown in Fig. 1 decreased to about one-seventh of that in the absence of triphenylphosphine. Acrylonitrile as well as butadiene strongly inhibited the ethylene dimerization, while a trace amount of hexadiene was detected on addition of butadiene.

Whether the olefin reacts with the aryl ligand of the nickel complex or not was examined by using a large amount of σ-arylnickel(II) compound. It can be expected that the reaction of olefin with the aryl ligands results in the formation of vinylnaphthalene, vinyltoluene, butenylnaphthalene *etc.* However, none of them was detected by gas chromatography and only a small amount of decomposed products of the complex such as naphthalene, 1,1'-dinaphthyl and triphenylphosphine were detected in the solution after dimerization, as is shown in Table 1 (Run 5, 6, 7, and 8). This means that the aryl ligand remains in the nickel complex during the course of dimerization.

Effect of Trifluoroboron Etherate. When bis(triphenylphosphine)nickel(II) dibromide was used as a catalyst, no activity for ethylene dimerization was observed in the absence of trifluoroboron etherate. However, it was found with bis(triphenylphosphine)σ-arylnickel(II) bromide that it slowly catalyzes ethylene dimerization even in the absence of trifluoroboron etherate. The rate of ethylene absorption was, for example, 1.8×10^{-2} (m*l* min^{-1}mmol-cat^{-1}) at 0°C under atmospheric pressure, when a methylene chloride solution (30 m*l*) of bis(triphenylphosphine)1-naphthylnickel(II) bromide (1 mmol) was used as a catalyst. Under the same conditions, the rate was surprisingly accelerated up to 44.9 [m*l* min^{-1}mmol-cat^{-1}] by the addition of trifluoroboron etherate (1 mmol), *viz*, the rate is increased to 2.6×10^3 times as much with one mole of trifluoroboron etherate and increases linearly with the mole ratio of trifluoroboron etherate to σ-arylnickel(II) complex as shown in Fig. 1.

We examined sodium tetraphenyl borate in place of trifluoroboron etherate to get information on the interaction between σ-arylnickel(II) compound and trifluoroboron etherate. Sodium tetraphenyl borate is known to take off anionic ligand from dihalide complexes of platinum(II) and nickel(II) giving cationic complexes as follows. $2M(P\phi_3)_2X_2+2NaB\phi_4 \rightarrow [M_2(P\phi_3)_4X_2][B\phi_4]_2+2NaX$ (M=Pd(II), Pt(II), Ni(II); X=Cl, Br).[11,13] Dried bis(triphenylphosphine)-1-naphthyl nickel(II) bromide (1 mmol) and sodium tetraphenyl borate (2 mmol) were dissolved in methylene chloride (50 m*l*) and the solution was kept at 0°C for 10 hr with stirring. It was filtered to separate the sodium bromide formed and the residual sodium tetraphenyl borate. Ethylene (40 cmHg) was introduced into the filtrate at 0°C and kept at the temperature for 2 hr with vigorous stirring. No dimerization was observed. The solution no longer showed any activity for dimerization in the presence of trifluoroboron etherate.

Isotopic Exchange of C_2H_4–C_2D_4 and Dimerization of C_2D_4. We examined the isotopic exchange of C_2H_4–C_2D_4 to investigate the active species of the catalyst system of σ-arylnickel compound-trifluoroboron etherate. The isotopic distribution (mol fraction) in the residual ethylene is given in Table 2.

Table 2. Isotopic exchange[a] of C_2H_4-C_2D_4

No		1	2	3
Ni complex[b]	(mmol)	0.01	0.21	0.2
$BF_3 \cdot OEt$	(mmol)	0.01	0.29	0
$C_2H_4+C_2D_4$[c]	(mmol)	2.14	1.05	1.12
Time	(min)	10	10	30
Conv. into C_4'	(%)	0	46.5[d]	0
Isotopic distribution in residual ethylene (%)	d_0	34.3	7.4	43.9
	d_1	8.1	26.4	5.4
	d_2	6.7	36.8	1.1
	d_3	12.7	23.4	9.1
	d_4	38.2	6.0	40.5

a) CH_2Cl_2 10 m*l*, Temp. 0°C.
b) 1-$C_{10}H_7NiBr(P\phi_3)_2$.
c) C_2H_4/C_2D_4=1.0 (isotopic distribution of reactant ethylene, d_0=50, $d_1=d_2$=0, d_3=4.0, d_4=46.0).
d) Isomer distribution; 1-C_4', 55.8%; *trans*-2-C_4', 29.9%; *cis*-2-C_4', 14.3%

In Run 2, 46.5% of the ethylene used is dimerized into butenes, where the isomer distribution is far from its equilibrium, whereas the isotopic distribution is in good agreement with the equilibrium distribution (d_0=6.7, d_1=25.9, d_2=37.5, d_3=24.0, d_4=5.9) in the residual ethylene as well as in the butenes formed. In Run 1 where the catalyst concentration was extremely small and Run 3 where no trifluoroboron etherate was added, only isotopic exchange and no butene was detected. This shows that the isotopic exchange between C_2H_4 and C_2D_4 is sufficiently faster than ethylene dimerization or butene isomerization and that one hydrogen atom undergoes exchange in one act. Thus there should be an active hydrogen atom which catalyzes the exchange reaction.

The source of active hydrogen was examined by means of dimerization using C_2D_4 (atomic fraction of hydrogen (f_H)=0.020). If the active hydrogen is supplied from the substances contained in the catalyst system except for ethylene, hydrogen would be taken up into butene and ethylene, leading to the result that f_H becomes higher than that of the starting ethylene. f_H's of olefins obtained under the various reaction conditions are shown in Table 3, where the amount of C_2D_4 used is approximately fixed. No appreciable increase of f_H is observed, independent of reaction time, the amount of catalyst and that of solvent. This means that no hydrogen is supplied from the solvent, diethylether, triphenylphosphine, or 1-naphthyl ligand present in the catalyst system.

11) H. C. Clark and K. K. Dixon, *J. Amer. Chem. Soc.*, **91**, 596 (1969).
12) J. Powell and B. L. Shaw, *J. Chem. Soc., A*, **1968**, 774.
13) P. M. Druce, M. F. Lappert, and P. N. K. Riley, *Chem. Commun.*, **1967**, 486.

TABLE 3. ATOMIC FRACTION OF HYDROGEN (f_H) IN ETHYLENE OR BUTENES AFTER DIMERIZATION OF C_2D_4[a)]

Ni[b)] complex (mmol)	$BF_3 \cdot OEt_2$ (mmol)	React time	f_H
0.20[c)]	0.79	3 hr	0.022[e)]
0.20[c)]	0.72	10 hr	0.024[e)]
0.20[c)]	0.72	150 hr	0.023[e)]
0.20[d)]	0.72	5 min	0.020[f)]
1.0[d)]	0.72	5 min	0.021[f)]
2.0[d)]	0.72	5 min	0.020[e,f)]
1.0[d)]	3.6	5 min	0.020[f)]
2.0[d)]	7.2	5 min	0.022[f)]

a) React. temp., 0°C; C_2D_4=24 m*l* (at STP).
b) (1-naphthyl)NiBr($P\phi_3$)$_2$.
c) 20 m*l* of CH_2Cl_2.
d) 30 m*l* of CH_2Cl_2.
e) Calculated from the butenes formed.
f) Calculated from the residual ethylene.

Discussion

Effect of Trifluoroboron Etherate. It is known that boron trifluoride reacts with $PdCl_2(PR_3)_2$ or $PtCl_2(PR_3)_2$ (R=alkyl, aryl) in organic solvent to give an ionized species such as $[Pd_2Cl_2(P\phi_3)_4]2BF_4$[11-13)] or $[(Pt_2Cl_2(P\phi_3)_4]2BF_4$,[11-14)] respectively. The corresponding ionized species will be formed from nickel compounds and boron trifluoride. In the case of Ni(π-TMCB)Cl_2-$AlEtCl_2$ (TMCB=tetramethylcyclobutadiene) catalyst, for example, the following equilibrium is usually assumed during the course of olefin dimerization.[5)]

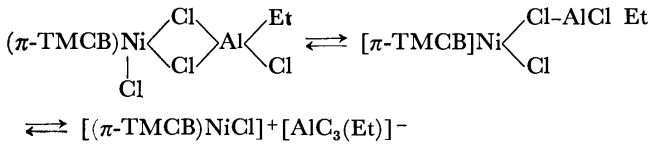

$\rightleftharpoons$ $[(\pi\text{-TMCB})NiCl]^+[AlC_3(Et)]^-$

Similar ionized intermediates have also been suggested for the other nickel halides-ethyl aluminium compounds systems.[3,6)] An ionized species, $[Ni(\sigma\text{-aryl})(P\phi_3)_2]^+$ might be formed in the present catalyst system. Thus $Ni(\sigma\text{-aryl})(P\phi_3)_2Br$ was treated with $NaB\phi_4$ for preparation of the species. However, no activity for ethylene dimerization was found even in the presence of trifluoroboron etherate. This indicates that such ionized species which has no halogen ligand is inactive for ethylene dimerization. It might be concluded that the active species should have at least one halogen ligand through which boron trifluoride can interact with nickel atom.

Boron trifluoride has so far been regarded as an acceptor for halide ion. However, it is more probable that it acts as an acceptor for phosphine ligand. It is known that a tertiary phosphine can coordinate to a Lewis acid to give salts such as $AlCl_3 \cdot P(Et)_3$ and $AlEtCl_2 \cdot P(Et)_3$[5)] and that the coordinated tertiary phosphine, such as triethylphosphine of $PdI_2 \cdot (PEt_3)_2$, can also be removed by a strong Lewis acid, boron trifluoride,[10)] as follows. $2[PdI_2(PEt_3)_2]+2BF_3 \rightarrow [Pd_2I_4(PEt_3)_2]+2BF_3 \cdot PEt_3$. Thus the addition of triphenylphosphine to the catalyst solution reduces the rate of dimerization, and the activity increases linearly with the mole ratio of $BF_3 \cdot OEt_2$ to σ-arylnickel compound as shown in Fig. 1. This suggests that the presence of trifluoroboron etherate is favorable for the dissociation of triphenylphosphine from bis(triphenylphosphine)σ-arylnickel(II) halide to give free coordination site on nickel available for the coordination of ethylene molecule. The role of trifluoroboron etherate can be summarized by the following scheme (Scheme 1).

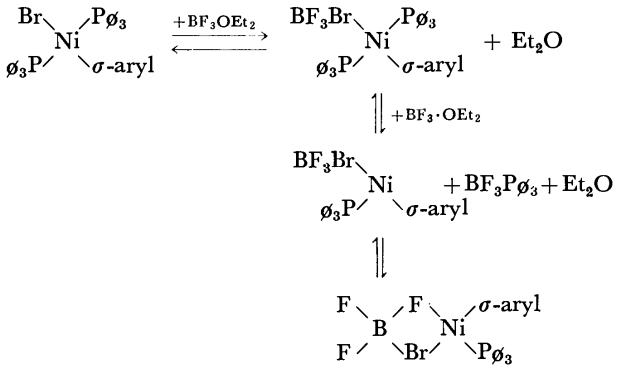

Scheme 1.

Reaction Scheme. The dimerization of lower olefin by the catalyst composed of nickel(II) complex and alkylaluminum has been explained in terms of a nickel-hydride-complex formed by catalyst components.[4,5)] No alkyl aluminum compound, however, is involved in the present catalyst system. There are two points to be clarified; (a) whether a nickel hydride acts as an intermediate, and (b) what substance supplies hydrogen to nickel. The result of isotopic exchange of C_2H_4–C_2D_4 as shown in Table 2 indicates that a nickel hydride has to be taken into account as an intermediate in the course of ethylene dimerization. Neither cyclobutane intermediate accepted in olefin metathesis,[15)] nor carbonium ion observed in acid catalysis[7)] offers satisfactory explanation for one hydrogen atom being exchanged in one act of the exchange and its rate being exceedingly faster than the isomerization of butenes formed.

The equilibrium values of f_Hs of total olefins in the dimerization of C_2D_4 are calculated by assuming that hydrogen is supplied to nickel from one of the substances involved in the reaction mixture, *i.e.* methylene chloride, triphenylphosphine, diethylether, and 1-naphthyl. They are given in Table 4. It is shown that the f_H value should increase, at lowest to 0.07, if isotopic scrambling is accomplished between these substances. However, since f_H remains at the starting value 0.02 within experimental error as shown in Table 3, it is clear that hydrogen is supplied to nickel from ethylene molecule.

Two processes can be expected for the formation of nickel hydride from ethylene molecule, one is an inser-

14) H. C. Clark, K. R. Dixon, and W. J. Jacobs, *Chem. Commun.*, **1968**, 93.

15) N. Calderon, E. A. Ofstead, J. P. Ward, W. A. Judy, and K. W. Scotto, *J. Amer. Chem. Soc.*, **90**, 4133 (1968).

Table 4. Calculated values[a] of f_Hs in olefin assuming the occurence of isotopic scrambling of C_2D_4

Substances supplying hydrogen	f_H
Solvent (CH_2Cl_2)	1
$P\phi_3$	0.40[b]
$(C_2H_5)_2O$	0.19[c]
1-naphthyl	0.07[d]
C_2D_4	0.02[e]

a) Calculated values, when (1-naphthyl)NiBr($P\phi_3$)$_2$ (0.20 mmol), $BF_3 \cdot OEt_2$ (0.8 mmol) and C_2D_4 (1 mmol) are used CH_2Cl_2 solvent.
b) With orthohydrogen atom of phenyl in $P\phi_3$ ligand.
c) With one hydrogen atom per one diethylether molecule.
d) With one hydrogen atom per one naphthyl ligand.
e) f_H of the C_2D_4 used.

tion process in which ethylene is inserted between nickel-carbon bond of 1-naphthyl nickel complex to give Ni–CH_2–CH_2–$C_{10}H_7$, followed by elimination of β-hydrogen to give Ni–H and 1-vinyl naphthalene. However, this seems to be unlikely, because neither vinylnaphthalene nor butenylnaphthalene was detected, and σ-aryl ligand was proved to remain in the nickel complex after ethylene dimerization. The other process is a dissociative addition of ethylene to give H–Ni–CH=CH_2. A similar addition was proposed by one of the authors (A.O.) for the mechanism of ethylene dimerization catalyzed by NiO–SiO_2 catalyst,[1] or by bis(benzonitrile) palladium(II) dichloride.[16]

The following course of reaction would account for the rapid hydrogen exchange of ethylene and its dimerization. The dissociative addition of ethylene takes place on the nickel complex shown in scheme 1, and another ethylene then attacks the nickel hydride to form a σ-ethyl-nickel complex reversibly, which is responsible for the rapid hydrogen exchange. 1-Butene may be formed from σ-ethyl-nickel complex by two processes. One is the coupling of ethyl and vinyl attached to the complex. The other is the insertion of another ethylene molecule into ethyl-nickel bond to form primary butyl-nickel complex followed by elimination of β-hydrogen to give 1-butene and nickel hydride. In the former, nickel hydride must be renewed or the next dimerization, while in the latter the hydride is always reproduced the vinyl being kept behind. Discrimination between these two processes is difficult at present.

The variation in activity among σ-aryl nickel compounds supports the view that the σ-aryl ligand is effectively involved in the catalytic species. A combination of steric and inductive factors seems to be responsible for the activity and selectivity for the dimerization. The exact function of the σ-aryl ligands, however, is obscure.

16) T. Kitamura, K. Maruya, Y. Moro-oka, and A. Ozaki, This Bulletin, **45**, 1457 (1972).

BULLETIN OF THE CHEMICAL SOCIETY OF JAPAN, VOL. 45, 2259—2265 (1972)

Magnetic Susceptibilities and Broad-Line PMR Spectra of Dichloro(pyridazine)copper(II) and Related Compounds

Shuji EMORI, Motomichi INOUE, and Masaji KUBO

Department of Chemistry, Nagoya University, Chikusa, Nagoya

(Received February 14, 1972)

The magnetic susceptibilities of CuX_2L (X: halide ion, L: 1,2,4-triazole, pyridazine, phthalazine, 4-amino-1,2,4-triazole) conform to the linear Ising model or Heisenberg model, indicating the presence of linear magnetic chains in the crystals. Fermi contact shift observed in the broad-line PMR spectrum indicates the diffusion of a positive hole from a copper atom to the molecule of heterocycles. The magnitude of the exchange integrals is related to the spin densities on the atoms of the heterocycles.

In the crystals of dichloro(1,2,4-triazole)copper(II), $CuCl_2$(tr), each copper atoms has a distorted octahedral coordination of four chlorine atoms and two nitrogen atoms.[1] The octahedra are joined with one another by sharing chlorine edges and are also linked by 1,2,4-triazole molecules, constituting an infinite linear chain as the structural unit. The magnetic susceptibility of the compound conforms to the linear Ising model.[2] From contact shifts in PMR spectrum, spin densities on atoms in 1,2,4-triazole have been evaluated.[3] From these, it was concluded that superexchange interaction operates between copper atoms through the heterocycle. From the same steric reason as for 1,2,4-triazole in $CuCl_2$(tr), a bidentate heterocyclic ligand having two neighboring nitrogen atoms (for example, pyridazine and phthalazine) is expected to coordinate to two copper atoms.[4] Therefore, in the crystals of CuX_2L type complexes (X: halide ion, L: bidentate nitrogen heterocycle), the magnetic unit is presumed to be an infinite linear chain, –Cu–L–Cu—, analogous to that in $CuCl_2$(tr). In this linear chain, superexchange

1) J. A. J. Jarvis, *Acta. Crystallogr.*, **15** 964 (1962).

2) M. Inoue, S. Emori, and M. Kubo, *Inorg. Chem.*, **7**, 1427 (1968).

3) M. Inoue and M. Kubo, *ibid.*, **5**, 70 (1966).

4) K. Hyde, G. F. Kokozska, and G. Gordon, *J. Inorg. Nucl. Chem.*, **31**, 1993 (1969).

interaction can operate between copper atoms through the molecules of the heterocycles, its magnitude depending on the electronic state of bridging ligands.[5] Therefore, we have measured the magnetic susceptibilities of this type of complexes in order to estimate exchange integrals and also recorded broad-line PMR spectra to evaluate the spin densities on atoms in the heterocycles.

Experimental

$CuCl_2L$ was prepared by modifying the method of Hyde *et al.*[4] A solution of an appropriate nitrogen heterocycle in 1 N hydrochloric acid was added in slight excess to a solution of copper(II) chloride in 3 N hydrochloric acid. On standing, green powder crystals separated. They were recrystallized from 3 N hydrochloric acid. $CuBr_2L$ was prepared in the same manner as for $CuCl_2L$ using hydrobromic acid in place of hydrochloric acid. The results of chemical analysis are listed in Table 1.

Table 1. Analytical data for CuX_2L

Compound		Cu, %	C, %	H, %	N, %	Cl or Br %
$CuCl_2$(pid)	Found	29.34	21.71	1.58	12.89	33.02
	Calcd	29.62	22.39	1.88	13.06	33.05
$CuCl_2$(pht)	Found	24.21	36.19	1.96	10.54	26.89
	Calcd	24.02	36.31	2.29	10.59	26.80
$CuCl_2$(atr)	Found	29.11	10.91	1.55	25.85	32.41
	Calcd	29.08	10.99	1.85	25.64	32.44
$CuBr_2$(tr)	Found	21.76	8.22	0.85	14.34	54.51
	Calcd	21.73	8.21	1.04	14.37	54.64
$CuBr_2$(pid)	Found	20.79	15.84	1.17	9.18	52.15
	Calcd	20.94	15.83	1.33	9.23	52.67
$CuBr_2$(pht)	Found	17.81	27.07	1.53	7.77	44.33
	Calcd	17.98	27.18	1.71	7.92	45.21
$CuBr_2$(atr)	Found	20.61	7.82	1.13	17.98	51.86
	Calcd	20.67	7.81	1.31	18.23	51.98

pid: pyridazine, pht: phthalazine, tr: 1,2,4-triazole, atr: 4-amino-1,2,4-triazole.

Magnetic susceptibility was determined by means of magnetic balances described in our previous paper.[2] The molar susceptibilities were corrected for diamagnetic contributions (in 10^{-6} emu/mol) from copper ions (-11),[6] chloride ions (-26),[6] bromide ions (-36),[6] 1,2,4-triazole (-38),[7] pyridazine (-38), phthalazine (-75), and 4-amino-1,2,4-triazole (-46). The value for pyridazine was assumed to be equal to that of pyrazine.[7] The values for phthalazine and 4-amino-1,2,4-triazole were evaluated on the basis of those for pyridazine and 1,2,4-triazole, respectively, by use of the Pascal constants. The temperature-independent paramagnetism was assumed to be equal to 60×10^{-6} emu/mol.[8]

The PMR spectra of the powder crystals were recorded at 25°C by means of a Model JNS-B broad-line NMR spectrometer from JEOLCO operating at 29.7 MHz with an amplitude of magnetic field modulation equal to 1.0 Oe. Water was employed as an external standard.

Results

The susceptibilities corrected for diamagnetic contributions and the temperature-independent paramagnetism obey the Curie-Weiss law at high temperatures as shown in Fig. 1. The Weiss constants and g-values evaluated from the Curie constants are listed in Table 2. The susceptibilities in the low-temperature region are plotted against the temper-

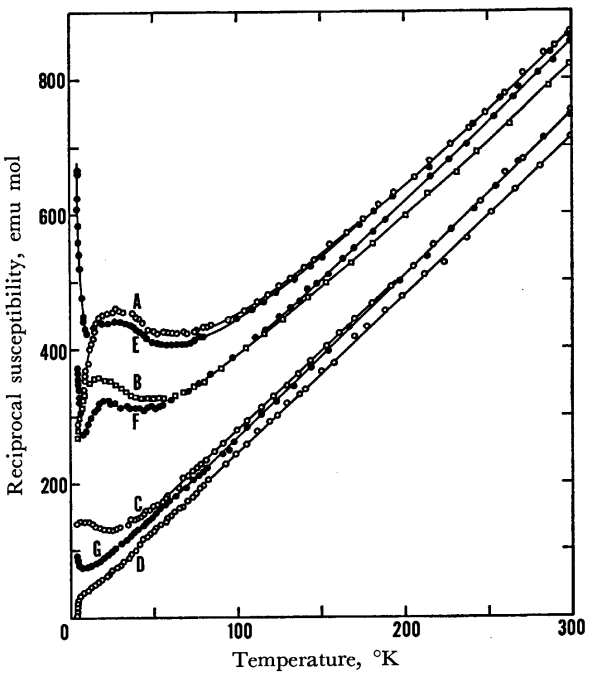

Fig. 1. Reciprocal susceptibilities of $CuCl_2$(pid) (A), $CuCl_2$(pht) (B), $CuCl_2$(atr) (C), $CuBr_2$(tr) (D), $CuBr_2$(pid) (E), $CuBr_2$(pht) (F), and $CuBr_2$(atr) (G) plotted against the temperature.

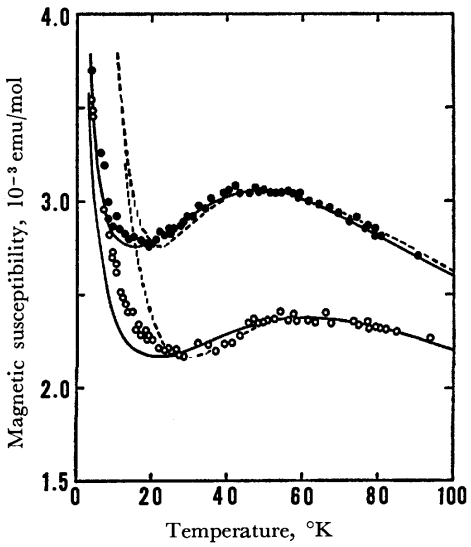

Fig. 2. Magnetic susceptibilities of $CuCl_2$(pid) (white circles) and $CuCl_2$(pht) (black circles). Solid curves: linear Heisenberg model. Broken curves: linear Ising model.

5) M. Inoue and M. Kubo, *Inorg. Chem.*, **9**, 2310 (1970).
6) P. W. Selwood, "Magnetochemistry," 2nd ed., Interscience Publishers, New York, N. Y. (1956), p. 78.
7) G. Foëx, "Constantes Sélectionées, Diamagnétisme et Paramagnétisme," Masson, Paris (1957).
8) B. N. Figgis and R. L. Martin, *J. Chem. Soc.*, **1956**, 3837.

Table 2. Weiss constant, θ, g-value evaluated from the Curie constant, g_C, and parameters, J/k, g, C_{low}, based on the Heisenberg model and the Ising model

Compound	θ, °K	g_C	Heisenberg model			Ising model		
			J/k, °K	g	C_{low}	J/k, °K	g	C_{low}
$CuCl_2$(tr)[a]	−19.0	2.13	—	—	—[b]	−17.9	2.07	0.027[d]
$CuCl_2$(pid)	−61.5	2.10	−51.7	2.06	0.000135	−87.3	2.13	0.000478
$CuCl_2$(pht)	−61.2	2.17	−40.6	2.08	0.000151	−68.0	2.16	0.000603
$CuCl_2$(atr)	−18.3	2.13	−17.6	2.17	0.000377	−29.4	2.26	0.00153
$CuBr_2$(tr)	−6.7	2.13	—	—	—[b]	−8.3	2.10	0.046[e]
$CuBr_2$(pid)	−69.0	2.13	−45.8	1.98	0.000129	−76.4	2.05	0.000492
$CuBr_2$(pht)	−47.4	2.08	−36.0	1.98	0.000274	−63.4	2.09	0.000714
$CuBr_2$(atr)	−10.1	2.10	−7.58	1.93	—[c]	−9.36	1.92	—[c]

a) Ref. 2. b) The Heisenberg model does not give good agreement with experimental data. c) No paramagnetic behavior was observed at low temperature. d) $\theta_{low}=2.5$°K. e) $\theta_{low}=2.8$°K.

ature in Figs. 2—6.

The observed PMR absorption derivative curves are shown in Figs. 7—10. Dibromo(1,2,4-triazole)-copper(II), $CuBr_2$(tr), dichloro(pyridazine)copper-(II), $CuCl_2$(pid), dibromo(pyridazine)copper(II), $CuBr_2$(pid), and dibromo(phthalazine)copper(II), $CuBr_2$(pht), show asymmetric curves, each of which can be decomposed into two simple derivative curves, one shifted to the low-field side and the other shifted to the high-field side. The shifts, $\Delta H/H$, are listed in Table 3. The curve of dichloro(phthalazine)copper-(II), $CuCl_2$(pht), is made up of a broad component

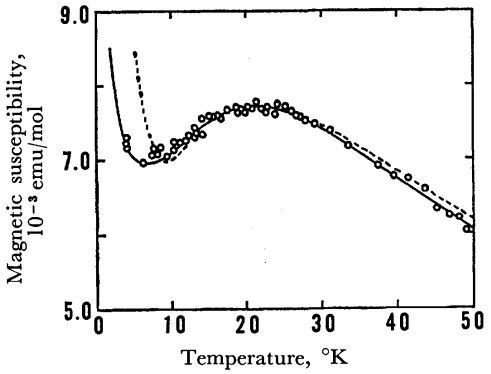

Fig. 3. Magnetic susceptibility of $CuCl_2$(atr). Solid curve: linear Heisenberg model. Broken curves: linear Ising model.

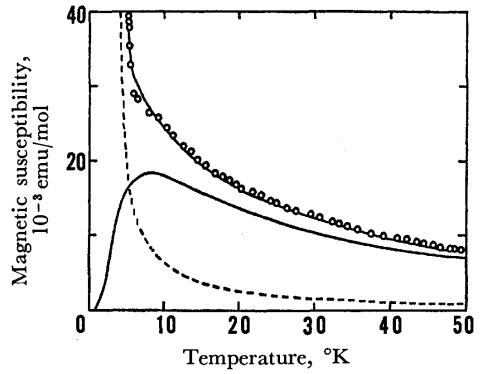

Fig. 4. Magnetic susceptibility of $CuBr_2$(tr) resolved into a low-temperature Curie-Weiss curve (broken curve) and a curve for the linear Ising model.

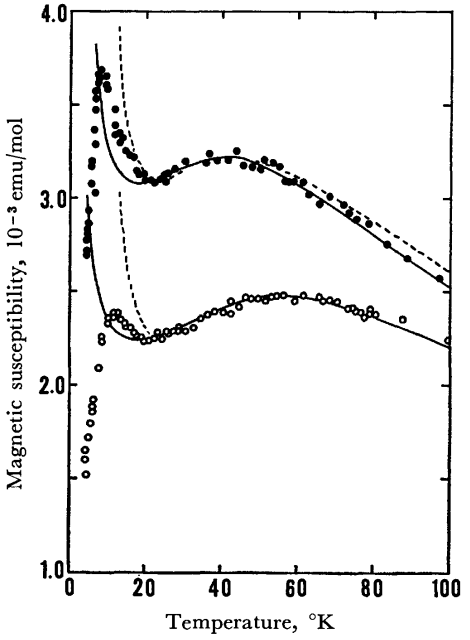

Fig. 5. Magnetic susceptibilities of $CuBr_2$(pid) (white circles) and $CuBr_2$(pht) (black circles). Solid curves: linear Heisenberg model. Broken curves: linear Ising model.

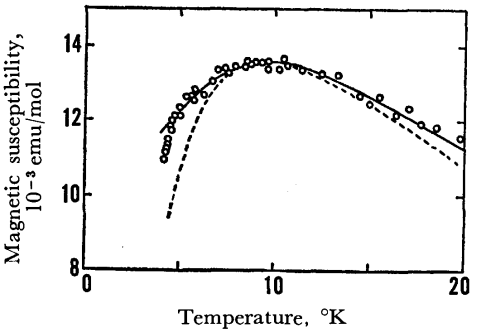

Fig. 6. Magnetic susceptibility of $CuBr_2$(atr). Solid curve: linear Heisenberg model. Broken curve: linear Ising model.

having a low-field shift, another broad component having a high-field shift, and a sharp component. The integrated intensity of the sharp component amounted to less than 0.1% of the total intensity and fluctuated among different preparations. Therefore,

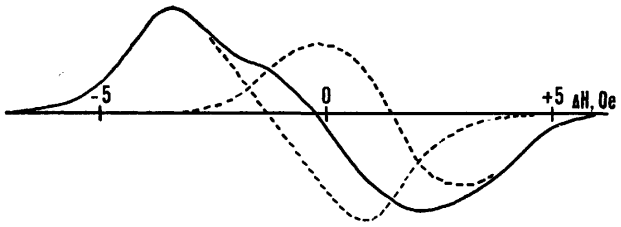

Fig. 7. PMR absorption derivative curve (full curve) of $CuBr_2$(tr) decomposed into two simple derivative curves (broken curves).

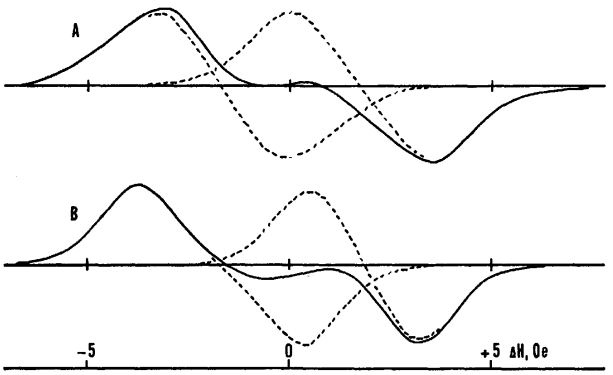

Fig. 8. PMR absorption derivative curves of $CuCl_2$(pid) (A) and $CuBr_2$(pid) (B). Each curve (full curve) is decomposed into two simple derivative curves (broken curves).

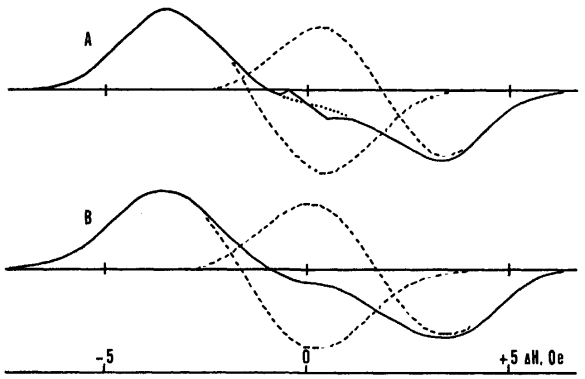

Fig. 9. PMR absorption derivative curves (full curves) of $CuCl_2$(pht) (A) and $CuBr_2$(pht) (B). The dotted curve in (A) shows the superposition of two derivative curves. A sharp unshifted component appears. The intrinsic absorption derivative curve of each compound is decomposed into two simple derivative curves(broken curves).

the unshifted curve is attributable to impurities or protons in randomly tumbling molecules. The dotted curve in Fig. 9A shows the superposition of the two broad curves and agrees with the observed curve except for a region near the unshifted component. The PMR absorption curves of dichloro(4-amino-1,2,4-triazole)copper(II), $CuCl_2$(atr), and dibromo-(4-amino-1,2,4-triazole)copper(II), $CuBr_2$(atr), also yield a sharp unshifted component, the integrated intensity of which is less than 1% and 0.5% of the total intensity, respectively. The intrinsic absorption curve of each of these compounds can be decomposed into two components.

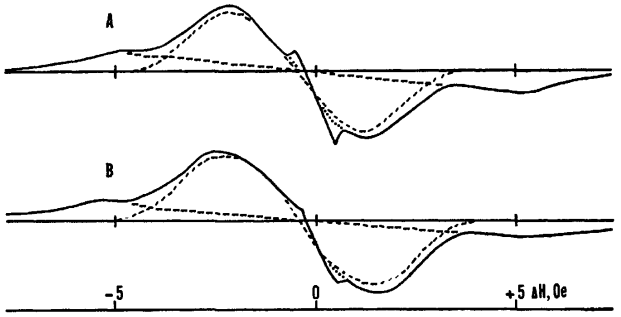

Fig. 10. PMR absorption derivative curves (full curves) of $CuCl_2$(atr) (A) and $CuBr_2$(atr) (B). Each of the dotted curves represent the superposition of two derivative curves (broken curves). In addition, a sharp component appears near the origin.

Table 3. Contact shift, $\Delta H/H$, contact interaction constant, a_i, and spin density, ρ_i

Compound	$\Delta H/H$ $\times 10^4$	Relative intensity	a_i, Oe	ρ_i
$CuCl_2$(tr)[a]	−1.3	2(3,5-CH)	+1.8	−0.08
	+1.4	1(4-NH)	−1.9	+0.06
$CuCl_2$(pid)	−2.5	1(3,6-CH)	+3.9	−0.16
	+2.5	1(4,5-CH)	−3.9	+0.16
$CuCl_2$(pht)	−2.1	2(1,4,5,8-CH)	+3.1	−0.13
	+2.6	1(6,7-CH)	−3.9	+0.16
$CuCl_2$(atr)	−0.7	(3,5-CH)	+0.9	−0.04
	—[b]	($N-NH_2$)	+	+
$CuBr_2$(tr)	−1.9	2(3,5-CH)	+2.5	−0.11
	+2.1	1(4-NH)	−2.7	+0.08
$CuBr_2$(pid)	−2.5	1(3,6-CH)	+3.9	−0.16
	+2.7	1(4,5-CH)	−4.2	+0.18
$CuBr_2$(pht)	−2.4	2(1,4,5,8-CH)	+3.6	−0.15
	+2.5	1(6,7-CH)	−3.8	+0.16
$CuBr_2$(atr)	−0.6	(3,5-CH)	+0.8	−0.03
	—[b]	($N-NH_2$)	+	+

a) In ref. 3, a_i and ρ_i were evaluated assuming $g=2.00$. The values in this table are based on g_C. b) The absolute value could not be determined.

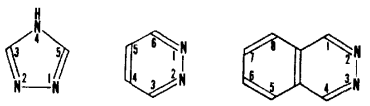

Discussion

The susceptibility *versus* temperature curve observed for $CuCl_2$(pid) exhibits a broad maximum at about 60°K and a paramagnetic behavior below about 20°K as shown in Fig. 2. $CuCl_2$(pht) and $CuCl_2$-(atr) shows a magnetic behavior resembling that of $CuCl_2$(pid) (Figs. 2 and 3). These magnetic properties are characteristic of linear antiferromagnets, typical examples of which are $CuCl_2$(tr),[2] potassium trifluorocuprate(II),[9] and 2,5-dihydroxy-*p*-benzoquinonatocopper(II).[10]

The susceptibility of $CuCl_2$(tr) has already been determined between 4.2 and 300°K (Fig. 3 in Ref. 2). With decreasing temperature, the susceptibility passes

through a maximum at about 11°K and increases sharply obeying the Curie-Weiss law below about 8°K. The behavior below 8°K is due either to the effect of magnetically isolated copper(II) ions existent in a small quantity or to interaction between linear chains. Susceptibility attributable to these effects was subtracted from the observed values. The resulting intrinsic susceptibility conforms to the parallel susceptibility, χ, of a linear Ising chain.[11]

$$\chi = \frac{Ng^2\beta^2}{4kT} \exp \frac{J}{kT} \quad (1)$$

Here apart from obvious notations, J denotes the exchange integral between the nearest neighbors in a chain. Therefore, the susceptibility of $CuCl_2$(tr) can be expressed by

$$\chi = \frac{Ng^2\beta^2}{4kT} \exp \frac{J}{kT} + \frac{C_{low}}{T-\theta_{low}} \quad (2)$$

where C_{low} and θ_{low} are the Curie constant and the Weiss constant in the low temperature region, respectively. From the susceptibility of $CuCl_2$(pid), C_{low} and θ_{low} cannot be determined accurately, because the temperature range of the paramagnetic effect is narrow. However, θ_{low} is estimated to be almost equal to 0°K (see Fig. 1). Therefore, the value of θ_{low} was assumed to be 0°K and g, J, and C_{low} were varied to get the best fit to the observed susceptibility especially near the temperature of the maximum susceptibility. The broken curve in Fig. 2 shows the result of calculation carried out with parameters listed in Table 2. Fisher[12] has pointed out that the perpendicular susceptibility given by

$$\chi = \frac{Ng^2\beta^2}{4|J|}\left[\tanh \frac{|J|}{2kT} + \frac{|J|}{2kT} \operatorname{sech}^2 \frac{|J|}{2kT}\right] \quad (3)$$

should be taken into account as well in the linear Ising model. However, all attempts to calculate curves involving both parallel and perpendicular components failed to reproduce the observed relative susceptibility as well as the absolute susceptibility. Bonner and Fisher[13] have calculated the susceptibility of a one-dimensional Heisenberg spin lattice. The observed susceptibility agrees well with the Bonner-Fisher curve corrected for the paramagnetic behavior in the low temperature region (see Fig. 2). For $CuCl_2$(pht) and $CuCl_2$(atr), the exchange integrals and the g-values were evaluated by the same procedure as employed for $CuCl_2$(pid) (see Table 2 and Figs. 2 and 3). The g-values are almost equal to those evaluated from the Curie constants and also to a value, 2.13±0.03, determined by ESR[4] (see Table 2). These support a presumption that –Cu–L–Cu— chains are formed in the crystals of the chlorine compounds. Hyde *et al.*[4] have carried out an ESR measurement on $CuCl_2$(pid) and suggested that the Heisenberg model rather than the Ising model is adequate because the value of $|D/J|$ is very small (D is the dipole-dipole interaction constant for spins in an axially symmetric crystal field). In fact, the observed susceptibility agrees with the theoretical curve for the Heisenberg model more closely than that for the Ising model.

The crystal of $CuBr_2$(tr) is expected to be isostructural with $CuCl_2$(tr). The susceptibility *versus* temperature curve can be reproduced by Eq. 2 in a manner similar to the case of $CuCl_2$(tr) (see Table 2 and Fig. 4). However, the Heisenberg model gives poor agreement with experimental data as in the case of $CuCl_2$(tr).[2]

The susceptibility *versus* temperature curve observed for $CuBr_2$(pid) exhibits two maxima at 12 and 55°K (see Fig. 5). The broad maximum at the higher temperature is undoubtedly due to a short-range magnetic interaction within a linear chain. Another maximum at the lower temperature is attributable to a three-dimensional long-range ordering existing below the temperature owing to interaction between chains.[14] The magnetic behavior of $CuBr_2$(pht) resembles that of $CuBr_2$(pid) as shown in Fig. 5. The susceptibilities of $CuBr_2$(pid) and $CuBr_2$(pht) at high temperature can be analyzed in the same way as for $CuCl_2$(pid). The g-values obtained from the Ising model are nearly equal to those evaluated from the Curie constants (see Table 2). On the other hand, the g-values based on the Heisenberg model are smaller than 2.00, whereas the g-value of a copper ion should be greater than 2.00 owing to spin-orbit interaction. This inconsistency indicates that the susceptibilities calculated with the Heisenberg model can hardly be fitted to the observed absolute susceptibilities despite an apparent qualitative agreement as in Fig. 5. Presumably this discrepancy is due to a strong magnetic interaction between chains suggested by the appearance of two maxima in the susceptibility *versus* temperature curves. The susceptibility of $CuBr_2$(atr) can be explained with difficulty by the Ising model as well as by the Heisenberg model (see Table 2 and Fig. 6) presumably because interaction exists between chains. A coupled-double-chain model[15,16] gives an approximation to the susceptibility of a crystal consisting of infinite chains, each of which is weakly coupled with neighboring chains. However, curves calculated with this model fail to agree with the observed susceptibility. Table 2 lists exchange integrals evaluated on the basis of the Heisenberg and Ising models for an isolated linear chain. The J/k values of the bromine compounds have some significance for the comparison of exchange interaction among the compounds. The effect of magnetic interaction between chains appears markedly in the bromine compounds, suggesting that the interaction takes place through bromine atoms.

An asymmetric PMR absorption curve observed for

9) S. Kadota, I. Yamada, S. Yoneyama, and K. Hirakawa, *J. Phys. Soc. Japan*, **23**, 751 (1967).
10) H. Kobayashi, T. Haseda, E. Kanda, and S. Kanda, *ibid.*, **18**, 349 (1963).
11) G. F. Newell and E. W. Montroll, *Rev. Mod. Phys.*, **25**, 353 (1953).
12) M. E. Fisher, *J. Math. Phys.*, **4**, 124 (1963).
13) J. C. Bonner and M. E. Fisher, *Phys. Rev.*, **135**, A640 (1964).
14) S. Emori, M. Inoue, and M. Kubo, *Inorg. Chem.*, **8**, 1385 (1969).
15) M. Inoue and M. Kubo, *J. Mag. Resonance*, **4**, 175 (1971).
16) S. Emori, M. Inoue, and M. Kubo, *This Bulletin*, **44**, 3299 (1971).

$CuBr_2$(tr) bears a striking resemblance to that of $CuCl_2$(tr) (see Fig. 7). This supports a presumption that $CuBr_2$(tr) is isostructural with $CuCl_2$(tr) and that all 1,2,4-triazole molecules are equivalent in the crystals.[1] From the intensity ratio, 2 : 1, of the two components, the stronger one on the low-field side is assigned to protons, 3-CH and 5-CH, bonded to carbon at positions 3 and 5, while the curve shifted to the high-field side is attributable to a proton, 4-NH, bonded to nitrogen at position 4. Undoubtedly, the shifts are due to the isotropic contact hyperfine interaction field and are given by[5,17]

$$\frac{\Delta H}{H} = -a_i\left(\frac{\gamma_e}{\gamma_N}\right)\frac{\chi}{g\beta N} \tag{4}$$

where H is the NMR field, a_i is the contact interaction constant of a proton bonded to carbon or nitrogen at position i, γ_e is the magnetogyric ratio of an electron, and γ_N is that of a nucleus. The constants, a_i, listed in Table 3 were calculated from the observed shifts, $\Delta H/H$, the susceptibility at room temperature, and the g-value evaluated from the Curie constant. For an aromatic radical species, in which spin density localized on the pπ orbital of a carbon atom interacts with a proton bonded to the carbon atom, a_i is related to the spin density, ρ_i, on the adjacent carbon atom by the McConnell relation:[17,18]

$$a_i = Q_{CH}\rho_i \tag{5}$$

where Q_{CH} is a proportionality constant, the value of which has been determined empirically as -22.5 Oe. This relation is expected to hold for protons bonded to nitrogen as well.[19] However, few data are available for Q_{NH}. Barton and Fraenkel[20] have carried out an ESR experiments on dihydropyrazine cation radicals and found that $Q_{NH}=-33.7$ Oe by use of $Q_{CH}=-23.7$ Oe. The values of Q_{CH} and Q_{NH} may vary to a considerable extent among different bonding types.[19] Using Barton and Fraenkel's values, we evaluated spin densities, $\rho_{3,5}$ and ρ_4 as listed in Table 3. Negative and positive spin densities are distributed alternately on atoms in a triazole ring: $\rho_{3,5}<0$ and $\rho_4>0$. The alternation in sign of the spin density indicates that ρ_1 and ρ_2 are positive. Accordingly, it is concluded that the migration of an unpaired electron from copper creates a positive spin density on nitrogen atoms bonded to copper.

For $CuCl_2$(pid), a_i and ρ_i were evaluated in the same manner as for $CuBr_2$(tr) and are listed in Table 3. In the crystals of $CuCl_2$(pid), all pyridazine molecules are presumed to be equivalent, because the crystal consists of linear chains, –Cu–(pid)–Cu–, as units. Hence, there are two kinds of protons in equal amounts in agreement with the result of PMR absorption. Since a positive spin density is expected to exist on nitrogen atoms bonded to copper as in CuX_2(tr), carbon atoms at positions 3 and 6 bear a negative spin density (see Table 2). Therefore, the absorption curve on the low-field side is attributable to protons, 3-CH and 6-CH, whereas the curve shifted to the high-field side is assigned to 4,5-CH protons, indicating that ρ_4 and ρ_5 are positive. For pyridazine anion radicals, the interaction constants, a_i, have been determined as $|a_{3,6}|=0.16$ Oe and $|a_{4,5}|=6.45$ Oe by ESR measurements.[21] A molecular-orbital calculation on the radical has shown that $a_{3,6}$ is positive whereas $a_{4,5}$ is negative (therefore, $\rho_{3,6}<0$ and $\rho_{4,5}>0$)[22] in support of our assignment. The ratio, $|a_{3,6}/a_{4,5}|=1.0$, for $CuCl_2$(pid) is much greater than 0.025 for a pyridazine anion radical. An odd electron in the radical is attracted to nitrogen owing to the difference between the electronegativities of carbon and nitrogen. Accordingly negative spin densities are induced on carbon atoms bonded to nitrogen. On the other hand, in the copper(II) complex positive spins are mostly localized on nitrogen atoms bonded to copper, because unpaired electrons migrate from copper to the molecules of the heterocycle. In π-bond conjugation, negative spin density on an atom increases with increasing positive spin density on adjacent atoms. This is the reason why the ratio, $|a_{3,6}/a_{4,5}|$, is larger in the copper complex than in the radical.

The observed absorption curve of $CuCl_2$(pht) can be decomposed into two simple curves of intensity ratio equal to 2 : 1 (see Fig. 9). In $CuCl_2$(pht), ρ_1 and ρ_4 are expected to be negative for the same reason as in $CuCl_2$(pid). In addition, an assumption of alternation in sign of the spin density leads to a conclusion that $\rho_{5,8}<0$ and $\rho_{6,7}>0$. These conform to the intensity ratio and the shifts of the two components (see Table 3). Although $\rho_{1,4}$ and $\rho_{5,8}$ must differ from each other, the stronger curve on the low-field side is difficult to resolve owing almost complete overlap. Table 3 gives average values. A molecular-orbital calculation carried out on a phthalazine anion radical has indicated the absence of a negative spin density on any carbon atoms.[22] However, in $CuCl_2$-(pht), an unpaired electron migrating from copper gives rise to a strong polarization in the π-bond system of the heterocyclic ligand. Owing to this effect, negative spin densities are distributed on carbon atoms at positions, 1, 4, 5, and 8.

The intrinsic absorption curve of $CuCl_2$(atr) consists of a curve with a peak-to-peak width of 3.3 Oe and a broad curve with a width of 10 Oe (see Fig. 10). The narrower one can be assigned to protons, 3,5-CH, by comparing the curves with those of CuX_2(tr). Therefore, the broad curve is attributable to protons in N-NH_2. The shift, $\Delta H/H$, of the broad curve cannot be determined accurately because the curve is very broad and an absorption curve due to impurities is superposed on it. The shift, however, suggests that the nitrogen atom at position 4 carries a positive spin density, in conformity with the results of CuX_2(tr).

17) H. M. McConnell and D. B. Chesnut, *J. Chem. Phys.*, **28**, 107 (1958).
18) T. H. Brown, D. H. Anderson, and H. S. Gutowsky, *ibid.*, **33**, 720 (1960).
19) J. R. Bolton, "Radical Ions," ed. by E. T. Kaiser and L. Kevan, John Wiley & Sons, New York, N. Y. (1968), p. 19.
20) B. L. Barton and G. K. Fraenkel, *J. Chem. Phys.*, **41**, 1455 (1964).
21) E. W. Stone and A. H. Maki, *ibid.*, **39**, 1635 (1963).
22) J. A. Pople and D. L. Beveridge, "Approximate Molecular Orbital Theory," McGraw Hill, New York, N. Y. (1970), p. 134.

For $CuBr_2$(pid), $CuBr_2$(pht), and $CuBr_2$(atr), the spin densities can be evaluated in a manner similar to that for the corresponding chlorine compounds (see Table 3).

The magnitude of the exchange integrals depends on the kind of heterocycles rather than halide ions (see Table 2). This indicates the predominance of superexchange interaction through the heterocycles. CuX_2(pid) and CuX_2(pht) carry larger spin densities on the atoms of the heterocycles than do CuX_2(tr) and CuX_2(atr). Large spin densities on the atoms of bridging ligands favor the migration of positive holes and, consequently, superexchange interaction between copper atoms. In conformity with this expectation, the exchange integrals of CuX_2(pid) and CuX_2(pht) are greater than those of CuX_2(tr) and CuX_2(atr).

Our grateful thanks are due to Dr. M. Iwasaki and Dr. B. Eda of the Government Industrial Research Institute, Nagoya, for giving us facilities to use a broad-line NMR spectrometer in the Institute.

BULLETIN OF THE CHEMICAL SOCIETY OF JAPAN, VOL. 45, 2265—2269 (1972)

The Second CMC of the Aqueous Solution of Sodium Dodecyl Sulfate. II. Viscosity and Density

Michiko KODAMA and Masaji MIURA

Department of Chemistry, Faculty of Science, Hiroshima University, Higashisenda-machi, Hiroshima

(Received December 20, 1971)

Our viscosity and density studies of an aqueous solution of sodium dodecyl sulfate have revealed that the 2nd critical micelle concentration (CMC) exists in addition to the 1st CMC and that the 2nd CMC is greatly influenced by such additives as sodium chloride, dodecyl alcohol, and benzene; these results are in good agreement with those obtained from the conductivity measurements described in the previous paper. The reduced viscosity of the micelle ($\eta_{sp.m}/C_m$) *vs.* C_m curve showed a knick at the concentration corresponding to the 2nd CMC as obtained by Tyuzyo and his co-workers. The molar volume of the hydrated micelle was calculated by using the equation: $\eta_{r.m}=1+2.5\phi_m+14.1\phi_m^2$; it has been found to decrease at about the 2nd CMC, similarly to the partial specific volume ($\bar{v}$) of SDS obtained from the density measurement. This may be attributed to a change in the micelle structure at the 2nd CMC, caused by a variation in the type of aggregation and by a decrease in the counter-ion binding by the micelle.

In our previous paper (Part 1), the micelle structure of an aqueous solution of sodium dodecyl sulfate (SDS), mainly in the concentration region above the 1st critical micelle concentration (CMC), has been studied from the point of view of conductivity measurements.[1] It was revealed by the conductivity studies that a so-called 2nd CMC exists at about 65 mM in addition to the 1st CMC at 8.3 mM, and also that the 2nd CMC is greatly influenced by such additives as sodium chloride, dodecyl alcohol, and benzene.

In the present study, density and viscosity measurements were carried out in order to obtain some more information about the micelle structure of the aqueous solution of SDS. This study can be expected to afford a new clue for clarifying the micelle structure above the 2nd CMC.

Experimental

Materials. The SDS, sodium chloride, dodecyl alcohol, and benzene used in this study were the same as those described in our previous paper,[1] and the aqueous solutions of SDS, both in the absence and presence of the additives, were prepared in the same manner as in the above work.

Procedures. A capillary viscometer of the Ubbelohde type was designed and employed to minimize the effect of the surface tension. Since dust has a great influence upon the flow time, particular attention was given to protect the solution from contamination with dust; the entrances of the viscometer were equipped with glass-filters, the viscometer was carefully cleaned and rinsed with dust-free, distilled water and alcohol, and the solution was introduced into the viscometer through a glass-filter. The flow time was determined by repeating the measurements at least four times, using a stop-watch, in a water-thermostat of 25.000±0.005°C after the temperature equilibrium had been established. The flow time of pure water was 570.00 sec. The density was measured by using pycnometers of the improved Ostwald type,[2] with capacities of 9—10 ml.

Results and Discussion

Viscosity, No Additive. The relative viscosity (η_r) of the aqueous solution of SDS is plotted against the concentration of SDS in Fig. la. As may be seen from this figure, a break point appears at about 65 mM in addition to that at 8.3 mM; the latter corresponds to the 1st CMC, while the former, the so-called 2nd CMC, agrees fairly well with the results obtained by other methods.[1,3,4]

1) M. Miura and M. Kodama, This Bulletin, **45**, 428 (1972).

2) Hennion, *Ind. End. Chem., Anal. Ed.*, **9**, 479 (1937).

3) T. Yasunaga, H. Oguri, and M. Miura, *J. Colloid Interface Sci.*, **23**, 352 (1967).

4) M. Miura, Y. Kubota, J. Miyahara, and I. Takeuchi, Abstract of the 20th Annual Meeting of the Chemical Society of Japan, Vol. I, p. 200 (1967).

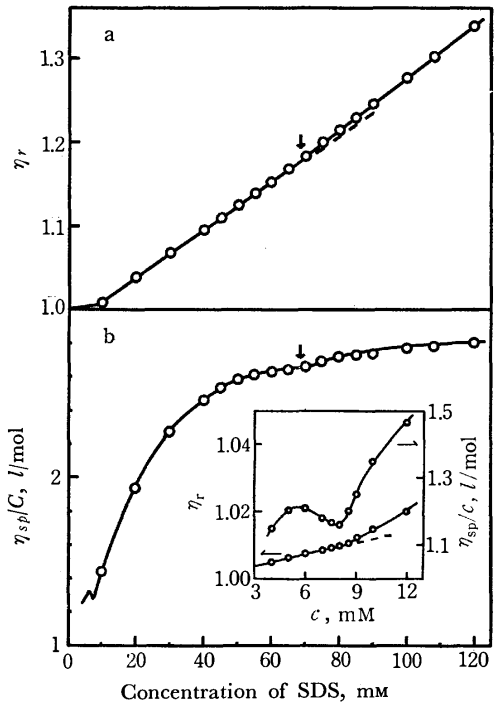

Fig. 1. Relative and reduced viscosities of SDS solution. The arrow in the figure indicates the 2nd CMC. a: Relative viscosity. b: Reduced viscosity. The viscosities in the neighborhood of the 1st CMC are shown under enlargement in Fig. 1b.

The reduced viscosity (η_{sp}/C) is also plotted against the concentration in Fig. 1b ; the results in the neighborhood of the 1st CMC are also shown in an enlarged form in Fig. 1b. As can be seen in Fig.1b, the reduced viscosity shows a minimum at the 1st CMC, as was found by Tyuzyo and his co-workers,[5,6] and then increases markedly above the 1st CMC. Tyuzyo and his co-workers did the following operations, presuming that above the 1st CMC the concentration of the detergent monomer in a solution which is in equilibrium with the micelle is almost constant:—

$$C_m = C - C_{cmc(I)}, \tag{1}$$

$$C_m^\circ = C_{cmc(II)} - C_{cmc(I)}, \tag{2}$$

$$\eta_{sp\cdot m}/C_m = (\eta_{r\cdot m} - 1)/C_m = (\eta_r/\eta_{r\cdot cmc(I)} - 1)/C_m, \tag{3}$$

$$[\eta_1]_m = \lim_{C_m \to 0}(\eta_{sp\cdot m}/C_m), \tag{4}$$

$$[\eta_2]_m = \lim_{C_m \to C_m^\circ}(\eta_{sp\cdot m}/C_m), \tag{5}$$

where C is the total concentration of SDS; C_m is the concentration of a micellar substance; $C_{cmc(I)}$ and $C_{cmc(II)}$ are the 1st and 2nd CMC's as obtained from viscosity measurements respectively; $\eta_{r\cdot cmc(I)}$ is the relative viscosity of the solution against water at the 1st CMC; $\eta_{r\cdot m}$ and $\eta_{sp\cdot m}/C_m$ are the relative and reduced viscosities of the micellar substance respectively, and $[\eta_1]_m$ and $[\eta_2]_m$ are the intrinsic viscosities of the micellar substance at the 1st and 2nd CMC's respectively.

The reduced viscosity of micellar SDS, as obtained from Eq. (3), is plotted against the concentration of micellar SDS in Fig. 2, where a knick corresponding to the 2nd CMC appears as in the experiments done

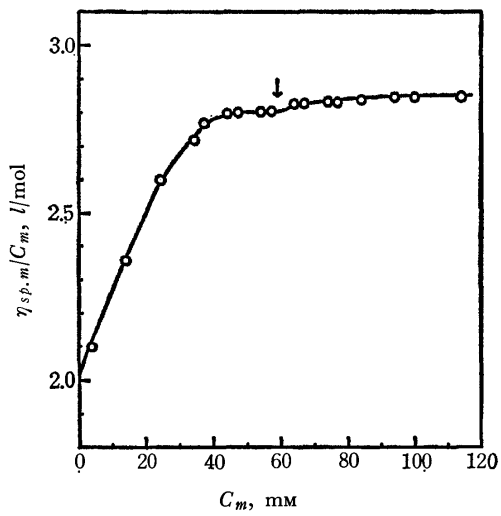

Fig. 2. Reduced viscosity of SDS micelle.

by Tyuzyo and his co-workers.[5,6] The values of $[\eta_1]_m$ and $[\eta_2]_m$ obtained from Fig. 2 by means of Eqs. (4) and (5) are, respectively, 2.0 and 2.8; those values agree fairly well with the reference values.[6]

The Guth and Simha equation,[7] which is a form of the Einstein equation extended for use with more concentrated solutions, was used in the present case:

$$\eta_r = 1 + 2.5\phi + 14.1\phi^2. \tag{6}$$

In this equation, ϕ is the volume fraction occupied by particles. It may be necessary to discount the detergent monomer, which play no role as a micellar substance, in the application of Eq. (6) to a micelle system. Therefore, on the assumption that the monomer concentration remains constant above the 1st CMC, the following equation can be obtained for the concentrated solutions containing the spherical micelles:

$$\eta_{r\cdot m} = 1 + 2.5\phi_m + 14.1\phi_m^2, \tag{7}$$

where ϕ_m is the volume fraction of hydrated micelles. The value of ϕ_m was calculated by the use of Eq.(7). The molar volume of the hydrated micelle (V_m) was obtained from this relation: $V_m = \phi_m/C_m$. The values of ϕ_m and V_m obtained in this manner are plotted against C_m in Figs. 3a and 3b respectively. It may be seen from these figures that ϕ_m increases linearly with C_m up to the 2nd CMC at about C=55 mM, while, in the range above the 2nd CMC, the curve bends toward the C_m axis, and that this phenomenon is reflected in the V_m *vs.* C_m curve—that is, V_m takes a nearly constant value up to the 2nd CMC and then decreases gradually. The values of V_m in the (I) and (II) parts in Fig. 3b are 0.91 *l*/mol and 0.80 *l*/mol respectively. These results may support the view that, in the concentration range between the 1st CMC and the 2nd CMC, the SDS micelle is spherical with a nearly constant volume ($V_{m(I)}$), while above the 2nd CMC it is deformed from the spherical shape to an asymmetric one, accompanied by a decrease in the

5) N. Sata and K. Tyuzyo, This Bulletin, **26**, 177 (1953).
6) H. Okuyama and K. Tyuzyo, *ibid.*, **27**, 259 (1954).
7) E. Guth and R. Simha, *Kolloid-Z.*, **74**, 266 (1936).

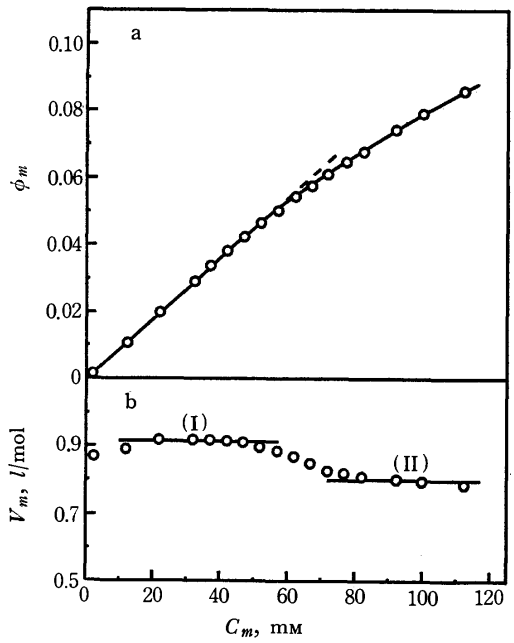

Fig. 3. a: Volume fraction of SDS micelle. b: Molar volume of the hydrated micelle of SDS.

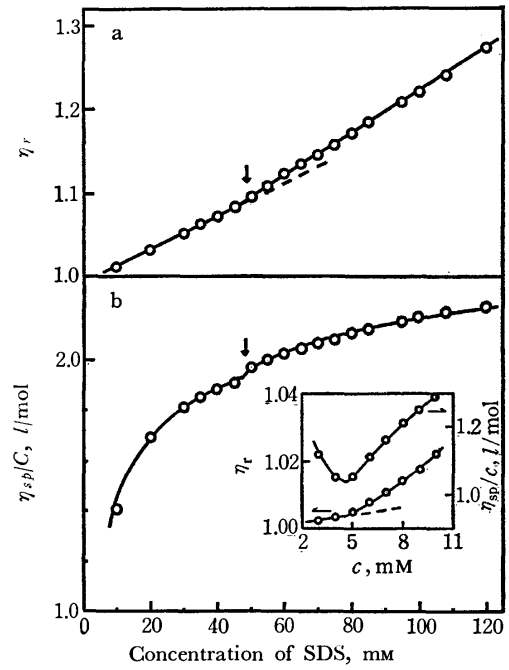

Fig. 4. Relative and reduced viscosities of SDS solution in the presence of 0.01 M NaCl. a: Relative viscosity. b: Reduced viscosity. The viscosities in the neighborhood of the 1st CMC are shown under enlargement in Fig. 4b.

8) K. Shinoda, T. Nakagawa, B. Tamamushi, and T. Isemura, "Colloidal Surfactants," Academic Press, New York (1963), p. 115.
9) D. C. Robins and I. L. Thomas, *J. Colloid Interface Sci.*, **26**, 415 (1968).
10) F. Iwadare and T. Suzawa, *Nippon Kagaku Zasshi*, **90**, 50 (1969).
11) P. Ekwall and P. Holmberg, *Acta Chem. Scand.*, **19**, 455, 573 (1965).
12) P. Ekwall, L. Mandell, and P. Solyom, *J. Colloid Interface Sci.*, **35**, 519 (1971).

molar volume ($V_{m(II)}$)[8-12]

Effect of Sodium Chloride. The results of the viscosity measurements of the SDS solution containing 0.01 M sodium chloride are shown in Fig. 4, while those in the neighborhood of the 1st CMC are shown in the same figure in an enlarged form. The 2nd CMC as well as the 1st CMC is lowered and at the same time the slope of the curve above the 2nd CMC is raised, compared with the results shown in Fig. 1a; this is in agreement with the results obtained by the conductivity measurements. The reduced viscosity of micellar SDS containing 0.01 M sodium chloride is shown in Fig. 5. It may also be seen from this figure that the knick at the concentration corresponding to the 2nd CMC is more remarkable than that in the absence of sodium chloride. The values of $[\eta_1]_m$ and $[\eta_2]_m$ are, respectively, 1.4 and 2.0; each of those values is lower than the value in the absence of an additive. In the presence of sodium chloride, the decrease in the $[\eta_1]_m$ or $[\eta_2]_m$ value may be due to the electroviscus effect predicted for charged systems.[13-16]

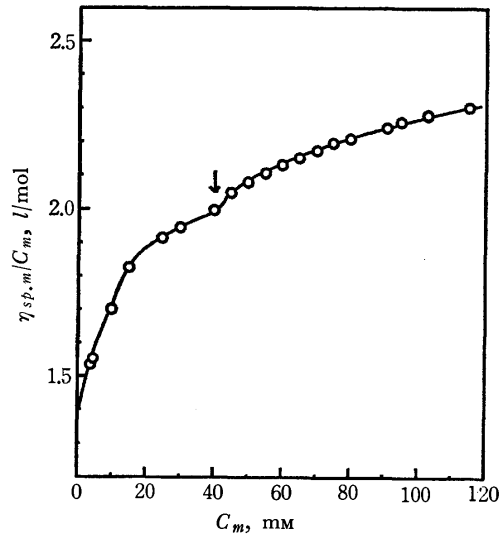

Fig. 5. Reduced viscosity of SDS micelle in the presence of 0.01 M NaCl.

Effect of Dodecyl Alcohol (DA). The results of the viscosity measurements of the SDS solution containing DA in a 1/10 molar ratio of DA to SDS are shown in Fig. 6, where the relative and reduced viscosities are plotted against the concentration of the SDS solution. It may be seen from this figure that no change appears at the concentration corresponding to the 2nd CMC. In this case, there may be no 2nd CMC. It can be concluded from the viscosity measurements, much as in the case of the conductivity measurements, that the presence of a proper amount of DA stabilizes the micelle in the region of low concentrations.

Effect of Benzene. The viscosity measurements of the SDS solution containing benzene in a molar

13) F. Booth, *Proc. Roy. Soc.* (London), **A 203**, 514, 533 (1950).
14) R. A. Rarker and S. P. Wasik, *J. Phys. Chem.*, **62**, 967 (1958).
15) P. Mukerjee, *J. Colloid Sci.*, **19**, 722 (1964).
16) C. Tanford and J. G. Buzzell, *J. Phys. Chem.*, **60**, 225(1956).

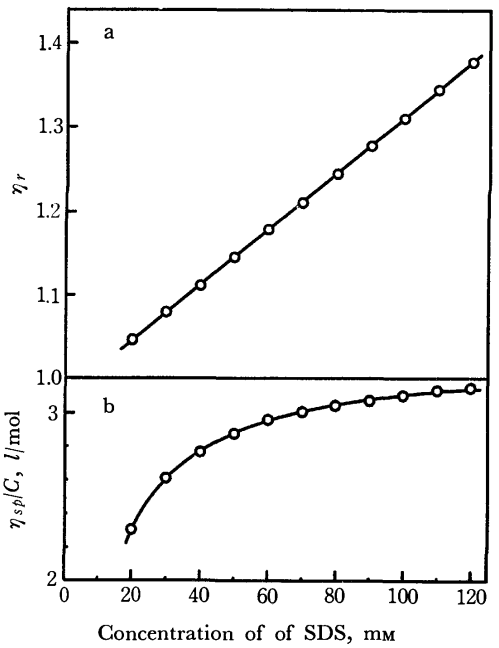

Fig. 6. Relative and reduced viscosities of SDS solution in the presence of DA in a molar ratio of DA to SDS, 1/10. a: Relative viscosity. b: Reduced viscosity.

of 1/4 were also carried out. The results obtained were almost the same as those obtained in the absence of additives, represented in Fig. 1; benzene has no remarkable influence upon the 2nd CMC, a finding in agreement with the results obtained by the conductivity measurements.

Density. The partial specific volume of SDS ($\bar{v}$) is calculated on the basis of the following equation (8):[17,18]

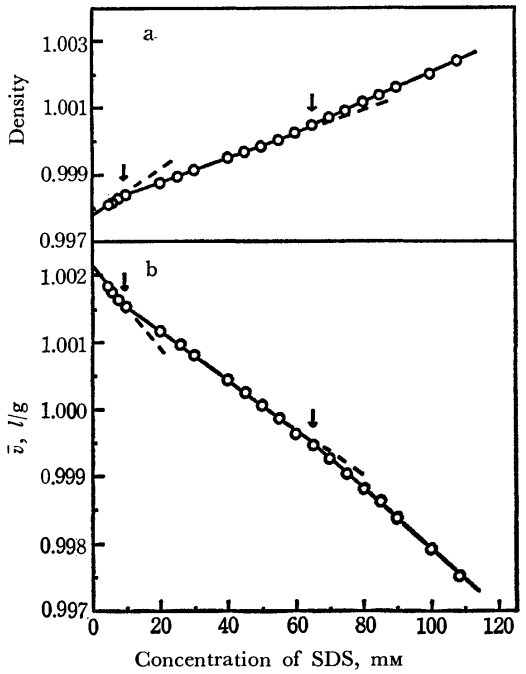

Fig. 7. a: Density of SDS solution. b: Specific volume of SDS solution.

17) H. Lal, *J. Colloid Sci.*, **8**, 414 (1953).
18) P. Mukerjee, *J. Phys. Chem.*, **66**, 1733 (1962).

$$\bar{v} = v + (1-x)\mathrm{d}v/\mathrm{d}x, \quad (8)$$

where v is the specific volume of the solution and x, the concentration of the solute per gram of the solution. The value of $\mathrm{d}v/\mathrm{d}x$ can be evaluated graphically from the v *vs.* x curve. The density and the specific volume of the aqueous solution of SDS in the absence of an additive are plotted against the concentration in Figs. 7a and 7b respectively. As may be seen from this figure, a break point exists at the 2nd CMC in addition to that at the 1st CMC. The partial specific volume of SDS is shown in Fig. 8;

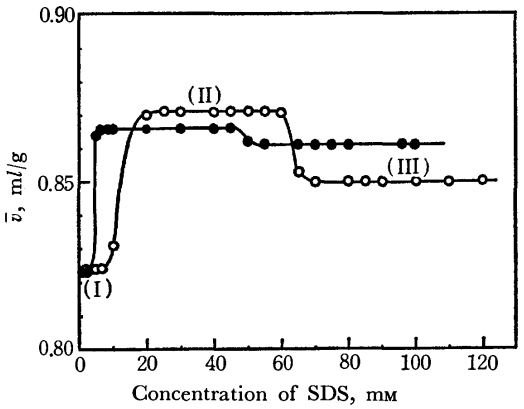

Fig. 8. Partial specific volume of SDS. ○: No additive, ●: 0.01 M NaCl.

after taking a practically constant value (I) in the concentration range below the 1st CMC, the partial specific volume increases rapidly at about the 1st CMC, remains constant (II) again over a wide concentration range up to the 2nd CMC, then decreases at about the 2nd CMC, and again remains constant (III) above the 2nd CMC. The values of v were estimated from the figure to be 0.871 ml/g and 0.851 ml/g in the (II) and (III) parts respectively. It may be noted that the behavior of the partial specific volume is quite similar to that of the hydrated molar volume obtained from the viscosity measurements shown in Fig. 3b. The partial specific volume and the hydrated molar volume both remain constant in the concentration range between the 1st CMC and the 2nd CMC. This may imply that the micelle structure — that is, the micelle size and shape — does not change in this concentration range.[19] The marked decreases in the partial specific volume and the hydrated volume at the 2nd CMC may be attributed to the change in the micelle structure; the SDS molecules, of which the micelle is composed, occupy a smaller space above the 2nd CMC than below the 2nd CMC as a result of a change in the type of aggregation.

Ekwall and his co-workers have observed, from their measurements of the viscosity[12] and density[19] of sodium caprylate solutions, that both the hydrated molar volume and the partial specific volume increased at about the 2nd CMC; they have concluded that these phenomena may be attributed to an increase

19) P. Ekwall, H. Eikrem, and L. Mandell, *Acta Chem. Scand.*, **17**, 111 (1963).

in the binding force between the micelle and the counter ion above the 2nd CMC. It is interesting to note that these two kinds of volumes of SDS decrease at the 2nd CMC, contrary to the results obtained by Ekwall and his co-workers. It was revealed from the conductivity measurements of the SDS solutions that the specific conductivity-concentration curve breaks upward at the 2nd CMC.[1] On the assumption that this conductivity behavior may be caused at least partly by an increase in the free counter ion (Na^+) as a result of a decrease in the counter-ion binding by the micelle, the decrease in the hydrated molar volume or the partial specific volume is explicable; the former may be ascribed to the dehydration of the SDS micelle resulting from a decreased counter-ion binding of the micelle, while the latter may be ascribed to a decrease in the volume of the SDS solution due to the interaction between the free counter ion and water, because the partial volume can be regarded as the sum of the volume of the ions themselves and that of the volume change of the solvent associated with the solvent-solute interaction.[18] The partial specific volume of SDS in the presence of 0.01 M sodium chloride is also represented in Fig. 8. The degree of decrease in the partial specific volume above the 2nd CMC is much smaller than that in the absence of sodium chloride. These problems will be discussed in detail later, with more experimental data.

BULLETIN OF THE CHEMICAL SOCIETY OF JAPAN, VOL. 45, 2269—2273 (1972)

The Quenching of Hg(6^3P_1) Atoms by Molecular Hydrogen as Investigated by ESR Spectroscopy

James B. FARMER and Kazuo SHIMOKOSHI*

Department of Chemistry, University of British Columbia, Vancouver 8, British Columbia, Canada

(Received March 11, 1972)

The gas phase electron spin resonance technique has been applied to study the quenching efficiency of Hg(6^3P_1) mercury atoms by molecular hydrogen. The concentration of hydrogen atoms produced by the mercury photosensitized decomposition of molecular hydrogen in a flow apparatus was followed as a function of the partial pressure of hydrogen with argon, neon, and hydrogen as carrier gases. The kinetic equations derived from the reaction mechanism proposed was shown to be in agreement with the experimental observations. The total quenching rate k_H was evaluated from the experimental results.

The quenching of excited mercury atoms Hg (6^3P_1) was first observed by Cario and Franck[1] and since that time this process has been the subject of numerous detailed investigations. Several comprehensive reviews of the literature have appeared.[2,3] Most investigators have devoted their attention to studying the quenching of excited Hg($^3P_1$) mercury atoms by hydrogen,[1-9] or hydrocarbons,[2-4,10-13] though many detailed studies have been made of the quenching processes caused by other molecules.[7,12-14] Undoubtedly the reaction of this type which has been most extensively investigated is that of the mercury photosensitized decomposition of molecular hydrogen. These extensive studies have been carried on not only because of the intrinsic importance of the quenching process itself, but because the mercury photosensitized decomposition of molecular hydrogen has proven to be a clean source of hydrogen atoms of considerable importance in the study of hydrogenation processes.

The quenching of excited mercury Hg(6^3P_1) atoms has been measured by both physical and chemical methods. Thus Thomas and Gwinn[5] studied the quenching efficiency of molecular hydrogen by measuring the pressure changes in the reaction cell. Cvetanovic[2] developed a chemical method for the estimation of quenching efficiencies. This method is based on chemical analysis of the reactants. Generally mixtures of nitrous oxide and hydrocarbons were used to quench the excited Hg*(6^3P_1) atoms, and subsequent product analysis enabled relative values for the quenching efficiencies to be estimated. Both physical[12,13] and chemical methods[2,6,10] have been used to study the quenching of excited mercury Hg (6^3P_1) atoms by alkanes and related compounds. The

* Present address: Department of Chemistry, Tokyo Institute of Technology, Ohokayama, Meguro, Tokyo.

1) G. Cario and J. Franck, *Z. Phys.*, **11**, 161 (1922).
2) R. J. Cvetanovic, "Progress in Reaction Kinetics" ed. G. Porter, Perganon Press Ltd., Oxford, Vol. **2**, (1964), p. 69.
3) H. E. Gunning and O. P. Strausz, "Advances in Photochemistry," Interscience Publishers, New York, Vol. **1**, (1962), p. 209.
4) A. B. Callear and R. G. W. Norrish. *Proc. Roy. Soc.*, **A266**, 299 (1962).
5) L. B. Thomas and W. D. Gwinn, *J. Amer. Chem. Soc.*, **70**, 2643 (1948).
6) K. Yang, J. D. Paden, and C. L. Hassell, *J. Chem. Phys.*, **47**, 3824 (1967).
7) A. B. Callear and R. E. M. Hedges, *Trans. Faraday Soc.*, **66**, 605 (1970).
8) A. B. Callear and R. E. M. Hedges, *ibid.*, **66**, 615 (1970).
9) A. B. Callear and J. McGurk, *Nature* **226**, 844 (1970).
10) K. Yang, *J. Amer. Chem. Soc.*, **89**, 5344 (1967).
11) A. C. Vikis and H. C. Moser. *J. Chem. Phys.*, **53**, 2333 (1970).
12) S. Penzes, A. J. Yarwood, O. P. Strausz, and H. E. Gunning, *ibid.*, **43**, 4524 (1965).
13) S. Penzes, O. P. Strausz, and H. E. Gunning, *ibid.*, *Phys.*, **45**, 2322 (1966).
14) A. C. Vikis, G. Torrie, and D. J. Le Roy, *Can. J. Chem.*, **48**, 3771 (1970).

flash photolysis technique was first used by Callear and Norrish[4] to investigate mercury photosensitized reactions and in particular to study the role of $Hg(^3P_0)$ atoms. Callear and Williams[15,16] studied mixtures of mercury vapour and various gases when subjected to a single pulse of uv radiation. A microwave pulse method was developed by Callear and Hedges[7,8] and applied particularly to study the role of HgH as an intermediate in $Hg(6^3P_1)$ photosensitized reactions. More detailed studies of the formation of HgH in the mercury photosensitized decomposition of molecular hydrogen were reported by Callear and McGurk[9]. Many workers have studied the importance of complex formation as an intermediate in the quenching of excited mercury $Hg(6^3P_1)$ atoms by molecules other than hydrogen. Thus Homer and Lossing[18] as the result of studies using a mass spectrometric technique postulated the formation of a HgCO* complex with a life-time of about 3×10^{-5} sec to account for the results of their study of the reaction $Hg(6^3P_1)$ atoms with CO. This same system was studied extensively by Karl, Kruss, and Polanyi[19-21] who recorded the infrared emission of vibrationally excited carbon monoxide to its ground state. The results were also interpretated in terms of the formation of a HgCO* complex. Later, in an extensive physical and chemical study[22] of the Hg/CO system, by London, Vikis, and Le Roy, it was stated that the results failed to yield any substantial additional evidence for the existence of the HgCO* complex.

Recently electron spin resonance spectroscopy has been used to study atom concentrations in reacting systems. In the case of certain reactions it has proved possible to detect atomic hydrogen in the gas phase at concentrations as low as 10^{10}-10^{11} atom/cc, and to estimate the concentrations of such atomic species quantitatively.[23] This method has been applied to the study of the mercury photo-sensitized reaction between hydrogen and oxygen.[24] In this paper we describe a somewhat improved experimental method using electron spin resonance spectroscopy and a flow system to study in greater detail this photosensitized reaction.

Experimental

The pure cylinder hydrogen used in these experiments was further purified by passage through a catalytic deoxygenator unit (Deoxo), and through a cold trap held at liquid nitrogen temperature. The other gases used, namely argon and neon, were obtained from the Matheson Company and were stated to be better than 99.998% pure. Before use these were passed through a cold trap held at liquid nitrogen temperature.

Figure 1 shows a schematic diagram of the experimental arrangement. The gaseous mixtures containing hydrogen were introduced to the reaction vessel after passing through the thermostated mercury saturator. The vapour pressure of the mercury was varied by changing the temperature of the circulating water cooling the saturator. The temperature could readily be controlled to ±0.2°C. After passing the radiation zone the gases entered the ESR cavity operating in a TE_{102} mode. The partial pressure of the gases was determined by measuring the flow rate of each gas which was accurately controlled by needle valves at the inlet and outlet of the system. The capillary flow meters were carefully calibrated before use.

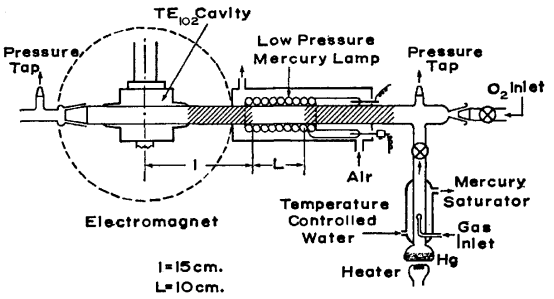

Fig. 1. Diagrammatic sketch of the experimental apparatus.

The irradiations were carried out using a Hanovia low pressure mercury vapour lamp which was spiral in form and having a diameter of 5 cm, and was 15 cm in length. The flow tube was 2 cm o.d. quartz coated on the inside with DuPont Teflon to reduce the rate of recombination of the hydrogen atoms at the surface. It is well known that without such wall coatings it is difficult to observe ESR signals due to H atoms because of high efficiency of the recombination due to wall collisions when uncoated quartz is used. A X-band homodyne ESR spectrometer using a modulating frequency of 100 kHz was used to determine the hydrogen atom concentrations. The H atom concentrations being

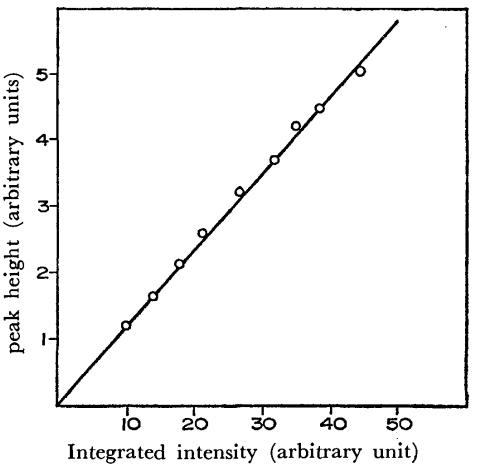

Fig. 2. Relationship between the integrated intensity and peak height of the ESR spectrum of H atoms in a flow system at mean pressures of 0.3 to 0.2 torr.

15) A. B. Callear and G. J. Williams, *Trans. Faraday Soc.*, **60**, 2158 (1964).
16) A. B. Callear, J. A. Green, and G. J. Williams, *ibid.*, **61**, 1831 (1965).
17) A. B. Callear and J. McGurk, *Chem. Phys. Lett.*, **7**, 491 (1970).
18) J. B. Homer and F. P. Lossing, *Can. J. Chem.*, **44**, 143 (1966).
19) G. Karl and J. C. Polanyi, *J. Chem. Phys.*, **38**, 271 (1963).
20) G. Karl, P. Kruus, and J. C. Polanyi. *ibid.*, **46**, 224 (1967).
21) G. Karl, P. Kruus, P. C. Polanyi, and I. W. M. Smith, *ibid.*, **46**, 244 (1967).
22) G. London, A. C. Vikis, and D. J. Le Roy, *Can. J. Chem.*, **48**, 1420 (1970).
23) A. A. Westenberg and N. de Haas, *J. Chem. Phys.*, **40**, 3087 (1964); **47**, 1393 (1967).
24) K. Shimokoshi, Y. Mori, and I. Tanaka, This Bulletin, **40**, 254 (1967).

estimated by comparing the integrated intensities with lines in the ESR spectrum of molecular oxygen whose concentrations in the reaction zone was known. The integration was achieved by using two successive operational amplifiers which provided respectively, the first and second integrals of the original derivative spectrum. A plot of the integrated intensity of the atomic hydrogen ESR signal against the peak heights is shown in Fig. 2. These data were obtained at mean pressures of hydrogen of 0.3 to 2.2 torr in the flow system.

Results and Discussion

As will be clear from the above, our experimental technique yields values for the variation of the concentration of the hydrogen atoms as a function of pressure. These data can be used to develop a kinetic analysis of the processes which occur when excited Hg (6^3P_1) atoms are quenched by molecular hydrogen.

When ground state mercury atoms $Hg(6^1S_0)$ absorb radiation of wavelength 2537Å the following initial processes occur:

$$Hg(6^1S_0) + h\nu \xrightarrow{k_1} Hg(6^3P_1) \quad (1)$$

$$Hg(6^3P_1) \xrightarrow{k_2} Hg(6^1S_0) + h\nu \quad (2)$$

Collision of the excited $Hg(6^3P_1)$ atoms with molecular hydrogen leads to a number of processes, all of which are of importance in understanding the nature of the complex reactions involved in the overall quenching phenomena.

The first reaction leading to the production of hydrogen atoms which obviously occurs is

$$Hg(6^3P_1) + H_2 \xrightarrow{k_3} HgH + H \quad (3)$$

Indirect evidence for the formation of HgH was obtained by Thomas and Gwinn.[5] Various workers[6,10,25,26] have discussed the possibility of this process both in terms of studies of potential surfaces correlating the $Hg(6^3P_1)$ atom and molecular hydrogen energy states, and phase-space theory in which reactive scattering is assumed to occur when the relative energy of translation exceeds the hump in the effective interaction potential curve. The observation of the spectrum of HgH in flash spectroscopic studies of mixtures of mercury and H_2, D_2, by Callear and Hedges[7,8], and by Callear and McGurk[9] clearly established that reaction (3) does occur. We should perhaps mention that Callear and McGurk[9] have suggested that the interaction of $Hg(6^3P_1)$ atoms and molecular hydrogen is somewhat more complicated than has been indicated in Eq. (3). They suggested that the following sequence of reactions occur,

$$Hg(6^3P_1) + H_2 \longrightarrow HHgH^* \text{ (insertion)}$$

$$HHgH^* \longrightarrow HHgH \text{ (crossing)}$$

$$HHgH \longrightarrow HgH + H \text{ (dissociation)}$$

In the present studies, however, we are of the opinion that Eq. (3) is an adequate representation of the interaction. The HgH formed in reaction (3) was found[8] to decay in less than 200 μsec.

Various mechanisms have been suggested for the subsequent reactions of the HgH produced in reaction (3). It may for example simply dissociate rapidly as follows

$$HgH + M \longrightarrow Hg(6^1S_0) + H + M$$

since the bond dissociation energy of HgH is only 8.6 kcal mol^{-1}. Another possible reaction is, of course,

$$HgH + H \longrightarrow Hg(6^1S_0) + H_2$$

which was postulated by Thomas and Gwinn[5] and subsequently adopted by a number of workers.[6-9,22]

Apart from reaction (3) there are two other quenching processes which must be considered to be of some importance, namely

$$Hg(6^3P_1) + H_2 \xrightarrow{k_4} Hg(6^3P_0) + H_2 \quad (4)$$

$$Hg(6^3P_1) + H_2 \xrightarrow{k_5} Hg(6^1S_0) + H_2 \quad (5)$$

The role of spin-orbit relaxation (reaction (4)) in the quenching of excited mercury (6^3P_1) atoms has been studied in some detail[4,7-9,12-14,22] and it is clear that in the case of hydrogen reaction (4) is an important process. Corresponding processes must occur when a carrier gas is used in the experiments using hydrogen mixtures so we must, in these cases, also include the following processes

$$Hg(6^3P_1) + M \xrightarrow{k_6} Hg(6^3P_0) + M \quad (6)$$

$$Hg(6^3P_1) + M \xrightarrow{k_7} Hg(6^1S_0) + M \quad (7)$$

many authers[1-5,7-9,12-14,29,30,32,33] have considered the role of metastable $Hg(6^3P_0)$ atoms in mercury photosensitized reactions. Callear and Hedges[7,8] showed conclusively that both molecular hydrogen and deuterium, in the presence of large excess of nitrogen react with $Hg(6^3P_0)$ atoms in the manner analogous to reaction (3), namely:-

$$Hg(6^3P_0) + H_2 \longrightarrow HgH + H \quad (3^1H)$$

$$Hg(6^3P_0) + D_2 \longrightarrow HgD + D \quad (3^1D)$$

and that the yields of HgH (or HgD) were slightly higher from $Hg(6^3P_0)$ than from $Hg(6^3P_1)$ atoms. Earlier, however, Callear and Norrish[4] had shown that the cross-section for quenching of $Hg(6^3P_0)$ by molecular hydrogen is 0.08Å^2, whereas that for $Hg(^3P_1)$ and hydrogen is 6Å^2. More recently London *et al.*[22] and Callear and McGurk[17] have confirmed that the rate of deactivation or reaction of $Hg(6^3P_0)$ atoms by hydrogen is very small. For these reasons it is unlikely that reaction (3^1H) is of any major significance in our case. The only reactions of $Hg(6^3P_0)$ atoms with hydrogen which need be considered are therefore,

25) K. J. Laidler, "The Chemical Kinetics of Excited States," Oxford University Press, 1955.
26) K. J. Laidler, *J. Chem. Phys.*, **10**, 43 (1942).
27) P. H. Garrett. *Phys. Rev.*, **20**, 779 (1932).
28) J. E. McAlduff and D. J. Le Roy. *Can. J. Chem.*, **43**, 2279 (1965).
29) G. H. Kimbell and D. J. Le Roy. *Can. J. Chem.*, **38**, 1714 (1960).
30) G. H. Kimbell and D. J. Le Roy. *ibid.*, **40**, 1229 (1962).
31) H. W. Webb and H. A. Messenger, *Phys. Rev.*, **33**, 319 (1929).
32) A. B. Callear and W. P. D. Pereira, *Trans. Faraday Soc.*, **59**, 2758 (1963).

$$Hg(6^3P_0) + H_2 \longrightarrow Hg(6^1S_0) + 2H \quad (8)$$

$$Hg(6^3P_0) + H_2 \longrightarrow Hg(6^1S_0) + H_2 \quad (9)$$

The corresponding reaction to (9) may also occur with a non-chemically reacting atom or molecule, *i.e.*,

$$Hg(6^3P_0) + M \xrightarrow{k_{10}} Hg(6^1S_0) + M \quad (10)$$

Because the life-time of the $Hg(6^3P_0)$ atoms is long, the radiative transition to the ground state

$$Hg(6^3P_0) \longrightarrow Hg(6^1S_0) + h\nu'$$

is also not likely to be of importance in our case.

The termination reactions involving hydrogen atoms are:—

$$H + H + H_2(M) \longrightarrow H_2 + H_2[M] \quad (11)$$

$$H \text{ (wall)} \longrightarrow \tfrac{1}{2}H_2 \quad (12)$$

Since the life-time of $Hg(6^3P_1)$ is quite short and the quenching processes k_3, k_4, and k_5 (and k_2) are fast, we can assume that a steady state concentration of $Hg(6^3P_1)$ and $Hg(6^3P_0)$ will quickly be established. Applying the normal steady state approximations we obtain the following equation for the rate of formation of hydrogen atoms:—

$$d[H]/dt = 2k_3[Hg(6^3P_1)]_{ss}[H_2] + 2k_8[Hg(6^3P_0)]_{ss}[H_2] - k_{12}[H] - k_{11}[H]^2[H_2] \quad (13)$$

As the total pressure in the flow tube was lower than 5 torr, and the concentration of hydrogen atoms was also so low, the termolecular recombination process (11) can be neglected, particularly as the transit time from the irradiation zone to the cavity is probably only 10^{-3} sec. Equation (13) therefore can be simplified to

$$d[H]/dt = A - k_{12}[H], \quad (14)$$

where

$$A = \frac{2I_0[H_2]}{k_2 + k_H[H_2] + k_M[M]}\left\{k_3 + k_8\frac{k_4[H_2] + k_6[M]}{k_H^\circ[H_2] + k_{10}[M]}\right\}. \quad (15)$$

In Eq. (15) we have written k_H for $k_3+k_4+k_5$, k_M for k_6+k_7, and k_H° for k_8+k_9.

Outside the illumination region the rate of formation of H atoms can be neglected so in those regions Eq.(14) has the form

$$d[H]/dt = -k_{12}[H]. \quad (16)$$

Under our experimental conditions when $[H_2] \gg [H]$, then the hydrogen atom concentration $[H]_c$ in the cavity given by the expression

$$[H]_c = \frac{A}{k_{12}}\{1 - \exp(-k_{12}L/v)\}\exp(-k_{12}l/v). \quad (17)$$

Where L is the length of the illumination zone, l the distance from the end of the illumination zone to the ESR cavity, and v is the linear flow velocity. The effect of the flow velocity on the hydrogen atom concentration in the cavity $[H]_c$ at constant pressure of hydrogen of 0.374 torr is shown in Fig. 3. If we assume that $k_{12}L/v$ and $k_{12}l/v$ are both $\ll 1$, then from Eq. (17) we obtain the result

$$[H]_c = \frac{AL}{v}\left(1 - \frac{k_{12}l}{v}\right)$$

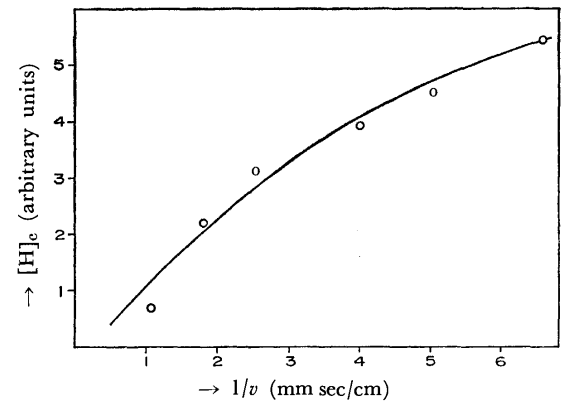

Fig. 3. Plot of hydrogen atom concentration $[H]_c$ as a function of $1/v$ at pressure of hydrogen of 0.374 torr.

which is in agreement with the experimental results as shown in Fig. 3.

From Eqs.(13)—(17) we can obtain the expression

$$\frac{B}{[H]_c} = \left(k_H + \frac{k_2}{[H_2]} + \frac{k_M[H]}{[H_2]}\right) \times \left\{\frac{k_H^\circ[H_2] + k_{10}[M]}{(k_3k_M^\circ + k_8k_4)[H_2] + (k_3k_{10} + k_8k_6)[M]}\right\}, \quad (18)$$

where $B=(2I/k_{12})\{1-\exp(-k_{12}L/v)\}\exp(-k_{12}l/v)$ which is constant under the conditions of our experiments where L, v, and I were kept constant. To evaluate $k_H=k_3+k_4+k_5$ we proceed as follows. Eq. (18) can be rewritten as

$$\frac{C}{[H]_c} = \left(k_H + \frac{k_2}{[H_2]}\right) \quad (19)$$

where $C=Bk_H^\circ/(k_3k_H^\circ+k_8k_4)$ if we neglect the quenching by inert gases used as carriers. A series of experiments were carried out using Ar, Ne, and H_2 as carrier gases at constant flow rate. Plots of the function $1/[H]_c$ obtained from the measurements of $[H]_c$, the hydrogen atom function in the cavity against $1/[H_2]$ are shown in Figs. 4, 5, and 6. Least squaring the data gave the values of k_H/k_2 at 20°C listed in Table 1. The ratio k_H/k_2 was evaluated because the method was thought not to be accurate enough to determine the parameters separately.

To evaluate k_H we need to have an estimate of k_2

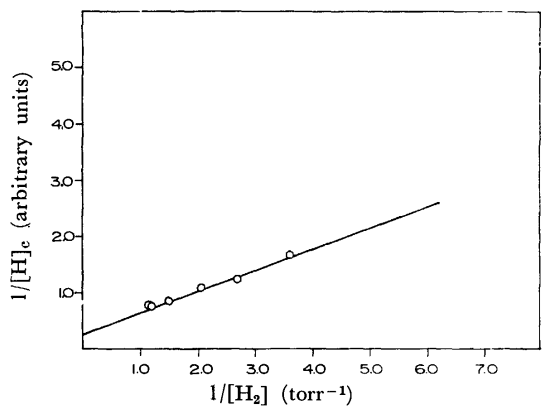

Fig. 4. Plot of $1/[H]_c$ against $1/[H_2]$ at total pressure of 1.0 torr with argon as the carrier gas.

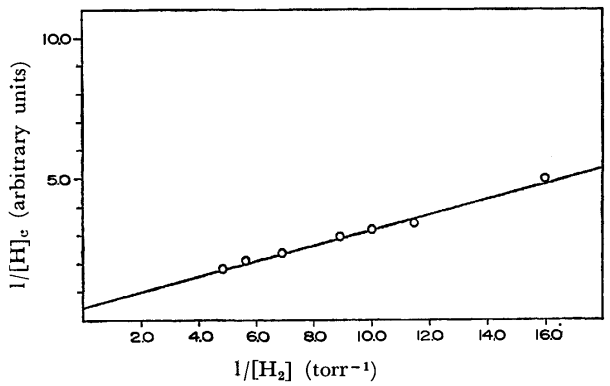

Fig. 5. Plot of $1/[H]_c$ against $1/[H_2]$ at total pressure of 2.0 torr with neon as the carrier gas.

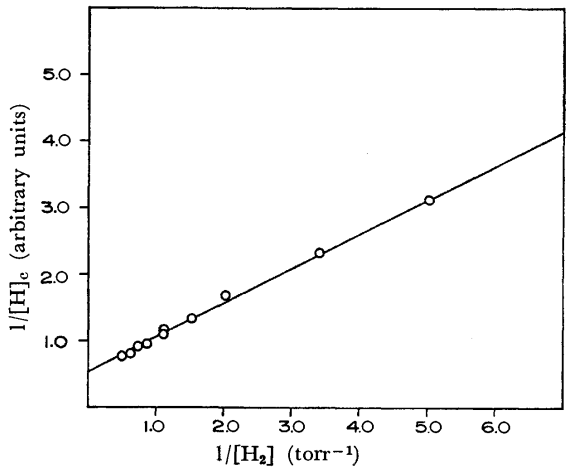

Fig. 6. Plot of $1/[H]_c$ against $1/[H_2]$ with hydrogen as carrier gas.

under the conditions of our experiments. The true lifetime of Hg(6^3P_1) atoms with respect to radiation has been reported by Garrett[27] as being 1.08×10^{-7} sec. This value may, however, need correction because of the possible imprisonment of the resonance radition, which has the effect of decreasing this value as the mercury vapour pressure is increased. For the range of mercury vapour pressure used in our experiments, we may make use of the expression (20) proposed by McAlduff and LeRoy[28]

$$k_2 = (1-q[\mathrm{Hg}])/\tau \qquad (20)$$

when q is a constant. As has been pointed out by many authors[29-31] radiation imprisonment effects depend on the geometry of the cell as well as the nature of the light source used. Under our experimantal conditions it was difficult to measure the concentration of the mercury atoms with high precision. This difficulty was, however, circumvented to an acceptable degree by the following method. The concentration in the reactor region was assumed to be linearly related to that in the saturator. If we assume there was little change in I_0 then by reducing the concentration of mercury atoms by one half, we carried out a determination of k_H/k_2 with the temperature of the reactor at 12°C at which point the vapour pressure of mercury is one half the value at 20°C. The value of the ratio $(k_H/k_2)_{20°}/(k_H/k_2)_{12°}$ was found to be 0.91, and substituting this value into Eg.(20) we obtain the result that $k_2=1.2/\tau$. This enables us to calculate k_H from the data in column 2 of Table 1. The resulting values of k_H are given in column 3 of Table 1. The only other data available for comparison is given in column 4 which are obtained by a chemical method.[1,22] The chemical method for determining the kinetic parameters is possibly subject to several inherent errors. The ESR method is more direct and may be more accurate. The agreement between the two sets of values is, however, satisfactory.

Table 1. Summary of the rate constants at 20°C

Carrier gas	k_H/k_2 (torr^{-1})	$10^{-10}\times k_H$ (l mol^{-1} sec^{-1}) this work	Literature values
H_2	1.11±0.20	22.5±4.0	30.7 (Ref. 22)
Ar	1.05±0.41	21.2±8.2	29.0 (Ref. 1)
Ne	0.98±0.33	20.9±5.7	

We wish to thank Professor C. A. McDowell for many interesting discussions and for his extensive help in writing this paper. This work was supported by grants from the Natinal Research Council of Canada.

The Crystal and Molecular Structure of Butein Monohydrate, Isolated from *Dahlia variabilis*

Norio SAITO*, Katsuhiko UENO,** and Yoshio SASADA

Laboratory of Chemistry for Natural Products, Tokyo, Institute of Technology, Ookayama, Meguro-ku, Tokyo, 159

(Received January 5, 1972)

The crystals of butein monohydrate isolated from *Dahlia variabilis* are monoclinic. The unit cell, with dimensions of $a=10.89$, $b=28.88$, $c=4.29$ Å, and $\beta=96.7°$, contains four molecules, and the space group is $P2_1/n$. An approximate structure was obtained by applying the symbolic addition procedure. The structural parameters were refined by the block-diagonal least-squares method, and the final R factor for 1063 observed reflexions was 0.171. In the molecule, the C(7)-C(8) double bond and the C(9)-O(3) carbonyl group take the *s-cis* conformation with respect to the C(8)-C(9) single bond. The A phenyl group and the exocyclic atoms (C(7)~O(3)) are nearly coplanar, and this plane makes a dihedral angle of 15.6° with that of the B phenyl group. The molecules build up a three-dimensional net through the hydrogen bonds. There is also an intramolecular hydrogen bond between O(3) and O(4).

From the experiment of feeding labelled acetate, phenylalanine, cinnamic acid, or shikimic acid to, for example, red cabbage, Neish *et al.*[1] have demonstrated conclusively that the C15-skeleton of flavonoids is biosynthesized through two separate pathways. One of the aromatic rings of flavonoids arises from the malonyl-CoA unit, whereas the other arises from the compounds in the prephenic-acid pathway. The C15-intermediate formed is then modified in various ways to give different types of flavonoid compounds. However, the problem has remained of whether the C15-intermediate is an activated flavanone or chalcone. Grisebach *et al.*[2] observed that ^{14}C-labelled chalcones are incorporated into flavonols, anthocyanins, and isoflavones, supporting the idea that chalcones are C15-intermediates of flavonoids. This is not conclusive, however, because the degree of the incorporation of chalcone is very low.

In order to carry out a study of flavonoids, it is necessary to have more detalied information on the structure of natural chalcones. Price[3] has reported that the chemical structure of butein from a yellow variety of species of dahlia is 3,4,2',4'-tetrahydroxychalcone (I). The present paper will deal with the X-ray structure determination of butein, isolated from the scarlet variety of the species of dahlia, as one of the major components of flavonoids.[4]

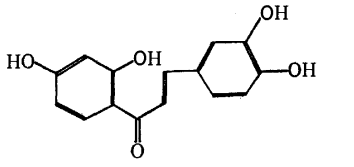

I

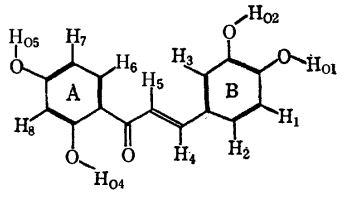

II

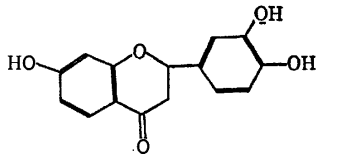

III

Experimental

Crystals were prepared by slow evaporation from a water-acetone mixture. They were yellow-orange needle crystals, showing a predominant (0 0 1) face. The crystal data obtained from the oscillation and Weissenberg photographs are summarized in Table 1. The reflexions were recorded, using Cu-K_α radiation, on equiinclination Weissenberg photographs for 0—3 layers around the c axis and for 0—2 layers around the b. The dimensions of the crystals used were $0.05\times0.03\times0.50$ mm. A total of 2217 independent reflexions were collected, of which 1154 were too weak to be measured, perhaps because of the small size of the crystals. Lorentz, polarization, and Phillips corrections were made as usual, but the absorption correction was omitted. The overall temperature factor obtained at this stage was 4.90 Å^2.

TABLE 1. CRYSTAL DATA OF BUTEIN MONOHYDRATE

Formula:	$C_{15}H_{12}O_5\cdot H_2O$
	M.W.=290.3; $F(0\ 0\ 0)=608$
Monoclinic,	$a=10.89$, $b=28.88$, $c=4.29$Å
	$\beta=96.7°$
Volume of the unit cell,	1393.9Å^3
Density (by flotation)	1.42 g·cm^{-3}
Density (calculated)	1.42 g·cm^{-3}
$Z=4$	
Absent spectra:	$h0l$ when $h+l$ is odd.
	$0k0$ when k is odd.
Space group is	$P2_1/n$

* Present address: Chemical Laboratory, Meiji Gakuin University, Shiroganedai, Minato-ku, Tokyo.

** Research Institute for Polymers and Textiles, Kanagawa-ku, Yokohama.

1) A. C. Neish, *Ann. Rev. Plant Physiol.*, **11**, 55 (1960).

2) H. Grisebach, In "Chemistry and Biochemistry of Plant Pigments," ed. by T. W. Goodwin, Academic Press, London and New York (1965), pp. 279—308.

3) J. R. Price, *J. Chem. Soc.*, **1939**, 1017.

4) N. Saito, K. Ishizuka, and Y. Osawa, *Bot. Mag. Tokyo*, **83**, 229 (1970).

Structure Determination

The symbolic addition procedure[5] was applied for sign-determination. The starting set for applying the Σ_2 formula, in which three phases define the point of origin, is shown in Table 2. The SIGMA program was utilized to list the reflexion triplets with the associated probabilities. The signs of 161 reflexions out of 282 with $|E| \geq 1.5$ were determined, although 53 of them were later found to be incorrect. The E map computed with these signs (A+, B−) has shown the molecular skeleton clearly.

Table 2. Starting set of the symbolic addition procedure

h	k	l	$\|E\|$	Phase or symbol
−10	6	1	4.42	+
− 7	14	1	4.93	+
− 6	11	2	3.71	+
− 8	16	2	4.88	A
− 8	15	1	3.99	B

A structure factor calculation based on this approximate structure gave an R factor of 0.46. Six cycles of block-diagonal matrix least-squares refinement decreased the R to 0.36. The water of crystallization was located from a difference Fourier synthesis.

Four subsequent cycles of refinement reduced the R to 0.23. Anisotropic thermal factors were then introduced; the R dropped to 0.183 after three cycles. At this stage, hydrogen atoms were located by assuming a suitable geometry and were included in the least-squares refinement. The R factor was reduced to 0.171 after three cycles. The atomic scattering factors were taken from International Tables for X-ray

Table 3. Final atomic coordinates and temperature factors

The anisotropic temperature factors are expressed in the form of $\exp\{-(B_{11}h^2+B_{22}k^2+B_{33}l^2+B_{12}hk+B_{13}hl+B_{23}kl)\}$

Atom	x/a	y/b	z/c	B_{11} or B	B_{22}	B_{33}	B_{12}	B_{13}	B_{23}
C(1)	0.2284	0.0653	1.4473	0.00386	0.00065	−0.01087	0.00092	0.01649	0.00799
C(2)	0.3083	0.0294	1.3943	0.00816	0.00062	0.03446	−0.00026	0.03397	0.00073
C(3)	0.4145	0.0376	1.2613	0.00489	0.00030	−0.00532	−0.00031	0.01923	0.00175
C(4)	0.4369	0.0829	1.1601	0.00600	0.00072	0.00657	0.00108	0.04229	0.00151
C(5)	0.3571	0.1192	1.2022	0.00317	0.00052	0.01863	−0.00165	0.02110	−0.00227
C(6)	0.2483	0.1096	1.3240	0.00516	0.00026	0.01675	−0.00030	0.03555	−0.00024
C(7)	0.5510	0.0892	1.0270	0.00686	0.00065	−0.01462	0.00052	0.00941	−0.00184
C(8)	0.5853	0.1274	0.8762	0.00544	0.00088	0.00373	0.00294	0.02849	0.00328
C(9)	0.7048	0.1305	0.7681	0.00488	0.00047	0.04155	0.00036	0.02585	0.00303
C(10)	0.7368	0.1719	0.5978	0.00371	0.00090	−0.00591	0.00112	0.01188	0.00002
C(11)	0.6566	0.2089	0.5235	0.00420	0.00105	0.00424	0.00245	0.03271	0.00703
C(12)	0.6894	0.2476	0.3728	0.00983	0.00074	0.00240	0.00338	0.06557	−0.01009
C(13)	0.8080	0.2490	0.2859	0.00515	0.00084	−0.01893	−0.00014	0.01405	0.00459
C(14)	0.8915	0.2140	0.3441	0.00571	0.00141	−0.03526	−0.00040	0.19587	0.00615
C(15)	0.8563	0.1750	0.5019	0.00399	0.00112	0.01432	0.00335	0.02048	0.01196
O(1)	0.1231	0.0597	1.5831	0.00687	0.00080	0.03290	−0.00037	0.07234	0.00788
O(2)	0.1758	0.1461	1.3935	0.00678	0.00044	0.11271	0.00047	0.06585	−0.00071
O(3)	0.7817	0.0975	0.8151	0.00753	0.00067	0.09377	0.00402	0.03736	0.01395
O(4)	0.9441	0.1411	0.5726	0.00496	0.00084	0.11951	0.00409	0.04841	0.01865
O(5)	0.8431	0.2875	0.1269	0.00666	0.00093	0.01648	−0.00025	0.03447	0.00894
O(6)	0.8975	0.0267	1.1927	0.00788	0.00134	0.09180	0.00084	0.00546	0.01417
H(1)	0.2882	0.9977	1.4633	3.26					
H(2)	0.4851	0.0107	1.2439	5.25					
H(3)	0.3673	0.1539	1.1261	1.92					
H(4)	0.6275	0.0729	1.1200	5.24					
H(5)	0.5371	0.1529	0.8569	1.50					
H(6)	0.5704	0.2046	0.5809	0.79					
H(7)	0.6322	0.2714	0.3290	4.53					
H(8)	0.9656	0.2129	0.2329	−0.41					
H(O1)	0.1059	0.0385	1.6794	5.60					
H(O2)	0.1128	0.1442	1.4328	5.54					
H(O4)	0.8911	0.1193	0.5416	0.94					
H(O5)	0.8367	0.2848	−0.0713	5.12					
H(O6A)	0.9789	0.0324	0.3431	−1.25					
H(O6B)	0.8664	0.0489	0.1120	1.99					

5) J. Karle and I. L. Karle, *Acta Crystallogr.*, **21**, 849 (1966).

Crystallography.[6] The final atomic coordinates and temperature factors are given in Table 3. The observed structure factors may be obtained on request to the authors. The computations were done on a HITAC 5020E computer with programs written by Tamaichi Ashida.

Discussion

Molecular Shape. The C(7)–C(8) double bond and the C(9)–O(3) carbonyl group are in the *s-cis* conformation with respect to the C(8)–C(9) bond. A similar conformation is observed in 4-methoxychalcone[7] and chalcone[8]. This cisoidal conformation is considered to be more stable than the transoidal conformation, because it does not suffer from repulsion between H(4) and H(6).

Table 4. Normal distances from the least-squares planes (Å)

	P(1)	*P*(2)	*P*(3)	*P*(4)	*P*(5)
C(1)	0.029			−0.046	
C(2)	0.288			0.021	
C(3)	0.276		0.219*	0.002	
C(4)	0.082		−0.016	0.002	
C(5)	−0.143		−0.333*	−0.028	
C(6)	−0.068			0.050	
C(7)	0.061	−0.078*	0.023		−0.014
C(8)	0.070	−0.088*	0.009		−0.038
C(9)	−0.026	−0.035*	−0.020		0.004
C(10)	0.027	−0.008	0.005		0.016
C(11)	0.208	0.009	0.095*		0.028
C(12)	0.218	−0.003			0.002
C(13)	0.066	−0.005			−0.010
C(14)	−0.090	0.005			0.003
C(15)	−0.113	0.001	−0.068*		0.013
O(1)	0.001			−0.057*	
O(2)	−0.419			−0.112*	
O(3)	−0.140		−0.049		0.048
O(4)	−0.340	−0.059*			−0.043
O(5)	0.099	0.010*			−0.010*
O(6)	−1.174				

P(1), the plane of all atoms; *P*(2), the plane of the ring A; *P*(3), the plane of the exocyclic atoms; *P*(4), the plane of the ring B; *P*(5), the plane of the ring A and exocyclic atoms. The atom with asterisk is not included in the plane evaluation.

Dihedral angle between the planes *P*(2) and *P*(3) 3.7°
P(2) and *P*(4) 15.6°
P(5) and *P*(4) 15.8°

As is shown in Table 4, the two phenyl rings, A and B, are planar within 0.01 Å and 0.05 Å respectively. The C(4), C(7), C(8), C(9), C(10), and O(3) atoms are also on a plane, within deviations of 0.05Å. The A ring and the plane of the exocyclic atoms (C(4)~O(3)) are nearly coplanar (±0.05Å). On the other hand, this plane makes a dihedral angle of 15.8° with the plane of the B phenyl group, mainly because of the rotation around the C(4)–C(7) bond. This may be due to the interaction of H(5) and H(3). The dihedral angle between the A and B rings is 15.6°. Thus, the molecule can be expressed to be nearly planar as a whole.

Bond Lengths and Angles. Figure 1 shows the bond lengths and angles in butein monohydrate calculated from the coordinates in Table 3. The estimated standard deviations are 0.02-0.03Å for the lengths and 1.0-2.0° for the angles. The average bond length in the two benzene rings is 1.39Å. The C–C single bond lengths–C(4)–C(7), 1.44, C(8)–C(9), 1.43, and C(9)–C(10), 1.47Å—are rather shorter than those in 4-methoxy chalcone (1.47, 1.49, and 1.47Å) and in chalcone (1.50,1.48, and 1.46Å). On the other hand, the doble bonds, C(7)–C(8) (1.35Å) and O(3)–C(9) (1.27Å), are somewhat long; the corresponding bond lengths are 1.33 and 1.23Å in 4-methoxychalcone, and 1.32 and 1.20Å in chalcone. The average bond length of four C–O(hydroxy) bonds is 1.37Å, which is slightly shorter

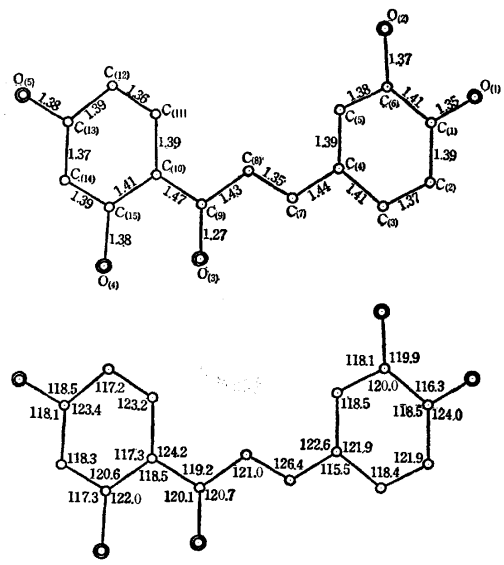

Fig. 1. Bond lengths (Å) and bond angles (°).
◎: O, ○: C

than the usual value. These bond lengths and the approximate planarity of the whole molecule mentioned above suggest that the π-electrons are delocalized, to some extent, throughout the whole molecule. The fluctuation in the C–C–C angles in two benzene rings is rather large. The C(4)–C(7)–C(8) angle is quite large (126.2°); similar values, 127.2° and 127.6°, are found in 4-methoxychalcone and chalcone respectively.

Hydrogen Bond. The O(4)–H hydroxyl group is hydrogen-bonded to the carbonyl oxygen atom, O(3), in the same molecule with the length of 2.49Å. Similar intramolecular hydrogen bonds are observed in obtusifolin (2.53Å),[9] salicylic acid (2.62Å),[10] 4-

6) "International Tables for X-ray Crystallography," Vol. 3, Kynoch Press, Birmingham, England (1962), p. 202.
7) D. Rabinovich and G. M. J. Schmidt, *J. Chem. Soc. B*, **1970**, 6.
8) D. Rabinovich, *ibid.*, *B*, **1970**, 11.
9) P. Narayanan, K. Zechmeister, M. Rohre, and W. Hoppe, *Acta Crystallogr.*, **B27**, 718 (1971).
10) M. Sundaralingam and L. H. Jensen, *ibid.*, **18**, 1053 (1965).

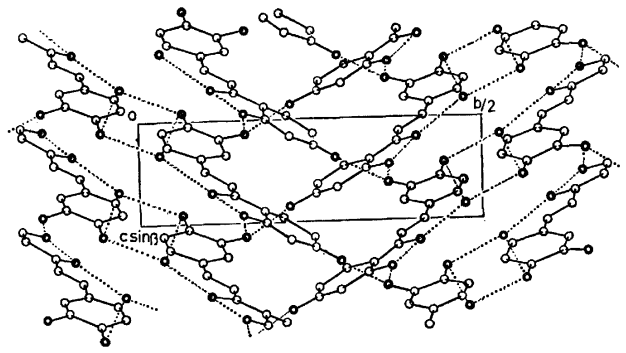

Fig. 2. The crystal structure projected along the *a* axis. The broken lines indicate the presumed hydrogen bonds.
◎: O, ○: C

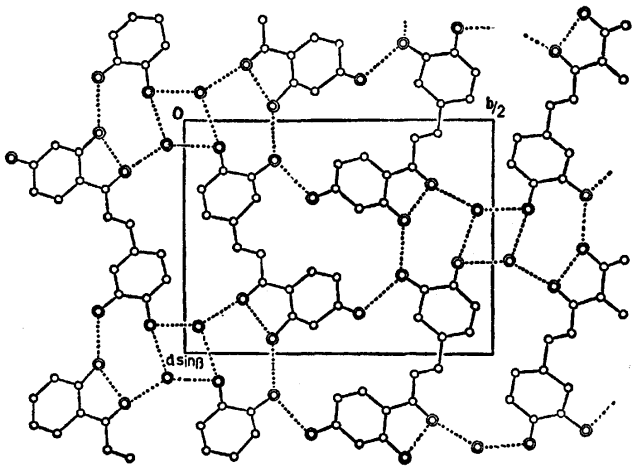

Fig. 3. The crystal structure projected along the *c* axis. The broken lines indicated the presumed hydrogen bonds.
◎: O, ○: C

aminosalicylic acid (2.62Å),[11] and salicylamide (2.49 Å).[12]

The arrangements of the molecules viewed along the *a* and *c* axes are shown in Figs. 2 and 3 respectively. The presumed hydrogen bonds are indicated with broken lines and are listed in Table 5. Six hydrogen bonds connect the molecules so as to form a three-dimensional net-work.

Table 5. Hydrogen bond distances

Bonds	Distance (Å)	Acceptor at
O(3)···O(6)	2.82	(x, y, z)
O(3)···O(4)	2.49	(x, y, z)
O(6)···O(1)	2.97	$(1+x, y, z)$
O(5)···O(2)	2.75	$(1/2+x, 1/2-y, -3/2+z)$
O(4)···O(2)	2.73	$(1+x, y, -1+z)$
O(6)···O(1)	2.69	$(1-x, -y, 3-z)$

Interconversion of Chalcone to Flavanone. As is well known, the chalcone-flavanone transformation is reversible, the equilibrium being shifted in favour of the flavanones.[13] Actually, chalcones can be converted to flavanones upon prolonged heating in an alcoholic acid or alkaline solution. From the structural characteristics revealed in the present study, the interconversion may be considered to occur through the following steps; the rotation of the A ring around the C(9)–C(10) single bond, accompanied by the breaking of the intramolecular hydrogen bond, the rotation of the A ring around the C(8)–C(9) single bond (the *s-trans* conformation (I)), and the cyclization of chalcone into flavanone (III).

The authors wish to thank Dr. Hirotaka Shimanouchi and Mr. Yuji Ohashi for their valuable discussions.

11) F. Bertinotti, G. Giacomello and A. M. Liquori, *Acta Crystallogr.*, **7**, 808 (1954).
12) Y. Sasada, T. Takano, and M. Kakudo, This Bulletin, **37**, 940 (1964).
13) T. R. Seshadri, In "The Chemistry of Flavonoid Compounds," ed. by T. A. Geissman, Pergammon, New York (1962), pp. 156—196.

On the Emission Spectra of the Unimolecular Reaction of Methylamine by Electron Impact

Kiyoshi FUKUI, Iwao FUJITA, and Keiji KUWATA

Department of Chemistry, Faculty of Science, Osaka University, Toyonaka, Osaka

(Received January 20, 1972)

The emission spectra of the following excited species produced from methylamine by electron impact (the energy of 150 eV) at a low pressure were observed: NH($A^3\Pi - X^3\Sigma$), CN($B^2\Sigma - X^2\Sigma$), CH($A^2\Delta - X^2\Pi$), and H(Balmer series). It was confirmed that the excited species are produced by a unimolecular reaction of methylamine. The replacement by deuterium decreases the production of the excited hydrogen atom from methylamine by about 40%, this supports the idea that the excited hydrogen atom is produced through a superexcited state of methylamine. It was also determined that the production of the excited hydrogen atom of the methyl group was less than that of the amino group by about 20%. This is in contrast to the findings on the mass spectrum of CD_3NH_2, where the peak of $CD_2NH_2^+$ was much higher than that of CD_3NH^+. The NH radical in the $A^3\Pi$ state was produced from methylamine and dimethylamine, while the NH radicals in the $A^3\Pi$ and the $c^1\Pi$ states were produced from ammonia.

The probability of the bond-scission of amines in a mass spectrometer has been studied by Hirota *et al.* In their study, it was pointed out that the skeletal bond-scission of the molecules proceeds through a superexcited state. On the other hand, the contribution of the superexcited state has been verified by a study of the isotope effect on the ionization yield.[2] In the present study, the possibility of superexcited state for the primary process of the bond-scission in a simple amine is examined.

The authors presumed that the contribution of the superexcited state can be verified by observing the Balmer-β line (the transition from $n=4$ to 2 of hydrogen) under electron impact. The excited hydrogen atom should be produced through a state with a higher energy than the ionization potential of methylamine (8.97 eV),[3] *i.e.*, a superexcited state, because the atom is in a higher energy state than 8.97 eV. In addition, the isotope effect on the dissociation of the C–H or the N–H bond in the molecule through such a superexcited state is studied.

Futhermore, the primary process of the ionization and dissociation of methylamine by electron impact will be discussed on the basis of the results on both the emission spectra and the mass spectra. The relative scission probavility of the C–H and N–H bond of methylamine as well as the isotope effect will be examined. It should be noticed that the electronic states of the NH radical produced from ammonia differ from those of hydrazine,[4] methylamine, and dimethylamine This problem will be discussed briefly in the present paper.

Experimental

Methylamine hydrochloride ($CH_3NH_2 \cdot HCl$, $CD_3NH_2 \cdot HCl$, or $CH_3ND_2 \cdot DCl$) was mixed with an excess of CaO which had been dried at 400°C in a vacuum to liberate the methylamine in the gas phase. Furthermore, the purification of methylamine by vacuum distillation was repeated at −90°C until it was about 99.9%, as determined by gas chromatography. In the present experiments, all the reagents used were of a guaranteed grade.

The $CH_3ND_2 \cdot DCl$ was prepared by the exchange of the amino hydrogen with heavy water. For the isotopic analysis of the deuterated methylamines, mass spectrometry was done by means of a Hitachi RMU-5 mass spectrometer. The CH_3ND_2 contained CH_3NDH of 34%, and the CD_3NH_2 contained CD_3NHD of 2% and CD_2HNH_2 of 2%. The mass spectrometry of CD_3NH_2 was done by means of the mass spectrometer in order to estimate the scission probabilities of the C–H bond and the N–H bond in $CD_3NH_2^+$ with the electron impact energy of 80 eV.

The principle of our apparatus for observing the emission spectra in the gas phase was the same as that used by Ogawa *et al.*[5] To observe the emission spectra, a Narumi RM-23 grating monochromator with an EMI-6256B photomultiplier was used. In the present study, the emission spectra from the fragments of methylamine were observed in the region from 300 nm to 500 nm. The dependence of the intensity of the Balmer-β line and the (0, 0) band of NH($A^3\Pi - X^3\Sigma$) on both the electron-beam current (target current) and the pressure in the collision chamber was examined. The pressure was measured by means of an ionization gauge connected to the chamber. The ratio of the intensity of the D_β line (the transition from $n=4$ to 2 of deuterium) to that of the H_β line (the transition from $n=4$ to 2 of hydrogen) was observed (the difference in the wave lengths was about 0.13 nm) by means of a Shimadzu GE-100 grating monochromator of a higher resolution equipped with a photomultiplier.

Results and Discussion

The emission spectrum of the fragments of methylamine in electron impact (energy of electron: 150 eV) is shown in Fig. 1, where the 336 nm and 337 nm bands were assigned to the (0,0) and (1,1) bands of NH($A^3\Pi - X^3\Sigma$) respectively. The sequence of (0,0), (1, 1), (2, 2), (3, 3), and (4, 4) bands of CN($B^2\Sigma -$

1) For example, K. Hirota, I. Fujita, M. Yamamoto, and Y. Niwa, *J. Phys. Chem.*, **74**, 410 (1970).

2) R. L. Platzman, *Vortex*, **23**, 372 (1962); W. P. Jesse and R. L. Platzman, *Nature*, **195**, 790 (1962); W. P. Jesse, *J. Chem. Phys.*, **38**, 2774 (1963); R. L. Platzman, *ibid.*, **38**, 2775 (1963); J. C. Person, *ibid.*, **43**, 2553 (1965); J. C. Person and P. P. Nicole, *ibid.*, **53**, 1767 (1970).

3) K. Watanabe, *ibid.*, **24**, 623 (1956).

4) H. Bubert and F. W. Froben, *J. Phys. Chem.*, **75**, 769 (1971).

5) T. Ogawa, I. Fujita, M. Hatada, and K. Hirota, This Bulletin, **44**, 659 (1971).

$X^2\Sigma$) was found in the region from 388 nm to 385 nm, and the emissions at 431 nm and 432 nm were assigned to the (0, 0) and (2, 2) bands of CH($A^2\Delta - X^2\Pi$) respectively. Moreover the emissions at 397, 410, 434, and 486 nm were assigned to the ε, δ, γ, and β lines of the Balmer series respectively.

The intensity of emission from the excited hydrogen atom and the (0, 0) band of the triplet NH radical depends linearly on the target current, as is shown in Fig. 2, when the pressure in the collision chamber is 5×10^{-4} Torr. This result shows that the excited species are produced by a single collision of the parent molecule with an electron. As is shown in Fig. 3, the intensity of the emission seems to depend linearly on the pressure of the collision chamber when the energy of the electron impact is 150 eV. This result could indicate that the excited species are produced directly through the unimolecular dissociation of the original molecule.

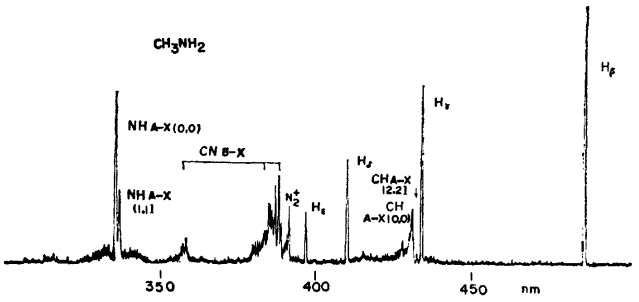

Fig. 1. Emission spectrum observed in electron impact of CH_3NH_2. The energy of electron impact is 150 eV. The pressure of the collision chamber is 3×10^{-4} Torr.

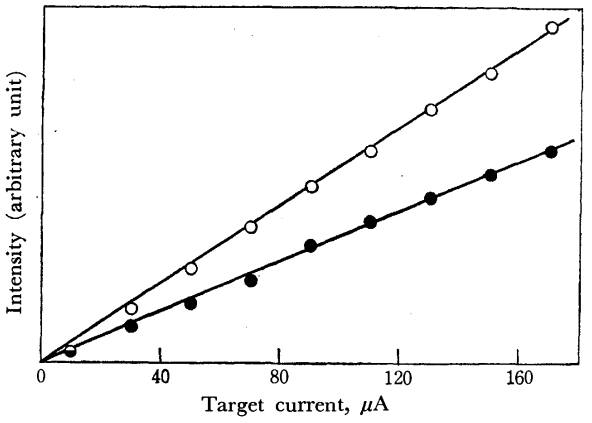

Fig. 2. Dependency of emission intensities on the target current. ○: Balmer-β line. ●: (0, 0) band of NH($A^3\Pi$-$X^3\Sigma$). The energy of electron impact is 150 eV. The pressure of the collision chamber is 5×10^{-4} Torr.

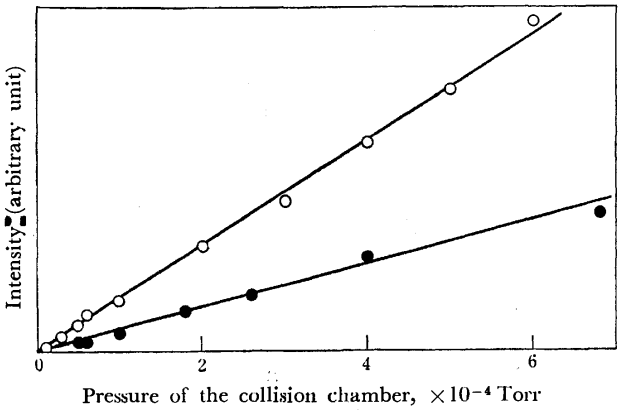

Fig. 3. Dependency of emission intensities on the pressure of the collision chamber. ○: Balmer-β line. ●: (0, 0) band of NH($A^3\Pi$-$X^3\Sigma$). The energy of electron impact is 150 eV. Target current is 100 μA for Balmer-β and 190 μA for NH.

Both results show that the excited species are produced in the primary processes of the decomposition of methylamine. It is also established in the case of NH_3 that the excited hydrogen atom and the triplet NH radical are produced through a unimolecular reaction. It is also presumed that other species, *e.g.*, CH($A^2\Delta$) and CN($B^2\Sigma$), are produced in a similar process.

Putting the pressure, the temperature in the collision chamber, and the radius of methylamine at 10^{-4} Torr, 300°K, and 5×10^{-8} cm[6] respectively, the collision time of an ideal gas for methylamine in the system is about 6×10^{-4} sec. Hence, the excited species emit the photon within a shorter peroid than the collision time under the given conditions.

As for the production of excited hydrogen atoms from methylamine, it may be presumed as a necessary condition that they are produced through a superexcited state of methylamine, because they have a higher energy than the ionization potential of methylamine (8.97 eV). Therefore, the following mechanism of bond-scission for methylamine under electron impact seems reasonable:

$$CH_3NH_2 \xrightarrow{e^-} CH_3NH_2^{**} \begin{cases} \xrightarrow{(1)} H^* + CH_3\dot{N}H \\ \xrightarrow{(2)} H^* + \dot{C}H_2NH_2 \end{cases}$$
$$CH_3NH_2^{**} \xrightarrow{(3)} CH_3NH_2^+ + e^-$$

In this mechanism, H* shows an excited hydrogen atom, and CH_3NH_2** shows a superexcited state of methylamine whose lifetime is known to be shorter than or in the same order as the period of one vibration. A dissociation process, (1) and/or (2), competes with the ionization process (3) from the superexcited state. If the mechanism is valid, substitution by the heavier isotope may decrease the probability of the (1) and (2) dissociations and may increase the probability of ionization (3). By the use of CD_3NH_2 and CH_3ND_2 the isotope effect on the dissociation, and also the ratio of the probability of dissociation (1) to that of (2) can be found.

Letting the observed intensity ratios of D_β to H_β be I_D/I_H for CD_3NH_2 and I_D'/I_H' for CH_3ND_2, the relations:

$$\frac{I_D}{I_H} = \frac{3\lambda\varepsilon_C}{2\varepsilon_N} \quad \text{and} \quad \frac{I'_D}{I'_H} = \frac{2\lambda\varepsilon_N}{3\varepsilon_C}$$

are obtained, where ε_N and ε_C represent the effects of the difference in the kind of bonding on the scission probability— *i.e.*, the N–H and C–H bonds of methylamine, respectively, and λ repersents the isotope

6) This value is a rough one.

effect on the bond-scission. As CH_3NH_2 contained CH_3NDH, and as CD_3NH_2 contained small amounts of CD_3NDH and CD_2HNH_2, in the above calculation corrections of I_D/I_H and I_D'/I_H' were made on the basis of the results of mass spectrometery. Putting the corrected values of 0.7 and 0.5 into I_D/I_H and I_D'/I_H' respectively, $\varepsilon_C/\varepsilon_N$ and λ were determined to be 0.8 and 0.6 respectively. From these results, the contribution of the (2) pathway to the production of the excited hydrogen atom is less than that of the (1) pathway by about 20% for each bond, and the isotope effect of deuteration on the dissociation process is shown to be a decrease of about 40%.

This isotope effect is consistent with the decrease in the (1) and (2) dissociations by the replacement by a heavier isotope, as is to be expected from the above mechanism including the superexcited state.

Contrary to the dissociation process of the neutral methylamine, the $CH_3NH^+/CH_3NH_2^+$ ratio of 0.2 was smaller than the ratio $CH_2NH_2^+/CH_3NH_2^+$ of 2.4 in the mass spectrum.

$$CH_3NH_2^+ \begin{cases} \nearrow CH_3NH^+ + H \\ \searrow CH_2NH_2^+ + H \end{cases}$$

However, we can not say which of bonds, the C–H bond or the N–H bond, in $CH_3NH_2^+$ dissociates more easily, because there are two possibilities: the scission of the C–H bond may occur more easily than the N–H bond, and the CH_3NH^+ may decompose further and so be little detected. It should be noticed that, in the decomposition of the positive ion, the hydrogen atom in the ground state is, in view of the energy, more favorable than that in the excited state. Thus, the hydrogen atom produced from $CH_3NH_2^+$ may contribute little to the emission.

The similar facts that the CH_3O^+/CH_3OH^+ and CH_2OH^+/CH_3OH^+ ratios were 0.2 and 1.6[7] respectively in mass spectrum (electron imapct energy: 80eV) should also be noticed. $\varepsilon_C/\varepsilon_O$ and λ had the same values of 0.8 in the case of CH_3OH[8].

Last, the production of the NH radical from methylamine may be discussed in relation to that from ammonia and dimethylamine. The emission spectra of the NH radical produced from methylamine and ammonia by electron impact are shown in Fig.4. Both the $c^1\Pi$ and $A^3\Pi$ state of the NH radical appeared in the emission spectrum of ammonia, while only the $A^3\Pi$ state of the NH radical appeared in those of methylamine and dimethylamine in the present study.

In a former study,[9] the NH radical in the $A^3\Pi$ state is not produced from ammonia by photon impact with energies up to about 11.87 eV (λ=105 nm), a value which is higher than the ionization potential of ammonia (10.15 eV).[10] Hence, if the $A^3\Pi$ state of the NH radical is supposed to be produced from ammonia in a triplet excited state, the ratio of the emission intensity of the $A^3\Pi$ state to that of the $c^1\Pi$ state should depend on the energy of the impact electron,

Fig. 4. The spectra of NH (the energy of electron impact: 150 eV). a) CH_3NH_2. b) NH_3. An arrow (↓) at 323 nm indicates R-head of (0, 0) band of NH($c^1\Pi$-$a^1\Delta$). Sharp bands at 336 and 337 nm are (0, 0) and (1, 1) bands of NH($A^3\Pi$-$X^3\Sigma$).

because the spin-forbidden transition is possible in the case of excitation by an electron impact with a lower energy. However, in the present study it did not depend on the impact energy in the region from 40 eV to 150 eV. Therefore, it can be supposed that the $A^3\Pi$ state of the NH radical is produced only through a superexcited state of ammonia with a higher energy than 11.87 eV.

The fact that the electronic state of the NH radical produced from methylamine and dimethylamine as well as hydrazine[4] differs from that produced from ammonia by electron impact can be explained by the spin conservation rule and redistribution of the excitation energy in the parent molecule. In addition, the type of the decomposition of the substituent group to ammonia probably determines the electronic state of the NH radical produced from the molecules.

In the present study, it can not be mentioned whether or not the NH($A^3\Pi$), CH($A^2\Delta$), and CN($B^2\Sigma$) radicals are produced through a superexcited state of methylamine, because the energy of these species does not exceed the ionization potential of methylamine and because the threshold energy which is needed to form the excited species is not known.

The authors would like to express their gratitude to Professors Shigero Ikeda and Yu Yokoyama for use of their Shimadzu GE-100 monochromator. The authors also wish to thank Dr Motoyoshi Hatada for his technical advice as constructing the collision chamber and Professor Kozo Hirota for his encouragement throughout this work.

7) Unpublished result by I. Fujita.
8) I. Fujita, M. Hatada, T. Ogawa, and K. Hirota, This Bulletin, **44**, 1751 (1971).
9) H. Okabe and M. Lenzi, *J. Chem. Phys.*, **47**, 5241 (1967).
10) K. Watanabe, *ibid.*, **26**, 542 (1957).

The Normal Magneto-Optical Rotatory Dispersion and the Magnetic Moment of Benzene

Yoshiya TAKENOSHITA

Department of Chemistry, Faculty of Science, Kyushu University, Fukuoka

(Received February 21, 1972)

The magneto-optical rotatory dispersion in the absorptionless region has been investigated with liquid benzene, and the related magnetic moment has been discussed theoretically. It has been concluded that the main contribution to the magneto-optical rotatory dispersion consists of an A term through the $^1A_{1g}\rightarrow{}^1E_{1u}$ transition and that the contribution from σ-electrons is never negligible. The magnetic moment in the excited state, $^1E_{1u}$, of benzene has been obtained as $-1.72\,\beta$ (Bohr magneton), which is about 2 or 4 times greater than the value of $-1.0\,\beta$ calculated with the FEN-model or the value of $-0.396\,\beta$ calculated by the LCAO-MO method.

The anomalous magneto-optical rotatory dispersion (MORD) and the magnetic circular dichroism (MCD) of porphyrine and other organic compounds have been studied by Shashoua and others.[1-3] The MCD's of benzene, triphenylene and coronene have been studied by Stephens *et al.*,[4] and the magnetic moment has been discussed in detail with triphenylene and coronene. No discussion has been made with benzene, however, since they did not succeed in observing the MCD of benzene in the region below 2300 Å because of the limitations of these experiments.

However, it could be possible to discuss the magnetic properties of benzene in the excited states if the normal magneto-optical rotatory dispersion (or the normal Faraday effect in an absorptionless region) would be simple enough to analyze. In 1955, Garner *et al.*[5] observed the normal MORD of liquid benzene. However, they had no intention of studying the magnetic properties of benzene itself, but those of several solute compounds dissolved in benzene. Already, in the period between 1896 and 1906, Perkin had made an extensive study of the Faraday effects of various organic compounds for the Na-D line.[6] Although his excellent experimental data have never been examined from the viewpoint of modern molecular physics, π-electrons may be expected to make an important contribution to the magnetic properties of benzene. No direct information has been obtained so far concerning the magnetic properties of benzene in the excited states.

We will try here to analyze the normal MORD of benzene and estimate its magnetic moment. The estimated value will be compared with the theoretical one, which will also be developed in this paper.

Theoretical Results of MORD

The contribution of the $a\rightarrow j$ transition to the normal MORD of isotropic molecules in a longitudinal magnetic field, H, along the $+z$ axis may be expressed as follows:[2,7,8]

$$[\phi(a\rightarrow j)]_M = -\frac{24NH}{\hbar c}\left[\frac{2\nu_{ja}\nu^2}{h(\nu_{ja}^2-\nu^2)^2}A(a\rightarrow j) + \frac{\nu^2}{\nu_{ja}^2-\nu^2}\{B(a\rightarrow j)+C(a\rightarrow j)/kT\}\right], \quad (1)$$

where $[\phi]_M$ is a molar magnetic rotation defined for natural optical activity,[9] where N is the Avogadro number, and where $h\nu_{ja}=W_j-W_a$ is the energy difference between the a and j states.

Assuming a random orientation of rotating anisotropic molecules, one obtains the Faraday parameters, A, B, and C, as follows:

$$A(a\rightarrow j) = (2d_a)^{-1}\sum[(j|\boldsymbol{\mu}|j)-(a|\boldsymbol{\mu}|a)] \times \mathrm{Im}\{(a|\boldsymbol{m}|j)\times(j|\boldsymbol{m}|a)\}, \quad (2a)$$

$$B(a\rightarrow j) = (2d_a)^{-1}\sum \mathrm{Im}\{\sum_{k\neq a}(k|\boldsymbol{\mu}|a)\cdot(a|\boldsymbol{m}|j) \times (j|\boldsymbol{m}|k)/(W_k-W_a)+\sum_{k\neq j}(j|\boldsymbol{\mu}|k)\cdot(a|\boldsymbol{m}|j) \times (k|\boldsymbol{m}|a)/(W_j-W_k)\}, \quad (2b)$$

$$C(a\rightarrow j) = (2d_a)^{-1}\sum(a|\boldsymbol{\mu}|a)\cdot\mathrm{Im}\{(a|\boldsymbol{m}|j)\times(j|\boldsymbol{m}|a)\}, \quad (2c)$$

where d_a is the degeneracy of the ground state, a, (the summations are taken over all the transitions degenerate with $a\rightarrow j$), where $\boldsymbol{m}$ and $\boldsymbol{\mu}$ $(=(\beta/\hbar)\sum(\boldsymbol{l}_i+\boldsymbol{s}_i))$ are the electric and magnetic dipole operators respectively, and where β stands for a Bohr magneton. The A, B, and C terms of Eq. (1) arise, respectively, from the Zeeman splitting of $a\rightarrow j$, the mixing of a and j with other states, k, by means of the magnetic field, and the change in the populations of the component levels of the ground state, a, due to its Zeeman splitting. Hence, A is different from zero only when a or j is degenerate, and C is different from zero only when a is degenerate.

If an imaginary term, $\mathrm{Im}\{(a|\boldsymbol{m}|j)\times(j|\boldsymbol{m}|a)\}$, in Eqs. (2a) and (2c) can be defined with a real dipole strength, D, one obtained the following:

$$D(a\rightarrow j) = (d_a)^{-1}|(a|\boldsymbol{m}|j)|^2 = 2.126\times10^6(d_a)^{-1}f_{ja}/\omega_{ja} \text{ (square of the Debye unit)}, \quad (3)$$

1) V. E. Shashoua, *J. Amer. Chem. Soc.*, **86**, 2109 (1964); *ibid.*, **87**, 4044 (1965); *Arch. Biochem. Biophys.*, **111**, 550 (1965).

2) P. J. Stephens, W. Suëtaak, and P. N. Schatz, *J. Chem. Phys.*, **44**, 4592 (1966).

3) B. Briat, D. A. Schooley, R. Records, E. Bunnenberg, and C. Djerassi, *J. Amer. Chem. Soc.*, **89**, 6170 (1967).

4) P. J. Stephens, P. N. Schatz, A. B. Retchie, and A. J. McCaffery, *J. Chem. Phys.*, **48**, 132 (1968).

5) F. H. Garner, O. B. E., C. W. Nutt, and A. Labbauf, *J. Inst. Petrol.*, **41**, 329 (1955).

6) W. H. Perkin, *J. Chem. Soc.*, **69**, 1025 (1896); *ibid.*, **81**, 292 (1902); *ibid.*, **89**, 849 (1906).

7) R. Serber, *Phys. Rev.*, **41**, 489 (1932).

8) A. D. Buckingham and P. J. Stephens, *Ann. Rev. Phys. Chem.*, **17**, 399 (1966).

9) Formerly, molar Verdet's constant $V_M(=-600[\phi]_M/H)$ was used as a technical term, but recently Stephens and coworkers have been using this term.

where f_{ja} is an oscillator strength[10] and where ω_{ja} is the energy difference between j and a in cm^{-1}. Accordingly, the magnetic moment of a diamagnetic organic molecules can be estimated as follows:

$$-\mu = 2A/D, \tag{4}$$

since $(a|\boldsymbol{\mu}|a)=0$, and since, then, $C=0$.

However, the normal MORD for an arbitary wave number in the absorptionless region is naturally expressed as the summation of $[\phi(a\rightarrow j)]_M$ over j. In a system with only one allowed electronic transition as benzene, the MORD in the absorptionless region is given as follows:

$$[\phi(\omega)]_M = -\frac{24NH}{c\hbar}\frac{2\omega^2}{c\hbar(\omega_{ja}^2-\omega^2)^2}A(a\rightarrow j) + \sum_{k\neq j}[\phi(a\rightarrow j)]_M, \tag{5}$$

where k consists of the excited states with π and/or σ excited electrons. As the first and second terms in Eq. (1) are proportional to ω^2, the last part in Eq. (5) can be regarded for $\omega_{ka}\gg\omega$ $(k>j)$ as:

$$\sum_{k>j}[\phi(a\rightarrow k)]_M = E\omega^2, \tag{6}$$

where E is constant and is expressed as $\sum_{k>j}2A(a\rightarrow j)/h\omega_{ka}{}^3$ and $\sum_{k>j}(B(a\rightarrow k)+C(a\rightarrow k)/\boldsymbol{k}T)/\omega_{ka}{}^2$. Then, one can estimate the values of the A term and the μ on the basis of an analysis of the normal MORD.

Magnetic Moment and Orbital Angular Momentum

The magnetic moment and electronic orbital angular momentum make discussed in 1966 by Stephens *et al.*[2] and in 1968 by Bishop and Dingle.[11] Now, the magnetic moment of benzene will be discussed. For convenience, we will take all the molecular orbital functions of benzene as real. The benzene is a regular hexagon molecule with a diamagnetic ground state, $^1A_{1g}$. The angular momentum vector operator can have only one non-zero component $(^1E_{1u}x|L_z|^1E_{1u}y)$ in excited states which involve two allowed electric dipole transitions, $(^1A_{1g}|m_x|^1E_{1u}x)$ and $(^1A_{1g}|m_y|^1E_{1u}y)$.[12] Therefore, the magnetic moment of the excited state, $^1E_{1u}$, may be defined by:

$$\mu = -(i\beta/\hbar)(^1E_{1u}x|L_z|^1E_{1u}y), \tag{7}$$

where z is the principal molecular axis; x and y, the mean basis functions transforming like the two coordinates, x and y respectively, and $\boldsymbol{L}(=\sum\boldsymbol{l}_i)$ is a total orbital angular momentum operator.

In the singly-excited configuration approximation of the MO theory, the $^1E_{1u}$ state $(e_{1g}{}^3, e_{2u})$ of benxene[13] is:

$$|^1E_{1u}x) = \frac{1}{2}[\{y\bar{y}x\bar{\xi}\}+\{y\bar{y}\xi\bar{x}\}+\{y\bar{\eta}x\bar{x}\}+\{\eta\bar{y}x\bar{x}\}],$$
$$|^1E_{1u}y) = \frac{1}{2}[\{y\bar{y}x\bar{\eta}\}+\{y\bar{y}\eta\bar{x}\}+\{y\bar{\xi}x\bar{x}\}+\{\xi\bar{y}x\bar{x}\}], \tag{8}$$

where x and y denote e_{1g}, ξ and η e_{2u} MO's, and where the braces symbolize anti-symmetrization. By substituting Eq. (8) into Eq. (7), one obtains:

$$\mu = -(i\beta/\hbar)[(\xi|l_z|\eta) - (x|l_z|y)]. \tag{9}$$

The calculation of the magnetic moments resolves itself into the problem of the estimation of the angular momentum of each electronic molecular orbital. An electronic angular momentum is generally equal to zero for non-linear molecules, but equal to a non-zero value, $\zeta_e\hbar$,[14] corresponding to a rotation around the molecular axis, for planar cyclic molecules, which are deemed intermediate between highly symmetric molecules and less symmetrical or asymmetrical ones. In the FEN model,[15] the wave functions of the degenerate states, $\psi_n{}^+$ and $\psi_n{}^-$ with quantum numbers, $\pm|n|$, are $a_{Bn}\cos(k_n, x)$ and $a_{Bn}\sin(k_n, y)$ respectively, where $a_{Bn}=\sqrt{2/L}$ for $n\geq 1$ or $1/\sqrt{2}$ for $n=0$, and where $k_n=2n\pi/L$. The x, y, ξ, and η in Eqs. (6) and (7) correspond to $n=1$, -1, 2, and -2 respectively. The matrix elements of l_z are equal to $(\psi_n{}^+|l_z|\psi_n{}^-)=-in\hbar$. In the LCAO-MO treatment, on the other hand, a new problem occurs when one operates l_z on each atomic orbital. If the atomic orbitals, χ_a, are expressed with $2p$-Slater AO's and if the molecular orbitals are taken as $\psi_k=\sum C_{ka}\chi_a$, the matrix elements of l_z are given as:

$$(\psi_2|l_z|\psi_1) = \sum_{a,b}C_{1a}C_{2b}(\chi_b|l_z|\chi_a). \tag{10}$$

If the origin of l_z is then transferred from the center of the molecular skeleton to the middle point, P, of a

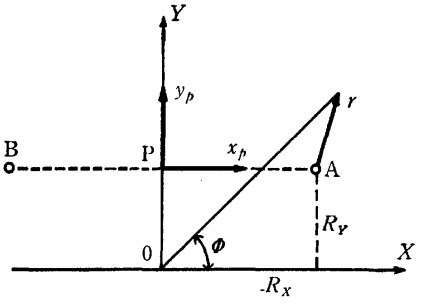

Fig. 1. A relation of an angular momentum operator with the coordinates.

bond between the A and B nuclei, as is shown in Fig. 1, one obtains:

$$l_z = l_z^p + i\hbar R_Y(\partial/\partial x_p). \tag{11}$$

Since $(\chi_b|l_z^p|\chi_a)=0$, one obtains:

$$(\chi_b|l_z|x_a) = i\hbar R_Y(\chi_b|\partial/\partial x_p|\chi_a). \tag{12}$$

The $R_Y\partial/\partial x_p$ operator corresponds to an infinitesimal rotation, $R_Y\delta\Phi$, and an effective component of l_z in

10) C. Sandorfy, "Electronic Spectra and Quantum Chemistry," Prentice-Hall Inc., New Jersey (1964), p. 100.
11) D. M. Bishop and T. W. Dingle, *J. Chem. Phys.*, **48**, 541 (1968).
12) P. S. Pershan, M. Gouterman, and R. L. Fulton, *Mol. Phys.*, **10**, 397 (1966).
13) W. E. Moffitt, *J. Chem. Phys.*, **22**, 320 (1954); R. Pariser and R. G. Parr, *ibid.*, **21**, 767 (1953).
14) G. Herzberg, "Molecular Spectra and Molecular Structure III. Electronic Spectra and Electronic Structure of Polyatomic Molecules," D. Van Nostrand Co., New York, (1966), p. 12.
15) K. Ruedenberg and C. W. Scherr, *J. Chem. Phys.*, **21**, 1565 (1953).

the multicenter field (see Appendix); therefore, it may express an electronic motion on a circle with a radius, R_Y, through the middle points between the A and B nuclei. For benzene, two circles are possible, since $R_Y=0$ on a connecting line through the point of origin.

If the coordinate system (x_p, y_p, z_p) is transformed to the elliptic coordinates (ξ, η, φ), one obtains:

$$R_Y\frac{\partial}{\partial x_p}|\chi_a) = \frac{1}{2}Z_{eff}R_Y\frac{\xi\eta-1}{\xi-\eta}|\chi_a), \quad (13)$$

and then:

$$(\chi_b|l_z|\chi_a) = \frac{\hbar}{i}\frac{p^2}{10}\frac{R_Y}{R_X}\exp(-p)\left(1+p+\frac{p^2}{3}\right), \quad (14)$$

where $p=Z_{eff}R_{ab}/2$ in atomic units.

Consequently, we can estimate and compare both the magnetic moments calculated experimentally from Eq. (6) and those calculated theoretically from Eqs. (9), (10), and (14) for some planar molecules. We shall discuss a normal MORD and a magnetic moment in the next section.

Results and Discussion

The normal MORD of liquid benzene, which is observed at 10°C with the same apparatus as was described in one of the present author's previous paper,[16] is shown in Fig. 2, which also gives the result estimated from the Verdet constant by Garner *et al.*[5] assuming a temperature of 20°C.

Assuming the contribution from only one electronic transition to the normal MORD and modifying Eqs. (1), (5), and (6), one can obtain:

$$\omega^2 = \omega_{ja}^2 - (A_0+B_0)^{1/2}\omega/[\phi]_M^{1/2}, \quad (15)$$

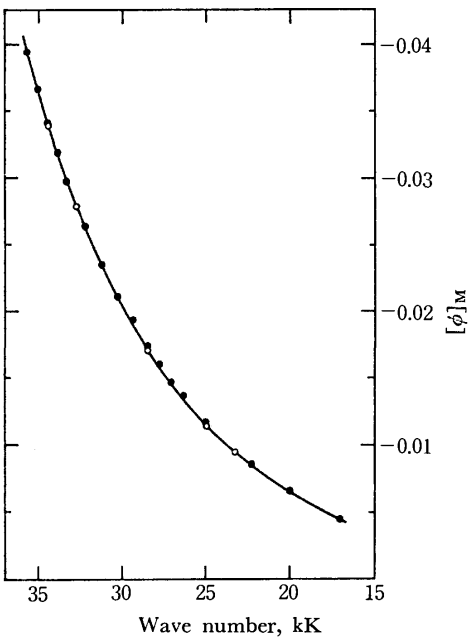

Fig. 2. The MORD (deg·l/m·mol·gauss) of benzene; dark circles are taken in this work and white ones show the data by Garner *et al.* (Ref. 5).

16) Y. Takenoshita and Y. Kanda, This Bulletin, **44**, 2293 (1971).

$$\omega^2 = \omega_{ja}^2 - A_0^{1/2}\omega/([\phi]_M - E\omega^2)^{1/2}, \quad (16)$$

where $A_0=21.346\times 2\omega_{ja}|A(a\rightarrow j)|$, where $B_0=21.346\times B(a\rightarrow j)(\omega_{ja}{}^2-\omega^2)+\sum_{k>j}[\phi(a\rightarrow k)]_M(\omega_{ja}{}^2-\omega^2)^2$, where ω is expressed in cm^{-1}, and where the factor 21.346 is the value of $(24N/c\hbar)$ when m stands for the Debye unit, and μ, the Bohr magneton.

From Eq. (15), it may be seen that the curve of $\omega/[\phi]_M^{1/2}$ *vs.* ω^2 is nearly a straight line; it is shown in Fig. 3(a). The deviation, increasing with a decrease in the ω^2 value from the straight line, shows that no terms except for $A(a\rightarrow j)$ are always completely negligible because of the behavior of B_0. A tangent, $A_0^{1/2}$, of the line becomes apparently greater, so the extrapolated resonance absorption, 59,500 cm^{-1}, may be assigned to the $^1A_{1g}\rightarrow{}^1E_{1u}$ transition (54,500 cm^{-1}).[17] It should, however, be stressed that the contributions of σ-electrons to the MORD are never negligible.

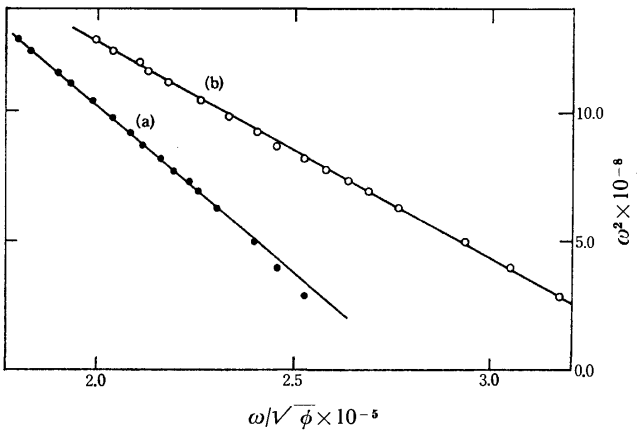

Fig. 3. Diagrams plotted (*a*) $\omega/([\phi]_M)^{1/2}$ and (*b*) $\omega/([\phi]_M - E\omega^2)^{1/2}$ *vs.* ω^2 for benzene.

According to the method of Perkin,[6] we can approximately estimate the ratio of the contribution by π and σ electrons. Perkin reported that, from the results of the Faraday effects of various organic compounds, the molecular rotation can be assumed to consist of rotations of constituent atoms. For example, the molecular rotation of the benzene skeleton, $[C_6H_6{}^{6+}]_M^D$, is proportional to the difference, $[C_6H_{12}]_M^D-6[H^+]^D=4.140$,[18] and the ratio of the contributions of the π and σ electrons is approximately equal to 7 : 4. Then, let us assume that the contributions of the electrons correspond to the E term in Eqs. (6) and (16). When $E=5.74\times10^{-12}$ for $E\omega_D^2=0.165\times10^{-2}$ (deg·l/m·mol·gauss), the curve of $\omega/([\phi]_M-E\omega^2)^{1/2}$ *vs.* ω^2 becomes almost straight, as is shown in Fig. 3(b). Since the straightness of the curve is very good, it is confirmed that the normal MORD of benzene has a large A term with one transition and that the other

17) H. B. Klevens and J. R. Platt, *J. Chem. Phys.*, **17**, 470 (1949).

18) $[C_6H_6]_M^D=11.284$, $[C_6H_{12}]_M^D=5.664$ and $[H]^D=0.254$. See Ref. 6. These values are defined with a dimensionless term, $V_M=[V]_M d_w/M_w r_w$, where r_w, d_w and M_w are the magnetic rotation per cm per gauss and the density and the molecular weight of water respectively. The MORD $[\phi]_M$ values are obtained through the multiplication of a factor, $-M_w r_w/600d_w=0.0003938$, to V_M.

TABLE 1. FARADAY PARAMETERS OF BENZENE

A_0 $\times 10^{-7}$	Res. abs. cm^{-1}	A $(d^2\beta)$[a]	D (d^2)[a]	Magnetic moment (β)[a]		
				Exp.	FEN	LCAO-MO
7.04	54280	30.4	35.3[b]	−1.72	−1.0	−0.396

a) d is expressed in Debye unit and β is a Bohr magneton.
b) Calculated from $f=0.94$ and $\omega=56{,}300\ cm^{-1}$ in Ref. 17.

terms are negligible in $([\phi]_M - E\omega^2)$. The extrapolated resonance absorption 54,280 cm^{-1}, is closer to 54,500 cm^{-1} than to the 59,500 cm^{-1} obtained by Eq. (15); therefore, the transition may be assigned to $^1A_{1g} \rightarrow {}^1E_{1u}$. The normal MORD of benzene, certainly, depends mainly on the π electronic structures. According to Stephens *et al.*,[4] this can naturally be predicted for coronene, which has a much greater value of the circular dichroism of the $^1A_{1g} \rightarrow {}^1E_{1u}$ transition than that of the $^1A_{1g} \rightarrow {}^1B_{2u}$ or $^1B_{1u}$ transition.

Therefore, the magnetic moment is given as -1.72β, with an f value of 0.94[19] (Table 1), and may be assigned to the excited degenerate state, $^1E_{1u}$. This observed moment is rather greater than the values of -1.0β for the FEN model or -0.396β for LCAO-MO when $r_{CC}=1.39$ Å, $Z_{eff}=3.25$, and the molecular orbitals without zero-differential overlap approximation[20] are used. This means that the observed magnitude of the A term is much greater than the theoretical values. Therefore, this probably means that the ratio, 7.144/11.284, of the contributions to the MORD by π-electrons used is too great, or that the observed A value consists of not only $A(^1A_{1g} \rightarrow {}^1E_{1u})$ but also of some terms for the other transitions. However, it is confirmed at last that there is a large A value. The existence of the large A value proves that the absorption band at 54,500 cm^{-1} has two symmetrical doublet transition moments, $(0|m_x|x)$ and $(0|m_y|y)$; this supports the conventional assignment of the β-band to $^1E_{1u}$.[4,12,21,22] It may be predicted that both the abnormal MORD and the MCD of the $^1A_{1g} \rightarrow {}^1E_{1u}$ transition of benzene may be assigned to the positive A type in Stephens' classification[2] or to the III type of Shashousa's[1].

It should be noted that the main component of the MORD is estimated experimentally in spite of difficulties in analyzing normal MORD. We shall not discuss further the magnetic properties of benzene, especially its magnetic moment, until the MCD or the abnormal MORD of benzene has been measured in its absorption regions. The normal MORD of benzene is never simple to analyze in its structure since a normal MORD depends on many transitions.

Finally, it should be noted that the MORD in the S-T absorptional region of benzene[23] has never been observed either with or without O_2-gases.

The author would like to thank Professor Yoshiya Kanda of his laboratory for his guidance, and Professor On Matsumura and Professor Yoshio Shibuya of the Department of Physics, Kyushu University, for providing him with the electric magnet.

Appendix

According to Bishop and Dingle, an electronic angular momentum operator[11] in the multicenter field of molecular orbitals has an effective component to atomic orbital, $|\chi_a)$ as follows:

$$\partial/\partial\phi\,|\chi_a) = -\frac{1}{2}Z_a \sin\theta_a(R_X \sin\varphi_a - R_Y \cos\varphi_a)\,|\chi_a), \tag{A.1}$$

where r_a, θ_a, and φ_a denote the polar coordinates at the nuclei A; the other notations are shown in Fig. 4. This

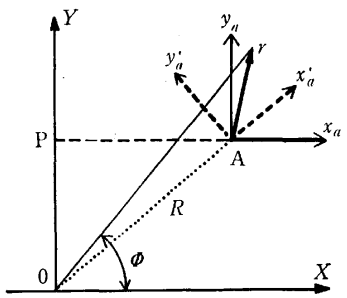

Fig. 4. A relation of the coordinates x_a and y_a by Bishop and Dingle with the x_a' and y_a' by Stephens *et al.*

can be easily proved to coincide with the operator reported by Stephens *et al.*[2] In Eq. (A. 1), as $\sin\theta_a \cos\varphi_a$ and $\sin\theta_a \sin\varphi_a$ can be put at x_a/r_a and y_a/r_a respectively, one obtaines:

$$\frac{\partial}{\partial\phi}|\chi_a) = -\frac{Z_a}{2r_a}(R_X y_a - R_Y x_a)\,|\chi_a) = R\frac{\partial}{\partial y_a'}|\chi_a). \tag{A.2}$$

If the atomic orbitals are expressed with Slater orbitals, which have no factor for φ in the confocal elliptic coordinate system, the integration of Eq. (A. 2) for φ agreeds with Eq. (13). In the multicenter field of molecular orbitals, therefore, the effective component of l_z may be obtained with Eq. (12).

19) K. Kimura and S. Nagakura, *Mol. Phys.*, **2**, 117 (1965).
20) If the MO's calculated with a zero-differential overlap approximation are used, the expected value $(\psi_i|l_z|\psi_i)$ is zero when the bond-length is limited to zero and is, therefore, physically meaningless.
21) E. Clar, "Aromatiche Kohlenwasserstoffe," 2nd ed. Julius Springer Verlag, Berlin, (1952).
22) J. R. Platt, *J. Chem. Phys.*, **17**, 484 (1949); R. C. Nelson and W. T. Simpson, *ibid.*, **23**, 1146 (1955); J. Petruska, *ibid.*, **34**, 1111 and 1121 (1961); E. W. Thulstrup, *Int. J. Quantum Chem.*, **3s**, 641 (1970).
23) A. Sklar, *J. Chem. Phys.*, **5**, 699 (1937); G. Lewis and M. Kasha, *J. Amer. Chem. Soc.*, **69**, 994 (1945); A. Pitts, *J. Chem. Phys.*, **18**, 1416 (1950); D. Evans, *J. Chem. Soc.*, **1957**, 1351; *Nature*, **176**, 777 (1955); D. Craig, J. Hollas, and G. King, *J. Chem. Phys.*, **29**, 974 (1958).

The Vibrational Spectra of Water of Crystallization in Barium Chlorate Monohydrate, Calcium Sulfate Dihydrate and Copper Chloride Dihydrate Crystals

Kunio FUKUSHIMA and Tsutomu YANAGIDA

Department of Chemistry, Faculty of Science, Shizuoka University, Oya, Shizuoka

(Received October 22, 1971)

Infrared spectra of water of crystallization and heavy water of crystallization were mesasured for $Ba(ClO_3)_2 \cdot H_2O$, $CaSO_4 \cdot 2H_2O$, $CuCl_2 \cdot 2H_2O$, $Ba(ClO_3)_2 \cdot D_2O$, $CaSO_4 \cdot 2D_2O$, and $CuCl_2 \cdot 2D_2O$, in which the divalent metal ion lies on the bisector line of H–O–H angle or D–O–D angle. From a comparison of the spectra, assignment of the infrared absorption bands was made for the rotational and the translational vibrations of the water of crystallization.

Water of crystallization is classified into several types by the mode of bonding with surrounding atoms and ions.[1] It was reported[2-4] that the optically active lattice vibration frequencies associated with water of crystallization change sensitively with the change of its state of bonding. In the present study, barium chlorate monohydrate. $Ba(ClO_3)_2 \cdot 2H_2O$, calcium sulfate dihydrate, $CaSO_4 \cdot 2H_2O$, copper chloride dihydrate, $CuCl_2 \cdot 2H_2O$ (type D in Chidambaram's classification[1]) were chosen as representatives of the crystals in which water of crystallization coordinates with a divalent metal ion on the bisector line of H–O–H angle,[5-7] and their bands due to water of crystallization were measured and assigned on the basis of the spectral change on deuteration.

Experimental

The sample were obtained by recrystallization of $Ba(ClO_3)_2 \cdot H_2O$ of guaranteed grade, Kanto Chemical Co., Inc., $CaSO_4 \cdot 2H_2O$ of guaranteed grade, Wako Pure Chemical Industries Ltd., and $CuCl_2 \cdot 2H_2O$ of guaranteed grade, Kanto Chemical Co., Inc. from their aqueous solutions. The deuterates of $Ba(ClO_3)_2 \cdot 2H_2O$ and $CaSO_4 \cdot 2H_2O$ were prepared as residues obtained by vacuum distillation of their heavy water solutions. The duterate of $CuCl_2 \cdot 2H_2O$ was obtained by exposure of $CuCl_2$ to D_2O vapor overnight in a small sealed bottle.

IR spectra in the region 4000—400 cm^{-1} were measured with the Nujol mulls of $Ba(ClO_3)_2 \cdot H_2O$, $CaSO_4 \cdot 2H_2O$, and their deuterates, and those of $CuCl_2 \cdot 2H_2O$ and its deuterate with the Nujol mulls placed between KBr plates covered with thin polyethylene sheets to avoid reaction of the samples with KBr plates. Far IR spectra (400—30 cm^{-1}) of $CaSO_4 \cdot 2H_2O$, $CuCl_2 \cdot 2H_2O$ and their deuterates were measured with their Nujol mulls placed between two polyethylene plates of 2 mm thickness, while those of $Ba(ClO_3)_2 \cdot H_2O$ and its deuterate were measured with a solid paraffin-sample mixture prepared by dispersing the sample powder into molten paraffin and solidifying the mixture cast on a polyethylene plate. The spectra are shown in Figs. 1—6.

Infrared spectra of $CaSO_4 \cdot 2H_2O$ above 300 cm^{-1} have been reported by many investigators.[8-10] The spectra of $CaSO_4 \cdot 2H_2O$ above 300 cm^{-1} in Figs. 3 and 4 are given mainly for the sake of comparison with those of its deuterate. A Hitachi EPI-G3 Infrared Spectrophotometer and a FIS-3 Far Infrared Spectrometer were used.

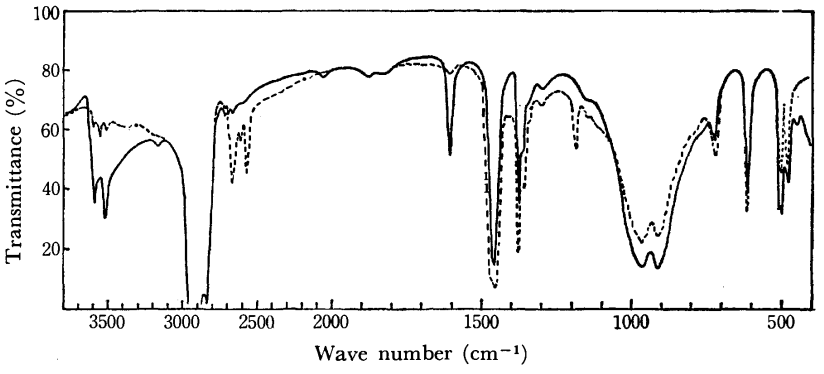

Fig. 1. Infrared spectra of barium chlorate monohydrate in Nujol mull (solid line) and its deuterate in Nujol mull (broken line).

1) R. Chidambaram, A. Sequeira, and S. K. Sikka, *J. Chem. Phys.*, **41**, 3616 (1964).
2) K. Fukushima, This Bulletin, **43**, 39 (1970).
3) K. Fukushima and H. Kataiwa, *ibid.*, **43**, 690 (1970).
4) K. Fukushima, *ibid.*, **43**, 1313 (1970).
5) S. W. Petersen and H. A. Levy, *J. Chem. Phys.*, **26**, 220 (1957).
6) M. Atoji and R. E. Rundle, *ibid.*, **29**, 1306 (1958).
7) G. Kartha, *Acta Crystallogr.*, **5**, 845 (1952).
8) M. Hass, G. B. B. M. Sutherland, *Proc. Roy. Soc., Ser. A*, **236**, 427 (1956).
9) R. J. Morris, Jr., *Anal. Chem.*, **35**, 1489 (1963).
10) F. A. Miller, G. L. Carlson, F. F. Bentley, W. H. Jones, *Spectrochim. Acta*, **16**, 135 (1960).

Discussion

The relative intensities of O—H stretching and H-O-H bending bands are much weaker than those of O-D stretching and D-O-D bending bands as shown in Figs. 1, 3, and 5. This indicates that the major component of each deuterate is $Ba(ClO_3)_2 \cdot D_2O$ $CaSO_4 \cdot 2D_2O$, or $CuCl_2 \cdot 2D_2O$.

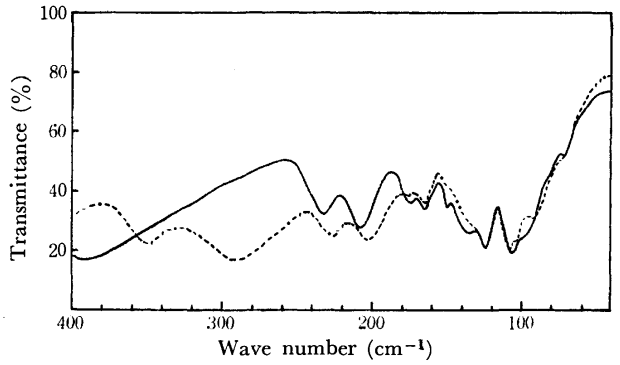

Fig. 2. Far infrared spectra of barium chlorate monohydrate dispersed into solid paraffin (solid line) and its deuterate dispersed into solid paraffin (broken line).

As shown in Fig. 6, the band of deuterated copper chloride dihydrate at 223 cm^{-1} corresponds to that of $CuCl_2 \cdot 2H_2O$ at 243 cm^{-1}. The asymmetrical band of $CuCl_2 \cdot 2H_2O$ at 298 cm^{-1} is interpreted to be composed of two overlapped bands at about 310 cm^{-1} and at 298 cm^{-1} from the fact that two bands appear at 295 cm^{-1} and 255 cm^{-1} for the deuterate and from a comparison of 310/255 value with the ν_H/ν_D values in Table 2. Similarly, the band of $CaSO_4 \cdot 2H_2O$ at 306 cm^{-1} corresponds to that of the deuterate at 259 cm^{-1}.

Comparing the spectra of the crystals with those of their deuterates, a correspondence can be set up between the observed frequencies of the former and of the latter as shown in Table 1. For $Ba(ClO_3)_2.2H_2O$,

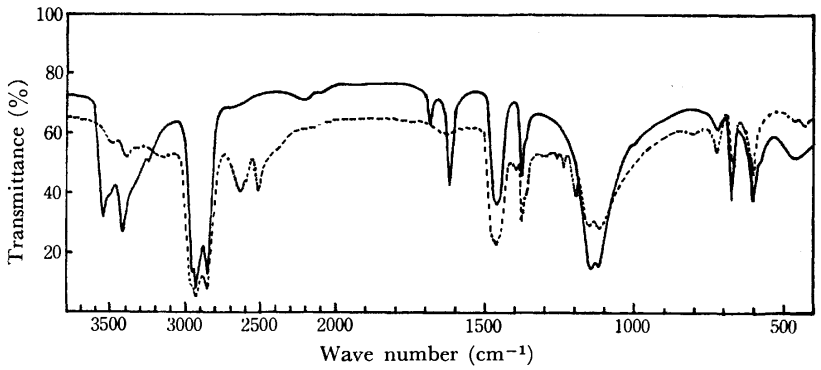

Fig. 3. Infrared spectra of calcium sulfate dihydrate in Nujol mull (solid line) and its deuterate in Nujol mull (broken line).

TABLE 1. FREQUENCIES IN cm^{-1} OF IR BANDS OF WATER OF CRYSTALLIZATION

$Ba(ClO_3)_2 \cdot H_2O$ ν_H	$Ba(ClO_3)_2 \cdot D_2O$ ν_D	ν_H/ν_D	$CaSO_4 \cdot 2H_2O$ ν_H	$CaSO_4 \cdot 2D_2O$ ν_D	ν_H/ν_D	$CuCl_2 \cdot 2H_2O$ ν_H	$CuCl_2 \cdot 2D_2O$ ν_D	ν_H/ν_D
451	350	1.29	576	432	1.33	*	360	
390	290	1.34	460	345	1.33	430	315	1.36
*	*		306	259	1.18	310	255	1.22
			271	212	1.28	243	223	1.09
233	226	1.03						
207	203	1.02						

* Not observed because of weak intensity and overlapping with other bands.

TABLE 2. CALCULATED MOMENTS OF INERTIA OF H_2O AND D_2O MOLECULES IN $CaSO_4 \cdot 2H_2O$ AND $CuCl_2 \cdot 2H_2O$ AND THEIR DEUTERATES[a] (IN 10^{-40} g·cm²)

	I_A	I_B	I_C	$\sqrt{I_{A,D_2O}/I_{A,H_2O}}$	$\sqrt{I_{B,D_2O}/I_{B,H_2O}}$	$\sqrt{I_{C,D_2O}/I_{C,H_2O}}$
$CaSO_4 \cdot 2H_2O$	1.067	2.089	3.157	1.34	1.41	1.39
$CaSO_4 \cdot 2D_2O$	1.919	4.174	6.093			
$CuCl_2 \cdot 2H_2O$	0.922	1.970	2.892	1.34	1.41	1.39
$CuCl_2 \cdot 2D_2O$	1.658	3.936	5.594			

a) The moments of inertia in the table were calculated using the bond length and bond angle of water of crystallization.[5,6] The same bond length and bond angle as H_2O molecule in the crystals were assumed for D_2O molecule in the deuterate crystals.

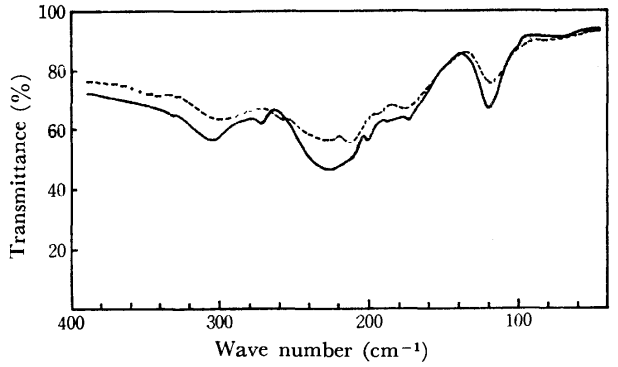

Fig. 4. Far infrared spectra of calcium sulfate dihydrate in Nujol mull (solid line) and its deuterate in Nujol mull (broken line).

Prask and Boutin observed[11] neutron scattering peak frequencies of 458 cm^{-1}, 390 cm^{-1}, 318 cm^{-1}, 238 cm^{-1}, 212 cm^{-1}, 149 cm^{-1}, 81 cm^{-1}, and 67 cm^{-1} as those due to water of crystallization. The observed IR band frquencies, which were found to shift on deuteration, correspond to the frequencies observed by Prask and Boutin except for the frequencies 318 cm^{-1}, 81 cm^{-1}, and 67 cm^{-1}. As shown in Table 1, the ν_H/ν_D values of 1.29 and 1.34 for the bands at 451 cm^{-1} and 390 cm^{-1}, respectively, lead to an assignment of the bands to the rotational vibrations of crystallization, while those of 1.03 and 1.02 for the bands at 233 cm^{-1} and 207 cm^{-1}, respectively, lead to an assignment of the bands to the translational vibartions of water of crystallization.

In the case of $CaSO_4 \cdot 2H_2O$ and $CuCl_2 \cdot 2H_2O$, the

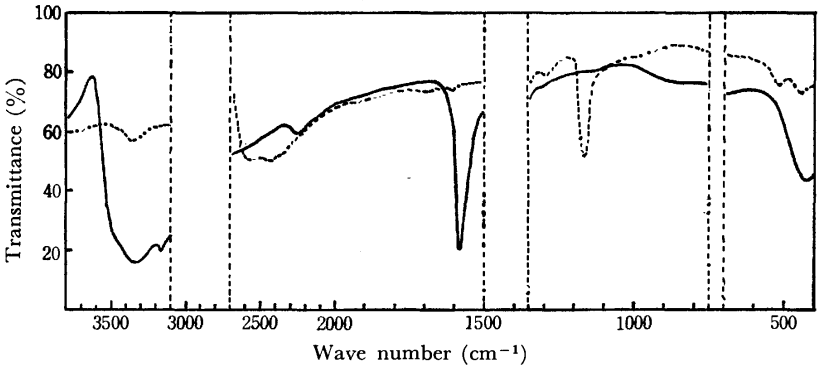

Fig. 5. Infrared spectra of copper chloride dihydrate in Nujol mull (solid line) and its deuterate in Nujol mull (broken line).

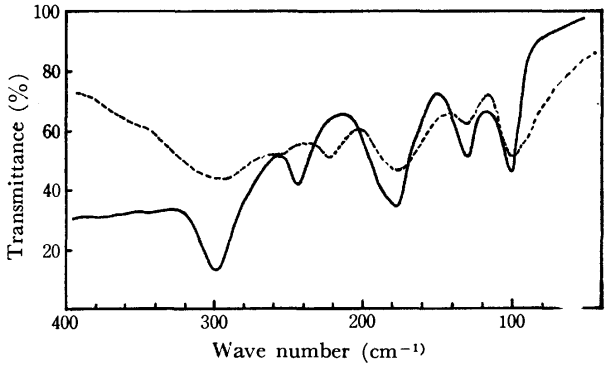

Fig. 6. Far infrared spectra of copper chloride dihydrate in Nujol mull (solid line) and its deuterate in Nujol mull (broken line).

bands at 576 cm^{-1} 460 cm^{-1}, and 430 cm^{-1}, are assigned to the rotational vibrations of water of crystallization on the basis of ν_H/ν_D values of 1.33, 1.33, and 1.36, respectively. The values are in accordance with the calculated values of $\sqrt{I_{A,D_2O}/I_{A,H_2O}}$ and $\sqrt{I_{C,D_2O}/I_{C,H_2O}}$ in Table 2. It is expected that ν_H/ν_D values of the translational vibrations of water of crystal lization in $CaSO_4 \cdot 2H_2O$ and $CuCl_2 \cdot 2H_2O$ crystals differ from those of $Ba(ClO_3)_2 \cdot H_2O$ crystal since the reduced masses of $Ca^{2+} \cdots OH_2$ and $Cu^{2+} \cdots OH_2$ systems differ from the mass of $Ba^{2+} \cdots OH_2$ system which is close to that of H_2O molecule. Thus, the bands at 271 cm^{-1} and 243 cm^{-1}, which have different ν_H/ν_D values higher than those of the bands at 233 cm^{-1} and 207 cm^{-1} of $Ba(ClO_3)_2 \cdot H_2O$ can be assigned to the translational vibrations of water of crystallization. The bands at 306 cm^{-1} and 310 cm^{-1} have very close ν_H/ν_D values. This indicates that these bands can be assigned to the rotational rather than the translational vibrations.

It has been reported that the spectra of the rotational vibrations of water of crystallization change remarkable with the change of bound state of water of crystallization.[2-4] Our results show that the spectra of water of crystallization having a coordinated divalent metal ion on the bisector line of H–O–H angle has a characteristic pattern, that is, the spectra consist of a broad band with medium intensity having two weaker bands on both sides, the characteristic spectra showing the difference corresponding to the different bound states of water of crystallization in the crystals. Interatomic distances in the crystals differ with the crystals. ($Ba(ClO_3)_2 \cdot H_2O$, $O_w \cdots Ba^{2+}$ 2.60 Å, $H_w \cdots O(ClO_3)$ 2.77 Å; $CuCl_2 \cdot 2H_2O$, $O_w \cdots Cu^{2+}$ 1.925 Å, $H_w \cdots Cl^-$ 2.258 Å; $CaSO_4 \cdot 2H_2O$, $O_w \cdots Ca^{2+}$ 2.34 Å and 2.35 Å, $H_w \cdots O(SO_4^{2-})$ 2.816 Å and 2.824 Å). These distances suggest that the water of crystallization of $CuCl_2 \cdot 2H_2O$ and $CaSO_4 \cdot 2H_2O$ is more strongly bound than that of $Ba(ClO_3)_2 \cdot H_2O$. This seems to cause the shift of frequencies of the weak band and the broad band having higher freuqncies than the other weak band.

11) H. J. Prask and H. Boutin, *J. Chem. Phys.*, **45**, 699 (1966).

The Molecular and Crystal Structures of Two Isomeric Dihydrofukinolidol Sulfites, $C_{15}H_{22}O_5S$

Akio FURUSAKI* and Tokunosuké WATANABÉ
Faculty of Science, Kwansei Gakuin University, Nishinomiya
(Received November 12, 1971)

The molecular and crystal structures of two isomeric dihydrofukinolidol sulfites, $C_{15}H_{22}O_5S$, have been studied by means of an X-ray analysis. The two sulfites, called S-1 and S-2, both crystallize in the orthorhombic space group $P2_12_12_1$, with four molecules in each unit cell. The cell dimensions are $a=12.544$, $b=14.457$, and $c=8.545$ Å for S-1, and $a=12.919$, $b=14.375$, and $c=8.496$ Å for S-2. The reflection intensities were measured visually from equi-inclination integrating Weissenberg photographs taken with Cu$K\alpha$ radiation. The structures were solved by the tangent formula procedure and refined by the block-diagonal-matrix least-squares method, the anisotropic thermal motions being assumed for all the atoms. The final R factor was 10.8% for S-1 and 11.2% for S-2. The absolute configurations of the molecules were determined by using the anomalous dispersion effects of the sulfur atoms for Cu$K\alpha$ radiation. It was found that the six-membered ring containing the sulfite group in S-1 takes the chair conformation, while the same ring in S-2 has the twist boat form. The exocyclic S–O bond in the two sulfites are both axially oriented, and the other corresponding parts of the two isomers are closely similar to each other.

Fukinolidol, $C_{15}H_{22}O_4$, is a hydrolysis product of the sesquiterpenoids, named fukinolide, fukinanolide, and S-fukinolide, which are isolated from the flower stalks of wild butterburs, *Petasites japonicus* Maxim. (Japanese name, "Fuki").[1] The molecular structure of the substance has already been studied by the X-ray method as well as by organic chemical means.[1,2] It has been found that the dihydro derivative of the substance is converted into two isomeric sulfites, $C_{15}H_{22}O_5S$, by the drop-by-drop addition of its pyridine at −35°——45°C over a two-hour period, followed by standing at room temperature for two hours.[3] The isomers, called hereafter S-1 and S-2, are similar in their UV and IR spectra, while they are considerably different in their NMR spectra and solubilities; S-2 is more soluble in polar solvents, such as methanol and chloroform. These facts suggest that the difference in the structure of the two isomers may arise solely from the configuration of the part containing the sulfur atom. Figure 1 shows the structural formula applicable to the two isomers. With respect to the sulfite group, this formula gives four different stereostructures shown in Fig. 2. The purpose of the present work is to determine which of the four structures S-1 and S-2 actually have.

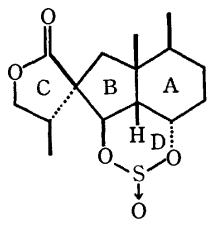

Fig. 1. The molecular structure of dihydrofukinolidol sulfites.

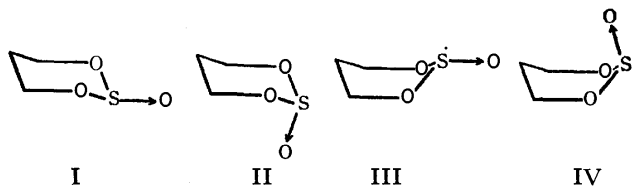

Fig. 2. The four possible stereostructures for the sulfite group.

Experimental

Single crystals of S-1 and S-2 were kindly supplied by Professor Keizo Naya of this university. The crystal data were derived from oscillation and Weissenberg photographs taken with CuK_α radiation; the results are summarized in Table 1. The reflection intensities were measured visually from equi-inclination integrating Weissenberg photographs taken with CuK_α radiation around the a and c axes. For the reflections whose α_1-α_2 doublets were completely split, 1.5 times α_1 spot intensities were used. The Lorentz-polarization and spot-size corrections were made, while the absorption effect was not taken into account, since the crystals used were sufficiently small. These data were then put on an

TABLE 1. CRYSTAL DATA

	S-1	S-2
Formula	$C_{15}H_{22}O_5S$	$C_{15}H_{22}O_5S$
MW	314.40	314.40
Mp	190.5—191.5°C (dec.)	187.5—188.5°C (dec.)
Shape	prism	needle
System	orthorhombic	orthorhombic
Cell dimensions		
a	12.544±0.002 Å	12.919±0.002 Å
b	14.457±0.001	14.375±0.002
c	8.545 ±0.002	8.496 ±0.001
Space group	$P2_12_12_1$	$P2_12_12_1$
Z	4	4
V	1549.6±0.5 Å^3	1577.8±0.4 Å^3
D_x	1.347 g/cm^3	1.323 g/cm^3

* Present address: Department of Chemistry, Faculty of Science, Hokkaido University, Sapporo.

1) K. Naya, I. Takagi, M. Hayashi, S. Nakamura, M. Kobayashi, and S. Katsumura, *Chem. Ind.* (London), **1968**, 318.
2) C. Katayama, A. Furusaki, I. Nitta, M. Hayashi, and K. Naya, This Bulletin, **43**, 1976 (1970).
3) K. Naya, I. Takagi, and T. Kasai, *ibid.*, **44**, 3204 (1971).

absolute scale by means of Wilson's method: the overall temperature factors obtained were 4.59 Å^2 for S-1 and 4.66 Å^2 for S-2. Thus, the structure factors of 1773 and 1754 independent reflections were derived for S-1 and S-2 respectively.

Structure Determination

The crystal structures of the two sulfites were both elucidated easily by using the tangent formula proce-

Table 2. The weighting scheme for S-1 and the distribution of $\langle W\Delta|F_o|^2\rangle$ values

$A=0.9170\times10^{-3}$ $C=0.2156$ $E=-0.2750\times10^{2}$
$B=0.2351\times10^{2}$ $D=-0.4331\times10^{-1}$ $F=0.6764$

$\sin\theta/\lambda$	0.00	0.30	0.42	0.49	0.55	0.60	0.64
0.0							
5.0	0.380 (4)	0.598 (27)	1.007 (50)	0.882 (138)	0.786 (187)	0.922 (180)	
10.0	0.426 (19)	0.974 (92)	1.282 (108)	1.151 (127)	0.909 (96)	1.119 (61)	
15.0	1.164 (27)	0.840 (101)	1.031 (92)	1.454 (33)	0.023 (6)		
25.0	0.929 (56)	0.621 (93)	0.562 (47)	0.221 (1)			
40.0	0.906 (60)	0.499 (30)	0.798 (1)				
80.0	0.649 (32)	0.409 (1)					
$\|F_o\|$							

The corresponding numbers of reflections are given in parentheses.

Table 3. The weighting scheme for S-2 and the distribution of $\langle W\Delta|F_o|^2\rangle$ values

$A=0.5503\times10^{-3}$ $C=0.7144\times10^{-1}$ $E=-0.2420\times10^{2}$
$B=0.2064\times10^{2}$ $D=0.5462\times10^{-2}$ $F=0.6049\times10$

$\sin\theta/\lambda$	0.00	0.30	0.42	0.49	0.55	0.60	0.64
0.0							
5.0	0.350 (7)	0.330 (41)	0.909 (63)	0.830 (155)	1.004 (186)	0.764 (172)	
10.0	0.700 (24)	0.989 (66)	1.045 (112)	1.227 (139)	1.260 (80)	0.985 (54)	
15.0	1.398 (31)	0.981 (104)	1.066 (88)	0.617 (19)	0.952 (8)		
25.0	0.800 (62)	0.621 (110)	0.668 (45)	3.761 (2)			
40.0	0.881 (58)	0.668 (22)	0.192 (1)				
80.0	1.069 (33)						
$\|F_o\|$							

The corresponding numbers of reflections are given in parentheses.

dure.[4] For the reflections whose E-values were larger than 1.20, the structure factors were calculated with sulfur atom positions obtained from sharpened Patterson functions and with the overall temperature factors previously described. Phase angles with $|F_c|$ values larger than $0.4\times|F_o|$ were selected for the starting set of phases necessary for the tangent formula calculation. This phase calculation was repeated under the condition that the corresponding phases were accepted only when the α-values and the numbers of the correlation terms were larger than 5.0 and 5 respectively. After three cycles of calculation, the accepted phases were increased from 202 to 375 for S-1, and from 204 to 385 for S-2. For both crystals, E-maps calculated with these phases showed clearly the positions of all the atoms except hydrogen.

The structures thus obtained were refined by the block-diagonal-matrix least-squares method, first with isotropic temperature factors and then with anisotropic thermal parameters. The following weighting scheme was introduced at this stage:

$$W = \exp(-AX^2-BY^2-CXY-DX-EY-F)$$
$$X = |F_o|,\ Y = \sin\theta/\lambda$$

The intensity data were made into groups with constant intervals along two coordinates, $|F_o|$ and $\sin\theta/\lambda$. The coefficients, A, B, C, D, E, and F, were determined by the least-squares method, so as to give as equal values of $\langle W\Delta|F_o|^2\rangle$ for all the reflection groups as possible. The coefficients thus obtained for S-1 and S-2 and the distributions of $\langle W\Delta|F_o|^2\rangle$ evaluated with these values are, respectively, given

Table 4. The final atomic parameters and their estimated standard deviations of S-1

(a) The atomic coordinates

Atom	x/a	σ	y/b	σ	z/c	σ	Atom	x/a	σ	y/b	σ	z/c	σ
S	0.2055	1	0.1190	1	0.7452	1	C(6)	0.0959	4	0.3379	3	0.3380	5
O(1)	0.2336	4	0.0692	2	0.5827	5	C(7)	0.1280	3	0.3456	2	0.5122	4
O(2)	0.2020	3	0.2269	2	0.6920	3	C(8)	0.2381	4	0.3886	3	0.5275	6
O(3)	0.0988	5	0.0950	3	0.7888	5	C(9)	0.1342	3	0.2427	2	0.5561	4
O(4)	0.2416	4	0.4470	4	0.6511	8	C(10)	0.1796	3	0.1951	3	0.4134	5
O(5)	0.3155	3	0.3750	4	0.4503	7	C(11)	0.0593	4	0.4079	2	0.6147	6
C(1)	0.1794	4	0.0914	3	0.4323	6	C(12)	0.1399	6	0.4444	5	0.7335	11
C(2)	0.0720	5	0.0481	3	0.4134	7	C(13)	−0.0331	5	0.3628	4	0.6960	9
C(3)	0.0245	5	0.0795	4	0.2631	7	C(14)	−0.0523	6	0.2137	6	0.1134	7
C(4)	0.0094	4	0.1846	4	0.2570	6	C(15)	0.1840	5	0.2348	5	0.1300	6
C(5)	0.1149	4	0.2367	3	0.2799	4							

(b) The anisotropic temperature factors are in form of $\exp(-B_{11}h^2-B_{22}k^2-B_{33}l^2-B_{12}hk-B_{23}kl-B_{31}lh)$

Atom	$B_{11}\times10^5$	$B_{22}\times10^5$	$B_{33}\times10^5$	$B_{12}\times10^5$	$B_{23}\times10^5$	$B_{31}\times10^5$
S	1222(10)	401(4)	1485(13)	224(11)	469(14)	−607(22)
O(1)	1128(30)	408(13)	1815(52)	504(34)	38(45)	−333(69)
O(2)	927(22)	321(10)	1167(34)	83(27)	230(32)	−515(51)
O(3)	1526(43)	569(18)	1470(51)	−194(46)	284(49)	669(78)
O(4)	1096(35)	643(22)	3371(113)	−563(47)	−937(87)	−716(107)
O(5)	795(24)	788(25)	2725(84)	−377(42)	1064(80)	21(74)
C(1)	900(32)	352(15)	1560(59)	350(36)	−144(51)	280(75)
C(2)	1091(41)	348(15)	1792(69)	−99(42)	−348(59)	271(92)
C(3)	1005(38)	551(21)	1685(70)	−186(47)	−621(71)	222(97)
C(4)	782(27)	633(22)	1054(44)	102(41)	−388(59)	−108(67)
C(5)	751(26)	483(17)	967(47)	107(36)	148(44)	252(57)
C(6)	977(33)	461(18)	1014(47)	108(41)	387(50)	−181(68)
C(7)	628(21)	290(12)	1188(45)	0(28)	216(42)	−83(54)
C(8)	665(24)	443(17)	1980(72)	−256(37)	458(64)	−235(71)
C(9)	598(20)	282(12)	934(40)	103(26)	116(38)	−46(48)
C(10)	713(25)	352(14)	1034(43)	158(30)	−25(42)	199(57)
C(11)	848(29)	287(14)	1543(58)	83(33)	−233(47)	−354(70)
C(12)	1144(49)	677(30)	2916(140)	−157(65)	−1417(120)	−538(143)
C(13)	933(37)	658(27)	2378(98)	2(53)	−987(89)	788(101)
C(14)	1000(43)	1106(49)	1452(72)	217(78)	−162(99)	−498(98)
C(15)	1040(43)	983(39)	989(53)	18(71)	267(76)	696(82)

The standard deviations are given in parentheses.

4) J. Karle and I. L. Karle, *Acta Crystallogr.*, **21**, 849 (1966).

TABLE 5. THE FINAL ATOMIC PARAMETERS AND THEIR ESTIMATED STANDARD DEVIATIONS OF S-2

(a) The atomic coordinates

Atom	x/a	σ	y/b	σ	z/c	σ	Atom	x/a	σ	y/b	σ	z/c	σ
S	0.2310	1	0.1266	1	0.7429	1	C(6)	0.1115	4	0.3392	3	0.3372	6
O(1)	0.1639	4	0.0650	2	0.6259	5	C(7)	0.1357	3	0.3468	2	0.5173	5
O(2)	0.1765	3	0.2266	2	0.7152	3	C(8)	0.2457	4	0.3795	4	0.5456	8
O(3)	0.3354	4	0.1327	4	0.6799	7	C(9)	0.1269	3	0.2445	2	0.5653	4
O(4)	0.2478	5	0.4363	4	0.6727	9	C(10)	0.1758	3	0.1906	3	0.4317	4
O(5)	0.3213	4	0.3618	4	0.4711	8	C(11)	0.0719	5	0.4157	3	0.6111	7
C(1)	0.1610	4	0.0870	3	0.4532	6	C(12)	0.1465	8	0.4426	5	0.7434	12
C(2)	0.0583	5	0.0499	3	0.3991	8	C(13)	−0.0316	6	0.3829	6	0.6772	9
C(3)	0.0316	5	0.0855	5	0.2339	9	C(14)	−0.0152	7	0.2292	8	0.0771	8
C(4)	0.0260	4	0.1918	4	0.2357	7	C(15)	0.2118	6	0.2337	7	0.1518	7
C(5)	0.1306	4	0.2369	4	0.2820	4							

(b) The anisotropic temperature factors are in form of $\exp(-B_{11}h^2-B_{22}k^2-B_{33}l^2-B_{12}hk-B_{23}kl-B_{31}lh)$

Atom	$B_{11}\times10^5$	$B_{22}\times10^5$	$B_{33}\times10^5$	$B_{12}\times10^5$	$B_{23}\times10^5$	$B_{31}\times10^5$
S	1082(9)	489(4)	1326(12)	337(11)	520(14)	−35(22)
O(1)	1284(35)	382(13)	1836(56)	−112(36)	488(46)	−171(84)
O(2)	902(22)	478(13)	933(33)	384(30)	109(36)	−385(50)
O(3)	815(25)	815(25)	2556(80)	435(45)	47(81)	−340(80)
O(4)	1274(45)	672(23)	3957(139)	−613(54)	−577(99)	−1885(139)
O(5)	779(24)	806(25)	3382(112)	−512(44)	1239(98)	−568(93)
C(1)	750(26)	373(15)	1505(58)	141(35)	−387(55)	63(75)
C(2)	843(31)	427(18)	2381(101)	−148(43)	−655(76)	97(105)
C(3)	969(39)	664(28)	2327(105)	197(55)	−1097(104)	−548(126)
C(4)	803(30)	698(26)	1346(62)	31(46)	−685(74)	−269(90)
C(5)	624(21)	643(22)	833(42)	106(38)	67(52)	141(59)
C(6)	738(27)	534(20)	1293(54)	31(40)	559(61)	−400(73)
C(7)	659(22)	309(13)	1376(52)	−114(30)	95(46)	−467(68)
C(8)	775(30)	481(19)	2636(101)	−450(43)	473(80)	−898(102)
C(9)	620(19)	316(13)	958(39)	33(28)	−22(42)	−193(57)
C(10)	585(20)	405(15)	907(40)	57(29)	−100(44)	31(58)
C(11)	1139(42)	343(16)	1778(72)	144(45)	−354(60)	−877(103)
C(12)	1520(70)	612(29)	3063(154)	216(73)	−1363(125)	−1732(204)
C(13)	947(40)	944(42)	2105(98)	722(70)	−1500(116)	−165(111)
C(14)	1125(50)	1407(69)	1407(79)	709(150)	−868(128)	−1027(119)
C(15)	926(40)	1298(57)	1202(61)	290(85)	359(104)	720(91)

The standard deviations are given in parentheses.

in Tables 2 and 3. After several cycles of the refinement using this weighting scheme, the R factor reached a value of 0.108 for S-1 and one of 0.112 for S-2. The final atomic parameters and their standard deviations are given in Tables 4 and 5. The tables of the observed and calculated structure factors are preserved by the Chemical Society of Japan.

The determination of the absolute configurations of the two sulfites was attempted by using the anomalous disperison effect of sulfur atoms for CuK_α radiation ($\Delta f_s''=0.6$). The comparison of the pairs of intensities, hkl and $h\bar{k}l$, was made on the Weissenberg photographs around the a axis already mentioned in the Experimental section. From the data shown in Tables 6 and 7, it can be concluded without any uncertain that the atomic parameters given in Tables 4 and 5, expressed in terms of a right-handed set of axes, correspond to the actual absolute configuration for either of the two sulfites. The absolute configurations of the two isomers thus obtained are both consistent with that of another derivative of fukinolidol.[2)]

The calculations necessary for the present work were carried out on a FACOM 270—20 computer in this university, using programs written in our laboratory.

Results and Discussion

Molecular Structures. The absolute configurations of the S-1 and S-2 molecules are, respectively, illustrated in Figs. 3(a) and 3(b) where each atom is represented as an ellipsoid, in conformity with the thermal parameters listed in Tables 4 and 5. From these figures, it is found that S-1 and S-2 correspond to II and IV respectively out of the four possible stereostructures given in Fig. 2. The bond distances and

Table 6. Bijvoet inequalities for S-1

h k l	$\lvert F_c(hkl)\rvert$	$\lvert F_c(\bar{h}\bar{k}\bar{l})\rvert$	Observations	h k l	$\lvert F_c(hkl)\rvert$	$\lvert F_c(\bar{h}\bar{k}\bar{l})\rvert$	Observations
1 16 1	2.76	2.46	>	3 15 3	3.20	2.64	>
1 16 2	1.07	0.78	>	3 16 3	5.26	5.97	<
1 6 6	1.87	1.56	>	3 12 4	6.49	7.21	<
1 7 6	5.35	6.43	<	3 5 5	3.05	4.01	<
1 8 6	3.05	2.73	>	3 1 7	5.83	4.91	>
1 1 7	7.37	5.90	>	3 5 7	3.74	4.50	<
1 7 7	7.34	6.56	>	3 1 9	2.19	2.75	<
1 9 7	2.43	2.96	<	4 6 1	3.86	2.42	<
1 1 8	5.55	4.32	>	4 7 1	8.12	9.25	<
1 2 9	3.34	3.70	<	4 13 1	7.93	6.64	>
1 4 9	2.09	1.71	>	4 12 2	6.86	7.81	<
1 1 10	2.08	2.44	<	4 5 3	5.26	7.61	<
1 3 10	2.60	2.32	>	4 1 4	9.74	7.96	>
1 6 10	3.11	2.71	>	4 5 5	3.68	1.82	>
2 13 1	4.76	3.81	>	4 8 6	3.12	2.45	>
2 14 1	6.44	5.77	>	4 9 6	2.29	3.06	<
2 16 1	5.27	4.67	>	4 2 9	2.48	2.02	>
2 14 2	5.17	4.54	>	5 13 1	2.95	3.26	<
2 16 2	4.97	4.40	>	5 14 1	3.41	2.75	>
2 17 3	3.78	4.43	<	5 2 2	27.29	30.25	<
2 5 4	7.21	6.16	>	5 12 2	5.39	6.06	<
2 11 4	3.02	3.94	<	5 4 3	5.48	2.69	>
2 16 4	3.48	4.15	<	6 3 2	13.11	11.00	>
2 6 5	9.67	11.56	<	6 11 2	10.63	11.99	<
2 9 6	5.16	5.83	<	6 15 2	5.90	5.22	>
2 7 8	2.63	3.08	<	6 12 3	1.82	2.14	<
3 5 1	10.93	9.43	>	6 3 5	10.38	9.11	>
3 7 1	17.33	15.39	>	6 1 10	3.31	2.95	>
3 8 1	4.65	6.50	<	7 12 1	7.00	6.24	>
3 11 1	4.53	3.27	>	7 14 2	4.71	4.21	>
3 1 2	7.41	9.35	<	7 13 4	1.53	1.89	<
3 2 2	6.98	9.84	<	7 14 4	2.49	1.70	>
3 8 3	17.09	19.04	<	7 12 5	5.60	6.30	<
3 12 3	10.80	11.96	<				

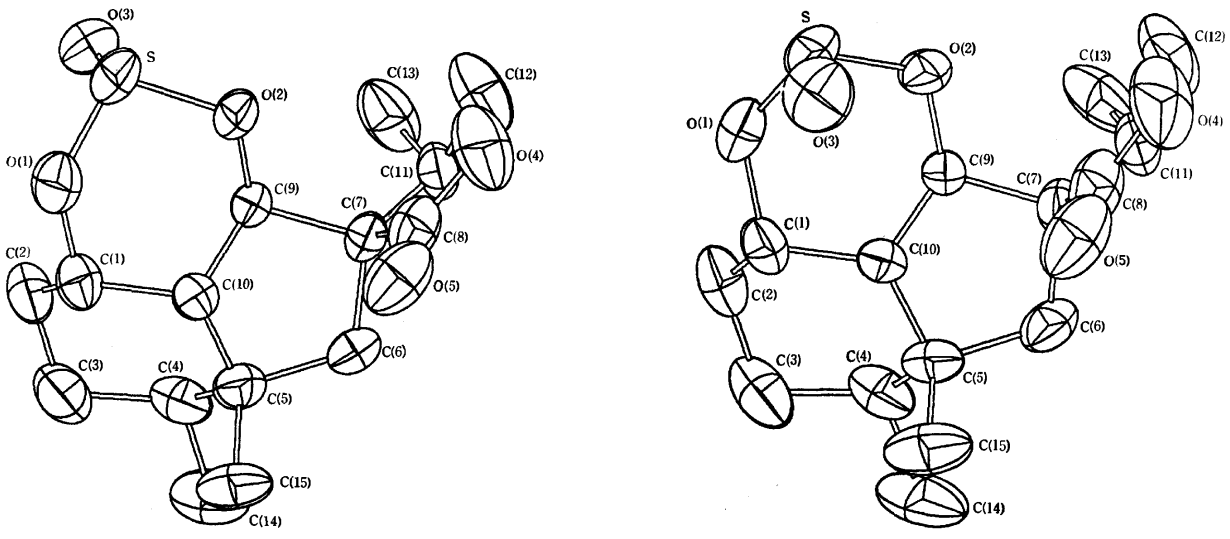

(a) S—1 (b) S—2

Fig. 3. The molecular frameworks.
The thermal ellipsoids enclose 50% probability.

TABLE 7. BIJVOET INEQUALITIES FOR S-2

h k l	$\lvert F_c(hkl)\rvert$	$\lvert F_c(\bar{h}\bar{k}\bar{l})\rvert$	Observations	h k l	$\lvert F_c(hkl)\rvert$	$\lvert F_c(\bar{h}\bar{k}\bar{l})\rvert$	Observations
1 5 1	2.28	4.74	<	4 5 4	2.12	1.13	>
1 11 1	4.77	5.91	<	4 11 4	5.12	4.42	>
1 13 2	4.21	3.45	>	4 15 4	1.74	2.20	<
1 7 3	12.58	10.70	>	4 1 5	3.50	4.35	<
1 8 3	2.18	1.67	>	4 5 5	6.01	6.85	<
1 9 3	10.96	12.21	<	4 9 6	4.01	3.41	>
1 15 3	2.12	2.63	<	4 13 6	2.92	2.45	>
1 17 3	3.96	3.44	>	4 7 7	3.45	2.77	>
1 1 4	13.65	11.19	>	5 9 1	10.92	12.22	<
1 5 4	8.43	7.61	>	5 13 1	2.61	3.80	<
1 13 4	3.60	4.16	<	5 15 1	2.94	3.40	<
1 15 4	1.85	0.92	>	5 16 1	2.55	3.00	<
1 16 4	2.29	2.03	>	5 2 2	3.00	1.85	>
1 17 4	2.27	1.81	>	5 14 2	1.88	2.39	<
1 3 5	7.22	5.91	>	5 3 3	8.72	7.11	>
1 5 6	4.90	6.15	<	5 5 3	4.25	6.13	<
1 9 6	8.36	9.41	<	5 11 3	5.12	4.55	>
1 10 6	2.95	2.47	>	5 11 4	4.24	5.15	<
1 5 7	6.59	7.36	<	5 13 4	4.95	4.45	>
1 6 7	3.17	3.75	<	5 3 6	1.21	2.46	<
1 9 7	4.36	3.93	>	5 6 6	6.83	7.74	<
1 11 7	1.67	2.21	<	6 10 1	10.65	9.36	>
1 12 7	2.17	2.62	<	6 8 2	9.14	7.91	>
1 13 7	4.88	5.43	<	6 15 2	3.47	4.07	<
2 17 2	1.91	2.16	<	6 10 3	6.19	7.28	<
2 16 4	4.31	5.06	<	6 13 3	4.44	4.93	<
2 6 5	7.74	9.38	<	6 15 3	1.95	1.49	>
2 6 7	13.87	12.12	>	6 1 4	4.84	3.93	>
3 14 2	3.69	4.12	<	6 6 5	5.27	3.87	>
3 3 3	10.96	8.65	>	6 7 5	8.29	7.49	>
3 11 3	2.68	1.64	>	6 9 5	6.00	6.81	<
3 13 3	3.72	5.02	<	6 7 6	5.78	6.47	<
3 15 3	2.18	1.54	>	6 1 7	3.27	4.07	<
3 3 4	14.65	16.93	<	6 5 8	3.47	3.96	<
3 6 5	1.23	1.73	<	7 9 1	4.41	5.33	<
3 3 6	8.85	10.35	<	7 1 2	6.33	7.37	<
3 4 8	5.06	5.65	<	7 3 2	5.21	4.69	>
4 12 1	3.30	3.66	<	7 11 2	4.36	3.53	>
4 13 1	6.22	5.56	>	7 9 3	2.95	1.85	>
4 16 1	1.69	1.47	>	8 2 1	4.71	3.90	>
4 3 2	3.96	5.15	<	8 9 1	8.27	7.25	>
4 8 2	14.58	12.65	>	8 2 3	4.17	3.59	>
4 11 2	5.91	6.63	<	8 1 6	4.86	4.36	>
4 12 2	8.77	10.45	<	8 4 6	5.66	4.90	>
4 1 3	8.30	9.49	<				

angles calculated with the final parameters are given in Tables 8 and 9, together with their standard deviations. The correction for the thermal motions of the atoms has been made, on the assumption of the riding motion, by means of the Busing-Levy method.[5] If the standard deviations are taken into consideration, the corresponding values of the bond distances and angles in the S-1 and S-2 molecules are in good agreement with each other, in particular for parts remote from the sulfite group. In both S-1 and S-2 molecules, the D rings containing the sulfite group are *cis*-fused with the A ring and *trans*-fused with the B ring, while the A and B rings are joined to each other in the *cis* configuration. On the other hand, the D ring makes a spiro-union with the B ring, the spiro-atom being C(7).

It has been already reported that the six-membered ring of trimethylene sulfite (TSU), like that of 2,2′-dichlorotrimethylene sulfite (DCT), has the chair conformation with the exocyclic S–O bond pointing

5) W. R. Busing and H. A. Levy, *Acta Crystallogr.*, **17**, 142 (1964).

Table 8. The bond distances (Å) in the S-1 and S-2 molecules

	S-1		S-2	
Bond	Distance	e.s.d.	Distance	e.s.d.
S-O(1)	1.603 (1.607)[a]	0.004	1.588 (1.598)	0.005
S-O(2)	1.625 (1.637)	0.003	1.618 (1.626)	0.004
S-O(3)	1.432 (1.448)	0.006	1.455 (1.476)	0.005
O(1)-C(1)	1.489 (1.502)	0.007	1.502 (1.521)	0.006
O(2)-C(9)	1.457 (1.470)	0.005	1.449 (1.464)	0.005
O(4)-C(8)	1.353 (1.394)	0.008	1.354 (1.393)	0.010
O(4)-C(12)	1.457 (1.459)	0.010	1.443 (1.450)	0.012
O(5)-C(8)	1.190 (1.215)	0.007	1.192 (1.215)	0.008
C(1)-C(2)	1.495 (1.504)	0.008	1.502 (1.517)	0.008
C(1)-C(10)	1.508 (1.519)	0.005	1.514 (1.525)	0.005
C(2)-C(3)	1.487 (1.490)	0.008	1.533 (1.544)	0.010
C(3)-C(4)	1.533 (1.545)	0.007	1.530 (1.546)	0.009
C(4)-C(5)	1.535 (1.542)	0.007	1.549 (1.562)	0.007
C(4)-C(14)	1.510 (1.536)	0.008	1.545 (1.579)	0.010
C(5)-C(6)	1.563 (1.567)	0.006	1.562 (1.566)	0.007
C(5)-C(10)	1.524 (1.528)	0.006	1.550 (1.558)	0.006
C(5)-C(15)	1.547 (1.573)	0.007	1.526 (1.560)	0.008
C(6)-C(7)	1.546 (1.560)	0.006	1.566 (1.574)	0.006
C(7)-C(8)	1.521 (1.538)	0.006	1.516 (1.540)	0.007
C(7)-C(9)	1.536 (1.540)	0.005	1.530 (1.537)	0.005
C(7)-C(11)	1.524 (1.533)	0.006	1.515 (1.532)	0.007
C(9)-C(10)	1.512 (1.520)	0.005	1.512 (1.515)	0.005
C(11)-C(12)	1.527 (1.561)	0.010	1.531 (1.564)	0.012
C(11)-C(13)	1.500 (1.525)	0.008	1.525 (1.542)	0.010

a) The numerical values in parentheses show the bond lengths corrected for the thermal motion effect.

Table 9. The valency angles (°) in the S-1 and S-2 molecules

	S-1		S-2			S-1		S-2	
	Angle	e.s.d.	Angle	e.s.d.		Angle	e.s.d.	Angle	e.s.d.
O(1)-S-O(2)	101.2	0.2	99.6	0.2	C(5)-C(6)-C(7)	109.5	0.3	109.1	0.4
O(1)-S-O(3)	108.8	0.3	108.0	0.3	C(6)-C(7)-C(8)	110.5	0.3	111.4	0.4
O(2)-S-O(3)	106.3	0.3	107.3	0.2	C(6)-C(7)-C(9)	100.3	0.3	100.3	0.3
S-O(1)-C(1)	123.4	0.3	120.6	0.3	C(6)-C(7)-C(11)	116.7	0.3	116.8	0.4
S-O(2)-C(9)	113.0	0.2	118.5	0.3	C(8)-C(7)-C(9)	109.2	0.3	109.0	0.3
C(8)-O(4)-C(12)	109.5	0.5	110.6	0.6	C(8)-C(7)-C(11)	102.8	0.3	102.9	0.4
O(1)-C(1)-C(2)	114.5	0.4	104.3	0.4	C(9)-C(7)-C(11)	117.4	0.3	116.6	0.4
O(1)-C(1)-C(10)	107.8	0.4	108.7	0.4	O(4)-C(8)-O(5)	120.7	0.5	122.4	0.6
C(2)-C(1)-C(10)	114.0	0.4	115.1	0.4	O(4)-C(8)-C(7)	110.6	0.5	109.5	0.6
C(1)-C(2)-C(3)	109.0	0.5	111.1	0.5	O(5)-C(8)-C(7)	128.7	0.4	128.2	0.5
C(2)-C(3)-C(4)	112.5	0.5	109.6	0.6	O(2)-C(9)-C(7)	112.1	0.3	111.8	0.3
C(3)-C(4)-C(5)	112.0	0.4	112.3	0.5	O(2)-C(9)-C(10)	110.5	0.3	112.6	0.3
C(3)-C(4)-C(14)	111.6	0.5	110.8	0.5	C(7)-C(9)-C(10)	105.2	0.3	105.1	0.3
C(5)-C(4)-C(14)	114.1	0.4	112.1	0.5	C(1)-C(10)-C(5)	118.1	0.3	118.3	0.3
C(4)-C(5)-C(6)	111.6	0.3	109.4	0.4	C(1)-C(10)-C(9)	111.4	0.3	111.1	0.3
C(4)-C(5)-C(10)	111.2	0.4	111.0	0.4	C(5)-C(10)-C(9)	102.9	0.3	103.8	0.3
C(4)-C(5)-C(15)	111.6	0.4	113.8	0.4	C(7)-C(11)-C(12)	102.3	0.4	102.1	0.5
C(6)-C(5)-C(10)	102.3	0.3	102.6	0.3	C(7)-C(11)-C(13)	116.5	0.4	118.0	0.5
C(6)-C(5)-C(15)	111.4	0.4	110.8	0.4	C(12)-C(11)-C(13)	110.7	0.5	111.1	0.6
C(10)-C(5)-C(15)	108.3	0.4	108.8	0.4	O(4)-C(12)-C(11)	105.5	0.6	104.5	0.7

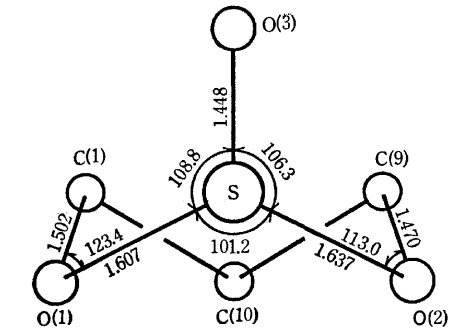

(a) S-1

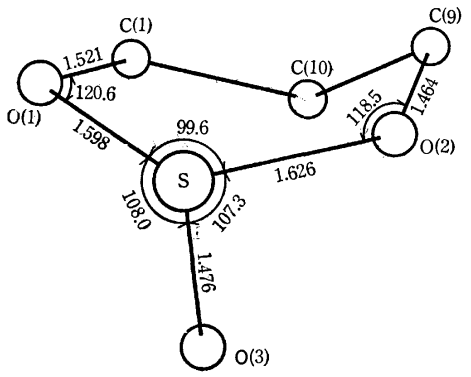

(b) S-2

Fig. 4. The geometry of the sulfite group.

in the axial direction.[6,7] It is interesting to see that S-1 closely resembles the two simple sulfites mentioned above with respect to both the ring conformation and the S–O orientation. On the other hand, the D ring in S-2 has the twist boat form, although the exocyclic S–O bond is also axial. The geometries of the sulfite group in S-1 and S-2 are shown in Figs. 4(a) and 4(b) respectively. These bond distances and angles are nearly the same as those in TSU and DCT; the four sulfites are compared in Table 10. In this table, it may be seen that the average C–O distances in S-1 and S-2, 1.486 and 1.493 Å, are somewhat longer than those in TSU and DCT, 1.46 and 1.462 Å, and that the S–O(3) bond in S-2 is slightly lengthened as compared with those in other, similar compounds.

It is noteworthy that, in both S-1 and S-2, the C(1)-O(1) and C(9)-O(2) distances, especially the former (1.502 Å in S-1 and 1.521 Å in S-2) are significantly longer than the accepted values for C–O bonds in ethers and alcohols, 1.43—1.44 Å. An elongation of the C–O bond has already been found in TSU (1.49 and 1.42 Å) and DCT (1.471 and 1.453 Å), but the deviation from the normal value was taken as hardly significant.[7] The large deviation for the C(1)-O(1) bonds found in the two isomeric sulfites can, though, be taken as significant and can be explained as follows. We may suppose that the lone-pair electrons on the sulfur atom are delocalized. It follows that a portion of the electrons on the sulfur atom, distributed over the tetrahedral directions, will be displaced towards the anti-bonding σ-orbital of the C–O grouping. This picture will explain not only the elongation of the C–O bond, but also the fact that the endocyclic S–O bonds are somewhat shortened in comparison with the S–O single bond distance calculated by using Schomaker-Stevenson's method, 1.69 Å. If this view is accepted, and if we compare the lengths of the S–O and C–O bonds for the sulfite groups, it can be concluded that the outflow of the lone-pair electrons on the sulfur atom will be somewhat more in S-2 than in S-1. Consequently, the sulfur atom in S-2 will become more electronegative and will form a weaker dative bond, S→O(3).

It is of great interest to examine why the two dative bonds, S→O(3), in S-1 and S-2 are formed not in the equatorial orientation, but in the axial orientation. There are several conceivable reasons for this. First, the equatorial orientation of the lone-pair orbital on

Table 10. The comparison of the trimethylene sulfite rings in the S-1, S-2, TSU, and DCT molecules

Bond, Angle	S-1	σ	S-2	σ	DCT	σ	TSU
S-O(1)	1.607	0.004	1.598	0.005	1.615	0.006	1.59
S-O(2)	1.637	0.003	1.626	0.004	1.631	0.006	1.60
S-O(3)	1.448	0.006	1.476	0.005	1.442	0.006	1.45
C(1)-O(1)	1.502	0.007	1.521	0.006	1.453	0.010	1.49
C(9)-O(2)	1.470	0.005	1.464	0.005	1.471	0.010	1.42
C(1)-C(10)	1.519	0.005	1.525	0.005	1.523	0.012	1.51
C(9)-C(10)	1.520	0.005	1.515	0.005	1.522	0.011	1.52
O(1)-S-O(2)	101.2	0.2	99.6	0.2	97.8	0.3	100
O(1)-S-O(3)	108.8	0.3	108.0	0.3	107.8	0.3	—
O(2)-S-O(3)	106.3	0.3	107.3	0.2	107.4	0.3	—
S-O(1)-C(1)	123.4	0.3	120.6	0.3	115.8	0.5	116
S-O(2)-C(9)	113.0	0.2	118.5	0.3	116.6	0.5	116
O(1)-C(1)-C(10)	107.8	0.4	108.7	0.4	109.0	0.6	106
O(2)-C(9)-C(10)	110.5	0.3	112.6	0.3	108.5	0.6	111
C(1)-C(10)-C(9)	111.4	0.3	111.1	0.3	110.6	0.6	110

6) C. Altona, H. J. Geise, and C. Romers, *Rec. Trav. Chim. Pays-Bas*, **85**, 1197 (1966).

7) J. W. L. van Oyen, R. C. D. E. Hasekamp, G. C. Verschoor, and C. Romers, *Acta Crystallogr.*, **B24**, 1471 (1968).

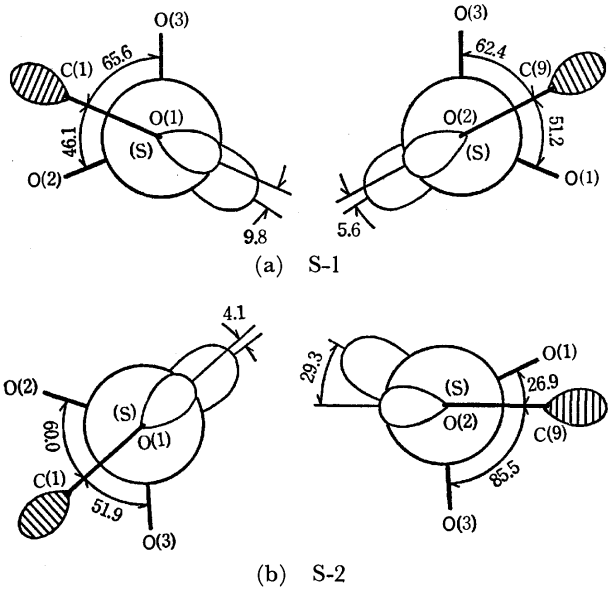

Fig. 5. The overlapping of the lone-pair orbital on S and the C–O anti-bonding orbitals.

the sulfur atom is more suitable for the overlapping with the anti-bonding σ-orbital of the C–O groups, as is shown in Fig. 5. Second, if the O(3) atom were equatorially bonded to the sulfur atom, this oxygen atom, carrying a considerable amount of negative charge, would be subjected to a stronger repulsion from the lone-pair electrons on the two oxygen atoms, O(1) and O(2), which, for the major part, would be localized in the sp^3 orbitals and extended axially and equatorially. Third, the attractive interaction between the negatively-charged oxygen atom, O(3), and the more or less positively-charged hydrogen atoms in the neighborhood of the oxygen would make the axial configuration of the S–O(3) bond stable. The distances from the O(3) atom to these hydrogen atoms are: 2.51 Å for H at C(9) and 2.61 Å for H at C(2) in S-1, and 2 54 Å for H at C(10) and 3.12 Å for H at C(1) in S-2 These values are calculated by assuming that the four bonds of the carbon atoms are in the tetrahedral direction and that the C–H distances are 1.08 Å.

It has already been mentioned that the D ring in S-1 takes the chair form. The dihedral angles around the endocyclic bonds in this ring and the internal valency angles are shown in Fig. 6(a). The average dihedral angle, ψ, and the average valency angle, θ, are calculated to be 54.9° and 111.2° respectively, while they are 59.2° and 109.8° in TSU and 59.6° and 109.7° in DCT. The values for the latter two substances are in good agreement with the normal values for cyclohexane, 60.0° and 109.5°. On the other hand, both of the ψ and θ values for S-1 deviate from the normal values in such a way that the ring becomes less puckered. The two C–O bonds make an angle of about 9° with each other, while the angle formed by the same bonds is found to be about 20° before the formation of the sulfite ring.[2] This shows that the sulfite ring is more or less strained. In fact, the valency angles at the O(1) and O(2) atoms differ from each other by no less than about 10°. Even

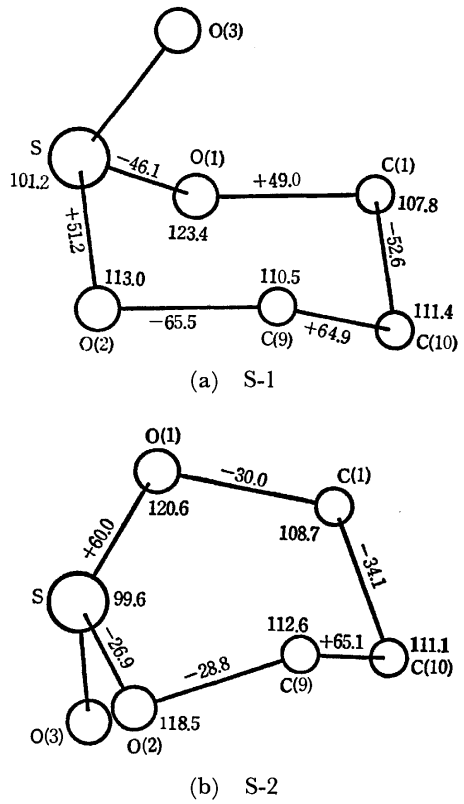

Fig. 6. The valency and torsional angles in D ring.

for such a deformed heterocyclic ring, Altona's relation, $\cos\psi = -\cos\theta/(1+\cos\theta)$, holds approximately; the calculated value is 55.5°, while the average of the observed dihedral angles is 54.9°.[7]

On the other hand, the twist boat form of the corresponding ring in S-2 is not only the most stable of the flexible forms, but is also suitable for the fusion with the bicyclononane system; the two C–O bond directions make an angle of about 25° with each other differing by only 5° from the angle found before the cyclization. Further, the valency angles at the O(1) and O(2) atoms, 120.6° and 118.5° respectively, are not so different from each other as those in S-1. From the symmetry of the torsional angles shown in Fig. 6(b), it may be seen that the heterocyclic ring in S-2 has roughly a two-fold rotation axis through the O(2) and C(1) atoms, though it is somewhat more flattened than the ideal twist boat form of cyclohexane, where the dihedral angels are 70°39′ or 33°10′.

The conformation of the B ring in S-1 differs from that in S-2; the former takes almost the half-chair form, while the latter has nearly the envelope form. The two ring conformations are illustrated in Fig. 7. In S-1, the C(9) and C(10) atoms deviate above and below from the plane containing the C(5), C(6), and C(7) atoms; the deviations are about 0.39 Å for the C(9) atom lying on the side opposite to the C(15) and about −0.30 Å for the C(10) atom. On the other hand, in S-2, the C(5), C(6), C(7), and C(10) atoms are nearly coplanar, and the C(9) atom deviates by about 0.63 Å toward the same side as the C(4) atom from the mean plane through the first four atoms. Though the five-membered rings in

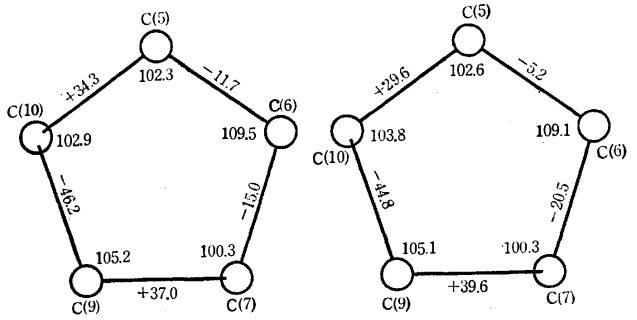

(a) (b)

Fig. 7. The valency and torsional angles in B rings; (a) S-1, (b) S-2.

fukinolidol di-bromoacetate as well as in S-2 are found to be approximately of the envelope form, in the former the C(10) atom is considerably displaced from the mean plane through the other four atoms. Thus, the conformation of the five-membered ring varies not only with the fusion of a heterocyclic ring containing the sulfite group, but also with the conformation of the sulfite ring itself.

The conformations of the A rings in S-1 and S-2 are shown in Figs. 8(a) and 8(b) respectively. These two conformations are quite close to each other. This shows that, in the two sulfites, the conformation of the cyclohexane rings is less influenced than that of the cyclopentane rings by the fusion of the sulfite group. The same conclusion can also be drawn from an examination of the conformations around the C(1)-C(10), C(5)-C(10), and C(9)-C(10) bonds. These can be explained by the rigidness of the chair form of the cyclohexane ring. However, a closer examination shows that the A ring is, in fact, affected to some extent by the conformation of the D ring; for example, the difference between the dihedral angles for the C(1)–C(10) bond is found to be about 5.8°. The six-membered rings in the bicyclononane system of S-1 and S-2 are somewaht more flattened than the normal ring of cyclohexane. The averages of the

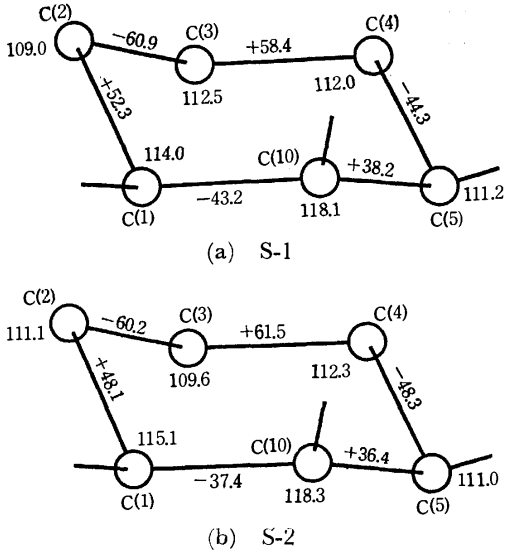

(a) S-1

(b) S-2

Fig. 8. The valency and torsional angles in A ring.

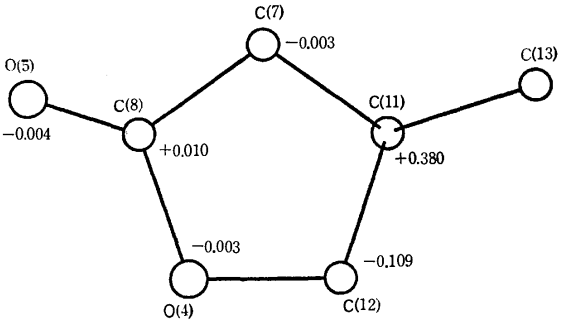

(a) S-1

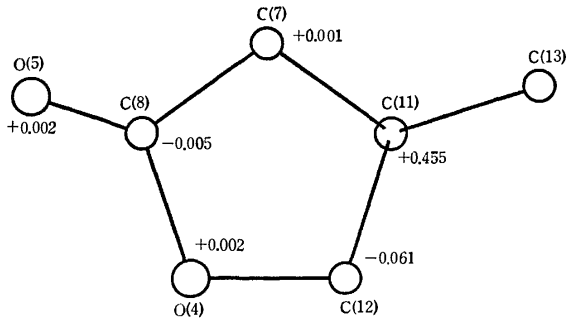

(b) S-2

Fig. 9. The deviations of the atoms from the carbonyl plane.

internal valency angles, θ, are 112.8° for S-1 and 112.9° for S-2. The mean values of the dihedral angles, ψ, as calculated by Altona's equation, are 50.8° and 50.4° for S-1 and S-2 respectively, while the observed values are 49.6° and 47.8° respectively.

Out of the four rings present in the S-1 and S-2 molecules, the remaining one is a γ-lactone C ring, which makes a spiro-union with the B ring and takes the envelope form for both of the two isomers. The corresponding bond lengths, valency angles, and torsional angles for the lactone rings of the two molecules are in good agreement with each other within the present limits of experimental error. This may show that the lactone ring is located too far from the sulfite group to be influenced by the conformational

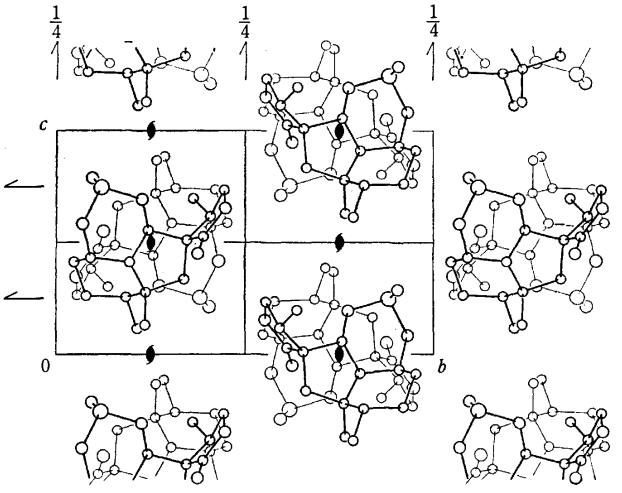

Fig. 10. The crystal structure of S-1 viewed along the *a* axis.

change of this group. The C(7), C(8), C(12), and O(4) atoms lie nearly on a plane, and the C(11) atom is displaced from the mean plane through the four atoms by about 0.47 Å for S-1 and 0.50 Å for S-2. The deviations of the atoms from the carbonyl plane are illustrated in Fig. 9.

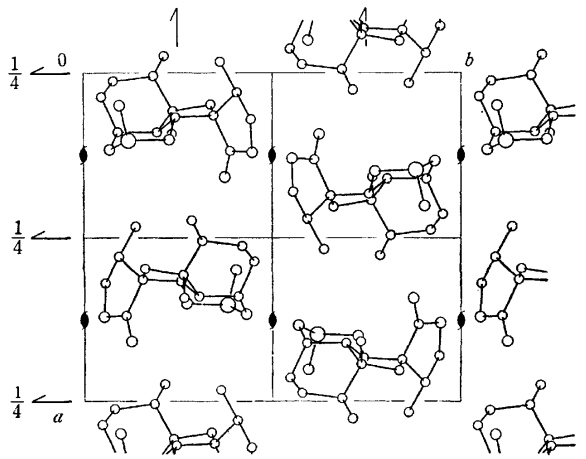

Fig. 11. The crystal structure of S-1 viewed along the *c* axis.

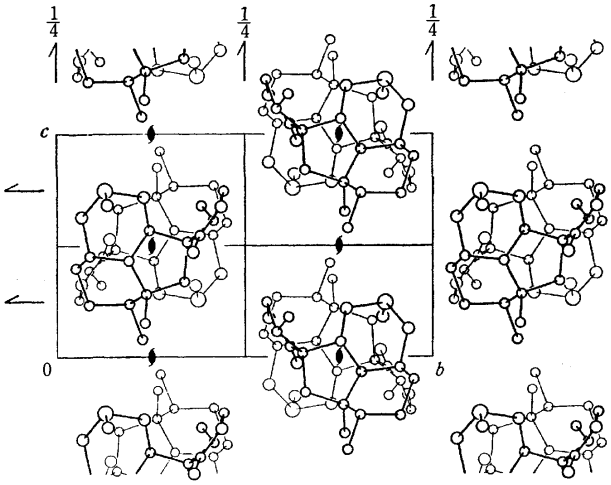

Fig. 12. The crystal structure of S-2 viewed along the *a* axis.

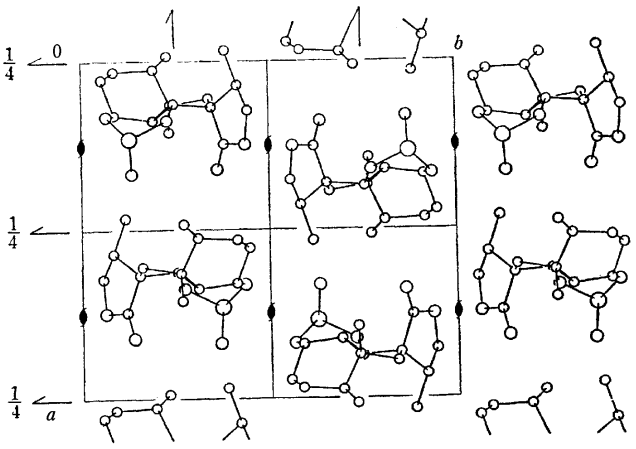

Fig. 13. The crystal structure of S-2 viewed along the *c* axis.

Table 11. The intermolecular contacts in the S-1 crystal

(1)	I···II (III···I)		(4)	I···VIII (XII···I)	
	O (5)···C (4)	3.59 Å		O (3)···C (11)	3.45 Å
	O (5)···C (2)	3.60		O (3)···C (13)	3.46
	C (10)···C (13)	3.82		C (2)···C (12)	4.29
	C (1)···C (13)	3.83	(5)	I···IX (XIII···I)	
	C (8)···C (4)	4.01		C (3)···C (6)	3.90 Å
	C (8)···C (3)	4.04		C (3)···C (11)	4.21
	C (15)···C (13)	4.10		C (2)···C (6)	4.28
(2)	I···IV (V···I)		(6)	I···X (XI···I)	
	S···C (15)	3.70 Å		C (12)···O (5)	3.25 Å
	C (13)···C (14)	4.17		C (12)···C (8)	3.81
(3)	I···VI (VII···I)				
	S···C (1)	3.73 Å			
	S···C (2)	3.96			

I: x/a, y/b, z/c (given in Table 4)
II: $1/2+x/a$, $1/2-y/b$, $1-z/c$
III: $-1/2+x/a$, $1/2-y/b$, $1-z/c$
IV: x/a, y/b, $1+z/c$
V: x/a, y/b, $-1+z/c$
VI: $1/2-x/a$, $-y/b$, $1/2+z/c$
VII: $1/2-x/a$, $-y/b$, $-1/2+z/c$
VIII: $-x/a$, $-1/2+y/b$, $3/2-z/c$
IX: $-x/a$, $-1/2+y/b$, $1/2-z/c$
X: $1/2-x/a$, $1-y/b$, $1/2+z/c$
XI: $1/2-x/a$, $1-y/b$, $-1/2+z/c$
XII: $-x/a$, $1/2+y/b$, $3/2-z/c$
XIII: $-x/a$, $1/2+y/b$, $1/2-z/c$

Table 12. The intermolecular contacts in the S-2 crystal

(1)	I···II (III···I)		(3)	I···VI (VII···I)	
	O (3)···C (14)	3.45 Å		O (3)···C (2)	3.50 Å
	O (3)···C (13)	3.49		S···C (1)	3.82
	O (5)···C (2)	3.49		S···C (2)	3.95
	O (3)···C (6)	3.59	(4)	I···VIII (XII···I)	
	O (3)···C (4)	3.60		O (1)···C (13)	3.55 Å
	C (15)···C (13)	3.99	(5)	I···IX (XIII···I)	
	C (10)···C (13)	4.03		C (3)···C (6)	4.04 Å
	C (1)···C (13)	4.15		C (3)···C (11)	4.04
	C (8)···C (3)	4.17		C (2)···C (6)	4.24
	C (8)···C (2)	4.19	(6)	I···X (XI···I)	
	C (8)···C (4)	4.20		C (12)···O (5)	3.44 Å
(2)	I···IV (V···I)			C (12)···C (8)	3.88
	S···C (15)	3.81 Å			
	C (13)···C (14)	4.06			

I: x/a, y/b, z/c (given in Table 5)
II~XIII: see Table 11.

Crystal Structures. The molecular arrangements viewed along the *a* and *c* axes are, respectively, shown in Figs. 10 and 11 for S-1 and in Figs. 12 and 13 for S-2. As may be seen in these figures, the two crystal structures are so similar to each other that they may be said to be isostructural. It is interesting to see that, notwithstanding the remarkable variation in the structure of the sulfite group, the molecular arrangments do not differ much from each other. The arrangement of the molecular centers is close to a face-centered lattice. The intermolecular contacts of a molecule with its nearest neighbors are listed in

Tables 11 and 12 for S-1 and S-2 respectively. In the S-1 crystal, there are several contacts somewhat closer than the usual van der Waals ones—for example, 3.25 Å for O(5)···C(12′) and 3.73 Å for S···C(1). From the comparison of the intermolecular distances, it may be said that S-1 has a closer molecular packing than S-2, corresponding to the higher density and the higher melting point.

In conclusion, the authors wish to express their thanks to Professor Keizo Naya and Dr. Ichiro Takagi** of this university, for providing them with the samples.

** Present address: Department of Chemistry, Faculty of Education, Wakayama University, Wakayama.

BULLETIN OF THE CHEMICAL SOCIETY OF JAPAN, VOL. 45, 2299—2303 (1972)

Vapor Pressure of a Mixed System of Asphaltene and Organic Solvent

Shinji SAKANOUE and Mitsuo ENDO

Faculty of General Education, The Tokyo University of Agriculture and Technology, Saiwai-cho, Fuchu, Tokyo

(Received December, 1971)

The vapor pressure of a system in which it is assumed that the maltene component in petroleum asphalt has been replaced by an organic solvent, *i.e.*, a mixed system of an asphaltene component and an organic solvent, was measured over a wide range of composition. The experimental results were then analyzed on the assumption that such a system is a binary system and that the equation $\mu_1=\mu_1^\circ+\boldsymbol{R}T\ln(1-v_2)+(1-1/z)v_2+\chi_1 v_2^2$ which Flory and Huggins derived for the chemical potential of a solvent of a linear, high-polymer solution which is not relatively dilute is applicable; the volumetric ratio, z, of the asphaltene particle and solvent molecule and the value of the parameter, χ_1, of the interaction of the asphaltene and solvent molecules were obtained. The above results made it clear that mixed systems of asphaltene plus chloroform and carbon tetrachloride all form a homogeneous phase over the entire composition range, but in the case of a cyclohexane system, separation into 2 phases occurs in the mixed composition range of 3.0 vol%—40 vol% asphaltene and a dilute phase of 3.0 vol% asphaltene and a concentrated phase of 40.0 vol% coexist. It may be assumed from the above results that there is a possibility of the presence of a state in which separation into 2 phases is also present in the case of asphalt.

The petroleum asphalt is composed of three components, which are called "asphaltene", "asphaltic resin," and "asphaltic oil," and it is generally accepted that it has a colloidal structure in which the asphaltene molecules or the micelles which absorb or adsorp the asphaltic resin disperse in asphaltic oil. However, there has been no study confirming such a colloidal structure of asphalt experimentally.

Here, we measured the vapor pressures of mixtures asphaltene with various organic solvents and examined the dissolved states of the asphaltene in the systems, the sizes of the asphaltene molecules or particles, and the interaction between the asphaltene and the organic solvent molecule. It can be considered that this examination is the first step in elucidating the structure of asphalt, since the above-mentioned system can be regarded as one in which a maltene component which is the mixture of asphaltic oil and resin is replaced by an organic solvent.

Experimental

Materials. Straight asphalt manufactured by the Nippon Sekiyu Co., Ltd., was used as the sample from which the asphaltene component was separated. The values of the penetration degree[1] and the ring and ball softening point[2] of this asphalt were 73 and 49 respectively.

Cyclohexane, benzene, chloroform, and carbon tetrachloride which had been purified according to the common method were used as the solvents to dissolve the asphaltene.

Separation of Asphaltene from Asphalt. The straight asphalt described above was mixed with 3 volumes of *n*-hexane, shaken, and left to stand for a long time; then the supernatant solution of the mixture was removed by decantation. The insoluble component separated from the mixture was mixed again with 3 volumes of *n*-hexane; this mixture was shaken and filtered, and the residue was used as the sample of asphaltene in the experiments.

Method for the Measurement of the Vapor Pressure. A quartz spring, on which a small glass basket containing the

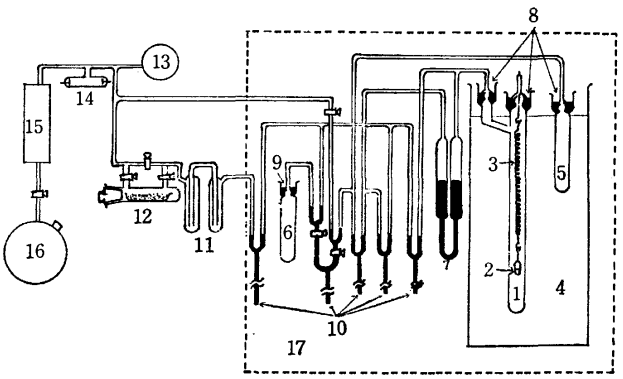

Fig. 1. Apparatus.
1. Glass tube 2. Glass basket 3. Quartz spring balance 4. Liquid thermostat 5, 6. Solvent stock container 7. Mercury manometer 8, 9. Mercury seal 10. Mercury cut 11. Trap 12. Desiccating agent 13. Macleod gauge 14. Geissler tube 15. Mercury diffusion pump 16. Rotary pump 17. Air thermostat

1) JIS K 2530.
2) JIS K 2531.

sample was hung, was placed in a long glass tube which was connected to a mercury manometer and a mercury diffusion pump and placed in a liquid thermostat.

The glass tube was evacuated, and then it was closed by shutting a mercury cut; a solvent vapor was introduced into the tube, and after giving a suitable length of time for the temperature equilibration to be reached, the vapor pressure of the sample mixture was read on the mercury manometer to within 0.001 cm. This apparatus is drawn schematically in Fig. 1. The pressure inside of this vacuum line without a sample, as measured by a Macleod gauge, was 10^{-5} mmHg. The compositions by the volume fractions of the systems were determined by means of the weight of the sample mixture, which was measured by means of the quartz-spring balance, and the densities of the asphaltene and the solvent. The dried asphaltene powder did not show the vapor pressure; accordingly, the asphaltene was treated as a non-volatile material.

Results and Discussion

Many difficulties arose in the theoretical treatment of the experimental results, for the asphaltene is not a single compound, but a mixture of several kinds of compounds; further, our information about these compounds and the molecular forms is sparse. Consequently, we will discuss the experimental results on the basis of two assumptions. The first is that the mixture of the asphaltene and organic solvent is a binary system, and the second is that the equation for a chemical potential of the solvent of a relatively concentrated solution of linear high polymers;

$$\mu_1 = \mu_1^\circ + \boldsymbol{R}T\ln(1-v_2) + \left(1-\frac{1}{z}\right)v_2 + \chi_1 v_2^2 \qquad (1)$$

which was derived by Flory[3] and by Huggins[4], can be applied to the system of the asphaltene and an organic solvent. In the above equation, μ_1 and μ_1° are the chemical potentials of the solvent in the system and the pure solvent respectively; z, the ratio of the molar volume of the solute molecule to the solvent molecule; χ_1, the parameter of the interaction between a solute and solvent molecules; v_2, the volume fraction of the solute in the system; $\boldsymbol{R}$, the gas constant, and T, the absolute temperature of the system.

On the other hand, when the vapor is assumed to be an ideal gas, the activity, a_1, of a solvent in the solution of a non-volatile material is given by;

$$a_1 = \frac{p}{p_0} \qquad (2)$$

where p and p_0 are the vapor pressures of the solvent over, respectively, a solution and a pure solvent. When the vapor is assumed to be an imperfect gas, a_1 is represented by;

$$a_1 = \frac{p}{p_0}\exp\left[\frac{-B}{\boldsymbol{R}T}(p_0-p)\right] \qquad (3)$$

where B is the second virial coefficient of the vapor of a pure solvent at T°K. In Eq. (3), $\exp[(-B/\boldsymbol{R}T)(p_0-p)]$ is the factor for the gas-imperfection correction. The relative deviation from 1 of this value is estimated to be 1.5% at most, and about 0.5% in mean value, in relation to the data of this experiment. Here, however, we ignored these gas-imperfection corrections and used Eq. (2), because we could not find the accurate values of B for the vapors at every measuring temperature of every solvents. The chemical potential of the solvent in solution can, therefore, be represented by the following equation:

$$\mu_1 = \mu_1^\circ + \boldsymbol{R}T\ln\frac{p}{p_0} \qquad (4)$$

A comparison of Eq. (1) with (4) gives:

$$\ln a_1 = \ln\frac{p}{p_0} = \ln(1-v_2) + \left(1-\frac{1}{z}\right)v_2 + \chi_1 v_2^2$$

or

$$a_1 = \frac{p}{p_0} = (1-v_2)\exp\left[\left(1-\frac{1}{z}\right)v_2 + \chi_1 v_2^2\right] \qquad (5)$$

In general, the interaction parameter, χ_1, can be determined by using the observed a_1 and z values, which are evaluated by means of the molecular weight. However, as the molecular weight of asphaltene has not been found, it was necessary to determine the values of both z and χ_1 at the same time, Eq. (5) was, therefore, rewritten as follows:

$$Y = \frac{\ln\frac{p}{p_0} - \ln(1-v_2)}{v_2} = \left(1-\frac{1}{z}\right) + \chi_1 v_2 \qquad (6)$$

If neither the z value nor the χ_1 value depends on the volume fraction, the plots of Y *vs.* v_2 should be linear. The intercept and the slope of the straight line will, then, give the values of $(1-1/z)$ and χ_1 respectively.

The plots of Y *vs.* v_2 for the four kinds of systems are shown in Figs. 2—5. As can be seen in these figures, the relation of Y to v_2 was found to be linear; accordingly, the values of χ_1 and z could be determined simultaneously. The values thus obtained for each system are shown in Table 1.

The above results show that χ_1 does not depend on v_2. Furthermore, the plot points of Y *vs.* v_2 at the different equilibrium temperatures were found to be on the same straight line. It may be thought that χ_1 does not depend on the temperature, either. Ac-

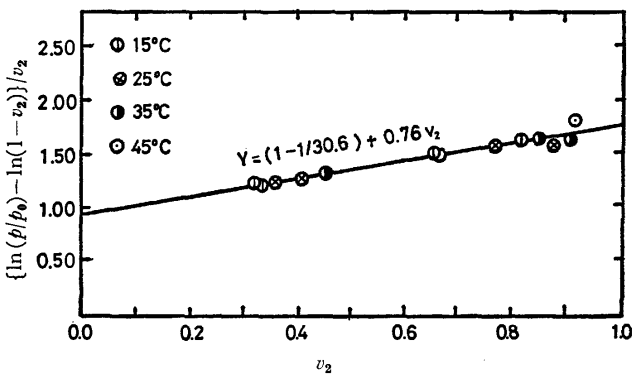

Fig. 2. A plot of $\{\ln(p/p_0) - \ln(1-v_2)\}/v_2$ *versus* volume fraction of asphaltene v_2 for the mixed system of asphaltene and cyclohexane.

3) P. J. Flory, *J. Chem. Phys.*, **9**, 660 (1941); **10**, 51 (1942).
4) M. L. Huggins, *ibid.*, **9**, 440 (1941); *J. Phys. Chem.*, **46**, 151 (1942).

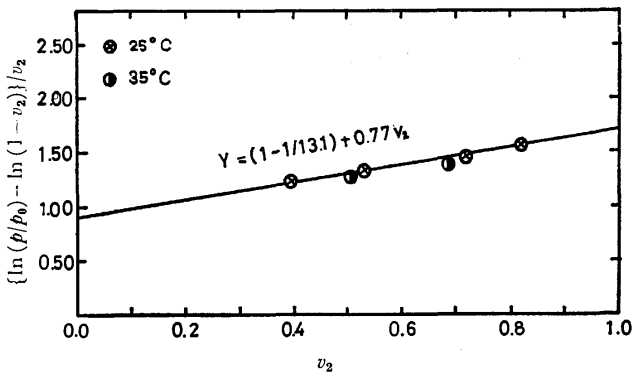

Fig. 3. A plot of $\{\ln(p/p_0)-\ln(1-v_2)\}/v_2$ *versus* volume fraction of asphaltene v_2 for the mixed system of asphaltene and benzene.

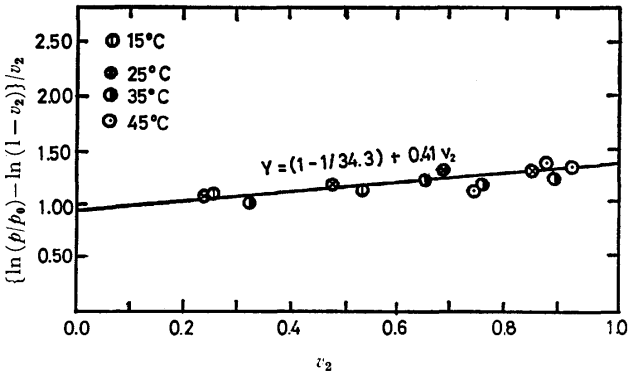

Fig. 4. A plot of $\{\ln(p/p_0)-\ln(1-v_2)\}/v_2$ *versus* volume fraction of asphaltene and chloroform.

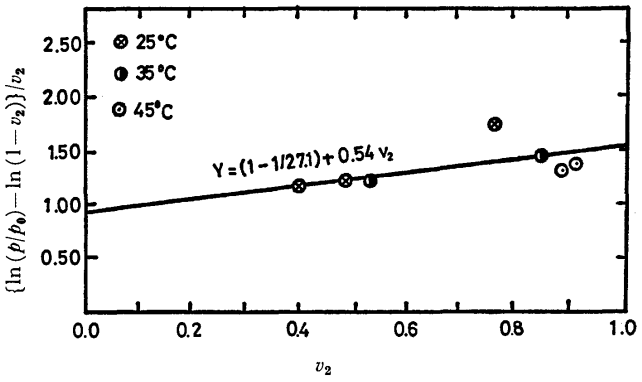

Fig. 5. A plot of $\{\ln(p/p_0)-\ln(1-v_2)\}/v_2$ *versvs* volume fraction of asphaltene v_2 for the mixed system of asphaltene and carbon tetrachloride.

cording to Flory,[3] χ_1 is a dimensionless quantity formally defined by:

$$\chi_1 = \frac{qx_{12}\Delta w_{12}}{kT} \tag{7}$$

where Δw_{12} is the exchange interaction energy per molecule; k, the Boltzmann constant, T, the absolute temperature; q, the coordination number about a lattice in solution and x_{12}, the number of segments in a solvent molecule. The mixing enthalpy change, ΔH_m, is represented by:

$$\Delta H_m = -kT^2\left(\frac{\partial \chi_1}{\partial T}\right)n_1 v_2 \tag{8}$$

Table 1. The volumetric ratio z of solute and solvent molecules, the interaction parameter χ_1 and the critical volume fraction and χ_1 value for phase separation

Solvent	Volumetric ratio	Interaction parameter	Critical values	
			Volume fraction	Interaction parameter
	z	χ_1	$(v_2)_c$	$(\chi_1)_c$
Cyclohexane	30.6	0.76	0.18	0.68
Benzene	13.1	0.77	0.27	0.78
Chloroform	34.3	0.41	0.17	0.67
Carbon tetrachloride	27.1	0.54	0.19	0.69

where n_1 is the mole number of the solvent in a solution. If the Δw_{12} does not depend on the temperature, it follows, by virture of Eq. (7), that χ_1 should be proportional to $1/T$. However, if χ_1 does not depend on the temperature, as here, it may be concluded from Eq. (8) that Δw_{12} should be proportional to T and that ΔH_m should become zero. These conclusions include the contradiction that such a solution is athermal; besides, the interaction parameter, χ_1, consists only of a configurational entropy change due to a solvent-solute interaction. Therefore, it is reasonable to assume that the variation in the value of χ_1 with the temperature is so slight in the temperature range of this experiment that the difference in the slope of the straight line for the different temperature could not be found.

Next, as the value of z is the ratio of the size of an asphaltene particle to that of a solvent molecule, if the molecular sizes of the solvents do not differ from one another, these values for the different systems should not differ from one another, either. The molecular sizes of benzene and the other solvents do not differ greatly; nevertheless, values of z for the asphaltene-benzene system are smaller than the others. This can probably be attributed to the fact that the values of z obtained from the intercepts of the straight lines in Figs. 2—5 are very sensitive to the length of the intercepts; we can not expect to obtain highly accurate values of z by this method. However, in order to know the order of magnitude of the molecular weight of asphaltene, we did attempt to estimate it roughly by multiplying the molecular weight of the solvent by z. For example, it was 2500 for the asphaltene-cyclohexane system and 1020 for the asphaltene-benzene system.

The lower the value of χ_1, the better the solvent. Consequently, as is shown in Table 1, chloroform is the best solvent among those used, while benzene and cyclohexane are relatively poor solvents.

The solid lines in Figs. 6—9 show the curves of the functions, which were obtained by substituting the values of χ_1 and z shown in Table 1 into Eq. (5). The observed values of activities, $a_1=p/p_0$, are also plotted

5) P. J. Flory, "Principles of Polymer Chemistry," Cornell Univ. Press, New York (1953) Chapt. 13.
6) P. J. Flory, *J. Chem. Phys.*, **10**, 51 (1942).

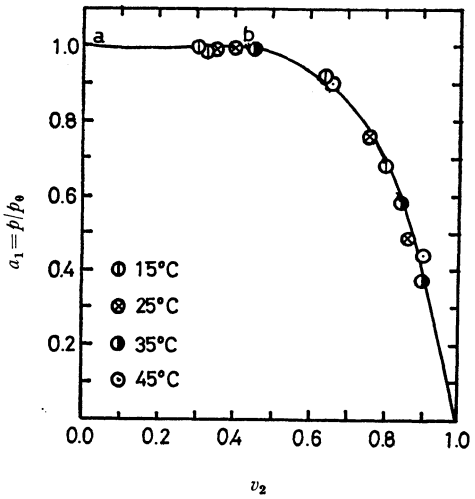

Fig. 6. An activity of cyclohexane $a_1(=p/p_0)$ in the system of asphaltene and cyclohexane *versus* the volume fraction of asphaltene v_2.

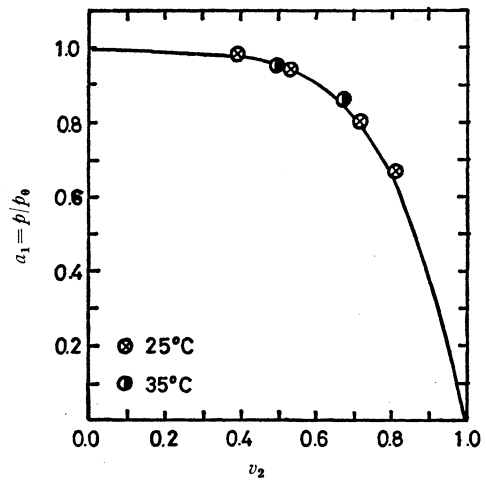

Fig. 7. An activity of benzene $a_1(=p/p_0)$ in the system of asphaltene and benzene *versus* the volume fraction of asphaltene v_2.

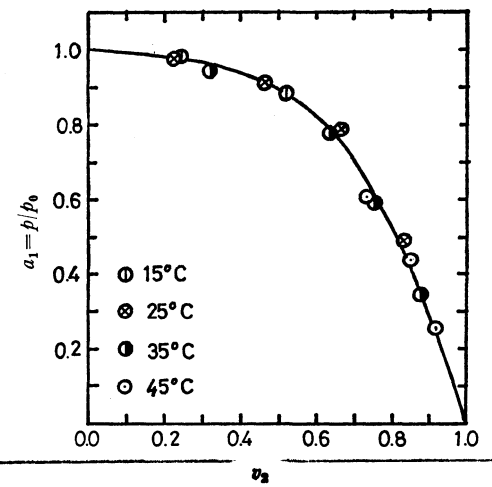

Fig. 8. An activity of chloroform $a_1(=p/p_0)$ in the system of asphaltene and chloroform *versus* the volume fraction of asphaltene v_2.

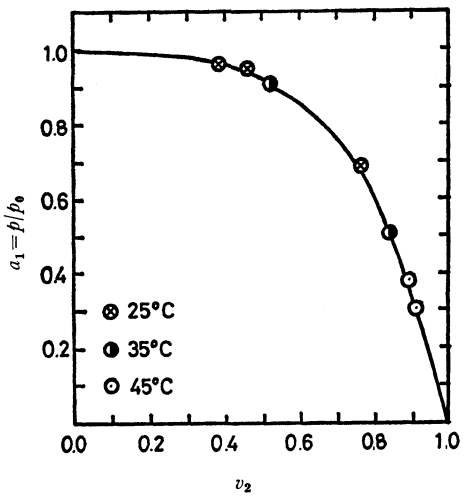

Fig. 9. An activity of carbon tetrachloride $a_1(=p/p_0)$ in the system of asphaltene and carbon tetrachloride *versus* the volume fraction of asphaltene v_2.

in these figures. Among these results, it is noteworthy that a phase separation occurs in the asphaltene-cyclohexane system, as is shown in Fig. 6, where the two different compositions of the separating phases are indicated by the symbols a and b.

The critical volume fraction and the critical interaction parameter of a phase separation are given by:

$$(v_2)_c = \frac{1}{(1+z)^{1/2}}$$

$$(\chi_1)_c = \frac{1}{2} + \frac{1}{z^{1/2}}$$

The values of $(v_2)_c$ for each system are also shown in Table 1, together with the actual values of χ_1. When $\chi_1 > (\chi_1)_c$, the phase separation occurs in a certain region of some mixture compositions. As is shown in Table 1, $\chi_1 > (\chi_1)_c$ only in the case of the asphaltene-cyclohexane system (that is, a phase separation should occur in this system), while all the other systems except the asphaltene-benzene system should be homogeneous over the range of composition. In the case of the asphaltene-benzene system, as the value of χ_1 is close to the value of $(\chi_1)_c$, and as the difference between the two values is in the range of experimental error of the values, we could not decide whether or not this system is homogeneous over the range of composition. In the case of the asphaltene-cyclohexane system, the compositions of the two separated phases were obtained by the following method. Corresponding to Eq. (1), the chemical potential of the solute is given by:

$$\mu_2 = \mu_2^\circ + \boldsymbol{R}T \ln v_2 - (z-1)(1-v_2) + \chi_1 z(1-v_2)^2 \quad (9)$$

where μ_2° is the chemical potential of the pure solute, while the relation between the volume fraction and the molar fraction of the solute is given by:

$$v_2 = \frac{zx_2}{1+(z-1)x_2} \quad (10)$$

From Eqs. (1), (9), and (10), the mean molar Gibbs energy of mixing in units of $\boldsymbol{R}T$ is represested by;

$$\frac{g-g^\circ}{RT} = (1-x_2)\ln\frac{(1-x_2)}{1+(z-1)x_2} + x_2\ln\frac{zx_2}{1+(z-1)x_2} + \frac{\chi_1 z(1-x_2)x_2}{1+(z-1)x_2}$$

when g and g° are the mean molar Gibbs free energies of the system after and before mixing respectively, and x_2 is the molar fraction of the solute. When a separation into two phases occurs, a double tangent with two contact points can be drawn to the curve of the plots of $(g-g^\circ)/RT$ *vs.* x_2, and the two contact points represent the two different compositions of the two phases.[7]

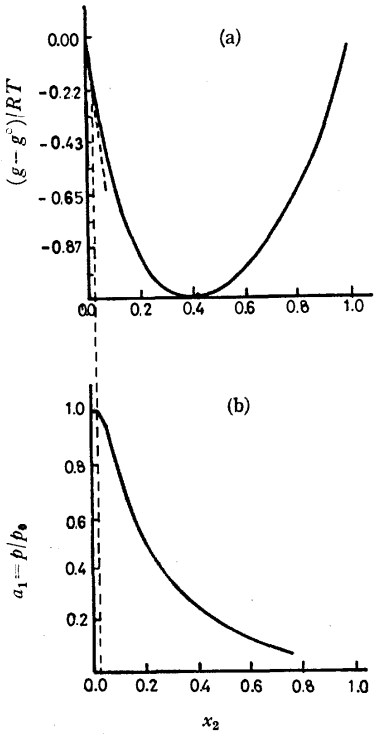

Fig. 10. Mean molar free energy of mixing asphaltene with cyclohexane, in units of RT, $(g-g^\circ)/RT$ *versus* the mole fraction of asphaltene x_2.

7) H. Tompa, "Polymer Solutions," Butterworths Scientific Publications, London (1956), Chap. 2.

The curves of these plots for the asphaltene-cyclohexane system are shown in Fig. 10(a), while the plots of $a_1=p/p_0$ *vs.* the molar fraction of the solute, x_2, are shown in Fig. 10 (b). A double tangent can be drawn to the curve in Fig. 10 (a), and it has become apparent that the composition of the dilute phase is 0.001 asphaltene relative to the molar fraction, or 3.0 vol%, while that of the concentrated phase is 0.021 relative to the molar fraction, or 40.0 vol%.

We attempted to confirm the presence of two separated phases in this system by using another method as well. That is, a mixture of asphaltene and cyclohexane (8.5% asphaltene by volume) was prepared; it was centrifuged, and then the concentration of the supernatant solution was determined. This concentration was 5.1% asphaltene by volume. This value is slightly different from that obtained from the contact point of the double tangent drawn to the curve in Fig. 10 (a), but it is evidence of the presence of a phase separation that the concentration of the supernatant solution is different from the composition of the total mixture.

As has been mentioned above, it has become apparent that separation into two phases occurs in a mixture of asphaltene with a saturated hydrocarbon such as cyclohexane; therefore, if the maltene component of asphalt, which is regarded as a solvent of asphaltene in a real asphalt, has an abundance of saturated hydrocarbon compounds, it can be guessed that the separation into the concentrated and dilute phases of asphaltene is possible at equilibrium in a real asphalt, too. Furthermore, in many cases the content of asphaltene in a straight asphalt is about 10—25% by weight; this agrees with the region of compositions in which a phase separation occurs in the asphaltene-cyclohexane system. If the fine drops of the concentrated phase of asphaltene disperse in its dilute phase, these states shall be relatively stable, because the difference in the specific weights of their phases is small and the viscosity of the dilute phase is considerably high. These states inside the asphalt can be described by saying that the asphaltene particles which adsorp a maltene component disperse in a maltene phase in which a slight quantity of asphaltene is dissolved.

Kinetic Study of the Formation and Decomposition of Amylose-iodine-iodide Complex

Akihiko YAMAGISHI, Taira IMAMURA, and Masatoshi FUJIMOTO

Department of Chemistry, Faculty of Science, Hokkaido University, Sapporo

(Received January 5, 1972)

The complex formation reaction among amylose, iodine and iodide ion in aqueous solution was investigated with a stopped-flow apparatus. The forward reaction rate was found to be expressed as $v=k[\text{Amylose}]([I_3^-]-\theta)$ for $[I_3^-]>\theta$, where θ is a critical value determining the mechanism. For $[I_3^-]>\theta$, the rate was considered to be determined by the process between a free amylose unit and free I_3^-. For $[I_3^-]<\theta$, the rate-determining step is considered to be intramolecular conversion from an intermediate to a final product. The rate of the reaction between amylose units and I_3^- is close to that of a diffusion-controlled process (7×10^8 M^{-1} sec^{-1}). These conclusions are supported by the study of the decomposition reaction of complex, using $Na_2S_2O_3$ or $Ce(SO_4)_2$.

The blue complex of amylose and iodine has been the subject of many investigators since its discovery in the last century. Recently a few investigations proved that a kinetic study, using stopped-flow technique, is a powerful approach to look into the formation mechanism and the structure of the amylose-iodine complex.[1,2] Hiromi *et al.* pointed out in his excellent paper that there exists an intermediate form of a complex before the final stable product appears.[1] Since the intermediate complex has an absorption maximum at a shorter wavelength than that of a final product, it is thought to be a short poly-iodine-chain randomly distributed in the amylose helix. The intermediate complex rearranges intramolecularly to the stable product. The growth of the triiodide chain was undoubtedly confirmed by the shift of an absorption peak and also by the fact of the high order dependence (about five) of the formation rate on triiodide ion concentration. These observations are a definite proof to show that a kinetic approach is powerful to study this complicated phenomena. There are, however, several problems left unsettled. For example, the magnitude of the rate constant of the initial attack of triiodide ion on the amylose helix is yet to be determined. If this rate constant is obtained, it will help us to consider what is happening in the initial stage of the reaction. It is also important to discriminate the role of iodide ions from that of iodines. This will explain why iodide ion is necessary for the complex formation in aqueous solution.[3] Another problem is about the effect of temperature on the reaction, since temperature is known to have a large influence over the amount of the complex in equilibrium.[4]

We tried to settle these questions under the appropriate conditions of amylose, iodide ion and iodine amounts.

Experimental

Materials. Commercial corn amylose (Sigma) was recrystallized twice from *n*-butanol under nitrogen atmosphere. Fractional precipitation was made, using dimethylsulfoxide and ethanol as solvents according to Everett and Forster.[5] Precipitates were dried *in vacuo*. The molecular weights of five fractions were determined by viscosity measurements, following Potter and Hassid.[6] A fraction with MW 1.0×10^4 was used for kinetic studies.

All inorganic reagents were commercial reagent grade and used without further purification.

Solutions. About 5 mg of amylose was dissolved in 1 m*l* of 1 M KOH solution, and neutralized by 1 M $HClO_4$ solution. The solution was diluted to 100 m*l* and used as a stock solution. This solution was freshly prepared before use.

About 1 g of iodine was added into a 250 m*l* aqueous solution containing 1.4×10^{-6} M KIO_3 and 0.1 M $HClO_4$, where KIO_3 and $HClO_4$ were added in order to suppress the hydrolysis of iodine.[7] After this mixture was stirred at room temperature for about 10 hr, it was filtered through sintered glass. The concentration of iodine and triiodide ion were determined spectrophotometrically from the molar extinction coefficients given by Awtrey and Connick;[7] 746 at 460 mμ for iodine and 26400 at 352 mμ for triiodide ion. The typical value of iodine concentration in a stock solution was about 1×10^{-3} M, and the upper limit of triiodide ion concentration 2×10^{-7} M.

Number of Amylose Equivalents. The concentration of amylose equivalents present in a solution was calculated from the spectra of an amylose-iodine complex. In Fig. 1 is shown an optical density of the complex at 620 mμ under the condition of excess iodine over amylose. Seeing that the optical density increases linearly with the concentration of amylose and that it stays constant in the range from 10 to 25°C, it was concluded that amylose was complexed to its maximum capacity. Using the molar extinction coefficient for one bound-iodine in case of $(0.1-0.3)[I^-]/[I_2]$, given by Schneider *et al.*,[4] we obtained that 7.8 glucose units take up one iodine molecule. This is in good agreement with the generally accepted value.[4] Therefore, we used this relationship to calculate the number of amylose equivalents from the weight percentage of amylose.

Kinetic Measurements. The rate of formation reaction between amylose and iodine was measured by following the rise of optical density at 620 mμ in a Yanagimoto stopped-flow apparatus. Iodide ions were added in an iodine solution before mixing. The rate of decomposition reaction was

1) K. Hiromi, T. Shibaoka, and S. Ono, *J. Biochem.*, **68**, 205 (1970).
2) J. Thompson and E. Hamori, *J. Phys. Chem.*, **75**, 272 (1971).
3) J. A. Thoma and D. French, *J. Amer. Chem. Soc.*, **82**, 4144 (1960).
4) C. L. Cronan and F. W. Schneider, *J. Phys. Chem.*, **73**, 3900 (1969).
5) W. W. Everett and J. F. Foster, *J. Amer. Chem. Soc.*, **81**, 3460 (1959).
6) A. L. Potter and W. Z. Hassid, *ibid.*, **73**, 593 (1951).
7) A. D. Awtrey and R. E. Connick, *ibid.*, **73**, 1842 (1951).

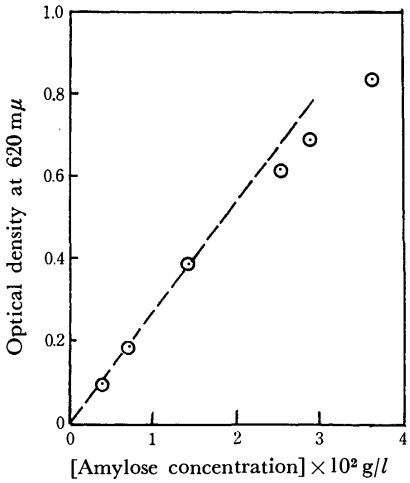

Fig. 1. The dependence of the optical density at 620 mμ on the concentration of amylose.
$[I_2]=7.4\times10^{-5}$ M, $[I^-]=1.0\times10^{-5}$ M. Temperature 10—25°C.

measured by mixing a solution containing amylose-iodine-iodide complexes with a solution containing decomposing reagents ($Ce(SO_4)_2$ or $Na_2S_2O_3$). The decrease of optical density was followed at 620 mμ. In both experiments, a 10 mm observation cell was used. Temperature was maintained within ±0.1°C.

Results and Discussion

(A) Dependence of Amount of Complex on the Concentration of Iodide Ions. It is known that the complex is not produced when no iodide ion is present in aqueous solution.[3] In order to obtain the dependence of the amount of the complex on the concentration of iodide ion, we mixed the solution of amylose with that of iodide ion and iodine in a stopped-flow apparatus, varying the concentration of iodide ion, $[I^-]$. The time course of the rise of the optical density is shown in Fig. 2 for several values of $[I_2]$ and $[I^-]$. As $[I_2]$ and $[I^-]$ decrease, it changes from an exponential curve to non-exponential one. Non-exponential curves consist of at least two relaxations. We call the first and the second relaxations the relaxation (I) and (II) respectively. In Fig. 3, the amount of the complex formed in the relaxation (I) is plotted against the initial value of $[I_2]$, where we assumed that in the exponential curves the product is formed only through the relaxation (I). In Fig. 4 the same result is also plotted against the initial concentration of triiodide ion, $[I_3^-]$, which was calculated from an equilibrium constant given by Awtrey and Connick.[7] The latter plot shows that the amount of complex seems to be determined uniquely by the initial $[I_3^-]$ in spite of various values of $[I^-]$ and $[I_2]$. Thus from the figure, 1.0×10^{-5} equivalents of amylose are all complexed when 6×10^{-7} M of $[I_3^-]$ is present. In other words one molecule of I_3^- is required for about 17 equivalents of amylose to form the complex by a single relaxation. Another conclusion is that the complex contains a smaller number of iodide ions in comparison with amylose equivalents, since nearly all amylose equivalents become complexed for sufficiently high $[I_2]$ under the condition of $[I^-]/[\text{Amylose Equivalent}]=0.125$ as shown in Fig. 3.

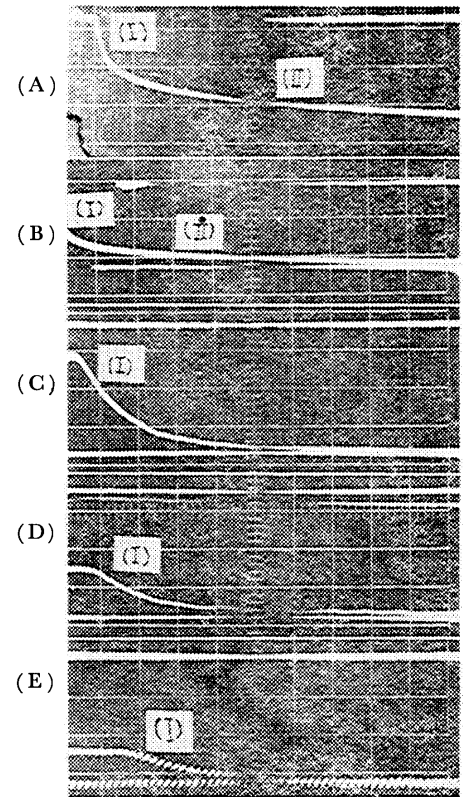

Fig. 2. The increase of the optical density at 620 mμ with time for various concentration of iodine and iodide ion at 25°C.
The initial values of $[I_2]$ and $[I^-]$ and the time scale are: (A) 5.5×10^{-5} M, 1.25×10^{-6} M, 5 sec/div., (B) 1.1×10^{-4} M, 1.25×10^{-6} M, 2 sec/div., (C) 1.6×10^{-4} M, 2.0×10^{-6} M, 50 msec/div., (D) 2.6×10^{-4} M, 3.0×10^{-6} M, 2 msec/div., (E) 2.6×10^{-4} M, 4.5×10^{-6} M, 1 msec/div. The vertical scale 0.1 ΔO.D./div. Amylose concentration 1.0×10^{-5} eq. The horizontal line above each signal shows the initial position of the optical density.

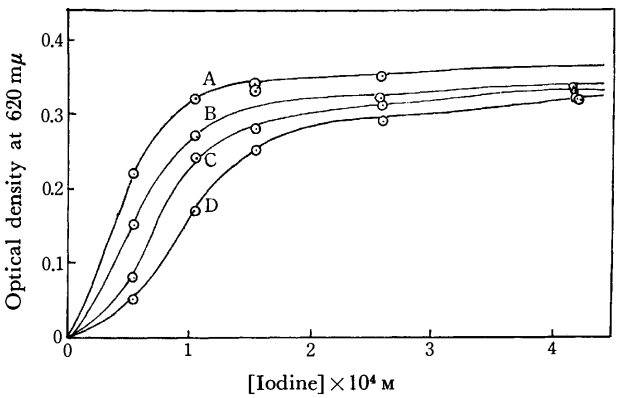

Fig. 3. The dependence of the optical density at 620 mμ on the iodine concentration for various values of iodide ion concentrations at 25°C.
$[I^-]$ is (A) 4.50×10^{-6} M, (B) 3.0×10^{-6} M, (C) 2.0×10^{-6} M, (D) 1.25×10^{-6} M. Amylose concentration 1.0×10^{-5} eq.

(B) Dependence of the Rate of Complex Formation on the Initial Concentration of Amylose. The rate of formation was measured, varying the initial number of amylose equivalents, [Am.]. The result is shown in

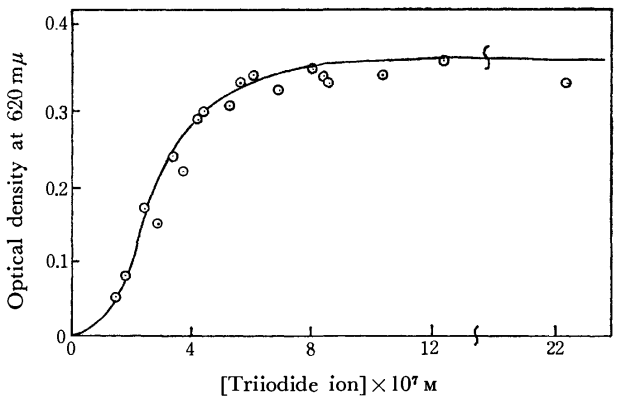

Fig. 4. The dependence of the optical density at 620 mμ on the triiodide ion concentration at 25°C.

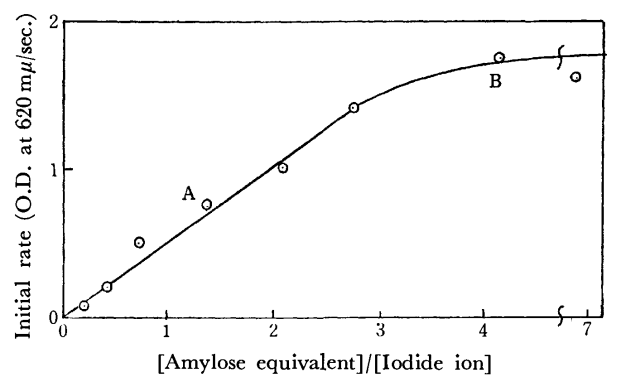

Fig. 5. The dependence of the initial rate of the complex formation on the ratio of the number of amylose equivalents to the iodide ion concentration at 10°C.
$[I_2]=2.6\times10^{-5}$ M, $[I^-]=5.0\times10^{-6}$ M. The region A denotes a linear portion, and the region B a staturated portion.

Fig. 5. As expected from the assumption that a certain unit of amylose polymer behaves independently in the course of formation reaction, the initial rate increases in proportion to [Am.] for small [Am.]. However, the rate becomes saturated to a constant value as [Am.] becomes comparable to $[I^-]$. In this region the time dependence of the rise of optical density becomes non-exponential, coinciding with the results in section (A). The result means that, although we called the initial stage of complex formation the relaxation (I) over all amylose range, the mechanism itself changes as the amylose amount passes through a critical value. Taking the results reported by Hiromi into account,[1] we concluded that, for small [Am.] (region A), the formation rate is determined by the reaction between a free amylose unit and free I^- or I_2 or its variants. On the other hand, for large [Am.] (region B), the rate is determined by the intramolecular process of an intermediate. The rise of optical density was followed in the wavelength range from 700 mμ to 300 mμ in order to find the spectra of a transient compound. However, no shift of the absorption peak was observed in both region A and B. Therefore, it is assumed that the process following the rate-determining step is too rapid to be observed, and that the transient compound has no absorption in the visible region.

(C) Dependence of the Rate of Complex Formation on the Concentration of Iodine and Iodide Ion. The rate of formation was measured for various values of $[I^-]$ and $[I_2]$. The results are shown in Fig. 6, in which the reciprocal of the half-life of the relaxation (I), $t_{1/2}$, is plotted against the initial $[I_3^-]$. The reason to choose $[I_3^-]$ as a parameter is that this plot is found to give a single curve in the wide range of $[I^-]$ and $[I_2]$. For small $[I_3^-]$, corresponding to region B in section (B), the rate is extremely slow and depends crucially on $[I_3^-]$. For large $[I_3^-]$, corresponding to region A, the rate increases linearly with $[I_3^-]$. Therefore, $t_{1/2}$ is expressed approximately as

$$t_{1/2}^{-1} = k([I_3^-]-\theta) \quad (1)$$

where θ is a value of the $[I_3^-]$ at the intercept obtained by extrapolating the linear portion of the curve. In section (B) it was suggested that in the region of $[I_3^-]<\theta$, the rate of complex formation is determined by the intramolecular process and that in the region of $[I_3^-]>\theta$, the rate is determined by the reaction between free amylose units and I^- or I_2 or its variants. From the relationship of Eq. (1), one of the possibilities for the rate-determining step is a reaction between an amylose unit and I_3^-,

$$Am + I_3^- \rightarrow Am\cdot I_3^-. \quad (2)$$

Since the complex $Am\cdot I_3^-$ is thought to have no absorption in the wavelength longer than 600 mμ,[8] reaction (2) may be followed by chain growth reaction. This later step which is too fast to be observed as stated in section (B) involves a reaction between an intermediate complex and I_2, *e.g.*

$$Am\cdot I_3^- + I_2 \rightarrow Am\cdot I_3^-\cdot I_2. \quad (3)$$

Thus the final product contains many I_2 molecule as concluded in section (A). In the region $[I_3^-]>\theta$, since $[I_2]$ and $[I^-]$ are in excess over amylose equivalents, they are assumed to be kept constant during the reaction. Supposing the equilibration $I^-+I_2 \rightleftarrows I_3^-$ is much faster than the formation rate,[9] $[I_3^-]$ is also kept constants. In reaction (2), therefore, the decrease of amylose units is expressed as below, neglecting a reverse reaction

$$d[Am.]/dt = -k[Am.][I_3^-],$$

where [Am.] represents the number of free amylose units, and k a second-order rate constant. From the slope of a linear portion in Fig. 6, k can be calculated as

$$k = 7\times10^8\ \text{M}^{-1}\text{sec}^{-1} \quad \text{at } 25°\text{C}.$$

This value is so large that it is close to the rate of a diffusion-controlled reaction.[10] Ono *et al.* concluded that amylose should be in helical form so as to form a complex with iodine.[11] Thus the above result means

8) H. Murakami, *J. Chem. Phys.*, **22**, 367 (1954).
9) O. E. Myers, *ibid.*, **28**, 1027 (1958).
10) Here we assume that a free amylose unit moves in liquid just as a free particle. However another extreme assumption that the unit is restricted to one position in medium will not affect the result very much. (*cf.* A. A. Frost and R. G. Pearson, "Kinetics and Mechanism," John Wiley and Sons, Inc., N. Y., 1961, p. 221).
11) S. Ono, T. Watanabe, K. Ogawa, and N. Okazaki, This Bulletin, **38**, 643 (1965).

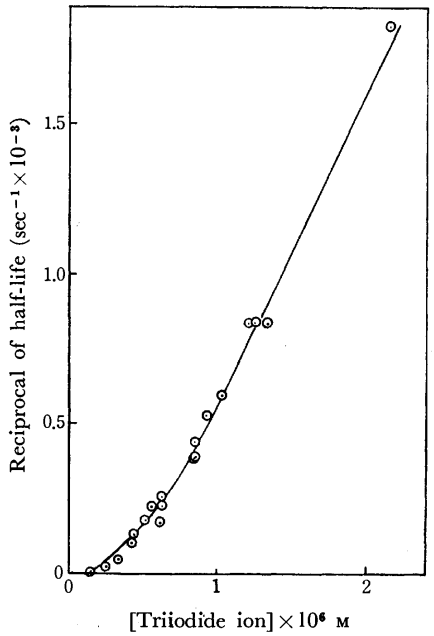

Fig. 6. The dependence of the rate of the complex formation on the triiodide ion concentration at 25°C.
This results are from the same experiments for Fig. 3.
$[I_2]=(1-4)\times10^{-4}$ M, $[I^-]=(1-5)\times10^{-6}$ M, and the amylose concentration 1.0×10^{-5} eq.

that the reaction between a triiodide ion and helical amylose is nearly a diffusion-controlled process.

The origin of the θ term in equation (2) is not clear. Apparently owing to this term, the dependence of the rate on $[I_3^-]$ is very crucial in the region of $[I_3^-]<\theta$. Also θ depends greatly upon temperature. Figure 7 shows the plot of the initial rate against $[I_3^-]$ at various temperatures. As temperature decreases, the linear portion becomes larger. Therefore in the region of $[I_3^-]<\theta$, the formation rate is greatly affected by $[I_3^-]$ and temperature. Under the present assumption of intramolecular process, it is suggested that the stability and the concentration of an intermediate depends very much on $[I_3^-]$ and temperature.

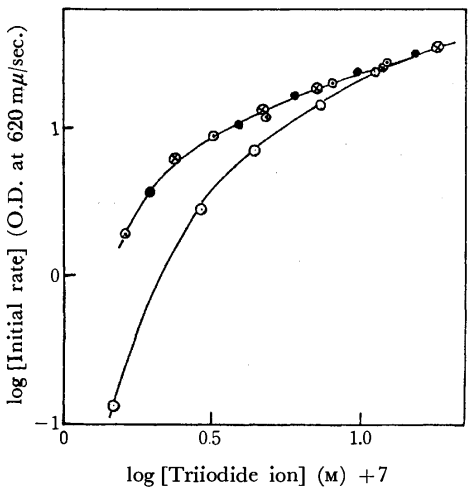

Fig. 7. The dependence of the initial rate of the complex formation on the triiodide ion concentration at various temperatures.
$[I_2]=5.4\times10^{-5}$ M, and amylose concentration 1.0×10^{-5} eq.
$[I^-]=(1.5-11)\times10^{-7}$ M. Temperature ○ 20°C, ⊙ 15°C, ● 10°C, ⊗ 5°C respectively.

(D) Decomposition of the Complex by Thiosulfate Ion and Cerium(IV). The amylose-iodine-iodide complex was found to decompose by adding sodium thiosulfate solution or cerium(IV) sulfate solution.

First the rate of decomposition was measured, using a $Na_2S_2O_3$ solution. At the sufficiently high concentration of $Na_2S_2O_3$, the decomposition occurs so rapidly within a dead time (about 1.5 msec). This is a surprising result, since this means that the decomposition rate is larger than that of formation. This is very unbelievable seeing that the formation constant is rather high.[4] One of the possible explanation is that the reversible equilibrium exists between the transient complex $Am\cdot I_3$ in Eq. (2) and the final products. They may be

$$Am\cdot I_3 + I_2 \rightleftharpoons Am\cdot I_3\cdot I_2. \quad (4)$$

By adding $Na_2S_2O_3$, I_2 is reduced to I^- and the above equilibrium moves toward the decomposition. The fact that the equilibrium (3) is very rapid coincides well with the direct appearance of a final product as stated in section (B).

Next the rate of decomposition was measured, using a $Ce(SO_4)_2$ solution. The rate was measurable this time even at 0.05 M Ce(IV). The example is shown in

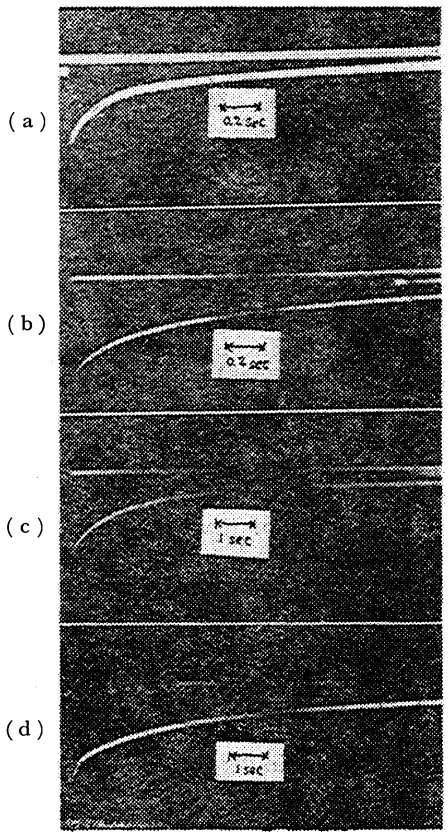

Fig. 8. The decrease of the optical density at 620 mμ with time at various temperatures, induced by the addition of $Ce(SO_4)_2$.
$[Ce(SO_4)_2]=2.8\times10^{-2}$ M, and [Complex] $=3.5\times10^{-6}$ eq.
Temperature and time scale: (a) 25°C, 0.2 sec/div., (b) 20°C, 0.2 sec/div., (c) 15°C, 1 sec/div., (d) 10°C, 1 sec/div., The vertical scale 0.05 ΔO.D./div.

Fig. 8. Since the decrease of the complex was found independent of $[Ce(SO_4)_2]$, we concluded that the decomposition occurs by the oxidation of free I^- by Ce(IV). The rate is considered to be determined by the reverse reaction of Eq. (2). The time dependence of decomposition is not exponential in spite that the formation is exponential in an appropriate condition. This means that triiodide ion is bound to amylose helix with various degrees of strength. In this sense, it is impossible to obtain the unique value for the equilibrium constant in this complexation reaction. Interestingly the reverse reaction is greatly temperature dependent as shown in Fig. 8. Therefore, the large temperature dependence of the stability of the amylose-iodine-iodide complex arises from the reverse reaction not from the forward reaction.

Summarizing these results, the forward, and the reverse reaction rate constants for the reaction,

$$Am + I_3^- \rightleftharpoons Am \cdot I_3^-,$$

are given as below.

Temperature	Forward	Reverse[a)]
25°C	7×10^8 M^{-1} sec^{-1}	4 sec^{-1}
20	same	2
15	same	0.5
10	same	0.3

a) The approximate value of a unimolecular reaction rate for the initial stage of decomposition.

BULLETIN OF THE CHEMICAL SOCIETY OF JAPAN, VOL. 45, 2308—2312 (1972)

Energy Transfer in the γ-Irradiated Benzene Solutions of Carbonyl Sulfide, Nitrous Oxide, and Carbon Dioxide

Shin SATO, Kiyoshi HOSOYA, Seishi SHISHIDO, and Shun-ichi HIROKAMI

Department of Applied Physics, Tokyo Institute of Technology, Ookayama, Meguro-ku, Tokyo

(Received January 21, 1972)

The γ-radiolysis of benzene solutions containing carbonyl sulfide, nitrous oxide, and carbon dioxide has been investigated at room temperature and at 0°C. Carbonyl sulfide was shown to be an effective electron scavenger and to give carbon monoxide as the product. By comparing the solute concentration dependences of $G(N_2)$ and $G(CO)$, it was concluded that the collision of secondary electrons with benzene does not efficiently produce the first excited singlet state, the G-value of which is less than 0.2 if it is produced at all. The concentration dependences of the $G(CO)$ and G(phenol) from the benzene solution of carbon dioxide also suggested that the superexcited state or the highly-excited state of benzene is too short-lived to transfer its energy to the solute.

When a benzene solution containing a small amount of a solute is irradiated by γ-rays, the solute molecules are subject to the attack of active species produced in the solvent and an "energy transfer from solvent to solute" occurs. Various mechanisms have been proposed for this energy transfer. The mechanisms may be classified into three categories. (1) The real energy transfer. The active species in this case are the first excited singlet ($^1B_{2u}$) and the lowest teiplet state ($^3B_{1u}$) of benzene. These states may be formed by the neutralization of benzene cations or by the direct excitation of secondary electrons. This type of energy transfer has been studied by many photochemists.[1,2] Our laboratory has also studied this type of energy transfer and shown that the benzene-photosensitized *cis-trans* isomerization of butene-2 in cyclohexane occurs through the triplet-triplet energy transfer when the concentration of the solute is less than 10^{-2} mol/l,[3] and that the benzene photo-sensitized decomposition of carbonyl sulfide through the singlet-singlet energy transfer.[4] (2) Ionic reactions. The active species in this case are electrons and benzene cations, whose reactions have been studied as an important subject of radiation chemistry. An example is the nitrogen formation from a γ-irradiated benzene solution of nitrous oxide.[5,6] It is believed that this reaction is initiated by the electron capture of nitrous oxide. As an example of the reaction of benzene cations, the formation of anisole in the γ-irradiated benzene-methanol mixture may be taken.[7] (3) The energy transfer from the superexcited state of benzene. This process has not been established by direct evidence, but its possibility has been discussed by theoretical radiation chemists.[8] Recently, Voltz quoted our data on the quenching effect of nitrous oxide on the scintillation from the *p*-terphenyl–benzene system as an example of this type of energy transfer.

The present paper will report the results of the γ-radiolysis of benzene solutions of carbonyl sulfide,

1) W. A. Noyes, Jr. and I. Unger, "Advances in Photochemistry," Vol. 4, ed. by W. A. Noyes, Jr., G. S. Hammond, and J. N. Pitts, Jr., Interscience Publishers, New York and London, (1966), p. 49.

2) P. J. Wagner and G. S. Hammond, *ibid.*, Vol. 5, (1968), p. 21.

3) S. Sato, H. Kobayashi, and K. Fukano, *Kogyo Kagaku Zasshi*, **72**, 209 (1969).

4) S. Sato, H. Miyamoto, S. Hirokami, and S. Tsunashima, This Bulletin, **45**, 754 (1972).

5) S. Sato, R. Yugeta, K. Shinsaka, and T. Terao, *ibid.*, **39**, 156 (1966).

6) S. Hirokami, S. Shishido, and S. Sato, *ibid.*, **44**, 1511 (1971).

7) J. A. Ward and W. H. Hamill, *J. Amer. Chem. Soc.*, **89**, 5116 (1967).

8) R. Voltz, "Progress and Problems in Contemporary Radiation Chemistry," Vol. 1, ed. by Teply, (1971), p. 139.

nitrous oxide, and carbon dioxide and will discuss the reaction mechanism for the formation of the products. The discussion will inevitably include the energy trasfer described above.

Experimental

Tokyo Kagaku Seiki Co. benzene (purest grade) was used as supplied. Further purification was not made.[6] The carbonyl sulfide (Merck Co.), nitrous oxide (Matheson Co.), and carbon dioxide (Takachiho Chemical Co.) were distilled bulb-to-bulb, and the head and tail fractions were rejected.

All the mixtures were sealed into small sampling tubes (about 3 m*l*) with a breakable seal attached. The subsequent procedure was the same as that reported in a previous paper.[6] Ostwald's solubility coefficients of carbonyl sulfide and nitrous oxide in benzene at room temperature are 12.5 and 3.8 respectively.

The samples were irradiated by ^{60}Co γ-rays at a dose rate of about 0.8×10^6 R/hr. In order to analyze the gases noncondensable at the temperature of liquid nitrogen, a Toepler pump with a gas buret and a cuprous oxide furnace attached was used. For the analysis of the products in the solution, we made use of a gas chromatograph, the column of which was 1-m dioctylphthalate at 130°C.

Results

COS–Benzene System. Table 1 shows the *G*-values of carbon monoxide and hydrogen as a function of the concentration of COS in benzene. The presence of the benzenethiol as one of the products could be detected by gas chromatography. However, the *G*-value at the COS concentration of 0.6 mol/*l* was as low as 0.12. No other products could be detected.

Since the dependence of $G(CO)$ on the concentration of COS was very similar to that of $G(N_2)$ on the concentration of N_2O, as reported in a previous paper,[6] the radiolysis at 0°C was carried out for the sake of comparison, for at that temperature any ratio of COS to benzene can be obtained. The result is shown in Fig.1, along with the $G(N_2)$ from the benzene solution of N_2O. Within the limit of experimental error, the two series of measurements coincide with each

Table 1. *G*-values of CO and H_2 from the benzene solution of COS

COS mol/*l*	$G(CO)$	$G(H_2)$	COS mol/*l*	$G(CO)$	$G(H_2)$
0.0053	0.206	—	0.420	3.31	—
0.0078	0.567	—	0.472	3.45	0.032
0.0108	0.567	—	0.558	3.58	—
0.0113	0.591	0.036	0.562	3.67	—
0.0315	1.22	—	0.938	4.06	—
0.0570	1.47	0.033	1.07	4.62	—
0.0955	1.96	0.043	1.26	4.69	0.034
0.123	2.13	0.032	1.54	4.96	—
0.156	2.17	0.038	1.70	4.92	—
0.210	2.40	—	2.04	4.97	—
0.256	2.74	0.034	2.22	5.61	—
0.404	3.46	—	3.34	5.52	—
0.410	3.38	—	4.23	6.07	—

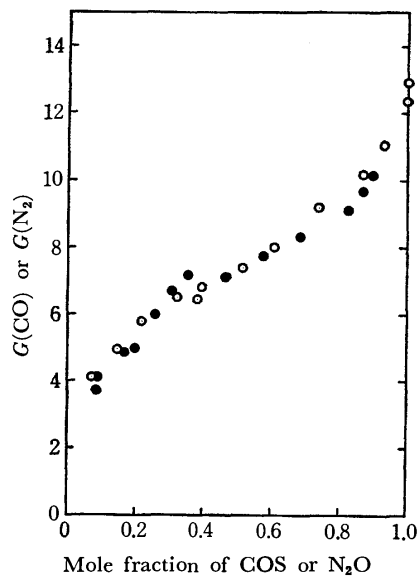

Fig. 1. *G*-values of CO and N_2 from the liquid phase mixtures of benzene-COS and benzene-N_2O at 0°C.
○: CO, ●: N_2

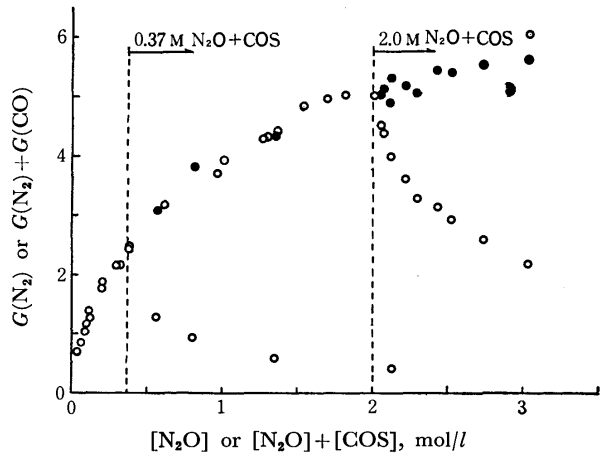

Fig. 2. *G*-values of N_2 from the benzene solution of N_2O at room temperature and the effect of the addition of COS.
○: $G(N_2)$, ●: $G(N_2)+G(CO)$

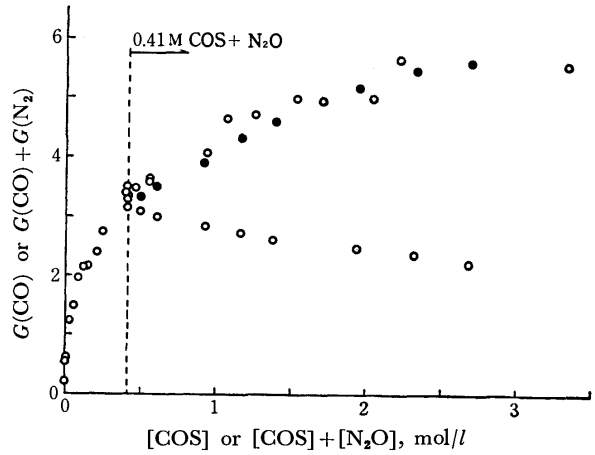

Fig. 3. *G*-values of CO from the benzene solution of COS at room temperature and the effect of the addition of N_2O.
○: $G(CO)$, ●: $G(N_2)+G(CO)$

other.

COS–N_2O–Benzene System. In order to study the competition of COS and N_2O as electron scavengers, benzene solutions containing the two solutes were γ-irradiated. Figures 2 and 3 show the results. Some of the results in Fig. 2 have already been reported.[9] In each figure, it is noticeable that the sum of $G(CO)$ and $G(N_2)$ at a certain concentration of $[COS]+[N_2O]$ is almost equal to the $G(CO)$ or $G(N_2)$ value obtained at the same concentration of COS or N_2O.

CO_2–Benzene System. In place of COS and N_2O, CO_2 was also used as a solute. Figure 4 shows the G-values of CO, phenol, and biphenyl as a function of the mole fraction of CO_2. The temperature was 0°C; no CO_2 mole fraction higher than 0.9 could be attained because of the fragility of the breakable seal attached to the reaction vessel.

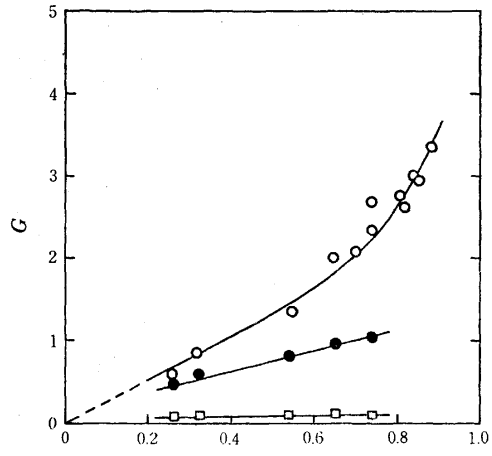

Fig. 4. G-values of CO, phenol, and biphenyl from the liquid phase mixture of benzene-CO_2.
○: CO, ●: phenol, □: biphenyl

Discussion

In the previous paper on the γ-radiolysis of the benzene solution of N_2O,[6] the reactions initiated by the electron capture of N_2O were described as follows:

$$e^- + N_2O \rightarrow N_2 + O^- \quad (1)$$

$$O^- + C_6H_6 \rightarrow C_6H_6O^- \quad (2)$$

$$C_6H_6O^- + N_2O \rightarrow N_2 + C_6H_6O_2^- \quad (3)$$

$$C_6H_6O_2^- + C_6H_6^+ \rightarrow C_6H_6O + C_6H_5OH \quad (4)$$

As was stated in the Results section, the behavior of COS as the solute in the γ-irradiated benzene solution was very similar to that of N_2O. Therefore, the reactions of COS may be written as follows:

$$e^- + COS \rightarrow CO + S^- \quad (5)$$

$$S^- + C_6H_6 \rightarrow C_6H_6S^- \quad (6)$$

$$C_6H_6S^- + COS \rightarrow CO + C_6H_6S_2^- \quad (7)$$

$$C_6H_6S_2^- + C_6H_6^+ \rightarrow 2\,C_6H_6 + S_2 \quad (8)$$

In Reaction (8), the formation of benzenethiol was not assumed, because the G-value of this compound was very small. The product, S_2, in this reaction probably polymerizes to S_8.[10] When the two solutes, N_2O and COS, are present together in a solution, the following two reactions must be taken into account for the formation of CO and N_2:

$$C_6H_6O^- + COS \rightarrow CO + C_6H_6OS^- \quad (9)$$

$$C_6H_6S^- + N_2O \rightarrow N_2 + C_6H_6SO^- \quad (10)$$

As is shown in Fig.2, when COS is added to the benzene solution containing N_2O, the $G(N_2)$ rapidly decreases with the increase in the COS concentration, while the sum of $G(N_2)$ and $G(CO)$ is almost equal to the $G(N_2)$ obtained at the N_2O concentration corresponding to $[COS]+[N_2O]$. The reverse situation is shown in Fig. 3, where N_2O is added to the COS–benzene solution. In this case, the decrease in $G(CO)$ with the concentration of added N_2O is not so rapid as the decrease in $G(N_2)$ on the addition of COS to the N_2O solution. These results may be explained as follows.

The electrons ejected in the solution are captured by N_2O or COS, the rate constants of which may be almost equal.

$$k_1 = k_5 \quad (I)$$

Otherwise, the curves for $G(N_2)+G(CO)$ in Fig. 2 and 3 should differ considerably from each other. On the other hand, the second steps of the formation of N_2 and CO are strongly dependent upon the rate constants; $k_3<k_9$ and $k_{10}<k_7$.

For the further analysis of these data, we may tentatively divide the G-values of noncondensable gases into two parts:

$$\begin{aligned} G(N_2) &= G_1(N_2) + G_2(N_2) \\ G(CO) &= G_1(CO) + G_2(CO) \end{aligned} \quad (II)$$

Here, G_1 denotes the G-value of the noncondensable gas resulting from Reaction (1) or (5), and G_2, that resulting from Reactions (3) and (10) or (7) and (9). Therefore, the following relation should hold:

$$\frac{G_1(N_2)}{G_1(CO)} = \frac{k_1[N_2O]}{k_5[COS]} = \frac{[N_2O]}{[COS]} \quad (III)$$

Since the solute concentration under present consideration is higher than 0.4 mol/l, the $C_6H_6O^-$ and and $C_6H_6S^-$ species may react further with the solutes before being neutralized. In other words, all the electrons captured by scavengers will produce two molecules of N_2 or CO:

$$G(N_2) + G(CO) = 2\{G_1(N_2) + G_1(CO)\} \quad (IV)$$

Then, if the $[N_2O]/[COS]$ ratio is known, we can calculate $G_2(N_2)$ and $G_2(CO)$.

On the other hand, if we can assume:

$$k_3/k_9 = k_{10}/k_7 = K \quad (V),$$

then we can easily derive the following equation:

9) S. Hirokami, S. Shishido, and S. Sato, This Bulletin, **43**, 973 (1970).

10) H. E. Gunning and O. P. Strausz, "Advances in Photochemistry," Vol. 4, ed. by W. A. Noyes, Jr., G. B. Hammond, and J. N. Pitts, Jr., Interscience Publishers, New York and London, (1966), p. 143.

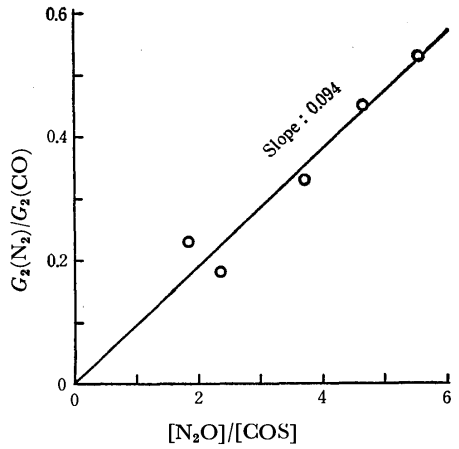

Fig. 5. $G_2(N_2)/G_2(CO)$ as a function of $[N_2O]/[COS]$ calculated from Fig. 2.

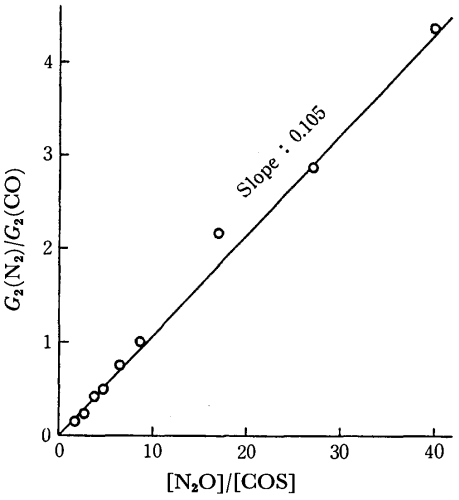

Fig. 6. $G_2(N_2)/G_2(CO)$ as a fuuction of $[N_2O]/[COS]$ calculated from Fig. 3.

$$\frac{G_2(N_2)}{G_2(CO)} = K\frac{[N_2O]}{[COS]} \qquad \text{(VI)}$$

Figure 5 was drawn from the data in Fig.2, and Fig.6, from those in Fig.3. Obviously, we could obtain the linear relationships expected from Eq. (VI) and a constant slope:

$$K = 0.10 \pm 0.005 \qquad \text{(VII)}$$

The agreement of these two slopes seems to support the reasoning presented above. We have tried to a more general relationship between the G-values of N_2 and CO, and the concentrations of N_2O and COS on the basis of the proposed reaction scheme, but no simple equations have so far been derived because of the inhomogeneous kinetics involved in the neutralization processes of ions in the system.

So far, we have stressed that the two curves of $G(N_2)+G(CO)$ in Figs. 2 and 3 are similar: however, a detailed comparison reveals that the two curves do not coincide with each other exactly especially, at the lower concentrations of the solutes. In the previous paper,[6] we showed that the $G(N_2)$ from the N_2O benzene solution is proportional to the square root of the N_2O concentration up to 2 mol/l:

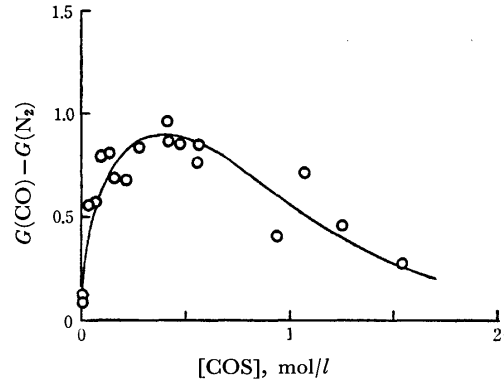

Fig. 7. The difference between $G(CO)$ and $G(N_2)$ as a function of the concentration of the solute.

$$G(N_2) = 3.78\sqrt{[N_2O]} \qquad \text{(VIII)}$$

By using this relation, the difference between $G(N_2)$ in Fig. 2 and $G(CO)$ in Fig. 3 was plotted as a function of the concentration of the solute. The results are shown in Fig.7. This difference may be partly due to the difference in the electron-scavenging efficiencies of N_2O and COS, but we believe that the main part result from the difference between the two compounds in sensitivity to the excited state of benzene. As has already been reported, N_2O and COS show quite different behaviors in the benzene-photosensitization; that is, the quantum yield of the formation of N_2 in the benzene-photosensitized decomposition of N_2O in cyclohexane is very small (<0.01 at 0.06 mol/l N_2O),[6] while COS is easily decomposed into CO and S by the benzene photo-sensitization ($\phi_{CO}=0.4$ at 0.06 mol/l COS).[4] Therefore, if the first excited singlet state of benzene ($^1B_{2u}$) is efficiently formed by the direct excitation of the secondary electrons in the radiolysis of the benzene solution, the $G(N_2)$ curve in Fig.2 should differ considerably from the $G(CO)$ curve in Fig. 3. In fact, the difference is small, as is shown in Fig. 7, and may be explained as follows. The electrons not scavenged by COS return to the parent benzene cations and produce the excited states of benzene, which can decompose COS. This process may be schematically described as follows:

$$e^- + C_6H_6^+ \rightarrow C_6H_6^*(^1B_{2u}) \qquad (11)$$

$$\searrow\ C_6H_6^{**}(^3B_{1u} \text{ or others}) \qquad (12)$$

$$C_6H_6^* + COS \rightarrow C_6H_6 + CO + S \qquad (13)$$

If this reasoning is correct, the following conclusion can be drawn—that the secondary electrons produced in the γ-radiolysis of benzene do not produce the first excited singlet state of benzene by direct collision. This statement, of course, does not mean that collisions of the secondary electrons with benzene give no electronically-excited states of benzene. Rather, the truth is probably that a large number of the electronically-excited states are produced, but their states are so high compared with the $^1B_{2u}$ state that the

conversion to the $^1B_{2u}$ state is not efficient.[11] Although the experimental error precludes an accurate estimation, the G-value of the $^1B_{2u}$-state benzene produced directly by the collision of secondary electrons cannot be higher than 0.2, if it is produced at all.

Fighure 4 shows the G-values of CO, phenol, and biphenyl from the benzene solution of CO_2. The yields of CO and phenol are almost linearly dependent upon the concentration of CO_2 at its lower concentrations. This suggests that CO and phenol are produced by the reactions of the active species formed from CO_2. It is known that oxygen atoms in the ground state do not efficiently produce phenol in the reaction with benzene. One possible mechanism for the formation of phenol, therefore is as follows:

$$C_6H_6 \rightsquigarrow C_6H_6^+ + e^-$$

$$CO_2 \rightsquigarrow CO + O$$

$$CO_2^+ + e^-$$

$$O + e^- \rightarrow O^-$$

$$O^- + C_6H_6 \rightarrow C_6H_6O^-$$

$$CO_2^+ + C_6H_6 \rightarrow CO_2 + C_6H_6^+$$

$$C_6H_6^+ + C_6H_6O^- \rightarrow C_6H_5OH + C_6H_6$$

This reaction scheme is very tentative, but it explains the linear dependence of G(CO) and G(phenol) on the CO_2 concentration.

Recently, much interest has been taken in the superexcited state produced in the radiolysis.[12] According to Voltz's estimation,[8] the energy transferred from the superexcited state or highly-excited state of aromatic compounds in the liquid phase is, very roughly, 20 eV. Moreover, he quoted our data regarding the quenching effect of N_2O in the scintillation from the p-terphenyl-benzene system as an example of the energy transfer from the superexcited state or the highly-excited state of benzene to the solute.[8] However, if the energy of 20 eV is transferred from the superexcited state of benzene to the solute, CO_2 should be decomposed as was N_2O if the solute used is CO_2 instead of N_2O. Figure 4 obviously shows that this is not likely. Therefore, it may safely be said that superexcited state or the highly-excited state of benzene is too short-lived to transfer its energy to the solute molecules.

11) C. L. Braun, S. Kato, and S. Lipsky, *J. Chem. Phys.*, **39**, 1645 (1963).

12) Y. Hatano, S. Shida, and S. Sato, This Bulletin, **41**, 1120 (1968).

BULLETIN OF THE CHEMICAL SOCIETY OF JAPAN, VOL. 45, 2312—2318 (1972)

The Orientation Overgrowth of Polycyclic Aromatic Quinones on the Cleavage Surface of Alkali Halide Single Crystals

Michio ASHIDA, Akihiko HAMADA, and Teizo WATANABE
Department of Industrial Chemistry, Faculty of Engineering, Kobe University, Nada-ku, Kobe

(Received November 15, 1971)

Vacuum-condensed films of polycyclic aromatic quinones (flavanthrone, indanthrone, and pyranthrone) were found to grow epitaxially on the cleavage faces of NaCl and KCl. Electron microscopy studies have shown that all the films on NaCl were composed of small, needle-like crystallites crossing orthogonally. The needle axis of the crystals coincides with the ⟨110⟩ directions of NaCl. When a cleavage surface of KCl was used as the substrate, vacuum-condensed films of flavanthrone and indanthrone were composed of dendroid crystals which assumed the standing *b*-axis orientation with an apparent C_{4v} symmetry. On the other hand, a pyranthrone film on KCl was composed of wedge-like crystals which assumed the standing *b*-axis orientation. The electron-diffraction pattern of the film revealed that the *b*-axis of each crystal tilts against the normal of the substrate face at an angle of 29° and takes a random orientation. When the films assume the standing *b*-axis orientation, the planar molecule in the crystal comes into parallel contact with the cleavage face of KCl. It may be presumed that the nitrogen atoms in both flavanthrone and indanthrone molecules are placed on potassium ions in the (001) plane of KCl.

The epitaxial crystallization of organic compounds on a cleavage face of alkali halides has been observed by many investigators. The orientation overgrowth of polyethylene,[1,2] *p*-aminobenzoic acid and sulfonicamide,[3] polyethylene and various other polymers,[4,5] poly γ-benzyl L-glutamate[6] and five oligopeptides[7] has been reported in little more than a decade. In these experiments, epitaxial deposits were formed on alkali halide surfaces from a supersaturated solution of the crystallizing substances.

In a previous paper, condensed polycyclic aromatic compounds were found to grow epitaxially when they

1) J. Willems, *Discuss. Faraday Soc.*, **25**, 111 (1957).
2) E. W. Fischer, *ibid.*, **25**, 204 (1957).
3) H. Seifert and L. Kuhn, *Naturwissenschaften*, **49**, 537 (1962).
4) J. A. Koutsky, A. G. Walton, and E. Baer, *J. Polym. Sci., Part A-2*, **4**, 611 (1966).
5) J. A. Koutsky, A. G. Walton, and E. Bare, *Polym. Lett.*, **5**, 177 (1967).
6) S. H. Carr, A. G. Walton, and E. Baer, *Biopolymers*, **6**, 469 (1968).
7) S. H. Carr and W. C. Colket, *J. Colloid Interfac. Sci.*, **31**, 328 (1969).

were condensed onto a cleavage face of a muscovite crystal *in vacuo*.[8] These molecules consist largely of flat benzene rings. In the crystals they are stacked together to form a column, in which the molecules are parallel to one another. The normal of the molecular plane is slightly tilted against the column axis. Thin films of copper-phthalocyanine, one of polycyclic aromatic compounds, when vacuum-sublimated on muscovite had two sorts of orientation according to the conditions of sublimation.[9,10] Similarly, phthalocyanine crystals deposited on a cleavage face of alkali halides took two types of orientation in compliance with the sort of substrate crystal.[11] These two orientations were called the parallel *b*-axis and the standing *b*-axis orientation, according to the direction of the *b*-axis of the crystal relative to the substrate face. In the crystal with the parallel *b*-axis orientation, the flat molecule stands obliquely on the substrate face and touches it at several points. On the contrary, in the case of the standing *b*-axis orientation the molecular planes are in contact parallel to the substrate face and the apparent symmetry of the oriented crystals is determined by the molecular symmetry. The basic orientation taken by a single molecule is determined by the molecular interaction between substrate atoms and adsorbed gas on the cleavage face. The molecules of polycyclic aromatic quinones have lower symmetry than that of phthalocyanine, and their way of packing in the crystal is remarkably similar to that of the latter. In order to establish that two such kinds of orientation occur also for other condensed polycyclic aromatic compounds, similar polycyclic aromatic quinones were vacuum-sublimated onto a cleavage face of alkali halides and the orientation overgrowth of these crystals was investigated by means of electron microscopy as well as by means of electron diffraction.

Experimental

The polycyclic aromatic quinones used in this work were flavanthrone ($C_{28}H_{12}O_2N_2$), indanthrone ($C_{28}H_{14}O_4N_2$), and pyranthrone ($C_{30}H_{14}O_2$); their constitutional formulas are shown in Fig. 1. These compounds were purified by repeated sublimation in a low-pressure stream of carbon dioxide at a temperature above 400°C and were examined by means of an X-ray diffractometer. The purified materials were sublimated from a tungsten basket onto a clean surface of alkali halide in a vacuum evaporator, as has been described in a previous paper.[10] Single crystals of rock salt and sylvine were used as the substrate. They were cleaved in air and immediately placed in the vacuum evaporator. The temperature of the substrate was kept in the range from 100 to 200°C.

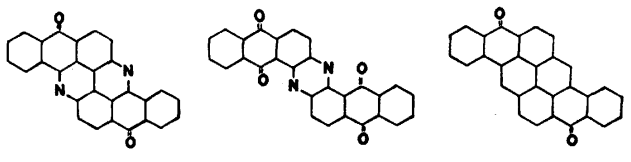

Flavanthrone Indanthrone Pyranthrone

Fig. 1. Constitutional formulas of quinones.

The specimens used for electron microscopy were prepared by the wet-stripping method after they had been reinforced with evaporated carbon film. Thallium chloride prepared by deposition *in vacuo* was used as a standard calibration material for the spacing measurements.

Results

A) Epitaxial Growth on Rock Salt. When flavanthrone was sublimated onto a cleavage face of rock salt at 150°C, certain areas of the film showed the well-defined, sngle-directional orientation whose electron micrograph and electron-diffraction pattern are shown in Figs. 2(a) and (b) respectively. The film was composed of laminar crystal strips giving rise to a raft structure as a whole. The fiber diagram obtained from the film reveals that the meridian coincides with the needle axis of the crystal strips. The maximum lattice spacing along this direction turned out to be 3.81 Å, which is in good agreement with the unit cell length of the *b*-axis. The diffraction spots on the equator have an equidistance of 8.10Å, which

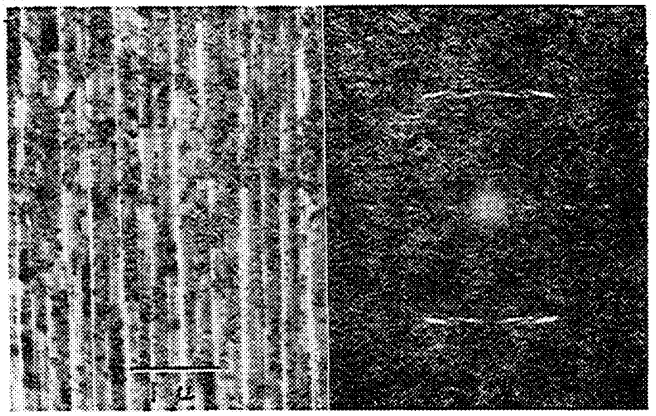

(a) (b)

Fig. 2. Electron micrograph (a) and electron diffraction pattern (b) of flavanthrone film vacuum-condensed onto the (001) plane of NaCl. Crystals assume the parallel *b*-axis orientation with single direction.

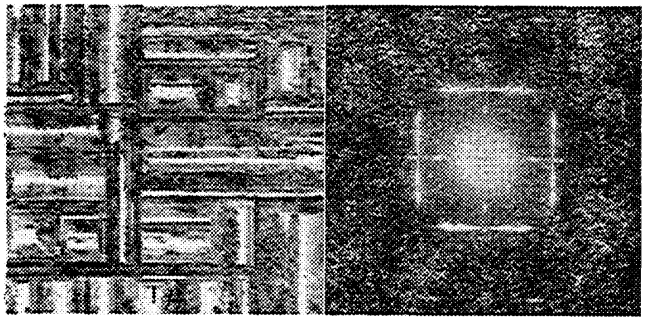

(a) (b)

Fig. 3. Electron micrograph (a) and electron diffraction pattern (b) of flavanthrone film vacuum-condensed onto the (001) plane of NaCl. Crystals assume the parallel *b*-axis orientation with double direction.

8) E. Suito, N. Uyeda, and M. Ashida, *Nature*, **194**, 273 (1962).
9) N. Uyeda, M. Ashida, and E. Suito, *J. Appl. Phys.*, **36**, 1453 (1965).
10) M. Ashida, This Bulletin, **39**, 2625 (1966).
11) M. Ashida, *ibid.*, **39**, 2632 (1966).

corresponds to 001 and its higher-order reflections. Thus, each crystal strip grows along the *b*-axis and its (001) plane lies parallel to the substrate face. The other areas of the flavanthrone film were composed of two groups of slender crystal strips crossing each other orthogonally, as is shown in Fig. 3 (a). Corresponding to such a configuration of the film, the diffraction pattern also had an orthogonal appearance, as Fig. 3(b) shows. This pattern is a superposition of two identical fiber diagrams, each of which is essentially the same as that of the single-directional orientation mentioned above. In order to establish the orientation of the deposited crystals relative to the substrate rock salt, well-developed crystals on the cleavage face were observed by means of an optical microscope. The needle axis of the deposited crystals was found to be parallel to the <110> direction of the substrate crystal.

When indanthrone was sublimated onto a cleavage face of rock salt, the film was built up of quite the same networks of laminar crystal strips crossing orthogonally as those of flavanthrone film. The electron-diffraction pattern in Fig. 4(a) also shows that the film assumes a double-directional orientation with strips crossing each other rectangularly. Each fiber spacing with a distance of 3.83 Å coincides with the unit length of the *b*-axis, and the series of the spots on the equator with a interplanar spacing of 15.4 Å corresponds to 200 and its higher-order reflections. The individual *b*-axis of the crystal was parallel to the <110> direction of rock salt.

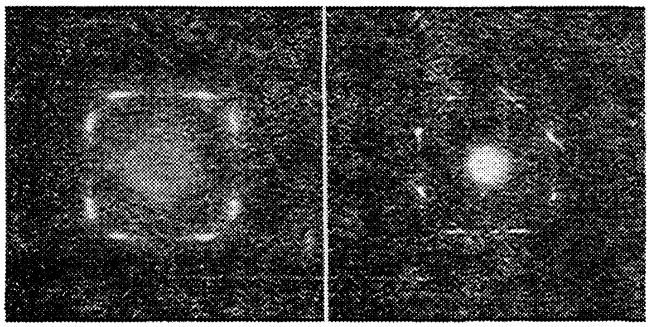

(a) (b)

Fig. 4. (a): Electron diffraction pattern of indanthrone film vacuum-condensed onto the (001) plane of NaCl at 150°C. (b): Electron diffraction pattern of pyranthrone film vacuum-condensed onto the (001) plane of NaCl at 200°C.

Pyranthrone films sublimated on rock salt took the same double-directional orientation as flavanthrone and indanthrone when the substrate was held to under 150°C. On the other hand, a triple-directional orientation was observed when the temperature of the substrate was raised to 200°C. An electron-diffraction pattern of the resulting film is a superposition of three identical fiber diagrams, as is shown in Fig. 4(b). The two dominant directions coincide with both the [110] and [1$\bar{1}$0] directions of rock salt, while the other faint direction runs parallel to the [100] direction of the substrate crystal. It should be noted that there are a few crystallites of pyranthrone growing along the [100] direction of the substrate rock salt as the temperature is raised to 200°C.

The characteristic behavior of the crystals deposited on rock salt is that their *b*-axes run parallel to the substrate face and that, consequently, they assume the parallel *b*-axis orientation.

B) Epitaxial Growth on Sylvine. When a cleavage face of sylvine was used as the substrate, vacuum-condensed films of polycyclic aromatic quinones showed quite a different orientation from those on the rock salt.

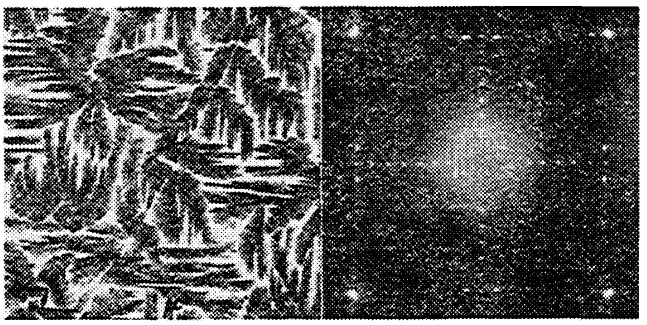

(a) (b)

Fig. 5. Electron micrograph (a) and electron diffraction pattern (b) of flavanthrone film vacuum-condensed onto the (001) plane of KCl. Crystals assume the standing *b*-axis orientation.

Flavanthrone crystals sublimated onto sylvine grow well-defined dendrites and form a discrete film, as is shown in Fig. 5(a). The electron-diffraction pattern of the film shown in Fig. 5(b) appears to overlap two single crystal patterns crossing orthogonally each other in spite of the reflections from many crystallites. This finding suggests that all the crystals deposited on sylvine take a well-defined orientation. Since the series of spots on the equator is equidistant corresponding to the interplanar spacing of 13.9 Å, they are clearly 200 and its higher-order reflections. On the contrary, the spacing of 1.75 Å, which is obtained from the distance between the first layer line and the equator, does not agree with any unit length of the crystallographic axes. The appearance of such layered lines should be ascribed to the position of the main zone axes of the deposited crystals, which are tilted against the substrate face and, consequently, against the electron beam. Because the equatorial spots have the indices of *h*00, all the spots within each layer line should have indices with the same *k* and *l* values. The spacing of the (014) plane is 1.78 Å. Thus, the spots on the layer lines above and below the equator correspond to *h*14 (or *h*1$\bar{4}$) and *h*$\bar{1}$4 (or *h*$\bar{1}$$\bar{4}$) respectively, and the *b*-axis of the crystal makes an angle of about 28° with the normal of the substrate face. The diffraction spots were indexed as is shown schematically in Fig. 6, in which the white circles represent the basic single crystal pattern. The total pattern is obtained by a superposition of this elementary pattern by the symmetry operation of C_{4v}, whose major axes are XX′ and YY′. By relating the orientation to the substrate crystal, the *a*-axis of flavanthrone was found to run along the <110> direction of sylvine.

In the case of indanthrone, the deposited film on

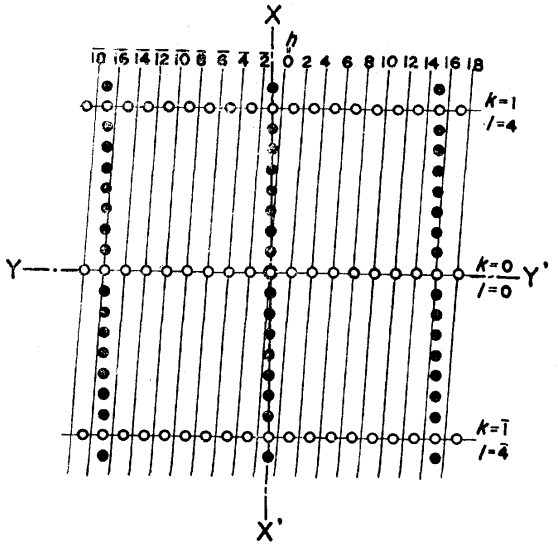

Fig. 6. The interpretation of the diffraction pattern shown in Fig. 5. White circles are the representation of the basic single pattern.

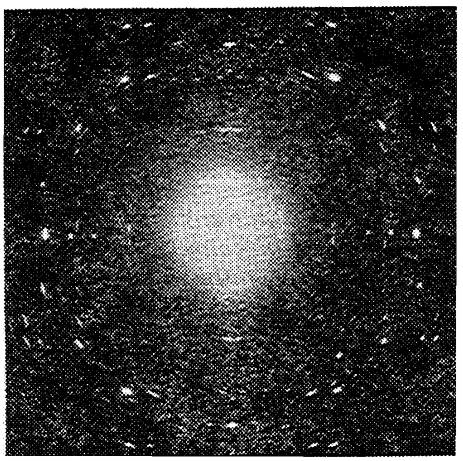

Fig. 7. Electron diffraction pattern of indanthrone film vacuum-condensed onto the (001) plane of KCl.

sylvine was composed of dendroid crystals similar to those of flavanthrone. The electron-diffraction pattern of the film shows a complicated pattern with the C_{4v} symmetry, as is represented in Fig. 7. Therefore, the film turned out to include eight groups of crystals, in each of which the crystals had the same orientation. Each elementary cross-grating pattern consits of three parallel regions. The unit length of the *b*-axis is more shorter than those of the *a*- and *c*-axes, so the reciprocal lattice plane with $k=1$ is located at a far distance compared with the other reciprocal lattice planes. Therefore, the spots in the region which includes the origin are the *h*0*l* reflections. They appear as at the intersection of the reciprocal lattice points as well as in their elongated intensity regions with the Ewald sphere. The other regions, which do not pass through the point of origin, correspond to the reciprocal lattice planes of $k=\pm1$. Thus, the total diffraction pattern is as is schematically reproduced in Fig. 8, in which the white circles indicate the basic single crystal pattern associated with one of two groups of crystals which have an apparent C_2 symmetry. Although the total pattern appears to be complicated, it can be illustrated by the systematic superposition of this elementary pattern with the major axes of C_{4v} symmetry, XX′ and YY′, which further coincide with the [110] and [1$\bar{1}$0] directions of sylvine respectively. From a consideration of the observed and calculated spacings as well as the intensities, the reciprocal lattice points, 804 and 91$\bar{2}$, were found to lie directly on the Ewald sphere. Consequently, the *a*-, *b*-, and *c*-axes of the crystal are inclined to the normal of the substrate face at angles of about 120°, 35°, and 76° respectively. As the AB line is the reciprocal *c** axis in the elementary pattern, the other lines, CD, EF, and GH, are similar *c** axes associated with individual crystal groups. Each reciprocal *c** axis was found to make an angle of about 5° with the nearest major axis of C_{4v} symmetry.

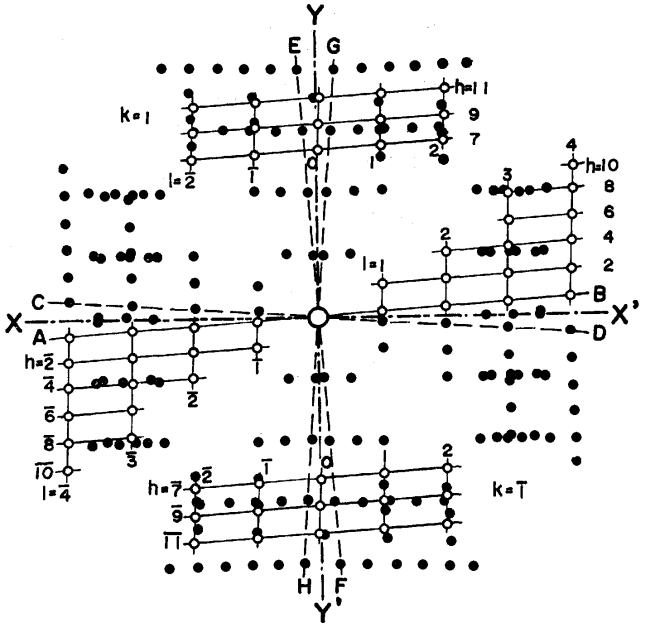

Fig. 8. The interpretation of the diffraction pattern shown in Fig. 7. White circles are the representation of the basic single crystal pattern.

Well-developed crystals of pyranthrone sublimated on sylvine had a definite wedge-like form, as is shown in Fig. 9(a). The electron-diffraction pattern of Fig. 9(b) represents an imperfect ring diagram, which indicates a random orientation. However, a selected area electron-diffraction pattern from one of the crystals, such as the one circled in Fig. 9(a), gave a single net pattern composed of three separate regions, as Fig. 9(c) shows. The diffraction spots were indexed as is schematically shown in Fig. 10. Considering the interplanar spacings and the intensities of the diffraction spots, it is found that the reciprocal lattice points, 105 and 10,1,$\bar{3}$, lie directly on the Ewald sphere. Consequently, the *b*-axis of the crystal tilts against the normal of the substrate surface at an angle of about 29°. If this single net pattern rotates around the point of origin, the resulting diagram coincides with the ring pattern of Fig. 9(b). Therefore, the random orientation seen in Fig. 9(b) arises from the differences in the tilting directions of the *b*-axes of the individual

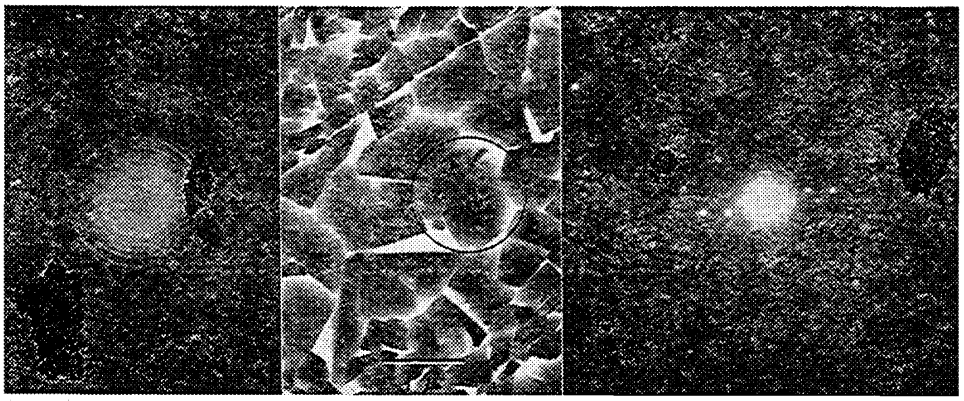

(b) (a) (c)

Fig. 9. Electron micrograph (a) and electron diffraction pattern (b) of pyranthrone film vacuum-condensed onto the (001) plane of KCl. Selected area diffraction pattern (c) of the crystal indicated by the circle in (a).

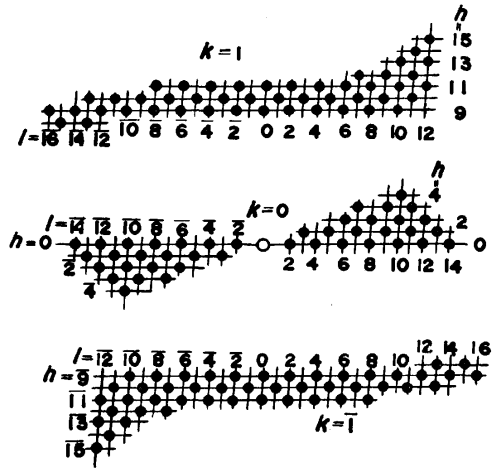

Fig. 10. The interpretation of the diffraction pattern shown in Fig. 9 (c).

crystallites, though the inclination angle of each *b*-axis to the normal of the substrate face is always a constant value of 29°.

Discussion

The crystal data of indanthrone, flavanthrone, and pyranthrone reported by Bailey,[12] Stadler,[13] and Maitland and Stadler[14] are summarized in Table 1. The molecules of polycyclic aromatic quinones are composed of many condensed benzene rings and form a flat plane, or a nearly flat one, as a whole. These flat molecules are closely packed together in a column, giving rise to a tilt against the column axis. The inclination angles of the molecular plane against the orthogonal *a*-, *b*-, or *c**-axis of each crystal are also shown in Table 1. When flavanthrone was sublimated on rock salt, the (001) face of the deposited crystal lay parallel to the substrate surface and its *b*-axis ran along either the [110] or [1$\bar{1}$0] axis of the substrate crystal. Since the planar molecules are not parallel to the (001) plane, they stand obliquely on the substrate surface so that they come in contact with the interface at several points. It is a problem which ion of sodium chloride attracts the deposited molecule and which atom of the flavanthrone molecule touches the substrate face. However, if a particular part in one molecule is located on the top of one Na^+ or Cl^- ion, it is likely that the same part of the adjacent molecule along the *b*-axis comes near to the top of the other like-charged ion and the crystal grows along the *b*-axis to form rod-like outward. In the cleavage face of rock salt, the distance between like-charged ions is 5.63 Å and 3.97 Å along the [100] and [110] axes respectively. Comparing these values with the length of the *b*-axis of the flavanthrone crystal, it seems reasonable that the preferential orientation of the deposits in the <110> directions occurs in the cleavage face of rock salt. The same characteristic behavior of other quinones, indanthrone, and pyranthrone was found in their epitaxial growth on rock salt. When the strips assume a cross-directional raft structure, the mutual orientation is uniquely defined and the needle axis of individual strips, essentially the *b*-axis, coincides with the <110> directions of rock salt. In the case of pyranthrone, in addition to these directions, a small number of crystallites oriented their *b*-axis parallel to the [100] direction of rock salt at high temperatures above 200°C. The different orientation observed in the pyranthrone film may be due to a weaker interaction between the deposit and substrate ions than those in the other quinones studied. If the energy of thermal vibration is not very high, the orientation in the <110> direction caused by this interaction will be favored. If the substrate temperature is raised and the energy of thermal vibration becomes high, the effect of the interaction will be reduced relatively and the alignment of the crystal will not be entirely specific in the <110> directions. Recently, Koutsky *et al.*[4,5] have reported that some polymers which crystallized epitaxially from a solution on alkali halide surfaces grew small, rod-like crystallites with an orientation in the <110> directions of the substrates. They also concluded that the polymer epitaxy was dependent on rows of like-charged ions in the

12) M. Bailey, *Acta Crystallogr.*, **8**, 182 (1955).
13) H. P. Stadler, *ibid.*, **6**, 540 (1953).

Table 1. Crystal data of quinones

		Flavanthrone	Indanthrone	Pyranthrone
Unit cell constants	a (Å)	27.9	30.8	22.0
	b (Å)	3.80	3.83	3.84
	c (Å)	8.10	7.84	21.2
	β	95°	92°	90°
	z	2	2	4
Space group		$P2_1/a$	$P2_1/a$	$P2_1/n$
Angles between crystal axes and the normal of molecular plane				
	a-axis	105°, 75°	110°, 80°	
	b-axis	26°	26°	26°
	c^*-axis	72°, 108°	75°, 105°	

substrate surfaces.

On the contrary, when sylvine was used as the substrate, the deposited films showed quite a different orientation, one giving rise to various morphological features. In the case of the flavanthrone crystal on sylvine, its b-axis is inclined to the normal of the substrate face at an angle of 28° and the a-axis runs along the <110> directions of sylvine. Because the molecular plane of flavanthrone is inclined against the (010) plane at an angle of 26°, the standing b-axis orientation suggests that the planar molecule nearly comes in contact parallelly with the substrate face. In heterocyclic compounds the charge is distributed on nitrogen atoms with a high density.[15] Therefore, in the planar molecule facing the substrate, it seems reasonable to assume that the nitrogen atoms of the molecule come in contact with K^+ ions, as is schematically shown in Fig. 11. A projection of the above molecules facing parallel along the b-axis on a molecular plane shifts in either the b_p or b_p' direction, which coincides with the [110] direction of sylvine, depending upon the staggering of the overlapping molecule. This configuration results in two different crystals which are related by a two-fold rotation axis. As sylvine has a four-fold rotation axis perpendicular to its (001) plane, the same relative orientation between the deposited and substrate crystals is obtained by the rotation of 90° in the deposited molecule. This gives rise to two different crystals, the projection of whose b-axis coincides with the $[1\bar{1}0]$ direction of sylvine. Thus, the total film consists of four groups of oriented crystals and the electron-diffraction pattern from them gives two overlapping diagrams crossing orthogonally. However, when we compare the inclination angles of the crystal axes to molecular plane with the tilting angle of the oriented crystal, it is clear that the flat molecule does not lie strictly parallel to the substrate face. Presumably each molecule is initially adsorbed parallelly to the (001) plane of sylvine, but the intermolecular force among neighboring molecules pulls the lying molecule slightly up, so that a perfect three-dimensional configuration builds up within the crystal.

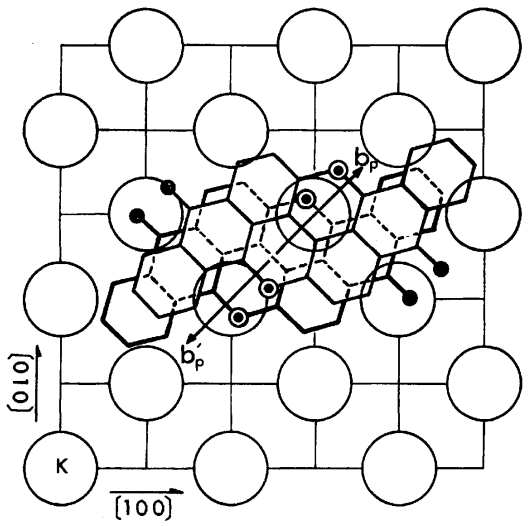

Fig. 11. The lattice structure of the (001) plane of KCl and the relative orientation of the deposited flavanthrone.
●: oxygen atom
⊙: nitrogen atom

The crystal of indanthrone sublimated on sylvine took the standing b-axis orientation, in which the a-, b-, and c-axes are inclined to the normal of the substrate face at angles of about 120°, 35°, and 76° respectively. When we compare these values with the inclination angles of the molecular plane against the crystal axes, it seems reasonable to conclude that the molecular plane comes into parallel contact with the substrate face. If the nitrogen atoms of the molecule are assumed to lie on K^+ ions, as is schematically shown in Fig. 12, a projection of the above molecule facing parallel along the b-axis on a molecular plane shifts in either the b_p or b_p' direction, which makes an angle of 30° with the $[1\bar{1}0]$ direction of sylvine. A projection of the c-axis on a molecular plane makes an angle of 125° with that of the b-axis, as is shown by the OA and OB lines concerned with b_p and b_p' and, consequently, makes an angle of 5° with the $[1\bar{1}0]$ direction of sylvine; this results in two different crystals related by the two-fold rotation axis. It should be noted that this angle coincides with that between the projection of the reciprocal c^*-axis of the indanthrone crystal and the [110] direction of sylvine as revealed by the electron-diffraction pattern. If a molecule is rotated about the XX′ axis by 180°, the molecule lies at the same position relative to the substrate ions. In this case, a projection

15) H. C. Longuet-Higgins and C. A. Coulson, *Trans. Faraday Soc.*, **43**, 87 (1947).

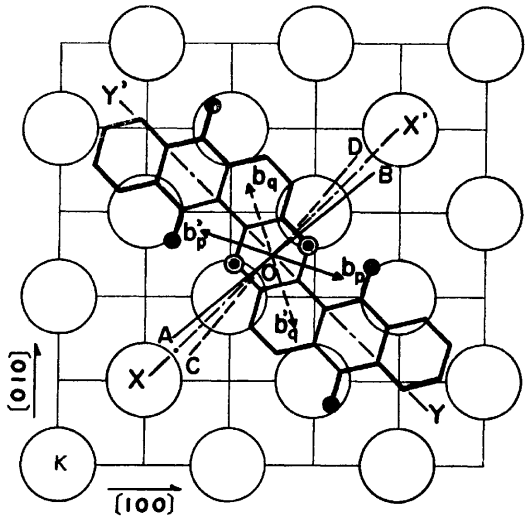

Fig. 12. Schematic diagram of the relative orientation of indanthrone to the (001) plane of KCl.
●: oxygen atom
⊙: nitrogen atom

of the *b*-axis on the surface makes an angle of 30° with the [1$\bar{1}$0] direction of sylvine, as is shown by b_q and b_q', and the projection of the *c*-axis is as is represented by the CD line. Consequently, such a molecular orientation gives rise to four sets of crystals with an apparent C_{2v} symmetry, whose mirror plane is perpendicular to the [110] direction, as is represented by the XX′ line. Moreover, the same relative orientation between the deposited and substrate crystals is obtained by the rotation of 90° in the deposited molecule. The orientation of the resulting crystals has a symmetry of C_{2v} as a whole, whose mirror plane is perpendicular to the [1$\bar{1}$0] direction, as is represented by the YY′ line. Thus, the total film involves eight sets of oriented crystals and shows an apparent C_{4v} symmetry, as far as the orientation of individual crystallites is concerned.

In the pyranthrone film vacuum-sublimated on sylvine, the individual crystals assumed the standing *b*-axis orientation, in which the *b*-axis tilted against the substrate face with an angle of 29°. However, the ring pattern from the total film suggested that the individual tilting *b*-axis took a random direction independent of the alignment of ions in the cleavage face of sylvine. When the inclination of the molecular plane to the crystal axes is considered, it is clear that the molecular plane is parallel to the substrate face, but no strictly preferential location of the component atoms in the deposited molecule seems to occur in this case. Pyranthrone is closely related to flavanthrone, in which the two C-H groups are replaced by N atoms. Both flavanthrone and indanthrone belong to the same structure type with the $P2_1/a$ space group, and their molecular planes are tilted about the C–O bond as an axis. On the other hand, pyranthrone belongs to a different structure type which contains two independent molecules per asymmetric unit. Perhaps there is a difference in the intermolecular forces of pyranthrone and the other quinones studied.

The various orientations on the cleavage faces of alkali halides may be caused by the complex combination of mutual interaction between the deposited and substrate crystals and the intermolecular force within the crystal. The condensed polycyclic aromatic compounds include π electrons out of the molecular plane. These electrons may affect the way of molecular adsorption by interaction with the gas which is adsorbed on the substrate face in advance, as been described in previous papers.[10,16] Therefore, the mode of molecular adsorption, the parallel *b*-axis or the standing *b*-axis orientation, is perhaps primarily determined by the interaction between these π electrons and the substrate face. The position of the individual component atoms relative to the substrate ions is determined by the charge distribution in the molecule itself. The influence of adsorption gas on orientation overgrowth will be described in a future report. For organic crystals composed of large flat molecules, we may suppose that both the charge distribution and the configuration of the molecules themselves, as well as the total lattice dimensions of the deposited and substrate crystals, are important in determining epitaxial growth.

The authors wish to thank Professor Eiji Suito and Dr. Natsu Uyeda of the Institute for Chemical Research, Kyoto University, for their many helpful discussions during this work.

16) N. Uyeda, M. Ashida, and E. Suito, Sixth Intern'l Cong. Electron Microscopy, Kyoto, **1**, 485 (1966).

The Dehalogenation of Haloalkanes on SiO_2-supported Metals

Yasuhide ANJU, Isao MOCHIDA, Hiroko YAMAMOTO, Akio KATO, and Tetsuro SEIYAMA

Department of Applied Chemistry, Faculty of Engineering, Kyushu University, Fukuoka

(Received November 25, 1971)

The dehalogenations of haloethanes and halopropanes over metals (Cu, Ag, Au, Fe, Co, Ni, Pd, and Pt) supported by silica gel were studied by means of the microcatalytic pulse technique in order to elucidate the mechanism of dehalogenation. The dechlorination reactivities of *cis*- and *trans*-1,2-dichloroethylenes and the dechlorination products from *dl*- and *meso*-2,3-dichlorobutanes were observed from the viewpoint of stereoselectivity. The order of catalytic activities among the metals for the dehalogenation of haloethanes was: Pt>Cu≈Ni>Ag≈Co≈Pd>Fe≈Au. Dehalogenation proceeded exclusively in the 1,2-dihaloethanes. However, dehydorhalogenation took place in the 1,2-dihalopropanes to an appreciable extent when the product distributions of dehydrohalogenation were similar to those on solid acids. Both 1,1,2-trichloroethane and 1,2-dichloropropane were more reactive than 1,2-dichloroethane. 1,2-dichloroethylenes from 1,1,2,2-tetrachloroethane and 2-butenes from *dl*- and *meso*-2,3-dichlorobutanes were nearly in an equilibrium ratio of *cis*/*trans* forms. From a comparison of these results with those of the dehydrohalogenation on solid acids, it is concluded that the dehalogenation of haloalkanes on metals proceeds through a radical-step-by-step mechanism.

It has been reported that the dechlorination of chloroethanes on chromia proceeds through an E2-concerted mechanism.[1] The dechlorination on metal sulfates has interest in connection with the stereoselectivity and activity which depend on the kind of metal ion.[2] It may be expected that the dehalogenation takes place selectivity on metals because of the nonpolar nature of their surfaces.

In the liquid phase, the reactions of *vic*-dibromoalkanes with metals such as Mg and Zn were studied, and an E2-concerted mechanism or a carbanion mechanism has been proposed on the basis of the product distribution.[3] It is interesting to compare the gas-phase dehalogenation on metals with the liquid-phase reaction.

In the present study, the dehalogenation of haloethanes and halopropanes on metals (Cu, Ag, Au, Fe, Co, Ni, Pd, and Pt) was investigated in order to elucidate the characteristics of metals compared with compound catalysts with regard to halogen-metal interaction. The activities of metals and the reactivities of several chloroalkanes were analyzed on the basis of the δ_C and δ_R LFER approaches.[1,2,4]

Additional information was obtained from the dechlorinations of 1,2-dichloroethylenes and 2,3-dichlorobutanes on several metals.

Experimental

Reagents. The reagents used in this work were obtained from the Tokyo Kasei Co. They were of an E.P. grade and were used without further purification. The *dl*- and *meso*-2,3-dichlorobutanes were obtained by the resolution of their mixture by using a DIDP (2 m, 20°C) column.

Catalysts. The metal catalysts supported by silica gel were obtained by impregnating silica gel (Wako) with an aqueous solution of metal salt (Cu, Ag, Co, Ni : nitrate, Au, Pd, Pt : chloride, Fe : hydroxide); then they were dried at 120°C in the atmosphere. Each catalyst contained 0.4 mg-atom/g-silica gel. Before use, all of them except Fe, Co, and Ni (Fe, Co : 450°C, Ni : 400°C) were reduced at 300°C by the hydrogen in the reactor.

Procedures. The reaction rates and selectivities were measured by the microcatalytic gas chromatographic technique in the temperature range from 200 to 450°C. TCP was used in an analytical column (60 or 120°C, 2 m). Silicon SF (4 m, room temperature) was also used for the separation of the butenes. Hydrogen gas was used as the carrier. Hydrogenolysis was very small, even on Pt, Ni, and Pd, in the reaction of 1,2-dihaloethane. However, decompositions other than dechlorination took place to a considerable extent in the reactions of 1,1,2,2-tetrachloroethane and 1,1,2-trichloroethane on Pd and Pt, so helium gas was used in these cases. The activities decreased from pulse to pulse (the second pulse conversion was *ca.* 50% of the first), so the reaction rates were obtained from the first pulse. This deactivation by reaction products means that the reaction observed in the present study is the halogenation of metals by haloalkanes. The reaction rates (ml/g·min) were measured below a 20% conversion. The details of the experiments have been described in previous papers.[1,2,5]

Results

Dehalogenation Activities of Metal Supported by Silica Gel. As for 1,2-dihaloethanes, dehalogenation took place exclusively on the metals supported by silica gel, except for 1,2-dibromoethane on Fe, where dehydrobromination took place to a considerable extent. The catalytic activities of metals for 1,2-dichloroethane are shown in Fig.1 as a function of the reaction temperature. The results for 1,2-dibromoethane are shown in Fig.2. The activities of the meatls at 300°C were in the order of Pt>Cu≈Ni>Co≈Ag≈Pd>Fe≈Au in both dehalogenations. The reactivities of the two haloethanes are compared in Fig.3. The rates of debromination were larger than those of dechlorination. This difference was pronounced on Pt, Pd, and Fe. The apparent activation energies were smaller for debromination than for dechlorination, corresponding to the higher re-

1) I. Mochida and Y. Yoneda, *J. Org. Chem.*, **33**, 2163 (1968).

2) a) I. Mochida, A. Kato, and T. Seiyama, *J. Catal.*, **18**, 33 (1970). b) I. Mochida, Y. Anju, H. Yamamoto, A. Kato, and T. Seiyama, This Bulletin, **44**, 3305 (1971).

3) L. Crombie and S. Harper, *J. Amer. Chem. Soc.*, **72**, 1707 (1950), H. O. House and R. S. Ro, *ibid.*, **80**, 182 (1958).

4) I. Mochida and Y. Yoneda, *J. Catal.* **8**, 223 (1967).

5) I. Mochida, Y. Anju, A. Kato, and T. Seiyama, This Bulletin, **45**, 1635 (1972).

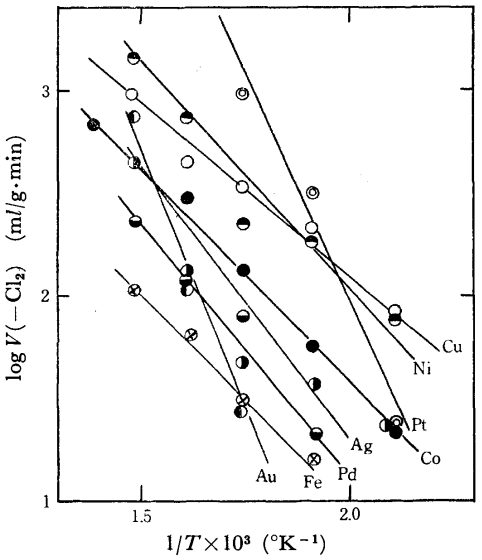

Fig. 1. Arrhenius plots of dechlorination of 1,2-dichloroethane on metals supported by silica gel.

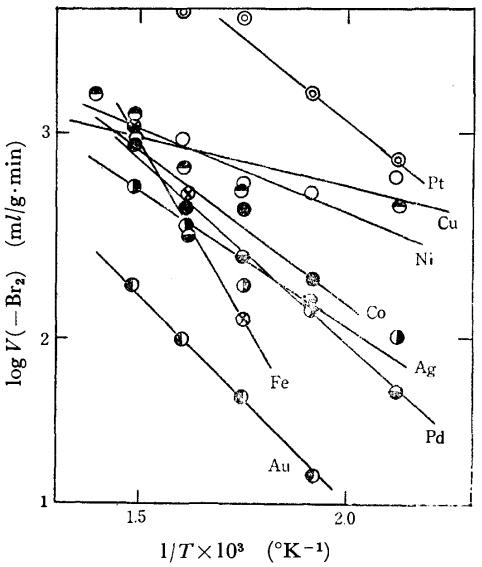

Fig. 2. Arrhenius plots of debromination of 1,2-dibromoethane on metals supported by silica gel.

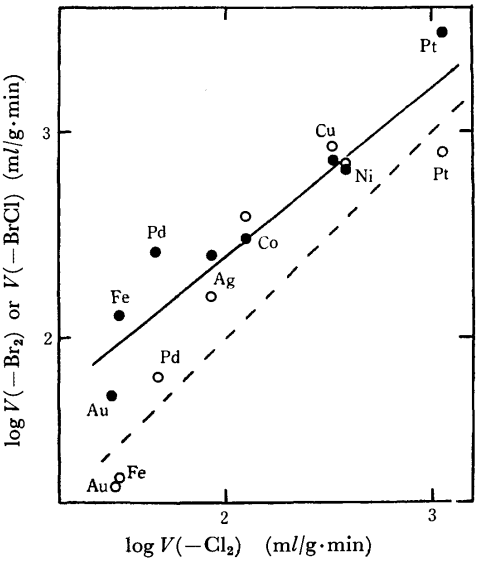

Fig. 3. Dehalogenation-reactivities of 1,2-dihaloethane at 300°C, abscissa; dechlorination of 1,2-dichloroethane, ordiate; debromination of 1,2-dibromoethane(●), and dechlorobromination of 1-bromo-2-chloroethane(○). Dotted line indicates the rate equal to dechlorination of 1,2-dichloroethane.

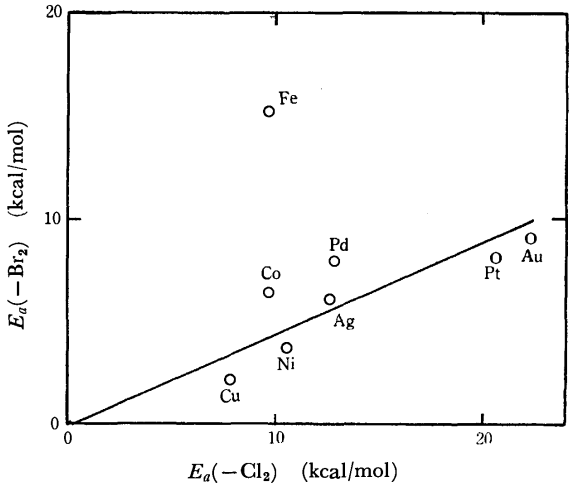

Fig. 4. Apparent activation energies of dehalogenation, abscissa; dechlorination of 1,2-dichloroethane, ordiate; debromination of 1,2-dibromoethane.

activity of the bromoethane. One can observe a correlation between the values of the apparent activation energies for the two dehalogenations. This correlation, together with the correlation of reactivities shown in Fig.3, indicates a similarity in the mechanisms between the two reactions.

On the other hand, the reactivity order among the three dihaloethanes, 1,2-dichloroethane, 1,2-dibromoethane and 1-bromo-2-chloroethane, varied according to the kind of metal as may be seen in Fig.3. The debromochlorination-reactivity of 1-bromo-2-chloroethane was near the debromination-reactivity of 1,2-dibromoethane on Cu, Ni, Co, and Ag, but was rather close to the dechlorination-reactivity on Pt, Pd, Au, and Fe. The first metal group shows a small activation energy, as may be seen in Fig.4. These results may reflect the difference between the two groups in the affinity of the metal to chlorine and bromine.

Substituent Effects on the Dechlorination Reactivity. The reactivities of three chloroethanes and 1,2-dichloropropane on some metals at 300°C are shown in Table1. The order of the reactivity was 1,1,2,2-tetrachloroethane > 1,1,2-trichloroethane > 1,2-dichloropropane > 1,2-dichloroethane. This order is different from that in dehydrohalogenation on solid acids, where 1,1,2-trichloroethane is much more reactive than 1,1,2,2-tetrachloroethane.[6] The above order is rather similar to that of dehydrochlorination on solid bases, but the reactivity differences among these reactants are not so large as in the dehydrochlorination on solid bases.[6]

6) I. Mochida, J. Take, Y. Saito, and Y. Yoneda, *J. Org. Chem.*, **32**, 3894 (1967).

TABLE 1. THE RATES OF DECHLORINATION OF SOME CHLOROETHANES AND 1,2-DICHLOROPROPANE ON METALS AT 300°C

Metal	Reactant			
	1,2-dichloro-propane	1,2-dichloro-ethane	1,1,2-tri-chloroethane	1,1,2,2-tetra-chloroethane
Cu	580	340	630	950
Ag	89	87	141	185
Au	98	89	109	140
Fe	18[a]	30	46	110
Co	186[a]	130	250	310
Ni	550	380	970	990
Pd[b]	19	6.7	20	19
Pt[b]	68	43	49	153

a) The rate of dehydrochlorination was very large as shown in Table 2.
b) Helium was used as a carrier gas.

TABLE 2. ELIMINATION OF 1,2-DIHALOPROPANE ON METALS SUPPORTED BY SILICA GEL AT 300°C[a] THE RESULTS WITH REGARD TO SOLID ACIDS WERE SHOWN FOR COMPARISON

Cat.	Reactant									
	1,2-dichloropropane					1,2-dibromopropane				
	$-Cl_2$(A)	$-HCl$(B)[b]	B/A	all./1[d]	t/c[e]	$-Br_2$(C)	$-HBr$(D)[c]	D/C	all./1[d']	t/c[e']
SA[f]	16.8	948	56.2	0.608	0.140	91	1575	17.3	3.86	0.390
Ag[g]	16.3	247	15.1	0.184	0.024	212	391	1.84	0.634	0.134
Fe	18.5	420	22.7	0.499	0.132	459	1248	2.75	0.805	0.377
Co	186	215	1.15	0.107	0.084	438	539	0.965	0.809	0.162
Ni	554	101	0.182	0	0.233	740	197	0.266	0.989	0
Cu	583	178	0.305	0.022	0.317	818	236	0.289	0.243	0
Ag	88.9	29	0.326	0.544	0.027	395	176	0.446	1.07	0.162
Au	98.2	6.2	0.070	0	0	67	30.7	0.458	—	—
Pd[h]	19.4	0	0			185	0	0		
Pt[h]	68.4	0	0			990	0	0		

a) Dehydrohalogenation did not proceed on Pd and Pt at all.
b) 2-chloropropylene was not detected at all except on Ni.
c) 2-bromopropane was detected on Fe, Co, Ni, but the mount was very small except Ni.
d, d') The ratio of allylchloride/1-chloropropylene and that of allylbromide/1-bromopropylene, respectively.
e, e') The ratio of *trans*-1-chloropropylene/*cis*-1-chloropropylene and that of *trans*-1-bromopropylene/*cis*-1-bromopropylene, respectively.
f) Silica alumina (13% Al_2O_3)
g) Alumina (calcined at 550°C)
h) Helium was used as a carrier gas.

The dehydrohalogenation of 1,2-dihalopropanes took place simultaneously with the dehalogenation to various extents, according to the kind of metal. The ratios of dehydrohalogenation/dehalogenation are shown in Table 2. The ratio is high on Fe and Co. The dehydrohalogenation-activities of metals were in the following order: Fe>Co>Cu, Ag, Ni, Au≫Pt, Pd. Allyl chloride, and 1-chloropropylenes, mainly *cis*-1-chloropropylene, were formed by the dehydrochlorinaiton of 1,2-dichloropropane. These product distributions are similar to those on solid acids.[7]

Stereoselectivity in Dechlorination. The products of dechlorination of 1,1,2,2-tetrachloroethane were *trans*- and *cis*-1,2-dichloroethylenes. 1,1-dichloroethylene was not detected. The ratios of *trans*-1,2/*cis*-1,2 obtained were near to the equilibrium value (0.654 at 300°[8]) on most metals except for Cu and Au, where the ratios were nearly unity. These selectivities were considered to be those for the primary product, since the rates of the isomerization of 1,2-dichloroethlyene were small compared with those of the dechlorination. It is interesting that the ferric and cupric sulfates on silica gel also gave, respectively, the equilibrium value and unity for this selectivity.

The *meso*- and *dl*-forms of 2,3-dichlorobutane have been used to investigate the stereospecificity in the eliminations: the dechlorination on zinc and magnesium metals in the liquid phase[3] and the dehydrochlorination on alkali- and alkali earth-metal salts.[9] In the present dechlorination on metals in the vapor

7) H. Tominaga, T. Nakamura, H. Arai, and T. Kunugi, *Kogyo Kagaku Zasshi*, **74**, 199 (1971).

8) A. S. Pitzer and J. L. Hollenberg, *J. Amer. Chem. Soc.*, **67**, 1493 (1954).

9) H. Noller, P. Andreu, and M. Hunger, *Angew. Chem. Int. Ed.*, (*Engl.*), **10**, 172 (1971).

Table 3. The ratio of 2-butenes, that is the ratio of dechlorination products from *dl*- and *meso*-2,3-dichlorobutanes

Metal	Reaction temperature	*trans*/*cis*[a]	*trans*/*cis*[b]
Cu[c]	100°C	1.9	2.0
Pt[d]	300°C	1.4	1.6

a) The ratio of 2-butenes, from *dl* form.
b) The ratio of 2-butenes, from *meso* form.
c) Hydrogen was used as a carrier gas.
d) Helium was used as a carrier gas. *i*-Butene was the main dechlorination product.

Table 4. The rates of *trans*- and *cis*-elimination ($-Cl_2$) of 1,2-dichloroethylenes at 300°C

Metal	Rate of *trans*-elim.[a] (ml/g·min)	Rate of *cis*-elim.[b] (ml/g·min)	Ratio $\left(\frac{\text{trans-elim.}}{\text{cis-elim.}}\right)$
Cu[c]	91	78	1.2
Pt[d]	15	52	0.3

a) $\begin{matrix}H\\Cl\end{matrix}\!\!>\!C\!=\!C\!<\!\!\begin{matrix}Cl\\H\end{matrix} \longrightarrow H\text{-}C\equiv C\text{-}H + Cl_2$
b) $\begin{matrix}H\\Cl\end{matrix}\!\!>\!C\!=\!C\!<\!\!\begin{matrix}H\\Cl\end{matrix} \longrightarrow H\text{-}C\equiv C\text{-}H + Cl_2$
c) Hydrogen was used as a carrier gas.
d) Helium was used as a carrier gas.

phase, both *meso*- and *dl*-2,3-dichlorobutanes produced *trans*- and *cis*-2-butenes to the same degree, as is shown in Table 3; this is in contrast to the dechlorination on zinc and magnesium metals in the liquid phase, where *meso*- and *dl*-forms gave *trans*- and *cis*-2-butenes respectively.[3] The rates of the isomerization of the 2-butenes were negligibly small on these metals under the same conditions. The lack of stereospecificity in the dechlorination of 2,3-dichlorobutanes indicated that the dechlorination took place through an intermediate in which the rotation of the C–C bonds was free. Therefore, a similar situation might occur in the dechlorination of 1,1,2,2-tetrachloroethane to 1,2-dichloroethylene.

Discussion

Mechanism of the Dehalogenation of Haloalkanes on Metal. In contrast to the selective occurence of dehydrohalogenation on solid acids and bases, the dehalogenation of haloethanes took place predominantly on the metals examined in the present study. Solid acids and bases have polar sites on their surface, whereas there are no such polar sites on matel surfaces. This difference between metals and solid acids or bases in the nature of the surface may be responsible for the variation in the elimination products. An ionic-step-by-step mechanism has been proposed for the dehydrohalogenation on solid acids,[2b] in this mechanism, the first step is the abstraction of a halogen atom as a halide ion. Judging from the nonstereospecific dechlorination of 2,3-dichlorobutanes, the dehalogenation of haloalkanes on metal may also occur by a step-by-step mechanism. The difference in elimination products, however, shows that the manner in the halogen abstraction is different between metals and solid acids. From the nonpolar nature of the metal surface, a non-ionic mechanism may be considered likely for the dehalogenation on matels. The small substituent effect on the dehalogenation reactivity on metals, compared with the dehydrohalogenation-reactivity on solid acids and bases, indicates a non-ionic intermediate in the dehalogenation on metals.[10]

A similar difference between metals and solid acids or bases was observed in the elimination reaction of 1,2-dichloroethylenes. On solid acids and bases, *cis*- and *trans*-1,2-dichloroethylenes underwent dehydrochlorination when the *cis*-form showed a much higher reactivity than the *trans*-form.[11] On the other hand, the dichloroethylenes underwent dechlorination on metals, as was observed on haloalkanes, and the reactivity difference of both isomers was not very large, as is shown in Table 4. The higher reactivity of *cis*-1,2-dichloroethylene is characteristic of an ionic medium, such as solid acids or bases and basic solutions. The comparable reactivity of the two isomers on metals, accordingly, shows that the dechlorination occurs through a non-ionic mechanism on metals.

From these comparisons between metals and solid acids or bases, it can be concluded that the dehalogenation of haloalkanes on metals proceeds though a radical-step-by-step mechanism.

The interaction between the halogen atom and a metal surface may result from the coordination of a lone pair of the halogen atom to the unoccupied orbitals. In the above mechanism, the first step of the dehalogenation of haloalkanes on metals is the abstraction of the halogen atoms by a metal surface. The fact that 1-bromo-2-chloroethane shows a close reactivity to 1,2-dibromoethane on Cu, Ni, Co, and Ag can be easily understood by the above radical-step-by-step mechanism, provided that the weaker C–Br bond is broken in the first step on both reactants. 1-bromo-2-chloroethane showed, on the other hand, a lower reactivity than 1,2-dibromoethane on Pt, Pd, and Au. This may be related to the large back-donating powers of these metals in M–Br coordination.[12]

The dehydrohalogenation which was observed with regard to 1,2-dihalopropane may proceed *via* an El carbonium ion mechanism, as is indicated by the product distribution being similar to that on the solid acids.[7] This mechanism can explain the high dehydrohalogenation reactivity of 1,2-dihalopropane from the electron-donating effect of the methyl group, as has been described previously.[2] High ratios of $-HX/-X_2$ were observed on Fe and Co, showing that these metals have a considerable ability to abstract the halogen atom as a halide ion besides a radical. The metals with a high value of dehydrohalogenation/

10) J. E. Leffler and E. Grunwald, "Rates and Equilibrium of Organic Reactions," Wiley, New York (1963), p. 226.

11) Y. Anju, H. Yamamoto, I. Mochida, A. Kato, and T. Seiyama, unpublished observations.

12) R. Pearson and J. Songstad, *J. Amer. Chem. Soc.*, **89**, 1827 (1967), H. Matsumoto, Y. Saito, and Y. Yoneda, *J. Catal.* **19**, 101 (1970).

dehalogenation selectivity (Fe and Co) and the metals with a low ratio (Pt and Pd) also showed a high activity for acetaldehyde formation and ethylene formation respectively from ethylene chlorohydrin.[5] The former was considered to proceed through a carbonium-ion mechanism, and the latter, through a radical mechanism.[5]

BULLETIN OF THE CHEMICAL SOCIETY OF JAPAN, VOL. 45, 2323—2326 (1972)

Origin of the Fine Structure of the Electronic Spectra of Pyrazine in Benzene Crystals

Isamu SUZUKA and Mitsuo ITO

Department of Chemistry, Faculty of Science, Tohoku University, Katahira-cho, Sendai, Japan

(Received December 2, 1971)

The absorption, fluorescence, and phosphorescence spectra of pyrazine doped in benzene crystal have been observed at 4.2°K. It was found that the 0-0 band and the main vibronic bands are accompanied by the fine structures consisting of several very sharp bands and few broad bands. A detailed examination of the fine structures has suggested that the sharp bands arise from the differently oriented guest molecules in the host crystal, and the broad bands come from coupling of the host crystal phonon with the guest molecule.

Low temperature electronic spectra of aromatic compounds doped in host crystal often exhibit fine structure in $0\sim200\ cm^{-1}$ region near main vibronic band. As the fine structure is in most cases very different for the same guest spectra on different host crystals, a coupling of the host crystal phonons with the electronic state of the guest molecule has been suggested to be the cause of the fine structure. Many workers have attempted to explain the fine structure with the $k=0$ phonons. However, the attempt seems unsuccessful because of lack of definite correspondence with the Raman and IR active phonon frequencies. Recently, Zahlan[1] and Ostertag[2] *et al.* have suggested that the $k\neq0$ phonons also play an important role and the fine structure represents more or less the frequency distribution of phonon density of the host crystal. Hochstrasser and Small[3] have pointed out, on the other hand, that the fine structure is partly explained by existence of several differently oriented guest molecules in the host lattice.

In the present investigation, the absorption, fluorescence and phosphorescence spectra of pyrazine in benzene crystal have been observed at 4.2°K. It was found that the main vibronic bands of these spectra are accompanied by the fine structures consisting of several very sharp bands and a few broad bands. Comparison among the fine structures of the absorption, fluorescence and phosphorescence spectra and effects of changing the host crystal from benzene to benzene-d_6 on their features revealed possible causes of the fine structure.

Experimental

The absorption, fluorescence and phosphorescence spectra were measured photographically with a Shimadzu GE-100 grating spectrograph in the second and third orders, the linear reciprocal dispersions being 4.1 and 2.7Å/mm, respectively. Exposure time ranged from 1 min to 4 hours with slit width of 50 μ.

Wave numbers of the sharp and broad bands were determined within accuracies of 0.5 and 1.0 cm^{-1}, respectively. Photoelectric spectral measurements were also carried out by using a Narumi grating double monochromator having a linear reciprocal dispersion in the first order of 11 Å/mm and an EMI 9558 BQ photomultiplier. The optical arrangement for taking the spectra at low temperatures is essentially the same as that described by Mikami.[4] The emission spectra were excited by Hg line of 3130Å from a Ushio high pressure mercury lamp, which was isolated by a Shimadzu Baush & Lomb high intensity monochromator as well as a Corning CS-75 filter.

Pyrazine (Tokyo Kasei, GR grade) was sublimated several times in vacuum. Benzene (Wako, GR grade) was purified by the procedure recommended by Kanda *et al.*[5] Benzene-d_6 (E. Merck, spectro-grade) was vacuum distilled. Concentration of the sample solutions were 10^{-2}—10^{-4} mol/*l*. The solution was degassed several times and transferred to a quartz cell of 1 mm path length in vacuum. The sample inserted in a cryostat was slowly cooled until 77 °K by cooled nitrogen gas, then, immersed in liquid He.

Results and Discussion

The absorption, fluorescence, and phosphorescence spectra of pyrazine in benzene crystal at 4.2°K are shown in Fig.1. These spectra are all due to an n-π^* transition of pyrazine. The spectra were sharp in benzene crystal compared with those in other host

1) A. B. Zahlan, in "Excitons, Magnons and Phonons in Molecular Crystals", ed. A. B. Zahlan, Cambridge Univ. Press (1968), p. 153.

2) R. Ostertag and H. C. Wolf, *Phys. Stat., Sol.* **31**, 139 (1969).

3) R. M. Hochstrasser and G. J. Small, *Chem. Commun.*, **5**, 87 (1965).
R. M. Hochstrasser and G. J. Small, *ibid.*, **45**, 2270 (1966).
R. M. Hochstrasser and G. J. Small, *ibid.*, **48**, 3612 (1968).

4) N. Mikami, *J. Mol. Spectry.*, **37**, 147 (1971).

5) Y. Kanda and R. Shimada, *Spectrochim. Acta*, **17**, 7 (1961).

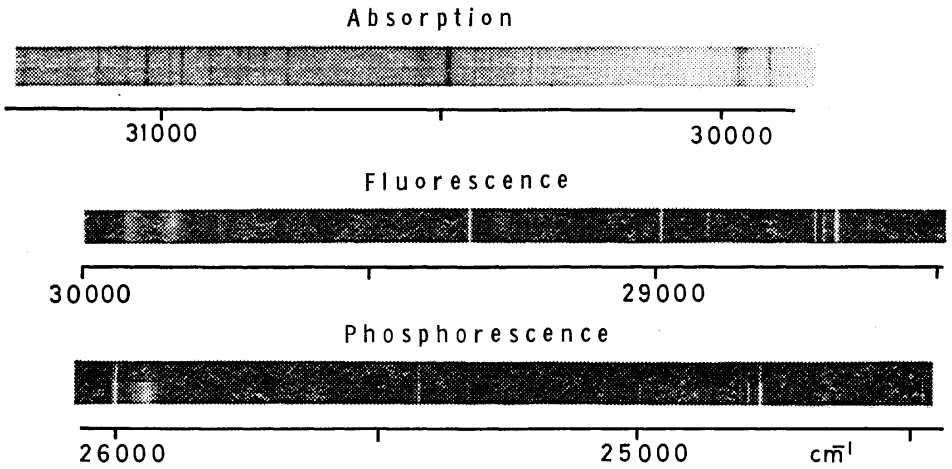

Fig. 1. The n-π^* absorption, fluorescence, and phosphorescence spectra of pyrazine crystal at 4.2°K.

Table 1. Frequency differences of the main bands near the 0-0 bands measured from the strongest reference

Host	Absorption		Fluorescence		Phosphorescence	
	C_6H_6	C_6D_6	C_6H_6	C_6D_6	C_6H_6	C_6D_6
Sharp band					−22.8	−22.2
	−9.2	−11.4	−8.1	−8.1	−5.7	−5.6
	0	0	0	0	0	0
	7.6	5.9	11.4	11.0	36.0	36.5
Broad band	77.0	44.0	49.0	48.0	48.0	45.5
	56.0	53.0	57.0	54.5	57.0	55.0
	62.0	58.5	64.0	60.0	63.5	60.0

crystal such as cyclohexane.[6] The essential feature of the spectra did not change when temperatrue and concentration of the sample were varied in the ranges of 4.2°K—77°K and 10^{-2}—10^{-4} mol/l, respectively.

The fine structures of the 0-0 bands of the absorption, fluorescence and phosphorescence spectra in benzene are reproduecd in Fig.2.[7] It is seen that the 0-0 bands are composed of very sharp bands and broad bands. A good mirror image relationship is seen between the absorption and fluorescence. Table 1 gives the frequency differences of the individual main bands measured from the strongest band in each spectrum selected as reference. It is seen that a good correspondence exists among the three spectra, especially the broad bands. Such broad bands are often observed in the electronic spectra of aromatic molecules doped in host crystal as side bands of the main vibronic bands. They are usually interpreted as "lattice or phonon bands" of the host crystal without evidence. If this interpretation would be correct, the broad bands should shift as a whole relative to the reference band when the host crystal is changed from C_6H_6 to C_6D_6. It is seen from Table 1 that the frequency differences between the broad bands and the reference band decrease in changing the host crystal from C_6H_6 to C_6D_6. The ratio of the frequency differences between C_6H_6 and C_6D_6 hosts is in average 1.05. This is close to the ratio of the lattice vibrational frequencies of C_6H_6 and C_6D_6 crystals, which is about 1.11 and 1.04 for optical active rotational and translational phonon modes, respectively.[8] It is

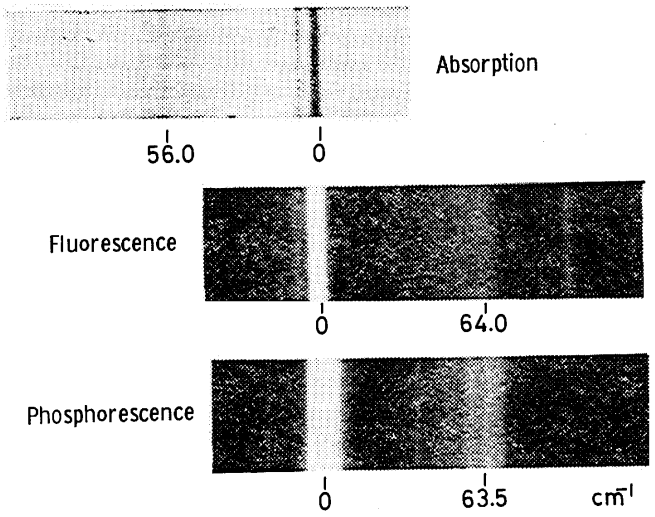

Fig. 2. Fine structures near the 0-0 bands of the absorption, fluorescence, and phosphorescence spectra of pyrazine in benzene crystal at 4.2°K.

6) I. Suzuka and M. Ito, unpublished data.

7) The 0-0 band of the fluorescence spectrum was not observed because of reabsorption. The fine structure shown in the figures and the tables of this paper is for 0-596 cm^{-1} band which was assumed to have same structure as that of the 0-0 band.

8) M. Ito and T. Shigeoka, *Spectrochim. Acta*, **22**, 1029 (1966).

suggested therefore that the broad bands arise from coupling with the host crystal phonons. Broadness of the bands is reasonable because all the phonons of various wave vectors k having quasi-continuous frequencies are able to contribute to intensity of the phonon bands.

Now, we shall consider the origin of the sharp bands. In Table 2 the frequencies of the sharp bands near the 0-0 bands of the absorption spectra of pyrazine in C_6H_6 and C_6D_6 are compared with the corresponding frequencies of the fluorescence spectra, the latter being estimated from the observed frequencies of the sharp bands near the 0—596 cm^{-1} vibronic bands of the fluoresence by adding a constant frequency of 596 cm^{-1} to them.

TABLE 2. THE FREQUENCIES OF THE SHARP BANDS NEAR THE 0-0 BANDS

	Absorption		Fluorescence[a]	
	cm^{-1}	Int.	cm^{-1}	Int.
Pyrazine in C_6H_6	29918	w	29917	w
	29912	s	29919	s
	29904	v. s	29904	v. s
	29895	m	29894	m
Pyrazine in C_6D_6	29916	w	29916	w
	29913	w		
	29908	s	29911	s
	29902	v. s	29902	v. s
	29890	m	29891	w
	29871	w	29873	w

a) see the footnote in text.

Assuming the same structure for the 0-0 and 0-596 cm^{-1} bands, the fluorescence frequencies listed in Table 2 may be regarded as representing the sharp bands near the 0-0 bands of the fluorescence spectrum which would be observed in absence of reabsorption. It is seen from the table that the sharp bands of the absorption and fluorescence agree very well within 2 cm^{-1}. Furthermore, the relative intensities are parallel between the two spectra. Similar results were found also for the absorption and fluorescence spectra of pyrazine in cyclohexane crystal.[6] We may conclude therefore that the individual sharp bands represent common origins of the absorption and fluorescence spectra. Recently, Small[9] reported the mixed crystal spectrum of anthracene in terphenyl, in which he found three fluorescence bands coinciding in frequency with the absorption bands. He interpreted them as due to the guest molecules differently oriented in the host lattice. This interpretation seems to be applied to our present case. In Fig.3, the fine structures associated with several main vibronic bands of the phosphorescence spectrum of pyrazine in benzene crystal are compared. The spectral pattern of the sharp bands which occur mainly on higher frequency side of the most intense band in each vibronic band is considerably different for different vibronic bands. This may also be taken as an evidence supporting the above interpretation that the sharp bands arise from

9) G. J. Small, *J. Chem. Phys.*, **52**, 656 (1970).

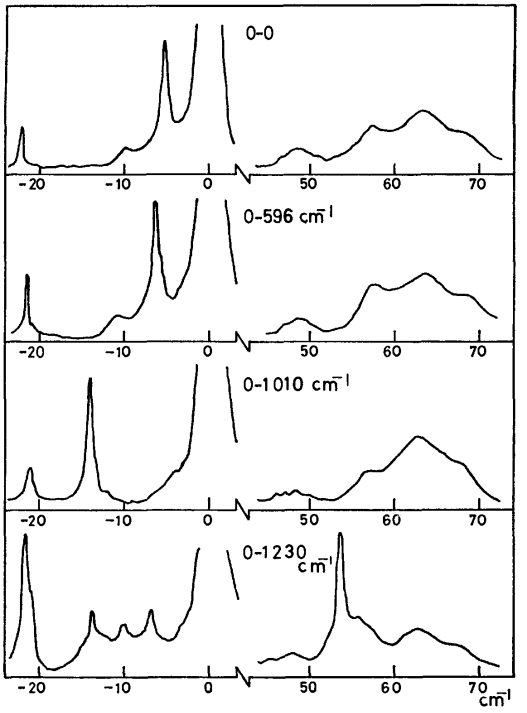

Fig. 3. Fine structures accompanied by several main vibronic bands of the phosphorescence spectrum of pyrazine in benzene crystal at 4.2°K.

different guest molecules situated in different circumstances in the host crystal. The molecules situated at different sites will have different frequencies of the molecular vibrations depending on degree of distortion of the guest molecules induced by crystal field of the host lattice. Since these guest molecules give rise to their own spectra having different 0-0 bands and different vibrational structures, different patterns of the fine structures are expected for different vibronic bands. The sharp bands associated with the main vibronic bands of the fluorescence spectrum also showed different spectral patterns similar to that of the phosphorescence spectrum.

In contrast to the sharp bands, the broad bands associated with the main vibronic bands of the phosphorescence spectrum, which occur mainly on lower frequency side of the strongest band in each vibronic band, are very similar in spectral feature to each other (Fig.3). As described before, when the host is replaced from benzene to benzene-d_6, these broad bands shift as a whole toward the strongest bands (hereafter, referred to as "reference band"), and this was taken as evidence supporting that the broad bands are host phonon bands. In this interpretation, we implicitly assumed that the broad bands are resulting from coupling of the host crystal phonons with the vibronic states of the guest molecule which gives the reference bands. The host crystal phonons will be able to couple also with other guest molecules which give the sharp bands other than the reference bands.

However, intensities of the phonon bands resulting from the sharp bands other than the reference bands will be much smaller than intensities of the phonon bands associated with the reference bands, because the

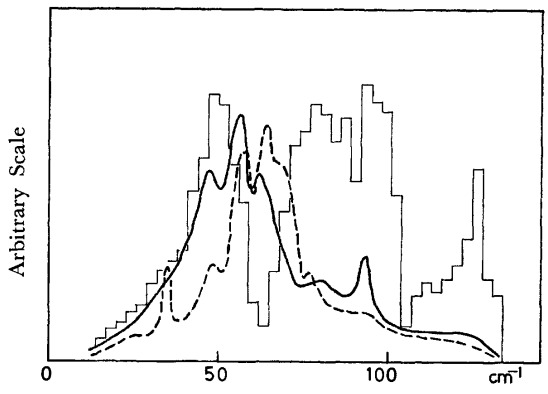

Fig. 4. Typical phonon bands of the absorption (—) and phosphorescence (----) of pyrazine in benzene at 4.2°K compared with the calculated D(ν) (—) of benzene at 135°K (taken from ref. (9)).

former are much weaker in intensity than the latter. Thus, the observed broad bands may be regarded as the phonon bands belonging mainly to the reference bands.

It may be worthwhile to mention here that the spectral pattern of the phonon bands seems not to depend on symmetry species of the molecular vibrations involved in the vibronic bands. For example, in the fluorescence spectrum we found two kinds of vibronic bands involving totally symmertric and nontotally symmetric molecular vibrations which give the same pattern of the phonon bands. This suggests that no specific selection rule is operative in coupling between the vibronic states of guest molecule and the phonons of host crystal. If it would be the case, the phonon bands should represent the density of states of the phonon, $D(\nu)$. Recently, Nakamura and Miyazawa[10] calculated $G(\nu)$ ($D(\nu)$ weighted with squared amplitude) of benzene crystal, which agrees well with that obtained from the neutron inelastic scattering experiment[11]. In Fig. 5, the $D(\nu)$ calculated by Nakamura and Miyazawa is compared with typical phonon structures of the phosphorescence and absorption spectra. According to Nakamura and Miyazawa, the peak near 50 cm^{-1} and the long tail in the region less than 50 cm^{-1} is mainly contributed from the acoustic phonons. The fact that greater part of intensity of the phonon bands is concentrated in the above frequency range suggests that the acoustic phonons of the host lattice play an important role in coupling of the electronic state of the guest molecule with the lattice vibrations of the host crystal.

The authors express their sincere thanks to Dr. N. Mikami for helpful discussions and advice throughout this work.

10) M. Nakamura and T. Miyazawa, *J. Chem. Phys.*, **51**, 3146 (1969). T. Miyazawa and M. Nakamura, *ibid.*, **52**, 5972 (1970).
11) K. W. Logan, S. F. Trevino, H. J. Prask, and J. D. Gault, *ibid.*, **53**, 3417 (1970).

BULLETIN OF THE CHEMICAL SOCIETY OF JAPAN, VOL. 45, 2326—2329 (1972)

On the Equivalence of Two Expressions for Potentiometric Titration of Polyelectrolytes

Hiroshi MAEDA

Department of Chemistry, Faculty of Science, Nagoya University, Nagoya

(Received December 3, 1971)

Two expressions for potentiometric titrations of polyelectrolytes are proved to be equivalent, being derived from a common basis. A thermodynamic interpretation of the term representing the non-ideality of polyelectrolyte solutions is also explicitly given.

It has been well known that potentiometric titrations of polyelectrolyte solutions can be described by the equation,[1-4]

$$\mathrm{pH} = \mathrm{p}K_0 + \log(\alpha/1-\alpha) + \Delta\mathrm{p}K \qquad (1)$$

Here K_0 and α denote the intrinsic dissociation constant of dissociable sites and the degree of ionization respectively. The last term in Eq.(1) represents the non-ideality of the solution and in ordinary cases arises solely from the electrostatic work accompanying ionization.

On the other hand, the following thermodynamic expression has been presented.[5]

$$(\partial\mu_p/\partial\mu_{\mathrm{H}})_{m_p,m_s} = \alpha x \qquad (2)$$

Here μ_p and μ_{H} denote the chemical potentials of polymer component and of hydrogen ions, and m_p and m_s the concentrations of ploymer and salt components. Futher x denotes the number of the dissociable sites on a polyion.

However, the equivalence of the two expressions, Eq.(1) and Eq.(2), has not been presented. The purpose of the present study is to derive the two expressions from a common basis and thus to show their equivalence.

1) A. Katchalsky and J. Gillis, *Rec. Tarv. Chim.*, **68**, 879 (1949).
2) R. Arnold and J. Th. G. Overbeek, *ibid.*, **69**, 192 (1950).
3) A. Katchalsky and S. Lifson, *J. Pholymer Sci.*, **11**, 409 (1953).
4) F. E. Harris and S. A. Rice, *J. Phys. Chem.*, **58**, 725 (1954).
5) A. Shatkay and I. Micheali, *ibid.*, **70**, 3777 (1966).

Theory

For the sake of simplicity, let us take a poly (weak) acid neutralized to various degrees by alkali as a polyelectolyte. Let us consider a solution containing n_w, n_p, n_s, and n_a moles of water, polyacid, simple salt (uni-uni valent), and alkali. We take a fully protonated species as a polymer component here. Concentrations of solutes are expressed in m's. The counter ions from alkali and those from simple salt are assumed to be of the same species. Since we consider the changes at a constant temperature and pressure, these variables do not appear explicitly in the present formulation.

Let us denote the average number of charged sites on a polyion as i, that is $i=\alpha x$. At equilibrium, i should be determined from the condition of minimum free energy.

$$(\delta G/\delta i)_{n_w,\ m_p,\ m_s,\ m_a} = 0. \tag{3}$$

Here G denotes the Gibbs free energy of the solution. The equation is just the equation for potentiometric titrations. The expression, however, corresponds to an infinitesimal virtual change δi. If the corresponding free energy change can be evaluated, we can obtain Eq.(1). On the other hand we can derive Eq.(2), if we can express the free energy due to a virtual change in terms of some thermodynamic quantities corresponding to quasi-static changes.

We denote the free energy arising from the electrostatic interaction between charges as G^{el}. Self-energy of a polyion, the electrostatic interaction between charged sites on a polyion, is also included in G^{el}. The remaining part of G will be further divided into two parts, G^p and G^s, where G^p represents the contribution from polyions and G^s from all other species. The unitary part of G^p can be divided into three parts; $G_0{}^p$ which is independent of i, $G_1{}^p$ which contains the contributions from the standard free energy of charged and uncharged sites and from their ideal mixing entropy, and $G_2{}^p$ which involves any other contributions depending on i. The cratic part of G^p can be expressed in terms of the ideal term in m_p when neither association nor conformational change occurs. However, it is designated here as $G_3{}^p$ for the purpose of wider applicability.

Let us consider the changes which actually occur in the solution accompanying the virtual change under consideration. At equilibrium, G may be written in terms of species as follows, if we take into account a relation demonstrating the dissociation equilibrium of water, $\mu_w=\mu_H+\mu_{OH}$.

$$G = (n_w+n_a)\mu_w + n_p\mu_{p,i} + (n_a+n_s)\mu_+ + n_s\mu_- + (n_H-n_{OH})\mu_H. \tag{4}$$

Here $\mu_{p,i}$ denotes the chemical potential of a polyion having i charged sites, and μ_+ and μ_- those of counter ions and coions. The equation implies that the contribution from excess hydrogen ions n_H^{ex} rather than that from total hydrogen ions is necessary to be taken into account when we consider the contribution from hydrogen ion species to the change of G associating with some process. Here the excess hydrogen ions are defined as the remainder resulting from the subtraction of hydroxyl ions from hydrogen ions, $n_H^{ex}=n_H-n_{OH}$. From the condition of electroneutrality,

$$n_p\delta i = \delta n_a + \delta n_H^{ex}. \tag{5}$$

The virtual change under consideration thus leads to the increase of the excess hydrogen ions by $n_p\delta i$ moles, since the change occurs at constant n_a. The result should not be interpreted as demonstrating that the hydrogen ions produced by the virtual change do not interact with hydroxyl ions and thus do not participate in the dissociation equilibrium of water. In fact, part of hydrogen ions released may be consumed by means of the combination with hydroxyl ions. But as a result of this reaction, exactly the same amount of the latter is also consumed and thus the amount of excess hydrogen ions is not altered. Practically the same result can be obtained, if we notice that except the extremely narrow region near pH 7, either hydrogen or hydroxyl ions are present in great excess so that the difference between the amount of excess ions and that of total ions becomes quite insignificant.

Therefore, corresponding to the virtual change, the number of charged sites on each polyion increases by δi, and $n_p\delta i$ moles of hydrogen ions are released into a solution from these polyions.

Let us evaluate the free energy change G involved in Eq. (3). For the calculation of the free energy other than electrostatic part, we may calculate it in two independent processes. For the process corresponding to the increase of charged sites, the free energy change can be expressed by the change of chemical potentials, since the process does not involve any variation of the number of particles in the system. We may reasonably assume that the interionic interaction other than electrostatic one is negligible except that between polyions. The exception is made here to leave room for the possibility that association of polyions occurs by short range interactions such as hydrogen bonding. According to this assumption, the unitary part of G^s is clearly independent of i and the cratic part can be expressed in terms of the ideal term $\boldsymbol{R}T\ln m$. Therefore G^s remains unchanged under the process considered. As to the remaining part G^p, it can be written as $n_p(\mu_{p,i}-\mu_{p,i}^{el})$. Here $\mu_{p,i}^{el}$ represents the electrostatic part of the chemical potential of a polyion. Corresponding to an increase of $n_p\delta i$ moles of hydrogen ions, the free energy change becomes $n_p\delta i(\mu_H-\mu_H^{el})$. Thus the free energy change except the electrostatic one amounts to,

$$\delta(G-G^{el}) = n_p\delta(\mu_{p,\,i}-\mu_{p,i}^{el})+n_p(\mu_H-\mu_H^{el})\delta i. \tag{6}$$

For the calculation of the change of electrostatic free energy, we regard the process as such that n_p moles of polyions having i charged sites are removed from the solution and exactly the same amount of polyions having $i+\delta i$ charged sites as well as $n_p\delta i$ moles of hydrogen ions are introduced into the solution. Then the total change becomes.

$$\delta G^{el} = n_p\mu_H^{el}\delta i + n_p(\mu_{p,i+\delta i}^{el}-\mu_{p,i}^{el}) = n_p\mu_H^{el}\delta i + n_p\delta\mu_{p,i}^{el}. \tag{7}$$

Adding Eqs. (6) to (7), we obtain

$$(\delta G/\delta i)_{n_w,\, m_p,\, m_s,\, m_a} = n_p[(\delta\mu_{p,i}/\delta i)_{m_p,\, m_s,\, m_a} + \mu_H]. \quad (8)$$

From Eq. (3), the r.h.s. of Eq. (8) should be zero at equilibrium.

Potentiometric Equation. In order to evaluate the derivative on the r.h.s. of Eq. (8), we examine various constituent contributions to $\mu_{p,i}$. In analogy with the classification of G^p, $\mu_{p,i}$ is also divided in the corresponding manner.

$$\mu_{p,i} = \mu_p^0 + \mu_{p,i}^1 + \mu_{p,i}^2 + \mu_{p,i}^3 + \mu_{p,i}^{el}. \quad (9)$$

Since G_0^p is defined as being independent of i, μ_p^0 is also independent of i. As to $\mu_{p,i}^1$, the term can be explicitly written as follows.

$$\mu_{p,i}^1 = -(\boldsymbol{R}T \ln K_0 + \mu_H^0)i + \boldsymbol{R}T[i \ln(i/x) + (x-i)\ln(x-i)/x].$$

Hence,

$$\delta u_{p,i}^1 = \delta i(-\boldsymbol{R}T \ln K_0 - \mu_H^0) + \boldsymbol{R}T(\delta i) \ln(i/x-i). \quad (10)$$

Substituting Eq. (10) into Eq. (8) and rearranging it a little, we obtain

$$\mathrm{pH} = \mathrm{p}K_0 + \log(\alpha/1-\alpha) + (0.434/\boldsymbol{R}T) \times [\delta(\mu_{p,i}^2 + \mu_{p,i}^3 + \mu_{p,i}^{el})/\delta i]. \quad (11)$$

Thus we have derived a potentiometric equation. Comparing Eq. (11) with Eq. (1), we have

$$\Delta\mathrm{p}K = (0.434/\boldsymbol{R}T)[\delta(\mu_{p,i}^2 + \mu_{p,i}^3 + \mu_{p,i}^{el})/\delta i]. \quad (12)$$

It can be seen from Eq. (12) that the non-ideal term depends on the non-ideal part of the chemical potential of a *polyion* and not of a *polymer component*. This result has not been explicitly given, though essentially equivalent statements were implicitly presented.[3,4] It may be somewhat significant to give the result in an explicit form, since a confusing expression about the thermodynamic interpretation of the non-ideal term has been reported recently.[6]

For ordinary polyelectrolytes, where a transition between discrete conformations is absent and polymer concentration remains unchanged during ionization, the term $\delta\mu_{p,i}^3$ vanishes. In this case, involved in the term $\mu_{p,i}^2$ are such contributions that the deviation of the mixing entropy of charged and uncharged sites from that of ideal behavior or the free energy due to the expansion of polymer chains. However, these contributions have been considered to be small compared with those involved in the term $\mu_{p,i}^{el}$.[7] Hence in this case the non-ideal term reduces to

$$\Delta\mathrm{p}K = (0.434/\boldsymbol{R}T)(\delta u_{p,i}^{el}/\delta i). \quad (13)$$

If conformational transition depending on ionization occurs, including the association of polymers, then the effect may be involved in the terms $\mu_{p,i}^2$ and $\mu_{p,i}^3$. Thus $\Delta\mathrm{p}K$ should be expressed in a general form as Eq. (12).[8-10]

Thermodynamic Expression. Since we have derived an ordinary potentiometric equation in the preceding section, it becomes necessary to deduce a thermodynamic expression represented by Eq. (2) in terms of the same model consideration.

It should be noted that the change of the chemical potential of polyions associating with an infinitesimal change δi is independent of whether the change occurs as a virtual one or as a quasi-static one. The difference between these two changes resides in the respect whether the increase of charges on polyions is neutralized by hydrogen ions alone or by both counter ions and hydrogen ions. On account of this, the derivative involved in Eq. (8) can be replaced with one corresponding to quasi-static change.

$$(\delta\mu_{p,i}/\delta i)_{m_p,\, m_s,\, m_a} = (\partial\mu_{p,i}/\partial i)_{m_p, m_s}. \quad (14)$$

Thus from Eq. (8),

$$(\partial\mu_{p,i}/\partial i)_{m_p, m_s} + \mu_H = 0. \quad (15)$$

Changing a variable from i to μ_H, we obtain the equation,

$$(\partial\mu_{p,i}/\partial\mu_H)_{m_p,\, m_s}(\partial\mu_H/\partial i)_{m_p,\, m_s} + \mu_H = 0. \quad (16)$$

According to the definition employed in the present treatment, the chemical potential of a polymer component can be written in terms of the constituent species.

$$\mu_p = \mu_{p,i} + i\mu_H. \quad (17)$$

Differentiation of Eq. (17) with respect to μ_H yields,

$$(\partial\mu_p/\partial\mu_H)_{m_p,\, m_s} = (\partial\mu_{p,i}/\partial\mu_H)_{m_p,\, m_s} + i + \mu_H(\partial i/\partial\mu_H)_{m_p,\, m_s}. \quad (18)$$

After Eq. (16) is taken into account, Eq. (18) finally reduces to

$$(\partial\mu_p/\partial\mu_H)_{m_p,\, m_s} = i = \alpha x. \quad (2)$$

Thus we have presented the equivalence of the two expressions, Eq. (2) and Eq. (11), by deriving them from a common basis.

Discussion

A brief comment should be added about the implication of the equations and averages under the situation of conformational changes. For the sake of brevity, we consider a solution where two discrete conformations "a" and "b" are present in equilibrium. In this case, three parameters are necessary to describe the system, which are taken to be i_a, i_b, and i. Here i_a and i_b denote average degrees of ionization of the respective conformations. The fraction of polymers in the "a"-conformation, f_a, is given as $(i-i_b)/(i_a-i_b)$. Two parameters i_a and i_b as well as f_a can be generally considered to be solved as the functions of $[m]$ and i from the equations

$$(\delta G/\delta i_a)_{[m],\, i,\, i_b} = 0, \quad (19)$$

and

$$(\delta G/\delta i_b)_{[m],\, i,\, i_a} = 0. \quad (20)$$

Here $[m]$ represents a set of variables n_w, m_p, m_s, and m_a. Hence, a virtual change δi consists of corresponding changes in δi_a, δi_b, and δf_a, which are uniquely determined if δi is given. The equilibrium value of i will be given by Eq. (3) as before. However, the implication of the equation in this case is,

$$(\delta G/\delta i)_{[m]} = (\delta G/\delta i_a)_{[m],\, i,\, i_b}(\delta i_a/\delta i)_{[m]} + (\delta G/\delta i_b)_{[m],\, i,\, i_a}(\delta i_b/\delta i)_{[m]} + (\delta G/\delta i)_{[m],\, i_a,\, i_b} = 0. \quad (21)$$

6) G. Torrence, S. Amdur, and J. A. Marinsky, *J. Phys. Chem.*, **75**, 2144 (1971).
7) L. Kotin and M. Nagasawa, *J. Chem. Phys.*, **36**, 873 (1962).
8) B. H. Zimm and S. A. Rice, *Mol. Phys.*, **3**, 391 (1960).
9) M. Nagasawa and A. Holtzer, *J, Amer. Chem. Soc.*, **86**, 538 (1964).
10) M. Nagasawa and A. Holtzer, *ibid.*, **93**, 606 (1971).

Subsequent equations, except the expressions for $\mu^{1}_{p,i}$ and $\delta\mu^{1}_{p,i}$ (Eq. (10)), can be interpreted similarly, if we take into account the relations,

$$\mu_{p,\,i} = f_a\mu_{p,\,i_a} + (1-f_a)\mu_{p,\,i_b} \tag{22}$$

and

$$\mu_{p,\,a} = \mu_{p,i_a} + i_a\mu_{\mathrm{H}} = \mu_{p,i_b} + i_b\mu_{\mathrm{H}} = \mu_p \tag{23}$$

since the conformational equilibrium is attained. Expressions for $\mu^{1}_{p,i}$ and $\delta\mu^{1}_{p,i}$ should be regarded as the definitions of them in this case.

From the discussion presented above, most of the equations are proved to hold in the case of conformational changes. However, the implication of averaged quantities such as $\mu_{p,i}$ or i may differ in both situations. Fluctuations from averages are considered to be relatively small in ordinary polyelectrolyte solutions, whereas they become considerably large in solutions where discrete conformations are present in equilibrium.

BULLETIN OF THE CHEMICAL SOCIETY OF JAPAN, VOL. 45, 2329—2331 (1972)

Studies on Microcapsules. XIII. Effect of Span 85 and pH of Aqueous Phase on the Formation of Polyamide Microcapsules

Tomoharu OGAWA*, Kouichi TAKAMURA, Masumi KOISHI, and Tamotsu KONDO**

* *Research Laboratory, Pentel Co., Ltd., Soka, Saitama*

Faculty of Pharmaceutical Sciences, Science University of Tokyo, Shinjuku-ku, Tokyo

(Received December 10, 1971)

The effects of the pH of aqueous phase containing piperazine and the concentration of Span 85, a nonionic surfactant with chemical description of sorbitan trioleate (Atlas Power Co., U.S.A) on the formation of polyphthalamide microcapsules were systematically investigated by the interfacial polycondensation method in the organic phase containing *p*-phthaloyl dichloride. The presence of Span 85 facilitated the formation of microcapsules by increasing the transfer of undissociated diamine molecules into the organic phase in the pH range 9.0–12.0, outside of which Span 85 did not significantly contribute to the formation of microcapsules. An increase in the pH in this range gives rise to an increase in the number of undissociated diamine molecules, promoting the transfer of diamine.

It is known that the partition of diamines between water and a water-immiscible organic liquid is important for the formation of polymers by interfacial polycondensation reaction.[1] The same holds for the formation of microcapsules by the interfacial polycondensation method.[2-4]

On the other hand, the partition coefficients of diamines were found to be affected favorably in an organic phase in the presence of Span 85, a nonionic surfactant.[2] Diamine molecules should exist in an undissociated form so that they can be transferred into an organic phase. This indicates that the partition might be significantly reduced near a pH equal to the pK value of diamines. Actually, when $NaHCO_3$ was present instead of Na_2CO_3 the partition of diamines was unfavorably affected, and hardly any microcapsules were formed.[5]

Since the findings are still scanty, a systematic study is needed to understand the effects of the pH of aqueous phase and the Span 85 concentration in organic phase on the formation of microcapsules. Thus, the effects of the pH of aqueous phase containing piperazine, a diamine, and the Span 85 concentration in a chloroform-cyclohexane mixture containing *p*-phthaloyl dichloride on the formation of polyphthalamide microcapsules were systematically examined.

Experimental

Determinarion of Apparent Partition Coefficient of piperazine. The apparent partition coefficient of piperazine was determined at various pH in the same way as in the preparation of micrlcapsules.[2] Ten milliliters of 0.40 M piperazine (diethylenediamine) was added to 10 ml of 0.90 N Na_2CO_3–$NaHCO_3$ in a 500 m*l* round bottom flask surrounded by ice. The Na_2CO_3–$NaHCO_3$ mixture was used with varying the mixing ratio but keeping constant the total concentration at 0.90 N. One hundred milliliters of mixed organic solvent (cholroform-cyclohaxane, 1 : 3 vol), containing 0–7 vol% Span 85 was added to the solution as an emulsifying agent. The mixed solution was then mechanically emulsified with a Chemistirrer (Tokyo Rika Kikai Co., Tokyo, Model B-100) at 521 r. p. m. for 5 min to yield a water-in-oil emulsion.

Immediately after stirring was stopped the emulsion was centrifuged at 13000 g for 10 min to remove the aqueous phase from the organic phase. The concentration of piperazine in the organic phase was then determined by titration with HCl solution in an isopropanol-ethyleneglycol mixture (1 : 1 vol) using BTB-BCG mixed indicator.[6] The

** To whom all inquiries should be addressed.

1) P. W. Morgan, and S. L. Kwolek, *J. Polymer Sci.*, **40**, 299 (1959)

2) M. Koishi, N. Fukuhara, and T. Kondo, *Chem. Pharm. Bull.* (Tokyo), **17**, 804 (1969).

3) M. Shiba, S. Tomioka, M. Koishi, and T. Kondo, *ibid*, **18**, 803 (1970).

4) Y. Shigeri, M. Koishi, and T. Kondo, *Can. J. Chem.*, **48**, 2047 (1970).

5) S. Suzuki, T. Kondo, and S. G. Mason, *Chem. Pharm. Bull.* (Tokyo), **16**, 1629 (1968).

6) S. Siggia, "Quantitative Organic Analysis *via* Functional Groups", 2nd Edition, John Wiley & Sons, Inc. New York. (1954).

partition coefficient of piperazine was calculated from its initial concentration in the aqueous phase and final concentration in the organic phase.

Determinarion of the percentage of Reacted Piperazine. The determination was carried out as follows. The mixture of the aqueous phase and the organic phase was mechanically emulsified under the same conditions as in the determination of apparent partition coefficient. One hunderd milliliters of 0.04 *M* *p*-phthaloyl dichloride solution in the mixed organic solvent was added to the emulsion obtained, and the resulting microcapsule suspension was centrifuged at 29000 g for 10 min after stirring was continued for 3 min. Centrifugation caused the breakdown of microcapsules and a clear aqueous phase was obtained.

A 5 m*l* portion of the aqueous phase was mixed with an equal volume of *p*-dimethylaminobenzaldehyde solution in methanol containing 30 vol% H_2SO_4. The amount of piperazine remaining unreacted was determined by measuring the absorption of colored complex at 425 mμ spectrophotometrically.[7] The percentage of reacted piperazine was calculated from its initial and final concentrations in the aqueous phase.

Measurement of Viscosity of Ploymer Solution. The measruement of viscosity of polymer solution was carried out in a way similar to that described previously.[4] Each microcapsule suspension prepared under various conditions was centrifuged to break down the microcapsules and the microcapsule membrane obtained was collected, washed, and dried under reduced pressure. The dried sample was dissolved in *m*-cresol. For each sample solution thus prepared, the relative viscosity was measured at 30 °C with a dilution type Ubbelohde viscometer. The reduced viscosity was then plotted against the polymer concentration and the intrinsic viscosity was graphically estimated by extrapolation to zero conecntration.

Determination of CMC of Span 85. The determination of critical micelle concentration of Span 85 was carried out by the method of Ross and Olivier.[8] 5m*l* of iodine solution (70 mg/*l*) in the mixed organic solvent was added to an equal volume of each Span 85 solution of various concentrations around its CMC in the same solvent. The transmittance of the solutions was then measured at a wavelength of 360 mμ using the mixed solvent as a reference. The CMC was graphically determined as the break point of transmittance *versus* concentration curve.

Results and Discussion

Apparent Partition Coefficient. The dependence of apparent partition coefficient of piperazine on the pH of aqueous phase at several Span 85 concentrations in the organic phase is shown in Fig. 1.

At any concentration of Span 85 in the organic phase, the apparent partition coefficient decreased first and then levelled off as the pH of aqueous phase increased, indicating that the transfer of piperazine from the aqueous to the organic phase initially inincreases but approaches a saturation value as the hydrogen ion concentration in the aqueous phase decreases.[9] This results from the fact that the pK values of piperazine are 5.57 and 9.81. Increases in the pH of aqueous phase will cause an increase in the number

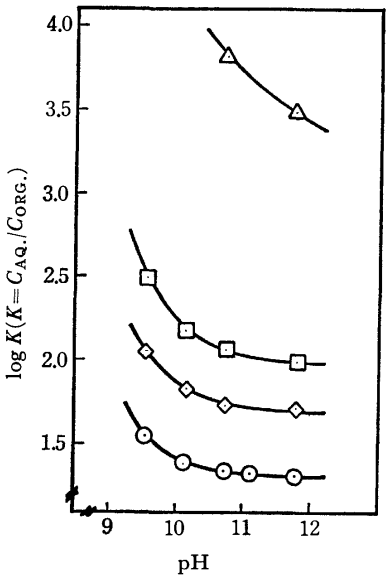

Fig. 1. The dependence of apparent partition coefficient of piperazine on the pH of aqueous phase at several Span 85 concentrations in the organic phase. Span 85 concentrations: (△) 0%, (□) 1%, (◇) 2%, and (○) 5%.

of unprotonated piperazine molecules and a transfer would be favored. The transfer would stop increasing when all the piperazine molecules in the aqueous phase take the unprotonated form above pH 10.0. This trend of a transfer of substances with pH-dependent dissociable groups in their molecules is frequently observed.[10–12]

It was reported that the transfer of piperazine or 1,6-hexamethylenediamine from aqueous Na_2CO_3 solution to a chloroform-cyclohexane mixture is facilitated by the presence of Span 85 in the organic solvent.[2] We see from Fig. 1 that the presence of Span 85 in the organic phase increases the transfer of piperazine irrespective of the pH of aqueous phase and the amount transferred increases as the Span 85 concentration increases. Although the exact role of Span 85 in facilitating the transfer of piperazine is not yet fully understood, a portion of piperazine transferred should exist in the solubilized form in Span 85 micelles since the concentrations of Span 85 we used lie beyond its CMC (9.3×10^{-2}%).

Percentage of Reacted Piperazine. The percentage of reacted piperazine with *p*-phthaloyl dichloride at

Table 1. Percentage of reacted piperazine

pH / Span 85 (vol%)	9.54	10.13	11.77
0	8	—	34
1.0	42	75	87
2.0	54	74	90
5.0	79	—	89
7.0	87	—	—

7) C. Menzie, *Anal. Chem.*, **28**, 1321 (1956).
8) S. Ross and J. P. Olivier, *J. Phys. Chem.*, **63**, 1671 (1959).
9) Transfer of piperazine was not noticeable below pH 9.0.
10) A. L. Misra, A. Hungei, and H, Keberle, *J. Pharm. Pharmac.*, **18**, 531 (1966).
11) G. Levy, and E. J. Mroszezak, *J. Pham. Sci.*, **57**, 235 (1966),
12) M. Nakano, *J. Pham. Sci.*, **60**, 571 (1971).

various pH and Span 85 concentrations is given in Table 1.

The percentage was greatly affected by both the pH of aqueous phase and the Span 85 concentration in organic phase. Since the interfacial polycondensation reaction occurs on the organic solvent side of the interface of water and organic solvent,[1] the percentage of reacted piperazine should be related to its apparent partition coefficient. The relation between the percentage and its apparent partition coefficient is illustrated in Fig. 2. The relation is linear for all the pH values and the slope of straight line increases with increasing pH. At a pH of about 12, the straight line becomes vertical, suggesting that the percentage is practically independent of the transferred amount of piperazine above this pH.

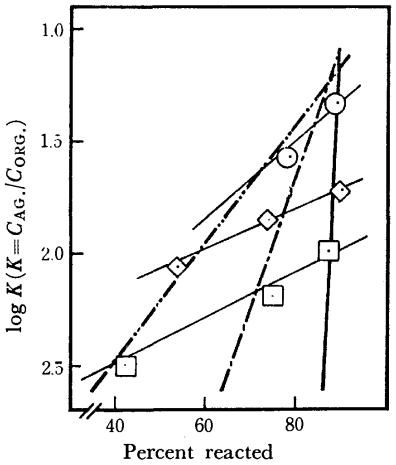

Fig. 2. The relation between the percent reacted of piperazine and its apparent partition coefficient. Span 85 concentrations: (□) 1%, (◇) 2%, and (○) 5%. pH of aqueous phase: (—··—) pH 9.54, (—·—) pH 10.13, and (—) pH 11.77.

We see also that the apparent partition coefficient increases, and consequently, the percentage decreases as the pH of aqueous phase lowers at any Span 85 cancentration in the organic phases. Since the apparent partition coefficient drastically rises below pH 9.0 irrespective of Span 85 concentration (Fig. 1), it would be inferred that the percentage greatly falls below this pH. In fact, polyphthalamide microcapsules were not formed appreciably below pH 9.0, however high the Span 85 concentration. This indicates a very low percentage. This would mean that the lower limit of pH for the formation of microcapsules making use of polycondensation reaction between a diamine and an acid dichloride lies around a value equal to the pK of the diamine used.

Intrinsic Viscosity of Polymers Constituting Microcapsules. The intrinsic viscosities of polymers constituting polyphthalamide microcapsules prepared under various conditions are given in Table 2.

A close relation is clearly observed between the intrinsic viscosity of polyphthalamide and the percentage by comparison with Table 1. A polymer with high intrinsic viscosity or high molecular weight is obtained at high percentage while a low intrinsic viscosity corresponds to a low percentage. Typical photomicrographs of microcapsules prepared under the conditions pH 9.54 of aqueous phase and 1 vol% of Span 85 in the organic phase, and pH 11.77 and 5 vol% of Span 85, are shown in Photos. 1 and 2, respectively.

Table 2. Intrinsic viscosity of polymers constituting microcapsules

pH / Span 85 (vol%)	9.54	10.31	11.77
1.0	0.20	0.31	0.56
2.0	—	0.35	0.43
5.0	0.53	—	0.55

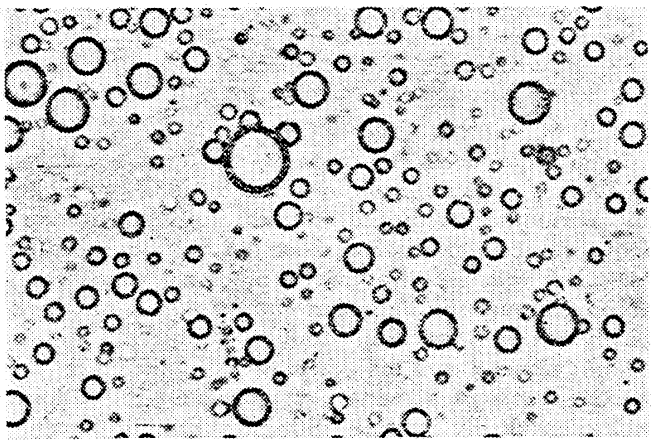

Photo. 1. Photomicrograph of polyphthalamide microcapsules prepared at pH 9.54 of aqueous phase and 1 vol% of Span 85 in the organic phase (×600).

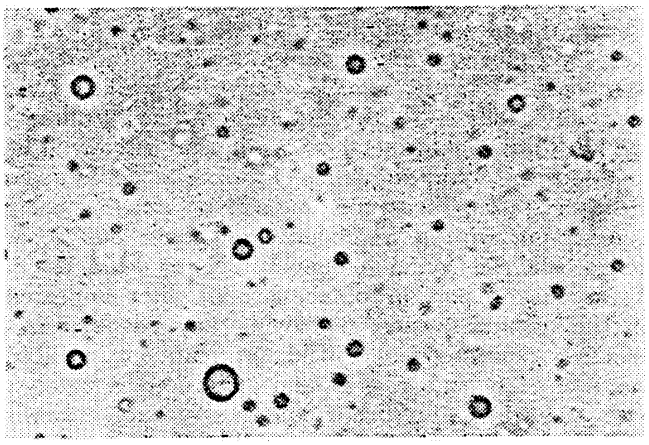

Photo. 2. Photomicrograph of polyphthalamide microcapsules prepared at pH 11.77 of aqueous phase and 5 vol% of Span 85 in the organic phase (×600).

Microcapsules were generally larger in size if they were prepared at low pH and Span 85 concentration as compared with those prepared at high pH and Span 85 concentration. Formation of large microcapsules was also reported[4] for the case in which the oil soluble reactant concentration in organic phase was reduced or the temperature at which polycondensation reaction takes place was lowered. It might be concluded that large microcapsules are formed by the mechanism discussed[4] whenever polymers with low intrinsic viscosity are produced.

The Formation of Metallic Silver in Silver-Form Zeolites

Kazuo TSUTSUMI and Hiroshi TAKAHASHI

Institute of Industrial Science, The University of Tokyo, Roppongi, Minato-ku, Tokyo

(Received December 23, 1971)

The formation of silver crystallites in silver-form zeolites was investigated, mainly by means of X-ray diffraction analysis. Silver ions were reduced to the zero-valent state; they aggregated to metals in three cases in this study—first, when silver-form zeolites were heated in a helium flow at above 600°C; secondly, when they were reduced by hydrogen, and lastly, when they were treated with the alkyl benzenes or alcohols above 300°C. The silver crystallites had sizes of 150—400, 150—200, and 200—300Å respectively when Ag(31.6%)-Na-$Y_{4.6}$ was re-reduced in the three cases mentioned above. If the silver ions are reduced, the zeolite becomes decationated-form, in which metallic silver is dispersed. The silver metals formed in the zeolite have peculiar interactions with oxygen.

Zeolite has been known to be useful as a catalyst in various organic reactions,[1] since it is so highly crystalline that theoretical studies of its activity and active site seem easier than those of many other catalysts. Furthermore, the activity is much higher than that of conventional silica-alumina catalysts, so it has been widely used as a practecal catalyst.

The present authors previously found that the cumene-cracking activities of transition metal-form zeolites gradually increase with each slug of cumene, eventually attaining maximum values.[2] The data of magnetic susceptibility indicate that paramagnetic nickel-form zeolite becomes ferromagnetic during the reaction as a result of the formation of metallic nickel. Thus, transition metal cations, such as Ni^{2+}, Fe^{3+}, Co^{2+}, Cd^{2+}, and Cr^{3+}, incorporated into the zeolite were reduced to the metals when these zeolites were used for catalysts in the cumene-cracking reaction.

The formation of metal in zeolite has already been reported by many authors. Lawson *et al.* studied nickel-crystallite formation in a Ni-Y zeolite using a reduction with a hydrogen flow above 300°C, as detected by electronmicroscope and X-ray diffraction.[3] A significant portion of these crystallites appeared on the outside surface, destroying any possible size-selective characteristics. Mild pretreatment reduced the rate of crystal growth and produced a catalyst with a slightly improved poison resistance. Lewis reported on the platinum crystallite formation in a Pt-Y zeolite.[4] The X-ray absorption edge data showed that all the platinum was reduced to a zero-valent state, and that, on the average, this platinum was smaller in size than that found in conventional reforming catalysts. Sixty percent of the reduced platinum was estimated to be 10Å size or less. Yates found that reducible metal cations such as Cd^{2+}, Mg^{2+}, and Zn^{2+} can be removed from zeolites by hydrogen treatment.[5] The reduced nickel and silver were held loosely in the zeolite lattice because of their low vapor pressures. The average nickel crystallite size was 240Å. In each case, no free metals were formed when the samples were heated in a vacuum. Rabo *et al.* investigated, by ESR, the oxidation state of nickel ions contained in Ni-Y which had been treated by either sodium vapor or by hydrogen; they found the formation of Ni^0 at 575°C.[6] Gioia has reported the reduction of Ni-X by hydrogen.[7]

Alloy fromation on zeolite Y was reported by Reman *et al.*[8] If two types of metal ions were present, for instance Ni^{2+} and Cu^{2+}, reduction by hydrogen, under favorable circumstances, led to the formation of crystals of alloys. Alloy formation was found to have a profound influence on the type of conversion of *n*-hexane.

In almost all the cases mentioned above, the reductions were performed by hydrogen.

In this paper, the formation of silver crystallites in Ag-form zeolites with reduction by hydrocarbons, mainly cumene, and other substances were investigated by X-ray diffraction analysis.

Experimental

The starting materials were synthetic sodium faujasite (Na-$Y_{4.6}$,$Na_2O \cdot Al_2O_3 \cdot 4.6SiO_2 \cdot nH_2O$) and synthetic mordenite (Na-M,$Na_2O \cdot Al_2O_3 \cdot 10SiO_2 \cdot nH_2O$).

The ion exchange of sodium ions for the silver ion was performed by stirring an aqueous suspension of the Na-form zeolite in the presence of a proper amount of silver nitrate. This treatment was done in the dark to prevent the silver ion being reduced. The degree of ion exchange was determined from chemical analysis.

Hydrocarbons were guaranteed-grade samples which had been dehydrated with a molecular sieve 4A before use.

For studying the catalytic activity, a pulse microreactor was used. The details were described in a previous paper.[9] The reactants (or the reducing agents), alkylbenzene, alcohol, or hydrogen, were injected by means of a syringe and were fed to the catalyst with a flow of dry helim, the flow rate of which was 60 cc/min. The products were trapped and analyzed by gas chromatography.

The electronmicrographs were taken by means of a Hitachi HU-11A-type electronmicroscope.

1) P. B. Venuto and P. S. Landis, *Advan. Catal. Relat. Subj.*, **18**, 259 (1968).
2) K. Tsutsumi, S. Fiji, snd H. Takahashi, *J. Catal.*, **24**, 8 (1972).
3) J. D. Lawson, and H. F. Rase, *Ind. Eng. Chem. Prod. Res. Develop.*, **9**, 317 (1970).
4) P. H. Lewis. *J. Catal.*, **11**, 162 (1968).
5) D. J. C. Yates, *J. Phys. Chem.*, **69**, 1676 (1965).
6) J. A. Rabo, C. L. Angell, P. H. Kasai, and V. Schomaker, *Disc. Faraday Soc.*, **41**, 328 (1966).
7) F. Gioia, G. Greco, Jr., and E. Drioli, *Chem. Ind.* (Milan) **71**, 457 (1969).
8) W. G. Reman, A. H. Ali, and G. C. A. Schuit, *J. Catal.*, **20**, 374 (1971).
9) K. Tsutsumi and H. Takahashi, *ibid.*, **24**, 1 (1972).

The X-ray powder diagrams were recorded by means of a X-ray diffractometer. The experimental conditions were as follows. Copper radiation was used; the scanning speed was 1° or 1/4° 2θ/min; the time constant was 2 sec; the receiving slit was 0.15 mm; the angular aperture was 1°. Silicon was used as the internal standard for the measurement of the crystallite size.

Results and Discussion

In Fig.1, the change in the cumene-cracking activities over Ag–Na–$Y_{4.6}$ with an increase in the Ag^+ exchange is shown in relation to the pulse number of the added cumene. The pretreatment was carried out at 450°C, and the reaction temperature was 350°C. As is clearly, the activities

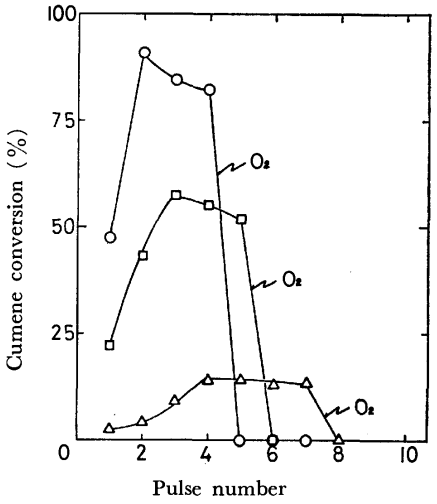

Fig. 1. Conversion of cumene over Ag-Na-$Y_{4.6}$ as a function of cumene pulse number and effect of oxygen addition.
—○— Ag(86.1%)-Na-$Y_{4.6}$
—□— Ag(31.6%)-Na-$Y_{4.6}$
—△— Ag(14.4%)-Na-$Y_{4.6}$

gradually increase with each slug of cumene until they attain a maximum value. The higher the extent of ion exchange or the reaction temperature, the greater the saturated activity. These tendencies are similar to those of transition metal-form zeolites such as Ni, Fe, Co, Cd, and Cr.[2] Therefore, the silver ion must be reduced to zero-valent silver, which aggregates to metal, during the reaction. At the same time, an active site, a decationated site, is newly formed. The activity was greatly decreased by the addition of oxgen at 450°C, and it could not be restored even if excess cumene was fed in. This behavior was surely connected with the formation of metallic silver.

Table 1 shows the cumene-cracking activity of Ag (31.6%)–Na–$Y_{4.6}$ at 350°C after various hydrocarbons, alcohols, and water were added at 450°C. The addition of hydrocarbons and alcohols clearly induces the activity increase; thus, the reduction of the silver ion by such reagents must occur in the zeolite. Water molecules, however, have no influence on the catalytic activity.

The X-ray diffraction diagrams of Ag(31.6%)–Na–$Y_{4.6}$ treated in various ways are illustrated in Fig.2. The B, C, E and F samples have a new prominent peak at about $2\theta = 37.5°$ and 44.0° which is not observed in the original. Since these peaks correspond to the (111) and (200) reflections of crystalline silver, it is confirmed that silver ions are reduced to Ag, which then aggregates to metal. Metallic silver can be formed even by heat treatment in a helium

Table 1. Effects of the additives on the cumene conversion rate on Ag(31.6%)-Na-$Y_{4.6}$[a]

Additives	Conversion rate (mol%)
Without addition	23.0
Toluene	46.0
Ethylbenzene	57.6
Cumene	60.7
t-Butylbenzene	56.9
p-Xylene	45.0
Mesitylene	34.1
Ethyl alcohol	22.1
i-Propyl alcohol	51.0
t-Butyl alcohol	54.2
Water	23.0

a) After 60 mg of Ag(31.6%)-Na-$Y_{4.6}$ was pretreated at 450°C and followed by addition of 5.7×10^{-5} mol of hydrocarbons, alcohol or water, the conversion rate of 5.7×10^{-5} mol cumene pulse was examined.

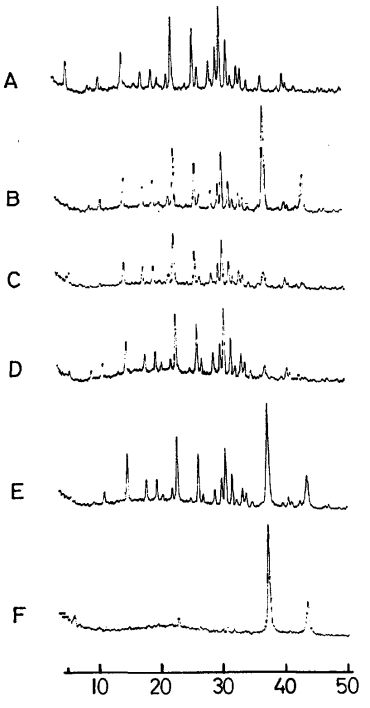

Fig. 2. X-ray diffraction patterns of Ag(31.6%)-Na-$Y_{4.6}$.
A: original.
B: treated in He at 750°C.
C: treated in He at 600°C.
D: pretreated in He at 450°C and followed by addition of cumene at 250°C.
E: pretreated in He at 450°C and followed by addition of cumene at 350°C.
F: pretreated in He at 450°C and followed by addition of cumene at 350°C and oxygen at 450°C.

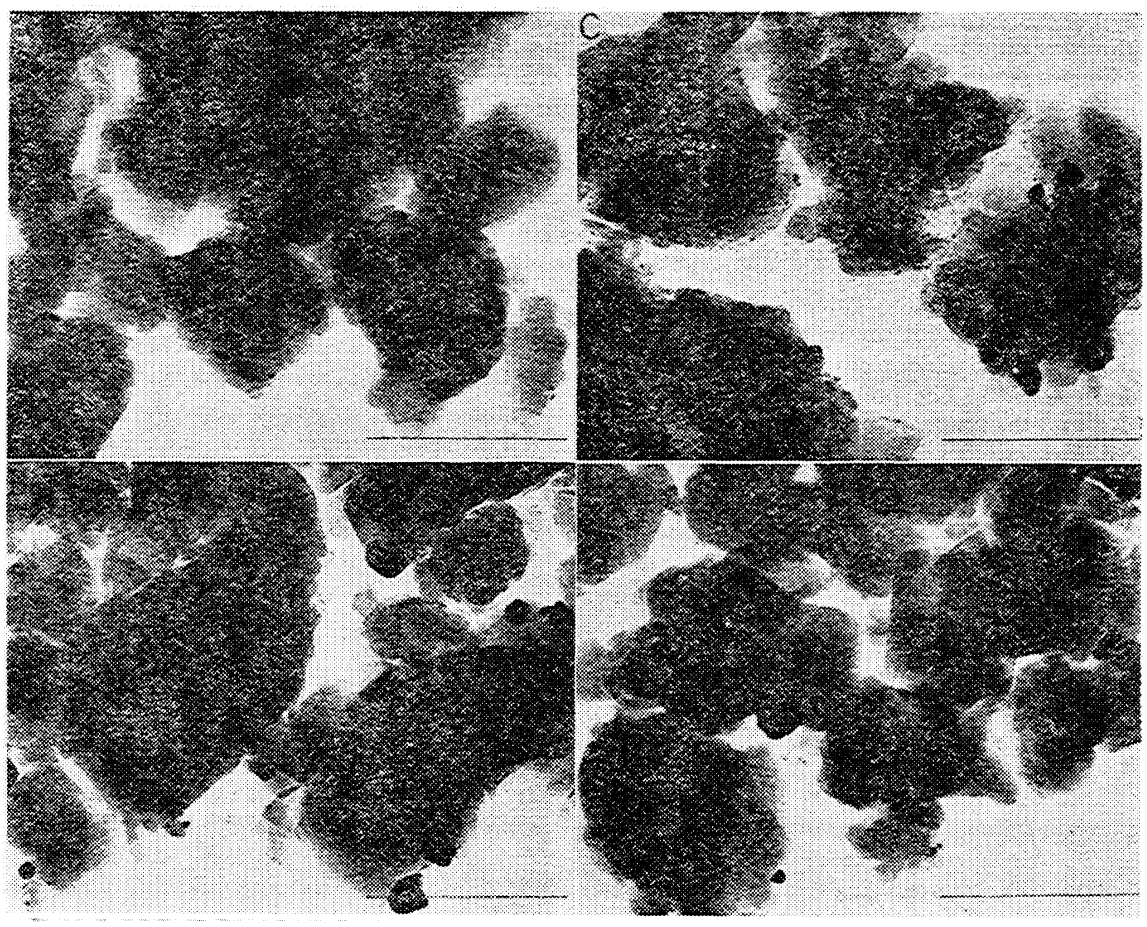

Fig. 3. Electronmicrographs of Ag(31.6%)-Na-$Y_{4.6}$. The linear dimension on electronmicrographs represents 0.5 μ.
A: original.
B: treated in He at 750°C.
C: pretreated in He at 450°C and followed by addition of cumene at 350°C.
D: pretreated in He at 450°C and followed by addition of cumene at 350°C and oxygen at 450°C.

flow at above 600°C; no such formation was observed in the case of Ni-form zeolites. The conversion of cumene and the formation of silver metal did not occur during the reaction below 250°C when the catalyst had been pretreated at 450°C. The oxygen addition destroyed the structure of the zeolite, as is shown in F: this agrees with the decrease in catalytic activity. The water addition under similar conditions induced no destruction of the structure and no decrease in the catalytic activity of zeolite.

The electronmicrographs of Ag(31.6%)-Na-$Y_{4.6}$ under various conditions are shown in Fig.3. There was no metallic silver in the original sample; however, its formation can be clearly observed in the B, C, and D species. The particle-size distribution in B is comparably uniform. The crystallite size of B is measured as 363Å by X-ray diffraction analysis, so the particle consists of several crystallites. The particle sizes in C are widely distributed. As is shown in D, the oxygen addition makes the particle size larger.

Judging from the particle size of metallic sliver, silver atoms which are formed with the reduction of ions are mobile and grow to the metallic state on the external surface.

Crystallite sizes of (200) faces of silver metals formed in Ag–Na–$Y_{4.6}$ under various conditions are listed in Table 2. The change in the crystallite sizes of the silver metals formed in Ag(31.6%)–Na–$Y_{4.6}$ with the heat treatment tempteature in the He flow is illustrated in Fig. 4. No formation of silver metal

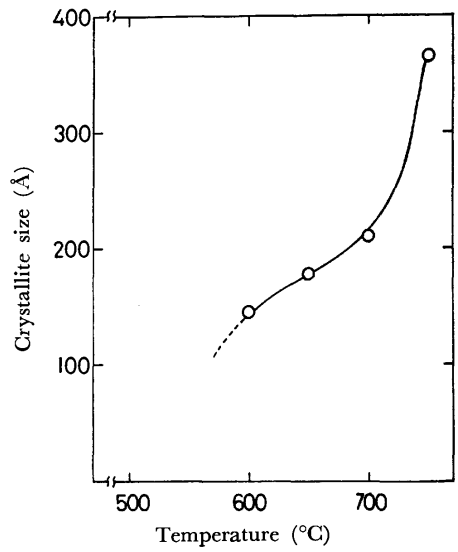

Fig. 4. Change of crystallite size of silver formed in Ag (31.6%)-Na-$Y_{4.6}$ with heat treatment temperature.

Table 2. Crystallite sizes (L_{200}) of silver formed in Ag-Na-$Y_{4.6}$ under various conditions

Degree of Ag-exchange (mol%)	Pretreatment temperature (°C)	Reactant	Reaction temperature (°C)	L_{200} (Å)
31.6	450			—
31.6	550			trace
31.6	600			146
31.6	650			178
31.6	700			211
31.6	750			363
14.4	450	Cumene[a)]	350	179
22.3	450	Cumene	350	216
31.6	450	Cumene	350	253
86.1	450	Cumene	350	298
31.6	450	Cumene	250	—
31.6	450	Cumene	300	213
31.6	450	Cumene	450	285
31.6	750	Cumene	250	416
31.6	750	Cumene	300	436
31.6	750	Cumene	350	439
31.6	750	Cumene	450	428
31.6	450	Cumene 1[b)]	350	176
31.6	450	Cumene 3	350	219
31.6	450	Cumene 5	350	225
31.6	450	Cumene 7	350	226
31.6	450	Cumene 9	350	253

a) More than 1.4×10^{-3} mol-cumene was added to 200 mg of Ag-Na-$Y_{4.6}$.
b) One pulse of 1.4×10^{-4} mol-cumene was added to 200 mg of Ag-Na-$Y_{4.6}$.

is observed under a heat treatment at temperatures lower than 600°C. The higher the temperature, the larger the crystallite. The mechanism of metal formation under heat treatment is thought to be as follows:

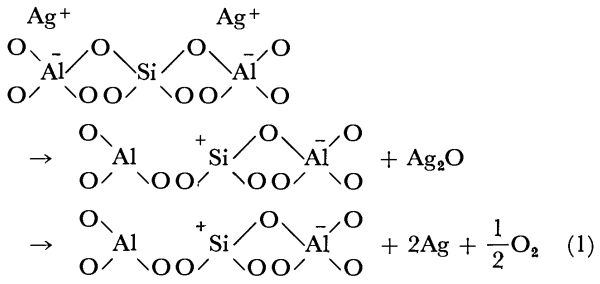

Since Ag_2O could not be detected by X-ray diffraction analysis, Ag_2O probably exists in the transition state.

An increase in the degree of silver-exchange facilitates the formation of comparably large crystallites, as is shown in Fig.5. In view of the relation between the degree of exchange and the crystallite size, the number of crystallites formed seems to be nearly constant regardless of the degree of exchange. The number of cages necessary for the formation of one crystallite are 1.7, 1.9, 2.2, and 1.6×10^5 in the samples of Ag-Na-$Y_{4.6}$ where the degrees of exchange are 14.4, 22.3, 31.6, and 81.6% respectively.

The change in crystallite size with the pulse number

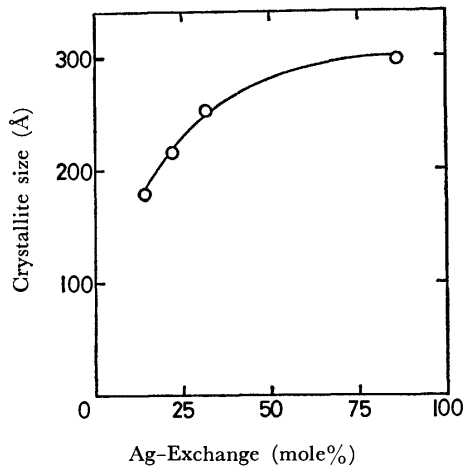

Fig. 5. Change of crystallite size of silver formed in Ag-Na-$Y_{4.6}$ with degree of Ag-exchange.

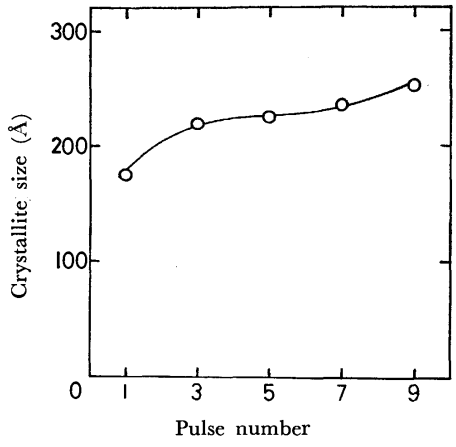

Fig. 6. Change of crystallite size of silver formed in Ag (31.6%)-Na-$Y_{4.6}$ with cumene pulse number.

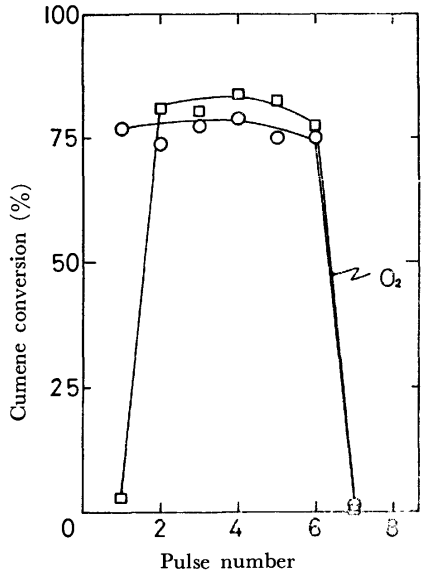

Fig. 7. Conversion of cumene over Ag (31.6%)-Na-$Y_{4.6}$ as a function of pulse number and effect of oxygen addition.
—○— pretreated in He at 450°C and followed by addition of hydrogen at 450°C before the reaction.
—□— pretreated in He at 750°C.

in Ag(31.6%)–Na–$Y_{4.6}$ is illustrated in Fig.6. The figure shows that the growth of the crystallite is related to the amount of cumene converted.

The dependence of the crystallite formation upon the reaction temperature in Ag(31.6%)–Na–$Y_{4.6}$ which has been pretreated at 450°C or 750°C is also shown in Table 2. When the zeolite is pretreated at 450°C, the crystallite size depends remarkably upon the reaction temperature; however, when it is pretreated at 750°C, the crystallite size formed in the reaction as 250°C is relatively large even though no cumene conversion occurred, and it merely changes at higher temperatures.

The crystallite size was increased to 261 or 320Å when oxgen was added to Ag(31.6%)–Na–$Y_{4.6}$ at 350 or 450°C after a cumene-cracking reaction at 350°C.

In Fig.7, the cumene conversion rates at 350°C are plotted against the pulse number over two Ag(31.6%)–Na–$Y_{4.6}$ samples; one was pretreated at 750°C, while the other was pretreated and then hydrogen was added at 450°C before the reaction. Although silver was formed in both samples, the activities differed greatly from each other. Since the transition from a Brønsted acid to a Lewis acid associated with the formation of metallic silver occurred upon the heat treatment at 750°C, the conversion of the first cumene pulse over the former was low. However, an increase in activity was observed upon the subsequent addition of cumene; this increase presumably resulted from the transition from a Lewis acid to a Brønsted acid by the cumene reacted. Over the zeolites which had been pretreated from 500 to 600°C, the conversions of the first cumene pulse were 15—20%; this reflected a few transitions from a Brønsted acid to a Lewis acid, and the saturated activities, 70—80%, resemble independently upon the pretreatment temperatrue. In the latter zeolite, Brønsted-acid sites were formed, accompanied by the formation of metallic silver, as in Equation (2):

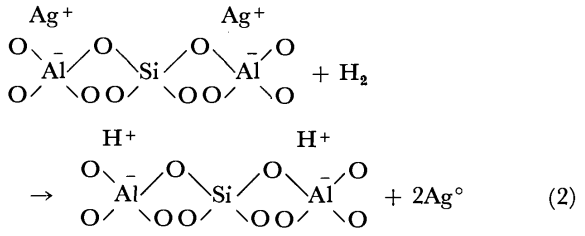

(2)

Therefore, the reduction by cumene and the increase in activity no longer occurred. The crystallite size of the silver formed in this zeolite before the reaction was 176Å, much smaller than that of the silver formed in the earlier case. This fact suggests that the catalytic activity is not essentially influenced by the formation and the size of silver crystallite, but by the formation of the Brønsted acid site.

The radiation by ultraviolet rays did not facilitate reduction of silver ions in Ag–Na–$Y_{4.6}$ under various conditions—that is, at 35, 200°C in air or at 300°C in a vacuum.

In Fig.8, the conversion rates of cumene at 350°C over silver-exchanged mordenite-type zeolite pretreated at 450°C are shown. The silver formed in Ag (35.1%)–Na–Mord. by cumene addition at 350°C after pretreatment at 450°C has a relatively large crystallite size, though the pore diameter of mordenite is smaller than that of faujasite. The heat treatment at 750°C also induced the formation of large crystallites of silver. However, since the X-ray diffraction peak of the (200) face of silver is overlapped by the peak of mordenite, the measurement of the crystallite size by X-ray-diffraction analysis is difficult The conversion of cumene was decreased with each slug of cumene over Ag(35.0%)–H(64.7%)–Na-Mord. and only traces of silver formation were found. In Ag (68.6%)–H(26.8%)–Na–$Y_{4.6}$, no formation of silver was observed. In these cases, H-form sites contribute to the activity and cumene molecules interact more strongly with H^+ than with Ag^+. This behavior agrees with the finding of Richardson that the reducibility of supported nickel was small if the support had an increased acidity.[10]

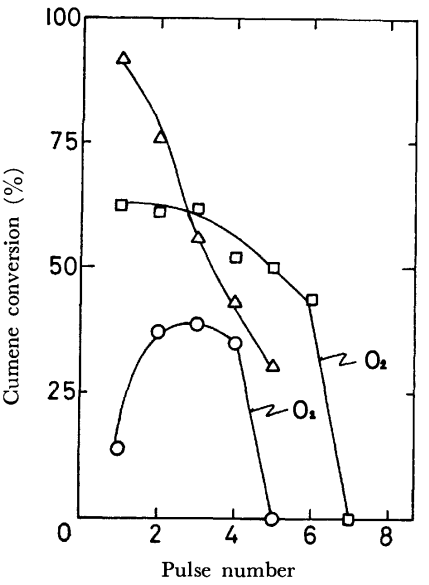

Fig. 8. Conversion of cumene over Ag-exchanged mordenite as a function of pulse number and effect of oxygen addition.
—○— Ag(35.1%)-Na-M pretreated at 450°C.
—□— Ag(35.1%)-Na-M pretreated at 750°C.
—△— Ag(35.0%)-H(64.7%)-Na-M pretreated at 450°C.

Some work has been done on the reducibility of Ag(36.1%)–Ni(50.6%)–Na–$Y_{4.6}$ zeolite. The reduction of silver was preferred to that of nickel, and the

Table 3. Crystallite sizes (L_{200}) of silver formed in Ag(36.1%)-Ni(50.6%)-Na-$Y_{4.6}$

Condition	L_{200} (Å)
Pretreated in He at 750°C	343
Pretreated in He at 450°C and followed by addition of cumene at 350°C	295
Pretreated in He at 450°C and followed by addition of hydrogen at 450°C	161

10) J. T. Richardson, *J. Catal.*, **21**, 122 (1971).

formation of alloy, which was reported by Reman *et al.* in the case of Ni–Cu–Y,[8] was not observed. The crystallite sizes of the silver in this zeolite are shown in Table 3. The sizes are similar to those of silver formed in Ag–Na–$Y_{4.6}$ under similar conditions.

We wish to thank Mr. Takashi Akeboshi for his assistance in carrying out the experiments.

BULLETIN OF THE CHEMICAL SOCIETY OF JAPAN, VOL. 45, 2337—2343 (1972)

The Formation of High-boiling By-products in the Isomerization and Disproportionation of *m*-Xylene over a Silica-alumina Catalyst under Pressure

Haruo TAKAYA, Naoyuki TODO, Tadasuke HOSOYA, Hideki ŌSHIO,* and Toshio MINEGISHI

National Chemical Laboratory for Industry, Mita, Meguro-ku, Tokyo

* *The Research Laboratory, Central Glass Company, Ltd., Imafuku, Kawagoe-shi, Saitama*

(Received December 10, 1971)

Continuous liquid-phase isomerization and disproportionation reactions over silica-alumina catalysts were carried out using *m*-xylene with varying concentration of water. The reactions were conducted at 290°C and 400°C under a pressure of 300 kg/cm². The results showed that the concentration of water required to attain a maximum activity for the isomerization was higher than that needed for the disproportionation reaction. The high-boiling by-products produced at 400°C comprized 2—5 per-cent of the weight of the total products, and the main component, polymethyldiphenylmethane, amounted to 70—80 per-cent of the by-products. The yield of polymethyldiphenylmethane was linearly correlated with that of toluene. This result appears to suggest that the disproportionation reaction and the polymethyldiphenylmethane formation proceed at a common active site and through the same intermediate.

In an earlier paper[1] the present authors reported that, in the liquid-phase isomerization of *m*-xylene, a silica-alumina catalyst revealed higher activity than in the vapor-phase reaction; moreover, even after 20 days no practical decline in the activity was observed. This superior ability of the catalyst in the liquid phase can be ascribed to the cleaning effects of the liquid reactant: in the liquid-phase reaction, the high-boiling by-product which, in the vapor-phase reaction, causes the activity to diminish due to its strong adsorptivity on the surface sites, is successively dissolved into the reactant; therefore, more surface sites are available for the isomerization.

As was shown in an earlier paper,[1] some components in the high-boiling by-product exhibit a temporary inhibiting effect, and these seem to be transformed into higher boiling compounds which exert a permanent poisoning effect on the catalytic activity. Hence, the decline in activity can not be avoided even in the liquid phase when the high-boiling by-product is produced to a great extent. On the basis of such considerations, it will be valuable, for the sake of the improvement of the catalyst life, to discover some means to reduce the yield of the high-boiling by-product.

The liquid-phase reaction can be characterized from another point of view—the yields of the high-boiling by-product can be measured rather quantitatively. Therefore, for the purpose of examining the possibility of reducing the high-boiling by-product or the disproportionation reaction products in the isomerization of *m*-xylene, the correlation between the yield of the high-boiling by-product and that of the disproportionation product, as well as the correlation between the yield of the isomerization product and that of the disproportionation product, will be studied in this paper. Practically, the correlations were studied over silica-alumina catalysts calcined at various temperatures by using *m*-xylene containing various amounts of water. It is well-known that a small amount of water influences the catalytic activity of silica-alumina.[2,3]

Experimental

The catalysts employed were two kinds of silica-alumina: one (I) was synthesized from aluminum isopropoxide and ethyl silicate,[4] while the other (II) was Nikki N633L. Both of these catalysts were calcined at 400°C or at 600°C for 20 hours. The equipment and the procedure for carrying out the continuous liquid-phase xylene isomerization under a high pressure were shown in previous papers.[1,5] In this study, all the experiments were carried out at a contact time (W/F) of 0.5 g-cat. h/g under a pressure of 300 kg/cm².

The reactant *m*-xylene (produced by Japan Gas Chemical Co. Inc.) was 99.6% pure and contained 100—130 ppm of water. Therefore, the concentration of water in the *m*-xylene was adjusted to the desired extent by drying with metallic sodium or calcium chloride and was determined by means of the Kaal-Fisher method.

The product was analyzed by gas chromatography. Two kinds of columns were used: one was 4 m in length, 1 mm in dia., and was packed with 5 per-cent Benton 34+DIDP

1) H. Takaya, N. Todo, T. Hosoya, T. Minegishi, M. Yoneoka, and H. Ōshio, This Bulletin, **44**, 2296 (1971).

2) A. Ozaki, "Catalyst Handbook," ed. by A. Ozaki, K. Tamaru, K. Tanabe, and S. Nishimura, Chijinshokan, Tokyo, Japan. (1967) p. 204.

3) T. Iwasaki and R. Hatta, *Kogyo Kagaku Zasshi*, **63**, 1975 (1960).

4) S. Yamadaya and H. Uchida, *Tokyo Kogyo Shikenjo Hokoku*, **61**, 254 (1966).

5) H. Takaya, N. Todo, T. Hosoya, T. Minegishi, and M. Yoneoka, *Kogyo Kagaku Zasshi*, **73**, 1831 (1970).

on diasolid L (100—200 mesh), while the other was 2 m in length, 3 mm in dia. and was packed with 20 per-cent silicone grease on celite 545.

The high-boiling by-product was separated by distilling the product at 100°C under a reduced pressure of 5 mmHg. Its composition was determined from the parent peaks of the mass spectra obtained by means of a Hitachi double-beam mass spectrometer.

Results and Discussion

Under the liquid-phase reaction conditions, the silica-alumina catalyst pretreated at a moderate temperature showed a considerably high activity for the isomerization reaction.[1,5] Accordingly, in order to detect the effects of water content on the activity, the reaction had to be carried out at a low temperature of 290°C where the equilibria among xylene isomers had not been established. On the other hand, at this temperature the rate of the production of the high-boiling compounds was very slow. Hence, in order to get information about the high-boiling by-product formation, the reaction was carried out at a higher temperature of 400°C, where measurable amounts of these compounds could be obtained.

3.1 Results at the Reaction Temperature of 290°C. The effects of water on both the isomerization and the disproportionation reaction were studied by using the II catalyst calcined at 600°C; the results are shown in Figs. 1-a, 2-a, and 3-a. In addition, it is known that the yield of toluene is approximately equal to that of trimethylbenzene at the reaction temperature of 290°C; hence, the yield of toluene can be considered as the disproportionation activity.[5] In these figures, the yield for neither the isomerization nor the disproportionation reaction in the first sample taken after 4 hours' reaction was obtained with a good reproducibility. As will be described below, however, this study aimed to follow only the manner of variation in the yields of the isomerization products and the disproportionation-reaction products with time. Thus, the lack of the reproducibility of the first yields of the products was not taken into account. The figures show that when the concentration of water in *m*-xylene was changed, the yields of the isomerization products varied with time in a different manner from those of the disproportionation. This fact suggests that different active sites may be available for the two reactions. This consideration was more clearly supported by the result shown in Fig. 1-b: when the reactant was changed from the *m*-xylene containing water below 5 ppm to the *m*-xylene containing 100—130 ppm, the yields of the isomerization products were recovered to about 50 per-cent of the initial ones, while the yield of the disproportionation product was decreased monotonously.

The variations in the activities for the isomerization and the disproportionation with the reaction time, as are shown in Figs. 1—3, appear to be attributable to the gradual adsorption of water in the reactant *m*-xylene in the cases of Figs. 2-a and 3-a, and to the deactivation due to the adsorption of undesirable high-boiling by-

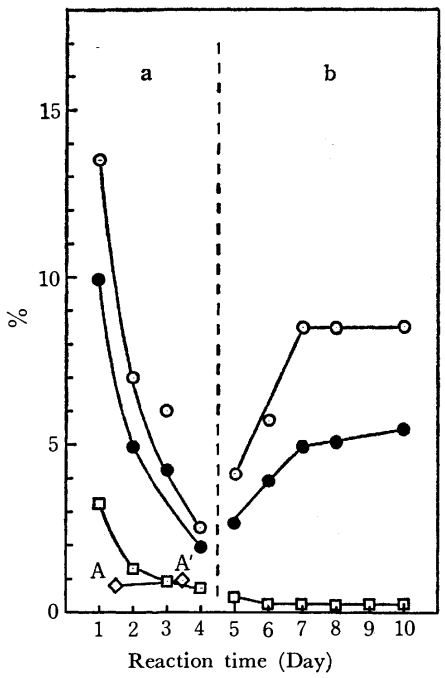

Fig. 1. Variation of activity with reaction time.
Catalyst: II. Calcining temperature of the catalyst: 600°C. Reaction temperature: 290°C. Concentration of water in *m*-xylene: below 5 ppm and 100—130 ppm in the regions designated by a and b respectively.
○: *p*-Xylene. ●: *o*-Xylene. □: Toluene.
◇: High-boiling by-products.

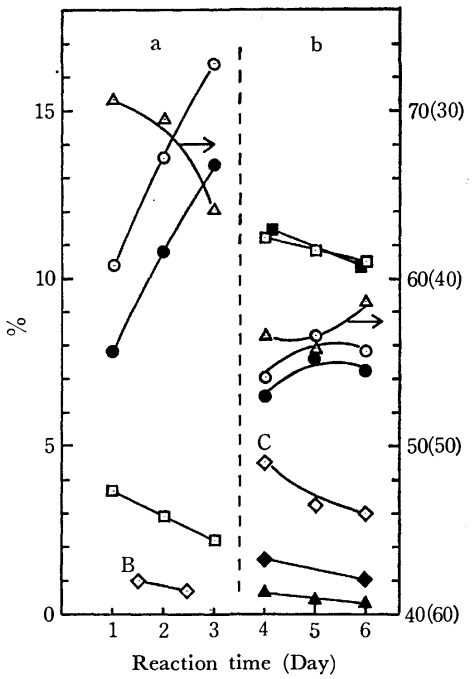

Fig. 2. Variation of activity with reaction time.
Catalyst: II. Calcining temperature of the catalyst: 600°C. Reaction temperature: 290°C and 400°C in the regions designated by a and b respectively. Concentration of water in *m*-xylene: 20—30 ppm. The figures in parentheses along the right ordinate show the conversions of *m*-Xylene: the conversion = 100% − an amount of unreacted *m*-xylene %.
△: *m*-Xylene. ○: *p*-Xylene. ●: *o*-Xylene.
□: Toluene. ■: Trimethylbenzene. ▲: Benzene.
◆: Tetramethylbenzene. ◇: High-boiling by-products.

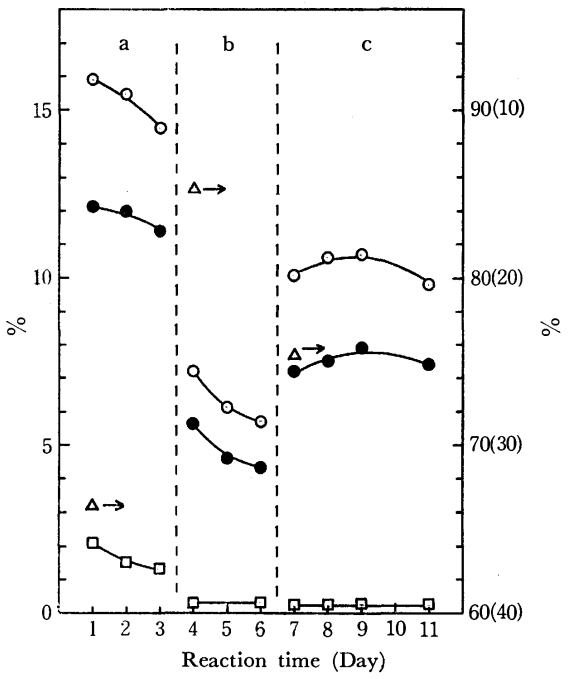

Fig. 3. Variation of activity with reaction time.
Catalyst: II. Calcining temperature of the catalyst: 600°C. Reaction temperature: 290°C. Concentration of water in *m*-xylene: 100—130 ppm and 20—30 ppm in the regions designated by a and c respectively. In the region designated by b, 1000 ppm of methanol was added to *m*-xylene.
△: *m*-Xylene. ○: *p*-Xylene. ●: *o*-Xylene.
□: Toluene.

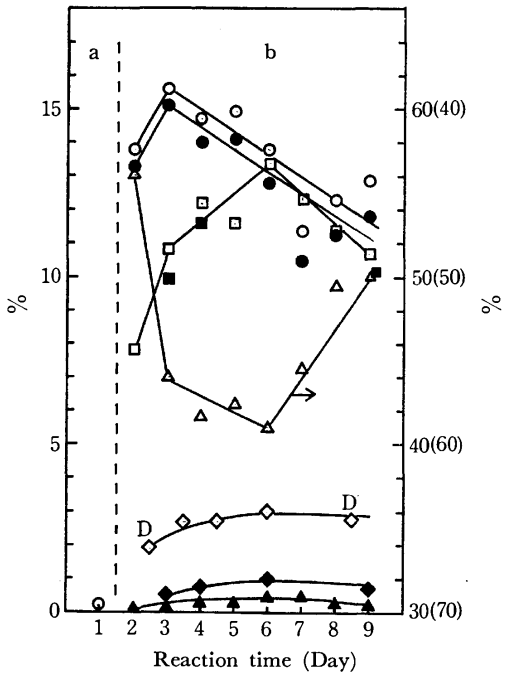

Fig. 4. Activity of Catalyst II.
Calcining temperature: 400°C. Reaction temperature: 290°C and 400°C in the regions designated by a and b respectively. Concentration of water in *m*-xylene: 20—30 ppm.
△: *m*-Xylene. ○: *p*-Xylene. ●: *o*-Xylene.
□: Toluene. ■: Trimethylbenzene. ▲: Benzene.
◆: Tetramethylbenzene. ◇: High-boiling by-products.

products in the case of Fig. 1-a. Also, Figs. 3-b and 3-c show the effects of the adsorption and desorption of water on the activities. In Fig. 3-b, methyl alcohol was decomposed to water and methyl ether. These results show that there was an amount of water adequate for the maximum activity for the isomerization, but that the activity for the disproportionation increased with a decrease in the concentration of water in *m*-xylene.

Figure 4-a illustrates that the II catalyst calcined at 400°C showed practically no activity in the two reactions. However, the I catalyst calcined at the same temperature revealed a low but measurable activity, as is shown in Fig. 5. This difference between the two catalysts may be related to the content of water in the catalysts, since the results obtained by the use of TGA and DTA showed that the dehydration of the II catalyst took place at a higher temperature than that of the I catalyst.

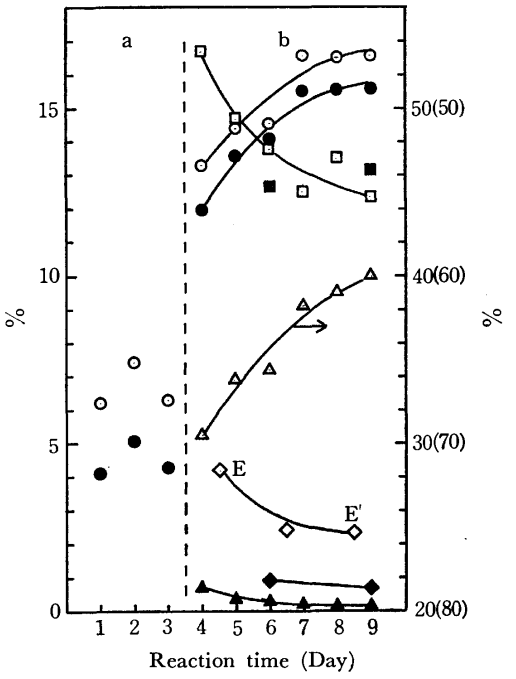

Fig. 5. Activity of catalyst I.
Calcining temperature: 400°C. Reaction temperatures: 290°C and 400°C in the regions designated by a and b respectively. Concentration of water in *m*-xylene: 20—30 ppm.
△: *m*-Xylene. ○: *p*-Xylene. ●: *o*-Xylene.
□: Toluene. ■: Trimethylbenzene. ▲: Benzene.
◆: Tetramethylbenzene. ◇: High-boiling by-products.

3.2 The Results at a Reaction Temperature of 400°C.
3.2.1 The Results Using II Catalyst: The results obtained at a reaction temperature of 400°C are shown in Figs. 2-b, 4-b, 6-b, and 7. These results can be divided into three groups, depending on the yields of the isomerization products and the disproportionation reaction products. In the first group (Figs. 6-b and 7), the equilibria among xylene isomers were established; also, the disproportionation products were produced in high yields. It can be said such results were obtained for the cases where the catalysts calcined at 600°C were used and where the reaction systems involved

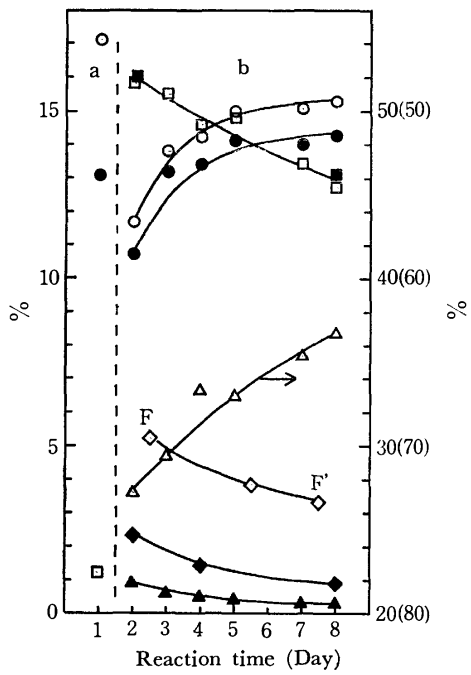

Fig. 6. Activity of catalyst II.
Calcining temperature: 600°C. Reaction temperatures: 290°C and 400°C in the regions designated by a and b respectively. Concentration of water in *m*-xylene: 100—130 ppm.
△: *m*-Xylene. ○: *p*-Xylene. ●: *o*-Xylene.
□: Toluene. ■: Trimethylbenzene. ▲: Benzene.
◆: Tetramethylbenzene. ◇: High-boiling by-products.

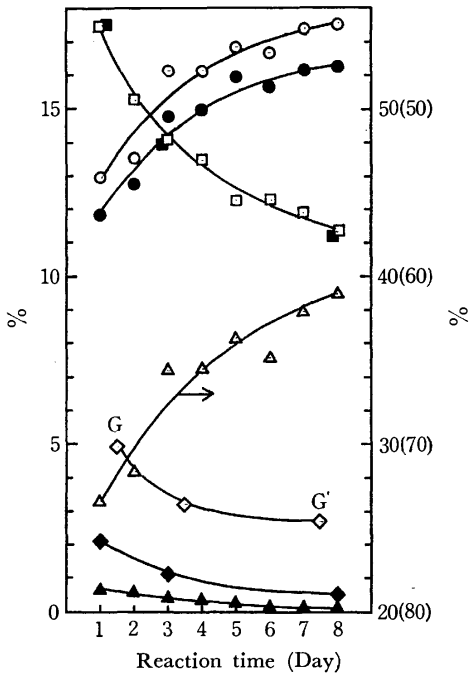

Fig. 7. Activity of catalyst II with using *m*-xylene containing 1000 ppm of methanol.
Calcining temperature of catalyst: 600°C. Reaction temperature: 400°C.
△: *m*-Xylene. ○: *p*-Xylene. ●: *o*-Xylene.
□: Toluene. ■: Trimethylbenzene. ▲: Benzene.
◆: Tetramethylbenzene. ◇: High-boiling by-products.

comparatively high concentrations of water; the reactant *m*-xylene contained a high concentration of water or 1000 ppm of methyl alcohol. On the other hand, the characteristic feature of the second group (Fig. 2-b) is that the yield of the disproportionation-reaction product was higher than that of the isomerization product in spite of the low conversion of *m*-xylene. In this group, the equilibria among xylene isomers were not established. This feature can be seen more clearly by comparing Fig. 2-b (obtained at a reaction temperature of 400°C) with Fig. 2-a (obtained at a reaction temperature of 290°C); the yields of the isomerization products at a reaction temperature of 290°C were more than those of the disproportionation, though the conversion of *m*-xylene was approximately equal to that at a reaction temperature of 400°C. The results of Fig. 2 were obtained using a catalyst calcined at 600°C and *m*-xylene containing a low concentration of water. The third was a group which showed a medium activity (Fig. 4-b). This was the case where a catalyst calcined at 400°C for 20 hours was used. It seems that the relatively lower activity than that of the first group may result from the insufficiency of the dehydration of the catalyst; the pretreatment of the II catalyst at 400°C for 20 hours was insufficient for the catalyst to reveal a high activity. The increasing activity up to the fourth day appears to correspond to the increase in the extension of the dehydration.

3.2.2 The Results with Using I Catalyst: According to the yields of the isomerization products and the disproportionation-reaction products, it may be said that the results shown in Figs. 5-b and 8-b belong to the first group and the second group respectively. The I catalyst calcined at 400°C revealed a high activity, as is shown in Fig. 5, where the reactant *m*-xylene contained 20—30 ppm of water. This result differs from that with using the II catalyst calcined at 400°C (Fig. 4-b). This discrepancy in activity may also be attributed to the greater ease of the dehydration of the I catalyst. The results shown in Fig. 8-b, where the catalyst was calcined at 600°C and where the reactant, *m*-xylene, contained 20—30 ppm of water, are the same

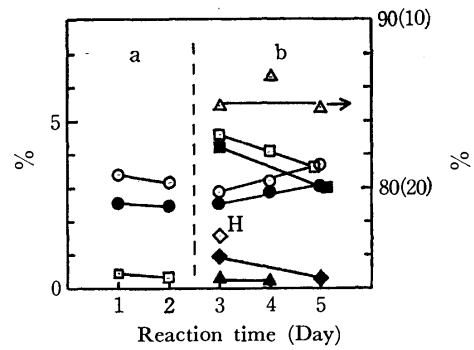

Fig. 8. Activity of catalyst I.
Calcining temperature of catalyst: 600°C. Reaction temperatures: 290°C and 400°C in the regions designated by a and b respectively. Concentration of water in *m*-xylene: 20—30 ppm.
△: *m*-Xylene. ○: *p*-Xylene. ●: *o*-Xylene.
□: Toluene. ■: Trimethylbenzene. ▲: Benzene.
◆: Tetramethylbenzene. ◇: High-boiling by-products.

as those in Fig. 2-b.

3.3 High-boiling By-product. The product for 23 hours' operation (about 130 g) was distilled at a reduced pressure of 5 mmHg and at a temperature of 100°C; the residue thus obtained was regarded as comprising the high-boiling by-products. As is shown in Figs. 1—8, the yields of the high-boiling by-products were in the range of 2—5 per-cent and seemed to be correlated with the yields of toluene. However, as to the isomerization products, the correlation with the high-boiling by-products could not be examined because, in most of cases, the equilibria of the isomerization were established.

The decline in activity observed in most cases at the reaction temperature of 400°C might be attributed to the large yields of high-boiling by-products. Two per-cent of the weight of the by-products was sufficient to lower the catalyst activity.[1)]

The compositions of the high-boiling by-products were analyzed by means of a mass spectrometer under the conditions described in a previous paper.[1)] The mass spectra of the samples designated by A—H in Figs. 2—8 were observed; three representative spectra are shown in Fig. 9. It can be seen that all the spectra consist of three homologous series differing in mass number by 14, corresponding to the replacement of a hydrogen atom by a methyl group. The three series correspond to polymethylnaphthalene, polymethyldiphenylmethane, and polymethylanthracene. The compositions and the yields are shown in Table 1. This table shows that polymethyldiphenylmethanes amounted to 70—80 per-cent and were the main components of the high-boiling by-product at the reaction temperature of 400°C. In the case of the reaction at 290°C, tetramethyldiphenylmethane, the mass number of which is 224, was the main product, and the amount of anthracene was small.

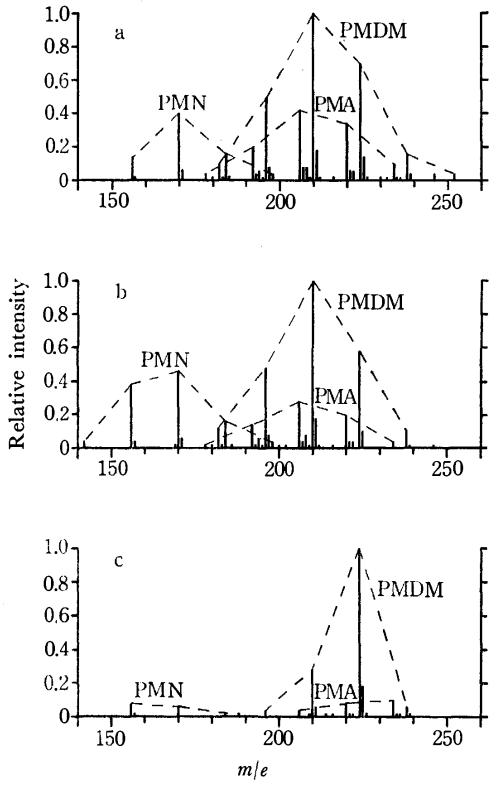

Fig. 9. Mass spectra of the high-boiling by-products.
These mass spectra were obtained at ionization voltages as low as 15 V in order to allow only the parent peaks of the components to appear.
a: Sample F shown in Figs. 6 and 10, and in Table 1.
b: Sample C shown in Figs. 2 and 10, and in Table 1.
c: Sample B shown in Figs. 2 and 10, and in Table 1.
PMN: Polymethylnaphthalene.
PMDM: Polymethyldiphenylmethane.
PMA: Polymethylanthracene or polymethylphenanthrene.

3.4 The Active Sites for the Isomerization and the Disproportionation. The results presented in Section 3.2 show that, at a reaction temperature of 400°C, the high activity for the isomerization and the disproportionation reaction was obtained under the reaction conditions of the first group, where an adequate amount of water existed in the reaction systems. This suggests that an adequate concentration of water is required to attain a maximum activity not only for the isomerization but also for the disproportionation reaction. However, considering the finding at 290°C that the activity for the disproportionation increased with a decrease in the concentration of water the required concentration for the disproportionation appears to be lower than that for the isomerization.

In connection with the active sites available for the isomerization, it has been generally accepted that the reaction is catalyzed by a protonic acid.[6,7,8,9,10)] The present results related with the effect of water concentrations on the isomerization activity really coincide with this view. As for disproportionation or transalkylation, however, the active sites proposed by several authors are not entirely consistent. From the correspondency of the catalytic activity to the Brønsted acidity, Izumi and Shiba[11)] concluded that the disproportionation of toluene over an alumina-boria catalyst proceeds mainly on protonic-acid sites. Matsumoto *et al.*[8)] reached the same conclusion with regard to the active sites for the disproportionation of *o*-xylene over a calcium-exchanged NaX-zeolite catalyst. On the other hand, according to Csicsery,[9)] the ratio of the isomerization to the transalkylation of 1-methyl-2-ethylbenzene over a silica-alumina catalyst increased with an increase in the water content of the reactant. They suggested, therefore, that transalkylation is catalyzed predominantly by a Lewis acid or by a protonic acid and Lewis acid pair.

If we assume that the disproportionation occurs at the protonic acid site, the present results can be interpreted as indicating that the acid strength of the site available for the disproportionation should be stronger than that for the isomerization, because the increasing concentration of water in the reaction system would reduce the mean acid strength due to the adsorption of water, which has a basic property. On the other

6) V. C. F. Holm and A. Clark, *J. Catal.*, **2**, 16 (1963).
7) T. Iwasaki, *Waseda Daigaku Oyokagakukaiho*, **30**, 4 (1963).
8) H. Matsumoto and Y. Morita, *Bull. Japan Petroleum Institute*, **11**, 40 (1969). *Kogyo Kagaku Zasshi*, **70**, 1674 (1967), *ibid.* **71**, 1004 (1968), *ibid.* **71**, 1496 (1968).
9) S. M. Csicsery and D. A. Hickson, *J. Catal.*, **19**, 386 (1970).
10) J. W. Ward, *ibid.*, **17**, 355 (1970).

Table 1. The yields and the composition of high-boiling by-products

Sample[a]		A	A′	B	C	D	D′	E	E′	F	F′	G	G′	H
Catalyst		II		II	II	II		I		II		II		I
Calc. temp of Cat. °C		600		600	600	400		400		600		600		600
React. temp °C		290		290	400	400		400		400		400		400
Concentration of water in *m*-xylene ppm		below 5		20–30	20–30	20–30		20–30		100–130		1000[g]		20–30
Yield[b], %	PMN[c]	0.1			1.0	0.2	0.3	0.7	0.2	0.8	0.3	0.9	0.2	0.1
	PMDM[d]	0.7	0.9	0.8	3.1	1.5	2.2	2.9	1.9	3.7	2.7	2.9	2.3	1.3
	PMA[e]				0.4	0.2	0.2	0.5	0.2	0.6	0.2	0.4	0.2	0.2
Composition[f], %	PMN	6	2	6	21	13	11	16	10	15	10	20	8	7
	PMDM	90	94	89	69	77	78	69	80	71	83	68	84	79
	PMA	4	4	5	8	9	9	12	9	12	6	10	7	12

a) These samples were shown also in Figs. 1—8 by the signs of A, A′,··· and H. b) Ratios to total products.
c) Polymethylnaphthalene. d) Polymethyldiphenylmethane. e) Polymethylanthracene.
f) Compositions of high-boiling by-products. g) Concentration of methyl alcohol.

hand, if we assume that the disproportionation reaction would be catalyzed by a Lewis acid, the role of water may be interpreted as promoting the desorption of undesirable products, polymethyldiphenylmethanes, due to the strong affinity of water with the acid sites. Up to an adequate content of water for the disproportionation, the produced polymethyldiphenylmethanes are desorbed successively without any formation of higher condensation products; thus, the effective sites could be prevented from permanent poisoning. A further increase in the water content, however, may result in a decrease in the effective active sites.

In conclusion, a full designation of the active sites available for the disproportionation seems to be beyond our reach at present; thus, further investigations must be made from a different point of view.

3.5 High-boiling By-products and Toluene. As is indicated in Fig. 10, the yield of polymethyldiphenylmethane, the main component of the high-boiling by-products, shows an approximately linear relation with that of toluene. This appears to suggest that the disproportionation reaction and the polymethyldiphenylmethane formation proceed at a common active site

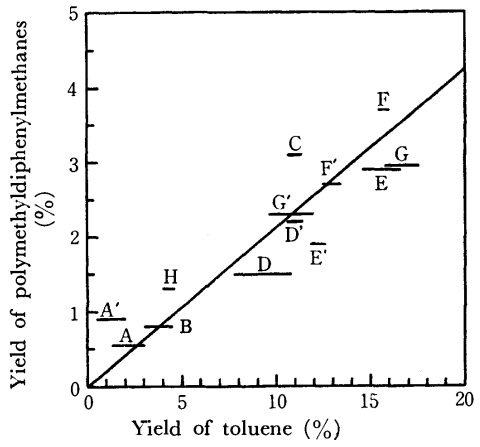

Fig. 10. Yield of polymethyldiphenylmethane *versus* that of toluene.
The letters indicate the samples shown in Table 1.
The width of the yield of toluene was caused by the fact that the deactivation occurred during 23 hr operation to obtain high-boiling by-products.

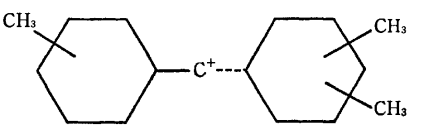

Fig. 11. A probable intermediate for the disproportionation reaction and the formation reaction of the polymethyldiphenylmethane.

and through the same intermediate. Therefore, it may be reasonable to think that the intermediate is similar to diphenylmethane, as is shown in Fig. 11. Lanewala[12] and Csicsery[13] proposed an intermediate similar to Fig. 11 for the transalkylation of alkylbenzenes over zeolite catalysts. Polymethyldiphenylmethanes seem to be produced by the release of a hydrogen molecule or methane from the intermediate.

As is shown in Fig. 9-c, tetramethyldiphenylmethane is the main component of the high-boiling by-product at the reaction temperature of 290°C. Considering the intermediate shown in Fig. 11, trimethyldiphenylmethane may be expected to be the main component at that reaction temperature, since the xylenes in the product amounted to more than 90 per-cent. This conflict can be resolved by considering the occurrence of a rapid exchange reaction between a reactant xylene and an aromatic ring of diphenylmethane.[14]

In addition, as is shown in Figs. 9-a and 9-b, the composition of the high-boiling by-product at 400°C was independent of the water concentration in *m*-xylene. In connection with the high-boiling by-products, another finding was that the product distribution of parent peaks of polymethylanthracene, which exert a stronger poisining effect on the catalyst activity than does diphenylmethane,[14] is similar to that of polymethyldiphenylmethane. This result leads us to think that polymethylanthracene would be formed dominantly from polymethyldiphenylmethane. However, poly-

11) A. Izumi and T. Shiba, *Nippon Kagaku Zasshi*, **84**, 699 (1963).
12) M. A. Lanewala and A. P. Bolton, *J. Org. Chem.*, **34**, 3107 (1969).
13) S. M. Csicsery, *ibid.*, **34**, 3338 (1969).
14) H. Takaya, N. Todo, T. Hosoya, H. Ōshio, and T. Minegishi, This Bulletin, in press.

methylanthracene or polymethylphenanthrene formation may occur through polymethylnaphthalene, since a small amount of polymethylnaphthalene was found in the products.

On the basis of the suggested mechanism concerning the formation of high-boiling by-products, it may be concluded that, under reaction conditions or a reaction system where the disproportionation products are required to be produced in high yields, a decline in the catalytic activity is unavoidable.

BULLETIN OF THE CHEMICAL SOCIETY OF JAPAN, VOL. 45, 2343—2346 (1972)

The Surface Properties of Rutile Prepared by the Hydrolysis of Titanium Tetrachloride. I. The Heat of Immersion in Water

Toru IWAKI, Masayoshi KOMURO, and Masaji MIURA

Department of Chemistry, Faculty of Science, Hiroshima University, Higashisenda-machi, Hiroshima

(Received January 17, 1972)

The surface properties of rutile prepared by hydrolyzing titanium tetrachloride have been studied by measuring the heat of immersion in water as a function of the outgassing temperature. The heat of immersion showed an extremely large value at outgassing temperatures between 300 and 400°C. However, when the rutile was calcined at 800°C, it showed a heat-of-immersion curve similar to those hitherto reported. In order to examine the phenomenon found on uncalcined rutile, the amounts of water physically and chemically adsorbed on the surface were estimated by measuring the water-vapor adsorption. We found that hydroxyl groups were formed in bulk as well as on the surface by means of the chemisorption, resulting in the formation of a hydrous structure because of the low crystallinity of the sample at temperatures below 400°C.

It is well known that the surface hydroxyl groups on such metal oxides as SiO_2, TiO_2, and Al_2O_3 are removed by thermal treatment *in vacuo*, resulting in the formation of an activated oxide structure, $Me\langle^{O}_{O}\rangle Me$, as a result of the condensation of the adjacent hydroxyl groups. The activated site may be rehydrated easily by the adsorptiom of water or may be stabilized by calicing at an elevated temperature. From our examinations of the heat of immersion, the water content, and the features of the adsorption of water, it seems that the nature of the activated site depends also on the nature of the substrate oxide.[1] So far, a number of studies on the heat of immersion of titanium dioxide have been performed by many workers. As for rutile, some studies have been done on samples calcined at high temperatures,[2-4] but none on uncalcined samples.

In the present work, the surface properties of titanium dioxide pretreated at various temperatures from 100 to 800°C *in vacuo* were examined by measuring the heats of immersion in water for uncalcined-rutile samples as well as for calcined ones. The uncalcined samples gave a relation between the heat of immersion and the outgassing temperature different from the results hitherto reported on calcined samples;[1-4] that is, an extremely large maximum occurred at about 300°C. In order to investigate the phenomenon in detail, the adsorption of water was measured for those samples. As a result, it was revealed that the hydroxyl groups were formed in bulk as well as on the surface by means of the chemisorption of water.

1) T. Omori, J. Imai, M. Nagao, and T. Morimoto, This Bulletin, **42**, 2198 (1969).

2) W. H. Wade and N. Hackerman, *J. Phys. Chem.*, **65**, 109 (1961).

3) A. C. Zettlemoyer, R. D. Iyengar, and P. Scheidt, *J. Colloid Interface Sci.*, **22**, 172 (1966).

4) T. Morimoto, M. Nagao, and T. Omori, This Bulletin, **42**, 943 (1969).

Experimental

Material. Three kinds of rutile samples were prepared by the hydrolysis of titanium tetrachloride as follows. An aqueous solution of 1 M titanium chloride was heated at 90°C for 12 hr with vigorous stirring until the deposition of the precipitate had stopped. The precipitate was then washed with distilled water, purified further by means of electrodialysis in order to remove the chloride ions, and then dried at 100°C for two days in air (Sample I). By X-ray analysis this sample was proved to be a rutile modification. The second sample was prepared by calcining Sample I at 800°C for 1 hr in air; then it was exposed to saturated water vapor for a week at room temperature (Sample II). The third sample was obtained by heating Sample II again to 800°C and by then keeping it at that temperature for 1 hr in air. The resulting product was steeped in water and dried at room temperature (Sample III).

The measurements of the differential thermal analysis of Samples I and II were carried out at various temperatures, from 20 to 800°C, in air. A large endothermic peak appeared around 110°C on Sample I, but did not on Sample II. This peak is considered to be connected with the dehydration.

Prior to carrying out the following measurements, each sample was pretreated at various temperatures between 100 and 800°C for 3 hr in a vacuum of 10^{-5} Torr.

Surface Area. The surface areas of the samples were determined from the nitrogen adsorption at 77°K by the conventional B.E.T. method, assuming the area of a nitrogen molecule to be 16.2 Å^2.

Water Content. The water vapor desorbed from the sample by evacuating at a given temperature was condensed in a trap cooled by liquid nitrogen, evaporated in a given system, and then recondensed in a trap cooled by dry ice. The water content of the sample was determined by

measuring the amount of reevaporated water volumetrically, assuming the water content at 800°C to be zero.

Heat of Immersion. The heats of immersion of the samples in water were measured at 25°C by using a calorimeter equipped with an automatic recorder; the details have been described elsewhere.[5] In order to prevent the effect of organic contaminants, the sample was outgassed with a liquid nitrogen trap just before the sample.[6]

Water-vapor Adsorption. The adsorption of water vapor on the surface was measured at 25°C gravimetrically by using a Cahn RG electrobalance. After the first adsorption isotherm had been obtained on the sample, this sample was outgassed at 25°C for 24 hr in a vacuum of 10^{-5} Torr in order to remove all the physically-adsorbed water. Then the second adsorption isotherm was determined at 25°C. A series of the first and second adsorption isotherms of water vapor on Sample I outgassed at various temperatures was obtained.

Results and Discussion

Surface Area. The specific surface areas of the three samples are shown in Fig.1 as a function of the outgassing temperature. The surface area of Sample I decreases remarkably as the outgassing temperature rises from 200 to 800°C, whereas that of Sample II is almost constant. The surface area of Sample III was determined at only one temperature because it was considered to be independent of the outgassing temperature, as was the case of Sample II. The progressive decrease in the surface area of Sample I suggests that sintering occurs even at low temperatures such as 300°C. The particle size of Sample I, estimated by using the Scherrer equation from the half-value breadth of the X-ray diffraction line from the (110) plane, increased from 33 to 186 Å with a rise in the outgassing temperature from 100 to 800°C. The surface area was calculated by assuming the shape of the particle to be spherical in order to compare it with the results of nitrogen adsorption, S_N. The resulting values, which are shown in Fig. 1, have the same tendency with regard to the effect of the temperature as in the case of S_{N_2}. However, these values are considerably larger than the nitrogen area. This implies that Sample I does not take as characteristically porous a structure as a result of the removal of water molecules as does Al_2O_3.[7] Therefore, outgassing at higher temperatures may make the particle grow in size, resulting in a decrease in the surface area.

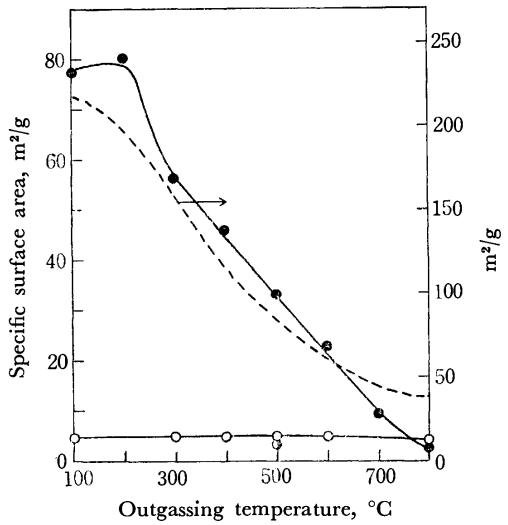

Fig. 1. Specific Surface area obtained from the adsorption of nitrogen as a function of the outgassing temperature; ●: Sample I, ○: Sample II, ◑: Sample III. Dotted line shows the specific surface area of the sample I estimated from the particle size.

Water Content. The water contents of Samples I and II are shown in Fig. 2, where the amounts of water are expressed by the number of hydroxly groups per unit of surface area, S_N. The fact that the amount of water in Sample I was much larger than that in Sample II was supported by the endothermic peak in the differential thermal analysis. The smaller surface area of Sample I at 100°C than at 200°C in Fig.1 may be due to the insufficient desorption of the water which may be present in the capillary, such as in the contacting zone among particles. The large water content may be one of the factors in the sintering at low temperatures.

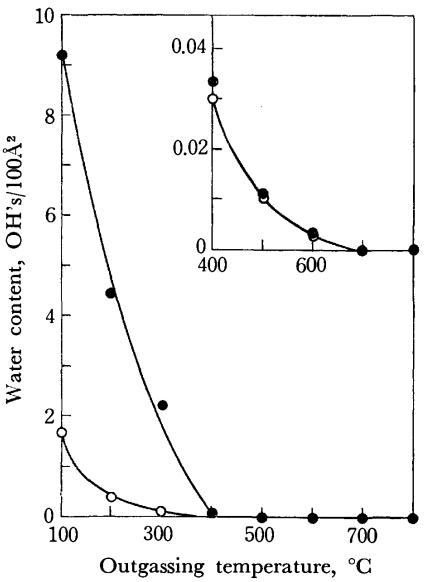

Fig. 2. Water content of rutile as a function of the outgassing temperature; ●: Sample I, ○: Sample II.

Heat of Immersion. Figure 3 shows the relation between the heats of immersion of the three samples in water and the outgassing temperature. Sample I revealed an extremely large heat-of-immersion value at temperatures between 300 and 400°C. The heat of immersion of Sample II was approximately constant above 400°C and did not reveal a maximum. Sample III, however, showed a maximum in its heat-of-immersion curve at a temperature between 400 and 500°C; this curve is similar to that reported by Morimoto *et al.*[3] From these results it is clear that

5) M. Miura, H. Naono, T. Iwaki, T. Kato, and M. Hayashi, *Kogyo Kagaku Zasshi*, **69**, 1623 (1966).
6) T. Iwaki and M. Miura, This Bulletin, **44**, 1754 (1971).
7) D. Aldcroft, G. C. Bye, J. G. Robinson, and K. S. W. Sing, *J. Appl. Chem.*, **18**, 301 (1968).

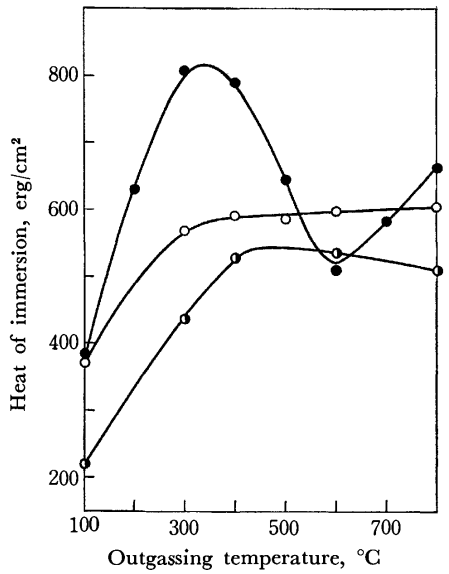

Fig. 3. Heat of immersion of rutile in water as a function of the outgassing temperature; ●: Sample I, ○: Sample II, ◑: Sample III.

the heat of immersion depends remarkably on the initial calcination of the sample.

The appearance of a maxiumm in the heat-of-immersion curve has generally been explained as being caused by the stabilization of the surface oxo-structure during the treatment at high temperatures *in vacuo*. This explanation is applicable to the behavior of Sample III, since it was calcined at a high temperature and may have a well-defined surface oxo-structure. However, it seems strange that an extremely large maximum in the heat-of-immersion curve was found for the sample treated at a low temperature. In order to investigate this phenomenon in detail, the adsorption of water on the surface of Sample I was examined as follows.

Water Adsorption. Figures 4a and 4b show, respectively, the first and second adsorption isotherms of water vapor on the surface of Sample I outgassed at various temperatures between 100 and 800°C. The ordinate in the figure represents the amount of water adsorbed per unit of area, S_{N_2}. The second isotherm obtained lies below and nearly parallel to that of the first run. The difference between these two curves is regarded as the amount of the water adsorbed chemically on the surface as hydroxyl groups. The second isotherm indicates the water adsorbed physically on the hydroxyl groups formed on the surface.

Both the first and second isotherms of the sample outgassed at 300°C indicate the largest adsorbed amounts of all; this phenomenon is similar to that of the heat of immersion, where the maximum occurs at a temperature between 300 and 400°C. By applying the BET method to the second isotherm, the monolayer volume of the physically adsorbed water was calculated. The amount of the hydroxyl groups formed by the chemisorption was estimated from the difference in the initial weights of the two samples on which the first and second adsorption runs were performed. This amount is almost consistent with that obtained

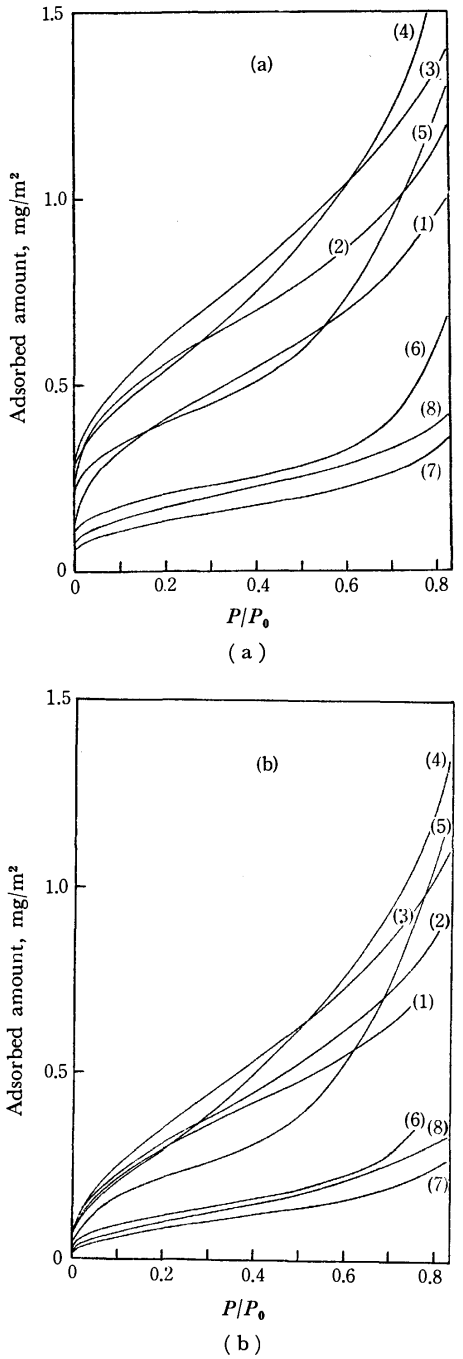

Fig. 4. Adsorption isotherms of water on rutile (Sample I) outgassed at various temperatures; (1) 100, (2) 200, (3) 300, (4) 400, (5) 500, (6), 600, (7) 700, (8) 800°C.
(a) First adsorption isotherms, (b) Second adsorption isotherms.

from the difference in the amounts of water adsorbed at a high pressure in the two isotherms. The number of the physically-adsorbed water molecules and that of the hydroxyl groups per unit of area obtained from the nitrogen adsorption are plotted in Fig.5 as functions of the outgassing temperature. In the figure there is also plotted the total number of hydroxyl groups per nitrogen area, which is the sum of the amount of the chemisorbed water and the water content. From this figure, it may be considered that the large heat of immersion at about 300°C is attributable

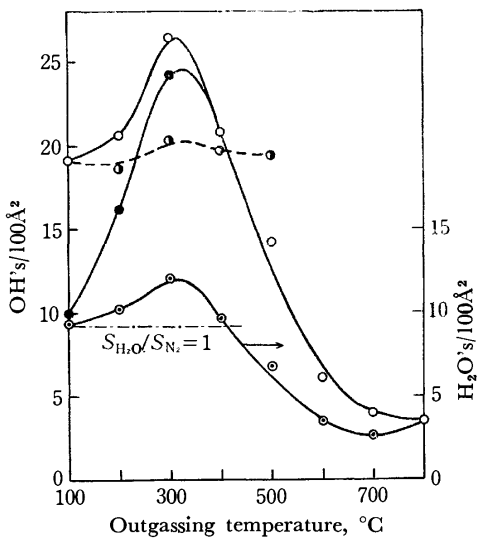

Fig. 5. Amounts of physically and chemically adsorbed water on the surface as a function of the outgassing temperature; ●: the number of hydroxyl groups formed by chemisorption per nitrogen area, ⊙: the number of physically adsorbed water per nitrogen area, ○ and ◑: total hydroxyl groups obtained by summing the chemically adsorbed water and water content per nitrogen area and water area respectively. Dotted line (—·—·—) shows that water area, S_{H_2O}, coincides with nitrogen area, S_{N_2}, at the amount of 9.3 H_2O's/100 Å².

mainly to the chemisorbed water.

It should be noted that the total number of hydroxyl groups per unit of area at temperatures between 100 and 500°C is too large to be accommodated to the monolayer coverage because the number of the hydroxyl groups corresponding to the monolayer coverage is 12/100 Å², which is calculated by assuming the radius of the hydroxyl group to be 1.45 Å.[8] There is the possibility that the true surface area of the sample is not evaluated by the nitrogen adsorption. Therfore, the surface area, S_{H_2O}, was estimated from the monolayer volume of the physically-adsorbed water by assuming the cross-sectional area of the water molecule to be 10.8 Å². The ratio of the water area, S_{H_2O}, to the nitrogen area, S_{N_2}, is related to the amount of the physically-adsorbed water per nitrogen area, as is indicated in Fig. 5. The water area exceeds the nitrogen area in the outgassing temperature range from 100 to 400°C and shows a maximum at about 300°C. The total number of hydroxyl groups per unit of water area is also plotted in Fig. 5; the number at 300°C is about 20/100 Å².

The surface of Sample I, when evacuated at a low temperature, may have an ill-defined oxo-structure because of the low crystallinity of the surface. When water molecules adsorb on such a surface, the hydroxyl groups may be formed in bulk as well as on the surface, resulting in the formation of hydrous titanium dioxide in part as in the following scheme:

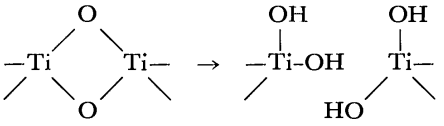

This reaction is irreversible; in other words, the unhydrated state produced by evacutaion does not return to the original unevacuated state, since the evacuation destroys the structure of the latter state. As the average number of titanium atoms exposed on the surface of rutile modification is 8/100 Å²,[9] it is calculated that about two or three hydroxyl groups combine with one titanium atom at temperatures below 400°C. This reaction may not occur on the stabilized surface oxo-groups, since the number of hydroxyl groups and also the heat of immersion decrease remarkably above 400°C. Above this temperature, the sample will form the more stable rutile structure in bulk and stabilized oxo-groups on the surface. As a consequence, the rehydration of the surface titanium atoms may be retarded, resulting in a decrease in the heat of immersion. The surface area of S_{H_2O} larger than S_{N_2} around 300°C may be responsible for the large number of hydroxyl groups on the surface, since water molecules adsorb physically on the hydroxyl groups.

Smaple I was tinged bluish gray when evacuated above 600°C. This color change has been considered to be caused by the removal of oxygen atoms from the surface.[10] Samples II and III also underwent a color change at high temperature, but it was slight compared with that of Sample I. The increase in the heat of immersion of Sample I above 600°C may be due to the contribution of the oxygen vacancy and the resulting distorted structure of the surface to the heat value.

8) J. A. A. Ketellar, "Chemical Constitution," Elsevier Pub. Co., Amsterdam (1958), p. 29.

9) T. Morimoto, M. Nagao, and F. Tokuda, *J. Phys. Chem.*, **73**, 243 (1969).

10) C. M. Hollabaugh and J. J. Chessick, *ibid.*, **65**, 109 (1961).

Behavior of Positive Hole in a γ-Irradiated 3-Methylpentane Glass at 77°K

Masahiro IRIE, Hiroshi YOSHIDA, Koichiro HAYASHI, and Seizo OKAMURA*

Faculty of Engineering, Hokkaido University, Sapporo

**Research Reactor Institute, Kyoto University, Kumatori-cho, Osaka*

(Received July 13, 1971)

In order to elucidate the behavior of a positive hole in irradiated alkane glasses, the effect of solutes having ionization potential lower than that of a glass matrix molecule upon the decay of a trapped electron was examined in a 3-methylpentane glass at 77°K by means of electron spin resonance. The decay was found to be explained in terms of the superposition of two exponentially decaying processes, as in the absence of a solute. Although the fast process was not affected by a solute, the slow process was further slowed by the addition of a solute. The effect of a solute is described by the empirical relation, $k/k_0=1/(1+fN)$, where k and k_0 are the rate constants of the slow decay in the presence and in the absence of a solute, respectively. N is the mole fraction of a solute. The observed values of the slowing-down efficiency, f, increase in parallel with the decreasing values of ionization potential of solutes: 2-methyltetrahydrofuran, diethylether, methylvinylether, 2-methylpentene-1 and *n*-butylvinylether. The results are interpreted in terms of trapping of a positive hole by a solute molecule and positive hole tunneling from a hole trap to a trapped electron.

Several investigations have been reported on the trapping process of an electron and its reactions in saturated hydrocarbon glasses irradiated by ionizing radiations at 77°K.[1] Little consideration, however, has been given to the behavior of a positive hole in the glasses. Louwrier and Hamill reported the absorption spectra attributable to the positive hole trapped by higher alkane solutes, a radical cation of higher alkanes, in a 3-methylpentane glass at 77°K, the behavior of which suggested that the charge recombination process involved hole migration by fast resonant charge transfer in a neat glass and by slow electron tunneling in a doped glass.[2,3] The hole migration was elucidated also by an electron spin resonance (ESR) study of the radical cation of tetramethylethylene in a 3-methylpentane glass by Ichikawa and Ludwig.[4]

The present authors studied the behavior of a trapped electron in an irradiated 3-methylpentane glass at 77°K and found that its decay was expressed by the superposition of fast and slow exponential decays.[5] The slow decay was found to be dependent on the 2-methylpentene-1 added to the glass, which suggests that it is due to the migration of positive charge. On the other hand, the fast decay was thought to be due to the migration of an electron. Recently, they have observed the ESR spectra attributable to a trapped positive hole in irradiated 3-methylpentane and 3-methylhexane glasses at 77°K.[6] The spectra were replaced by that of a solute cation when vinylethers were added to the glasses.[7] These facts also imply that migration and trapping of the positive hole are involved in ionic processes in an irradiated 3-methylpentane glass.

In the present investigation, the effect of several solutes on the slow decay of a trapped electron in a 3-methylpentane glass is studied in order to elucidate the behavior of a positive hole in detail. The results obtained confirm the previous interpretation that the slow decay of a trapped electron is caused by the migration of the positive hole in the glass.

Experimental

3-Methylpentane, 2-methylpentene-1, and *n*-butylvinylether were purified by the same treatment as described previously.[7] Ethylether and 2-methyltetrahydrofuran were fractionally distilled three times over sodium and distilled *in vacuo* into a sodium–potassium mirrored vessel repeatedly until the mirror was no longer damaged. Methylvinylether was passed through a column of potassium hydroxide, dried with calcium hydride and distilled into a sodium-potassium mirrored vessel five times *in vacuo*.

The samples were distilled into ESR sample tubes of pure quartz and sealed under the pressure less than 10^{-4} mmHg. The amount of a solute was estimated from the volume and gas pressure.

Irradiation was carried out at 77°K in the dark to a dose of 5.2×10^{18} eV/g. ESR measurements were carried out with the aid of a conventional X-band spectrometer with 100 kHz magnetic field modulation and at the low microwave power of 0.3 milliwatts, at 77°K in the dark.

Ionization potentials were measured by means of a conventional mass spectrometer, by determining the threshold of appearance potentials with a linear extraporation method.

Results

The ESR signal of a neat 3-methylpentane glass irradiated at 77°K is composed of three spectra: a sextet spectrum due to a 3-methylpentyl radical, a broad unresolved spectrum due to a trapped positive hole (the cation radical of 3-methylpentane) and a sharp singlet spectrum due to a trapped electron, as reported previously.[5,6] The trapped electron decays rapidly at 77°K in the dark. The decay includes two exponentially decaying processes; the rate constants are 0.2 and 0.04 min^{-1} for the fast decay and the slow

1) See for example, W. H. Hamill, "Radical Ions," ed. Keiser and Kevan, Intersci. Publ., New York, (1968), p. 321; J. E. Willard, "Fundamental Processes in Radiation Chemistry," ed. Ausloos, Intersci. Publ., New York, (1968), p. 599.

2) P. W. F. Louwrier and W. H. Hamill, *J. Phys. Chem.* **72**, 3878 (1968).

3) P. W. F. Louwrier and W. H. Hamill, *ibid.*, **74**, 1418 (1970).

4) T. Ichikawa and P. K. Ludwig, *J. Amer. Chem. Soc.* **91**, 1023 (1969).

5) M. Irie, K. Hayashi, S. Okamura. and H. Yoshida, *J. Chem. Phys.* **48**, 922 (1968).

6) H. Yoshida, T. Shiga, and M. Irie, *ibid.*, **52**, 4906 (1970).

7) M. Irie, K. Hayashi, S. Okamura, and H. Yoshida, *Intern. J. Radiat. Phys. Chem.* **1**, 297 (1969).

8) K. Watanabe, T. Nakamura, and J. Mottl, *J. Quant. Spectrosc.* **2**, 369 (1962).

one, respectively.[5]

Even if a small amount of a hole scavenger is added, the decay of the trapped electron is still caused by the two processes, as shown in Fig. 2 of Ref. 5. However, the rate constant of the slow decay decreases with the increasing concentration of the added solute. Fig. 1 shows the effect of an added solute, representatively of *n*-butylvinylether. The yield of a slowly decaying electron increases very slightly with the addition of a solute. These facts imply that a small amount of a solute (less than 10^{-1} mol%) provides few additional physical trapping sites for an electron but interrupts the charge neutralization process. It should be noted that the fast decay of a trapped electron is not affected by the addition of a small amount of a solute.

As to the dependence of the rate constant of the slow decay of a trapped electron upon the concentration of a solute, representative results are shown in Fig. 2. Changes in the rate constant follow the empirical relation,

$$k/k_0 = 1/(1+fN) \quad (1)$$

where k_0 and k are the rate constants in the absence and in the presence of a solute, respectively.

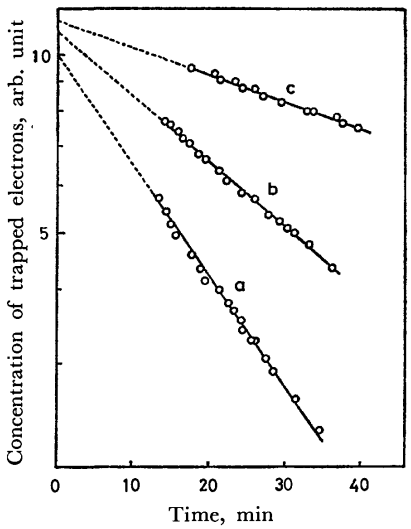

Fig. 1. Decay of trapped electrons in 3-methylpentane glass at 77°K in the presence and in the absence of *n*-butylvinylether. Radiation dose: 5.2×10^{18} eV/g. Concentration of *n*-butylvinylether: (a) 0, (b) 6.6×10^{-3} mol% and (c) 3.2×10^{-2} mol%.

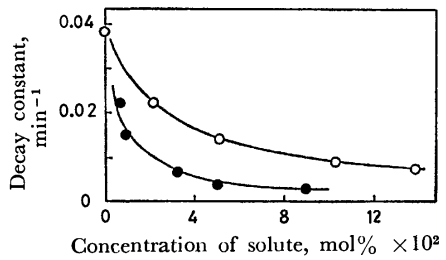

Fig. 2. Relation between the first order rate constant of the slow decay of trapped electrons at 77°K in 3-methylpentane glass irradiated to a dose of 5.2×10^{18} eV/g and the concentration of added solutes, (○) methylvinylether and (●) *n*-butylvinylether. Curves are derived from the relation (1). See text.

N and f are the mole fraction of a solute and the slowing-down efficiency proper to each solute, respectively.

The slowing-down efficiency of several solutes thus determined and their values of ionization potential are listed in Table 1. All the solutes have ionization potential lower than that of 3-methylpentane. The slowing down efficiency increases with the increasing difference of ionization potential between a solvent molecule and a solute. This is illustrated in Fig. 3.

Table 1. Relation between the slowing-down efficiency and the ionization potential of solutes added to the irradiated 3-methylpentane glass

Solute	Slowing-down efficiency f	Ionization potential (eV)	
		This work	Reported value[a]
n-Butylvinylether	1.4×10^4	8.44	——
2-Methylpentene-1	5.4×10^3	8.94	——
Methylvinylether	3.4×10^3	9.14	8.93
Diethylether	3.2×10^3	9.43	9.53
2-Methyltetrahydrofuran	2.7×10^3	——	9.54[b]
3-Methylpentane	——	10.20	10.08

a) See Ref. 8. b) Ionization potential of tetrahydrofuran.

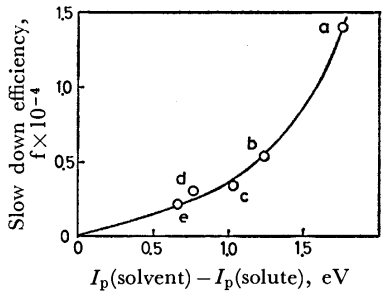

Fig. 3. Relation between the slowing-down efficiency and the difference of ionization potential between the glass matrix molecule and the added solutes, (a) *n*-butylvinylether, (b) 2-methylpentene-1, (c) methylvinylether, (d) diethylether, and (e) 2-methyltetrahydrofuran.

The ionization potential has not yet been reported for some of the solutes. Therefore, it was determined by the conventional mass spectrometric method, being shown in the third column of Table 1. Although the method seems unfortunately not to give the absolute values of significance, the difference between them may be enough significant to be related with the slowing-down efficiency. The ionization potential previously reported for some solutes is cited in the fourth column for comparison.

Discussion

The solutes examined have ionization potential lower than that of 3-methylpentane and negative electron affinity. Therefore, they are able to stabilize the positive hole in the glass forming a radical cation, whereas they do not capture electrons chemically. The results shown in Fig. 3 provide the evidence that the slow decay of a trapped electron is caused by the

migration of a positive hole to the immobile deeply trapped electron. If the decay resulted from the migration of an electron itself, the slowing-down efficiency might depend on the nature of a solute molecule such as dipole moment (dielectric constant) and electron affinity, rather than on ionization potential. However, this is not the case. For example, the slowing-down efficiency of 2-methylpentene-1 is found to be larger than that of methylvinylether, though the dipole moment of the former is evidently smaller than that of the latter.

The above argument leads also to the conclusion that the fast decay of a trapped electron is thought to be caused independently of a solute by the migration of an electron, as suggested previously.[5] This necessarily requires electron population in two kinds of traps, a shallow trap and a deep trap. The shallow trap is intrinsic to non-polar hydrocarbon glasses formed by preferably oriented C–H bond dipoles,[9] while the deep trap involves a solute molecule or an impurity molecule which can not be removed by the purification of 3-methylpentane.

What is to be considered is why the positive hole trapped by the solute still moves, bringing about the slow decay of a trapped electron. In order to account for the slow dark decay of a trapped hole in a 3-methylpentane glass containing a higher alkane solute, Louwrier and Hamill postulated hole migration involving electron tunneling from a solute molecule to a solute radical cation.[2,3] In their case where the concentration of a solute was rather high (~1 mol %), the tunneling occurred more readily with the increasing concentration of a solute. In the present experiment for low concentration of a solute (less than 10^{-1} mol %), the slow decay of a trapped electron may be interpreted in terms of hole tunneling from a trapped positive hole to the trapped electron, rather than that between solute molecules.

A rough estimation of the rate of tunneling can be made by assuming a one-dimensional potential barrier as shown in Fig. 4, where the region A is the potential well formed by a solute molecule which traps a positive hole. In the region C, there is a trapped electron which the hole tunnels to and recombines with. If one takes the potential in this region as zero, U_0 and V_0 are approximated by the values of ionization potential of solute and glass matrix molecules, respectively. If one assumes that the trapped positive hole has the same energy eigenvalue as that in the potential well of infinite height and length of a, the flow of probability at the region C is expressed by the following relation,

$$\lambda = \frac{2(E-U_0)\sqrt{2mE}}{maV_0} \exp\left(-2\hbar^{-1}l\sqrt{2m(V_0-E)}\right) \quad (2)$$

which is identical with the rate of charge neutralization.[10] The mass of a hole is taken to be the same as that of an electron, m. $E-U_0$ is the kinetic energy of a positive hole in the ground state, being estimated to be 0.1 eV. V_0-E can be approximated with the difference of ionization potential between glass matrix and solute molecules, ~1 eV. The widths of a well, and of a barrier l, are taken to be 5×10^{-8} (molecular dimension) and 4×10^{-7} cm (charge separation distance), respectively. These numerical estimates lead to $\lambda\sim10^{-4}$ sec^{-1}, which is consistent with the observed rate constant of the slow decay of a trapped electron in the presence of a solute.

The absolute value obtained above is somewhat arbitrary, because it is rather sensitive to the estimated values, especially those of V_0 and l. However, equation (2) accounts for the experimental results well at least qualitatively. If the ionization potential of a solute is lower and therefore V_0-E is larger, the trapped electron decays more slowly. Consequently, the slowing-down efficiency is expected to be larger. This agrees qualitatively to what was observed.

With the increasing concentration of a solute, the positive hole is more readily trapped, on the way back to the electron in a deep trap, by a solute molecule. This results in a trend that the average distance between a trapped positive hole and an electron (the average value of l in Eq. (2)) is lengthened by an increase of concentration, as far as the tunneling occurs between a solute molecule and a trapped electron. The above argument accounts for qualitatively the observed dependence of the rate constant of the slow decay of a trapped electron upon the concentration of a solute as shown in Fig. 2. The reason why the effect of a solute follows the empirical relation (1) still remains unknown, because of lack of knowledge on the distribution of distance l.

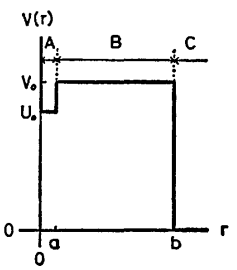

Fig. 4. A simplified one-dimensional trapping potential of positive hole. Region A is the potential well formed by a solute molecule which traps a positive hole. An electron is trapped in region C. V_0 and U_0 are ionization potential of solvent molecule and solute molecule, respectively.

9) H. Yoshida and T. Higashimura, *Can. J. Chem*, **48**, 504 (1970).

10) According to the potential shown in Fig. 4, the wave function in the region C is easily obtained by a usual treatment, as

$$\Psi_C = \frac{k_1\cos k_1a - \kappa\sin k_1a}{\sqrt{2\pi a}\,(ik_3-\kappa)} \exp(-\kappa l) \exp\{ik_3(r-b)\},$$

where

$$k_1=\sqrt{\frac{2m}{\hbar^2}(E-U_0)},\ k_3=\sqrt{\frac{2m}{\hbar^2}E},\ i\kappa=\sqrt{\frac{2m}{\hbar^2}(E-V_0)},$$

and

$$l = b - a.$$

Using the approximation $k_1a=\pi$, the wave function is reduced to

$$\Psi_C = \frac{k_1}{\sqrt{2\pi a}\,(\kappa-ik_3)} \exp(-\kappa l) \exp\{ik_3(r-b)\}.$$

Therefore, the flow of probability is obtained as Eq. (2). See for example, G. Araki, "Quantum Chemistry," Baifukan, Tokyo, (1961), p. 505.

The Structural Transformation of Ferric Oxyhydroxides and Their Activity to Sulfur Dioxide

Tatsuo Ishikawa and Katsuya Inouye

Department of Chemistry, Faculty of Science, Chiba University, Chiba

(Received January 20, 1972)

α-, β-, and γ-FeOOH calcined at various temperatures up to 500°C have been examined by determining adsorption isotherms in order to relate the reactivity to SO_2 with the structural transformation. For each ferric oxyhydroxide, the amount of chemisorbed SO_2 per unit surface area (A_c), a measure of reactivity to SO_2, decreases with the progress of transformation into α-Fe_2O_3. At temperatures of calcination below 200°C the A_c value of β-FeOOH is larger than that of α-FeOOH or γ-FeOOH. It is shown by thermogravimetric analysis that the weight loss of β-FeOOH caused by heating is larger than the theoretical value corresponding to the dehydration of hydroxyl groups; $2FeOOH \rightarrow Fe_2O_3 + H_2O$. Changes in the X-ray diffraction patterns and Cl content of β-FeOOH with calcination indicate that β-FeOOH is transformed into α-Fe_2O_3 with elimination of inherently contained Cl at a higher temperature than other oxyhydroxides. The high reactivity to SO_2 and large weight loss of β-FeOOH caused by heating have been discussed with respect to the particular crystal structure of β-FeOOH containing Cl and molecular H_2O, in addition to hydroxyl groups.

It is known that SO_2 in the atmosphere and stack gases accelerates the corrosion of iron. Various oxides and oxyhydroxides of iron, composing the corrosion products of iron, play important roles in the corrosion process and consequently determine the physical and chemical properties of corroded metal surfaces. It seems significant to clarify the mechanism of the acceleration of corrosion by studying the interaction of SO_2 with those oxidized compounds.

Ferric oxyhydroxide is transformed into α-Fe_2O_3 by heating, through courses differing with environmental conditions and the crystal structures of ferric oxyhydroxides in question,[1] although the transformation mechanism has been proposed by several workers.[2,3,4]

The surface activity also changes during the course of transformation. Jurinak[5] reported from water adsorption measurement on α-FeOOH heated at various temperatures that the adsorbability decreases at the temperature range where the conversion occurs from α-FeOOH to α-Fe_2O_3. It is well-known that hydroxyl groups contained in ferric oxyhydroxide are eliminated as H_2O at approximately 300°C according to the reaction; $2FeOOH \rightarrow Fe_2O_3 + H_2O$. Okamoto, Furuichi and Sato[4] have reported that ferric oxyhydroxide releases the "bound" water at approximately 170°C and the "crystallization" water is evolved at approximately 300°C, the former appearing to affect the chemical reactivity of ferric oxyhydroxide.

If we assume that the reactivity of ferric oxyhydroxide to SO_2 mainly depends on hydroxyl groups in ferric oxyhydroxide, it would be interesting to see whether the reactivity changes with the removal of hydroxyl groups in the transformation into α-Fe_2O_3. In the preceding paper,[6] the authors reported on the SO_2 adsorption on ferric oxyhydroxides (α-, β- and γ-FeOOH) to show that each oxyhydroxide chemisorbs a considerable amount of SO_2; the amount of chemisorption is especially larger for β-FeOOH than other oxyhydroxides. Furthermore, by the kinetic treatment of the reaction between SO_2 and ferric oxyhydroxides, it was suggested that β-FeOOH is more reactive to SO_2 than other oxyhydroxides.

The purpose of the present investigation is to study the interaction of SO_2 with α-, β- and γ-FeOOH at various temperatures of calcination and to relate the reactivity to SO_2 with the structural transformation.

Experimental Procedures

Materials. α-FeOOH (α-1) was precipitated by the hydrolysis of 0.1 M ferric oxalate solution at 100°C for 45 minutes and at the initial pH of 6.6, regulated by adding 1 M $NaHCO_3$ solution. The precipitate produced was washed repeatedly and dried at 100°C.[7] More crystalline α-FeOOH (α-2) prepared similarly by the hydrolysis of ferric sulfate solution, the pH being adjusted at 13.6 with 0.1 M KOH solution, was stirred at 50°C for 30 hours. After filtering the suspension, the α-FeOOH precipitates obtained were washed until no sulfate ions were detected. They were then dried at 100°C for 5 hr.[8]

The hydrolysis of 1 liter of 0.1 M ferric chloride solution containing 100 g urea at 100°C for 15 hours gave crystalline β-FeOOH (β-1). The precipitates of β-FeOOH were washed with water and dried at 100°C for 2 hr.[9] Less crystalline β-FeOOH (β-2) was prepared by hydrolysing 0.1 M ferric chloride solution at 75°C for 6 hours. The precipitates were washed with 1 N ammonium chloride until no Fe ions were detected with thiocyanate solution. They were finally washed with methanol and with ether, and dried in an air oven at 100°C for 2 hours.[10].

Crystalline γ-FeOOH (γ-1) was prepared by the method

1) A. L. Mackay, "Reactivity of Solids", ed. by J. H. De Boer, Elsevier Publishing Co., Amsterdam, (1961), p. 571.

2) J. D. Bernal, D. R. Dasgupta and A. L. Mackay, *Nature*, **180**, 645 (1957).

3) H. B. Weiser and W. O. Milligan, *J. Amer. Chem. Soc.*, **57**, 238 (1935).

4) G. Okamoto, R. Furuichi and N. Sato, *Electrochim. Acta*, **12**, 1287 (1967).

5) J. J. Jurinak, *J. Colloid Sci.*, **19**, 477 (1964).

6) T. Ishikawa and K. Inouye, *Nippon Kagaku Zasshi*, **91**, 935 (1970).

7) K. J. Gallagher and D. N. Phillips, *Trans. Faraday Soc.*, **64**, 785 (1968).

8) W. Feitknecht, A. Wyttenbach and W. Buser, "Reactivity of Solids," ed. by J. H. De Boer, Elsevier Publishing Co., Amsterdam, (1961), p. 1234.

9) E. R. Nightingale Jr. and R. E. Benk, *Anal. Chem.*, **32**, 566 (1960).

10) I. M. Kolthoff and B. Moskoviz, *J. Amer. Chem. Soc.*, **58**, 777 (1936).

of Baudisch and Albrecht.[11] The ferrous hydroxide suspension, obtained by mixing 1 liter of ferrous chloride aqueous solution containing 40 g $FeCl_2 \cdot 4H_2O$ with 200 m*l* of 2 M hexamethylenetetramine solution, was treated with 27 m*l* of 1 M sodium nitrate, and then kept at 60°C for 45 minutes. γ-FeOOH (γ-1) was collected by filtering the suspension. Amorphous γ-FeOOH (γ-2) was prepared by adding 400 m*l* of 0.25 M potassium iodate to the mixture of 800 m*l* ferrous sulfate aqueous solution containing 56 g $FeSO_4 \cdot 7H_2O$ and 800 m*l* of sodium thiosulfate aqueous solution containing 90 g $Na_2S_2O_3 \cdot 5H_2O$, and then by stirring the resulting suspension at 45°C for 1 hr.[12] Preparation of γ-FeOOH samples was performed in a stream of nitrogen, and the resulting precipitates were thoroughly washed with water and dried at 60°C for 10 hr.

Methods. The amount of adsorbed SO_2 was determined gravimetrically at 30°C by means of a quartz spring balance with an accuracy of 0.20 mg. Before the adsorption measurement, approximately 200 mg of the sample was outgassed under 10^{-5} Torr, heated up to 110, 150, 200, 300, 400, and 500°C at a heating rate of 8°C/min and kept for 5 hours at each temperature under 10^{-5} Torr. Pure SO_2 dried with $CaCl_2$ was then introduced to the adsorption apparatus to measure the elongation of quartz spring by a cathetometer. The adsorption equilibrium was attained within 1 hr for each sample. Desorption was carried out immediately after the adsorption experiment. The desorption equilibrium was attained within 2 hours.

The BET surface area determination was made by a conventional volumetric nitrogen adsorption measurement. The pretreatment of the sample was similar to that in the SO_2 adsorption.

The X-ray diffraction patterns were obtained by the powder method with a diffractometer Geigerflex 2001 (Rigaku Denki Co. Ltd.) by use of Mn-filtered FeK_α (30 kV, 10 mA). The samples, calcined at 110, 150, 200, 300, 400 and 500°C under 10^{-5} Torr for 5 hours, were examined by means of X-ray diffraction.

Differential thermal analysis was carried out in air by Thermoflex 8001 S (Rigaku Denki Co. Ltd.) using α-Al_2O_3 as a reference sample. The enthalpy change in the structural transformation of the sample was measured by a differential scanning calorimeter DSC-1 (Perkin-Elmer Co.), at a heating rate of 8°C/min. The weight loss of the sample by heating was determined gravimetrically with a quartz balance, at a heating rate of 8°C/min.

The Volhald method was employed to determine the chlorine content of β-FeOOH. A solution of 100 mg of the sample in 30 m*l* concentrated nitric acid was diluted with water to 50 m*l* and an aliquot was titrated with 0.1 N $AgNO_3$ solution.

The iron content in the sample was determined by the following method; Fe^{3+} in hydrochloric acid solution, reduced to Fe^{2+} with $SnCl_2$, was titrated against a standard 0.05 N $K_2Cr_2O_7$ solution in the presence of sodium 4-diphenylammine sulfonate as an indicator.

Results

The thermogravimetric analysis (TGA) curves for α-FeOOH samples (α-1 and α-2) are given in Fig. 1. Both samples show rapid weight losses in the temperature range 200—300°C, but the weight loss of α-1 occurs in a temperature range lower than α-2. However, the total weight loss of each sample is consistently 12%, which is somewhat higher than the theoretical value (10%) corresponding to the change; $2FeOOH \rightarrow Fe_2O_3 + H_2O$. Similar curves were obtained for γ-FeOOH. The TGA curves of β-FeOOH in Fig. 2 differ from those of α-FeOOH in a gradual loss in the temperature range 100—450°C. The total weight loss is 20% for β-1 and 18% for β-2. The sublimed $FeCl_3$ was observed in the inner wall of the TGA apparatus during the course of heating around 400°C, where a stepwise drop of weight also took place for β-1 as shown in Fig. 2.

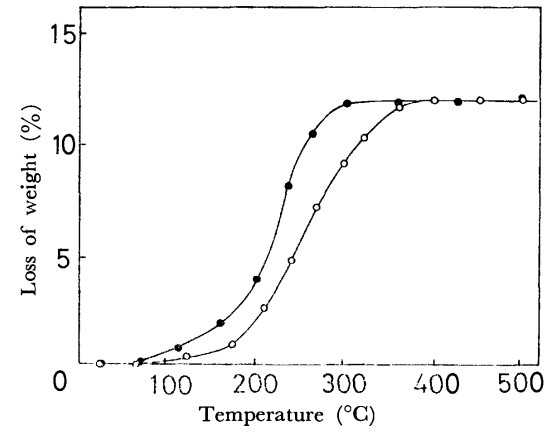

Fig. 1. TGA curves for α-1 and α-2: ●, α-1; ○, α-2.

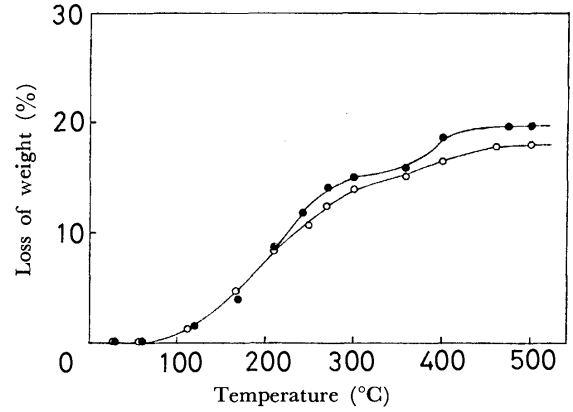

Fig. 2. TGA curves for β-1 and β-2: ●, β-1; ○, β-2.

The differential thermal analysis (DTA) curves of α-2, β-1 and γ-1 are given in Fig. 3. The curves of crystalline α-FeOOH (α-2) involves an endothermic peak at 110°C caused by the desorption of adsorbed water and an endothermic peak at 295°C by the dehydration of "crystallization" water.[13] For β-FeOOH, endothermic and exothermic peaks overlap each other at nearly 300°C. The endothermic peak of the sublimation of $FeCl_3$ appears at 400°C as found in the TGA curves. An endothermic peak at 170°C is probably caused by the elimination of molecular water embraced in β-FeOOH crystal. γ-FeOOH shows the exothermic peak at 430°C, which is considered to be due to the transformation of γ-Fe_2O_3 to α-Fe_2O_3.[13]

11) O. Baudich and W. H. Albrecht, *J. Amer. Chem, Soc.*, **54**, 943 (1932).

12) E. B. Seidman, *Anal. Chem.*, **30**, 1680 (1958).

13) W. Lodding and L. Hammel, *ibid.*, **32**, 657 (1960).

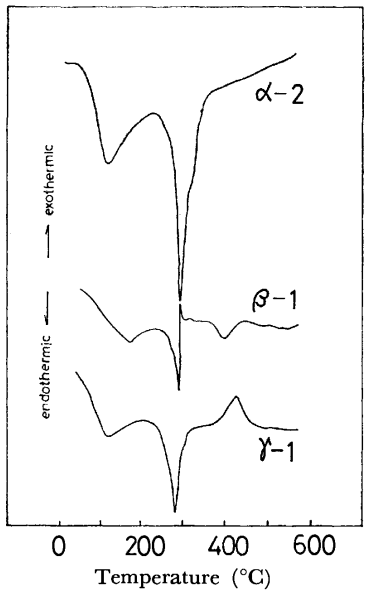

Fig. 3. DTA curves for α-2, β-1 and γ-1.

The endothermic peaks in the differential scanning calorimeter (DSC) curves in Fig. 4 correspond to dehydration. However, the samples used for DSC determinations kept in a desiccator for a long time adsorb less water than the samples used for DTA. No endothermic peaks caused by the desorption of physically adsorbed water are observed in DTA curves. The heat of dehydration obtained from the endothermic DSC peaks is 49, 75, 45 and 36 cal/g for α-1, α-2, γ-1 and γ-2, respectively. These results indicate that the more crystalline oxyhydroxide has a higher heat of dehydration than the less crystalline oxyhydroxide.

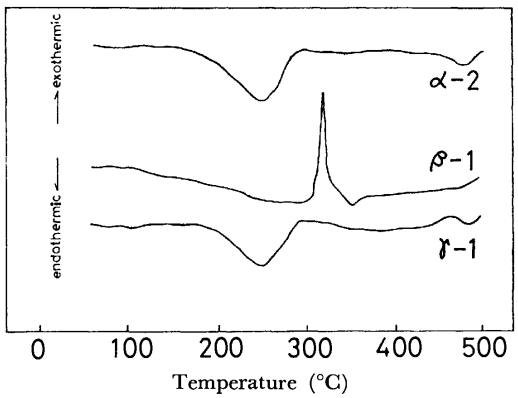

Fig. 4. DSC curves for α-2, β-1 and γ-1.

As demonstrated by the change of X-ray diffraction patterns in Fig. 5, α-2 is transformed into α-Fe_2O_3 at 200°C. The crystallinity of resulting α-Fe_2O_3 is seen to be gradually improved with further appearance of additional diffraction peaks of α-Fe_2O_3 at 400°C. On the other hand, β-1 (Fig. 6) changes to an amorphous mixture, composed of β-FeOOH and α-Fe_2O_3, in the temperature range 200—300°C. At 400°C, however, the amorphous mixture is suddenly transformed into the crystalline α-Fe_2O_3. γ-1 (Fig. 7) is transformed into amorphous γ-Fe_2O_3 at 200°C and is suddenly converted to crystalline α-Fe_2O_3 at 400°C. However, the TGA, DTA and DSC curves

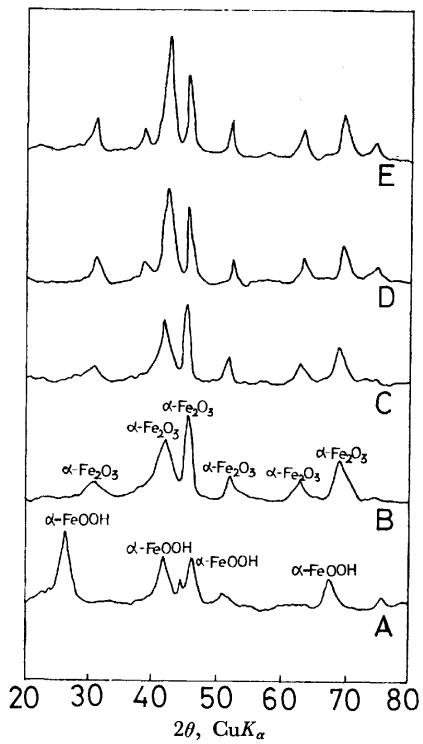

Fig. 5. X-ray diffraction patterns of α-2 at various temperatures of calcination: A, 150°C; B, 200°C; C, 300°C; D, 400°C; E, 500°C.

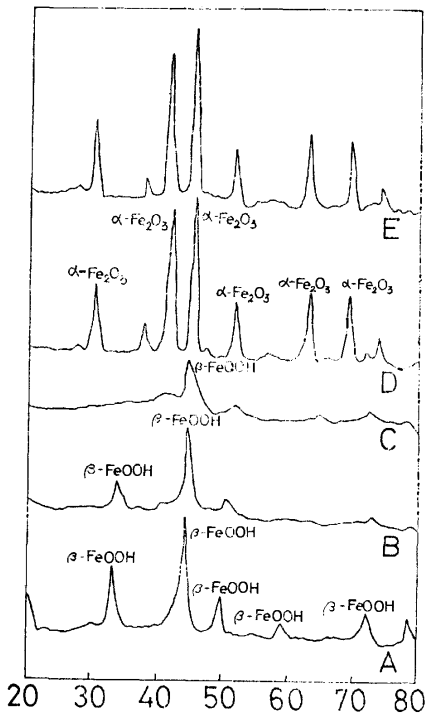

Fig. 6. X-ray diffraction patterns of β-1 at various temperatures of calcination: A, 150°C; B, 200°C; C, 300°C; D, 400°C; E, 500°C.

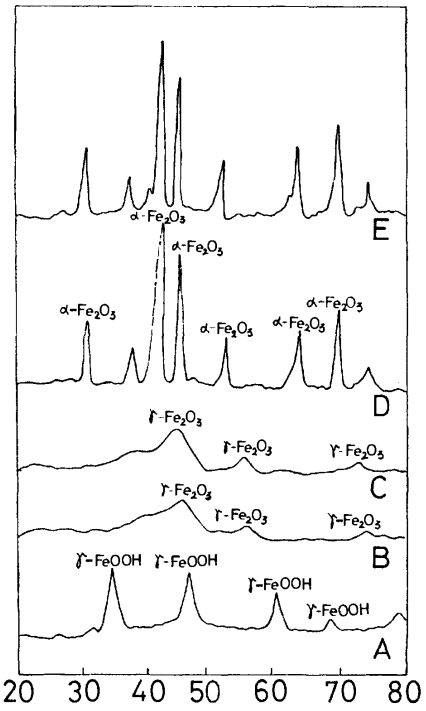

Fig. 7. X-ray diffraction patterns of γ-1 at various temperatures of calcination: A, 150°C; B, 200°C; C, 300°C; D, 400°C; E, 500°C.

shown in Figs. 1, 3 and 4 indicate that α-2 and γ-1 are transformed into α-Fe_2O_3 and γ-Fe_2O_3 at temperatures higher than the transformation temperatures obtained by X-ray diffraction. The discrepancy in transformation temperature is considered to be due to different heat treatments; the X-ray samples were outgassed for 5 hours at various temperatures under 10^{-5} Torr, whereas the DTA, TGA and DSC curves were obtained in air at a fixed rate of heating.

The variation of specific surface area with the temperature of calcination given in Fig. 8 shows a maximum between 200 and 300°C for each sample.

The SO_2 adsorption isotherm obtained at 30°C is of the BET-II type for each sample. Figure 9 shows the isotherm for α-2. The monolayer capacity of the

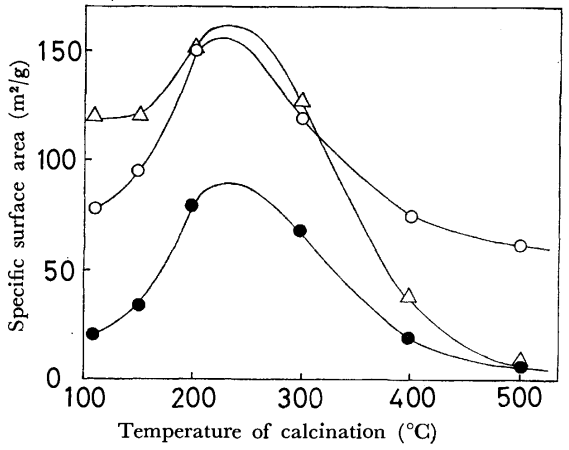

Fig. 8. Specific surface area plotted against temperature of calcination: ○, α-2; ●, β-1; △, γ-1.

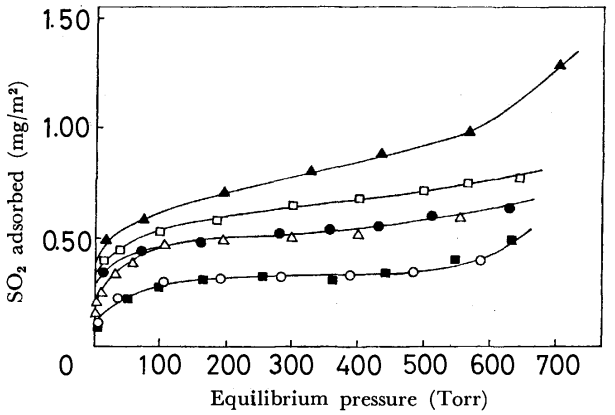

Fig. 9. Adsorption isotherms for α-2 at various outgassing temperatures: △, 110°C; ●, 150°C; □, 200°C; ▲, 300°C; ■, 400°C; ○, 500°C.

SO_2 adsorption per unit surface area (A_m), calculated by the BET method, is illustrated in Fig. 10 as a function of the outgassing temperature. Below 150°C, the A_m values are almost constant and no differences in A_m are observed between ferric oxyhydroxides examined. The adsorbed SO_2, remaining on the surface after desorption under 10^{-5} Torr at 30°C for 24 hr, is regarded as the chemisorbed SO_2.[6] The relationship between the amount of the chemisorbed SO_2 per unit surface area (A_c) and the temperature of calcination is given

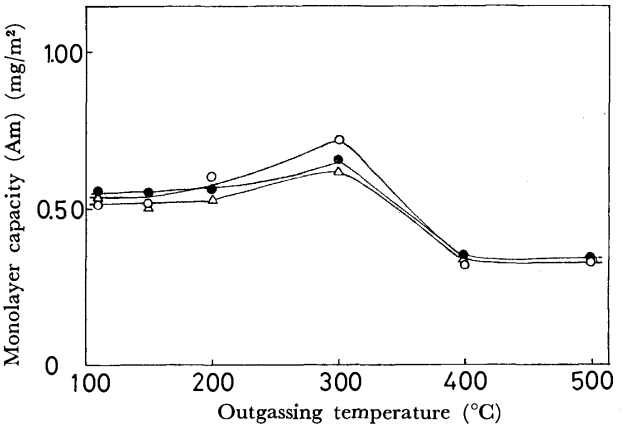

Fig. 10. Effect of outgassing temperatnre on monolayer capacity: ○, α-2; ●, β-1; △, γ-1.

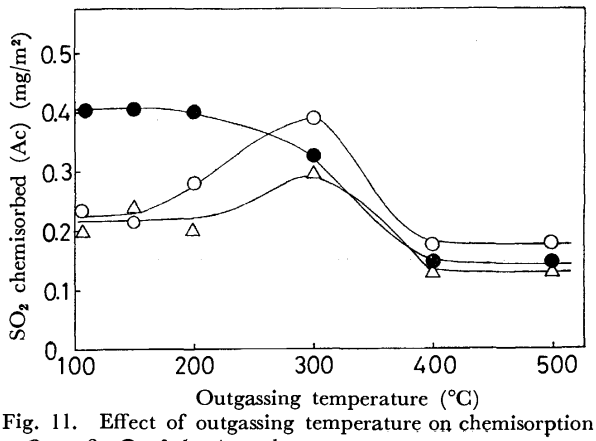

Fig. 11. Effect of outgassing temperature on chemisorption; ○, α-2; ●, β-1; △, γ-1.

in Fig. 11. The A_c value of β-FeOOH is larger than those of other ferric oxyhydroxides below 200°C. However, in the temperature range 200—400°C, the A_c of β-FeOOH drops with the formation of crystalline α-Fe_2O_3 and is nearly equal to the A_c of α-FeOOH and γ-FeOOH above 400°C.

The content of chlorine, which is characteristic of β-FeOOH, was found to be 4.6 wt% for β-1. As illustrated in Fig. 12, the chlorine content of β-FeOOH expressed in the atomic ratio (Cl/Fe) is constant below 200°C and decreases rapidly with increasing temperature in the range 200—400°C.

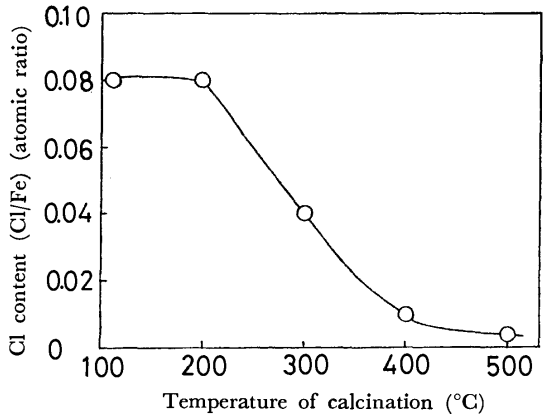

Fig. 12. Cl content in β-1 against temperature of calcination.

Discussion

The weight loss of α-FeOOH and γ-FeOOH by heating, which is larger than the stoichiometric value of water content, indicates that α-FeOOH and γ-FeOOH contain a small amount of "bound" water which is eliminated at a lower temperature range. As shown in Fig. 1, the crystalline sample (α-2) is dehydrated at a higher temperature than the less crystalline sample (α-1). A similar tendency was also observed for γ-FeOOH. Furthermore, the higher heat of dehydration calculated from the DSC curves was obtained for the crystalline sample. These results imply that the crystalline ferric oxyhydroxide is more difficult to be dehydrated as compared with the less crystalline ferric oxyhydroxide.

Dasgupta and Mackay[14,15] suggested that β-FeOOH has the hollandite ($BaMn_8O_{16}$) or α-MnO_2 structure with Cl and H_2O in the Ba^{2+} position. It is known that the Cl content in β-FeOOH varies with the extent of washing, since the Cl can be replaced by H_2O molecule.[3] In our experiments, the DTA curve for β-1 (Fig. 3) shows that H_2O is released from the crystal at approximately 170°C. Chlorine begins to be eliminated at 200°C as shown in Fig. 12, and DTA and TGA curves show that $FeCl_3$ is sublimed at 400°C. Thus the large total weight loss of β-FeOOH is obviously associated with the evolution of Cl_2 and H_2O in the crystal. It is therefore presumed that β-FeOOH contains two kinds of Cl; one which can be easily replaced by H_2O molecule, and the other which is strongly bound to Fe and removed as $FeCl_3$ by heating at 400°C. Figures 6 and 12 show the structural changes of β-FeOOH to α-Fe_2O_3, with elimination of Cl as $FeCl_3$ at approximately 400°C. From our results, the strongly bound Cl seems to stabilize the crystal structure of β-FeOOH with regard to transformation into α-Fe_2O_3. Thus the higher temperature is observed for the transformation of β-FeOOH into α-Fe_2O_3.

The relations between the specific surface area and temperature of calcination (Fig. 8) indicate that each ferric oxyhydroxide becomes amorphous and porous during the course of dehydration. After showing the maximum, the surface area decreases with the rise in temperature owing to crystallization and sintering.

The almost constant value of A_m below 150°C shown in Fig. 10 is referred to the fact that X-ray diffraction patterns are identical up to 150°C. It may be further assumed that the decrease of A_m with transformation is due to the disappearance of hydroxyl groups. On the other hand, the maximum monolayer capacity observed for each sample at 300°C seems to be due to the maximum chemisorption at 300°C as shown in Fig. 11. The maxima of chemisorption observed for α-2 and γ-1 appear to be caused by the higher surface activity in the temperature range, in which the samples undergo transformation into crystalline α-Fe_2O_3 and their crystals are distorted. As illustrated in Fig. 11, β-FeOOH chemisorbs a larger amount of SO_2 than other oxyhydroxides below 200°C. It is considered from the extraordinarily high activity of β-FeOOH to SO_2 that the vacancies formed by the removal of the molecular water by outgassing may be the chemisorption sites for SO_2. The number of such sites decreases with the destruction of the β-FeOOH structure with heating.

These results indicate that the reactivity to SO_2 decreases with the transformation from ferric oxyhydroxide into α-Fe_2O_3, and β-FeOOH in particular has a higher reactivity to SO_2 than other ferric oxyhydroxides at the temperature of calcination below 200°C. The characteristic behavior of β-FeOOH in the transformation process to α-Fe_2O_3 and the higher reactivity to SO_2 would be due to the crystal structure containing molecular water and chlorine which do not exist in other ferric oxyhydroxides.

The authors wish to thank Professor H. Kambe of Tokyo University for the DSC measurements.

14) D. R. Dasgupta and A. L. Mackay, *J. Phys. Soc. Japan*, **14**, 932 (1959).
15) A. L. Mackay, *Miner. Mag.*, **32**, 545 (1960).

Calculation of the Reduced Partition Function Ratios of α-, β-Quartzs and Calcite

Yuji SHIRO and Hitoshi SAKAI*

Department of Education, Hiroshima University, Shinonome, Hiroshima

**Institute for Thermal Spring Research. Okayama University, Misasa, Tottori*

(Received January 22, 1972)

The reduced partition function ratios (r.p.f.r.) of α, β-quartz and calcite were calculated for oxygen isotopic substitution, using the force fields. Optical vibrations are represented by factor group mode ($k=0$) and acoustic contributions were approximated by the Debye mode of vibration. The theoretical calculation predicts that the r.p.f.r. of quartz could have a discrete gap of about 0.8‰ at the α-β-transition temperature (573°C), the r.p.f.r. of α-quartz being larger in magnitude and in temperature-dependency. This implies that the isotopic fractionation factors between quartz and other materials such as water, could be significantly affected by the transition. A comparison of the calculated r.p.f.r. of quartz and calcite with the experimental fractionation factors between these minerals and water yields a fairly consistent value of the r.p.f.r. of water, supporting the force field models used for calculations. The comparison also revealed that the r.p.f.r. of water in the temperature interval 300—800°C and under a hydrostatic pressure of 2 Kb should deviate from those of ideal water vapor at the same temperatures by as much as 1‰ due to the non-ideality of the compressed water fluid.

Distribution of oxygen isotopes in nature is largely controlled by the equilibrium partitioning of the isotopes among coexisting phases. Detailed knowledge on the isotopic fractionation factors between major rock-forming minerals and water is essential in order to understand the isotopic ratios of the various substances in nature. The isotopic fractionation factors have been experimentally determined for a wide range of temperature for systems such as quartz-water, feldspar-water and calicte-water (*e.g.*, O'Neil and Clayton[1], O'Neil and Taylor[2]). On the other hand, the theoretical calculation of the isotopic fractionation factors has been developed by Urey[3], Bigeleisen and Mayer[4], and Bigeleisen[5]. However, application of the theory to condenced materials has been rather limited because of the complicated nature of the calculation. The fractionation factors between calite and water were first studied by McCrea[6], but his model was two simple to explain the experimental results. More refined calculations on the system were made by Bottinga[7] and O'Neil *et al.*[8] and the agreement between the experimental and theoretical values was greatly improved. The present authors calculated the reduced partition function ratios of α-quartz, β-quartz and calcite, using the force fields reported by Shiro[9,10] and Yamaguchi.[11] The present paper will describe the calculation in some detail and the results will be compared with the experimental fractionation factors obtained by other investigators. The effect of the non-ideality of water vapor at high temperatures and pressures on the isotopic fractination factors between water and these minerals will also be discussed.

Calculation of the Reduced Partition Function Ratios of α-, β-Quartz and Calcite. For the isotopic exchange reactions

$$1/2\ Si^{16}O_2 + H_2{}^{18}O = 1/2\ Si^{18}O_2 + H_2{}^{16}O, \quad (1)$$

$$1/3\ CaC^{16}O_3 + H_2{}^{18}O = 1/3\ CaC^{18}O_3 + H_2{}^{16}O, \quad (2)$$

the fractionation factors, α_{q-w} and α_{c-w}, are defined as follows.

$$\alpha_{q-w} = (^{18}O/^{16}O)_{quartz}/(^{18}O/^{16}O)_{water}, \quad (3)$$

and

$$\alpha_{c-w} = (^{18}O/^{16}O)_{calcite}/(^{18}O/^{16}O)_{water}, \quad (4)$$

These fractionation factors can be calculated from the relations

$$\alpha_{q-w} = f_q{}^{1/2}/f_w, \quad (5)$$

and

$$\alpha_{c-w} = f_c{}^{1/3}/f_w, \quad (6)$$

where f represents the reduced partition function ratios (r.p.f.r.) of the subscript substance.

The r.p.f.r. is generally defined by[4]

$$f = (Q^*/Q)_{qm}/(Q^*/Q)_{cl}, \quad (7)$$

where the numerator is the quantum mechanical partition function ratio and the denominator is the classical partition function ratio. The asterisk represents the heavy isotopic species. The partition function ratios of a crystalline solid are related to vibrational frequencies as follows.

$$(Q^*/Q)_{qm} = \prod_i \frac{e^{-u_i^*/2}(1-e^{-u_i})}{e^{-u_i/2}(1-e^{-u_i^*})}, \quad (8)$$

and

$$(Q^*/Q)_{cl} = \prod_i \frac{u_i}{u_i^*} = \left(\frac{m^*}{m}\right)^{3n/2}, \quad (9)$$

where $u_i = h\nu_i/kT$, ν_i=vibrational frequencies, h=Planck's constant, k=Boltzman constant, m=mass of light isotope, m^*=mass of heavy isotope, n=number of atoms involved in the substitution, and T=absolute temperature.

The r.p.f.r. of quartz and calcite were calculated

1) J. R. O'Neil and R. N. Clayton, "Isotopic and Cosmic Chemistry," edited by Craig et al, North-Holland Pub. Co., 1964, p. 157.
2) J. R. O'Neil and H. P. Taylor, Jr., *Amer. Mineralogist*, **52**, 1414 (1967).
3) H. C. Urey, *J. Chem. Soc.*, **1947**, 562.
4) J. Bigeleisen and M. G. Mayer, *J. Chem. Phys.*, **15**, 261 (1947).
5) J. Bigeleisen, *ibid.*, **34**, 1485 (1961).
6) J. M. McCrea, *ibid.*, **18**, 846 (1950).
7) Y. Bottinga, *ibid.*, **72**, 800 (1968).
8) J. R. O'Neil, R. N. Clayton, and T. K. Mayeda, *ibid.*, **51**, 5547 (1969).
9) Y. Shiro, *J. Sci. Hiroshima Univ.*, **A-II 32**, 69 (1968).
10) Y. Shiro, *ibid.*, **A-II 32**, 77 (1968).
11) H. Yamaguchi, *et al.*, to be submitted.

under the following assumptions: (1) all vibrations are harmonic oscillations, (2) crystal vibrations can be divided into optical and acoustic modes, and (3) the vibrational phases of all unit cells in the optical mode are the same, or $k=0$. The r.p.r.f. due to the optical mode are the same, or $k=0$. The r.p.f.r. due to the mode of vibration, f_{opt}, is then obtained by

$$\ln f_{opt} = \sum_{i=1}^{3N-3} \{[u_0(i)-u_0^*(i)]/2 + \ln[1-e^{-u_0(i)}]/[1-e^{-u_0^*(i)}] - \ln[u_0(i)/u_0^*(i)]\}, \quad (10)$$

where N=number of atoms in a unit cell, $u_0=h\nu_0/kT$ and ν_0=optically active vibration frequency (k=0).

The r.p.f.r. due to the acoustic vibrations can be calculated from the following equation if the Debye approximation of the acoustic vibration is valid.[12]

$$\ln f_{acoust} = \frac{3}{40}(\Theta^2-\Theta^{*2})/T^2, \quad (11)$$

$$= \sum_{j=1}^{3} \frac{h^2}{40k^2T^2}[\nu_a^2(j)-\nu_a^{*2}(j)], \quad (11)'$$

where Θ and ν_a represent the Debye temperature and acoustic (Debye) frequencies. Since acoustic vibration is a periodic translation of all atoms in a unit cell, acoustic frequency of the heavy isotopic crystal is assumed to be

$$\nu_a^*/\nu_a = \Theta^*/\Theta = (M/M^*)^{1/2} \quad (12)$$

where M denotes the mass of unit cell.

The observed values of ν_0 (i) of α-quartz were taken from Scott and Porto[13] and Saksena[14] and are given in Table 1. Since β-quartz belongs to factor group D_3, the vibrations of B_1- and B_2-symmertry groups are infrared- and Raman-inactive and only the frequencies of vibrations belonging to A_1, A_2, E_1, and E_2 have been measured[15] (Table 1). The missing frequencies were estimated as follows. Inspection of the observed frequencies of α- and β- quartz indicates that the latter are, on the average, 0.990 of the corresponding frequencies of the former in the region above 600 cm^{-1} and 0.924 below 600 cm^{-1}. This implies that the vibrations of lower frequencies are more strongly affected by the transition than those of higher frequencies. Assuming that the frequency ratios are the same for the B_1 and B_2 vibrations, the "observed frequencies" of the missing vibrations were estimated by multiplying the corresponding freuqencies of α-quartz by the ratios mentioned above (Table 1). The optical frequencies of α- and β- ^{18}O-quartzs were calculated by using the force fields obtained by Shiro[9] and Yamaguchi.[11] The calculated frequencies ν_{cal}^* were then converted into the "observed values" ν_0^*, assuming the following relationship.

$$\nu_0^*/\nu_0 = \nu_{cal}^*/\nu_{cal} \quad (13)$$

The acoustic frequencies of calcite can be calculated by means of the Giulotto-Loinger model[7,16], since carbonate ions are relativaly independent of each other in calcite crystals. However, the structure of quartz is too complicated to apply thier method. Thus,

TABLE 1. OPTICAL VIBRATIONAL FREQUENCIES (cm^{-1}) AND THE DEBYE TEMPERATURES (°K) OF ^{16}O AND ^{18}O QUARTZ

α- quartz			β- quartz		
D_3	ν_0 [a]	ν_0^* [b]	D_6	ν_0 [c]	ν_0^* [b]
	464	439.9	A_1	453	427.0
	1085	1037.5		1074 [f]	1028.8
A_1	356	345.8	B_1	329 [f]	320.9
	207	196.9		191 [f]	181.6
	1080	1037.3		1072	1027.9
	495	474.9	A_2	490	468.9
A_2	778	772.0		770 [f]	769.5
	364	344.3	B_2	336 [f]	316.9
	1072	1020.3		1060	1017.3
	795	780.8		785	773.0
	475	457.7	E_1	470	454.9
	128	120.8		97	91.8
E	1162	1115.9		1154	1096.7
	696	682.8		686	676.7
	394	376.0	E_2	395	372.4
	265	251.1		250	237.0
	Θ [d]	Θ^* [e]		Θ [d]	Θ^* [e]
	204	197.5		204	197.5

a) Observed optical frequency of α-$Si^{16}O_2$, see Refs. 13, 14.
b) Hypothetical optical frequency of α-$Si^{18}O_2$, see text.
c) Observed optical frequency of β-$Si^{16}O_2$, see Ref. 15.
d) Observed Debye temperature of $Si^{16}O_2$, see Ref. 14.
e) Calculated Debye temperature of $Si^{18}O_2$, see text.
f) Hypothetical optical frequency of $Si^{16}O_2$, see text.

TABLE 2. OPTICAL AND ACOUSTIC VIBRATIONAL FREQUENCIES (cm^{-1}) OF ^{16}O AND ^{18}O CALCITE

D_{3d}	ν_0 [a]	ν_0^* [b]	D_{3d}	ν_0 [a]	ν_0^* [b]
A_{1g}	1086	1023.7		1434	1412.4
			E_g	712	673.7
A_{1u}	1086 [e]	1023.8		284	267.8
	222	214.4		156	148.8
	803 [e]	795.8		1484	1461.9
A_{2g}	234 [e]	229.8		706	668.1
	72 [e]	68.1	E_u	330	314.3
	885	877.4		182	178.6
A_{2u}	357	347.1		106	104.9
	106	100.6			
	ν_a [c]	ν_a^* [d]		ν_a [c]	ν_a^* [d]
A_{2u}	142.1	138.0	E_u	104.3	101.3

a) Observed optical frequency of $CaC^{16}O_3$, see Ref. 17.
b) Hypothetical optical frequency of $CaC^{18}O_3$, see text.
c) Calculated acoustic frequency of $CaC^{16}O_3$, see Ref. 16.
d) Calculated acoustic frequency of $CaC^{18}O_3$, see text.
e) Calculated optical frequency of $CaC^{16}O_3$, see Ref. 10.

12) H. Sakai, *Geochem. J.*, **2**, 29 (1968).
13) J. F. Scott and S. P. S. Porto, *Phys. Rev.*, **161**, 903 (1966).
14) B. D. Saksena, *Proc. Ind. Acad. Sci.*, **12A**, 93 (1940).
15) a) I. Shimon and H. O. McMahon, *J. Chem. Phys.*, **21**, 23 (1953); b) P. K. Narayanaswamy, *Proc. Ind. Acad. Sci.*, **A28**, 417 (1948).
16) L. Giulotto and A. Loinger, *Nuovo Cimento*, **8**, 475 (1951).

the Debye temperature obtained by specific heat measurement of α-quartz[14] was used to calculate the acoustic portion of the r.p.f.r. of both α- and β-quartz (Table 1). Contribution of the acoustic vibrations to the total reduced partition function ratios is less than 0.5% and the assumption made above will not seriously affect the results.

The observed optical frequencies of calcite were taken from Ramdas results.[17] The optically inactive frequencies of A_{1u}- and A_{2g}-symmetry groups were calculated by Shiro.[10] The "observed frequencies" of ^{18}O-calcite were obtained as described above by using the force field given by Shiro.[10] The Debye temperatures of ^{16}O-calcite were taken from the calculation of Giulotto and Loinger.[16] The values are given in Table 2.

Results

The r.p.f.r. of α-, β-quartz and calcite are given in Table 3. The r.p.f.r. of calcite were obtained by using the same frequencies of the free carbonate ion and the lattice vibrations as used by Bottinga.[7] Our "Bottinga's values" are approximately 1.5‰ larger than his at all temperatures. The reason for this is not clear at present. The values quoted as "Bottinga's values" are those we re-calculated using the vibrational frequencies presented by Bottinga[7], and the value of 3/2 $\ln(m^*/m) = 3/2 \ln \frac{17.999167}{15.99491} = 0.17708$.

Table 3. Reduced partition function ratios of quartz and calcite

Temp (°C)	$1/2\frac{1}{3}\ln f_q$		$1/3 \ln f_c$	
	α-quartz	β-quartz	Ours	Bottinga's
0	123.04	(118.95)	112.50	115.47
25	106.99	(103.41)	97.96	100.54
50	93.83	(90.67)	86.03	88.29
75	82.92	(80.11)	76.12	78.11
100	73.77	(71.24)	67.80	69.56
150	59.42	(57.34)	54.71	56.11
200	48.82	(47.07)	45.02	46.15
250	40.78	(39.27)	37.64	38.56
300	34.55	(33.23)	31.89	32.66
350	29.63	(28.45)	27.35	27.98
400	25.69	(24.62)	23.70	24.22
500	19.84	(18.95)	18.26	18.62
600	15.78	15.01	14.47	14.72
700	12.85	12.17	11.74	11.91
800	10.68	10.05	9.69	9.81
900	9.01	8.44	8.14	8.20
1000	7.72	7.18	6.92	6.94

Discussion

The oxygen isotopic fractionation factors between calcite and water have been experimentally studied by McCrea[6] and Epstein *et al.*[8] at higher temperatures. The observed fractionation factors were found to be well approximated by an equation of the form $10^3 \ln \alpha_{c-w} = a/T^2 + b$, for a wide range of temperature, although the deviation from the linear equation becomes large at temperatures above 800°C. The experimental fractionation factors employed in this paper for calcite-water system is that given by O'Neil *et al.*[8]:

$$10^3 \ln \alpha_{c-w} = 2.78 \times 10^6/T^2 - 3.39 \qquad (14)$$

The experimental range of temperature was 0—500°C for equation (14). The calculation was extended to 800°C for the purpose of comparison with the fractionation factors between quartz and water. A slightly different equation, $10^3 \ln \alpha_{c-w} = 2.71 \times 10^6/T^2 - 1.84$, was also given by the same authors[1] for a temperature rage 0–750°C. The former equation gives a value about 0.6‰ higher at room temeprature and about 1.5‰ higher at 1000°C than that given by the latter equation.

The experimental fractionation factors in the system quartz-water have been subjected to significant revision since the first experimental work of O'Neil and Clayton.[1] The value of $\ln \alpha_{q-w}$ =used in the following discussion was taken from Fig.1 of Epstein and Taylor[19] and approximated by the least square fit equation[20],

$$10^3 \ln \alpha_{q-w} = 3.57 \times 10^6/T^2 - 2.71 \qquad (15)$$

The applicable temperature range of equation (15) would be 300–800°C. However, the equation gives about 2‰ larger fractionation factors in the temperature range 500–800°C than those reported by O'Neil and Clayton.[1] These discrepancies are apparently due to experimental difficulty in determination of the fractionation factors, suggesting that a comparison of theory and experimental rseults can not be free from uncertainty arising not only from the theory, but also from the experimental estimation of the fractionation factors.

The difference between the calculated r.p.f.r. of quartz and the observed values of $\ln \alpha_{q-w}$ is shown in Table 4. Similar values for calcite-water system are also shown. The differences (denoted as $f_{1w(q)}$ and $f_{1w(c)}$), should be equal to the r.p.f.r. of water and can be compared to the r.p.f.r. of water obtained independently by other methods.

The r.p.f.r. of liquid water may be obtained from the theoretically calculated r.p.f.r. of gaseous water and the observed isotopic vapor pressure ratios of water by means of the relationship

$$\ln f_{1w} = \ln f_{vw} + \ln \alpha_{1w-vw}, \qquad (16)$$

where subscripts 1w and vw stand for liquid and vapor water, respectively. The latest values of $\ln f_{vw}$ (Table 4) were claculated by Bottinga[7] who took into account the anharmonicity of the vibrations of water molecules. The values of $\ln \alpha_{1w-vw}$ have been mesaured by several

17) A. K. Ramdas, *Proc. Ind. Acad. Sci.*, **37A**, 441 (1953).

18) S. Epstein, R. Buchsbaum, A. Lowenstam and H. C. Urey, *Bull. Geol. Soc. Amer.*, **64**, 1315 (1953).

19) S. Epstein and H. P. Taylor, Jr., "Researches in Geochemistry" II, New York, John Wiley, P. H. Abelson ed., (1966) p. 32 Fig. 1.

20) H. P. Taylor, Jr., Personal communication (1971).

Table 4. Reduced partition function ratios of water

Temp °C	$\ln f_{vw}$ ‰	$\ln \alpha_{1w-vw}$ ‰	$\ln f_{1w}$ ‰			
			$\ln \alpha_{vw-1w} + \ln f_{vw}$	$\ln f_{CO_2} - \ln \alpha_{CO_2-1w}$	$1/2 \ln f_q - \ln \alpha_{q-w}$	$1/3 \ln f_c - \ln \alpha_{c-w}$
0	68.22	11.19	79.41	80.20	(77.18)	(78.59)
25	61.64	8.86	70.50	71.25	(68.96)	70.05
50	56.08	6.88	62.96	63.68	(61.89)	62.77
75	51.33	5.19	56.52	57.20	(55.80)	56.55
100	47.21	3.73	50.94	51.58	(50.53)	51.21
150	40.46	1.32	41.78	(42.35)	(41.98)	42.56
200	35.16	−0.58	34.58	(35.07)	(35.44)	35.98
250	30.90	(−2.11)	(28.79)	(29.18)	(30.36)	30.87
300	27.40	(−3.38)	(24.02)	(24.32)	(26.34)	26.81
350	24.49				23.13	23.58
400	22.03				20.53	20.95
500	18.11				16.61	17.00
600	15.15				13.10	14.21
700	12.86				11.19	12.19
800	11.04				9.75	10.67

authors in a temperature range below 100°C.[21-24] Unfortunately, agreement between the values reported by these authors was rather poor, the maximum discrepancy being as much as 1‰. Values were obtained from the least square fit equation of the form $\ln p/p^* = a/T+b$ to the data given by Uvarov *et al.*[23] Theoretical verification of the equation was given by Bigeleisen.[5] We selected the data of Uvarov *et al.*[23] because only their measurements were extended to temperatures above 100°C, but in the least square fit calculation, the three highest temperature points were excluded for the reason that their data show a significantly different temperature dependency as compared to the lower temperature data. O'Neil and Adami[25] computed the values of $\ln f_{1w}$ from the observed isotopic fractionation factor between carbon dioxide and water and the calculated reduced partition function ratios of carbon dioxide. Their results are represented by the least square fit equation, $10^3 \ln f_{1w} = 29.14 \times 10^3/T - 26.54$ as shown in Table 4. The values of $\ln \alpha_{1w-vw}$ reported by Uvarov *et al.*[23] are essentially the lowest among those reported by other investigators, while the values of O'Neil and Adami[25] would rather represent a highest estimation of this kind. Hence, the two sets of data could define a possible range of values of $\ln f_{1w}$. We see from Table 4 that in spite of many uncertainties involved in the experimental and theoretical estimations, the values of $\ln f_{1w(c)}$ and $\ln f_{1w(q)}$ at a temperature range below 600°C are fairy close to each other, especially those of $\ln f_{1w(c)}$ being within a possible range of the values presented above.

Above the α-β transition point of quartz (573°C) the values of $\ln f_{1w(q)}$ deviate significantly from those of $\ln f_{1w(c)}$, because the r.p.f.r. of β-quartz is about 0.8‰ smaller at the transition point. The temperature dependency is also smaller than for α-quartz. This is a reflection of the fact that β-quartz is characterized by a less dense crystal structure than α-quartz: the unit cell of the former being appeoximately 0.1Å

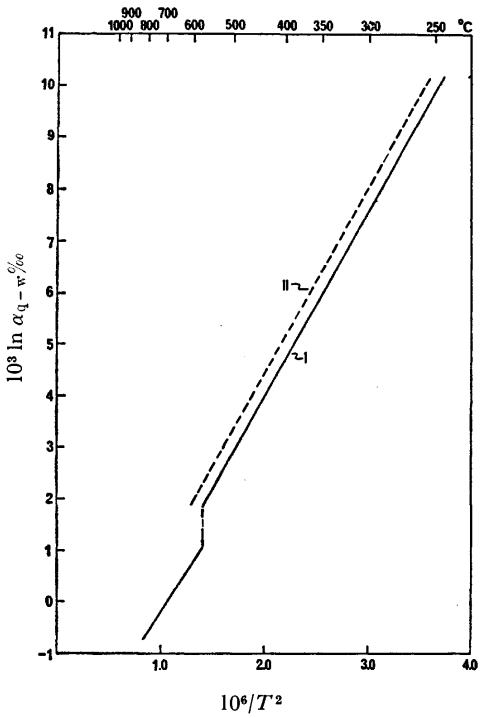

Fig. 1. Isotopic fractionation factors between quartz and water.
I: Theoretical values obtained by the calculated values of $1/2 \ln f_q$ and those of $\ln f_{1w(c)}$.
II: Experimental values by equation (18).

21) I. Dostrovsky and A. Raviv., *Proc. Intern. Symp. Isotope Separation*, Amsterdam, **1957**, 336 (1958).
22) S. Szapiro and F. Steckel, *Trans. Faraday Soc.*, **63**, 883 (1967).
23) O. V. Uvarov, N. M. Sokolov, and N. M. Zavoronkov, *Kernenergie*, **5**, 323 (1962).
24) P. Baertschi and M. Thürauf, *Helv. Chim. Acta*, **43**, 80 (1960).
25) J. R. O'Neil and L. H. Adami, *J. Phys. Chem.*, **73**, 1553 (1969).

longer than the latter in both the a and c axes.[26] Yamaguchi[11] also demonstrated that the strecthing force constant of Si-O bond in β-quartz is about 0.2 mdyn/Å smaller than that in α-quartz on normal coordinate treatment. The "theoretical" values of $\ln \alpha_{q-w}$, calculated by the relationship $\ln \alpha_{q-w} = 1/2 \ln f_q - \ln f_{iw(c)}$, are plotted against $10^6/T^2$ in Fig. 1. The experimental values represented by equation (15) are also shown for comparison (dotted line). It is seen that the α-β transition of quartz should have a significant effect on the isotopic fractionation factors between quartz and water, although the experimental results so far obtained do not support the prediction. The calculated discontinuity at the transition point may be made smaller by adjusting the vibrational frequencies of α-quartz, while the uncertainty in the experimental determinations of the fractionation factor may also be large. Thus we feel that an exact comparison between theory and experiments is rather difficult at present.

The experimental data of quartz-water and calcite-water system at higher temperatures were determined under a hydrostatic pressure of 2 Kbar.[1] The values of $f_{iw(q)}$ and $f_{iw(c)}$ in Table 4 are, therefore, those of supercritical water at 2 Kbar. A good agreement between $f_{iw(q)}$ and $f_{iw(c)}$ below the α-β transition temperature of quartz allows us to say with some confidence that the difference between $f_{iw(c)}$ and the r.p.f.r. of gaseous water calculated by Bottinga above the critical temperature of water is ascribed to the non-ideality of water fluid under the experimental conditions. The non-ideality in the r.p.f.r. is about 1‰ at temperatures around 600°C and then decreases rapidly above 700°C. It should be noted that the compressed supercritical water fluid is "isotopically lighter" than the freely expanded water vapor at the same temperature. The cross-over point of the liquid-vapor water system lies somewhere around 150–200°C.[23] Above this temperature the heavy water ($H_2{}^{18}O$) possesses a higher vapor pressure than that of $H_2{}^{16}O$. The cross-over phenomena are qualitatively ascribed to the difference between $H_2{}^{16}O$ and $H_2{}^{18}O$ of the zero-point energy change by condensation of water.[5] The non-ideality in the r.p.f.r. of the compressed supercritical water fluid would also be due to the same effect, although a quantitative explanation is not possible at the present time.

Table 3 indicates that "Bottinga's values" of the r.p.f.r. of calcite ($1/3 \ln f_c$) are about 3% larger than our values. In our model, the carbonate ions in calcite crystals are not independent of each other, while in Bottinga's model, they vibrate freely without interaction.[7] As a result of mutual interaction of carbonate ions in our model, the ν_3 vibration at 1467 cm^{-1} a free carbonate ion[27] splits into two broad lines at 1434 and 1484 cm^{-1}. In general, the vibration of higher frequency makes more contribution to the r.p.f.r., hence the neglect of this unsymmetric splitting in Bottinga's model could be a cause of the discrepancy mentioned above.

The authors would like to express thier thanks to Professor T. Miyazawa, Osaka University, for his critical reading of the manuscript and helpful discussion. One of the authors(Y.S.) is indepted to the Sakkokai Foundation for financial help.

Added in Proof: The experimental equation of high temperature liquid-vapor fractionation factor for $H_2{}^{16}O$-$H_2{}^{18}O$ by Y. Bottinga and H. Craig (*Amer. Geophys. Union Trans.* **49**, 356 (1968)) is $\ln \alpha_{1w-vw} = -7.174 + 4.716 \times 10^3/T - 0.058 \times 10^6/T^2$. Due to their values, our obtained values $\ln \alpha_{q-w}$ become 6.3‰, 11.1‰, and 21.1‰, at 300°C, 200°C, and 100°C, respectively. The values are *ca.* 2‰ smaller than the Talor's results.[20]

26) R. W. G. Wyckoff, "Crystal Structures" (1948) Interscience, New York.

27) S. D. Ross and J. Goldsmith, *Spectrochim. Acta*, **2**, 781 (1964).

Steady-Light Irradiation and Flash Photolysis Studies of [2.2]Metacyclophane-Iodine Systems. Mechanistic Implications of Transannular Dehydrogenation Reaction

Shigenari HAYASHI and Takeo SATO*

Department of Chemistry, Nihon University, Sakurajosui, Setagaya-ku, Tokyo

**Department of Chemistry, Faculty of Science, Tokyo Metropolitan University, Fukazawa, Setagaya-ku, Tokyo*

(Received January 25, 1972)

Irradiation of cyclohexane solutions of [2.2]metacyclophane in the presence of iodine is shown to yield 4,5,-9,10-tetrahydropyrene as the initial product. In order to clarify the mechanism of the cyclodehydrogenation reaction, steady-light irradiation, and flash photolysis experiments have been carried out. The rate of formation of 4,5,9,10-tetrahydropyrene is followed by UV spectra measurements using a characteristic band maximum at 292 nm. The rate of appearance of 4,5,9,10-tetrahydropyrene is found to be proportional to the absorption of light. The reaction is a one photon process. The reaction rate is almost constant when the concentration of iodine is less than 7×10^{-4} mol/*l*, but decreases gradually with higher concentrations. A long-lived species, whether radical or excited triplet, can not be detected by flash techniques. It is most likely that the first step involves the excited singlet. Involvement of CT-complex is proposed.

Due to the proximity of two benzene rings, [2.2]-metacyclophane (MCP) shows transannular interaction which causes spectral anomalies and results in transannular reactions to give pyrene derivatives.[2] Spectral studies of the charge transfer complexes involving TCNE and other electron acceptors were reported.[3]

Sato *et al.* reported on a photochemical transannular reaction of MCP induced by iodine.[4] Examination of the photoreaction using a high-pressure mercury lamp gave the following results:[5] a) Irradiation of degassed MCP-I_2-cyclohexane solutions results in a spectral change indicative of the formation of 4,5,9,10-tetrahydropyrene (4HP), which can be isolated in a fair yield. b) When photolysis is continued, further dehydrogenation occurs to give 4,5-dihydropyrene (2HP) and pyrene. c) No appreciable reaction occurs when the solution is photolyzed in air in the absence of iodine. d) Besides an oxidant, iodine appears to play a special role in the photoreaction. e) A light source with 253.7 nm line is the most effective one.

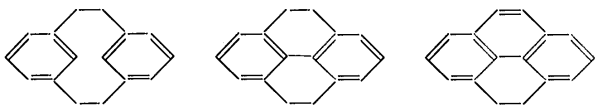

MCP 4HP 2HP

A mechanistic study of the transannular reaction is especially attractive in comparison with the related photocyclization reactions such as the formation of phenanthrene from *cis*-stilbene,[6] photolytic cleavage of [2.2]paracyclophane,[7] and photoequilibrium in certain metacyclophane compounds.[8]

In order to reveal the initial stage of the reaction, to account for acceleration of the reaction with iodine and to provide mechanistic implications, this paper records spectral studies under steady-light conditions and flash photolysis experiments.

Experimental

Materials and Procedures. [2.2]Metacyclophane (MCP)[9,10] was purified by combining recrystallization and column chromatography. 4,5,9,10-Tetrahydropyrene (4HP) and 4,5-dihydropyrene (2HP) were recrystallized three times from ethanol and sublimed. Cyclohexane (Wako Junyaku G.R. grade) was purified by the ordinary method. Purity was confirmed by UV spectrum and gas chromatography. Apparatus similar to that reported[11] was used for the steady-light illumination. The light source is a Ushio U12-1E low pressure mercury lamp operating at 100 V, supplied through a voltage stabilizer. The reaction temperature was 30°C. The sample solutions were degassed 7—8 times by the freeze-pump-thaw method *in vacuo* (the degassed solution). Aerated solutions were also used. At various time intervals, the sample cell was taken out and the absorption spectra were measured with a Hitachi EPU-2A spectrophotometer or a Shimadzu RM autorecording spectrophotometer. The effect of wavelength on the quantum yields was studied by choosing monochromatic light selected from a Toshiba SHL-100UV mercury lamp with a suitable

1) Photochemistry of [2.2]Metacyclophanes, Part II, for Part I see Ref. 3. Photo-Aryl Coupling and Related Reactions. X: Part IX, T. Sato, K. Nishiyama, S. Shimada, and K. Hata, This Bulletin, **44**, 2858 (1971).

2) Reviews: R. W. Griffin, Jr., *Chem. Rev.*, **63**, 45 (1963); T. Sato, *Kagaku no Ryoiki*, **23**, 672, 765 (1969); T. Sato, *Nippon Kagaku Zasshi*, **92**, 277 (1971).

3) S. Hayashi, and T. Sato, *Nippon Kagaku Zasshi*, **91**, 950 (1970).

4) T. Sato, E. Yamada, Y. Okamura, T. Amada, and K. Hata, This Bulletin, **38**, 1049 (1965).

5) T. Sato, M. Wakabayashi, S. Hayashi, and K. Hata, *ibid.*, **42**, 773 (1969).

6) F. B. Mallory, C. S. Wood, and J. T. Gordon, *J. Amer. Chem. Soc.*, **84**, 4361 (1962); *ibid.*, **85**, 828 (1963); *ibid.*, **86**, 3094 (1964). N. J. Turro, "Molecular Photochemistry," W. A. Benjamin. Inc., New York (1965), p. 234; F. R. Stermitz in O. L. Chapman ed., "Organic Photochemistry," Vol. 1, Mercel Dekker Inc., New York (1967), p. 249.

7) R. C. Helgeson and D. J. Cram, *J. Amer. Chem. Soc.*, **88**, 509 (1966).

8) H. R-Blattman, D. Menche, E. Heilbronner, R. J. Molyneus, and V. Boekelheide, *ibid.*, **87**, 130 (1965).

9) M. Fujimoto, T. Sato, and K. Hata, This Bulletin, **40**, 600 (1967).

10) S. Akabori, T. Sato, and K. Hata, *J. Org. Chem.*, **33**, 3277 (1968); T. Sato, S. Akabori, S. Muto, and K. Hata, *Tetrahedron*, **24**, 5557 (1968).

11) M. Koizumi, H. Obata, and S. Hayashi, This Bulletin, **37**, 108 (1964).

combination of Hoya or Toshiba glass filters, an aqueous solution of nickel sulfate (100 g/300 m*l*, 1 cm) and an interference filter. The quantity of light absorption was measured by a potassium ferrioxalate actinometer,[12] or a calibrated Kipp & Zonen thermopile and a Shimadzu K-2 potentiometer.

Main xenon flash lamp (96J, duration time of 15 μ sec) of the flash photolysis apparatus was followed by a second flash after 50 μsec and the transmitted light, after being passed through a Nalumi RM spectrography/monochromator, was led to a dry-plate. Alternatively, transmitted light was received by a Hamamatu photomultiplier and observed with the aid of an Iwasaki oscilloscope.

Results and Discussion

Steady Light Experiments. General Features of the Photooxidation: A spectral change occurs when a degassed MCP-I_2-cyclohexane solution is irradiated using 253.7 nm light as shown in Fig. 2. When irradiation is continued new maxima appear at 260, 268, 280, 292, 320, and 334 nm, which are ascribed to 4HP (see Fig. 1). The structure of 4HP was confirmed by IR and NMR spectra, and by direct comparison with the authentic material. The formation of 4HP is almost quantitative.

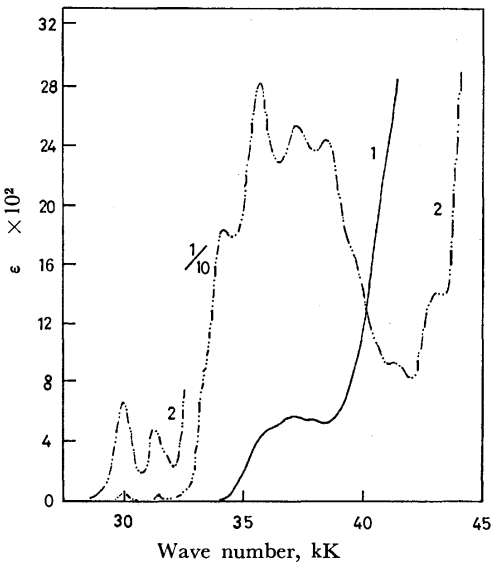

Fig. 1. Absorption spectra in cyclohexane.
(1): [2.2]Metacyclophane,
(2): 4, 5, 9, 10-Tetrahydropyrene.

On further irradiation, 4HP is converted in to 2HP and eventually to pyrene.[5] The reaction occurs successively. The secondary dehydrogenation steps are, however, much slower than the formation of 4HP from MCP and can be neglected. No thermal reactions occur with dilute solution. The transannular bonding is possible only under photolytic conditions.

An absorption maximum due to iodine, occurring at 525 nm diminished during the course of irradiation (Fig. 2). Conversion of iodine to hydrogen iodine could be inferred, but attempts to characterize it failed.

12) C. A. Parker, *Proc. Roy. Soc.* (London), **220A**, 104 (1953).

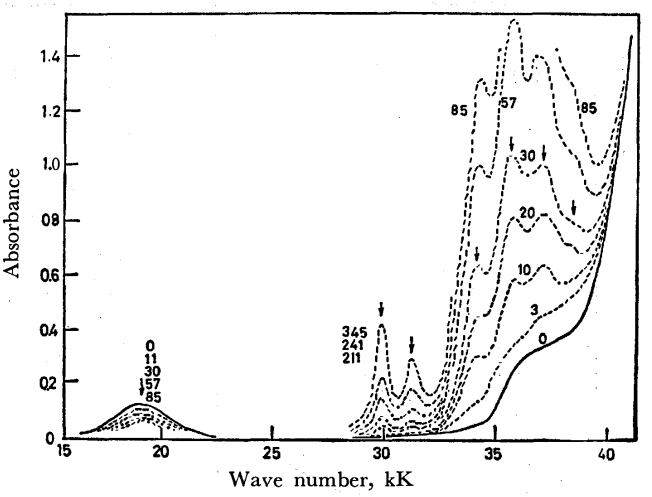

Fig. 2. Change of absorption spectra of the mixed solution of [2.2]metacyclophane and iodine by UV-irradiation (degassed cyclohexane solution).
[MCP]: 5.1×10^{-4}mol/*l*, [I_2]: 1.44×10^{-4}mol/*l*
Numbers denote the time of illumination (min).

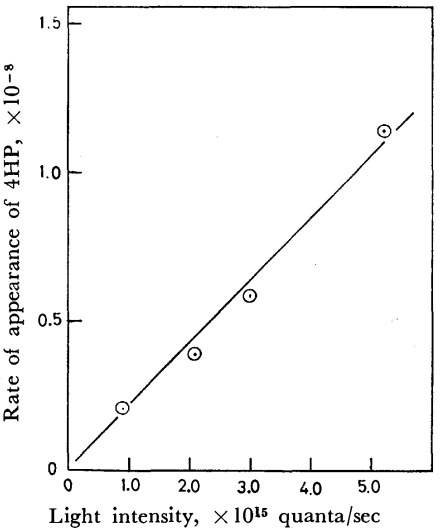

Fig. 3. Effect of the incident light intensity on the rate of appearance of 4HP.

Quantum yields of the reaction are summarized in Table 1. The results indicate that the most efficient

Table 1. The quantum yield
[MCP]: 5.5×10^{-4} M; [I_2]: 1.6×10^{-4} M

Exciting light, nm	Quantum yield
253.7	6.2×10^{-3}
296.7, 280.2	
302.2—302.8	5.3×10^{-3}
312.6—313.2	
546.1	
577.0—579.0	0
No Filter	5.5×10^{-3}

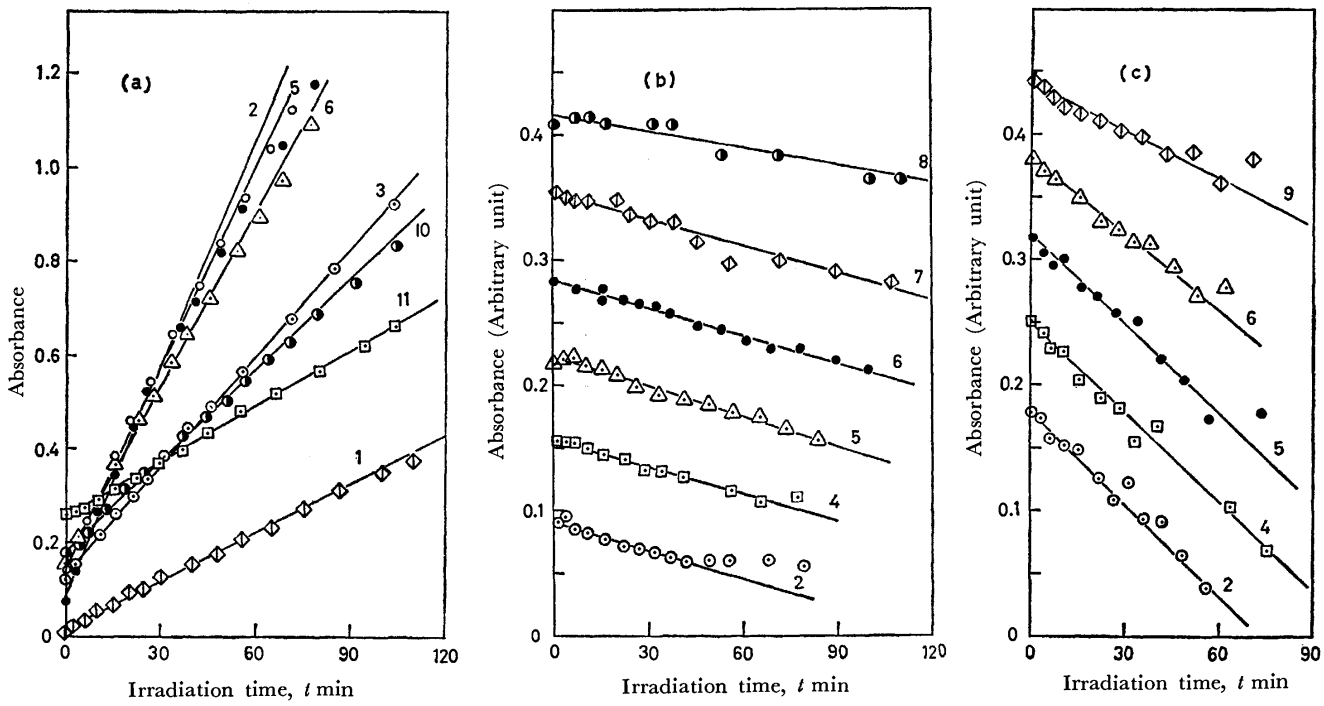

Fig. 4. Effect of iodine initial concentration.
a): Absorbance at 292 nm *vs.* *t* plot. b): Absorbance at 520 nm *vs.* *t* plot. c): Absorbance at 272 nm *vs.* *t* plot.
[MCP]: 5.1×10^{-4} mol/*l*
[I_2]: 1) 0 4) 3.26 7) 10.5 10) 17.6
2) 0.99×10^{-4} mol/*l* 5) 4.31 8) 11.5 11) 25.0
3) 1.05 6) 6.46 9) 13.5

light is 253.7 nm line. Excitation of iodine absorption in the visible region using a 500 W tungsten lamp was not effective. The experiments described hereafter were carried out with a low pressure lamp. The reaction rate was determined by UV spectra following absorbance changes at 292 nm with appropriate time intervals.[13]

Effect of Light Intensity: A satisfactory linear correlation was obtained from plots absorbance *vs.* *t* at the initial stage. We see from Fig. 3 that the rate of appearance of 4HP (evaluated from the initial slope of the run for reaction) is proportional to light intensity. The main reaction is a one photon process.

Effect of Initial Iodine Concentration on the Rate: Since absorbing species at 253.7 nm are MCP, 4HP, and iodine, the light absorption can be expressed as follows.

$$I_{abs} = (I_0/d)(1-\exp(-2.303\mathrm{d}D_t)) \times 10^3$$
$$D_t = \varepsilon_{MCP}C_{MCP} + \varepsilon_I C_I + \varepsilon_{4HP}C_{4HP} \quad (1)$$

In the present studies, however, the conversion of MCP does not exceed 15%. For treatment of the initial stage of the reactions the term due to 4HP can be neglected.

$$I_{abs} = (I_0/d)(1-\exp(-2.303\mathrm{d}(\varepsilon_{MCP}C_{MCP}+\varepsilon_I C_I))) \times 10^3$$
$$= 2.303I_0(\varepsilon_{MCP}C_{MCP}+\varepsilon_I C_I) \times 10^3 \quad (2)$$

where C_{MCP}, C_I, C_{4HP}, ε_{MCP}, ε_I, and ε_{4HP} represent concentration and molar absorptivity of MCP, iodine, and 4HP, I_0 and d are light intensity and sample path length, respectively. Molar absorptivity of 4HP is more than ten times that of MCP and iodine, and would cause inner filter effects but only at a later stage. Assuming that only MCP takes part in reaction and that the rate of disappearance is proportional to light absorption, the following formula is obtained.

$$-\frac{\mathrm{d}C_{MCP}}{\mathrm{d}t} = \frac{\mathrm{d}C_{4HP}}{\mathrm{d}t} = kI_{abs}\frac{\varepsilon_{MCP}C_{MCP}}{\varepsilon_{MCP}C_{MCP}+\varepsilon_I C_I}$$
$$C_{4HP} = 2303kI_o\varepsilon_{MCP}C_{MCP}t = k_{4HP}t \quad (3)$$

Eq. (3) indicates that the formation of 4HP is proportional to the reaction time. This was satisfied experimentally (Fig. 4-a).

The reaction rate changes with iodine concentration[5]. For the sake of quantitative study, reaction mixtures with various iodine concentration were subjected to photolytic reaction. A good linear relationship was observed between C_{4HP} and reaction time (t) for several sets of mixtures (Fig. 4-a), although at very low iodine concentration some discrepancies were found except for the initial stage of the reaction. The rate of formation of 4HP(k_{4HP}) can be calculated from the slope.

At 253.7 nm iodine behaves also as an absorbing species and its decay being observed. Cleavage of iodine to radicals $I_2 \rightarrow 2I\cdot$ occurs, making it an attacking species. The relation between iodine concentration and rate of 4HP formation is shown in Fig. 5. When iodine concentration exceeds 7×10^{-4} mol/*l*, the reaction rate decreases gradually, possibly due to an innerfilter

13) At 292 nm, $\varepsilon_3 \gg \varepsilon_1$, ε_2, $\varepsilon_1+\varepsilon_2$, where ε_1, ε_2, and ε_3 are molar absorptivities for MCP, I_2, and 4HP, respectively. Therefore, absorbance increase in this region is assumed to be due to 4HP.

effect of iodine. This indicates that the following scheme is not the sole path.

$$\left.\begin{aligned} &I_2 \xrightarrow{h\nu} I_2^* \rightarrow 2I\cdot \\ &MCP + 2I\cdot \rightarrow 4HP + 2HI \end{aligned}\right\} \quad (4)$$

The fact that the dehydrogenation reaction proceeds with a significant rate even at very low iodine concentration ($<7\times10^{-4}$ mol/l) suggests two possibilities involving either a CT-complex between MCP and iodine or a rather long-lived intermediate subjected to iodine attack. For the latter case MCP can be excited to a triplet state, which may undergo electron and proton transfer reactions

$$\left.\begin{aligned} &MCP^* + I_2 \rightarrow MCP^+ + I_2^- \\ &MCP^+ + I_2^- \rightarrow 4HP + 2HI \end{aligned}\right\} \quad (5)$$

From flash photolysis experiments, however, such species could not be detected.

The rate of disappearance of iodine (k_I) determined at 525 nm also depends on the initial iodine concentration, as for k_{4HP}. Decrease of MCP leads to 4HP formation. The rate is in a complimentary relation

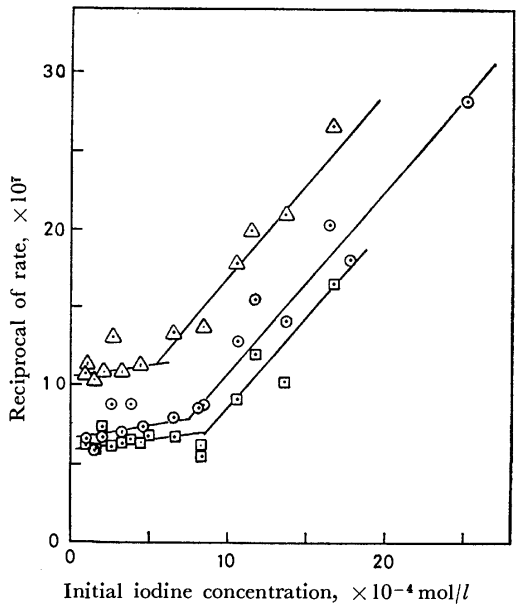

Fig. 5. Reaction rates (k_{4HP}, k_{MCP}, k_I) *vs.* initial iodine concentration plot.
⊙: 4HP, △: MCP, ⊡: Iodine

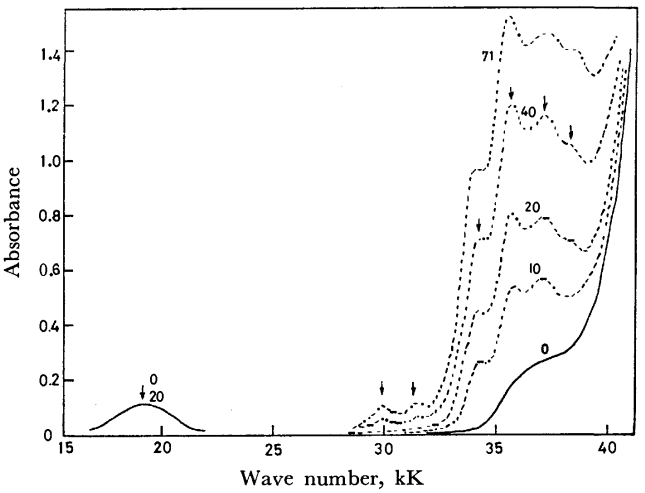

Fig. 6. Spectral change when the MCP containing iodine in the aerated solution was irradiated by 253.7 nm.
[MCP]: 5.1×10^{-4} mol/l, [I_2]: 1.4×10^{-4} mol/l
Numbers denote the time of illumination (min).

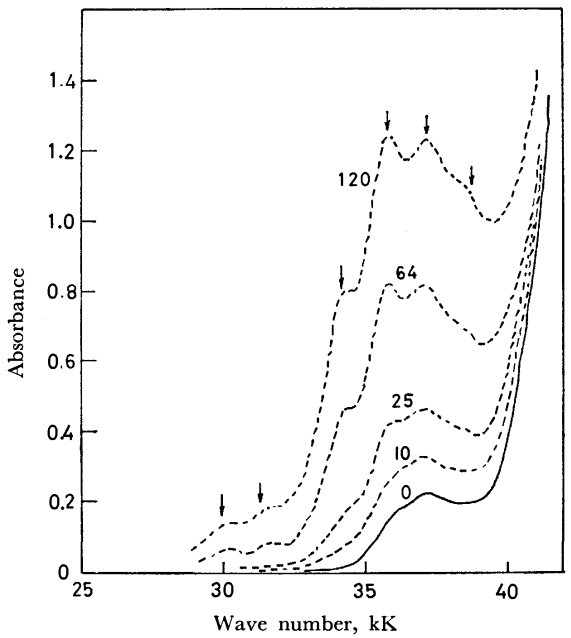

Fig. 7. Change of absorption spectra of MCP by UV-Irradiation (aerated cyclohexane solution).
[MCP]: 5.0×10^{-4} mol/l
Numbers denote the time of illumination (min).

(Fig. 4-b, Fig. 5).

Spectral changes observed by illuminating an aerated MCP-I_2-cyclohexane system are shown in Fig. 6. Recently, Sorimachi, Shizuka, and Morita[14] reported that the photolytic reaction of MCP to 4HP occurred in the absence of iodine. Photodehydrogenation with oxygen is, however, much slower than with iodine. Even slower rate of reaction was observable with degassed cyclohexane solutions (Fig. 7). Although the ability of hydrogen abstraction in *cis*-stilbene-phenanthrene reactions is considered to be in the order $I\cdot > O_2 > I_2$,[6] it does not hold in the present case. This suggests that an essentially different mechanism is involved in the photolytic reaction of MCP. Irradiation of *cis*-stilbene gives 4*a*,4*b*-dihydrophenanthrene in a reversible process, which in the dark reaction is oxidized by an added oxidant. On the other hand MCP is subjected to irreversible oxidation on irradiation. Even with the lack of unsaturation connecting two aromatic moieties, MCP undergoes photodehydrogenation by virtue of favorable molecular geometry, proximity of coupling positions and great strain energy.

14) H. Shizuka, K. Sorimachi, and T. Morita, Abstracts of Papers, the 24 th Annual Meeting of the Chemical Society of Japan, Osaka, April, 1971.

Apparent activation energy of the reaction is 5.5 kcal/mol which can be compared with 5.0 kcal/mol found for stilbene.

The Effect of MCP Initial Concentration. Experiments carried out with MCP concentrations show that the rate of 4HP formation is proportional to MCP concentration. The relation between MCP concentration and k_0 which can be calculated from k_{4HP} assuming $k_{4HP}/C_{MCP}=k_0$, is shown in Fig. 8. The values represent approximate quantum yields. For [MCP]$\geqq 5\times10^{-4}$ mol/l, k_0 is almost constant. No such linear correlation exists with more dilute solutions.

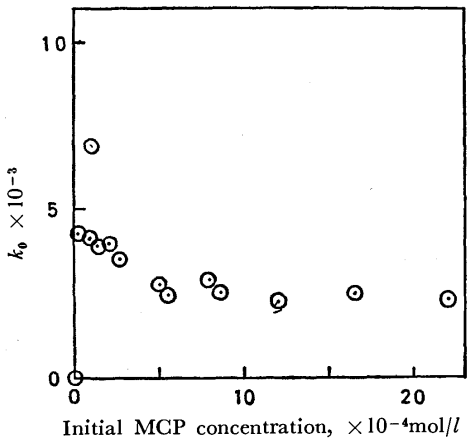

Fig. 8. k_0 *vs.* MCP concentration plot.
[I_2]: 3.3×10^{-4}mol/l

Flash Technique Experiments. Although the overall process of the I_2-induced dehydrogenation of MCP can be written as $MCP+I_2 \xrightarrow{h\nu} 4HP+2HI$, it is necessary to know whether it is such a simple reaction or a multistep reaction going through some intermediates. Muszkat and Fisher[15] presented a free radical mechanism involving radical species such as PH·, formed by hydrogen abstraction from dihydrophenanthrene PH_2, and HO_2· in the *cis*-stilbene-phenanthrene reaction. In order to solve the problems flash photolysis experiments were carried out for degassed cyclohexane solutions of MCP-I_2, MCP and I_2.

No absorption spectra suggesting the presence of an intermediate was observed. If an intermediate with a lifetime longer than 5×10^{-5} sec had been involved, the corresponding absorption could have been observed. For several wavelength regions, the diminishing absorption after main flash was followed by oscilloscope observation. Although absorption due to the product was observed, no diminishing absorption characteristic of an intermediate was detected.

Formation of Molecular Complex. The results of flash photolysis eliminate the possibility that the reaction proceed through a long-lived intermediate such as triplet species. As an alternative, we can postulate an intermediacy of the CT complex between MCP and iodine. The UV spectrum of a mixture of MCP ($\sim10^{-2}$ mol/l) and iodine ($\sim10^{-3}$ mol/l) in cyclohexane showed the presence of a band maximum at 334 nm which was absent in the individual spectra (Fig. 9). The band position is in agreement with the expected maximum[16] 336 nm, calculated from the ionization potential of MCP, 8.41 eV.[3]

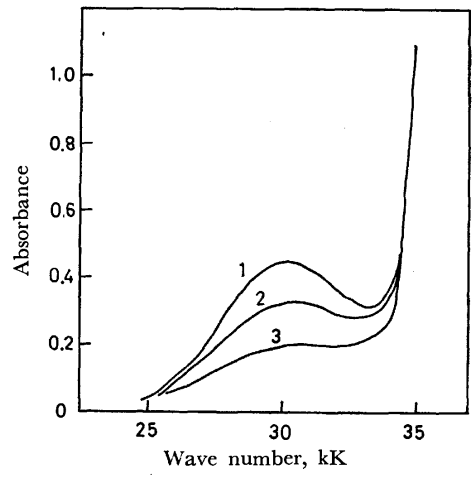

Fig. 9. Absorption spectra of the molecular complex between MCP and iodine in cyclohexane solution.
[I_2]: 2.21×10^{-3}mol/l, [MCP]: 1) 1.44×10^{-2}mol/l, 2) 0.931, 3) 0.508

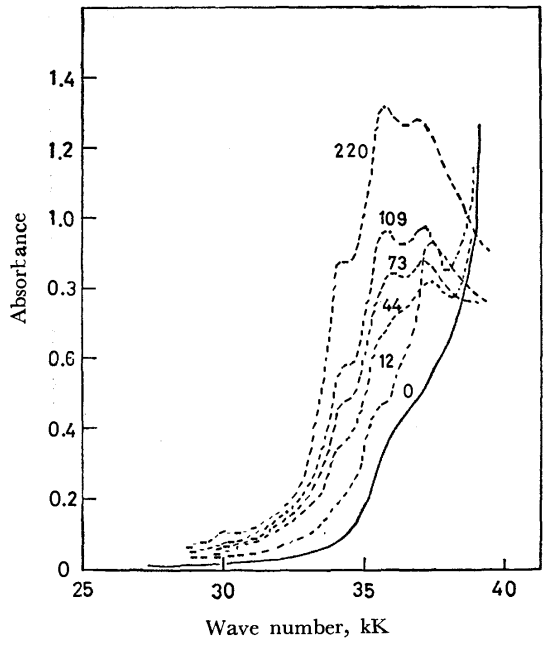

Fig. 10. Change of the absorption spectra of the solution containing MCP and *p*-benzoquinone by UV-irradiation.
[MCP]: 5.0×10^{-4}mol/l
[BQ]: 5.0×10^{-4}mol/l
Numbers denote the time of illumination (min).

15) K. A. Muszkat and E. Fisher, *J. Chem. Soc., B*, **1967**, 662.

16) Briegleb[18] presents the relation between the ionization potential (I_D) of the electron donor and the transition energy($h\nu_{CT}$) of CT-band as follows.

$$h\nu_{CT} = I_D - C_1 + \frac{C_2}{I_D - C_1}$$

Since $C_1=5.20$ eV, $C_2=1.5$ eV in iodine, calculation gives $h\nu_{CT}$ using $I_D=8.41$ eV.

TABLE 2. PHYSICAL PROPERTIES FOR THE MCP-I_2 COMPLEX (20.2°C)

Hydrocarbon	$\lambda_{CT.\ max.}$ nm	ε_{max}	K l/mol	$-\Delta H$ kcal/mol	$-\Delta S$ cal/mol/deg	$-\Delta G$ kcal/mol
MCP	334	1050	16.7	1.83	3.9	0.69
m-Xylene[18]	318	12500	—	—	—	—

The equilibrium constant K and the molar absorptivity ε of the complex calculated from the Rose-Drago equation[17] are in agreement with experimental values. This suggests the possibility that the photocyclodehydrogenation of MCP proceed by complexing with iodine.

As compared with the *m*-xylene-I_2 complex, the MCP complex absorbs at a longer wavelength region with intensity of about one-tenth. The difference is caused by a transannular electronic interaction which delocalize electron density in a charged structure, and also by bent benzene structure.[2] The equilibrium constant is larger than that of *m*-xylene, which is about 3 l/mol, but smaller than that of the MCP-TCNE complex.

Experiments with p-*Benzoquinone and Others.* *p*-Benzoquinone (BQ) and benzophenone (BP)[19] were also found to be effective as an oxidant.

The spectral change indicating the formation of 4HP upon irradiation with MCP–BQ–cyclohexane solutions is shown in Fig. 10. The reaction is rather complex since both MCP and BQ absorb at 253.7 nm. The formation of 4HP appears to be slower compared with iodine.

With BP as an oxidant, 4HP was formed when both MCP and BP were excited although no reaction occurred when BP alone was excited.[19] Abstraction of aryl hydrogens with BP and BQ is interesting when we consider the fact that they are usually photo-reduced only with good hydrogen donors.

On the other hand, irradiation of MCP-TCNE complex gave no indication of 4HP formation. Electon affinity[20] increases in the order O_2(0.7—0.9 eV) < iodine(1.7—1.8 eV) < BQ(2.0 eV) < TCNE-(2.89 eV). A stronger complex can be formed in this order. No relation exists between reactivity and this order.

General Discussion

Photolysis reaction of MCP differs in many ways with respect to the cyclization reaction of *cis*-stilbene, in which oxidation of the dihydrophenenthrene intermediate is accomplished both with oxygen and iodine in the dark reaction. It also differs from the photolysis reaction of [2.2]paracyclophane case since no ring cleavage product could be obtained. In the presence of iodine the rate of formation of 4HP is rapid as compared with other oxidants. This suggests that iodine plays a special role in the photocyclization. Mechanistic considerations, however, reveal that the action of iodine is not simple and appears to involve complicated processes.

From the results of flash photolysis study and the fact that photodehydrogenation was not scavenged by oxygen, one could eliminate the possibility of involvement of MCP triplet (Eq. (5)).

If the reaction comprises uncomplexed MCP in the excited singlet state as given by

$$\left.\begin{aligned} &\text{MCP} \xrightarrow{h\nu} \text{MCP*} \\ &\text{MCP*} + I_2 \rightarrow \text{4HP} + \text{2HI} \end{aligned}\right\} \quad (6)$$

one can expect the dependence of iodine concentration on the rate of formation of 4HP. The results given in Fig. 5, however, clearly indicate that the formation of 4HP is not affected by iodine concentration, if $[I_2] <$ *ca.* 7×10^{-4} mol/l. On the same basis, one can deny that iodine radical is involved in Eq. (4).

We propose the following scheme involving a molecular complex for the initial stage of the photolysis

$$\text{MCP} + I_2 \rightleftarrows (\text{MCP}\cdots I_2) \quad \text{(complex formation)} \quad (7)$$

$$(\text{MCP}\cdots I_2) \xrightarrow{h\nu} (\text{MCP*}\cdots I_2) \quad (8)$$

$$(\text{MCP*}\cdots I_2) \rightarrow (\text{MCP}\cdots I_2) \text{ or } \text{MCP} + I_2 \quad (9)$$

$$(\text{MCP*}\cdots I_2) \rightarrow \text{4HP} + \text{2HI} \quad (10)$$

where MCP* denotes excited state of MCP. It is highly probable that the excited singlet MCP is reactive. This formulation fits nicely the experimental results.

No intermediate compound corresponding to 4*a*,4*b*-dihydrophenanthrene formulated in *cis*-stilbene cyclization can be postulated in the MCP case, since two benzene rings are not in conjugation. The fact that no long-lived species can be detected by flash photolysis and oxygen has little effect on the reaction suggests the absence of any free-radical intermediate such as the one lacking one hydrogen atom from MCP.

Whether step(10) is such a simple process or consists of multi-step reactions is not known. However, it might be attractive to assume electron transfer processes followed by dehydroiodination:

$$\left.\begin{aligned} &(\text{MCP*}\cdots I_2) \rightarrow (\text{MCP}^+\cdot I_2^-) \\ &(\text{MCP}^+\cdot I_2^-) \rightarrow \text{4HP} + \text{2HP} \end{aligned}\right\} \quad (11)$$

The importance of such electron transfer processes and charge-transfer resonance configuration (CT configuration) might be suggested as follows: a) Photolysis of [2.2]paracyclophane in methanol with

17) N. J. Rose and R. S. Drago, *J. Amer. Chem. Soc.*, **81**, 6138, 6141 (1959).

18) G. Briegleb, "Elektronen-Donator-Acceptor-Komplexe," Springer-Verlag, Berlin-Göttingen-Heidelberg (1961).

19) T. Sato, K. Nishiyama, S. Shimada, and K. Hata, This Bulletin **44**, 2858 (1971).

20) "Kagaku Binran (Handbook of Chemistry)," Chem. Soc. Japan (ed.), Maruzen, Tokyo (1966), p. 1132.

253.7 nm light can best be explained by assuming a CT configuration.[7] b) With [2.2]paracyclophane, the contribution of CT configuration caused by transannular interaction can be seen even with molecules in the neutral ground state. With the anion radical the contribution can be assumed to be about 50%. Energy of the CT configuration was considered to be several eV.[21] c) A similar interaction was observed with MCP and a delocalized configuration helps to form CT-complex. d) On contact with potassium film, MCP is shown to form 4HP anion radical instead of MCP anion radical. Martin and Gerson[22] interpreted the result by assuming initial formation

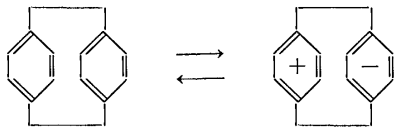

Ground configuration CT configuration
Neutral [2.2]Paracyclophane[21]

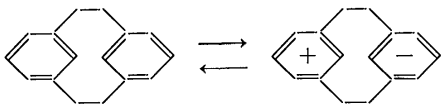

Ground configuration CT configuration
Neutral MCP

of MCP anion radical which undergoes transannular dehydragenation reaction. Kowata, Hoshino, and Koizumi,[23] on the other hand, presented evidence that 4HP is formed first on the surface of the metal, and is then reduced to 4HP anion radical. Regardless of the mode of formation, hydrogen abstraction $C_{8,16}$ occurs very rapidly. The facile oxidation can be explained in terms of the large strain energy, calculated by Boyd *et al.*[24] to be *ca.* 13 kcal/mol. The role of iodine is dual; it helps to increase delocalized configuration and acts as a hydrogen abstractor.

One of the authors (S. H.) wishes to thank Professor Masao Koizumi, Tohoku University, for many helpful discussions and suggestions during this work. Flash photolysis was carried out in the Institute of Physical and Chemical Research. The author (S. H.) is also grateful to Dr. Akira Kira for use of the flash apparatus and valuable discussions.

Appendix

The rate of disappearance of MCP is followed by calculating absorbance change of MCP, D^{272}_{MCP}, at 272 nm. After appropriate time intervals, the observed absorbance at 272 nm, D^{272}, can be expressed as follows.

$$D^{272} = D^{272}_{MCP} + D^{272}_{I} + D^{272}_{4HP}$$

where D^{272}_{I} and D^{272}_{4HP} are the absorbances due to iodine alone, and 4HP at 272 nm, respectively. Thus D^{272}_{MCP} is calculated as follows.

$$D^{272}_{MCP} = D^{272} - \frac{\varepsilon^{272}_{4HP}}{\varepsilon^{292}_{4HP}} D^{292}_{4HP} - \frac{\varepsilon^{272}_{I}}{\varepsilon^{520}_{I}} D^{520}_{I}$$

where D^{292}_{4HP} and D^{520}_{I} are the observed absorbances at 292 nm and 520 nm, respectively. The reaction rate of MCP, k_{MCP} is evaluated from the initial slopes (Fig. 4-c).

21) A Ishitani and S. Nagakura, *Mol. Phys.*, **12**, 1 (1967).
22) W. B. Martin and F. Gerson, *J. Amer. Chem. Soc.*, **91**, 1883 (1969).
23) H. Kowata, M. Hoshino, and M. Koizumi, Abstract, the 24 th Annual Meeting of the Chemical Society of Japan, Osaka (1971).
24) Chyi-fend Shieh, D. Mcnally, and R. H. Boyd, *Tetrahedron*, **25**, 3653 (1969).

Studies of Built-up Films by Means of the Polarized Infrared ATR Spectrum. III. Elaidic Acid Films[1]

Tohru TAKENAKA and Kazuko NOGAMI

Institute for Chemical Research, Kyoto University, Uji, Kyoto

(Received January 31, 1972)

Attenuated total reflection studies with polarized infrared radiation have been made of multilayers of elaidic acid built up on a germanium plate by the Blodgett technique. It is concluded that the built-up films prepared from the tap-water substrate are made of calcium elaidate monohydrate. From the intensity changes in the regularly-spaced peaks (progression bands) in the region from 1350 to 1180 cm^{-1}, the planarity of the chain segment between the carboxylate group and the double bond is found to be dependent upon the surface pressure applied in the process of monolayer transfer onto the germanium plate. Studies of the anisotropy of the absorption index in the films show that the molecules assume a uniaxial orientation with respect to the axis normal to the germanium-sample interface (the *z*-axis), with an angle from 30° to 33° (in average) between the *z*-axis and the molecular axes. Furthermore, from the changes in the reflectivity with the number of layers, the film thickness per layer is estimated to be *ca.* 21.9 Å, a value which is in good agreement with the half-value of the long spacing, 44.16 Å, of the films as determined by X-ray diffraction studies. This apparently indicates that the films appear as the Y type.

In previous papers[2,3] of this series, attenuated total reflection (ATR) studies[4-6] have been made of multilayers of stearic acid and mixed multilayers of stearic acid and barium stearate built up on a germanium plate by the Blodgett technique.[7] It has been found that they are made of microcrystallites in the monoclinic or triclinic form, and that the hydrocarbon chains of stearic acid assume a uniaxial orientation on the axis normal to the germanium-sample interface, whereas the hydrocarbon chains of barium stearate give rise to a specific orientation in the interface with respect to the polishing direction of the germanium plate in its cleaning procedure. The film thickness per layer has been estimated to be 23.8 Å for the stearic acid films and 24.3 Å for the mixed films of stearic aicd and barium stearate; both values are in good agreement with the value previously reported.[7,8]

Since elaidic acid has the double bond in the *trans* form at the center of the C_{18} hydrocarbon chain, it is worth studying the multilayers of elaidic acid by the same method and discussing the effect of the double bond on the structure of the films as well as on their molecular orientation. Thus, in the present work, the polarized infrared ATR method was extended to studies of the multilayers of elaidic acid built up on the germanium plate by the Blodgett technique.[7] Unfortunately, attempts to compare the results of this study with those of oleic acid, which is the *cis* isomer, were unsuccessful, for the transfer of the oleic acid monolayer onto the germanium plate was incomplete and reproducible results could not be obtained, although Alexander[9] has prepared "excellent" multilayers of oleic acid (much less readily than the *trans* form) from the Cambridge tap-water substrate.

Theoretical

A full discussion of the theory used in this study has been given in the previous paper,[2] and so it will not be repeated here.

Experimental

The elaidic acid was a material of the highest purity (99%); it was purchased from the Sigma Chemical Co., and was used without further purification. It melted at 44.0°C, the melting point being in good agreement with the value in the literature.[10]

The multilayers of elaidic acid were formed by transferring the monolayer spread on a substrate (from a 0.04% solution in benzene) onto a germanium trapezoidal ATR plate, 50 mm long, 18 mm high, and 2 mm thick, by the Blodgett technique.[7] As Alexander[9] has pointed out, the best substrate was found to be ordinary tap water, filtered before use. Its pH was *ca.* 7.7, and it contained approximately 5×10^{-5} mol of calcium bicarbonate per liter of water. A synthetic substrate of the same pH and calcium concentration was comparatively poor for multilayer building, but the reason for this marked difference has not been investigated. The plate was slowly dipped in the water and then withdrawn, with its large faces (50 mm long × 18 mm high) vertical through the monolayer, at the fixed rate of 5 mm/min maintained with the use of a motor and reduction gear. Rapeseed oil (spreading pressure: 10.5 dyn/cm) or triolein (15 dyn/cm) was employed as the piston oil, with reference to the surface pressure-area isotherm of the elaidic acid monolayer reported by Marsden and Rideal.[10]

The germanium plate was cleaned by the same procedure as that reported in the previous paper.[2] The main step was the repolishing of the plate on a plane ground pitch plate covered with a silk cloth by the use of a polishing material (Linde) and a detergent solution. The plate was then thoroughly rinsed with water. This was followed by ultrasonic cleaning in alcohol and in chloroform.

1) Presented at the 24th Symposium of Colloid and Surface Chemistry, Gifu, October, 1971.

2) T. Takenaka, K. Nogami, H. Gotoh, and R. Gotoh, *J. Colloid Interfac. Sci.*, **35**, 395 (1971).

3) T. Takenaka, K. Nogami, and H. Gotoh, *ibid.*, **39**, (1972) in press.

4) N. J. Harrick, *J. Phys. Chem.*, **64**, 1110 (1960).

5) J. Fahrenfort, *Spectrochim. Acta*, **17**, 698 (1961).

6) N. J. Harrick, "Internal Reflection Spectroscopy," Interscience publishers, New York (1967).

7) K. B. Blodgett, *J. Amer. Chem. Soc.*, **57**, 1007 (1935).

8) A. Müller, *Proc. Roy. Soc., Ser. A*, **114**, 542 (1927).

9) A. E. Alexander, *J. Chem. Soc.*, **1939**, 777.

10) J. Marsden and E. K. Rideal, *ibid.*, **1938**, 1163.

The polarized infrared ATR spectra of the multilayers were recorded by a Perkin-Elmer model 521 grating spectrophotometer equipped with a multiple ATR attachment as well as a wire grid polarizer.[2] The ATR attachment has been designed so that the radiation can be reflected between the germanium-plate faces 25 times at the average angle of incidence of 45°. The semiangle of the radiation cone incident upon the ATR plate is *ca.* 3°. The error due to this beam convergence was estimated to be relatively small and was ignored in this study. The X-ray diffraction patterns of the multilayers were obtained with the aid of a Rigaku Denki X-ray diffractometer through the reflection method using the copper-K_α line.

All the experiments were carried out in a room of a constant temperature (20±0.2°C) and a constant humidity (45±2%).

Results and Discussion

The Polarized ATR and Transmission Spectra. In Fig.1 the infrared absorption specturm of elaidic acid obtained by the KBr pellet technique is reproduced for reference. Figures 2A and 2B represent the polarized ATR spectra of the 3-layer and 31-layer films, respectively, of elaidic acid prepared by the use of rapeseed oil as the piston oil. The solid line refers to the orientation of the electric vector parallel to the plane of incidence ($R_\parallel$), while the broken line refers to the electric vector perpendicular to it ($R_\perp$). Unfortunately, the latter line could not be recorded in the region lower than *ca.* 850 cm^{-1}, since the intensity of this particular polarized radiation was largely reduced in this region by various causes, such as the polarization characteristics of the grating in the monochromator and the absorption by the germanium plate. The transmission spectrum of the 31-layer films is also given (by the dotted line) in Fig. 2B. Apparently, the peaks are much stronger in the ATR spectra than in the transmission specturm.

It should be noticed that the C=O stretching band observed at 1710 cm^{-1} in the specturm of elaidic acid itself (Fig. 1) disappears in Fig. 2A and 2B, and that a pair of new peaks appears at 1550 and 1522 cm^{-1} in the spectra of the 3-layer film (Fig. 2A). With an increase in the number of layers, another pair of peaks appears at 1573 and 1537 cm^{-1}; these peaks are enhanced, while the intensities of the 1550 and 1522 cm^{-1} peaks are kept unchanged (Fig. 2B). Since the pair of bands at 1572 and 1536 cm^{-1} observed in the spectra of calcium salts (monohydrates) of long-chain fatty acids has been assigned to the antisymmetrical stretching vibration of the carboxlyate group,[11-13] the pair of peaks at 1573 and 1537 cm^{-1} observed in this

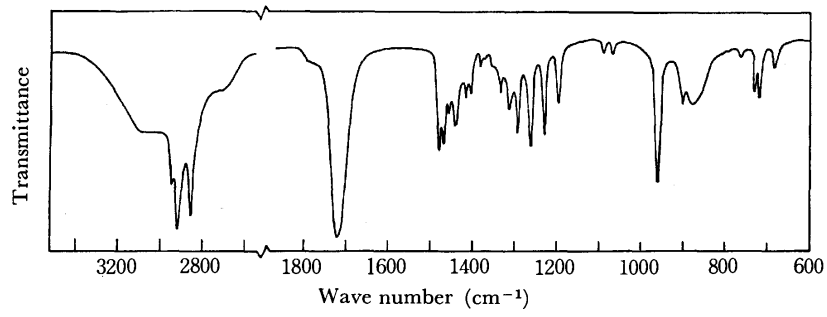

Fig. 1. Infrared absorption spectrum of elaidic acid obtained by the KBr pellet technique.

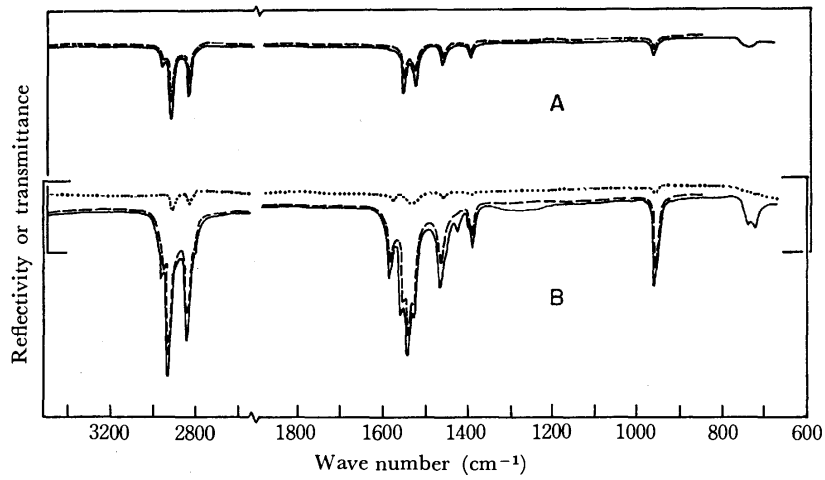

Fig. 2. Polarized infrared ATR and transmission spectra of the 3-layer (A) and 31-layer films (B) of elaidic acid (piston oil; rapeseed oil):
——: $R_\parallel$ } ATR spectra, -----: transmission spectrum.
——: $R_\perp$ }

11) B. Ellis and H. Pyszora, *Nature*, **181**, 181 (1958).
12) M. Kawano, *Nippon Kagaku Zasshi*, **81**, 1805 (1960).
13) Y. Koga and R. Matuura, *Memo. Fac. Sci., Kyushu Univ., Ser. C.* **4**, 1 (1961).

study (Fig. 2B) can confidently be attributed to the same vibration of calcium elaidate monohydrate. In other words, the multilayers of elaidic acid are prepared in the form of calcium salt (monohydrate) from the tap-water substrate. The disappearance of the peaks of elaidic acid itself at *ca.* 3100 cm^{-1} (the OH stretching vibration) and at 870 cm^{-1} (the OH out-of-plane deformation vibration) in Fig. 2B can also be interpreted in the same way. The first pair, at 1550 and 1522 cm^{-1}, observed in the spectra of the very thin-layer films (Fig. 2A) may be ascribed to calcium salts interacting with the germanium surface. Corresponding to the pair of peaks assigned to the antisymmetrical stretching vibration of the carboxlate group, the two peaks at 1432 and 1398 cm^{-1} can be attributed to the symmetrical strecthing vibration of the same group in calcium elaidate monohydrate.

Another marked difference in the spectra between the elaidic acid crystal and films is seen in the region from 1350 to 1180 cm^{-1}. In the spectrum of the elaidic acid crystal (Fig.1), regularly-spaced peaks of a medium intensity are found in this region, but only traces are observed in the spectra of the elaidic acid films (Fig. 2B). This is different from the cases of the multilayers of stearic acid[2] and of barium stearate,[3] for which the progression bands have been observed in the ATR spectra as in the spectra of their crystals. According to Susi,[14] the bond progression of the elaidic acid crystal is to be ascribed to the coupled wagging and/or twisting vibrations of the methylene groups in the chain segment between the carboxyl group and the double bond,[15] and it appears only when the segment is in the planar *trans*-zigzag configuration. The above-mentioned finding, therefore, suggests that the first chain segment of elaidic acid is scarcely in the planar configuration in the films prepared with rapeseed oil (spreading pressure: 10.5 dyn/cm).

When, however, the multilayers of elaidic acid are formed with triolein (spreading pressure: 15 dyn/cm), the weak progression bands appear as shown in Fig. 3. The positions of the bands are identical with those of the progression bands in the crystal spectrum (Fig. 1). The high parallel polarization of the progression bands can be interpreted in terms of an orientation of the planar chain segment toward the *z*-axis (Fig. 4), because the transition moments of the wagging and/or twisting modes of the methylene groups lie along the chain axes.[2,3] The other parts of the spectra are the same as those in Fig. 2B. It is apparent from these facts that the planarity of the chain segment is largely dependent upon the surface pressure applied in the process of monolayer transfer onto the germainum plate. The presumption that the multilayers prepared at higher surface pressures will give rise to stronger progression bands could not be ascertained, because of the collapse of the monolayer at such a surface pressure. The poor planarity of the chain segment of elaidic acid in the films may arise from the expanded structure of its monolayer which is seen in the surface pressure–area isotherm.[10]

The intense peak at 963 cm^{-1} is assigned to the CH out-of-plane deformation vibration of the *trans*-vinylene group, and the peak at *ca.* 720 cm^{-1}, to the rocking vibration of the methylene groups.[16] The other major peaks will be dicussed below.

The Molecular Orientation. The orientation of the elaidic acid molecules in the films was discussed by calculating three components of their absorption indices[5,17] (κ_x, κ_y, and κ_z) from Eqs. [5] and [8] in Ref. 2. Three axes, *x*, *y*, and *z*, of the germanium plate are shown in Fig. 4. The plane of incidence is the *yz*-plane. The dipping direction of the plate during the course of the film transfer and the polishing direction of the plate in its cleaning procedure are parallel to the *x*- and *y*-axes, respectively. The reflectivities ($R_\parallel$ and $R_\perp$) were obtained from the polarized ATR spectra. Some typical results are shown in Fig. 2 for the 3-layer and 31-layer films. The coefficients, *A*, *B*, and *C*, of Eq. [5] in the previous paper[2] were evaluated from Eq. [6] as $A=18.0$, $B=15.2$, and $C=20.7$ using the above-mentioned number of reflections ($q=25$) and the angle of incidence ($\theta_1=45°$), on the assumption that the refractive indices of the germanium plate (n_1) and the elaidic acid films (n_2) were 4.00 and 1.46,[18] respectively, at room temperature.

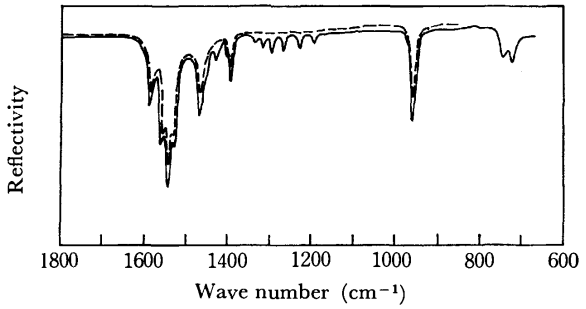

Fig. 3. Polarized infrared ATR spectra of the 31-layer film of elaidic acid (piston oil; triolein):
——: $R_\parallel$, ——: $R_\perp$.

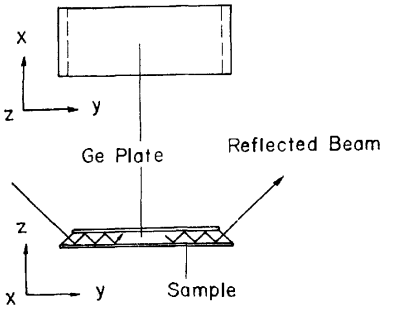

Fig. 4. Three axes of the germanium ATR plate.

14) H. Susi, *Anal. Chem.*, **31**, 910 (1959).

15) The terminal chain segment (from the double bond to the methyl group) does not give rise to regularly spaced, medium intensity bands, and may cause some weak, irregular bands occuring among the main progression bands.[14]

16) L. J. Bellamy, "The Infrared Spectra of Complex Molecules," Methuen, London (1958).

17) P. A. Flournoy and W. J. Schaffers, *Spectrochim. Acta*, **22**, 5, 15 (1966).

18) "Yushi Kagaku Binran," ed. by Nippon Yukagaku Kyokai Maruzen, Tokyo (1958), Chap. 3.

Table 1. Molecular orientation in the elaidic acid films

	Wave number (cm^{-1})	$\kappa_x(=\kappa_y)$	κ_z	D_{xz}	F	α
31 layers	2920	0.071	0.022	3.26	−0.301	31°
	2850	0.044	0.012	3.83	−0.327	29°
163 layers	2920	0.123	0.041	3.01	−0.286	32°
	2850	0.080	0.028	2.89	−0.279	33°

The polarized transmission measurements were also carried out for the thicker films with more than 31 layers, because they are sufficient for the detection of the absorption bands in the 2900-cm^{-1} region. For all the films examined, no difference was found between the transmission spectra obtained by the use of polarized radiations with the electric vectors parallel to the x- and y-axes, as in the case of the stearic acid films.[2] This apparently indicates that $\kappa_x=\kappa_y$, suggesting that the molecules in the films give rise to a random orientation on the z-axis, in other words, to a uniaxial orientation with respect to the z-axis, irrespective either of the dipping direction or of the polishing direction during the film preparation. From these discussions, we obtain, for example, the values of $\kappa_x(=\kappa_y)$ and κ_z shown in Table 1 for the peaks at 2920 and 2850 cm^{-1} (the antisymmetrical and symmetrical stretching vibrations of the methylene groups, respectively) of the 31-layer and 163-layer films.

In the case of the uniaxial orientation, the orientation of the molecules is evaluated by the orientation function, F,[19] calculated from:

$$F = \frac{1-D_{xz}}{1+2D_{xz}} \tag{1}$$

with:

$$D_{xz} = \kappa_x/\kappa_z. \tag{2}$$

Here, F defines the degree of the orientation of the transition moments with respect to the z-axis, as has been described in the previous paper.[2] The values of D_{xz} and F are given in Table 1 for 31-layer and 163-layer films. As a model of uniaxial orientation, if we assume that the molecular axis is uniformly oriented with an angle of α around the z-axis and that, further, the transition moment of the peak is uniformly oriented with an angle of β around the molecular axis, F can be expressed by the following equation:[13]

$$F = \frac{1}{2}(3\overline{\cos^2\alpha}-1)\cdot\frac{1}{2}(3\cos^2\beta-1), \tag{3}$$

where $\overline{\cos^2\alpha}$ denotes the average value of $\cos^2\alpha$. Since it is well known that the antisymmetrical and symmetrical stretching modes of the methylene guoups do not mix with the other modes, and that both their transition moments are perpendicular to the molecular axis ($\beta=90°$), while they are normal to each other, the values of α can be obtained for the 31-layer and 163-layer films as is shown in the last column of Table 1. The results are in agreement with the corresponding values of stearic acid,[2] suggesting that the inclination of the molecular axes in the elaidic acid films is nearly the same, on the average, as that in the stearic acid films.[2] In other words, the effect of the double bond in the *trans* form on the molecular orientation can virtually be ignored.

Film Thickness per Layer. In Fig.5, the reflectivity, $R_\perp$, is plotted against the number of layers, m, for five major peaks at 2920, 2850, 1537, 1465, and 1398 cm^{-1}. In the process of calculating the reflectivity, the effect of the absorption of radiation by the sample films on both sides of the germanium trapezoidal plate upon the polarized ATR spectra was corrected by the method described in the previous paper.[2] For each peak, $R_\perp$ decreases first with the increase of m and attains a constant value at a certain number of layers, m_c (indicated by an arrow in Fig. 5), which is characteristic of the peak. The larger $R_\perp$ values for the 1537 cm^{-1} peak at the small m values are interpreted as resulting from the peak shift in the very thin films as a result of the interaction between the carboxylate group and the germanium surface described previously.

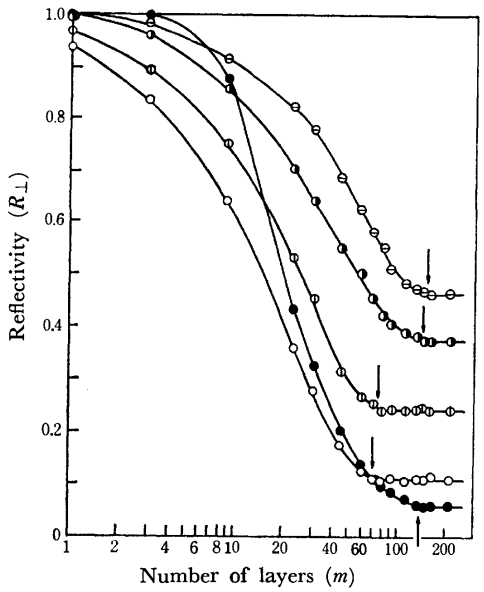

Fig. 5. Reflectivity $R_\perp$ as a function of the number of layers m:
—○—: 2920 cm^{-1}, —◑—: 2850 cm^{-1}, —●—: 1537 cm^{-1},
—◑—: 1465 cm^{-1}, —⊖—: 1398 cm^{-1}.

Since, from the discussions in the previous paper,[2] m_c is thought to be the number of layers which gives the penetration depth,[4] d, of the radiation (into the sample films) expressed by Eq. [1] of the previous paper,[2] we can obtain the film thickness per layer, d_0, by dividing d by m_c. The results are summarized

19) R. Zbinden, "Infrared Spectroscopy of High Polymers," Academic Press, New York (1964), Chap. V.

Table 2. Film thickness per layer of the elaidic acid films

Wave number (cm^{-1})	Assignment	d (Å)	m_c	d_0 (Å)
2920	CH_2 antisym. stretching	1560	70	22.3
2850	CH_2 sym. stretching	1600	75	21.3
1537	COO^- antisym. stretching	2960	135	21.9
1465	CH_2 scissoring	3110	140	22.2
1398	COO^- sym. stretching	3260	150	21.7
			Mean	21.9 Å

in Table 2 for all the peaks examined, together with their assignments.

The X-ray diffraction pattern of the 163-layer films is shown in Fig.6. An analysis of the main peaks in Fig.6 gives the value of 44.16 Å as the long spacing of the films. The fact that half of this value, 22.08 Å, is in good agreement with the mean value of d_0, 21.9 Å, suggests that the elaidic acid films appear as the Y type,[7] as Alexander[9] has pointed out.

In the case of stearic acid, the long spacing of the film has been found to be equal to that of the crystal.[3] In the case of elaidic acid, however, the above-mentioned value of the long spacing of the film is apparently shorter than that of the crystal, 48.9 Å.[20] This may correspond to the finding that the chain segment of elaidic acid is not in a clear planar configuration in the films.

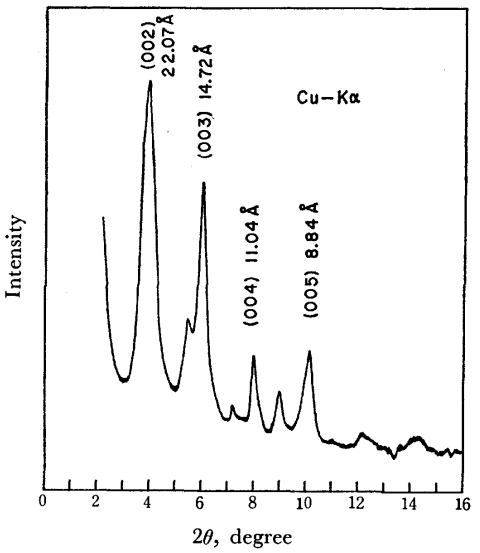

Fig. 6. X-Ray diffraction pattern of the 163-layer film of elaidic acid.

The authors wish to express their thanks to Dr. Rempei Gotoh, Professor Emeritus of Kyoto University, for his encouragement and guidance. Thanks are also due to Dr. Masayuki Tabushi [21] of this Institute for his analysis of the tap water used.

20) J. H. Benedict and B. F. Daubert, *J. Amer. Chem. Soc.*, **71**, 4113 (1949).

21) Present address: Tohoku Women's University, Hirosaki, Aomori.

BULLETIN OF THE CHEMICAL SOCIETY OF JAPAN, VOL. 45, 2371—2383 (1972)

Vibrational Spectra of Propionamide and Its C- and N-Deuterated Compounds

Yoshihiro KURODA, Yutaka SAITO, Katsunosuke MACHIDA, and Toyozo UNO

Faculty of Pharmaceutical Sciences, Kyoto University, Sakyo-ku, Kyoto

(Received February 3, 1972)

The infrared and Raman spectra of $CH_3CH_2CONH_2$, $CH_3CD_2CONH_2$ and their *N*-deuterated compounds in the solid state have been measured. The normal coordinate analysis has been made by assuming the molecular symmetry of C_s. A Urey-Bradley force field was used for the in-plane vibrations and a valence force field for the out-of-plane vibrations of the amide group. The ethyl group was treated by a Urey-Bradley type force field as well as a valence type force field. The assignments of the fundamental frequencies have been made by referring to the infrared and Raman intensities, isotopic frequency shift and the calculated frequencies by using the force constants which were taken from *n*-paraffins and acetamide. The agreement between the observed and the calculated frequencies in the initial calculation was good for the CH_3 and the amide group vibrations but was not good enough for some vibrations involving the α-carbon atom. Only the force constants related to these vibrations were refined by the least squares method in order to obtain the best fit. The calculated frequencies in this way fit to the observed satisfactorily.

Recently, we reported the infrared spectra of *n*-fatty acid amides, $CH_3(CH_2)_nCONH_2$ (n=1—16), and discussed the effect of the end amide group on the band progression frequencies arising from vibrations of the alkyl chain.[1] By assuming the invariance of the force field of the chain part, the shifts of band progressions on going from *n*-paraffins to amides were elucidated satisfactorily to arise from the change in the fashion of the vibrational coupling between the alkyl chain and the end groups. The force constants related to the α-methylene group are expected, however, to differ more or less from those of the *n*-paraffins, reflecting the change in the electronic structure induced by the polar end group. The present work has been undertaken to see if such difference in the force con-

1) K. Machida, S. Kojima and T. Uno, *Spectrochim. Acta*, **28**, 235 (1972).

stants between amides and *n*-paraffins can be estimated from the vibrational analysis of propionamide.

Besides our previous work,[1] the infrared and Raman spectra of propionamide have been reported by several investigators,[2-6] but there have remained many fundamental frequencies yet unassigned. In order to discuss the vibrational spectra of propionamide more precisely and to examine the transferability of force constants, we synthesized $CH_3CD_2CONH_2$ and $CH_3CD_2COND_2$, and measured the infrared and Raman spectra of these compounds together with those of usual species, $CH_3CH_2CONH_2$ and $CH_3CH_2COND_2$. The infrared spectrum of the 50 per cent *N*-deuterated sample of propionamide was also recorded for comparison. The normal coordinate analysis based on the GF matrix method[7] has been made by using the force constants transferred from acetamide[8-9] and *n*-paraffins.[10] By comparing the observed spectra with the result of the initial calculation, reasonable assignments have been given to all the fundamental frequencies of four isotopic species of propionamide. The agreement between the observed and the initially calculated frequencies was not good enough for some vibrations of the joint part of the ethyl and amide groups, but an appreciable improvement of frequency fits was attained soon by the least squares refinement of the related force constants.

Experimental

Materials. Methylmalonic acid was prepared by the saponification of commercially available diethyl methylmalonate,[11] and was submitted to the exchange reaction with D_2O in a sealed tube twice. After the removal of the excess D_2O, methylmalonic-d_1-acid-d_2 was thermally decomposed at 140—150°C and the product was distilled at the same time.[12] Thus obtained propionic-α,α-d_2 acid-*d* (CH_3CD_2COOD) was purified by distillation under reduced pressure. The deuterium content at the α-position of this acid was estimated to be about 92 per cent by the NMR spectrum. Propionyl-α,α-d_2 chloride (CH_3CD_2COCl) was prepared from propionic-α,α-d_2 acid-*d* and benzoyl chloride,[13] and was converted into propion-α,α-d_2 amide ($CH_3CD_2CONH_2$) by the reaction with NH_3 gas in ether at about -15°C. Similarly, propionamide ($CH_3CH_2CONH_2$) was synthesized from commercially available propionyl chloride. The amides were purified by the recrystallization from benzene. The NH_2 compounds were converted into the corresponding ND_2 compounds by the exchange reaction with

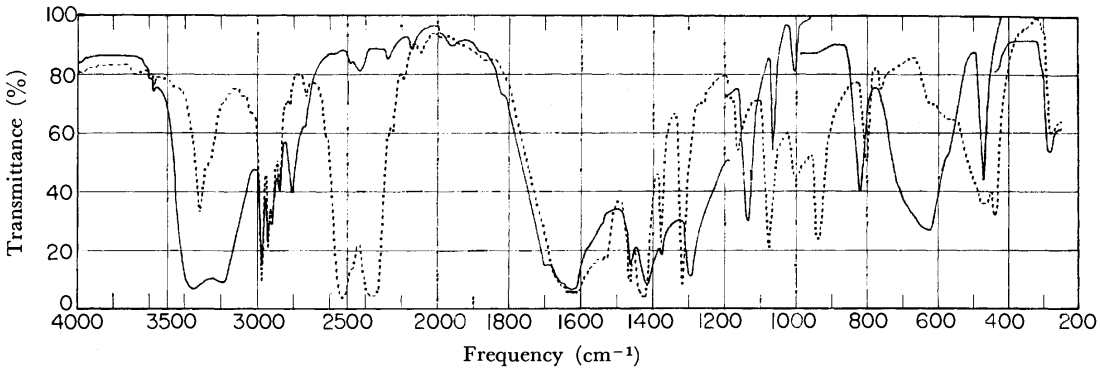

Fig. 1. Infrared spectra of $CH_3CH_2CONH_2$ (——) and $CH_3CH_2COND_2$ (----) in the region between 4000 and 250 cm^{-1}.

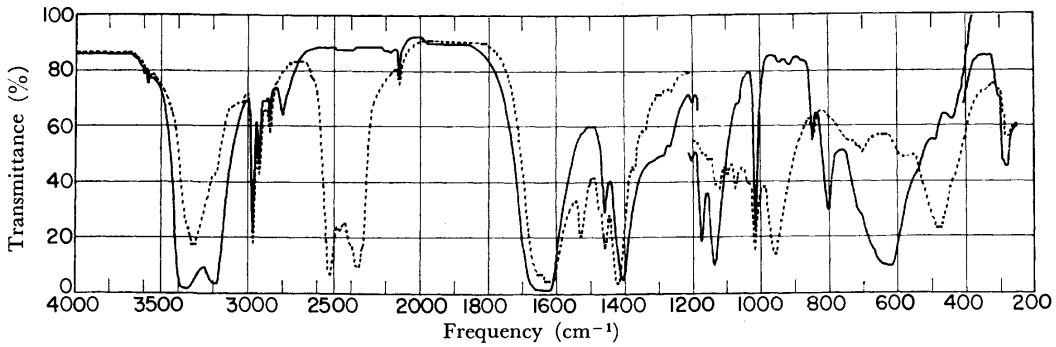

Fig. 2. Infrared spectra of $CH_3CD_2CONH_2$ (——) and $CH_3CD_2COND_2$ (----) in the region between 4000 and 250 cm^{-1}.

2) J. E. Katon, W. R. Feairheller, Jr., and J. V. Pustinger, Jr. *Anal. Chem.*, **36**, 2126 (1964).
3) K. W. F. Kohlrausch and A. Pongratz, *Ber. Dtsch. Chem. Ges.*, **67**, 976 (1934).
4) R. Ananthakrishnan, *Proc. Indian Acad. Sci., A*, **5**, 200 (1937).
5) A. W. Reitz and J. Wagner, *Z. Phys. Chem.*, **B43**, 339 (1939).
6) K. Venkata Ramiah, V. Venkata Chalapathi and C. A. I. Chary, *Current Sci.*, (India), **35**, 350 (1966).
7) E. B. Wilson Jr., *J. Chem. Phys.*, **7**, 1047 (1939); **9**, 76 (1941).
8) T. Uno, K. Machida and Y. Saito, This Bulletin, **42**, 897 (1969).
9) T. Uno, K. Machida and Y. Saito, *Spectrochim. Acta.*, **27**, 833 (1971).
10) J. H. Schachtschneider and R. G. Snyder, *ibid.*, **19**, 117 (1963).
11) W. J. Gensler and E. Berman, *J. Amer. Chem. Soc.*, **80**, 4949 (1958).
12) P. Hölemann and K. Clusius, *Ber.*, **70**, 819 (1937).
13) H. C. Brown, *J. Amer. Chem. Soc.*, **60**, 1325 (1938).

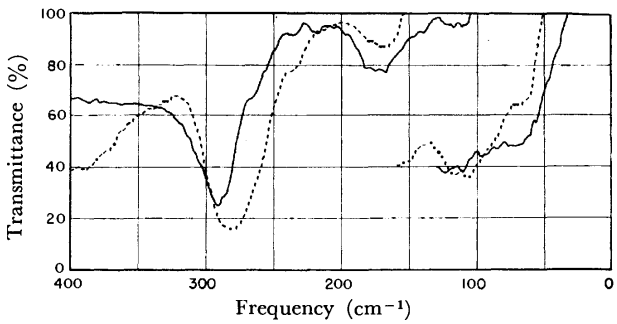

Fig. 3. Infrared spectra of $CH_3CH_2CONH_2$ (——) and $CH_3CH_2COND_2$ (----) in the region between 400 and 33 cm^{-1}.

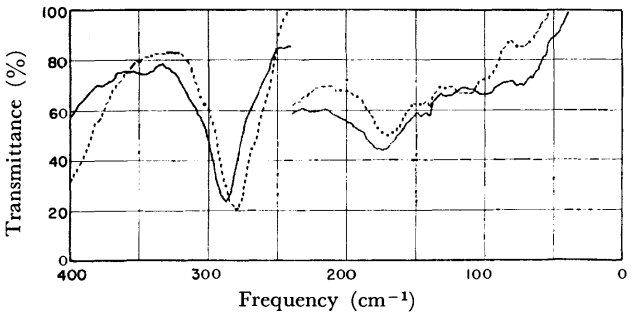

Fig. 4. Infrared spectra of $CH_3CD_2CONH_2$ (——) and $CH_3CD_2COND_2$ (----) in the region between 400 and 33 cm^{-1}.

D_2O. The partially *N*-deuterated samples were prepared by using mixtures of H_2O and D_2O.

Measurement. The infrared spectra were recorded on a Perkin-Elmer Model 521 grating spectrophotometer (4000—250 cm^{-1}, Figs. 1 and 2) and on a Hitachi FIS-3 grating spectrophotometer (400—33 cm^{-1}, Figs. 3 and 4). The samples were measured as mulls with Nujol or hexachlorobutadiene. The wave number was calibrated by the standard absorptions of polystyrene, indene and ammonia. The Raman spectra were measured for the crystalline samples obtained from the melt sealed in a capillary tube on a SPEX RAMALOG laser Raman spectrophotometer (Figs. 5 and 6). The exciting line (4880 Å) was generated by an argon ion laser at an approximate output power of 200 mW. The observed frequencies are listed in Table 1 together with the relative intensities and assignments.

Normal Coordinate Analysis

The molecular symmetry of propionamide adopted in the present calculation is that of the point group C_s with the C_α-C_β bond at the *trans* position of the C–N bond (hereafter, the alkyl carbon atoms are specified by greek subscripts if necessary). Although the structure determination by the X-ray analysis has not yet been made for propionamide, the assumption of the C_s structure may be justified from the crystallographic data for a number of long chain *n*-fatty acid amides.[14-17] It has been shown that the cell di-

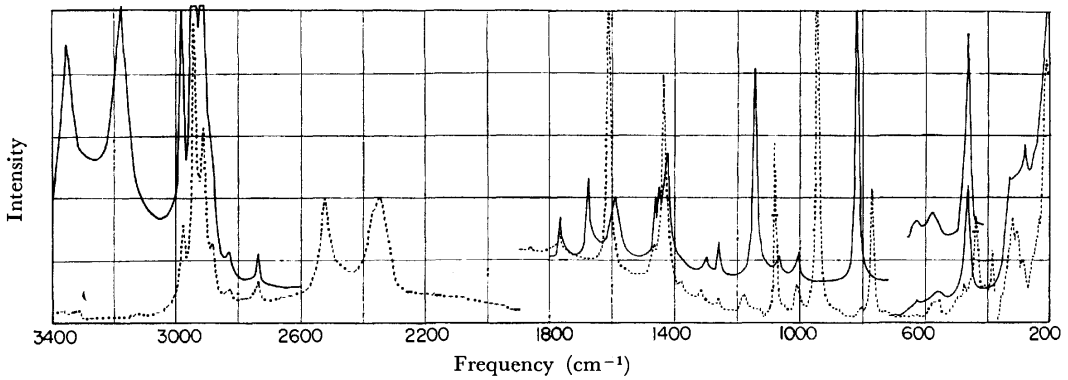

Fig. 5. Raman spectra of $CH_3CH_2CONH_2$ (——) and $CH_3CH_2COND_2$ (----) in the region between 3400 and 200 cm^{-1}.

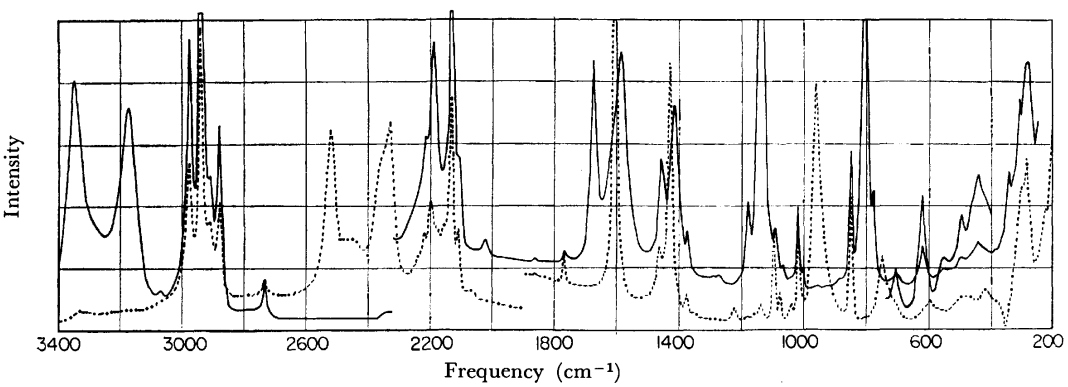

Fig. 6. Raman spectra of $CH_3CD_2CONH_2$ (——) and $CH_3CD_2COND_2$ (----) in the region between 3400 and 200 cm^{-1}.

14) J. D. Turner and E. C. Lingafelter, *Acta Crystallogr.*, **8**, 551 (1955).
15) J. R. Brathovde and E. C. Lingafelter, *ibid.*, **11**, 729 (1958).
16) S. Kurokawa, This Bulletin, **28**, 660 (1955).
17) J. D. Turner and E. C. Lingafelter, *Acta Crystallogr.*, **8**, 549 (1955).

TABLE 1. INFRARED AND RAMAN FREQUENCIES OF $CH_3CH_2CONH_2$, $CH_3CH_2COND_2$, $CH_3CD_2CONH_2$, AND $CH_3CD_2COND_2$ IN cm^{-1}

$CH_3CH_2CONH_2$		$CH_3CH_2COND_2$		$CH_3CD_2CONH_2$		$CH_3CD_2COND_2$	
Infrared	Raman	Infrared	Raman	Infrared	Raman	Infrared	Raman
3350 vs	3350 vs			3350 vs	3350 vs		
3190 vs	3175 vs			3190 vs	3172 vs		
2980 m	2978 vs	2980 m	2978 m	2970 m	2978 vs	2970 m	2974 s
2940 w	2942 vs	2940 w	2942 vs	2935 w	2940 vs	2935 w	2940 vs
2920 sh	2912 vs	2920 vw	2912 vs				
2880 w		2880 w	2884 w	2870 w	2880 s	2870 w	2877 s
2820 sh	2825 vw	2820 vw	2825 vw				
2805 m				2795 w			
2740 sh	2733 w	2730 w	2733 vw		2733 w		2733 w
2435 w		2530 vs	2525 s			2520 vs	2525 vs
		2370 vs	2350 s			2360 vs	2335 vs
2280 vw		2250 vw					
		2190 vw		2180 vw	2190 vs	2180 vw	2190 vs
2150 w		2100 vw		2120 w	2130 vs	2120 w	2130 vs
1960 w					2023 w		2110 sh
	1762 w		1762 w		1765 vw		1765 w
1665 vs	1674 s			1665 vs	1674 vs		
1625 vs	1590 s	1630 vs	1610 vs	1625 vs	1585 vs	1630 vs	1605 vs
1465 m	1460 sh	1466 m	1462 sh	1462 w	1457 s	1462 w	1460 sh
	1450 sh						
1418 vs	1422 s	1425 vs	1435 vs	1409 vs	1416 vs	1425 vs	1428 vs
1382 vw		1382 m	1380 vw	1378 sh	1372 w	1377 vw	1376 w
1296 vs	1300 vw	1318 vs	1327 vw				
	1260 w		1260 vw				
		1165 m	1180 w	1174 m	1179 m		1224 w
1142 s	1148 vs			1136 s	1143 vs	1152 sh	1138 vw
						1120 w	
1068 m	1070 w	1078 s	1078 vs	1093 sh	1095 w	1096 vw	1095 m
				1070 sh	1073 sh	1070 w	1073 w
1004 w	1009 w	1006 w	1009 m			1036 sh	1040 vw
				1016 s	1020 m	1014 s	1018 m
		942 s	945 vs	948 w	1000 sh	956 s	960 vs
				918 w			
				850 w	850 s	845 vw	850 s
821 m	820 vs	808 m	806 vw	803 m	807 vs		
		765 w	769 s		780 sh	740 sh	750 m
				710 sh	703 vw	700 vw	
680 sh				670 sh			
640 vs	630 vw	625 sh		625 vs	618 m	575 sh	600 w
570 sh	570 vw	580 sh	570 vw	550 sh	550 vw	525 sh	
		475 m	470 vw	495 vw	492 vw	470 s	480 w
472 m	470 s	443 m	438 m	442 vw	440 w	420 sh	420 w
			380 w		342 sh		
	320 m		318 m		310 sh		
			308 m				
292 m	285 w	281 m	282 vw	288 m	280 s	280 w	280 s
175 w		170 w		175 w		170 w	
120 vw		117 vw					
110 vw		107 vw					
70 vw		70 vw		70 vw		70 vw	

mension c_0 increases but a_0 and b_0 remain almost constant on going from $CH_3CH_2CONH_2$ to $CH_3(CH_2)_{14}CONH_2$, and that the N, C, C_α and C_β atoms of $CH_3(CH_2)_nCONH_2$ (n=8 and 12) are nearly coplanar.

The structure parameters used in the calculation are shown in Table 2, where the bond lengths and angles concerned with hydrogen atoms are assumed values. The other parameters were taken from the results of X-ray analysis of related molecules.[18-19] In the C_s

Table 2. Structure parameters used for the calculation

Bond length in Å		Bond angles	
r(C=O)	1.260[a]	ϕ(CCN)	117°12'[a]
r(C-N)	1.334[a]	ϕ(CCO)	119°36'[a]
r(C-C=O)	1.527[b]	ϕ(NCO)	123°12'[a]
r(C-CH_2)	1.546[b]	ϕ(CCH)	109°28'
r(C-H)	1.08	ϕ(HCH)	109°28'
r(N-H)	1.02	ϕ(CNH)	120°
		ϕ(HNH)	120°
		ϕ(CCC)	109°28'

a) Taken from Ref. 18.
b) Taken from Ref. 19.

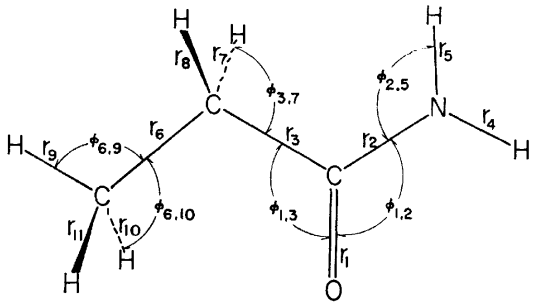

Fig. 7. Molecular structure and internal coordinates.

Table 3. Symmetry coordinates for propionamide

Symmetry coordinates[a]	Description of modes (Abbr.)
(a) In-plane vibrations (a')	
$S_1 = \Delta r_1$	C=O str. (νC=O)
$S_2 = (2\Delta\phi_{4,5} - \Delta\phi_{2,4} - \Delta\phi_{2,5})/\sqrt{6}$	NH_2 bend. (βNH_2)
$S_3 = (\Delta\phi_{2,4} - \Delta\phi_{2,5})/\sqrt{2}$	NH_2 rock. (ρNH_2)
$S_4 = \Delta r_2$	CN str. (νCN)
$S_5 = (\Delta\phi_{1,3} - \Delta\phi_{1,2})/\sqrt{2}$	C=O def. (δC=O)
$S_6 = (2\Delta\phi_{2,3} - \Delta\phi_{1,3} - \Delta\phi_{1,2})/\sqrt{6}$	CCN def. (δCCN)
$S_7 = (\Delta r_4 - \Delta r_5)/\sqrt{2}$	NH_2 asym. str. ($\nu_{as}NH_2$)
$S_8 = (\Delta r_4 + \Delta r_5)/\sqrt{2}$	NH_2 sym. str. (ν_sNH_2)
$S_9 = \Delta r_3$	C-C=O str. (νCC_α)
$S_{10} = \Delta r_6$	C-C str. ($\nu C_\alpha C_\beta$)
$S_{11} = (2\Delta\phi_{10,11} - \Delta\phi_{9,10} - \Delta\phi_{9,11})/\sqrt{6}$	CH_3 asym. def. ($\delta_{as}CH_3$)
$S_{12} = (\Delta\phi_{9,10} + \Delta\phi_{9,11} + \Delta\phi_{10,11} - \Delta\phi_{6,9} - \Delta\phi_{6,10} - \Delta\phi_{6,11})/\sqrt{6}$	CH_3 sym. def. (δ_sCH_3)
$S_{13} = (2\Delta\phi_{6,9} - \Delta\phi_{6,10} - \Delta\phi_{6,11})/\sqrt{6}$	CH_3 rock. (ρCH_3)
$S_{14} = (\Delta\phi_{3,7} + \Delta\phi_{3,8} - \Delta\phi_{6,7} - \Delta\phi_{6,8})/2$	CH_2 wag. (ωCH_2)
$S_{15} = (4\Delta\phi_{7,8} - \Delta\phi_{3,7} - \Delta\phi_{3,8} - \Delta\phi_{6,7} - \Delta\phi_{6,8})/\sqrt{20}$	CH_2 bend. (βCH_2)
$S_{16} = (5\Delta\phi_{3,6} - \Delta\phi_{3,7} - \Delta\phi_{3,8} - \Delta\phi_{6,7} - \Delta\phi_{6,8} - \Delta\phi_{7,8})/\sqrt{30}$	CCC def. (δCCC)
$S_{17} = (2\Delta r_9 - \Delta r_{10} - \Delta r_{11})/\sqrt{6}$	CH_3 asym. str. ($\nu_{as}CH_3$)
$S_{18} = (\Delta r_9 + \Delta r_{10} + \Delta r_{11})/\sqrt{3}$	CH_3 sym. str. (ν_sCH_3)
$S_{19} = (\Delta r_7 + \Delta r_8)/\sqrt{2}$	CH_2 sym. str. (ν_sCH_2)
(b) Out-of-plane vibration (a'')	
$S_{20} = (\Delta\phi_{6,10} - \Delta\phi_{6,11})/\sqrt{2}$	CH_3 rock. (ρCH_3)
$S_{21} = (\Delta\phi_{9,10} - \Delta\phi_{9,11})/\sqrt{2}$	CH_3 asym. def. ($\delta_{as}CH_3$)
$S_{22} = (\Delta\phi_{3,8} - \Delta\phi_{3,7} - \Delta\phi_{6,7} - \Delta\phi_{6,8})/2$	CH_2 rock. (ρCH_2)
$S_{23} = (\Delta\phi_{3,8} - \Delta\phi_{3,7} + \Delta\phi_{6,7} - \Delta\phi_{6,8})/2$	CH_2 twist. ($t CH_2$)
$S_{24} = (\Delta r_{10} - \Delta r_{11})/\sqrt{2}$	CH_3 asym. str. ($\nu_{as}CH_3$)
$S_{25} = (\Delta r_7 - \Delta r_8)/\sqrt{2}$	CH_2 asym. str. ($\nu_{as}CH_2$)
$S_{26} = (\Delta\tau_{3,6,9} + \Delta\tau_{3,6,10} + \Delta\tau_{3,6,11} + \Delta\tau_{7,6,9} + \Delta\tau_{7,6,10} + \Delta\tau_{7,6,11} + \Delta\tau_{8,6,9} + \Delta\tau_{8,6,10} + \Delta\tau_{8,6,11})/3$	CH_3 torsion (τCH_3)
$S_{27} = (\Delta\tau_{1,2,4} + \Delta\tau_{1,2,5} + \Delta\tau_{3,2,4} + \Delta\tau_{3,2,5})/2$	NH_2 torsion (τNH_2)
$S_{28} = (\Delta\tau_{1,2,4} + \Delta\tau_{1,2,5} - \Delta\tau_{3,2,4} - \Delta\tau_{3,2,5})/2$	C=O def. (πC=O)
$S_{29} = (-\Delta\tau_{1,2,4} + \Delta\tau_{1,2,5} - \Delta\tau_{3,2,4} + \Delta\tau_{3,2,5})/2$	NH_2 wag. (ωNH_2)
$S_{30} = (\Delta\tau_{1,3,7} + \Delta\tau_{1,3,8} + \Delta\tau_{1,3,6} + \Delta\tau_{2,3,7} + \Delta\tau_{2,3,8} + \Delta\tau_{2,3,6})/\sqrt{6}$	C-C=O torsion (τCC_α)

a) $\phi_{i,j}$ means the angle formed by the bonds r_i and r_j.
$\tau_{i,j,k}$ means the dihedral angle formed by the planes $r_i - r_j$ and $r_j - r_k$.

18) W. C. Hamilton, *ibid.*, **18**, 866 (1965).
19) T. Uechi, T. Watanabé, and K. Osaki, *Sci. Rep. (Osaka Univ.)*, **15**, 1 (1966).

TABLE 4. FORCE CONSTANTS

(a) Calculation A[a)]

No.	Force constant		No.	Force constant		No.	Force constant	
1	K(NH)	5.728	17	$f_{30,30}$	0.0069	33	$F(CC_\alpha C_\beta)$	0.324
2	H(HNH)	0.375	18	$f_{27,28}$	−0.0160	34	$F(CC_\alpha H)$	0.548
3	H(CNH)	0.406	19	$f_{27,29}$	−0.0061	35	$F(HC_\alpha H)$	0.046
4	H(NCO)	0.521	20	$f_{28,29}$	0.0235	36	$F(C_\beta C_\alpha H)$	0.548
5	$H(C_\alpha CN)$	0.625	21	K(CO)	7.233 (7.438)[b)]	37	$F(C_\alpha C_\beta H)$	0.548
6	$H(C_\alpha CO)$	0.247	22	K(CN)	5.580 (5.525)	38	$F(HC_\beta H)$	0.046
7	F(HNH)	0.0	23	$K(CC_\alpha)$	2.700 (3.187)	39	$f_{4,9}$	−0.2475 (0.000)
8	F(CNH)	0.376	24	$K(C_\alpha C_\beta)$	2.229	40	$\kappa(CH_2)$	−0.016 (0.002)
9	F(NCO)	1.228	25	$K(C_\alpha H)$	4.023	41	$\kappa(CH_3)$	−0.014
10	$F(C_\alpha CN)$	0.137	26	$K(C_\beta H)$	4.425	42	$f_{\beta\omega}{}^t$	0.036
11	$F(C_\alpha CO)$	0.563	27	$H(CC_\alpha C_\beta)$	0.492 (0.290)	43	$f_{\beta\omega}{}^g$	−0.004
12	P(NH-NH)	−0.149	28	$H(CC_\alpha H)$	0.217 (0.195)	44	$f_{\beta\gamma}{}^t$	0.087
13	$f_{26,26}$	0.0069	29	$H(HC_\alpha H)$	0.416 (0.438)	45	$f_{\beta\gamma}{}^g$	−0.009
14	$f_{27,27}$	0.1392	30	$H(C_\beta C_\alpha H)$	0.156 (0.195)	46	$f'_{\beta\gamma}{}^t$	−0.022
15	$f_{28,28}$	0.3825	31	$H(C_\alpha C_\beta H)$	0.191	47	$f'_{\beta\gamma}{}^g$	−0.002
16	$f_{29,29}$	0.0898	32	$H(HC_\beta H)$	0.438	48	$f_{2,14}$	−0.0108 (0.000)

(b) Calculation B[c,d)]

No.	Force constant		No.	Force constant		No.	Force constant	
21	K(CO)	7.376 (7.438)[b)]	31	$F'_{R\gamma}$	−0.004	41	H_ω	1.351 (0.901)
22	K(CN)	5.764 (5.525)	32	$F_{R\omega}$	0.351	42	$f_{\beta\omega}{}^t$	0.072
23	K_r	4.704	33	H_α	0.540	43	$f_{\beta\omega}{}^g$	−0.058
24	F_r	0.039	34	H_δ	0.504 (0.550)	44	$f_{\beta\gamma}{}^t$	0.106
25	K_d	4.546	35	H_β	0.637	45	$f_{\beta\gamma}{}^g$	−0.024
26	F_d	0.016	36	F_β	−0.017	46	$f'_{\beta\gamma}{}^t$	−0.002
27	$K_R{}^1(CC_\alpha)$	3.248 (4.329)	37	H_γ	0.643 (0.666)	47	$f'_{\beta\gamma}{}^g$	0.002
28	$K_R{}^1(C_\alpha C_\beta)$	4.329	38	F_γ	−0.008 (−0.016)	48	$f_{4,9}$	−0.2549 (0.000)
29	F_R	0.064	39	F'_γ	0.001 (0.023)	49	$f_{2,14}$	−0.0276 (0.000)
30	$F_{R\beta}$	0.261	40	$F_{\gamma\omega}$	−0.124			

a) Force constants Nos. 1—12 and Nos. 21—39 in units of mdyn/Å.
Force constants Nos. 13—20 and Nos. 40—48 in units of mdyn·Å/(rad)²
b) ( ): initial value
c) The force constants Nos. 1–20 are the same as those in the Calculation A.
d) The force constants of ethyl group were taken from Calculation V in Ref. 10: Stretching constants in units of mdyn/Å. Stretch-bend interaction constants in units of mdyn/rad. Bending constants in units of mdyn·Å/(rad)².

model, the 30 fundamental vibrations of propionamide are classified into 19 in-plane (a′) and 11 out-of-plane (a″) modes. The internal coordinates and the internal symmetry coordinates are shown in Fig. 7 and Table 3, respectively. In order to avoid missassignments due to any inadequacy of force constants, the calculation was carried out in two ways, in which the CH_3-CH_2-group was treated by a modified Urey-Bradley force field (Calculation A) and by a general valence force field (Calculation B). In both Calculations A and B, the amide group was treated by a simple Urey-Bradley force field for the a′ vibrations and a valence force field for the a″ vibrations. In the initial calculations, the force constants of the amide group were transferred from our earlier results for acetamide.[8-9] and those of the ethyl group from Schachtschneider and Snyder's work on *n*-paraffins; see Table 4.[10] Calculations A and B by the transferred force constants gave essentially the same results as each other, reproducing well the observed fundamental frequencies of $CH_3CH_2CONH_2$ and $CH_3CH_2COND_2$ for the vibrations of the CH_3 and the $CONH_2$ ($COND_2$) groups. The initial calculation failed, however, to give satisfactory fits for the C_α–C stretching, the CH_2 bending and the C_β–C_α–C deformation frequencies. By taking account of these results together with the observed infrared and Raman intensities and isotopic frequency shifts, vibrational assignments have been made for the remaining fundamentals of four isotopic species of propionamide.

Vibrational Assignment

There is no question on the assignment of the NH_2 asymmetric and symmetric stretching frequencies (*ca.* 3350 and 3190 cm^{-1}) and their ND_2 counterparts (2530 and 2370 cm^{-1}). They were observed as strong bands in both the infrared and Raman spectra. For the NH_2 and ND_2 symmetric stretching vibrations, we observed an apparent difference by about 20 cm^{-1}

between the infrared and the Raman frequencies. This difference is attributable to the intermolecular interaction by hydrogen bonds in the crystalline state, where the infrared active and the Raman active vibrations may belong to different symmetry species of the factor group. In Figs. 1 and 2, the band at 3310 cm^{-1} and the shoulder at 3200 cm^{-1} are assigned to the NH stretching vibrations of the NHD compounds. In order to distinguish between the bands due to the NHD compounds and those of the ND_2 compounds clearly, the infrared spectra of 50 per cent *N*-deuterated samples were measured and the normal coordinate analysis was also made for the *trans* and the *cis* isomers of CH_3CH_2-CONHD. The observed and the calculated frequencies, the relative intensities and the assignments are summarized in Table 5. The assignments of the CH_3 and CH_2 stretching vibrations are easily made by comparing the infrared and Raman spectra of the CH_2 compounds with those of the CD_2 compounds. Following Nolin and Jones,[20] the strong Raman band at 2940 cm^{-1} observed for each isotope of propionamide may be assigned to the first overtone of the CH_3 asymmetric deformation vibration at about 1460 cm^{-1}, enhanced by the resonance with the CH_3 symmetric stretching vibration. The CD_2 asymmetric and symmetric stretching frequencies were observed, respectively, at about 2180 and 2120 cm^{-1} for $CH_3CD_2CONH_2$ and $CH_3CD_2COND_2$. They are not immediately obvious in the infrared, but are definitely found as sharp strong bands in the Raman spectra.

In the region between 1800 and 1550 cm^{-1}, the infrared spectra of $CH_3CH_2CONH_2$ and CH_3CD_2-$CONH_2$ show two strong and broad bands centered at about 1665 and 1625 cm^{-1} which almost overlap with each other, but the Raman spectra of these compounds show two clearly separated bands at about 1674 and 1590 cm^{-1} (see Figs. 5 and 6). These bands arise certainly from the C=O stretching and the NH_2 bending vibrations. According to the normal coordinate analysis, both S_1 (C=O stretching) and S_2 (NH_2 bending) are important in the potential energy distribution for each of these fundamentals. The infrared band at 1418 cm^{-1} of $CH_3CH_2CONH_2$ shifts to 1425 cm^{-1} on the *N*-deuteration (see Fig. 1). This band is assigned to two fundamentals, *viz.*, the CH_2 bending and the C–N stretching vibrations, the high frequency shift on the *N*-deuteration being associated only with the latter. A distinct evidence for the contribution of the C–N stretching vibration to this band is that CH_3CD_2-$CONH_2$ shows the corresponding band at 1409 cm^{-1}, which shifts also to a high frequency on the *N*-deuteration (Fig. 2). The assignment of the α-CH_2 bending frequency has been established for a number of *n*-acyl compounds.[21]

The infrared band of $CH_3CH_2CONH_2$ observed at 1296 cm^{-1} was assigned previously to the CH_2 wagging mode. The N-deuteration causes an upward shift of this band by about 22 cm^{-1}, in accordance with the removal of the NH_2 bending frequency from its high-frequency side. The corresponding Raman band at 1300 cm^{-1} is very weak, but it is easily assigned to the CH_2 wagging mode since it shifts to a higher frequency on the N-deuteration similar to that of the infrared counterpart. In the Raman spectrum CH_3-CH_2CONH_2 shows a weak band at 1260 cm^{-1} which does not shift on the *N*-deuteration and is assignable to the CH_2 twisting vibration. The corresponding infrared band was not observed. In the region between 1300 and 1200 cm^{-1}, neither the infrared nor the Raman spectrum of $CH_3CD_2CONH_2$ shows noticeable bands, but a weak Raman band is observed at 1224 cm^{-1} for $CH_3CD_2COND_2$. According to the normal coordinate analysis, this band is assigned to the ND_2 bending vibration, which gives rise to the medium infrared band at 1165 cm^{-1} and the weak Raman band at 1180 cm^{-1} for $CH_3CH_2COND_2$.

In the infrared spectrum between 1200 and 900 cm^{-1} (see Fig. 1), $CH_3CH_2CONH_2$ shows three bands at 1142, 1068, and 1004 cm^{-1}, the first arising from the NH_2 rocking vibration. Its Raman counterpart appears at 1148 cm^{-1} very strongly. The 1068 cm^{-1} band was assigned previously to the C_α–C_β stretching vibration. The normal coordinate analysis in this work indicates that the C_α–C_β stretching and the a′ CH_3 rocking vibrations couple strongly with each other, and give rise to the two bands at 1068 and 1004 cm^{-1}. On the *N*-deuteration the 1068 cm^{-1} band shifts to 1078 cm^{-1} but the 1004 cm^{-1} band remains unshifted. The very strong Raman band at 945 cm^{-1} of $CH_3CH_2COND_2$ is easily assigned to the ND_2 rocking vibration by taking account of the isotope shift and its characteristic intensity. The infrared and Raman spectra of the CD_2 compounds in this region are much more complicated than those of the CH_2 compounds. As shown in Fig. 6, the Raman bands corresponding to the infrared bands at 1136 cm^{-1} of $CH_3CD_2CONH_2$ and at 956 cm^{-1} of $CH_3CD_2COND_2$ are very strong and are easily assigned to the NH_2 and ND_2 rocking vibrations, respectively. The assignments of the other bands have been made by referring to the calculated

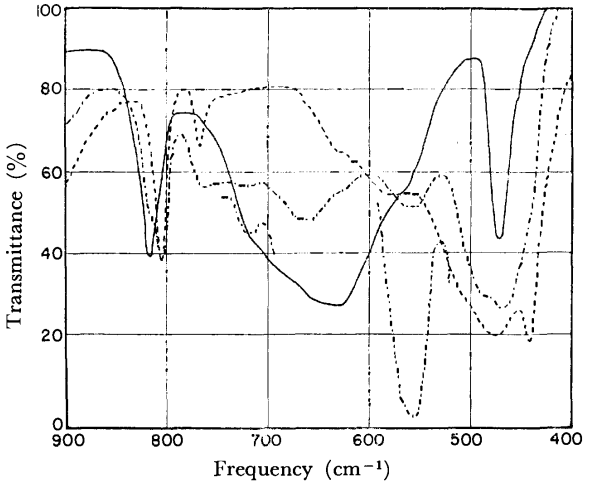

Fig. 8. Infrared spectra of $CH_3CH_2CONH_2$ (——), CH_3-CH_2CONHD (·—·) and $CH_3CH_2COND_2$ (----) in the region between 900 and 400 cm^{-1}.

20) B. Nolin and R. Norman Jones, *J. Amer. Chem. Soc.*, **75**, 5626 (1953).

21) L. J. Bellamy, "The Infrared Spectra of Complex Molecules," 2nd ed. Methuen & Co. Ltd., London, p. 23.

frequencies. According to the normal coordinate analysis, the coupling among the CH_3 rocking, C_α–C_β stretching, $NH_2(ND_2)$ rocking and the CD_2 bending vibrations seems to be considerable.

Three fundamental frequencies are expected for $CH_3CH_2CONH_2$ in the region between 900 and 700 cm^{-1}, *viz.*, the C–C_α stretching, the CH_2 rocking and the NH_2 torsional frequencies, but the infrared spectrum of this compound shows only one medium absorption band at 821 cm^{-1}. We assigned this band to a composite absorption contributed by the above three modes. On the *N*-deuteration, this band is replaced by a medium band at 808 cm^{-1} due certainly to the CH_2 rocking vibration, and a weak band assignable to the C–C_α stretching vibration appears at 765 cm^{-1}. The contribution of the NH_2 torsional

TABLE 5. OBSERVED AND CALCULATED FREQUENCIES OF CH_3CH_2CONHD AND CH_3CD_2CONHD IN cm^{-1}

CH_3CH_2CONHD						CH_3CD_2CONHD					
	Calc. A						Calc. A				
Obs.	*trans*	Δ(%)	*cis*	Δ(%)	Assign.	Obs.	*trans*	Δ(%)	*cis*	Δ(%)	Assign.
(a) In-plane vibrations (a')											
3310 vs	3291	0.6			νNH	3310 vs	3291	0.6			νNH
3200 sh			3278	2.4	νNH	3200 sh			3278	2.4	νNH
2980 m	2958	0.7	2958	0.7	$\nu_{as}CH_3$	2970 m	2958	0.4	2958	0.4	$\nu_{as}CH_3$
2880 w	2891	0.4	2891	0.4	ν_sCH_3	2870 w	2885	0.5	2885	0.5	ν_sCH_3
2820 w	2855	1.2	2855	1.2	ν_sCH_2	2465 vs			2399	2.7	νND
2465 vs			2399	2.7	νND	2410 vs	2387	0.9			νND
2410 vs	2387	0.9			νND	2120 vw	2078	2.0	2078	2.0	ν_sCD_2
1640 vs	1634	0.4	1644	0.2	νC=O	1640 vs	1628	0.7	1640	0.0	νC=O
1528 w	1536	0.5			Amide II	1528 w	1536	0.5			Amide II
1479 sh			1475	0.3	δNH	1474 sh			1472	0.1	δNH
1465 m	1469	0.2	1471	0.4	$\delta_{as}CH_3$	1462 m	1466	0.3	1467	0.3	$\delta_{as}CH_3$
1418 s	1424	0.4	1425	0.5	βCH_2	1409 s			1420	0.7	νCN
1418 s			1417	0.0	νCN	1377 vw	1388	0.8	1387	0.8	δ_sCH_3
1382 w	1388	0.4	1388	0.4	δ_sCH_3	1346 sh	1334	0.9			Amide III
	1339				Amide III	1166 w			1147	1.6	$\rho CH_3+\omega CD_2$
1318 m			1289	2.2	ωCH_2	1155 w	1138	1.5			$\rho CH_3+\omega CD_2$
1295 m	1281	1.0			ωCH_2	1096 vw	1109	1.2	1112	1.4	$\nu C_\alpha C_\beta$
1078 s	1086	0.8	1086	0.8	$\nu C_\alpha C_\beta+\rho CH_3$	1036 sh	1048	1.2			ρNHD
1045 sh	1048	0.3			ρNHD	1016 s	998	1.8	1000	1.6	βCD_2
1003 m	1010	0.7	1018	1.5	$\nu C_\alpha C_\beta+\rho CH_3$	956 s			954	0.2	ρNHD
948 sh			955	0.7	ρNHD	845 w	860	1.7	860	1.7	ωCD_2
818 sh			839	2.5	νCC_α				827		νCC_α
767 vw	799	4.2			νCC_α		785				νCC_α
			616		δC=O				604		δC=O
565 w	597	5.6			δC=O		587				δC=O
455 sh	452	0.6	441	3.2	δCCN	430 sh	444	3.2	433	0.6	δCCN
285 w	274	4.0	273	4.3	δCCC	281 w	273	3.0	272	3.3	δCCC
(b) Out-of-plane vibrations (a'')											
2980 m	2967	0.4	2967	0.4	$\nu_{as}CH_3$	2970 m	2966	0.1	2966	0.1	$\nu_{as}CH_3$
2920 vw	2900	0.7	2900	0.7	$\nu_{as}CH_2$	2180 vw	2143	1.7	2143	1.7	$\nu_{as}CD_2$
1465 m	1465	0.0	1465	0.0	$\delta_{as}CH_3$	1462 m	1464	0.2	1464	0.2	$\delta_{as}CH_3$
1265 vw	1267	0.1	1267	0.1	tCH_2	1070 w	1091	2.0	1091	2.0	ρCH_3
1066 sh	1083	1.6	1083	1.6	$\rho CH_3+\rho CH_2$		911		911		tCD_2
818 sh	805	1.6	802	1.9	$\rho CH_2+\rho CH_3$				772		τNHD+ωNHD
767 vw			773	0.0	τNHD+ωNHD		735				τNHD+ωNHD
721 vw	721	0.0			τNHD+ωNHD	718 vw			703	2.1	ρCD_2+tCD_2
660 w	636	3.6			πC=O+ωNHD	690 vw	692	0.2			ρCD_2+tCD_2
			599		πC=O	615 vw	597	3.0			ωNHD+ρCD_2
553 w	521	5.8	519	6.1	ωNHD+πC=O	535 sh			539	0.7	ωNHD+τNHD +ρCD_2
171 w	192	12.4	192	12.7	τCH_3	485 m	486	0.1	507	4.4	πC-O+ρCD_2 +ωNHD
70 w	69	1.4	69	1.4	τCC_α		191		191		τCH_3
							65		65		τCC_α

vibration to the 821 cm^{-1} band of $CH_3CH_2CONH_2$ is suggested from the fact that the infrared spectrum of the 50 per cent *N*-deuterated sample of propionamide shows two weak bands at 767 and 721 cm^{-1} (Fig. 8). These bands may be assigned to the NH out-of-plane deformation vibrations of the NHD compounds.[9] The initially calculated C–C_α stretching frequencies of $CH_3CH_2CONH_2$ and $CH_3CH_2COND_2$ were about 50 cm^{-1} higher than the observed values, but the assignment of these fundamentals was substantiated by the appearance of strong Raman bands at 820 and 769 cm^{-1} for $CH_3CH_2CONH_2$ and $CH_3CH_2COND_2$,

Table 6. The CH_2 and C-C_α-C_β deformation frequencies of propane and propionamide

	Propane			Propionamide		
	Obs.[a]	Calc. A[a]	Calc. B[b]	Obs.	Calc. A	Calc. B
CH_2 bend.	1449	1452	1449	1418	1457	1469
CH_2 wag.	1332	1347	1333	1296 (1318)[c]	1324 (1330)[c]	1308 (1317)[c]
CH_2 twist.	1278	1282	1275	1260	1279	1279
CH_2 rock.	748	747	729	821	827	819
CCC def.	375	383	383	292	248	251

a) Taken from Ref. 10.
b) Calculated from the force constants of Calc. V in Ref. 10.
c) The frequencies of the ND_2 compound are shown in parentheses.

Table 7. Observed and calculated frequencies of $CH_3CH_2CONH_2$ in cm^{-1}

	Obs.	Calc. A	Δ(%)[a]	Calc. B	Δ(%)[a]	P.E.D.[b] (Calc. A)	Assign.[c]
(a)	In-plane vibrations (a′)						
ν_2	3350	3366	0.5	3366	0.5	S_7(100)	$\nu_{as}NH_2$
ν_2	3190	3185	0.2	3185	0.2	S_8(99)	ν_sNH_2
ν_3	2980	2958	0.7	2955	0.8	S_{17}(99)	$\nu_{as}CH_3$
ν_4	2880	2891	0.4	2877	0.1	S_{18}(82), S_{19}(16)	ν_sCH_3
ν_5	2820	2855	1.2	2856	1.3	S_{18}(17), S_{19}(84)	ν_sCH_2
ν_6	1665	1662	0.2	1668	0.2	S_1(24), S_2(53), S_4(25)	$\nu C{=}O+\beta NH_2$
ν_7	1625	1622	0.2	1626	0.1	S_1(38), S_2(41)	$\nu C{=}O+\beta NH_2$
ν_8	1465	1471	0.4	1478	0.9	S_{11}(79), S_{13}(10)	$\delta_{as}CH_3$
ν_9	1418	1425	0.5	1421	0.2	S_9(11), S_{15}(68)	βCH_2
ν_{10}	1418	1418	0.0	1414	0.3	S_3(12), S_4(32), S_5(14), S_9(14), S_{15}(26)	$\nu CN+\beta CH_2$
ν_{11}	1382	1388	0.4	1394	0.9	S_{12}(104)	δ_sCH_3
ν_{12}	1296	1289	0.5	1304	0.6	S_{14}(85)	ωCH_2
ν_{13}	1136	1148	1.1	1147	0.9	S_1(19), S_3(63)	ρNH_2
ν_{14}	1068	1086	1.7	1084	1.5	S_{10}(56), S_{13}(25), S_{16}(10)	$\nu C_\alpha C_\beta+\rho CH_3$
ν_{15}	1004	1012	0.8	1001	0.3	S_{10}(35), S_{13}(34)	$\nu C_\alpha C_\beta+\rho CH_3$
ν_{16}	821	846	3.0	820	0.1	S_4(11), S_9(39), S_{13}(18)	νCC_α
ν_{17}	630	622	1.3	616	2.3	S_5(59), S_{16}(16)	$\delta C{=}O$
ν_{18}	472	460	2.5	462	2.2	S_6(54), S_9(17), S_{10}(11), S_{16}(10)	δCCN
ν_{19}	292	275	5.8	276	5.3	S_5(23), S_6(25), S_{16}(54)	δCCC
(b)	Out-of-plane vibrations (a″)						
ν_{20}	2980	2967	0.4	2963	0.6	S_{24}(99)	$\nu_{as}CH_3$
ν_{21}	2920	2900	0.7	2919	0.0	S_{25}(100)	$\nu_{as}CH_2$
ν_{22}	1465	1465	0.0	1476	0.8	S_{21}(89)	$\delta_{as}CH_3$
ν_{23}	1260	1267	0.6	1271	0.9	S_{23}(83)	tCH_2
ν_{24}	1068	1083	1.4	1082	1.3	S_{20}(49), S_{22}(29), S_{23}(10)	$\rho CH_3+\rho CH_2$
ν_{25}	821	807	1.7	805	2.0	S_{20}(31), S_{22}(39), S_{27}(24)	$\rho CH_3+\rho CH_2$
ν_{26}	821	791	3.8	792	3.7	S_{22}(10), S_{27}(67), S_{28}(11), S_{29}(11)	τNH_2
ν_{27}	680	699	2.8	699	2.8	S_{27}(10), S_{29}(84)	ωNH_2
ν_{28}	570	580	1.8	581	2.0	S_{22}(14), S_{28}(70)	$\pi C{=}O$
ν_{29}	175	193	10.1	193	10.1	S_{26}(95)	τCH_3
ν_{30}	70	70	0.0	70	0.0	S_{30}(98)	τCC_α

a) $\Delta(\%)=|\nu_{obs.}-\nu_{calc.}|\times 100/\nu_{obs.}$
b) Those less than 10 per cent are omitted.
c) ν: stretching; β: bending; δ: deformation; ω: wagging; ρ:rocking; t: twisting; τ: torsion; π: out-of-plane deformation.

respectively. In the infrared spectrum of $CH_3CD_2CONH_2$, a medium band assignable to the C–C_α stretching and the NH_2 torsional vibrations is observed at 803 cm^{-1}. The corresponding Raman band at 807 cm^{-1} is again very strong and is replaced by a medium band at 750 cm^{-1} on the *N*-deuteration. Besides these bands, $CH_3CD_2CONH_2$ shows a weak band at 850 cm^{-1} which hardly shifts on the *N*-deuteration and is assignable to the CD_2 wagging vibration.

The NH_2 and ND_2 wagging and the skeletal deformation frequencies are expected in the region between 700 and 250 cm^{-1}. For the infrared spectrum of $CH_3CH_2CONH_2$, we assigned previously the very strong and broad band centered near 640 cm^{-1} to the NH_2 wagging vibration, the shoulder band at 570 cm^{-1} to the C=O a'' deformation vibration and the band at 472 cm^{-1} to the C=O a' deformation vibration.[1] The asymmetrical contour of the first of these bands indicates, however, the presence of an implicit absorption with the maximum near 680 cm^{-1}. Furthermore, the 50 per cent *N*-deuterated sample of propionamide shows a weak infrared band at 660 cm^{-1}, which is not observed in the spectrum of $CH_3CH_2COND_2$ (see Fig. 8). If this band is due to a fundamental vibration of *trans* or *cis* CH_3CH_2CONHD, the NH_2 wagging frequency of $CH_3CH_2CONH_2$ should be higher than 660 cm^{-1} in order that the isotopic shifts fulfil the Rayleigh condition.[22] Accordingly we assigned the implicit absorption near 680 cm^{-1} of $CH_3CH_2CONH_2$ to the NH_2 wagging vibration. The strong absorption giving rise to the peak near 640 cm^{-1} was then attributed to the C=O a' deformation vibration by referring to the normal coordinate analysis, which led also to the revised assignment of the band at 472 cm^{-1} to the C_α–C–N deformation vibration. In the Raman spectrum of $CH_3CH_2CONH_2$, there is no noticeable band assignable to the NH_2 wagging vibration, but two weak bands arising from the C=O a' and a'' deformation vibrations are observed at 630 and 570 cm^{-1}, respectively. The shifts of these bands on the C_α- and *N*-deuterations were found to agree well with the initial calculation, and the assignments of the infrared and Raman bands of the CD_2 compounds in this region were made without much difficulty by referring to the calcu-

Table 8. Observed and calculated frequencies of $CH_3CH_2COND_2$ in cm^{-1}

	Obs.	Calc. A	Δ(%)	Calc. B	Δ(%)	P.E.D. (Calc. A)	Assign.
(a)	In-plane vibrations (a')						
ν_1	2980	2958	0.7	2955	0.8	$S_{17}(99)$	$\nu_{as}CH_3$
ν_2	2880	2891	0.4	2877	0.1	$S_{18}(82), S_{19}(16)$	ν_sCH_3
ν_3	2820	2855	1.2	2856	1.3	$S_{18}(17), S_{19}(84)$	ν_sCH_2
ν_4	2530	2498	1.3	2498	1.3	$S_7(100)$	$\nu_{as}ND_2$
ν_5	2370	2303	2.8	2303	2.8	$S_8(98)$	ν_sND_2
ν_6	1635	1626	0.5	1636	0.0	$S_1(63), S_4(24), S_6(14)$	νC=O
ν_7	1466	1470	0.3	1478	0.8	$S_{11}(80), S_{13}(10)$	$\delta_{as}CH_3$
ν_8	1425	1426	0.0	1420	0.4	$S_4(33), S_5(10), S_9(24), S_{15}(20)$	$\nu CN+\nu C_\alpha C_\beta+\beta CH_2$
ν_9	1418	1423	0.3	1413	0.4	$S_4(12), S_{15}(74)$	βCH_2
ν_{10}	1382	1388	0.4	1394	0.9	$S_{12}(104)$	δ_sCH_3
ν_{11}	1318	1299	1.5	1327	0.7	$S_{14}(83)$	ωCH_2
ν_{12}	1165	1182	1.5	1173	0.7	$S_2(73)$	βND_2
ν_{13}	1078	1086	0.7	1084	0.6	$S_{10}(55), S_{13}(24), S_{16}(10)$	$\nu C_\alpha C_\beta+\rho CH_3$
ν_{14}	1006	1010	0.4	1000	0.4	$S_{10}(33), S_{13}(40)$	$\nu C_\alpha C_\beta+\rho CH_3$
ν_{15}	942	946	0.4	948	0.6	$S_1(18), S_3(48), S_4(10)$	ρND_2
ν_{16}	765	795	3.9	764	0.2	$S_3(22), S_9(44), S_{13}(15)$	$\nu CC_\alpha+\rho ND_2$
ν_{17}	580	593	2.3	593	2.3	$S_5(59), S_{16}(14)$	δC=O
ν_{18}	443	435	1.9	436	1.5	$S_6(50), S_9(16), S_{16}(11)$	δCCN
ν_{19}	281	271	3.5	272	3.1	$S_5(21), S_6(29), S_{16}(53)$	δCCC
(b)	Out-of-plane vibrations (a'')						
ν_{20}	2980	2967	0.4	2963	0.6	$S_{24}(99)$	$\nu_{as}CH_3$
ν_{21}	2920	2900	0.7	2919	0.0	$S_{25}(100)$	$\nu_{as}CH_2$
ν_{22}	1465	1465	0.0	1476	0.8	$S_{21}(89)$	$\delta_{as}CH_3$
ν_{23}	1260	1267	0.6	1271	0.9	$S_{23}(82)$	tCH_2
ν_{24}	1078	1082	0.4	1082	0.4	$S_{20}(49), S_{22}(29), S_{23}(10)$	$\rho CH_3+\rho CH_2$
ν_{25}	808	802	0.7	801	0.9	$S_{20}(36), S_{22}(53), S_{28}(16)$	$\rho CH_3+\rho CH_2$
ν_{26}	625	636	1.7	636	1.7	$S_{22}(13), S_{27}(15), S_{28}(53), S_{29}(28)$	πC=O+ωND_2
ν_{27}	580	554	4.5	555	4.5	$S_{27}(84)$	τND_2
ν_{28}	475	505	6.3	505	6.3	$S_{28}(19), S_{29}(69)$	$\omega ND_2+\pi$C=O
ν_{29}	170	192	13.0	192	13.0	$S_{26}(95)$	τCH_3
ν_{30}	70	68	2.9	68	2.9	$S_{30}(97)$	τCC_α

22) D. Steele, E. R. Lippincott, and J. Xavier, *J. Chem. Phys.*, **33**, 1242 (1960).

lated frequencies. For the C–C_α–C_β deformation frequency of $CH_3CH_2CONH_2$, the initially calculated values are about 40 cm^{-1} lower than the observed frequency of the infrared band (292 cm^{-1}), but we are quite confident on the assignment of this fundamental from the previous analysis of the band progression of *n*-fatty acid amides as well as the intensity of the Raman counterpart.

In the region below 200 cm^{-1}, $CH_3CH_2CONH_2$ and its *N*- and C_α-deuterated compounds show several infrared bands assignable to the torsional vibrations about the C–C_α–C_β skeleton, but unambiguous assignments of these fundamentals are difficult since the bands due to lattice vibrations may overlap with them. According to the normal coordinate analysis, the C_α–C_β and C–C_α torsional vibrations of the CH_2 compounds are thought to contribute to the bands at about 170 and 70 cm^{-1}, respectively. No appreciable shifts of these bands were observed on the C_α-deuteration.

Refinement of Force Constants

There are two factors which may affect the shifts of the CH_2 group frequescies on going from propane to propionamide, *viz.*, the change in the fashion of mechanical couplings with the rest of molecules and the change in the force constants within the CH_2 group. How these two factors participate in the observed shifts may be estimated from a comparison of the experimental results with the initially calculated frequencies, since the force constants for the CH_3CH_2-group used in the initial calculation have been known to reproduce the observed frequencies of *n*-paraffins very well.[10] Table 6 shows the observed and the calculated values of the CH_2 group frequencies of propane and propionamide; the results for the C–C_α–C_β deformation frequency are also listed. From the failure of the calculation to reproduce the observed difference in the CH_2 bending frequency between propane and propionamide, it is seen that the observed shift stems from the change of the force constants related to this frequency. Contrarily, the agreement between the calculated and the observed shifts of the CH_2 rocking frequency suggests that the nature of the shift is essentially mechanical. The calculated shift of the C–C_α–C_β deformation frequency is too large and the mechanical effect on this shift should be cancelled partly by the change in appropriate force constants. For the

Table 9. Observed and calculated frequencies of $CH_3CD_2CONH_2$ in cm^{-1}

	Obs.	Calc. A	Δ(%)	Calc. B	Δ(%)	P.E.D. (Calc. A)	Assign.
(a)	In-plane vibrations (a′)						
ν_1	3350	3366	0.5	3366	0.5	$S_7(100)$	$\nu_{as}NH_2$
ν_2	3190	3185	0.2	3185	0.2	$S_8(99)$	ν_sNH_2
ν_3	2970	2958	0.4	2955	0.5	$S_{17}(100)$	$\nu_{as}CH_3$
ν_4	2870	2885	0.5	2877	0.3	$S_{18}(99)$	ν_sCH_3
ν_5	2120	2078	2.0	2092	1.3	$S_{19}(99)$	ν_sCD_2
ν_6	1665	1661	0.3	1666	0.1	$S_1(21), S_2(58), S_4(24)$	$\nu C{=}O+\beta NH_2$
ν_7	1625	1617	0.5	1617	0.5	$S_1(42), S_2(36), S_6(10)$	$\nu C{=}O+\beta NH_2$
ν_8	1462	1468	0.4	1477	1.0	$S_{11}(84)$	$\delta_{as}CH_3$
ν_9	1409	1420	0.8	1418	0.7	$S_3(16), S_4(41), S_5(17), S_9(24)$	$\nu CN+\nu CC_\alpha$
ν_{10}	1378	1387	0.7	1394	1.1	$S_{12}(106)$	δ_sCH_3
ν_{11}	1174	1165	0.8	1179	0.4	$S_3(39), S_9(15), S_{13}(20), S_{14}(15)$	$\rho NH_2+\rho CH_3$
ν_{12}	1136	1128	0.7	1133	0.3	$S_1(19), S_3(19), S_{13}(22), S_{15}(11)$	$\rho NH_2+\rho CH_3$
ν_{13}	1093	1107	1.3	1086	0.6	$S_{10}(64), S_{14}(19), S_{15}(22)$	$\nu C_\alpha C_\beta+\beta CD_2$
ν_{14}	1016	998	1.8	1005	1.1	$S_{10}(15), S_{13}(17), S_{15}(60)$	βCD_2
ν_{15}	850	861	1.2	845	0.6	$S_{10}(12), S_{13}(15), S_{14}(61)$	ωCD_2
ν_{16}	803	836	4.1	812	1.1	$S_4(11), S_9(36), S_{13}(13)$	νCC_α
ν_{17}	618	608	1.6	603	2.4	$S_5(57), S_{16}(17)$	$\delta C{=}O$
ν_{18}	442	452	2.2	453	2.5	$S_6(53), S_9(17), S_{16}(10)$	δCCN
ν_{19}	288	274	4.8	276	4.3	$S_5(23), S_6(25), S_{16}(55)$	δCCC
(b)	Out-of-plane vibrations (a″)						
ν_{20}	2970	2966	0.1	2963	0.2	$S_{24}(100)$	$\nu_{as}CH_3$
ν_{21}	2180	2143	1.7	2180	0.0	$S_{25}(102)$	$\nu_{as}CD_2$
ν_{22}	1462	1464	0.2	1475	0.9	$S_{21}(90)$	$\delta_{as}CH_3$
ν_{23}	1070	1091	2.0	1110	3.8	$S_{20}(68)$	ρCH_3
ν_{24}	918	912	0.7	887	3.4	$S_{22}(14), S_{23}(62), S_{28}(18)$	tCD_2
ν_{25}	803	795	1.1	794	1.1	$S_{27}(92)$	τNH_2
ν_{26}	710	721	1.5	722	1.6	$S_{20}(12), S_{22}(12), S_{23}(21), S_{28}(23), S_{29}(47)$	$\omega NH_2+\pi C{=}O+tCD_2+\rho CD_2$
ν_{27}	670	671	0.2	673	0.4	$S_{22}(26), S_{29}(47)$	$\omega NH_2+\rho CD_2$
ν_{28}	495	517	4.4	517	4.4	$S_{22}(42), S_{28}(50)$	$\pi C{=}O+\rho CD_2$
ν_{29}	175	191	9.3	191	9.3	$S_{26}(96)$	τCH_3
ν_{30}	70	65	7.7	65	7.7	$S_{30}(98)$	τCC_α

TABLE 10. OBSERVED AND CALCULATED FREQUENCIES OF $CH_3CD_2COND_2$ IN cm^{-1}

	Obs.	Calc. A	Δ(%)	Calc. B	Δ(%)	P.E.D. (Calc. A)	Assign.
(a)	In-plane vibrations (a')						
ν_1	2970	2958	0.4	2955	0.5	$S_{17}(100)$	$\nu_{as}CH_3$
ν_2	2870	2885	0.5	2877	0.3	$S_{18}(99)$	ν_sCH_3
ν_3	2520	2498	0.9	2498	0.9	$S_7(100)$	$\nu_{as}ND_2$
ν_4	2360	2303	2.4	2303	2.4	$S_8(98)$	ν_sND_2
ν_5	2120	2078	2.0	2092	1.3	$S_{19}(99)$	ν_sCD_2
ν_6	1630	1621	0.6	1628	0.1	$S_1(64), S_4(25), S_6(14)$	$\nu C{=}O$
ν_7	1462	1468	0.4	1477	1.0	$S_{11}(83), S_{13}(10)$	$\delta_{as}CH_3$
ν_8	1425	1425	0.0	1417	0.6	$S_2(10), S_4(43), S_5(14), S_9(26)$	$\nu CN+\nu CC_\alpha$
ν_9	1377	1387	0.8	1394	1.2	$S_{12}(106)$	δ_sCH_3
ν_{10}	1224	1205	1.5	1221	0.2	$S_2(61), S_9(15), S_{14}(11)$	βND_2
ν_{11}	1120	1129	0.8	1135	1.4	$S_2(12), S_{13}(37), S_{14}(10), S_{15}(14)$	ρCH_3
ν_{12}	1096	1107	1.0	1087	0.8	$S_{10}(61), S_{14}(20), S_{15}(21)$	$\nu C_\alpha C_\beta$
ν_{13}	1014	998	1.6	1004	1.0	$S_{10}(14), S_{13}(16), S_{15}(61)$	βCD_2
ν_{14}	956	946	1.1	948	0.8	$S_1(18), S_3(46), S_4(10)$	ρND_2
ν_{15}	845	859	1.7	843	0.2	$S_{10}(12), S_{13}(20), S_{14}(63)$	ωCD_2
ν_{16}	740	779	5.3	750	1.3	$S_3(25), S_9(41)$	$\nu CC_\alpha+\rho ND_2$
ν_{17}	577	585	1.7	585	1.7	$S_5(59), S_{16}(15)$	$\delta C{=}O$
ν_{18}	420	427	1.6	428	1.9	$S_6(48), S_9(16), S_{16}(11)$	δCCN
ν_{19}	280	270	3.5	271	3.2	$S_5(21), S_6(29), S_{16}(53)$	δCCC
(b)	Out-of-plane vibrations (a'')						
ν_{20}	2970	2966	0.1	2963	0.2	$S_{24}(100)$	$\nu_{as}CH_3$
ν_{21}	2180	2143	1.7	2180	0.0	$S_{25}(102)$	$\nu_{as}CD_2$
ν_{22}	1462	1464	0.2	1475	0.9	$S_{21}(90)$	$\delta_{as}CH_3$
ν_{23}	1070	1091	2.0	1110	3.8	$S_{20}(68)$	ρCH_3
ν_{24}	918	911	0.8	886	3.5	$S_{22}(14), S_{23}(62), S_{28}(18)$	tCD_2
ν_{25}	700	705	0.6	707	0.9	$S_{20}(20), S_{22}(30), S_{23}(30), S_{28}(33)$	$\rho CD_2+tCD_2+\pi C{=}O$
ν_{26}	575	602	4.7	601	4.5	$S_{22}(17), S_{27}(47), S_{28}(13), S_{29}(25)$	$\tau ND_2+\omega ND_2$
ν_{27}	525	535	1.9	536	2.0	$S_{22}(12), S_{27}(52), S_{29}(38)$	$\tau ND_2+\omega ND_2$
ν_{28}	470	482	2.6	483	2.7	$S_{22}(21), S_{28}(34), S_{29}(32)$	$\pi C{=}O+\omega ND_2$
ν_{29}	170	191	12.3	191	12.3	$S_{26}(96)$	τCH_3
ν_{30}	70	64	9.4	64	9.4	$S_{30}(98)$	τCC_α

CH_2 wagging frequency, Calculation B gave a much better result than Calculation A, but both the calculations failed to give sufficient shift of this frequency on the *N*-deuteration of propionamide.

Taking account of these results as well as the discrepancies in the C–C_α stretching frequencies, we tried to improve the force field of propionamide by the least squares refinement of the deformation constants related to the valence angles around the C_α atom and the C–C_α, C=O, and C–N stretching constants. In addition to the adjustment of the last two constants, the introduction of an interaction constant $f_{4,9}$ was found necessary to suppress the influence of the C–C_α stretching constant on the C=O and the C–N stretching frequencies. Another interaction constant, $f_{2,14}$ was introduced to amplify the calculated shift of the CH_2 wagging frequency on the *N*-deuteration. The other force constants were fixed to the transferred values. In the course of the refinement in Calculation A, the C–C_α stretching constant, $K(CC_\alpha)$, became smaller than the fixed C_α–C_β stretching constant, $K(C_\alpha C_\beta)$. This result is physically unacceptable, since the bond order of the C–C bond adjoining a double bond is expected to be higher than that of an isolated C–C bond. Accordingly, we fixed $K(CC_\alpha)$ to the mean value of those of acetamide (3.187)[8] and *n*-paraffins (2.229)[10], and refined the remaining constants until they converged. A similar diminishing of the C–C_α stretching constant, $K_R^I(CC_\alpha)$, occurred also in Calculation B. In this case the diagonal *F* matrix element for the C–C_α stretching coordinate is contributed not only from $K_R^I(CC_\alpha)$ but also from the Urey-Bradley type repulsion constants of the amide group, $F(C_\alpha CO)$ and $F(C_\alpha CN)$, and it is difficult to correlate the force constants to the bond order directly. Accordingly, the refinement was carried through with no restriction on $K_R^I(CC_\alpha)$.

The final sets of force constants are given in Table 4, and the results obtained from these constants are summarized together with the observed frequencies in Tables 7—10. The discrepancies between the observed and the calculated values of the C–C_α stretching frequencies in Calculation A are larger than those in Calculation B, because of fixing $K(CC_\alpha)$ to a value which perhaps is not optimum. In other respects, the results of Calculations A and B are not much different

from each other, the fits between the observed and the calculated frequencies being fairly good.

The authors wish to express their thanks to Prof. K. Nakamoto of Marquette University for the use of laser Raman spectrophotometer and Prof. T. Takenaka of Kyoto University for the use of Perkin-Elmer 521 and Hitachi FIS-3 grating infrared spectrophotometers. Thanks are due to Dr. T. Shingu of Kyoto University for the NMR measurement. Throughout this work, FACOM 230-60 computer of Kyoto University Computer Center was used.

BULLETIN OF THE CHEMICAL SOCIETY OF JAPAN, VOL. 45, 2383—2385(1972)

On the Mechanism of H-Atom Formation by Reaction of Electrons in Frozen Acidic Solutions at 77°K[1]

Shin-ichi OHNO, Teikichi SASAKI, and Mitsuru KOIKE
Japan Atomic Energy Research Institute, Tokai-mura, Ibaraki-ken

(Received November 13, 1971)

A model for the reaction of radiation-produced electrons in frozen acidic solutions is presented to explain anomalies. It does not assume the inertness of the hydrogen ion as an electron scavenger in the solid phase but involves a process in which an H-atom, the product of the ($e^- + H^+$) reaction, is transferred to an adjacent water molecule through an H-bonded network until it finds a suitable site where it can be trapped or a species with which to react. Results from ESR-measurements on photolysed frozen solutions of ferrocyanide ions in the presence of nitrate ions and 2-propanol as well as the data on H/D isotope effects were used as evidence supporting the model.

It is generally believed that radiation-produced electrons are converted into hydrogen atoms on reacting with the hydrogen ion in both liquid[2] and gas phases.[3]

$$e^- + H_3O^+ \longrightarrow H_3O \longrightarrow H + H_2O \qquad (1)$$

However, the above mechanism does not seem to hold in the solid phase, because of three anomalies: (1) The yield of H-atoms in ice is not as high as might be expected from the experimental results in the liquid phase.[4] (2) In a solvent consisting of D_2O and H_2O where both H- and D-atoms are produced, the product ratio H/D in the solid phase is quite different from that in gas or liquid phase.[5] (3) Paramagnetic relaxation experiments on γ-irradiated frozen aqueous systems have shown that the trapped H-atoms are distributed uniformly in the irradiated sample,[6] while the trapped electrons are non-uniformly distributed.

Some authors assume that the electron does not react with the hydrogen ion at 77°K,[4,7] but the trapped H-atoms found in irradiated acidic ice result from the reactions of the electron either with undissociated acids or with water molecules in the hydration layer of the added solute.[4,7] However, many other solutes, inorganic and organic, react with the electron as effectively in the solid as in the liquid phase.[4,8,9] The hydrogen ion would be the only exception for which no reason was given.[8]

The purpose of this paper is to present a model for the reaction of electrons in acidic ice which would reasonably explain the anomalies, not assuming the exceptional inertness of the hydrogen ion as an electron scavenger.

Experimental and Results

Electrons were generated from ferrocyanide ions by photolysis at 254 nm. The merit of this method over the radiolysis method is that other reactive species (*e.g.* OH, H, H_2O^+, or H_2O_2) are not produced, thus eliminating the complex reaction sequences. Details of the experimental procedures were the same as described.[5] ESR spectra of UV-irradiated frozen solutions (at 77°K) of 10^{-2}M potassium ferrocyanide containing various concentrations of sodium nitrate and 2-propanol are shown in Fig. 1. In the liquid phase, the electron (e_{aq}^-) reacts rapidly with both H_3O^+ and NO_3^- (rate constants$\approx 10^{10}$M^{-1}s^{-1}) but not with 2-propanol,[10] while the H-atom reacts with both NO_3^- and 2-propanol (rate constants$\approx 10^7$M^{-1}s^{-1}) but only slowly with H_3O^+.[10] Thus, one might expect that, in a frozen solution containing 10^{-3}M NO_3^- and 10^{-1}M 2-propanol, the electron reacts only with NO_3^- to

1) Presented at 4th Intern. Conf. Radiation Res., Evian, 1970.
2) E. J. Hart, "Actions Chemiques et Biologiques des Radiations," Ed. by M. Haissinsky, Masson & Cie., (1966). Ser. **10**, Chap. 1.
3) G. R. A. Johnson and M. Simic, "The Chemistry of Ionization and Excitation," Ed. by G. R. A. Johnson and G. Scholes, Taylor & Francis Ltd., (1967), p. 211.
4) L. Kevan, "Radiation Chemistry of Aqueous Systems," Ed. by G. Stein, Weizmann Science Press, (1968), p. 21.
5) S. Ohno, This Bulletin, **41**, 1301 (1968).
6) J. Zimbrick and L. Kevan, *J. Chem. Phys.*, **47**, 5000 (1967).
7) L. Kevan, P. N. Moorthy, and J. J. Weiss, *J. Amer. Chem. Soc.*, **86**, 771 (1964).
8) B. G. Ershov and A. K. Pikaev, *Radiation Res. Rev.*, **2**, 1 (1969).
9) L. Kevan, *J. Amer. Chem. Soc.*, **89**, 4238 (1967).
10) M. Anbar and P. Neta, *Intern. J. Appl. Radiation Isotopes*, **18**, 493 (1967).

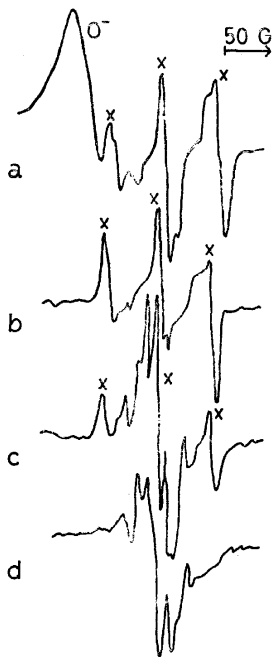

Fig. 1. ESR spectra of UV-irradiated frozen solutions (at 77°K) of 10^{-2} M $K_4[Fe(CN)_6]$ containing various concentrations of $NaNO_3$ and 2-propanol.

Medium	$[NO_3^-]$, M	[2-propanol], M
(a): 5N NaOH	0.001	0.1
(b): 1N H_2SO_4	0.01	0.01
(c): 1N H_2SO_4	0.001	0.1
(d): 1N H_2SO_4	0	0.2

Lines (×) refer to the signals due to the NO_2 radical.

give NO_2 radical. This was found to be the case with an alkaline medium (Fig. 1, a), but not with an acidic medium (Fig. 1, c) where the signals due to the NO_2 radicals are largely replaced by one due to the 2-propanol radical.[11] This suggests that the electron is converted into an H-atom on going from an alkaline to an acidic medium.

One of us (S. O.) observed[5] the product ratio H/D arising from the reaction between the electron and the hydrogen ion in a solvent composed of light and heavy water (the atom ratio in the solvent $(H/D)_{water}=1$) in the liquid phase as a function of temperature (2—40°C) and also in the solid phase at 77°K. Since it is known that H-atoms are fractionated over D-atoms in the hydronium ion, the observed isotope effect (S_{all}) will comprise two consecutive isotope effects; the equilibrium isotope effect (K) in the formation of hydronium ion from water and the kinetic isotope effect (S_{ion}) in the formation of hydrogen atom from the hydronium ion.

$$S_{all} = K \times S_{ion} \qquad (2)$$

11) ESR signals ascribed to NO_2 and 2-propanol radicals are identical with those reported by Chachaty and Hayon.[12]

Figure 1, a, shows the presence also of O^- radical ion. They can be formed as follows:

$$e^- + NO_3^- \longrightarrow NO_3^{2-}$$
$$\begin{cases} NO_3^{2-} + H_2O \longrightarrow NO_2 + 2OH^- \\ NO_3^{2-} \longrightarrow NO_2^- + O^- \end{cases}$$

The value of the equilibrium isotope effect at various temperatures can be calculated with data by Heinzinger and Weston.[13] The observed overall isotope effects together with the kinetic isotope effects thus calculated for the liquid phase system are plotted in Fig. 2 against the reciprocal of absolute temperature. The value obtained at 85°C by Meyerstein[14] and the gas phase datum at 140°C reported by Johnson and Simic[3] are also given.

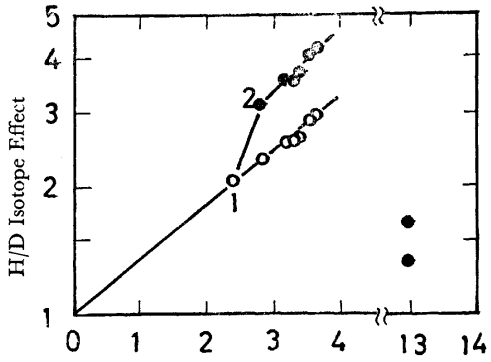

Fig. 2. Temperature dependence of the isotope effects on H/D atom production.
Point (1) refers to the gas phase datum obtained by Johnson and Simic at 140°C (Ref. 3). Point (2) is that due to Meyerstein (Ref. 14). The other values of S_{ion} (●) are from Ref. 5. For S_{all} (○), see text.

Discussion

The straight line (in Fig. 2) throughout the liquid and gas phase regions which is obtained when $\log(S_{ion})$ is plotted against $1/T$ indicates that the same reaction mechanism holds in both phases and that the relative rates of O–H and O–D bond breakages k_H/k_D can be given by

$$\frac{k_H}{k_D} = \exp\left(\frac{E_D - E_H}{RT}\right) \qquad (3)$$

where E_H and E_D are the activation energy of O–H and O–D breakages, respectively. The slope of the straight line in Fig. 2 gives $E_D - E_H = 0.6$ kcal/mol. A value of this order of magnitude might be appropriate for the difference in zero-point energy between O–H and O–D bonds in the intermediate complex such as H_2DO.

On the other hand, the observed isotope effect in the solid phase is strikingly low ($S_{all} \approx 1.5$), suggesting that the H-atom trapping process in the solid differs a great deal from liquid phase reactions.

12) C. Chachaty and E. Hayon, *J. Chim. Phys.*, **60**, 1115 (1964).
13) K. Heinzinger and R. E. Weston, *J. Phys. Chem.*, **68**, 744 (1964).
14) D. Meyerstein, Ph. D. Thesis, Hebrew Univ. 1965, quoted by M. Anbar and D. Meyerstein, in Ref. 4, p. 109,

The results shown in Fig. 1 indicate that photodetached electrons from ferrocyanide ions are converted into H-atoms in sulfuric acid ice. Fletcher and Freeman observed that the trapped H-atom yields, $G(H_t)$, found in γ-irradiated sulfuric acid glasses can be reduced from 1.3 to 0.24 by the presence of 10^{-3} mol fraction of ethanol.[15] This demonstrates that the precursor of H_t in the acid glass which can react with ethanol might be an H-atom rather than an electron. Recent observations that the presence of sulfuric acid in frozen aqueous solutions of a number of organic compounds enhances the yield of the radiation-produced organic radical[16] also suggest the conversion of the electron into an H-atom in acidic ice.

Concerning H-atom trapping in irradiated ice, the following facts are well-known. H-atoms are not stabilized in pure water at 77°K, though they are stable near 4°K.[4] At 77°K, only aqueous systems containing ions of a certain type such as ClO_4^-, SO_4^{2-}, or PO_4^{3-} can stabilize H-atoms.[17] Acids such as HF, CCl_3COOH, H_2SO_3 do not give stabilized H-atoms when irradiated at 77°K.[17] This would indicate that at 77°K H-atoms can migrate through the water structure until they reach a trapping site which can stabilize an H-atom. The structure of this particular trap in the ice cannot be precisely visualized as yet, but it is probably associated with an oxyanion. According to Ultee and Kepford,[17] the site involves a hydrated MO_4^--type ion, which in aqueous solution should provide a tight three-dimensional lattice, destroying the open structure of ice rather than providing a specific site.

We feel that reaction (1) takes place irrespective of the phase, *i.e.*, even in the solid phase. An H-atom, the product of reaction (1) in the solid phase, will be transferred through the hydrogen-bonded network of the ice and be trapped stably at the site which can stabilize the H_t.

$$H_m\cdots O(H)-H \longrightarrow H-O(H)\cdots H_m \qquad (4)$$

Here, a moving H-atom is designated by H_m. An H-atom transfer of this type can be caused by the thermal vibration of the lattice at 77°K, but not at 4°K. The process may be so slow that in the liquid phase the H-atom would predominantly diffuse about in the usual sense to be scavenged by the solute added. Such a transfer would prevail only in the solid phase where all the atoms can be assumed to be immobilized.

Our model would explain the three anomalies associated with the solid phase. Assuming that the observed H_t is caused by reaction (1) alone, not including an H-atom transfer, an H/D isotope effect as large as 50 would be expected at 77°K if Eq. (3) holds. In fact, a value of about 1.5 was obtained. The value of H_t/D_t by the present model would be a consequence of the H/D atom ratio eventually present in the trapping site. The isotope effect of this kind does not arise from competing reactions and will not make the value of H/D largely differ from unity. It is thus not surprising that a marked difference in the magnitude of the isotope effect is found between the solid and the liquid phases.

One may expect that, in an acidic ice, competition occurs between the solute(S) and the trapping site(T) for the moving H-atom through the H-bonded chain-(H_m):

$$e^- + H_3O^+ \longrightarrow H_m \begin{cases} + T \longrightarrow H_t \\ + S \longrightarrow [SH] \end{cases} \qquad (5)$$

[SH] would decompose to give more stable species in the matrix. If as an example NO_3^- and 2-propanol are taken for S, the decomposition would be:

$$[NO_3H^-] \longrightarrow NO_2 + OH^- \text{ or } NO_2^- + OH \qquad (6)$$

$$[(CH_3)_2CHOH_2] \longrightarrow (CH_3)_2COH + H_2 \qquad (7)$$

Reaction (7) is a possible process producing the alcohol radical by an attack of a diffusing H-atom.[18] If we assume that the order of magnitude for the concentration of T in an acidic glass to be 10^{-2}M, any solute which is involved in the H-bonded chain and which can scavenge H_m could reduce the yield of H_t, even though its concentration is small compared to that of the acid. This is why the hydrogen ion does not apparently react with the electron in frozen matrices.

The wider distribution from the point of energy deposit of the trapped H-atoms than that of the trapped electrons may also be understood.

It is of interest to note that the mobile energy in 5.3M H_2SO_4 glass, assumed by Dainton and Gopinathan,[21] which can liberate Cl^- ion from chloracetic acid (with a G-value of about 2), and which is incapable of reacting with nitrous oxide is possibly the mobile H-atom through hydrogen bonds.

15) J. W. Fletcher and G. R. Freeman, *Can. J. Chem.*, **45**, 635 (1967).

16) P. N. Moorthy, G. Gopinathan, and K. N. Rao, *Radiation Effects*, **2**, 175 (1970).

17) C. J. Ultee and C. R. Kepford, *J. Chem. Phys.*, **52**, 3462 (1970).

18) Hagopian and Johnsen showed that thermal energy H-atoms produced by a heated tungsten-filament do not abstract α-H from ethanol at 77°K,[19] whereas many other authors observed that the H_t in sulfuric acid glass disappears, in the presence of organic substances, to be replaced by organic radicals.[15,16,20] The latter observation may be explained in terms of the H_m-scavenging process by organic compounds.

19) A. K. E. Hagopian and R. H. Johnsen, *J. Phys. Chem.*, **72**, 1949 (1968).

20) W. Köhnlein and D. Schulte-Frohlinde, *Radiation Res.*, **38**, 173 (1969).

21) F. S. Dainton and C. Gopinathan, *Trans. Faraday Soc.*, **65**, 143 (1969).

The Primary Photochemical Process of 4-Nitropyridine *N*-Oxide II. Decay Kinetics of the Photochemical Intermediates[1]

Norisuke HATA, Isao ONO, and Tamio TSUCHIYA

Department of Chemistry, College of Science and Engineering, Aoyama Gakuin University, Chitosedai, Setagaya-ku, Tokyo

(Received February 4, 1972)

In order to clarify the primary photochemical process of 4-nitropyridine *N*-oxide in solution, kinetic flash spectrophotometric studies were carried out under various conditions. The flash excitation of 4-nitropyridine *N*-oxide in alcoholic solution resulted in three transient species in the spectral region between 360 nm and 580 nm; one of them was a weak absorption at about 530 nm (transient species A and A'), and the other, a stronger one around 380 nm (transient species B). The experiments on the decay kinetics of these transients revealed that the photochemical reaction of 4-nitropyridine *N*-oxide in an alcoholic solution proceeded through these intermediate species originating from the excited singlet state; Process I (the photochemical formation of 4-hydroxypyridine *N*-oxide nitrate) involved the bimolecular interaction between an intermediate A' and unexcited molecule, while Process II (the photochemical formation of 4-hydroxylaminopyridine *N*-oxide) was initiated by a hydrogen-atom abstraction from a solvent molecule by an intermediate B which was produced from another intermediate A. The two intermediates A and A' were reasonably assumed to be formed concurrently from the excited singlet state of 4-nitropyridine *N*-oxide.

4-Nitropyridine *N*-oxide changes upon irradiation of 313 nm light in ethanol to give 4-hydroxypyridine *N*-oxide nitrate (Process I) or 4-hydroxylaminopyridine *N*-oxide (Process II), depending on the reaction conditions.[2-5] As has been described in a previous paper,[5] the observation of the transient absorption in the region between 360 nm and 580 nm and the measurements of the quantum yields under various conditions led to the conclusions that Processes I and II both proceed *via* some intermediate species originating from the excited singlet state of 4-nitropyridine *N*-oxide; Process I being due to a bimolecular interaction between an intermediate and an unexcited molecule, and Process II involving a hydrogen abstraction of an intermediate from an alcoholic solvent.

The purpose of the present investigation is to clarify whether or not the transient species observed in a flash photolysis of 4-nitropyridine *N*-oxide are actually responsible for Processes I and II, and then to obtain some information on the primary process.

Experimental

Materials. The 4-nitropyridine *N*-oxide used in this experiment was synthesized by nitrating the pyridine *N*-oxide according to the method given in the literature,[6] and the product was purified by recrystallization from acetone several times. The solvents used for the flash experiments were reagent-grade methanol, ethanol, isopropanol, and glycerol, all of which were used without further purification.

Flash Spectrophotometric Experiment. A sample solution contained in a quartz reaction cell (8 cm in length and 2 cm in diameter) was deaerated by flushing the cell with nitrogen. A quartz flash photolysis lamp (10 cm in length and 2 cm in diameter) filled with xenon gas was operated at 11 kV and 2 μF, dissipating an energy of 120 J; the duration of the flash was 10 μsec. The absorption spectra of transient species and their decays were determined with a xenon lamp (Toshiba 500 W) or a tungsten lamp (60 W), a plane grating spectrograph (Shimadzu GE-100), a photomultiplier tube (RCA 1P28), and a synchroscope (Toshiba 3054).

Results and Discussion

Figures 1 and 2 show the absorption spectra of the transient species produced by a flash excitation of 4-nitropyridine *N*-oxide in deaerated ethanol or glycerol at room temperature; the spectrum was plotted immediately after the flash and also at some specified time interval following the flash. As can be seen from the figures, two absorption systems were observed in the region between 360 nm and 580 nm; one of them was a weak absorption at about 530 nm, and the other, stronger one around 380 nm. Both absorptions were reduced to some extent in their intensity

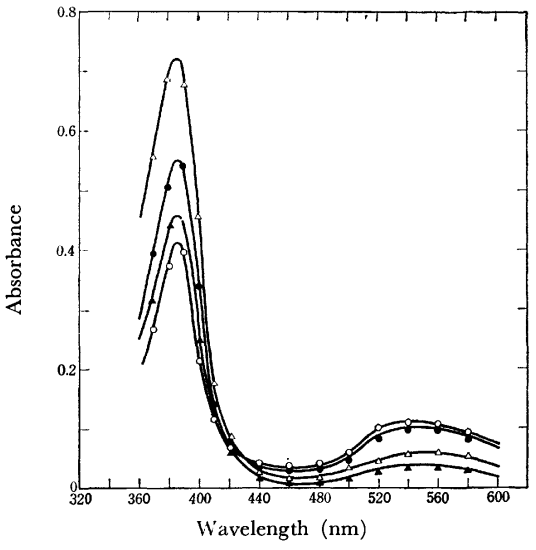

Fig. 1. Absorption spectrum of the transient species in 3.0×10^{-5}M 4-nitropyridine *N*-oxide in ethanol at room temperature.
(1) -○-, (2) -●-, (3) -△-, and (4) -▲- indicate the spectrum taken at 40 μsec, 60 μsec, 200 μsec, and 1 msec, respectively, after the flash.

1) Part I: N. Hata, E. Okutsu, and I. Tanaka, This Bulletin, **41**, 1769 (1968).
2) C. Kaneko, S. Yamada, I. Yokoe, N. Hata, and Y. Ubukata, *Tetrahedron Lett.*, **1966**, 4729.
3) C. Kaneko, S. Yamada, and I. Yokoe, *Chem. Pharm. Bull.* (Tokyo), **15**, 356 (1767).
4) C. Kaneko, I. Yokoe, and S. Yamada, *Tetrahedron Lett.*, **1967**, 775.
5) N. Hata, E. Okutsu, and I. Tanaka, This Bulletin, **41**, 1769 (1968).
6) E. Ochiai, *J. Org. Chem.*, **18**, 535 (1953).

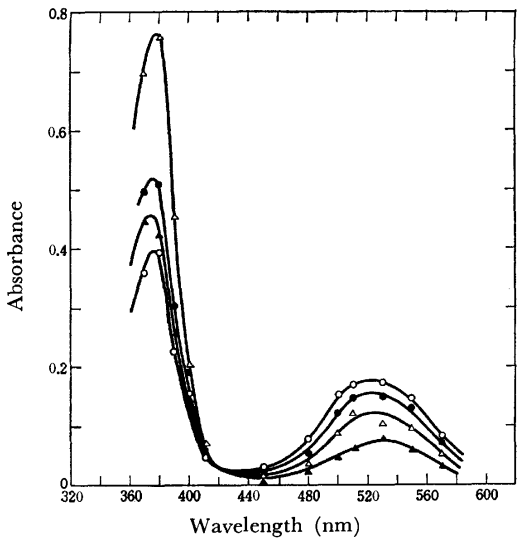

Fig. 2. Absorption spectrum of the transient species in 3.0×10^{-5} M 4-nitropyridine *N*-oxide in glycerol at room temperature.
(1) -○-, (2) -●-, (3) -△-, and (4) -▲- indicate the spectrum taken at 40 μsec, 60 μsec, 200 μsec, and 1 msec, after the flash.

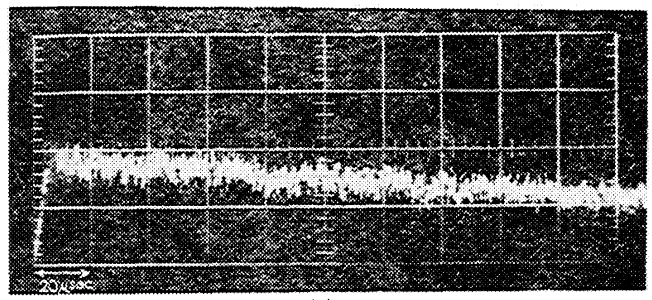

(a)

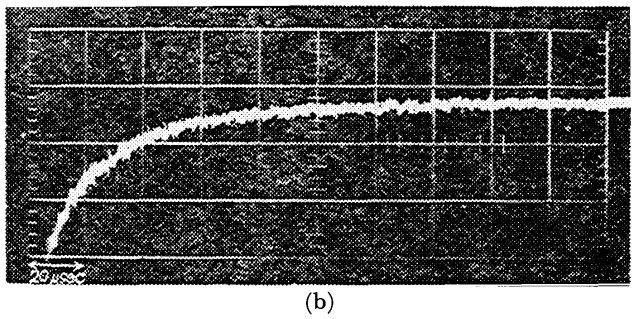

(b)

Fig. 3. Oscilloscope traces of transient absorption at 530 nm and 380 nm in ethanol (3.0×10^{-5} M) at room temperature. Horizontal scale, 20 μsec/division; Vertical scale, transmitted light intensity (downward).
(a): at 530 nm, (b) at 380 nm

in an oxygen-saturated solution, but they were not quenched completely. In addition, it may be inferred from these figures that the decay of the 530-nm species was followed by the formation of the 380-nm species. Figure 3 presents some typical pictures of oscilloscope traces taken at 530 nm and 380 nm after flash illumination of a 3.0×10^{-5} M solution of 4-nitropyridine *N*-oxide in deaerated ethanol. It is clear that an appreciable time was required for the appearance of the 380-nm species, while the formation of the 530-nm species was instantaneous-within the time of the flash. Quite similar results were also obtained in a methanol or an isopropanol solution. These observations indicate that the transient absorption which appeared around 530 nm was due to species different from those of the 380 nm absorption.

Next, kinetic examinations of the transients produced by flash illumination in deaerated solutions such as methanol, ethanol, isopropanol, and glycerol were carried out by measuring photoelectrically the time dependence of the absorption intensity (D) at 530 nm and 380 nm under various conditions.

Figure 4(a) shows the results when the first-order rate law was applied for the decay of the transients at 530 nm, while the second-order rate plots are shown

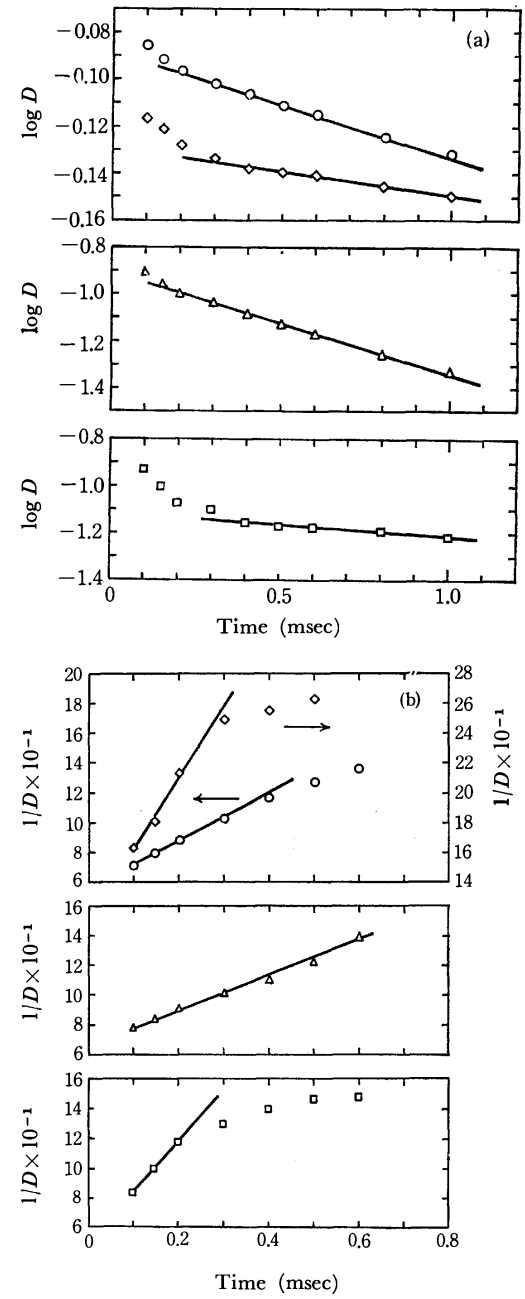

Fig. 4. First- and second-order rate plots for the decay of the transient absorption at 530 nm in various solvents at room temperature.
-◇-: in methanol, -○-: in ethanol, -△-: in isopropanol, -□-: in glycerol.
(a) first-order rate plots, (b) second-order rate plots.

in Fig.4(b). There, the second-order rate plot in Fig. 4(b) seems to require some considerations, because the slope at the first (initial) stage of decay is greater than that at the second stage in the cases of methanol, ethanol, and glycerol solution.

Generally, when any transient species, say X, is able to decay according to both the first- and second-order processes, the decay rate is expressed as follows:

$$-\mathrm{d}[\mathrm{X}]/\mathrm{d}t = k_1[\mathrm{X}] + k_2[\mathrm{X}]^2 \quad (1)$$

where k_1 and k_2 represent, respectively, the first- and second-order rate constants. The slope of the first-order rate plot is given by Eq. (2). Thus, the slope at the first stage of decay must be greater than that at the second stage.

$$-\mathrm{d}(\ln[\mathrm{X}])/\mathrm{d}t = k_1 + k_2[\mathrm{X}] \quad (2)$$

Equation (3) gives a slope of the second-order rate plot, indicating that the slope at the second stage of decay can be expected to be greater than that of the first stage.

$$\mathrm{d}(1/[\mathrm{X}])/\mathrm{d}t = k_1/[\mathrm{X}] + k_2 \quad (3)$$

These general relations were applied to the present experimental results. Tentatively, let us suppose that the transient absorption around 530 nm is due to a single species which decays according to both the first- and second-order rate laws. On this assumption, the first-order rate plot in Fig.4(a) is consistent with Eq.(2), whereas the second-order rate plot in Fig.4(b) is in conflict with Eq.(3). For this reason, it seems most reasonable to conclude that the 530 nm absorption should be ascribed to two transient species which decay with different first-order rate constants. Therefore, the faster species is referred to as the intermediate A (rate constant, k_A) and the slower one as the intermediate A′ (rate constant, $k_{A'}$). The values of these rate constants, as evaluated from the decay curve in Fig. 4(a), are given in Table 1.

TABLE 1. RATE CONSTANTS OF THE INTERMEDIATE SPECIES A, A′, AND B IN VARIOUS SOLVENTS AT ROOM TEMPERATURE

Solvent	k_A(sec^{-1}) $\times 10^{-4}$	$k_{A'}$(sec^{-1}) $\times 10^{-2}$	k_B(sec^{-1}) $\times 10^{-1}$	k_B^f(sec^{-1}) $\times 10^{-4}$
Methanol	2.4	2.3	0.17	5.0
Ethanol	0.90	9.2	1.2	1.5
Isopropanol	0.48	9.2	3.1	0.82
Glycerol	1.0	2.0	0.25	1.1

Figures 5 and 6 show the first- and second-order rate plots for the transient absorption around 380 nm. There, a single straight-line relation was obtained by plotting log D against the time in an isopropanol or glycerol solution, while in a methanol or ethanol solution the decay curve followed, at the first stage of decay, the second-order rate law and, at the second stage, the first-order kinetics. Moreover, in the case of a methanol or ethanol solution, the first- and second-order rate plots were fairly consistent with Eqs.(2) and (3). From these results, it may be concluded that the transient absorption around 380 nm is due to a single species which decays according to the first-order kinetics, but that there is a small contribution from the second-order process in the case of a methanol

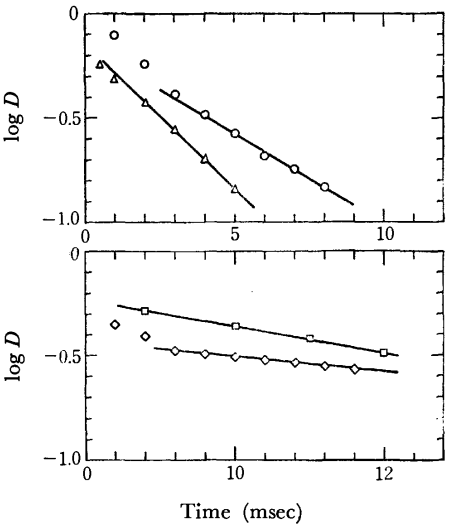

Fig. 5. First-order rate plots for the decay of the transient absorption at 380 nm in various solvents at room temperature.
-◇-: in methanol, -○-: in ethanol, -△-: in isopropanol, -□-: in glycerol.

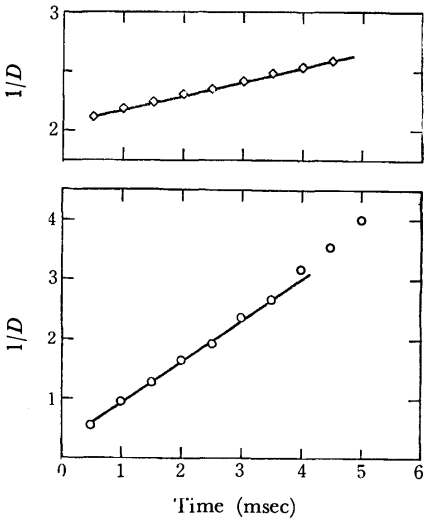

Fig. 6. Second-order rate plots for the decay of the transient absorption at 380 nm in methanol (-◇-) and in ethanol (-○-).

or ethanol solution. Therefore, the transient species is referred to as the intermediate B, and the first-order rate constants, k_B, estimated from the straight-line portion of the curve in Fig. 5 are given in Table 1.

The rate constant of the formation of the intermediate B, k_B^f, was evaluated from the rise in the transient absorption at 380 nm (Fig.3). The values thus obtained of k_B^f in various solutions are listed in Table 1. In Table 1 the decay rate of the intermediate A may be found to agree closely with that of the formation of the intermediate B. This suggests that the species B is produced directly from the intermediate A.

Although the decay rate of the intermediate B increased when the solvent was changed from methanol to ethanol and then to isopropanol, such a solvent dependency of the decay rate was not found in the case of the intermediate A or A′ (Table 1). The data imply that the intermediate B is probably responsible

for Process II, which involves a hydrogen-atom abstraction from the solvent alcohol, as has been reported previously.[5] Generally, when any transient species can abstract a hydrogen atom from a hydrogen donor, its decay rate may be expected to increase in proportion to the concentration of the hydrogen donor. In order to confirm which intermediate, A, A′, or B, is involved in the hydrogen-atom abstraction from the solvent alcohol, therefore, the decay rates of these species were determined as a function of the concentration of isopropanol added as a hydrogen donor in a methanol solution; the results are shown in Fig.7. The decay

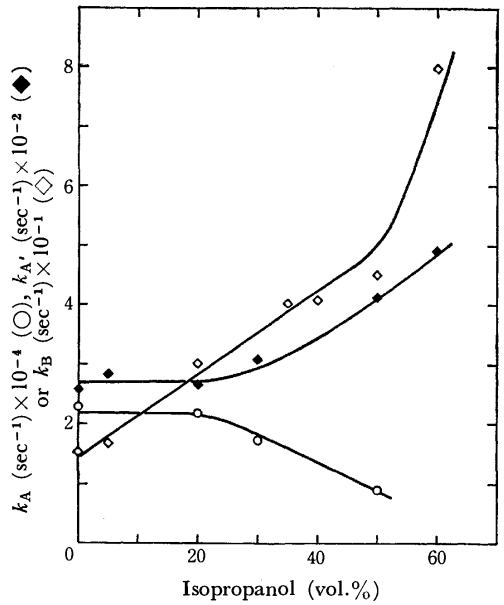

Fig. 7. Effect of an addition of isopropanol on the first-order decay rates of the intermediate species A, A′, and B in methanol.
-○-: intermediate species A, -◆-: intermediate species A′, -◇-: intermediate species B.

rate of the intermediate B increased proportionately with the amounts of isopropanol added, while the decay of the intermediate A or A′ was independent of the addition of isopropanol up to about 20 vol.%. Consequently, it appears plausible that the intermediate B is responsible for Process II. When the amounts of isopropanol added exceeded *ca* 40% in volume, however, the decay rates of these species showed a great change and approached the value in the case of the isopropanol solution.

In a previous paper,[5] on the basis of the concentration and temperature dependences of the quantum yield of the 4-nitropyridine *N*-oxide disappearance, Process I has been inferred to proceed *via* a transient complex formed from the interaction of an intermediate, say Y, originating from the excited singlet state (S_1) with an unexcited molecule (S_0), as described in the following sequence:

	Rate
$Y \rightarrow S_0$ (or chemical change)	$k_Y^a[Y]$
$S_0 + Y \rightarrow (S_0Y)$	$k_Y^b[S_0][Y]$
$(S_0Y) + S_0 \rightarrow Y + S_0 + S_0$	$k_Y^c[(S_0Y)][S_0]$
$(S_0Y) \rightarrow$ Process I	

If these steps are actually involved in Process I, and if one of the three transients, A, A′, and B, observed here corresponds to the intermediate Y described above, then its decay rate (k_Y) may be expected to vary with an increased concentration of 4-nitropyridine *N*-oxide following Eq.(4).

$$k_Y = k_Y^a + k_Y^b[S_0] - k_Y^c[(S_0Y)][S_0]/[Y] \quad (4)$$

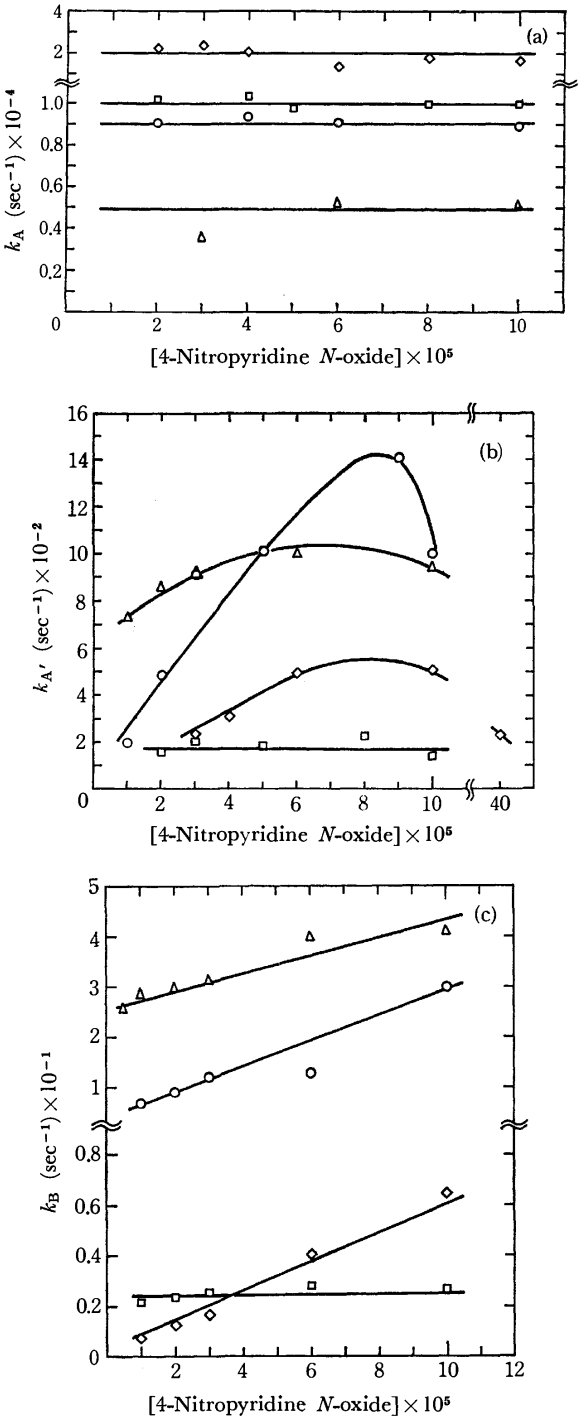

Fig. 8. First-order decay rates of the intermediate species A, A′, and B *versus* initial concentration of 4-nitropyridine *N*-oxide.
-◇-: in methanol, -○-: in ethanol, -△-: in isopropanol, -□-: in glycerol.
(a) intermediate species A, (b) intermediate species A′, (c) intermediate species B.

For this reason, the effect of the initial concentration of 4-nitropyridine *N*-oxide on the decay rates of the intermediates, A, A′, and B, was examined in deaerated ethanol. With an increase in the concentration of 4-nitropyridine *N*-oxide, as Fig. 8 shows, the decay rate of the intermediate A′ increased until it approached a steady value, and then decreased; such a concentration-dependence of the decay rate is consistent with Eq.(4). On the other hand, the decay rate of the intermediate B increased linearly with an increase in the concentration of 4-nitropyridine *N*-oxide, while that of the intermediate A remained unchanged, in the range of concentrations used in this experiment. These resluts support the idea that the intermediate A′ is responsible for Process I, and that this process proceeds through the formation of a transient complex (S_0A').

From the experimental results presented above, the following scheme seems to be reasonable for the primary photochemical process of 4-nitropyridine *N*-oxide in an alcoholic solution;[7] a partial modification is made of a scheme proposed in a previous paper.[5] The 4-nitropyridine *N*-oxide excited into the S_1 state by absorbing the ultraviolet light (>300 nm) is converted into the intermediate A (530nm), followed by transformation to the intermediate B (380 nm),

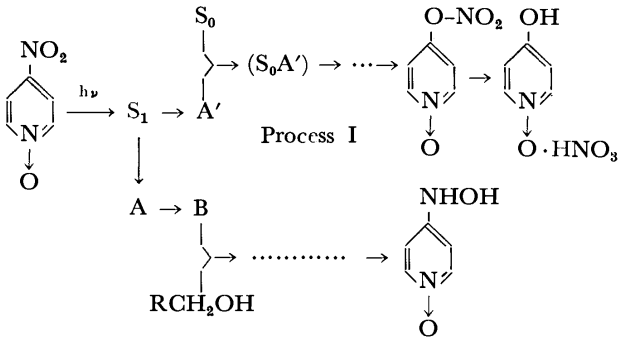

which then abstracts a hydrogen atom from an alcoholic solvent to lead to Process II. Here, it seems to be of particular interest that 4-nitropyridine *N*-oxide is photochemically reduced *via* some intermediates originating from the excited singlet state, since the photochemical reduction of aromatic nitro compound generally proceeds through the lowest triplet state.[8] As will be reported in a later paper,[9] however, it has become apparent from the studies of the biacetyl sensitization that the photoreduction of 4-nitropyridine *N*-oxide is also capable of proceeding *via* the lowest triplet state. The intermediate A′ (530 nm), which is also considered to result from the S_1 state, would interact with the ground state molecule, S_0, to give a transient complex (S_0A'), through which Process I proceeds. The end product of Process I, the 4-hydroxypyridine *N*-oxide nitrate, has been demonstrated to result from a hydrolysis of the nitric acid ester of 4-hydroxypyridine *N*-oxide generated during the photoreactions.[3] Accordingly, certain reactions taking place within the transient complex (S_0A') appear to lead to the formation of this nitric acid ester, although the mechanism is entirely ambiguous at present. The 4-hydroxylaminopyridine *N*-oxide formed by Process II may be converted photochemically to 4-nitropyridine *N*-oxide under an oxygen atmosphere.[10] Hence, the ultraviolet irradiation of the 4-nitropyridine *N*-oxide in an atmosphere of oxygen is expected to give 4-hydroxypyridine *N*-oxide nitrate as the major product; in fact, its yield has been reported to be 60–65% in an ethanol solution.[3] On the contrary, the 4-hydroxylaminopyridine *N*-oxide is expected to be the main product under a nitrogen atmosphere, particularly in the case of a concentrated solution of 4-nitropyridine *N*-oxide, because most of the transient complex (S_0A') is quenched by collision with an unexcited *N*-oxide molecule; Process II thus becomes more likely. The experiments performed under such conditions support this idea.[2,5]

Meanwhile, as has been suggested by Kaneko *et al.*[3,4] the Nef-type mechanism is also anticipated to be responsible to some extent for the formation of 4-hydroxypyridine *N*-oxide nitrate; especially, the photoreaction of 3,5-dimethyl 4-nitropyridine *N*-oxide has been considered to be due to this mechanism.[4] It seems, therefore, that further studies are necessary in order to elucidate the mechanism of Process I.

As to the structure of the intermediates, A, A′, and B, involved in Process I or II, we could not draw any conclusions from only the present experimental results. As judged from the facts that 4-nitropyridine *N*-oxide undergoes a photochemical change in a moiety of the nitro group, but not of the N→O group, however, it may be assumed that the nitro group in each of these intermediates is considerably different from a normal one in structure. In addition, the fact that the absorption spectrum of the intermediate A (530 nm) exists in the same region as that of the intermediate A′ suggests that their electronic structures are quite similar to each other. On the other hand, the absorption band of the intermediate B (380 nm) is located rather close to that of 4-nitropyridine *N*-oxide (330 nm), which probably means

7) Considered from the fact that the transient absorptions are always observed regardless of the presence or absence of oxygen in solution, the intermediate species A, A′, and B are assumed to originate from the excited singlet state (S_1) but not the lowest triplet state.

8) a) Nitrobenzene and 1-nitronaphthalene : R. Hurley and A. C. Testa, *J. Amer. Chem. Soc.*, **88**, 4330 (1966), *ibid.*, **89**, 6917 (1967), S. Hashimoto, J. Sunamoto, H. Fujii, and K. Kano, This Bulletin, **41**, 1249 (1968), J. A. Barltrop, and N. J. Bunce, *J. Chem. Soc., C*, **1968** 1467, W. Trotter and A. C. Testa, *J. Amer. Chem. Soc.*, **90**, 7044 (1968), R. Hurley and A. C. Testa, *ibid.*, **90**, 1949 (1968), S. Hashimoto and K. Kano, *Kogyo Kagaku Zasshi*, **72**, 188 (1969), W. Trotter and A. C. Testa, *J. Phys. Chem.*, **74**, 845 (1970); b) 4-Nitropyridine : S. Hashimoto, K. Kano, and K. Ueda, *Tetrahedron Lett.*, **1969**, 2733. This Bulletin, **44**, 1102 (1971). c) About the photochemistry of aromatic nitro compounds see, for example, H. A. Morrison, "The Chemistry of the Nitro and Nitroso Groups," Part 1, ed. by H. Feuer, Interscience Publishers, New York, (1969), Chapter 4.

9) I. Ono and N. Hata, This Bulletin, in press.

10) The photochemical conversion of 4-hydroxylaminopyridine *N*-oxide to 4-nitropyridine *N*-oxide in ethanol under an oxygen atmosphere has been reported by Kaneko *et al.*[3]

that the nitro group of the intermediate B structurally a little resembles that of unexcited 4-nitropyridine *N*-oxide. In order to clarify the structure of the intermediates, A, A′, and B, it seems to be important to elucidate in detail the reaction mechanism for both Processes I and II; along this line further studies are now in progress.

In conclusion, the authors wish to express their hearty thanks to Professor Ikuzo Tanaka of Tokyo Institute of Technology for his encouragement and Professor Shiro Matsumoto of this university for his permission to use a flash-photolysis apparatus.

BULLETIN OF THE CHEMICAL SOCIETY OF JAPAN, VOL. 45, 2391—2397 (1972)

Studies of the Properties of the Basic Sites on the Silica-alumina Surface through the Reaction of the Basic Sites with Copper(II) Complexes Containing 2,2′-Bipyridine

Kazuto TAKIMOTO

Department of Chemistry, Faculty of Science, Hiroshima University, Higashisenda-machi, Hiroshima

(Received February 14, 1972)

The substitution reactions of complexes with basic sites on the surfaces of silica-alumina and alumina and the properties of the basic sites were studied through the adsorption of the complexes onto the surfaces. The hydroxyl groups with basic strengths of two kinds, $H_0 > 9.3$ and $7.2 < H_0 < 9.3$, exist on the silica-alumina surface pretreated at 300°C. They are present in a cluster state. The basic strength becomes higher as the outgassing temperature becomes lower. The complexes predominantly interact with the O^{2-} ions on the surface pretreated at a relatively high temperature, resulting in new chemical species. The basic strength of the O^{2-} ions is lower than that of the hydroxyl groups on the surface pretreated at a lower temperature. The hydroxyl groups on the alumina surface outgassed at 300°C are distributed, on the whole, homogeneously in comparison with those of the silica-alumina surface, and their basic strength is $H_0 > 9.3$. The nature of the basic sites on the alumina surface tends to vary with the outgassing temperature, similarly to those on the silica-alumina surface. These analyses were performed on the basis of the ESR spectra for complexes in basic solutions.

The acidic properties of the silica-alumina surface have been extensively studied by various techniques[1-4] because the catalytic action of silica-alumina is closely correlated with its acidic properties.[5,6] The nature and the structure of the acidic sites and such reactions as isomerization and polymerization on the surface have been reviewed by Tanabe and Takeshita.[7]

On the other hand, Krylov *et al.* have found, by the phenol-vapor adsorption method, that the basic sites are present on the surface of silica-alumina.[8] It is of great interest from the viewpoint of acid-base bifunctional catalysis that the basic sites as well as the acidic sites exist on the surface. The basic properties of the silica-alumina surface have been investigated by several means,[8,9] but the nature and structure of the basic sites have scarcely been revealed. However, the basic properties of alumina[10] as well as those of calcium oxide [11] and magnesium oxide[12] have been fairly well elucidated in comparison with those of silica-alumina. It has been reported that weakly basic sites are present on the surface of silica gel on the basis of the measurement of the amounts of phenol vapor retained on this surface at various elevated temperatures.[8] Peri[13] and Yamadaya[14] have proposed a mechanism of the formation of the basic sites which include hydroxyl groups and/or negatively-charged oxygen ions, O^{2-}.

We found, from our ESR measurements, that the coordinated water molecules in the copper(II) complexes with 2,2′-bipyridine were replaced by one or two hydroxyl ions in aqueous solutions at pH values higher than 8.[15] Such a phenomenon was also observed in basic methanol solutions. Thus, these complexes were adsorbed as so-called indicators in order to elucidate the basic properties of the hydroxyl groups on the surfaces of silica-alumina and alumina. The ESR spectra for the complexes adsorbed on the surfaces were quite similar to those in the basic solutions; the hydroxyl groups contribute to the formation of the chemical species on the surfaces. However, in

1) O. Johnson, *J. Phys. Chem.*, **59**, 827 (1955).
2) H. Uchida and M. Temma, *Shokubai*, **4**, 353 (1962).
3) W. K. Hall, *J. Catal.*, **1**, 53 (1962).
4) M. R. Basila, J. R. Kantner, and K. H. Rhee, *J. Phys. Chem.*, **68**, 3197 (1964).
5) K. Tarama, S. Teranishi, H. Honda, and S. Yoshida, *Shokubai*, **6**, 268 (1964).
6) J. W. Ward and R. C. Hansford, *J. Catal.*, **13**, 154 (1969).
7) K. Tanabe and T. Takeshita, "San Enki Shokubai (Acid-Base Catalysis)," Sangyo Tosho, Tokyo (1966).
8) O. V. Krylov and E. A. Hokina, *Probl. Kinetiki i Kataliza, Acad. Nauk. USSR*, **8**, 248 (1955).
9) K. Tanabe and T. Yamaguchi, *J. Res. Inst. Catalysis, Hokkaido Univ.*, **14**, 93 (1966).
10) G. M. Schwab and H. Kral, *Proc. Intern. Congr. Catalysis, 3rd, Amsterdam*, **1**, 433 (1964).
11) K. Saito and K. Tanabe, *Shokubai*, **11**, (25th Symp. Catalysis, Preprints of Paper), 206 (1969).
12) J. Take, N. Kikuchi, and Y. Yoneda, *ibid.*, **10**, (23rd Symp. Catalysis, Preprints of Papers), 127 (1968).
13) J. B. Peri, *J. Phys. Chem.*, **69**, 220 (1965).
14) M. Yamadaya, K. Shimomura, T. Konoshita, and H. Uchida, *Shokubai*, **7**, 313 (1965).
15) K. Takimoto and M. Miura, This Bulletin, in press.

addition to these hydroxyl groups, it is also necessary to take negatively-charged oxygen ions into consideration as basic sites when the samples are treated at relatively high temperatures; α sites which contain a negatively-charged oxygen ion in close proximity to an exposed aluminum ion are formed by the condensation of Al-OH groups in the course of the dehydration of the surface.[16] These sites are acid-base rather than Lewis-acid sites. This method can differentiate to some extent which of the basic sites is mainly bound to these complexes, as will be discussed later. In this paper, the substitution reaction of the complexes with the basic sites on the surfaces of silica-alumina and alumina, and the properties of the basic sites, as estimated from an analysis of the chemical species which are generated by these reactions, will be reported.

Experimental

Materials. The cupric sulfate, methanol, and 2,2′-bipyridine, all obtained from the Wako Pure Chemical Co., were of a guaranteed reagent grade and were used without further purification. The indicators,[17] bromothymol blue ($pK_a=7.2$), and phenolphthalein ($pK_a=9.3$) from the Yoneyama Co., were also of a guaranteed reagent grade. The copper(II) complexes with 2,2′-bipyridine, the 1 : 1 complex (or $[Cu(bip)(H_2O)_4]SO_4$) and the 1 : 2 complex (or $[Cu(bip)_2(H_2O)_2]SO_4$), were synthesized in methanol and were recrystallized repeatedly from methanol. The alumina, 50% silica-alumina, and silica gel were the same as those used in our preceding work.[18]

Procedures. These complexes were adsorbed from water-free methanol solutions onto surfaces which had previously been treated at 100, 300, 500, and 800°C for 3 hr. After the methanol had been eliminated, the ESR spectra were measured at 77°K. These experiments were carried out in a dark room because these complexes are photosensitive.

Apparatus. The ESR spectra were obtained by using a spectrometer described elsewhere.[19] The chemical species were determined from the ESR spectra of the 1st and 2nd derivatives.

Results and Discussion

Chemical Species in the Solutions. The ESR spectra in methanol solutions were measured in order to be compared with those obtained on the surfaces. The ESR spectrum for the 1:1 complex is shown in Fig. 1. The spin Hamiltonian can be described as:

$$\mathscr{H} = \beta[g_{//}H_zS_z+g_\perp(H_xS_x+H_yS_y)] + A_{//}S_zI_z + A_\perp(S_xI_x+S_yI_y)$$

where β is the electron Bohr magneton, where $g_{//}$ and $g_\perp$ are the components of the axial g tensor, and where $A_{//}$ and $A_\perp$ are the components of the copper nuclear hyperfine (hf) interaction. This spectrum is axially symmetrical. Four peaks were observed in the lower

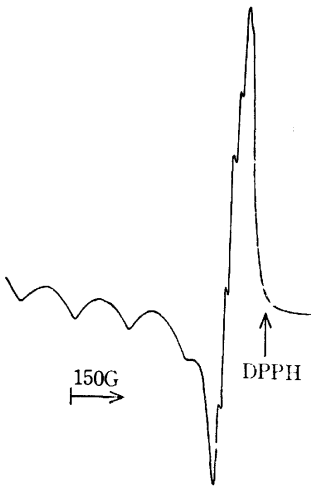

Fig. 1. ESR spectrum for the 1 : 1 complex in methanol at 77°K.

magnetic field. These are ascribed to the parallel component of the hf interaction due to the nuclear spin of copper, $I=3/2$. The superhyperfine (shf) structure was observed in the perpendicular component in the higher magnetic field. When the 1:1 complex is prepared in methanol, the following chemical equilibrium may be established:

$$Cu^{2+} + bip + 4H_2O \rightleftarrows \underset{I}{[Cu(bip)(H_2O)_4]^{2+}} \quad (1)$$

Only the I species was observed, probably because the equilibrium lies almost completely to the right. According to the Jahn-Teller effect, the long or distortion axis is frozen in different orientations at low temperatures. The stable state is the one in which the distorted z axis is perpendicular to the plane containing ligands. Thus, two nitrogen atoms in a bipyridine molecule predominantly coordinate with the copper ion in the xy plane.[20,21]

The ESR parameters for the 1:1 complex are plotted against the concentration of sodium hydroxide in a methanol solution in Fig. 2. With an increase in the basic concentration, three sets of $g_{//}$ and $A_{//}$ values were observed. The reactions of this complex with the hydroxyl ion may be represented as:[22]

$$\underset{I}{[Cu(bip)(H_2O)_4]^{2+}} + OH^- \rightleftarrows \underset{II}{[Cu(OH)(bip)(H_2O)_3]^{1+}} + H_2O \quad (2)$$

$$2\underset{II}{[Cu(OH)(bip)(H_2O)_3]^{1+}} \rightleftarrows \underset{II'}{[(H_2O)_2(bip)Cu\langle^{OH}_{OH}\rangle Cu(bip)(H_2O)_2]^{2+}} + 2H_2O \quad (3)$$

16) J. B. Peri, *J. Phys. Chem.*, **70**, 3168 (1966).
17) K. Tanabe and T. Yamaguchi, *J. Res. Inst. Catalysis, Hokkaido Univ.*, **11**, 179 (1964).
18) M. Miura, Y. Kubota, T. Iwaki, K. Takimoto, and Y. Muraoka, This Bulletin, **42**, 1476 (1969).
19) A. Hasegawa and M. Miura, *ibid.*, **40**, 2553 (1967).
20) W. B. Lewis, M. Alei, and L. O. Morgan, *J. Chem. Phys.*, **45**, 4003 (1966).
21) M. Noack and G. Gordon, *J. Chem. Phys.*, **48**, 2689 (1968).
22) R. B. Ryland, G. S. Ronay, and F. M. Fowkes, *ibid.*, **62**, 798, 867 (1958).

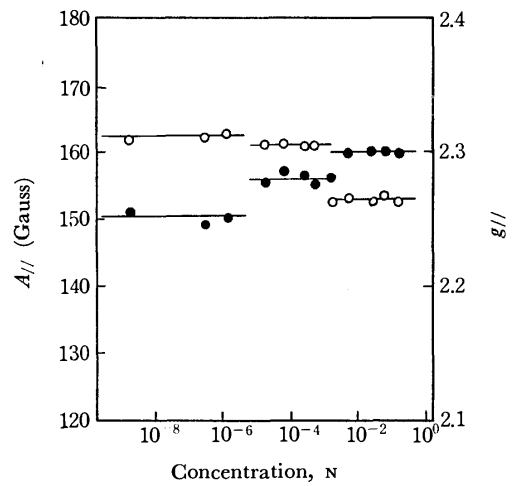

Fig. 2. Variations of the ESR parameters for the 1 : 1 complex with the concentration of sodium hydroxide in methanol solution.
●: $A_{//}$; ○: $g_{//}$

$$\frac{1}{2}[(H_2O)_2(bip)Cu\langle^{OH}_{OH}\rangle Cu(bip)(H_2O)_2]^{2+} + OH^-$$
II′
$$\rightleftarrows [Cu(OH)_2(bip)(H_2O)_2]^0 \quad (4)$$
III
$$[Cu(OH)(bip)(H_2O)_3]^{1+} + OH^-$$
II
$$\rightleftarrows [Cu(OH)_2(bip)(H_2O)_2]^0 + H_2O \quad (5)$$
III

It is well known that the value of $g_{//}$ decreases, and that of $A_{//}$ increases, with an increase in the ability of eletron donation of a ligand, which can be represented by pK_a;[23] the covalency of the bonding of the copper ion with the ligand increases. The covalency depends mainly upon the value of $g_{//}$, as has been reported by Maki and McGarvey[24] and by Kivelson and Neiman.[25] When the ligand is replaced by a more basic one, the values of $g_{//}$ and $A_{//}$ change with the number of the latter ligands.[26] Thus, the species with the highest value of $g_{//}$ (2.313) corresponds to I. On the other hand, the species with the middle and lowest values of $g_{//}$ (2.306 and 2.263) correspond to II and III respectively. However, the dimer species II′ could not be observed in the methanol solution; the coupling constant of the hf interaction was not one-half of that of the II species, and furthermore the signal due to the $\Delta M_s = \pm 2$ transitions could not be detected in a much lower field, *ca.* 1600 gauss. On the contrary, the formation of the dimer species was confirmed in a basic aqueous solution by Ryland[22] and by Harris.[27]

When the 1:2 complex is prepared in methanol, the chemical equilibrium may be established as follows:

$$[Cu(bip)(H_2O)_4]^{2+} + bip$$
I
$$\rightleftarrows [Cu(bip)_2(H_2O)_2]^{2+} 2H_2O \quad (6)$$
IV

The IV species was overwhelmingly observed, probably because the equilibrium lies almost to the right. Figure 3 shows the ESR parameters for the 1:2 complex, also with the basic concentration of the methanol solution. The following chemical equilibria for the 1:2 complex in the basic methanol solution are considered to be established by taking those in the basic aqueous solutions into account:[28]

$$[Cu(bip)_2(H_2O)_2]^{2+} + OH^-$$
IV
$$\rightleftarrows [Cu(OH)(bip)(H_2O)_3]^{1+} + bip \quad (7)$$
II
$$2[Cu(OH)(bip)(H_2O)_3]^{1+}$$
II
$$\rightleftarrows [(H_2O)_2(bip)Cu\langle^{OH}_{OH}\rangle Cu(bip)(H_2O)_2^{2+} + 2H_2O$$
II′ (8)
$$[Cu(OH)(bip)(H_2O)_3]^{1+} + OH^-$$
II
$$\rightleftarrows [Cu(OH)_2(bip)(H_2O)_2)]^0 + H_2O \quad (9)$$
III
$$\frac{1}{2}[(H_2O)_2(bip)Cu\langle^{OH}_{OH}\rangle Cu(bip)(H_2O)_2]^{2+} + OH^-$$
II′
$$\rightleftarrows [Cu(OH)_2(bip)(H_2O)_2]^0 \quad (10)$$
III

Two sets of ESR parameters were observed, as can be seen in Fig. 3. The species with the higher value

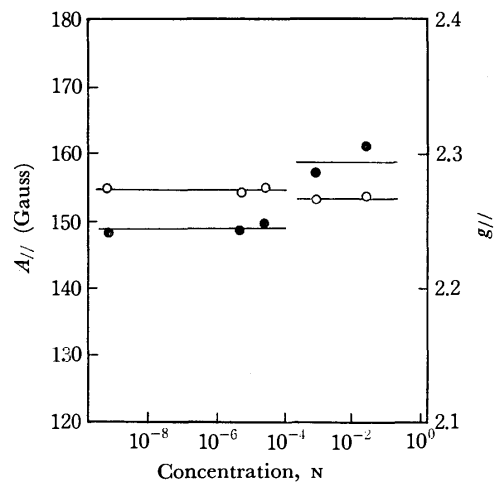

Fig. 3. Variations of the ESR parameters for the 1 : 2 complex with the concentration of sodium hydroxide in methanol solution.
●: $A_{//}$; ○: $g_{//}$

23) H. Yokoi, U. Otagiri, M. Sai, and T. Isobe, Symp. ESR, 10th, Tokyo, Preprints of Papers, 62 (1971).
24) A. H. Maki and B. R. McGarvey, *J. Chem. Phys.*, **29**, 31 (1958).
25) D. Kivelson and R. Neiman, *ibid.*, **35**, 149 (1961).
26) K. Takimoto, A. Hasegawa, and M. Miura, in press.
27) C. M. Harris, E. Sinn, W. R. Walker, and P. R. Woolliams, *Aust. J. Chem.*, **21**, 631 (1968).
28) H. Ojima, *Nippon Kagaku Zasshi*, **84**, 787 (1963).

of $g_{//}$ corresponds to IV. The II species in Eq. (7) could not be observed, although that in Eq. (2) could be detected. This may indicate that the equilibrium of Eq. (7) lies almost completely to the left. On the contrary, the II species in Eq. (7) could be observed in the aqueous solution. The dimer species II′ could not be observed either, as in the case of the 1:1 complex.

When the 1:2 complex was dissolved in 40% ethanol-60% water and measured at 77°K, two chemical species were observed by Noack and his co-worker.[21] One is a *trans* isomer which is the same as the IV species observed in methanol at 77°K. The other species, with a much lower value of $g_{//}$ and a smaller value of $A_{//}$, is the *cis* isomer (Species V). Two bipyridine molecules coordinate with the copper ion, on the *xy* and *xz* or *yz* planes respectively. The *cis* isomer is predominant at room temperature.

The ESR spectra were also measured in the basic aqueous solution, since the chemical species in the aqueous solution had been determined by means of the absorption-spectra and conductometric-titration methods.[22,28] The $g_{//}$ value in a methanol solution was almost the same as that in an aqueous solution, while the $A_{//}$ value varied somewhat; the chemical species of the former are the same as the latter. However, the perpendicular component of the ESR spectra obtained in the methanol solution was a single line, while that in the aqueous solution was split. This may be ascribed to the effect of the linewidth. The over-all spectra obtained on the surface are rather similar to those in methanol solutions

Chemical Species on the Surfaces. Since the acitve sites on the surface are largely influenced by water molecules, an adsorbate is usually adsorbed on the surface from a solution of a nonpolar solvent. In this study, however, these complexes were adsorbed on the surface from water-free methanol solutions because they scarcely dissolved at all in any nonpolar solvent. The complex and methanol competitively react with surface hydroxyl groups, so that an ester may be formed by the reaction of methanol with the hydroxyl groups. If the 1:1 complex is present on the esterified surface, the values of $g_{//}$ and $A_{//}$ may be similar to those of the I species, since the electron-donation ability of the $-OCH_3$ group is much lower than that of the hydroxyl group. Such a species, however, could not be observed on the surfaces. Thus, the basic hydroxyl group on the surfaces may be considered to react with the complexes in preference to methanol. The comparison of the ESR parameters in the solutions with those obtained on the surfaces is reasonable, since the axial symmetry of the latter is also approximately maintained.

The properties of the basic sites on the surfaces, the distribution and the strengths of the basic sites, were determined in the following way. The qualitative distribution of the basic sites was estimated from the distance between the neighboring ligands replaced by two hydroxyl ions or hydroxyl groups, which can be calculated from the data of the X-ray analysis of the 1:2 complex;[29,30] the complex is a measure for determining the distribution of the basic sites. It is presumed that the distance is about 3 Å. The distance between the neighboring ligands of the 1:1 complex may be slightly different from that of the 1:2 complex.[21] On the other hand, the strengths of the basic sites on the surfaces were deduced from the pK_a value corresponding to the pH value of the aqueous solution, in which the complexes begin to react with hydroxyl ions. For the 1:1 complex, the coordinated water molecule begins to be replaced by the hydroxyl ion at pH≒8. The color of bromothymol blue ($pK_a=7.2$) begins to change from yellow to green at pH≒ 8. Thus, the basic strength of the aqueous solution at pH≒8 appreximately corresponds to $H_0=7.2$.[31] The basic strength of the aqueous solution at pH≒ 9.6 corresponds to $H_0=9.3$, since the color of phenolphthalein ($pK_a=9.3$) begins to change at pH≒9.7. The coordinated water molecule in the 1:2 complex begins to be replaced by the hydroxyl ion at pH≒9.6; it resists the substitution reaction more than the 1:1 complex. This tendency becomes larger with an increase in the number of the bipyridine molecule coordinated to the copper ion.[28] Thus,

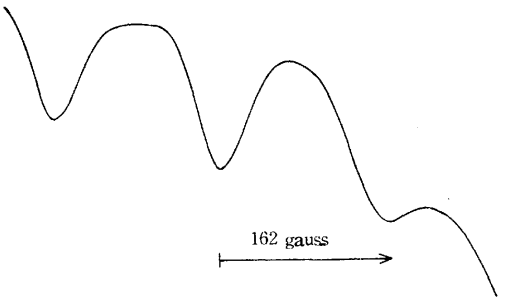

Fig. 4. Parallel component of the ESR spectra for the 1 : 1 complex adsorbed on the surface of 50% silica-alumina pretreated at 300°C.

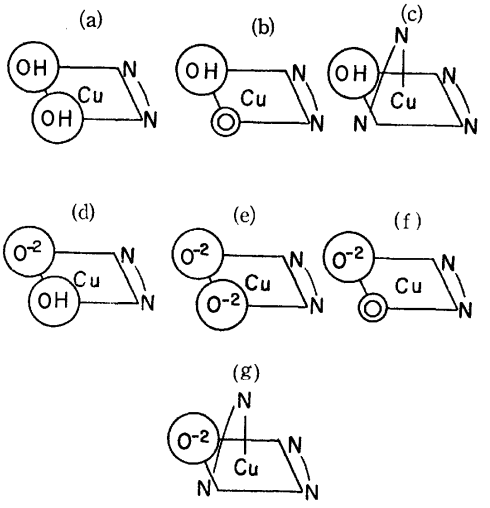

Fig. 5. Chemical species which are possibly generated by the interaction between the complexes and the basic sites of the surfaces.
◎: solvent molecule

29) H. Nakai, S. Ooi, and H. Kuroya, This Bulletin, **43**, 577 (1970).
30) I. M. Procter and F. S. Stephens, *J. Chem. Soc.*, *A*, **1969**, 1248.
31) Reference 7, p. 73—76.

the formation of the II or III species by the adsorption of the 1:1 and 1:2 complexes suggests that basic sites with at least $H_0>7.2$ and $H_0>9.3$ exist on the surfaces.

Figure 4 shows the parallel component of the ESR spectrum for the 1:1 complex adsorbed on the surface of 50% silica-alumina treated at 300°C for 3 hr. By comparison with the values of $g_{//}$ and $A_{//}$ in the solutions, only one species formed on this surface was determined to be III. The chemical species which are possibly generated by the interaction between the complexes and the surfaces are represented in Fig. 5. The III species can be illustrated by (a) in the figure. The basic strength of the hydroxyl groups participating in the formation of the (a) type is at least $H_0>7.2$. The distance between the neighboring hydroxyl groups on the surface is estimated to be about 3 Å.[29,30] Thus, the (a) type is generated on only two contacted hydroxyl groups. The maximum number of hydroxyl groups which can be present on the surface is calculated to be 11 OH's per 100 Å. On the other hand, Morimoto *et al.*[32] have reported that the number of hydroxyl groups on the 50% silica-alumina surface pretreated at 300°C is 3.5 OH's per 100 Å. These facts may indicate that the hydroxyl groups exist in a cluster rather than homogeneously.

Figure 6 shows the parallel components of the ESR spectrum for the 1:2 complex adsorbed on the surface of 50% silica-alumina which had previously treated at 300°C for 3 hr. This spectrum indicates that another type exists in addition to the (a) type. The spectrum with the values of $g_{//}=2.224$ and $A_{//}=138$ gauss is the *cis* isomer, represented as the (c) type; only the hydroxyl groups of $H_0>9.3$ can expel one bipyridine molecule from the 1:2 complex, while those of $7.2<H_0<9.3$ can not, as can be understood from the substitution reaction in the basic aqueous solution. The (b) type could not be observed, either. Certainly, then, basic sites with basic strengths of two kinds are present on the 50% silica-alumina.

Figure 7 shows the parallel components of the ESR

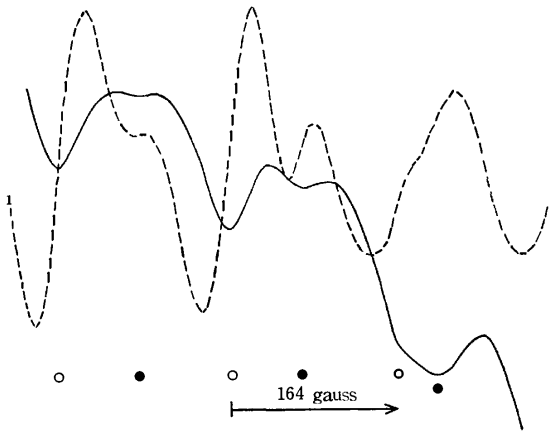

Fig. 6. Parallel component of the ESR spectra for the 1:2 complex adsorbed on the surface of 50% silica-alumina pretreated at 300°C.
——: the 1st derivative, ----: the 2nd derivative;
○: type (a), ●: type (c)

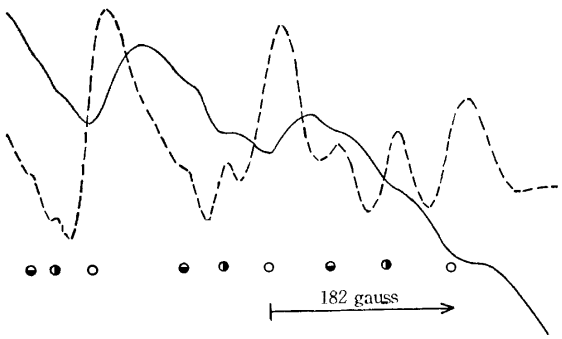

Fig. 7. Parallel component of the ESR spectra for the 1:1 complex adsorbed on the surface of alumina pretreated at 300°C.
——: the 1st derivative, ----: the 2nd derivative;
○: type (a), ◑: type (b), ◒: unknown

spectrum for the 1:1 complex adsorbed on the surface of alumina pretreated at 300°C for 3 hr. Three chemical species were observed. The species with the lowest value of $g_{//}$ (2.265) corresponds to the (a) type, while that of the middle value of $g_{//}$ (2.306) is assigned to the (b) type by comparison with those in the solutions. In additon to these two species, a third species ($g_{//}=2.340$) exists. Its structure is still uncertain. It is necessary for the formation of the (a) type that the distance between the neighboring basic hydroxyl groups of $H_0>7.2$ is at least 3 Å, as has been described previously. Furthermore, the presence of the (b) type suggests that the distance between the neighboring hydroxyl groups of $H_0>7.2$ is larger than 3 Å. That is, the basic hydroxyl groups may, as a whole, be distributed homogeneously without forming a cluster, unlike the case of 50% silica-alumina. When the 1:2 complex was adsorbed on the alumina surface, the ESR spectrum was exactly the same as that for the 1:1 complex. Three types are present on this surface, while the (c) type could not be observed. This suggests that the basic hydroxyl groups of $H_0>9.3$ predominate over those of $7.2<H_9<9.3$.

The ESR parameters on the surface of 50% silica-alumina are plotted against the outgassing temperature in Fig. 8. When the 1:2 complex was adsorbed on a surface pretreated at 100°C for 3 hr, the (c) type could hardly be detected. This probably reflects the lack of basic hydroxyl groups of $7.2<H_0<9.3$. The basic strength of the hydroxyl groups became higher as the outgassing temperature was lowered; the value of $g_{//}$ increased and that of $A_{//}$ decreased with a rise in the outgassing temperature from 100 to 300°C. O'Reilley *et al.* have indicated, from their NMR studies, that the majority of protons are present as Si-OH groups on the surface.[33] Basila has reported that the isolated Si-OH groups on the silica-alumina surface increase as the outgassing temperature is raised.[34] The appearance of the stronger hydroxyl groups, with a decrease in the outgassing temperature seems, therefore, to be due to the weakly-bonded hydroxyl group attached to the aluminum atom. This me-

32) T. Morimoto, M. Nagao, and J. Imai, This Bulletin, **44**, 1282 (1971).

33) D. E. O'Reilley, H. P. Leftin, and W. K. Hall, *J. Chem. Phys.*, **29**, 970 (1958).

34) M. R. Basila, *J. Phys. Chem.*, **66**, 2223 (1962).

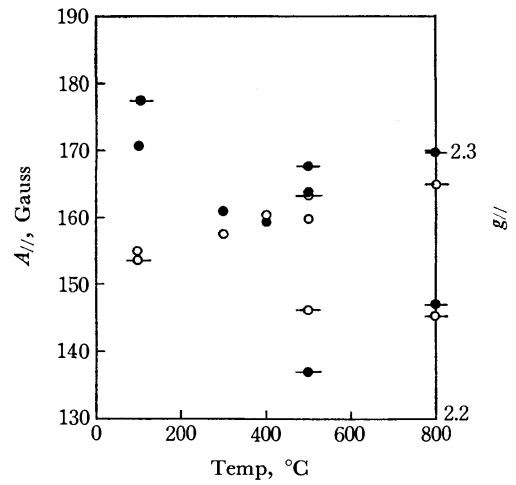

Fig. 8. Variations of the ESR parameters for the complexes adsorbed on the surface of 50% silica-alumina with the outgassing temperature.
●: $g_{//}$, ○: $A_{//}$ for the 1:1 complex;
●: $g_{//}$, ○: $A_{//}$ for the 1:2 complex

chanism is similar to that for the alumina surface, as will be described later. When the surface is pretreated at a relatively high temperature, it is considered that the negatively-charged oxygen ions play an important role in the substitution reaction. It has been reported that α sites which contain a negatively-charged oxygen ion in close proximity to an exposed aluminum atom are present on the surface pretreated between 300 and 500°C at a concentration of less than 10^{13} sites/cm^2.[16] Above this outgassing temperature, the O^{2-} ions are closely connected with the formation of the chemical species of the (d)-(g) types.

The 1:2 complex was adsorbed on the surface pretreated at a much higher temperature, 800°C, in order to investigate whether or not the O^{2-} ions reacted with the complex. Two chemical species were observed on this surface. However, they were different from the two types, (a) and (c), generated on the surface pretreated at 300°C. The value of $g_{//}$ for one species was somewhat higher than that of the (a) type. The other was slightly different from that of the (c) type. The absorption band at 3745 cm^{-1} which is due to an isolated Si-OH group appears on the surface pretreated at 500°C and is quite similar to that on the the silica gel surface.[34] Linear relationships have been found between the electronegativities of elements bonded to the hydroxyl groups and the vibrational frequencies of the hydroxyl groups;[35] the charge density of the hydroxyl groups becomes larger and the wave number shifts upward as the electronegativities of the elements decrease. The wave number of the Si-OH group on the surface of silica-alumina is approximately the same as that on silica gel. Thus, the hydroxyl groups on the silica-alumina surface pretreated at higher temperatures are not basic, since the silica gel sufrace is not basic, as will be discussed later. The (e) and (g) types, therefore, seem to be present on the surface pretreated at 800°C. Judging from the $g_{//}$ value, the basic strength of the O^{2-} ions formed at relatively high temperatures is rather weaker than that of the hydroxyl groups retained on the surface pretreated at a lower temperature. The values of $g_{//}$ for the complex adsorbed on the surface pretreated at 400–800°C were approximately constant. This may indicate that the O^{2-} ions predominantly react as basic sites on the surface, while the hydroxyl groups mainly react as basic sites on the surface pretreated below 300°C.

In order to compare them with those of the silica-alumina surface, the ESR spectra were also measured on the calcium oxide surface since the basic properties of the latter surface have been fairly well established. The basic strength of the hydroxyl groups on the surface of calcium hydroxide is quite different from that of the O^{2-} ions on the surface of calcium oxide. When the 1:2 complex was adsorbed on the surface of calcuim hydroxide pretreated at 100°C for 3 hr, the (a) type was observed. On the other hand, when the 1:2 complex was adsorbed on the surface of calcium oxide pretreated at 600°C for 3 hr, the observed species was quite different from the (a) type. The O^{2-} ions are responsible for the formation of this species, since scarcely no hydroxyl groups exist on this surface.[36] The parallel components of the ESR spectrum consist of four peaks. This spectrum is rather similar to that of cupric sulfate in methanol. All the bipyridine molecules in the 1:2 complex, therefore, seem to be expelled through the reaction with the surface. However, no such phenomenon was observed in the basic solutions These facts suggest that the basic strength of the O^{2-} ions is much higher than that of hydroxyl ions or hydroxyl groups. This is aslo in good agreement with the fact that the basic strength of the O^{2-} ions on the surface of calcium oxide is quite great, as determined by the phenol-vapor adsorption method.[8,12]

The ESR parameters for the surface of alumina are plotted against the outgassing temperature in Fig. 9. When the complexes were adsorbed on the surface of alumina pretreated at 100°C, the (a) and (b) types were observed. The value of $g_{//}$ for the (a) type was low in comparison with that on the alumina surface pretreated at 300°C. This supports the mechanism of the formation of the basic sites proposed by Yamadaya *et al.*; [14] they attributed the basic property of alumina to weakly-adsorbed hydroxyl groups rather than to strongly-adsorbed ones. The 1:2 complex was adsorbed on the surface of alumina pretreated at 800°C in order to determine whether the complex reacts with the hydroxyl groups or with O^{2-} ions. Two chemical species were observed. The $g_{//}$ values for these two species ($g_{//}$=2.270 and 2.316) were somewhat higher than those of the (a) and (b) types respectively. The α sites which contain negatively-charged oxygen ions begin to appear at about 400°C.[24] Thus, the O^{2-} ions are considered to be responsible for the formation of three chemical species, the (d), (e), and (f) types. The surface of alumina pretreated at 800°C has well-defined absorption maxima at 3700, 3733,

35) R. West, *J. Phys. Chem.*, **64**, 822 (1960).

36) S. Malinowski, S. Szczepanska, and J. Sloczynski, *J. Catal.* **7**, 67 (1964).

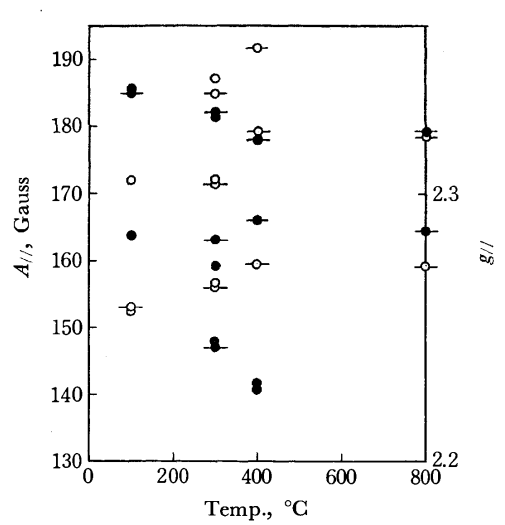

Fig. 9. Variations of the ESR parameters for the complexes adsorbed on the surface of alumina with the outgassing temperature.
●: $g_{//}$, ○: $A_{//}$ for the 1:1 complex;
●: $g_{//}$, ○: $A_{//}$ for the 1:2 complex

3744, 3780, and 3800 cm^{-1}.[13] These correspond to the isolated hydroxyl groups. Peri has reported that the basic strength of the hydroxyl group becomes higher as the number of negatively-charged oxygen ions surrounding its hydroxyl group increases;[13] some of these isolated hydroxyl groups can act as basic sites. The species with the value of $g_{//}$ (2.270) may be ascribed to the (d) or (e) type, and that with the value of $g_{//}$ (2.316) may correspond to the (b) or (f) type. On the whole, the basic strengths of both the hydroxyl groups and O^{2-} ions on this surface are lower than those of hydroxyl groups on the surface pretreated at a very low temperature, as can be seen in Fig. 9. The value of $g_{//}$ increased to 400°C and thereafter was approximately constant. This may indicate that the strengths of the basic sites on the surface of alumina pretreated below 400°C mainly depend on the hydroxyl groups, while those of sites on the surface evacuated above this temperature predominantly depend upon the the hydroxyl groups and/or the O^{2-} ions.

When the 1:1 complex was adsorbed on the surface of silica gel pretreated at 300°C for 3 hr, only one species was observed. The shf structure at the higher magnetic field coincided in position with that observed in the acidic methanol solution. The hydroxyl groups on the surface of silica gel, therefore, seem to be acidic rather than basic, though it has been reported, on the basis of the phenol-vapor adsorption method,[8] that those on the surface are weakly basic.

Conclusion. Hydroxyl groups with basic strengths of two kinds, $H_0>9.3$ and $7.2<H_0<9.3$, are present on the 50% silica-alumina surface pretreated at 300°C for 3 hr. They exist in a cluster state on the surface. The negatively-charged oxygen ions play an important role as basic sites on the silica-alumina surfaces pretreated at relatively high temperatures. The basic strengths of the hydroxyl groups become higher as the outgassing temperature is lowered. This seems to be due to the weakly-bonded Al-OH groups on the silica-alumina surface. The hydroxyl groups of $H_0>9.3$ are present on the alumina surface pretreated at 300°C, and they are distributed, as a whole, homogeneously in comparison with those on the silica-alumina surface. The basic strengths of the hydroxyl groups get higher as the outgassing temperature is lowered. This seems to be ascribable to the weakly-bonded hydroxyl groups rather than to the strongly-bonded ones. The negatively-charged oxygen ions and/or the hydroxyl groups act as basic sites on the alumina surface pretreated above 400°C. The hydroxyl groups on the silica gel surface are acidic rather than basic.

The author wishes to express his hearty thanks to Professor Masaji Miura for his continuous encouragement and guidance throughout this work.

Calorimetric and Magnetic Studies of Crystalline and Glassy Bis[*N*-(3-methoxysalicylidene)isopropylamine]nickel(II)[1]

Naoto Arai, Michio Sorai, and Syûzô Seki

Department of Chemistry, Faculty of Science, Osaka University, Toyonaka, Osaka

(Received March 1, 1972)

Thermal and magnetic properties of Ni(3-CH_3O-SAL·*iso*-C_3H_7)$_2$ were investigated by measuring thermograms, infrared and electronic spectra, heats of solution, magneitc susceptibilities, and heat capacities around glass transition temperature. In addition to the known paramagnetic crystalline phase III and the diamagnetic crystalline phase IV, two new crystalline phases (I and II) were discovered. Phase I was found to be paramagnetic, its molecular geometry being of a tetrahedral four-coordinated form like that of phase III, while phase II, similar to phase IV, is diamagnetic and has a square-planar four-coordinated form. Although the order of thermodynamic stability of these four crystalline phases was not determined, they were isolated stably at room temperature. The supercooled liquid and glassy states of this compound were realized for the first time by quenching the sample in the molten state. Unusual magnetic behaviors of these two states were satisfactorily accounted for by assuming an equilibrium between the diamagnetic and the paramagnetic species. In the supercooled liquid state, the paramagnetic species was partially converted into the diamagnetic one with decreasing temperature. Below the glass transition temperature T_g, however, this conversion process was prevented and the magnetic susceptibility obeyed apparently Curie's law with a 26% paramagnetic content. The heat capacity measurement revealed a typical glass transition phenomenon at 297.5 K and the heat capacity jump at T_g was determined to be 172 $JK^{-1}mol^{-1}$. Detailed discussions were given for the relationship between molecular geometry and its associated magnetic property and also for the phase relationship between various phases.

Extensive studies have been carried out on the magnetic properties of the Schiff base metal complexes. An interesting problem in this field might be the elucidation of the relationship between the geometry of molecules and their associated magnetic properties. Bis(*N*-R-X-salicylidene)nickel(II) is a typical example. The molecular formula of this compound is illustrated in Fig.1 and abbreviated as Ni(X-SAL·R)$_2$

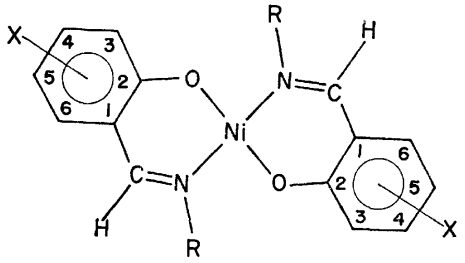

Fig. 1. Molecular formula of Ni(X-SAL·R)$_2$.

hereafter. By varying the substituent groups X and/or R, this coordination compound can possess the following four molecular forms; (i) square planar four-coordinated form, (ii) tetrahedral four-coordinated one, (iii) binuclear five-coordinated one, and (iv) polymeric octahedral six-coordinated chain form.[2-4]

In the solutions in inert solvents, Ni(X-SAL·R)$_2$ exists as an equilibrium mixture consisting of two or more species of the four forms. The magnetic properties of these solutions depend on both temperature and concentration. This phenomenon is well known as "solution paramagnetism."

In a solid state, however, a given Ni(X-SAL·R)$_2$ can possess only one form. Rare exceptions are the cases of Ni(H-SAL·CH_3)$_2$,[5,6] Ni(5-Cl-SAL·CH_3)$_2$,[7] and Ni(5-Br-SAL·CH_3)$_2$,[7] where the additional paramagnetic forms have been obtained by heating the stable diamagnetic form in a solid state.

Recently Yamada *et al.*[8] reported the new finding of a pair of isomers for crystalline Ni(3-CH_3O-SAL·*p*-Cl-C_6H_4)$_2$ and Ni(3-CH_3O-SAL·*p*-Br-C_6H_4)$_2$, where the binuclear five-coordinated as well as the polymeric six-coordinated forms have been stably isolated as a crystalline state. A similar isolation has been also reported for the present material by the same authors.[9] In this case brown and green crystals were obtained from methanol and ethylether solutions, respectively. The electronic spectra and magnetic susceptibility measurements at room temperature revealed that the brown crystal shows paramagnetism and its central Ni^{2+} ion is coordinated tetrahedrally, while the green crystal is diamagnetic with a square-planar form. These authors also reported transformation of the green form into the brown one at 430—431 K followed by melting at 460—461 K.

The main purpose of the present work is to investigate the relationship between molecular geometry and magnetism in Ni(3-CH_3O-SAL·*iso*-C_3H_7)$_2$ and also to elucidate the relative thermodynamic stability among different crystalline forms by means of precise heat of solution and magnetic susceptibility measurements as well as spectroscopic methods. In addition to the green and the brown forms mentioned above, we found two other new crystalline phases which exist stably at room temperature. We also found that both the supercooled liquid and the glassy states can

1) A part of this paper was read before the 6th Japanese Calorimetry Conference, November (1970), Yokohama.

2) R. H. Holm, G. W. Everett, Jr., and A. Chakarvorty, *Progr. Inorg. Chem.*, **7**, 83 (1966).

3) B. O. West, "New Pathways in Inorganic Chemistry," Cambridge Univ. Press (1968), p. 303.

4) E. K. Barefield and D. H. Busch, *Quart. Rev.*, **22**, 456 (1968).

5) C. M. Harris, S. L. Lenzer, and R. L. Martin, *Austral. J. Chem.*, **11**, 331 (1958).

6) L. Sacconi, P. Paoletti, and R. Cini, *J. Amer. Chem. Soc.*, **80**, 3583 (1958).

7) H. C. Clark and R. J. O'Brien, *Can. J. Chem.*, **37**, 436 (1959); **39**, 1030 (1961).

8) S. Yamada, K. Iwasaki, and A. Takeuchi, *Inorg. Chim. Acta*, **2**, 395 (1968).

9) A. Takeuchi and S. Yamada, This Bulletin, **42**, 3046 (1969).

be realized by quenching the molten state. The brown and green forms will be designated as crystalline phases III and IV, respectively, and the two new forms as crystalline phases I and II, respectively, following the order of magnitude of heat of solution of each phase (see Fig.5).

For the sake of comparison, the magnetic structure of Ni(H-SAL·$CH_3)_2$ crystal was also investigated by measuring the infrared and electronic spectra as well as the thermograms.

Experimental

Material. *(A) Ni(3-CH_3O-SAL·iso-$C_3H_7)_2$*: Of the four isomers of the present complex, crystalline phases III and IV were prepared by following the method of Takeuchi and Yamada[9] and phases I and II were obtained from III or IV on heating in the solid state. Preparation of each crystalline phase, the supercooled liquid and the glassy state was carried out as follows:

(i) Crystalline phase III. The crude material was recrystallized from methanol solution to give brown prism crystals. *(ii) Crystalline phase IV.* Evaporation of a solvent from a green ethylether solution of the brown crystal yielded a green prism crystal which was purified by recrystallization from the same solvent. *(iii) Crystalline phase I.* Heating the crystalline phase III up to 443—448 K for *ca.* 15 minutes or phase IV up to 403—438 K for *ca.* 30 minutes under the atmosphere of helium gas converted the respective phases into a brown colored phase I, which was easily supercooled down to room temperature. *(iv) Crystalline phase II.* By keeping the supercooled liquid of the present complex at 343—363 K for *ca.* 30 minutes, crystallization took place to give a green solid phase II, which was also supercooled easily to room temperature. *(v) Supercooled liquid and glassy states.* These phases were obtained by quenching the molten substance at a cooling rate greater than 10 K min^{-1}. Results of chemical and elementary analyses of each crystalline phases are given in Table 1.

Table 1. Elementary and chemical analyses of Ni(3-CH_3O-SAL·*iso*-$C_3H_7)_2$ and Ni(H-SAL·$CH_3)_2$

		C(%)	H(%)	N(%)	Ni(%)
	Ni(3-CH_3O-SAL·*iso*-$C_3H_7)_2$				
Calcd		59.62	6.37	6.32	13.25
Found	Phase I	59.49	6.28	6.32	—
	Phase II	59.67	6.39	6.29	—
	Phase III	59.75	6.47	6.34	13.16
	Phase IV	59.70	6.37	6.32	—
	Ni(H-SAL·$CH_3)_2$				
Calcd		58.77	4.93	8.57	17.95
Found	Phase I	58.61	4.94	8.56	17.83
	Phase II	58.73	4.95	8.56	17.82

(B) Ni(H-SAL·$CH_3)_2$: Diamagnetic green form (phase II) and paramagnetic buff-colored form (phase I) were prepared according to the methods by Klemm and Raddatz[10] and others.[5,6] The results of elementary and chemical analyses of both forms are also shown in Table 1.

Thermal Analysis. Prior to precise calorimetric investigation, thermal analysis was made by using a differential scanning calorimeter (Perkin-Elmer, DSC-1B) at 173—473 K. The scanning rate was 10 K min^{-1}.

Infrared Absorption Spectra. The infrared spectra of Ni(3-CH_3O-SAL·*iso*-$C_3H_7)_2$ and Ni(H-SAL·$CH_3)_2$ were recorded on a Grating-type Infrared Spectrophotometer Model DS-402G (Japan Spectroscopic Co., Ltd.) in the range 4000—400 cm^{-1} at room temperature and 120 K. The far-infrared spectra of both compounds were also obtained by a Spectrophotometer No.FIS-001 (Hitachi Ltd.) in the range 500—80 cm^{-1} at the same temperatures. The Nujol mull method was employed for preparation of the samples.

Electronic Spectra. In order to get more insight into the coordination schemes in each phase of Ni(3-CH_3O-SAL·*iso*-$C_3H_7)_2$ we measured the electronic spectra. For the sake of comparison the electronic spectra of Ni(H-SAL·$CH_3)_2$ were also measured. The electronic reflection spectra of both compounds in solid state were recorded on a spectrophotometer model EPU-2A (Hitachi Ltd.) in the range 23,000—10,000 cm^{-1} at room temperature.

Heat of Solution. The heat of solution of Ni(3-CH_3O-SAL·*iso*-$C_3H_7)_2$ into chloroform was measured by using a LKB-8700 Precision Calorimetry System at 18—30°C. The calorimeter was standardized on an international scale in our laboratory by measuring the heat of solution of tris(methylhydroxy)aminomethane into 0.1 N HCl solution. The amount of sample used in each measurement varied from 90 to 620 mg but the amount of solvent was always about 100 cm^3.

Heat Capacity. The heat capacities of phase II and the glassy state of Ni(3-CH_3O-SAL·*iso*-$C_3H_7)_2$ at 230—343 K were measured by using an adiabatic calorimeter.[11] The amount of specimen was 24.3532 g(=0.0549502 moles). A small quantity of helium gas was sealed into the calorimeter cell along with the sample to aid in the heat transfer. The experimental errors were within ±0.3% in all cases.

The glassy state was prepared by quenching the molten substance in the calorimeter cell to dry-ice temperature. In this case the cooling rate was estimated to be about −100 K min^{-1}. After quick setting of the calorimeter cell to the cryostat, the temperature of the cell was maintained at 273 K during the course of evacuation of the equipment. This procedure prevented the transformation of the supercooled liquid into phase II.

The sample of phase II was prepared by complete transformation of the supercooled liquid into this phase by keeping the sample at 339.4 K (just above the crystallization temperature) for *ca.* 12 hr.

Magnetic Susceptibility. The magnetic susceptibilities of Ni(3-CH_3O-SAL·*iso*-$C_3H_7)_2$ were measured at the field-strength of 7.65 kG by use of the Faraday method in the temperature region 120—530 K. The amount of specimen employed was 400—500 mg.

Phase Relationships

Thermal analysis is one of the most effective methods for determining phase relations. Run 1 in Fig.2 shows the DSC curve of the brown paramagnetic phase III of Ni(3-CH_3O-SAL·*iso*-$C_3H_7)_2$. In heating direction the DSC curve showed an endothermic peak with a small subsequent exothermic effect at 433—443 K. Phase III was transformed into a new high-temperature phase. This phase (mp 460 K) was easily supercooled down to 173 K (see Run 2). The thermal behavior of the green phase IV is shown in Run 3. Phase IV was transformed into a high-temperature phase at 383 K, which was also supercooled down to 173 K and

10) W. Klemm and K. H. Raddatz, *Z. Anorg. Allgem. Chem.*, **250**, 207 (1942).

11) H. Suga and S. Seki, This Bulletin, **38**, 1000 (1965).

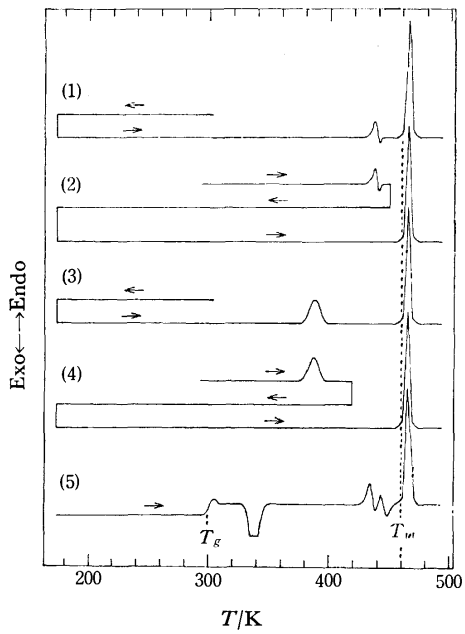

Fig. 2. DSC curves; (1) phase III, (2) a new high-temperature phase obtained from phase III, (3) phase IV, (4) a new high-temperature phase obtained from phase IV, and (5) the glassy state.

melted at 460 K (see Run 4). The thermal behavior of the molten substance of phase IV was exactly the same as that of phase III. By cooling the molten substance at the rate -10 K min^{-1} the liquid state was quenched to the lowest temperature investigated. Run 5 shows the heating curve of the quenched substance, which exhibited a thermal anomaly similar to that in a glass transition at *ca.* 298 K. The anomaly was confirmed to be a real glass transition through the enthalpy relaxation effects observed by auxiliary experiments. On further heating an exothermic peak due to crystallization was observed at *ca.* 333 K where the supercooled liquid state was irreversibly transformed into another crystalline phase, which we designate crystalline phase II. The phase showed rather complicated thermal behaviors at 423—453 K and melted at 460 K. It should be noticed that both high-temperature phases obtained by heating phases III and IV were recognized as the same crystalline phase, which we designate crystalline phase I. The colors of phases I and II were brown and green, respectively.

Infrared absorption spectra can provide useful information on molecular structure. Although quantitative assignments have not been made, noticeable differences in absorption peaks were observed among each crystalline phases. In the case of Ni(3-CH_3O-SAL·*iso*-$C_3H_7)_2$, the infrared spectrum of phase I was, on the whole, similar to that of phase III. However, extra absorption peaks characteristic of phase I were observed especially in the range 800—700 cm^{-1} and at 1045 cm^{-1}. The spectra of phases II and IV, on the other hand, resembled each other except for a slight differences in the range 400—350 cm^{-1}. The spectra of phases I and III were, however, quite unlike those of II and IV. The four spectra might be grouped into two classes, one consisting of the spectra of phases I and III, and the other the spectra of phases II and IV. One of the most characteristic peaks which can be distinguished from

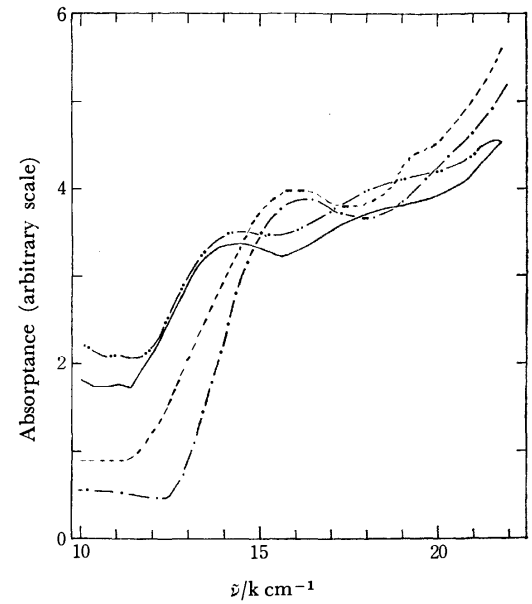

Fig. 3. The electronic spectra at room temperature; ——, phase I; ----, phase II; —·—, phase III; —·—, phase IV.

each class is the C=N stretching vibration near 1600 cm^{-1}. The single peak due to the C=N stretching in the first class was found to split into a doublet in the case of the second class; *i. e.*, 1607 cm^{-1} (strong) for phase I; 1607 cm^{-1} (strong) for phase III; 1602 (shoulder) and 1615 cm^{-1} (strong) for phase II; 1603 (moderate) and 1622 cm^{-1} (strong) for phase IV. Another characteristic band probably due to one of the metal-ligand coordinate bonds appeared in the far-infrared region; 304 cm^{-1} (phase I), 346 cm^{-1} (phase II), 301 cm^{-1} (phase III), and 347 cm^{-1} (phase IV).

In general, infrared spectra reflect the difference in molecular structure as well as the local symmetry in which a relevant absorption mode will be excited. Appreciable differences observed between the two classes indicate that remarkable differences exist in the molecular structure and the local symmetry. There is, however, little distinction between phases I and III and also between II and IV.

Similar situations were also observed in the electronic spectra of the four crystalline phases. The electronic spectra of Ni(3-CH_3O-SAL·*iso*-$C_3H_7)_2$ at room temperature are shown in Fig.3. The absorption maxima due to the crystal-field bands appeared at 11100 (weak), 14330 (strong), and 17830 cm^{-1} (broad) for phase I and at 11050 (weak), 14500 (strong), and 18300 cm^{-1} (broad) for phase III. These spectra have the closest resemblance to those of the other Schiff base nickel complexes with tetrahedral configuration. On the other hand, phases II and IV showed the crystal-field band at 16000 cm^{-1} and at 16200 cm^{-1}, respectively. These features are similar to the spectrum of the square planar phase II in Ni(H-SAL·$CH_3)_2$. It is therefore safely concluded that the coordination scheme in phases I and III of Ni(3-CH_3O-SAL·*iso*-$C_3H_7)_2$ is tetrahedral and in phases II and IV square planar.

Heat of Solution

If the precise heat capacity data from sufficiently

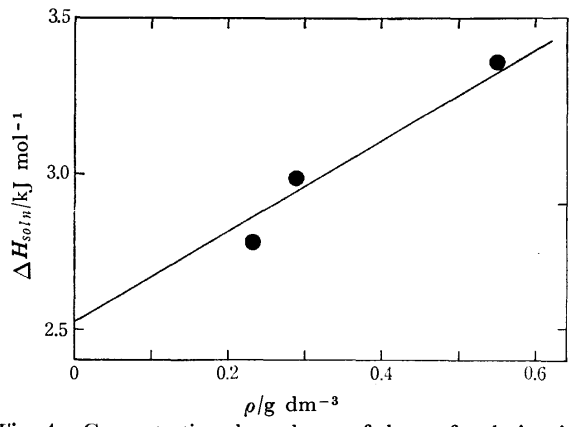

Fig. 4. Concentration dependence of heat of solution into chloroform at 24°C.

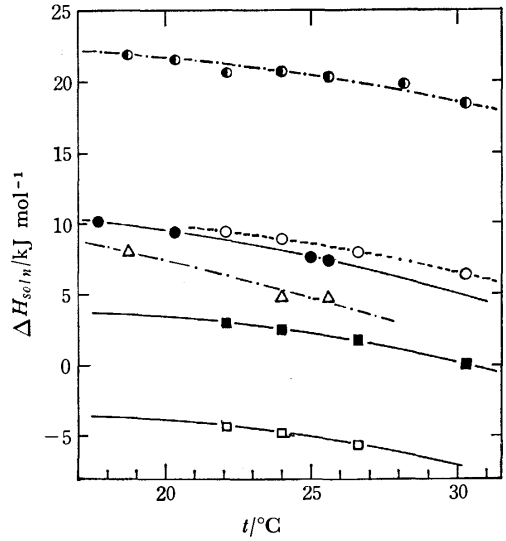

Fig. 5. Temperature dependence of the heat of solution; ○, phase I obtained from phase III; ●, phase I obtained from phase IV; △, phase II; ■, phase III; □, phase IV; and ◐, supercooled liquid state.

low temperatures are combined with the data of heat of solution, the difference in standard Gibbs energy between the phases might be obtained. The values enable us to determine the order of thermodynamic stability among various crystalline phases which remain "stable" at room temperature. We have measured the heat of solution of four crystalline phases and the supercooled liquid state of Ni(3-CH_3O-SAL·*iso*-$C_3H_7)_2$ at 18–30 °C. In order to confirm a possible concentration dependence on the heat of solution in advance, the data for the brown phase III was measured at 24°C by varying the amount of specimen. As is shown in Fig.4, an approximately linear dependence exists in the concentration region investigated. In determining the heat of solution, the following two assumptions were made; (i) the final state of the solution is identical in all cases and (ii) the correction to the infinitely diluted state of any sample is regarded as the same as the result given in Fig.4. The heats of solution thus obtained for each phase and the supercooled liquid state are plotted in Fig.5 as a function of temperature. The experimental error was estimated to be within ±0.62%. The ordinate ΔH_{soln} corresponds to the enthalpy difference between the infinitely diluted solution and solid phase.

We have regarded two high-temperature phases obtained by heating both phases III and IV as the identical phase (phase I), based on the results of infrared spectra. It was found, however, that there exists a slight but significant discrepancy in the heat of solution between the two kinds of samples of phase I prepared from phases III and IV (Fig.5). The discrepancies are beyond experimental error. This could be accounted for by close examination of each transition behavior revealed by the DSC curves. As shown in Fig.2, phase IV is transformed into phase I at 383 K accompanied by an endothermic peak, while phase III is transformed into phase I at a higher temperature *via* a metastable phase. The endothermic peak at 433 K corresponds to the transition from phase III to a metastable phase and the subsequent exothermic peak corresponds to that of metastable phase to phase I. In this two-step transition a sintering phenomenon was observed directly in the sample glass tube. The temperature range for phase I obtained from phase III is quite narrow compared with that formed from phase IV. Thus, severe control of temperature and complete transformation are necessary for the preparation of pure and stable phase I from phase III. The differences in the heat of solution of phase I can be attributed to the incomplete transformation from a metastable phase to phase I.

On the other hand, the heat of solution data for a supercooled liquid state and for phase II is not so accurate compared with those for phases I, III, and IV for the following reasons. The heat capacity measurement revealed that partial crystallization occurred in the supercooled liquid region even at temperatures far below the exothermic peak in the DSC curve. Thus the supercooled liquid samples used for the measurement of heat of solution seem to involve a certain amount of phase II arising from a partial crystallization at these temperatures, while the samples of phase II can involve partially the supercooled liquid state since the crystallization was too sluggish to attain completion.

It should be pointed out that there is a fundamental difference between thermal and various spectroscopic investigations. Only a slight difference was observed between phases I and III, and also between phases II and IV both in the infrared as well as in the electronic spectra. We have thus grouped these four phases into two classes; one consisting of phases I and III with the tetrahedral molecular form and the other of phases II and IV with the square-planar molecular form. The heat of solution, however, revealed large differences between phases I and III, and also between phases II and IV. These results imply that thermal investigations such as the measurement of heat of solution are more useful than spectroscopic analysis in the study of intermolecular interaction in relation to molecular arrangement or phase problem in the solid state.

Heat Capacity around Glass Transition Temperature

In order to obtain more quantitative insight into the glass transition phenomenon, the heat capacities

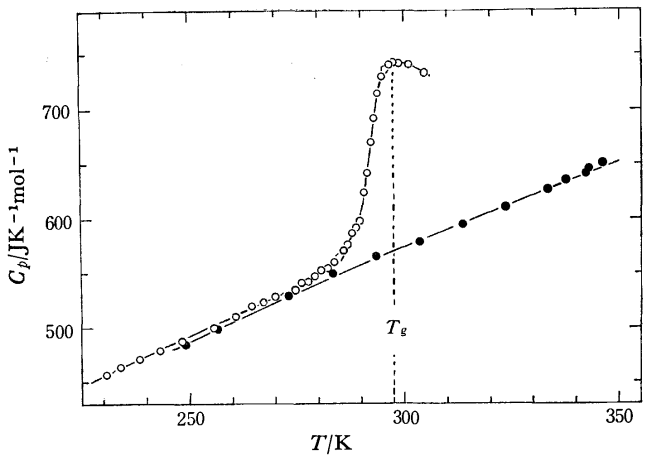

Fig. 6. Heat capacity around T_g; ○, glassy state and ●, phase II.

Table 2. The heat capacity of Ni(3-CH_3O-SAL·*iso*-$C_3H_7)_2$ (Molecular weight 443.187)

T/K	C_p/J K^{-1}mol^{-1}	T/K	C_p/J K^{-1}mol^{-1}
Glassy state		292.374	670.11
230.747	457.22	293.229	691.80
233.948	463.53	294.072	715.63
238.278	470.86	294.925	730.23
243.188	479.28	295.784	736.37
248.349	487.84	296.645	740.75
255.724	499.94	297.614	743.28
260.712	510.34	299.010	741.87
264.548	519.72	301.359	740.91
267.276	523.23	304.847	733.60
269.982	527.98	337.524	635.09
272.827	530.73	342.273	641.37
274.666	534.66	346.030	650.56
276.198	541.15		
277.722	542.11		
279.238	547.13	Phase II	
280.745	552.55	249.000	484.78
282.237	554.30	256.506	499.93
283.715	559.98	264.139	504.20
284.930	564.47	273.187	529.05
285.903	570.49	283.473	549.43
286.879	576.29	293.502	565.19
287.845	587.17	303.569	578.93
288.799	591.66	313.699	594.67
289.732	598.35	323.651	611.00
290.639	624.30	333.426	626.95
291.527	642.05	343.002	646.12

of the glassy state and phase II were measured at 230—343 K. The results are plotted in Fig .6 and listed in Table 2. A typical glass transition was observed at 297.5 K. The ratio of the glass transition temperature T_g to the melting point amounted to 0.648. This value falls within the range 0.50—0.67, which is favorable to a number of glass-forming materials. The heat capacity jump ΔC_p at T_g was 172 JK^{-1}mol^{-1} and the ratio of ΔC_p to the heat capacity of phase II at this temperature was found to be 0.309. The exothermic effect due to crystallization was observed just above T_g and the heat capacity in the narrow supercooled liquid region decreased with increasing temperature, even after correction of a temperature drift in the computation of the heat capacities. We were not able to measure the heat capacity of the supercooled liquid state above 305 K because the great evolution of heat due to the crystallization effect disturbed the measurements. Due to this gradual heat evolution effect even above T_g, we were not able to estimate the heat of crystallization directly from the heat capacity data. We can, however, evaluate this heat effect from the difference of heats of solutions for phase II and supercooled liquid state which amounts to *ca.* 15.7 kJ mol^{-1}.

Magnetic Properties

Extensive studies have been carried out on the magnetic susceptibility measurements of the Schiff base metal complexes. However, almost all the data are restricted to those obtained at room temperature. More quantitative information on the magnetic properties could be provided by varying the temperature.

We measured the magnetic susceptibility of the various phases of Ni(3-CH_3O-SAL·*iso*-$C_3H_7)_2$ over a wide temperature range of 120—530 K. The molar susceptibilities χ_m are plotted in Figs. 7—10. To make clear their correspondence to thermal behaviors, the results of DSC curves are also given. Although the general aspect of magnetic susceptibility coincided with the results of thermal data, slight mismatches in some anomalous parts were observed because of the different scanning rate of temperature, *i.e.*, 4—6 K min^{-1} in the magnetic measurement and 10 K min^{-1} in the thermal analysis, and also because of the uncertainty involved in temperature measurement for

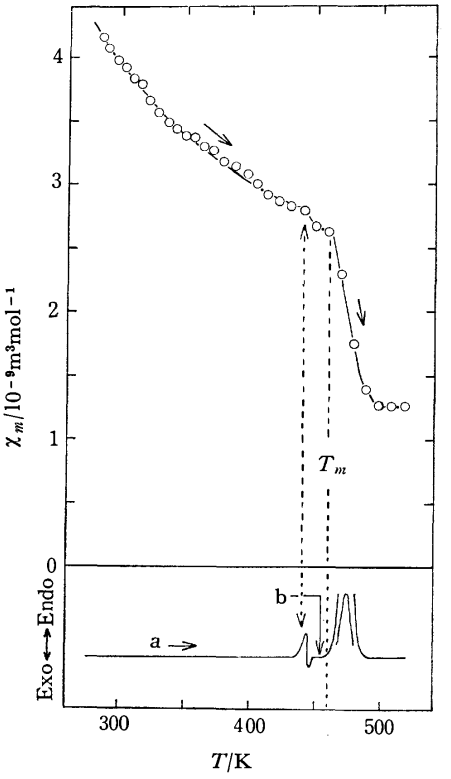

Fig. 7. Magnetic susceptibility χ_m *versus* temperature for phase III; (a) phase III and (b) phase I. In this and in Figs. 8—10, the DSC curves are also shown for comparison.

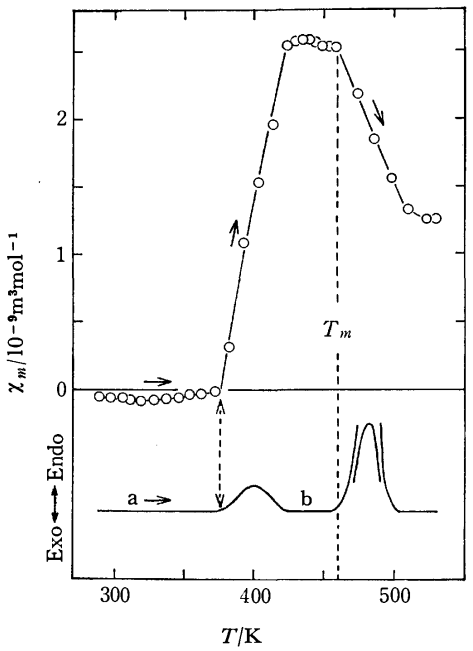

Fig. 8. χ_m *versus* T for phase IV; (a) phase IV and (b) phase I.

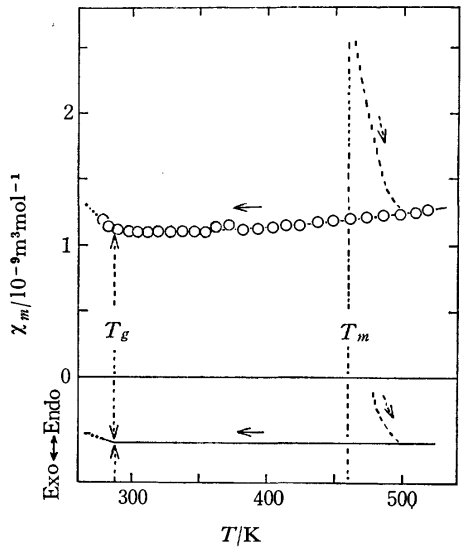

Fig. 9. χ_m *versus* T for supercooled liquid state.

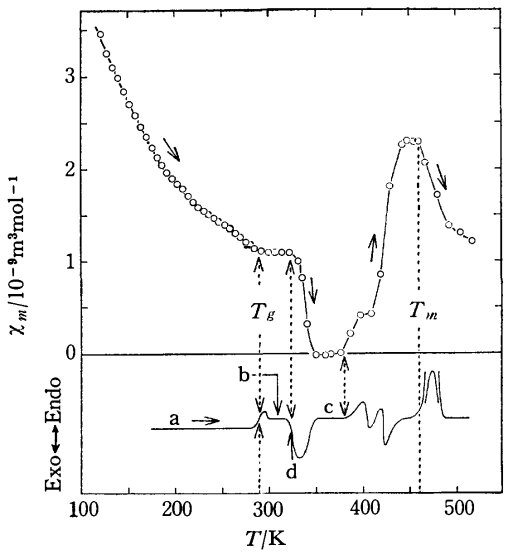

Fig. 10. χ_m *versus* T for the glassy state; (a) glassy state, (b) supercooled liquid state, (c) phase II, and (d) crystallization.

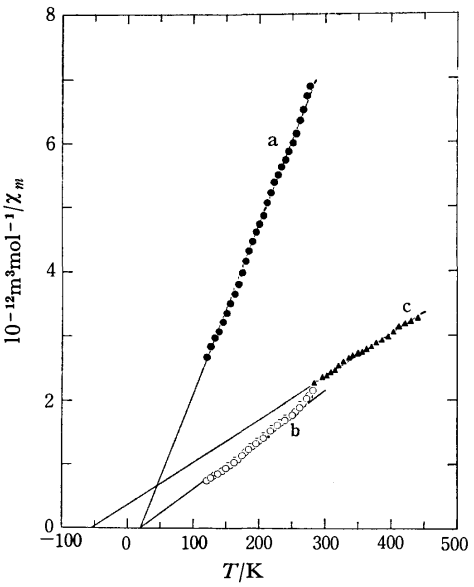

Fig. 11. $1/\chi_m$ *versus* T relationship; (a) glassy state, (b) paramagnetic species in glassy state, and (c) phase III.

magnetic data. In the figures the melting points of each sample obtained from the magnetic study are fitted to those from the thermal study.

χ_m of phase III decreases with increasing temperature according to the characteristic behavior of paramagnetic substances (Fig. 7). Although a slight fall in χ_m occurred at the transition point corresponding to phase III→I, the magnetic property of the new phase I was found to be paramagnetic similar to phase III. At melting point T_m, the value of χ_m decreased abruptly by one half, but in the liquid state χ_m was nearly independent of the temperature.

In the heating curve of χ_m for phase IV (Fig. 8), the value of χ_m increases sharply at the transition point and the diamagnetic phase IV is transformed into a paramagnetic phase I. The melting behavior is quite the same as that shown in Fig. 7.

In the cooling curve of χ_m for the molten substance (Fig.9), the liquid and the supercooled liquid states show paramagnetism but the magnetic behavior is peculiar. Upon cooling to the glass transition point T_g, the values of χ_m decrease but are almost independent of temperature. Below T_g, however, χ_m seems to obey roughly the Curie law.

In the heating curve of χ_m for the glassy state (Fig.10), magnetic susceptibility up to T_g, shows an ordinary paramagnetism except in the vicinity of T_g. Above T_g, the behavior of χ_m is characteristic of the supercooled liquid state. The value χ_m, however, decreases suddenly at crystallization temperature and shows diamagnetism in the new phase II. On further heating, the diamagnetic phase II is transformed into a paramagnetic phase *via* complicated steps of transition and finally melts at 460 K.

The effective Bohr magneton number μ_{eff} of phases I, III, and the glassy state is given in Table 3. It

Table 3. Effective Bohr magneton number of Ni(3-CH_3O-SAL·*iso*-$C_3H_7)_2$ $\mu_{eff}=2.83\sqrt{\chi_a(T-\theta)}$

T/K	μ_{eff}/μ_B		T/K	μ_{eff}/μ_B		T/K	μ_{eff}/μ_B	
	Phase I			Apparent μ_{eff} of glassy state			μ_{eff} of paramagnetic species	
	$\theta=0$			$\theta=0$	$\theta=+21$		in glassy state	
437	3.15		133	1.89	1.74		$\theta=0$	$\theta=+21$
449	3.18		151	1.90	1.74	133	3.59	3.25
			169	1.88	1.74	151	3.58	3.25
	Phase III		185	1.85	1.74	169	3.54	3.25
	$\theta=0$	$\theta=-54$	201	1.84	1.74	185	3.46	3.25
297	3.17	3.46	218	1.82	1.74	201	3.42	3.25
331	3.17	3.46	234	1.82	1.74	218	3.37	3.25
342	3.18	3.46	251	1.83	1.74	234	3.36	3.25
363	3.21	3.46	267	1.81	1.74	251	3.35	3.25
387	3.24	3.46	282	1.78	1.74	267	3.30	3.25
412	3.24	3.46				282	3.23	3.25

has been calculated on the basis of both the Curie law, $\mu_{eff}=2.83\sqrt{\chi_a T}$, and the Curie-Weiss law, $\mu_{eff}=2.83\sqrt{\chi_a(T-\theta)}$, the atomic magnetic susceptibility χ_a being determined by correcting the underlying diamagnetism of all constituent atoms (-267×10^{-12} m^3mol^{-1}). The Weiss constants of phase III and of the glassy state were determined from Fig.11 to be -54 K and $+21$ K, respectively. It was impossible to estimate the Weiss constant of phase I because of the limited temperature region. The signs of the constant imply that the intermolecular interactions in the glassy state and in phase III have a ferromagnetic and antiferromagnetic nature, respectively. The values of the Weiss constants for both cases, however, seem to be extraordinarily large in view of the fact that the Weiss constant is proportional to the interaction between magnetic ions in molecular field theory. In the glassy state, the packing of molecules may be somewhat loose as compared with a crystalline phase and the regular superexchange paths established in a crystalline phase may be disturbed randomly in the glassy state. Therefore, a small value for the Weiss constant is expected for the glassy state. The interpretation for the large Weiss constant obtained by the present experiment will be a further problem. The Weiss constant for phase III, $\theta=-54$ K, indicates the existence of a heat capacity anomaly or a magnetic phase transition at a temperature of several tens degree-Kelvin. However, such a heat capacity anomaly was not found down to 13 K. Further discussions concerning the magnetic interaction will not be given, since a small uncertainty in temperature and a large extrapolation from the high temperature will lead to errors.

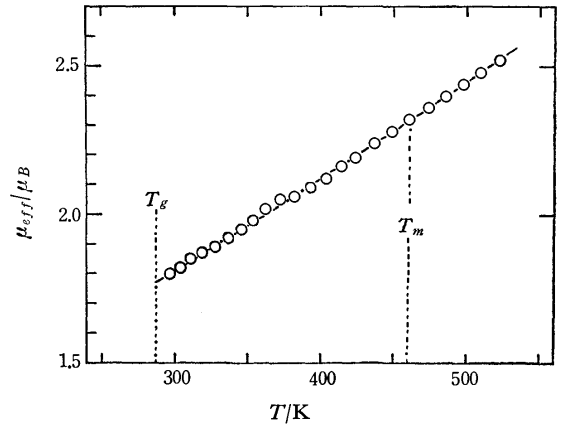

Fig. 12. Effective Bohr magneton number of supercooled liquid against temperature.

The effective Bohr magneton number of the supercooled liquid state is shown in Fig.12 as a function of temperature. An explanation of the magnetic susceptibilities of the molten nickel(II) complexes based on the existing equilibrium between the diamagnetic and the paramagnetic species has already been given.[12] We have applied a similar discussion to the present supercooled liquid and the glassy states of Ni(3-CH_3O-SAL·*iso*-$C_3H_7)_2$. In the supercooled liquid state, an equilibrium between two species seems to be established since the magnetic susceptibility shows a curious behavior and does not obey the Curie law. It is assumed here that a certain equilibrium may be reached between the paramagnetic tetrahedral molecule of phase III and the diamagnetic planar molecule of phase II and/or phase IV. The molar fraction of the paramagnetic species x in the supercooled liquid state is related to the effective Bohr magneton number of phase III and that of the supercooled liquid state as follows.

$x=\chi_a$(supercooled liquid state)/χ_a(phase III)
$=[\mu_{eff}$(supercooled liquid state)$]^2/[\mu_{eff}$(phase III)$]^2$.

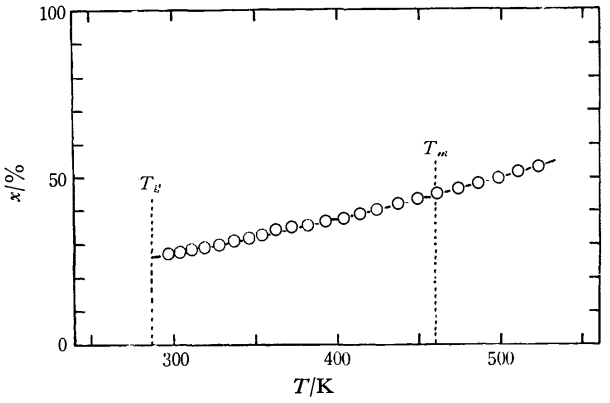

Fig. 13. Temperature dependence of the paramagnetic content in the liquid and the supercooled liquid states.

12) L. Sacconi, R. Cini, and F. Maggio, *J. Inorg. Nuclear Chem.*, **8**, 489 (1958).

The temperature dependence of x is shown in Fig.13. Upon cooling down to T_g, the paramagnetic species are partially converted into a diamagnetic one according to the following equilibrium relationship.

$$\underset{(1-x)}{\text{diamagnetic species}} \rightleftarrows \underset{(x)}{\text{paramagnetic species.}}$$

The equilibrium constant K_p was determined from the relation

$$K_p = [\text{paramagnetic species}]/[\text{diamagnetic species}] = x/(1-x).$$

The thermodynamic quantities ΔG, ΔH, and ΔS associted with this equilibrium can be calculated from the plot of $\ln K_p$ against $1/T$ as shown in Fig.14. The numerical values are listed in Table 4. As was expected the free energy difference between the two species is rather small. This may be one reason why two crystalline forms can be obtained stably from different solvents. The free energy data also show that at lower temperatures the diamagnetic planar form is more stable than the paramagnetic tetrahedral one, but at higher temperatures such as 510 K, the order of stability is reversed. Both ΔH and ΔS are considerably small compared with those of other solutions of Schiff base metal complexes.[4] Steric effects of the substituent groups and solvent effect will be responsible for this difference.

In the glassy state, however, the conversion of the paramagnetic species into the diamagnetic one seems to be frozen because of a long relaxation time required. The content of the paramagnetic species in the glassy state was estimated from Fig.13 to be about 26%. The magnetic susceptibility of the glassy state obeys the Curie law in keeping the paramagnetic content at 26%. This behavior seems to be consistent with the thermodynamic nonequilibrium condition in the glassy state. By using the paramagnetic content of *ca.* 26% the experimental susceptibility data in the glassy state was reduced to the molar paramagnetic susceptibility. In this case the Weiss constant also becomes +21 K (Fig. 11).

As is shown in Fig.10, the magnetic susceptibility around the glass transition temperature varies continuously with temperature with no jump. This is in contrast to other phase transition regions. In the temperature range from about 232 K to T_g, an approximately linear relationship holds between the magnetic susceptibility and temperature for the glassy state. This may be partially due to the enthalpy relaxation effect, which is generally observed just below the glass transition point. In other words, in setting the sample at this temperature region for a long time, its magnetic susceptibility decreases gradually to the extrapolated value from the supercooled liquid state.

Table 4. Thermodynamic quantities for diamagnetic ⇄ paramagnetic equilibrium in the supercooled liquid state of Ni(3-CH_3O-SAL·*iso*-$C_3H_7)_2$

T / K	ΔG / kJ mol^{-1}	ΔH / kJ mol^{-1}	ΔS / J K^{-1} mol^{-1}
304	2.43	3.82	4.56
337	2.27	3.89	4.81
404	1.72	7.15	13.5
437	1.19	8.83	17.5
474	0.552	9.50	18.9
510	−0.238	11.3	22.6

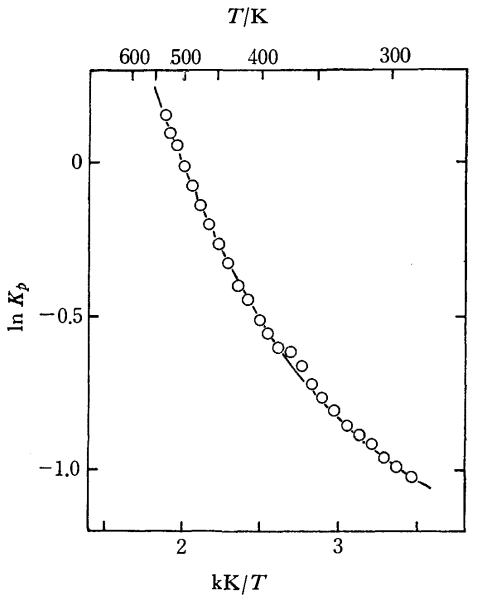

Fig. 14. Temperature dependence diamagnetic ⇄ paramagnetic equilibrium constant in the supercooled liquid state.

Conclusion

Thermal and magnetic properties of Ni(3-CH_3O-SAL·*iso*-$C_3H_7)_2$ were investigated by means of various methods. In addition to the known crystalline phases III and IV, two new crystalline phases I and II and the existence of the supercooled liquid and the glassy states were found. The molecular structure and its associated magnetic properties in phases I and II were determined to be of paramagnetic tetrahedral form and diamagnetic square-planar one, respectively. The infrared and electronic spectra elucidated that the molecular configuration in phase I resembles that in phase III and that the molecular form in phase II is similar to that in phase IV. However, remarkable differences were observed in the heat of solution data between phases I and III, and between phases II and IV. These facts imply that the spectroscopic methods reflect the local symmetry in a molecule, or that information on short-range effects can be obtained from the spectroscopic methods. The calorimetric methods reveal the intermolecular or the long-rang effects in a condensed system.

The unusual magnetic behavior observed in the supercooled liquid state was well accounted for by assuming that an equilibrium between the paramagnetic and the diamagnetic species is established. In decreasing temperature the paramagnetic species was partially converted into the diamagnetic one. But further cooling below glass transition temperature prevented the conversion between two species because of a much longer relaxation time. In the glassy state the para-

magnetic content was found to be about 26% and its magnetic susceptibility obeyed the Curie-Weiss law.

From the viewpoint of statistical mechanics the paramagnetic glass will provide an interesting problem. The present glassy state may be regarded as a random-system in which the paramagnetic species are distributed randomly. The question, whether any phase transition will occur or not in such a random-system, remains unsolved. To obtain more insight into this problem it will be necessary to measure exactly the magnetic susceptibility of the glassy state down to a further low temperature region.

The magentic measurements of the paramagnetic phases I and III at lower temperature will also provide the detailed knowledges about the Weiss constants and the nature of the intermolecular interactions.

The authors would like to express their sincere thanks to Professor Y. Shimura and Dr. S. Kaizaki who kindly permitted use of the spectrophotometer to obtain the electronic spectra, and to Professor A. Tazaki and Mr. G. Kaji, Faculty of Engineering Science, for the use of the apparatus for magnetic susceptibility measurements.

BULLETIN OF THE CHEMICAL SOCIETY OF JAPAN, VOL. 45, 2406—2412 (1972)

The Crystal Structure of μ-Oxo-bis{pentamminechromium(III)} Chloride Monohydrate, $[(NH_3)_5Cr\text{-}O\text{-}Cr(NH_3)_5]Cl_4 \cdot H_2O$[1]

Akio URUSHIYAMA

Department of Chemistry, Faculty of Science, Rikkyo University, Nishi-Ikebukuro, Toshima-ku, Tokyo

(Received March 13, 1972)

The crystal structure of μ-oxo-bis{pentamminechromium(III)} chloride (basic rhodochromic chloride) monohydrate, $[(NH_3)_5Cr\text{-}O\text{-}Cr(NH_3)_5]Cl_4 \cdot H_2O$, has been determined from the three-dimensional X-ray data. The crystals are orthorhombic. The cell dimensions are: $a=11.94\pm0.01$, $b=11.71\pm0.01$, and $c=13.40\pm0.02$ Å. The space group is *Pbca*, with four formula units in a unit cell. The structure was refined by the least-squares method, with anisotropic temperature factors, to $R=0.14$. A bridging oxygen atom of the basic rhodochromic complex ion is situated on the inversion center. Therefore, the complex has a center of symmetry and, accordingly, a linear Cr–O–Cr system. The N–Cr–O angles are nearly 90° or 180°, and the Cr–N bond distances are in the range from 2.09 to 2.14 Å (average 2.11 Å). The complex ion has approximately a D_{4h} symmetry. The Cr–O distance is 1.80 Å, which is quite short compared with that found in the other Cr(III) complexes. The linear Cr–O–Cr system and its short bond distance suggest the presence of an extensive π-bonding in this system. The single-crystal polarized absorption spectra in the visible and ultraviolet regions were also measured. It was found that the characteristic sharp absorption bands of the basic rhodochromic complex ion are all polarized along the four-fold rotation axis of the complex.

Since the rhodochromic (μ-hydroxo-bis{pentamminechromium(III)} ion: rhodochromic ion, μ-oxo-bis{pentamminechromium(III)} ion: basic rhodochromic ion) and erythrochromic (μ-hydroxo-aquotetramminechromium(III) pentamminechromium(III) ion: erythrochromic ion, μ-hydroxo-hydroxo-tetramminechromium(III) pentamminechromium(III) ion: basic erythrochromic ion) series of compounds were first prepared by Jørgensen[2] in 1882, their correct constitutions and their interesting transformation relationships have been discussed in several studies.[3,4] Wilmarth *et al.*,[5] in 1955, on the basis of their careful analyses, determination of pK values, and cleavage-reaction studies of these compounds, proposed the following formulae and relationships for these binuclear complexes of chromium(III):

$$[(NH_3)_5Cr\text{-}OH\text{-}Cr(NH_3)_5]^{5+} \underset{H^+}{\overset{OH^-}{\rightleftharpoons}} [(NH_3)_5Cr\text{-}O\text{-}Cr(NH_3)_5]^{4+}$$

rhodochromic ion — basic rhodochromic ion

$$[(NH_3)_5Cr\text{-}OH\text{-}Cr(H_2O)(NH_3)_4]^{5+} \underset{OH^-}{\overset{H^+}{\rightleftharpoons}} [(NH_3)_5Cr\text{-}OH\text{-}Cr(OH)(NH_3)_4]^{4+}$$

erythrochromic ion — basic erythrochromic ion.

1) A short communication including the present X-ray work has been reported: a) A. Urushiyama, T. Nomura, and M. Nakahara, This Bulletin, **43**, 3971 (1970). Subsequently, correspondence on the structures of the binuclear complexes of chromium(III), including the basic rhodochromic complex ion, has appeared: b) M. Yevitz and J. A. Stanko, *J. Amer. Chem. Soc.*, **93**, 1512 (1971). The results obtained by these arthors were essentially consistent with our X-ray studies. The polarized absorption spectra of the basic rhodochromic salt have also been reported in a short communication: c) A. Urushiyama, M. Nakahara, and Y. Kondo, This Bulletin, **44**, 2290 (1971).

2) S. M. Jørgensen, *J. Prakt. Chem.*, **25**, 231 (1882).

3) A. Werner, "Neuere Anschauungen auf dem Gebiete der anorganischen Chemie," 5 Aufl. (1923), p. 273.

4) K. A. Jensen, *Z. Anorg. Chem.*, **232**, 257 (1937).

5) W. K. Wilmarth, H. Graff, and S. T. Gustin, *J. Amer. Chem. Soc.*, **78**, 2683 (1956).

Subsequently, a variety of the μ-hydroxo-acidotetramminechromium(III)pentamminechromium(III) (acidoerythrochromic) complexes, $[(NH_3)_5Cr\text{-}OH\text{-}CrX(NH_3)_4]^{4+}$ ($X=F^-$, Cl^-, Br^-, I^-, NCS^-, and NO_2^-),[6,7] have been synthesized from the erythrochromic complex, and $[(NH_3)_5Cr\text{-}OH\text{-}Cr(NH_3)_4enH]^{6+}$ [8] from the thiocyanato-erythrochromic complex (en= ethylenediamine).

In these binuclear complexes of chromium(III), the chracteristic "blue" basic rhodochromic salts have been reported to have very different properties from the other compounds in the series. That is, the remarkably reduced magnetic susceptibilities of these salts and their variation with the temperature have been investigated by several workers.[9-12] Schwarzenbach and Magyar[13] investigated the hydrolysis reaction of the rhodo- and erythrochromic series of complexes in an aqueous solution, and reported that the basic rhodochromic complex ion in a basic aqueous solution is transformed very rapidly into the red basic etythrochromic complex with a half-lifetime of 44 sec at 25°C. The visible and ultraviolet absorption spectra of the basic rhodochromic salts show one broad band in the 16600 cm^{-1} region and several unfamiliar sharp bands in the near-ultraviolet region[9,14-16] which have never been found in the spectra of the ordinary chromium(III) complexes.

These unusual properties of the basic rhodochromic complex have been ascribed to the fact that the Cr–O–Cr system of the basic rhodochromic complex may be linear and, hence, may contain an extensive π-bond character, while the other red binuclear complexes in these series may have the bent Cr–OH–Cr bridging system.[1a]

Therefore, it is important to know the structural features of the basic rhodochromic complex, *i.e.*, the Cr–O–Cr angle, the Cr–O and Cr–N bond distances, *etc.* In the present work, in order to determine the structure of the basic rhodochromic complex, the relatively stable crystal of the basic rhodochromic chloride monohydrate, $[(NH_3)_5Cr\text{-}O\text{-}Cr(NH_3)_5]Cl_4\cdot H_2O$, was subjected to three-dimensional X-ray analysis. The single-crystal polarized absorption spectra of the basic rhodochromic perchlorate monohydrate, $[(NH_3)_5Cr\text{-}O\text{-}Cr(NH_3)_5](ClO_4)_4\cdot H_2O$, were also measured and found to be related to the orientation of the complex.

Experimental

X-ray Studies. Crystals of basic rhodochromic chloride monohydrate, $[(NH_3)_5Cr\text{-}O\text{-}Cr(NH_3)_5]Cl_4\cdot H_2O$, were prepared by Jørgensen's method.[2] When 7g of the rhodochromic chloride monohydrate, $[(NH_3)_5Cr\text{-}OH\text{-}Cr(NH_3)_5]Cl_5\cdot H_2O$, were dissolved in 50 m*l* of an ice-cold 2 N NH_3 aqueous solution, almost black crystals of basic rhodochormic chloride monohydrate were soon produced. Because the hydrolysis reaction of the complex takes place immediately in an aqueous solution, the crystallization has to be hastened, and so it is difficult to obtain large crystals. However, a few crystals with dimensions as large as about $0.15\times0.15\times0.10$ mm were found upon a carefull examination under a microscope of the crystals produced. The crystals exhibited some dichroism (blue—greenish blue)and were unstable to even ordinary levels of humidity, turning to red after a few days in the atmosphere of the laboratory. Therefore, the crystals were sealed in a Lindemann glass capillary and mounted on a goniometer. The changes in their color could not be observed for at least a week under these conditions. The oscillation and Weissenberg photographs indicated the crystals are orthorhombic, with unit cell dimensions of $a=11.94\pm0.01$, $b=11.71\pm0.01$, and $c=13.40\pm0.02$ Å, and that the Laue symmetry is mmm. The systematic absences—$0kl$ for $k=2n+1$, $h0l$ for $l=2n+1$, and $hk0$ for $h=2n+1$—are compatible with the *Pbca* space group. The density of the crystals observed by the flotation method was 1.58 g cm^{-3}, and the calculated one was 1.59 g cm^{-3} for $z=4$. The schematic drawing of the crystal related to its crystallographic axes is shown in Fig.1. For the intensity data collection, multiple-film equi-inclination Weissenberg photographs were taken around the *a* axis from zero through the 7th layer and around the *c* axis from zero through the 5th layer, changing the crystals, whose approximate dimensions were $0.15\times0.15\times0.10$ mm, for each layer. Ni-filtered CuK_α radiation was used. The intensities were estimated visually with a standard film strip; 811 independent reflections were thus obtained. Lorentz and polarization corrections were applied.

Spectroscopic Studies. For the measurement of the visible and ultraviolet absorption spectra of single crystals of a microscopic size, an apparatus was used constructed of a Hitachi EPS-3T spectrophotometer and a Nippon Kogaku POH polarizing microscope, together with two Olympus M090 reflecting-type objectives (×90). The microscope part of the apparatus was sealed in a stainless steel box and was evacuated to 10^{-3} mmHg for the studies at low temperatures. A thin plate of a single-crystal of the basic rhodochromic perchlorate monohydrate, prepared by Linhard's method[6] and of the approximate dimensions of 0.5×0.6 mm, was

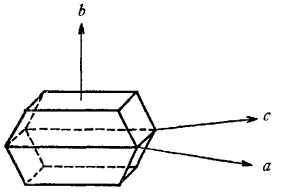

Fig. 1. Schematic drawing of a single crystal of $[(NH_3)_5Cr\text{-}O\text{-}Cr(NH_3)_5]Cl_4\cdot H_2O$ with reference to its crystallographic axes.

6) M. Linhard and M. Weigel, *Z. Anorg. Allg. Chem.*, **299**, 15 (1959).
7) M. Nakahara and Y. Kondo, *Nippon Kagaku Zasshi*, **92**, 571 (1971).
8) G. Schwarzenbach and B. Magyar, *Helv. Chim. Acta*, **45**, 1454 (1962).
9) C. E. Schäffer, *J. Inorg. Nucl. Chem.*, **8**, 149 (1958).
10) A. Eanshaw and J. Lewis, *J. Chem. Soc.*. **1961**, 396.
11) H. Kobayashi, T. Haseda, and E. Kanda, *J. Phys. Soc. Jap.*, **15**, 1646 (1960).
12) E. Pedersen, private communication.
13) G. Schwarzenbach and B. Magyar, *Helv. Chim. Acta*, **45**, 1425 (1962).
14) M. Mori, S. Ueshiba, and H. Yamatera, This Bulletin, **32**, 88 (1959).
15) L. Dubicki and R. L. Martin, *Aust. J. Chem.*, **23**, 215 (1970).
16) T. Uemura, Y. Kondo, and I. Otabe, presented at the 8th Symposium on Coordination Chemistry, Tokyo, November 1958; Y. Kondo, "Coordination Bond (in Japanese)," ed. by R. Tsuchida and M. Kotani, Tokyo Kagakudojin, Tokyo (1961), p. 106.

TABLE 1. OBSERVED AND CALCULATED STRUCTURE FACTORS

L	Fo	Fc	L	Fo	Fc	L	Fo	Fc	L	Fo	Fc	L	Fo	Fc	L	Fo	Fc	L	Fo	Fc	L	Fo	Fc
H, K = 0, 0			5	140	132	6	94	85	3	22	-21	12	53	-64	5	203	207	3	0	-14	3	26	-52	3	60	27
2	111	110	6	130	148	7	52	33	4	177	-156	H, K = 4, 4			6	43	56	4	75	-67	4	0	6	4	84	-60
4	486	-503	7	52	43	8	0	-76	5	133	123	0	80	-68	7	75	77	5	0	-20	5	0	13	5	72	65
6	85	-81	8	71	65	H, K = 2, 4			6	179	161	1	104	-100	8	42	38	6	57	57	H, K = 6, 9			6	0	-6
8	163	161	14	73	-83	0	211	-210	H, K = 3, 4			2	0	5	9	80	-80	7	0	2	0	84	75	7	16	21
10	134	138	H, K = 1, 4			1	58	-68	1	43	-24	3	48	-42	10	33	21	8	57	62	1	98	-96	8	34	53
12	56	44	1	21	-41	2	89	-79	2	0	-7	4	97	85	11	110	-102	9	0	9	2	51	37	H, K = 8, 0		
H, K = 0, 2			2	31	35	3	97	-103	3	25	-28	5	22	25	12	0	-3	10	32	20	3	131	-128	0	57	-45
0	189	174	3	43	51	4	284	286	4	206	195	6	0	-23	13	0	0	H, K = 6, 0			4	93	-82	2	72	-74
1	260	-238	4	61	57	5	30	32	5	202	181	7	68	62	14	32	-29	0	109	-110	5	51	44	4	144	156
2	56	77	5	128	146	6	137	140	6	34	35	8	0	9	15	59	56	2	0	-12	6	91	-92	6	167	187
3	247	-257	6	57	-37	7	88	89	7	125	116	9	45	38	H, K = 5, 3			4	128	130	7	74	65	8	0	-2
4	140	-127	7	33	25	8	66	-69	8	188	-180	H, K = 4, 5			1	53	53	6	61	66	H, K = 6, 10			10	66	-88
5	12	-11	8	26	-32	9	31	24	9	62	-55	0	82	-74	2	52	36	8	0	14	6	60	52	H, K = 8, 1		
6	165	-155	H, K = 1, 5			10	42	-43	10	56	-45	1	239	243	3	114	103	10	21	-10	H, K = 6, 11			0	121	-127
7	246	218	1	83	-85	H, K = 2, 5			11	113	-113	2	0	-17	4	42	-35	12	32	-29	0	0	14	1	36	39
8	77	63	2	36	34	0	85	67	12	112	107	3	300	302	5	66	65	14	0	13	1	0	-34	2	29	-35
9	145	152	3	120	133	1	87	81	H, K = 3, 5			4	33	28	6	23	-34	16	27	37	2	0	-5	3	40	-38
10	107	97	4	79	-79	2	75	-64	1	81	-61	5	53	-45	7	131	-118	H, K = 6, 1			3	85	-104	4	96	103
11	34	-34	5	273	278	3	185	177	2	60	-45	6	0	21	8	82	75	0	186	-196	4	0	20	5	57	-45
12	27	-32	6	30	-37	4	96	-84	3	64	-63	7	187	-185	9	60	67	1	178	-191	5	43	-38	H, K = 8, 2		
13	85	-96	7	18	-5	5	0	11	4	29	-18	8	0	2	10	42	-1	2	0	-22	6	47	49	0	195	-215
H, K = 0, 4			8	75	60	6	108	94	5	136	128	9	75	-64	11	105	80	3	245	-285	7	69	87	1	55	47
0	420	390	9	0	-13	7	50	-53	6	0	7	10	0	-10	H, K = 5, 4			4	207	223	8	33	10	2	0	-7
1	126	122	10	0	6	8	35	40	7	113	109	11	43	54	1	176	-161	5	95	98	9	52	69	3	127	125
2	115	-130	11	65	-51	9	33	-50	8	21	-10	12	0	1	2	236	224	6	66	64	H, K = 7, 0			4	137	153
3	82	-81	12	45	-25	10	93	-86	9	39	-54	13	70	69	3	74	69	7	175	181	2	40	-56	5	38	31
4	71	-60	15	56	54	11	0	-11	10	0	15	14	0	0	4	61	52	H, K = 6, 2			4	282	-262	6	0	0
5	103	-96	H, K = 1, 6			12	0	0	11	116	-106	H, K = 4, 6			5	101	99	0	165	163	6	25	21	7	89	-85
6	295	270	1	54	-76	13	85	77	15	59	60	0	81	88	6	64	-63	1	77	73	8	162	163	H, K = 8, 3		
7	101	95	2	177	183	14	0	32	H, K = 3, 6			1	130	136	7	0	9	2	0	-18	10	62	60	0	83	-90
8	121	109	3	75	79	15	63	43	1	78	61	2	66	-63	8	86	-78	3	93	89	12	104	-104	1	133	109
9	87	88	4	39	-8	H, K = 2, 6			2	275	234	3	68	57	9	73	-71	4	0	1	14	61	-58	2	34	-30
10	118	-114	5	57	-54	0	246	-225	3	38	-8	4	0	-16	10	0	-20	5	0	9	H, K = 7, 1			3	123	100
11	39	-47	6	81	-77	1	10	6	4	80	95	5	74	-68	11	81	-61	6	16	32	1	0	-19	H, K = 8, 4		
12	92	-77	7	87	-96	2	81	-72	5	139	-151	6	116	120	12	28	33	7	71	-57	2	123	132	0	173	160
13	81	-97	H, K = 1, 7			3	72	61	6	62	-49	7	0	-16	13	0	-15	8	0	16	3	0	-18	1	96	94
14	71	85	1	32	-40	4	228	233	7	50	-55	8	37	37	14	57	50	9	70	-52	4	43	37	2	0	24
15	0	3	2	46	62	5	72	61	8	117	-94	9	0	3	15	39	32	H, K = 6, 3			5	119	132	3	81	83
16	28	41	3	24	-24	6	122	127	H, K = 3, 7			10	53	-49	H, K = 5, 5			0	125	-132	6	62	-54	7	61	-66
H, K = 0, 6			4	96	107	7	29	-33	1	0	12	H, K = 4, 7			1	0	-21	1	19	-25	7	91	97	8	0	-2
0	62	-71	5	72	90	8	40	-44	2	182	173	0	123	125	2	148	-134	2	138	-124	11	72	-85	9	74	-53
1	0	-13	6	0	-8	9	76	-66	3	0	42	1	83	97	3	0	0	3	0	8	15	36	56	12	67	50
2	36	-48	7	61	54	H, K = 2, 7			4	0	19	2	78	72	4	35	18	4	35	-3	H, K = 7, 2			H, K = 8, 5		
3	92	92	8	98	-119	0	69	58	5	110	103	3	77	91	5	37	26	5	77	66	1	75	-97	0	85	-66
4	120	118	H, K = 1, 8			1	62	-56	6	104	-75	4	87	-80	6	81	81	6	204	196	2	108	-103	1	105	76
5	62	44	1	35	52	2	55	59	H, K = 3, 8			5	26	-26	7	0	0	7	47	35	3	0	24	2	0	0
6	88	81	2	51	43	3	65	-67	1	196	192	6	133	-149	8	60	-52	8	22	31	4	29	22	3	76	51
7	37	-29	H, K = 1, 9			4	82	-70	2	67	-75	7	78	-88	9	10	-14	9	39	-49	5	146	157	4	42	46
8	68	55	1	67	87	5	91	82	3	112	-105	8	0	-6	10	0	-15	10	182	-168	6	58	41	5	80	-13
12	83	-87	2	148	149	6	108	-131	4	0	-3	9	21	-33	11	0	14	11	28	-13	7	61	66	H, K = 9, 0		
H, K = 0, 8			3	38	40	7	37	-15	5	117	-113	10	98	115	12	33	42	12	53	-41	8	0	-6	2	82	-101
0	102	110	4	58	61	8	0	-5	H, K = 3, 9			11	44	44	H, K = 5, 6			13	54	43	9	64	-63	4	0	-31
1	178	213	5	36	-32	9	95	-91	1	95	84	12	57	53	1	111	105	14	59	56	10	0	24	6	55	74
2	41	-52	6	40	-39	10	93	88	H, K = 4, 0			H, K = 4, 8			2	126	139	H, K = 6, 4			11	82	-89	8	0	1
3	154	186	7	76	-88	H, K = 2, 8			0	78	-59	0	38	56	3	0	-4	0	66	81	H, K = 7, 3			10	0	-6
4	85	-94	8	75	-90	0	0	-33	2	31	47	1	0	-17	4	111	117	1	16	-20	1	88	82	H, K = 9, 1		
5	68	-81	9	67	69	1	90	72	4	0	4	2	0	25	5	60	-48	2	44	40	2	100	104	1	80	-90
6	49	50	10	51	-37	2	0	-23	6	120	-110	3	39	35	6	0	-20	3	0	14	3	62	-70	2	101	119
7	91	-95	11	67	72	3	105	119	8	0	5	4	53	40	7	32	-22	4	0	5	4	80	79	3	76	74
8	41	56	H, K = 1, 10			4	51	73	10	68	74	5	41	41	8	133	-137	5	14	26	5	0	-21	4	0	29
H, K = 1, 0			1	49	-66	5	43	37	H, K = 4, 1			6	29	-32	9	33	34	6	54	-50	6	0	-37	5	141	139
2	93	-75	H, K = 2, 0			6	0	30	0	119	-119	10	60	61	10	22	-26	7	0	-5	7	67	37	6	61	-64
4	10	10	2	86	107	7	94	-84	1	95	87	H, K = 4, 9			11	44	38	8	0	15	8	104	-88	7	0	10
6	12	-25	4	108	100	8	0	-18	2	39	-41	0	86	82	12	58	65	9	0	-18	H, K = 7, 4			8	0	18
8	67	76	6	164	-166	9	76	-98	3	37	-34	1	0	-3	13	0	15	10	39	61	1	95	-83	H, K = 9, 3		
10	61	56	8	90	-90	H, K = 2, 9			4	53	43	2	50	42	14	40	42	H, K = 6, 5			2	186	200	8	177	-164
12	25	-19	10	148	157	0	118	125	5	119	-109	3	50	-48	H, K = 5, 7			0	69	-75	3	67	57	H, K = 9, 5		
14	52	-47	12	95	89	1	64	-15	6	107	97	4	41	-43	1	21	22	1	0	8	4	0	-16	1	151	123
H, K = 1, 1			14	0	-24	H, K = 2, 10			7	73	76	5	43	-49	2	0	18	2	0	-1	5	18	21	2	45	45
1	271	260	H, K = 2, 1			0	94	93	8	0	11	6	93	-82	3	93	81	3	24	16	6	73	-65	3	27	21
2	114	-91	1	167	-164	H, K = 3, 0			9	133	141	7	34	33	4	0	-19	4	49	44	H, K = 7, 5			4	0	1
3	37	-20	2	83	-93	2	419	-437	10	77	-72	8	0	-6	5	64	46	5	129	108	1	140	123	5	92	-84
4	164	-182	3	168	-179	4	63	46	11	0	1	9	66	64	6	0	3	6	0	-3	2	86	80	6	0	-11
5	58	-80	4	248	-232	6	183	165	12	0	-18	10	61	58	7	95	-88	7	79	-68	3	29	-20	7	111	-101
6	21	-24	5	49	58	H, K = 3, 1			13	92	-98	H, K = 5, 0			8	0	0	8	0	9	4	0	-19	8	0	10
7	127	-130	6	94	103	1	190	192	H, K = 4, 2			2	136	-139	9	39	50	9	161	-151	5	30	-39	9	102	95
8	206	241	7	146	147	2	155	-159	0	558	574	4	240	-267	10	17	-18	10	21	18	6	31	-37	10	0	-11
9	153	153	8	21	29	3	142	-146	1	77	66	6	50	53	11	61	56	11	40	34	7	32	-7	11	95	101
10	42	40	9	50	36	4	44	-39	2	15	-15	8	176	186	H, K = 5, 8			12	21	-19	8	31	18	H, K = 10, 0		
11	124	142	10	128	-136	5	50	-41	3	26	-25	10	29	54	1	81	74	13	87	73	9	79	67	0	0	30
12	77	-86	H, K = 2, 2			6	90	73	4	106	-106	12	104	-105	2	0	17	H, K = 6, 6			H, K = 7, 6			2	67	-62
H, K = 1, 2			0	54	-60	7	16	39	5	30	-36	H, K = 5, 1			3	0	0	0	111	120	1	83	80	4	0	11
1	129	-137	1	168	-155	8	24	-23	6	84	98	1	14	-45	4	0	-9	1	34	21	2	66	57	6	103	120
2	177	219	2	34	50	9	82	80	7	32	27	2	52	-70	5	138	-132	2	0	4	3	55	-39	8	46	45
3	76	74	3	200	-204	H, K = 3, 2			8	76	75	3	67	74	6	0	16	3	0	-10	4	79	73	10	58	-73
4	236	-238	4	227	230	1	167	-155	9	50	24	4	61	51	7	80	-91	4	53	-28	5	0	-6	12	42	-52
5	33	29	5	36	18	2	45	-34	H, K = 4, 3			5	86	85	8	0	27	H, K = 6, 7			6	0	-3	H, K = 10, 1		
6	86	-99	6	44	-49	3	42	46	0	331	-337	6	76	71	9	68	58	0	197	196	7	0	16	4	52	-67
7	0	-20	7	149	151	4	194	-200	1	180	169	7	57	-50	10	0	0	1	31	33	8	105	-92	H, K = 10, 2		
8	120	135	8	90	-85	5	108	96	2	104	-106	8	124	-135	11	76	83	2	18	17	H, K = 7, 7			0	44	-35
9	33	-37	9	78	81	6	62	50	3	118	115	9	18	19	H, K = 5, 9			3	47	38	1	74	59	3	109	101
10	56	60	10	87	81	7	63	55	4	220	213	10	19	-21	1	38	37	4	119	-122	H, K = 7, 8			H, K = 10, 4		
11	0	-11	H, K = 2, 3			8	79	66	5	52	-67	11	67	46	2	92	-87	8	48	43	1	0	35	0	228	216
12	85	-96	0	311	-296	9	95	-76	6	142	152	12	74	48	3	47	-33	12	35	30	2	60	70	1	87	89
H, K = 1, 3			1	109	-108	10	0	0	7	75	-71	H, K = 5, 2			4	0	6	13	35	39	5	105	-102	2	35	26
1	102	-87	2	37	-32	11	85	-80	8	41	-20	1	148	-149	5	0	-4	H, K = 6, 8			7	83	-71	3	98	98
2	359	-384	3	223	-181	H, K = 3, 3			9	0	13	2	134	-128	H, K = 5, 10			0	63	47	11	71	64	4	116	-118
3	21	-17	4	306	287	1	117	-95	10	91	-83	3	81	66	1	34	28	1	43	-52	H, K = 7, 9					
4	176	-159	5	111	107	2	36	-40	11	51	40	4	72	-53	2	114	-109	2	0	9	2	0	-9			

mounted on a fused quartz slide. This slide was placed on a copper stage and cooled to near the temperature of liquid nitrogen, and the absorption spectra were measured through the crystal on the aperture of the copper stage. By using a small amount of grease on the slide, the crystal was fixed with its faces upright; its thickness was estimated with a micrometer eyepiece to be about 2μ. A thermocouple indicated that the crystal was cooled to 90°K in the low-temperature studies.

Structure Determination

As there are four formula units, $[(NH_3)_5Cr\text{–}O\text{–}Cr(NH_3)_5]Cl_4\cdot H_2O$, in a unit cell, the space group symmetry (*Pbca*) requires the bridging oxygen atom of the complex to lie on a special position with inversion symmetry. Therefore, the binuclear basic rhodochromic complex should have a center of symmetry, and the Cr–O–Cr group should be strictly linear. The position of the chromium atom was deduced from a three-dimensional Patterson map. The chloride ions and the nitrogen atoms were easily located by a series of three-dimensional Fourier syntheses. After these atomic positions were refined by several cycles of block-diagonal-matrix least-squares refinement, the discrepancy factor, R, defined as $R=\Sigma||F_o|-|F_c||/\Sigma|F_o|$ was reduced to 0.21. At this stage, a difference Fourier synthesis was calculated to search for the position of the water molecule of crystallization, whose presence was also confirmed by infrared spectroscopy. A relatively low electron density peak was found at the general position of $x=0.04$, $y=0.44$, and $z=0.06$. Thus, the oxygen atom of the water molecule with a multiplicity of 0.5 was placed at this position, and after several cycles of the block-diagonal-matrix least-squares refinement with isotropic temperature factors, R was reduced to 0.15. Finally, a refinement using the anisotropic temperature factors for all atoms led to $R=0.14$ (0.11 for non-zero reflections). In the final least-squares refinement, the weights were assumed to be $w=1$ for $F_o\geq 3.6$ and $w=0.5$ for $F_o<3.6$. The final atomic coordinates and the temperature factors are given in Table 2, and their standard deviations are in Table 3. The observed and calculated structure factors are listed in Table 1. The atomic scattering factors used in the calculations were taken from the International Tables for X-ray Crystallography.[17] All the computations were done on a HITAC 5020E computer at the Computer Center of the University of Tokyo, using the library program system UNICS.

Results and Discussion

Crystal Structure. A perspective drawing of the basic rhodochromic ion is shown in Fig. 2. The bond distances and angles, with their standard deviations, are listed in Tables 4 and 5. The basic rhodochromic ion has the center of symmetry as already described;

Table 2. Final atomic coordinates and temperature factors

Anisotropic temperature factors are expressed in the form $\exp\{-(B_{11}h^2+B_{22}k^2+B_{33}l^2+B_{12}hk+B_{13}hl+B_{23}kl)\}$

Atom	x/a	y/b	z/c	B_{11}	B_{22}	B_{33}	B_{12}	B_{13}	B_{23}
Cr	0.0514	0.0956	0.0950	0.00286	0.00297	0.00296	0.00044	−0.00043	0.00018
Cl(1)	0.2938	0.4841	0.3661	0.00789	0.01125	0.00607	0.00635	0.00233	0.00421
Cl(2)	0.3844	0.2312	0.1487	0.00604	0.00615	0.00515	−0.00045	−0.00030	0.00139
N(1)	0.2031	0.0083	0.1063	0.00664	0.00180	0.00523	0.00216	0.00265	0.00037
N(2)	−0.0174	−0.0055	0.2078	0.00629	0.00688	0.00573	−0.00027	0.00454	0.00653
N(3)	−0.0992	0.1899	0.0926	0.00247	0.00229	0.00488	0.00185	0.00141	−0.00132
N(4)	0.1227	0.2052	−0.0131	0.00800	0.00426	0.00695	0.00051	0.00643	0.00256
N(5)	0.1112	0.2086	0.2092	0.00624	0.01278	0.00528	−0.00620	0.00353	−0.00787
H_2O	0.0376	0.4355	0.0598	0.00683	0.00510	0.00851	−0.00539	−0.00385	0.00200
O	0.0000	0.0000	0.0000	0.00463	0.00700	0.00385	0.00089	−0.00484	−0.00179

Table 3. Estimated standard deviations

$\sigma(x)$, $\sigma(y)$, and $\sigma(z)$ in Å, (B) in Å^2)

Atom	$\sigma(x)$	$\sigma(y)$	$\sigma(z)$	$\sigma(B_{11})$	$\sigma(B_{22})$	$\sigma(B_{33})$	$\sigma(B_{12})$	$\sigma(B_{13})$	$\sigma(B_{23})$
Cr	0.0034	0.0030	0.0029	0.00024	0.00024	0.00015	0.00047	0.00041	0.00037
Cl(1)	0.0067	0.0072	0.0064	0.00064	0.00073	0.00041	0.00117	0.00086	0.00098
Cl(2)	0.0059	0.0059	0.0058	0.00052	0.00054	0.00037	0.00090	0.00076	0.00073
N(1)	0.0167	0.0151	0.0161	0.00168	0.00135	0.00112	0.00250	0.00227	0.00213
N(2)	0.0184	0.0192	0.0171	0.00183	0.00174	0.00126	0.00280	0.00239	0.00250
N(3)	0.0131	0.0144	0.0162	0.00128	0.00131	0.00102	0.00209	0.00200	0.00204
N(4)	0.0194	0.0159	0.0189	0.00194	0.00166	0.00138	0.00275	0.00267	0.00246
N(5)	0.0194	0.0205	0.0179	0.00177	0.00239	0.00132	0.00344	0.00259	0.00288
H_2O	0.0312	0.0270	0.0309	0.00297	0.00270	0.00241	0.00482	0.00436	0.00401
O	0.0000	0.0000	0.0000	0.00175	0.00199	0.00124	0.00304	0.00241	0.00275

17) International Table for X-ray Crystallography Vol. III, Kynoch Press, Birmingham (1952).

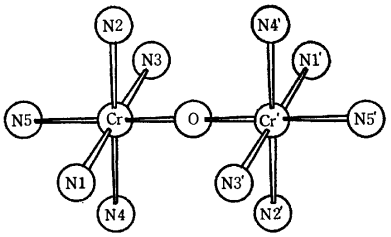

Fig. 2. Perspective drawing of the basic rhodochromic complex ion, $[(NH_3)_5Cr\text{-}O\text{-}Cr(NH_3)_5]^{4+}$.

TABLE 4. INTERATOMIC DISTANCES IN THE COMPLEX CATION, $[(NH_3)_5Cr\text{-}O\text{-}Cr(NH_3)_5]^{4+}$
(e.s.d.'s are given in parentheses)

Cr-O	1.803(3) Å	N(1)-N(2)	2.97(2)
Cr-Cr	3.607(4)	N(1)-N(3)	4.19(2)
Cr-N(1)	2.09(2)	N(1)-N(4)	2,97(2)
Cr-N(2)	2.09(2)	N(1)-N(5)	2.93(3)
Cr-N(3)	2.11(2)	N(1)-N(3)'	3.75(3)
Cr-N(4)	2.11(2)	N(2)-N(3)	2.93(2)
Cr-N(5)	2.14(2)	N(2)-N(4)	4.20(3)
Cr-N(1)'	4.24(2)	N(2)-N(5)	2.94(3)
Cr-N(2)'	4.23(2)	N(2)-N(4)'	3.72(3)
Cr-N(3)'	4.22(2)	N(3)-N(4)	3.01(2)
Cr-N(4)'	4.24(2)	N(3)-N(5)	2.97(2)
Cr-N(5)'	5.75(2)	N(3)-N(1)'	3.75(3)
O-N(1)	2.81(2)	N(4)-N(5)	2.98(3)
O-N(2)	2.79(2)	N(4)-N(2)'	3.72(3)
O-N(3)	2.81(2)		
O-N(4)	2.82(2)		
O-N(5)	3.95(2)		

TABLE 5. BOND ANGLES IN THE COMPLEX CATION, $[(NH_3)_5Cr\text{-}O\text{-}Cr(NH_3)_5]^{4+}$
(e.s.d.'s are given in parentheses)

O-Cr-N(1)	92.4(4)°	N(2)-Cr-N(3)	88.5(7)
O-Cr-N(2)	91.4(5)	N(2)-Cr-N(4)	176.8(7)
O-Cr-N(3)	91.4(4)	N(2)-Cr-N(5)	88.0(7)
O-Cr-N(4)	91.7(5)	N(3)-Cr-N(4)	90.8(7)
O-Cr-N(5)	179.4(5)	N(3)-Cr-N(5)	88.4(7)
N(1)-Cr-N(2)	90.6(7)	N(4)-Cr-N(5)	88.9(7)
N(1)-Cr-N(3)	176.1(6)		
N(1)-Cr-N(4)	89.9(7)		
N(1)-Cr-N(5)	87.8(7)		

therefore, the Cr–O–Cr oxygen bridging system is linear. Each N_1–Cr–N_2, N_2–Cr–N_3, N_3–Cr–N_4, and N_4–Cr–N_1 angle is nearly 90°, and the N_5–Cr–O angle is approximately 180°, as is shown in Table 5, the complex roughly has a four-fold rotation axis passing through a sequence of the N_5–Cr–O–Cr'–N'_5 atoms. Hence, the basic rhodochromic complex ion must have an approximately D_{4h} symmetry. Hewkin and Griffith[18] have reported, in their infrared spectroscopic studies of the binuclear transition metal complexes, that the basic rhodochromic complex chloride shows the absorption band assigned to the asymmetric stretching vibration of the Cr–O–Cr group at almost the same position as in the similar oxo-bridged binuclear complexes, $K_4[Cl_5Ru\text{-}O\text{-}RuCl_5]$[19] and $K_4[Cl_5Re\text{-}O\text{-}ReCl_5]$,[20] both of which have been confirmed to be of the D_{4h} symmetry by the X-ray method (Table 6). They also suggested that, in the case of the linearly oxygen-bridged transition metal binuclear complexes, the asymmetric stretching vibrations of the bridge atoms are almost independent of the mass of the metal atoms involved, assuming that the Cr–O–Cr group in the basic rhodochromic complex is linear. The results of the present X-ray work are consistent with these findings.

TABLE 6. INFRA-RED ABSORPTION DATA[a]

Complex	M-O-M asym. str.	M-O-M sym. str.
$K_4[Cl_5Ru\text{-}O\text{-}RuCl_5]\cdot H_2O$	866 cm^{-1}	226 cm^{-1}
$K_4[Cl_5Re\text{-}O\text{-}ReCl_5]\cdot H_2O$	885	230
$[(NH_3)_5Cr\text{-}O\text{-}Cr(NH_3)_5]Cl\cdot H_2O$	873	215

a) Date from ref. 18.

The Cr–O distance is 1.80 Å, which is quite short compared with the values found in the rhodochromic complex ion, $[(NH_3)_5Cr\text{-}OH\text{-}Cr(NH_3)_5]^{5+}$, (Cr–O 2.00 Å);[1a] it is comparable to that in $K_4[Cl_5Ru\text{-}O\text{-}RuCl_5]$ (Ru–O 1.80 Å) and in $K_4[Cl_5Re\text{-}O\text{-}ReCl_5]$ (Re–O 1.86 Å). Dunitz and Orgel[21], to explain the diamagnetic properties of $[Cl_5Ru\text{-}O\text{-}RuCl_5]^{4+}$, elucidated its electronic structure by means of a molecular orbital model, which allowed the unpaired electrons of ruthenium(IV) to couple through the bridging oxygen. The linear Cr–O–Cr system and its short bond distance certainly suggest the presence of an extensive π-bonding in this system, as in the ruthenium complex. The remarkably reduced magnetic susceptibilities and the unusual electronic spectra of the basic rhodochromic complex are certainly due to this π-bonding.

The basic aqueous solutions of the acido-erythrochromic complex salts show a characteristic blue color, although it fades out rapidly. The absorption spectra of these blue solutions,[13] similar to those of the basic rhodochromic complex ion, are characterized by one broad band in the visible region and several sharp bands in the near-ultraviolet region, indicating that these blue chemical species also contain the linear Cr–O–Cr system.

Several other binuclear transition metal complexes have been known to have a linear M–O–M group, as confirmed by the X-ray method. They are listed in Table 7, along with their M–O distances and M–O–M angles. All of them show the distinctive feature of the short M–O distance, strongly indicating the presence of the π-bonding character in these systems.

Some Cr–N bond distances of the basic rhodochro-

18) D. J. Hewkin and W. P. Griffith, *J. Chem. Soc.*, **1966**, 472.

19) A. G. Mathieson, D. P. Mellor, and N. C. Stephenson, *Acta Crystallogr.*, **5**, 185 (1952).

20) L. C. Morrow, *ibid.*, **15**, 851 (1962).

21) J. D. Dunitz and L. E. Orgel, *J. Chem. Soc.*, **1953**, 2594.

Table 7. Binuclear complexes containing linear M-O-M

Complex	M-O distance	M-O-M angle	Ref.
$K_4[Cl_5Ru\text{-}O\text{-}RuCl_5]\cdot H_2O$	1.80Å	180°	19
$K_4[Cl_5Re\text{-}O\text{-}ReCl_5]\cdot H_2O$	1.86	180	20
$[(NH_3)_5Cr\text{-}O\text{-}Cr(NH_3)_5]Cl_4\cdot H_2O$	1.80	180	present work
$[(C_5H_5)Cl_2Ti\text{-}O\text{-}TiCl_2(C_5H_5)]$	1.78	180	22
[pyPcMn-O-MnPcpy][a]	1.71	178	23
$[Mo_2O(O)_2(C_2H_5OCS_2)_4]$	1.851, 1.872	178.03	24
$K_2[Mo_2O(O_2)_2(C_2O_4)_2(H_2O)_2]$	1.876	180	25
$K_2[Ti_2O_5(H_3NC_7O_4)_2]\cdot 5H_2O$	1.825	178.1	26
$[(H_2O)BFe\text{-}O\text{-}FeB(H_2O)](ClO_4)_4$[b]	1.8	180	28
$K_3[(H_2O)Cl_4Ru\text{-}N\text{-}RuCl_4(H_2O)]$	1.718 (M-N)	180	27

a) py: pyridine Pc: phthalocyanine
b) B: 2,13-dimethyl-3,6,9,12,18-pentaazabicyclo[12.3.1]octadeca-1(18),2,12,14,16-pentaene

mic complex ion had been expected to be significantly longer than others, since a transformation reaction from the basic rhodochromic complex to the red basic erythrochromic complex takes place very rapidly in an aqueous solution, substituting an OH^- group for one of the ammonia molecules. Indeed, the $Cr\text{–}N_5$ distance (2.14 Å) was observed to be somewhat longer than the others. However, its difference from the other Cr–N distances (average value 2.10 Å) did not exceed three times the estimated standard deviation.

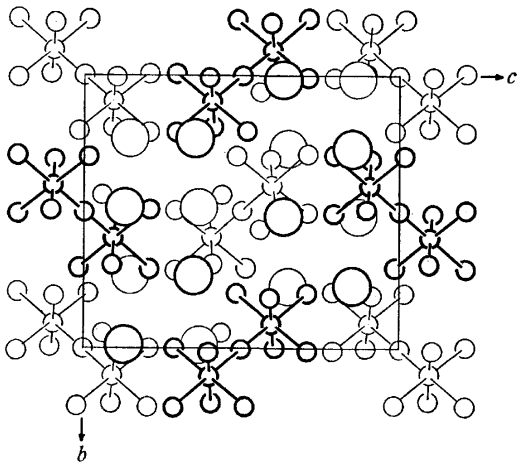

Fig. 3. Crystal structure viewed along the *a* axis.

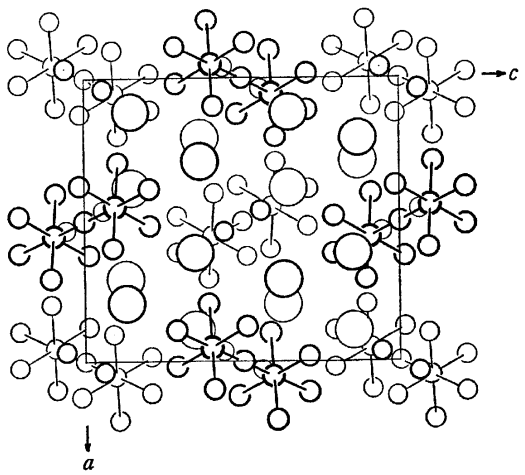

Fig. 4. Crystal structure viewed along the *b* axis.

The crystal structures viewed along the *a* and *b* axes are shown in Figs. 3 and 4 respectively. The complexes are arranged as shown in Fig. 4 by bold lines or fine lines, retaining the bridging oxygen atoms on the same planes, which are alternately piled up back to back, sliding along the *b* axis with a half unit for each layer. The chloride ions are packed into channels elongated along the *b* axis between these piles. The water of crystallization is located in the space surrounded by the six complex ions. The shortest $Cl^{-}\cdots N(NH_3)$ approach appears at a distance of 3.32 Å.

Visible and Ultraviolet Absorption Spectra. The visible and ultraviolet absorption spectra of the basic rhodochromic complex salts, which cannot be measured easily in an aqueous solution because of their rapid hydrolysis, have been studied by several methods, *e.g.*, the extrapolation of the aqueous solution spectrum,[14] the diffuse reflectance method,[9,15] the rapid-flow method,[13] and the microspectroscopic technique.[16,29]

As has already been stated, it has been found in these spectroscopic studies that the basic rhodochromic complex ion shows some unfamiliar sharp absorption bands in the near-ultraviolet region. Furthermore, Kondo[16] has pointed out that these sharp bands are strongly polarized, and recently Dubicki *et al.*[15] have found that some of these sharp bands disappear at the temperature of liquid nitrogen.

The crystal structure of the basic rhodochromic chloride monohydrate has been determined in the present X-ray studies; hence, it has become possible to relate the single-crystal polarized absorption spectra

22) P. Corrakini and G. Allegra, *J. Amer. Chem. Soc.*, **81**, 5510 (1959).
23) L. H. Vogt, Jr., A. Zalkin, and D. H. Templeton, *Inorg. Chem.*, **6**, 1725 (1967).
24) A. B. Blake, F. A. Cotton, and J. S. Wood, *J. Amer. Chem. Soc.*, **86**, 3024 (1964).
25) F. A. Cotton, S. M. Morehouse, and J. S. Wood, *Inorg. Chem.*, **3**, 1603 (1964).
26) D. Schwarzenbach, *Inorg. Chem.*, **9**, 2391 (1970).
27) M. Ciechanowicz and A. C. Skapski, *Chem. Commn.*, **1969**, 574.
28) E. Fleischer and S. Hawkinson, *J. Amer. Chem. Soc.*, **89**, 720 (1967).
29) M. Morita and S. Shionoya, *J. Phys. Soc. Jap.*, **28**, 134 (1970).

of the complex salt to the orientation of the dimeric unit. Unfortunately, single-crystals of basic rhodochromic chloride monohydrate, although they exhibit a dichroism (blue through light polarized parallel to the *a* axis, greenish-blue through light polarized parallel to the *c* axis), are unsuitable for study by means of the microspectroscopic technique because of their shape (Fig. 1). However, a similar dichroism can be observed more distinctly in thin plates of the crystals of the perchlorate, and they *are* suitable for microspectroscopic study. As the color of the chloride crystal has already been related to the orientation of the complex. it seems reasonable to say that the absorption parallel to the four-fold rotation axis of the complex contributes greatly to the polarized absorption spectrum along the extinction direction of the perchlorate crystal that shows greenish-blue with polarized light having a parallel electric vector.

The single-crystal polarized absorption spectra of the basic rhodochromic perchlorate monohydrate along two extinction directions are shown in Fig. 5.

The absorption spectra at room temperature consist of two broad bands in the 16600 and 22000 cm^{-1} regions, of three strong sharp bands at 25350, 26630, and 29830 cm^{-1}, and of at least four weak sharp bands at 14320, 23920, 28010, and 28320 cm^{-1}. These sharp bands were found to be all polarized along the four-fold rotation axis of the complex, while the broad band in the 16600 cm^{-1} region seems to be slightly reduced in intensity along the four-fold rotation axis. When the crystal was cooled to about 90°K, a new band was revealed at 32400 cm^{-1}; it was found also to be polarized along the four-fold rotation axis. The intensity of the strong sharp band at 26630 cm^{-1} was considerably sensitive to the temperature, as has already been pointed out by Dubicki *et al.* It had almost disappeared in the 90°K spectrum, implying that this band originated from the thermally-excitable electronic level above the ground state.

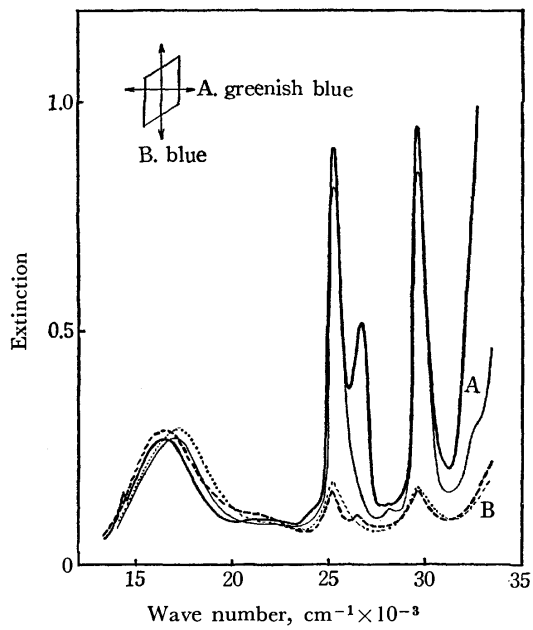

Fig. 5. Polarized absorption spectra of the basic rhodochromic perchlorate, $[(NH_3)_5Cr\text{-}O\text{-}Cr(NH_3)_5](ClO_4)_4 \cdot H_2O$. —— and ----: at room temperature, —— and ·····: at 90°K

The electronic spectra of the basic rhodochromic complex are very difficult to characteriz. Furthermore, no other polynuclear transition metal complexes have been found to show sharp absorption bands similar to those of the basic rhodochromic complex. If the electronic structure of the basic rhodochromic complex can be described in terms of the molecular orbital model,[15,21] the ordering of the molecular orbitals of the binuclear complex of D_{4h} symmetry can be expected to be;

$$e_u,\ (b_{2g},\ b_{1u},\ e_g),\ e_u^*.$$

These orbitals should be filled with ten electrons in the case of the basic rhodochromic complex. That the relative energies of the non-bonding b_{2g}, b_{1w}, and e_g orbitals are not known makes the problem very complicated. Recently, Schmidtke[30] has described the electronic structure of the basic rhodochromic complex in further detail, assuming the complex to have a D_{4h} or D_{4d} symmetry; he has pointed out that the d_z^2 orbitals of the metals should be coupled with the oxygen p_z orbital in either symmetry case to produce a higher-energy anti-bonding a_{2u} orbital than these molecular orbitals. He assigned the sharp band at 25350 cm^{-1} to the electronic transition from the metal-localized b_{2g} or b_{1u} orbital to the delocalized a_{2u}^* orbital with some vibrational structures, and the band at 29830 cm^{-1} to that from the metal-localized e_g orbital to the delocalized a_{2u}^* orbital.

However, that the intensity of the band at 26630 cm^{-1} is considerably sensitive to the temperature compared with that of the band at 25350 cm^{-1} leads to some confusion. If the same excited state is concerned, the "hot" band should appear on the lower-wavenumber side of the band from the ground state. Thus, as Dubicki has suggested, it seems that some selection rule, perhaps the spin one,[31] has a strong influence upon the appearance of the absorption spectra in this region. These electronic transitions are possibly coupled with some vibrational modes of the complex. The results of the present polarized spectroscopy indicate that each direct product of the representations of the (vibronic) wavefunctions of the ground state and the excited state concerned with these sharp bands should contain not E_u but A_{2u}. Only such conditions can lead to the *z* polarization of the absorption bands of the complex in the D_{4h} symmetry.

The author wishes to express his thanks to Professor Yukio Kondo, Professor Masayoshi Nakahara, and Dr. Teruo Nomura of Rikkyo University for their helpful discussions and encouragement throughout the course of this work.

30) H. H. Schmidtke, *Theor. Chim. Acta*, **20**, 92 (1971).
31) B. Jezowska-Trzebiato ska and W. Wojciechoeski, "Theory and Structure of Complex Compounds," Wroclaw (1962), p. 375.

Vibrational Spectra of *trans-trans* Diacetamide and Its C- and N-Deuterated Compounds

Yoshihiro KURODA, Yutaka SAITO, Katsunosuke MACHIDA, and Toyozo UNO
Faculty of Pharmaceutical Sciences, Kyoto University, Sakyo-ku, Kyoto,
(Received March 24, 1972)

The infrared spectra of $CH_3CONHCOCH_3$, $CD_3CONHCOCH_3$, $CD_3CONHCOCD_3$, and their N-deuterated compounds have been recorded for the unstable crystalline modification in which the molecules are in the *trans-trans* conformation (form B). The Raman spectra of $CH_3CONHCOCH_3$ in the form B crystal and in the complex with KI have also been recorded. Vibrational assignments have been given by referring to the characteristic group frequencies of related compounds, the infrared dichroic measurement for $CH_3CONHCOCH_3$ and the isotopic frequency shifts. The normal coordinates analysis has been made by assuning the planar *trans-trans* conformation of the –CONHCO– (–CONDCO–) group. The calculated frequencies fit to the observed satisfactorily.

The rotational isomerism of the imide (–CONHCO–) group has been found for diacetamide, the first member of the homologous series of aliphatic acyclic imides.[1,2] In the usually occuring crystalline modification, form A, and in the concentrated solutions in non-polar solvents, diacetamide takes the *trans-cis* conformation, in which one of the C=O bonds is at the *trans* position and the other at the *cis* position with respect to the central NH bond. The more symmetric *trans-trans* conformation is taken, on the other hand, by molecules in another crystalline modification, form B, which is unstable at room temperature. Previously, the in-plane normal frequencies of *trans-trans* diacetamide and the corresponding *N*-deuterated derivatives were calculated on a simplified model in which the methyl groups were taken as point masses.[3] However, more detailed investigations for both the *trans-trans* and the *trans-cis* conformations are necessary to discuss how the force constants of the –CONHCO– group are affected by the change of molecular environments on the interconversion of the conformation. In succession to the recently reported vibrational analysis of *trans-cis* diacetamide,[4,5] the present paper deals with the infrared and Raman spectra of *trans-trans* diacetamide and the infrared spectra of its C- and N-deuterated derivatives. Most of the fundamental frequencies have been assigned and the normal coordinate calculation has been made by assuming a Urey-Bradley force field supplemented by the general valence force constants for C–C and C–N torsions and the C=O and N–H out-of-plane deformations. The force constants have been refined by the least squares method to give the best agreement between the observed and the calculated frequencies. The C=O and C–N stretching force constants of the *trans-trans* and *trans-cis* molecules reflect well the difference in the type of hydrogen bonds between the form A and form B crystals.

Experimental

The preparation and N-deuteration of $CH_3CONHCOCH_3$ and $CD_3CONHCOCD_3$ were described in our preceding paper.[4] In the present work, $CD_3CONHCOCH_3$ was also synthesized from CH_3COND_2 and CD_3COCl by the same method that was used to synthesize $CD_3CONHCOCD_3$.[4] The NMR spectrum of the obtained specimen revealed that it contained a small amount of the CHD_2 and CH_2D species. However, this specimen exhibited no indication of infrared absorptions due to such isotopic impurities, and the infrared spectra of $CD_3CONHCOCH_3$ and $CD_3CONDCOCH_3$ were used as references for the interpretation of the vibrational spectra of diacetamide. The recrystallization from water, which is the previously described method to prepare the form B crystal,[1] resulted mostly in the formation of the form A crystal for the material used in this work. Instead, the slow crystallization from the melt in a sealed glass tube was found to lead effectively to the formation of the form B crystal. For Nujol mulls of the samples prepared as described above, the infrared spectra were measured on a Koken DS-301 infrared spectrophotometer (4000—700 cm^{-1}), on a Perkin-Elmer Model-521 grating spectrophotometer (900–250 cm^{-1}) and on a Hitachi FIS-3 grating spectrophotometer (400—33 cm^{-1}). In the region where the absorptions of Nujol appear, hexachlorobutadiene was used as the mulling medium for $CH_3CONHCOCH_3$ and $CH_3CONDCOCH_3$,

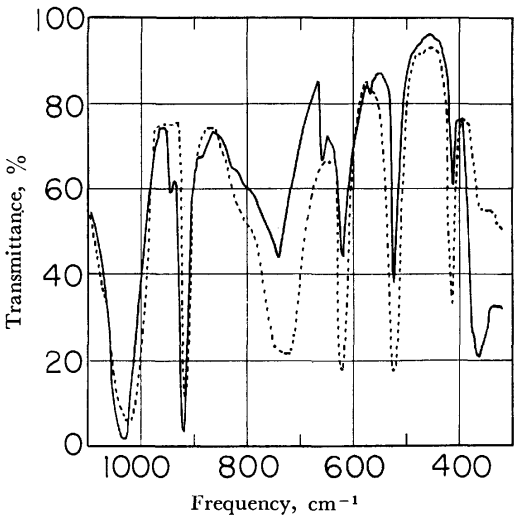

Fig. 1. Polarized infrared spectra of $CH_3CONHCOCH_3$ in the region between 1100 and 350 cm^{-1}.
Solid line: electric vector parallel to the direction of crystal growth.
Dotted line: electric vector perpendicular to the direction of crystal growth.

1) T. Uno and K. Machida, This Bulletin, **34**, 545 (1961)
2) T. Uno and K. Machida, *ibid.*, **35**, 1226 (1962)
3) T. Uno and K. Machida, *ibid.*, **36**, 427 (1963)
4) Y. Kuroda, Y. Saito, K. Machida, and T. Uno, *Spectrochim. Acta*, **27**, 1481 (1971).
5) Y. Kuroda, Y. Saito, K. Machida, and T. Uno, *ibid.*, in press.

but hexachlorobutadiene could not be used for the C-deuterated compounds since the transition to the form A crystal took place very quickly in this medium. It was found previously that diacetamide mixed with NaBr, NaI, and KI shows similar infrared spectra to the form B crystal.[6] Recently, Roux *et al.* have confirmed by the X-ray analysis that diacetamide takes the *trans-trans* conformation on forming the complex with NaBr and KI.[7] Since the form B crystal of the C-deuterated compounds were found to be very unstable even in Nujol mulls, infrared spectra of the complex with KI were used to check the absorptions due to the *trans-cis* molecules. Occasionally, the form B crystal was obtained by the slow crystallization form the melt inserted between two KBr plates. One of these solid films of CH_3-

TABLE 1. OBSERVED FREQUENCIES OF $CH_3CONHCOCH_3$, $CH_3CONDCOCH_3$, $CD_3CONHCOCH_3$, $CD_3CONDCOCH_3$, $CD_3CONHCOCD_3$, AND $CD_3CONDCOCD_3$

$CH_3CONHCOCH_3$		CH_3CONH-$COCH_3$-KI	CH_3COND-$COCH_3$	CD_3CONH-$COCH_3$	CD_3COND-$COCH_3$	CD_3CONH-$COCD_3$	CD_3COND-$COCD_3$
Infrared	Raman	Raman	Infrared	Infrared	Infrared	Infrared	Infrared
3260 s		3245		3260 s		3260 s	
3180 s		3163		3180 s		3170 s	
3015 m		3001				3015 w	
2995 vw		2968	2995 vw	2995 vw	2995 vw		
2915 vw		2935	2915 vw	2915 vw	2915 vw		
		2920	2405 vs		2415 vs		2420 vw
1841 vw		1763		2230 vw	2230 vw	2230 vw	2230 vw
		1750		2110 vw	2110 vw	2110 vw	2110 vw
1730 vs	1734	1733	1730 vs	1728 vs	1726 vs	1720 vs	1720 vs
1695 sh		1705	1672 sh			1690 sh	1665 sh
		1523[a]					
1513 s		1488		1510 vs		1508 vs	
1428 w		1427	1428 w	1421 w	1421 w		
1369 m		1378	1369 s				1353 s
1327 vw			1327 sh	1324 vw		1324 w	1324 sh
		1250[a]				1260 vs	
1236 vs		1224		1243 vs		1175 sh	
			1120 vw		1110 sh	1122 vw	1120 m
1070 sh (⊥)[b]			1094 w	1079 m	1098 m	1087 w	1087 w
1030 s (∥)[b]	1033	1037	1028 m	1038 w	1037 w	1030 w	1030 sh
1027 s (⊥)				1018 m	1018 m		1011 m
945 vw (∥)	976[a]	979[a]	947 m	959 w	992 m	972 m	955 m
					924 m		
920 s (∥, ⊥)	923	921	900 w	910 m	910 m	909 m	909 m
		836[a]		890 w	883 w	868 w	842 w
				805 vw	796 w	819 m	816 m
737 s (⊥)		751		737 s		734 m	734 m
661 vw (∥)	673	673					
		650[a]					
626 s (⊥)			626 s	627 vw	627 vw		
				603 m	605 w		550 sh
			546 s		546 s	542 m	540 s
526 s (⊥)	532	533	523 s	498 s	498 s	485 s	485 s
418 s (⊥)	420	420	412 w	408 w	402 w		379 vw
368 m (∥)	380	382	368 s	349 m	347 m	343 m	343 s
250 vw		227	240 vw				230 vw
160 vw		177	160 vw				
		120					
95 m	109		95 m				80 m
65 m	74		65 m				63 m
	55						
	38						

a) These frequencies may be due to the *trans-cis* diacetamide.
b) Infrared dichroism. ⊥, ∥ : Electric vector perpendicular and parallel to the direction of crystal growth, respectively.

6) T. Uno and K. Machida, This Bulletin, **34**, 1448 (1961).

7) J. P. Roux and J. C. A. Boeyens, *Acta Crystallogr.*, **B25**, 1700, 2395 (1969)

$CONHCOCH_3$ was found to contain a small portion of the oriented crystal by the inspection under a polarization microscope. The infrared dichroic measurement for this sample has been made on a Perkin-Elmer Model-521 grating spectrophotometer with a wire-grid polarizer in the region between 1100 and 350 cm^{-1} (Fig. 1). All the wave numbers were calibrated by the standard absorptions of polystyrene, indene, ammonia, and 1, 2, 4-trichlorobenzene. The Raman spectrum of the form B crystal of $CH_3CONHCOCH_3$ obtained from the melt sealed in a capillary tube was recorded on a JEOL JRS-O1A laser Raman spectrophotometer. The exciting line (4880Å) was generated by an argon-ion laser at an approximate output power of 250 mW. The Raman spectrum of a mixed pellet of $CH_3CONHCOCH_3$ and KI was measured on a JRS-U1 laser Raman spectrophotometer with the excitation source of a 400 mW argon-ion laser (4880Å). The observed infrared and Raman frequencies are listed in Table 1.

Vibrational Assignment

On the assumption of the *trans-trans* planar conformation, the C-undeuterated and the fully C-deuterated diacetamides belong to the point group C_{2v}, and should contain 30 infrared active fundamental transitions, $12(a_1)+11(b_2)+7(b_1)$, while the remaining $6(a_2)$ normol modes are infrared inactive. All of the fundamental transitions of the half C-deuterated diacetamides, which have the C_s symmetry, should be infrared active. There is no Raman inactive transition for both the C_{2v} and the C_s molecules. The X-ray analysis by Roux and Boeyens[7] has revealed that the –CONHCO– group of diacetamide in the diactamide-KI (2 : 1) complex is only slightly distorted from the *trans-trans* planar conformation. Since the infrared spectrum of this complex and that of the form B crystal of diacetamide are almost identical with each other, it is reasonable to assume that diacetamide molecules in the form B crystal have essentially the same conformation as those in the KI complex.

The characteristic infrared absorptions of the *trans*-CONHCO-group observed in the region above 1150 cm^{-1} are the NH stretching doublet at 3260 and 3180 cm^{-1}, the imide I (a_1 C=O stretching) band at 1730 cm^{-1} and the imide II and III bands.[2] The last two bands arise from the coupled vibrations of the NH in-plane bending and CN stretching. All these bands were observed similarly for the C-deuterated compounds, and were used to check the formation of the form B crystal throughout this work. The diminishing of the imide II and III bands and the appearance of the imide II′ band (CN stretching) on the N-deuteration are clearly recognized for the fully C-deuterated compounds, for which no interference by the CH_3 absorptions is expected in the region between 1450 and 1350 cm^{-1} (see Fig. 2).

The assignment of infrared absorptions of *trans-trans* $CH_3CONHCOCH_3$ below 1150 cm^{-1} were much facilitated by the dichroism observed for the thick oriented specimen of the form B crystal described in the experimental section. By analogy with the X-ray analysis of dipropionamide, which takes the *trans-trans* conformation in the crystlline state,[8] *trans-trans* diacetamide is thought to form chain polymers by means of the bifurcated hydrogen bond, retaining the two-fold axis in the direction of chains along which the crystal grows. We may accordingly expect that the direction of crystal growth is parallel to the transition moment of a_1 vibrations but is perpendicular to those of b_1 and b_2 vibrations. The medium band at 1030 cm^{-1} of $CH_3CONHCOCH_3$ was assigned previously to the a_1, b_1, and b_2 CH_3 rocking vibrations.[3] In accord with this assignment, the dichroic measurement disclosed three components, one of which was observed at 1030 cm^{-1} for the parallel polarization of the incident radiation, while the others, a peak at 1027 cm^{-1} and a shoulder at 1070 cm^{-1}, for the perpendicular polarization. Since the initial calculation in the normal coordinate analysis gave the b_1 CH_3 rocking frequency about 50 cm^{-1} higher than the b_2 frequency, we assigned the shoulder near 1070 cm^{-1} and the peak at 1027 cm^{-1} to the b_1 and b_2 CH_3 rocking vibrations, respectively. On the N-deuteration, the intensity of the 1030 cm^{-1} band is reduced appreciably, and two weak bands

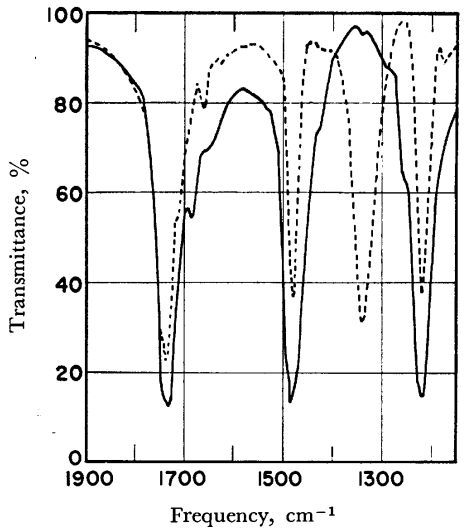

Fig. 2. Infrared spectra of $CD_3CONHCOCD_3$-KI complex (solid line) and $CD_3CONDCOCD_3$-KI complex (dotted line) in the region between 1900 and 1150 cm^{-1}.

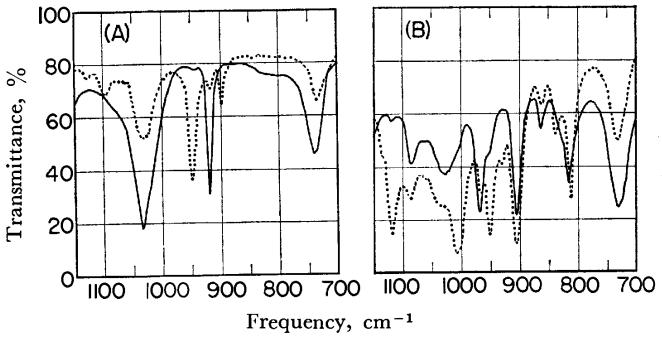

Fig. 3. (A) Infrared spectra of $CH_3CONHCOCH_3$ (solid line) and $CH_3CONDCOCH_3$ (dotted line) in the region between 1150 and 700 cm^{-1}. (B) Infrared spectra of $CD_3CONHCOCD_3$ (solid line) and $CD_3CONDCOCD_3$ (dotted line) in the region between 1150 and 700 cm^{-1}.

8) T. Uechi, T. Watanabé, and K. Osaki, *Sci. Rep.* (*Osaka Univ.*) **15**, 1 (1966)

appear nearly at 1094 and 947 cm^{-1}. This spectral change has been ascribed to the coupling between the b_2 CH_3 rocking and the ND in-plane deformation vibrations.[3] The b_1 CH_3 rocking absorption of $CH_3CONDCOCH_3$ could not be identified (Fig. 3).

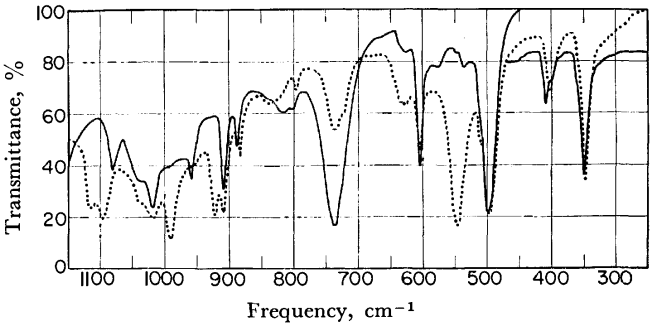

Fig. 4. Infrared spectra of $CD_3CONHCOCH_3$ (solid line) and $CD_3CONDCOCH_3$ (dotted line) in the region between 1150 and 250 cm^{-1}.

From analogy with the cases of CD_3CONH_2 and *trans-cis* $CD_3CONHCOCD_3$,[4,9] the infrared bands at 1087 and 1030 cm^{-1} of *trans-trans* $CD_3CONHCOCD_3$ are assigned to the CD_3 symmetric (a_1 and b_2) and asymmetric (a_1, b_1, and b_2) deformation vibrations, respectively. The *N*-deuteration gives rise to two additional bands at 1120 and 1011 cm^{-1}, which indicate that one of the b_2 CD_3 deformation vibrations couples with the ND in-plane deformation vibration. The half C-deuterated compound, $CD_3CONHCOCH_3$ shows two weak bands at 1079 and 1018 cm^{-1} and a shoulder band at 1038 cm^{-1} (see Fig. 4). According to the normal coordinated analysis, there is no appreciable coupling between the CH_3 and the CD_3 group vibrations, and the band at 1079 cm^{-1} and the shoulder at 1038 cm^{-1} are assigned respectively to the a' CD_3 symmetric and asymmetric deformation vibrations, while the band at 1018 cm^{-1} is assigned to both the a' CH_3 rocking and the a'' CD_3 asymmetric deformation vibrations. On the N-deuteration, the half *C*-deuterated compound shows a spectral change between 1150 and 950 cm^{-1} which is similar to that observed for the fully C-deuterated compound. The occurence of the coupling between the ND in-plane deformation vibration and the CH_3 or CD_3 deformation vibrations of $CH_3CONDCOCH_3$, $CD_3CONDCOCH_3$, and $CD_3CONDCOCD_3$ was confirmed by the normal coordinates analysis, and the assignments of the infrared absorptions of the N-deuterated compounds in this region were given reasonably by referring to the calculated frequencies.

Diaceamide has two C–C stretching vibrations, the intrinsic frequency of which is estimated to be near 900 cm^{-1} from analogy with acetamide[9] and *N*-methylacetamide.[10] So we assigned first the parallel and perpendicular components of the band at 920 cm^{-1} of $CH_3CONHCOCH_3$ to the a_1 and b_2 C–C strecthing vibrations, respectively. According to the mormal coordinates analysis, however, the a_1 mode responsible for this band is rather complex, consistimg of the CN stretching, the CH_3 rocking and the C–N–C deformation vibrations. The calculated a_1 and b_2 frequencies are very close to each other just as are observed. On the N-deuteration, the band at 920 cm^{-1} is replaced by a weak band at 900 cm^{-1}, which may be assigned to analogous vibrations. The infrared spectrum of $CD_3CONHCOCD_3$ between 1000 and 700 cm^{-1} is much more complicated than that of $CH_3CONHCOCH_3$, since the CD_3 rocking frequencies occur in this region. There are five bands in all, among which the bands at 972 and 868 cm^{-1} shift to 955 and 842 cm^{-1}, respectively, while those at 909 and 819 cm^{-1} shift hardly on the N-deuteration. By referring to the calculated frequencies, we assigned the 972 cm^{-1} band to the complicated a_1 vibration corresponding to that related to the 920 cm^{-1} band of $CH_3CONHCOCH_3$, and the 868 cm^{-1} band to the b_2 C–C stretching vibration. The N-deuteration insensitive bands at 909 and 819 cm^{-1} were assigned to the b_1 and b_2 CD_3 rocking vibrations, respectively. The remaining a_1 CD_3 rocking frequency was calculated to be 756 cm^{-1}. The corresponding absorption seems to be overlapped by the broad band at 734 cm^{-1} due to the NH out-of-plane deformation (imide V) vibration. For $CH_3CONHCOCH_3$, this imide V band shows the perpendicular dichroism just as expected for the b_1 species.

In the region between 700 and 300 cm^{-1}, *trans-trans* diacetamide is expected to have five infrared active fundamentals due to the a_1, b_1, and b_2 C=O deformations and the a_1 and b_2 C–C–N deformations, but the form B crystal of $CH_3CONHCOCH_3$ shows only four bands at 626, 526, 418, and 368 cm^{-1} for the unpolarized radiation. Previously, the band at 626 cm^{-1} was assigned to the a_1 and b_1 C=O deformation vibrations, based on the appearance of an additional band at 640 cm^{-1} on the N-deuteration.[1] The band at 640 cm^{-1} observed previously for the form B crystal of $CH_3CONDCOCH_3$ is missing, however, in the newly recorded spectra in this work, and is considered to be due to the contaminated *trans-cis* compound. Instead, the Raman spectra of the form B crystal and the KI-complex of $CH_3CONHCOCH_3$ recorded

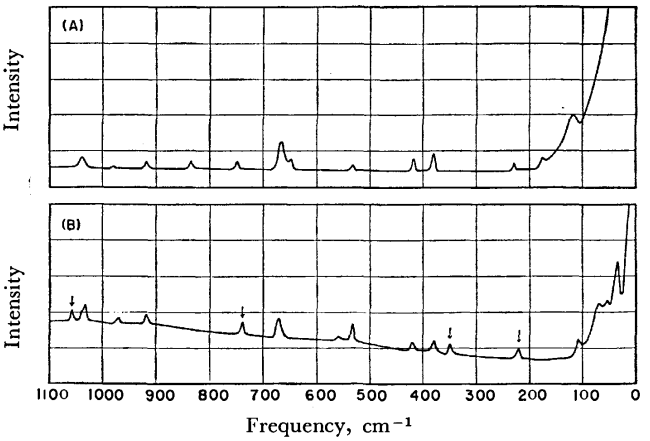

Fig. 5. (A) Raman spectrum of $CH_3CONHCOCH_3$-KI complex in the region between 1100 and 0 cm^{-1}. (B) Raman spectrum of $CH_3CONHCOCH_3$ in the region between 1100 and 0 cm^{-1}. (↓): Ar^+

9) T. Uno, K. Machida, and Y. Saito, This Bulletin., **42**, 897 (1969).

10) J. Jakes and B Schneider, *Collect. Czech. Chem. Commun.* **33**, 643 (1968).

in this work (Fig. 5) exhibited a very strong band near 673 cm^{-1} hardly assignable to non-totally symmetric fundamentals. Correspondingly, the infrared dichroic measurement revealed the presence of a weak band at 661 cm^{-1} appearing only for the parallel polarization of the incident radiation(Fig.1). The difference of 12 cm^{-1} between the Raman and infrared frequencies may be ascribed to a factor group splitting. Based on this result, the assignment of the a_1 C=O deformation (imide IV) frequency in the infrared spectrum should be revised from 626 cm^{-1} to 661 cm^{-1}. According to the normal coordinates analysis, the contribution of the C-C stretching vibration to this fundamental is also large, explaining well the prominent intensity of the Raman band at 673 cm^{-1}.

The infrared bands at 626, 526, and 418 cm^{-1} show the perpendicular dichroism and are assigned to the b_1 C=O deformation (imide VI), b_2 C=O deformation (imide IV) and the b_2 C–C–N deformation vibrations, respectively. The assignments of the bands at 526 and 418 cm^{-1} to b_2 fundamentals are supported by the appearance of a weak infrared band at 945 cm^{-1}, which shows the parallel dichroism and is assignable to the combination tone, 526+418. The remaining infrared band at 368 cm^{-1} shows the parallel dichroism and is assigned undoubtedly to the a_1 C–C–N deformation vibration. In the Raman spectra, three bands are observed near 530, 420, and 380 cm^{-1} corresponding to the infrared bands at 526, 418, and 368 cm^{-1}, but no Raman counterpart is observed for the infrared band at 626 cm^{-1}. This result is reasonable since out-of-plane fundamentals are usually weak in Raman spectra. It is difficult to explain why the infrared band at 626 cm^{-1} does not shift on the N-deuteration, whereas the normal coordinates analysis predicts a high-frequency shift of 10 cm^{-1} for the b_1 C=O deformation vibration. For the $CH_3CONHCOCH_3$-KI complex, the corresponding infrared band at 621 cm^{-1} shifts to 626 cm^{-1} on the N-deuteration, reflecting a small interaction between the ND and the C=O deformation vibrations in the b_1 species. The assignments of the infrared bands due to the skeletal deformation vibrations of the C- and N-deuterated diacetamide were made by referring to the result for $CH_3CONHCOCH_3$ and taking account of the isotope shifts. The infrared band due to the a_1 imide IV vibration of the C- and the N-deuterated compounds could not be identified probably because of its extreme weakness. In the infrared spectrum of the form B crystal of $CD_3CONHCOCD_3$ in Fig. 6, the bands at 587 and 523 cm^{-1} are due to the *trans-cis* molecules formed by the partial transition from the form B to the form A crystal. Similarly, the bands of *trans-cis* $CD_3CONDCOCD_3$ appear at 620, 587, and 521 cm^{-1} in Fig. 6.

In analogy with the case of *trans-cis* diacetamide, the infrared bands due to the C–N and the C–C torsional and C–N–C deformation vibrations are expected in the region below 300 cm^{-1}. We assigned the broad band centered at about 250 cm^{-1} and the very weak band at 160 cm^{-1} of the form B crystal of $CH_3CONHCOCH_3$ to the b_1 C–N torsional and the a_1 C–N–C deformation vibrations, respectively (Fig. 7). In consistent with the calculated isotope effect, the former band undergoes a low-frequency shift by about 10 cm^{-1}, while the latter remains unshifted on the *N*-deuteration. In the Raman spectrum of $CH_3CONHCOCH_3$-KI complex, the corresponding bands were observed at 227 and 177 cm^{-1}. For both $CH_3CONHCOCH_3$ and $CH_3CONDCOCH_3$, the infrared absorption due to the b_1 C–C torsional vibration is thought to overlap with a lattice absorption, giving rise to the peak at 95 cm^{-1}, since the form B crystal of CD_3COND-

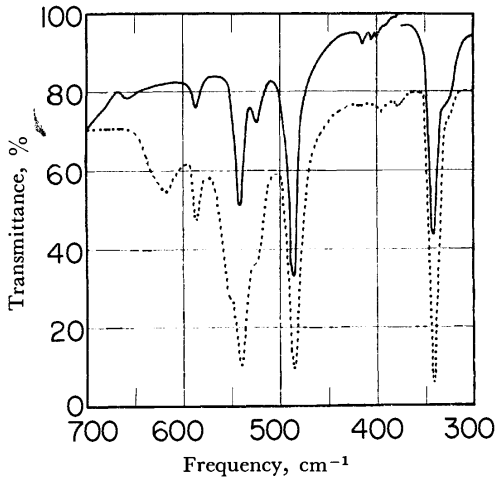

Fig. 6. Infrared spectra of $CD_3CONHCOCD_3$ (solid line) and $CD_3CONDCOCD_3$ (dotted line) in the region between 700 and 300 cm^{-1}.

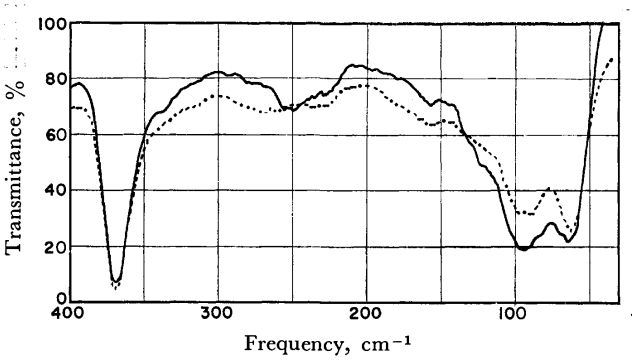

Fig. 7. Infrared spectra of $CH_3CONHCOCH_3$ (solid line) and $CH_3CONDCOCH_3$ (dotted line) in the region between 400 and 33 cm^{-1}.

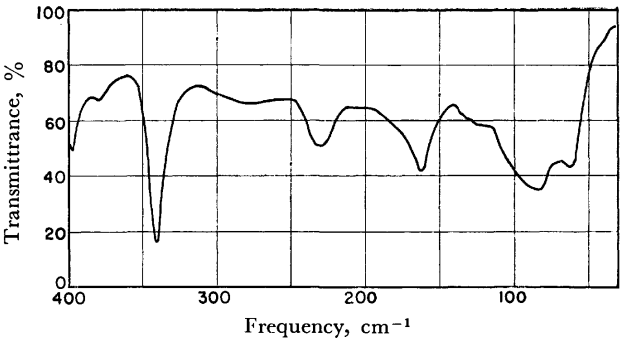

Fig. 8. Infrared spectrum of $CD_3CONDCOCD_3$ in the region between 400 and 33 cm^{-1}.

$COCD_3$ shows the corresponding peak at 80 cm^{-1} (Fig. 8). No isotope shift is observed for the infrared band at 65 cm^{-1} of the form B crystal. This band is missing in the spectra of the form A crystal, and is assigned undoubtedly to lattice vibrations. The infrared band due to the C–N torsional and the C–N–C deformation vibrations of the C-deuterated diacetamides in the *trans-trans* conformation could not be detected because of the interference of the bands due to the *trans-cis* molecules.

Normal Coordinates Analysis

In order to check the internal consistency of the present assignments of the fundamental frequencies of various isotopic molecules and to obtain a reliable set of force constants, the normal coordinates treatment has been made for *trans-trans* diacetamide and its C- and N-deuterated compounds. The internal symmetry coordinates were written down in the same way as the case of *trans-cis* diacetamide,[4,5] since we included the half C-deuterated molecules having the C_s symmetry in the calculation. The meanings of the symmetry coordinates are listed in Table 2. The secular equations were set up according to the GF matrix method.[11] We used a Urey-Bradley force field for the in-plane vibrations and the out-of-plane vibrations concerning the methyl groups and a valence force field for the remaining out-of-plane vibrations. The starting set of the Urey-Bradley force constants was the same as that used in the calculation for *trans-cis* diacetamide.[4] The diagonal valence force constants were transferred from acetamide[12] and *trans-cis* diacetamide,[5] while the off diagonal valence force constants were assumed to be zero first. The isotope shifts predicted by the initial calculation were useful to pick up some of the empirically unassignable fundamentals of the N- and the C-deuterated compounds. The force constants for the in-plane vibrations were refined in an analogous way to the case of *trans-cis* diacetamide,[4] until an overall

Table 2. The meanings of the internal symmetry coordinates

	Description of modes			Description of modes			Description of modes	
S_1	CC str.	(νCC)	S_{13}	CH_3 rock.	(ρCH_3)	S_{25}	CH_3 asym. def.	($\delta_{as}CH_3$)
S_2	C=O str.	(νC=O)	S_{14}	C=O def.	(δC=O)	S_{26}	CH_3 rock.	(ρCH_3)
S_3	CN str.	(νCN)	S_{15}	CCN def.	(δCCN)	S_{27}	CH_3 asym. str.	($\nu_{as}CH_3$)
S_4	CN str.	(νCN)	S_{16}	CNC def.	(δCNC)	S_{28}	CH_3 asym. def.	($\delta_{as}CH_3$)
S_5	C=O str.	(νC=O)	S_{17}	C=O def.	(δC=O)	S_{29}	CH_3 rock.	(ρCH_3)
S_6	CC str.	(νCC)	S_{18}	CCN def.	(δCCN)	S_{30}	CH_3 torsion	(τCH_3)
S_7	CH_3 sym. def.	($\delta_s CH_3$)	S_{19}	NH str.	(νNH)	S_{31}	CH_3 torsion	(τCH_3)
S_8	CH_3 asym. def.	($\delta_{as}CH_3$)	S_{20}	CH_3 sym. str.	($\nu_s CH_3$)	S_{32}	CN torsion	(τCN)
S_9	CH_3 rock.	(ρCH_3)	S_{21}	CH_3 asym. str.	($\nu_{as}CH_3$)	S_{33}	CN torsion	(τCN)
S_{10}	NH def.	(δNH)	S_{22}	CH_3 sym. str.	($\nu_s CH_3$)	S_{34}	C=O def.	(πC=O)
S_{11}	CH_3 sym. def.	($\delta_s CH_3$)	S_{23}	CH_3 asym. str.	($\nu_{as}CH_3$)	S_{35}	C=O def.	(πC=O)
S_{12}	CH_3 asym. def.	($\delta_{as}CH_3$)	S_{24}	CH_3 asym. str.	($\nu_{as}CH_3$)	S_{36}	NH def.	(πNH)

Table 3. Force constants

(A) Urey-Bradley type force constants in mdyn/Å (*KAPPA* is given in mdyn·Å/(rad)²)

	Force constant			Dispersion		Force constant			Dispersion
1.	K(CH)	4.53_7	(4.62)*	0.033	11.	H(CCH)	0.21_1	(0.358)	0.030
2.	K(NH)	5.42_0	(5.74)	0.074	12.	H(HCH)	0.40_6	(0.401)	0.007
3.	K(CO)	8.71_9	(9.8)	0.267	13.	F(NCO)	0.91_8	(1.20)	0.162
4.	K(CN)	3.77_9	(4.0)	0.161	14.	F(NCC)	0.41_2	(0.70)	0.177
5.	K(CC)	3.23_1	(3.2)	0.256	15.	F(CCO)	0.56_9	(0.50)	0.169
6.	H(NCO)	0.11_4	(0.2)	0.068	16.	F(HNC)	0.36_2	(0.35)	0.073
7.	H(NCC)	0.79_3	(0.3)	0.148	17.	F(CNC)	1.78_9	(1.70)	0.222
8.	H(CCO)	0.24_1	(0.25)	0.091	18.	F(CCH)	0.48_9	(0.372)	0.062
9.	H(HNC)	0.29_9	(0.31)	0.020	19.	F(HCH)	0.05_6	(0.083)	0.013
10.	H(CNC)	0.26_8	(0.50)	0.108	20.	*KAPPA*	-0.01_4	(−0.104)	0.018

* ( ); initial value

(B) Valence type force constants in mdyn·Å/(rad)²

1. $f_{30,30}=f_{31,31}$	0.0033	4. $f_{36,36}$	0.087	7. $f_{32,36}=-f_{33,36}$	−0.019	10. $f_{26,34}=f_{29,35}$	−0.044
2. $f_{32,32}=f_{33,33}$	0.085	5. $f_{32,34}=f_{33,35}$	−0.018	8. $f_{34,35}$	−0.047		
3. $f_{34,34}=f_{35,35}$	0.417	6. $f_{32,35}=f_{33,34}$	0.004	9. $f_{34,36}=-f_{35,36}$	0.059		

11) E. B. Wilson Jr., *J. Chem. Phys.*, **7**, 1047 (1939); **9**, 76 (1941).

12) T. Uno, K. Machida, and Y. Saito, *Spectrochim. Acta* **27**, 833 (1971).

TABLE 4. OBSERVED AND CALCULATED FREQUENCIES OF $CH_3CONHCOCH_3$ IN cm^{-1}

(a) In-plane vibrations (a_1, b_2)

	Obsd.	Calcd.	Δ(%)[a]	P.E.D. (%)[b]	Assignment
ν_1 (a_1)	3215	3238	0.7	$S_{19}(100)$	νNH
ν_2 (a_1)	2995	2997	0.1	$S_{21}(50), S_{23}(50)$	$\nu_{as}CH_3$
ν_{13}(b_2)	2995	2997	0.1	$S_{21}(50), S_{23}(50)$	$\nu_{as}CH_3$
ν_3 (a_1)	2915	2922	0.3	$S_{20}(50), S_{22}(50)$	ν_sCH_3
ν_{14}(b_2)	2915	2922	0.3	$S_{20}(50), S_{22}(50)$	ν_sCH_3
ν_4 (a_1)	1730	1727	0.2	$S_2(35), S_5(35)$	Imide I
ν_{15}(b_2)	1695	1700	0.3	$S_2(34), S_5(34), S_{10}(17)$	Imide I
ν_{16}(b_2)	1513	1512	0.1	$S_3(19), S_4(19), S_{10}(69)$	Imide II
ν_5 (a_1)	1428	1428	0.0	$S_8(44), S_{12}(44)$	$\delta_{as}CH_3$
ν_{17}(b_2)	1428	1425	0.2	$S_8(44), S_{12}(44)$	$\delta_{as}CH_3$
ν_6 (a_1)	1369	1375	0.4	$S_7(50), S_{11}(50)$	δ_sCH_3
ν_{18}(b_2)	1369	1374	0.4	$S_7(52), S_{11}(52)$	δ_sCH_3
ν_7 (a_1)	1327	1326	0.1	$S_1(18), S_3(18), S_4(18), S_6(18)$	νCN
ν_{19}(b_2)	1236	1238	0.2	$S_1(17), S_3(31), S_4(31), S_6(17), S_{10}(12)$	Imide III
ν_8 (a_1)	1030	1015	1.4	$S_2(12), S_5(12), S_9(19), S_{13}(19)$	$\rho CH_3+\nu C{=}O$
ν_{20}(b_2)	1027	1005	2.2	$S_9(38), S_{13}(38)$	ρCH_3
ν_9 (a_1)	920	934	1.5	$S_3(10), S_4(10), S_9(22), S_{13}(22), S_{16}(17)$	$\rho CH_3+\delta$CNC$+\nu$CN
ν_{21}(b_2)	920	933	1.4	$S_1(27), S_3(12), S_4(12), S_6(27)$	νCC
ν_{10}(a_1)	661	661	0.0	$S_1(18), S_6(18), S_{14}(12), S_{16}(13), S_{17}(12)$	Imide IV
ν_{22}(b_2)	526	542	3.0	$S_{14}(12), S_{15}(30), S_{17}(12), S_{18}(30)$	Imide IV
ν_{23}(b_2)	418	407	2.6	$S_{14}(33), S_{15}(12), S_{17}(33), S_{18}(12)$	$\delta C{=}O+\delta$CCN
ν_{11}(a_1)	368	367	0.3	$S_{14}(18), S_{15}(17), S_{17}(18), S_{18}(17)$	$\delta C{=}O+\delta$CCN
ν_{12}(a_1)	177	184	3.9	$S_{14}(12), S_{15}(12), S_{16}(62), S_{17}(12), S_{18}(12)$	δCNC

(b) Out-of-plane vibrations (b_1)

	Obsd.	Calcd.	Δ(%)[a]	P.E.D. (%)[b]	Assignment
ν_{24}(b_1)	2995	2996	0.0	$S_{24}(50), S_{27}(50)$	$\nu_{as}CH_3$
ν_{25}(b_1)	1428	1427	0.1	$S_{25}(44), S_{28}(44)$	$\delta_{as}CH_3$
ν_{26}(b_1)	1070	1063	0.7	$S_{26}(38), S_{29}(38)$	ρCH_3
ν_{27}(b_1)	737	738	0.2	$S_{32}(32), S_{33}(32), S_{36}(63)$	πNH$+\tau$CN
ν_{28}(b_1)	626	613	2.1	$S_{34}(41), S_{35}(41), S_{36}(61)$	$\pi C{=}O+\pi$NH
ν_{29}(b_1)	250	255	1.8	$S_{32}(22), S_{33}(22)$	τCN
ν_{30}(b_1)	95	105	10.5	$S_{30}(49), S_{31}(49)$	τCH_3

a) $\Delta(\%)=|\nu_{obsd}-\nu_{calcd}|\times 100/\nu_{obsd}$
b) Those less than 10% are omitted.

TABLE 5. OBSERVED AND CALCULATED FREQUENCIES OF $CH_3CONDCOCH_3$ IN cm^{-1}

(a) In-plane vibrations (a_1, b_2)

	Obsd.	Calcd.	Δ(%)[a]	P.E.D. (%)[b]	Assignment
ν_1 (a_1)	2995	2997	0.1	$S_{21}(50), S_{23}(50)$	$\nu_{as}CH_3$
ν_{13}(b_2)	2995	2997	0.1	$S_{21}(50), S_{23}(50)$	$\nu_{as}CH_3$
ν_2 (a_1)	2915	2922	0.3	$S_{20}(50), S_{22}(50)$	ν_sCH_3
ν_{14}(b_2)	2915	2922	0.3	$S_{20}(50), S_{22}(50)$	ν_sCH_3
ν_3 (a_1)	2405	2373	1.3	$S_{19}(100)$	νND
ν_4 (a_1)	1730	1723	0.4	$S_2(36), S_5(36)$	Imide I′
ν_{15}(b_2)	1672	1677	0.3	$S_2(40), S_5(40)$	Imide I′
ν_{16}(b_2)	1428	1429	0.1	$S_8(42), S_{12}(42)$	$\delta_{as}CH_3$
ν_5 (a_1)	1428	1428	0.0	$S_8(44), S_{12}(44)$	$\delta_{as}CH_3$
ν_6 (a_1)	1369	1375	0.4	$S_7(50), S_{11}(50)$	δ_sCH_3
ν_{17}(b_2)	1369	1374	0.4	$S_7(51), S_{11}(50)$	δ_sCH_3
ν_{18}(b_2)	1353	1358	0.4	$S_3(44), S_4(44), S_{10}(26)$	Imide II′
ν_7 (a_1)	1327	1325	0.2	$S_1(18), S_3(18), S_4(18), S_6(18)$	νCN$+\nu$CC
ν_{19}(b_2)	1094	1076	1.6	$S_1(15), S_6(15), S_9(11), S_{10}(39), S_{13}(11)$	δND$+\nu$CC$+\rho CH_3$
ν_8 (a_1)	1028	1010	1.8	$S_2(10), S_5(10), S_9(23), S_{13}(23)$	ρCH_3

TABLE 5. Continued

	Obsd	Calcd	Δ(%)[a]	P.E.D. (%)[b]	Assignment
$\nu_{20}(b_2)$	947	984	3.9	$S_9(29), S_{13}(29)$	ρCH_3
$\nu_9\ (a_1)$	900	920	2.3	$S_3(11), S_4(11), S_9(18), S_{13}(18), S_{16}(18)$	$\rho CH_3+\nu CC+\delta CNC$
$\nu_{21}(b_2)$	900	892	0.9	$S_1(12), S_3(18), S_4(18), S_6(12), S_{10}(21)$	$\delta ND+\nu CN+\nu CC$
$\nu_{10}(a_1)$		658		$S_1(18), S_6(18), S_{14}(13), S_{16}(14), S_{17}(13)$	Imide IV'
$\nu_{22}(b_2)$	523	534	2.1	$S_{14}(12), S_{15}(29), S_{17}(12), S_{18}(29)$	Imide IV'
$\nu_{23}(b_2)$	412	407	1.2	$S_{14}(33), S_{15}(12), S_{17}(33), S_{18}(12)$	$\delta C{=}O+\delta CCN$
$\nu_{11}(a_1)$	368	367	0.4	$S_{14}(19), S_{15}(17), S_{17}(19), S_{18}(17)$	$\delta C{=}O+\delta CCN$
$\nu_{12}(a_1)$	160	183	14.4	$S_{14}(12), S_{15}(12), S_{16}(62), S_{17}(12), S_{18}(12)$	δCNC

(b) Out-of-plane vibrations (b_1)

	Obsd	Calcd	Δ(%)[a]	P.E.D. (%)[b]	Assignment
$\nu_{24}(b_1)$	2995	2996	0.0	$S_{24}(50), S_{27}(50)$	$\nu_{as}CH_3$
$\nu_{25}(b_1)$	1428	1427	0.1	$S_{25}(44), S_{28}(44)$	$\delta_{as}CH_3$
$\nu_{26}(b_1)$		1063		$S_{26}(38), S_{29}(38)$	ρCH_3
$\nu_{27}(b_1)$	626	623	0.5	$S_{34}(39), S_{35}(39), S_{36}(11)$	$\pi C{=}O+\pi ND$
$\nu_{28}(b_1)$	546	547	0.2	$S_{32}(18), S_{33}(18), S_{36}(117)$	$\pi ND+\tau CN$
$\nu_{29}(b_1)$	240	243	1.4	$S_{32}(28), S_{33}(28)$	τCN
$\nu_{30}(b_1)$	95	105	10.5	$S_{30}(49), S_{31}(49)$	τCH_3

a) $\Delta(\%)=|\nu_{obsd}-\nu_{calcd}|\times 100/\nu_{obsd}$
b) Those less than 10% are omitted.

TABLE 6. OBSERVED AND CALCULATED FREQUENCIES OF $CD_3CONHCOCH_3$ IN cm^{-1}

(a) In-plane vibrations (a')

	Obsd	Calcd	Δ(%)[a]	P.E.D. (%)[b]	Assignment
$\nu_1\ (a')$	3215	3238	0.7	$S_{19}(100)$	νNH
$\nu_2\ (a')$	2995	2997	0.1	$S_{23}(100)$	$\nu_{as}CH_3$
$\nu_3\ (a')$	2915	2922	0.3	$S_{22}(100)$	$\nu_s CH_3$
$\nu_4\ (a')$	2230	2228	0.1	$S_{21}(100)$	$\nu_{as}CD_3$
$\nu_5\ (a')$	2110	2099	0.5	$S_{20}(99)$	$\nu_s CD_3$
$\nu_6\ (a')$	1728	1725	0.2	$S_2(30), S_5(41), S_{18}(10)$	Imide I
$\nu_7\ (a')$		1698		$S_2(40), S_5(28), S_{10}(17)$	Imide I
$\nu_8\ (a')$	1510	1511	0.0	$S_3(19), S_4(20), S_{10}(70)$	Imide II
$\nu_9\ (a')$	1421	1427	0.4	$S_{12}(88)$	$\delta_{as}CH_3$
$\nu_{10}(a')$		1375		$S_6(11), S_{11}(102)$	$\delta_s CH_3$
$\nu_{11}(a')$	1324	1326	0.1	$S_1(25), S_3(19), S_4(18), S_6(18)$	νCN
$\nu_{12}(a')$	1243	1239	0.3	$S_1(21), S_3(30), S_4(31), S_6(17), S_{10}(12)$	Imide III
$\nu_{13}(a')$	1079	1081	0.1	$S_1(13), S_3(13), S_7(74)$	$\delta_s CD_3$
$\nu_{14}(a')$	1038	1030	0.8	$S_8(87)$	$\delta_{as}CD_3$
$\nu_{15}(a')$	1018	1006	1.2	$S_5(14), S_{13}(50)$	ρCH_3
$\nu_{16}(a')$	959	958	0.2	$S_4(19), S_{13}(26), S_{15}(11), S_{16}(15)$	$\rho CH_3+\nu CN$
$\nu_{17}(a')$	890	895	0.6	$S_1(14), S_3(10), S_6(24), S_7(16)$	νCC
$\nu_{18}(a')$	805	785	2.5	$S_9(71)$	ρCD_3
$\nu_{19}(a')$	627	632	0.8	$S_1(19), S_6(15), S_{16}(11), S_{17}(17)$	Imide IV
$\nu_{20}(a')$	498	510	2.4	$S_9(13), S_{14}(10), S_{15}(18), S_{17}(14), S_{18}(32)$	Imide IV
$\nu_{21}(a')$	408	401	1.7	$S_{14}(39), S_{17}(25), S_{18}(15)$	$\delta C{=}O+\delta CCN$
$\nu_{22}(a')$	349	348	0.4	$S_{14}(17), S_{15}(23), S_{17}(21)$	$\delta C{=}O+\delta CCN$
$\nu_{23}(a')$		180		$S_{14}(11), S_{15}(14), S_{16}(61), S_{17}(11), S_{18}(12)$	δCNC

(b) Out-of-plane vibrations (a'')

	Obsd	Calcd	Δ(%)[a]	P.E.D. (%)[b]	Assignment
$\nu_{24}(a'')$	2995	2996	0.0	$S_{27}(100)$	$\nu_{as}CH_3$
$\nu_{25}(a'')$	2230	2223	0.3	$S_{24}(100)$	$\nu_{as}CD_3$
$\nu_{26}(a'')$	1421	1427	0.4	$S_{28}(89), S_{29}(10)$	$\delta_{as}CH_3$
$\nu_{27}(a'')$	1038	1061	2.2	$S_{28}(10), S_{29}(78)$	ρCH_3

TABLE 6. Continued

	Obsd	Calcd	Δ(%)[a]	P.E.D. (%)[b]	Assignment
$\nu_{28}(a'')$	1018	1023	0.5	$S_{25}(92)$	$\delta_{as}CD_3$
$\nu_{29}(a'')$	910	886	2.7	$S_{26}(61), S_{34}(27)$	$\rho CD_3+\pi C{=}O$
$\nu_{30}(a'')$	737	733	0.5	$S_{32}(31), S_{33}(30), S_{36}(73)$	$\pi NH+\tau CN$
$\nu_{31}(a'')$	603	596	1.2	$S_{34}(13), S_{35}(66), S_{36}(48)$	$\pi C{=}O+\pi NH$
$\nu_{32}(a'')$	498	502	0.8	$S_{26}(22), S_{34}(61), S_{35}(28)$	$\pi C{=}O+\rho CD_3$
$\nu_{33}(a'')$		247		$S_{32}(20), S_{33}(24), S_{34}(10)$	$\tau CN+\pi C{=}O$
$\nu_{34}(a'')$		114		$S_{31}(28), S_{32}(34), S_{33}(36)$	$\tau CN+\tau CH_3$
$\nu_{35}(a'')$		101		$S_{31}(70), S_{32}(17), S_{33}(11)$	$\tau CH_3+\tau CN$
$\nu_{36}(a'')$		74		$S_{30}(96)$	τCD_3

a) $\Delta(\%)=|\nu_{obsd}-\nu_{calcd}|\times 100/\nu_{obsd}$
b) Those less than 10% are omitted.

TABLE 7. OBSERVED AND CALCULATED FREQUENCIES OF $CD_3CONDCOCH_3$ IN cm^{-1}

(a) In-plane vibrations (a')

	Obsd	Calcd	Δ(%)[a]	P.E.D. (%)[b]	Assignment
$\nu_1(a')$	2995	2997	0.1	$S_{23}(100)$	$\nu_{as}CH_3$
$\nu_2(a')$	2915	2922	0.3	$S_{22}(100)$	ν_sCH_3
$\nu_3(a')$	2415	2373	1.7	$S_{19}(99)$	νND
$\nu_4(\alpha')$	2230	2228	0.1	$S_{21}(100)$	$\nu_{as}CD_3$
$\nu_5(a')$	2110	2099	0.5	$S_{20}(99)$	ν_sCD_3
$\nu_6(a')$	1726	1721	0.3	$S_2(32), S_5(40)$	Imide I'
$\nu_7(a')$		1675		$S_2(45), S_5(36)$	Imide I'
$\nu_8(a')$	1421	1429	0.5	$S_{12}(86)$	$\delta_{as}CH_3$
$\nu_9(a')$		1375		$S_6(10), S_{11}(101)$	δ_sCH_3
$\nu_{10}(a')$		1359		$S_3(45), S_4(47), S_{10}(27)$	Imide II'
$\nu_{11}(a')$		1325		$S_1(26), S_3(19), S_4(17), S_6(18)$	νCN
$\nu_{12}(a')$	1110	1110	0.0	$S_1(29), S_5(10), S_7(49), S_{10}(17)$	$\delta_sCD_3+\delta$ND$+\nu$CC
$\nu_{13}(a')$	1037	1030	0.7	$S_7(11), S_8(60), S_{10}(10)$	$\delta_{as}CD_3$
$\nu_{14}(a')$	1018	1027	0.8	$S_7(24), S_8(30), S_{10}(19), S_{13}(10)$	$\delta_{as}CD_3+\delta_sCD_3+\delta$ND
$\nu_{15}(a')$	992	999	0.7	$S_5(13), S_6(13), S_{13}(42)$	ρCH_3
$\nu_{16}(a')$	924	934	1.1	$S_4(15), S_{13}(21), S_{15}(10), S_{16}(17)$	$\rho CH_3+\delta$CNC
$\nu_{17}(a')$	883	870	1.4	$S_1(10), S_3(11), S_4(15), S_6(17), S_{10}(12)$	νCC
$\nu_{18}(a')$	796	779	2.1	$S_9(71)$	ρCD_3
$\nu_{19}(a')$	627	630	0.4	$S_1(18), S_6(15), S_{16}(11), S_{17}(17)$	Imide IV'
$\nu_{20}(a')$	498	504	1.2	$S_9(12), S_{14}(10), S_{15}(18), S_{17}(14), S_{18}(32)$	Imide IV'
$\nu_{21}(a')$	402	401	0.3	$S_{14}(39), S_{17}(25), S_{18}(16)$	$\delta C{=}O+\delta$CCN
$\nu_{22}(a')$	347	347	0.0	$S_{14}(17), S_{15}(24), S_{17}(21)$	$\delta C{=}O+\delta$CCN
$\nu_{23}(a')$		179		$S_{14}(11), S_{15}(14), S_{16}(62), S_{17}(11), S_{18}(12)$	δCNC

(b) Out-of-plane vibrations (a'')

	Obsd	Calcd	Δ(%)[a]	P.E.D. (%)[b]	Assignment
$\nu_{24}(a'')$	2995	2996	0.0	$S_{27}(100)$	$\nu_{as}CH_3$
$\nu_{25}(a'')$	2230	2223	0.3	$S_{24}(100)$	$\nu_{as}CD_3$
$\nu_{26}(a'')$	1421	1427	0.4	$S_{28}(89), S_{29}(10)$	$\delta_{as}CH_3$
$\nu_{27}(a'')$	1037	1060	2.2	$S_{28}(10), S_{29}(78)$	ρCH_3
$\nu_{28}(a'')$	1018	1023	0.5	$S_{25}(92)$	$\delta_{as}CD_3$
$\nu_{29}(a'')$	910	883	2.9	$S_{26}(62), S_{34}(27)$	$\rho CD_3+\pi C{=}O$
$\nu_{30}(a'')$	605	602	0.5	$S_{29}(10), S_{32}(10), S_{34}(12), S_{35}(62)$	$\pi C{=}O$
$\nu_{31}(a'')$	546	547	0.2	$S_{32}(18), S_{33}(18), S_{36}(117)$	πND$+\tau$CN
$\nu_{32}(a'')$	498	502	0.8	$S_{26}(22), S_{34}(61), S_{35}(29)$	$\pi C{=}O+\rho CD_3$
$\nu_{33}(a'')$		236		$S_{32}(25), S_{33}(29)$	τCN
$\nu_{34}(a'')$		114		$S_{31}(28), S_{32}(34), S_{33}(36)$	$\tau CN+\tau CH_3$
$\nu_{35}(a'')$		101		$S_{31}(70), S_{32}(17), S_{33}(11)$	$\tau CH_3+\tau CN$
$\nu_{36}(a'')$		74		$S_{30}(96)$	τCD_3

a) $\Delta(\%)=|\nu_{obsd}-\nu_{calcd}|\times 100/\nu_{obsd}$
b) Those less than 10% are omitted.

TABLE 8. OBSERVED AND CALCULATED FREQUENCIES OF $CD_3CONHCOCD_3$ IN cm^{-1}

(a) In-plane vibrations (a_1, b_2)

	Obsd	Calcd	Δ(%)[a]	P.E.D. (%)[b]	Assignment
ν_1 (a_1)	3200	3238	1.2	$S_{19}(100)$	νNH
ν_2 (a_1)	2230	2228	0.1	$S_{21}(50), S_{23}(50)$	$\nu_{as}CD_3$
ν_{13}(b_2)	2230	2228	0.1	$S_{21}(50), S_{23}(50)$	$\nu_{as}CD_3$
ν_3 (a_1)	2110	2099	0.5	$S_{20}(50), S_{22}(50)$	ν_sCD_3
ν_{14}(b_2)	2110	2099	0.5	$S_{20}(50), S_{22}(50)$	ν_sCD_3
ν_4 (a_1)	1720	1722	0.1	$S_2(36), S_5(36)$	Imide I
ν_{15}(b_2)	1690	1696	0.4	$S_2(34), S_5(34), S_{10}(17)$	Imide I
ν_{16}(b_2)	1508	1509	0.1	$S_3(20), S_4(20), S_{10}(70)$	Imide II
ν_5 (a_1)	1324	1326	0.1	$S_1(25), S_3(19), S_4(19), S_6(25)$	νCN
ν_{17}(b_2)	1260	1240	1.6	$S_1(21), S_3(30), S_4(30), S_6(21), S_{10}(11)$	Imide III
ν_{18}(b_2)	1087	1089	0.2	$S_7(36), S_{11}(36)$	δ_sCD_3
ν_6 (a_1)	1087	1069	1.6	$S_7(39), S_{11}(39)$	δ_sCD_3
ν_7 (a_1)	1030	1030	0.0	$S_8(43), S_{12}(43)$	$\delta_{as}CD_3$
ν_{19}(b_2)	1030	1027	0.3	$S_8(47), S_{12}(47)$	$\delta_{as}CD_3$
ν_8 (a_1)	972	964	0.8	$S_2(11), S_5(11), S_{16}(22)$	δCNC+νC=O
ν_{20}(b_2)	868	865	0.4	$S_1(16), S_3(10), S_4(10), S_6(16), S_7(12), S_{11}(12)$	νCC
ν_{21}(b_2)	819	815	0.5	$S_9(34), S_{13}(34)$	ρCD_3
ν_9 (a_1)	734	756	3.1	$S_9(39), S_{13}(39)$	ρCD_3
ν_{10}(a_1)		605		$S_1(16), S_6(16), S_{14}(10), S_{17}(10)$	Imide IV
ν_{22}(b_2)	485	479	1.2	$S_9(11), S_{13}(11), S_{14}(14), S_{15}(21), S_{17}(14), S_{18}(21)$	Imide IV
ν_{23}(b_2)		393		$S_{14}(29), S_{15}(14), S_{17}(29), S_{18}(14)$	δC=O+δCCN
ν_{11}(a_1)	343	334	2.6	$S_{14}(20), S_{15}(14), S_{17}(20), S_{18}(14)$	δC=O+δCCN
ν_{12}(a_1)		175		$S_{14}(10), S_{15}(10), S_{16}(61), S_{17}(10), S_{18}(14)$	δCNC

(b) Out-of-plane vibrations (b_1)

	Obsd	Calcd	Δ(%)[a]	P.E.D. (%)[b]	Assignment
ν_{24}(b_1)	2230	2223	0.3	$S_{24}(50), S_{27}(50)$	$\nu_{as}CD_3$
ν_{25}(b_1)	1030	1024	0.6	$S_{25}(46), S_{28}(46)$	$\delta_{as}CD_3$
ν_{26}(b_1)	909	895	1.6	$S_{26}(28), S_{29}(28)$	$\rho CD_3+\pi$C=O
ν_{27}(b_1)	734	729	0.7	$S_{32}(29), S_{33}(29), S_{36}(83)$	πNH+τCN
ν_{28}(b_1)	542	565	4.2	$S_{26}(16), S_{29}(16), S_{34}(31), S_{35}(31), S_{36}(42)$	πC=O+πNH
ν_{29}(b_1)		240		$S_{32}(21), S_{33}(21)$	τCN
ν_{30}(b_1)		75		$S_{30}(49), S_{31}(49)$	τCD_3

a) $\Delta(\%)=|\nu_{obsd}-\nu_{calcd}|\times 100/\nu_{obsd}$
b) Those less than 10% are omitted.

TABLE 9. OBSERVED AND CALCULATED FREQUENCIES OF $CD_3CONDCOCD_3$ IN cm^{-1}

(a) In-plane vibrations (a_1, b_2)

	Obsd	Calcd	Δ(%)[a]	P.E.D. (%)[b]	Assignment
ν_1 (a_1)	2420	2373	1.9	$S_{19}(99)$	νND
ν_2 (a_1)	2230	2228	0.1	$S_{21}(50), S_{23}(50)$	$\nu_{as}CD_3$
ν_{13}(b_2)	2230	2228	0.1	$S_{21}(50), S_{23}(50)$	$\nu_{as}CD_3$
ν_3 (a_1)	2110	2099	0.5	$S_{20}(50), S_{22}(50)$	ν_sCD_3
ν_{14}(b_2)	2110	2099	0.5	$S_{20}(50), S_{22}(50)$	ν_sCD_3
ν_4 (a_1)	1720	1718	0.1	$S_2(36), S_5(36)$	Imide I'
ν_{15}(b_2)	1665	1672	0.4	$S_2(40), S_5(40)$	Imide I'
ν_{16}(b_2)	1353	1360	0.5	$S_3(48), S_4(48), S_{10}(28)$	Imide II'
ν_5 (a_1)	1324	1325	0.1	$S_1(25), S_3(19), S_4(19), S_6(25)$	νCN
ν_{17}(b_2)	1120	1124	0.4	$S_1(24), S_6(24), S_7(28), S_{10}(15), S_{11}(28)$	$\delta_sCD_3+\nu$CC+δND
ν_6 (a_1)	1087	1068	1.8	$S_7(41), S_{11}(41)$	δ_sCD_3
ν_7 (a_1)	1030	1030	0.0	$S_8(45), S_{12}(45)$	$\delta_{as}CD_3$
ν_{18}(b_2)	1030	1027	0.3	$S_8(47), S_{12}(47)$	$\delta_{as}CD_3$
ν_{19}(b_2)	1011	1007	0.4	$S_7(14), S_{10}(44), S_{11}(14)$	δND+δ_sCD_3

TABLE 9. Continued

	Obsd	Calcd	Δ(%)[a]	P.E.D. (%)[b]	Assignment
ν_8 (a_1)	955	949	0.6	$S_2(11), S_5(11), S_{15}(10), S_{16}(21), S_{18}(10)$	δCNC+νC=O
ν_{20}(b_2)	842	845	0.4	$S_1(14), S_3(10), S_4(10), S_6(14)$	νCC+νCN
ν_{21}(b_2)	816	807	1.2	$S_9(34), S_{13}(34)$	ρCD_3
ν_9 (a_1)	734	753	2.6	$S_9(39), S_{13}(39)$	ρCD_3
ν_{10}(a_1)		603		$S_1(16), S_6(16), S_{14}(10), S_{17}(10)$	Imide IV′
ν_{22}(b_2)	485	474	2.3	$S_9(11), S_{13}(11), S_{14}(14), S_{15}(21), S_{17}(14), S_{18}(21)$	Imide IV′
ν_{23}(b_2)	379	393	3.7	$S_{14}(28), S_{15}(15), S_{17}(28), S_{18}(15)$	δC=O+δCCN
ν_{11}(a_1)	343	334	2.6	$S_{14}(20), S_{15}(14), S_{17}(20), S_{18}(14)$	δC=O+δCCN
ν_{12}(a_1)		175		$S_{14}(10), S_{15}(14), S_{16}(61), S_{17}(10), S_{18}(14)$	δCNC

(b) Out-of-plane vibrations (b_1)

	Obsd	Calcd	Δ(%)[a]	P.E.D. (%)[b]	Assignment
ν_{24}(b_1)	2230	2223	0.3	$S_{24}(50), S_{27}(50)$	$\nu_{as}CD_3$
ν_{25}(b_1)	1030	1024	0.6	$S_{25}(46), S_{28}(46)$	$\delta_{as}CD_3$
ν_{26}(b_1)	909	891	2.0	$S_{32}(29), S_{29}(29)$	$\rho CD_3+\pi$C=O
ν_{27}(b_1)	550	568	3.3	$S_{26}(16), S_{29}(16), S_{32}(13), S_{33}(13), S_{34}(27), S_{35}(27)$	πC=O+ρCD_3
ν_{28}(b_1)	540	547	1.3	$S_{32}(15), S_{33}(15), S_{36}(123)$	πND+τCN
ν_{29}(b_1)	230	229	0.4	$S_{32}(26), S_{33}(26)$	τCN
ν_{30}(b_1)	80	75	6·7	$S_{30}(49), S_{31}(49)$	τCD_3

a) $\Delta(\%)=|\nu_{obsd}-\nu_{calcd}|\times 100/\nu_{obsd}$
b) Those less than 10% are omitted.

convergence of force constants was attained. On the refinement of the out-of-plane force constants, the Urey-Bradley force constants for the methyl groups were fixed to the converged values in the in-plane calculation, and the valence force constants were adjusted by referring to the Jacobian matrix and repeating the least squares method by parts. The final values of force constants are given in Table 3, and the calculated frequencies are listed in Tables 4—9 together with the dominant terms in the potential energy distribution and the assignments. The reliability of the presently obtained force constants may be ascertained from the agreement between the observed and the calculated frequencies. The potential energy distributions in Tables 4—9 show that the coupling among the skeletal deformation vibrations is considerable. For the C-deuterated compounds, the CD_3 rocking vibrations also participate in this coupling, explaining well the fact that the C-deuteration gives rise to much larger shifts of the skeletal deformation frequencies than the N-deuteration. In Table 10, the stretching force constants obtained in the present work are compared with those of the *trans-cis* diacetamide reported before (Calculation II in Ref. 4). In the form A crystal, only the *cis*-CONH- group of *trans-cis* diacetamide is involved in the hydrogen bonds, and accordingly K(CO)(*trans*) is larger than K(CO)(*cis*) and K(CN)(*trans*) is smaller than K(CN)(*cis*). The presently obtained values of K(CO) and K(CN) of *trans-trans* diacetamide fall between the values of the corresponding *trans-* and *cis-*constants of *trans-cis* diacetamide. This result is reasonable since the C=O and the C–N bonds involved in the bifurcated hydrogen bonds of the form B crystal are expected to have intermediate bond orders between the unassociated and the normally hydrogen-bonded cases.

TABLE 10. STRETCHING FORCE CONSTANTS OF *trans-cis* AND *tans-trans* DIACETAMIDES (mdyn/Å)

	trans-cis	*trans-trans*
K(CH)	4.40	4.54
K(NH)	5.46	5.42
K(CO)	8.92 (*trans*) 8.09 (*cis*)	8.72
K(CN)	3.50 (*trans*) 4.12 (*cis*)	3.78
K(CC)	3.36	3.23

The authors wish to express their thanks to Prof. T. Takenaka of Kyoto University for the use of Perkin-Elmer 521 and Hitachi FIS-3 grating infrared spectrophotometers. Thanks are also due to Prof. T. Miyazawa and Dr.H.Sugeta of Osaka University, Dr. T. Kajiura of Japan Electron Optics Laboratory Co., Ltd. for the measurements of laser Raman spectra and to the staff of the Kyoto University Computer Center for use of the FACOM 230-60 computer.

A Molecular Orbital Calculation of Chemically Interacting Systems. Addition of Singlet Methylene to Ethylene

Hiroshi FUJIMOTO, Shinichi YAMABE, and Kenichi FUKUI

Faculty of Engineering, Kyoto University, Sakyo-ku, Kyoto

(Received March 31, 1972)

A semi-empirical self-consistent-field molecular orbital calculation of the addition of singlet methylene to ethylene was carried out on the basis of an isolated molecule approximation. The calculation was made with respect to two modes of approaches of methylene to ethylene which were proposed by Hoffmann. A calculation of the electron populations by use of the configuration interaction wave function showed that singlet methylene added to ethylene double bond in an electrophilic fashion with a quasi-synchronous formation of two σ bonds to yield cyclopropane. The present calculation revealed the important roles of the interaction between the highest occupied molecular orbital of ethylene and the lowest unoccupied molecular orbital of methylene and of the interaction between the highest occupied molecular orbital of methylene and the lowest unoccupied molecular orbital of ethylene, in interpreting the formation of new σ bonds between ethylene and methylene and the disappearance of the π bond of ethylene.

Molecular orbital (MO) theory has achieved a fair success in interpreting the orientation and stereoselection in various sorts of chemical reactions.[1,2] In dealing with chemical reactions by MO methods, there exist two kinds of approaches. One is to apply MO methods, regarding the whole system composed of two reacting species as if it were one molecule, while the other intends to express the energy and the electron populations of a reacting system by use of the MO's which are obtained with respect to the two reactants in their isolated states. Although the application of the latter approach is usually limited to the cases of weak interaction, it is capable of providing us with some basic information on the nature of chemical reactions. Murrell and his collaborators extended the theory of long range force to the interaction with small orbital overlap and divided the interaction energy into several terms.[3] Their theory has been applied to some weak interactions, such as hydrogen bonding and molecular complexes.[4,5] In one of our previous papers, we have discussed the interaction energy between two reacting systems, by partitioning it into the Coulomb, exchange, delocalization, and polarization terms and have pointed out the importance of the delocalization interaction in promoting reactions.[6] An investigation of the delocalization energy has led us to a supposition that the interaction between the highest occupied (HO) MO of one reactant and the lowest unoccupied (LU) MO of the other reactant is almost solely responsible for the determination of the favorable paths of a majority of chemical reactions.[7] The concept of the HOMO-LUMO interaction now seems to be a well established and powerful means to disclose the detailed mechanisms of chemical reactions.[8-10] It is interesting to examine how such particular orbital interaction explains bond formation, bond loosening and charge-transfer, since these are characteristics of chemical reactions.

In this paper, we show the results of calculation on the addition of singlet methylene to ethylene. This reaction was studied by Hoffmann mainly from an energetic viewpoint, using the extended Hückel MO method.[11] Therefore, it will be a test of our configuration interaction (CI) approach to chemical reactions to compare our result with that of Hoffmann.

Interaction between Two Systems

In order to calculate the electron distribution of chemically interacting system of two molecules, by use of the MO's obtained for each of them in an isolated state, we proceed in the following way; (1) we make a self-consistent-field (SCF) calculation on each of the two reactants separately and determine the MO's, (2) we construct the Slater determinantal wave functions for the combined system which represent the original and charge-transferred electron configurations, using the MO's obtained in (1), and (3) then we calculate the wave function for the lowest energy state of the interacting system by solving the secular equation by the usual CI procedure of the electron configurations given in (2), with respect to a given nuclear framework of the system composed of the two reactants.[12]

The wave function of the interacting system is ap-

1) (a) K. Fukui, "Molecular Orbitals in Chemistry, Physics, and Biology," P.-O. Löwdin and B. Pullman, Eds., Academic Press, New York, N. Y. (1964). (b) K. Fukui, "Modern Quantum Chemistry. Istanbul Lectures, Part I," O. Sinanoğlu, Ed., Academic Press, New York, N. Y. (1965). (c) K. Fukui, "Sigma Molecular Orbital Theory," O. Sinanoğlu and K. B. Wiberg, Eds., Yale University Press, New Haven, Conn. (1970).

2) (a) R. B. Woodward and R. Hoffmann, *J. Amer. Chem. Soc.* **87**, 395, 2511 (1965). (b) R. Hoffmann and R. B. Woodward, *ibid.*, **87**, 2046, 4388, 4389 (1965). (c) R. B. Woodward and R. Hoffmann, *Angew. Chem. Int. Ed. (Engl).*, **8**, 781 (1969). (d) M. J. S. Dewer, *Tetrahedron Suppl.*, **8**, *Part I*, 75 (1966). (e) L. Salem, *J. Amer. Chem. Soc.*, **90**, 543, 553 (1969). (f) K. Fukui, *Fortschr. Chem. Forsch.*, **15**, 1 (1970). (g) K. Fukui and H. Fujimoto, This Bulletin, **40**, 2018 (1967).

3) J. N. Murrell, M. Randić, and D. R. Williams, *Proc. Roy. Soc., Ser. A.* **284**, 566 (1965).

4) F. B. van Duijneveldt and J. N. Murrell, *J. Chem. Phys.*, **46**, 1759 (1967).

5) J. L. Lippert, M. W. Hanna, and P. J. Trotter, *J. Amer. Chem. Soc.*, **91**, 4035 (1969).

6) K. Fukui and H, Fujimoto, This Bulletin, **41**, 1989 (1968).

7) K. Fukui and H. Fujimoto, *ibid.*, **42**, 3399 (1969).

8) G. Klopman, *J. Amer. Chem. Soc.*, **90**, 223 (1968).

9) R. G. Pearson, *Theor. Chim. Acta.* **16**, 107 (1970).

10) K. Fukui, *Accounts Chem. Res.*, **4**, 57 (1971).

11) R. Hoffmann, *J. Amer. Chem. Soc.*, **90**, 1475 (1968).

12) H. Fujimoto, S. Yamabe, and K. Fukui, This Bulletin, **44**, 2936 (1971).

proximately given by;

$$\Psi = C_0\Psi_0 + \sum_i^{occ}\sum_l^{uno} C_{i\to l}\Psi_{i\to l} + \sum_k^{occ}\sum_j^{uno} C_{k\to j}\Psi_{k\to j} \quad (1)$$

where Ψ_0 is the original electron configuration with the adiabatic interaction, $\Psi_{i\to l}$ is the charge-transferred state in which an electron in the ith occupied MO of one reactant is shifted into the lth unoccupied MO of another, and $\Psi_{k\to j}$ is the charge-transferred state in the converse fashion. The symbols $\sum^{occ}$ and $\sum^{uno}$ imply the summation over all the occupied and unoccupied MO's respectively. The local-excited states are less important than the charge-transferred states and can be neglected in a first approximation.[12]

Calculation on Isolated Reactants

The MO's of ethylene and methylene were calculated by a semi-empirical all valence-electrons SCF MO method as before.[13] The nuclear configurations of these species were chosen as the same as those adopted by Hoffmann.[11] The calculated MO energy levels of ethylene and methylene are shown in Fig. 1. The

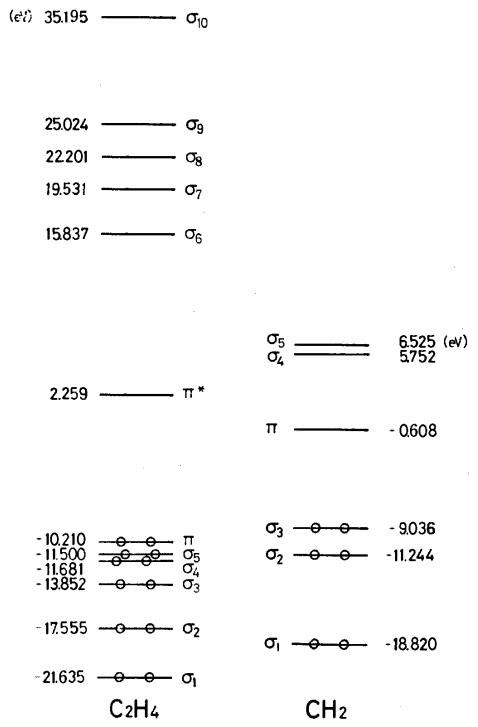

Fig. 1. MO energy levels of ethylene and methylene.

calculated ionization potential of ethylene is 10.2 eV, which is 0.2~0.4 eV smaller than the observed values.[14] The HOMO of methylene is a lone-pair like orbital and the LUMO is a purely p atomic orbital (AO) of the carbon atom. We tentatively term the MO's as shown in Fig. 1.

13) K. Fukui, H. Fujimoto, and S. Yamabe, *J. Phys. Chem.*, **76**, 232 (1972).
14) (a) K. Watanabe, *J. Chem. Phys.*, **26**, 542 (1957).
(b) W. C. Walker and G. L. Weissler, *ibid.*, **23**, 1547 (1955).

Electron Populations

Hoffmann proposed two modes of approaches of methylene to ethylene.[11] Those are schematically illustrated in Fig. 2 in order to define the variables and

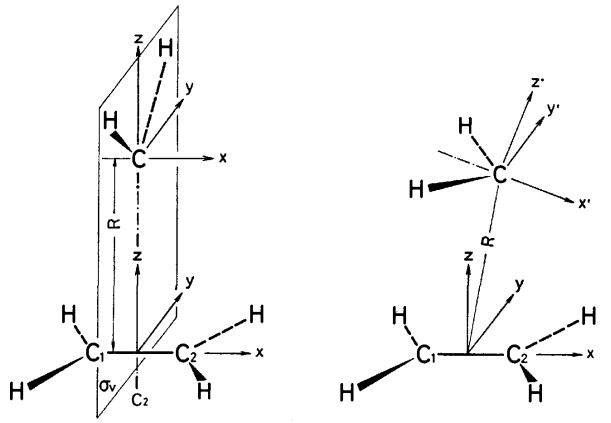

Fig. 2. A schematic representation of assumed reaction models.

coordinates. In Model I, methylene approaches ethylene on the C_2 principal axis, directing the lone-pair orbital toward ethylene. In Model II, the carbon atom of methylene locates away from the bisecting axis of the ethylene C–C bond. We follow the paths suggested by Hoffmann.[11] In this context, we distinguish each model only by specifying the value of R in Fig. 2. It is convenient to choose different Cartesian coordinate systems for methylene and for ethylene in Model II as shown in Fig. 2. The integrals which are necessary for the calculation of the matrix elements of the secular equation were estimated in the same way as in our previous calculation.[13]

Table 1 gives the coefficients of the CI wave function, C_0, $C_{i\to l}$'s and $C_{k\to j}$'s in Eq. (1), for the lowest root of the secular equation, with respect to Models Ia (R=3.0 Å), IIa (R=3.0 Å), and IIb (R=2.85 Å). By comparing Models Ia and IIa, it is clear that the mixing in of charge-transferred electron configurations is much more effective in the latter than in the former. In Models IIa and IIb, the most dominant term except Ψ_0 is the charge-transferred electron configuration from the HOMO of ethylene to the LUMO of methylene, and the next dominant is the one from the HOMO of methylene to the LUMO of ethylene. Comparison of these two models elucidates that the mixings of the charge-transferred electron configuration from the HOMO of ethylene to the LUMO of methylene and of the one from the HOMO of methylene to the LUMO of ethylene become more and more dominant over other charge-transferred electron configurations with the progress of the reaction.

The electron densities of the combined system of ethylene and methylene are given by

$$\rho(1) = M\int \Psi^*(1,2,\cdots,M)\Psi(1,2,\cdots,M)d\xi_1 d\tau_2\cdots d\tau_M \quad (2)$$

where M is the total number of electrons of the system

Table 1. The coefficients of the ground-state CI wave function

Model Ia			$C_0=0.9967$					
			i					
			σ_1	σ_2	σ_3	σ_4	σ_5	π
$\lvert C_{i\to l}\rvert$	l	π	0	0.0240	0	0	0	0
		σ_4	0.0130	0	0	0.0013	0	0.0313
		σ_5	0	0	0.0104	0	0	0
			j					
			π_*	σ_6	σ_7	σ_8	σ_9	σ_{10}
$\lvert C_{k\to j}\rvert$	k	σ_1	0	0	0	0.0021	0	0
		σ_2	0	0.0008	0	0	0	0
		σ_3	0	0	0	0.0013	0	0

Model IIa			$C_0=0.9555$					
			i					
			σ_1	σ_2	σ_3	σ_4	σ_5	π
$\lvert C_{i\to l}\rvert$	l	π	0.0406	0.0185	0	0.0062	0	0.1947
		σ_4	0.0072	0.0011	0	0.0086	0	0.0048
		σ_5	0	0	0.0014	0	0.0091	0
			j					
			π^*	σ_6	σ_7	σ_8	σ_9	σ_{10}
$\lvert C_{k\to j}\rvert$	k	σ_1	0.0121	0	0.0008	0.0015	0	0.0002
		σ_2	0	0.0023	0	0	0.0002	0
		σ_3	0.0600	0	0.0025	0.0015	0	0.0000

Model IIb			$C_0=0.9215$					
			i					
			σ_1	σ_2	σ_3	σ_4	σ_5	π
$\lvert C_{i\to l}\rvert$	l	π	0.0493	0.0173	0	0.0001	0	0.2650
		σ_4	0.0070	0.0003	0	0.0102	0	0.0027
		σ_5	0	0	0.0039	0	0.0110	0
			j					
			π^*	σ_6	σ_7	σ_8	σ_9	σ_{10}
$\lvert C_{k\to j}\rvert$	k	σ_1	0.0130	0	0.0011	0.0009	0	0.0003
		σ_2	0	0.0039	0	0	0.0003	0
		σ_3	0.0851	0	0.0042	0.0024	0	0.0005

i and j denote the MO's of ethylene and k and l stand for those of methylene.

composed of ethylene and methylene (=18). By calculating the terms appearing in Eq. (2) separately, we can disclose the origin of the formation of the intermolecular σ bonds between ethylene and methylene and of the disappearance of the π bond of ethylene. This is an advantage of the present CI method over the usual variational approaches to chemically interacting systems. In order to visualize this circumstance, we show the results of calculation on Models Ib and IIc in which R is 2.7 Å. Figure 3 shows the electron densities of Model IIc in the x–z cross section at $y=0$. Figure 3 (a) indicates the simple sum of the electron densities of ethylene and methylene without interaction and Fig. 3 (b) shows the electron densities of the state of adiabatic interaction, ρ_0. It is noted that the electron densities in the intermolecular region between ethylene and methylene in the Ψ_0 state decrease in comparison with $\rho_{CH_2}+\rho_{CH_2CH_2}$, due to the electron exchange interaction in that state. This is essential to the interaction between two closed shell systems.[12,15] Figure 4 demonstrates ρ. By comparing Figs. 3 and 4, it is clear that the mixing of charge-transferred electron configurations into Ψ_0 is of importance in interpreting the chemical bond formation

15) V. Magnasco, *Theor. Chim. Acta*, **21**, 267 (1971),

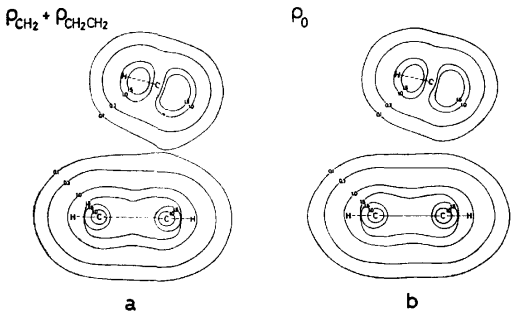

Fig. 3. Electron densities of Model II in the $x-z$ cross section at $y=0$ ($e^-/Å^3$).
(a): the simple sum of the electron densities of ethylene and methylene.
(b): without charge-transfer interaction.

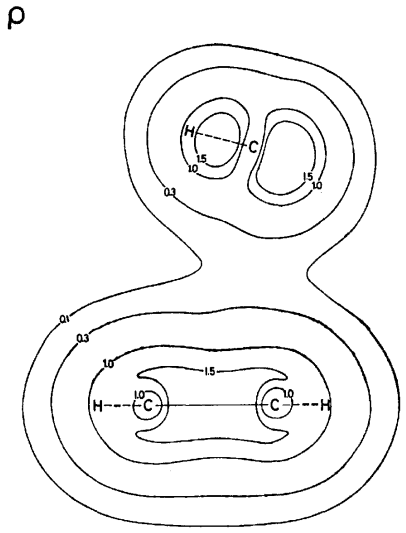

Fig. 4. Electron densities of Model II in the $x-z$ cross section at $y=0$, with charge-transfer interaction.

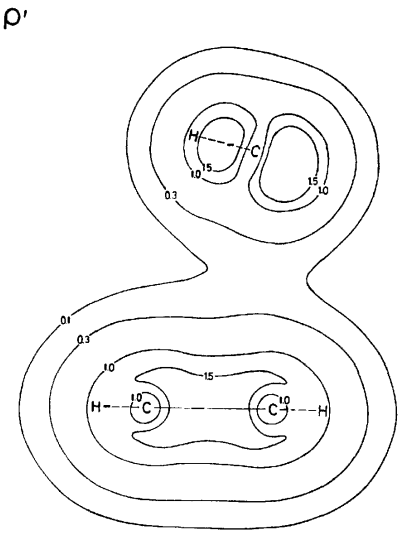

Fig. 5. Electron densities of Model II in the $x-z$ cross section at $y=0$, in which only the HOMO-LUMO interactions are included.

between ethylene and methylene, as well as the weakening of the π bond of ethylene. Figure 5 shows the electron densites in Ψ' state, in which only the charge-transfer interaction from the HOMO of ethylene into the LUMO of methylene and that from the HOMO of methylene into the LUMO of ethylene are taken into consideration. Comparison of Figs. 4 and 5 indicates that the changes in the electron densities due to the mixing in of charge-transferred electron configurations are almost covered by only introducing the HOMO-LUMO interactions. This signifies the mobility of π electrons in case of chemical reactions and suggests the pertinency of the π electrons approximation in discussing the chemical reactivity of conjugated molecules.[1,2] In this calculation, the nuclear configuration of ethylene was kept unchanged. As ethylene loses its planarity with the progress of the reaction, the $\sigma-\pi$ interaction takes place.[16] The σ part and the π part of ethylene will also mix through the orbital overlap interaction with the MO's of methylene.

Figure 6 shows the electron densities of Model Ib. The left of the vertical line presents the simple sum of the electron densities of ethylene and methylene and the right gives the electron densities of the interacting state, ρ. We can see that the bond formation between ethylene and methylene is not effective, indicating the disadvantage of such an approach of methylene to ethylene as Model I. This conclusion is consistent with the results of the extended Hückel MO calculation by Hoffmann.[11]

Figure 7 shows the changes in atomic populations and in atomic bond populations of ethylene and methylene due to the interaction with respect to Models Ia and IIa. We can see that ethylene becomes positively charged, while methylene gets negatively charged in Model II. This agrees with the experimental observations that singlet methylenes add to olefinic double bonds in an electrophilic fashion.[17] Both of the atomic bond populations between the carbon of methylene and the carbons 1 and 2 of ethylene are positive, demonstrating a synchronous character of

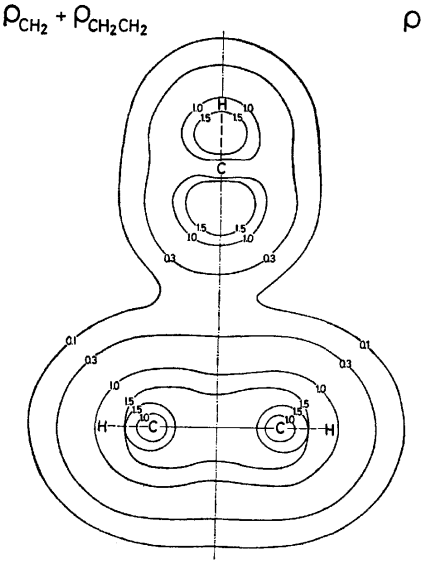

Fig. 6. Electron densities of Model I in the $x-z$ cross section at $y=0$.

16) K. Fukui and H. Fujimoto, This Bulletin, **39**, 2116 (1966).

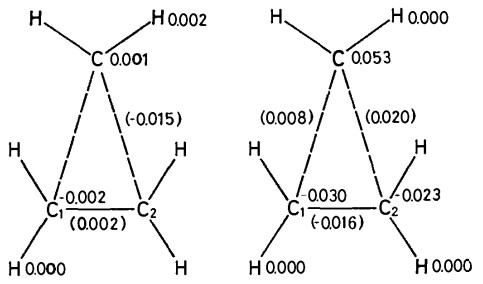

Fig. 7. Changes in atomic populations and in atomic bond populations due to the interaction (the values in parentheses denote the changes in atomic bond populations).

this reaction.

Here let us investigate the mode of charge-transfer in some details. As has been mentioned above, there exist two modes of charge-transfer, *i.e.*, from ethylene to methylene and the converse. Tables 2 and 3 give the changes in AO populations of ethylene and of methylene, due to the charge-transfer from ethylene to methylene and from methylene to ethylene, with respect to Model IIa. The values in the second column in Table 2 indicate the changes in the electron populations of the AO's of ethylene by the charge-transfer from ethylene to methylene, and those in the third column are the changes in the AO populations due to the charge-transfer from methylene to ethylene. Table 3 can be similarly understood. The negative values in the columns of accepted electrons in Tables 2 and 3 may appear strange at first sight. This is

TABLE 2. THE CHANGES IN THE AO POPULATIONS OF ETHYLENE DUE TO THE ELECTRON DELOCALIZATION INTERACTION IN MODEL IIa

AO	Electrons donated	Electrons accepted	Net change
$1C_s$	0.0028	−0.0001	−0.0029
$1C_x$	0.0003	0.0000	−0.0003
$1C_y$	0.0000	0.0000	0.0000
$1C_z$	0.0290	0.0023	−0.0267
$2C_s$	0.0016	0.0000	−0.0016
$2C_x$	0.0004	0.0001	−0.0003
$2C_y$	0.0001	0.0000	−0.0001
$2C_z$	0.0248	0.0036	−0.0212

TABLE 3. THE CHANGES IN THE AO POPULATIONS OF METHYLENE DUE TO THE ELECTRON DELOCALIZATION INTERACTION IN MODEL IIa

AO	Electrons donated	Electrons accepted	Net change
C_s	0.0003	−0.0008	−0.0011
$C_{x'}$	0.0048	0.0001	−0.0047
$C_{y'}$	0.0000	0.0002	0.0002
$C_{z'}$	0	0.0585	0.0585

17) (a) P. S. Skell and A. Y. Garner, *J. Amer. Chem. Soc.*, **78**, 5430 (1956). (b) W. von E. Doering and W. A. Henderson, *ibid.*, **80**, 5274 (1958).

TABLE 4. THE INTERMOLECULAR AO BOND POPULATIONS BETWEEN METHYLENE AND ETHYLENE IN MODEL IIa

		Methylene			
		C_s	$C_{x'}$	$C_{y'}$	$C_{z'}$
Ethylene	$1C_s$	−0.0008	−0.0003	0	0.0008
	$1C_x$	0.0003	0.0000	0	0.0000
	$1C_y$	0	0	−0.0002	0
	$1C_z$	−0.0048	0.0010	0	0.0116
	$2C_s$	−0.0032	−0.0001	0	0.0032
	$2C_x$	0.0001	0.0000	0	−0.0001
	$2C_y$	0	0	−0.0001	0
	$2C_z$	−0.0015	0.0017	0	0.0200

TABLE 5. THE CHANGES IN THE AO BOND POPULATIONS OF THE CARBON-CARBON BOND OF ETHYLENE DUE TO THE INTERACTION IN MODEL IIa

	$1C_s$	$1C_x$	$1C_y$	$1C_z$
$2C_s$	−0.0008	0.0002	0	0
$2C_x$	−0.0001	0.0000	0	0
$2C_y$	0	0	0.0001	0
$2C_z$	0	0	0	−0.0151

caused by the negative intermolecular overlap population of the AO t (t belongs to the molecule A), which is not recovered by the increase in intramolecular populations of that AO, in case of the electron delocalization from the molecule B to the molecule A.[12] We can recognize that the apparent changes in AO populations are only overall results of mutual electron donating and electron accepting interactions. This may be a characteristic feature of chemical interaction between two electronically neutral systems. The AO bond populations between the AO's of ethylene and the AO's of methylene are given in Table 4 with respect to Model IIa. The results indicate that the most contributing term to the bond formation is the combination of the $p\pi$ orbitals of ethylene and the vacant p orbital of methylene. Table 5 shows the changes in the AO bond populations of the C–C bond of ethylene. We can see that the weakening of the π bond is conspicuous, although the σ bond remains almost unchanged. Tables 4 and 5 may be helpful to understand how the double bond of ethylene is converted into the single bonds with methylene in the course of the addition of singlet methylene to ethylene.

Conclusion

We have made an approximate MO calculation on the addition of singlet methylene to ethylene by an isolated molecule CI method. The electron populations of the system, composed of ethylene and methylene, have been calculated by use of the SCF MO's of the two species. The results of the present calculation have proved the important role of the HOMO-LUMO interactions in determining the favorable path of the addition of singlet methylene to ethylene. The analysis of the electron populations

has demonstrated an interesting feature of chemical interactions between two electronically neutral systems that stronger electron donating and electron accepting interactions take place than simply expected from the apparent changes in electron populations. The present calculation suggests that the CI approach to chemically reacting systems is promising for a better understanding of the mechanisms of chemical reactions.

It is a pleasure to express our gratitude to the Data Processing Center, Kyoto University for its generous permission to use the FACOM 230-60 computer.

BULLETIN OF THE CHEMICAL SOCIETY OF JAPAN, VOL. 45, 2429—2433 (1972)

Dipole Moment Functions of CO and HCl

Isao SUZUKI

Department of Chemistry, Faculty of Science, The University of Tokyo, Bunkyo-ku, Tokyo

(Received April 11, 1972)

A general formalism is presented for the least-squares determination of dipole moment functions of diatomic molecules in which the radial part wave functions obtained as numerical solutions of vibration and vibration-rotation Hamiltonian matrix are used. Although this approach is purely numerical, the advantage of using orthonormal basis and perturbed wave functions is retained. Attempts have been made on the determination of the cubic dipole moment functions for the CO and HCl molecules. All the available data of dipole as well as transition moments and the Herman-Wallis factors for these molecules are considered in the refinement process. The following cubic dipole moment functions are obtained (in Debye): $M(\Delta r)=0.1243-3.0722(\Delta r)+0.1909(\Delta r)^2+2.1856(\Delta r)^3$ for CO and $M(\Delta r)=1.093+0.949(\Delta r)+0.034(\Delta r)^2-0.78(\Delta r)^3$ for HCl.

Dipole moment of a diatomic molecule in a given electronic state solely depend on its internuclear distance and can be expressed as $M(r)$. It is customary to expand $M(r)$ in a power series around the equilibrium distance r_e,

$$M(r)=\sum_{k=0} M_k(r-r_e)^k=\sum_{k=0} M_k(\Delta r)^k \qquad (1)$$

Equation (1) may be rewritten by using dimensionless normal coordinate $q=(\omega_e/2B_e)^{1/2}(\Delta r/r_e)$

$$M(q)=\sum_{k=0} p_k q^k, \qquad (2)$$

where $p_k=M_k r_e \gamma^{1/2}$ and $\gamma=(2B_e/\omega_e)$. The diagonal matrix element

$$\mu_{vJ}=\langle v, J|M(q)|v, J\rangle \qquad (3)$$

represents the dipole moment of a vibration-rotation state (v,J), where $|v,J>$ is the wave function for the radial part Schrödinger equation, while the intensity of a vibration-rotation line $(v,J\rightarrow v',J')$ is proportional to the square of matrix element

$$R_{vJ}^{v'J'}=\langle v' J'|M(q)|v, J\rangle. \qquad (4)$$

The total intensity of a vibrational transition $(v\rightarrow v')$ is related with the rotationless matrix element

$$R_v^{v'}=\langle v'|M(q)|v\rangle, \qquad (5)$$

where $|v>=|v,0>$. Similarly, Eq. (3) is reduced to

$$\mu_v=\langle v|M(q)|v\rangle. \qquad (6)$$

Therefore, the coefficients p_k in Eq. (2) can be determined from the measured infrared intensities or dipole moments, provided that accurate wave functions are known for the vibration-rotation states involved. In a previous paper,[1] a method was given in which the vibration or vibration-rotation levels of a diatomic molecule are related with the harmonic and anharmonic force constants by solving the vibrational Hamiltonian numerically. It was emphasized that a set of orthonormal wave functions is readily obtained as linear combinations of the harmonic oscillator basis functions through numerical diagonalization,[2]

$$|v\rangle=\sum_{n=0} a_{vn}|n\rangle \text{ and } \sum_{n=0} a_{vn}a_{v'n}=\delta_{vv'} \qquad (7)$$

As described in I, the coefficients a_{vn}'s for the low lying vibrational states have been determined very accurately from the hexic and octic potential functions respective for the CO and HCl molecules. These results are combined with the recent measurements of infrared line intensities and of dipole moments to determine the dipole moment functions for these molecules. An effort has been made to collect and evaluate as many relevant data as possible.

Determination of Dipole Moment Function

A number of attempts have been made to determine the dipole moment functions of diatomic molecules. The previous works have been summarized by Young and Eachus,[3] who calculated the dipole moment matrix elements for the CO molecule by a purely numerical method, in which the radial part Schrödinger equation is solved by a computer program. The resultant wave functions were used to compute $R_v^{v'}$ and $R_{vJ}^{v'J'}$. Recently, Toth, Hunt, and Plyler[4] have calculated the same matrix elements by

1) I. Suzuki, This Bulletin, **44**, 3277 (1971); Hereafter referred to as I.

2) The indices n and m are used to indicate the harmonic oscillator wave functions $\varphi_n^0(q)$ and $\varphi_m^0(q)$, and v and v' refer to the true (perturbed) vibrational states. Symbols and notations used in this paper are given in I.

3) L. A. Young and W. J. Eachus, *J. Chem. Phys.*, **44**, 4195 (1966).

4) R. A. Toth, R. H. Hunt, and E. K. Plyler, *J. Mol. Spectrosc.*, **32**, 74, 85 (1969).

an analytical method with the cubic dipole moment function and the quintic potential function, the second-order perturbation method being used. These authors have extended their calculation to the HCl molecule, the third-order perturbation theory was used in this case.[5] More recently, Kaiser[6] has analyzed the molecular beam electric resonance spectra of HCl and and DCl, and obtained very precise values of dipole moments for a few vibration-rotation states. He has used the 'wave function approximation' to compute the coefficients M_0—M_4 from the RKR potential.

Our present approach is to use the coefficients a_{vn}'s ($v \leq 4$) for CO and HCl which have been determined precisely by the numerical diagonalization of the vibrational Hamiltonian matrix. Although this method is purely numerical as the RKR approach, we can take full advantage of the orthonormal property of the basis and the perturbed wave functions. This seems to be very useful for practical purpose. It will be shown later that the radial part wave function for the vibration-rotation state (v,J) is also expressed as

$$|v, J> = \sum_{n=0} b_{vn}{}^J |n>. \tag{8}$$

Equations (3)—(6) may be written by using Eqs. (7) and (8),

$$\mu_{vJ} = \sum_{k=0} p_k \sum_{n=0} \sum_{m=0} b_{vn}{}^J b_{vm}{}^J \langle m|q^k|n\rangle, \tag{9}$$

$$R_{vJ}{}^{v'J'} = \sum_{k=0} p_k \sum_{n=0} \sum_{m=0} b_{vn}{}^J b_{v'm}{}^{J'} \langle m|q^k|n\rangle, \tag{10}$$

$$\mu_v = \sum_{k=0} p_k \sum_{n=0} \sum_{m=0} a_{vn} a_{vm} \langle m|q^k|n\rangle, \tag{11}$$

$$R_v{}^{v'} = \sum_{k=0} p_k \sum_{n=0} \sum_{m=0} a_{vn} a_{v'm} \langle m|q^k|n\rangle, \tag{12}$$

The matrix element $<m|q^k|n>$ is well-known (see, for example, Table A-1 in I), and its value can be generated in a computer by a subroutine OPERQ ($k \leq 8$). The coefficients a_{vn} and $b_{vn}{}^J$ are evaluated through numerical diagonalization, it is much simpler to use Eqs. (9)—(12) for the evaluation of the dipole and transition moments. This is the method we have used throughout this study.

Herman-Wallis Factors $C_v{}^{v'}$ and $D_v{}^{v'}$. It was first recognized by Herman and Wallis[7] that the vibration-rotation transition moment, $R_{vJ}{}^{v'J'}$ is related with the rotationless transition moment $R_v{}^{v'}$ as

$$\begin{aligned} |R_{vJ}{}^{v'J'}|^2 &= |R_v{}^{v'}(m)|^2 = |R_v{}^{v'}|^2 F_v{}^{v'} \\ &= R_v{}^{v'}|^2 (1 + C_v{}^{v'} m + D_v{}^{v'} m^2 + \cdots), \end{aligned} \tag{13}$$

where $m = -J$ for P-branch and $m = J+1$ for R-branch. In the present study, the Herman-Wallis factors are used as input data, instead of using numerous vibration-rotation transition moments.

Numerical Computations. The numerical computations have been carried out on a HITAC 5020E computer of the Computer Centre in the University of Tokyo, double precision arithmetic (64 bits) being used.

Input Data. For the determination of the dipole moment function, *i.e.* the coefficients M_k's, we

5) R. A. Toth, R. H. Hunt, and E. K. Plyler, *J. Mol. Spectrosc.*, **35**, 110 (1970).
6) E. W. Kaiser, *J. Chem. Phys.*, **53**, 1686 (1970).
7) R. Herman and R. F. Wallis, *ibid.*, **23**, 637 (1955).

TABLE 1. EXPERIMENTAL AND CALCULATED TRANSITION MOMENTS ($R_v{}^{v'}$), DIPOLE MOMENTS (μ_v) AND HERMAN-WALLIS FACTORS ($C_v{}^{v'} : D_v{}^{v'}$) FOR CO

	Expl.	Weight	Calcd(1)	Calcd(2)	Ref.
$R_0{}^1$	−0.104	0.025	−0.1035	−0.1038	a
$R_0{}^2$	0.00653	1.0	0.00632	0.00624	b
$R_0{}^3$	−0.000424	290.0	−0.000419	−0.000611	c
μ_0	0.112	1.0	0.112	0.112	d
$C_0{}^1$	0.0	1.0	0.0002	0.0002	a
$C_0{}^2$	0.0054	0.0625	0.0051	0.0052	b
$C_0{}^3$	0.0118	0.02	0.0114	0.0078	c
$D_0{}^1$	0.0	1.0	7×10^{-6}	7×10^{-6}	a
$D_0{}^2$	0.00004	0.02	0.00003_4	0.00002_2	b
$D_0{}^3$	0.00018	1.0	0.00008_8	0.00004_3	c

$p_0 = 0.1243 \pm 0.0002$, $p_1 = -0.1465 \pm 0.0002$, $p_2 = 0.000434 \pm 0.000015$, $p_3 = 0.000237 \pm 0.000009$ Debye.
a) Ref. 3.
b) C. L. Korb, R. H. Hunt, and E. K. Plyler, *J. Chem. Phys.*, **48**, 4252 (1968).
c) Ref. 4.
d) C. A. Burros, *J. Chem. Phys.*, **28**, 427 (1958).

TABLE 2. EXPERIMENTAL AND CALCULATED TRANSITION MOMENTS ($R_v{}^{v'}$), DIPOLE MOMENTS (μ_v) IN DEBYE, AND HERMAN WALLIS FACTORS ($C_v{}^{v'} : D_v{}^{v'}$) FOR HCl AND DCl

HCl	Expl.	Weight	Calcd(a)	Calcd(b)	Ref.
$R_0{}^1$	0.068	0.6	0.071	0.071	a
$R_0{}^2$	−0.0080	39.0	−0.0076	−0.0083	a
$R_0{}^3$	0.00051	0.0	0.00051	0.00090	a
$R_1{}^2$	0.0971	0.01	0.0999	0.0986	b
$R_2{}^3$	0.1187	0.01	0.1203	0.1188	b
μ_0	1.1085	4.0	1.1083	1.1086	c
μ_1	1.1390	1.0	1.1386	1.1373	c
μ_2	1.1685	1.0	1.1679	1.1653	c
$C_0{}^1$	−0.026	0.25	−0.027	−0.027	a
$C_0{}^2$	−0.0086	0.44	−0.0058	−0.0057	a
$C_0{}^3$	0.017	0	0.0102	0.007	a, b
$D_0{}^1$	0.00045	25.0	0.00027	0.00024	a
$D_0{}^2$	0.00041	25.0	0.00036	0.00023	a
$D_0{}^3$	—	0	0.00106	0.00045	—
DCl	**Expl.**	**Weight**	**Calcd(a)**	**Calcd(b)**	**Ref.**
$R_0{}^1$	0.0563	0.01	0.0606	0.0600	b
$R_0{}^2$	−0.0050	0.01	−0.0053	−0.0058	b
$R_0{}^3$	0.00031	0.01	0.00028	0.00054	b
μ_0	1.1033	4.0	1.1040	1.1045	c
μ_1	1.1256	1.0	1.1258	1.1252	c

Debye	Set(a)	Set(b)
p_0	1.0930 ± 0.0004	1.0940 ± 0.0005
p_1	0.1018 ± 0.0004	0.1008 ± 0.0006
p_2	0.00039 ± 0.00033	-0.00099 ± 0.00047
p_3	-0.00096 ± 0.00029	-0.00068 ± 0.00040

a) Ref. 5. b) W. S. Benedict, R. Herman, G. E. Moore, and S. Silverman, *J. Chem. Phys.*, **26**, 1671 (1957). c) Ref. 6.

have tried to use all the available data on the dipole and transition moments, those on the isotopic species being included.[8] The data used in the present study for the CO and HCl molecules are listed respectively in Tables 1 and 2. The relative weights of these data are estimated from the quoted values of error limits and are also included in Tables 1 and 2.

Potential Functions. Throughout the present study, the results with the hexic potential function for CO (Set 9) and the octic potential function for HCl (Set 10) given in I are used. The coefficients a_{vn}'s were obtained numerically from the above potentials, and the matrix elements of the form

$$\langle v|q^k|v'\rangle = \sum_{n=0} \sum_{m=0} a_{vn}a_{v'm}\langle n|q^k|m\rangle \qquad (14)$$

are computed. Numerical values of the relevant matrix elements are listed in Tables 3 and 4 respective for CO and HCl, the values of force constants are reproduced at the bottom of each table.

Table 3. Matrix elements $\langle v|q^k|v'\rangle$ for CO

v	v'	$k=0$	$k=1$	$k=2$	$k=3$
0	0	1.0	0.085720	0.511891	0.159313
0	1	0.0	0.709445	0.203138	1.123690
0	2	0.0	−0.040501	0.697083	0.363200
0	3	0.0	0.003883	−0.097995	0.810633

ω_e=2169.9191, k_3=−123.5529, k_4=8.7314, k_5=−0.46782, k_6=0.01579, B_e=1.931241 cm^{-1}.

Evaluation of Coefficient $b_{vn}{}^J$. In order to calculate $R_{vJ}{}^{v'J'}$ and μ_{vJ},$b_{vn}{}^J$ in Eq. (8) must be known. This may be done by two different ways. Since the wave function $|v>=|v,0>$ is known, the perturbation method may be applied;

$$|v,J> = |v> + \sum_{v'\neq v}{}' H_{vv'}{}^{(1)}|v'>/(E_v{}^o - E_{v'}{}^o) \qquad (15)$$

Table 4. Matrix elements $\langle v|q^k|v'\rangle$ for HCl and DCl

	v	v'	$k=0$	$k=1$	$k=2$	$k=3$
HCl	0	0	1.0	0.151165	0.535999	0.288249
	1	1	1.0	0.459392	1.767420	1.982410
	2	2	1.0	0.777172	3.249080	6.713190
	0	1	0.0	0.712683	0.361166	1.254500
	0	2	0.0	−0.071234	0.673832	0.634534
	0	3	0.0	0.012203	−0.166867	0.691510
	1	2	0.0	1.016060	1.045050	4.058170
	2	3	0.0	1.254770	1.967090	8.498830
DCl	0	0	1.0	0.108159	0.377024	0.146278
	1	1	1.0	0.327420	1.211693	0.987922
	0	1	0.0	0.602222	0.217985	0.727798
	0	2	0.0	−0.050963	0.490239	0.326599
	0	3	0.0	0.007398	−0.102399	0.450480

ω_e=2991.8183, k_3=−299.0935, k_4=39.0356, k_5=−3.88475, k_6=0.27635, k_7=−0.01859, k_8=0.00125, B_e=10.593553 cm^{-1}.

where

$$H_{vv'}{}^{(1)} = \langle v'|H_{ROT}|v\rangle = B_eJ(J+1)\times \sum_{k=1} R_k \sum_{n,m=0} a_{vn}a_{v'm}\langle m|q^k|n\rangle, \qquad (16)$$

from which $b_{vn}{}^J$ is obtained after appropriate normalization.[9] Another method to obtain the coefficients $b_{vn}{}^J$ is the direct diagonalization of each vibration-rotation submatrix. The coefficients are directly obtained by solving the J-submatrices.[10] The above methods have been applied to evaluate the coefficients $b_{vn}{}^J$ for the CO and HCl molecules. The coefficients $b_{0n}{}^J$ and $b_{1n}{}^J$ calculated for the J=0, 10, 20, and 30 levels of the HCl molecule are listed in Table 5. Apparently, the perturbation technique breaks down about J=10. The coefficients obtained by the direct numerical diagonalization method are used in the present investigation. No significant discrepancies

Table 5. Radial part of vibration-rotation wave functions for HCl

The Coefficients $b_{vn}{}^J$'s are given (Eq. 8). *D*: Direct Method. *P*: Perturbation Method.

v=0	n=	0	1	2	3	4	5	6	7	8	9	10	11	12
J=0		0.994	0.105	0.010	0.029	0.007	0.001	0.002	0.001					
J=10	*D*	0.988	0.150	0.020	0.031	0.009	0.002	0.002	0.001					
	P	0.988	0.150	0.018	0.030	0.009	0.002	0.002	0.001					
J=20	*D*	0.960	0.270	0.062	0.040	0.018	0.006	0.003	0.002	0.001				
	P	0.960	0.274	0.041	0.032	0.017	0.004	0.002	0.001	0.000				
J=30	*D*	0.880	0.435	0.166	0.081	0.042	0.020	0.010	0.005	0.003	0.001	0.001		
	P	0.886	0.456	0.076	0.035	0.027	0.007	0.003	0.002	0.001	0.000	0.000		
v=1														
J=0		−0.105	0.949	0.284	0.058	0.065	0.028	0.008	0.006	0.003	0.001	0.001		
J=10	*D*	−0.159	0.915	0.350	0.089	0.073	0.037	0.013	0.008	0.004	0.002	0.001	0.001	
	P	−0.159	0.915	0.351	0.086	0.071	0.036	0.012	0.008	0.004	0.002	0.001	0.000	
J=20	*D*	−0.285	0.797	0.483	0.183	0.107	0.062	0.029	0.015	0.009	0.004	0.002	0.001	
	P	−0.280	0.802	0.497	0.148	0.083	0.052	0.021	0.010	0.006	0.003	0.001	0.001	
J=30	*D*	−0.447	0.530	0.580	0.344	0.204	0.126	0.073	0.041	0.024	0.013	0.007	0.004	0.002
	P	−0.416	0.590	0.646	0.216	0.091	0.071	0.031	0.013	0.009	0.004	0.002	0.001	0.001

8) The treatment for the isotopic species was described in I.

9) See Eq. (4) in I. The term with k=0 vanishes from orthogonality.

10) The entire vibration-rotation Hamiltonian matrix is factored into a number of submatrices characterized with the quantum number J, since no cross terms occur in H_{ROT} with regard to J.

have been found for the coefficients of the CO molecule, and the both methods yield almost identical results up to $J=30$.

Results and Discussion

It was reported by Toth *et al.*[4] that their analytical method for the CO molecule gave the identical results with those calculated by the numerical method of Young and Eachus.[3] We have also checked our method by feeding the M_k values given by Young and and Eachus, and obtained the identical results for the transition moments R_0^1, R_0^2, and R_0^3. The M_k values given by Toth *et al.*[6] for the HCl molecule have also been tested. Again we can reproduce their calculated results with the exceptions of C_0^3 and D_0^3. This is, however, somewhat expected, since we included higher order force constants in our potential, and as we reported in I, this effects is prominent in the wave function related with the $v=3$ level : $|3,J>$.

The least-squares adjustment for the coefficients p_0—p_3 has been done for the CO and HCl molecules by using the experimental data in Tables 1 and 2, the results being included in the same tables.[11] Table 1 shows that the four parameter dipole moment function can fit the ten experimental data of CO with an exception of D_0^3, to which the contributions of the neglected higher terms in the dipole moment function are large. In the last column of Table 1, indicated as calcd(2), are listed the calculated values when the p_3 term is omitted from the dipole moment function. This is done to demonstrate the effect of the p_3 term, and it is easily seen that the p_3 term contributes significantly to the moments related with the $v=3$ level. The converged values of p_0 through p_3 are not very much different from those obtained previously. However, one comment must be made on the value of p_0.

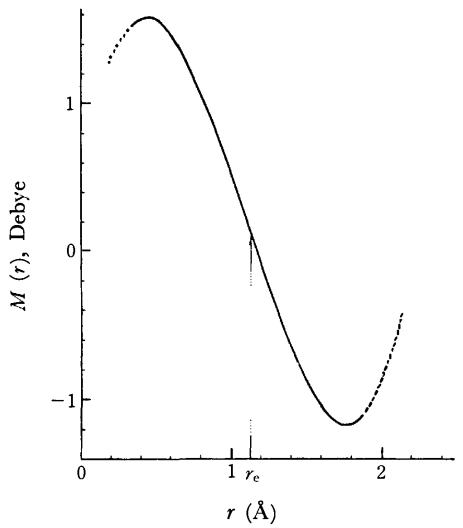

Fig. 1. The cubic dipole moment function of CO.
$M(\Delta r)=0.1243-3.0722(\Delta r)+0.1909(\Delta r)^2+2.1856(\Delta r)^3$
$M(q)=0.1243-0.1465\,q+0.000434\,q^2+0.000237\,q^3$

11) The value p_0 is taken as positive in the present calculation, since only the relative signs among the coefficients $p_k(M_k)$ have physical significance.

The previous calculations were made on the assumption of $p_0=\mu_0$, the dipole moment of the ground vibrational state. As seen from Eq. (9) and Tables 3 and 4, this assumption is obviously incorrect, the higher coefficients also contribute to μ_0. Consideration of this fact makes the value of p_0 about 10% higher than given previously, since p_1 has an opposite sign in CO. The dipole moment function around its equilibrium distance r_e is plotted in Fig. 1.

In the case of HCl and DCl, we have also used the cubic dipole moment function with four parameters to fit the eighteen independent data listed in Table 2. The agreement between the calculated and experimental data is much improved as compared with those previously done. As expected, the discrepancies are rather large for the values of C_0^3 and D_0^v's to which, again, the larger contributions from the neglected higher terms are expected. The converged values of p_k are converted to coefficients M_k and are listed in Table 6 along with those obtained by previous work-

Table 6. The coefficients of dipole moment function, M_k, of HCl determined by several investigators

	Present		Kaiser (Ref. 6)		THP (Ref. 5)
	(a)	(b)	HCl	DCl	
M_0(D)	1.093	1.094	1.093_3	1.092_2	1.095
M_1(D/A)	0.949	0.939	0.925	0.935	0.905
M_2(D/A^2)	0.034	−0.087	0.08	0.07	−0.066
M_3(D/A^3)	−0.78	−0.55	−0.64	−0.63	−0.73
M_4(D/A^4)	—	—	−0.39	−0.32	—

ers. There is a discrepancy in the previous works as to the sign of M_2; Toth *et al.*[5] gave the value of −0.066 D/A^2 to M_2, whereas Kaiser[6] gave 0.08 and 0.07 D/A^2 respectively for HCl and DCl. As we started the least squares procedure with $M_0=1.095$ D, $M_1=1.0$D/A, $M_2=M_3=0$, we have obtained a converged set, Set(a), given in the first column of Table 6. However, if we started from the values given in Ref. 5, we obtain the second converged set, Set(b), in the second column. The calculated dipole and transition moments as well as the Herman-Wallis factors are given respectively in Columns 3 and 4 in Table 2. Overall fit of the calculated results with the experiment is better in Set (a), which seems to be a natural choice. In order to draw firmer conclusion, however, more experimental data are necessary, because most disagreements between the calcd(b) and experimental values occur in the constants to which the higher terms in the dipole moment function which are neglected in the present study may well contribute significantly. The present calculation is performed within the framework of the Born-Oppenheimer approximation, although the deviations from the Born-Oppenheimer behavior are detected in Kaiser's precise measurement of dipole moments for HCl and DCl, this effect is too small for the separate determination of dipole moment functions of both species. In addition, more complex treatment is necessary for the potential functions.[12] The present

12) P. R. Bunker, *J. Mol. Spectry.*, **35**, 306 (1970).

calculation gives the somewhat averaged results for p_k's.

Finally, the dipole moment function for HCl, Set (a), is plotted against the internuclear distance in Fig. 2. Figure 3 is also the plot of the same function close to the equilibrium distance in an enlarged scale. The positions of the average internuclear distances in the $v=0$, 1, and 2 levels: $\langle\bar{r}\rangle_0$, $\langle\bar{r}\rangle_1$, and $\langle\bar{r}\rangle_2$, and the dipole moments of μ_0, μ_1, and μ_2 are indicated by arrows. Since in the linear dipole moment function,

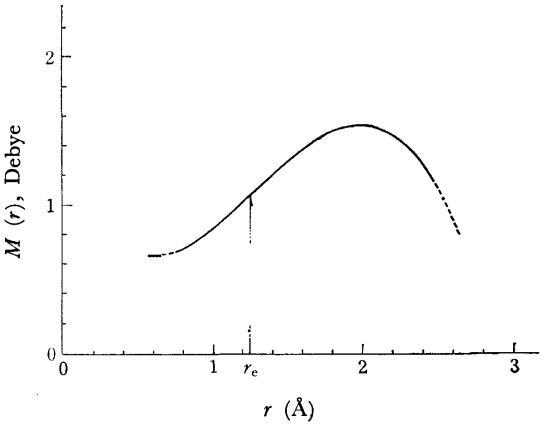

Fig. 2. The cubic dipole moment function of HCl, Set (a).
$M(\Delta r)=1.093+0.949(\Delta r)+0.034(\Delta r)^2-0.78(\Delta r)^3$
$M(q)=1.093+0.1018\,q+0.00039\,q^2-0.00096\,q^3$

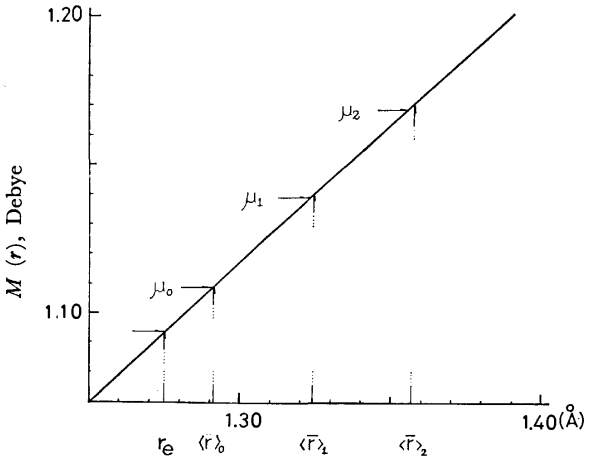

Fig. 3. The cubic dipole moment function of HCl, Set (a), around its equilibrium distance: The average internuclear distances, $\langle\bar{r}\rangle_0$, $\langle\bar{r}\rangle_1$, and $\langle\bar{r}\rangle_2$, and dipole moments μ_0, μ_1, and μ_2 of HCl are indicated by arrows.

$$\mu_v = M_0 + M_1(\langle\bar{r}\rangle_v - r_e), \tag{15}$$

the mismatch of the arrows shows the effect of quadratic and cubic terms.

The author wishes to thank Prof. Takehiko Shimanouchi for his encouragement and helpful discussion throughout this study.

BULLETIN OF THE CHEMICAL SOCIETY OF JAPAN, VOL. 45, 2433—2437 (1972)

Photochemical Reactions of *p*-Benzoquinone Complexes with Aromatic Molecules

Satoshi ARIMITSU* and Hiroshi TSUBOMURA

Department of Chemistry, Faculty of Engineering Science, Osaka University, Toyonaka, Osaka

(Received April 14, 1972)

Electronic absorption spectra and ESR spectra have been measured for the photolyzed charge transfer complexes between *p*-benzoquinone and aromatic donors in low temperature matrices. When the *p*-benzoquinone complex with toluene or *p*-xylene was irradiated at 77°K, an electronic absorption spectrum attributable to the semiquinone radical was obtained together with that of the benzyl-type radical. The spectral shape and position of the former are somewhat different from those of the semiquinone radicals obtained by the photolysis of *p*-benzoquinone or hydroquinone. These differences indicate the presence of interaction between semiquinone and benzyl-type radicals. The ESR spectra obtained from these systems show that these radicals form pairs in the triplet ($S=1$) state. It is concluded that the radical pairs are produced as a result of intermolecular hydrogen atom transfer from the aromatic donor molecule to *p*-benzoquinone in the excited states of the CT complexes formed between them. The irradiations of various *p*-benzoquinone complexes were carried out in the wavelength regions corresponding to the lowest CT absorption bands at 77°K, and the reactivities were discussed in relation to the electronic structures and geometrical configurations of the CT complexes in the excited states. From the analysis of ESR spectra, the fine structure constant was evaluated for each of the radical pairs, from which the average distance between interacting unpaired electrons was calculated.

Studies on the chemical behaviors of charge transfer (CT) complexes have presented some informations for understanding the reaction paths in which CT complex are involved.[1] In view of the electronic nature of the CT interaction, it is understood that the complexes in the states are generally the precursors of ionic reactions. It was found by Leonhardt and Weller that flash illumination of a solution of peryline and *N,N*-dimethylaniline in a polar solvent leads to the formation of perylene anion.[2] Thereafter, it has been shown for

* Present address: Sagami Chemical Research Center, 3100 Ohnuma, Sagamihara, Kanagawa.

1) E. M. Kosower, *Prog. Phys. Org. Chem.*, **3**, 81 (1965); T. Nogami, K. Yoshihara, and S. Nagakura, *J. Phys. Chem.*, **73**, 2670 (1969); T. Nogami, T. Yamaoka, K. Yoshihara, and S. Nagakura, This Bulletin, **44**, 380 (1971); S. Tazuke, *J. Phys. Chem.*, **74**, 2390 (1970).

2) H. Leonhardt and A. Weller, *Z. Phys. Chem. N. F.*, **29**, 277 (1961); *Ber. Bunsenges. Phys. Chem.*, **67**, 791 (1963).

aromatic donor-acceptor systems that the formation of ionic species *via* the CT complexes in the excited states is a general phenomenon.[3] Recently, the ionic dissociation processes of excited CT complexes were studied by the nano-second laser photolysis.[4]

We have found that the photoreduction of benzophenone proceeds easily in low temperature rigid matrices containing aniline derivatives, leading to the formation of radical-pair between ketyl and aromatic amine radicals in the triplet state.[5] Since the photoreduction of benzophenone does not take place apprecibly in ordinary organic matrices at 77° K, we have proposed that the formation of electron donor-acceptor complexes of benzophenone with aromatic amines enhances the photoreduction of benzophenone. In order to obtain further information on the roles of CT interactions in such chemical reactions, we have made a detailed study on the photochemistry of *p*-benzoquinone complexes in low temperature rigid matrices.

It is well known that *p*-benzoquinone forms stable CT complexes with various aromatic compounds.[6] Photoreductions of *p*-benzoquinone and its derivatives yield the semiquinone radicals in the hydrogen-donating solvents.[7] In the present paper, we have examined the photo-chemical reactivity of *p*-benzoquinone complexed with various electron donors. The electronic absorption and emission spectra of these complexes and the ESR spectra of the photolysis products have also been studied.

Experimental

Materials. Both *p*-benzoquinone (BQ) and hydroquinone were purified by repeated recrystallization from ethanol and sublimation in vacuum. Toluene, *p*-xylene, mesitylene, *p*-methylanisole, α-methylnaphthalene, and *N,N*-dimethyl-*p*-toluidine were purified by fractional distillation under ordinary or reduced pressure. β-Methylnaphthalene and *p*-toluidine were purified by vacuum sublimation. The organic solvents used in the present work, 2-methyltetrahydrofuran (2-MTHF), ether, ethanol, and isopentane, were purified by the methods described in our previous papers.[5,8]

Apparatus. Photolysis was carried out with a 500-W super high pressure mercury lamp combined with various Toshiba glass filters in order to select the excitation wavelengths corresponding to the first CT absorption band of BQ complexes. All samples examined in this work were degassed by the usual freeze-pump-thaw technique. All experiments were performed at the temperature of liquid nitrogen. The instruments used for the measurements of emission and absorption spectra in the ultraviolet and visible region, and the ESR spectra are the same as described in our earlier paper.

Results

Electronic Absorption and Emission Spectra of BQ Complexes. The electronic spectrum of BQ shows an (n,π^*) band in the visible region and the lowest (π,π^*) band in the near ultraviolet region.[9] Apart from these bands, the electron donor-acceptor interactions between BQ and aromatic donors cause CT absorption bands. Both the maxima and the onset positions for the CT bands observed in 2-MTHF matrix at 77° K are summarized in Table 1, showing clearly that they shift to lower frequencies with decreasing ionization potentials of donor molecules.

The emission spectra of BQ complexes with toluene, mesitylene, and *p*-methylanisole are shown in Fig. 1. In the low temperature rigid matrix containing only BQ, a weak emission was found visually by high intensity excitation, but the emission was so weak that no spectrum could be recorded. As is seen in Fig.1, the

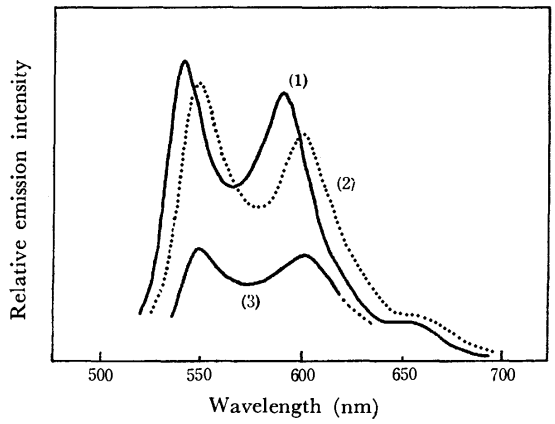

Fig. 1. Emission spectra of BQ complexes with aromatic donors in 2-MTHF at 77°K: 1) toluene; 2) mesitylene; 3) *p*-methylanisole.

emission maximum shifts slightly to longer wavelength as the ionization potential of donor molecules decreases. The phosphorescence spectra of BQ and its complexes with toluene and mesitylene were measured at low temperature by Briegleb *et al.*[10] The results obtained in the present work agree well with theirs. Since the shapes and band positions of the emission spectra obtained for the CT complexes are very much similar to those of BQ, the phosphorescent states of these complexes are most probably the modified locally excited $^3(n,\pi^*)$ state of BQ. Similar phosphorescence spectra have been observed for the BQ complexes with *p*-xylene, α-methylnaphthalene, and β-methylnaphthalene. In the case of CT complexes with *p*-toluidine and *N,N*-dimethyl-*p*-toluidine, no emission could be observed.

3) K. Kawai, N. Yamamoto, and H. Tsubomura, This Bulletin, **42**, 369 (1969); D. Rehen and A. Weller, *Ber. Bunsenges. Phys. Chem.*, **73**, 839 (1970); T. Okada, H. Oohari, and N. Mataga, This Bulletin, **43**, 2750 (1970).

4) R. Potashnik and M. Ottolenghi, *Chem. Phys. Lett.*, **6**, 525 (1970); C. R. Goldschmidt and M. Ottolenghi, *ibid.*, **6**, 570 (1970); H. Masuhara and N. Mataga, *ibid.*, **6**, 608 (1970).

5) S. Arimitsu and H. Tsubomura, This Bulletin, **44**, 2288 (1971); *ibid.*, **45**, 1357 (1972).

6) L. Michaelis and S. Granick, *J. Amer. Chem. Soc.*, **66**, 1023 (1944); R. Foster and T. J. Thomson, *Trans. Faraday Soc.*, **59**, 296 (1963); R. S. Becker and E. Chen, *J. Chem. Phys.*, **45**, 2403 (1966).

7) H. Linschitz, J. Rennert, and T. M. Kon, *J. Amer. Chem. Soc.*, **76**, 5839 (1954); N. K. Bridge and G. Porter, *Proc. Roy. Soc.*, **A244**, 259, 279 (1958); G. Porter and M. W. Windsor, *ibid.*, **A245**, 238 (1958).

8) S. Arimitsu, K. Kimura, and H. Tsubomura, This Bulletin, **42**, 1858 (1969).

9) J. W. Sidman, *J. Chem. Phys.*, **27**, 820 (1957); A. Kuboyama, This Bulletin, **35**, 295 (1962).

10) G. Briegleb, W. Herre, and D. Wolf, *Spectrochim. Acta*, **25**, 39 (1969).

Absorption Spectra of BQ Complexes Irradiated at 77°K. Electronic absorption spectrum obtained after the photolysis of BQ in an ethanol rigid matrix is shown by curve a in Fig.2. A similar spectrum was observed after the photolysis of hydroquinone in ethanol.[11] Therefore, it is unambiguously concluded that these absorptions are ascribed to the semiquinone radical, in agreement with the assignment of previous authors.[12] When hydroquinone in a mixed (1:1) solvent of toluene and ethanol was photolyzed at 77° K, the absorption spectrum of semiquinone radical as shown by curve b in Fig.2 was obtained. The spectrum is a little broader than that in pure ethanol at 77°K. When BQ-toluene complex was irradiated in the wavelength region corresponding to the CT absorption band at 77° K, a spectrum shown by curve c in Fig.2 was obtained, by subtracting the absorption before irradiation. It seems reasonable to attribute the visible absorption to the semiquinone radical and the near ultraviolet absorption to the benzyl radical.

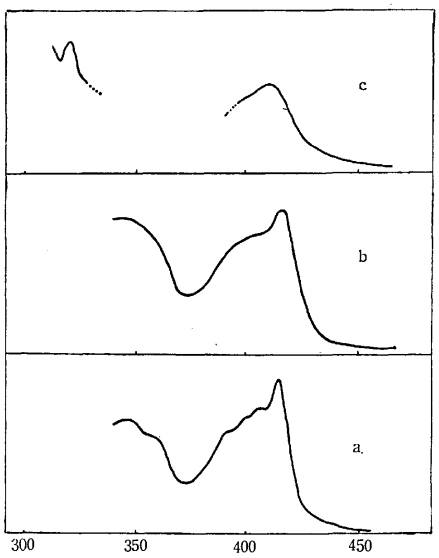

Fig. 2. Electronic absorption spectra of semiquinone radicals obtained after the photolysis of BQ and hydroquinone in low temperature rigid matrices: a, BQ in ethanol at 77°K; b, hydroquinone in toluene and ethanol (1 : 1) at 77°K; c, BQ in toluene and ethanol (1 : 1) at 77°K.

BQ–*p*-xylene complex shows a CT absorption maximum at 360 nm in an EPA (5 parts ether, 5 parts isopentane, 2 parts ethanol) rigid matrix. When it was subjected to irradiation in the range from 350 to 400 nm at 77° K, the absorption of semiquinone radical appeared gradually. At the same time, the CT absorption faded and the absorption attributable *p*-methylbenzyl radical also appeared. No spectral change was detected by the illumination of *p*-xylene in an EPA solution at the same wavelength region at 77° K.

ESR Spectra of BQ Complexes Irradiated at 77°K. A typical ESR spectrum obtained after the photolysis of the CT complex of BQ and *p*-methylanisole is shown in Fig.3. The spectrum consists of a weak band at a low magnetic field and stronger bands showing large splittings centered at a magneitc field twice as large as that for the weak one. In our previous study on the photochemistry of benzophenone in aromatic amine solutions, we found that the ESR spectra obtained after the irradiation of benzophenone–aromatic amine systems can be attributed to the radical pair in the triplet state ($S=1$).[5] The ESR spectrum shown in Fig. 3, together with those obtained from other BQ complexes, agrees well with them, and unambigously indicates that similar radical pairs are produced.

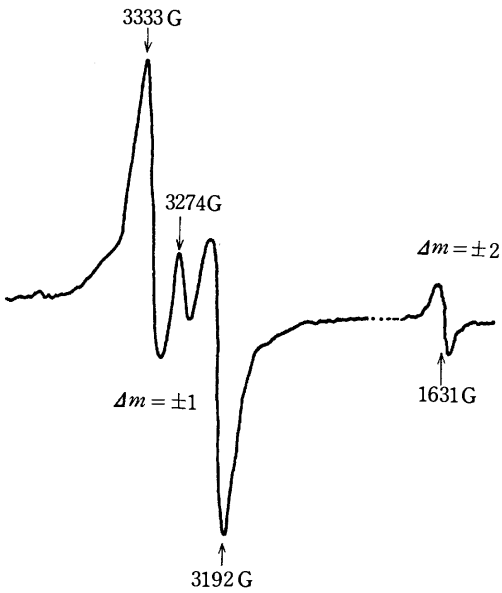

Fig. 3. An ESR spectrum of BQ-*p*-methylanisole complex in 2-MTHF irradiated at 77°K. ($\nu=9147$ MHz.)

When BQ was irradiated at 77° K, the ESR spectrum obtained shows only the absorption signals due to free radicals at the $g=2$ region, attributable to the semiquinone and solvent radicals. From these experimental results, it is established that the absorption spectra are due to radical pairs produced by the intermolecular hydrogen transfer from donors to BQ. Photolysis of the BQ complexes with toluene, *p*-xylene, mesitylene, and α-methylnaphthalene also showed similar ESR spectra. In the case of BQ–β-methylnaphthalene, it has been suggested by the ESR measurement that the hydrogen transfer reaction does not take place appreciably, only radical absorption appearing at the $g=2$ region. In BQ–*p*-toluidine and BQ–*N*,*N*-dimethyl-*p*-toluidine systems, no ESR signal could be found by excitation of the lowest CT absorption band, indicating no photochemical reaction. From the electronic absorption measurements, it was also established that

11) K. Kimura, K. Yoshinaga, and H. Tsubomura, *J. Phys. Chem.*, **71**, 4485 (1967).

12) G. Porter and E. Strachan, *Trans, Faraday Soc.*, **54**, 1595 (1958); G. Porter and F. Wilkinson, *Proc. Roy. Soc.*, **A264**, 1(1961); G. Porter, and P. Suppan, *Trans. Faraday Soc.*, **61**, 1664 (1965).

13) Y. Kurita, H. Ohigashi, and M. Kashiwagi, *Bussei*, **9**, 87 (1968).

Table 1. CT spectral characteristics of the complexes of *p*-benzoquinone and various aromatic donors at 77°K and the appearance of the ESR spectra of their irradiation products

Donor	CT band maxima, $\times 10^3$ cm^{-1}	CT band onset $\times 10^3$ cm^{-1}	Phosphorescence onset, $\times 10^3$ cm^{-1}	Donor I_p[15] eV	Total spin	D, gauss	*R*, Å
Toluene	~31.3	~25.0	18.5	8.82	1	135	5.9_1
p-Xylene	29.4	~23.8		8.45	1	142	5.8_1
Mesitylene	28.6	~22·7	18.3	8.39	1	137	5.8_8
α-Methylnaphthalene	25.3	~19.2		7.96	1	118	6.1_8
p-Methylanisole	24.6	~19.2	18.2		1	141	5.8_2
p-Toluidine	19.3	~14.3			—		
N,N-Dimethyl-*p*-toluidine	18.7	<14.3			—		

the absorption intensity of the CT bands of these systems did not change detectably throughout the irradiation.

We can evaluate the fine structure constants (D) from the spin-spin splittings of the $\Delta m = \pm 1$ transitions of the ESR spectra obtained. The fine structure constants obtained from the separation corresponding to D are listed in Table 1, together with the average distance (R) between two unpaired electrons, calculated from these constants by using a point-charge-density approximation.[13]

Discussion

It can be seen in Table 1 that the frequencies of the charge-transfer bands arising from the interaction between the aromatic donor and BQ shift to the longer wavelength with decreasing ionization potentials of the donor molecules. As to the photochemical behaviors, the CT complexes of BQ can be classified into two groups. The complexes with toluene, *p*-xylene, mesitylene, α-methylnaphthalene, and *p*-methylanisole belong to group A and those with *p*-toluidine and *N,N*-dimethyl-*p*-toluidine to group B. The photoreduction of BQ takes place in group A, but not in group B. In group A, the CT state is higher than the lowest triplet state in each system, characterized as the locally excited $^3(n,\pi^*)$ state of BQ, as indicated by the measurements of emission spectra. The lowest excited singlet states of BQ complexes in group A have mainly the nature of either the CT state or the locally excited $^1(n,\pi^*)$ state of BQ. In group B, on the other hand, the lowest triplet state is not the $^3(n,\pi^*)$ state of BQ but mostly of the CT nature, as suggested by the emission spectral measurements, and the lowest excited singlet state is also the CT state. Therefore, it can safely be concluded that the distinction between photochemical behaviors of group A and B can be explained on the basis of the different electronic structures in the lowest triplet states of these complexes. Consequently, it is concluded that the hydrogen trasnfer reaction of BQ complexes occurs in the lowest triplet states of the CT complexes characterized by the (n,π^*) state of BQ.

Another possible alternative for the photochemical reaction mechanism for the BQ complexes is the initial electron transfer from the donor molecule to BQ, followed by the proton transfer. This seems unlikely, however, because such a reaction should be favorable in the cases of stronger CT complexes such as BQ–*p*-toluidine and BQ–*N,N*-dimethyl-*p*-toluidine systems, contrary to our experimental results.

As shown in Table 1, the fine structure constants of radical pairs are different from complex to complex. It can be concluded from these results that the intermolecular hydrogen transfer occurs from the donors, not from the solvent, to BQ in the low temperature matrices, leading to the formation of the radical pair in the triplet spin state, because, if the hydrogen transfer reaction were to occur from the solvent molecule to BQ, the fine structure constant should be the same in all cases.

It is interesting to note that the photochemical reaction of these complexes is affected critically by the position of the methyl-group in the donor molecules. For example, the CT complex of BQ–α-methylnaphthalene excited in the wavelength region of the CT absorption band shows an ESR spectrum arising from the triplet radical pair, but the spectrum attributable to the semiquinone and solvent radicals were obtained from the photolysis of BQ–β-methylnaphthalene system. Therefore, no hydrogen atom transfer reaction from the donor to BQ is shown to take place in the latter system. The distinction in the photochemical reaction between the above two complexes is not explained by the electronic natures of the lowest excited triplet states, since they have both the locally excited $^3(n,\pi^*)$ levels of BQ as the lowest triplet level as suggested by the emission measurements. Thus it seems more reasonable to conclude that the distinction is caused by the different geometric conditions between the two complexes, leading probably to the changes of $CH_3\cdots O$ distance, there are some theoretical arguments on the geometrical configuations of molecular complexes in the excited states.[14] The present results and those of the similar studies might provide bases for

14) T. Kobayashi, S. Iwata, and S. Nagakura, This Bulletin, **43**, 713 (1970); T. Kobayashi, K. Yoshihara, and S. Nagakura, *ibid.*, **44**, 2603 (1971); H. Masuhara and N. Mataga, *Z. Phys. Chem. N. F.*, to be published.

15) K. Watanabe, T. Nakayama, and J. Mottl, *J. Quant. Spectrosc. Radiat. Transfer*, **2**, 369 (1962).

the elucidation of the geometries of CT complexes in the excited states as well as in the ground states.

In conclusion, it has been established in the present work that the photochemical hydrogen abstraction reaction of BQ in the complexes with aromatic donors occurs in low temperature rigid matrices, only in cases where the lowest triplet state is mainly of the $^3(n,\pi^*)$ character of BQ. In cases where the donor is so strong that the ^{3}CT state is lower than the $^3(n,\pi^*)$ state of BQ, no hydrogen abstraction takes place. These results indicate that the reactions proceed from such states as those in which the oxygen atom has an unpaired electron in its non-bonding atomic orbital. These results also clearly indicate that the initial electron transfer followed by proton tunnelling is not the route for the hydrogen abstraction reaction irrespective of the strengths of the donor-acceptor interactions.

BULLETIN OF THE CHEMICAL SOCIETY OF JAPAN, VOL. 45, 2437—2439 (1972)

Self-Diffusion Coefficients and Interdiffusion Coefficient in Acetone-Benzene System

Yoshinobu KAMEI and Yasumichi OISHI

Department of Nuclear Engineering, Faculty of Engineering, Kyushu University, Fukuoka, Japan

(Received May 1, 1972)

Self-diffusion coefficients of acetone and benzene have been determined in the whole composition range of the binary system at 25°C by a capillary-cell method using the ^{14}C-marked tracer. The results were in a good agreement with those determined by the NMR spin-echo method by McCall and Douglass. The products of the respective self-diffusion coefficients and the viscosity of this system showed a relatively constant compositional dependence. Bearman's relation was shown to hold between the self-diffusion coefficients and the partial molar volumes for the system. The validity of Darken's equation was confirmed for the self-diffusion coefficients and the interdiffusion coefficient of the system.

The relationship between the self-diffusion coefficients of the components and the interdiffusion coefficient for a binary system has been described by Darken[1] and by Hartley and Crank[2] as Eq. (1):

$$D_{12} = (N_1 D_2^* + N_2 D_1^*)\ (\mathrm{d} \ln a_1 / \mathrm{d} \ln N_1) \qquad (1)$$

where D_{12} is the interdiffusion coefficient, D^* the self-diffusion coefficient, N the mole fraction, a the activity, and the subscript i refers to component i. In the present work, the self-diffusion coefficients of both components were determined for the whole composition range of the acetone–benzene system to test the validity of Eq. (1) for this system by comparing the interdiffusion coefficient experimentally determined and that theoretically calculated with Eq. (1).

Experimental

The capillary-cell method was used for determining self-diffudion coefficients. The employed apparatus and technique have been described elsewhere.[3] All the determinations were made at 25±0.02°C. The acetone and benzene used were of spectrum analysis reagent grade. The radioactivity of the tracer in the sample solution in the capillary was adjusted so as to be about 0.06 μCi/cc with ^{14}C-labelled $(CH_3)_2CO$ or C_6H_6. The radioactivity of the tracer was determined in a toluene solution of 2,5-diphenyloxazole with a liquid scintillation counter.

1) L. S. Darken, *Trans. Amer. Isnt. Min. Met. Ent.*, **175**, 184 (1948).

2) G. S. Hartley and J. Crank, *Trans. Faraday Soc.*, **45**, 801 (1949).

3) A. Nishi, Y. Kamei, and Y. Oishi, This Bulletin, **44**, 2855 (1971).

Results

Figure 1 shows the self-diffusion coefficients of acetone, $D^*((CH_3)_2CO)$ and benzene, $D^*(C_6H_6)$ determined at 25°C as a function of mole fraction of acetone.

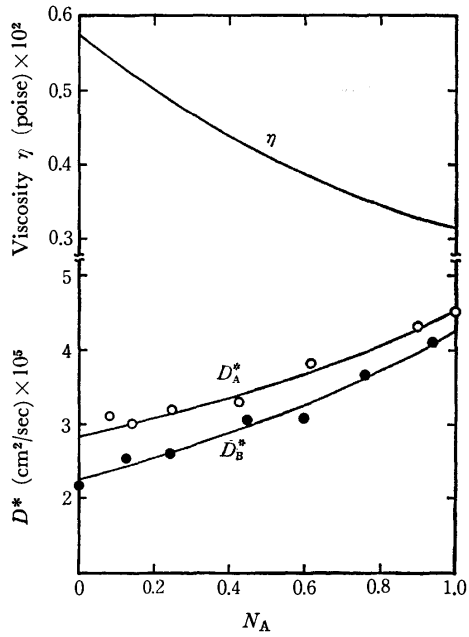

Fig. 1. Self-diffusion coefficients and viscosity for acetone-benzene system as a function of mole fraction of acetone at 25°C. D_A^* and D_B^* are self-diffusion coefficients of acetone and benzene. η is viscosity.

All are the averaged values of more than three determinations. The self-diffusion coefficients of pure acetone[4] and benzene[5-9] were taken from the literatures. Both self-diffusion coefficients show similar and relatively linear compositional dependence.

Discussion

(1) *Comparison of the Results with Those by NMR Spin-Echo Method.* Self-diffudion coefficients of both components for the acetone–benzene system have been determined by McCall and Douglass using the NMR spin-echo method.[10] They confirmed the accuracy of their method by comparing their results with Mills data determined by a diaphragm-cell method for the benzene–cyclohexane system.[11] For the acetone–chloroform system, the results by McCall *et al.* and those by Hardt *et al.* by a capillary-cell method[12] are in a good agreement only for the self-diffusion coefficients of acetone, but show a large discrepancy of about 18% for chloroform. For the acetone–benzene system, however, our results by the capillary-cell method are in good agreement with McCall and Douglass's results by the NMR spin-echo method for both components.

(2) *Products of Self-Diffusion Coefficient and Viscosity.* The compositional dependence of both self-diffusion coefficients and that of the viscosity, η[13] are in reverse trends as seen in Fig. 1. Figure 2 shows the products of the viscosity and the respective self-diffusion coefficients as a function of composition where $\eta \cdot D^*((CH_3)_2CO)$ and $\eta \cdot D^*(C_6H_6)$ remain constant for the whole composition range of the system. The similar results have been showed previously for the carbon tetrachloride–cyclohexane[3] and acetone–water[4] systems.

(3) *Bearman's Relation.* The relationship between the self-diffusion coefficients and the partial molar volumes for a binary regular solution has been described by Bearman[14] as Eq. (2):

$$D_1^*/D_2^* = \bar{V}_2/\bar{V}_1 \qquad (2)$$

where $\bar{V}_1$ and $\bar{V}_2$ are the partial molar volumes of components 1 and 2, respectively. $D^*((CH_3)_2CO)/D^*(C_6H_6)$ is shown as a function of compositon in Fig. 2. $\bar{V}(C_6H_6)/\bar{V}((CH_3)_2CO)$ ranges within 1.19 to 1.24 for the whole composition range of the system and in a good agreement with $D^*((CH_3)_2CO)/D^*(C_6H_6)$ shown in Fig.2. This means that Bearman's relation holds for this system.

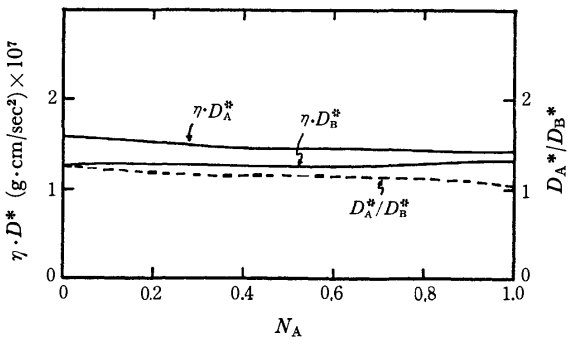

Fig. 2. Compositional dependence of $\eta \cdot D_A^*$, $\eta \cdot D_B^*$, and D_A^*/D_B^*.

(4) *Darken's Equation.* The theoretical interdiffusion coefficient calculated by Eq. (1) is compared with those determined experimentally by Anderson, Hall, and Babb[15] and by Cullinan and Toor[16] in Fig.3 as a function of mole fraction of acetone. The ther-

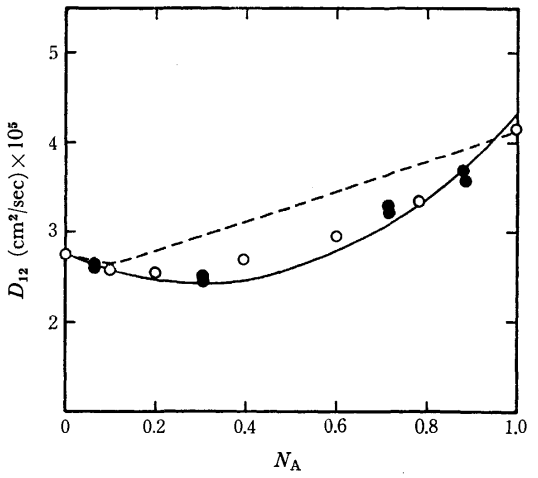

Fig. 3. Comparison of theoretical and experimental interdiffusion coefficients for acetone-benzene system at 25°C.
—— theoretical, present work
- - - theoretical, McCall and Douglass (Ref. 10)
○ experimental, Anderson et al (Ref. 15)
● experimental, Cullinan and Toor (Ref. 16)

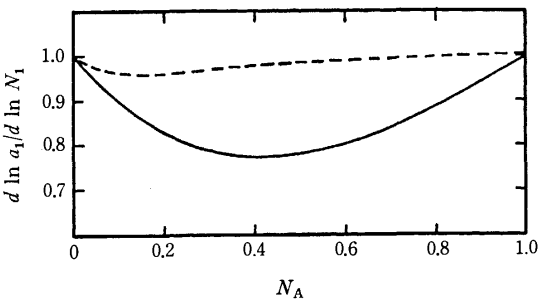

Fig. 4. Thermodynamic factor for acetone-benzene system as a function of acetone mole fraction.
—— present work
- - - McCall and Douglass (Ref. 10)

4) Y. Kamei and Y. Oishi, *Nippon Kagaku Zasshi*, **91**, 403 (1970).
5) K. Graupner and E. R. S. Winter, *J. Chem. Soc.*, **1952**, 1145.
6) P. A. Johnson and A. L. Babb, *J. Phys. Chem.* **60**, 14 (1956).
7) H. Hiraoka, J. Osugi, and W. Jono, *Rev. Phys. Chem. Jap.* **28**, 52 (1958).
8) R. E. Rathbun and A. L. Babb, *J. Phys. Chem.*, **65**, 1072 (1961).
9) R. Mills, *ibid.*, **67**, 600 (1963).
10) D. W. McCall and D. C. Douglass *ibid.*, **71**, 987 (1967).
11) R. Mills, *ibid.*, **69**, 3116 (1965).
12) A. P. Hardt, D. K. Anderson, R. Rathbun, B. W. Mar. and A. L. Babb, *ibid.*, **63**, 2059 (1959).
13) "International Critical Table," McGrow Hill (1929), Vol.5 p. 39.
14) R. J. Bearman, *J. Chem. Phys.*, **32**, 1308 (1960).
15) D. K. Anderson, J. R. Hall, and A. L. Babb, *J. Phys. Chem.*, **62**, 404 (1958).
16) H. T. Jr. Cullinan and H. L. Toor, *ibid.*, **69**, 3941 (1965).

modynamic factor for the system necessary for the calculation was estimated from the excess free energy calculated from equilibrium vapour pressure at 45°C determined by Brown and Smith[17] and shown in Fig.4. The theoretical and experimental interdiffusion coefficients are in a good agreement within ±6%. This confirms the validity of Darken's equation for the acetone–benzene system. A similar comparison of the theoretical and experimental interdiffusion coefficients has been made by McCall and Douglass.[10] Their results, however, showed a fairly large discrepancy between the experimental and theoretical values as shown together in Fig.3. As described already, the self-diffusion coefficients of the respective components determined by them are close to our determinations. The cause of their discrepancy is in their thermodynamic factors, shown in Fig.4, which they estimated from the vapour-liquid equilibrium at boiling points for varied compositions.[18]

The authors thank M. Kurokawa for his assistance in experimental works.

17) I. Brown and F. Smith, *Australian J. Chem.*, **10**, 423 (1957).

18) W. Reinders and C. H. de Minjer, *Rec. Trav. Chim.*, **59**, 369 (1940).

BULLETIN OF THE CHEMICAL SOCIETY OF JAPAN, VOL. 45, 2439—2444 (1972)

Temperature Dependence of Corona-charging Properties on TiO_2-Polymer Dispersion Layers

Takeaki IIDA, Toyokazu NONAKA, and Hiroshi NOZAKI

Institute of Industiral Science, University of Tokyo, Roppongi, Minato-ku, Tokyo, 106

(Received September 3, 1971)

The corona-charging properties of TiO_2-polymer dispersion layers were determined in the dark at temperatures 0°—35°C by the turn-table method. Dispersion layers of TiO_2 (rutile) and polyvinyl acetate, coated on an aluminum foil to about 15 μ thickness, were used. The results showed the rising rate of the surface potential has a maximum at around 20°C. The saturation potential decreases slightly with a rise in temperature. The decay potentials were represented by the plot log V *vs.* $\sqrt{t}$. The relation between log V and $\sqrt{t}$ is linear in certain range of the surface potential, and the gradient increases in proportion to the rise in temperature. This is discussed with the use of an equivalent-circuit model.

Studies have been made on the corona-charging properties of electrophotographic sensors with respect to change with the contents of the photoconductor,[1] sensitization of the corona-charging,[2] and effects of the relative humidity.[3] The results were summarized by Schaffert,[4] Yoshida,[5] and Ionue.[6]

Amick's model for the corona-charging mechanism,[7] and Inoue's empirical equation for the dark decay[8] are often used to explain the behaviors of the corona-charging properties.

Inoue's equation is convenient for representing the experimental results of surface potential decay. The surface potential $V(t)$ at decay period is approximated by the following equation in a certain range of surface potential.

$$V(t) = V_0 e^{-\alpha\sqrt{t}} \quad (1)$$

where V_0 is the initial potential, α is the decay constant, and t is the time from the instant at which corona discharge is turned off. Taking the logarithm of (1), we get

$$\log V(t) = \log V_0 - 0.43\,\alpha\sqrt{t} \quad (2)$$

This means that the decay curve is linear when the log V is plotted against $\sqrt{t}$. According to Inoue's experiments, the gradient depends on such factors as the initial potentials, binder to photocondutcor weight-ratio and amounts of additives.

In this study the corona-charging properties of the sensors were found to depend a great deal on temperature. The results obtained will be of use not only for studying the mechanism of the corona-charging but also for controlling the surface potentials in commercial machines operating at various temperatures.

Experimental

Titanium dioxide of the rutile type was prepared by the hydrolysis of titanium tetrachloride distilled several times, and ignited at 500°C for 2 hrs. The average diameter of the power was about 0.5μ, and the specific surface area as determined by BET was 1.57m²/g. Polyvinyl acetate (PVAc) of the average polymerization degree of 1400 was used as a binder.

Preparation of the dispersion layers was as follows. The ratio of binder to titanium dioxide in weight was chosen to

1) I. Tashiro, T. Kimura, M. Kuwahara, and G. Ohno, *Electrophotography*, **8**, 9 (1969).
2) E. Inoue and T. Yamaguchi, *ibid.*, **5**, 65 (1964).
3) S. Kikuchi, H. Nozaki, and S. Sakata, *ibid.*, **1**, 39 (1959).
4) R. M. Schaffert, "Electrophotography" Focal Press (1965).
5) K. Yochida, "Electrophotography and its Apparatus" Nikkankohgyo (1967).
6) E. Inoue, K. Kikuchi, K. Sayanagi, M. Mori, and S. Wada, "Image Science and Engineering" Kyoritsushuppan (1970), Vols. I, II, III.
7) J. A. Amich, *RCA Rev.*, **20**, 753, 770 (1962).
8) E. Inoue, H. Kokado, T. Yamaguchi, S. Nagashima, and K. Takahashi, *Electrophotography*, **1**, 27 (1962).

be 100/0, 90/10, 70/30, 50/50, 20/80. The materials were mixed in a ball-mill crasher for 10 hr, using ethyl acetate as a solvent. The mixture was coated on an aluminium foil with a film coater, and the samples were dried at 110°C for 2 hr. The thickness of the layers was around 15 μ.

The layers cut out in the size of 12 cm × 7 cm were fixed on an aluminiun plate and kept in a chamber where the relative humidity was kept at 30%—35% for 48hr or more.

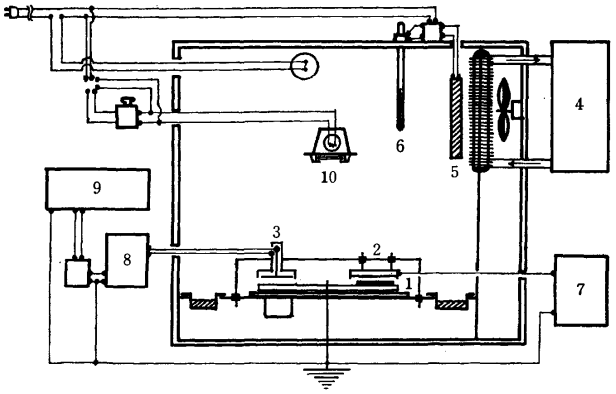

Fig. 1. A schematic illustration of the experimental equipment.
(1) dispersion layer, (2) corona discharger, (3) detecter, (4) refrigerator, (5) cooling fin, (6) relay thermometer, (7) high voltage battery, (8) surface potential meter, (9) recorder, (10) infrared light.

Measurement of the surface potentials at low temperatures was carried out in a chamber where the air was cooled by a cooler to which a cooling medium was circulated from a refrigerator, as shown in Fig. 1. Measurement at high temperatures was carried out with a heater regulated by a relay thermometer. The temperature was raised from 0°C to 35°C by each 5°C. To avoid air leakage from outside, all operations were performed with a pair of rubber gloves attached to the chamber wall.

When the chamber was insulated from the outside, the humidity inside decreased with the rise in temperature. A small amount of humid air was then introduced to the chamber to keep the relative humidity constant at 35%.

The negative corona discharge was carried out by applying −5kV on three steel wands, 0.1mm in diameter, fixed 5mm the turn-table. The corona current was controlled at around 5×10^{-6}A. The turn-table was rotated at 78 rpm. Measurements of the surface potential on the layers were carried out with a surface potential meter of a chopper type.

A typical surface potential change against time is shown in Fig. 2. The slow potential-rise during the initial few seconds is attributed to the charging period of space charges in the layer.[7] After this period, the potential rises almost in proportion to the time from the point M to N in Fig.2, and is saturated to a certain surface potential. The rising rate of the corona potential was determined from the gradient of the line MN. The corona discharge was carried out for one minute, after that the potential gradually decreased to zero. The initial potential V_0 is defined to be the potential at one minute after the turn-off of the corona discharge.

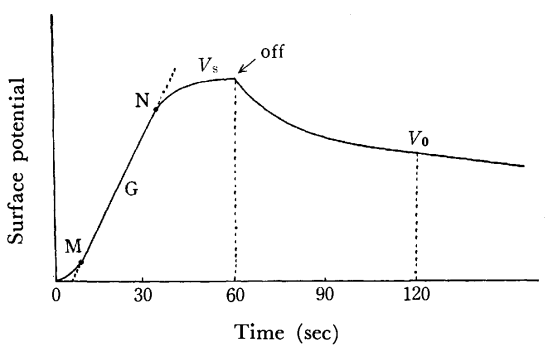

Fig. 2. The typical curve of the surface potential change against the time.

To eliminate the fatigue effect of the corona charging on the layer, an infrared light (200 W) was adjusted to the smaple for 10 minutes at 33°C and the sample was kept in the dark at room temperature for 48 hr between each measurements.

Measurements of the electrical resistivity and the electrocapacity of the dispersion layer were carried out by changing the temperature. A silver electrode (5 × 5 cm²) was evaporated in a vacuum on the layer. The specimen was fixed in a dark chamber in which temperature and relative humidity were controlled. A stainless-steel plate was placed on the sample surface with contact pressure 10.0g/cm². The electrical resistivity was directly measured with a 610-B Keithley electrometer. The electrostatic capacity was measured with a Wheatstone brige applying an alternative current of 1kHz.

Results

The rising rate of the corona potential G (volt/sec) is plotted against the temperature in Fig. 3. From the results it can be said that G for 0–30% TiO_2-contents increases with a rise in temperature, through its maximum at around 20°C, and suddenly decreases from 25 to 35°C. For 10% and 30% TiO_2-contents, G at 35°C is lower than that at 0°C. However, for 50% and 80% TiO_2-contents, G decreases gradually from 5 to 10°C, becoming almost constant from 10 to 35°C.

The temperature dependence of the asturation potential V_s is shown in Fig.4. The saturation potentials for 0–30% TiO_2-contents are almost constant at 0°–

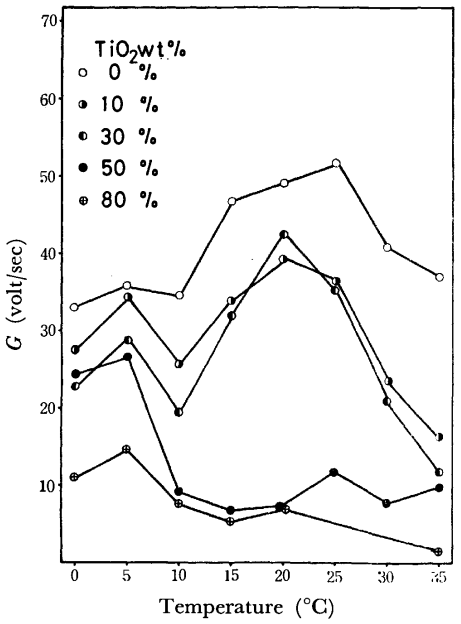

Fig. 3. The rising rate of the surface potential, G (volt/sec), were plotted against the temperature.

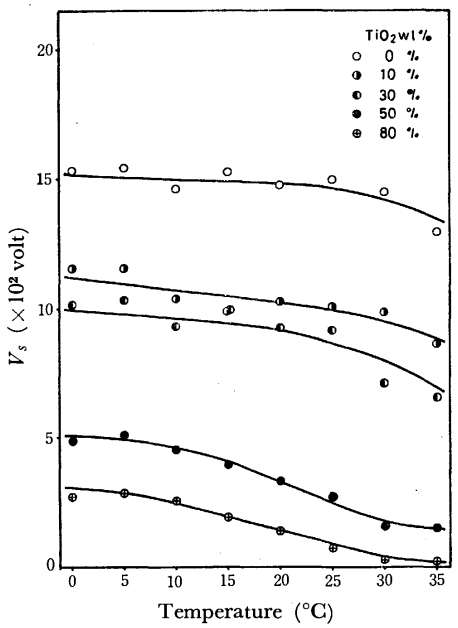

Fig. 4. The temperature dependence of the saturation potential.

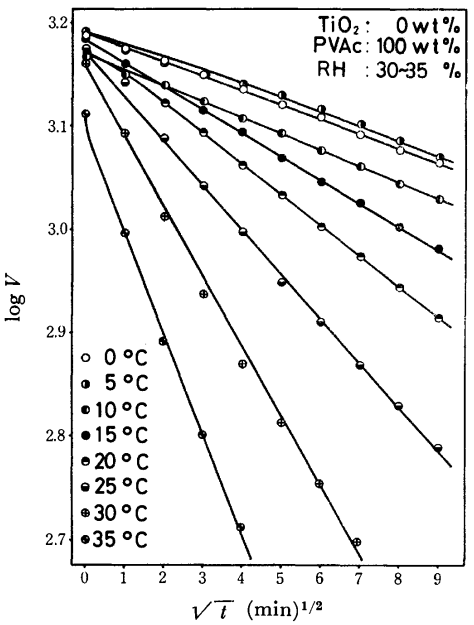

Fig. 6. The logarithm of the dark decay potential on the polyvinyl acetate layer is plotted against the square root of the time at various temperatures.

25°C, decreasing slightly at 25°–35°C. The saturation potentials for 50–80% TiO_2-contents decrease gradually with the rise in temperatures.

The temperature dependence of velocity of the dark-decay is shown in Fig.5. The velocity defined by $(V_s-V_o)/V_s$ increases considerably with the rise in temperature. This tendency is greater for the high percentage of TiO_2-contents.

The dark-decay of the surface potential at various temperatures for long duration was studied by changing the titanium-dioxide contents. The results are represented by the relation between log V and $\sqrt{t}$ in Figs. 6—10.

A good linear relation is given on the polyvinyl acetate layer for a long duration of the decay (Fig.6). However, the linearity between log V and $\sqrt{t}$ at higher TiO_2-contents does not hold at the initial steps (Figs. 7–8). The decay velocities for 50–80% TiO_2-contents are so rapid that the linearity holds for a short range of the decay period (Figs. 9–10). It can be said that the potential decay increases with the rise in temperature. The temperature dependence of the gradients of the linear lines in the plots between log V and $\sqrt{t}$, *viz.*, the decay constant α, is shown in Fig. 11. The decay

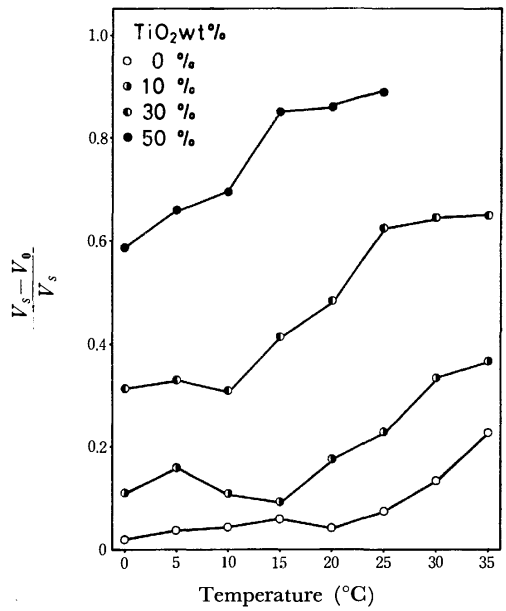

Fig. 5. The temperature dependence of the velocity of the dark decay, where V_0 is the surface potential at one minute after the turn-off of the corona discharge.

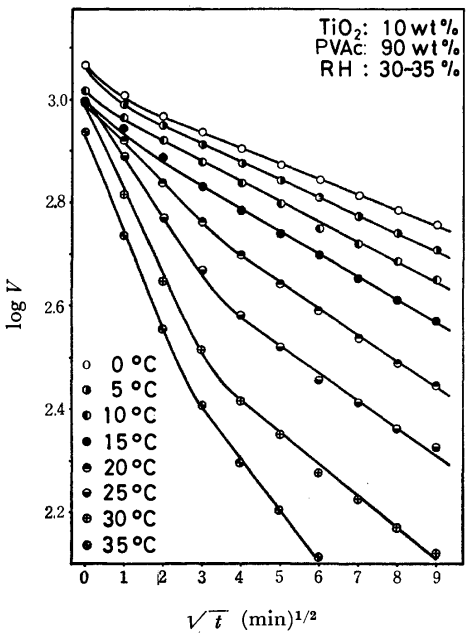

Fig. 7. The logarithm of the dark decay potential on the dispersion layer containing 10 wt% of titanium dioxide is plotted against the square root of the time at various temperatures.

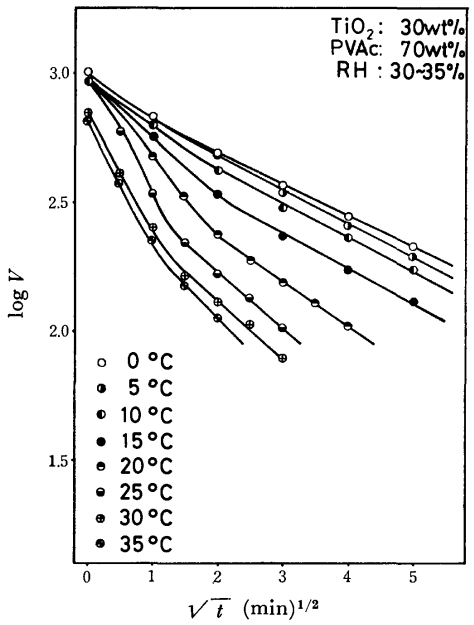

Fig. 8. The logarithm of the dark decay potential on the dispersion layer containing 30 wt% of titanium dioxide is plotted against the square root of the time at various temperatures.

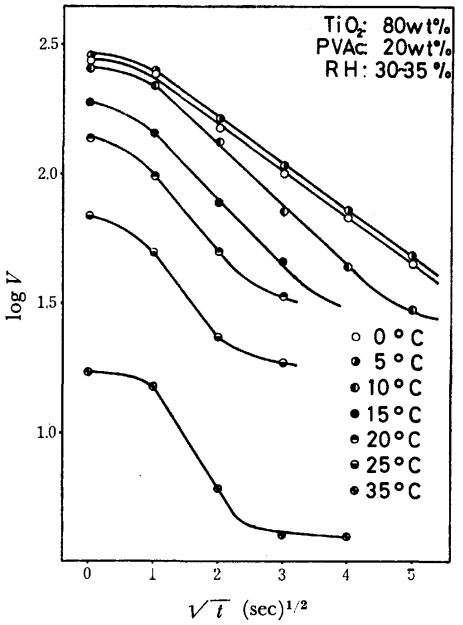

Fig. 10. The logarithm of the dark decay potential on the dispersion layer containing 80 wt% of titanium dioxide is plotted against the square root of the time at various temperatures.

constant increases in proportion to the rise in temperature, and with the increase in the percentage of TiO_2-contents.

The temperature dependence of the air-gap conductivity between the corona and the turn-table at corona-discharging which corresponds to the corona current at the applied voltage of -5kVi sre presented by a dotted line in Fig.12. The solid line represents the resistance of the air gap calculated from the values of the corona current. It can be said that the corona current gradually increases with the rise in temperature.

The resistivity of the layer at various TiO_2-contents is shown as a function of the temperature in Fig.13. The layer of 0% of TiO_2-contents has the highest resistivity, and the resistivity decreases with the increase in TiO_2-contents. In general the resistivity of the layer greatly decreases with the rise in temperature.

The capacitance (per one square centimeter) of the layer at various TiO_2-contents is shown as a funtion of the temperature in Fig.14. The layer of 80% of TiO_2-contents has the highest capacitance, and the capacitance of the layer slightly increases with the rise in temperature.

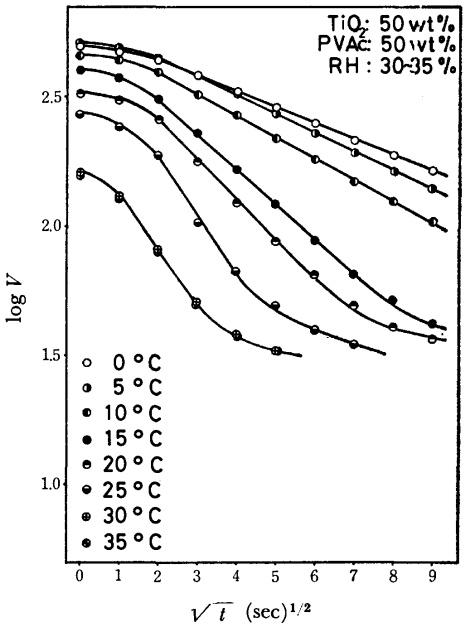

Fig. 9. The logarithm of the dark decay potential on the dispersion layer containing 50 wt% of titanium dioxide is plotted against the square root of the time at various temperatures.

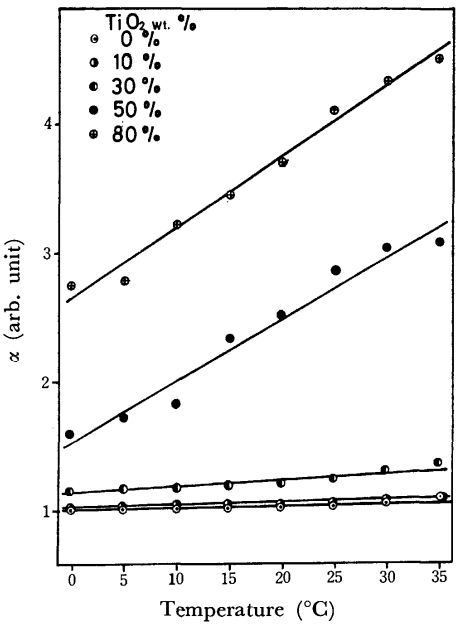

Fig. 11. The temperature dependence of the potential-decay constant, α (in Eq. 2) is shown at various percentage of the titanium-dioxide contents.

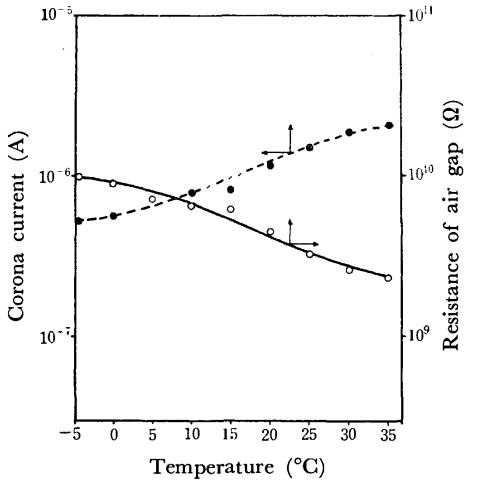

Fig. 12. The dotted line represents the temerature dependence of the corona current, and the solid line represents the resistance of air gap at corona discharging calculated by the corona current.

Discussion

The corona-charging properties of titanium-dioxide dispersion layers were studied by changing the temperature from 0 to 35°C. To interpret the temperature dependence with the use of an equivalent-circuit model shown in Fig.15, the corona current, the resistance of the layer, and the capacitance of the layer were mesaured by changing the temperature. It is reasonable that the corona current (Fig.12) increases with the increase in temperature, since not only the electron emission from the corona electrodes but also the mean free-path of corona ions increase with the rise in temperature. It is also reasonable that the resistivity of the layer decreases with the rise in temperature, since the free electrons in the layer increases with the rise

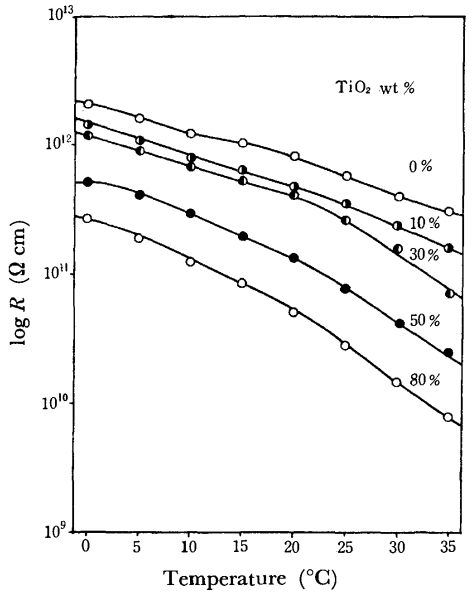

Fig. 13. The temperature dependence of the specific resistivity of the dispersion layer.

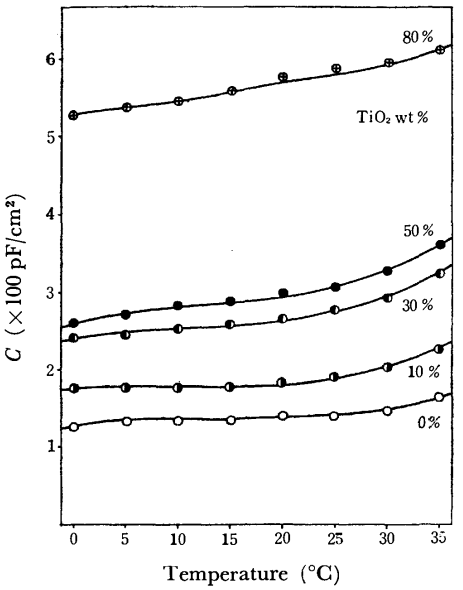

Fig. 14. The temperature dependence of the capacitance of the dispersion layer.

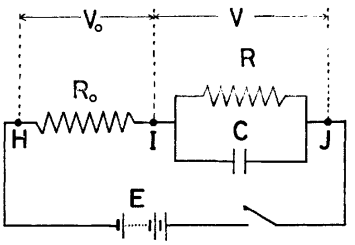

Fig. 15. An equivalent circuit of the dispersion layer.
V_0: Potential difference between H and I
V: Potential difference between I and J
R_0: Resistance of the air gap at corona discharging
R: Resistance of the dispersion layer
C: Capacitance of the dispersion layer

in temperature as shown in Fig.14. Würstlin[10] reported that the dielectric constant of polyvinly acetate increases with a rise from 25°C to 80°C. On the other hand, the dielectric constant of TiO_2-ceramics (rutile) decreases with a rise from 25 to 70°C.[11] In the case of the dispersion layer, the capacitance of the layer increases with a rise in temperature (Fig.14). It can thus be said that the temperature dependence of the capacitance is dominantly governed by the dependence of the dielectric constant of polyvinyl acetate.

In the equivalent-circuit given in Fig.15, when the switch is turned on and a voltage E is applied to the circuit, the change in potential between I and J is given by the equation

$$V = \frac{ER}{R_0+R}\left[1-\exp\left\{-\frac{1}{C}\left(\frac{1}{R_0}+\frac{1}{R}\right)t\right\}\right]. \quad (3)$$

Differentiating V with time, the rising rate of the surface potential is obtained:

$$G = \frac{dV}{dt} = \frac{E}{R_0C}\left[\exp\left\{-\frac{1}{C}\left(\frac{1}{R_0}+\frac{1}{R}\right)t\right\}\right]. \quad (4)$$

9) T. Iida and H. Nozaki, This Bulletin, **42**, 2820 (1969).

10) F. Würstlin, *Kolloid-Z.*, **134**, 143 (1953),

11) L. J. Berberich and M. E. Bell, *J. Appl. Phys.*, **11**, 681 (1940).

Since G is a function of three independent variables of R_0, R, and C, we can not satisfactorily explain the temperature dependence of G only by means of the partial differentiation of G with R_0, R, or C. We thus calculated G directly with the use of the observed values of R_0, R, and C. The rising rate of the surface potential calculated by Eq. (4), in which time was taken at ten seconds, with the use of the data, R_0, R, and C in Figs.12—14, is shown in Fig.16. It can be said that G for 0% TiO_2-contents has a maximum at around 25°C, and the maximum shifts to lower temperature range with the increase in TiO_2-contents. Consequently, G for 80% TiO_2-contents has a maxiumm at around 10°C. The agreement between the calculated values and the observed values (Fig.3) is fairly good.

The saturation potential is given by $ER/(R_0+R)$ from Eq. (3). Figure 4 shows that V_s depends on the temperature of the layer. V_s was calculated with the use of the data R_0 and R in Figs. 12—13 as a function of temperature. In this case the agreement between the calculated values and the observed values (Fig. 4) is also fairly good.

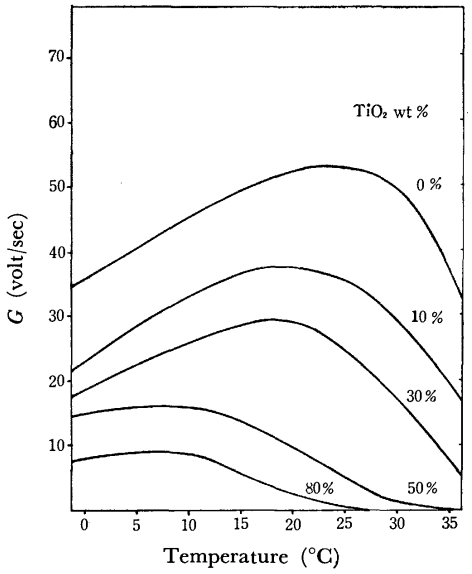

Fig. 16. The rising rate of the surface potential calculated by the equation (4) with the use of the data, R_0, R, and C in Figs. 12—14.

In the case of the discharging process, when the switch is turned off, the discharging current flows only through the resistance of the layer. Therefore, the speed of the dark decay depends greatly on the resistance of the layer. Figure 5 shows that the velocity of the dark decay depends greatly on the temperature of the layer, since R of the layer decreases with a rise in temperature (Fig.13)

The results in Figs.6—10 show that the logarithm of the decay potential decreases in proportion to the square root of the time at a certain range of the decay period. It is not possible to derive directly such a relation with the use of the simple qeuivalent-circuit shown in Fig. 15. Inoue[8] and Papazian[12] proposed a more complex empirical equation in which the summation of the exponential terms of $V_i \exp(-t_i/R_iC_i)$ is considered, where V_i, R_i, and C_i are the potential, resistance and capacitance at the time t_i, respectively. However, it is rather difficult to calculate the potential decay with the use of V_i, R_i, and C_i, since R_i and C_i are not easily measured in actual cases.

We should point out that the decay constant α increases in proportion to the temperature rise from 0° to 35°C. It is not possible to derive such a relation with the use of the simple equivalent-circuit model shown in Fig.15. A more complex model will be needed.

The authors wish to thank Mr. T. Watabe, Mr. H. Ishii, and Mr. T. Takayama for their experimental assistance in this work.

12) H. A. Papazian, P. A. Flinn, and D. Trivich, *J. Electrochem. Soc.*, **104**, 84 (1957).

Photochemical Reaction of 9-Chloroacridine in Aerated and Deaerated Ethanol. II. Studies by Means of a Flash Technique

Katsumi NAKAMARU, Shigeya NIIZUMA, and Masao KOIZUMI

Dapartment of Chemistry, Faculty of Science, Tohoku University, Katahira, Sendai

(Received September 3, 1971)

Studies were made on the transient species produced when the aerated and deaerated ethanol solutions of 9-Cl-acridine (9-Cl-A) are flashed. In the deaerated solution, triplet state of 9-Cl-A and a long-lived radical species of unknown structure were detected. It was established that the latter is produced by a reatcion in the singlet excited state of 9-Cl-A (and possibly in the higher triplet ($T_{n-\pi}$*)) and that it produces biacridyl by a bimolecular reaction. In the aerated solution, another radical species of a long life of which structure is still unknown, was detected. It was established that this radical species reacts bimolecularly and produces acridone.

In a previous paper,[1] we have established that irradiation of 9-Cl-acridine in ethanol by 365 nm, produces acridone (A) in the aerated solution, while in the absence of oxygen, mainly biacridan (BAH_2) is produced *via* biacrydyl (BA). The proposed scheme is as follows.

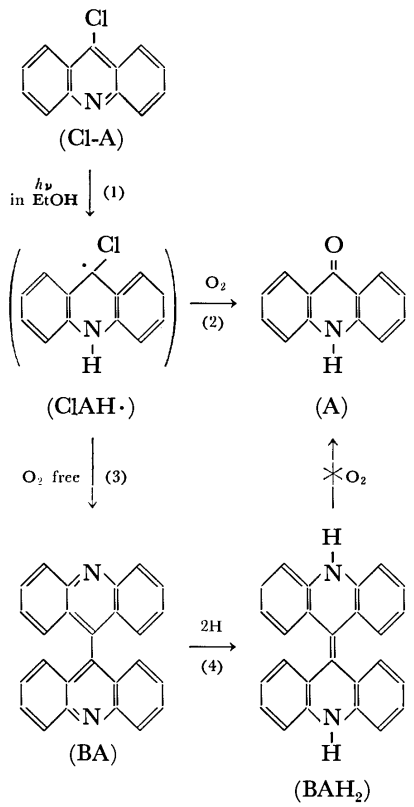

The identification of BA and BAH_2 was established in the previous paper, and there is no doubt on the occurence of process (4). But it is quite unknown how processes (1) and (3) occur, or in other words, whether the splitting of HCl preceeds or follows the dimerization reaction. Still less unknown is the detailed mechanism of the production of acridone. The only information obtained experimentally is that the presence of reductive medium and of oxygen is necessary for the reaction to occur.

In order to elucidate the detailed mechanism of these reactions, we have performed flash photolysis studies for both the aerated and deaerated solutions. For the aerated solution, a certain transient intermediate was detected which produces acridone by a bimolecular reaction. In the deaerated solution, two transient species, long-lived and short-lived were detected and it was established that the long-lived species produces biacridyl bimolecularly. Although we did not succeed in identifying the transient species, the present results are consistent with the conclusion given in the previous paper and are helpful for elucidating the mechanisms of the reactions.

Experimental

Materials. All the materials were purified as described in the previous paper.

Apparatus and Procedures. The apparatus for the flash photolysis is an usual one employed in our laboratory.

Results and Discussion

Deaerated Solution. Two kinds of transient intermediates, short-lived M_1, and long-lived M_2, were detected. It was established that the photoproduct is biacridyl by measuring its spectrum after flashing the sample several times. Although the absorption spectra of M_1 and M_2 overlap with each other to some extent, they can be distinguished rather easily because of their great difference in their lifetimes.

Figure 1 gives the plot of $1/D$ (D, optical density at 460 nm) against time. As will be verified below, the later stage obeys the second order, while the earlier stage deviates greatly from the second order plot. The order of reaction in an early stage was examined by the following procedures; 1) extrapolation of the later linear portion, 2) substraction of the D-value on the extrapolated line (D_{ext}) from D at various time points and 3) plotting of $\log(D-D_{ext})$ or $1/(D-D_{ext})$ against time. As shown in Fig. 1b the $\log(D-D_{ext})$ *vs.* t plot gives a straight line irrespective of the wavelengths. Hence one can conclude that the decay in the early stage obeys the first order. To check the reliability of this procedure and to obtain the correct spectral shape, we plot $(D-D_{ext})$ at various wavelengths against $(D-D_{ext})_{440}$. As shown in Fig. 2 all of them give good linear plots, and the spectral shape could thus be determined accurately. This is given in Fig. 3. All the transient spectra reported below were obtained or checked by the similar

1) K. Nakamaru, S. Niizuma, and M. Koizumi, This Bulletin, **44**, 1256 (1971).

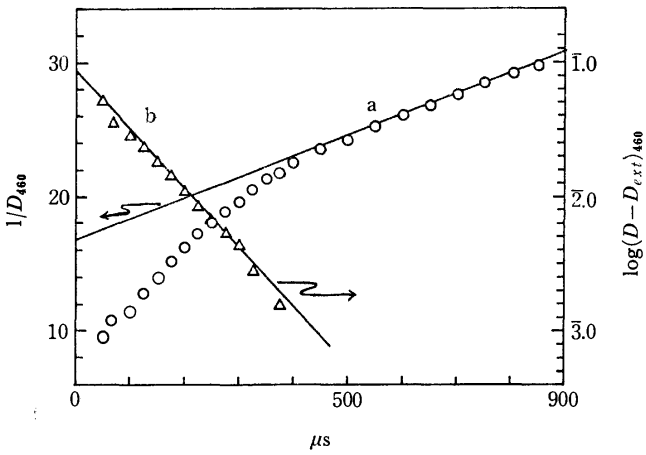

Fig. 1. Analysis of the decay of the two intermediates produced in the degassed solution of 9-Cl-A in ethanol (1×10^{-4} M), at 460 nm (See text).
a: decay of M_2 (long-lived intermediate)
b: decay of M_1 (short-lived intermediate)

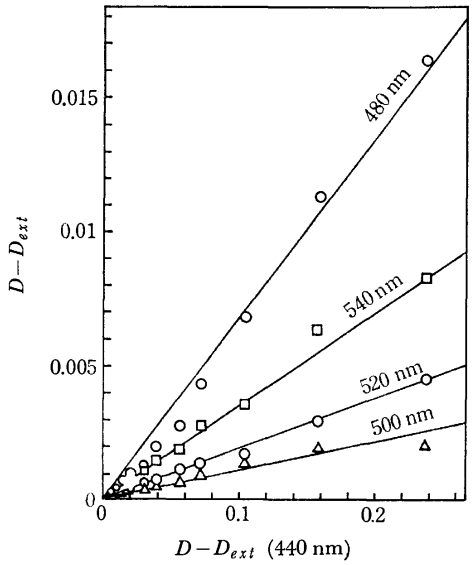

Fig. 2. Plot of $D-D_{ext}$ (at various wavelengths) *vs.* $D-D_{ext}$ (at 440 nm). Degassed solution of 9-Cl-A in ethanol (1×10^{-4} M).

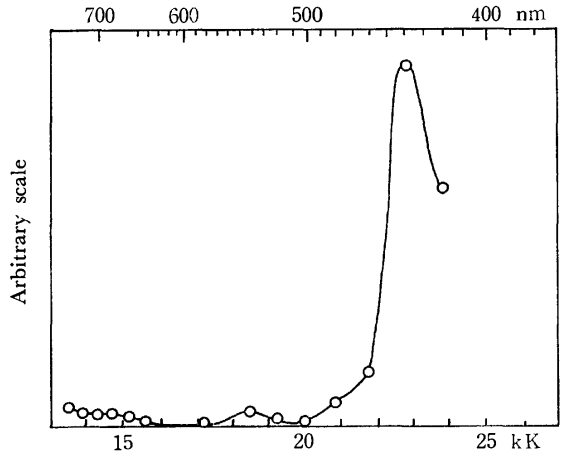

Fig. 3. Spectrum of short-lived intermediate, M_1 obtained in the degassed solution of 9-Cl-A (1×10^{-4} M).

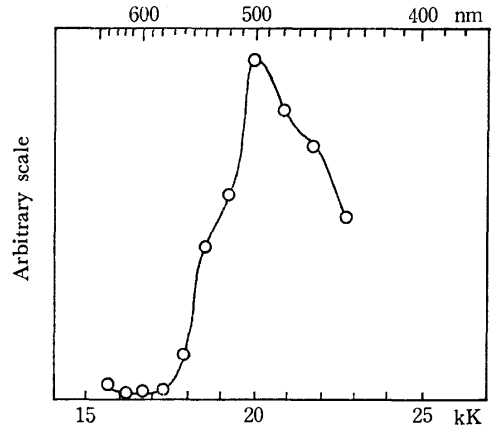

Fig. 4. Spectrum of long-lived intermediate, M_2 obtained in the degassed solution of 9-Cl-A (1×10^{-4} M).

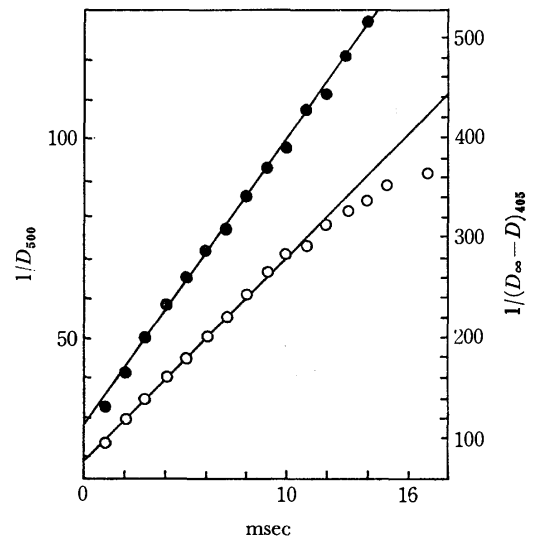

Fig. 5. Second-order plot for the decay of M_2 (at 500 nm) and for the build-up of BA (at 405 nm). Degassed solution of 9-Cl-A in ethanol (1×10^{-4} M).
○: $1/D_{500}$, ●: $1/(D_\infty-D)_{405}$

method as described above. The success of the above procedure implies that there is no interrelation between M_1 and M_2. M_1 may safely be identified as the triplet state on the basis of its lifetime (rate constant, 7.4×10^3 sec^{-1}) and a somewhat similar spectral shape as that of acridine triplet. Hence it is likely that M_2 is produced by a reaction in the singlet excited state of 9-Cl-A(and possibly in the high triplet (n-π^*)).

Figure 4 gives the spectral shape of M_2 as obtained by the similar method as described above. Figure 5 gives the decay of M_2 and the build-up of BA plotted according to the second order rate formula. The former was measured at 500 nm while the latter at 405 nm. The inclinations of the plots which give $k/\varepsilon d$ are for the former 1.8×10^4 sec^{-1} and for the latter 2.8×10^4 sec^{-1}. Figure 6 gives the relation between the decrease of M_2 and the increase of BA, as measured by the change in the optical densities respectively at 500 nm and at 405 nm. It is seen that the plot of D_{500} *vs.* $(D_\infty-D)_{405}$ gives a good straight line passing through the origin. We can conclude from Figs. 5 and 6 that BA is produced from M_2 accord-

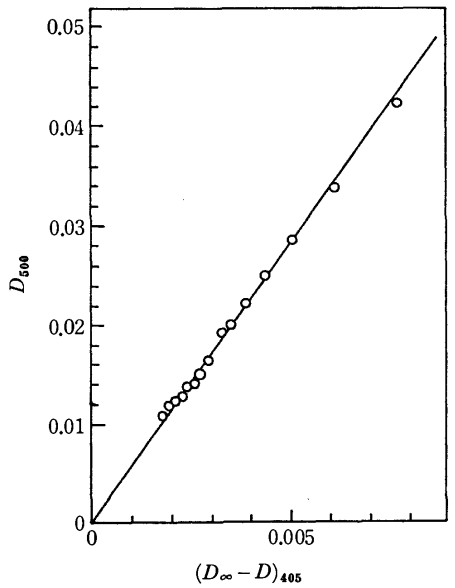

Fig. 6. Relation between the quantity of the intermediate M_2 and that of BA in the degassed solution of 9-Cl-A in ethanol (1×10^{-4} M).

ing to a bimolecular reaction. As to the identification of M_2, there are two possibilities. One is a half-reduced 9-Cl-acridine (I). In this case splitting of hydrogen

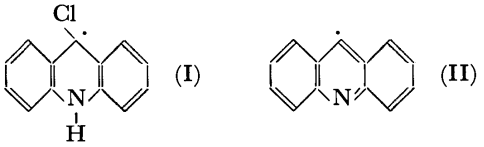

chloride occurs during or after dimerization. Another possible structure is (II). This is produced when the splitting of HCl from (I) preceeds dimerization. Discrimination of the two will be possible if we undertake the similar experiments using other 9-halogenated acridines.

The Aerated Ethanol Solution. Only one transient species with a rather long lifetime was detected. The product after flashing was identified as acridone by measuring the UV spectrum. A transient species has a spectral shape as given in Fig. 7. Since it is common that no T-T absorption is observed in the aerated solution, this transient species is attributed to some kind of radical species. Comparing Fig. 7 with Fig. 4, we can conclude that this radical species is different from M_2. We call it M_3 for the sake of convenience.

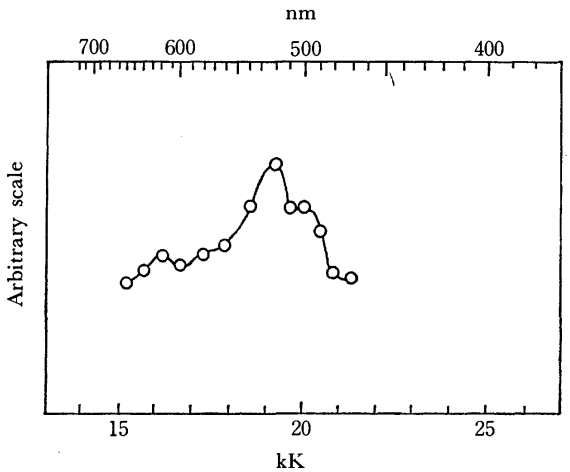

Fig. 7. Spectrum of intermediate M_3 obtained in the aerated solution of 9-Cl-A in ethanol (1×10^{-4} M).

In Fig. 8 the decay of M_3 measured at 520 nm and the build-up of acridone as measured at 400 nm are plotted as a second order process. Since at 400 nm, the spectra of M_3 and acridone overlap to some extent, $(D_\infty - D)_{400}$ was plotted against time. It is evident that the decay of M_3 and the build-up of acridone run parallel. This was confirmed further by Fig. 9 where $(D_\infty - D)_{400}$ and D_{520} at corresponding time points are plotted. The plot is a good straight line. We can conclude therefore, that acridone is produced from some unknown radical species M_3 bimolecularly.

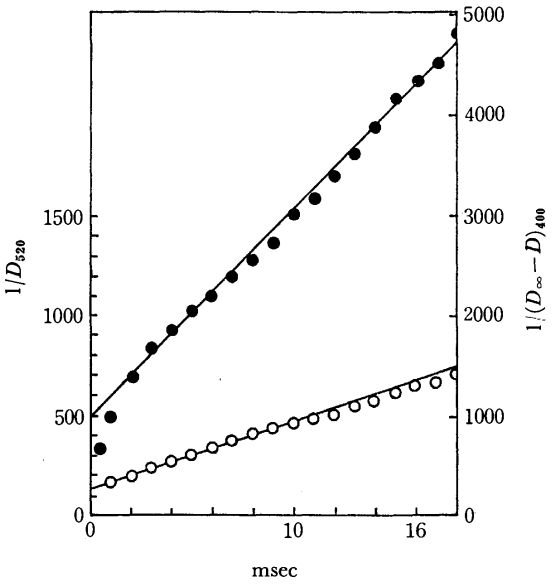

Fig. 8. Second-order plot for the decay of M_3 (at 520 nm) and for the build-up of acridone (at 400 nm). Aerated solution of 9-Cl-A in ethanol (1×10^{-4} M).
○: $1/D_{520}$, ●: $1/(D_\infty - D)_{400}$

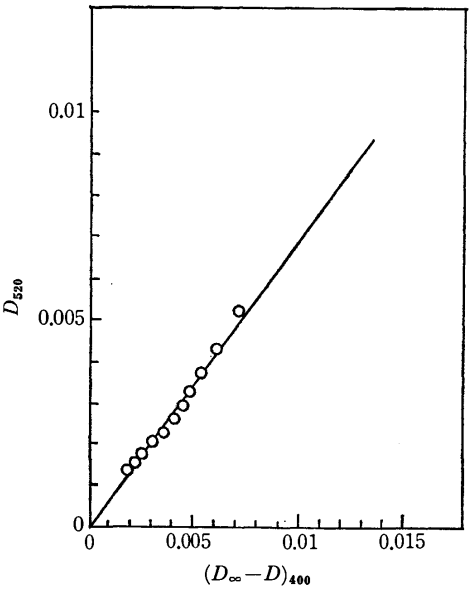

Fig. 9. Relation between the quantity of the intermediate M_3 and that of acridone in the aerated solution of 9-Cl-A in ethanol (1×10^{-4} M).

The identification of M_3 will become easier when M_2 is identified and so was not attempted at the present stage. Only provisional discussions will be given below. Judging from the fact that M_3 gives rise to acridone bimolecularly and that oxygen is involved in the reaction, it seems very probable that HO_2 group is attached to acridine structure in some way. If one assumes M_2 has a structure (II) and further assumes that (II) is formed even in the presence of exygen, then it is conceivable that (II) reacts with oxygen, and the resulting peroxiradical deprives hydrogen atom from ethanol producing the following hydroper-

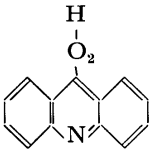

oxide. This will produce acridone bimolecularly. On the other hand, if M_2 has structure (I), it is expected to be oxidized back to 9-Cl-acridine from analogy to acridine, rather than attacked by oxygen at 9-position. Another possibility is primary production of 9-Cl-acridan *via* molecular mechanism and the attack of oxygen at 9-position. But this is also im-

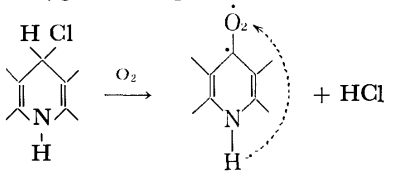

probable because acridan type product was not detected in the steady light reaction of 9-Cl-acridine.[1]

The identification of M_2 and M_3 is most desirable to establish the mechanism of the general photoreaction of 9-Cl-acridine. Furthermore it will be interesting to investigate the transient radical species of photoreaction of BA at various acidities in view of great difference of stability in $BAH_2^{+}\cdot$ and $BAH\cdot$ reported in a previous paper.[2] These studies will be made in near future.

2) S. Niizuma, K. Nakamaru, and M. Koizumi, *Chem. Lett.*, **1972**, 59.

BULLETIN OF THE CHEMICAL SOCIETY OF JAPAN, VOL. 45, 2448—2451 (1972)

Fluorinated Ligands. I. Chelating Behavior of 1-Amino-3,3,3-trifluoro-2-propanol with Copper(II) Ion and Preparation of Copper(II)-, Cobalt(III)-, and Nickel(II) Complexes*

Isao YOSHIDA and Hiroshi KOBAYASHI

Department of Organic Synthesis, Faculty of Engineering, Kyushu University, Fukuoka, 812

(Received October 5, 1972)

In the reaction of 1-amino-3,3,3-trifluoro-2-propanol (LOH) with cupric ion in aqueous solutions two kinds of complex species were found to be formed: One was a complex ion of $[Cu(LO)(H_2O)_2]^{+1}$, which was of major abundance in the solutions where mole ratio of the ligand to the metal ion was less than 3, and the other was an inner complex of $[Cu(LO)_2]$ predominating in the solutions which contained a large excess of the ligand or a small amount of alkali. The structures of the species in the solution phases were assigned by the spectral data. Chelate compounds of inner complex type, $[Cu(LO)_2(H_2O)]$, $[Co(LO)_3]$, and $[Ni(LO)_2]$, were synthesized from the present ligand and corresponding metal ion. These are insensitive to moisture in the air. Structures of the chelates are discussed on the basis of spectroscopic observations.

In connection with studies on coordinating behaviors of hydroxyl group of aminoalcohols and of their *N*-alkylated derivatives, various preparative and spectral studies have been carried out. In the early preparative studies by Hieber and Levy[1] and by Brintzinger and Hase,[2] the isolated products were complex salts containing the neutral ligands accompanied by counter anions. Complex formation with copper(II) in aqueous solution was studied by means of the spectroscopic method by Ojima and Sone,[3] who concluded that a tetraaminocopper(II) complex, $[Cu(amine)_4]^{+2}$, was formed in the region of lower concentration of the ligand, which behaved therein as a monodentate ligand, and that an increase in the ligand concentration or an addition of a strong base afforded a 1:2 (Cu: ligand) inner complex chelate. These complexes, however, could not be isolated as a stable form from such solutions. Yoneda and Kida[4] also isolated a neutral trisethanolaminecoblat(III), $[Co(NH_2CH_2CH_2O)_3]$, from a strongly alkaline aqueous solution. Subsequently Kida[5] obtained copper(II) chelates of inner complex type, $[Cu(NH_2CH_2CH_2O)_2(H_2O)]$ and $[Cu(NH_2CH(C_6H_5)CH(C_6H_5)O)_2]$, from anhydrous alkaline ethanol solutions. In every case, the isolated metal chelates of inner complex type were unstable and readily affected by moisture.

In this paper, we discuss the chelating behavior of

* Contribution No. 259 from the Department of Organic Synthesis, Kyushu University.

1) W. Hieber and E. Levy, *Z. Anorg. Allgem. Chem.*, **219**, 225 (1934).

2) H. Brintzinger and B. Hase, *ibid.*, **252**, 293 (1944).

3) H. Ojima and K. Sone, *ibid.*, **309**, 110 (1961).

4) H. Yoneda and S. Kida, *J. Amer. Chem. Soc.*, **82**, 2139 (1960).

5) S. Kida, *Nippon Kagaku Zasshi*, **85**, 428 (1964).

1-amino-3,3,3-trifluoro-2-propanol [$CF_3CH(OH)CH_2NH_2$; LOH] with copper ion in aqueous phases and the structures of copper(II)-, cobalt(III)-, and nickel(II) chelates of the present ligand in solid phase, in comparison with some other ethanolamine type ligands.

Experimental

Apparatus. All melting points measured were uncorrected. Visible absoprtion and reflectance spectra were measured with a Hitachi ESP-2 and a Hitachi EPU-2 spectrophotometers, respectively. The IR spectra were recorded with a JASCO DS-403G spectrophotometer. Molecular weights were determined on a Vapor Pressure Osmometer (Mechrolab Inc.) with 2-methyloxine as a standard substance for the copper complex in absolute ethanol, and *p*-bromonitrobenzene for the nickel complex in absolute methanol. Copper(II) acetate monohydrate (an extrapure grade from the Wako Pure Chemicals Co., Ltd.) was used without further purification for the reaction equilibrium study in aqueous media.

Synthesis of 1-amino-3,3,3-trifluoro-2-propanol. The aminofluoropropanol hydrochloride was prepared according to Jones.[6] Into a solution of the hydrochloride in as a small amount of water as possible, was added a saturated aqueous sodium bicarbonate up to pH 8. The freed aminopropanol was extracted with ethylether. The ethereal solution was dried and concentrated slowly on a water bath to give precipitates, which were recrystallized from ethylether, melting at 97—98°C.

Found: C, 27.77; H, 46.6; N, 8.22; Cu, 10.82%. Calcd for $C_3H_6ONF_3$: C, 27.95; H, 4.65; N, 10.82%.

Synthesis of Bis(1-amino-3,3,3-trifluoro-2-propanolato)copper(II) Monohydrate. One gram of copper acetate monohydrate was dissolved into 50 m*l* of water containing 1.3 g of the ligand, and then 0.2 M aqueous sodium hydroxide was added slowly up to pH being 8. The solution was kept at about 40°C for 12 hr on a water bath. The resulting mixture, when cooled to 0°C, gave a red-violet crystalline precipitate, which was recrystallized from an ethyl acetate-ethanol mixture, to give red-purple needles decomposing at 199—200°C.

Found: C, 21.44; H, 3.60; N, 8.22; Cu, 18.81%; mol wt, 324. Calcd for $C_6H_{12}O_3N_2F_6Cu$: C, 21.38; H, 3.56; N, 8.30; Cu, 18.81%; mol wt, 337.5.

Synthesis of tris(1-amino-3,3,3-trifluoro-2-propanolato)cobalt(III). One and three tenth gram of cobaltous perchlorate was added into 20 m*l* of ethanol containing 0.32 g of the ligand and then 0.2 M aqueous sodium hydroxide was added slowly into the mixture until its pH became 9. The solution was maintained at about 50°C on a water bath for about 24 hr. A pink powdery precipitate, which was obtained from the resulting mixture when cooled to 0°C, was washed with ethanol, and then dried *in vacuo*, decomposing at 240°C. The product was insoluble in donating solvents such as ethanol and water, whereas being soluble in inert organic solvents such as benzene.

Found: C, 24.52; H, 3.45; N, 9.99; Co, 13.63%. Calcd for $C_9H_{15}O_3N_3F_9Co$: C, 24.38; H, 3.39; N, 9.48; Co, 13.29%.

Synthesis of bis(1-amino-3,3,3-triffuoro-2-propanolato)nickel(II). A saturated ethanol solution of 0.45 g of nickel(II) perchlorate was added into a saturated ethanol solution of 0.32 g of the ligand. Light-blue crystals which precipitated immediately, were collected by filtration and recrystallized from ethanol, to give light-blue plates decomposing at 170—173°C. The complex was insoluble in an inert organic solvent such as benzene, while being soluble in a donating solvent such as methanol.

Found: C, 22.62; H, 3.48; N, 8,87% mol wt (in methanol), 312. Calcd for $C_6H_{10}O_2N_2F_6Ni$: C, 22.81; H, 3.18; N, 8.88; mol wt, 314.89.

Paper Electrophoresis. Paper electrophoresis of the copper complex was performed in a solvent immersion method on a filter paper strip soaked in a 0.1 M sodium chloride electrolyte. Potential applied between both ends (14 cm distant) was 640 V (45.7 V/cm) and current 3 mA. A copper spot of the fluoro-ligand complex did not migrate when the potential was applied for 5 min, while those of bis(ethylenediamine)copper(II) perchlorate and of copper(II) perchlorate travelled 20 mm respectively toward the negative electrode in 5 min under the same operation conditions. Diphenyl-carbazone was used as a chromogenic indicator for copper ion.

Results and discussion

Spectrophotometric Studies on the Chelating Behavior of the Ligand (LOH) with Copper(II) Ion. Figure 1 shows absorption spectra of aqueous solutions containing copper(II) ion and various amouts of the ligand (LOH). When the mole ratio of copper ion to the ligand in the solution is less than 1:2 (Cu:LOH), copper(II) ion precipitates in a form of hydroxide. A 1:3 (Cu:LOH) mixture gives a clear solution showing an absorption peak at 14500 cm^{-1}. An increase in the ligand concentration causes a blue shift of the absorption peak up to 16600 cm^{-1} until the mole ratio becomes as much as 1:6. Further increase in the ligand concentration does not produce any more shift in the absorption band. The 1:6 or 1:8 solution shows the absorption curve superimposable to that of the red-violet copper chelate in aqueous solution phases which is shown in Fig. 3. Figure 2 indicates that an addition of an equimole of aqueous sodium hydroxide to the 1:1 (Cu:LOH) mixture results in dis-

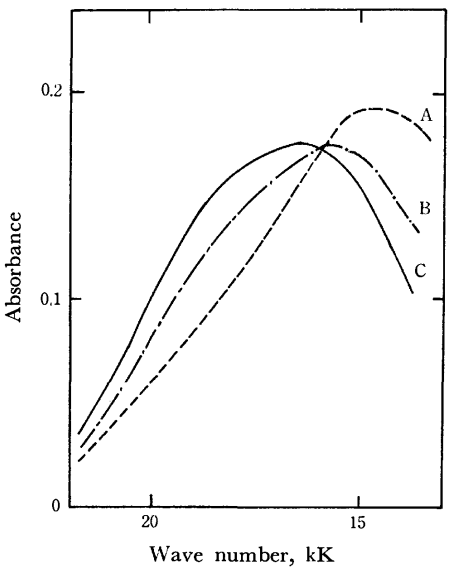

Fig. 1. The absorption spectra of Cu(II)-LOH mixture, the mole ratio being (A); 1:3, (B); 1:4, (C); 1:6, and 1:8, Cu(II) concn.; 5×10^{-3}M.

6) R. C. Jones, *J. Amer .Chem. Soc.*, **70**, 143 (1948).

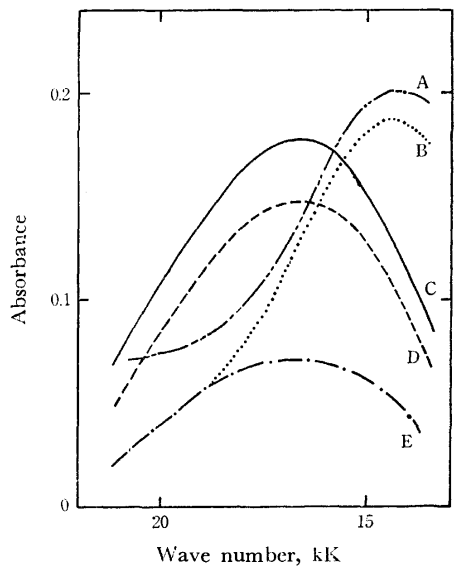

Fig. 2. The absorption spectra of a $Cu(LO)_2(H_2O)$-Cu(II) (1 : 1) mixture (A), and of Cu(II)-LOH-NaOH mixtures, the mole ratio being (B), 1 : 1 : 1, (C); 1 : 4 : 5, (D); 1 : 2 : 5 and (E); 1 : 2 : 2, Cu(II) concn.; 5×10^{-3}M.

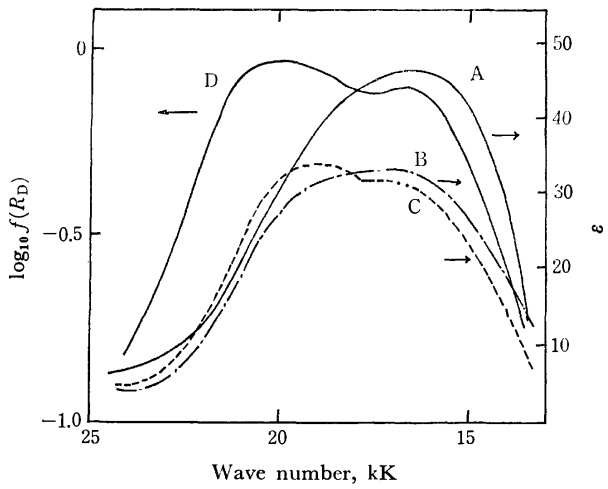

Fig. 3. The absorption spectra in water (A), methanol (B) and ethanol (C), and the reflectance spectrum (D) of $Cu(LO)_2(H_2O)$.

solution of the precipitates of copper hydroxide, giving a clear blue solution, an absorption peak of which is at 14500 cm^{-1} in good agreement with that of the 1 : 3 mixture in Fig. 1. Dissolution of the solid copper chelate, $Cu(LO)_2(H_2O)$, in an equimole of aqueous copper acetate also gives a blue solution showing the absorption curve B in Fig. 2, absorption maximum of which is also in good agreement with the above 1 : 3 mixture in Fig. 1. This value of the absorption peak corresponds to that of a 1:1 copper chelate of ethylenediamine at 15200 cm^{-1} [7] or that of *N*-hydroxyethylethylenediamine at 14500 cm^{-1},[8] and is most likely to be ascribed to the formation of a 1 : 1 ($Cu:LO^{-1}$) chelate in the aqueous solutions. An ddition of alkali into the 1 : 2 (Cu : LOH) mixture in which precipitates of copper hydroxide are formed, affords a clear red-violet solution, which shows an absorption peak at 16600 cm^{-1}, as illustrated by Curve E in Fig. 2, in agreement with that of the 1 : 6 mixture in Fig. 1. Further addition of alkali or the ligand does not produce any shift of the absorption band.

In a region of the mole ratio higher than 1 : 6, the 1 : 2 inner complex is formed. An excess of the ligand is likely to play a role of an agent deprotonating from the hydroxyl group upon the chelate formation. Presence of the 1 : 2 inner complex is also indicated by the results of high voltage paper electrophoresis, which show that the copper chelate is of zero charge in aqueous media. In contrast with isopropanolamine which produced a 1:2 chelate in a region of the mole ratio higher than 1 : 10,[3] the present ligand readily forms the neutral 1 : 2 chelate under much milder conditions.

Complexing behavior of the present fluoro-ligand, therefore, seems to be quite different from that of an ordinary ethanolamine type ligand. The latter causes precipitation of copper hydroxide in a 1:3 (Cu:ligand) aqueous mixture and gives a tetraammine type complex in a range of mole ratio slightly higher than 1 : 4, forming no 1 : 1 chelate.[3] The trifluoromethyl group affects the donating power of the adjacent hydroxyl group presumably by its strong electron-withdrawing effect, favoring the dissociation of proton from hydroxyl oxygen. Consequently chelate formation with copper ion is more easily attained.

Spectral Studies on the Chelate Compounds of Copper(II)-, Cobalt(III)-, and Nickel(II) ions. IR spectral results on the ligand and its metal chelates are summarized in Table 1, including assignments of the bands according to Brannon.[9] The free ligand shows a broad band diffused between 3200 and 2400 cm^{-1} due to a strongly hydrogenbonded hydroxyl group, and a sharp doublet at 3330 and 3280 cm^{-1} related to a primary amino group involved in the hydrogen bonding. The hydrochloride of the ligand shows also a broad strong band centered at 3220 cm^{-1} due to a hydroxyl group, N–H stretching bands due to the ammonium group being probably hidden under the hydroxyl absortion.

Copper Complex, $Cu(LO)_2(H_2O)$. IR spectrum of the copper chelate shows a prominent absorption band spread over from 3260 to 3100 cm^{-1} due to lattice water in agreement with the result of elemental analysis, N–H absorptions again being hidden under the strong water band. The absorption peak due to ν(C–F) is observed at 1123 cm^{-1}. Figure 3 shows the visible reflectance and absorption spectra of the chelate in some donating solvents respectively. The reflectance spectrum exhibits an absorption peak and a shoulder at 20200 and about 16600 cm^{-1} respectively, indicating a square planar structure with respect to the central metal ion in the chelate molecule.[10,11]

7) H. B. Jonassen and T. H. Dexter, *J. Amer. Chem. Soc.*, **71**, 1553 1949).

8) J. L. Hall and W. E. Dean, *ibid.*, **80**, 4183 (1958).

9) D. G. Brannon, R. H. Morrison, J. L. Hall, G. L. Humphrey, and D. N. Zimmerman, *J. Inorg. Nucl. Chem.*, **33**. 981 (1971).

10) J. P. Fackler, Jr., F. A. Cotton, and D. W. Barnum, *Inorg. Chem.*, **2**, 97 (1963).

11) A. E. Martell, R. L. Belford, and M. Calvin, *J. Ionrg. Nucl. Chem.*, **5**, 170 (1958).

Table 1. Chracteristic IR frequencies for ligand and its metal chelates[a)]

Compound	ν(OH)	ν_a(NH)	ν_s(NH)	$\delta(NH_2)$	ν(CN)	ν(CF)	ν(CC)
LOH	3200—2400 m	3330 m	3280 m	1612 m	1160 s	1135 s	1076 m
LOH.HCl	3220 s, br	b)	b)	1602 m	1161 s	1150 s, sh	1120 m
$Cu(LO)_2.H_2O$	3260—3100 s	b)	b)	1620 s	1165 s	1123 s	1100 s
$Co(LO)_3$		3300 m	3220 m	1616 m	1165 s	1120	1100 s
$Ni(LO)_2$		3400 w	3376 w	1600 m	c)	c)	c)

a) In Nujol mulls. Frequencies are given in $K(cm^{-1})$. Intensity designations: w, weak; m, medium; s, strong; br, broad; sh, shoulder.
b) Obscured by hydroxyl bands.
c) Unable to be assigned due to much complicated spectrum in these region.

On the other hand, the paper electorphoresis of the chelate indicates that the complex is present as a zerocharged, neutral complex in aqueous media. Combined with the result of molecular weight determination, these observations indicate consistently the copper chelate to be an inner complex type, excluding a possibility of an ion-pair type complex such as $[Cu(LO)(LOH)]^+[OH]^-$.

Absorption spectrum in water shows at 16400 cm^{-1} a broad peak, which is at much lower wave-number with a narrower half-band width than those of the corresponding band observed in the solid reflectance spectrum. These spectral evidences indicate an existence of axial ligation of the solvent molecules on the planar tetracoordinate copper chelate to form the penta- or hexacoordinations.[12,13)]

While the spectral characteristics in methanol and in ethanol in the region between 15000 and 21000 cm^{-1} are rather resemblant to those observed in the reflectance spectrum, and the effect of axial ligation of the solvent molecules in such alcohol solutions is, therefore, considered to be in a small extent, though comparisons of the absorption intensities suggesting the slightly stronger effect of methanol than that of ethanol.

Cobalt complex, $Co(LO)_3$. A strong IR absorption band at 3220 cm^{-1} due to ν(O–H) of the present aminofluoropropanol hydrochloride disappears in the spectrum of the cobalt chelate, while the absorption peak due to ν(C–F) remains at 1120 cm^{-1}. Curve A in Fig. 4 shows the spectrum of the chelate in a benzene solution. Two absorption maxima at 25200 and 18200 cm^{-1} indicate an octahedral hexacoordination structure in respect to the central cobalt(III) ion.[14)] The solubility of the chelate in inert organic solvents also supports to be of an inner complex type.

Nickel Complex, $Ni(LO)_2$. Curve B in Fig. 4 shows the reflectance spectrum of the nickel chelate. General feature of three absorption peaks at 27000, 16200, and 9700 cm^{-1} indicates[15)] an octahedral coordination structure of the chelate in respect to the central metal ion, whereas the analytical data indicate the mole ratio of 1:2 for nickel ion to the ligand and the IR spectrum shows no absorption band due to hydroxyl group or water. The nickel chelate is, therefore, considered to be of a polymeric structure at least in a solid phase. On the other hand, the chelate takes a monomeric form in a donating solvent such as methanol. The absorption spectrum in the solvent, as shown in the curve C of Fig. 4, indicates an octahedral coordination structure regarding the central metal ion. Therefore solid polymeric chelate complex cleaves to give a monomeric form by donating of two molecules of methanol upon dissolution.

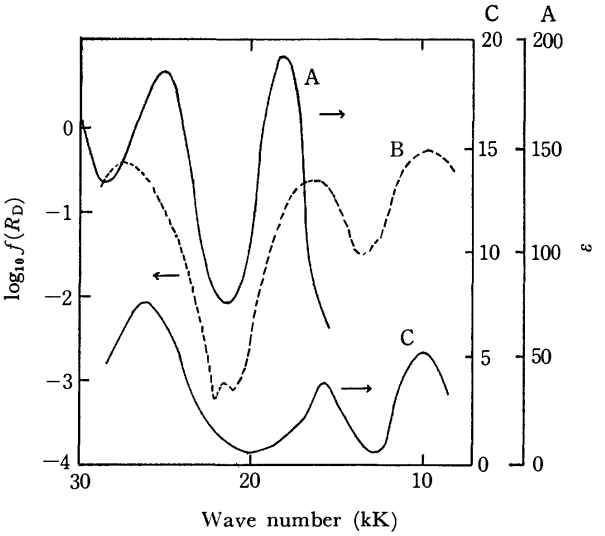

Fig. 4. The absorption spectrum of $Co(LO)_3$ in benzene (A), and the reflectance (B), and absorption (C) spectra of $Ni(LO)_2$

The metal chelates of the present ligand were isolated as stable forms without any precautions, forming a striking contrast to those of monoethanolamine which were highly sensitive to moisture.

The authors are grateful to Prof. Keihei Ueno for his valuable advices and to the Ministry of Education for a grant-in-aid for scientific research.

12) L. L. Funck and T. R. Ortolano, *Inorg. Chem.*, **7**, 567 (1968).
13) a) I. Yoshida, Y. Oono, H. Kobayashi, and K. Ueno, This Bulletin, **45**, 174 (1972).
b) D. P. Graddon and K. B. Heng, *Aust. J. Chem.*, **24**, 1059 (1971).
14) F. A. Cotton and G. Wilkinson, "Advanced Inorganic Chemistry," Interscience Publish, Inc., New York, (1966), p. 875.
15) F. A. Cotton and G. Wilkinson, *ibid.*, p 881.

Schiff Bases Derived from Heptane-2,4,6-trione and Ethylenediamine, and Its Copper(II) and Oxovanadium(IV) Chelates*

Tairoku YANO, Tetsuaki USHIJIMA, Masaomi SASAKI, Hiroshi KOBAYASHI, and Keihei UENO

Department of Organic Synthesis, Faculty of Engineering, Kyushu University, Fukuoka, 812

(Received October 6, 1971)

The copper(II) and oxovanadium(IV) complexes of a new Schiff base derived from heptane-2,4,6-trione and ethylenediamine were prepared. Of a macrocyclic two-to-two and an open jaw-shaped two-to-one (trione to diamine) condensation product, only the latter gave mononuclear copper(II) and oxovanadium(IV) complexes. The coordinating sites to the metal ion in each complex are discussed referring to the spectroscopic results.

In the course of an investigation of the chelate complexes of heptane-2,4,6-trione with various metal ions,[1,2] we have been interested in the Schiff base derived from the trione and diamines, in an analogous manner to the Schiff bases of pentane-2,4-dione and diamines.[3] In the case of heptane-2,4,6-trione and ethylenediamine, however, two kinds of the Schiff bases can be formed. One is DAADEN (5,9,14,18-tetramethyl-1,4,10,13-tetraazacyclooctadeca-5,8,14,17-tetraene-7,16-dione) (structure I) which is a two-to-two condensation product of the trione and the diamine. The other is DAAEN (6,11-dimethyl-7,10-diazahexadeca-6,10-diene-2,4,13,15-tetraone) (structure II) which is a two-to-one condensation product. As seen from their structures, both can behave either as a sexadentate or as a quadridentate ligand, and macrocyclic DAADEN may be less flexible upon complex formation than open jaw-shaped DAAEN. Thus, it is of great interest to investigate the chelating behavior of these multidentate ligands.

This paper is to report on the synthesis of a new macrocyclic Schiff base ligand, DAADEN, as well as the syntheses and structural studies on the mononuclear open jaw-shaped DAAEN chelates of copper(II) and oxovanadium(IV) ions.

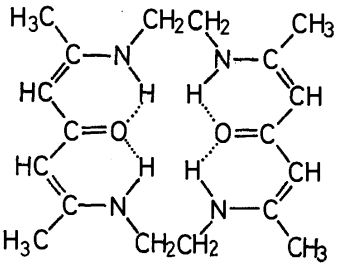

Structure I

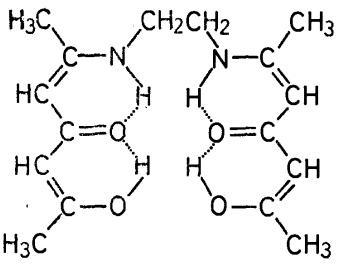

Structure II

Experimental

Synthesis of the Ligand. DAADEN. To 60 ml of a methanolic solution containing 10.0 g (0.07 mol) of heptane-2,4,6-trione, was added 10 ml of methanolic solution of 4.6 g (0.074 mol) of 98% ethylenediamine, and the mixture was warmed at 30—40°C for a few minutes. Resulting precipetate was collected by filtration, and recrystallized from a methanol-chloroform mixture to give pale yellow needles. Yield was 10.7 g; mp 215—216°C. NMR($CDCl_3$): 1.88 ppm (12H), 3.23—3.40 ppm(8H), 4.77 ppm(4H), 10.70—11.50 ppm(4H). IR: 1625 cm^{-1} $\nu_{C=O}$(hydrogen bonded); 1580 and 1520 cm^{-1}, $\nu_{C=C}$ and $\nu_{C=N}$.

Found: C, 64.76; H, 8.53; N, 16,69%. Calcd for $C_{18}H_{28}N_4O_2$: C, 65.03; H, 8.49; N, 16.85%.

Syntheses of the Metal Chelates. Copper(II)-DAAEN Chelates: Into 250 ml of a chloroform solution containing 3.32 g (0.01 mol) of DAADEN, was added with stirring 100 ml of an aqueous solution of 2.0 g (0.01 mol) of cupric acetate monohydrate, and the mixture was stirred for 30 min at 18°C until a green precipitate appeared in an aqueous layer and a chloroform layer became dark violet. The green precipitate in the aqueous layer was collected by filtration, recrystallized from pyridine and dried under reduced pressure to yield green powder (1.48 g, 36.3%) which was found to be bis(heptane-2,4,6-trionato)dicopper(II), by elemental analysis and infrared spectral comparison with an authentic sample.[2]

The dark violet chloroform layer was evaporated under reduced pressure to remove the solvent, and the residual oil was dissolved again into a small amount of chlorofrom. The chloroform solution was eluted on a column of activated alumina (50 g) with the same solvent. After the solvent was distilled off from the eluate, the residual solid was recrystallized from a *n*-hexane-chloroform mixture, to yield red-violet crystalline powder, Complex A, (0.94 g, 25.5%). IR: 1720 and 1705 cm^{-1}, $\nu_{C=O}$(free); 1590 and 1520 cm^{-1}, $\nu_{C=O}$, $\nu_{C=C}$ and provably $\nu_{C=N}$.[4]

Found: C, 52.66; H, 6.20; N, 7.39%. Calcd for $C_{16}H_{22}N_2O_4Cu$: C, 52.00; H, 5.95; N, 7.30%.

Oxovanadium(IV)-DAAEN Chelate. Into a solution of 2.84 g (0.02 mol) of heptane-2,4,6-trione in 70 ml of methanol, were added a solution of 0.6 g (0.01 ml) of 98%

* Contribution No. 260 from the Department of Oragnic Synthesis, Kyushu University

1) F. Sagara, H. Kobayashi, and K. Ueno, This Bulletin, **41**, 266 (1968).

2) F. Sagara, H. Kobayashi, and K. Ueno, This Bulletin, **45**, 794 (1972).

3) For example, K. Ueno and A. E. Martell, *J. Amer.Chem. Soc.*, **59**, 998 (1955).

4) K. Nakamoto, "Infrared spectra of inorganic and coordination compounds" 2nd Ed., Wiley-Interscience, New York, 1970.

ethylenediamine in 20 ml of methanol and 1.01 g (0.01 mol) of finely powdered oxovanadium hydroxide. The mixture was refluxed under a nitrogen atmosphere for 1.5 hr. The resulting green precipitate and unreacted oxovanadium hydroxide were collected by filtering the reaction mixture, and the solid mixture was treated with chloroform to dissolve the chelate. After evaporating the solvent from the chloroform solution, the green residue was recrystallized from pyridine to yield brown needles (2.07 g). When this product was dried at 64°C under 10^{-3}—10^{-4} mmHg, green needles, VO-DAAEN, (1.7 g, 49.5%) were obtained. IR: 3220 cm^{-1}, ν_{N-H}(hydrogen bonded); 1627 cm^{-1}, $\nu_{C=O}$(coordinated); 1595, 1555, and 1538 cm^{-1}, $\nu_{C=O}$, $\nu_{C=C}$, and $\nu_{C=N}$ of chelate ring; 980 cm^{-1}, $\nu_{V=O}$.

Found: C, 52.11;H, 6.05; N, 7.51%. Calcd for $C_{16}H_{22}N_2O_5V$: C, 51.49; H, 5.94; N, 7.51%.

Apparatus and Measurement. IR spectra were measured with JASCO DS-301 and DS-403G spectrophotometers. The NMR spectra were recorded on a Varian A-60 instrument using TMS as an internal reference. Thermogravimetric analysis on the pyridine adduct of the oxovanadium chelate was conducted with a Shimadzu automatic recording thermobalance. The furnace temperature was raised at a rate of 3°C per minute under a nitrogen atmosphere and the weight loss was recorded automatically up to 367°C.

Results and Discussion

Quadridentate ligands derived from 1,2- or 1,3-diamines and β-dicarbonyl compounds have been investigated extensively, and their coordinating structure has been well established to be *N,N,O,O*,-tetracoordinate square planar. In this connection, our first attempt was to synthesize a macrocyclic sexadentateligand (DAADEN) which was a two-to-two condensation product of ethylenediamine and heptane-2,4,6-trione. The condensation reaction took place very easily in methanol, yielding an expected compound. The infrared absorption spectrum of the product does not show any band due to ν_{N-H} of free amino group, indicating that both amino groups on ethylenediamine are involved with the condensation reaction. On the other hand, the reaction of heptane-2,4,6-trione and methylamine gave 1,2,6-trimethylpyridone in a high yield,[5] and the above fact suggests the inactivity of the carbonyl group at 4-position of the trione against the condensation with amines. It is very likely, therefore, that the condensation of heptane-2,4,6-trione with diamines also takes place on the both terminal carbonyl groups of the trione, but not on the central one. These presumptions, combined with the empirical formula from the elemental analysis, indicate the structure I for DAADEN.

Our second attempt was to synthesize an open jaw-shaped sexadentate ligand (DAAEN) which was a two-to-one (trione to diamine) condensation product. However, our trials under various reaction conditions have not been successful yet. On the other hand, this particular ligand was found to be only obtainable in a form of metal chelate as described below.

Copper Chelates. Contrary to our expectation, the reaction of DAADEN with cupric ion gave no macrocyclic copper(II) chelate, but bis(heptane-2,4,6-trionato)dicopper(II) and the complex A (Cu-DAAEN). The fact that the chelate of the parent trione is obtained in a considerable yield even under such mild reaction conditions is indicative of the relative easiness of hydrolysis of DAADEN. The ligand itself is, however, fairly stable in an aqueous solution, and therefore copper(II) ion may catalyze to accelerate such hydrolysis reaction.

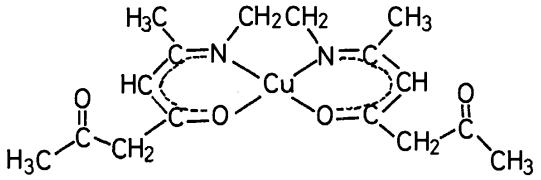

Structure III

As to the complex A, the infrared spectrum shows a coordinated carbonyl band at 1590 cm^{-1} and two peaks related to uncoordinated carbonyl groups at 1720 and 1705 cm^{-1}, the presence of the latter band indicating that not all of the carbonyl groups are engaged in coordination with copper ion. The result of elemental analysis also suggests the one-to-one mononuclear DAAEN chelate. Electronic spectrum of the complex A in chloroform is shown in Fig.1 along with those of the model compounds of similar coordination structures; bis(acetylacetonato)copper(II) ($Cu(acac)_2$) and bis(acetylacetone)ethylenediiminato-copper(II) (Cu-ACEN), in the same solvent. It is well known that the absorption maxima and intensity of *d-d* transition band are sensitive to the number and symmetry of donor atoms around the central metal ion, and to the ligand field strength. Thus, the close similarity of the absorption spectrum of the complex A to that of bis(acetylacetone)ethylenediiminato-copper(II), strongly suggests the N_2O_2-tetracoordinate planar structure III for the complex A. Analytical

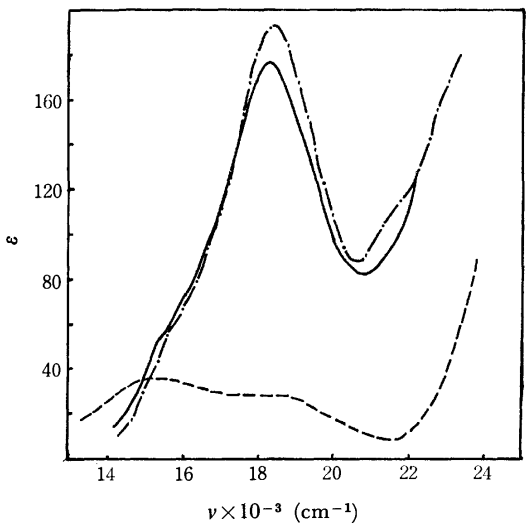

Fig. 1. Electronic absorption spectra in chloroform.
—— Complex A, Cu-DAAEN, —·— Cu-ACEN,
- - - $Cu(acac)_2$.

5) S. Hunig and G. Kobrich, *Ann.*, **617**, 181 (1958).

result and infrared spectra are also consistent with this structure.

It is interesting to note that DAAEN could not be formed without the presence of copper ion and could be isolated only in a form of the metal chelate, though in a low yield. Copper(II) ion in this case may stabilize the Schiff base ligand against hydrolysis in a similar manner as in the case of bis(acetylacetone)ethylenediiminatocopper(II). This behavior of DAAEN forms a striking contrast to the macrocyclic DAADEN, of which we have been unsuccessful in obtaining the copper(II) chelate.

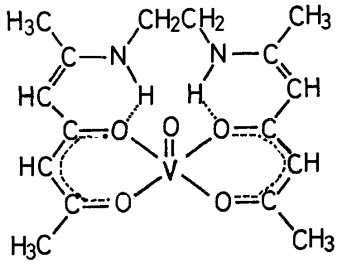

Structure IV

Oxovanadium(IV) Chelate. The reaction of DAADEN with oxovanadium(IV) salts in aqueous media did not give any product of definite composition. However, the reaction of heptane-2,4,6-trione and ethylenediamine with oxovanadium(IV) hydroxide under a nitrogen atmosphere yielded the metal chelate of DAAEN presumably *via* a template reaction.

The result of elemental analysis suggests the one-to-one oxovanadium(IV) chelate of DAAEN. Infrared spectrum is characterized with absorption bands due to an imino group, a coordinated carbonyl group and a V=O bond at 3220,1628, and 980 cm^{-1} respectively. The bands assignable to uncoordinated carbonyl groups are not observed.

Electronic spectrum of the VO-DAAEN chelate in chloroform is shown in Fig. 2 along with those of bis(acetylacetonato)oxovanadium(IV) ($VO(acac)_2$) and bis(acetylacetone)ethylenediiminatooxovanadium(IV) (VO-ACEN) in the same solvent. In contrast to the copper chelate, close similarity of thes pectra is noticed between the DAAEN- and the acetylacetonato-chelate, suggesting that an O_5-pentacoordinate square pyramidal structure IV is preferable to an N_2O_3 type coordination for the VO-DAAEN chelate. The structure IV is consistent with the infrared spectral

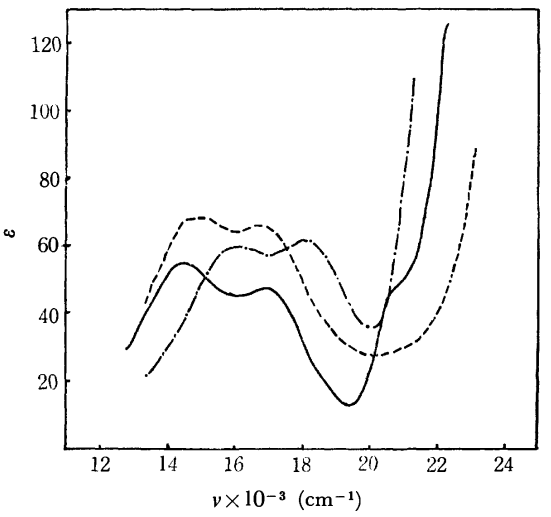

Fig. 2. Electronic absorption spectra in chloroform.
—— VO-DAAEN, —·— VO-ACEN,
--- $VO(acac)_2$.

evidence that no frec carbonyl group is left in the chelate.

The reversible addition of one mole of pyridine to one mole of the chelate also indirectly supports the square pyramidal structure. When the green VO-DAAEN chelate is recrystallized from pyridine, a brown DAAEN-VO-Py, which is presumably an octahedral coordination sturcture, is obtained. Thermogravimetric analysis on the pyridine adduct showed a sudden weight decrease corresponding to the loss of one mole of pyridine per mole of the adduct at a temperature between 199 and 201°C. The substance remaining after the thermal analysis was identical with the green VO-DAAEN.

The reason why the coordination site of DAAEN differs depending upon the kind of metal ions can be explained by the soft and hard acid and base concept.[6] If one reminds that oxovanadium(IV) ion is a harder acid than copper(II) ion, and that oxygen is a harder base than nitrogen, then it is reasonable that oxovanadium(IV) ion prefers an O_4 type coordination, while copper(II) ion prefers an N_2O_2 coordination.

The authors are grateful to Messrs. Hiroshi Yamachika and Shûzo Kano for their laboratory work during the early stage of this work. They also thank the Ministry of Education for a financial support.

6) R. G. Pearson, *J. Amer. Chem. Soc.*, **85**, 3533 (1963).

Polarographic Behavior of Nickel(II) in Propionitrile and Benzonitrile in the Presence of Thiocyanate Ions

Eiki ITABASHI*

Department of Chemistry, Faculty of Science, Osaka University, Toyonaka, Osaka.

(Received November 24, 1971)

The effect of the cation of the supporting electrolyte on the electrode reaction of nickel(II) in propionitrile and benzonitrile solutions containing thiocyanate ion was investigated by DC polarography and *i-t* curve analysis. In the absence of thiocyanate ion, a propionitrile solution of nickel(II) gives a single irreversible wave in $LiClO_4$ and $NaClO_4$ supporting electrolytes and a double wave in Et_4NClO_4 and n-Bu_4NClO_4, and a benzonitrile solution of nickel(II) gives a double wave in alkali metal and quaternary ammonium perchlorates. Nickel(II) in these nitrile solvents in the presence of thiocyanate ion exhibits a catalytic pre-wave in alkali metal perchlorates and a catalytic maximum wave in quaternary ammonium perchlorates. The double wave of nickel(II) in the absence of thiocyanate ion is due to the inhibition of the charge transfer process by the relatively weak adsorption of quaternary ammonium cations and not to the presence of two electroactive species. A mechanism which involves the cyclic regeneration of adsorbed thiocyanate ion for the catalytic pre-wave and the catalytic reduction of thiocyanate ion with the electroreduced metallic nickel for the maximum wave has been presented.

The adsorption effect of the foreign substance on the electrode reaction in non-aqueous media has received less considerable attention, although that in aqueous media is well known. This could be the result of a weak adsorption of substance from non-aqueous solvents. Specific adsorption of quaternary ammonium cations from acetonitrile solution seems to be considerably weaker than from aqueous solution.

The electrode reaction of nickel(II) at the dropping mercury electrode in acetonitrile has previously been reported to be inhibited by the adsorption of quaternary ammonium cations[1] and to be accelerated by the adsorption of halide ions[2] as well as thiocyanate ions.[3] An acetonitrile solution of nickel(II) in the presence of thiocyanate ion exhibits two kinds of catalytic polarographic current.

Nickel(II) in $LiClO_4$ and $NaClO_4$ supporting electrolytes gives a catalytic pre-wave which arises at less negative potentials than that for the usual nickel(II) reduction wave, and in $(C_2H_5)_4NClO_4$ (Et_4NClO_4) and $(n\text{-}C_4H_9)_4NClO_4$ (n-Bu_4NClO_4) electrolytes a catalytic maximum wave over a wide range of potentials at which the usual nickel(II) reduction wave reaches its limiting plateau. It was proposed in a previous paper[3] that the electrode reaction mechanism for the maximum wave of nickel(II) was due to the catalytic reduction of thiocyanate ion with the electroreduced metallic nickel, and not to the catalytic hydrogen evolution.

In order to investigate the adsorption effect of quaternary ammonium cations on the electrode reaction of nickel(II) and the properties of the catalytic polarographic current of nickel(II) in the presence of thiocyanate and quaternary ammonium ions in non-aqueous solvents, some experiments were carried out in propionitrile and benzonitrile solvents. The present paper describes the experimental results on the above-mentioned systems.

Experimental

Purified propionitrile[4] and benzonitrile[5] were obtained by the procedures given in the literatures. All the other chemicals were prepared by the procedures described previously.[1,3] The total water content of the polarographic solution containing nickel(II) perchlorate and supporting electrolyte was found to be 10—20 mM by Karl Fisher titration. All solutions were *deaerated* with nitrogen gas.

Direct current (D. C.) polarograms and current-time (*i-t*) curves of individual drops at constant potential were obtained with the potentiostat previously described[2] and made from operational amplifiers. In the following section and in the figures, "current" means them aximum current observed just before the fall of a mercury drop. The potential of the DME was measured against a saturated calomel electrode (SCE). The cell equipment for the polarographic measurements was the same as previously reported.[1] The dropping mercury electrode (DME) had an m value of 1.44_6 mg/sec and a drop time of 5.01 sec in a *deaerated* 0.1 M lithium perchlorate acetonitrile solution at −0.70 V *vs.* SCE and 60 cm mercury height. All measurements were made at 25.0±0.1°C.

Results

Propionitrile System. Larson and Iwamoto[4] have reported that a propionitrile solution of nickel(II) in 0.1 M Et_4NClO_4 supporting electrolyte gave an irregular reduction wave. The reduction wave of nickel(II) in propionitrile solution is influenced by the nature of the cation of the supporting electrolyte. The resultant polarograms are shown in Fig. 1. Nickel(II) gives an irreversible wave in $LiClO_4$ electrolyte and a double wave in Et_4NClO_4 and n-Bu_4NClO_4 electrolytes. A similar single reduction wave was also observed in 0.1 M $NaClO_4$ solution. Nickel(II) in alkali metal perchlorate solutions containing LiSCN gives a pre-wave, where it is reduced with greater reversibility. Figure 2 shows the effect of the thiocyanate concentration on the reduction waves of nickel(II) in $LiClO_4$ solution. The pre-wave increases in height

* Present address: Department of Chemistry, Miyagi University of Education, Aoba, Sendai.

1) E. Itabashi and S. Ikeda, *J. Electroanal. Chem.*, **26**, 97 (1970).
2) E. Itabashi and S. Ikeda, *ibid.*, **26**, 103 (1970).
3) E. Itabashi and S. Ikeda, *ibid.*, **36**, 189 (1972).
4) R. C. Larson and R. T. Iwamoto, *J. Amer. Chem. Soc.*, **82**, 3526 (1960).
5) R. C. Larson and R. T. Iwamoto, *ibid.*, **82**, 3239 (1960).

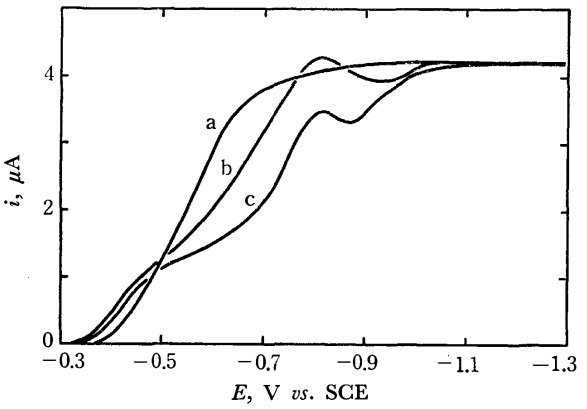

Fig. 1. Effect of electrolyte on the polarograms of 0.5 mM nickel(II) in propionitrile. (a), 0.1M $LiClO_4$; (b), 0.1M Et_4NClO_4; (c), 0.1M n-Bu_4NClO_4.

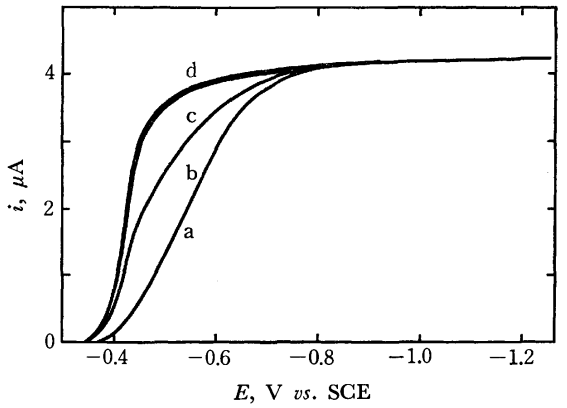

Fig. 2. Polarograms of 0.5 mM nickel(II) in propionitrile solutions containing 0.1 M $LiClO_4$ and various concns. of LiSCN: (a), 0; (b), 0.1 mM; (c), 0.3 mM; (d), 0.5 mM.

and becomes a more appreciable portion of the total limiting current of nickel(II) species as the thiocyanate concentration increases. There was no further essential change in the shape of the reduction wave when the thiocyanate concentration exceeded 0.5 mM. The effect of the thiocyanate concentration on the reduction waves of nickel(II) in n-Bu_4NClO_4 solution is shown in Fig. 3. Nickel(II) in n-Bu_4NClO_4 solution in the presence of small amounts of LiSCN exhibits a maximum wave over a wide range of potentials rather than a limiting plateau. The maximum wave increases in height with increase in concentration of LiSCN up to about 0.5 mM. Table 1 presents the exponents of the i-t curves for the reduction waves of nickel(II) in n-Bu_4NClO_4 solution containing various concentrations of LiSCN. The first step of the double wave of nickel(II) in the absence of LiSCN has a mixed diffusion-kinetic character, and the second step has the characteristics of normal diffusion control. In the presence of LiSCN, the exponents of the i-t curves for the maximum wave at the whole potential region examined are very close to the value of 0.67 expected for a kinetic-controlled electrode mechanism. The exponents of the i-t curves for the limiting current observed at the most negative potentials at which

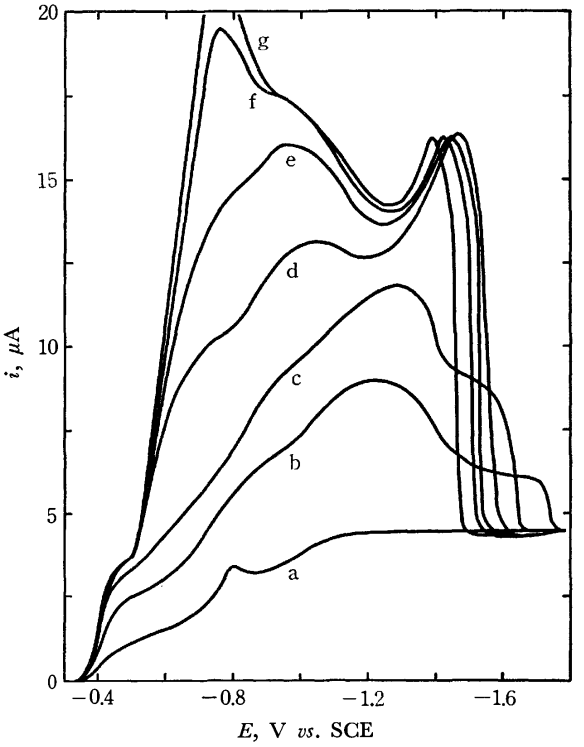

Fig. 3. Polarograms of 0.5 mM nickel(II) in propionitrile solutions containing 0.1 M n-Bu_4NClO_4 and various concns. of LiSCN: (a), 0; (b), 0.05 mM; (c), 0.1 mM; (d), 0.2 mM; (e), 0.3 mM; (f) 0.5 mM; (g), 1.0 mM.

TABLE 1. EFFECT OF CONCENTRATION OF LiSCN ON THE EXPONENT OF i-t CURVES FOR THE REDUCTION WAVES OF 0.5 mM NICKEL(II) IN 0.1 M n-Bu_4NClO_4 PROPIONITRILE SOLUTION

LiSCN mM	E V vs. SCE	x in $i_l=kt^x$	LiSCN mM	E V vs. SCE	x in $i_l=kt^x$
0	−0.50	0.53	0.5	−0.48	0.30
0	−1.20	0.19	0.5	−0.80	0.67
0.1	−0.48	0.27	0.5	−1.45	0.63
0.1	−1.20	0.60	1.0	−0.76	0.71
0.2	−0.48	0.27	1.0	−1.00	0.68
0.2	−1.00	0.61	1.0	−1.20	0.65
0.2	−1.46	0.64	1.0	−1.40	0.67

the maximum wave disappeared were found to be close to the value of 0.17 expected for a diffusion-controlled mechanism, whereas the limiting current of the pre-wave observed at potentials less negative than −0.5 V *vs.* SCE had a mixed diffusion-kinetic character.

Benzonitrile System. The reduction wave of nickel(II) in benzonitrile has been investigated by Larson and Iwamoto,[5] who reported that nickel(II) gave a two-step reduction wave, and the second step was accompanied by a peak-type of maximum. Figure 4 shows the typical reduction waves of nickel(II) in benzonitrile containing various supporting electrolytes.

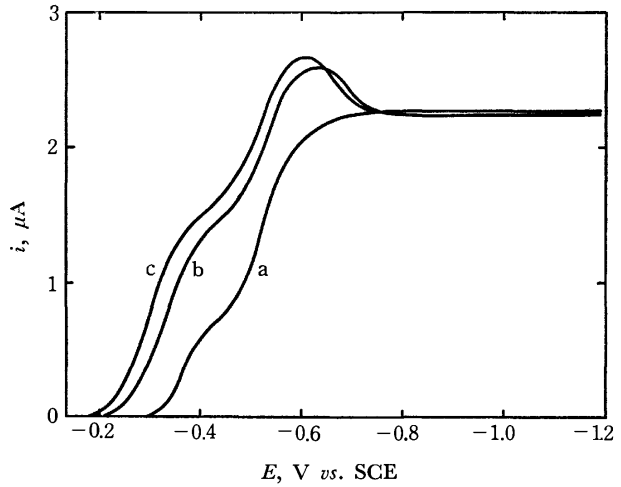

Fig. 4. Effect of electrolyte on the polarograms of 0.5 mM nickel(II) in benzonitrile. (a), 0.1 M $LiClO_4$; (b), 0.1 M Et_4NClO_4; (c), 0.1 M n-Bu_4NClO_4.

In any case, a two-step reduction wave was observed. The second step in quaternary ammonium percholrate solutions exhibits a round maximum at around −0.6 V *vs.* SCE. The limiting current of the first step was found to have a mixed diffusion-kinetic character from the results of the *i-t* curve measurements. In order to investigate the form of the electrocapillary curve, drop time measurements were made for benzonitrile solution. Drop time *vs.* potential curve exhibited a plateau in the potential region between −0.1 V and −0.7 V *vs.* SCE in 0.1 M $LiClO_4$ electrolyte solution, and irregularities which appeared as increase or decrease of drop time in the potential region between −0.2 V and −0.7 V *vs.* SCE in 0.1 M n-Bu_4NClO_4. Similar irregularities of drop time were also observed in benzonitrile solutions containing Et_4NClO_4, $C_6H_5N(CH_3)_3ClO_4$, and $C_6H_5CH_2N(CH_3)_3ClO_4$. The fact that drop time *vs.* potential curves in benzonitrile solution exhibits a slight irregularity has also been reported by Larson and Iwamoto.[5]

With small amounts of LiSCN present, the first step in $LiClO_4$ solution increased in height with increase in concentration of LiSCN. When the concentration of LiSCN exceeded 0.5 mM, the second step merged with the first step to give a single wave with the half-wave potential corresponding to the first step of the double wave. Figure 5 shows the effect of the thiocyanate concentration on the reduction waves of nickel(II) in 0.1 M n-Bu_4NClO_4 solution. In the presence of LiSCN, two maxima are observed in the potential region between −0.5 V and −1.5 V *vs.* SCE. The heights of the double maxima increase with increase in concentration of LiSCN up to about 1.0 mM. The limiting current observed at the most negative potentials at which the maximum wave disappeared was also enhanced by the presence of LiSCN. A similar enhancement of the limiting current at the most negative potentials was observed in benzonitrile solution containing the other quaternary ammonium perchlorates as supporting electrolyte. The resultant reduction waves are shown in Fig. 6. The increment of the limiting current caused by the addition of LiSCN was

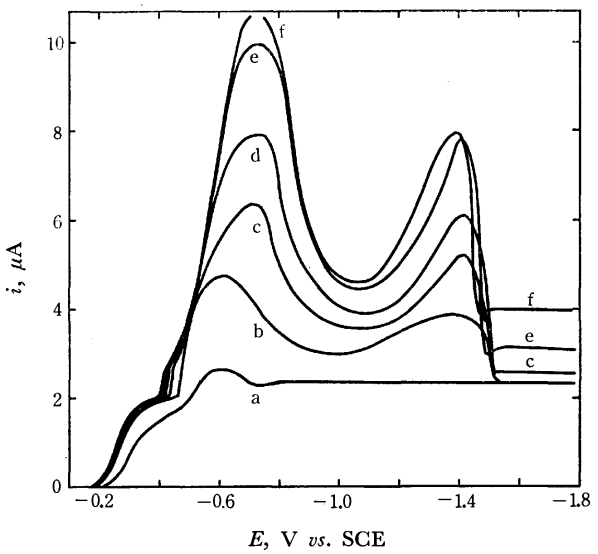

Fig. 5. Polarograms of 0.5 mM nickel(II) in benzonitrile solutions containing 0.1 M n-Bu_4NClO_4 and various concns. of LiSCN: (a), 0; (b), 0.05 mM; (c), 0.1 mM; (d), 0.2 mM; (e), 0.5 mM; (f), 1.0 mM.

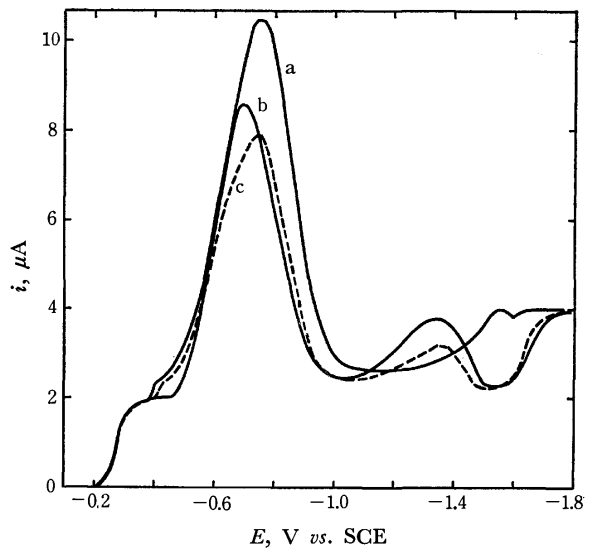

Fig. 6. Effect of electrolyte on the polarograms of 0.5 mM nickel(II) in benzonitrile solutions containing 1.0 mM LiSCN. (a), 0.1 M Et_4NClO_4; (b), 0.1 M $C_6H_5N(CH_3)_3ClO_4$; (c), 0.1 M $C_6H_5CH_2N(CH_3)_3ClO_4$.

Table 2. Effect of concentration of LiSCN on the exponent of *i-t* curves for the reduction waves of 0.5 mM nickel(II) in 0.1 M n-Bu_4NClO_4 benzonitrile solution

LiSCN mM	E V *vs.* SCE	x in $i_t=kt^x$	LiSCN mM	E V *vs.* SCE	x in $i_t=kt^x$
0	−0.40	0.31	0.5	−1.10	0.63
0	−1.20	0.18	0.5	−1.76	0.18
0.1	−0.40	0.24	1.0	−0.78	0.65
0.1	−0.70	0.59	1.0	−1.38	0.66
0.1	−1.40	0.60	1.0	−1.76	0.18

found to be proportional to the concentration of LiSCN. Table 2 presents the exponents of the *i-t* curves for the reduction wave of nickel(II) in 0.1 M n-Bu_4NClO_4 solution in the presence of LiSCN. When the thiocyanate concentration exceeds 0.1 mM, the double maxima have the characteristics of kinetic control. While the exponents of the *i-t* curves of the limiting plateau observed at the most negative potentials are very close to the value of 0.17 expected for a diffusion controlled electrode mechanism.

Discussion

The double wave of nickel(II) in propionitrile and benzonitrile solutions containing quaternary ammonium cations could be explained by considering the adsorption of cations.

The kinetic property of the first step of the doublet is the result of the relatively weak adsorption of quaternary ammonium cations from nitrile solvents. The weakly surface active substance at consideravely higher concentrations causes the limiting current to decrease and also the drop life dependence of the instantaneous current to change[6,7] from $t^{1/6}$ to $t^{2/3}$. The appearance of the double wave in benzonitrile solution containing $LiClO_4$ is attributable to the adsorption of benzonitrile molecules on the mercury surface. Drop time *vs.* potential curve for benzonitrile solution containing 0.1 M $LiClO_4$ exhibited a plateau having no apparent change of drop time over a wide range of potentials at which the double wave of nickel(II) appeared. This finding could indicate the specific adsorption of benzonitrile molecules on the mercury surface. Benzonitrile differs from acetonitrile and propionitrile; it has delocalized electrons in the phenyl ring which are capable of interacting with mercury electrode.

The reaction mechanism of the pre-wave and the maximum wave for the nickel(II)-thiocyanate systems in propionitrile and benzonitrile can be written as the following sequence.[4]

$$Ni(NCS)^+ \overset{K}{\rightleftharpoons} Ni(II) + NCS^- \quad (1)$$

$$NCS^-_{bulk} \rightleftharpoons NCS^-_{ads} \quad (2)$$

$$R_4N^+_{bulk} \rightleftharpoons R_4N^+_{ads} \quad (3)$$

$$Ni(II) + NCS^-_{ads} \overset{k_1}{\longrightarrow} Ni(NCS)^+_{ads} \quad (4)$$

$$Ni(NCS)^+_{ads} + 2\,e \xrightarrow[fast]{} Ni(0)metal + NCS^-_{ads} \quad (5)$$

$$Ni(0)metal + NCS^-_{ads} \overset{k_2}{\longrightarrow} Ni(II) + CN^- + S^{2-} \quad (6)$$

where R_4N^+ refers to quaternary ammonium cation, K is the effective formation constant of the nickel(II)-thiocyanate complex in the bulk of the solution. k_1 and k_2 are the rate constants of reactions (4) and (6). The reactions (2) and (3) represent the adsorption equilibria of NCS^- and R_4N^+ ions, respectively. The cyclic regeneration of the adsorbed thiocyanate ion in the sequence of reactions (4) and (5) accounts for the catalytic enhancement of the pre-wave, and the cyclic regeneration of electroactive nickel(II) in the sequence of reactions (5) and (6) accounts for the catalytic process of maximum wave. The reaction mechanism of the maximum wave might be explained by considering the direct reduction of the adsorbed thiocyanate ion at the surface of electrodeposited nickel as the working electrode instead of reaction(6).

If the maximum wave is caused by the direct reduction thiocyanate ion at the deposited nickel, the height of the maximum wave would be close to the value of the diffusion controlled current to be expected. It is reasonable to postulate that the catalytic enhancement of the limiting current is due to the chemical reduction of thiocyanate ion with the deposited metallic nickel, and not to the direct reduction of thiocyanate ion at the deposited nickel.

The peaking of the catalytic current of the nickel(II)-thiocyanate system in the presence of quaternary ammonium cations could be the result of a slight polarographic maximum or it could indicate that the electrode reaction mechanism involves some adsorbed species. It is well known that the catalytic hydrogen waves of some organic sulfur-containing compounds and amines exhibit peaks which have been attributed to a mechanism involving adsorbed species.

Although this study has not provided any conclusive evidence as to the exact role of quaternary ammonium cations involved in the mechanism of the catalytic maximum wave, the fact that the catalytic maximum wave is observed in quaternary ammonium solutions and not in alkali metal solutions suggests that the nature of the electrodeposited metallic nickel is strongly dependent on the electrolyte present in the solution. If the reduction of nickel(II) proceeds at the part of the electrode covered with quaternary ammonium cations the amalgamation of the electrodeposited metallic nickel would be inhibited and the deposit remains on the surface of mercury electrode. The amalgamation of the electrodeposited iron-group metals in aqueous solutions is inhibited by the adsorption of several surface active substances.[8-10]

If the deposited metallic nickel in nitrile solvents in the presence of quaternary ammonium cations is an active species, it could react with thiocyanate ion. At the most negative potentials, the catalytic maximum wave disappears as a result of decreasing adsorption of quaternary ammonium cations and hence of decreasing concentration of the active metallic nickel. No appearance of the catalytic maximum wave of nickel(II) in alkali metal solutions is caused by the quick amalgamation of metallic nickel.

The limiting current observed at the most negative potentials in benzonitrile solution containing quaternary ammonium cations is enhanced by the presence of LiSCN. The total limiting current has the characteristics of normal diffusion control, and the increment of the limiting current caused by the addition of LiSCN is proportional to the concentration of LiSCN. The diffusion-current constant, I_D, for the increment

6) R. W. Schimd and C. N. Reilley, *J. Amer. Chem. Soc.*, **80**, 2087 (1958).

7) H. Matsuda, *Rev. Polarog. Kyoto*, **14**, 87 (1967).

8) V. F. Ivanov and Z. A. Iofa, *Russ. J. Phys. Chem. English Transl.*, **36**, 571 (1962); **38**, 1026 (1964).

9) S. P. Perone and W. F. Gutknecht, *Anal. Chem.*, **39**, 892 (1967).

10) I. M. Kolthoff and P. Mader, *ibid.*, **41**, 924 (1969).

of the limiting current was found to be nearly equal to the value expected for the one-electron reduction of various alkali metal ions in benzonitrile. When experiments were carried out using the benzonitrile solution containing 0.5 mM $(n\text{-}Bu_4N)_2Ni(NCS)_4$ and 0.1 M $n\text{-}Bu_4NClO_4$, the height of the limiting current at the most negative potentials at which the catalytic maximum wave disappeared was found to be equal to the magnitude of the diffusion current of nickel(II). Therefore, it is reasonable to postulate that the enhancement of the limiting current at the most negative potentials in benzonitrile solution containing quaternary ammonium cations is due to the discharge of lithium ions. The half-wave potentials of lithium ions in benzonitrile solutions containing 0.1 M $n\text{-}Bu_4NClO_4$ and 0.1 M $C_6H_5N(CH_3)_3ClO_4$ were found to be -1.80 V and -1.82 V *vs.* SCE, respectively. In the potential region where the specific adsorption of quaternary ammonium cations is absent, the electrodeposited metallic nickel is unstable and quickly amalgamates and reacts further with mercury to give the stable nickel amalgam. If a slight amount of deposited stable nickel still remains on the mercury surface in the potenital region where the catalytic maximum wave disappears in benzonitrile solution, this deposited nickel aids in reducing the overvoltage of lithium ions.

The reduction potential of sodium ions was also displaced towards less negative potentials in benzonitrile solution containing nickel(II), quaternary ammonium cations and NaSCN.

However, no apparent displacement of the reduction potentials of alkali metal ions was observed in acetonitrile and propionitrile solvents. This could be the result of the delocalized electrons in the phenyl ring of benzonitrile molecule facilitating electron transfer in the bridge mechanism of the electrode process.

The auther wishes to thank Professor Shigero Ikeda for his encouragement throughout this study.

BULLETIN OF THE CHEMICAL SOCIETY OF JAPAN, VOL. 45, 2459—2464 (1972)

An NMR Study of Metal Complexes Containing Acetylacetone and Related Compounds. III. The Preparation and Determination of the Configurations of Cobalt(III) Complexes Containing *N,N'*-Ethylenebis(acetylacetonimine) and *N,N'*-Ethylenebis(salicylideneimine)

Yuki Fujii, Akio Osawa, Yoichiro Furukawa, Fujio Ebina, and Sozo Takahashi*

Department of Chemistry, Ibaraki University, Bunkyo-cho, Mito, Ibaraki

**Department of Chemistry, Ibaraki Technical College, Fukayatsu, Nakane, Katsuta, Ibaraki*

(Received December 14, 1971)

A series of *cis-β*-form cobalt(III) complexes containing *N,N'*-ethylenebis(acetylacetonimine) dianion (baen) or *N,N'*-ethylenebis(salicylideneimine) dianion (salen) were prepared—*cis-β*-[Co(X)(Y)] and *cis-β*-[Co(X)(Z)]ClO_4 (where X=baen or salen, Y=anions of acetylacetone, benzoylacetone, 8-hydroxyquinoline, and Z=ethylenediamine, 1,10-dipyridyl, 1,10-phenanthroline). The synthetic methods and characterization data are given. Also prepared were a series of *trans*-form cobalt(III)-bean complexes—*trans*-[Co(X)$(A)_2$]ClO_4 and *trans*-K[Co(X)$(NO_2)_2$] where X=baen, and A=ammonia, methylamine, pyridine, aniline). The isolation of only *cis-β*-form complexes in reactions between [Co(X)$(H_2O)_2$] and the bidentate ligands contrasts with the isolation of only *trans*-form ones in those between [Co(X)$(H_2O)_2$] and the monodentate ligands. This result was explained in terms of the relative stabilities of the three configurations of the coordinated baen and salen. On the basis of the configurational analysis, the relative stabilities of the three configurations were determined to be *trans*-planar form > *cis-β* form > *cis-α* form.

Cobalt(II) and Cobalt(III) complexes containing *N,N'*-ethylenebis(acetylacetonimine) dianion (baen) or *N,N'*-ethylenebis(salicylideneimine) dianion (salen) have been known for some time.[1-15] All the reported

1) G. T. Morgen and J. D. Smith, *J. Chem. Soc.*, **127**, 2030 (1925).
2) P. Pfeiffer, E. Breith, E. Lübbe, and T. Tsumaki, *Ann. Chem.*, **503**, 84 (1933).
3) K. Ueno and A. E. Martell, *J. Phys. Chem.*, **59**, 998 (1955); **60**, 1270 (1956).
4) P. J. McCarthy, R. I. Hovey, K. Ueno, and A. E. Martell, *J. Amer. Chem. Soc.*, **77**, 5820 (1955).
5) S. Yamada, H. Nishikawa, and E. Yoshida, *Proc. Japan Acad.*, **40**, 211 (1964).
6) S. Yamada, *Coord. Chem. Rev.*, **1**, 415 (1966).
7) H. Nishikawa and S. Yamada, This Bulletin, **37**, 8 (1964).
8) G. W. Everett, Jr., and R. H. Holm, *J. Amer. Chem. Soc.*, **88**, 2442 (1966).
9) G. Costa, G. Mestroni, and L. Stefani, *J. Organometal. Chem.*, **7**, 473 (1967); G. Costa, G. Mestroni, G. Tauzher, and L. Stefani, *ibid.*, **6**, 181 (1966); G. Costa and G. Mestroni, *ibid.*, **11**, 325, 333 (1968).
10) G. Costa and G. Mestroni, *Tetrahedron Lett.*, 1783 (1967).
11) G. Costa, G. Mestroni, and G. Pellizer, *J. Organometal. Chem.*, **15**, 187 (1968).
12) G. Costa, A. Puxeddu, and G. Tauzher, *Inorg. Nucl. Chem. Lett.*, **4**, 319 (1968).
13) H. Yoneda and Y. Morimoto, This Bulletin, **41**, 2544 (1968).
14) A. L. Crumbliss and F. Basolo, *J. Amer. Chem. Soc.*, **92**, 55 (1970); B. M. Hoffman, D. L. Diemente, and F. Basolo, *ibid.*, **92**, 61 (1970).
15) A. L. Crumbliss and F. Basolo, *Irong. Chem.*, **10**, 1676 (1971).

complexes have a planar configuration except for the complexes described in Reference 1). In a previous paper,[16] we reported the preparation and the halogenation reaction of the [Co(baen)(acac)] complex, and we mentioned that we could obtain only a *cis*-β-form complex, not a *cis*-α one. In this paper, we will report the preparation and the determination of the structures of two series of *cis*-β and *trans-planar*-forms cobalt(III)-baen, -salen complexes, and will describe the reason for isolating only *cis*-β-form complexes in the reactions of $[Co(X)(H_2O)_2]$ (where X=baen or salen) and the bidentate ligands.

Experimental

Preparation of Complexes. *1)* trans-N,N'-*ethylenebis(acetylacetoniminato)diamminecobalt(III) perchlorate Dihydrate*, trans-$[Co(baen)(NH_3)_2]ClO_4\cdot 2H_2O$ *(I)*: Five milliliters of 18 N ammonia were added to *trans-N,N'*-ethylenebis(acetylacetoniminato)diaquocobalt(II)[1] (3.2 g, 0.01 mol) in 200 m*l* of methanol, and then, to the resultant solution, a hydrogen peroxide solution was added. When sodium perchlorate monohydrate (5 g) in methanol was added to the above solution, yellowish-brown crystals were separated out. They were subsequently recrystallized from methanol. Yield, about 90%.

2) trans-N,N'-*ethylenebis(acetylacetoniminato)dimethylaminecobalt(III) perchlorate Dihydrate*, trans-$[Co(baen)(CH_3NH_2)_2]ClO_4\cdot 2H_2O$ *(II)*: This complex was prepared by using the method employed for the preparation of Complex I. Brown crystals were obtained in about a 90% yield.

3) trans-N,N'-*ethylenebis(acetylacetoniminato)dipyridinecobalt(III) perchlorate*, trans-$[Co(baen)(py)_2]ClO_4$ *(III)*: This complex was also prepared by using the method employed for the preparation of Complex I. Brown crystals were obtained in about a 90% yield.

4) trans-N,N-*ethylenebis(acetylacetoniminato)dianilinecobalt(III) perchlorate*, trans-$[Co(bean)(aniline)_2]ClO_4$ *(IV)*: This complex was also prepared by the method used for Complex I. Brown crystals were obtained in about an 80% yield.

5) Sodium trans-*dinitro*-N,N'-*ethylenebis(acetylacetoniminato)cobalt(III)*, trans-$Na[Co(baen)(NO_2)_2]$ *(V)*: *N,N'*-ethylenebis(acetylacetoniminato)diaquocobalt(II) (6.3 g, 0.02 mol) was dissolved in 200 m*l* of methanol, and then sodium nitrite (4 g, 0.06 mol) in 50 m*l* of water was added to this solution. The resulting solution was heated on a water bath and was concentrated to about 150 m*l* by evaporating the solvent. When the solution was cooled to 0°C, brown crystals were separated out. They were recrystallized from methanol. Yield, about 70%. From the IR spectrum, the coordination of the nitro groups was confirmed.

6) trans-*nitro*-N,N'-*ethylenebis(acetylacetoniminato)aquocobalt(III)*, trans-$[Co(baen)(NO_2)(H_2O)]$ *(VI)*: Complex V was dissolved in water, and the solution was heated on a water bath for one hour. When the resulting solution was cooled to 0°C, dark green crystals were separated out. They were subsequently recrystallized from methanol. Yield, about 30%. From the IR spectrum, the coordination of the nitro group was confirmed.

7) trans-*nitro*-N,N'-*ethylenebis(acetylacetoniminato)pyridinecobalt(III)*, trans-$[Co(baen)(NO_2)(py)]$ *(VII)*: Complex VI was dissolved in methanol, and then an equimolar amount of pyridine was added to the solution. When the resultant solution was slowly concentrated at room temperature, reddish-brown crystals were separated out. They were washed with methanol. Yield, about 60%.

8) cis-β-N,N'-*ethylenebis(acetylacetoniminato)acetylacetonatocobalt(III)*, cis-β-$[Co(baen)(acac)]$ *(VIII)*: This complex was prepared by means of the known method given in Ref.16). Green crystals were obtained in about an 80% yield.

9) cis-β-N,N'-*ethylenebis(acetylacetoniminato)benzoylacetonatocobalt(III)*, cis-β-$[Co(baen)(bzac)]$ *(IX)*: Benzoylacetone (1.8 g, 0.011 mol) in 100 m*l* of methanol neutralized by potassium hydroxide (0.6 g, 0.011 mol) was added to a methanol (200 m*l*) solution of *N,N'*-ethylenebis(acetylacetonimonato)-diaquocobalt(II) (3.2 g, 0.01 mol). After air had been sucked through the solution for two hours, it was concentrated to about 100 m*l* by evaporating the solvent under reduced pressure. When the solution was then allowed to stand for two or three days, green crystals were separated out. They were recrystallized from methanol. Yield, about 70%.

10) cis-β-N,N'-*ethylenebis(acetylacetoniminato)-8-oxyquinolinatocobalt(III)*, cis-β-$[Co(baen)(oxin)]$ *(X)*: This complex was prepared by the method employed for the preparation of Complex IX, but using 8-hydroxyquinoline in place of benzoylacetone. Green crystals were obtained in a 40% yield.

11) cis-β-N,N'-*ethylenebis(acetylacetoniminato)ethylenediaminecobalt(III) Perchlorate Dihydrate*, cis-β-$[Co(baen)(en)]ClO_4\cdot 2H_2O$ *(XI)*. An equimolar amount of ethylenediamine was added to a methanol solution of *N,N'*-ethylenebis(acetylacetoniminato)diaquocobalt(II). Then, to the resultant solution hydrogen peroxide solution was added. When sodium perchlorate monohydrate in methanol was added to the above solution, brown power was separated out. This was washed thoroughly with methanol. Yield, about 90%.

12) cis-β-N,N'-*ethylenebis(acetylacetoniminato)-1,10-dipyridylcobalt(III) Perchlorate*, cis-β-$[Co(baen)(dip)]ClO_4$ *(XII)*: This complex was prepared by using the method employed for complex XI. Recrystallized from methanol, green crystals were obtained in about an 80% yield.

13) cis-β-N,N'-*ethylenebis(acetylacetoniminato)-1,10-phenanthrolinecobalt(III) Perchlorate*, cis-β-$[Co(baen)(phen)]ClO_4$ *(XIII)*: This complex was prepared by the method employed for the preparation of Complex XII. Green crystals were obtained in about an 80% yield.

14) cis-β-N,N'-*ethylenebis(salicylideneiminato)acetylacetonatocobalt(III)*, cis-β-$[Co(salen)(acac)]$ *(XIV)*: *N,N'*-ethylenebis(salicylideneiminato)cobalt(II)[2] (1.5 g) was dissolved in 200 m*l* of methanol, and potassium acetylacetonate was added to the solution. The resulting solution was heated on a water bath for fifteen minutes. When the resulting solution was concentrated to about 50 m*l*, yellowish-green crystals were separated out. They were subsequently recrystallized from methanol. Yield, about 90%.

15) cis-β-N,N'-*ethylenebis(salicylideneiminato)benzoylacetonatocobalt(III)*, cis-β-$[Co(salen)(bzac)]$ *(XV)*: This complex was prepared by using the method employed for Complex XIV. Yellowish-green crystals were obtained in about a 90% yield.

16) cis-β-N,N'-*ethylenebis(salicylideneiminato)ethylenediaminecobalt(III) Perchlorate Dihydrate*, cis-β-$[Co(salen)(en)]ClO_4\cdot 2H_2O$ *(XVI)*: This complex was prepared by using the method used for Complex XI. A brown powder was obtained in an 80% yield.

17) cis-β-N,N'-*ethylenebis(salicylideneiminato)-1,10-dipyridylcobalt(III) Perchlorate*, cis-β-$[Co(salen)(dip)]ClO_4$ *(XVII)*: This complex was prepared by using the method employed for the preparation of Complex XII. Green crystals were obtained in about an 80% yield.

18) cis-β-N,N'-*ethylenebis(salicylideneiminato)-1,10-phenanthrolinecobalt(III) Perchlorate*, cis-β-$[Co(salen)(phen)]ClO_4$ *(XVIII)*. This complex was prepared by using the method employed for Complex XIII. Green crystals were obtained in about

16) Y. Fijii, This Bulletin, **43**, 1722 (1970).

TABLE 1. ELEMENTAL ANALYSES DATA OF THE COMPLEXES

Complex		C (%) Found	C (%) (Calcd)	H (%) Found	H (%) (Calcd)	N (%) Found	N (%) (Calcd)
$[Co(bean)(NH_3)_2]ClO_4 \cdot 2H_2O$	(I)	31.76	(31.97)	6.36	(6.27)	12.43	(12.43)
$[Co(bean)(CH_3NH_2)_2]ClO_4 \cdot 2H_2O$	(II)	35.25	(35.11)	6.65	(6.75)	11.82	(11.70)
$[Co(bean)(py)_2]ClO_4$	(III)	49.15	(49.02)	5.32	(5.25)	10.33	(10.40)
$[Co(bean)(aniline)_2]ClO_4$	(IV)	50.98	(51.02)	5.66	(5.72)	9.83	(9.92)
$Na[Co(bean)(NO_2)_2]$	(V)	36.41	(36.37)	4.55	(4.58)	14.01	(14.14)
$[Co(bean)(NO_2)(H_2O)]$	(VI)	41.72	(41.74)	6.13	(5.85)	12.19	(12.17)
$[Co(bean)(NO_2)(py)]$	(VII)	50.27	(50.24)	6.01	(5.71)	13.94	(13.79)
[Co(bean)(acac)]	(VIII)	53.68	(53.55)	6.80	(6.63)	7.36	(7.35)
[Co(bean)(bzac)]	(IX)	59.58	(59.72)	6.23	(6.16)	6.19	(6.33)
Co(bean)(oxin)]	(X)	59.31	(59.29)	5.53	(5.69)	9.76	(9.88)
$[Co(bean)(en)]ClO_4 \cdot 2H_2O$	(XI)	35.14	(35.26)	6.60	(6.36)	12.00	(11.75)
$[Co(bean)(dip)]ClO_4$	(XII)	49.12	(49.22)	4.68	(4.89)	10.52	(10.43)
$[Co(bean)(phen)]ClO_4$	(XIII)	51.33	(51.39)	4.69	(4.68)	9.99	(9.98)
[Co(salen)(acac)]	(XIV)	59.21	(59.43)	6.56	(6.60)	4.74	(5.00)
[Co(salen)(bzac)]	(XV)	63.64	(63.93)	5.58	(5.73)	4.88	(4.76)
$[Co(salen)(en)]ClO_4 \cdot 2H_2O$	(XVI)	41.39	(41.35)	5.54	(5.80)	11.02	(10.72)
$[Co(salen)(dip)]ClO_4$	(XVII)	53.48	(53.57)	3.61	(3.81)	9.58	(9.61)
$[Co(salen)(phen)]ClO_4$	(XVIII)	54.53	(54.51)	3.42	(3.60)	9.20	(9.08)

TABLE 2. NMR SPECTRAL DATA OF *trans* FORM COMPLEXES

Complex	Solvent	Peaks of baen δ (ppm) C=CH	CH_2–CH_2	CH_3 (C=O)	CH_3 (C=N)	Peaks of others δ (ppm)
$[Co(bean)(NH_3)_2]ClO_4$	D_2O	5.13	3.61	2.25	2.08	
	d-DMSO	4.94	3.47	2.12	1.98	
$[Co(bean)(CH_3NH_2)_2]ClO_4$	D_2O	5.13	3.62	2.25	2.08	1.55 (CH_3NH_2)
	d-DMSO	4.93	3.47	2.13	2.00	1.50, 1.40, 1.30 (Triplet of CH_3NH_2)
$[Co(bean)(py)_2]ClO_4$	D_2O	5.02	3.73	2.26	2.04	7.2—8.2 (Multiplet of py)
$[Co(bean)(aniline)_2]ClO_4$	*d*-DMSO	4.93	3.60	2.18	2.08	6.6—7.2 (Multiplet of aniline)
$Na[Co(bean))NO_2)_2]$	D_2O	5.32	3.63	2.22	2.11	
$[Co(bean)(NO_2)(H_2O)]$	*d*-DMSO	4.97	3.61	2.16	2.05	
$[Co(bean)(NO_2)(py)]$	*d*-DMSO	4.95	3.62	2.15	1.99	7.2—8.2 (Multiplet of py)
$[Co(salen)(NH_3)_2]ClO_4$	*d*-DMSO	8.15 (CH=N of salen)	ca. 3.7	(CH_2–CH_2)		6.5—7.5 (Multiplet of phenyl group)
$[Co(salen)(CH_3NH_2)_2]ClO_4$	*d*-DMSO	8.22 (CH=N of salen)	ca. 3.7	(CH_2–CH_2)		6.5—7.5 (Multiplet of phenyl group)
						1.50, 1.40, 1.30 (Triplet of CH_3NH_2)

an 80% yield.

The elemental analyses data of all the complexes are summarized in Table 1.

Measurements. The NMR spectra of the complexes were recorded with a Hitachi R-20 spectrometer (60 MHz) at 35°C, using D_2O, $CDCl_3$, or deuterated dimethylsulfoxide as the solvent. In all the NMR measurements, TMS or NaTMS was used as the internal reference.

Results anb Discussion

NMR Spectra of Complexes I, II, III, IV, V, VI, and VII. The NMR spectra of the *trans* complexes are summarized in Table 2, together with those of *trans*-form Co(III)-salen complexes. Some typical NMR spectra of *trans*-form complexes are shown in Fig. 1.

Complexes I, II, III, IV, V, VI, and VII, all of which involve unidentate ligands, show NMR spectra having one C=CH and two CH_3 signals with relative intensities of 1 : 3 : 3. Generally, three geometrical isomers, *trans-planar*, *cis-*α, and *cis-*β, are possible for these complexes.[1] Complexes VI and VII, in which two unidentate ligands are present, show the typical NMR spectral pattern corresponding to the *trans* isomer. Therefore, these complexes, VI and VII, can be assigned a *trans*-form structure. Considering that the well-known oxygen carriers, Co(II)-baen complexes,[3,8–10,14] also have a *trans*-form structure, all the complexes, I, II, III, IV, V, VI, and VII, can be concluded to have *trans-planar* structures.

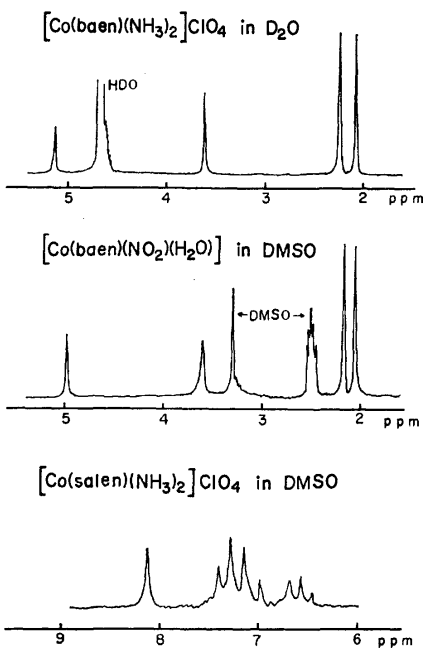

Fig. 1. Typical NMR spectra of *trans* form Co(III)-baen, -salen complexes.

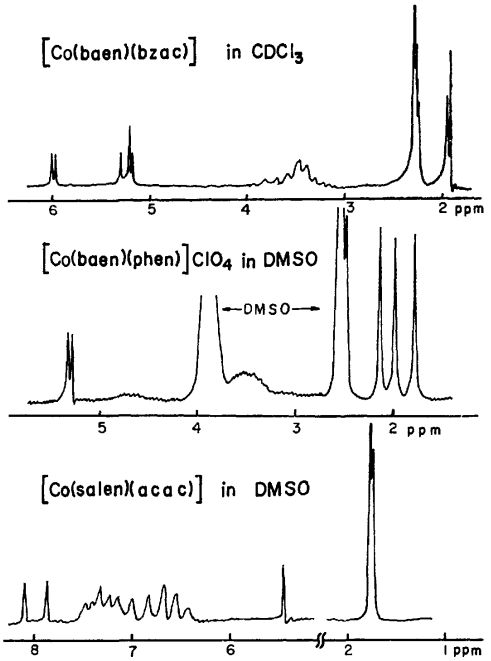

Fig. 2. Typical NMR spectra of *cis-β* form Co(III)-baen, -salen complexes.

The Co(III)-salen complexes containing ammonia or methylamine, which were prepared by using the well-known method described in Ref. 5), show NMR spectra with one CH=N signal; it is confirmed form study of their NMR spectra that these Co(III)-salen complexes take the *trans-planar* structure.

NMR Spectra of Complexes VIII, IX, X, XI, XII, and XIII. The data of the NMR spectra of *cis-β*-form Co(III)-bean, -salen complexes are listed in Tables 3 and 4, while some typical NMR spectra of these complexes are also shown in Fig. 2.

The baen complexes VIII, X, XI, XII, and XIII, show NMR spectra with two C=CH and four CH_3 signals for baen (the relative intensities of their peaks are 1 : 1 : 3 : 3 : 3 : 3). Since these spectral patterns correspond to the structure of the *cis-β*-form, as has been mentioned in a previous paper,[16] Complexes VIII, X, XI, XII, and XIII are assigned *cis-β*-form structures. On the other hand, Complex IX shows three C=CH signals with relative intensities of 1 : 2 : 1 for baen, two C=CH signals with relative intensities of 1 : 1 for bzac, and six CH_3 signals with relative intensities of 9 : 6 : 3 : 3 : 3 : 6 for baen and bzac. Although all the signals are not clearly resolved in this NMR spectrum, it can easily be understood that Complex IX does not contain only one species of the three

Table 3. NMR spectral data oe *cis-β* form cobalt(III)-baen complexes

Complex	Solvent	Peaks of baen (ppm)				Peaks of others (ppm)
		C=CH	CH_2-CH_2	CH_3 (C=O)	CH_3 (C=N)	
VIII	$CDCl_3$	5.21(1) 5.19(1)	*ca.* 3.4*	2.25(6)	2.32(3) 1.98(3)	5.36(1) (C=CH of acac) 2.11(3), 1.75(3) (CH_3 of acac)
IX	$CDCl_3$	5.29(1) 5.21(2) 5.18(1)	*ca.* 3.4*	2.29(9), 2.25(6), 2.23(3) 2.20(3), 1.95(3), 1.91(6)		(two of them are CH_3 of bzac) 6.00(1), 5.97(1) (C=CH of bzac)
X	$CDCl_3$	5.25(1) 5.03(1)	*ca.* 3.5*	2.37(3) 2.13(3)	2.05(6)	6.8—8.2 (multiplet of oxin)
XI	*d*-DMSO	5.19(1) 5.04(1)	*ca.* 3.5*	2.18(3) 2.16(3)	2.00(3) 1.71(3)	
XII	*d*-DMSO	5.27(1) 5.24(1)	*ca.* 3.5*	2.40(3) 2.06(3)	2.01(3) 1.87(3)	7.5—8.8 (multiplet of dip)
XIII	*d*-DMSO	5.31(1) 5.26(1)	*ca.* 3.5*	2.45(3) 2.11(3)	1.96(3) 1.75(3)	7.9—9.0 (multiplet of phen)

( ) represents No. of H's. * shows the complicated band.

TABLE 4. NMR SPECTRA OF *cis-β* FORM COBALT(III)-SALEN COMPLEXES

Complex	Solvent	Peaks of salen δ (ppm)		Peaks of others δ (ppm)
		CH=N	CH_2-CH_2	
XIV	*d*-DMSO	8.07(1) 7.87(1)	*ca.* 3.8[a](4)	5.43(1) (C=CH of acac) 1.74(3) 1.72(3) (CH_3 of acac)
XV	*d*-DMSO	8.15(1) 7.88(1)	*ca.* 4.1[a](4)	6.13(1) (C=CH of bzac) 1.89(3) (CH_3 of bzac)

( ) represents No. of H's.
a) The complicated band.

possible geometrical isomers—*cis-α*, *cis-β*$_1$, and *cis-β*$_2$, but that it is either a 1 : 1 mixture of two *cis-β* isomers or a 1 : 1 mixture of *cis-α* and one of the two *cis-β* isomers. However, as the NMR spectra expected for the two cases are thought to be nearly identical with each other, we can not distinguish whether the observed NMR spectrum corresponds to the former case or to the latter one. Since Complexes VIII, X, XI, XII, and XIII take only the *cis-β*-form structure, as has been mentioned above, and since all the above Co(III)-baen complexes are synthesized by using nearly the same reaction conditions, Complex IX is also thought to have the *cis-β*-form structure. Thus, Complex IX can be assummed to be a 1 : 1 mixture of two *cis-β* isomers.

Despite the fact that Complex IX contains two *cis-β*-form isomers in a relative ratio of 1:1, Complex X contains only one *cis-β*-form isomer, though two *cis-β* isomers are also possible in this case. As will be mentioned later, this can be mainly ascribed to the steric nature of these complexes.

NMR Spectra of Complexes XIV, XV, XVI, XVII, and XVIII. Complexes XIV and XV show two CH=N signals and one C=CH signal. Therefore, we can safely assign the *cis-β* structure to these complexes. However, in the cases of Complexes XVII and XVIII, the CH=N signal overlaps with the signals of the coordinated dipyridyl or phenanthroline. Therefore, it is difficult to determine the structure of these complexes from the NMR spectra only. Also it is difficult to determine the structure of Complex XVI because of its low solubility in a solvent. However, since the baen complexes containing bidentate ligands have *cis-β*-form structures, and since the salen complexes of acac and bzac have also *cis-β*-form structures, we can assign a *cis-β*-form structure to Complexes XVI, XVII, and XVIII, too. The reason for isolating only one *cis-β*-form isomer in Complex XV can be ascribed to the steric interaction of this complex, which will be discussed later.

The Preference of the trans-*Planar Structure in [Co(baen)(A)$_2$]ClO$_4$ and the Preference of a* cis-*β Structure in [Co(baen)(Y)]ClO$_4$.* In the reaction between *trans*-[Co(baen)(H_2O)$_2$] and the monodentate ligands, we can obtain only the *trans*-planer-form complexes in high yields. On the other hand, in the reaction between *trans*-[Co(baen)(H_2O)$_2$] and the bidentate ligands, we can obtain only *cis-β*-form complexes in high yields. In both cases, as we used the *trans*-[Co(baen)(H_2O)$_2$] as the starting material, it is thought possible that the configuration of the reaction products depends strongly on the reaction mechanism. In order to confirm this point, we prepared the complexes starting from the coblat(II) ion. The complex which was prepared by mixing the cobalt(II) ion, ammonia, and baen (in this order) gives the same NMR spectrum as that of Complex I. The complex which was prepared by mixing the cobalt(II) ion, phenanthroline, and baen (in this order) gives a NMR spectrum corresponding to the *cis-β*-form structure. From these observations, it can be concluded that the formation of the *trans*-form complex in the case of the unidentate ligands and the formation of only the *cis-β*-form complex in the case of the bidentate ligands do not depend on only the reaction mechanism.

Relative Stability of the Configuration. It has been established that baenH_2 takes the ketamine structure in solution.[17] On the other hand, although two resonance structures, ketamine and ketimine, are possible, the coordinated baen is thought to take the ketimine structure exclusively.[4] In the cases of the coordinated salen, it is clear that the salen takes the ketimine structure, because free salenH_2 takes the ketimine structure and the resonance from ketimine to ketamine structures in salen complexes is almost impossible because of the phenyl group.[3,18] Therefore, it can be thought that the C=N bonds of the coordinated baen and salen have mainly a double-bond character; therefore, their nitrogen atoms take the electronic configuration of the sp^2 hybridization. From the above structual restrictions, and the fact that the O—⟩ N=⟩ group of baen and salen is planar in nature, it is expected that the coordinated baen and salen will prefer the planar to all other configurations, corresponding to the *trans*-planar structure of octahedral complexes. The reason why only *trans*-form complexes isolated in the reaction between *trans*-[Co(baen)-(H_2O)$_2$] and the unidentate ligands is thought to be mainly based on the above facts.

In the cases of the baen and salen complexes which contain a bidentate ligand, baen and salen can not take a *trans*-planar configuration, but only a *cis-α* or *cis-β* form. When baen and salen take a *cia-α*

17) G. O. Dudek and R. H. Holm, *J. Amer. Chem. Soc.*, **83**, 2099 (1961).
18) G. N. Weinstein, M, J. O'Connor and R. H. Holm. *Inorg. Chem.*, **9**, 2104 (1970).

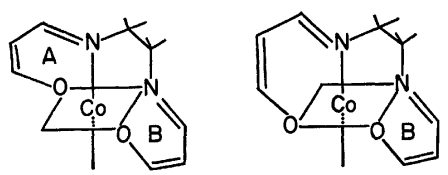

cis-α *cis-β*

Fig. 3. The geometrical structures of *cis-α* and *cis-β* forms Co(III)-baen, -salen backbones.

or *cis-β*-form, it can be concluded form the molecular model test that the chelate rings A, B and B in Fig. 3 are distorted from the plane of $Co\langle^{O}_{N}$ by about 30°. This distortion will cause the decrease in the π-bond-formation ability of baen and salen with the cobalt(III) ion as compared with that in the *trans*-planar complexes. From this point of view, it is concluded that the relative stabilities among three configurations are as follows: planar>*cis-β*>*cis-α*.

In the cases of the *cis-β*-form complexes, some steric interaction between the coordinated baen, salen, and the bidentate ligands is observed in their molecular model tests. Since the chelate ring B is distorted from the plane of $Co\langle^{O}_{N}$ by about 30°, as is shown in Fig. 3, when the sterically bulky groups such as benzoylacetone and 8-oxyquinoline are coordinated to the cobalt(III)-baen, salen backbone, some steric interaction between the bulky groups and the methyl, phenyl groups of the distorted $^{O-}_{N=}\rangle$ group occurs. This steric hindrance is thought to be much larger in salen than in baen, and much larger in 8-oxyquinoline than in benzoylacetone. This steric hindrance is thought to be the main reason why only one *cis-β*-form isomer is siolated in the cases of Complexes X and XV.

The authors wish to express their deep thanks to Dr. M. Kodama of Ibaraki University for his encouragement.

BULLETIN OF THE CHEMICAL SOCIETY OF JAPAN, VOL. 45, 2464—2468 (1972)

Mixed Solvent Deuterium Isotope Effects on the Hydrolysis of UO_2^{2+} and Be^{2+} Ions

Masunobu MAEDA,[1] Toshihiko AMAYA*, Hitoshi OHTAKI, and Hidetake KAKIHANA*

Department of Electrochemistry, Faculty of Engineering, Tokyo Institute of Technology, O-okayama, Meguro, Tokyo

**Research Laboratory of Nuclear Reactor, Tokyo Institute of Technology, O-okayama, Meguro, Tokyo*

(Received February 8, 1972)

Stability constants of the hydrolysis species of UO_2^{2+} ion were determined in pure light water and 80% heavy water containing 3M $NaClO_4$ as an ionic medium at 25°C, and the results were compared with those in pure heavy water. The decrease of the stability constants in hydrolysis reactions of UO_2^{2+} ion, as well as of Be^{2+} ion, was discussed in terms of the equilibrium theory of the solvent deuterium isotope effects, which is based on the assumptions that activity coefficients of chemical species in isotopic exchange equilibria remain unchanged with the change in the deuterium atom fraction in the solvent, that the solvated hydrogen ion possesses three equivalent lyons, and that the isotopic equilibria are subject to the rule of the simple geometric mean. Satisfactory agreements were found between the observed and calculated values for the relative stability constants of the hydrolysis species of UO_2^{2+} and Be^{2+} in water of various hydrogen isotopic compositions.

In the preceding papers,[2-5] we have studied on the hydrolysis reactions of Be^{2+}, UO_2^{2+}, Cu^{2+}, and Y^{3+} ions in pure heavy water and have found that the compositions of complexes formed by hydrolysis in heavy water are the same as those in light water, and that the stability constants of the complexes in heavy water are smaller than those in light water. In the study of the hydrolysis of Be^{2+} ion in mixtures of light and heavy water, it has been found that the stability constants decrease monotonously with the increase in the deuterium atom fraction.[6]

In the present paper are included results on the hydrolysis of UO_2^{2+} ion in 80%(deuterium atom fraction) heavy water as well as in light water, and a quantitative interpretation is attempted for the variation of the stability constants for hydrolysis species of UO_2^{2+} and Be^{2+} ions in H_2O-D_2O mixtures in terms of the equilibrium theory of solvent deuterium isotope effects, which have so far been applied to acid-base equilibria in light and heavy water by a number of investigators.[7]

Symbols.

Z Average number of lyonium ions split off per metal ion

B Total concentration of metal ion

1) To whom correspondence should be addressed.

2) H. Kakihana and M. Maeda, This Bulletin, **43**, 109 (1970).

3) M. Maeda and H. Kakihana, *ibid.*, **43**, 1097 (1970).

4) H. Kakihana, T. Amaya, and M. Maeda, *ibid.*, **43**, 3155 (1970).

5) H. Kakihana, T. Amaya, and M. Maeda, *Trans. Royal Inst. Technol., Pure and Appl. Chem.*, **34**, 49 (1972).

6) H. Kakihana and M. Maeda, This Bulletin, **42**, 1458 (1969).

7) L. L. Schaleger, P. Salomaa, and F. A. Long, "Chemical Physics of Ionic Solutions," Ed. by B. E. Conway and R. G. Barradas, John Wiley & Sons, Inc., New York (1966), p. 237.

E emf (mV), E_0 constant (mV), E_j a liquid junction potential (mV)
n Deuterium atom fraction {D/(D+H)}
L Lyon, H or D
$\beta_{p,q}$ Equilibrium constant for the hydrolysis reaction
$qM^{z+}+2pL_2O=M_q(OL)_p^{(zq-p)+}+pL_3O^+$
Superscripts, H, D, and n represent light water, heavy water, and their mixture with the deuterium atom fraction of n.
(p,q) Complex, $M_q(OL)_p^{(zq-p)+}$.
l Total concentration of free lyonium ion.

Results

Values of Z, average number of lyonium ion split off per metal ion by hydrolysis, and log l at each series of B, the total concentration of the metal ion, are shown graphically in Figs. 1 and 2, respectively. A generalized least squares method was applied to determine the most probable values of stability constants of the minimum number of hydrolysis species which would suffice to account for the experimental data. Values of stability constants were so chosen that the error square sum ($\Sigma(Z_{calc}-Z)^2$) becomes minimum, where Z_{calc} denotes calculated values of Z with a particular set of the constants, $\beta_{p,q}$. Among some combinations of complexes, the assumptions of formation of (2, 2), (4, 3) and (5, 3) complexes, the (4, 3) complex being a minor component, gave the most satisfactory agreement between experimental and calculated values of Z in both systems of 80% heavy water and light water. These complexes have also been found in heavy water.[3] The final values of stability constants of the complexes are listed in Table 1, together with those in pure heavy water.

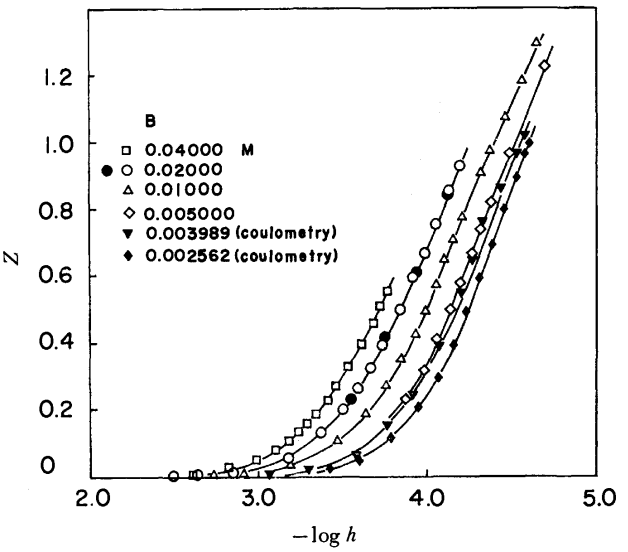

Fig. 1. Average number, Z, of OH bound per UO_2^{2+}, as a function of log h for the system of light water. Drawn curves were calculated with the stability constants given in Table 1. Open symbols denote the forward titrations and filled symbols the back titrations.

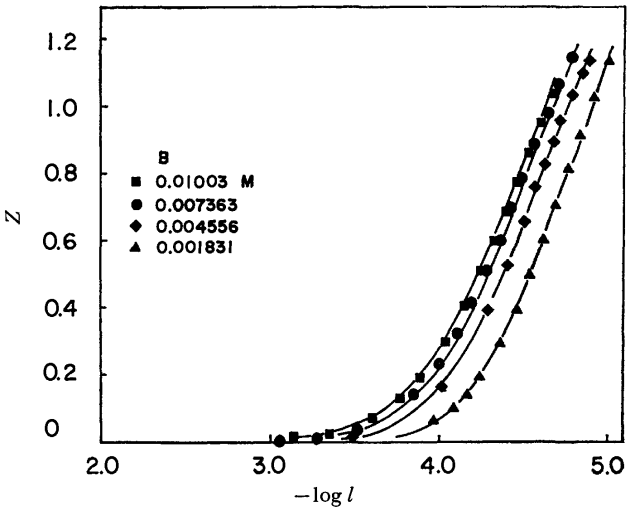

Fig. 2. Average number, Z, of OL bound per UO_2^{2+}, as a function of log l for the system of 80% heavy water. Drawn curves were calculated with the stability constants given in Table 1.

Table 1. Stability constants of uranyl hydroxo complexes in light and heavy water and 80% heavy water

	Light water[a]	80% Heavy water[a]	Heavy water[a]
$-\log \beta_{2,2}$	6.17±0.02	6.61±0.03	6.80±0.02
$-\log \beta_{4,3}$	$12.92\pm0.1_5$	$14.28\pm0.2_0$	$14.00\pm0.1_5$
$-\log \beta_{5,3}$	17.04±0.03	18.16±0.04	18.63±0.02

a) The uncertainties of the constants were estimated as 3σ.

The present results for the light water system were compared with those obtained by Sillén *et al.*[15] in the same ionic medium(3 M $NaClO_4$). Values for $\beta_{p,q}$ they obtained were $-\log \beta_{1,1}\simeq6.10$, $-\log \beta_{2,2}=6.04\pm0.02$, $-\log \beta_{4,3}\simeq13.21$ and $-\log \beta_{5,3}=16.53\pm0.02$. For the (4, 3) complex almost the same stability constant was found in the present study. For the (2, 2) and (5, 3) complexes, on the other hand, the smaller stability constants were obtained in this work than those of their work. No (1, 1) complex found by Sillén *et al.* was detected.

Discussion

As has been seen from results in systems of Be^{2+},[2,6] Cu^{2+},[4] and Y^{3+},[5] the compositions of complexes formed by hydrolysis in heavy water are the same as those in light water, while the stability constants of the complexes are smaller in heavy water than in light water. Essentially the same results were found in the system of uranyl ions.

The first attempt of interpretation of the solvent deuterium isotope effect was made by Gross and his co-workers[8] for acid catalyzed reactions, and the Gross' treatment has been applied to acid dissociation equilibria of water itself[9] and some acids such as am-

8) P. Gross, H. Steiner, and F. Krauss, *Trans. Faraday Soc.*, **32**, 877 (1936); P. Gross and H. Wischler, *ibid.*, **32**, 879 (1936); P. Gross, H. Steiner, and H. Suess, *ibid.*, 863 (1936).

9) P. Salomaa, L. L. Schaleger, and F. A. Long, *J. Amer. Chem. Soc.*, **86**, 1 (1964).

monium ion[10] and phosphoric acid,[9] as well as to reaction kinetics.[11]

Since hydrolysis reactions are regarded as acid dissociation reactions of aquated metal ions, essentially similar treatments as Gross' may be used for analysis of hydrolysis schemes of metal ions in H_2O-D_2O mixtures. In the equilibrium theory first proposed by Gross,[8] the following assumptions are made; (1) Activity coefficients of chemical species do not change through the exchange of protons in a molecule with deuterons, (2) a solvated hydrogen ion possesses three lyons, and (3) isotopic disproportionation equilibria are subject to the rule of the simple geometric mean. Under these assumptions and with knowledge of values of stability constants of hydrolysis species in light and heavy water, variations of stability constants of hydrolysis species of UO_2^{2+} and Be^{2+} ions with the deuterium atom fraction in the solvent were discussed.

(1) Solvent Deuterium Isotope Effects on the Hydrolysis of UO_2^{2+}. On the basis of the above assumptions, prevailing equilibria among the various solvent species, protons, and deuterons along with their equilibrium constants are written as follows.

$$H_2O + D_2O = 2HDO \ ; \ 4 \tag{1}$$

$$2H_3O^+ + D_3O^+ = 3H_2DO^+ \ ; \ 27 \tag{2}$$

$$H_3O^+ + 2D_3O^+ = 3HD_2O^+ \ ; \ 27 \tag{3}$$

$$1/3H_3O^+ + 1/2D_2O = 1/3D_3O^+ + 1/2H_2O \ ; \ \psi \tag{4}$$

From Eq.(1), the concentrations of waters in a solvent mixture of a deuterium atom fraction n become

$$[H_2O] = (1-n)^2 \tag{5}$$

$$[HDO] = 2n(1-n) \tag{6}$$

$$[D_2O] = n^2 \tag{7}$$

The total concentration of lyonium ions, $\sum[L_3O^+]$ is expressed by Eq. (8) in terms of $[H_3O^+]$, n and ψ by means of Eqs. (1)—(7).

$$\sum[L_3O^+] = [H_3O^+] + [H_2DO^+] + [HD_2O^+] + [D_3O^+] = [H_3O^+](1-n+n\psi)^3(1-n)^{-3} \tag{8}$$

Let us consider a solution of the (2, 2) complex in a mixed H_2O-D_2O solvent. There are three different types of complexes, $(UO_2)_2(OH)_2^{2+}$, $(UO_2)_2(OH)(OD)^{2+}$ and $(UO_2)_2(OD)_2^{2+}$. The following two deuterium fractionation factors are defined;

$$(UO_2)_2(OH)_2^{2+} + D_2O = (UO_2)_2(OD)_2^{2+} + H_2O \ ; \ \Phi_{20}$$

$$(UO_2)_2(OH)_2^{2+} + 1/2D_2O = (UO_2)_2(OH)(OD)^{2+} + 1/2H_2O \ ; \ \Phi_{21}$$

and they are given as

$$\Phi_{20} = \{[(UO_2)_2(OD)_2^{2+}]/[(UO_2)_2(OH)_2^{2+}]\} \times \{(1-n)/n\}^2 = (\beta^D_{2,2}/\beta^H_{2,2})\psi^{-6} \tag{9}$$

$$\Phi_{21} = \{[(UO_2)_2(OH)(OD)^{2+}]/[(UO_2)_2(OH)_2^{2+}]\} \times \{(1-n)/n\} = K(\beta^D_{2,2}/\beta^H_{2,2})\psi^{-3} \tag{10}$$

Here, K is the isotopic disproportionation factor for the reaction,

$$1/2(UO_2)_2(OH)_2^{2+} + 1/2(UO_2)_2(OD)_2^{2+} = (UO_2)_2(OH)(OD)^{2+} \ ; \ K \tag{11}$$

From Eqs. (8)—(10), the total concentration of the (2, 2) complexes is given as follows.

$$\sum[(UO_2)_2(OL)_2^{2+}] = [(UO_2)_2(OH)_2^{2+}] \times \{1 + \Phi_{20}(n/(1-n))^2 + \Phi_{21}(n/(1-n))\} \tag{12}$$

The equilibrium constant, $\beta_{2,2}$ in a mixed solvent, which is accessible to experimental measurement is made up of the total concentrations of the various isotopic species involved.

$$\beta^n_{2,2} = \{\sum[(UO_2)_2(OL)_2^{2+}] \cdot \sum[L_3O^+]^2\} / \{[UO_2^{2+}]^2 \sum[L_2O]^4\} \tag{13}$$

Introducing the expressions for the total concentration of the (2, 2) complexes (Eq. (12)) and of lyonium ions (Eq.(8)) into Eq. (13), we obtain

$$\beta^n_{2,2} = [\{[(UO_2)_2(OH)_2^{2+}][H_3O^+]^2\}/\{[UO_2^{2+}]^2(1-n)^6\}] \times \{1 + \Phi_{20}(n/(1-n))^2 + \Phi_{21}(n/(1-n))\}(1-n+n\psi)^6 \tag{14}$$

If we assume that the equilibrium constant of the reaction $2UO_2^{2+} + 4H_2O = (UO_2)_2(OH)_2^{2+} + 2H_3O^+$ in a mixed solvent with a deuterium atom fraction n is equal to that of the same reaction in pure light water, the following equation is readily obtained.

$$\beta^n_{2,2}/\beta^H_{2,2} = (1-n+n\psi)^6 \times \{(1-n)^2 + \Phi_{20}n^2 + \Phi_{21}n(1-n)\} \tag{15}$$

The application of the rule of the geometric mean to the equilibrium(11) leads to K=2.[12] As the values for $\beta^H_{2,2}$ and $\beta^D_{2,2}$ have been obtained experimentally and the value for ψ has been reported to be 0.69,[13] the relative stability constant, $\beta_{2,2}/\beta_{2,2}$ can be calculated using Eqs.(9) and (10).

The relative stability constant, $\log(\beta^n_{2,2}/\beta^H_{2,2})$ at $n=0.8$ thus calculated is shown in Table 2. The agreement between the experimental and calculated values is satisfactory.

TABLE 2 CALCULATED AND OBSERVED RELATIVE STABILITY CONSTANTS, $\log(\beta^n_{p,q}/\beta^H_{p,q})$ AT $n=0.8$

Complex	$\log(\beta^n_{p,q}/\beta^H_{p,q})$	
	Calcd	Obsd
$(UO_2)_2(OL)_2^{2+}$	−0.46	−0.44
$(UO_2)_3(OL)_5^+$	−1.17	−1.12

In general, Eq. (15) can be written, for the (p,q) complex, as follows;

$$\beta^n_{p,q}/\beta^H_{p,q} = (1-n+n\psi)^{3p} \cdot \{\sum_m \Phi_{pm} n^{(p-m)}(1-n)^m\} \tag{16}$$

and Φ_{pm} is given as

$$\Phi_{pm} = K_m(\beta^D_{p,q}/\beta^H_{p,q})^{(p-m)/p} \cdot \psi^{-3(p-m)} \tag{17}$$

where K_m denotes the equilibrium constant of the following isotopic disproportionation reaction (charges are omitted);

10) P. Salomaa, L. L. Schaleger, and F. A. Long, *J. Phys. Chem.*, **68**, 416 (1964).

11) C. G. Swain and E. R. Thornton, *J. Amer. Chem. Soc.*, **83**, 3890 (1961).

12) J. Bigeleisen, *J. Chem. Phys.*, **23**, 2264 (1955).

$$\frac{m}{p}M_q(OH)_n + \frac{p-m}{p}M_q(OD)_p = M_q(OH)_m(OD)_{p-m} \; ; \; K_m \quad (18)$$

Φ_{pp}, K_0, and K_p are defined as 1.

Variation of the stability constant of the $(UO_2)_3(OL)_5^+$ complex, $\log(\beta^n{}_{5,3}/\beta^H{}_{5,3})$, can be calculated from Eq. (16); in this case $K_1=5$, $K_2=10$, $K_3=10$, and $K_4=5$ are given under the assumption of the geometric mean.[12]

The calculated results at $n=0.8$ are represented in Table 2.

For the $(UO_2)_3(OL)_4^{2+}$ complex, the formation of which is quite small, uncertainties of the stability constants are so large that the discussion of the variation of the stability constant with the solvent composition can hardly be made.

(2) Solvent Deuterium Isotope Effects on the Hydrolysis of Be^{2+}. In the previous studies for the hydrolysis of Be^{2+} ion in light water,[2,14] heavy water,[2] and their mixtures,[6] we found that the main product of the reaction is $Be_3(OL)_3^{3+}$ in all systems examined and the stability constant of the species decreases with the increase of the deuterium atom fraction in the solvent. The continued variation of the relative stability constant of the (3, 3) species with the change in the deuterium atom fraction in the solvent has been determined experimentally as follows.[6] If only the (3, 3) species is present in appreciable amounts in mixed H_2O-D_2O solvents, the following equation can be derived:

$$1/2\log Z - 3/2\log(1-Z) = 1/2\log 3 + 1/2\log\beta_{3,3} + \log B - 3/2\log l \quad (19)$$

Differentiation of Eq.(19) with respect to the deuterium atom fraction at constant B and Z values gives the equation:

$$\partial\log\beta_{3,3} = 3\,\partial\log l \quad (20)$$

The variation of the stability constant can be determined according to Eq.(20) if the change in l with the deuterium atom fraction is measured. In order to determine the variation of l with the deuterium atom fraction, the change in emf, ΔE, with the solvent composition was measured at constant B (0.02 and 0.04 M) and Z values ($Z\simeq0.5$, where the (3, 3) species has been found to be predominant), and the change in E_0, that is ΔE_0, with the deuterium atom fraction was also measured by the similar titration procedure without beryllium ions. From the values for ΔE and ΔE_0 at any given solvent composition the change in l, $\Delta\log l$, could be evaluated by the equation $\Delta\log l=(\Delta E-\Delta E_0)/59.15$. The observed changes in $\beta_{3,3}$ with varying deuterium atom fraction from 0 to 0.8 are shown in Fig. 3.

Calculation of the relative stability constant of the $Be_3(OL)_3^{3+}$ complex in water of different hydrogen isotopic compositions was carried out by substituting the relation $K_1=K_2=3$[12] into Eq.(16). The results are compared with the experimental ones in Fig. 3. We see that the agreement is satisfactory.

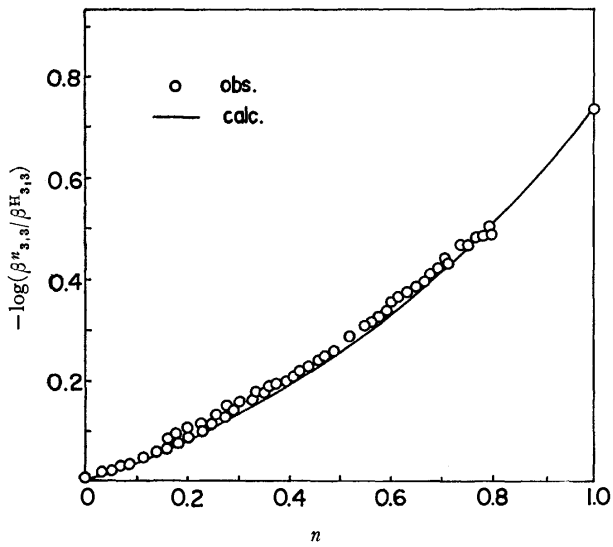

Fig. 3. Observed and calculated values of $-\log(\beta^n{}_{3,3}/\beta^H{}_{3,3})$ for the (3, 3) complex of Be^{2+} in H_2O-D_2O mixtures.

Conclusion

1) Stability constants of hydrolysis species of UO_2^{2+} ion were determined in light and 80% heavy water containing 3 M $NaClO_4$ as an ionic medium at 25°C. The results are tabulated in Table 1.

2) Relative stability constants of hydrolysis species of UO_2^{2+} and Be^{2+} ions in various H_2O-D_2O mixtures were estimated by application of the equilibrium theory of solvent deuterium isotope effects. Satisfactory agreements were found between the observed and calculated values.

Experimental

Reagents. Reagents used were, unless otherwise stated, prepared and analyzed as have been described in Refs. 2 and 3.

Uranyl percholrate solution was prepared and analyzed with the same procedures as those described in Ref. 15. *Uranyl perchlorate in* 80% *heavy water* was prepared by the repeated evaporation of uranyl perchlorate solution under an infrared lamp, while adding 80% heavy water.

NaOL solution in 80% *heavy water* was prepared by electrolysis of sodium perchlorate in 80% heavy water.

Apparatus. *A Wilhelm type half-cell*[17] was used for emf measurements, and a modified one for constant-current coulometry.

Glass electrodes of Beckman No. 40498 were used in combination with *a Radiometer PHM-4C pH-meter (Copenhagen).*

A coulometric analyzer(Leeds & Northrup Co., Philadelphia) was used as a constant current power source.

Procedures. Hydrolysis of uranyl ions in 80% heavy water and in light water was investigated by measurements of the total concentration of free lyonium ion using a glass electrode. Sodium perchlorate was used as an ionic medium in order to keep the total concentration of perchlorate ion to be 3 M. The total concentration of uranyl ion was kept constant in each series of experiments.

The lyonium ion concentration was measured by means

13) P. Salomaa, *Acta Chem. Scand.*, **23**, 2095 (1969).
14) H. Kakihana and L. G. Sillén, *ibid.*, **10**, 985 (1956).
15) H. S. Dunsmore, S. Hietanen, and L. G. Sillén, *ibid.*, **17**, 2644 (1963).
16) S. Hietanen, B. R. L. Row, and L. G. Sillén, *ibid*, **17**, 2735 (1963).

of the cell;

$$\text{GE}|\text{Test Solution}|\text{Ref} \qquad \text{(A)}$$

where GE denotes a glass electrode and Ref, the reference half cell containing 2.99 M $NaClO_4$—0.01 M $AgClO_4$ solution and a silver-silver chloride electrode. The liquid junction between the reference half cell and the test solution was constructed with 3 M $NaClO_4$ in 80% heavy water or in light water.

For the system of light water, both coulometric and ordinary titrations were employed. Since no difference has been observed between the results by these two methods, a coulometric titration was used for the system of 80% heavy water.

The emf of the cell(A) is given, at 25°C, as follows:[18]

$$E = E_0 + 59.15 \log l + E_j \qquad (21)$$

E_j, a liquid junction potential was negligible under the present experimental condition.

17) W. Forsling, S. Hietanen, and L. G. Sillén, *ibid.*, **6**, 901 (1952).

18) H. Kakihana, M. Maeda, and T. Amaya, This Bulletin, **43**, 1377 (1970).

BULLETIN OF THE CHEMICAL SOCIETY OF JAPAN, VOL. 45, 2468—2472 (1972)

Some Metal Complexes Containing Ethyl Acetoacetate or Ethyl Malonate as a Neutral Ligand

Hideyoshi MORITA,* Yukio NAKAMURA, and Shinichi KAWAGUCHI

Department of Chemistry, Faculty of Science, Osaka City University, Sumiyoshi-ku, Osaka

(Received February 23, 1972)

The following metal complexes containing ethyl acetoacetate (etacH) or ethyl malonate (etmalH) as a neutral ligand have been prepared: $CoCl_2L$, $CoBr_2L$, $ZnCl_2L$ (L=etacH or etmalH), and $MnBr_2$(etmalH). These compounds are all hygroscopic and unstable, releasing the ester ligand below 100°C *in vacuo* or in donor solvents. The infrared spectra show that the ratio of keto and enol tautomers in etacH complexes is similar to that for the free ligand. The ν(C=O) band attributable to the enol tautomer of etmalH is observed in the complexes, though not in the free ligand. The electronic spectra measured in Nujol suggest that the cobalt(II) complexes are tetrahedral. The structure of $MnBr_2$(etmalH) is not yet certain.

Acetylacetone is one of the most versatile ligand; it usually coordinates to the metal atom as a bidentate anion,[1] although in some cases it serves as a unidentate anion, forming a metal-carbon bond[2] or an ether type metal-oxygen[3] linkage. In a previous paper we reported on several metal complexes containing acetylacetone as a neutral ligand.[4]

The neat liquid of acetylacetone (acacH) is a mixture of keto and enol tautomers; the equilibrium content of the latter was determined by the NMR method to be 81.4% at 25°C.[5] However, in the above metal complexes of neutral acetylacetone, such an equilibrium composition is not maintained; rather, one of the two tautomers is incorporated exclusively. Thus, $MnBr_2(acacH)_2$ involves enolic molecules as unidentate ligands,[6] but $NiBr_2(acacH)_2$,[7] $ZnCl_2$-(acacH), CoX_2(acacH), and CrX_2(acac)(acacH) (X=Cl, Br) all contain the keto tautomer as a bidentate ligand.[4] Similarly, $UO_2(acac)_2(acacH)$ has been reported to have an enol molecule,[8] and] [Ni-$(acacH)_3](ClO_4)_2$ and other related Ni(II) complexes, the keto tautomer.[9] Proton magnetic resonance studies of $[Mg(acacH)_2(H_2O)_2](ClO_4)_2$ in CD_3NO_2 have also revealed that the keto tautomer is the dominant species bonded to the magnesium ions in solution.[10]

As an extension of the previous work, we have tried to synthesize several metal complexes containing ethyl acetoacetate or ethyl malonate as a neutral ligand. In contrast with acetylacetone, the keto tautomer is the major component in these esters; the enol content has been reported to be about 8% in ethyl acetoacetate[11] and seems to be negligible in ethyl malonate. Thus, it was expected that metal complexes of these ester molecules involve the keto tautomer exclusively.

Experimental

Materials. The anhydrous metal halides were prepared by the following methods. About 50 ml of freshly-distilled thionyl chloride was added to 25 g of cobalt(II) chloride hexahydrate, and the mixture was refluxed for about 2 hr. After the vacuum distillation of the excess thionyl chloride, the residual anhydrous cobalt(II) chloride was dried for three days in a vacuum desiccator containing po-

* Present address: Faculty of Pharmaceutical Sciences, The University of Tokushima.

1) J. P. Fackler, Jr., *Progr. Inorg. Chem.*, **7**, 361 (1966); E. C. Lingafelter, *Coord. Chem. Rev.*, **1**, 151 (1966).

2) D. Gibson, *ibid.*, **4**, 225 (1969).

3) T. J. Pinnavaia, W. T. Collins, and J. J. Howe, *J. Amer. Chem. Soc.*, **92**, 4544 (1970), and references cited therein.

4) Y. Nakamura, K. Isobe, H. Morita, S. Yamazaki, and S. Kawaguchi, *Inorg. Chem.*, **11**, 1573 (1972).

5) L. W. Reeves, *Can. J. Chem.*, **35**, 1351 (1957).

6) S. Koda, S. Ooi, H. Kuroya, Y. Nakamura, and S. Kawaguchi, *Chem. Commun.*, **1971**, 280.

7) S. Koda, S. Ooi, H. Kuroya, K. Isobe, Y. Nakamura, and S. Kawaguchi, *ibid.*, **1971**, 1321.

8) J. M. Haigh and D. A. Thornton, *Inorg. Nucl. Chem. Lett.*, **6** 231 (1970).

9) P. W. N. M. van Leeuwen, *Rec. Trav. Chim.*, **87**, 396 (1968); K. Anzenhofer and T. G. Hewitt, *Z. Kristallogr.*, **134**, 54 (1971).

10) P. W. N. M. van Leeuwen and A. P. Praat, *Inorg. Chim. Acta*, **4**, 101 (1970).

11) J. L. Burdett and M. T. Rogers, *J. Amer. Chem. Soc.*, **86**, 2105 (1964).

TABLE 1. METAL COMPLEXES CONTAINING ETHYL ACETOACETATE OR ETHYL MALONATE AS A NEUTRAL LIGAND

Complex[a]	Color	Found (Calcd), %				Magnetic moment BM (°K)
		M	X	C	H	
$CoCl_2$(etacH)	pale blue	23.07 (22.67)	26.96 (27.27)	26.59 (27.72)	4.12 (3.88)	5.01 (291)
$CoCl_2$(etmalH)	deep blue	21.17 (20.32)	24.19 (24.45)	28.08 (28.98)	4.12 (4.17)	4.98 (295)
$CoBr_2$(etacH)	light blue	16.19 (16.89)	43.63 (45.81)	22.02 (20.66)	3.30 (2.89)	
$CoBr_2$(etmalH)	deep blue	15.69 (15.55)	41.98 (42.18)	22.06 (22.19)	3.29 (3.19)	4.85 (293)
$MnBr_2$(etmalH)	pale pink	14.64 (14.65)	42.73 (42.63)	22.12 (22.42)	3.31 (3.23)	5.51 (293)
$ZnCl_2$(etacH)	white	24.27 (24.54)	26.56 (26.61)	26.91 (27.05)	3.98 (3.78)	
$ZnCl_2$(etmalH)	white	21.75 (22.05)	24.03 (23.92)	28.11 (28.36)	4.32 (4.08)	

a) etacH: ethyl acetoacetate, $CH_3COCH_2COOC_2H_5$. etmalH: ethyl malonate, $C_2H_5OCOCH_2COOC_2H_5$.

tassium hydroxide.[12] Anal. Found: Co, 45.59; Cl, 54.32%. Commercial zinc(II) chloride was also dried by a similar method to yield an anhydrous compound.[12] Anal. Found: Zn, 47.14; Cl, 52.42%. The anhydrous cobalt(II) bromide was obtained by the dehydration of the commercial hexahydrate by heating at 130°C for 10 hr and by evacuating at the same temperature for 2 hr. Anal. Found: Co, 27.12; Br, 72.61%. The anhydrous manganese(II) bromide was prepared according to Watt and Manhas[13] by a reaction between manganese(II) carbonate and hydrobromic acid. Anal. Found: Mn, 25.48; Br, 74.23%.

Ethyl acetoacetate and ethyl malonate were distilled under reduced pressure, and the distillates, collected at 83—86°C and 99—102°C respectively, were used in this study. Mercury(II) tetraisothiocyanatocobaltate(II) was prepared according to Figgis and Nyholm.[14] Anal. Found: C, 9.73; N, 11.43%. Calcd for $HgCo(NCS)_4$: C, 9.77; N, 11.39%.

Syntheses and Analyses of the Ester Complexes. About a 40-m*l* portion of ethyl acetoacetate or ethyl malonate was added to about 1 g of an anhydrous metal halide, and the mixture was stirred for about 48 hr. The precipitate was filtered, washed with petroleum ether, and dried *in vacuo*. The complexes thus prepared are all hygroscopic; special care was taken to exclude atmospheric moisture in the preparation and filtration procedures.[4]

The cobalt and manganese in these complexes were determined gravimetrically as sulfates, and zinc, as ammonium phosphate. The halide contents were also measured gravimetrically as silver salts. The results of the elemental analysis of these compounds are tabulated in Table 1, together with some properties.

Measurements. No solvent is available in which these complexes are dissolved without decomposition. A solid specimen was ground with Nujol and placed between two plates of opal glass, and its transmission spectrum was measured[15] with a Hitachi-Perkin Elmer 139 spectrophotometer. The infrared spectra were measured in Nujol by means of Hitachi EPI-2 (700—4000 cm^{-1}) and EPI-L (200—700 cm^{-1}) infrared spectrophotometers.

A thermo-spring balance (C-282) of Hamada Denki Seisaku-sho, Ltd., was used for the thermogravimetric analysis of the ethyl malonate complexes; the temperature of a sample was raised at a rate of 20°/hr. The decomposition residue was dissolved in water and analyzed.

The magnetic susceptibility was determined at room temperature by the Gouy method with an automatically-recording magnetic balance of Shimadzu Seisakusho, Ltd. Mercury(II) tetraisothiocyanatocobaltate(II) was used as the reference.

Results

Infrared Spectra. In Table 2 are summarized the infrared absorption spectra of metal complexes of ethyl acetoacetate (etacH) and ethyl malonate (etmalH) in the regions of the carbonyl, metal-oxygen, and metal-halogen stretching vibrations. The carbonyl stretching frequencies of the free ligands were assigned by reference to the literature;[16] they are included in the table. In the infrared spectrum of the free ligand etacH, the ν(C=O) band for the keto tautomer is very strong and that for the enol tautomer is weak, reflecting the equilibrium composition of the two tautomers. The ν(C=O) band for the enol tautomer is hardly detectable in the spectrum of etmalH.

The infrared spectra of acetylacetone complexes showed the carbonyl stretching absorption solely due to either the keto or the enol tautomer, revealing that either one of the tautomers was incorporated exclusively in each complex.[4] On the contrary, carbonyl stretching bands attributable to both tautomers are observed in each of the present ester complexes (Table 2), indicating that each compound is a mixture of complex molecules containing the keto tautomer as a ligand and those having the enol tautomer. Although the carbonyl stretching region of these complexes is very broad and exact estimation is difficult, the rough intensity ratio of the carbonyl bands of the two tautomers in each ethyl acetoacetate complex is near to that for the free ligand. This observation suggests that the formation constants of keto and enol complexes are similar in these cases. Since the carbonyl stretching band of the enol tautomer of free ethyl malonate can hardly be identified, it is not certain whether the bands observed at 1618—1658 cm^{-1} for the metal complexes are assignable to the coordinated enol tautomer. If this is indeed the case, though, it must be concluded that the complex formation constant of the enol tautomer is much larger than that

12) T. Moeller (ed.), "Inorganic Syntheses," Vol.5, McGraw-Hill, New York (1957), p. 153.
13) G. W. Watt and B. S. Manhas, *J. Inorg. Nucl. Chem.*, **28**, 1945 (1966).
14) B. N. Figgis and R. S. Nyholm, *J. Chem. Soc.*, **1958**, 4190.
15) K. Shibata, "Methods of Biochemical Analyses," Vol.7 edited by D. Glick, Interscience, New York (1959), p. 77.
16) W. Gordy, *J. Chem. Phys.*, **8**, 516 (1940); R. S. Rasmussen and R. R. Brattain, *J. Amer. Chem. Soc.*, **71**, 1073 (1949); R. W. Hay and B. P. Caughley, *Aust. J. Chem.*, **20**, 1829 (1967).

Talle 2. Characteristic infrared spectra (cm^{-1}) of metal complexes containing ethyl acetoacetate or ethyl malonate as a neutral ligand

L=etacH				L=etmalH					Assignment
L	$CoCl_2L$	$CoBr_2L$	$ZnCl_2L$	L	$CoCl_2L$	$CoBr_2L$	$MnBr_2L$	$ZnCl_2L$	
1738 vs	1717 sh	1720 sh		1750 vs	1750 sh	1755 sh	1753 sh	1737 vs	keto ν(C=O)
1717 vs	1702 vs	1703 vs	1730 vs	1736 vs	1729 vs	1726 vs	1726 vs	1715 vs	
		1685 vs	1706 vs		1698 vs	1690 vs		1683 sh	
1643 m	1657 m	1650 m	1625 m		1657 w	1655 m	1658 m	1618 w	enol ν(C=O)+ν(C=C)
	250	250	233		243			230	ν(M-O)
						235	230		
	242	240	218		232			218	
	343	272	335		340	265	258(?)	330	ν(M-X)
	310	230	300		318	230		305	

of the keto tautomer in the case of ethyl malonate.

Distinct absorption bands appearing in the 377—397 cm^{-1} region were attributed to the metal-oxygen stretching vibrations in the complexes of the keto tautomers. On the other hand, the ν(M–O) bands of the enol tautomers are obscure because of their minor abundances; they will not be assigned here.

The metal-halogen stretching absorptions were assigned according to the literature;[17,18] they are listed in Table 2. These exist in the range of frequencies attributable to the non-bridging metal-halogen stretching vibration in tetrahedral complexes of the MX_2L_2 type, where L respresents a unidentate ligand.

Electronic Spectra and Magnetic Data. The absorption spectra of $CoCl_2$(etacH) and $CoCl_2$(etmalH) in Nujol (Fig. 1) exhibit three maxima, at 600, 675, and 717 nm, and at 598, 680, and 722 nm, respectively. These spectra unequivocally indicate that those are tetrahedral complexes,[19] although their magnetic moments are a little higher than the values usually observed for tetrahedral cobalt(II) complexes.[19]

The observed magnetic moment (5.51 B. M.) of $MnBr_2$(etmalH) certifies that this is a high-spin complex, but we can not distinguish whether it is tetrahedral or octahedral. The absorption spectrum can not be observed by the opal glass method due to the low absorption intensity. However, the pale pink color might reflect an octahedral structure, since manganeses(II) usually has a green-yellow color in tetrahedral environments.[20]

Thermogravimetric Data. The negative shifts of the carbonyl stretching frequencies of etacH and etmalH caused by ligation to metal atoms are minute, suggesting the weakness of these bonds. This is also revealed by the thermogravimetric data of etmalH complexes depicted in Fig. 2 and summarized in Table 3. The zinc complex is most unstable and begins to decompose at 40°C. The weight loss coincides

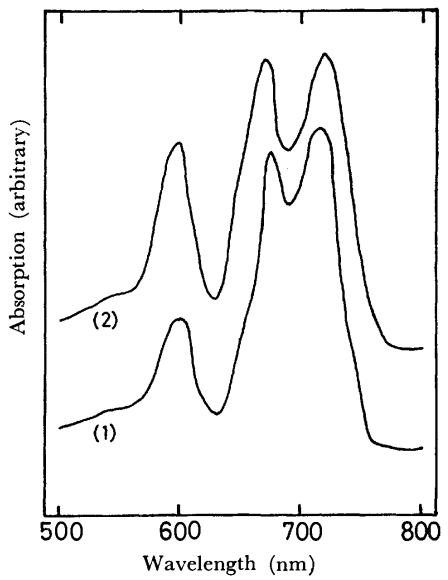

Fig. 1. Absorption spectra of $CoCl_2$(ethyl acetoacetate) (1) and $CoCl_2$(ethyl malonate) (2) in Nujol.

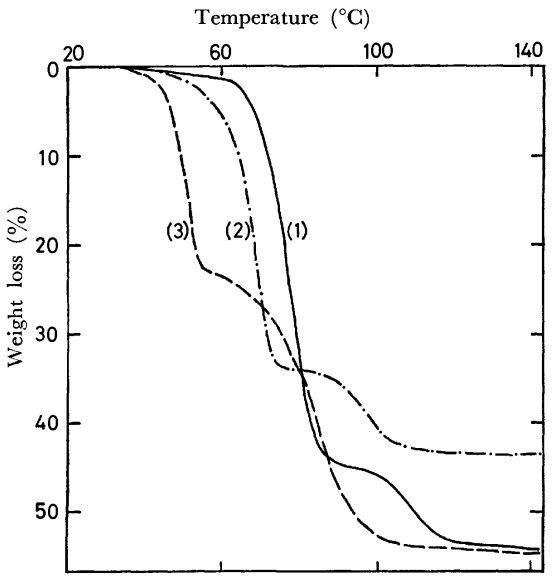

Fig. 2. Thermogravimetric analyses of ethyl malonate (L) complexes: (1) $CoCl_2L$, (2) $MnBr_2L$, (3) $ZnCl_2L$.

17) R. Colton and J. H. Canterford, "Halides of the First Row Transition Metals," Wiley-Interscience, New York (1969), p. 327.
18) C. Postmus, J. R. Ferraro, A. Quattrochi, K. Shobatake, and K. Nakamoto, *Inorg. Chem.*, **8**, 1851 (1969).
19) R. L. Carlin, "Transition Metal Chemsitry," Vol. 1, Marcel Dekker, New York (1965), p. 1.
20) F. A. Cotton and G. Wilkinson, "Advanced Inorganic Chemistry," 2nd ed., Interscience, New York (1966), p. 837.

TABLE 3. THERMOGRAVIMETRIC ANALYSIS OF METAL COMPLEXES CONTAINING ETHYL MALONATE AS A NEUTRAL LIGAND

Complex	Beginning of decomposition °C	Wt loss, %		Analysis of residue, %			
				Found		Calcd[b]	
		Found	Calcd[a]	M	X	M	X
$CoCl_2$(etmalH)	60	54.07	55.23	45.85	53.96	45.39	54.61
$MnBr_2$(etmalH)	50	42.78	42.72	25.66	74.22	25.58	74.42
$ZnCl_2$(etmalH)	40	54.62	54.03				

a) Calcd for the loss of etmalH. b) Calcd for the anhydrous metal halide.

with the calculated content of the ligand in each complex, while the composition of the residue coincides with that of the metal halide.

Although the final decomposition residue is thus the metal halide, a plateau-like portion is observed in each decomposition curve, suggesting the presence of some metastable intermediate. The composition corresponds to $CoCl_2$: etmalH=6 : 1, $MnBr_2$: etmalH =5 : 1, and $ZnCl_2$: etmalH=5 : 3. Allan *et al.*[21] studied the thermal decomposition of adducts of cobalt(II) chloride and manganese(II) bromide with pyridine and its methyl derivatives; they found $CoCl_2$·2/3 py and $MnBr_2$·2/3 (Me-py) as intermediates. Much more effort will be needed to characterize the decomposition intermediates in the present case.

Discussion

In a previous paper acetylacetone complexes were synthesized by three alternative methods:[4] (1) the direct addition of acetylacetone to anhydrous metal halides, (2) the reaction of the usual acetylacetonate chelate with dry hydrogen bromide in dichloromethane containing free acetylacetone, and (3) the reaction of trichlorotris(tetrahydrofurn)chromium(III) with acetylacetone. The ester complexes were prepared by the first method. In order to succeed in getting solid complexes by this method, the metal halide should have an appropriate solubility in the free ligand. Anhydrous nickel(II) chloride is insoluble in etacH and etmalH, and does not give either complex. On the other hand, the solubility of manganeses(II) bromide in etacH is too high and the isolation of a solid complex was unsuccessful.

The thermodynamic stabilities of ester complexes are relatively low, but those listed in Table 1 were stable enough to be analyzed and characterized. Anhydrous manganese(II) chloride reacted with both etacH and etmalH, giving solid products, but their decomposition pressures were so large that they easily decomposed to the starting materials without affording any complexes of a definite composition. On the contrary, the cobalt(II) bromide complex with etacH held the ligand in excess of the 1 : 1 composition. As is shown in Table 1, even after prolonged evacuation at 50°C the analytical data showed some contamination with the free ligand. The function of the slight excess of etacH in this complex is not at all clear.

As to the structures of these ester complexes, any conclusive discussion is impossible, since no adequate solvent is available for the molecular-weight determination and since no suitable crystal has yet been obtained for the X-ray analysis. The infrared spectra indicate that both the keto and the enol tautomers are incorporated in these ester complexes, while the electronic spectra of solid specimens of cobalt(II) chloride complexes in Nujol suggest the tetrahedral structure for these complexes. The ketonic complex may be presumed to be monomeric, two halogen atoms and two carbonyl oxygen atoms of the keto tautomer surrounding the metal atom tetrahedrally. It is not certain whether the structure of the minor enolic complex is reflected in the absorption spectra. If this is indeed the case, and if the enolic complex also assumes a tetrahedral structure, some polymeric structure containing the Co-Br chain must be formed, since the enol tautomer of etacH or etmalH does not seem to act as a bidentate.

The octahedral structure might be assigned to $MnBr_2$(etmalH) on the basis of its pale pink color. This structure may be realized if the keto tautomer of the ester occupies two adjacent coordination sites and if the $MnBr_2$ unit constructs an infinite spiral chain. On the other hand, two enolic molecules of acetylacetone are used in $MnBr_2(acacH)_2$ to complete the octahedral structure around each manganese atom in the infinite linear $MnBr_2$ chain.[6] Such a difference in the tautomeric form of the ligand molecule incorporated might be the reason why acetylacetone forms the 2 : 1 complex with $MnBr_2$, while ethyl malonate froms the 1 : 1 complex. Recently Kemula and Iwamoto[22] investigated the complex formation equilibria in a solution of $SnCl_4$ and various esters. Ethyl acetate, ethyl glutarate, and ethyl adipate act as monodentate ligands and form 1 : 1 and 2 : 1 complexes with $SnCl_4$, depending on the ratio of the ester to $SnCl_4$, but ethyl oxalate and ethyl malonate serve as chelating agents and form only 1 : 1 complexes.

The relative bonding strengths of acacH, etacH, and etmalH to metal might be worth noting. The metal-oxygen stretching frequencies for zinc complexes nearly coincide ($ZnCl_2(acacH)$[4] 230, 210; $ZnCl_2$-(etacH) 233, 218; $ZnCl_2$(etmalH) 230, 218 cm^{-1}), but some difference is noticed for cobalt(II) complexes

21) J. R. Allan, D. H. Brown, R. H. Nuttall, and D. W. A. Sharp, *J. Inorg. Nucl. Chem.*, **26**, 1895 (1964); **27**, 1865 (1965).

22) A. Kemula and R. T. Iwamoto, *J. Phys. Chem.*, **72**, 1334 (1968).

($CoCl_2$(acacH)[4] 264, 248; $CoCl_2$(etacH) 250, 242; $CoCl_2$(etmalH) 243, 232 cm^{-1}). The latter results might reflect the relative bonding strengths of these ligands in the order of acacH > etacH > etmalH. The amounts of the nagative shift in the carbonyl stretching frequencies of these complexes from those of free ligands are so small that they do not permit the differentiation of their bonding strengths.

The magnetic measurements were carried out at Kyoto University, and the authors are indebted to Dr. H. Kobayashi for providing facilities for them. Acknowledgement is made to Mr. J. Gohda for the elemental analysis, and also to the Ministry of Education for its financial support.

BULLETIN OF THE CHEMICAL SOCIETY OF JAPAN, VOL. 45, 2472—2475 (1972)

Isotopic Exchange Kinetics between Trisacetylacetonatocobalt(III) and Acetylacetone-^{14}C in Organic Solvents

Kazuo SAITO and Mizue MURAKAMI

Chemistry Department, Faculty of Science, Tohoku University, Sendai

(Received February 26, 1972)

The isotopic exchange proceeds faster than the decomposition of the complex at more than 80°C and below 120°C. McKay plot gives a linear diagram at the initial stage of isotopic exchange. The rate is expressed by $R=[\text{complex}](k_1+k_2[\text{acacH}])$, where acacH stands for free acetylacetone. The Arrhenius activation energy decreases in the order anisole (25 kcal per mole), chlorobenzene (21), and toluene (18) and is subject to acid catalysis with a strong acid as trichloroacetic. Comparison of the data with those of racemization of this complex, and isomerization and inversion of tris(benzoylacetonato)cobalt(III) suggested that k_1 represents dissociation mechanism through a five coordinate intermediate containing a unidentate acetylacetonate anion, and the k_2 an association mechanism involving association of free acacH with the intermediate.

In order to extend our studies of isotopic exchange kinetics of β-diketonato complexes,[1,2] exchange reaction between tris(acetylacetonato)cobalt(III) [Co(acac)$_3$] and acetylacetone (acacH) labelled with ^{14}C has been examined in organic solvents. This complex was claimed to be substitution inert on a qualitative experiment,[3] and to undergo decomposition at higher temperatures.[4] We have found that this complex decomposes to bis(acetylacetonato)-cobalt(II) at more than 130°C in gaseous state within several minutes. On the other hand, in organic solvents the cobalt(III) complex gave brown precipitate on prolonged heating at more than 70°C (*e.g.* after 30 hr at 90°C). Infrared absorption spectrum of the precipitate in KBr pellet disclosed that it consists mainly of polymeric acetylacetonatocobalt(III) complex and does not contain cobalt(II) complex. The visible and ultraviolet absorption spectrum of the remaining reaction mixture suggested that [Co(acac)$_2$] is appreciable, when the reaction mixture was heated so long as to give the precipitate.

McKay plot[5] in toluene and anisole at 80 to 97°C (Fig. 1) gave a straight line at the initial stage of the exchange reaction, where the absorption spectrum remained unchanged. With progress of the reaction, however, the apparent rate gradually decreased accompanied by change in absorption spectrum and eventually with formation of the brown precipitate. The apparent rate of exchange (R) was reproducible in the initial stage at 85 to 100°C and seemed to suit for kinetic studies.

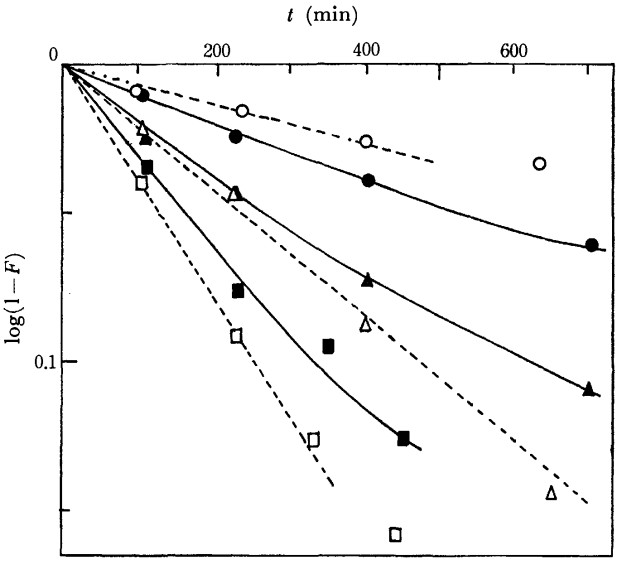

Fig. 1. McKay plots in toluene and anisole.
[complex]=[acacH]=0.05 M, ○ 80; △ 90; □ 97°C.
Open marks in anisole and solid marks in toluene.

Results

Figure 2 shows the relationship between the log of initial concentration of the complex and log R values in anisole and toluene. The diagram has a gradient

1) K. Saito and K. Masuda, This Bulletin, **43**, 119 (1970).
2) K. Saito and M. Takahashi, *ibid.*, **42**, 3462 (1969).
3) R. W. Kluiber, *J. Amer. Chem. Soc.*, **82**, 4839 (1960).
4) R. C. Fay, A. Y. Girgis, and U. Klabunde, *ibid.*, **92**, 7056 (1970).
5) H. A. C. McKay, *Nature*, **142**, 997 (1938).

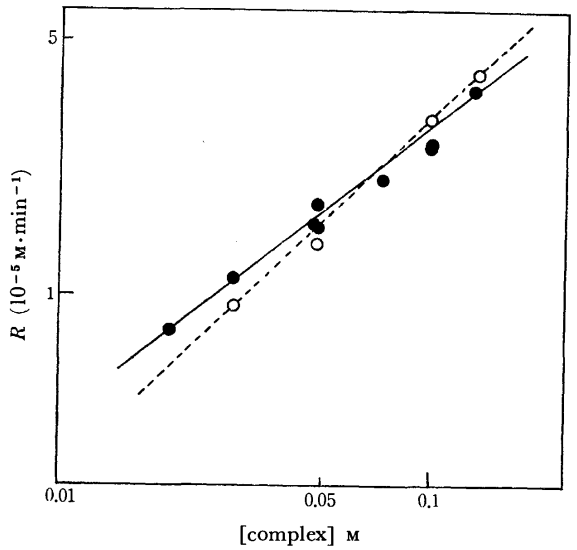

Fig. 2. Relationship between R and the initial concentration of complex.
90°C, —●— in toluene, --○-- in anisole, [acacH] =0.05 M.

near to unity in both solvents and the rate is expressed by Eq. (1).

$$R = k_0[\text{complex}] \quad (1)$$

Figure 3 gives the relationship between R and the concentration of the free ligand in anisole and toluene. The diagram indicates that the k_0 consists of two terms, one of which is independent of and the other dependent on the concentration of acacH. (Eq. 2)

$$R = [\text{complex}](k_1 + k_2[\text{acacH}]) \quad (2)$$

The k_1 and the k_2 are known from the intercept and the gradient of the lines, respectively, and listed in Table 1. The Arrhenius activation energy is known from the data in Table 1 and listed together. Because of the big error involved in the determination of k_1 and k_2 values by extrapolation, only overall E_a values are significant. The influence of acid and base on the

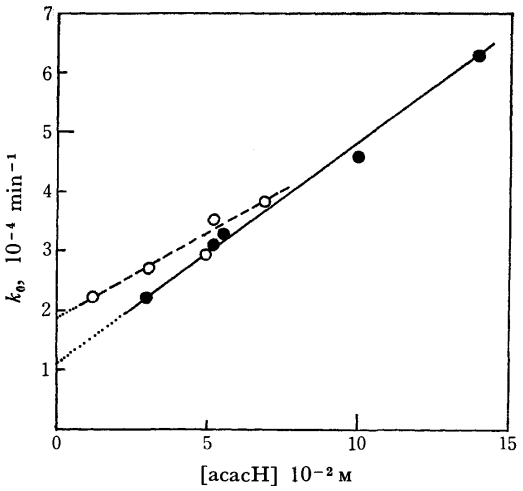

Fig. 3. Relationship between k_0 and the initial concentration of free acetylacetone-^{14}C.
90°C, —●— in toluene, --○-- in anisole.

exchange rate in toluene and anisole is shown in Table 2. Addition of the bivalent cobalt(II) complex [Co(acac)$_2$] did not affect the rate. Toluene was almost saturated with water, and its content was changed within a limited range (0.008 to 0.019 M) in the given temperature region. However, no significant change in R values was observed. The water content remained practically unchanged (within ±0.001 M) during kinetic runs.

Discussion

As the McKay plot indidates, isotopic exchange reaction predominates at the early stage of reaction without being involved by the irreversible decomposition. It appears as if the linear range on the McKay plot is larger at a higher temperature. It is presumably because the temperature coefficients of the rates of isotopic exchange and the decomposition differ from each other.

Table 1. First order rate constants and the Arrhenius activation energy[a)]

Solvent	Temp. °C	k_0 min^{-1}	E_a kcal/mol
Toluene	80	1.6×10^{-4}	
	85	2.2×10^{-4}	
	90	3.2×10^{-4} [b)]	18
	97	4.6×10^{-4}	
Anisole	80	1.1×10^{-4}	
	90	2.8×10^{-4} [c)]	25
	97	6.0×10^{-4}	
Chlorobenzene	80	1.2×10^{-4}	
	90	2.4×10^{-4}	21
	97	5.0×10^{-4}	
(Racemization)	98.2	4.8×10^{-3}	34.8 [d)]
(Isomerization of [Co(bzac)$_3$])	96.1	7.6×10^{-3}	33 [e)]
(Inversion of [Co(bzac)$_3$])	96.1	1.3×10^{-2}	33 [e)]
(Ligand interchange of [Co(bzac)$_3$])	96.1	4×10^{-6}	48 [f)]

a) [complex]=[acacH]=0.05 M. b) $k_1=1.85\times10^{-4}$ min^{-1}, $k_2=3.05\times10^{-3}$ M^{-1} min^{-1}. c) $k_1=1.1\times10^{-4}$, $k_2=3.2\times10^{-3}$. d) Ref. 4. e) Average of *cis*- and *trans*-isomers, Ref. 6. f) Exchange of benzoylacetonate between [Co(bzac)$_3$] and [Co(bzac-d_4)$_3$], Ref. 6.

Table 2. Influence of acids and base upon the rate

Solvent	Acid or base	Concn (M)	R mol·min^{-1}	k_0 min^{-1}
Toluene	*m*-Toluic acid	0.01	1.1×10^{-5}	4.2×10^{-4}
	Trichloroacetic acid	0.01	8.3×10^{-5}	16.6×10^{-4}
	Pyridine	0.02	1.2×10^{-5}	2.4×10^{-4}
	(None)		1.6×10^{-5}	3.6×10^{-4}
Anisole	*m*-Toluic acid	0.01	1.8×10^{-5}	3.6×10^{-4}
	Trichloroacetic acid	0.01	12.5×10^{-5}	25.0×10^{-4}
	Pyridine	0.02	1.2×10^{-5}	2.4×10^{-4}
	(None)		1.4×10^{-5}	2.4×10^{-4}

[complex]=[acacH]=0.05 M, 90°C.

The k_1 Path. The first term of Eq. (2) seems to represent a mechanism in which the break of metal-ligand bond is the rate-determining step. This path can be interpreted in two ways. In one of them, break of the first metal-oxygen bond at one of the chelate rings is the rate-determining step, and the remaining metal-oxygen bond breaks fast. The second way is to consider that the first bond breaks and forms rapidly so that an intermediate state involving unidentate acetylacetonate can survive for a significant lapse of time, and the break of the remaining bond is the rate-determining step.

Girgis and Fay[6] studied the kinetics of ligand interchange between tris(benzoylacetonato)cobalt(III) [Co(bzac)$_3$] with the same complex labelled with ^{2}H in chlorobenzene at 96.1°C, and compared the rate and activation parameters with those of the inversion and isomerization of this complex (Table 1). The ligand interchange proceeds slower by one order or two, and they proposed a predominating intermediate involving axial trigonal bipyramidal structure with a unidentate ligand. Their k_0 value for ligand interchange was obtained in the absence of excessive ligand, and can be compared with our k_1 values. Although the experimental conditions are different, our k_1 values are larger than theirs by *ca.* two orders. This fact would be due to the smaller basicity of acetylacetonate than benzoylacetonate.

Fay, Girgis, and Klabunde measured the rate of racemization of partly resolved [Co(acac)$_3$] in chlorobenzene at 78 to 108°C.[4] The results are included in Table 1. Although their experimental condition is not exactly equal to ours, the isotopic exchange rate is smaller than the rate of racemization by one order.

In order to account for the mechanisms of isotopic exchange and racemization in consonance, we tend to consider an intermediate involving a unidentate ligand. Fig. 4 gives a probable scheme for the mechanism of the present isotopic exchange. One of the cobalt(III)-oxygen bonds in one of the three ligands can break and restore rapidly. The vacant coordination site could be occupied either by the solvent molecule or free acetylacetone. The latter case will be discussed later. The intermediate can also rearrange to give trigonal bipyramidal structure. Whenever the remaining bond of the unidentate ligand

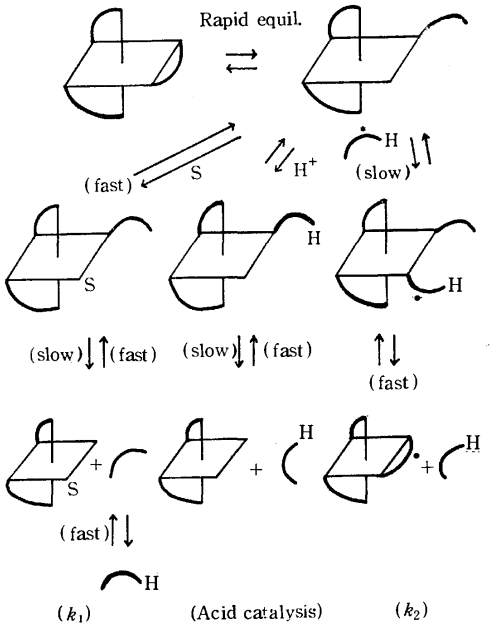

Fig. 4. Probable mechanism for the isotopic exchange. S, solvent molecule; the arc-form represents acac$^-$.

breaks spontaneously, the ligand would be liberated and the labelled free acetylacetone would combine with cobalt(III) rapidly to give a first order rate term corresponding to k_1. Contribution of this term would depend on how easily the free end of unidentate ligand recombines with cobalt(III). A polar solvent such as anisole would occupy the vacant site more easily than less polar solvents (*e.g.* toluene) do, and retard the recombination to increase the contribution of k_1. This is what was experimentally found.

An alternative explanation could be encountered by considering the role of water in the solvent. However, water content did not affect the rate, although the examined range of concentration was rather small, and its participation could be excluded.

The acid catalysis could be understood by considering the protonation at the free end of unidentate ligand, which increases the difficulty with which the free end recombines with cobalt(III) to restore the original complex. Only a strong acid such as trichloroacetic acid seems to be eligible of bringing about such an effect. Contribution of free acetylacetone (p$K\simeq6$) as acid catalyst is ruled out, because a stronger acid, *m*-toluic acid (pK=4.27) is not useful as acid catalyst.

6) A. Y. Girgis and R. C. Fay, *J. Amer. Chem. Soc.*, **92**, 7061 (1970).

If an acetylacetonate ligand were liberated whenever its first bond with cobalt(III) was broken, this would result in simultaneous racemization and isotopic exchange. Hence the fact that racemization is faster than isotopic exchange (Table 1) should be interpreted by an intra-molecular twist mechanism without liberation of the ligand. The activation enthalpy of the racemization is close to those of inversion and isomerization of $[Co(bzac)_3]$, and there seems to be no reason to exclude such a twist mechanism for the racemization of $[Co(acac)_3]$.

The k_2 Term. The second term of Eq. (2) is also interpreted in two ways. One is to reckon a rate-determining nucleophilic attack of acetylacetone upon the intermediate containing a unidentate acetylacetonate. The other is to consider a preliminary equilibrium between free acetylacetone and the intermediate, and regard the break of remaining cobalt(III)-oxygen bond of the original ligand as rate-determining step. In this case the k_2 term is written as $k_2'K_2$[acacH], where K_2 and k_2' stand for the apparent association constant and the rate of bond break in the adduct, respectively.

Such an interaction was first proposed by Graziano and Harris,[7] and later modified by Llewellyn, O'Connor and Odell[8] for the isotopic exchange of trioxalatochromate(III) with oxalic acid-^{14}C. Neither of them, however, distinguished these two mechanisms. It is generally understood that a dissociative mechanism gives higher E_a values than an associative mechanism does. The E_a values in Table 1 decreases in the sequence, anisole, chlorobenzene, and toluene. Because of experimental difficulty E_a values for the k_1 and the k_2 path were not obtained separately. Anisole, with the biggest contribution of the k_1 term, gives the biggest E_a, whilst toluene with the smallest contribution of k_1 gives the smallest E_a. Chlorobenzene will have less affinity toward cobalt(III) than anisole despite of its bigger dipole moment.

This fact seems to be in favor of the first mechanism reckoning rather associative nature of the k_2 term. Dielectric constants of organic compounds decrease with rise of temperature, and the rather ionic interaction involved in the preliminary equilibrium between free acetylacetone and the intermediate will be facilitated at a higher temperature. This would give rise to increase in K_2 values with rise of temperature and the the dissociative $k_2'K_2$ values might bring about bigger temperature coefficient for the k_2 term. Such a tendency does not seem to suit for interpretation of the experimental results, and we tend to reckon the rather associative interpretation more appropriate, although nothing decisive can be stated at the present stage.

7) F. D. Graziano and G. M. Harris, *J. Phys. Chem.*, **63**, 330 (1959).

8) D. R. Llewellyn, C. O'Connor, and A. L. Odell, *J. Chem. Soc.*, **1964**, 4627.

Experimental

Materials. The labelled compound, acetylacetone-^{14}C was prepared as reported before.[1] The specific activity was 0.02 mCi per mg. Tris(acetylacetonato)cobalt(III) was synthesized from cobalt(II) carbonate, commercial acetylacetone, and hydrogen peroxide, and recrystallized from hot benzene by addition of petroleum ether and cooling.[8] When the recrystallized $[Co(acac)_3]$ was sublimed at 3 mmHg at 120°C, the product gave the same kinetic result. Hence the product was regarded sufficiently pure. Impure complex can give erroneous results.

Toluene was shaken with concentrated sulfuric acid, washed with water and sodium hydroxide solution, dried with calcium chloride and then with metallic sodium and distilled. Anisole was washed with sodium hydroxide solution and water, dried with calcium chloride and then with sodium and distilled. Chlorobenzene was washed with 1% sodium carbonate solution and water, dried with calcium chloride and distilled. The water contents of these solvents were *ca.* 0.012, 0.035, and 0.0046 M, respectively, on Karl Fischer titration in a mixture of pyridine and propyleneglycol. *m*-Toluic and trichloroacetic acid were sublimed *in vacuo*, and pyridine was distilled by the usual method.

Measurement. A known amount of labelled acetylacetone was added to the thermostated complex solution ($\simeq 10^{-2}$ M, 10 or 15 ml) to produce $\simeq 10^{-2}$ M solution and kept in a thermostat. Aliquots ($\simeq 2$ ml each) were taken out of the solution at appropriate intervals, added to cold petroleum ether (*ca.* 20 ml), and set aside in a cold Dewar vessel. Green needles appeared within 3 hr. The mother liquor was decanted, the precipitate washed with petroleum ether and dried at 80°C. A portion (3 to 7 mg) was dissolved in anisole containing 0.4% *p*-terphenyl and 0.01% POPOP (30 ml) to prepare liquid scintillator and the counting rate measured by use of the photomultiplier pulse due to β rays.[1] The quenching effect of the colored solution was corrected by use of a calibration curve. (*e.g.* the apparent counting rate decreases to 72% in the liquid scintillator containing 3 mg of $[Co(acac)_3]$ per 30 ml.) Acids and bases were added to the original complex solution in advance.

The authors wish to thank Nishina Memorial Foundation for the Grant-in-aid.

Synthesis of Tengerite Type Rare Earth Carbonates[1]

Hisanobu WAKITA* and Kozo NAGASHIMA

Department of Chemistry, Faculty of Science, Tokyo Kyoiku University, Bunkyo-ku, Tokyo, 112

(Received March 28, 1972)

Rare earth carbonates which give the same X-ray powder diffraction pattern as tengerite were prepared by heating aqueous solutions containing rare earth chlorides and ammonium trichloroacetate. Y, Er, Ho, and Gd gavee xactly the same X-ray powder pattern as tengerite, while Nd and Sm were similar to tengerite but with a few additional diffractions. X-ray powder data of the tengerite type rare earth carbonate were indexed and cell parameters of $a_0=9.20\pm0.02$ Å, $b_0=11.32\pm0.03$ Å, and $c_0=7.59\pm0.01$ Å for $Y_2(CO_3)_3\cdot nH_2O$ ($n=2$—3), with 4 moles of formula units per cell and orthorhombic symmetry were established. Linear correlations were demonstrated between refractive indices or cell parameters of the synthesized carbonates and their respective rare earth element atomic numbers.

The compositions and structures of rare earth carbonates have been the subject of numerous recent studies.[2] Some of the results reported in these studies are inconsistent. Most mineralogists consider the existence in nature of only three normal carbonates: lanthanite $La_2(CO_3)_3\cdot 8H_2O$,[3] calkinsite $(La,Ce)_2(CO_3)_3\cdot 4H_2O$,[4] and tengerite $Y_2(CO_3)_3\cdot nH_2O$ ($n=2$—3),[5] and several double carbonates such as burbankite $Na_2(Ca, Sr, Ba, Ce, La)_4(CO_3)_5$,[4] and sahamalite $(Ce, La, Nd)_2(Mg, Fe)(CO_3)_4$.[6]

Shinn and Eick[7] studied the structure of lanthanite and indicated that it contains 4 formula units in an orthorhombic unit cell of space group Pccn, with lattice parameters of $a_0=8.984\pm0.004$, $b_0=9.580\pm0.004$, and $c_0=17.00\pm0.01$ Å ($\rho_{obsd}=2.72\pm0.02$ g cm^{-3}; $\rho_{calcd}=2.732$ g cm^{-3}). Pecora and Kerr[4] examined calkinsite X-ray crystalographically and determined the following cell parameters; $a_0=9.57\pm0.02$, $b_0=12.65\pm0.08$, $c_0=8.94\pm0.02$ Å, space group $P2_122_1$ or D_2,[4] 4 formula units per cell. Among these rare earth carbonates, rather little has been known of the characteristics of tengerite, a very rare hydrous yttrium carbonate mineral, despite its early discovery at Ytterby, Sweden.

Regarding the composition of tengerite, Iimori[8] suggested the formula of a hydrous basic double carbonate of yttrium and calcium, $Y_3Ca(OH)_3(CO_3)_4\cdot 3H_2O$-(?) based on the analysis of the material from Suishoyama, Iisaka, Fukushima, Japan. On the other hand, the material from Baringer Hill, Texas, USA, was described as a hydrous double carbonate of yttrium and beryllium.[9]

To study the composition, a hydrated yttrium carbonate was synthesized by precipitation from a homogeneous aqueous solution containing yttrium chloride and ammonium trichloroacetate and digestion of the precipitate in the mother liquor for an extended period. The X-ray diffraction pattern of the precipitated carbonate agreed with that of tengerites from Suishoyama[10] and from Iveland, Norway (ASTM-16-698). The similarity between the sample from Suishoyama and the synthesized carbonate was also confirmed by DTA, TGA, and IR absorption data.[5] The analysis of the synthesized carbonate established the following molecular ratio; $Y_2O_3=1.00$: $CO_2=3.01$: $H_2O=2.35$ (average). This ratio is close to the normal carbonate of yttrium.

Experimental and Results

Preparation of the Tengerite Type Rare Earth Carbonates. Rare earth carbonates may be conveniently prepared by precipitation from homogeneous solution by hydrolysis of the trichloroacetates of rare earth elements.[11]

$$2M(C_2Cl_3O_2)_3 + (x+3)H_2O \rightarrow M_2(CO_3)_3\cdot xH_2O + 3CO_2 + 6CHCl_3$$

Rare earth carbonates thus obtained are usually coarse and easily filtered. However, the precipitates generally appear amorphous when examined by X-ray powder diffractometry. (This is probably the explanation for the many different results reported for the compositions of artificially prepared rare earth carbonates.) Crystalline precipitates of excellent quality were obtained by heating the solutions containing the precipitates for several days. As will be described in the following section, the crystalline yttrium carbonate prepared by this procedure has the tengerite structure.

The procedure applied throughout the study is as follows: Four g of trichloroacetic acid were added

1) Presented in part at the 23rd annual meeting of the chemical society of Japan, Tokyo, 1969.

* Present address: Department of Chemistry, Faculty of Science, Fukuoka University, Fukuoka, 814.

2) R. G. Charles, *J. Inorg. Nucl. Chem.*, **27**, 1498 (1965); E. L. Head and C. E. Holley, Jr., "Rare Earth Research III," Gordon and Breach, New York, N.Y. (1964), p. 51; E. L. Head and C. E. Holley, Jr., "Rare Earth Research IV," Gordon and Breach, New York, N.Y. (1965), p. 707.

3) A.S.T.M.; Alphabetical and Grouped Numerical Index of X-ray diffraction Data, 14—190.

4) W. T. Pecora and Joe H. Kerr, *Am. Mineral.*, **38**, 1169 (1953).

5) K. Nagashima and H. Wakita, *Nippon Kagaku Zasshi*, **89**, 856 (1968).

6) H.W. Jaffe, R. Meyrowitz, and H. T. Evans, Jr., *Am. Mineral.* **38**, 741 (1953).

7) D. B. Shinn and H. A. Eick, *Inorg. Chem.*, **7**, 1340 (1968).

8) T. Iimori, *Sci. Papers Inst. Phys. Chem. Res.* (Tokyo), **38**, 832 (1938).

9) C. Palache, H. Berman, and C. Frondel, "Dana's System of Mineralogy," Vol. II, 7th ed., John Wiley & Sons, Inc., New York, N.Y. (1951), p. 275.

10) A. Kato, "X-ray Powder Data for Radioactive Minerals," No. 11, Geological Survey of Japan, Tokyo, Japan, 1958, p. 127.

11) M. L. Salutsky and L. L. Quill, *J. Amer. Chem. Soc.*, **72**, 3306 (1950).

to 250 m*l* of aqueous solution containing 6 mM yttrium chloride. The pH of the solution was adjusted between 4 and 5 with dilute ammonium hydroxide, then the solution was heated on a steam bath for two days.

Figure 1 shows a typical micrograph of yttrium carbonate prepared by this procedure.

Fig. 1. Hydrated yttrium carbonate.

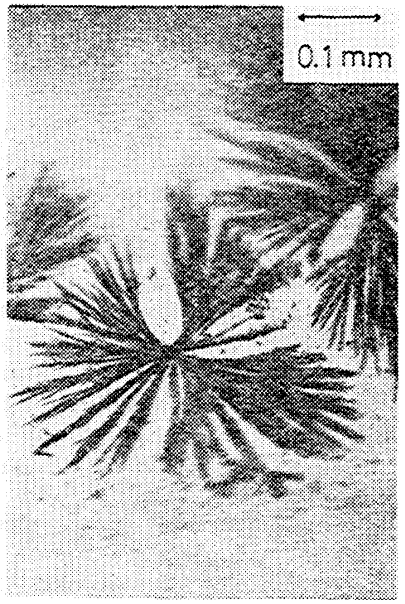

Fig. 2. Hydrated yttrium carbonate (prepared in a sealed tube).

Figure 2 is also a micrograph of yttrium carbonate prepared by maintaining the solution (YCl_3+CCl_3-COOH+NH_4OH, pH=4—5) in a sealed glass ampoule for about one week at 70°C. Carbonates of the other rare earth elements were synthesized by applying the same procedure. Most of the specimens were in the form of radial aggregates of fine fibers as seen in Fig. 1. Carbonates samples other than yttrium exhibited admixed larger amorphous particles in addition to the crystalline particles.

X-Ray Powder Diffraction and Optical Properties. The X-ray powder diffraction data for the synthesized yttrium carbonate are tabulated in Table 1, in which those for tengerite from Iveland, Norway (ASTM 16-698(1966)) are also represented for comparison.

The X-ray powder data of the synthesized sample are virtually identical with those of natural tengerite.

TABLE 1. X-RAY POWDER DATA AND THEIR INDICES FOR NATURAL TENGERITE AND SYNTHESIZED HYDRATED YTTRIUM CARBONATE

I		II				
d_{obs} Å	I/I_0	d_{obs} Å	I/I_0	$Q(1/d^2)_{obs}$	Probable *hkl*	$Q(1/d^2)_{calc}$
7.54	60	7.589	90	0.017	001	0.017
5.60	60	5.673	70	0.031	020	0.031
4.57	70	4.604	100	0.047	200	0.047
3.86	100	3.890	70	0.066	201	0.065
3.77	20	3.782	30	0.070	030	0.070
3.55	60	3.573	50	0.078	220	0.079
		3.046	5	0.108	300	0.106
2.95	70	2.967	40	0.114	310	0.114
		2.919	8	0.117	230	0.118
2.68	20	2.696	15	0.136	320	0.138
2.59	10	2.598	10	0.148	222	0.148
2.53	50	2.537	30	0.155	321	0.155
		2.520	10	0.158	003	0.156
		2.406	10	0.173	240	0.172
		2.372	10	0.178	330	0.177
		2.334	5	0.184	312	0.184
2.29	30	2.295	10	0.190	241	0.190

I: Iveland, Norway (ASTM). Fe/Mn rad.=1.9373 Å.
II: Synthesized hydrated yttrium carbonate, Cu/Ni rad.=1.5418 Å.

Under the microscope the synthesized sample shows a straight extinction and positive axial character. The refractive indices of the synthesized yttrium carbonate are

$\gamma=1.624\pm0.002$, $\alpha=1.612\pm0.001$ and $\gamma-\alpha=0.012\pm0.003$

Those of natural tengerite from Suishoyama, Japan measured by Kato[10] are

$\gamma=1.642$, $\alpha=1.622$, and $\gamma-\alpha=0.020$

The small difference between the two materials may be due to the compositional difference. The other optical properties could not be measured accurately, because the synthesized sample is too finely grained. The above data lead the assignment of tetragonal or orthorhombic (or hexagonal) symmetry to the carbonate.

The indexing to the X-ray powder data for tengerite was accomplished through the application of Battelle indexing charts,[12] since a literature survey, did not reveal an index to the X-ray powder data for tengerite.

In Table 1 the probable indices are given, and good agreement is shown between the observed and calculated Q values when an orthorhombic cell with $a_0=9.20\pm0.02$, $b_0=11.32\pm0.03$, $c_0=7.59\pm0.01$ Å was assumed. Applying these cell parameters and measured density (3.3—3.1 g cm^{-3}), the number of the formula units in a cell was calculated as 4. The results of electron diffraction studies were used to determine the crystal system and cell parameters.

12) J. C. Bell and A. E. Austin, "Battelle Indexing Charts for Diffraction Patterns of Tetragonal, Hexagonal and Orthorhombic Crystals," Battelle Memorial Institute, Columbus 1, Ohio, U.S.A.

Chemical Analysis of Rare Earth Carbonates. The results of the chemical analyses of air dried carbonates are given in Table 2. Table 2 also shows that the molar ratios, $R_2O_3 : CO_2$ ($: H_2O$) are not whole numbers except in the case of yttrium carbonate which corresponds to $Y_2(CO_3)_3 \cdot nH_2O$ ($n=2$—3, a part of H_2O may be zeolitic). This apparent anomaly may be attributed to the admixed amorphous particles and to the instability of the carbonates. Concerning the instability of rare earth carbonates, Shinn and Eick[7] mentioned two bonding positions of carbonate ions in the lanthanite structure, one coordinates as a unidentate ligand and one as a bidentate ligand. Water molecules behave similarly; one coordinates to a metal ion and one does not, therefore some of the carbonate ions and water molecules may be expected to be rather easily lost from the structure.

Table 2. Chemical analyses of synthesized rare earth carbonate

	M_2O_3 : CO_2 : H_2O (molar ratio)		
$Y_2(CO_3)_3 \cdot nH_2O$	1.00	3.01	2.35
Yb- [a]	1.00	2.05	3.87
Er- [b]	1.00	3.01	2.25
Ho-	1.00	2.43	4.58
Dy-	1.00	2.84	2.79
Gd-	1.00	2.92	2.58
Sm-	1.00	2.87	2.34
Nd-	1.00	2.79	2.29
La-	1.00	2.97	8.04

a) Amorphous by X-ray examination.
b) Prepared in a sealed tube.

Proton magnetic resonance of the synthesized hydrated lanthanum carbonate (lanthanite type) and hydrated yttrium carbonate (tengerite type) were run at room temperature using a broad-line NMR spectrometer. A spectrum composed of a broad and a sharp absorption indicating two bonding positions for water molecules, was obtained for the lanthanum compound, while a signal with one sharp absorption was obtained for the yttrium compound.

X-Ray Powder Diffraction of Some Rare Earth Carbonates. By the procedure described in the prior section, hydrated carbonates were obtained from lanthanum, neodymium, samarium, gadolinium, dysprosium, holmium, erbium and ytterbium. The X-ray powder diffraction patterns and the powder data of these carbonates are shown in Fig. 3 and Table 3 respectively. Figure 3 indicates the X-ray powder patterns of gadolinium, dysprosium, and holmium carbonates are almost identical with that of yttrium carbonate. The increase in d values with increasing ionic radii of the metals is well recognized (Table 3).

As for neodymium and samarium compounds, although several additional diffractions, for example at 5.529(Nd) and 5.481Å(Sm), were observed, the arrangements and intensities of most of the diffractions are almost the same as those of yttrium carbonate. The lanthanum compound given an X-ray powder pattern quite different from that of yttrium carbonate

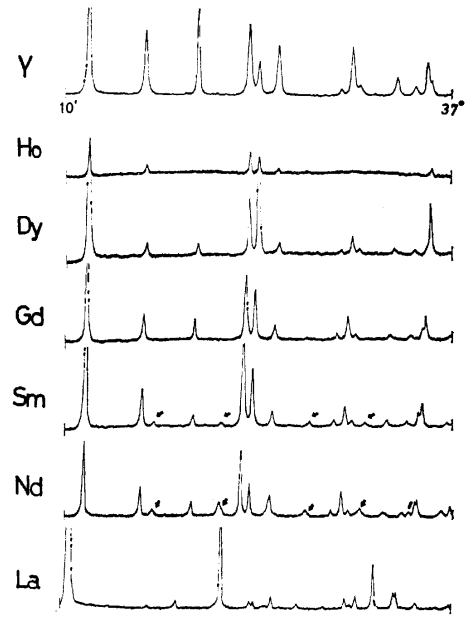

Fig. 3. X-ray powder diffraction patterns of hydrated rare earth carbonates.
Arrows indicate peaks not observed in the diffractions of tengerite

and similar to that of lanthanite.[3] The pattern and powder data for ytterbium and scandium compounds are not listed in the figure and table, because only an amorphous phase for ytterbium and a hydroxide for scandium were obtained by the present procedure. These results may indicate the fact that La^{3+} is too large and Yb^{3+} and Sc^{3+} are too small for the tengerite structure.

In Table 3, in addition to the powder data, cell parameters a_0, b_0, c_0 and refractive indices γ and α of

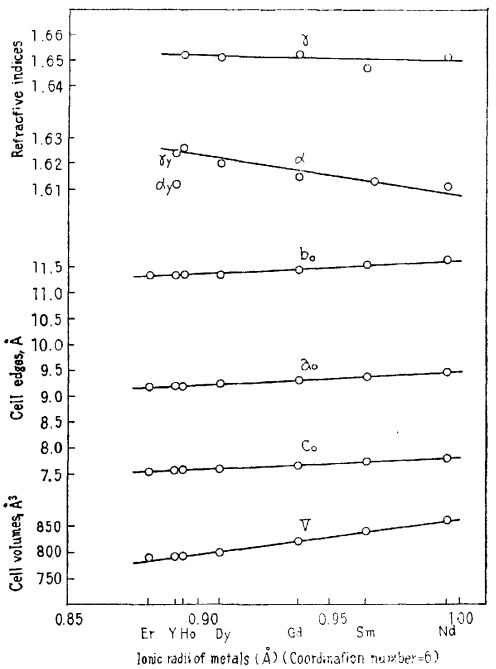

Fig. 4. Lattice parameters, refractive indices *vs.* ionic radii of rare earth metals.

TABLE 3. X-RAY POWDER DATA, CELL PARAMETERS[a] AND REFRACTIVE INDICES FOR SYNTHESIZED RARE EARTH CARBONATES

$Y_2(CO_3)_3 \cdot H_2O$			Er-	Ho-	Dy-	Gd-	Sm-	Nd-	La-
d (Å)	I/I_0	probable hkl	d (Å)	d (Å)	d (Å)	d (Å)	d (Å)	d (Å)	d (Å)
7.589	90	001	7.563	7.589	7.609	7.681	7.755	7.823	8.588
5.673	70	020	5.673	5.673	5.684	5.731	5.780	5.825	6.800
							5.481[b]	5.529[b]	5.627
4.604	100	200	4.601		4.618	4.659	4.695	4.738	5.001
							4.254[b]	4.295[b]	4.066
3.890	70	201	3.887	3.893	3.897	3.933	3.965	4.001	3.890
3.782	30	030	3.778	3.784	3.789	3.824	3.858	3.897	3.850
3.573	50	220	3.576	3.579	3.580	3.616	3.645	3.678	3.651
							3.295[b]	3.334[b]	3.403
3.046	5	300	3.045		3.045	3.079	3.104	3.131	3.184
2.967	40	310	2.965		2.975	3.000	3.026	3.050	3.021
2.919	8	230	2.915		2.930	2.952	2.979	3.006	2.988
							2.889[b]	2.929[b]	2.988
2.696	15	320	2.699		2.714	2.734	2.759	2.780	
2.598	10	222	2.595		2.607	2.626	2.648	2.675	
								2.637[b]	
2.537	30	321	2.517			2.564	2.585	2.607	

$Y_2(CO_3)_3 \cdot nH_2O$	Er-	Ho-	Dy-	Gd-	Sm-	Nd-	La-
$a_0=9.20\pm0.02$ Å	9.20	9.21	9.24	9.32	9.39	9.48	
$b_0=11.32\pm0.03$ Å	11.35	11.35	11.37	11.46	11.56	11.65	
$c_0=7.59\pm0.01$ Å	7.56	7.59	7.61	7.68	7.76	7.82	
$\gamma=1.624$		1.652	1.651	1.652	1.647	1.651	
$\alpha=1.612$		1.626	1.620	1.615	1.613	1.611	

a) Except for yttrium compound, calculated from 001, 020, and 200.
b) Additional diffractions. In calculation of a_0, b_0, c_0, these diffractions were neglected.

the compounds are listed. The values of a_0, b_0, and c_0 for samarium and neodymium compounds were calculated by applying the indices of tengerite to most of the diffractions and neglecting the weak diffractions to which indices of tengerite could be given.

Relations between Lattice Parameters and Refractive Indices of Rare Earth Carbonates and the Ionic Radii of Rare Earth Elements. In Fig. 4, cell parameters a_0, b_0, and c_0 and refractive indices γ and α, of the synthesized carbonates are plotted *versus* ionic radii of rare earth metals.[13] It is observed in Fig. 4 that cell parameters a_0, b_0, and c_0 and unit cell volumes of tengerite type rare earth carbonates increase linearly with increasing ionic radii of the metals, while refractive indices, (which closely follow the densities) decrease with increasing ionic radii of the metals.

13) R. D. Shannon and C. T. Prewitt, *Acta Crystallogr.*, (1969), B25, 925.

The authors wish to express their thanks to Dr. Y. Kuroda and Dr. S. Shimoda, Geological and Mineralogical Institute, Tokyo Kyoiku University, Dr. A. Kato, National Science Museum, Dr. K. Harada, Exploration Department, Sumitomo Metal Mining Co., and to Mr. K. Furuhashi of this department for their generous helps.

Binuclear Metal Complexes. IV.[1] The Preparation and Properties of Binuclear Copper(II) Complexes of Schiff Bases Derived from 2,6-Diformyl-4-methylphenol and Glycine or Alanine[2]

Hisashi OKAWA, Sigeo KIDA, Yoneichiro MUTO,* and Tadashi TOKII*

Department of Chemistry, Faculty of Science, Kyushu University, Hakozaki, Fukuoka

**Department of Chemistry, Saga University, Saga*

(Received April 10, 1972)

A new series of binuclear copper(II) complexes with different bridging groups, Fsal(=gly)$_2$Cu$_2$X (X=OH, Cl, Br) and Fsal(=ala)$_2$Cu$_2$X (X=Cl), were synthesized, Fsal(=gly)$_2$ and Fsal(=ala)$_2$ being the Schiff bases prepared by condensation of 2,6-diformyl-4-methylphenol with glycine and alanine, respectively. The copper(II) ions are bridged by the phenolic oxygen in the organic moiety and also the X. The properties of the complexes were studied by IR spectra, visible spectra, and magnetic susceptibility measurements at various temperatures. From the cryomagnetic data it was concluded that the effect of the bridging group X upon magnetic exchange interaction decreases in the order: OH>Cl~Br.

It is known that 1,3,5-triketones[3-5] and diethyl cyclopentanone-2,5-diglyoxylate[6,7] form binuclear copper(II) complexes composed of two ligands and two copper(II) ions. Although 2,6-diformyl-4-methylphenol is similar to the ligands in structure, its complex-forming behavior is markedly different. The ligand and copper(II) chloride form a binuclear complex, dichloro-μ-chloro-μ-2,6-diformyl-4-methylphenolatodicopper(II)[8] (Fig. 1, (a)), in which the ratio of copper to the ligand is 2 : 1. Thus the use of 2,6-diformyl-4-methylphenol makes it possible to prepare binuclear copper(II) complexes bridged with two different groups, i.e., the phenolic oxygen (the first bridging group) and a monoatomic or polyatomic anion such as chloride, bromide, hydroxide, or methanolate ion (the second bridging group). Okawa prepared dihalogeno-μ-hydroxo-μ-2,6-bis-(*N*-alkyliminomethyl)-4-methylphenolatodicopper(II)[8] (Fig. 1, (b)), by the reaction of 2,6-diformyl-4-methylphenol, an alkyl amine and copper(II) chloride or copper(II) bromide. A binuclear copper(II) complex of the Schiff base with *o*-aminophenol, in which a methanolate ion acts as the second bridging group, was also prepared[9] (Fig. 1, (c)).

It is clear that the second bridging group is variable depending upon the nature of the four coordinating atoms other than the bridging atoms. It appears that there is a certain relation between the coordinating and bridging atoms closely associated with

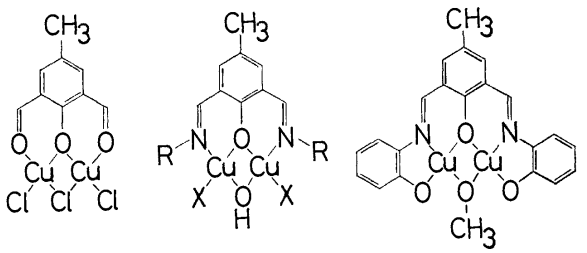

R=alkyl
X=Cl or Br

(a) (b) (c)

Fig. 1.

the stability of the binuclear copper(II) complex. In order to find the relation, we attempted to synthesize binuclear copper(II) complexes of the Schiff bases derived from 2,6-diformyl-4-methylphenol and α-amino acids. We obtained a series of Fsal(=gly)$_2$-Cu$_2$X (X=OH, Cl or Br) and Fsal(=ala)$_2$Cu$_2$X (X=Cl), where Fsal(=gly)$_2$ and Fsal(=ala)$_2$ indicate the Schiff bases with glycine and alanine, respectively, and the X is the second bridging group(Fig. 2).

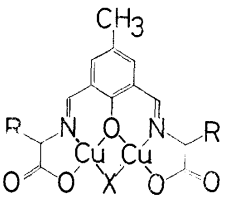

R=H: Fsal(=gly)$_2$Cu$_2$X (X=OH, Cl or Br)
R=CH$_3$: Fsal(=ala)$_2$Cu$_2$X (X=Cl)

Fig. 2. Structure of complexes.

These complexes are the first series of planar binuclear copper(II) complexes bridged with two different groups.

The magnetic exchange between a pair of copper(II) ions has also been studied. In Fsal(=gly)$_2$Cu$_2$X only the second bridging group, X, varies. Thus the complexes are very suitable for a study of the effects of the bridging groups upon the spin-spin coupling interaction.

1) Part III, H. Okawa and S. Kida, This Bulletin, **45**, 1759 (1972).

2) This work was presented at the 24th Annual Meeting of the Chemical Society of Japan, Suita, April, 1971. A part of the work was reported by H. Okawa and S. Kida, This Bulletin, **44**, 1172 (1971).

3) Y. Taguchi, F. Sagara, H. Kobayashi, and K. Ueno, *ibid.*, **43**, 2470 (1970).

4) D. Baker, C. W. Dudley, and C. Oldham, *J. Chem. Soc., A*, 2608 (1970).

5) D. P. Murtha and R. L. Lintvedt, *Inorg. Chem.*, **9**, 1532 (1970).

6) D. P. Graddon and I. T. Townsend, *Aust. J. Chem.*, **22**, 505 (1969).

7) A. D. Toy, T. D. Smith and J. R. Pilbrow, *J. Chem. Soc., A*, 2600 (1970).

8) H. Okawa, This Bulletin, **43**, 3019 (1970).

9) R. Robson, *Inorg. Nucl. Chem. Lett.*, **6**, 125 (1970).

Experimental

Syntheses. The synthesis of 2,6-diformyl-4-methylphenol has been described previously.[1]

Fsal(=gly)$_2$Cu$_2$Cl. An aqueous solution of glycine (300.3 mg) was added to a solution of 2,6-diformyl-4-methylphenol (330 mg) and copper(II) chloride dihydrate (681 mg) in ethanol (75 m*l*). The clear solution was heated at 70°C for ten minutes and left standing overnight. The separated green needles were collected and washed with ethanol.

Found: C, 35.42; H, 2.67; N, 6.11; Cl, 7.82%; mol wt, 430 (methanol). Calcd for $C_{13}H_{11}N_2O_5ClCu_2$: C, 35.67; H, 2.53; N, 6.40; Cl, 8.10%; mol wt, 437.78.

Fsal(=gly)$_2$Cu$_2$Br. An aqueous solution of glycine (300.3 mg) was added to a dark solution of 2,6-diformyl-4-methyl-phenol (330 mg) and anhydrous copper(II) bromide (893.5 mg) in ethanol (100 m*l*). The resulting green solution was heated on a water-bath and then cooled to give green needles, which were collected and washed with ethanol.

Found: C, 32.74; H, 2.41; N, 5.51; Br, 16.71%. Calcd for $C_{13}H_{11}N_2O_5BrCu_2$: C, 32.38; H, 2.30; N, 5.81; Br, 16.57%.

Fsal(=gly)$_2$Cu$_2$(OH)·H$_2$O: An aqueous solution of glycine (300.3 mg) was added to an ethanolic solution of 2,6-diformyl-4-methylphenol (330 mg) and copper(II) acetate monohydrate (800 mg) or copper(II) sulfate pentahydrate (1 g). A yellowish green by-product was separated by decantation and the remaining blue product was collected and thoroughly washed with ethanol. Contamination by the yellow by-product was avoided by employing anhydrous copper(II) fluoride as the source of metal ions.

Found: C, 35.88; H, 3.25; N, 6.33%. Calcd for $C_{13}H_{12}N_2O_6Cu_2\cdot H_2O$: C, 35.70; H, 3.23; N, 6.41%.

The water of crystallization could be removed by heating at 110°C/2 mmHg for 8 hours.

Fsal(=ala)$_2$Cu$_2$Cl. This complex was obtained by treating 2,6-diformyl-4-methylphenol (330 mg), *dl*-alanine (360 mg) and copper(II) chloride dihydrate (681 mg) in ethanol. The green solution was concentrated to 30 m*l*, and 20 m*l* of acetone was added. After the reaction mixture was left standing overnight, the separated deep green needles were collected and washed with cold ethanol.

Found: C, 38.88; H, 3.72; N, 5.76; Cl, 7.70%. Calcd for $C_{15}H_{15}N_2O_5ClCu_2$: C, 38.68; H, 3.25; N, 6.01; Cl, 7.61%.

Measurements. Magnetic susceptibilities were determined in the range from liquid nitrogen temperature to room temperature by the Gouy method with a magnetic field strength of about 7000 Oersted. The apparatus was similar in design to the one described by Figgis and Nyholm;[10] an electromagnet (Nihon-Komitsu Model 350) and a vacuum semimicro balance with a reading accuracy of ±0.02 mg (Chyo Balance Co.). Temperature control was carried out by an electrically regulated system with an accuracy of ±0.2°K at 150°K. Temperature measurements were carried out by means of a copper-constantan thermocouple. The effective magnetic moment μ_{eff} was calculated from the expression

$$\mu_{eff}=2.83\sqrt{(\chi_A-N\alpha)T}\ ,$$

where χ_A is the atomic susceptibility corrected by use of Pascal's constants[11,12] for diamagnetism and $N\alpha$ is the temperature independent paramagnetism associated with copper(II) ions.

The infrared spectra of the complexes were measured with a Hitachi EPI-S2 spectrophotometer in the region 4000—650 cm^{-1} on a KBr disk. In some cases the hexachlorobutadiene mull method was used for the measurements in the region 4000—2000 cm^{-1}. The reflectance spectra and solution spectra of the complexes in water, methanol, and pyridine were measured with a Hitachi EPS-3T spectrophotometer in the near-infrared and visible regions.

Results and Discussion

The complexes Fsal(=gly)$_2$Cu$_2$Cl and Fsal(=gly)$_2$-Cu$_2$Br were obtained quantitatively but the yield of Fsal(=gly)$_2$Cu$_2$(OH)·H$_2$O was low. Only Fsal-(=ala)$_2$Cu$_2$Cl was isolated from Fsal(=ala)$_2$ in a very low yield. The syntheses of binuclear copper(II) complexes of the Schiff bases with other α-amino acids such as valine, leucine, isoleucine, and phenylalanine were unsuccessful. A deep green solution was formed when 2,6-diformyl-4-methylphenol, an amino acid and a copper(II) salt were mixed in

Table 1. IR absorption bands of complexes (cm^{-1}).

Fsal(=gly)$_2$Cu$_2$X			Fsal(=ala)$_2$-Cu$_2$Cl	Assignment
X=OH	X=Cl	X=Br		
3370 w				O-H
3040 w	3050 w	3050 w	3050 w	C-H
2990 w			2990 w	CH_3
2940 w	2950 w	2950 w	2950 w	CH_3
1645 s	1650 s	1650 s	1650 s	C=O
1625 s	1630 s	1630 s	1630 s	C=N
1600 w	1600 m	1595 m	1595 m	skeletal
1555 s	1555 s	1555 s	1560 s	skeletal
1455 m	1455 m	1455 m	1455 m	skeletal
1418 w	1415 w	1415 w	1410 w	
			1390 m	
1357 s	1375 s	1377 s	1360 s	C-O (phenol)
1335 s	1312 m	1315 m	1315 m	
1295 m	1293 m	1290 m	1280 m	
1240 m	1245 w	1258 w	1247 w	
	1235 w	1233 w		
1185 w	1197 w	1200 w	1195 w	
			1120 w	
1085 s	1077 s	1085 s	1085 s	C-N
			1045 w	
1020 w	1007 w	1010 w	1000 w	
990 w	990 w	990 w	990 w	
922 m	940 m	935 m	940 m	
883 w	890 w	868 w	885 w	
837 s	828 s	822 s	825 s	CH out of plane
			782 m	
768 s	762 s	762 s	770 m	
758 s			750 m	

s=strong, m=medium, and w=weak.

10) B. N. Figgis and R. S. Nyholm, *J. Chem. Soc.*, **1959**, 331.

11) G. Foëx, G. J. Gorter, and L. J. Smits, "Constantes Sélectionneés, Diamagnétisme et Paramagnétisme, Relaxation Paramagnétique," Masson & Cie, Paris (1957), p. 222.

12) P. W. Selwood, "Magnetochemistry," Interscience Publishers, New York (1956), pp. 78, 91.

ethanol, but only 2,6-diformyl-4-methylphenol was recovered from the concentrated reaction mixture. The marked differences in isolating the complexes are difficult to explain at present. The molecular weight determination for Fsal(=gly)$_2$Cu$_2$Cl supports the binuclear structure shown in Fig. 2.

The IR spectra of Fsal(=gly)$_2$Cu$_2$X (X=OH, Cl and Br) and Fsal(=ala)$_2$Cu$_2$Cl are very similar to each other (Table 1), suggesting similar structures of the complexes. The spectra in the region 1700—1400 cm^{-1} resemble those of the copper(II) complex of the Schiff base derived from salicylaldehyde and glycine.[13] The complicated bands at 1650—1630 cm^{-1} may be assigned to the C=O and C=N stretching vibrations, while the bands at 1600 and 1455 cm^{-1} have been assigned to the aromatic skeletal vibration.[14,15] Okawa and Kida[9] pointed out that the new band around 1555 cm^{-1} can be attributed to a skeletal vibration of the aromatic ring. The band appears on the low-frequency side of 1550 cm^{-1} in the mononuclear copper(II) complexes of the Schiff bases derived from salicylaldehyde, and on the high-frequency side of 1550 cm^{-1} in the complexes where a phenolic oxygen acts as a bridge.[16] The present complexes are therefore expected to have a binuclear structure bridged with a phenolic oxygen. The very strong band at 1380—1350 cm^{-1} might be assigned to the C–O vibration.[14,15,17] Ueno and Martell[18] assigned the strong band near 1085 cm^{-1} to the C–O stretching vibration. We found that the corresponding band in dichloro-μ-hydroxo-μ-2,6-bis(*N*-alkyliminomethyl)-4-methylphenolatodicopper(II)[7] depends markedly upon the alkyl group (CH_3, 1030; C_2H_5, 1040; *iso*-C_3H_7, 1065; *tert*-C_4H_9, 1080 cm^{-1}). Consequently this band can be assigned to the C–N stretching vibration. In anhydrous Fsal(=gly)$_2$Cu$_2$(OH) the O–H vibration was found at 3370 cm^{-1}.

The ligand field bands of the complexes are given in Table 2. The reflectance spectrum of Fsal(=gly)$_2$Cu$_2$(OH)·H$_2$O showed the ligand field band at 650 mμ, which is higher in energy than those of other complexes. The complexes except for Fsal(=gly)$_2$Cu$_2$(OH)·H$_2$O are likely to keep their binuclear structures in polar solvents such as water, methanol, and pyridine, since they can be recrystallized from these solvents and their visible spectra in them are similar. On the other hand, Fsal(=gly)$_2$Cu$_2$(OH)·H$_2$O is hardly soluble in most solvents though it is soluble in pyridine. However, it is clear that the complex decomposes in pyridine since the green prisms isolated from the concentrated solution were found to be bis(glycinato)copper(II) by IR spectrum. The thermal decomposition temperatures for Fsal(=gly)$_2$Cu$_2$Cl, Fsal(=gly)$_2$Cu$_2$Br and Fsal(=gly)$_2$Cu$_2$(OH)·H$_2$O are 220—225°, 223—225°, and 217—220°C, respectively. Though the difference in the decomposition temperature of the complexes is small, the results indicate that in the series of complexes Fsal(=gly)$_2$Cu$_2$X (X=OH, Cl, and Br) the relative stability increases with X=Cl~Br>OH, in spite of the lower bridging ability of the halide atoms.[19] This is in contrast to that found for the series of binuclear copper(II) complexes of the Schiff bases derived from 2,6-diformyl-4-methylphenol and N,N-dialkylethylenediamines.[20] The remarkable stability of the present complexes may be explained by the fact that the organic moieties are suitable for forming binuclear complexes and consequently strongly combine two copper(II) ions.

The χ_A and μ_{eff} values at various temperatures are given in Table 3. It was found that Fsal(=gly)$_2$Cu$_2$(OH)·H$_2$O is antiferromagnetic. The experimental data could be explained in terms of the Bleaney-Bowers equation[21]

$$\chi_A=\frac{Ng^2\beta^2}{3kT}\left[1+\frac{1}{3}\exp(-2J/kT)\right]^{-1}+N\alpha \quad ,$$

where $-2J$ is the energy separation between the singlet and triplet states, k the Boltzmann constant, N the Avogadro number, β the Bohr magneton and g the Lande g-factor (Fig. 3). The $-2J$, g and $N\alpha$ values were obtained by the best fit of susceptibility data to the Bleaney-Bowers equation. The results are given in Table 3.

Fsal(=gly)$_2$Cu$_2$Cl, Fsal(=gly)$_2$Cu$_2$Br and Fsal(=ala)$_2$Cu$_2$Cl obey the Curie-Weiss law (Fig. 4). Approximate values of the Weiss constant θ were obtained by extrapolating the curves $1/(\chi_A-N\alpha)$ *vs.* T assuming 60×10^{-6} cgs. emu for $N\alpha$.[22] Since all

Table 2. Ligand field bands of complexes (mμ)

	Solutions			Powder
	H_2O	CH_3OH	Py	
Fsal(=gly)$_2$Cu$_2$Cl	680	680	680	695
Fsal(=gly)$_2$Cu$_2$Br	675	675	675	695
Fsal(=gly)$_2$Cu$_2$(OH)·H$_2$O			(663)[a]	650
Fsal(=ala)$_2$Cu$_2$Cl	670	670	668	690

a) Decomposed in pyridine.

13) A. Nakahara, This Bulletin, **32**, 1195 (1959).
14) B. D. Sarma and J. C. Bailar, Jr., *J. Amer. Chem. Soc.*, **77**, 5476 (1955).
15) B. D. Sarma, K. R. Ray, R. E. Sievers, and J. C. Bailar, Jr., *ibid.*, **86**, 14 (1964).
16) E. Sinn and C. M. Harris, *Coord. Chem. Rev.*, **4**, 391 (1969).
17) C. S. Marvel, S. A. Aspey, and E. A. Dudley, *J. Amer. Chem. Soc.*, **78**, 4905 (1956).
18) K. Ueno and A. E. Martell, *J. Phys. Chem.*, **60**, 1270 (1956).
19) B. Jozowska-Trizebiatowska, In W. Schneider, G. Anderegg and Gut (Eds.), Essays in Coordination Chemistry, Exp. Suppl, Verlag Birkhauser, Basel-Stuttgart (1964), p. 128.
20) H. Okawa, S. Kida, Y. Muto, and T. Tokii, to be reported.
21) B. Bleaney and K. D. Bowers, *Proc. Roy. Soc. Ser. A*, **214**, 451 (1952).
22) B. N. Figgis and R. L. Martin, *J. Chem. Soc.*, **1956**, 3837.

TABLE 3. MOLAR MAGNETIC SUSCEPTIBLITIES (cgs. emu) AND EFFECTIVE MAGNETIC MOMENTS (B. M.) OVER A TEMPERATURE RANGE

$Fsal(=gly)_2Cu_2(OH)\cdot H_2O$			$-2J=447\ cm^{-1}$; $g=2.16$; $N\alpha=70\times10^{-6}$					
T (°K)	76.2	92.7	118.4	140.6	160.5	179.2	199.1	
$\chi_A\times10^6$	79	92	140	201	265	323	384	
μ_{eff}	0.07	0.13	0.26	0.40	0.50	0.60	0.71	
T (°K)	229.1	249.2	283.0					
$\chi_A\times10^6$	461	499	553					
μ_{eff}	0.85	0.93	1.05					
$Fsal(=gly)_2Cu_2Cl$		$\theta\simeq-22$°K						
T (°K)	76.2	95.2	125.2	142.6	159.6	197.9	218.4	
$\chi_A\times10^6$	3837	3368	2726	2491	2273	1910	1716	
μ_{eff}	1.52	1.59	1.64	1.67	1.68	1.71	1.70	
T (°K)	250.6	283.3	289.8					
$\chi_A\times10^6$	1508	1346	1343					
μ_{eff}	1.71	1.71	1.71					
$Fsal(=gly)_2Cu_2Br$		$\theta\simeq-7$°K						
T (°K)	76.2	97.3	139.8	180.5	219.1	259.9	288.3	
$\chi_A\times10^6$	4775	3918	2813	2265	1807	1559	1396	
μ_{eff}	1.70	1.73	1.75	1.78	1.75	1.76	1.76	
$Fsal(=ala)_2Cu_2Cl$		$\theta\simeq-48$°K						
T (°K)	76.3	94.4	123.4	158.9	195.5	222.4	256.0	285.3
$\chi_A\times10^6$	3515	3123	2566	2149	1844	1665	1498	1362
μ_{eff}	1.45	1.52	1.57	1.63	1.67	1.69	1.72	1.72

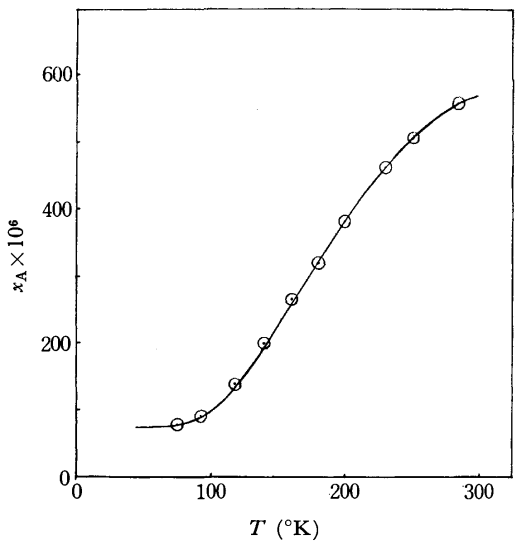

Fig. 3. Variation of molar magnetic susceptibilities with temperature for $Fsal(=gly)_2Cu_2(OH)\cdot H_2O$. The curve was calculated from the Bleaney-Bowers equation using the sets of parameters listed in Table 3.

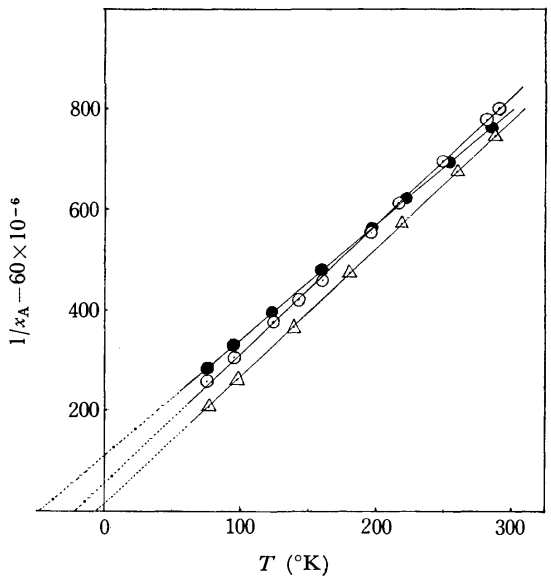

Fig. 4. Variation of reciprocal molar magnetic susceptibilities with temperature.
○: $Fsal(=gly)_2Cu_2Cl$, △: $Fsal(=gly)_2Cu_2Br$,
●: $Fsal(=ala)_2Cu_2Cl$.

these complexes possess negative Weiss constants, it is evident that there is antiferromagnetic exchange interaction between the copper(II) ions in the complexes. In most oxygen-bridged copper(II) complexes,[23-26] the Cu-O bond lengths and the Cu-O-Cu bond angles are in the ranges 1.8—2.0 Å and 100—115°, respectively. If the Cu-O bond length and the Cu-O-Cu bond angle in the present complexes are assumed to be 1.9 Å and 110° respectively, then the copper-copper interatomic distance is about 3.4 Å. Since this interatomic distance is much greater than

23) J. A. Bertrand, J. A. Kelley, and J. L. Breece, *Inorg. Chim. Acta*, **4**, 247 (1970).
24) J. A. Bertrand and J. A. Kelley, *ibid.*, **4**, 203 (1970).
25) J. A. Barnes, W. E. Hatfield, and D. J. Hodgson, *Chem. Commun.*, 1593 (1970).
26) G. A. Barclay, C. M. Harris, B. F. Hoskins, and E. Kokot, *Proc. Chem. Soc.*, **1961**, 264.

the 2.56 Å of metallic copper, a direct exchange interaction between copper(II) ions is not likely to occur. Thus the superexchange through the bridging groups is most important in the magnetic interaction in the complexes.

The powder X-ray diffraction spectra of Fsal(=gly)$_2$Cu$_2$Cl and Fsal(=gly)$_2$Cu$_2$Br are quite similar to each other, but differ from that of Fsal(=gly)$_2$Cu$_2$(OH)·H$_2$O. This implies that the crystal structures of Fsal(=gly)$_2$Cu$_2$Cl and Fsal(=gly)$_2$Cu$_2$Br are very similar to each other but differ from the structure of Fsal(=gly)$_2$Cu$_2$(OH)·H$_2$O. Nevertheless, in the present discussion we regard the molecular structures of all these complexes as practically the same, since the 5–6–6–5 condensed ring system makes a rigid skeleton for each of the complexes. This is supported by the consideration on the series of tetranuclear copper(II) complexes[27-31] of the type Cu$_4$OX$_6$L$_4$ (X is chloride or bromide atom and L is a unidentate ligand), in which the bond angles and bond lengths in one bridge are fixed and another bridging group is replaceable.

We assume that the spin-spin coupling through the phenolic oxygen is the same in all complexes. Consequently, the difference in magnetic behavior of the complexes reflects the effect of the second bridging groups upon the spin exchange interaction. From the data given in Table 3 the effect is found to be in the order: OH>Cl~Br. As it is known that most binuclear copper(II) complexes with phenolic oxygen bridges show demagnetisation,[16] it is remarkable that Fsal(=gly)$_2$Cu$_2$Cl, Fsal(=gly)$_2$Cu$_2$Br, and Fsal(=ala)$_2$Cu$_2$Cl have relatively large magnetic moments close to the spin-only value of 1.73 B.M. This might be due to the out-of-plane distortion of the Cu-O-Cu plane of the complexes.

From the Weiss constants of the complexes it can be assumed that the chloride bridge is more effective than the bromide bridge in spin coupling. It is usually found that the spin exchange interaction in binuclear complexes bridged with bromide ions is greater than that in the corresponding complexes bridged with chloride ions. For example, anhydrous copper(II) bromide has a lower magnetic moment (1.31 B.M.) than anhydrous copper(II) chloride (1.75 B.M.).[32] In the binuclear copper(II) complexes[14] of the Schiff bases derived from 2,6-diformyl-4-methylphenol and *N*,*N*-dialkylethylenediamines, the complexes bridged with a bromide ion exhibit a greater antiferromagnetic interaction than the complexes bridged with a chloride ion. Lever *et al.*[33] prepared some tetrahedral binuclear cobalt(II) complexes of a phthalazine derivative containing one halide bridge. From cryomagnetic measurements they found that the bromide-bridged complex shows a larger $-2J$ value than the corresponding chloride-bridged complex. However, the difference of effect between chloride and bromide bridging groups is usually small, and insofar as our complexes are concerned, it is reasonable to say that the chloride and bromide bridges exert a comparable effect on the spin exchange interaction.

27) J. A. Bertrand, *Inorg. Chem.*, **6**, 495 (1967).
28) J. A. Bertrand and J. A. Kelley, *ibid.*, **8**, 1982 (1969).
29) N. S. Gill and M. Stern, *ibid.*, **9**, 1619 (1970).
30) B. T. Kilbourn and J. D. Dunitz, *Inorg. Chim. Acta*, **1**, 209 (1967).
31) J. A. Bertrand and J. A. Kelley, *ibid.*, **4**, 526 (1970).
32) M. Kato, H. B. Jonassen, and J. C. Fanning, *Chem. Rev.*, **64**, 99 (1964).
33) A. B. P. Lever, L. K. Thompson, and W. M. Reiff, *Inorg. Chem.*, **11**, 104 (1972).

Magnetic Circular Dichroism of Nickel(II) and Copper(II) Complexes with 1,4,8,11-Tetraazacyclotetradecane Derivatives

Hiroshi KOBAYASHI and Bohdan KORYBUT-DASZKIEWICZ*

Department of Chemistry, Tokyo Institute of Technology, Ookayama, Meguro-ku, Tokyo

(Received April 10, 1972)

The magnetic circular dichroism (MCD) spectra of nickel(II) and copper(II) complexes with 1,4,8,11-tetraazacyclotetradecane derivatives were measured. An anomalous MCD dispersion was observed in a (*d*, *d**) band at 22000 cm^{-1} for the copper(II) complexes and at 22000—23000 cm^{-1} for the nickel(II) complexes. In the ultraviolet region, the nickel(II) complexes show a normal MCD dispersion in the 35500 cm^{-1} band which appears only for the ligands with >C=N- double bonds, while the copper(II) complexes show an anomalous dispersion in the 39000 cm^{-1} band which appears even if the ligand lacks >C=N- double bonds. The 35500 cm^{-1} band of the nickel(II) complexes is assigned to a "metal to ligand" charge-transfer transition $1e_g \rightarrow \pi^*$ and the 39000 cm^{-1} band of the copper(II) complexes to a "ligand to metal" charge-transfer transition $1e_u \rightarrow 2b_{1g}$. In the nickel(II) complex of a ligand with two isolated and two conjugated double bonds shows a normal MCD dispersion in the 25000 cm^{-1} band. The absorption band is assigned to a "metal to ligand conjugated double bonds" charge-transfer transition rather than a (*d*, *d**) transition.

Macrocyclic coordination compounds formed by condensation of metal-amine complexes with aliphatic carbonyl compounds are of great interest.[1] Recent magnetic circular dichroism (MCD) measurements have furnished various information on the electronic characteristics of the low energy electronic excitations of planar complexes.[2-5] So far, however, the MCD spectra were only briefly discussed with respect to the planar complexes with macrocyclic ligands.[6] In the present work, nickel(II) and copper(II) complexes with different tetraazacyclotetradecane derivatives in various steps of oxidation as well as in different conformations were chosen for the MCD measurements in order to get more general information on the low energy electronic excitations.

TABLE 1. LIST OF COMPLEXES

Complex	Abbreviation	Preparation
5,12-dimethyl-1,4,8,11-tetraazacyclotetradecanecopper(II) diperchlorate (prepared from an isomer ligand of mp 110°C)	IACu	1
5,12-dimethyl-1,4,8,11-tetraazacyclotetradecanecopper(II) diperchlorate (prepared from an isomer ligand of mp 145°C)	IBCu	1
5,12-dimethyl-1,4,8,11-tetraazacyclotetradecanenickel(II) diperchlorate (prepared from an isomer ligand of mp 110°C)	IANi	2
5,12-dimethyl-1,4,8,11-tetraazacyclotetradeca-4,11-dienecopper(II) diperchlorate	IICu	1
N-dl-5,7,7,12,14,14-hexamethyl-1,4,8,11-tetraazacyclotetradeca-4,11-dienecopper(II) diperchlorate (racemic isomer)	IIICuα	3
C-meso-N-dl-5,7,12,14-tetramethyl-1,4,8,11-tetraazacyclotetradeca-4,11-dienenickel(II) diperchlorate	IVANiα	4
C-meso-N-meso-5,7,12,14-tetramethyl-1,4,8,11-tetraazacyclotetradeca-4,11-dienenickel(II) diperchlorate	IVANiβ	4
C-dl-N-dl-5,7,12,14-tetramethyl-1,4,8,11-tetraazacyclotetradeca-4,11-dienenickel(II) diperchlorate	IVBNi	4
meso-5,7,12,14-tetramethyl-1,4,8,11-tetraazacyclotetradeca-1,4,8,11-tetraenenickel(II) diperchlorate	VANi	5
5,7,7,12,14,14-hexamethyl-1,4,8,11-tetraazacyclotetradeca-1,4,8,10-tetraenenickel(II) diperchlorate	VINi	6

1. B. Jezowska-Trzebiatowska, R. Kolinski, B. Korybut-Daszkiewicz, J. Mrozinski, and W. Wojciechowski, *Bull. Acad. Polon. Sci., Ser. Sci. Chim.*, **17**, 411 (1969).
2. R. A. Kolinski and B. Korybut-Daszkiewicz, *ibid.*, **17**, 13 (1969).
3. N. F. Curtis, Y. M. Curtis, and H. K. Y. Powell, *J. Chem. Soc., A*, **1966**, 1015.
4. R. A. Kolinski and B. Korybut-Daszkiewicz, "Proceedings of the XIII ICCC," September 1970, Poland, I 320.
5. Oxidation of the complex IVANiα by analogy to Curtis' preparative method of the complex VINi.[6]
6. N. F. Curtis, *Chem. Commun.*, **1966**, 882; N. F. Curtis, *Coord. Chem. Rev.*, **3**, 3 (1968).

* A UNESCO International Post-graduate Scholar from the Instytut Chemii Organicznej, Polskiej Akademii Nauk, Warozawa (Institute of Organic Chemistry, Polish Academy of Sciences, Warsaw) Poland.

1) N. F. Curtis, *Coord. Chem. Rev.*, **3**, 3 (1968).
2) D. S. Martin, Jr., J. G. Foss, M. E. McCarville, M. A. Tucker, and A. J. Kassman, *Inorg. Chem.*, **5**, 491 (1966).
3) A. J. McCaffery, P. N. Schatz, and P. J. Stephens, *J. Amer. Chem. Soc.*, **90**, 5730 (1968).
4) P. J. Stephens, A. J. McCaffery, and P. N. Schatz, *Inorg. Chem.*, **7**, 1923 (1968).
5) S. B. Piepho, P. N. Schatz, and A. J. McCaffery, *J. Amer. Chem. Soc.*, **91**, 5994 (1969).
6) Q. Looney and B. E. Douglas, *Inorg. Chem.*, **9**, 1955 (1970).

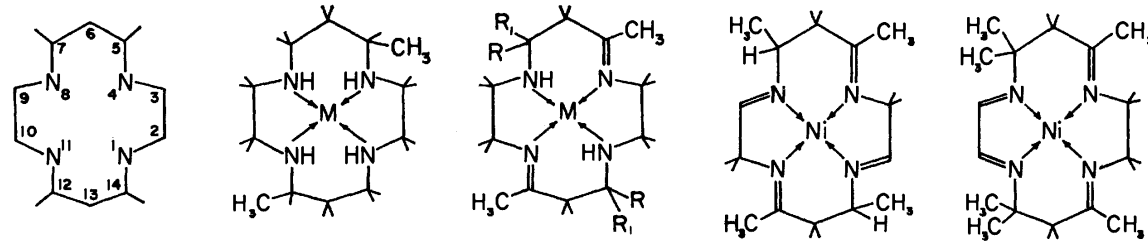

M=Cu(II) IACu
IBCu
M=Ni(II) IANi

M=Cu(II)
R=R$_1$=H II Cu
R=R$_1$=CH$_3$ III Cuα
M=Ni(II)
R=H, R$_1$=CH$_3$
IVANiα, IVANiβ, IVBNi

VA Ni

VI Ni

Fig. 1. Structures of the complexes studied.

Experimental

Materials. Preparation of the complexes was described elsewhere.[7-9] Samples obtained from the original preparative works were used without further purification. The names, notations, preparation, and structures of the complexes used in the present work are summarized in Table 1 and Fig. 1. Two isomeric 5,12-dimethyl-1,4,8,11-tetraazacyclotetradecanes [denoted by IA (mp 110°C) and IB (mp 145°C)] were complexed with copper(II) perchlorate (Table 1). The free ligand 5,7,12,14-tetramethyl-1,4,8,11-tetraazacyclotetradeca-4,11-diene was obtained by the condensation of ethylenediamine monohydroperchlorate with methyl propenyl ketone in water-methanol solution and complexed with nickel(II) acetate. Three isomers IVANiα, IVANiβ, and IVBNi (Table 1) were separated by fractional recrystallization. The complexes IVANiα and IVANiβ are an interconvertible pair, while the complex IVBNi is a nonconvertible isomer.

Measurements. The measurement technique of magnetic circular dichroism was given previously.[10] All measurements were carried out with a JASCO ORD/UV-5 spectropolarimeter with its CD attachment and an electromagnet. The magnetic field was set at 10000 Gauss. The visible and ultraviolet absorption spectra were taken on a Shimadzu automatic recording spectrophotometer Model MPS-50 and the infrared spectra of Nujol mull were recorded with a Hitachi spectrophotometer Model EPI-G3.

The organic solvents used were nitromethane and pyridine. In the case of aqueous solution, an acidic solution (0.05 N $HClO_4$) was used in order to prevent a possible isomerization of the complexes.

Results and Discussion

Magnetic circular dichroism (MCD) and absorption spectra are shown in Figs. 2—6. An apparent single absorption band was observed at about 20000 cm^{-1} (ε=100) for the copper(II) complexes and at 22000—23000 cm^{-1} (ε=80) for the nickel(II) complexes except the complex VINi. The single weak band is composed of an envelope with several overlapping (d, d^*) bands. The diamagnetic ground states of the nickel complexes were established by magnetic susceptibility measurements. They are all diamagnetic in the solid state as in nitromethane solution.[1,7,9] Both the nickel(II) and copper(II) complexes show an asymmetric anomalous MCD dispersion in the (d, d^*) band. The asymmetric shape of the MCD spectra in the visible region should be interpreted as a superposition of B term extremes of the excitations $d_{z^2}\rightarrow d_{x^2-y^2}$ and $d_{xy}\rightarrow d_{x^2-y^2}$ and an A term dispersion of a degenerate excitation $d_{zx}, d_{yz}\rightarrow d_{x^2-y^2}$ in term of Ste-

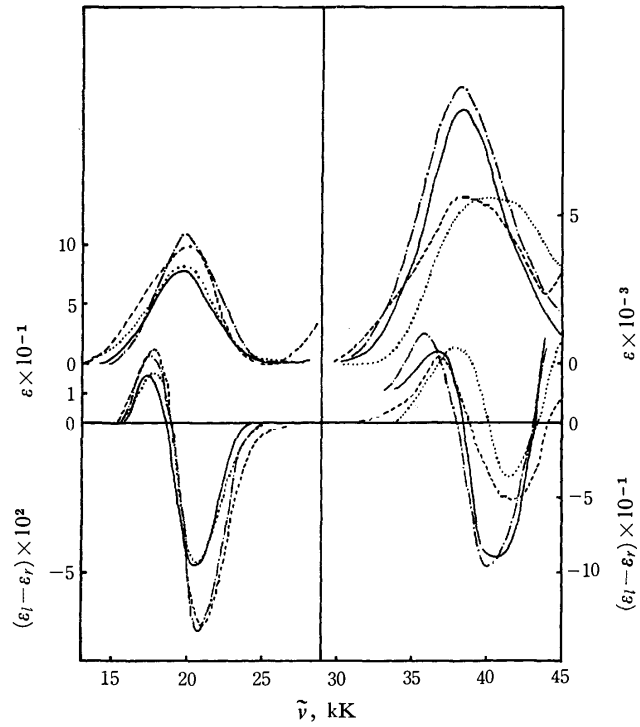

Fig. 2. Absorption and MCD spectra of the copper(II) complexes in acidic water.
——: IACu, —·—: IBCu, ·····: IICu, ----: IIICuα

7) R. A. Kolinski and B. Korybut-Daszkiewicz, *Bull. Acad. Polon. Sci., Ser. Sci. Chim.*, **17**, 13 (1969).
8) B. Jezowska-Trzebiatowska, R. Kolinski, B. Korybut-Daszkiewicz, J. Mrozinski, and W. Wojciechowski, *ibid.*, **17**, 411 (1969).
9) R. A. Kolinski and B. Korybut-Daszkiewicz, "Proceedings of the XIII ICCC," September 1970, Poland, **1** 320.
10) H. Kobayashi, M. Shimizu, and I. Fujita, This Bulletin, **43**, 2335 (1970).

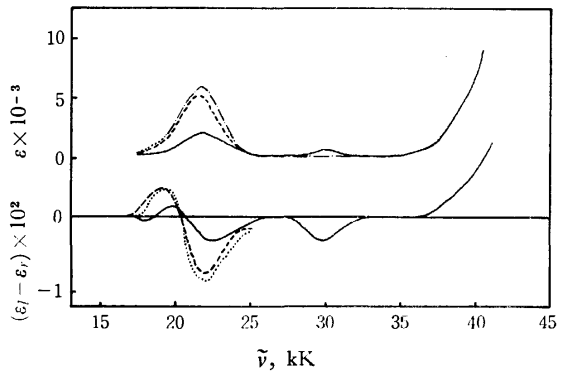

Fig. 3. Absorption and MCD spectra of the nickel(II) complex IANi.
——: in acidic water, —·—: in methanol,
·····: in nitromethane, ----: in pyridine

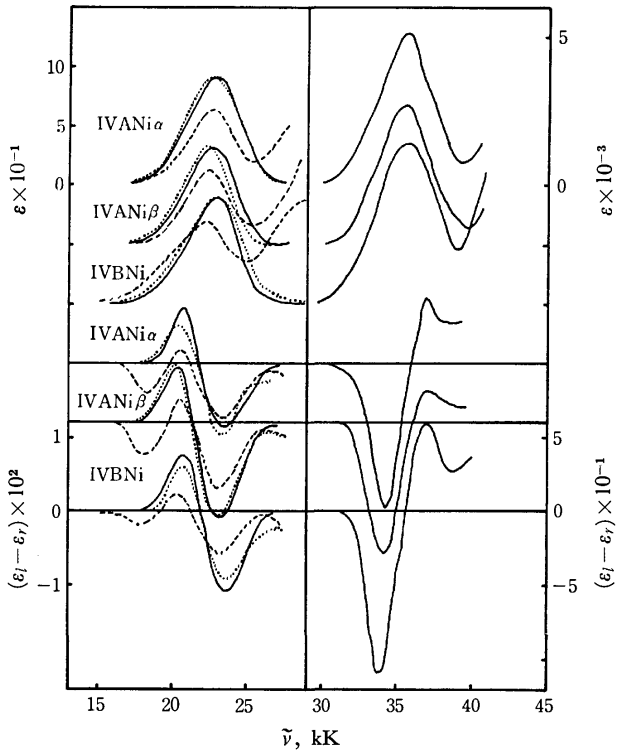

Fig. 4. Absorption and MCD spectra of the nickel(II) complexes IVANiα, IVANiβ, and IVBNi.
——: in acidic water, ·····: in nitromethane,
----: in pyridine

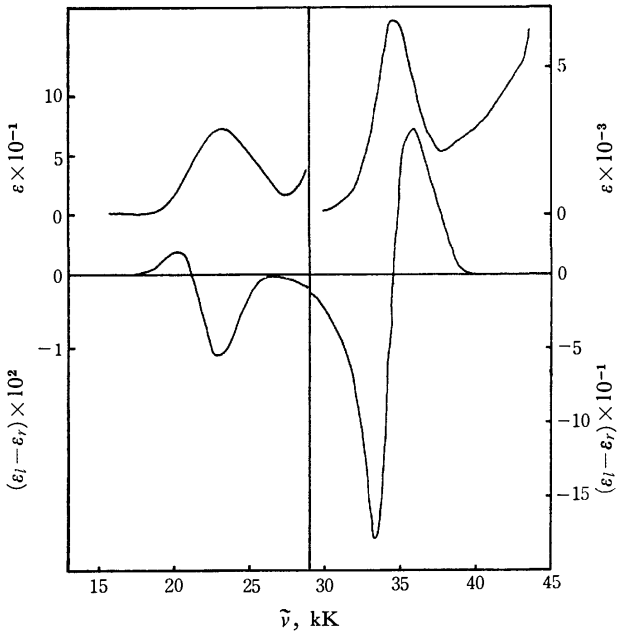

Fig. 5. Absorption and MCD spectra of the nickel(II) complex VANi in H_2O.

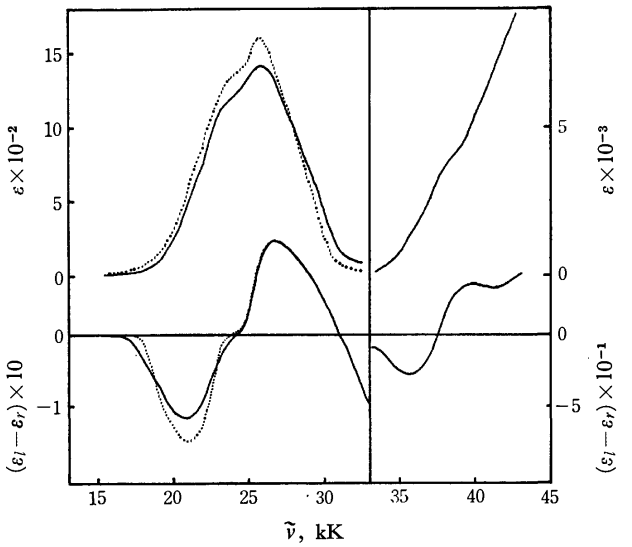

Fig. 6. Absorption and MCD spectra of the nickel(II) complex VINi.
——: in acidic water, ·····: in nitromethane

phens' theory of MCD.[11-13] Such a superposition of (d, d^*) bands can also be confirmed by the measurements of optical rotatory dispersion (ORD) or circular dichroism (CD) of the optically active isomers of the complex IVBNi. The CD curve extremes, in fact, were not coincident with the observed absorption maximum. Similar phenomena have been observed.[14,15] An MCD dispersion observed in the (d, d^*) bands of the nickel(II) and copper(II) complexes evidently reveals the location of a degenerate excitation $d_{zx}, d_{yz} \rightarrow d_{x^2-y^2}$.

When the solvent was changed, a red-shift and intensity enhancement of the absorption band of the copper(II) complexes were observed in the ordering nitromethane<water<pyridine. The solvent effect is shown in Fig. 7. In the case of the nickel(II) complexes, however, no such red-shift and intensity enhancement were observed. In pyridine solution a remarkable splitting and intensity reduction were found in the visible band of the nickel(II) complexes IVANiα, IVANiβ, and IVBNi and an appreciable enhancement of the absorption intensity was observed in near-ultraviolet region. As evidenced by magnetic

11) P. J. Stephens, "Theoretical Studies of Magneto-Optics Phenomena," Thesis, Oxford University, 1964.
12) A. D. Buckingham and P. J. Stephens, *Ann. Rev. Phys. Chem.*, **17**, 399 (1966).
13) P. J. Stephens, *J. Chem. Phys.*, **52**, 3489 (1970).
14) H. Ito and J. Fujita, This Bulletin, **44**, 741 (1971).
15) Y. Nishida and S. Kida, *ibid.*, **43**, 3814 (1970).

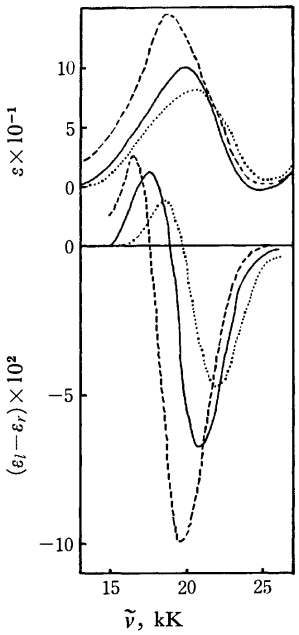

Fig. 7. Absorption and MCD spectra of the copper(II) complex IIICuα.
——: in acidic water, ·····: in nitromethane,
----: in pyridine

susceptibility and NMR measurements, these complexes in pyridine solution exist partially in a paramagnetic state. An axial coordination of pyridine sufficiently reduces an energy gap between the diamagnetic and triplet ground states, thus giving rise to a thermal equilibrium between the states. The MCD minima at 18000—19000 cm^{-1} are assigned to the second (d, d^*) transition $^3A_2 \rightarrow a^3T_1$ in the paramagnetic octahedral nickel(II) complexes. Enhancement of absorption intensity in near-ultraviolet is also interpreted as arising from the third (d, d^*) transition $^3A_2 \rightarrow b^3T_1$ of the paramagnetic species. This is in good agreement with the recent observations by Harding *et al.* on paramagnetic trisethylenediamine nickel(II) and tris-2,2′-bipyridine nickel(II) complexes.[16] The complex IANi shows this type of spectral behavior even in aqueous solution as shown in Fig. 3, whereas in pyridine, alcohol and nitromethane it shows a single absorption band at 22000 cm^{-1} characteristic of the diamagnetic square-planar nickel complexes. In organic solvents, the counter perchlorate ion tends to disturb the coordination of solvent donors. Furthermore a steric hindrance against axial coordination arising from a conformation of two methyl groups in one side of the macrocyclic ligand of the complex IANi should be noted. On the contrary, a similar complex prepared by reduction of 2,4,4,10,12,12-hexamethyl-1,5,9,13-tetraazacyclohexadeca-1,9-dienenickel(II) perchlorate shows a coexistence of the triplet and singlet ground states in such donor solvents as dimethylsulfoxide, dimethylformamide and methyl cyanide, whereas in aqueous solution it gives rise to only a single absorption band at 22500 cm^{-1} of the diamagnetic species.[17]

16) M. J. Harding, S. F. Mason, D. J. Robbins, and A. J. Thomson, *J. Chem. Soc., A*, **1971**, 3058.

In the ultraviolet region the nickel(II) complex with isolated >C=N- double bonds shows an absorption band of intermediate intensity (ε=5000) at 35500 cm^{-1}, which increases with the number of isolated double bonds. The other bands appear around 44000 cm^{-1} and 47500 cm^{-1} (ε=12000). The copper(II) complexes, even if the ligand lacks the >C=N- double bonds, show an absorption band around 39000 cm^{-1} (ε=5000—10000) with a similar shape as observed in the nickel(II) complexes. The nickel(II) complexes of the ligands with no >C=N- double bands show no absorption band up to the 44000 cm^{-1} band. Non-existence of the >C=N- double bonds in the complexes IACu, IBCu and IANi was confirmed by IR spectrum. The A term dispersion of MCD is observed in the ultraviolet region as shown in Figs. 2, 4, and 5. However, the A term dispersion in ultraviolet region of the nickel(II) complexes has a sign opposite to that of the A term dispersion in visible region observed for both nickel(II) and copper(II) complexes and also to that of the A term dispersion in ultraviolet region of the copper(II) complexes.

The ultraviolet band at 39000 cm^{-1} of the copper(II) complexes observed even when the ligand lacks >C=N- double bonds is assigned to a degenerate charge-transfer transition from a degenerate molecular orbital pair σ_x and σ_y, predominantly localized on nitrogen lone-pair orbitals, a vacant copper(II) antibonding orbital x^2-y^2. In the case of the nickel(II) complexes, the ultraviolet band at 35500 cm^{-1} is assigned to a degenerate charge-transfer transition from a degenerate non-bonding $d\pi$ orbital pair zx and yz to the lowest antibonding molecular orbital π^*. When the number of isolated >C=N- double bonds in the ligand is increased, the ultraviolet charge-transfer band makes no shift but the intensity is enhanced. However, a complex of the ligand with two isolated double bonds and two conjugated ones gives rise to an intense absorption band around 25000 cm^{-1} (ε= 1400) with a shoulder on the lower wave number side around 24100 cm^{-1} as shown in Fig. 6. The sign of term dispersion in the 25000 cm^{-1} band is opposite to that in (d, d^*) bands, which are usually observed in the same region, and the same as the sign observed at the 35500 cm^{-1} band of the nickel(II) complexes with isolated double bonds. The shoulder at 24100 cm^{-1} might be due to a (d, d^*) transition. The absorption band at 25000 cm^{-1} should be assigned to a degenerate charge-transfer transition from a degenerate non-bonding $d\pi$ orbital pair to the antibonding molecular orbital π^* predominantly delocalized over the conjugated double bonds.

A schematic molecular orbital diagram of the diamagnetic d^8 planar complex is given in Fig. 8. There are three spin-allowed (d, d^*) transitions corresponding to the one-electron transitions $1b_{2g} \rightarrow 2b_{1g}$ ($^1A_{1g} \rightarrow {}^1A_{2g}$), $2a_{1g} \rightarrow 2b_{1g}$ ($^1A_{1g} \rightarrow {}^1B_{1g}$), and $1e_g \rightarrow 2b_{1g}$ ($^1A_{1g} \rightarrow {}^1E_g$). An A term dispersion is anticipated for the (d, d^*) transition $1e_g \rightarrow 2b_{1g}$ ($^1A_{1g} \rightarrow {}^1E_g$). Because of

17) L. G. Warner and D. H. Busch, *J. Amer. Chem. Soc.*, **91**, 4092 (1969), and also E. K. Barefield and D. H. Busch, *Inorg. Chem.*, **10**, 1216 (1971).

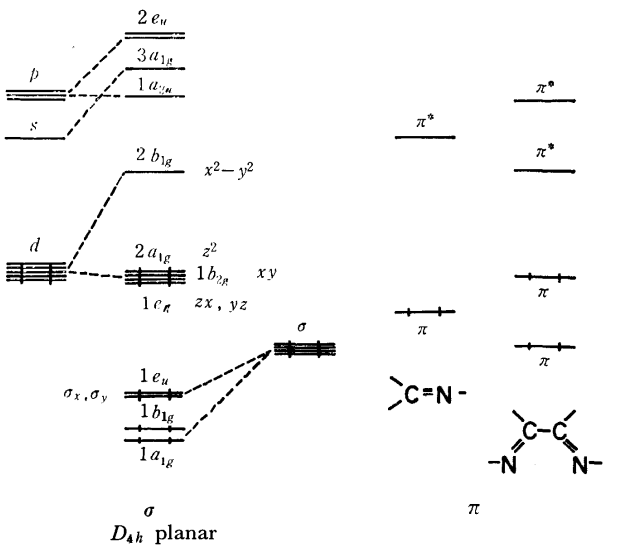

Fig. 8. Molecular orbital diagrams (schematic).

the Laporte forbidden character, the transition should borrow a spectral intensity by vibronic coupling from the allowed charge-transfer transition $1e_u \rightarrow 2b_{1g}$ ($^1A_{1g} \rightarrow {}^1E_u$ x, y polarized), $1e_g \rightarrow 1a_{2u}$ ($^1A_{1g} \rightarrow {}^1E_u$ x, y polarized) and/or $1e_g \rightarrow 1e_u$ ($^1A_{1g} \rightarrow {}^1A_{2u}$ z polarized). Since the transition $1e_g \rightarrow 1e_u$ is z polarized, it can not participate in the MCD observed in (d, d^*) band. As shown in the Appendix, A/D of the transition $1e_u \rightarrow 2b_{1g}$ is negative, while A/D of the transition $1e_g \rightarrow 1a_{2u}$ is positive. Since the MCD dispersion observed in (d, d^*) band is an anomalous one, the allowed transition granting spectral intensity to the (d, d^*) transition is a charge-transfer transition with negative A/D, namely $1e_u \rightarrow 2b_{1g}$. The same theory can also be applied to the (d, d^*) transition of the copper(II) complexes. Molecular vibrations which can mix the Laporte forbidden transition $1e_g \rightarrow 2b_{1g}$ with the allowed transition $1e_u \rightarrow 2b_{1g}$ are out of plane deformation vibrations ν_3 (a_{2u}) and ν_5 (b_{2u}) rather than any other stretching vibrations. These vibrations give rise to a temporary overlapping between zx, yz and nitrogen lone-pair orbitals and thus a non-zero off-diagonal term $(1e_g|\hat{h}'|1e_u)$.

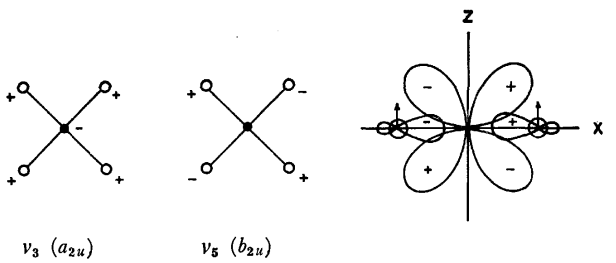

Fig. 9. Out of plane deformation vibrations which mix a Laporte forbidden transition $1e_g \rightarrow 2b_{1g}$ with the allowed transition $1e_u \rightarrow 2b_{1g}$.

The copper(II) complexes, even when the ligand lacks >C=N- double bonds, show an ultraviolet band of intermediate intensity at 39000 cm^{-1} and an anomalous MCD dispersion in the band. Thus the band is assigned to a symmetry allowed transition with a character of charge-transfer from the degenerate molecular orbital pair $1e_u$ to the vacant copper(II) antibonding orbital $2b_{1g}$. The transition $1e_u \rightarrow 2b_{1g}$ gives negative A/D and thus an anomalous MCD dispersion. In the case of the nickel(II) complexes, however, the ultraviolet band of intermediate intensity at 35500 cm^{-1}, is observed only when the ligand has isolated >C=N- double bonds and shows a normal MCD dispersion. The band is assigned to a "metal to ligand" charge-transfer transition from the degenerate nickel(II) $d\pi$ orbitals zx, yz to a vacant antibonding molecular orbital of exciton-coupling >C=N- double bonds π^*. The charge-transfer transition should borrow spectral intensity from a strongly allowed coupling (π, π^*) transition in the isolated >C=N- double bonds or the Laporte allowed transition $1e_g \rightarrow 1a_{2u}$.

(a) (b)

Fig. 10. Normal and anomalous dispersions.
(a) normal dispersion
(b) anomalous dispersion

An exciton coupling between isolated π systems in the coordinating ligand is possible and thus the resultant allowed (π, π^*) oscillator can be a planar oscillator in the case of the complexes VANi and VINi, whereas it gives only a linear oscillator in the case of the complexes with two *trans* >C=N- double bonds such as IVANiα, IVANiβ, and IVBNi. Thus the allowed (π, π^*) transitions in the double bond systems in the coordinating ligand could grant an MCD dispersion intensity to the "metal to ligand" charge-transfer transition only in the cases of the complexes VANi and VINi. In such a planar molecular environment, the allowed degenerate excitation $1e_g \rightarrow 1a_{2u}$ principally localized on the central metal ion is a planar oscillator rather energetically low. Since the molecular orbital $1a_{2u}$ can conjugate with two *trans* >C=N- double bonds in the complexes IVANiα, IVANiβ and IVBNi, the transition $1e_g \rightarrow 1a_{2u}$ can grant a spectral intensity and also an MCD dispersion intensity to the charge-transfer transition $1e_g \rightarrow \pi^*$. Although the possibility of spectral intensity borrowing in the "metal to ligand" charge-transfer transition from the allowed (π, π^*) transitions can not be eliminated, some spectral intensity should surely be stolen from the intrametal allowed transition $1e_g \rightarrow 1a_{2u}$. As shown in the Appendix, the excitation $1e_g \rightarrow 1a_{2u}$ gives rise to a normal MCD dispersion. In fact, the "metal to ligand" charge-transfer transition in the nickel complexes IVANiα, IVANiβ, IANi, and VINi constantly shows a normal MCD dispersion which indicates a borrowing of spectral intensity from the planar oscillator $1e_g \rightarrow 1a_{2u}$.

The authors would thank Profs. K. Saito and J. Fujita, Department of Chemistry, Tohoku University, for their helpful discussions, and Dr. H. Kato, Kobe University, for his kind advice. One of the authors

(B. K-D.) wishes to express his gratitude to the Japanese Government for a UNESCO fellowship and also to the Polish Academy of Sciences which made his stay in this country possible. This work was also supported by a grant from the Ministry of Education.

Appendix

A degenerate transition from the ground state $|o\rangle$ to a degenerate excited state pair $|\pm j\rangle$ is accompanied by an A term dispersion of MCD. The molecular constant A in the transition $|o\rangle \rightarrow |\pm j\rangle$ is defined as follows:[11-13]

$$A = 6\langle +j|\mu_z|+j\rangle \mathrm{Im}\{\langle o|\hat{m}_x|+j\rangle\langle +j|\hat{m}_y|o\rangle\}$$

where $\hat{\mu}$ and $\hat{m}$ are magnetic and electric dipole operators, respectively, and

$$\langle \pm j|\hat{\mu}_z|\pm j\rangle = -\beta/\hbar\langle \pm j|\hat{l}_z|\pm j\rangle .$$

MCD spectrum shows a normal dispersion when $A/D>0$, where

$$D = 6\{|\langle o|\hat{m}_x|+j\rangle|^2+|\langle o|\hat{m}_y|+j\rangle|^2\} .$$

It shows an anomalous dispersion when $A/D<0$.

The state wave functions $|o\rangle$ and $|\pm j\rangle$ are given in terms of a degenerate molecular orbital pair $|\pm j)$ and a non-degenerate molecular orbital $|a)$ as follows:

$$\begin{array}{ll} |o\rangle & |+j)|\overline{+j})|-j)|\overline{-j}) \\ |+j\rangle & |+j)|\overline{+j})[|-j)|\overline{a}) - |\overline{-j})|a)]/\sqrt{2} \\ |-j\rangle & |-j)|\overline{-j})[|+j)|\overline{a}) - |\overline{+j})|a)]/\sqrt{2} \end{array}$$

where no bar implies spin α, a bar implies spin β and

$$(\pm j|\hat{\mu}_z|\pm j) = -\beta/\hbar(\pm j|\hat{l}_z|\pm j) = \mp j'\beta.$$

Since

$$\langle \pm j|\hat{\mu}_z|\pm j\rangle = (\pm j|\hat{\mu}_z|\pm j) = \mp j'\beta,$$

it follows that

$$A = 6(-j'\beta)\mathrm{Im}\{2(-j|\hat{m}_x|a)(a|\hat{m}_y|-j)\}$$

and

$$D = 6\{2|(-j|\hat{m}_x|a)|^2+2|(-j|\hat{m}_y|a)|^2\}.$$

The degenerate transition $1e_g \rightarrow 1a_{2u}$, for example, is rewritten $|\pm j) \rightarrow |a)$, in terms of $|\pm j) = \{|xz) \pm i|yz)\}/\sqrt{2}$ and $|a) = |z)$. Since

$$(-j|\hat{m}_x|a) = \frac{1}{\sqrt{2}}(zx+iyz|\hat{m}_x|z) = \frac{1}{\sqrt{2}}(zx|\hat{m}_x|z) \equiv \frac{1}{\sqrt{2}}m$$

and

$$(a|\hat{m}_y|-j) = \frac{1}{\sqrt{2}}(z|\hat{m}_y|zx-iyz) = -\frac{i}{\sqrt{2}}(z|\hat{m}_y|yz) \equiv -\frac{i}{\sqrt{2}}m$$

it follows that

$$A/D = (1/2)j'\beta.$$

This gives a normal dispersion. For the degenerate transition $1e_u \rightarrow 2b_{1g}$ given in terms of $|\pm j) = \{|\sigma_x) \pm i|\sigma_y)\}/\sqrt{2}$ and $|a) = |x^2-y^2)$, we have

$$(-j|\hat{m}_x|a) = \frac{1}{\sqrt{2}}(\sigma_x+i\sigma_y|\hat{m}_x|x^2-y^2) = \frac{1}{\sqrt{2}}(\sigma_x|\hat{m}_x|x^2-y^2) \equiv \frac{1}{\sqrt{2}}m'$$

$$(a|\hat{m}_y|-j) = \frac{1}{\sqrt{2}}(x^2-y^2|\hat{m}_y|\sigma_x-i\sigma_y) = \frac{-i}{\sqrt{2}}(x^2-y^2|\hat{m}_y|\sigma_y) \equiv \frac{i}{\sqrt{2}}m'$$

and thus $A/D = -(1/2)j'\beta$. The gives an anomalous dispersion.

Preparation and Circular Dichroism Spectra of Bis(amino-acidato)ethylenediaminecobalt(III) Complexes

Nobuko MATSUOKA, Jinsai HIDAKA, and Yoichi SHIMURA

Department of Chemistry, Faculty of Science, Osaka University, Toyonaka, Osaka

(Received April 26, 1972)

Cis(O) and *trans(O)* complexes of bis(L-serinato)ethylenediaminecobalt(III) ion have been prepared and completely separated into six possible isomers by ion-exchange column chromatography. These isomers have been assigned to *Λ-trans(O)*, *Λ-trans(O)*, *Λ-C_2-cis(O)*, *Λ-C_1-cis(O)*, *Λ-C_1-cis(O)* and *Λ-C_2-cis(O)* in the elution order, on the basis of their absorption and circular dichroism spectra. *Trans(O)*- and *C_1-cis(O)*-bis(glycinato)ethylene-diaminecobalt(III) complexes have been resolved into their optically active isomers, and *trans(O)*-bis(L-alaninato)-ethylenediaminecobalt(III) ion has been prepared and separated into two configurationally active isomers. The absorption and circular dichroism data of six isomers of $[Co(L\text{-ser})_2en]^+$, two isomers of $[Co(L\text{-ala})_2en]^+$ and two isomers of $[Co(gly)_2en]^+$ have been discussed in being compared with those of the corresponding isomers of oxalatobis(L-serinato)cobaltate(III) complex.

Recently a number of reports[1-8] have been presented for the stereochemistry of cobalt(III) complexes with α-aminoacidato ligand and these studies have mainly been developed on the basis of their absorption and circular dichroism (CD) spectra. In a previous paper,[7] we reported the spectral and stereochemical properties of six isomers of oxalatobis(L-serinato)cobaltate(III) complex, with which are compared those of the corresponding isomers of oxalatobis(glycinato)cobaltate(III) complex. It is interesting to compare the results for such $[Co(O)_4(N)_2]$ type complexes with those for $[Co(O)_2(N)_4]$ type complexes. The present work is concerned with the absorption and CD spectra of six isomers of bis(L-serinato)-ethylenediaminecobalt(III) complex and optical isomers of *trans(O)*- and *C_1-cis(O)*-bis(glycinato)-ethylenediaminecobalt(III) complexes, all of which belong to a general type, $[Co(O)_2(N)_4]$. This may be the first study reported for the CD of bis(amino-acidato)ethylenediaminecobalt(III) type complexes.

Experimental

1) Resolution of Bis(glycinato)ethylenediaminecobalt(III) Iodide. By using an aqueous solution of sodium perchlorate as an eluting agent, we obtained three kinds of racemic perchlorates, *trans(O)*, *C_1-cis(O)* and *C_2-cis(O)*, of this complex, more easily than by using the potassium bromide solution as in a previous paper.[9] A large excess of sodium iodide was added to the concentrated solution of each the perchlorate; then the corresponding racemic iodides deposited. When the crystallization was not easy, they were obtained by adding an appropriate amount of ethanol to the solution. The red crystals were filtered off, washed with ethanol-water mixture and ethanol, and dried in air.

$(+)_{589}$-trans(O)-[Co(gly)$_2$en]I·H_2O. An aqueous suspension of 2.0 g (0.0048 mol) of racemic *trans(O)* iodide[10] was stirred well with 0.8 g (0.0048 mol) of silver acetate. The resulted yellow precipitate of silver iodide was removed. To the filtrate, 1.0 g (0.0024 mol) of $(-)_{546}$-K[Co(edta)]·$2H_2O$ was added, and a small amount of insoluble material formed was filtered out. From this solution the reddish violet diastereomer was obtained by concentrating it in a vacuum desiccator, and was recrystallized from aqueous solution by adding acetone. Pure crystals were filtered, washed with acetone-water mixture and acetone, and dried in air. Then the diastereomer was converted to iodide by dissolving it in a small amount of water and by adding an excess of sodium iodide. The red crystals deposited were filtered, washed with ethanol and dried in air.

$(+)_{589}$-C_1-cis(O)-[Co(gly)$_2$en]I·$2H_2O$. Racemic *C_1-cis(O)* iodide (2.6 g, 0.006 mol) and silver acetate (1.2 g, 0.007 mol) were stirred well in 20 m*l* of water. After the silver iodide formed was removed, a saturated solution of 1.0 g (0.003 mol) of potassium antimony(III) L-tartrate 1½-hydrate was added to the filtrate. The red crystals of diastereomer deposited when the solution was evaporating in a vacuum desiccator. If a colorless compound was formed before deposition of the diastereomer, it was removed. The red crystals were filtered, washed with ethanol-water mixture and ethanol, and dried in air. To a concentrated solution of the diastereomer a large excess of sodium iodide was dissolved and the solution was cooled in an ice-bath. The optically active iodide was recrystallized from water by adding ethanol. The red crystals were filtered, washed with ethanol-water mixture and dried in air.

2) Preparation and Separation of Two Isomers of trans(O)-*Bis(L-alaninato)ethylenediaminecobalt(III) Perchlorate.* To a solution of 12.0 g (0.05 mol) of cobalt(II) chloride hexahydrate in 40 m*l* of water, a mixed solution of 9.0 g (0.10 mol) of L-alanine and 3.0 g (0.05 mol) of ethylenediamine in 50 m*l* of water was added. The resulting solution was oxidized by mechanical stirring with 10 g of lead dioxide at 70°C for about 20 min, and cooled to room temperature. After removing a bulky insoluble material, a large amount of acetone was added to the filtrate. The supernatant was decanted out and the residual dark-red oil was dissolved in a small amount of water. Insoluble material was filtered out and the filtrate was poured into a column (30 mm × 900 mm) containing strong anion-exchange resin (Dowex 50 W × 8, 200~400 mesh, hydrogen form). The neutral

1) C. T. Liu and B. E. Douglas, *Inorg. Chem.*, **3**, 1356 (1964); S. K. Hall and B. E. Douglas, *ibid.*, **8**, 372 (1969).
2) T. Yasui, J. Hidaka, and Y. Shimura, This Bulletin, **39**, 2417 (1966); T. Yasui, J. Fujita, and Y. Shimura, *ibid.*, **42**, 2081 (1969).
3) R. G. Denning and T. S. Piper, *Inorg. Chem.*, **5**, 1056 (1966).
4) J. Hidaka and Y. Shimura, This Bulletin, **40**, 2312 (1967).
5) M. Shibata, H. Nishikawa, and Y. Nishida, *Inorg. Chem.*, **7**, 9 (1968).
6) Y. Kojima and M. Shibata, *ibid.*, **9**, 238 (1970).
7) N. Matsuoka, J. Hidaka, and Y. Shimura, *ibid.*, **9**, 719 (1970).
8) T. Yasui and B. E. Douglas, *ibid.*, **10**, 97 (1971).
9) N. Matsuoka, J. Hidaka, and Y. Shimura, This Bulletin, **40**, 1868 (1967).

species was swept out with water. By eluting with 0.1 N $NaClO_4$ solution, the adsorbed bands were gradually separated to a violet, two kinds of dark-red, and a broad red bands in this order. From the measurements of the visible absorption spectra of eluants, it was confirmed that the species in the violet band was *mer*-$[Co(O)_3(N)_3]^+$ type by-product, and that complexes in the dark red bands were two kinds of isomers of *trans(O)*-$[Co(L\text{-ala})_2en]^+$, and that one in the red band was a mixture of isomers of C_1- and C_2-*cis(O)*-$[Co(L\text{-ala})_2en]^+$. As for the *trans* isomers it was also shown that the earlier eluted species was $(-)_{589}$-isomer and the later eluted $(+)_{589}$-isomer, by measurements of their ORD. The eluates of the two *trans(O)* isomers were independently concentrated in a vacuum evaporator, and the obtained crystals were filtered, washed with ethanol-water mixture and ethanol, and dried in air.

3) Preparation and Separation of Six Isomers of Bis(L-serinato)ethylenediaminecobalt(III) Complexes. A solution containing 12.0 g (0.05 mol) of cobalt(II) chloride hexahydrate in 30 m*l* of water was mixed with a solution of 3.0 g (0.05 mol) of ethylenediamine and 10.5 g (0.10 mol) of L-serine in 40 m*l* of water. The resulting brown solution was mechanically stirred with 20 g of lead dioxide at 70°C for about 30 min; then the solution became violet-red. The solution was cooled to room temperature and kept in a refrigerator overnight. After the bulky insoluble material precipitated was filtered out, ethanol-ether mixture was added to the filtrate, until an oily substance settled and the supernatant became colorless. The supernatant was decanted out and dark red oil was dissolved in a small amount of water. If an insoluble compound was formed, it was filtered out. The resulting solution was poured into a column (30 mm × 150 mm) containing strong cation exchange resin (Dowex 50W × 8, 200~400 mesh, hydrogen form), and the violet and pink neutral species, which were *mer*- and *fac*-$[Co(L\text{-ser})_3]$ respectively, were swept out with water. By elution with $NaClO_4$ aqueous solution (0.02 N in the first stage, then 0.05, 0.1, 0.2, and 0.5 N in the later stage of elution, successively) at a rate of 3 m*l*/min, the adsorbed bands were gradually separated into several violet and blue violet bands, two dark red bands, and four red bands in this order. Of the last four red bands the first and the fourth bands were of faint color as compared with the other two. It was confirmed from the measurements of absorption spectra and ORD that there were some by-products in the violet and blue violet bands. There were $(+)_{589}$-*trans(O)*- and $(-)_{589}$-*trans(O)*-$[Co(L\text{-ser})_2en]^+$ isomers in the two dark red bands in the elution order, and $(+)_{589}$-C_2-*cis(O)*-, $(-)_{589}$-C_1-*cis(O)*, $(+)_{589}$-C_1-*cis(O)*- and $(-)_{589}$-C_2-*cis(O)*-$[Co(L\text{-ser})_2en]^+$ isomers in the four red bands in the elution order. In top region of the column, brownish red bands of some higher charged complexes stayed. Each eluate of six isomers was concentrated to less than 50 m*l* in a vacuum evaporator at 30°C, and the perchlorate or iodide was crystallized from the concentrated solution as follows.

$(+)_{589}$-trans(O)-$[Co(L\text{-ser})_2en]ClO_4$. To the concentrated eluate containing this isomer, about two times volume of ethanol was added. Red needles deposited. This was recrystallized from water by adding ethanol. Yield: 0.5 g.

$(-)_{589}$-trans(O)-$[Co(L\text{-ser})_2en]I$. This isomer did not deposit by adding ethanol to the concentrated eluate. So that an appropriate amount of ether was added to the mixture of the eluate and ethanol. Then an oily substance was separated, and it was dissolved in a methanol-water mixture. To solution ether was added once more. If the substance formed was oily again, this treatment was repeated until crystals began to appear. Thus a crude perchlorate was obtained. By adding an excess of sodium iodide (solid) and an appropriate amount of ethanol to an aqueous solution of the crude perchlorate, the red crystals of iodide were deposited. The pure crystals were filtered, washed with ethanol-water mixture and ethanol, and dried in air. Yield: 0.6 g.

$(+)_{589}$-C_2-cis(O)-$[Co(L\text{-ser})_2en]I$. A saturated aqueous solution of potassium iodide was added to the concentrated eluate until a white precipitate of potassium perchlorate was no more produced, and then the precipitate was filtered out. To remove of iodine formed in the solution, following procedure was carried out. To a mixture of the filtrate and a little amount of ethanol, an appropriate amount of ether was added until two layers were formed. The resultant was transferred into a separatory funnel and was shaken well. A yellow ether layer, in which iodine dissolved, was removed, and the red aqueous solution containing the complex was more several times shaken with ether, until the ether layer became nearly colorless. Then the red solution was kept in a refrigerator overnight. The crystals deposited were filtered and washed well with methanol until impure colorless crystals were washed away. The crude complex was recrystallized from water by adding ethanol and ether. The red crystals were filtered, washed with ethanol-water mixture and ethanol, and dried in air. Yield: 0.07 g.

$(-)_{589}$-C_1-cis(O)-$[Co(L\text{-ser})_2en]I$. By adding a large amount of ethanol and ether to the concentrated eluate, the dark red oily substance was separated. The supernatant was decanted out, and the oily substance was stirred well with a large amount of ethanol until it became powdery. After kept in a refrigerator overnight, the red powder was filtered, washed with ethanol-water mixture and ethanol, and dried in air. When a small amount of acetone was added to an aqueous solution of the crude compound, a red crystalline substance was formed. After filtering out this substance, an excess of sodium iodide and ethanol were added to the mother liquor. Then the complex iodide deposited as red crystals. It was filtered, washed with ethanol-water mixture and ethanol, and dried in air. Yield 0.2 g.

$(+)_{589}$-C_1-cis(O)-$[Co(L\text{-ser})_2en]ClO_4$. A crude perchlorate was prepared by a similar method to that used for the isolation of $(-)_{589}$-C_1-*cis(O)*-isomer. It was recrystallized from water by adding acetone. The red crystals were filtered, washed with acetone-water mixture and acetone, and dried in air. Yield: 0.2 g.

$(-)_{589}$-C_2-cis(O)-$[Co(L\text{-ser})_2en]I \cdot 2H_2O \cdot 1/2serH$. This complex was isolated as pinkish red crystals from a concentrated sixth eluate by the same method as that used for the isolation of $(+)_{589}$-C_2-*cis(O)*-isomer. Yield: 0.04 g.

4) Measurements. The electronic absorption spectra were measured with a Beckman DU spectrophotometer. The CD spectra were recorded on a Roussel-Jouan Dichrograph and the ORD curves were checked with a Yanagimoto recording spectropolarimeter, Model-185. All measurements were made in aqueous solutions at room temperature.

Results and Discussion

Three geometrical isomers, *trans(O)*, C_2-*cis(O)*, and C_1-*cis(O)*, are possible for the bis(glycinato)-ethylenediaminecobalt(III) complex (Fig. 1). Of these isomers, *trans(O)* and C_1-*cis(O)* isomers were optically resolved with $(-)_{546}$-K[Co(edta)] and

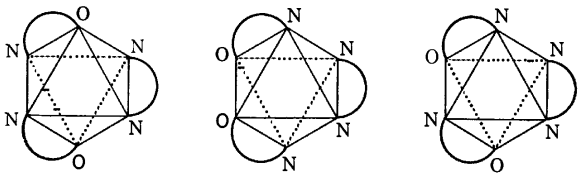

Fig. 1. The three geometrical isomers of Λ-$[Co(gly)_2en]^+$.

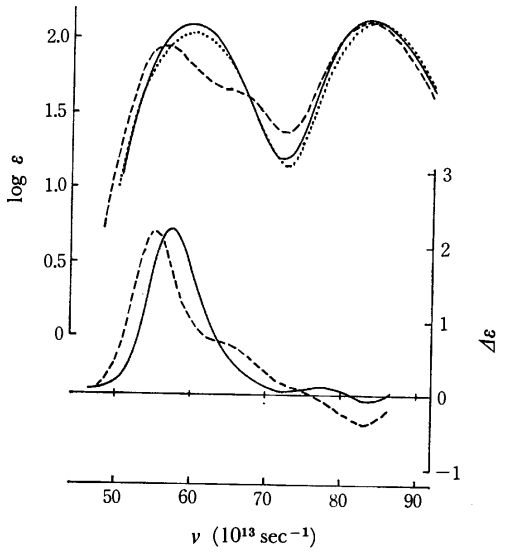

Fig. 2. Absorption and CD curves of $(+)_{589}$-*trans*(*O*) (----) and $(+)_{589}$-C_1-*cis*(*O*)-$[Co(gly)_2en]^+$ (——); and absorption curve of C_2-*cis*(*O*)-$[Co(gly)_2en]^+$ (·····).

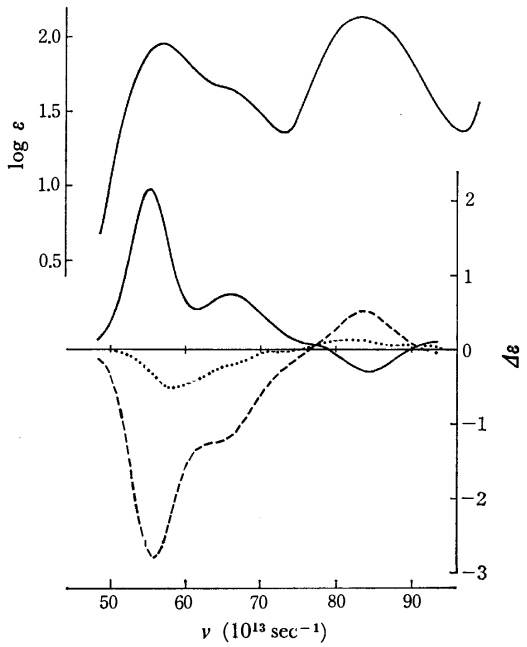

Fig. 3. Absorption and CD curves of $(+)_{589}$-*trans*(*O*)-[Co(L-ser)$_2$en]$^+$ (——); CD curve of $(-)_{589}$-*trans*(*O*)-[Co(L-ser)$_2$en]$^+$ (----); and vicinal effect (2L) curve of *trans*(*O*)-[Co(L-ser)$_2$en]$^+$ (·····).

potassium antimony(III) L-tartrate, respectively, as resolving agents. Their absorption and CD curves are shown in Fig. 2 with the absorption curve of the

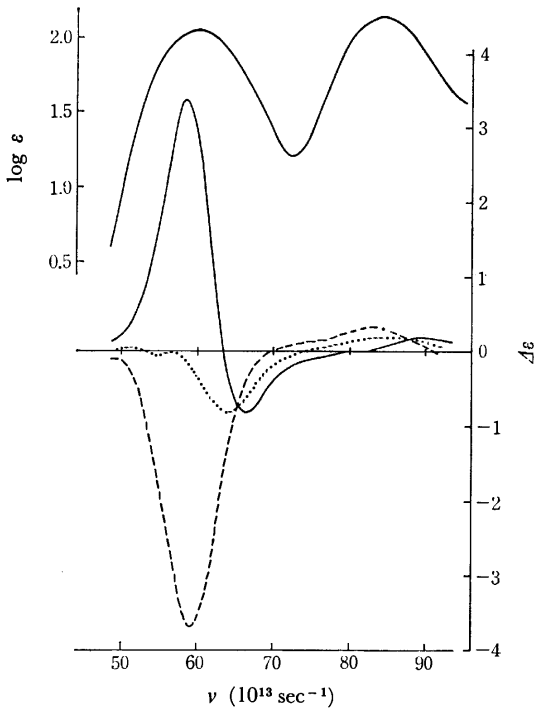

Fig. 4. Absorption and CD curves of $(+)_{589}$-C_2-*cis*(*O*)-[Co(L-ser)$_2$en]$^+$ (——); CD curve of $(-)_{589}$-C_2-*cis*(*O*)-[Co(L-ser)$_2$en]$^+$ (----); and vicinal effect (2L) curve of C_2-*cis*(*O*)-[Co(L-ser)$_2$en]$^+$ (·····).

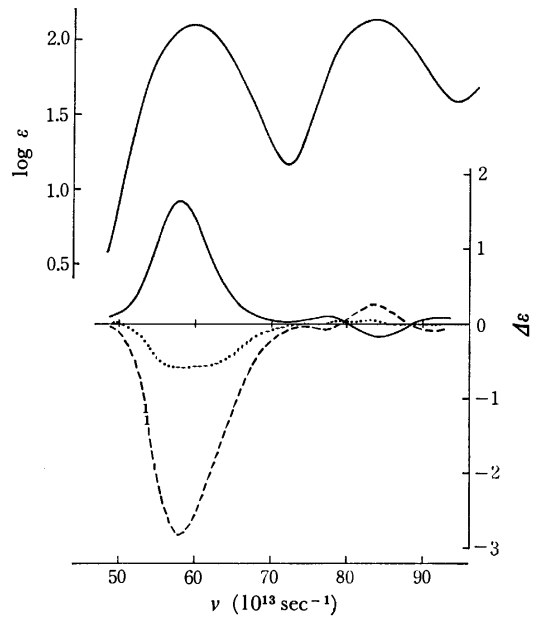

Fig. 5. Absorption and CD curves of $(+)_{589}$-C_1-*cis*(*O*)-[Co(L-ser)$_2$en]$^+$ (——); CD curve of $(-)_{589}$-C_1-*cis*(*O*)-[Co(L-ser)$_2$en]$^+$ (----); and vicinal effect (2L) curve of C_1-*cis*(*O*)-[Co(L-ser)$_2$en]$^+$ (·····).

C_2-*cis*(*O*) isomer. The six possible isomers of the bis(L-serinato)ethylenediaminecobalt(III) complex, Δ- and Λ-*trans*(*O*), Δ- and Λ-C_2-*cis*(*O*) and Δ- and Λ-C_1-*cis*(*O*), were completely separated by ion-exchange column chromatography. Their absorption and CD curves are shown in Figs. 3—5 and the curves of *trans*(*O*) isomers of bis(L-alaninato)ethylene-

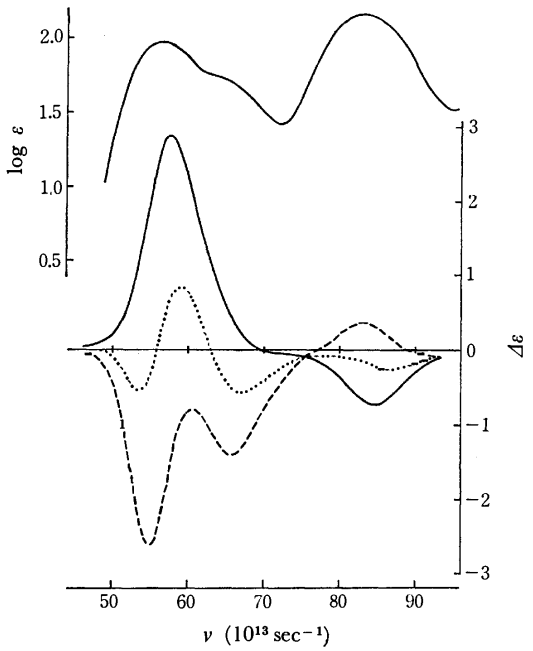

Fig. 6. Absorption and CD curves of $(+)_{589}$-*trans(O)*-[Co(L-ala)$_2$en]$^+$ (——); CD curve of $(-)_{589}$-*trans(O)*-[Co(L-ala)$_2$en]$^+$ (----); and vicinal effect (2L) curve of *trans(O)*-[Co(L-ala)$_2$en]$^+$ (·····).

diaminecobalt(III) complex in Fig. 6. The analytical data of the isomers obtained in this work are summarized in Table 1 and the spectral data in Tables 2 and 3.

Characterization of Isomers. The isomers from the first and second eluates in column chromatography of bis(L-serinato) complex can be assigned confidently to the *trans(O)* structure from the remarkable splitting of their first absorption bands (Fig. 3 and Table 2).[9] The isomers from the remaining four eluates are of *cis(O)* structure because of the symmetrical pattern of their first absorption bands (Figs. 4 and 5 and Table 2) and of the ion-exchange chromatographic behavior as described in "Experimental section." In a previous work,[9] we found that the second absorption band maximum of the C_2-*cis(O)* isomer of bis(glycinato)-ethylenediamine complex locates at higher energy than that of the C_1-*cis(O)* isomer and that the $\log(D_I/D_{II})$ value in the C_2-*cis(O)* isomer is larger in absolute value than that in the C_1-*cis(O)* isomer, where D_I and D_{II} are the optical densities at the absorption maxima of the first and the second absorption bands, respectively. The C_1-*cis(O)* and C_2-*cis(O)* structures of the bis(glycinato) complexes have been confirmed by PMR.[9] The second absorption bands of the present four *cis(O)* isomers are at 84.3, 83.3, 83.6, and 85.1×10^{13} sec^{-1} for the 3rd, 4th, 5th, and 6th eluates, respectively. From these values, it is assumed that the isomers from the 3rd and 6th eluates are C_2-*cis(O)* and the 4th and 5th C_1-*cis(O)*. This assignment brings about that the $\log(D_I/D_{II})$ value is −0.09 for each of the two C_2-*cis(O)* isomers, −0.02 for one C_1-*cis(O)* (from 4th eluate) and −0.04 for another C_1-*cis(O)* isomer (from 5th eluate).

It is well known that the absolute configuration of the cobalt(III) complexes with chelated α-aminoacidato ligands can be assigned from the sign of major CD band in the first absorption band region, *i.e.*, the Λ[12] complex has (−) major CD band and the Λ one (+).[7] The assignment was supported by Dabrowiak and Cooke[11] from their PMR study on several α-aminoacidato complexes including *trans(O)*-[Co(L-ala)$_2$en]$^+$. Therefore each of the $(+)_{589}$-isomers in the present work has Λ-configuration and each of the $(-)_{589}$-isomers Λ-configuration (Figs. 2—6 and Table 3). According-

Table 1. Analytical data of [Co(aminoacidato)$_2$en]X type complexes

Complex	Found			Calcd		
	C	H	N	C	H	N
trans(O)-[Co(gly)$_2$en]ClO$_4$	19.48	4.45	15.07%	19.66	4.40	15.28%
$(+)_{589}$-*trans(O)*-[Co(gly)$_2$en][Co(edta)]	30.76	4.86	13.49	31.18	4.91	13.64
$(+)_{589}$-*trans(O)*-[Co(gly)$_2$en]I·H$_2$O	17.46	4.49	13.55	17.49	4.40	13.60
C_1-*cis(O)*-[Co(gly)$_2$en]ClO$_4$·2H$_2$O	18.02	4.91	13.79	17.90	5.01	13.92
C_1-*cis(O)*-[Co(gly)$_2$en]I·2H$_2$O	17.06	4.78	12.96	16.76	4.69	13.03
$(+)_{589}$-C_1-*cis(O)*-[Co(gly)$_2$en]I·2H$_2$O	16.78	4.74	12.82	16.76	4.69	13.03
C_2-*cis(O)*-[Co(gly)$_2$en]ClO$_4$	19.37	4.32	14.82	19.66	4.40	15.28
C_2-*cis(O)*-[Co(gly)$_2$en]I	18.28	4.05	14.82	18.29	4.09	15.28
$(+)_{589}$-*trans(O)*-[Co(L-ala)$_2$en]ClO$_4$	24.12	5.12	14.47	24.35	5.11	14.20
$(-)_{589}$-*trans(O)*-[Co(L-ala)$_2$en]ClO$_4$	24.24	5.11	13.98	24.35	5.11	14.20
$(+)_{589}$-*trans(O)*-[Co(L-ser)$_2$en]ClO$_4$	22.42	4.89	13.01	22.52	4.72	13.13
$(-)_{589}$-*trans(O)*-[Co(L-ser)$_2$en]I	20.71	4.45	12.11	21.16	4.44	12.34
$(+)_{589}$-C_1-*cis(O)*-[Co(L-ser)$_2$en]ClO$_4$	23.21	4.90	13.02	22.52	4.72	13.13
$(-)_{589}$-C_1-*cis(O)*-[Co(L-ser)$_2$en]I	21.18	4.46	12.12	21.16	4.44	12.34
$(+)_{589}$-C_2-*cis(O)*-[Co(L-ser)$_2$en]I	21.30	4.57	12.15	21.16	4.44	12.34
$(-)_{589}$-C_2-*cis(O)*-[Co(L-ser)$_2$en]I·2H$_2$O·1/2 serH	21.23	5.12	11.41	21.03	5.11	11.61

10) N. Matsuoka, J. Hidaka, and Y. Shimura, This Bulletin, **39**, 1257 (1966).
11) J. C. Dabrowiak and D. W. Cooke, *J. Amer. Chem. Soc.*, **92**, 1097 (1970).
12) Absolute configurations are designated by the IUPAC tentative rule: *Inorg. Chem.*, **9**, 1 (1970).

TABLE 2. ABSORPTION DATA OF [Co(aminoacidato)$_2$en]$^+$ TYPE COMPLEXES

Complex	I-Band		II-Band		Ref.
	ν_{max}[a]	(log ε_{max})	ν_{max}[a]	(log ε_{max})	
trans(O)-[Co(gly)$_2$en]I·H_2O	56.6	(1.94)	83.3	(2.12)	9
	ca. 66	(*ca.* 1.64)			
C_2-*cis(O)*-[Co(gly)$_2$en]Br·H_2O	59.8	(2.04)	84.0	(2.11)	9
C_1-*cis(O)*-[Co(gly)$_2$en]Br·$3H_2O$	59.9	(2.09)	83.1	(2.13)	9
Λ-(+)$_{589}$-*trans(O)*-[Co(L-ala)$_2$en]ClO_4	56.4	(1.97)	83.1	(2.17)	
	ca. 66	(*ca.* 1.70)			
Δ-(−)$_{589}$-*trans(O)*-[Co(L-ala)$_2$en]ClO_4	56.6	(1.98)	82.9	(2.13)	
	ca. 66	(*ca.* 1.67)			
Λ-(+)$_{589}$-*trans(O)*-[Co(L-ser)$_2$en]ClO_4	56.7	(1.95)	83.1	(2.13)	
	ca. 66	(*ca.* 1.64)			
Δ-(−)$_{589}$-*trans(O)*-[Co(L-ser)$_2$en]I	56.7	(1.95)	83.3	(2.13)	
	ca. 66	(*ca.* 1.70)			
Λ-(+)$_{589}$-C_2-*cis(O)*-[Co(L-ser)$_2$en]I	60.0	(2.05)	84.3	(2.14)	
Δ-(−)$_{589}$-C_2-*cis(O)*-[Co(L-ser)$_2$en]I·$2H_2O$·1/2 serH	60.1	(2.10)	85.1	(2.19)	
Λ-(+)$_{589}$-C_1-*cis(O)*-[Co(L-ser)$_2$en]ClO_4	59.9	(2.11)	83.6	(2.15)	
Δ-(−)$_{589}$-C_1-*cis(O)*-[Co(L-ser)$_2$en]I	60.0	(2.12)	83.3	(2.14)	

a) In the unit of 10^{13} sec^{-1}.

TABLE 3. CIRCULAR DICHROISM DATA OF [Co(aminoacidato)$_2$en]$^+$ TYPE COMPLEXES

Complex	I-Band		II-Band	
	ν_{ext}[a]	($\Delta\varepsilon_{ext}$)	ν_{ext}[a]	($\Delta\varepsilon_{ext}$)
Λ-(+)$_{589}$-*trans(O)*-[Co(gly)$_2$en]I·H_2O	55.3	(+2.19)	83.3	(−0.32)
	ca. 66	(+0.64)		
Λ-(+)$_{589}$-C_1-*cis(O)*-[Co(gly)$_2$en]I·$2H_2O$	57.1	(+2.21)	77.4	(+0.11)
			83.8	(−0.08)
Λ-(+)$_{589}$-*trans(O)*-[Co(L-ala)$_2$en]ClO_4	57.7	(+2.88)	84.7	(−0.74)
Δ-(−)$_{589}$-*trans(O)*-[Co(L-ala)$_2$en]ClO_4	54.8	(−2.63)	83.3	(+0.36)
	65.7	(−1.40)		
Λ-(+)$_{589}$-*trans(O)*-[Co(L-ser)$_2$en]ClO_4	55.1	(+2.13)	84.3	(−0.30)
	65.7	(+0.75)		
Δ-(−)$_{589}$-*trans(O)*-[Co(L-ser)$_2$en]I	55.7	(−2.81)	84.3	(+0.51)
	63.8	(−1.26)		
Λ-(+)$_{589}$-C_2-*cis(O)*-[Co(L-ser)$_2$en]I	58.4	(+3.38)	89.6	(+0.18)
	66.2	(−0.83)		
Δ-(−)$_{589}$-C_2-*cis(O)*-[Co(L-ser)$_2$en]I·$2H_2O$·1/2 serH	59.2	(−3.67)	83.3	(+0.33)
Λ-(+)$_{589}$-C_1-*cis(O)*-[Co(L-ser)$_2$en]ClO_4	58.0	(+1.64)	77.9	(+0.09)
			84.3	(−0.18)
			92.3	(+0.08)
Δ-(−)$_{589}$-C_1-*cis(O)*-[Co(L-ser)$_2$en]I	58.0	(−2.84)	77.5	(−0.08)
			84.0	(+0.24)
			91.5	(−0.11)

a) In the unit of 10^{13} sec^{-1}.

ly, it is concluded that the six L-serinato isomers obtained are *Λ-trans(O)*, *Λ-trans(O)*, *Λ-C_2-cis(O)*, *Δ-C_1-cis(O)*, *Λ-C_1-cis(O)*, and *Δ-C_2-cis(O)* in the elution order, which agrees also with that found in the case of [Co(ox)(L-ser)$_2$]$^-$.

The iodide of *Δ-C_2-cis(O)*-[Co(L-ser)$_2$en]$^+$ isomer was isolated with L-serine (Table 1). This fact suggests that the coordinated L-serinate ion is partly freed from the coordination sphere in the isolation process. This suggestion is supported from the fact that the yield of C_2-*cis(O)* isomer was considerably low in comparison with that of C_1-*cis(O)* isomer in the case of [Co(gly)$_2$en]$^+$ or [Co(L-ser)$_2$en]$^+$ and that the optical resolution of C_2-*cis(O)*-[Co(gly)$_2$en]$^+$ was unsuccessful because of the partial decomposition. Similar low yields were also reported for the C_2-*cis(O)*-isomers of bis(glycinato)(D-propylenediamine)cobalt(III)[6] and bis(L-hydrogenaspartato)(D-propylenediamine)cobalt(III)[13] complexes. Though it seems from these facts that the C_2-*cis(O)* structure is less stable than the

13) Y. Kojima and M. Shibata, *ibid.* **10**, 2382 (1971).

C_1-cis(O) structure, further studies should be carried out for substantiation of this remark.

Circular Dichroism Spectra. In the first absorption band region, the *trans(O)* isomer shows two CD bands of same sign whose dominant peak is in the lower energy side. This agrees well with the pattern, which is predicted from the CD spectra of the *trans(N)* oxalatobis(α-aminoacidato) complexes.[4,7] It appears that, of the *trans(O)* isomers here studied, *Λ-trans(O)*-[Co(L-ala)$_2$en]$^+$ somewhat deviates from the group behavior in CD (Fig. 6). It has been known that the configurational and vicinal contributions to CD are almost separable and additive for the cobalt(III) complexes with optically active α-aminoacidato ligands.[1,7] From this viewpoint, the following relationships were applied for the CD curves of L-serinato and L-alaninato isomers.

$$\Delta\varepsilon(2\text{L}) = 1/2\{\Delta\varepsilon(\Lambda_{2\text{L}}) + \Delta\varepsilon(\Delta_{2\text{L}})\}$$
$$\Delta\varepsilon(\Lambda) = 1/2\{\Delta\varepsilon(\Lambda_{2\text{L}}) - \Delta\varepsilon(\Delta_{2\text{L}})\}$$

Each calculated configurational curve agrees with the observed curve of the corresponding glycinato isomer (Fig. 7). For this reason, there is nothing strange about the CD curve of *Λ-trans(O)*-[Co(L-ala)$_2$en]$^+$, whose configurational CD also consists of two bands in the first absorption band region.

The CD patterns of C_1- and *C_2-cis(O)* isomers are not so distinctive in the first absorption band region (Figs. 4, 5 and 7). In the second absorption band region, however, the CD pattern of the *C_1-cis(O)* isomer differs significantly from that of the *C_2-cis(O)* isomer. That is, the *C_1-cis(O)* isomer shows well split three CD bands whose signs are +, −, and +, listing from lower energy for the *Λ* isomer (Figs. 2 and 5), whereas the *C_2-cis(O)* and *trans(O)* isomers show one or two CD bands in appearance. The same relationship was also observed for the CD spectra of the C_1 and C_2 isomers of oxalatobis(α-aminoacidato) complexes.[7] These facts suggest that the CD pattern in the second band region favorably reflects the symmetry of the complex ion.

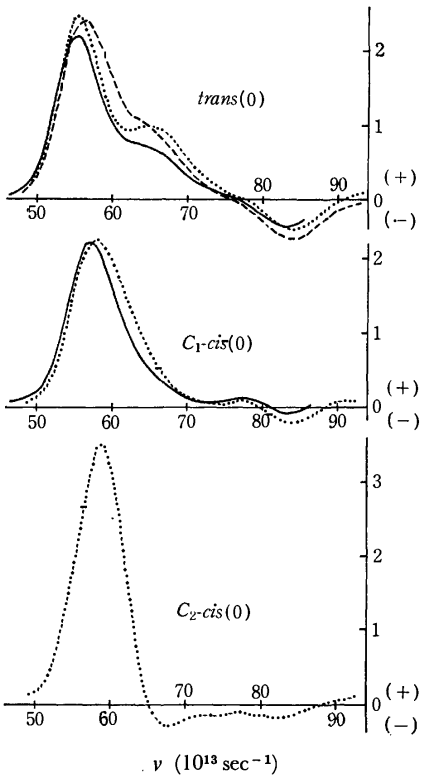

Fig. 7. Configurational effect curve of *Λ-trans(O)*-, *Λ-C_1*- and *Λ-C_2-cis(O)*-[Co(L-ser)$_2$en]$^+$ (·····) and *trans(O)*-[Co(L-ala)$_2$en]$^+$ (----); and observed curves of *Λ-trans(O)*- and *Λ-C_1-cis(O)*-[Co(gly)$_2$en]$^+$ (——).

Studies on New Derivatives of 8-Quinolinol as Chelating Agents. II. Chelate Formation of Some Aminomethyl Derivatives Derived from 8-Hydroxyquinoline-2-carbaldehyde with Metal Ions

Takehisa HATA and Toyozo UNO

Faculty of pharmaceutical Sciences, Kyoto University, Yoshida, Sakyo-ku, Kyoto

(Received October 30, 1971)

The reactions of new oxine derivatives with additional coordinative sites, 8-hydroxyquinoline-2-carbaldehyde, 2-(*p*-chlorophenylaminomethyl)-, 2-(naphthylaminomethyl)-, 2-(*p*-tolylaminomethyl)-, and 2-(*o*-hydroxyphenylaminomethyl)-8-hydroxyquinoline, and *N,N'*-bis(8-hydroxy-2-quinolylmethyl)ethylenediamine (abbreviated as HQA, CAMHQ, NAMHQ, TAMHQ, PAMHQ, and BHQED respectively), with Cu^{2+}, Co^{2+}, Ni^{2+}, Zn^{2+}, Cd^{2+}, Mn^{2+}, Mg^{2+}, and Ca^{2+} were investigated by potentiometric and spectrophotometric methods. The stability constants of the metal chelates were determined in a 50 v/v % aqueous dioxane solution at 25°C. The stability constants of metal chelates of HQA, NAMHQ, CAMHQ, and TAMHQ with a ligand-to-metal ratio of 2 : 1 are lower than those of oxine. In these ligands, steric hindrance due to the aminomethyl group results in lower stability constants of the metal chelates. PAMHQ reacts as a terdentate ligand with Cu^{2+}, Mn^{2+}, Mg^{2+}, and Ca^{2+} to form 1 : 1 chelates by coordination with quinoline nitrogen and two phenolate oxygens. BHQED reacts with Cu^{2+}, Co^{2+}, Ni^{2+}, Cd^{2+}, and Mn^{2+} to form a protonated chelate, MHL^+, in the acid region, while, in the neutral region, one proton is released from the protonated chelate to form a deprotonated chelate, ML, by coordination with six donor groups, namely, two imino and hydroxyl groups, and two quinoline nitrogens. BHQED acts as a sexadentate ligand to form the most stable chelates among these oxine derivatives.

In a previous paper,[1] we reported the syntheses of new oxine derivatives, such as 8-hydroxyquinoline-2-carbaldehyde(HQA), 2-(*p*-chlorophenylaminomethyl)-8-hydroxyquinoline(CAMHQ), 2-(naphthylaminomethyl)-8-hydroxyquinoline(NAMHQ), 2-(*p*-tolylaminomethyl)-8-hydroxyquinoline(TAMHQ), 2-(*o*-hydroxyphenylaminomethyl)-8-hydroxyquinoline(PAMHQ), and *N,N'*-bis-(8-hydroxy-2-quinolylmethyl)ethylenediamine(BHQED), with additional coordinative sites. Their color reactions with metal ions and acid dissociation constants were also reported.

The influence of the introduction of the additional groups into these ligands may be reflected in the stability of the metal chelates in the following way. If additional coordinative groups, such as aminomethyl, imino, and hydroxyl groups, participate in the coordination, the formation of stable multidentate chelates may be expected. On the contrary, the steric hindrance of these groups at the 2 position may lower the stability of the metal chelates. In this case, the effect of these groups may be greater than that of the alkyl and aryl groups, which have been known to lower the stability of the metal chelates by their steric hindrance. The effect of the additional coordinative groups on the chelate formation may be discussed through a comparison of the stability of the metal chelates formed from these ligands with that of the metal chelates of oxine. From these points of view, we investigated the chelate formation of the oxine derivatives in a 50 v/v % aqueous dioxane solution by potentiometric and spectrophotometric methods.

Experimental

Reagents. The preparations of 8-hydroxyquinoline-2-carbaldehyde, 2-(*p*-chlorophenylaminomethyl)-, 2-(naphthylaminoethyl)-, 2-(*p*-tolylaminomethyl)-, 2-(*o*-hydroxyphenylaminomethyl)-8-hydroxyquinoline, and *N,N'*-bis-(8-hydroxy-2-quinolylmethyl)ethylenediamine were described in the previous paper.[1] Stock solutions of metal chlorides and and perchlorates were standardized by titration with EDTA. All the other compounds used were of a reagent-grade purity.

Potentiometric Titration. The details of the experimental conditions and the method have been described previously.[1] As the ligands and the metal chelates are in soluble in water, the titrations were carried out in a 50 v/v % aqueous dioxane. A solution containing a ligand (10^{-3} M), perchloric acid (10^{-3} M for HQA, CAMHQ, NAMHQ, TAMHQ, and PAMHQ, and 2×10^{-3} M for BHQED), and metal chloride or perchlorates (from 5×10^{-4} M to 10^{-2} M) was titrated with a standard KOH solution.

Spectrophotometric Measurements. The absorption spectra were measured with a Hitachi recording spectrophotometer model 124, and measurements were made in a 50 v/v% aqueous dioxane solution. The pH of the solutions was adjusted with KOH and $HClO_4$ solutions or a Walpole buffer (CH_3COOH–CH_3COONa).

Results and Discussion

HQA, NAMHQ, CAMHQ, and TAMHQ. The results of the molar-ratio method showed that HQA, CAMHQ, and NAMHQ react with metal ions to form 2 : 1 ligand-to-metal chelates. Accordingly, the titration was carried out in the molar ratio of 2 : 1. With HQA, CAMHQ, and NAMHQ, similar curves were obtained. The titration curves of HQA in the presence and the absence of metal ions are shown in Fig. 1. In the cases of Co^{2+}, Ni^{2+}, Zn^{2+}, Cd^{2+}, Mn^{2+}, Mg^{2+}, and Ca^{2+}, each titration curve of the three ligands gives an inflection at $a=1$, indicating that the dissociation reaction of the proton from the ligand occurs between $a=0$ and $a=1$, and that the formation of metal chelates occurs between $a=1$ and $a=2$. However, as is shown in Fig. 2, the titration curves of TAMHQ-metal systems differ from those of HQA-, CAMHQ-, and NAMHQ-metal systems. With all the metal ions except for Cu^{2+} and Ni^{2+}, the titration curves

1) T. Hata and T. Uno, This Bulletin, **45**, 477 (1972)

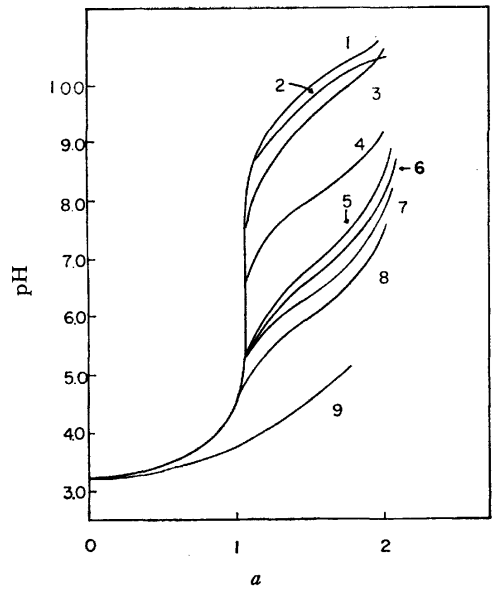

Fig. 1. Potentiometric titration curves of molar ratio of HQA to metal ions 2 : 1 in 50 v/v% aqueous dioxane solution at 25°C μ=0.1(KCl); abscissa a represents moles of KOH added per mole of ligand; curve 1, ligand; 2, Ca^{2+}; 3, Mg^{2+}; 4, Mn^{2+}; 5, Cd^{2+}; 6, Ni^{2+}; 7, Co^{2+}; 8, Zn^{2+}; 9, Cu^{2+}.

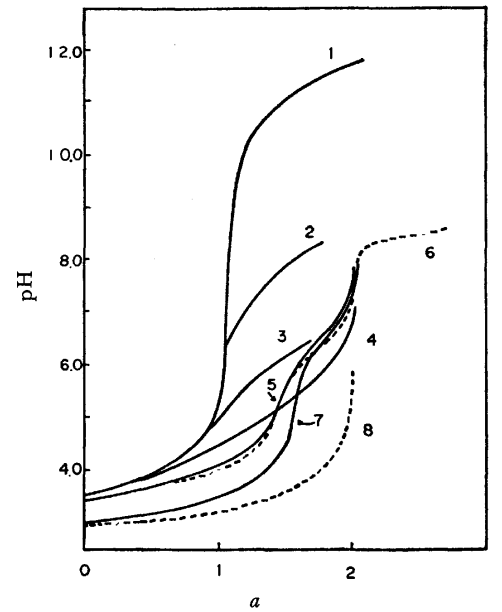

Fig. 2. Potentiometric titration curves of molar ratio of TAMHQ to metal ions 2 : 1 and 1 : 1; the solid line and broken line represent the curves of molar ratio 2 : 1 and 1 : 1, respectively; curve 1, ligand; 2, Mn^{2+}; 3, Cd^{2+}; 4, Zn^{2+}; 5 and 6, Ni^{2+}; 7 and 8, Cu^{2+}.

are analogous to those of HQA, CAMHQ, and NAMHQ, and they show an inflection at a=1. However, with Cu^{2+}, the curve of the 2 : 1 molar ratio gives an inflection at a=1.5, while in the curve of the 1 : 1 molar ratio, an inflection is no longer observed at a=1.5. The titration curves for the Cu^{2+} ion suggest the following reaction process. The dissociation reaction of the proton from the ligand and the formation reaction of the 1 : 1 chelate CuL^+ occur

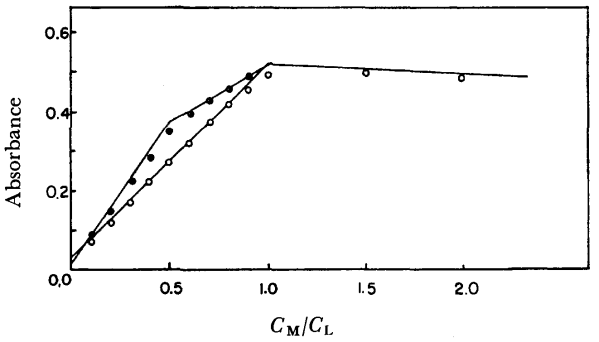

Fig. 3. The determination of molar ratio of TAMHQ to Cu^{2+} in 50 v/v% aqueous dioxane solution; abscissa represents the molar ratio of metal to ligand; ○, pH 4.80; ◑, pH 6.92.

simultaneously between a=0 and a=1.5, and this chelate reacts with the second ligand to form the 2 : 1 chelate ML_2 in the 2 : 1 molar ratio solution. On the other hand, in the 1 : 1 solution, the ligand reacts with the Cu^{2+} ion to release two protons and form the 1 : 1 chelate in one step.

$$H_2L^+ \rightleftharpoons HL + H^+ \qquad K_2=\frac{[HL][H^+]}{[H_2L^+]} \tag{1}$$

$$Cu^{2+} + L^- \rightleftharpoons CuL^+ \qquad K_{ML}=\frac{[CuL^+]}{[Cu^{2+}][L^-]} \tag{2}$$

$$CuL^+ + L^- \rightleftharpoons CuL_2 \qquad K_{ML_2}=\frac{[CuL_2]}{[CuL^+][L^-]} \tag{3}$$

In fact, the results of the molar-ratio method given in Fig. 3 show that TAMHQ forms the 1 : 1 chelate below pH 4.80 and the 2 : 1 chelate together with the 1 : 1 chelate at about pH 6.90. With Ni^{2+}, the titration curves of the 2 : 1 and 1 : 1 molar ratios are identical between a=0 and a=2, but the hydrolysis of the Ni^{2+} ion occurs at about a=2 in the 1 : 1 solution. From these facts, it is considered that TAMHQ reacts with the Ni^{2+} ion to form a protonated chelate, M·HL·L between a=0 and a=1.5; then one proton is released to form a deprotonated 2 : 1 chelate, ML_2, between a=1.5 and a=2 in both solution:

$$Ni^{2+} + HL + L^- \rightleftharpoons Ni\cdot HL\cdot L \qquad K=\frac{[Ni\cdot HL\cdot L^+]}{[Ni^{2+}]\cdot[HL]\cdot[L^-]} \tag{4}$$

$$Ni\cdot HL\cdot L^+ \rightleftharpoons NiL_2 + H^+ \qquad K_C=\frac{[NiL_2]\cdot[H^+]}{[Ni\cdot HL\cdot L^+]} \tag{5}$$

The equilibrium constants, K and K_C, given in Reactions (4) and (5) are calculated from the data in the regions between a=0.3 and a=1.2, and between a=1.6 and a=1.9, respectively. The results obtained from the 2 : 1 and 1 : 1 curves coincide to give log K=13.45 and pK_C=6.62 respectively.

The stability constants of 2 : 1 ligand-to-metal chelates were calculated by Bjerrum's method,[2] as modified by Irving and Rossotti,[3] from the following equations:

2) J. Bjerrum, "Metal Ammine Formation in Aqueous solution," P. Haase and Sons, Copenhagen, 1941.

3) G. Irving and H. S. Rossoti, *J. Chem. Soc.*, **1953**, 3397.

$$[L]=\frac{C_L+[HClO_4]+[OH^-]-[KOH]-[H^+]}{[P]} \quad (6)$$

$$\bar{n}=\frac{C_L-Q\cdot[L]}{C_M} \quad (7)$$

where $P=[H^+]/K_1+2\cdot[H^+]^2/K_1\cdot K_2$, and $Q=1+[H^+]/K_1+[H^+]^2/K_1\cdot K_2$; n is the average number of ligands bound per metal ion, C_L and C_M are the total ligand concentration and the total metal concentration respectively, and K_1 and K_2 are acid dissociation constants. The values of $\bar{n}$ and [L] at each point of the titration curves were calculated from Eqs. (6) and (7). From these data, the formation curves were plotted. The step-by-step stability constants, K_{ML} and K_{ML_2}, were calculated by the least-squares method by the use of Eq. (8):

$$\frac{\bar{n}}{(\bar{n}-1)\cdot[L]}=\frac{(2-\bar{n})\cdot[L]}{(\bar{n}-1)}K_{ML}\cdot K_{ML_2}-K_{ML} \quad (8)$$

When the precipitation was observed in the course of titration, the stability constants were estimated apporoximately from the values of pL at $\bar{n}=0.5$ and $\bar{n}=1.5$. From the values of K_{ML}, K_{ML_2}, and [L], $\bar{n}$ was recalculated by Eq. (9) and theoretical formation curves were plotted:

$$\bar{n}=\frac{K_{ML}\cdot[L]+2\cdot K_{ML}\cdot K_{ML_2}\cdot[L]^2}{1+K_{ML}\cdot[L]+K_{ML}\cdot K_{ML_2}\cdot[L]^2} \quad (9)$$

The theoretical curve and the experimental plots of the TAMHQ metal chelates are shown in Fig. 4. The theoretical curve is in good agreement with the experimental plots. The stability constants are summarized in Table 1, along with the acid dissociation constants, and are compared with those of oxine.

As may be seen in Table 1, the stability constants of the metal chelates of four ligands, HQA, CAMHQ, NAMHQ, and TAMHQ, are lower than those of oxine. These results can be explained as follows. The basicity of these ligands is lower than that of oxine. These ligands do not behave as terdentate ligands, but as bidentate ligands toward metal ions; that is, the quinoline nitrogen and phenolate oxygen for four ligands participate in coordination to metal ions to form 2 : 1 chelates. Moreover, the aminomethyl group introduced at the 2 position induces a large steric hindrance. Accordingly, their metal chelates should be lower in stability than those of oxine, as is observed in the cases of 2-aryl- and 2-alkyl-8-hydroxyquinoline.[4,5]

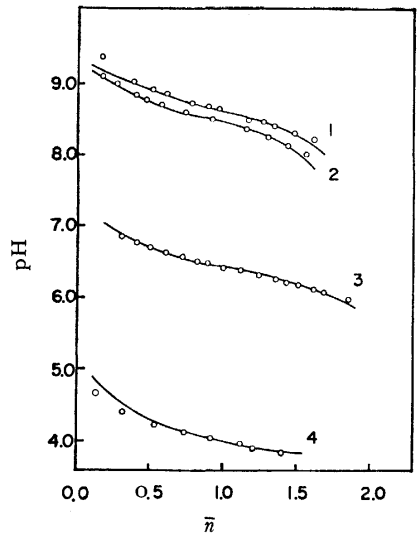

Fig. 4. The formation curves of TAMHQ-metal chelates; solid line represents the theoretical formation curves; curve 1, Zn^{2+}; 2, Co^{2+}; 3, Mn^{2+}; 4, Mg^{2+}.

The stability of metal chelates in these ligands decreases in the order of $Cu^{2+}>Zn^{2+}>Co^{2+}\sim Ni^{2+}>Cd^{2+}>Mn^{2+}$. It is noteworthy that this order is in agreement with that in 2-alkyl-8-hydroxyquinoline and is different from that of oxine, that is, Mellor-Mallery's order[6]: $Cu^{2+}>Ni^{2+}>Co^{2+}>Zn^{2+}>Cd^{2+}>Mn^{2+}$.

PAMHQ. The titration curves of the 1 : 1 and 2 : 1 molar ratios are shown in Fig. 5. In the presence of any metal ion except Zn^{2+}, the titration curves of the 2 : 1 molar ratio are almost identical

Table 1. The stability constants of metal chelates of HQA, TAMHQ, CAMHQ, and NAMHQ $\mu=0.1$, 25°C

Ligand	Oxine[a]		HQA		TAMHQ		CAMHQ		NAMHQ	
Cation	log K_{ML}	log K_{ML_2}	log K_{ML}	log K_{ML_2}	log K_{ML}	log K_{ML_2}	log K_{ML}	log K_{ML_2}	log K_{ML}	log K_{ML_2}
Cu^{2+}	13.49	12.73	8.97	8.46	<12.00	8.06			10.7[b]	
Zn^{2+}	9.96	8.90	7.25	7.14	8.92	8.22	9.24	8.63	9.21	8.62
Ni^{2+}	11.43	9.94	6.58	6.62			8.9[b]		8.07	7.98
Co^{2+}	10.55	9.11	7.12	6.43	8.78	8.06	8.6[b]		8.6[b]	
Cd^{2+}	7.78		6.63	6.17	8.5[b]		8.4[b]			
Mn^{2+}	8.28	7.17	5.49	4.92	6.67	6.20	6.8[b]			
Mg^{2+}	6.38	5.43	3.45		4.2		4.5		4.6	
Ca^{2+}	3.2		4.0	2.6					3.5	
	pK_1	pK_2	pK_1	pK_2	pK_1	pK_2	pK_1	pK_2	pK_1	pK
H^+	11.54	3.97	9.92	<3	11.11	3.62	11.10	3.19	11.11	3.39

a) W. D. Johnston and H. Freiser, *J. Amer. Chem. Soc.*, **74**, 5239 (1952). b) Precipitation occured.

4) W. D. Johnston and H. Freiser, *J. Amer. Chem. Soc.*, **74**, 5239 (1952).
5) H. Kaneko and K. Ueno, This Bulletin, **39**, 1910 (1966).
6) D. P. Mellor and L. Malley, *Nature*, **159**, 370 (1947); **161**, 436 (1948).

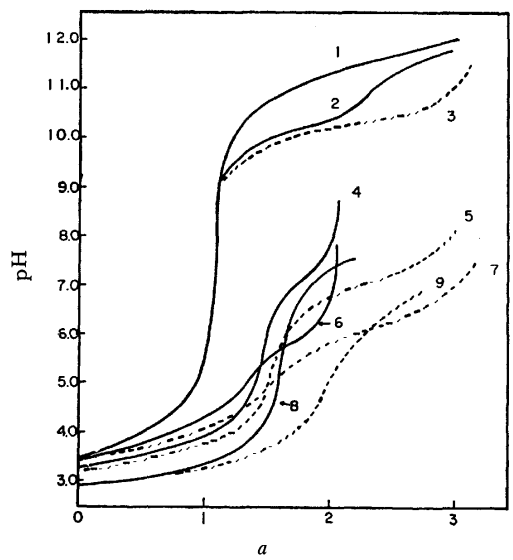

Fig. 5. Potentiometric titration curves of molar ratio of PAMHQ to metal ions 2 : 1 and 1 : 1; solid line and broken line represent the curves of molar ratio 2 : 1 and 1 : 1, respectively; curve 1, ligand; 2 and 3, Ca^{2+}; 4 and 5, Ni^{2+}; 6 and 7, Zn^{2+}; 8 and 9, Cu^{2+}.

TABLE 2. THE STABILITY CONSTANTS OF METAL CHELATES OF 2-(*o*-HYDROXYPHENYLAMINOMETHYL)-8-HYDROXYQUINOLINE(PAMHQ) $\mu=0.1$, 25°C

Cation	log K_{MHL}	log $K_{M(HN)_2}$	log K_{ML}	
Cu^{2+}		8.07	17.44	log $K_{CuHL^+}=12.47$
Co^{2+}	8.06	8.02		$pK^{H^+}_{CuHL^+}=6.54$
Cd^{2+}	6.80	6.70		
Mn^{2+}	6.36	5.94	9.50	
Mg^{2+}	4.52		5.17	
Ca^{2+}	4.51		6.10	
	pK_1	pK_2	pK_3	
H^+	11.53	10.86	3.72	

with the curves for TAMHQ. This observation indicates that PAMHQ reacts with metal ions to form 2 : 1 protonated chelates by the coordination of metal ions with quinoline nitrogen and phenolate oxygen in the quinoline ring in the same manner as TAMHQ. In fact, as is apparent from Table 2, the stability constants of 2 : 1 protonated chelates of PAMHQ are comparable with those of the four ligands described above, and are lower than those of oxine.

However, the curves of the 1 : 1 molar ratio differ from those of the 2 : 1 molar ratio. With Cu^{2+}, the titration curve gives an inflection at $a=2$, and at this point the color of the 1 : 1 molar ratio solution changes from green to a brownish red, while the color of the 2 : 1 molar ratio solution changes from light green to a brownish yellow. The absorption spectra of the 1 : 1 molar ratio solution at the various pH values given in Fig. 6 show that in the low pH region, only one band is observed, with an absorption maximum at 380 nm, whereas the absorption spectra change in accordance with the increase in pH to show two absorption bands with absorption maxima at 480 and 580 nm in the region above pH 6.0. From these facts, it is clear

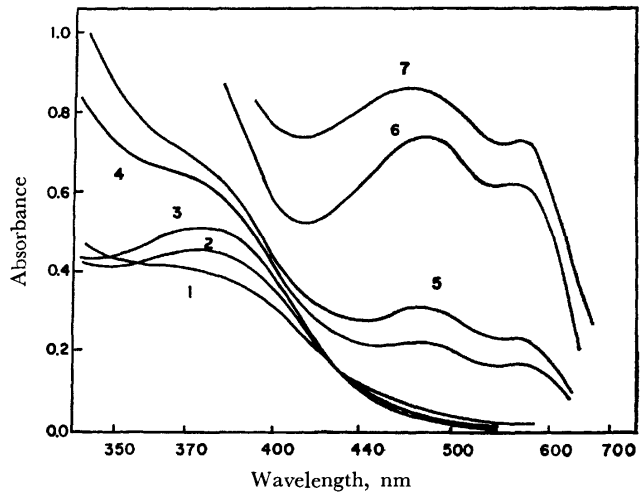

Fig. 6. Absorption spectra of molar ratio of PAMHQ to Cu^{2+} 1 : 1 solution in 50 v/v% aqueous dioxane at various pH; PAMHQ=$Cu^{2+}=2\times10^{-4}$ M; curve 1, pH 3.60; 2, 4.20; 3, 5.95; 4, 7.10; 5, 7.90; 6, 8.00; 7, 8.88.

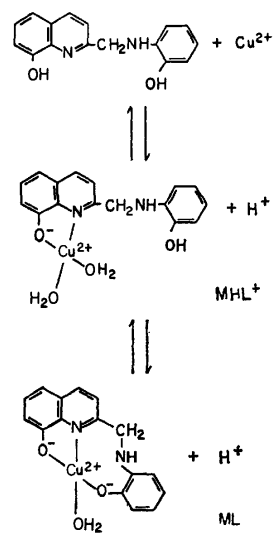

Chart 1. PAMHQ-Cu^{2+} chelate.

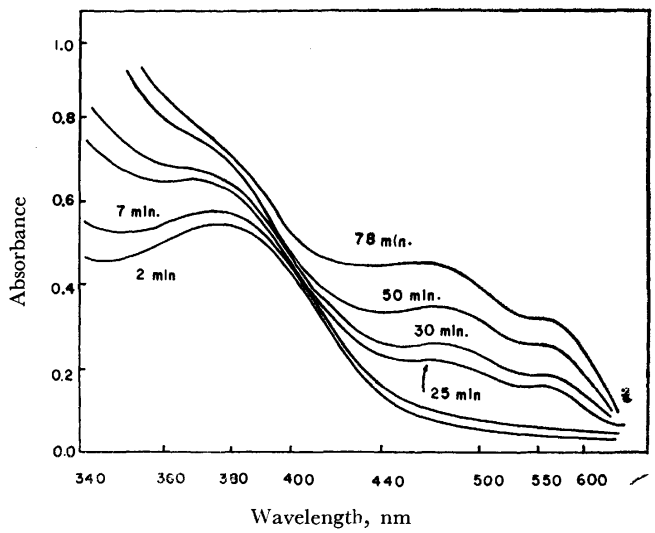

Fig. 7. Spectral change of molar ratio of PAMHQ to Cu^{2+} 1 : 1 solution with time at pH 7.40 (Walpole buffer) in 50 v/v% aqueous dioxane.

that two different chelating species exist in the 1 : 1 solution. That is, as may be seen in Chart 1, PAMHQ reacts with the Cu^{2+} ion to form the protonated chelate $CuHL^+$ between $a=0$ and $a=2$ by the coordination of the Cu^{2+} ion with quinoline nitrogen and phenolate oxygen in the quinoline ring, and then one proton is released from the protonated chelate and the CuL chelate is formed by coordination with phenolate oygen in benzene ring. The spectral change with the time shown in Fig. 7 reveals that the equilibrium of Reaction (10) is rapid, but Reaction (11), the conversion of $CuHL^+$ into CuL, is slow.

$$Cu^{2+} + HL^- \rightleftarrows CuHL^+ \quad K_{CuHL^+} = \frac{[CuHL^+]}{[Cu^{2+}]\cdot[HL^-]} \tag{10}$$

$$CuHL^+ \rightleftarrows CuL + H^+ \quad K^{H^+}_{CuHL^+} = \frac{[CuL]\cdot[H^+]}{[CuHL^+]} \tag{11}$$

Accordingly, the stability constants were calculated from the data of the curve which was obtained by the titration for 2.25 hr. The results are given in Table 2, together with the over-all stability constant, K_{CuL}; it is clear that the stability constants are higher than that of oxine.

However, with Ni^{2+}, and Zn^{2+}, the titration curves of the 1 : 1 and 1 : 10 molar ratios exhibit an inflection at $a=1.5$, indicating that three protons are displaced from the ligand in two steps. Judging from the fact that the three curves of the 2 : 1, 1 : 1, and 1 : 10 molar ratios give an inflection at $a=1.5$, it is considered that the same reaction occurs between $a=0$ and $a=1.5$ in each solution. That is, as was observed for the TAMHQ–Ni^{2+} system, PAMHQ reacts first with the Ni^{2+} ion to form a 2 : 1 protonated chelate, $Ni\cdot H_2L\cdot HL$, between $a=0$ and $a=1.5$, and then this chelate reacts with the free Ni^{2+} ion to release 1.5 protons and to form a 1 : 1 chelate, NiL, between $a=1.5$ $a=3$ in the 1 : 1 solution.

With Mn^{2+}, Mg^{2+}, and Ca^{2+}, the initial reaction, that is, the one-proton dissociation reaction from the ligand, is followed by the two-proton displacement reaction in the 1 : 1 and 1 : 10 molar ratios solutions. This fact indicates that PAMHQ reacts with these metal ions to form a 1 : 1 terdentate chelate by coordination with two phenolate oxygens and quinoline nitrogen. The stability constants of 1 : 1 deprotonated chelates are higher than those of oxine, as is shown in Table 2.

Although the reaction mechanism of PAMHQ–Ni^{2+} and Zn^{2+} has not been completely clarified, it is obvious from the above discussion that PAMHQ reacts with Cu^{2+}, Mn^{2+}, Mg^{2+}, and Ca^{2+} to form terdentate chelates and that their stabilities are higher than those of the chelates of oxine.

BHQED. This ligand has two hydroxyl and imino groups, and two quinoline nitrogens, and is expected to act as a multidentate ligand toward metal ions to form 1 : 1 ligand-to-metal chelates. The titration curves obtained in the equivalent (1 : 1) and excess (1 : 10) molar ratios of ligand to metal are shown in Fig. 8. The shapes of the curves clearly show the different types of reactions observed, involving the formation of deprotonated chelates as well as various protonated chelates.

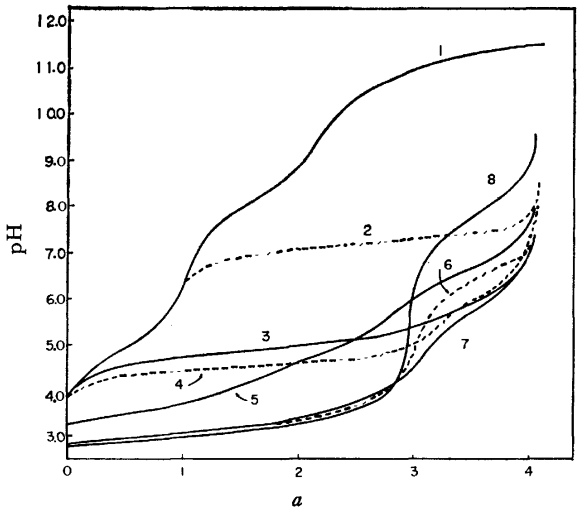

Fig. 8. Potentiometric titration curves of the equivalent and the excess molar ratio of BHQED to metal ions; solid line and broken line represent the equivalent and excess curves, respectively; curve 1, ligand; 2, Mg^{2+}; 3 and 4, Mn^{2+}; 5 and 6 Ni^{2+}; 7, Co^{2+}; 8, Cu^{2+}.

In the cases of Cu^{2+} and Mn^{2+}, the equivalent curves have an inflection at $a=3$ and, moreover, a flat buffer region between $a=0$ and $a=3$. These facts indicate that three protons are displaced from the ligand in one step to form a monoprotonated chelate, MHL^+, and that one proton is then dissociated from this chelate to form a deprotonated chelate, ML:

$$M^{2+} + HL^- \rightleftarrows MHL^+ \quad K^{M}_{ML_2} = \frac{[MHL]}{[M^{2+}]\cdot[HL^-]} \tag{12}$$

$$MHL^+ \rightleftarrows ML + H^+ \quad K^{H^+}_{MHL^+} = \frac{[ML]\cdot[H^+]}{[MHL^+]} \tag{13}$$

The equilibrium constants were calculated by the use of Eqs. (14) and (15) from the data in the regions between $a=0.5$ and $a=2.5$, and between $a=3.2$ and $a=3.9$, respectively.

$$K_{MHL^+} = \frac{C_L\cdot(\varepsilon-\sigma)\cdot\varepsilon+\alpha\cdot\sigma\cdot\varepsilon}{\{\varepsilon\cdot(C_M-C_L)+\sigma(C_L-\alpha)\}\cdot(C_L-\alpha)} \tag{14}$$

$$K^{H^+}_{MHL^+} = \frac{(\alpha-C_M)\cdot[H^+]}{(2\cdot C_M-\alpha)} = \frac{(\alpha-C_L)\cdot[H^+]}{(2\cdot C_L-\alpha)} \tag{15}$$

Where $\varepsilon=[H^+]/K_2+2\cdot[H^+]^2/K_2\cdot K_3+3\cdot[H^+]^3/K_2\cdot K_3\cdot K_4$, $\sigma=1+[H^+]/K_2+[H^+]^2/K_2\cdot K_3+[H^+]^3/K_2\cdot K_3\cdot K_4$, and $\alpha=[KOH]+[H^+]-[OH^-]-[HClO_4]$; C_M and C_L are the total ligand concentration and the total metal concentration respectively, and K_2, K_3, and K_4 are the respective acid dissociation constants. With Co^{2+}, Ni^{2+}, and Cd^{2+}, the initial reaction is a two-proton displacement to form a diprotonated chelate:

$$M^{2+} + H_2L \rightleftarrows MH_2L^{2+} \quad K^{M}_{ML_2} = \frac{[MH_2L^{2+}]}{[M^{2+}]\cdot[H_2L]}$$

This is followed by a dissociation reaction:

$$MH_2L^{2+} \rightleftarrows MHL^+ + H^+ \quad K^{H^+}_{MH_2L} = \frac{[MHL^+]\cdot[H^+]}{[MH_2L^{2+}]}$$

$$MHL^+ \rightleftarrows ML + H^+ \quad K^{H^+}_{MHL^+} = \frac{[ML]\cdot[H^+]}{[MHL^+]}$$

The equilibrium constants for each step can be calculated because there is a suitable buffer region.

With Mg^{2+}, the excess curve shows that Mg^{2+} is not bound until at least one proton is displaced from the ligand because of the weaker binding ability of this metal ion to the ligand; this follows the displacement of three protons to form a deprotonated chelate between $a=1$ and $a=4$. The data of the excess curve were employed in the previous paper for the evaluation of the stability constants by the use of Schwarzenbach's method.[7] The equilibrium constants are summarized, along with the overall stability constants, in Table 3.

TABLE 3. THE STABILITY CONSTANTS OF METAL CHELATES OF *N,N'*-BIS(8-HYDROXY-2-QUINOLYLMETHYL)ETHYLENEDIAMINE(BHQED), $\mu=0.1$, 25°C

Cations	log $K^{H^+}_{MH_2L}$	log $K^{H^+}_{MHL^+}$	log $K^{M}_{MH_2L}$	log $K^{M}_{MHL^+}$	log K_{ML}
Cu^{2+}		7.89		20.0	23.5
Co^{2+}	3.59	5.99	12.49	19.0	22.5
Ni^{2+}	5.20	6.79	9.59	14.2	18.9
Cd^{2+}	3.91	7.78	10.62	17.4	22.0
Mn^{2+}		6.20		12.4	17.6
Mg^{2+}					10.2
	pK_1	pK_2	pK_3	pK_4	
H^+	11.38	10.81	8.15	5.12	

In the presence of Cu^{2+}, Co^{2+}, Ni^{2+}, Cd^{2+}, and Mn^{2+}, but not Mg^{2+}, BHQED reacts with these metal ions to form a monoprotonated chelate, MHL^+, and this reaction is followed by the dissociation of one proton from this chelate to form a deprotonated chelate, ML. As is shown in Table 3, the dissociation constants, $K^{H^+}_{MHL^+}$ of these metal chelates decrease in the order: $Cu^{2+}>Cd^{2+}>Ni^{2+}>Mn^{2+}>Co^{2+}$. This order shows that the $K^{H^+}_{MHL^+}$ values of Co^{2+} and Mn^{2+} chelates, which are considered to have an octahedral structure, are lower than those of the Cu^{2+}, Ni^{2+}, and Cd^{2+}

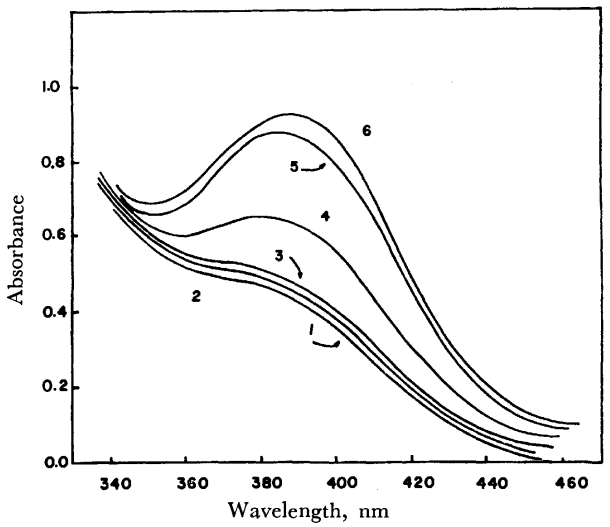

Fig. 9. Absorption spectra of BHQED-Cu^{2+} chelate at various pH in 50 v/v% aqueous dioxane solution; BHQED=$Cu^{2+}=2\times10^{-4}$ M; curve 1, pH 3.12; 2, 3.72; 3, 6.00; 4, 7.32; 5, 8.08; 6, 10.66.

7) G. Schwarzenbach, *Helv. Chem. Acta*, **33**, 947 (1950).

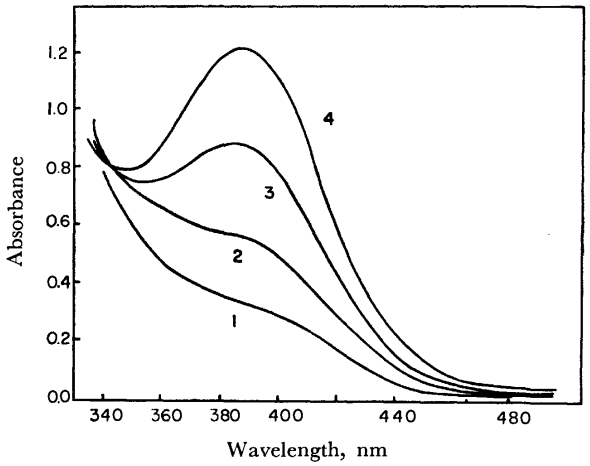

Fig. 10. Absorption spectra of BHQED-Co^{2+} chelate at various pH in 50 v/v% aqueous dioxane solution; BHQED=$Co^{2+}=2\times10^{-4}$ M; curve 1, pH 3.09; 2, 3.92; 3, 5.45; 4, 8.05.

chelates, which have square planar, or tetrahedral structures. As is indicated in Figs. 9 and 10, in the BHQED-Cu^{2+} system the spectral change is not observed in the region from pH 3.1 to 6.0, but as the pH is increased above 6.0 the intensity of the band (max. 389 nm) increases with an increase in the pH and remains constant above pH 9.0. In the BHQED-Co^{2+} system, the absorption band changes gradually with the change of pH in the region from pH 2.0 to 4.0 and greatly at about pH 6.0. These facts indicate that the one-proton displacement reaction is not the dissociation of the proton from the coordinated water, but the dissociation of the proton from the free hydroxyl group in the quinoline ring. Moreover, with Cu^{2+}, the conversion of MHL^+ into ML does not occur with ease in the acid region from about pH 2.5 to 6.0 because the protonated chelate exists stably in this pH region as a square planar chelate by coordination of the Cu^{2+} ion with two imino nitrogens and phenolate oxygen. Above pH 6.0, this chelate rearranges to have a distorted octahedral structure by coordination with another phenolate oxygen and also by weaker coordination with two quinoline nitrogens in the fifth and the sixth positions above and below the plane. The reaction scheme is given in Chart 2. With Co^{2+}, the conversion occurs readily in a lower pH region than Cu^{2+}, because the Co^{2+} chelate tends to be arranged

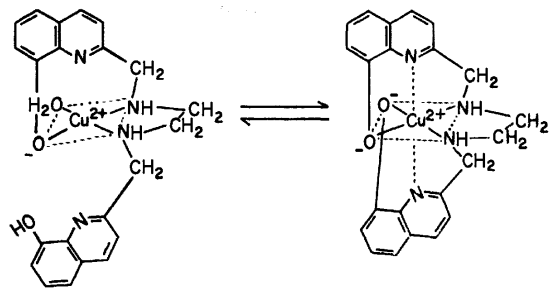

Chart 2. BHQED-Cu^{2+} chelate.

Table 4. Comparison of stability constants of BHQED, HBED, EDAMP, and Trien metal chelates

Cation	BHQED log K_{ML}	HBED log K_{ML}	EDAMP log K_{ML}	Trien log K_{ML}	ΔK (BHQED-HBED)	ΔK (BHQED-EDAMP)	ΔK (BHQED-Trien)
Cu^{2+}	23.5	21.38	16.3	20.5	2.1	7.3	8.1
Co^{2+}	22.5	19.89	12.8	11.0	2.7	11.0	12.8
Ni^{2+}	18.8	19.31	12.7	14.1	−0.4	6.1	4.7
Cd^{2+}	22.0	17.52	9.9	10.0	4.5	12.1	12.0
Mn^{2+}	17.6	14.78	5.9	4.9	3.8	11.7	6.6

from the structure formed by coordination with three donor groups to a more stable octahedral structure by coordination with two imino nitrogens and phenolate oxygens and by equivalent coordination with two quinoline nitrogens in the fifth and the sixth positions above and below the plane. From the above discussion, it is clear that BHQED behaves as a sexadentate ligand toward metal ions.

This conclusion is supported by a comparison of the BHQED-metal chelate with triethylenetetramine (trien),[8] ethylenebis-(2-aminomethyl)pyridine (EDAMP)-,[9] and *N,N'*-di(2-hydroxybenzyl)ethylenediamine-*N,N'*-diacetic acid(HBED)[10]-metal chelates. The stability constants of these metal chelates are given in Table 4. From the increment of the stability constants of BHQED-metal chelates over the trien and EDAMP metal chelates seen in Table 4, the importance of the contribution of quinoline nitrogens to the stabilities of the chelates may be roughly estimated. The metal ions of a higher coordination number, Co^{2+}, Cd^{2+}, and Mn^{2+}, show a large increment of the stability for the BHQED-metal chelates, causing the more favorable steric arrangement of the quinoline nitrogens. On the other hand, the smaller increment observed for the Cu^{2+} ion indicates that these three ligands react with the Cu^{2+} ion to form a stable, square, planar chelate, although there is also a contribution of the quinoline nitrogens in the BHQED chelate, as is shown in Chart 3. Moreover, HBED acts as a sexadentate ligand toward metal ions in the same manner as does BHQED. With Cu^{2+}, HBED forms a stable, distorted, octahedral chelate by coordination with two amino nitrogens and two phenolate oxygens and by weaker coordination with two carboxylate oxygens in the fifth and the sixth positions above and below the plane. In fact, the stability constant of the BHQED-Cu^{2+} chelate is slightly higher than that of the HBED-Cu^{2+} chelate compared with that of the trien- and EDAMP-Cu^{2+} chelates.

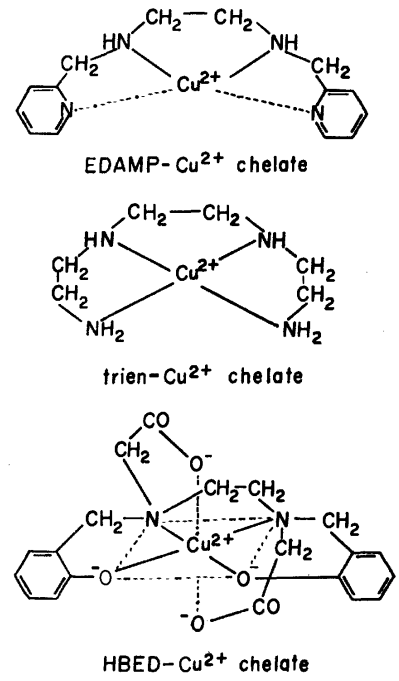

Chart 3. Cu^{2+} chelate of EDAMP, trien, and HBED.

The fact that BHQED forms the most stable chelates among various oxine derivatives is probably due to the sterically-favorable arrangement of bonds when all six donor groups of the ligand are involved in the coordination of metal ion.

8) F. Nakashima and K. Sakai, *Bunsekikagaku*, **10**, 89 (1961).
9) R. G. Lacoste and A. E. Martell, *Inorg. Chem.*, **3**, 881 (1964).
10) F. L'Epilattennier, I. Murase, and A. E. Martell, *J. Amer. Chem. Soc.*, **89**, 837 (1967).

Spectra and *Keto-Enol* Equilibrium of Benzoylacetanilides

Ahmad Sami A. S. Shawali, Magdi M. Naoum, and Saad A. Ibrahim
Department of Chemistry, Faculty of Science, University of Cairo, Giza, Egypt, UAR

(Received September 6, 1971)

A series of twelve monosubstituted benzoylacetanilides have been prepared by condensation of acetoacetanilide with substituted benzoylchlorides. IR and UV spectral data are presented and discussed. The benzoyl CO stretching frequencies were correlated with σ^+ ($\bar{\nu}=34.97\sigma^+ + 1705$; $r=0.983$). The effect of substituents in the benzoyl moiety on the *keto-enol* equilibrium, has also been investigated. The data were correlated by the equation: $\log K=0.865\sigma^+ - 0.615$; $r=0.988$.

While several investigations on benzoylacetanilides have been made concerning their reactions[1] and acidities,[2] meagre data are available on their spectral characteristics. Furthermore, although there are several reports dealing with the effects of substituents on the *keto-enol* equilibria in systems such as benzoylacetones,[3] 2-benzoylcyclanones,[4] and ethyl benzoylacetates,[5] benzoylacetanilides (I) have not been included in these analyses.

In the present communication, we wish to present a convenient method for the preparation of substituted benzoylacetanilide together with their spectral (IR and UV) characteristics. This report also contains the results of a study of the *keto-enol* equilibrium of such compounds and the effect of substituents on it.

Synthesis. Of the various methods that have been reported[6] for the synthesis of aroylacetanilides, the only generally useful one has been the condensation of equimolecular amounts of ethyl aroylacetate with the appropriate arylamine at elevated temperatures. Since most of the ethyl esters of aroylacetic acids are not commercially available, it was of interest to find an alternate short and general method that could be employed for the synthesis of aroylacetanilides. The conversion of ethyl benzoylacetoacetate to ethyl benzoylacetate[7] with ammonium chloride and ammonium hydroxide suggests that acylation of acetoacetanilide and the decomposition of the resulting 2-aroylacetoacetanilide might be a general reaction which has been long overlooked. We have, in fact, found that aroylacetanilides (I) can be conveniently prepared from acetoacetanilide according to the reaction sequence outlined in Scheme 1. Twelve compounds (Ia—l), four of which are new, were prepared this way.

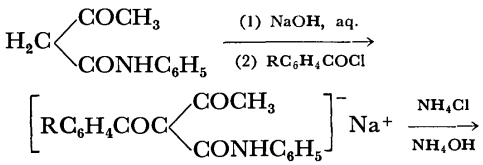

$RC_6H_4COCH_2CONHC_6H_6 + CH_3COOH$

I

a, R=4-CH_3O	g, R=4-Br
b, R=4-CH_3	h, R=3-Cl
c, R=3-CH_3	i, R=3-Br
d, R=H	j, R=4-CN
e, R=3-CH_3O	k, R=3-NO_2
f, R=4-Cl	l, R=4-NO_2

Scheme 1

Infrared Spectra. The infrared absorption maxima of aroylacetanilides (Ia—l) and their assignments are given in Table 1. The most significant feature of these spectra is the presence and location of the carbonyl stretching bands. In the carbonyl region, benzoylacetanilide (Id) possesses two strong bands, one near 1705 and the second 1669 cm^{-1}. By analogy to acetoacetanilide[8] these bands are assigned to the benzoyl and anilide carbonyl groups, respectively. The appearance of the bonzoyl CO group and the complete absence of any OH band suggest that benzoylacetanilide and its substituted derivatives, under the conditions of measurement, exist almost in the *keto* form. The data indicate also that the position of the aroyl CO band depends, to a large extent, upon the nature of the substituent present. As shown in Table 1, as the character of the substituent (*meta* or *para* to the CO group) changes progressively from electron donating to electron withdrawing, the value of ν_{CO} increases.

Good correlations of carbonyl stretching frequencies with Hammett constants have been reported for acetophenones,[9] benzophenones,[10] benzoyl chlorides,[11] and chalcones.[12] The application of the Hammett

1) H. Lund, *Ber.*, **67**, 937 (1934); K. Sano, *J. Org. Chem.*, **34**, 2076 (1969); M. M. Naoum, M. Sc. Thesis, University of Cairo, 1970.

2) P. van Brandt, E. De Hoffmann, and A. Bruylants, *Bull. Soc. Chim. Belges*, **73**, 782 (1964).

3) R. D. Campbell and W. L. Harmer, *J. Org. Chem.*, **28**, 379 (1963); R. D. Campbell and H. M. Gilow, *J. Amer. Chem. Soc.*, **82**, 5426 (1960).

4) D. J. Sardella, D. H. Heinert, and B. L. Shapiro, *J. Org. Chem.*, **34**, 2817 (1969).

5) M. R. Gelin, S. Gelin, and M. C. Zambratas, *C. R. Acad Sci., Paris*, **270**, 832 (1970).

6) C. J. Kibler and A. Weissberger, "Organic Synthesis," Coll. Vol. III, p. 108 (1955); C. R. Hauser and G. A. Rynolds, *J. Amer. Chem. Soc.*, **70**, 4250 (1948); G. H. Brown, *et al.*, *ibid.*, **79**, 2919 (1957); B. Satskun and S. S. Israelstram, *J. Org. Chem.*, **26**, 3191 (1961); A. J. Hodgkinson and B. Staskun, *ibid.*, **34**, 1709 (1969).

7) C. Bulow and E. Hailer, *Ber.*, **35**, 915 (1902).

8) D. N. Sen and P. Umpathy, *Indian J. Chem.*, **6**, 516 (1968).

9) R. N. Jones, W. F. Forbes, and W. A. Mueller, *Cand. J. Chem.*, **35**, 504 (1957); H. C. Brown and Y. Okamoto, *J. Amer. Chem. Soc.*, **80**, 4979 (1958).

10) N. Fuson, M. L. Josien, and F. M. Shelton, *ibid.*, **76**, 2526 (1954).

11) M. St. C. Flett, *Trans. Faraday Soc.*, **44**, 767 (1948).

12) N. L. Silver and D. W. Jr., Boykin, *J. Org. Chem.*, **35**, 759 (1970).

Table 1. Characteristic infrared bands (cm^{-1}) of substituted benzoylacetanilides

Ia	Ib	Ic	Id	Ie	If	Ig	Ih	Ii	Ij	Ik	Il	Assignment
3260	3300	3300	3260	3290	3290	3290	3280	3270	3350	3375	3400	N-H stretch
3175	3185	3200	3200	3180	3200	3200	3120	3180	3120	3340	3320	
3045	3050	3050	3065	3060	3060	3040	3040	3040	3050	3075	3050	=C-H stretch
3020		3100	3045							3040		
2950	2920	2930	2900	2950	2925	2940	2940	2925	2925	2950	2930	-C-H stretch
2830	2850	2875	2840	2840	2850	2850	2830	2850	2910	2850	2850	
1683	1689	1700	1705	1703	1710	1710	1720	1722	1726	1730	1734	Aroyl CO
1666	1666	1666	1669	1668	1662	1662	1666	1665	1670	1652	1650	Amide-I
1600	1600	1590	1605	1604	1600	1609	1608	1600	1610	1608	1600	C=C skeletal
1580	1570	1575	1560		1570			1575		1560	1570	stretching
1510	1510	1515	1515	1500	1500	1500	1510	1500	1500	1500	1510	vibrations
1450	1460	1465	1450	1455	1455	1440	1450	1455	1450	1460		
1540	1540	1550	1550	1557	1541	1543	1550	1547	1550	1552	1563	Amide-II
1430	1420	1430	1415	1425	1415	1415	1420	1425	1425	1410	1410	C-H scissoring
1325	1300	1315	1310	1325	1300	1315	1310	1310	1315	1310	1315	Amide-III
1265	1265	1275	1265	1280	1275	1275	1220	1220	1250	1280	1290	
1225	1250	1225	1230		1225	1225			1225	1260	1215	
840					845	845				865	870	Aromatic C-H
835												bending
820	810				825	825			830		855	
	790	790		785			790	780		780	775	
760	760	755	755	765	760	760	770	750	765	750	762	
740			725		730	720	750	740		730	755	
	700		700	700			700		702		725	
695		695	690	690	069	690	685	960	695	698	700	

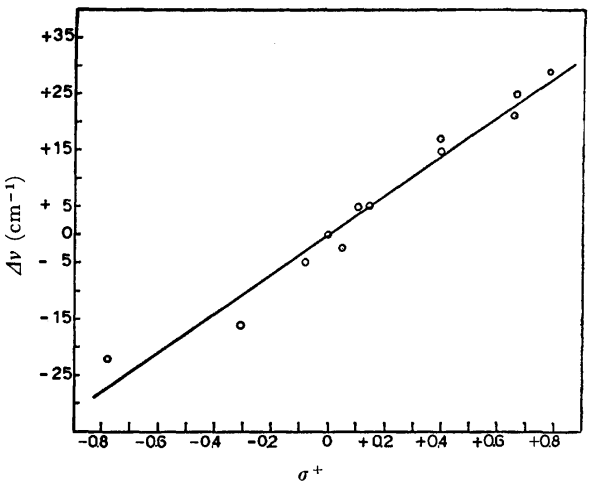

Fig. 1. Plot of $\Delta\nu$ *vs.* the substituent σ^+ for benzoylacetanilides.

equation to the CO frequencies of aroylacetanilides (Ia—l) is shown in Fig. 1, in which $\Delta\bar{\nu}$ is plotted against σ^+ values; $\Delta\bar{\nu}=\bar{\nu}_R-\bar{\nu}_H$. The values of the slope and intercept were calculated by the least-squares method.[15] The best straight line fit corresponds to the equation:

$$\bar{\nu}=34.97\sigma^+ +1705;\ r=0.983$$

The ρ of value ~35 obtained for benzoylacetanilides indicates a shift of ~35 cm^{-1} per unit of σ^+ constant, which is, within statistical limits, three times as much as the ρ for acetophenones series ($\rho=12.33$).[9,12] This relatively high sensitivity of the strength of the CO double bond to substituents suggests strongly that there is appreciable orbital overlap between the phenyl and carbonyl groups of the present series in solid state.

Table 2. Ultraviolet spectra of substituted benzoylacetanilides

Compound No.	Ethanol λ_{max}, nm(log ε)		Cyclohexane λ_{max}, nm (log ε)	
	Band A	Band B	Band A	Band B
Ia	323(3.69)	272(4.29)	318(3.73)	278(4.30)
Ib	311(3.83)	251(4.30)	309(3.96)	254(4.44)
Ic	310(3.81)	244(4.19)	303(3.92)	244(4.21)
Id	308(3.97)	242(4.35)	306(4.07)	243(4.37)
Ie	311(4.13)	242(4.35)	305(3.97)	245(4.11)
If	314(4.06)	251(4.30)	306(4.24)	254(4.30)
Ig	315(4.08)	251(4.29)	311(4.23)	260(4.24)
Ih	312(4.07)	237(4.24)	307(4.14)	237(4.16)
Ii	312(4.06)	239(4.24)	308(4.15)	237(4.21)
Ij	324(4.12)	244(4.26)	321(4.16)	243(4.20)
Ik	312(4.14)	230(4.29)	309(3.95)	240(3.98)
Il	345(4.15)	257(4.29)	334(4.19)	248(4.23)

Ultraviolet Spectra. The ultraviolet spectral data for benzoylacetanilides in cyclohexane and ethanol are presented in Table 2. The absorption pattern was, in each case, characterized by the presence of two bands: Band A usually is located in the region of 305—350 nm, and Band B in the 240—280 nm region. The data also indicate that for the compounds studied Band A exhibits a bathochromic displacement as the solvent is varied from cyclohexane to ethanol.

It has been reported that λ_{max} values (log ε 4 to 5 in every case) for the chromophoric systems: Ar–C=C–C=O, Ar–CO–C=C–, Ar–CO–CH_2–CO–, and Ar–C(=O)–CH=C(–O–H···O)– are 281—307, 248—283, 253 and 300 nm, respectively.[13] Accordingly, the A and B bands in the electronic absorption spectra of benzoylacetanilides can be assigned to the cinnamoyl and benzoyl chromophoric groups of the *enol* and *keto* forms respectively. Further, the fact that the λ_{max} values of the A bands are all larger than 300 nm provides evidence that the aroyl carbonyl rather than the anilide carbonyl is involved in enolization of the benzoylacetanilides as shown in structure II.

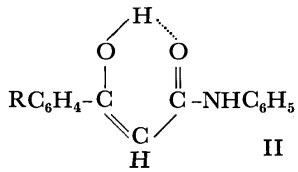

II

The position of λ_{max} of band A of benzoylacetanilides cannot be attributed to a bathochromic effect of the OH on the Ar–C=C–CO– system because it has been observed that the auxochromic effect of the OH and CH_3O groups on such a system does not shift λ_{max} beyond the 300 nm region.[13]

The shift of λ_{max} with a change of solvent is in the direction expected for a transition in which absorption produces a more polar excited state.

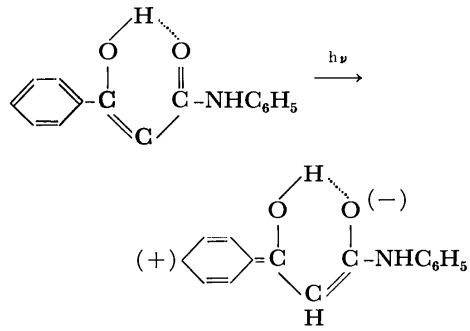

The Keto-Enol *Equilibrium.* As expected, the lowest *enol* per cent (Table 3) is observed for the *p*-methoxyl group and the highest for the nitro group. The values of the equilibrium data as $\log(K/K_0)$ for the enolization reaction have been correlated with the substituent constant σ^+ as taken from Ritchie and Sager.[14] Figure 2 illustrates such a correlation. It is seen that the *meta*- and *para*-substituted benzoylacetanilides follow the Hammett equation closely.

A computer program was written to carry out the least-squares and statistical treatment of the date with the sigma constants according to the method of Jaffé.[15] The twelve values set of K in Table 3 best fit a straight line indicated by the equation: $\log K = 0.865\,\sigma^+ - 0.615$; ($r=0.988$; $s=0.033$). The magnitude of the reaction constant ρ of value 0.865 is, within statistical limits, very close to the reaction constant for ethyl benzoylacetates (0.967).[5] This suggests that in the compounds studied the effects of coplanarity, resonance, inductive, and dipole interactions appear to be parallel to the same effects in ethyl benzoylacetate tautomeric equilibrium.

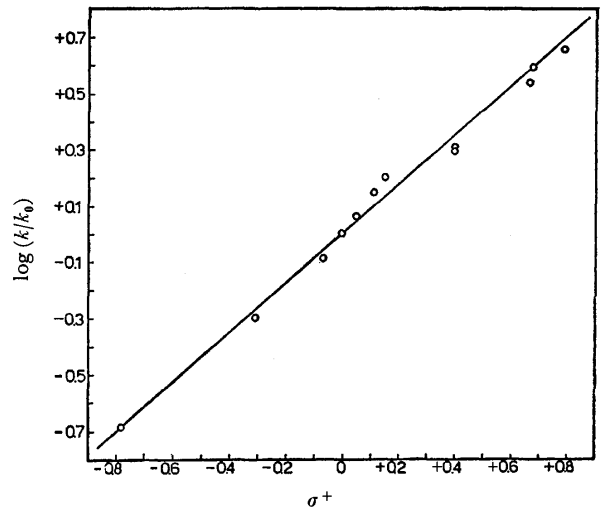

Fig. 2. Plot of $\log(k/k_0)$ *vs.* the substituent σ^+ for benzoylacetanilides.

TABLE 3. TAUTOMERIC EQUILIBRIUM AND SIGMA SUBSTITUENT CONSTANTS

Compound No.	*Enol*, %	K	$\log K/K_0$	σ^+
Ia	5.00	0.0523	−0.690	−0.78
Ib	11.58	0.131	−0.294	−0.31
Ic	17.28	0.209	−0.088	−0.07
Id	20.40	0.256	0.000	0.00
Ie	18.20	0.222	−0.062	0.05
If	26.4	0.358	0.146	0.11
Ig	24.3	0.320	0.097	0.15
Ih	33.4	0.501	0.292	0.40
Ii	34.8	0.534	0.300	0.40
Ij	46.8	0.879	0.536	0.66
Ik	49.8	0.993	0.589	0.67
Il	54.06	1.176	0.662	0.79

Furthermore, the data indicate that *enol* stability is determined by both mesomeric electronic delocalization[16a,b] and inductive electron withdrawal.[16c] From the value and sign of ρ, it is clear that electron donor substituents (methyl and methoxyl) lend more stability to the *keto* form than the enol form. It is logical, therefore, to conclude that the *enol* system is less electron deficient (electron demanding) than is the single carbonyl group.

Experimental

Melting points were determined on a Fischer-Johns hot stage. Elemental analyses were performed by microanalysis

13) J. U. Lowe, Jr., and N. L. Fergusen, *J. Org. Chem.*, **30**, 3000 (1965).

14) C. D. Ritchie and W. F. Sager, "Progress in Physical Organic Chemistry," Vol. 2, Interscience Publishers Inc., New York, (1964).

15) H. H. Jaffé, *Chem. Rev.*, **53**, 191 (1953).

16) a) S. Forsen, *Arkim. Kemi*, **20**, 1, 25 (1962); b) R. L. Lintvedt and H. F. Holtzclaw, *Inorg. Chem.*, **5**, 239 (1966); J. L. Burdett and M.T. Rogers, *J. Amer. Chem. Soc.*, **86**, 2105 (1964).

Laboratory, National Research Center, Dokki, Giza, Egypt. All solvents employed in this study were of spectral quality. Acetoacetanilide was prepared from ethyl acetoacetate and aniline by a method previously described[18] All yields reported relate to the recrystallized material.

Preparation of Aroylacetanilides. Acetoacetanilide (0.1 mol) was dissolved in 60 m*l* of 20% aqueous sodium hydroxide solution. The resulting solution was externally cooled by an ice bath and stirred by a magnetic stirrer. When the temperature of the solution reaches 2°C aroyl chloride (0.1 mol) was added from a dropping funnel, if liquid or in 0.1 g increments if solid, while the temperature of the reaction mixture was kept below 5°C. After all the acid chloride was added, the mixture was stirred for half an hour at 5°C; and for additional 30 min at room temperature. The reaction mixture was then diluted with 15 m*l* of 25% aqueous ammonium hydroxide solution containing 5.4 g (0.1 mol) of ammonium chloride and stirred for 5 minutes. The resulting mixture was heated to 40—50°C, left to stand overnight at room temperature, and filtered. Recrystallisation of the crude product from ethanol or dilute ethanol gave aroylacetanilide in 40—50% yield. The mp of the previously reported compounds agree with the literature values. The following aroylacetanilides ($RC_6H_4COCH_2CONHC_6H_5$) are new: R=4-Br, mp 144—145°C, Found: C, 56.61; H, 3.95; N, 4.10; Br, 24.98%. Calcd for $C_{15}H_{12}BrNO_2$: C, 56.60; H, 3.77; N, 4.40; Br, 25.16%. R=3-Cl, mp 127—128°C. Found: C, 66.17; H, 4.57; N, 5.20; Cl, 12.96 %. Calcd for $C_{15}H_{12}ClNO_2$: C, 65.81; H, 4.39; N, 5.12; Cl, 12.98%. R=3-Br, mp 123—124°C, Found: C, 56.60; H, 3.90; N, 4.01; Br, 25.32%. Calcd for $C_{15}H_{12}BrNO_2$: C, 56.60; H, 3.77; N, 4.40; Br, 25.16%. R=4-CN, mp 140—142°C, Found: C, 72.75; H, 4.39; N, 10.58%. Calcd for $C_{16}H_{12}N_2O_2$: C, 72.72; H, 4.54; N, 10.60%.

Measurement of Spectra. The IR spectra were measured using a Perkin-Elmer model 377 double beam recording spectrophotometer, with sodium chloride optics. All compounds were recorded as potassium bromide pellets.

The UV spectra were determined using a Beckmann DK recording spectrophotometer. Matched quartz cells were used. Stock solutions for each compound were prepared by dissolving an accurately weighed amount of the sample in 50 m*l* of ethanol or cyclohexane. Solution with concentrations of 10^{-3} to 10^{-5} M were prepared by dilution of the stock solution using certified National Bureau of Standards 2- and 5-m*l* pipets and 10-m*l* volumetric flasks. In all cases solutions were allowed to equilibrate at least 24 hr in the dark before spectra were measured. Data determined are listed in Tables 1 and 2.

Determination of Percentage of Enol. The *enol* content was determined at equilibrium. A weighed sample of benzoylacetanilide (approximately 0.2 g) was dissolved in 50 m*l* of anhydrous absolute methanol. The solution was allowed to stand for 24 hr in a constant temperature water bath at 25±1°C in the dark. After this time, the modified bromine titration procedure[19] was used to determine the percentage of *enol*, with results given in Table 3. That the equilibrium is attained, is ensured by the fact that the *enol* per cent determined after extending the equilibrium time to 48 and 72 hr is similar to that determined after 24 hr. The maximum deviation of single determinations from the average of three to five determinations for each compounds was ±1 or less.

17) G. O. Dudeck and G. P. Volpp, *J. Org. Chem.*, **30**, 50 (1965).

18) H. Pfeiffer, *J. Prakt. Chem.*, **111**, 240 (1925).

19) S. R. Cooper and R. P. Barners, *Anal. Chem.*, **60**, 379 (1938); A. Gero, *J. Org. Chem.*, **19**, 1960 (1954).

BULLETIN OF THE CHEMICAL SOCIETY OF JAPAN, VOL. 45, 2507—2509 (1972)

Studies on Benzoquinolines [*f*] and [*h*]. Part I

Rameshwar P. TIAGI and Bhuwan C. JOSHI

Chemical Laboratories, University of Rajasthan, Jaipur-4, India

(Received March 8, 1971)

2-Chloro-4-methyl and 2-methyl-4-chloro-benzo[*h*]quinolines, 1-chloro-3-methyl- and 1-methyl-3-chloro-benzo[*f*]quinolines were converted into corresponding hydrazino derivatives. Structural studies of the hydrazino compounds and their derivatives were carried out. Chlorine atom in a position adjacent to nitrogen of the ring was found to be more reactive than in that away from nitrogen in benzo[*f*] and [*h*]quinolines. Cyclisation of hydrazino derivatives by nitrous and formic acids occurred at position 2 in 1-methyl-3-hydrazinobenzo[*f*]-quinoline and at position 3 in the case of 2-hydrazino-4-methylbenzo[*h*]quinoline, respectively, while in the case of 1-hydrazino-3-methylbenzo[*f*]quinoline, at position 10 and in 4-hydrazino-2-methylbenzo[*h*]quinoline, at position 5, respectively.

1-Methyl-3-chloro- and 1-chloro-3-methyl-benzo[*f*]-quinolines (IA and IB), and 2-chloro-4-methyl- and 2-methyl-4-chloro-benzo[*h*]quinolines (IC and ID) were prepared by the usual methods.[1-3] The chloro compounds IA—ID did not react with hydrazine hydrate (80%) when the reactions were carried out in low boiling solvents such as alcohol and dioxane. However, in hot glycerol the corresponding hydrazino derivatives (IIA—IID) were obtained. The hydrazino derivatives IIA and IIC were obtained under refluxing for 6—8 hr, while compounds IIB and IID were obtained when the time of refluxing was extended to 10—12 hr. This indicates the greater reactivity of chlorine at a position adjacent to nitrogen as compared to that away from nitrogen. Such differences in reac-

1) L. Knorr, *Ber.*, **17**, 540, (1884).
2) M. Conrad and L. Limpach, *ibid.*, **21**, 531 (1888); L. Limpach, *Ber.*, **64**, 969, (1931).
3) A. Albert, D. J. Brown, and H. Duewell, *J. Chem. Soc.*, **1948**, 1284.

Table 1. NMR chart (Chemical shifts given in ppm (δ))

Compound	-NH Proton broad		Aromatic proton		Proton as singlet		N=CH proton		$-C-CH_3$ proton as singlet		$-NH-NH_2$ proton	
	Position	No. of proton	Position	No. of proton	Position	No. of proton	Position	No. of proton	Position	No. of proton	position	No. of proton
IIA	—	—	7.6 —8.05	6	7.05 at 2	1	—	—	2.50	3	1.55, 1.2	3
IIB	—	—	7.6 —8.05	6	7.05 at 2	1	—	—	2.60	3	1.6, 1.2	3
IIC	—	—	7.6 —8·05	6	7.05 at 3	1	—	—	2.50	3	1.55, 1.2	3
IID	—	—	7.6 —8.05	6	7.05 at 3	1	—	—	2.65	3	1.6, 1.2	3
IIIA	8.70	1	7.6 —8.05	6	—	—	—	—	2.50	3	—	—
IIIB	8.35	1	7.6 —8.05	5	7.05 at 2	1	—	—	2.65	3	—	—
IIIC	8.75	1	7.6 —8.05	6	—	—	—	—	2.50	3	—	—
IIID	8.30	1	7.6 —8.05	5	7.05 at 3	1	—	—	2.65	3	—	—
IVA	8.85	1	7.6 —8.05	6	—	—	6.5	1	2.50	3	—	—
IVB	8.40	1	7.6 —8.05	6	7.05 at 2	1	—	—	2.55	3	—	—
IVC	8.80	1	7.6 —8.05	6	—	—	6.5	1	2.50	3	—	—
IVD	8.25	1	7.45—8.05	6	7.05 at 3	1	—	—	2.60	3	—	—

tivities were observed in the quinoline compounds.[4]

4-Chloroquinaldine with hydrazine under drastic conditions gave 3-methyl-5-(*o*-aminophenyl)pyrazole, an isomer of 2-methyl-4-hydrazinoquinoline.[5] However, this was not observed in the case of the above compounds (IA—ID) wherein hydrazino derivatives (IIA—IID) were obtained.

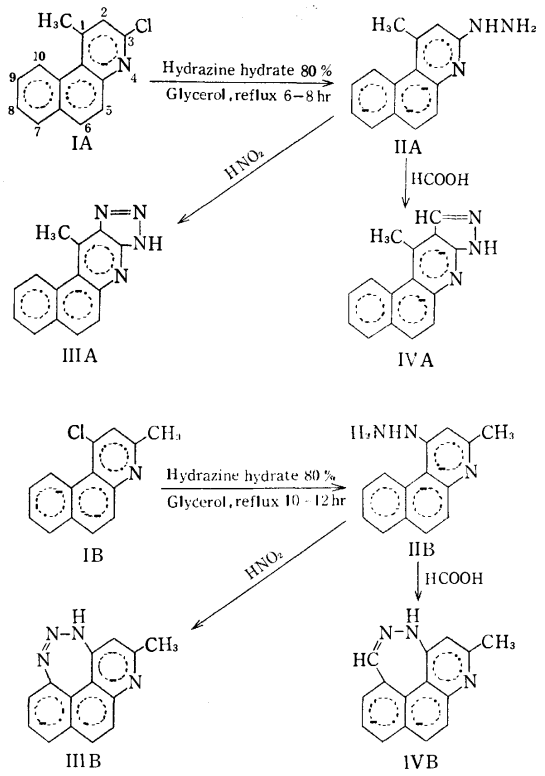

IA IIA IIIA IVA IB IIB IIIB IVB

Elemental analysis of the compounds IIA—IID suggested the formula $C_{14}H_{13}N_3$. NMR spectrum of IIB indicated the presence of six aromatic protons (δ 7.6—8.05 ppm) and one aromatic proton as singlet (δ 7.05 ppm). Protons at nitrogen were found at δ 1.6 and δ 1.2 ppm, while methyl protons ($C-CH_3$) as a singlet at δ 2.60 ppm. All the data supported hydrazino structure for IIB. The positions of various protons in compounds IIA, IIC, and IID were more or less similar to IIB.

Hydrazino derivatives (IIA—IID) reacted with nitrous acid to give compounds IIIA—IIID ($C_{14}H_{10}N_4$). NMR studies of IIIB indicated the presence of methyl (δ 2.65 ppm), -NH(δ 8.35 ppm), five aromatic (δ 7.6—8.05 ppm) and one aromatic (δ 7.05 ppm) protons. The absence of the protons of $-NH-NH_2$ (δ 1.2, 1.6 ppm) as indicated in the NMR spectrum of IIB, along with the presence of a -NH proton at δ 8.35 ppm, indicated the formation of 3-methylbenzo[*f*]-1′,2′,3′-triazepino[4′,7′:1,10]quinoline.

It appeared that the intermediate $RNHN_2^+Cl^-$ from IIB to IIIB must have cyclised at position 10 instead of position 2 as there was still an indication of the aromatic proton as a singlet (δ 7.05 ppm) in IIIB which was also present in IIB. But in IIIA, no proton was found at position 2 as there was no indication of the aromatic proton at δ 7.05 ppm in the NMR spectrum. However, the positions of six aromatic protons (at positions 5, 6, 7, 8, 9, and 10), methyl and -NH protons were found to be more or less similar to those in IIA.

When the hydrazino derivatives (IIA—IID) were treated with formic acid, compounds of molecular formula $C_{15}H_{11}N_3$ (IVA—IVD) were obtained. NMR spectrum of IVA indicated the absence of the proton at 2 (as singlet at δ 7.05 ppm), along with the presence of methyl protons (δ 2.5 ppm singlet), -NH proton (δ 8.85 ppm) and N=CH (δ 6.5 ppm) proton. This also indicated the presence of methyl and six aromatic protons almost in similar positions as in IIA. In the NMR spectrum of IVB, the presence of methyl protons (δ 2.55 ppm singlet), one aromatic proton (δ 7.05 ppm), six aromatic protons (δ 7.5—8.05 ppm), NH proton (δ 8.4 ppm) and the absence of a proton at δ 6.5 ppm were evident. It appears that the cyclisation occurred at 10 and not at 2, since the aromatic proton at the position 2 was found as a singlet (δ 7.05 ppm).

4) R. J. Rowlett and R. E. Lutz, *J. Amer. Chem. Soc.*, **68**, 1288, (1946).

5) E. Koenigs and J. Freund, *Chem. Ber.*, **80**, 143, (1947).

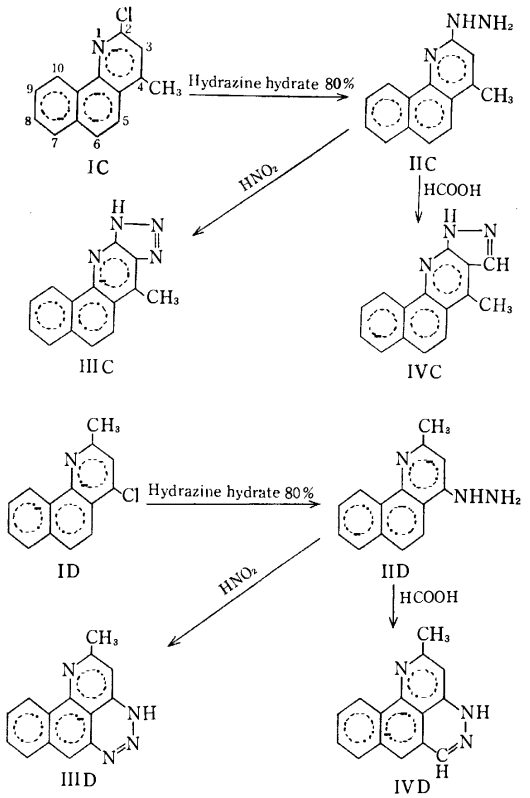

Formation of IIIC, IIID, IVC, and IVD could be explained similarly.

Experimental

All the melting points are uncorrected. Micro analyses were performed by C.D.R.I., Lucknow. NMR spectra were made on a Varian A-60 model in $CDCl_3$ as a solvent and TMS as an internal indicator. Chemical Shifts are given in ppm (δ).

1-Methyl-3-hydrazinobenzo[f]*quinoline(IIA).* 2.27 g (0.01 mol) of 1-methyl-3-chlorobenzo[*f*]quinoline (IA) was dissolved in glycerol and the solution was refluxed. To the hot reaction mixture, hydrazine hydrate (80%, 0.06 g, 0.015 mol) was gradually added with constant stirring. After the addition of hydrazine hydrate was completed, the reaction mixture was refluxed for 6—8 hr. The mixture was cooled and poured into ice-cold water. The solid was filtered and dissolved in the least amount of methanol. The methanolic solution was filtered and was kept at 0°C for 24 hr. The compound (mp 141—142°C; yield, 1.36 g, 60%) thus obtained showed no chlorine. Tlc examination gave one spot (R_f, 0.54) using dioxane as a solvent and Silica Gel G as an adsorbent.

Found: C, 74.98%; H, 6.02%; N, 19.04%. Calcd for $C_{14}H_{13}N_3$: C, 75.33%; H, 5.82; N, 18.83%.

Similarly, IB yielded 1-hydrazino-3-methylbenzo[*f*]-quinoline (IIB) with a refluxing time of 10—12 hr. Yield 51%, mp 161—162°C (R_f, 0.72).

Found: N, 19.28%. Calcd for $C_{14}H_{13}N_3$: N, 18.83%.

2-Hydrazino-4-methylbenzo[*h*]quinoline(IIC) was prepared from IC mp 116—117°C, yield 58% (R_f 0.79).

Found: N, 19.32%. Calcd for $C_{14}H_{13}N_3$: N, 18.83%.

ID yielded 2-methyl-4-hydrazinobenzo[*h*]quinoline (II-D) with a refluxing time of 10—12 hr in 48% yield mp 170—171°C (R_f, 0.68).

Found: N, 19.02%. Calcd for $C_{14}H_{13}N_3$: N, 18.83%.

1-Methylbenzo[f]*-1,2,3-triazolo*[*4,5*-b]*quinoline (IIIA).* 0.5 g of 1-methyl-3-hydrazinobenzo[*f*]quinoline(IIA) was dissolved in dilute hydrochloric acid. The ice-cold solution was kept at 0—2°C. The ice-cold saturated solution of sodium nitrite was added cautiously till brown fumes were evolved. The reaction mixture was shaken well during the course of addition, and was then decomposed with cold water. The solid was filtered and washed 3—4 times with water (till washings gave no positive test for ionic chlorine). It was crystallized from ethanol (mp 214—215°C).

Found: C, 71.5; H, 4.52; N, 23.62%. Calcd for $C_{14}H_{10}N_4$: C, 71.78; H, 4.27; N, 23.93%.

Similarly, IIB yielded 3-methyl-1′-*H*-benzo[*h*]-1′,2′,3′-triazepino[4′,7′ : 1, 10]quinoline (IIIB) (mp 180—181°C).

Found: N, 23.62%. Calcd for $C_{14}H_{10}N_4$: N, 23.93%. IIC yielded 4-methylbenzo[*h*]-1,2,3-triazolo[4,5-*b*]quinoline (IIIC) (mp 160—161°C).

Found: N, 23.68%. Calcd for $C_{14}H_{10}N_4$: N, 23.93%. and IID, yielded 2-methyl-1′-*H*-benzo[*h*]-1′,2′,3′-triazino-[4′, 6′ : 4, 5]quinoline (IIID): (mp 189—190°C).

Found: N, 23.58%. Calcd for $C_{14}H_{10}N_4$: N, 23.93%.

1-Methylbenzo[f]*-1,2-pyrazolo*[*4,5*-b]*quinoline (IVA).* To a well stirred hot solution of 0.5 g of 1-methyl-3-hydrazinobenzo[*f*]quinoline in redistilled dioxane (with a little sodium acetate), formic acid in excess was cautiously added. The mixture was then refluxed for 4—5 hr on a sand bath. The reaction mixture was cooled and poured into ice-cold water and kept overnight at 0°C. The solid obtained was filtered, washed 3—4 times with water and was crystallised from acetone (mp 260—261°C).

Found: C, 74.07%; H, 4.82%; N, 17.28%. Calcd for $C_{15}H_{11}N_3 \cdot 1/2H_2O$; C, 74.38%; H, 4.95%, N, 17.35%. Similarly, IIB yielded 3-methyl-1′-*H*-benzo[*f*]-1′,2′-diazepino[4′, 7′ : 1, 10]quinoline (IVB), mp (215—216°C).

Found: N, 17.02%. Calcd for $C_{15}H_{11}N_3 \cdot 1/2H_2O$: N, 17.35%. IIC yielded 4-methylbenzo[*h*]-1,2-pyrazolo-[4,5-*b*]quinoline(IVC) (mp 204—205°C).

Found: N, 16.88%. Calcd for $C_{15}H_{11}N_3 \cdot 1/2H_2O$: N, 17.35%, IID, yielded 2-methyl-2′-*H*-benzo[*h*]-1′,2′-pyrazino[3′,5′:4,5]quinoline (IVD) (mp 224—225°C).

Found: N, 16.82%. Calcd for $C_{15}H_{11}N_3 \cdot 1/2H_2O$: N, 17.35%.

The authors express their thanks to the Head of the Chemistry Department for providing the necessary facilities and to Dr. (Mrs.) Reena Ramchandran for making available NMR spectra of the compounds.

The CNDO/2 Study of Barbararyl Cation and Its Isomeric $C_9H_9^+$ Systems

Shigeo YONEDA,[1a,c] Saul WINSTEIN,[1b] and Zen-ichi YOSHIDA[1c,d]

Department of Chemistry, University of California, Los Angeles, California, 90024, U.S.A. and Department of Synthetic Chemistry, Kyoto University, Yoshida, Kyoto

(Received July 16, 1971)

The geometrical and electronic structures of $C_9H_9^+$ systems have been studied applying CNDO-2 method. The calculated results are used to discuss the stabilities of the structures for $C_9H_9^+$ system and their electronic states. It is suggested that the carbonium ion which has a D_{3h} symmetry (IV) enjoys much stabilization energy, whereas bicyclo[3.2.2]nonatrienyl cation (I) is less stable than IV. The stability of IV can be explained by unusual delocalization of its electrons over the molecule.

A considerable amount of attention has been recently focussed on $C_9H_9^+$ systems such as bicyclo[3.2.2]-nonatrienyl (I), 9-barbararyl (II) and bishomotropylium (III) cations.[2-5] The direct observation of II and III by NMR at low temperature was recently reported by Winstein and his co-workers.[4b] On the other hand, based on the results of deuterium scrambling reaction, Schleyer[3] has proposed the presence of the reaction intermediate species (or the transition state) as presented in IV, which undergoes effective threefold symmetrization.

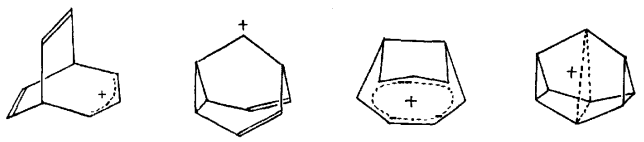

(I) (II) (III) (IV)

The approach using molecular orbital calculations is helpful in investigating the stabilities and the electronic states of these systems. Although experiences with semiempirical molecular orbital methods suggest that they are capable of yielding very satisfactory geometrical data, it seems to be almost impossible to apply semiempirical MO method to $C_9H_9^+$ systems because of their large number of internal degrees of freedom (3N−6).

We have succeeded in carrying out the complete MO treatment for IV and I by considering the appropriate symmetry properties. First of all, all the bond angles and the bond lengths for the symmetrical structure (IV) were varied, and the most stable symmetrical structure was obtained. After that, the energy change by the possible deformations was examined. As a result, the calculated potential energy surface clearly indicates that the structure IV represents an energy minimum.

For the structure at the energy minimum, a population analysis[6] was carried out. The electron densities and the overlap populations demonstrated unusual delocalization in the structure IV. The similar MO treatment for I was carried out, even though much computing time was required due to the large number of internal degrees of freedom compared with the case of IV. The energy minimum obtained for I was much higher than that for IV, as expected from the theory of "bicycloaromaticity" proposed by Goldstein,[3a,3b] indicating I to be bicycloantiaromatic.

Method of Calculation

Our treatment is fundamentally composed of the following two steps; 1) the determination of the most stable structure by minimizing the molecular energy with respect to internal coordinates, 2) the estimation of the electron densities and the overlap populations in the structure of energy minimum.

The method of calculation employed in this study is CNDO-2 by Pople and Segal.[7] The model initially chosen has a D_{3h} symmetry [IV] as depicted in Fig. 1.

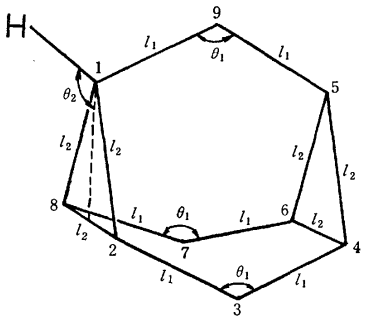

Fig. 1. Geometrical parameters for IV.

In the D_{3h} symmetrical structure, variable geometrical parameters are the bond lengths, $l_1(C_2C_3=C_3C_4=C_6C_7=C_7V_8=C_1C_9=C_9C_5)$, $l_2(C_1C_2=C_2C_8=C_8C_1=C_4C_5=C_5C_6=C_6C_4)$ and the bond angle $\theta_1(\angle C_2C_3C_4=\angle C_1C_9C_5=\angle C_8C_7C_6)$. The bond angle θ_2 is also a geometrical parameter to whose change, however, molecular energy is fairly insensitive. A bond length of 1.09 Å assumed for all C–H bonds. The calculation was

1) a) Postdoctrate Fellow (UCLA) 1969–1970, Department of Chemistry, University of California, Los Angeles. b) Deceased, November 23, 1969. c) Department of Synthetic Chemistry, Kyoto University. d) To whom the correspondence should be addressed.

2) W. von E. Doering, B. M. Ferrier, E. T. Fossel, J. H. Hartenstein, M. Jones, Jr., G. Klumpp, R. M. Rubin, and M. Saunders, *Tetrahedron*, **23**, 3943 (1967).

3) a) M. J. Goldstein, and B. G. Odell, *J. Amer. Chem. Soc.*, **89**, 6356 (1967). b) M. J. Goldstein, *ibid.*, **89**, 6357 (1967),

4) a) P. von R. Schleyer, J. J. Harper, G. L. Dunn, V. J. Di Pasquo, and J. R. E. Hoober, *ibid.*, **89**, 698 (1967). b) P. von R. Schleyer and R. E. Leone, *ibid.*, **90**, 4164 (1968). c) J. C. Barborak, J. Daub, D. M. Follweiser, and P. von R. Schleyer, *ibid.*, **91**, 7760 (1969). d) J. C. Barborak and P. von R. Schleyer, *ibid.*, **92**, 3184 (1969).

5) a) P. Ahlberg, D. L. Harris, and S. Winstein, *ibid.*, **92**, 2146 (1970). b) P. Ahlberg, D. L. Harris, and S. Winstein, *ibid.*, **92**, 4454 (1970).

6) R. S. Mulliken, *J. Chem. Phys.*, **23**, 1833 (1935).

7) J. A. Pople and G. A. Segal, *ibid.*, **44**, 3289 (1966).

organized as follows. The bond length l_1 was first calculated by minimizing the molecular energy, assuming $l_2=1.54$ Å and $\theta_1=\theta_2=120°$. Using the calculated value for l_1(1.40 Å), the value of 115° for θ_1 was obtained, and then with these value of l_1 and θ_1, the bond length l_2 was calculated. With the new values for θ_1 and l_2, l_1 was recalculated. This process was repeated until an absolute minimum in energy with respect to l_1, l_2 and θ_1 was obtained. Fixing the final values for l_1, l_2 and θ_1, the best bond angle θ_2 was obtained.

Thus, after the most stable symmetrical structure was obtained by changing all the bond lengths and the bond angles, the change of the molecular energy with respect to several possible deformations was examined. All the bond angles and bond lengths were varied independently or simultaneously as shown in the examples below.

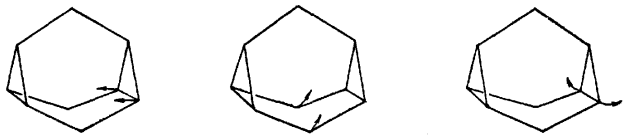

A B C

A similar treatment of bicyclo[3.2.2]nonatrienyl cation (I) was carried out. In this case, main geometrical parameters are the bond angles θ_1, θ_2, θ_3 and θ_4 as shown in Fig. 2. The coordinates of C_6, C_7, C_8 and C_9 was first calculated for changes in θ_1 and θ_2, assuming $\theta_3=120°$, $C_2C_3=C_3C_4=1.40$Å, $C_1C_2=C_4C_5=C_1C_7=C_1C_8=C_5C_6=C_5C_9=1.52$ Å and $C_6C_7=C_8C_9=1.34$Å according to the literature.[8] The coordinates for the protons H_2, H_3, H_4, H_6, H_7, H_8 and H_9 are calculated on the assumption that they lie in each corresponding plane and the C_1H_1 and the C_5H_5 bonds are at equal angles from the other bonds at C_1 and C_5, respectively. Using θ_1 and θ_2 obtained from the first computation (both 70°), the bond angles θ_3 and θ_4 were varied and determined by minimizing the molecular energy. This process was repeated until the energy minimum was obtained with respect to θ_1, θ_2, θ_3 and θ_4. Finally, using this set of bond angles, the changes in the molecular energy were tested by varying each bond length. In the present calculations the angles were calculated to within 1° and the bond lengths within 0.01 Å, respectively.

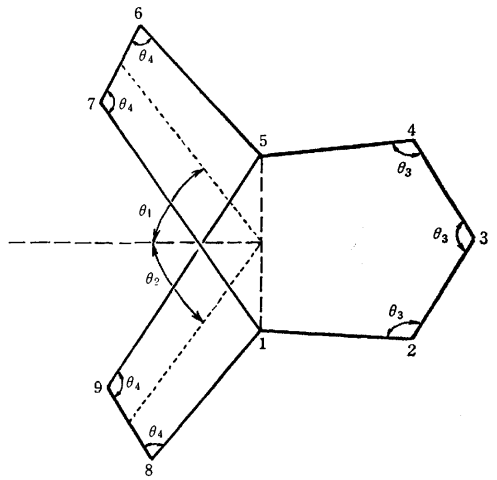

Fig. 2. Geometrical parameters for I.

8) J. A. Pople and M. Gordon, *J. Amer. Chem. Soc.*, **89**, 4253 (1967).

The electron densities and the overlap populations for the structure (IV) and (I) were calculated and presented in Fig. 3 and 4, respectively.

Results and Discussion

From the calculation for (IV) changing all the geometrical parameters, the molecular energy for the most stable symmetrical structures was calculated to be −70.0733 a.u. In this structure, the bond lengths $l_1=1.41$ Å, $l_2=1.52$ Å and the bond angles $\theta_1=115°$ and $\theta_2=120°$. Any small geometrical deformation did not lower the energy of the symmetrical structure. It is clear that the structure IV is at least one of the minima on the potential energy surface. The electronic densities and the overlap populations for this structure are shown in Fig. 3. The positive

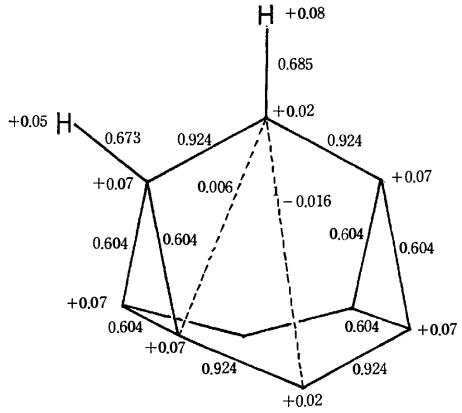

Fig. 3. The electronic charges and the overlap populations for IV.

charge was delocalized over all the carbon atoms as might be expected. An important aspect for this D_{3h} symmetrical structure is that the overlap populations for l_1 correspond to that for an aromatic bond, since the value of 0.924 for l_1 is comparable to that of benzene (0.960), whereas the value of 0.604 for l_2 is smaller than that of a typical sp^3 C–C bond, 0.704, which is obtained for the C–C bond in neopentane. Accordingly, the electronic state of IV could be visualized in (IV'). It is immediately obvious from this representation that IV is stabilized by cyclopropylcarbinyl resonance. There are six equivalent cyclopropylcarbinyl fragments, $C_8C_2C_1C_9$, $C_1C_8C_2C_3$, $C_2C_1C_8C_7$, $C_4C_5C_6C_7$, $C_5C_6C_4C_3$ and $C_6C_4C_5C_9$, as is seen in IV'. In other words, IV is a highly homoconjugated system.

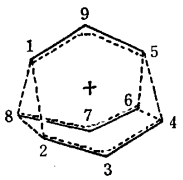

(IV')

The prediction of much stability in IV supports the observation by Schleyer *et al.*[4c] that deuterium distributed almost exclusively between C_3, C_7 and C_9 in the solvolysis of 9-D-barbararyl tosylate. In the study of the direct observation of II by NMR, Winstein and his coworkers[5b] suggested a facile divinylcyclopropylcarbinyl-divinylcyclopropylcarbinyl rearrangement as given in the following mechanism, with which Schleyer

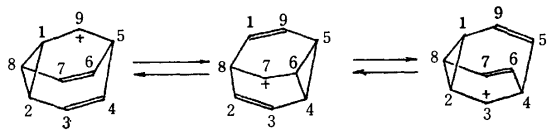

IIa IIb IIc

et al. also agreed in their recent paper.[4b] According to the present calculation, this rearrangement can be facilitated through the symmetrical intermediate IV'.

The calculation of the energy of the species derived from IV by simultaneous large deformations (A, B and C) might approach that for II. The computations were attempted several times, but a lower molecular energy was not obtained. As an attempt to find an energy minimum of II on the potential surface seemed to consume too much time, a laborious complete treatment was not carried out.

A similar theoretical treatment for another $C_9H_9^+$ system, bicyclo[3.2.2]nonatrienyl cation (I), yielded the bond angles, 69°, 69°, 126° and 119° for θ_1, θ_2, θ_3 and θ_4, respectively, and the bond lengths, 1.52 Å, 1.40 Å and 1.34 Å for $C_1C_2=C_1C_7=C_1C_8=C_4C_5=C_5C_6=C_5C_9$, $C_2C_3=C_3C_4$ and $C_6C_7=C_8C_9$, respectively, at its energy minimum geometry. The calculated molecular energy of −70.0361 a.u. was much higher than that

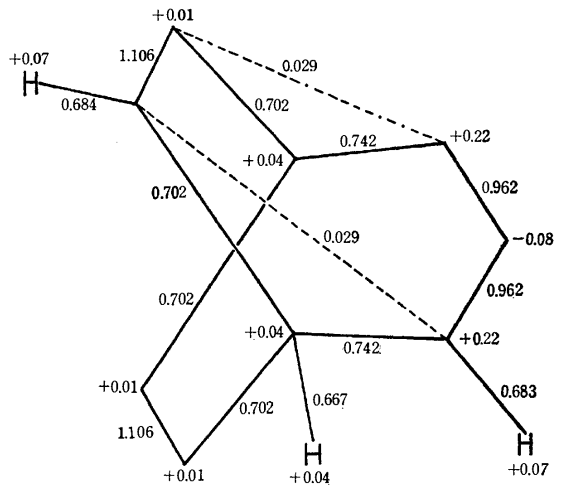

Fig. 4. The electronic charges and the overlap populations for I.

for IV, in accordance with the antibicycloaromaticity of I. In the five membered systems such as $C_2C_3C_4$-C_9C_8 and $C_2C_3C_4C_6C_7$ in Fig. 4, the small overlap populations (0.029) clearly indicate that the systems are antihomoaromatic.

A similar MO calculation for bishomotropylium ion (III), which should be the most stable $C_9H_9^+$ system, is now under investigation.[9]

We should like to thank Dr. P. Ahlberg and Dr. D. Blagdon for assistance in many illuminating discussions.

9) From a calculation for III choosing an appropriate set of geometrical parameters, an molecular energy (−70.0691 a.u.), much more stable than I and comparable to IV, has already been obtained.

The 9-Barbaralyl Cation

Roald HOFFMANN, W.-D. STOHRER, and M. J. GOLDSTEIN
Department of Chemistry, Cornell University, Ithaca, N.Y., U.S.A.

(Received August 12, 1971)

We find that the 9-barbaralyl cation assumes a structure with 3-fold symmetry in which there is an interesting orbital pattern caused by strong conjugative interaction of the central *p* orbitals with the cyclopropane rings. We think this symmetrical cation is identical with the transition state for the Cope rearrangement of 9-barbaralyl cation.

At −135°C, in super acid media, the 9-barbaralyl cation **1** undergoes a sequence of rapid rearrangements which renders all protons equivalent on the NMR time scale.[1] Under solvolytic conditions evidence for a somewhat faster and less degenerate rearrangement

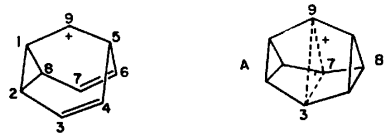

1 **2**

has been obtained.[2] In this process positions 3,7,9 are made equivalent, as are 1,2,4,5,6, and 8.

Several mechanisms may be written for both the partially degenerate and totally degenerate rearrangements.[1-3] For the former process an attractive transition state or intermediate which in its molecular symmetry reflects the degeneracy of the rearrangement is the D_{3h} $C_9H_9^+$ cation **2** suggested by Schleyer and coworkers.[2a,b] It also accidentally represents a confluence of four areas of our interest: the ability of a cyclopropyl group to enter into conjugation,[4] the concept of through-bond coupling,[5] the modification of the Cope rearrangement,[6] the structure and rearrangements of $(XH)_n$ species.[7] We present here an analysis of its electronic structure.

Consider the interaction of the Walsh orbitals[4,8] of cyclopropane rings A and B of **2** with the set of three *p* orbitals at C_3, C_7 and C_9. These latter three orbitals

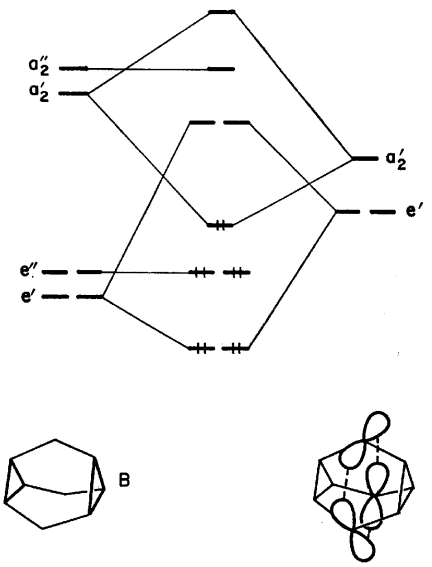

Fig. 1. Interaction of cyclopropane ring orbitals (left) with orbitals of carbons 3, 7, and 9 (right).

also generate a Walsh set, with a doubly degenerate e′ orbital below a nondegenerate a_2', but the splitting between e′ and a_2' must be much smaller than in a normal cyclopropane because the C_3–C_7 distance is long. Figure 1 shows the interaction of the orbitals of rings A and B with this inner set. The following points emerge:

1) The highest occupied MO is a_2'. Interaction of the inner set with the Walsh orbitals of rings A and B reverses the direct overlap determined ordering e′ below a_2'. This is because the overlap of a C_3 *p* orbital with the optimally aligned Walsh orbitals of rings A and B is greater than its overlap with C_7 or C_9 *p* orbitals. In an extended Hückel calculation on **2** with CCC angles of 120° at C_3, C_7, and C_9 the a_2' orbital emerges 2.0 eV below e′.

2) The shape of the a_2' orbital is given in **3** below. Since it is composed of the a_2' combination of inner orbitals mixed in a bonding way with the antibonding a_2' combination of outer ring orbitals it leads to stronger C_1–C_9, weaker C_1–C_2 bonds (only one member of the symmetry related set is given). a_2' is 3–7, 3–9, 7–9 antibonding, and so representation **2**, if it implies any such bonding, is inappropriate.[9]

1) P. Ahlberg, D. L. Harris, and S. Winstein, *J. Amer. Chem. Soc.*, **92**, 4454 (1970).

2) a) J. C. Barborak, J. Daub, D. M. Follweiler, and P. von R. Schleyer, *ibid.*, **91**, 7760 (1969); b) J. C. Barborak and P. von R. Schleyer, *ibid.*, **92**, 3184 (1970); c) J. B. Grutzner and S. Winstein, *ibid.*, **92**, 3186 (1970).

3) R. E. Leone and P. von R. Schleyer, *Angew. Chem.*, **82**, 889 (1970).

4) a) R. Hoffmann, *J. Chem. Phys.*, **40**, 2480 (1964); b) R. Hoffmann, *Tetrahedron Lett.*, **1965**, 3819; c) R. Hoffmann, *ibid.*, **1970**, 2907.

5) a) R. Hoffmann, A. Imamura, and W. J. Hehre, *J. Amer. Chem. Soc.*, **90**, 1499 (1968); b) R. Hoffmann, E. Heilbronner, and R. Gleiter, *ibid.*, **92**, 706 (1970); c) R. Hoffmann, *Accounts Chem. Res.*, **4**, 1 (1971).

6) R. Hoffmann and W. -D. Stohrer, *J. Amer. Chem. Soc.*, **93**, 6941 (1971).

7) a) R. Hoffmann and W. N. Lipscomb, *J. Chem. Phys.*, **36**, 2179 (1963); b) R. Hoffmann and W. N. Lipscomb, *Inorg. Chem.*, **2**, 231 (1963). c) W. -D. Stohrer and R. Hoffmann, *J. Amer. Chem. Soc.*, **94**, 1661 (1972). d) M. J. Goldstein, *ibid.*, **89**, 3657 (1967). e) M. J. Goldstein and R. Hoffmann, *ibid.*, **93**, 6193 (1971).

8) A. D. Walsh, *Trans. Faraday Soc.*, **45**, 179 (1949).

9) Similar results have been obtained by S. Yoneda, S. Winstein, and Z. Yoshida, This Bulletin, **45**, 2510 (1972). We are grateful to Dr. Yoneda for communicating his results to us prior to publication.

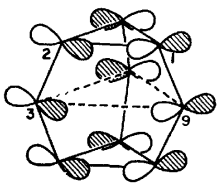

3

3) The collapse of **2** to **4** is a symmetry forbidden process. This is perhaps easiest seen by noting that the new 3–7 σ bond in **4** is symmetric with respect

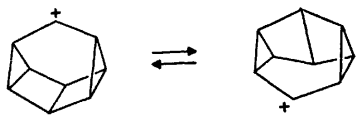

4 **4'**

to reflection in the symmetry plane perpendicular to that bond, but the occupied a_2' orbital of **2** is antisymmetric. Thus the hypothetical rearrangement of **4** to **4'** where the cationic center shifts from say C_7 to C_3 cannot proceed *via* the transition state or intermediate **2**. A less symmetrical circumvention, like that we have discovered in $C_5H_5^+$,[7c] is here made geometrically unlikely.

We now turn to the relationship of cation **2**, its electronic structure described in Fig. 1, to the transition state **5** for the degenerate Cope rearrangement of **1**⇌**1'**. This rearrangement was considered but dis-

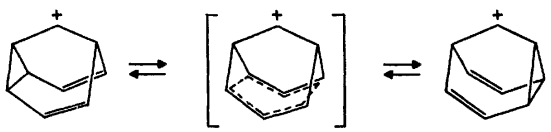

1 **5** **1'**

carded as a source of degeneracy in the rearrangements of the 9-barbaralyl and 9-methyl-9-barbaralyl cations by Ahlberg, Grutzner, Harris, and Winstein.[1,10] The basis for discounting the occurrence of a Cope rearrangement was apparently the trend in Cope rearrangement activation energies on going from barbaralone to protonated barbaralone.[10] However we would like to reconsider the transition state **5** in view of its geometrical similarity to cation **2**.

The interconversion of **2** and **5** is a symmetry allowed process. Let us classify levels with respect to the mirror plane containing carbons 1, 9, and 5. The occupied levels in transition state **5** (or collapsed cation **1**) are two symmetric levels and one antisymmetric, shown schematically below.[6] (The view is along the

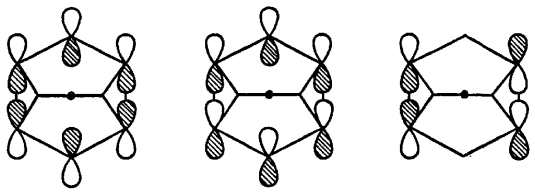

S_1 A S_2

C_2 axis, from the top toward C_9). These correlate directly to the occupied levels of **2**: S_1 and S_2 go to form the 2–8 and 4–6 σ bonds, while A by mixing with the empty p orbital at C_9 goes over into the crucial a_2' orbital of **2**.

Given the structural similarities of **2** and **5** and the fact that they have similar electronic configurations we think it is highly likely that they are not distinct molecules but one and the same species. Whether this is a transition state or intermediate can be only decided by calculations better than the ones at our command. But we propose that the rearrangement of the 9-barbaralyl cation merges with the Cope rearrangement of the same molecule—the midpoint of that reaction is of D_{3h} symmetry and simply has three possible collapse channels.

We are grateful to P. v. R. Schleyer for a discussion this problem and R. Platt for assistance with some calculations. The stay of W. -D. S. at Cornell was made possible by a grant from the Deutsche Forschungsgemeinschaft. Our work was supported by the National Science Foundation and the National Institutes of Health.

10) P. Ahlberg, J. B. Grutzner, D. L. Harris, and S. Winstein, *J. Amer. Chem. Soc.*, **92**, 3478 (1970).

Syntheses of Substituted Phenyl-2-thienyliodonium Halides and Their Pyrolysis Reactions

Yorinobu YAMADA and Makoto OKAWARA

Research Laboratory of Resources Utilization, Tokyo Institute of Technology, Ookayama, Meguro-ku, Tokyo

(Received October 2, 1971)

Various substituted phenyl-2-thienyliodonium halides were prepared by the reaction of thiophene with substituted phenyliodoso acetates in acetic anhydride–concentrated sulfuric acid. In the pyrolysis reaction of substituted phenyl-2-thienyliodonium chlorides it was found that the chloride ion selectively attacked the 1-carbon of the phenyl group. The product ratios in the pyrolysis reaction of substituted phenyl-2-thienyliodonium bromides can be explained on the basis of a bimolecular aromatic nucleophilic substitution except for *p*-chlorophenyl-2-thienyliodonium bromide. In the case of *p*-chloro substituted derivative an interesting effect of *p*-chloro group was observed. The pyrolysis reaction of substituted phenyl-2-thienyliodonium iodides gave substituted phenyl iodides and 2-iodothiophene. The solution reaction of phenyl-2-thienyliodonium halides in *N,N*-dimethylformamide gave halobenzene and 2-iodothiophene. These results suggest that the reaction proceeds *via* an interaction between the halide ion and the phenyl group in a trigonal-bipyramidal structure.

Many reactions of diaryliodonium salts with various nucleophiles have been studied.[1] However, scarcely any reactions of phenyl-2-thienyliodonium salts containing the thienyl group as a ligand of iodonium salts have been reported except for the electroreduction and the nucleophilic displacement with sulfite ion in water by Beringer and his co-workers.[2] They reported that the replacement of the phenyl group in diphenyliodonium cation by the 2-thienyl group increases the ease of electroreduction and the susceptibility to nucleophilic attack. When phenyl-2-thienyliodonium cation was cleaved by sulfite ion in water, the ratio of attack on the thiophene ring to that on the benzene ring was 2: 1.

$$\mathrm{Ph\text{–}I^{+}\text{–}Th} + \mathrm{SO_3^{2-}} \longrightarrow \begin{cases} \mathrm{PhSO_3^-} + \mathrm{ThI} \\ \mathrm{ThSO_3^-} + \mathrm{PhI} \end{cases} \quad (1)$$

They attributed such a result to the predominant resonance interaction between the iodine and the phenyl ring or to the difference in electronegativity between the phenyl and 2-thienyl groups.

We have investigated the synthesis of polymeric iodonium salt ($\mathrm{PSJ^+X^-}$) containing the polystyryl structure as one of the ligands and the possibility of their application to synthetic chemistry.[3]

Various substituted phenyl-2-thienyliodonium halides (I) were synthesized and allowed to react in the molten state for investigation of the difference in reactivity between the substituted phenyl and thienyl groups.

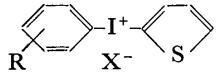

(I)

Results and Discussion

Syntheses of Substituted Phenyl-2-thienyliodonium Halides. Phenyl-2-thienyliodonium salts can be synthesized in three ways. The first method is the reaction of iodosobenzene with thiophene in acetic acid–acetic anhydride–sulfuric acid (Yield 49%).[2]

$$\mathrm{PhIO} + \mathrm{ThH} + \mathrm{H_2SO_4} + \mathrm{Ac_2O} \longrightarrow \mathrm{Ph\text{–}I^{+}\text{–}Th} + \mathrm{HSO_4^-} + 2\mathrm{AcOH} \quad (2)$$

The second method is the reaction of iodosobenzene diacetate with thiophene in acetic acid–acetic anhydride–trifluoroacetic acid (Yield 92%).[2]

$$\mathrm{PhI(OAc)_2} + \mathrm{ThH} + \mathrm{CF_3COOH} \longrightarrow \mathrm{Ph\text{–}I^{+}\text{–}Th} + \mathrm{CF_3COO^-} + 2\mathrm{AcOH} \quad (3)$$

The third is the reaction of 2-thienyllithium with phenyl(*trans*-chlorovinyl)iodonium chloride in toluene giving phenyl-2-thienyliodonium salt in 38% yield.[4]

$$\mathrm{ThLi} + \begin{matrix} \mathrm{H} \\ \mathrm{Cl} \end{matrix}\!\!\diagdown\!\!\diagup\!\!\begin{matrix} \mathrm{I^{+}\text{–}Ph} \\ \mathrm{H} \end{matrix} \mathrm{Cl^-} \longrightarrow \mathrm{Th\text{–}I^{+}\text{–}Ph\ Cl^-} + \mathrm{LiCl} + \mathrm{CH{\equiv}CH} \quad (4)$$

We prepared the substituted phenyl-2-thienyliodonium salts by modifying the reaction (3), *viz.*, the substituted phenyliodoso diacetate was allowed to react in the presence of concentrated sulfuric acid in acetic anhydride.

$$\mathrm{ArI(OAc)_2} + \mathrm{ThH} + \mathrm{H_2SO_4} \longrightarrow \mathrm{Ar\text{–}I^{+}\text{–}Th\ HSO_4^-} + 2\mathrm{AcOH} \quad (5)$$

The desired iodonium halides were precipitated by adding the aqueous solution of corresponding metal halides to the reaction mixture obtained. The results are summarized in Table 1. The structures were confirmed by elemental analysis and infrared spectrum. The solubility in polar solvents such as water, methanol, and *N,N*-dimethylformamide (DMF) decreases in the order, chloride>bromide>iodide.

Pyrolysis Reactions of Iodonium Halides in the Molten State. There are two paths as shown below in the nucleophilic displacement of substituted diphenyliodonium salt in the solution.

1) F. M. Beringer and R. A. Falk, *J. Chem. Soc.*, **1964**, 4442; O. A. Ptitsyana, G. G. Lyatiev, and O. A. Reutov, *Zh. Org. Khim.*, **6**, 1353 (1970); *Chem. Abstr.*, **73**, 87551j (1970).

2) F. M. Beringer, H. E. Bachofner, R. A. Falk, and M. Leff, *J. Amer. Chem. Soc.*, **80**, 4279 (1958).

3) Y. Yamada and M. Okawara, *Markomol. Chem.*, **152**, 153 (1972); *ibid.*, **152**, 163 (1972).

4) F. M. Beringer and R. A. Nathan, *J. Org. Chem.*, **35**, 2095 (1970).

TABLE 1. PREPARATION OF SUBSTITUTED PHENYL-2-THIENYLIODONIUM HALIDES

Substituted group R–	Counter anion X^-	Mp (°C)	Yield (%)	Elemental analysis (%) Found C	Found H	Calcd C	Calcd H
p-MeO[d]	Br^-	180—185	38.4	33.11	2.46	33.27	2.54
	I^-	150—155	39.4	29.67	2.19	29.75	2.27
p-Me[d]	Br^-	180—185	58.3	34.50	2.78	34.67	2.65
	I^-	138—143	58.3	30.46	2.32	30.86	2.35
m-Me	Cl^-	210—213	71.5	38.85	3.14	39.25	2.99
	Br^-	215—217	98.0	34.44	2.64	34.67	2.65
	I^-	155—157	98.0	30.31	2.44	30.86	2.35
p-Cl	Cl^-	170—177	55.4	33.13	1.94	33.64	1.98
	Br^-	180—185	57.1	30.08	1.68	29.92	1.76
	I^-	145—148	58.5	26.76	1.45	26.78	1.57
m-Cl	Cl^-	195—210	20.6	33.53	2.13	33.63	1.98
	Br^-	185—187	28.5	29.59	1.69	29.92	1.76
	I^-	135—143	48.6	26.58	1.33	26.78	1.57
H	Cl^-	220—225[a]	—	35.73	2.62	37.23	2.49
	Br^-	200—205[b]	20.6	32.80	2.27	32.72	2.20
	I^-	142—144[c]	—	29.16	1.80	29.00	1.94
	ClO_4^-	157—162	64.0	31.21	1.97	31.07	2.09

a) Lit. gives 217—225°C.
b) Lit. gives 170—174°C.
c) Lit. gives 129—132°C: F. M. Beringer, R. A. Falk, and M. Leff, *J. Amer. Chem. Soc.*, **80**, 4279 (1958).
d) The corresponding iodonium chlorides were not isolated because of their poor crystallizability.

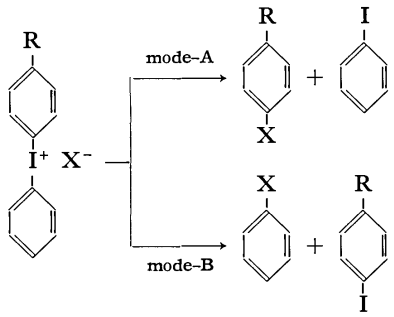

When the substituent of phenyl group is electron-releasing, the reaction of mode-B predominates and *vice versa*, and the rate of the reaction is always faster in the latter than in the former. Similarly, there are two paths conceivable for the reaction of substituted phenyl-2-thienyliodonium salts as follows.

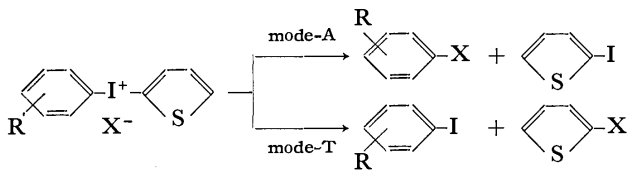

The results of a number of pyrolysis reactions conducted for 5 min. at 235°C are summarized in Table 2. It is clear that the product ratios show a selective nucleophilic attack of the chloride ion on the phenyl ring regardless of the effect of substituent group. However, the product ratios in the case of the iodonium bromide can be explained on the basis of a bimolecular aromatic nucleophilic substitution except for the reaction of *p*-chlorophenyl-2-thienyliodonium bromide. In the case of phenyl-2-thienyliodonium iodide substituted phenyl iodide and 2-thienyliodide alone were obtained.

TABLE 2. CLEAVAGE TENDENCY OF SUBSTITUTED PHENYL-2-THIENYLIODONIUM HALIDES

Substituted group	Counter anion	Mode-A : Mode-T (mol %)	
H	Cl^-	100	0
m-Cl	Cl^-	100	0
p-Cl	Cl^-	100	0
m-Me	Cl^-	100	0
H	Br^-	100	0
m-Cl	Br^-	100	0
p-Cl	Br^-	76.1	23.9
m-Me	Br^-	100	0
p-Me	Br^-	70.7	29.3
p-MeO	Br^-	60.0	40.0

In every case biaryl, bithienyl, and 2-thienylarene which are considered to be produced in a free radical process were not found by glc analysis. It is of interest that the pyrolysis reaction of the iodonium chloride proceeds *via* the reaction of mode-A alone.

In general, the thiophene ring is more susceptible to the nucleophilic substitution than the benzene ring.[5] As an example, it was reported that the nucleophilic substitution on 2-bromo-5-nitrothiophene was more than one hundred times faster than that on *p*-bromonitrobenzene.[6] Therefore, some factors other than electronic effect should be taken into account for the predominant reactivity of benzene ring obtained in our experiment.

5) L. Melander, *Arkiv Förmkem.*, **8**, 361 (1955).
6) R. Motoyama, S. Nishimura, Y. Murakami, K. Hari, and E. Imoto, *Nippon Kagaku Zasshi*, **78**, 954 (1957).

Khotsyanova has studied the crystal structure of diphenyliodonium chloride.[7] The molecular is T-shaped, containing a linear C_1 (1-carbon at one phenyl ring) –I–Cl group perpendicular to a C_2 (1-carbon at another phenyl ring) –I group as shown in II.

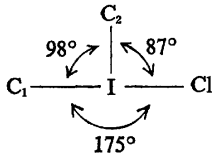

$C_1-I=C_2-I=2.08$ Å
$I-Cl=3.08$ Å

(II)

Taking into account the two lone pairs the molecule should have trigonal-bipyramidal structure (III), the one phenyl ring and two lone pairs on the equatorial position, another phenyl ring and the chloride ion at the apices.

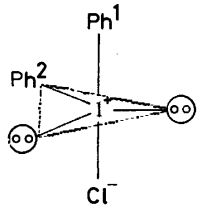

(III)

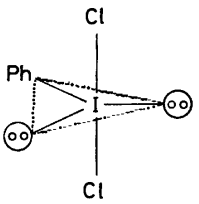

(IV)

Such a trigonal-bipyramidal structure has also been reported for the case of iodobenzene dichloride as shown in IV.[8]

In view of these facts the substituted phenyl-2-thienyliodonium halide should have a trigonal-bipyramidal structure (Va), the phenyl ring and two lone pairs on the equatorial position and the thienyl ring and halogen atom at the apices. On the basis of this assumption the reaction is considered to proceed *via* the overlap of π-orbital of the aryl group and

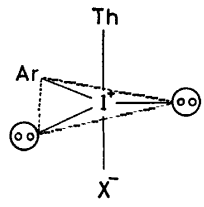

(Va)

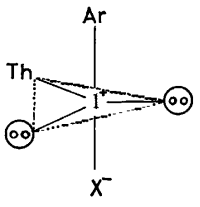

(Vb)

the *p*-orbital of halide ion with concomitant cleavage of the bond between the 1-carbon of the aryl group and iodine atom. A similar type of reaction which proceeds through the orbital interaction of the halide ion and the aryl group has been reported for the pyrolysis reaction of triarylsulfonium halides.[9] If the aryl-2-thienyliodonium halide exists in a structure such as Vb, it is expected that the formation of 2-halothiophene predominates. However, hardly any 2-chlorothiophene was produced in the case of the iodonium chlorides. Furthermore, 2-bromothiophene was not produced except for *p*-chloro-, *p*-methyl-, and *p*-methoxy-substituted derivatives in the case of the iodonium bromides. It is reasonable to assume that the more electronegative thienyl ring compared to phenyl ring is located in the site opposite to the halide anion because of their electronic repulsion.[10] These results suggest a structure such as Va rather than Vb in the transition state.

The proton chemical shifts (δ-value) of substituted phenyl-2-thienyliodonium bromides are greater (0.01—0.27 ppm) than those of the corresponding chlorides.[11] Thus, the chloride ion is found to be situated in the position more closely to the iodine atom than the bromide ion (that is, the I–Cl bond occupies more covalent character in comparison with the I–Br bond,[12] and the positive charge on the iodine atom of the iodonium bromide is greater than that of the iodonium chloride. The preferred chloride-aryl coupling over bromide-aryl coupling arises since the bond between aromatic-1-carbon and iodine atom of the iodonium bromide acquires a double bond character through the resonance of the substituent as compared with that of the iodonium chloride. Thus, the reaction of mode-A is liable to occur in the case of the iodonium chlorides compared to that of mode-T by the effective orbital interaction between the aryl ring and the chloride ion. On the other hand, the bromide ion attacked not only the aryl ring (mode-A) but also the thienyl ring (mode-T) in the case of *p*-chloro-, *p*-methyl-, and *p*-methoxyphenyl-2-thienyliodonium bromides. *p*-Methyl and *p*-methoxy substituents prevent the reaction of mode-A owing to their electron-releasing effect. In the *p*-chloro substituent, however, the occurence of the reaction of mode-T could not be explained on the basis of the inductive effect of the *p*-chloro group. The resonance structure (VI) participating with the lone pair of the chlorine atom makes the reaction of mode-T possible. The bond linking the $-I^+$-2-thienyl group to the aromatic ring acquires a double

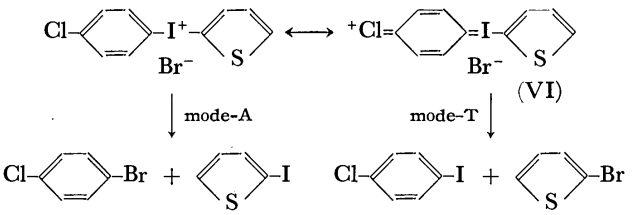

bond character, making it more difficult to be broken. As shown in Table 3, the increase in λ_{max} in going from *m*-substituted or unsubstituted to *p*-chlorophenyl-

7) T. L. Khotsyanova, *Kristallografiya*, **2**, 51 (1957); *Chem. Abstr.*, **52**, 1704b (1958).

8) E. M. Archer and T. G. D. van Schalkwyk, *Acta Crystallogr.*, **6**, 88 (1953); D. F. Banks, *Chem. Rev.*, **66**, 260 (1966).

9) G. H. Wiegand and W. E. McEwen, *J. Org. Chem.*, **33**, 2671 (1968).

10) Imoto and his co-workers have reported the aryl value (σ_a) on various aromatic compounds. According to them, the aryl values of phenyl and 2-thienyl groups have been reported as 0.00 and 0.30, respectively. Y. Otsuji, K. Kubo, and E. Imoto, *Nippon Kagaku Zasshi*, **80**, 1300 (1959).

11) Y. Yamada and M. Okawara, unpublished data.

12) Petrosyan has reported from the NMR spectra of diphenyliodonium halides that the bond between chloride ion and iodine atom occupies more covalent character than that between bromide ion and iodine atom. V. S. Petrosyan, *Dokl. Acad. Nauk SSSR*, **175**, 613 (1967); *Chem. Abstr.*, **68**, 7940u (1968).

TABLE 3. UV SPECTRA OF SUBSTITUTED PHENYL-2-THIENYLIODONIUM HALIDES (in Methanol)

Substituted group	Counter anion	λ_{max} (nm)	log ε
H	Cl^-	241	4.03
m-Cl	Cl^-	240	3.98
p-Cl	Cl^-	241	4.20
m-Me	Cl^-	239	4.02
H	Br^-	238	3.88
m-Cl	Br^-	240	3.97
p-Cl	Br^-	244	4.13
m-Me	Br^-	239	4.17
p-Me	Br^-	242	4.11
p-MeO	Br^-	254	4.19

2-thienyliodonium bromide suggests the presence of such a conjugated system. If the resonance structure such as VI contributes to the reaction, the iodine atom and the bromide ion become far apart in contrast to the case of absence of such a resonance structure and orbital interaction will occur between not only the bromide ion and the aryl ring but also between the bromide ion and the thienyl ring. Thus, the reaction of not only mode-A but also of mode-T occurs. In the case of *m*-chloro substituted derivative the reaction of mode-T did not occur since the resonance structure due to the lone pair of the chlorine atom was not possible. It is also understandable from the small difference in λ_{max} between phenyl- and *m*-chlorophenyl-2-thienyliodonium bromide. In the case of the iodonium chloride, the contribution of the resonance structure such as VII is neglected from the ultraviolet spectra data. The λ_{max} in *p*-chlorophenyl-2-thienyliodonium chloride is much the same as that in *m*-chlorophenyl-2-thienyliodonium or phenyl-2-thienyliodonium chloride.

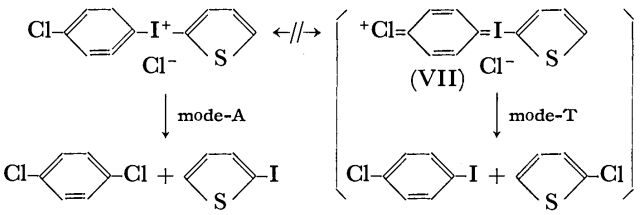

In view of the results of *p*-chlorophenyl-2-thienyliodonium bromide it is considered that the cleavage tendencies of *p*-methoxy- and *p*-methyl-phenyl-2-thienyliodonium bromide are ascribed not only to the inductive effect of the substituent group but also to the conjugated structure:

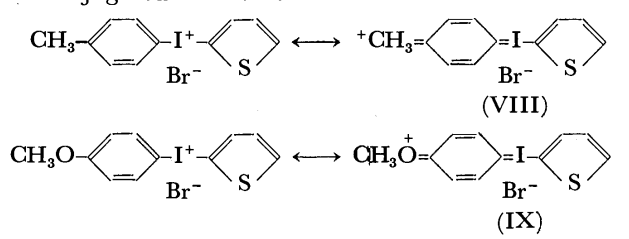

The difference in λ_{max} between *m*- and *p*-methylphenyl-2-thienyliodonium bromide suggests the presence of the hyperconjugated system such as VIII. The absence of the reaction of mode-T in the case of *m*-methylphenyl-2-thienyliodonium bromide suggests a larger contribution of the resonance effect to the occurrence of the reaction than that of the inductive effect. The significant increase in λ_{max} in going from the unsubstituted phenyl-2-thienyliodonium bromide to *p*-methoxyphenyl-2-thienyliodonium bromide suggests the presence of the conjugated system such as IX. The large difference in λ_{max} between *p*-methyl- and *p*-methoxyphenyl-2-thienyliodonium bromide reflects on the mode of reaction *viz.*, the reaction of mode-T is liable to take place in the case of *p*-methoxy substituted derivative in comparison with *p*-methyl substituted derivative.

Beringer and his co-worker also reported on the possibility of the conjugation on *p*-methoxy and *p*-methyl groups in diphenyliodonium salt from the study of ultraviolet spectra.[13] Such a conjugated system has also been reported in the case of *p*-methyl- and *p*-methoxyphenyl diazonium salts.[14]

When the halide ions (Cl^-, Br^-) were allowed to react with phenyl-2-thienyliodonium ion in DMF, the results were similar to that of pyrolysis reaction, *viz.*, only the reaction of mode-A occurred. When the nitrite or thiocyanate ion was used as a nucleophile in DMF, only the reaction of mode-A occurred to give nitrobenzene or phenyl isothiocyanate and 2-iodothiophene, respectively. In the reaction of phenyl-2-thienyliodonium ion with sulfite ion, the ratio of mode-A to mode-T is 1 : 2.

It was found that the iodonium halides containing the thienyl group as a ligand exhibited high activity against a variety of microorganisms, especially against pseudomonas aeruginosa. It has been reported that 2,5-thiophenediyl-bis(phenyliodonium salts) are bioactive against various microorganisms.[15] While the question in toxicity remains unsettled, these distinctive bioactivities resulting from a combination of iodonium and thienyl structures are very interesting.

Experimental

All the melting points are uncorrected. The electronic spectra were obtained on a Hitachi EPS-3T Spectrometer at room temperature using a well-matched pair of 1 cm-cells. Gas chromatographic analysis was carried out with a Hitachi Gas Chromatograph 023-5051 at 100°C using chlorobenzene as an internal standard. Column used was placed with Silicon DC 703 (20%) on Celite 545 (stainless tube 1 m).

Materials. Thiophene of commercial grade was used without further purification. Substituted phenyl iodides were prepared by standard procedure from the corresponding aniline derivatives. 2-Iodothiophene was prepared from thiophene and iodine in the presence of mercuric oxide.[16] 2-Bromothiophene was prepared from thiophene and bro-

13) F. M. Beringer and I. Lillien, *J. Amer. Chem. Soc.*, **82**, 5135 (1960).

14) Z. Jezic, presented at the 161st ACS National Meeting, Division of Medicine Chemistry, Los Angeles, March, 1971; Preprint, 34.

16) W. Minnis, "Organic Syntheses", Coll. Voll. II, (1943) p. 357.

mine.[17] Substituted phenyl iodine diacetates were prepared by modification of the method of Leffler and Story.[18] The other substituted phenyl iodine diacetates were prepared by a procedure similar to that given for *m*-chlorophenyl iodine diacetate as follows. To a mixture of 51.6 g (0.22 mol) of *m*-chloroiodobenzene and 140 m*l* of purified acetic acid was added dropwise with stirring 110 g (0.43 mol) of 30%-peracetic acid. The flask was chilled with an ice–water bath during the course of slow addition (0.5 hr). The solution was stirred at 10°C for three additional hours and then allowed to stand overnight at room temperature. The solvent was evaporated *in vacuo*. The remaining white crystals were washed with petroleum ether and dried under reduced pressure to give 66.7 g (85.2%) of the product. Purity was estimated iodometrically to be better than 99.8%.

Syntheses of Substituted Phenyl-2-thienyliodonium Halides. Substituted phenyl-2-thienyliodonium halides were prepared by a procedure similar to that given for *p*-chlorophenyl-2-thienyliodonium halides. To a well-stirred mixture of 10.8 g (0.03 mol) of *p*-chlorophenyliodoso diacetate, 5 g (0.06 mol) of thiophene, and 100 m*l* of acetic anhydride kept below 5°C was added 4 m*l* of concentrated sulfuric acid over one hour. After having been stirred under 10°C for 2 hr, the reaction mixture was diluted with 200 m*l* of water, extracted with ether until color was no longer removed and treated with activated carbon. Addition of 10 g of potassium iodide in water gave a colorless precipitate, which was collected, washed with water and methanol and dried to yield 7.88 g of *p*-chlorophenyl-2-thienyliodonium iodide. From similar reaction mixtures *p*-chlorophenyl-2-thienyliodonium bromide and *p*-chlorophenyl-2-thienyliodonium chloride were also obtained. The bromide and the chloride were recrystallized from methanol but the iodide was not recrystallized because of its poor solubility. The results are shown in Table 1.

Pyrolysis Reactions of Substituted Phenyl-2-thienyliodonium Halides. Each iodonium halide in Table 1 was pyrolyzed in a 15 mm Pyrex tube about 15 cm long, sealed at one end at 245±5°C until the reaction was complete. About 10 cm of the sealed end of the tube was immersed into an oil bath, the remainder of the tube being used as an air condenser. In all cases the composition of the pyrolyzates were determined by means of gas chromatograph. Identification of the products was accompanied by means of retention time. In no case was any significant amount of unexpected product found. All the iodonium halides, when pyrolyzed, gave the products expected from their thermal decomposition. Resolution and appropriate shape of the halide peaks obtained in the chromatograms of the pyrolyzates were sufficient to permit determination of the relative ratios of the halides formed in each pyrolyzate. Approximate peak areas were obtained by multiplying the peak height by the peak width at half height. In the case of the bromide the reaction mode was determined from the amounts of 2-iodothiophene and 2-bromothiophene, and in the case of the chloride from the amounts of 2-iodothiophene and the corresponding substituted phenyl iodide, respectively.

Reaction of Phenyl-2-thienyliodonium Ion with Various Nucleophiles in DMF. The mixture of 0.97 g (0.0025 mol) of phenyl-2-thienyliodonium perchlorate and 0.65 g (0.005 mol) of sodium sulfite dissolved in 50 m*l* of DMF and 30 m*l* of water was held at 100°C for 5 hr. At the end of the reaction the reaction mixture was poured into cold water, extracted with ether two times and the extract was dried over anhydrous sodium sulfate. On removing the solvent by distillation, the residual mixture was redissolved in a small quantity of ether and then the amounts of iodobenzene and 2-iodothiophene were determined by glc analysis. When chloride or bromide ion was used as a nucleophile, 0.97 g (0.0025 mol) of the iodonium perchlorate and 0.29 g (0.005 mol) of sodium chloride or 0.52 g (0.005 mol) of sodium bromide dissolved in 50 m*l* of DMF was held at 100°C for 5 hr. When nitrite or thiocyanate ion was used as a nucleophile, 0.97 g (0.0025 mol) of the iodonium perchlorate and 0.35 g (0.005 mol) of sodium nitrite or 0.49 g (0.005 mol) of potassium thiocyanate dissolved in 40 m*l* of DMF and 10 m*l* of water was held at 100°C for 5 hr. In each case the subsequent experiment was carried out in the same way as mentioned above.

17) D. A. Shirley, "Preparation of Organic Intermediates", John Wiley & Sons Inc., London (1951), p. 60.

18) J. E. Leffler and L. J. Story, *J. Amer. Chem. Soc.*, **89**, 2333 (1967).

The Reaction of Dicarbonyl Compounds with Potassium in the Presence of Trimethylsilyl Chloride

Takashi MURAKAWA, Koji FUJII, Shinji MURAI, and Shigeru TSUTSUMI

Department of Petroleum Chemistry, Faculty of Engineering, Osaka University, Suita, Osaka

(Received February 24, 1972)

The reaction of dicarbonyl compounds with potassium in the presence of trimethylsilyl chloride was studied. The carbonyl compounds were benzil (II), 9,10-phenanthroquinone (III), *p*-benzoquinone (IV), disodium salt of tetrahydroxy-*p*-benzoquinone (V), and *trans*-dibenzoylethylene (VI), as well as benzophenone (I). I and II gave bistrimethylsiloxy compounds in good yields, but III did not react under the same conditions. 1,4-Bistrimethylsiloxybenzene and 1,4-diphenyl-1,4-bistrimethylsiloxybutadiene were obtained from IV and VI respectively. A similar conjugate reductive silylation was successful with V affording hexakistrimethylsiloxybenzene in 35% yield.

In the presence of trialkylsilyl chlorides, monoketones undergo reductive dimerization to pinacol bissilyl ethers with magnesium or alkali metals.[1-3] 1,2-Bistrimethylsiloxy alkenes were obtained when acyloin condensation was carried out in the presence of trimethylsilyl chloride.[4,5] Since the modified acyloin condensation is very likely to involve reductive silylation of 1,2-diketone intermediates,[6] it seems to be of interest to study the reduction of dicarbonyl compounds with alkali metal in the presence of trimethylsilyl chloride. A few studies have been reported on the reductive silylation of diketones. Rühlman treated benzil with alkali metal and trimethylsilyl chloride to give two isomeric enediol-disilyl ethers. However, no effort was made to establish the structure of each isomer.[4a] Recently Bouas-Laurent reported the reductive silylation of quinones with magnesium, bistrimethylsiloxy arenes being obtained.[7]

The present work deals with the reaction of dicarbonyl compounds with potassium in the presence of trimethylsilyl chloride. The compounds studied were benzil (II), 9,10-phenanthroquinone (III), *p*-benzoquinone (IV), disodium salt of tetrahydroxy-*p*-benzoquinone (V),[8] and *trans*-dibenzoylethylen (VI), as well as benzophenone (I). The following conjugate reductive silylation would be expected for the 1,2- and 1,4-dicarbonyl compounds:

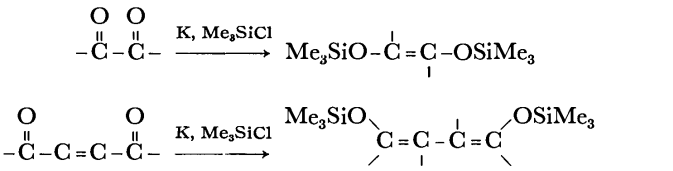

Potassium was used as a reducing metal because it melts above 64°C and can provide a clean metal surface during the course of reaction. The standard procedure of the reaction is as follows. Trimethylsilyl chloride in a slight excess was added to a mixture of a ketone, melted potassium and a solvent over a period of 2 hr at 60—70°C. When the total amount of trimethylsilyl chloride was added at the beginning of the reaction, the same products were obtained but in a lower yield probably because of impurities formed on the metal surface. The results are shown in Table 1.

Benzophenone (I) gave VII which was identical with that prepared separately by the trimethylsilylation of benzopinacol. The observed wide range of melting point might be attributed to the dissociation of VII into diphenyl(trimethylsiloxy)methyl radical as suggested by Calas *et al.*[1] From benzil (II), *cis*- and *trans*-1,2-bistrimethylsiloxy-1,2-diphenylethylene (VIIIa and VIIIb respectively) were obtained in good yields. The assignment of the isomer was based on the IR spectra. The *cis*-isomer VIIIa showed an absorption due to the double bond at 1620 cm^{-1}, while the *trans*-isomer VIIIb showed no double bond absorption usually observed for a double bond at the center of symmetry.[9] The high melting point of VIIIb might also support this assignment. The ratio of VIIIa to VIIIb was 70: 30. The predominant formation of VIIIa could be explained by the stabilization of *cis*-radical-anion.[10] 9,10-Phenanthroquinone (III) which is considered to have *s-cis* configuration of II resisted completely to react under the present con-

1) R. Calas, N. Duffaut, C. Bourges, F. Pisiotti, and J. Dunognes, *Acad. Sci., Paris, Ser, C*, **267**, 322 (1968).

2) C. L. Fryl, R. M. Salinger, and T. J. Patin, *J. Amer. Chem. Soc.*, **88**, 2343 (1966).

3) a) R. A. Calas, J. Dunogues, N. Duffant, and C. Biran, *Acad. Sci., Paris, Ser, C*, **267**, 494 (1968). b) K. Rühlmann, A. Sitzki, and C. Michael, *Chem. Ber.*, **101**, 285 (1968).

4) a) K. Rühlmann and S. Poredda, *J. Prakt. Chem.*, **12**, 18 (1960). b) U. Schrapler and K. Rühlmann, *Chem. Ber.*, **96**, 2780 (1963). c) *ibid.*, **97**, 1383 (1964). d) *ibid.*, **98**, 1352 (1965). e) K. Rühlmann, H. Seefluth, and H. Becker, *ibid.*, **100**, 3820 (1967).

5) a) J. J. Bloomfield, *Tetrahedron Lett.*, **1968**, 587. b) *ibid*,. **1968**, 591. c) *ibid.*, **1968**, 5647. d) G. E. Green and S. Worthley, *ibid.*, **1968**, 3319. e) J. M. Conia and J. M. Denis, *ibid.*, **1969**, 3545. f) G. A. Russell and G. W. Holland, *J. Amer. Chem. Soc.*, **91**, 3968 (1969). g) T. Mori, T. Nakahara, and H. Nozaki, *Can. J. Chem.*, **47**, 3266 (1966). h) C. Ainsworth and F. Chen, *J. Org. Chem.*, **35**, 1272 (1970).

6) S. M. McElvain, "Organic Reactions," Vol. 4, p. 257. (1949).

7) H. Bouas-Laurent, R. Lapouyade, C. Brigand, and J. P. Desvergne, *Acad. Sci., Paris, Ser, C*, **270**, 2167 (1970).

8) A preliminary result obtained for V has been reported. S. Murai, T. Murakawa, and S. Tsutsumi, *Chem. Commun.*, **1970**, 1329.

9) L. J. Bellamy, "The Infrared Spectra of Complex Molecules," John Wiley & Sons, Inc., New York, N. Y. (1958), p. 38.

10) a) N. L. Bauld, *J. Amer. Chem. Soc.*, **84**, 4345 (1962). b) *ibid.*, **87**, 4748 (1965).

TABLE 1. REDUCTIVE SILYLATION OF CARBONYL COMPOUNDS

Exp. No.	Material	Solvent	Product	Yield (%)
1	$C_6H_5CC_6H_5$ (I)	Toluene	$(Me_3Si-O-C(C_6H_5)_2-)_2$ (VII)	72
2	$C_6H_5C-CC_6H_5$ (II)	Benzene	$C_6H_5(Me_3SiO)C=C(C_6H_5)OSiMe_3$ (VIIIa) and $Me_3SiOC(C_6H_5)=C(C_6H_5)OSiMe_3$ (VIIIb)	88 *cis/trans*=70/30
3	(III)	Benzene	No reaction	
4	(IV)	Benzene	No reaction	
		THF	$Me_3SiO-C_6H_4-OSiMe_3$ (IX)	28
5	(V)	THF	$(Me_3SiO)_3C_6H_3-OSiMe_3$ (X)	35
6	(VI)	Benzene	$C_6H_5(Me_3SiO)C=C(H)-C(OSiMe_3)=C(H)-C_6H_5$ (XIa) or $Me_3SiOC(H)=C(C_6H_5)-C(H)=C(H)-OSiMe_3$ (XIb)	12

ditions.[11] The double bond in the dianion of ene-diol formed by reduction in the case of II might bring the originally separated two phenyl groups into one π-net work increasing *ca.* 18 kcal/mol of the delocalization energy of the system.[10] On the other hand, two phenyl groups of III are originally coupled and the effect of introducing a double bond at 9,10-position by the reduction with alkali metal might decrease the delocalization energy as compared with that of III.[12] The reaction of *trans*-dibenzoylethylene (VI), a 1,4-diketone, gave a bistrimethylsiloxybutadine (XI) whose NMR spectra showed one sharp singlet due to the trimethylsilyl group. Of the three possible isomers for XI, *trans-trans-* or *cis-cis*-1,4-diphenyl-1,4-bistrimethylsiloxybutadine (XIb or XIa) is consistent with the NMR data, but not for the *cis-trans* isomer with two nonequivalent trimethylsilyl groups. The low yield of XI might be due to polymerization of the product.

The 1,6-conjugate reductive silylation was extended to *p*-quinones. The reaction of *p*-benzoquinone (IV) in benzene gave 1,4-bistrimethylsiloxybenzene (IX) when tetrahydrofuran was used as a solvent. A similar conjugate reductive silylation was successful with disodium salt of tetrahydroxy-*p*-benzoquinone (V) affording hexakistrimethylsiloxybenzene (X) is 35% yield. Inspection of a model of X revealed the existence of two representative structures; one with

11) However, III was reported to undergo reductive silylation with magnesium.[7] The difference from potassium and magnesium is not clear.

12) A. Streitwieser, Jr., "Molecular Orbital Theory for Organic Chemist," John Wiley & Sons, Inc., New York, N. Y. (1961), p. 251.

Table 2. Properties of silylated products

Products	Mp °C (Bp °C/mmHg)	Formula	Analyses (%) Found (Calcd) C	H	NMR[a] τ	IR cm^{-1}
VII	130—135[d]	$C_{32}H_{38}O_2Si_2$	75.28 (75.29)	7.43 (7.45)	9.98 (*s*, 18H) 2.89 (*s*, 20H)	1250, 830 (Me_3Si) 1105 (C–O–Si)
VIIIa	(160—161/8)[e]	$C_{20}H_{28}O_2Si_2$	67.74 (67.41)	8.18 (7.87)	9.95 (*s*, 18H) 3.20 (*s*, 10H)	1250, 850 (Me_3Si) 1150 (C–O–Si) 1620 (C=C)
VIIIb	108—110[f]	$C_{20}H_{28}O_2Si_2$	67.55 (67.41)	7.97 (7.87)	10.23 (*s*, 18H) 2.07 (*s*, 10H)	1250, 850 (Me_3Si) 1150 (C–O–Si)
IX	48—50[g]	$C_{12}H_{22}O_2Si_2$	56.76 (56.65)	8.69 (8.65)	9.76 (*s*, 18H) 3.36 (*s*, 4H)	1225, 1255, 840 (Me_3Si) 925 (C–O–Si)
X	220[c]	$C_{24}H_{54}O_6Si_6$	47.39 (47.47)	9.12 (8.96)	9.86 (*s*)	1250, 840 (Me_3Si)[b] 1040 (C–O–Si)
XI	128—130	$C_{22}H_{30}O_2Si_2$	68.73 (69.07)	7.82 (7.73)	9.75 (*s*, 18H) 3.63 (*s*, 2H) 2.70 (*m*, 10H)	1245, 870 (Me_3Si) 1580, 1555 (C=C–C=C) 1060 (C–O–Si)

a) Obtained in CCl_4. *s*: singlet, *m*: multiplet. b) There was an additional strong absorption at 890 cm^{-1}. c) The mass and UV spectroscopic data were reported elsewhere.[8] d) Lit,[1] 158°C decomp. e) Lit,[4a] bp 142—143.5/2 mmHg f) Lit,[4a] 109.5—110°C. g) Lit[7] 49—50°C.

all the silicon and oxygen atoms in the same plane of benzene ring and the other in which only the six oxygen atoms lie in the plane of the ring leaving the six silicon atoms outside (alternatively above and below) the plane. Low temperature NMR study was carried out in the hope of obtaining information on the non-equivalent methyl groups which might arise. However, the one sharp singlet (τ 9.86 in CCl_4 at room temperature) remained unchanged even at −100°C (in ether-pentane). This could be accounted for in different way, such as (a) as being due to the methyl protons lying too far apart to be affected by aromatic π-electrons or (b) to free rotation about the bonds in trimethylsilyl groups. No conclusive evidence of the structure of X has so far been obtained.

The reductive silylation has been proven to be a good synthetic method for compounds such as X and XI which might be otherwise difficult to obtain.

Experimental

The starting materials, ketone, diketones, and quinones were commercially available except for *trans*-1,2-dibenzoylethylene.[13] All the reactions were carried out under dry nitrogen. Boiling and melting points were uncorrected.

General Procedure. To a rapidly stirred mixture of 0.1 mol of carbonyl compound and potassium (0.1 g atom for I and 0.2 g atom for II—IV, and VI, and 0.4 g atom for V) in an appropriate solvent was added a slight excess of trimethylsilyl chloride (above the amount of potassium used) over a period of 2 hr at 60—70°C. The reaction mixture was then cooled to room temperature and left to stand overnight. Filtration of potassium chloride followed by evaporation of the solvent afforded the product mixture. This was found to contain merely starting carbonyl compounds in the case of Expts. 3 and 4 (in benzene). In Expts. 1, 4 (in THF), 5, and 6, the resulting product mixture was solids and was recrystallized from hexane to give pure silylated compounds VII, IX, X, and XI, in the yields shown in Table 1. In Expt. 2, the product mixture was a yellow liquid which on standing partially crystallized. The solids were collected by filtration and crystallized from hexane to give VIIIb, colorless rhombic crystals. The filtrate was distilled under reduced pressure and afforded VIIIa, a colorless liquid, bp 160—161°C/8 mmHg. The *cis*/*trans* ratio was determined from the NMR spectrum of the mixture.

The authors are indebted to Shin-etsu Kagaku Kogyo Co. Ltd. for the supply of trimethylsilyl chloride.

13) R. E. Lutz, "Organic Syntheses," Coll. Vol. III, p. 248 (1955).

Bromine Addition to Cyanonorbornene Derivatives[1]

Shōichi KIKKAWA, Masakatsu NOMURA, Yōichirō UNO,
Masaaki MATSUBARA, and Yūji YANAGIDA
Department of Applied Chemistry, Faculty of Engineering, Osaka University, Yamadakami, Suita
(Received October 30, 1971)

The addition reactions of *endo*-5-cyanonorbornene, *trans-endo,exo*-5,6-dicyanonorbornene, *cis-endo*-5,6-dicyanonorbornene, and *cis-exo*-5,6-dicyanonorbornene with bromine have been studied. The assignments of the configurations of bromine adducts were determined mainly on the basis of the NMR spectra. As to *trans-endo,exo*-5,6-dicyanonorbornene, reaction mixtures have been found to contain *trans* and *exo-cis* adducts. The reaction conditions involving the proportions of these isomers and a rationale for the formation of the *exo-cis* adduct are discussed. *cis-endo*-5,6-Dicyanonorbornene and *cis-exo*-5,6-dicyanonorbornene gave the *exo-cis* adduct and the *trans* adduct respectively. The stereochemistry of bromine atoms may be explained in terms of a steric factor. A kinetic study showed that these addition reactions in solution in acetic acid obey the second-order rate law and that the magnitudes of the rate constants are in the order; *cis-exo*-5,6-dicyanonorbornene>*trans-endo,exo*-5,6-dicyanonorbornene>*cis-endo*-5,6-dicyanonorbornene.

Recently Traylor[2] noted that *cis*-electrophilic additions to a wide variety of bicycloheptene structures have been established and that several explanation have been proffered for the observation of *exo-cis* additions to norbornenes—the twist-strain theory, molecular electrophilic addition, torsional effects, and so on.

However, concerning halogen additions to norbornene derivatives bearing electronegative substituents, much attention has been paid only to the bromination of the cyclopentadiene–maleic anhydride adduct.[3-5] Kwart and Kaplan[5] explained the *exo-cis* addition of bromine to the *endo*-adduct on the basis of steric hindrance or *endo*-carbonyl participation.

As part of a study of the electronic and steric effects in the stereochemistry of halogen additions to norbornene derivatives, we have investigated the halogenation of four cyanonorbornenes, *endo*-5-cyanonorbornene, *trans-endo, exo*-5,6-dicyanonorbornene, *cis-endo*-5,6-dicyanonorbornene, and *cis-exo*-5,6-dicyanonorbornene. First, the confirmation of the halogen adduct and the structural assignment have been studied; secondly, in order to study the reactivity of bromine to four substrates, the kinetics of bromination in dry acetic acid have been investigated and the magnitudes of the rate constants have been deduced by the second-order approximate treatment of the resulting kinetic data.

Experimental[6]

Reagents. *a)* endo-*5-Cyanonorbornene (Substrate I)*: The procedure of Alder, Heimbach, and Reubke[7] was followed, using 1 mol of freshly-distilled cyclopentadiene (67 g) and 1 mol of acrylonitrile (53 g). The resulting reaction mixture was separated into the *exo*-adduct (bp 81—84°C/10.5 mmHg, 18 g; lit,[7] 80—85°C/12 mmHg) and the *endo*-adduct (bp 99°C/26 mmHg, 37 g; lit,[7] 88°C/12 mmHg) by fractional distillation. Both adducts were confirmed to be more than 99% pure by glc analysis.

b) trans-endo,exo-*5,6-Dicyanonorbornene (Substrate II)*: The procedure of Blomquist and Winslow[8] was followed. From 0.1 mol (7.8 g) of fumaronitrile prepared in the usual way and 0.11 mol (9 m*l*) of cyclopentadiene in 50 m*l* of ethanol, we obtained 11.5 g (83%) of the substrate II, which showed a mp of 103—104°C (lit,[8] 95.5—96°C) on recrystallization from ethanol. (Found: C, 74.77; H, 5.59; N, 19.08%.)

c) cis-endo-*5,6-Dicyanonorbornene (Substrate III) and* cis-exo-*5,6-Dicyanonorbornene (Substrate IV)*: As the crude malenitrile prepared from maleamide as described by Blomquist[8] contained considerable amounts of fumaronitrile and another component, malenitrile (mp 30—32°C, lit,[8] 30—31°C) was purified by liquid-column chromatography (elute, benzene; silica gel, 100 mesh). Gas chromatography indicated a purity of 99%. The procedure of Blomquist[8] was followed using 0.02 mol (1.56 g) of malenitrile and 0.024 mol (2 m*l*) of cyclopentadiene. The fractional recrystallization of the resulting reaction mixture gave 2.0 g of the *endo* adduct, which was also confirmed to be pure by a comparison with the NMR spectrum of the crude adduct in d_6-DMSO (mp 163—165°C; Found: C, 74.77; H, 5.52; N, 19.33%; lit,[8] 155—156°C) and 0.2 g of the *exo* adduct (mp 108—110°C; lit,[9] 108—110°C).

Bromination of Substrate I with Bromine. A solution of bromine (8.0 g, 0.05 mol) in 25 m*l* of carbon tetrachloride was stirred, drop by drop, into a solution of Substrate I (6.0 g, 0.05 mol) in 50 m*l* of carbon tetrachloride over a 30-min period at 0°C. After the stirring had been continued for an additional 3 hr, a solid separated. This material[10] weighed 10.5 g; it was recrystallized from ethanol (mp 154—156°C) and confirmed to be dibromide by elemental analysis

1) Presented at the 24th Annual Meeting of the Chemical Society of Japan, Osaka, April, 1971; Proceedings, Vol. III, p. 1562.
2) T. G. Traylor, *Accounts Chem. Res.*, **2**, 152 (1969).
3) H. Kwart and L. Kaplan, *J. Amer. Chem. Soc.*, **75**, 3356 (1953).
4) J. A. Berson, *ibid.*, **76**, 4060 (1954).
5) H. Kwart and L. Kaplan, *ibid.*, **76**, 4078 (1954).
6) All the melting points were determined on a Yanagimoto micromelting point apparatus and are uncorrected. The infrared spectra were recorded on a Hitachi EPI-2G apparatus, while the NMR spectra were obtained with a JNM-3H-60 spectrometer, using TMS as the internal standard. The mass spectra were measured with a Hitachi-RMU-6E instrument operating at 70 eV.
7) K. Alder, K. Heimbach, and R. Reubke, *Chem. Ber.*, **91**, 1516 (1958).
8) A. T. Blomquist and E. C. Winslow, *J. Org. Chem.*, **10**, 149 (1945).
9) J. Sauer, H. Wiest, and A. Mielert, *Chem. Ber.*, **97**, 3183 (1964).
10) Abbreviated as I-*t* hereafter.

and by a study of its mass spectrum. The stereochemistry of the bromine atoms was estimated to be *trans* by studying the NMR spectrum. Found: C, 34.64; H, 2.98; N, 5.20%; Calcd for $C_8H_9NBr_2$: C, 34.45; H, 3.25; N, 5.20%; M^+: 277 (1), 279 (2), 281 (1).[11]

NMR spectrum (in $CDCl_3$): τ: 6.35 [2H, m, W_h (band width at half-height)]=*ca.* 4 Hz, H-*endo* 5 and H-*endo* 6,[12] 7.00 (2H, d,q,. J=4.6, 5.4, and 1.8 Hz, H-*exo* 5 and H-*exo* 6), (in d_6-DMSO): τ: 5.65 (2H, m, W_h=*ca.* 4 Hz) 5.88 (2H, d,t,. J=4.6, 5.4, and 1.8 Hz).

Chlorination of Substrate I with Chlorine. Chlorine gas (3.6 g, 0.05 mol) was passed through a solution of Substrate I (8.0 g, 0.05 mol) in 50 m*l* of carbon tetrachloride with stirring over a period of about one hour at 0°C.

The crystalline product (5.0 g) was separated by filtration on a glass filter, and the filtrate was evaporated to dryness; this afforded a small amount of an oily product (about 1.0 g). The crystalline product purified by means of liquid-column chromatography (elute, chloroform; silica gel, 100 mesh) (mp 141—143°C) was confirmed to be dichloride by elemental analysis and by a study of the mass spectrum. The stereochemistry of chlorine atoms of the dichloride was identified as *trans* on the basis of the similarity of its NMR spectrum with that of the dibromide. Found: C, 50.75; H, 4.70; N, 7.30%; Calcd for $C_8H_9NCl_2$: C, 50.75; H, 4.77; N, 7.36%. M^+: 189 (9), 191 (6), 193 (1).

The oily product when distilled yielded a distillate boiling at 93°C/10^{-3} mmHg (0.6 g). The gas-chromatographic separation of the distillate afforded a colorless liquid which was estimated to consist of *endo*-5-cyano-*anti* or *syn*-7-chloronorbornene (23%) and 5-chloro-2-cyano-nortricyclene (77%) by means of elemental analysis and a study of the mass spectrum and NMR spectrum ($CDCl_3$). Found: C, 62.30; H, 4.75; N, 9.23%. Calcd for C_8H_8NCl: C, 62.56; H, 5.25; N, 9.12%. M^+: 153 (3), 155 (1).

Assignments of the Spectral Data of the Liquid Product. *endo*-5-Cyano-*anti* or *syn*-7-chloronorbornene; H_1, H_2 protons, 3.84 ppm, H_7 proton, 5.85 ppm. $C_5H_5Cl^+$: 110 (3), 112 (1), retro Diels-Alder fraction.[16] 5-Chloro-2-cyano-nortricyclene; H_5 proton, 5.67 ppm. IR, 805 cm^{-1} (800—810 cm^{-1})[17] characteristic absorption of nortricyclene.

Bromination of Substrate II with Bromine. A few milliliters of a bromine solution containing 8.0 g of bromine in 25 m*l* of carbon tetrachloride was stirred into a solution of Substrate II (7.5 g, 0.05 mol) in 50 m*l* of carbon tetrachloride, but the bromine color did not disappear immediately; therefore, the residual bromine solution was added under reflux over a period of 30 min, and the stirring was continued for an additional 4 hr. The separated crystalline compound (10.0 g) was filtered from a hot reaction solution and recrystallized from benzene; mp 205—206°C.[18] The stereochemistry of bromine atoms was estimated to be *exo-cis* on the basis of NMR spectrum in the d_6-DMSO solution. Found: C, 35.64; H, 2.68; N, 9.20%; Calcd for $C_9H_8Br_2N_2$: C, 35.56; H, 2.65; N, 9.22%; M^+: 302 (1), 304 (2), 306 (1).

The above procedure was also followed on the same scale in an acetic acid solution at 30°C. The residue resulting after the evaporation of the acetic acid was recrystallized from benzene; mp 150—180°C (9.7 g). This material (2.0g) was dissolved in 20 m*l* of hot ethanol, and the less soluble material filtered while still hot was recrystallized from toluene (mp 206.5—207.5°C (0.2 g)), corresponding to the *exo-cis* adduct. Then the crystalline compound which separated on standing from the ethanol mother liquor was once more dissolved in about 15 m*l* of hot ethanol. The less soluble material was removed by filtration, whereupon about 0.8 g of crystals separated from the ethanol mother liquor. The resulting solid was recrystallized from ethanol; mp 138—140°C (0.5 g). The stereochemistry of bromine atoms in this adduct[19] was estimated to be *trans* on the basis of the NMR spectrum in the d_6-DMSO solution. [τ: 5.22 (1H, d, d,. J=3.8 and 4.5 Hz, H-*exo* 5 or H-*exo* 6), 5.89 (1H, t, J=~3.0 Hz, H-*endo* 6 or H-*endo* 5), 6.16 (1H, t, J=4.5 Hz, H-*exo* 2), 6.50 (1H, d, d,. J=2.1 and 5.0 Hz), 7.06 (2H, m, H-1 and 4), 7.81 (1H, forming the one part of the AB system, H-7a), 8.10 (1H, forming the other part of the AB system, H-7b)]. Found: C, 35.75; H, 2.63; N, 9.37%. Calcd for $C_9H_8Br_2N_2$: C, 35.56; H, 2.65; N, 9.22%.

Bromination of Substrate III with Bromine. Substrate III (1.44 g, 0.01 mol) dissolved in 90 m*l* of acetic acid was treated with 1.9 g (0.012 mol) of bromine dissolved in 30 m*l* of acetic acid. After stirring had been continued for three days at room temperature, a crystalline product separated. This material weighed 2.2 g and was identified as a crude *exo-cis* adduct (mp 289—290°C[20] (recrystallized from 1-propanol)). Found: C, 35.83; H, 2.60; N, 9.04%. Calcd for $C_9H_8N_2Br_2$: C, 35.56; H, 2.65; N, 9.22%. The mother liquor was evaporated to dryness, leaving a further quantity (0.2 g) of the *exo-cis* adduct, as was confirmed by the NMR spectrum (see Table 3).

Bromination of Substrate IV with Bromine. A solution of bromine (0.019 g, 0.012 mol) in 5 m*l* of acetic acid was added to a dark brown measured flask containing a solution of Substrate IV (0.145 g, 0.01 mol) in 17 m*l* of acetic acid, and then the mixture was allowed to stand at 30°C for 3 hr. After the end of the reaction, the solvent was evaporated and the resulting product was recrystallized from ethanol; mp 179—182°C[21] (0.15 g). The stereochemistry of bromine atoms was confirmed to be *trans* on the basis of the NMR spectrum of the d_6-DMSO solution (see Table 3). Found: C, 35.63; H, 2.66; N, 9.33%. Calcd for $C_9H_8N_2Br_2$: C, 35.56; H, 2.65; N, 9.22%.

Determination of the Rate of Addition. The rate of addition was determined by the titration method which was similar to that of Buckles and his co-workers.[22]

Solutions of the substrate in about 80 m*l* of acetic acid were warmed to bath temperature in a 100-m*l*, dark brown, measured flask, into which a stock solution of bromine in acetic acid was then pipetted and mixed. The acetic acid was then rapidly added to make a vloume of 100 m*l*. At appropriate intervals, 5.0-m*l* samples were pipetted into a

11) The number in brackets shows the ratio of the peak strength.

12) If the stereochemistry of the two bromine atoms is assumed to be *exo-cis*, the broad absorption (W_h=4 Hz) at 6.35 ppm can not be explained on the basis of the reported magnitude of the *endo-endo* coupling constants (approximately 6—7 Hz);[13-15] therefore, the stereochemistry was suggested to be *trans*.

13) P. Laszlo and R. Schlever, *J. Amer. Chem. Soc.*, **86**, 1171 (1964).

14) C. Davis, Jr., and T. V. Van Auken, *ibid.*, **87**, 3900 (1965).

15) L. M. Jackman and S. Sternhell, "Applications of Nuclear Magnetic Resonance Spectroscopy in Organic Chemistry," ed. by D. H. R. Barton and W. Doering, Pergamon Press, New York, N. Y. (1969), p. 289.

16) S. J. Cristol, R. A. Sanchez, and T. C. Morrill, *J. Org. Chem.*, **31**, 2738 (1966).

17) J. D. Roberts, E. R. Trumbull, J. W. Bennett, and R. Armstrong, *J. Amer. Chem. Soc.*, **72**, 3116 (1950).

18) Abbreviated as II-*c* hereafter.

19) Abbreviated as II-*t* hereafter.

20) Abbreviated as III-*c* hereafter.

21) Abbreviated as IV-*t* hereafter.

22) R. E. Buckles, J. L. Miller, and R. J. Thurmaier, *J. Org. Chem.*, **32**, 888 (1967).

flask containing 50 ml of a 2.5% KI methanol solution. The flask was swirled 5 times and then allowed to stand for 1 min, after which the iodine was titrated with a standard thiosulfate solution (1/50N) with a starch indicator.

The time for the start of the reaction was taken as the time at which half of the bromine solution was out of the pipet. The time for the stop of the reaction was determined in a manner similar to that used for the start of the reaction.

In the case of Substrate IV, rate-measurements experiments were carried out on the scale of one-fifth, as in the above description.

Assignment of Spectral Lines. In Fig. 1 are shown the decoupled spectra of compound II-*c* (mp 206.5—207.5°C) in the d_6-DMSO solution obtained using the frequency-sweep technique (Hitachi-R 20—60 spectrophotometer).[23] Part A shows the normal spectrum. The absorption at τ 7.05 is readily identified as the result of the bridge-head protons by means of the broad patterns resulting from several coupling interactions. The low-field absorption centered at τ 5.35 (doublet of quartets) is also identified as the result of two hydrogens attached to the brominated carbons on the basis of its chemical shifts[24] and integrated areas. The absorption at τ 8.03 shows the C_7 AB pattern. On the basis of the discussion presented above, the two residual absorptions at τ 6.30 and τ 6.63 are assigned as 2-*endo* or 3-*exo* hydrogens. Part B shows the spectrum obtained upon the irradiation of the C_1, C_4 protons at τ 7.05. First, the appearance of the upfield part of the C_7 AB pattern changes to a triplet of doublets. The coupling constant values (1.8 Hz) are reasonable as a zigzag, long-range coupling. Secondly, the irradiation at τ 7.05 alters the pair of doublets at τ 6.30 to only one doublet in order to remove 4.5 Hz coupling. The value of 4.5 Hz corresponds to the coupling between the bridge proton C_1 or C_4 and the C_2 *exo* or C_3 *endo* proton respectively, since the absorption at τ 6.30 may be assigned to either the 2-*exo* or 3-*endo* proton. The magnitude of the coupling between the C_4 proton and the C_3 *endo* proton was expected to be almost zero because of the unfavorable vicinal dihedral angle,[25] so the resonance at τ 6.30 is confirmed as the 2-*exo* proton. Thus the 4.5 Hz coupling between the C_1 and C_2 *exo* protons is established. The irradiation of the upper-field part of the C_7 AB pattern (Part C in Fig. 1) eliminates the splitting, 1.8 Hz, of C_5, C_6 hydrogens at τ 5.35. By combining the results of Part B and Part C, the 1.8 Hz splitting is established as a zigzag, long-range coupling between C_5 *endo* or C_6 *endo* hydrogen[26] and C_{7b} hydrogen. Thus, $J_{5\text{-}endo,\ 6\text{-}endo}$ and $J_{7b,7a}$ are confirmed to be 6.3 Hz and 11.7 Hz respectively. Therefore, the stereochemistry of bromine atoms is established as *exo-cis*.

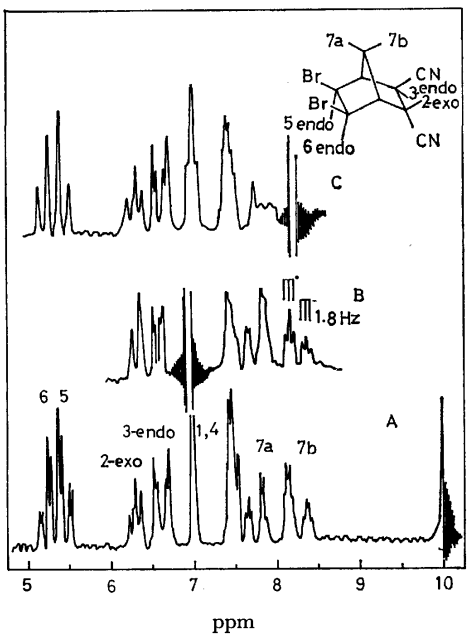

Fig. 1. NMR spectra of compound II-*c* in solution in d_6-DMSO A: normal; B: decoupled from protons 1,4; C: decoupled from proton 7b.

The stereochemistry of compound II-*t* is established as *trans* on the basis of the decoupling experiments involving

Table 1. Chemical shifts[a] and coupling constants (Hz)

Compound	2	3	1, 4[b]	5	6	7a	7b
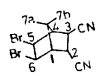	6.31	6.61	7.05	5.44	5.26	7.80	8.26
	$J_{7a,\ 7b}$=11.7, $J_{5\text{-}endo,\ 6\text{-}endo}$=6.3, $J_{2\text{-}exo,\ 3\text{-}endo}$=5.7, $J_{2\text{-}exo,\ 1}$=4.5, $J_{7b,\ 5\text{- or }6\text{-}endo}$=1.8.						
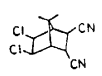	6.25	6.62	7.13	5.50	5.31	7.89	8.29
	$J_{7a,\ 7b}$=12.0, $J_{5\text{-}endo,\ 6\text{-}endo}$=6.3, $J_{2\text{-}exo,\ 3\text{-}endo}$=5.4, $J_{2\text{-}exo,\ 1}$=5.4, $J_{7b,\ 5\text{- or }6\text{-}endo}$=2.1.						
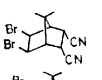	6.31	6.31	7.03	5.28	5.28	7.87	8.38
	$J_{7a,\ 7b}$=10.8, $J_{7b,\ 5\text{- or }6\text{-}endo}$=2.4.						
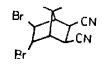	6.37	6.37	7.05	5.84	5.30	7.75	8.01
	$J_{7a,\ 7b}$=11.8, $J_{7b,\ 5\text{-}endo}$=2.1, $J_{5\text{-}endo,\ 6\text{-}exo}$=3.9, $J_{6\text{-}exo,\ 1}$=3.9.						

a) Values are shifts in τ-units.
b) Chemical shifts represent the positions of band centers.
c) The stereochemistry was estimated on the basis of the similarity of NMR spectrum of the material (small quantity, broad range of mp near 124°C) obtained from chlorination of substrate II in hot CCl_4 solution to that of compound II-*c*.

23) Measurements were carried out by Mr. Yoshio Takai of The Institute of Scientific and Industrial Research, Osaka University.
24) P. M. Subramanian, M. T. Emerson, and N. A. Lebel, *J. Org. Chem.*, **30**, 2624 (1965).
25) M. Karplus, *J. Chem. Phys.*, **30**, 11 (1959).
26) The low-field peak (τ 5.26) among C_5, C_6 *endo* protons may be assigned to the C_6 *endo* proton since the C_6 *endo* proton is favorably situated for shielding by the C_2 *endo* cyano group;[27] this explanation seems to be in good agreement with the fact that two C_5, C_6 *endo* protons of III-*c* show a signal at τ 5.28 (in d_6-DMSO).
27) J. M. Jackman and G. Y. Sarkis, This Bulletin, **42**, 1179 (1969).

trans-5-chloro-6-iodo-*trans*-2,3-norbornanedicarbonitrile[28] and the arguments presented in Footnote[12], but the question of whether the C_6 proton is *exo* or *endo* remains unresolved and is now under investigation. Therefore, the absorptions of the appearance of a triplet at τ 5.89 and τ 6.16 (described before) are substantially duplicates of two doublets, so the coupling constants, 5.0, 2.1, 4.5, and 3.8 Hz, can be assigned to $J_{2\text{-}exo,3\text{-}endo}$, $J_{7a,3\text{-}endo}$, $J_{5\text{-}exo,4}$ (or $J_{6\text{-}exo,1}$), and $J_{5\text{-}exo,6\text{-}endo}$ (or $J_{5\text{-}endo,6\text{-}exo}$) respectively.

The stereochemistry of compound III-*c* is confirmed to be *exo-cis* as follows. The doublet (1.8 Hz splitting) at τ 5.28 corresponds to C_5, C_6 hydrogens attached to the carbons bearing bromine atoms, as is shown by the chemical shifts and integrated areas, so it is reasonable to consider that the 1.8 Hz coupling may be attributed to the long-range coupling between C_5 *endo* or C_6 *endo* and C_{7b} hydrogen. The stereochemistry of compound IV-*t* is confirmed *trans* in a way similar to that used for compound II-*t*. The assigned chemical shifts and coupling constants are listed in Table 1.

Discussion

Fortunately, the rates of bromine addition to Substrates II, III, and IV in the measurable region could be obtained by the conventional titration method. The concentrations of bromine against the reaction time are plotted in Fig. 2 for the addition reactions of bromine to Substrates II, III, and IV. The finding on *cis-endo*-5,6-norbornene-carboxylic anhydride (Substrate V) is also plotted for the sake of comparison. Figure 2 shows that the reactivity falls in this sequence; Substrate IV>II>III≃V, indicating that the *endo* orientation of cyano groups retards the addition reactions of bromine. The stereochemical results obtained here would seem to suggest that, in this addition reaction, *exo*-substituents exert such a steric influence on the rate-determining transition state as to reduce the rate of addition; that is, it may be considered that the entering bromide ion in the transition state may be sterically hindered by the *endo*-cyano group so

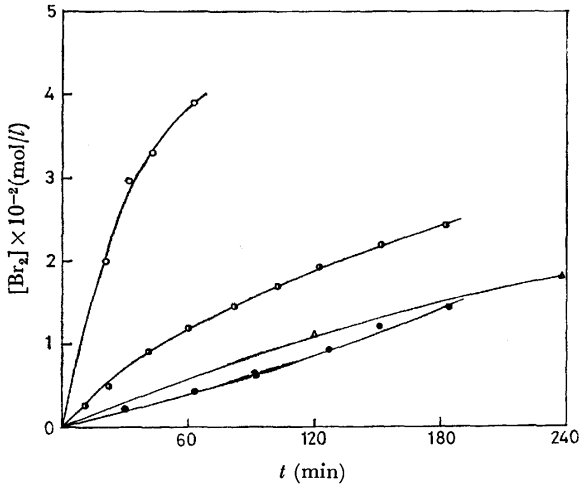

Fig. 2. Plots of consumed bromine against time for bromine addition reactions
○: Substrate IV (29.8°C); △: Substrate III (29.9°C);
◑: Substrate II (30.1°C); ●: Substrate V (30.0°C).

28) The NMR spectrum of this compound will be discussed in detail elsewhere.

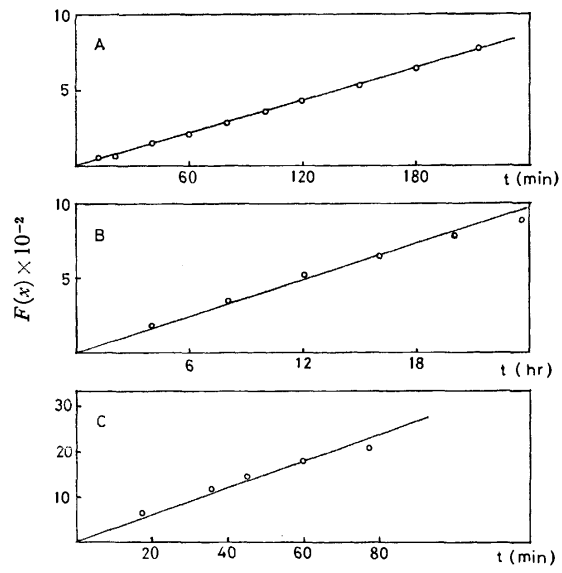

Fig. 3. Typical plots of second-order bromination rates
A: Data for substrate II at 30.1°C (*a*: 6.072×10^{-2} mol/*l* *b*: 4.995×10^{-2} mol/*l*) B: Data for substrate III at 29.9°C (*a*: 5.991×10^{-2} mol/*l*, *b*: 4.960×10^{-2} mol/*l*) C: Data for substrate IV at 29.8°C (*a*: 5.994×10^{-2} mol/*l*, *b*: 4.970×10^{-2} mol/*l*) $F(x)=\log[b(a-x)/a(b-x)]$ a=initial bromine concentration, b=initial substrate concentration, x=bromine reacted at time t.

that the *endo* orientation of substituents may produce a much greater rate reduction. This explanation[29] does not contradict the kinetic results to be described below.

Figure 3 shows the rate data treated by a second-order rate equation ($dx/dt=k\times[Br_2]\times[Sub]$).

Table 2. Rate constants for bromination of substrates (II, III, and IV) in acetic acid

Substrate	Temp (°C)	10^4 k (*l*/mol sec)	Concentration (mol/*l*)
II	30.1	12.78 (52.0)[a]	0.05
	29.9	16.90 (52.0)	0.05
	19.9	8.84 (42.7)	0.05
	20.0	17.07 (80.8)	0.1
	30.1	26.32 (89.0)	0.1
III	29.9	6.05 (60.0)	0.05
	19.9	1.59 (32.8)	0.05
IV	29.8	121.5 (79.0)	0.05
	28.9	122.3 (78.1)	0.05
V	30.0	5.17 (27.4)	0.05
	29.9	7.28 (37.9)	0.05

a) Numbers in brackets indicate the percentage of completion where plots of log $[b(a-x)/a(b-x)]$, *versus* time were linear.

29) Kwart and Miller,[30] in a kinetic study of the addition of 2,4-dinitrobenzenesulfenyl chloride to *cis-exo*-5,6-norbornene-carboxylic anhydride and Substrate V in glacial acetic acid, have explained the lower reactivity of the latter in terms of the field effect, by which they suggested that the nucleophilic character of the double bond may be reduced preferably in the case of the *endo*-anhydride. This view corresponds to the situation in which the *exo*-side attacking of a reagent and the formation of the intermediate cation may be the rate-determining steps.

30) H. Kwart and L. J. Miller, *J. Amer. Chem. Soc.*, **83**, 4552 (1961).

Table 3. Bromination of substrates (II, III, and IV)

Substrate	Solvent	Reaction time	Temp (°C)	Yield (%)	*cis* (%)	*trans* (%)
II	CCl_4	2 hr	76.8	89	67	33
	CCl_4	24 hr	30.0	96[a)]	54	46
	AcOH	6 hr	20.0	100[a)]	23	77
	AcOH	2.5 hr	28.9	90[a)]	24	76
	AcOH	5.5 hr	39.5	100[a)]	45	55
III	AcOH	3 days	room temp	80	100	0
IV	AcOH	3 hr	30.0	55	11	89

a) A solution of bromine (1.76 g 0.011 mol) in 90 m*l* acetic acid and substrate II (1.44 g, 0.01 mol) were introduced in a dark brown measured flask immersed in the aquarium provided with a mercury thermoregulator. The crude product obtained after removal of acetic acid was washed with *n*-hexane to remove a trace of acetic acid and submitted to quantitative analysis.

As to Substrate II, the data were best fitted by the second-order rate law, but the plots of the rate data of Substrate III treated by the second-order rate law show a slight downward trend while the plots of the rate data of Substrate IV treated by the second-order rate law also show a downward trend. However, in the present study, it is considered reasonable, in attempting to know the order of magnitude of rate constants, to assume that the rate approxinately fits the second-order rate law.[31)]

The rate constants deduced above are summarized in Table 2. The bromination of Substrate II was also carried out in carbon tetrachloride, but in this solvent no such clean-cut results were obtained. A relatively rapid consumption of bromine was observed after an arbitrary interval from the start of reaction, suggesting that the reaction in this solvent was homolytic. This trend (homolytic) was also observed in the bromination of Substrate II in acetic acid at 39.5°C.

Table 3 summarizes the approximate compositions of the dibromide mixtures obtained under various reaction conditions; they were calculated on the basis of a NMR-spectra analysis in the d_6-DMSO solution.

Table 3 shows that, in a carbon tetrachloride solution, the *exo* adduct of Substrate II predominates over the *trans* adduct of Substrate II, and this reaction in carbon tetrachloride is found to show a partial homolytic character, as was discussed in the part concerning rate study. In acetic acid at 39.5°C, where the bromination was considered to be partially homolytic on the basis of the rate study, the proportion of the *exo-cis* adduct increased. This type of observation of an *exo-cis* adduct increase with an increase in the homolytic character has been reported by Berson and his coworkers[4,32,33)] for the bromination of the maleic anhydride adduct of furan and cyclopentadiene. As to the bromination of the anhydride adduct of furan, only a *trans* adduct was obtained in a polar solvent such as acetic acid.

However, in the present study, the *exo-cis* adduct (23—24%) has been obtained with a residual *trans* adduct in acetic acid at 20 or 30°C.

Judging from the rate data at 20 or 30°C, the reaction in acetic acid may be considered to proceed by the heterolytic mechanism, so the formation of the *exo-cis* adduct may be explained by the steric concept that the attacking reagent bromide ion suffers a repulsive, non-bonded interaction with the *endo* cyano group of Substrate II in the *endo* direction. The stereochemistry of the bromine addition of Substrates III and IV shown in Table 3 may be explained in terms of the steric hindrance described above.

31) When treated by a third-order rate equation ($dx/dt = k \times [Br_2]^2 \times [Sub]$), the rate data gave less precise results.

32) J. A. Berson and R. Swiuler, *J. Amer. Chem. Soc.*, **75**, 4366 (1953).

33) J. A. Berson, *ibid.*, **76**, 5748 (1954).

Peptides Containing Aminophosphonic Acids. I. Reactivity of α-Aminobenzylphosphonic Acid

Kiyoshi YAMAUCHI, Masayoshi KINOSHITA, and Minoru IMOTO*

Department of Applied Chemistry, Osaka City University, Sumiyoshi-ku, Osaka

(Received January 14, 1972)

The chemical reactivity of α-aminobenzylphosphonic acid was investigated in order to survey the methods for incorporating aminophosphonic acids into a peptide chain. The investigation revealed that i) a dipeptide analog linked with a phosphonamide bond could be produced by the reaction of *C*-protected amino acid with the *N*-protected aminophosphonomonochloridate, and that ii) amino groups of the aminophosphonic acid possessed a reactivity similar to those of amino acids, and were capable of coupling with *N*-protected amino acids by means of dicyclohexylcarbodiimide.

Since the recent discovery of β-aminoethylphosphonic acid from sea animals, such as rumen protozoa and anthopleura elegantissima,[1,2] the aminophosphonic acids have attracted considerable biological interest not only because of their structural similarity to amino acids, but also because of their excellent metal-chelating properties, especially for calcium and ferric ions.[3]

This paper is concerned with the reactivity of aminophosphonic acids, and α-aminobenzylphosphonic acid was employed as a model compound to search the route for the preparation of phosphorus analogs of enzymes or peptides, which are chemically modified by replacing some amino acids with their phosphonic acid analogs or by inserting aminophosphonic acids into a peptide chain, as is shown below (I). α-Aminobenzylphosphonic acid can be obtained in a sizable quantity from a simple reaction of benzaldehyde, diethyl phosphite, and ammonia.[4]

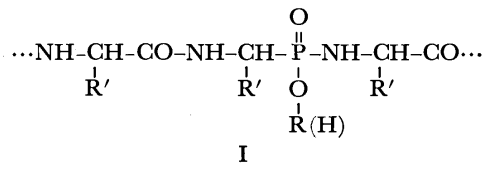

I

Results and Discussion

As in peptide synthesis, the reactivity of aminophosphonic acids for the following four steps must be studied in order to construct peptides with aminophosphonic acids; i) the protection of the amino and the phosphonic acid groups, ii) the activation of the phosphonic acid group, iii) coupling reactions to form an amide bond or a phosphonamide bond, and iv) the removal of the protecting groups.

For Step i, when diethyl α-aminobenzylphosphonate (II), in which the phosphonic acid function is already blocked by ethyl groups, was treated with the usual

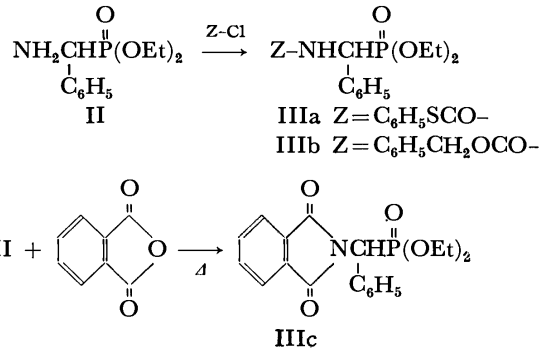

masking reagents for the amino group[5] (*e.g.* thiophenoxycarbonyl chloride, benzyloxycarbonyl chloride, and phthalic anhydride), the corresponding *N*-protected derivatives (IIIa—c) were produced in 79%, 98%, and 51% yields respectively. These results and a coupling reaction with a free carboxyl group, which will be described later, indicate that amino groups of aminophosphonic acids have reactivity similar to those of amino acids.

The removal of ethyl groups was then attempted from phosphonic acid groups of these compounds. Thus, IIIa, upon treatment with HCl-acetic acid, produced IVa, whereas upon alkaline hydrolysis IIIa only underwent decomposition.

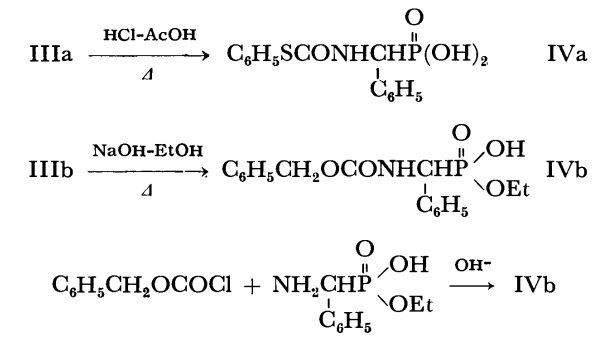

On the other hand, when IIIb was treated with an ethanolic sodium hydroxide solution, the half ester (IVb) was generated; this half ester could also be synthesized through the reaction of ethyl hydrogen α-aminobenzylphosphonate with benzyloxycarbonyl chloride.

These *N*-protected aminobenzylphosphonic acid

* Present address: Department of Applied Chemistry, Kansai University, Suita, Osaka.

1) M. Horiguchi and M. Kandatsu, *Nature*, **184**, 901 (1959).

2) J. S. Kettredge, E. Roberts, and D. G. Simmon, *Biochemistry*, **1**, 624 (1963).

3) A. D. F. Toy and E. Uhing, Div. of Organic Chemistry, American Chemical Society Meeting, New York, September, 1963.

4) M. E. Chalmers and G. M. Kosolapoff, *J. Amer. Chem. Soc.*, **75**, 5278 (1953).

5) J. P. Greenstein and M. Winitz, "Chemistry of the Amino Acids", Vol. 2. John Wiley & Sons Inc., New York, N.Y. (1961).

derivatives, however, did not condense to form any phosphonamide with ethyl glycinate by means of dicyclohexylcarbodiimide (DCC).

$$\text{IVa or IVb} + NH_2CH_2CO_2C_2H_5 \xrightarrow{DCC} \text{No reaction}$$

Therefore, another route was estimated–the activation of the phosphonic acid group of II (Step ii) through its conversion to its phosphonochloridate. This transformation was easily accomplished by the reaction of IIIc with a slight excess of phosphorus pentachloride, thus producing ethyl phthalimidobenzylphosphonochloridate (V). The process is quite similar to that used for chlorination of phthalylamino acids with the same reagent.[6]

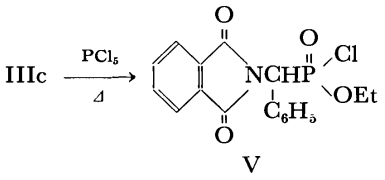

V

When the chloride (V) was subsequently allowed to react with ethyl glycinate, the dipeptide (VI) was formed in a 70% yield (Step iii), showing the extension of peptides from phosphinyl to amino groups.

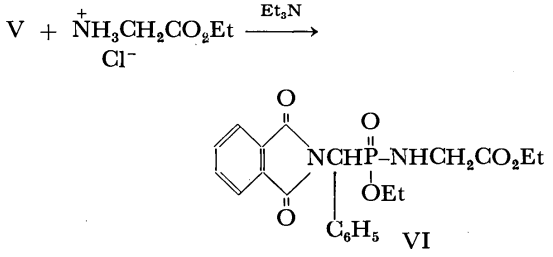

VI

The remaining step necessary for the introduction of aminophosphonic acids into a peptide chain is to place an amino acid to the left of the aminophosphonic acid. This process was examined by the reaction of II with *N*-protected amino acids, using DCC. The successful formation of the dipeptide analogs (VIIa—b) in 74—95% yields ensures that a peptide linkage can be obtained by procedures similar to those employed in the usual peptide synthesis.[5,7]

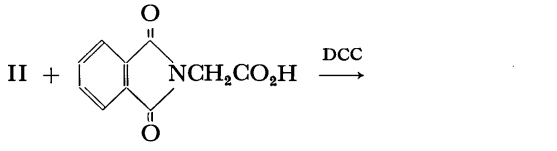

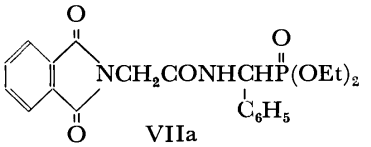

VIIa

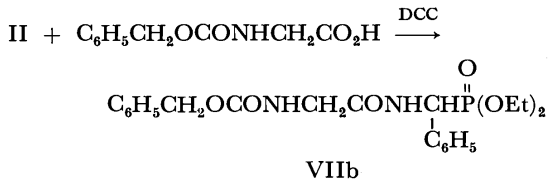

VIIb

Using the experimental results above obtained, we have studied the synthesis of tripeptides with aminomethylphosphonic acid in the center. These results and the attempted removal of the protecting groups (Step iv) will be discussed in a subsequent paper.

Experimental

The melting points (mp) are uncorrected. The infrared spectra were measured by means of a Jasco, Model IR-G spectrometer. The nuclear magnetic resonance spectra (NMR) were recorded with a Hitachi-Perkin-Elmer appratus, Model R-20.

Preparation of Diethyl α-Aminobenzylphosphonate (II). The hydrochloride of II was synthesized according to the procedure of Chalmers and Kosolapoff[4] using benzaldehyde (25.4 g, 0.24 mol), diethyl phosphite (33.0 g, 0.24 mol), and ammonia (excess); mp 158—159°C, 26.4 g, 40% (lit,[4] 159—160°C, 31%).

To the hydrochloride of II (10.0 g, 0.036 mol) suspended in ether (70 m*l*) was added 4N sodium hydroxide, keeping the temperature of the mixture below 3°C with an ice–water bath. Enough anhydrous potassium carbonate was then added to the mixture until the water layer disappeared. The ether layer gave a clear liquid of II (6.13 g, 70%) after the evaporation of the solvent. The decomposition of II took place during vacuum distillation. IR (neat), 3350 (w), 3275 (w), 3030 (w), 2980 (m), 1600 (w), 1490 (w), 1235 (s), 1030 (s), 960 (s), 690 (m) cm^{-1}; NMR ($CDCl_3$), τ 2.7 (complex m, 5, phenyl), 5.89 (d, 1, C<u>H</u>), 4.20 (complex m, 4, C<u>H</u>$_2$), 8.85 (qua, 6, C<u>H</u>$_3$). The ester was found pure from thin-layer and gas chromatographies.

Protection of Amino Group of II. *A) With Thiophenoxycarbonyl Chloride*: Thiophenoxycarbonyl chloride (3.50 g, 20.4 mmol) was added to a solution of II (9.50 g, 39.0 mmol) in THF (70 m*l*). After the mixture had been stirred at room temperature overnight, the resulting white crystals of the hydrochloride of II were filtered out, and the solvent was removed from the filtrate. The addition of petroleum ether to the residue produced diethyl *N*-thiophenoxycarbonyl-α-aminobenzylphosphonate (IVa) as white needle crystals; 6.0 g, 80%; mp 136—137°C (THF–petroleum ether); IR (KBr), 3350 (m), 3150 (m), 2950 (m), 1670 (s), 1540 (s), 1240 (s), 1020 (s), 970 (m), 700 (m) cm^{-1}; NMR ($CDCl_3$), τ 1.9 (broad d, N<u>H</u>), 2.5 (complex m, 5, phenyl), 4.67 (qua, 1, C<u>H</u>C$_6$H$_5$), 5.76 (qui, 2, C<u>H</u>$_2$CH$_3$), 6.13 (complex six, 2, C<u>H</u>$_2$CH$_3$), 8.64 and 8.91 (t, 3, CH$_2$C<u>H</u>$_3$).

Found: C, 56.95; H, 5.90; N, 3.84%. Calcd for $C_{18}H_{22}NO_4PS$: C, 56.98; H, 5.85; N, 3.69%.

B) With Benzyloxycarbonyl Chloride: To amine (II) (7.00 g, 28.8 mmol) dissolved in tetrahydrofuran (THF) (100 m*l*) was added benzyloxycarbonyl chloride (2.50 g, 14.7 mmol) at room temperature with stirring vigorously. Soon after the addition, the hydrochloride of II precipitated as white crystals. After stirring at room temperature overnight, the reaction mixture was filtered to remove the hydrochloride of II (3.80 g). The filtrate was then concentrated to give a yellow residue which was crystallized from ether to give needle crystals of IVb; 5.30 g, 98%; mp 108—109°C (from ether); IR (KBr); 3200 (m), 3050 (m), 1705 (s), 1550 (s), 1260 (s), 1020 (s), 970 (s), 690 (m) cm^{-1}; NMR ($CDCl_3$)

6) C. Sheehan and S. Frank, *J. Amer. Chem. Soc.*, **71**, 1856 (1949).

7) G. T. Young, "Peptides, Preceedings of the 5th European Symposium (1962)", Pergamon Press, Oxford, p. 1063.

τ 2.62 (complex m, 5, phenyl), 3.80 (broad, 1, NH), 4.80 (qua, 1, $C\underline{H}C_6H_5$), 4.85 (s, 2, $C\underline{H}_2C_6H_5$), 5.6—6.5 (complex m, 4, $C\underline{H}_2CH_3$), 8.75 and 8.94 (two t, 6, $CH_2C\underline{H}_3$).

Found: C, 60.44; H, 6.56; N, 3.93%. Calcd for $C_{19}H_{24}NO_5P$: C, 60.47; H, 6.41; N, 3.70%.

C) With Phthalic Anhydride: A mixture of II (6.51 g, 26.6 mmol) and phthalic anhydride (3.94 g, 26.6 mmol) was heated at 170—180°C for 2 hr. The resulting viscous liquid was dissolved in chloroform (7 m*l*) and chromatographed on alumina. Diethyl phthalimidobenzylphosphonate (IIIc) was eluted with ethyl acetate; 5.0 g, 51%; mp 101—103°C (ether); IR (KBr), 2990 (w), 1770 (w), 1710 (s), 1380 (s), 1255 (s), 1050 (s), 730 (m) cm^{-1}; NMR ($CDCl_3$), τ 2.20 (complex m, 5, phenyl), 2.65 (complex m, 4, phthalyl), 6.20 (d, 1, C$\underline{H}$), 5.75 (six, 4, two $C\underline{H}_2$), 8.75 (t, 6, $C\underline{H}_3$).

Found: C, 61.30; H, 5.41; N, 3.75%. Calcd for $C_{19}H_{20}NO_5P$: C, 61.12; H, 5.40; N, 3.75%.

Hydrolysis of IIIa. A mixture of IIIa (1.65 g, 4.20 mmol), concentrated hydrochloric acid (3 m*l*), and acetic acid (3.5 m*l*) was refluxed for 30 min. The reaction mixture was then diluted with water (8 m*l*) and the solution was stored in an ice-box. The resulting crystals (IVa) were separated, washed with water and dried; 150 g, 75%; mp 142—143°C ($CHCl_3$–acetone); IR (KBr), 3350 (w), 1650 (s), 1620 (m), 1520 (m), 1200 (s), 1050 (m), 950 (m), 750 (w) cm^{-1}; NMR (DMSO-d_6), τ 0.9 (broad, 1, POH), 2.60 (complex m, 10, two phenyl), 3.30 (broad, 1, NH), 4.90 (qua, 1, $C\underline{H}C_6H_5$).

Found: C, 50.93; H, 4.85; N, 4.25%. Calcd for $C_{14}H_{14}NO_4PS\cdot 0.5H_2O$: C, 50.61; H, 4.55; N, 4.21%.

Hydrolysis of IIIb. Compound IIIb (1.0 g, 2.65 mmol) was dissolved in a mixture of 0.4N sodium hydroxide (10 m*l*) and ethanol (10 m*l*), after which the solution was heated at 80°C for one hour. The solvent was then evaporated under reduced pressure, giving a white paste-like residue, which was dissolved in 20 m*l* of water, and pH of the solution was adjusted to about 3 by the addition of concentrated hydrochloric acid. The white solid (IVb) obtained was separated and recrystallized from petroleum ether–chloroform, 0.59 g, 64%, mp 182—183°C; IR (KBr), 3250 (w), 1710 (s), 1540 (s), 1250 (s), 1040 (m), 700 (m) cm^{-1}; NMR ($CDCl_3$), τ 2.5 (complex m, 10, two phenyl), 7.40 (broad s, 1, NH), 6.80 (qua, 1, C$\underline{H}$), 5.15 (s, 2, $C\underline{H}_2C_6H_5$), 5.95 (qua, 2, $C\underline{H}_2$), 8.75 (t, 3, $C\underline{H}_3$).

Found: C, 57.24; H, 5.81; N, 4.47%. Calcd for $C_{17}H_{20}NO_5P\cdot 0.5H_2O$: C, 56.98; H, 5.90; N, 3.91%.

Reaction of Ethyl Hydrogen α-Aminobenzylphosphonate with Benzyloxycarbonyl Chloride. To the ester (1.58 g, 0.075 mol) suspended in water (30 m*l*) was mixed with benzyloxycarbonyl chloride (1.5 g, 0.088 mol) at room temperature. 4N Sodium hydroxide (5 m*l*) was then added to the mixture and a solution was stirred for 10 min. After the unreacted chloride had been removed by extraction with ether, the pH of the aqueous solution was adjusted to 5 by the addition of concentrated hydrochloric acid, the solution was then concentrated as much as possible under reduced pressure. The extraction of the residue with chloroform and the evaporation of the solvent from the organic layer gave a clear substance which upon mixing with petroleum ether afforded IVb as white crystals; 0.8 g, 31%; mp 183—184°C (acetone). The IR and NMR spectra were identical with those of an authentic sample produced from the hydrolysis of IIIb.

Attempted Coupling of IVa or IVb with Ethyl Glycinate. A mixture of IVa (0.64 g, 1.9 mmol) or IVb (0.40 g, 0.11 mmol), an equivalent amount of ethyl glycinate, and DCC (2 equivalents) in DMF (10 m*l*) was stored at room temperature for a week. No precipitate of dicyclohexylurea appeared, showing that the coupling reaction did not take place in this system.

O-Ethyl Phthalimidobenzylphosphonochloridate (V). A mixture of IIIc (2.70 g, 7.25 mmol), phosphorus pentachloride (1.52 g, 7.30 mmol) and benzene (5 m*l*) was heated for 6.5 hr. The light-boiling substances were then removed under reduced pressure. The residue[8] was mixed with petroleum ether–ether (1:1) and cooled in a methanol–dry ice bath to give a white solid (V); 2.1 g, 80%; mp up to 85°C; IR (0.1 mm $CHCl_3$ liquid cell), 3030 (w), 1770 (m), 1725 (s), 1470 (m), 1370 (s), 1275 (s), 1030 (s), 970 (s), 545 (m) cm^{-1}; NMR ($CDCl_3$) τ 2.2 (complex m, 5, phenyl), 2.6 (complex m, 4, phthalyl), 4.05 (qua, 1, CH), 5.70 (m, 2, CH_2), 8.70 (qua, 3, CH_3). The elemental analysis of V was replaced with that of *O*-ethyl hydrogen phthalimidobenzylphosphonate, which had been obtained from the reaction of V with an excess of water in an 80% yield; mp 181—183°C; IR (KBr), 2980 (w), 1760 (w), 1710 (s), 1375 (s), 1200 (s), 1020 (s), 720 (m) cm^{-1}: NMR ($CDCl_3$), τ 1.8—3.0 (complex m, 9, phthalyl and phenyl), 4.20 (d, 1, C$\underline{H}$), 5.87 (qua, 2, $C\underline{H}_2$), 8.80 (qua, 3, $C\underline{H}_3$).

Found: C, 59.42; H, 4.68; N, 3.81%. Calcd for $C_{17}H_{16}NO_5P$: C, 59.13; H, 4.67; N, 4.05%.

Preparation of VI. Compound (IIIc) (2.22 g, 5.95 mmol) was allowed to react with phosphorus pentachloride (1.23 g, 5.90 mmol) in benzene (10 m*l*) to give the chloride as an oily substance, it was dissolved in THF (10 m*l*) and added to a chloroform (30 m*l*) solution of ethyl glycinate hydrochloride (0.9 g, 6.5 mmol) containing triethylamine (5.0 g, 50 mmol) at room temperature. The solution was then stirred overnight and washed with water. The chloroform layer was dried over Drierite and concentrated to about 5 m*l*. Column chromatography on silicic acid was then carried out on the solution. Elution with ether afforded VI (1.8 g, 70%) as a clear oil. The distillation of the product failed because of decomposition, its IR and NMR spectra were however, consistent with the assigned structure; IR (neat), 3350 (w), 3050 (w), 2980 (m), 1765 (w), 1710 (s), 1620 (w), 1495 (w), 1375 (s), 1250 (s), 1030 (s), 750 (m), 710 (s) cm^{-1}; NMR ($CDCl_3$) τ 2.2 (complex m, 5, phenyl), 2.65 (complex m, 4, phthalyl), 4.20 (qua, 1, CH), 5.5—6.3 (complex m, 7, $POC\underline{H}_2$, $N\underline{H}C\underline{H}_2CO_2C\underline{H}_2$), 8.78 and 8.85 (two t, 6, $C\underline{H}_3$).

Preparation of VIIa. A mixture of phthalyl-glycine (0.95 g, 0.467 mmol), II (1.13 g, 0.467 mmol), DCC (1.50 g, 0.73 mmol), and THF (15 m*l*) was stirred overnight at room temperature. Acetic acid (1 m*l*) and water (2 m*l*) were then added to the reaction mixture, and stirring was continued for 2 hr. The resulting dicyclohexylurea was filtered out, and the solvent was removed from the filtrate by means of a rotary evaporator at a water-bath temperature below 50°C. Chloroform (30 m*l*) was added to the residue, and the solution was washed with 10% sodium bicarbonate and water. The organic solution was concentrated to about 2.5 m*l*, giving a viscous oil which was subsequently crystallized from benzene to generate clear crystals; 1.90 g, 95%; mp 195—196°C; IR 3250 (m), 3030 (w), 2980 (m), 1730 (s), 1555 (m), 1420 (m), 1230 (s), 1030 (s), 720 (m) cm^{-1}; NMR ($CDCl_3$) τ 0.80 (d, 1, NH), 1.9—2.7 (complex m, 9, phenyl and phthalyl), 4.33 (qua, 1, $C\underline{H}C_6H_5$), 5.50 (s, 2, $C\underline{H}_2CO$), 5.60—6.60 (complex m, 4, $C\underline{H}_2CH_3$), 8.55 and 8.92 (two, t, 6, $C\underline{H}_3$).

Found: C, 58.82; H, 5.40; N, 6.30%. Calcd for $C_{21}H_{23}$-

8) The successive reactions were carried out using the oily residue directly, since which was almost pure according to the NMR spectrum but showed considerable difficulty in crystallization.

N_2O_6P: C, 58.60; H, 5.38; N, 6.51%.

Preparation of VIIb. A procedure similar to that used for the preparation of VIIa was carried out for a mixture of *N*-benzyloxycarbonylglycine (1.50 g, 7.18 mmol), II (1.75 g, 7.18 mmol), DCC (3.19 mmol), and THF (15 m*l*) to form VIIb as white crystals; 2.30 g, 74%; mp 88—89°C (ether); IR (KBr), 3250 (m), 3050 (w), 1720 (s), 1680 (s), 1550 (s), 1220 (s), 1160 (m), 1020 (s), 700 (m) cm^{-1}. NMR ($CDCl_3$) τ 1.45 (broad d, 1, N$\underline{H}$), 2.7 (complex m, 10, two, phenyl), 4.20 (broad t, 1, CON$\underline{H}C\underline{H}_2$), 4.42 (qua, 1, PC$\underline{H}C_6H_5$), 4.92 (s, 2, C$\underline{H}_2C_6H_5$), 5.85 (qui, 2, C$\underline{H}_2CH_3$), 6.10 (qui, 2, C$\underline{H}_2CH_3$), 8.72 and 8.96 (two t, 6, C$\underline{H}_3$).

Found: C, 58.28; H, 6.48; N, 6.45%. Calcd for $C_{21}H_{27}N_2O_6P$: C, 58.19; H, 6.78; N, 6.46%.

BULLETIN OF THE CHEMICAL SOCIETY OF JAPAN, VOL. 45, 2531—2534 (1972)

Peptides Containing Aminophosphonic Acids. II. The Synthesis of Tripeptide Analogs

Kiyoshi YAMAUCHI, Masayoshi KINOSHITA, and Minoru IMOTO*

Department of Applied Chemistry, Osaka City University, Sumiyoshi-ku, Osaka

(Received January 14, 1972)

The synthesis of tripeptides containing aminophosphonic acid was attempted as follows. Diethyl phthalylimidomethyl phosphonate (I) was chlorinated with phosphorus pentachloride to the phosphonomonochloridate (II), which was then coupled with amino acid ethyl esters to give the corresponding dipeptides (IIIa—c). The phthalyl groups of III were removed with hydrazine, and the resulting free amines were subsequently combined with phthalyl-amino acids by means of dicyclohexylcarbodiimide to produce the tripeptide analogs (IVa—c) in good yields.

In the preceding paper[1] we described the reactivity of α-aminobenzylphosphonic acid in connection with exploring a synthetic route for incorporating aminophosphonic acids into a peptide chain; we found that i) the reaction of *C*-protected amino acids with the *N*-protected aminophosphonomonochloridate could produce the corresponding dipeptide analogs linked through the phosphonamide bond, and ii) the amino group of aminophosphonic acids possessed a reactivity similar to that of amino acids and was capable of coupling with carboxyl groups of amino acids by means of dicyclohexylcarbodiimide (DCC).

In this paper we wish to report the synthesis of tripeptide analogs containing aminomethylphosphonic acid in the center. Aminophosphonic acid may be considered as the simplest phosphonic acid analog of glycine, and it would give readily crystallizable products than those obtained from α-aminobenzylphosphonic acid[1] because of less steric hindrance and the lack of an asymmetric carbon. Furthermore, the synthesis of tripeptides may offer a suitable guideline for the preparation of phosphorus analogs of higher peptides.

Results and Discussion

On the basis of the results of the previous work,[1] aminomethylphosphonic acid, the amino and phosphonic acid groups of which were blocked with phthalyl and ethyl groups respectively, was prepared by the following route. *N*-Hydroxylmethylphthalimide was brominated by phosphorus tribromide to produce *N*-bromomethylphthalimide in a 78% yield, the latter substance was then allowed to react with triethyl phosphite to generate diethyl phthalimidomethylphosphonate (I) in an 82% yield (Eq. (1)).

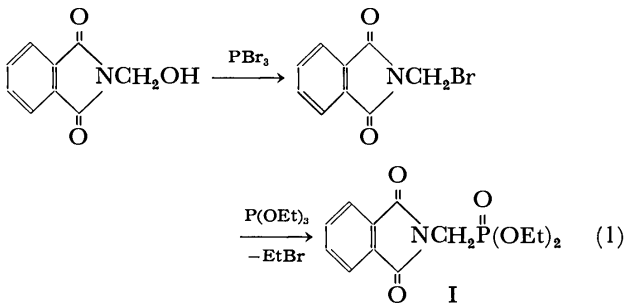

(1)

I

To activate the phosphonic-acid function for coupling with amino acids, compound I was treated with a slight excess of phosphorus pentachloride in benzene, giving crystalline ethyl phthalimidomethylphosphonochloridate (II) quantitatively (Eq. (2)). The chloride (II) showed a typical acid chloride character.[2]

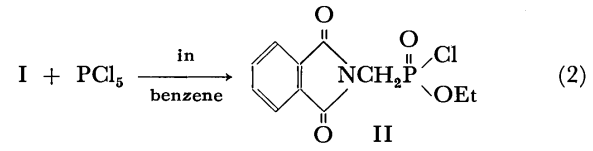

(2)

II

Amino acid ethyl ester hydrochlorides were then coupled with II in the presence of triethylamine,

* Present address: Department of Applied Chemistry, Kansai University, Suita, Osaka.

1) K. Yamauchi, M. Kinoshita, and M. Imoto, This Bulletin, **45**, 2528 (1972).

2) The chloride (II) showed the typical acid chloride character. Thus, when II was allowed to react with water, amines, and alcohols, the corresponding products, *e.g.*, ethyl hydrogenphosphonate, phosphonamides, and esters, were obtained in good yields.

thus producing dipeptide analogs (IIIa—c) in 70—88% yields (Eq. (3)).

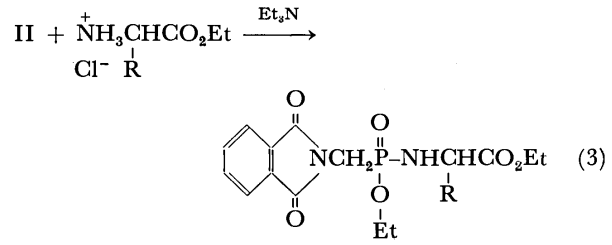

(3)

IIIa: R=H (PHT-gly-gly-OEt)
IIIb: R=*d*, *l*-CH_3 (PHT-gly-ala-OEt)
IIIc: R=*l*-$CH_2C_6H_5$ (PHT-gly-phe-OEt)

The attempted reactions of II with plain amino acids failed, though the procedure used was similar to that employed in the reactions of *N*-protected amino acid chlorides with amino acids, which has been reported to produce dipeptides.[3]

For the transformation of III into tripeptides which have aminomethylphosphonic acid in the center, the phthalyl group of III must be removed to give the corresponding free amines. This process was easily accomplished through the treatment of III with one equivalent of ethanolic hydrazine under mild conditions. The resulting amines were subsequently allowed to couple with phthalyl-amino acids, using DCC as the condensing agent, and produced tripeptide analogs (IVa—c) in 70—75% yields, (Eq. (4)). The procedure employed here was similar to those used in peptide synthesis.[4]

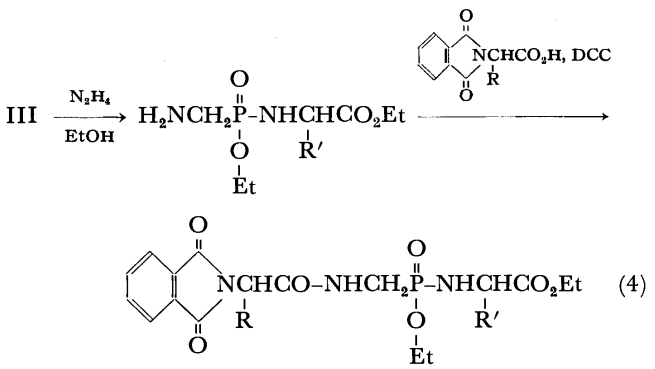

(4)

IVa: R=H, R′=H (PHT-gly-gly-gly-OEt)
IVb: R=H, R′=*l*-$CH_2C_6H_5$ (PHT-gly-gly-phe-OEt)
IVc: R=*l*-$CH_2C_6H_5$, R′=H (PHT-phe-gly-gly-OEt)

Concerning the removal of protecting groups, the phthalyl groups of the above compounds may be deblocked by hydrazine, as shown in the conversion of III to IV. The removal of the ethyl groups from carboxylic and phosphonic acid groups, however, was difficult, since P–N bond cleavage took place exclusively upon a mild acid treatment (Eq. (5)). Thus, when heated in a mixture of hydrochloric acid and acetic acid, IIIa produced the half ester (V) after 20 min, whereas IVa gave the phosphonic acid derivative (IV) within 40 min.

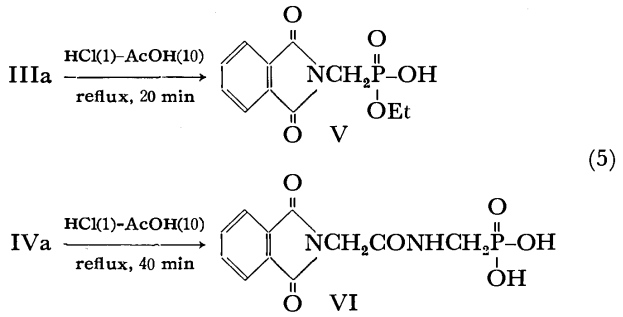

(5)

For the extension of the peptide chain, however, the presence of the carbonyl ester part does not provide any obstacles when the phthalyl groups is replaced with other *N*-protecting groups in the –CONH-bond-forming step (Eq. 4) and when an azide method is employed for the activation of carboxylic acid group. Work on these problems is now in progress and will be described later.

Experimental

The melting points (mp) are uncorrected. The infrared spectra (IR) were run on a Jasco Model IR-G spectrometer. The nuclear magnetic resonance spectra (NMR) were recorded with a Hitachi-Perkin-Elmer appratus, Model R-20. The optical rotations were obtained using a Yanagimoto Photomagnetic Polarimeter, Model OR-10.

Preparation of Diethyl Phthalimidomethylphosphonate (I). A) N-*Bromomethylphthalimide*: A mixture of *N*-hydroxymethylphthalimide (50.0 g, 0.282 mol) and phosphorus tribromide (77.0 g, 0.285 mol) was warmed until a dark-orange solution resulted. The cooled reaction mixture was poured into ice water to give a gray solid, which was then washed with water, dried, and crystallized from chloroform to produce *N*-bromophthalimide; 53.0 g, 78%; mp 149—150°C (lit,[5] 148°C).

B): *N*-Bromomethylphthalimide (39.5 g, 0.165 mol) and triethyl phosphite (27.4 g, 0.165 mol) were placed in a 200 m*l* round-bottom flask equipped with a distilling column, and then heated gently to initiate a reaction. After the exothermic reaction had subsided, the heating of the flask was continued for one hour, during which time the distillation of ethyl bromide stopped. Chloroform (100 m*l*) was added to the cooled reaction mixture, and the solution was washed with water (100 m*l*×3). The organic solution was dried over Drierlite and concentrated. The addition of petroleum ether to the residue gave white crystals (I); 40.0 g, 82%; mp 67°C (*n*-hexane); IR (KBr), 1770 (w), 1715 (s), 1240 (s), 1050 (s), 980 (m) cm^{-1}; NMR ($CDCl_3$) τ 1.85 (s, 4, phthal), 5.58 (qui, 4, $C\underline{H}_2$), 5.70 (d, 2, $C\underline{H}_2PO$), 8.60 (t, 6, $C\underline{H}_3$).

Found: C, 52.74; H, 5.44; N, 4.76%. Calcd for $C_{13}H_{16}NO_5P$: C, 52.52; H, 5.42; N, 4.71%.

Preparation of O-*Ethyl Phthalimidomethylphosphonochloridate (II)*. Compound I (6.27 g, 21.0 mmol), phosphorus pentachloride (4.67 g, 22.5 mmol), and dry benzene (20 m*l*) were refluxed for 15 hr. The solvent was then distilled out under reduced pressure to give a clear residue which, upon standing at

3) J. C. Sheehan and V. S. Frank, *J. Amer. Chem. Soc.*, **71**, 1856 (1949).

4) J. P. Greenstein and M. Winitz, "Chemistry of the Amino Acids," Vol. 2. John Wiley & Sons Inc., New York, N.Y. (1961).

5) G. W. Pucher and T. B. Johnson, *J. Amer. Chem. Soc.*, **44**, 817 (1922).

room temperature, solidified as white crystals. Recrystallization from dry tetrahydrofuran(THF)–ether gave needle crystals; 5.6 g, 93%; mp 92—94°C; IR ($CHCl_3$), 1780 (w), 1725 (s), 1600 (w), 1385 (s), 1300 (m), 1250 (m), 710 (m) cm^{-1}; NMR ($CDCl_3$), τ 1.8 (complex m, 4, phthalyl), 5.40 (d, 2, $C\underline{H}_2P$), 5.50 (complex m, 2, $POC\underline{H}_2$), 8.55 (qua, 3, $C\underline{H}_3$).

Found: C, 46.21; H, 4.03; N, 5.10; Cl, 12.76%. Calcd for $C_{11}H_{11}ClNO_4P$: C, 45.93; H, 3.85; N, 4.87; Cl, 12.33%.

Since the chloride (II) was produced quantitatively in an almost pure state, it was used for the successive reactions directly, without recrystallization.

Preparation of Phosphorus Analogs of Dipeptide (III). *PHT-gly-gly-OEt (IIIa)*: To a chloroform (70 m*l*) solution of ethyl glycinate hydrochloride (4.65 g, 0.033 mol) was added triethylamine (15 m*l*) with cooling by an ice-water bath. Chloride (II) (9.65 g, 0.034 mol), which was dissolved in THF (70 m*l*), was then added drop by drop over 15 min with stirring vigorously. After the completion of the addition, the reaction mixture was stirred for 10 hr. The resulting triethylamine hydrochloride was filtered out; the filtrate was concentrated to about 20 m*l* and diluted with chloroform to 100 m*l*, after which the solution was washed once with 10% sodium bicarbonate and then with water. The evaporation of the solvent and the addition of ether to the residue yielded white crystals. Recrystallization from ether–THF gave 10.5 g (88%) of IIIa; mp 132—133°C; IR (KBr), 3200 (w), 1750 (w), 1710 (s), 1220 (s) cm^{-1}; NMR ($CDCl_3$); τ 1.8 (complex m, 4, phthalyl), 5.6 (complex m, 4, $POC\underline{H}_2$, $CO_2C\underline{H}_2$), 5.77 (s, 2, $NC\underline{H}_2CO$), 4.02 (d, 2, $NC\underline{H}_2P$), 8.75 (two t, 6, $POCHCH_3$, $COCH_2C\underline{H}_3$).

Found: C, 51.09; H, 5.20; N, 7.68%. Calcd for $C_{15}H_{19}N_2O_6P$: C, 50.84; H, 5.40; N, 7.90%.

PHT-gly-ala-OEt (IIIb): The procedure similar to that used for the preparation of IIIa was employed, using II (5.80 g, 0.020 mol) and *d,l*-alanine ethyl ester hydrochloride (3.10 g, 0.020 mol) to produce IIIb as clear crystals; 5.1 g, 70%; mp 126—127°C) petroleum ether–THF); IR (KBr), 3150 (w), 1740 (w), 1710 (s), 1400 (s), 1200 (s), 1150 (s), 1040 (s), 720 (s) cm^{-1}. NMR ($CDCl_3$) τ 2.15 (complex m, 4, phthalyl), 5.6—6.2 (complex m, 7, $NC\underline{H}_2POC\underline{H}_2$, $C\underline{H}CH_3$, $COC\underline{H}_2$), 6.4 (broad, 1, $PN\underline{H}$), 8.55 (d, 3, $CHC\underline{H}_3$), 8.70 and 8.73 (t, 3, $COCH_2C\underline{H}_3$, or $POCH_2C\underline{H}_3$).

Found: C, 52.24; H, 5.66; N, 7.57%. Calcd for $C_{16}H_{21}N_2O_6P$: C, 52.19; H, 5.75; N, 7.61%.

PHT-gly-l-phe-OEt (IIIc): The chloride (7.00 g, 0.0243 mol) was allowed to react with *l*-phenylalanine ethyl ester hydrochloride (5.60 g, 0.025 mol) in a manner similar to that used in the synthesis of IIIa to form IIIc as clear crystals; 9.2 g, 83%; mp 94—95°C (ether–THF); IR (KBr), 3350 (w), 1760 (w), 1710 (s), 1390 (s), 1220 (s), 1110 (s), 960 (s) cm^{-1}; NMR ($CDCl_3$), τ 2.20 (complex m, 4, phthalyl), 5.6—6.5 (complex m, 7, $NC\underline{H}_2P$, $POC\underline{H}_2$, $C\underline{H}CO_2C\underline{H}_2$), 6.90 (d, 2, $C\underline{H}_2C_6H_5$), 8.80 (two t, 6, $POCH_2C\underline{H}_3$, $COCH_2C\underline{H}_3$); $[\alpha]_D^{21}$ +8.97° ($CHCl_3$, *c* 4.2).

Found: C, 58.15; H, 5.55; N, 6.16%. Calcd for $C_{22}H_{25}N_2O_6P \cdot 0.5H_2O$: C, 58.27; H, 5.78; N, 6.17%.

Preparation of Phosphorus Analogs of Tripeptide. *PHT-gly-gly-gly-OEt (IVa)*: Compound IIIa (1.50 g, 4.22 mol) was dissolved in ethanol (15 m*l*) and the solution was mixed with 1N ethanolic hydrazine (4.5 m*l*). After the reaction mixture had been kept at room temperature overnight, the resulting solid was filtered out and the filtrate was concentrated by a rotary evaporator at the water-bath temperature below 45°C. Since a white solid appeared upon the addition of THF to the residue, the solution was again filtered. The evaporation of the solvent from the filtrate gave gly-gly-OEt as a liquid. The amine thus obtained and phthalyl-glycine (0.83 g, 4.05 mmol) were dissolved in dry THF (10 m*l*), with which dicyclohexylcarbodiimide (1.0 g, 4.85 mmol) had been mixed. The solution was then kept at room temperature overnight. Water (1 m*l*) and acetic acid (0.5 m*l*) were subsequently added to the reaction mixture, after which it was allowed to stand at room temperature for 2 hr. The resulting dicyclohexylurea was removed, and the remaining solution was concentrated as much as possible. The residue was diluted with chloroform (20 m*l*) and neutrallized with 10% sodium bicarbonate. After the organic solution had then been dried over Drierite, the solvent was removed to give a light-yellow liquid. Upon the addition of ether, IVa appeared as white crystals; 1.1 g, 70%; mp 186—187°C (THF); IR (KBr), 3300 (w), 3200 (w), 1770 (w), 1710 (s), 1660 (m), 1560 (m), 1420 (m), 1200 (s), 1040 (m), 960 (m) cm^{-1}; NMR ($CDCl_3$), τ 2.3 (m, 4, phthalyl), 5.50 (s, 2, $C\underline{H}_2$-phthalyl), 5.90 (qua, 4, $COC\underline{H}_2$, $POC\underline{H}_2$), 6.0—6.6 (complex m, 5, $NHC\underline{H}_2PN\underline{H}C\underline{H}_2$), 8.70 (t, 3, $COCH_2C\underline{H}_3$), 8.76 (qua, 3, $POCH_2C\underline{H}_3$).

Found: C, 49.60; H, 5.28; N, 10.07%. Calcd for $C_{17}H_{22}N_3O_7P$: C, 49.63; H, 5.39; N, 10.21%.

PHT-gly-gly-phe-OEt (IVb): The phthalyl group was removed from IIIc (1.58 g, 3.50 mmol) with 1N ethanolic hydrazine (4.0 m*l*) in a manner similar to the procedure described in the preparation of IVa. The amine (about 1.59 g) was then coupled with phthalyl-glycine (0.70 g, 3.4 mmol) by DCC (1.0 g). The reaction mixture was processed as described above to produce IVb; 1.45 g, 75%; mp 164—166°C (THF); IR (KBr), 3250 (w), 3200 (w), 1715 (s), 1660 (m), 1550 (w), 1410 (m), 1190 (s), 1030 (s), 700 (m) cm^{-1}; NMR ($CDCl_3$), τ 2.1 (complex m, 5, phthalyl, CONH), 2.6 (complex m, 5, phenyl), 5.5—7.2 (complex m, 12, $C\underline{H}_2$ phthalyl, $C\underline{H}_2P(OC\underline{H}_2-)N\underline{H}C\underline{H}C\underline{H}_2C_6H_5$, $COC\underline{H}_2$), 8.5—9.2 (complex m, 6, $POCH_2C\underline{H}_3$, $COCH_2C\underline{H}_3$); $[\alpha]_D^{19}$ −27.3° ($CHCl_3$, *c* 6.1).

Found: C, 58.23; H, 5.50; N, 8.43%. Calcd for $C_{24}H_{28}N_3O_7P$: C, 57.48; H, 5.62; N, 8.37%.

PHT-l-phe-gly-gly-OEt (IVc): After IIIa (2.0 g, 5.65 mmol) had been treated with 1N hydrazine (6 m*l*), the resulting amine (1.22 g) was coupled with phthalyl-*l*-phenylalanine (1.67 g, 5.65 mmol) by DCC (1.5 g) in THF (20 m*l*). The mixture was handled in a way similar to that used with IVa to generate a light-yellow oil; this oil was then column-chromatographed on silicic acid to give IVc as a clear oil; 2.0 g, 70%; IR ($CHCl_3$); 3200 (m), 1770 (w), 1740 (m), 1710 (s), 1670 (m), 1520 (m), 1375 (s), 1190 (s), 1130 (s), 960 (m), 710 (s) cm^{-1}; NMR ($CDCl_3$) τ 2.0 (broad m, 1, $CON\underline{H}$), 2.3 (complex m, 4, phthalyl), 2.78 (s, 5, phenyl), 4.80 (qua, 1, $PON\underline{H}$), 5.6—6.7 (complex m, 11, $C\underline{H}C\underline{H}_2$-$C_6H_5$, $C\underline{H}_2POC\underline{H}_2$, $C\underline{H}COC\underline{H}_2$), 8.6—9.0 (two t, 6, $COCH_2$-$C\underline{H}_3$, $POCH_2C\underline{H}_3$); $[\alpha]_D^{19}$ −75.47° ($CHCl_3$, *c* 14.5).

Found: C, 57.10; H, 5.91; N, 8.12%. Calcd for $C_{24}H_{28}N_3O_7P$: C, 57.48; H, 5.62; N, 8.37%.

Acid Hydrolysis of IIIa. Compound IIIa (0.67 g, 18.9 mmol) was dissolved in 7 m*l* of a mixture of concentrated hydrochloric acid and acetic acid (1: 10), and then the solution was refluxed for 20 min. Water was added to the cooled reaction mixture, and the resulting solution was concentrated under a reduced pressure to give a white solid, this solid subsequently crystallized from THF to produce ethyl hydrogen phthalimidomethylphosphonate; 0.3 g, 59%; mp 205°C; IR (KBr), 3000—2500 (broad w), 1775 (w), 1725 (s), 1400 (m), 1205 (m), 1035 (s), 720 (s) cm^{-1}.

Found: C, 48.92; H, 4.54; N, 5.01%. Calcd for $C_{11}H_{12}NO_5P$: C, 49.07; H, 4.49; N, 5.20%.

Acid Hydrolysis of IVa. A similar procedure was employed for IVa (0.055 g, 0.13 mmol) using 5 m*l* of the

acid solution and taking a refluxing time of 40 min to produce phthalyl-glycylaminomethylphosphonic acid; 0.03 g, 75%; mp 192—194°C, IR (KBr), 3250 (w), 1770 (w), 1725 (s), 1660 (m), 1420 (m), 1100—1200 (m), 1000 (m), 960 (m), 720 (m) cm^{-1}; NMR (D_2O), 2.30 (s, 4, phthalyl), 5.70 (s, 2, $NC\underline{H}_2CO$), 6.55 (d, 2, $C\underline{H}_2P$).

Found: C, 44.62; H, 3.98; N, 9.05%. Calcd for $C_{11}H_{11}N_2O_6P$: C, 44.30; H, 3.71; N, 9.40%.

BULLETIN OF THE CHEMICAL SOCIETY OF JAPAN, VOL. 45, 2534—2537 (1972)

Products from the Reaction of Dinitrotetramethylbenzenes with Fuming Nitric Acid. A New Route to Some Polynitro Carbonyl Compounds[1)]

Hitomi SUZUKI* and Kiyomi NAKAMURA

Department of Chemistry, Faculty of Science, Kyoto University, Sakyo-ku, Kyoto

(Received January 22, 1972)

Reaction of dinitrotetramethylbenzenes with fuming nitric acid has been investigated. 5,6-Dinitro-1,2,3,4-tetramethylbenzene undergoes a slow oxidation to give 2,3,4,5-tetranitro-2,3,6,6-tetramethylcyclohex-4-enone in 82—87% yield, which is thermally unstable and upon heating readily converted into 4,5-dinitro-2,3,6,6-tetramethylcyclohexa-2,4-dienone losing two molecules of nitrogen dioxide. 4,6-Dinitro-1,2,3,5-tetramethylbenzene reacts readily with cold fuming nitric acid, giving 2,6-dinitro-3,4,5-trimethylbenzaldehyde in 76—84% yield, together with small amounts of 2,6-dinitro-3,4,5-trimethylphenylnitromethane, 2,6-dinitro-3,4,5-trimethylbenzoic acid, and 2,6-dinitro-3,4,5-trimethylbenzyl alcohol. 3,6-Dinitro-1,2,4,5-tetramethylbenzene is stable towards the action of fuming nitric acid, but is slowly converted into 3,6-dinitro-2,4,5-trimethylbenzyl nitrate on being heated with mixed acid at 40—50°C. The mode of formation of unusual products is briefly discussed.

On treatment with an excess of ordinary nitrating agent, tetraalkylbenzenes give dinitrotetraalkylbenzenes as the final product. Because of good crystallization and moderate melting range, dinitro derivatives are often used for the characterization of liquid hydrocarbons. We have reported that fuming nitric acid nitrooxylated the alkyl side-chain of fully substituted derivatives of polyalkylbenzenes to yield the benzylic compounds.[2)] The reaction is of electrophilic character and remarkably retarded by the presence of deactivating substituents such as nitro or carboxyl groups, although pentamethylnitrobenzene and pentamethylbenzoic acid can undergo a slow side-chain nitrooxylation at ortho methyl groups.[3,4)] It is expected, therefore, that the doubly deactivated dinitrotetramethylbenzenes are quite stable towards further action of the nitrating agent. However, dinitro derivatives of 1,2,3,4-tetramethylbenzene (prehnitene) and 1,2,3,5-tetramethylbenzene (isodurene) are found to react with fuming nitric acid with moderate ease to produce a tetranitrocyclohexenone or a dinitrobenzaldehyde, respectively, in good yields.

When a solution of 5,6-dinitro-1,2,3,4-tetramethylbenzene (5,6-dinitroprehnitene, DNP) in cold fuming nitric acid (d=1.50) was stood at room temperature for several days, it reacted with the nitrating agent with gentle liberation of nitrogen dioxide. Quenching with water, followed by careful crystallization of the precipitate from a mixture of dichloromethane and light petroleum (bp 40—50°C) gave nearly colorless prisms (I), $C_{10}H_{12}N_4O_9$, in 82—87% yield, which melted at 111—114°C with complete decomposition. Its mass spectrum showed fragment ion peaks derived from the non-detectable molecular ion at m/e 286 ($M-NO_2$), 256 ($M-NO_2-NO$), and 240 ($M-2NO_2$). Its infrared spectrum suggested the formation of an unsaturated nitro carbonyl compound (1742 (C=O), 1674 (C=C), 1540—1580 (NO_2, broad), 1328—1337 (NO_2, broad), and 846 cm^{-1} (NO_2)). Its ^1H NMR spectrum (100 MHz, $CDCl_3$) with four singlets at 8.71, 8.51, 8.11, and 7.67 τ indicated the presence of four methyl groups. The possibility of formation of the conjugated carbonyl compound was ruled out by the absence of ultraviolet maximum (in MeOH) above 220 nm.

Nitro carbonyl compound (I) was thermally unstable and, when heated gently in carbon tetrachloride, it readily released nitrogen dioxide and was converted into a bright yellow substance (II), $C_{10}H_{12}N_2O_5$, mp 94—96°C. The mass spectrum was very similar to that of I, except for the lack of two minor peaks at m/e 286 and 256. The peak at m/e 240 indicated the formation of II from I by the loss of two molecules of nitrogen dioxide. Its infrared spectrum showed the conjugated carbonyl bands at 1684, 1644 (C=O), and 1617 cm^{-1} (C=C), and absorption bands due to the conjugated nitro groups at 1533—1543 and 1365 cm^{-1}. The ultraviolet spectrum (in MeOH) had a maximum at 296—298 nm ($\log \varepsilon$=3.66) in accord with the

* Present address: Department of Chemistry, Faculty of Science, Hiroshima University, Hiroshima.

1) The Reaction of Polysubstituted Aromatics. XXVII. Part XXVI: This Bulletin, **45**, 1270 (1972). Preliminary account has been published in *Chem. Commun.*, **1972**, 340.

2) H. Suzuki, This Bulletin, **43**, 879 (1970); H. Suzuki, K. Nakamura, and M. Takeshima, *ibid.*, **44**, 2248 (1971).

3) H. Suzuki and K. Nakamura, *ibid.*, **44**, 227 (1971).

4) K. Nakamura, *ibid.*, **44**, 133 (1971).

presence of a 2,4-cyclohexadienone system.[5] The ^1H NMR spectrum of II consisted of three singlets at 8.56, 7.94 and 7.81 τ, with relative areas 2 : 1 : 1. The signal at 8.56 τ was due to the *gem*-dimethyl on C-6. If we make a reasonable assumption that the vicinal disposition of two nitro groups in DNP remains intact during the course of reaction, the two *gem*-methyl groups should be located next to the *vic*-dinitro grouping; otherwise they will absorb at around 8.7—8.9 τ.[6] The significant low-field shift is attributed to the location of the methyl groups in a deshielding region of the neighboring nitro group.[7] The inductive and electric field effects would also contribute. The two signals at 7.81 and 7.94 τ could be assigned to the methyl groups on C-2 and C-3, respectively. Examination of a scale model shows that the most preferred conformation of the two nitro groups in II is the one in which the C-5 nitro group is nearly coplanar with the ring to minimize steric crowding, while the C-4 nitro group is twisted considerably out of the ring plane to decrease unfavorable electrostatic interaction between two polar functionalities.[8] The C-3 methyl will then be placed out of the center of the deshielding region of the C-4 nitro group and be subject to reduced deshielding. The C-2 methyl group would be deeply deshielded by the combined effect of the nitro and carbonyl groups. These spectral evidences allowed for II the formulation of *4,5-dinitro-2,3,6,6-tetramethylcyclohexa-2,4-dienone*. Further proof of the structure is obtained from the mass spectrum, which showed prominent peaks at *m/e* 194 (M−Me−NO−H), 166 (M−Me−NO−CHO), 152 (M−2Me−NO−CO), 150 (M−2Me−2NO), 148 (M−2NO_2), and a peak cluster at *m/e* 119—124, Very strong peaks at *m/e* 108, 105, 93, 91, 79, 78, and 77 indicate a structure closely related to the benzenoid compound.

Nitro carbonyl compound (I) was, therefore formulated as *2,3,4,5-tetranitro-2,3,6,6-tetramethylcyclohex-4-enone*, whose most preferred structure was suggested from the molecular model shown in Fig. 1, two molecules of nitrogen dioxide being added to the unsaturated bond of II in a *trans* manner. The marked non-equivalence of the geminal methyl groups at 8.71 and 8.51 τ is probably due to the anisotropic effect of the neighboring carbonyl and nitro groups. The easy elimination of two nitrogen dioxide molecules from I suggests the crowding of the nitro and carbonyl groups in half-chair conformer.

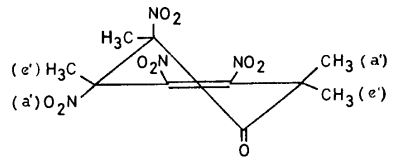

Fig. 1.

Formation of ketone (I) could be accounted for by the following sequence involving the addition-elimination process and the Wagner-Meerwein migration of methyl group (Scheme 1). Since the *vic*-dinitro

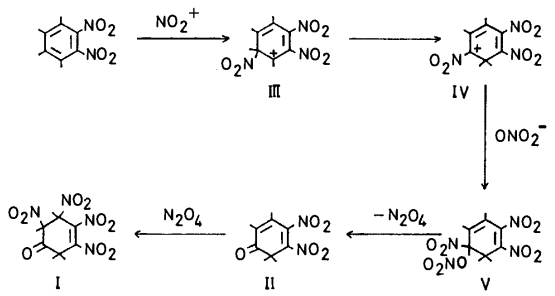

Scheme 1.

grouping deactivates the neighboring positions strongly, the initial attack of the nitronium ion would occur at the 2-position of DNP to form benzenonium ion (III), in which the methyl group at the attacking site will migrate to the more positively charged carbon atom at the 1-position. The nitrate anion will add to ion (IV) thus formed to give an unstable nitro nitrate (V), from which nitrogen dioxide is eliminated to yield ketone (II). Addition of nitrogen dioxide to II, probably in a homolytic fashion, will give I as the final product. This is probably the first example of the intramolecular migration of the ring methyl group observed in nitration. The migration of the methyl group from side-chain to nucleus has been reported by Myhre in the nitration of 1,3,5-tri-*t*-butylbenzene.[9]

4,6-Dinitro-1,2,3,5-tetramethylbenzene (4,6-dinitroisodurene, DNI) dissolved in cold fuming nitric acid soon began to react with active liberation of nitrogen dioxide. The major product, mp 163—164°C, had a molecular formula $C_{10}H_{10}N_2O_5$ and was identified as 2,6-dinitro-3,4,5-trimethylbenzaldehyde (XI) on the basis of its spectral data. In addition to XI, small amounts of 2,6-dinitro-3,4,5-trimethylphenylnitromethane (XII), 2,6-dinitro-3,4,5-trimethylbenzoic acid, and 2,6-dinitro-3,4,5-trimethylbenzyl alcohol were obtained as by-products. Aldehyde (XI) might be formed by the acid-catalyzed decomposition of the initially fromed 2,6-dinitro-3,4,5-trimethylbenzyl nitrate (IX). Similar reactions have been observed in our previous work.[10] Several mechanistic routes could explain the fromation of XI, high regio-selectivity suggesting the ionic character of the reaction. One of the possible pathways is shown in Scheme 2.

5) A. I. Scott, "Interpretation of the Ultraviolet Spectra of Natural Products", Pergamon Press, London (1964).

6) Polymethylcyclohexa-2,4-dienones are known to have ^1H NMR peaks for 2-methyl at 8.12—8.17, 3-methyl at 7.75—7.98, 4-methyl at 8.12—8.14, 5-methyl at 8.17—8.26, and 6-methyl at 8.72—8.89 τ, respectively. H. Hart, P. M. Collins, and A. J. Waring, *J. Amer. Chem. Soc.*, **88**, 1005 (1966); A. J. Waring, M. R. Morris, and M. M. Islam, *J. Chem. Soc., C*, **1971**, 3274. Reduction of ketone II gave an amino compound, which reacted with 1,2-diketone to form a condensation product of an unidentified structure in accord with the vicinal disposition of two nitro groups.

7) R. W. Frank and S. M. A. Williamson, *J. Org. Chem.*, **31**, 2420 (1966).

8) Analogous situation has been reported for 1,2-dinitrobenzene. K. E. Calderbank, R. J. W. Le Févre, and G. L. D. Ritchié, *J. Chem. Soc., B*, **1968**, 503.

9) P. C. Myhre, M. Beug, K. S. Brown, and B. Östman, *J. Amer. Chem. Soc.*, **93**, 3452 (1971), and previous papers cited therein.

10) H. Suzuki, M. Sawaki, and R. Sakimoto, This Bulletin, **45**, 1515 (1972).

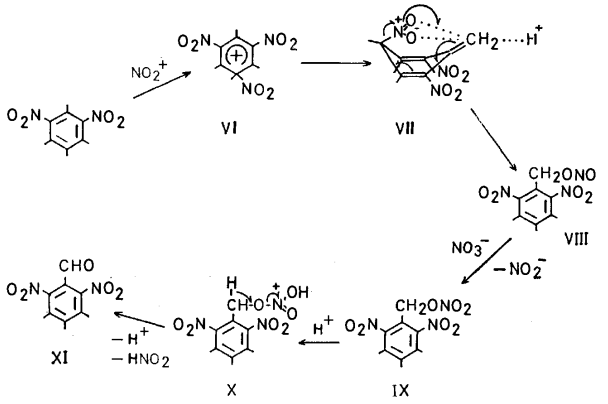

Scheme 2.

The initial attack of the nitronium ion will occur mainly at 2-position of DNI to give ion VI, which can be most effectively stabilized by three methyl groups. Proton release will take place preferentially from the most highly activated C-5 methyl group flanked both sides by nitro groups, leading to the intermediate stage (VII), in which the C-2 nitro group and the C-5 methylene group are not so far apart as to exclude the presence of *any* interaction between the oxygen atom of the C-2 nitro group and the methylene carbon atom. Fission of the C-2–NO_2 bond, followed by the redistribution of electrons in the activated complex will result in the transfer of the nitro group from the C-2 to the methylene carbon, yielding benzyl ester (VIII). Migration of the nitro group to the remote *para* position in preference to the neighboring *ortho* position may be rationalized by assuming that the transition state of the migration resembles the benzylic intermediate rather than the methylenecyclohexadiene, and is stabilized more effectively by the electron-donating methyl group at para position. This interpretation is in agreement with the fact that the nitration of polymethylbenzenes carried out in a dilute acetic acid solution affords a considerable amount of benzyl nitrate along with benzyl acetate at a very early stage of the reaction, and that the ratio of side-chain nitrooxylation and ring nitration is nearly independent of the concentration of nitric acid and added electrolyte.[4] A sort of tight-associated ion-pair may intervene and play some role in the process. The process is formally analogous to the thermal isomerization of 4-methylene-1-ethyl-1,2,3,5,6-pentamethylcyclohexa-2,5-diene to pentamethyl-*n*-propylbenzene, although the latter reaction is known to proceed through radical mechanism.[11] In the presence of excess nitric acid, benzyl nitrite (VIII) is not hightly stable and is readily converted into nitrate (IX). IX will then be protonated to form the conjugated acid (X), in which the fission of the N–O bond will give rise to the formation of benzaldehyde (XI) and the nitrous acid. The sulfuric acid-catalyzed transformation of the benzyl nitrate into the benzaldehyde has been reported to form some amounts of the benzoic acid as a by-product.[12]

Both the ionic mechanism and the one-electron transfer process could explain the formation of phenylnitromethane (XII) (Scheme 3). At present we prefer the view that nitromethane (XII) is derived from the benzyl ester through the nucleophilic displacement on the benzylic carbon of the conjugate acid (X′), although the situation is not clear as yet.[13]

Of three isomeric dinitrotetramethylbenzenes, 3,6-dinitro-1,2,4,5-tetramethylbenzene (3,6-dinitrodurene, DND) was the least soluble in fuming nitric acid. It was quite stable towards the oxidative action of the nitrating agent and mostly recovered unchanged even after a fortnight on being left to stand at room temperature. Protonation of the nitro group seems to have been the major reaction that had occurred. The infrared spectrum of the recovered material indicated the presence of some carbonyl compounds, but the product could not be identified because of the very small quantity. On being heated with a large excess of mixed acid (H_2SO_4:HNO_3=1:1 v/v) at 40—50°C, DND underwent a slow side-chain nitrooxylation to give 3,6-dinitro-2,4,5-trimethylbenzyl nitrate in good yield. Reduced reactivity of 1,4-dinitro system towards the electrophilic attack was well observed.

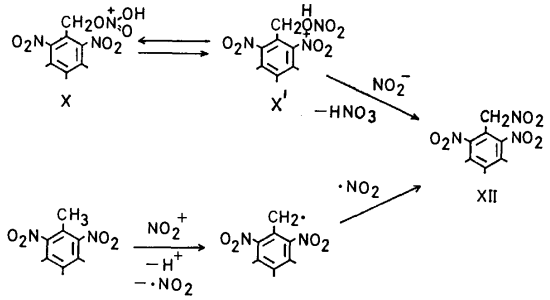

Scheme 3.

The present unusual reaction seems to provide a novel, simple route to some polynitro carbonyl compounds which are otherwise not readily accessible. The reaction is closely dependent on the orientation of the alkyl groups in the ring, and a facile destruction of the aromatic ring upon nitration may be characteristic of the vicinal polyalkylbenzene derivatives.

Experimental

All melting points were determined with a hot-stage apparatus and are uncorrected. Infrared spectra were run as Nujol on a Jasco DS-402G spectrophotometer and only prominent peaks were recorded. ^1H NMR measurements were carried out on a JEOLCO PS-100 spectrometer with deuteriochloroform as solvent and tetramethylsilane as an internal standard. Ultraviolet spectra were recorded in methanol solution of a Shimadzu QV-50 spectrophotometer. The mass spectra were obtained by Dr. A. Ohno of Sagami

11) R. N. Berezina, V. G. Schubin, and V. A. Koptyug, *Zh. Vses. Khim. Obshchest.*, **1968**, 356; V. G. Schubin, R. N. Berezina, and V. A. Koptyug, *Zh. Org. Khim.*, **6**, 2262 (1970).

12) S. D. Ross, E. R. Coburn, and M. Finkelstein, *J. Org. Chem.*, **33**, 589 (1968).

13) In view of the high propensity that the nitro compounds have to undergo protonation on nitro groups rather than release of one electron from the deactivated nucleus, the intermediary formation of the radical cation from DNI seems to be less probable in the strong protogenic acid medium.

Chemical Research Center, to whom the authors are indebted.

5,6-Dinitro-1,2,3,4-tetramethylbenzene (mp 178—179°C), 4,6-dinitro-1,2,3,5-tetramethylbenzene (mp 181—182°C), and 3,6-dinitro-1,2,4,5-tetramethylbenzene (mp 210—211°C) were prepared from the corresponding hydrocarbons by the ordinary procedure.

Reactions of Dinitrotetramethylbenzenes with Fuming Nitric Acid. 5,6-Dinitro-1,2,3,4-tetramethylbenzene (DNP). DNP (7.5 g) was dissolved in small portions in cold fuming nitric acid (d=1.5, 60 m*l*) to give a clear yellow solution. The color of the solution gradually turned dark red and a fume of nitrogen dioxide began to evolve slowly. The mixture was allowed to stand under hood at room temperature for several days, during the course of which the initial dark color faded to a light yellow. On being diluted with an excess of water, a pasty precipitate was obtained which, on being left to stand, gradually solidified to a white crystalline cake. The product was filtered, thoroughly washed with water, and dissolved into a minimum amount of dichloromethane. The solution was warmed at 35—40°C, light petroleum (bp 40—50°C) was added drop by drop until the solution became slightly cloudy, and the solution was left to cool under cover. Care should be taken to avoid excess heating. Faintly yellow prisms soon began to separate (8.8—9.4 g). Any attempt to crystallize the product from the hot solvent led to extensive decomposition of the product. On the basis of elemental analysis, infrared, ultraviolet, ^{1}H NMR, and mass spectral data, the product was formulated as *2,3,4,5-tetranitro-2,3,6,6-tetramethylcyclohex-4-enone (I)*. IR: 697, 732, 763, 785, 824, 846, 912, 976, 995, 1024, 1032, 1066, 1084, 1126, 1155, 1182, 1240, 1328—1337, 1540—1580, 1674, and 1742 cm^{-1}.

Found: C, 36.23; 36.42; H, 3.58; 3.78; N, 16.76; O, 43.37%. Calcd for $C_{10}H_{12}N_4O_9$: C, 36.16; H, 3.64; N, 16.87; O, 43.34%.

The ketone was thermally unstable and melted at 111—114°C with complete decomposition. When crystallization was attempted by dissolving I in hot carbon tetrachloride, nitrogen dioxide was liberated and a bright yellow substance, mp 94—96°C, was obtained. This was identified as *4,5-dinitro-2,3,6,6-tetramethylcyclohexa-2,4-dienone (II)* on the basis of spectral evidences. IR: 714, 736, 777, 849, 999, 1048, 1198, 1245, 1272, 1299, 1533—1540, 1617, 1644, and 1684 cm^{-1}.

Found: C, 49.92; H, 5.02%. Calcd for $C_{10}H_{12}N_2O_5$: C, 50.00; H, 5.04%.

4,6-Dinitro-1,2,3,5-tetramethylbenzene (DNI). A solution of DNI (7.2 g) in fuming nitric acid (60 m*l*), when stood at room temperature, soon began to liberate red fume. After the cease of reaction, the solution was diluted with water and a white crystalline precipitate was filtered, washed with dilute aqueous sodium hydrogen carbonate, and dissolved in a mixture of dichloromethane and light petroleum, from which the major product was readily separated as large prisms (5.9—6.4 g), mp 163—164°C after recrystallization several times, and identified as *2,6-dinitro-3,4,5-trimethylbenzaldehyde (XI)*. IR: 699, 778, 861, 896, 1023, 1052, 1285, 1359, 1532, and 1712 cm^{-1}; ^{1}H NMR: 7.66 (2 Me), 7.52 (Me), and 0.16 τ (CHO).

Found: C, 50.12; H, 4.29%. Calcd for $C_{10}H_{10}N_2O_5$: C, 50.42; H, 4.23%.

The aldehyde was stable towards spontaneous oxidation, but soon became yellow or light brown on storage under diffused light.

A less soluble minor part was fractionally recrystallized from ligroin to give fine needles (*ca.* 0.5 g), $C_{10}H_{11}N_3O_6$, mp 158—159°C. It showed ^{1}H NMR peaks at 7.65 (2 Me), 7.56 (Me), and 4.58 τ (CH_2), and IR bands at 711, 766, 785, 855, 878, 898, 1057, 1288, 1317, 1360, 1535, and 1567 cm^{-1}, and was identified as *2,6-dinitro-3,4,5-trimethylphenylnitromethane.*

Found: C, 44.69; H, 4.18%. Calcd for $C_{10}H_{11}N_3O_6$: C, 44.61; H, 4.12%.

Another minor product, mp 193—195°C, was *2,6-dinitro-3,4,5-trimethylbenzyl alcohol.* IR: 776, 857, 868, 1010, 1043, 1055, 1365, 1535, and 3530 cm^{-1}.

Found: C, 50.08; H, 5.09%. Calcd for $C_{10}H_{12}N_2O_5$: C, 50.00; H, 5.04%.

The aqueous sodium hydrogen carbonate washing of the product was neutralized with hydrochloric acid to give a white precipitate, which on recrystallization several times from aqueous ethanol gave fine needles (*ca.* 0.5 g), mp 233—236°C with decomposition, and was identified as *2,6-dinitro-3,4,5-trimethylbenzoic acid.* IR: 662, 721, 781, 857, 896, 1168, 1360, 1535, 1753, and 3300 cm^{-1}.

Found: C, 47.43; H, 3.76%. Calcd for $C_{10}H_{10}N_2O_6$:C, 47.25; H, 3.97%.

3,6-Dinitro-1,2,4,5-tetramethylbenzene (DND). DND (4.5 g) was dissolved in a large excess of mixed acid (40 m*l*; H_2SO_4: HNO_3 (d=1.5) =1: 1 v/v), and the solution was kept at 40—50°C for several hours and then at around 60°C for 0.5 hr. This was poured onto crushed ice followed by the usual work-up, and gave *3,6-dinitro-2,4,5-trimethylbenzyl nitrate* as pale yellow needles (3.5 g, 61%), mp 139—140°C. IR: 676, 752, 853, 886, 983, 1212, 1222, 1273, 1365, 1535, and 1645 cm^{-1}; ^{1}H NMR (in CCl_4): 7.73 (2 Me), 7.65 (Me), and 4.59 τ (CH_2).

Found: C, 41.93; H, 3.60; N, 14.57%. Calcd for $C_{10}H_{11}N_3O_7$: C, 42.11; H, 3.89; N, 14.73%.

A Kinetic Study of the Polymerization of Acrylic Acid in the Presence of Polyvinylpyrrolidone

Ryo MURAMATSU and Takeo SHIMIDZU

Department of Hydrocarbon Chemistry, Faculty of Engineering, Kyoto University, Kyoto

(Received January 25, 1972)

The polymerization of acrylic acid (AA) in a dilute aqueous solution in the presence of polyvinylpyrrolidone (PVP) has been studied kinetically, with the extent of polymerization followed by a bromometric titration method. The rate of the polymerization changed characteristically with the amount of PVP in the solution and went through a maximum at a certain initial mole ratio of PVP and AA, $[PVP]_0/[AA]_0$, under a constant $[AA]_0$ value. The mole ratio which gave the maximum rate was almost proportional to the reciprocal of $[AA]_0$. In the course of the polymerization, a polymer complex consisting of PVP and polymerized AA was precipitated. Its composition, $(PAA)_c/(PVP)_c$, has been found to be different as the polymerization conditions are varied. Hardly no comparable data between the bromometric method and a turbidimetric method used to measure the rate were obtained. The influence of PVP on the polymerization was assumed to be caused by the local concentration of AA in the vicinity of PVP. A mechanism based on the effect of the local concentration, the "polymer atmosphere binding mechanism," has been found to explain the experimental results well.

Ferguson and Shah have described that the polymerization of acrylic acid (AA) in the presence of polyvinylpyrrolidone (PVP) in a dilute aqueous solution exhibits kinetically the characteristics of a "replica polymerization."[1] In their study, the rate of the polymerization was observed to go through a maximum at an equimolar ratio of PVP and AA under a constant AA concentration. Such a phenomenon has been explained as a "replica polymerization," a "matrix polymerization," or a "template polymerization." Many polymerization systems have been investigated in connection with the matrix polymerization—for example, the polymerizations of 4-vinylpyridine in the presence of polystyrenesulfonic acid or polyacrylic acid by Kabanov *et al.*,[2] that of acrylic acid in the presence of polyethylenimine by Bamford and Shiiki[3] and by Ferguson and Shah,[4] that of methacrylic acid in the presence of polyvinylpyrrolidone by Sakaguchi *et al.*,[5] that of methacrylic acid in the presence of poly-*N*-vinyl-5-methyl-2-oxazolidone by Okawara *et al.*,[6] that of 4-vinylpyridine in the presence of polymaleic anhydride by Kinoshita *et al.*,[7] and that of methacrylic acid or acrylic acid in the presence of polyethylene glycol by Osada.[8]

The interactions between the monomer and the polymer in those polymerization systems are various and multiform in their qualities and strengths. As regards the interaction between a simple electrolyte and a polyelectrolyte, for example, the site binding of simple electrolytes to polyelectrolytes and also the local concentration of simple electrolytes in the vicinity of polyelectrolytes have been considered.[9] These things have also been dealt with in ionic reactions in the presence of polyelectrolytes.[10] Except for the perfect replica polymerization shown in the polymerization of methacrylic acid or acrylic acid using Novolak resins by Kämmerer *et al.*,[11] the replica polymerization could not be declared until the exact duplication of such information on a polymer templates as the molecular weight has been proved, as Kinoshita has reported.[7]

In the present experiment, the polymerization of acrylic acid (AA) in the presence of polyvinylpyrrolidone (PVP) in a dilute aqueous solution, a similar polymerization system which Ferguson and Shah have studied kinetically by a turbidimetric method,[1] has been investigated, with the rate of the polymerization followed by measuring the quantities of an unreacted monomer, AA. In connection with the result concerning the peculiar influence of PVP on the rate of the polymerization of AA, the local concentration of AA in the vicinity of the PVP molecule in the polymerization will be discussed.

Experimental

Materials. Acrylic acid (AA) was purified by sublimation at a pressure below 10^{-1} mmHg. Quantities of double bonds more than 97 mol% in the sublimate were detected by bromometric titration analysis. The polyvinylpyrrolidone (PVP) was of a commercial origin and was purified with water and acetone. The PVP of M.W. 24500 was used unless otherwise stated. The polyacrylic acid (PAA) was obtained by the acidification of a commercial sodium polyacrylate with HCl or by the polymerization of AA in an aqueous solution, and was purified by dialysis. The potassium persulfate ($K_2S_2O_8$), used as an initiator, *N*-methylpyrrolidone (MP), and propionic acid (PA) were all of commercial origin, and they were purified in the usual manners.

1) J. Ferguson and S. A. O. Shah, *Eur. Polym. J.*, **4**, 343 (1968).
2) O. V. Kargina, V. A. Kabanov, and V. A. Kargin, *J. Polym. Sci. Part C*, **22**, 339 (1968); V. A. Kabanov, V. A. Petrovskaya, and V. A. Kargin, *Vysokomol. Soedin.*, **A 10**, 925 (1968).
3) C. H. Bamford and Z. Shiiki, *Polymer*, **9**, 595 (1968).
4) J. Ferguson and S. A. O. Shah, *Eur. Polym. J.*, **4**, 611 (1968).
5) Y. Sakaguchi, K. Tamaki, T. Shimizu, and J. Nishino, *Kobunshi Kagaku*, **27**, 284 (1970).
6) T. Endo, R. Numazawa, and M. Okawara, *ibid.*, **28**, 541 (1970).
7) K. Shima, Y. Sumii, and M. Kinoshita, 18th Annual Meeting of the Society of Polymer Science Japan (1969), 1F03; Y. Sumii, M. Kinoshita, and M. Imoto, 19th Symposium of the Society of Polymer Science Japan (1970), 22B06.
8) Y. Osada, *Kagaku no Ryoiki*, **25**, 9 (1971).
9) "Encyclopedia of Polymer Science and Technology," Vol. 10, Interscience Publishers, New York (1968), p. 781.
10) H. Morawetz, *Accounts Chem. Res.*, **3**, 4152 (1970).
11) H. Kämmerer and S. Ozaki, *Markomol. Chem.*, **91**, 1 (1966); H. Kämmerer and A. Jung, *ibid.*, **101**, 284 (1966); H. Kämmerer and N. Önder, *ibid.*, **111**, 67 (1968).

Polymerization Reaction. The polymerizations of AA were carried out in sealed ampules. Each aqueous solution of AA, PVP, and $K_2S_2O_8$ was charged in an ampule (10 m*l*) and frozen in turn without mixing those portions, and then sealed under nitrogen. The sealed ampules were shaken in a thermostat maintained at 74±0.1°C for a given time.

Measurement of the Rate of the Polymerization. The rate of the polymerization of AA was followed by measuring the quantities of the unreacted AA by the Lucass-Pressman method, a bromometric titration method.[12] The additions of bromine were carried out at 40—50°C for 5 min. The effects of $[K_2S_2O_8]$ and [PVP] on the addition of bromine to the unreacted AA were negligible.

Analysis of the Composition of the Polymer Complex. A polymer complex which was precipitated in the course of the polymerization of AA in the presence of PVP, the polymer complex (A), was separated by the centrifugation of the reaction solution and then washed with water three times. The composition of the polymer complex (A) was determined by elemental analysis. It was difficult to find any solvent system which could dissociate or dissolve the polymer complex (A) completely. Therefore, the molecular weight of PAA polymerized in the presence of PVP could not be detected. On the other hand, a polymer complex which was formed in mixing PAA and PVP, the polymer complex (B), was purified and analyzed by the same method in order to compare it with the polymer complex (A).

Examination of a Turbidimetric Method Used in Following the Extent of the Polymerization. Both the change in the turbidity with the extent of the polymerization of AA in the presence of PVP and the turbidity caused by mixing PAA and PVP were measured in a jacketed turbidity cell (glass; optical path, 2.20 cm; volume, 35 m*l*) or a standard cell (optical path, 1.00 cm), using a hand-made turbidimeter and a Beckman DB-G spectrophotometer.

Results

Some typical time-conversion curves are shown in Fig. 1. The time-conversion curve of the polymerization of AA in the presence of PVP could be treated as a straight line at the range of 30—60% conversion, as may be seen in Fig. 1, Curve A. As the temperature of this reaction system did not reach a given temperature at the early stage of the polymerization, it is difficult to measure the initial rate accurately. The rate of the polymerization was obtained from the slope of the linear part in the time-conversion curve. The time-conversion curve of the polymerization of AA without PVP is shown as Curve B. In both cases, *N*-methylpyrrolidone (MP), which would be a monomeric analog of PVP, was found to have no effect on the rate of the polymerization, so it is assumed that the pyrrolidone group does not affect the reactivity of AA and the decomposition of $K_2S_2O_8$.

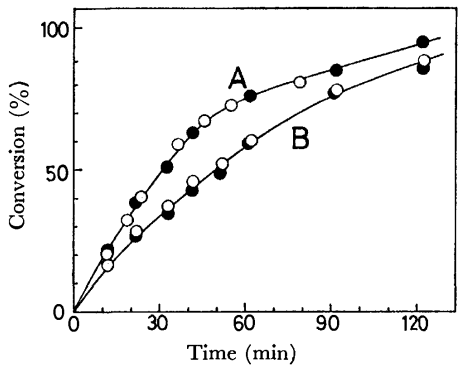

Fig. 1. Typical time-conversion curves of the polymerization of AA.
$[AA]_0=5.0\times10^{-2}$ (mol/*l*); $[K_2S_2O_8]_0=7.4\times10^{-3}$ (mol/*l*); 74±0.1°C.

Curve		$[PVP]_0$ (mol/*l*)	$[MP]_0$ (mol/*l*)
A	○	2.5×10^{-2}	0
	●	2.5×10^{-2}	2.5×10^{-2}
B	○	0	0
	●	0	5.0×10^{-2}

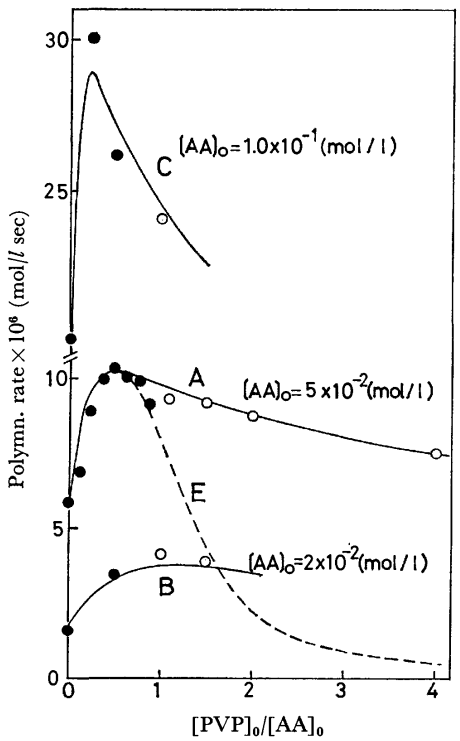

Fig. 2. Influence of $[PVP]_0$ on the rate of the polymerization of AA.
$[K_2S_2O_8]_0=7.4\times10^{-3}$ (mol/*l*);
●, presence of MP ($[MP]_0+[PVP]_0=[AA]_0$);
○, absence of MP; 74±0.1°C.
Curves A, B, C, calcd. by Eq. (B) (Polymer atmosphere binding mechanism).
Curve E, calcd. by Eq. (A-3) (Specific site binding mechanism).

The influence of PVP on the rate of the polymerization is shown in Fig. 2. Under constant initial concentrations of AA, $[AA]_0$, and $K_2S_2O_8$, $[K_2S_2O_8]_0$, the rate of the polymerization went through a maximum at a certain ratio of PVP and AA, $[PVP]_0/[AA]_0$. A similar tendency has been described in, for instance, the studies of the polymerizations of AA in the presence of polyethylenimine,[3,4] of that of methacrylic acid in the presence of poly-*N*-vinyl-5-methyl-2-oxazolidone,[6] and of that of *N*-vinyl-2-oxazolidone in the presence of polymethacrylic acid.[13]

12) H. J. Lucass and D. Pressman, *Ind. Eng. Chem. Ana. Ed.*, **10**, 140 (1938).

13) T. Endo, R. Numazawa, and M. Okawara, *Makromol. Chem.*, **146**, 247 (1971).

The ratios of $[PVP]_0/[AA]_0$ at which the rates were maximum, $\{[PVP]_0/[AA]_0\}_{max}$, were almost proportional to the reciprocal of $[AA]_0$. Moreover, the concentrations of PVP at $\{[PVP]_0/[AA]_0\}_{max}$ were about 2.5×10^{-2} mol/l. As for the viscosity of the reaction solution, $\eta_{sp}/[PVP]_0$, it did not change remarkably in the vicinity of the PVP concentration of 2.5×10^{-2} mol/l, as is shown in Fig. 3. From those results, the theory that the acceleration of the rate is caused by a conformational change in PVP can be rejected.

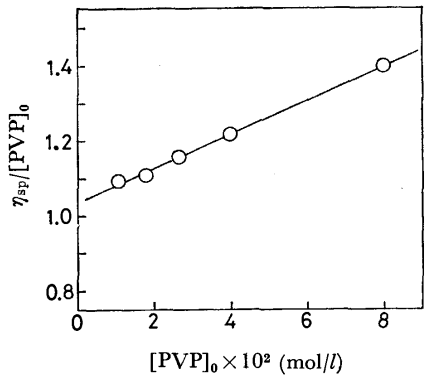

Fig. 3. Viscosity of the reaction solution.
$[PA]_0=2.0\times10^{-2}$ (mol/l);
$[K_2S_2O_8]_0=7.4\times10^{-3}$ (mol/l); 74±0.1°C.

If this polymerization system were a "replica polymerization system," $\{[PVP]_0/[AA]_0\}_{max}$ would be a constant under different $[AA]_0$ values and would not decrease as $[AA]_0$ becomes higher. It seems rather unlikely, then, that the present polymerization is the "replica polymerization," although there is no direct evidence on this point. Ferguson and Shah have described that the rate of the polymerization went through a maximum rate of 14.7×10^{-4} mol/l·sec at almost the same PVP concentration as AA when $[AA]_0$ was 2×10^{-2} mol/l.[1] This rate was remarkably different from the 4.2×10^{-6} mol/l·sec found in our work. This difference will be discussed later. In Fig. 4, the rate calculated from the AA consumption

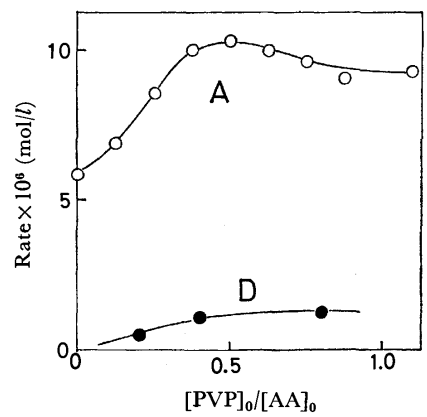

Fig. 4. Comparison of the rates by the titration method and by the polymer complex (A) weighing method.
$[AA]_0=5.0\times10^{-2}$ (mol/l); $[K_2S_2O_8]_0=7.4\times10^{-3}$ (mol/l); $[PVP]_0+[MP]_0=[AA]_0$; 74±0.1°C.
○: polymerization rate by the bromometric titration
●: precipitation rate of the polymer complex (A)

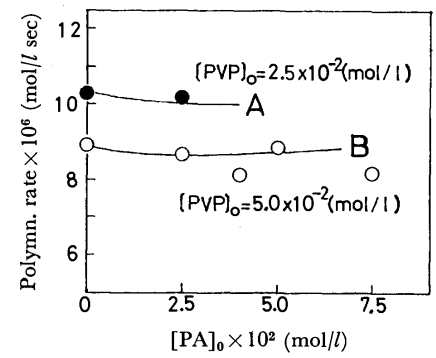

Fig. 5. Influence of PA on the rate of the polymerization of AA.
Conditions as given for Fig. 4.
Curves A, B; calcd. by Eq. (B′), (polymer atmosphere binding mechanism)

as measured by the bromometric titration method, and the rate calculated from the yield of the polymer complex (A) formed in the course of the polymerization of AA in the presence of PVP are shown. The rate obtained by the polymer-complex weighing method differs from that obtained by the titration method; this difference will also be discussed later.

The influence of propionic acid (PA), a non-polymerizable analog of the AA monomer, on the rate of the polymerization is shown in Fig. 5. PA had no effect on the rate of polymerization. This result also leads to a negation of hypothesis of the "replica polymerization" for this polymerization system.

Figure 6 shows the dependence of $[AA]_0$ on the rate of the polymerization. Apparently, the rate of the polymerization of AA with PVP was proportional to the 1.9 powers of $[AA]_0$, while the rate without PVP was proportional to the 1.5 powers of $[AA]_0$.

The dependence of the initiator concentration, $[K_2S_2O_8]_0$, on the rate of the polymerization was also studied, as is shown in Fig. 7. The rate was almost proportional to the 0.5 power of $[K_2S_2O_8]_0$

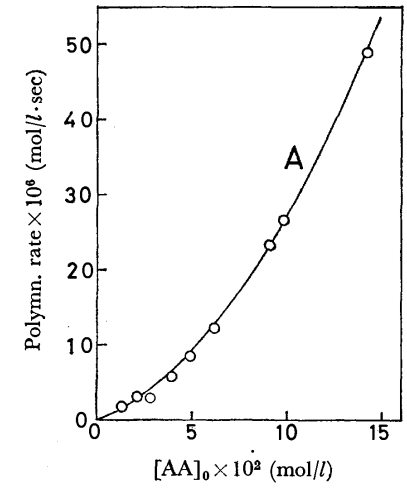

Fig. 6. Influence of $[AA]_0$ on the rate of the polymerization of AA.
$[PVP]_0=5.0\times10^{-2}$ (mol/l); $[K_2S_2O_8]_0=7.4\times10^{-3}$ (mol/l) 74±0.1°C
Curve A; calcd. by Eq. (B), (Polymer atmosphere binding mechanism)

Table 1. Yield and composition of the polymer complex (A)

No.	Monomer $[AA]_0$ (mol/l)	Polymer $[PVP]_0$ (mol/l)	Initiator $[K_2S_2O_8]_0$ (mol/l)	Yield $(PAA)_c/[AA]_0$	Composition $(PAA)_c/(PVP)_c$	Complexes PVP $(PVP)_c/[PVP]_0$
1	5×10^{-2}	2×10^{-2} (No. 1)	7.4×10^{-3}	22.6 (%)	1.183	48.0 (%)
3	5×10^{-2}	2×10^{-2} (No. 2)	7.4×10^{-3}	24.7	1.191	51.8
4	5×10^{-2}	2×10^{-2} (No. 3)	7.4×10^{-3}	23.5	1.006	58.3
5	5×10^{-2}	4×10^{-2} (No. 1)	7.4×10^{-3}	26.1	1.004	32.4
6	5×10^{-2}	1×10^{-2} (No. 1)	7.4×10^{-3}	9.1	1.365	33.5
7	5×10^{-2}	2×10^{-2} (No. 1)	3.7×10^{-3}	29.0	1.244	58.3
8	10×10^{-2}	2×10^{-2} (No. 1)	7.4×10^{-3}	18.2	1.800	52.3
9	5×10^{-2}	5×10^{-2} (No. 1)	7.4×10^{-3}	—	0.851	—
10	5×10^{-2}	5×10^{-2} (No. 3)	7.4×10^{-3}	—	0.626	—

Reaction time, 3 hr; 74±0.1°C.
M.W. of PVP; No. 1, 24500; No. 2, 40000; No. 3, 700000.
$(PAA)_c$ shows the quantity of PAA found in the complex.
$(PVP)_c$ shows the quantity of PVP found in the complex.

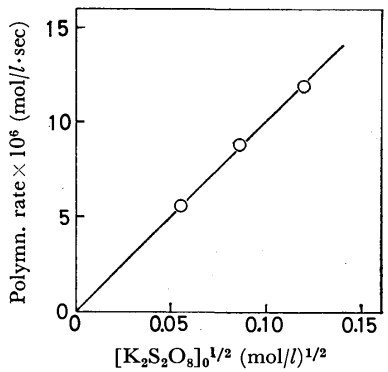

Fig. 7. Influence of $[K_2S_2O_8]_0$ on the rate of the polymerization of AA.
$[AA]_0=[PVP]_0=5.0\times10^{-2}$ (mol/l); 74±0.1°C.

at constant AA and PVP concentrations. The rate of the polymerization of AA without PVP has been reported to be proportional to the 0.5 power of the persulfate initiator.[14] These results indicate that the acceleration of the rate of the polymerization of AA in the presence of PVP was not caused by the trapping of radicals in the precipitated phase, the so-called "gel-effect."

Table 1 shows the yield and composition, $(PAA)_c/(PVP)_c$, of the polymer complex (A) precipitated in the course of the polymerization of AA in the presence of PVP. Fig. 8 shows the influence of $[PVP]_0$ on $(PVP)_c/(PAA)_c$ in the polymer complex (A). Even at a constant $[AA]_0$, value where the amounts of PAA formed were similar, the $(PVP)_c/(PAA)_c$ ratios in the polymer complexes (A) were different from one another, and they became smaller as $[PVP]_0$ became smaller. The concentrations of PVP and AA also affected the composition of the polymer complex (A), $(PAA)_c/(PVP)_c$, even though the $[PVP]_0/[AA]_0$ ratios were the same (No. 6, No. 8, in Table 1). Even when the $[AA]_0/[PVP]_0$ ratio was large and the amount of polymerized AA was larger than $[PVP]_0$, not all of the PVP was found in the polymer complex (A) (No. 1—8 in Table 1). These results indicate that not all the polymerized AA formed the polymer complex (A) with an equimolar ratio of PAA and PVP and that the polymer complex (A) formation was not complete. The difference between the rate calculated from the yield of the polymer complex (A) and that calculated from the consumption of AA, as is seen in Fig. 4, can explained as a non-quantification in the formation of the polymer complex (A). The molecular weight of the PVP used also affects the formation of the polymer complex (A) (No. 1, 4, 9, and 10 in Table 1).

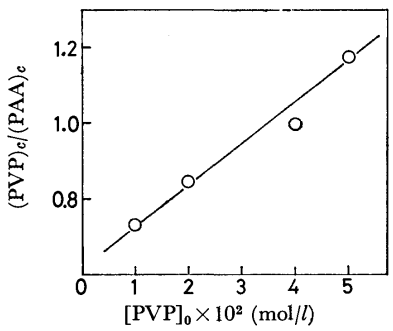

Fig. 8. Composition of the polymer complex (A).
No.'s 1, 5, 6, and 9 in Table 1; M.W. of PVP, 24500

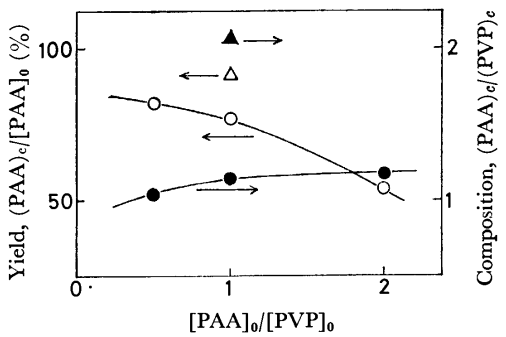

Fig. 9. Yield and composition of the polymer complex (B).
$[PVP]_0=5.0\times10^{-2}$ (mol/l); $[K_2S_2O_8]_0=7.4\times10^{-3}$ (mol/l); Mixing temperature, 74±1°C.
PAA No. 5; ○, yield; ●, composition
PAA No. 1; △, yield; ▲, composition
M.W. of PAA No. 5, 5300; M.W. of PAA No. 1, fairly higher than that of PAA No. 5.

14) H. Ito, S. Shimizu, and S. Suzuki, *Kogyo Kagaku Zasshi*, **58**, 194 (1955).

Figure 9 shows the yield of the polymer complex (B) formed by mixing PAA and PVP, $(PAA)_c/[PAA]_0$, and the composition of the polymer complex (B), $(PAA)_c/(PVP)_c$. Much as in the discussion of the polymer complex (A), it can be said that the PAA and PVP which did not take part in the formation of the polymer complex (B) still remained in the solution phase. Further, the yield and the composition of the polymer complex (B) depended on the molecular weight of PAA. The ratio in the polymer complex (B), $(PAA)_c/(PVP)_c$, formed with the PAA of a higher molecular weight was larger than that formed with the PAA of a lower molecular weight. The ratio in the polymer complex (A) (No. 9 in Table 1) was smaller than that of the polymer complex (B) formed with the PAA of M.W.=5300. These results suggest that the molecular weight of the polymerized AA in the presence of PVP is probably lower than 5300.

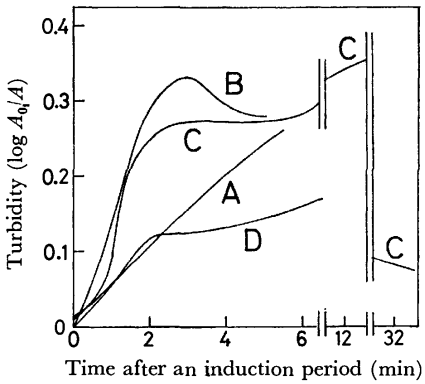

Fig. 10. Variation of turbidity with extent of the polymerization of AA.
$[AA]_0=[PVP]_0=2.0\times10^{-2}$ (mol/l);
$[K_2S_2O_8]_0=7.4\times10^{-3}$ (mol/l); 74±1°C.
Stirring; A, non; B, gentle; C, moderate; D, vigorous.

The turbidimetric method for measuring the extent of the polymerization of AA was examined. After an induction period of 7—13 min the turbidity of the polymerization system increased greatly, went through a maximum, and then decreased, as is shwon in Fig. 10. The variation in the turbidity depended on the stirring of the polymerization system. To compare the bromometric titration method with the turbidimetric method, an aliquot of the reaction mixture, which is shown as Curve C in Fig. 10, was provided for the bromometric titration. From the titration, the conversions in the polymerization of AA were found to increase (conversions of 64% at 12 min and 86% at 32 min, respectively) in spite of the decrease in the turbidity. This shows that the correlation between the turbidity and the conversion was not simple.

The change in the turbidity observed when a concentrated PAA solution was added to a PVP solution in the turbidity cell was also studied (Fig. 11). The turbidity increased greatly within 10 sec after the addition of the PAA solution, went through a maximum, then decreased and reached an equilibrium 2—3 min later. To this solution, a portion of the PAA solution was additionally introduced; the turbidity then changed as before. A linear relationship between the amount

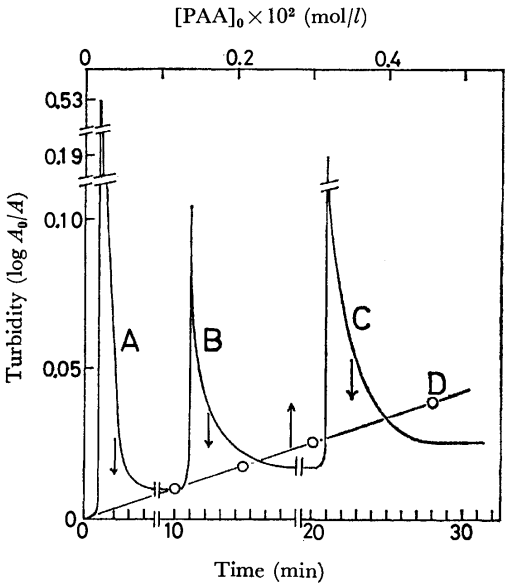

Fig. 11. Variation of turbidity with the amount of $[PAA]_0$.
Reaction solution, 20.0 ml; $[PVP]_0=2.0\times10^{-2}$ (mol/l), $[K_2S_2O_8]_0=7.4\times10^{-3}$ (mol/l).

Curve	Added PAA
A	0.04 ml
B	+0.03 ml
C	+0.03 ml

$[PAA\ (M.W.=5300)]=6.0\times10^{-1}$ (mol/l)
Curve D, equilibrium turbidity. 74±1°C.

of PAA and the equilibrium turbidity was observed; *cf.* the D line in Fig. 11. If the D line is adopted as a calibration curve of the polymerized AA in the polymerization, the rate of the polymerization, shown as Curve C in Fig. 10, should be 5×10^{-4} mol/l·sec. This value is similar to that Ferguson and Shah obtained (14.7×10^{-4} mol/l·sec). However, if we adopt the data at the maximum turbidity, the corresponding PAA should be about 200% to the fed-in AA. From these results, it may be considered that it is unreliable to measure the rate of the polymerization by following the turbidity.

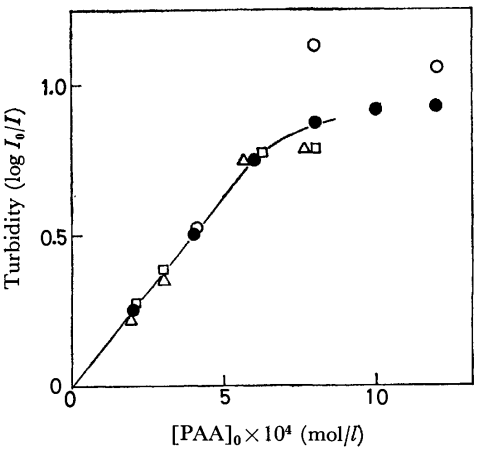

Fig. 12. Variation of turbidity with the amount of $[PAA]_0$.
$[K_2S_2O_8]_0=7.4\times10^{-3}$ (mol/l);
○, □: $[PVP]_0=2.0\times10^{-2}$ (mol/l);
△: $[PVP]_0=5.0\times10^{-2}$ (mol/l);
●: $[PVP]_0=[PA]_0=2.0\times10^{-2}$ (mol/l);
M.W. of PAA, 1900; light source, 500 mμ; 74±0.1°C.

Figure 12 shows the turbidity observed when a PAA solution was added to a PVP solution under various conditions. In this case, the turbidity was observed through a photocell (optical path, 1.00 cm) after mixing and shaking the PVP-$K_2S_2O_8$ solution and the PAA solution. As the linear relationship between the turbidity and $[PAA]_0$ was not obtained in the range of over 5×10^{-4} mol/l of $[PAA]_0$, this method could not be applied in our study.

Dscussion

The polymerization in the present study can not be explained as a "replica polymerization," because the mole ratio, $[PVP]_0/[AA]_0$, at which the rate of the polymerization was at its maximum changed with the $[AA]_0$ value (as is shown in Fig. 2), PA did not affect the rate of the polymerization (as is shown in Fig. 5), and the composition of the polymer complex (A) varied with the complex-forming conditions (Table 1).

Here, two simple model mechanisms may be considered:

A) specific-site binding mechanism ("replica polymerization"-AA adsorbed on PVP polymerizes) and B) polymer-atmosphere binding mechanism (AA drawn atmospherically by PVP polymerizes).

A) Mechanisms of Specific-site Binding. *Case A-1*): The adsorption of AA on PVP follows Langmuir's adsorption isotherm, and both adsorbed AA and not-adsorbed AA polymerize. The adsorption may be expressed as follows:

$$[P] + [M_f] \overset{K}{\rightleftarrows} [PM],$$
$$\theta = [PM]/[P]_0 = [M_f]/([M_f]+1/K)$$

where $[M_f]$ and $[PM]$ are not-adsorbed and adsorbed AA respectively and where $[M]_0$ and $[P]_0$ are volume-average concentrations of AA and PVP respectively (they are defined as $[PM]+[M_f]=[M]_0$, $[PM]+[P]=[P]_0$). K is an equilibrium constant of adsorption, and θ is the fraction of the adsorbed sites.

i) An adsorbed AA can migrate freely on PVP, and the rate of the polymerization of PVP is proportional to the adsorbed AA, (θ); the rate of the polymerization, V, can be expressed as:

$$V = [P]_0k_3\theta + k_4[M_f]^{1.5} = k_3[PM] + k_4[M_f]^{1.5} \quad \text{(A-1-1)}$$

where k_3 and k_4 are the rate constants of the polymerization of adsorbed AA on PVP and of not-adsorbed AA respectively.

ii) The rate of the polymerization of the adsorbed AA is proportional to the average length of the continuous sequence of AA molecules adsorbed on PVP, which is expressed as:

$$\nu = (1-\theta)\sum_{p=1}^{\infty}P\theta^{p-1} = 1/(1-\theta)$$

where p is the length of the continuous sequence of the AA adsorbed on PVP. The rate can, then be expressed as:

$$V = k_3[PM]/(1-\theta) + k_4[M_f]^{1.5} \quad \text{(A-1-2)}$$

Case A-2): An adsorption of AA on PVP follows Freundlich's adsorption isotherm ($n=2$)

$$\theta = [PM]/[P]_0 = a[M_f]^{1/2}$$

similar to i), then,

$$V = k_3[PM] + k_4[M_f]^{1.5} \quad \text{(A-2-1)}$$
$$V = k_3[PM]/(1-\theta) + k_4[M_f]^{1.5} \quad \text{(A-2-2)}$$

The calculated rates followed by (A-1-1), (A-1-2), (A-2-1), and (A-2-2) were all monotonous increasing functions with respect to $[PVP]_0$ and did not agree with the characteristics of the experimental results shown in Fig. 2.

Case A-3): Bamford *et al.* have presented the following expression for the polymerization on a template.[3]

$$V = C\exp(-\alpha Z^{\beta}/kT)[X]$$

where α and β are arbitrary constants, where C is the total radical concentration, where Z is $[P]/[PM]$, and where $[X]$ is $[PM]$. The total rate should be considered to be the sum of the rates of polymerization on and apart from the template. Accordingly, the following equation can be obtained:

$$V = C\exp\{-\alpha([P]/[PM]^{\beta}/kT\}[PM] + k_4[M_f]^{1.5} \quad \text{(A-3)}$$

The rate curve calculated by Eq. (A-3) using the numerical values of $K=22.2$ (l/mol) (K is Langmuir's adsorption constant), $C\exp(-\alpha/kT)/k_4=4.0375$, and $\beta=1.81946$, which were obtained from the initial and the optimum conditions of the experimental data, is shown as Curve E in Fig. 2. This curve deviates much from the experimental results obtained at higher concentrations of PVP. In addition, the fact that Eq. (A-3) gave similar values of $\{[PVP]_0/[AA]_0\}_{max}$ at different $[AA]_0$ values differs from the experimental results.

It is difficult to obtain an expression which agrees well with the characteristics of the experimental data in the present study, considering the mechanisms of specific-site binding.

B) A Mechamism of Polymer-Atmosphere Binding. A local concentration of AA can be expected to be distributed continuously in the reaction system. However, to simplify the discussion, the reaction system is assumed to be divided into two domains. One is a polymer domain where AA is concentrated in the vicinity of PVP (the volume fraction is f, the concentrations of PVP and AA in the polymer domain are $[P_p]$ and $[M_p]$ respectively), and the other is a free domain (the volume fraction is $1-f$, and the concentration of AA is $[M_f]$). Because MP did not affect the rate of the polymerization (Fig. 1), and because the dependence of the initiator on the rate of the polymerization of AA differed little in either the presence or absence of PVP (Fig. 7), the fundamental reaction mechanisms in both domains are assumed to be the same as in a homogeneous reaction system. As the PVP is a linear vinyl polymer, the shape of this polymer domain can be considered to be a cylinder along the chain of PVP. The total length of this cylinder is proportional to $[PVP]_0$. The $f/(1-f)$, ratio will increase with $[PVP]_0$ and decrease with $[AA]_0$. The contribution of $[AA]_0$ to the ratio is not simple, since the domain, f, will be set through an interdependence of $[M_f]$ and $[M_p]$. Thus, the following expression may be assumed:

$$f/(1-f) = [P]_0/a$$

where a is a function of the monomer and where $[P]_0$ is the volume average concentration of PVP. Considering the equilibrium and the stoichiometry:

$$[M_f] + [P_p] \overset{K}{\rightleftarrows} [M_p] \quad (K;\ \text{equilibrium constant})$$

$$f[M_p] + (1-f)[M_f] = [M]_0, \quad f[P_p] = [P]_0$$

where $[M]_0$ is the volume-average concentration of AA. Then, the overall rate of polymerization of AA, V can be expressed as follows:

$$V = fk[M_p]^{1.5} + (1-f)k[M_f]^{1.5}$$
$$= k[M]_0^{1.5}\{[P]_0([P]_0+a)^2+a([P]_0+a)^{0.5}(1/K)^{1.5}\}/$$
$$([P]_0^2+a[P]_0+a/K)^{1.5} \qquad (B)$$

As to the influence of PVP on the rate of the polymerization when $[AA]_0$ is 5×10^{-2} mol/l, the rate curve calculated by means of Eq. (B) with $K=64.7$ (l/mol) and $a=0.2$ is shown as Curve A in Fig. 2. The calculated rate curves with $a=0.38$ ($[AA]_0=2\times10^{-2}$ mol/l) and $a=0.19$ ($[AA]_0=10\times10^{-2}$ mol/l) are also shown as Curves B and C respectively. These curves agree well with the experimental data. Thus, a was found to be a function of $[AA]_0$, and it increased as $[AA]_0$ decreased. According to these results, the following empirical formula of a was obtained:

$$a = 1.2[M]_0 + 0.007/[M]_0$$

Using this formula, the relation between $[AA]_0$ and f was found to be as is shown in Fig. 13. At higher concentrations of $[AA]_0$, f decreased with $[AA]_0$. Regarding this phenomenon, two tentative considerations will be made. One is a shrinking of PVP by AA; the other is a shielding of PVP by AA according to a Debye-Hückel theory. As to the dependence of $[AA]_0$ on the rate of the polymerization the rate curve calculated by means of Eq. (B) with $K=64.7$ (l/mol) and $a=1.2[M]_0+0.007/[M]_0$ is shown as Curve A in Fig. 6. This calculated rate curve was found to agree with the experimental data and to be apparently proportional to the 1.9 powers of $[AA]_0$. As to the influence of PA on the rate of the polymerization, if the influence of PA to PVP is similar to that of AA to PVP, the rate V', may be expressed as follows:

$$V' = ([M_{AA}]_0/[M]_0)^{1.5}V \qquad (B')$$

where $[M]_0$ is $[M_{AA}]_0+[M_{PA}]_0$ and where $[M_{AA}]_0$, and $[M_{PA}]_0$ are the volume-average concentrations of AA and PA respectively. The calculated rate, V', defined by Eq. (B') with $K=67.4$ (l/mol) and $a=1.2[M]_0+0.007/[M]_0$ was apparently independent of the $[PA]_0$ values, which are shown as Curves A and B ($V'_{(B)PA=0}=9\times10^{-6}$ mol/l·sec) in Fig. 5. As has been mentioned above, the polymerization of AA in the presence of PVP in the present study can be explained well by a mechanism considering the locally-concentrated AA in the vicinity of PVP. Moreover, this consideration can also be applied to the other reaction system. Endo, Numazawa, and Okawara[6] have described that the rate of the polymerization of methacrylic acid (MAA) in the presence of poly-*N*-vinyloxazolidone (PNVOx) went through a maximum at [PNVOx]/[MAA] being unity. By applying Eq. (B) to their results without any further consideration, the calculated rate curve was found rather to fit their experimental data with $K=300$ (l/mol) and $a=0.07$. The larger K value obtained in their polymerization system can be explained reasonably as arising from a different magnitude of the interactive fource.

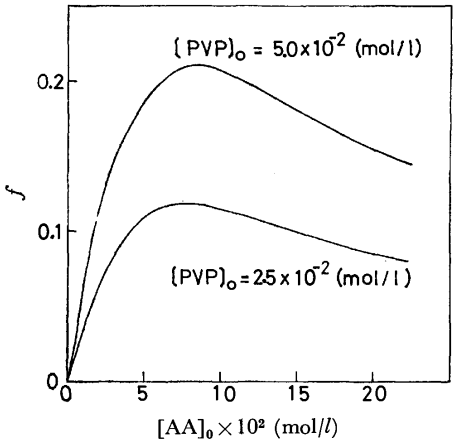

Fig. 13. Relation between $[AA]_0$ and f.

The authors are very grateful to Professor Kenichi Fukui, head of their laboratory, for his unfailing encouragement. Also, the authors are indebted to Mr. Teiji Kobayashi for his help in part of the measurements.

Asymmetric Hydrogenation of C=O Double Bond with Modified Raney Nickel. XXI. The Effect of Water on the Asymmetric Activity of the Catalyst

Toshio NINOMIYA*

Division of Organic Chemistry, Institute for Protein Research, Osaka University, Kita-ku, Osaka

(Received January 26, 1972)

The effect of water added to the hydrogenation system of methyl acetoacetate was investigated on catalysts modified with L-amino acids, their derivatives, and D- or L-hydroxy acids. In the absence of water, catalysts modified with all L-amino acids except L-serine and L-proline gave methyl $D_s(-)$-3-hydroxybutyrate, and in the presence of water all the catalysts modified with L-amino acids gave methyl $L_s(+)$-3-hydroxybutyrate. On the other hand, the catalysts modified with L- or D-hydroxy acids were not affected by the addition of water and gave an $L_s(+)$ or $D_s(-)$ hydrogenation product respectively. In the presence of water, the catalyst modified with the L-valine methyl ester gave an $L_s(+)$ product, while the catalysts modified with *N*-acetyl L-amino acids were not affected by water. As a whole, it was concluded that water added to the hydrogenation system affected the amino group of the modifying reagent on the catalyst surface, which might play an important role in the asymmetric control of the substrate approaching the catalyst surface. The water in the hydrogenation system also promoted the hydrogenation rate, regardless of the modifying reagents.

In a previous report on the investigation of asymmetric hydrogenation with Raney nickel catalysts modified with optically-active amino acids or hydroxy acids,[1] the catalysts modified with L-glutamic acid, L-valine, and L-alanine were demonstrated to show (+) asymmetric activities upon the addition of water, and it was concluded that water affected the asymmetric site of the catalyst rather than the position of the keto-enol equilibrium of the substrate, methyl acetoacetate.[2]

It seemed that an investigation of the effect of water on the asymmetric site of the catalyst would be important and informative in connection with the clarification of the asymmetric hydrogenation mechanism. The present work is intended to make clear the effect of the water.

The present paper will report on the effect of water on the asymmetric activities of the catalysts modified with L-amino acids, *N*-acetyl L-amino acids, L-amino acid methyl ester, L-amino acid nickel chelate, and L- or D-hydroxy acids. Also, the role of the amino group of the modifying reagent, L-amino acid, will be discussed in connection with the effect of water.

As as whole, it can be deduced that the amino group of L-amino acid plays an important role in the asymmetric control of the substrate approaching the catalyst surface.

The influence of water on the hydrogenation rate will also be referred to.

Experimental

The preparation and the modification of the Raney nickel catalyst, the hydrogenation of methyl acetoacetate, the addition of water to the hydrogenation system, and the measurement of the asymmetric activity of the catalyst were performed in the manner described in the previous paper.[1]

As the Raney nickel alloy, 1.5 g of R-Ni ND (from Kawaken Fine Chemicals Co., Ltd., lot 1949) was used, and as the substrate for hydrogenation was used 0.15 mol of methyl acetoacetate (from the Nippon Synthetic Chemical Industry Co., Ltd., lot 70).

Results and Discussion

Figures 1-1 and 1-2 shows the asymmetric activities of the catalysts modified with L-leucine (L-Leu), L-phenylalanine (L-Phe), L-tryptophan (L-Try), L-methionine (L-Met), L-threonine (L-Thr), L-serine

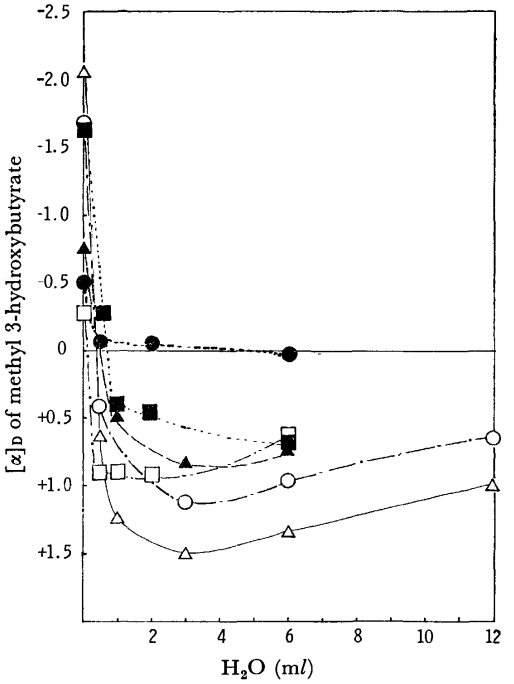

Fig. 1-1. Effect of added water on asymmetric activity of catalyst modified with L-amino acids at 0°C.
○: L-leucine △: L-methionine
△: L-phenylalanine ■: L-tryptophan
□: L-threonine ●: L-histidine

* Present address: Dai Nippon Toryo Co., Ltd., Nishinoshimonocho, Konohana-ku, Osaka.

1) Part XX: F. Higashi, T. Ninomiya, and Y. Izumi, This Bulletin, **44**, 1333 (1971).

2) The + or − asymmetric activity of the catalyst is represented by the optical rotatory sign (+ or −) of the hydrogenation product, methyl 3-hydroxybutyrate.

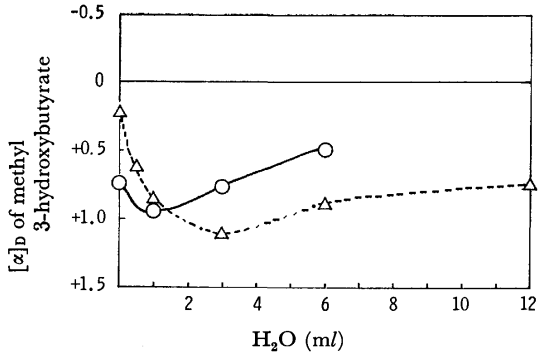

Fig. 1–2. Effect of added water on asymmetric activity of catalyst modified with L-serine and L-proline at 0°C.
—○—: L-serine ---△---: L-proline

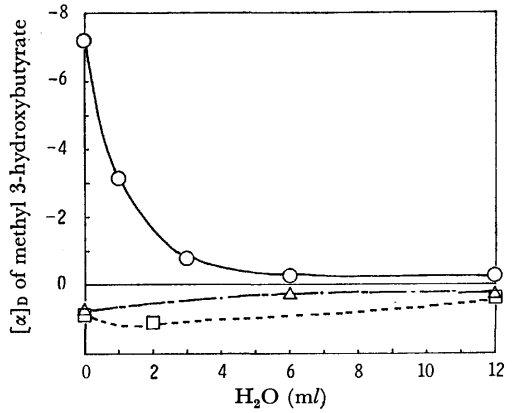

Fig. 2. Effect of added water on asymmetric activity of the catalyst modified with optically active hydroxy acids at 0°C.
—○—: D-tartaric acid
·-△-·: L-2-hydroxy-3-methylbutyric acid
—□—: L-2-hydroxy-3-phenylpropionic acid

(L-Ser), L-proline (L-Pro) and L-histidine (L-His) in the hydrogenation of methyl acetoacetate (MAA) with the addition of water. As is shown in Fig. 1, with the addition of water the catalysts modified with L-Leu, L-Phe, L-Try, L-Met, L-Thr, and L-His showed (+) asymmetric activity, while without any addition of water these catalysts showed (−) asymmetric activity. The catalysts modified with L-Ser and L-Pro, having (+) asymmetric activities in the absence of water, showed higher (+) asymmetric activities in the presence of water. Compared with the catalysts modified with other L-amino acids, the catalyst modified with L-His was little affected by water and showed only (+) asymmetric activity with the addition of 6 m*l* of water.

Figure 2 shows the effect of water on the catalysts modified with D-tartaric acid, L-2-hydroxy-3-methylbutyric acid, and L-2-hydroxy-3-phenylpropionic acid. The added water did not cause the inversion of the asymmetric direction when the catalysts were modified with these hydroxy acids.

As can be seen in Figs. 1 and 2, the catalysts modified with L-amino acids showed (+) asymmetric activities in the presence of water, while the catalysts modified with D- or L-hydroxy acids were not affected by water.

The above facts clearly show that the effect of water is characteristic of the catalysts modified with L-amino

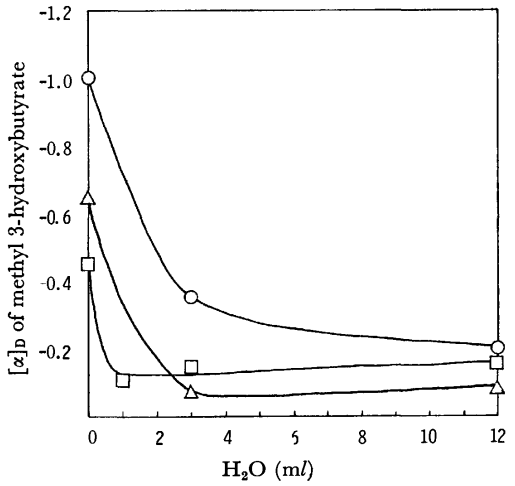

Fig. 3. Effect of additional water on asymmetric activity of catalyst.
—○—: Modification with *N*-acetyl L-isoleucine at 0°C
—△—: Modification with *N*-acetyl L-phenylalanine at 0°C
—□—: Modification with *N*-acetyl L-alanine at 0°C

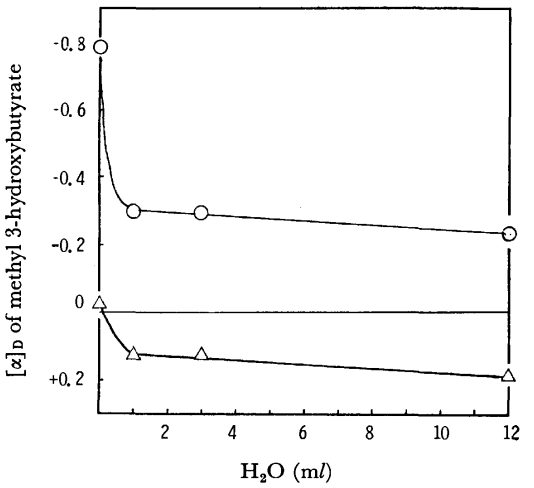

Fig. 4. Effect of additional water on asymmetric activity of catalyst.
—○—: Modification with *N*-acetyl-L-valine at 0°C
—△—: Modification with L-valine methyl ester at 0°C

acids. In the previous paper,[1] the water added to the hydrogenation system was demonstrated to influence the asymmetric sites of the catalysts modified with L-amino acids.

In order to investigate in detail the effect of water on the asymmetric site of the catalyst modified with L-amino acids, the effect of water on the catalysts modified with *N*-acetyl L-amino acids and the L-amino acid methyl ester was examined.

Figure 3 shows the effect of water on the catalysts modified with *N*-acetyl L-isoleucine, *N*-acetyl L-phenylalanine, and *N*-acetyl L-alanine. As may be seen in Fig. 3, even in the presence of water these catalysts showed (−) asymmetric activities and did not show (+) asymmetric activities; this was in striking contrast to the catalysts modified with L-Ileu, L-Phe, and L-Ala. The above facts suggest that the sensitivities of the catalyst to water may be decreased by the acetylation of the amino group.

Figure 4 shows the effect of water on the asymmetric activities of catalysts modified with the L-valine methyl ester and *N*-acetyl L-valine. As may be seen in Fig. 4, in the presence of water the catalyst modified with the L-valine methyl ester showed (+) asymmetric activity, while the catalyst modified with *N*-acetyl L-valine showed (−) asymmetric activity. The above facts make it clear that the free amino group may be affected by water and bring the catalyst (+) asymmetric activity. From the standpoint of the above discussion, the effect of the water on the asymmetric activity of the catalyst modified with L-histidine shown in Figs. 1–1 can be explained as follows; L-histidine, well known as a strong chelating reagent, can be adsorbed as a tridentate on the catalyst surface, and, because of both the steric and electrostatic effects of the imidazole group neighboring the amino group, the amino group may be hardly affected at all by a small amount of water added to the hydrogenation system.

Figure 5 illustrates the effect of water on the catalyst modified with the L-valine nickel chelate. As is illustrated in Fig. 5, the catalyst modified with the L-valine nickel chelate, which showed a much higher (−) asymmetric activity than the catalyst modified with L-valine in the absence of water, also gave (+) asymmetric activity in the presence of water, as did the catalyst modified with L-valine. The amino group of the L-valine nickel chelate is considered to be in a nearly free state, because, as is shown in Fig. 6, the nickel L-valine complex had adsorption bands corresponding to the ν_s and ν_{as} of NH_2 around 3300 cm^{-1}, while crystalline L-valine showed absorption bands around 3000 cm^{-1} assigned to the ν_s and ν_{as} of NH_3^+. Accordingly, the catalyst modified with the L-valine nickel chelate is considered to be easily affected by water to show (+) asymmetric activity.

The above discussion shows that water can affect the free amino group of the L-amino acid used as the modifying reagent and cause the inversion of the asymmetric activity and/or give higher (+) asymmetric activity to the catalyst modified with L-amino acid. From the fact that the catalyst modified with the L-valine methyl ester behaved toward water like that modified with L-valine, as is shown in Fig. 4, but showed a far lower (−) asymmetric activity than that modified with L-valine, it seems that the carboxyl group of the modifying reagent is independent of the effect of water and probably participates in the stable

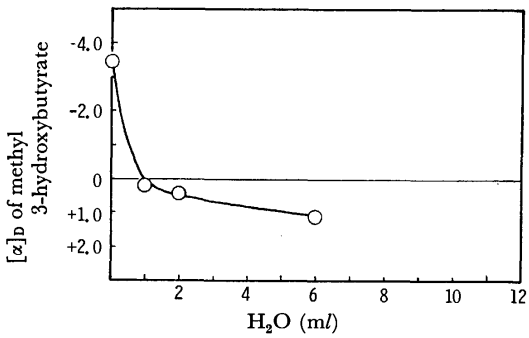

Fig. 5. Effect of additional water on asymmetric activity of catalyst. (Modification with L-valine nickel chelate at 0°C)

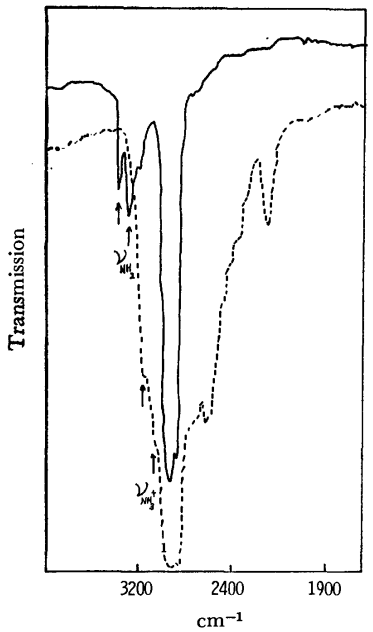

Fig. 6. IR spectra of Ni[L-Val]$_2$ (Nujol, ——) and L-Val (Nujol, ——).

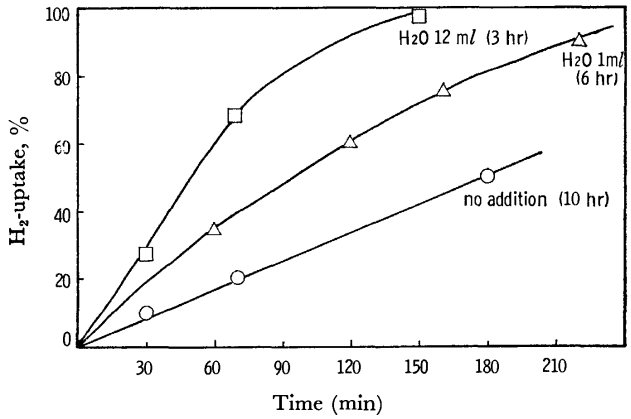

Fig. 7. Effect of additional water on hydrogenation rate. (Modified with D-tartaric acid at 0°C, pH 5.0)

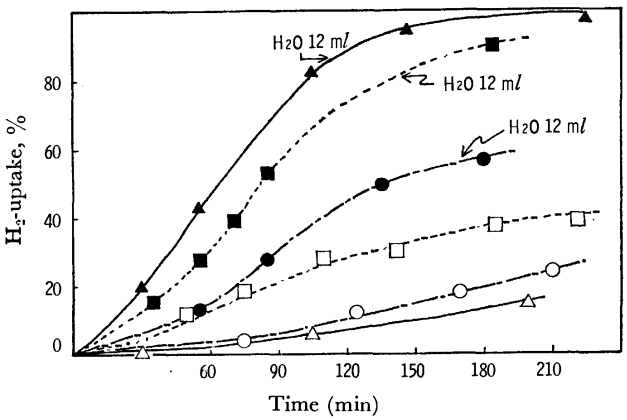

Fig. 8. Effect of additional water on hydrogenation rate.
—△—: Modification with L-valine at 0°C
—○—: Modification with L-3-methyl-2-hydroxybutyric acid at 0°C
—□—: Modification with *N*-acetyl L-isoleucine at 0°C

adsorption of the modifying reagent on the catalyst surface. As a whole, it can be concluded that the amino group of L-amino acid plays an important role in the asymmetric control of the substrate approaching the catalyst surface.

In Fig. 7 the hydrogenation rate is plotted against the amount of water added to the hydrogenation system in the modification with D-tartaric acid. As is illustrated in Fig. 7, the addition of 12 m*l* of water brought about the promotion of the hydrogenation rate and carried the hydrogenation to completion in about 3 hr, while the standard hydrogenation, without any addition of water, took about 10 hr.

A similar promotion of the hydrogenation rate was also observed when the catalysts were modified with L-valine, L-2-hydroxy-3-methylbutyric acid, and *N*-acetyl L-isoleucine, as is shown in Fig. 8.

From the above facts it can be concluded that the water added to the hydrogenation system promotes the hydrogenation rate, independent of the kind of modifying reagent used in the asymmetric hydrogenation of methyl acetoacetate.

The author wishes to express his thanks to Professor Yoshiharu Izumi for his valuable advice and encouragement throughout this work.

BULLETIN OF THE CHEMICAL SOCIETY OF JAPAN, VOL. 45, 2548—2550 (1972)

Asymmetric Hydrogenation of C=O Double Bond with Modified Raney Nickel. XXII

Toshio NINOMIYA*

Division of Organic Chemistry, Institute for Protein Research, Osaka University, Kita-ku, Osaka

(Received January 26, 1972)

The state of the amino acid molecule used as a modifying reagent on a catalyst surface was investigated. From the relationship between the asymmetric activities of the catalysts modified with L-valine and its derivatives and the stability constants of the nickel chelates of L-valine and its derivatives, it was concluded that L-valine adsorbs like a ligand of the chelate on the catalyst surface. This conclusion was also supported by the finding that the asymmetric activity of the catalyst modified with the nickel L-valine chelate was higher than those of the catalysts modified with L-valine and its derivatives. Also, the asymmetric activities of the catalysts modified with L-histidine, L-serine, and L-proline, and with the nickel chelates of the above three L-amino acids were discussed on the basis of the stability constants of the nickel chelates of the above three L-amino acids, it was concluded that two conditions at least are necessary for the modifying reagent to be effective; it must adsorb stably on the catalyst surface, and it must have a structure affording effective asymmetric control of the substrate.

In a series of investigations of asymmetric hydrogenation by our research group, it has been reported that the catalysts modified with *O*-acetyl D-tartaric acid, *O*-benzoyl D-tartaric acid, and the D-tartaric acid diethyl ester show lower (−) asymmetric activities than the catalyst modified with D-tartaric acid, and also that the catalysts modified with *N,N*-dimethyl-L-glutamic acid and *N*-cyanoethyl-L-glutamic acid have lower (−) asymmetric activities than the catalyst modified with L-glutamic acid.[1] From the above results, it was conclusively inferred that a hydroxyl group or an amino group and a carboxyl group are desirable modifying reagents to produce the high asymmetric activity of the catalyst.

However, no systematic information about the adsorption state of the modifying reagent on the catalyst surface has been obtained. The present work was undertaken in order to elucidate the adsorption state of the modifying reagent, L-amino acid, on the catalyst surface. As the modifying reagents, monoamino monocarboxylic acids were mainly used by virtue of the ease of analysis of the state of the modifying reagent on the catalyst surface.

The adsorption form of amino acid formed by the chelation on the catalyst surface is discussed on the correlation between the asymmetric activity of the catalyst and the stability constant of the nickel chelate of the modifying reagent. Furthermore, the essential chemical character of the modifying reagent in the asymmetric hydrogenation is discussed.

Experimental

The preparation of the modified Raney nickel catalyst, the hydrogenation of methyl acetoacetate, and the measurement of the asymmetric activity of the catalyst were done as described in a previous paper.[2]

Results and Discussion

Table 1 indicates the asymmetric activities of the catalysts modified with L-valine and its derivatives. As Table 1 indicates, the catalyst modified with L-valine showed a higher (−) asymmetric activity than the

* Present address: Dai Nippon Toryo, Co., Ltd., 38 Nishino-shimonocho, Konohana-ku, Osaka.

1) S. Tatsumi, M. Imaida, Y. Fukuda, Y. Izumi, and S. Akabori, This Bulletin, **37**, 846 (1964).

2) Y. Izumi, T. Harada, T. Tanabe, and K. Okuda, This Bulletin, **44**, 1418 (1971).

Table 1. The asymmetric activities of the catalysts modified with L-valine and L-valine derivatives

Modifying reagent	Solvent	concn. %	Modifying condition Temp. (°C)	Time (min)	$[\alpha]_D$ of Methyl 3-hydroxybutyrate
L-Valine	H_2O	2	0	90	−2.47
L-Valine·Na	H_2O	2	0	90	−0.33
L-Valine·HCl	H_2O	2	0	90	−1.79
N-Acetyl L-Valine	H_2O	1	0	90	−0.79
N-Benzoyl-L-valine	MeOH	1	0	90	−0.27
L-Valine methyl ester	H_2O	1	0	90	−0.20
L-Valinol	H_2O	1	0	90	−0.15
trans-Ni[L-Val]$_2$ ·H_2O	MeOH	1	0	90	−3.42
trans-Cu[L-Val]$_2$	MeOH	0.2	0	90	−3.10
Zn[L-val]$_2$	MeOH	0.8	0	90	−2.32

R–Ni ND (Kawaken Fine Chemicals Co., Ltd.) lot 1949 1.5 g.
MAA (The Nippon Synthetic Chemical Industry Co., Ltd.) lot 70, 0.15 mol.

catalysts modified with *N*-acetylated L-valine, L-valine methyl ester, and L-valinol.

From the information provided by co-ordination chemistry, L-amino acids are well known as usual chelating reagents for transition metals, and it is also known that the stability constants of the metal chelates of L-amino acids are depressed by the chemical derivation of the amino group or carboxyl group.[3)]

On the basis of the above facts, the decrease in the (−) asymmetric activity of the catalyst by the chemical derivation of the amino or carboxyl group of the modifying reagent, as is shown in Table 1 seems to depend on the depression of the stability of the chemical adsorption of the modifying reagent on the catalyst surface by the chemical derivation, and the modifying reagent, L-valine, seems to be adsorbed as a ligand of the chelate on the catalyst surface.

Table 2. The asymmetric activities of the catalysts modified with L-Ileu, L-Phe, L-Met and their metal chelates

Modifying reagent	Solvent	concn. %	Modifying condition Temp. (°C)	Time (min)	$[\alpha]_D$ of Methyl 3-hydroxybutyrate
trans-Ni[L-isoleu]$_2$ ·$2H_2O$	MeOH	1	0	90	−2.98
cis-Cu[L-isoleu]$_2$ ·$2H_2O$	MeOH	1	0	90	−2.44
L-Isoleucine	H_2O	1	0	90	−2.84
Ni[L-Phe]$_2$·$2H_2O$	$PhCH_2OH$	1	0	90	−1.89
L-Phenylalanine	H_2O	1	0	90	−2.11
Ni[L-Met]$_2$·$1/2H_2$	H_2O	0.8	0	90	−0.86
L-Methionine	H_2O	1	0	90	−0.72

R–Ni ND (Kawaken Fine Chemicals Co., Ltd.) lot 1949, 1.5 g.
MAA (The Nippon Synthetic Chemical Industry Co., Ltd.) lot 70, 0.15 mol.

3) a) R. B. Martin and J. T. Edsall, *J. Amer. Chem. Soc.*, **82**, 1107 (1960); b) J. M. White, R. A. Manning, and N. C. Li, *ibid.*, **78**, 2367 (1956).

Table 2 lists the asymmetric activities of the catalysts modified with L-isoleucine (L-Ileu). L-phenylalanine (L-Phe), and L-methionine (L-Met) and those nickel chelates. As is listed in Table 2, the asymmetric activities of the catalysts modified with the nickel chelates of the above three L-amino acids were nearly equal to or higher than those of the catalysts modified with the corresponding L-amino acids. The catalysts modified with *N*-acetyl L-isoleucine and *N*-acetyl L-phenylalanine showed far lower (−) asymmetric activities than those modified with L-Ileu and L-Phe respectively. The low (−) asymmetric activities of the catalysts modified with *N*-acetyl L-isoleucine and *N*-acetyl L-phenylalanine probably result from the less stable adsorption of *N*-acetyl L-isoleucine and *N*-acetyl L-phenylalanine on the catalyst surface than that of L-Ileu and L-Phe. These results also support the above-mentioned deduction that the L-amino acid used as the modifying reagent adsorbs like a ligand of the chelate on the catalyst surface.

Table 2 also shows that the catalyst modified with the *trans* nickel L-isoleucine chelate and a higher (−) asymmetric activity, while, the catalyst modified with the *cis* copper L-isoleucine chelate had a lower (−) asymmetric activity, than the catalyst modified with L-Ileu. These results may be interpreted as follows: in the modification of the *trans* nickel L-isoleucine chelate, both secondary butyl groups of the nickel L-Ileu chelate stretch out on the same side from the chelate-ring plane and the chelate adsorbs through the *d*-electron as the less sterically-hindered side on the catalyst surface, as is illustrated in Fig. 1.

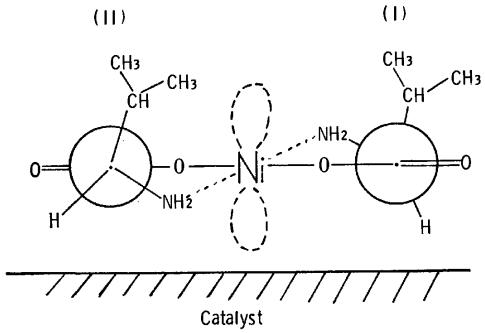

Fig. 1. Proposed adsorption state of *trans* nickel L-isoleucine chelate.

When the substrate, methyl acetoacetate, approaches the catalyst surface, if the interaction of the substrate with the right modifying reagent molecule (I) in Fig. 1, fit for the asymmetric hydrogenation, the left molecule (II) should strongly reject the substrate, and *vice versa*.

Consequently, in the modification of *trans* nickel L-isoleucine chelate, the push-pull effect by both modifying molecules, I and II, on the asymmetric control of the substrate would cause higher (−) asymmetric activity than in the modification with L-Ileu, which produces mixture of *cis* and *trans* forms on the

catalyst surface. On the other hand, in the case of modification with the *cis* copper L-isoleucine chelate naturally hinders the adsorption of the chelate, so that the *cis* chelate adsorbs less stably than L-Ileu and the *trans* chelate. The catalyst modified with the *cis* chelate would give a lower (−) asymmetric activity than those modified with the *trans* nickel L-isoleucine chelate and L-Ileu.

The above discussion is also supported by the fact that the catalyst modified with the nickel L-valine chelate shows far more (−) asymmetric activity than that catalyst modified with L-valine. The high asymmetric activities of the catalysts modified with the *trans* nickel L-valine chelate and the *trans* copper L-valine chelate, shown in Table 1, seem to be due to stable adsorption by the *d*-electron of nickel or copper metal on the catalyst surface.

TABLE 3. THE ASYMMETRIC ACTIVITIES OF THE CATALYSTS MODIFIED WITH L-Ser, L-Thr, L-Pro, L-His AND THEIR NICKEL CHELATES

Modifying reagent	Solvent	concn. %	Modifying condition		$[\alpha]_D$ of Methyl 3-hydroxybutyrate
			Temp. (°C)	Time (min)	
Ni[L-Ser]$_2$·2H$_2$O	H$_2$O	1	0	90	+0.39
L-Serine	H$_2$O	2	0	90	+0.72
Ni[L-Thr]$_2$·2H$_2$O	H$_2$O	1	0	90	±0.00
L-Threonine	H$_2$O	1	0	90	−0.27
Ni[L-Pro]$_2$·2H$_2$O	H$_2$O	1	0	90	+0.12
L-Proline	H$_2$O	1	0	90	+0.18
Ni[L-His]$_2$·H$_2$O	H$_2$O	1	0	90	±0.00
L-Histidine	H$_2$O	1	0	90	−0.48

R-Ni ND (Kawaken Fine Chemicals Co., Ltd.) lot 1949, 1.5 g.
MAA (The Nippon Synthetic Chemical Industry Co., Ltd.) lot 70, 0.15 mol.

Table 3 lists the asymmetric activities of the catalysts modified with L-serine (L-Ser), L-threonine (L-Thr), L-proline (L-Pro), and L-histidine (L-His) and the nickel chelates of those L-amino acids.

As is listed in Table 3, all the catalysts modified with L-His, L-Ser, L-Thr, and L-Pro showed smaller asymmetric activies than the catalysts modified with L-Val, L-Ileu, and L-Phe, shown in Tables 1 and 2, and they did not always show the (−) asymmetric direction.

The stability constants of nickel chelates of Pro, Ser, and His are known to be equal or greater than that of Val,[3,4] and the above discussion suggests that the stable adsorption of the modifying reagent, *i.e.*, chelation, on the catalyst surface can cause a high asymmetric activity in the catalyst. However, contrary to expectation, the asymmetric activities of the catalysts modified with L-Pro, L-Ser, L-His and L-Thr are less than that of the one modified with Val. The above phenomena can be explained as follows: though Pro, Ser, His and perhaps Thr can adsorb stably on the catalyst surface, their asymmetric control ability to the substrate would be far less effective than that of L-Val, L-Ileu, and L-Phe.

Also, as is shown in Table 3, catalysts modified with nickel chelates of L-His, L-Ser, L-Thr and L-Pro gave lower asymmetric activities than catalysts modified with L-His, L-Ser, L-Thr, and L-Pro respectively. In according for the above fact, it can be considered that all the six bonding electrons of nickel metal are completely occupied by two tridentate-ligand molecules and that the nickel chelate of those ligands will be attached to the catalyst surface only by weak physical adsorption, so that the catalysts modified with these nickel chelates show low asymmetric activities.

On the basis of the above discussion as a whole, it can be concluded that the modifying reagent, L-monoamino monocarboxylic acid, should adsorb like a ligand of the chelate on the catalyst surface and that two conditions at least are necessary in a desirable modifying reagent in the asymmetric hydrogenation; it must adsorb stably on the catalyst surface and it must have a structure affording effective asymmetric control of the substrate.

The author wishes to express his sincere thanks to Professor Yoshiharu Izumi for his valuable advice and encouragement throughout this work.

4) A. Albert, *Biochem. J.*, **47**, 531 (1950); R. Leberman and B. R. Rabin, *Trans. Faraday Soc.*, **55**, 1660 (1959).

Asymmetric Hydrogenation of C=O Double Bond with Modified Raney Nickel Catalyst. XXIII

Toshio NINOMIYA*

Division of Organic Chemistry, Institute for Protein Research, Osaka University, Kita-ku, Osaka

(Received January 26, 1972)

The ultraviolet spectra of acetylacetone and methyl acetoacetate adsorbed on evaporated nickel film modified with amino or hydroxy acid were measured. The spectroscopic data suggested that the adsorbed species of acetylacetone was affected by the modifying pH, that the interaction between acetylacetone and the hydroxy acid was different from that between acetylacetone and the amino acid, and also that methyl acetoacetate, similar to acetylacetone, chemisorbed with a pseudo aromatic ring on the nickel surface. Consequently, the above results strongly support the theory that in the asymmetic hydrogenation, the substrate, acetylacetone or methyl acetoacetate, approaches the catalyst surface in a form like a pseudo aromatic ring, that it is asymmetrically controlled by the modifying reagent adsorbed on the catalyst surface, and, further, that the ease of the adsorption of the substrate onto the catalyst determines the rate of asymmetric hydrogenation.

In the course of the investigation of asymmetric hydrogenation with modified Raney nickel catalysts, many kinds of ketones have been used as the substrate for the asymmetric hydrogenation; β-ketoester and β-diketone have been demonstrated to be the most suitable substrates.[1] However, the approach mechanism of the substrate to the catalyst surface has not been made clear. The clarification of the approach-mechanism of the substrate to the catalyst surface would give important information for solving the mechanism of the asymmetric hydrogenation.

The present work is intended to make clear the approach-mechanism of the acetylacetone (Hacac) and methyl acetoacetate (MAA) substrates to the catalyst surface.

In a previous short communication[2] the absorption spectra of Hacac adsorbed on evaporated nickel film modified with D-tartaric acid have been reported. The present paper will report, in detail, on the adsorption state of the substrate, Hacac or MAA, onto evaporated nickel film modified with optically-active amino or hydroxy acid.

The experimental procedure developed by Kishi *et al.*[3] was improved. The adsorption spectra of Hacac adsorbed on the nickel film modified at various modifying pH values suggested that the adsorbed species of Hacac on the nickel film can be changed by changing the modifying pH and that Hacac can be adsorbed with ease on the nickel surface with an increase in the modifying pH.

Moreover, from the fact that, at the same modifying pH the absorption spectra of Hacac on the nickel film modified with tartaric acid were different from those of Hacac on the nickel film modified with glutamic acid, it was concluded that the substrate, in approaching the nickel surface, is affected characteristically by the asymmetric control of the modifying reagent adsorbed on the nickel surface and that the asymmetric control mechanism by hydroxy acid for the substrate was different from that by amino acid because of the difference in the chemical interaction between the hydroxy group and the amino group with the substrate.

As for MAA, which is similar to Hacac, it was made clear that MAA chemisorbs like a chelate with a pseudo aromatic ring on the nickel surface, and the ease of the adsorption of MAA on the evaporated nickel film modified with an optically-active compound was parallel with the asymmetric hydrogenation rate of MAA in the presence of a catalyst modified by the corresponding modifying reagent.

Experimental

The experimental apparatus developed by Kishi[3] was improved and used; *cf.* Fig. 1. The evaporation conditions of nickel onto the quartz windows was the same as the conditions reported by Kishi.[3] After the nickel had been evaporated onto the quartz windows, the break-off seal (G) was broken by means of the glass-coated magnet (H) and a 2% modifying aqueous solution (I), which had been degassed, was gently introduced into the quartz cell. At 0°C for 30 min, the nickel surface was modified by the modifying aqueous solution. Then, the modifying aqueous solution was transported into I, the modified nickel film was washed twice with water, and the water was evaporated from the ultraviolet cell. The substrate, acetylacetone or methyl acetoacetate, was introduced into the cell, and then the ultraviolet spectra were recorded on a Hitachi EPS-2 spectrophotometer equipped with a liquid nitrogen trap.

The GR-grade acetylacetone was obtained from Nakarai Pure Chemicals, while the methyl acetoacetate was obtained from The Nippon Synthetic Chemical Co., Ltd., both were distilled several times under a vacuum. The purity of the nickel wire is 99.5%.

Results and Discussion

1) Adsorption of Acetylacetone (Hacac). Figure 2 illustrates the absorption spectra of Hacac adsorbed on the evaporated nickel film modified with D-tartaric acid at pH 2.0, 5.0, and 9.0. As is illustrated in Fig. 2, in the modification at pH 2.0 a weak band was observed around 280 mμ after a 30-min exposure

* Present address: Dai Nippon Toryo, Co., Ltd., 38 Nishinoshimonocho, Konohana-ku, Osaka.

1) Y. Izumi, M. Imaida, T. Harada, T. Tanabe, S. Yajima, and T. Ninomiya, This Bulletin, **42**, 241 (1969); T. Tanabe, *ibid.*, to be published.

2) T. Ninomiya, K. Kishi, and S. Ikeda, *ibid.*, **43**, 2270 (1970).

3) K. Kishi, S. Ikeda, and K. Hirota, *J. Phys. Chem.*, **71**, 4384 (1967).

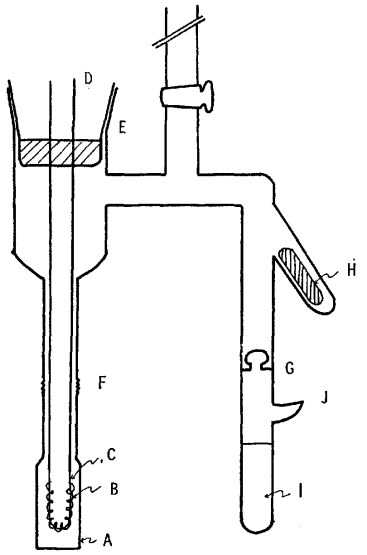

Fig. 1. Dirgram of the ultraviolet cell.

A: quartz cell	F: graded seal
B: nickel metal wire	G: break-off seal
C: tungsten filament	H: glass-coated magnet
D: heavy tungsten leads	I: tartaric acid solution
E: taper joint	J: fused seal

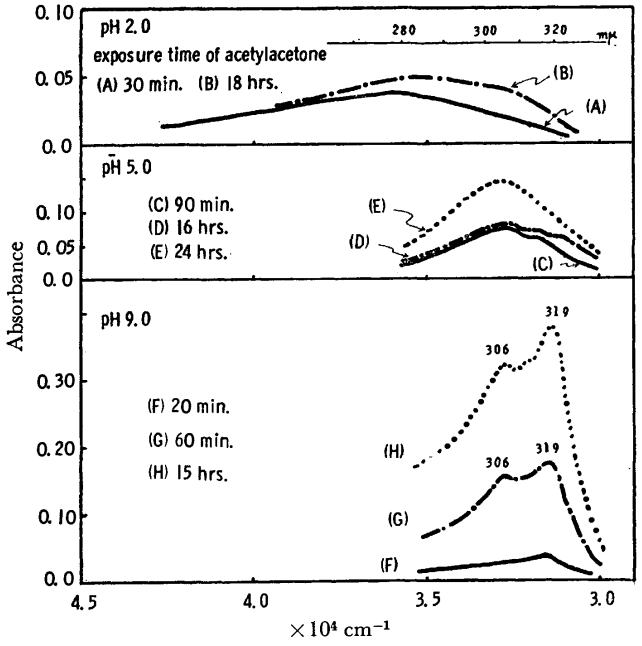

Fig. 2. Ultraviolet spectra of acetylacetone adsorbed on nickel film with preadsorbed D-tartaric acid at pH 2.0, 5.0, and 9.0.

to acetylacetone, and the band maximum shifted to a longer wavelength after 18 hr. In the modification at pH 5.0, absorption peaks were observed at 306, 316, and 322 mμ after 16 hr; these peaks became one at 303—306 mμ after 24 hr. In the treatment at pH 9.0, three intensive bands were observed at 306, 313, and 319 mμ after 15 hr.

The maximum peak at 303 mμ was assigned to an absorption peak of the π-π^* transition of adsorbed $acac^-$ in the study by Kishi *et al.*[2] of the absorption spectrum of Hacac adsorbed on the unmodified nickel film.

Tanabe,[4] one of our research group, suggested that, in the modification with a free tartaric acid aqueous solution (pH 2.0), one of the carboxyl groups of tartaric acid is bound to the catalyst surface, while the other, being undissociated, stretches out from the nickel surface and is dissociated by the neutralization, with an increase in the modifying pH.

On the basis of the above information, the results in Fig. 2 can be explained by the following proposition. In the modification at pH 2.0, the acidic β-carboxyl group stretching out from the nickel surface could hinder the enolization of Hacac, which would favor Hacac making a stable adsorption with a chelation from on the nickel surface; consequently, enol-form Hacac could hardly adsorb on the nickel surface. Hence, we observed the shift of adsorption maximum at 303 mμ, which was seen in the adsorption of Hacac on the unmodified nickel surface, to at shorter wavelength position.

In the modification at pH 5.0, the acidity of the β-carboxyl group of tartaric acid should be mostly neutralized; therefore, acetylacetone can adsorb with a stable pseudo aromatic ring on the nickel surface because there is little hindrance by the acidity of the β-carboxyl group, and the absorption band can be considered to show a maximum peak at 303—306 mμ.

In the treatment at pH 9.0, both carboxyl groups of tartaric acid were mostly neutralized, the amounts of tartaric acid adsorbed were moderately small compared with the amounts adsorbed in the modification at pH 5.0,[5] and acetylacetone would adsorb more easily

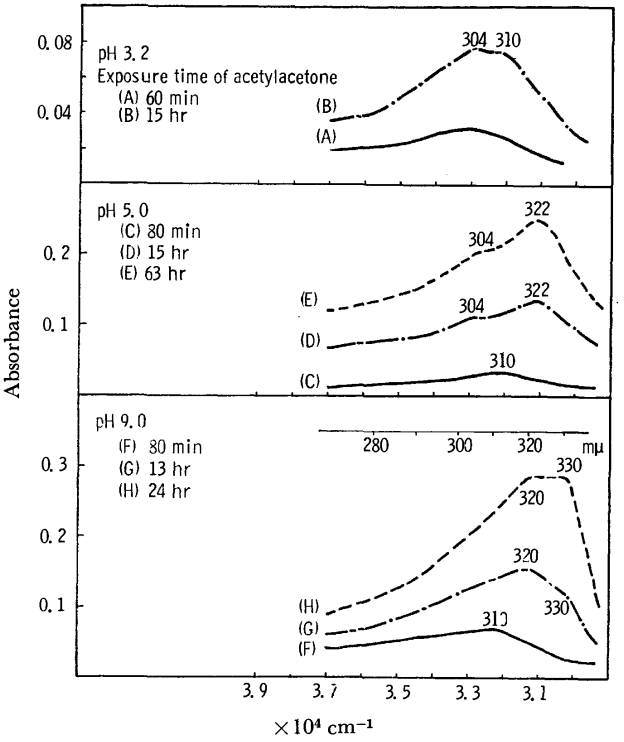

Fig. 3. Ultraviolet spectra of acetylacetone adsorbed on nickel film with preadsorbed L-glutamic acid at pH 3.2, 5.0, and 9.0.

4) T. Tanabe, This Bulletin, to be published.
5) S. Tatsumi, This Bulletin, **41**, 408 (1968).

than at pH 5.0. Thus, the chemical circumstances on the catalyst surface at pH 9.0 were different from those at pH 5.0. Therefore, the absorption spectrum of Hacac at pH 9.0 is considerably different from that at pH 5.0 as is shown in Fig. 2.

Figure 3 displays the absorption spectra of Hacac adsorbed on the nickel film modified with L-glutamic acid at pH 3.2, 5.0, and 9.0. As is illustrated in Fig. 3, in the modification at pH 3.2 two weak bands, at 304 mμ and 310 mμ, were observed after 15 hr's exposure to acetylacetone.

With an increase in the modifying pH value, the bands of adsorbed Hacac shifted to longer wavelength positions and their intensities increased. The above shift of the adsorption bands with an increase in the modifying pH must be due to the effect or γ-carboxyl group of L-glutamic acid, as in the modification with tartaric acid.

On the basis of the above facts and discussion, it is clear that the approaching form of the substrate was affected by the chemical circumstances of the modifying reagent on the nickel surface; that is, in acidic circumstances acetylacetone could hardly take the enol form while in neutral or basic circumstances acetylacetone could take the enol form and could stably adsorb with a pseudo aromatic ring on the nickel surface.

Moreover, a remarkable difference between Figs. 2 and 3 was observed at the same modifying pH. That is, at both pH 5.0 and pH 9.0 the absorption spectra in the modification with tartaric acid were different from those in the modification with glutamic acid. This important difference in the absorption spectra is due to the difference in chemical interaction between the substrate and the modifying reagent, probably because of the difference in reactivity to the substrate between the amino group of amino acid and the hydroxy group of hydroxy acid. For example, the amino group can behave as a base to the substrate, acetylacetone, the enol form of which may act as an acid, and can also form a Schiff base with the ketone group of the substrate, while the hydroxy group acting as an acid can make a hydrogen bond with the ketone group of the substrate.

This difference in chemical interaction between the amino and the hydroxy groups and the carbonyl group of the substrate seems to result in a difference in asymmetric direction between the catalysts modified with L- (or D-) amino acid and L- (or D-) hydroxy acid. As a matter of fact, the catalysts modified with L-aspartic acid show (−) asymmetric activity, while the catalysts modified with L-malic acid show (+) asymmetric activity, in the asymmetric hydrogenation of methyl acetoacetate.[6]

In conclusion, the above phenomenon supports strongly the idea that, in the asymmetric hydrogenation, the substrate approaching the catalyst surface is perturbed and affected asymmetrically by the modifying reagent on the catalyst surface.

2) Adsorption of Methyl Acetoacetate. Figure 4 illustrates the absorption spectra of methyl acetoacetate (MAA) adsorbed on the unmodified nickel film. As is illustrated in Fig. 4, a broad band was observed at 285 mμ. The band did not disappear upon the use of a liquid nitrogen trap, although the band at 239 mμ due to vapor MAA disappeared upon the use of a liquid nitrogen trap. In addition, the intensity of the band increased with an increase in the time of exposure to MAA, and upon exposure to acetic acid vapor the band disappeared instantly.

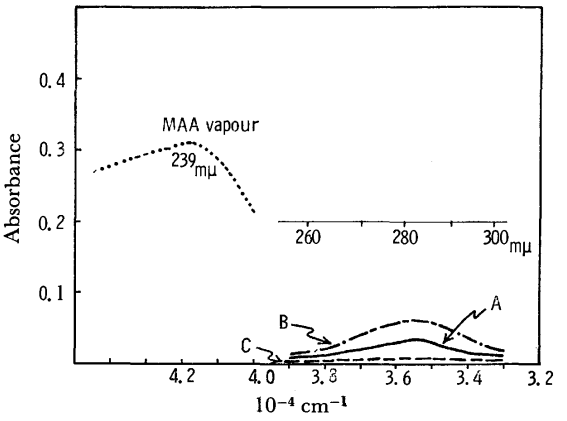

Fig. 4. Ultraviolet spectra of methyl acetoacetate adsorbed on nickel film (without preadsorption).
A: 60 min B: 18 hr C: 30 sec after AcOH

The above facts support the idea that the band at 285 mμ is to be ascribed to the chemisorbed species of MAA on the nickel film. Further, from the fact that the position of the band maximum of chemisorbed MAA (285 mμ) is near that of nickel methyl acetoacetate (278 mμ in methanol), MAA can be concluded to chemisorb like a chelation form with a pseudo aromatic ring on the nickel surface.

Figure 5 shows the absorption spectra of MAA adsorbed on nickel film modified with L-valine, L-glutamic acid, L-histidine, and D-tartaric acid. As is shown in Fig. 5, the intensities of the absorption spectra originating from MAA adsorbed on the nickel surfaces modified with valine, glutamic acid, and histidine

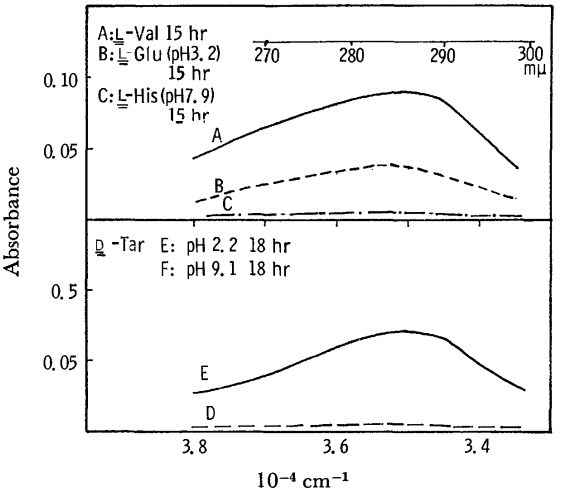

Fig. 5. Ultraviolet spectra of methyl acetoacetate adsorbed on nickel film with preadsorbed L-valine, L-glutamic acid, L-histidine, and D-tartaric acid.

6) Y. Izumi, S. Yajima, K. Okubo, and K. K. Babievsky, *ibid* **44**, 1416 (1971).

decreased in the following order; valine>glutamic acid≫ histidine. This order seems to be related to the hydrogenation rate of MAA in the presence of a catalyst modified with L-valine, L-glutamic acid, or L-histidine. That is, the hydrogenation of MAA with the catalyst modified with L-histidine took at least 2 times as long as the hydrogenation with catalysts modified with neutral L-amino acids.

Histidine can chelate strongly on the nickel surface because histidine can act as a tridentate chelating reagent,[7] while neutral L-amino acids acts as bidentate reagents. As a result, it can be considered that a nickel atom of the catalyst surface on which a histidine molecule should absorb strongly can hardly attract the substrate, while a nickel atom on which a neutral amino acid should adsorb can attract the substrate rather easily.

Therefore, the MAA substrate will probably approach the nickel surface modified with L-histidine with more difficulty than that modified with neutral L-amino acids.

In the modification with D-tartaric acid, the adsorption intensity at pH 2.2 was far weaker than that at pH 9.1. The phenomenon is probably due to the reason mentioned in the case of acetylacetone; that is, at pH 2.2, the β-carboxyl group, being undissociated, should hinder the enol-form adsorption of MAA, while at pH 9.1 the β-carboxyl group of D-tartaric acid is mostly neutralized and MAA can adsorb easily with the enol from on the nickel surface. The above results correspond to the facts shown in Fig. 6.

In Fig. 6, the percentage of hydrogenation is plotted against the hydrogenation time in the asymmetric hydrogenation with the catalysts modified with D-tartaric acid at pH 2.2 and pH 9.5 at 0°C. As is shown in Fig. 6, the hydrogenation rate in the modification at pH 2.2 is smaller than that as pH 9.5. From the above discussion, it is clear that the asymmetric hydrogenation rate of MAA depends on the degree of hindrance of the modifying reagent, which probably contains at least two factors, the strength of the chelation ability for amino acids and the acidity of the β-carboxyl group for a tartaric acid, in relation to a the substrate approaching the catalyst surface.

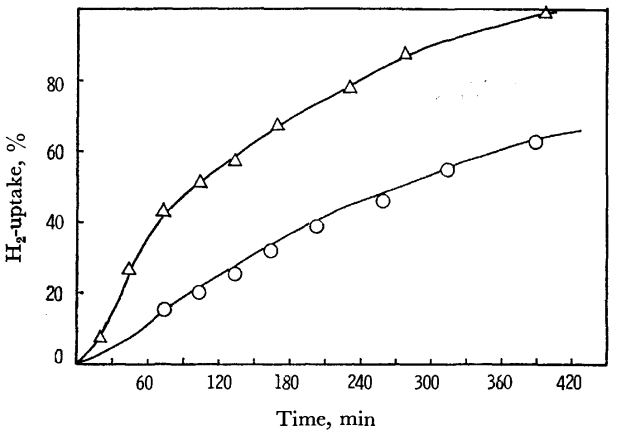

Fig. 6. Effect of modifying pH on hydrogenation rate. (modification with D-tartaric acid at 0°C)
—△—: pH 9.5; —○—: pH 2.2

The author wishes to express his sincere thanks to Professor Yoshiharu Izumi, Professor Shigero Ikeda, and Dr. Kosaku Kishi for their valuable advice and encouragement throughout this work.

7) R. Leberman and B. R. Rabin, *Ttans. Faraday Soc.*, **55**, 1660 (1959).

Asymmetric Hydrogenation of C=O Double Bond with Modified Raney Nickel. XXIV. The Effect of Unsaturated Compounds on the Asymmetric Activity of the Catalyst

Toshio NINOMIYA*

Division of Organic Chemistry, Institute for Protein Research, Osaka University, Kita-ku, Osaka

(Received January 26, 1972)

Dehydroacetic acid and methyl *cis*-3-acetoxycrotonate were picked out as trace impurities of the substrate, methyl acetoacetate. The effects of dehydroacetic acid, methyl *cis*-3-acetoxycrotonate, and diketene, which is the starting material for the preparation of methyl acetoacetate, on the asymmetric activities of catalysts modified with L-amino acids were examined in the hydrogenation of methyl acetoacetate. The above three compounds, when added to the hydrogenation system, raised the asymmetric activity of the catalyst. Also, simple unsaturated compounds, such as acetone and diethyl maleate, has a similar effect on the catalyst. The effects of the above unsaturated compounds on the asymmetric activities of the catalysts modified with L-amino acids were discussed, and it was suggested that the unsaturated compounds adsorb on the catalyst surface and might scavenge the asymmetrically uncontrolled active hydrogen absorbed on the catalyst surface.

In the course of an investigation of asymmetric hydrogenation with Raney nickel catalysts modified with optically-active amino or hydroxy acids, it was often observed that a difference in the lot number of the substrate, methyl acetoacetate, caused an indefinite asymmetric activity in the catalyst. As one of the reasons for the above phenomenon, the contaminant components in the substrate can be considered to have an influence on the asymmetric activity of the catalyst.[1] The present investigation was carried out in order to confirm the trace components in the substrate and in order to clarify the effect of those trace components on the asymmetric activity of the catalyst.

As the trace components in methyl acetoacetate (The Nippon Synthetic Chemical Industry, Co., Ltd., lot 70), dehydroacetic acid (DHA) and methyl *cis*-3-acetoxycrotonate (MAC) were picked out from the substrate, and the effects of DHA, MAC, and diketene, which is the starting material for the preparation of the substrate, on the asymmetric activity of the catalysts modified with L-amino acids were tested.

From the fact that DHA, MAC, and diketene, being unsaturated compounds or hydrogen acceptors, have a great effect on the asymmetric activity of the catalyst, the effect of simple unsaturated compounds, such as acetone and diethyl maleate, on the asymmetric activities of the catalysts modified with L-amino acids was investigated further.

As a whole, the unsaturated compounds, which have ketone groups or C=C double bonds, caused a rise in the asymmetric activities of the catalysts modified with L-amino acids. The effect of unsaturated compounds on the asymmetric activity of the catalyst was discussed on the basis of the above results.

Results and Discussion

The gas chromatograms of three kinds of methyl acetoacetate, lot A, lot B, and lot 70, are shown in Fig. 1. As is indicated in Fig. 1, the contents of the trace components in methyl acetoacetate were different from one another. To confirm the trace component, in methyl acetoacetate (MAA), lot 70, the lot was rectified under reduced pressure and the trace components of the substrate were concentrated. As trace components, DHA and MAC were isolated and identified.

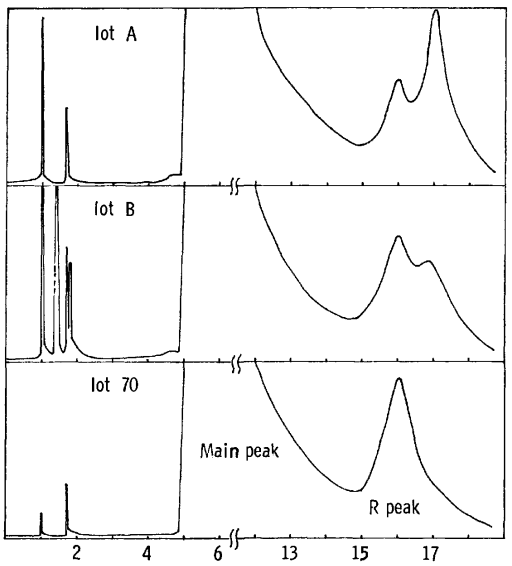

Fig. 1. Gas chromatogram of methyl acetoacetate.
Apparatus: Shimadzu GC-4HPF
Column: PEG 20M 1.5% Chromosorb W 60—80 mesh
Column temperature: 80°C
Injection temperature: 100°C
Sens. 10^4M Ω; Range 1.6 V; Injection 0.2 μ

Figures 2 and 3 show the effect of DHA and MAC, when added to the hydrogenation system, on the assymmetric activities of the catalysts modified with L-glutamic acid and L-valine. The addition of DHA and MAC to the hydrogenation system raises, the (−) asymmetric activities of the catalysts modified with L-glutamic acid and L-valine.

Figure 3 also shows that, in the presence of the catalyst modified with L-valine, a more purified sub-

* Present address: Dai Nippon Toryo, Co., Ltd., 38 Nishinoshimonocho, Konohana-ku, Osaka.

1) The report about the impurities contained in methyl acetoacetate was published by Motoda and Yoshie. [T. Motoda and Y. Yoshie, *Kogyo Kagaku Zasshi*, **68**, 41 (1965)].

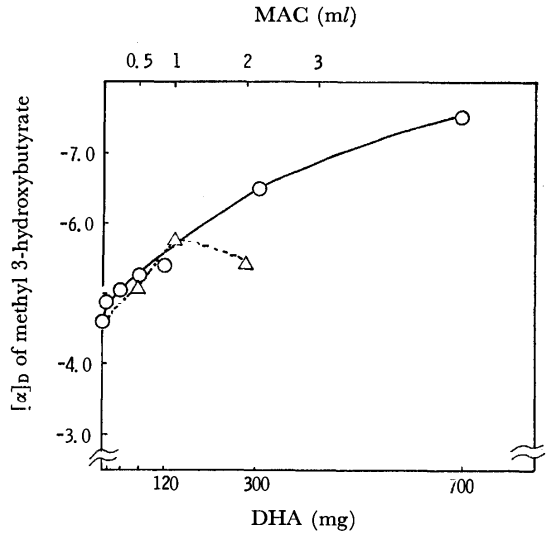

Fig. 2. Effect of added methyl 3-acetoxycrotonate and dehydroacetic acid on asymmetric activity of catalyst.
(modified with L-glutamic acid at 0°C, pH 5.0)
—○—: Dehydroacetic acid (DHA)
--△—: Methyl 3-acetoxycrotonate (MAC)

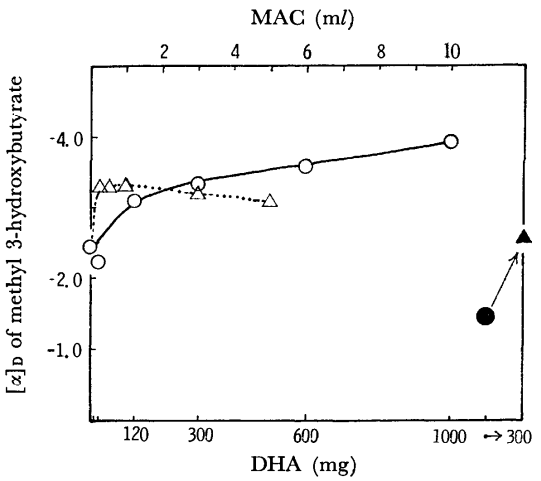

Fig. 3. Effect of added methyl 3-acetoxycrotonate and dehydroacetic acid on asymmetric activity of catalyst.
(modified with L-valine at 0°C)
—○—: Dehydroacetic acid (DHA)
—△—: Methyl 3-acetoxycrotonate (MAC)
—●—: Without addition, redistilled MAA being used
—▲—: DHA, redistilled MAA being used

strate, one which had been obtained by the rectification of MAA lot 70, was hydrogenated in a lower asymmetric yield ($[\alpha]_D = -1.48$), while the addition of 300 mg of DHA to the above purified substrate caused a high asymmetric activity ($[\alpha]_D = -2.56$).

The above facts clearly indicate that the asymmetric activity of the catalyst shown in the hydrogenation of MAA lot 70 was intrinsically affected by the trace components of MAA lot 70, DHA, or MAC.

Furthermore, the possibility that MAA includes a small amount of diketene, because diketene is the starting material of MAA, led us to examine the effect of diketene on the asymmetric activity of the catalyst.

Figure 4 indicates the effect of diketene on the asymmetric activities of the catalysts modified with L-

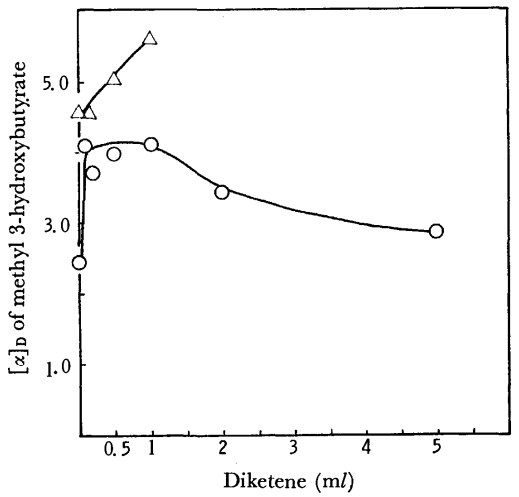

Fig. 4. Effect of added diketene on asymmetric activity of catalyst.
—△—: Modification with L-glutamic acid at 0°C, pH 5.0
—○—: Modification with L-valine at 0°C

glutamic acid and L-valine. As is illustrated in Fig. 4, diketene, when added to the hydrogenation system, raised the asymmetric activities of the catalysts modified with L-glutamic acid and L-valine.

From the results shown in Figs. 2, 3, and 4, it is clear that DHA, MAC, and diketene affect the asymmetric activities of the catalysts modified with L-amino acids in a similar manner. The above three substances have reducible groups, C=O and/or C=C in commons and it can be supposed that the treatment of the catalyst with simple unsaturated compounds, containing ketone groups or C=C double bonds may raise the asymmetric activities of the catalysts modified with L-amino acids.

The effect of simple unsaturated compounds on the asymmetric activities was examined with the catalysts modified with L-valine and L-alanine.

TABLE 1. EFFECT OF VARIOUS REDUCIBLE REAGENTS ON THE ASYMMETRIC ACTIVITIES OF THE CATALYSTS

Reagent (ml)	Immersion time (sec)	$[\alpha]_D$ of methyl 3-hydroxybutyrate: Modification with L-val at 0°C	$[\alpha]_D$ of methyl 3-hydroxybutyrate: Modification with L-ala at 0°C
No treatment	—	−2.47	+0.04
Acetone (18)	90	−3.06	−0.03
Methylethylketone (18)	90	−3.63	−0.18
Cyclohexanone (18)	90	−2.46 −2.47	—
Methylacetoacetate (lot 70) (18)	90	−4.15	−0.32 −0.30
Cyclohexene (18)	90	−3.75	+0.53
Diethyl maleate (18)	90	−4.14	−0.56
Diethyl fumarate (18)	90	no H uptake	no H uptake
Acrylonitrile (18)	90	—	−0.19
Nitromethane (18)	90	—	±0.00

R-NiND (Kawaken Fine Chemical Co., Ltd.) lot 1949, 1.5 g. Substrate; Methyl acetoacetate (The Nippon Synthetic Chemical Industry Co. Ltd.) lot 70 0.15 mol.

Table 1 shows the effect of various reducible compounds on the asymmetric activities of the catalysts modified with L-valine and L-alanine. As is shown in Table 1, the treatment with various ketones and olefins raised the asymmetric activities of the catalysts in most cases. An interesting, remarkable difference was observed between the cases of diethyl maleate and diethyl fumarate; that is, the treatment of the catalyst with diethyl maleate gave a high asymmetric activity to the catalyst, while the treatment of the catalyst with diethyl fumarate lowered and strongly inhibited the hydrogenation.

On the basis of the above results it is clear that unsaturated compounds with ketone groups or C=C double bonds played an important role in raising the asymmetric activities of the catalysts modified with L-amino acids. Then, the unsaturated compounds which gave a high asymmetric activity to the catalyst were hydrogenated under asymmetric hydrogenation conditions.

As was reported in a previous paper,[2] saturated compounds, for example, ethanol and *n*-hexane, are known not to cause a rise in the asymmetric activities of the catalysts modified with L-amino acids. As a result, the effect of the hydrogenated products of the above unsaturated compounds can be disregarded. Moreover, as is shown in Table 1, the 90-sec pretreatment of the catalyst with the substrate, MAA iteself, as an unsaturated compound brought a higher asymmetric activity to the catalyst than no pretreatment, which is the standard asymmetric hydrogenation procedure. On the other hand, the present author has previously made it clear that MAA adsorbs with a pseudo aromatic ring on the catalyst surface.[3]

Therefore, the effect of unsaturated compounds might be associated with the absorbed hydrogen on the catalyst surface. On the whole, it can be concluded that the unsaturated compounds adsorb on the catalyst surface and that, at that stage, they might scavenge asymmetrically uncontrolled active hydrogen absorbed on the catalyst surface. Therefore, with regard to the above phenomenon, Izumi, one of our research group, has attempted to explain it by the hypothesis of a "Quasi liquid hydrogen layer."[4]

Experimental

The preparation and modification of the Raney nickel catalyst, the hydrogenation of methyl acetoacetate, and the measurement of the asymmetric activity of the catalyst were performed in the manner described in a previous paper.[5]

As the Raney nickel alloy, 1.5 g of R-Ni ND, lot 1949 (Kawaken Fine Chemicals Co., Ltd.), was used, and as the substrate we used 0.15 mol of methyl acetoacetate (MAA), lot 70, from the Nippon Synthetic Chemical Industry Co., Ltd.

Isolation and Identification of DHA and MAC. MAA, lot 70 (600 m*l*), was rectified under reduced pressure (15 mmHg) with a Podbielniak 13-mm Heli-Grid column and was then concentrated to 30 m*l*. The yellowish brown residue was cooled overnight in a refrigerator, and the yellowish precipitate was separated by filtration. The precipitate was recrystallized from an ethanol solution. Yield, 0.3 g; mp 105—110°C (capillary).

NMR: δ (10%, $CDCl_3$) 2.26 (3H, s, $CH_3 \cdot \underset{\underset{O}{|}}{C}=C$), 2.62 (3H, s, $CH_3 \cdot \underset{\underset{O}{|}}{C}-$), 5.93 (1H, s, C=CH–C), and 16.84 (1H, s, $\underset{\underset{O}{\|}}{C}-CH-\underset{\underset{O}{\|}}{C}=O$). IR: (KBr) 1720 (ketone), 1620—1640 and 1550 cm^{-1} (pyrone ring).

Found: C, 56.41; H, 4.83; N, 1.16%. Calcd for $C_8H_8O_4$: C, 57.14; H, 4.80; N, 0.00%.

From the above physicochemical data, the crystals were identified as dehydroacetic acid.

The filtrate was suspended in a nickel chloride aqueous solution ($NiCl_2 \cdot 6H_2O$ (24 g) in H_2O (50 m*l*)). To the above suspension solution, we slowly added a caustic soda solution (NaOH (8 g) in H_2O (50 m*l*)) under ice-water cooling, and the pH was adjusted about 7.

After the mixture had been stirred for 2 hr, the nickel methyl acetoacetate was filtered off and the filtrate was introduced into a gas-chromatogram apparatus, Varian 90-P3; the peak, R, shown in Fig. 1 was separately collected.

NMR: δ (1%, CCl_4) 2.04 (3H, s, CH_3–C), 2.21 (3H, s, CH_3–$\underset{\underset{O}{\|}}{C}$–), 3.57 (3H, s, O–$CH_3$), 6.49 (1H, s, C=CH–C). IR: (liquid film) 1710 and 1760 (esters) and 1660 cm^{-1} (C=C).

From the IR and NMR data and by identification[6] with synthetic *cis*-3-acetoxycrotonate, the R peak was identified as methyl *cis*-3-acetoxycrotonate (MAC).[1] Gas-chromatographic calculation showed the MAA lot 70 to contain 0.3% MAC.

Addition of DHA, MAC, and Diketone. A chemically pure grades of DHA and diketene (Wako Pure Chemical Industries, Ltd.) were used. The MAC was prepared by the method of Claisen.[6] DHA, MAC and diketene were all added to the substrate, MAA, which was then introduced into autoclave, and the reduction product, methyl 3-hydroxybutyrate, was fractionally distilled.

Treatment of the Catalyst with Simple Ketones or Olefins. The catalyst modified with an L-amino acid was immersed for 90 sec in 18 m*l* of a ketone or an olefin; by decantation the catalyst was separated from the ketone or the olefin with the aid of a magnet to retain the catalyst, and the catalyst was introduced with the substrate into the autoclave.

The author wishes to express his thanks to Professor Yoshiharu Izumi for his valuable advice and encouragement throughout this work, to Miss Kiku Koike and Mrs. Nobuko Okuhara for the elemental analysess to Drs. Yoshimoto Ohta and Kiichi Nishimura for their permission to use the fine distillation apparatus, and also to the Nippon Synthetic Chemical Industry Co., Ltd., for giving him information on the impurities contained in methyl acetoacetate.

2) Part XX: F. Higashi, T. Ninomiya, and Y. Izumi, This Bulletin, **44**, 1333 (1971).
3) T. Ninomiya, *ibid.*, to be published.
4) Y. Izumi, *Shokubai (Catalyst)*, **12**, 201 (1970).
5) Y. Izumi, T. Harada, T. Tanabe, and K. Okuda, This Bulletin, **44**, 1418 (1971).
6) L. Claisen and E. Haase, *Ber.*, **33**, 3778 (1900).

The Autoxidation of Phenols Catalyzed by Phthalocyanine-Fe(II) and Salcomine-pyridine

Masaru TADA and Takashi KATSU

Department of Chemistry, School of Science and Engineering, Waseda University, Shinjuku, Tokyo, 160

(Received February 4, 1972)

The autoxidation of 2,4,6-tri-*t*-butylphenol (**1**), 2,6-di-*t*-butylphenol (**2**), and 2,4-di-*t*-butylphenol (**3**) is catalyzed by phthalocyanine-Fe(II) (PC-Fe(II)) and salcomine-pyridine (SAL-Py). PC-Fe(II) gives, preferentially, the coupling product of such phenoxy radicals as **4**, **7**, and **8**. SAL-Py, on the other hand, gives *o*- and *p*-benzoquinones, such as **5** and **6**, resulting from the coupling of the phenoxy radical and the hydroperoxy radical. Metal phthalocyanines including Mn(II), Co(II), Ni(II), or Cu(II) as the central metal ion are inactive as catalysts for the oxidation. PC-Fe(II) does not catalyze the autoxidation of phenol itself and mono-alkylated phenols.

The autoxidation of phenols catalyzed by salcomine and its derivatives has drawn much attention in connection with the relation between the mode of oxidation and the states of the oxygen-adducts of salcomine.[1,2] On the other hand, the autoxidation of phenols catalyzed by ion complexes, which are assumed to be carriers of molecular oxygen, has not been reported except for the preliminary result on the autoxidation of poly-phenol catalyzed by phthalocyanine-Fe(II) (PC-Fe(II) hereinafter).[3] Our attention was directed to the catalytic activity of PC-Fe(II) in the autoxidation of organic compounds in connection with the structual similarity of PC-Fe(II) to a biologically-important hemin. In this paper we will report on the autoxidation of phenols catalyzed by PC-Fe(II). The autoxidation of phenols catalyzed by salcomine-pyridine (SAL-Py hereinafter) was also carried out in order to compare the modes of catalysis of the two catalysts.

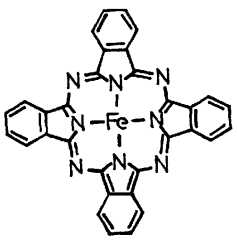

PC-Fe(II)

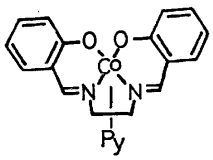

SAL-Py

Results and Discussion

Several metal phthalocyanines including Mn(II), Co(II), Ni(II), or Cu(II) as the central metal ion were tested as catalysts for the oxidation 2,4,6-tri-*t*-butylphenol (**1**) and 2,6-di-*t*-butylphenol (**2**), but they were nearly all inactive; only PC-Fe(II) showed a strong catalytic activity. In contrast, Vogt *et al.* reported that the oxidation of 2,6-dimethylphenol was catalyzed by salcomines and not by the complexes in which the central metal ion of salcomine was replaced by Mn(II), Fe(II), Ni(II), or Cu(II).[1]

The distributions of the products from the oxidation of 2,4,6-tri-*t*-butylphenol (**1**), 2,6-di-*t*-butylphenol (**2**), and 2,4-di-*t*-butylphenol (**3**) are shown in Tables 1, 2, and 3 respectively.

The oxidation products from the three phenols **1**, **2**, and **3**, originate almost exclusively from the coupling of two phenoxy radicals when the oxidations are catalyzed by PC-Fe(II). The peroxide, **4**, must be formed by the coupling of two phenoxy radicals from **1** at a para-position through the bridge of molecular oxygen, as a result of the steric hindrance of a direct coupling. The biphenoquinone, **7**, must be formed by the further oxidation of biphenol **9**. On the oxidation of **3**, the biphenol **8** is not further oxidized[4] and an appreciable amount of the starting phenol, **3**, is recovered; the yield of **8** is improved to 88% by changing the solvent from methanol to tetrahydrofuran.

On the oxidations of **1**, **2**, and **3** catalyzed by SAL-Py, the coupling of a phenoxy radical and a hydroperoxy radical becomes more important. Thus two quinones, **5** and **6**, from the phenol **1** must be formed through the intermediates, **10** and **11** respectively, by the elimination of *t*-butyl alcohol. The first oxidation products, **12** and **13**, from the phenols **2** and **3** respectively, must be further transformed to afford the quinones **5** and **6**.

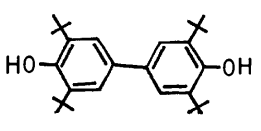

9

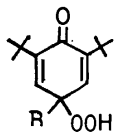

10: R=*t*-C$_4$H$_9$ **12**: R=H

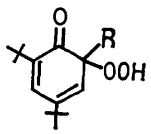

11: R=*t*-C$_4$H$_9$ **13**: R=H

The mode of the autoxidation of *t*-butyl-substituted phenols catalyzed by PC-Fe(II) is similar to that of oxidations by a one-electron-transfer oxidizing agent, such as $K_3Fe(CN)_6$, PbO_2, or Ag_2O.[5,6,7] The autoxi-

1) a) L. H. Vogt, Jr., J. G. Wirth, and H. L. Eisenbeiner, *J. Org. Chem.*, **34**, 273 (1969). b) D. J. Tamaja, L. H. Vogt, Jr., and J. G. Wirth, *ibid.*, **35**, 2029 (1970).

2) T. Matsuura, K. Watanabe, and A. Nishinaga, *Chem. Commun.*, **1970**, 163.

3) A. H. Cook, *J. Chem. Soc.*, **1938**, 1768.

4) A different product becomes the major one upon the catalysis of PC-Fe(II) which has been purified freshly by precipitation from a sulfuric-acid solution of PC-Fe(II) by adding water. The structure of this product is now under investigation.

5) C. D. Cook and R. C. Woodworth, *J. Amer. Chem. Soc.*, **75**, 6242 (1953).

6) H. Blanchard, *J. Org. Chem.*, **25**, 264 (1960).

7) C. D. Cook, *ibid.*, **18**, 261 (1953).

Table 1. Autoxidation of 2,4,6-tri-*t*-butylphenol (**1**)

Catalyst	Product		
	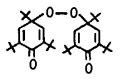		
	4	**5**	**6**
PC–Fe(II)	87%	4%	2%
SAL–Py	40%	28%	4%

Table 2. Autoxidation of 2,6-di-*t*-butylphenol (**2**)

Catalyst	Product	
	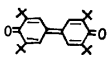	
	7	**5**
PC–Fe(II)	*ca.* 100%	
SAL–Py	11%	75%

Table 3. Autoxidation of 2,4-di-*t*-butylphenol (**3**)

Catalyst	Product		
	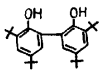		
	8	**6**	recovered
PC–Fe(II)[D]	57%	trace	36%
SAL–Py	3%	29%	58%

dation catalyzed by SAL-Py, on the other hand, gives quinones preferentially; this characteristic is rather similar to that of cobalt- or copper-complexes, such as salcomine or CuCl-amine which have a high potential to combine with molecular oxygen.[1,8,9]

PC-Fe(II) does not catalyze the autoxidation of phenol itself and mono-alkylated phenols including *o*- and *p*-*t*-butylphenol, and *o*-, *m*-, and *p*-cresol. PC-Fe(II) catalyzes only the oxidation of phenols giving stable phenoxy radicals, including di- and tri-*t*-butylphenols, and gives the products derived from the coupling of two phenoxy radicals, either directly or through an oxygen bridge.

Experimental

Materials. Commercially available 2,4,6-tri-*t*-butylphenol (**1**), 2,6-di-*t*-butylphenol (**2**), and 2,4-di-*t*-butylphenol (**3**) were used after purification by recrystallization from ethanol; **1**, mp 131°C, or distillation under reduced pressure; **2**, 132—133°C/18 mmHg. **3**, 141—142°C/18 mmHg.

Catalysts. Metal phthalocyanines were prepared by the method of Dent-Linstead[10] from the chlorides of the corresponding metal and phthalonitrile, or by Gattermann's procedure[11] from the corresponding chlorides, phthalic anhydride, and urea. The crude phthalocyanines were successively washed with boiling methanol, hot diluted sulfuric acid, methanol, and ether. The phthalocyanines thus obtained were dried and kept in a desiccator until their use.

Salcomine-pyridine was prepared by the procedure of Bails-Calvin[12] from cobalt acetate, ethylenediamine, salicylaldehyde, and pyridine; the complex was kept in a vacuum desiccator until its use.

A General Procedure of Autoxidation. A methanol solution (100 m*l*) of one of the phenols (0.015 mol) was exposed to oxygen for 18 hr at room temperature in the presence of metal phthalocyanine (0.015 mol) or salcomine-pyridine (0.015 mol). The reaction mixture was magnetically stirred during the reaction period. After the evaporation of the solvent, the product was taken into ether and was purified by preparative layer chromatography on silica gel eluted with benzene.

Oxidation of 2,4,6-Tri-t-butylphenol (1). The oxidation products from 0.393 g of **1** were seperated by preparative layer chromatography to give three bands on the chromatogram. The extraction of the top, middle, and bottom bands gave peroxide **4** (0.341 g, 87%), *p*-quinone **5** (0.016 g, 4%) and *o*-quinone **6** (trace) respectively when catalyzed by PC-Fe(II). The autoxidation of the phenol **1** by SAL-Py gave the same products as those from the PC-Fe(II) catalysis, but the product distribution was different, as is shown in Table 1. The structures of the products were deduced to be **4**,[13] **5**,[14] and **6**[15] from a comparison of their melting points and infrared spectra.

Oxidation of 2,6-Di-t-butylphenol (2). The oxidation product of 0.309 g of the phenol **2** catalyzed by PC-Fe(II) showed only one spot on an analytical thin-layer chromatogram without any purification; it was identified as biphenoquinone **7**[16] (0.306 g, *ca.* 100%) by a comparison of the melting points and infrared spectra. The oxidation product of 0.309 g of **2** catalyzed by SAL-Py showed two bands on a preparative layer chromatogram; the lower band gave *o*-quinone **5** (0.232 g, 75%) as the major product, while biphenoquinone **7** (0.033 g, 11%) was given from the upper band.

Oxidation of 2,4-Di-t-butylphenol (3). The oxidation product of 0.309 g of **3** catalyzed by PC-Fe(II) gave two spots on an analytical thin-layer chromatogram; the lower spot corresponded to the starting phenol **3** (0.111 g, 36%). The oxidation product, the upper spot, was seperated by preparative layer chromatography to give biphenol **8** (0.176 g, 57%), which was found to be identical with the authentic sample[17] by a comparison of the melting points and infrared spectra. Preparative layer chromatography of the product from the reaction catalyzed by SAL-Py showed another band at the bottom of the chromatogram. The extraction of that band afforded *o*-quinone **6** (0.089 g, 29%) as the major product.

8) A. Nishinaga, K. Watanabe, and T. Matsuura, 4th Symposium on Oxidation, Chemical Society of Japan, October 1970, Tokyo, Abstract p. 48.
9) C. M. Orland, Jr., *J. Org. Chem.*, **33**, 2516 (1968).
10) C. E. Dent and R. P. Linstead, *J. Chem. Soc.*, **1934**, 1027.
11) L. Gattermann, "Die Praxis des Organischen Chemikers" 40 Auflage, Walter de Gruyter & Co., Berlin (1961), p. 288.
12) R. H. Bails and M. Calvin, *J. Amer. Chem. Soc.*, **69**, 1886 (1947).
13) E. Müller and K. Ley, *Chem. Ber.*, **87**, 922 (1954).
14) E. Müller and K. Ley, *ibid.*, **88**, 601 (1955).
15) K. Ley and E. Müller, *ibid.*, **89**, 1402 (1956).
16) M. S. Kharasch and B. S. Jhose, *J. Org. Chem.*, **22**, 1439 (1957).
17) J. H. Fookes, E. L. Pelton, and M. W. Long, Jr., U. S. Patent 2885444 (1959), *Chem. Abstr.*, **54**, 5579i (1970).

Polar Substituent Constants for Substituted Phenyl Groups. The Extended Taft Equation.

Yoichiro NAGAI, Hideyuki MATSUMOTO, Taichi NAKANO, and Hamao WATANABE
Department of Chemistry, Gunma University, Kiryu, Gunma

(Received February 17, 1972)

Values of the σ* constants have been defined for some *m*- and *p*-substituted phenyl groups from the ^{29}Si–H coupling constants for a series of *m*- and *p*-substituted phenylsilanes, phenylmethylsilanes, and phenyldimethylsilanes. The σ* constants for the groups, XC_6H_4, were found to be directly related to the Hammett σ constants for the ring substituents, X. From this correlation the σ* constants for a number of other substituted phenyl groups have also been calculated. Examples have been presented in which a simple relationship holds between the Taft polar substituent constants including the newly derived σ* constants and molecular properties for a series of compounds covering both aliphatic and aromatic substances. Correlations of reactivities with the extended σ* values have been illustrated and the implications of the results are discussed.

It is well known that there exist two important quantitative relationships of very great generality between structure and reactivity, *i.e.*, the Hammett and Taft equations.[1,2] The former applies within

$$\log K/K_0 = \rho\sigma \quad (1)$$

$$\log K/K_0 = \rho^*\sigma^* \quad (2)$$

a great number of reaction series of *m*- and *p*-substituted benzene derivatives, while the latter is followed by a considerable body of aliphatic reaction series involving a wide variety of functional groups, mechanisms, attacking reagents, experimental conditions, *etc.* Both of the two general relationships are based on a rather simple idea that the effect of structure on reaction rates, equilibrium constants, physical properties, *etc.*, is nearly always determined by a single principal factor, the polar effect of the substituent. Although this idea holds, of course, only when other factors such as resonance and steric effects are absent or negligible or vary linearly, there leaves no doubt that numerous instances indeed follow the linear free energy equations. The two relationships are thus associated with very nearly the same physical implications, but it is generally believed that Eq. (1) is applicable only to aromatic reaction series whereas the use of Eq. (2) is limited only to aliphatic reactions. In effect, the scales of the two sets of substituent constants differ much from each other. Since, however, the two linear polar energy relationships have almost identical physical meanings and mathematical forms, it would be anticipated that the two equations could be extended to merging if the two sets of substituent constants are directly related to one another.

An attempt has been made in this work to define Taft σ* values for some *m*- and *p*-substituted phenyl groups and to determine whether the Taft σ* constants so derived are linearly related to the Hammett σ constants. It was hoped that such relations would prove to be of value in studying polar effects of substituents on various molecular properties and that a comparison of these properties with the use of the extended Taft equation would indicate the presence or absence of other structural factors.

Polar Substituent Constants for Substituted Phenyl Groups

In order to obtain Taft's polar substituent constant (σ* values) for substituted phenyl groups, Nagai and coworkers selected NMR values of the ^{29}Si-H coupling constant for series of substituted phenylsilanes, phenylmethylsilanes, and phenyldimethylsilanes.[3] Evidence has been presented that a good correlation exists between reported values[4,5] of $J(^{29}\text{Si-H})$ for hydrosilanes of the general formula $R_1R_2R_3SiH$, where R's could be a phenyl(s), an alkyl(s) and a hydrogen(s), and the sum of the σ* constants for R_1, R_2, and R_3. The coupling constants follow the equation,

$$J(^{29}\text{Si-H}) = -10.21\sum\sigma^* - 182.9$$

with a correlation coeffecient of 0.994. It is thus possible to evaluate the polar substituent constant for a substisuted phenyl group in question by fitting its NMR parameter to the equation above. The σ* values so obtained for several substituted phenyl groups are listed in Table 1 in which probable errors are included. Since it has also been shown that the ^{29}Si-H coupling constants for each series of the arylhydrosilanes correlate well with Hammett's σ con-

Table 1. Polar substituent constants (σ*) for substituted phenyl groups as determined from the J (^{29}Si–H) values

Group	σ*	Probable error
p-$N(CH_3)_2C_6H_4$	0.16	±0.01
p-$CH_3OC_6H_4$	0.36	±0.01
p-$CH_3C_6H_4$	0.46	±0.01
m-$CH_3C_6H_4$	0.48	±0.002
p-ClC_6H_4	0.75	±0.01
m-ClC_6H_4	0.85	±0.02

1) a) L. P. Hammett, "Physical Organic Chemistry", McGraw-Hill, N. Y. (1940), p. 184. b) H. H. Jaffe, *Chem. Rev.*, **53**, 191 (1953).

2) R. W. Taft, Jr., "Steric Effects in Organic Chemistry", ed. by M. S. Newman, John Wiley, N. Y. (1956), p. 556.

3) Y. Nagai, M. Ohtsuki, T. Nakano, and H. Watanabe, *J. Organometal. Chem.*, **35**, 81 (1972).

4) B. K. Hunter and L. W. Reeves, *Can. J. Chem.*, **46**, 1399 (1968).

5) M. A. Jensen, *J. Organometal. Chem.*, **11**, 423 (1968).

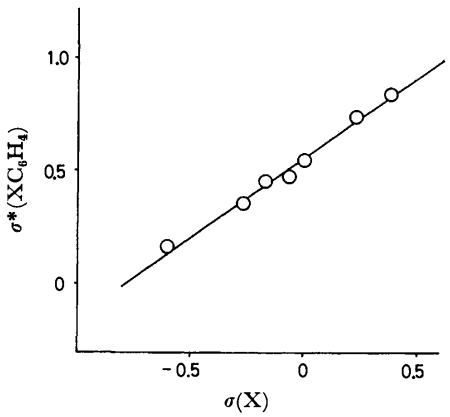

Fig. 1. Relationship between σ and σ^* constants.
σ^* $(XC_6H_4)=0.720\ \sigma(X)+0.575$

stants,[3] the σ^* constants listed in Table 1 are expected to be related to σ constants; two sets of substituent constants are plotted against each other in Fig. 1 which exhibits an excellent linear relationship with a correlation coefficient of 0.995. The regression line can be expressed in terms of the following equation.

$$\sigma^*(XC_6H_4) = 0.72\sigma(X) + 0.58 \qquad (3)$$

The value of the intercept, 0.58, agrees well within experimental error with the σ^* value for a phenyl group, 0.60. It follows then that with the use of Eq. (3) one can further proceed to define the σ^* values for a number of other XC_6H_4 groups by scaling σ values of substituents X to fit this expression. Some selected σ^* values thus calculated are summarized in Table 2.[6]

All the substituted phenyl groups listed in Table 2 are more electron-withdrawing than the methyl group as indicated by positive signs of the σ^* values. It is of interest to note that σ^* values of some of the substituted phenyl groups are lower than that of hydrogen, *i.e.*, 0.49. Thus such a substituted phenyl group is shown to be a weaker electron attractor than hydrogen. This is not unexpected since they contain substituents, X, which are +R (by Gould's classification[9]) in nature.

The correctness of the σ^* values for substituted phenyl groups presented in Table 2 can be tested by giving an example of their use for prediction purposes. Taft[2] has quoted the ionization of aliphatic carboxylic acids, RCOOH, in water at 25°C as a typical example of reactions following his equation. For this particular correlation, log $K=1.721\sigma^*$ -4.65. Values of the polar substituent constants for *m*- and *p*-substituted benzyl groups can readily be obtained from the values listed in Tables 1 and 2 taking the fall-off factor per methylene group to be 2.8 as suggested by Taft. From the correlation above together with the σ^* values for the benzyl groups, it is possible to predict values of the ionization constant for substituted phenylacetic acids which have been determined by Dippy and Williams.[10] The calculated and observed values of the ionization constant are given in Table 3 for comparison. The agreement between the two sets of values is excellent, thus confirming the σ^* values defined in this work to be quite satisfactory.

Table 2. σ^* values for some substituted phenyl substituents calculated by Eq. (3)

X	σ [a]	σ^*
p-OPh	−0.32	0.35
p-*t*-Bu	−0.20	0.43
p-Et	−0.15	0.47
m-Et	−0.07	0.53
p-Ph	−0.01	0.57
p-F	0.06	0.62
m-OMe	0.12	0.66
p-Br	0.23	0.74
m-OPh	0.25	0.76
m-F	0.34	0.82
m-Br	0.39	0.86
m-CF_3	0.43	0.89
p-CO_2R	0.45	0.90
p-CF_3	0.54	0.96
m-CN	0.56	0.98
p-CN	0.66	1.05
m-NO_2	0.71	1.09
p-NO_2	0.78	1.14

a) See C. D. Ritchie and W. F. Sager, "Progress in Physical Organic Chemistry, Vol. 2" Interscience, N. Y. (1964), p. 323.

Table 3. Predicted and observed values of ionization constants for substituted phenylacetic acids at 25°C in water

Substituent	log K (calcd)	log K (obsd)
p-*t*-Bu	−4.38	−4.42
p-*i*-Pr	−4.36	−4.39
p-Et	−4.36	−4.37
p-Me	−4.37	−4.37
p-MeO	−4.43	−4.36
H	−4.28	−4.31
p-Cl	−4.19	−4.19
p-Br	−4.19	−4.19
p-I	−4.18	−4.18
m-I	−4.14	−4.16
m-Cl	−4.13	−4.14
m-NO_2	−3.98	−3.97
p-NO_2	−3.95	−3.85

6) The use of σ° (Ref. 7) or σ^n (Ref. 8) values also gives good correlations with the $J(^{29}Si\text{-}H)$ values, so that the σ° or σ^n values for substituted phenyl groups may be evaluated in a similar fashion. These substituent constants might provide a better choice since they represent inductive constants for the substituted phenyl groups relative to the unsubstituted phenyl group, although in general their values do not differ significantly from σ values. Nevertheless the authors prefer the correlation with σ because of its fundamental importance and of the greater number of substituents for which σ values are available.

7) R. W. Taft, Jr., *J. Phys. Chem.*, **64**, 1805 (1960).

8) H. Van Bekkum, P. E. Verkade, and B. M. Wepster, *Rec. Trav. Chim.* Pays-Bas, **78**, 815 (1959).

9) E. S. Gould, "Mechanism and Structure in Organic Chemistry", Holt-Rinehart-Winston, N. Y. (1964), p. 212.

10) J. F. J. Dippy and F. R. Williams, *Chem. Rev.*, **25**, 151 (1939).

Application of the New σ^* Constants

It is a matter of course that the σ^* values for *m*- and *p*-substituted phenyl groups can be used to correlated a vast number of reaction series with reasonable precisions since they are linearly related to Hammett's σ values. Their utility manifests itself, however, when properties of compounds R–Y are compared, where the groups, R, contain both aliphatic and aromatic substituents. Although not many investigations have been carried out covering such a wide range of compounds under a single set of experimental conditions, Nagai and coworkers have found two typical examples[3] following the extended Taft equation. The NMR ^{29}Si-H coupling constants for 30 aliphatic and aromatic hydrosilanes were correlated nicely with $\sum\sigma^*$, where $\sum\sigma^*$ is the sum of σ^* values for the groups on the central silicon atom (Fig. 2). In this relationship the slope is equal to -10.3 Hz/σ^* with a correlation coefficient of 0.996. Figure 3 illustrates a correlation of the methyl ^{13}C–H coupling constants for series of arylmethylsilanes and aryldimethylsilanes with σ^*. In this case $\rho^*=1.68$ Hz/σ^* and $\gamma=0.966$.

The correlation of the ionization of aliphatic[2] and aromatic[1] carboxylic acids gave a somewhat different picture as shown in Fig. 4. The two independent relationships found in this figure have comparable slopes, the aromatic line being below the aliphatic line by *ca.* 0.5 log unit. These findings furnish convincing justification for the concept that there is a substantial resonance stabilization in the reactant state of aromatic acids that is undoubtedly due to the interaction between an aromatic ring and the carbonyl function.

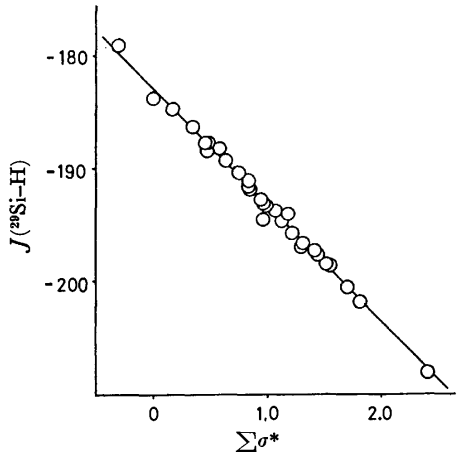

Fig. 2. Correlation of $J(^{29}Si-H)$ for 30 hydrosilanes of general formula $R_1R_2R_3SiH$ with σ^*.
$J(^{29}Si-H)=-10.21\sum\sigma^*-182.9$

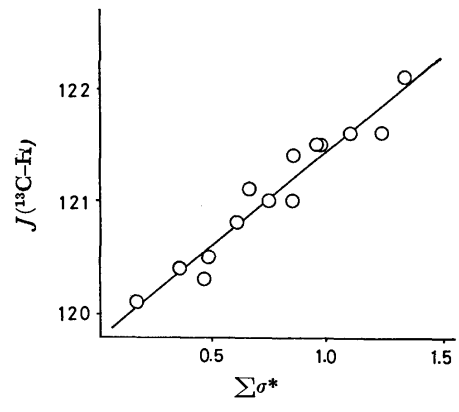

Fig. 3. Correlation of methyl $J(^{13}C-H)$ for phenylmethylsilanes and phenyldimethylsilanes.
$J(^{13}C-H)=1.678\sum\sigma^*+119.8$

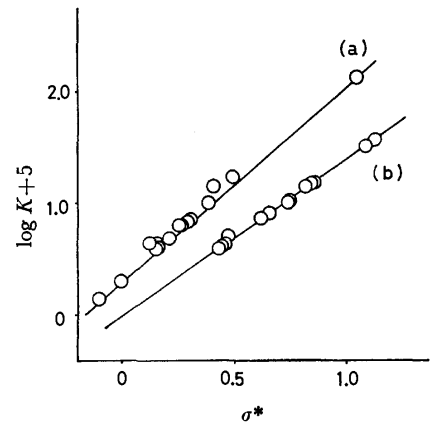

Fig. 4. Correlation of ionization constants for aliphatic and aromatic carboxylic acids with σ^*.
(a) Aliphatic acids; $\log K=1.721\,\sigma^*-4.65$
(b) Aromatic acids; $\log K=1.389\,\sigma^*-5.00$

Perhaps the most interesting generalization concerning the use of the σ^* values for substituted phenyl groups may be drawn from the rate data on the hydrogen abstraction from nuclear substituted aralkylhydrocarbons by polar radicals. In actuality, it has long been recognized that various electron-poor radicals display rather pronounced polar effects in their attack on hydrogens to be abstracted. This general trend has been frequently verified by a number of rate data on the benzylic hydrogen abstractions from series of substituted alkylbenzenes that have been treated within the framework of the Hammett relationship.[11] It is

11) It might be argued that reactivities of benzylic hydrogens toward abstracting polar reagent such as halogens, alkoxy, and trichloromethyl radicals are better correlated with σ^+ derived by Brown and Okamoto[12] than with σ. This idea has been first proposed by Russell[13] and supported later on by several other workers.[14–18] However, a survey of the existing rate data on the hydrogen abstraction revealed that there are also many instances[17] giving a somewhat better fit to the ordinary σ function rather than σ^+. Furthermore, even for some cases in which a better correlation with σ^+ has been reported with emphasis, the difference in the magnitude of correlation coefficient is not significant enough to warrant a definite adoption of the σ^+ correlation.[20]

12) H. C. Brown and Y. Okamoto, *J. Amer. Chem. Soc.*, **80**, 4979 (1958).
13) G. A. Russell, *J. Org. Chem.*, **23**, 1407 (1958).
14) J. A. Howard and K. U. Ingold, *Can. J. Chem.*, **41**, 1744 (1963).
15) C. Walling, A. L. Rieger, and D. D. Tanner, *J. Amer. Chem. Soc.*, **85**, 3129 (1963).
16) R. E. Pearson and J. C. Martin, *ibid.*, **85**, 354 (1963).
17) E. S. Huyser, *ibid.*, **82**, 394 (1960), "Free-Radical Chain Reactions", John Wiley, N. Y. (1970), p. 89.
18) H. Sakurai and A. Hosomi, *J. Amer. Chem. Soc.*, **89**, 458 (1967).
19) J. Hardil and V. Chvalovsky, *Coll. Czech. Chem. Commun.*, **33**, 2029 (1968). See also Ref. 20.
20) Y. Nagai, "Modern Organic Chemistry", ed. by S. Ito *et al.*, Hirokawa, Tokyo, in press.

generally accepted that few if any steric effects are observable on the rate of the hydrogen abstraction processes for a wide variety of structural change in substrate.[21] It is therefore expected that reactivities for benzylic hydrogens toward a given attacking radical species are related only to the polar effects of substituents if resonance effects are absent or constant.

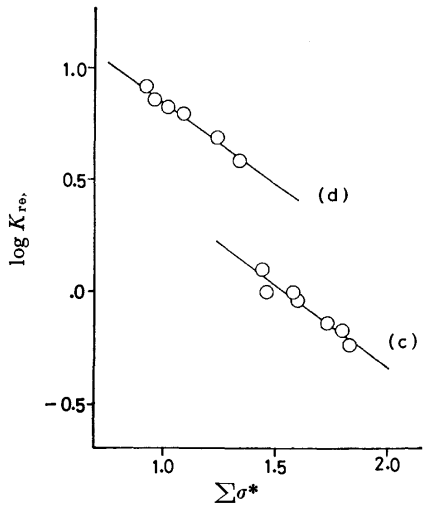

Fig. 5. Plots of relative reactivities for substituted toluenes and ethylbenzenes toward sulfuryl chloride *versus* σ^*.
(c) Toluenes; $\log k_{rel} = -0.741 \sum\sigma^* + 1.14$
(d) Ethylbenzenes; $\log k_{rel} = -0.731 \sum\sigma^* + 1.58$

Treatment of the relative reactivities (on a per hydrogen available basis) at 40°C for two series of alkylbenzenes, substituted toluenes and ethylbenzenes, toward sulfuryl chloride in carbon tetrachloride[22] by the Taft equation again gave two independent correlations as shown in Fig. 5. The ρ^* values for the two reaction series are essentially identical. However, the entire body of the rate data cannot be accomodated by a single line. The difference in positions of the two lines is likely to be accounted for by the accelerating hyperconjugation effects of the α-methyl group in ethylbenzene in the transition state which more or less resembles the product state, the benzylic radical. With regard to this point it seemed appropriate to inquire whether the rate data of silicon analogs of alkylbenzenes such as phenylsilane, phenylmethylsilane and phenyldimethylsilanes are incorporated with the extended Taft equation, since the contributing hybrid structures in the transition state of the hydrogen abstraction would require at least partly a silicon-carbon double bond which, unlike a carbon-carbon double bond, has never been positively detected.[23] Relative rate constants for these arylhydrosilanes at 80°C toward the trichloromethyl radical have been obtained in our previous work[24] and a plot of the relative rates *versus* σ^* is shown in Fig. 6. In this case there are once

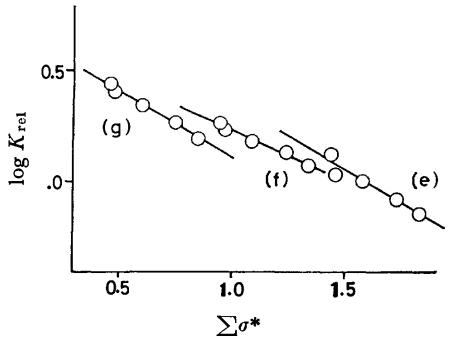

Fig. 6. Plots of relative reactivities for substituted phenylsilanes toward carbon tetrachloride *versus* σ^*.
(e) Phenylsilanes; $\log k_{rel} = -0.595 \sum\sigma^* + 0.943$
(f) Phenylmethylsilanes; $\log k_{rel} = -0.429 \sum\sigma^* + 0.652$
(g) Phenyldimethylsilanes; $\log k_{rel} = -0.601 \sum\sigma^* + 0.702$

again found three independent straight lines which are closely located each other with comparable σ^* values. However, the whole range of rate data can also be accommodated by a single relationship with an acceptable correlation coefficient, 0.98. This observation is in keeping with the expectation deduced from the inability of silicon to make a double bond and leads to a conclusion that the reactivities for the silicon series thus apparently depend upon solely the polar effects of substituents.

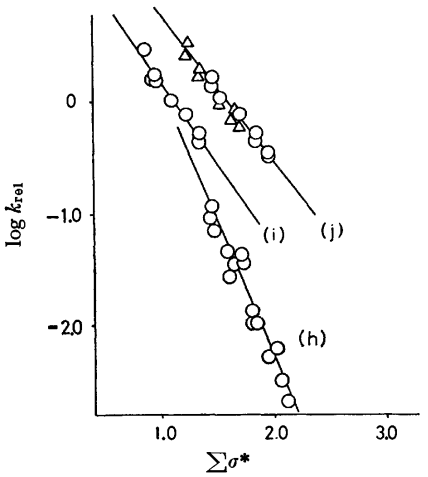

Fig. 7. Plots of relative reactivities for $XC_6H_4CH_2R$ toward the bromine atom in carbon tetrachloride at 80°C *versus* σ^*.
(h) R=hydrogen; $\log k_{rel} = -2.497 \sum\sigma^* + 2.652$
(i) R=methyl; $\log k_{rel} = -1.441 \sum\sigma^* + 1.606$
(j) R=phenyl (circles), R=vinyl (triangles); $\log k_{rel} = -1.309 \sum\sigma^* + 2.034$

Figure 7 shows correlations between $\sum\sigma^*$ and rates of hydrogen abstraction by the bromine atom from *m*- and *p*-substituted toluenes,[15] ethylbenzenes,[25] diphenylmethanes,[26] and allylbenzenes[26] in carbon tetrachloride at 80°C. To obtain the relative rates expressed in terms of k(toluene)=1, the rate ratio of toluene: ethylbenzene: diphenylmethane: allylbenzene was set to be 1: 23: 18: 25, the value being taken from a table compiled by Low and Lee.[26] Also the σ^* value for the vinyl group was calculated as

21) G. A. Russell and P. G. Haffley, *J. Org. Chem.*, **31**, 1869 (1966).
22) K. H. Lee, *Tetrahedron*, **25**, 4363 (1969).
23) C. Eaborn, "Organosilicon Compounds", Butterworths, London (1960), p. 86.
24) Y. Nagai, H. Matsumoto, M. Hayashi, E. Tajima, M. Ohtsuki, and N. Sekikawa, *J. Organometal. Chem.*, **29**, 209 (1971).
25) R. L. Huang and K. H. Lee, *J. Chem. Soc., C*, **1966**, 935.
26) T. P. Low and K. H. Lee, *J. Chem. Soc., B*, **1970**, 535.

follows.

$$\sigma^*(CH_2{=}CH) = \sigma^*(CH_3CH{=}CH) - \{\sigma^*(CH_3CH_2CH_2) - \sigma^*(CH_3CH_2)\}$$
$$= +0.360 - (-0.115+0.100) = +0.375$$

As seen in Fig. 7, for the last three series ρ^* values are actually not distinguishable from each other. Among them diphenylmethanes and allylbenzenes seem to be correlated by a single line. The line formed by points for all of the ethylbenzenes is about 0.5 log unit below that defined by series of diphenylmethanes and allylbenzenes. Obviously the accelerating effects of the phenyl and vinyl groups due to resonance interaction with the odd electron developing in the transition state are of the same order of magnitude. The ρ^* value for reactions of toluenes is distinctly larger, in the absolute magnitude, than those for other series. The difference in structural dependence in the hydrogen abstraction from aralkylhydrocarbons has been one of the central subjects for recent years and results regarding this point have been explained mainly in terms of the degree of bond breaking in the transition state.[27] Thus the greater ρ^* values for the toluenes is reflected by the greater ratio of k_H/k_D[28] for the reaction of toluene (4.9) with the bromine atom compared to that for the reaction of ethylbenzene (2.7). Such an explanation advanced for the observed variation in the reaction constant for benzylic hydrogen reactivities toward free radicals implies that the linear free energy relationship would hold only within limited class of compounds. Such is found to be the case not only in this instance but also in many other reactions of the hydrogen abstraction which follow, but even in these cases one may obtain useful informations as to the detailed structure of the transition state.

Figure 8 refers to a similar treatment for bromination rates in chlorobenzene for toluenes (Br_2, 80°C),[19] cumenes (NBS, 70°C),[27] and neopentylbenzenes (NBS, 70°C).[29] Totherow and Gleicher[29] reported a value of 0.45 for the ratio of reactivities of k(neopentylbenzene)/k(toluene) at 70°C while Russell and coworkers[30] obtained a value of 14 for k(cumene)/k(toluene) at 40°C. Although these relative reactivities were determined under different conditions, these are fairly close to allow for direct comparison. The treatment yielded three straight lines with different slopes and this is expected for reactions which involve large differences in the degree of bond breaking in the transition state. It seems significant that the reaction of neopentylbenzenes with the bromine atom shows the smaller substituent dependence than that of toluenes in spite of the fact that neopentylbenzene has a relative rate of one-half that of toluene.[29] In general the ρ values for aralkylhydrocarbons appear to be related to the relative rates of reaction of the parent compounds;[14,31] the faster the reaction of a parent compound, the smaller the ρ value for the reaction series. For this reason the observed tendency for reactions of neopentylbenzenes is anomalous and in keeping with an explanation proposed by Totherow and Gleicher based on unfavorable steric interactions between a substrate and an attacking reagent.[29]

Comparison of chlorination rates for aliphatic and aromatic series of compounds with the aid of the Taft equation discloses yet another interesting point. Extensive studies have been made by Migita, Nagai, and Kosugi[32,33] of the chlorination of systematized series of aliphatic compounds under certain conditions,

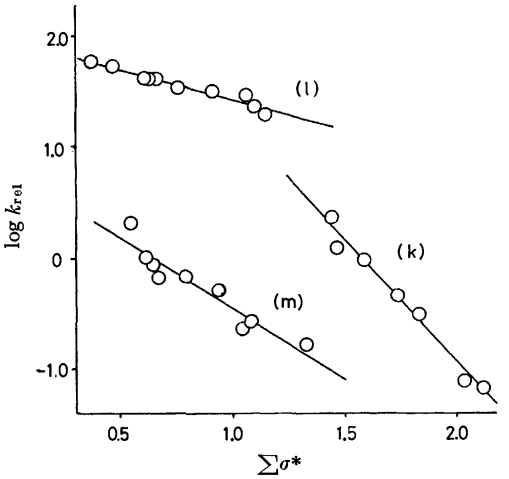

Fig. 8. Plots of relative reactivities for substituted toluenes, cumenes and neopentylbenzenes toward the bromine atom *versus* σ^*.
(k) Toluenes; $\log k_{rel} = -2.198 \sum\sigma^* + 3.462$
(l) Cuments; $\log k_{rel} = -0.542 \sum\sigma^* + 1.971$
(m) Neopentylbenzenes; $\log k_{rel} = -1.280 \sum\sigma^* + 0.831$

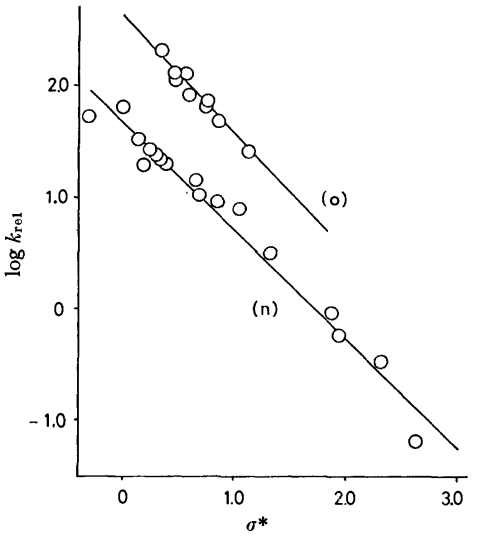

Fig. 9. Plots of relative reactivities of R–CH_3 toward photochlorination at 40C° *versus* σ^*.
(n) R=alkyl; $\log k_{rel} = -0.955\,\sigma^* + 1.698$
(o) R=aryl; $\log k_{rel} = -1.050\,\sigma^* + 2.647$

27) G. J. Gleicher, *J. Org. Chem.*, **33**, 332 (1968).
28) K. B. Wiberg and L. H. Slaugh, *J. Amer. Chem. Soc.*, **80**, 3033 (1958).
29) W. D. Totherow and G. J. Gleicher, *ibid.*, **91**, 7150 (1969).
30) G. A. Russell, C. DeBoer, and K. M. Desmond, *ibid.*, **85**, 365 (1963).
31) M. M. Martin and G. J. Gleicher, *ibid.*, **86**, 233 (1964).
32) M. Kosugi, T. Migita, and Y. Nagai, *Nippon Kagaku Zasshi*, **92**, 477 (1971).
33) Y. Nagai, M. Kosugi, K. Takeuchi, and T. Migita. *Tetrahedron*, **26**, 2791 (1970).

while Russell and Williamson[34] have obtained relative rate data for the chlorination of a series of substituted toluenes including a wide range of substituents. Since both of the measurements were conducted under very nearly the same conditions, relative reactivities for compounds of either types can be readily compared with a considerable degree of reliability, if the two sets of rate data are combined. This can immediately be done since a reactivity ratio of k(toluene)/k(t-BuCl) was found by Russell[35] to be 1.1 : 0.12. The results were treated using the Taft equation to give correlations shown in Fig. 9. Strikingly enough, there were found two parallel lines and this finding indicates that the stabilization by resonance interaction between an aromatic ring and the reaction site amounts to about 0.5 log unit corresponding 0.7 kcal/mol. That is, this value holds regardless of the substituents present on the phenyl group.

34) G. A. Russell and R. C. Williamson, Jr., *J. Amer. Chem. Soc.*, **86**, 2357 (1964).
35) G. A. Russell, *ibid.*, **80**, 4997 (1958).

Conclusions

Many useful informations as to the effect of structure on molecular properties can be obtained by correlating reactivities or physical measurements with a set of Taft polar substituent constants including values for substisuted phenyl groups which we have defined. Some instances following the extended Taft equation have been illustrated. The treatment of this type is especially instructive when comparing reactivities or physical properties of groups of benzylic type. The new polar substituent constants have general utility in the identification of the specific resonance or steric effects. Deviations from the extended Taft relationship provide a measure of such effects and this use of the σ^* values has been exemplified.

The authors are grateful to Professor T. Migita of Gunma University who made a number of valuable suggestions on this topic.

BULLETIN OF THE CHEMICAL SOCIETY OF JAPAN, VOL. 45, 2565— 2570 (1972)

Restricted Rotation in Aromatic Ketones. I. Substituent Effects on the Barrier to Rotation about the Benzene-to-Carbonyl Bond[1)]

Nobuo NAKAMURA and Michinori ŌKI

Department of Chemistry, Faculty of Science, The University of Tokyo, Hongo, Tokyo

(Received February 23, 1972)

Several aryl isopropyl ketones and aryl benzyl ketones were synthesized and their NMR spectra were recorded at various temperatures. Their temperature dependence was accounted for in terms of the restricted rotation about the benzene-to-carbonyl bond, whose free energies of activation at the coalescence temperatures varied from 9 to 15 kcal/mol according to the steric effect of ortho substituents, the buttressing effect of meta substituents, and the steric effect of the side-chain groups.

Nuclear magnetic resonance spectroscopy has proved to be a powerful and convenient tool for the study of the relatively slow internal rotations, the representative being the PMR spectroscopic studies on amides, biphenyls, aromatic aldehydes, and diazoketones.[2)]

When the torsional process is slow enough and if the process produces the mirror images, there should exist a pair of optical antipodes even at the room temperature. Thus many successful results are to be seen in the resolution into the stable atropisomers whose pivot bonds are the sp^2-sp^2 hybridized. However, no example for which carbonyl carbon is involved as a carbon of sp^2-hybridization has been claimed to be resolved,[3)] though carbonyl group has been the subject of a large number of studies in organic chemistry because of its variety of reactions and reactivities.

The concept and the continuous interest in the torsional stereoisomerism led us to explore to what extent the rotation about the benzene-to-carbonyl bond could be hindered by the ortho substituents and to estimate whether the stable rotational isomers could be isolated at room temperature.

We now wish to report our results about the steric effects on the barrier to rotation about the benzene-to-carbonyl bond in some aromatic ketones using the

1) A part of this article was presented at the 21st anual meeting of the Chemical Society of Japan, Osaka, 1968.

2) a) M. T. Rogers and J. C. Woodbrey, *J. Phys. Chem.*, **66**, 540 (1962). b) W. L. Meyer and R. B. Meyer, *J. Amer. Chem. Soc.*, **85**, 2170 (1963). c) F. A. L. Anet and M. Ahmad, *ibid.*, **86**, 119 (1964). d) F. Kaplan and G. K. Meloy, *Tetrahedron Lett.*, **1964**, 2427. F. Kaplan and G. K. Meloy, *J. Amer. Chem. Soc.*, **88**, 950 (1966). e) N. Nakamura, *Kagaku no Ryoiki*, **23**, 154 (1969); N. Nakamura, *ibid.*, **23**, 262 (1969); H. Kessler, *Angew. Chem.*, **82**, 237 (1970).

3) During the course of our study, the cinchonine salt of *t*-butyl 3-carboxy-2,4,6-trimethylphenyl ketone was reported to exibit a mutarotation in solution, and the half-life time of the reacmization of the ketone was estimated to be 6.2 min at 0°C. See A. G. Pinkus, J. I. Riggs, Jr., and S. M. Broughton, *J. Amer. Chem. Soc.*, **90**, 5043 (1968).

variable temperature NMR technique which does not need the prior optical resolution.

It is well known that in *o*-substituted and *o,o'*-disubstituted aromatic ketones carbonyl group is not coplanar with the benzene ring at the ground state as a consequence of the steric requirements. When the rotation in question is sufficiently restricted, there should result the following two conformers A and $\bar{A}$, the latter being the mirror image of the former when X and Y are different from the each other.

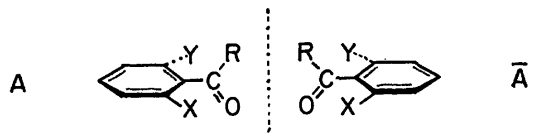

Fig. 1. Conformations of 2,6-disubstituted phenyl ketone.

Then, if R carries a methylene group or geminal methyl groups, the nonequivalence of the protons concerned is expected as in the case of a biphenyl[2] and an ansanoid compound.[4] Thus isopropyl and benzyl groups were chosen for the side chain groups for the convenience of the synthesis. If the coalescence or the change in line-shapes of these signals is observed in the NMR spectra, it should be possible to derive the kinetic data involving the internal rotation.

As for X and Y, they should provide magnetic environments of large difference in order to facilitate the distinguishing of the enantiomeric protons. Thus methyl, chlorine, bromine or methoxy groups were used in this study.

Syntheses

The following six compounds were prepared by the routes shown in the scheme 1.

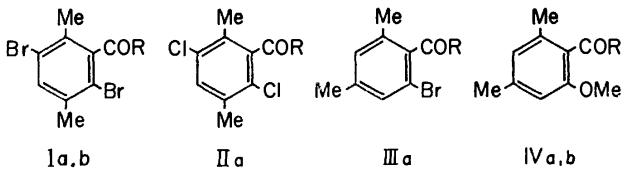

Ia,b IIa IIIa IVa,b

a, R = $CH(CH_3)_2$: b, R = CH_2Ph

The appropriate nitriles which had been obtained by the several steps were hydrolysed in two steps to afford in relatively high yields the corresponding carboxylic acids, which were then converted to the acid chlorides by the action of thionyl chloride.

Treatment of the acid chloride with an ethereal solution of excess of isopropylmagnesium bromide gave after one distillation a mixture of the desired ketone and the corresponding secondary alcohol in a molar ratio of about 1 : 3 as clarified by vpc analysis. This mixture was oxidized with chromic acid in aqueous acetic acid at 0°C, and the oxidation product was purified by distillation and/or column chromatography on silica gel to give Ia, Ib, IIa, and IIIa.

4) M. Nakazaki, K. Yamamoto, and S. Okamoto, *Tetrahedron Lett.*, **1969**, 4597.

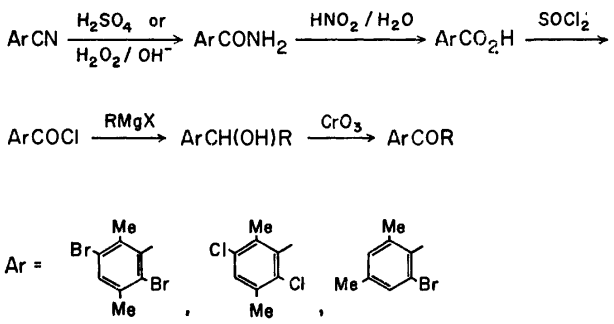

Scheme 1.

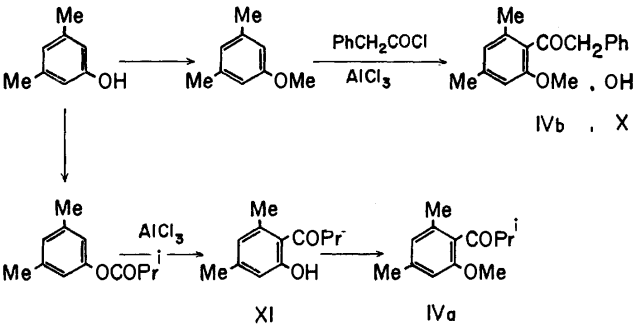

Scheme 2.

3,5-Xylenol was converted to the isobutyrate, which was treated with anhydrous aluminum chloride without solvent to rearrange to the phenolic ketone. The latter was then methylated to afford IVa. IVb was prepared by the Friedel-Crafts reaction of 3,5-dimethylanisol with phenylacetyl chloride in the presence of aluminum chloride (see Scheme 2).

Results

The NMR spectra of Ia in carbon tetrachloride, benzene, and pyridine were recorded at the ambient temperature, and the results were summarized in Table 1.

The methyl groups of isopropyl residue appeared as a sharp doublet (J=7 Hz, half-width 1.5 Hz) in carbon tetrachloride. However, when the solvent was changed to benzene and further to pyridine, the signals of isopropyl-methyl groups decreased in their heights, whose values relative to the methyl group attached directly to the aromatic ring were 1.0 in carbon tetrachloride, 0.54 in benzene, and 0.48 in pyridine. These figures apparently indicated that there were the chemical-shift differences between two methyl groups of the isopropyl-side-chain. That is, the rotation about the benzene-to-carbonyl bond was relatively slow on NMR time scale.

When the temperature of the pyridine solution was lowered to 18—20°C, the signal changed in its appearance to a single broad peak, which split into four peaks on further cooling and finally into the two sets of doublets at −35°C, the chemical-shift difference and the coupling constant being 13.5 Hz and 7.1 Hz, respectively. On the contrary, the signal increased in its height as the temperature was raised and at

Table 1. NMR Spectra of Ia in three solvents[a)]

Solvent	Chemical-shift[b)]			Peak-height Ratio (1/2)
	$CH(C\underline{H}_3)_2\cdots 1$	$C\underline{H}(CH_3)_2$	$Ar\text{–}C\underline{H}_3\cdots 2$	
CCl_4	1.19[d]	3.07[sep]	2.21[s], 2.37[s]	1.0
C_6H_6	1.03[d]	2.88[sep]	1.88[s], 2.07[s]	0.54
C_5H_5N	1.16[d]	3.12[sep]	2.24[s]	0.48

a) The spectra were taken at 23°C in about 10% soln.
b) δ in ppm unit from TMS as an internal standard. d, sep, and s refer to doublet, septet and singlet, respectively.

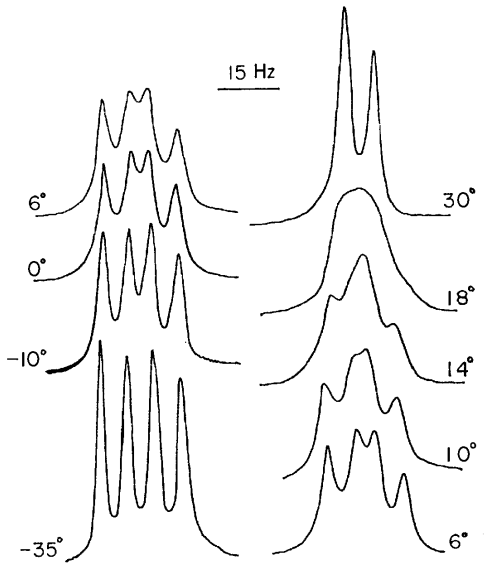

Fig. 2. Methyl signals of isopropyl group at various temperatures.

last a sharp doublet resulted at 60°C.

From these temperature dependence of the spectra shown in Fig. 2, the rates and free energies of activation for rotation were evaluated using the following approximation methods.[5)] For the isopropyl ketones, the approximate rates k_c at the coalescence temperatures T_c were calculated by

$$k_c = \frac{\pi\delta\nu}{\sqrt{2}} \quad (1)$$

and the free energies of activation by

$$\Delta G_c^{\ddagger} = 4.57\,T_c\left(9.97+\log_{10}\frac{T_c}{\delta\nu}\right) \quad (2)$$

whereas for the benzyl ketones, k_c and $\Delta G_c^{\ddagger}$ at T_c were calculated by

$$k_c = \frac{\pi\sqrt{\delta\nu^2+6J^2}}{\sqrt{2}} \quad (3)$$

and

$$\Delta G_c^{\ddagger} = 4.57\,T_c\left(9.97+\log_{10}\frac{T_c}{\sqrt{\delta\nu^2+6J^2}}\right) \quad (4)$$

The variable-temperature spectra of the other compounds were also taken and the results together with those of Ia were sammarized in Tables 2 and 3.

In each case, the coalescence temperature for the isopropyl ketone was assigned to the temperature at which a single broad peak was observed ($\delta\nu > J_{CH_3CH}$) or at which two broad peaks were observed ($\delta\nu < J_{CH_3CH}$).

As the chemical-shift difference of the two methyls in IIIa could not obtained experimentally, $\delta\nu$ of 13.5 Hz was assumed for IIIa because the free energy of activation at the coalescence temperature was mainly decided by the T_c value as shown in Eq. (2), and because the two ortho substituents of IIIa were the same as those of Ia, for which $\delta\nu$ of 13.5 Hz had been obtained experimentally. Substitution of $T_c=-77$°C and $\delta\nu=13.5$ Hz in Eq. (2) gave the $\Delta G_c^{\ddagger}$ value of 10 kcal/mol for IIIa. Similarly, the free energy of activation for IVa was estimated to be about 9 kcal/mol at the experimental coalescence temperature of −95°C, the same chemical-shift difference and coupling constant being assumed for compound IVb with those of Ib.

Discussion

Comparison of the free energies of activation gives the following sequence in the decreasing order:

Ia > IIa—Ib > IIIa > IVa—IVb

The free energies of activation of the ketones studied here are equal or greater than those of benzaldehyde studied by Anet. This fact is apparently ascribed to the steric effects of the ortho substituents and side chain. When Ia is compared with IIIa, that is, when the compounds with the same pair of substituents at 2,6-positions but with the different substitution patterns, the former being 2,3,5,6-tetrasubstituted and the latter 2,4,6-trisubstituted, are compared with each other, the barrier to rotation in the former is greater than that in the latter by 5 kcal/mol.

This surprisingly large value can be best accounted for by the idea that the buttressing effect of the meta substituents is operating substantially in Ia. Such an effect is well known especially for biphenyl derivatives, where 10—2000 times of the slow-down effect on the rate of racemization are reported.[6)]

5) J. A. Pople, W. G. Schneider, and H. J. Bernstein, "High-Resolution Nuclear Magnetic Resonance", McGraw-Hill Book Co., Inc., New York (1959); J. W. Emsley, J. Feeney, and L. H. Sutcliff, "High Resolution Nuclear Magnetic Resonance Spectroscopy", Pergamon Press (1965).

6) L. N. Ferguson, "The Modern Structural Theory of Organic Chemistry", Japanese language ed., Tokyo Kagaku Dojin, Tokyo (1965), p. 286. See also M. Rieger and F. H. Westheimer, *J. Amer. Chem. Soc.*, **72**, 19 (1950), where about 10^5 times of the slow-down effect of the 5,5′-diiodo substituents on the racemization of 3,3′-dicarboxy-5,5′,6,6′-tetraiodobiphenyl is reported. This effect corresponds to the about 7 kcal/mol difference of the free energies of activation.

TABLE 2. NMR PARAMETERS AND FREE ENERGIES OF ACTIVATION FOR ROTATION

Compound	Solvent	T_c, °C	$\delta\nu$, Hz	$\Delta G_c^{\neq}$, kcal/mol	k_c, sec^{-1}
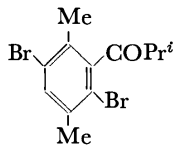	C_5H_5N	20	13.5	15.0±0.2	30
	$(CD_3)_2CO$	−3	4.8	14.5±0.2	11
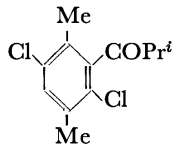	$(CD_3)_2CO$	−40	3.6	12.5±0.2	11
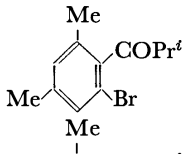	C_5H_5N–CS_2	−77	13.5	10.1	—
	$(CD_3)_2CO$	−73	4.8		—
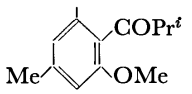	C_5H_5N–CS_2	−95	13.5	9.0	—

TABLE 3. NMR PARAMETERS AND FREE ENERGIES OF ACTIVATION FOR ROTATION

Compound	Solvent	T_c,°C	$\delta\nu$, Hz	J, Hz	$\Delta G_c^{\neq}$, kcal/mol	k_c, sec^{-1}
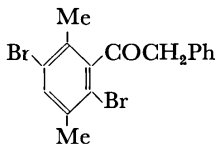	C_5H_5N–CS_2	−27	7.9	9.0	12.4±0.2	52
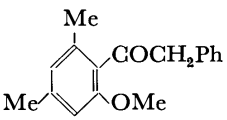	C_5H_5N–CS_2	−95	7.9	9.0	8.8	—

Comparison of the data of Ia and IIa gives the difference of the barriers by 2.5 kcal/mol, which clearly shows the effectiveness of the steric hindrance, the former having a larger substituent in an ortho position than the latter.[7]

The difference between IIIa and VIa is much lesser than that expected from the ground of van der Waals' radii. However, it may be necessary to obtain more accurate data to discuss the similarness or dissimilarness of the steric effect of the substituents in detail.

The steric effect of the side-chain groups may be also shown when Ia and Ib are compared. The magnitude of the difference in this case amounts to *ca.* 2.5 kcal/mol to indicate that the side-chain group is also involved in slowing down the rotation about the benzene-to-carbonyl bond.[8] It is, of course, understandable if the coplanar transition state for rotation is assumed, where the steric interference between the ortho substituents and the side-chain is playing the main role in determining the energy barrier.

Experimental

NMR spectra were recorded on either a Jeol Model JNM-C-60H, or a HITACHI Model R-20B spectrometer both operating at 60 MHz. Samples were run as dilute solutions in an apropriate solvent indicated using TMS as an internal reference. Chemical shifts are recorded as parts per million downfield from TMS on the δ scale. Sample temperatures were measured and calibrated by the chemical shift differences between the hydroxyl protons and the methylene protons of ethylene glycol for the higher temperatures, or by those between the hydroxyl proton and the methyl protons of methanol for the lower temperatures. IR spectra were taken with a HITACHI Model G-2 grating spectrophotometer. The purities of the oily final compounds were checked by analytical vpc using a Shimadzu GC-4APF gas chromatograph equipped with flame ionization detectors using nitrogen as carrier gas, the flow rate of which was set to 40 ml/min. Glass tubing columns, designed for on-column injection, 2 m in length and 3 mm of inner diameter, and packed with 10% SE-52 on Diasolid M of 60—80 mesh, were used. Melting points are uncorrected.

7) The van der Waals radii of bromine, chlorine and methyl groups are 1.95, 1.80, and 2.0 Å, respectively. L. Pauling, "Nature of the Chemical Bond", 3rd ed., Cornel U. P., Ithaca, N. Y. (1960), pp. 260, 263. The bond lengths of C(sp^3)–Br and C(sp^2)–Cl are 1.875 and 1.711 Å, respectively. M. G. Brown, *Trans. Faraday Soc.*, **55**, 694 (1959).

8) Slow-down of the internal rotation of amides due to the side-chain groups has been also reported. See A. Mannschreck, *Tetrahedron Lett.*, **1965**, 1341.

2,5-Dibromo-3,6-dimethylbenzonitrile (V). *(a)*: Diazotization of 2,5-Dibromo-3,6-dimethylaniline. To a solution of 42 g of the aniline in 360 m*l* of ethanol, 36 m*l* of concentrated sulfuric acid was added dropwise below 0°C, and the mixture was cooled to −10°C. To this mixture 20.5 g of butyl nitrite was added with vigorous stirring over a period of 30 min and the stirring was continued at this temperature for an additional 1 hr, at the end of which time 180 m*l* of cold ether was added and the mixture was stirred for 30 min to complete the separation of solid. The diazonium sulfate was collected on a glass filter, washed with cold anhydrous ethanol and finally dissolved in ice-water.

(b): The Sandmeyer Reaction. To a cuprous cyanide solution obtained from 100 g of cupric sulfate according to the standard method, the diazonium salt solution prepared in (*a*) was added slowly with vigorous stirring. The stirring was continued for 10 hr at room temperature and then at 50°C for 2 hr. After cooling, the organic layer was separated, washed with water, and dried over anhydrous sodium sulfate. The solvent was evaporated *in vacuo* and the crystalline residue was recrystallized from ethanol to yield 20.5 g (47% of the theoretical) of the desired product, mp 123°C.

Found: C, 37.20; H, 2.44; N, 4.85%. Calcd for $C_9H_7Br_2N$: C, 37.40; H, 2.88; N, 4.64%.

2,5-Dichloro-3,6-dimethylbenzonitrile (VII). VII was prepared in a similar way as described for (V), mp 109.5—111.0°C.

Found: C, 53.84; H, 3.81; N, 6.82%. Calcd for $C_9H_7Cl_2N$: C, 54.03; H, 3.53; N, 7.00%.

2,5-Dibromo-3,6-dimethylbenzoic Acid (VI). A mixture of 5.0 g of 2,5-dibromo-3,6-dimethylbenzonitrile, 10 m*l* of water and 30 m*l* of concentrated sulfuric acid was heated at 160°C for 1 hr, cooled to room temperature, and poured into 70 m*l* of cold water. The resulting solid was collected and recrystallized from ethanol to yield 3.0 g of 2,5-dibromo-3,6-dimethylbenzamide, mp 214—217°C. The half of the amide was dissolved in dilute sulfuric acid (obtained from 15 g of concentrated sulfuric acid and 7.6 g of water) and treated with 1 g of sodium nitrite in 1.5 m*l* of water at 0°C. The mixture was then maintained at 80—90°C for 10 min and again cooled to 0°C. The carboxylic acid was collected and dissolved in sodium bicarbonate solution, which was then acidified to give 1.3 g of the desired compound, mp 160°C. NMR ($CDCl_3$): 2.42 (3H, singlet), 2.49 (3H, singlet), 7.53 (1H, singlet), 9.08 (1H, singlet).

Found: C, 34.97; H, 2.40; Br, 52.56%. Calcd for $C_9H_8Br_2O_2$: C, 35.10; H, 2.62; Br, 51.89%.

6-Bromo-2,4-dimethylbenzoic Acid (IX). Starting from 2.5 g of 6-bromo-2,4-dimethylbenzonitrile,[9] 1.9 g of 6-bromo-2,4-dimethylbenzamide, mp 178—180°C, was obtained in a similar way as described for (VI). IR (Nujol): $\nu_{N=H}$ 3400, 3170 cm^{-1}, $\nu_{C=O}$ 1690 cm^{-1}. NMR ($CDCl_3$): 2.27 (3H, singlet), 2.33 (3H, singlet), 5.96 (1H, singlet), 6.48 (1H, singlet), 6.92 (1H, singlet), 7.15 (1H, singlet).

A mixture of 1.5 g of the amide, 14 g of concentrated sulfuric acid, and 7.6 g of water was treated with 1 g of sodium nitrite in 2 m*l* of water as described for (VI) to yield 1.3 g of the carboxylic acid, mp 153—155°C. IR (Nujol): $\nu_{C=O}$ 1700 cm^{-1}. NMR ($CDCl_3$): 2.27 (3H, singlet), 2.38 (3H. singlet), 6.93 (1H, singlet), 7.20 (1H, singlet), 9.64 (1H, singlet).

Found: C, 47.06; H, 4.16; Br, 35.21%. Calcd for $C_9H_9BrO_2$: C, 47.19; H, 3.96; Br, 34.88%.

2,5-Dichloro-3,6-dimethylbenzoic Acid (VIII). To a solution of 10 g of 2,5-dichloro-3,6-dimethylbenzonitrile in 140 m*l* of 95% ethanol, 4 m*l* of 6N sodium hydroxide solution was added followed by 60 m*l* of 30% hydrogen peroxide solution at 50°C. After heating for 2 hr at 50°C, the reaction mixture was neutralized with 5% sulfuric acid and diluted with water. The precipitated amide was collected, dissolved in 50% (v/v) sulfuric acid and treated with a saturated sodium nitrite solution as described for (VI). Yield 7 g, mp 145.5—148.0°C. NMR ($CDCl_3$): 3.31 (3H, singlet), 3.37 (3H, singlet), 7.26 (1H, singlet), 9.22 (1H, singlet). For the elemental analysis, the acid was methylated with diazomethane to the corresponding methyl ester, mp 36.5—37.0°C. NMR ($CDCl_3$): 2.28 (3H, singlet), 3.31 (3H, singlet), 3.94 (3H, singlet), 7.27 (1H, singlet).

Found: C, 51.37; H, 4.27; Cl, 30.62%. Calcd for $C_{10}H_{10}Cl_2O_2$: C, 51.53; H, 4.32; Cl, 30.42%.

2,5-Dibromo-3,6-dimethylphenyl Isopropyl Ketone (Ia). To an ethereal solution of isopropyl magnesium bromide prepared from 21 g of isopropyl bromide, 4.0 g of magnesium ribbon, and 70 m*l* of anhydrous ether under nitrogen atmosphere, a solution of 2,5-dibromo-3,6-dimethylbenzoyl chloride in anhydrous ether, prepared from 5.0 g of 2,5-dibromo-3,6-dimethylbenzoic acid and thionyl chloride, was added dropwise at room temperature. The stirring was continued for 2 hr after the addition was completed, at the end of which time the reaction mixture was poured into the mixture of crushed ice and hydrochloric acid. The organic layer was separated, washed and dried over anhydrous magnesium sulfate. The solvent was evaporated and the residual oil was chromatographed on silica gel to yield the desired ketone, yield 1.4 g, mp 24°C. The vpc analysis of the product showed only a single peak, whose retention time was 11.5 min at the column temperature of 180—200°C with the program rate being 2°C/min.

Found: C, 43.04; H, 3.95; Br, 48.01%. Calcd for $C_{12}H_{14}Br_2O$: C, 43.15; H, 4.22; Br, 47.84%.

2,5-Dibromo-3,6-dimethylphenyl Benzyl Ketone (Ib). A mixture of 4.0 g of 2,5-dibromo-3,6-dimethylbenzoic acid and 5 m*l* of thionyl chloride was heated. After the evolution of gases ceased, the excess of thionyl chloride was evaporated *in vacuo* and the residual solid was dissolved in 5 m*l* of anhydrous ether. The solution was again evaporated *in vacuo* to remove any thionyl chloride or hydrogen chloride. The acid chloride was dissolved in 80 m*l* of anhydrous ether, and added over a 1 hr period to an ethereal solution of benzyl magnesium chloride prepared from 25.5 g of benzyl chloride, 4.0 g of magnesium ribbon, and 100 m*l* of anhydrous ether under nitrogen atmosphere. The product was distilled under reduced pressure to give a fraction boiled at 200—210°C/2 mmHg. The distillate solidified and recrystallized from petroleum ether to afford the desired ketone, yield 2.0 g, mp 108—109°C. IR: $\nu_{C=O}$ 1713 cm^{-1} (liq.), 1705 cm^{-1} (solid). NMR (CCl_4): 1.92 (3H, singlet), 2.36 (3H, singlet), 3.99 (2H, singlet), 7.14 (5H, singlet), 7.35 (1H, singlet).

Found: C, 50.49; H, 3.64; Br, 42.02%. Calcd for $C_{16}H_{14}Br_2O$: C, 50.29; H, 3.69; Br, 41.83%.

2,4-Dimethyl-6-bromophenyl Isopropyl Ketone (IIIa). The reaction between 2,4-dimethyl-6-bromobenzoyl chloride from 6.9 g of the corresponding acid and isopropyl magnesium bromide from 37 g of isopropyl bromide afforded 4.5 g of an oil boiling at 113—116°C/2 mmHg, which was proved by vpc analysis to be a 1:3 mixture of the ketone and the corresponding secondary alcohol.

To a solution of the above mixture in 10 m*l* of acetic acid, a solution of 0.93 g of chromic anhydride in 40 m*l* of acetic acid and 13 m*l* of water was added at 0°C with vigorous stirring, which was continued for 30 min after the addition

9) A. S. Wheeler and R. E. Thomas, *J. Amer. Chem. Soc.*, **50**, 2287 (1928).

was completed. The reaction mixture was poured into ice-water and extracted with ether. The ether extract was washed with saturated sodium bicarbonate solution and with water and then dried over magnesium sulfate. The solvent was evaporated and the residual oil (*ca.* 4.3 g) was chromatographed on 129 g of silica gel and eluted with petroleum ether–benzene (5: 1). The yield of the ketone was 3.2 g. The vpc analysis of the product showed only a single peak, whose retention time was 9.3 min at the column temperature of 160—200°C with the program rate being 4°C/min. IR (neat): $\nu_{C=O}$ 1700 cm^{-1}. NMR (CCl_4): 1.16 (6H, doublet, J=7 Hz), 2.15 (3H, singlet), 2.26 (3H, singlet), 3.13 (1H, septet, J=7 Hz), 6.88 (1H, singlet), 7.11 (1H, singlet).

Found: C, 56.29; H, 5.98; Br, 31.54%. Calcd for $C_{12}H_{15}BrO$: C, 56.49; H, 5.93; Br, 31.32%.

2,5-Dichloro-3,5-dimethylphenyl Isopropyl Ketone (IIa). 2,5-Dichloro-3,6-dimethylbenzoyl chloride prepared from 6.6 g of the corresponding acid was treated similarly as above. Chromic acid oxidation of the products followed by chromatography on silica gel yielded 2.8 g of the desired ketone, the vpc analysis of which showed only a single peak; retention time, 8.2 min at the column temperature of 180—200°C with the program rate being 2°C/min. IR (neat): $\nu_{C=O}$ 1700 cm^{-1}. NMR (CCl_4): 1.18 (6H, doublet, J=7.5 Hz), 2.17 (3H, singlet), 2.34 (3H, singlet), 3.02 (1H, septet, J=7.5 Hz), 7.23 (1H, singlet).

Found: C, 58.93; H, 5.97; Cl, 28.81%. Calcd for $C_{12}H_{14}Cl_2O$: C, 58.79; H, 5.76; Cl, 28.92%.

2,4-Dimethyl-6-methoxyphenyl Benzyl Ketone (IVb). To 14.7 g of anhydrous aluminum chloride covered with 30 m*l* of carbon disulfide, a solution of 13.6 g of 3,5-dimethylanisole and 15.4 g of phenylacetyl chloride in 70 m*l* of carbon disulfide was added dropwise with vigorous stirring. The mixture was stirred at room temperature for 1 hr and then kept at the reflux temperature for an additional 1 hr. The mixture was cooled to room temperature and the solvent was removed by decantation. The residual complex was decomposed by the addition of 150 g of crushed ice and 50 m*l* of hydrochloric acid, and the mixture was extracted with benzene. The combined extract was washed with 5% sodium hydroxide solution, then with water, and dried over calcium chloride. After the removal of the solvent the residual oil was distilled under reduced pressure. Yield 7.5 g, bp 157—159°C/1 mmHg, $n_D^{23.2}$ 1.5685. IR (neat): 1670 cm^{-1}. NMR (CS_2): 1.82 (3H, singlet), 2.17 (3H, singlet), 3.64 (3H, singlet), 3.88 (2H, singlet), 6.40 (2H, singlet), 7.04 (5H, singlet).

Found: C, 80.44; H, 7.27%. Calcd for $C_{17}H_{18}O_2$: C, 80.28; H, 7.13%.

2,4-Dimethyl-6-hydroxyphenyl Benzyl Ketone (X). The alkaline wash of the benzene extract of (IVb) was acidified and the product extracted with ether. The ether extract was washed with water and dried over sodium sulfate. After the evaporation of the solvent, the residual oil was distilled to yield the *o*-hydroxy ketone. Yield 10.2 g, bp 168—173°C/1 mmHg, $n_D^{23.2}$ 1.5921. IR (neat): ν_{O-H} 3300 cm^{-1}, $\nu_{C=O}$ 1650 cm^{-1}. NMR (CS_2): 2.10 (3H, singlet), 2.33 (3H, singlet), 4.04 (2H, singlet), 6.35 (1H, singlet), 6.40 (1H, singlet), 7.08 (5H, singlet), 11.24 (1H, singlet).

Found: C, 79.71; H, 6.82%. Calcd for $C_{16}H_{16}O_2$: C, 79.97; H, 6.71%.

2,4-Dimethyl-6-hydroxyphenyl Isopropyl Ketone (XI). To 24 g of 3,5-dimethyl phenyl isobutyrate, bp 95°C/2 mmHg, was added 22 g of anhydrous aluminum chloride at once, and the mixture was heated at 90°C for a few minutes, at he end of which time the reaction temperature was raisetd to 120°C as fast as possible and maintained at 120°C for 10 min. The reaction was completed by heating the mixture at 140°C for 30 min. After cooling the reaction mixture was treated with 50 g of crushed ice and 30 m*l* of hydrochloric acid and steamdistilled. The *o*-hydroxy ketone was recrystallized from petroleum ether. Yield 6.0 g, mp 82—82.5°C and 91—91.5°C (dual mp). IR (Nujol): ν_{O-H} 3330 cm^{-1}, $\nu_{C=O}$ 1680 cm^{-1}. NMR (CCl_4): 1.15 (6H, doublet, J= 7.1 Hz), 2.20 (3H, singlet), 2.45 (3H, singlet), 3.40 (1H, septet, J=7.1 Hz), 6.40 (1H, singlet), 6.46 (1H, singlet), 10.62 (1H, singlet).

Found: C, 74.78; H, 8.31%. Calcd for $C_{12}H_{16}O_2$: C, 74.97; H, 8.39%.

2,4-Dimethyl-6-methoxyphenyl Isopropyl Ketone (IVa). The corresponding *o*-hydroxy ketone was methylated with dimethyl sulfate to afford the desired product. Bp 109—110°C/2 mmHg, $n_D^{23.2}$ 1.5118. IR (neat): $\nu_{C=O}$ 1680 cm^{-1}. NMR (CCl_4): 1.05 (6H, doublet, J=7.1 Hz), 2.08 (3H, singlet), 2.25 (3H, singlet), 3.00 (1H, septet, J=7.1 Hz), 3.74 (3H, singlet), 6.43 (1H, singlet), 6.49 (1H, singlet).

Found: C, 75.63; H, 8.97%. Calcd for $C_{13}H_{18}O_2$: C, 75.69; H, 8.80%.

Decarboxylative Alkylation in the Photolysis of Benzhydryl Esters

Shinsaku FUJITA, Yoshimi OZAKI, and Hitosi NOZAKI

Department of Industrial Chemistry, Kyoto University, Yoshida, Kyoto

(Received February 29, 1972)

The photolysis of benzhydryl esters (**1a**—**1b**) results in decarboxylation, thus affording 1,1-diphenylalkanes, diphenylmethane, and 1,1,2,2-tetraphenylethane. The photochemistry of trityl and benzyl esters is also examined. The photochemical solvent incorporation proceeds in both radical and ionic senses. Most characteristically, the irradiation of **1a** in toluene gives 1,1,2-triphenylethane, whereas that of **1a** in methanol produces benzhydryl methyl ether. Such a dual nature of the photolysis is explained in terms of the intimate ion-radical pair hypothesis proposed by Walling.

Previously, we reported that the photoreaction of 1-phenylcycloalkenes in acetic acid gave 1-acetoxy-1-phenylcycloalkanes, and that further irradiation yielded 1-methyl-1-phenylcycloalkanes under decarboxylation.[1] The present report will describe an extension of the latter reaction to esters of mono-, di-, and triphenylated carbinols.[2]

The irradiation of 0.06—0.08 M solutions of benzhydryl esters (**1**) in benzene was effected by the use of a high-pressure mercury lamp. The photolysates were then subjected to gas-chromatographic (GC) analysis; the results are summarized in Table 1. Each component was separated by preparative-scale GC and was identified by comparing it with an authentic sample. The decarboxylation was the main process giving the corresponding 1,1-diphenylalkane (**2**).[4-7]

TABLE 1. PHOTOLYSIS OF **1a**—**1e** IN BENZENE[a)]

Ester	R	Irrad. time hr	Conv. %	Product, %		
				2[b)]	**3**	**4**
1a[8)]	Me	48	40	70	7	10
1b	Et	48	39	49	7	12
1c	Pr	48	46	48	7	6
1d		48	61	48	11	20
1e[9)]	$PhCH_2$	48	67	66	4	18

a) Irradiation was effected on 0.06 M—0.08 M solutions placed in quartz tubes (1.5ϕ×18 cm) with an external 200-W, high-pressure mercury lamp under nitrogen at room temperature.

b) Authentic samples of **2a**—**2c** (Ref. 4) were prepared by the hydrogenolysis of the corresponding alkyldiphenylcarbinol under acidic conditions (Ref. 5). The structures of **2d** (Ref. 6) and **2e** (Ref. 7) were established by means of their IR, NMR, and mass spectra. The yields were calculated on the basis of the consumed esters (**1**) and of the GC peak areas.

In each case, diphenylmethane (**3**)[10] and 1,1,2,2-tetraphenylethane (**4**)[11] were obtained as by-products.

This type of decarboxylation was a general process in the photolysis of other phenylcarbinyl esters. The alkylation was observed in the photolysis of benzyl cyclohexanecarboxylate (**5**), affording benzylcyclohexane (**6**) in a fair yield, **7** and **8** being by-products. The irradiation of trityl acetate (**9a**)[12] and propionate (**9b**)[12] gave 1,1,1-triphenylethane (**10a**)[13] and -propane (**10b**)[13] respectively. Triphenylmethane (**11**)[14] was detected as a by-product among the photolysates. Remarkably, however, the formation of the known stable trytyl "free" radical[15] was not supported by product analysis; neither the dimer[16] nor the peroxide arising therefrom was detected.[15] This is

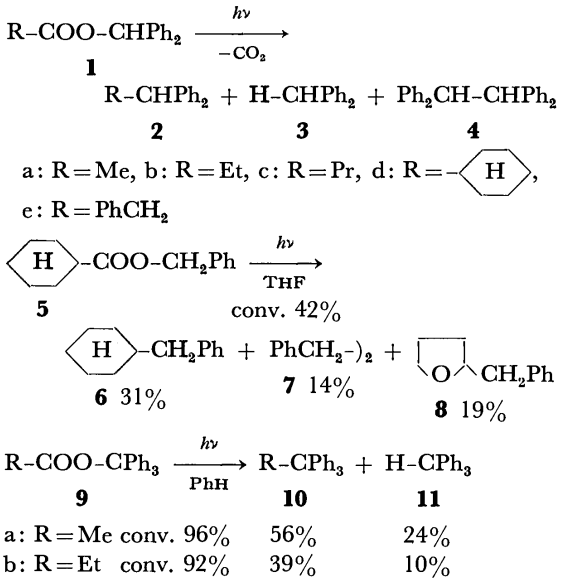

1) a) S. Fujita, T. Nômi, and H. Nozaki, *Tetrahedron Lett.*, **1969**, 3557. b) S. Fujita, Y. Hayashi, T. Nômi, and H. Nozaki, *Tetrahedron*, **27**, 1607 (1971). c) S. Fujita, Y. Hayashi, and H. Nozaki, This Bulletin, **44**, 1970 (1971).

2) When the present investigation was almost completed, Givens and Oettle reported similar photodecarboxylation of benzyl esters (Ref. 3). This communication prompted us to report independent results using benzhydryl esters.

3) R. S. Givens and W. F. Oettle, *J. Amer. Chem. Soc.*, **93**, 3301 (1971).

4) A. Klages and S. Heilman, *Ber.*, **37**, 1447 (1904).

5) A. C. Cope, S. S. Hecht, *J. Amer. Chem. Soc.*, **89**, 6920 (1967).

6) K. Ziegler and B. Schnell, *Ann. Chem.*, **437**, 251 (1924).

7) W. Schlenk and E. Bergmann, *ibid.*, **463**, 45 (1928).

8) N. T. Farinacci and L. P. Hammette, *ibid.*, **59**, 2542 (1937).

9) E. Hardegger, Z. E. Hewihi, and F. G. Robinet, *Helv. Chim. Acta*, **31**, 442 (1948).

10) C. Friedel and J. M. Crafts, *Bull. Soc. Chim. Fr.*, [2], **41**, 324 (1884).

11) C. R. Kinney and M. L. Mayhue, *J. Amer. Chem. Soc.*, **53**, 198 (1931).

12) K. D. Berlin, L. H. Gower, J. W. White, D. E. Gibbs, and G. P. Sturm, *J. Org. Chem.*, **27**, 3595 (1962).

13) M. Gomberg and L. H. Cone, *Ber.*, **39**, 2957 (1906).

14) R. F. Nystrom and C. A. Berger, *J. Amer. Chem. Soc.*, **80**, 2896 (1958).

15) M. Gomberg, *Ber.*, **33**, 3150 (1900).

16) a) H. A. Staab, H. Brettschneider, and H. Brunner, *Chem. Ber.*, **103**, 1101 (1970). b) H. Lankamp, W. Th. Nauta, and C. MacLean, *Tetrahedron Lett.*, **1968**, 249.

Table 2. The photolysis of **1a** and **1b** in various solvents (48 hr, at room temperature)[a]

Run	Ester	Solvent (S-H)	Recovered **1a**, %	Recovered **1b**, %	Product, % **2a**	**2b**	**3**	**4**	S-CHPh$_2$, % S
1		benzene	60	—	28 (70)	—	3 (7)	4 (10)	
2		toluene	87	—	5 (39)	—	1 (6)	2 (14)	PhCH$_2$, 2 (13)
3		ether	67	—	10 (30)	—	2 (6)	2 (5)	
4	**4a**	THF	38	—	17 (27)	—	4 (6)	5 (8)	, 11 (18)
5		MeOH	9	—	16 (18)	—	3 (3)	3 (3)	MeO, 34 (37)
6		AcOH	8	—	25 (27)	—	3 (3)	3 (3)	
7		EtCOOH	12	7 (8)	15 (17)	9 (10)	2 (3)	2 (3)	
8		benzene	—	61	—	19 (49)	3 (7)	5 (12)	
9		ether	—	54	—	20 (43)	4 (8)	3 (6)	
10	**4b**	AcOH	4 (4)	2	8 (9)	30 (31)	5 (6)	2 (2)	
11		EtCOOH	—	19	—	31 (38)	4 (5)	2 (3)	

a) Yields are determined by GC analysis and values in parentheses refer to the ones based on the consumed **1a** or **1b**.

in sharp contrast with the formation of **4** and **7** in the photolysis of **1** and **5**.

To gain insight into the mechanics involved, the photolysis of benzhydryl acetate (**1a**) or propionate (**1b**) was effected in various solvents (Table 2). (1) With toluene as the solvent, 1,1,2-triphenylethane (**12**) was obtained, along with **2a**—**4** products (Run 2). The photolysis in tetrahydrofuran gave 2-benzhydryltetrahydrofuran (**13**) (Run 4). (2) The irradiation of **1a** in methanol gave benzhydryl methyl ether (**14**), a methanolysis product (Run 5).[17] The photolysis of the **1a** acetate in propionic acid gave a mixture of the unchanged **1a** and the transesterification product or the propionate (**1b**), as well as the hydrocarbons, **2a** and **2b**, arising from **1a** and **1b** respectively (Run 7). Similarly, **1b** in acetic acid gave **2a** along with **2b** on UV irradiation (Run 10). Benzhydryl acetate (**1a**) was also detected in the photolysate. Thus, photochemical solvolysis[17] *via* the benzhydryl cation preceded the decarboxylation in protic solvents. (3) The irradiation of (*S*)-(+)-benzhydryl 2-methylbutanoate ($[\alpha]_D$ +5.65) afforded 1,1-diphenyl-2-methylbutane ($[\alpha]_D$ +0.65), together with **3** and **4**. As all attempts to prepare an optically-pure sample of the hydrocarbon proved unsuccessful, the degree of the retention (or inversion) could not be estimated.[18]

Apparently, no complete dichotomy can be demonstrated between "radical" and "polar" photodecompositions. This reminds us of the hypothesis of intimate ion pair-radical pair intermediate proposed by Walling *et al.* for the thermolysis of diacyl peroxides.[20] An adaptation of this hypothesis to the present photolysis would account for the observed results indicated in Scheme 1. Very probably, the decarboxylative coupling products (**2**, **6**, and **10**) and the formal hydrogenolysates (**3** and **11**) are "polar"

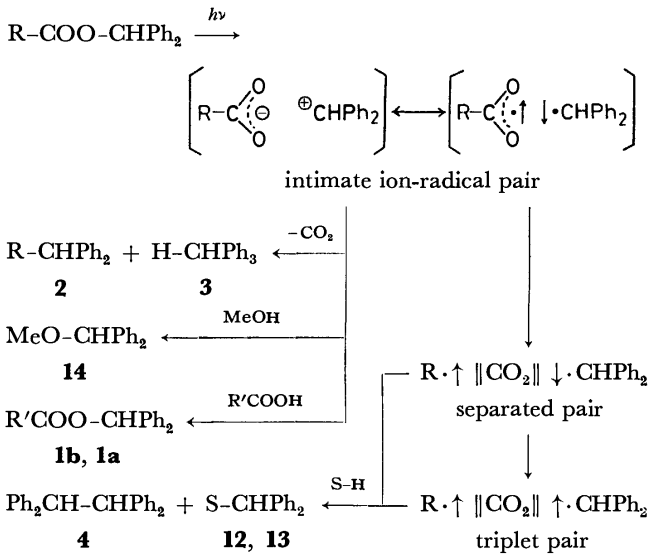

Scheme 1.

products arising from the "intimate" ion-radical pair, which also gives rise to solvolysates (**14**, **1b**, and **1a**).[21] The "radical" products, such as **4**, **7**, **8**, **12**, and **13**, can be ascribed to the separated pair, the triplet pair, or, alternatively, to the "leaked" free radical. The absence of such "radical" products in the photolysis of trityl esters is explicable on the basis of a dominant contribution of the triphenylcarbonium-ion structure to the intimate ion pair-radical pair "resonance" and the facile collapse to the "polar" products. Such a dualistic nature of the photolysates is reminiscent of our previous observations[22] of the photochemical nucleophilic alkylation of benzopyridines by alkanoic acids proceeding under decarboxylation to give alkyl-

17) a) H. E. Zimmerman and V. R. Sandel, *J. Amer. Chem. Soc.*, **85**, 915 (1963). b) S. von Kostanecki and V. Lampe, *Ber.*, **39**, 4019 (1906).

18) The photo-Fries rearrangement of aryl esters is accompanied by the decarboxylation process, which has been accounted for by a concerted mechanism. See Ref. 19.

19) R. A. Finnegan and D. Knutson, *J. Amer. Chem. Soc.*, **89**, 1970 (1967).

20) C. Walling, H. P. Waits, J. Milovanovic, and C. G. Pappiannou, *ibid.*, **92**, 4927 (1970).

21) However, a concerted mechanism cannot be excluded in the decarboxylative alkylation. See footnote 18.

22) R. Noyori, M. Kato, M. Kawanisi, and H. Nozaki, *Tetrahedron*, **25**, 1125 (1969).

dihydro-derivatives. The reaction would also possibly involve several similar ion-radical pair intermediates:

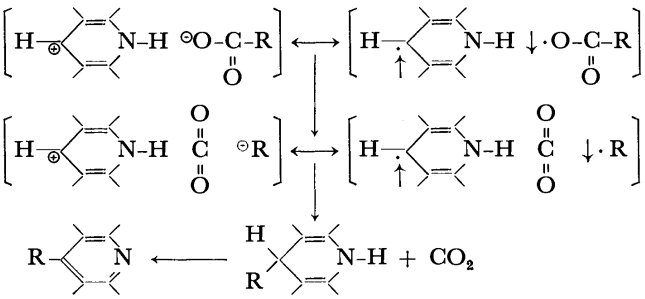

Experimental

All the melting points are uncorrected. The NMR spectra were taken on a JEOL C-60-H spectrometer, the mass spectra, on a Hitachi RMU-6L, and the IR, on a Shimadzu IR-27G spectrometer. The optical rotations were determined on a Yanagimoto OR-50 polarimeter. The preparative GC was performed on High-vacuum Silicone Grease 30% on Celite 545 (2 m), using helium as the carrier gas. The product distributions were determined by GC (Silicone Grease SE 30, 5% on Celite 545, 0.75 m, flame-ionization detector, with nitrogen as the carrier), using benzophenone, tetraphenylethylene, benzhydryl propionate, and benzhydryl phenylacetate as internal standards.

*Benzhydryl Propionate (**1b**).* Propionic acid (18 m*l*, 0.24 mol), benzhydrol (16.0 g, 0.09 mol), and sulfuric acid (1 m*l*) were dissolved in ethylene chloride (60 m*l*), and the solution was heated to reflux for 23 hr. The reaction mixture was neutralized with aqueous sodium bicarbonate, extracted with ether, and washed with a saturated sodium chloride solution. The combined ethereal extracts were dried over sodium sulfate and concentrated. The residue was distilled to give **1b** (13.1 g, 63%); bp 122°C/1 mmHg. IR (neat): 3030, 1737, 1495, 1455, 1167, 1010, 741, 700 cm^{-1}. NMR (CCl_4): δ 7.23 (10H, s, Ph), 6.85 (s, 1H, $Ph_2C\underline{H}$), 2.35 (q, 2H, $CH_3C\underline{H}_2$), 1.10 (t, 3H, $C\underline{H}_3CH_2$). MS *m/e* (relative abundance): 240 (9), 184 (23), 167 (52), 166 (100), 165 (72), 77 (27).

Found: C, 79.9; H, 6.9%. Calcd for $C_{16}H_{16}O_2$: C, 80.0; H, 6.7%.

*Benzhydryl Butyrate (**1c**).* A mixture of butyric acid (4.4 g, 0.05 mol), benzhydrol (9.2 g, 0.05 mol), *p*-toluenesulfonic acid (1.1 g), and benzene (80 m*l*) was heated for 23 hr under reflux using a Dean-Stark separator. The usual subsequent work-up gave **1c** (6.9 g, 54%); bp 129°C/2 mmHg. IR (neat): 3026, 1735, 1495, 1249, 1168, 980, 742, 700 cm^{-1}. NMR (CCl_4): δ 7.23 (s, 10H, Ph), 6.85 (s, 1H, $Ph_2C\underline{H}$), 2.78 (t, 2H, $C\underline{H}_2CO$), 1.63 (m, 2H, $CH_3C\underline{H}_2$), 0.88 (t, 3H, CH_3). MS *m/e* (relative abundance): 254 (14), 184 (34), 167 (64), 166 (100), 165 (84), 77 (27), 43 (36).

Found: C, 80.4; H, 7.3%. Calcd for $C_{17}H_{18}O_2$: C, 80.3; H, 7.1%.

*Benzhydryl Cyclohexanecarboxylate (**1d**).* This was prepared from cyclohexanecarboxylic acid (3.2 g, 0.03 mol) and benzhydrol (4.6 g, 0.03 mol) as above. Yield: 6.0 g (82%); mp 52—53.5°C (*n*-hexane). IR (Nujol): 3026, 1729, 1496, 1241, 1190, 1163, 1130, 750, 697 cm^{-1}. NMR (CCl_4): δ 7.33 (s, 10H, Ph), 6.90 (s, 1H, $Ph_2C\underline{H}$), 2.66—1.00 (m, 11H, cyclohexyl). MS *m/e* (relative abundance): 294 (7), 184 (24), 167 (72), 166 (100), 165 (47), 83 (23), 55 (21).

Found: C, 81.3; H, 7.4%. Calcd for $C_{20}H_{22}O_2$: C, 81.6; H, 7.5%.

*Photolysis of Benzhydryl Esters (**1a**—**1e**) in Benzene. General Procedure.* A 0.06—0.08M solution (16 m*l*) of **1** in benzene was placed in a quartz tube and irradiated with a 200-W, high-pressure mercury lamp under nitrogen for 48 hr. The photoproducts were separated by preparative GC (190—200°C), purified by distillation or recrystallization and identified by comparison with authentic samples. The products isolated were 1,1-diphenylalkane (**2a**—**2e**), diphenylmethane (**3**), and 1,1,2,2-tetraphenylethane (**4**). The latter compound was precipitated from the reaction mixtures when they were left standing. The results are summarized in Table 1.

*Photolysis of Benzyl Cyclohexanecarboxylate (**5**).* A 0.1M solution (10 m*l*) of **5** in tetrahydrofuran was placed in a quartz tube and irradiated under a nitrogen atmosphere with a 200-W, high-pressure mercury lamp for 48 hr. Subsequent separation by GC afforded dibenzyl, benzylcyclohexane (**6**),[23] and 2-benzyltetrahydrofuran (**8**).[24] The results are found in the text.

*Photolysis of Trityl Esters (**9a** and **9b**) in Benzene.* A 0.06M solution (16 m*l*) of the ester in benzene was placed in a quartz tube and irradiated with a 200-W, high-pressure mercury lamp under a nitrogen atmosphere for 48 hr. The photoproducts were separated by GC and identified by comparison with authentic samples. The irradiation of **9a** gave 1,1,1-triphenylethane (**10a**) and triphenylmethane (**11**). The **9b** ester gave 1,1,1-triphenylpropane (**10b**) and **11** on UV irradiation. The dimer of triphenylmethyl could not be isolated in either case. The results are found in the text.

*Photolysis of **1a** and **1b** in Various Solvents. General Procedure.* Solutions (0.08M, 16 m*l*) of **1** in different solvents were placed in quartz tubes and irradiated at the same time with a 200-W, high-pressure mercury lamp under nitrogen for 48 hr. The photolysates in the case of acidic solvents were neutralized with aqueous sodium bicarbonate, extracted with ether, and dried over sodium sulfate. The photoproducts were then separated by GC; the results are summarized in Table 2.

2-Benzhydryltetrahydrofuran (**13**) was isolated in the photolysis in tetrahydrofuran; bp 140°C (bath temperature)/3 mmHg. IR (neat): 3024, 1600, 1495, 1454, 1065, 1030, 743, 700 cm^{-1}. NMR (CCl_4): δ 7.14 (s, 10H, Ph), 4.65—4.21 (m, 1H, α-methine), 3.73 (d, 1H, $Ph_2C\underline{H}$), 4.00—3.39 (m, 2H, α-methylene), 2.14—1.06 (m, 4H, methylenes). MS *m/e* (relative abundance): 238 (1), 167 (19), 71 (100), 44 (94).

Found: C, 85.8; H, 7.7%. Calcd for $C_{17}H_{18}O$: C, 85.7; H, 7.6%.

(+)-Benzhydryl 2-Methylbutanoate. Optically-active 2-methylbutanoic acid ($[\alpha]_D^{29}$ +15.35° (neat)), which was obtained by the oxidation of commercially-available, optically-active amyl alcohol ($[\alpha]_D^{29}$ −4.4° (neat), optical purity: 93%), was converted to its acid chloride.[19] The acid chloride (3.2 g, 0.03 mol) was slowly added to a solution of benzhydrol (4.0 g, 0.02 mol) in pyridine (5 m*l*) and benzene (5 m*l*). The mixture was heated to reflux for 1.5 hr, and the excess pyridine was removed by dil. hydrochloric acid and extracted with ether. The combined extracts were washed with aqueous sodium chloride and dried over sodium sulfate. Subsequent condensation and distillation gave the title ester as a slightly yellow liquid (5.9 g, 92%); bp 113°C/0.08 mmHg. $[\alpha]_D^{29}$ +5.65° (0.0397 g/m*l* CCl_4). IR (neat): 3030, 1739, 1498, 1446, 1173, 1142 cm^{-1}. NMR (CCl_4): δ 7.23 (s, 10H, Ph), 6.85 (s, 1H, $Ph_2C\underline{H}$), 2.75—2.10 (m, 1H, CH–CO), 2.00—1.15 (m, 2H, CH_2), 1.12 (d, 3H, $C\underline{H}_3CH$), 0.81 (t, 3H,

23) N. G. Ssidorova and I. P. Zuckervanik, *Z. Obsc. Chim.*, **10**, 2073 (1940); *Chem. Centbl.*, **1941**, I. 2930.

24) T. Kariyone, *Yakugaku Zasshi*, **515**, 6 (1925).

$C\underline{H}_3CH_2$).

Found: C, 80.6; H, 7.6%. Calcd for $C_{18}H_{20}O_2$: C, 80.6; H, 7.5%.

Photolysis of (+)-Benzhydryl 2-Methylbutanoate. A 0.07M solution (16 m*l*) of the ester in benzene was irradiated for 48 hr. As well as diphenylmethane and 1,1,2,2-tetraphenylethane, 1,1-diphenyl-2-methylbutane (48%, $[\alpha]_D^{27}$ +0.65° (0.0214 g/m*l* CCl_4)) was obtained. IR (neat), 3026, 2960, 1495, 1455, 1028, 742, 700 cm^{-1}. NMR (CCl_4): 7.19 (s, 10H, Ph), 3.42 (d, 1H, $Ph_2C\underline{H}$), 2.55—1.65 (m, 1H, methine), 1.55—0.60 (m, 8H, other protons). MS *m/e* (relative abundance): 224 (6), 168 (22), 167 (100), 165 (25).

Found: C, 91.0; H, 8.8%. Calcd for $C_{17}H_{20}$: C, 91.0; H, 9.0%.

The financial support of the Ministry of Education, the Japanese Government, and the Toray Science Foundation is acknowledged with pleasure.

BULLETIN OF THE CHEMICAL SOCIETY OF JAPAN, VOL. 45, 2574—2577 (1972)

Thermolysis and Photolysis of Benzopinacol Dicarboxylates

Tamio SHIRAFUJI, Yasusi YAMAMOTO, and Hitosi NOZAKI
Department of Industrial Chemistry, Kyôto University, Yosida, Sakyô-ku, Kyôto
(Received April 1, 1972)

Thermal decomposition of benzopinacol dicarboxylates (I) results in the cleavage of the central carbon-carbon bond to afford benzhydryl esters (II) and benzophenone (III). Benzopinacol diacetate (Ia) in benzyl alcohol–benzene solution produces benzyl acetate *via* ionic reaction path, whereas Ia in THF–benzene or in toluene gives radical products such as 2-diphenylmethylenetetrahydrofuran and bibenzyl, respectively. Photolysis of I proceeds in the similar manner as thermolysis to afford II and III. The ester II is further decarboxylated photochemically to give 1,1-diphenylalkane, diphenylmethane, and 1,1,2,2-tetraphenylethane. The photochemical solvent incorporation of II proceeds in both radical and ionic sense. Such dual nature of the reaction products in thermolysis and photolysis of I and of the photodecarboxylation of II is explained in terms of the intimate ion-radical pair hypothesis proposed by Walling.

In continuation of the studies on copper carbenoids in a homogeneous system, we have found that Cu(II) carboxylates in aqueous DMF catalyze the decomposition of diphenyldiazomethane to afford benzopinacol dicarboxylates (I).[1] The reaction constitutes the only available approach to the novel class of ester I. The present report describes thermolysis and photolysis of these esters.

The Thermal Decomposition of I. Heating of 0.02—0.05 M benzene solutions of I in a sealed tube at 150—160°C under nitrogen atmosphere gave benzhydryl esters (II) and benzophenone (III). The results were summarized in Table 1. The similar reaction of I in benzene–2-propanol (1 : 1) afforded II as the main product besides III and acetone pinacol (IV). This is explained by assuming the homolysis of

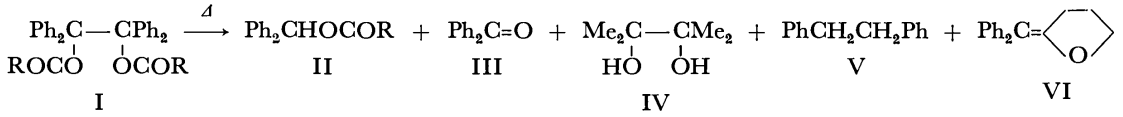

I II III IV V VI

TABLE 1. THERMOLYSIS OF I IN VARIOUS SOLVENTS (150—160°C)

I	R	Solvents	Reaction time hr	Products (Yield in %)[a]		
				II	III	others
a	Me	PhH	10	12	78	—
		PhMe	5	10	70	V (tr)
		PhH–MeOH (1 : 1)	22	17	66	—
		PhH–THF (1 : 1)	17	27	51	VI (11)
		PhH-*iso*PrOH (1 : 1)	14	70	12	IV (19)
b	Et	PhH	15	22	58	—
		PhH-*iso*PrOH (1 : 1)	15	62	24	IV (24)
c	*n*-Pr	PhH	20	24	64	—
		PhH-*iso*PrOH (1 : 1)	20	70	14	IV (25)

a) Each value is based on the glc peak area and the recovery of I was negligible. The yields of IV are based on the starting amount of I.

1) T. Shirafuji, Y. Yamamoto, and H. Nozaki, *Tetrahedron*, **27**, 5353 (1971).

the central carbon-carbon bond of I and the subsequent hydrogen-transfer from 2-propanol to the resulting acetoxydiphenylmethyl radical.[2] The thermal decomposition of Ia in toluene gave bibenzyl (V) and the one in benzene–THF (1 : 1) 2-diphenylmethylenetetrahydrofuran (VI), respectively, along with IIa and III. Probably VI is ascribed to the loss of acetic acid from 2-acetoxydiphenylmethyltetrahydrofuran (VII) during the isolation process (distillation or column chromatography).[6] The isolation of V and VI is indicative of the homolysis of the carbon-carbon bond of I. Remarkably a product of ionic nature was isolated in the thermolysis of Ia in benzene–benzyl alcohol (1 : 1). Benzyl acetate was obtained, although in a trace amount, besides IIa and III. The ester is accounted for by assuming the intermediacy of acetyl cation arising from acetoxydiphenylcarbonium ion as formulated in Scheme 1.[7]

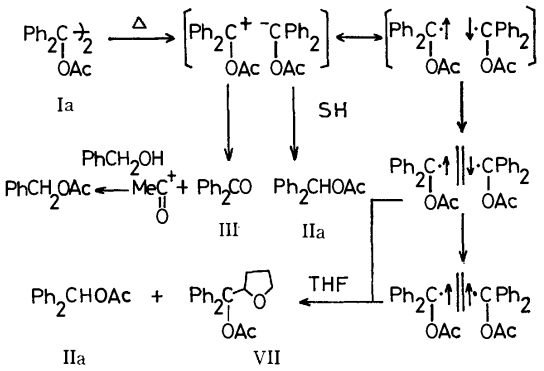

Scheme 1.

Such novel carbon-carbon bond cleavage of I in both radical and ionic sense may be explained by the adaptation of the hypothesis of intimate ion pair-radical pair intermediates as proposed by Walling *et al.* in the thermolysis of diacyl peroxides.[8] We may assume that a part of II and III,[9] and benzyl acetate are "polar" products arising from the intimate ion-radical pair. "Radical" products such as IV, V, VI, and therefore VII are ascribed to the separated pair, the triplet pair, or alternatively to the "leaked" free radical.

In each run described above, a trace amount of tetraphenylethylene was obtained.

The Photolysis of I. The irradiation of 0.02—0.05 M solutions of I in benzene was effected with a high pressure mercury lamp. The products were II, III, and 1,1-diphenylalkane (VIII) in addition to a trace each of diphenylmethane (IX) and 1,1,2,2-tetraphenylethane (X) as shown in Table 2. The irradiation of I in benzene–2-propanol (1 : 1) or in benzene–methanol (1 : 1) gave the respective benzhydryl ethers XI or XII along with II, VIII, IX, and X. On the other hand, the photolysis of Ia in benzene–THF gave VI and 2-benzhydryltetrahydrofuran (XIII) as well as IIa, III, VIIIa, IX and X. Compound VI is again ascribed to the thermal decomposition of VII in the glc separation process. With toluene as a solvent, V and 1,1,2-triphenylethane (XIV) were obtained besides IIa, III, VIIIa, IX, and X.

Presumably the photolysis of Ia gives the same "intimate" ion-radical pair as shown in Scheme 1 first.[8] The formation of IIa, III, and VII is explained analogously as above. The complication is due to further photodecomposition of II.[10]

It should be added that the above mentioned photodecomposition of II occurs in the presence of III, as both are produced in the photolysis of I. When a benzene solution of IIa and III in a mole ratio of 3 : 1 was irradiated, the result was only slightly reduced yield of VIIIa (9%) under 87% recovery of IIa in comparison with the photolysis of IIa in the absence of III affording VIIIa (15%) and 75% recovery of IIa. The photolysis of a mixture of IIa and III in a mole ratio of 1 : 5 did not proceed at all and resulted in the recovery of completely unchanged IIa and III. This is explained by assuming that benzophenone quenches the S_1 state of IIa effectively.[12] In fact, the fluorescence spectrum of IIa measured in 0.04 M ethanol solution indicated a band with max at 280 and 290 nm. Addition of equimolar amount of III

2) For the thermolysis, photolysis and related reactions of such polyphenylated ethanes as benzopinacol and *sym*-bis(trimethylsiloxy)tetraphenylethane, see Ref. 3, 4, and 5.

3) a) S. G. Cohen and N. M. Stein, *J. Amer. Chem. Soc.*, **93**, 6542 (1971); b) M. B. Rubin and J. M. Ben-Bassat, *Tetrahedron Lett.*, 3403 (1971); c) M. B. Rubin, *ibid.*, 3931 (1969); d) B. M. Monroe and S. A. Weiner, *J. Amer. Chem. Soc.*, **91**, 450 (1969); e) D. C. Neckers and D. P. Colenbrander, *Tetrahedron Lett.*, 5045 (1968).

4) a) R. Calas, J. Dunogues, N. Duffaut, and C. Biran, *C. R. Acad. Sci. Paris. Ser. C*, **267**, 494 (1968); b) R. Calas, N. Duffaut, C. Biran, P. Bourgeois, F. Piscotti, and J. Dunogues, *ibid.*, **267**, 322 (1968); c) E. J. Corey and R. L. Carney, *J. Amer. Chem. Soc.*, **93**, 7318 (1971); d) E. J. Louis and G. Urry, *Tetrahedron Lett.*, 3295 (1968).

5) For so-called "hexaphenylethane" or triphenylmethyl dimer, see: a) H. A. Staab, H. Brettschneider, and H. Brunner, *Chem. Ber.*, **103**, 1101 (1970); b) H. Lankamp, W. Th. Nauta, and C. Maclean, *Tetrahedron Lett.*, 249 (1968). For a genuine hexaphenylethane, see: H. A. Staab, K. S. Rao, and H. Brunner, *Chem. Ber.*, **104**, 2634 (1971).

6) A mixture (*ca.* 1 : 5) of VI and probably VII was eluted from silica gel column and showed an intense IR absorption at 1747 cm^{-1}. Compound VII could not be isolated in a pure form.

7) This acetoxydiphenylmethyl radical or cation was supposed to be present in the reaction of diphenyldiazomethane with $Cu(OAc)_2$ in aqueous DMF at room temperature under nitrogen atmosphere and this gives rise to benzophenone as a deacetylation product besides benzopinacol diacetate. See Ref. 1.

8) C. Walling, H. P. Waits, J. Milovanovic, and C. G. Pappiaonnou, *J. Amer. Chem. Soc.*, **92**, 4927 (1970).

9) 2-Phenoxyprop-2-yl radical gives acetophenone and methane *via* phenyl-migration. See A. Ohno, N. Kito, and Y. Ohnishi, This Bulletin, **44**, 467, 470 (1971).

10) Photodecarboxylation of II to give VIII, IX, and X was already recorded. See Ref. 11a.

11) a) S. Fujita, Y. Ozaki, and H. Nozaki, This Bulletin, **45**, 2571 (1972); b) S. Fujita, Y. Hayashi, T. Nomi, and H. Nozaki, *Tetrahedron*, **27**, 1607 (1971); c) R. Noyori, M. Kato, M. Kawanisi, and H. Nozaki, *ibid.*, **25**, 1125 (1969).

12) The role of benzophenone as a singlet quencher has been observed in the cyclodimerization of anethole occurring *via* the S_1 state. See Ref. 13.

13) H. Nozaki, I. Otani, R. Noyori, and M. Kawanisi, *ibid.*, **24**, 2183 (1968).

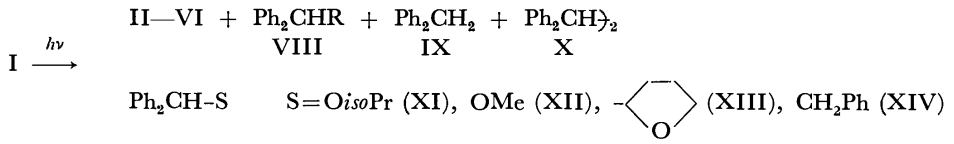

TABLE 2. PHOTOLYSIS OF I IN VARIOUS SOLVENTS (quartz vessel, 200 W high pressure Hg lamp)

I	R	Solvents	Irradiation time hr	Recovery of I (%)	Products (yield in %)[a] II	III	VIII	others
a	Me	PhH	62	0	25	70	tr	—
		PhH-*iso*PrOH (1: 1)	15	0	6	—	26	XI (33), IV (20)
		PhH-MeOH (1: 1)	22	0	—	—	11	XII (30)
		PhH-THF (1: 1)	15	0	22	tr	22	XIII (28), VI (15)
		PhMe	21	0	21	—	3	V (39), XIV (8)
b	Et	PhH	18	15	34	18	6	—
		PhH-*iso*PrOH (1: 1)	18	20	—	—	7	XI (21), IV (16)
c	*n*-Pr	PhH	22	35	5	28	tr	—
		PhH-*iso*PrOH (1: 1)	20	20	4	—	4	XI (22), IV (17)

a) A trace amount of IX and X was obtained in every run.

to this solution completely quenched the fluorescence.[14]

Experimental

All the melting points and the boiling points are uncorrected. The microanalyses were performed by Mrs. K. Fujimoto. The IR spectra were obtained on a Shimadzu IR-27-G spectrophotometer, and the mass spectra on a Hitachi RMU-6L machine. The NMR spectra were taken in $CDCl_3$ or CCl_4 solution at 60 MHz on a JEOL C-60-H spectrometer and chemical shifts were given in ppm from TMS internal standard. NMR signals in singlet are designated as s, doublet as d, triplet as t, and multiplet as m. glc analyses and separations were performed with columns (1 m) packed with HVSG (30%) on Celite 545 or SE 30 (5%) on Chromosorb. Unless otherwise stated, irradiation was effected externally by means of a 200 W high pressure mercury lamp (quartz jacket) from a distance of 2 cm under nitrogen atmosphere at room temperature.

The General Procedure for Thermolysis of Benzopinacol Dicarboxylates (I). A benzene solution (20 m*l*) of I (1.0 mmol) in a sealed tube was heated at 150—160°C for 10—20 hr under nitrogen atmosphere. After distillation *in vacuo*, the reaction mixture was separated by glc to give benzhydryl carboxylate (II) and benzophenone (III). Each product was identical with the authentic samples (IR, MS, and glc retention times).[11] The yields of II and III, estimated on glc, were summarized in Table 1. The following description is concerned with the cases which cannot be covered sufficiently by Table 1.

The Thermolysis of Benzopinacol Diacetate (Ia) in Benzene–THF. A benzene–THF (1: 1) solution (20 m*l*) of Ia (0.30 g, 0.67 mmol) in a sealed tube was heated at 150—160°C for 17 hr under nitrogen atmosphere. Distillation of the reaction mixture *in vacuo* followed by glc separation gave benzhydryl acetate (IIa) (0.081 g, 27%), III (0.12 g, 51%) and 2-diphenylmethylenetetrahydrofuran (VI) (0.036 g, 11%). Compound VI formed an oil, bp 155—160°C/0.06 mmHg (bath temperature). IR (neat): 1645, 1600, 1176, 1075, 1040, 1028, 992 cm^{-1}. NMR (CCl_4, 10%): δ 7.50—7.10 (m, 10H, aromatic), 4.22 (t, 2H, $-OC\underline{H}_2-$), 2.50 (m, 2H, $=C(-O-)-C\underline{H}_2-$), and 1.97 (m, 2H, $-OCH_2C\underline{H}_2-$). MS (relative abundance): *m/e* 236 (M^+ 86), 180 (57), 165 (100), 77 (48).

Found: *m/e* 236.117 (M^+). Calcd for $C_{17}H_{16}O$: *m/e* 236.120.

The Thermolysis of Ia in Benzene–Benzyl Alcohol. A benzene–benzyl alcohol (1:1) solution (20 m*l*) of Ia (0.20 g, 0.44 mmol) in a sealed tube was heated at 150—160°C for 15 hr under nitrogen atmosphere. Distillation of the reaction mixture followed by glc separation gave IIa (0.17 g, 85%), III (0.008 g, 5%) and benzyl acetate (trace).

The General Procedure for Photolysis of Diester I. A benzene solution (20 m*l*) of I (1.0 mmol) in a quartz vessel was irradiated for 15—22 hr or more prolonged irradiation time (62.5 hr). The solvent was evaporated and the residue was washed with ether to give the recovery of I. The filtrate was again concentrated *in vacuo* and the residue was washed with methanol to give 1,1,2,2-tetraphenylethane (X). The filtrate was distilled and subjected to glc separation to give II, III, 1,1-diphenylalkane (VIII), and diphenylmethane (IX). Each product was identified by the comparison with the authentic samples[16-18] (IR, MS, and glc retention times). The yields of each product were estimated on glc as shown in Table 2. The following description is concerned with the cases which cannot be covered sufficiently by Table 2.

The Irradiation of Ia in Benzene–2-Propanol. A solution of Ia (0.20 g, 0.44 mmol) in benzene–2-propanol (1:1) (20 m*l*) was irradiated for 15 hr. Separation of the reaction mixture by distillation and by glc afforded acetone pinacol (0.006 g, 20%), IIa (0.012 g, 6%), VIIIa (0.042 g, 26%), IX (trace),

14) For the photolysis of *sym*-tetraphenylethane, see Ref. 15. The presence of *vic*-acetoxyls completely changes the reaction course.

15) J. A. Ross, W. C. Schumann, D. B. Vasi, and R. W. Binkley, *Tetrahedron Lett.*, 3283 (1971).

16) W. W. Hartmann and P. Phillips, "Org. Syntheses", Coll. Vol., **2**, (1943), p. 232.

17) J. S. Reichert and J. A. Nieuwland, *ibid.*, Coll. Vol., **1**, (1941), p. 229.

18) A. C. Cope and S. S. Hecht, *J. Amer. Chem. Soc.*, **89**, 6920 (1967).

X (trace), and benzhydryl isopropyl ether (XI) (0.066 g, 33%). The ether XI formed an oil, bp 110—115°C/0.1 mmHg (bath temperature). IR (neat): 1295, 1255, 1180, 1170, 1135, 1118, 1080, 1057, 1028, 935, 920, and 905 cm^{-1}. NMR (CCl_4, 15%): δ 7.40—7.00 (m, 10H, aromatic), 5.36 (s, 1H, $Ph_2C\underline{H}$–O–), 3.59 (m, 1H, –$C\underline{H}Me_2$), and 1.15 (d, 6H, methyl). MS (relative abundance): *m/e* 226 (M^+, 11), 182 (12), 167 (100), 152 (23), 107 (68), 105 (66), 77 (46).

Found: C, 84.8; H, 7.9%. Calcd for $C_{16}H_{18}O$: C, 84.9; H, 8.0%.

Independent synthesis of XI was performed according to the method similar to the reported one.[19] The IR spectrum and glc retention time were completely identical with those of the photoreaction product XI.

The Irradiation of Ia in Benzene–THF. A solution of Ia (0.20 g, 0.44 mmol) in benzene–THF (1:1) (20 m*l*) was irradiated for 15 hr. After distillation *in vacuo*, the reaction mixture was separated by glc to give IIa (0.044 g, 22%), III (trace), VI (0.044 g, 15%), VIIIa (0.036 g, 22%), IX (trace), X (trace), and 2-benzhydryltetrahydrofuran (XIII) (0.060 g, 28%). Compound XIII was identified by the comparison with the authentic sample (IR, NMR, MS, and glc retention time).[11a]

The Irradiation of Ia in Toluene. A solution of Ia (0.20 g, 0.44 mmol) in toluene (20 m*l*) was irradiated for 21 hr. Distillation of the reaction mixture *in vacuo* followed by glc separation gave bibenzyl (0.038 g, 39%), IIa (0.041 g, 21%), VIIIa (0.005 g, 3%), IX (trace), X (trace), and 1,1,2-triphenylethane (XIV) (0.017 g, 8%). Compound XIV was identical with the authentic sample (IR, NMR, MS, and glc retention time).[20]

The Irradiation of IIa in the Presence of Benzophenone. A solution of IIa (0.040 g, 0.18 mmol) and benzophenone (0.010 g, 0.06 mmol) in benzene (10 m*l*) was irradiated for 24 hr to afford VIIIa, IX, X, and recovered IIa. The yields of each component were shown in the text.

The authors are grateful to Mr. Yoshimi Ozaki for his assistance. Financial support from the Ministry of Education, Japanese Government, and from Toray Science Foundation is acknowledged with pleasure. They are grateful to Prof. G.W. Griffin at Louisiana State University in New Orleans for valuable suggestions.

19) S. von Kostanecki and V. Lampe, *Ber. Deut. Chem. Ges.*, **39**, 4019 (1906).

20) W. von Schlenk and E. Bergmann, *Ann. Chem.*, **463**, 45 (1928).

BULLETIN OF THE CHEMICAL SOCIETY OF JAPAN, VOL. 45, 2577—2579 (1972)

Synthesis of Some Nucleoside Analogs of Substituted 1,2,3-Triazole

Osamu MAKABE, Shunzo FUKATSU, and Sumio UMEZAWA

Department of Applied Chemistry, Faculty of Engineering, Keio University, Hiyoshi, Kohoku-ku, Yokohama

(Received March 28, 1972)

1-(β-D-Ribofuranosyl)-1,2,3-triazole-4-carboxamide (**4**) and 4-amino-1-(β-D-ribofuranosyl)-1,2,3-triazole-5-carboxamide (**7**) have been synthesized as an approach to obtain bioisosteres of pyrazomycin, an antiviral agent. The synthesis has been accomplished by condensation of blocked triazoles with tri-*O*-benzoyl-D-ribofuranosyl chloride in the presence of mercuric cyanide in nitromethane. UV spectral studies revealed the orientation of *N*-glycosidation in the substituted triazoles.

Current research in nucleoside antibiotics has stimulated an interest in synthesizing nucleoside analogs of a variety of heterocyclic bases. We interested in synthesizing some compounds related to pyrazomycin which was recently discovered by Gerzon *et al.*[1] Pyrazomycin (3-(β-D-ribofuranosyl)-4-hydroxypyrazole-5-carboxamide) is one of the rare *C*-nucleosides and an inhibitor of virus multiplication.

In this paper the syntheses of 1-(β-D-ribofuranosyl)-1,2,3-triazole-4-carboxamide (**4**) and 4-amino-1-(β-D-ribofuranosyl)-1,2,3-triazole-5-carboxamide (**7**) are described. In these compounds, the CH= group in pyrazomycin is replaced by ring nitrogen (an isosteric ring equivalent).

In the present synthesis, the coupling of blocked triazoles with a poly-*O*-acylribosyl halide was effected with mercuric cyanide in nitromethane[2] to give the blocked nucleosides. Another purpose of the present investigation was to study the orientation of *N*-glycosidation in substituted 1,2,3-triazole.

Condensation of 2,3,5-tri-*O*-benzoyl-D-ribofuranosyl chloride[3] (**2**) with 4-ethoxycarbonyl-1,2,3-triazole[4] (**1**) or 5-acetamido-1,2,3-triazole-4-carboxamide[5] (**5**) in the presence of mercuric cyanide in nitromethane gave 1-(β-D-2′,3′,5′-tri-*O*-benzoylribofuranosyl)-4-ethoxycarbonyl-1,2,3-triazole (**3**) or 4-acetamido-1-(β-D-2′,3′,5′-tri-*O*-benzoylribofuranosyl)-1,2,3-triazole-5-carboxamide (**6**).

1) K. Gerzon, R. H. Williams, M. Hoehn, M. Gorman, and D. C. DeLong, 2nd Intern. Cong. Heterocyclic Chemistry, Monptpellier, France, July 10, 1969, Abstract C-30.

2) N. Yamaoka, K. Aso, and K. Matsuda, *J. Org. Chem.*, **30**, 149 (1965).

3) H. M. Kissman, C. Pidacks, and B. R. Baker, *J. Amer. Chem. Soc.*, **77**, 18 (1955).

4) S. Yamada, T. Mizoguchi, and A. Ayata, *J. Pharm. Soc. Japan, Yakugaku Zasshi*, **77**, 452 (1957).

5) S. Yamada, T. Mizoguchi, and A. Ayata, *ibid.*, **77**, 455 (1957).

Treatment of **3** with methanolic ammonia gave 1-(β-D-ribofuranosyl)-1,2,3-triazole-4-carboxamide (**4**). This compound proved to be identical to that recently prepared by G. Alonso *et al.*[6] by an alternative synthesis from a glycosyl azide and methyl propiolate.

Similar treatment of **6** with methanolic ammonia gave crude 4-acetamido-1-(β-D-ribofuranosyl)-1,2,3-triazole-5-carboxamide (**7'**). Further hydrolysis of crude **7'** with methanolic ammonia in a sealed tube at 80°C for 20 hr afforded 4-amino-1-(β-D-ribofuranosyl)-1,2,3-triazole-5-carboxamide (**7**).

In accord with expectation based on participation[7] of the *C*-2 benzoyl group of the halogenosugar (**2**), the above-mentioned condensations afforded β-anomers (**3** and **6**) respectively. The anomeric nature was established by their NMR spectra. The anomeric protons of **3** and **6** appeared as doublets with $J_{1',2'}$ values of 2.8 and 1.8 (in DMSO-d_6) respectively, indicating their β-configuration.[8]

Positions of substitution of the ribosyl moiety in the triazole bases were established by comparison of the ultraviolet spectra of **4** and **7** with those of *N*-methyl derivatives **12**, **8**, **9**, **10** of 1,2,3-triazole-4-carboxamide and 5-amino-1,2,3-triazole-4-carboxamide. The former *N*-methyl derivative (**12**) was prepared from 4-carboxy-1-*N*-methyl-1,2,3-triazole which was reported by Pedersen.[9] The latter three *N*-methyl derivatives (**8**, **9**, **10**) were prepared by the method reported by Albert and Tratt[10] and their UV spectra have here been determined. The absorption maxima and extinctions of **4** and **7** were compatible with those of 1-*N*-methyl-1,2,3-triazole-4-carboxamide (**12**) and 5-amino-3-*N*-methyl-1,2,3-triazole-4-carboxamide (**10**), respectively, as shown in Table 1. It should be noted that the ribosyl group is introduced to *N*-1 of the triazole ring in case of **1**, whereas, in case of **5**, the sugar group is introduced to *N*-3 of the triazole ring.

Table 1. Ultraviolet spectral data

Compd No.	Solvents, absorption spectra mμ (ε) 0.1N-HCl		pH 7 water		0.1N-NaOH	
	λ_{max}	λ_{min}	λ_{max}	λ_{min}	λ_{max}	λ_{min}
12[a]	215 (11400)		212 (10400)		221 (9000)	
4	213 (12200)		211 (12700)		220 (11100)	
8[a]	228 (7990)	242 (4620)	228 (8630)	242 (5040)	228 (7770)	242 (4550)
	262 (7560)		262 (8180)		262 (7480)	
9[a]	218 (6700)	240 (1970)	218 (6310)	240 (1790)	228 (5250)	240 (1550)
	274 (5840)		274 (6350)		274 (6280)	
10[a]	206 (7620)	243 (2020)	201 (9400)	241 (2250)	221 (4370)	240 (2220)
	275 (4280)		273 (5020)		273 (5070)	
7	206 (10500)	239 (2800)	200 (11000)	241 (1900)	220 (6600)	240 (1800)
	277 (6400)		279 (6200)		280 (6400)	

a) 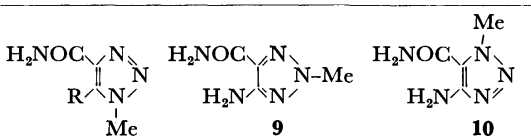

8: R=NH_2
12: R=H

9 **10**

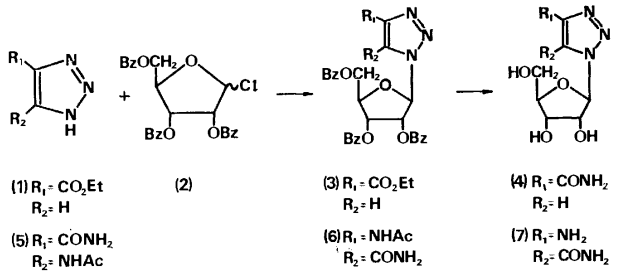

(1) R_1=CO_2Et, R_2=H; (2); (3) R_1=CO_2Et, R_2=H; (4) R_1=$CONH_2$, R_2=H; (5) R_1=$CONH_2$, R_2=NHAc; (6) R_1=NHAc, R_2=$CONH_2$; (7) R_1=NH_2, R_2=$CONH_2$

Chart 1.

Experimental

Thin-layer chromatography (tlc) was carried out on microscope slides coated with silica gel, and the spots were visualized with sulfuric acid. The NMR spectra were measured with a Varian A-60D spectrometer. Tetramethylsilane (τ 10.00; for the solution of deuteriodimethylsulfoxide) and sodium 4,4-dimethyl-4-silapentane-1-sulfonate (τ 10.00; for the solution of deuterium oxide) were used as internal standards.

1-(2',3',5'-Tri-O-benzoyl-β-D-ribofuranosyl)-4-ethoxycarbonyl-1,2,3-triazole (3). 2,3,5-Tri-*O*-benzoyl-D-ribofuranosyl chloride (**2**) (prepared[3] from 4.63 g (9.2 mmol) of 1-*O*-acetyl-2,3,5-tri-*O*-benzoyl-D-ribofuranose) was dissolved in nitromethane (25 ml) and the solution was added to a hot mixture of 4-ethoxycarbonyl-1,2,3-triazole (**1**) (1.31 g, 9.29 mmol), mercuric cyanide (2.33 g, 9.2 mmol), and Drierite (5 g) in nitromethane (70 ml). The mixture was refluxed for 2.5 hr with stirring. The hot suspension was filtered and the filter cake was washed thoroughly with ethylacetate. The filtrate and washings were combined and evaporated to dryness. The residue was dissolved in ethylacetate (5 ml) and silica gel (5 g) was added; the mixture was evaporated and the residue was chromatographed on a column of silica gel (150 g) with benzene and benzene–ethylacetate (19:1). The main portion eluted with the latter solvent system was evaporated to give **3**. Recrystallization from benzene, colorless needles, 2.99 g (54.9%); mp 168—170°C; $[\alpha]_D^{22}$ −74.8° (*c* 1.47, chloroform); UV: λ_{max} (methanol) 229 mμ (ε 48800); IR (KBr): 1730 (C=O), 710 cm^{-1} (phenyl); NMR (DMSO-d_6, τ): 0.93 (s, H-5), 3.17 (d, $J_{1',2'}$ 2.8 Hz, H-1'), 5.61 (q, *J* 7.0 Hz, $CO_2CH_2CH_3$), 8.68 (t, *J* 7.8 Hz, $CO_2CH_2CH_3$).

Found: C, 63.80; H, 4.62; N, 7.32%. Calcd for $C_{31}H_{27}$-

6) G. Alonso, M. T. Garcia-Lòpez, G. Garcia-Munoz, R. Madronero, and M. Rico, *J. Heterocycl. Chem.*, **7**, 1269 (1970).

7) B. R. Baker, *Ciba Foundation Symposium, Chem. and Biol. of Purines*, **1957**, 120; J. J. Fox and I. Wempen, *Advances in Carbohydrate Chem.*, **14**, 283 (1959); J. A. Montgomery and H. J. Thomas, *ibid.*, **17**, 301 (1962).

8) R. U. Lemieux and D. R. Lineback, *Ann. Rev. Biochem.*, **32**, 155 (1963).

9) C. Pedersen, *Acta Chem. Scand.*, **13**, 888 (1959).

10) A. Albert and K. Tratt, *J. Chem. Soc.*, **1968**, 344; A. Albert, *ibid.*, **1968**, 2076.

O_9N_3: C, 63.58; H, 4.65; N, 7.18%.

1-(β-D-Ribofuranosyl)-1,2,3-triazole-4-carboxamide (4). A solution of **3** (0.96 g, 1.6 mmol) in absolute methanol (40 m*l*) saturated with ammonia was kept at 0°C for 3 days. The solution was evaporated and the resulting syrup was chromatographed on a column of 40 g of silica gel (2.1×30 cm) with benzene–ethanol (10: 1), (6: 1), (4: 1), (1: 2), and ethanol. The last fraction gave a chromatographically homogeneous **4**. Recrystallization from water, colorless needles; 0.32 g (80%); mp 208°C (lit,[6] mp 204°C); $[\alpha]_D^{20}$ −57.3° (*c* 1.43, water) (lit,[6] $[\alpha]_D$ −51.5° (*c* 0.45, water)); UV: λ_{max} (water) 211 mμ (ε 12700); IR (KBr): 3420, 3300 (OH), 1637, 1615, 1560 cm^{-1} (amide); NMR (D_2O, τ): 1.17 (s, H-5), 3.92 (d, $J_{1',2'}$ 3.9 Hz, H-1').

Found: C, 39.23; H, 4.82; N, 22.41%. Calcd for $C_8H_{12}O_5N_4$: C, 39.34; H, 4.95; N, 22.94%.

4-Acetamido-1-(2',3',5'-tri-O-benzoyl-β-D-ribofuranosyl)-1,2,3-triazole-5-carboxamide (6). To a hot mixture of 5-acetamido-1,2,3-triazole-4-carboxamide (**5**) (0.97 g, 5.7 mmol), mercuric cyanide (1.45 g, 5.7 mmol) and Drierite (5.5 g) in nitromethane (140 m*l*), a solution of 2,3,5-tri-*O*-benzoyl-D-ribofuranosyl chloride (**2**) (prepared from 2.87 g (5.7 mmol) of 1-*O*-acetyl-2,3,5-tri-*O*-benzoyl-D-ribofuranose) in nitromethane (30 m*l*) was added and the mixture was refluxed for 3 hr with stirring. The hot mixture was filtered, the filter cake was thoroughly washed with ethylacetate, and the filtrate and washings were combined and evaporated to dryness. The resulting gum was dissolved in methanol (5 m*l*), silica gel (5 g) was added and the suspension was evaporated to dryness. The residue was placed on a column of silica gel (140 g) and eluted successively with benzene–ethylacetate (19: 1, 440 m*l*), (9: 1, 960 m*l*), (4: 1, 1330 m*l*), and (2: 1, 1560 m*l*). Evaporation of the last fraction gave **6**, colorless glass, 1.63 g (48%). The product could not be crystallized, but it was chromatographycally homogeneous; $[\alpha]_D^{20}$ −73.0° (*c* 1.54, chloroform); UV: λ_{max} (methanol) 231 mμ (ε 10400); IR (KBr): 1730 (C=O, benzoyl), 1673, 1603, 1561 (amide), 713 cm^{-1} (phenyl); NMR (DMSO-d_6, τ): 3.32 (d, $J_{1',2'}$ 1.8 Hz, H-1').

Found: C, 60.59; H, 4.82; N, 11.26%. Calcd for $C_{31}H_{27}O_9N_5$: C, 60.68; H, 4.44; N, 11.42%.

4-Amino-1-(β-D-ribofuranosyl)-1,2,3-triazole-5-carboxamide (7). A solution of **6** (1.38 g, 2.25 mmol) in absolute methanol (200 m*l*) was saturated with ammonia at 0°C, kept at the same temperature for 3 days, and evaporated under diminished pressure at 40°C. A mixture of the residue and silica gel (1 g) in methanol was placed on a column of silica gel (40 g, 2.1×30 cm) and eluted successively with benzene and benzene–ethanol (9: 1). The latter fraction was evaporated to dryness. A solution of the residue (crude **7'**) in absolute methanol (10 m*l*) saturated with ammonia was placed in a sealed tube and kept at 80°C for 20 hr. After removal of the solvent under diminished pressure, the residue was taken in methanol and silica gel (500 mg) was added. The mixture was placed on a column of silica gel (30 g, 2.0×25 cm; packed with ethylacetate) and successively eluted with ethylacetate (70 m*l*) and ethylacetate–acetone (1: 1, 100 m*l*). Evaporation of the latter fraction gave **7**, colorless glass, chromatographycally homogeneous, 0.309 g (54%); $[\alpha]_D^{23}$ −52.4° (*c* 1.29, water); UV: λ_{max} (water) 200, 270 mμ (ε 11000, 6200); λ_{min} (water) 241 mμ (ε 1900); IR (KBr): 3340 (OH), 1660, 1605 cm^{-1} (amide); NMR (D_2O, τ): 4.27 (d, $J_{1',2'}$ 3.8 Hz, H-1').

Found: C, 36.92; H, 5.54; N, 26.55%. Calcd for $C_8H_{13}O_5N_5$: C, 37.07; H, 5.06; N, 27.02%.

1-Methyl-4-ethoxycarbonyl-1,2,3-triazole (11). A solution of 1-methyl-4-carboxy-1,2,3-triazole[8] (2.50 g, 16.1 mmol) in absolute ethanol (40 m*l*) saturated with dry hydrogen chloride was refluxed for 4 hr. After removal of the solvent, the resulting syrup was triturated with water (5 m*l*). Filtration yielded colorless powder, 2.00 g (65.4%). Recrystallization from water; mp 93—94.5°C.

Found: C, 46.50; H, 5.74; N, 27.22%. Calcd for $C_6H_9O_2N_3$: C, 46.44; H, 5.85; N, 27.08%.

1-Methyl-1,2,3-triazole-4-carboxamide (12). A suspension of **11** (1.01 g, 6.52 mmol) in absolute methanol (40 m*l*) saturated with ammonia was placed in a sealed tube and kept at 90°C for 5 hr. After cooling, the precipitate was filtered, 616 mg (75.0%). Recrystallization from 50% aqueous ethanol; sublimes at 150—220°C.

Found: C, 38.02; H, 4.45; N, 44.27%. Calcd for $C_4H_6ON_4$: C, 38.09; H, 4.80; N, 44.43%.

The authors wish to thank Mr. Saburo Nakada of our laboratory for microanalysis and Mr. Hiroshi Suzuki for technical assistance. We are also thankful to the Ministry of Education for a Scientific Research Grant-in-aid.

A Salt Effect on the Reaction of Zinc Carbenoid

Nariyoshi KAWABATA,* Shigeyoshi NODA, and Shinzo YAMASHITA
Department of Chemistry, Kyoto Institute of Technology, Matsugasaki, Sakyo-ku, Kyoto
(Received April 10, 1972)

Bicyclo[4.1.0]heptane (norcarane) was obtained as the major product of the reaction of cyclohexene with diethylzinc and methylene iodide. In the presence of lithium halide or magnesium halide, however, the yield of norcarane considerably decreased. Large amounts of *n*-propyl and *n*-butyl iodides were formed which was interpreted in terms of an insertion mechanism, *viz.*, insertion of zinc carbenoid into the carbon-iodine bond of ethyl and *n*-propyl iodides.

Reports were given on the synthesis of cyclopropane derivatives by the reaction of olefins with diethylzinc and *gem*-diiodoalkanes such as methylene, ethylidene and benzal iodides.[1]

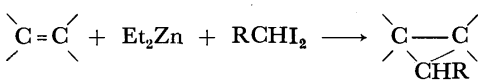

(1)

(R=H, CH_3, C_6H_5)

The reaction presumably proceeds *via* an intermediate zinc carbenoid species,[1e] and is closely related to the Simmons-Smith reaction:[2]

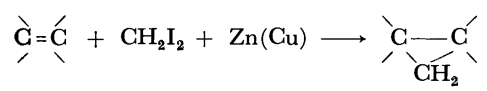

(2)

However, reaction (1) proceeds much more rapidly and *gem*-diiodoalkane should be added slowly to moderate the reaction. Reaction (1) was modified by the use of ethylidene and benzal iodides instead of methylene iodide. Diethylzinc is inflammable in air, making the reaction impracticable. In order to get rid of this inconvenience, we tried to use diethylzinc prepare *in situ* from zinc halide and ethyllithium or ethylmagnesium halide *i.e.*, to carry out the reaction in the presence of lithium or magnesium halide, and found a remarkable effect of these metal halides on the mode of reaction (1).

The reaction of cyclohexene with diethylzinc and methylene iodide in benzene or ether gave bicyclo-[4.1.0]heptane (norcarane) in good yield.[1a,1b]

TABLE 1. REACTION OF CYCLOHEXENE WITH DIETHYLZINC AND METHYLENE IODIDE IN THE PRESENCE OF METAL HALIDE[a]

Cyclohexene (mmol)	CH_2I_2 (mmol)	Et_2Zn[b] (mmol)	Metal	Halide (mmol)	Solvent	Products (%)[c]			
						Norcarane	n-C_3H_7I	n-C_4H_9I	n-$C_5H_{11}I$
20.0	20.0	13.3	—	—	Benzene	64.5	8.0	3.0	—
15.0	15.0	10.0	—	—	Ether	41.3	12.0	6.7	trace
15.0	15.0	10.0	LiCl	0.07	Ether	41.3	20.1	8.0	trace
14.9	15.0	10.0	LiBr	1.26	Ether	28.4	24.4	12.0	trace
15.0	15.0	10.0	LiBr	2.22	Ether	10.0	24.7	14.7	trace
15.0	15.0	10.0	LiBr	3.83	Ether	4.0	21.3	18.7	trace
7.5	7.5	5.0	LiI	0.52	Ether	12.7	27.3	20.3	trace
15.0	15.0	10.0	LiI	2.04	Ether	2.7	17.3	6.7	trace
7.5	7.5	5.0	LiI	4.78	Ether	trace	23.6	14.1	trace
15.0	15.0	10.0[d,e]	$MgCl_2$	20.0	Ether	trace	22.7	21.3	trace
15.1	15.0	10.0[d]	$MgBr_2$	20.0	Ether	2.7	22.7	10.7	2.0
15.0	15.0	10.0	MgI_2	2.77	Ether	28.0	17.5	6.0	trace
15.0	15.0	10.0	MgI_2	4.21	Ether	26.9	17.9	8.0	trace
15.0	15.0	10.0	MgI_2	8.42	Ether	13.5	19.5	9.1	trace
15.1	15.0	10.0[d]	MgI_2	20.0	Ether	7.5	20.4	13.9	trace
15.0	15.0	10.0	ZnI_2	2.19	Ether	40.0	18.7	10.7	trace

a) Reactions were carried out at 35°C for 14 hr under a nitrogen atmosphere.
b) Used as a 1.00 mol/*l* solution.
c) Based on methylene iodide.
d) Diethylzinc was prepared *in situ* from ethylmagnesium halide and zinc halide.
e) Diethylzinc was used as a 0.50 mol/*l* solution.

* To whom inquiries should be directed.

1) a) J. Furukawa, N. Kawabata, and J. Nishimura, *Tetrahedron Lett.*, **1966**, 3353; b) J. Furukawa, N. Kawabata, and J. Nishimura, *Tetrahedron*, **24**, 53 (1968); c) J. Furukawa, N. Kawabata, and J. Nishimura, *Tetrahedron Lett.*, **1968**, 3495; d) J. Furukawa, N. Kawabata, Y. Ueda, and J. Nishimura, *Kogyo Kagaku Zasshi*, **71**, 164 (1968); e) J. Furukawa, N. Kawabata, S. Taniguchi, and J. Nishimura, *ibid.*, **72**, 1963 (1969); f) J. Nishimura, N. Kawabata, and J. Furukawa, *Tetrahedron*, **25**, 2647 (1969); g) J. Nishimura, J. Furukawa, N. Kawabata, and T. Fujita, *ibid.*, **26**, 2229 (1970); h) J. Nishimura, J. Furukawa, and N. Kawabata, This Bulletin, **43**, 2195 (1970); i) J. Nishimura, J. Furukawa, N. Kawabata, and H. Koyama, *ibid.*, **44**, 1127 (1971); j) J. Nishimura, J. Furukawa, N. Kawabata, and M. Kitayama, *Tetrahedron*, **27**, 1799 (1971).

2) a) H. E. Simmons and R. D. Smith, *J. Amer. Chem. Soc.*, **80**, 5323 (1958); b) H. E. Simmons and R. D. Smith, *ibid.*, **81**, 4256 (1959); c) E. P. Blanchard and H. E. Simmons, *ibid.*, **86**, 1337 (1964); d) H. E. Simmons, E. P. Blanchard, and R. D. Smith, *ibid.*, **86**, 1347 (1964).

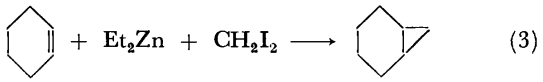

(3)

However, in the presence of lithium halide or magnesium halide, the yield of norcarane decreased considerably and large amounts of *n*-propyl and *n*-butyl iodides were formed.

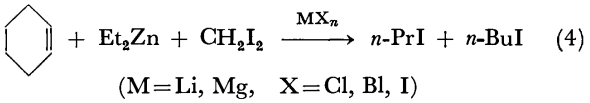

(4)

(M=Li, Mg, X=Cl, Bl, I)

Results are given in Table 1.

Hydrolysis of the reaction mixture at an early stage of reaction (3) produced large amounts of methyl and ethyl iodides,[1e] while the amount of norcarane was small at this stage. The formation of methyl iodide after hydrolysis indicates the presence of iodomethylzinc compounds[3] in the reaction mixture. Thus, the first step was concluded to be the formation of ethyl iodide and iodomethylzinc compounds, *e.g.*, $EtZnCH_2I$ (I). The reaction of iodomethylzinc compounds with cyclohexene to form norcarane is slower than the first step.

$$Et_2Zn + CH_2I_2 \xrightarrow{fast} EtI + \underset{I}{EtZnCH_2I} \quad (5)$$

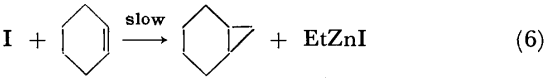

(6)

$$EtZnI + CH_2I_2 \longrightarrow EtI + \underset{II}{IZnCH_2I} \quad (7)$$

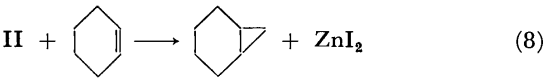

(8)

The formation of *n*-propyl and *n*-butyl iodides can be ascribed to the reaction of iodomethylzinc compounds with ethyl and *n*-propyl iodides, respectively.

$$I + EtI \longrightarrow n\text{-}PrI + EtZnI \quad (9)$$

$$I + n\text{-}PrI \longrightarrow n\text{-}BuI + EtZnI \quad (10)$$

$$II + EtI \longrightarrow n\text{-}PrI + ZnI_2 \quad (11)$$

$$II + n\text{-}PrI \longrightarrow n\text{-}BuI + ZnI_2 \quad (12)$$

In the presence of lithium halide or magnesium halide, reactions (9), (10), (11), and (12) predominated over (6) and (8). Zinc iodide also showed the same sort of effect as that given in Table 1. The yield of norcarane was lower and that of *n*-propyl and *n*-butyl iodides higher in ether than in benzene. The difference can be attributed partly to the difference of solubility of zinc iodide formed by (11) and (12).

Two mechanisms are possible for reactions (9) to (12), one is a coupling reaction between iodomethylzinc compounds and ethyl iodide or *n*-propyl iodide. This mechanism is conceivable since the presence of magnesium halide enhances the coupling reaction of dialkylcadmium with acyl halide.[4] Dialkylcadmium prepared *in situ* from alkylmagnesium halide and cadmium halide in ether reacts with acyl halide to form ketone. However, isolated (salt-free) dialkylcadmium does not react with acyl halide.

$$R_2Cd + R'COX \xrightarrow{MgX'_2} RCOR' \quad (13)$$

The other mechanism is an insertion reaction of iodomethylzinc compounds into the carbon-iodine bond of ethyl iodide or *n*-propyl iodide.

In order to distinguish the two mechanisms, we carried out the reaction of cyclohexene with diethylzinc and bromoiodomethane, giving a small amount of norcarane, and large amounts of *n*-propyl, *n*-butyl, and ethyl iodides. However, ethyl, *n*-propyl, and *n*-butyl bromides were not detected. The results are given in Table 2.

The presence of a large amount of ethyl iodide and the absence of ethyl bromide indicate that the first step is (14) rather than (15).

$$Et_2Zn + ICH_2Br \longrightarrow EtI + BrCH_2ZnEt \quad (14)$$

$$Et_2Zn + ICH_2Br \longrightarrow EtBr + ICH_2ZnEt \quad (15)$$

The formation of *n*-propyl and *n*-butyl iodides instead of *n*-propyl and *n*-butyl bromides makes the insertion mechanism preferable to the coupling mechanism.

Coordination of lithium or magnesium halide to organozinc compounds during the reaction is conceivable. However, extensive physicochemical studies may be necessary before proposing a definite mechanism of this salt effect.

Experimental

Materials. Diethylzinc was prepared by the conventional method.[5] Ethylmagnesium halides were prepared from ethyl halide and magnesium turnings in ether. Concentration of ethylmagnesium halide was determined by an acid-base titration. Commercial products of anhydrous zinc

Table 2. Reaction of cyclohexene with diethylzinc and bromoiodomethane in the presence of metal halide[a]

Et_2Zn[b] (mmol)	Metal	Halide (mmol)	Products (%)[c]			
			Norcarane	n-C_3H_7I	n-C_4H_9I	n-$C_5H_{11}I$
5.0	—	—	2.7	31.1	7.4	trace
5.0[d]	$MgBr_2$	10.0	trace	12.3	2.0	trace

a) Reactions were carried out at 35°C for 14 hr in ether under a nitrogen atmosphere with 7.5 mmol of cyclohexene, 7.0 mmol of bromoiodomethane, and 5.0 mmol of diethylzinc.
b) Diethylzinc was used as a 1.00 mol/*l* solution.
c) Based on bromoiodomethane.
d) Diethylzinc was prepared *in situ* from ethylmagnesium bromide and zinc bromide.

3) Iodomethylzinc compounds would be $EtZnCH_2I$, $Zn(CH_2I)_2$, $IZnCH_2I$ and/or their associated molecules.

4) a) J. Kollonitsch, *Nature*, **188**, 140 (1960); b) J. Kollonitsch, *J. Chem. Soc., A*, **1966**, 453, 456.

5) C. R. Noller, "Organic Syntheses," Coll. Vol. II, (1943), p. 184.

chloride and bromide were dried by rapidly heating *in vacuo*. Commercial anhydrous zinc iodide was dissolved in ether, dried by calcium hydride; the clear supernatant layer was transferred to a flask and ether was removed *in vacuo* at room temperature. All the zinc halides purified in this manner were completely soluble in ether. Commercial anhydrous lithium chloride was dried by heating *in vacuo*. Anhydrous lithium bromide was prepared by heating its monohydrate *in vacuo*. Anhydrous lithium iodide was prepared by dehydration of its trihydrate, *i.e.*, lithium iodide trihydrate was dissolved in ether, dried with calcium hydride; the clear supernatant layer was transferred to a flask, and ether was removed *in vacuo* at room temperature. Anhydrous magnesium iodide was prepared from magnesium trunings and iodine in ether. Bromoiodomethane was prepared by the conventional method.[6] Commercial cyclohexene, methylene iodide, ethyl bromide, ethyl iodide, *n*-propyl bromide, *n*-propyl iodide, *n*-butyl bromide, and *n*-butyl iodide were purified by distillation. Authentic sample of norcarane was prepared from cyclohexene, methylene iodide and diethylzinc.[1a] Purity was confirmed by vapor phase chromatography. Solvents were purified by the usual method.[7] Nitrogen was purified as described previously.[1b]

Procedure. A three-necked flask equipped with a thermometer, dropping funnel, three-way cock and magnetic stirring bar was evacuated and filled with dry nitrogen. Metal halide was dissolved in ether and added to the flask *via* a hypodermic syringe. Diethylzinc was then added similarly. The concentration of diethylzinc was made to be 1.00 or 0.50 mol/*l* at this stage by controlling the amount of solvent. Cyclohexene was added *via* a hypodermic syringe to this solution. Methylene iodide was then added through a dropping funnel over a period of half an hour while stirring at room temperature. After the addition the reaction mixture was allowed to stand at 35°C for 14 hr. The reaction mixture was successively poured into a saturated aqueous solution of ammonium chloride. The organic layer was analyzed by vapor phase chromatography. Yields of products were determined by vapor phase chromatography with calibration curves.

6) S. Miyano and H. Hashimoto, This Bulletin, **44**, 2864 (1971).

7) J. A. Riddick and W. B. Bunger, "Organic Solvents," Wiley-Interscience, New York (1970).

BULLETIN OF THE CHEMICAL SOCIETY OF JAPAN, VOL. 45, 2582—2586 (1972)

N,N,N′,N′-Tetramethylethylenediamine-Copper Salt-catalysed Coupling of Aryl Grignard Reagents with Alkyl and Aralkyl Halides

Kazuhiko ONUMA and Harukichi HASHIMOTO*

Department of Synthetic Chemistry, The University of Tokyo, Bunkyo-ku, Tokyo
**Department of Applied Chemistry, Faculty of Engineering, Tohoku University, Sendai*

(Received October 30, 1971)

In the presence of *N,N,N′,N′*-tetramethylethylenediamine (TMEDA) and a small amount of copper salt, phenyl- and *p*-tolylmagnesium bromides react with alkyl or benzyl halide to give cross-coupling products in benzene or in a benzene–diethyl ether solvent. Among the alkyl iodides, normal iodides are most reactive, while secondary iodides do not react under our conditions. As copper salts, CuCl, $CuCl_2$, $CuCl_2$(TMEDA), and CuBr are all efficient for catalysis. This newly-developed catalytic system of TMEDA-copper salt is thought to be useful for the syntheses of polyalkyl-substituted aromatic hydrocarbons. As the reaction mechanism, the intermediate formation of TMEDA-coordinated organocopper(I) species and the nucleophilic displacement is proposed.

In general, Grignard reagents react very slowly, or not at all, with organic halides, except for some activated molecules, such as allylic halides.[1] On the other hand it is well known that some transition metal salts catalyse these reactions efficiently for example, in the cobalt salt-catalysed "Kharasch reaction."[3] Recent works[4] have shown that, in these cobalt salt-catalysed reactions, zero-valent cobalt is a real catalytic species and that free radicals from organic halides are involved. In most of these metal salt-catalysed reactions, however, the cross coupling between the Grignard reagent and organic halide is not a predominant reaction.[5]

1) In some cases, reactions do occur by the use of a high temperature in high-boiling solvents or in neat, though the yields are generally low. It is also said that, in these high-temperature reactions, free radicals are involved.[2]

2) "Methods of Elemento-Organic Chemistry," Vol. 2, ed. by A. N. Nesmeyanov and K. A. Kocheshkov, North-Holland, Amsterdam (1967) Chaps. 17 and 19.

3) M. S. Kharasch and O. Reinmuth, "Grignard Reagents of Nonmetallic Substances" Prentice-Hall, New York (1954).

4) F. W. Frey, Jr., *J. Org. Chem.*, **26**, 5187 (1961); J. Morizur, *Bull. Soc. Chim. Fr.*, **1964**, 1331; D. I. Davies, D. H. Hey, and M. J. Tiecco, *J. Chem. Soc.*, **1965**, 7062; M. H. Abraham and M. J. Hogarth, *J. Organometal. Chem.*, **12**, 1 (1968); D. I. Davies, J. N. Done, and D. H. Hey, *J. Chem. Soc., C*, **1969**, 1392.

5) a) Products from homocoupling, disproportionation, hydrogen abstraction or other radical involved reactions are major products. b) Of course there are special cases where cross couplings take place efficiently, for example: copper salt catalysed reaction of acetylenic Grignard reagent with allyl halide,[6] vinyl halides react with Grignard reagents in the presence of iron affording cross coupling products in good yield,[7] alkyl Griganrd reagents react with alkyl halides by the catalysis of copper(I) halide.[8]

6) R. Ya. Levina and V. K. Daukshas, *Zh. Obshch. Khim.*, **30**, 1758 (1960).

7) M. Tamura and J. Kochi, *J. Amer. Chem. Soc.*, **93**, 1487 (1971).

8) M. Tamura and J. Kochi, *ibid.*, **93**, 1485 (1971).

We previously reported that the copper(I)-ethylenediamine complex can reduce benzyl chloride (Eq. (1)[9,10]), and aryl Grignard reagents are known to be easily oxidised by high-valent transition metal salts, such as copper(II),[11] and iron(III)[12,13] (Eq. (2)):

$$PhCH_2Cl + Cu(I)(en)_n \longrightarrow PhCH_2CH_2Ph + Cu(II)(en)_n \quad (1)$$

$$RX \xrightarrow{Me^{(n-1)+}} R\text{-}R \quad (1')$$

$$ArMgX \xrightarrow{Me^{n+}} Ar\text{-}Ar \quad (2)$$

The combination of these two sets of reactions (Eqs. 1 and 2) suggests that the bidentate amine-copper salt system may be a good catalyst for the reaction between Grignard reagents and organic halides. From this point of view, we investigated the copper salt-*N,N,N',N'*-tetramethylethylenediamine(TMEDA)-catalysed reaction of aryl Grignard reagnets with alkyl and aralkyl halides. In this paper we will report that this system is a good catalyst for *cross* couplings.

$$ArMgX + RX' \xrightarrow[\text{copper salt}]{\text{TMEDA}} Ar\text{-}R \quad (3)$$

Experimental

Materials. The *N,N,N',N'*-tetramethylethylenediamine was prepared according to the method in the literature[14] and was cautiously distilled in nitrogen after having been refluxed on sodium. Commercial triethylamine was distilled on sodium. The reagent-grade alkyl iodides were used after distillation. The isobutyl and *sec*-butyl iodides were prepared from the corresponding alcohols.[15] All the substituted benzyl chlorides and benzyl chloride were used without further purification. Reagent-grade anhydrous cuprous chloride and bromide were further purified by the usual method. Anhydrous cupric chloride was obtained from the product of the dehydration of the dihydrate by heating *in vacuo* at 100°C for several days. $CuCl_2$ (TMEDA) was prepared by Bertini's method[16] in butanol.

The standard substances for glc, propyl-, isobutyl-, *sec*-butyl-, amyl- and isoamylbenzene, and *p*-methyl-, *p,p'*-dimethyl- and *p*-chlorodiphenylmethane were prepared by the method described in this paper on a larger scale. They were identified by NMR, IR, and elemental analysis.

The benzene solution of the Grignard reagent-TMEDA complex was prepared by dropping phenyl- or *p*-tolylmagnesium bromide into a benzene sloution of TMEDA in the presence of magnesium turnings at 50°C;[17] afterward the solution was filtered and stored under a nitrogen atmosphere. The concentration was determined by chelate titration, mostly about $2.2—2.9\times10^{-1}$ mol/*l*; 20—30 m*l* of the solution was used for a separate run. The Grignard reagent in diethyl ether was prepared in the usual manner and stored. The concentration was determined by acid-base titration.

Reaction Procedures. *Method A*: All the reactions were made under a nitrogen atmosphere. In a four-necked, round-bottomed flask equipped with a condenser, a thermometer, a nitrogen inlet, a dropping funnel, and a magnetic stirrer, 40 m*l* of benzene, organic halide, and a small amount of copper salt were placed. Then the reaction was started at 80°C by adding a benzene solution of the Grignard-TMEDA complex (25—30 m*l*) through the funnel. After completion, the reaction mixture was hydrolysed and extracted with ether, and the extract was condensed. The product analysis was made by glc with a 2 m Silicone DC550 column.

Method B: To the solution of organic halide, TMEDA, and copper salt in 40 m*l* of benzene, we dropped an ether solution of the Grignard reagent (20—25 m*l*) at 60°C. The other procedures were the same as in Method A.

Results and Discussion

As expected, cross coupling occurred between aryl Grignard reagents and alkyl or benzyl halides as a result of the use of the catalytic system of TMEDA-copper salt in benzene or in a benzene–ether solvent. As an amine ligand, TMEDA, is chosen because TMEDA has no active hydrogen and is known to be a good coordinating ligand not only for copper but also for a Grignard reagent.[18] The mole ratio of TMEDA to the Grignard reagent should be above one-to-one to obtain good results. On the other hand, the appropriate quantity of copper salt is around 5 mole percent. The use of an excess of copper salt usually increases unfavorable by-products. It should be noted that if one of pair of this catalytic system (TMEDA and copper salt) is absent, the reaction does not take place at all.

There are two methods for the reaction. In "Method A," a Grignard reagent-TMEDA complex prepared in benzene is allowed to react with organic halide in the presence of copper salt in benzene at 80°C. In "Method B," a Grignard reagent prepared in diethyl ether is dropped into a benzene solution of organic halide, TMEDA, and copper salt at 60°C. The ratio of benzene to ether is about 2:1.

$$\text{Method A}\quad ArMgBr(TMEDA) + RX \xrightarrow[\text{benzene}]{\text{copper salt}} Ar\text{-}R + MgBrX(TMEDA) \quad (4)$$

$$\text{Method B}\quad ArMgBr + RX \xrightarrow[\text{benzene-ether}]{\text{TMEDA, copper salt}} Ar\text{-}R + MgBrX \quad (5)$$

In THF or in diethyl ether, the reaction does not proceed.

Reactions with Alkyl Halides. Tables 1 and 2 show the results of the reaction of phenyl and *p*-tolylmagnesium bromide with a variety of alkyl halides. These results may be summarized as follows. i) The yields of cross-coupling products from the reaction of phenyl Grignard reagent with normal alkyl iodides

9) K. Wada and H. Hashimoto, This Bulletin, **41**, 3601 (1968); K. Onuma, J. Yamashita, and H. Hashimoto, *ibid.*, **43**, 836 (1970).
10) Chromium(II)-ethylenediamine complex is known more powerful reductant: J. K. Kochi and J. W. Powers, *J. Amer. Chem. Soc.*, **92**, 137 (1970).
11) E. Sakellarios and Th. Kyrimis, *Ber.*, **57**, 322 (1924).
12) G. Champetier, *Bull. Soc. Chim. Fr.*, **47**, 1131 (1930).
13) W. B. Smith, *J. Org. Chem.*, **26**, 4206 (1961); also see Ref. 2.
14) R. W. Moshier and L. Spialter, *ibid.*, **21**. 1050 (1956).
15) H. Stone and H. Shechter, "Organic Syntheses," Coll. Vol. IV, (1963), p. 323.
16) I. Bertini and F. Mani, *Inorg. Chem.*, **6**, 2032 (1967).
17) E. C. Ashby and R. Reed, *J. Org. Chem.*, **31**, 971 (1966).
18) In the presence of TMEDA Grignard reagent can be prepared in nonpolar solvent, see Ref. 17.

TABLE 1. REACTION WITH ALKYL HALIDE, METHOD A
PhMgBr·TMEDA: 6×10^{-3} mol or 7.5×10^{-3} mol, RX: 5×10^{-3} mol, CuCl: 5.3±0.1 mol %, in benzene, 24 hr.

RX	Temp. °C	PhMgBr/RX	Yield[a] of Ph–R (%)
n-BuBr[b]	80	1.2	44
n-BuI	80	1.2	65
n-BuI	80	1.5	79
n-PrI	80	1.5	64
n-PrI	80	1.5	69
EtI	70	1.5	85
MeI	40	1.5	93
n-AmI	80	1.5	73
i-BuI	80	1.5	33
i-AmI	80	1.5	62

a) Based on alkyl halide.
b) 10 hr.

TABLE 2. REACTION WITH ALKYL HALIDE, METHOD B
ArMgBr: 6×10^{-3} mol, R'X: 5×10^{-3} mol, TMEDA: 8.5×10^{-3} mol (TMEDA/R'X~1.7), CuCl: 5.3± 0.1 mol %, in benzene–ether (2:1), 60°C, 24 hr.

R–C$_6$H$_4$–MgBr	R'I	Yield[a] of R–C$_6$H$_4$–R' (%)
H	*n*-PrI	81
H	*n*-BuI	85
H	*i*-PrI	7
H	EtI	83
H	MeI[b]	9[c]
H	*n*-AmI	83
H	*sec*-BuI	4
H	*i*-BuI	61
H	*i*-BuI	68[d]
H	*i*-AmI	71
CH_3	EtI	82
CH_3	*n*-BuI	80

a) Based on alkyl halide.
b) At 40°C.
c) Methyl iodide reacts with TMEDA before Grignard reagent is added.
d) 48 hr.

are generally good, and alkyl substitution on the aromatic ring does not affect the yields. This provides a useful synthetic procedure for a variety of alkyl-substituted aromatics. ii) Among alkyl halides, alkyl iodides are most reactive. iii) The steric effect is rather significant; that is, secondary iodides do not react, and the yields with alkyl iodides which are branched at the β or γ position are considerably decreased. iv) Method A is more susceptible to this steric effect.[19] v) In the case of methyl iodide, which is very reactive toward TMEDA,[20] Method B is not

19) This may be due to the fact that TMEDA is more tightly held to the complex in benzene than in benzene–ether solution.
20) TMEDA is fairly basic amine, especially in nonpolar solvent: P. Paoletti, R. Barbucci, A. Vacca, and A. Dei, *J. Chem. Soc., A*, **1971**, 310.

TABLE 3. EFFECT OF ADDED TMEDA IN METHOD B
PhMgBr: 6×10^{-3} mol, *n*-BuI: 5×10^{-3} mol, CuCl: 5.3±0.1 mol %, in benzene–ether (2:1), 60°C.

TMEDA/*n*-BuI	Reaction time hr	Yield[a] of C$_6$H$_5$–Bu^n (%)
1.0	5	35
1.0	24	52
1.3	24	77
1.6	24	86
1.9	24	85
2.1	24	86

a) Based on alkyl halide.

applicable, but in Method A an ordinary reaction takes place smoothly, suggesting that coordinated TMEDA reacts no more with the iodide.

As the large steric hindrance may be partly attributable to the bulky TMEDA molecule, we tried to use triethylamine instead of TMEDA, but in the presence of triethylamine even normal alkyl iodides do not react. In Method B, as is shown in Tables 2 and 3, more than 1.6 times as much TMEDA as alkyl halide is necessary.[21]

The formation of biphenyl (or *p,p'*-bitolyl), which is the homocoupling product of Grignard reagent, as a by-product in the reaction is unavoidable; the yield is 10—25% in Method A and 2—4% in Method B. The increased percentage in Method A may be due to the relatively high reaction temperature.

Reactions with Benzyl Chlorides. The results of the reactions of phenyl and *p*-tolylmagnesium bromide with *p*-substituted benzyl chlorides are tabulated in Tables 4 and 5. Though the yields of the diphenylmethane derivatives are satisfactory, the *p*-methyl

TABLE 4. REACTION WITH BENZYL CHLORIDE, METHOD A
R_1–C$_6$H$_4$–MgBr·TMEDA: 6×10^{-3} mol or 7.5×10^{-3} mol, R_2–C$_6$H$_4$–CH_2Cl: 5×10^{-3} mol, CuCl: 5.3±0.1 mol %, in benzene, 80°C, 5 hr

R_1–C$_6$H$_4$–MgBr·TMEDA (I)	R_2–C$_6$H$_4$–CH_2Cl (II)	Yield[a] of R_1–C$_6$H$_4$–CH_2–C$_6$H$_4$–R_2 (%)	
		(I)/(II) =1.2	1.5
H	H	74	81
H	CH_3	79	84
H	Cl	78	79
CH_3	H	58	64
CH_3	CH_3	73	73

a) Based on benzyl chloride.

21) In our conditions alkyl iodides do not react with free TMEDA except for methyl iodide.

TABLE 5. REACTION WITH BENZYL CHLORIDE, METHOD B

R_1-C$_6$H$_4$-MgBr: 6×10^{-3} mol, R_2-C$_6$H$_4$-CH_2Cl: 5×10^{-3} mol, TMEDA: 6×10^{-3} mol, CuCl: 5.3± 0.1 mol%, in benzene–ether (2: 1), 60°C, 10 hr.

R_1-C$_6$H$_4$-MgBr	R_2-C$_6$H$_4$-CH_2Cl	Yield[a] of R_1-C$_6$H$_4$-CH_2-C$_6$H$_4$-R_2 (%)
H	H	81
H	CH_3	89
H	Cl	85
CH_3	H	68, 78[b]
CH_3	CH_3	76

a) Based on benzyl chloride.
b) 20 hr.

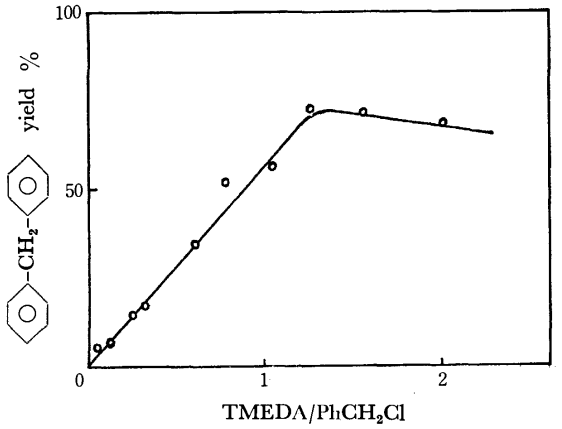

Fig. 1. Effect of added TMEDA in Method B PhMgBr: 6×10^{-3} mol, $PhCH_2Cl$: 5×10^{-3} mol, CuCl: 5.3±0.1 mol % in benzene–ether (2: 1) 60°C, 5 hr.

substitution of a Grignard reagent reduces the reactivity somewhat.

The elucidation of the substituent effect on benzyl chloride is rather difficult, because a side reaction between benzyl chloride and TMEDA takes place. Concerning this, there are some experimental facts. a) In Method B, the optimum ratio of TMEDA to benzyl chloride is around 1.2:1 (Fig. 1) and the presence of an excess of TMEDA reduces the yield, in keen contrast to the case of alkyl iodide. b) Also, in Method A, the further addition of TMEDA can not increase the yield, but such a further addition of TMEDA evidently shortens the necessary reaction time. c) In the presence of an excess of TMEDA, scarcely no unreacted benzyl choride is recovered, suggesting that it disappeared as a quaternary ammonium salt after the treatment. It is clear form these results that active benzyl chloride reacts with a non-coordinated excess TMEDA molecule to form ammonium salt. Therefore, an excess of TMEDA can not increase the yield of the cross-coupling product. As alkyl iodides do not react with free TMEDA, an excess of TMEDA can serve only for the promotion of the reaction.

In the reaction with benzyl chloride, biphenyl, bibenzyl, and a small amount of toluene are also obtained as by-products. The rough percentages of these by-products are as follows. In Method A, the biphenyl derivatives are 5—25% and the bibenzyl derivatives are 1—10%. In Method B. the biphenyl derivatives are 3—7% and the bibenzyl derivatives are 1—4%. Generally speaking, Method B gives a little better results.

Copper Salts. The cupric chloride-TMEDA complex ($CuCl_2$TMEDA) was prepared and used as a catalyst, but the yield of cross coupling is only around 10%. In the presence of a large amount of TMEDA, that is, under ordinary reaction conditions, the catalytic activity of the $CuCl_2$TMEDA complex is just the same as that of cuprous chloride. This suggests that the coordination of TMEDA not only to copper but also to a Grignard reagent is important. The coordination of TMEDA must increase the carbanion character of the organic moiety of the Grignard reagent.[22]

$CuCl_2$ and CuBr as well as CuCl and $CuCl_2$TMEDA have similar reactivity. The use of copper(II) salt, however, increases the formation of biphenyl, only a little but obviously.

Other transition metal salts, such as ferric chloride, cobaltous chloride, and chromous chloride, can also bring about the reaction, but homocouplings are predominant, as in an ordinary "Kharasch reaction."

Reaction Mechanism. Some features of the reaction with alkyl halide can be summarized as follows: (i) The order of the reactivity of alkyl halide is $I \gg Br \gg Cl$. (ii) The steric hindrance is relatively large. iii) CH_3I and C_2H_5I are excellently reactive. These results suggest that the reaction type is very similar to the bimolecular nucleophilic displacement.

The addition of cyclohexene (a mild radical scavenger) or acrylonitrile does not affect it at all, showing that the formation of a free radical is unlikely. It can be said, therefore, that the mechanism of copper catalysis is different from that of cobalt,[4] silver,[23] or iron[7] salt, where the formation of a free radical by the reduction of an organic halide by a zero-valent metal is observed.

Tamura and Kochi[8] reported recently that, in the copper salt-catalysed coupling of an alkyl Grignard reagent with alkyl halide in THF, the formation of organocopper, followed by its nucleophilic displacement, is the key step in the catalysis; the results obtained here support this idea.

To make sure that the copper metal is not operative, the Grignard reagent was first allowed to react with a catalytic amount of cuprous chloride. When the deposition of copper metal began after 1 hr, alkyl iodide was added to this solution. The yield of the cross-coupling product by this procedure was significantly lowered. On the other hand, as has been mentioned already, the use of copper(II) salt as a

22) In case of organolithium compounds such polarizing effect is apparent: M. D. Rausch and D. J. Ciappenelli, *J. Organometal. Chem.*, **10**, 127 (1967); A. J. Chalk and T. J. Hoogeboom, *ibid.*, **11**, 615 (1968).

23) M. Tamura and J. Kochi, *J. Amer. Chem. Soc.*, **93**, 1483 (1971).

catalyst increases the biphenyl formation from the Grignard reagent, which means that copper(II) is first reduced to the copper(I) state by the Grignard reagent. The intermediate formation of the organocopper species from the Grignard reagent and copper(I) is, therefore, most probable. Organocuprate complexes are known to be very reactive toward alkyl and aryl halides.[24]

Thus, we propose as the reaction mechanism the formation of organocopper and its nucleophilic displacement;

$$(L)CuX + PhMgBr(L) \longrightarrow (L)CuPh + MgBrX(L)^{25)} \quad (6)$$

$$(L)CuPh + RI \longrightarrow Ph\text{-}R + (L)CuI^{26)} \quad (7)$$

L: TMEDA

The displacement may be assisted by copper:

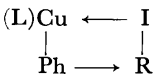

Finally, we want to emphasize again that this reaction takes place only when the catalytic system of TMEDA-copper salt is present. TMEDA plays an important role as a coordinating ligand on both the Grignard reagent and copper.

24) E.J. Corey and G.H. Posner, *J. Amer. Chem. Soc.*, **89**, 3911 (1967); E.J. Corey and G.H. Posner, *ibid.*, **90**, 5615 (1968); G.M. Whitesides, W. F. Fischer, Jr., J. S. Filippo, Jr., R. W. Bashe, and H. O. House, *ibid.*, **91**, 4871 (1969).

25) It is possible that real organocopper species is not (L)CuPh but complexes with magnesium like LCuPh(MgBrXL): R. J. Depasquale and C. Tamborski, *J. Org. Chem.*, **34**, 1736 (1969).

26) Considering the effect of TMEDA coordination which can stabilize high valent state there can not be excluded the possibility of reaction path of Eq. 8:

$$LCuPh+RI \rightarrow ILCu(III)\cdot Ph\cdot R \rightarrow R\text{-}Ph+LCuI \quad (8)$$

such redox cycle is probable in copper catalysis but there are no evidence at present: H. O. House and W. F. Fischer, Jr., *J. Org. Chem.*, **33**, 949 (1968).

BULLETIN OF THE CHEMICAL SOCIETY OF JAPAN, VOL. 45, 2586—2590 (1972)

The Codimerization of Butadiene and Ethylene Catalyzed by Cobaltous Chloride-Ditertiary Phosphine Complexes-Grignard Reagent-ROH. Effects of Ditertiary Phosphine Ligands and Alcohols

Teruhiko KAGAWA and Harukichi HASHIMOTO*

Department of Synthetic Chemistry, The University of Tokyo, Bunkyo-ku, Tokyo
**Department of Applied Chemistry, Faculty of Engineering, Tohoku University, Sendai*

(Received November 18, 1971)

Butadiene-ethylene codimerization is accomplished by means of the catalyst derived from the reactions of $CoCl_2(Ph_2P(CH_2)_nPPh_2)_m$ with a Grignard reagent and then with appropriate amounts of alcohols to obtain 1,4-*cis*-hexadiene selectively. The yield of 1,4-hexadiene depends on the number of ditertiary phosphine ligands (m), the methylene-chain length of the ligand (n), and the kind of alcohol. A hydride complex, $HCo(Ph_2P(CH_2)_2PPh_2)_2$ also has codimerization activity in the presence of both *n*-PrMgCl and alcohols. It is considered that the resulting alkoxymagnesium chloride activates the catalyst.

A number of transition-metal catalyst systems in the codimerization of ethylene and 1,3-butadiene have been investigated by many worker.[1a–j] These catalysts usually consist of a transition-metal salt or complex and organoaluminum compounds as the reducing agents, similar to the Ziegler-type polymerization catalysts,[2] and low valent organo-transition metal complexes have been suggested as the active intermediates. Codimerization catalyst systems, in which Grignard reagents are contained as reducing agents, have, however, been much less studied. It has been found in a patent[3] that 1,4-hexadiene can be prepared by the reaction of ethylene and butadiene in the presence of Fe (II) and a Grignard reagent. Greco and Carbonaro[4] reported that the $FeCl_3$–*i*-PrMgCl system was an active catalyst of butadiene dimerization and of butadiene-norbornadiene codimerization.

In earlier papers dealing with ethylene-butadiene codimerization reactions catalyzed by $CoCl_2(Ph_2P(CH_2)_nPPh_2)$–$AlEt_3$[5] and $NiCl_2$–$Ph_2P(CH_2)_nPPh_2$–

1) a) D. Wittenberg, *Angew. Chem.*, **75**, 1124 (1963). b) G. Hata, *J. Amer. Chem. Soc.*, **86**, 3903 (1964). c) T. Alderson, E. L. Jenner, and R. V. Lidsey, Jr., *ibid.*, **87**, 5638 (1965). d) M. Iwamoto and S. Yuguchi, *J. Org. Chem.*, **31**, 4290 (1966). e) R. Cramer, *J. Amer. Chem. Soc.*, **89**, 1633 (1967). f) R. G. Miller, T. J. Kealy, and A. L. Barney, *ibid.*, **89**, 3756 (1967). g) A. Carbonaro, A. Greco, and G. Dall'Asta, *Tetrahedron Lett.*, **1967**, 2037. h) M. Iwamoto and S. Yuguchi, *Kogyo Kagaku Zasshi*, **70**, 1221, 1505 (1967). M. Iwamoto and S. Yuguchi, *ibid.*, **71**, 133, 233, 237 (1968), M. Iwamoto and S. Yuguchi, This Bulletin, **41**, 150, (1968). i) G. Hata, This Bulletin, **41**, 2443, 2762 (1968). j) C. A. Tolman, *J. Amer. Chem. Soc.*, **92**, 6777 (1970).

2) 1) b, d, f, h, and i.

3) T. Yoshida and S. Yuguchi, Japan. 25964 (1968); *Chem. Abstr.*, **71**, 30037n (1969).

4) a) A. Greco, A. Carbonaro, and G. Dall'Asta, *J. Org. Chem.*, **35**, 271 (1970). b) A. Carbonaro and A. Greco, *J. Organometal. Chem.*, **25**, 477 (1970).

5) T. Kagawa, Y. Inoue, and H. Hashimoto, This Bulletin, **43**, 1250 (1970).

$AlEt_3$,[6] the present authors described how the ditertiary phosphine ligand affects product distribution in a striking manner.

In the present investigation, it will now be shown that, in the codimerization of ethylene and butadiene by $CoCl_2(Ph_2P(CH_2)_nPPh_2)_m$, Grignard reagent can be used as the reducing agent instead of organoaluminum compounds, provided that an appropriate amount of alcohol or acetone is present, and that 1,4-hexadiene is formed selectively by these catalyst systems. The effects of alcohols and ligands on the 1,4-hexadiene formation have also been studied.

Experimental

Reagents. Ethereal solutions of *n*-propylmagnesium chloride and phenylmagnesium bromide were prepared from Mg chips and *n*-propyl chloride, and from bromobenzene, respectively and were used after filtration. The concentrations of both Grignard reagents were determined by acid-base titration (1.5—2.0 mmol/g solution). Anhydrous cobaltous chloride and triphenylphosphine were obtained commercially, while ditertiary phosphines ($Ph_2P(CH_2)_nPPh_2$, n=2,3,4, and 6)[7] were prepared by the method described by Hewertson and Watson[8] and their purity confirmed by elementary analysis and a melting-point determination. DPE: mp 140—141°C (143—144°C),[8] Found: C, 78.25; H, 6.21%. Calcd: C, 78.39; H, 6.07%. DPP: mp 63.3—65.3°C (61—62°C),[9] Found: C, 78.66; H, 6.08%. Calcd: C, 78.62; H, 6.36%. DPB: mp 134°C (137—139°C),[10] Found: C, 78.78; H, 6.81%. Calcd: C, 78.85; H, 6.62%. DPH: mp 126—127°C, Found: C, 78.50; H, 6.86%. Calcd: C, 79.26; H, 7.11%. The cobalt complexes with the above ditertiary phosphines were prepared according to the reported methods.[11]

A hydride complex, $HCo(DPE)_2$, was obtained by the reduction of $CoCl_2(DPE)_2$ with $NaBH_4$ in ethanol and was used after the recrystallization of a benzene solution.[12] IR ν_{Co-H} 1884 cm^{-1} (KBr). Elementary analysis; Found: C, 72.79; H, 5.59%. Calcd: C, 72.89; H, 5.78%.

1,3-Butadiene (Nippon Petroleum Chem. Co., Ltd.) was dehydrated by passing it through anhydrous calcium chloride and molecular-sieve columns and was condensed in a measuring vessel in order to measure its volume. Ethylene (of the grade for polyethylene) was used with no further purification. The toluene, ether, alcohols, and acetone were purified by conventional methods, and were distilled and stocked in an atmosphere of nitrogen.

Procedure. Every operation was carried out under a vacuum or in an atmosphere of nitrogen.

Catalyst Preparation. Some typical experiments were carried out as follows. $CoCl_2$DPP–*n*-PrMgCl–ROH System. A 108 mg, (0.20 mmol) of $CoCl_2$DPP was suspended in 8 m*l* of toluene, and then 1.52 g portion of an ethereal solution of *n*-PrMgCl (2.91 mmol, Mg/Co=14.5) was added by a syringe; this solution was stirred with a magnetic stirrer at room temperature until reduction had proceeded completely to form a black solution. A calculated amount of an ethanol–toluene solution (0.572 g, 2.51 mmol of EtOH, EtOH/Co=12.5) was then added with agitation, whereupon an exothermic reaction occurred. This solution was used as the catalyst. Some other catalysts were made in a similar way.

$HCo(DPE)_2$–n-PrMgCl–ROH System. 0.943 g of an *n*-PrMgCl ether solution (1.92 mmol, Mg/Co=17.8) and 0.943 g of a *t*-butyl alcohol–toluene (1.92 mmol of *t*-BuOH, *t*-BuOH/Co=17.8) were added to a toluene suspension of 92 mg (0.11 mmol) of $HCo(DPE)_2$ (in this order), and this mixture was warmed to 40—50°C. The color stayed red throughout the reaction.

Oligomerization Reaction. A 100-m*l* stainless steel autoclave equipped with a magnetic stirrer was charged with the above catalyst solution and a calculated amount of butadiene (in this order). The temperature was then raised to 90—100°C, ethylene was injected to a pressure of approximately 50 kg/cm^2, and the reaction was carried out with agitation under a constant ethylene pressure. After 2.5 hr, the autoclave was cooled to room temperature and the catalyst was quenched by adding 2 m*l* of a methanol–HCl solution. The reaction solution was then washed with distilled water and dried on anhydrous sodium sulfate. After distillation, the products were analyzed by glc. The main product was 1,4-*cis*-hexadiene, which was identified by IR and NMR.

Isolation and Identification of $HCo(DPB)_2$. An ethereal solution of *n*-PrMgCl (6.72 mmol) was added at room temperature, to a stirred suspension of $CoCl_2$DPB (1.11 g, 2.00 mmol) and DPB (0.856 g, 2.01 mmol) in toluene (10 m*l*). The solution gradually became red. After filtration, *n*-hexane was added to the filtrate in order to precipitate the crystals. The resulting crystals were filtered off, dried, and recrystallised from the toluene solution by adding *n*-hexane. The dark-red crystalline compound was dried *in vacuo* at 40—50°C. Mp 158—159°C; Found: C, 73.99; H, 6.33%. Calcd for $C_{56}H_{57}P_4Co$: C, 73.76; H, 6.18%. Its proton magnetic spectrum in benzene shows a chemical shift at τ=27.2 assigned to the hydridic hydrogen of $HCo(DPB)_2$, which consists of a quintet with an intensity ratio of 1:4:6:4:1 and with a J_{PH} value of 28 Hz. However, its IR spectrum does not show any clearly-defined absorptions due to the cobalt-hydrogen stretching vibrations.

Result and Discussion

Butadiene-ethylene codimerization was catalyzed by adding appropriate amounts of alcohols to the reaction mixture of $CoCl_2$–$(Ph_2P(CH_2)_nPPh_2)_m$ (n=2, 3, and 4; m=1, 2) with ethereal *n*-propylmagnesium chloride in toluene, thus forming 1,4-hexadiene. In most cases, the selectivity of 1,4-hexadiene is so significantly high that the catalytic activity can be evaluated by means of the yield of 1,4-hexadiene based on the charged butadiene.

$CoCl_2(Ph_2P(CH_2)_nPPh_2)_m$–n-PrMgCl–Alcohol Systems. When *n*-propylmagnesium chloride was allowed to react with a cobaltous chloride-suspended toluene solution, the solution gradually turned black and a black precipitate was formed. This solution had no catalytic activity for 1,4-hexadiene formation. The reduction of cobaltous chloride with a Grignard reagent

6) Y. Inoue, T. Kagawa, and H. Hashimoto, *Tetrahedron Lett.*, **1970**, 1099.

7) Abbreviations: DPE, 1,2-bis(diphenylphosphino)ethane; DPP, 1,3-bis(diphenylphosphino)propane; DPB, 1,4-bis(diphenylphosphino)butane; DPH, 1,6-bis(diphenylphosphino)hexane.

8) W. Hewertson and H. R. Watson, *J. Chem. Soc.*, **1962**, 1490.

9) G. R. Van Hecke and W. D. Horrocks, Jr., *Inorg. Chem.*, **5**, 19 (1966).

10) L. Sacconi and Gelsomini, *ibid.*, **7**, 291 (1968).

11) a) W. D. Horrocks, Jr., G. R. Van Hecke, and D. D. Hall, *ibid.*, **6**, 694 (1967). b) 10).

12) A. Sacco and R. Ugo, *J. Chem. Soc.*, **1964**, 3274.

has been known as the outset of a Kharasch reaction[13] and has been considered to proceed as follows;

$$2RMgX + CoX_2 \longrightarrow R_2Co + 2MgX_2$$

$$R_2Co \longrightarrow Co + 2R\cdot$$

In this reaction sequence, the formations of organocobalt and of metallic cobalt are assumed as intermediate steps, but it has also been suggested by several workers[14] that a magnesium-coordinated intermediate with a different composition depending upon the molar ratio of Mg/Co is formed.

The addition of an *n*-PrMgCl ether solution to $CoCl_2$DPP in toluene at room temperature brought about a rapid reaction, and the mixture became black. This solution had only a low activity (*ca.* 5% yield of 1,4-hexadiene). On the other hand, when an appropriate amount of alcohol or acetone was added to the above solution, the catalytic activity was drastically increased and the yield of 1,4-hexadiene rose to 70% or more. This behavior is shown in Fig. 1, in which the effect of the amounts of alcohols and acetone at a constant *n*-PrMgCl concentration is illustrated. Among alcohols, ethyl alcohol has a high activity over a wide range of EtOH/Co molar ratios. As can be seen from Fig. 1, the highest activity of 1,4-hexadiene formation is revealed at almost the same amount of alcohol as in the Grignard reagent, while at lower and higher molar ratios of alcohol/Co, the catalyst was deactivated. Acetone was effective in the same manner. Further, in the system of $CoCl_2$DPP–*n*-PrMgCl–large excess *t*-BuOH(*n*-PrMgCl/Co=2.2, *t*-BuOH/Co=34), the codimerization reaction proceeded only slightly. The above facts show that the remaining *n*-PrMgCl reacts with the added alcohol or acetone to give alkoxymagnesium chloride; the catalyst may be activated by the resulting ROMgCl,

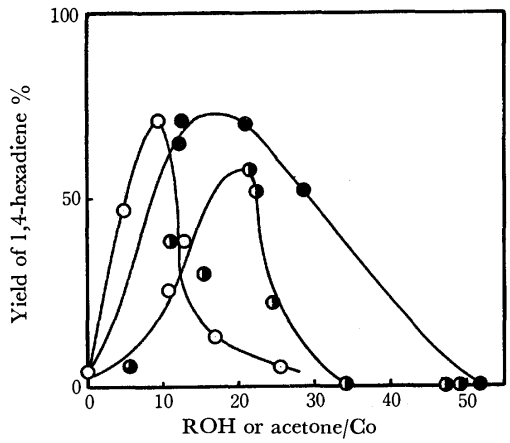

Fig. 1. Effect of molar ratio of ROH/Co or acetone/Co on yield of 1,4-hexadiene at constant concentration of *n*-PrMgCl $CoCl_2$DPP: 0.20 mmol. Reaction temperature: 90—100°C Reaction time: 2—2.5 hr
○ MeOH (*n*-PrMgCl/Co=11)
● EtOH (*n*-PrMgCl/Co=15)
◑ acetone (*n*-PrMgCl/Co=21)

13) Mechanism of Kharasch reaction is reviewed in Ref. 14 b.
14) a) G. Costa, G. Mestroni, and G. Boscarato, *Ric. Sci. Rend., Sez. A*, **7**, 315 (1964) *Chem. Abstr.*, **63**, 18145h. b) M. H. Abraham and M. J. Hogarth, *J. Organometal. Chem.*, **12**, 1, 497 (1968).

not by the added alcohol itself.

On the other hand, using a mixture of a $CoCl_2$DPP-*n*-PrMgCl (1:2) reaction solution and *t*-BuOMgCl prepared previously from *t*-BuOH and *n*-PrMgCl as the catalyst, the yield of 1,4-hexadiene was found to be 14% (*t*-BuOMgCl/Co=12), but at a higher molar ratio (*t*-BuOMgCl/Co=20) the products were viscous liquids and higher oligomerization compounds were probably formed. The mixing order of catalyst components seems to be important in obtaining a highly active catalyst for butadiene-ethylene codimerization.

The temperature dependency of the codimerization reaction catalyzed by $CoCl_2$DPP–*n*-PrMgCl–*t*-BuOH system was studied and significant activity was revealed over 90°C; this tendency is similar to the case of the $CoCl_2(DPE)_2$–$AlEt_3$ system.[15]

The effects of the ligand, that is, the number of ditertiary phosphine ligands, "*m*", that of the methylene chain length between two phosphorus atoms, "*n*", and the kind of added alcohols (ROH; R=Me, Et, *i*-Pr and *t*-Bu) on the yield of 1,4-hexadiene in the system of $CoCl_2(Ph_2P(CH_2)_nPPh_2)_m$–*n*-PrMgCl–ROH are given in Table 1. The length of the methylene chain, "*n*", slightly affected the formation of 1,4-hexadiene except in the case of DPH, which had no catalytic activity; the following orders are obtained;

Table 1. Effect of ditertiary phosphine ligands and alcohols in $CoCl_2L_{(2)}$–*n*-PrMgCl–ROH systems

Complex	ROH	*n*-PrMgCl/Co	ROH/Co	Yield of 1,4-hexadiene[a] (%)
$CoCl_2$DPE	MeOH	11.2	9.6	36
	EtOH	12.4	10.4	61
	EtOH	12.6	22.7	45
	i-PrOH	12.8	11.1	53
	t-BuOH	13.0	11.3	58
$CoCl_2(DPE)_2$	MeOH	12.5	10.5	18
	EtOH	12.2	10.2	67
	EtOH	12.2	22.0	58
	i-PrOH	13.8	12.1	70
	t-BuOH	14.8	12.8	78
$CoCl_2$DPP	MeOH	11.2	9.4	71
	EtOH	14.5	12.5	71
	EtOH	15.2	20.9	70
	i-PrOH	13.3	11.5	50
	t-BuOH	13.9	11.7	63
$CoCl_2$DPP[b]	MeOH	12.8	11.2	11
+ DPP	*t*-BuOH	13.1	11.4	72
$CoCl_2$DPB	MeOH	10.9	8.6	59
	EtOH	14.5	12.5	71
$CoCl_2$DPB[b]	MeOH	15.2	13.2	trace
+ DPB	*t*-BuOH	15.0	12.9	65
$CoCl_2$DPH	EtOH	12.1	10.1	—

$CoCl_2L_{(2)}$=0.20 mmol. Reaction temperature: 90—100°C. Reaction time: 2.5 hr.
a) Based on charged butadiene
b) $CoCl_2$L: L=1:1

15) M. Iwamoto and S. Yuguchi, This Bulletin, **41**, 150 (1968).

$$CoCl_2DPP(n=3) \approx CoCl_2DPB(n=4) \gtrsim CoCl_2DPE(n=2) \gg CoCl_2DPH(n=6)$$

$$CoCl_2(DPE)_2 \gtrsim CoCl_2DPP + DPP \gtrsim CoCl_2DPB + DPB$$

The first order is the same as in the reported $CoCl_2(Ph_2P(CH_2)_nPPh_2)$–$AlEt_3$ system.[15] It shows that these ditertiary phosphine ligands (n=2, 3, and 4) stabilize the active intermediate by the formation of a chelate ring. The number of ditertiary phosphine ligands, "m", was closely related to the kinds of alcohol in activating the catalyst; the catalysts of $CoCl_2(DPE)_2$ and $CoCl_2L+L$ (L=DPP and DPB) (m=2) had a highly active character in combination with t-BuOH, but with MeOH only a small amount of 1,4-hexadiene was produced, while in the case of $CoCl_2L$ (L=DPE, DPP, and DPB) (m=1) the activity was roughly independent of the king of alcohol. In other words, the resulting t-BuOMgCl is a better co-catalyst than MeOMgCl in the $CoCl_2L_2$ and $CoCl_2L+L$ systems.

These results suggest that this catalytic codimerization reaction consists of two steps: one is the reduction of Co(II) complexes by the Grignard reagent, and the other is the activation of the resulting low-valent cobalt complex by alkoxymagnesium chloride. Therefore, a further investigation of butadiene-ethylene codimerizations catalyzed by low-valent cobalt complexes would be useful in accounting for these two steps.

Codimerization Reaction Catalyzed by a Hydride Complex $HCo(DPE)_2$. As low-valent cobalt complexes coordinated by the ditertiary phosphine, $HCo(DPE)_2$[16] and $Co(DPE)_2$[17] have been known. The hydride complex $HCo(DPE)_2$ shows codimerization activity only in the presence of both n-PrMgCl and alcohols, as is shown in Table 2. The order of activation is as follows:

$$t\text{-BuOH} > i\text{-PrOH} \approx \text{EtOH} > \text{MeOH}$$

This behavior is the same as in the $CoCl_2L_2$ (or $CoCl_2L+L$) + n-PrMgCl system described above, and the possibility of hydride-complex formation seems to be present in the later system.

On the other hand, a number of σ-bonded organo-transition-metal complexes stabilized by phosphine ligands[18] have been obtained in reactions of transition-metal complexes with Grignard reagents containing no β-hydrogen. With Grignard reagents having β-hydrogen, the σ-alkylmetal complexes formed may decompose to hydride-metal complexes because of their instability. In the reaction of $CoCl_2(DPE)_2$ or $CoCl_2L+L$ (L=DPP and DPB) with n-PrMgCl also, low-valent cobalt complexes must be formed. In fact, a new hydride complex, $HCo(DPB)_2$, was isolated from the reaction mixture of $CoCl_2DPB$, DPB and n-PrMgCl in a toluene–ether solvent at room temperature; it was later identified. In the case of $CoCl_2L$ (m=1), which has a ligand-deficient structure, there may be present another type of low-valent complex, which may be coordinated by a magnesium compound or a solvent.

The facts that $HCo(DPE)_2$ itself has no activity for codimerization reaction and that there is no influence on its activity by adding t-BuOH alone, while in the presence of both n-PrMgCl and t-BuOH a high activity is obtained (Table 2), show that the resulting ROMgCl also plays an important role in this system. It is said that a vacant coordination site is a major factor in influencing catalytic behavior in a homogeneous transition-metal catalyst. Iwamoto and his co-workers[19] reported that $HCo(DPE)_2$ reveals catalytic activity in the presence of some kinds of phenol, and they assumed an interaction between phosphorus atoms and phenol to make a vacant coordination site. Recently, Tolman[20] described how a nickel hydride $HNi(P(OEt)_3)^+_4$ catalyzed an ethylene-butadiene codimerization to give 1,4-hexadiene and that the rate-determining step in this system was ligand dissociation from $HNiL_4^+$ (L=$P(OEt)_3$). Therefore, alkoxymagnesium chloride may cause ligand dissociation in these cobalt-based catalysts.

$CoCl_2(Ph_2P(CH_2)_nPPh_2)_m$–PhMgBr–ROH Systems. When phenylmagnesium bromide was used as the reducing agent instead of n-propylmagnesium chloride, the 1,4-hexadiene formation reaction proceeded in the same way, but the yield was lower than that of the n-PrMgCl system. The results are listed in Table 3.

Table 2. Ethylene-butadiene codimerization reaction catalyzed by $HCo(DPE)_2$–n-PrMgCl–ROH

ROH	n-PrMgCl/Co	ROH/Co	Yield of 1,4-hexadiene (%)
MeOH	—	30.5	none
	17.1	17.2	trace
EtOH	—	21.7	none
	17.0	17.3	34
	17.8	21.8	34
i-PrOH	18.8	18.7	33
t-BuOH	17.8	17.8	53

$HCo(DPE)_2$=0.1 mmol.
Reaction condition: see footnote in Table 1.

Table 3. $CoCl_2L_{(2)}$–PhMgBr–ROH catalyst system

Complex	ROH	PhMgBr/Co	ROH/Co	Yield of 1,4-hexadiene (%)
$CoCl_2DPE_2$	EtOH	11.9	9.9	15
$CoCl_2(DPE)_2$	EtOH	8.7	7.6	45
$CoCl_2DPP$	EtOH	11.7	9.7	65
$CoCl_2DPP$ + DPP	EtOH	11.4	9.4	53
$CoCl_2DPB$	EtOH	10.6	9.2	15
$CoCl_2DPB$ + DPB	EtOH	11.2	9.4	trace
	t-BuOH	11.1	9.1	trace

$CoCl_2L_{(2)}$=0.20 mmol.
Reaction condition: see footnote in Table 1.

16) a) F. Zingales, F. Canziani, and A. Chiesa, *Inorg. Chem.*, **2**, 1303. b) 12).
17) A. Sacco and R. Rossi, *Chem. Commun.*, **1965**, 602.
18) G. W. Parshall and J. J. Mrowca, "Advances in Organometallic Chemistry" ed. by F. G. A. Stone and R. West, Academic Press Inc. New York, Vol. 7, (1968), p. 157.
19) Y. Iwamoto and S. Yuguchi, *Kogyo Kagaku Zasshi*, **71**, 233 (1968).
20) C. A. Tolman, *J. Amer. Chem. Soc.*, **92**, 4217, 6777 (1970).

A diphenyl-complex may be formed in this catalyst system, since Chatt and his associates[21] isolated a diaryl-complex from the reaction solution of $CoBr_2(PEt_2Ph)_2$ with mesitylmagnesium bromide. No further details of the mechanism of 1,4-hexadiene formation are yet clear in these systems.

21) J. Chatt and B. L. Shaw, *J. Chem. Soc.*, **1961**, 285.

BULLETIN OF THE CHEMICAL SOCIETY OF JAPAN, VOL. 45, 2590—2593 (1972)

Base-catalyzed Condensation of *o*-Nitroacetophenone. V. Hydrogenation of Compound A, a Condensation Product. Formation of a 4-Quinolone from an Indoline System

Toshio MIWA

Faculty of Science, Osaka City University Sumiyoshiku, Osaka

(Received January 24, 1972)

The catalytic hydrogenation of compound A, a base-catalyzed condensation product of *o*-nitroacetophenone, followed by treatment of the product with acid gave a 4-quinolone. The quinolone proved to be 2-[1-(*o*-aminophenyl)-1-hydroxyethyl]-4-quinolone by the oxidative degradation of the corresponding quinoline derivative.

In an attempt to isolate the basic fraction from the catalytic reduction mixture of compound A,[1] $C_{17}H_{14}O_5N_2$, a base-catalyzed condensation product of *o*-nitroacetophenone, there was obtained an amphoteric compound, $C_{17}H_{16}O_2N_2$, (I). Measurement of the *C*-methyl group of this compound gave a value of 0.71. Its ultraviolet spectrum shows an intensive maximum at 238 nm and characteristic twin maxima at 317 and 329 nm (Fig. 1). These absorption features are typical of 4-quinolones;[2] especially, the shape and location of the twin maxima and the disappearance of the bifurcation in acid solution suggest that a 2-substituted 4-quinolone structure is seemingly preferable to a 3-substituted one for this compound.[3]

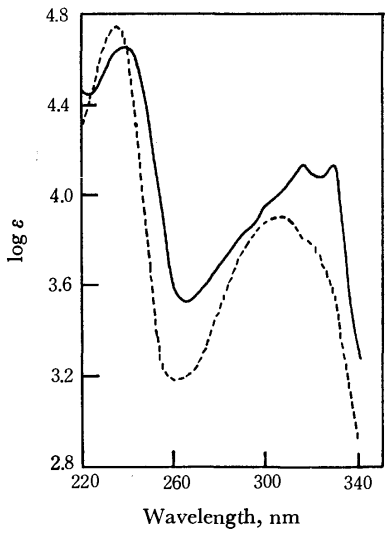

Fig. 1. UV spectra of the 4-quinolone I in ethanol (——) and in 0.1N hydrochloric acid (-----).

Acetylation of the compound I with acetic anhydride in aqueous alkali gave a monoacetyl derivative II, $C_{19}H_{18}O_3N_2$. Its infrared spectrum ($\nu_{C=O}$ 1667 cm^{-1}) indicated the compound to be an *N*-acetyl derivative. The ultraviolet absorption was similar to that of the compound I.

On the other hand, treatment of the alkaline solution of compound I with benzoyl chloride gave a dibenzoyl derivative III, $C_{31}H_{24}O_4N_2$. Its infrared spectrum ($\nu_{C=O}$ 1748 and 1667 cm^{-1}) showed that, besides the amino group, a phenolic hydroxyl group had been acylated. From the ultraviolet spectrum (Fig. 2), which lacks the bifurcation near 320 nm and resembles

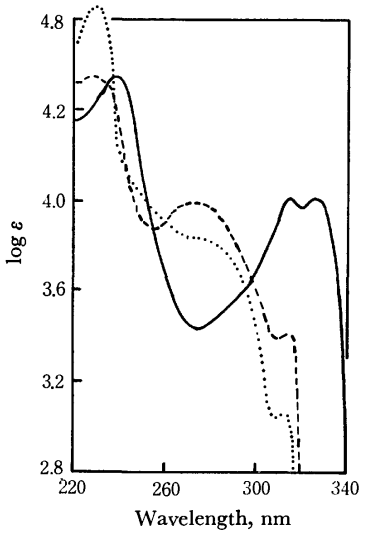

Fig. 2. UV spectra of the *N*-acetyl (——), *O,N*-dibenzoyl (-----), and *N*-acetyl (····) derivatives.

1) T. Sakan, K. Kusuda, and T. Miwa, This Bulletin, **37**, 1678 (1964).

2) R. S. Beer, L. McGroth, and A. Robertson, *J. Chem. Soc.*, **1950**, 3283. B. Witkop, J. B. Patrick, and M. Rosenblum, *J. Amer. Chem. Soc.*, **73**, 2641 (1951).

3) G. W. Ewing and E. A. Steck, *ibid.*, **68**, 2181 (1946); E. A. Steck, G. W. Ewing, and F. C. Nachod, *ibid.*, **71**, 238 (1949).

those of quinolines,[4] apparently the 4-hydroxyl group of the 4-quinolone nucleus was acylated. Methylation of the *N*-acetyl derivative II with diazomethane yielded a methyl ether IV, $C_{20}H_{20}O_3N_2$,[5] having an ultraviolet spectrum similar to the compound III.

From these observations, structures I, II, III, and IV were assigned to the compound I, its *N*-acetyl, *O*,*N*-dibenzoyl, and *N*-acetyl-*O*-methyl derivatives, respectively, the remaining inert oxygen function being tentatively assumed to be a tertiary alcohol.

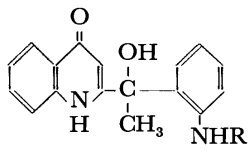

I: R=H
II: R=$COCH_3$

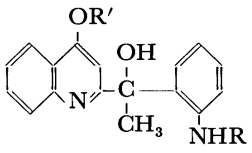

III: R, R'=COC_6H_5
IV: R=$COCH_3$, R''=CH_3

To confirm these structures, attempts were made to convert the 4-quinolone system to a quinoline nucleus, which was seemingly suitable to oxidative degradation. Transformation of 4-quinolones to the corresponding quinolines has been effected usually through the 4-chloro compounds.[6]

For replacement of the 4-hydroxyl group by chlorine, refluxing with phosphorus oxychloride is recommended as the best method.[7] Treatment of the *N*-acetyl derivative II with the reagent led to a chloride V, $C_{19}H_{15}ON_2Cl$, with evolution of hydrogen chloride. Ultraviolet absorption (Fig. 3) of the chloride supported the formation of a quinoline nucleus sufficiently. Simultaneous formation of an oxazine ring,[8] consequently the presence of an *o*-acylamidobenzylalcohol system in II, was proved by lack of the 3000-cm^{-1} band, disappearance of the amide I band and existence of a C=N stretching band (1631 cm^{-1}) in the infrared spectrum as well as by appearance of a new maximum at 268 nm in the ultraviolet absorption.[9]

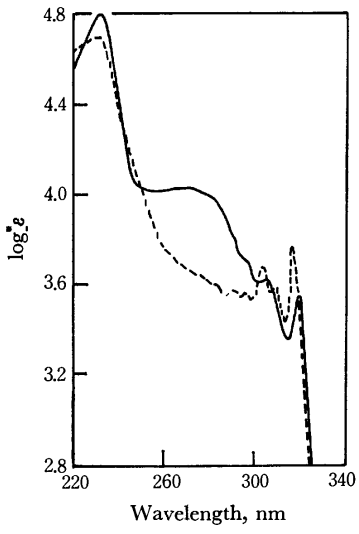

Fig. 3. UV spectra of the chloride V (——) and its hydrogenolysis product VI (– – –).

Hydrogenation of the chloride V over palladium-on-carbon in the presence of potassium acetate produced a chlorine-free compound VI, $C_{19}H_{18}ON_2$, infrared spectrum of which showed an amide I band at 1686 cm^{-1}, indicating re-formation of an amide function by hydrogenolysis of the oxazine ring.

The quinoline VI was hydrolyzed with dilute sulfuric acid and the resulting amine was immediately oxidized by addition of the Beckmann solution. From the basic volatile fraction, a methyl ketone was isolated as a semicarbazone, which decomposed at the same temperature as those of both 2- and 3-acetylquinolines; however, comparison of the infrared spectra established the semicarbazone from the oxidation product to be that of 2-acetylquinoline. Consequently, the compound I was confirmed to be 2-[1-(*o*-aminophenyl)-1-hydroxyethyl]-4-quinolone (I).

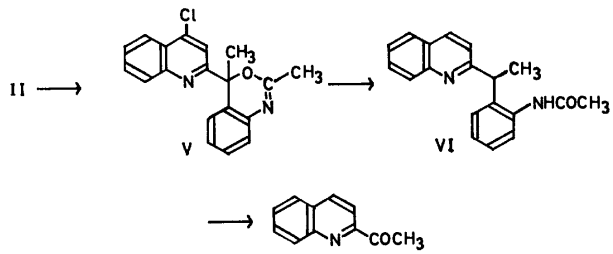

The acid catalysis in the rearrangement of the reduction product was verified by the spectral tracing of the reaction. The ultraviolet absorption of the crude reduction mixture showed a strong absorption at 380 nm reminiscent of compound A. Addition of one drop of dilute hydrochloric acid into the photometrical cell caused a momentary, striking change of the spectrum into one similar to that of the compound I in acid solution (see Experimental). The mechanism proposed in Chart 1 is obvious when the carbon skeleton of the 4-quinolone is compared with that of compound A.

This rearrangement provides a novel type of ring enlargement of a nitrogen heterocycle, different nitrogen atoms participating in the ring formation. Formation of the β-diaminoketone from the reduction product might be reversible; however, stabilization by the formation of the quinolone nucleus makes the last step

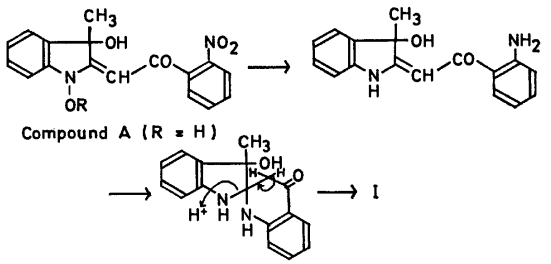

Chart 1.

4) D. Sutherland and C. Compton, *J. Org. Chem.*, **17**, 1257 (1952).

5) Methylation of 4-quinolone with diazomethane gives 4-methoxyquinoline: H. Meyer, *Monatsh. Chem.*, **27**, 987 (1906).

6) E. g., E. Späth and J. Pikl, *Ber.*, **62**, 2244 (1929).

7) A. Albert, "Heterocyclic Chemistry," Essential Books, London (1959), p. 80.

8) J. B. Patrick and B. Witkop, *J. Org. Chem.*, **19**, 1824 (1954).

9) 4-Chloromethyl-2,4-dimethyl-4*H*-3,1-benzoxazine has its absorption maximum at 259 nm (log ε 3.87). [C. W. Rees and C. E. Smithen, *J. Chem. Soc.*, **1964**, 928.

irreversible and the cleavage of the indoline ring is apparently the acid-catalyzed step.

Hydrogenation of compound A and its methyl ether in the presence of hydrochloric acid gave the compound I directly as expected.

Experimental

All melting points are not corrected. Unless otherwise noted, ultraviolet spectra were taken in ethanol and infrared spectra in Nujol mull; they are expressed in λ_{max} nm ($\log \varepsilon$) and ν_{max} cm^{-1}, respectively.

Hydrogenation of the Compound A Methyl Ether. 2-[1-(2-aminophenyl)-1-hydroxyethyl]-4-quinolone (I). An ethanol solution of 340 mg (1 mmol) of compound A methyl ether was shaken in the presence of 5% palladium-on-carbon under atmospheric pressure of hydrogen for 4 hr, during which 115 m*l* (*ca.* 18°C) of hydrogen was absorbed. Ultraviolet absorption taken immediately after the reduction (unknown concentration): λ_{max} ($-\log T$): 236 (0.818), 305 (0.150), and 403 (0.663). After addition of one drop of N hydrochloric acid (the same concentration): λ_{max} ($-\log T$): 235 (3.85), 304 (0.520), and 389 (0.320). After removal of the catalyst, followed by evaporation of the solvent *in vacuo*, the resulting residue was taken in N sulfuric acid and washed with ether. The aqueous solution was treated with active carbon, filtered and made faintly alkaline with aqueous ammonia to separate amorphous precipitates, which were collected by filtration, washed with water and dried; yield 195 mg. This material was used without further purification for formation of derivatives.

In one run, the precipitates were dissolved in ether and the ethereal solution was re-extracted with N sodium hydroxide. Neutralization of the alkaline solution with 2N hydrochloric acid produced precipitates again. After filtration of the precipitates, the mother liquor containing some ether was left to evaporate to deposit crystals, decomposing at 122°C. λ_{max} 238 (4.66), 317 (4.14), and 329 (4.13). $\lambda_{max}^{0.1N\ HCl}$ 235 (4.75) and 306 (3.91).

Found: C, 66.29; H, 6.35; N, 8.77%; *C*-methyl group:[10] 0.71. Calcd for $C_{17}H_{16}O_2N_2 \cdot 1.5H_2O$: C, 66.43; H, 6.23; N, 9.12%.

Hydrogenation of both compound A and its methyl ether over 5% palladium-on-carbon in the presence of equimolecular amount of hydrochloric acid gave similar results.

2-[1-(2-Acetamidophenyl)-1-hydroxyethyl]-4-quinolone (II). Crude compound I (159 mg) was dissolved in 4.2 m*l* of 2N sodium hydroxide. After removal of a little amount of insoluble material, the clear solution, chilled in an ice-bath, was treated with 0.2 m*l* of acetic anhydride. Trituration caused crystallization. Filtration, followed by washing with water and drying, yielded 128 mg of crystals, which, after recrystallization from aqueous ethanol, decomposed at 198—201°C. λ_{max} 239 (4.55), 315 (4.02), and 327 (4.03). ν_{max} 1664 and 1621 (C=O).

Found: C, 66.62; H, 5.58; N, 8.73%. Calcd for $C_{19}H_{18}O_3N_2 \cdot H_2O$: C, 67.04; H, 5.92; N, 8.23%.

2-[1-(2-Benzamidophenyl)-1-hydroxyethyl]-4-benzoyloxyquinoline (III). A solution of 168 mg of the crude compound I in 1.5 m*l* of 0.2N sodium hydroxide, chilled in ice, was treated with 0.1 m*l* of benzoyl chloride and triturated to deposit crystals, which weighed 100 mg. Recrystallization from methanol gave crystals melting at 169—170°C. λ_{max} 229 (4.55), 276 (3.99), and 315 (3.42). ν_{max} 1751 and 1669 (C=O). This material was analyzed after drying at 80°C for 1 hr.

Found: C, 75.51; H, 4.96; N, 5.80%. Calcd for $C_{31}H_{24}O_4N_2$: C, 76.21; H, 4.95; N, 5.73%.

2-[1-(2-Acetamidophenyl)-1-hydroxyethyl]-4-methoxyquinoline (IV). A suspension of 300 mg of the *N*-acetyl derivative II in 10 m*l* of methanol was treated with an ethereal solution of diazomethane prepared from 1.0 g of nitrosomethylurea. Evaporation of the solvent left crystals, which were recrystallized from 50% methanol to give *ca.* 170 mg of crystals melting at 168°C. λ_{max} 230 (4.86) and 313 (3.07). ν_{max} 1684 (C=O).

Found: C, 71.75; H, 6.18; N, 8.31%. Calcd for $C_{20}H_{20}O_3N_2$: C, 71.41; H, 5.99; N, 8.33%.

4-(4-Chloro-2-quinolyl)-2,4-dimethyl-4H-3,1-benzoxazine (V). A mixture of 0.80 g of the *N*-acetyl derivative II (monohydrate) and about 5 m*l* of phosphorus oxychloride was heated on a water bath, yielding a yellow solution immediately with evolution of hydrogen chloride. After being heated for 15 min, the mixture was removed from phosphorus oxychloride under reduced pressure and the residue poured into a mixture of ice and aqueous ammonia to separate brown precipitates. The mixture was extracted with ether; the extract was washed with sodium bicarbonate solution, dried and evaporated. Trituration of the residue with petroleum benzine yielded crystals, which, after filtration and subsequent washing with petroleum benzine, weighed 0.36 g. The crystals, after recrystallization from methanol–petroleum ether, melted at 125°C. λ_{max} 232 (4.80), 268 (4.03), 307 (3.62), and 320 (3.56). ν_{max} 1631 (C=N).

Found: C, 70.79; H, 4.98; N, 8.48%. Calcd for $C_{19}H_{15}ON_2Cl$: C, 70.69; H, 4.68; N, 8.68%.

2-[1-(2-Acetamidophenyl)ethyl]quinoline (VI). A mixture of 0.36 g of the chloride V, 0.20 g of sodium acetate trihydrate and 0.40 g of 5% palladium-on-carbon in 20 m*l* of ethanol containing 10 drops of water was hydrogenated at atmospheric pressure, absorbing 73 m*l* of hydrogen. After removal of the catalyst, evaporation of the solvent left a residue, which was taken in ether and washed with water. Evaporation of the dried ethereal solution left crystals, which, after recrystallization from ether–petroleum ether, weighed 0.21 g and melted at 115.5—116.5°C. λ_{max} 232 (4.70), 291 (3.58), 297 (3.56), 304 (3.68), 310 (3.57), and 317 (3.77). ν_{max} 1686 (C=O).

Found: C, 78.73; H, 6.35; N, 9.79%. Calcd for $C_{19}H_{18}ON_2$: C, 78.59; H, 6.25; N, 9.65%.

Oxidative Degradation into 2-Acetylquinoline. A mixture of 140 mg of the amide VI, 5 m*l* of water and 15 m*l* of N sulfuric acid was heated on a water bath for 8 hr. Into the cooled mixture, 8 m*l* of the Beckmann solution (prepared by dissolving 2.94 g of potassium dichromate in a little amount of water, adding 2.5 m*l* of concentrated sulfuric acid, and diluting to 25 m*l*) was added and stirred at the room temperature for 8 hr. After decomposition of the excess dichromate with ethanol, the mixture was made alkaline and extracted with ether. Evaporation of the ethereal solution gave a residue, which was distilled under a 5 Torr-pressure to give a fraction boiling at a bath temperature below 100°C. The distillate (λ_{max} 243 and 290), which gave a positive iodoform test, was converted into a semicarbazone (10 mg), decomposing at 239°C after recrystallization from ethanol. The infrared spectrum of the semicarbazone was not identical with that of 3-acetylquinoline[11] semicarbazone [mp 245°C

10) E. J. Eisenbraun, S. M. McElvain, and B. F. Aycock, *J. Amer. Chem. Soc.*, **76**, 607 (1954). The measurement was carried out by Dr. Shōji Hayashi, to whom the author is indebted.

11) V. Boekelheide and J. Weinstock, *J. Amer. Chem. Soc.*, **74**, 660 (1952).

(decomp.); lit, 236—236.5°C[12]], but completely idendical with that of 2-acetylquinoline[13] (λ_{max} 244 (4.51) and 293 (3.75)] semicarbazone [mp 242°C (decomp.). Found: C, 63.34; H, 5.31; N, 23.64%. Calcd for $C_{12}H_{12}ON_4$: C, 63.14; H, 5.30; N, 24.55%].

The author wishes to express his thanks to Mr. Jun'ichi Gōda and his associates for their elementary analyses and to Mrs. Hiromi Aotani for her infrared determinations.

12) S. Yamada and I. Chibata, *Chem. Pharm. Bull.* (Tokyo), **3**, 21 (1955).

13) R. B. Woodward and E. C. Kornfeld, *J. Amer. Chem. Soc.*, **70**, 2508 (1948).

BULLETIN OF THE CHEMICAL SOCIETY OF JAPAN, VOL. 45, 2593—2597 (1972)

Aminocyclitols. XXVIII. Bromination of Inosamines and Inosadiamines

Tetsuo SUAMI, Seiichiro OGAWA, Shinichi YANAGIDA, and Kazuhiro NOJIMA

Department of Applied Chemistry, Faculty of Engineering, Keio University, Hiyoshi, Yokahama

(Received January 22, 1972)

Bromination of four inosamines (*myo*-2 (**1**), *chiro*-1 (**2**), *muco*-1 (**3**), and *scyllo* (**4**)) and three inosadiamines (*neo*-1,4 (**11**), *muco*-1,5 (**14a,b**), and *muco*-1,4 (**19**)) with acetyl bromide and acetic anhydride in a sealed tube at 130—160°C has been studied. 2,5-Dibromo-2,5-dideoxy-*chiro*-inosamine-3 tetraacetate (**8**), was obtained from **1**, **2**, and **3**, and, as a monobromide, only 2-bromo-2-deoxy-*chiro*-inosamine-3 pentaacetate (**7**) could be isolated from the bromination product of **3**. From **11**, monobromide (**12**) and dibromide (**13**) were obtained. From **14a** or **14b**, 2-bromo-2-deoxy-*chiro*-inosadiamine-3,5 pentaacetate (**15**) was obtained, and, under a more drastic condition, **15** was further brominated to afford 1,5-dibromo-1,5-dideoxy-*chiro*-inosadiamine-2,4 tetraacetate (**16**). The bromo compounds so obtained were converted into the corresponding deoxy or dideoxy derivatives by hydrogenolysis. All the structures of the new compounds have been confirmed on the basis of proton magnetic resonance (PMR) spectroscopy using their acetyl derivatives. Considering from the structures of the bromides, a mechanism of a bromination reaction has been proposed.

In connection with the previous paper,[1] we wish to report the bromination of inosamines and inosadiamines with acetyl bromide and acetic anhydride at high temperature. Bromo-deoxyinosamines and -deoxy-inosadiamines are useful precursors for a preparation of the corresponding deoxy derivatives. We had already described the facile synthesis of 2-deoxy-streptamine from the key intermediary compound, 2-bromo-2-deoxystreptamine, which was obtained in a high yield by bromination of *myo*-inosadiamine-1,3.[2] In all the cases studies so far,[1-3] the hydroxyl groups vicinal and in *cis* position to an amino or acetamido group in aminocyclitols are preferentially displaced by bromine in a mixture of acetyl bromide and acetic anhydride. However, in the present report, it has been shown that, when there is a possibility of a displacement of more than one hydroxyl groups by bromine, a bromine atom was previously introduced in aminocyclitols following observed rule, whereas, the displacement of the second hydroxyl group was much influenced by a stereochemical and electronic environments.

When *myo*-inosamine-2 hydrochloride (**1**)[4] was treated with acetyl bromide in a sealed tube at 155—160°C for 8 hr, followed by acetylation, dibromo-dideoxyinosamine tetraacetate (**8**) was obtained mainly as a sole crystalline product in 32% yield. On treatment with acetyl bromide similarly as described above, both *N*-acetyl-*chiro*-inosamine-1 (**2**) and *N*-acetyl-*muco*-

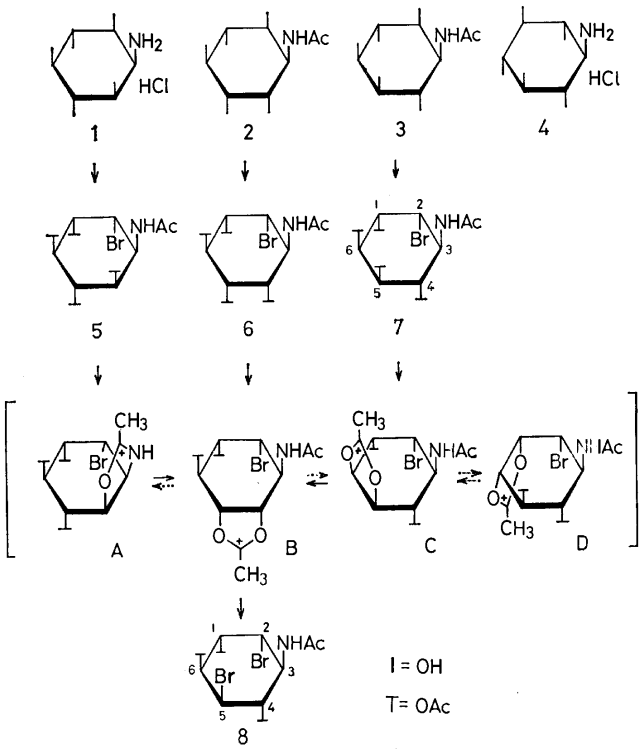

1) T. Suami, S. Ogawa, and H. Sano, This Bulletin, **43**, 1843 (1970).

2) T. Suami, F. W. Lichtenthaler, S. Ogawa, Y. Nakashima, and H. Sano, *ibid.*, **41**, 1014 (1968).

3) T. Suami, S. Ogawa, Y. Nakashima, and H. Sano, *ibid.*, **40**, 2958 (1967).

4) H. E. Carter, R. K. Clark, B. Lytle, and G. E. McCasland, *J. Biol. Chem.*, **175**, 684 (1948).

inosamine-1 (**3**)[5] gave **8** in 16 and 11% yield, respectively. While, the reaction of **3** with acetyl bromide at 135—140°C for 4 hr gave bromo-deoxyinosamine pentaacetate (**7**) in 45% yield, along with a small amount of **8**. Hydrogenolysis of **7** and **8** in the presence of Amberlite IR-4B (OH^-) and Raney nickel T-4[6] afforded deoxy- (**9**) and dideoxy-inosamine (**10**) in 65 and 56% yield, respectively.

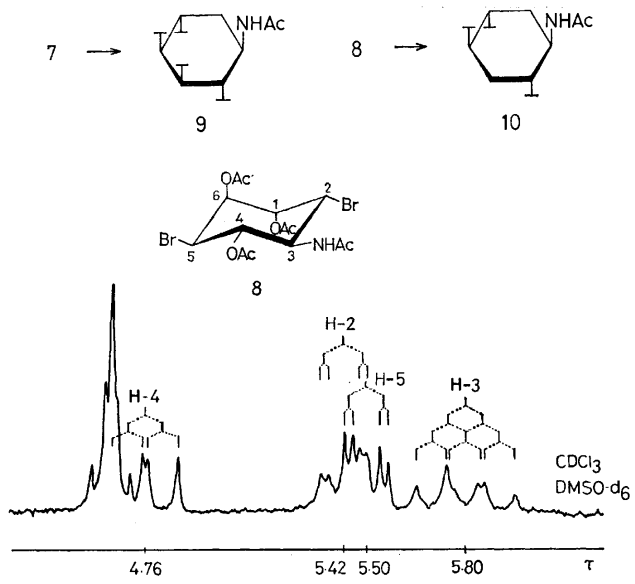

Fig. 1. Partial PMR spectrum of 2,5-dibromo-2,5-dideoxy-*chiro*-inosamine-3 tetraacetate (**8**) in a mixture of $CDCl_3$ and DMSO-d_6 at 100 MHz.

The structural elucidation of **7**, **8**, **9**, and **10** was carried out by means of the PMR spectroscopy. The PMR spectrum of **8** in a mixture of $CDCl_3$ and dimethylsulfoxide-d_6 (DMSO-d_6) at 100 MHz (Fig. 1) was in good accord with the structure, 2,5-dibromo-2,5-dideoxy-*chiro*-inosamine-3 tetraacetate. The wide sextet at τ 5.80 (J=9.5, 11.0, and 11.0 Hz) was assigned to C-3 proton that has two vicinal axial protons and indicated an axial-axial-axial arrangement for H-2, H-3, and H-4. Both H-2 and H-5 appeared as a quartet at τ 5.42 and 5.50, showing $J_{2,3}=J_{4,5}=11.0$ Hz and $J_{1,2}=J_{5,6}=2.0$ Hz, which was indicative of an equatorial-equatorial arrangement for H-1 and H-6. The wide doublet of doublet at τ 4.76 (J=9.5 and 11.0 Hz) was attributed to C-4 proton which demonstrated that one of the two bromine atoms is located at C-5. While, in the spectrum measured in $CDCl_3$, four acetyl methyl protons appeared at τ 7.78, 7.80, 7.88, and 8.00, which were assigned to an axial, an axial and an equatorial acetoxy, and an equatorial acetamido group, respectively.[7] Furthermore, the PMR spectrum of **10** in $CDCl_3$ at 100 MHz showed an octet at τ 5.75 which was assignable to H-3, since on deuteration it collapsed to a sextet. This result again indicated a diaxial arrangement for H-3 and H-4 and another bromine atom should attach equatorially to C-2. Therefore, the proposed structure of **8** was confirmed evidently.

In the PMR spectrum of **7** in $CDCl_3$, signals due to two protons attached to the carbon atoms having the acetamido group and bromine atom appeared around τ 5.50 as a complex multiplet, which probably suggested that they are located on a vicinal position. The acetyl methyl protons appeared as fine singlets at τ 7.83, 7.85, 7.92, 7.98, and 8.04, which were attributed to an axial, an axial, an equatorial and an equatorial acetoxy, and an equatorial acetamido group, respectively. Since **7** might be considered as the intermediary compound for **8** in the bromination reaction, its structure, taking an epimerization into account, should be either 2-bromo-2-deoxy-*chiro*-inosamine-3 or -*muco*-inosamine-3 pentaacetate. The latter might be likely the intermediary bromo-deoxy compound (**6**) from **2**, however, the formation of **6** could not be observed on bromination of **2** under a mild condition. Consequently, **7** was assigned to the former structure.

According to the results obtained, the mechanism of the bromination reaction might be proposed as follows. Initially, cyclic oxazolinium ions are formed between *cis* arranged acetamido and acetoxy groups by a front-side participation reaction.[8] Then they are opened by S_N2 attack of bromide ion to produce the bromo-deoxy compound (**5**, **6**, and **7**). Then, cyclic acetoxonium or oxazolinium ions are formed between remaining *cis* arranged groups and the cyclic ions are cleaved by nucleophlic attack of bromide ions or *trans*-situated adjacent groups.[9] The existence of an equilibrium (A⇄B⇄C⇄D) resulted from a rearrangement of a cyclic intermediary ion may be substantiated by the formation of the same dibromide **8** from **1**, **2**, and **3**, which additionally indicated that a bromide ion can only attack them in the most favorable configuration (B) satisfying the stereochemical and electronic requirement to afford one dibromide predominantly. For instance, in the similar halogenation reaction of cyclitols studied so far,[10] a vicinal dihalide has never been obtained.

Attempted bromination of *scyllo*-inosamine hydrochloride (**4**)[4] under a vigorous condition failed. Thus, even though the reaction temperature was raised up to 180°C, **4** was recovered as the hexaacetate from the reaction mixture. This result, like in the case of streptamine,[2] demonstrated that a formation of an intermediary oxazolinium ion initiates a nucleophilic attack of bromide ion.

Then the bromination of readily available *N*,*N*'-diacetyl-*neo*-inosadiamine-1,4 (**11**)[11] was attempted. On similar treatment with acetyl bromide and acetic anhydride (2: 1) at 145—150°C for 7 hr, **11** gave the acetates of bromodeoxyinosadiamine (**12**) and dibromo-

5) T. Suami and S. Ogawa, This Bulletin, **37**, 1238 (1964); T. Suami, F. W. Lichtenthaler, and S. Ogawa, *ibid.*, **39**, 170 (1966).

6) S. Nishimura, *ibid.* **32** 61 (1959).

7) F. W. Lichtenthaler and P. Emig, *Carbohyd. Res.*, **7**, 121 (1968).

8) R. Boschan and S. Winstein, *J. Amer. Chem. Soc.*, **78**, 4921 (1956).

9) S. J. Angyal, P. A. J. Gorin, and M. E. Pitman, *J. Chem. Soc.*, **1965**, 1807; H, Paulsen and C-P. Herold, *Chem. Ber.*, **104**, 1311 (1971).

10) G. E. McCasland, *Advans. Carbohyd. Chem.*, **20**, 11 (1965).

11) F. W. Lichtenthaler and H. O. L. Fischer, *J. Amer. Chem. Soc.*, **83**, 2005 (1961).

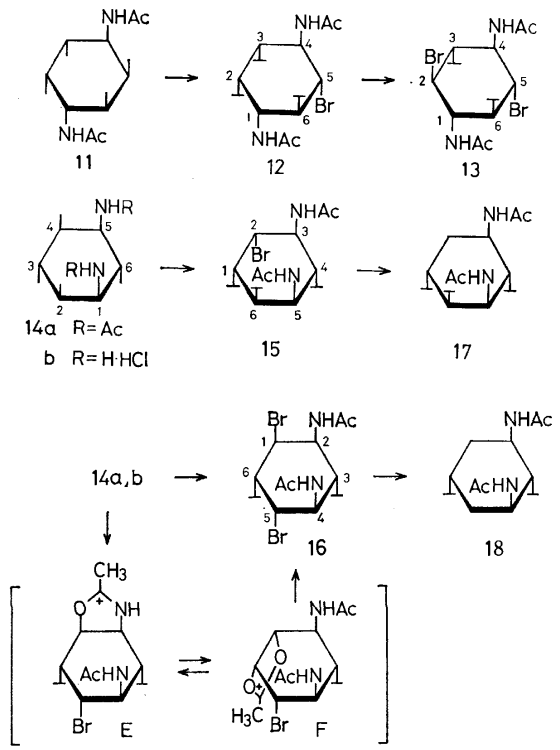

dideoxyinosadiamine (**13**) in a yield of 29 and 14%, respectively. By analogy with the proposed reaction mechanism, the structure of **12** and **13** may be deduced to be 5-bromo-5-deoxy-*myo*-inosadiamine-1,4 pentaacetate and 2,5-dibromo-2,5-dideoxy-*scyllo*-inosadiamine-1,4 tetraacetate, respectively. In the PMR spectrum of **12**, the signal due to one axial acetoxy group diminished and this accounted for one of the axial hydroxyl groups in **11** being replaced by bromine atom. The PMR spectrum of **13** gave two singlets in τ 8 region, indicating the symmetrical configuration of **13**. These PMR spectroscopic evidences are consistent with the proposed structures of **12** and **13**.

Secondarily, *N,N'*-diacetyl-*muco*-inosadiamine-1,5 (**14a**)[5] was subjected to the bromination reaction. It gave the bromo-deoxyinosadiamine pentaacetate (**15**) in 33% yield, on treatment with acetyl bromide and acetic anhydride (2: 1) at 140°C for 3 hr. While, when the same reaction was conducted at 145—150°C for 6 hr, the dibromo-dideoxyinosadiamine tetraacetate (**16**) was obtained mainly in 32% yield. From *muco*-inosadiamine-1,5 dihydrochloride (**14b**),[5] **16** was also obtained in 31% yield by a drastic condition. Hydrogenolysis of **15** and **16** afforded the corresponding deoxy- (**17**) and dideoxy-derivative (**18**) in 85 and 72% yield, respectively.

On the basis of the following PMR spectroscopic data, the structures of **15** and **16** were assigned to 2-bromo-2-deoxy-*chiro*-inosadiamine-3,5 pentaacetate and 1,5-dibromo-1,5-dideoxy-*chiro*-inosadiamine-2,4 tetraacetate, respectively, and **17** and **18** were assigned to the corresponding deoxy- and dideoxy-compound. The PMR spectrum of **15** in DMSO-d_6 revealed two singlets in an axial region of an acetoxy group, hence, one axial hydroxyl group in **14** must be replaced by bromine atom. Had the bromine atom been located at

Table 1. Chemical shifts of acetyl methyl protons[a]

Compound	Solvent	Acetoxy ax.	Acetoxy eq.	Acetamido eq.
7	A	7.75 7.83	7.93 7.99	8.00
	B	7.80 7.85	8.05 8.09	8.20
8[c]	A	7.78 7.80	7.88	8.00
	B	7.82[b]	7.98	8.20
9	A	7.83 7.85	7.92 7.98	8.04
10[c]	A	7.89 7.92	7.93	8.05
12	B	7.82	7.96 8.13	8.16 8.20
13	B		8.00[b]	8.20[b]
15	B	7.81 7.85	8.08	8.21[b]
16	B	7.80	8.07	8.13 8.20
17	B	7.85[b]	8.08	8.18 8.23
18	B	7.91	8.10	8.25[b]
neo-Inosadiamine-1,4 hexaacetate	B	7.89[b]	8.11[b]	8.25[b]
muco-Inosadiamine-1,5 hexaacetate[5]	B	7.87 7.90[b]	8.08	8.21[b]

a) PMR spectra were measured at 60 MHz, unless otherwise noted. Solvents were: A $CDCl_3$, B DMSO-d_6. The peak positions are given in τ-values.
b) Signal due to two equivalent methyl protons.
c) Measured at 100 MHz.

C-3, both **15** and **17** should have a symmetrical structure and their PMR spectra had to be simpler than those observed herein. Nonequivalence of the signals due to two axial acetoxy groups in **15** and two acetamido groups in **17** evidently indicated their unsymmetrical structures and the location of the bromine atom at C-2 (C-4) of **14**. The PMR spectrum of **18** showed three singlets (1 : 1 : 2) at τ 8 region, that were assigned to an axial and an equatorial acetoxy, and two equatorial acetamido groups, respectively. The signals due to ring protons were amenable to the first order analysis, that is, a narrow quintet at τ 4.97 (J=2.5 Hz) and a wide triplet at τ 5.93 (J=10.0 Hz) were readily assigned to H-6 and H-3 proton, respectively. A two protons octet at τ 5.73 (J=11.5, 10.0, 10.0, and 6.5 Hz) assignable to two equivalent protons at C-2 and C-4 showed that two acetamido groups were equivalent each other and adjacent to the equatorial acetoxy group and methylene protons. On the other hand, in the PMR spectrum of **16**, two singlets at τ 8.13 and 8.20 were assigned to the equatorial two acetamido groups. The presence of nonequivalent acetamido groups indicated that the arrangement of two bromine atoms adjacent to them should be 1,3-*trans* position. Therefore, the configuration of the bromine atom in **15** only remained equivocal. Since, in the PMR spectrum of **15** in DMSO-d_6, the signals corresponding to the ring protons attached to the carbon atoms having the acetamido groups and bromine atom appeared as a complex multiplet at τ 5.5—6.0, the configuration of the bromine

atom could not be determined by the first order analysis of them. However, by analogy with the proposed reaction mechanism of the bromination reaction, it might be reasonable that the cyclic oxazolinium ion initially formed is opened by a rearside attack of bromide ion and therefore the bromine atom in **15** is in *trans* configuration to the neighboring acetamido group. Then the second oxazolinium ion (E) seemed to be attacked by the adjacent *trans*-situated acetoxy group to produce another ion (F), which only undergoes nucleophilic attack of bromide ion to give **16**.

Bromination of *muco*-inosadiamine-1,4 dihydrochloride (**19**)[12] gave a complex mixture (at least four components were detected by tlc analysis) and no further isolation has been attempted.

Experimental

Melting points were determined on a Mitamura Riken micro hot stage and are uncorrected. PMR spectra were measured with a Varian A-60D (60 MHz) or HA-100D (100 MHz) spectrometer with tetramethylsilane as internal standard. IR spectra were recorded in KBr disks with Jasco IR-E infrared spectrophotometer. Tlc was performed on silica gel plates (Wakogel B-10) using methyl ethyl ketone–toluene (1 : 5 or 1 : 10) as the solvent system. The compounds were detected by heating with 30% sulfric acid. Evaporations were performed below 50°C under diminished pressure. Whenever pyridine was employed in a reaction, the residual pyridine was removed by repeated codistillation with dry toluene. All the compounds described in this paper are racemic.

N-*Acetyl*-chiro-*inosamine-1 (2).* *chiro*-Inosamine-1 hexaacetate[13] (3.0 g) was treated with methanol (20 m*l*), saturated with ammonia at 0—5°C, overnight at room temperature. Then the mixture was evaporated and the residue was recrystallized from 80% aqueous methanol to give colorless prisms (1.42 g, 41%) of **2**, mp 225—226°C (a transition was observed at 168—169°C). IR: 1640 and 1560 cm^{-1} (NHAc).

Found: C, 43.43; H, 6.84; N, 6.33%. Calcd for $C_8H_{15}NO_6$: C, 43.56; H, 7.06; N, 6.17%.

2-Bromo-2-deoxy-chiro-*inosamine-3 Pentaacetate (7).* A mixture of *N*-acetyl-*muco*-inosamine-1 (**3**)[5] (100 mg) and acetyl bromide (5 m*l*) was heated in a sealed tube at 135—140°C for 4 hr. After cooling to room temperature, the reaction mixture obtained from six sealed tubes was poured into ethanol (200 m*l*) and evaporated to dryness. The residue was treated with acetic anhydride (15 m*l*) and pyridine (15 m*l*) overnight at room temperature. Then an insoluble material was filtered off and the filtrate was evaporated to give crude crystals, which was recrystallized from ethanol to give crystals (602 mg, 45%) of **7**, mp 188—189°C. IR: 1750 (OAc), 1660 and 1575 cm^{-1} (NHAc).

Found: C, 42.73; H, 5.17; N, 3.45; Br, 18.04%. Calcd for $C_{16}H_{22}NO_9Br$: C, 42.50; H, 4.87; N, 3.10; Br, 17.70%.

2,5-Dibromo-2,5-dideoxy-chiro-*inosamine-3 Tetraacetate (8).* (a) A mixture of *myo*-inosamine-2 hydrochloride (**1**)[4] (150mg) and acetyl bromide (5 m*l*) was heated in a sealed tube at 155—160°C for 8 hr. The reaction mixture obtained from five sealed tubes was processed similarly as described under the preparation of **7**. The crude product was chromatographed on a column of activated aluminum oxide with chloroform. The eluates were evaporated to give an oily product which crystallized upon addition of ethanol to give crystals (615 mg, 32%) of **8**, mp 240—245°C. Recrystallization from ethanol afforded colorless needles (590 mg), mp 247—248°C. IR: 3240 (NH), 1755 (OAc), 1660 and 1580 cm^{-1} (NHAc).

Found: C, 35.72; H, 4.43; N, 3.08; Br, 33.52%. Calcd for $C_{14}H_{19}NO_7Br_2$: C, 35.56; H, 4.02; N, 2.96; Br, 33.90%.

(b) A mixture of **2** (220 mg) and acetyl bromide (4 m*l*) was heated in a sealed tube at 145—150°C for 6 hr. The reaction mixture obtained from three sealed tubes was processed as described in (a) to give crystals (223 mg, 16%) of **8**, mp 243—244°C.

(c) A mixture of **3** (100 mg) and acetyl bromide (5 m*l*) was heated in a sealed tube at 155—160°C for 8 hr. The reaction mixture obtained from ten sealed tubes was processed as described in (a) to give crystals (113 mg, 11%) of **8**, mp 244—245°C.

(d) Compound **2** was treated with acetyl bromide similarly as described under the preparation of **7**. *chiro*-Inosamine-1 hexaacetate was obtained in a high yield and tlc of the resulting reaction product showed one main component (*chiro*-inosamine-1 hexaacetate) along with two minor ones, one of which was shown to be corresponding to a reference sample of **8**. The unidentified component was considered to be the bromo-deoxy compound probably.

2-Deoxy-chiro-*inosamine-3 Pentaacetate (9).* A solution of **7** (350 mg) in 50% aqueous ethanol (20 m*l*) was catalytically hydrogenated in a Parr shaker type apparatus (4 kg/cm^2 of the initial hydrogen pressure) in the presence of Raney nickel T-4[6] and Amberlite IR-4B (OH^-) at 40—45°C for 20 hr. The catalyst and resin were removed by filtration and the filtrate was evaporated to give crude crystals (206 mg) which was recrystallized from ethanol to afford colorless needles (189 mg, 65%) of **9**, mp 208—209°C. IR: 1750 (OAc), 1660, 1640, and 1585 cm^{-1} (NHAc).

Found: C, 51.80; H, 6.29; N, 3.84%. Calcd for $C_{16}H_{23}NO_9$: C, 51.47; H, 6.21; N, 3.75%.

2,5-Dideoxy-chiro-*inosamine-3 Tetraacetate (10).* Compound **8** (297 mg) was hydrogenated similarly as described under the preparation of **9**. The crude crystals were recrystallized from ethanol to afford colorless crystals (110 mg 56%) of **10**, mp 149—151°C. IR: 1745 (OAc), 1640, and 1570 cm^{-1} (NHAc).

Found: C, 53.55; H, 7.24; N, 4.49%. Calcd for $C_{14}H_{23}NO_7$: C, 53.10; H, 7.26; N, 4.42%.

5-Bromo-5-deoxy-myo-*inosadiamine-1,4 Pentaacetate (12) and 2,5-Dibromo-2,5-dideoxy*-scyllo-*inosadiamine-1,4 Tetraacetate (13).* A mixture of *N,N'*-diacetyl-*neo*-inosadiamine-1,4 (**11**) (mp 324—326°C, lit,[11] 325—328°C) (104 mg), acetyl bromide (5 m*l*) and acetic anhydride (2 m*l*) was heated in a sealed tube at 145—150°C for 7 hr. Then the brown reaction mixture obtained from two sealed tubes was poured into cold ethanol (50 m*l*) and allowed to stand at room temperature overnight. The resulting precipitates were collected, dried and treated with acetic anhydride (3 m*l*) and pyridine (3 m*l*) overnight at room temperature. The acetate (13 mg) so obtained was identified with an authentic sample of *neo*-inosadiamine-1,4 hexaacetate[11] by IR spectral comparison. The alcoholic mother liquor was evaporated to dryness and the residue was acetylated as described above to give an oily product which crystallized upon addition of ethanol to afford crystals (54 mg, 15%) of **13**, mp 268—269°C. Recrystallization from ethanol gave an analytical sample of **13**, mp 272—273°C (decomp.). IR: 1750 (OAc), 1660, and 1540 cm^{-1} (NHAc).

Found: C, 35.78; H, 4.51; N, 6.11; Br, 33.31%. Calcd

12) T. Suami, F. W. Lichtenthaler, and S. Ogawa, This Bulletin, **40**, 1488 (1967).

13) T. Suami, S. Ogawa, and M. Uchida, *ibid.*, **43**, 3577 (1970).

for $C_{14}H_{20}N_2O_6Br_2$: C, 35.62; H, 4.27; N, 5.94; Br, 33.85%.

The mother liquor of **13** was condensed to a small volume and settled in a refrigerator overnight to give crystals (101 mg, 29%) of **12**, mp 257—259°C (decomp.). Recrystallization from ethanol gave colorless plates of **12**, mp 261—262°C (decomp.). IR: 1760 (OAc), 1655 and 1555 cm^{-1} (NHAc).

Found: C, 43.05; H, 5.64; N, 6.07; Br, 17.44%. Calcd for $C_{16}H_{23}N_2O_8Br$: C, 42.59; H, 5.14; N, 6.21; Br, 17.71%.

1,5-Dibromo-1,5-dideoxy-chiro-*inosadiamine-2,4 Tetraacetate (16).* (a) A mixture of *N,N'*-diacetyl-*muco*-inosadiamine-1,5 (**14a**)[5] (250 mg), acetyl bromide (4 m*l*) and acetic anhydride (2 m*l*) was heated in a sealed tube at 145—150°C for 6.5 hr. After keeping in a refrigerator overnight, the tube was opened carefully and the resulting precipitates were collected by filtration. The crude crystals were recrystallized from ethanol to afford crystals (420 mg, 32%) of **16**, mp 228—229°C (decomp.). IR: 1755 (OAc), 1660 and 1540 cm^{-1} (NHAc).

Found: C, 35.85; H, 4.53; N, 5.96; Br, 33.75%. Calcd for $C_{14}H_{20}N_2O_6Br_2$: C, 35.62; H, 4.27; N, 5.94; Br, 33.85%.

The filtrate of the reaction mixture was processed similarly as described under the preparation of **7** to give an oily product. Tlc showed a small proportion of a faster moving component along with **16** and *muco*-inosadiamine hexaacetate.[5]

(b) A mixture of *muco*-inosadiamine-1,5 dihydrochloride (**14b**)[5] (391 mg), acetyl bromide (4 m*l*) and acetic anhydride (2 m*l*) was heated in a sealed tube at 145—150°C for 6.5 hr. Then the reaction mixture was processed similarly as described in (a) to give crystals (226 mg, 31%) of **16**, mp 227—231°C (decomp.).

2-Bromo-2-deoxy-chiro-*inosadiamine-3,5 Pentaacetate (15).* A mixture of **14a** (209 mg), acetyl bromide (4 m*l*) and acetic anhydride (2 m*l*) was heated in a sealed tube at 140°C for 3 hr. After cooling to room temperature, the tube was opened and the precipitates were collected by filtration. Tlc of the reaction solution showed one main component along with one minor one, corresponding to a reference sample of **16**. The crude crystals were fractionally crystallized from ethanol to give crystals (104 mg, 29%) of **15**, mp 235—236°C, and crystals (15 mg, 4%) of **16**.

Found: C, 42.53; H, 5.30; N, 6.24; Br, 18.05%. Calcd for $C_{16}H_{23}N_2O_8Br$: C, 42.59; H, 5.14; N, 6.21; Br, 17.71%.

2-Deoxy-chiro-*inosadiamine-3,5 Pentaacetate (17).* Compound **15** (152 mg) was hydrogenated in 90% aqueous ethanol (30 m*l*) similarly as described under the preparation of **9**. The crude product was recrystallized from aqueous ethanol to give crystals (90 mg, 72%) of **17**, mp 290—293°C. IR: 1755 (OAc), 1650 and 1555 cm^{-1} (NHAc).

Found: C, 51.68; H, 6.74; N, 7.37%. Calcd for $C_{16}H_{24}N_2O_8$: C, 51.60; H, 6.50; N, 7.52%.

1,5-Dideoxy-chiro-*inosadiamine-2,4 Tetraacetate (18).* Compound **16** (675 mg) was hydrogenated similarly as described under the preparation of **17**. The crude crystals were recrystallized from ethanol to give colorless crystals (381 mg, 85%) of **18**, mp 260—262°C. IR: 1745 (OAc), 1660 and 1560 cm^{-1} (NHAc).

Found: C, 53.60; H, 7.29; N, 9.24%. Calcd for $C_{14}H_{22}N_2O_6$: C, 53.49; H, 7.05; N, 8.91%.

The authors are grateful to Professor Sumio Umezawa for his kind advice, to Mr. Saburo Nakada for his elementary analyses, and to Messrs. Hayashi Uchino, Yasutaro Yasuda, and Toshihide Ikeda for their assistance in the preparative experiments. The financial support from the Ministry of Education for this work is gratefully acknowledged.

BULLETIN OF THE CHEMICAL SOCIETY OF JAPAN, VOL. 45, 2597—2602 (1972)

Inositol Derivatives. IV.[1] Synthesis of Anhydro Derivatives of 1,2-*O*-Cyclohexylidene-inositol

Tetsuo SUAMI, Seiichiro OGAWA, Shuichi OKI, and Kumiko OHASHI
Department of Applied Chemistry, Faculty of Engineering, Keio University, Hiyoshi, Yokohama
(Received March 1, 1972)

A reaction of 1,2-*O*-cyclohexylidene-*myo*-inositol tosylates with sodium methoxide in an appropriate solvent gave nine anhydro derivatives (mono- 6 and di-epoxide 3). The structures of new compounds were determined by proton magnetic resonance (PMR) spectroscopy and the reaction sequences.

Recent discovery of cyclohexane diepoxide tumor inhibitor, crotepoxide,[2] stimulated us to investigate a preparation of anhydro derivatives of inositols, which are also useful intermediary compounds for a synthesis of inositol derivatives.

In 1947, Schöpf and Arnold[3] first reported a synthesis of 2,3-anhydro-*allo*-inositol from conduritol A by a treatment with peracid. Later, Nakajima *et al.*[4] described six inositol epoxides (conduritol epoxides) which were obtained from five conduritols derived from benzene-glycol. Very recently, Gero *et al.*[5] have described the preparation of 1L- and DL-1,2-anhydro-*chiro*- and 1L-1,2-anhydro-*myo*-inositol, and their biological activities were

1) Previous reports on inositol derivatives: T. Suami, S. Ogawa, T. Tanaka, and T. Otake, This Bulletin, **44**, 835 (1971); T. Suami, S. Ogawa, and S. Oki, *ibid.*, **44**, 2820 (1971); T. Suami, S. Ogawa, and S. Oki, *ibid.*, **44**, 2824 (1971).

2) S. M. Kupchan, R. J. Hemingway, P. Coggon, A. T. McPhail, and G. A. Sim, *J. Amer. Chem. Soc.*, **90**, 2982 (1968).

3) C. Schöpf and W. Arnold, *Ann. Chem.*, **558**, 123 (1947).

4) M. Nakajima, I. Tomida, N. Kurihara, and S. Takei, *Chem. Ber.*, **92**, 173 (1959); M. Nakajima and N. Kurihara, *ibid.*, **94**, 515 (1961).

5) D. Mercier, A. Olesker, and S. D. Gero, *Carbohyd. Res.*, **18**, 227 (1971).

examined. However, inositol diepoxide has never been described until now.

In the present paper, we wish to report a synthesis of mono- and di-epoxides of inositols from 1,2-*O*-cyclohexylidene-*O*-*p*-toluenesulfonyl-*myo*-inositols[6] by a treatment with sodium methoxide in an appropriate solvent. The structures of new compounds were established mainly by way of their PMR spectroscopy and the reaction sequences.

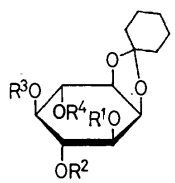

	R^1	R^2	R^3	R^4
1	Ts	H	H	H
2	Ts	H	H	Ts
3	Ts	H	Ts	H
4	Ts	Ts	H	H
5	Bz	Ts	H	Ts
6	Bz	Ts	Ts	Ac
7	Ts	H	Ts	Ts
8	Ts	Ts	H	Ts
9	Bz	Ts	Ts	Ts

When 1,2-*O*-cyclohexylidene-3-*O*-*p*-toluenesulfonyl-*myo*-inositol (**1**) was treated with a slight excess of sodium methoxide in methanol at room temperature for 3 hr, 1,2-anhydro-5,6-*O*-cyclohexylidene-*chiro*-inositol (**10a**) was obtained almost exclusively in 80—90% yield.

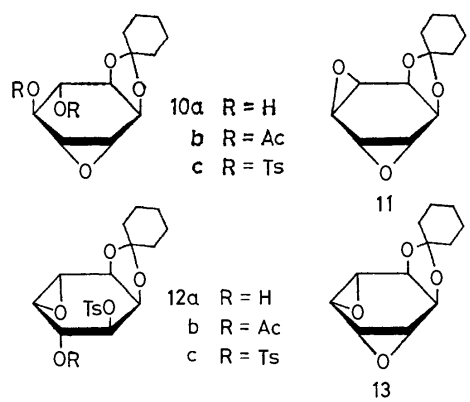

Acetylation of **10a** with acetic anhydride and pyridine afforded the diacetate (**10b**). On treatment with *p*-toluenesulfonyl chloride in pyridine, **10a** gave the di-*O*-*p*-toluenesulfonate (**10c**). The PMR spectrum of **10b** in deuteriochloroform ($CDCl_3$) at 60 MHz (Fig. 1) was fully resolved by a first-order method and all signals were assigned unambiguously to the protons. The two protons (H-1 and H-2) attached to the epoxide ring appeared as two doublets ($J_{1,2}$ 3.0 Hz) at τ 6.73, and 6.51. Also small coupling constants ($J_{2,3}$ and $J_{1,6}$) were observed, which indicated that the epoxide ring was situated *trans* to the vicinal substituents.[7] The two protons (H-5 and H-6) appeared as double doublet and doublet ($J_{4,5}$ 8.0 Hz, $J_{5,6}$ 5.5 Hz) at τ 5.98 and 5.35, respectively. Therefore, the epoxide ring was shown to be located on C-1 and C-2. The remaining doublet and triplet ($J_{3,4}$ 8.0 Hz) at τ 5.06 and 4.80 were ascribed to H-3 and H-4, respectively. While, in the spectrum of **10c**, the two protons (H-1 and H-2) appeared as 2-proton singlet at τ 6.66. The triplet, 2-proton doublet, and triplet (J 6.0 Hz) appeared at τ 5.98, 5.33, and 5.16, which could be attributed to H-5, H-3 and H-6, and H-4, respectively. Consequently, the proposed structure was evidently confirmed by the PMR spectral data, and it was shown that a migration of an oxide-ring did not occur under the condition used.

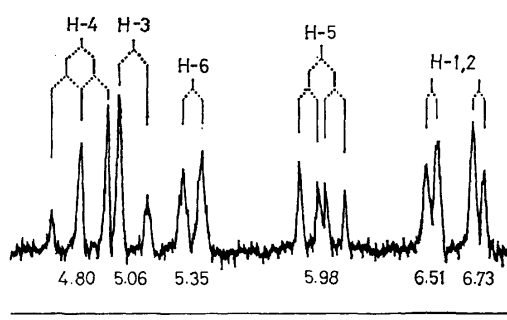

Fig. 1. Partial PMR spectrum of 3,4-*O*-acetyl-1,2-anhydro-5,6-*O*-cyclohexylidene-*chiro*-inositol (**10b**) in $CDCl_3$ at 60 MHz.

Five di-*O*-*p*-toluenesulfonyl derivatives of 1,2-*O*-cyclohexylidene-*myo*-inositol were then treated successively with sodium methoxide. The 3,6-di-*O*-*p*-toluenesulfonate (**2**)[6] was reacted with a slight excess of sodium methoxide in methanol overnight at room temperature to give the diepoxide (**11**) in 87% yield. The PMR spectrum of **11** in $CDCl_3$ (Fig. 2) revealed three multiplets (τ 6.73, 6.53, and 6.40) due to four protons attached to two epoxide rings, which was indicative of the unsymmetrical structure of **11**, hence, the epoxide rings were in *trans* arrangement each other. The two protons (H-3 and H-4) attached to the carbon atoms bonding to the cyclohexylidene group appeared at τ 5.59 and 5.36 as double doublet and broad doublet ($J_{3,4}$ 6.0 Hz, $J_{2,3}$ 3.0 Hz), respectively. Therefore, **11** was assigned to 1,2: 5,6-dianhydro-3,4-*O*-cyclohexylidene-*allo*-inositol.

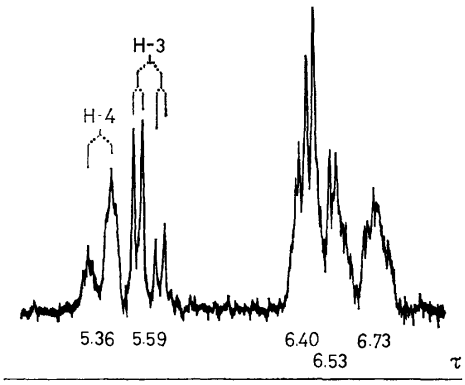

Fig. 2. Partial PMR spectrum of 1,2: 5,6-dianhydro-3,4-*O*-cyclohexylidene-*allo*-inositol (**11**) in $CDCl_3$ at 60 MHz.

By the similar treatment with sodium methoxide, the monoepoxide (**12a**) was obtained in a yield of 76% from the 3,5-di-*p*-toluenesulfonate (**3**).[6] A more drastic condition was needed for converting **3** into the

6) T. Suami, S. Ogawa, T. Tanaka, and T. Otake, This Bulletin, **44**, 835 (1971).

7) F. Sweet and R. K. Brown, *Can. J. Chem.*, **46**, 1481 (1968).

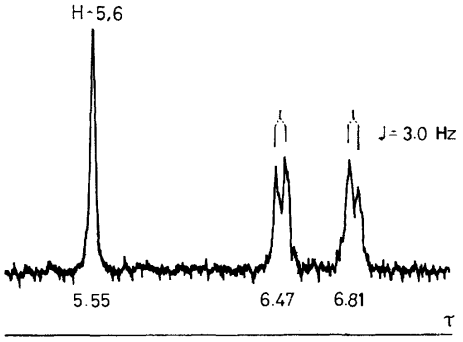

Fig. 3. Partial PMR spectrum of 1,2: 3,4-dianhydro-5,6-*O*-cyclohexylidene-*allo*-inositol (**13**) in $CDCl_3$ at 60 MHz.

diepoxide **13**. Thus, **3** was treated with an excess of sodium methoxide in boiling 2-methoxyethanol for 10 min to afford **13** in 28% yield. Monitoring the reaction using thin layer chromatography (tlc), **12a** was found to be an intermediate compound for further epoxidation to **13**. Compound **12a** was transformed into the monoacetate (**12b**) and di-*p*-toluenesulfonate (**12c**), respectively, by the usual way. Since **12c** was shown to be different from **10c**, **12a** must be either 1,2-anhydro-5,6-*O*-cyclohexylidene-4-*O*-*p*-toluenesulfonyl- or 1,2-anhydro-4,5-*O*-cyclohexylidene-6-*O*-*p*-toluenesulfonyl-*neo*-inositol. The latter can not give the diepoxide and could be excluded, therefore, **12a** was assigned to the former structure. And **13** was deduced to be 1,2: 3,4-dianhydro-5,6-*O*-cyclohexylidene-*allo*-inositol. The PMR spectrum of **13** in $CDCl_3$ (Fig. 3) revealed a simple pattern of signals for the ring protons, showing a symmetrical 1,3-*cis* diepoxide structure of **13**. The signals for H-4 and H-3 protons of **12b** appeared as two double doublets ($J_{3,4}$ 9.0 Hz, $J_{4,5}$ 2.0 Hz, and $J_{2,3}$ 1.5 Hz) at τ 5.17 and 4.43, respectively. In **12c**, the lower double doublet (H-3) upshifted[6] relatively by *ca.* 0.3 ppm (τ 4.78), comparing with that of **12b**, which showed that the acetoxy group was located at C-3 position in **12b**.

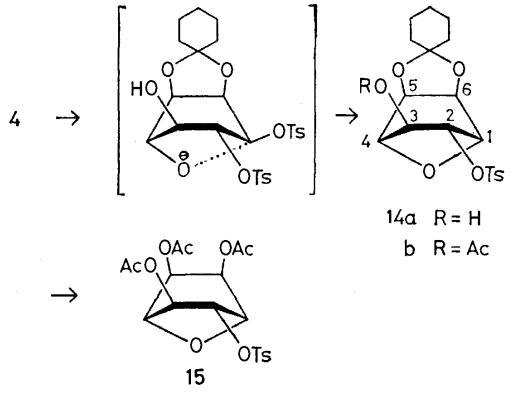

On a similar treatment, the 3,4-di-*p*-toluenesulfonate (**4**)[6] gave the monoepoxide (**14a**) in 67% yield. Compound **14a** was converted into the oily acetate (**14b**). Removal of the cyclohexylidene group of **14a** with boiling 80% aqueous acetic acid, followed by acetylation, afforded the triacetate (**15**) in 69% yield. By analogy, a structure of **14a** was initially considered to be 1,2-anhydro-4,5-*O*-cyclohexylidene-3-*O*-*p*-toluenesulfonyl-*epi*-inositol. However, the PMR spectra of **14a**, **14b**, and **15** in $CDCl_3$ lacked the signals of 1,2-epoxide ring protons in the region of τ 6.40—6.90[8] (Fig. 4). Furthermore, when **4** was treated with an excess of sodium azide in boiling 2-methoxyethanol for 20 hr, **14a** was surprisingly obtained in 73% yield almost exclusively. Under the azidation condition described above, all the *p*-toluenesulfonates studied so far[9] were smoothly converted into the expected azido compounds *via* intermediate 1,2-epoxides. Since the 1,2-epoxide structure could not account for both the unusual stability for the powerful nucleophilic reagent and the spectral data, **14a** was assumed to be 1,4-anhydro-5,6-*O*-cyclohexylidene-2-*O*-*p*-toluenesulfonyl-*chiro*-inositol. Therefore, it might be considered that in the compound **4** an attack of 5-hydroxyl group on C-4 is restricted by a stereochemical environment, and then, another hydroxyl group on C-6 attacks rear-side of C-3 in a boat conformation to form a transannular epoxide (1,4-anhydro ring).

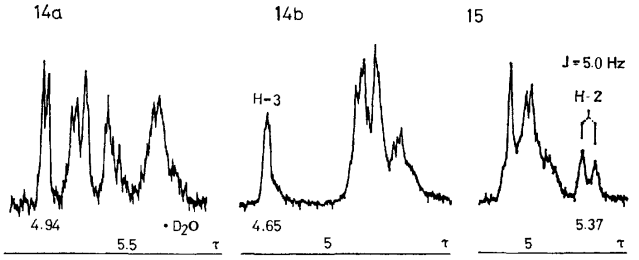

Fig. 4. Partial PMR spectra of 1,4-anhydro-5,6-*O*-cyclohexylidene-2-*O*-*p*-toluenesulfonyl-*chiro*-inositol (**14a**), its 3-*O*-acetate (**14b**), and 3,5,6-tri-*O*-acetyl-1,4-anhydro-2-*O*-*p*-toluenesulfonyl-*chiro*-inositol (**15**) in $CDCl_3$ at 60 MHz.

1-*O*-Benzoyl-2,3-*O*-cyclohexylidene-4,6-di-*O*-*p*-toluenesulfonyl-*myo*-inositol (**5**), which was obtained by a selective *p*-toluenesulfonylation of 1-*O*-benzoyl-2,3-*O*-cyclohexylidene-*myo*-inositol,[10] was subjected to an epoxidation to give the diepoxide (**16**) in 19% yield.

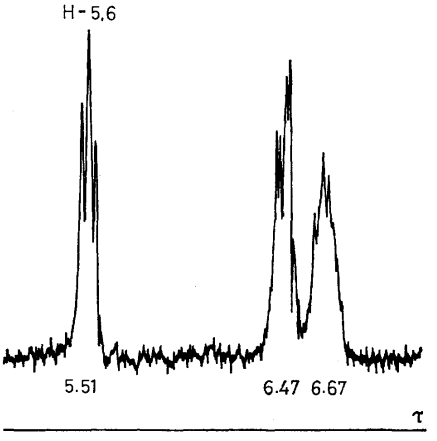

Fig. 5. Partial PMR spectrum of 1,2: 3,4-dianhydro-5,6-*O*-cyclohexylidene-*cis*-inositol (**16**) in $CDCl_3$ at 60 MHz.

8) Observed in the PMR spectra of eleven epoxides prepared in this study.

9) T. Suami, S. Ogawa, T. Tanaka, and S. Oki, in preparation. A part of the work had been reported at the Annual Meeting of the Chemical Society of Japan, Osaka, April, 1971.

10) T. Suami, S. Ogawa, K. Ohashi, and S. Oki, This Bulletin, in press.

Monitoring the reaction by tlc, it was found that **5** was slowly converted into **16** and **16** so formed gradually reacted with methoxide ion to give rise to a monomethyl ether (**17**). Thus, when **5** was treated with 7 molar equivalent of sodium methoxide in methanol at room temperature for 2 days, **17** was obtained mainly in 48% yield. Considering from the reaction sequence, **16** was assigned to 1,2:3,4-dianhydro-5,6-*O*-cyclohexylidene-*cis*-inositol. The PMR spectrum of **16** in $CDCl_3$ (Fig. 5) revealed symmetrical three multiplets due to three pairs of equivalent protons at τ 6.67, 6.47, and 5.51, supporting the *cis*-1,3-diepoxide structure. Compound **17** was assigned to 2,3-anhydro-4,5-*O*-cyclohexylidene-6-*O*-methyl-*epi*-inositol by the PMR spectral data. In the PMR spectrum of **17**, all the signals could not be well resolved by a first-order method, except those due to the two protons on C-4 and C-5. Thus, the double doublet at τ 5.39 was assigned to H-4 proton ($J_{3,4}$ 3.0 Hz, $J_{4,5}$ 7.0 Hz), which was closely related to that of **20** (τ 5.40, $J_{3,4}$ 2.5 Hz, $J_{4,5}$ 7.0 Hz). The broad doublet at τ 5.74 (H-5) seemed to be corresponding to that of **20** (τ 5.89).

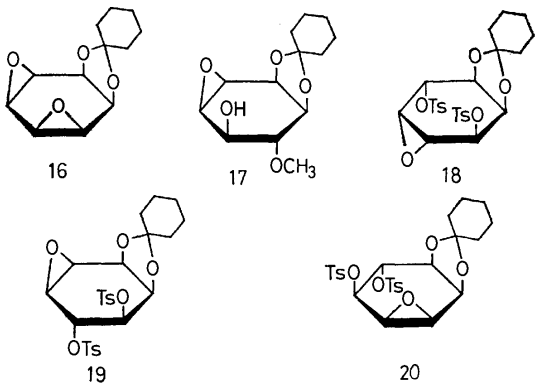

From 4-*O*-acetyl-1-*O*-benzoyl-2,3-*O*-cyclohexylidene-*myo*-inositol (**6**),[10] **11** was obtained in a yield of 69% by similar treatment with sodium methoxide.

Three tri-*O*-*p*-toluenesulfonyl derivatives of 1,2-*O*-cyclohexylidene-*myo*-inositol were treated analogously with sodium methoxide. The 3,5,6-tri-*p*-toluenesulfonate (**7**)[6] gave the monoepoxide (**18**) in 60% yield, which was shown to be different from **10c**. And, **18** was assigned to 1,2-anhydro-4,5-*O*-cyclohexylidene-3,6-di-*O*-*p*-toluenesulfonyl-*neo*-inositol. In **7**, an oxide anion at C-4 seemed to attack preferentially the 5-carbon atom to give rise to the 4,5-epoxide derivative. The PMR spectrum of **18** in $CDCl_3$ showed three multiplets at τ 6.46, 5.81, and 4.91, which were ascribed to H-1 and H-2, H-4 and H-5, and H-3 and H-6, respectively.

While, the 3,4,6-tri-*p*-toluenesulfonate (**8**)[6] gave, on a similar treatment, the monoepoxide (**19**) in 84% yield. Two structures were possible for **19**: 1,2-anhydro-3,4-*O*-cyclohexylidene-5,6-di-*O*-*p*-toluenesulfonyl- and 1,2-anhydro-4,5-*O*-cyclohexylidene-3,6-di-*O*-*p*-toluenesulfonyl-*epi*-inositol. If **19** had the latter structure, its PMR spectrum should rather resemble that of **18** than that of **12c**, but, substantially the resemblance between the spectra of **19** and **12c** was observed. An oxide anion at C-5 was also expected to attack 6-carbon atom favorably, considering from the result obtained in the case of **4**. Then **19** was assigned to the former structure.

The similar treatment of 1-*O*-benzoyl-2,3-*O*-cyclohexylidene-4,5,6-tri-*O*-*p*-toluenesulfonyl-*myo*-inositol (**9**)[10] with sodium methoxide afforded 2,3-anhydro-4,5-*O*-cyclohexylidene-1,6-*O*-*p*-toluenesulfonyl-*epi*-inositol (**20**) in 82% yield. The proposed structure was supported not only by the reaction sequence, but also by the PMR spectrum.

Experimental

Melting points were determined on a Mitamura Riken micro hot stage and are uncorrected. IR spectra were measured on a Jasco IR-E spectrophotometer in KBr disks. PMR spectra were measured on a Varian A-60D spectrometer at a concentration of *ca.* 10% deuteriochloroform ($CDCl_3$) or dimethyl sulfoxide-d_6 (DMSO-d_6) with tetramethylsilane as an internal standard. Chemical shifts are expressed in τ-values and signals are expressed as s (singlet), dd (double doublet), t (triplet), and m (complex multiplet). Values given for coupling constants are first-order. Tlc was performed using silica gel (Wakogel B-10, Wako Pure Chemical Industries Ltd.) using methyl ethyl ketone and toluene or benzene and ethyl acetate as the solvent system. The compounds were detected by heating at 100°C after spraying 30% sulfuric acid. Evaporation was performed by a rotary evaporator below 50°C under diminished pressure. Unless otherwise noted, methanol solution of sodium methoxide (0.1 M) used in this experiment was prepared by dissolving sodium (0.23 g) in absolute methanol (100 m*l*). All the compounds described in this paper are racemic.

*1,2-Anhydro-5,6-*O*-cyclohexylidene-*chiro*-inositol (**10a**).* 1,2-*O*-Cyclohexylidene-3-*O*-*p*-toluenesulfonyl-*myo*-inositol (**1**)[6] (5.0 g) was dissolved in hot methanol (100 m*l*) and cooled to room temperature. To the solution was added methanol (20 m*l*) containing 1.5 molar equivalent of sodium methoxide, and the mixture was kept at room temperature for 3 hr. Then the solution was evaporated to dryness and the residue was partitioned between chloroform and water. The organic layer was washed with water, dried over anhydrous sodium sulfate and evaporated to give practically pure crystals (2.63 g, 90%) of **10a**, mp 91—98°C. Recrystallization from ethanol-ether gave analytically pure needles (1.69 g, 58%), mp 109—110°C. PMR ($CDCl_3$): τ 6.68 (1-proton dd, $J_{1,2}$= 4.0 Hz, $J_{1,6}$=1.0 Hz, H-1), 6.50 (1-proton m, H-2), 5.90 (2-protons m, H-3,4), 5.60 (1-proton dd, $J_{4,5}$=4.0 Hz, $J_{5,6}$= 6.0 Hz, H-5), and 5.32 (1-proton d, H-6).

Found: C, 59.40; H, 7.29%. Calcd for $C_{12}H_{18}O_5$: C, 59.49; H, 7.49%.

*3,4-*O*-Acetyl-1,2-anhydro-5,6-*O*-cyclohexylidene-*chiro*-inositol (**10b**).* Compound **10a** (100 mg) was treated with acetic anhydride (0.5 m*l*) and pyridine (1 m*l*) overnight at room temperature. Then the mixture was poured into ice and water (25 m*l*), and the resulting colorless needles were collected by filtration: yield 124 mg (92%), mp 102—103°C. Recrystallization from ethanol afforded colorless prisms, which showed the same melting point.

Found: C, 59.25; H, 7.02%. Calcd for $C_{16}H_{22}O_7$: C, 58.88; H, 6.80%.

*1,2-Anhydro-5,6-*O*-cyclohexylidene-3,4-*O*-toluenesulfonyl-*chiro-*inositol (**10c**).* To a solution of **10a** (100 mg) in dry pyridine (2 m*l*) was added *p*-toluenesulfonyl chloride (0.24 g, 3 molar equivalent) and the mixture was kept at room temperature for 2 days. Tlc indicated two main components, probably two mono-*p*-toluenesulfonates, together with **10a**.

Then an additional portion of *p*-toluenesulfonyl chloride (470 mg, 6 molar equivalent) in dry pyridine (2 m*l*) was added to the mixture and the solution was kept at 25°C for 3 days. Then the reaction mixture was poured into ice and water and the resulting oily product was extracted with chloroform several times. The combined extracts were washed with water, dried over anhydrous sodium sulfate and evaporated to give an oily residue which crystallized upon addition of chloroform–ethanol to afford colorless crystals, (90 mg, 40%) of **10c**, mp 110—111°C. Recrystallization from the same solvent gave an analytical sample, mp 115—117°C. PMR ($CDCl_3$): τ 7.55 (6-protons s, 2 OTs), 6.66 (2-protons s, H-1,2), 5.98 (1-proton t, $J_{4,5}=J_{5,6}=6.0$ Hz, H-5), 5.33 (2-protons d, $J_{2,3}=J_{1,6}=0$ Hz, $J_{3,4}=6.0$ Hz, H-3,6), and 5.16 (1-proton t, H-4).

Found: C, 56.60; H, 5.37; S, 11.78%. Calcd for $C_{26}H_{30}O_9S_2$: C, 56.70; H, 5.49; S, 11.64%.

*1,2: 5,6-Dianhydro-3,4-*O*-cyclohexylidene*-allo-*inositol (11).* (a) To a solution of 1,2-*O*-cyclohexylidene-3,6-di-*O*-*p*-toluenesulfonyl-*myo*-inositol (**2**)[6] (2.0 g) in methanol (40 m*l*) was added methanolic sodium methoxide (7.3 m*l*, 2 molar equivalent) and the reaction mixture was kept overnight at room temperature. The residue remaining on evaporation of the solvent was extracted several times with ethyl acetate, and the combined extracts were evaporated to give a crystalline product. The crystals were digested with methanol and collected by filtration: yield 0.70 g (87%), mp 142—144°C. Recrystallization from chloroform–ethanol gave an analytical sample, mp 143—144°C.

Found: C, 64.64; H, 7.46%. Calcd for $C_{12}H_{16}O_4$: C, 64.26; H, 7.19%.

(b) Treatment of 4-*O*-acetyl-1-*O*-benzoyl-2,3-*O*-cyclohexylidene-5,6-di-*O*-*p*-toluenesulfonyl-*myo*-inositol (**6**)[10] (146 mg) with methanolic sodium methoxide (1.1 m*l*, 5 molar equivalent) in a mixture of chloroform (3 m*l*) and methanol (2 m*l*) similarly as described above afforded colorless plates (32 mg, 69%) of **11**, mp 141.5—143.5°C.

*1,2-Anhydro-5,6-*O*-cyclohexylidene-4-*O*-p-toluenesulfonyl-*neo-*inositol (12a).* To a solution of 1,2-*O*-cyclohexylidene-3,5-di-*O*-*p*-toluenesulfonyl-*myo*-inositol (**3**)[6] (0.20 g) in a mixture of chloroform (10 m*l*) and methanol (2 m*l*) was added methanolic sodium methoxide (1.1 m*l*, 3 molar equivalent) and the reaction mixture was kept overnight at room temperature. Then the mixture was processed similarly as described under the preparation of **11** to give the oily product, which crystallized upon addition of methanol. The crystals were digested with petroleum ether and collected by filtration: colorless needles, yield 0.11 g (76%), mp 142—144°C. An analytical sample was obtained by recrystallization from chloroform–ethanol: colorless prisms, mp 154—155°C.

Found: C, 57.75; H, 5.99; S, 8.38%. Calcd for $C_{19}H_{24}O_7S$: C, 57.55; H, 6.10; S, 8.09%.

*3-*O*-Acetyl-1,2-anhydro-5,6-*O*-cyclohexylidene-4-*O*-p-toluenesulfonyl-*neo-*inositol (12b).* Compound **12a** (62 mg) was acetylated with acetic anhydride (1 m*l*) and pyridine (2 m*l*) overnight at room temperature. The reaction mixture was then poured into ice and water and the precipitates were collected by filtration. Recrystallization from chloroform–ethanol gave colorless rods (58 mg, 85%) of **12a**, mp 149—150°C. PMR ($CDCl_3$): τ 8.14 (3-protons s, OAc), 7.53 (3-protons s, OTs), 6.82 and 6.55 (1-proton d, $J_{1,2}=4.0$ Hz, H-1 and H-2), 5.48 (2-protons m, H-5,6), 5.17 (1-proton dd, $J_{3,4}=9.0$ Hz, $J_{4,5}=2.0$ Hz, H-4), and 4.43 (1-proton dd, $J_{2,3}=1.5$ Hz, H-3).

Found: C, 57.53; H, 5.86; S, 7.44%. Calcd for $C_{21}H_{26}O_8S$: C, 57.50; H, 5.98; S, 7.31%.

*1,2-Anhydro-5,6-*O*-cyclohexylidene-3,4-di-*O*-p-toluenesulfonyl-*neo-*inositol (12c).* Compound **12a** (51 mg) in dry pyridine (2 m*l*) was treated with *p*-toluenesulfonyl chloride (74 mg, 3 molar equivalent) at room temperature for 3 days and then at 80—85°C for 10 min. The reaction mixture was poured into water (50 m*l*) and extracted with chloroform (20 m*l*) several times. The combined extracts were washed with water, dried over anhydrous sodium sulfate and evaporated to give an oily product. Tlc showed a main component together with several minor ones. Then the crude product was chromatographed on a column of silica gel (Wakogel C-200, 20 g) and eluted with methyl ethyl ketone–toluene (1:4). The main fractions were combined and evaporated to give a crystalline residue. Crystallization from chloroform–ethanol gave colorless prisms (48 mg, 47%) of **12c**, mp 168—168.5°C. PMR ($CDCl_3$): τ 7.55 (6-protons s, 2 OTs), 6.85 and 6.45 (1-proton dd, $J_{1,2}=4.0$ Hz, H-1 and H-2), 5.53 (2-protons s, H-5,6), 5.26 (1-proton dd, $J_{3,4}=9.0$ Hz, $J_{4,5}=1.5$ Hz, S-4), and 4.78 (1-proton dd, $J_{2,3}=1.5$ Hz, H-3).

Found: C, 56.66; H, 5.38; S, 11.71%. Calcd for $C_{26}H_{30}O_9S_2$: C, 56.70; H, 5.49; S, 11.64%.

*1,2: 3,4-Dianhydro-5,6-*O*-cyclohexylidene-*allo-*inositol (13).* To a solution of **3** (0.50 g) in 2-methoxyethanol (30 m*l*) was added methanolic sodium methoxide (2.7 m*l*, 3 molar equivalent) and the mixture was refluxed for 10 min. Monitoring the reaction by tlc, it was found that **12a**, as well as **3**, completely disappeared and **13** formed gradually underwent nucleophilic attack of methoxide ion to give rise to the slower moving component, probably a monomethyl ether. The brown reaction mixture was evaporated to dryness and the residue was extracted with ethyl acetate. Evaporation of the extracts gave a crystalline product which was chromatographed on a silica gel (20 g) and eluted with methyl ethyl ketone–toluene (1:4). The fractions containing the faster moving component were combined and evaporated to give colorless plates (56 mg, 28%) of **13**, mp 104—110°C. Recrystallization from ethyl acetate afforded an analytical sample, mp 111.5—112.5°C.

Found: C, 64.27; H, 6.95%. Calcd for $C_{12}H_{16}O_4$: C, 64.26; H, 7.19%.

*1,4-Anhydro-5,6-*O*-cyclohexylidene-2-*O*-p-toluenesulfonyl-*chiro-*inositol (14a).* (a) To a solution of 1,2-*O*-cyclohexylidene-3,4-*O*-*p*-toluenesulfonyl-*myo*-inositol (**4**)[6] (100 mg) in a mixture of chloroform (3 m*l*) and methanol (4 m*l*) was added methanolic sodium methoxide (0.36 m*l*, 2 molar equivalent) and the reaction mixture was kept overnight at room temperature. The mixture was processed similarly as described under the preparation of **11** to give an oily product which crystallized upon addition of ethanol to give colorless prisms (47 mg, 67%) of **14a**, mp 114—115°C. Recrystallization from ethanol afforded an analytical sample. The melting point did not change. PMR ($CDCl_3$): τ 7.53 (3-protons s, OTs).

Found: C, 57.57; H, 6.23; S, 8.07%. Calcd for $C_{19}H_{24}O_7S$: C, 57.30; H, 6.06; S, 8.08%.

(b) A mixture of **4** (1.08 g), sodium azide (1.09 g) and 90% aqueous 2-methoxyethanol (20 m*l*) was refluxed for 20 hr. Then the reaction mixture was evaporated to dryness and dried by repeated co-distillation with toluene. The residue was extracted with hot ethyl acetate and the extracts were evaporated to give colorless crystals (0.55 g, 73%) of **14a**, mp 114—116°C. This compound was identified with the product obtained in (a) by IR and PMR spectral comparison.

Compound **14a** was acetylated with acetic anhydride and pyridine in the usual way to give the oily acetate (**14b**). Tlc indicated a single spot in methyl ethyl ketone–toluene (1:4). PMR ($CDCl_3$): τ 8.08 (3-protons s, OAc) and 7.55 (3-protons s, OTs).

3,5,6-Tri-O-acetyl-1,4-anhydro-2-O-p-toluenesulfonyl-chiro-inositol (**15**). Compound **14a** (0.21 g) was refluxed with 80% aqueous acetic acid (10 ml) for 3 hr. The reaction mixture was evaporated to dryness and the residue was treated with acetic anhydride (5 ml) and pyridine (5 ml) overnight at room temperature. Then the mixture was evaporated with toluene to give a yellow oil, which was dissolved in ethyl acetate and chromatographed on a column of aluminum oxide (5 g). The eluate was evaporated to give a oily product which crystallized by trituration with ethanol: colorless crystals, yield 0.16 g (69%), mp 124.5—125.5°C. An analytical sample was obtained by recrystallization from ethanol, mp 125—126°C. PMR ($CDCl_3$): τ 7.98 (6-protons s, 2 OAc), 7.86 (3-protons s, OAc) and 7.53 (3-protons s, OTs).

Found: C, 51.51; H, 5.14; S, 7.52%. Calcd for $C_{19}H_{22}O_{10}S$: C, 51.60; H, 4.98; S, 7.24%.

*1,2: 3,4-Dianhydro-5,6-O-cyclohexylidene-*cis*-inositol* (**16**). To a solution of 1-*O*-benzoyl-2,3-*O*-cyclohexylidene-4,6-di-*O*-*p*-toluenesulfonyl-*myo*-inositol (**5**)[10] (0.30 g) in a mixture of methanol (4 ml) and methyl ethyl ketone (6 ml) was added methanolic sodium methoxide (1.6 ml, 3.5 molar equivalent) and the mixture was kept overnight at room temperature. Then the reaction mixture was processed similarly as described under the preparation of **11** to give an oily product. Tlc indicated two main components. The crude mixture was then chromatographed on a column of silica gel (20 g) and eluted with methyl ethyl ketone-toluene (1:3). The fractions containing the slower moving component were combined and evaporated to give colorless plates (19 mg, 19%) mp 129—131°C. An analytical sample was obtained by recrystallization from ethyl acetate–petroleum ether, mp 130—131°C.

Found: C, 64.04; H, 7.29%. Calcd for $C_{12}H_{16}O_4$: C, 64.26; H, 7.19%.

*2,3-Anhydro-4,5-O-cyclohexylidene-6-O-methyl-*epi*-inositol* (**17**). (a) To a solution of **5** (0.30 g) in a mixture of methanol (4 ml) and methyl ethyl ketone (6 ml) was added methanolic sodium methoxide (1.6 ml, 3.5 molar equivalent) and the solution was kept overnight at room temperature. Then an additional amount of methanolic sodium methoxide (1.6 ml) was added and, after 24 hr, the mixture was evaporated to dryness and the residue was processed similarly as described under the preparation of **11** to give crude crystals (66 mg, 48%). It was recrystallized from ethyl acetate–petroleum ether to afford colorless needles (48 mg) of **17**, mp 96—98°C. PMR ($CDCl_3$): τ 6.51 (2-protons m, H-2,3), 6.45 (3-protons s, OCH_3), and 6.10 (2-protons broad s, H-4,5).

Found: C, 61.16; H, 7.52%. Calcd for $C_{13}H_{20}O_5$: C, 60.91; H, 7.87%.

(b) Compound **5** (0.40 g) was dissolved in a mixture of chloroform (8 ml) and methanol (4 ml) and methanolic sodium methoxide (1.12 ml, 3.5 molar equivalent) was added. The mixture was kept at room temperature for 17 days and then processed similarly as described in (a) to give colorless crystals (40 mg, 20%) of **17**.

*1,2-Anhydro-4,5-O-cyclohexylidene-3,6-di-O-p-toluenesulfonyl-*neo*-inositol* (**18**). To a solution of 1,2-*O*-cyclohexylidene-3,5,6-tri-*O*-*p*-toluenesulfonyl-*myo*-inositol (**7**)[6] (0.20 g) in a mixture of chloroform (4 ml) and methanol (2 ml) was added methanolic sodium methoxide (0.56 ml, 2 molar equivalent) and the reaction mixture was kept at room temperature for 1 hr. Then the mixture was processed similarly as described under the preparation of **11** to give crude crystals. It was digested with methanol and collected by filtration: colorless needles, yield 91 mg (60%), mp 190—191°C. Recrystallization from chloroform–ethanol gave an analytical sample. The melting point did not change. PMR ($CDCl_3$); τ 7.57 (6-protons s, 2 OTs).

Found: C, 56.48; H, 5.39; S, 11.31%. Calcd for $C_{26}H_{30}O_9S_2$: C, 56.70; H, 5.49; S, 11.64%.

*1,2-Anhydro-3,4-O-cyclohexylidene-5,6-di-O-p-toluenesulfonyl-*epi*-inositol* (**19**). To a solution of 1,2-*O*-cyclohexylidene-3,4,6-tri-*O*-*p*-toluenesulfonyl-*myo*-inositol (**8**)[6] (0.10 g) in a mixture of chloroform (2 ml) and methanol (1 ml) was added methanolic sodium methoxide (0.14 ml, 1 molar equivalent) and the mixture was kept overnight at room temperature. Then the reaction mixture was processed similarly as described under the preparation of **11**. The crude crystals was recrystallized from chloroform–methanol to give colorless needles (64 mg, 84%) of **19**, mp 184—184.5°C. Recrystallization from the same solvent gave an analytical sample. PMR ($CDCl_3$): τ 7.53 (6-protons s, 2 OTs), 6.76 (1-proton t, $J_{1,2}$= 3.5 Hz, $J_{2,3}$=4.0 Hz, H-2), 6.61 (1-proton d, $J_{1,6}$=0 Hz, H-1), 5.34 (1-proton dd, $J_{4,5}$=3.0 Hz, $J_{5,6}$=8.0 Hz, H-5), and 5.08 (1-proton d, H-6).

Found: C, 57.07; H, 5.83; S, 11.37%. Cacld for $C_{26}H_{30}O_9S_2$: C, 56.70; H, 5.49; S, 11.64%.

*2,3-Anhydro-4,5-O-cyclohexylidene-1,6-di-O-p-toluenesulfonyl-*epi*-inositol* (**20**). To a solution of 1-*O*-benzoyl-2,3-*O*-cyclohexylidene-4,5,6-tri-*O*-*p*-toluenesulfonyl-*myo*-inositol (**9**)[10] (0.35 g) in a mixture of chloroform (5 ml) and methanol (5 ml) was added methanolic sodium methoxide (1.1 ml, 3 molar equivalent) and the mixture was kept at room temperature. After 15 min, colorless needles were crystallized out from the solution and the crystals were collected by filtration: yield 0.19 g (82%), mp 215.5—216°C. An analytical sample was obtained by recrystallization from chloroform-ethanol. The melting point did not change. PMR ($CDCl_3$): τ 7.56 and 7.53 (3-protons s, OTs), 6.52 (1-proton dd, $J_{2,3}$=4.0 Hz, $J_{3,4}$=2.5 Hz, H-3), 6.27 (1-proton d, $J_{1,2}$=0 Hz, H-2), and 5.40 (1-proton dd, $J_{4,5}$=7.0 Hz, H-4). (DMSO-d_6): τ 6.45 (2-protons m, H-2,3), 5.90 (1-proton t, $J_{4,5}$=$J_{5,6}$=7.5 Hz, H-5), 5.37 (1-proton dd, $J_{3,4}$=2.5 Hz, H-4), 5.33 (1-proton dd, $J_{1,6}$=9.5 Hz, H-6), and 4.79 (1-proton d, $J_{1,2}$=0 Hz, H-1).

Found: C, 56.36; H, 5.26; S, 11.50%. Calcd for $C_{26}H_{30}O_9S_2$: C, 56.70; H, 5.49; S, 11.64%.

The authors are grateful to Professor Sumio Umezawa for his kind advice, to Mr. Saburo Nakada for his elementary analyses, and to Mr. Tsunehisa Ueda for his preparative experiment. The financial support from the Ministry of Education for this work is gratefully acknowledged.

The Synthesis and Reaction of Monohalogeno-*t*-butyloxycarbonylamino Acids

Takanobu OHNISHI, Hiroshi SUGANO, and Muneji MIYOSHI

Research Laboratory of Applied Biochemistry, Department of Synthetic Chemistry, Tanabe Seiyaku Co., Ltd. Kashima-cho, Higashiyodogawa-ku, Osaka

(Received January 29, 1972)

Monohalogeno-*t*-butyloxycarbonylamino acids (XBOC-amino acids) were synthesized by the use of the corresponding chloroformates in a basic aqueous solution. Several dipeptides containing XBOC-amino acid were also prepared. The cleavage of the XBOC group was successfully carried out not only under some acidic conditions, but also by heating in methanol or ethanol. In order to demonstrate the usefulness of this group in peptide synthesis, Z-Gly-Lys(Z)-Gly-OEt was synthesized *via* BrBOC-Lys(Z)-Gly-OEt, which had been treated by hot ethanol. Side reaction during the synthesis of XBOC-amino acids will also be described.

The *t*-butyloxycarbonyl (BOC) group is of considerable importance in peptide chemistry, especially in solid-phase synthesis. Since our collaborators reported a method in which the BOC group was introduced by reacting *t*-butyl chloroformate (BOC–Cl) with amino acids in an aqueous alkaline solution,[1] BOC-amino acids have been prepared as a commercial scale. Unfortunately, BOC–Cl is unstable even in inert organic solvents, such as ether, dichloromethane, and tetrahydrofuran, and it can not be stored for a long time at −20°C. Also, the BOC–Cl content in the solution can not be precisely estimated. For these reasons, many investigators have attempted to develop a new protecting group which can be easily synthesized.[2–5] Carpino *et al.* recently reported on the α-halogeno-*t*-butyloxycarbonyl (XBOC) group.[6] They found that α-bromo- and α-chloro-*t*-butyl chloroformate (BrBOC–Cl, ClBOC–Cl) were significantly more stable than BOC–Cl, and that, on treatment with anilines, the corresponding urethans were obtained, while the acylation reaction was generally unsuccessful with amino acid derivatives.

In the present paper, the authors will report on the synthesis, properties and application of BrBOC- and ClBOC-amino acids.[7]

Results

Synthesis of XBOC-amino Acids. α-Bromo- and α-chloro-*t*-butyl alcohol were prepared by Carpino's method, which had been employed for the preparation of α,α-dibromo-*t*-butyl alcohol.[6] These alcohols were converted into the corresponding chloroformates as the usual manner and were purified by distillation. The characterizations of the alcohols and the chloroformates were identical with those previously reported.[6]

The chloroformates were treated with amino acid esters in water–chloroform–tetrahydrofuran and with amino acids in an aqueous alkaline solution.

In order to confirm the structures of the BrBOC- and ClBOC-amino acid benzyl esters thus obtained, the esters were converted into the acids by saponification or hydrogenolysis; the yields were moderate (Eq. (1)).

$$\text{XBOC-Cl} + \underset{\displaystyle \underset{\displaystyle R}{|}}{\text{C}_6\text{H}_5\text{CH}_2\text{OCO-CH-NH}_2} \xrightarrow[\text{H}_2\text{O-CHCl}_3\text{-THF}]{\text{Et}_3\text{N}} \underset{\displaystyle \underset{\displaystyle R}{|}}{\text{XBOC-NHCHCO}_2\text{CH}_2\text{C}_6\text{H}_5} \xrightarrow[\text{or } \text{H}_2/\text{Pd}]{\text{OH}^-} \underset{\displaystyle \underset{\displaystyle R}{|}}{\text{XBOC-NHCHCOOH}} \quad (1)$$

R: amino acid side chain
X: Br, Cl

The results are shown in Tables 1 and 2.

XBOC-amino acids show IR spectra similar to those of BOC-amino acids (Fig. 1).

Cleavage of the XBOC Group. A relatively high stability of BrBOC and ClBOC groups is shown in the acidic reagents. Neither of them is completely cleaved when left standing in 10% hydrogen chloride in dioxane or anhydrous trifluoroacetic acid at room temperature for an hour.

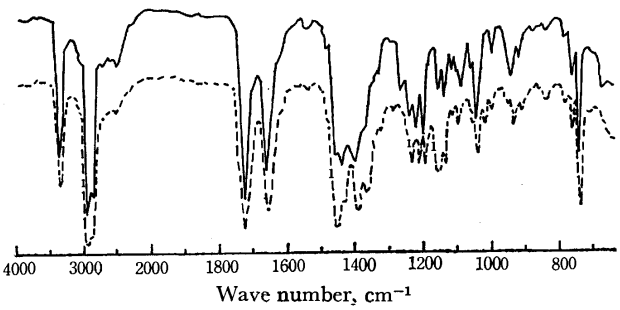

Fig. 1. IR spectra of BrBOC-Trp-OH (——) and BOC-Trp (– – –) in Nujol.

1) S. Sakakibara, I. Honda, K. Takada, M. Miyoshi, T. Ohnishi, and K. Okumura, This Bulletin, **42**, 809 (1969).

2) G. A. Olah and S. J. Kuhn, *J. Amer. Chem. Soc.*, **82**, 2308 (1960).

3) G. A. Olah and S. J. Kuhn, *J. Org. Chem.*, **26**, 237 (1961).

4) S. Nakanishi, T. C. Myers, and E. V. Jensen, *J. Amer. Chem. Soc.*, **77**, 3099 (1955).

5) E. Schnabel, H. Herzog, P. Hoffman, E. Klauke, and I. Ugi, *Ann. Chem.*, **716**, 175 (1968); *Angew. Chem.*, **80**, 396 (1968).

6) L. A. Carpino, K. N. Parameswaran, R. K. Kirkley, J. W. Spiewak, and E. Schmitz, *J. Org. Chem.*, **35**, 3291 (1970).

7) All amino acid residues are of the L-configuration. The abbreviated designation of amino acids, peptides and their derivatives is in accordance with the proposal of the IUPAC-IUB Commission of Biochemical Nomenclature, which appeared in *Biochemistry*, **5**, 2485 (1966); *ibid.*, **6**, 362 (1967).

8) C. M. Suter and H. D. Zook, *J. Amer. Chem. Soc.*, **66**, 738 (1944).

Table 1. α-Bromo-*t*-butyloxycarbonylamino acids

Amino acids	Yield (%)	Mp °C	$[\alpha]_D^{20}$	Analysis (Calcd) C %	H %	N %	Br %
Gly	55	103	—	33.32 (33.09)	4.82 (4.75)	5.43 (5.49)	31.53 (31.44)
Pro	78	117	−38.0°a)	40.88 (40.80)	5.43 (5.48)	4.77 (4.76)	27.24 (27.17)
Trp	63	110	+27.0°a)	49.83 (50.14)	5.19 (4.99)	6.85 (7.30)	20.58 (20.85)
Phe·DCHA	79	268	+ 4.6°b)	59.30 (59.38)	7.96 (7.82)	5.27 (5.30)	14.65 (15.20)
Val·DCHA	47	291	−17.0°b)	55.54 (55.34)	8.62 (8.65)	5.82 (5.86)	16.50 (16.73)
Met·DCHA	48	266	−26.5°b)	51.77 (51.85)	8.10 (8.11)	5.51 (5.49)	15.75 (15.68)
Ile·DCHA	41	286	− 6.7°b)	56.99 (56.20)	8.83 (8.82)	5.68 (5.69)	15.14 (15.26)
Ala·DCHA	60	286	−31.5°b)	53.34 (53.44)	8.25 (8.29)	6.12 (6.23)	17.74 (17.77)

a) *c* 1, AcOEt b) *c* 1, AcOH

Table 2. α-Chloro-*t*-butyloxycarbonylamino acids

Amino acids	Yield (%)	Mp °C	$[\alpha]_D^{20}$a)	Analysis (Calcd) C %	H %	N %	Cl %
Gly	81	104.0	—	40.40 (40.10)	5.78 (5.77)	6.77 (6.68)	16.55 (16.91)
Pro	86	102.0	−54.9°	48.22 (47.90)	6.61 (6.83)	5.54 (5.58)	14.24 (14.14)
Trp	76	140.2	− 8.5°	56.67 (56.55)	5.78 (5.93)	8.25 (8.24)	10.56 (10.43)
Ala·DCHA	72	124.0	−14.3°	59.36 (59.45)	9.07 (8.98)	6.95 (6.93)	8.90 (8.77)
Leu·DCHA	72	106.7	−16.6°	61.96 (61.78)	9.73 (9.69)	6.33 (6.26)	7.54 (7.93)
Ile·DCHA	60	120.0	− 2.0°	61.94 (61.78)	9.76 (9.69)	6.35 (6.26)	7.41 (7.92)
Val·DCHA	63	130.0	− 6.0°	61.02 (61.02)	9.50 (9.54)	6.59 (6.46)	8.12 (8.18)
Phe·DCHA	65	248.5	+ 1.5°	64.59 (64.90)	8.49 (8.58)	5.73 (5.82)	7.39 (7.37)
N,*S*-di-Cys ·DCHA	60	106.4	−16.1°	52.27 (52.53)	7.78 (7.75)	4.96 (4.90)	12.24 (12.40)
Met·DCHA	69	128.3	−14.3°	56.93 (56.81)	8.87 (8.88)	6.09 (6.02)	7.81 (7.62)
Glu·$(DCHA)_2$	68	188.0	− 5.9°	63.36 (63.33)	9.65 (9.76)	6.58 (6.51)	5.86 (5.49)

a) *c* 1, AcOH

The reduction of the XBOC-group to the BOC group by means of sodium borohydride in water, by means of hydrogenolysis in methanol over a palladium catalyst, or by means of electrolytic reduction does not proceed.

However, the BrBOC group is completely removed under the following conditions: heating in methanol or ethanol; borontrifluoride etherate in trifluoroacetic acid at room temperature for an hour; 4N hydrogen bromide in acetic acid, and sodium in liquid ammonia. The ClBOC group is completely cleaved by borontrifluoride etherate in trifluoroacetic acid, by 4N hydrogen bromide in acetic acid, and by sodium in liquid ammonia.

The cleavage of the BrBOC group by heating in methanol or ethanol is a unique deprotection technique. This reaction, named "self-cleavage" by Carpino, may proceed similarly to the self-cleavage of BrBOC-aniline (Eq. (2)).[6]

The selective cleavage of the BrBOC group may be possible, since other amino-protecting groups such as BOC and the benzyloxycarbonyl (Z) group are stable under heating in methanol or ethanol.

Peptide Synthesis. XBOC-amino acids were converted into dipeptides by the mixed anhydride (M.A.) method, which was the better than dicyclohexylcarbodiimide (DCCD) method (Table 3).

The tripeptide sequence, Z–Gly–Val–Gly–OMe, was then synthesized by the M.A. method, couplingZ–Gly–OH with H–Val–Gly–OMe prepared from BrBOC–

Table 3. Dipeptides containing α-halogeno-*t*-butyloxycarbonylamino acids

Products	Method	Yield (%)	Mp °C	$[\alpha]_D^{20a)}$	Analysis (Calcd) C %	H %	N %	Br or Cl %
BrBOC–Phe–Gly–OEt	DCCD	29	93	— 9.4°	50.56 (50.35)	6.02 (5.87)	6.40 (6.52)	18.46 (18.61)
BrBOC–Val–Gly–OMe	M.A.	61	100	—13.6°	42.26 (42.53)	6.29 (6.27)	8.15 (7.63)	21.56 (21.76)
ClBOC–Phe–Gly–OEt	DCCD	63	79	— 7.7°	56.04 (56.17)	6.63 (6.54)	7.17 (7.27)	9.52 (9.21)
ClBOC–Ala–Gly–OEt	DCCD	59	65	—17.4°	46.87 (46.67)	6.88 (6.85)	9.40 (9.06)	11.05 (11.45)
ClBOC–Val–Gly–OMe	M.A.	65	89	—13.0°	48.16 (48.36)	7.09 (7.18)	8.96 (8.67)	10.53 (10.99)

a) *c* 1, AcOEt

Table 4. Tripeptides obtained from various dipeptides

Starting compound	Deprotection technique	Yield (%)	Tripeptide Mp °C	Tripeptide $[\alpha]_D^{20}$ (*c* 1, MeOH)
BrBOC–Val–Gly–OMe	Reflux in MeOH	65	145—147	—34.0°
ClBOC–Val–Gly–OMe	4 N HBr–AcOH	59	144—146	—34.2°
Z–Val–Gly–OMe	Hydrogenolysis	66	146—148	—33.9°

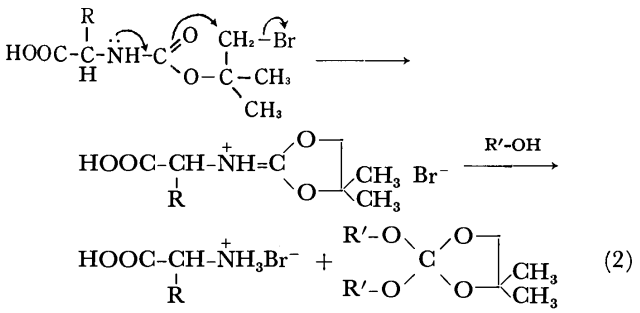

(2)

R : amino acid side chain
R′: CH_3, C_2H_5

Val–Gly–OMe and ClBOC–Val–Gly–OMe.

The BrBOC group was removed on heating in methanol, and the ClBOC group was removed by the use of 4N hydrogen bromide in acetic acid. These tripeptides were identical with that obtained from Z–Val–Gly–OMe (Table 4).

The utility of the BrBOC group as an α-amino-protecting group of lysine is demonstrated as follows:

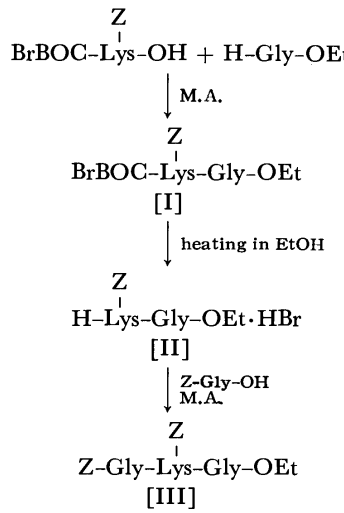

BrBOC–Lys(Z)–OH was coupled with H–Gly–OEt to yield BrBOC–Lys(Z)–Gly–OEt *via* the mixed anhydride in 69%. I was stirred under reflux in ethanol for an hour; dipeptide hydrobromide II was thus obtained in a pure state in a yield of 89%. II was condensed with Z–Gly–OH by the M.A. method to afford Z–Gly–Lys(Z)–Gly–OEt.

The characteristics of the tripeptide are identical with those previously reported.[9]

Thus, the BrBOC group is cleaved selectively by heating in ethanol, so it may be possible to use this group for the protection of amino acids in the synthesis of long, complicated peptides.

Side Reaction. In the reaction of the BrBOC–Cl with amino acids or amino acid esters, Carpino did not obtain the urethane derivatives, but the amine hydrobromides and the urea derivatives were isolated. The urea formation in the reaction of *t*-amyl chloroformate with amino acid esters in the presence of triethylamine in an anhydrous organic solvent has been described by Sakakibara and Itoh.[10] We have also found that the urea is largely formed by reacting BOC–Cl or benzyl chloroformate with amino acid esters under the same anhydrous conditions, and that the urea formation decreased when the reaction is carried out in an aqueous solvent. From this point of view, we tried to react the XBOC–Cl with amino acids and amino acid esters under aqueous conditions.

Although the desired XBOC-amino acids and esters were formed quantitatively under those conditions, it was found that the XBOC-amino acids or esters formed in the basic reaction solution were transformed into 2-oxazolidinones to a large extent if the solution was allowed to stand overnight. This phenomenon was also observed when pure BrBOC-amino acid dissolved in a 2N sodium hydroxide solution was stored for 24 hr

9) H. Zahn and H. R. Falkenburg, *Ann. Chem.*, **636**, 117 (1960).
10) S. Sakakibara and M. Itoh, This Bulletin, **40**, 646 (1967).

Table 5. 2-Oxazolidinones derived from α-bromo-*t*-butyloxycarbonylamino acids

Amino acids	Yield (%)	Mp °C	$[\alpha]_D^{20}$ (*c* 1, AcOEt)	Calcd (%)			Found (%)		
				C	H	N	C	H	N
Phe	42	103	−26.5°	63.86	6.50	5.31	63.52	6.48	5.31
Met	32	109	− 2.0°	48.57	6.92	5.66	48.83	6.88	5.59
Leu	44	102	+10.5°	57.61	8.35	6.60	57.76	8.41	6.16

(Eq. (3)).

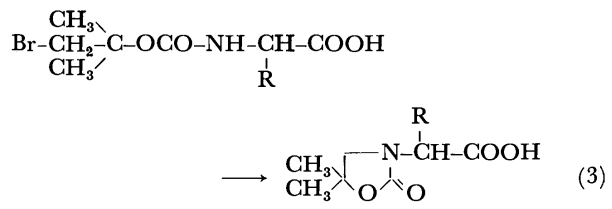

R: amino acid side chain

ClBOC-amino acids were transformed into 2-oxazolidinones to a smaller extent under the same conditions. This structure is confirmed by IR, elementary analysis, and NMR. The results are shown in Table 5. The NMR spectrum of the 2-oxazolidinone derived from BrBOC-phenylalanine are shown in Fig. 2.

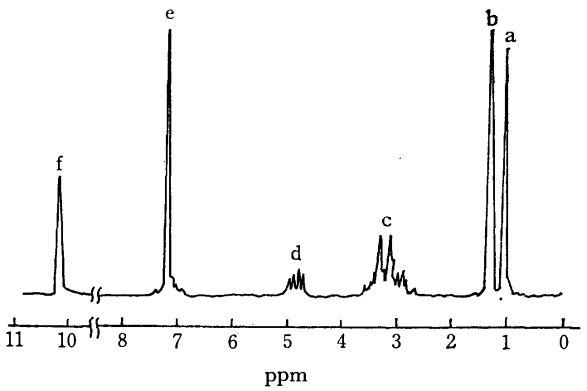

Fig. 2. NMR spectrum of (S)-5,5-dimethyl-3-(α-carboxyphenethyl)-2-oxazolidinone in $CDCl_3$.
a: CH_3, b: CH_3, c: CH_2, d: -CH–, e: ring-CH=, f: OH

Experimental

α-Bromo-t-butyl Alcohol. To a slurry of *N*-bromosuccinimide (178 g) in water (400 m*l*), isobutene gas was bubbled under vigorous stirring at 15—20°C. After 30 min, all of the *N*-bromosuccinimide disappeared; stirring was then continued for an additional 30 min. The mixture was extracted several times with ether, the ether extract was dried over magnesium sulfate, and the solution was evaporated. The remaining oil was distilled to give the alcohol; yield, 105 g (70%); bp 55—56°C/25 mmHg. NMR δ (CCl_4): 1.28 (s, 6H, CH_3), 3.28 (s, 1H, OH), 3.42 (s, 2H, CH_2).

α-Chloro-t-butyl Alcohol. This was obtained from *N*-chlorosuccinimide (100 g), water (380 m*l*), and isobutene as described above except that isobutene was introduced at 60—65°C; yield, 45 g (59%); bp 51—52°C/55 mmHg.

α-Bromo-t-butyl Chloroformate. Into a solution of phosgene (65 g, 0.65 mol) and α-bromo-*t*-butyl alcohol (103 g, 0.65 mol) in ether (1000 m*l*), a solution of pyridine (51 g, 0.65 mol) in ether (500 m*l*) was added under stirring at −20——30°C. The mixture was stirred for 2 hr at −20°C and was then allowed to stand overnight at room temperature. The salt was filtered, and the ethereal solution was washed with ice-cold water and with a 3% sodium bicarbonate solution, and dried over magnesium sulfate. The solvent was distilled off, and the remaining oil was distilled to give the chloroformate; yield, 100 g (72%); bp 60—61°C/10 mmHg. IR: cm^{-1} (liq. film) 1770 (C=O); NMR δ ($CDCl_3$): 1.62 (s, 6H, CH_3), 3.63 (s, 2H, CH_2).

α-Chloro-t-butyl Chloroformate. This was obtained from phosgene (32 g, 0.32 mol), α-chloro-*t*-butyl alcohol (35 g, 0.32 mol), pyridine (25 g, 0.32 mol), and ether (600 m*l*) as described above; yield, 37 g (68%); bp 50—51°C/10 mmHg.

α-Bromo-t-butyloxycarbonylglycine Benzyl Ester (General Procedure for the Synthesis of BrBOC- and ClBOC-amino Acid Esters). To a solution of H-Gly-OBzl·TsOH[11] (17 g, 50 mmol) and triethylamine (14 m*l*) in chloroform (200 m*l*) and water (50 m*l*), a solution of α-bromo-*t*-butyl chloroformate (11 g, 50 mmol) in chloroform (100 m*l*) was added at −1—0°C over a 30-min period. After the mixture had been stirred for 1 hr at the same temperature, it was washed successively with N hydrochloric acid, a 4% sodium bicarbonate solution, and water, and then dried over magnesium sulfate in a refrigerator. The solvent was distilled off, and the remaining oil was crystallized by the addition of ethyl acetate and petroleum ether. The crystal (3 g (17%)) was shown to be the urea derivative by IR; mp 105—106°C. From the filtrate, after the removal of the solvent, there was obtained the α-bromo-*t*-butyloxycarbonylglycine benzyl ester, yield of oil, 11 g (61%). IR: cm^{-1} (liq. film) 1755, 1725 (C=O).

α-Bromo-t-butyloxycarbonylglycine From the Benzyl Ester.

a) By Catalytic Hydrogenolysis: A mixture of the α-bromo-*t*-butyloxycarbonylglycine benzyl ester (8 g) obtained above and a 5% palladium-carbon catalyst (500 mg) in methanol (50 m*l*) was hydrogenated for 2 hr at room temperature. After the removal of the catalyst and the solvent, the white crystals were filtered and recrystallized from ethyl acetate and petroleum ether; yield, 3.0 g (55%); mp 102—103°C.

Found: C, 33.32; H, 4.82; N, 5.45; Br, 30.53%. Calcd for $C_7H_{12}NO_4Br$: C, 33.09; H, 4.75; N, 5.49; Br, 31.44%.

b) By Alkaline Hydrolysis: A solution of the α-bromo-*t*-butyloxycarbonylglycine benzyl ester (3 g, 12 mmol) and N sodium hydroxide (12 m*l*) in tetrahydrofuran (50 m*l*) was stirred for 30 min at 0°C. The mixture was then acidified with N hydrochloric acid and was extracted several times with ethyl acetate. The ethyl acetate solution was washed with water and was dried over magnesium sulfate. It was treated as had been described above to give white crystals; yield, 1 g (33%); mp 102—103°C.

Found: C, 33.15; H, 4.95; N, 5.50; Br, 31.03%. Calcd for $C_7H_{12}NO_4Br$: C, 33.09; H, 4.75; N, 5.49; Br, 31.44%.

α-Bromo-t-butyloxycarbonyl-L-proline (General Procedure for the Synthesis of BrBOC- and ClBOC-amino Acids). A solution of α-bromo-*t*-butyl chloroformate (10.75 g, 50 mmol) in tetrahydrofuran (20 m*l*) was added slowly to a solution of L-proline (5.75 g, 50 mmol) in a mixture of tetrahydrofuran (30 m*l*)

11) L. Zervas, M. Winitz, and J. P. Greenstein, *J. Org. Chem.*, **22**, 1515 (1957).

and 2N sodium hydroxide (70 ml) at 0—2°C. The mixture was stirred vigorously during the addition of the chloroformate. The stirring was continued for a further hour at 0°C. At the end of this period, the reaction mixture was adjusted to pH 2—3 with N hydrochloric acid, and the product was extracted with ethyl acetate. The extract was washed with water and dried over magnesium sulfate in a refrigerator. After the solvent had been distilled off *in vacuo*, crystals were obtained; those crystals were then recrystallized from ethyl acetate and petroleum ether; yield, 11.5 g (78%). The physical constants of the material are shown in Table 1.

BrBOC-Val-Gly-OMe (General Procedure for the Synthesis of α-BrBOC- and α-ClBOC-dipeptides). To a solution of BrBOC-Val-OH (2.5 g, 10 mmol) and triethylamine (1.4 ml) in chloroform (50 ml), ethyl chloroformate (1.2 g, 11 mmol) was added drop by drop at −15——10°C. After 15 min a solution of H-Gly-OMe·HCl[12] (1.38 g, 11 mmol) and triethylamine (1.5 ml) in chloroform (50 ml) was added at −10——5°C. The mixture was stirred for a further hour at 0—10°C and then washed successively with N hydrochloric acid, a 4% sodium bicarbonate solution, and water. After drying over magnesium sulfate in a refrigerator, the solvent was distilled off *in vacuo* and the remaining oil was crystallized by the addition of petroleum ether. It was recrystallized from ethyl acetate and petroleum ether; yield, 2.1 g (65%). The physical constants of the material are shown in Table 3.

Z-Gly-Val-Gly-OMe. *a) From BrBOC-Val-Gly-OMe*: BrBOC-Val-Gly-OMe (3.6 g, 10 mmol) was refluxed in methanol for 1 hr. The solvent was distilled off, and the remaining H-Val-Gly-OMe·HBr was used without purification. To a solution of Z-Gly-OH[13] (2.1 g, 10 mmol) and triethylamine (1.5 ml) in chloroform (50 ml), ethyl chloroformate (1.1 g, 10 mmol) was added drop by drop at −15——10°C. After 15 min a solution of the H-Val-Gly-OMe·HBr obtained above and triethylamine (1.4 ml) in chloroform was added at −10——5°C. The mixture was stirred for 1 hr at 0—10°C and then washed successively with 3N hydrochloric acid, a 4% sodium bicarbonate solution, and water. After drying over magnesium sulfate, the solvent was distilled off and the remaining solid was recrystallized from ethyl acetate and petroleum ether; yield, 2.5 g (65%). The value of specific rotation and the melting point are shown in Table 4.

Found: C, 56.63; H, 6.48; N, 10.71%. Calcd for $C_{18}H_{25}N_3O_6$: C, 56.98; H, 6.64; N, 11.08%.

b) From ClBOC-Val-Gly-OMe: ClBOC-Val-Gly-OMe (1.6 g, 5 mmol) was dissolved in 4N hydrogen bromide in acetic acid (10 ml) at room temperature. After 1 hr, the solution was evaporated and the remaining oil was triturated with ether. The H-Val-Gly-OMe·HBr thus obtained was coupled with Z-Gly-OH (1.1 g, 5 mmol) as had been described above; yield, 1.1 g (59%). The data of this product are shown in Table 4.

c) From Z-Val-Gly-OMe: Z-Val-Gly-OMe[14] (1.6 g, 5 mmol) was hydrogenated over palladium black in methanol in the presence of 2.5 ml of a methanolic solution of 2N hydrogen chloride. The solution was filtered from the catalyst, and the filtrate was evaporated to dryness. The oily residue was coupled with Z-Gly-OH (1.1 g, 5 mmol) as had been described above, yield, 1.2 g (66%). Its properties agreed with those of the products obtained from ClBOC-Val-Gly-OMe or BrBOC-Val-Gly-OMe (see Table 4).

BrBOC-Lys(Z)-Gly-OEt (I). BrBOC-Lys(Z)-OH was obtained from BrBOC-Cl (11 g, 50 mmol) and H-Lys(Z)-OH[15] (14 g, 50 mmol) in a manner similar to that described for the preparation of BrBOC-Pro-OH. It was not crystallized and was used without purification; yield of oil, 20 g (87%). The oily BrBOC-Lys(Z)-OH (18.5 g, 40 mmol) thus obtained was coupled with H-Gly-OEt·HCl[12] (5.6 g, 40 mmol) by the mixed anhydride method described for the preparation of BrBOC-Val-Gly-OEt. The resultnig BrBOC-Lys(Z)-Gly-OEt was recrystallized from ethyl acetate and petroleum ether; yield, 16 g (80%); mp 91—93°C, $[\alpha]_D^{25}$ −10.5° (*c* 1, AcOEt).

Found: C, 50.78; H, 5.94; N, 7.75; Br, 14.44%. Calcd for $C_{23}H_{34}N_3O_7Br$: C, 50.83; H, 6.12; N, 7.73; Br, 14.70%.

H-Lys(Z)-Gly-OEt·HBr (II). I (5.4 g) was refluxed in EtOH (100 ml) for 1 hr. The solution was then evaporated, and the residue was recrystallized from ethanol and ether; yield, 4.0 g (89%); mp 137—140°C; $[\alpha]_D^{25}$ +13.0° (*c* 1, EtOH).

Found: C, 47.81; H, 6.41; N, 9.30; Br, 17.58%. Calcd for $C_{18}H_{28}N_3O_5Br$: C, 48.11; H, 6.29; N, 9.38; Br, 17.83%.

Z-Gly-Lys(Z)-Gly-OEt (III). To a solution of Z-Gly-OH (2.1 g, 10 mmol) and triethylamine (1.4 ml) in chloroform (50 ml), ethyl chloroformate (1.1 g, 10 mmol) was added at −12——10°C. After 15 min, a solution of (II) (4.5 g, 10 mmol) and triethylamine (1.4 ml) in chloroform (30 ml) was added, and the reaction mixture was stirred for 1 hr at 0—10°C. Then, it was washed with N hydrochloric acid, a 4% sodium bicarbonate solution, and water. After drying over magnesium sulfate, the solution was evaporated *in vacuo*, and the remaining oil was crystallized by the addition of petroleum ether. The crystal was recrystallized from ethyl acetate and petroleum ether; yield, 2.8 g (50.5%); mp 156—159°C; $[\alpha]_D^{25}$ −17.2° (*c* 1, AcOH). Lit,[9] mp 155—158°C, $[\alpha]_D^{25}$ −17.0° (*c* 1, AcOH).

Found: C, 60.12; H, 6.66; N, 9.99%. Calcd for $C_{28}H_{36}N_4O_8$: C, 60.36; H, 6.52; N, 10.07%.

(S)-5,5-dimethyl-3-(α-carboxyphenethyl)-2-oxazolidinone (General Procedure for the Preparation of 2-Oxazolidinone Derivatives).

a) From L-Phenylalanine and BrBOC-Cl: A solution of α-bromo-*t*-butyl chloroformate (11 g, 50 mmol) in tetrahydrofuran (20 ml) was added slowly to a solution of L-phenylalanine (8.2 g, 50 mmol) in a mixture of tetrahydrofuran (30 ml) and 2N sodium hydroxide (80 ml) at 0—2°C under stirring. The stirring was continued for a further 2 hr at 0°C, and then overnight at room temperature. The mixture was acidified with N hydrochloric acid and was extracted with ethyl acetate. The extract was dried over magnesium sulfate. After the solvent had been distilled off, crystals were obtained; they were recrystallized from ether and petroleum ether; yield, 4 g (42%). The data of this product are shown in Table 5.

b) From BrBOC-L-Phenylalanine: BrBOC-Phe-OH (3.44 g, 10 mmol) was dissolved in a mixture of N sodium hydroxide (12 ml) and MeOH (50 ml) at room temperature. After 24 hr, the solution was acidified with N hydrochloric acid and extracted with ethyl acetate. The extract was dried and evaporated to dryness. The residue was recrystallized from ether and petroleum ether; yield, 1.6 g (60%). Its properties agreed with those of the product described above.

12) T. Curtius and F. Geebel, *J. Prakt. Chem.*, (2) **37**, 150 (1888).

13) D. F. Detar, R. Silverstein, and F. F. Rogers, *J. Amer. Chem. Soc.*, **88**, 1024 (1966). F. H. C. Stewart, *Aust. J. Chem.*, **18**, 1699 (1965).

14) C. H. Li, J. Ramachandran, D. Chung, and B. Gorup, *J. Amer. Chem. Soc.*, **86**, 2703 (1964).

15) A. Neuberger and F. Sanger, *Biochem. J.*, **37**, 515 (1943).

A Simple Protecting Group Protection-Purification "Handle" for Polynucleotide Synthesis. II.

Kiyohiko TAJIMA and Tsujiaki HATA

Department of Chemistry, Tokyo Institute of Technology, Ookayama, Meguro-ku, Tokyo

(Received January 31, 1972)

A new method for the synthesis of oligonucleotides by employing a protecting group protection-purification "handle" was investigated. It was found that 3′-*O*-acetylthymidylyl(5′→3′)thymidine 5′-phosphor[*p*-*N*,*N*-dimethylamino]anilidate (NpTpTOAc) was prepared in 65% yield from thymidine 5′-phosphor[*p*-*N*,*N*-dimethylamino]anilidate (NpT) and 3′-*O*-acetylthymidine 5′-phosphate (pTOAc) in the presence of triisopropylbenzenesulfonyl chloride (TPS). The NpTpTOAc was selectively isolated by the use of Dowex 50W-X2 and Amberlite IR-45 resins. After treatment of NpTpTOAc with 80% acetic acid, pTpTOAc was obtained in 60% yield based on pTOAc. Similarly, trinucleotide derivative, pTpTpTOAc, was isolated in 31% yield based on pTpTOAc.

Application of the solid phase method to oligonucleotide synthesis has recently been studied.[1] However, the desired sequence of oligonucleotides obtained is accompanied with several truncated and failure sequences as the purity of the product depends on the yield of coupling reactions on polymer supports, and only 100% yield in every coupling can prevent the formation of truncated and failure sequences.[2] Separation of oligonucleotides prepared by the present method seems to be more difficult than the usual method because the contents of truncated and failure sequences are uniformly much more than those of a true sequence. Especially, higher yields of coupling reactions except in the case of 100% yield would cause much difficulty. In order to remove the restriction of solid phase synthesis, a new synthetic method of oligonucleotides, in which true sequence of oligonucleotide may be selectively prepared without using column chromatography, has been established.[3]

The results of experiments for the preparation of oligothymidylates designed by a new method are described in this paper. The coupling reactions of nucleotide were carried out in solution in the absence of polymer. In the next stage, the desired oligonucleotide was seaprated from the other by-products using an ion exchange resin utilizing salt formation or molecular adsorption between the protecting group and the ion exchange resin by taking advantage of the separation on solid phase.

The protecting group (N) on nucleoside 5′-phosphate end is of importance, since during the course of the experiment the group acts as a protecting group of phosphate in the coupling reactions and also functions as a "handle" for separation. A basic *N*,*N*-dimethyl-*p*-phenylenediamino group was chosen as the protecting group on the nucleoside 5′-phosphate end. This was introduced to form a phosphoroanilidate linkage which could be cleaved easily by treatment with 80% acetic acid at 80°C for 3 hr.

Thymidine 5′-phosphoroanilidate (NpT) was prepared in 90% yield when thymidine 5′-phosphate was treated with *N*,*N*-dimethyl-*p*-phenylenediamine in the presence of dicyclohexylcarbodiimide (DCC) according to a modification of the procedure of Moffatt.[4] The NpT was purified and isolated from the reaction mixture by treatment with Dowex 50W-X2 (H^+ form) since the resin adsorbs NpT by a salt formation between sulfonic acid group of Dowex 50W-X2 and *N*,*N*-dimethyl anilino group of NpT, which excluded the formation of the inner salt of NpT.

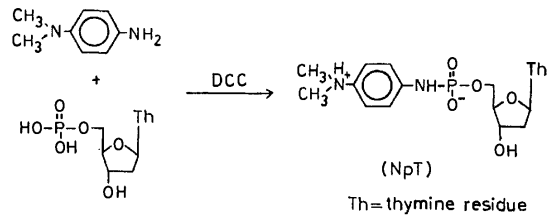

NpT is stable pink oil and can be stored in dry pyridine at 0°C for more than one month. The possible self-condensation reaction[5] into the corresponding pyrophosphate, P^1,P^2-dithymidine 5′-pyrophosphate, was not observed even when it was treated with Dowex 50W-X2 (H^+ form).

When a mixture of 1.3 equivalent of NpT and 1 equivalent of 3′-*O*-acetylthymidine 5′-phosphate (pTOAc) was treated with 3 equivalent of triisopropylbenzenesulfonyl chloride (TPS) in dry pyridine at room temperature for 13 hr, the corresponding dinucleotide derivative, NpTpTOAc, was formed in 65% yield along with P^1,P^2-di-3′-*O*-acetylthymidine 5′-pyrophosphate $(pTOAc)_2$, the starting materials pTOAc and NpT being recovered. These compounds were detected by paper chromatography and the yield was determined spectrophotometrically.

After passing the mixture through a column of Dowex 50W-X2 (H^+ form), NpT was selectively adsorbed on the resin as described in the preparation

1) a) R. L. Letsinger and V. Mahadevan, *J. Amer. Chem. Soc.*, **87**, 3526 (1965); **88**, 5319 (1966). b) F. Cramer, R. Helbig, H. Hettler, K. H. Scheit, and H. Seliger, *Angew. Chem.*, **78**, 640 (1966); F. Cramer and H. Köster, *ibid.*, **80**, 488 (1968). c) H. Hayatsu and H. G. Khorana, *J. Amer. Chem. Soc.*, **88**, 3182 (1966); **89**, 3880 (1967). d) L. R. Melby and D. R. Strobach, *ibid.*, **89**, 450 (1967); *J. Org. Chem.*, **34**, 421, 427 (1969). e) G. M. Blackburn, M. J. Brown, and M. R. Harris, *J. Chem. Soc., C*, **1967**, 2483. f) T. Kusama and H. Hayatsu, *Chem. Pharm. Bull.* (Tokyo), **18**, 319 (1970).

2) E. Bayer, H. Eckstein, K. Hägele, W. A. König, W. Brüning, H. Hagenmaier, and W. Parr, *J. Amer. Chem. Soc.*, **92**, 1735(1970).

3) T. Hata, K. Tajima, and T. Mukaiyama, *ibid.*, **93**, 4928 (1971).

4) J. G. Moffatt and H. G. Khorana, *ibid.*, **83**, 649 (1961).

5) V. M. Clark, G. W. Kirby, and A. R. Todd, *J. Chem. Soc.*, **1957**, 1497.

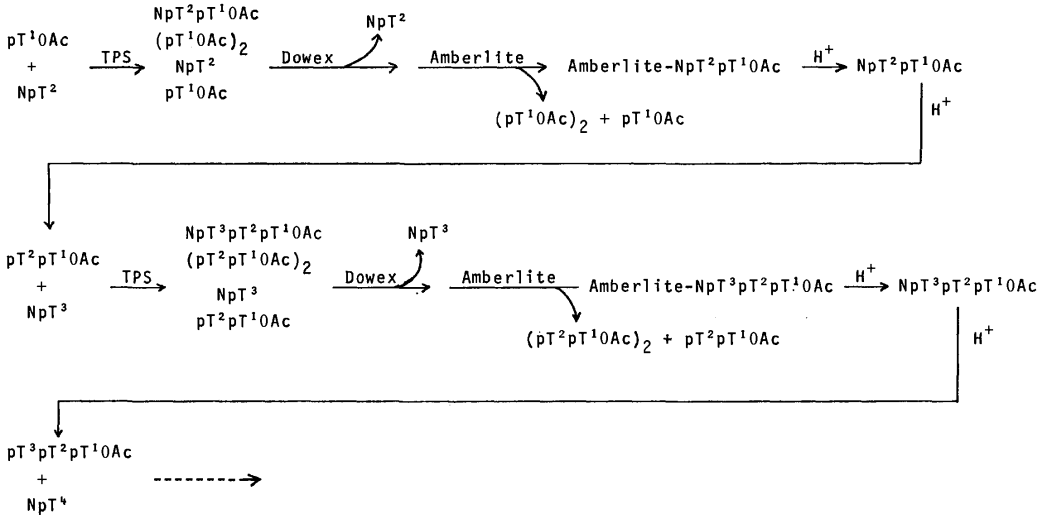

Chart 1. General synthetic scheme.

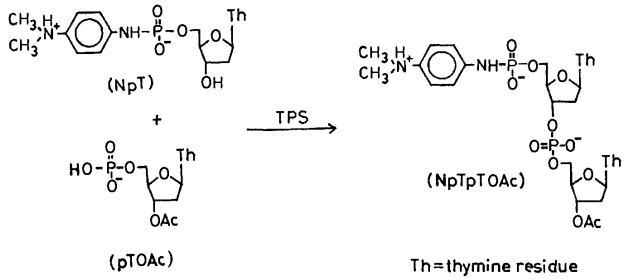

of NpT. The eluate containing NpTpTOAc, $(pTOAc)_2$ and pTOAc was neutralized with 0.1N sodium hydroxide. When the solution was passed through a column of Amberlite IR-45 (free base), NpTpTOAc was selectively adsorbed on the resin excluding adsorption of the other compounds, pTOAc and $(pTOAc)_2$. After washing the resin with neutral water, the resin was treated with 80% acetic acid and the eluate containing NpTpTOAc was heated at 80°C for 3 hr. The solution was concentrated under reduced pressure for removal of acetic acid, and the residue was dissolved in water. *N,N*-Dimethyl-*p*-phenylenediamine was removed by treatment of the aqueous solution with Dowex 50W-X2 (H^+ form). The eluate was lyophilized to remove a trace of moisture and stored in dry pyridine. pTpTOAc was isolated in 60% yield based on pTOAc.[6]

It is most probable that Amberlite IR-45 having anilino group includes *N,N*-dimethyl-*p*-phenylenediamino group of NpTpTOAc by a force of molecular adsorption. This was supported by the adsorption of the base *N,N*-dimethyl-*p*-phenylenediamine on the IR-45 resin. Further, when a mixture of 1 equivalent of pTpTOAc and 3 equivalent of NpT was treated with 3 equivalent of TPS in dry pyridine at room temperature for 14 hr, the corresponding trinucleotide derivative, NpTpTpTOAc, was obtained in 34% yield along with NpT and $(pTpTOAc)_2$.[7] pTpTpTOAc was isolated by means of a similar procedure (see Experimental) to that described for pTpTOAc.

A general synthetic scheme developed for oligothymidylate derivatives is outlined in Chart 1.

In conclusion, it should be noted that the use of the basic protecting group in oligonucleotide synthesis resulted in the selective preparation of oligonucleotides. The chain of oligomer propagates from the head, whereas in the solid phase method it propagates from the tail, *i.e.*, in the former, the oligonucleotide can be purified at each step where the protecting group N enacts the role of handle for separation. This is why the oligomer is selectively prepared. The principle of this method could be applied for the synthesis of polypeptides and other complex molecules.

Experimental

General Procedure. Paper chromatography was performed by a descending technique using Toyo Roshi No. 51 paper. Solvent systems used were: 2-propanol, concentrated ammonium hydroxide, water (7:1:2 v/v) (Solvent 712); ethanol, 1M ammonium acetate (7:3 v/v, pH=7.5) (Solvent 73). Pyridine was purified as follows; Commercial pyridine was distilled over *p*-toluenesulfonyl chloride, phosphorus pentoxide and over potassium hydroxide and stored over calcium hydride. 2,4,6-Triisopropylbenzenesulfonyl chloride (TPS) was prepared by a procedure in literature.[8] *N,N*-Dimethyl-*p*-phenylenediamine was purified by distillation (bp 79—82°C/0.7 mmHg), before use and stored in dry pyridine.

Preparation of NpT. A mixture of pyridinium salt of thymidine 5′-phosphate (0.5 mmol) and *N,N*-dimethyl-*p*-phenylenediamine (3 mmol) was combined with a mixture of water (1 ml) and *t*-butyl alcohol (5 ml). DCC (2.5 mmol) was then added. The mixture was heated under gentle reflux on a glycerin bath at 93—94°C for 3 hr and concentrated to dryness under reduced pressure. The residue was suspended in water (10 ml) and the suspension was washed with three portions of ether (3×10 ml). The aqueous layer was then extracted with three portions of chloroform and concentrated *in vacuo* (1 ml). This was applied to a column

6) Hydrolysis of the acetyl group from pTpTOAc was observed under acidic conditions. Acetylation with acetic anhydride afforded pure pTpTOAc in quantitative yield.

7) $(pTpTOAc)_2$ refers to P^1,P^2-di-3′-*O*-acetylthymidylyl(3′→5′)-thymidine 5′-pyrophosphate. No pTpTOAc was detected from the reaction mixture.

8) R. Lohrmann and H. G. Khorana, *J. Amer. Chem. Soc.*, **88**, 8296 (1966).

TABLE 1. CHROMATOGRAPHIC AND SPECTRAL PROPERTIES OF THE REPORTED COMPOUNDS

Compound	Pc[a] solvent		Spectral data[c] (in H_2O, pH=9)	
	712	73	λ_{max} (10^{-3} ε)	λ_{min} (mμ)
pT	0.20	0.22		
NpT	0.58		251 (17.2)	230
pTOAc	0.22	0.33		
NpTpTOAc	0.45		255 (25.0)	235
pTpTOAc	0.12	0.29		
pTpT[b]	0.09	0.19		
NpTpTpTOAc	0.24		266 (33.0)	236
pTpTpTOAc	0.05	0.12		
pTpTpT[b]	0.04	0.10		

a) Pc=paper chromatography.
b) The compound has been reported by Khorana and co-workers.[9] The R_f values of the compounds agree well with those given in literature. The oligothymidylates prepared by the present method were characterized by degradation to pT with snake *venom* phosphodiesterase and by mobility of the oligothymidylates relative to pT on paper electrophoresis (phosphate buffer, pH 8).
c) The ε_{max} values were obtained and calculated from those of the corresponding free thymidylates.

(1.5×15 cm) of Dowex 50W-X2 (H^+ form). The column was washed first with water (150 m*l*) and then eluted with 0.2N aqueous triethylamine. The eluate was concentrated to dryness under reduced pressure. NpT was obtained in 90% (7740 O.D.$_{251}$ units at pH 9) yield as pink oil which was chromatographically pure. Spectral data are given in Table 1.

Preparation of NpTpTOAc. Triethylammonium salt of NpT (0.13 mmol) and 3′-*O*-acetylthymidine 5′-phosphate (pTOAc) (0.1 mmol) were dissolved in pyridine (1 m*l*) and the mixture was concentrated to dryness. This was repeated five times for complete removal of moisture. The residue was dissolved in pyridine (0.3 m*l*) and TPS (0.3 mmol)was added. The mixture was allowed to stand at room temperature for 13 hr and water (0.3 m*l*) was added. After 3 hr, the solvent was removed *in vacuo* and the residue was suspended in water (3 m*l*). The aqueous solution was washed with ether and then with chloroform and concentrated to *ca.* 0.5 m*l*. The solution was applied to a column (1.5×5 cm) of Dowex 50W-X2 (H^+ form). The column was washed with water (300 m*l*). The eluate contains NpTpTOAc, $(pTOAc)_2$ and pTOAc. It was concentrated to *ca.* 2 m*l* and neutralized with 0.1N sodium hydroxide and then Amberlite IR-45 (free base) (3 m*l*) was added. After 30 min, the mixture was applied to a column (1.5×6 cm) of Amberlite IR-45 (free base). The column was washed with water (100 m*l*) for removal of $(pTOAc)_2$ and pTOAc and then 50% acetic acid (10 m*l*) was added. It was allowed to stand for 30 min. The column was eluted and washed with water. This was repeated once more. Eluate and washings were combined and concentrated *in vacuo*. NpTpTOAc was obtained in 65% (1625 O.D.$_{255}$ units at pH 9) yield as colorless oil which was chromatographically pure. The spectral data are given in Table 1.

Preparation of pTpTOAc. NpTpTOAc (0.06 mmol) was dissolved in 80% acetic acid (5 m*l*). The solution was allowed to stand at 80°C for 3 hr and concentrated to dryness. The residue was dissolved in water (1 m*l*) and applied to a column (1.5×2 cm) of Dowex 50W-X2 (H^+ form). The column was eluted with water and the eluate was concentrated. pTpTOAc was obtained in 92% yield based on NpTpTOAc and stored in dry pyridine. When hydrolysis of the acetyl group from pTpTOAc was observed, acetylation with acetic anhydride afforded pure pTpTOAc in quantitative yield.

Preparation of NpTpTpTOAc. pTpTOAc (0.015 mmol) and triethylammonium salt of NpT (0.045 mmol) were dissolved in pyridine (1 m*l*) and the mixture was concentrated to dryness. This was repeated five times for complete removal of moisture. The residue was then dissolved in pyridine (0.15 m*l*) and TPS (0.045 mmol) was added. The mixture was allowed to stand at room temperature for 14 hr and water (0.5 m*l*) was then added under cooling. It was allowed to stand at room temperature for 3 hr and then concentrated *in vacuo*. The residue was suspended in water (3 m*l*). The aqueous solution was washed with ether and with chloroform and then concentrated to *ca.* 0.5 m*l*. It was applied to a column (1.5×5 cm) of Dowex 50W-X2 (H^+ form). The column was eluted with water (150 m*l*). The eluate contains NpTpTpTOAc, $(pTpTOAc)_2$ and pTpTOAc. It was concentrated to *ca.* 1 m*l* and neutralized with 0.1N sodium hydroxide. Amberlite IR-45 (free base) was added to the solution. After being left to stand at room temperature for 30 min, it was applied to a column (1.5×5 cm) of Amberlite IR-45 (free base). The column was washed with water for removal of $(pTpTOAc)_2$ and pTpTOAc and then 50% acetic acid (10 m*l*) was added. The column was allowed to stand for 30 min, then eluted and washed with water. This was repeated once more. Eluate and washings were combined and concentrated under reduced pressure. NpTpTpTOAc was obtained in 31% (153 O.D.$_{266}$ units at pH 9) yield as colorless oil which was chromatographically pure. The spectral data are given in Table 1.

Preparation of pTpTpTOAc. NpTpTpTOAc (0.047 mmol) was dissolved in 80% acetic acid (2 m*l*). The solution was allowed to stand at 80°C for 3 hr and concentrated to dryness. The residue was dissolved in water (1 m*l*) and 1 m*l* of Dowex 50W-X2 (H^+ form) was added and allowed to stand at room temperature for 10 min. Dowex 50W-X2 was filtered and washed with water. Filtrate and washings were combined and concentrated *in vacuo*. pTpTpTOAc was obtained in 91% yield based on NpTpTpTOAc and stored in dry pyridine.

The authors heartily thank Professor Teruaki Mukaiyama for his encouragement and discussion throughout the investigation.

9) a) P. T. Gilham and H. G. Khorana, *J. Amer. Chem.* Soc., **80**, 6212 (1958). b) H. G. Khorana and J. P. Vizsolyi, *ibid.*, **83**, 675 (1961).

Total Syntheses of Carbohydrates. I. Dihydroxyacetone and DL-Erythrulose

Takashi ANDO,* Sachiko SHIOI, and Masazumi NAKAGAWA**

Department of Chemistry, Faculty of Science, Osaka University, Toyonaka, Osaka, 560

(Received January 24, 1972)

An improved method of preparation of halopropargyl alcohol is described. Hydration of halopropargyl alcohol followed by hydrolysis gave dihydroxyacetone which was identified as its dibenzoate. 2-Butyne-1,4-diol was converted into acetoxymethyl vinyl ketone. 1,4-Diacetoxy-3-bromobutan-2-one obtained by the addition of acetyl hypobromite to the vinyl ketone was treated with silver acetate to yield tri-*O*-acetyl-DL-erythrulose. Hydrolysis of the triacetate afforded DL-erythrulose which was identified as phenylhydrazone.

Since the pioneering work of R. Lespieau,[1] a number of papers have appeared on total syntheses of carbohydrates. Stereoselective synthesis of carbohydrates involves two problems; the construction of asymmetric centers bearing hydroxyl group with particular configuration, and the introduction of formyl- or keto-function at a desired position. The former can be solved in principle by (1) a stereoselective synthesis of an open chain olefinic compound followed by stereospecific hydroxylation, (2) stereospecific reactions of cyclic compounds such as reduced furans or pyrans, or (3) a combination of (1) and (2). Open chain compounds can usually be obtained by stereoselective half-reduction of acetylenic compounds. Construction of more than three asymmetric centers with a particular configuration in an open chain olefinic compound is usually difficult, but the versatile reactivity of an acetylenic compound, the precursor of an olefinic compound, provides various routes for the introduction of carbonyl function. Thus, the total syntheses of DL-erythrulose,[2] DL-apiose,[3] 2-deoxy-DL-*erythro*-pentose,[4,5] 2-deoxy-DL-*threo*-pentose,[5] the four isomers of DL-aldopentose,[6] ethyl glycoside of 3-amino-3-deoxy-DL-arabinose,[7] L-mycarose[8] and ethyl glycoside of DL-picrocin[9] were achieved starting from various acetylenic compounds.

We have studied total syntheses of carbohydrates starting from simple acetylenic or olefinic compounds, and wish to report on the total syntheses of dihydroxyacetone and DL-erythrulose.[10]

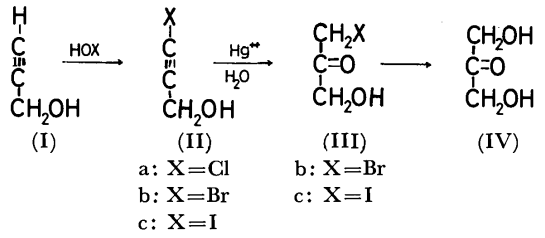

Scheme 1. Synthesis of dihydroxyacetone (IV).

The reported methods of preparation of dihydroxyacetone by chemical means such as isomerization of glyceraldehyde,[11] bromine oxidation of glycerol,[12] alkaline treatment followed by acid hydrolysis of 1,2-isopropylideneglyceryl chloride[13] and hydrolysis of 1,3-dichloroacetone[14] do not seem to be very satisfactory. As is shown in Scheme 1, we carried out the synthesis of dihydroxyacetone (IV) employing propargyl alcohol (I) as a starting material. Treatment of an ethynyl compound with hypohalite under strongly alkaline conditions is the usual method of preparation of haloacetylene.[15] However, the reaction conditions can not be applied to propargyl alcohol (I), since I and II are sensitive to strong base. Since the prolonged treatment of I with calcium hypohalite and calcium hydroxide in water resulted in recovery of I, alcohol (I) was converted into α-methoxyethyl ether derivative by the reaction with methyl vinyl ether. Treatment of the ether derivative with sodium hydroxide-calcium hypohalite in water followed by acid hydrolysis of the protective group afforded chloropropargyl alcohol (IIa) in a 53% yield. Bromopropargyl alcohol (IIb) could be prepared in a 65% yield by rapid addition of I to a mixture of calcium hypobromite, calcium hydroxide, water and ether at a temperature below −5°C.[16] When the reaction temperature is higher than this an appreciable amount of bromopropiolic acid is formed accompanied by a significant decrease in the yield of IIb. It is to be noted that calcium hypobromite can oxidize primary acetylenic alcohol to carboxylic acid leaving the acetyl-

* Present address: The Institute of Scientific and Industrial Research, Osaka University, Yamadakami, Suita, Osaka.

** To whom inquiries should be addressed.

1) R. Lespieau, "Advances in Carbohydrate Chemistry," Vol. 2, ed. by W. W. Pigman and M. L. Wolfrom, Academic Press Inc. Publishers, New York, N. Y. (1946), p. 107.

2) R. A. Raphael, *J. Chem. Soc.*, **1952**, 401.

3) R. A. Raphael, *Angew. Chem.*, **69**, 516 (1957).

4) M. M. Fraser and R. A. Raphael, *J. Chem. Soc.*, **1955**, 4280.

5) F. Weygand and H. Leube, *Chem. Ber.*, **89**, 1914 (1956).

6) I. Iwai and T. Iwashige, *Chem. Pharm. Bull.* (Tokyo), **9**, 316 (1961); T. Iwashige, *ibid.*, **9**, 492 (1961); T. Iwashige and K. Tomita, *ibid.*, **9**, 976 (1961); I. Iwai and K. Tomita, *ibid.*, **11**, 184 (1963); I.Iwai, T. Iwashige, M. Asai, K. Tomita, T. Hiraoka, and J. Ide, *ibid.*, **11**, 188 (1963).

7) T. Iwashige, M. Asai, and I. Iwai, *ibid.* **11**, 1569 (1963).

8) D.M. Lemal, P.D. Pacht, and R, B, Woodward, *Tetrahedron*, **18**, 1275 (1962).

9) V. B. Mochalin, Yu. N. Porshnev, and G. I. Samokhvalov, *J. Gen. Chem. USSR*, **39**, 665 (1969).

10) Part of this study was presented before the Annual Meeting of the Chemical Society of Japan (1960 and 1962).

11) H. O. L. Fischer, C. Tanbe, and E. Baer, *Ber.*, **60**, 479 (1927).

12) H. P. den Otter, *Rec. Trav. Chim. Pays-Bas*, **56**, 474 (1937).

13) H. O. L. Fischer, E. Baer, and L. Feldmann, *Ber.*, **63**, 1732 (1930).

14) E. Waldmann and V. Prey, *Monatsh. Chem.*, **82**, 861 (1951).

15) F. Strauss, L. Kollek, and W. Heyn, *Ber.*, **63**, 1868 (1930).

16) The reported method of preparation of IIb [L. F. Hatch, W. E. Blankenstein, and S. H. Chu, *J. Org. Chem.*, **23**, 397 (1958)] gave a much lower yield.

enic bond intact under weak alkaline conditions at a low temperature. The procedure of preparation of iodopropargyl alcohol (IIc) had to be modified because of the unstable nature of hypoiodite, *i.e.*, an aqueous solution of iodine–potassium iodide was added to an aqueous suspension of calcium hydroxide containing I. By this procedure, iodopropargyl alcohol (IIc) was obtained in a 56% yield.

Halopropargyl alcohols (IIa, IIb, and IIc) thus prepared were found to be rather unstable. The stability decreases with the increase in the atomic weight of halogen atom. Iodopropargyl alcohol (IIc) could be recrystallized from ether or petroleum ether to yield pure crystals (mp 39.5—41.0°C). Recrystallization of IIc from methanol or ethanol, however, gave a different substance (mp 153°C), which was assigned to be 2,3,3-triiodo-2-propen-1-ol on the basis of IR spectrum and the elemental analysis.

The hydration of halopropargyl alcohols (IIa, IIb, and IIc) was examined with two catalysts, an aqueous sulfuric acid containing mercuric sulfate (Reagent A)[17] and mercury-impregnated Dowex-60 (Reagent B).[18] Bromo- and iodopropargyl alcohols (IIb and IIc) gave smoothly corresponding haloketones (IIIb, 69% and IIIc, 53%) on treatment with Reagent A. On the other hand, the chloro-compound (IIa) gave no ketone under the same reaction conditions. Treatment of IIa under more drastic conditions resulted in a minor amount of a mercury containing substance, which seems to be an intermediate complex of hydration. Although the hydration of IIa and IIb could not be accomplished by Reagent B, IIc gave iodoketone (IIIc) in an 84% yield under these conditions. The marked difference in reactivity of halopropargyl alcohols (IIa, IIb, and IIc) may be explained in terms of the difference in electron donating power of halogen atoms. The hydration of acetylenic linkage is regarded as an electrophilic addition reaction catalyzed by mercuric ion.[17] Thus, the reaction is considered to be retarded by the presence of an electron attractive substituent and enhanced by an electron donating group. Haloacetylene can be regarded as a resonance hybrid of V and VI.

$$\underset{\text{(V)}}{RC{\equiv}C\text{–}X} \longleftrightarrow \underset{\text{(VI)}}{R\bar{C}{=}C{=}\overset{+}{X}}$$

The increase of contribution of VI in the sequence Cl<Br<I has been confirmed by the measurement of dipole moment of arylhaloacetylenes.[19] The IR spectra of halopropargyl alcohols (IIa, IIb, and IIc) exhibit absorptions due to $\nu_{C\equiv C}$ at 2250, 2240, and 2195 cm^{-1}, respectively, and the absorption intensity was found to be in the sequence IIa≈IIb>IIc. The IR spectral behavior observed in IIa—c is consistent with the conclusion obtained from the dipole moment measurement.

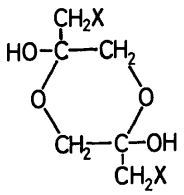

(VII)

The crystalline halogenohydroxyacetones (IIIb and IIIc) showed no carbonyl absorption in their IR spectra. This suggests that the halohydroxyacetones (IIIb—c) exist in the dimeric form (VII) in the solid state as in the case of dihydroxyacetone (IV). However, the IR spectrum of IIIc in liquid state exhibits absorption due to carbonyl group (1700 cm^{-1}) and ethylenic linkage (1620 cm^{-1}), which indicates that IIIc in solution exists in monomeric state at equilibrium of keto- and enol-forms. IIIb was found to be extremely unstable. Complete decomposition took place within about 1 hr at 30°C. IIIb could be kept in a refrigerator for a long time without change in appearance, but the melting point (75—76°C) lowered rapidly to *ca.* 50°C.

Dihydroxyacetone (IV) is extremely sensitive to acid and base. It decomposes or polymerizes easily in the presence of acid or alkali. Rearrangement to methylglyoxal or glyceraldehyde is also easily caused by acid or alkali. Consequently, the preparation of IV from its ester or ether derivative is difficult. It has been reported that the hydrolysis of diacetate of IV by means of weak alkali or water alone, or the hydrogenolysis of dityrityl or dibenzyl ether of IV gave fruitless results.[14] The hydrolysis of monoacetate IV with barium carbonate also gave only a trace of IV.[13] We have therefore employed an ester-exchange method which has been successfully applied to the conversion of bromoacetone to acetol[20] or 1-alkoxy-3-halogenopropan-2-one to 1-alkoxy-3-hydroxypropan-2-one.[21] Treatment of both IIIb and IIIc with anhydrous sodium formate in boiling anhydrous methanol gave a syrup. All attempts to crystallize the syrup were unsuccessful. However, the absence of methylglyoxal or glyceraldehyde was confirmed by various color reactions.[22] The syrup gave crystalline dibenzoate which gave a superimposable IR spectrum with that of an authentic specimen and showed no depression in mixed melting point. Syrupy IV obtained from IIIc was contaminated with potassium iodide and its removal was found to be difficult owing to the solubility of the salt in organic solvent. The best results were obtained with the use of bromo-compound (IIIb).

In 1952, Raphael reported on the synthesis of DL-erythrulose (XIII) starting from butynediol (VIII) *via* bromoketone (X).[2] In order to improve the preparation of bromoketone (X), a key substance of the present synthesis, we have studied the conversion of

17) R. A. Raphael, "Acetylenic Compounds in Organic Synthesis," Butterworth, London (1955), p. 40.
18) M. S. Newman, *J. Amer. Chem. Soc.*, **75**, 4740 (1953); J. D. Billimoria and N. F. Maclagan, *J. Chem. Soc.*, **1954**, 3257.
19) C. J. Wilson and H. H. Wenzke, *J. Amer. Chem. Soc.*, **56**, 2025 (1934).
20) P. A. Levene and A. Walti, "Organic Syntheses," Coll. Vol. II, p. 5 (1948).
21) A. Grün and W. Stoll, U. S. 2374283 (1945).
22) C. Neuberg, *Biochem. Z.*, **71**, 150 (1915).

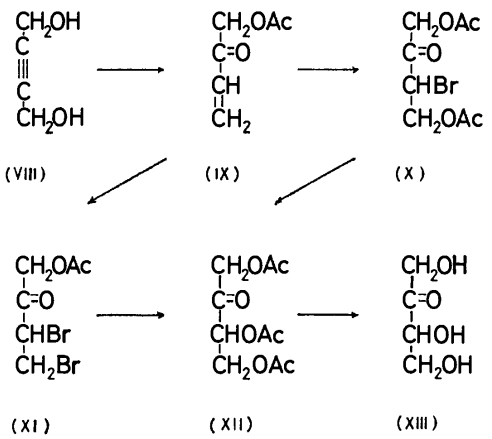

Scheme 2. Synthesis of DL-erythrulose (XIII).

acetoxymethyl vinyl ketone (IX) into bromoketone (X) (Scheme 2). Vinyl ketone (IX) was prepared according to a reported method.[23] It has been pointed out that a terminal double bond usually has low reactivity to electrophilic addition.[24,25] A double bond conjugated with an electron withdrawing group such as carbonyl is also inert to peracid oxidation.[26] Hydroxylation by means of alkaline hydrogen peroxide which is usually applied to double bond conjugated with carbonyl group can not be used, since the ester linkage in IX might be cleaved and the product is considered to be sensitive to alkali. The formation of bromohydrin by the reaction of *N*-bromoacetamide[27] or *N*-bromosuccinimide[2,24] in water is well-known. Bromohydrin acetates have been obtained by the reaction of *N*-bromoacetamide[28] or *N*-bromosuccinimide[29] in acetic acid. However, it is recognized that an ethylenic bond conjugated with carbonyl function except for α,β-unsaturated carboxylic acid reacts sluggishly with these reagents.[27,30]

In was found that the vinyl ketone (IX) is stable in acetic acid and a prolonged treatment with *N*-bromosuccinimide at room temperature affords the desired bromoketone (X) in a 46% yield. Bromoketone (X) which has been reported as a liquid[2] was obtained as fairly unstable crystals and gave a reasonable IR spectrum and satisfactory data of elemental analysis. As so far this seems to be the first instance of addition of acryl hypohalite to a double bond conjugated with carbonyl group. By the Raphael method,[2] bromoketone (X) was treated with silver acetate in acetic acid to yield tri-*O*-acetyl-DL-erythrulose (XII). Hydrolysis of triacetate (XII) by means of barium hydroxide[2] gave DL-erythrulose (XIII) as a syrup, which was identified as phenylhydrazone. Treatment of dibromoketone (XI) obtained by the addition of bromine to IX with silver acetate in acetic acid gave unsatisfactory results, and XIII could not be isolated in pure state.

Experimental

All the melting points are uncorrected. IR spectra were obtained on a Hitachi EPI-2 Spectrophotometer by Nujol mull method unless otherwise stated. Anhydrous acetic acid was prepared by the fractionation of acetic acid containing 5% of acetic anhydride which had been refluxed for 1 hr.

1-Methoxyethyl Propargyl Ether. Propargyl alcohol (I, 56 g) was added over a period of 50 min to methyl vinyl ether (110 m*l*) containing phosphoryl chloride (2—3 drops) at 0—8°C. After the mixture had been stirred for 3.5 hr at this temperature, it was left to stand overnight at room temperature. Excess methyl vinyl ether was removed by distillation, and the residue was washed successively with 10% sodium carbonate, 4N sodium hydroxide and water and dried (potassium carbonate). The propargyl ether was obtained as colorless liquid, 120.5 g (70%), bp 47—48°C/32—33 mmHg.

3-Chloro-2-propyn-1-ol (IIa). To a stirred mixture of sodium hydroxide (173 g), bleaching powder (85.2 g, corresponding to 0.72 molar equivalent of hypochlorite) and water (100 m*l*), was added 1-methoxyethyl propargyl ether (68.4 g, 0.6 mol) over a period of 25 min at 0°C. The mixture was stirred for 3.5 hr at room temperature and then left to stand overnight. After excess hypochlorite had been reduced by addition of sodium hydrogen sulfite (30 g), concentrated hydrochloric acid (430 m*l*) was added under cooling. The mixture was kept overnight at room temperature to complete hydrolysis of the protective group. The mixture was extracted with ether. The extract was washed with 1% sodium hydrogen carbonate solution and water and dried (sodium sulfate). The residue obtained by evaporation of the solvent was distilled twice *in vacuo* under nitrogen stream. IIa was obtained as colorless liquid, 29.2 g (53%), bp 49.5—50.5°C/13 mmHg, n_D^{20} 1.46916 [lit,[31] bp 68°C/35 mmHg, n_D^{20} 1.4727], IR (neat): 3300, 2920, 2870, 2250, 1420, 1360, 1225, 1080, 1005 cm^{-1}.

Found: C, 40.14; H, 3.40%. Calcd for C_3H_3OCl: C, 39.81; H, 3.38%.

p-*Nitrobenzoate*: Colorless rods, mp 113.4—114°C [lit,[32] mp 112°C].

3-Bromo-2-propyn-1-ol (IIb). Bromine (77 m*l*, 1.5 mol) was added over a period of 30 min to a stirred suspension of calcium hydroxide (185 g, 2.5 mol) in water (2 *l*) maintained at 0°C. An appreciable drop in temperature of the mixture was observed. Ether (800 m*l*) was added to the hypobromite solution (again the temperature decreased to −8°C) and propargyl alcohol (I, 72.9 g, 1.3 mol) was added over a 7 min-period under vigorous agitation. After the mixture had been stirred for 30 min below −5°C, the cooling bath was removed and stirring was continued for 3.5 hr. Sodium hydrogen sulfite (52 g, 0.5 mol) was added under cooling. After 20 min, concentrated hydrochloric acid (250 m*l*) was added to dissolve calcium hydroxide, and the organic layer was extracted with ether repeatedly (total 1700 m*l*). The combined ether solution was washed with a solution of ferrous sulfate (22 g) in dilute sulfuric acid (concd. sulfuric acid,

23) G. F. Hennion and F. P. Kupiecki, *J. Org. Chem.*, **18**, 160 (1953).
24) R. A. Raphael, *J. Chem. Soc.*, **1949**, s 44.
25) *Inter alia*, D. Swern, *J. Amer. Chem. Soc.*, **69**, 1692 (1947).
26) For theoretical explanation, see F. L. Weisenborn and D. Taub, *ibid.*, **74**, 1329 (1952); I. M. Roitt and W. A. Waters, *J. Chem. Soc.*, **1949**, 3060.
27) I. Salamon and T. Reichstein, *Helv. Chim. Acta*, **30**, 1616 (1957).
28) E. Schmidt, W. V. Knilling, and A. Ascherl, *Ber.*, **59**, 1279 (1926).
29) A. Jovtscheff, *Chem. Ber.*, **93**, 2045 (1960).
30) C. O. Guss and R. Rosenthal, *J. Amer. Chem. Soc.*, **77**, 2549 (1955).
31) M. Julia and J. M. Surzur, *Bull. Soc. Chim. Fr.*, **1956**, 1614.
32) H. G. Viehe, *Chem. Ber.*, **92**, 1950 (1959).

12 ml in water, 220 ml), and then with 10% aqueous solution of sodium carbonate. The residue obtained by evaporating the solvent was distilled to give IIb, colorless liquid, 114.8 g (65.4%), bp 42—46°C/2 mmHg. Redistillation of this material gave pure IIb, bp 45—46°C/2 mmHg, n_D^{25} 1.51486 [lit,[16] bp 41—42°C/1.5 mmHg, n_D^{25} 1.5146]. Pure IIb crystallized in a refrigerator. IR (neat): 3350—3400 (O–H), 2240 (C≡C), 1050 (C–O) cm^{-1}.

Found: C, 26.48; H, 2.45; Br, 58.77%. Calcd for C_3H_3OBr: C, 26.69; H, 2.24; Br, 59.21%.

3,5-Dinitrobenzoate: Yellow rods, mp 122—123°C (from ether) [lit,[16] mp 115—116°C].

Bromopropiolic acid, mp 85—86°C (from benzene followed by vacuum sublimation) [lit,[15] mp 84—86°C] was obtained from the washing (sodium carbonate solution) on acidification. When the reaction mixture was acidified with hydrochloric acid without reduction of hypobromite ion, 2,3,3-tribromo-2-propenoic acid, mp 119—120°C (from benzene followed by a vacuum sublimation) [lit,[33] mp 118°C] was obtained.

3-Iodo-2-propyn-1-ol (IIc). To a stirred mixture of calcium hydroxide (43 g, 0.58 mol), propargyl alcohol (I, 16.8 g, 0.3 mol) and water (500 ml) was added at 0°C a solution of iodine (76 g, 0.3 mol) and potassium iodide (76 g) in water (70 ml) over a period of 13 hr. Sodium hydrogen sulfite (10 g) and then concentrated hydrochloric acid (60 ml) were added to the reaction mixture. Extraction was carried out with ether. After washing (2% sodium hydrogen sulfite and then 10% sodium carbonate solutions) and drying (sodium sulfate), the solvent was removed. The residue, 30.6 g (56%), crystallized in a refrigerator. The crystals were recrystallized twice from petroleum ether to give pure IIc, colorless rods, mp 39.5—41°C [lit,[34] mp 43—44°C], IR: 3150, 2920, 2860, 2195, 1460, 1380, 1355, 1230, 1040, 1030, 980, 965 cm^{-1}.

Found: C, 19.75; H, 1.66; I, 70.45%. Calcd for C_3H_3OI: C, 19.80; H, 1.66; I, 69.75%.

IIc was found to be unstable and could not be kept without decomposition for a long time even in a refrigerator.

1-Bromo-3-hydroxypropan-2-one (IIIb). Mercuric oxide (16 g) was dissolved in a mixture of sulfuric acid (40 g) and water (200 ml) (Reagent A). Bromopropargyl alcohol (IIb, 81.0 g, 0.6 mol) was added under stirring to the solution at such a rate to maintain the temperature of reaction mixture at 40—50°C. The mixture was then stirred for further 1 hr. The insoluble material was filtered and washed with water. The combined washing and filtrate were nearly neutralized by gradual addition of sodium hydrogen carbonate, and repeatedly extracted with ether (total 2.5 l). The extract was washed with a saturated solution of sodium chloride and dried (sodium sulfate). The solvent was removed under reduced pressure at room temperature. Crystalline IIIb thus obtained was washed with ether (63.3 g, 68.7%). The crude material was dissolved in ethanol at 40°C and a small amount of insoluble material was removed by filtration. Concentration of the filtrate under reduced pressure at room temperature yielded IIIb, mp 75—76°C, contaminated with a trace of mercury compound which could not be removed by treatment with ion exchange resin. IR: 3430 (O–H) cm^{-1}. The absorption due to carbonyl group could not be observed.

Found: C, 23.30; H, 3.26; Br, 51.15%. Calcd for $C_3H_5O_2Br$: C, 23.55; H, 3.29; Br, 52.24%.

IIIb reduced Fehling's solution at room temperature, and was found to be extremely heat sensitive.

Benzoate: Fine needles, mp 133.5—134.5°C (from benzene). Found: C, 47.06; H, 3.54; Br, 30.79%. Calcd for $C_{10}H_9O_3Br$: C, 46.72; H, 3.53; Br, 31.08%.

1-Iodo-3-hydroxypropan-2-one (IIIc). *a) By Means of Reagent A*: Iodopropargyl alcohol (IIc, 3.6 g, 0.02 mol) was added over a period of 40 min to Reagent A prepared from mercuric oxide (0.5 g), concentrated sulfuric acid (2 g) and water (10 ml). The mixture was stirred for further 2 hr at 30°C. The reaction mixture was extracted repeatedly with ether and the extract was washed with 5% sodium hydrogen carbonate, 5% potassium iodide and a saturated sodium chloride solutions, successively and dried (sodium sulfate). The residue obtained by evaporation of the solvent under reduced pressure was kept in a refrigerator to give crystals, 2.1 g (53%). The crystals were recrystallized from ethyl acetate to yield pure IIIc, colorless hexagonal plates, mp 99.5—101°C. IR (liquid): 3420 (O–H) broad, 1700 (C=O), 1620 (C=C); IR (Nujol mull of the crystals): 3300 (O–H) cm^{-1}.

Found: C, 17.90; H, 2.45; I, 64.13%. Calcd for $C_3H_5O_2I$: C, 18.02; H, 2.52; I, 63.46%.

b) By Means of Reagent B: Mercury-impregnated Dowex-60 (Reagent B) was prepared according to the reported method.[18] Iodopropargyl alcohol (IIc, 36.4 g, 0.2 mol) was added over 30 min-period in a stirred mixture of Reagent B (12 g) and water (60 ml) at 35°C. After the mixture had been stirred for further 1.5 hr at the same temperature, the mixture was saturated with sodium chloride and extracted with ether. The extract was washed with 5% potassium hydroxide and a saturated sodium chloride solutions successively and dried (sodium sulfate). The solvent was removed under reduced pressure. The residue crystallized in a refrigerator (33.5 g, 84%). Pure material, 99.5—101°C was obtained according to the above procedure and gave an identical IR spectrum.

Dihydroxyacetone (IV). *a) From 1-Bromo-3-hydroxypropan-2-one (IIIb)*: A mixture of potassium formate (7.6 g, 0.09 mol), 1-bromo-3-hydroxypropan-2-one (IIIb, 9.2 g, 0.06 mol) and methanol (100 ml) was refluxed for 5 hr. The reaction mixture was concentrated to *ca.* 60 ml and mixed with ether (100 ml). The inorganic material deposited was removed by filtration. The filtrate was concentrated under reduced pressure to afford dihydroxyacetone (IV) as a syrup. The syrup was dissolved in ether–methanol and the insoluble material was removed. The syrup obtained by evaporation of the solvent under diminished pressure reduced Fehling's solution at room temperature, and gave positive color reactions characteristic of dihydroxyacetone with sodium nitroprusside, resorcinol, phloroglucinol and orcinol,[22] thus proving the absence of methylglyoxal or glyceraldehyde. Since the syrupy dihydroxyacetone (IV) could not be crystallized after treatment with ion exchange resin (Dowex 50WX8 and Dowex 3), it was converted into a dibenzoate by the usual method. The crude dibenzoate was recrystallized from ethanol to yield colorless needles, mp 120.5—121°C [lit,[11] mp 121°C].

Found: C, 68.49; H, 4.71%. Calcd for $C_{17}H_{14}O_5$: C, 68.45; H, 4.73%.

The dibenzoate showed no depression of melting point on admixture with a benzoate (mp 120.5°C) prepared from an authentic specimen of IV. The IR spectra of both were found to be superimposable.

b) From 1-Iodo-3-hydroxypropan-2-one (IIIc): By the procedure used in the case of bromo-hydroxypropanone (IIIb), IIIc could be converted into a crude IV as a red syrup con-

33) H. B. Hill, *J. Amer. Chem. Soc.*, **3**, 178 (1881).

34) R. Lespieau, *Ann. Chim.*, **11**, 269 (1897); A. M. Sladkov, L. Y. Ukhin, G. N. Gorshkova, M. A. Chubarova, A. G. Makhsumov, and V. I. Kasatochkin, *Zh. Org. Khim.*, **1**, 415 (1965); [*Chem. Abstr.*, **63**, 1718 (1965)].

taining a minor amount of potassium iodide. The crude material gave positive color reactions characteristic of IV[22] and reduced cold Fehling's solution. The crude IV gave a dibenzoate, mp 119—120°C, which was proved to be identical with that of an authentic dibenzoate of IV.

1-Acetoxy-3-buten-2-one (IX). Acetoxybutenone (IX) was prepared according to the reported method[23] with modification. The reaction mixture obtained from 2-butyne-1,4-diol (VIII, 21.5 g, 0.25 mol) was filtered and the filtrate was concentrated under reduced pressure to remove the major part of acetic acid and acetic anhydride. The concentrate was mixed with ether and the insoluble material was removed by filtration. The residue obtained by evaporation of the solvent was distilled *in vacuo*. Acetoxybutenone (IX) was obtained as a colorless liquid, 18.6 g (58%), bp 63—66°C/3.5 mmHg, n_D^{20} 1.43136 [lit,[23] bp 70°C/4 mmHg, n_D^{25} 1.4355].

IX was subjected immediately to the subsequent reaction.

1,4-Diacetoxy-3-bromobutan-2-one (X). Freshly prepared *N*-bromosuccinimide (33.5 g, 0.188 mol) was added to a solution of the vinyl ketone (IX, 18.6 g, 0.145 mol) in dry acetic acid (120 m*l*). The mixture was stirred at room temperature until the crystals of *N*-bromosuccinimide disappeared (3—4 days). The resulting solution was mixed with ether (700 m*l*), and a saturated solution of sodium hydrogen carbonate and then solid sodium hydrogen carbonate were added in small portions. The alkaline aqueous layer was extracted with ether (150 m*l*). The combined ether layer was dried and evaporated under reduced pressure, thus yielding a pale yellow liquid. The colorless crystals, 17.7 g (45.7%) obtained by trituration of the liquid with a small amount of ether were recrystallized from methanol or methanol-water to yield pure X, mp 49.0—49.5°C [lit,[2] bp 100—102°C/10^{-4} mmHg].

Found: C, 36.07; H, 4.24; Br, 29.82%. Calcd for $C_8H_{11}O_5Br$: C, 35.98; H, 4.15; Br, 29.92%.

It was found that X decomposes rapidly on a metal surface and should be handled with a glass spatula. An interesting difference was observed between the IR spectrum of crystalline X by Nujol mull method and that of liquid X by liquid film method. Liquid X exhibits a broad absorption in carbonyl region (1765—1740 cm^{-1}), but the absorption splits into two peaks (1767 and 1725 cm^{-1}) in the spectrum of crystalline X. The sharp absorption observed below 1500 cm^{-1} in the spectrum of crystalline X could not be observed in that of liquid X.

1-Acetoxy-3,4-dibromobutan-2-one (XI). Bromine (17.3 g, 0.108 mol) was added dropwise into an ice-cooled solution of IX (13.9 g, 0.108 mol) in carbon tetrachloride (40 m*l*). The mixture was left to stand overnight and the solvent was removed under diminished pressure. Distillation of the residue *in vacuo* yielded XI as a viscous yellow liquid, 24.0 g (76.7%), bp 103—105°C/1 mmHg, n_D^{25} 1.51567, IR (neat): 1765—1735 (C=O of ketone and ester), 1225 (C-O of ester) cm^{-1}.

Found: C, 25.36; H, 2.77; Br, 54.92%. Calcd for $C_6H_8O_3Br_2$: C, 25.06; H, 2.80; Br, 55.50%.

Tri-O-acetyl-DL-erythrulose (XII). *a) From 1,4-Diacetoxy-3-bromobutan-2-one (X):* A mixture of diacetoxybutanone (X, 15.4 g, 0.058 mol), dry silver acetate (16.5 g, 0.099 mol) and anhydrous acetic acid (140 m*l*) was refluxed for 6 hr. The reaction mixture was cooled and the solid deposited was filtered and washed with acetic acid. The combined filtrate and washing were mixed with dry sliver acetate (16.5 g, 0.099 mol). After the mixture had been refluxed for 3 hr, the solvent was removed under reduced pressure and the residue was extracted with ether. The residue obtained by evaporation of the solvent was distilled *in vacuo* to yield a light yellow viscous liquid, 3.4 g (23.9%), bp 73—124°C/6×10^{-4} mmHg. Redistillation of this material afforded XII as a viscous liquid, bp 90°C/3×10^{-4} mmHg, n_D^{18} 1.44946 [lit,[2] bp 108—110°C/10^{-4} mmHg, n_D^{18} 1.4545], IR (neat): 2940, 1770—1740 (C=O of ketone and ester), 1143, 1085, 1055, 1020, 975, 928, 875, 838 cm^{-1}.

Found: C, 48.49; H, 5.77%. Calcd for $C_{10}H_{14}O_7$: C, 48.78; H, 5.73%.

b) From 1-Acetoxy-3,4-dibromobutan-2-one (XI): A mixture of XI (14.4 g, 0.05 mol), dry silver acetate (28.4 g, 0.17 mol) and dry acetic acid (200 m*l*) was treated according to the procedure used in the case of X. A minor amount of viscous yellow liquid, bp 80—125°C/10^{-4} mmHg was obtained. Although the liquid gave a weak positive Beilstein test, the IR spectrum was found to be closely related to that of the product obtained from X [IR: 2920, 1760—1700 (C=O of ketone and ester), 1135, 1075, 1050, 1020, 935, 910, 875, 835 cm^{-1}]. Presumably the liquid contains XII as a major component. Further purification was not performed.

DL-Erythrulose (XIII). A mixture of barium hydroxide octahydrate (8 g), water (80 m*l*) and the triacetate (XII, 2.5 g) was kept at 0°C for 90 min with occasional shaking, after which the mixture was saturated with carbon dioxide and the barium carbonate formed was removed by filtration. 4N Sulfuric acid was added to the filtrate in a slight excess. After the barium sulfate precipitated had been removed by means of a centrifuge, the solution was concentrated *in vacuo* at a temperature below 23°C to one fourth in volume. The concentrated solution was treated with Dowex 30 and again concentrated *in vacuo* at a temperature below 20°C. The syrupy residue was placed in an evacuated desiccator containing phosphorus pentoxide, yielding DL-erythrulose (XIII) as viscous syrup, 0.8 g. The syrup reduced cold Fehling's solution instantaneously.

A mixture of XIII (0.2 g) and a solution of phenylhydrazine in 50% aqueous acetic acid was kept at room temperature for 10 days to give deep brown precipitate. This material was crystallized from benzene to yield DL-erythrulose osazone as yellow needles, mp 168—169°C [lit, mp 166—168°C;[2] mp 167°C[35]].

Financial support from Mr. Tokusuke Egawa, president of Kofuku-sogo Bank, is gratefully acknowledged.

35) H. J .H. Fenton and H. Jackson, *J. Chem. Soc.*, **75**, 1 (1899).

Total Syntheses of Carbohydrates. II. DL-Erythrose and DL-Threose

Kenkichi SONOGASHIRA* and Masazumi NAKAGAWA**

Department of Chemistry, Faculty of Science, Osaka University, Toyonaka, Osaka

(Received January 24, 1972)

Propargyl alcohol was converted into 4-acetoxy-*cis*-crotonaldehyde diethyl acetal (III) *via* three steps. *cis*-Hydroxylation of III with potassium permanganate followed by acetylation yielded tri-*O*-acetyl-DL-erythrose diethyl acetal (IV). Hydrolysis of IV afforded syrupy DL-erythrose (VI) which could be converted into erythritol (VII) and its dibenzylidene derivative. An acid hydrolysis of III gave 4-acetoxy-crotonaldehyde (VIII) which was converted into triacetyl-DL-threose diethyl acetal (XI) or DL-threose pentaacetate (XII). Hydrolysis of XI and XII gave syrupy DL-threose which could be identified as di-benzylidenethreitol.

The total syntheses of dihydroxyacetone and DL-*glycero*-tetrulose (DL-erythrulose) have been reported.[1] The present paper deals with the total syntheses of DL-etythrose (VII) and DL-threose (XIV). The syntheses were achieved by Glattfeld and Kribben by the Rosenmund reduction of the corresponding aldonic acid chloride derivative which had been derived from allyl alcohol using stereospecific reactions.[2] An excellent total synthesis of DL-threose (XIV) was reported by Schmid and Grob[3] by the *cis*-hydroxylation of *trans*-1,1,4-triacetoxy-2-butene which can be prepared from crotonaldehyde.

cis- and *trans*-Ethylenic compounds have now became readily available from acetylenic precursors by stereoselective half-reduction. Various methods of stereospecific *cis*- and *trans*-hydroxylation of ethylenic bond are also known. A combination of these two seems to offer a new possibility of stereospecific syntheses of carbohydrates.[4] In the present study, propargyl alcohol was used as a starting material.

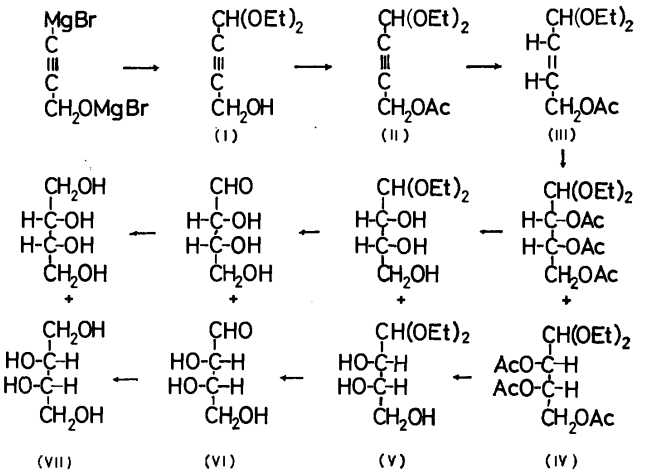

Scheme 1. Synthesis of DL-erythrose (VII).

The reaction sequence of total synthesis of DL-erythrose (VII) is shown in Scheme 1. *Erythro*-configuration was accomplished by *cis*-hydroxylation of the *cis*-olefinic compound (III) with potassium permanganate. The reaction of ethyl orthoformate with bis-Grignard derivative of propargyl alcohol was carried out according to the reported method[5] with modification to afford C_4-acetal (I). C_4-acetal (I) gave *cis*-olefinic acetoxy-acetal (III) in a high yield by acetylation followed by half-reduction over the Lindlar catalyst.[6] The reduction of C_4-acetal (I) using the same catalyst gave *cis*-olefinic hydroxy-acetal only in a low yield presumably owing to the cleavage of acetal bond.

cis-Hydroxylation of III was carried out in the usual way with aqueous potassium permanganate at temperatures of 0—5°C. Introduction of carbon dioxide into the reaction mixture to neutralize the potassium hydroxide formed during the course of reaction gave no appreciable effect. The crude reaction product was acetylated with acetic anhydride and pyridine. The acetylated product was distilled *in vacuo* to give 2,3,4-tri-*O*-acetyl-DL-erythrose diethyl acetal (IV) in a 28% yeild together with a recovery of III. The results of elemental analysis and IR spectrum were found to be consistent with the assigned structure (IV). Treatment of IV with sodium methoxide in methanol at a low temperature afforded DL-erythrose diethyl acetal (V) as a fairly pure syrup. Syrup V was hydrolyzed with dilute sulfuric acid to yield colorless syrup of DL-erythrose (VI). Paper chromatography of VI thus obtained produced a spot exactly corresponding to

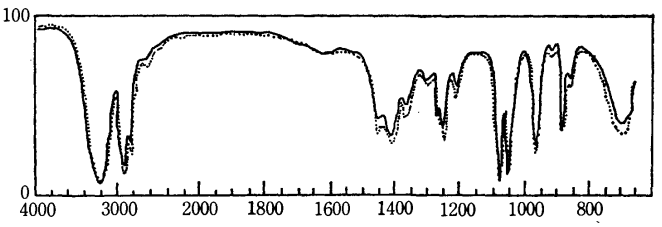

Fig. 1. IR spectra of erythritol. Synthesized material (——); authentic specimen (·····), (KBr-disk).

* Present address: The Institute of Scientific and Industrial Research, Osaka University, Yamadakami, Suita, Osaka.

** To whom inquiries should be addressed.

1) T. Ando, S. Shioi, and M. Nakagawa, This Bulletin, **45**, 2611 (1972).

2) a) J. W. E. Glattfeld and B. D. Kribben, *J. Amer. Chem. Soc.*, **61**, 1720 (1939); b) J. W. E. Glattfeld and E. Rietz, *ibid.*, **62**, 974 (1940); c) W. W. Lake and J. W. E. Glattfeld, *ibid.*, **66**, 1091 (1944).

3) H. Schmid and E. Grob, *Helv. Chim. Acta*, **32**, 77 (1949).

4) R. A. Raphael, "Acetylenic Compounds in Organic Synthesis," Butterworth Scientific Publications, London (1955), p. 92.

5) R. G. Jones and M. J. Mann, *J. Amer. Chem. Soc.*, **75**, 4048 (1953).

6) H. Lindlar, *Helv. Chim. Acta*, **35**, 446 (1952).

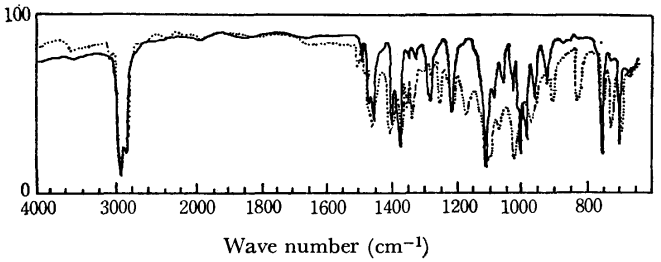

Fig. 2. IR spectra of di-*O*-benzylidene-erythritol (——) and di-*O*-benzylidene-threitol (·····), (KBr-disk).

that of authentic D-erythrose.[7] Hydrogenation of VI over platinum catalyst yielded crystalline erythritol (VII) which gave a superimposable IR spectrum with that of an authentic specimen (Fig. 1). The mixed melting point of VII with an authentic erythritol showed no depression. Di-*O*-benzylidene derivative obtained from VII (mp 201—202°C) showed an identical melting point with the reported value (mp 201—202°C).[8] The IR spectrum of di-*O*-benzylidene erythritol is shown in Fig. 2 toghether with that of threitol derivative.

trans-Hydroxylation of *cis*-ethylenic linkage affords *threo*-configuration. However, all attempts at *trans*-hydroxylation of *cis*-acetoxy acetal (III) with performic, peracetic or perbenzoic acid were unsuccessful. 4-Acetoxy crotonic acid was isolated from the reaction product of performic or peracetic acid oxidation. This indicates that the hydrolysis of acetal bond may occur prior to the epoxidation of the ethylenic linkage. Consequently, an inverse route to *threo*-configuration, *i.e.*, *trans*-hydroxylation of *trans*-olefin, was investigated. Reduction of acetylenic alcohol (I) or its 4-*O*-tetrahydro-2-pyranyl derivative in liquid ammonia with sodium[9,10] and reduction of I with lithium aluminum hydride[11] were found to be infeasible for preparative

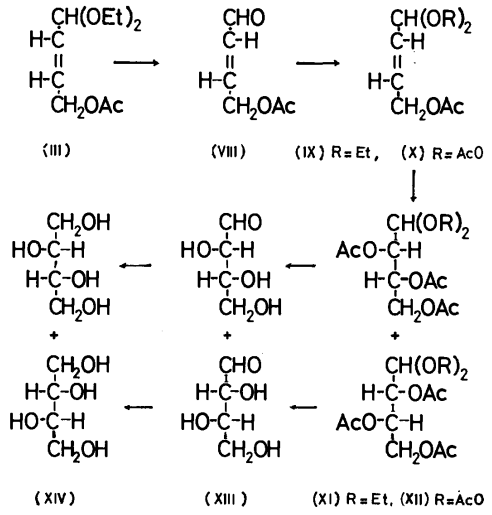

Scheme 2. Synthesis of DL-threose (XIV).

purposes owing to the poor yield of *trans*-ethylenic compound. *cis*-Ethylenic acetal (III) was hydrolyzed at room temperature (Scheme 2) with 70% aqueous formic or 50% aqueous acetic acid to give *trans*-ethylenic aldehyde (VIII),[12] which could be converted into *trans*-ethylenic acetal (IX, 64%) by the usual method.[13] *trans*-Ethylenic aldehyde diacetate (X, 71%) was also obtained by the actions of acetic anhydride and sulfuric acid on VIII. *cis*-Hydroxylation of *trans*-ethylenic acetal (IX) was carried out with an aqueous potassium permanganate at a low temperature introducing carbon dioxide into the reaction mixture. The product was acetylated without purification. The resulting acetylated material was distilled *in vacuo* to yield DL-threose derivative (XI, 14%) together with a recovery of IX. DL-Threose derivative (XI) thus prepared was treated successively with sodium methoxide in methanol and sulfuric acid to yeild DL-threose (XIII) as a syrup. The syrupy XIII was reduced over platinum catalyst, and the product was converted into crystalline di-*O*-benzylidene derivative. The benzylidene derivative showed an identical melting point (mp 218—219.5°C) with the reported value of di-*O*-benzylidene-DL-threitol (mp 220.5°C).[3] Di-*O*-benzylidene-erythritol has a much lower melting point than that of threitol derivative, and the IR spectra of these two dibenzylidene derivatives also show the difference seen in Fig. 2. The above results confirm the *threo*-configuration of XIII and XIV.

trans-Ethylenic triacetate (X) prepared by Schmid and Grob[3] from crotonaldehyde diacetate and used as an intermediate of the synthesis of DL-threose could be converted into DL-threose pentaacetate (XII) by their method on treatment with the Milas reagent[14] followed by acetylation. The hydrolysis of XII with sodium methoxide in methanol afforded syrupy DL-threose (XIII) which could be identified as di-*O*-benzylidene derivative of threitol (XIV).

The overall yield of DL-threose (XIII) from propargyl alcohol was found to be *ca.* 3.3% *via* acetal and 2.7% *via* triacetate (X).

Experimental

All the melting points are uncorrected. The IR spectra were obtained on a Hitachi EPI-2 Spectrophotometer.

1,1-Diethoxy-2-butyn-4-ol (I). A solution of propargyl alcohol (39.2 g, 0.7 mol) in tetrahydrofuran (50 m*l*) was added to a solution of ethylmagnesium bromide (prepared from magnesium, 36.5 g, 1.5 g-atom, ethyl bromide, 163.5 g. 1.5 mol and tetrahydrofuran, 400 m*l*) over a period of 1 hr. After the mixture had been refluxed for 3 hr, ethyl orthoformate (104 g, 0.7 mol) was added to the cooled mixture in one portion. The mixture was refluxed for 8 hr under stirring and stood overnight at room temperature. After a part of the solvent (*ca.* 200 m*l*) has been distilled off, the mixture was added to an ice-cooled solution of ammonium

7) A. S. Perlin and C. Brice, *Can. J. Chem.*, **34**, 541 (1956).
8) E. Fischer, *Ber.*, **27**, 1535 (1894).
9) L. Crombie, *J. Chem. Soc.*, **1952**, 4338.
10) M. M. Fraser and R. A. Raphael, *ibid.*, **1955**, 4280.
11) J. Attenburrow, A. F. B. Cameron, J. H. Chapman, R. M. Evans, B. A. Hems, A. B. A. Jansen, and T. Walker, *ibid.*, **1952**, 1094.
12) R. A. Raphael and F. Sondheimer, *ibid.*, **1951**, 2693.
13) P. H. Williams, G. B. Payne, W. J. Sullivan, and P. R. Van Ess, *J. Amer. Chem. Soc.*, **82**, 4883 (1960); H. O. L. Fischer and E. Baer, *Helv. Chim. Acta*, **18**, 514 (1935).
14) N. A. Milas and S. Sussman, *J. Amer. Chem. Soc.*, **58**, 1302 (1936).

acetate (200 g) in water (700 ml) and shaken with ether. The emulsion formed was broken by filtering through a layer of celite. The celite layer was washed with ether and the aqueous layer was extracted with the same solvent. The combined extracts and washings were dried (sodium sulfate) and the solvent was removed under reduced pressure. Distillation of the residue *in vacuo* afforded colorless liquid, bp 113—115°C/3 mmHg as main fraction. This material was redistilled to give pure I, 49.5 g (45%), bp 100—102°C/1.5 mmHg, n_D^{25} 1.4491 [lit,[5] bp 118—122°C/9 mmHg, bp 88°C/0.5 mmHg; n_D^{25} 1.4495, IR (neat): 3400 (O–H) cm^{-1}].

Found: C, 60.90; H, 8.97%. Calcd for $C_8H_{14}O_3$: C, 60.73; H, 8.92%.

Diethoxybutynol (I) was found to be unstable and turned pale yellow after several hours at room temperature, but could be kept without decomposition in a tightly stoppered flask in a refrigerator.

4-Acetoxy-1,1-diethoxy-2-butyne (II). A mixture of acetic anhydride (90 ml) and hydroxy acetal (I, 57.9 g, 0.365 mol) was heated to 95—100°C for 2 hr. The residue obtained by evaporation of acetic acid and acetic anhydride under reduced pressure was distilled *in vacuo* to give II as colorless liquid, bp 86—89°C/2.5 mmHg, 62.3 g (85.3%), n_D^{20} 1.4413, IR (neat): 1735, 1235 (CH_3CO_2–) cm^{-1}. An analytical specimen was obtained by redistillation of this material, bp 84°C/2.2 mmHg.

Found: C, 59.98; H, 8.06%. Calcd for $C_{10}H_{16}O_4$: C, 59.98; H, 8.05%.

II was found to be unstable and turned pale yellow on standing a few hours at room temperature. Acetylation of I with pyridine-acetic anhydride gave II in a low yield (56.2%).

*4-Acetoxy-*cis*-crotonaldehyde Diethyl Acetal (III).* II (20.0 g, 0.1 mol) in benzene (100 ml) was reduced over a Lindlar catalyst[6] (3.5 g) at 16°C. Uptake of 1 mol of hydrogen was observed over a period of 1.5 hr. The catalyst was removed by filtration and the solvent was distilled off under reduced pressure. Distillation of the residue *in vacuo* afforded III as colorless liquid, 19.2 g (96%), bp 91—93°C/4 mmHg, n_D^{20} 1.4318, IR (neat): 1730, 1235 (CH_3CO_2–), 1650 (–CH=CH–) cm^{-1}.

Found: C, 59.42; H, 8.95%. Calcd for $C_{10}H_{18}O_4$: C, 59.38; H, 8.97%.

*2,3,4-Tri-*O*-acetyl-*DL*-erythrose Diethyl Acetal (IV).* To a vigorously stirred suspension of III (10 g, 0.050 mol) in water (100 ml) was added an aqueous solution (420 ml) of potassium permanganate (7.5 g) over a period of 1.25 hr at 0—5°C. After the addition had been completed, the reaction mixture was warmed to 35°C to coagulate the manganese dioxide formed. The dioxide collected on a sintered glass filter was washed with methanol and water, successively. The washings were combined with the filtrate and concentrated to *ca.* 115 ml under reduced pressure at a temperature below 35°C. The concentrated solution (pH 6.0) was saturated with sodium chloride and repeatedly extracted with ether, and dried (sodium sulfate). The residue obtained by evaporation of the solvent under diminished pressure was mixed with anhydrous methanol and benzene, and the solvent were again removed under reduced pressure. The procedure was repeated twice, giving a syrupy residue (4.6 g, IR (neat): 3450 (O–H) cm^{-1}). The residue was mixed with acetic anhydride (10 ml) and pyridine (10 ml). The mixture was kept at room temperature for 24 hr and then at 40°C for 18 hr. The reaction mixture was concentrated under reduced pressure at a temperature below 30°C. The ice-cooled residue was poured onto ice-water (100 ml) and extracted with ether. The extract was washed successively with 1N hydrochloric acid saturated with sodium chloride, a saturated aqueous solution of sodium hydrogen carbonate and a saturated sodium chloride solution and dried (sodium sulfate). The viscous liquid obtained by evaporation of the solvent under reduced pressure was subjected to high vacuum distillation. Acetoxy-crotonaldehyde diethyl acetal (III) was recovered as a forerun, bp 60°C/10^{-4} mmHg. Triacetyl-erythrose diethyl acetal (IV) was obtained as colorless viscous liquid, bp 94—100°C/10^{-4} mmHg, 4.4 g (28%). The material was redistilled to give pure IV, bp 97—98°C/10^{-4} mmHg, n_D^{20} 1.4327.

Found: C, 52.57; H, 7.53%. Calcd for $C_{14}H_{24}O_8$: C, 52.49; H, 7.55%.

DL-Erythrose Diethyl Acetal (V). A solution of IV (2.4 g) in anhydrous methanol (15 ml) was chilled to −13°C and mixed with 0.10N solution of sodium methoxide in methanol (10.0 ml) which had been cooled to the same temperature. After the mixture had been kept at −20°C for 24 hr, it was exactly neutralized with 1N sulfuric acid. The mixture was concentrated under reduced pressure at 20—25°C. The residue containing crystals of sodium sulfate and sodium acetate was extracted with anhydrous ethanol (10 ml). The extract was evaporated again under reduced pressure. The procedure was repeated twice, yielding DL-erythrose diethyl acetal (V) as colorless syrup, IR (neat): 3420 (O–H) cm^{-1}. An analytical specimen was prepared on standing a small portion of the syrup in a highly evacuated desiccator containing phosphorus pentoxide.

Found: C, 49.31; H, 9.22%. Calcd for $C_8H_{18}O_5$: C, 49.47; H, 9.34%.

All attempts to crystallize V failed.

DL-Erythrose (VI). The syrupy diethyl acetal (IV) was dissolved in 1N sulfuric acid (20 ml) and the solution was left standing for 5 days at room temperature. After the solution had been neutralized with 1N sodium hydroxide solution, water was removed under reduced pressure at a temperature below 20°C. Anhydrous methanol was added to the residue and the sodium sulfate deposited was removed by filtration. The filtrate was evaporated *in vacuo*, and the residue was extracted with the same solvent. Evaporation of the solvent *in vacuo* gave colorless syrup, 2.5 g (95%). A small portion of the syrup was dried in a highly evacuated desiccator over phosphorus pentoxide and subjected to elemental analysis.

Found: C, 40.91; H, 6.80%. Calcd for $C_4H_8O_4$: C, 40.00; H, 6.71%.

The syrup reduced Fehling's solution at room temperature. Descending paper chromatography (Filter paper: Toyo Roshi No. 51; solvent system: (A) upper layer of *n*-butyl alcohol–benzene–pyridine–water (5:1:3:3) or (B) methyl ethyl ketone saturated with water; detection reagent: anilinium oxalate) of the syrup gave a spot (R_f 0.51 (A); R_f 0.85 (B)). An authentic D-erythrose prepared by the method of Perlin and Brice[7] gave a spot at the same R_f-value (R_f 0.51 (A); R_f 0.85 (B))

Syrupy DL-erythrose (VI, 0.3 g) dissolved in a small amount of water was mixed with a solution of phenylhydrazine (1.5 g) in 50% aqueous acetic acid. The mixture was placed on a water-bath kept at 50°C for 1 hr. The yellow crystalline mass deposited was recrystallized once from water and then twice from benzene to give pure osazone, mp 166—167°C (decomp.) [lit,[2c] mp 166—167°C (decomp.)].

Found: C, 64.50; H, 6.10; N, 18.29%. Cacld for $C_{16}H_{18}O_2N_4$: C, 64.41; H, 6.08; N, 18.78%.

*Erythritol and Di-*O*-benzylidene-erythritol.* Syrupy DL-erythrose (VI, 0.41 g) in methanol was reduced over platinum catalyst (prepared from platinum oxide, 25 mg) at 100°C for 2 hr (initial pressure of hydrogen: 44 atm.). The catalyst was removed by filtration and the filtrate was evaporated

under diminished pressure to give colorless crystals, 0.39 g. The crystals were recrystallized twice from a small amount of methanol to yield pure erythritol, mp 116.5—118.5°C, which showed no depression of melting point on admixture with an authentic specimen of erythritol, mp 117—118°C.

Found: C, 39.24; H, 8.22%. Calcd for $C_4H_{10}O_4$: C, 39.34; H, 8.25%.

Erythritol thus obtained was converted into di-*O*-benzylidene-erythritol according to the method of Fischer.[8] The benzylidene derivative showed melting point identical with that of reported value, mp 201—202°C [lit,[8] 201—202°C].

4-Acetoxy-crotonaldehyde (VIII). Acetoxy-*cis*-ethylenic acetal (III, 3.8 g) dissolved in a mixture of formic acid (5 m*l*) and water (2 m*l*) was kept at room temperature for 24 hr. Benzene was added to the residue obtained by evaporation of the mixture and benzene was again removed under reduced pressure. The residue was distilled *in vacuo* to give colorless liquid, bp 54—57°C/1 mmHg. Redistillation of this substance afforded pure 4-acetoxy-crotonaldehyde (VIII) as colorless liquid, 1.4 g (60%), bp 73—76°C/3 mmHg, n_D^{20} 1.4518, IR (neat): 1730, 1225 (CH_3CO_2–), 1680, 2760 (–CHO), 1640, 960 (*trans* –CH=CH–) cm^{-1}.

Found: C, 56.39; H, 6.89%. Calcd for $C_6H_8O_3$: C, 56.24; H, 6.29%.

2,4-Dinitrophenylhydrazone: mp 158—161°C (decomp.) (from ethanol).

Found: C, 46.28; H, 3.98; N, 18.04%. Calcd for $C_{12}H_{12}O_6N_4$: C, 46.76; H, 3.92; N, 18.18%.

4-Acetoxy-crotonaldehyde Diethyl Acetal (IX). Ethyl orthoformate (2.7 g, 0.02 mol) and ammonium nitrate (0.1 g) were added to a solution of *trans*-aldehyde (VIII, 2.65 g, 0.02 mol) in anhydrous ethanol (10 m*l*). The mixture was heated to 100°C and ethyl formate and ethanol were gradually distilled off through a Widmer column. Distillation of the residue *in vacuo* afforded colorless liquid, 1.55 g (37.2%), bp 77—80°C/1.5 mmHg. This material was redistilled to give pure IX, bp 74—75°C/1 mmHg, n_D^{20} 1.4328, IR (neat): 1765, 1230 (CH_3CO_2–), 1650, 950 (*trans* –CH=CH–) cm^{-1}.

Found: C, 59.10; H, 8.93%. Calcd for $C_{10}H_{18}O_4$: C, 59.38; H, 8.97%.

IX could be obtained in a much higher yield without isolation of VIII. After a solution of *cis*-acetal (III, 11.0 g, 0.055 mol) in 50% aqueous acetic acid (20 m*l*) had been kept at 40°C for 48 hr, the solvent was removed under reduced pressure. The residue was mixed with benzene and the solvent was again distilled off *in vacuo*. This procedure was repeated twice. Acetalization of the residue according to the above method yielded IX, 7.0 g (63.6%).

2,3,4-Tri-O-*acetyl*-DL-*threose Diethyl Acetal (XI).* An aqueous solution of potassium permanganate (6.65 g in 220 m*l* of water) was added dropwise to a vigorously stirred suspension of *trans*-acetal (IX, 9.4 g, 0.047 mol) in water (60 m*l*) over a period of 70 min. The mixture was kept at 0°C and carbon dioxide was continuously introduced into the mixture. The reaction mixture was worked up according to the method used for the preparation of tri-*O*-acetyl-erythrose diethyl acetal (IV). The crude acetoxy-dihydroxy-acetal (5.7 g) thus obtained was mixed with pyridine (12 m*l*) and acetic anhydride (12 m*l*). The mixture was allowed to stand at room temperature for 27 hr and then at 35°C for 21 hr. Deep brown liquid obtained by concentration of the mixture under reduced pressure was dissolved in ether. The ice-cooled ether solution was poured onto ice-water (100 m*l*). The mixture was saturated with sodium chloride and repeatedly extracted with ether. The extract was washed twice with 1N hydrochloric acid saturated with sodium chloride, once with a saturated sodium hydrogen carbonate solution and water and then dried (sodium sulfate). The residue obtained by evaporation of the solvent gave on a vacuum distillation a forerun (recovered IX, bp 60—70°C/6×10^{-4} mmHg, 3.2 g) and XI, colorless syrup, 1.4 g (14% based on consumed IX), n_D^{25} 1.4368.

4-Acetoxy-crotonaldehyde Diacetate (X). A solution of *cis*-ethylenic acetal (III, 15.8 g, 0.077 mol) in 50% aqueous acetic acid was kept at 40°C for 48 hr. The residue obtained by evaporation of the solvent under reduced pressure was mixed with acetic anhydride (30 m*l*). A few drops of concentrated sulfuric acid was added to the mixture under cooling with water. After the mixture had been kept at room temperature for 20 hr, powdered sodium acetate (0.6 g) was added and distilled to yield X as colorless viscous liquid, 12.6 g (71%), bp 122—124°C/1.8 mmHg [lit,[3] bp 102—104°C/1×10^{-2} mmHg], n_D^{20} 1.4414.

Found: C, 52.43; H, 6.41%. Calcd for $C_{10}H_{14}O_6$: C, 52.17; H, 6.13%.

DL-*Threose Pentaacetate (XII).* Acetoxy-crotonaldehyde diacetate (X, 4.4 g, 0.02 mol) was treated with Milas' reagent[14] according to the reported method.[3] Acetylation of the reaction product (IR: 3400 (O–H) cm^{-1}) by means of acetic anhydride (12 m*l*) and pyridine (12 m*l*) yielded XII as colorless liquid, 0.7 g (11%), bp 92—100°C/1×10^{-4} mmHg [lit,[3] bp 115—122°C/5×10^{-3} mmHg].

Found: C, 49.05; H, 5.90%. Calcd for $C_{14}H_{20}O_{10}$: C, 48.27; H, 5.79%.

DL-*Threose (XIII).* *a) By Hydrolysis of 2,3,4-Tri*-O-*acetyl*-DL-*threose Diethyl Acetal (XI)*: Hydrolysis of XI (14 g) according to the method used for triacetyl-DL-erythrose diethyl acetal (IV) afforded DL-threose (XIII) as light brown syrup (0.5 g). The syrup reduced cold Fehling's solution. The crude XIII was subjected to the reduction without purification.

b) By Hydrolysis of DL-*Threose Pentaacetate (XII)*: DL-Threose pentaacetate (0.7 g) in anhydrous methanol (30 m*l*) was mixed with 2% solution of sodium methoxide in anhydrous methanol (10 m*l*) at −10°C. The mixture was kept at the same temperature for 24 hr, and then was neutralized with 1N sulfuric acid. Sodium sulfate deposited was removed by filtration. The filtrate was concentrated under reduced pressure. The residue was mixed with anhydrous methanol and the sulfate was again removed. Concentration of the filtrate *in vacuo* afforded DL-threose (XIII) as a light brown syrup (0.2 g). The syrup reduced Fehling's solution at room temperature.

Di-O-*benzylidene-threitol.* *a) From* DL-*Threose Obtained from XI*: Syrupy DL-threose (XIII) obtained from XI in 75% aqueous ethanol was reduced over platinum catalyst (initial pressure: 70 atm; 100°C; 3 hr). The reduction product worked up according to the procedure employed in the preparation of erythritol (VII) gave threitol (XIV, 0.25 g) as a syrup. The syrup was mixed with benzaldehyde (0.75 m*l*) and hydrochloric acid (0.9 m*l*). After the mixture was kept at room temperature for 1 hr, it was extracted with chloroform. The extract was washed successively with a sodium hydrogen carbonate solution and water and dried. The residue obtained by evaporation of the solvent was dissolved in hot ethanol and treated with active charcoal to yield di-benzylidene-threitol as colorless needles, 200 mg, mp 218—219.5°C [lit,[3] 220.5°C], IR: *Cf.*, Fig. 2.

Found: C, 72.78; H, 6.12%. Calcd for $C_{18}H_{18}O_4$: C, 72.46; H, 6.08%.

b) From DL-*Threose Obtained from XII*: Crude DL-threose (XIII) obtained by the hydrolysis of XII was reduced according to the procedure for the preparation of VII. The light brown syrupy threitol (XIV) obtained was converted into

di-benzylidene-threitol, colorless needles, mp 218—219°C. This material showed no depression of melting point on admixture with di-benzylidene-threitol derived from XI. The IR spectrum was found to be superimposable with that of the benzylidene derivative obtained from XI.

The financial support extended by Mr. Tokusuke Egawa, president of Kofuku-sogo Bank, is gratefully acknowledged.

BULLETIN OF THE CHEMICAL SOCIETY OF JAPAN, VOL. 45, 2620—2624 (1972)

Total Syntheses of Carbohydrates. III. DL-Glyceraldehyde and 2-Deoxy-DL-*erythro*-pentose

Kosuke MIMAKI, Michihiko MASUNARI, Gen NAKAMINAMI, and Masazumi NAKAGAWA*

Department of Chemistry, Faculty of Science, Osaka University, Toyonaka, Osaka

(Received January 31, 1972)

The synthesis of DL-glyceraldehyde (III) by the Barton's oxidation of DL-isopropylideneglycerol (I) was described. 2-Deoxy-DL-*erythro*-pentose (IX) (2-deoxy-DL-ribose) has been synthesized by the Barton's oxidation of 2-deoxy-3,4-*O*-isopropylidene-5-*O*-(tetrahydro-2-pyranyl)-DL-*erythro*-pentitol (VIII) and by the hydroboration of DL-*erythro*-4-pentyn-1,2,3-triol (XI) followed by hydrogen peroxide oxidation. The latter method gave crystalline 2-deoxy-DL-*erythro*-pentose (IX) in a reasonable yield.

In the previous papers, we have reported the syntheses of dihydroxyacetone,[1] DL-*glycero*-tetrulose,[1] DL-threose[2] and DL-erythrose[2] starting from simple acetylenic compounds. Selective synthesis of *cis*- and *trans*-ethylenic compounds followed by stereospecific hydroxylation of ethylenic linkage and introduction of carbonyl function played important roles in the syntheses of these carbohydrates. In the present paper, we wish to report a new syntheses of DL-glyceraldehyde (III) and the syntheses of 2-deoxy-DL-*erythro*-pentose (IX) according to two different routes.

The Pfitzner-Moffatt reagent[3] has been proved to be adequate for the conversion of primary alcohol to aldehyde. However, disadvantage of application of this reagent[4] or the dimethylsulfoxide-acetic anhydride reagent[5] for carbohydrate synthesis has been pointed out by several authors. We have carried out the synthesis of DL-glyceraldehyde (III) by means of the Barton's oxidation[6] proving the usefulness of this procedure for carbohydrate synthesis. As is illustrated in Scheme 1, DL-isopropylideneglycerol (I) in dry ether was treated with phosgene in the presence of quinoline to give chloroformate (II) in a good yield. Purification of chloroformate (II) was achieved by a distillation under reduced pressure. However, the crude II could be used in the subsequent reaction without difficulty. Crude chlorofomate (II) was mixed with dimethyl sulfoxide resulting in evolution of carbon dioxide. After treatment with triethylamine, the protective group was hydrolyzed by means of ion-exchange resin. DL-Glyceralehyde (III) was obtained as syrupy liquid, and gave a single spot on tlc which corresponds exactly with that of an authentic specimen. The syrupy glyceradehyde (III) partly crystallized on standing. 2,4-Dinitrophenylhydrazone of III was obtained in a yield of 33% based on DL-isopropylideneglycerol (I).

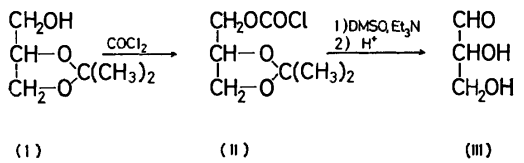

(I) (II) (III)

Scheme 1. Synthesis of DL-glyceraldehyde (III). DMSO=dimethyl sulfoxide

The successful result of the Barton's oxidation prompted the present authors to the synthesis of 2-deoxy-DL-*erythro*-pentose (IX) employing the same oxidation reaction.

The total syntheses of 2-deoxy-*erythro*-pentose (IX) have been reported by Fraser and Raphael[7] and Weygand and Leube.[8] In the former case, the yield of the pentose was found to be unsatisfactory, however, anilide of 2-deoxy-*erythro*-pentose (IX) was obtained in an overall yield of 2.5% in the latter case using commercially available 1-methoxy-1-buten-3-yne as starting meterial.

The reaction sequence we have employed was shown in Scheme 2.

The reaction of lithium acetylide of tetrahydropyranyl ether derivative of propargyl alcohol (IV) in refluxing liquid ammonia with ethylene oxide gave

* The author to whom inquiries should be addressed.

1) T. Ando, S. Shioi, and M. Nakagawa, This Bulletin, **45**, 2611 (1972).

2) K. Sonogashira and M. Nakagawa, *ibid.*, **45**, 2616 (1972).

3) K. E. Pfitzner and J. G. Moffatt, *J. Amer. Chem. Soc.*, **87**, 5661, 5670 (1965).

4) D. Horton, M. Nakadate, and J. M. J. Tronchet, *Carbohyd. Res.*, **7**, 56 (1968).

5) J. L. Godman and D. Horton, *ibid.*, **6**, 229 (1968).

6) D. H. R. Barton, B. J. Garner, and R. H. Wightman, *J. Chem. Soc.*, **1964**, 1855.

7) M. M. Fraser and R. A. Raphael, *ibid.*, **1955**, 4280.

8) F. Weygand and H. Leube, *Chem. Ber.*, **89**, 1914 (1956).

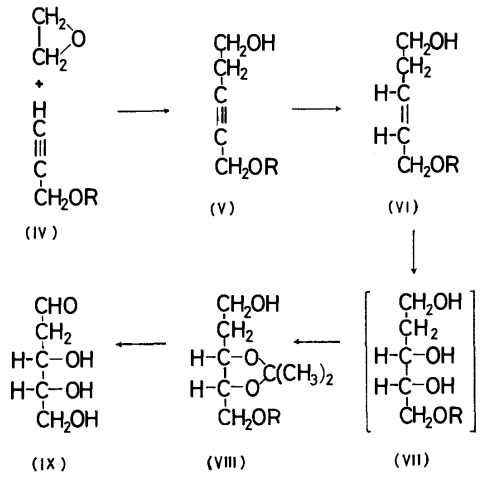

Scheme 2. Synthesis of 2-deoxy-DL-*erythro*-pentose (IX).
R=tetrahydropyranyl
The formulae of D-isomers are shown for brevity.

C_5-acetylenic compound (V) in a high yield. A half-reduction of V by means of Lindlar catalyst[9] afforded C_5-*cis*-ethylenic compound (VI). VI was treated with potassium permanganate to cause *cis*-hydroxylation of the *cis*-ethylenic bond. 3,4-*erythro*-Compound (VII) was obtained as a viscous syrup. Syrupy VII, which was proved to be fairly homogeneous by tlc, was subjected to the following reaction without purification. A difficulty was encountered in the conversion of VII to the corresponding acetonide (VIII). The reaction of VII with acetone in the presence of anhydrous cupric sulfate was followed by IR spectroscopy and tlc. The change of IR spectra indicated that the cleavage of tetrahydropyranyl group occurred accompanying an anomalous increase in the amount of dimethyldioxolane ring on heating the mixture under reflux. Therefore, the reaction was carried out at room temperature, and the reaction was quenched as soon as the spot of VII in tlc disappeared. Chromatographic purification of the reaction product on alumina gave crude isopropylidene derivative (VIII) in a low yield. The Barton's oxidation[6] of the crude VIII followed by acid hydrolysis of the protective groups resulted in a syrupy product, which gave a spot corresponding to that of authentic 2-deoxy-D-*erythro*-pentose. The crude 2-deoxy-DL-*etythro*-pentose (IX) thus obtained gave crystalline anilide in a low yield. The preparation of 2-deoxy-DL-*erythro*-pentose (IX) according to the reaction sequence indicated in Scheme 2 resulted in a rather unsatisfactory consequence. However, the usefulness of the Barton's oxidation in carbohydrate chemistry seems to remain for further investigation.

Preparation of aldehyde by addition of bis(1,2-dimethylpropyl)borane to terminal ethynyl group followed by oxidation with hydrogen peroxide has been reported by Brown and Zweifel.[10] Application of this method to a poly-ol having an ethynyl group is a conceivable route of synthesis of 2-deoxyaldose. DL-*erythro*-4-Pentyn-1,2,3-triol (XI),[11] a precursor for the synthesis of DL-*erythro*-pentose (IX), is a known compound prepared by *trans*-hydroxylation of *trans*-2-penten-4-yn-1-ol (X)[12] by means of performic acid. According to the reaction sequence illustrated in Scheme 3, the triol (XI) was treated with an excess of bis(1,2-dimethylpropyl)borane and the reaction product was oxidized with hydrogen peroxide under careful addition of 1N sodium hydroxide solution to neutralize the resulting boric acid, and to keep the pH of medium at 7.0—7.5. The control of pH is essential in this reaction. An appreciable decrease in the yield of IX was observed when the pH of medium increased to *ca.* 9. The reaction mixture was mixed with sodium hydrogen sulfite solution, and then deionized with ion-exchange resin. The syrup obtained by removing boric acid as methyl ester was treated with aniline according to the usual manner. The anilide thus obtained was found to be identical with that of an authentic D-IX and that of DL-IX which was prepared by another synthetic route.[13] The IR spectra of anilide derived from DL-IX and an authentic D-IX are recorded in Fig. 1. The yield of anilide of IX on the basis of ethynyl compound (XI) was found to be 20%, and the overall yield from epichlorohydrin was 3.8%. The free pentose (IX) obtained from anilide crystallized completely on seeding with a piece of crystal of an authentic D-isomer. The elemental analysis and the comparison of tlc with that of an authentic D-IX indicate that the crystals are 2-deoxy-*erythro*- pentose (IX). The pentose (IX) showed no optical activity over a wide range of wavelength indicating the crystallization of DL-isomer. This is the

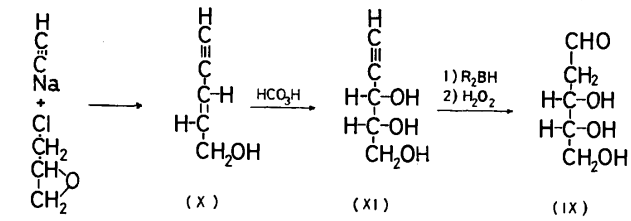

Scheme 3. Another synthesis of 2-deoxy-DL-*erythro*-pentose (IX).
R=$(CH_3)_2CH-\underset{\displaystyle CH_3}{\underset{|}{CH}}-$
The formulae of D-isomers are shown for brevity.

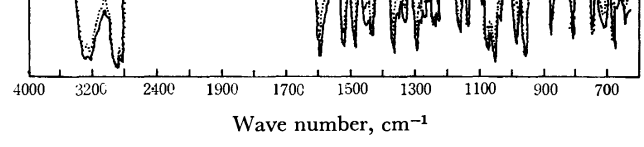

Wave number, cm^{-1}

Fig. 1. IR spectra of anilide of DL-IX (——) and anilide of an authentic D-IX (·····), (Nujol mull).

9) H. Lindlar, *Helv. Chim. Acta*, **35**, 446 (1952).
10) H. C. Brown and G. Zweifel, *J. Amer. Chem. Soc.*, **81**, 1512 (1959); **83**, 3834 (1961).
11) R. A. Raphael, *J. Chem. Soc.*, **1949**, S 44.
12) L. J. Haynes, I. M. Heilbron, E. R. H. Jones, and F. Sondheimer, *ibid.*, **1947**, 1583.
13) G. Nakaminami, S. Shioi, Y. Sugiyama, S. Isemura, M. Shibuya, and M. Nakagawa, This Bulletin, **45**, 2624 (1972).

first instance of crystalline 2-deoxy-DL-*erythro*-pentose (IX).

After completion of this study, an independent paper on the application of hydroboration for the synthesis of α,β-ethylenic aldose derivatives was published.[14]

Experimental

Silica Gel G (E. Merck, Darmstadt, Germany) was used for tlc. Anisaldehyde-sulfuric acid-acetic acid-ethanol[15a] (A), concentrated sulfuric acid[15b] (B) and diphenylamine-sulfuric acid-acetic acid[16] (C) were used as detection reagents. In the case of reagent (C), the splayed tlc plate was covered with another glass plate and baked at 90—100°C to develop the color. IR spectroscopy was performed with a Hitachi EPI-2 or a Japan Spectroscopic DS-402G Spectrophotometer. NMR spectra were obtained on Varian A-60 Spectrometer operated at 60 MHz using TMS as internal standard. All the melting points are uncorrected.

*1-O-Chloroformyl-2,3-O-isopropylidene-*DL*-glycerol (II).* A solution of DL-isopropylideneglycerol[17] (I, 13.2 g, 0.1 mol) and quinoline (12.9 g, 0.1 mol) in anhydrous ether (150 ml) was strongly chilled on an ice-salt bath. Phosgene passed through linseed oil and concentrated sulfuric acid was introduced for 2 hr into the chilled solution under stirring. Further stirring was continued for 30 min under cooling, and then for 2 hr at room temperature. The reaction mixture was filtered to remove quinoline hydrochloride with the aid of slight excess air pressure avoiding atmospheric moisture. Evaporation of the filtrate under reduced pressure yielded viscous light yellow liquid [15.6 g, 80%, IR (neat): 1784 (Cl-C=O), 1383, 1375, 842 (dimethyl dioxolane) cm^{-1}]. The crude chloroformate (II) could be used without purification in the subsequent reaction. Crude II turned to brown in a few days on standing at room temperature. A vacuum distillation of the crude material afforded pure II as colorless liquid, bp 75°C/7 mmHg, n_D^{25} 1.4381, NMR (CCl_4): δ 1.32 (3H, s) CH_3; δ 1.39 (3H, s) CH_3.

Found: C, 43.93; H, 5.75; Cl, 17.99%. Calcd for $C_7H_{11}O_4Cl$: C, 43.20; H, 5.70; Cl, 18.22%.

DL-*Glyceraldehyde (III).* Dimethyl sulfoxide (5 ml) was added to chloroformate (II, 973 mg, 5 mmol) at 10—15°C under vigorous evolution of carbon dioxide. After 2 min, the cooling bath was removed, and the mixture was stirred for 15 min at room temperature (>20°C). The mixture was then chilled on an ice-bath and mixed with triethylamine (607 mg, 6 mmol). After the mixture had been stirred for 3 min at the temperature, stirring was continued for 20 min at room temperature (>20°C). Triethylammonium chloride deposited was removed by filtration. The filtrate was mixed with a cation exchange resin [Amberlite IR-200 (H^+) in water (10 ml)]. After the mixture had been stirred for 2 hr under ice cooling, an anion exchange resin [Dowex-3 (OH^-)] was added to remove chloride ion. The resins were removed by filtration and washed with water. The combined filtrate and washing, which gave negative silver nitrate and Beilstein tests, were concentrated under reduced pressure at a temperature below 35°C. After most of the water had been distilled off, remaining dimethyl sulfoxide was removed under high vacuum at the same temperature. The resulting syrup reduced strongly the Tollens' and the Fehling's solutions. The absorption arising from dimethyldioxolane ring completely disappeared in the IR spectrum of the syrupy material. The syrup gave one spot (R_f 0.36) on tlc (solvent: acetone; detection reagent: A or B), and the spot of isomeric dihydroxyacetone (R_f 0.64) or another spot could not be observed. An acetone solution of the syrup was placed for a long time in a refrigerator, resulting in deposition of a small amount of colorless rods, mp 127—135°C [lit, mp 138°C,[18] mp 142.5°C[19]]. The colorless crystals gave identical tlc with that of an authentic specimen. An acetone solution of syrupy III obtained by another run gave a small amount of colorless powder. The substance showed no definite melting point, but underwent color change to brown at *ca.* 200°C. However, tlc and IR spectrum of the colorless solid were found to be identical with those of an authentic specimen (*Cf.*, Fig. 2). It has been reported that the melting point of DL-glyceraldehyde (III) varies widely depending on the rate of heating and the method of measurement.[20] Our observation seems to be related with this phenomenon.

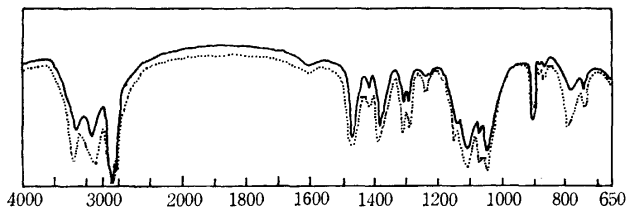

Fig. 2. IR spectra of DL-glyceraldehyde [mp *ca.* 200°C (decomp.)] (——) and an authentic DL-glyceraldehyde (·····), (Nujol mull).

2,4-Dinitrophenylhydrazone of DL*-Glyceraldehyde.* Syrupy DL-glyceraldehyde (III, 180 mg) was converted to the 2,4-dinitrophenylhydrazone (105.5 mg, 33% based on II) according to the reported method.[21] The hydrazone was recrystallized from ethyl acetate to give pure material, mp 169—169.5°C [lit,[21] mp 170°C]. 2,4-Dinitrophenylhydrazone thus prepared showed no depression of melting point on admixture with that of an authentic DL-glyceraldehyde, and the IR spectrum was superimposable with that of authentic specimen.

Found: C, 40.06; H, 3.85; N, 20.72%. Calcd for $C_9H_{10}O_6N_4$: C, 40.00; H, 3.73; N, 20.74%.

5-(Tetrahydro-2-pyranyloxy)-3-pentyn-1-ol (V). A solution of tetrahydropyranyl ether of propargyl alcohol[22] (IV, 60 g, 0.429 mol) in ether (36 ml) was added over a period of 1 hr to a stirred solution of lithium amide (prepared from lithium, 0.6 g, 0.87 g-atom) in liquid ammonia (600 ml). After the mixture had been stirred for 2 hr, ethylene oxide (60 ml, 1.2 mol) was added in a portion. The mixture was refluxed for 14.5 hr at a temperature of −26——30°C using a cold-finger reflux condenser containing dry ice-ethanol. After addition of a concentrated aqueous ammonia solution (6 ml), the ammonia was allowed to evaporate. The residue was mixed with water and extracted with ether. The extract

14) D. Horton, J. B. Hughes, and J. M. J. Tronchet, *Chem. Commun.*, **1965**, 481.
15) K. Randerath, translated by D. D. Libman, "Thin-layer Chromatography," Academic Press, New York and London (1963), a) p. 200; b) p. 56.
16) Z. Dische, *Mikrochemie*, **8**, 4 (1930).
17) M. Renoll and M. S. Newman, "Organic Syntheses," Coll. Vol. III, p. 502 (1955).
18) A. Wohl and C. Neuberg, *Ber.*, **33**, 3095 (1900).
19) Footnote 14 in H. O. Fischer, C. Taube, and E. Baer, *Ber.*, **60**, 482 (1927).
20) W. F. Gresham and W. E. Grigsby, *J. Org. Chem.*, **14**, 1103 (1949).
21) H. Reich and B. K. Samuels, *ibid.*, **21**, 68 (1956).
22) H. B. Henbest, E. R. H. Jones, and I. M. S. Walls, *J. Chem. Soc.*, **1950**, 3646.

was washed with a saturated sodium chloride solution and dried (sodium sulfate). The residue obtained by evaporation of the solvent under reduced pressure was subjected to a vacuum distillation to give pure V as colorless liquid, bp 123—128°C/2 mmHg, n_D^{20} 1.4864, 57.9 g (73.5%) [lit,[23] bp 125—126°C/0.7 mmHg, n_D^{21} 1.4873]. IR (neat): 3440 (O–H), 2230 (–C≡C–), 902, 870, 815 (tetrahydropyranyl) cm^{-1}.

Found: C, 65.00; H, 8.72%. Calcd for $C_{10}H_{16}O_3$: C, 65.19; H, 8.75%.

*5-(Tetrahydro-2-pyranyloxy)-3-*cis*-penten-1-ol (VI).* The acetylenic alcohol (V, 27.6 g, 0.15 mol) in ethyl acetate (150 m*l*) was reduced over Lindlar catalyst[9] (5.75 g) under an atomspheric pressure of hydrogen at room temperature. The uptake of hydrogen ceased after 4.5 hr (3520 m*l*, Calcd 3480 m*l*). The liquid obtained by evaporation of the solvent under diminished pressure was distilled *in vacuo* to yield pure VI as colorless liquid, bp 120—125°C/3 mmHg, n_D^{20} 1.4774, 25.0 g (90%), IR (neat): 3420 (O–H), 3015 (=C–H), 1662 (–C=C–), 902, 868, 814 (tetrahydropyranyl) cm^{-1}.

Found: C, 64.47; H, 9.71%. Calcd for $C_{10}H_{18}O_3$: C, 64.49; H, 9.74%.

*2-Deoxy-5-O-(tetrahydro-2-pyranyl)-*DL-erythro-*pentitol (VII).* To a solution of the ethylenic alcohol (VI, 45 g, 0.24 mol) in ethanol (450 m*l*) maintained at —40°C was added under vigorous agitation a solution of potassium permanganate (37.9 g, 0.24 mol) in water (700 m*l*) over a period of 13.5 hr. During this period, the temperature of reaction mixture was raised gradually to —20°C. After standing overnight, the reaction mixture was stirred at 35°C for 1 hr. Manganese dioxide was collected by filtration and washed with hot water. The combined filtrate and washings were salted out by the addition of anhydrous potassium carbonate. The organic layer was separated, and the aqueous layer was extracted with ether. The aqueous layer was then extracted with the same solvent for 24 hr using a continuous extractor. The organic layer was combined with the extracts and washed with a saturated solution of sodium chloride and dried (sodium sulfate). Evaporation of the solvent under reduced pressure afforded a light brown viscous syrup, 27.4 g (61%), tlc (solvent: ethyl acetate; detection reagent: A): R_f 0.15 (strong), 0.27 (weak), 0.35 (weak), 0.55 (medium), IR (neat): 3370 (O–H), 910, 870, 810 (tetrahydropyranyl) cm^{-1}. The spots at R_f 0.15 and 0.55 seem to be attributable to VII and VI, respectively. Since the purification was found to be difficult, the crude VII thus prepared was subjected to the following reaction.

*2-Deoxy-3,4-O-isopropylidene-5-O-(tetrahydro-2-pyranyl)-*DL-erythro-*pentitol (VIII).* A mixture of the crude VII (3.518 g), anhydrous cupric sulfate (17.6 g) and anhydrous acetone (352 m*l*) was stirred at room temperature. At 2 hr intervals, small samples of the solution were took out and examined by tlc (solvent: ethyl acetate; detection reagent: A). As soon as the spot of VII had disappeared (usually after 4—8 hr), cupric sulfate was removed by filtration to halt the reaction. The filtrate was concentrated under reduced pressure to give a pale yellow liquid (3.394 g). Tlc of the liquid exhibits a main spot at R_f *ca.* 0.7 and a minor spot at R_f *ca.* 0.9 (solvent: ethyl acetate; detection reagent: A). A 1 g-portion of the pale yellow liquid was chromatographed on alumina (E. Merck, activity III—IV, 100 g). The column was eluted with ethyl acetate and the eluant was fractionally collected (each 7 m*l*). The fractions 8 and 9 were homogeneous on tlc (R_f 0.9). The fraction 11 gave one spot at R_f 0.7, whereas the fractions 12—17 were found to be a mixture of two components (R_f 0.7 and 0.65). On evaporating the solvent under reduced pressure, the fraction 11 gave fairly pure VIII as a syrup (96 mg), IR (neat): 3420 (O–H), 1389, 1378, 845 (dimethyldioxolane), 907, 870, 810 (tetrahydropyranyl) cm^{-1}. NMR (DMSO-d_6): δ 1.26 (3H, s) CH_3, δ 1.31 (3H, s) CH_3, 4.55 (1H, broad s) $-CH\langle^{O}_{O}$.

Found: C, 60.99; H, 9.27%. Calcd for $C_{13}H_{24}O_5$: C, 59.98; H, 9.29%.

*2-Deoxy-*N*-phenyl-*DL-erythro-*pentosylamine.* *a) By the Barton's Oxidation*: Syrupy crude VIII (286 mg) obtained from the fractions 11—17 and quinoline (171 mg) were dissolved in anhydrous ether (20 m*l*). The solution was chilled on an ice-salt bath, into which a rapid stream of purified phosgene was introduced for 10 min. The reaction mixture was then stirred for 1 hr at 20°C. Quinoline hydrochloride deposited was filtered with the aid of slightly elevated air pressure avoiding atmospheric humidity. Concentration of the filtrate under reduced pressure yielded chloroformate as light yellow liquid [IR (neat): 1780 (Cl–C=O) cm^{-1}]. The crude chloroformate (355 mg) was mixed with dimethyl sulfoxide (5 m*l*) under stirring and external cooling (bath temperature: 10—15°C). After the exothermic reaction with evolution of carbon dioxide had subsided, the cooling bath was removed and the mixture was stirred at 20°C for 15 min. Then the ice-cooled reaction mixture was mixed with triethylamine (0.185 m*l*) and kept for 3 min at the same temperature. After stirring for 20 min at 20°C, amine hydrochloride deposit was removed. The filtrate was mixed with water (15 m*l*) under cooling, and extracted repeatedly with ether and dried (sodium sulfate). Evaporation of the solvent under diminished pressure gave a pale yellow liquid (205 mg). A mixture of the liquid (203 mg) and 0.1N hydrochloric acid (5 m*l*) was stirred overnight at room temperature. The liquid gradually dissolved in aqueous layer. After 18 hr, the mixture was treated with Dowex-3 (OH^-) to remove chloride ion, and 2-hydroxytetrahydropyran formed was extracted with ether. The aqueous layer was concentrated under reduced pressure at a temperature below 35°C. The syrupy residue was dried *in vacuo* over phosphorus pentoxide, yielding crude 2-deoxy-DL-*erythro*-pentose (IX, 89 mg). Tlc (solvent: acetone; detection reagent: B or C) gave a spot at R_f 0.60 which corresponds with that of an authentic D-isomer. A mixture of the syrupy IX (76 mg), aniline (0.103 m*l*), methanol (0.2 m*l*) and water (0.2 m*l*) was seeded with a trace amount of crystals of the anilide obtained from an authentic DL-IX and the mixture was kept in a refrigerator for a week. The crystals deposited were collected by filtration and washed with 50% aqueous methanol and ether, and then dried to yield the anilide of DL-IX as colorless leaflets (1 mg), mp 157—162°C (decomp.). The anilide thus obtained gave identical IR spectrum with that of the anilide by the method (b). (see, below).

b) By Hydroboration of DL-erythro-*4-Pentyn-1,2,3-triol (XI)*: A solution of bis(1,2-dimethylpropyl)borane was prepared according to the usual manner from a solution of 2-methyl-2-butene (4.6 g, 62.4 mmol) in tetrahydrofuran (20 m*l*) and a diborane stock solution (26.9 m*l*, 15.6 mmol). To the stirred solution of bis(1,2-dimethylpropyl)borane which was strongly cooled on an ice-salt bath was added in an atmosphere of nitrogen a solution of pentyn-triol (XI, 697 mg, 6 mmol) in tetrahydrofuran (5 m*l*) accompanying with evolution of hydrogen. The mixture was stirred for 30 min under ice-cooling, then for 2 hr at room temperature. After standing overnight at room temperature, water (120 m*l*) was added under ice-cooling and stirring. Hydrogen peroxide (15%, 13.6 m*l*) was then added dropwise over a period of 20 min to the

23) L. P. Wells, Istraeli 9220, *Chem. Abstr.*, **52**, 20058 (1958).

vigorously stirred mixture, simultaneously 1N sodium hydroxide solution was added in amall drops to keep the pH of mixture at 7.0—7.5. Further stirring was continued for 30 min under ice-cooling, then for 4 hr at room temperature. In order to decompose the excess of hydrogen peroxide, 1N sodium hydrogen sulfite solution was added to the ice-cooled mixture in 1 m*l* portion until the mixture gave negative iodine-starch test. The resulting solution was treated with Amberlite IR 200 (H^+) and Dowex-3 (OH^-) to remove sodium and sulfate ions. The deionized solution was evaporated *in vacuo* at a temperature below 35°C. The residue, a mixture of syrupy liquid and crystalline boric acid, was mixed with methanol, and evaporated under reduced pressure. The procedure was repeated 3 times to remove boric acid as methyl ester. The residue was dried *in vacuo* over phosphorus pentoxide to yield crude 2-deoxy-DL-*erythro*-pentose (IX) as a syrup (750 mg). The syrupy IX (369 mg) was mixed with aniline (0.256 m*l*), ethanol (2.13 m*l*) and waer (0.99 m*l*) and kept in a refrigerator. After 2 days, 90 mg of crystals of the anilide deposited, and second crop of the anilide (36 mg) was obtained from the mother liquor. [Total yield: 20% based on the acetylenic triol (XI)]. The crystals were recrystallized from methanol to afford colorless plates, mp 157—160°C (decomp.). [lit,[8] mp 154—155°C]. The IR spectrum of the anilide was found to be identical with those of anilides derived from an authentic D-IX and DL-IX prepared by a different route.[13] IR (Nujol mull): 3330, 3260 (OH, NH), 1606, 1500, 1445, 760, 698 (aromatic) cm^{-1} (*Cf.*, Fig. 1).

2-Deoxy-erythro-*pentose (IX).* According to the usual method,[24] a mixture of anilide (75 mg), benzaldehyde (0.075 m*l*), benzoic acid (7.5 mg) and water (2.25 m*l*) was stirred at room temperature for 22 hr, and then extracted 3 times with ether. The aqueous layer was concentrated *in vacuo* at a temperature below 35°C, thus yielding a colorless syrup. After the syrup had been kept over phosphorus pentoxide *in vacuo*, a small amount of ethyl acetate was added. The mixture crystallized on seeding with a trace of crystals of an authentic D-IX. The crystalline DL-IX (44 mg, 92%) was recrystallized from ethyl acetate to yield pure DL-IX, mp 86—89°C, tlc (detection reagent: C): R_f 0.60 (solvent: acetone); R_f 0.74 (solvent: methanol). The R_f values were found to be identical with those of authentic DL-IX and D-IX prepared by a different method.[13]

Found: C, 45.03; H, 7.52%. Calcd for $C_5H_{10}O_4$: C, 44.77; H, 7.52%.

The authors gratefully acknowledge to Mr. Tokusuke Egawa, the president of Kofuku-sogo Bank, for financial support.

24) E. Hardegger, "Methods in Carbohydrate Chemistry," Vol. 1, ed. by R. L. Whistler and M. L. Wolfrom, Academic Press, New York and London (1962), p. 178.

BULLETIN OF THE CHEMICAL SOCIETY OF JAPAN, VOL. 45, 2624—2634 (1972)

Total Syntheses of Carbohydrates. IV. 2-Deoxy-DL-, L- and D-*erythro*-pentoses and Related Sugars

Gen NAKAMINAMI, Sachiko SHIOI, Yoko SUGIYAMA, Satoko ISEMURA, Mikio SHIBUYA, and Masazumi NAKAGAWA*

Department of Chemistry, Faculty of Science, Osaka University, Toyonaka, Osaka

(Received January 31, 1972)

5-Bromo-2,5-dideoxy-*threo*-pentono-γ-lactone (III) could be obtained stereoselectively from 3-hydroxy-4-pentenoic acid (I) by the reaction with *N*-bromosuccinimide in water. On successive treatment with an aqueous potassium hydroxide and an acid type cation exchange resin, bromolactone (III) gave stereoselectively 2-deoxy-*erythro*-pentono-γ-lactone (IV). Reduction of IV by means of bis(1,2-dimethylpropyl)borane afforded 2-deoxy-*erythro*-pentose (V). 3-Hydroxy-4-pentenoic acid (I) could be optically resolved. The (+)-acid yielded 2-deoxy-D-*erythro*-pentose (D-V) and the (−)-acid could be converted to 2-deoxy-L-*erythro*-pentose (L-V). 2,5-Dideoxy-*threo*-pentose (VIII) and 5-bromo-2,5-dideoxy-*threo*-pentose (IX) were obtained from bromo-lactone (III). Diethyl mercaptal of IX gave azido-compound (XI) in a low yield by the reaction with sodium azide. The conformation of γ-lactones (III, IV, and VII) and the mechanistic aspects of stereoselective reactions are discussed.

In the previous paper we reported the total synthesis of *rac*-2-deoxy-*erythro*-pentose.[1] The present paper deals with the syntheses of optically active forms of the carbohydrate. In spite of remarkable development of the total syntheses of carbohydrates, only two reports on total syntheses of optically active carbohydrates have been published. Fischer has reported the total syntheses of D- and L-mannoses, D- and L-glucoses and D-fructose starting from mannonic acid which had been derived from acrolein dibromide *via* DL-glucosazone.[2] After about 80 years, L-(−)-mycalose which is a constituent of various macrolide antibiotics was synthesized by Lemal, Pacht, and Woodward.[3] After the publication of preliminary report of the present paper,[4] the total synthesis of optically active kasuga-

* The author to whom inquiries should be addressed.

1) K. Mimaki, M. Masunari, G. Nakaminami, and M. Nakagawa, This Bulletin, **45**, 2620 (1972).

2) For summary, see, E. Fischer, *Ber.*, **23**, 2114 (1890).

3) D. M. Lemal, P. D. Pacht, and R. B. Woodward, *Tetrahedron*, **18**, 1275 (1962).

4) G. Nakaminami, M. Nakagawa, S. Shioi, Y. Sugiyama, S. Isemura, and M. Shibuya, *Tetrahedron Lett.*, **1967**, 3983.

mycin has been briefly reported by two groups.[5]

The following scheme illustrates the reaction sequence of total synthesis of 2-deoxy-L-*erythro*-pentose, however, the same scheme will be used in the description of syntheses of DL- and D-forms of the carbohydrate.

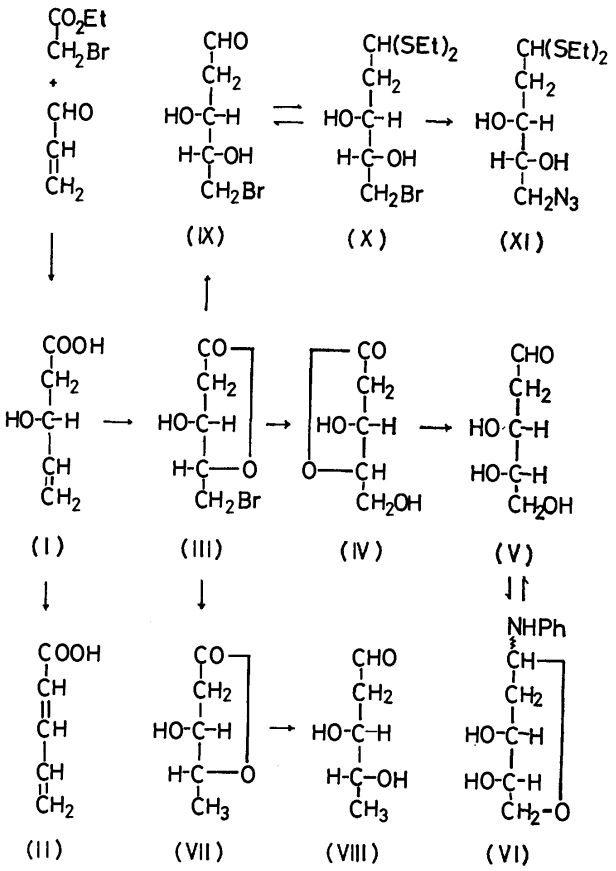

Scheme 1. Syntheses of 2-deoxy-L-*erythro*-pentose (L-V) and related sugars.

The Reformatsky reaction of acrolein with ethyl bromoacetate followed by alkaline hydrolysis afforded DL-β-hydroxy acid (I). Owing to ready dehydration to form pentadienoic acid (II), β-hydroxy acid (I) should be handled with care. Treatment of DL-β-hydroxy acid (I) with 0.5 equivalent of quinine followed by decomposition of the salt afforded (−)-β-hydroxy acid [(−)-I] which gave ultimately 2-deoxy-L-*erythro*-pentose (L-V). The hydroxy acid (I) obtained from the mother liquor of the quinine salt was resolved by means of quinidine salt to give (+)-β-hydroxy acid [(+)-I] which could be converted to 2-deoxy-D-*erythro*-pentose (D-V). The subsequent reactions were carried out with DL-compounds in the first place and then with optically active forms. It has been well-known that a terminal mono-substituted double bond is resistant to peracid oxidation.[6] Therefore, hydroxylation by means of potassium permanganate[7] was first attempted. The acetyl derivative of β-hydroxy acid (I) was treated with an aqueous solution of potassium permanganate under a neutral condition. In spite of the consumption of permanganate, no identifiable product could be isolated from the reaction mixture. Consequently, indirect hydroxylation *via* halohydrin[8] was applied to the hydroxy acid (I). Treatment of β-hydroxy acid (I) with *N*-bromosuccinimide in water followed by a chromatographic purification on silica gel[9] yielded syrupy bromolactone (III) in a yield of 57%. The (−)-acid [(−)-I] gave (+)-III and the (+)-acid [(+)-I] resulted in (−)-III. The by-products were found to be a complex mixture of highly polar compounds and could not be purified. Bromolactone (III) thus obtained was found to be homogeneous without contamination with *erythro*-isomer on the basis of tlc and NMR spectroscopy. The tlc and NMR spectra of IV and VII which were derived from III (see, below) indicate that these lactones are free from their epimers. This fact also supports the homogenity of bromolactone (III). The analytical data of III and its phenylhydrazide, and the IR (C=O, 1795 cm^{-1} in $CHCl_3$: γ-lactone) and NMR spectral data (see, following part) of III are consistent with the assigned structure. The fact that an aqueous solution of optically active III showed practically no change of rotation over a period of 2 weeks affords an additional evidence for γ-lactone structure of III. The immediate change of rotation of (+)-bromolactone (III, $[\alpha]_D$ +51°, H_2O) to $[\alpha]_D$ −3.4° on addition of a drop of concentrated aqueous sodium hydroxide indicates that the configuration of $C_{(4)}$ should belong to D-series according to the Hudson's lactone rule.[10] Consequently, the *O*-function at $C_{(4)}$ should be written in the right side in Fischer's projection formula. As is stated below, because the configuration of $C_{(3)}$ in bromolactone (III) is undoubtedly retained during the course of derivation to 2-deoxy-L-*erythro*-pentose (V), the hydroxyl group at $C_{(3)}$ in (+)-bromolactone (III) which gave the L-form of V, should be written in the left side in Fischer's projection formula indicating that bromolactone (III) has *threo*-configuration. Further evidence for *threo*-configuration of III was obtained by the preparation of 2,5-dideoxy-pentono-lactone (VII). Reduction by means of tri-*n*-butyltin hydride,[11] which had not yet been used in the field of carbohydrate chemistry,[12] was successfully adopted for the conversion of bromolactone (III) to dideoxy-pentono-lactone (VII)

5) Y. Suhara, F. Sasaki, K. Maeda, H. Umezawa, and M. Ohno, *J. Amer. Chem. Soc.*, **90**, 6559 (1968); S. Yasuda, T. Ogasawara, S. Kawabata, I. Iwataki, and T. Masumoto, *Tetrahedron Lett.*, **1969**, 3969.

6) J. Böseken and J. S. P. Blumberger, *Rec. Trav. Chim. Pays-Bas*, **44**, 90 (1925); H. Meerwein, *J. Prak. Chem.*, **113**, 9 (1926); T.W. Findley, D. Swern, and J. T. Scanlan, *J. Amer. Chem. Soc.*, **67**, 412 (1945); D. Swern, G. N. Billen, and J. T. Scanlan, *ibid.*, **68**, 1504 (1946).

7) E. J. Witzemann, W. L. Evans, H. Hass, and E. F. Schroeder, "Organic Syntheses," Coll. Vol. II, p. 307 (1958).

8) R. A. Raphael, *J. Chem. Soc.*, **1949**, S 44.

9) Chromatography on silica gel was found to be superior to that on neutral alumina reported in the preliminary report.[4]

10) J. Stanĕk, M. Černy, J. Kocourek, and J. Pacák, translated by K. Mayer, "The Monosaccharides," Academic Press, New York and London, (1963), p. 55.

11) L. F. Fieser and M. Fieser, "Reagents for Organic Synthesis," John Wiley and Sons, Inc., New York, London, and Sydney, (1967), p. 1192.

12) Cf., for example, S. Hanessian, *Advan. Carbohyd. Chem.*, **21**, 143 (1966); J. E. G. Barnett, *ibid.*, **22**, 177 (1967).

instead of the usual hydrogenolysis.[13] The isolation of dideoxy-lactone (VII) from the reaction mixture could be performed easily owing to the high solubility of VII in water. The spectroscopic data of 2,5-dideoxy-pentono-lactone (VII) were found to be consistent with the structure of VII [IR: 1783 cm^{-1} (γ-lactone); NMR: δ 1.25 (doublet, methyl H)]. Dideoxy-lactone obtained from (+)-bromolactone [(+)-III] showed dextrorotation in an aqueous solution and no change of rotation could be observed over 2 weeks supporting γ-lactone structure. The specific rotation of (+)-dideoxy-lactone [(+)-VII, $[\alpha]_D$ +58°] immediately changed to +13° on addition of a drop of concentrated aqueous solution of sodium hydroxide. This fact suggests that (+)-VII belongs to D-series. The NMR spectrum of VII could

TABLE 1. NMR SPECTRUM OF DIDEOXY-LACTONE (VII) (60 MHz in DMSO-d_6)

Proton	Multiplicity	δ (ppm)	J (Hz)
$C_{(2)}$-H	double d	2.21	J_{2-3} 1.5
$C_{(2)}$-H′	double d	2.84	$J_{2'-3}$ 5.3
$C_{(3)}$-H	m	4.25	$J_{2-2'}$ 17
$C_{(3)}$-OH	d	5.19	J_{3-4} 3.6
$C_{(4)}$-H	o	4.5	J_{3-OH} 4.5
$C_{(5)}$-H_3	d	1.25	J_{4-5} 6.3

d=doublet; m=multiplet; o=octet.

be analyzed employing decoupling technique (Table 1). The coupling constants between hydrogen atoms attached to the lactone ring (J_{2-3}, $J_{2'-3}$, J_{3-4}) could be explained most satisfactory on the assumption that dideoxylactone (VII) belongs to *threo(cis)*-series and D-form of VII holds a conformation and configuration shown in Fig. 1. All of the conformation derived from

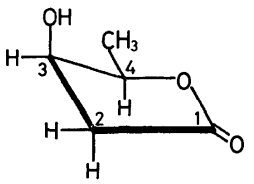

Fig. 1. Probable configuration and conformation of 2,5-dideoxy-D-*threo*-pentono-γ-lactone (D-VII).

erythro(trans)-configuration of VII gave no relevant explanation of the coupling constants. An examination of the Dreiding model of conformer shown in Fig. 1 indicates that the dihedral angles (ϕ) between neighboring hydrogen atoms should be as follows: $\phi_{2,3}$ 85—90°, $\phi_{2',3}$ 35—40°, and $\phi_{3,4}$ 40—50°. The calculation of J-values according to the method of Karplus[14] using modified J_0-value[15] and the estimated dihedral angles was performed. A fairly good agreement between observed and calculated J-values was obtained. The calculated J-values were found to be J_{2-3}=−0.28—−0.21, $J_{2'-3}$=5.94—5.2, and J_{3-4}=5.1—3.6. The unusual large dihedral angle between neighboring hydrogen atoms of *cis*-configuration in five membered ring ($\phi_{3,4}$ 40—50°) has been observed also in sugar derivatives.[15-17] Considering the presence of bulky methyl group in equatorial position and the planar shape of lactone grouping (C–CO–O–C),[18] the conformation illustrated in Fig. 1 seems to be highly probable.

The assignment of NMR spectrum of bromolactone (III) is summarized in Table 2, though there remains some uncertainty owing to poor resolution of the signals of $C_{(3)}$–H and $C_{(4)}$–H and overlap of the signal of water with them. The closely related coupling constants of bromolactone (III) with those of dideoxy-lactone (VII) indicate that D-bromolactone (D-III) has a similar conformation to D-VII shown in Fig. 1.

TABLE 2. NMR SPECTRUM OF BROMOLACTONE (III) (60 MHz in D_2O)

Proton	Multiplicity	δ (ppm)	J (Hz)
$C_{(2)}$-H	double d	2.57	J_{2-3} 1.5
$C_{(2)}$-H′	double d	3.12	$J_{2'-3}$ 5.3
$C_{(3)}$-H	m	*ca.* 4.7	$J_{2-2'}$ 18.5
$C_{(4)}$-H	sextet. (?)	*ca.* 4.85	J_{3-4} 3.8(?)
$C_{(5)}$-H	d	3.67	J_{4-5} 6.4

d=doublet; m=multiplet.

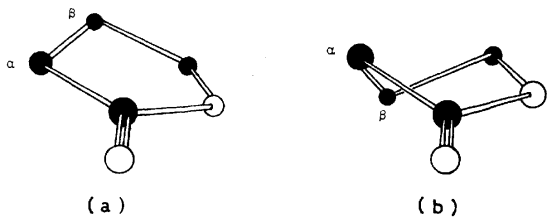

Fig. 2. Stable conformations of γ-lactone.

Mathieson[18] has pointed out that the stable conformation of γ-lactone is restricted to (a) and (b) in Fig. 2 in which C_β is either above or below the lactone plane owing to the preference of co-planarity of the five atoms of lactone group (C–CO–O–C). The location of C_β with respect to the lactone plane is related to the configuration at C_α. Considering the stable conformation of γ-lactone, a general rule has been proposed by Beecham[19] on the relation of the sign of Cotton effect of circular dichroism of $n\rightarrow\pi^*$ region of γ-lactone such as aldonolactone to the conformation of lactone ring. He has concluded that the sign of circular dichroism of aldono-γ-lactone is governed by the conformation of lactone ring independent on the configuration of substituent group other than C_α-position, and the conformation (a) and (b) are associated respectively with (+)- and (−)-Cotton effect. The lactones III and VII have no substituent

13) For example, F. H. Newth, W. G. Overend, and L. F. Wiggins, *J. Chem. Soc.*, **1947**, 10; P. W. Kent, M. Stacey, and L. F. Wiggins, *ibid.*, **1949**, 1232; N. K. Kochetkov, L. I. Kudryashow, A. I. Usov, and B. A. Dmitriev, *J. Gen. Chem. USSR*, **31**, 3081 (1961).

14) M. Karplus, *J. Chem. Phys.*, **30**, 11 (1959).

15) R. J. Abraham, L. D. Hall, L. Hough, and K. A. McLauchlan, *J. Chem. Soc.*, **1962**, 3699.

16) L. D. Hall, *Chem. Ind.*, **1963**, 950.

17) For review, see, L. D. Hall, *Advan. Carbohyd. Chem.*, **19**, 51 (1964).

18) A. McL. Mathieson, *Tetrahedron Lett.*, **1963**, 81.

19) A. F. Beecham, *Tetrahedron Lett.*, **1968**, 2355, 3591.

Table 3. CD and ORD spectra of D-III, D-VII, and L-IV

	ORD in H_2O [ϕ]	CD in H_2O $\Delta\varepsilon_{max}$
D-III	max: 220 nm, +2940°; min: 213 nm, +2820°	213 nm, +0.480
D-VII	max: 222 nm, +2560°; min: 210 nm, +2130°	213 nm, +0.502
L-IV	max: 222 nm, +1370°; min: 199 nm, −1480°	210 nm, +0.597

group at C_α, however, as stated above, D-III and D-VII seem to hold conformation (a). Consequently, D-III and D-VII should exhibit (+)-Cotton effect in their circular dichroism spectra. As is shown in Table 3, the observed results agreed with the anticipation affording a further evidence for the conformation of D-III and D-VII.

Treatment of bromolactone (III) with aqueous 1N potassium hydroxide at room temperature followed by standing at pH 1 for 24 hr afforded 2-deoxy-*erythro*-pentono-γ-lactone (IV) as a syrup in fairly high yield (63%). The syrupy γ-lactone (IV) was proved to be free from impurity on the basis of tlc, paper chromatography and NMR spectroscopy. The IR spectrum of IV and the elemental analysis of its phenylhydrazide were found to be consistent with the assigned structure. Although the syrupy IV derived from D- and L-bromolactones (III) showed somewhat lower $[\alpha]_D$-values as compared with a reported value,[20] the syrupy D- and L-IV could be used without purification in the subsequent reaction. D(+)-III and L(−)-III afforded L(−)-IV and D(+)-IV, respectively. Positive Cotton effect observed in the ORD and CD spectra of L(−)-IV (Table 3) indicates that L(−)-IV has conformation (a) in Fig. 2. Both of the bulky groups in IV, the hydroxyl group at $C_{(3)}$ and the hydroxymethyl group at $C_{(4)}$, take axial position in the conformation (a). An analogous rather unusual situation has been found in the conformation of D-ribono-γ-lactone.[21] The NMR spectrum of IV is recorded in Table 4. A confirmative information could not be obtained from the NMR data owing to the overlap of signal of $C_{(3)}$–H with that of $C_{(4)}$–H. The value of $J_{2'-3}$ is consistent with the conformation (a), however, the value of J_{2-3} is larger than the expected one. Accordingly, the possibility of the presence of a small fraction of conformation (b) can not be excluded. Inspection of the Dreiding model of conformation (b) revealed that the dihedral angles should be $\phi_{2,3}$ 160° and $\phi_{2',3}$ 35°. The coupling constants calculated using these angles are found to be as follows: J_{2-3} 8.87 and $J_{2'-3}$ 5.94.

Table 4. NMR Spectrum of 2-deoxy-*erythro*-pentono-γ-lactone (IV) (60 MHz in DMSO-d_6)

Proton	Multiplicity	δ (ppm)	J (Hz)
$C_{(2)}$–H	double d	2.19	J_{2-3} 2.5
$C_{(2)}$–H′	double d	2.83	$J_{2'-3}$ 6
$C_{(3)}$–H	broad m	4.26	$J_{2-2'}$ 18
$C_{(4)}$–H			J_{4-5} 3.8
$C_{(3)}$–OH	d	5.43	J_{3-OH} 4
$C_{(5)}$–H_2	double d	3.54	
$C_{(5)}$–OH	t	5.0	J_{5-OH} 5.3

d=doublet, t=triplet, m=multiplet.

Reduction by means of sodium borohydride has been widely used for the conversion of aldono-γ-lactone to the corresponding aldose. However, treatments of 2-deoxy-lactone (IV) with the hydride under the usual conditions resulted in the recovery of IV. In view of the ease of reduction of α-hydroxy- and α-amino-esters to aldehydes,[22] the unsuccessful reduction of IV seems to be attributable to the absence of such substituent at α-position of IV. The reduction of IV could be achieved by the use of bis(1,2-dimethylpropyl)-borane (disiamylborane) which has been proposed by Brown and Bigley.[23] The reagent has been successfully applied for acylated aldono-lactones by Kohn, Samaritano, and Lerner.[24] The syrupy IV in anhydrous tetrahydrofuran was mixed with a large excess of disiamylborane. After the mixture had been stood over *ca.* 20 hr at room temperature, water was added to decompose the excess of reducing agent and to hydrolyze the borinate ester (XII) presumably formed. The

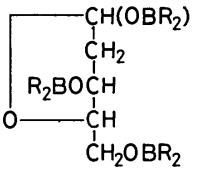

(XII)

R=-CH(CH$_3$)·CH(CH$_3$)$_2$

aqueous mixture was extracted with ether to remove dialkylborinic acid. Evaporation of the resulting aqueous layer afforded a syrup. Tlc of the syrup gave a spot which exactly corresponds to that of an authentic sample of 2-deoxy-*erythro*-pentose (V), and no other distinct spots could be observed. Treatment of the syrupy V with aniline according to the usual procedure[25] gave crystalline aniline derivative (61% based on lactone, IV). D-, L-, and DL-anilides thus prepared gave superimposable IR spectra with that of the anilide prepared from an authentic 2-deoxy-D-*erythro*-pentose. As summarized in Table 5, good coincidence of the melting points and specific rotations with those of reported values were found. The anilide (VI) yielded 2-deoxy-*erythro*-pentose (V) in a high yield (*ca.* 90%)

20) R. E. Deriaz, W. G. Overend, M. Stacey, E. G. Teece, and L. F. Wiggins, *J. Chem. Soc.*, **1949**, 1879.

21) R. J. Abraham, L. D. Hall, L. Hough, K. A. McLauchlan, and H. J. Miller, *ibid.*, **1963**, 748.

22) O. Baeyer, "Methoden der Organischen Chemie," (Houben-Weyl), Bd. 7, Teil 1, Georg Thieme Verlag, Stuttgart (1954), p. 279.

23) H. C. Brown and D. B. Bigley, *J. Amer. Chem. Soc.*, **83**, 486 (1961); H. C. Brown, D. B. Bigley, S. K. Arora, and M. M. Yoon, *ibid.*, **92**, 7161 (1970).

24) P. Kohn, R. H. Samaritano, and L. M. Lerner, *ibid.*, **86**, 1457 (1964); **87**, 5475 (1965).

25) E. Hardegger, "Methods in Carbohydrate Chemistry," Vol. 1, ed. by R. L. Whistler and M. L. Wolfrom, Academic Press, New York and London (1962), p. 177.

Table 5. Melting points and specific rotations of V and VI

		Found	Lit. values
Mp	D-VI	170—173°C (decomp.)	170—172°C (decomp.)[26]
	L-VI	174—176°C (decomp.)	174—175°C[27]
	DL-VI	158—159°C (decomp.)	154—155°C[28]
$[\alpha]_D^{a)}$	D-VI	+56°	+46°[25,29]; +64°[30]
	L-VI	−55°	−58°[27]
$[\alpha]_D^{b)}$	D-V	−56°	−56°[30,31]; −57～−58°[25]
	L-V	+60°	+59°[20]

a) The value at equilibrium in pyridine.
b) The value at equilibrium in water.

on treatment with benzoic acid, benzaldehyde and water according to the usual procedure.[25] 2-Deoxy-D- and L-*erythro*-pentose (D- and L-V) initially obtained as syrup crystallized on standing for a few days. On the other hand, syrupy DL-V could be crystallized only after seeding with a small piece of crystal of an authentic D-V. 2-Deoxy-*erythro*-pentoses (D-, L-, and DL-V) showed no definite melting points indicating that they are mixture of α- and β-anomers. Tlc of crystalline 2-deoxy-*erythro*-pentoses gave spots just corresponding to that of authentic specimen. Also as recorded in Table 5, the specific rotations of D- and L-V were found to be identical with those of literature values. As a matter of course, D- and L-IV afforded D- and L-V, respectively. It should be noted that all the reactions proceed stereoselectively without any detectable formation of 2-deoxy-*threo*-pentose, an epimer of V. In view of the quite different physical properties of 2-deoxy-*threo*-pentose [D-isomer: $[\alpha]_D^{19}=-2°$ (H_2O)[32]] and its anilide [D-isomer: mp 137°C, $[\alpha]_D^{19}=-20°$ (H_2O);[32] DL-isomer: mp 145—146°C[28]] and the homogeneous nature of syrupy V as revealed by tlc, the formation of epimeric 2-deoxy-*threo*-pentose can be ignored. The over-all yields of DL-, L-, and D-V were found to be 9.3, 3.8, and 3.0%, respectively.

Independently and about the same time with the publication of preliminary report of the present study,[4] reduction of free aldonolactone to aldose by means of disiamylborane was reported.[33] The present authors have carried out the reduction of DL-bromolactone (III) and DL-dideoxy-lactone (VII) by the use of disiamylborane. DL-Dideoxy-lactone (VII) yielded 2,5-dideoxy-DL-*threo*-pentose (VIII) as a syrup. The syrup gave a strong spot on tlc accompanied by a few very weak spots. The syrup was converted to 2,4-dinitrophenylhydrazone (48% based on VII) which gave satisfactory elemental analysis and IR spectrum. Reduction of DL-bromolactone (III) afforded syrupy 5-bromo-2,5-dideoxy-DL-*threo*-pentose (IX). The syrupy IX was converted to crystalline diethylmercaptal (X, 38% based on III). Hydrolysis of X gave crystalline DL-IX. Bromopentose (IX) was found to be very unstable and decomposed at room temperature in a few days forming a black material. Mercaptal (X) was also rather unstable compound, but could be kept without decomposition in a refrigerator.

Because bromopentose (IX) seemed to be a potential precursor of aminopentose, bromomercaptal (X) was treated with sodium azide in boiling methanol to give 5-azido-compound (XI). After 30 hr, tlc of the reaction product gave no spot of bromomercaptal (X), but exhibits two main spots together with two minor spots. 5-Azido-compound (XI) could be obtained from one of the minor spot in a poor yield (9%). Conversion of XI to aminopentose had to be abandoned owing to the poor yield. The substances obtained from the two main spots gave no characteristic absorption other than hydroxyl group in their IR spectra. The same substances were obtained when bromomercaptal (X) was refluxed in methanol in the presence of sodium hydrogen carbonate. Therefore, the substances presumably concern with the anomer mixture of XIII.[34]

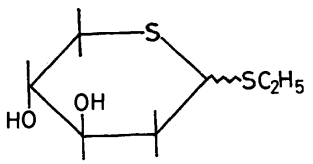

(XIII)

Treatment of bromomercaptal (X) with ammonia resulted in the formation of complex mixture and definite compound could not be identified.

Finally, we wish to give a brief account on the nature of stereoselectivety of the above-mentioned reactions.

26) H. W. Diehl and H. G. Fletcher, Jr., *Arch. Biochem. Biophys.*, **78**, 386 (1958).
27) K. Butler, S. Laland, W. G. Overend, and M. Stacey, *J. Chem. Soc.*, **1950**, 1433.
28) F. Weygand and H. Leube, *Chem. Ber.*, **89**, 1914 (1956).
29) J. C. Sowden, *J. Amer. Chem. Soc.*, **76**, 3541 (1954).
30) L. Hough, *J. Chem. Soc.*, **1953**, 3066.
31) W. G. Overend, M. Stacey, and L. F. Wiggins, *ibid.*, **1949**, 1358.
32) F. Weygand, Ref. 25), p. 185.
33) T. A. Giudici and A. L. Fluharty, *J. Org. Chem.*, **32**, 2043 (1967). Other instances of disiamylborane reduction of aldonolactone derivatives, see, P. Kohn, L. M. Lerner, A. Cahn, Jr., S. D. Ginodrio, and C. A. Zitrin, *Carbohyd. Res.*, **7**, 21 (1968) and references cited therein.
34) Recently, J. Harness and N. A. Hugher (*Chem. Commun.*, **1971**, 811) have reported the formation of furanose derivative (C) instead of cyclic sulfide (B) on heating an acetone solution of 5-*O*-*p*-toluenesulfonyl-L-arabinose diethyl or dibenzyl dithioacetal (A, R=Et or benzyl). Consequently, the possibility that the substance obtained from bromoacetal (X) has a structure analogous to C can not be excluded. Further investigation about this point is now in progress.

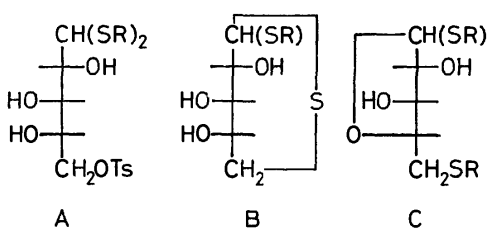

As previously described, reaction of β-hydroxy-γ,δ-ethylenic acid (I) with *N*-bromosuccinimide in water gave exclusively *threo*-isomer (III) and unexpectedly the formation of epimeric *erythro*-isomer could not be observed. Beacuse the intramolecular nucleophilic attack of carboxyl group has been recognized in the electrophilic addition reaction of γ,δ-ethylenic acid,[35] bromo-γ-lactone (III) may be formed directly by the participation of carboxyl group without intermediacy of bromo-dihydroxy acid. Therefore, it seems to be likely that hydroxy-ethylenic acid (I) holds preferentially the conformation XIV or XV in which the

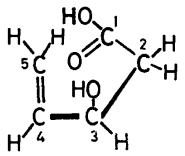

(XIV)

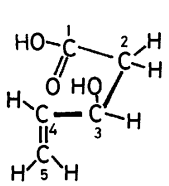

(XV)

carboxyl group situates in a proximity of the ethylenic bond. The hydroxyl group at $C_{(3)}$ and $C_{(5)}$ in conformation XIV are located in the same side with respect to the plane defined by $O-C_{(1)}-C_{(2)}-C_{(3)}-C_{(4)}$. On the contrary, the hydroxyl groups at $C_{(3)}$ and $C_{(5)}$ in conformation XV are situated in opposite side of the plane. Consequently, an additional stability would be rendered to the conformer XIV, because a hydrogen bonding between the hydroxyl group at $C_{(3)}$ and π-electron of the ethylenic bond[36] is possible only in XIV. If hydroxy-ethylenic acid (I) has the conformation XIV and bromonium ion attacks $C_{(5)}$ from the back side of carboxyl group being accompanied by simultaneous attack of carboxyl oxygen to $C_{(4)}$, the resulting bromolactone (III) should have *threo*-configuration.

threo-Bromolactone (III) affords solely *erythro*-lactone (IV) without contamination of *threo*-isomer by the reaction with an aqueous potassium hydroxide followed by acid. This fact indicates that the ring opening of *threo*-epoxide (XVI) which is a possible reaction intermediate should occur at $C_{(4)}$ instead of $C_{(5)}$ with complete inversion of configuration. This is in accord with the general tendency of ring opening of epoxide, *i.e.*, usually epoxide ring is cleaved by acid at secondary carbon with inversion of configuration.[37] However, such a clear-cut result observed in the conversion of III into IV is rather unusual in saturated aliphatic epoxides. An intramolecular participation of carboxyl group again might have an important role in this reaction, *i.e.*, the carboxyl oxygen in XVI preferentially attacks $C_{(4)}$ to give γ-lactone (IV) rather than $C_{(5)}$ which leads to the formation of δ-lactone. The complete inversion at $C_{(4)}$ seems to be attributable to

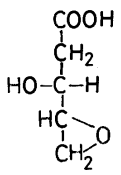

(XVI)

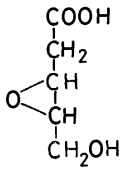

(XVII)

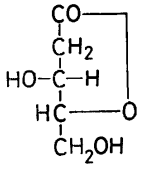

(XVIII)

the intramolecular nature of attack and the rather high nucleophilicity of carboxyl group. The possibility of formation of epoxide (XVII) as a reaction intermediate which might be formed from XVI by the attack of hydroxyl group at $C_{(3)}$[38] can be ruled out, because the ring opening at either $C_{(3)}$ or $C_{(4)}$ of *erythro*-type XVII should result in the formation of 2-deoxy-*threo*-pentono-γ-lactone (XVIII) being in conflict with the observation. Therefore, it can be concluded that the configuration of $C_{(3)}$ in hydroxyethylenic acid (I) is kept intact throughout the reaction sequence. Accordingly, *R*-configuration of (−)-hydroxyethylenic acid [(−)-I] which gave 2-deoxy-L-*erythro*-pentose (L-V) and *S*-configuration of (+)-ethylenic acid [(+)-I], the precursor of 2-deoxy-D-*erythro*-pentose (D-V) are concluded.

Experimental

Melting points were measured on a Mettler EP2 apparatus and uncorrected. The IR spectra were obtained on a Hitachi EPI-2, EPI-S or a JACSO DS-402G spectrophotometer. The ORD and CD spectra were measured on a Yanagimoto ORD-185 and a JASCO ORD/UV-5 spectropolarimeters, and the NMR spectra, with a Varian A-60 or T-60, using tetramethylsilane or sodium 4,4-dimethylsilapentane sulfonate as internal standard. Double irradiation was performed on a JEOL JNM-4H-100 or JNM-C-60HL spectrometer. A commercial silica gel (E. Merck, Darmstadt, Germany, 70—325 mesh) was immersed in 60% aqueous acetic acid overnight and washed thoroughly with water until the filtrate gave a neutral test. After the washed silica gel had been kept at 120°C for 15 hr, it was used in the chromatography. Silica gel G (E. Merck, Darmstadt, Germany) was used as adsorbent in tlc. Benzene-ethyl acetate (1: 1) (A), acetone (B), methanol (C) and ethyl acetate-95% ethanol (20: 1) (D) were used as solvents. Iodine[39a] (a), hydroxamic acid reagent[39b] (b), Tollens' reagent[40] (c) and Dische's reagent[41] (d) were used as detection reagents. In the case of reagent (d), the sprayed glass was covered with another plate of glass and heated at 90—100°C to develop color reaction.

Ethyl 3-Hydroxy-4-pentenoate. In a nitrogen atmosphere, a 30 m*l* portion of a solution of ethyl bromoacetate (111 m*l*, 1 mol)[41] and acrolein (87 m*l*, 1.3 mol) in anhydrous benzene (250 m*l*) was added to zinc powder[43] (142 g, 2.17 g-atom)

35) See, for example, P. B. de la Mare and R. Bolton, "Electrophilic Additions to Unsaturated Systems," Elsevier, Amsterdam, London and New York (1966), p. 140.

36) M. Ōki and H. Iwamura, This Bulletin, **32**, 567 (1959).

37) Cf., E. L. Eliel, "Steric Effects in Organic Chemistry," ed. by M. S. Newman, John Wiley and Sons, Inc., New York (1956), p. 106.

38) On the neighboring-group participation of hydroxyl group under acidic conditions, see, L. Goodman, *Advan. Carbohyd. Chem.*, **22**, 109 (1967).

39) K. Randerath, translated by D. D. Libman, "Thin-layer Chromatography," Academic Press, New York and London (1963), a) p. 56, b) p. 203.

40) Reference 10, p. 869.

41) Z. Dische, *Mikrochemie*, **8**, 4 (1930).

42) S. Natelson and S. Gottfried, "Organic Syntheses," Coll. Vol. III, p. 381 (1955).

43) The quality of zinc powder is essential in this reaction. Only the zinc powder of Mitsuwa Chemicals Co. gave satisfactory result.

activated with hydrochloric acid[44] and the mixture was stirred under careful heating. After the initial vigorous reaction had subsided, the remaining solution was added to the stirred mixture under careful heating in such a rate to maintain gentle reflux. After the addition of solution had been completed, the mixture was refluxed for further 30 min under stirring. The hot reaction mixture was poured into an ice-cooled 4N sulfuric acid (600 ml) under stirring. Greyish viscous insoluble material was removed by filtration and washed with ether. The washings were combined with the organic layer. The aqueous layer was extracted 6 times with ether. The total organic layer was washed once with a saturated sodium chloride solution and twice with a saturated solution of sodium chloride containing sodium hydrogen carbonate and dried (sodium sulfate). The residue obtained by evaporation of the solvent under reduced pressure was distilled under nitrogen atmosphere *in vacuo*. Ethyl 3-hydroxy-4-pentenoate was obtained as colorless liquid, 72 g (50%), bp 63—64°C/2 mmHg, n_D^{25} 1.4393. IR (neat): 3470 (O–H); 1735 (C=O); 995, 925 (–CH=CH_2) cm^{-1}.

Found: C, 58.60; H, 8.33%. Calcd for $C_7H_{12}O_3$: C, 58.31; H, 8.39%.

When the reaction was carried out in other solvents of low boiling points such as ether, diisopropyl ether or tetrahydrofuran, the control of exothermic reaction was difficult resulting in a poor yield.

N-Phenyl-3-hydroxy-4-pentenoamide. According to the reported method,[45] ethyl hydroxy-pentenoate was converted to crystalline anilide. To an ice-cooled solution of ethylmagnesium bromide [from magnesium (2 g), ethyl bromide (10 g) and ether (60 ml)] was added aniline (8 g) and then the pentenoate (6 g) under stirring. After the mixture had been stirred for 30 min at room temperature and then further 30 min at 40°C, the reaction mixture was poured into 2N hydrochloric acid (50 ml). The crystals obtained upon work-up of the ethereal layer were recrystallized twice from benzene, thus yielding pure anilide as colorless needles, mp 127.5—128.5°C. IR (Nujol mull): 3300, 3210, 3140, 3080 (OH and NH); 1665 (amide I), 1550 (amide II), 1315 (amide III); 1603, 757, 690 (C_6H_5–) cm^{-1}.

Found: C, 69.14; H, 6.87; N, 7.27%. Calcd for $C_{11}H_{13}NO_2$: C, 69.09; H, 6.85; N, 7.33%.

3-Hydroxy-4-pentenoic Acid (I). Ethyl 3-hydroxy-4-pentenoate (92.8 g, 0.644 mol) was added over a period of 45 min into an ice-cooled and stirred solution of potassium hydroxide (38.1 g, 0.68 mol) in water (635 ml). The mixture was stirred for 14 hr at room temperature and then stood over 12 hr at the same temperature. The reaction mixture was extracted 3 times with ether. The ice-cooled aqueous layer was made just acid to Congo red with concentrated hydrochloric acid (59 ml) and then saturated with sodium chloride. The aqueous layer was extracted 5 times with ether. The extract was washed 3 times with a saturated sodium chloride solution. The washings were combined with the aqueous layer and extracted with ether using a continuous extractor for 20 hr. The extract was washed according to the above-stated procedure. The total aqueous layer was again extracted by means of a continuous extractor for 20 hr. After washing procedure, the extract was combined with other ethereal extracts. The total extract was dried over sodium sulfate. The residue obtained by evaporating the solvent was distilled *in vacuo* under nitrogen atmosphere to give 3-hydroxy-4-pentenoic acid (I) as viscous colorless liquid, 63.5 g (85%), bp 95°C/1 mmHg, n_D^{30} 1.4630. IR (neat): *ca.* 3500—2500 (OH); 1715 (C=O); 995, 930 (–CH=CH_2) cm^{-1}.

Found: C, 51.56; H, 7.06%. Calcd for $C_5H_8O_3$: C, 51.72; H, 6.94%.

It was found that hydroxy-pentenoic acid (I) is easily dehydrated to give crystalline pentadienoic acid (II).[46] When the hydrolysis of I was carried out with 2N potassium hydroxide at room temperature for 2 days, II was obtained as main product.

Optical Resolution of 3-Hydroxy-4-pentenoic Acid (I). Hydroxy-pentenoic acid (I, 25.7 g, 0.222 mol) was added to a suspension of quinine (36 g, 0.111 mol) in hot water (295 ml) and shaken for a few min on a boiling water-bath. A slightly turbid solution thus obtained was treated with active charcoal. Crystals deposited mostly on standing the clear filtrate, otherwise the filtrate was seeded to cause crystallization. After standing in a refrigerator for 3 days, the crystals were collected by filtration and washed with water. The mother liquor was concentrated to one-half volume and stood over 8 days in a refrigerator, thus yielding second crop of crystals. The combined crystals (32 g) were recrystallized from water (295 ml), yielding colorless needles, 26.2 g, $[\alpha]_D^{24}=-137°$ ($c=1.1$, H_2O). The crystals showed no definite melting point, but most of the crystals melted at 117—122°C. The mother liquor of recrystallization gave second crop of crystals, 2.7 g, $[\alpha]_D^{18}=-134°$ ($c=1.1$, H_2O). The total yield was 57%. IR (Nujol mull): 1550, 1410 (–CO_2^-) cm^{-1}.

Found: C, 65.67; H, 7.54; N, 6.10%. Calcd for $C_{25}H_{32}O_5N_2 \cdot H_2O$: C, 65.48; H, 7.47; N, 6.11%.

The crystals lost its water of crystallization of heating to 65°C *in vacuo*, but the anhydrous crystals still showed no definite melting point (most of the crystals melted at 119—124°C).

Found: C, 67.92; H, 7.44; N, 6.33%. Calcd for $C_{25}H_{32}O_5N_2$: C, 68.16; H, 7.32; N, 6.36%.

Quinine salt monohydrate (25.1 g, 0.0548 mol) thus obtained was placed in a separatory funnel and mixed with sodium hydrogen carbonate (6 g, 0.071 mol), water (130 ml) and chloroform (500 ml). The mixture was shaken to dissolve the quinine salt. The organic layer was washed twice with water. The washings were combined with the aqueous layer and made just acid to Congo red with 6N hydrochloric acid under ice-cooling. The aqueous solution was treated according to the procedure used in the preparation of *rac*-hydroxy-pentenoic acid (I). (—)-I was obtained as pale yellow liquid, 4.6 g, (72%), $[\alpha]_D^{25}=-9.8°$ ($c=0.81$, H_2O). Ths material could be used without further purification in the subsequent reaction. A vacuum distillation of the crude material gave pure (—)-I as colorless viscous liquid, bp 107—109°C/3 mmHg, n_D^{20} 1.4658, $[\alpha]_D^{20}=-9.6°$ ($c=1.03$, H_2O), $[\alpha]_D^{17}=-26°$ ($c=1.35$, C_2H_5OH). Pure (—)-I crystallized in a refrigerator. The IR spectrum of (—)-I was found to be superimposable with that of racemic I.

Found: C, 51.57; H, 6.99%. Calcd for $C_5H_8O_3$: C, 51.72; H, 6.94%.

The initial mother liquor was concentrated to *ca.* 50 ml and mixed with sodium hydrogen carbonate (15 g). The crystals of quinine deposited were removed by filtration and washed with water. Partially resolved (+)-hydroxy-pentenoic acid, light yellow liquid, 12.8 g (50% recovery), $[\alpha]_D^{25}=+4.5°$ ($c=2.08$, H_2O) was obtained from the combined aqueous layer according to the previously described procedure. The specific rotation indicates that the optical

44) R. L. Shriner, "Organic Reactions," Vol. 1, John Wiley and Sons, Inc., New York (1942), p. 16.

45) D. V. N. Hardy, *J. Chem. Soc.*, **1936**, 398.

46) E. R. H. Jones, G. H. Whitham, and M. C. Whiting, *ibid.*, **1954**, 3201.

purity of the (+)-hydroxy-pentenoic acid should be 47%. In another run, partially resolved (+)-I having optical purity of 54% was obtained. Purified quinidine[47] (18.1 g, 0.056 mol) was mixed with partially resolved (+)-I [8.4 g, $[\alpha]_D=+14°$ (C_2H_5OH), optical purity=54%, corresponds to 0.056 mol of pure (+)-I] and water (25 m*l*). The mixture was heated to give a homogeneous solution. The solution was seeded with crystals of qunidine salt of I and kept at room temperature for 4 days. The crystals deposited were collected by filtration and washed with acetone. The crystals were recrystallized from acetone to give pure quinidine salt, colorless rods, 11.4 g (46%), $[\alpha]_D^{17}=+180°$ ($c=0.11$, H_2O). The crystals showed no definite melting point (130—149°C). IR (Nujol mull): 1594; 1404 ($-CO_2^-$) cm^{-1}.

Found: C, 68.00; H, 7.47; N, 6.32%. Calcd for $C_{25}H_{32}O_5N_2$: C, 68.16; H, 7.32; N, 6.36%.

Sodium hydrogen carbonate (2.5 g, 0.03 mol) was added to a solution of pure qunidine salt (11.4 g, 0.0259 mol) in water (40 m*l*). Quinidine initially deposited as liquid could be crystallized on seeding and removed by filtration. Treatment of the aqueous layer according to the procedure used in the preparation of (−)-I afforded slightly crude (+)-I as liquid, 2.8 g (93%), $[\alpha]_D^{17}=+26°$ ($c=1.01$, C_2H_5OH). The IR spectrum of this material was found to be superimposable with that of DL-isomer. This material was used in the following reaction without further purification. Vacuum distillation under nitrogen atmosphere of crude (+)-I obtained by another run yielded (+)-I as colorless liquid, bp 104—106°C/2 mmHg which crystallized on standing in a refrigerator, n_D^{25} 1.4633, $[\alpha]_D^{25}=+24°$ ($c=1.03$, C_2H_5OH).

Found: C, 51.13; H, 6.90%. Calcd for $C_5H_8O_3$: C, 51.72; H, 6.94%.

Second crop of qunidine salt was obtained from the aqueous mother liquor. Recrystallization of the crude salt from water gave 5.4 g of qunidine salt, $[\alpha]_D^{19}=+173°$ ($c=0.11$, H_2O).

Attempts to resolve (±)-I by means of cinchonine, cinchonidine, brucine, strychnine, and ephedrine gave fruitless results.

DL-*3-Acetoxy-4-pentenoic Acid.* A mixture of hydroxy-pentenoic acid (I, 24 g, 0.2 mol) and acetic anhydride (50 m*l*) was heated on a boiling water-bath for 2.5 hr. After the acetic anhydride and acetic acid formed had been removed under reduced pressure, water (40 m*l*) was added to the residue and kept at 60°C for 1 hr. The reaction mixture was saturated with sodium chloride and extracted with ether. The extract was dried over sodium sulfate. The residue obtained by evaporation of the solvent under reduced pressure was distilled *in vacuo* in a stream of nitrogen, yielding acetoxy-pentenoic acid as colorless liquid, 26.5 g (83%), bp 96.5—98°C/1.5 mmHg, n_D^{25} 1.4445, IR (neat): *ca.* 3600—2400 (OH): 1745, 1720 (C=O); 990, 935 ($-CH=CH_2$) cm^{-1}.

Found: C, 53.15; H, 6.34%. Calcd for $C_7H_{10}O_4$: C, 53.16; H, 6.37%.

Acetylation of I by means of pyridine-acetic anhydride gave predominantly pentadienoic acid.

5-Bromo-2,5-dideoxy-DL-, D-, *and* L-threo-*Pentono-γ-lactones (III).* A mixture of DL-β-hydroxy acid (I, 10.4 g, 0.09 mol), finely powdered *N*-bromosuccinimide[48] (17.7 g, 0.099 mol) and water (180 m*l*) was stirred at room temperature for 17 hr in a dark place. The resulting orange yellow clear solution was saturated with sodium chloride (55 g) and extracted with ether (50 m*l*×5). The ethereal extract was washed with a saturated sodium chloride solution containing 5% of sodium hydrogen sulfite (30 m*l*) and a saturated sodium chloride solution (20 m*l*×3), successively and dried (sodium sulfate). The residue obtained by evaporating the solvent under reduced pressure was placed in an evacuated desiccator containing phosphorus pentoxide. The yellowish brown syrup thus obtained (5.8 g) exhibited satisfactory IR spectrum and gave a strong spot of III at R_f 0.55 (solvent system: A, detection reagent: a or b) in the tlc accompanied with a faint coloration near the starting point.

The combined aqueous layer and washings were mixed with a saturated sodium chloride solution containing 5% of sodium sulfite (2 m*l*) to reduce liberated bromine and extracted with ether for 24 hr employing a continuous extractor. The ethereal extract containing crystals and oily material was chilled on an ice-bath. The crystals were collected by filtration and washed successively with ether and ethyl acetate which could be identified as succinimide on the basis of IR spectroscopy. Ethyl acetate was added to the combined filtrate and washings to dissolve separated oily material and dried (sodium sulfate). The residue obtained by evaporation of the solvent under diminished pressure was placed in an evacuated desiccator over phosphorus pentoxide, thus yielding second crop of yellow syrup (12.6 g). Because tlc (solvent system: A, detection reagent: a or b) of the syrup revealed that the main constituents of the syrup are bromolactone (III, R_f 0.55) and succinimide (R_f 0.4), the syrup (10 g) was subjected to a chromatography on silica gel (300 g) employing benzene-ethyl acetate (1: 1) as eluting solvent. The eluate was fractionated into 100 m*l* portions. Bromolactone (III, 5.2 g) contaminated with a small amount of succinimide was obtained from the fractions 3—10, which gave pure bromolactone (III, 3.34 g) on re-chromatography on silica gel. The total yield of pure III was found to be 57%, n_D^{20} 1.5214, IR ($CHCl_3$): 3610 (OH); 3460 (hydrogen bonded OH); 1795 (C=O) cm^{-1}. IR (neat): 3460 (hydrogen bonded OH); 1775 (C=O) cm^{-1}.

Found: C, 30.17; H, 3.92; Br, 40.72%. Calcd for $C_5H_7O_3Br$: C, 30.79; H, 3.62; Br, 40.97%.

A chromatography of the second crop of III on neutral alumina (Woelm, activity III) gave less satisfactory result.

Treatment of DL-bromolactone (III) in ethanol with phenylhydrazine gave phenylhydrazide which was recrystallized from ethanol to give pure material as colorless needles. The phenylhydrazide sintered at 135°C and decomposed at 137—138°C.

Found: C, 43.82; H, 5.04; N, 9.02; Br, 26.46%. Calcd for $C_{11}H_{15}BrN_2O_3$: C, 43.58; H, 4.99; N, 9.24; Br, 26.36%.

According to the procedure used in the preparation of DL-bromolactone (III), (−)-β-hydroxy-pentenoic acid [(−)-I, 7.275 g, 0.0627 mol], *N*-bromosuccinimide (12.3 g, 0.069 mol) and water (130 m*l*) gave D-bromolactone (D-III). The first crop [4.15 g, $[\alpha]_D^{25}=+45°$ (initial)→+44° (after 2 weeks) ($c=0.65$, H_2O)] gave an identical IR spectrum with that of pure DL-III and could be used in the following reaction without further purification. Chromatography of the second crop (9.89 g) on silca gel or neutral alumina afforded pure D-III. The total yield of pure D-III was 56%, n_D^{25} 1.5207, $[\alpha]_D^{25}=+54°$ (after 24 hr)→+50° (after 2 weeks) ($c=0.081$, H_2O).

Found: C, 30.95; H, 3.68; Br, 40.48%. Calcd for $C_5H_7O_3Br$: C, 30.79; H, 3.62; Br, 40.97%.

Phenylhydrazide of D-III was recrystallized from 2-propanol to give aggregate of colorless needles or plates, mp 132—135°C (decomp.) [with a pre-heated bath (115°C) and a rapid temperature increase, 6°C/min].

47) R. T. Major and J. Finkelstein, *J. Amer. Chem. Soc.*, **63**, 1368 (1941).

48) E. Campaigne and B. F. Tullar, "Organic Syntheses," Coll. Vol. IV, p. 921 (1963).

Found: C, 43.84; H, 5.06; N, 9.07; Br, 25.96%. Calcd for $C_{11}H_{15}BrN_2O_3$: C, 43.58; H, 4.99; N, 9.24; Br, 26.36%.

The reaction of (+)-hydroxy-pentenoic acid (2.8 g, 0.024 mol) with *N*-bromosuccinimide (4.7 g, 0.027 mol) in water (50 m*l*) afforded L-bromolactone (L-III). The first crop [1.54 g, $[\alpha]_D^{17}=-46°$ (initial)$\rightarrow[\alpha]_D^{20}=-46°$ (after 2 weeks) ($c=0.54$, H_2O)] could be used without purification in the subsequent reaction. The second and third crops (total 3.27 g) were subjected to chromatography on silica gel to give pure L-III. The total yield of pure L-III was found to be 2.47 g (52%).

2-Deoxy-DL-, L-, *and* D-erythro-*Pentono-γ-lactones (IV).* A mixture of DL-III (860 mg, 4.41 mmol) and 1N potassium hydroxide (9 m*l*, 9 mmol) in a tightly stoppered flask was swirled for 30 min in an ice-bath, and then kept at room temperature for 23 hr. The reaction mixture was treated with Amberlite IR 120 (H^+) to remove potassium ion and the resulting acid solution (pH *ca.* 1) was stood over 22 hr at room temperature. The solution was chilled on an ice-bath and treated with Dowex 3 (OH^-). The solution which gave negative Beilstein's test was concentrated under reduced pressure at a temperature below 30°C. The residue was placed in an evacuated desiccator containing phosphorus pentoxide, thus yielding 2-deoxy-DL-*erythro*-γ-lactone (DL-IV) as almost colorless syrup, 346 mg, (59%), n_D^{20} 1.4900, IR (neat): 3380 (OH); 1765 (C=O) cm^{-1}. The syrup gave one spot (R_f 0.58) on a paper chromatogram (solvent system: 1-butanol: acetic acid: water=4:1: 5,[47] detection reagent: silver nitrate-sodium hydroxide-ammonia,[49] filter paper: Toyo Roshi No. 51). Tlc (solvent: B, detection reagent: b or c) of the syrup gave a main spot at R_f 0.75 and in some cases very weak spots at R_f 0.6 and 0.42 were observed.

According to the usual manner, phenylhydrazide was obtained from the syrup (95 mg, 0.72 mmol) and phenylhydrazine (84 mg, 0.78 mmol) in ethanol (1 m*l*). The hydrazide was recrystallized from 2-propanol and then from acetone to give pure material, aggregate of colorless leaflets. The crystals were found to be a mixture of two dimorphic forms, mp 134—135°C and mp 140—142°C.

Found: C, 54.94; H, 6.73; N, 11.55%. Calcd for $C_{11}H_{16}O_4N_2$: C, 54.99; H, 6.71; N, 11.66%.

Treatment of D(+)-bromolactone (D-III, 260 mg, 1.33 mmol) according to the procedure used in the case of DL-isomer gave 2-deoxy-L-*erythro*-pentono-γ-lactone (L-IV, 109 mg, 62%) as a colorless syrup which showed a superimposable IR spectrum with that of DL-IV, n_D^{20} 1.4870, $[\alpha]_D^{15}=-8.5°$ (initial)$\rightarrow-9.8°$ (after 2 weeks) ($c=1.08$, H_2O). Phenylhydrazide obtained from L-IV also showed dimorphism, mp 122—123°C and mp 146—146.5°C [lit,[31] mp 145—146°C].

Found: C, 54.84; H, 6.66; N, 11.57%. Calcd for $C_{11}H_{16}O_4N_2$: C, 54.99; H, 6.71; N, 11.66%.

L(−)-Bromolactone (L-III, 1.5 g, 7.7 mmol) afforded 2-deoxy-D-*erythro*-pentono-lactone (D-IV, 647 mg, 63%), $[\alpha]_D^{20}=+4.9°$ (initial)$\rightarrow+6.8°$ (after 13 days) ($c=1.04$, H_2O). The spectrum of D-IV was found to be identical with that of DL-form.

2-Deoxy-N-*phenyl*-DL-, L-, *and* D-erythro-*Pentosylamine (VI).* A solution of bis(1,2-dimethylpropyl)borane was prepared according to the usual procedure from 2-methyl-2-butene (1.9 g, 27 mmol) in anhydrous tetrahydrofuran and a stock solution of diborane in the same solvent (concentration: 0.85 mmol/m*l*, 8 m*l*, 6.8 mmol). To the ice-cooled and stirred solution of bis(1,2-dimethylpropyl)borane was added a solution of slightly crude 2-deoxy-DL-*erythro*-pentono-γ-lactone (IV, 160 mg, 1.2 mmol) in anhydrous tetrahydrofuran (7 m*l*) in an atmosphere of nitrogen. Evolution of hydrogen was observed. After the mixture had been stirred at room temperature for 21 hr, water (30 m*l*) was added under cooling on an ice-bath, and then further stirring was continued for 40 min at room temperature. Ether was added to the reaction mixture and the ether layer was extracted twice with water. The second aqueous extract gave a negative test for the Dische's reagent.[42] The combined aqueous layer was extracted 3 times with ether. All ethereal layers were combined, and again extracted with water. Total aqueous layer was concentrated under reduced pressure at a temperature below 30°C. The resulting syrup was mixed with methanol and the solvent was removed under diminished pressure. This procedure was repeated 3 times. The syrup thus obtained was dried in an evacuated desiccator over phosphorus pentoxide. Tlc (solvent: B, detection reagent: d) of the pale yellow syrup thus prepared (154 mg) produced a strong spot at R_f 0.51 corresponding to that of an authentic D-V and a very weak spot at R_f 0.58. The syrup was mixed with an aniline solution (1.4 m*l*) prepared from aniline (1.8 m*l*), ethanol (15 m*l*) and water (7 m*l*), and the mixture was placed in a refrigerator. The crystals deposited were collected by filtration and washed successively with 50% aqueous methanol and ether, thus yielding fairly pure DL-VI as almost colorless needles, 153 mg (61% based on DL-IV). The crystals were recrystallized from ethanol to give pure DL-VI, colorless plates, mp 158—159°C (decomp.) (with a pre-heated bath (140°C)). The IR spectrum (Nujol mull) of DL-VI [3320, 3250 (OH, NH); 1605, 1500, 1445, 760, 695 (C_6H_5–) cm^{-1}] was found to be identical with that of an authentic D-VI.

Found: C, 62.98; H, 7.37; N, 6.55%. Calcd for $C_{11}H_{15}O_3N$: C, 63.14; H, 7.23; N, 6.69%.

Treatment of L-lactone (L-IV, 124 mg, 0.94 mmol) with 2-methyl-2-butene (1.7 g, 24 mmol) and the stock solution of diborane (6 mmol) according to the above-mentioned procedure resulted in L-VI (120 mg, 61% based on L-IV). Pure L-VI was obtained upon recrystallization from ethanol, mp 174—176°C (decomp.) (with a pre-heated bath (*ca.* 155°C) and a heating rate of 4°C/min), $[\alpha]_D^{14}$ ($c=1.28$, pyridine): −140° (after *ca.* 20 min); −81° (after 2 hr); −70° (after 7 hr); −55° (after 24 hr); −55° (after 29 hr). L-VI gave a superimposable IR spectrum (Nujol mull) with those of DL-VI and authentic D-VI.

Found: C, 63.21; H, 7.34; N, 6.69%. Calcd for $C_{11}H_{15}O_3N$: C, 63.14; H, 7.23; N, 6.69%.

D-Anilide (D-VI, 184 mg, 58%) was obtained from D-lactone (D-IV, 202 mg, 1.53 mmol), 2-methyl-2-butene (2.6 g, 37 mmol) and the stock solution of diborane (9 mmol). Slightly crude D-VI obtained was recrystallized from ethanol, thus yielding pure D-VI as colorless plates, mp 170—173°C (decomp.) (with a pre-heated bath (150°C) and a heating rate of 3—4°C/min), $[\alpha]_D^{20}$ ($c=1.02$, pyridine): +150° (after 10 min); +77° (after 4.5 hr); +56° (after 24 hr); +56° (after 28.5 hr). D-VI thus obtained showed an identical IR spectrum (Nujol mull) with that of an authentic D-VI.

Found: C, 63.19; H, 7.27; N, 6.62%. Calcd for $C_{11}H_{15}O_3N$: C, 63.14; H, 7.23; N, 6.69%.

2-Deoxy-DL-, L-, *and* D-erythro-*Pentoses (V).* A mixture of slightly crude DL-anilide (DL-VI, 193 mg, 0.923 mmol), benzaldehyde (0.2 m*l*, 1.9 mmol), benzoic acid (19 mg) and water (5.8 m*l*) was placed in a tightly stoppered flask and stirred for 24 hr at room temperature. Disappearance of crystals was observed after 1.5 hr resulting in separation of an oily material. After the mixture had been extracted

49) S. M. Partridge, *Biochem. J.*, **42**, 238 (1948).

3 times with ether, the aqueous layer was evaporated under reduced pressure at a temperature below 35°C. The residue was placed in an evacuated desiccator containing phosphorus pentoxide to give colorless syrup (133 mg, 88%). The syrup mixed with a small amount of ethyl acetate crystallized completely upon seeding with a tiny piece of crystal of an authentic 2-deoxy-D-*erythro*-pentose (D-V). The crystals were recrystallized from ethyl acetate to yield pure D-V, aggregate of colorless needles or plates. Fluctuation of melting point of D-V between 85—91°C was observed. D-V thus prepared gave identical tlc with that of an authentic specimen of 2-deoxy-D-*erythro*-pentose (R_f 0.52, solvent: B, detection reagent: d; R_f 0.73, solvent: C, detection reagent: d).

Found: C, 44.67; H, 7.42%. Calcd for $C_5H_{10}O_4$: C, 44.77; H, 7.52%.

Similar treatment of L-anilide (L-VI, 49 mg, 0.23 mmol) with benzaldehyde (0.05 m*l*) and benzoic acid (5 mg) in water (1.5 m*l*) afforded L-V as colorless syrup (32 mg). The syrup was triturated with a small amount of acetone-2-propanol (6: 1) and placed in a refrigerator. The colorless crystals deposited were filtered and washed successively with ethyl acetate and ether, thus yielding pure 2-deoxy-L-*erythro*-pentose (L-V, 26 mg, 84%), $[\alpha]_D^{15}$ ($c=1.06$, H_2O): +63° (after 19 min); +61.5° (after 26 min); +60° (after 1.25 hr); +60° (after 3 hr); +60° (after 4.75 hr). Tlc of L-V produced a spot (R_f 0.5, solvent: B, detection reagent: d) which exactly coincided with that of an authentic specimen of D-V.

Found: C, 44.76; H, 7.50%. Calcd for $C_5H_{10}O_4$: C, 44.77; H, 7.52%.

D-Anilide (D-VI, 91 mg, 0.44 mmol) was treated according to the above described procedure with benzaldehyde (0.1 m*l*), benzoic acid (9 mg) and water (2.8 m*l*). 2-Deoxy-D-*erythro*-pentose (D-V) was obtained in a yield of 91% (53 mg), $[\alpha]_D^{23}$ ($c=1.12$, H_2O): −56° (after 50 min); −56° (after 1.5 hr).

Found: C, 44.68; H, 7.52%. Calcd for $C_5H_{10}O_4$: C, 44.77; H, 7.52%.

2,5-Dideoxy-DL- *and* D-threo-*Pentono-γ-lactones (VII).* A mixture of DL-bromolactone (DL-III, 2.2 g, 0.011 mol), tri-*n*-butyltin hydride[50] (7.2 g, 0.025 mol) and anhydrous tetrahydrofuran (25 m*l*) was refluxed for 8 hr and then stood overnight at room temperature. The residue obtained by evaporation of the solvent under reduced pressure was mixed with water (50 m*l*) and petroleum benzine (bp 60—80°C, 15 m*l*). The benzine layer was washed with water (20 m*l*× 2). The aqueous layer was filtered and combined with the washings. The combined aqueous layer was washed with petroleum benzine. Total benzine layer was extracted twice with water. The extract was added to the combined aqueous layer and treated with a mixture of active charcoal and celite. The resulting clear solution was evaporated under reduced pressure at a temperature below 35°C. The residue was dried in an evacuated desiccator over phosphorus pentoxide to give colorless syrup, 1.1 g (85%). Tlc of the syrup produced a spot at R_f 0.2 (solvent system: A, detection reagent: a or b). Dideoxy-γ-lactone (VII) could be distilled *in vacuo*, bp 109°C/0.1 mmHg, n_D^{25} 1.4606 [lit,[51] bp 139—141°C/0.6 mmHg, n_D^{25} 1.4632], IR ($CHCl_3$): 3620, 3450 (OH); 1780 C=O) cm^{-1}.

Found: C, 50.91; H, 6.86%. Calcd for $C_5H_8O_3$: C, 51.72; H, 6.94%.

Phenylhydrazide of DL-VII was prepared according to the usual procedure and recrystallized from 2-propanol to give pure material, colorless plates, mp 120—122°C.

Found: C, 58.77; H, 7.23; N, 12.33%. Calcd for $C_{11}H_{16}O_3N_2$: C, 58.91; H, 7.19; N, 12.49%.

A mixture of D(+)-bromolactone (D-III, 2.04 g, 10.5 mmol), tri-*n*-butyltin hydride (6.7 g, 23 mmol) and anhydrous tetrahydrofuran (25 m*l*) was refluxed for 18 hr and then allowed to stand overnight at room temperature. Treatment of the reaction mixture according to the procedure used in the case of DL-isomer afforded dideoxy-D-*threo*-pentono-γ-lactone (D-VII), 1.14 g (93%), bp 107°C/0.3 mmHg, n_D^{20} 1.4583, $[\alpha]_D^{20}=+57°$ (after 4 hr)→+58° (after 2 weeks) ($c=0.98$, H_2O). D-VII gave an identical IR spectra (neat or in $CHCl_3$) with those of DL-VII.

Found: C, 51.98; H, 7.01%. Calcd for $C_5H_8O_3$: C, 51.72; H, 6.94%.

2,5-Dideoxy-DL-threo-*pentose (VIII).* Reduction of DL-dideoxy-pentono-lactone (DL-VII, 485 mg, 4.18 mmol) by means of bis(1,2-dimethylpropyl)borane prepared from 2-methyl-2-butene (6.4 g, 92 mmol) and a tetrahydrofuran solution of diborane (23 mmol) according to the procedure used in the reduction of 2-deoxy-pentono-lactone (IV) afforded DL-2,5-dideoxy-pentose (DL-VIII) as pale yellow syrup (575 mg). This substance reduced the Tollens' reagent and gave a positive test for the Dische's reagent.[40] Tlc (solvent system: D) of the syrup gave main spot at R_f 0.48 accompanying faint spots at R_f 0.68, 0.42, 0.34, and 0.18 (detection reagent: C). Only the main spot (R_f 0.48) could be observed when detection reagent d was used.

The syrupy DL-dideoxy-pentose (DL-VIII, 60 mg) was mixed with ethanol (1 m*l*) and a few small crystals of 2,4-dinitrophenylhydrazine was added to the refluxing solution, and when the crystals had dissolved, an additional small amount of the hydrazine was added to the solution. This procedure was repeated until no more dissolution of the hydrazine could be observed. Further reflux was continued (total 3 hr), and then the mixture was cooled. The resulting crystals were filtered and washed with ethanol. The filtrate gave second crop of crystals on addition of water. The crude crystals thus obtained (62 mg, 48% based on lactone, VII) were recrystallized successively from ethanol and ethyl acetate to give pure 2,4-dinitrophenylhydrazone of VIII, tiny yellow plates, mp 144.5—146.5°C. IR (KBr-disk): 3300, 3090 (OH, NH); 2970 (CH_3–); 1520, 1330 (–NO_2) cm^{-1}.

Found: C, 44.02; H, 4.90; N, 18.80%. Calcd for $C_{11}H_{14}O_6N_4$: C, 44.30; H, 4.73; N, 18.79%.

5-Bromo-2,5-dideoxy-DL-threo-*pentose Diethyl Dithioacetal (X).* The reaction of DL-bromolactone (DL-III, 585 mg, 3 mmol) with bis(1,2-dimethylpropyl)borane prepared from 2-methyl-2-butene (4.6 g, 66 mmol) and diborane (15.5 mmol) in tetrahydrofuran according to the method used in the case of 2-deoxy-pentono-lactone (IV) afforded a colorless syrup which gave positive test for the Dische's reagent (first crop: 427 mg; second crop was obtained from the ether extract containing disiamylborinic acid by extraction with water: 127 mg). The syrup (first crop, 255 mg) was mixed with ethanethiol (0.3 m*l*) and concentrated hydrochloric acid (1 m*l*) at room temperature resulting in instantaneous deposition of crystals with evolution of heat. After the mixture had been shaken for 15 min in an ice-bath, the slurry was mixed with water and the crystals were collected by filtration, washed thoroughly with water until neutral filtrate was obtained, and then washed with petroleum benzine, thus yielding thioacetal (X, 191 mg) as colorless needles. The second crop of syrup was treated according to the above

50) M. Ohara and R. Okawara, *J. Organometal. Chem.*, **3**, 484 (1965).

51) E. E. van Tamelen, F. M. Strong, and U. C. Quarck, *J. Amer. Chem. Soc.*, **81**, 750 (1959).

described procedure to give 20 mg of X. Total yield of X was 38% (based on III). Recrystallization of the crystals from petroleum benzine yielded pure X as white silky needles, mp 92.5—95°C (decomp.) (with a pre-heated bath (85°C) and a heating rate of 2°C/min), NMR ($CDCl_3$): δ 1.28 (6H, triplet, $J_{CH_3-CH_2}$ 7.6, CH_3). IR (KBr-disk): 3360 (OH); 2960 (CH_3–); 1415 (S–CH_2–) cm^{-1}.

Found: C, 35.81; H, 6.40; Br, 26.66; S, 21.13%. Calcd for $C_9H_{19}O_2BrS_2$: C, 35.64; H, 6.31; Br, 26.34; S, 21.14%.

5-Bromo-2,5-dideoxy-DL-threo-*pentose (IX).* DL-Thioacetal (DL-X, 97 mg, 0.32 mmol) in acetone (1 m*l*) and mercuric chloride (349 mg, 1.28 mmol) in acetone-water (1.5—0.2 m*l*) were mixed at room temperature with finely powdered cadmium carbonate (349 mg, commercial material had been washed with water and dried). After the mixture had been stirred for 24 hr, the insoluble material was removed by filtration and washed with acetone. The combined filtrate and washings were evaporated under reduced pressure in the presence of a small amount of cadmium carbonate. The residue was extracted 3 times with water (total 5 m*l*). The extract was treated with a mixture of Amberlite IR 120 (H^+) and Dowex 3 (OH^-) under ice-cooling. The ion exchange resins were removed by filtration and washed thoroughly with water. Concentration of the combined filtrate and washings *in vacuo* at a temperature below 35°C yielded a syrup. The syrup was dried in an evacuated desiccator over phosphorus pentoxide. The dried syrup (39 mg, 62%) was triturated with a small amount of ethyl acetate and kept in a refrigerator, resulting in complete crystallization. The crystals were recrystallized from ethyl acetate to give pure bromo-dideoxy-DL-*threo*-pentose (DL-IX) as colorless fine needles, mp 81.5—83.5°C (decomp.).

Found: C, 30.28; H, 4.49; Br, 41.76%. Calcd for $C_5H_9O_3Br$: C, 30.48; H, 4.60; Br, 40.56%.

DL-IX was found to be fairly unstable and in certain cases decomposition of DL-IX at room temperature to form black material was observed in a day.

5-Azido-2,5-dideoxy-DL-threo-*pentose Diethyl Dithoiacetal (XI).* A mixture of bromo-pentose mercaptal (X, 50 mg, 0.17 mmol) in methanol (5 m*l*) and sodium azide (87 mg, 1.3 mmol) in water (1.5 m*l*) was refluxed for 48 hr. The reaction mixture was evaporated under reduced pressure. The residue was mixed with methanol and again the solvent was removed *in vacuo*. This procedure was repeated to remove water completely. The residue thus obtained was extracted thoroughly with ethyl acetate. The residue obtained by evaporation of the solvent under reduced pressure was placed in an evacuated desiccator containing phosphorus pentoxide to give pale yellow syrup (30 mg). Preparative tlc of the syrup [silica gel G, thickness 0.5 mm; solvent system: chloroform-acetone (9: 1); detection reagent: iodine] resulted in the separation of the following substance: (a) R_f 0.6, almost colorless syrup, 8 mg, (b) R_f 0.35, colorless syrup, 11 mg, (c) R_f 0.17, colorless syrup, 4 mg (9%), IR (neat): 2100 ($-N_3$) cm^{-1}, (d) R_f 0.04, pale yellow syrup, 2 mg.

The financial support of Mr. Tokusuke Egawa, the President of Kofuku-sogo Bank is gratefully acknowledged.

Study of Across-Space Intramolecular Charge-Transfer Interaction by Absorption and Fluorescence Spectroscopy

Kiyoshi MUTAI

Department of Chemistry, College of General Education, University of Tokyo, Komaba, Meguro, Tokyo

(Received July 21, 1971)

Across-space (through-space) intramolecular charge-transfer (CT) interaction has been observed in homologous series of p-$O_2NC_6H_4(CH_2)_nNHAr$ (I) and p-$O_2NC_6H_4(CH_2)_nNRAr$ (II). Introduction of an alkyl group to the amino nitrogen of I, thus producing II, generally increases the intensity of the CT absorption band. It also induces the red-shift of the band position in most cases owing to the increase of the basicity of the donor, while the blue-shift is observed in *ortho* substituted derivatives. The latter effect is explained by the steric inhibition of the delocalization of nitrogen lone-pair electrons. The CT fluorescence has been observed at room temperature in the lower homologs ($n=1$, 2, and rarely 3) of I and II. Higher intensity of the fluorescence is generally observed in $n=1$. The increase of intensity is observed when a small amount of benzene is added to a cyclohexane solution. The excitation spectrum shows two peaks; one at the ^1L_b transition wavelength of the amine moiety and the other at the CT absorption. The former suggests the possibility that an excited donor collides intramolecularly with a ground state acceptor part (p-nitrophenyl group) to form an excited CT state, and the latter presents a strong evidence for the origin of the fluorescence being the excited CT state.

Of the modes of intermolecular and intramolecular interactions arousing the interest of chemists, hydrogen bonding seems to have been studied most extensively in the past. However, during the last few years interest has grown in the study of intramolecular charge-transfer (CT) interaction.[1,2] This paper deals with the across-space[3] intramolecular CT effect, studied hitherto mainly by absorption spectroscopy with particular attention paid to the CT ground state. The present study is intended to provide information on the excited state of the intramolecular CT interaction with the aid of fluorescence spectroscopy as well as on the ground state.

Since the *intramolecular* CT interaction is subject to conformational restrictions, one can expect to observe spectral features differing from those of the *intermolecular* interaction in which the energetically most favorable conformation is exclusively assumed. Thus the characteristic aspects in the *intramolecular* interaction may provide valuable data for grasping the CT phenomenon. In *intramolecular* interaction the equilibrium constant between interacting and non-interacting molecules is independent of concentration so far as intermolecular interaction is negligible, and enables one to observe purely 1 : 1 interaction at low concentration even if the interaction is hardly detectable in an *intermolecular* case. This condition, of course, simplifies the interpretation of the spectral features.

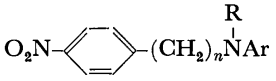

I, R=H
II, R=Me or Et

a, Ar=C_6H_5
b, Ar=4-MeC_6H_4
c, Ar=2,4-$Me_2C_6H_3$
d, Ar=2,4,6-$Me_3C_6H_2$
e, Ar=4-$MeOC_6H_4$
f, Ar=2,5-$(MeO)_2C_6H_3$
g, Ar=1-$C_{10}H_7$
h, Ar=2-$C_{10}H_7$

The compounds used for the present study are the homologous series of the type, p-$O_2NC_6H_4(CH_2)_nNHAr$ (I) and p-$O_2NC_6H_4(CH_2)_nNRAr$ (II), where R denotes methyl or ethyl groups, and Ar phenyl, p-tolyl, 2,4-dimethylphenyl, mesityl, p-anisyl, 2,5-dimethoxyphenyl or naphthyls. The CT interaction is expected between p-nitrophenyl (acceptor) and arylamino (donor) groups.

Results and Discussion

Absorption Spectra. Absorption spectra of the compounds of type I in carbon tetrachloride solution have been reported.[2] In the present study, a mixture of benzene–cyclohexane (1:4) was used as a common solvent for the measurement of absorption and fluorescence spectra. Addition of benzene to cyclohexane increases both the dissolving power of the solvent system and the intensity of the CT fluorescence. In order to show the effect of the number of methylene groups (n) and the difference between I and II series, some absorption curves are reproduced in Figs. 1 through 3. The data of the CT bands are summarized in Table 1. The CT band is obtained by subtracting a reference or standard spectrum from the spectrum of I or II. There are two ways for setting up the reference spectrum;[2] one is to adopt the spectrum of a sufficiently higher homolog (generally, a homolog with $n\geqq5$), and the other to adopt the sum of the spectra of the compounds having similar chromophores and simple struc-

1) a) W. N. White, *J. Amer. Chem. Soc.*, **81**, 2912 (1959); b) S. Shifrin, *Biochim. Biophys. Acta*, **96**, 173 (1966); c) J. W. Verhoeven, I. P. Dirks, and Th. J. de Boer, *Tetrahedron Lett.*, **1966**, 4399; d) A. J. de Gee, J. W. Verhoeven, I. P. Dirks, and Th. J. de Boer, *Tetrahedron*, **25**, 3407 (1969); e) J. W. Verhoeven, I. P. Dirks, and Th. J. de Boer, *ibid.*, **25**, 4037 (1969); f) H. A. H. Craenen, J. W. Verhoeven, and Th. J. de Boer, *Tetrahedron Lett.*, **1970**, 1167; g) R. Carruthers, F. M. Dean, L. E. Houghton, and A. Ledwith, *Chem. Commun.*, **1967**, 1206; h) M. Ōki and K. Mutai, *Tetrahedron Lett.*, **1968**, 2019; i) M. Itoh and E. M. Kosower, *J. Amer. Chem. Soc.*, **90**, 1843 (1968); j) J. P. Carrión, D. A. Deranleau, B. Donzel, K. Esko, P. Moser, and R. Schwyzer, *Helv. Chim. Acta*, **51**, 459 (1968); k) P. Moser, *ibid.*, **51**, 1831 (1968); l) K. Mutai, *Tetrahedron Lett.*, **1971**, 1125.

2) M. Ōki and K. Mutai, *Tetrahedron*, **26**, 1181 (1970).

3) The word "across-space" is used in order to distinguish the effect from "through-bond" intramolecular CT interaction.[4,5] "Through-space" may be used instead.

4) a) S. Nagakura and J. Tanaka, *J. Chem. Phys.*, **22**, 236 (1954); b) S. Nagakura, *ibid.*, **23**, 1441 (1955); c) S. Nagakura, *Pure Appl. Chem.*, **7**, 79 (1963).

5) H. A. Bent, *Chem. Rev.*, **68**, 588 (1968).

Table 1. Charge-transfer bands of p-$O_2NC_6H_4(CH_2)_n$ NHAr (I) and p-$O_2NC_6H_4(CH_2)_n$ NRAr (II) in benzene-cyclohexane (1 : 4)

Ar	R	$n=1$ λ_{max} (nm)	ε	$n=2$ λ_{max} (nm)	ε	$n=3$ λ_{max} (nm)	ε
C_6H_5 (Ia)	H	333	360	325	1030	317	530
(IIa)	Me	356	480	340	1750	329	450
	Et	357	380	347	1430		
4-MeC_6H_4 (Ib)	H	339	380	333	930		
(IIb)	Me	364	455	347	1580		
2,4-$Me_2C_6H_4$ (Ic)	H	350	285	339	785		
(IIc)	Me	321	440	313	1040		
2,4,6-$Me_3C_6H_2$ (Id)	H	326	855	316	1035		
(IId)	Me	323	680	313	1225		
4-$MeOC_6H_4$ (Ie)	H	355	380	347	710		
(IIe)	Et	370	325	361	990		
2,5-$(MeO)_2C_6H_3$ (If)	H	351	260	338	810		
(IIf)	Et	335	565	322	1210		

tures. For practical reasons both methods are adopted. The latter is applied, to some derivatives of I and most of II, since their higher homologs are liquid at room temperature and difficult to be isolated in pure state because of their high boiling points. p-Nitrobutylbenzene and $ArNR-CH_2CH_3$ (R is hydrogen or alkyl) were used as model compounds. Thus the application of the different methods does not yield any significant difference in the CT band characteristics.[2)]

It is generally accepted that alkylation of the nitrogen of aniline or its derivative increases the π-basicity of the compound. Thus when I and II with the same Ar group are compared, II has a stronger electron-donor than I and is expected to have higher population of the CT interacting molecule, the situation leading to a higher intensity of the CT band of II at a longer wavelength than I. Hence, the introduction of an alkyl group to the amine nitrogen of I is a means to confirm the origin of the band as CT interaction.

As regards the band position, however, the prediction does not necessarily hold. We see from Table 1 that there are two groups of derivatives in which one reveals the shift of the band position to the long-wavelength side by the introduction of an alkyl goup to the amino nitrogen, as is observed in the cases of Ia, Ib, and Ie, and the other to the short-wavelength side as is observed in Ic, Id, and If. The effect observed in the latter group is contrary to expectation, but it can be understood if we note that all the Ar's in this group contain *ortho* substituent; that is, the *ortho* substituent hinders the orbital axis of the nitrogen lone-pair electrons from being pararell with p_π orbital axis of benzene, inducing less increase or even decrease of the π-basicity of NRAr group in comparison with the corresponding NHAr group. The group NH-2,4,6-$Me_3C_6H_2$ containing two

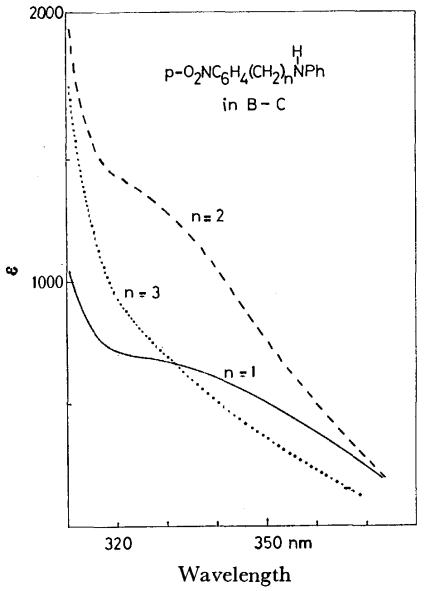

Fig. 1. Absorption spectra of p-$O_2NC_6H_4(CH_2)_n$NHPh (Ia) in long wavelength region in benzene-cyclohexane (1 : 4) mixture. Numerals attached to the curves denote the number of methylene group (n).

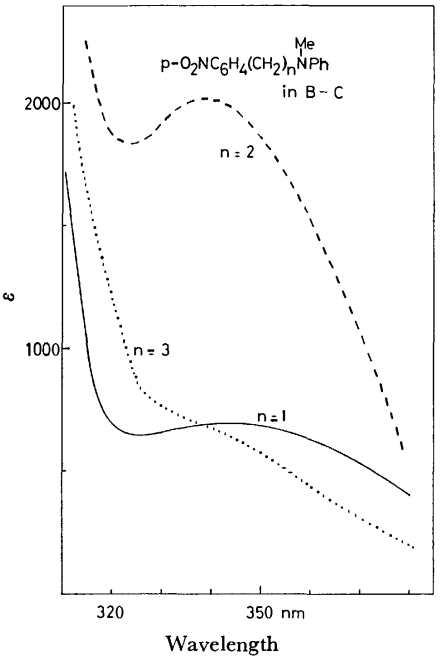

Fig. 2. Absorption spectra of p-$O_2NC_6H_4(CH_2)_n$NMePh (IIa) in long wavelength region in benzene-cyclohexane (1 : 4) mixture. Numerals attached to the curves denote the number of methylene group (n).

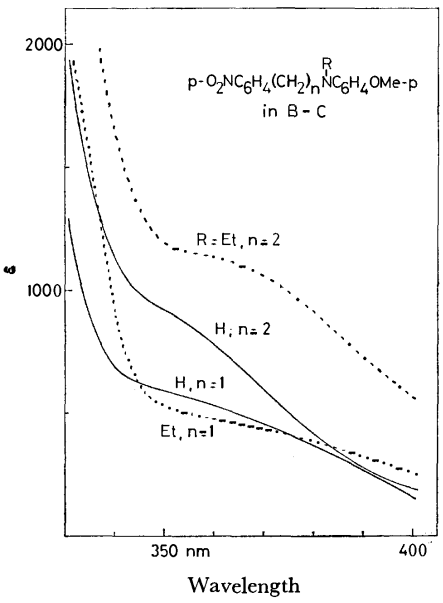

Fig. 3. Absorption spectra of p-$O_2NC_6H_4(CH_2)_nNRC_6H_4O$-Me-$p$ (Ie and IIe, R=Et) in long wavelength region in benzene–cyclohexane (1:4) mixture.

ortho methyls undergoes this steric effect (λ_{max} of Id at 326 and 316 nm $n=1$ and 2, respectively),[2] which is insignificant for NH-2,4-$Me_2C_6H_3$ group with one *ortho* methyl (λ_{max} of Ic at 350 and 339 nm in $n=1$ and 2, respectively). This steric inhibition of resonance has also been detected by means of the N–H stretching vibration,[2] dipole moment,[6] and ultraviolet absorption spectra of *N,N*-dimethylaniline derivatives.[7] Thus further introduction of a methyl group to the nitrogen of Id causes no further remarkable effect (only 3 nm of blue-shift in both $n=1$ and 2 of IId). On the other hand, we see from band positions of the derivatives of Ic and If that the steric effect makes no appreciable contribution when the nitrogen is a secondary amine type. Consequently it can be said that the introduction of an alkyl group to I increases the π-basicity of the donor only when the Ar group has no *ortho* substituent.

It seems strange that the decrease of the π-basicity of the donor is accompanied by an increase of intensity. However, examination of the CT band data shows a general relationship between the peak position and intensity; the shorter the λ_{max}, the higher the intensity. This phenomenon has also been observed in other solvents[2] and in some intermolecular CT complexes.[8-11] Although no satisfactory explanation has been given to this effect,[12] the abnormal increase of the intensity accompanied by blue-shift is in line with the general rule, and probably not with the increase of the number of interacting molecules.

Fluorescence Spectra. In the fluorescence spectra of I and II at room temperature, a fluorescence peak due to the excited state of the across-space intramolecular CT interaction was observed at 500—550 nm. Some CT fluorescence spectra are shown in Figs. 4 through 9 with excitation spectra. The peak was assigned as above for the following reasons. (1) The concentration of the solution used for measurement was less than 2×10^{-4} mol/l, which is dilute enough to exclude intermolecular interacting species. (2) The peak was observed only in the lower homologs and did not appear when the number of the methylenes (n) exceeds three. It should be remembered that the CT absorption band was observed in the lower homologs of $n\leqq4$. (3) Generally, the increase of the π-basicity of the donors owing to the introduction of electron-donating group(s) into the benzene ring or the nitrogen induced red-shift of the fluorescence peak (especially in $n=1$ homolog of I), reflecting the similar feature observed in the CT absorption spectrum. (4) The excitation spectrum showed a maximum at the λ_{max} of the corresponding CT absorption (Figs. 4—9). (1) and (2) provide evidences for intramolecular process. (3) and (4) suggest a close relationship between appearance of peak and CT interaction. The peak positions and their intensities are summarized in Tables 2 and 3.

a) Solvent Effects: The solvents used for the measurement of CT fluorescence are cyclohexane and benzene–cyclohexane (1:4, v/v) mixture. A slight blue-shift of the CT fluorescence is observed (Tables 2 and 3), when the solvent was changed from the latter to the former, and the effect is consistent with the shift of the CT absorption band[2] and also with that observed for intermolecular CT fluorescence.[13] In most cases addition of benzene to cyclohexane increased the intensity. The most significant effect is observed in the spectra of Ia ($n=1$ and 2) and Ib ($n=1$ and 2) which show no peak in cyclohexane. For these derivatives with weak donors the addition of benzene seems to be extraordinarily effective.

It is surprising, however, that the higher homolog of Ia ($n=3$) shows a peak in cyclohexane but not in benzene–cyclohexane system. The peak might be due to impurity, but this can be denied for the following reasons; a similar effect was observed in the series of Ib and IIa ($n=3$ shows the largest peak height), and the presence of an impurity which exhibits fluorescence even at a concentration less than 10^{-6} mol/l (since no impurity was detected by any other spectroscopic method, its concentration must be, at most, a few per cent to the sample compound) is incredible.

It is also noteworthy that the addition of benzene does not always result in the increase of intensity.

6) J. W. Smith, *J. Chem. Soc.*, **1961**, 81.
7) H. B. Klevens and J. R. Platt, *J. Amer. Chem. Soc.*, **71**, 1714 (1949).
8) A. Bier, *Rec. Trav. Chem. Pays-Bas*, **75**, 866 (1956).
9) R. E. Merrifield and W. D. Phillips, *J. Amer. Chem. Soc.*, **80**, 2778 (1958).
10) L. J. Andrews and R. M. Keefer, *ibid.*, **74**, 4500 (1952).
11) M. Tamres, D. R. Virzi, and S. Searles, *ibid.*, **75**, 4358 (1953).
12) It has not yet been elucidated to what extent the spectra of the original chromophores undergo modifications in their band shapes on interaction. It is therefore difficult to discriminate whether the trend is "artificial" or inherent in CT interaction, as long as the CT band is obtained by subtraction of the reference spectrum, or the apparent peak position and intensity in the absorption curve are regarded as "true" as is often the case for intermolecular interaction.
13) K. Kaneta and M. Koizumi, This Bulletin, **40**, 2254 (1967).

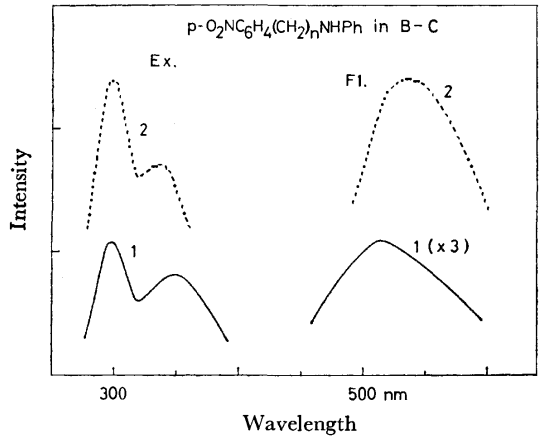

Fig. 4. Fluorescence (Fl.) and excitation (Ex.) spectra of *p*-$O_2NC_6H_4(CH_2)_nNHPh$ (Ia) in benzene–cyclohexane (1 : 4) mixture. Numerals attached to the curves denote *n*.

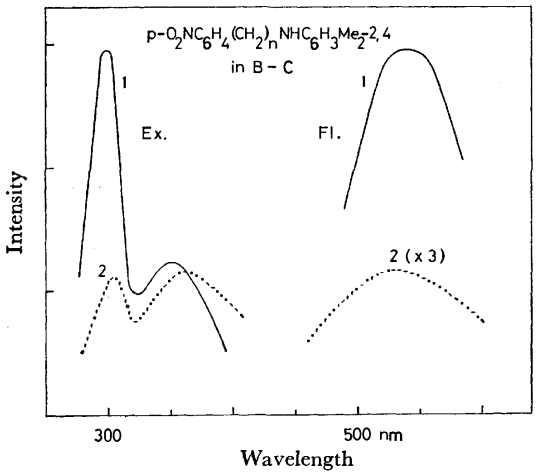

Fig. 5. Fluorescence (Fl.) and excitation (Ex.) spectra of *p*-$O_2NC_6H_4(CH_2)_nNHC_6H_3Me_2$-2,4 (Ic) in benzene–cyclohexane (1 : 4) mixture. Numerals attached to the curves denote *n*.

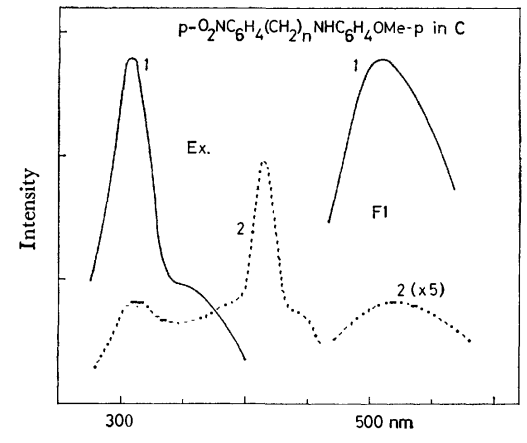

Fig. 6. Fluorescence (Fl.) and excitation (Ex.) spectra of *p*-$O_2NC_6H_4(CH_2)_nNHC_6H_4OMe$-*p* (Ie) in cyclohexane. Numerals attached to the curves denote *n*.

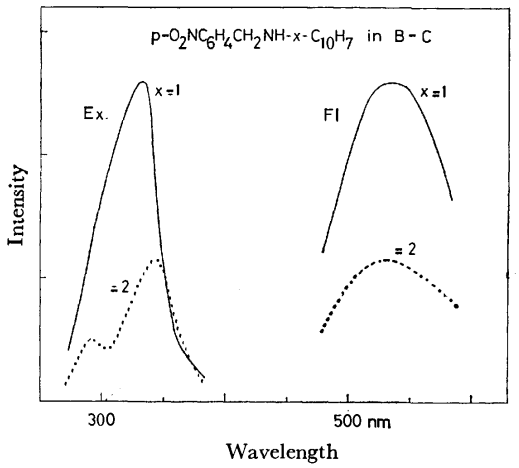

Fig. 7. Fluorescence (Fl.) and excitation (Ex.) spectra of *N*-(*p*-nitrobenzyl)naphthylamines in benzene–cyclohexane (1 : 4) mixture. Numerals attached to the curves denote the position of amino group in naphthalene nucleus.

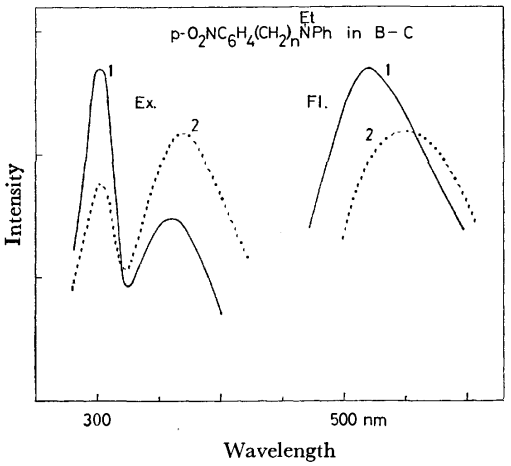

Fig. 8. Fluorescence (Fl.) and excitation (Ex.) spectra of *p*-$O_2NC_6H_4(CH_2)_nNEtPh$ (IIa) in benzene–cyclohexane (1 : 4) mixture. Numerals attached to the curves denote *n*.

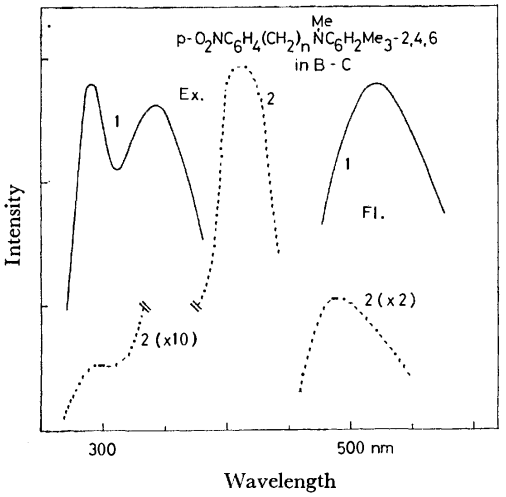

Fig. 9. Fluorescence (Fl.) and excitation (Ex.) spectra of *p*-$O_2NC_6H_4(CH_2)_nNMeC_6H_2Me_3$-2,4,6 (IId) in benzene–cyclohexane (1 : 4) mixture. Numerals attached to the curves denote *n*.

Table 2. Intramolecular charge-transfer fluorescence of p-$O_2NC_6H_4(CH_2)_n$ NHAr (I)

Ar	n	Benzene–cyclohexane (1: 4)		Cyclohexane	
		λ_{max} (nm)	Relative intensity[a]	λ_{max} (nm)	Relative intensity[a]
C_6H_5 (Ia)	1	512	3.3	—	
	2	540	21	—	
	3	±		545	3.1
	4	—		—	
4-MeC_6H_4 (Ib)	1	525	42	—	
	2	535	3.6	500	2.5
	3	—		550±10	
2,4-$Me_2C_6H_3$ (Ic)	1	536	29	492[b]	2.9
	2	530	3.8	510	5.5
	3	—		—	
2,4,6-$Me_3C_6H_2$ (Id)	1	554	31	502	24
	2	525	3.6	523	2.5
	3	—		—	
4-$MeOC_6H_4$ (Ie)	1	>550[c]		510	83
	2	525	5.4	518	4.8
	3	+		—	
2,5-$(MeO)_2C_6H_3$ (If)	1	560±5[c]	3.7	522	10
	2	527	2.5	±	
1-$C_{10}H_7$ (Ig)	1	535	100	493[b]	17
	2	570	15	535	33
	3	—		—	
2-$C_{10}H_7$ (If)	1	527	51	485±10[b]	2.1
	2	570	18	527	13

a) The intensity of p-$O_2NC_6H_4CH_2NH$-1-$C_{10}H_7$(Ig) is taken as 100.
b) Owing to the overlap with stray light in short wavelength region, the exact maximum position is difficult to be determined.
c) Owing to the low sensitivity of the photomultiplier (1P28) in long-wavelength region, the maximum does not appear in the range measured.

Table 3. Intramolecular charge-transfer fluorescence of p-$O_2NC_6H_4(CH_2)_n$ NRAr (II)

Ar	R	n	Benzene–cyclohexane (1: 4)		Cyclohexane	
			λ_{max} (nm)	Realtive intensity[a]	λ_{max} (nm)	Relative intensity[a]
C_6H_5 (IIa)	Me	1	522	51		
		2	545	64	504	2.5
		3	560±10	7.3	560±10	3.0
	Et	1	522	77	496	2.4
		2	550	61	500	3.8
4-MeC_6H_4 (IIb)	Me	1	548	230	490	35
		2	515	7.0	510	4.0
2,4-$Me_2C_6H_3$ (IIc)	Me	1	545	62	490	11
		2	525	6.1	520±5	2.5
2,4,6-$Me_3C_6H_2$ (IId)	Me	1	522	60	492	2.2
		2	490	12	505	3.7
4-$MeOC_6H_4$ (IIe)	Et	1	>550[b]		530	250
		2	525	10	500	12
2,5-$(MeO)_2C_6H_4$ (IIf)	Et	1	>550[b]		525	65
		2	502	6.1	497	4.0
1-$C_{10}H_7$ (IIg)	Et	1	543	160	498	74

a) The intensity of p-$O_2NC_6H_4CH_2NH$-1-$C_{10}H_7$ (Ig) is taken as 100.
b) Owing to the low sensitivity of the photomultiplier (1P28) in long-wavelength region, the maximum does not appear in the range measured.

For instance, $n=1$ homologs of Id, Ie, and Ig exhibited no peak when dissolved in pure benzene as well as in 96% ethanol, while Ia showed the CT peak in benzene.

So far there is no satisfactory explanation for these phenomena caused by the added benzene and sufficient evidence to assign the effects to electronic origin (*e.g.* energy-transfer process) or to environmental origin (*e.g.* solvation), or both.

b) Peak Position and Intensity: A comparison of Tables 2 and 3 with Table 1 shows that there is no simple relationship between the maximum positions of the CT absorption band and the fluorescence. As regards CT absorption, it has been found that the longer the n ($n \leqq 3$), the shorter the wavelength of its λ_{max}, irrespective of solvent.[2] In benzene–cyclohexane system, most of the homologous series reveal the same tendency in their CT fluorescence bands. However, the tendency is reversed when the solvent was changed to cyclohexane. This might be due to the change of the potential energy curves of the CT ground and excited states caused by different solvation.

It is noteworthy that the peak position and intensity of $n=1$ homolog are generally more affected by solvent than $n=2$. A scale model shows only partial overlap of π-electron clouds of the donor and acceptor is allowed in $n=1$ because of the short methylene chain, but parallel plane conformation of the benzene rings is possible for $n=2$, the situation being the same both in I and II. The latter face-to-face conformation which permits sufficient overlap of the π-electron clouds is expected to be more stable than the conformation of $n=1$ and less susceptible to environmental factors. Probably this is the main reason for the fluorescence characteristics of $n=1$ being more sensitive to solvent.

For the series I ($n=1$) in benzene–cyclohexane, the CT fluorescence λ_{max} is in the order Ia<Ib<Ic<Id<Ie, which reflects the order of the electron-donating ability of Ar group and also nearly that of the λ_{max} of the CT absorption. The exception is Id, the CT absorption band of which is at the shortest wavelength due to the steric inhibition of delocalization of the nitrogen lone-pair electrons by two *ortho* methyls. Thus the fluorescence λ_{max} is expected at a shorter wavelength than Ia. However, since the most stable conformation of the excited state is achieved during much longer life time of fluorescence (about 10^{-9} sec) than conformational readjustment (about 10^{-12} sec) and the CT absorption observed is merely a vertical transi-

Table 4. Excitation spectra of the CT fluorescence of p-$O_2NC_6H_4(CH_2)_n$ NHAr (I)

Ar	n	Benzene-cyclohexane (1: 4) λ_I (nm)	λ_{II} (nm)	Intensity ratio λ_I/λ_{II}		Cyclohexane λ_I (nm)	λ_{II} (nm)	Intensity ratio λ_I/λ_{II}	^1L_b[a] (nm)	CT λ_{max} (nm)
C_6H_5 (Ia)	1	298	345	0.75		—	—		295	333
	2	300	335	0.73		—	—			325
4-MeC_6H_4 (Ib)	1	300	350	0.52		—	—		304	339
	2	308	350	0.95	+400	305	350	0.87		333
2,4-$Me_2C_6H_3$ (Ic)	1	298	350	0.42		297	352	0.74	299	350
	2	303	360	1.1	+405	300	350	0.69		339
2,4,6-$Me_3C_6H_2$ (Id)	1	290	340	1.1		290	340	1.1	286	326
	2	300—355	Broad			290	325	0.62		316
4-$MeOC_6H_4$ (Ie)	1	313	355	0.44		310	355sh[c]	0.34	308	355
	2	315	415[b]	0.81		315	415	1		347
2,5-$(MeO)_2C_6H_3$ (If)	1	300	355	0.47		300	355	0.37	298	351
	2	305	350	0.9		±				

a) The ^1L_b transition of ArNHEt in cyclohexane. b) A sharp peak (see Figs. 6 and 9). c) Shoulder.

Table 5. Excitation spectra of the CT fluorescence of p-$O_2NC_6H_4(CH_2)_n$ NRAr (II)

Ar	R	n	Benzene-cyclohexane (1: 4) λ_I (nm)	λ_{II} (nm)	Intensity ratio λ_I/λ_{II}	Cyclohexane λ_I (nm)	λ_{II} (nm)	Intentity ratio λ_I/λ_{II}	^1L_b[a] (nm)	CT λ_{max} (nm)
C_6H_5 (IIa)	Me	1	300	360	0.68				300	356
		2	303	358	0.92	303	365	1.2		340
		3	303	350	0.52	305	355	0.52		329
	Et	1	302	362	0.55	302	365	0.72	303	357
		2	303	370	1.3	307	375	1.6		347
4-MeC_6H_4 (IIb)	Me	1	306	365	0.55	305	365	0.62	307	364
		2	312	360	1.4	310	360	0.91		347
2,4-$Me_2C_6H_3$ (IIc)	Me	1	290	340sh[b]	0.52	287	330sh[b]	0.73	285±5	321
		2	300	415[c]	4.2	290	415[c]	1.3		313
2,4,6-$Me_3C_6H_2$ (IId)	Me	1	290	345	1.1	290sh[b]	355	1.9		323
		2	295	412	54	310	405	14		313
4-$MeOC_6H_4$ (IIe)	Et	1	320	Plateau	0.26	315	365	0.33	318	370
		2	330	415[c]	4.0	325	410[c]	1.4		361
2,5-$(MeO)_2C_6H_4$ (IIf)	Et	1	312	355[c]	0.70	302	350	0.41	297	335
		2	307	410[c]	8.1	305	410[c]	2.6		322

a) The ^1L_b transition of ArNREt in cyclohexane. b) Shoulder. c) A sharp peak (see Figs. 6 and 9).

tion from the ground state, the "abnormal" behavior of Id might not be surprising if it is admitted that the most stable conformation of these two states differs.

c) Excitation Spectra of CT Fluorescence: Some typical examples of the excitation spectral curves are shown in Figs. 4 through 9. We see at a glance that a curve consists of two bands. One peak at shorter wavelength approximately agrees with the position of ^1L_b transition of ArNR-group, and the other with the CT absorption (see Tables 4 and 5). Agreement of these values can be said to be satisfactory, if we take into consideration some uncertainties possibly involved in both the excitation and absorption spectra (no correction has been made for the wavelength dependence of the sensitivity of the spectrometer).

The fact that the light having the same wavelength as CT absorption is effective for fluorescence is a strong evidence for the CT fluorescence.

It is interesting but puzzling that the excitation spectra of $n=2$ homologs of IIc—IIf showed a narrow but intense peak at about 410 nm (Fig. 9). The same phenomenon is also observed in some derivatives of I (Fig. 6). Appearance of this extra peak is restricted only to the $n=2$ homologs in both I and II series. No corresponding absorption is found in the absorption spectra of these compounds, and no convincing explanation has been obtained.

It is also interesting that the mere excitation of the amine moiety is effective for CT fluorescence. This suggests at least two processes possible for the appearance of the excited CT state; (1) only an amine moiety in a CT interacting molecule is excited and falls to the lowest excited singlet level of CT interaction releasing the excess energy nonradiatively. (2) An amine moiety free from the interaction absorbs light, and in its excited state during the stay collides with the *p*-nitrophenyl group at the other end of the methylene chain to form a CT interacting molecule in excited state. The processes are described in the following scheme, where A and D are the acceptor (*p*-nitrophenyl) and the donor (NRAr) groups, respectively (for λ_I and λ_{II}, see Tables 4 and 5).

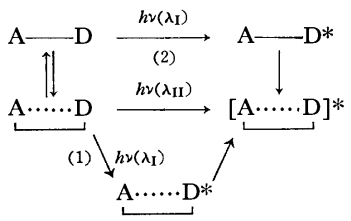

From the viewpoint of energy level, ^1L_a band of *p*-nitrophenyl group at 265 nm (in heptane)[14] is higher than the ^1L_b of the amine moieties and the excitation of the nitrophenyl group should be effective in either process. Contrary to expectation no peak could be detected at the wavelength corresponding to this absorption. In this respect, it is notable that in 1,4-dimethoxybenzene — trinitrobenzene or — chloranil system the excitation of an acceptor results in the formation of donor cation,[15] suggesting that the encounter of the excited acceptor with the donor leads to the transient acceptor anion and donor cation likely to be formed when a CT complex is excited in polar solvent. Although there is no reason why this intermolecular process should not be observed in an intramolecular case, no satisfactory explanation has been found as yet.

Of the two processes, (2) is considered as more probable, since an excimer and an exciplex are formed in a similar process. The same process has been considered possible for the intermolecular CT interaction between anilines and oxygen molecule,[16] and between *N,N*-dimethylnaphthylamine and methyl benzoate.[17] As an evidence, it may be cited that the ratio of the apparent peak heights of the excitation spectrum, λ_{II}/λ_I, is in almost all the cases larger in $n=2$ than $n=1$ (for typical example, see Figs. 5 and 8). The ratio is independent of the quantum yield of the fluorescence and of the intensity distribution of light source, and, therefore, represents the relative effectiveness of two types of excitations. The larger value of $n=2$ homolog shows that the excitation of the CT state is more effective than that of the same band of $n=1$ homolog, or, in other words, the excitation of the amine moiety is less effective in $n=2$. According to process (2), the effect is explained as follows. The excited donor in $n=2$ homolog has a smaller chance to encounter the acceptor before transition to the ground state due to its longer chain length than $n=1$, the situation leading to the relative inefficiency of ^1L_b excitation and the increase of the relative effectiveness of CT band excitation.

Conclusion

It was suggested[2] that the interaction might be "contact charge-transfer",[18] but the occurrence of CT fluorescence indicates the presence of energy minimum in the excited energy level of the CT interaction. It might be said that in the interacting species some stable and unstable complexes are present whose stability depends mostly on conformational factors of the interacting groups.

Intramolecular excimer formation has been studied by several investigators,[19] who showed that strict conditions are required for the occurrence of the phenomenon. As an example, the number of methylene groups in Ar–$(CH_2)_n$–Ar system must be three for the observation of intramolecular excimer fluorescence. When the number is two, insufficient overlap of π-electron clouds in the aromatic rings prevents the radiative

14) W. M. Schubert and J. Robins, *J. Amer. Chem. Soc.*, **80**, 559 (1958).

15) K. Kawai, N. Yamamoto, and H. Tsubomura, This Bulletin, **42**, 369 (1969).

16) M. Hori, H. Itoi, and H. Tsubomura, *ibid.*, **43**, 3765 (1970).

17) T. Miwa and M. Koizumi, *ibid.*, **39**, 2588 (1966).

18) E. Orgel and R. S. Mulliken, *J. Amer. Chem. Soc.*, **89**, 6056 (1967).

19) a) F. Hirayama, *J. Chem. Phys.*, **42**, 3136 (1965); b) M. T. Vala, Jr., J. Haebig, and S. A. Rice, *ibid.*, **43**, 886 (1965); c) J. W. Longworth and F. A. Bovey, *Biopolymers*, **4**, 115 (1966); d) D. T. Browne, J. Eisinger, and N. J. Leonard, *J. Amer. Chem. Soc.*, **90**, 7302 (1968); e) E. A. Chandross and C. J. Dempster, *ibid.*, **92**, 3586 (1970).

Table 6. Elemental analyses and yields of new compounds used in this study
p-$O_2NC_6H_4(CH_2)_n$ NRAr

Ar	R	n	Yield, %	Mp or (bp/mmHg), °C	Formula	C %		H %		N %	
						Calcd	Found	Calcd	Found	Calcd	Found
4-MeC_6H_4	H	1	61	67—68	$C_{14}H_{14}N_2O_2$	69.40	69.45	5.83	5.65	11.56	11.71
		2	27	76—77	$C_{15}H_{16}N_2O_2$	70.29	70.10	6.29	6.12	10.93	10.92
2,5-$(MeO)_2C_6H_3$	H	1	66	118—118.5	$C_{15}H_{16}N_2O_4$	62.49	62.67	5.59	5.49	9.72	9.92
		2	26	63—64	$C_{16}H_{18}N_2O_4$	63.56	63.77	6.00	5.87	9.27	9.40
C_6H_5	Me	3	37	(185—190/2)[a]	$C_{16}H_{18}N_2O_2$	71.09	70.81	6.71	6.49	10.36	10.34
	Et	1	53	65—66	$C_{15}H_{16}N_2O_2$	70.29	70.34	6.29	6.19	10.93	10.69
		2	23	(187—190/1)[b]	$C_{16}H_{18}N_2O_2$	71.09	70.93	6.71	6.68	10.36	10.53
4-MeC_6H_4	Me	1	43	48—49	$C_{15}H_{16}N_2O_2$	70.29	70.54	6.29	5.99	10.93	11.20
		2	35	59—60	$C_{16}H_{18}N_2O_2$	71.09	70.99	6.71	6.53	10.36	10.60
2,4-$Me_2C_6H_3$	Me	1	37	72—73	$C_{16}H_{18}N_2O_2$	71.09	70.90	6.71	6.91	10.36	10.22
		2	34	(189—192/3)[c]	$C_{17}H_{20}N_2O_2$	71.88	71.80	7.34	7.09	10.09	9.85
2,4,6-$Me_3C_6H_2$	Me	1	30	61—62	$C_{17}H_{20}N_2O_2$	71.88	71.66	7.34	6.99	10.09	10.08
		2	47	(180—187/2)[d]	$C_{18}H_{22}N_2O_2$	72.45	72.26	7.43	7.30	9.39	9.52
4-$MeOC_6H_4$	Et	1	20	64—65	$C_{16}H_{18}N_2O_3$	67.11	66.84	6.34	6.18	9.78	10.03
		2	11	(197—200/2)	$C_{17}H_{20}N_2O_3$	67.98	68.28	6.71	6.80	9.33	9.58
2,5-$(MeO)_2C_6H_3$	Et	1	34	85—86	$C_{17}H_{20}N_2O_4$	64.54	64.53	6.37	6.46	8.86	8.99
		2	16	(186—190/1.5)[e]	$C_{18}H_{22}N_2O_4$	65.44	65.26	6.71	6.45	8.48	8.37
1-$C_{10}H_7$	Et	1	34	91—92	$C_{19}H_{18}N_2O_2$	74.49	74.61	5.92	5.85	9.15	8.98

a) n_D^{23} 1.6018. b) n_D^{25} 1.6079. c) n_D^{20} 1.5838. d) n_D^{28} 1.5795. e) n_D^{23} 1.5815.

process. If we compare the *number of atoms* separating donor and acceptor allowed for excimer fluorescence (only 3) with that allowed for CT fluorescence (2, 3, and in some cases 4), it is clear that the CT excited state depends to a smaller extent on conformational requirements as expected from its larger stabilizing energy.

Experimental

Electronic Absorption Studies. Spectra were recorded on a Shimadzu MPS-50L automatic recording spectrophotometer. Quartz cells of 1.0 cm in length were used. The concentration of benzene-cyclohexane solution was less than 2×10^{-3} mol/*l*.

Emission Studies. Fluorescence spectra were recorded at room temperature on an Aminco-Bowman spectrophotofluorometer. The concentration of both benzene-cyclohexane and cyclohexane solution was always in the range $1-2\times10^{-4}$ mol/*l*. In every measurement, the peak height of the CT fluorescence band p-$O_2NC_6H_4CH_2NH$-1-naphthyl (Ig, $n=1$) was determined in order to obtain a factor necessary for the adjustment of intensity fluctuation of incident light. The CT fluorescence intensities were given relative to that of this compound (relative intensity=100) in Tables 2 and 3. The fluorescence peak height of *N*-ethyl-1-naphthylamine is 8.5×10^4 (at 390 nm, corrected for the sensitivity of 1P28) in this scale. The excitation wavelength was 313 nm. The data in Tables 2 and 3, and fluorescence curves in Figs. 4—9 are corrected for the sensitivity of photomultiplier (1P28).[20] As a result, in some compounds ($n=1$ of Ie, IIe, and IIf) no peak was found in their corrected spectral curve, on account of large and uncertain correction factors in long wavelength region.

Excitation spectra were determined with the same spectrophotofluorometer equipped with an "off-axis ellipsoidal mirror condensing" system. No correction for the wavelength dependence of the sensitivity of the instrument was made.

Solvents. Spectrograde or guaranteed reagents were used after careful distillation.

Materials. Both types of compounds (I and II) were prepared as described in a previous paper.[2] The physical constants and results of elemental analyses of the new products are given in Table 6.

The author wishes to thank Dr. Akira Kuboyama, Government Chemical Industrial Research Institute, for permitting him to use the spectrophotofluorometer. He also wishes to express his gratitude to Professor Yoshiya Harada (University of Tokyo) and Dr. Jun-ichi Aihara (University of Hokkaido) for their valuable discussions and suggestions. Thanks are also due to the Matsunaga Science Foundation for financial support of this work.

20) C. E. White, M. Ho, and E. Q. Weimer, *Anal. Chem.*, **32**, 32, 438 (1960).

NOTES

BULLETIN OF THE CHEMICAL SOCIETY OF JAPAN, VOL. 45, 2643—2644 (1972)

Application of Factor Analysis to Polarography

Darryl G. HOWERY

Department of Chemistry, Brooklyn College of The City University of New York, Brooklyn, N. Y., U.S.A.

(Received May 9, 1972)

Chemical problems in which the observable is measurably dependent upon several variables are seldom amenable to detailed analysis. Recent applications of the mathematical method of factor analysis to some multidimensional chemical problems have led to new insights in the fields of nuclear magnetic resonance spectroscopy[1,2] and gas-liquid chromatography.[3,4] The results of factor analyzing a data matrix of polarographic half-wave potentials for five alkaline and four alkaline-earth metals in five polar solvents are presented here.

Any function being factor analyzed must be a linear sum of factors, where in addition each factor must be in the form of a separable product term.[1] For the half-wave potential of the i-th ion in the α-th solvent, we assume therefore that

$$E^0_{1/2,i,\alpha} = \sum_j I_{ij} V_{j\alpha} \qquad (1)$$

where I_{ij} is the j-th ion factor for the i-th ion, $V_{j\alpha}$ is the j-th solvent factor for the α-th solvent, and the sum is taken over the minimum number of abstract eigenvectors or controlling factors, j, necessary to span the data-matrix space. The reproduction portion of the factor analysis scheme allows one to find the minimum number of abstract eigenvectors, and the least-squares rotational portion of the scheme allows individual physically significant properties of both ions and solvents to be tested for possible identification with the abstract eigenvectors.

Procedure

The data matrix was taken from the compilation of Gutmann,[5] with the half-wave potentials measured relative to aqueous saturated calomel electrode being selected for factor analysis. Ions and solvents are listed in Table 1. All computations were performed on a FACOM 230-60 digital computer using the Fortran IV program developed by Malinowski and coworkers.[1]

Results and Discussion

Number of Controlling Factors. The reproduction portion of the factor analysis program enables one to reproduce the data matrix stepwise using the largest abstract eigenvector, the two largest eigenvectors, and so forth. When the agreement between the measured and the predicted half-wave potentials is overall reasonable considering the uncertainty of the measurement, the number of abstract eigenvectors used for that reproduction is taken to be equal to the number of independent controlling factors in the problem. The minimum number of factors required to adequately characterize the data space, information ordinarily not obtainable in complex problems, is thus determined. Examination of the error in the various reproductions leads one to conclude that the half-wave potential space is probably a three-factor space since with the three largest eigenvectors only seven points in the reproduced matrix are in error by more than 30 mV, the largest error being 58 mV. If the data for lithium and magnesium are ommitted from the matrix, the reproduction with three factors is not improved implying that the factors which account for irreversibility are still operative in the reduced-matrix space.

Test of Physically Significant Factors. The least-squares rotational part of the factor analysis scheme furnishes valuable insights into the factors governing the reduction process and in particular the ion-solvent interactions. A suspected chemical or physical property can be tested for identification as a fundamental factor of the space by seeing if a test vector composed of the values of that property associated with the row elements of the data matrix can be rotated mathematically onto an abstract eigenvector of the space. In a successful test the values for the property predicted by the factor analysis method must agree reasonably well with the corresponding points on the test vector. Even if some values of the property are not known or are suspect, the test can still be made since the program includes provisions for free-floating, *i.e.*, leaving blank, some points on the test vector.

A) Ion Factors: The ionic charge (see Table 1 for the results) and the reciprocal of the crystalline ionic radius both gave moderately good agreement between the test and the predicted vector. The lithium ion, the charge for which was free-floated in the ionic charge test, appears to behave more like a divalent ion. A test for the ionic potential, *i.e.*, the ionic charge divided by the crystalline ionic radius, gave the fair fit shown in Table 1. The values for Li^+ and Mg^{2+} were free-floated since the effective ionic potential quite possibly might differ from the conventional ionic potential for ions known to have high overvoltages in

1) P. H. Weiner, E. R. Malinowski, and A. R. Levinstone, *J. Phys. Chem.*, **74**, 4537 (1970).

2) P. H. Weiner and E. R. Malinowski, *ibid.*, **75**, 1207, 3160 (1971).

3) P. H. Weiner and D. G. Howery, *Can. J. Chem.*, **50**, 448 (1972).

4) P. H. Weiner, C. Dack, and D. G. Howery, *J. Chromatogr.*, in press.

5) V. Gutmann, "Co-ordination Chemistry in Non-aqueous Solutions," Springer-Verlag, Vienna (1968), p. 33.

Table 1. Tests for physically significant parameters

Ion	Ionic charge		Ionic potential	
	Test	Predicted	Test	Predicted
Li^+	(1.00)	2.03	(1.47)	1.88
Na^+	1.00	1.16	1.03	0.92
K^+	1.00	1.25	0.75	1.02
Rb^+	1.00	0.92	0.68	0.63
Cs^+	1.00	0.87	0.60	0.57
Mg^{2+}	2.00	2.17	(3.02)	2.07
Ca^{2+}	2.00	2.06	2.02	1.94
Sr^{2+}	2.00	1.76	1.78	1.62
Ba^{2+}	2.00	1.78	1.50	1.67

Solvent	ΔH_{vap}		$1/R'$		Donor number	
	Test	Predicted	Test	Predicted	Test	Predicted
DMSO	12.6	12.3	1.47	1.45	2.98	2.72
DMA	12.7	13.5	1.45	1.45	2.78	2.82
Water	10.5	11.4	1.39	1.41	1.80	2.19
PDC	11.9	11.5	1.22	1.21	1.51	1.43
MeCN	7.8	7.8	1.22	1.21	1.41	1.30

PDC=propylene dicarbonate. Three-factor space assumed for tests. Points in parenthesis on the test vectors were free-floated. Values for the crystalline ionic radius (A) were taken from "Handbook of Chemistry and Physics," ed. by R. C. Weast 46th Edition, Chemical Rubber Co., Cleveland (1964), p. F89; for the molar enthalpy of vaporization (kcal/mol), from reference 5 and from "Techniques of Organic Chemistry," ed. by A. Weissberger Vol. II, 3rd Edition, Wiley, New York, (1970); for the radial correction factor, from Ref. 7; and for the donor number, from Ref. 5.

water. Crystalline ionic radius, equivalent weight, solubility of the metal in mercury (g/100 g) and ionic polarizability do not appear to be factors since the fit was quite poor for each of the tests. A test for the solubility expressed as a mole fraction showed the proper trends but the fit was still rather poor.

B) Solvent Factors: Since mathematically in a three-factor space test points for all five solvents must be specified on a test vector, the lack of reported physical properties for PDC somewhat restricted the solvent properties which could be tested. Three solvent parameters tested moderately well (see Table 1 for the results): the molar enthalpy of vaporization, the donor number as defined by Gutmann,[6] and the reciprocal of a radial correction factor, R', proposed by Matsuura *et al.*[7] Boiling point (°K), dipole moment, molar polarization, dielectric constant, viscosity, Trouton's constant and the Hildebrand solubility parameter all gave sufficiently poor fits to be excluded as fundamental factors.

Since so little is known about the mathematical formulation of ion-solvent interactions especially when expressed in the form required by Eq. 1), speculation on the implications of the ion and solvent tests reported here seems premature. A major advantage of the method of factor analysis is that one can test an individual parameter in a many-factor space though lacking a theoretical model for the interaction.

If three independent ion factors or solvent factors are discovered, one can attempt to reproduce the data matrix using physically significant test vectors.[2,4] The reproduction using the set molar enthalpy of vaporization, donor number and $1/R'$ was surprisingly good, with the average of the column average errors being 28 mV. The solvent-factor space would appear to be spanned fairly well with these three factors.

The application of factor analysis to new areas of chemistry is being severely limited by the lack of large, complete, and accurate data matrices. At present, extensive data of the type required for comprehensive factor analysis studies are available as far as we know only in the field of gas-liquid chromatography.[8] The matrix employed in this study severely tested the factor analysis method since the number of solvents was so small compared to the number of factors required to span the space. Since experience has indicated that the number of rows and columns should preferably be at least twice the number of factors, the reproduction of the data matrix with three eigenvectors and the fit of the test vectors given in Table 1 are encouraging. More definitive conclusions to this complex problem should be possible if a larger data matrix were available.

Dr. K. Izutsu suggested this problem and furnished much valued advice. J. Okuda's help on programming, Professor T. Fujinaga's financing of the computer work, and the use of the Computer Center of Kyoto University are gratefully acknowledged.

6) Ref. 5., p. 19.

7) J. Matsuura, K. Umemoto, and Y. Kakeuchi, 16th Polarographic Symposium, Kyoto, 1970.

8) W. O. McReynolds, "Gas Chromatographic Retention Data," Preston Technical Abstracts Co., Evanston, Illinois (1966).

BULLETIN OF THE CHEMICAL SOCIETY OF JAPAN, VOL. 45, 2645—2646 (1972)

Carbon-14 Isotope Effect on sp^2-sp^3 Hybridization in the Prototropic Equilibrium of *N*-Benzylidenebenzylamine

Yasuhide YUKAWA, Takashi ANDO, and Tetsuo OTSUBO

The Institute of Scientific and Industrial Research, Osaka University, Yamadakami, Suita, Osaka

(Received January 29, 1972)

Isotope effects on equilibria can be calculated exactly on the basis of mechanical properties of two stable states involved, which can be observed directly. Accurate determination and theoretical consideration of these effects serve to elucidate the more complex problem of inferring from observed kinetic isotope effects something about transition state structure. *N*-Benzylidenebenzylamine system is known to show a prototropic equilibrium (Eq. (1)) in the presence of a strong base.[1]

$$\mathrm{Ar\text{-}CH{=}N\text{-}CH_2\text{-}Ar' \rightleftarrows Ar\text{-}CH_2\text{-}N{=}CH\text{-}Ar'} \quad (1)$$

Substitution of an aliphatic carbon with a carbon-14 isotope should cause a carbon isotope effect on equilibrium (I⇄II).

$$\mathrm{Ph\text{-}{*}CH{=}N\text{-}CH_2\text{-}Ph \rightleftarrows Ph\text{-}{*}CH_2\text{-}N{=}CH\text{-}Ph}$$
$$\text{(I)} \qquad\qquad \text{(II)}$$

It is the effect accompanying the change in sp^2-sp^3 hybridization of a carbon atom.

Gamboa and coworkers reported the isotope fractionation of 60—70% in the equilibrium of the 1,3-diphenyl-1-propene system (Eq. (2)), but it seems

$$\mathrm{Ph\text{-}{*}CH{=}\overset{\displaystyle CH_3}{\overset{|}{C}}\text{-}CH_2\text{-}Ph \rightleftarrows Ph\text{-}{*}CH_2\text{-}\overset{\displaystyle CH_3}{\overset{|}{C}}{=}CH\text{-}Ph} \quad (2)$$

abnormally large.[2] On the other hand, Kresge and coworkers[3] observed a small reverse isotope effect in the ionization of triphenylmethyl chloride-1-^{13}C. In these respects, the carbon-14 isotope effect on the equilibrium (I⇄II) was measured and compared with a theoretically calculated value.

Results and Discussion

N-Benzylidenebenzylamine(methine-^{14}C) (I) was prepared by condensation of benzaldehyde(carbonyl-^{14}C) with benzylamine. The equilibrium was effected by the action of 30 parts of 1.45N alcoholic sodium ethoxide at 40.0 and 82.0°C. Definite portions of the reaction mixture were added into 2N hydrochloric acid solution of saturated 2,4-dinitrophenylhydrazine at appropriate time intervals. Precipitates of benzaldehyde 2,4-dinitrophenylhydrazone (III) were collected and purified by recrystallisation. Samples of III were oxidized with the Van Slyke-Folch mixture and the radioactivity of the carbon dioxide generated was measured by the ionization chamber counting method.

Table 1. Specific radioactivity data for the methyleneazomethine equilibrium at 40.0±0.1 and 82.0±0.1°C

No.	Compound	Temp (°C)	Time (hr)	Specific activity (mCi/mol)
1	I			1.0492±0.0011
2	III	40.0	0	1.0419±0.0009
3			1	0.9663
4			2	0.8237
5			4	0.6721
6			8	0.5798
7			24	0.5323±0.0007
8			36	0.5302±0.0005
9			50	0.5284±0.0003
10		82.0	0	1.0457±0.0001
11			0.5	0.5276±0.0008
12			1.0	0.5286±0.0005

The results are summarized in Table 1.

The small difference between the radioactivity of the starting material (I) and that of the 2,4-dinitrophenylhydrazone (III) at initial stage in each of thest two experiments can be attributed to the partial isomerization of I to II during the course of the preparation under mild basic conditions. It is apparent that the equilibrium was reached within 36 hr at 40°C and 30 min at 82°C. The equilibrium constant K, whose value corresponds to that of the isotope effect in this case, is calculated by Eq. (3);

$$K = [\mathrm{II}]/[\mathrm{I}] = (\mathrm{A}-\mathrm{B})/\mathrm{B} \quad (3)$$

where A is the specific activity of the starting material (I) and B is that of the 2,4-dinitrophenylhydrazone (III) at equilibrium. The results thus obtained show small isotope effects on the equilibrium: K=0.983±0.002 at 40.0°C and K=0.986±0.002 at 82.0°C. The equilibrium constants smaller than unity indicate that the equilibrium is in favor of the carbon-14 atom at the sp^2-position.

Theoretical values of isotope effects on equilibrium can be calculated by the Bigeleisen equation (Eq. (4)),[4]

$$K = 1 + \sum_i \left(\frac{1}{2} - \frac{1}{u_i} + \frac{1}{e^{u_i}-1}\right)\Delta u_i \quad (4)$$

where $u_i = \boldsymbol{h}c\omega_i/\boldsymbol{k}T$, Δu_i is the difference in u_i between isotopes, and ω_i is the wave number of the ith normal mode. For calculation of Eq. (4), only stretching vibrations were used, which are usually considered as the most effective factors of isotope effects. An observed infrared spectrum was analyzed and vibrational fre-

1) C. K. Ingold, "Structure and Mechanism in Organic Chemistry", 2nd ed., Cornell University Press, Ithaca, N. Y. (1969), p. 808.

2) J. M. Gamboa, R. P. Ossorio, and R. Rapún, *Anales Real Soc. Espan. Fis. Quim.*, **57B**, 607 (1961).

3) A. J. Kresge, N. N. Lichtin, K. N. Rao, and R. E. Weston, Jr., *J. Amer. Chem. Soc.*, **87**, 437 (1965).

4) J. Bigeleisen and M. G. Mayer, *J. Chem. Phys.*, **15**, 261 (1947).

quencies were determined as follows:[5] C=N, 1640; C–N, 1200; C–H (in =CH–), 3030; C–H (in $-CH_2-$), 2865 and 2835 cm^{-1}. Stretching frequencies for carbon-carbon single bonds in =CH–Ph and $-CH_2-Ph$ were arbitrarily taken as 1050 and 1000 cm^{-1}, respectively. Frequencies for a carbon-14 isotope were calculated by the following relationship: $\omega_1/\omega_2=(\mu_2/\mu_1)^{1/2}$, where μ means a reduced mass. The equilibrium constants K calculated as above are 0.986 at 40°C and 0.987 at 82°C. Although inclusion of bending vibrations may give a better result, these calculated values are in fair agreement with the observed values, considering the errors in measurement of radioactivity and the simple approximation used for theoretical calculation.

Experimental

Material. Benzaldehyde(carbonyl-^{14}C) was prepared according to the procedure of Ott.[6]

N-Benzylidenebenzylamine(methine-^{14}C) (I). Benzaldehyde(carbonyl-^{14}C) was treated with 5.0 m*l* of benzylamine for 30 min at 80—90°C. After being cooled, the reaction mixture was diluted with 20 m*l* of ether. The ether solution was washed with 10 m*l* of 2% acetic acid, 10 m*l* of saturated sodium bicarbonate solution, and 20 m*l* of distilled water, successively, and finally dried over anhydrous potassium carbonate. The solvent was removed and the colorless oil remained was distilled under reduced pressure; bp 158.5°C/4.8 mmHg, yield 5.85 g (78.5%).

Methyleneazomethine Rearrangement. *N*-Benzylidenebenzylamine(methine-^{14}C) (I, 1.847 g) was added all at once into 60.204 g of 1.45N alcoholic sodium ethoxide in a reaction vessel preheated in a constant temperature bath at 40.0±0.1°C. Six m*l* aliquot of the reaction mixture was pipetted into 50 m*l* of 2N hydrochloric acid solution containing saturated 2,4-dinitrophenylhydrazine at appropriate time intervals. The solutions were kept to stand for 24 hr at 50°C for complete precipitation of 2,4-dinitrophenylhydrazone (III). After being cooled to room temperature, 10 m*l* of distilled water was added. Crystals of III were filtered, washed thoroughly with 2N hydrochloric acid and distilled water, successively, and then dried for 12 hr at 80—90°C. Samples of III purified by recrystallization three or four times from acetone were assayed for radioactivity.

In the same manner, 0.991 g of I was rearranged in 29.243 g of 1.45N alcoholic sodium ethoxide solution at 82.0±0.1°C.

Measurement of Radioactivity. About 10 mg of accurately weighed III was oxidized with the Van Slyke-Folch mixture[7] in a Nuclear-Chicago Model GW1 carbon glassware system, and the carbon dioxide generated was swept into a Model DC 250 ion chamber with tank carbon dioxide. The ion current was measured with a Nuclear-Chicago Model 6010 Dynacon electrometer system.

5) Infrared spectra were recorded on a JASCO Model DS-402G IR Spectrophotometer in carbon tetrachloride (4000—1300 cm^{-1}) and in carbon disulfide (1300—660 cm^{-1}).

6) *cf.* A. Murray, III and D. L. Williams, "Organic Syntheses with Isotopes", Part I, Interscience Publishers, New York, N. Y. (1958), p. 626.

7) D. D. Van Slyke, J. Plazin, and J. R. Weisiger, *J. Biol. Chem.*, **191**, 299 (1951).

BULLETIN OF THE CHEMICAL SOCIETY OF JAPAN, VOL. 45, 2646—2648 (1972)

An MO-Theoretical Account of the Catalytic Decomposition of Alkyl Hydroperoxides by Transition-metal Ions

Katsutoshi OHKUBO and Hirokazu KANAEDA

Department of Synthetic Chemistry, Faculty of Engineering, Kumamoto University, Kurokami-machi, Kumamoto

(Received April 14, 1971)

Many chemical studies of the decomposition reactions of alkyl hydroperoxides with or without catalysts have been done during the last decade. The mechanism of the catalytic decomposition of the hydroperoxides by transition-metal ions has, however, been established on the basis of the Haber-Weiss mechanism,[1] and some aspects of the process of the reactions are still veiled. The present study has been undertaken in an attempt to elucidate the processes of the decomposition reactions, using the all-valence-electron ASMO SCF and extended Hückel (EHMO) methods involving metal *d*-orbitals of transition metals.

Method of Calculation

Three systems were investigated in this work: (a) the monomers and dimers of alkyl hydroperoxides (ROOH: R=H, CH_3, C_2H_5, n-C_3H_7, i-C_3H_7, and t-C_4H_9), (b) the nucleophilic attack of the transition-metal ion (Cr(II), Co(II), or Fe(II)) on CH_3OOH, and (c) the electrophilic attack of Co(III) on CH_3OOH. The zero-differential overlap approximated ASMO SCF[2] and EHMO methods were used in this paper; the one-center and two-center Coulomb repulsion integrals were estimated by the Pariser[3] and the Ohno[4] approximations respectively. In the EHMO method, the resonance integrals were evaluated by

1) F. Haber and P. Weiss, *Proc. Roy. Soc., Ser. A*, **147**, 233 (1939).

2) The ionization energies (and electron affinities) of Cr, Co, and Fe are cited from Ref. 8 (Ref. 10), Ref. 8 (Ref. 10), and Ref. 9 (Ref. 10) respectively. The ASMO SCF method used was almost the same as the method reported by H. Kato, H. Konoshi, and T. Yonezawa (This Bulletin, **40**, 1017 (1967)).

3) R. Pariser, *J. Chem. Phys.*, **21**, 568 (1953).

4) K. Ohno, *Theoret. Chim. Acta*, **2**, 568 (1953).

means of the Wolfsberg-Helmholtz approximation.[5]

Results and Discussion

First, we will interpret the unimolecular or the bimolecular decomposition[6] of ROOH in connection with the association of ROOH.[7] Figure 1 shows the changes in the total energies of ROOH dimers, together with those of monomers (R=H, CH_3, C_2H_5, n-C_3H_7, i-C_3H_7, and t-C_4H_9), due to the stretching of the O–H bonds, which resulted from the EHMO calculations. The ROOH monomers are slightly less stable than the ROOH dimers. In addition, the reactivity of the former to nucleophiles such as low-valent metal ions is higher than that of the latter; notice, for example, the reactivity indices ($^1/_2N^{LU}_{p\sigma}$), *i.e.*, the partial AO bond population in the lowest unoccupied (LU) MO, which is strongly localized in the O–O $p\sigma$-type orbital (see Table 1). Consequently, it is probable, at low concentrations of ROOH, that the unimolecular decomposition occurs predominantly either with or without catalysts.

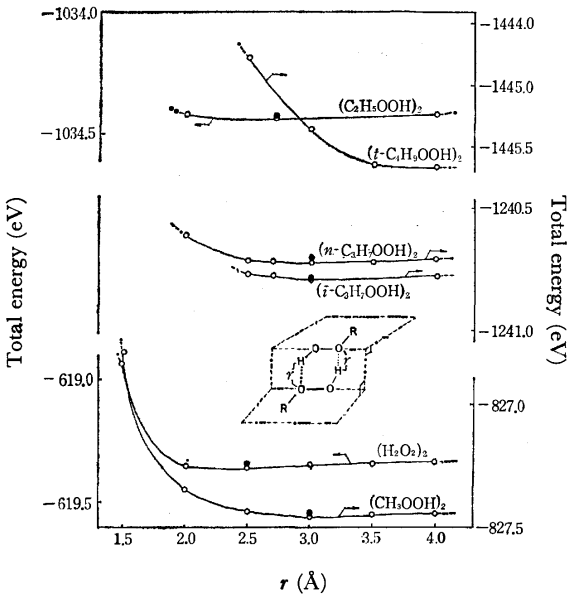

Fig. 1. Changes in the total energies of ROOH dimers as a function of the O–H distance (denoted by r), together with those of ROOH monomers.
(○: ROOH dimer; ●: ROOH monomer.)

Secondly, let us discuss the catalytic decomposition of ROOH by the transition-metal ions from the viewpoint of our experimental findings; about 95 mol% of the quantity of cumene hydroperoxide (the initial amount was 22.5 mmol) disappeared after 0.5 hr at 80°C in cumene (50 ml) containing Co(II) supplied by its stearate (0.33 mol/l), although, thermally, the hydroperoxide decomposed little even after 9.0 hr. Under the same reaction conditions, Ni(II), Fe(II), and Cr(III) lessened the quantity of the hydroperoxide

Table 1. Electronic properties and reactivities of ROOH and their dimers

ROOH and $(ROOH)_2$	O–H (Å)	Bond population of the O–O	$\frac{1}{2}N^{LU}_{p\sigma}$	Total energy (eV)
H_2O_2		0.359	−0.309	−309.671
$(H_2O_2)_2$	2.5	0.358	−0.155	−619.359
CH_3OOH		0.360	−0.309	−413.716
$(CH_3OOH)_2$	3.0	0.361	−0.154	−827.455
C_2H_5OOH		0.358	−0.309	−517.211
$(C_2H_5OOH)_2$	2.7	0.358	−0.153	−1034.428
n-C_3H_7OOH		0.357	−0.308	−620.387
$(n$-$C_3H_7OOH)_2$	3.0	0.357	−0.154	−1240.791
i-C_3H_7OOH		0.356	−0.307	−620.356
$(i$-$C_3H_7OOH)_2$	3.0	0.356	−0.153	−1240.728
t-C_4H_9OOH		0.354	0.308	−722.831
$(t$-$C_4H_9OOH)_2$	(4.0)	0.354	−0.153	−1445.664

These results were obtained from the EHMO calculations.

by *ca.* 6, 4, and 17 mol% respectively. The order of the catalytic abilities of the low-valent transition metal ions for the hydroperoxide decomposition, *i.e.*, Co(II)>Ni(II)>Fe(II), can be well explained by the parallelism with that of the energy required for the electron-releasing from the metal ion to the antibonding O–O $p\sigma$ orbital, namely, with that of the orbital energies of the highest occupied (HO) AO of the metal ions (−7.84,[8] −9.24,[8] and −11.0 eV[9] respectively).

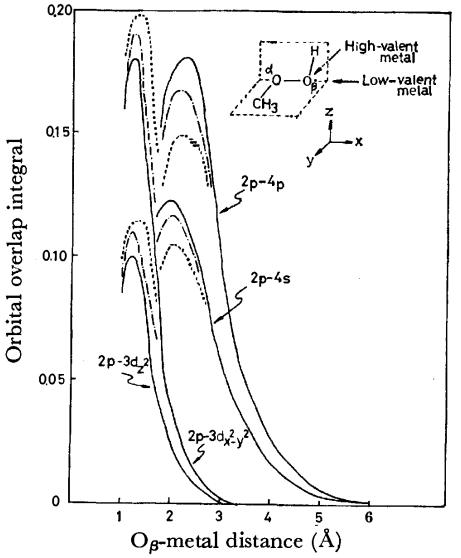

Fig. 2. Changes in orbital overlaps between oxygen p-orbitals and metal d-, s-, and p-orbital due to the variation of the O_β-metal distance. (——: Co; ·····: Cr; ——: Fe)

A more precise discussion should be made here with respect to the catalytic decomposition of ROOH by the metal ions. From the orbital overlaps between oxygen 2p and metal 3d AOs indicated in Fig. 2, the following two reactions can be expected in the O_β-metal region below 3.0 Å: the nucleophilic attack of a low-valent metal on the O–O $p\sigma$ orbital in the direction

5) M. Wolfsberg and L. Helmholtz, *J. Chem. Phys.*, **20**, 837 (1952).
6) Bateman, *Quart. Rev.*, **8**, 147 (1954).
7) C. Walling and H. Heaton, *J. Amer. Chem. Soc.*, **87**, 48 (1965).
8) F. A. Cotton and T. E. Haas, *Inorg. Chem.*, **3**, 1004 (1964).
9) L. L. Lohr, Jr., and W. N. Lipscomb, *ibid.*, **3**, 22 (1964).

TABLE 2. CHANGES IN THE ELECTRONIC STATES OF TRANSITION METAL IONS AND CH_3OOH ATTACKED BY LOW-VALENT METAL IONS

O_β-Metal ion distance (Å)	Atom population of metal	AO populations					
		Transition metal			CH_3OOH		
		$d_{x^2-y^2}$	d_{z^2}	d_{xy}	$O_\beta-p_y$	$O_\beta-p_x$	$O_\alpha-p_x$
	4.000(6.000)				1.996(1.996)	1.050(1.050)	0.983(0.983)
1.6	3.243(6.0)	0.327(1.615)	0.109(1.855)	0.038(0.037)	1.869(1.885)	1.558(1.189)	1.388(1.149)
1.5	(5.323)	(1.111)	(1.697)	(0.076)	(1.870)	(1.378)	(1.613)
1.4	3.218	0.315	0.135	0.089	1.813	1.639	1.490

These results were obtained from the ASMO SCF calculations.
Values and those in parentheses indicate the cases of Cr(II) and Fe(II) respectively.

of the O–O axis from the O_β side[10] and the electrophilic attack of a high-valent metal on the nonbonding lone-pair O_β $2p_y$-orbital (note the larger population and delocalizability to nucleophiles[11] of O_β as compared with those of O_α). In these attacks, the wholly unoccupied $4s$ and $4p$ orbitals situated at high-energy levels may not play an important direct role in the interaction of the metal ion with ROOH.

Thirdly, it is of interest to notice the changes in the electronic states of the transition-metal ions and ROOH by the interaction, which predominantly occurs near the maximum overlaps between oxygen $2p$ orbitals and metal d-orbitals, *i.e.*, near 1.5 Å (see Fig. 2). The orbital symmetry allows two pairs of overlaps: the dp-σ overlap between the O–O $p\sigma$ and $d_{x^2-y^2}$ and/or d_{z^2} and that between the nonbonding lone-pair O_β, p_y, and d_{xy}. In both attacks we recognized an electron-inflowing from the $d_{x^2-y^2}$ metal to the O–O $p\sigma$ and an electron-backdonation from the lone-pair, O_β p_y, to the d_{xy} metal, as can be seen from Table 2. It is necessary to mention here that the negative value of the bond population of the O–O in ROOH attacked by the metal ion within the O_β-metal distance of 2.0 Å indicates a scission of the O–O linkage, while, even at the O_β–S distance of 1.47 Å, the bond population of the O–O is positive in the case of the nucleophilic interaction of $(CH_3)_2S$ with CH_3OOH.[12] The remarkable ability of the transition-metal ions for the hydroperoxide decomposition was, for instance, thus reflected in the change in the electronic state of ROOH attacked by the metal ion.

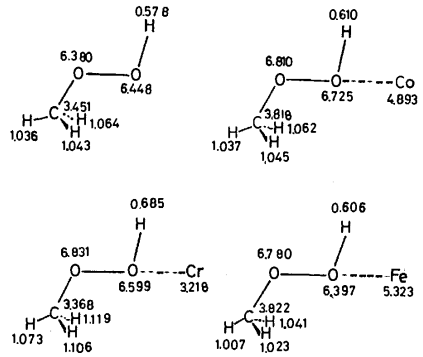

Fig. 3. Valence electron distributions of the systems of CH_3OOH–transition metal ion. (O_β–Co or Cr=1.5 Å; O_β–Fe=1.4 Å)

Finally, the valence-electron distributions of the CH_3OOH-metal ion systems are indicated in Fig. 3.

The calculations were carried out on the FACOM 230-60 computer at the Computer Center of Kyushu University.

10) J. Hinze and H. H. Jaffé, *Can. J. Chem.*, **41**, 1315 (1963).
11) T. Yonezawa, O. Yamamoto, H. Kato, and K. Fukui, *Nippon Kagaku Zasshi*, **87**, 26 (1966).
12) K. Ohkubo, T. Ninomiya, and H. Kanaeda, *Tetrahedron*, **28**, 2969 (1972).

BULLETIN OF THE CHEMICAL SOCIETY OF JAPAN, VOL. 45, 2649—2651 (1972)

Theoretical Consideration on the Electronic Structures of *trans*- and *cis*-Isomers of Acrolein and 2,4-Pentadienal

KOZO INUZUKA

Department of Applied Science, Tokyo Electrical Engineering College, Kanda, Chiyoda-ku, Tokyo

(Received February 7, 1972)

In the previous paper[1] an approach to n,π^*-state energy calculation was presented and the electronic structures of lower n,π^* and π,π^* states of several carbonyl molecules in the planar *trans* form were studied within the framework of the SCF–MO–CI approximation. Theoretical considerations suggest the possibility of the existence of *cis*-acrolein,[2] but its existence is not experimentally clear. Generally, no experimental evidence of the *cis*-form is known for such short polyene aldehydes as acrolein and pentadienal, but such longer ones as retinal, which corresponds to 2,4,6,8,10-dodecapentaenal in the π-electron system, have several *cis*-isomers.[3] In the case of retinal, its isomers play an important role in the vision mechanism of rhodopsin, and they have specific features in their optical behavior;[4] nevertheless, theoretical consideration of the electronic structure of *cis*-isomers of polyene aldehyde is still scarce. Therefore, it is of interest to make clear the electronic structure of *trans*- and *cis*-isomers of polyene aldehydes. The UV spectra of the conjugated enones and dienones have been well studied, and the empirical correlations of the UV absorption with the structure have become evident.[5,6] However, the band position of the n,π^* absorption spectrum for such a conjugated system as *trans*- and *cis*-polyene aldehydes is still unclear. In this paper the band positions of n,π^* and π,π^* states for *trans*- and *cis*-forms of acrolein and 2,4-pentadienal were studied by the same approach as was developed previously within the framework of the Pariser-Parr-Pople SCF–MO–CI method.[7,8] The P-P-type two-center repulsion integral[7] was used for the calculation of the π-electron system. The Mataga-Nishimoto approximation[9] was adopted for two-center repulsion integrals between n and π electrons.

In the previous paper[1] the value of -14.75 eV[10] was used for the parameter, U_n, in Eq. (7) corresponding to the n-orbital energy calculation. In this paper the value of -14.60 eV will tentatively be used for the U_n parameter in order to improve the calculated n,π^*-state energy.

The following numerical values[11] were used for the skeletal structures of acrolein and 2,4-pentadienal; 1.34 Å for the carbon double bond, 1.46 Å for the single bond, and 1.22 Å for the carbonyl group. The value of 120° was assigned to the C–C–C and C–C–O bond angles. All the calculations were carried out on the assumption of a planar structure for the present molecules.

Results and Discussion

The calculated results are listed in Table 1.

The intense absorption spectrum of acrolein is observed at 5.96 eV (208 nm), while the weak absorption band is observed at 3.71 eV (334 nm),[12] in an n-hexane solution. These observed values are assigned to the lowest π,π^* and n,π^* singlet states of acrolein.[12] These state energies correspond to the present calculated values, 5.960 eV (208 nm, $f=0.803$) for the π,π^* singlet state energy and 3.767 eV (329 nm) for the n,π^* singlet state energy.

On the other hand, the theoretical π,π^* and n,π^* singlet state energies of *cis*-acrolein are 5.608 eV (221 nm, 0.381) and 3.800 eV (326 nm). These results suggest that the π,π^* singlet state of *trans*-acrolein is higher than that of *cis*-acrolein and that the intensity of the former is larger than that of the latter. Those theoretical results correspond well with the observed results of the conjugated enones (from a to d)[13] shown in Fig. 1. The location of the n,π^* singlet state of

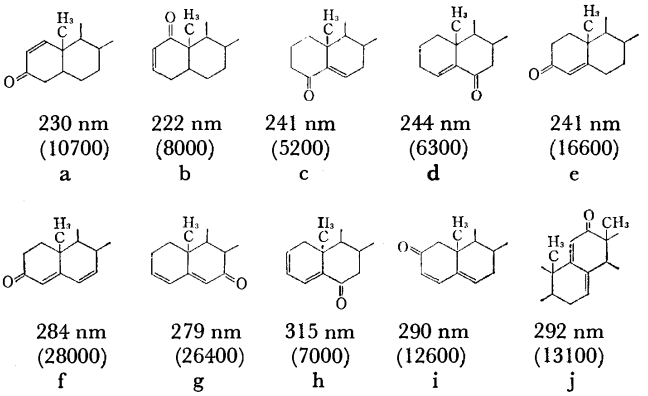

Fig. 1. Conjugated enones and dienones with the values of λ_{max} and intensities of their UV.[13]

1) K. Inuzuka and R. S. Becker, This Bulletin, **45**, 1557 (1972).
2) R. S. Becker, K. Inuzuka, and J. King, *J. Chem. Phys.*, **52**, 5164 (1970).
3) R. S. Becker, K. Inuzuka, and D. E. Balke, *J. Amer. Chem. Soc.*, **93**, 38 (1971).
4) R. S. Becker, K. Inuzuka, J. King, and D. E. Balke, *ibid.*, **93**, 43 (1971).
5) R. B. Woodward, *ibid.*, **63**, 1123 (1941) and **64**, 72, 76 (1942).
6) L. K. Evans and A. E. Gillam, *J. Chem. Soc.*, **1941**, 815, **1943**, 565.
7) R. Pariser and R. G. Parr, *J. Chem. Phys.*, **21**, 466, 767 (1953).
8) J. A. Pople, *Trans. Faraday Soc.*, **49**, 1375 (1953).
9) N. Mataga and K. Nishimoto, *Z. Phys. Chem.*, **13**, 140 (1957).
10) J. M. Parks and R. G. Parr, *J. Chem. Phys.*, **32**, 1657 (1960).
11) H. Mackle and L. E. Sutton, *Trans. Faraday Soc.*, **47**, 691 (1951).
12) K. Inuzuka, This Bulletin, **34**, 6 (1961).
13) L. F. Fieser and M. Fieser, "Steroids," Reinhold Publishing Corp., New York (1959).

TABLE 1. CALCULATED LOWEST SINGLET AND TRIPLET STATE ENERGIES AND f NUMBERS OF *trans*- AND *cis*-ISOMERS OF ACROLEIN AND 2,4-PENTADIENAL WITH THE OBSERVED VALUES

Molecule		Sym	Singlet				Triplet	
			E_{cal}[a]	f_{cal}	E_{obs}	f_{obs}	E_{cal}	E_{obs}
trans-Acrolein		A'	5.960(208)	0.803	5.96(208)	0.10	2.935(422)	3.05(406)
		A''	3.767(329)		3.71(334)		3.255(381)	3.01(412)
cis-Acrolein		A'	5.608(221)	0.381			2.969(418)	
		A''	3.800(326)				3.300(376)	
2,4-Pentadienal	**A**	A'	4.745(261)	1.245	4.79(259)	0.58[b]	2.048(605)	
		A''	3.651(340)		3.81(325)		3.161(392)	
	B	A'	4.426(280)	0.612			2.072(598)	
		A''	3.661(339)				3.172(391)	
	C	A'	4.603(269)	0.859			2.098(591)	
		A''	3.679(337)				3.204(387)	
	D	A'	4.737(262)	1.173			2.046(606)	
		A''	3.650(340)				3.162(392)	
	E	A'	4.376(283)	0.595			2.120(585)	
		A''	3.681(337)				3.205(387)	
	F	A'	4.497(276)	0.639			2.052(604)	
		A''	3.657(339)				3.189(389)	
	G	A'	4.312(288)	0.382			2.056(603)	
		A''	3.615(343)				3.127(396)	

a) eV in units; numbers in parentheses are in units of nm.
b) This f number corresponds to that of 2,4-hexadienal which was calculated from the data in Ref. 21.

cis-acrolein is a little bit higher than that of *trans*-acrolein, but there is no significant difference between the two n,π^* state energies; the difference may be within the range of accuracy of the present approximation.

The theoretical π,π^* triplet state energy of *trans*-acrolein, 2.935 eV is in good agreement with the observed value, 3.05 eV.[14] The corresponding value of *cis*-acrolein, 2.969 eV, is very close to that of *trans*-acrolein.

The calculated n,π^* triplet state energy of the *trans*-isomer, 3.255 eV, is still higher than the corresponding observed value, 3.01 eV,[15-17] although the present value is an improvement over the previous value, 3.405 eV.[1] According to the experimental results, the lowest triplet state of acrolein may be assigned to the n,π^* state, but both states are nearly degenerate. Therefore, the vibronic mixing of these states may be dominant.

The π,π^* singlet state of 2,4-pentadienal is observed at 4.79 eV (259 nm), and its n,π^* absorption spectrum is observed at 3.81 eV (325 nm), in an ethyl alcohol solution.[18] However, the n,π^* absorption spectrum of pentadienal appears at a shorter wavelength than that of acrolein, probably because of the solvent effect. The value of 4.79 eV may be assigned to the calculated π,π^* singlet state energy, 4.745 eV (261 nm, $f=1.245$), of the *trans*-isomer **A**. The calculated π,π^* singlet state energy and the oscillator strength of *trans*-pentadienal **A** are the largest of any other *cis*-isomers, as in the case of acrolein. This theoretical result is in harmony with the experimental results on the dienones (from f to j)[13] shown in Fig. 1. Figure 1 shows that the π,π^* singlet state and the intensity of *trans*-isomer are higher and larger than those of any *cis*-isomers. The calculated π,π^* singlet state energy and oscillator strength for the **D** isomer, 4.737 eV (262 nm) and 1.173, are larger than those of the **E** isomer, 4.376 eV (283 nm) and 0.595. Those results correspond well with the experimental results of the i or j and h compounds shown in Fig. 1.

The calculated n,π^* singlet energy of *trans*-2,4-pentadienal, 3.651 eV (340 nm), corresponds to the observed value, 3.81 eV (325 nm). The calculated n,π^* singlet state energies of *cis*-isomers lie within the range from 3.615 to 3.681 eV, as is shown in Table 1. It is interesting that there is no significant difference in the calculated n,π^* singlet state energy of *trans*- and *cis*-pentadienal isomers as there is in their π,π^* singlet state energy.

The calculated values of the π,π^* triplet state energies of pentadienal isomers lie within the range from 2.046 to 2.120 eV. The calculated lowest n,π^* triplet state energy of *trans*-pentadienal is 3.161 eV. The corresponding values of the *cis*-isomers range from 3.162 to 3.205 eV. These results suggest that the lowest π,π^* and n,π^* triplet states are almost constant in all the isomers.

The UV and optical rotatory dispersion curves of keto steroids containing *trans*- and *cis*-conjugated polyene aldehyde skeletal structures in their molecules may become experimental data for the comparison of the location of the n,π^* states of *trans*- and *cis*-isomers.

14) J. M. Hollas, *Spectrochim. Acta*, **19**, 1425 (1963).
15) J. C. D. Brand and D. G. Willamson, *Discuss. Faraday Soc.*, **35**, 184 (1963).
16) K. Inuzuka, This Bulletin, **34**, 729 (1961).
17) W. H. Eberhardt and H. Renner, *J. Mol. Spectrosc.*, **6**, 483 (1961).
18) E. L. Pippen and M. Nonaka, *J. Org. Chem.*, **23**, 1580 (1958).

However, the conjugated system of the keto steroid as a model compound of an acrolein or pentadienal isomer may be different from the present model assumed for an acrolein or pentadienal isomer because of some twisting around a certain single or double bond, because of some deviation from planarity, and because of the effect of the other parts of the keto steroid attached to the conjugated system. Especially, the comparison of the theoretical values of the acrolein and pentadienal isomers with the spectroscopic data of the corresponding keto steroids for the n,π^* singlet- and triplet-state energies and the π,π^* triplet energy should be done carefully, because there is no such significant difference in the energy states of *trans*- and *cis*-isomers with respect to the n,π^* states and the π,π^* triplet state respectively. Also, their n,π^*- and π,π^*-state energies are affected by the twisting of the single or double bond. The twisting about the single bond brings about a blue shift of the π,π^* state, while the double-bond twisting brings about a red shift.[2,3] The same theoretical result[19,20] is also obtained for the n,π^* state.

This work was supported by a grant from Tokyo Electrical Engineering College (T. E. E. C.) Research Fund. The author wishes to acknowledge the assistance of staffs of T. E. E. C. Computing Center for present work.

19) J. J. McCullough, H. Ohorodnyk, and D. P. Santry, *Chem. Commun.*, **1969**, 570.
20) K. Inuzuka, (unpublished).
21) E. R. Blout and M. Fields, *J. Amer. Chem. Soc.*, **70**, 189 (1948).

BULLETIN OF THE CHEMICAL SOCIETY OF JAPAN, VOL. 45, 2651—2652 (1972)

The Crystal and Molecular Structure of *p*-Bromobenzoic Acid

Kenji OHKURA*, Setsuo KASHINO, and Masao HAISA

Department of Chemistry, Faculty of Science, Okayama University, Tsushima, Okayama

(Received May 1, 1972)

In the course of X-ray crystallographic study of the 1:1 addition compound of *p*-bromobenzoic acid and piperidine,[1] it became desirable to determine the molecular structure of the parent acid itself. The unit cell dimensions and space group of *p*-bromobenzoic acid have already been determined by Toussaint,[2] who has also shown that the (*hk*0) Patterson projection closely resembles that of *p*-chlorobenzoic acid.[2] However, no further refinement of the structure has yet been undertaken. This paper presents the three-dimensional X-ray structure analysis of *p*-bromobenzoic acid.

Experimental

Crystals obtained by slow evaporation from ether solution were monoclinic needles elongated along the *c*-axis. Cell constants were determined from Weissenberg and oscillation photographs, and calibrated with sodium chloride.

Crystal data: *p*-bromobenzoic acid, $C_7H_5O_2Br$; M=201.0; mp=251°C, monoclinic, a=29.59(5), b=6.15(1), c=3.98(1) Å, β=95.5(1)°, U=720.4 Å^3, D_m=1.859, D_x=1.854 g·cm^{-3}, Z=4.

Linear absorption coefficient for Cu $K\alpha$(λ=1.5418 Å); μ=76.5 cm^{-1}. $F(000)$=392.

Absent spectra: *h*0*l* when *h* is odd, 0*k*0 when *k* is odd. Space group is $P2_1/a$.

The cell dimensions are substantially identical with those of Toussaint.[2]

Reflections were recorded with Cu $K\alpha$ radiation (1.5418 Å) by means of the equi-inclination Weissenberg technique, for the layers of *hk*0 to *hk*2, using a crystal of 0.19×0.20×1.5 mm. 837 independent non-zero reflections were measured visually, whose intensities ranged from 1 to 10165. The spot shape of the Weissenberg photographs of the *h*0*l* layer was unsuitable for intensity measurement so that these reflections were omitted in the refinement. Corrections were made for the Lorentz and polarization factors, and for the spot shape.

Structure Determination

Approximate positional parameters of all non-hydrogen atoms were obtained from two-dimensional sharpened Patterson projections onto (010) and (001). The structure thus obtained was refined by the block-diagonal least-squares method,[3] first with isotropic thermal parameters and then with anisotropic ones for the bromine and oxygen atoms. The weighting scheme used was:

$$\sqrt{w} = 0.0, \text{ if } F_o \leq F_{min}(2.0),$$

and

$$\sqrt{w} = 1.0, \text{ if } F_{min} < F_o \leq F_{max}(20.25),$$
$$\sqrt{w} = F_{max}/F_o, \text{ if } F_o > F_{max},$$

but zero weight was given for two strong reflections, 201 and 211, because they were seriously affected by extinction.

The R index became 0.102. At this stage, no atomic parameters shifted by as much as 0.3 σ, hence the refinement was terminated. The difference synthesis

* Present address: Kyowa Carbon Co., Ltd., Ushimado, Okayama, Japan.

1) S. Kashino, Y. Sumida, and M. Haisa, *Acta Crystallogr.*, **B28**, 1374(1972).

2) J. Toussaint, *Mém. Soc. Sci. Liège*, **12** (3), 1 (1952).

3) Y. Okaya and T. Ashida, "HBLS IV, The Universal Crystallographic Computing System (I)," Japanese Crystallographic Association (1967), p. 65.

revealed only broad peaks corresponding to five hydrogen atoms.

Finally structure factors were calculated for all atoms including the hydrogen atoms, on the assumption of the C–H bond length of 1.08 Å, the O–H bond length of 1.05 Å, the normal bond angles, and the same isotropic temperature factors as those of the carbon or oxygen atoms to which they are attached. The final R index was 0.096 for 837 non-zero reflections.

The atomic scattering factors used in the calculation were those of Hanson, Herman, Lea, and Skillman.[4] The numerical calculations were performed with the aid of a HITAC 5020E computer of the Computer Center of The University of Tokyo.

Results and Discussion

The final atomic parameters are given in Table 1 and bond lengths and angles are listed in Table 2. Arrangement of molecules in a crystal, the selected intermolecular contacts, and the numbering of atoms are shown in Fig. 1.

Table 1. Final atomic parameters along with their estimated standard deviations within parentheses

Atom	x/a	y/b	z/c	B(Å^2)
C(1)	0.0900(3)	0.3165(15)	0.8197(32)	2.24(15)
C(2)	0.0814(3)	0.5151(15)	0.6558(33)	2.67(17)
C(3)	0.1178(3)	0.6452(16)	0.5907(32)	2.79(18)
C(4)	0.1619(3)	0.5780(15)	0.6691(32)	2.48(16)
C(5)	0.1710(3)	0.3743(15)	0.8370(32)	2.49(17)
C(6)	0.1348(4)	0.2460(15)	0.9149(39)	2.93(19)
C(7)	0.0508(3)	0.1713(17)	0.8938(33)	2.78(17)
O(8)	0.0579(2)	0.0056(11)	1.0602(24)	a)
O(9)	0.0103(3)	0.2388(12)	0.7786(32)	a)
Br(10)	0.2115(1)	0.7577(2)	0.5769(4)	a)

a) The anisotropic thermal parameters are expressed as: $\exp(-B_{11}h^2-B_{22}k^2-B_{33}l^2-B_{12}hk-B_{13}hl-B_{23}kl)$. All values of B_{ij} should be multiplied by 10^{-4}.

	B_{11}	B_{22}	B_{33}	B_{12}	B_{13}	B_{23}
O(8)	8(1)	224(19)	701(98)	6(6)	−35(13)	371(62)
O(9)	6(8)	293(25)	1316(151)	3(7)	−23(16)	539(76)
Br(10)	10(0)	328(4)	690(25)	−36(1)	25(3)	37(11)

Table 2. Bond lengths (Å) and angles (°) along with their estimated standard deviations within parentheses

Bond	Length	Bond	Angle
Br(10)–C(4)	1.902(10)	C(2)–C(1)–C(6)	121.3(9)
O(8)–C(7)	1.225(14)	C(2)–C(1)–C(7)	119.8(8)
O(9)–C(7)	1.307(13)	C(6)–C(1)–C(7)	118.9(9)
C(1)–C(7)	1.517(14)	C(1)–C(2)–C(3)	118.8(9)
C(1)–C(2)	1.400(14)	C(2)–C(3)–C(4)	121.4(9)
C(2)–C(3)	1.388(14)	Br(10)–C(4)–C(3)	120.9(8)
C(3)–C(4)	1.377(13)	Br(10)–C(4)–C(5)	119.1(7)
C(4)–C(5)	1.436(14)	C(3)–C(4)–C(5)	120.0(9)
C(5)–C(6)	1.391(15)	C(4)–C(5)–C(6)	119.2(8)
C(6)–C(1)	1.411(14)	C(1)–C(6)–C(5)	119.3(10)
		O(8)–C(7)–O(9)	124.0(10)
		O(8)–C(7)–C(1)	120.1(9)
		O(9)–C(7)–C(1)	115.8(9)

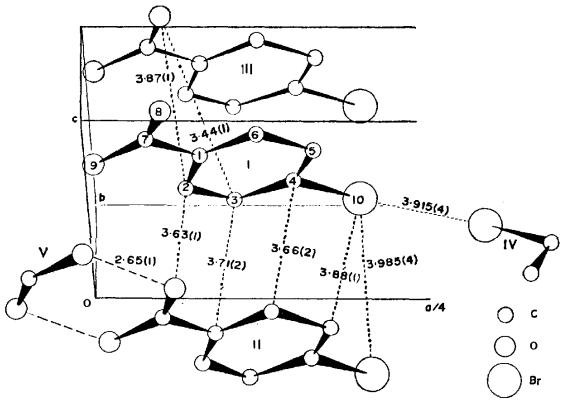

Fig. 1. Arrangement of the molecules in the crystal, the selected intermolecular contacts (Å), and the numbering of atoms.
Key for molecules I: x, y, z II: $x, y, z-1$
III: $x, 1+y, z$ IV: $1/2-x, 1/2+y, 1-z$
V: $-x, -y, 1-z$
Molecules unnecessary for illustration are omitted.
------ Intermolecular contact, —— Hydrogen bond.

Pairs of molecules are linked through O–H–O hydrogen bonds (2.646±0.012 Å) forming dimers, and are stacked along the c-axis. Values for the O–H–O hydrogen bond length of *para*-substituted benzoic acids[5-9] range from 2.61 Å for *p*-aminobenzoic acid[5] to 2.65 Å for *p*-nitrobenzoic acid,[6] but no influence of *para*-substituents on the hydrogen bond length is discernible.

Unlike aliphatic carboxylic acids, *para*-substituted benzoic acids have no remarkable difference between the two C–O bond lengths in the carboxyl group. For example, those of terephthalic acid,[7] benzoic acid,[8] and *p*-toluic acid[9] are 1.262 and 1.272 Å, 1.24 and 1.29 Å, and 1.292 and 1.292 Å, respectively. However, *p*-bromobenzoic acid has two significantly different C–O bond lengths (1.225±0.014 and 1.307±0.013 Å) as found in *p*-nitrobenzoic acid[6] (1.222 and 1.319 Å), while *p*-bromobenzoate ion[1] has nearly equal bond lengths (1.255±0.011 and 1.281±0.011 Å).

Except the carboxyl C–O bond length, the remaining structural features of a *p*-bromobenzoic acid molecule are very similar to those of a *p*-bromobenzoate ion in the addition compound of *p*-bromobenzoic acid and piperidine.[1] The bond length of C(1)–C(7) (1.517 Å) is significantly shortened compared with the standard single bond value of 1.54 Å. The aromatic C–Br distance (1.902 Å) is slightly longer than the normally accepted value of 1.85 Å.[10] The carboxyl group is twisted out of the plane of the benzene ring by 5.8°.

Including intermolecular Br–Br distances (3.92 and 3.98 Å), all the intermolecular contacts correspond to normal van der Waals distances. The bromine atoms are in the *bc* cleavage plane.

4) H. H. Hanson, F. Herman, J. D. Lea, and S. Skillman, *Acta Crystallogr.*, **17**, 1040 (1964).
5) T. F. Lai and R. E. Marsh, *ibid.*, **22**, 885 (1967).
6) T. D. Sakore and L. M. Pant, *ibid.*, **21**, 715 (1966).
7) M. Bailey and C. J. Brown, *ibid.*, **22**, 387 (1967).
8) G. A. Sim, J. M. Robertson, and T. H. Goodwin, *ibid.*, **8**, 157 (1955).
9) M. G. Takwale and L. M. Pant, *ibid.*, **B27**, 1152 (1971).
10) "International Tables for X-ray Crystallography," Vol. III, The Kynoch Press, Birmingham (1962), p. 275.

BULLETIN OF THE CHEMICAL SOCIETY OF JAPAN, VOL. 45, 2653—2654 (1972)

Polarized Absorption Spectrum of Acridone

Hiroyasu INOUE, Toshihiko HOSHI,* and Junko YOSHINO*

Department of Applied Chemistry, Faculty of Technology, Kanagawa University, Kanagawa-ku, Yokohama
**Department of Chemistry, College of Science and Engineering, Aoyama Gakuin University, Chitosedai, Setagaya-ku, Tokyo*

(Received December 25, 1971)

In previous papers, we reported the polarized absorption spectra of several aromatic compounds in stretched PVA sheets, and discussed the assignment of the electronic bands. Especially, as for a molecule of C_{2v} or D_{2h}, we could divide the absorption spectrum into two components, polarized parallel to and perpendicularly to the C_2-axis of the molecule.[1]

In the present paper, the divided spectra of acridone are determined, and the assignments of the electronic bands are established by a comparison of the observed results with theoretical ones.

Kokubun[2] measured the absorption and fluorescence spectra of acridone in various solvents, and discussed the assignment of the electronic bands. Zanker and Wittwer[3] compared the absorption and fluorescence polarization spectra of acridone with those of some hydroxyacridines.

Experimental

Materials. Commercially-available acridone was purified by repeated recrystallizations from ethanol.

Measurement of the Polarized Absorption Spectrum. The measurement and analysis of the polarized absorption spectrum were carried out following a method described elsewhere.[1,4]

Notations. The notations used in the figures of the polarized absorption spectrum and the divided spectra are as follows.

$D_{\parallel}$ and $D_{\perp}$: Absorbances measured for incident light polarized respectively parallel to and perpendicular to the stretched direction of the PVA sheet.

R_d: Ratio between $D_{\parallel}$ and $D_{\perp}$, $D_{\parallel}/D_{\perp}$.

R_s: Degree of stretching of the PVA sheet.

θ: Orientation angle, which means an angle between a transition moment for an electronic transition and an orientation axis of the molecule.

D: Absorbance in an unstretched PVA sheet.

D_x and D_y: Absorbances whose transition moments are along the X- and Y-axes of the molecule respectively. The D_x and D_y curves are called divided spectra.

Method of Calculation

The electronic transition energies and the oscillator strengths for acridone were calculated by means of the PPP approximation,[5] including the variable β method.[6] The valence-state ionization potentials and the electron affinities for carbon, oxygen, and nitrogen atoms were taken as $I_p(C)=11.42$ eV, $E_a(C)=0.58$ eV, $I_p(O)=33.0$ eV, $E_a(O)=11.47$ eV, $I_p(N)=14.16$ eV, and $E_a(N)=1.34$ eV. The two-center electron repulsion integrals were evaluated by using the Nishimoto-Mataga equation.[7] The resonance integrals, β_{rs}, were obtained by the equations:[6] $\beta_{CC}=-1.84-0.51P_{CC}$, $\beta_{CN}=-2.02-0.53P_{CN}$, and $\beta_{CO}=-2.20-0.56P_{CO}$, where P_{rs} is the bond order. All singly-excited configurations associated with the transitions between each of the five highest occupied levels and each of the five lowest vacant levels were included in the CI calculation. The geometry of the molecule used here is shown in Fig. 1. All the bond angles were assumed to be 120°.

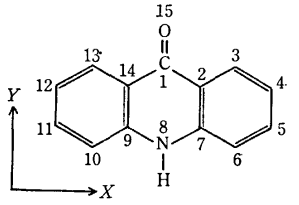

Fig. 1. The geometry of acridone.
$d_{1-15}=1.210$ Å $d_{1-2}=d_{2-3}=\cdots\cdots=d_{1-14}=1.395$ Å

Results and Discussion

Figure 2 shows the polarized absorption spectrum of

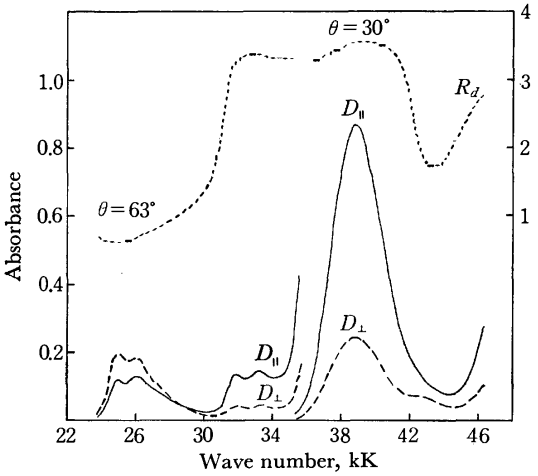

Fig. 2. The polarized absorption spectrum of acridone.

1) H. Inoue, T. Hoshi, T. Masamoto, J. Shiraishi, and Y. Tanizaki, *Ber. Bunsenges. Phys. Chem.*, **75**, 441 (1971); T. Hoshi, H. Inoue, J. Shiraishi, and Y. Tanizaki, This Bulletin, **44**, 1743 (1971).

2) H. Kokubun, *Z. Elektrochem.*, **62**, 599 (1958).

3) V. Zanker and A. Wittwer, *Z. Phys. Chem. N.F.*, **24**, 183 (1960).

4) Y. Tanizaki and S. Kubodera, *J. Mol. Spectrosc.*, **24**, 1 (1967).

5) R. Pariser and R. G. Parr, *J. Chem. Phys.*, **21**, 466, 767 (1953).

6) K. Nishimoto and L. S. Forster, *Theoret. Chim. Acta*, **3**, 407 (1965).

7) N. Mataga and K. Nishimoto, *Z. Phys. Chem. N. F.*, **13**, 140 (1957).

acridone. The R_d values are the largest around 38.8 kK and the smallest around 24.9 kK in the observed wave number region. The orientation angles of the 38.8 kK and the 24.9 kK bands are, respectively, 30° and 63°. These bands seem to be polarized perpendicularly to each other, because the sum of the orientation angles mentioned above is nearly a right angle (30°+63°=93°). As in the cases of anthraquinones,[8] it is considered that the angle of the orientation axis against the X-axis is smaller than that against the Y-axis; therefore, the bands with large R_d values are considered to be polarized along the X-axis, and the bands with small R_d values, along the Y-axis. Since the 24.9 kK band is isolated from the other bands and since the R_d values of this band are almost constant, we can determine the divided spectra of this compound by using the polarization direction of the 24.9 kK band as the standard. As may be seen from the divided spectra in Fig. 3, the absorption spectrum of acridone below 50 kK consists of three X-polarized bands, at 31.8, 38.8, and 45.9 kK, and three Y-polarized bands, at 24.9, 38.2, and 42.6 kK.

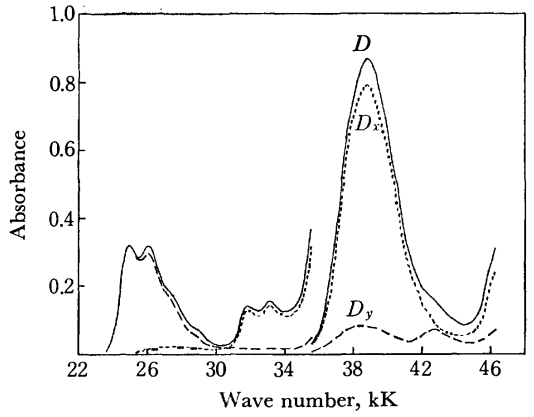

Fig. 3. The divided spectra of acridone.

According to Kokubun,[2] the two bands at 24.9 and 31.8 kK are to be assigned to the ^1L_a and the ^1L_b bands respectively; this assignment is not contradictory with the present results concerning the polarization directions. The observed results described above are compared with the theoretical ones in Fig. 4. The observed and the theoretical results are in good agreement, except for the position of the I transition. The two peaks of the D_y curve at 38.2 and 42.6 kK are due to different electronic transitions; they may correspond to two calculated transitions, IV and VII respectively. The 24.9 kK band is polarized along the Y-axis, and the >NH and >C=O groups have, respectively, electron-donating and electron-accepting characters, so the 24.9 kK band is expected to have a considerable intramolecular charge-transfer character. The calculated transition I is related to the electronic excitation from the ground state to the first excited state Ψ_I, $\Psi_I = -0.179\Psi_{5,11} + 0.328\Psi_{6,10} + 0.211\Psi_{7,12} + 0.890\Psi_{8,9} - 0.101\Psi_{8,12}$, where $\Psi_{i,j}$ is a configuration wave function associated with an one-electron excitation from the ith MO (ϕ_i) to the jth MO (ϕ_j). As is shown above, the coefficient of the $\Psi_{8,9}$ is relatively large; therefore, Ψ_I can be approximately represented by $\Psi_{8,9}$. The coefficients for the MO's, ϕ_8 and ϕ_9, are shown pictorially in Fig. 5. As may be seen from this figure, the electronic transition from ϕ_8 to ϕ_9 results in a considerable charge migration from the >NH group to the >C=O group. Hence, it can be deduced that the I transition is of the intramolecular charge-transfer type.

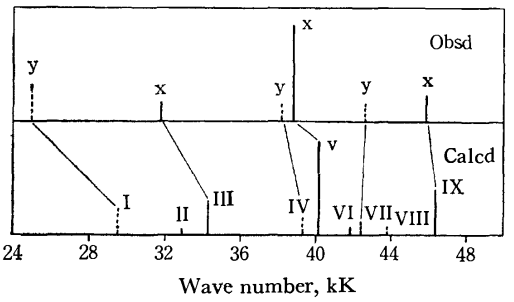

Fig. 4. Comparison of the observed and the calculated results.

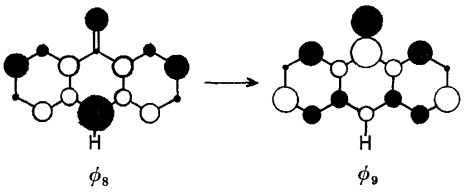

Fig. 5. The coefficients for the MO's ϕ_8 and ϕ_9.

8) H. Inoue, T. Hoshi, and Y. Tanizaki, *Nippon Kagaku Zasshi*, **92**, 501 (1971).

BULLETIN OF THE CHEMICAL SOCIETY OF JAPAN, VOL. 45, 2655—2656 (1972)

Spectrophotometric Studies of the Reaction of 2,2′,4,4′-Tetranitrodiphenylmethane with Bases in Various Solvents

Hiroyasu INOUE and Tadamitsu SAKURAI

Department of Applied Chemistry, Faculty of Technology, Kanagawa University, Kanagawa-ku, Yokohama

(Received February 5, 1972)

A methylene group between two electron-withdrawing moieties is active and is easily subjected to the elimination of a proton from the methylene group, thus yielding a carbanion. For several compounds of this category, the pK_a values have been determined by optical and electrometric measurements.[1-3] For example, 4,4′-dinitrodiphenylmethane has a fairly small pK_a value, 15.8.[2,3] Thus, 2,2′,4,4′-tetranitrodiphenylmethane (abbreviated hereafter to TND) can be expected to be a stronger carbon acid than 4,4′-dinitrodiphenylmethane, in view of the larger number of the nitro groups in TND. At present, however, few reports concerning the carbanion formation of TND have been published.

In this paper, the reaction of TND with such bases as NaOH and triethylamine (TEA) is investigated by means of optical measurements. Especially, solvent effects on the reaction are studied.

Experimental

Materials. The TND was prepared according to the method of Schöpff[4] and was recrystallized twice from acetic acid and several times from a benzene-ethanol mixed solvent; mp 171°C (lit,[4] 172°C). The solvents used here were purified by the standard procedure for each solvent. The TEA was distilled twice just before its use.

Measurements of Absorption Spectra. The ultraviolet and visible absorption spectra were measured with a Shimadzu Spectrophotometer QV-50, using 1-cm quartz cells. The temperature of the cell compartment was kept constant by circulating water from a constant-temperature bath.

Results and Discussion

When NaOH was added to solutions of TND in mixed solvents of organic solvent–water (4:1 in volume), the solutions immediately showed a blue color. The absorption spectra in a mixed solvent of methanol–water are shown in Fig. 1. If the basic solution is neutralized, the original spectrum (Curve I in Fig. 1) can be reproduced. The spectral change can safely be attributed to the carbanion formation of TND. The following equilibrium is considered to be established;

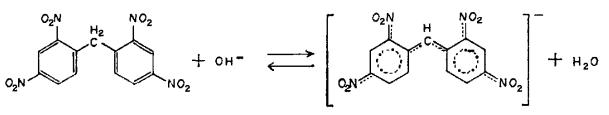

Some carbanions are known to cause disproportionation or electron transfer to the neutral species, thus giving radical anions.[5] In the case of TND, however no signal was observed in the ESR spectrum of the basic solution, so it was not necessary to consider any radicals of TND.

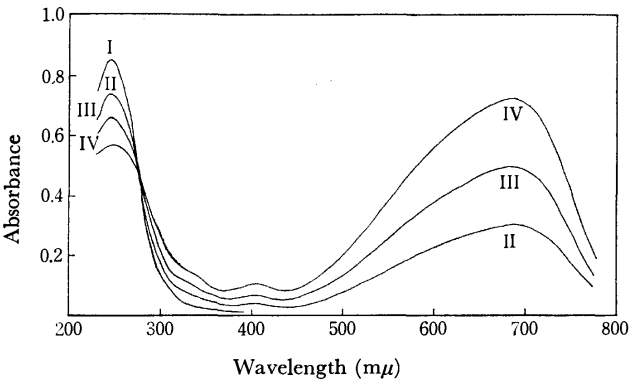

Fig. 1. The absorption spectra of the TND–NaOH system in a methanol–water (4:1) mixed solvent; [TND]=2.74×10⁻⁵M.
I; pH=5.8, II; 12.1, III; 12.6, IV; 13.0.

The equilibrium constant for the base-catalyzed reaction was determined by applying the Benesi-Hildebrand equation,[6] while the value of pK_a was obtained by the use of the following equation;

$$pK_a = pH - \log \frac{\frac{D}{\varepsilon}}{[AH]_0 - \frac{D}{\varepsilon}}$$

where $[AH]_0$ is the initial concentration of TND and where D and ε are, respectively, the absorbance and the molar extinction coefficient of the carbanion band

Table 1. The equilibrium constant, pK_a and the carbanion band for the TND–NaOH system in mixed solvents of organic solvent–water (4:1) at 25°C

Solvent	Dielectric constant[a]	K ($l \cdot mol^{-1}$)	pK_a	λ_{max} (mμ)	ε
Methanol+H_2O	32.6	34	12.6	685	33300
Dioxane+H_2O	2.21	1.96×10^4	9.69	715	47000
Acetone+H_2O	20.5	4.90×10^4	9.37	700	46700
Dimethyl sulfoxide+H_2O	48.9	6.80×10^4	9.08	695	38500

a) The values are of the organic solvents.

1) F. Hashimoto, J. Tanaka, and S. Nagakura, *J. Mol. Spectry.*, **10**, 401 (1963).
2) R. L. Burwell and C. H. Langford, *J. Amer. Chem. Soc.*, **82**, 1503 (1960).
3) K. Bowen and R. Stewart, *Tetrahedron*, **21**, 261 (1965).
4) M. Schöpff, *Ber.*, **27**, 2316 (1894).
5) G. A. Russell and E. G. Janzen, *J. Amer. Chem. Soc.*, **84**, 4153 (1962); **89**, 300 (1967).
6) H. A. Benesi and J. H. Hildebrand, *ibid.*, **71**, 2703 (1949).

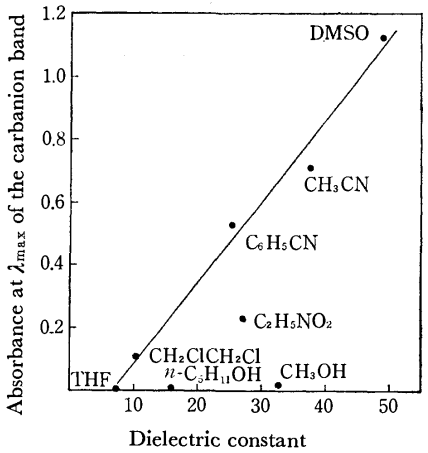

Fig. 2. Relation between the absorbances of the carbanion bands around 700 mμ and dielectric constants of the solvents; [TND]=2.5×10^{-5}M, [TEA]=0.143M.

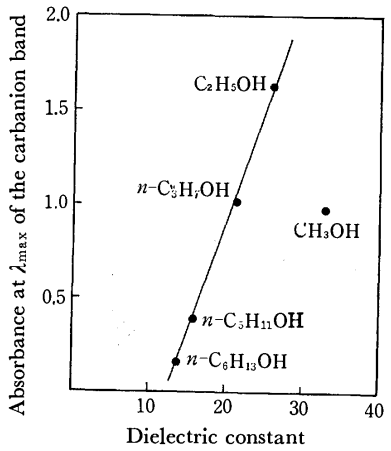

Fig. 3. Relation between the absorbances of the carbanion bands around 700 mμ and dielectric constants of the alcohols; [TND]=3.5×10^{-4}M, [TEA]=1.19M.

appearing around 700 mμ. The results are presented in Table 1.

Obviously, TND is a stronger carbon acid than 4,4′-dinitrodiphenylmethane. The results in Table 1 indicate that the polarity of the solvent used significantly influences the carbanion formation. Therefore, we considered a TND–TEA system in various solvents. TND reacts with TEA, showing a spectral change similar to that shown in Fig. 1. However, it was found that the reaction occurred only in solvents with dielectric constants larger than 7.39 (THF). A linear relationship was found to hold between the absorbance of the carbanion band around 700 mμ and the dielectric constant of the solvent used, as is shown in Fig. 2. This seems to indicate that the stabilization of the carbanion, probably by solvation, plays an important role in the reaction. As for the reaction in nitroethane or alcohols, factors other than the polarity of the solvent must be took into account, for their behavior is exceptional. Since these solvents can cause an interaction with TEA, the concentrations of the free TEA molecule decrease in these solvents. Nevertheless, in alcohols also the absorbance is related linearly to the dielectric constant, except in the case of methanol, as is shown in Fig. 3. The lower absorption intensity in methanol may indicate that the interaction of methanol with TEA is stronger than those of the other alcohols.

In the solvents with dielectric constants smaller than 7.39, the absorption spectrum changes only in the ultraviolet region upon the addition of TEA. From the relation between the concentration of TEA and the change in absorbance, it can be said that TND forms a 1 : 1 complex with TEA through hydrogen-bonding between the methylene group of TND and the N atom of TEA.

In 1,2-dichloroethane, the rate of the reaction was much slower than that in a solvent with a higher dielectric constant, in which the carbanion was formed immediately after the addition of TEA. Since the absorbance at 700 mμ increases quadratically with respect to time in the initial stage, an intermediate reaction step may exist between the reactants and the product.[7] At present, the hydrogen-bonded complex is inferred to be the intermediate, because the spectral change in the initial stage is similar to that observed in the less polar solvents.

7) T. Nogami, K. Yoshihara, H. Hosoya, and S. Nagakura, *J. Phys. Chem.*, **75**, 2670 (1969).

BULLETIN OF THE CHEMICAL SOCIETY OF JAPAN, VOL. 45, 2657—2658 (1972)

Electrical Resistivity of Ternary Compounds, Graphite-Aluminum Bromide-Bromine

Tadashi SASA, Yoichi TAKAHASHI, and Takashi MUKAIBO

Department of Nuclear Engineering, The University of Tokyo, Hongo, Bunkyo-ku, Tokyo

(Received March 24, 1972)

The formation of graphite lamellar compounds is believed to be accompanied with a transfer of electrons between graphite and reactant molecules. Electronic properties of various graphite lamellar compounds have been studied for investigating the nature of the chemical bonding and degree of charge-transfer between reactants and graphite layers.[1] It was found that the charge-transfer did not proceed to the complete ionization of reactant molecules in graphite layer interstices in many cases, and that the ratio of the number of transferred electrons to that of reactant molecules remained fractional. Hennig,[1] and Dzurus and Hennig[2] introduced a model in which only a part of the reactant molecules is completely ionized, making an ionic bonding between graphite layers, while the other molecules remain neutral and stabilize the ions by acting as spacers between them. The case of ternary compounds such as graphite–$AlCl_3$–Cl_2[2] was interpreted as follows: All the chlorine atoms in the compound are completely ionized while $AlCl_3$ molecules remain neutral and act as spacers of Cl^- ions. The mole ratio of $AlCl_3$ to Cl is found to be three for all the reactant concentrations, the chemical formula of the ternary compound being given as $C_n^+ \cdot Cl^- \cdot 3AlCl_3$ or $C_n^+ \cdot AlCl_4^- \cdot 2AlCl_3$.[2]

A mixture of $AlBr_3$ and Br_2 also formed a ternary lamellar compound with graphite, the ratio of $AlBr_3$ to Br in the compound being nearly three up to the bromine content of Br/C=0.014.[3,4] We measured the electrical resistivity of the ternary compound by changing the amount of reactants. The charge-transfer between the reactants and graphite is discussed.

Experimental

Pyrolytic graphite deposited at 1700°C and heat-treated at 2100°C was used as the sample. *C*-spacing and specific resistivity of the graphite were 3.417 Å and 6.0×10^{-4} Ω·cm, respectively. The graphite sample was cut into $1.5 \times 20 \times 0.2$ mm specimens. Platinum wires 0.2 mm in diameter were fixed tightly into small holes drilled on the specimen to make good electrical contacts.

The ternary lamellar compound, graphite–$AlBr_3$–Br_2, was prepared as follows: A controlled amount of bromine was doped in each graphite specimen resulting in the formation of a bromine residue compound. The bromine-doped graphite specimen was then allowed to react with $AlBr_3$ at 120°C in an evacuated reaction tube. After the reaction, the electrical resistivity of the specimen along the direction perpendicular to *c*-axis was measured *in situ* at room temperature by the four contact potentiometric method. Temperature dependence of the resistivity of the compound was found to be very small as compared with that of original graphite.

Results and Discussion

The electrical resistivity of graphite–$AlBr_3$–Br_2 is shown in Fig. 1 by a solid line (open circles). That of the graphite–bromine residue compound with different bromine concentrations measured prior to the reaction with $AlBr_3$ is shown by a dashed line (open triangles). The horizontal axis represents the concentration of free bromine in the ternary compound, in which Br in $AlBr_3$ is not included. The point shown by arrow II is the concentration at which a compound of the second stage structure (compound II, Ref. 4) is formed. The composition of the ternary compounds below this point is represented by $C_n 3AlBr_3 \cdot Br$.[3,4] The resistivity of the saturation compound of the ternary system (compound I, Ref. 4, with the first stage structure and the composition $C_9AlBr_3 \cdot Br_2$) prepared from the same graphite sample was also measured. Although the value of the ratio Br/C of this compound is far beyond the scale, the electrical resistivity indicated by arrow I is nearly the same as that of compound II.

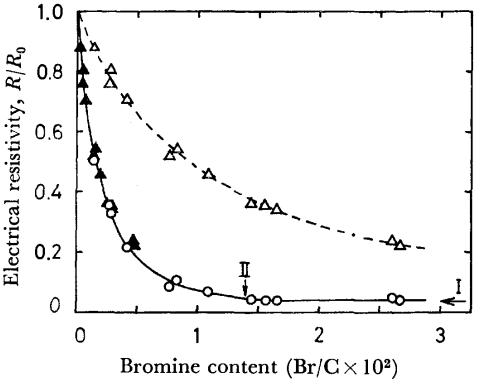

Fig. 1. Electrical resistivity of the graphite compound.
△: graphite bromine residue compound
○: graphite–$AlBr_3$–Br_2 ternary lamellar compound
▲: relation between the electrical resistivity and the assumed concentration of transferred electrons

The electrical resistivity of the bromine residue compound is lower than that of the original graphite. The absorption of $AlBr_3$ by the residue compound led to further decrease of resistivity. Thus it is considered that the addition of $AlBr_3$ in the interstices of graphite layers caused further transfer of electrons from graphite to reactants. With an increase of reactant concentra-

1) G. R. Hennig, "Progress in Inorganic Chemistry," Vol. 1, Interscience Publishers, New York, N. Y. (1959), p. 125.
2) M. L. Dzurus and G. R. Hennig, *J. Amer. Chem. Soc.*, **79**, 1051 (1957).
3) T. Sasa, Y. Takahashi, and T. Mukaibo, This Bulletin, **45**, 937 (1972).
4) T. Sasa, Y. Takahashi, and T. Mukaibo, *ibid.*, **45**, 2250 (1972).

tion in the ternary compound, the electrical resistivity decreased sharply down to the value of compound II. On the contrary, at concentrations beyond that for compound II up to that for compound I, the resistivity showed little change while the reactant contents increased greatly. Thus the fraction of the charge-transferred molecules in the intercalated reactant is considered to decrease considerably when the composition approaches that of compound I.

Hennig[1] reported that the ratio of the number of transferred electrons to that of bromine atoms was 1:5.5 in a graphite-bromine residue compound. A modified plotting of the electrical resistivity of the compound based on this assumption is also given in Fig. 1. Solid triangles show the relation of the electrical resistivity of bromine residue compound *vs.* $Br/C \times 1/5.5$, which represents the assumed concentration of transferred electrons. These plots agree quite well with the solid line representing the relation between he electrical resistivity and the bromine concentration in the ternary compound.

This agreement suggests that all the bromine molecules in the ternary compound are ionized. However, it should be pointed out that there is also a possibility of partial donation of electrons from graphite layers to $AlBr_3$ molecules. In the case of graphite–$FeCl_3$ compound,[5,6] the measurements of Mössbauer spectra suggest that all the intercalated $FeCl_3$ molecules equally take an active part in the charge-transfer.

It is difficult at present to determine whether the chemical formula of the compound is $C_n^+ \cdot Br^- \cdot 3AlBr_3$, or $C_n^+(Br)^{-\delta}(3AlBr_3)^{-\delta'}$. However, from our results it is concluded that bromine assumes a substantially large part in the charge-transfer between the reactants and graphite layers in the ternary compound, graphite–$AlBr_3$–Br_2.

5) B. V. Liengme, M. W. Bartlett, J. G. Hooley, and J. R. Sams, *Phys. Lett.*, **A25**, 127 (1967); *Carbon*, **6**, 681 (1968).
6) A. G. Freeman, *Chem. Commun.*, **1968**, 193.

BULLETIN OF THE CHEMICAL SOCIETY OF JAPAN, VOL. 45, 2658—2659 (1972)

Silyl Radicals. X. On the Mechanism of Uncatalyzed Reduction of Carbon Tetrachloride with Polysilicon Hydride[1]

Hideki SAKURAI, Mineo YAMAGATA, and Masashi MURAKAMI
Department of Chemistry, Faculty of Science, Tohoku University, Sendai, 980

(Received February 7, 1972)

Gilman and Harrell have reported first that polysilicon hydride such as tris(trimethylsilyl)silane reacted smoothly with carbon tetrachloride to give the corresponding chlorosilane without any added catalyst.[2]

The mechanism of the uncatalyzed reduction may be either a molecular reduction involving a four-centered transition state[3,4] or a free-radical chain reactions typically shown in the case of peroxide-catalyzed reduction of carbon tetrachloride with hydrosilanes.[5] The following evidence reported in this paper indicates the latter to be the case.

Both pentamethyldisilane and 1*H*-heptamethyltrisilane, dissolved in carbon tetrachloride, respectively, were converted quantitatively to the corresponding chlorosilanes by heating at 50°C for 38 hr. Addition of a small amount of a free-radical scavenger such as galvinoxyl[6] resulted in complete inhibition of the reduction of carbon tetrachloride with pentamethyldisilane even at 135°C. This is a strong indication of a free-radical nature of the uncatalyzed reaction.

$$Me_3SiSiMe_2H + CCl_4 \longrightarrow Me_3SiSiMe_2Cl + CHCl_3 \quad (1)$$

$$Me_3SiSiMe_2SiMe_2H + CCl_4 \longrightarrow Me_3SiSiMe_2SiMe_2Cl + CHCl_3 \quad (2)$$

Uncatalyzed reduction of carbon tetrachloride with monosilanes, such as *n*-propyldimethylsilane and triethylsilane, did not occur at 50°C. However, while triethylsilane alone did not react with an excess of carbon tetrachloride on heating at 80°C, addition of pentamethyldisilane resulted in conversion of both silanes to the corresponding chlorosilanes in good yields, and again the reaction was inhibited by galvinoxyl. These facts suggest a free-radical mechanism for the reaction. The co-chlorination of triethylsilane and pentamethyldisilane may be interpreted by the following sequence of reactions.

$$Me_5Si_2H \longrightarrow Me_5Si_2\cdot + (H\cdot) \quad (3)$$

$$Me_5Si_2\cdot + CCl_4 \longrightarrow Me_5Si_2Cl + CCl_3\cdot \quad (4)$$

$$Me_5Si_2H + CCl_3\cdot \longrightarrow Me_5Si_2\cdot + CHCl_3 \quad (5)$$

$$Et_3SiH + CCl_3\cdot \longrightarrow Et_3Si\cdot + CHCl_3 \quad (6)$$

$$Et_3Si\cdot + CCl_4 \longrightarrow Et_3SiCl + CCl_3\cdot \quad (7)$$

Pentamethyldisilane functions as an initiator in this scheme. The reaction of pentamethyldisilane with carbon tetrachloride could not be completed, when the mixture was degassed as thoroughly as possible. Therefore, oxygen plays some role at the initiation

1) For part IX, see Ref. 7.
2) H. Gilman and R. L. Harrell, *J. Organometal. Chem.*, **5**, 199 (1966).
3) J. Y. Corey and R. West, *J. Amer. Chem. Soc.*, **85**, 2430 (1963).
4) J. D. Austin and C. Eaborn, *J. Chem. Soc.*, **1964**, 2279.
5) Y. Nagai, K. Yamazaki, I. Shiojima, N. Kobori, and M. Hayashi, *J. Organometal. Chem.*, **9**, 21 (1967).
6) P. D. Bartlett and T. Funahashi, *J. Amer. Chem. Soc.*, **84**, 2596 (1962).

step, although the precise mechanism is uncertain.

Pentamethyldisilane can also initiate the S_H2 reaction between an organodisilane and 1,2-dibromoethane.[7] Addition of a small amount of pentamethyldisilane to a mixture of hexamethyldisilane and 1,2-dibromoethane at 80°C resulted in complete conversion of hexamethyldisilane to trimethylbromosilane.

The relative reactivity of pentamethyldisilane to triethylsilane towards chlorination with carbon tetrachloride was determined in the presence and absence of an initiator, respectively. Since it is well established that reactions of silyl radicals with carbon tetrachloride (steps 4 and 7) are very rapid,[8] the steps 5 and 6 determine the relative reactivity which should be invariable regardless of the nature of initiation.

The reactivity ratio of pentamethyldisilane to triethylsilane in the uncatalyzed reaction was found to be 8.3 and 6.5 at 80.0°C. The dibenzoyl peroxide catalyzed reaction gave the value of 6.3 at 80.0°C. These two sets of values agree with each other fairly well although not perfectly.[13]

It is worthwhile to note that pentamethyldisilane is several times more reactive than triethylsilane toward carbon tetrachloride. The difference in the reactivity may arise from the more electron-positive nature of the pentamethyldisilanyl group than the monosilyl group,[9] which may play a role in a possible polar effect in the transition state of chlorine abstraction.[10]

Experimental

Materials. Pentamethyldisilane,[11] 1*H*-heptamethyltrisilane,[11] triethylsilane,[12] and galvinoxyl[6] were prepared according to literatures.

Uncatalyzed Reaction of Pentamethyldisilane with Carbon Tetrachloride in the Absence or the Presence of Galvinoxyl. A mixture of pentamethyldisilane (0.109 g, 0.83 mmol) and carbon tetrachloride (1.19 g, 7.73 mmol) in a sealed tube was placed in a thermostatted oil bath kept at 135±1°C for 1 hr. Inspection of the mixture by glc after addition of *m*-xylene (internal standard) revealed that it contained pentamethylchlorodisilane (0.85 mmol, 102%), chloroform and unchanged carbon tetrachloride. On the other hand, only a trace amount of pentamethylchlorodisilane was detected by glc with another mixture of pentamethyldisilane (0.119 g, 0.90 mmol) and carbon tetrachloride (1.12 g, 7.28 mmol), which contained 0.0057 g (0.014 mmol) of galvinoxyl, after heating at 135±1°C for 1 hr.

Competitive Chlorination of Pentamethyldisilane and Triethylsilane. *a) Uncatalyzed Thermal Reaction*: In small glass ampules (*ca.* 3 ml) were placed a solution of pentamethyldisilane and triethylsilane in carbon tetrachloride. Dry nitrogen was bubbled gently through the capilary for about 5 min and then ampules were sealed. These were immersed in an oil bath thermostatted at 80.0°C. After given intervals, ampules were picked up and mixtures were analyzed on glc.

b) Dibenzoyl Peroxide Catalyzed Reactions: Similarly mixtures of pentamethyldisilane, triethylsilane, and dibenzoyl peroxide in carbon tetrachloride were subjected to reaction.

c) Analytical Procedure: Products were identified by glc and NMR. For quantitative analyses an internal standard (*e.g.* *m*-xylene) was used. The relative reactivity was calculated by the equation.

$$(k_A/k_B) = \log([A_0]/[A_t])/\log([B_0]/[B_t])$$

where $[A_0]$ and $[A_t]$ are the concentrations of pentamethyldisilane (A) at the initial and a given time, respectively, and $[B_0]$ and $[B_t]$ have a similar significance for triethylsilane (B). Relative rates were calculated by the least squares method. Data are listed in Table 1.

Table 1. Competitive chlorination of Me_5Si_2H (A) and Et_3SiH (B) with CCl_4 at 80.0°

Reactants (mmol)				Reaction time (hr)	$[A_t]$	$[B_t]$	k_A/k_B
$[A_0]$	$[B_0]$	CCl_4	BPO				
2.07	2.10	19.6[a]		12	1.54	2.01	
				18	1.41	1.99	8.2_6
				24	1.37	2.00	
				30	0.93	1.91	
1.04	4.09	19.8		12	0.93	4.04	
				18	0.79	3.04	
				24	0.87	3.99	6.5_2
				30	0.79	3.97	
				36	0.75	3.91	
1.04	4.09	19.8	0.09	10 (min)	0.56	3.81	
				20 (min)	0.14	3.10	6.3_1
				30 (min)	0.13	2.92	

a) Reaction with this mixture in the presence of BPO was too rapid to determine the relative rates.

The authors are indebted to Toshiba Silicone Co., Ltd. for a gift of chlorosilanes.

7) A. Hosomi and H. Sakurai, *ibid.*, **94**, 1384 (1972).
8) A. Hudson and H. A. Hussain, *Mol. Phys.*, **16**, 199 (1969).
9) H. Sakurai, S. Deguchi, M. Yamagata, S. Morimoto, M. Kira, and M. Kumada, *J. Organometal. Chem.*, **18**, 285 (1969).
10) R. A. Jackson, *Advan. Free-Radical Chem.*, **3**, 231 (1969).
11) M. Kumada, M. Ishikawa, and S. Maeda, *J. Organometal. Chem.*, **2**, 478 (1964).
12) F. P. Price, *J. Amer. Chem. Soc.*, **69**, 2600 (1947).
13) **Note Added in Proof**: L. H. Sommer and L. A. Ulland, *J. Amer. Chem. Soc.*, **94**, 3803 (1972), reported recently the rate of hydrogen abstraction from $Ph_3SiPhSiMeH$ by trichloromethyl radicals relativeto α-NpPhMeSiH to be 7.1.

BULLETIN OF THE CHEMICAL SOCIETY OF JAPAN, VOL. 45, 2660—2661 (1972)

Photolytic Addition of Trichlorosilane to Acetone in the Gas Phase

Takaaki DOHMARU, Yoshio NAGATA, and Jitsuo TSURUGI
Radiation Center of Osaka Prefecture, Shinke-cho, Sakai, Osaka

(Received May 1, 1972)

Although silyl radicals have long been known to add to a C=O bond of ketones,[1-5] detailed kinetics of this reaction has never been studied. Our previous works[6,7] on the reduction of alkyl aliphatic carboxylates with trichlorosilane (TCS), reported that the first step of this reaction is addition of trichlorosilyl radical to carbonyl of carboxylates. In connection with these works, we have examined the kinetic behavior of the photolytic addition of TCS to acetone in the gas phase. Using a gaschromatograph directly attached to a vacuum line, the reaction mixture was kept completely free from contact with air during analyses.

Experimental

Apparatus and Procedure. Photolyses and analyses were carried out on a conventional Pyrex vacuum line. The full light from a 50 W medium pressure mercury arc was admitted into a Pyrex reaction vessel of 5.88 cc which cuts off the light of a wavelength region shorter than about 2700 Å to prevent absorption by TCS. The reaction vessel was heated in an electrical furnace controlled to better than ±1°C. After the photolysis, the reaction mixture was transferred by a Toepler pump to a gas sampler which is directly connected to a gaschromatograph equipped with a Gow-Mac thermister detector. A 1 m glass column of 30% SE-30 on Chromosorb W was used at 43°C. Before a series of runs, the column was siliconized by TCS until a reproducible peak height of TCS was obtained.

Material. TCS was treated with quinoline to remove hydrogen chloride and distilled under atmospheric pressure. The distillate (bp 31.8—32.2°C) was further purified by vacuum distillation. Acetone was dried with anhydrous magnesium sulfate and distilled through a 50 cm fractionation column packed with glass Raschig rings. Isopropoxytrichlorosilane prepared previously in this laboratory[6] was used after degassing. All the materials were stored on the vacuum line at −78°C.

Results and Discussion

Rates, and hence quantum yields for product formation and reactant consumption were determined from concentration-time curves at various temperatures. A typical analytical curve at 253°C is shown in Fig. 1.

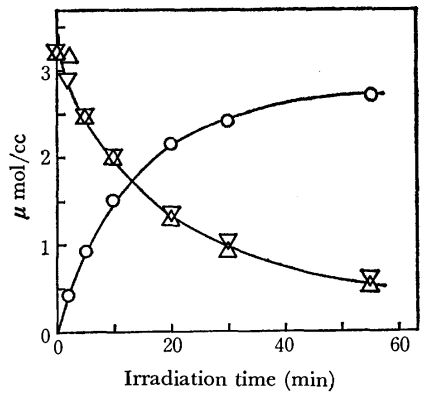

Fig. 1. Plots of the concentration of adduct, $(CH_3)_2CHO\text{-}SiCl_3$ (○) and of reactants, TCS (△) and acetone (▽) with irradiation time at 253°C.

From Fig. 1, each one mole of acetone and TCS is consumed and one mole of adduct (isopropoxytrichlorosilane) is formed; the following stoichiometric relation holds within the experimental error.

$$(CH_3)_2CO + HSiCl_3 = (CH_3)_2CHOSiCl_3 \qquad (A)$$

The initial rate of reaction was obtained from the initial slope of a concentration-time curve of adduct at a given temperature. The results were summerized in Table 1. Activation energy was calculated to be 6.7 kcal/mol.

In order to obtain the kinetic orders of the reaction, the variations in rate with the reactant concentration were examined at 125°C. The results are presented in Fig. 2 in which (a) shows a run with a constant TCS pressure of 50 Torr (2.01 μmol/cc) and acetone pressure of 50—150 Torr, and (b) with a constant acetone pressure of 50 Torr and TCS pressure of 50—150 Torr. Fairly good linear plots were obtained in both runs and the slopes of (a) and (b) were calculated to be 0.40 and 1.0, respectively. The rate of

TABLE 1. RATES OF REACTION AT VARIOUS TEMPERATURE

$[TCS]_0 = [Acetone]_0 = 3.27$ μmol/cc

Temp. (°C)	253[a]	188	138	78
Rate (μmol/cc min)	0.202	0.071	0.032	0.0075
Quantum Yield[b]	90	32	14	3

a) At this temperature, the mixture was allowed to stand in the reaction cell for about 30 min without irradiation, but no detectable reaction product was observed in spite of the possible molecular reaction between acetone and TCS.[8]

b) Acetone photolysis was used for actinometry.[9]

1) For a reviw see for example, R. A. Jackson, *Adv. Free Radical Chem.*, **3**, 231 (1969).
2) R. Calas and N. Duffant, *Compt. Rend.*, **245**, 906 (1957).
3) R. Calas, J. Valade, and J. C. Miléo, *Bull. Soc. Chim. France*, **1961**, 2213.
4) H. Sakurai, A. Hosomi, and M. Kumada, This Bulletin, **40**, 1551 (1967).
5) A. G. Beaumont, C. Eaborn, and R. A. Jackson, *J. Chem. Soc., B*, **1970**, 1624.
6) J. Tsurugi, R. Nakao, and T. Fukumoto, *J. Amer. Chem. Soc.*, **91**, 4587 (1969).
7) Y. Nagata, T. Dohmaru, and J. Tsurugi, submitted for publication.
8) J. A. Kerr, D. H. Slater, and J. C. Young, *J. Chem. Soc., A*, **1966**, 104.
9) J. G. Calvert and J. N. Pitts, Jr., "Photochemistry", John Wiley & Sons, Inc. New York (1966), p. 782.

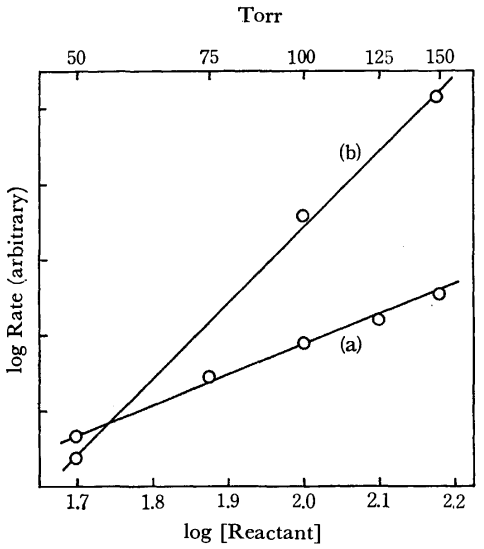

Fig. 2. Variation of rates of adduct formation with acetone concentration (a), and with TCS concentration (b) at 125°C.

adduct formation may be expressed by Eq. (B);

$$R_{adduct} \propto [\text{Acetone}]^{0.4}[\text{TCS}] \quad \text{(B)}$$

The results mentioned above are consistent with the following mechanism.

$$CH_3COCH_3 \longrightarrow 2\cdot CH_3 + CO \quad (1)$$

$$\cdot CH_3 + HSiCl_3 \longrightarrow CH_4 + \cdot SiCl_3 \quad (2)$$

$$\cdot SiCl_3 + CH_3COCH_3 \longrightarrow (CH_3)_2\dot{C}OSiCl_3 \quad (3)$$

$$(CH_3)_2\dot{C}OSiCl_3 + HSiCl_3 \longrightarrow (CH_3)_2CHOSiCl_3 + \cdot SiCl_3 \quad (4)$$

$$2(CH_3)_2\dot{C}OSiCl_3 \longrightarrow \text{products} \quad (5)$$

In our experimental conditions, TCS does not absorb light and only acetone contributes to an initiation reaction (1). Reactions (3) and (4) constitute chain propagating steps. Reaction (5) was assumed as a termination step, and will be seen to lead to the correct kinetic behavior. The steady-state treatment of the

$$R_{adduct} = k_4 k_5^{-1/2} I_a^{1/2}[\text{TCS}] \quad \text{(C)}$$

scheme leads to rate Eq. (C), where k_x denotes a rate constant of a reaction (x) and I_a does a rate of absorption of light. I_a may be considered to be directly proportional to an acetone concentration. Then, Eq. (C) leads to Eq. (D), which is in reasonable agreement

$$R_{adduct} \propto [\text{Acetone}]^{0.5}[\text{TCS}] \quad \text{(D)}$$

with the observations. The reaction chain is adequately long at 253°C, so that the overall variations of the concentration of the reactants and product may be explained in terms of reactions (3) and (4), the inspection of which leads to the stoichiometric Eq. (A). This was also confirmed by the result of Fig. 1. From Eq. (C), overall activation energy E_0 is equal to $E_4 - {}^1/_2 E_5$. The activation energy of a radical combination reaction such as reaction (5) may be generally assumed to be ~0 in the gas phase, so $E_4 \simeq E_0 = 6.7$ kcal/mol.

SHORT COMMUNICATIONS

Formation of Myrcene in the Sodium-catalyzed Oligomerization of Isoprene[1]

Kunihiko TAKABE, Takao KATAGIRI, and Juntaro TANAKA

Department of Synthetic Chemistry, Faculty of Engineering, Shizuoka University, Hamamatsu-shi

(Received September 6, 1971)

Recently investigations[2] have been carried out on the metal complex-catalyzed oligomerization of isoprene. However, no information was obtained on the formation of myrcene (I) (7-methyl-3-methylene-1,6-octadiene), a very important monoterpene occurring in nature, directly from isoprene.

We have investigated the sodium-catalyzed polymerization of isoprene already reported,[3,4] under improved conditions, and found that the oligomers contained significant amounts of myrcene(I) and 6-isopropenyl-9-methyl-3-methylene-1,8-decadiene (II).

Isoprene reacted smoothly with sodium metal in benzene solution and the oligomers were obtained (Table 1). For example, isoprene (15 g) in benzene (20 m*l*) was allowed to react with lumps of sodium (0.5 g, about 1.5 mm cubes) at 40°C for 5 hr with stirring in a pressure bottle. The reaction mixture was then cooled and treated with 15 m*l* ethanol to decompose sodium and organosodium compounds. Distillation of the reaction products gave C_{10} fraction (0.7 g) at 55—60°C/15 mmHg, C_{15} fraction (0.3 g) at 60—63°C/1.0 mmHg and the residue[5] (0.7 g). The first fraction was found to contain 85% of I and the second 76% of II by IR, NMR, and mass spectrometry after gas chromatographic fractionation.[6]

TABLE 1. THE REACTIONS OF ISOPRENE WITH SODIUM

Isoprene (g)	Solvent	(m*l*)	Na (g)	Temp (°C)	Time (hr)	Fractions (g) C_{10}	C_{15}	Residue
15	C_6H_6	20	0.5	40	5	0.7	0.3	0.8
10	C_6H_6	30	0.4	40	5	0.2	t[a]	0.9
20	C_6H_6	20	2.0	40	5	0.6	0.3	1.7
15	C_6H_6	20	0.5	40	10	0.9	0.3	3.3
20	C_6H_6	20	1.0	50	6	t[a]	—	4.6
15	Et_2O	20	0.5	40	3	—	—	12.5[b]
15	THF	20	0.5	40	1.5	—	—	13.0[b]

a) t; trace. b) Distillation was impossible.

Myrcene (I):[7] Mass; *m/e* 136 (M^+). IR (cm^{-1}); 1650, 1600, 990, 910, 890, 825. NMR (CCl_4); δ, 4.80—6.50 (4H, m, $-CH=CH_2$ and $-\dot{C}=CH-$), 4.90 (2H, broad-s, $-\dot{C}=CH_2$), 2.03—2.30 (4H, m, $=\dot{C}-CH_2-CH_2-\dot{C}=$), 1.65 (3H, s, $CH_3\dot{C}=$), 1.57 (3H, s, $CH_3\dot{C}=$).

6-Isopropenyl-9-methyl-3-methylene-1,8-decadiene (II): Mass; *m/e* 204 (M^+). IR (cm^{-1}); 1650, 1600, 990, 910, 890, 835. NMR (CCl_4); δ, 4.82—6.50 (4H, m, $-CH=CH_2$ and $-\dot{C}=CH-$), 4.88 (2H, broad-s, $-\dot{C}=CH_2$), 4.65 (2H, broad-s, $-\dot{C}=CH_2$), 1.80—2.50 (5H, m, $-CH_2-\dot{C}=$ and $-CH-\dot{C}=$), 1.60 (9H, broad-s, $CH_3C=$), 1.20—1.52 (2H, m, $-CH_2-$).

1) Syntheses of Terpenoids by Telomerization. VII. Part VI; T. Katagiri, K. Takabe, K. Ono, and J. Tanaka, *Nippon Kagaku Zasshi*, **92**, 811 (1971).

2) a) C. W. Bird, "Transition Metal Intermediate in Organic Synthesis", Logos Press, London, (1967), p. 30. b) A. Misono, Y. Uchida, K. Furuhata, S. Yoshida, This Bulletin, **42**, 1383, 2303 (1969); S. Watanabe, K. Suga, H. Kikuchi, *Aust. J. Chem.*, **23**, 385 (1970); Y. Uchida, K. Furuhata, H. Ishikawa, This Bulletin, **44**, 1118 (1971).

3) The sodium catalyzed polymerization of isoprene in tetrahydrofuran has been known to form mainly 1,4- and 3,4-polymers. [A. V. Tobolsky, C. E. Rogers, *J. Polym. Sci.*, **40**, 73 (1959).]

4) It has been reported by Suga that the reactions of isoprene with lithium- or sodium-naphthalene gave the linear dimers of isoprene (dimethyloctadienes and trimethylheptadiene). [K. Suga, S. Watanabe, This Bulletin, **40**, 1257 (1967); S. Watanabe, K. Suga, T. Fujita, *Synthesis*, **7**, 375 (1971).]

5) The residue was a very viscous fluid and considered to be a mixture of 1,4- and 3,4-bonded higher oligomers of isoprene by IR. [IR(cm^{-1}); 885, 835.]

6) Glc conditions; Apiezon L, 0.5 mmϕ×90 m, 110°C for C_{10} fraction and 150°C for C_{15} fraction.

7) The data of I agreed completely with those of authentic myrcene.

ENDOR Study of Radical Mixture Formed on the Reduction of *p*-Xyloquinone[4]

Yashige KOTAKE and Keiji KUWATA

Department of Chemistry, Faculty of Science, Osaka University, Toyonaka, Osaka

(Received May 25, 1972)

The central line of the ESR spectrum of a radical mixture may be very complicated when the spectra both contain odd numbers of lines centered at almost the same *g* value. But in this central line all the information of the system is contained. ENDOR is capable of extracting hyperfine splitting constants (hfsc) and the intensity change of the lines in both spectra independently because ENDOR detects the enhancement of an ESR line intensity when the radio frequency hits the NMR frequency of the proton in a radical. Only a couple of ENDOR lines above and below the NMR frequency of free proton appear for each group of equivalent protons. The assignment of the hfsc and the identification of the radical can be made clear from inspection of the ESR spectra. Moreover the kinetic behavior of the system may be studied much more easily than by using ESR technique.

Mixing C_2H_5ONa–C_2H_5OH with *p*-xyloquinone (2,5-dimethylbenzoquinone) produced radicals which showed ESR spectra as Figs. 1a—1c. In dilute ethanolic solution of C_2H_5ONa the spectrum was that of *p*-xylosemiquinone anion radical.[1] In the case that C_2H_5ONa concentration was high the spectra changed with time.

The ENDOR spectra at several reaction stages measured at the top of the first derivative ESR spectrum for the center line at −10°C are shown in Figs. 1d, 1e, and 1f. The ENDOR spectrometer used was constructed in our laboratory which consists of ordinary ESR spectrometer with 200 Hz field modulation and high power ENDOR attachment. This unit delivers maximum output of peak 600 watts sinusoidally modulated radio frequency power and its modulation frequency can be varied from 5 to 15 kHz. The field frequency lock was also used.[2] The comparison between Fig. 1b and 1e may show the advantage of ENDOR technique. Figure 1b consists of overlapped lines of two radicals except weak side lines, while the ENDOR spectrum shows three peaks above free proton frequency quite clearly. The hfsc's can be determined accurately. From the change in relative intensity, it is easy to tell that from which radical the line comes. In Table 1 accurate hfsc's are shown which were determined by the analysis of ENDOR spectra.

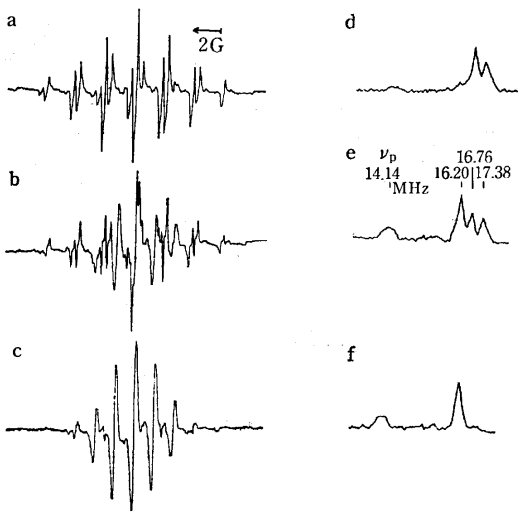

Fig. 1. ESR (a, b, c) and ENDOR (d, e, f) spectra of *p*-xyloquinone–C_2H_5ONa–C_2H_5OH system (quinone and C_2H_5ONa were in 1 : 2 molar ratio). a and d: just after mixing, b and e: after 5 hr at room temperature, c and f: after 3 days at room temperature.

TABLE 1.

Radical	hfsc (gauss)	Assignment
1	$a_1=1.87$	*p*-xylosemiquinone anion
	$a_2=2.31$	a_1: ring protons
		a_2: methyl protons
2	$a_1=1.47$	diethoxy-*p*-xylosemiquinone anion
	$a_2<0.2$	a_1: methyl protons
		a_2: ethoxy protons

Radical 1 in Table 1 can be ascribed to *p*-xylosemiquinone anion radical.[1] Radical 2 has protons which have a large hf coupling and very small one. The large coupling considering about the binomial distribution of the ESR spectrum is assigned to two methyl groups. And remaining coupling is ascribed to ethoxy protons by considering the further reaction in alkali–alcohol media.[3] The fact that ENDOR lines of these groups are rather broad may show that there are two residual small hf coupling which come from the methylene and methyl protons of ethoxy group.

In this reaction system, the two radicals could be identified by their ESR spectra. But by use of ENDOR technique two radicals were identified without the isolation of ESR spectra and the hfsc's were determined accurately even in a radical mixture. This seems to be one of the useful applications of ENDOR.

1) B. Venkataraman, B. G. Segal, and G. K. Fraenkel, *J. Chem. Phys.*, **30**, 1006 (1959).

2) J. S. Hyde, *ibid.*, **43**, 1806 (1965).

3) K. Kuwata and Y. Shimizu, This Bulletin, **42**, 864 (1969).

4) **Note Added in Proof**: Similar kind of work by N. M. Atherson and A. J. Blackhurst appears in *J. Chem. Soc. (Faraday Trans. II)*, **1972**, 470.

A Novel Route to Mixed Transition-Metal Complexes

Katsutoshi YASUFUKU and Hiroshi YAMAZAKI
The Institute of Physical and Chemical Research, Wako-shi, Saitama
(Received March 21, 1972)

Preparation of complexes containing different transition metals has recently attracted much attention.[1,2] We report herewith on the preparation of mixed transition metal complexes in which metal atoms are joined by the alkynyl group.

Bis-π-cyclopentadienyl-bisphenylethynyltitanium (I)[3] reacted readily with nickel carbonyl in benzene at room temperature giving dark olive-green crystals (II) in good yield; mp 141—145°C (decomp.); NMR ($CDCl_3$, τ): 4.49 (s, C_5H_5) and 2.25—2.80 (m, C_6H_5); IR (KBr, ν, cm^{-1}): 1994 (vs, C≡O) and 1850 (C≡C coordinated). The data and the molecular weight (467.5 by vapor pressure osmometry and the molecular ion $[M]^+$ at *m/e* 466 followed by $[M-CO]^+$ at *m/e* 438 in the mass spectrum) suggest structure II.

$$(\pi\text{-}C_5H_5)_2Ti(C{\equiv}CC_6H_5)_2 + Ni(CO)_4 \longrightarrow$$

I

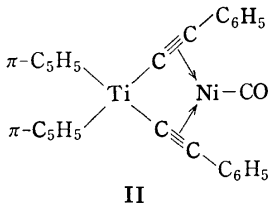

II

The propynyliron complex (IIIa)[4] reacted also readily with cobalt carbonyl giving black crystals

$$\pi\text{-}C_5H_5Fe(CO)(L)\text{-}C{\equiv}C\text{-}R + Co_2(CO)_8$$

IIIa-c

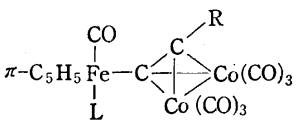

IVa-c

$\xrightarrow{-CO,\,L}$

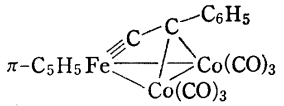

V

a (L: CO, R: CH_3)
b (L: CO, R: C_6H_5)
c (L: $PPhMe_2$, R: C_6H_5)

(IVa) in almost quantitative yield; mp 60—61°C; NMR: 5.01 (s, C_5H_5) and 7.32 (s, CH_3); IR (C_6H_{14}): 2065 (s), 2024 (vs), 1999 (s), and 1996 (sh) (terminal CO); Mass (*m/e*): 502 ($[M]^+$) and ions $[M-nCO]^+$ (n=1~8). The structure was assigned tentatively to IVa.

On the other hand, similar treatment of the phenylethynyliron complex (IIIb)[5] with the cobalt carbonyl afforded black crystals, $C_{19}H_{10}O_6FeCo_2$; mp 110—115°C (decomp.); Mass: 508 ($[M]^+$) and ions $[M-nCO]^+$ (n=1~6); IR: 2068 (s), 2026 (vs), 2000 (s), and 1986 (msh); NMR: 4.98 (s, C_5H_5) and 2.3—2.9 (m, C_6H_5). Structure V is postulated as a plausible one; unequivocal assignment being impossible with spectral data available at present. V might be formed *via* an intermediate IVb. Successful isolation of IVc, mp 91—94°C (decomp.), and its facile transformation into V support the above reaction sequence. Attempts to obtain a V analogue from IVa were not successful.

A similar triiron complex (VI), $C_{20}H_{10}O_7Fe_3$, mp 143—146°C, was obtained as brown crystals from the reaction of IIIb with iron nonacarbonyl in refluxing benzene; Mass: 530 ($[M]^+$) and ions $[M-nCO]^+$ (n=1~7); IR: 2053 (s), 2018 (vs), 2000 (s), 1996 (s), 1976 (s), and 1965 (s) (terminal CO) and 1870 (s, bridge CO).

$$IIIb + Fe_2(CO)_9 \longrightarrow$$

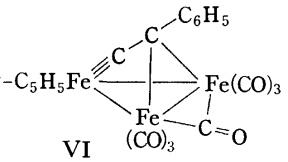

VI

Ethynylnickel complexes (VII) reacted also with the iron carbonyl giving mixed metal complexes. Reaction of VIIa with carbonyl gave the known olive-green crystalline compound VIII[6] and a new complex (IXa), mp 195—197°C, as brown crystals. Similarly, the carbomethoxy derivative (IXb), mp 202—204°C, was obtained from VIIb. Analysis of the mass and IR spectra support formula IX.

$$\pi\text{-}C_5H_5Ni(PPh_3)(C{\equiv}C\text{-}R) + Fe_2(CO)_9 \longrightarrow$$

VIIa, b

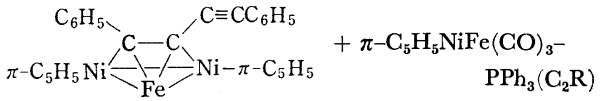

VIII

a (R:C_6H_5) b(R:CO_2CH_3)

Thus, the transition metal acetylide complexes exhibit high reactivity toward metal carbonyls and provide a new type of mixed transition metal clusters.

1) M. C. Baird, "Progress in Inorganic Chemistry," Vol. 9, ed. by F. A. Cotton, Interscience Publishers, N. Y. (1968), p. 1.
2) K. Yasufuku and H. Yamazaki, *Kagaku no Ryoiki*, **25**, 1022 (1971).
3) J. H. Teuben and H. J. de Liefde Meijer, *J. Organometal. Chem.*, **17**, 87 (1969).
4) P. W. Jolly and R. Pettit, *ibid.*, **12**, 491 (1968).
5) M. L. H. Green and T. Mole, *ibid.*, **12**, 404 (1968).
6) J. F. Tilney-Bassett, *J. Chem. Soc.*, **1963**, 4784.
* Satisfactory microanalyses have been obtained for these compounds.

The Nuclear Magnetic Resonance Spectra of 2-Formylaminopyridine and 2-Formylamino-γ-picoline

Nobuko ENOMOTO and Michio KONDO

Central Research Laboratories, Sankyo Co., Ltd., Hiromachi 1-chome, Shinagawa-ku, Tokyo

(Received November 10, 1971)

The NMR spectra of 2-formylaminopyridine and 2-formylamino-γ-picoline have been recorded under various conditions. At low temperatures, these compounds were found to exist in two forms. In these two forms, the chemical shifts of the ring proton-3 differ much from each other because of the difference in the orientation of the formylamino group, which has a large magnetic anisotropy. The difference in the chemical shifts of the formyl protons in the two forms are too large to be explained by the anisotropic shielding effect of the pyridine-ring currents. At higher temperatures, the signal coalescence of these protons in two forms have been observed. The molecular structures of these compounds have been concluded to be planar.

A large magnetic anisotropy is associated with the amide group. The acetylation effect on the *ortho* proton chemical shifts was studied for a number of anilines, and it was shown that pronounced downfield shifts of the protons at the 6-position were observed when the molecules had substituents at the 2-position capable of forming intramolecular hydrogen bonds with the amide proton.[1-5]

This kind of intramolecular hydrogen bonding would be rather easily disrupted in polar solvents, such as dimethyl sulfoxide, which is well known as an agent for interacting with amide protons.[6] The free rotation around the C_{ring}–N bond thus induced by the disruption of the intramolecular hydrogen bond is reflected in the upfield shifts of the proton-6 in 2,4-dichloroacetanilide[2] or of 2,4-dinitroacetoanilide[2,7] in dimethyl sulfoxide, for example, as compared to the signals observed in chloroform.

In acetylaminopyridines, the conjugation interaction between the substituent and the pyridine ring is dependent upon the position of substitution. A remarkable deshielding shift of the proton-3 of 2-acetylaminopyridine was considered to be indicative of the planarity of the molecule, probably in the *endo* form.

It has been reported that acetanilide exists in the *endo* form,[8] whereas formanilide in solution coexists in both forms, *endo* and *exo*.[2,9]

In this paper we will present the NMR spectra of 2-formylaminopyridines under various conditions and make it clear that the large deshielding shift of the proton-3 is associated with molecules in the *endo* form.

Experimental

2-Aminopyridine was refluxed with excess formic acid for 5 hr. The water produced and the excess formic acid were distilled off under reduced pressures. The 2-formylaminopyridine was distilled out last. This fraction was submitted to redistillation and finally to recrystallization from benzene; mp 71°C.

Found: C, 59.17; H, 5.17; N, 22.77%. Calcd for $C_6H_6N_2O$: C, 59.01; H, 4.95; N, 22.94%.

2-Formylamino-γ-picoline was prepared in a similar way; mp 89°C.

Found: C, 62.01; H, 6.06; N, 20.63%. Calcd for $C_7H_8N_2O$: C, 61.75; H, 5.92; N, 20.58%.

Reasonable mass spectra were obtained for these two compounds.

The NMR spectra were recorded on a Varian A-60D spectrometer under various conditions. Temperatures could be controlled within ±2°C at higher temperatures, but only within ±4°C at lower temperatures. The concentration dependence of the chemical shifts was found to be negligible for any protons but amide protons. The figures reported in this paper were read from the spectra of solutions with a concentration of 10 w/v%.

Results and Discussion

Assignment. The low-field part of the spectrum of 2-formylamino-γ-picoline in di-*n*-propyl ketone is shown in Fig. 1. It is clear that there are two molecular species in solution at low temperatures. Following the general concept that $J_{trans} > J_{cis}$, the sharp doublet with a coupling constant of 11 Hz at 9.50 ppm was assigned to the formyl proton in the *exo* form. Another doublet with a smaller splitting, 2 Hz, at 8.63 ppm was ascribed to the formyl proton in the *endo* form. The lower-field resonance of the formyl proton in the *exo* form could be attributed to its closer proximity to the pyridine ring than the same proton in the *endo* form. This chemical-shift difference is much larger than that observed for formanilide.[9]

Bourn *et al.* estimated the chemical-shift difference of the formyl protons of formanilide at the *exo* and *endo* positions as about 0.25 ppm, using reasonable values for the bond lengths and assuming that all bond angles are 120° and that the moleclule is planar.[9]

1) T. H. Siddall, III and W. E. Stewart, *J. Mol. Spectrosc.*, **24**, 290 (1967).
2) R. F. C. Brown, L. Radom, S. Sternhell, and I. D. Rae, *Can. J. Chem.*, **46**, 2577 (1968). B. D. Andrews, I. D. Rae, and B. E. Reichert, *Tetrahedron Lett.*, **1969**, 1859.
3) J. R. Bartels-Keith and R. F. H. Cieciuch, *Can. J. Chem.*, **46**, 2593 (1968).
4) B. M. Lynch, C. M. Chen, and Y. K. Wigfield, *ibid.*, **46**, 1141 (1968).
5) M. Zanger, W. W. Simons, and A. R. Gannaro, *J. Org. Chem.*, **33**, 3672 (1968).
6) a) L. A. LaPlanche and M. T. Rogers, *J. Amer. Chem. Soc.*, **86**, 337 (1964). b) R. H. Barker and G. J. Boudreaux, *Spectrochim. Acta*, **A23**, 727 (1967).
7) I. D. Rae, *Can. J. Chem.*, **46**, 2589 (1968).
8) B. F. Pedersen and B. Pedersen, *Tetrahedron Lett.*, **1965**, 2995.
9) a) A. J. R. Bourn, D. G. Gillies, and E. W. Randall, *Tetrahedron* **20**, 1811 (1964). b) A. J. R. Bourn, D. G. Gillies, and E. W. Randall, *ibid.*, **22**, 1821 (1966).

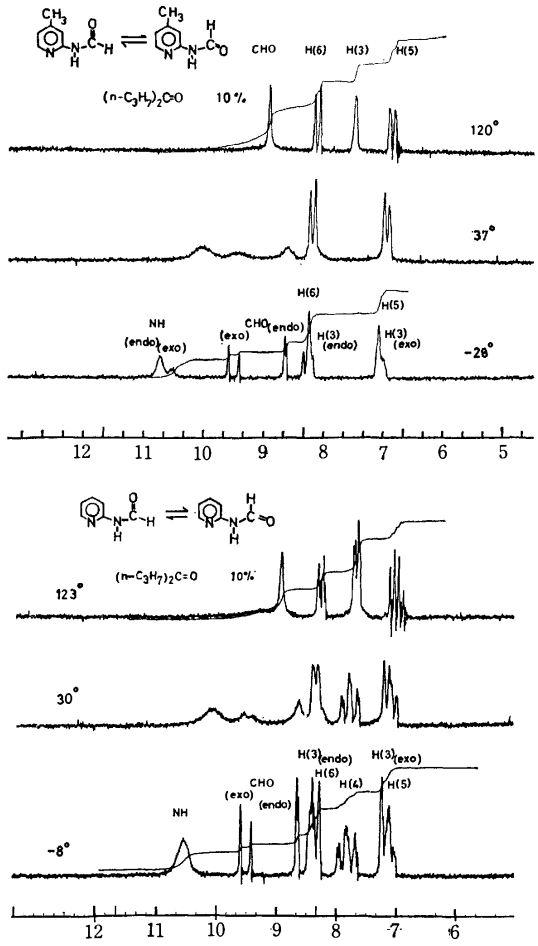

Fig. 1. The lowfield region of the NMR spectra of 2-formylamino-γ-picoline and 2-formylaminopyridine in di-*n*-propyl ketone at different temperatures.

The difference of 0.87 ppm observed in the present case is too large to be explained by the anisotropic effect of the pyridine ring, because the latter is similar in size to that of the benzene ring. The formyl proton in the *exo* form might be subjected to a strong deshielding effect due to the lone-pair electrons on the ring nitrogen in the D configuration, because the flip-rotation about the C_{ring}–N_{amide} bond, C⇌D, seems to be very probable.

There are two other signals, at 10.73 and 10.62 ppm, which are easily assigned to the amide protons in the *exo* and *endo* forms respectively on the basis of their temperature dependence. The amide-proton signal shifts to higher fields on an increase in the temperature of the solution; this shift is due to diminished intermolecular interactions through the amide group.[9] The signal then undergoes a pronounced broadening due primarily to the intermolecular exchange of the amide protons.

Roughly speaking, there are two multiplets, at 7.0 and 8.2 ppm, and each multiplet has an intensity corresponding to more than one proton. The multiplet at lower fields is attributable to the ring proton-6 and the proton-3 in the *endo* form. The other multiplet signal arises from the proton-5 and the proton-3 in the *exo* form. These assignments of the proton-5 and -6 are consistent with the NMR parameters of unsubstituted pyridine.[10] The assignment of the signals of the proton-3 is based on the signal intensity.

At elevated temperatures, the signal for the proton-3 coalesces and appears at 7.53 ppm as a singlet with a

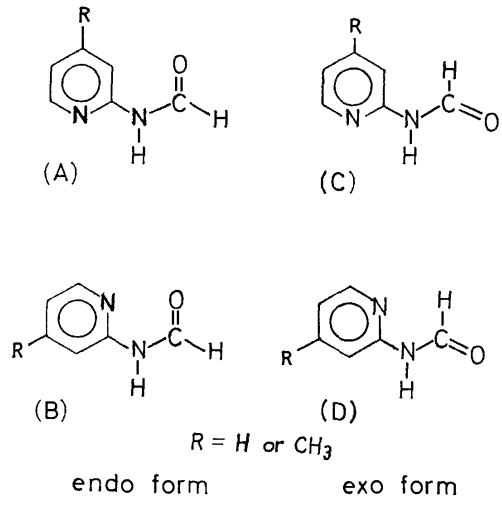

somewhat unresolved structure. A considerable rapid rotation around the amide bond, CO–NH, is responsible for this coalescence.[11] This rotation also causes the coalescence of the formyl proton signal with a linewidth comparable with that of the proton-3 signal.

From these observations, it is quite certain that the proton-3 experiences quite a different magnetic environment depending upon whether the molecules are in the *exo* form or in the *endo* form. On the other hand, the proton-5 or -6 has nearly the same value for the chemical shift in either form. Similarly, the signals of the methyl protons at the 4 position in the two rotamers almost overlap each other. These observation reflect a sharp distance-dependence of the anisotropy effect.

Arguments almost the same as those above are certainly applicable to the NMR spectrum of 2-formylaminopyridine at various temperatures, except for the fact that the ring-proton spectrum is somewhat complicated because of the presence of the proton-4.

Table 1 summarizes the results obtained under various conditions.

Chemical Shifts of Ring-proton-3 in the endo *and* exo *Forms.* In chloroform, acetone, and di-*n*-propyl ketone, the chemical shifts of the proton-3 in the two rotamers are nearly the same, suggesting that the molecular structures are also very similar in these solvents. In toluene, however, the chemical shift for the *exo* form is shifted to a field higher by about 0.6 ppm, whereas the *endo* form signal is shifted little with respect to those in chloroform solutions. This observation is also indicative of the reasonableness of the assumption that the lower-field signal of the proton-3 is associated with the *endo* form, for it is well known that the protons *trans* to the carbonyl oxygen with respect to the amide bond are more shielded than those in the *cis* position

10) S. Castellano, C. Sun, and R. Kostelnik, *J. Chem. Phys.*, **46**, 327 (1967).

11) J. A. Pople, W. G. Schneider, and H. J. Bernstein, "High Resolution Nuclear Magnetic Resonance," McGraw-Hill, New York (1959), p. 365.

TABLE 1. CHEMICAL SHIFTS OF RING PROTON-3, FORMYL PROTON AND AMIDE PROTON

Solvent	Temp.	CHO		NH		H(3)	
		endo	*exo*	*endo*	*exo*	*endo*	*exo*
2-Formylaminopyridine							
$CDCl_3$	−40°C	8.62	9.38	11.3	11.4	8.4	7.1
	37	8.63	9.87	10.1		8.3	7.1
Acetone-d_6	−31	8.62	9.47	10.3		8.3	7.1
	37	8.60	9.47	9.9		8.3	7.1
$(n\text{-}C_3H_7)_2CO$	− 8	8.70	9.52	10.6		8.4	7.2
	37	8.60	9.50	10.0		8.2	7.2
	123	8.92		9.3		7.7	
Toluene-d_8	12	8.28	9.30	10.5	11.7	8.4	6.4
	37		9.30	9.9	10.5	8.4	6.4
	103	8.67		8.9		7.33	
DMSO-d_6	37	8.33	9.23	10.5		7.8	7.0
	150	8.93		9.8		7.5	
2-Formylamino-γ-picoline							
$CDCl_3$	−41	8.63	9.37	11.70		8.22	6.88
	37	8.56	9.33	10.4		8.17	6.78
Acetone-d_6	−21	8.53	9.38	10.30		8.13	6.92
	37	8.53	9.37	9.35		8.07	6.87
$(n\text{-}C_3H_7)_2CO$	−28	8.63	9.50	11.15	11.03	8.20	7.00
	37	8.60	9.47	10.0		8.20	6.90
	117	8.97		8.9		7.53	
Toluene-d_8	13	8.33	9.30	10.65	11.10	8.25	6.33
	37	8.32	9.33	10.35	10.82	8.28	6.33
	100	8.67		9.00		7.25	
DMSO-d_6	37	8.37	9.25	10.47		7.97	6.93
	130	8.83		9.87		7.27	
DMSO-d_6–D_2O	−12	8.48	9.20			7.87	6.87
	37	8.50	9.20			7.83	6.97
	90	8.87				7.37	

when aromatic hydrocarbons are used as the solvents.[12] In a mixed solvent such as D_2O–DMSO-d_6, on the other hand, the chemical shift of the proton-3 in the *endo* form shows an upfield shift, probably due to a slight decrease in the deshielding effect of the amide group, which might be twisted slightly out of the plane of the pyridine ring, as has already been described in the introductory section for 2,4-dichloroacetanilide. This twisting could be attributed to the interactions of the amide group with the solvent molecules, water and dimethyl sulfoxide; both are representative solvents capable of interacting with solute molecules having polar groups through the formation of intermolecular hydrogen bonds.

Planarity of 2-Formylaminopyridine. The acetylation effect on the *ortho* protons is smaller in acetanilide than in 2-chloroacetanilide.[1] This difference is probably to be ascribed to the fact that the rotation around the C_{ring}–NH bond is free in the former, but is strongly restricted in the latter, which holds the molecule planar.

The chemical shift of the proton-3 of 2-formylaminopyridine in the *endo* form is about 8.2 ppm. Therefore, the "formylation" deshielding shift is about 1.85 ppm, because the chemical shift of the proton-3 in 2-aminopyridine is 6.35 ppm.[13] A similar value of 1.70 ppm has been reported as the "acetylation" shift for the proton-3 resonance of 2-aminopyridine.[2] Consistent with this, the proton-6 in 2,4-dichloroacetanilide, where the internal rotation around the C_{ring}–N_{amide} bond is strongly restricted by the intramolecular hydrogen bond, resonates at 8.32 ppm, lower by 1.66 ppm than the resonance of the corresponding proton in 2,4-dichloroaniline. The excellent agreement of these values seems to indicate a restricted rotation around the C_{ring}–N_{amide} in 2-formylaminopyridines.[14]

This is also supported by the fact that the chemical shifts of the 2 and 6 protons in *p*-formyltoluidide in chloroform are 7.37 and 7.11 ppm for the molecules in the *endo* and *exo* forms.[1] It is quite certain that this small difference in the chemical shifts for the two rotamers is attributable to the free rotation around the C_{ring}–N bond.

The downfield shift of the proton-3 in 2-acetylaminopyridine has been reported to be very large, suggesting that molecules have a planar structure. The

12) J. V. Hatton and R. E. Richards, *Mol. Phys.*, **3**, 253 (1960); *ibid.*, **5**, 139 (1962).

13) W. B. Smith and J. L. Roark, *J. Phys. Chem.*, **73**, 1049 (1969).

14) The authors have no idea about the flip-rotation about the C_{ring}–N_{amide} bond, A⇌B.

molecular planarity of this compound is reflected in other evidence wherein a weak, long-range coupling is observed between the amide proton and the proton-4.[15] Unfortunately, in the case of 2-formylaminopyridine, however, the corresponding long-range coupling could not be identified because of the superposition of the two signals corresponding to the two rotamers where the chemical shifts of the proton-4 are very similar to each other.

The large difference in the chemical shifts of the formyl protons in the *endo* and *exo* forms, already described, also strongly suggests the planarity of 2-formylaminopyridines.

From these facts, it seems very probable that 2-formylaminopyridines have planar structures near room temperature. The dipole interaction between the amide group at the position 2 and the pyridine ring is considered to be a main factor in keeping the molecule planar.[1] A similar situation occurs with α-dipyridyl, which has been determined to be planar and *trans* in chloroform.[16]

endo-exo *Equilibrium.* The *endo-exo* equilibrium can be evaluated only at low temperatures. Table 2 gives the *endo-exo* equilibrium constant, $R=I(endo)/I(exo)$, where $I(endo)$ and $I(exo)$ stand for the intensities of the signals from molecules in the *endo* and *exo* forms respectively. It is very interesting to note that the R value changes slightly with the change in solvent from chloroform to a mixed solvent of dimethyl sulfoxide and water (1 : 1). In the cases of thioacetanilide[17,18] and thioacetonaphthalide,[19] the corresponding R values are strongly dependent upon the polarity of solvents. In the case of formanilide, the addition of dimethyl sulfoxide to a chloroform solution caused an intensification of the *endo*-signal.[20] This trend is contrary to the present results.

Table 2. Population ratio of *endo/exo* in different solvents

Solvent	Temperature	Ratio (*endo/exo*)
Chloroform	−28 (°C)	1.4
Acetone	−28	1.3
Di-*n*-propyl ketone	−28	1.2
DMSO-water (1:1)	−12	0.93

In a chloroform solution of 2-chloro-*p*-formyltoluidide,[3] the proton-6 chemical shifts were found to be 7.0 and 8.13 ppm in the *exo* and *endo* form respectively, at 10°C and with the R value of 0.5. At 40°C, however, a partial coalescence occurred and the proton-6 signal appeared at 8.10 ppm, lower than the value estimated directly from the two chemical shifts and the R value at 10°C given above. This suggests that the equilibrium was shifted to the *endo* form with an increase in the temperature. In the present case, however, the resonance positions of the formyl protons and of the proton-3 at higher temperatures are almost the same as those evaluated from the R values and the chemical shifts of these protons obtained from the NMR spectra at low temperatures. This suggests a temperature independence of the population ratio of the two rotational isomers.

15) M. Kondo, unpublished data.
16) S. Castellano, H. Gunter, and S. Ebersole, *J. Phys. Chem.*, **69**, 4166 (1965).
17) I. Suzuki, M. Tsuboi, T. Shimanouchi, and S. Mizushima, *Spectrochim. Acta*, **16**, 471 (1960).
18) M. Kondo, unpublished data.
19) M. Kondo, unpublished data.
20) T. Nishiyama and F. Yamada, *Nippon Kagaku Zasshi*, **89**, 979 (1968).

Kinetic Studies of Intermolecular Hydrogen Bonding in Carboxylic Acids by Means of Ultrasonic Absorption Measurement. I. Fatty Acids

Takayuki SANO, Nobuhide TATSUMOTO, Toshio NIWA, and Tatsuya YASUNAGA

Department of Chemistry, Faculty of Science, Hiroshima University, Higashisenda-machi, Hiroshima

(Received November 15, 1971)

The ultrasonic absorptions in *n*-butyric, isobutyric, *n*-valeric, isovaleric, and *n*-caproic acids have been measured in the frequency range from 2.5 to 95 MHz in order to study the relationship between the ultrasonic absorption and the chemical structure of the alkyl group in carboxylic acids. The relaxation absorptions were observed for all the acids with relaxation frequencies in the range of 1.6—8.7 MHz. The kinetic parameters have been calculated on the basis of an assumption that the absorptions are associated with the breakage of one of the two hydrogen bonds in the dimer, as in the case of propionic acid. The values of the heat of reaction, ΔH, were calculated to be 4.7—6.4 kcal per mole of dimer. By an application of the results to Taft's equation, $\log K=\rho^*\sigma^*+sE_s$, it is deduced that the change in the ΔH in a series of monocarboxylic acids is due to variations in the inductive effect of each alkyl group. However, the change in the heat of activation, ΔH^*, can not be explained in terms of the inductive effect.

It is well known that an excess absorption of ultrasound exists in the frequency range from 0.5 to 10 MHz in such liquid monocarboxylic acids as acetic[1,2] and propionic[3,4] acids. As the origin of this absorption, the transition from monomeric to dimeric molecules of carboxylic acid has been assumed.[5]

However, the ultrasonic investigation for acetic acid in various solvents by Piercy and Lamb[6] raises the question of whether the above mechanism for the ultrasonic absorption is reasonable for acetic acid. Furthermore, Tabuchi[7] has suggested that the absorption in acetic acid might be associated with the transition from the cyclic dimer to the open dimer. Also, one of the present authors[4] has concluded that the ultrasonic absorption is associated with a perturbation of the following equilibrium:

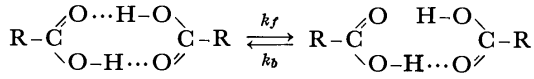

from his measurement of the ultrasonic absorption in methyl propionate solutions of propionic acid, and has calculated the kinetic parameters of this reaction.

Hitherto, the ultrasonic study of monocarboxylic acids has been done mainly for acetic and propionic acids. It is interesting to study the changes in the absorption with the increase in the carbon number and with the changes in the alkyl group of carboxylic acids in its structure.

Experimental

A pulse technique[4] was used to measure the ultrasonic absorption in the liquid monocarboxylic acids over the frequency range from 2.5 to 95 MHz. The velocity of the sound was measured by means of an ultrasonic interferometer[8] operated at 3.0 and 5.0 MHz. In order to observed the dependence of the relaxation frequency and the absorption on the temperature, measurements were made in the temperature range from 15 to 30°C for *n*-butyric, isobutyric, *n*-valeric, and isovaleric acids, and from 25 to 45°C for *n*-caproic acid. The relaxation absorption in *n*-caproic acid is relatively small in comparison with the others. The densities were measured with a pycnometer. An adiabatic-type calorimeter was used for the heat-capacity measurements. The chemicals used were all guaranteed grade and were used without further purification.

Results

The ultrasonic absorption spectra in a series of monocarboxylic acids are shown in Figs. 1—6. All the spectra can be represented by a single relaxation formula:

$$\frac{\alpha'}{f^2}=\frac{\alpha}{f^2}-B=\frac{A}{1+(f/f_{\max})^2} \qquad (1)$$

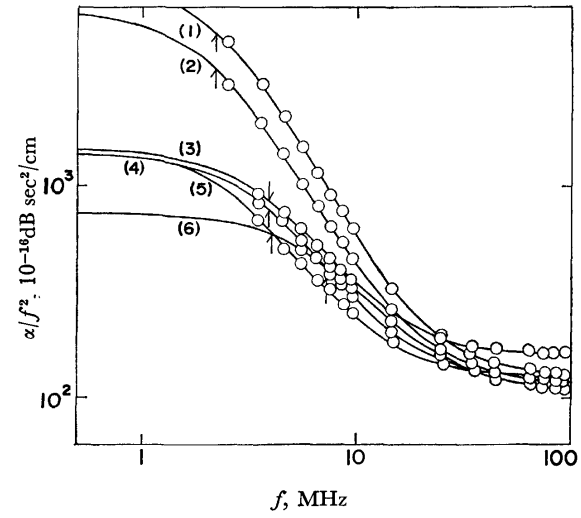

Fig. 1. Ultrasonic absorption spectra in monocarboxylic acids: (1), propionic; (2), butyric; (3), isovaleric; (4), valeric; (5), caproic; and (6), isobutyric acids at 25°C.

1) B. Spakowski, *C. R. Acad. Sci. URSS*, **18**, 169 (1938).
2) J. Lamb and J. M. M. Pinkerton, *Proc. Roy. Soc. Ser., A*, **199**, 114 (1949).
3) J. Lamb and J. Huddart, *Trans. Faraday Soc.*, **46**, 540 (1950).
4) N. Tatsumoto, *J. Chem. Phys.*, **47**, 4561 (1967).
5) E. Freedman, *ibid.*, **21**, 1784 (1953).
6) J. E. Piercy and J. Lamb, *Trans. Faraday Soc.*, **52**, 930 (1956).
7) D. Tabuchi, *Z. Elektrochem.*, **64**, 141 (1960).
8) T. Yasunaga, H. Oguri, and M. Miura, *J. Chem. Phys.*, **43**, 3512 (1965).

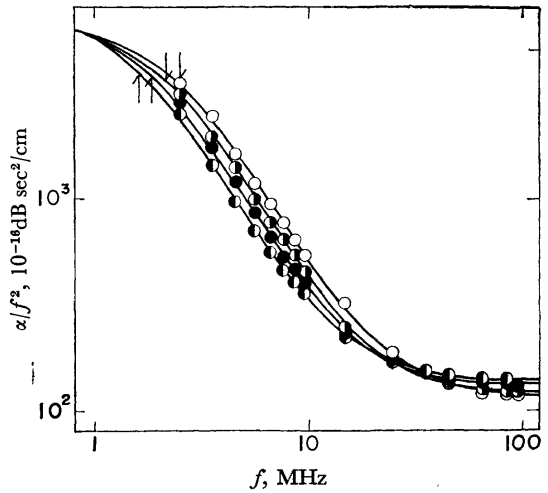

Fig. 2. Ultrasonic absorption spectra in butyric acid at various temperatutes: ◐: 15°C; ●: 20°C; ◑: 25°C; ○: 30°C.

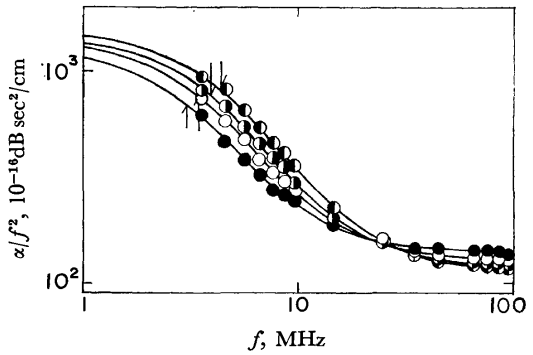

Fig. 3. Ultrasonic absorption spectra in valeric acid at various temperatures: ●: 15°C; ○: 20°C; ◑: 25°C; ◐: 30°C.

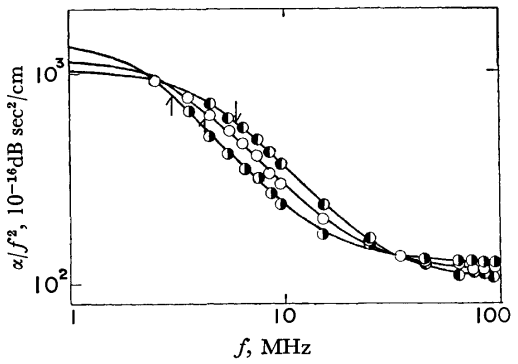

Fig. 4. Ultrasonic absorption spectra in caproic acid at various temperatures: ◑: 25°C; ○: 35°C; ◐; 45°C.

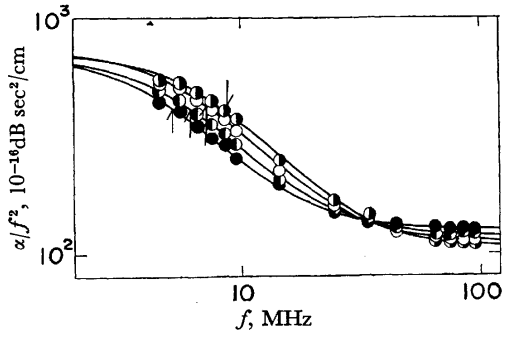

Fig. 5. Ultrasonic absorption spectra in isobutyric acid at various temperatures: ●: 15°C; ◐: 20°C; ○: 25°C; ◑: 30°C.

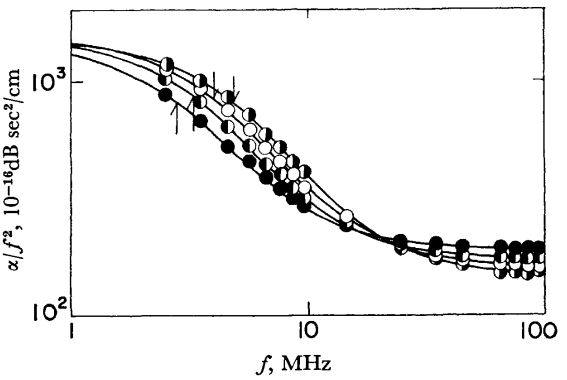

Fif. 6. Ultrasonic absorption spectra in isovaleric acid at various temperatures: ●: 15°C; ◐: 20°C; ○: 25°C; ◑: 30°C.

where α is the ultrasonic absorption coefficient; f, the frequency of sound; α', the excess absorption coefficient, and f_{max}, the relaxation frequency. A and B are the excess and the classical absorption respectively. The values of A, B, f_{max}, and the maximum of the absorption per wavelength $(\alpha'\lambda)_{max}$ are listed in Table 1. The uncertainties in A, B, and f_{max} are approximately ± 10, ± 5, and $\pm 5\%$ respectively. The other values required for the calculation of kinetic parameters, such as the sound velocity (u), the density (ρ), the thermal expansion coefficient (l), and the heat capacity at a constant pressure (C_p), are given in Table 2. The errors in u, ρ, l, and C_p are ± 0.01, ± 0.05, ± 0.5, and

TABLE 1. THE ACOUSTICAL CHARACTERISTICS OF MONOCARBOXYLIC ACIDS AT THE VARIOUS TEMPERATURES

T (°K)	f_{max} (MHz)	A (10^{-16} dB·sec cm^{-1})	B	$(\alpha'\lambda)_{max}$ (10^{-2} dB)
		Butyric acid		
288	1.6	7600	137	7.6
293	1.9	7300	130	8.3
298	2.2	7000	118	9.1
303	2.5	6700	115	10.0
		Isobutyric acid		
288	5.2	580	125	1.8
293	6.4	572	117	2.1
298	7.3	623	109	2.6
303	8.7	600	104	2.9
		Valeric acid		
288	3.0	1120	140	2.1
293	3.4	1280	129	2.7
298	3.8	1300	118	3.0
303	4.4	1380	114	3.7
		Isovaleric acid		
288	2.8	1330	190	2.2
293	3.5	1200	173	2.7
298	4.2	1139	159	3.2
303	5.0	1090	126	3.7
		Caproic acid		
298	2.9	1400	124	2.5
303	3.6	1250	122	2.8
308	4.3	1110	112	2.9
313	5.0	1050	110	3.3
318	5.9	980	102	3.4

Table 2. The thermodynamic parameters for the monocarboxylic acids

T (°K)	u (3MHz) (10^5 cm sec^{-1})	ρ[a] (g cm^{-3})	l[b] (10^{-4} deg^{-1})	C_p°[c] (cal g^{-1}. deg^{-1})
	Butyric acid			
288	1.2247	0.9634	9.77	0.526
293	1.2062	0.9584	9.77	0.526
298	1.1880	0.9534	9.77	0.526
303	1.1701	0.9485	9.77	0.526
	Isobutyric acid			
288	1.1747	0.9547	9.80	0.450
293	1.1562	0.9498	9.80	0.450
298	1.1363	0.9448	9.80	0.450
303	1.1179	0.9399	9.80	0.450
	Valeric acid			
288	1.2565	0.9430	8.82	0.590
293	1.2379	0.9386	8.82	0.590
298	1.2198	0.9342	8.82	0.590
303	1.2018	0.9298	8.82	0.590
	Isovaleric acid			
288	1.2020	0.9344	8.23	0.594
293	1.1839	0.9301	8.23	0.594
298	1.1658	0.9261	8.23	0.594
303	1.1480	0.9219	8.23	0.594
	Caproic acid			
298	1.2569[d]	0.9225	8.80	0.533
303	1.2405	0.9183	8.80	0.533
308	1.2233	0.9135	8.80	0.533
313	1.2064	0.9092	8.80	0.533
318	1.1876	0.9049	8.80	0.533

a), b), c) The values calculated from H. H. Landolt and R. Bornstein, "Physikalische Chemische Tabellen," Vol. III. Part 3. d) The sound velocities measured at 5 MHz.

$\pm 10\%$ respectively.

If one assumes that the excess absorption in a series of monocarboxylic acids is due to the same type of reaction as in the case of acetic[2] and propionic[4] acids, the general expression for this reaction type is:

$$A \underset{k_b}{\overset{k_f}{\rightleftarrows}} B$$

and:

$$K = \frac{k_f}{k_b} \tag{2}$$

$$2\pi f_{max} = k_f + k_b \tag{3}$$

where K is the equilibrium constant and where k_f and k_b are the forward and backward rate constants respectively. If it is assumed that the volume change in this reaction is zero, the relaxation heat capacities at a constant volume and pressure are represented by the equation:

$$C_p^r = C_v^r = \frac{(\Delta H)^2}{RT^2} \cdot \frac{K}{(1+K)^2} \tag{4}$$

where ΔH is the enthalpy change of reaction; T, the absolute temperature, and R, the gas constant.

The enthalpy change is calculated by means of van't Hoff's isochore:

$$\left(\frac{\partial \ln K}{\partial (1/T)}\right)_p = -\frac{\Delta H}{R} \tag{5}$$

$$K = \exp(-\Delta G/RT) \tag{6}$$

where ΔG is the free energy change of the reaction. Similarly, the temperature dependence of the rate constant is given by:

$$\left(\frac{\partial \ln k}{\partial (1/T)}\right)_p = -\frac{\Delta H^*}{R} \tag{7}$$

The activation free energy is given by the Eyring equation:

$$k = \frac{kT}{h} \exp\left(-\frac{\Delta G^*}{RT}\right) \tag{8}$$

where k is the Boltzman constant; h, the Planck constant, and ΔG^*, the activation free energy. The kinetic parameters, K, k_f, and k_b, and thermodynamic parameters, ΔH and ΔH^*, were calculated from Eqs. (2)—(6) by the same procedure as was used in a previous paper.[4] ΔG and ΔS were calculated by the relationship: $\Delta G = \Delta H - T\Delta S$. The values thus obtained are listed in Table 3. The uncertainties in K, ΔG, ΔH, ΔS, k_b, k_f, ΔH_b^*, and ΔH_f^* are approximately ± 30, ± 20, ± 20, ± 20, ± 5, ± 10, ± 10, and $\pm 20\%$ respectively.

Discussion

As can be seen in Table 3, ΔH increases monotonously with the increase in the carbon number for normal compounds, while it decreases for isocompounds. In order to explain this phenomenon quantitatively from the point of view of the structure of the alkyl group, the following Taft's[9] equation is used:

Table 3. The kinetic parameters for a series of monocarboxylic acids at 30°C

	K (10^{-2})	ΔG (kcal/mol)	ΔH (kcal/mol)	ΔS (cal/deg)	k_b (10^7/sec)	ΔH_b^* (kcal/mol)	k_f (10^5/sec)	ΔH_f^* (kcal/mol)
Acetic acid[a]	21.9	0.95	2.7	5.9	0.47	8.9	10.3	~12
Propionic acid[b]	3.3	2.0	4.3	7.3	1.7	6.8	5.9	~11
Butyric acid	3.0	2.1	4.7	8.5	1.5	5.3	4.6	~10
Valeric acid	1.4	2.5	5.4	9.3	2.7	5.5	3.9	~10
Caproic acid	1.0	2.7	5.7	9.7	2.3	6.0	2.3	~11
Isobutyric acid	0.35	3.3	6.4	9.9	5.5	5.0	1.9	~12
Isovaleric acid	0.74	2.9	6.0	10.0	3.0	5.8	2.2	~12

a), b) The values calculated from data in literatures.[2,4]

9) R. W. Taft, Jr., *J. Amer. Chem. Soc.*, **74**, 2729 (1952).

$$\log K_i = \rho^*\sigma^* + sE_s \quad (9)$$

where K_i is the rate constant or equilibrium constant; σ^*, the polarity parameter, and E_s, the steric parameter. ρ^* and s are proportionality constants and depend only on the type of reaction. The plots of log K against σ^* and E_s are represented in Figs. 7 and 8 respectively, where for the values of σ^* and E_s those found in the literature are used.[9,10] It can be seen in the figures that log K changes linearly with σ^*, while no simple relationship is found between log K and E_s. The value of ρ^* calculated from the plot is 13.8. From this fact and the linearity between log K and ΔH, as can be seen in Fig. 9, it can be deduced that the difference in the ΔH values of the series of monocarboxylic acids is due to variations in the polarity effect of each alkyl group in the molecules. A combination of Figs. 7 and 8 shows that ΔH increases

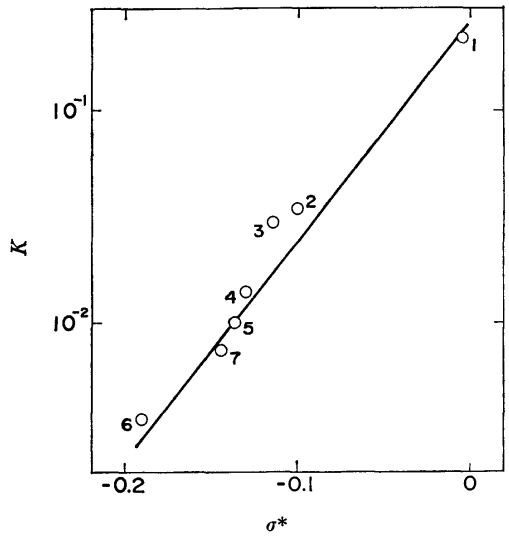

Fig. 7. The plot of ln K against σ^* for a series of carboxylic acids. Hereafter numbers denote the acids as (1), acetic; (2), propionic; (3), butyric: (4), valeric; (5), caproic; (6), isobutyric; and (7), isovaleric acids.

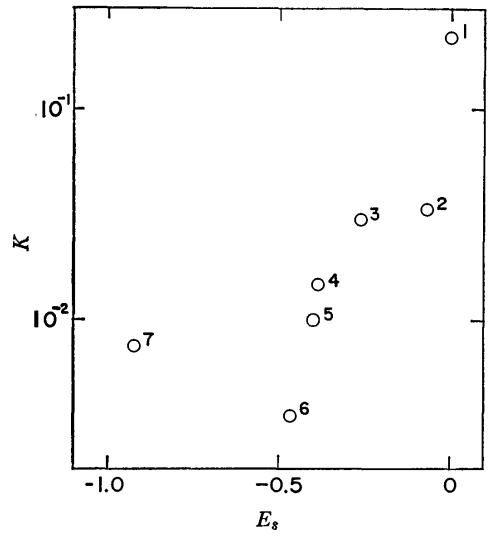

Fig. 8. The plot of ln K against E_s.

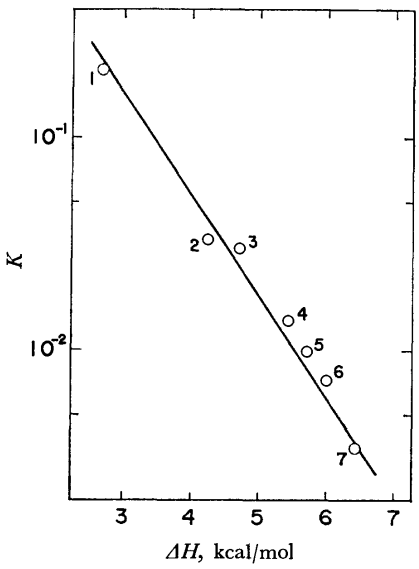

Fig. 9. The plot of ln K against ΔH.

with the strength of the polarity effect, *i.e.*, with the decrease in σ^*. The values of ΔH are in the range of 4.7—6.4 kcal per mole of dimer; this finding is consistent with the fact that these values are those of the breaking of one hydrogen bond, and there is a linear relationship[11] between σ^* and the inductive effect of the alkyl group on the carboxyl group. From these

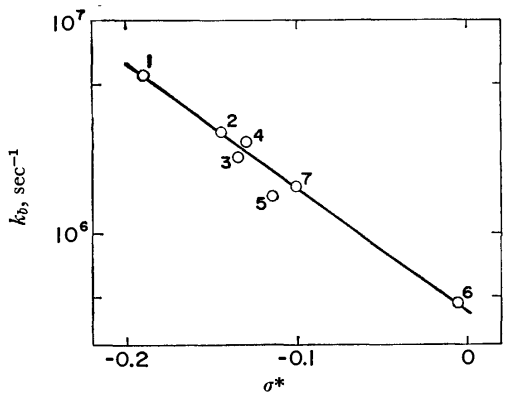

Fig. 10. The plot of ln k_b against σ^*.

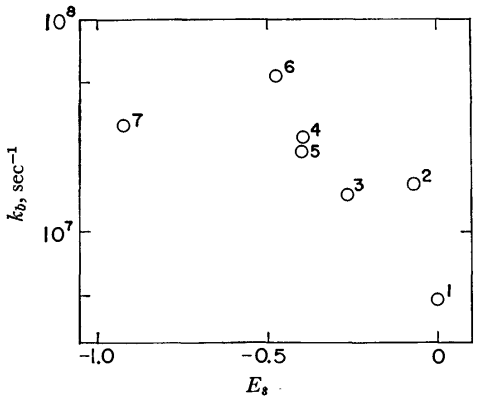

Fig. 11. The plot of ln k_b against E_s.

10) R.W. Taft, Jr., *J. Amer. Chem. Soc.*, **75**, 4538 (1953).

11) M. Chiang and T. Tai, *Scientia Sinica*, **12**, 785 (1963).

results, it can be concluded that the electron density of the carboxyl group increases with the increase in the inductive effect, so the hydrogen bond becomes more stable in the cyclic dimer than in the open dimer.

The relationships between the rate constant and the values of σ^* and E_s, are shown in Figs. 10 and 11, where the plot of $\log k_b$ against σ^* gives a straight line; no such relationship exists between $\log k_b$ and E_s, however the value of ρ^* calculated from the plot is -7.90. The change in ΔH_b^* cannot, however, be ascribed to the polarity effect, as can be seen in Table 3, where there exists no simple relationship between $\log k_b$ and ΔH_b^*.

As can be seen in Table 3, the ΔH_b^* values of acetic and propionic acids are greater than those of other acids. The abnormal ΔH_b^* values of these two acids may be ascribed to the formation of the polymer, as has been suggested by a study[12] of sound velocity and dipole moment. The liquid contains some linear polymer, and some excess energy is required to break the hydrogen bonds of the polymer.

From the above discussion, it may reasonably be concluded that the excess absorptions in the series of monocarboxylic acids are all associated with the perturbation of the equilibrium between the open dimer and the cyclic dimer, and that the cyclic dimer becomes more stable because of the inductive effect of the alkyl group, which increases the electron density in the carboxyl group.

More extensive measurements may be desirable to confirm the inductive effect mentioned above. A study of halogeno carboxylic acids is now in progress; the results will be reported.

12) M. Blinc and R. Blinc, *J. Polym. Sci.*, **32**, 506 (1958).

BULLETIN OF THE CHEMICAL SOCIETY OF JAPAN, VOL. 45, 2673—2677 (1972)

Kinetic Studies of Intermolecular Hydrogen Bonding in Carboxylic Acids by Means of Ultrasonic Absorption Measurement. II. Halogeno Carboxylic Acids

Takayuki SANO, Nobuhide TATSUMOTO, Yukio MENDE, and Tatsuya YASUNAGA

Department of Chemistry, Faculty of Science, Hiroshima University, Higashisenda-machi, Hiroshima

(Received December 21, 1971)

The ultrasonic absorptions in several halogeno carboxylic acids, such as monochloroacetic, dichloroacetic, trichloroacetic, trifluoroacetic, α-chloropropionic, and β-chloropropionic acids, have been measured in the frequency range from 2.5 to 95 MHz. Excess absorptions were observed in all the acids. The kinetic and the thermodynamic parameters based on the equilibrium between the open dimer and the cyclic dimer were calculated. An application of Taft's equation, $\log K=\rho^*\sigma^*+sE_s$, to the results suggests that neither the equilibrium constant nor the rate constant depends on the polarity effect of the alkyl group, but depends mainly on the steric effect, and that the reaction is controlled not only by the enthalpy change, but also by the entropy change.

In a previous paper[1] the mechanism of the ultrasonic absorption in the fatty acids has been attributed to a perturbation of the equilibrium between the cyclic dimer and the open dimer:

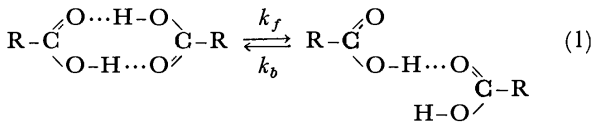

(1)

In view of the kinetic and thermodynamic characteristics based on the above reaction for a series of fatty acids, it has been concluded that the cyclic dimer becomes more stable because of an increase in the electron density in the carboxyl group with an increase in the inductive effect of the alkyl group. Since this conclusion has been deduced from the results for the fatty acids with only the hydrocarbon in the alkyl group, more extensive studies seemed desirable. The present study was undertaken in an attempt to confirm more completely this effect for some halogeno carboxylic acids with the help of ultrasonic absorption measurements. Because some halogeno carboxylic acids such as dichloroacetic acid[2] are occasionally used as the solvents of biopolymers, it seemed worthwhile to measure the ultrasonic absorption in halogeno carboxylic acids in order to understand the more complex biochemical and solvent interaction reactions.

Experimental

A pulse technique[3] was used to measure the ultrasonic absorptions in the liquid halogeno carboxylic acids, such as monochloroacetic, dichloroacetic, trichloroacetic, trifluoroacetic, α-chloropropionic, and β-chloropropionic acids, together with trimethylacetic acid in the frequency range from 2.5 to 95 MHz. The velocity of the sound was measured by an ultrasonic interferometer[4] operated at 3.0 MHz and

1) T. Sano, N. Tatsumoto, T. Niwa, and T. Yasunaga, This Bulletin, **45**, 2669 (1972).

2) G. Schwarz, *Ber. Bunsenges. Phys. Chem.*, **68**, 834 (1964).

3) N. Tatsumoto, *J. Chem. Phys.*, **47**, 4561 (1967).

4) T. Yasunaga, H. Oguri, and M. Miura, *ibid.*, **43**, 3512 (1965).

by the sing-around method[5] at 1.92 MHz. In order to observe the dependence of the relaxation frequency, the excess absorption, and other physical properties on the temperature, measurements were made at various temperatures over the melting point: monochloroacetic, 66.3, 70, 74, and 78°C; dichloroacetic, 20, 25, 30, 35, and 40°C; trichloroacetic, 65.4, 69.1, 73, and 77°C; trifluoroacetic, 15, 20, 25, and 30°C; α-chloropropionic, 20, 25, 30, 35, and 40°C; β-chloropropionic, 45, 50, 55, and 60°C; and trimethylacetic acids, 40 and 45°C. All the compounds are deliquescent, so the ultrasonic cell was designed to maintain a sample liquid in an inert and dry atmosphere. The densities were measured by a pycnometer, and the heat capacities, by an adiabatic-type calorimeter. The chemicals used were all of a guaranteed grade and were used without further purification.

Results

The ultrasonic absorption spectra for the monochloro-, dichloro-, trichloro-, trifluoro-, trimethylacetic, α-chloropropionic, and β-chloropropionic acids are shown in Fig. 1. In all these acids except the trimethylacetic acid, excess absorptions were observed. The relaxation spectra can all be represented by a single relaxation formula:

$$\frac{\alpha}{f^2} = \frac{A}{1+(f/f_{max})^2} + B \qquad (2)$$

where α is the ultrasonic absorption coefficient, f is the frequency of sound, f_{max} is the relaxation frequency, and A and B are the excess and classical absorptions respectively.

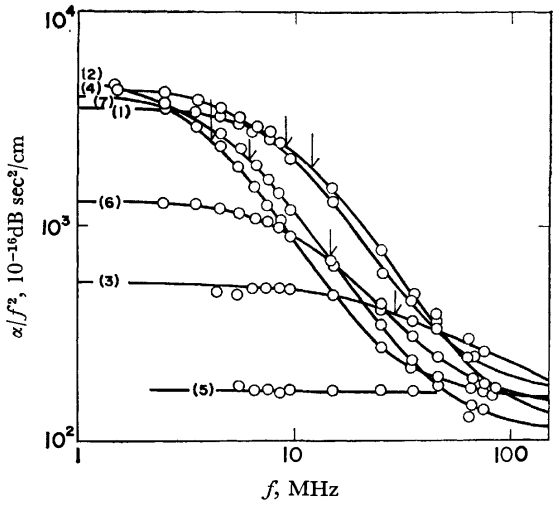

Fig. 1. Ultrasonic absorption spectra in some carboxylic acids: (1): monochloroacetic, 66.3°C; (2): dichloroacetic, 25°C; (3): trichloroacetic, 65°C; (4): trifluoroacetic, 30°C; (5): trimethylacetic, 40°C; (6): α-chloropropionic 25°C; and (7): β-chloropropionic acids, 50°C.

A least-squares computer program is routinely used to evaluate the three parameters, A, B, and f_{max}. The uncertainties in A, B, and f_{max} are approximately ±10, ±5, and ±5% respectively. These values are

5) T. Yasunaga, N. Tatsumoto, and M. Miura, This Bulletin, **37**, 1655 (1964).

TABLE 1. THE ACOUSTICAL CHARACTERISTICS OF HALOGENO CARBOXYLIC ACIDS AT THE VARIOUS TEMPERATURES

T (°K)	f_{max} (MHz)	A (10^{-16} dB·sec^2 cm^{-1})	B	$(\alpha'\lambda)_{max}$ (10^{-1} dB)
		Monochloroacetic acid		
339	12	3550	110	2.58
343	14	3301	100	2.77
347	16	2907	110	2.76
351	18	2618	100	2.77
		Dichloroacetic acid		
293	3.3	5300	165	1.10
298	4.1	4800	155	1.23
303	5.0	4400	140	1.36
308	6.1	3900	123	1.46
313	7.5	3500	120	1.60
		Trifluoroacetic acid		
288	6.5	4980	240	1.14
293	7.3	4571	220	1.15
298	8.1	4240	220	1.16
303	9.0	4293	164	1.27
		α-Chloropropionic acid		
293	12	1250	162	0.915
298	14.5	1150	145	1.00
303	17	1050	130	1.06
308	20	960	115	1.13
313	23	890	95	1.19
		β-Chloropropionic acid		
318	5.5	4400	130	1.51
323	6.0	4100	110	1.52
328	6.7	3950	110	1.61
333	7.3	3670	110	1.62

TABLE 2. THE THERMODYNAMIC PARAMETERS FOR THE HALOGENO CARBOXYLIC ACIDS

T (°K)	u (10^5 cm sec^{-1})	ρ (g cm^{-3})	l (10^{-4} deg^{-1})	C_p^0 (cal g^{-1}· deg^{-1})
		Monochloroacetic acid		
339	1.2117	1.4043	9.670	0.479
343	1.2009	1.3982	9.670	0.479
347	1.1901	1.3921	9.670	0.479
351	1.1793	1.3860	9.670	0.479
		Dichloroacetic acid		
293	1.2682	1.2963	9.780	0.382
298	1.2556	1.2902	9.780	0.382
303	1.2433	1.2841	9.780	0.382
308	1.2321	1.2780	9.780	0.382
313	1.2213	1.2720	9.780	0.382
		Trifluoroacetic acid		
288	0.7074	1.5031	7.219	0.464
293	0.6918	1.4905	7.219	0.464
298	0.6762	1.4788	7.219	0.464
303	0.6606	1.4670	7.219	0.464
		α-Chloropropionic acid		
293	1.2201	1.5633	6.469	0.350
298	1.2076	1.5583	6.469	0.350
303	1.1941	1.5535	6.469	0.350
308	1.1793	1.5486	6.469	0.350
313	1.1654	1.5436	6.469	0.350
		β-Chloropropionic acid		
318	1.2482	1.1822	10.25	0.555
323	1.2343	1.1776	10.25	0.555
328	1.2201	1.1730	10.25	0.555
333	1.2061	1.1684	10.25	0.555

listed in Table 1. On the other hand, in the trimethylacetic acid the value of α/f^2 remains constant at 165×10^{-16} dB sec^2/cm in the frequency range from 3.5 to 85 MHz, and the temperature dependence of the excess absorption in the trichloroacetic acid can not be measured because of the high relaxation frequency. The other values required for the calculation of the kinetic and thermodynamic parameters (*e.g.*, the sound velocity, u; the density, ρ; the thermal expansion coefficient, l, and the heat capacity at a constant pressure, C_p) are listed in Table 2. The experimental errors in u, ρ, l, and C_p are approximately ±0.01, ±0.05, ±0.5, and $\pm10\%$ respectively.

If the same type of reaction, which does not accompany any volume change, as that reported previously in the case of the fatty acids is considered to be the origin of the excess absorptions in the acid studied in this report, the reaction type can be given by:

$$A \underset{k_b}{\overset{k_f}{\rightleftarrows}} B \tag{3}$$

and the kinetic and thermodynamic parameters can be given by equations:

$$K = \frac{k_f}{k_b} \tag{4}$$

$$2\pi f_{max} = k_f + k_b \tag{5}$$

$$C_v^r = C_p^r = \frac{(\Delta H)^2}{RT^2}\cdot\frac{K}{(1+K)^2} \tag{6}$$

$$K = \exp(-\Delta G/RT) \tag{7}$$

$$\Delta G = \Delta H - T\Delta S \tag{8}$$

$$\frac{\partial \ln (k_i/T)}{\partial(1/T)} = -\frac{\Delta H_i^*}{R} \tag{9}$$

where K is the equilibrium constant, and where k_f and k_b are the forward and backward rate constants respectively. C_v^r and C_p^r are the relaxation heat capacities at a constant volume and a constant pressure respectively. ΔH is the heat of reaction; ΔG, the free energy, and ΔS, the entropy of reaction. k_i represents k_f or k_b, and ΔH_i^* is the heat of activation. The kinetic and thermodynamic parameters were calculated from Eqs. (4)—(9). However, the kinetic values, such as K, k_f, and k_b, cannot be compared directly with those of other cmpounds because the measurements had to be done at various temperatures over the melting point. Consequently, the kinetic parameters at 30°C are estimated by extrapolations of K, k_f, and k_b respectively *vs.* the temperature; they are listed in Table 3. The errors are approximately $\pm20\%$ in K, ΔG, ΔH, and ΔS, ±5 and $\pm10\%$ in k_b and ΔH_b^*, and ±10 and $\pm20\%$ in k_f and ΔH_f^*.

Discussion

As can be seen in Fig. 1, the halogeno carboxylic acids studied in the present paper show an ultrasonic absorption similar with regard to the position of the relaxation frequency and the magnitude of B to that in the fatty acids reported in the previous paper. This suggests that the ultrasonic absorptions in the halogeno carboxylic acids are associated with the same type of reaction as in the fatty acids.

In order to confirm the polarity effect of the alkyl group on Reaction (1), the following Taft's equation was used:

$$\log K_i = \rho_i^*\sigma^* + s_iE_s \tag{10}$$

where K_i is the rate constant or equilibrium constant, where σ^* and E_s are the polarity and steric parameters respectively, where ρ_i^* and s_i are the proportionality constants and depend only on the type of reaction, and where the subscript i represents K or k_b. The plots of $\log K$ against σ^* and E_s are represented in Figs. 2 and

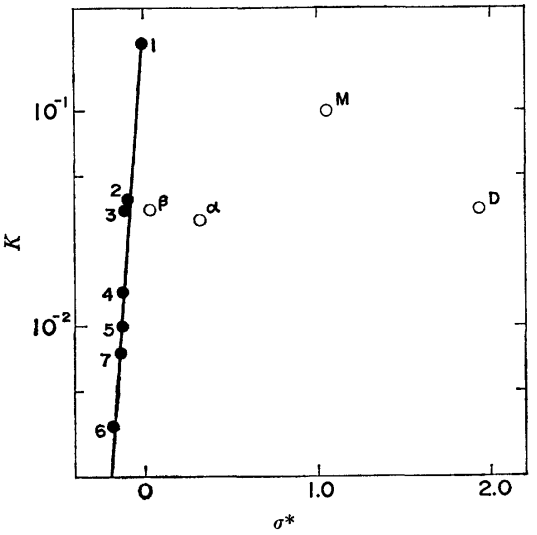

Fig. 2. The plot of ln K against σ^* for a series of carboxylic acids along with the aliphatic acids. Symbols identify the compounds corresponding to individual point as follows: (1): acetic; (2): propionic; (3): butyric; (4): valeric; (M): monochloroacetic; (D): dichloroacetic; (T), trifluoroacetic; (α): α-chloropropionic; and (β): β-chloropropionic acids. These symbols are used in the same way hereafter.

Table 3. The kinetic parameters for a series of carboxylic acids at 30°C

	K (10^{-2})	ΔG (kcal/mol)	ΔH (kcal/mol)	ΔS (cal/deg)	k_b (10^7/sec)	ΔH_b^* (kcal/mol)	k_f (10^5/sec)	ΔH_f^* (kcal/mol)
Acetic acid[a)]	21.9	0.95	2.7	5.9	0.47	8.9	10.3	~12
Monochloroacetic acid	9.8	1.4	2.9	4.9	1.4	7.1	11.5	~10
Dichloroacetic acid	0.75	1.5	3.6	6.7	10	5.5	7.45	~ 9
Trifluoroacetic acid	1.7	1.0	2.9	6.0	4.8	3.4	8.2	~ 7
Propionic acid[b)]	3.3	2.0	4.3	7.3	1.7	6.8	5.9	~11
α-Chloropropionic acid	3.2	3.4	4.4	7.7	3.1	7.7	10	~12
β-Chloropropionic acid	3.5	2.0	3.9	6.3	2.6	3.9	9.1	~11

a), b) The values calculated from data in leteratures.

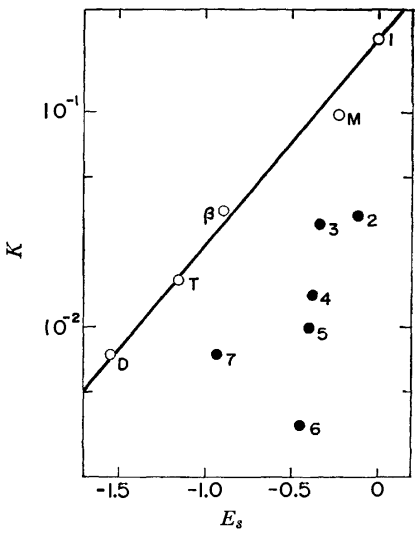

Fig. 3. The plot of ln K against E_s.

3 respectively, along with that of the fatty acids obtained in the previous report. The values of σ^* and E_s are found in the literature.[6] In Fig. 2, it can be seen that the relationship between log K and σ^* is linear in the case of the fatty acids, but is not linear in that of the halogeno carboxylic acids. With respect to the relationship between log K and E_s in Fig. 3, the halogeno carboxylic acids give a better straight line than the fatty acids. The value of s_K for the equilibrium constant calculated from the plot is 0.954. As to the relationships between log k_b and σ^* and E_s, similar explanations can also be given from Figs. 4 and 5. The value of s_{k_b} for the rate constant is calculated to be -0.869. Therefore, it can be deduced that both K and k_b depend mainly on the steric effect of the alkyl group in halogeno carboxylic acids; this is in contrast with the case of fatty acids.

Moreover, it can be seen in Table 3 that the relationship between log K and ΔH and that between log k_b and ΔH_b^* are not linear. Though the results are unfortunately, inconsistent with our expectations with regard to the behavior of the kinetic values, the difference may be ascribed to the large size of the halogen atom; that is, the substitution of the large halogen atoms for the hydrogen atom in the alkyl group of the acids may lead to an intermolecular steric interaction rather than to an intramolecular electrostatic effect. Because the relationship between log K and ΔS is also not linear, as can be seen in Table 3, it can be deduced that the reaction in the halogeno carboxylic acids is controlled not only by the enthalpy change, but also by the entropy change.

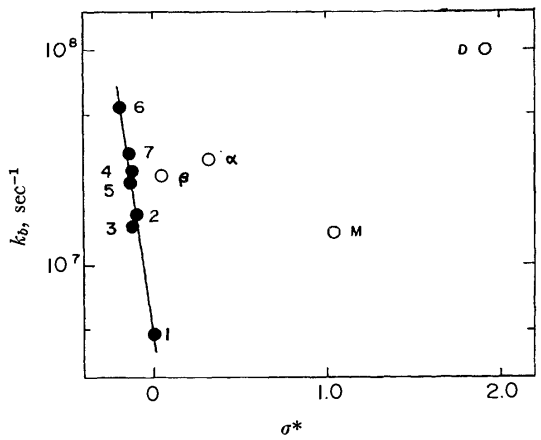

Fig. 4. The plot of ln k_b against σ^*.

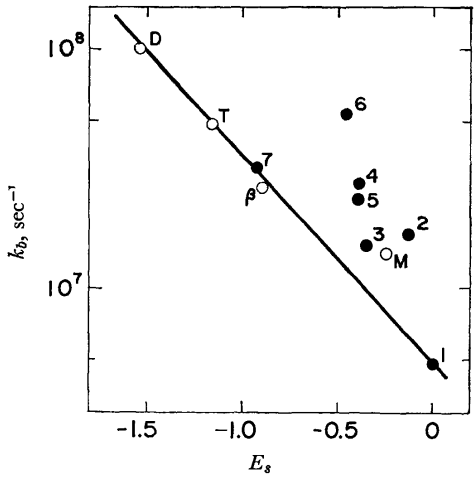

Fig. 5. The plot of ln k_b against E_s.

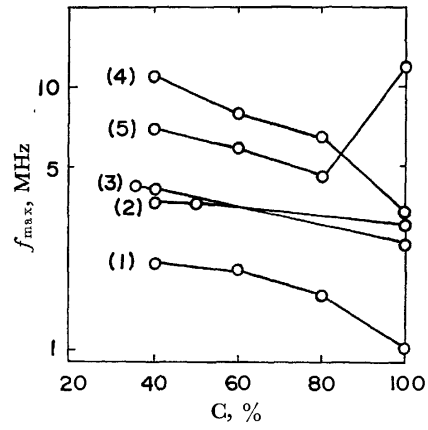

Fig. 6. The plot of the relaxation frequency against volume percent of the some carboxylic acids in dioxane solutions: (1): acetic; (2): propionic; (3): butyric; (4): dichloroacetic; and (5): α-chloropropionic acids.

In order to observe only the abnormal behavior of the relaxation frequency in solutions, ultrasonic absorption measurements were carried out in dioxane solutions of some carboxylic acids, such as acetic, propionic, butyric, dichloroacetic, and α-chloropropionic acids. The results are shown in Fig. 6. In all the acids, the relaxation frequencies shift to the higher-frequency side with a decrease in the concentration; they do this in spite of the existence of a concave point in the case of the α-chloropropionic acid. This fact may support the suggestion that the ultrasonic absorption mechanism in the halogeno carboxylic acids is the same reaction as in the fatty acids. From the above discussion and the quite recent investigations by

6) R. W. Taft, Jr., *J. Amer. Chem. Soc.*, **74**, 2729 (1952); R. W. Taft, Jr., *ibid.*, **75**, 4538 (1953).

Corsaro and Atkinson,[7,8] it is reasonable to conclude that the excess absorptions in the series of carboxylic acids studied in this and previous papers are to be attributed to the perturbation of the equilibrium between the cyclic dimer and the open dimer, and also that the reaction in the case of the halogeno carboxylic acids depends mainly on the steric effect rather than on the polarity effect of the alkyl group, and that it is controlled by both the enthalpy and the entropy changes. While it might be interesting to study the cause of the concave point in the α-chloropropionic acid, visible in Fig. 6, the investigation of such a solvent effect is beyond the scope of this discussion.

Finally, the presence of other excess absorptions is to be expected in the higher-frequency ranges over 100 MHz, because the carboxylic acids studied in this and previous papers all have similar values greater than about 100×10^{-16} dB·sec^2/cm of the classical absorption; B. Thus, the ultrasonic absorption measurements over a wider frequency range, and the interpretation of the overall absorptions, will lead to a final solution of the problem of the ultrasonic absorption in the carboxylic acids.

7) R. D. Corsaro and G. Atkinson, *J. Chem. Phys.*, **54**, 4090 (1971).

8) R. D. Corsaro and G. Atkinson, *ibid.*, **55**, 1971 (1971).

BULLETIN OF THE CHEMICAL SOCIETY OF JAPAN, VOL. 45, 2677—2683 (1972)

The Self-diffusion of Chloride Ions in Nickel Dichoride Crystallites and an Isotopic Exchange Reaction between Chlorine Gas and the Crystallites

Yoshihiro SENSUI

Institute for Atomic Energy, Rikkyo (St. Paul's) University, Yokosuka

(Received March 10, 1972)

The self-diffusion of chloride ions in the bulk of nickel dichloride crystallites was studied in the temperature range of 180—340°C in a carefully-evacuated vacuum system; the isotopic exchange reaction between gaseous chlorine and the crystallites was also studied. The activation energy for the migration of chloride ions was determined to be 1.01 eV (=23.3 kcal/mol). The exchange reaction proceeded with activation energies of 3.6 and 9 kcal/mol for the active and the less-active part of the surface first layer, 13 and 16 kcal/mol for the active and the less-active one of the second layer, and 21 kcal/mol for the third layer. (These activation energies converge to the value of the self-diffusion in the bulk.) The Θ-rule nearly holds good in the present case.[1]

The correlation between the surface reactivities of solids and the surface-structures is a very interesting theme in the field of surface science. Verwey[2] proposed that on the surface of ionic crystals, ions within the surface first layer change the degree of polarization and are displaced from the normal lattice position, in this way reducing their surface energies. Benson *et al.*[3] and Anderson and Scholz[4] extended this model by taking into consideration the relaxation of the first five layers in the crystal of alkali halides. The results of their calculation show that the several surface layers should be distorted.

The isotopic exchange reaction between crystal and gaseous molecules is one of the simplest surface reactions, and the method of this exchange reaction is very useful in the investigation of the self-diffusion of ions in crystals. Such reactions have been studied in the systems of $NaCl/Cl_2$,[5,6,10,12] KCl/Cl_2,[7,10] $RbCl/Cl_2$,[8] and KBr/Br_2.[9] Harrison and his co-workers[5] have investigated mainly the surface-exchange reaction. Barr *et al.*[9-11] and Laurent and Benard[12] have studied mainly the self-diffusion in the bulk of the crystals, while Takaishi and the present author[6-8] have studied that of chloride ions, along with the surface-exchange reaction, which shows, successively, the expected correlation between the surface structure and its reactivities of NaCl,[6] KCl,[7] and RbCl.[8] However, there have been few studies of higher valent metal halide crystals, except for the self-diffusion study of the $MnCl_2/Cl_2$ system by the present author[13] and

1) G. M. Schwab, *Advan. Catal.* **20**, 251 (1950).
2) E. J. Verwey, *Rec. Trav. Chim.*, **65**, 521 (1946).
3) G. C. Benson, P. I. Freeman, and E. Dempsey, *Advan. Chem. Ser.*, **33**, 26 (1961); *J. Chem. Phys.*, **39**, 302 (1963). G. C. Benson and T. A. Claxton, *ibid.*, **48**, 1356 (1968).
4) P. J. Anderson and A. Scholz, *Trans. Faraday Soc.*, **64**, 2973 (1968).
5) L. G. Harrison, J. A. Morrison, and G. S. Rose, "Solid/Gas-Interface" Butterworths, London (1957), p. 287. L. G. Harrison, J. A. Morrison, and G. S. Rose, *J. Phys. Chem.*, **61**, 1314 (1957). L. G. Harrison, I. M. Hoodless, and J. A. Morrison, *Discuss. Faraday Soc.*, **28**, 103 (1959). R. J. Adams and L. G. Harrison, *Trans. Faraday Soc.*, **60**, 1792 (1964).
6) T. Takaishi and Y. Sensui, *Surface Sci.*, **19**, 339 (1970).
7) T. Takaishi and Y. Sensui, *Trans. Faraday Soc.*, **63**, 1007 (1967).
8) T. Takaishi and Y. Sensui, *ibid.*, **65**, 131 (1969).
9) L. W. Barr and D. K. Dawson, "Phyiscs and Chemistry of Ceramic Surfaces, Proceeding 5 (British Ceramic Soc.)," (1965), p. 77.
10) L. W. Barr, I. M. Hoodless, J. A. Morrison, and R. Rudham, *Trans. Faraday Soc.*, **56**, 697 (1960).
11) L. W. Barr, J. A. Morrison, and P. A. Schroeder, *J. Appl. Phys.*, **32**, 624 (1965).
12) J. F. Laurent and J. Benard, *J. Phys. Chem. Solids.*, **3**, 7 (1957).
13) Y. Sensui, This Bulleitn, **45**, 359 (1972).

the qualitative studies by Willard and his co-workers.[14]

In this paper, results of a study of the exchange reaction between chlorine gas and nickel dichloride crystallites will be presented as well as the results concerning the self-diffusion of chloride ions in the crystallites. This material was chosen for a reason similar to that in the case of manganese dichloride; that is, it is relatively easy to handle because of its layer structure, its relatively low volatility, and its surface homogeneity, presumed from the results of the krypton adsorption study by Larher[15] and from the electron-microscopic data (Fig. 1).

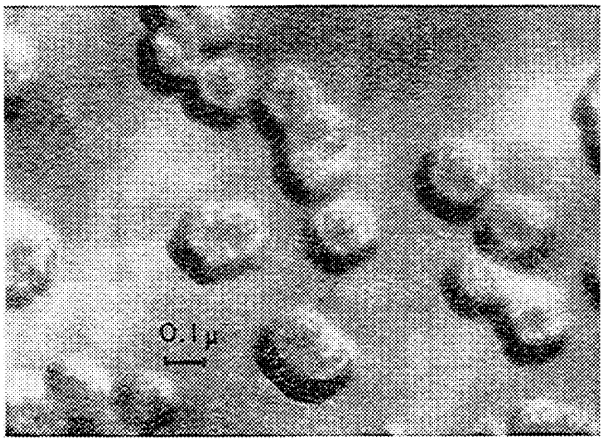

Fig. 1. The external shape of nickel dichloride crystallites used in the present experiment.

Experimental

Procedure. The apparatus used was the same as that described in the previous papers.[6-8] The system was all made of glass, except for two pieces of Teflon stopper in the circulation pump. The sample was dehydrated by baking at 60°C for about 10 hr in a vacuum. Then, the temperature was gradually raised to 200°C over 3 hr and kept at that temperature for about 7 hr. After this pre-baking, the system was sealed off from the main pumping line and thus made grease-free. Baking out at a temperature higher than 200°C was carried out with a Vac-Ion pump, which was isolated when the residual pressure was below 5×10^{-7} torr during the baking of the sample at 340°C.

Chlorine gas of a purity of 99.8%, contained in a glass cylinder (supplied from Takachiho Chemical Co.), was distilled and dehydrated by means of Linde-3A Molecular Sieves. The latter had been baked out prior to use in a vacuum of 5×10^{-7} torr at 400°C. This is a necessary procedure.[7] In the sealed-off vacuum system, purified chlorine gas was introduced, through a breakable seal, into a system containing carefully baked-out radioactive nickel dichloride crystallites. The reaction was followed by measuring the radioactivity of ^{36}Cl in gaseous chlorine, which was circulated by means of a circulation pump made of glass.[15] A thin-wall G.M. counter in a part of the system had a counting efficiency of 3% against 0.714 MeV γ-ray from ^{36}Cl.

Materials. Radioactive nickel dichloride was obtained by the isotopic-dilution method from radioactive hydrochloric acid which had been distilled in a vacuum and from nickel dichloride which had been prepared by a reaction between nickel sponge (Johnson-Matthey's spectrographically-standardised reagent, catalog No. J.M. 891) and distilled hydrochloric acid. The specific radioactivity of the resultant radioactive nickel dichloride was 5.2 μc/g. The precipitates of the radioactive dichloride were prepared by modifing Marshall's method[17] *i.e.*, by adding about 100 parts of distilled ethyl ether to one part of a saturated alcoholic solution of the dichloride. After the supernatant solution had been replaced with ethyl ether, the precipitates were transferred into the vacuum system. The crystallites were obtained by baking them out carefully by means of the procedure described above. The crystallites thus obtained have an even-grained external shape, as is shown in Fig. 1 and by the BET surface area of 26 m^2/g, which agrees with the geometric area calculated from the electron-microscopic data. This means that the crystallites are non-porous and that the roughness-factor of the surface is approximately unity.

Results and Discussion

Self-diffusion of Chloride Ions in the Bulk of the Crystallites. In the crystal of nickel dichloride with a $CdCl_2$ structure, chlorine atoms are arranged in cubic closest-packing, and a nickel atom occupies an octahedral hole made up of chlorine atoms, forming a sandwich-like layer of Cl–Ni–Cl, consisting of two adjacent layers of chlorine atoms with a layer of nickel atoms between them. Since the primary valencies of the nickel and chlorine atoms are satisfied within the sandwich-like layer, there being only van der Waals forces between adjacent layers, this may be regarded as a semi-infinite two-dimensional molecule in a first approximation.[18] However it should be mentioned that there may be some influences of nickel atoms on the configuration of adjacent chlorine layers, because of the cubic close-packed arrangement taking place in nickel dichloride crystals. Therefore, only on the basis of the structure of the crystal, we cannot predict that an anion vacancy migrates predominantly in either direction, either along or beyond the sandwich-like layer in the bulk of the crystal, by exchanging its site with the chlorine atom's. In the following paragraph, the experimental results on the self-diffusion of ^{36}Cl in the bulk of nickel dichloride crystallites will be described in some detail.

The mean length of the shorter sides of the crystallites used was estimated to be 0.06 μ from the electron-microscopic data (*cf.* Fig. 1); this corresponds to a few hundred layers in the direction along the *c*-axis of the crystal. In the present experiments, only the ^{36}Cl in the bulk of the near-surface region diffuses out into the gaseous phase and was measured; the region corresponds to less than 30 layers. Therefore, the diffusion data obtained may be analyzed on the basis of the model of semi-infinite media as a first approximation. For this model, the diffusion equation has the solution;[19]

14) M. Blau, W. T. Carnall, and J. E. Willard, *J. Amer. Chem. Soc.*, **74**, 5762 (1952). R. A. Howald and J. E. Willard, *ibid.*, **77**, 2046 (1955). J. R. Wilson and J. E. Willard, *J. Phys. Chem.*, **70**, 1665 (1966).
15) Y. Larher, *ibid.*, **72**, 1847 (1968).
16) T. Takaishi, *Shokubai (Catalyst)*, **9**, 127 (1967).
17) F. G. Marshall, *Phys. Rev.*, **58**, 642 (1940).
18) A. F. Wells, "Structural Inorganic Chemistry" Oxford University Press, Third Edition (1962).
19) A. B. Lidiard and K. Thermaligam, *Discuss. Faraday Soc.*, **28**, 64 (1959).

$$X_g = X_s + 2\alpha(Dt/\pi)^{1/2}$$

where X_g designates the amount of ^{36}Cl diffused out into the gaseous phase after time t; X_s that of ^{36}Cl in the surface region which diffused out into the gaseous phase at the initial stage of the reaction; D, the bulk diffusion constant, and α, the product of the surface area and the initial concentration of ^{36}Cl. Denoting the measured counting rate by C, we obtain;

$$C = K \cdot X_g \text{ and } C_s = K \cdot X_s,$$

where K is the conversion factor. Thus we obtain;

$$C = C_s + \frac{2\alpha}{K}(Dt/\pi)^{1/2}$$

in which the value for C_s cannot be obtained directly from the experiments. The exchange process, it is expected, may be rate-controlled by the bulk-diffusion, and the curve of C against $\sqrt{t}$ may be linear, except in the initial stage. However, there are some ambiguities with regard to the start of the reaction. The measured time t must be corrected; namely, it is replaced by $(t+\delta)$, where the value for δ is determined empirically so as to give a linear curve. The results are given in Fig. 2, which the intersection of the straight line with the ordinate gives the value for C_s.

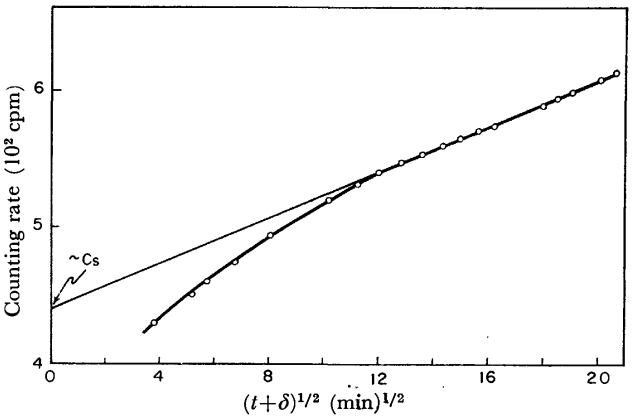

Fig. 2. The plots of C against the square-root of $(t+\delta)$. The data obtained from the specimen II at 180°C.

Next, we suppose that a first diffusion run is carried out at a temperature, T_1, for time t_1, in which the diffusion constant is D_1. If a second run is made at another temperature, T_2, for time t_2, in which the constant is D_2, the total counting rate, C, may be shown by;[19]

$$C = C_s + \frac{2\alpha}{K\sqrt{\pi}}(D_1t_1 + D_2t_2)^{1/2}.$$

This may be extended to further runs and be rewritten as follows;

$$(C - C_s)^2 = \left(\frac{4\alpha^2}{\pi K^2}\right)(D_1t_1 + D_2t_2 + \cdots).$$

The values of $(C-C_s)^2$ thus obtained are plotted against the time in Fig. 3.

The measured points fit well on the straight lines. If the crystallites had a large number of dislocations along which diffusion proceeded much faster, or it concomitant diffusions with different rate constants

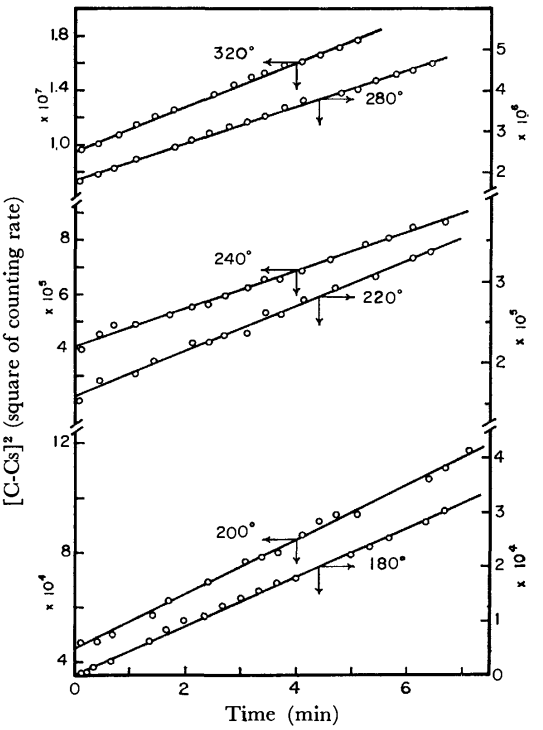

Fig. 3. The plots of $(C-C_s)^2$ against time. All of data in this figure are obtained from the specimen II.

proceeded, complex curves would be obtained; that is, the plots of $(C-C_s)^2$ against the time would not fit on a straight line when the temperature was changed. This is not observed in the present case, and so it may be concluded that the model used is adequately supported experimentally. When the self-diffusion of chloride ions or anion vacancies takes place uniformly both parallel with and perpendicular to the sandwich-like layers in the bulk of the crystallites, the values of C_s correspond to the amount of ^{36}Cl within about five layers which diffused out into the gaseous phase. Moreover if the diffusion has proceeded predominantly in either direction, the value of C_s agrees with the one which corresponds to nine layers. In the case of alkali chlorides, in which the surfaces are distorted remarkably by electrostatic forces,[3] the value of C_s corresponds to five layers or so.[6-8] Since it may generally be regarded that the degree of distortion in the surface region of covalent crystals is smaller than that of the distortion of ionic crystals, the value of C_s which correlates with the surface distortion may not be larger in the former than in the latter. Therefore, it may be concluded that the diffusion in the bulk of nickel dichloride crystallites proceeds uniformly in both of the directions in the temperature range used in the present experiment, 180—340°C. This presumption is consitent with the analytical results of the exchange reaction in the surface region, which will be presented below. From the slopes in Fig. 3, the values of $(4\alpha^2/\pi K^2)D$ can be obtained. The Arrhenius plots of these values are shown in Fig. 4.

The slope in this figure gives the activation energy for the migration of ^{36}Cl, ΔE_d, in the bulk of nickel dichloride crystallites. From this experimental results, we obtain;

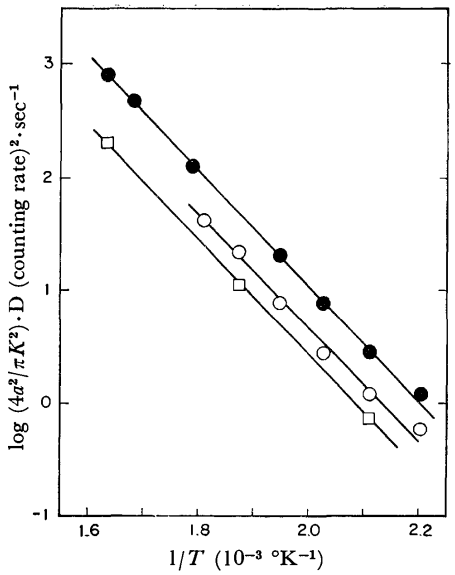

Fig. 4. The Arrhenius plots of apparent self-diffusion rates. ○, ●, and □ refer to different specimens, I, II, and III, respectively.

$$D = D_0 \exp(-\Delta E_d/kT),$$

$$\Delta E_d = 1.01 \text{ eV and } D_0 = \sim 3\times 10^{-8} \text{ cm}^2\cdot\text{sec}^{-1}.$$

Both of these values are slightly large in comparison with the corresponding values in the crystallites of manganese dichloride[13] with the same $CdCl_2$-structure, in which $\Delta E_d=0.95$ eV and $D_0=1\times 10^{-8}$ cm$^2\cdot$sec^{-1}.

The diffusion experiments in the present work were carried out in the temperature range of 180—340°C. Since ^{36}Cl in the region deeper than the near-surface region diffused out into the gaseous phase within an hour or so at temperatures higher than 340°C, the data obtained in the condition could not be analyzed on the basis of the model of semi-infinite media. No break in the Arrhenius curve was found in the present case, while one appeared obviously at about 330°C in the case of the manganese dichloride crystallites. This discrepancy may be ascribed to the narrow temperature range in which the present experiment was carried out. Hence, the present work was limited to determining the activation energy and the frequency factor of the migration of ^{36}Cl or an anion vacancy; these values for the formation of an anion vacancy or a pair of an anion and a cation vacancies were excluded.

Exchange Reaction in the Surface Region of the Crystallites. In the bulk of nickel dichloride crystallites, a stoichiometric configuration is satisfied by the octahedral coordination of chlorine atoms around a nickel atom, but on the surface the configuration can not always be satisfied. The electron-micrography of the crystallite shows that the surface of the crystal may be approximately regarded as consisting of two kinds of external planes, which are parallel with and perpendicular to the sandwich-like layers. The configuration of the chlorine atoms in the latter planes can not be satisfied by the octahedral configuration for a reason to be explained below. As a help to explanation, a bird's-eye view of the external side model of the sandwich-like layer[18] is shown in Fig. 5. Side I

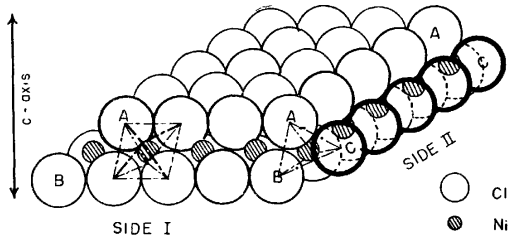

Fif. 5. A bird's-eye view of the side-model of the sandwich-like layer in nickel dichloride crystal. Chlorine atoms at the position of *A*, *B*, and *C* take the effective valencies of 1/3, 1/2, and unity, respectively.

in this figure shows a section of the octahedral configuration, in which a nickel atom is co-ordinated with three one-third-effectively-valent chlorine atoms (A) and two half-valent chlorine atoms (B).

On this side, there are no chlorine atoms at the apex positions of the octahedral structures. On the other hand, in the crystal side structure shown on Side II of Fig. 5, a nickel atom occupies a tetrahedral hole made up of an effectively uni-valent chlorine atom (C) and three one-third-valent chlorine atoms (A). It may thus be self-evident that the tetrahedral configuration shown on Side II of Fig. 5 is more stable thermodynamically than the vacant octahedral structure on Side I. Therefore, we may predict that, in the external plane perpendicular to the sandwich-like layer, chlorine atoms are arranged in a distorted tetrahedral configuration. Hence, it may be presumed that there are two kinds of domains in the first layer of the crystal surface. The ratio of these two domain areas can be estimated from the electronmicroscopic data as follows;

$$\frac{\text{(Domain I, perpendicular to the sandwich-layer)}}{\text{(Domain II, parallel with the sandwich-layer)}} = \frac{0.8}{1}.$$

The distortion appearing in the first layer of the surface may influence the configuration of the second layer. Hence, it should be considered that there are two kinds of parts in the second layer of the surface, much as in the first layer.

Below, the exchange reactions in the surface region will be analyzed kinetically on the basis of the conditions described above. The surface of nickel dichloride crystallites is highly reactive for chlorine gas; this situation is similar to that with the crystallites of alkali chlorides—that is, gaseous chlorine exchanges with chlorine atoms in the first layer of the surface, even at −21.2°C, and the exchange reaction between the first and the second layers at room temperature takes place rather gradually, as shown in Fig. 6.

Let C and $2C(s)$ be the counting rate at time t and at saturation respectively. Then, we can calculate the value of $C(s)$ from the surface area of the crystallites and the specific radioactivity of the chlorine atoms, if we assume that all of the ^{36}Cl atoms in the first and second layers are transferred into the gaseous phase. [This assumption is valid, since the chlorine atoms in the gaseous phase are about 500 times more than those in the surface monolayer of the crystallites, and the reverse reaction from the phase to the crystal may be neglected.] The calculated values of $C(s)$ are in

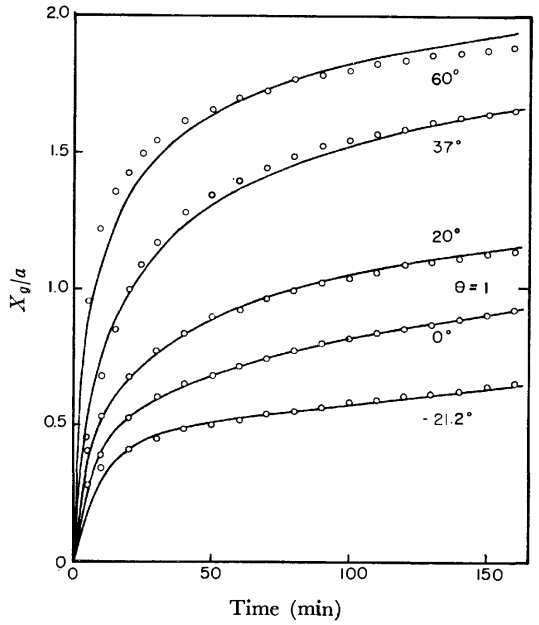

Fig. 6. Counting rates against time curve for the first and the second layer reaction. The line $\theta=1$, designates the monolayer capacity: Solid curves show the values calculated from Eq. (2).

good agreement with those from the measurement of the exchange reaction.

The initial portion of the curve at low temperatures can be analyzed tentatively without taking the second layer into consideration. Now, let us assume that there is a considerable difference between the reactivities of the two domains in the crystal surface. The plots of $\log[1-C/C(s)]$ against the time are shown in Fig. 7. These curves are graphically analyzed in a manner similar to the treatment of the decay of a mixture of radio-isotopes.

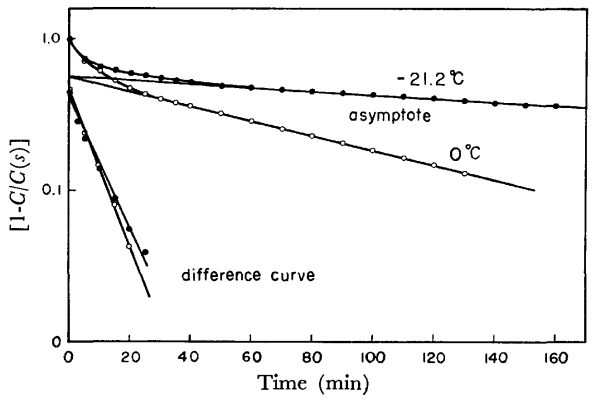

Fig. 7. The plots of log $[1-C/C(s)]$ against time for the reaction in the first and the second layer. The points in the difference curves are calculated from the smoothed experimental curves and the asymptote.

The asymptotes to the tail of the experimental curves give the curves of the relative counting rate against the time referred to the least relative part of the first layer. The difference between the experimental curve and the asymptote is shown as a difference curve, which is approximately linear. The intercepts of the asymptote and the difference curve with the ordinate give the relative values of the two kinds of domain area; the ratio of the active area to the less-active one has the value of 0.78—0.82, in agreement with the ratio estimated from the electron-microscopic data. The best-fitting values of the rate constants for the respective domains, $k_1(1)$ and $k_1(2)$, can be determined from the slopes of the difference curve and the asymptote. The above results indicate that the two-domains model is a good approximation. After the exchange reaction in the first and the second layers were completed at 60°C, the temperature was raised to 80°C, at which point the third-layer exchange reaction proceeded at a slow rate as shown in Fig. 9. The influence of ^{36}Cl in the third layer must be taken into consideration even in the first- and the second-layer exchange reactions at temperatures near 60°C, while the third-layer reaction may proceed at a very slow rate at that temperature.

The approximate reaction scheme is given by;

$$\begin{array}{l} \overset{k_1(1)}{\swarrow} \text{domain(1) of 1st layer} \overset{k_2(1)}{\rightleftharpoons} \text{2nd layer} \overset{k_3}{\rightleftharpoons} \text{3rd layer} \\ \qquad\quad \text{area} \propto a(1) \qquad\quad \text{area} \propto a(1) \qquad\quad \text{area} \propto a(1) \\ \text{gas} \\ \underset{k_1(2)}{\nwarrow} \text{domain(2) of 1st layer} \overset{k_2(2)}{\rightleftharpoons} \text{2nd layer} \overset{k_3}{\rightleftharpoons} \text{3rd layer} \\ \qquad\quad \text{area} \propto a(2) \qquad\quad \text{area} \propto a(2) \qquad\quad \text{area} \propto a(2) \end{array}$$

In this scheme, the reverse reaction from the gaseous phase to the solid is ignored for the reason mentioned above, and it is assumed that the rate constants for the (1) and (2) domains, $k_3(1)$ and $k_3(2)$, have the same value, k_3. The kinetic analysis, then, is given by;

$$\begin{aligned} &dX_g(j)/dt = k_1(j)x_1(j) \\ &dx_1(j)/dt = -k_1(j)x_1(j) - k_2(j)x_1(j) + k_2(j)x_2(j) \\ &dx_2(j)/dt = -k_2(j)x_2(j) + k_2(j)x_1(j) - k_3x_2(j) + k_3x_3(j) \\ &X_g + x_1(j) + x_2(j) + x_3(j) = 3a(j), \end{aligned} \tag{1}$$

and

$$X_g = \sum_{j=1}^{2} X_g(j),\ x_1 = \sum_{j=1}^{2} x_1(j),\ x_2 = \sum_{j=1}^{2} x_2(j),\ x_3 = \sum_{j=1}^{2} x_3(j),$$

$$a = \sum_{j=1}^{2} a(j),$$

where x_n designates the number of ^{36}Cl in the nth layer at time t; a, the number of ^{36}Cl contained in each layer at $t=0$; k_n, the apparent rate constant of the exchange reaction between the $(n-1)$th and the nth layers; the subscript g, the gaseous phase; and (j), the jth kind of domain.

To obtain a solution, an approximation is made;

$$x_3 = a \cdot \exp(-\lambda t),$$

where λ is the effective rate constant for the decrease in x_3. Then, using the boundary condition;

$$X_g(j) = 0, \text{ and } x_1(j) = x_2(j) = x_3(j) = a(j), \text{ at } t = 0,$$

we obtain the solution;

$$\begin{aligned} \frac{X_g(j)}{a(j)} = {} & \frac{k_1(j)}{\rho_+(j)\rho_-(j)}\left\{\frac{k_2(j)k_3}{\lambda} - \rho_+(j) - \rho_-(j) - k_1(j)\right\} \\ & - \frac{k_1(j)k_2(j)k_3}{\lambda[\lambda+\rho_+(j)][\lambda+\rho_-(j)]}\exp(-\lambda t) \\ & - \frac{k_1(j)}{\rho_+(j)[\rho_+(j)-\rho_-(j)]}\left\{\rho_-(j) + k_1(j)\right. \end{aligned}$$

$$-\frac{k_2(j)k_3}{\lambda+\rho_+(j)}\Big\}\exp[\rho_+(j)t]$$
$$-\frac{k_1(j)}{\rho_-(j)[\rho_-(j)-\rho_+(j)]}\Big\{\rho_+(j)+k_1(j)$$
$$-\frac{k_2(j)k_3}{\lambda+\rho_-(j)}\Big\}\exp[\rho_-(j)t]$$

with;

$$2\rho_\pm = -\{[k_1(j)+2k_2(j)+k_3] \pm [k_1(j)^2+4k_2(j)^2+k_3^2-2k_1(j)k_3]^{1/2}\}. \quad (2)$$

By a comparison of Eq. (2) with the experimental curves, the best-fitting values for $k_1(j)$, $k_2(j)$, and k_3 are determined with the aid of an electronic computer. The experimental results are well described by the theory, as is shown in Fig. 6. The Arrhenius plots of $k_1(j)$ and $k_2(j)$ are given in Fig. 8; from them, the activation energies for the exchange reaction can be obtained: 3.6 kcal/mol (=0.16 eV) for the active part of the first layer, 9 kcal/mol (=0.39 eV) for the less-active one, 13 kcal/mol (=0.57 eV) for the active part of the second layer, and 16 kcal/mol (=0.68 eV) for the less-active one.

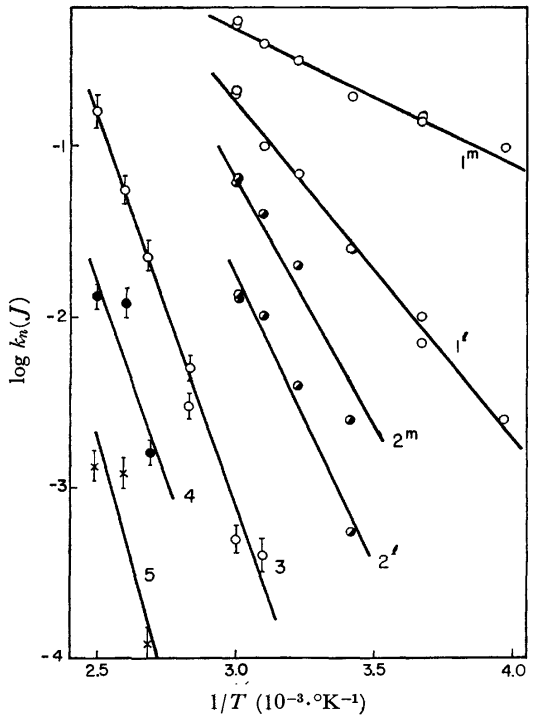

Fig. 8. The Arrhenius plots of the rate constants. The rate constants are given in units of min^{-1}; the numbers in this figure designate the layer's number; the superscripts for number 1 and 2, *m* and *l*, mean the active and the less-active domain, respectively.

In the second-layer exchange reaction, the values of the activation energies are close to each other between the active and less-active parts, and those of the rate constants for the respective parts approach one another with an increase in the temperature. From these results, we may assume that the exchange reaction in the inward layers deeper than the second layer proceeds at rates approximately equal between the two domains. From this point of view, the results of the exchange reaction in these layer may be analyzed as follows.

Since the rate of reaction in the third layer is much lower than that in the second, in analyzing the reaction in the inner layers exceeding the second, it may be assumed that the distribution of ^{36}Cl is in equilibrium between the gaseous phase and the first and second layers. The rates of the reaction in the fourth and fifth layers are similar to the rate in the third; hence, the successive reaction in these layers must be considered. A preliminary analysis of the initial stage of reaction in the third layer showed that the third layer behaves as a uniform one; that is, no remarkable difference in the reactions in the two domains is observed. Thus, the kinetic equation can be given by;

$$dX_g/dt = k_3x_3$$
$$dx_3/dt = -k_3x_3 - k_4x_3 + k_4x_4$$
$$dx_4/dt = k_4x_3 - k_4x_4 - k_5x_4 + k_5x_5, \quad (3)$$

and so on. To obtain a solution, an approximation is made;

$$x_5 = a\cdot\exp(-\gamma t),$$

where γ is an effective rate constant for the decrease in x_5. Then, using the boundary conditions;

$$X_g = 0, \text{ and } x_3 = x_4 = x_5 = a, \text{ at } t = 0,$$

we obtain a solution analogous with Eq. (2);

$$\frac{X_g}{a} = \frac{k_3}{\eta_+-\eta_-}\left\{\frac{k_4k_5}{\gamma}-\eta_+-\eta_--k_3\right\}$$
$$-\frac{k_3k_4k_5}{\gamma(\gamma+\eta_+)(\gamma+\eta_-)}\exp(-\gamma t)$$
$$-\frac{k_3}{\eta_+(\eta_+-\eta_-)}\left\{\eta_-+k_3-\frac{k_4k_5}{\gamma+\eta_+}\right\}\exp(\eta_+t)$$
$$-\frac{k_3}{\eta_-(\eta_--\eta_+)}\left\{\eta_++k_3-\frac{k_4k_5}{\gamma+\eta_-}\right\}\exp(\eta_-t), \quad (4)$$

with;

$$2\eta_\pm = -\{(k_3+2k_4+k_5)\pm(k_3^2+4k_4^2+k_5^2-2k_3k_5)^{1/2}\}.$$

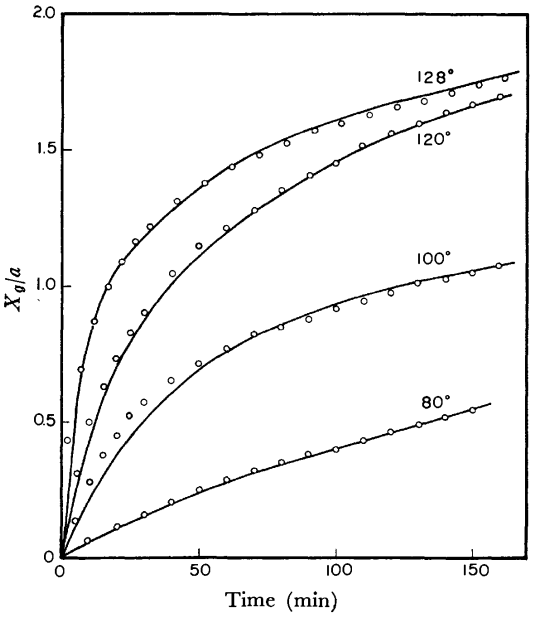

Fig. 9. Counting rates against time curve for the reaction in the third, fourth and fifth layers. Solid curves show the values calculated from Eq. (4).

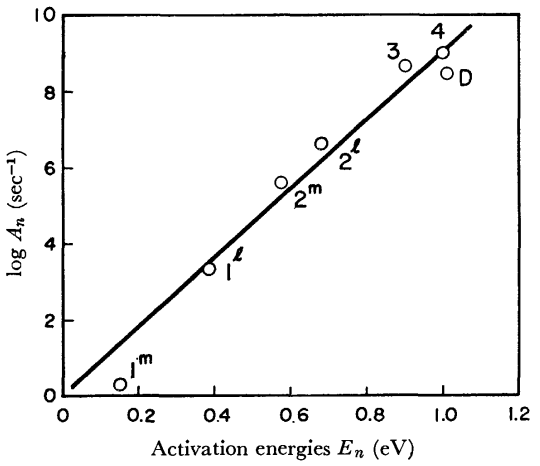

Fig. 10. Linear relationship between log A_n and ΔE_n. A_n is given in the unit of sec^{-1}.

By a comparison of Eq. (4) with the experimental curves obtained, the best-fitting values for k_3, k_4, and k_5 are determined with the aid of a computer. Most of the experimental results are well described by the theory, as is shown in Fig. 9. The Arrhenius plots of k_3, k_4, and k_5 are given in Fig. 8, from which the activation energies for the exchange reaction are obtained: 21 kcal/mol (=0.9 eV) for the third layer and about 23 kcal/mol (=1 eV) for the fourth layer, with some ambiguity.

The actifation energies of the exchange reaction in the surface region converge with that of the self-diffusion in the bulk of nickel dichloride crystallites. This is similar to the previous results on alkali chlorides,[6-8] while the properties of the crystal are remarkably different between nickel dichloride and alkali chlorides.

The relation between the diffusion coefficient, D, and the rate constant, k_d, is given by $D=\frac{1}{2}k_d l^2$, where k_d is the number of jumps per unit time, and l, the distance of a jump. Experssing k_d and k_n in the form $k=A\cdot\exp(-\Delta E/\boldsymbol{k}T)$, we obtain a linear relationship between log A_n and ΔE_n, as is shown in Fig. 10; that is, the Θ-rule holds nearly entirely good in the present case, as in many rate processes.[1]

The present author's sincere thanks are due to Professor T. Takaishi of Rikkyo University for his valuable discussions and to Dr. A. Nakamoto of Rikkyo University for his assistance in the computer calculation.

BULLETIN OF THE CHEMICAL SOCIETY OF JAPAN, VOL. 45, 2683—2687 (1972)

Mechanism of Charge-transfer Polymerization. III.[1] Flash Photolysis of *N*-Vinylcarbazole—Chloranil System

Yasuhiko SHIROTA, Kiyoshi KAWAI,* Naoto YAMAMOTO,** Kazuhiro TADA, Tadamasa SHIDA,*** Hiroshi MIKAWA, and Hiroshi TSUBOMURA**

Department of Applied Chemistry, Faculty of Engineering, Osaka University, Yamadakami, Suita, Osaka

(Received February 22, 1972)

Photochemical formation of transient *N*-vinylcarbazole cation and chloranil anion-radicals has been demonstrated by means of flash spectroscopy for the *N*-vinylcarbazole–chloranil–solvent systems. Identification and decay of the species formed by flash illumination are described.

The photochemical reaction of *N*-vinylcarbazole (VCZ) in the presence of an electron acceptor has currently been the subject of great interest. The reaction is complex involving cationic polymerization, cyclodimerization, and in certain cases radical polymerization or copolymerization with an electron-accepting monomer, the reaction course being strongly solvent dependent.[2] For example, in the system VCZ–chloranil(CA), cationic polymerization of VCZ occurs in benzene,[3] while in polar, basic solvents such as acetone, acetonitrile or methanol cyclodimerization of VCZ takes place to form *trans*-1,2-dicarbazylcyclobutane.[2,4] It has been postulated that the reaction proceeds *via* transient VCZ cation-radical formed by the photochemical electron transfer between the donor, VCZ, and an electron acceptor, and the reaction course is explained in terms of the dual reactivity, cationic and radical, of the VCZ cation-radical.[2] However, no direct evidence for the formation of ion-radical intermediates has so far been obtained.

The present study was undertaken to demonstrate the formation of VCZ cation and CA anion-radicals by means of flash spectroscopy for the VCZ–CA–

* Present address: Central Research Laboratory, Sumitomo Chem. Co., Ltd., Takatsuki, Osaka.

** Department of Chemistry, Faculty of Engineering Science, Osaka University, Toyonaka, Osaka.

*** The Institute of Physical and Chemical Research, Wako-shi, Saitama.

1) Part II: M. Fujimatsu, T. Natsuume, H. Hirata, Y. Shirota, S. Kusabayashi, and H. Mikawa, *J. Polymer Sci., Part A-1*, **8**, 3349 (1970).

2) K. Tada, Y. Shirota, S. Kusabayashi, and H. Mikawa, *Chem. Commun.*, **1971**, 1169.

3) M. Shimizu, K. Tanabe, K. Tada, Y. Shirota, S. Kusabayashi, and H. Mikawa, *ibid.*, **1970**, 1028.

4) R. A. Crellin, M. C. Lambert, and A. Ledwith, *ibid.*, **1970** 682.

solvent systems. We reported[5] on the flash photolysis of CA in various solvents, the results of which were utilized for the present analysis. Formation of VCZ cation and CA anion-radicals was confirmed and occurrence of the electron transfer in the photochemical reaction of VCZ in the presence of an electron acceptor has been verified for the first time.[6,7] VCZ cation-radical was confirmed by the radiolytic method established for the selective formation of ion-radicals.

Experimental

Materials. *N*-Vinylcarbazole (VCZ) (Nakarai Chemical Ltd., extra pure grade) was recrystallized twice from methanol, then twice from *n*-hexane and dried *in vacuo* for two or three days at room temperature, mp 65°C. Chloranil (CA) of reagent grade (Wako Pure Chemical Ind. Ltd.) was recrystallized from benzene, then passed through a column of freshly baked calcium carbonate using benzene as an eluent to remove acidic impurities,[8] and then recrystallized twice from benzene, followed by a fractional sublimation *in vacuo*. Acetone was refluxed with potassium permanganate for half a day, dried with calcium sulfate and distilled. Acetonitrile was refluxed over phosphorus pentoxide for 24 hr, distilled and then refluxed over anhydrous potassium carbonate and again distilled immediately before use. Methanol was refluxed with small amounts of sodium metal and distilled. Benzene was purified and dried in the usual way and distilled from sodium wire immediately before use. *sec*-Butyl chloride (*s*-BuCl) (Tokyo Chemical Ind. Co.) was used as received, purity being proved to be good enough for the radiolytic experiment.

Flash Spectroscopy. The concentration ranges of VCZ and CA were 2×10^{-4}—8×10^{-4}M and 1×10^{-4}—2×10^{-4}M, respectively. Freshly prepared solutions were evacuated at 10^{-5} mmHg by several freeze-pump-thaw cycles or bubbled with highly purified nitrogen gas for about 20 min to remove dissolved oxygen, and then poured into a cylindrical silica cell, 1.5 cm in diameter and 20 cm in length. The apparatus is almost the same as that described by Yamamoto *et al.*[9] The transient absorption spectra were obtained photographically with Fuji Neopan SSS film (ASA 200). A combined filter composed of a glass plate and a benzene solution of ethylcarbazole (2×10^{-4}M) was used to cut off the light of wavelength below 350 nm.

Absorption Spectroscopy of γ-Irradiated Rigid Solutions. *N*-Vinylcarbazole in *s*-BuCl was frozen at 77°K to a glassy rigid solution and γ-irradiated at the same temperature (total dose 1.6×10^{19} eV/g). The absorption appearing in the visible to near infrared region was measured with a Cary 14RI spectrophotometer. Further details of the experiment are described elsewhere.[10]

Results and Discussion

N-Vinylcarbazole forms a charge-transfer complex with CA in the ground state (λ_{CTmax} 506 nm, shoulder at 590 nm, in CCl_4). However, in the present experiment no donor-acceptor interaction in the ground state was observed because of the low concentration of the solutions, selective excitation of the acceptor, CA, thus being possible. Absorption of photoenergy by VCZ (*ca.* 2×10^{-4}M) was almost negligible in the wavelength region above 350 nm. When CA was selectively excited by the flash illumination ($h\nu>350$ nm) of a nitrogen-bubbled acetone solution containing 2×10^{-4}M VCZ and 1×10^{-4}M CA at room temperature, a transient absorption spectrum consisting of two band systems was obtained, one with a maximum at 446 nm and a shoulder at 421 nm, and the other a weak, broad band system in the region of wavelength longer than 550 nm (Fig. 1).

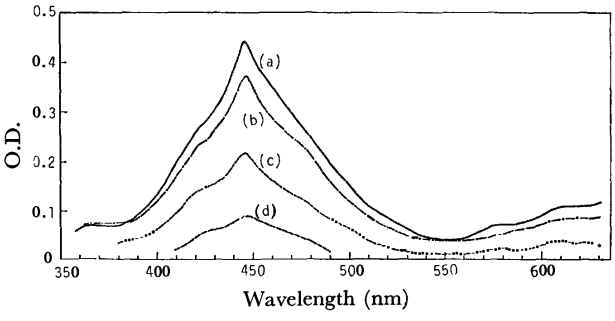

Fig. 1. The absorption spectra of transient species obtained by the flash photolysis of an acetone solution of VCZ (2×10^{-4} M) and CA (1×10^{-4} M). Delay time: (a) 3 μsec (b) 9 μsec (c) 26 μsec (d) 84 μsec. O. D. stands for the optical density.

The former was assigned to CA anion-radical from its identity with the spectrum of the chemically prepared CA anion-radical in acetone.[11] The latter was attributed to VCZ cation-radiacl as the most reasonable counterpart of the CA anion. Its intensity was found to decrease with increasing concentration of VCZ, which suggests the occurrence of the reaction of VCZ cation-radical formed with VCZ monomer. The assignment was substantiated by γ-irradiation of VCZ in *s*-BuCl at 77°K which is known to produce exclusively the solute cation.[10,12] The absorption spectrum of the VCZ cation observed for the irradiated frozen solution is shown in Fig. 2. The authenticity of the spectrum as due to VCZ cation would be supported by the fair agreement of the result of calculation shown by the sticks in Fig. 2. The result was obtained by using a computer program[13] for the SCF-MO calculation of open-shell molecules.[14] The absorption identified with the VCZ cation (Fig. 2) may be compared favorably with the absorption (Fig. 1) at wave-

5) K. Kawai, Y. Shirota, H. Tsubomura, and H. Mikawa, This Bulletin, **45**, 77 (1972).

6) Y. Shirota, K. Kawai, N. Yamamoto, K. Tada, H. Mikawa, and H. Tsubomura, *Chem. Lett.*, **1972**, 145.

7) Recently laser photolysis studies were made on the systems VCZ-tetracyanobenzene and VCZ-tetracyanoethylene. Y. Nishina, Y. Taniguchi, and N. Mataga, The 3rd Symposium on the Charge-transfer Complex, Sendai, October, 1971, Reprint p. 53.

8) T. Natsuume, M. Nishimura, M. Fujimatsu, M. Shimizu, Y. Shirota, H. Hirata, S. Kusabayashi, and H. Mikawa, *Polym. J.*, **1**, 181 (1970).

9) N. Yamamoto, Y. Nakato, and H. Tsubomura, This Bulletin, **39**, 2603 (1966).

10) T. Shida and W. H. Hamill, *J. Chem. Phys.*, **44**, 2369, 4372 (1966).

11) Y. Iida, This Bulletin, **43**, 2772 (1970).

12) C. David, P. Janssen, and G. Geuskens, *Spectrochim. Acta*, **27A**, 367 (1971).

13) The program was written by S. Iwata of the Institute of Physical and Chemical Research to whom the authors are indebted.

14) T. Shida and S. Iwata, *J. Phys. Chem.*, **75**, 2591 (1971).

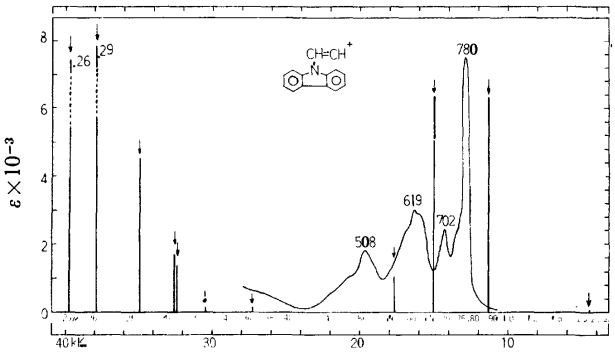

Fig. 2. The absorption spectrum of VCZ cation-radical produced by γ-ray irradiation of VCZ in *s*-BuCl matrix at 77°K. The sticks represent the theoretical spectrum obtained by an SCF-MO calculation for the cation. The left ordinate refers to the molar extinction coefficient of the experimental spectrum while the right refers to the oscillator strength of the theoretical spectrum. The numbers at peak are the wavelengths in unit of nm.

lengths longer than 550 nm (due to the limitation in the film, the absorption beyond 650 nm in Fig. 1 could not be measured).

For comparison with the VCZ–CA system the absorption spectrum obtained by the flash illumination of CA only in acetone solution is shown in Fig. 3. It should be noted that no pure absorption of CA anion-radical was obtained in this case. The *T-T'* absorption of CA appeared in the region 450—550 nm at the delay time of 3 μsec and faded away mostly at 17 μsec, and the bands at *ca.* 440 nm and *ca.* 370 nm which persisted after disappearence of *T-T'* absorption were regarded as due to the mixture of CA semiquinone radical and CA anion-radical.[5] The absorption spectra of CA semiquinone radical and CA anion-radical are similar, but the semiquinone radical has a second band at λ_{max} 357—375 nm,[5] while the anion-radical has none in this region. The absorption spectrum of CA semiquinone radical has been obtained by the flash photolysis of CA in tetrahydrofuran as a result of hydrogen abstraction reaction from the solvent by the excited CA, showing a band at λ_{max} 437 nm with a shoulder at 414 nm and a band at λ_{max} 375 nm.[5] Although a very weak, broad band system was also observed beyond 550 nm even with CA only in acetone solution, it decayed at nearly the same rate as for the triplet state of CA and was assigned to the charge-transfer band between the solvent as a donor and triplet CA as an acceptor. The same phenomenon was found in a benzene solution.[5]

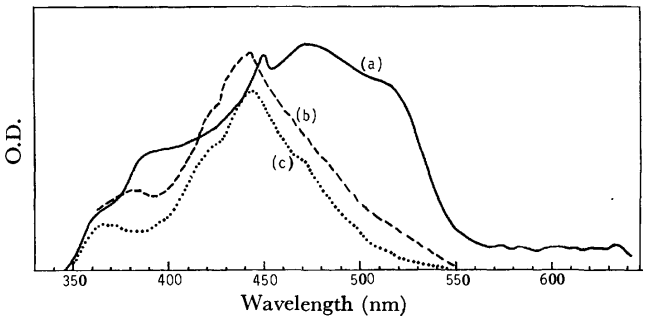

Fig. 3. The absorption spectra of transient species obtained by the flash photolysis of CA (2.3×10^{-4} M) in acetone. Delay time: (a) 3 μsec (b) 17 μsec (c) 56 μsec.

Chloranil anion-radical formed in an acetone solution of VCZ and CA decayed at a diffusion-controlled rate (Fig. 4). A rate constant $k=2.1\times10^{10}$M^{-1}sec^{-1} was obtained by using the molar extinction coefficient $\varepsilon=9\times10^{3}$ reported for CA anion-radical at its abosrption.[10]

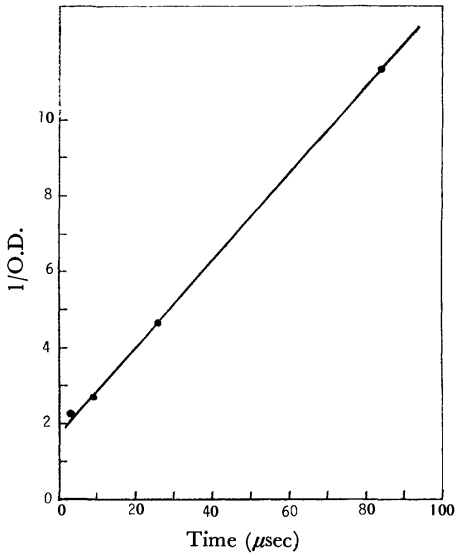

Fig. 4. Plots of second-order kinetics for the decay of CA anion-radical at 446 nm formed in an acetone solution of VCZ (2×10^{-4} M) and CA (1×10^{-4} M).

The second-order decay of CA anion-radical indicates a bimolecular recombination between VCZ cation and CA anion-radicals and/or between VCZ dimer cation-radical and CA anion-radical, which is consistent with the proposed mechanism for the cyclodimerization of VCZ,[2,4] if the reaction proceeds under the conditions of the present flash photolysis as in the preparatory scale reaction.

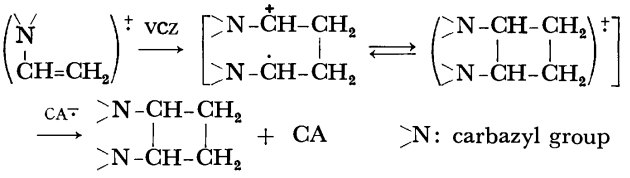

The kinetic observation in an acetone solution may be explained in terms of the following scheme of reactions.

$$VCZ + CA \xrightarrow{h\nu} VCZ^{+\cdot} + CA^{-\cdot} \quad (1)$$

$$VCZ^{+\cdot} + CA^{-\cdot} \xrightarrow{k_1} VCZ + CA \quad (2)$$

$$VCZ^{+\cdot} + VCZ \underset{k_{-2}}{\overset{k_2}{\rightleftharpoons}} VCZ_2^{+\cdot} \quad (3)$$

$$VCZ_2^{+\cdot} + CA^{-\cdot} \xrightarrow{k_3} VCZ_2 + CA \quad (4)$$

The rate equation of the decay of CA anion-radical is

$$-d[CA^{-\cdot}]/dt = k_1[CA^{-\cdot}]\{[VCZ^{+\cdot}] + (k_3/k_1)[VCZ_2^{+\cdot}]\}, \quad (5)$$

where

$$[VCZ^{+\cdot}] + [VCZ_2^{+\cdot}] = [CA^{-\cdot}] \quad (6)$$

$$[VCZ_2^+]/[VCZ^+][VCZ] = k_2/k_{-2} = K \quad (7)$$

Substituting Eqs. (6) and (7) into (5) we obtain

$$-d[CA^-]/dt = k_1[CA^-]^2\left\{\frac{1+(k_3/k_1)K[VCZ]}{1+K[VCZ]}\right\} = k_1C[CA^-]^2, \quad (8)$$

$([CA^-] \ll [VCZ])$ C: constant

which is the second-order decay equation. The following rate equation is derived from the above scheme of reactions where the process k_{-2} is not considered in Eq. (3), if the rate constant k_1 is assumed to be equal to k_3.

$$-d[CA^-]/dt = k_1[CA^-]^2 \quad (9)$$

If the absorption at longer wavelengths in Fig. 1 is due to the VCZ cation, it should be observed irrespective of solvent. When acetonitrile was used in place of acetone, the solution of VCZ (2.5×10^{-4}M) and CA (1×10^{-4}M) gave the spectrum shown in Fig. 5 which is similar to Fig. 1 and may be interpreted in terms of the formation of VCZ cation and CA anion-radicals. In contrast to the solution containing the two solutes CA only in acetonitrile showed the absorption shown in Fig. 6. This can be attributed to T-T' absorption of CA and the absorption mainly due to the semiquinone radical. No absorption appeared at the wavelength longer than 550 nm.

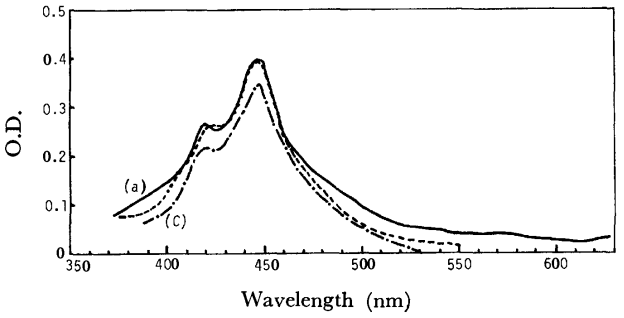

Fig. 5. The absorption spectra of transient species obtained by the flash photolysis of an acetonitrile solution of VCZ (2.5×10^{-4} M) and CA (1×10^{-4} M). Delay time: (a) 4 μsec, (b) 9 μsec, (c) 250 μsec.

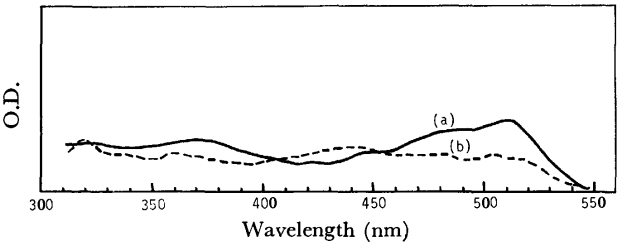

Fig. 6. The absorption spectra of transient species obtained by the flash photolysis of CA (1.4×10^{-4} M) in acetonitrile. Delay time: (a) 3 μsec. (b) 26 μsec.

The transient absorption spectrum obtained in methanol is shown in Fig. 7. In methanol the spectrum in the region 400—500 nm differs somewhat in shape from that observed in acetone or in acetonitrile, showing two bands at λ_{max} 426 and 451 nm. The absorption attributable to VCZ cation-radical appeared at a wavelength longer than 550 nm. The absorption bands in the region 400—500 nm are almost the same as those obtained by the flash photolysis of CA only in methanl and interpreted as an admixture of the absorption of CA anion-radical and CA semiquinone radical. The semiquinone radical is suggested to be formed by the protonation of the anion-radical initially formed.

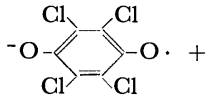

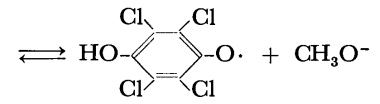

In the flash photolysis of CA only in methanol the spectrum obtained is composed of the T-T' absorption, the absorption of the semiquinone radical and of the anion-radical. No absorption appeared at a wavelength longer than 550 nm (Fig. 8). In this case the initially formed semiquinone radical by the hydrogen abstraction reaction of the excited CA from the solvent dissociates into the anion-radical and is in equilibrium with the latter species.

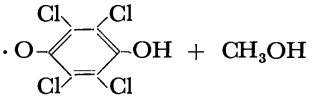

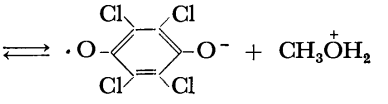

The acid-base equilibrium between the semiquinone radical and the anion-radical (semiquinone anion) in

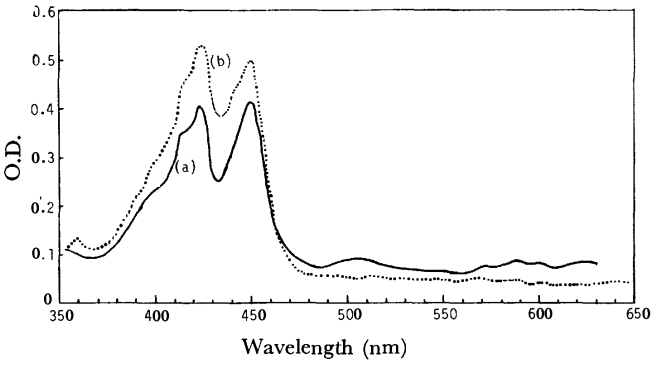

Fig. 7. The absorption spectra of transient species obtained by the flash photolysis of a methanol solution of VCZ (2×10^{-4} M) and CA (1×10^{-4} M). Delay time: (a) 3 μsec (b) 8.5 μsec.

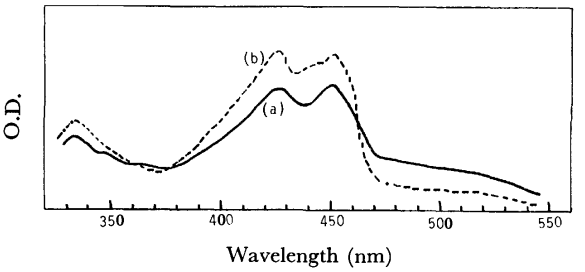

Fig. 8. The absorption spectra of transient species obtained by the flash photolysis of CA (1.8×10^{-4} M) in methanol. Delay time: (a) 3 μsec (b) 16 μsec.

methanol has also been shown by Bridge and Porter[15] in the flash photolysis of duroquinone.

Noticeably, CA anion-radical formed in acetonitrile or in methanol persisted for a much longer time than in acetone under comparable conditions. Details are not available at present and further studies are needed with respect to this point. Flash photolysis of the system VCZ–CA was also carried out in benzene solution, but the absorption bands obtained were very low in intensity and no definite conclusions were reached.

Transient CA anion and VCZ cation-radicals were detected in the VCZ–CA–solvent systmes by selective excitation of the acceptor, while in the absence of VCZ no pure absorption of CA anion-radical was obtained. This confirms the fact that photochemical electron transfer took place between VCZ and the excited CA in polar solvents. This seems to be the first example to demonstrate the occurrence of electron transfer in the photochemical reaction of VCZ in the presence of an electron acceptor.

15) N. K. Bridge and G. Porter, *Proc. Roy. Soc. Ser. A*, **244**, 259 (1958).

BULLETIN OF THE CHEMICAL SOCIETY OF JAPAN, VOL. 45, 2687—2692 (1972)

A New Theory of Melting at High Pressures

Hitoshi KANNO

Department of Chemistry, Faculty of Science, The University of Tokyo, Hongo, Bunkyo-ku, Tokyo

(Received March 14, 1972)

As an improvement of the significant structure theory, a new partition function of monatomic liquid was derived:

$$Z_l(T, V_l) = \left\{\prod_{i=1}^{3N_v}\left[2\sinh\left(\frac{h\nu_i}{2kT}\right)\right]^{-1}\right\}\left\{\left(\frac{2\pi mkT}{h^2}\right)^{3/2}\frac{eV_f}{N_t}\right\}^{N_t}\exp\left\{-\frac{\Phi_l(V_l)}{kT}\right\}$$

where $3N_v$ and $3N_t$, ($N_v+N_t=N$; Avogadro number), are the numbers of freedom in vibrational and translational motions, respectively, ν_i the i-th normal vibration in the vibrational motion, m the mass of molecule, V_f the free volume of liquid, and $\Phi_l(V_l)$ the configurational potential energy of liquid. Melting of argon at high pressures is successfully interpreted by means of the partition function.

Theoretical interpretations of melting in terms of the partition function have been made by a number of investigators.[1-3] Of the theories suggested, few can give a satisfactory quantitative description of melting. This is connected partly with the confused state of theory of melting and partly with the inadequacy and/or the mathematical difficulty of various proposed partition functions of liquid. A satisfactory interpretation of melting seems to be achieved by the finding of a good partition function for liquid.

Though the significant structure theory of liquid developed by Eyring and his co-workers[4] yields good numerical agreement with experiment for a number of the thermodynamic properties of many types of liquids, Tuerpe and Keeler[5] have shown that it does not give a satisfactory description of melting phenomenon at high pressures. The theory, however, suggests two important facts: (1) the liquid consists of both vibrational and translational degrees of freedom, and (2) the partition function of liquid must be analogous to that of solid near the melting point and to that of gas toward the gas region.

Bearing these concepts in mind it seems worthwhile to investigate the possibility of deriving the partition function of liquid which is applicable to the melting process at high pressures. The purposes of this study are to present a new partition function of liquid differing somewhat from Eyring's one,[4] and to apply it to the melting phenomenon, in particular the melting of argon at high pressures.

Theoretical

Adopting the concept of the significant structure theory[4] that both vibrational and translational degrees of freedom coexist in the liquid state, let us assume that the number of atoms in the vibrational motion is N_v and that the number in the translational motion is N_t ($=N-N_v$, N: Avogadro number). Accordingly the numbers of freedom $3N_v$ and $3N_t$ are distributed between the two motions in the liquid. The significant structure theory also considers that movable holes of mocleular size produced by volume increase accompanying fusion and thermal expansion confer the translational degrees of freedom on some fractions of molecules of the liquid.

1) J. E. Lennard-Jones and A. F. Devonshire, *Proc. Roy. Soc.* (London), **169**, 317 (1937); **170**, 464 (1939).

2) John. G. Kirkwood and Elizabeth Monroe, *J. Chem. Phys.*, **9**, 514 (1941).

3) G. A. Mansoori and F. B. Canfield, *ibid.*, **51**, 4958, 4967 (1969).

4) H. Eyring, T. Ree, and N. Hirai, *Proc. Nat. Acan. Sci., U. S.*, **44**, 683 (1958), E. J. Fuller, T. Ree, and H. Eyring, *ibid.*, **45**, 1594 (1959), H. Eyring and T. Ree, *ibid.*, **47**, 526 (1961), H. Eyring and Mu Shik Jhon, "Significant Liquid Structure", John Wiley, New York, (1969), and references contained therein.

5) D. R. Tuerpe and R. N. Keeler, *J. Chem. Phys.*, **47**, 4283 (1967).

If we assume that a hole in liquid moves about as freely as does a molecule in vapor, it is to be expected that a molecule in the translational motion can share the whole excess volume of the liquid. In other words, the molecules in the translational motion are statistically indistinguishable. Consider a molecule in the translational motion in the liquid. It may move randomly from one position into a neighboring hole by producing a hole behind and may be oscillatory there, but another molecule begins to make translational motion by jumping into the hole. So, as a whole, it may be visualized that a hole in the liquid moves freely from one position to another similar to a gas molecule in vapor. This view has been proposed and supported by many theoretical approaches and experimental evidences,[4,6-8] though not without a few objections.[9]

The energy level in the vibrational motion is given by

$$\varepsilon_i = h\nu_i\left(n_i+\frac{1}{2}\right) \tag{1}$$

where ν_i is the normal vibration of the i-th freedom in the vibrational motion, n_i the quantum number specifying vibrational state. The kinetic energy of the particle in the translational motion is

$$\frac{1}{2m}p_j^2 = \frac{1}{2m}(p_{xj}^2+p_{yj}^2+p_{zj}^2) \tag{2}$$

where p_{xj}, p_{yj}, and p_{zj} are, respectively, the x-, y-, and z-components of momentum p_j, and m the mass of molecule. Thus the energy state of the liquid is designated by the quantum numbers n_i ($i=1, 2, \cdots 3N_v$) of normal vibration, momenta p_j ($j=1, 2, \cdots N_l$) of atoms in the translational motion and the configurational potential energy arising from intermolecular forces $\Phi_l(V_l)$. Hence the total internal energy of the system is represented as follows.

$$E_l(V_l, n_i, p_j) = \Phi_l(V_l) + \sum_{i=1}^{3N_v}\left(n_i+\frac{1}{2}\right)h\nu_i + \sum_{j=1}^{N_l}\frac{p_j^2}{2m}. \tag{3}$$

Since the sum of states for one particle in the translational motion is given by

$$z_j = \int_{-\infty}^{+\infty}\int\int\int_{volume}\exp\left(-\frac{p_j^2}{2mkT}\right)\frac{1}{h^3}\mathrm{d}p_{xj}\mathrm{d}p_{yj}\mathrm{d}p_{zj}\mathrm{d}x\mathrm{d}y\mathrm{d}z \tag{4}$$

and the sum of states for the i-th vibrational motion is

$$z_i = \sum_{n_i=0}^{\infty}\exp\left\{-\frac{\left(n_i+\frac{1}{2}\right)h\nu_i}{kT}\right\} = \left\{2\sinh\left(\frac{h\nu_i}{2kT}\right)\right\}^{-1}, \tag{5}$$

the partition function for the liquid composed of N monatomic molecules is

$$Z_l(T, V_l) = \sum_{states}\exp\left\{-\frac{E_l(V_l, n_i, p_j)}{kT}\right\}$$
$$= \left\{\prod_{i=1}^{3N_v}z_i\right\}\frac{1}{N_l!}\left(\prod_{j=1}^{N_l}z_j\right)\exp\left\{-\frac{\Phi_l(V_l)}{kT}\right\}$$
$$= \left\{\prod_{i=1}^{3N_v}\left[2\sinh\left(\frac{h\nu_i}{2kT}\right)\right]^{-1}\right\}$$
$$\times\left\{\left(\frac{2\pi mkT}{h^2}\right)^{3/2}\frac{eV_f}{N_l}\right\}^{N_l}\exp\left\{-\frac{\Phi_l(V_l)}{kT}\right\}, \tag{6}$$

where V_f is the free volume of the liquid.[10] In this calculation it was assumed that each degree of freedom is separable. We also used Stirling's approximation $N_l! = (N_l/e)^{N_l}$ for the factorial $N_l!$ in the denominator of the partition function which arises from the indistinguishability of the particles in the translational motion. The condition for the validity of Eq. (6) is the separability of the internal energy into kinetic (vibrational and translational) and potential parts.

The Helmholtz free energy of the liquid becomes

$$F_l(T, V_l) = -kT\log Z_l(T, V_l)$$
$$= \Phi_l(V_l) + kT\sum_{i=1}^{3N_v}\log\left\{2\sinh\left(\frac{h\nu_i}{2kT}\right)\right\}$$
$$-N_lkT\log\left\{\left(\frac{2\pi mkT}{h^2}\right)^{3/2}\frac{eV_f}{N_l}\right\} \tag{7}$$

There are two efficient approximation methods for the vibrational term in Eq. (7); Debye's approximation[11] and Einstein's.[12] According to the former, the number of modes of vibration in the frequency range from ν to $\nu+\mathrm{d}\nu$ is given by

$$g(\nu) = \frac{9N_v}{\nu_m^3}\nu^2$$

where ν_m is the highest allowed frequency of the vibration of the system. Applying this approximation to the vibrational term in Eq. (7), we get

$$F_l(T, V_l) = \Phi_l(V_l)$$
$$+ 9kN_vT(T/\theta_l)^3\int_0^{\theta_l/T}x^2\log\left\{2\sinh\left(\frac{x}{2}\right)\right\}\mathrm{d}x$$
$$-N_lkT\log\left\{\left(\frac{2\pi mkT}{h^2}\right)^{3/2}\frac{eV_f}{N_l}\right\} \tag{8}$$

where $\theta_l(=h\nu_m/k)$ is the characteristic temperature of liquid. It is expected that θ_l is more strongly temperature dependent than that of solid.

Equation (8) has the same asymptotic behaviour as Eyring's equation:[4] When N_l approaches zero, Eq. (8) gives the Helmholtz free energy of a solid, and when N_v goes to zero, we have the Helmholtz free energy of a real gas.

In principle we can now derive all the thermodynamic properties of liquid from the usual thermodynamic equations, but in order to make further progress it is necessary to know the exact values of N_l (or N_v), θ_l, $\Phi_l(V_l)$, and V_f or their exact forms as functions of T and V_l.

According to the significant structure theory,[4] N_l, N_v, and V_f are represented by

$$N_l = N\left(\frac{V_l-V_s}{V_l}\right)$$

6) L. Cailletet and E. Mathias, *C. R. Acad. Sci., Paris*, **102**, 1202 (1886); **104**, 1563 (1887).
7) H. Eyring, *J. Chem. Phys.*, **4**, 283 (1936).
8) Dan McLachan, Jr., and Ernest G. Ehlers, *J. Geophys. Res.*, **76**, 2780 (1970).
9) J. H. Hildebrand and G. Archer, *Proc. Nat. Acad. Sci. U. S.*, **47**, 1881 (1961).
10) The term "free volume" is used in the free volume theory in a different meaning. In this theory, it is referred to as the sum volume of movable holes in the liquid.
11) P. Debye, *Ann. Physik.*, **39**, 789 (1912).
12) A. Einstein, *ibid.*, **22**, 180 (1970).

$$N_v = N\left(\frac{V_s}{V_l}\right) \tag{9}$$
$$V_f = V_l - V_s$$

where V_s and V_l are the volume of solid at melting point and the volume of liquid, respectively. These relations were derived on the assumption that in one mole of liquid there are $(V_l-V_s)/V_s$ moles of holes of molecular size and that the whole excess volume (the sum of the volumes of the movable holes) is communally utilized by the molecules in the translational motion. If we assume that a hole in the liquid completely surrounded by other molecules moves freely like a gas molecule in a vapor, the effective number of holes (the number of molecules in the translational motion) which behave like a gas molecule is obtained by multiplying the number of holes $N(V_l-V_s)/V_s$ by the probability of molecules occupying the positions around the hole V_s/V_l. The relation (9) are expected to be valid for the liquid forming closed packed crystal or nearly closed packed crystal and for the region not far from melting point. Adopting these relations to our formulation, we obtain the following expression for the Helmholtz free energy of liquid

$$F_l(T, V_l) = \Phi_l(V_l) + 9RT(V_s/V_l)(T/\theta_l)^3\int_0^{\theta_l/T} x^2 \log\left\{2\sinh\left(\frac{x}{2}\right)\right\}dx - RT\left(\frac{V_l-V_s}{V_l}\right)\log\left\{\left(\frac{2\pi mkT}{h^2}\right)^{3/2}\frac{eV_l}{N}\right\} \tag{10}$$

Now let us consider the melting process of monatomic molecule substances such as inert gas elements. From the thermodynamical point of view, fusion takes place when the Gibbs free energies of solid and of liquid intercept each other. This is expressed by the equation

$$F_s(T, V_s) + PV_s = F_l(T, V_l) + PV_l \tag{11}$$

where P is the pressure of the system.

In connection with the equation of liquid we formulated, we employ the partition function of Debye type for the solid phase. The Helmholtz free energy of the solid phase is thus given by

$$F_s(T, V_s) = \Phi_s(V_s) + 9RT(T/\theta_D)^3\int_0^{\theta_D/T} x^2 \log\left\{2\sinh\left(\frac{x}{2}\right)\right\}dx \tag{12}$$

where $\Phi_s(V_s)$ is the configurational potential energy of solid, and θ_D the Debye characteristic temperature of the solid.

The theory of melting is required to be capable of evaluating the temperature of melting, the change of volume and the latent heat of melting from intermolecular potential. In this paper, however, the reverse method is employed to test the applicability of the present model since the adoption of the crude theories for evaluating the values of $\Phi_l(V_l)$ and θ_l may obscure the applicability of Eq. (10).

We choose the entropy change upon fusion and the volumes of solid and liquid at the triple point as adjustable parameters and adjust the characteristic temperature (θ_l) and the configurational potential energy of liquid $\Phi_l(V_l)$ to the condition of Eq. (11) at the triple point. Then with the aid of Eq. (11) we calculate the melting point, entropy change upon fusion, internal energies and entropies of both phases at the pressure P and compare them with experimental data.

From Eq. (10), we get

$$S_l(T,\theta_l) = -\frac{\partial F_l(T,\theta_l)}{\partial T} = -9R\left(\frac{V_s}{V_l}\right)\left(\frac{T}{\theta_l}\right)^3\int_0^{\theta_l/T} x^2\log\left\{2\sinh\left(\frac{x}{2}\right)\right\}dx + 4.5R\left(\frac{V_s}{V_l}\right)\left(\frac{T}{\theta_l}\right)^3\int_0^{\theta_l/T} x^3\coth\left(\frac{x}{2}\right)dx + R\left(\frac{V_l-V_s}{V_l}\right)\log\left\{\left(\frac{2\pi mkT}{h^2}\right)^{3/2}\frac{eV_l}{N}\right\} + \frac{3}{2}R\left(\frac{V_l-V_s}{V_l}\right) \tag{13}$$

and for the solid we obtain

$$S_s(T,\theta_D) = -9R(T/\theta_D)^3\int_0^{\theta_D/T} x^2\log\left\{2\sinh\left(\frac{x}{2}\right)\right\}dx + 4.5R(T/\theta_D)^3\int_0^{\theta_D/T} x^3\coth\left(\frac{x}{2}\right)dx \tag{14}$$

Accordingly, the entropy change on fusion (ΔS_m) is given by

$$\Delta S_m = S_l(T_m,\theta_l) - S_s(T_m,\theta_D) \tag{15}$$

With the aid of Eqs. (13), (14), and (15), and the observed values of V_s, V_l, and θ_D, we can determine the value of θ_l by fitting the calculated ΔS_m to experiment at the triple point. At the triple point of argon (T_m=83.81 K), the observed values of V_s, V_l, and ΔS_m are 24.614,[13] 28.332 ml,[13] and 3.395 cal/mol K,[14] respectively. With the value of θ_D=80 K,[15] Eq. (15) gives the value θ_l of 54.8 K. Determination of $\Phi_l(V_l)$ at the triple point is a straightforward numerical problem: it is solved by utilizing the evaluated values of θ_l and $\Phi_s(V_s)$ and by satisfying Eq. (11). As the value of $\Phi_s(V_s)$ is -1955 cal/mol at the triple point,[16] the value of $\Phi_l(V_l)$ which is found to satisfy Eq. (11) is -1624 cal/mol. In this calculation we can neglect the terms PV_s and PV_l in Eq. (11) as they are small compared to $F_s(T, V_s)$ and $F_l(T, V_l)$ at ordinary pressures.

Next we proceed to consider the melting of argon at high pressures. We cannot now neglect the PV terms in Eq. (11), and several plausible approximations and estimations must be introduced to achieve numerical calculations. At high pressures the pressure effect on $\Phi_s(V_s)$, $\Phi_l(V_l)$, θ_D, and θ_l must be taken into account. For the configurational potential energy of the solid, we use the equation[16]

$$\Phi_s(V_s) = -\frac{z}{2}N\varepsilon\left\{2.4090\left(\frac{N\sigma^3}{V_s}\right)^2 - 1.0109\left(\frac{N\sigma^3}{V_s}\right)^4\right\} \tag{16}$$

13) K. Clusius and K. Weigand, *Z. Physik. Chem.*, **B46**, 1 (1940).
14) P. Flubacher, A. J. Leadbetter, and J. A. Morrison, *Proc. Phys. Soc.*, **78**, 1449 (1961).
15) K. Clusius, *Z. Physik. Chem.*, **B31**, 459 (1936).
16) R. H. Wentorf, R. J. Beuhler, J. O. Hirschfelder, and C. F. Curtiss, *J. Chem. Phys.*, **18**, 1484 (1950). The values $\varepsilon=165\times10^{-16}$ ergs and $\sigma=3.41\times10^{-8}$ cm obtained by E. Whalley and W. G. Schneider, *J. Chem. Phys.*, **23**, 1644 (1955) were used in numerical calculations.

where z is the number of nearest neighbor molecules, σ and ε are, respectively, the distance and energy characteristics of the system in the 6—12 Lennard-Jones potential, *i.e.*,

$$\phi(r) = 4\varepsilon\left\{\left(\frac{\sigma}{r}\right)^{12} - \left(\frac{\sigma}{r}\right)^{6}\right\} \tag{17}$$

To obtain the value of $\Phi_l(V_l)$ at the pressure P, we introduce the approximation

$$\Phi_l(V_l) = \left(\frac{V_s}{V_l}\right)A \cdot \Phi_s(V_s) \tag{18}$$

where A is an adjustable parameter and determined to fit the data at the triple point. For the sake of simplicity A is taken to be independent of pressure, *i.e.*, constant. This approximation is based on the facts that the change of configurational potential energy on melting is mainly due to the decrease of the number of nearest neighbor molecules and that in the case of inert gas elements the contribution to the configurational potential energy from the non-nearest neighbor molecules is not so large. Combining the observed values of $\Phi_s(V_s) = -1955$ and $\Phi_l(V_l) = -1624$ cal/mol at the triple point, the value of A is found to be 0.9564.

The Grüneisen law[17] may be used to take account of the pressure effect on the characteristic temperature of both phases:

$$\gamma = -\frac{\partial \log \theta}{\partial \log V} \tag{19}$$

where γ is the Grüneisen parameter and θ the characteristic temperature of the system. If we assume that the Grüneisen parameter is constant, Eq. (19) may be integrated at once to yield

$$\begin{aligned} \gamma_s \log\left(\frac{V_s}{V_s^0}\right) &= \log\left(\frac{\theta_D^0}{\theta_D}\right) \\ \gamma_l \log\left(\frac{V_l}{V_l^0}\right) &= \log\left(\frac{\theta_l^0}{\theta_l}\right) \end{aligned} \tag{20}$$

where θ_D^0 and θ_l^0 are respectively the Debye temperature of solid and the characteristic temperature of liquid at a reference melting point. V_s^0 and V_l^0 are the corresponding volumes of solid and liquid, γ_s and γ_l are the Grüneisen parameters of solid and liquid, respectively. It seems clear that in the case of liquid phase the accuracy of Eq. (20) is not very high.

Although some of these approximations are not rigorous enough for accurate computations, it is expected that they are valid enough to show the main feature of melting phenomenon at high pressures. Once the values of $\Phi_s(V_s)$, $\Phi_l(V_l)$, θ_D, and θ_l are known as functions of volume of the system, we can evaluate the melting point, latent heat of fusion, internal energy of the system at the pressure P with the aid of Eq. (11) and the observed values of V_s and V_l at the melting point corresponding to P.

Calculations and Discussion

The results of calculations together with the experimental data[18] are shown in Table 1. The calculation procedure was follows. At first the values of $\Phi_s(V_s)$, $\Phi_l(V_l)$, θ_D, θ_l, N_t, and V_f were calculated by use of Eqs. (9), (16), (18), and (20), and the observed values of V_s and V_l at the melting point T_m of the pressure P.[18] We adopted the triple point of argon as a reference point. The value of γ_s and γ_l were assumed to be 2.21 and 2.10, respectively. Then substituting these values into Eq. (11), we found the melting temperature of the system at the pressure P, and using this calculated temperature the entropies and the internal energies of both phases were evaluated. Though the value of γ_s was taken from the data (the value of 80 K) summarized by Pollack,[19] the value of γ_l was chosen so as to fit the calculations to the experimental data. The internal energy was calculated by use of the well-known thermodynamic relation

TABLE 1. COMPARISON OF CALCULATED AND OBSERVED THERMODYNAMIC PROPERTIES OF ARGON AT MELTING TEMPERATURES

P	T_m		ΔS_m		$S_s(T_m)$		$S_l(T_m)$		$E_s(T_m)$		$E_l(T_m)$		θ_D	θ_l
	Obsd	Calcd	Obsd	Calcd	Obsd	Calcd	Obsd	Calcd	Obsd	Calcd	Obsd	Calcd	Calcd	
0.687	100	$103._2$	12.1	11.4_3	41.3	39.0_0	53.4	50.4_2	−5750	−5610	−4733	−4624	82.9_0	60.9_2
1.146	110	$114._2$	11.5	10.5_4	42.8	41.0_0	54.3	51.5_4	−5580	−5393	−4590	−4467	84.9_1	63.6_1
1.630	120	$124._8$	11.0	10.0_1	44.1	42.4_6	55.2	52.4_7	−5380	−5190	−4415	−4304	87.3_0	66.2_2
2.136	130	$134._9$	10.5	9.4_9	45.3	43.7_4	55.9	53.2_2	−5180	−4984	−4243	−4139	89.6_3	68.8_2
2.662	140	$144._6$	10.4	9.2_7	45.9	44.7_1	56.3	53.9_8	−5070	−4789	−4126	−3965	92.3_1	71.2_1
3.210	150	$154._2$	10.2	8.9_6	46.7	45.6_3	56.9	54.6_0	−4870	−4584	−3929	−3788	94.7_5	73.6_0
3.781	160	$163._5$	10.0	8.7_1	47.8	46.4_5	57.8	55.1_6	−4610	−4378	−3660	−3604	97.1_8	75.9_1
4.374	170	$172._8$	9.9	8.4_8	48.4	47.2_4	58.3	55.7_2	−4420	−4164	−3454	−3412	99.4_0	78.0_6
4.987	180	$182._0$	9.6	8.3_0	48.7	48.0_1	58.3	56.3_1	−4270	−3943	−3319	−3210	101.5_1	80.0_0
5.614	190	$190._8$	9.4	8.0_8	48.8	48.6_8	58.2	56.7_6	−4130	−3727	−3187	−3016	103.5_7	82.0_3
6.250	200	$199._5$	9.1	7.9_3	49.2	49.3_0	58.3	57.2_2	−3950	−3510	−3016	−2816	105.5_8	83.9_1

a) Pressure is in kilobars, temperature in degrees Kelvin. Energies are in joules per mole and entropies are in joules per mole K.

b) All observed T_m, ΔS_m, $S_s(T_m)$, $S_l(T_m)$, $E_s(T_m)$, $E_l(T_m)$ values were obtained from R. K. Crawford and W. B. Daniels, *J. Chem. Phys.*, **50**, 3171 (1969). The values of V_l and V_s used in the calculations were also obtained from the same reference.

17) E. Grüneisen, "Handbuch der Physik," X, (1926), p. 1.

18) R. K. Crawford and W. B. Daniels, *J. Chem. Phys.*, **50**, 3171 (1969).

19) Gerald L. Pollack, *Rev. Mod. Phys.*, **36**, 748 (1964).

$$E(T) = -T^2\left\{\frac{\partial}{\partial T}\left(\frac{F}{T}\right)\right\} \tag{20}$$

Agreement between calculation and experiment[18] is excellent, but it is interesting to not that all the calculated ΔS_m, $S_l(T_m)$, $S_s(T_m)$, $E_l(T_m)$, and $E_s(T_m)$ values are systematically smaller in their absolute values than the corresponding observed values. This is considered to be in part due to the errors inherent in the various approximations introduced and to the neglect of anharmonic effect of vibrational motions in both solid and liquid. Bridgman[20] also reported the entropy change on fusion of argon at high pressures. The reported values of ΔS_m are 10.31, 8.64, 7.49, 6.64, 6.07, and 5.62 J/mol K at melting temperatures 106.3, 126.4, 144.9, 162.0, 178.0, and 193.1 K, respectively. They are all lower than the corresponding calculated values.

Table 2. Variation of $\gamma_l(T_m)$, ΔS_m, $E_l(T_m)$, and $S_l(T_m)$ with melting temperature[a]

T_m (Obsd)	T_m (Calcd)	$\gamma_l(T_m)$[b]	ΔS_m	$E_l(T_m)$	$S_l(T_m)$
100	$100._1$	1.79	11.7_4	−4698	50.1_1
110	$110._0$	1.85	10.9_7	−4568	51.0_5
120	$120._0$	1.91	10.4_3	−4417	51.9_4
130	$130._1$	1.96	9.8_6	−4255	52.7_7
140	$140._3$	2.00	9.5_8	−4070	53.5_3
150	$149._8$	2.02	9.2_4	−3893	54.1_7
160	$160._2$	2.05	8.9_1	−3684	54.8_5
170	$169._6$	2.06	8.6_5	−3488	55.4_4
180	$180._2$	2.08	8.3_9	−3255	56.1_5
190	$189._8$	2.09	8.1_3	−3042	56.6_7
200	$199._5$	2.10	7.9_3	−2816	57.2_2

a) Temperature is in degrees Kelvin (K). Entropies are in joules per mole K (J/mol K) and energies in joules per mole (J/mol).
b) The value of γ_l was chosen so as to give the observed melting temperature at pressure P. The value of γ_s was assumed to be 2.21.

Dugdale and Frank[21] showed that in the case of solid helium the Debye temperature depends only on volume to a first approximation and that the Grüneisen law, *i.e.*, $\gamma_s = -\mathrm{d}\log\theta_D/\mathrm{d}\log V_s$, holds well along the melting curve up to high pressures. By fixing γ_s constant, *i.e.*, $\gamma_s = 2.21$, we can determine the value of γ_l which gives observed melting temperature at P. The variation of γ_l with the increase in pressure is shown in Table 2 along with the entropy change upon fusion, internal energy and entropy of liquid. The fact that γ_l approaches the value of γ_s with the increase in pressure expects that thermodynamic properties of liquid resemble more and more those of solid with the increase in pressure. Although the value of γ_s was fixed constant throughout the calculations, γ_s also varies with volume and temperature.

From Eq. (20), the specific heat of liquid at constant volume is obtained as

Table 3. Specific heat of liquid inert gas element at melting point[a]

Element	Mp	θ_D	ΔH_m	θ_l (Calcd)	$CV_l(T_m,\theta_l)$ (Obsd)	$CV_l(T_m,\theta_l)$ (Calcd)
Ne	24.56	64	80.1	40.3	4.42[a]	4.92
Ar	83.81	80	284.5	54.8	5.50[b] 5.19[c]	5.46
Kr	115.78	63	392.0	44.0	5.38[d]	5.53
Xe	161.37	55	548.5	35.9	—	5.66

a) Melting temperature, θ_D and θ_l are in degrees Kelvin (K), ΔH_m (heat of fusion) is in calories per mole (cal/mol), $CV_l(T_m,\theta_l)$ is in calories per mole K (cal/mol K).
Sources of data: θ_D: K. Clusius, *Z. Phys. Chem.* (Leipzig), **B31**, 459 (1936). ΔH_m, V_s, and V_l: Gerald L. Pollack, *Rev. Mod. Phys.*, **36**, 748 (1964). $CV_l(T_m,\theta_l)$ observed; estimated from a) C. Gladun, *Cryogenics*, **6**, 27 (1966); b) A. Eucken and F. Hauk, *Z. Phys. Chem.*, **134**, 161 (1928); c) C. Gladun and F. Menzel, *Cryogenics*, **10**, 210 (1970); d) C. Gladun, *ibid.*, **11**, 205 (1971).

$$CV_l(T,\theta_l) = \left\{\frac{\partial E_l(T,\theta_l)}{\partial T}\right\}_V$$
$$= 9R\left(\frac{V_s}{V}\right)\left(\frac{T}{\theta_l}\right)^3\int_0^{\theta_l/T}\frac{x^4e^x}{(e^x-1)^2}\mathrm{d}x$$
$$+\frac{3}{2}R\left(\frac{V_l-V_s}{V_l}\right) \tag{21}$$

With the aid of the computed θ_l value, we can evaluate $CV_l(T_m, \theta_l)$. Comparison of the calculated $CV_l(T_m, \theta_l)$ with experiment is given in Table 3 together with the data of other inert gas elements. Though the calculated $CV_l(T_m, \theta_l)$ value deviates systematically from experimental value for all inert gas elements, the agreement is fairly good. The fact that deviation between calculation and experiment becomes larger from krypton (xenon) to neon is attributable to the underestimation of the number of freedom in the translational motion. In other words, Eq. (9) gives a lower value than the actual one for the N_l value. The reason is as follows. From classical theory one would expect the V_s value at 0 K and zero pressure to be equal to $N\sigma^3$. For krypton and xenon this holds within experimental error and for argon this is nearly true, but for neon and helium the actual molar volumes are very much larger than those given by the formula $N\sigma^3$. Accordingly the validity of Eq. (9) is lost in the cases of neon and helium.

We used a most simple form for evaluating configurational potential energy of liquid, but it is to be pointed out that Eq. (18) does not give asymptotic consistency: it does not yield the potential of solid when V_l approaches V_s. However, the good agreement with experiment leads to the conclusion that the approximation is rather adequate for the evaluation of $\Phi_l(V_l)$. Obviously a detailed theoretical study for the accurate calculation of the configurational potential energy of liquid is required to complete the present theory. It seems very likely that development of the

20) P. W. Bridgman, *Phys. Rev.*, **46**, 930 (1934).
21) J. S. Dugdale and J. P. Frank, *Phil. Trans. Roy. Soc.* (London) **A257**, 1 (1964).

radial distribution function method[22,23] and/or the Monte Carlo method[24,25] will suffice the requirement in near future.

At the present time some ambiguities exist in the present theory, especially in the calculations of $\Phi_l(V_l)$, N_l (or N_v), V_f, θ_l, and γ_l. Neverthless there is little doubt that the partition function of liquid given here will work well for the liquid composed of monatomic molecules. A more detailed application of the partition function is clearly bounded up with a better understanding of the volume and temperature dependencies of $\Phi_l(V_l)$, N_l, V_f, θ_l, and γ_l.

The author would like to thank Professor H. Hamaguchi for his interest and encouragement. Thanks also go to Professor T. Kihara for his criticism of the manuscript and helpful suggestions.

22) J. G. Kirkwood and E. M. Boggs, *J. Chem. Phys.*, **10**, 394 (1942); J. G. Kirkwood, E. K. Maun, and B. J. Alder, *ibid.*, **18**, 1040 (1950); J. G. Kirkwood, V. A. Lewinson, and B. J. Alder, *ibid.*, **20**, 929 (1952).

23) G. S. Rushbrooke, "Physics of Simple Liquids", edited by J. Rowlinson, G. S. Rushbrooke, and H. N. V. Temperley, North-Holland Publishing Co., Amsterdam (1968), Chapt II.

24) W. W. Wood, *ibid.*, Chapt V.

25) J. A. Barker, R. A. Fisher, and R. O. Watts, *Molec. Phys.*, **21**, 657 (1971).

BULLETIN OF THE CHEMICAL SOCIETY OF JAPAN, VOL. 45, 2692—2694 (1972)

On the Change of Electrical Conductivity of Metal on Melting

Hitoshi KANNO

Department of Chemistry, Faculty of Science, The University of Tokyo, Hongo, Bunkyo-ku, Tokyo

(Received April 4, 1972)

A partition function of liquid recently proposed by the present author[1] has been applied to the change of the electrical conductivity of metal at melting point. The relation between σ_s/σ_l and θ_D/θ_l is more successfully interpreted by this partition function than that used by Mott.[2]

It was previously reported that a partition function proposed by the author was successfully applied to the melting of argon at high pressures.[1] The partition function of N monatomic liquid is

$$Z_l(T, V_l) = \left\{ \prod_{i=1}^{3N_v} \left[2 \sinh\left(\frac{h\nu_i}{2kT} \right) \right]^{-1} \right\} \times \left\{ \left(\frac{2\pi mkT}{h^2} \right)^{3/2} \frac{eV_f}{N_l} \right\}^{N_l} \exp\left\{ -\frac{\Phi_l(V_l)}{kT} \right\} \quad (1)$$

where N_l and N_v, $(N_l+N_v=N)$, are respectively the numbers of molecules in translational and vibrational motions, ν_i is the normal mode of the i-th vibrational motion, m the mass of a molecule, V_f the free volume of the liquid, and $\Phi_l(V_l)$ the configurational potential energy of the liquid.

It is worthwhile applying the partition function to other systems in order to examine its applicability and validity. The application to liquid metals is described in this paper with special emphasis on the characteristic temperature of liquid (θ_l). Correlation between σ_s/σ_l (σ: electrical conductivity of metal at melting point, and subscripts s and l denote respectively solid and liquid phases) and θ_D/θ_l (θ_D: Debye temperature of a solid metal) is interpreted more successfully by means of the partition function than that used by Mott.[2]

Evaluation of Characteristic Temperature of Liquid

At present there is no well-defined theoretical model to evaluate the mean vibrational frequency of atoms in the vibrational motions in the liquid metal from their interatomic potentials. We adopt the same procedure as given previously[1] to evaluate the characteristic temperature of liquid at melting point.

The Helmholtz free energy of liquid metal is given, by

$$\begin{aligned} F_l(T, V_l) &= -kT \log Z_l(T, V_l) \\ &= \phi_l(V_l) + kT \sum_{i=1}^{3N_v} \log \left\{ 2 \sinh\left(\frac{h\nu_i}{2kT} \right) \right\} \\ &\quad - N_l kT \log \left\{ \left(\frac{2\pi mkT}{h^2} \right)^{3/2} \frac{eV_f}{N_l} \right\} \end{aligned} \quad (2)$$

Applying the Debye approximation to the vibrational part in Eq. (2), and adopting the Eyring presentations[3] for N_l, N_v, and V_f, *viz*

$$\begin{aligned} N_v &= \frac{NV_s}{V_l} \\ N_l &= \frac{N(V_l - V_s)}{V_l} \\ V_f &= V_l - V_s \end{aligned} \quad (3)$$

where V_s and V_l are the volumes of solid at the melting point and of liquid, respectively, we obtain

$$\begin{aligned} F_l(T, V_l) &= \phi_l(V_l) \\ &\quad + 9RT \left(\frac{V_s}{V_l} \right) \left(\frac{T}{\theta_l} \right)^3 \int_0^{\theta_l/T} x^2 \log \left\{ 2 \sinh\left(\frac{x}{2} \right) \right\} dx \\ &\quad - RT \left(\frac{V_l - V_s}{V_l} \right) \log \left\{ \left(\frac{2\pi mkT}{h^2} \right)^{3/2} \frac{eV_l}{N} \right\}, \end{aligned} \quad (4)$$

1) H. Kanno, This Bulletin, **45**, 2687 (1972).

2) N. F. Mott, *Proc. Roy. Soc. Ser.*, *A*, **146**, 465 (1934).

3) H. Eyring, T. Ree, and N. Hirai, *Proc. Nat. Acad. Sci. U. S.*, **44**, 683 (1958); H. Eyring and Mu Shik Jhon, "Significant Liquid Structure", John Wiley & Sons, New York (1969), and references contained therein.

where θ_l is the characteristic temperature of liquid (which corresponds to the Debye temperature of the solid). It should be pointed out that relations (3) are only approximate and are thought to be valid only for the low temperature region not far from melting point and for a close packed substance in its solid phase.

In correspondence to the partition function of liquid, we use the Debye equation for the solid phase

$$F_s(T, V_s) = \Phi_s(V_s) + 9RT\left(\frac{T}{\theta_D}\right)^3 \int_0^{\theta_D/T} x^2 \log\left\{2 \sinh\left(\frac{x}{2}\right)\right\} dx \quad (5)$$

where $\Phi_s(V_s)$ is the configurational potential energy of solid metal and θ_D the Debye temperature.

The entropy change on melting ΔS_m is represented by

$$\Delta S_m = \frac{\Delta H_m}{T_m} = S_l(T_m, V_l) - S_s(T_m, V_s) = -\left\{\frac{\partial F_l(T, V_l)}{\partial T}\right\}_{T=T_m} + \left\{\frac{\partial F_s(T, V_s)}{\partial T}\right\}_{T=T_m} \quad (6)$$

where ΔH_m is the latent heat of fusion, $S_l(T_m, V_l)$ and $S_s(T_m, V_s)$ are the entropies of liquid and solid phases at melting point, respectively.

With the aid of the observed values of θ_D, V_l, V_s, ΔS_m, and Eq. (6), we can determine the characteristic temperature of liquid (θ_l) at melting point by adjusting ΔS_m to give the experimental value.

Calculations and Discussion

The data used for calculations are tabulated in Table 1. Though the values T_m, V_l, V_s, and ΔS_m are in fair agreement in literature, the θ_D values show some difference according to the method (elastic or thermal) and temperature range at which determination was carried out. We used the Debye temperature of about 298 K obtained from specific heat data.[4]

As regards the characteristic temperature of liquid metal, Mott[2] has made an interesting comparison. He showed that the ratio of electrical conductivity of liquid metal to that of solid metal (both measured at melting point) is well correlated to the ratio of the mean frequencies of thermal vibrations of atoms in solid and liquid phases.

The electrical conductivity of solid metal is expressed as[5]

$$\sigma_s = \text{const} \cdot \frac{e^2}{m^*}\left(\frac{\beta}{C_D}\right)^2 \frac{m \cdot \theta_D^2}{V_s T} \quad (7)$$

where β/C_D and m^* (effective mass of electron) represent the magnitude of the binding of the electron to the lattice, e is the charge of electron.

When a metal melts, only a small percentage of volume increase is observed. Experimental evidences[6,7] show that structual configuration of liquid metal just above melting point retains most of the features of solid metal. Thus adopting Mott's hypothesis that electrical conductivity change at melting point is mainly due to the change of the electron scattering with phonon of high energy and utilizing the same formula as Eq. (7) for the electrical conductivity of liquid metal, we may easily derive the following formula

$$\frac{\sigma_s}{\sigma_l} = \left(\frac{\theta_D}{\theta_l}\right)^2 \cdot \frac{V_l}{V_s} \quad (8)$$

In Mott's theory a liquid metal is assumed to consist only of vibrational freedom. He derived the following formula giving the relation between σ_s/σ_l and θ_E/θ by applying the harmonic oscillator model of liquid to the liquid metal at the melting point:

$$\frac{\Delta H_m}{T_m} = 3R \log\left(\frac{\theta_E}{\theta}\right)[+R]^{8)} \quad (9)$$

where θ_E is the Einstein temperature and θ is a characteristic temperature of liquid state which corresponds

Table 1. Data used for the calculations

Metal	Mp (K)	V_s (ml)	V_l (ml)	θ_D (K)	ΔS_m (cal/mol·K)
Li	452	13.12[a]	13.48	448	1.59_0
Na	370.8	24.17[a]	24.80	155	1.67_7
K	336.6	46.43[a]	47.74	100	1.65_1
Rb	311.8	56.99_5[a]	58.42	59	1.80
Cs	301.8	69.98[a]	71.80	43	1.67_7
Cu	1356	7.610[b]	7.951	310	2.30_0
Ag	1234	11.16[c]	11.54	221	2.25_3
Au	1336.2	10.66[d]	11.34	178	2.21
Mg	923	14.85[e]	15.29	330	2.32
Zn	692.7	9.55[a]	9.94	237	2.54_8
Cd	594.2	13.48[a]	14.02	221	2.49
Hg	234.28	14.132[f]	14.64_9	92	2.34_1
Al	933.2	10.71[a]	11.39	390	2.74
In	429.76	15.99[g]	16.28	129	1.81
Tl	576.7	17.72[g]	18.10	96	1.77
Pb	600.58	18.70[h]	19.41	87	1.90

Sources of data: Melting point, Debye temp., and entropy of fusion—Ref. 4; volume of liquid at mp—Handbook of Chemistry and Physics, 50th ed., The Chemical Rubber Co. Pub., (1969) B255—259; volume of solid at mp—a) recalculated from the data tabulated in L. D. Lucas, *Mem. Sci. Rev. Met.*, **61**, 1 (1964), b) E. Widawaki and F. Sauerwald, *Z. Anorg. Allg. Chem.*, **192**, 145 (1930), c) F. Sauerwald, *Z. Metalk.*, **14**, 457 (1922), d) E. Gebhard and S. Dorner, *ibid.*, **42**, 353 (1951), e) P. J. McGonigal, A. D. Kirshenbaum, and A. V. Grosse, *J. Phys. Chem.*, **66**, 737 (1962), f) Ref. 12, see also Ref. a, g) A. Schneider and G. Heymer, *Z. Anorg. Allg. Chem.*, **286**, 118 (1956), h) cited in A. D. Kirshenbaum, J. A. Cahill, and A. V. Grosse, *J. Inorg. Nucl. Chem.*, **22**, 33 (1961).

4) K. A. Gschneider, Jr., in "Solid State Physics," Vol. **16**, F. Seitz and D. Turnbull Eds., Academic, New York, (1964), pp. 275—426.

5) H. Jones, in "Handbuch der Physik," Bd **XIX**, edited by S. Flügge, Springer-Verlag, (1956), pp. 227—315.

6) N. S. Gingrich, *Rev. Mod. Phys.*, **15**, 90 (1943).

7) "The Properties of Liquid Metals", edited by P. D. Adams, H. A. Davies, and G. Epstein, Taylor and Francis, London, (1967), and *Advan. Phys.*, **16**, (1967), pp. 147—307.

8) In Mott's original paper,[2] the term R was omitted. As first suggested by O. K. Rice, *J. Chem. Phys.*, **6**, 476 (1938) and shown by the significant structure theory[3] and the present theory, the communal entropy introduced on melting, which is the cause for the term R in Eq. (9), is in fact much smaller in most actual cases than R.

TABLE 2. COMPARISON OF CALCULATED σ_s/σ_l VALUES WITH OBSERVED CONDUCTIVITY CHANGES

Metal	σ_s/σ_l Observed	σ_s/σ_l Calcd by Mott[a)]	σ_s/σ_l Calcd by this theory
Li	1.59	1.75[a)]	1.65
Na	1.45	1.80	1.69
K	1.58	1.79	1.66
Rb	1.60	1.87	1.75
Cs	1.67	1.80	1.68
Cu	2.1	2.26	2.01
Ag	2.1	2.20	2.00
Au	2.3	2.23	1.85
Mg	1.8	2.24	2.08
Zn	2.2	2.44	2.18
Cd	2.0	2.40	2.07
Hg	3.7—4.9	2.27	2.00
Tl	2.1	1.85	1.73
Al	2.2	2.67	2.26
Pb	1.9	1.96	1.76
In	2.2	1.87	1.76

Source of data: Observed values are taken from the tabulated data in Ref. 9.

a) Calculated with Eqs. (8) and (9) using tabulated data in Table 1. In this calculation the term $\boldsymbol{R}$ in Eq. (9) was omitted after Mott.

to the Einstein temperature.

The values of σ_s/σ_l computed from Eqs. (6) and (8) compared with the values obtained by Mott's theory are given in Table 2. We see that the values σ_s/σ_l calculated by Eq. (6) give better agreement to experiment than those deduced from Eq. (9). This might be due to the fact that in Mott's theory all ΔS_m are ascribed to the change of vibrational frequency, neglecting the communal entropy. Actually a part of ΔS_m is caused by the introduction of the partial indistinguishability of the particles upon melting. It should be pointed out that as Eyring's relations for N_t and V_f, *i.e.*, Eq. (3), are not applicable to the open structure metals such as Bi, Sb, and Ga, it is impossible to evaluate the characteristic temperatures of these liquid metals by Eq. (6). The volume of the open structure metal contracts on melting and the σ_s/σ_l values also show anomalous changes.[9)]

9) T. E. Faber, in "The Physics of Metals, I Electrons", edited by J. M. Ziman, Cambridge University Press, (1969), pp. 282—316.

The general agreement of the calculated σ_s/σ_l values with the observed ones indicates that the translational motions of metal atoms in liquid phase and the holes introduced make a negligible contribution to the change of electrical conductivity because of their small fractions in the $3N$ degrees of freedom in the liquid metal just above melting point.

Carlson, Eyring, and Ree[10)] applied the significant structure theory to liquid metals such as Na and Hg to interpret the thermodynamic properties of these metals, including viscosity and self-diffusion. The theory, however, assumes that the mean frequency of thermal vibrations of atoms in liquid phase is the same as that of solid phase. Thus it can not applied to the present problem.

In recent years a new approach has been made for describing the electrical conductivity of liquid metal in terms of the pseudopotential approximation.[11,12)] Although the agreement between theory and experiment is encouraging, quantitative comparison is still premature.

Conclusion

Despite exceptions such as Hg, Ga, Sb, and Bi (some of them are semiconductors in the solid phase but ordinary metals when liquid), it is concluded in conjunction with Mott that most part of the change of electrical conductivity of metal on melting is ascribed to the change of the frequency of thermal vibrations in $3N$ degrees of freedom. The weakness of the liquid model used by Mott (communal entropy problem) was removed in the present model and a better agreement between theory and experiment was obtained.

The author wishes to thank Professor H. Hamaguchi for his kind encouragement.

10) C. M. Carlson, H. Eyring, and T. Ree, *Proc. Nat. Acad. Sci. U. S.*, **46**, 649 (1960).

11) J. M. Ziman, *Phil. Mag.*, **6**, 1013 (1961), *Advan. Phys.*, **13**, 89 (1964).

12) N. W. Ashcroft and J. Lekner, *Phys. Rev.*, **145**, 83 (1966).

The Powder ESR Spectra of Some Bis(amino acidato)copper(II) Complexes

Seizo MISUMI, Toshiyuki ISOBE, and Shinkichi KIMOTO

Inorganic Chemistry Laboratory, Faculty of Science, Kyushu University, Fukuoka

(Received December 28, 1971)

Copper(II) complexes with some natural amino acids were prepared, and their powder ESR spectra were measured. The pattern types of the ESR spectra of these Cu(II) complexes with amino acids were classified into four types, and by the pattern type, the *cis*- or *trans*-isomer was estimated.

Many X-ray crystallographic investigations of bis(amino acidato)copper(II) complexes[1-12] have revealed that the amino acids are usually bidentately-coordinated to the metal through the nitrogen (N) of the amino group and the oxygen (O) of the carboxyl group. Though there is the possibility of a *cis*- or *trans*-coordination for a bis-complex, the bis(glycinato)-copper(II) monohydrate reported by Tomita[13] was the first example of the *cis*-configuration. Since then other *cis*-complexes have been found[4,5,8,10] and many bis(amino acidato)copper(II) complexes have been investigated by X-ray crystallography,[1-12] infrared spectra,[14,15] visible diffuse reflectance spectra,[16] and ESR.[17-20]

In this paper, the powder ESR spectra of these complexes will be presented and discussed.

Experimental

Materials. The copper(II) complexes used in this study were as follows: $Cu(gly)_2 \cdot H_2O$-(I), $Cu(gly)_2 \cdot H_2O$-(II), $Cu(L\text{-val})_2$, $Cu(DL\text{-val})_2 \cdot H_2O$, $Cu(L\text{-ile})_2 \cdot H_2O$, $Cu(DL\text{-ile})_2 \cdot H_2O$, $Cu(L\text{-asn})_2$, $Cu(L\text{-arg})_2(NO_3)_2 \cdot 3H_2O$, $Cu(L\text{-trp})_2$, $Cu(L\text{-gln})_2$, $Cu(L\text{-ala})_2$, $Cu(DL\text{-ala})_2$, $Cu(L\text{-ser})_2$, $Cu(L\text{-thr})_2 \cdot H_2O$, $Cu(DL\text{-phe})_2$-(I), $Cu(DL\text{-phe})_2$-(II), $Cu(L\text{-phe})_2$, and $Cu(L\text{-leu})_2$, where the abbreviations used are gly : glycine, val : valine, ile : isoleucine, asn : asparagine, arg : arginine, trp : tryptophane, gln : glutamine, ala : alanine, ser : serine, thr : threonine, phe : phenylalanine, and leu : leucine.

Preparation. The $Cu(gly)_2 \cdot H_2O$-(I) and $Cu(gly)_2 \cdot H_2O$-(II) were prepared by the method of Tomita[13]; the $Cu(L\text{-val})_2$, $Cu(L\text{-ile})_2 \cdot H_2O$, and $Cu(L\text{-gln})_2$, by the method of Neuberg *et al.*[21] from basic $Cu(OH)_2 \cdot CuCO_3$, and the $Cu(DL\text{-val})_2 \cdot H_2O$, $Cu(DL\text{-ile})_2 \cdot H_2O$, $Cu(L\text{-asn})_2$, $Cu(L\text{-trp})_2$, $Cu(L\text{-ala})_2$, $Cu(DL\text{-ala})_2$, $Cu(L\text{-phe})_2$, and $Cu(L\text{-leu})_2$, by the method of Abderhalden and Schnitzler[22] from freshly-prepared $Cu(OH)_2$, while the $Cu(L\text{-arg})_2(NO_3)_2 \cdot 3H_2O$ was prepared by a method similar to that described by Dubois.[23] The $Cu(L\text{-ser})_2$ was prepared by the methods of both van der Helm and Franks[4] and of Abderhalden and Schnitzler[22]; the two complexes thus obtained were identical. The $Cu(DL\text{-phe})_2$-(I) and $Du(DL\text{-phe})_2$-(II) were prepared by the method of Herlinger *et al.*[14] All the ligand molecules were commercially available.

Each molecular formula was determined by elementary analysis and was confirmed by studying the far-infrared spectrum.

Measurements. The ESR spectra (powdered samples) of the complexes were measured at room temperature with a JEOL X-band ESR spectrometer, model JES-ME-3X, equipped with a 100 KHz field modulation unit.

Results and Discussion

1) $Cu(gly)_2 \cdot H_2O$-(I) and $Cu(gly)_2 \cdot H_2O$-(II).

Tomita[13] suggested that bis(glycinato)copper(II) monohydrate was a *cis*- and that dihydrate was a *trans*-complex. However, Yasui and Shimura[16] reported that the *trans*-complex was also a monohydrate, and the same result was obtained in this work. The separation of *cis*- and *trans*-complexes was confirmed by the methods of X-ray analysis,[2] infrared spectrum,[14,15] and visible diffuse reflectance spectrum.[16]

The powder ESR spectra of $Cu(gly)_2 \cdot H_2O$-(I) and $Cu(gly)_2 \cdot H_2O$-(II), checked by means of the infrared spectra, are shown in Fig. 1. It can be seen from Fig. 1 that, while the spectrum of *cis*-$Cu(gly)_2 \cdot H_2O$ is clearly axial in character, that of *trans*-$Cu(gly)_2 \cdot H_2O$ shows a distortion from the usual axial pattern. It is reasonable to expect that the *trans*-complex would display such a rhombic distortion due to the difference in Cu–O and Cu–N bond lengths. The ESR spectrum of *trans*-$Cu(gly)_2 \cdot H_2O$ was measured for the first time.

2) The Other Bis(amino acidato)copper(II) Complexes.

1) H. C. Freeman, *Adv. Protein Chem.*, **22**, 257 (1967).
2) H. C. Freeman, M. R. Snow, I. Nitta, and K. Tomita, *Acta Crystallogr.*, **17**, 1463 (1964).
3) A. Dijkstra, *ibid.*, **20**, 588 (1966).
4) D. van der Helm and W. A. Franks, *ibid.*, **B25**, 451 (1969).
5) C. M. Weeks, A. Cooper, and D. A. Norton, *ibid.*, **B25**, 443 (1969).
6) C. M. Gramaccioli and R. Marsh, *ibid.*, **21**, 594 (1966).
7) B. Evertsson, *ibid.*, **B25**, 30 (1969).
8) R. D. Gillard, R. Mason, N. C. Payne, and G. B. Robertson, *Chem. Commun.*, **1966**, 155.
9) S. Guha and N. N. Saha, *Acta Crystallogr.*, **B26**, 2073 (1970).
10) R. D. Gillard, R. Mason, N. C. Payne, and B. R. Robertson, *J. Chem. Soc., A*, **1969**, 1864.
11) A. M. Mathieson and H. K. Welsh, *Acta Crystallogr.*, **5**, 599 (1952).
12) D. van der Helm, M. B. Lawson, and E. L. Enwall, *ibid.*, **B27**, 2411 (1971).
13) K. Tomita, This Bulletin, **34**, 280 (1961).
14) A. W. Herlinger, S. L. Wenhold, and T. V. Long, *J. Amer. Chem. Soc.*, **92**, 6474 (1970).
15) R. A. Condrate and K. Nakamoto, *J. Chem. Phys.*, **42**, 2590 (1965).
16) T. Yasui and Y. Shimura, This Bulletin, **39**, 604 (1966).
17) W. Windsch and M. Welter, *Z. Naturforsch.*, **22A**, 1 (1967).
18) H. Yokoi and T. Isobe, This Bulletin, **42**, 2085 (1969).
19) A. L. Poznyak, V. N. Tadeush, and L. A. Il'yukevich, *Zh. Strukt. Khim.*, **6**, 779 (1965).
20) I. V. Miroshnichenko, G. M. Larin, and Ya. K. Syrkin, *ibid.*, **7**, 361 (1966).
21) C. Neuberg, H. Lustig, and I. Mandl, *Arch. Biochem. Biophys.*, **26**, 77 (1950).
22) E. Abderhalden and E. Schnitzler, *Z. Physiol. Chem.*, **163**, 94 (1927).
23) S. Valladas-Dubois, *Bull. Soc. Chim. France*, 967 (1961).

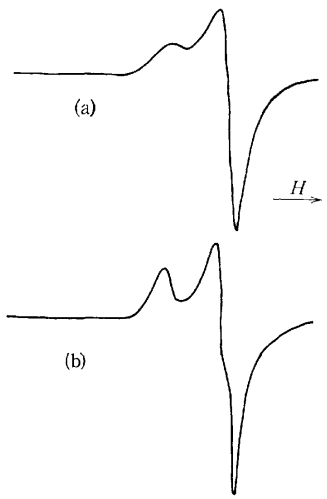

Fig. 1. The powder ESR spectra of *cis*-Cu(gly)$_2$·H$_2$O-(I) (a) and *trans*-Cu(gly)$_2$·H$_2$O-(II) (b).

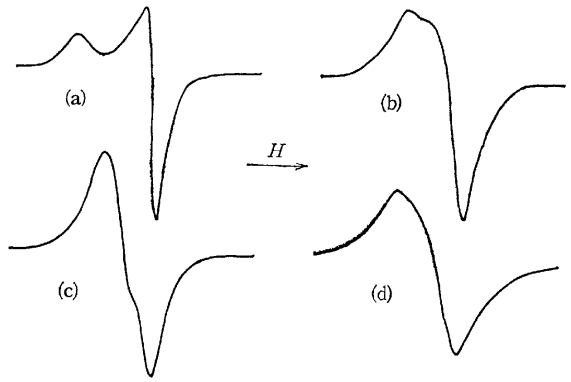

Fig. 2. The different types of the powder ESR spectra.
(a) Cu(L-val)$_2$-type, (b) Cu(L-trp)$_2$-type
(c) Cu(L-thr)$_2$·H$_2$O-type, (d) Cu(L-ala)$_2$-type

Figure 2 shows four typical polycrystalline ESR spectra of bis(amino acidato)copper(II) complexes: (a) Cu(L-val)$_2$, (b) Cu(L-trp)$_2$, (c) Cu(L-thr)$_2$·H$_2$O, and (d) Cu(L-ala)$_2$. Cu(L-val)$_2$, Cu(L-ile)$_2$·H$_2$O, Cu(DL-ile)$_2$·H$_2$O, Cu(L-asn)$_2$, Cu(L-arg)$_2$(NO$_3$)$_2$·3H$_2$O, and Cu(DL-phe)$_2$-(II) belong to the Cu(L-val)$_2$-type; Cu(L-trp)$_2$, Cu(DL-ala)$_2$, Cu(L-gln)$_2$, and Cu(DL-val)$_2$·H$_2$O belong to the Cu(L-trp)$_2$-type, and Cu(L-thr)$_2$·H$_2$O and Cu(L-ser)$_2$ belong to the Cu(L-thr)$_2$·H$_2$O-type, while Cu(L-ala)$_2$, Cu(DL-phe)$_2$-(I), Cu(L-phe)$_2$, and Cu(L-leu)$_2$ belong to the Cu(L-ala)$_2$-type.

The *cis*- and *trans*-complexes determined or estimated in this and other studies[2-5,12,14,16] are summarized in Table 1. The column for the ESR spectra in Table 1 shows the type of the powder ESR spectrum. Figure 2 shows that Cu(L-val)$_2$ gives an axial pattern, while Cu(L-trp)$_2$, Cu(L-thr)$_2$·H$_2$O, and Cu(L-ala)$_2$ give a non-axial pattern (clearly neither rhombic nor isotropic). From Table 1, the complexes of the Cu(L-val)$_2$-type can be found to be all *cis*-complexes except for the result of infrared spectra of Cu(L-val)$_2$.[14] On the other hand, the complexes of the Cu(L-trp)$_2$-type, the Cu(L-thr)$_2$·H$_2$O-type, and the Cu(L-ala)$_2$-type are all found to be *trans*-complexes except for the results of the X-ray analysis of Cu(L-ser)$_2$.[4] Therefore, the complexes of the Cu(L-val)$_2$-type are estimated to be *cis*-complexes, and the complexes of the Cu(L-trp)$_2$-type and the Cu(L-ala)$_2$-type, *trans*-complexes.

Although there is a difference between the results on Cu(L-val)$_2$ by Herlinger *et al.*[14] and those by Yasui and Shimura,[16] it may be believed to be a *cis*-complex on the basis of the above discussion.

According to van der Helm and Franks, Cu(L-ser)$_2$ forms a square pyramidal complex.[4] The four atoms (N_A, N_B, O_{1A}, O_{1B}) are not coplanar, but form a very flattened tetrahedron.[4] This is a complex with a lower symmetry than the other, so it may be supposed that this complex shows a non-axial pattern of the powder ESR spectrum. Only a coplanar *cis*-complex shows an axial pattern, while a non-coplanar *cis*-complex shows a non-axial pattern. Cu(L-thr)$_2$·H$_2$O is found to be the same type.

Bis(DL-phenylalaninato)copper(II) is a complex[14] which has *cis*- and *trans*-isomers, just as bis(glycinato)-copper(II)[13] and bis(L-alaninato)copper(II).[3,8] Cu(DL-phe)$_2$-(I) belongs to the Cu(L-ala)$_2$-type, and Cu(DL-phe)$_2$-(II) belongs to the Cu(L-val)$_2$-type; the

Table 1. Bis (amino acidato) copper (II) complexes determined or estimated by authors and other investigators

	Crystal structure	Infrared spectra[14]	Reflection spectra[16]	ESR spectra
Cu(gly)$_2$·H$_2$O-(I)	*cis*[2]	*cis*	*cis*	(*cis*)
Cu(gly)$_2$·H$_2$O-(II)	—	*trans*	*trans*	(*trans*)
Cu(L-ala)$_2$	*trans*[3]	*trans*	*trans*	L-ala (*trans*)
Cu(L-ser)$_2$	*cis*[4]	—	—	L-thr
Cu(L-ile)$_2$·H$_2$O	*cis*[5]	*cis*	*cis*	L-val (*cis*)
Cu(L-val)$_2$	—	*trans*	*cis*	L-val (*cis*)
Cu(DL-ile)$_2$·H$_2$O	—	*cis*	*cis*	L-val (*cis*)
Cu(DL-phe)$_2$-(II)	—	*cis*	—	L-val (*cis*)
Cu(DL-phe)$_2$-(I)	—	*trans*	—	L-ala (*trans*)
Cu(DL-ala)$_2$	—	*trans*	*trans*	L-trp (*trans*)
Cu(DL-val)$_2$·H$_2$O	—	*trans*	*trans*	L-trp (*trans*)
Cu(L-thr)$_2$·H$_2$O	—	—	*trans*	L-thr
Cu(L-phe)$_2$	*trans*[12]	*trans*	—	L-ala (*trans*)
Cu(L-leu)$_2$	—	*trans*	—	L-ala (*trans*)

former is found to be a *trans*-complex, and the latter, a *cis*-complex, from the results of the powder ESR spectra. These facts agree with those of the other infrared spectral study.[14] Thus, it supports our findings that a *cis*-complex or *trans*-complex found not only for bis(glycinato)copper(II), but also for bis(DL-phenylalaninato)copper(II), could be estimated by ESR. Table 1 shows the good agreement of our study with other studies.[2,3,5,12,14,16]

The geometrical isomers are believed to be classifiable as follows:

$Cu(gly)_2 \cdot H_2O$-(I)	*cis*
$Cu(gly)_2 \cdot H_2O$-(II)	*trans*
$Cu(\text{L-val})_2$	*cis*
$Cu(\text{DL-val})_2 \cdot H_2O$	*trans*
$Cu(\text{L-ile})_2 \cdot H_2O$	*cis*
$Cu(\text{DL-ile})_2 \cdot H_2O$	*cis*
$Cu(\text{DL-phe})_2$-(I)	*trans*
$Cu(\text{DL-phe})_2$-(II)	*cis*
$Cu(\text{L-asn})_2$	*cis*
$Cu(\text{L-arg})_2(NO_3)_2 \cdot 3H_2O$	*cis*
$Cu(\text{L-trp})_2$	*trans*
$Cu(\text{L-gln})_2$	*trans*
$Cu(\text{L-ala})_2$	*trans*
$Cu(\text{L-phe})_2$	*trans*
$Cu(\text{L-leu})_2$	*trans*

The authors wish to thank the Ministry of Education for its financial support given to this research.

BULLETIN OF THE CHEMICAL SOCIETY OF JAPAN, VOL. 45, 2697—2702 (1972)

Studies on the Interaction between Long Chain Alcohols and Alkyl Sulfates. II. Molecular Association between Dodecyl Alcohol and Dodecyl Sulfate of Divalent Metals

Yoshikiyo Moroi, Kinshi Motomura, and Ryohei Matuura
Department of Chemistry, Faculty of Science, Kyushu University, Fukuoka

(Received December 28, 1971)

Molecular interaction between dodecyl alcohol and dodecyl sulfate of divalent metal cations such as Mg^{2+}, Ca^{2+}, Sr^{2+}, Ba^{2+}, Mn^{2+}, Co^{2+}, Ni^{2+}, and Cu^{2+} was studied by measurement of heat of complex formation, differential thermal analysis and infrared spectroscopy. It was found that magnesium, manganese, cobalt, nickel, and copper dodecyl sulfates formed two or three kinds of complexes with dodecyl alcohol, differing in composition depending on temperature. On the other hand, no evidence of complex formation could be found by these experimental techniques for calcium, strontium and barium dodecyl sulfates, all of which are very small in solubility into water. For the former class of metal dodecyl sulfates the composition of complex was 3.5—4.0 in molar ratio of alcohol to sulfate at temperature below the melting point of alcohol, while it was 5.0—6.0 at temperature above it. The heat of complex formation above the melting point of alcohol was −40——44 kcal/mol-sulfate. Two or three characteristic absorption bands could be found over the range 3200—3500 cm^{-1}, suggesting that the complex formation is due to hydrogen bonding between two components.

Many papers concerning the interaction between long chain alcohols and alkyl sulfates have been published with viewpoints of emulsion and film stabilization due to complex formation and penetration. The results, however, have not been coincident with one another. Recently, Friberg has attempted to interrelate the molecular complexes as emulsion and foam stabilizer with phase diagram of the components;[1-3] in his papers the materials have not been confined to long chain compounds.

In our previous paper, it has been shown that there are two kinds of complexes, I and II, between dodecyl alcohol and sodium dodecyl sulfate, tetradecyl alcohol and sodium tetradecyl sulfate, hexadecyl alcohol and sodium hexadecyl sulfate, differing in the composition ratio of alcohol to sulfate.[4] The complex I was stable at temperature below the melting point of alcohol, the molar ratio of alcohol to sulfate being 0.55—0.63. The complex II was stable at temperature above the melting point of alcohol, its molar ratio being 1.0.

The object of this paper is to extend the previous work to divalent alkyl sulfates and to see the difference between monovalent and divalent cation complexes by the same methods as in the previous paper. Also it is our aim to investigate whether the mechanism of the complex formation could be elucidated by statistical thermodynamics.

The following abbreviations are used.
DOH: Dodecyl Alcohol
$Mg(DS)_2$, $Ca(DS)_2$, $Sr(DS)_2$, $Ba(DS)_2$, $Mn(DS)_2$, $Co(DS)_2$, $Ni(DS)_2$, $Cu(DS)_2$: Magnesium, Calcium, Strontium, Barium, Manganese, Cobalt, Nickel, and Copper Dodecyl Sulfate, respectively.

1) St. Friberg and L. Rydhag, *Kolloid-Z. Z. Polym.*, **244**, 233 (1971).
2) St. Friberg and S. I. Ahmad, *J. Colloid Interfac. Sci.*, **35**, 175 (1971).
3) St. Friberg, *Kolloid-Z. Z. Polym.*, **244**, 333 (1971).
4) Y. Moroi, K. Motomura, and R. Matuura, This Bulletin, **44**, 2078 (1971).

These are often represented as $M(DS)_2$.
DTA: Differential Thermal Analysis
IR: Infrared Spectroscopy

Experimental

Materials. DOH was the same as described in the previous paper.[4] $M(DS)_2$ was prepared by a double decomposition from divalent metal cation chloride or sulfate and purified sodium dodecyl sulfate (SDS) in aqueous media. The CMC value was 8.13×10^{-3} mol/*l* at 25°C. The precipitate of $M(DS)_2$ formed was purified by repeated recrystallizations from water, and was dried at 125°C for fifteen minutes under a reduced pressure. The purified $M(DS)_2$ did not show any characteristic endothermic peak of SDS at 104°C on a DTA curve. The absorption bands of water could hardly be found in their IR spectra.

The specimens of complexes of DOH and $M(DS)_2$ used for measurements of DTA, IR and heat of complex formation were prepared by the two methods, *i.e.*, the melt method and the crystallization method. These were quite the same as described in the previous paper. Most of these metal dodecyl sulfates were so hygroscopic that all operations were performed in an atmosphere of dried nitrogen gas.

Methods. A Shimadzu X-ray diffractometer (DV-1) with a Geiger counter was employed with a beam exit slit of 0.7 mm. The nickel filtered copper radiation was used in all cases. The apparatus was standardized at angles 28.44° of silicon. The scanning speed was 1 deg/min., and the chart speed was 20 mm/min.

The DTA apparatus and operational condition were the same as those in the preceeding paper.[4] In the present case, two or three endothermic peaks appeared in DTA curves of the complexes even after a long time. As a result, the ratio of alcohol to sulfate in the complex above the melting point of DOH was determined from the composition at which the exothermic peak due to freezing of excess free alcohol disappeared on cooling curve. On the other hand, below the melting point the ratio was determined from the composition at which the endothermic peak due to melting of excess free alcohol disappeared on heating curve. This method is different from the previous one,[4] and the reason will be made clear in the next section.

The IR apparatus and operational condition were the same as those in the preceeding paper[4] except replacing hexachlorobutadiene by Nujol.

The heat of complex formation was measured at 35°C with an Applied Electric Laboratory calorimeter, Model CM-204S1. The samples were so hygroscopic that they were sealed into a glass ampule. On mixing them with DOH the ampule was held in DOH and crushed in it by a small hammer, after having been thermally equilibriated. The sample weight was about 100 mg and DOH used was 50 ml. Sodium dodecyl sulfate, sodium tetradecyl sulfate, and sodium hexadecyl sulfate formed the complexes with their corresponding alcohols which are insoluble in the alcohols, while complexes of $M(DS)_2$ with DOH were very soluble in DOH. Consequently $M(DS)_2$ with DOH were very soluble in DOH. Consequently, the heat of complex formation could not be measured only through mixing the sulfate with the alcohol. Therefore, it was determined by subtracting the heat (ΔHs) evolved by solubilizing the complex into DOH from the heat (ΔHt) evolved by mixing the dried sulfate with DOH with subsequent solubilization of complex.

Results and Discussion

X-ray Diffraction. The characteristic data of $M(DS)_2$ are collected in Table 1. As $Co(DS)_2$, $Ni(DS)_2$, and $Cu(DS)_2$ are so hygroscopic that their characteristics change during operation, the values for these sulfates are those for the compounds with water of crystallization, *i.e.*, $M(DS)_2\cdot nH_2O$. The amounts of water of crystallization for hygroscopic $M(DS)_2$ determined by elementary analysis were identical with those in literature,[5] and the agreement between the calculated and observed values of elementary analysis was good.

Table 1. Results of DTA and X-ray diffraction for $M(DS)_2$

$M(DS)_2$	DTA (°C)		X-ray (Å)
	Dehydration	Transition	Long spacing
$Mg(DS)_2$		120	34.0
$Ca(DS)_2$		83	30.0
$Sr(DS)_2$			36.0
$Ba(DS)_2$		121	33.8
$Mn(DS)_2$		132	32.1
$Co(DS)_2\cdot6H_2O$	56, 85, 110		20.6
$Ni(DS)_2\cdot6H_2O$	57, 72, 85, 101		29.2
$Cu(DS)_2\cdot4H_2O$	44, 118		25.0
NaDS		104	31.6, 39.0

It can be said from this result that the X-ray long spacing of metal sulfates with water of crystallization are shorter than those without water. This fact indicates that the carbon chain axis of sulfates with water is more tilted than those without water.

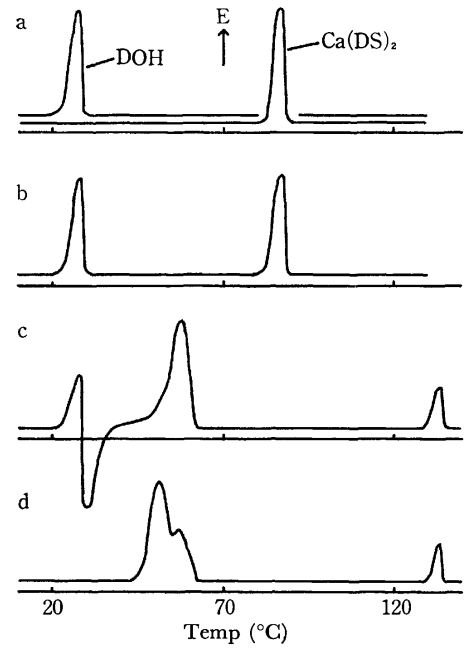

Fig. 1. DTA curves for detecting a complex formation. a: DOH and $Ca(DS)_2$ b: mixture of DOH and $Ca(DS)_2$, c: mixture of DOH and $Mn(DS)_2$, d: $Mn(DS)_2$-DOH complex, E: endothermic

5) R. Matuura and I. Satake, *Yushi*, **16**, 94 (1963).

DTA. The complex formation could easily be detected by DTA technique. The typical examples are shown in Fig. 1. When the mixture of $M(DS)_2$ and DOH in a solid phase is heated in a DTA cell from the temperature below the melting point of DOH to higher temperature, the DTA curve results merely in the superposition of their own DTA curves, unless they form a complex. On the other hand, the mixture which forms a complex shows a sharp exothermic peak in the heating curve just beyond the endothermic peak due to melting of DOH. This exothermic peak is followed by a new endothermic peak which corresponds to the characteristic peak of the complex. This phenomenon indicates that the mixture in solid state cannot undergo a reaction, while the melt of DOH can react with solid $M(DS)_2$ to form a complex accompanying heat evolution.

The sodium sulfate complexes were so stable that they kept up their own state during the operation without showing any peak in a DTA curve due to transition. On the contrary, divalent cation complexes are not so stable and have two or three more endothermic peaks even after being kept at a fixed temperature for a long time. Therefore, it was difficult to assign each endothermic peak to a complex. When the complexes formed above the melting point of DOH are cooled below it, they release the extra DOH at freezing state and transform to the other complexes. These complexes formed below the melting point of DOH are so unstable that they react again with the extra molten DOH on being heated above the melting point of DOH and show the exothermic peak due to complex formation in addition to the characteristic endothermic peak of the complex. However, it was possible, in some cases, to assign the peak to complex L or complex H, with the aid of the measurement of peak area on DTA curve, depending on the temperature at which the complex was kept. Complex L and complex H are complexes which formed below and above the melting point of DOH, respectively. The results of differential thermograms of these complexes are summarized in Table 2. Consequently, differing from the method in the previous paper, the following method was used in this study to determine the composition of the complex. The composition of complex L was determined from the ratio of DOH to $M(DS)_2$ in the state where the endothermic peak due to melting of extra free DOH disappears, and the composition of complex H was determined from the ratio in the state where the exothermic peak due to freezing of extra free DOH disappears. The typical DTA curves of manganese complex are shown in Fig. 1.

Table 2. Characteristic endothermic temperatures of complexes in DTA curves

Metal	Complex L (°C)	Complex H (°C)
Mg	40—43	53—55
Ca	—	—
Sr	—	—
Ba	—	—
Mn	40—41, 46—47	57—58
Co	38—40, 47—50	57—59
Ni	30—33, 38—40	
Cu	40—42, 48—50	

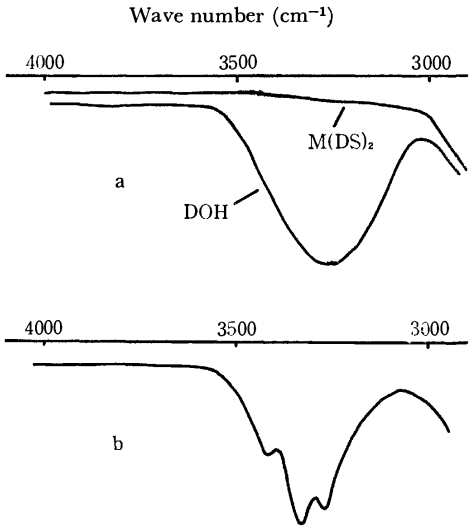

Fig. 2. IR spectra of complex formation. a: DOH and $M(DS)_3$, b: $Mn(DS)_2$-DOH complex

Infrared. Infrared spectroscopy as well as DTA are useful technique for detecting the complex formation. It is shown in Fig. 2 that the spectrum in the hydroxyl stretching region has sharper bands than those of DOH and is composed of two or three absorption bands. These bands, however, are broader in comparison with those of sodium sulfate complex. This might suggest that there are two or three kinds of (slightly diffused) bonding states between $M(DS)_2$ and DOH. The characteristic band region of complexes is the same as that of DOH, indicating that complexes are formed by the hydrogen bonding between two components in a manner similar to DOH. As will be mentioned later, it can also be confirmed from the magnitude of heat of complex formation that the complex formation is mainly due to the hydrogen bonding. The characteristic bands are summarized in Table 3.

Table 3. Characteristic absorption bands of complexes in IR spectra

Metal	Absorption band (cm^{-1})		
Mg	~3310	~3370	~3450
Mn	~3290	~3320	~(3460)
Co	~3280	~3320	~(3480)
Ni	~3290	~3340	~(3420)
Cu	~3200	~3300	

Heat of Complex Formation. As shown in Fig. 3, $M(DS)_2$ reacts with molten DOH to form a complex with heat evolution and then resolves in molten DOH with heat absorption. When particles of larger size, of $M(DS)_2$ were dropped into molten DOH, the rate of resolution is larger than that of complex formation, accompanying net heat absorption. The heat of complex H formation (ΔH_H) is shown in Table 4 together with the results of complex H composition. Complex H used to measure ΔH_S had the composition of $M(DS)_2 \cdot 6DOH$. Even if the ratio of alcohol to sulfate is less than six, the effect of excess DOH on ΔH_S should be

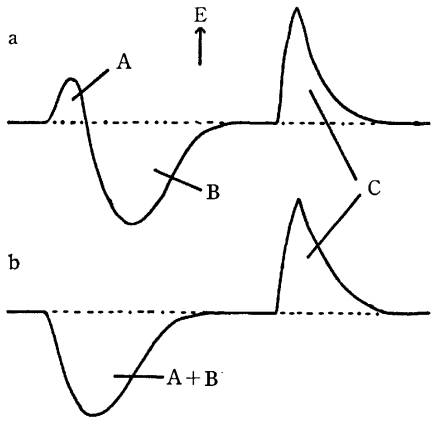

Fig. 3. Diagram of heat of complex formation and dissolution into DOH. a: $M(DS)_2$ in small size, b: $M(DS)_2$ in larger size, A: heat of complex formation, B: heat of dissolution of complex, C: standard heat, E: exothermic

Table 4. Heat of complex formation and composition of complex

Metal	ΔH_H (kcal/mol-sulfate)	Molar ratio of DOH to $M(DS)_2$	
		complex L	complex H
Mg	−41.0±2	3.8—4.0	5.8—6.0
Mn	−40.1±2	3.8—4.0	5.8—6.0
Co	−41.2±2	3.8—4.0	5.0—6.0
Ni	−41.5±2	3.8—4.0	5.0—6.0
Cu	−44.0±2	3.8—4.0	5.5—6.0

negligible because of very little solubilization of complex H in excess DOH. The values of ΔH_H are about −40 kcal/mol-sulfate. These values are five or six times as large as those of sodium sulfate complex formation (7—8 kcal/mol-sulfate). This is consistent with the fact that the ratio of alcohol to sulfate in complex H is 5 to 6, while that of complex II of sodium sulfate is 1.0.

Statistical Thermodynamical Consideration

It seems to be instructive in a further investigation to discuss the complex formation with the viewpoint of statistical thermodynamics. In analogy with the previous paper,[4] this discussion is intended to explain the composition of complexes, namely the molar ratio of alcohol to sulfate in a complex, which is nearly 4 below the melting point of alcohol and nearly 6 above it. As mentioned above, there are two or three complexes in total, differing from the case of sodium sulfates. Furthermore, a divalent metal sulfate has two radicals of alkyl sulfate in a molecule, and then the theoretical treatment comes to be a little more difficult.

The consideration is based on the concept of chapter XI in "mixture" by Guggenheim.[6] We denote alcohol and sulfate by A and B, respectively, and consider a binary mixture containing Nr molecules of alcohol and N molecules of sulfate on a lattice of $N(r+2)$ sites with a coordination number Z, where $M(DS)_2$ is regarded as a dimer and occupies two lattice sites. Since A and B molecules have ZNr and $(2Z-2)N$ contact number, respectively, the total number of intermolecular contact (Q) is given by

$$Q = \frac{ZN}{2}(r+q), \tag{1}$$

where q is defined so that the open chain r-mer containing r elements may have Zq contacts, and then q is in this case equal to $2-2/Z$. The ratios of Q from A and B are denoted by U and V, respectively.

$$U = \frac{r}{r+q} \tag{2}$$

$$V = \frac{q}{r+q} \tag{3}$$

There are four kinds of contacts, A-A, A-B, B-A, and B-B. We denote by $-2X/Z$ the energy for a pair of the same kind of molecules and further define W such that the contribution of A-B contact of configurational energy is

$$-\frac{X'_{A-A}+X'_{B-B}+W}{Z}. \tag{4}$$

What must be emphasized at this point is that the energy for a longitudinal pair should be different from that for a lateral one. Nevertheless, we used $-2X/Z$ as the mean value of them. Consequently, the discussion cannot be given in terms of individual item, but may be limited to the mean values as a whole.

From these definitions, we can construct Table 5 for a complete random distribution. The prime in Table 5 refers to the newly obtained complex, E_c being the total configurational energy.

Table 5. Number of pairs and certain related quantities

Kind of contact	Number of contacts	Energy of all such contacts
A-A	QU^2	$-\frac{2}{Z}\ QU^2X'_{A-A}$
A-B	QUV	$-\frac{1}{Z}\ QUV(X'_{A-A}+X'_{B-B}+W)$
B-A	QVU	$-\frac{1}{Z}\ QVU(X'_{B-B}+X'_{A-B}+W)$
B-B	QV^2	$-\frac{2}{Z}\ QU^2X'_{B-B}$
All	Q	$-\frac{2Q}{Z}\ (UX'_{A-A}+VX'_{B-B}+UVW)=E_c$

E_c can be rewritten as follows;

$$E_c = -N\left(rX'_{A-A}+qX'_{B-B}+\frac{rq}{r+q}W\right) \tag{5}$$

According to definition, the configurational partition function Ω is given by

$$\Omega = \sum \exp(-E_c/kT), \tag{6}$$

where the summation extends over the $g(Nr, N)$ distinguishable configurations. $g(Nr, N)$ is given by

6) E. A. Guggenheim, "Mixtures", ed. by R. H. Fowler, P. Kapitza, N. F. Mott, and E. C. Bullard, Oxford at the Clarendon Press (1952).

$$g(Nr, N) = \left(\frac{Z}{2}\right)^N \frac{(Nr+2N)!}{(Nr)!N!}\left\{\frac{(Nr+Nq)!}{(Nr+2N)!}\right\}^{1/(2-q)} \quad (7)$$

As the configurational free energies of pure substances containing the same number of molecules are $-NrX_{A-A}$ and $-NqX_{B-B}$, the molar free energy of mixing of the sulfate is given by

$$\Delta F_m = -Nr(X'_{A-A}-X_{A-A}) - Nq(X'_{B-B}-X_{B-B}) - \frac{Nrq}{r+q}W - RT\left[\ln 2Z - r\ln\frac{r}{r+2} - 2\ln\frac{2}{r+2} + \frac{1}{2-q} \times\left\{r\ln\frac{r+q}{r+2} + q\ln(r+q) - 2\ln(r+2)\right\}\right], \quad (8)$$

where N is Avogadro's number. Concerning a liquid or solid phase, we can, without serious error, replace internal energy and Helmholtz free energy by enthalpy and Gibbs free energy, respectively. Consequently the molar enthalpy of mixing of sulfate is given by

$$\Delta H = -Nr(X'_{A-A}-X_{A-A}) - Nq(X'_{B-B}-X_{B-B}) - \frac{Nrq}{r+q}W, \quad (9)$$

where we assume that the temperature changes of X'_{B-B}, X_{B-B}, and W are negligible, because of very limited temperature range 20—35°C in this case.

First, when $r=0$, we obtain the equation

$$\Delta H = -Nq(X'_{B-B}-X_{B-B}) \equiv \Delta H_0 \quad (10)$$

The new parameter ΔH_0 is hypothetically equivalent to the heat evolved when a sulfate is transformed into a complex whose lattice sites are all occupied by sulfate molecules.

Second, when $r=r_H$, which is the ratio of DOH to $M(DS)_2$ in complex H, ΔH_H is given by

$$\Delta H_H = -r_H(NX'^H_{A-A} - NX^1_{A-A}) + \Delta H_0 - \frac{Nr_Hq}{r_H+q}W, \quad (11)$$

where $X^1{}_{A-A}$ is the X_{A-A} of liquid alcohol and ΔH_H is equal to the heat of complex H formation measured above the melting point of alcohol.

We may obtain unknown parameters from the ratios of DOH to $M(DS)_2$ in complex L and complex H, imposing conditions consistent with the results on ΔG_m.

For complex L,

$$\frac{\partial \Delta G_{mL}}{\partial r} < 0 \text{ at } r = r_{L1},$$

$$\frac{\partial \Delta G_{mL}}{\partial r} > 0 \text{ at } r = r_{L2}, \quad (12)$$

and $$\Delta G_{mH} < 0 \quad \text{at } r_{L1} < r < r_{L2},$$

where r_{L1} and r_{L2} are lower and upper limit of r_L, respectively.

For complex H,

$$\frac{\partial \Delta G_{mH}}{\partial r} < 0 \text{ at } r = r_{H1},$$

$$\frac{\partial \Delta G_{mH}}{\partial r} > 0 \text{ at } r = r_{H2}, \quad (13)$$

and $$\partial \Delta G_{mH} < 0 \quad \text{at } r_{H1} < r < r_{H2},$$

where r_{H1} and r_{H2} are lower and upper limit of r_H, respectively.

We employed 1, 2, and 3 kcal/mol -$M(DS)_2$ as a reasonable value for ΔH_0, and 22.8 and 15.1 kcal/mol for NX_{A-A} and $NX^1{}_{A-A}$, respectively, according to the previous paper.[4] Thus NW and NX'_{A-A} can be obtained from Eqs. (11), (12), and (13), with Z to be an unknown parameter. A typical example for calculation is shown in Fig. 4 for $Mg(DS)_2$-DOH complex. The results obtained are summarized in Table 6. This shows that the values of NX'_{A-A} are 17—19 and 11—13 kcal/mol for NX'^L_{A-A} and NX'^H_{A-A} respectively.

In the previous paper, NX'_{A-A} was the average of those of complex I and II. On the other hand, in

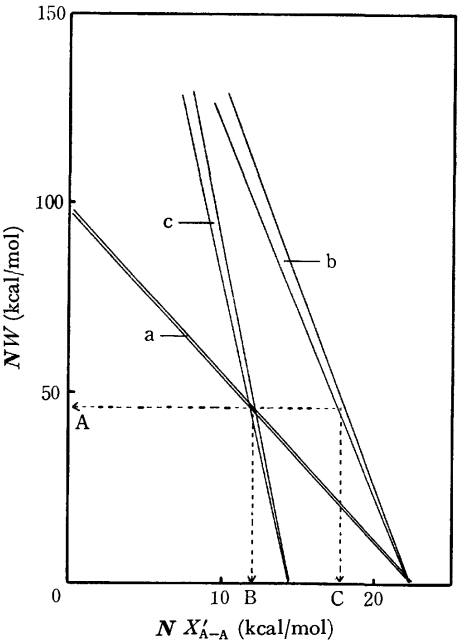

Fig. 4. Calculation of NW and NX'_{A-A} for $Mg(DS)_2$-DOH, $Z=8$. Extents obtained from equations: (a), Eq. (11); (b), Eq. (12); (c), Eq. (13).
A: value of NW, B: value of NX'^H_{A-A}, C: value of NX'^L_{A-A}

Table 6. Calculated values of unknown parameters

Metal	NX'^L_{A-A} (kacl/mol)	NX'^H_{A-A} (kcal/mol)	NW (kcal/mol)	H_L (kcal/mol-$M(DS)_2$)
		$Z=6$		
Mg	18.0±0.6	12.0±0.2	46±2	−35.0±10
Mn	18.0±0.6	12.0±0.2	46±2	−35.0±10
Co	18.6±0.6	12.2±0.6	47±2	−36.1±10
Ni	18.6±0.6	12.2±0.6	47±2	−36.1±10
Cu	18.4±0.6	12.2±0.3	49±2	−38.4±10
		$Z=8$		
Mg	18.0±0.3	12.2±0.2	46±2	−35.0± 9
Mn	18.0±0.3	12.2±0.2	46±2	−35.0± 9
Co	18.1±0.3	11.8±0.6	47±2	−36.6± 9
Ni	18.1±0.3	11.8±0.6	47±2	−36.6± 9
Cu	17.1±0.3	11.9±0.3	49±2	−37.4± 9
		$Z=12$		
Mg	17.4±0.3	11.9±0.2	45±2	−33.0± 9
Mn	17.4±0.3	11.9±0.2	45±2	−33.0± 9
Co	17.0±0.3	11.5±0.6	48±2	−35.4± 9
Ni	17.0±0.3	11.5±0.6	48±2	−35.4± 9
Cu	17.5±0.3	11.8±0.3	44±2	−32.3± 9

the present treatment the NX'_{A-A} is separated into NX'^{L}_{A-A} and NX'^{H}_{A-A} for complex L and complex H, respectively. Comparing these values with the previous ones, 14—16 kcal/mol, which is almost equal to the mean value of NX'^{L}_{A-A} and NX'^{H}_{A-A}, we arrive at the conclusion that the state of alcohol in monovalent cation complex is almost equal to that in divalent one.

Using the values of NX'^{L}_{A-A}, the heat of complex L formation can also be calculated with W in complex H also shown in Table 6. Thus, it is found that the absolute value of ΔH_L is smaller than that of ΔH_H and the effect of the alterations of ΔH_0 and Z on unknown parameters is rather small.

What is evident from these results is as follows; $M(DS)_2$ of divalent ion whose sulfate (MSO_4) is rather soluble in water is apt to form a complex with DOH, and *vice versa*.

For Ca, Sr, and Ba dodecyl sulfate, the intermolecular force in a crystal state is so strong that the complex cannot be formed. In other words, their own intermolecular force is stronger than that between $M(DS)_2$ and DOH in a complex state. On the other hand, the intermolecular force of dodecyl sulfate of such metals as Mg, Mn, Co, Ni, and Cu is weaker than that between $M(DS)_2$ and DOH in a complex state and leads to a negative enthalpy change on the complex formation that has a main effect on negative free energy change.

According to the above discussion, the dodecyl sulfate of divalent metals having larger solubility into a water must form a complex with DOH. The composition of it should depend on the metal ion and the temperature.

BULLETIN OF THE CHEMICAL SOCIETY OF JAPAN, VOL. 45, 2702—2708 (1972)

Oxygen Vacancies in the Perovskite-type Ferrites. II. Mössbauer Effect in the $SrFeO_{2.5}$-$LaFeO_3$ Solid-solution System

Hiroshi YAMAMURA and Ryôiti KIRIYAMA*

National Institute for Research in Inorganic Materials, Kurakake, Sakura-Mura, Niihari-Gun, Ibaraki
**The Institute of Scientific and Industrial Research, Osaka University, Yamadakami, Suita, Osaka*

(Received December 7, 1971)

The Mössbauer effect was studied for the solid-solution $Sr_{1-x}LaFeO_{2.5+x/2}$ system, prepared by firing in a vacuum. The intensity of the characteristic six absorption lines of the tetrahedral-iron site in the brownmillerite-type phase ($0.0 \leq x \leq 0.20$) was weakened with an increase in the La content because of an increasing incorporation of oxygen, while the Mössbauer parameters remained constant. $SrFeO_{2.5}$ with a brownmillerite-type structure, completely changed into a cubic perovskite-type structure at the composition with $x=0.30$; however, the original absorption peaks for the tetrahedral-iron site still exist even if the intensity is considerably decreased. Moreover, new peaks came out, with Mössbauer parameters different from those for the octahedral- or the tetrahedral-iron sites. On the basis of the values of their Mössbauer parameters, the origin of the new peak can be assigned to the presence of a five-coordinated iron site surrounded by a trigonal bipyramidal polyhedron of oxygen rather than a square pyramidal one. The three kinds of iron site lead to a single octahedral one when most of Sr is replaced with La ($x \geq 0.50$). The oxygen-deficient, perovskite-type phase with a cubic symmetry may be stabilized by the presence of the mixed-coordination scheme of Fe^{3+}, *i.e.*, the octahedral, trigonal bipyramidal, and tetrahedral sites.

In the previous paper,[1] we studied the role of oxygen vacancies in the stabilization of the perovskite-type structure in the $Sr_{1-x}M_xFeO_{3-\delta}$ solid-solution system ($M=Y^{3+}$, La^{3+}, Bi^{3+}, or In^{3+}). The X-ray diffraction measurements indicated that the end member $SrFeO_{2.5}$, which is isostructural with brownmillerite, which has an orthorhombic symmetry, changed to a cubic perovskite-type structure upon the addition of M^{3+} ($0.30 \leq x \leq 0.60$) as a result of a decrease in the concentration of oxygen vacancies. Throughout the previous study, however, we could not visualize the details of an oxygen-deficient structure only by means of X-ray diffractometry. The purpose of the present work is to further clarify the contents of the defect structure with the aid of such Mössbauer spectroscopic information, observed at iron sites, as the coordination state from the surrounding oxygens, the nature of the chemical bonding, and the electric-field gradient.

$LaFeO_3$, being isostructural with $GdFeO_3$ (the space group P_{bnm}-D_{2h}^{16}), consists of four distorted sub-cells,[2] and neutron-diffraction measurements[3] have shown that it has a G-type,[4] spin-ordered antiferromagnetic structure with its Neel temperature at 750°K. The Mössbauer spectrum was first observed by Eibschutz *et al.*[5] to show an isomer shift of +0.32 mm/sec and

1) H. Yamamura and R. Kiriyama, *Nippon Kagaku Kaishi*, **1972**, 343.

2) S. Geller and E. A. Wood, *Acta Crystallogr.*, **9**, 563 (1956).

3) W. C. Koehler and E. O. Wollan, *J. Phys. Chem. Solids*, **2**, 100 (1957).

4) E. O. Wollan and W. C. Koehler, *Phys. Rev.*, **100**, 545 (1955).

5) M. Eibschutz, G. Gorodetsky, S. Shtrikman, and D. Tres, *J. Appl. Phys.*, **35**, 1071 (1964).

an internal magentic field of 519 kOe. On the other hand, MacChesney *et al.*[6] studied the $SrFeO_{3-\delta}$ system, in which $SrFeO_{2.5}$ (prepared by firing in CO_2/H_2) was found to have a brownmillerite-type structure. The Mössbauer spectrum for $SrFeO_{2.5}$ was first reported by Gallagher *et al.*[7] without sufficient discussion. According to the results of Collvile's study, $CaFeO_{2.5}$,[8] being isostructural with $SrFeO_{2.5}$ (the space group P_{cmn}-D_{2h}^{16}), has an orthorhombic symmetry, are containing two types of iron sites, (Fe_I and Fe_{II}), both of which are alternatively drawn up along the *b*-axis. The Fe_I occupies an octahedral site surrounded by 6 O^{2-}, while the Fe_{II} occupies a tetrahedral site surrounded by 4 O^{2-} ions. The crystal lattice with a perovskite-type structure is deformed by the ordering of the oxygen vacancies. The neutron-diffraction measurements[9] revealed that $CaFeO_{2.5}$ also has a G-type antiferromagnetic structure with its Neel temperature at 720°K, where the spins of Fe^{3+} in both the octahedral and tetrahedral sub-lattices all lie along the *c*-axis. Grant,[10] after having studied the Mössbauer effect of $CaFeO_{2.5}$, concluded that the electric-field gradient is axially symmetric, in which the *z*-principal axis is parallel to the crystallographic *b*-axis, and that the large quadrupole splitting both the iron sites arises from the deformation of the corresponding oxygen-octahedron and -tetrahedron.

The Mössbauer effect for the $Sr_{1-x}La_xFeO_{3-\delta}$ system, prepared by firing under a high oxygen pressure, was studied by Shimony *et al.*[11] and by Gallagher *et al.*[12] In their investigation, however, attention was paid only to the mixed valencies of Fe^{3+} and Fd^{4+}, not to the generated lattice defect. On the other hand, only a few studies of the defect structure using Mössbauer spectroscopy have been published. Sawatzky *et al.*[13] determined the extent of the distribution of Fe^{3+} for octahedral and tetrahedral sites in the inverse spinel $CoFe_2O_4$. On the other hand, Elias *et al.*[14] successfully confirmed the occurrence of the tetrahedral Fe^{3+} site due to the presence of iron vacancies even in the wüstite phase ($Fe_{1-x}O$); their results are consistent with the results of the neutron-diffraction study.[15]

Experimental

Preparation of the Samples. The solid-solution samples were prepared by ball milling mixed particles of graduated pure reagents, (α-Fe_2O_3, $SrCO_3$ and La_2O_3) in the desired proportions, and by then firing at 900°C and 1000°C in air for 5 hr. The samples thus obtained were refired at 1100°C in a vacuum ($\sim 10^{-3}$ mmHg) and then cooled to room temperature, while the same degree of vacuum was maintained, after a given firing period. The method of preparation has been described in greater detail in the previous paper.[1]

X-Ray Diffractometry. X-ray powder diffractometry using cobalt-$K\alpha$ radiation was used for the assignment of the structure as well as for the determination of the lattice constant of the specimens.

Measurements and Analysis of Mössbauer Spectra. The Mössbauer spectrum was taken using a spectrometer equipped with 400-channel pulse-height analyzer (a RAH-403 type; Hitachi Co., Ltd.), calibration with either iron foil or α-Fe_2O_3. The source used was cobalt-57, with 14.4 keV γ-radiation, dispersed in either palladium or copper; it was driven at a constant accerelation speed ($\pm$10 mm/sec) for all the measurements at room temperature. The absorbers were prepared by grinding the oxide samples into fine particles and by then evenly spreading them on a square aluminium plate 0.50 mm thick with a circular hole 20 mm in internal diameter; both sides of the powder compact thus molded were sealed with cellophane. The thickness of the powder compact was chosen so that it contained about 15—20 mg of total iron per square centimeter of the cross section. The isomer shifts are given in values relative to metallic iron for all the samples.

The energy levels of magnetic hyperfine splitting between the ground state and first excited one of iron-57 under the presence of an axially symmetric electric-field gradient is given by the following equation:

$$E = -g\mu_n H m_I + (-1)^{|m_I|+1/2}\varepsilon, \qquad (1)$$

where μ_n, H, m_I, and ε are the nuclear magneton, the internal magnetic field, the magnetic quantum number, and the electric quadrupole parameter respectively. Fig. 1 shows

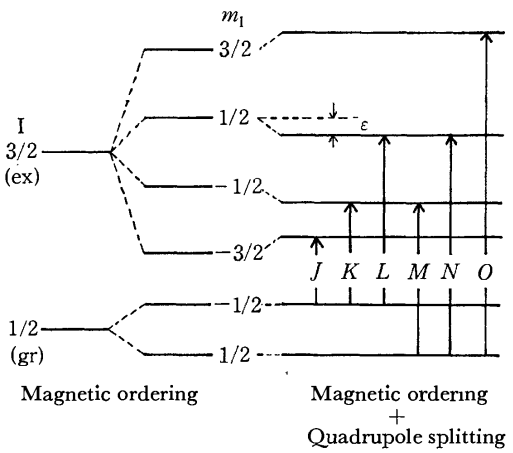

Fig. 1. Energy levels of iron-57 in the Mössbauer spectrum. I, m_I and ε are nuclear spin quantum number, magnetic quantum number of iron-57 and quadrupole parameter, respectively.

diagramatically the energy levels of iron-57. In this figure, each energy level is denoted as *J*, *K*, *L*, *M*, *N*, or *O*, in the order of ascending energy. Therefore, the quadrupole parameter (ε) is given by:

$$\varepsilon = \frac{1}{4}\{(O-N)-(K-J)\}. \qquad (2)$$

On the other hand, an isomer shift (I.S.) closely correlated

6) J. B. MacChesney, R. C. Sherwood, and J. F. Potter, *J. Chem. Phys.*, **43**, 1907 (1965).
7) P. K. Gallagher, J. B. MacChesney, and D. N. E. Buchanan, *ibid.*, **41**, 2429 (1964).
8) A. A. Colville, *Acta Crystallogr.*, **B26**, 1469 (1969).
9) T. Takeda, Y. Yamaguchi, S. Tomiyoshi, M. Fukase, M. Sugimoto, and H. Watanabe, *J. Phys. Soc. Japan*, **24**, 446 (1968).
10) R. W. Grant, *J. Chem. Phys.*, **51**, 1156 (1969).
11) U. Shimony and J. M. Knudsen, *Phys. Rev.*, **144**, 361 (1966).
12) P. K. Gallagher and J. B. MacChesney, Symposia of the Faraday Soc., No. 1, The Mössbauer Effect, (1968), p. 40.
13) G. A. Sawatzky, F. van der Woude, and A. H. Morrish, *J. Appl. Phys.*, **39**, 1204 (1968).
14) D. J. Elias and J. W. Linnett, *Trans. Faraday Soc.*, **65**, 2673 (1969).
15) W. L. Roth, *Acta Crystallogr.*, **13**, 140 (1960).

with the contribution of *s*-electron density manifests itself as a shift of the nuclear energy levels and, therefore, is given by the following equation:

$$\text{I.S.} = \frac{4}{5}\pi Ze^2R^2\left(\frac{\delta R}{R}\right)\{|\Psi_a(0)|^2-|\Psi_s(0)|^2\} \quad (3)$$

$$= \frac{1}{12}(3J+2K+L+M+2N+3O), \quad (4)$$

where $e|\Psi(0)|^2$ is an expression for the charge density at the nucleus and whose R and δR are, respectively, the ground-state radius of iron-57 and the difference in nuclear radius between the ground-state and the excited-one. The Mössbauer velocity was obtained by multiplying the respective pair peaks, *J*—*O*, *K*—*N*, and *L*—*M*, by the transition probabilities of 3, 2, and 1 respectively.

Results and Discussion

At first, the structural knowledge on the $Sr_{1-x}La_xFeO_{3-\delta}$ solid-solution system obtained by X-ray diffractometry will be briefly described. The content of oxygen vacancies (δ) varies with the content of La (x), as may be understood from the formula. The X-ray powder patterns of the sample with x=0.0—0.20 could be indexed on the basis of a brownmillerite-type structure with orthorhombic symmetry. It is noticeable that the intensity of fairly strong peaks with an even larger k number in Miller indices (*hkl*) (*e.g.*, (161), (080), and (280)) decreased with an increase in x. On the other hand, the respective pair peaks, such as (200)—(002), (240)—(042), and (341)—(143), in the brownmillerite-type phase approached each other with an increase in x, resulting in the appearance of the corresponding peaks of (110), (111), and (211) in the cubic perovskite-phase with a further increase in x.

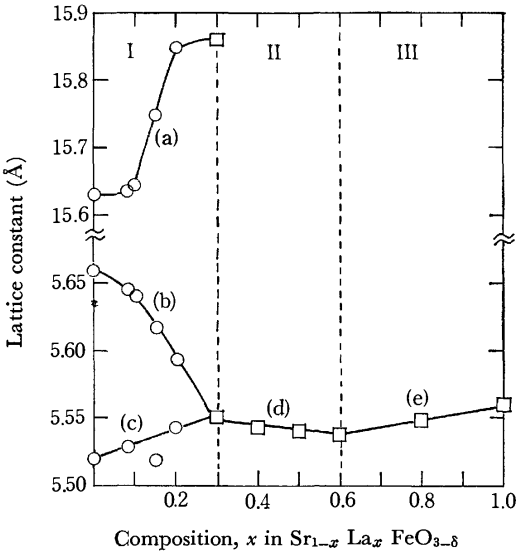

Fig. 2. Lattice constants in the system $Sr_{1-x}La_xFeO_{3-\delta}$ prepared by firing at 1100°C in vacuum: (a), (b), and (c) are the lattice constants of *b*-, *a*- and *c*-axis for the brownmillerite-type orthorhombic phase (region I), respectively and (d) and (e) are the lattice constants for the cubic perovskite-type phase (region II) and pseudocubic $LaFeO_3$-type one (region III).

The rather broad diffraction pattern and no splitting of the peak due to $K\alpha_1$ and $K\alpha_2$ radiation at a high diffraction angle for the cubic perovskite phase in the compositional range of x=0.30—0.60 suggest that the structure is a little random as a result of its vacancies. The lattice constant *versus* the composition is plotted in Fig. 2. In the unit-cell parameter of the brownmillerite-type phase, the *a*-axis decreased rapidly, whereas the *c*-axis increased slowly, with an increase in the La content, the two meeting at x=0.30. In Fig. 2, the lattice constant in the cubic perovskite-type phase is given, for comparison, as a value 2 times the actual lattice constant, a_0.[16] On the other hand, the tendency of the b_0 parameter to increase over the region with x=0.20 resulted in 15.85 Å, which was approximately equal to 15.94 Å ($=a_0\times4\sqrt{2}$).[16] This fact allows us to consider the phase with x=0.20 as a pseudotetragonal structure formed as an intermediate phase during the transformation between the two phases. Over the compositional range of x=0.30—0.60, the cubic perovskite-type structure was preferable; its lattice constant was 3.926 Å at the composition of x=0.30, larger than that of 3.850 Å for $SrFeO_3$ prepared by firing under a high oxygen pressure, after MacChesney *et al.*[6] The lattice constant in the cubic phase decreased linearly with an increase in the contents of La. The further addition of La (x=0.80—1.0) distorted the cubic lattice to a $LaFeO_3$-type structure with an orthorhombic symmetry. Thus, it seems likely that the presence of oxygen vacancies of the solid-solution plays an important role in the stabilization of a perovskite-type structure with cubic symmetry.

The Mössbauer spectrum of $SrFeO_{2.5}$ at room temperature is shown in Fig. 3(a). It is understandable in terms of a couple of six-line patterns arising from types of iron sites having both different magnetic hyperfine splitting and quadrupole splittings. The quadrupole splitting must occur as a result of the destruction of the spherical symmetry built by the surrounding ions around iron, because the Fe^{3+} ion itself is in a spherically symmetrical $^6A_1$ state. Generally, the relation between ΔE_Q, the quadrupole splitting observed above the Neel point, and ε, the quadrupole parameter observed below it, are given by the following equation:

$$\varepsilon = \frac{1}{4}\Delta E_Q(3\cos^2\theta-1), \quad (5)$$

where θ is the angle between the magnetic field and the principal axis of the electric-field gradient. The idea proposed by Grant[10] in his Mössbauer study on $CaFeO_{2.5}$ may be also true for $SrFeO_{2.5}$; that is, the electric-field gradient at both the iron tetrahedral and octahedral sites may be axially symmetric, with the *z*-principal axis parallel to the crystallographic *b*-axis. On the other hand, the antiferromagnetic spins of both the iron sites in $SrFeO_{2.5}$ are supposed to be along the

16) When the lattice constants for the brownmillerite-type phase with an orthorhombic symmetry and for the cubic perovskite-type one are assumed to be a_0, b_0, c_0, and a^* respectively, the relations among them are given by the following equations; $a_0\simeq c_0\simeq 2a^*$ and $b_0\simeq 4\sqrt{2}a^*$.

c-axis. Therefore, Eq. (5) may be simplified to:

$$\varepsilon = -\frac{1}{4}\Delta E_Q \qquad (6)$$

Since the Mössbauer spectra are measured below the Neel point in this work, ΔE_Q can be calculated using the observed values of ε with the aid of Eq. (6). The presently-observed absorption lines are here denoted as J, K, L, M, N, and O in the order of ascending energy, as has been described above, together with additional symbols showing the coordination numbers of the iron sites. Therefore, for example, the third line from the left in the tetrahedral iron site is expressed by 4L (Fig. 3(a)).

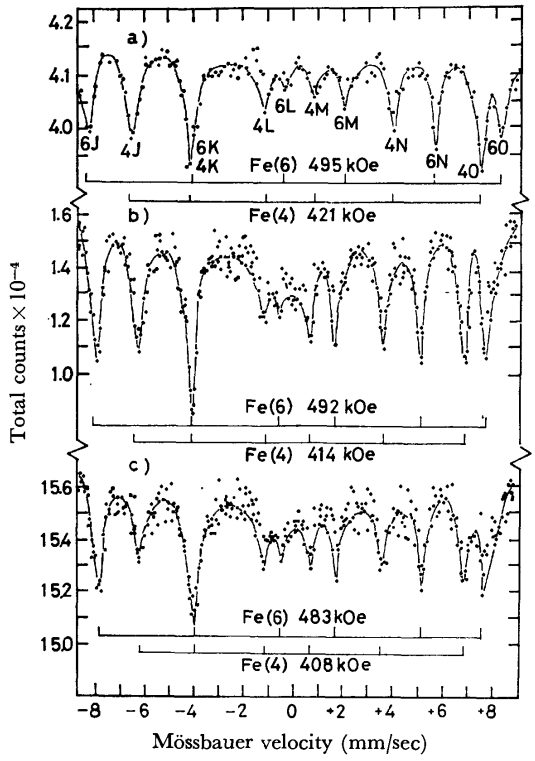

Fig. 3. Mössbauer spectra in the system $Sr_{1-x}La_xFeO_{3-\delta}$ ($0.0 \leq x \leq 0.10$) prepared by firing in a vacuum: a), b) and c) are the spectra for the composition of $x=0.0$, 0.07 and 0.10, respectively. Number in parentheses is coordination number of oxygen.

The Mössbauer parameters of $SrFeO_{2.5}$, *i.e.*, the isomer shifts, quadrupole splittings, and internal magnetic fields, were calculated to be +0.235 mm/sec, +0.391 mm/sec, and 495 kOe for the octahedral iron site, and +0.160 mm/sec, −0.280 mm/sec, and 421 kOe for the tetrahedral one, respectively. The higher velocity of the isomer shift, accompanied by a larger internal magnetic field, for the octahedral site than those for the tetrahedral one may be explained by the contribution of covalency in Fe–O bonding, this being also found in the cases of spinels[17] and garnets.[18] Both the values of the isomer shift indicate that two types of iron in this solid-solution are three valency states.

17) T. Mizoguchi and M. Tanaka, *J. Phys. Soc. Japan*, **18**, 1301, (1963).

18) W. J. Nicholson and G. Burns, *Phys. Rev.*, **133**, 1568 (1964).

Accordingly, the relation between the substituted La content and the oxygen one for the solid-solution system in the present study may be presented by x in the composition: $Sr_{1-x}La_xFeO_{2.5+x/2}$.

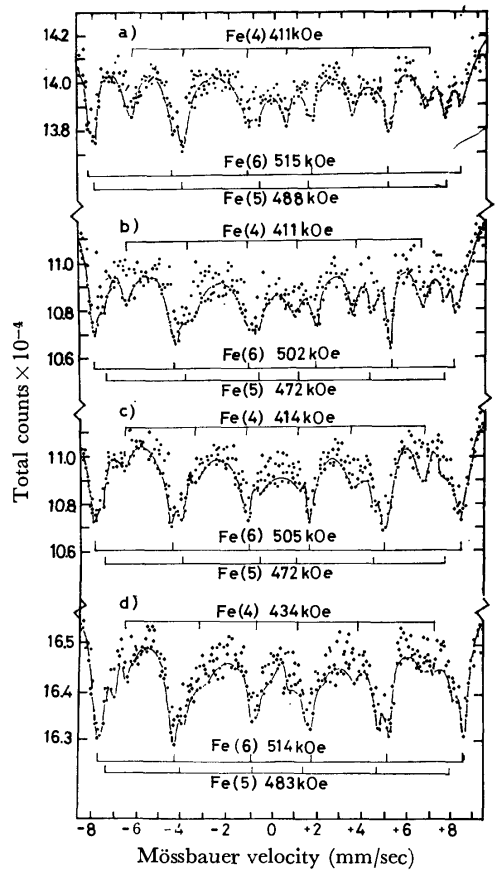

Fig. 4. Mössbauer spectra in the system $Sr_{1-x}La_xFeO_{3-\delta}$ ($0.15 \leq x \leq 0.40$) prepared by firing in a vacuum: a), b), c) and d) are the spectra for the composition of $x=0.15$, 0.20, 0.30 and 0.40, respectively. Number in parentheses is coordination number of oxygen.

The Mössbauer spectra for $x=0.07$ and $x=0.10$ are shown in Fig. 3(b) and 3(c) respectively. The respective intensities of the 4M-, 4N-, and 4O-peaks decreased with an increase in the La content. This fact may be attributed to a change in the coordination state of Fe^{3+} from a tetrahedral site to an octahedral one occurring as a result of the incorporation of oxygen due to La substitution. No change was observed in the values of the internal magnetic field and quadrupole splitting, whereas the isomer shift for the octahedral, Fe^{3+} site had a tendency to move toward the higher-velocity side when the content of Sr decreased in the compositional range from $x=0.0$ to 0.10.

The Mössbauer spectrum for the composition with $x=0.15$ revealed a broad line with an asymmetric form, as is shown in Fig. 4(a). In addition, new absorption lines appeared between the 4O and 6O lines, and between the 4K and 6K lines. This means the appearance of new six lines different from the lines for the octahedral and tetrahedral Fe^{3+} sites. If only the amount of oxygen incorporated by the addition of La controls the change from a tetrahedral site to an

octahedral one, the peak intensity for the tetrahedral site must be only two-thirds that for the octahedral site at the composition of $x=0.15$. Experimental evidence, however, indicated that the intensities for the two sites were nearly equal. The values of the isomer shift, the quadrupole splitting, and the internal magnetic field for the sample with $x=0.15$ were +0.380 mm/sec, +0.109 mm/sec, and 515 kOe for the octahedral site, +0.136 mm/sec, −0.150 mm/sec, and 411 kOe for the tetrahedral site and +0.326 mm/sec, +0.326 mm/sec, and 488 kOe for the new peak, respectively. It is noticeable that the isomer shift and the internal magnetic field for the new peak both fall between those for the octahedtal site and those for the tetrahedral site.

The Mössbauer spectrum for the sample with $x=0.20$, with a pseudotetragonal perovskite-type structure, is shown in Fig. 4(b); three kinds of six absorption line also appear, and a new line appears in the neighborhood of the 6*N* line besides the splitting which has already occurred in the sample with $x=0.15$. The sample with $x=0.30$ revealed an exact cubic perovskite-type structure. According to a discussion on the basis of the crystal structure, the central metal ion in the cubic perovskite-type structure must be surrounded by six oxygen ions. Nevertheless, it is interesting that the presently-observed oxygen-deficient perovskite-type phase with cubic symmetry possesses measurable amount of the tetrahedral iron site and the "X-site" in addition to the octahedral site (Fig. 4(c)).

In the sample with the composition of $x=0.40$ (Fig. 4(d)), the absorption line from the tetrahedral iron site was still recognized even if its intensity was weakened. For the sample with $x=0.50$ (Fig. 5(a)) and $x=0.80$ (Fig. 5(b)), however, broad six line arose only from the octahedral site, in which the half-height width values of the respective line were four times (for $x=0.50$) and two times (for $x=0.80$) the value in $LaFeO_3$ (Fig. 5(c)). In spite of such a situation regarding the intensity of the absorption lines of the octahedral site, little change for that of the tetrahedral site occurred. These facts allow us to say that an increase in the oxygen content in the solid-solution plays no role in the occurrence of change from the tetrahedral site to the octahedral one over the compositional range from $x=0.50$ to $x=1.0$.

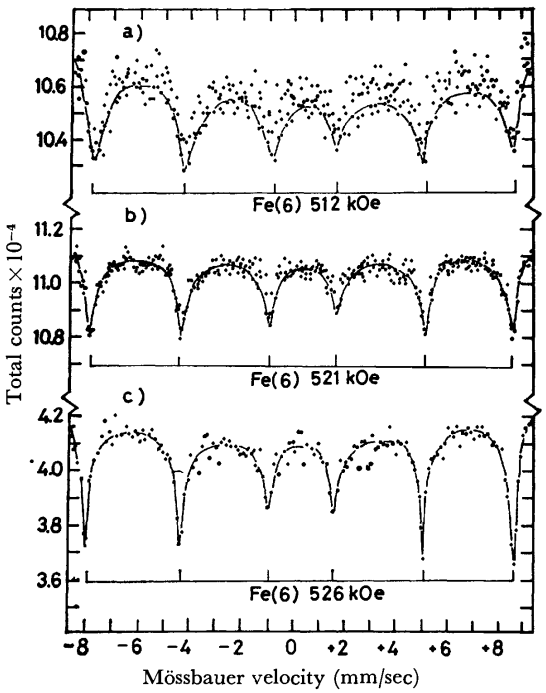

Fig. 5. Mössbauer spectra in the system $Sr_{1-x}La_xFeO_{3-\delta}$ ($0.50 \leq x \leq 1.0$) prepared by firing in a vacuum: a), b), and c) are the spectra for the composition of $x=0.50$, 0.80 and 1.0, respectively. Number in parentheses is coordination number of oxygen.

To clarify the details of the present oxygen-deficient structure, it seems important to discuss the assignment of the unknown peak for "X-iron site" which appeared in all the samples with the composition of $x=0.15$—0.40. The characteristics of the new unknown pattern may be summarized as follows:

(1) The value of the isomer shift falls between that for the octahedral site and that for the tetrahedral site, regardless of the composition.

(2) The value of the internal magnetic field is also between that for the octahedral site and that for the tetrahedral site.

(3) No measurable change in the intensity of the new peak is observed over the entire range of composition of the solid-soltuion presently treated.

(4) The magnitude and the direction of the quadrupole splitting in the brownmillerite-type phase are almost equal to those for octahedral site, the magnitude being decreased considerably in the cubic perovskite-type phase.

The possible origins for the occurrence of the new peaks are as follows:

(1) The presence of a different phase containing Fe^{3+}.

(2) The existence of Fe^{2+} occurring as a result of firing at a fairly high temperature in a vacuum and/or of the substitution of La^{3+}.

(3) The presence of a tetrahedral or octahedral site with an environment slightly different from the brownmillerite-type phase of $SrFeO_{2.5}$.

(4) The presence of Fe^{4+} remained unchanged even under a fairly high degree of vacuum.

(5) The formation of five-coordinated Fe^{3+} as an intermediate during the course of the transformation from a tetrahedral site to an octahedral one.

No different phase containing Fe^{3+} with magnetic ordering, however, was confirmed by either X-ray diffractometry or magnetic measurements. The possibility of (2) and (3) can also be ruled out because the value of the isomer shift is between those for the octahedral and tetrahedral Fe^{3+} sites. On the other hand, Fig. 2 shows that the length of the *b*-axis in the brownmillerite-type structure increased with an increase in the content of incorporated oxygen, suggesting an increase in the over-all coordination number of Fe^{3+}; thus, one more of the possibilities (4) may be ruled out. The most probable reason for the occurrence of the octahedral iron site may be the existence of small amounts of $LaFeO_3$ in the brownmillerite-type phase.

The values of the isomer shift and the internal magnetic field of $LaFeO_3$, however, indicate that it is different from the values for the "X-iron site". The above anomalies in the Mössbauer parameters may be explained by the fifth possibility, that is, the presence of the five-coordinated Fe^{3+}.

Van Loef,[19] in his Mössbauer study of spinels and garnets, suggested that the values of the isomer shifts and the internal magnetic fields have a close relation to the form of oxygen-coordinated polyhedron. The results in the present work support his idea. The possible form of the five-coordinated polyhedron may be a regular trigonal bipyramidal rather than a square pyramidal because of the fairly small quadrupole splitting.

Table 1. Mössbauer parameters in the system $Sr_{1-x}La_xFeO_{3-\delta}$ prepared by firing in a vacuum

Comp. (x)	C.N.	H_{int} (kOe)	I.S. (mm/sec)	ε (mm/sec)
0.0	6	495	0.235	0.391
	4	421	0.160	−0.287
0.07	6	492	0.339	0.340
	4	414	0.204	−0.285
0.10	6	483	0.367	0.340
	4	408	0.190	−0.298
0.15	6	515	0.380	0.109
	5	488	0.326	0.226
	4	411	0.136	−0.150
0.20	6	502	0.367	0.104
	5	472	0.284	0.066
	4	411	0.079	−0.025
0.30	6	505	0.380	0
	5	472	0.285	0.068
	4	414	0.136	−0.028
0.40	6	514	0.385	0
	5	483	0.275	0
	4	434	0.248	0
0.50	6	512	0.386	0
0.80	6	512	0.385	0
1.00	6	526	0.396	0.056

Remarks
C.N.: oxygen coordination number around iron
$H_{int.}$: internal magnetic field
I.S. : isomer shift relative to metallic iron
ε : quadrupole parameter

The Mössbauer parameters obtained in the present work are summarized in Table 1. The isomer shift and the quadrupole splitting for the three types of iron sites against the composition are also plotted in Fig. 6 and 7. The isomer shift for the octahedral Fe^{3+} site increased abruptly with an increase in the concentration of La and then stayed constant over the cubic perovskite-type phase, approaching that of $LaFeO_3$ when the concentration of La increased further. The isomer shift for the tetrahedral site showed a more complicated variation with the composition. It decreased rapidly up to $x=0.20$ and then increased linearly above $x=0.20$, nearly coinciding with the

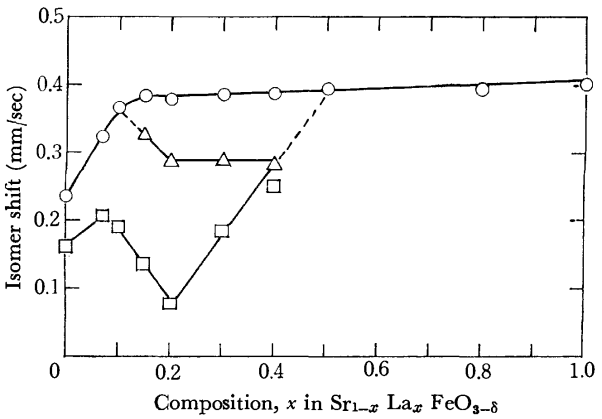

Fig. 6. Isomer shifts *vs.* composition in the system $Sr_{1-x}La_x$-$FeO_{3-\delta}$ prepared by firing in a vacuum.
○: isomer shift for the octahedral Fe^{3+} site
△: isomer shift for the trigonal bipyramidal Fe^{3+} site
□: isomer shift for the tetrahedral Fe^{3+} site

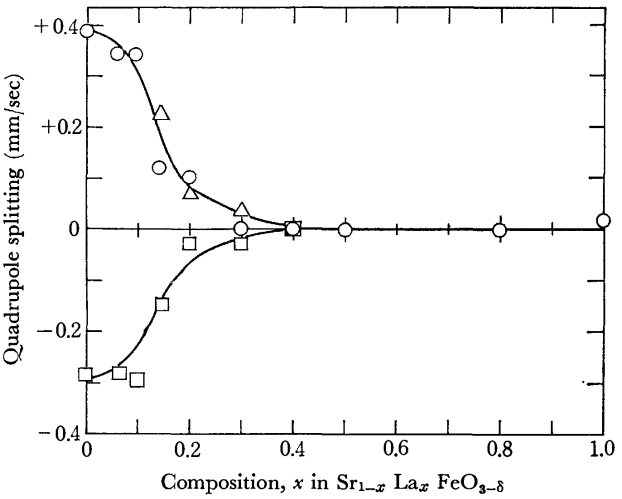

Fig. 7. Quadrupole splitting *vs.* composition in the system $Sr_{1-x}La_xFeO_{3-\delta}$ prepared by firing in a vacuum.
○: quadrupole splitting for the octahedral Fe^{3+} site
△: quadrupole splitting for the trigonal bipyramidal Fe^{3+} site
□: quadrupole splitting for the tetrahedral Fe^{3+} site

expected value for the octahedral site estimated by extraporation to $x=0.50$, where the Mössbauer pattern showed only a broad six-line pattern for the octahedral iron site.

The relation between the quadrupole splitting and the composition seems to be valuable enough to discuss on the basis of crystal symmetry. Though the values of the quadrupole splitting for all the sites over the entire compositional range of $x=0.0$—0.10, in which the brownmillerite-type phase was preferable, are comparable to that of $SrFeO_{2.5}$, they considerably decreased with the progress of the structural transformation from the orthorhombic phase to the tetragonal one, and then show no quadrupole splitting when the cubic perovskite-type is attained. No internal magnetic field dependence on the composition was observed; these values for octahedral, tetrahedral, and trigonal bipyramidal sites were found to be ~510, ~480, and ~410 kOe respectively.

It is necessarily uncommon for the trigonal bipyra-

19) J. J. Van Loef, *Physica*, **32**, 2102 (1966).

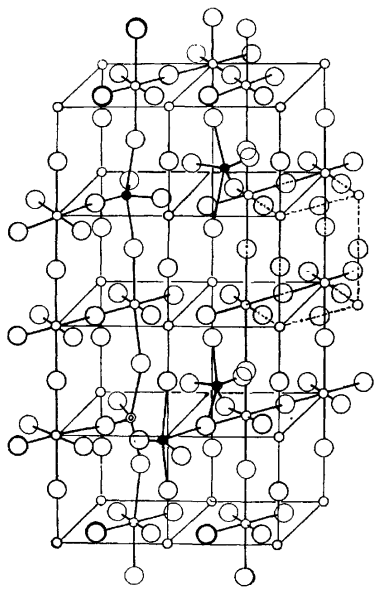

○: Oxygen, ○: iron (6), •: iron (5), ◎: iron (4)

Fig. 8. Imaginative oxygen-deficient cubic perovskite-type structure in the system $Sr_{1-x}La_xFeO_{3-\delta}$ prepared by firing in a vacuum, where large cation, Sr or La ion is omitted for simplicity. The primitive unit cell is represented in dashed line. Number in parentheses is coordination number of oxygen.

midal polyhedron of oxygen to be present as a result of the absence of oxygen along the direction [110] out of the cubic perovskite-type structure. The imaginative oxygen-deficient cubic perovskite-type structure with octahedral, trigonal bipyramidal, and tetrahedral iron site is shown in Fig. 8. The reported Mössbauer spectroscopic measurements, together with the nuclear ferromagnetic resonance spectroscopic measurements, however, have already indicated that magneto plumbite, $BaFe_{12}O_{19}$, with layer structure, has a trigonal bipyramidal iron site.[20-22] The isomer shift for the trigonal bipyramidal iron site in $BaFe_{12}O_{19}$ was found to be between that for the octahedral site and that for the tetrahedral site, as in the present study. On the other hand, the quadrupole splitting and the internal magnetic field were larger and smaller than the values for both the octahedral and tetrahedral sites. In this case, however, the presence of the five-coordinated iron site may be expected because one of the anion sites is replaced by barium in the $BaFe_{12}O_{19}$.

Wadsley[23] has studied the importance of transition metal-oxygen mixed coordination schemes associated with an anion-deficient phase. Negas and Roth[24] have discussed the stoichiometry and the stability of $SrMnO_{3-\delta}$ from the standpoint of variation in the coordination scheme of the manganese cation and suggested the presence of a trigonal bipyramidal manganese site in addition to a normal octahedral site, without, however, reporting any data on this idea. In summary, it may be shown that the presence of an ion deficiency in the crystal lattice contributes to the change in the coordination number. Accordingly, the traditional thinking that vacancies exist as simple holes is not applicable for an oxygen-deficient perovskite-type structure. This idea may be sometimes true for an oxide solution.

The authors would like to thank Dr. Ri-ichi Kikuchi for allowing them to use the apparatus for the Mössbauer effect at the Radio Isotope Laboratory in the Institute of Scientific and Industrial Research, Osaka University, and Dr. Shin-ichi Shirasaki for his helpful discussion while they were preparing this paper.

20) P. Raum, *Nature*, **170**, 708 (1952).
21) J. S. van Wieringen and J. G. Rensen, *Z. Angew. Phys.*, **21**, 69 (1966).
22) K. Hareyama, K. Kohen, and K. Umematsu, *J. Phys. Soc. Japan*, **29**, 791 (1970).
23) A. D. Wadsley, "Nonstoichiometric Compounds" (L. Mandecorn, Ed.), Academic Press Inc., New York, N. Y., 1964, Chap. 3.
24) T. Negas and R. S. Roth, *J. Solid State Chem.*, **1**, 407 (1970).

Electron Spin Resonance Study of Adduct Formation by Bis(trifluoroacetylacetonato)copper(II) with Phosphorus Donor Ligands

F. LEH and K. M. CHAN*

Air Pollution Research Center, University of California, Riverside, California 92502, U.S.A.
** California State University, Long Beach, California 90840, U.S.A.*

(Received September 6, 1971)

The study of the ESR spectra parameters of bis(trifluoroacetylacetonato)copper(II)-phosphorus complexes in chloroform solution at room temperature and 77°K shows that the g and hyperfine tensors change with the formation of 1 : 1 adduct. Such effect is more clearly exhibited by the parameters $A_{\parallel}$ and $g_{\parallel}$. A correlation is obtained between the spectral data and the basicity of the tertiary phosphine ligands.

High spin divalent transition metal ions usually have strong tendency to form compounds having a coordination number greater than four.[1] For example, the axial ligation of bis(acetylacetonato)copper(II) forms 1 : 1 adduct with heterocyclic bases.[2,3] However, such adduct formation depends on the relative electron withdrawing power of the β-diketones.[4] Successive trifluoromethylation of the acetylacetones will increase their affinity for the copper atom for axial ligation, which has been demonstrated by the formation of 1 : 1 and/or 1 : 2 addition complexes with donor solvent and nitrogen containing chelates by bis(trifluoroacetylacetonato)copper(II)[5] and bis(hexafluoroacetylacetonato)-copper(II).[6,7]

The preparation of the above complexes of σ-type nitrogen containing ligands are well documented, but not for π-type bases. This is primarily due to the fact that copper(II) salts react with tertiary phosphine and are reduced to copper(I) compounds.[8-10] Only recently the preparation of 1 : 1 adduct of bis(hexafluoroacetylacetonato)copper(II) with triphenylphosphine was reported.[11] This paper describes our work in ESR study of 1 : 1 adducts of bis(trifluoroacetylacetonato)copper(II) with tertiary phosphines.

Solvent Effect on Copper Complexes

Antosik *et al.*[12] analysed the effect of the solvent on axial ligations. Based on the ESR spectra of several square planar cupric β-ketoenolates, they concluded that the axial ligation arose from the two-axial dipoles acting on the two axes perpendicular to the plane of cupric complexes. First-order perturbation theory was used to obtain the relationships between the spin-Hamiltonian parameters for the 'isolated' complexes with those for the perturbed complexes. Greater values of the parallel components of the g tensors and numerically smaller values of the parallel components of the hyperfine tensor for the chloroform complexes than that of the corresponding components in the 'isolated' cupric chelates were predicted.

A systematic investigation of the ESR parameter $\langle A \rangle$ of bis(t-butylacetoacetato)copper(II) in different organic solvents such as cyclohexane, carbon tetrachloride, benzene, chloroform, pyridine-cyclohexane mixture, was carried out by Libutti, Wayland, and Garito.[13] Basic solvents, *e.g.* pyridine, caused a large decrease in $\langle A \rangle$ values and an increase in $\langle A \rangle$ values occurred if less coordinating solvents were used. Another study with ESR spectra of bis(acetylacetonato)-copper(II) in various solvents was reported by Adato and Eliezer,[7] and showed that the anisotropy of the nuclear hyperfine interaction tensor varied with different solvents. Such effect was claimed to be better obtained from the hyperfine splitting parameter $A_{\perp}$.

Experimental

Dark green bis(trifluoroacetylacetonato)copper(II)-phosphorus complexes, $Cu(tfac)_2 \cdot PR_3$ (where $PR_3 = (n\text{-}Bu)_3P$, Et_3P, Ph_3P, $PhPMe_2$, Ph_2PMe, $(PhO)_3P$) were prepared by mixing 1 : 1 ratio of bis(trifluoroacetylacetonato)copper-(II) with phosphine in chloroform solution under nitrogen. Bis(trifluoroacetylacetonato)copper(II)-phosphorus complexes are quite stable in vacuum at 0°C, but decompose rapidly when heated over 50°C.

ESR spectra were recorded with a Varian V-4502 EPR spectrometer equipped with a 100-kHz field modulation and control unit (Model V-4560). The g values were measured by comparison with the free radical standard diphenylpicryhydrazyl (DPPH) for which the g_0 value was accurately known to be 2.0036.

Results and Discussion

In chloroform solution, bis(trifluoroacetylacetonato)copper(II)-phosphorus complexes, $Cu(tfac)_2 \cdot PR_3$ ($PR_3 = Et_3P$, $(n\text{-}Bu)_3P$, Ph_2PMe, $PhPMe_2$) exhibit the

1) D. P. Graddon, *Coord. Chem. Rev.*, **4**, 1 (1969).
2) D. P. Graddon and E. C. Watton, *J. Inorg. Nucl. Chem.*, **21**, 49 (1961).
3) R. D. Gillard and G. Wilkinson, *J. Chem. Soc.*, **1963**, 5399.
4) W. Partenheimer and R. S. Drago, *Inorg. Chem.*, **9**, 47 (1970).
5) R. D. Gillard and G. Wilkinson, *J. Chem. Soc.*, **1963**, 5885.
6) D. E. Fenton, R. S. Nyholm, and M. R. Truter, *J. Chem. Soc., A*, **1971**, 1577.
7) I. Adato and I. Eliezer, *J. Chem. Phys.*, **54**, 1472 (1971).
8) W.E. Hatfield and R. Whyman, "Transition Metal Chemistry", ed. R. L. Calvin, Dekker, New York (1969), pp. 5, 47.
9) F. G. Moss and P. H. Op Het Veld, *J. Inorg. Nucl. Chem.*, **32**, 3225 (1970).
10) W. A. Anderson, A. J. Carty, G. J. Palenik, and G. Schreiber, *Can. J. Chem.*, **49**, 761 (1971).
11) M. Baird and R. A. Zaronka, *Chem. Commun.*, **1971**, 448.
12) S. Antosik, N. M. D. Brown, A. A. McConnell, and A. L. Porte, *J. Chem. Soc., A*, **1969**, 545.
13) B. L. Libutti, B. B. Wayland, and A. F. Garito, *Inorg. Chem.*, **8**, 1510 (1969).

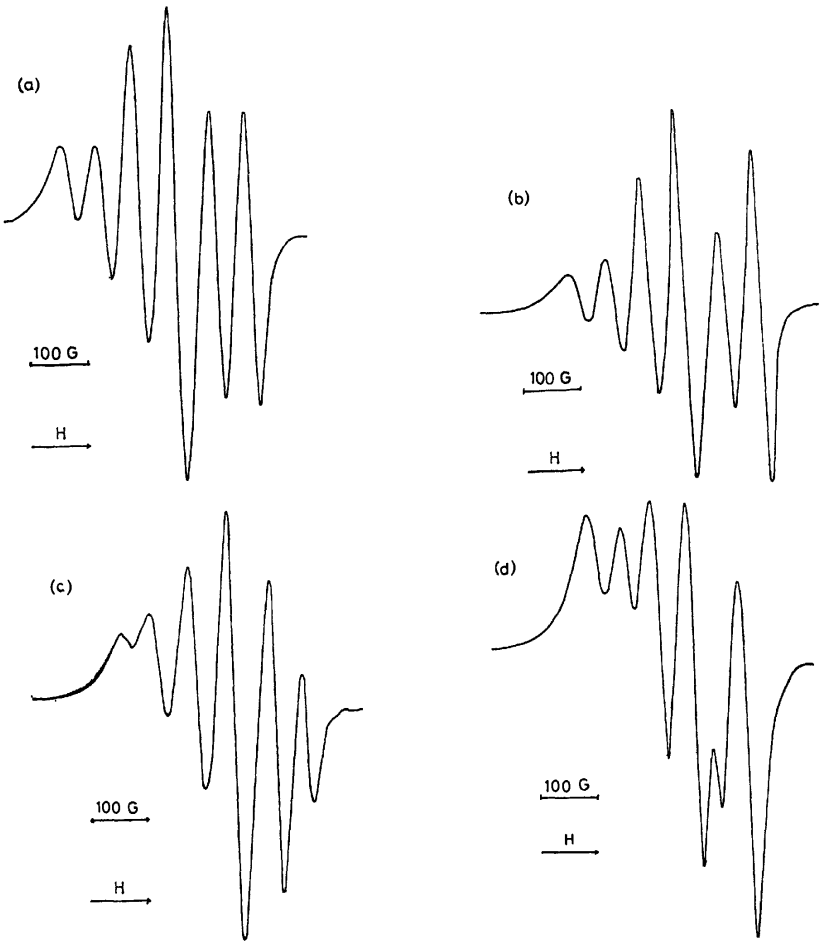

Fig. 1. ESR spectra of bis(trifluoroacetylacetonato)copper(II)-phosphorus complexes at room temperature in chloroform.
(a): triethylphosphine (b): *n*-tributylphosphine
(c): dimethylphenylphosphine (d): diphenylmethylphosphine

ESR spectra as shown in Fig. 1 (a), (b), (c), (d). In a polycrystalline sample, all molecules are assumed to be in an identical environment, and their microcrystalline axes randomly oriented. In a frozen solution spectra (Fig. 2), it is possible to obtain $g_{\parallel}$ and $A_{\parallel}$, and from these values we calculated $g_{\perp}$ and $A_{\perp}$ using the approximate equations $\langle g\rangle = g_{\parallel}/3 + 2g_{\perp}/3$ and $\langle A\rangle = A_{\parallel}/3 + 2A_{\perp}/3$, where $\langle A\rangle$ and $\langle g\rangle$ are obtained in solution assuming that the freezing of the solvent does not change the local crystal field in a manner that would affect the isotropic A and g values.

The spectra of bis(trifluoroacetylacetonato)copper-(II)-phosphorus complexes characterise the interaction of the unpaired electron of Cu(II) (nuclear spin $I=3/2$) with one ^{31}P nucleus ($I=1/2$), this interaction being responsible for the doublet splitting of the four copper lines. Due to the overlapping of $+3/2$ and $+1/2$ hyperfine lines of the one with $-3/2$ and $-1/2$

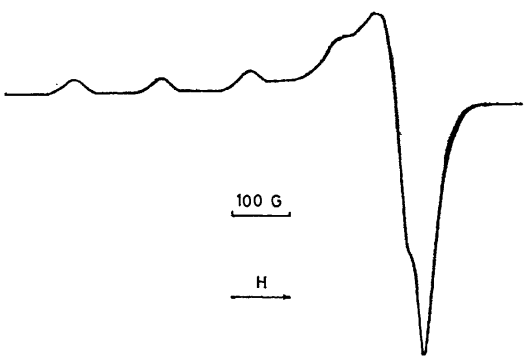

Fig. 2. ESR spectrum of bis(trifluoroacetylacetonato)copper-(II)-dimethylphenylphosphine complex at 77°K in chloroform.

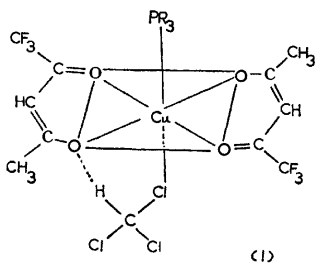

(1)

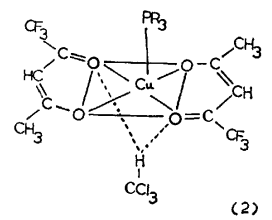

(2)

TABLE 1. ESR SPECTRA PARAMETERS OF 10^{-3}M SOLUTIONS OF BIS(TRIFLUOROACETYLACETONATO)-COPPER(II) AND BIS(TRIFLUOROACETYLACETONATO)COPPER(II)-PHOSPHORUS COMPLEXES IN CHLOROFORM. HYPERFINE TENSOR COMPONENTS ARE IN UNITS OF $10^{-4}cm^{-1}$

Ligand	$\langle g \rangle$	$\langle A \rangle$	$g_\parallel$	$g_\perp$	$A_\parallel$(Cu)	$A_\perp$(Cu)	$A_p(^{31}P)$	ΔHNP
$CHCl_3$[a]	2.128	69.9	2.300	2.042	168.2	20.8	—	
Et_3P	2.0901	54.2	2.1978	2.0363	127.8	14.5	119.1	111
$(n\text{-}Bu)_3P$	2.1128	54.0	2.1923	2.0231	119.5	19.9	116.9	131
Me_2PPh	2.0864	51.2	2.2113	2.0363	130.4	7.8	110.4	281
$MePPh_2$	2.0929	43.4	2.1985	2.0401	118.4	3.0	82.3	
Ph_3P	2.0942	59.4	2.2031	2.0397	124.4	24.2	—	573
$(PhO)_3P$	2.1067	51.2	2.2207	2.0497	128.1	9.5	—	875

a) from Ref. 13.

lines of the other, a typical six lines spectra are observed. When the phosphine is triphenylphosphine, the ESR spectra of the complexes in chloroform consist mainly of the unresolved four copper lines, but the greater g and smaller A compared with $Cu(tfac)_2$ imply the axial ligation of phosphorus ligand.[12] From the data in Table 1, we suggest the structure of (1) and (2) as in the following diagram, where the chloroform molecule is linked to the metal *via* one of its chlorines[4] or bonded to a pair of the ligand oxygen atoms *via* hydrogen atom.[16] The evidence for the formation of six coordinate bis adducts in bis(trifluoroacetylacetonato)-copper(II) has been found in other case[5] and bis adducts of square planar Ni(II) complexes are common.[14,15] Observations of the X-band spectra of a series of Cu(II) β-diketonates in chloroform-toluene glasses[12] have shown that the exhibition had twice the number of expected lines. This is due to the formation of weak chloroform complexes with some square planar compounds of copper(II).

Our results indicate that phosphines are better ligands towards bis(trifluoroacetylacetonato)copper(II) than the corresponding phosphites. Since phosphite is better π-bonder and poorer σ-donor than phosphine, it follows that the σ-bonding tendency of a ligand is a predominant factor in determining its reactivity. The data in Table 1 also indicate that in phosphine series, the A_P, decreases with increasing basicity of the ligand in the order $Et_3P > (n\text{-}Bu)_3P > Me_2PPh \gg MePPh_2 \gg PPh_3 > P(OPh)_3$. The relative basicities of the phosphines were measured by Streuli,[17] using nitromethane as a solvent and recording the difference in half-neutralization potentials, ΔHNP, with *N,N'*-diphenylguanidine as a standard. The electron involved in π and σ-bonding between transition metal and phosphine is shifted more toward the phosphorus atom. The highest occupied molecular orbital of the above complexes, which contain an unpaired electron, seems to reflect the general donor-acceptor properties of the ligands.

As predicted from the molecular orbital calculations,[12] the axial ligation results in decreasing separations of ΔE_{xy} and ΔE_{xz}, which yield the differences in the ESR parallel components of the g and hyperfine tensors. The decrease in both $A_\parallel$ and $g_\parallel$ values from bis(trifluoroacetylacetonato)copper(II) to 1:1 phosphine adduct illustrates the coordination effect. Such phenomena were previously attributed to the solvent effect. Dimerization is also expected to reduce the value of hyperfine tensor in a manner similar to the formation of 1:1 adduct. However, in a dimer, two copper(II) ions ($S=1/2$) are coupled together by a dipolar interaction, a singlet ($S=0$) and triplet ($S=1$) state will be formed and the dipolar interaction will cause a separation of the $M_s=1$ and $M_s=0$ levels in zero magnetic field. ESR transitions are observed within the triplet. These will be in either normal or allowed $\Delta M=1$ type centered about a resonance position H_0, and in addition one may find forbidden or $\Delta M=2$ transition occurring at about $H_0/2$. The absence of low field signal in ESR spectrum of bis-(trifluoroacetylacetonato)copper(II)-phosphorus complexes reveals that the changes in ESR parameters can thus be ascribed to differences in the monomer and not to partial dimer.

Attempts to synthesize 1:2 complexes of bis(trifluoroacetylacetonato)copper(II) and phosphine were unsuccessful. The reactions led to the formation of Cu(I) complexes as $Cu(tfac)(PR_3)_2$.

The above experimental evidence indicates the formation of 1:1 adduct of bis(trifluoroacetylacetonato)-copper(II) and tertiary phosphines. Further systematic investigations of interaction between β-diketone transition metal complexes and phosphorus ligands are in progress.

Partial financial support by the California State University at Long Beach Foundation is gratefully acknowledged.

14) G. N. La Mar, *Inorg. Chim. Acta*, **3**, 183 (1969).
15) R. L. Carlin and A. E. Siegel, *Inorg. Chem.*, **9**, 1587 (1970).
16) E. Sinn, *Inorg. Nucl. Chem. Lett.*, **6**, 811 (1970).
17) C. A. Streuli, *Anal. Chem.*, **32**, 985 (1960).

Infrared Spectrum and Normal Vibrations of *N,N*-Dimethylthioacetamide

Arabinda RAY and D. N. SATHYANARAYANA

Department of Inorganic and Physical Chemistry, Indian Institute of Science, Bangalore-12, India

(Received February 9, 1972)

Infrared spectrum of *N,N*-dimethylthioacetamide (DMTA) has been recorded in the region 250—4000 cm^{-1}. Normal vibration analysis has been carried out employing Urey-Bradley force field and assignments are made and supported by comparison with related molecules. The complexes of DMTA with cobalt(II), copper(I), and mercury(II) chlorides have been prepared and their infrared spectra recorded. The frequency shifts in metal complexes are in accord with the assignments of C=S and C–N frequencies.

Although the normal vibrations of primary and secondary thioamides have been well investigated,[1,2] no detailed study of tertiary thioamides seems to have been made. It is only recently we made a normal vibration analysis of *N,N*-dimethylthioformamide (DMTF) to know the detailed nature of the vibrations.[3] It was considered worthwhile to study the normal vibrations in the next higher thioamide, *N,N*-dimethylthioacetamide (DMTA). In this paper, the normal coordinate treatment of DMTA employing Urey-Bradley force field (UBF) is reported. The preparation of the complexes of DMTA with the chlorides of cobalt(II), copper(I), and mercury(II) and their infrared spectra are also included. The assignment of the infrared frequencies are discussed by comparison with related molecules and also from frequency shifts in metal complexes.

Experimental

Materials Employed. *N,N*-Dimethylthioacetamide was synthesized by treating "high purity" *N,N*-dimethylacetamide (obtained from National Chemical Laboratory, Poona, India) with phosphorus pentasulphide (Merck) in benzene (A. R. Grade) according to the general procedure of Hofmann.[4] It was repeatedly recrystallized from *n*-hexane. $CoCl_2 \cdot 6H_2O$, $CuCl_2 \cdot 2H_2O$, and $HgCl_2$ were of A. R. Grade quality. Distilled ethanol (99%) was used.

Preparation of Complexes. *Dichlorobis(DMTA) Cobalt-(II)*: It was prepared by mixing ethanol solutions of DMTA and cobalt(II) chloride according to the reported procedure[5] (Found: Co, 17.03; S, 18.66%. Calcd for $CoCl_2 \cdot 2DMTA$: Co, 17.54; S, 19.05%.).

Chloro-(DMTA) Copper(I): An ethanol solution of DMTA was mixed with copper(II) chloride in ethanol, when copper-(II) gets reduced to copper(I) and an yellow precipitate of the cuprous complex was obtained. It was filtered off, washed thoroughly with ethanol followed by carbon disulphide and dried in vacuum (Found: Cu, 31.23; S, 14.90%. Calcd for CuCl·DMTA: Cu, 31.43; S, 15.84%.).

Dichlorotetrakis(DMTA) Mercury(II): The above method was followed for its preparation. The resulting white precipitate was filtered, washed with ethanol and dried in vacuum (Found: Hg, 30.30; S, 18.41%. Calcd for $HgCl_2 \cdot 4DMTA$: Hg, 29.34; S, 18.72%.).

Analysis. The complexes were analysed for metal and sulfur by standard methods.

Infrared Spectra. The infrared spectra of DMTA and its complexes were taken in Nujol mull and KBr pellets on a Carl-Zeiss UR 10 spectrophotometer in the range 4000—400 cm^{-1}, and on a Perkin-Elmer grating spectrophotometer, 521 in the range 400—250 cm^{-1}.

Normal Coordinate Treatment

The molecule DMTA belongs to the point group C_s and its 39 fundamental vibrations are classified as 24 A′ and 15 A″ vibrations. The secular equation of the Wilson's GF matrix was solved for A′ vibrations only, which were of interest in the present study. Further, the six C–H stretching modes were split off for simplification. The internal coordinates are defined in Fig. 1 and the symmetry coordinates are listed in Table 1. The structural parameters were taken from DMTF.[3] The C–C′ bond length was assumed to be 1.54 Å and the angles around carbon, tetrahedral. An IBM computer 360/44 was used.

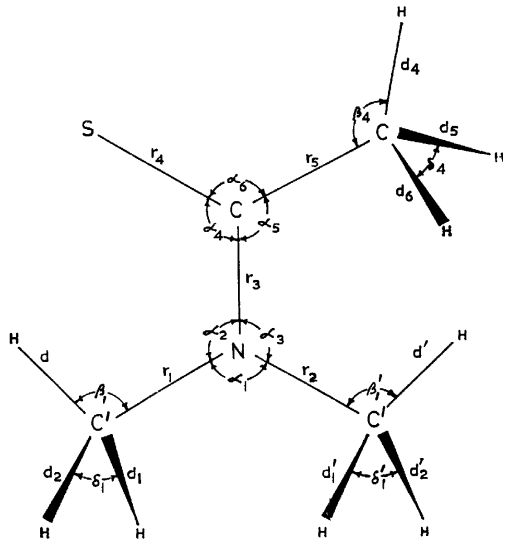

Fig. 1. Internal coordinates for DMTA.

Force Field. It is noteworthy that the UBF has been found to be very effective in the vibrational analysis of thioamide derivatives.[1-3,6] It is for this reason that UBF was chosen for our calculations.

1) I. Suzuki, This Bulletin, **35**, 1286, 1449, 1456 (1962).

2) C. N. R. Rao and G. C. Chaturvedi, *Spectrochim. Acta*, **27A**, 520 (1971).

3) G. Durga Prasad, D. N. Sathyanarayana, and C. C. Patel, This Bulletin, **44**, 316 (1971).

4) A. W. Hofmann, *Ber.* **11**, 338 (1878).

5) S. K. Madan and D. Mueller, *J. Inorg. Nucl. Chem.*, **28**, 177 (1966).

6) R. K. Gosavi, U. Agarwala, and C. N. R. Rao, *J. Amer. Chem. Soc.*, **89**, 235 (1967).

Table 1. Symmetry coordinates for DMTA

Symmetry coordinate	Description[a]
$S_1=(r_1+r_2)/\sqrt{2}$	Sym C'N str
$S_2=(r_1-r_2)/\sqrt{2}$	Asym C'N str
$S_3=r_3$	CN str
$S_4=r_4$	CS str
$S_5=r_5$	CC' str
$S_6=(2\alpha_1-\alpha_2-\alpha_3)/\sqrt{6}$	C'NC' bend
$S_7=(\alpha_2-\alpha_3)/\sqrt{2}$	C'NC bend
$S_8=(2\alpha_4-\alpha_5-\alpha_6)/\sqrt{6}$	NCS bend
$S_9=(\alpha_5-\alpha_6)/\sqrt{2}$	CCS bend
$S_{10}=(\delta_4+\delta_5+\delta_6-\beta_4-\beta_5-\beta_6)/\sqrt{6}$	Sym (C)CH_3 def
$S_{11}=(2\delta_4-\delta_5-\delta_6)/\sqrt{6}$	Asym (C)CH_3 def
$S_{12}=(2\beta_4-\beta_5-\beta_6)/\sqrt{6}$	(C)CH_3 rock
$S_{13}=(2\delta_1-\delta_2-\delta_3+2\delta_1'-\delta_2'-\delta_3')/\sqrt{12}$	Asym (N)CH_3 def
$S_{14}=(2\delta_1-\delta_2-\delta_3-2\delta_1'+\delta_2'+\delta_3')/\sqrt{12}$	Asym (N)CH def
$S_{15}=(\delta_1+\delta_2+\delta_3-\beta_1-\beta_2-\beta_3+\delta_1'+\delta_2'+\delta_3'-\beta_1'-\beta_2'-\beta_3')/\sqrt{12}$	Sym (N)CH_3 def
$S_{16}=(\delta_1+\delta_2+\delta_3-\beta_1-\beta_2-\beta_3-\delta_1'-\delta_2'-\delta_3'+\beta_1'+\beta_2'+\beta_3')/\sqrt{12}$	Sym (N)CH_3 def
$S_{17}=(2\beta_1-\beta_2-\beta_3+2\beta_1'-\beta_2'-\beta_3')/\sqrt{12}$	(N)CH_3 rock
$S_{18}=(2\beta_1-\beta_2-\beta_3-2\beta_1'+\beta_2'+\beta_3')/\sqrt{12}$	(N)CH_3 rock

a) Sym is symmetric, asym is asymmetric and def is deformation.

Table 2. Force constants (in md/Å) for DMTA

Stretching		Bending		Repulsion	
$K_{C'N}$	3.40	$H_{C'NC'}$	0.180	$F_{C'C'}$	0.25
K_{CN}	5.75	$H_{C'NC}$	0.20	$F_{CC'}$	0.55
K_{CS}	3.74	H_{SCN}	0.150	F_{NC}	0.75
K_{CC}	2.85	$H_{C'CN}$	0.390	F_{NS}	1.45
Intramolecular tension (md Å)		$H_{C'CS}$	0.390	F_{SC}	0.60
k_{CCH3}	−0.056	$H_{HC'N}$	0.30	F_{NH}	0.55
k_{NCH3}	−0.050	$H_{HC'(N)H}$	0.425	F_{CH}	0.50
		$H_{HC'C}$	0.255	F_{HH}	0.05
		$H_{HC'(C)H}$	0.410	F'	−0.1F

The initial set of UBF constants were taken from thioacetamide (TAM), *N*-methylthioacetamide (NMTA), and DMTF.[1-3] The force constants were progressively improved by an iterative procedure. Some of the bending force constants in DMTA differ from, and the stretching and repulsion force constants remain nearly the same as those in TAM, NMTA, and DMTF. Thus, the force field appears to be satisfactorily transferrable among related thioamide molecules. The frequency fit is satisfactory except the rocking frequencies which show comparatively large deviations as are usually the case in the UBF. The final set of force constants is given in Table 2.

Table 3. Observed and calculated frequencies of DMTA and their assignments

Frequencies, cm^{-1}			PED,[b] %
Obsd	Calcd	Δ[a]	
1540	1536	0.26	$S_3(46)$, $S_{13}(16)$, $S_{17}(15)$
1470	1475	0.34	$S_{14}(80)$, $S_{18}(19)$
	1462	0.54	$S_{13}(42)$, $S_{11}(30)$, $S_{12}(11)$
	1429	2.11	$S_{15}(50)$, $S_{11}(28)$, $S_{13}(10)$
1430	1422	0.56	$S_{16}(96)$
	1405	1.75	$S_{15}(44)$, $S_3(18)$, $S_{11}(15)$
1370	1373	0.22	$S_{10}(91)$
1284	1279	0.39	$S_5(28)$, $S_4(17)$, $S_8(15)$, $S_2(11)$, $S_7(10)$
1185	1154	2.62	$S_{17}(36)$, $S_{15}(14)$, $S_{16}(12)$
1130	1133	0.27	$S_2(26)$, $S_{18}(26)$, $S_5(24)$
1060	1004	5.28	$S_2(39)$, $S_{18}(38)$
1020	998	2.16	$S_{12}(38)$, $S_{17}(22)$, $S_3(11)$
870	867	0.34	$S_1(37)$, $S_4(24)$, $S_{12}(15)$
656	661	0.76	$S_1(44)$, $S_4(25)$, $S_5(17)$
495	495	0	$S_8(40)$, $S_7(21)$, $S_2(16)$
444	446	0.40	$S_9(59)$, $S_6(12)$, $S_4(10)$
300	300	0	$S_6(79)$, $S_9(13)$
—	202	—	$S_7(59)$, $S_8(33)$

a) $\Delta=|\nu\text{calc}-\nu\text{obs}|\times 100/\nu\text{obs}$; ν denotes frequency in cm^{-1}.
b) Contribution less than 10% is not included.

Table 4. Infrared frequencies in the range 250—1800 cm^{-1} for DMTA complexes and their assignment

$CoCl_2$ 2DMTA	CuCl DMTA	$HgCl_2$ 4DMTA	DMTA	Assignment[a]
1580 vs	1590 vs	1610 vs	1540 vs	ν(C-N)+δ_a(N-CH_3)+r(N-CH_3)
1465 s	1470 vs	1470 s	1470 s	δ_a(CH_3)N,C
1430 s	1430 vs	1410 s	1430 s	δ_s(N-CH_3)
1385 vs	1385 s	1370 s	1370 s	δ_s(C-CH_3)
1285 vs	1262 vs	1270 vs	1284 vs	ν(C-C')+ν_a(C'-N)+ν(C=S)+δ(NCS)
1192 vs	1190 m	1195 m	1185 s	r(N-CH_3)+δ(N-CH_3)
—	—	—	1160 vw	r(N-CH_3);(A'')
1130 s	1115 s	1130 s	1130 s	ν_a(C'N)+ν(C-C)+r(N-CH_3)
1060 s	1085 sh	1050 w	1060 w	ν_a (C'-N)+r(N-CH_3)
1030 vs	1025 s	1015 m	1020 vs	r(CH_3)N,C
862 s	845 m	860 vw 845 m	870 s	ν_s(C'-N)+ν(CS)
655 vs	635 s	640 s	656 s	ν_s(C'-N)+ν(C=S)+ν(C-C')
542 vw	540 vw	535 w	540 vw	π(C-C');(A'')
498 m	485 w	498 w	495 m	δ(NCS)+δ(CNC')
448 m	435 m	451 m	444 m	δ(CCS)
428 vw	400 w	428 w	402 vw	—
378 w	368 w	364 s	370 vw	—
336 vw	340 vw	350 m	349 vw	π(C'NC');(A'')
325 vw				
290 w	306 sh	284 sh	300 sh	δ(C'NC')

a) ν means stretching, δ=bending, r=rocking, π=out-of-plane bending; s=symmetric and a=asymmetric; A'' vibrations are tentatively assigned.

Results and Discussion

The observed and calculated frequencies along with the assignments from potential energy distribution (PED) are given in Table 3. The infrared frequencies of DMTA and its complexes in the region 250—1800 cm^{-1} and their assignments are presented in Table 4. A brief discussion of the assignment of the frequencies is given below.

C–N and C=S Stretching Modes. From valence bond concept, on coordination of the thiocarbonyl sulfur to metal, the C–N stretching frequency is expected to increase while the C=S stretching frequency show a decrease. The C–N stretching frequency occurring at 1540 cm^{-1} in DMTA increases to 1580 to 1610 cm^{-1} in metal complexes and the increase is apparently related to the metal ion. The C–N stretching frequency has been reported to increase to 1600 cm^{-1} on *S*-methylation as expected.[7] A band at 1560 cm^{-1} in DMTF has a similar assignment.[3]

Two bands at 870 and 656 cm^{-1} have large C=S stretching contribution, about 25% in each case. These frequencies decrease to 862—845 and 652—635 cm^{-1}, respectively, in metal complexes. The decrease in the 870 and 656 cm^{-1} bands is substantial in the case of copper(I) and mercury(II), while it is nominal in the case of cobalt(II). This is understandable since copper(I) and mercury(II) are known to form stronger coordination bonds with sulfur donors than cobalt(II). The 870 and 656 cm^{-1} bands have been found to shift to lower frequencies on "selenation", *i.e.*, in *N,N*-dimethylselenoacetamide,[7] to 834 and 606 cm^{-1}, respectively. Similar downward shift in these two frequencies has been noted on *S*-methylation.[7] These findings support the larger contribution from C=S stretching to 870 and 656 cm^{-1} bands. An earlier assignment[8] of C=S stretching for a band near 1100 cm^{-1} is thus not favoured.

Significant contribution of C=S stretching is seen in the 1284 cm^{-1} band also. This band also shows smaller shift to a lower frequency by 10—15 cm^{-1} in metal complexes except in the cobalt complex.

C'–N and C–C' Stretching Modes. The asymmetric C'–N stretching, unlike in DMTF and DMF[3] (*N,N*-dimethylformamide), is highly coupled and is distributed in the frequencies at 1284, 1130, and 1060 cm^{-1}. The C'–N symmetric stretching has contributions in the 870 and 656 cm^{-1} bands. Their occurrence is comparable with those of DMF and DMTF.[3]

Similarly, the C–C' stretching is highly mixed with other vibrations and has contributions in the frequencies at 1284, 1130, and 656 cm^{-1}. The assignment is comparable to that in NMTA[1] and *N*-methylacetamide.[9] The C–C stretching has been located at 954 cm^{-1} in *N,N*-dimethylacetamide.[10]

Skeletal Bending Modes. The bands at 495 and 444 cm^{-1} are predominantly due to NCS and CCS bending vibrations, respectively. The corresponding bands in thioacetamide have been found[1] at 470 and 380 cm^{-1}. No gradual change in frequencies has been

7) K. A. Jensen and P. H. Nielsen, *Acta Chem. Scand.*, **20**, 597 (1966).

8) C. Collard-Charon and M. Rensen, *Bull. Soc. Chem. Belges.*, **72**, 304 (1963).

9) T. Miyazawa, T. Shimanouchi, and S. Mizushima, *J. Chem. Phys.*, **29**, 611 (1958).

10) R. L. Jones, *J. Mol. Spectrosc.*, **11**, 411 (1963).

observed for these bands in complexes, probably because of their possible different structures.

C-CH_3 and N-CH_3 Bending Modes. The symmetric and asymmetric deformations at 1370 and 1470 cm^{-1}, respectively, and the rocking mode at 1020 cm^{-1} for C-CH_3 group compare well with those in related molecules.[1,9,12] Similarly, the symmetric and asymmetric bending modes of the N-CH_3 group are easily located at 1430 and 1470 cm^{-1}, respectively and the rocking modes at 1185 and 1060 cm^{-1}.[9-12]

Frequency Shifts in Metal Complexes. Although cobalt(II) complexes were known earlier,[5] no infrared study concerning DMTA has been reported. The complexes of copper(I) and mercury(II) chlorides are new. The effect of complex formation on C=S and C-N stretching frequencies was pointed out earlier. It is satisfying to note that the expected frequency shifts have been realised. The NCS bending frequency may be expected to show a small increase on coordination to metals. However, this band is nearly stationary, except for 3 cm^{-1} raise in mercury and cobalt complexes. This may be attributed to the complicated nature of coupling in the 495 cm^{-1} frequency and also to the different structures of the complexes.

The authors thank Prof. C. C. Patel, for helpful discussion and encouragement; and Mr. G. Durga Prasad for help in the initial stages of calculation and for preparing the cobalt complex.

11) Y. Mido and H. Murata, This Bulletin, **42**, 3372 (1969).
12) H. A. Szymanski, "Theory and Practice of IR Spectroscopy," Plenum Press, New York (1964), pp. 209—213.

BULLETIN OF THE CHEMICAL SOCIETY OF JAPAN, VOL. 45, 2715—2719 (1972)

Ultrasonic Study of Solute-Solvent Interaction in Aqueous Solutions of Tetraalkylammonium Salts

Fumio HIRATA and Kiyoshi ARAKAWA

Research Institute of Applied Electricity, Hokkaido University, Sapporo

(Received September 6, 1971)

Ultrasonic velocity of aqueous solutions of tetraalkylammonium chlorides was measured over wide ranges of concentration and temperature in order to study the nature of solute-solvent interactions. Adiabatic compressibility was obtained from the data of sound velocity and density. The results were discussed in terms of the influence of solutes upon the structure of liquid water. It has been shown that Me_4N^+ is a structure breaker, while n-Bu_4N^+ forms a structure or "icebergs" around the cations evidently, and that the ability of iceberg formation begins at n-Pr_4N^+. It was concluded that the icebergs have a more rigid structure than the ice-like structure in bulk water.

Aqueous solutions of tetraalkylammonium salts show abnormal behavior in various physico-chemical properties, such as partial molal volume,[1-3] activity coefficient,[4-6] heat of solution,[7-10] conductance,[11] and viscosity.[12]

The behavior has been discussed mainly in terms of water-hydrocarbon interactions leading to recognition of hydrophobic interactions.

In recent years, the important role of hydrophobic interaction for the maintenance of higher order structure of protein molecules with non-polar side chains in aqueous solutions has become increasingly clear.[13,14]

When hydrocarbon molecules are dissolved in water, the entropy of solution becomes much more negative than in corresponding non-aqueous solutions. On this basis Frank and Evans[15] postulated the formation of "icebergs" around non-polar solute molecules in water.

Recently, Wen and Saito[1] have obtained remarkable results in the measurement of partial molal volume of tetraalkylammonium bromides in aqueous solutions.

A deep minimum appears for the partial molal volume of tetrabutylammonium bromides at about 1 mol/l.

It ascends with rising temperature. For the sake of interpretation, formation of a *clathrate-like structure* of water molecules around tetrabutylammonium cations was suggested.

1) W. Y. Wen and S. Saito, *J. Phys. Chem.*, **68**, 2639 (1964).
2) F. Franks and H. Smith, *Trans. Faraday Soc.*, **63**, 2586 (1967).
3) B. E. Conway, R. E. Verral, and J. E. Desnoyer, *ibid.*, **62**, 2738 (1966).
4) R. M. Diamond, *J. Phys. Chem.*, **67**, 2513 (1963).
5) W. Y. Wen, S. Saito, and C. Lee, *ibid.*, **70**, 1244 (1966).
6) S. Lindenbaum and G. E. Boyd, *ibid.*, **68**, 911 (1964).
7) S. Lindenbaum, *ibid.*, **70**, 814 (1966).
8) W. Y. Wen and J. H. Hung, *ibid.*, **74**, 170 (1970).
9) T. S. Sarma, R. K. Mohanty, and J. C. Ahluwalia, *Trans. Faraday Soc.*, **65**, 2333 (1969).
10) C. V. Krishnan and H. L. Friedman, *J. Phys. Chem.*, **73**, 3934 (1969).
11) D. F. Evans and R. L. Kay, *ibid.*, **70**, 366 (1966), R. L. Kay and D. F. Evans, *ibid.*, **70**, 2325 (1966).
12) E. R. Nightingale, Jr., *ibid.*, **63**, 1381 (1959), *ibid.*, **66**, 894 (1962).
13) W. Kauzman, *Advances in Protein Chem.*, **14**, 1 (1959).
14) G. Nemethy, *Angew. Chem. Int. Ed.*, **6**, 195 (1967).
15) H. S. Frank and M. W. Evans, *J. Chem. Phys.*, **13**, 507 (1945).

Frank and Wen,[16] on the other hand, proposed a simple model for the modification of the structure of liquid water caused by the presence of ions.

A tetraalkylammonium cation is regarded as a fairly large spherical ion and a solute with hydrophobic surface. These two factors are supposed to influence the liquid structure of water. It is of interest to study the solute-solvent interaction in aqueous solutions of these salts.

The compressibility obtained from the measurement of sound velocity is determined primarily by intermolecular forces. It is useful to measure sound velocity for the purpose of studying the structural change of liquid water induced by solute molecules.

However, there have been very few studies along this line, except that reported by Conway and Verral which was made over a limited range of temperature at low concentrations[17] and also that by Allam and Lee.[18]

We have, thus, attempted to measure ultrasonic velocity of aqueous solutions of tetraalkylammonium chlorides over wide ranges of concentration and temperature.

Experimental

Samples of tetraalkylammonium chlorides, R_4NCl (R; Me, Et, Bu) were obtained from Wako Pure Chemical Industry Co., Ltd. and tetrapropylammonium chloride from Eastman Organic Chemicals, Rochester, New York. The samples were purified by recrystallization from ethanol-ether mixtures for tetramethylammonium chloride and chloroform-ether mixtures for tetraethylammonium chloride,[1] respectively.

All salts were dried in a vacuum at 60—70°C.

Concentrations of aqueous solutions of these four salts were determined by gravimetric analysis by precipitation with $AgNO_3$. The results agreed with the values calculated from the weight of dried samples before dissolution within small errors.

Sound velocity was measured using a crystal interferometer of the usual type at 3 MHz. The cell used was the same type as that previously described.[19]

Measurements were carried out at temperature from 20 to 35°C. Temperature was controlled within ± 0.05°C.

Density was measured using a pycnometer of the usual type.

Results

Ultrasonic Velocity. The ultrasonic velocity for aqueous solutions of tetraalkylammonium salts at 3 MHz is plotted against temperature and shown in Figs. 1 (a)—(d). We see that it increases linearly with the rise in temperature for tetramethylammonium chloride solutions, but temperature dependency is seen to be reversed at a certain concentration in the case of the other three salts.

Adiabatic Compressibility. Adiabatic compressibility κ_s is obtained from the sound velocity and density of solutions. Values of κ_s for aqueous solutions of tetraalkylammonium chlorides are plotted against temperature in Figs. 2 (a)—(d).

Similarly to sound velocity *vs.* temperature curves, the temperature dependence of κ_s is reversed at a certain concentration for solutions of Et_4NCl, Pr_4NCl, and Bu_4NCl, respectively. The values of κ_s at 25°C for each 1 mol/*l* solution is shown in Fig. 3 as a function of the number of carbon atoms in each salt. It is seen that adiabatic compressibility decreases with the number of carbon atoms and that the temperature dependence is reversed between Et_4NCl and Pr_4NCl.

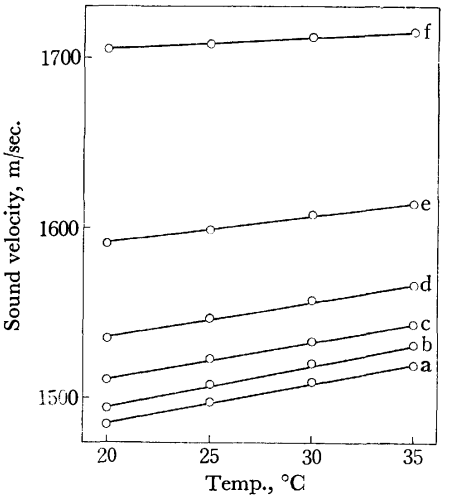

Fig. 1(a). Ultrasonic velocity of aqueous solutions of tetramethylammonium chloride. Concn. (M: mol/*l*) (a) Pure water, (b) 0.10 M, (c) 0.25 M, (d) 0.50 M, (e) 1.01 M, (f) 2.02 M.

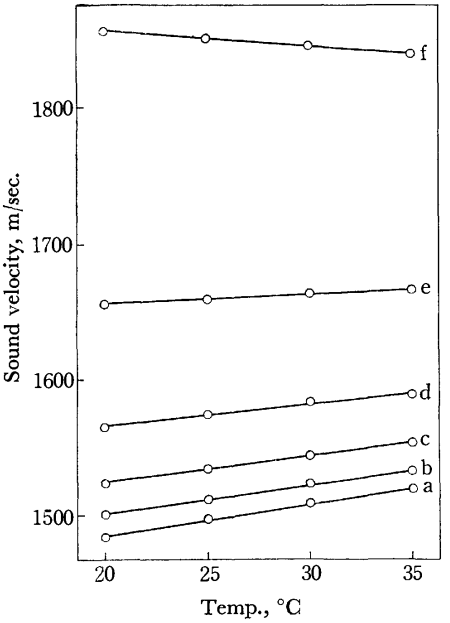

Fig. 1(b). Ultrasonic velocity of aqueous solutions of tetraethylammonium chloride. Concn. (M: mol/*l*) (a) Pure water (b) 0.13 M (c) 0.26 M, (d) 0.52 M, (e) 1.03 M, (f) 2.06 M.

16) H. S. Frank and W. Y. Wen, *Discuss. Faraday Soc.*, **24**, 133 (1957).
17) B. E. Conway and R. E. Verral, *J. Phys. Chem.*, **70**, 3952 (1966).
18) D. S. Allam and W. H. Lee, *J. Chem. Soc.*, *A*, 426 (1966).
19) O. Kiyohara and K. Arakawa, This Bulletin, **43**, 3037 (1970).

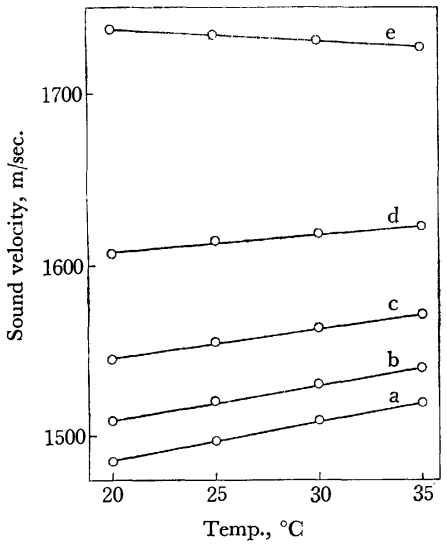

Fig. 1(c). Ultrasnonic velocity of aqueous solutions of tetrapropylammonium chloride. Concn. (M: mol/*l*) (a) Pure water, (b) 0.10 M, (c) 0.25 M, (d) 0.51 M, (e) 1.01 M.

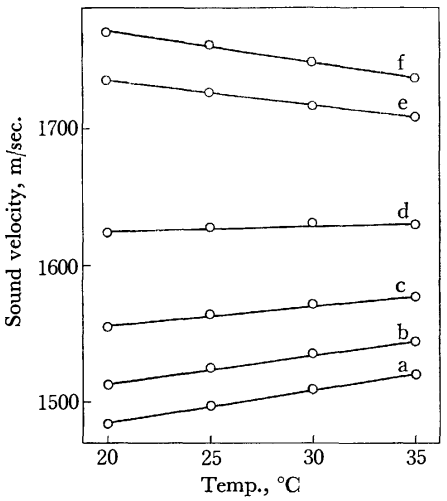

Fig. 1(d). Ultrasonic velocity of aqueous solutions of tetrabutylammonium chloride. Concn. (M: mol/*l*) (a) Pure water, (b) 0.08 M, (c) 0.22 M, (d) 0.44 M, (e) 0.88 M, (f) 1.15 M.

Discussions

Compressibility in Water. Water is regarded as an equilibrium mixture of two structures such as an *ice-like structure* and a *close packed structure.*[20,21]

Compressibility of liquid water is given by

$$\kappa = \kappa_\infty + \kappa_{relax.}/(1+\omega^2\tau^2) \qquad (1)$$

where κ_∞ is an instantaneous part of compressibility and $\kappa_{relax.}$ a relaxational part of compressibility.[20]

The relaxation time τ corresponding to $\kappa_{relax.}$ is of the order of 10^{-11} sec. The relation $\omega\tau \ll 1$ holds in the present experiment, where ω is the angular frequency. Thus, the adiabatic compressibility obtained is equal to $\kappa_\infty + \kappa_{relax.}$.

With the rise in temperature, κ_∞ increases due to thermal expansion, and $\kappa_{relax.}$ decreases due to thermal rupture of the ice-like structure.

Thus, the decrease of compressibility at temperatures 20—35°C is attributed to the decrease of $\kappa_{relax.}$, which is dominant over the increase of κ_∞.

Structure Breaking Effect of Tetramethylammonium Cations. Compressibility decreases rapidly from pure water to aqueous solutions of tetramethylammoium chloride (Fig. 3). This might be ascribed to three effects: (1) the effect of Cl^- on the structure of water, (2) the decrease of compressibility caused by the introduction of large incompressible cations Me_4N^+, (3) the influence of Me_4N^+ on the structure of the surrounding water.

The difference between partial molal volume, $\bar{V}$, and intrinsic volume, V^0, estimated from crystal radius of

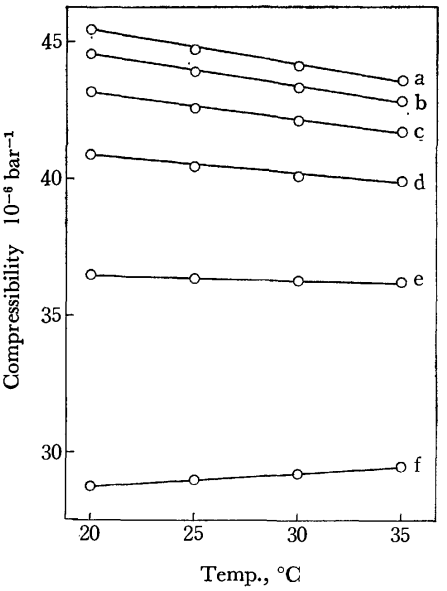

Fig. 2(a). Compressibility of aqueous solutions of tetramethylammonium chloride. Concn. (M: mol/*l*) (a) Pure water, (b) 0.10 M, (c) 0.25 M, (d) 0.50 M, (e) 1.01 M, (f) 2.02 M.

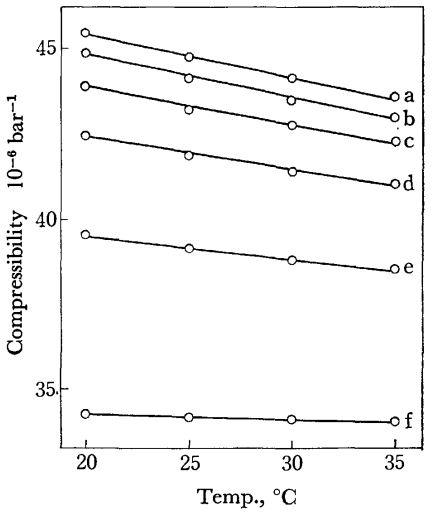

Fig. 2(b). Compressibility of aqueous solutions of tetraethylammonium chloride. Concn. (M: mol/*l*) (a) Pure water, (b) 0.13 M, (c) 0.26 M, (d) 0.52 M, (e) 1.03 M, (f) 2.06 M.

20) L. Hall, *Phys. Rev.*, **73**, 775 (1948).
21) K. Arakawa and K. Sasaki, This Bulletin, **42**, 303(1969).

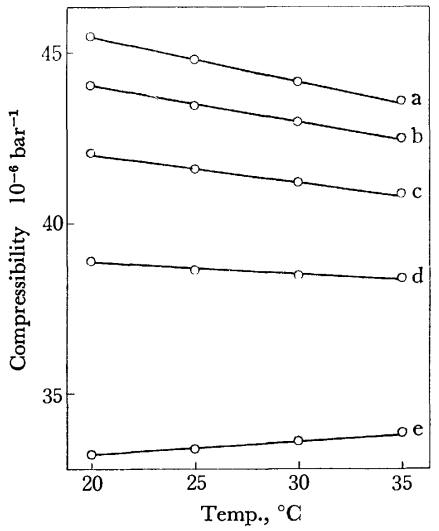

Fig. 2(c). Compressibility of aqueous solutions of tetrapropylammonium chloride. Concn. (M: mol/l) (a) Pure water, (b) 0.10 M, (c) 0.25 M, (d) 0.51 M, (e) 1.01 M.

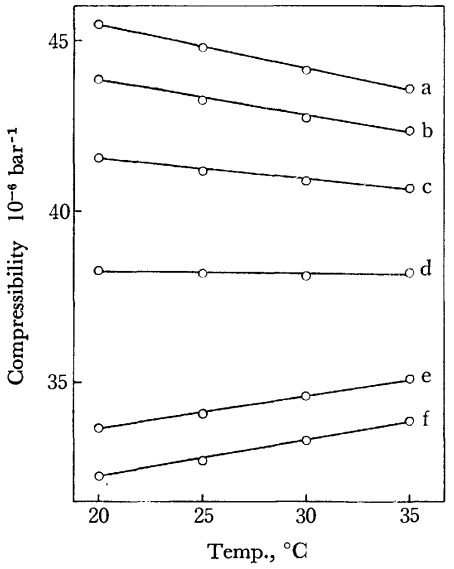

Fig. 2(d). Compressibility of aqueous solutions of tetrabutylammonium chloride. Concn. (M: mol/l) (a) Pure water, (b) 0.08 M, (c) 0.22 M, (d) 0.44 M, (e) 0.88 M, (f) 1.15 M.

ions represents the volume change of water caused by the action of ions. The values of $(V^0\text{-}\bar{V})$ of Cl^- and Me_4N^+ are estimated to be 1.7 and 21.4 cm^3/mol, respectively.[3] The effect of Cl^- is regarded to be negligible as compared with that of Me_4N^+.

Thus, only the contribution from Me_4N^+ might be taken into consideration.

The values of $(V\kappa_s)$ of an 1 mol/l solution of tetramethylammonium chloride is given by

$$V\kappa_s = N_1V_1\kappa_1 + N_2(V^0_{NMe_4^+}\kappa^0_{NMe_4^+} + V^0_{Cl^-}\kappa^0_{Cl^-}) \quad (2)$$

where

V; volume of an 1 mol/l aqueous solution
κ_s; adiabatic compressibility of 1 mol/l aqueous solution
κ_1; average compressibility of solvent water in the solution

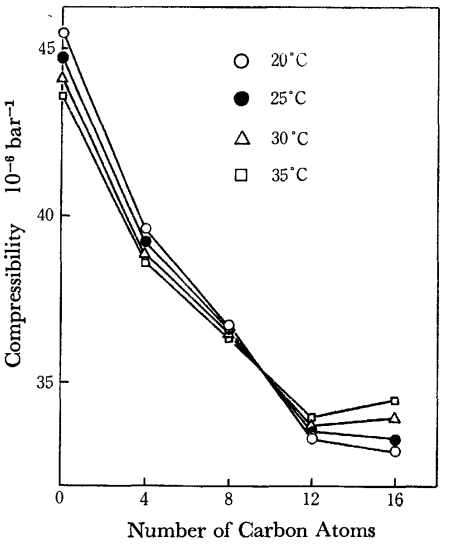

Fig. 3. Compressibility of 1 M aqueous solutions of tetraalkylammonium chlorides as a function of the number of carbon atoms in each salt.

V_1; volume of solvent water in the solution
N_1; number of moles of water in the solution
$V^0_{NMe_4^+}$; intrinsic volume of Me_4N^+
N_2; number of moles of Me_4NCl
$\kappa^0_{NMe_4^+}$; intrinsic compressibility of Me_4N^+
$V^0_{Cl^-}$; intrinsic volume of Cl^-
$\kappa^0_{Cl^-}$; intrinsic compressibility of Cl^-

In this equation, $(V^0_{Cl^-}\kappa^0_{Cl^-})$ is practically zero and can be neglected. Thus we obtain the magnitude of κ_1 by the equation

$$\kappa_1 = \frac{V\kappa_s - N_2V^0_{NMe_4^+}\kappa^0_{NMe_4^+}}{N_1V_1} \quad (3)$$

The intrinsic volume of Me_4N^+, $V^0_{NMe_4^+}$, is estimated with large uncertainty from 90 to 105 cm^3/mol.[1-3,12]

When we use the largest value[22] 105 cm^3/mol for $V^0_{NMe_4^+}$ and the value 3×10^{-6} bar^{-1} for $\kappa^0_{NMe_4^+}$ we find the average compressibility of water in the solution at 25°C to be smaller than the compressibility in pure water at the same temperature.[27] Thus, the sharp decrease of compressibility from pure water to a 1 mol/l aqueous solution of Me_4NCl is primarily ascribed to the structure-breaking effect of Me_4N^+.

22) The value V_{ion} was calculated from the ionic radius in crystal r_x by the equation

$$V^0_{ion} = \frac{4}{3}\pi N_A r_x^3 \quad (N\text{: Avogadro's number})$$

This value is supposed to be too large in the case of Me_4N^+, as compared with reported values of V_{ion}.[1-3,13,23-26]

23) L. G. Hepler, *J. Phys. Chem.*, **61**, 1426 (1957).

24) P. H. Stokes and R. A. Robinson, *Trans. Faraday Soc.*, **53**, 301 (1957).

25) R. Mukerjee, *J. Phys. Chem.*, **65**, 740, 744 (1961).

26) E. Gleuckauf, *Trans. Faraday Soc.*, **61**, 914 (1965).

27) The value of $\kappa_{NMe_4^+}$ has not been determined. It might be estimated to be larger than 3×10^{-6} bar^{-1} which is nearly equal to the value for fused quartz, flint glass, LiCl crystal (*cf.* Cho-onpa Gijutsu Binran (Handbook for Ultrasonic Technique), Nikkan Kogyo Shinbun Co., Ltd. (1966), p. 1325). When $\kappa_{NMe_4^+} \geq 3\times10^{-6}$ bar^{-1}, the value of $\kappa_1 < 44.7_5\times10^{-6}$ bar^{-1} which is the value for bulk water at 25°C.

This conclusion is also supported by the fact that the temperature dependence of compressibility of a 1 mol/l solution of Me_4NCl is smaller than that of pure water (Fig. 3).

Moreover, it is consistent with the results of studies for physico-chemical properties of the solution such as partial molal volume,[1] heat capacity[9], and conductivity.[11]

Iceberg Formation Around Tetrabutylammonium Cations. Several papers have peported that Bu_4N^+ ions form icebergs around themselves.

Wen and Saito[1] stated in 1964 that the structure of icebergs is "*clathrate like*". However, Wen and Hung[8] stated recently that "the nature of structure promotion by hydrocarbons or tetraalkylammonium salts is not well defined". Wicke[28] stated on the basis of NMR data that the icebergs around non-polar solutes have a "rigid" structure involving non-tetrahedral linking of H_2O molecules.

The values of κ_s of 1 mol/l solution of Bu_4NCl increase with rising temperature (Fig. 3).

The amount of icebergs is supposed to decrease with the rise in temperature. Thus, our result supports the idea that the icebergs around Bu_4N^+ cations have a smaller compressibility than bulk water, and that the structure of the icebergs is more rigid than ice-like structure.

The Nature of Icebergs. Conway and Verral discussed the molal adiabatic compressibility of solutes in aqueous solutions of tetraalkylammonium halides at infinite dilution.[17] They calculated the difference of molal values of κ_s at infinite dilution,

$$\phi^0_{K(s),Me,NX} - \phi^0_{K(s),Et,NX},\ \phi^0_{K(s),Et,NX} - \phi^0_{K(s),Pr,NX},\ \textit{etc.}$$

From the difference the contribution from co-anions to the compressibility of solutions was cancelled out.

We have calculated the difference of κ_s for solutions $\kappa_{Me,NCl,1M} - \kappa_{Et,NCl,1M}$, *etc.* at concentration 1 mol/l, and have compared the results with the values of Conway and Verral at infinite dilution (Table 1).

In the case of tetramethylammonium salt, tetraethylammonium salt and tetrapropylammonium salt solutions, the values of the difference at infinite dilution and those at 1 mol/l are nearly the same, but those between tetrapropylammonium salt solutions and tetrabutylammonium salt solutions at infinite dilution are much larger than the values at 1 mol/l.

The effect of solute to surrounding water per mole in the 1 mol/l solution is clearly less than the effect at infinite dilution owing to an overlapping effect (Fig. 4).[29]

Table 1. The difference of molal adiabatic compressibility

This work (10^{-6} bar^{-1} mol^{-1} l)		Conway and Verral (10^{-6} bar^{-1} mol^{-1} l)	
$\kappa_{Me_4NCl,\ 1M} - \kappa_{Et_4NCl,\ 1M}$,	2.6$_3$	$\phi^0_{K(s),\ Me_4NX} - \phi^0_{K(s),\ Et_4NX}$,	2.4
$\kappa_{Et_4NCl,\ 1M} - \kappa_{Pr_4NCl,\ 1M}$,	3.0$_6$	$\phi^0_{K(s),\ Et_4NX} - \phi^0_{K(s),\ Pr_4NX}$,	3.7
$\kappa_{Pr_4NCl,\ 1M} - \kappa_{Bu_4NCl,\ 1M}$,	0.2$_0$	$\phi^0_{K(s),\ Pr_4NX} - \phi^0_{K(s),\ Bu_4NX}$,	10.6

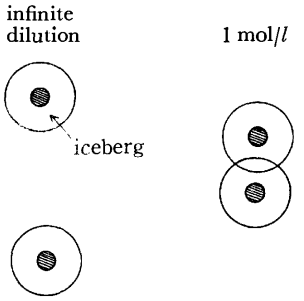

Fig. 4. Overlapping effect of solute-solvent interactions.

The fact that the difference between our data and those of Conway and Verral becomes appreciable (last row, Table 1) supports the idea that the overlapping effect appears typically in Bu_4N^+ ions. This is consistent with the above conclusion.

Dernell and Greyson[30] found that the tetraalkylammonium salts depress the temperature of maximum density of water T_m and the order of the effect increases in sequence $H_4N^+ < Me_4N^+ < Et_4N^+ < Pr_4N^+ < Bu_4N^+ < Am_4N^+$. They concluded that "the water structure-promoting characteristics of the species ordinarily found at room temperature do not manifest themselves in the neighborhood of T_m". Sarma and Ahluwalia,[31] however, rejected the conclusion from their measurements of heats of solution ΔH_s^0.

Heat capacity changes ΔC_p in aqueous solutions of Bu_4NBr, Pr_4NI, and $NaBPh_4$ derived from ΔH_s^0 values show no appreciable change as temperature falls from 30 to 4°C. They suggested that the hydration sheath around non-polar groups is not definitely ice-I-like but rather resembles a Pauling-type clathrate cage or some other polymorphic modification of ice. Our concept of rigid icebergs is consistent with this idea.

Relation between the Ability of Iceberg Formation and Ionic Size. As seen in Fig. 3, a marked difference appears in the temperature dependence of Pr_4NCl, where it is reversed, and the tendency is more remarkable in the solution of Bu_4NCl. Thus, the ability of iceberg formation seems to be appreciable at Pr_4N^+.

This agrees with the results obtained by Lindenbaum[7] from a study of thermodynamic excess functions in which the magnitude of excess enthalpy and entropy for Pr_4NCl solutions are very large in comparison with those for Me_4NCl and Et_4NCl solutions and the trend becomes more marked for Bu_4NCl solution.

On the other hand, several papers state that the behavior of Me_4N^+ differs from that of R_4N^+ (R; Et, *n*-Pr, *n*-Bu).[5,9,32]

This discrepancy may be at least partly ascribed to the difference of the nature of physico-chemical properties treated in those studies.

Our thanks are due to the kind cooperation of Mr. Nobuo Takenaka, Dr. Osamu Kiyohara, and Mr. Keiji Hasegawa.

28) E. Wicke, *Angew. Chem. Int. Ed.*, **5**, 106 (1966).
29) H. S. Frank, "Chemical Physics of Ionic Solutions" (ed., B. E. Conway and R. G. Barradas) p. 53, John, Wiley and Sons. Inc., (1966).
30) A. J. Darnell and J. Greyson, *J. Phys. Chem.*, **72**, 3021 (1968).
31) T. S. Sarma and J. C. Ahluwalia, *J. Phys. Chem.*, **74**, 3547 (1970).
32) E. R. Nightingale, Jr., "Chemical Physics of Ionic Solutions" (ed., B. E. Conway and R. G. Baradas) John, Wiley and Sons. Inc. (1966), p. 87.

Induced Optical Activity of Nucleic Acid-Toluidine Blue O Complex

Tomoyasu NAKAMURA and Yasumasa J. I'HAYA
Department of Materials Science, The University of Electro-Communications, Chofu-shi, Tokyo
(Received February 19, 1972)

The absorption, circular dichroism (CD) and optical rotatory dispersion spectra of DNA–toluidine blue O complexes were observed over the visible absorption spectral region. Effect of temperature on CD was examined at the temperatures 6—86°C. For the complex of a low DNA phosphate to dye ratio, the Krönig-Kramers transform was carried out and one positive and four successive negative CD bands were resolved. It is concluded that the shorter wavelength CD bands, one positive and one negative, are due to an exciton splitting of the dye dimers and that the rest may be induced by an asymmetric environment of the DNA deoxyribose residue.

In a previous paper,[1] we reported that the DNA- and RNA-thionine (Th) complexes show Cotton effects in the visible absorption region of the dye and that these Cotton effects may have two origins; one induced from the dye monomers bound to DNA (Optical Activity I) and the other caused by an interaction between the dimerically bound dyes (Optical Activity II). In a preliminary report on the study of the DNA-toluidine blue O (TBO) complexes,[2] we demonstrated that the usual exciton theory fails to predict the longer wavelength Cotton effects of the high *P*/*D* (DNA phosphate residue/dye concentration) complexes. In Optical Activity I, the dye monomers seem to be involved in a complicated interaction with the asymmetric environment due to deoxyriboses of DNA.

The most striking feature of the DNA-TBO complex at low *P*/*D* is the sign of each partial circular dichroism (CD) spectrum, which is completely the reverse of that found in the DNA-acridine orange (AO) complex. On the other hand, the general feature of the CD spectra of the DNA- and RNA-Th complexes resembles that of the DNA-AO complex including their signs.[1] In this paper, we report the absorption spectra and Cotton effects of the DNA-TBO complexes at low as well as at high *P*/*D* values, with particular reference to their temperature dependence. CD band resolution is carried out for the low *P*/*D* complex by means of the Krönig-Kramers transform. It is shown that both effects of exciton splitting and asymmetric field are necessary for inducing the longer wavelength Cotton effects.

Experimental

Commercial calf-thymus DNA (Sigma Type I) and toluidine blue O (3-amino-7-dimethylamino-2-methylphenazathionium chloride) (Merck) were used without further purification. Stock aqueous solutions of DNA and TBO were dessolved in 0.01M phosphate buffer (pH 6.84). Concentration of TBO was chosen to be 5×10^{-5}M. A Jasco ORD/UV-5 recording spectropolarimeter with CD attachment was used. Further experimental details were the same as given previously.[1]

Results

The intensity of the absorption spectrum of TBO in water changes with concentration. According to Rabinowitch and Epstein,[3] the absorption peak appearing at low concentration is called M-band (monomer band) and at high concentration D-band (dimer band). In our experiment, the M-band and the D-band of TBO are located at 637 nm ($\varepsilon=2.9\times10^4$) and 562 nm ($\varepsilon=1.1\times10^4$), respectively. Using the same method as theirs, we obtained the average equilibrium constant for dimerization $K=2.6\times10^{-4}\,l\cdot mol^{-1}$ at room temperature, the value being nearly equal to that of methylene blue.[3]

An analogous change in the visible absorption spectrum of the dye can be seen when DNA is added to the dye solution. This has been reported by Huse, Miyake, and Tsuboi.[4] Apart from a detailed charac-

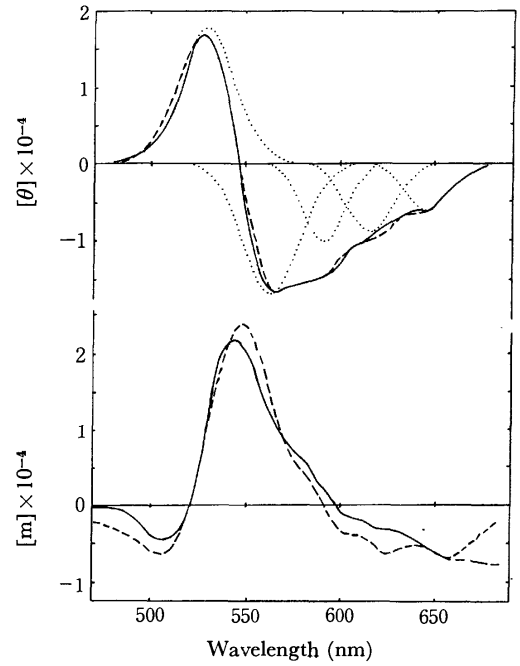

Fig. 1. The observed and calculated CD (upper) and ORD (lower) spectra of DNA–TBO *P*/*D*=0.26 complex; solid curve: observed; dotted curve: resolved components; broken curve: sum of the resolved components.

1) Y. J. I'Haya and T. Nakamura, This Bulletin, **44**, 951 (1971).
2) Y. J. I'Haya, T. Nakamura, Y. Yagi, T. Sano, and H. Ito, *Intern. J. Quantum Chem. Symposium*, **5**, 361 (1971).
3) E. Rabinowitch and L. F. Epstein, *J. Amer. Chem. Soc.*, **63**, 69 (1941).
4) Y. Huse, K. Miyake, and M. Tuboi, This Bulletin, **38**, 1039 (1965).

teristic, the changing profile of the absorption spectrum of DNA-TBO is similar to that of DNA-AO.[5] On the other hand, the optical rotatory dispersion (ORD) and CD spectra of DNA-TBO are quite different from those of DNA-AO.[6-8] The representative CD and ORD spectra of DNA-TBO are shown in Fig. 1 with their CD band components resolved by the Krönig-Kramers transform.[9] At low P/D values, one positive and four successive negative CD bands appear with maxima located at 529, 563, 590, 615, and 645 nm, respectively. They are hereafter referred to as Bands I, II, III, IV, and V. Band V (at 645 nm) is somewhat doubtful. At high P/D values, the positive CD maximum (Band I) disappears and the successive negative CD maxima (Bands II—V) shift a little to the shorter wavelength side, a newly developed positive CD band then coming out at about 650 nm (Fig. 2). The features of CD bands change with both temperature and P/D values (Fig. 3).

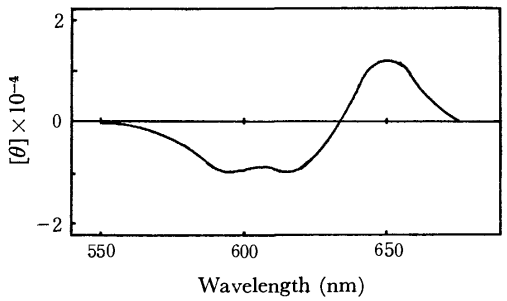

Fig. 2. CD spectrum of DNA-TBO P/D=2.6 complex.

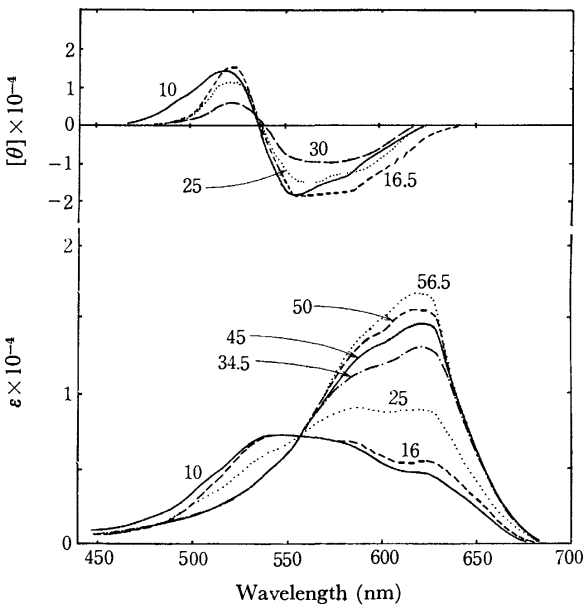

Fig. 3. Effect of temperature on CD (upper) and absorption (lower) spectra of DNA-TBO P/D=0.46 complex. Each figure shows temperature (°C).

5) H. Ito and Y. J. I'Haya, *Intern. J. Quantum Chem.*, **2**, 5 (1968).
6) B. J. Gardner and S. F. Mason, *Biopolymers*, **5**, 79 (1967).
7) K. Yamaoka and R. A. Resnik, *J. Phys. Chem.*, **70**, 4051 (1966).
8) M. Zama and S. Ichimura, *Biopolymers*, **9**, 53 (1970).
9) C. Djerassi, "Optical Rotatory Dispersion," McGraw-Hill, New York (1960), p. 159.

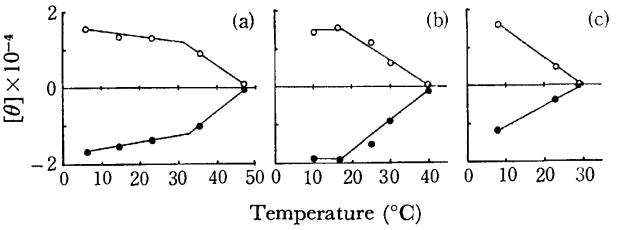

Fig. 4a. Temperature dependence of $[\theta]_{max}$ of DNA-TBO complexes; ○: positive maxima at 520—530 nm, ●: negative maxima at 555—560 nm.
(a): P/D=0.22, (b): P/D=0.46, (c): P/D=0.93

The change in molar ellipticity $[\theta]$ is plotted against temperature in Fig. 4a. It should be noted that the $[\theta]$ values of the positive CD maximum at about 524 nm (Band I) and the negative one at about 560 nm (Band II) diminish linearly with increasing temperature. Furthermore, the $[\theta]$ values of these CD bands do not change very much even at sufficiently low temperature when P/D is considerably low (<0.5), although a slight shift of the whole spectrum to the shorter wavelength side is observed (Fig. 3). It was difficult to observe a positive CD band located at about 650 nm, as the sensitivity of our photomultiplier was very low in the spectral region. The temperature effect of this band, therefore, was not examined. The temperature dependence of the negative CD band of the P/D=2.6 complex is shown in Fig. 4b. The effect of temperature on the absorption curves of TBO dissolved in 0.01 M phosphate buffer is given in Fig. 5a.

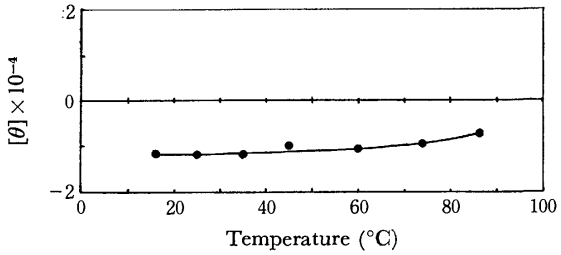

Fig. 4b. Temperature dependence of negative CD maximum (600—604 nm) of DNA-TBO P/D=2.6 complex.

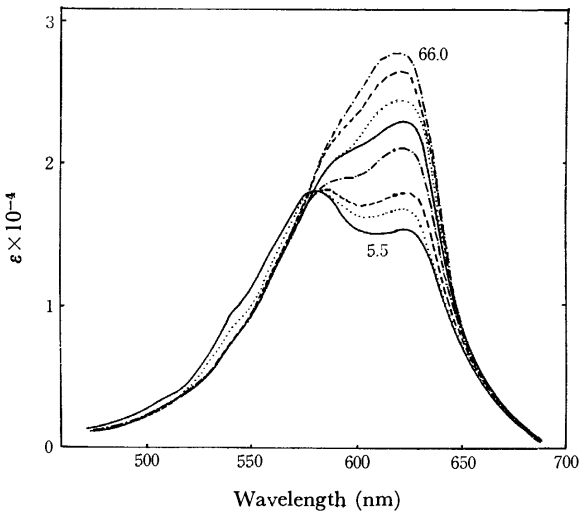

Fig. 5a. Absorption spectrum of TBO in 10^{-2} M phosphate buffer at various temperatures. Concentration of TBO, 5×10^{-5} M. Temperatures, from lower to upper, 5.5, 10, 15, 25.5, 36, 45.5, 56 and 66°C.

Discussion

According to Gardner and Mason,[6] dyes contributing to the optical activity of nucleic acid-dye complexes can be divided into two species, those bound to the nucleic acid helix monomerically and those bound dimerically. In our previous study on the DNA- and RNA-Th complexes, we confirmed the validity of their interpretation.[1] The present study on the DNA-TBO complexes also supports this conclusion. As shown in Fig. 1, the two resolved CD bands located at 529 and 563 nm are of nearly equal ellipticity and have signs opposite to each other (*vide infra*). Moreover, their $[\theta]_{max}$ wavelengths (Bands I and II) correspond to the shoulders, which may be thought to be split absorption bands due to a dye-dye interaction of each absorption spectrum of the complexes taken at various temperatures (Fig. 3).

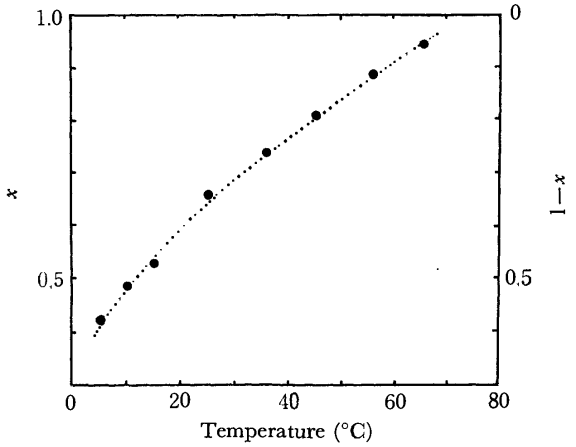

Fig. 5b. Plot of monomer (x) and dimer ($1-x$) fraction of TBO in aqueous solution against temperature.

These facts suggest that the optical activity appearing at 500—550 nm is induced by an exciton interaction in line with the works of Moffitt[10] and of Tinoco.[11] In addition to this, a comparison of the change in the dimer fraction ($1-x$ in Fig. 5b) and that in the maximum values of molar ellipticity with increasing temperature ($[\theta]$ in Fig. 4a) suggests that the intensities of these CD bands depend upon the amount of the dye dimers bound to the DNA helix. The numerical value of molar ellipticity should be constant if there is no conformational change in the dye-dye steric conformation. Actual molar ellipticity should then be evaluated using the concentration of the *dye dimers* bound to the DNA helix at appropriate sites. The actual molar ellipticities for bands I and II located at 529 and 563 nm, respectively, are thus evaluated and listed in Table 1. Here the following assumptions are made: (i) in the temperature range where $[\theta]_{max}$ is constant, there is no free dye[12] and the fraction of the bound dye dimers is constant; (ii) the fractions of monomer and dimer are estimated from the absorption spectrum of the dye in aqueous solution measured at the corresponding temperature.

Assumption (i) seems to be valid since in the temperature range where the $[\theta]$ value is constant (10—16°C for the complex of $P/D=0.46$) the absorption spectrum of the complex does not change its profile very much as seen in Fig. 3. Assumption (ii) is not justified but requisite, since estimation of monomer and dimer fractions from the absorption spectrum of the complex is not possible due to the shift in the absorption spectrum and the strong hyper- and/or hypo-chromisms. In order to evaluate actual $[\theta]$ values under Assumptions (i) and (ii), the dimer fraction of the dye must be estimated at the temperature where slope of the plot $[\theta]_{max}$ *vs.* temperature changes (Fig. 4a).

The rotational strengths for the resolved CD bands are also calculated by means of the relationship[9]

$$R_k \simeq 0.696 \times 10^{-42}\sqrt{\pi}[\theta_k]\frac{\Delta_k}{\lambda_k} \quad (k=\text{I—V})$$

where $[\theta_k]$, Δ_k, and λ_k are the molar ellipticity, the half band width and the wavelength of $[\theta_k]_{max}$ of the k-th CD band, respectively. The results are given in Table 1. The calculated $[\theta]_{max}$ and R for bands I and II are comparable with observed values. The absolute values of R_I and R_{II} are nearly equal to each other within experimental error. This suggests that the optical activity appearing in the neighborhood of 550 nm is due to just one origin as has been stated.

Table 1. Molar ellipticities and rotational strengths for resolved CD bands of DNA-TBO $P/D=0.26$ complex[a]

Band	λ_{max} (nm)	$\lambda_{shoulder}$ (nm)	$[\theta]_{max}\times10^{-4}$ Obsd	$[\theta]_{max}\times10^{-4}$ Calcd	$R\times10^{-40}$cgs Obsd	$R\times10^{-40}$cgs Calcd
I	529.1	~532	1.75	3.85	7.18	15.81
II	563.4	~554	−1.72	−3.78	−6.67	−14.73
III	590.7	~582	−1.05		−2.85	
IV	615.3	~620	−0.9		−2.60	
V	645.2	—	−0.6		−1.60	

a) Calculations of $[\theta]_{max}$ and R for Bands III—V have not been carried out since the origins of the bands are not due to the TBO dimers.

Three causes seem to be possible for Bands III, IV, and V. (1) They might be induced from an interaction between the monomerically bound dyes, since the wavelengths of the CD band maxima are located around the monomer absorption band. (2) A contribution from some higher energy levels may induce such successive CD bands as reported by Bush and Brahms in the case of oligonucleotides.[13] (3) They might be induced by an asymmetric environment attributed to the asymmetric carbons of deoxyriboses. It should be noted that for high P/D values a positive CD band located at about 650 nm appears as shown in Fig. 2. Previous results indicated that this band (called M(+)

10) W. Moffitt, *J. Chem. Phys.*, **25**, 407 (1956).

11) I. Tinoco, Jr., "Advances in Chemical Physics," Vol. 4, ed. by I. Prigogine, Interscience Publishers, New York (1962), p. 113.

12) An equilibrium dialysis experiment carried out in our laboratory shows that the value of P/D becomes less than one below 24°C.

13) C. A. Bush and J. Brahms, *J. Chem. Phys.*, **46**, 79 (1966).

in reference 2) results from the dye monomers, the type of interaction being probably not of an exciton type.[2] Thus, Bands III—V cannot be attributed to (1) alone, *i.e.* to the monomerically bound dyes.

The maxima of Bands III and IV correspond well with the absorption shoulders of the complex (Table 1). The bands can thus be attributed to a combination of (2) and (3), *i.e.* to vibrational levels of the dye (probably in its dimerically bound state), which become optically active by the influence of the asymmetric carbons of deoxyriboses.

We might conclude as follows. (1) The Cotton effects of the low *P*/*D* complexes in the wavelength region 500—580 nm (Optical Activity II) are induced from an exciton-type interaction between the dye dimers. (2) The Cotton effects of the high *P*/*D* complexes in the wavelength region 620—670 nm (Optical Activity I) result from the dye monomers through the asymmetric perturbation of deoxyriboses. (3) Three negative CD bands developed in the wavelength region 550—650 nm correspond to vibrational components of the dye, which become optically active due to the asymmetric environment of DNA. Characteristics of the DNA-TBO system are the signs of the CD bands of its low *P*/*D* complex, which are opposite to the corresponding CD bands of DNA-AO and DNA-Th complexes. This suggests that the steric conformations of DNA-dye complexes are not always the same, contrary to the conventional interpretation. Since AO, Th, and TBO have a similar molecular framework, there seems to be no big difference between the binding sites of the dye molecules to the DNA helices. The major factor determining the CD band signs, therefore, can not be the whole helical arrangement of the bound dyes but is probably the local arrangement and/or relative orientation of the neighboring dye molecules that form dimers.

This research was supported in part by a grant-in-aid from the Ministry of Education.

BULLETIN OF THE CHEMICAL SOCIETY OF JAPAN, VOL. 45, 2723—2730 (1972)

Hydrogenation by Cyanocobaltate. II.[1] Mechanisms of the Hydrogenations of 1,3-Butadiene and Isoprene Catalyzed by Pentacyanocobaltate(II) in Aqueous Solution

Takuzo FUNABIKI, Mitsuo MATSUMOTO, and Kimio TARAMA

Department of Hydrocarbon Chemistry, Faculty of Engineering, Kyoto University, Sakyo-ku, Kyoto

(Received January 5, 1972)

Hydrogenations of 1,3-Butadiene and isoprene catalyzed by pentacyanocobaltate(II) have been studied by the measurements of infrared and nuclear magnetic resonance spectra on the reaction solutions and by following the time-courses of the reactions. Infrared spectroscopy has revealed: (1) The aging reaction is promoted by CN^- ion and it hardly occurs at a low CN/Co ratio. (2) In the hydrogenation of butadiene the formation of a σ-but-2-enyl complex at a high CN/Co ratio is very rapid, but that of a *syn*-π-(1-methylallyl) complex at a low CN/Co ratio is generally slow. The rate of the formation of these complexes is affected by the relative concentration of butadiene to $Co(CN)_5H^{3-}$. (3) In the hydrogenation of isoprene a σ-3-methylbut-2-enyl complex is formed regardless of the CN/Co ratio. Nuclear magnetic resonance spectroscopy has confirmed the structures of these complexes and it also showed that the σ-but-2-enyl complex consists of simliar amounts of the *cis*- and *trans*-isomers. The reactions are explained by the mechanisms, in which intermediate complexes in the formation of alk-1-enes and alk-2-enes are the *cis*- and *trans* σ-but-2-enyl and the *syn*-π-(1-methylallyl) complexes in the case of butadiene, and the σ-2- and -3-methylbut-2-enyl and the π-(1,2-dimethylallyl) complexes in the case of isoprene. It is described that the reactivity and the selectivity in the hydrogenation of conjugated dienes are strongly controlled by the steric factor in the transition state.

Pentacyanocobaltate(II) is one of the typical transition metal complexes which hydrogenate conjugated dienes selectively to simple-olefins, and has been studied by many authors.[2] Two mechanisms have been proposed for the selective hydrogenation; the one involves organocobalt complexes as intermediates, and the other free radicals. In the former case it has been found that the selectivity depends on the CN/Co ratio. The hydrogenation of butadiene has been studied in most detail, because the effect of the CN/Co ratio is most remarkable,[3] and the reaction has been interpreted in terms of the following scheme.

1) Part I. T. Funabiki and K. Tarama, This Bulletin, **44**, 945 (1971).

2) See the review by J. Kwiatek, "Catalysis Reviews" Vol. 1, ed. by H. Heinemann, Marcel Dekker, New York (1968), p. 37.

3) (a) M. S. Spencer and D. A. Dowden, U. S., 3009969 (1961). (b) J. Kwiatek, I. L. Mador, and J. K. Seyler, *Advan. Chem. Ser.*, **37**, 201 (1963). (c) J. Kwiatek and J. K. Seyler, Proceedings of the 8th International Conference on Coordination Chemistry, Vienna, 1964 (V. Gutmann, ed.) Springer, Vienna (1968), p. 308. (d) J. Kwiatek and J. K. Seyler, *J. Organometal. Chem.*, **3**, 421 (1965). (e) T. Suzuki and T. Kwan, *Nippon Kagaku Zasshi*, **86**, 713 (1965).

$$2Co(CN)_5^{3-} + H_2 \rightleftarrows 2Co(CN)_5H^{3-}$$
$$Co(CN)_5H^{3-} + C_4H_6 \rightleftarrows Co(CN)_5(C_4H_7)^{3-}$$
$$Co(CN)_5(C_4H_7)^{3-} + Co(CN)_5H^{3-} \longrightarrow C_4H_8 + 2Co(CN)_5^{3-}$$

Kwiatek and Seyler[3c,3d] have proposed a mechanism in which σ-but-2-enyl pentacyanocobaltate [I] and π-methylallyltetracyanocobaltate [II] are the intermediates in the formations of 1- and *trans*-2-butenes, respectively. They isolated the complex [I] in an impure solid state and studied its reactivity with $Co(CN)_5H^{3-}$. Although the NMR spectrum observed at 60 MHz was not analyzed completely, [I] was assumed on the analogy with σ-but-2-enyl-π-cyclopentadienyldicarbonyliron. The equilibrium between the complexes [I] and [II] was assumed on the analogy with the equilibrium between σ- and π-allyl complexes which was demonstrated by NMR. This mechanism has been generally accepted, but the lack of any kinetical study would be its greatest defect. Afterwards, Burnett *et al.*,[4] tried kinetical treatments and proposed a mechanism in which the direct intermediate in the formation of 1-butene is not [I] but σ-1-methylprop-2-enyl pentacyanocobaltate [III] on the basis of the hypothesis that the additions of $Co(CN)_5H^{3-}$ to butadiene and intermediate complexes may proceed through a 1,2-addition mechanism. In spite of the detailed discussion, the proposed mechanism was not convincing because the variation of the amount of the intermediate complexes was not followed.

The hydrogenation of isoprene, on the other hand, has not been studied in detail and some complicating results have been reported: The selectivity depends not only on the CN/Co ratio but on the ratio of the concentration of isoprene to cobalt and on the presence of hydrogen.[2,5] No mechanism to explain satisfactorily these results has been proposed.

Recently the present authors have found a novel solvent effect on the selectivity in the hydrogenation of butadiene.[1,6] The formation of *cis*-2-butene, which is hardly observed in aqueous solution, is greatly promoted in the glycerol-methanol or ethylene glycol-water solvent in the presence of excess cyanide ion. In consideration of the solvent effect, it seemed essential to clarify the mechanism in aqueous solution. For this purpose, it is important to discuss on the hydrogenations of butadiene and isoprene at the same time, because the former can give one terminal and two internal olefins, while the latter gives two terminal and one internal olefins. In this paper, mechanisms of these reactions are proposed from the time-courses of the formations of the products and of the complexes including the intermediate complexes, and from the confirmation of the structures of the intermediate complexes. These were performed by the gaschromatographic analysis of gas samples and by the measurements of IR and NMR spectra on the reaction solution without isolating the unstable species.

Experimental

Infrared Spectral Measurements. IR spectra of the reaction solutions were recorded on a JASCO DS-403G spectrophotometer in the 2000—2200 cm^{-1}. To enable the quick and repeated samplings and measurements of the complexes sensitive to air and heat of an infrared ray, a polyethylene cell placed between two plates of rock salt was used. Frequency was accurate to within ± 1 cm^{-1}.[7]

Nuclear Magnetic Resonance Spectral Measurements. NMR spectra of the reaction solutions were recorded in most cases at 100 MHz with a Varian HR-100D spectrometer, but JEOL C-60HL and Varian HR-220 were also used. D_2O was usually used as a solvent, but H_2O was also used to confirm the proportion of the intensity of the bands corresponding to CH_2 and CH_3 groups. Measurements were performed either at room temperature or at 5°C.

Hydrogenation Procedure. The hydrogenation was carried out in a 100 m*l* flask containing a 25 or 50 m*l* solution with a cobalt concentration of 0.2M. Gases in the reaction vessel were circulated through the solution at a flow rate of about 500 m*l* per minute.[1] Gas and aqueous samples picked out by injection syringes were analyzed by glc and IR, respectively. In the case of butadiene, reactions were carried out under three different conditions: (A) In the absence of hydrogen, the reaction of $Co(CN)_5^{3-}$ was started under an atmosphere of butadiene, (B) The reaction of $Co(CN)_5H^{3-}$, which was previously prepared, was started under an atmosphere of butadiene and a small amount of hydrogen, (C) The reaction of $Co(CN)_5^{3-}$ was started under an atmosphere of hydrogen and butadiene. In the case of isoprene, reactions were carried out under the conditions similar to (A) and (B). For the NMR measurements reactions were carried out in 2 m*l* solutions at 0°C.

Results and Discussion

Reactions of Pentacyanocobaltate(II) with Water and Hydrogen. It has been well known that pentacyanocobaltate(II) reacts with water to form hydridopentacyanocobaltate (aging reaction), and the reaction has been explained in terms of the Eq. (1)[8] or (2).[2]

$$2Co(CN)_5^{3-} + H_2O \longrightarrow Co(CN)_5H^{3-} + Co(CN)_5OH^{3-} \quad (1)$$
$$2Co(CN)_5^{3-} + 2H_2O \longrightarrow Co(CN)_5H^{3-} + Co(CN)_5OH_2^{2-} + OH^- \quad (2)$$

As seen in Fig. 1a, the IR spectra of the pentacyanocobaltate(II) solution under an atmosphere of nitrogen at 0°C in the presence of excess cyanide ion (CN/

4) M. G. Burnett, P. J. Connoly, and C. Kemball, *J. Chem. Soc., A*, **1968**, 991.

5) (a) T. Suzuki and T. Kwan, *Nippon Kagaku Zasshi*, **86**, 1341 (1965). (b) J. Kwiatek and J. K. Seyler, *Advan. Chem. Ser.*, **70**, 207 (1968).

6) (a) K. Tarama and T. Funabiki, This Bulletin, **41**, 1744 (1968). (b) T. Funabiki and K. Tarama, *Tetrahedron Lett.*, **1971**, 1111.

7) T. Funabiki and K. Tarama, This Bulletin, **45**, 2945 (1972)

8) (a) N. K. King and M. E. Winfield, *J. Amer. Chem. Soc.*, **83**, 3366 (1961). (b) B. DeVries, *J. Catal.*, **1**, 489 (1962). (c) O. Piringer and A. Farcus, *Z. Phys. Chem. N. F.*, **46**, 190 (1965). (d) M. G. Burnett, P. J. Connoly, and C. Kemball, *J. Chem. Soc., A*, **1967**, 800.

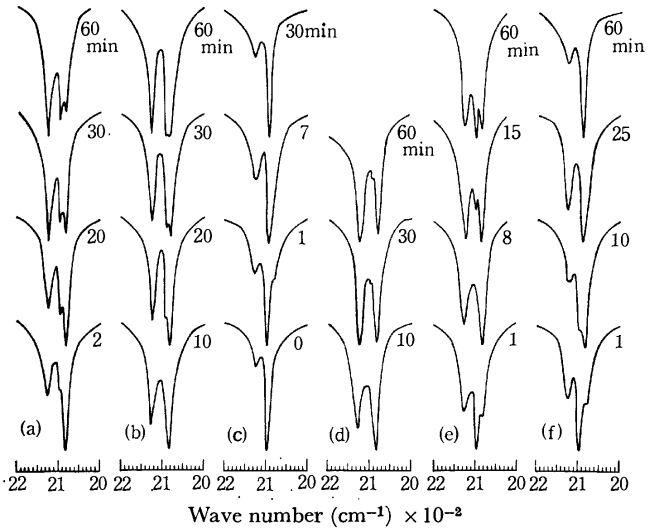

Fig. 1. IR spectra of the reaction solution in H_2O at 0°C in the hydrogenation of butadiene.
(a) Aging reaction at CN/Co=6.0, (b) Under condition (A) at CN/Co=6.0, (c) Under condition (B) at CN/Co=6.0, (d) Under condition (A) at CN/Co=4.5 (e) Under condition (B) at CN/Co=4.5, (f) Under condition (B) at CN/Co=5.0

Co=6.0) showed a gradual decay of the 2082 cm^{-1} band of $Co(CN)_5^{3-}$ in accompany with growths of the 2097 cm^{-1} band of $Co(CN)_5H^{3-}$ and of the band near at 2127 cm^{-1}. In the absence of excess cyanide ion (CN/Co=5.0), however, the reaction was so slow that only a weak shoulder band of $Co(CN)_5H^{3-}$ was observed even after one hour. In the presence of deficient cyanide ion (CN/Co=4.5), the formation of $Co(CN)_5H^{3-}$ was much slower. Although it has been reported that the aging reaction is promoted by alkali metal ions,[8c,9] the addition of KCl to the solution at CN/Co=5.0 had no effect. These results suggest that the cyanide ion rather than the potassium ion is responsible for the promotion of the aging reaction, and that the following reactions take place rather rapidly even at low temperatures in the presence of excess cyanide ion.

$$Co(CN)_5OH^{3-} + CN^- \longrightarrow Co(CN)_6^{3-} + OH^- \quad (3)$$

$$Co(CN)_5OH_2^{2-} + CN^- \longrightarrow Co(CN)_6^{3-} + H_2O \quad (4)$$

It has been supposed that these reactions are very slow at low temperatures,[2,8a] and the band near at 2127 cm^{-1} can not be corresponded exclusively to $Co(CN)_6^{3-}$ because $Co(CN)_5OH_2^{2-}$ shows a similar band, but the above proposals seem to be supported by the following results. (1) From the linear relationship between CN stretching frequencies and the Taft's σ_I function,[7] it is expected that $Co(CN)_5OH^{3-}$ shows the band near at 2110 cm^{-1}. (2) It has been reported that in the visible and ultraviolet spectroscopic study of the aging reaction, the formation of $Co(CN)_6^{3-}$ instead of $Co(CN)_5OH^{3-}$ was observed and it exceeded that of $Co(CN)_5OH_2^{2-}$ except in the initial stage.[8d]

When hydrogen was absorbed by pentacyanocobaltate(II) at 0°C, a strong $Co(CN)_5H^{3-}$ band together with a weak broad band near at 2125 cm^{-1} were observed regardless of the CN/Co ratio (*cf.* Fig. 1c). At 20°C, the $Co(CN)_5^{3-}$ band did not disappear completely, demonstrating that the reaction is reversible and the equilibrium constant depends on the reaction temperature.

Hydrogenation of Butadiene. (i) In the Presence of Excess Cyanide Ion (CN/Co=6.0) at 0°C. Under condition (A), a slow growth of a new band of the complex [I] at 2091 cm^{-1} was observed accompanied by a slow decay of the $Co(CN)_5^{3-}$ band (Fig. 1b). The formation of 1-butene as a main product was very slow but was continuous, reflecting that the aging reaction proceeds under this condition.

Under condition (B), the IR spectral changes as shown in Fig. 1c were observed. In the initial stage of the reaction, the $Co(CN)_5^{3-}$ band appeared in accompany with a decay of the $Co(CN)_5H^{3-}$ band, but both were rapidly replaced by the band of the complex [I]. The formation of butenes (1-(90%), *trans*-2-(8%), *cis*-2-(2%)) was remarkable in the initial stage, but it did not proceed any more after about 15 minutes when the formation of [I] was accomplished.[10]

Under condition (C), the accomplishment of the formation of [I] took place after 45 minutes when the ratio of butadiene to hydrogen was 1/1(vol). Under this condition, the formation of 1-butene was remarkable: 1-(98%), *trans*-2-(1%), *cis*-2-(1%). It appeared that the lower ratio of butadiene to hydrogen was advantageous for the product formation while the higher one was so for the formation of the complex [I]. The $Co(CN)_5H^{3-}$ band was not observed in the course of reaction.

(ii) In the Presence of Deficient Cyanide Ion (CN/Co=4.5) at 0°C. Under condition (A), a weak 2098 cm^{-1} band of the complex [II] barely appeared after 30 minutes, but its growth and a decay of the $Co(CN)_5^{3-}$ band were very slow (Fig. 1d). The yield of butenes (the main product was *trans*-2-butene) was much lower than that in (i), reflecting that the aging reaction hardly proceeds under this condition.

Under condition (B), a rapid decay of the $Co(CN)_5H^{3-}$ band and a growth of the $Co(CN)_5^{3-}$ band were observed in accompany with an initial rapid formation of *trans*-2-butene (1-(14%), *trans*-2-(82%), *cis*-2-(4%)).[10] Different from the mode in (i), the band of [II] appeared after the complete disappearance of the $Co(CN)_5H^{3-}$ band and grew gradually, whereas the $Co(CN)_5^{3-}$ band decayed (Fig. 1e).

Under condition (C), the formation of [II] was greatly affected by the ratio of butadiene to hydrogen and was remarkable at a high ratio. When the ratio was 6/1, a steady growth of the band of [II] and a decay of the $Co(CN)_5^{3-}$ band took place immediately. When the ratio was 1/1, a weak shoulder band of [II] which appeared in the initial stage did not grow, and the strong $Co(CN)_5^{3-}$ band hardly changed. On the other hand, the formation of butenes was more

9) N. K. King and M. E. Winfield, *J. Amer. Chem. Soc.*, **80**, 2060 (1958).

10) The mode of the time courses of the formation of butenes were similar to those at 20°C, which were reported in the previous paper (Ref. 1).

remarkable in the latter than in the former. The composition of butenes (1-, *trans*-2-, *cis*-2-) was: 15%, 84%, 1% in the former and 10%, 89%, 1% in the latter. (In the experiments (i) and (ii), the composition of butenes was nearly constant in the course of reaction.)

(iii) In the Presence of the Stoichiometric Amount of Cyanide Ion (CN/Co=5.0) at 0°C. The relation between the variation of the complexes and the composition of butenes was rather complicated. As seen in Fig. 1f, the IR spectral change under condition (B) was similar to that in Fig. 1c showing the formation of the complex [I], except an initial great growth of the $Co(CN)_5^{3-}$ band. *trans*-2-Butene was the main product as reported[1,3] (1-(12%), *trans*-2-(81%), *cis*-2-(7%) after 10 min.), but a slight increase of 1-butene was observed with the elapse of time (1-(18%), *trans*-2-(76%), *cis*-2-(6%) after 60 min).

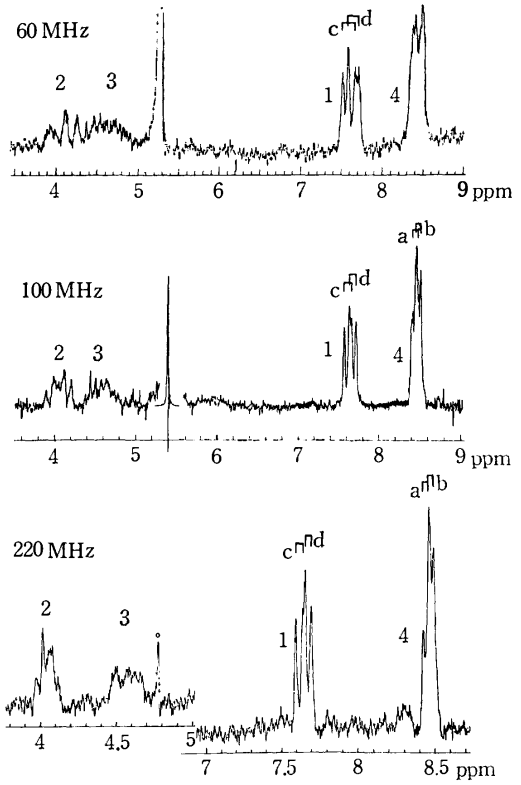

Fig. 2. NMR spectra of the reaction solution at CN/Co= 6.0 and D_2O in the hydrogenation of butadiene. Observed at 60, 100, and 220 MHz and at room temperature.
○, Side band of H_2O.

$$\overset{1}{CH_2}\text{–}\overset{2}{CH}\text{=}\overset{3}{CH}\text{–}\overset{4}{CH_3}$$
$$\underset{|}{Co(CN)_5^{3-}}$$

Confirmation of the Structures of the Intermediate Complexes in the Hydrogenation of Butadiene. Although Kwiatek and Seyler could not analyze the NMR spectra of the σ-butenyl complex observed at 60 MHz,[3d] the comparison of the NMR spectra measured directly on the reaction solution at 60, 100, and 220 MHz made it possible to reveal that the solution contained two complexes with very similar configurations (Fig. 2). They were assigned to the *cis*- and *trans*-isomers of [I].[11] Although it could not been determined clearly which signal corresponded to each isomer, slightly stronger bands (b and d) may correspond to the *trans*-isomer, because the *trans*-isomer may be more stable than the *cis*-isomer and because $J_{3,4}$ of the *trans*-isomer of the analogous compounds is in most cases smaller than that of the *cis*-isomer. It was also demonstrated that the proportion of the isomers did not depend on the CN/Co ratio so long as an excess cyanide ion was present. It is noteworthy that the proportion of the deuterium atom incorporated into the terminal methyl groups of the complexes prepared in D_2O under an atmosphere of hydrogen varied with the reaction condition. When the enough butadiene was added to the solution of the hydridocomplex under condition (B), one deuterium atom per mole of the complex was incorporated, but when the complex was prepared under condition (C), the proportion decreased greatly. It has been reported that the rate of the H–D exchange between $Co(CN)_5H^{3-}$ and D_2O is certainly very much faster than the addition reaction.[8d,12] A study on this problem is in progress.

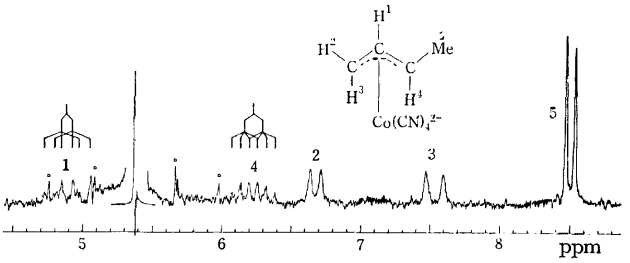

Fig. 3. NMR spectrum of the reaction solution at CN/Co= 4.5 in D_2O in the hydrogenation of butadiene. Observed at 100 MHz and at 5°C.
○, Side band of H_2O.

It has been considered that the complex [II] is too unstable to be observed,[3d] but the IR spectra showed the formation of an intermediate complex in the presence of deficient cyanide ion and made it possible to find an appropriate condition for its formation. The NMR spectrum observed after the separations of the residual $Co(CN)_5^{3-}$ by an addition of $BrCCl_3$ and of precipitates by filteration, revealed that the solution contained only a *syn*-π-(1-methylallyl) complex (Fig. 3).[11] It is noteworthy that an *anti*-complex was not contained. Deuterium atom was not incorporated into the complex in spite of the reaction in the D_2O solvent. It was also demonstrated by IR and NMR that [II] was converted to [I] and *vice versa* by the addition of either the KCN or $CoCl_2$ solution to the solution containing each complex. Chemical shifts and coupling constants are summarized in Table 1.

Hydrogenation of Isoprene. Figure 4 shows the typical results under condition (A) at 30°C with a cobalt concentration of 0.2M ($CoCl_2$=10 mmol) and with 10 mmol of isoprene. It shows clearly the dependence of product compositions on the reaction time and the CN/Co ratio. The results can be considered from

11) T. Funabiki and K. Tarama, *Chem. Commun.*, **1971**, 1177.
12) L. M. Jackman, J. A. Hamilton, and J. M. Lawlor, *J. Amer. Chem. Soc.*, **90**, 1914 (1968).

Table 1. Chemical shifts and coupling constants for the intermediate complexes

Complexes	Chemical shift τ (ppm)	Coupling constant J (Hz)
CH_2^1–CH^2=CH^3–CH_3^4 | $Co(CN)_5^{3-}$	H^4 (b) 8.46(d) (a) 8.43(d)	$J_{3,4}$ (b) 6.5 (a) 7.0
	H^3 4.30(m)	
	H^2 4.01(m)	
	H^1 (d) 7.67(d) (c) 7.61(d)	$J_{1,2}$ (d) 8.6 (c) 9.4
H^1 C H^2—C CH_3^5 H^3 H^4 $Co(CN)_4^{2-}$	H^5 8.50(d)	$J_{4,5}$ 6.2
	H^4 6.23(dq)	$J_{1,4}$ 12.3
	H^3 7.53(d)	$J_{1,3}$ 12.3
	H^2 6.68(d)	$J_{1,2}$ 7.8
	H^1 4.89(dt)	
CH_3^3 CH_2^1–CH^2=C^3–CH_3 | $Co(CN)_5^{3-}$	H^3 8.42(s)	
	H^2 4.30(t)	$J_{1,2}$ 9.5
	H^1 7.63(d)	

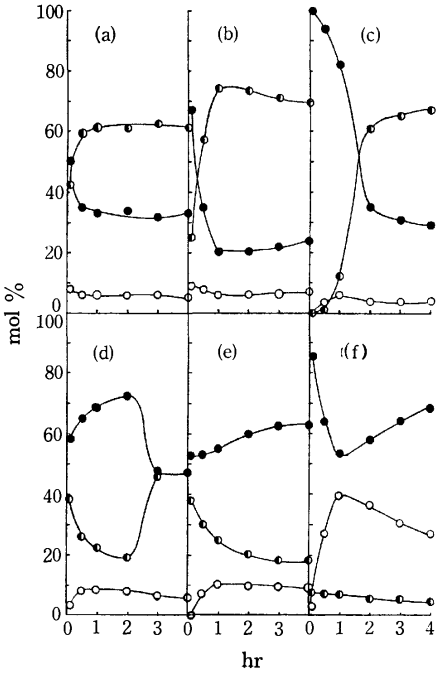

Fig. 4. Time-courses of the composition of products in the hydrogenation of isoprene in H_2O, at 30°C, and under condition (A).
●: 2-methyl-1-butene, ○: 3-methyl-1-butene,
◐: 2-methyl-2-butene
At CN/Co=(a) 5.0, (b) 5.2, (c) 5.4, (d) 5.6, (e) 5.8, (f) 6.0

the two different relations; (i) between 2-methyl-1- and 2-methyl-2-butenes, (ii) between 2-methyl-1- and 3-methyl-1-butenes.

(i) Figure 4 shows that 2-methyl-2-butene is produced even in the presence of excess cyanide ion and that the proportion of 2-methyl-1- and -2-butenes is abruptly replaced in the course of reaction. This change took place when green precipitates appeared in the solution and was caused by the abrupt formation of 2-methyl-2-butene in accompany with the stop of the formation of 2-methyl-1-butene (Fig. 5). The time

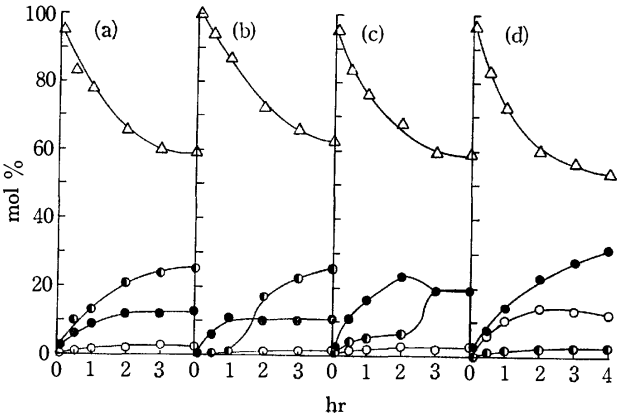

Fig. 5. Time-courses of the composition of products and isoprene in the hydrogenation of isoprene in H_2O, at 30°C, and under contition (A).
●: 2-methyl-1-butene, ○: 3-methyl-1-butene,
◐: 2-methyl-2-butene △: isoprene
At CN/Co=(a)5.0, (b) 5.4, (c) 5.6, (d) 6.0

when the change took place depended on the cyanide ion concentration and on the reaction temperature; the lower the concentration and the higher the temperature, the earlier the change took place. These results may be most reasonably explained by the following. The cyanide ion concentration decreases in the course of reaction owing to the aging reactions (1)—(4) or to the hydrolysis of the cyanide ion, and 2-methyl-2-butene is formed when the cyanide ion becomes deficient.

(ii) The mode of the formation of the two terminal olefins was remarkably different. The formation of 2-methyl-1-butene was always greater than that of 3-methyl-1-butene in an initial stage of the reaction. Although the formation of 3-methyl-1-butene was generally small, it became remarkable in the presence of a large excess cyanide ion. As the aging reaction was promoted by the excess cyanide ion, it was supposed that the increase in the relative concentration of $Co(CN)_5H^{3-}$ to isoprene might promote the formation of 3-methyl-1-butene. This was demonstrated by the result in Fig. 6, in which the effect of the relative concentration of isoprene to cobalt was examined.

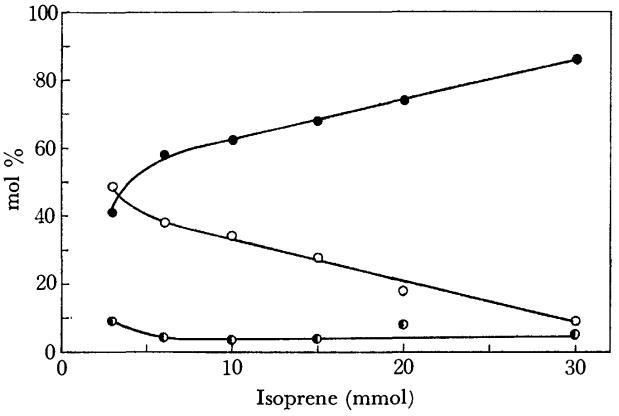

Fig. 6. Effect of the relative concentration of isoprene to $Co(CN)_5^{3-}$ in the hydrogenation of isoprene (Compositions after 3 hr) in H_2O, at 30°C, under condition (A), and with $CoCl_2$=10 mmol.
●: 2-methyl-1-butene, ○: 3-methyl-1-butene,
◐: 2-methyl-2-butene

Under condition (B), the formations of 3-methyl-1-butene at CN/Co=6.0 and of 2-methyl-2-butene at CN/Co=5.0, were greatly promoted. At CN/Co=6.0, the composition of the products (2-methyl-1-, 3-methyl-1-, 2-methyl-2-butenes) was 51%, 33%, 16% after 5 min and it became 2%, 70%, 9% after 20 min, which was maintained subsequently. It is noteworthy that the composition of 3-methyl-1-butene is greater than that of 2-methyl-1-butene. At CN/Co=5.0, the composition (8%, 9%, 83%) was nearly constant throughout the course of reaction.

The IR spectra of the reaction solutions in the presence of excess cyanide ion showed similar changes to the case of butadiene, showing the band of the intermediate complex at 2090 cm^{-1}. At CN/Co=4.5, however, the same band at 2090 cm^{-1} together with the shoulder band of $Co(CN)_5^{3-}$ was observed, contrary to the expectation that a new band may be observed at higher frequencies than 2090 cm^{-1}.

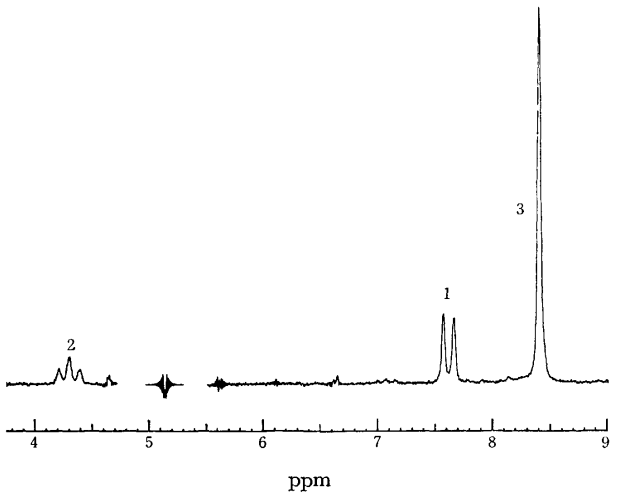

Fig. 7. NMR spectrum of the reaction solution at CN/Co=6.0 in D_2O in the hydrogenation of isoprene. Observed at 100 MHz and 5°C.

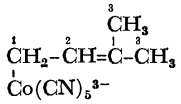

The NMR spectrum observed in the D_2O solution under condition (B) (Fig. 7) demonstrated that the solution at CN/Co=6.0 contained only a σ-3-methyl-but-2-enyl complex [VII],[13] and that the complex at CN/Co=4.5 was not a π-allylic complex but the σ-complex [VII].

Mechanisms of the Hydrogenations of Butadiene and Isoprene in Aqueous Solution. (i) Mechanism of the Initial Interaction of $Co(CN)_5H^{3-}$ with Substrates to form the Intermediate Complexes. In the hydrogenation by other transition metal complexes, the coordination of the substrate at a vacant site on the metal is mostly required, but in the case of pentacyanocobaltate(II) it has been proposed that the hydrogen of the hydridocomplex approaches the positive β-carbon of an activated double bond to form the four-center transition state [A][2,4] or the radical transition state [B].[13,14]

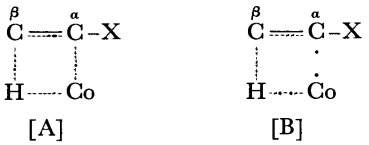

[A] has been proposed on the analogy with the transition state in the formation of $Co(CN)_5H^{3-}$ from $Co(CN)_5^{3-}$ and hydrogen,[4] but the kinetic trends in the addition of $Co(CN)_5H^{3-}$ to α,β-unsaturated compounds indicated that [B] best describes the initial interaction of $Co(CN)_5H^{3-}$ with most activated olefins.[13] The result that substituents on the β-carbon, regardless of their electron-donating (*e.g.* CH_3, CO_2^-)[12,13] or -attracting (*e.g.* C_6H_5)[15] properties, interfere with the reaction of $Co(CN)_5H^{3-}$ with substrates, and that the kinetic trends fail to parallel the stability of $CoC(CH_3)X$ adducts,[13] indicate that steric rather than electronic factors control the initial step and the C···H bonding rather than the C···Co is important in the transition state. Thus, [B] is preferable to [A].

Although it had been supposed that the hydridocomplex adds to activated olefins as though it were polarized Co^+–H^-,[2] it is well assumed from the infrared spectroscopic study that the polarization must be in a slight degree.[7] The view that the atomic hydrogen rather than the anionic hydrogen of $Co(CN)_5H^{3-}$ approaches the β-carbon, is supported by the result that the formation of 3-methyl-1-butene exceeds that of 2-methyl-1-butene in the presence of excess $Co(CN)_5H^{3-}$ in the hydrogenation of isoprene, because radicals approach more readily C^1 than C^4 in

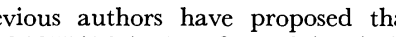

$C^1=C^2-C^3=C^4$ and *vice versa* in the case of anions.[16]

The previous authors have proposed that the 1,2-adduct $CoC(CH_3)X$ is first formed inevitably *via* the transition state [A] or [B] and it isomerizes readily to the more stable 1,4-adduct in the hydrogenation of conjugated dienes,[4,13,14] but the result of the hydrogenation of isoprene suggests that this may not necessarily be the case. Mechanism 1 shows the probable courses for the formation of the intermediate complexes and the products in the hydrogenation of isoprene.

It is well assumed that the rate of the reaction (6) is greater than that of (5), because the formation of 3-methyl-1-butene is greater than that of 2-methyl-1-butene in the presence of excess $Co(CN)_5H^{3-}$, under which condition intermediates are more completely converted to products. Even if the hydrogen atom of $Co(CN)_5H^{3-}$ approaches C^1 more readily than C^4, the mechanism, in which the 1,2-adducts [IV] and [VI] should be first formed, seems to be unfavorable to explain the rate difference, because the tertiary alkyl complex [VI] must be extremely less stable than [IV]. On the base that the thermodynamic stability

13) J. Halpern and L. Y. Wong, *J. Amer. Chem. Soc.*, **90**, 6665 (1968).

14) J. Kwiatek, "Transition Metals in Homogeneous Catalysis", ed. by G. N. Schrauzer, Marcel Dekker, Inc., N. Y. (1971), p. 13.

15) T. Funabiki, unpublished results.

16) K. Hayashi, T. Yonezawa, C. Nagata, S. Okamura, K, Fukui, *J. Polym. Sci.*, **20** 537 (1956); T. Yonezawa T. Higashimura. K. Katagiri, K. Hayashi, S. Okamura, and K. Fukui, *ibid.*, **26**, 311 (1957).

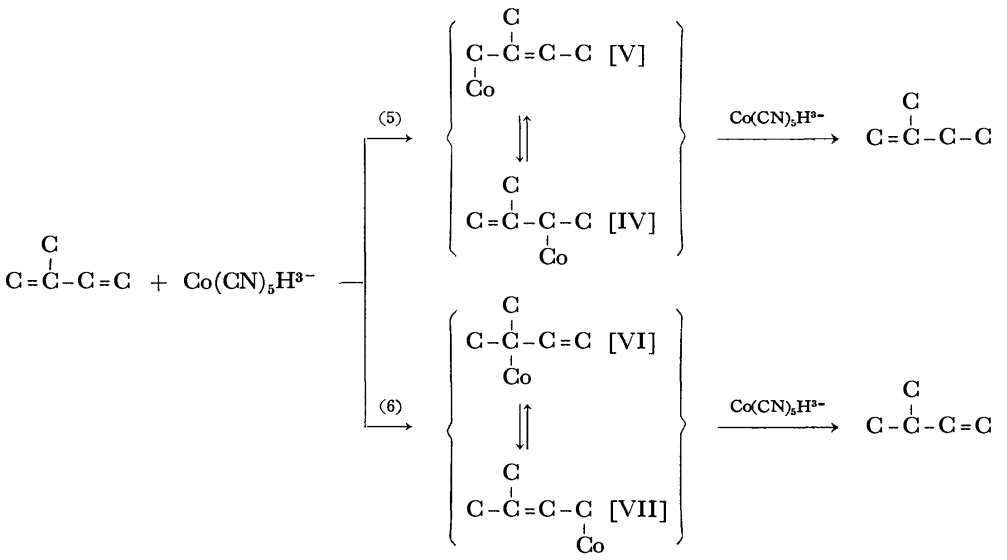

Mechanism 1.

may be in order of [VII]≥[V]>[IV]>[VI] and that the reactions (5) and (6) are reversible, the 1,4-addition mechanism may be probable so long as it is supposed that the C···Co bonding in the transition state is not important. This is supported by the following. From the point of view that the process consists of the radical addition to the radicals, $[C^1{=}\overset{\overset{C}{|}}{C^2}{=}C^3{-}C^4H_3]$ and $[H_3C^1{-}\overset{\overset{C}{|}}{C^2}{=}C^3{=}C^4]$, about the same probability is expected for the addition of Co to C^1 and to C^3 in the reaction (5), but the addition to C^4 must be greater than to C^2 in the reaction (6).[16] Similarly, in the hydrogenation of butadiene, the 1,2- and 1,4-additions seem to have the same probability, but the latter may be predominant on account of the greater stability of the 1,4-adducts.

(ii) Mechanisms of the Conversion of σ-Complexes to π-Allylic Complexes. The complexes [II], [II'], [VIII], [IX], and [X] are the possible π-allylic complexes in the hydrogenations of butadiene and isoprene.

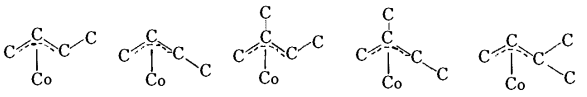

[II] [II'] [VIII] [IX] [X]

The present results that have demonstrated the formation of [II] and the equilibrium between [I] and [II] in the hydrogenation of butadiene are well explained by the mechanism 2, which have originally been proposed by Kwiatek and Seyler.[3c] In the hydrogenation of isoprene, none of [VIII], [IX], and [X] could be observed, but the relation between the 2-methyl-1- and -2-butenes in Fig. 4 indicates that the equilibrium in the mechanism 3 is taking place. [VIII] must be too unstable to have been observed on account of an additional methyl group to [II]. It is well assumed that the formations of [IX] and [X] may be negligible, because they must be less stable than [II']. The observation of the σ-complex [VII] in the deficient cyanide concentration indicates that the equilibrium in the mechanism 4 hardly takes place.

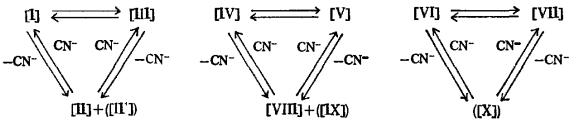

Mechanism 2 Mechanism 3 Mechanism 4

The isomerisation between [I] and [III] or [IV] and [V] may occur *via* the transition states which do not require ligand dissociation.[3c] The equilibrium [I]⇄[III] can explain the formation of similar amounts of the *cis*- and *trans*-isomers of [I] and the independence of the proportion on the CN/Co ratio. It is supposed that *cis*-[I] is slightly less stable than *trans*-[I] and it may be the origin of the selective formation of *cis*-2-butene in the presence of excess cyanide ion in the alcoholic solvents.[1,6]

(iii) Mechanisms of the Product Formation. The result that the formation of 2-methyl-1-butene is always greater than that of 3-methyl-1-butene in the initial stage of the hydrogenation of isoprene may arise from that the intermediate for the latter is more stable than that for the former. Although the mechanism in which the 1,2-adducts [IV], [VI] are the direct intermediates for these alk-1-enes may not be excluded only for the reason that [VI] is less stable than [IV], the mechanism seems implausible because the principle proposed in the mechanism[4] can not be applied in general, especially to the radical mechanism. Alternatively, the results are clearly explained by the mechanism in which the 1,4-adducts are the direct intermediates. As described previously, the thermodynamic stability of [V] and [VII] seems similar ([VII] may be slightly more stable than [V] because a methyl group is located at the β-position in [V] and at the γ-position in [VII]). When the hydrogen atom of $Co(CN)_5H^{3-}$ approaches the γ-carbon in [V] or [VII], the steric factor, which controls the initiation step, should control the reactivity. Two methyl groups on the γ-carbon in [VII] must

hinder more strongly the approach of the hydrogen atom of $Co(CN)_5H^{3-}$ than the single methyl group in [V], resulting in the greater kinetic stability of [VII] than [V]. Similarly, [I] should be the direct intermediate for the formation of 1-butene in the hydrogenation of butadiene. The dependence of the rate of the formation of [I] and 1-butene on the ratio of butadiene and hydrogen under condition (C) supports this mechanism. The steric factor can also explain that [VII] is kinetically more stable than [I] despite the thermodynamic stability seems reverse.

It is evident that the π-allylic complexes [II] and [VIII] are the direct intermediates for *trans*-2-butene and 2-methyl-2-butene, respectively. This is strongly supported by the result that the formations of [II] and of *trans*-2-butene depend greatly on the relative concentration of butadiene and hydrogen under condition (C). The difficulty of the formation of [II] compared with [I] may be attributable to the lower kinetic stability of [II] than [I], because their thermodynamic stability may be similar or reverse. The result at CN/Co=5.0 in the hydrogenation of butadiene is readily understood by this difference of the kinetic stability between these two complexes which must be formed in similar amounts. The difference of the kinetic stability is interpreted in terms of the steric factor. The hydrogen atom of $Co(CN)_5H^{3-}$ can approach more readily [II] than [I] because [II] has an unsubstituted carbon atom. This steric factor explains also that 1-butene is not formed from [II], because the hydrogen of $Co(CN)_5H^{3-}$ can approach the unsubstituted carbon more readily than the carbon substituted by a methyl group.

The explanation by the steric factor can be applied in general to the hydrogenation by pentacyanocobaltate(II) and excludes the mechanism in which the Co···Co bonding is included in the transition state.[4,5b]

In conclusion, the hydrogenations of butadiene and isoprene in aqueous solution are interpreted satisfactorily in terms of the mechanisms 5 and 6, respectively.

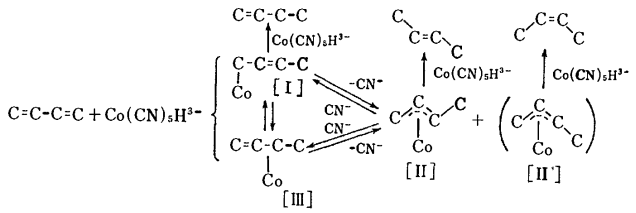

Mechanism 5

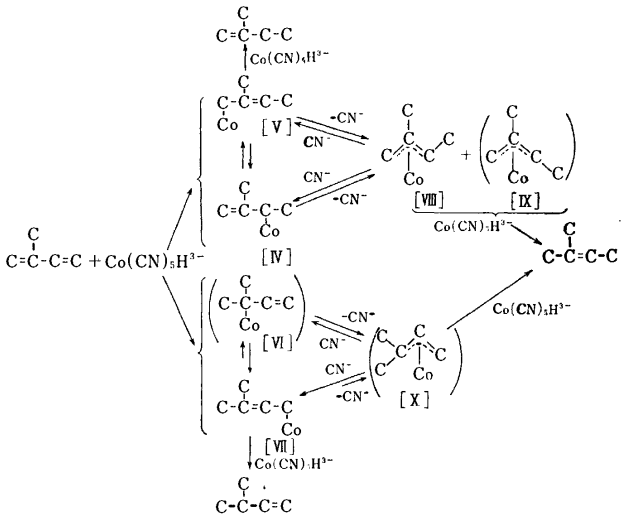

Mechanism 6

Order of Quencher Participation in Photochemistry. I. Proton Transfer from the Excited *p*-Hydroxybenzophenone in Mixed Solvents of Cyclohexane and Alcohols

Mikio Hoshino and Masao Koizumi

Department of Chemistry, Faculty of Science, Tohoku University, Katahira, Sendai

(Received January 20, 1972)

The change in the absorption spectrum of *p*-hydroxybenzophenone (HOBP) and relative quantum yields Φ_{rel} for the photoreduction of HOBP have been studied in mixed solvents consisting of cyclohexane and four kinds of alcohol. The change in absorption spectrum occurs in two steps with methanol, ethanol, and 2-propanol, suggesting the following equilibria, HOBP+S⇆A, and A+S⇆B (S, alcohol molecule). Φ_{rel} changes in two steps with methanol and ethanol and in one step with 2-propanol and amyl alcohol roughly in line with the spectral change. The changes in Φ_{rel} have been interpreted to be due to the deprotonation of HOBP. $\Phi_{rel}=1/(1+K[S]^n)$ holds for them with $n=5.5$ for 2-propanol and $n=7$ for other alcohols. A linear relation holds between $1/(n-1)\log K$ and Hammett's constant of alkyl group of alcohols, suggesting that the deprotonation tendency depends upon the specific interaction between alcohol molecules. The reactivity of A-species is considered to depend largely on the dielectric nature of the solvent.

We examined Porter and Suppan's mechanism[1,2] for the suppression of the photoreduction of *p*-hydroxybenzophenone (HOBP) in ethanol and obtained additional information.[3] The proton transfer from the excited HOBP, was reconfirmed as a cause for the non-occurrence of the photoreduction. It was found that a hydrogen-bonded species consisting of HOBP and ethanol does not necessarily undergo the ionic dissociation upon excitation. Such a species (A) is formed in cyclohexane when a small amount of ethanol is added, but under such conditions it does not undergo the proton transfer and accordingly it is photoreduced efficiently. This result is consistent with the finding of Matsuyama and Baba that a hydrogen-bonded species of HOBP and $(CH_3)_3N$ in cyclohexane–isopentane–ether (4: 4: 1) exhibits the phosphorescence from molecular $T(n\text{-}\pi^*)$ state at 77°K.[4] For the proton transfer to occur, a certain condition is necessary which is realized at higher ethanol concentrations. With an increase in ethanol concentration, it was suggested from the change of the absorption spectrum that in addition to A another species, perhaps HOBP with two C_2H_5OH attached to OH of HOBP (B) is formed in equilibrium with A. However, the proton transfer was found to occur much more rapidly with the increase of ethanol concentration than the formation of B. Therefore the proton transfer which occurs upon excitation is not directly concerned with the ground state equilibrium suggested by the absorption spectra. In fact, the decrease of the quantum yield of photoreduction with the increase of ethanol concentration caused by the proton transfer, was found to obey the equation

$$\Phi_{rel}=\frac{1}{1+K[\text{ethanol}]^n} \qquad (1)$$

wher $n=7$.

1) G. Porter and P. Suppan, *Trans. Faraday Soc.*, **61**, 1164 (1965).
2) T. S. Godfrey, G. Porter, and P. Suppan, *Discuss. Faraday Soc.*, **39**, 194 (1965).
3) M. Hoshino and M. Koizumi, *Chem. Lett.*, **1972**, 189.
4) A. Matsuyama and H. Baba, This Bulletin, **44**, 855 (1971).

The present paper reports on the previous communication in detail together with results obtained for methanol, 2-propanol and amyl alcohol. The relative quantum yields have been found to be reproduced by Eq. (1) in all cases.

Experimental

A 6W germicidal lamp was employed as a light source of the steady light experiments. Spectral change was measured with a Hitachi ESP-3T spectrophotometer. Apparatus and procedures for the flash experiment are the usual ones employed in our laboratory.

Alcohols and cyclohexane were purified by the usual methods. *p*-Hydroxybenzophenone of G.R. grade of Wako Junyaku was recrystallized three times from aqueous ethanol.

Results

Absorption Spectra of HOBP in the Mixed Solvents of Cyclohexane and Alcohols. The change in absorption spectrum of HOBP in cyclohexane is given in Fig. 1 as a function of the ethanol concentration. With the addition of ethanol the peak located at 272 nm in cyclohexane gradually shifts to longer wavelength. It is seen that the change occurs in two steps, the first

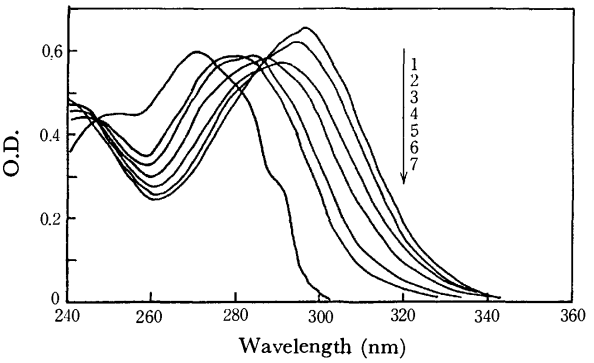

Fig. 1. Spectral change of HOBP in cyclohexane (3.65×10^{-5} M) with the addition of ethanol. Concentration of ethanol; 1) 3.4, 2) 8.5×10^{-1}, 3) 1.7×10^{-1} 4) 8.5×10^{-2}, 5) 3.4×10^{-2}, 6) 1.7×10^{-2}, 7) 0 M (Downward at 300 nm).

step ending at $\sim 3\times10^{-2}$M and the second occurring from 3×10^{-2}M to pure ethanol.

An isosbestic point is not observed in the first step. It appears in the second step, but not so clearly. Taking into account the superposition of the general solvent effect, which obscures the existence of the isosbestic point, one may safely assume the following equilibrium.

$$\text{HOBP} + \text{S} \rightleftarrows \text{A} \qquad \text{A} + \text{S} \rightleftarrows \text{B} \qquad (2)$$

where S denotes an ethanol molecule.

The equilibrium constant of the second step was estimated by the equation

$$(D_\infty - D)K[\text{S}] = D - \varepsilon_A C_0 \qquad (3)$$

which can be derived directly from

$$D = C_A\varepsilon_A + C_B\varepsilon_B \qquad C_A + C_B = C_0$$

$$K = C_B/C_A[\text{S}]$$

D; optical density of HOBP at a given ethanol concentration

D_∞; the optical density in pure ethanol

The plots of $(D_\infty - D)$ [S] against D at two wavelengths are shown in Fig. 2. Their slopes have the same magnitude giving $K = 1.2_3\times10\text{M}^{-1}$.

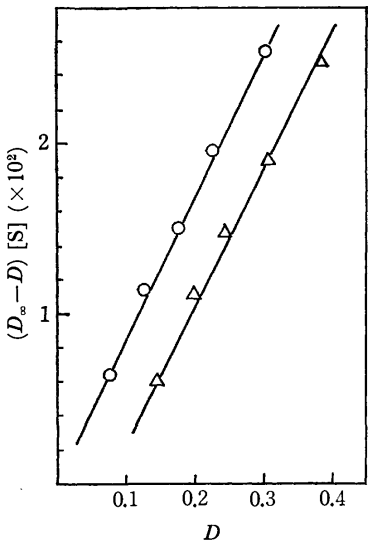

Fig. 2. Examples of the plots of $(D_\infty - D)$ [S] *vs.* D.
○: 310 nm △: 305 nm

The results for methanol, 2-propanol, and amyl alcohol are given in Figs. 3, 4, and 5. In the case of methanol and 2-propanol the change occurs in two steps as in ethanol and so the same type of equilibrium is thought to exist. The above analysis gives for 2-propanol the equilibrium constant for A+S⇄B, $K = 2\times10\text{M}^{-1}$. For methanol, the analysis was not successful. For amyl alcohol the two step change is not so distinguished. The degree of the shift is in the order, methanol>ethanol>2-propanol≈amyl alcohol.

Relative Quantum Yields as a Function of Alcohol Concentration. The spectral change of HOBP in cyclohexane upon irradiation is given in Fig. 6, which shows a gradual and monotonous decrease in optical density. This is due to the following reaction as in the

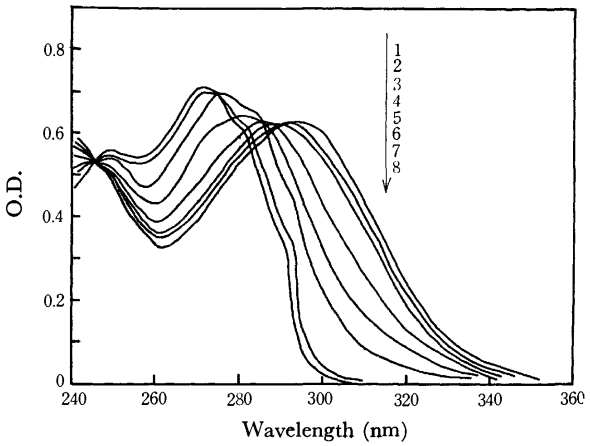

Fig. 3. Spectral change of HOBP in cyclohexane (4.27×10^{-5} M) with the addition of methanol. Concentration of methanol; 1) 1.22×10^{-1}, 2) 9.76×10^{-2}, 3) 6.10×10^{-2}, 4) 4.88×10^{-2}, 5) 4.66×10^{-2}, 6) 3.44×10^{-2}, 7) 1.12×10^{-2}, 8) 0 M (downward at 300 nm).

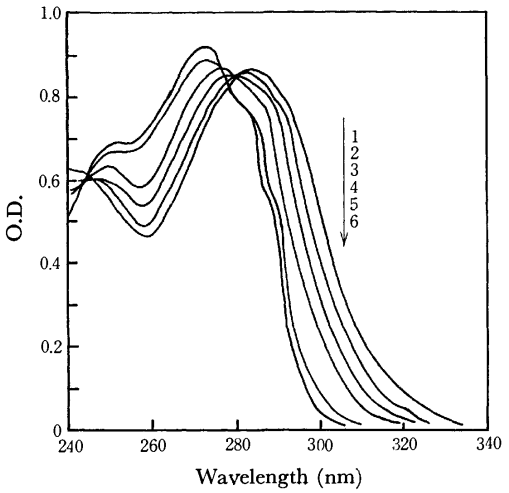

Fig. 4. Spectral change of HOBP in cyclohexane (5.60×10^{-5} M) with the addition of 2-propanol. Concentration of 2-propanol; 1) 5.24×10^{-2}, 2) 3.93×10^{-2}, 3) 2.62×10^{-2}, 4) 1.31×10^{-2}, 5) 6.54×10^{-3} 6) 0 M (downward at 300 nm).

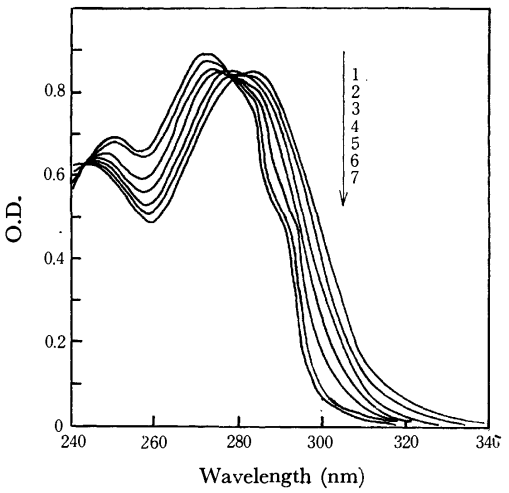

Fig. 5. Spectral change of HOBP in cyclohexane (5.42×10^{-5} M) with the addition of *n*-amyl acohol. Concentration of *n*-amyl alcohol; 1) 2.76×10^{-2}, 2): 2.3×10^{-2}, 3): 1.8×10^{-2}, 4): 1.4×10^{-2}, 5): 9.2×10^{-3}, 6): 4.6×10^{-3}, 7): 0 M (downward at 300 nm).

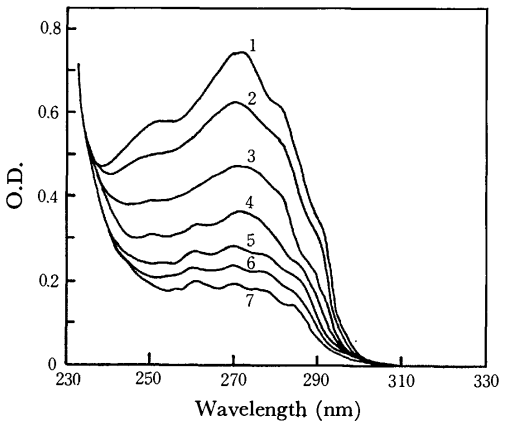

Fig. 6. Spectral change of HOBP in cyclohexane (4.57×10^{-5} M) upon irradiation at 2537 Å. Time of irradiation; 1): 0, 2): 0.5, 3): 1.0, 4): 1.5, 5): 2.0, 6): 2.5, 7): 3.0 min.

case of benzophenone.[5,6]

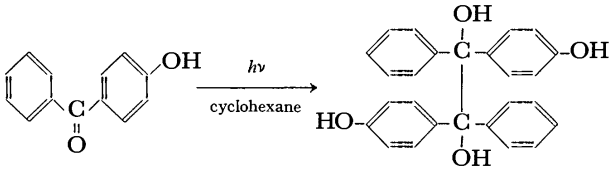

The rate was evaluated from the following equation, which takes the inner filter effect of the product pinacol into account.

$$-\frac{dC_A}{dt} = \Phi I_0(1-10^{-D})\frac{D_A}{D}$$

where C_A and D_A are the concentration of HOBP and the optical density due to HOBP, respectively. D is the total optical density experimentally obtained.

Integrating, we get

$$C_A^0 - C_A(t) = \Phi I_0\int_0^t (1-10^{-D})\frac{D_A}{D}dt.$$

By means of the relations

$$C_A^0 - C_A(t) = \frac{\Delta D}{(\varepsilon_A-\varepsilon_B)} \qquad D = D_A + \frac{\varepsilon_B}{(\varepsilon_A-\varepsilon_B)}\Delta D$$

(ε_B, the molar extinction coefficient of pinacol)

we obtain

$$\Delta D/(\varepsilon_A-\varepsilon_B) = \Phi I_0\int_0^t (1-10^{-D})D_A/D\,dt = \Phi I_0\int_0^t Y dt. \quad (4)$$

$\int_0^t Y\,dt$ can be obtained graphically.

An example of the analysis by Eq. (4) is shown in Fig. 7. The appearance of an induction period might be due to the incompleteness of the degassing. The relative quantum yields Φ_{rel} at various ethanol concentrations obtained by the above method are plotted against ethanol concentration in Fig. 8. The decrease of Φ_{rel} seems to occur in two steps, the first step being very small. A remarkable decrease from about 3×10^{-2}M of ethanol can not be reproduced either by Stern-Volmer or Perrin equations. It has been found that the following equation fits the results very well.

5) J. G. Calvert and J. N. Pitts, Jr., "Photochemistry," John Wiley & Sons, New York, (1966), p. 534.

6) A. Schonberg, "Preparative Organic Photochemistry," Springer-Verlag, New York Inc. (1968), p. 206.

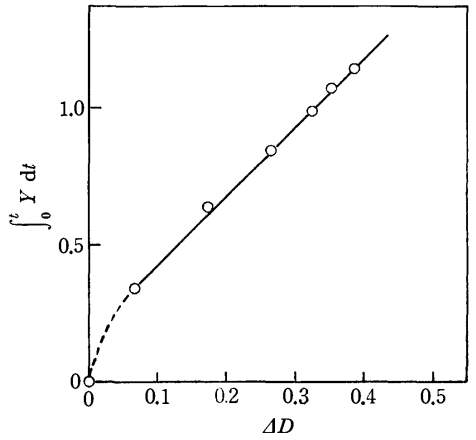

Fig. 7. An example of the plot of $\int_0^t Y\,dt$ *vs.* ΔD. HOBP in cyclohexane (4.57×10^{-5} M).

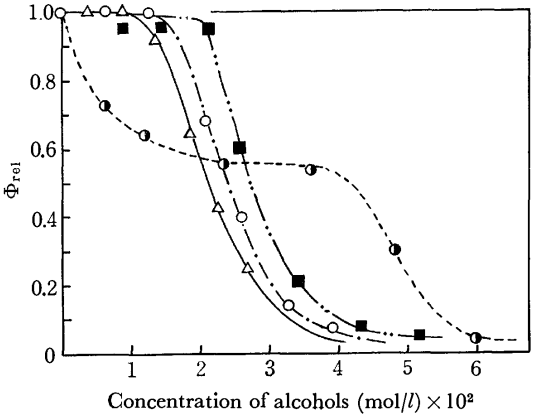

Fig. 8. Dependence of the relative quantum yield for the photoreduction of HOBP upon the concentration of alcohols. ◑: methanol, ○: 2-propanol, ■: ethanol, △: *n*-amyl alcohol.

$$\Phi_{rel} = \frac{1}{1+K[S]^n} \quad (1)$$

Thus by plotting log $(1/\Phi_{rel}-1)$ against log [S], we obtain a good straight line, which gives $n=7$ and $K=8\times10^{10}$. Hereafter the value of the order of quencher participation will be called n. The curve in Fig. 8 is a calculated one. We see from Figs. 1 and 8 that Φ_{rel} decreases very rapidly in the ethanol concentration region where the absorption spectrum begins to turn from species A to B.

The relative quantum yields obtained for 2-propanol, mechanol, and amyl alcohol by the same method of analysis are also given in Fig. 8.

In the case of methanol the results are conspicuous, the change occurring very clearly in two steps. This implies that species A in this case has much lower photoreactivity than that of HOBP itself. The first step seems to come to an end at about 3×10^{-2}M where the concentration of species B greatly predominates judging from the spectral change given in Fig. 3. The result for methanol ensures the reality of the small decrease of Φ in the low concentration region of ethanol.

The dependence of Φ_{rel} on isopropyl and amyl alcohol concentration is reproduced very satisfactorily

by Eq. (1). In the case of methanol, we assumed $\Phi_{rel}=0.58$ as a value at the end of the first step. The quantum yields in the second step were normalized in reference to this value.

The values of K and n and the related quantities are listed in Table 1. Some physical constants which will be referred to later are also included.

Table 1. The values of K and n and the related quantities

	n	K	$C_{1/2}$(M)[a]	DK at 25°C	Viscosity at 20C°
Methanol	7	2.5×10^{9}	4.7×10^{-2}	32.63	0.611
Ethanol	7	8.0×10^{10}	2.5×10^{-2}	24.30	1.19
2-Propanol	5.5	9.86×10^{8}	2.2×10^{-2}	18.3	2.39
Amyl alcohol	7	4.7×10^{11}	$2.0_7\times10^{-2}$	13.9	4.36

a) $C_{1/2}$, the concentration at which Φ decreases by one-half.

Studies on Primary Processes by means of Flash Technique. To obtain better insight into the proton transfer, flash photolysis studies have been performed on the HOBP solution in ethanol, cyclohexane and also in their mixture.

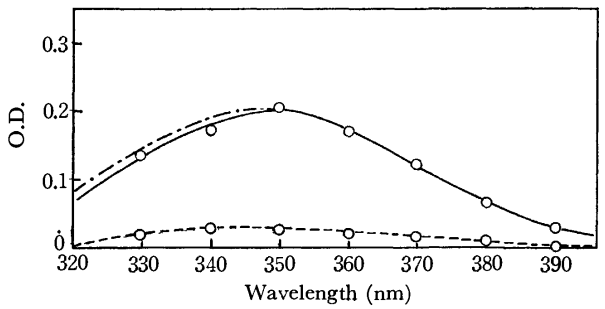

Fig. 9. Transient absorption spectrum of HOBP in ethanol.
—○—: immediately after flashing, --○--: after 500 μsec,
———: O⁻BP prepared chemically

The solution of HOBP 5.6×10^{-5}M in ethanol was subjected to a flash with a power of 80 J/flash. A transient spectrum immediately after the flash is given in Fig. 9. It has a peak at about 350 nm and the spectral shape agrees exactly with that of O⁻BP (alkaline alcoholic solution of HOBP). This is in complete agreement with Porter and Becket's result.[7] The decay obeys the second order with a rate constant of $1.6_2\times10^{9}$M^{-1}sec^{-1} which was evaluated by the use of $\varepsilon=2.25\times10^{4}$ at 340 nm. This value is a little smaller than the diffusion controlled rate constant.

The transient spectrum when 5.1×10^{-5}M HOBP in cyclohexane was subjected to a flash with a power of 150 J/flash is given in Fig. 10. The spectrum resembles very much that of ketyl radical of benzophenone reported by Porter and Wilkinson.[8] The spectrum is observed in the degassed solution but not in the aerated solution. The decay of the ketyl radical is of second order with a rate constant of 1.1×10^{9}M^{-1}sec^{-1}. This value was evaluated with the use of $\varepsilon=1.08\pm0.22\times10^{4}$ at 550 nm obtained from the optical density divided by

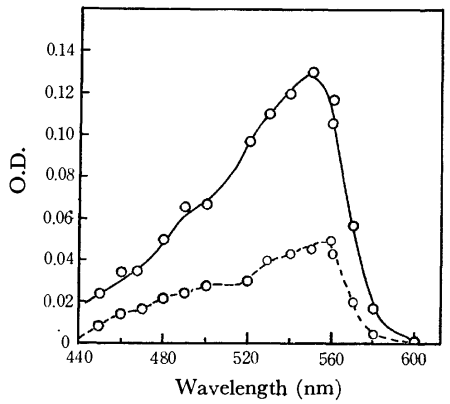

Fig. 10. Transient absorption spectrum of HOBP in cyclohexane.
—○—: immediately after flashing,
--○--: after 100 μsec

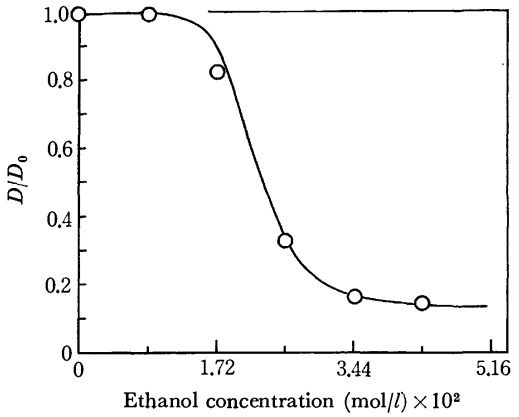

Fig. 11. Dependence of the relative quantum yield of ketyl radical (D/D_0) upon the ethanol concentration.

the yield of ketyl radical (evaluated from the decrease of HOBP).

The yield of ketyl radical immediately after flashing as a function of the ethanol concentration in cyclohexane is given in Fig. 11. The yield was determined by measuring the optical density of ketyl radical in the long wavelength region where there is no absorption of anion. The decline of the curve becomes prominent at about 2.1×10^{-2}M which is a little smaller than the concentration given in Fig. 8. This may be due to different experimental conditions. The agreement can be said satisfactory. It is concluded that the cause for the quenching of photoreduction occurs prior to the formation of ketyl radical. It is most likely that this is related to deprotonation. It should be added that the rate constant of the disappearance of ketyl radical is scarcely affected by the ethanol concentration.

Discussion and Supplementary Experiments

From the results, it is suggested that two types of molecular associates are formed between HOBP and alcohol in cyclohexane. Thus the change in absorption spectrum occurs in two distinct steps in methanol, ethanol, and 2-propanol. The quantum yield of photoreduction also changes in two steps in methanol

7) A. Becket and G. Porter, *Trans. Faraday Soc.*, **59**, 1686 (1963).
8) G. Porter and F. Wilkinson, *ibid.*, **57**, 1686 (1961).

and ethanol.

As regards the change in absorption spectrum the isosbestic point is not always observed, this being due to the superposition of the general solvent effect. Thus for methanol, whose dielectric constant is as large as 32.63, no clear isosbestic point is observed in both the first and second steps.

As regards the first step of the spectral change, it is most likely connected with the formation of a hydrogen-bonded species as follows.

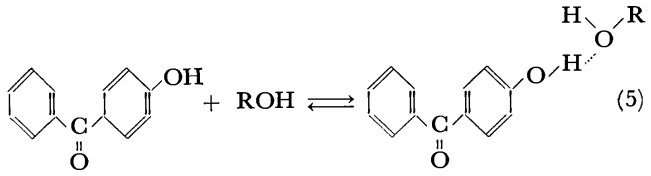

The hypothesis is supported by the absorption spectrum of HOBP in ether shown in Fig. 12 which also gives the spectral change due to the addition of ethanol. It is certain that ether forms a hydrogen bond with HOBP in the following way and a close resemblance

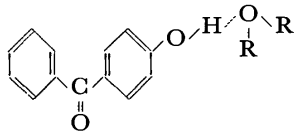

of the absorption spectrum of HOBP in ether to that of species A supports the existence of equilibrium (5). We see from Fig. 12 that the absorption spectrum changes gradually with the increase in ethanol concentration giving no isosbestic point.

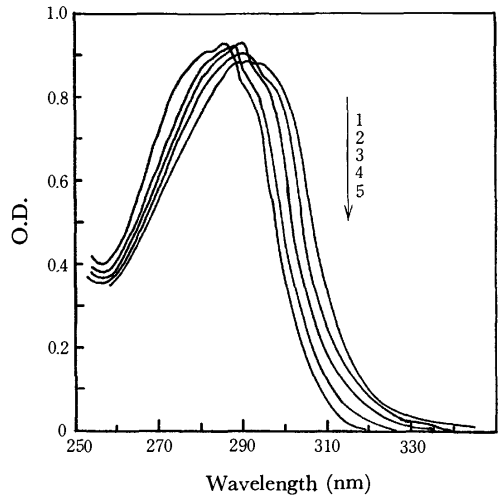

Fig. 12. Spectral change of HOBP in ether (5.50×10^{-5} M) with the addition of ethanol. Concentration of ethanol; 1) 5.1, 2) 3.4, 3) 1.7, 4) 0.85, 5) 0 M (downward at 310 nm).

As regards the second step, a detailed discussion was given on the nature of species B in ethanol-cyclohexane.[3] Some pieces of evidence were presented for the assumption that as long as the spectral behavior is concerned, the second ethanol molecule in species B is attached to the first one bonded to HO and not to the C=O group of HOBP. The present results obtained for other alcohols are also consistent with this view. Furthermore, the equilibrium constants for A+S⇌B are for ethanol and 2-propanol 1.2×10 and 2×10 respectively, which are not incompatible with the association constants of alcohols reported in literature.[9]

As to the spectral shift, two factors are considered to be important, (a) the general solvent effect represented by DK and (b) the specific interaction between solute and solvent molecules such as hydrogen-bonding. The former is the largest in methanol and decreases in the order ethanol, 2-propanol, amyl alcohol. The latter is considered to become larger from methanol to ethanol, amyl alcohol and to 2-propanol. No clear-cut isosbestic point and a large shift in case of methanol can be ascribed to a large DK. In the case of amyl alcohol for which DK is the smallest, the specific interaction only is an important factor, and this is why the two steps are not so distinctly separated.

The relative quantum yields in the mixed solvents clearly demonstrate that species A does not undergo the eventual deprotonation upon excitation and accordingly it is photoreduced efficiently. This is supported by the fact that HOBP is very efficiently photoreduced in ether.[10] Ether has no hydrogen to be detached as a proton and accordingly a hydrogen-bonded species can be reduced even in pure ether.

Analysis of the experimental results using Eq. (4) leads to the quantum yield of 1.35. This suggests the existence of a similar situation to that for the photoreduction of benzophenone in 2-propanol.[11]

A remarkable exception is methanol; in this case Φ_{rel} of species A is 0.58 with reference to free HOBP. Thus the reactivity of H-bonded species in methanol is about one half that of free HOBP. In the case of ethanol the difference in reactivity between free HOBP and hydrogen-bonded species is very small and in other alcohols there is no measureable difference.

The following analyiss supports the view that the above difference in the case of methanol (and perhaps in ethanol) is attributed to the nature of species A and not related with the transient proton transfer or other kinetic phenomena. On the basis of the following scheme involving equilibrium, HOBP+S⇌A

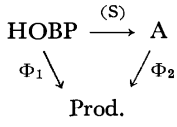

we obtain

$$\Phi = \frac{\Phi_1+\Phi_2\alpha[S]}{1+\alpha[S]} \qquad (6)$$

where

$$\alpha = \frac{\varepsilon_A}{\varepsilon_f}K, \qquad K = \frac{[A]}{[HOBP][S]}$$

(ε_f and ε_A are molar extinction coefficients of free HOBP and A-Species)

9) N. O. Coggeshall and E. L. Saier, *J. Amer. Chem. Soc.*, **73**, 5414 (1951).

10) The photoreduction of HOBP in ether seems to be somewhat anomalous; upon irradiation, a new absorption spectrum appears in the longer wavelength region in contrast to cyclohexane. This may be due to a trivial side reaction.

11) Φ for the photoreduction of benzophenone in 2-propanol varies from 0.80 to 2 according to the light intensity.[5]

It follows from (6) that

$$\frac{1-\Phi_{rel}}{[S]} = \alpha\Phi_{rel} - \alpha\frac{\Phi_2}{\Phi_1} \qquad (7)$$

In fact the plot of $1-\Phi_{rel}/[S]$ *vs.* Φ_{rel} gives a good straight line and from the slope and intercept we obtain $\Phi_2/\Phi_1 \approx 0.5$ which agrees fairly well with the experimental value.

However, in view of the fact that the specific interaction between ROH and HOBP or the strength of H-bond is the weakest for methanol and ethanol next, the dielectric nature of the solvent is considered to be an important factor for determining the reactivity of H-species. Perhaps the entity consisting of $O\text{-}H\cdots O\langle^{H}_{R}$ group and the surrounding solvation sphere of alcohol molecules may determine the reactivity.

On the other hand, the second step decrease in Φ_{rel} in methanol and ethanol and a single step decrease in other alcohols are considered to be closely related to the deprotonation of HOBP. It is regrettable that the yield of anion could not be examined as a function of ethanol concentration, since the absorption spectrum of anion was superposed by that of ketyl radical which has about ten times absorbance as that of the former. However, the approximate agreement between the two plots, Φ_{rel} and the yield of ketyl radical against [ethanol], implies that the cause of the quenching of photoreduction occurs prior to the formation of ketyl radical. It is very likely therefore, that the phenomenon is related to the proton transfer. Successful analysis by Eq. (1) also supports this view. If the decrease in Φ_{rel} were merely due to the difference in reactivity of species A and B existing in equilibrium, the decrease would not be so steep.

The result where the order of quencher participation (n) is as large as seven might be understood in the following way. For the proton transfer to suppress the reaction, the excited anion O⁻BP produced as a result of deprotonation would be reconverted to the ground state with no chance of recombining with the proton. This may be possible only if a proton transfer occurs from one alcohol molecule to its neighbour in a successive scheme of a relay type as shown below (Grotthus mechanism).

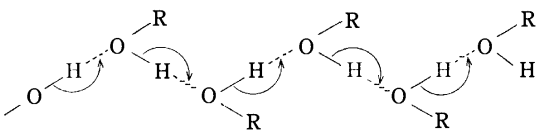

The order of the quencher participation may then be interpreted as the average number of alcohol molecules participating in the proton transfer, required for the quenching of reaction to occur. The result where n is seven for three alcohols except for 2-propanol is also in line with this view.

If such a model is accepted the value of K may be related to the association tendency of alcohol molecules. If one assumes that this tendency is measured by an equilibrium constant of dimerization and the same equilibrium constant for the successive association

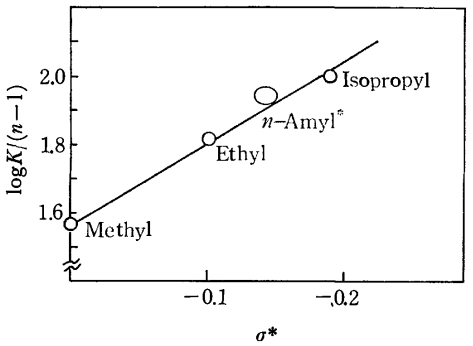

Fig. 13. A plot of log $K/(n-1)$ against σ^*.
σ^* value of n-amyl is assumed to be −0.130——0.145.

$$k = \frac{[A_2]}{[A]^2} = \frac{[A]^3}{[A_2][A]} = \frac{[A_4]}{[A_3][A]} = \cdots$$

then k is given by $K^{1/n-1}$. In fact, the relation between $\log K/(n-1)$ and the Hammett constant[12] is approximately linear as shown in Fig. 13. That the order of quencher participation is 5.5 for 2-propanol may be due to a large electron releasing power of isopropyl group, which enhances the accepting power of proton.

Thus we might say that the proton transfer efficiency in alcohols is closely related to the specific interaction between alcohol molecules and not to the dielectric nature or the viscosity of the solvent, as was found in Table 1.

It is of interest to add that for Φ_{rel} in the mixed solvent of ether and ethanol, the same type of equation as (1) holds but with $n=3$ and $K=2.8\times10^{-2}$. The smaller values of n and K are reasonable because the proton accepting power is considered to be larger for ether than for ethanol. It is possible that the following structure has a lifetime longer than that of the excited anion O⁻BP.

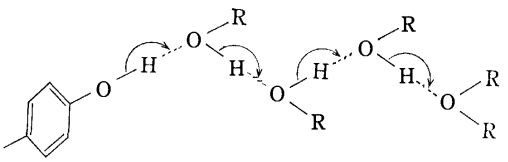

Thus all the results we obtained are consistently explained by the Grotthus mechanism of proton transfer.

Our thanks are due to Dr. K. Kikuchi for his help in the flash experiments.

12) R. W. Taft, Jr., in Steric Effects in "Organic Chemistry," ed. by Newman, John Wiley & Sons, New York, N. Y. (1956), p. 619.

On the First Singlet and Triplet Excited States of the Lithium Molecule

Susumu KOHDA,* Kimio OHNO,
and Hiroshi TAKETA

Department of Chemistry, Faculty of Science, Hokkaido University, Sapporo
General Education Department, Kyushu University, Ropponmatsu, Fukuoka

(Received December 6, 1971)

The first singlet and triplet excited states of Li_2 are studied by the MO and VB methods. As basis, only $1s$ and $2s$ AO's are used. In the MO description, the antibonding MO is more diffuse than the bonding MO and the difference is bigger in $^1\Sigma_u^+$ than $^3\Sigma_u^+$. In the VB description, splitting of the $2s$ orbital in the purely ionic ($^1\Sigma_u^+$) and covalent ($^3\Sigma_u^+$) wave functions does not lead to any energy lowering. An interpretation of this result is suggested. The calculated singlet-triplet separation is compared with previous calculations.

The lithium molecule is the simplest diatomic molecule with inner shells. In this paper, the first singlet and triplet excited states are studied by the molecular orbital (MO) and valence bond (VB) methods.

In conventional MO and VB calculations, only those atomic orbitals (AO's) which are occupied in the ground state of free atoms are usually used as a basis and the same basis is used to describe different excited states as well as the ground state. These conventional MO and VB calculations failed badly in predicting the V-T separation in C_2H_4[1] and the $^3\Sigma_u^- - ^3\Sigma_u^+$ separation in O_2[2]. In order to overcome this difficulty within the framework of the MO method, Huzinaga[3,4] advocated the use of different AO's for bonding and anti-bonding MO's and the view that these AO's could also be different in different states. He applied this idea to C_2H_4 and obtained a much better value for the V-T separation. His anti-bonding MO in the V state is very diffuse and the optimum orbital exponent of $2p\pi$ AO turns out to be as small as 0.2. This remarkable result was confirmed later by Goddard, Hunt, and Dunning,[5] who used a very flexible basis in their calculation. Ohno and Itoh[6,7], on the other hand, had attacked the same problem by the VB method. Their method is characterized by the use of different AO's for a neutral atom and for its positive and negative ions. Although their calculations were approximate, the V-T and $^3\Sigma_u^- - ^3\Sigma_u^+$ separations they obtained were fairly good.

In this work, the first singlet and triplet excitation energies of Li_2 are calculated both by Huzinaga's MO method and by the spirit of Ohno and Itoh's VB method. The aim of the work is not to achieve a numerical accuracy for these excited states but to gain qualitative idea about charcteristics of these states. Thus, only $1s$ and $2s$ Slater-type orbitals are used as the basic AO's. The orbital exponent of $1s$ is fixed at 2.685, which is the potimum value for the neutral Li atom.[8] The internuclear distance is also fixed at the observed value of 5.051 a.u.[9]

Molecular Orbital Treatment

In the MO treatment with the limited basis explained above, the wave functions for the first singlet and triplet excited states are written as

$$\Psi^{MO}(^1\Sigma_u^+) = 1/\sqrt{2}\,[\det|1\sigma_g\overline{1\sigma}_g 1\sigma_u\overline{1\sigma}_u 2\sigma_g\overline{2\sigma}_u| - \det|1\sigma_g\overline{1\sigma}_g 1\sigma_u\overline{1\sigma}_u\overline{2\sigma}_g 2\sigma_u|], \quad (2.1)$$

and

$$\Psi^{MO}(^3\Sigma_u^+) = 1/\sqrt{2}\,[\det|1\sigma_g\overline{1\sigma}_g 1\sigma_u\overline{1\sigma}_u 2\sigma_g\overline{2\sigma}_u| + \det|1\sigma_g\overline{1\sigma}_g 1\sigma_u\overline{1\sigma}_u\overline{2\sigma}_g 2\sigma_u|], \quad (2.2)$$

where spins α and β are associated with the orbitals with out and with a bar, respectively.

Following Huzinaga's procedure, we take the orbital exponents of the $2s$ orbitals used in $2\sigma_g$ and $2\sigma_u$ as two independent variational parameters. They are denoted by δ_g for $2\sigma_g$ and δ_u for $2\sigma_u$. The orbitals $2\sigma_g$ and $2\sigma_u$ are orthogonalized to $1\sigma_g$ and $1\sigma_u$, respectively, by the Schmidt procedure. The latter are constructed from the $1s_a$ and $1s_b$ AO's.

The energy is thus a function of two parameters, *i.e.*, δ_g and δ_u for each state. The results are collected in Table 1. When we use the same AO's in constructing the two MO's $2\sigma_g$ and $2\sigma_u$ (MO2=VB2), the optimum orbital exponents for $^1\Sigma_u^+$ and $^3\Sigma_u^+$ turned out to be close to the optimum value of Li^- and Li, respectively. The latter values are 0.547 for Li^-[10] and 0.637 for Li.[8] This could be expected since when the restriction $\delta_u=\delta_g$ is imposed, the MO functions Eq. (2.1) and Eq. (2.2) are identical with the VB functions which are inoic for $^1\Sigma_u^+$ and covalent for $^3\Sigma_u^+$.

When we use different AO's in different MO's (MO3), the antibonding $2\sigma_u$ becomes more diffuse than the bonding $2\sigma_g$. The degree of splitting is bigger in $^1\Sigma_u^+$ than in $^3\Sigma_u^+$. This is in accord with the observations made by Huzinaga,[11] and

* Present Address: Department of Chemistry, Faculty of Science, Hirosaki Uneversity, Hirosaki.

1) R. G. Parr and B. L. Crawford, Jr., *J. Chem. Phys.* **16**, 526 (1948).
2) W. Moffitt, *Proc. Roy. Soc*, **A210**, 224 (1951).
3) S. Huzinaga, *J. Chem. Phys.*,**36**, 453 (1962).
4) S. Huzinaga, *Theoret. Chim. Acta*, **15**, 12 (1969).
5) T. H. Dunning, W. J. Hunt, and W. A. Goddard III, *Chem. Phys. Lett.*, **4**, 147 (1969).
6) K. Ohno and T. Itoh, *J. Chem. Phys.*, **23**, 1468 (1955).
7) T. Itoh and K. Ohno, *ibid.*, **25**, 1098 (1956).
8) J. Ransil, *Rovs. Mod. Phys.*, **32**, 245 (1960).
9) G. Herzberg, "Spectra of Diatomic Molecules", Van Nostrand, Toronto, p 546 (1950).
10) S. Kohda (unpublished result).
11) S. Huzinaga, Prog. *Theoret. Phys.*, **19**, 125 (1957) and **20**, 15 (1958).

TABLE 1. ELECTRONIC ENERGY OF Li_2 AS A FUNCTION OF $2s$ ORBITAL EXPONENTS δ_g AND δ_u

Computational method	2s-Orbital exponents $^1\Sigma_g^+$		$^3\Sigma_g^+$		Total energy (a.u.)		$^1\Sigma_u^+ - ^3\Sigma_u^+$ (eV)
	δ_g	δ_u	δ_g	δ_u	$^1\Sigma_u^+$	$^3\Sigma_u^+$	
MO 1=VB 1[a]	0.637	0.637	0.637	0.637	−14.7130	−14.8079	2.58
MO 1′=VB 1′[b]	0.65	0.65	0.65	0.65	−14.7072	−14.8040	2.63
MO 2=VB 2[a]	0.582	0.582	0.647	0.647	−14.7173	−14.8079	2.46
MO 3[a,c]	0.737	0.437	0.702	0.612	−14.7350	−14.8109	2.06
MO+CI (5)[b]	0.65	0.65	0.65	0.65	−14.7912	−14.8145	0.63

a) Present work. $R=5.051$ a.u. $\delta_{1s}=2.6865$
b) Ref. 15. $R=5.00$ a.u. $\delta_{1s}=2.65$ $\delta_{2p}=0.65$
c) Variation with $\delta_u \neq \delta_g$.

Phillipson and Mulliken[12] on H_2, by Huzinaga[3,4] and Dunning *et al.*[5] on C_2H_4, and by Taketa *et al.* on O_2[13]. However, even the splitting between $2\sigma_g$ and $2\sigma_u$ in $^1\Sigma_u^+$ is smaller than that found in H_2, C_2H_4, and O_2. This is probably connected with the fact that the equilibrium internuclear distance is large in comparison with the radius of the valence orbital in the case of Li_2.

Valence Bond Treatment

In the VB treatment with the limited bais we employed, the wave functions for the first singlet and triplet excited states can be written as

$$\begin{aligned}\Psi^{VB}(^1\Sigma_u^+) = N[&\det|1s_a\overline{1s_a}1s_b\overline{1s_b}2s_a\overline{2s_a}|]\\ &-\det|1s_a\overline{1s_a}1s_b\overline{1s_b}\overline{2s_a}2s_a'|\\ &-\det|1s_a\overline{1s_a}1s_b\overline{1s_b}2s_b\overline{2s_b}'|\\ &+\det|1s_a\overline{1s_a}1s_b\overline{1s_b}\overline{2s_b}2s_b'|],\end{aligned} \tag{3.1}$$

and

$$\begin{aligned}\Psi^{VB}(^3\Sigma_u^+) = N'[&\det|1s_a\overline{1s_a}1s_b\overline{1s_b}2s_a\overline{2s_b}'|\\ &-\det|1s_a\overline{1s_a}1s_b\overline{1s_b}\overline{2s_a}2s_b'|\\ &-\det|1s_a\overline{1s_a}1s_b\overline{1s_b}2s_b\overline{2s_a}'|\\ &-\det|1s_a\overline{1s_a}1s_b\overline{1s_b}\overline{2s_b}2s_a'|].\end{aligned} \tag{3.2}$$

These wave functions correspond to the structures Li^+-Li^- for $^1\Sigma_u^+$ and Li-Li for $^3\Sigma_u^+$ and contain two variational parameters δ_{2s} and δ_{2s}'. All $2s$ orbitals $2s_a$, $2s_b$, $2s_a'$ and $2s_b'$ are orthogonalized to the $1s$ orbitals by the Schmidt procedure.

The energy again becomes a function of two parameters. Contrary to our expectation, the energy minima are found at $\delta_{2s}=\delta_{2s}'=0.582$ for $^1\Sigma_u^+$ and at $\delta_{2s}=\delta_{2s}'=0.647$ for $^3\Sigma_u^+$. When $\delta_{2s}=\delta_{2s}'$, the wave functions in Eqs. (3.1) and (3.2) are identical with those in Eqs. (2.1) and (2.2), respectively, under the restriction $\delta_u=\delta_g$. This means that no improvement over the simple VB function comes about by allowing the wave functions an extra freedom of $\delta_{2s} \neq \delta_{2s}'$. An exactly similar conclusion is reached in the VB treatment of the $^1\Sigma_u^+$ and $^3\Sigma_u^+$ states of H_2 with the two $1s$-type AO's.[14]

In these cases, the wave function is symmetric with respect to the two parameters and the energy must have a extremum at $\delta_{2s}=\delta_{2s}'$ when δ_{2s} and δ_{2s}' change along a line perpendicular to the line $\delta_{2s}=\delta_{2s}'$. The results we have obtained mean that the point where $\delta_{2s}=\delta_{2s}'=0.582$ ($^1\Sigma_u^+$) or 0.647 ($^3\Sigma_u^+$) is a minimum and not a saddle point. This may seem less strange when the valence bond wave functions in Eqs. (3.1) and (3.2) are expressed in the following way:

$$\Psi^{VB}(^1\Sigma_u^+) \propto \Psi^{MO}(^1\Sigma_u^+) + \Psi'^{MO}(^1\Sigma_u^+)$$
$$\Psi^{VB}(^3\Sigma_u^+) \propto \Psi^{MO}(^3\Sigma_u^+) + \Psi'^{MO}(^3\Sigma_u^+)$$

where Ψ^{MO} ($^1\Sigma_u^+$) and $\Psi^{MO}(^3\Sigma_u^+)$ have been given in Eqs. (2.1) and (2.2), respectively, and Ψ'^{MO} has the same functional form as Eq. (2.1) or Eq. (2.2) but δ_{2s} and δ_{2s}' are interchanged in $2\sigma_g$ and $2\sigma_u$. We have seen that the energies of the wave functions Ψ^{MO} ($^1\Sigma_u^+$) and $\Psi^{MO}(^3\Sigma_u^+)$ are quite low. However, $\Psi'^{MO}(^1\Sigma_u^+)$ and $\Psi'^{MO}(^3\Sigma_u^+)$ are expected to have very high energies, since they correspond to an unlikely model in which the bonding MO is diffuse and the anti-bonding MO is tight. The wave functions in Eqs. (3.1) and (3.2) are forced to contain equal amount of Ψ^{MO} and Ψ'^{MO}. This might be the reason why the extra degree of freedom introduced in the VB calculation turns out to be superfluous.

Summary

The calculated singlet-triplet separation is compared with other calculations in Table 1. Unfortunately, the $^3\Sigma_u^+$ state has not been observed. If we take the value of 0.63 eV obtained by the best calculation among the listed as a standard, the separation we obtained is only slightly better than the conventional calculation. However, the modification introduced here makes it clear that the $2\sigma_u$ orbital in the $^1\Sigma_u^+$ state is more diffuse than the $2\sigma_g$ orbital and both of the $2\sigma_u$ and $2\sigma_g$ orbitals in the $^3\Sigma_u^+$ state. It should also be noted that the use of two $2s$-type AO's in the ionic ($^1\Sigma_u^+$) and covalent ($^3\Sigma_u^+$) functions does not lead to any improvement over the conventional treatment.

The authors wish to express their hearty thanks to Professor S. Huzinaga for valuable discussions. Calculation of molecular integrals were carried out on the HITAC 5020E Computer at the University of Tokyo Computing Centre and the rest on the FACOM 270—20 Computer at the Chemistry Department, Hokkaido University.

12) P. E. Phillipson and R. S. Mulliken, *J. Chem. Phys.*, **28**, 1248 (1958).
13) H. Taketa, H. Tatewaki, O Nomura, and K. Ohno, *Theoret. Chim. Acta*, **11**, 369 (1968).
14) T. Noro, K. Tanaka, and K. Ohno (unpublished result).
15) E. Ishiguro, K. Kayama, M. Kotani, and Y. Mizuno, *J. Phys. Soc. Japan*, **12**, 1355 (1957).

Thermal Decomposition of Ammonium Salts of Transition Metal Oxyacids. I. Thermogravimetric Analysis of Ammonium Paramolybdate

Il-Hyun PARK*

Department of Chemistry, Faculty of Science, Kyoto University, Sakyo-ku, Kyoto

(Received August 5, 1970)

The decomposition of ammonium paramolybdate (APM) has been investigated by using a quartz spring balance in various ambient pressures. APM is decomposed in four or five stages, including a dehydration procedure, depending on the ambient pressures. However, these results do not agree with those of previous reports. This discrepancy may be attributed to the use of a sensitive quartz spring balance, a small amount of a sample, the application of a slow heating rate, or the utilization of DTG curves in the present study. The control of the ambient pressure was effective in investigating the thermogravimetric change in detail, especially in confirming the dehydration reaction. It is also concluded clearly that, in the course of the decomposition process, there is a final decomposition stage which has never been reported. The kinetics of the thermal decomposition was studied. The activation energies of the decomposition of APM under 760 Torr are 38.6, 194.8, 81.9, and 151.2 kcal·mol^{-1} respectively for the first to the fourth stages.

The thermal decomposition of ammonium paramolybdate tetra-hydrate (APM) has been studied by many investigators, and its decomposition process and the intermediates have been reported.[1-9] It was found by thermal analysis that APM decomposes in three stages. However, Rode and Tverdokhlebov reported that it decomposes in four stages, that is, they said there is a dehydration stage of all the hydrated water molecules. They also determined the composition of the intermediates by chemical analysis, by the X-ray diffraction method, *etc.* Their results, however, disagree with each other. Especially, the decomposition temperatures of the first stage and the third stage on their thermogravimetric curves (TGA) and the compositions of the intermediates are not in agreement with each other. This could be due to the differences in the experimental conditions and methods they adopted. Nevertheless, both of them forms a stable substance, $(NH_4)_2O\cdot 4MoO_3$, as a decomposition product up to the second stage.

In the present experiment, the ambient pressure was controlled in order to study the process of the first and third decomposition stages in detail, for about these stages the previous papers were not in agreement. The pressure-control method means to maintain a constant ambient pressure of a desired value during the decomposition.

The gases evolved by decomposition generally diffues slowly from the vicinity of the sample under normal atmospheric pressure, but the diffuse more rapidly when the ambient pressure decreases. As a result, changes in the decomposition process can be expected. If the evolving gases near the sample are continuously eliminated, we can expect to obtain different information.

The experiments were carried out by means of thermogravimetric analysis, using a highly-sensitive quartz spring balance calibrated for thermal agitation, in seven different ambient pressures: 760, 580, 130, 70, 20, 5, and 10^{-3} Torr (*in vacuo*). The final products of decomposition were identified by means of X-ray diffraction.

Experimental

Apparatus and Procedure. The thermogravimetric measurement was carried out by means of the apparatus shown in Fig. 1. A quartz crucible, containing the powdered

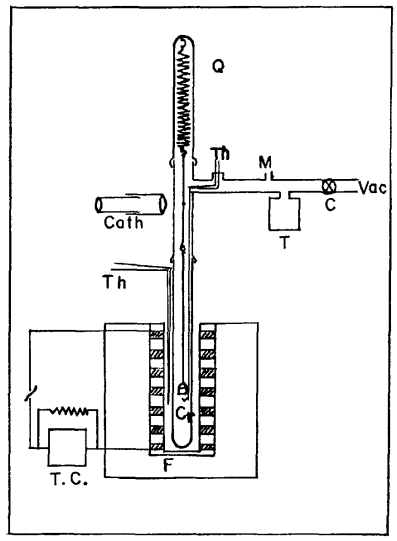

Fig. 1. Apparatus of TGA.

Q: quartz helix	Th: thermocouple
M: to manometer	Vac: to vacuum
C: cock	T: trap
Cath: cathetometer	Cr: crucible
F: furnace	T. C: temp. controller

* Present address: Department of Chemistry, College of Science & Engineering, Sung Kyun Kwan University, Seoul, Korea.

1) J. Schibata, This Bulletin, **47**, 242 (1926).
2) T. Dupuis, *C.R. Acad. Sci., Paris*, **228**, 841 (1949).
3) K. Funaki and T. Segawa, *J. Electrochem. Soc. Japan*, **18**, 152 (1950).
4) C. Duval, "Inorganic Thermogravimetric Analysis," Elsevier, Amsterdum, (1953), p. 332.
5) A. J. Hegedüs, K. Sasvari, and J. Neugebaure, *Z. Anorg. Allgem. Chem.*, **293**, 56 (1957).
6) E. Ya. Rode and V. N. Tverdokhlebov, *Zh. Neorg. Khim.*, **3**, 2343 (1958).
7) W. Romanowski, *Chem. Stosow* **7**(1), 105 (1963).
8) E. Ma, This Bulletin, **37**, 171 (1964).
9) E. Ma, *ibid.*, **37**, 648 (1964).

sample, was hung by means of a fine quartz rod to a quartz spring balance, and the shortening of the helix caused by the decrease in weight was measured by means of a cathetometer. The spring balance had a sensitivity of 0.391 mm/mg with 162 turns, and a maximum load of 1 g, including the weight of the sample crucible (about 0.2 g). The temperature was measured by means of two chromel-alumel thermocouples; one of them was set right under the crucible in the reaction tube in order to measure the decomposition temperature, while the other was set outside of the reaction tube at the same level as the crucible in order to control the heating rate. The control of the ambient pressure was attained by using a liquid nitrogen trap which condensed the evolved gases except a small amount of nitrogen, so that any large change in pressure in the reaction tube was suppressed. The experiments were carried out in a closed system in order to maintain a constant pressure except in the case of 760 Torr.

Samples. The sample was a Merck reagent of an extra pure grade (Germany) and was used without further purification. The sample was powdered to 150—200 mesh. The effect of the particle size on the thermogravimetric change was within the limits of experimental error. Considering the balance sensitivity, the sample weight of 50 mg was used. The final decomposition products in 760 Torr and 10^{-3} Torr were examined by means of the X-ray diffraction method.

Effects of Air Buoyancy and Convection. Before the measurements of the thermogravimetric change, the effects of air buoyancy and convection in the cylindrical decomposition tube must be considered. The temperature change in the spring balance should also be taken into account. Upon a change in temperature the crucible and the crucible with a sample will show an apparent weight change. Therefore, correction is essential in order to obtain an accurate thermogravimetric curve. The factors which cause the apparent weight changes are the air buoyancy, the convection effect in the cylindrical tube, the shape of the crucible, the temperature change in quartz helix, *etc.* In order to determine the above-mentioned correction, the apparent weight change for an inert sample (30 mg) in the crucible in an elevating temperature was measured by means of the apparatus used for the measurement. The correction curves thus obtained are shown in Fig. 2. It may be seen from the figure that the apparent weight increase was observed up to about 200°C regardless of the ambient pressures. The maximum weight increases were found to be about 0.2 mg. Above 200°C, the apparent weight loss was seen up to about 400°C, where the maximum weight loss of about 0.35 mg was observed. The observed weights during the decomposition were thus corrected. Although the corrections are not exact because the weight and volume of the sample change as the decomposition proceeds, the discrepancy is considered to be small and can be disregarded.

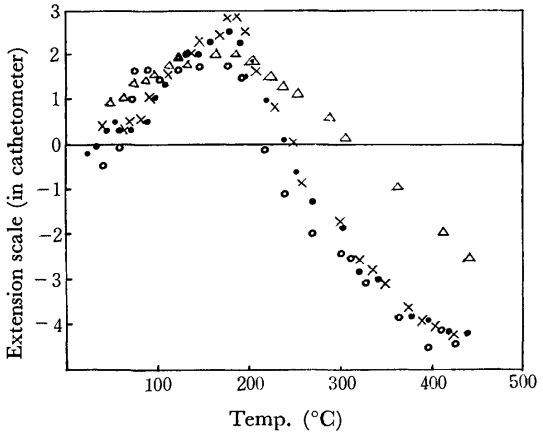

Fig. 2. Apparent weight change of crucible.
●: 760 Torr ×: 580 Torr
○: 130 Torr △: 20 Torr

Corrections of Temperature. Generally, it is difficult to measure directly the temperature of the sample which hangs from the helix during decomposition. The usual way is to measure the temperature in the furnace near the sample. However, this method often introduces a large error in the decomposition temperature. If the furnace temperature is increased at a constant rate, the temperature of the furnace is usually higher than the decomposition temperature. It is said that this thermal lag is about 3 to 14°C, and that it is approximately proportional to the heating rate.[10] The difference was examined by attaching one thermocouple directly to the sample crucible and the other to the outside of the reaction tube near the sample. The results are shown in Fig. 3. It may be seen from the figure that the difference in temperature decreases as the ambient pressure decreases.

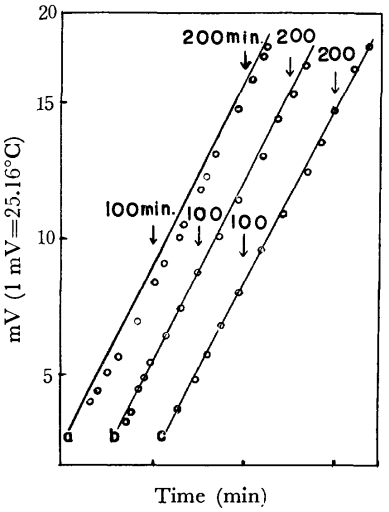

Fig. 3. Temperature correction curve.
○: Sample temp ———: Furnace temp
(a): 760 Torr (b): 130 Torr (c): 20 Torr

X-Ray Analysis. To identify the final products decomposed from APM at 760 Torr and 10^{-3} Torr, the X-ray analysis was carried out using a Schimadzu recording diffractometer with Cu-$K\alpha$ radiation.

Results and Discussion

Thermogravimetric Analysis. The TGA curves obtained by the thermogravimetric measurements in ambient pressures of 760, 580, 130, 70, 20, 5, and 10^{-3} Torr at a heating rate of 2°C/min are shown in Figs. 4 and 5, while the differential thermogravimetric curves (DTG curves) are shown in Figs. 6 and 7. It may clearly be seen from the curves that APM decomposes in four stages under higher pressures and in five stages under the pressures below 130 Torr. Here, the first stage of the decomposition splits into two stages, although the stable range of the intermediate is not very large. This is different from the results reported by other investigators,[1-9] who considered APM to

10) A. E. Newkirk, *Anal. Chem.*, **32**, 1558 (1960).

decompose in three stages under 760 Torr. Only Rode reported the decomposition in four stages, but his sample was $5(NH_4)_2O \cdot 12MoO_3 \cdot 12H_2O$.

Funaki and Rode reported that all the molecules of the water of hydration are removed during the first decomposition process (Duval, Hegedüs, and Ma did not show the dehydration step). This suggests that the removal of the water of hydration can occur independently of the removal of ammonia, and that the first decomposition process under pressures of 130 Torr or lower corresponds to a part of the dehydration. As will be described in the next paper, the analysis of the gases evolved by decomposition under low pressures confirms this process.

The DTG curve under 70 Torr shows that the maximum of dw/dt in the first decomposition process corresponds to 80°C and that the weight loss at the minimum is 23.5%, which approximately corresponds to three water molecules of APM. That is, the first stage in 70 Torr corresponds to the removal of three water molecules of APM, this is also true under 130 Torr. For the cases of 20 and 5 Torr, the elimination of two molecules of water corresponds to the first decomposition stage. By comparing the first minimum on DTG curves under 20 or 5 Torr with those under 130 or 70 Torr, it is seen that the trough of the former

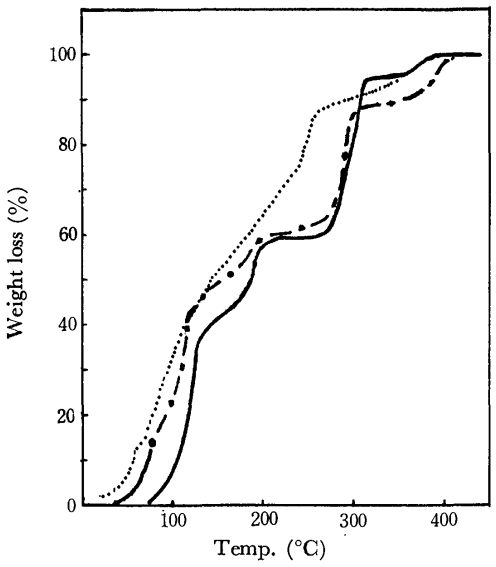

Fig. 4. TGA curve.
——: 760 Torr -·-·-: 130 Torr
------: 20 Torr ·····: 10^{-3} Torr

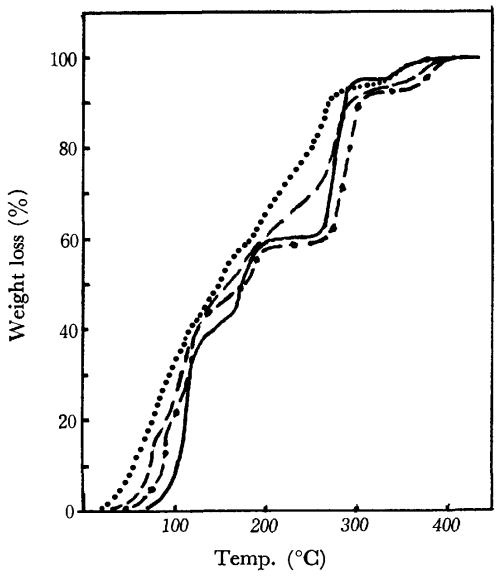

Fig. 5. TGA curve.
——: 580 Torr -·-·: 70 Torr ·····: 5 Torr

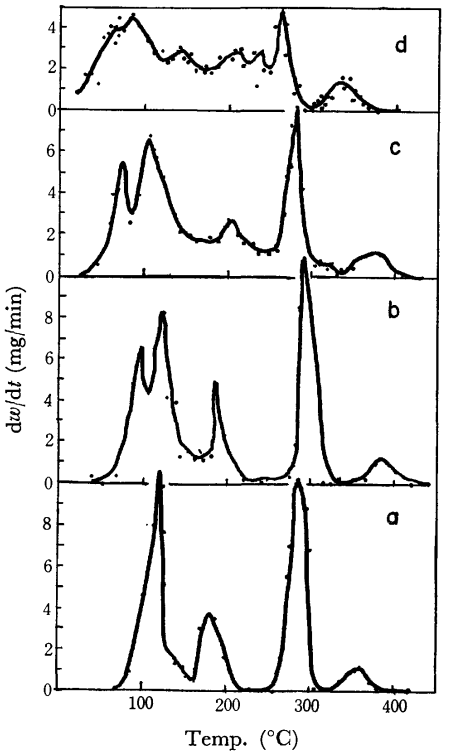

Fig. 6. DTG curve.
a: 760 Torr b: 130 Torr c: 20 Torr d: 10^{-3} Torr

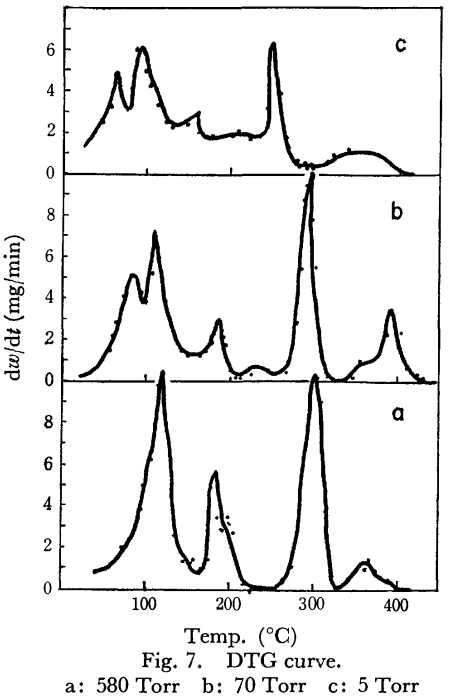

Fig. 7. DTG curve.
a: 580 Torr b: 70 Torr c: 5 Torr

is deeper than that of the latter. The depth of the trough on the DTG curve is considered to be related to the stability of the intermediate; that is, the height of the trough above the base line indicates the instability of the intermediate. The higher trough means that the intermediate is more unstable, and that two continuous reactions overlap considerably. Accordingly, by comparing Figs. 6 and 7 we can find that the intermediates under 20 or 5 Torr are more stable than those under 130 or 70 Torr. Therefore, it is not unreasonable to suppose that, also under 760 or 580 Torr, the dehydration reaction occurs prior to the removal of ammonium oxide, but the overlap of the two succeeding reactions is so large that the processes can not be observed separately, as they can under lower pressures. Judging from the tendency for the number of removed water molecules to decrease with a decrease in the ambient pressure, it will be expected that more than three water molecules can be removed in the first decomposition stage under 760 or 580 Torr and less than two under 10^{-3} Torr. Ma reported that, under 760 Torr APM begins to evolve ammonia at the temperature of about 120°C. The dehydration becomes rapid at around 115°C, and it is almost complete at 130°C. He concluded that, in the first stage in 760 Torr, four molecules of water are removed at first, and that then some ammonia is removed, without being any step resulting in $2(NH_4)_2O \cdot 5MoO_3$ at about 130°C. Lindqvist[11] showed, by crystallographic investigations, that the four hydrates were not included in the crystal structure of the discrete hepta-molybdate ion, $Mo_7O_{24}^{6-}$. This indicates that the water molecules of hydration exist independently in crystal lattice and that they are bonded with a weak bonding strength. Therefore, they can easily break away with a decrease in the atmospheric pressure before ammonium oxide evolves.

It is seen that both the first minimum under 760 and 580 Torr and the second minimum below 130 Torr on the DTG curve occur at the same temperature of about 160°C. However, the intermediates have different compositions and are comparatively unstable, with no horizontal portions being observed on the TGA curves. Different compositions for the intermediate have been reported by different investigators. Funaki and Rode decided it was a product of mere dehydration. On the other hand, Ma and others obtained the $2(NH_4)_2O \cdot 5MoO_3$ formula, but their TGA curves also suggest a lack of stability. Accordingly, it can be presumed that the intermediates in this region are so unstable that the compositions vary depending on the decomposition conditions.

From the TGA and DTG curves, it may be seen clearly that a stable intermediate, $(NH_4)_2O \cdot 4MoO_3$, is produced under any conditions except under pressures below 20 Torr. This is in good agreement with the conclusions described in the literature. However, even this stable compound could not be recognized in an ambient pressure below 20 Torr. This means that the two succesive reactions overlap very much and that the effect of the ambient pressure is large in the low-pressure range. The temperature range for the existence of this stable compound was around 220—260°C, which is in good agreement with the results reported by other workers.

It is of interest to note that a new intermediate was found at the third decomposition stage under 760 and 580 Torr and at the fourth decomposition stage under below 130 Torr. This stage exists between the stable compounds, $(NH_4)_2O \cdot 4MoO_3$, and the final product, MoO_3, and seems to be fairly stable. It may be seen from the DTG curves that the stable intermediate exists in the temperature range of 315—330°C under any conditions. From the weight loss data, the mole ratios, $(NH_4)_2O/MoO_3$ of this intermediate lie approximately in the range from 0.04 to 0.06. It converts into a final product, MoO_3, through another decomposition stage. According to Ma, the catalytic decomposition of ammonia to hydrogen and nitrogen by MoO_3 occurs at this stage. However, the reaction is not a catalytic decomposition but the oxidation of ammonia by Mo(VI) oxide, for no hydrogen was detected. The TGA data indicates that the weight loss percentage increases as the ambient pressure decreases. In the pressure below 70 Torr, the total weight loss was greater than the theoretical value. For example, under 10^{-3} Torr, the total weight loss percentage was 19.04%, this was 0.57% larger than the theoretical value, and the composition calculated from this value was approximately $MoO_{2.98}$ It seems to be reasonable to assume that the loss of oxygen was mainly due to the oxidation of ammonia. Moreover, the oxygen deficiency of MoO_3 was not observed upon decomposition under pressures above 130 Torr because of the reoxidation by the oxygen in the surrounding atmosphere. This conclusion will be confirmed by the analysis of the evolved gases in the succeeding paper.

From the above discussion, the following can be said to be the processes of the thermal decomposition in 760, 130, and 20 Torr:

760 Torr;

The color of the final product was a deep greenish gray.

$$3(NH_4)_2O \cdot 7MoO_3 \cdot 4H_2O \xrightarrow{90-130^\circ C} \underset{7.8-7.9\%(7.8\%)^{a)}}{5(NH_4)_2O \cdot 14MoO_3} \xrightarrow{175-210^\circ C} \underset{11.1\%(11.1\%)}{(NH_4)_2O \cdot 4MoO_3} \xrightarrow{285-315^\circ C} \underset{17.6\%(17.5\%)}{(NH_4)_2O \cdot 28MoO_3} \xrightarrow{360-395^\circ C} \underset{18.45\%(18.47\%)}{7MoO_3}$$

130 Torr;

The color of the final product was a grayish green.

$$3(NH_4)_2O \cdot 7MoO_3 \cdot 4H_2O \xrightarrow{65-105^\circ C} 3(NH_4)_2O \cdot 7MoO_3 \cdot H_2O \xrightarrow[4.3\%(4.4\%)]{105-145^\circ C} \underset{8.5-9.2\%(9.0\%)}{9(NH_4)_2O \cdot 28MoO_3} \xrightarrow{180-210^\circ C} \underset{11.0-11.1\%(11.1\%)}{(NH_4)_2O \cdot 4MoO_3} \xrightarrow{275-305^\circ C} \underset{16.6\%(16.5\%)}{(NH_4)_2O \cdot 15MoO_3} \xrightarrow{360-400^\circ C} \underset{18.56\%(18.47\%)}{7MoO_3}$$

a) The value of the observed weight-loss percentage, with the theoretical value in parentheses.

11) I. Lindqvist, *Ark. Kemi*, **2**, 325, 349 (1950).

20 Torr;
The color of the final product was a grayish green.

$$3(NH_4)_2O\cdot 7MoO_3\cdot 4H_2O \xrightarrow{50-85^\circ C}$$

$$3(NH_4)_2O\cdot 7MoO_3\cdot 2H_2O \xrightarrow{85-140^\circ C} 2(NH_4)_2O\cdot 7MoO_3$$
3.0—3.2%(2.9%) 9.7—10.4%(10.0%)

$$\xrightarrow{190-210^\circ C} 5(NH_4)_2O\cdot 28MoO_3 \xrightarrow{265-290^\circ C}$$
12.9—13.4%(13.2%)

$$(NH_4)_2O\cdot 15MoO_3 \xrightarrow{360-390^\circ C} 7MoO_3$$
17.3—17.5%(17.2%) 18.73%(18.47%)

The final product decomposed under 760 Torr was a light greenish gray. In the 10^{-3} Torr sample the color changed during decomposition; it was light green at 200°C, a light greenish gray at 250°C, and violet black at the final decomposition temperature.

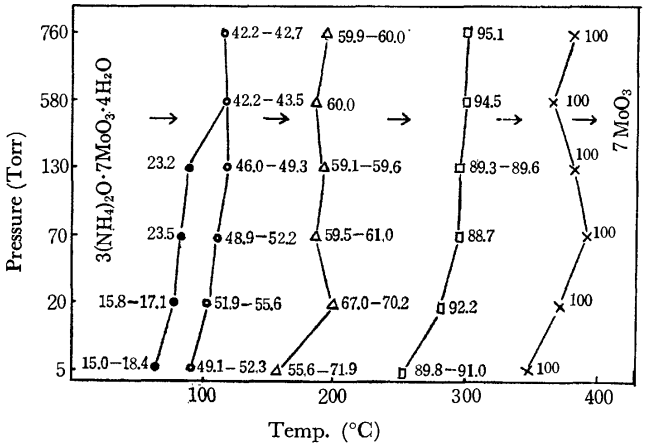

Fig. 8. Relationship between pressure and maximum decomposition temperature and percentage of decomposition.

Figure 8 shows the general relationship between the maximum temperatures of decomposition (corresponding to the peaks of the DTG curves) in various ambient pressures and the weight-loss percentage. The X-ray patterns of the final products (composition, MoO_3) obtained by decomposition are given in Table 1. They show a reasonable agreement with the X-ray patterns for MoO_3 reported in the literature,[12] but the present author could not enough investigate for the lower Mo(VI) oxides with the oxygen-deficient structure.

Table 1. X-Ray analysis of the final products prepared by decomposition of APM under 760 Torr (a) and 10 Torr (b) pressures

(a)		(b)	
d(Å)	I/I_0	d(Å)	I/I_0
6.97	0.1	3.80	0.70
3.79	0.57	3.44	0.38
3.44	0.43	3.24	1.00
3.25	1.00	2.54	0.38
2.54	0.13	2.30	0.325
2.30	0.37	1.84	0.375
1.97	0.17	1.656	0.25
1.95	0.21	1.625	0.225
1.84	0.28		
1.73	0.20		
1.66	0.19		
1.63	0.19		

Reaction Kinetics. The advantages of studying the reaction kinetics from the data obtained under a rising sample temperature are that considerably less experimental data are required than in the isothermal method, and that the kinetics can be continuously probed over the entire temperature range. However, it is necessary to measure the temperature accurately and also to avoid any change in the heating rate by an *endo-* or *exo*-thermic reaction. The latter effect can be avoided fairly well by suing a small amount of the sample. The reaction kinetics using the TGA data has been investigated by a number of workers. Freeman and Carroll[13] obtained the following equation applicable to the sample under heating and examined its applicability:

$$\frac{-\Delta E^*/2.3R\Delta(1/T)}{\Delta \log W_r} = -x + \frac{\Delta \log dw/dt}{\Delta \log W_r}$$

E^*: energy of activation.
R: gas constant.
T: absolute temperature.
x: the order of reaction.
$W_r = W_c - W$
W: total weight loss up to the time t.
W_c: weight loss at the completion of the reaction.

By using a plot of $(\Delta\log dw/dt)/(\Delta\log W_r)$ *vs.* $(\Delta 1/T)/(\Delta\log W_r)$ for each reaction, the activation energy can be calculated. For the purpose of this plot, dw and W_r were determined directly from the TGA values. The straight lines in Figs. 9 and 10 show the decomposition reaction from the first to the fourth stage under 760 Torr. From the slopes of these lines, the activation energies of the decomposition of APM

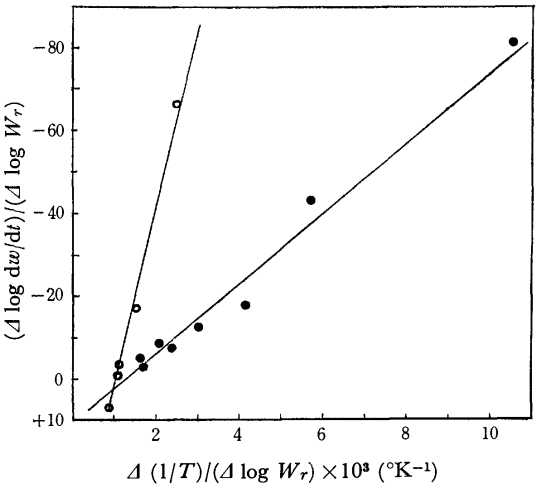

Fig. 9. Kinetics of 1st and 2nd decomposition.
●: First decomp. step
○: Second decomp. step

12) A. Magnélé, G. Anderson, B. Blomberg, and L. Kihlborg, *Anal. Chem.*, **24**, 1998 (1952).
13) E. S. Freeman and B. Carroll, *J. Phys. Chem.*, **62**, 394 (1958).

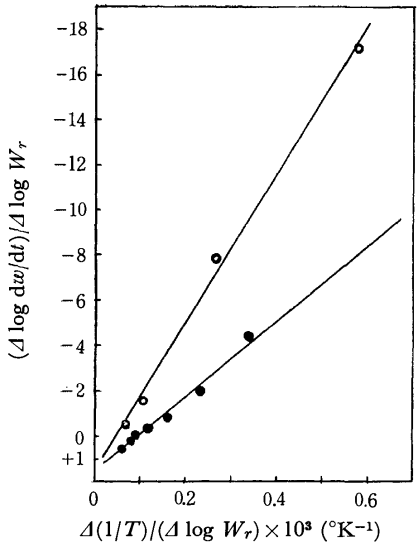

Fig. 10. Kinetics of 3rd and 4th decomposition.
●: Third decomp. step
○: Fourth decomp. step

in 760 Torr were found to be 38.6, 194.8, 81.9, and 151.2 kcal·mol^{-1} respectively from the first to the fourth stage. As has previously been described, there is a dehydration reaction stage in the decomposition process under the pressures below 130 Torr. By using the data obtained from the dehydration reaction, the activation energy was claculated for the dehydration process. Figure 11 shows the plot of $\Delta(1/T)/(\Delta \log W_r)$ *vs.* $(\Delta \log dw/dt)/(\Delta \log W_r)$ for the case of 70 Torr. The activation energy was found from its slope to be 17.3 kcal·mol^{-1}.

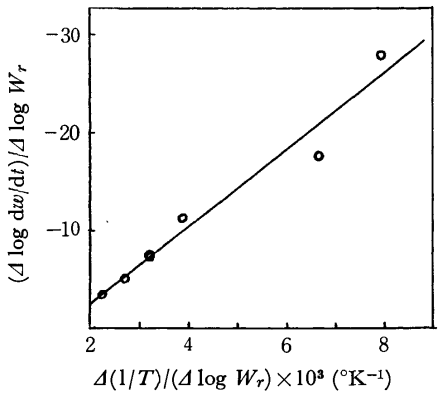

Fig. 11. Kinetics of water loss.

The author wishes to express his thanks to Professor Kumasaburo Kodera of Kyoto University for his valuable advice and continuous encouragement throughout this work. He is also grateful to Assistant Professor Norihiko Nakanishi of Kyoto University for his advice for X-ray analysis and to Mr. Isao Kusunoki of Kyoto University for his fruitful discussions and to Mr. Shinkichi Schimidzu for the measurement of TGA.

Thermal Decomposition of Ammonium Salts of Transition Metal Oxyacids. II. The Determination of the Gas Constituents Evolved by Ammonium Paramolybdate Decomposition

Il-Hyun PARK*

Department of Chemistry, Faculty of Science, Kyoto University, Sakyo-ku, Kyoto

(Received August 5, 1970)

Gases evolved by the decomposition of ammonium paramolybdate tetrahydrate have been analyzed by means of an omegatron mass spectrometer. Only water molecules of the hydration were eliminated during the first stage of decomposition, and the final stage was not the elimination reaction of ammonia but the oxidation reaction of ammonia by Mo(VI) oxide. Between 150 and 250°C, ammonia and water were evolved in a mole ratio of roughly 2:1, corresponding to the elimination of $(NH_4)_2O$. However, the range is not clear because of the overlap of the elimination of water at the lower limit and that of nitrogen at the upper limit. At higher temperatures, a small amount of NO was observed.

In a previous paper[1] it was described that ammonium paramolybdate tetrahydrate (APM) is decomposed in four stages under 760 Torr and in five stages under below 130 Torr; those results were based on thermogravimetric analyses.

Many published papers have discussed the gases evolved in each stage of decomposition simply on basis of the thermogravimetric analysis curves (TGA curves). It is said that in the first stage, ammonia and water are simultaneously removed as soon as four molecules of water are removed, and no separate stages have been observed in this process. The mole ratio of ammonia to water is 2:1; it corresponds to that of $(NH_4)_2O$. The second and the third decomposition stage are also considered to be the elimination of $(NH_4)_2O$ as ammonia and water.

Ma[2] carried out the analysis of evolved gases by means of an omegatron mass spectrometer and found that nitrogen began to come out around 250°C and reached a maximum around 320°C. He also found that hydrogen was evolved along with the nitrogen; he concluded that both were produced by the decomposition of ammonia on the surface of Mo(VI) oxide. He also measured the amount of evolved ammonia by chemical analysis and found a general agreement with the weight loss. He pointed out that any discrepancy is due to the formation of nitrogen from ammonia. In addition, he reported that water is evolved more than would be theoretically expected from the amount of ammonia. Therefore, it was considered worth while to study the gas evolution by thermal decomposition. Especially, the evolution of nitrogen observed by Ma and the dehydration stage described in the previous paper was confirmed by gas analysis. The present studies were carried out by means of an omegatron mass spectrometer.

Experimental

Apparatus and Procedure. Figure 1 shows a schematic diagram of the apparatus; it was constructed of molybdenum glass and was composed of a fused silica reaction tube coupled with a pressure-measuring device, an omegatron mass spectrometer, and two evacuating systems. The apparatus was bakable at 450°C, and its ultimate vacuum was 1×10^{-8} Torr. The main residual gas was carbon monoxide, accompanied by small amounts of carbon dioxide and water. Between the reaction tube and the omegatron, there was a copper seal metal valve and a capillary leak which reduced the pressure in the reaction tube to below 1×10^{-5} Torr for the operation of the omegatron. A McLeod gauge was used to measure the pressure of the noncondensable gases, while the total pressure of the omegatron system was measured by means of a Bayard-Alpert gauge. The evolving gases were analyzed by means of the omegatron mass spectrometer. The omegatron tube was of Mitsubishi Electric make, simple box type, and was placed in a magnetic field of 4500 gauss. The resonance ion current of the omegatron was measured by means of a Takeda TR-84H vibrating reed electrometer. The temperature of decomposition was measured by means of a chromel-alumel thermocouple.

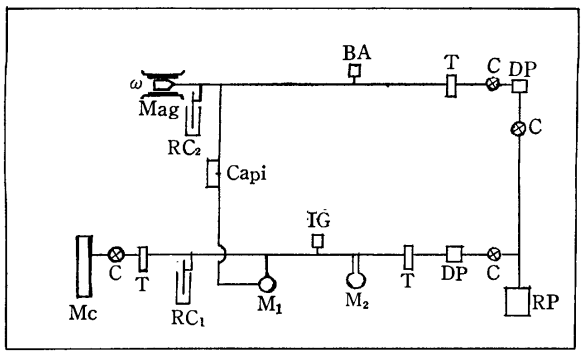

Fig. 1. Apparatus for gas analysis by omegatron.

RP: Rotary pump	DP: Oil diff. pump
C: Grease cock	T: Liq. N_2 trap
M_1 M_2: Metal valve	BA: BA gauge
IG: Ionization gauge	RC: React. cell
Capi: Capillary	ω: Omegatron
Mag: Magnet	Mc: McLeod gauge

Measurement of the Evolving Gases. The gases evolved in each decomposition stage were analyzed in the closed system and in the evacuating system. A powdered sample of Merck extra pure grade (50 mg) was placed in the decomposition cell, RC_1, in the case of the closed system. The measurement of the evolved gases was carried out from room temperature (20°C) to 500°C at intervals of 50°C. Usually, after about one hour the pressure of the evolved gases attained a stationary value. Then the gases were

* Present address: Department of Chemistry, College of Science & Engineering, Sung Kyun Kwan University, Seoul, Korea.

1) I. H. Park, This Bulletin, **45**, 2739 (1972).

2) E. Ma, *ibid.*, **37**, 171 (1964).

Table 1. Pattern coefficients of various gases

Gases	Mass									
	12	14	15	16	17	18	19	28	32	44
NH_3		1.2	4.2	7.0	100					
H_2O				1.8	21	100	10			
N_2		10						100		
CO	4—5	0.3-0.4		4				100		
CO_2	2			7					0.3	100

introduced into the omegatron through the capillary leak and were analyzed. After the measurements, the remaining gases were evacuated through a metal valve, M_2. After the pressure of the reaction system has attained 1×10^{-5} Torr, the constituents of the residual gases were checked. Then, the temperature of the cell was raised to the next decomposition temperature and the gases evolved were analyzed. The same procedure was repeated up to 500°C.

The observed intensities of the different gas ions were compared in the following way. At pressures lower than 10^{-5} Torr, the relationship of the ion current to the pressure may be represented by the following equation:

$$S \cdot P = i_+/i_-$$

where S is the sensitivity and can be treated much as the sensitivity in the ionization gauge, i_+, the ionic current produced by the electron current, i_-, and P, the pressure. The values of the sensitivity ratio for the ionization gauge for various gases determined by Wagener and Johnson[3] were used in estimating the relative amounts of N_2, H_2O, and CO_2. For the other gases, the relative sensitivities were estimated on the assumption that the sensitivity of the ionization gauge, S, and N_e, the total number of electrons per gas molecule, have a linear relationship.[4] Therefore, for the most important gases, NH_3 and H_2O, the sensitivities are nearly equal. The difference in the conductance of the gas should be considered in exact measurements, but as it is proportional to the square root of the molecular weight and as the main gases measured were ammonia and water, the correction is omitted here.

For the identification of the spectrum, the pattern coefficients of the relevant gases were determined to be as is shown in Table 1. They are in good agreement with Klopfer's[5] results. Hydrocarbons from the greased stop cock which connects the reaction system to the McLeod gauge might cause some trouble in the measurement; for instance, they might react with the sample. Therefore, to confirm whether or not there was any effect, another experiment was carried out by using an evacuating system free from grease vapor. This was carried out below 10^{-6} Torr under continuous evacuation. For this purpose, the sample cell, RC_2, near the omegatron was used. This procedure was carried out in order especially to investigate the gas constituents above 250°C.

Dehydration Process. The measurements were carried out in a closed system under an ambient pressure of 10^{-1} Torr in order to check the elimination of the hydrated molecules prior to the evolution of ammonia, under a low temperature as far as was possible. The evolved gases were measured at intervals of 10°C from room temperature to 100°C.

Oxidation of Ammonia by Molybdenum Oxide. Molybdenum oxides, obtained by the thermal decomposition of APM heated up to 450°C under 760 Torr and under 10^{-3} Torr, were used. The oxide sample was placed in RC_1 and was heated under 10^{-1} Torr ammonia. The gases produced by the reaction for 1 hr were investigated by means of the omegatron at intervals of 50°C from 300 to 500°C. Of course, the evolution of ammonia or nitrogen from the sample itself has previously been examined, but no ammonia or nitrogen was detected.

Results and Discussion

The relative amounts of the gases evolved by thermal decomposition in a closed system are shown in Fig. 2 as a function of the temperature. The mass spectra before and after the production of nitrogen, namely, at 250, 300, and 350°C, are shown in Fig. 3. Gas analysis was carried out at the temperature near the maximum of dw/dt on the DTG curve given in the previous paper. As was reported in that paper, it was assumed, from the results of TGA, that there was a dehydration process under pressures lower than 130 Torr, but its existence should be confirmed by gas analysis. Only Funaki[6] has pointed out the existence of the dehydration process of four molecules of water at 110°C. On the other hand, from the titration of

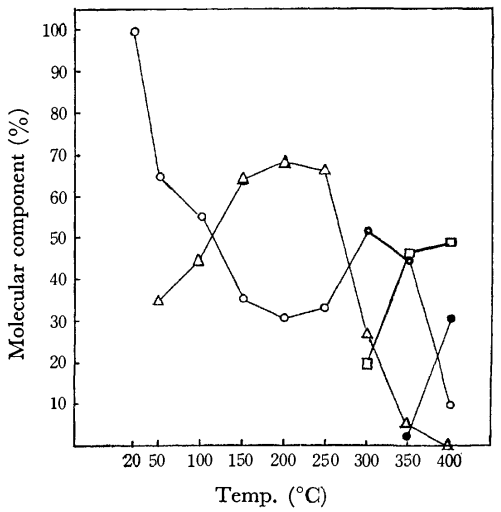

Fig. 2. Molecular component of decomposed gases.
○: H_2O △: NH_3 □: N_2 ●: CO_2

3) S. Wagener and C. B. Johnson, *J. Sci. Instr.*, **28**, 278 (1951).

4) Dushman-Lafferty, "Scientific Foundation of Vacuum Technique," 2nd edition, John Wiley & Sons Inc., (1962), p. 326.

5) A. Klopfer, S. Gorbe, and W. Schmidt, *Vacuum Symposium Transaction*, **27**, (1960).

6) K. Funaki and Segawa, *J. Electrochem. Soc. Jap.*, **18**, 152 (1950).

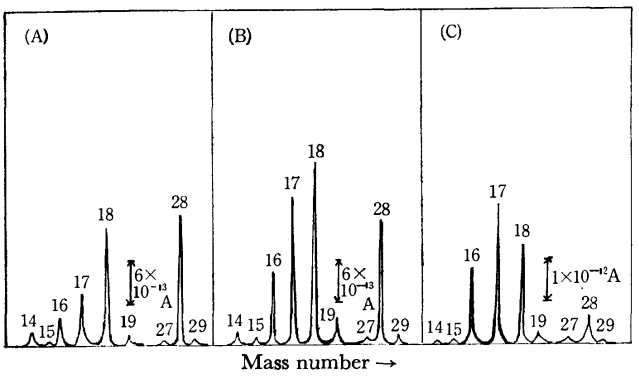

Fig. 3. Mass spectra of the evolved gases at 250—350°C.
(A): 350°C, $P=6.1\times10^{-7}$ Torr, $I_e=1.0$ μA, $V_{rf}=0.7$ V_{rms}
(B): 300°C, $P=9\times10^{-7}$ Torr, $I_e=1.0$ μA, $V_{rf}=0.7$ V_{rms}
(C): 250°C, $P=1\times10^{-6}$ Torr, $I_e=1.0$ μA, $V_{rf}=0.7$ V_{rms}

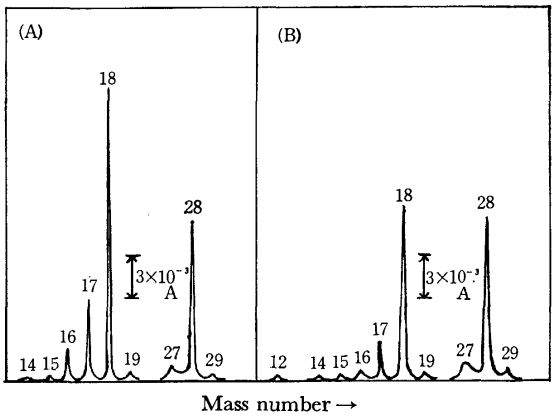

Fig. 4. Mass spectra of the evolved gases at 70 and 80°C.
(A): 80°C, $P=7\times10^{-7}$ Torr, $I_e=0.5$ μA, $V_{rf}=0.9$ V_{rms}
(B): 70°C, $P=7.3\times10^{-7}$ Torr, $I_e=0.5$ μA, $V_{rf}=0.9$ V_{rms}

evolved ammonia, Ma presumed the existence of a dehydration process just before the removal of $(NH_4)_2O$ within the first stage of the decomposition under 760 Torr. In his thermogram, however, the separation of the two processes is not seen. Also, by the present experiment, the separate dehydration process was not observed in the first decomposition process under 760 Torr. Figure 4 shows the limit of dehydration, *i.e.*, the beginning of ammonia evolution in an ambient pressure of 10^{-1} Torr. Under 10^{-1} Torr and below 70°C the peak of $m/e=17$ is considered to be almost entirely the fragment ion of H_2O, and the amount of ammonia is very small. However, at 80°C about one third of the peak may be attributed to ammonia. Therefore, the evolution of ammonia, *i.e.*, the removal of $(NH_4)_2O$, began at about 80°C; below this temperature only water of hydration was released. Thus, the existence of the dehydration stage under 10^{-1} Torr was confirmed. In Table 2, the temperatures at which ammonia began to be released in different ambient pressures are shown. From Table 2, it is clear that the temperature of ammonia production shifts to higher temperatures as the ambient pressure increases and that a part of the water molecules of hydration are removed at the beginning of decomposition, but the removal of the residual water overlaps with that of ammonia. The higher the pressure, the greater is the overlapping of the two procedures. Ammonia exists in the crystal as ammonium ions, and it is released with the water in the composition of $(NH_4)_2O$. Generally, it has been considered that the final product, MoO_3, is produced by the removal of only NH_3 and H_2O, although the analysis of the evolved gas has not been done. Ma analyzed the evolved gases for the first time and found out that, in the stage of the removal of $(NH_4)_2O$, the ratio of NH_3 and H_2O was not 2: 1. However, in the present study, it may be seen in Fig. 2 that the ratio of 2: 1 continued from 150 to 250°C; it is considered that this corresponds to the elimination of $(NH_4)_2O$. It was found by the thermogravimetric analysis that the intermediate obtained by the decomposition at this stage has the composition of $(NH_4)_2O\cdot4MoO_3$; it is an extremely stable compound. The TGA curve shows that this stable compound decomposes above 250°C. According to Figs. 2 and 3, the evolution of ammonia decreased suddenly at 300°C; simultaneously, the peak of $m/e=28$ appeared. This is clearly the peak of nitrogen. It may be seen from Table 3 that the pressure at 300°C measured by the McLeod gauge without a cold trap was below 1/10 of that at 250°C. The value of the total pressure is not very reliable because of the pressure of the condensable water vapor; nevertheless, it is true that the amounts of gases evolved are very small at this temperature.

The total pressure of gas evolved at 350°C again increased to twice that at 300°C and reached a maximum. Hydrogen was not observed at all; the main products at this stage were water and nitrogen, which

Table 2. Variation of dehydration temperature in various ambient pressure of decomposition

Ambient pressure (Torr)	760	130	70	20	5	10^{-1}	10^{-3}	10^{-5}
Temperature which NH_3 evolution begins	115[a)]	105[b)]	95[b)]	85[b)]	80[b)]	80[c)]	70[b)]	50[c)]

a) temperature proposed by Ma. b) temperature of dw/dt=min. in 1st decomposition process on Figs. 6 and 7 in previous paper. c) temperature determined by omegatron.

Table 3. Total pressure of evolved gases

Temperature (°C)	20	50	100	150	200	250	300	350	400
Pressure ($\times10^{-1}$ Torr)	0.26	1.13	4.8	6.8	11.9	10.6	1.3	2.5	0.41

was the oxidation product of ammonia with Mo(VI) oxide. However, the amount of water is considerably less than that which should be produced by the oxidation of ammonia. This discrepancy may be explained by the loss of water by adsorption on the inside wall of the glass apparatus, because the total amount of gas evolved was rather small.

The gases evolved at 400°C were mainly nitrogen and carbon dioxide of $m/e=44$, and no ammonia was observed. As the total pressure was very low at this temperature, the amounts of nitrogen and water were very small. Therefore, the thermal decomposition of APM was completed here. The carbon dioxide might be produced by the oxidation of the impurity carbon contained in the sample, or part of it might come from the grease vapor. As for the production of carbon dioxide, Onchi and Kusunoki[7] have reported that, by the thermal decomposition of MoO_3 *in vacuo*, the main gaseous product about 400°C was carbon dioxide, the production of oxygen-deficient oxide is attributable to the reduction by the impurity. The main gases observed at 450 and 500°C were carbon dioxide and carbon monoxide, plus a small amount of NO, $m/e=30$. Nitric oxide might be produced by the further oxidation of ammonia. Oxygen with $m/e=32$ has not observed throughout the decomposition up to 500°C.

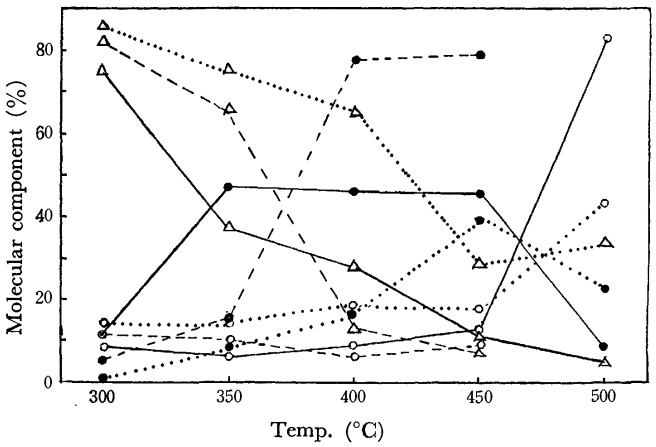

Fig. 5. Molecular component of N_2, H_2O, and NH_3, evolved by reaction of NH_3 with MoO_3.
——}MoO_3 prepared in vac.
····· MoO_3 prepared in air
●: N_2, ○: H_2O, △: NH_3

The experiment in the evacuating system confirmed that the evolution of ammonia, water, and nitrogen was similar to that in the closed system except that the temperature of nitrogen production was shifted to a slightly higher temperature. This fact suggests that the oxidation of ammonia takes place at the moment of its production, or that the collisions with the surface need not be repeated many times, though the produced NH_3 comes in contact with the oxide surface. The results of the oxidation of ammonia by the MoO_3 produced by the thermal decomposition of APM in air or *in vacuo* show that nitrogen was formed about 300°C and that the amount reached its maximum at 350—400°C for both samples (Fig. 5). The tendency of the reaction is similar to the case of APM but the temperature seems to be shifted to a higher value. However, no detailed discussion can be made because of the lack of reproducibility of the data. It was found that the evolution of H_2O came later than the production of N_2. The reason for this may be as follows: when NH_3 was oxidized on the surface of MoO_3, the O-H bond was perhaps produced in a crystal by binding the H of NH_3 and the O of MoO_3, and later, as the temperature rose, this O-H was perhaps eliminated by way of the formation of H_2O. Further examinations are needed to confirm this conclusion on the basis of the reproducibility of the experimental results. Nevertheless, it was proved that the ammonia produced in a crystal is actively oxidized to nitrogen on the surface of MoO_3 or on the interface of the crystal.

The author wishes to express his thanks to Professor Kumasaburo Kodera of Kyoto University for his valuable advice and continuous encouragement throughout the course of this work. He also wishes to thank Assistant Professor Masaru Onchi and Mr. Isao Kusunoki of Kyoto University for their continuing interest and helpful advice.

7) M. Onchi and I. Kusunoki, *Nippon Kagaku Zasshi*, **85**, 612 (1964).

Thermal Decomposition of Ammonium Salts of Transition Metal Oxyacids. III.[1] Thermogravimetric Analysis of Ammonium Chromate

Il-Hyun PARK*

Department of Chemistry, Faculty of Science, Kyoto University, Sakyo-ku, Kyoto

(Received February 1, 1971)

Thermal decomposition of ammonium chromate (AC) and ammonium dichromate (ADC) has been studied by means of TG, DTA, and DTG. It showed four steps in thermal decomposition of AC and three steps in that of ADC. Decomposition product in each step of the thermal decomposition was examined by X-ray diffraction method. From the results of both thermogravimetric analysis and X-ray study, it was concluded that the first decomposition product of AC was ADC, the second was CrO_3 and the final product was Cr_2O_3. The third product gave the X-ray patterns of the mixture of Cr_2O_3 and CrO_3, and the mole ratio of O/Cr in the temperature range for the existence of the product (300—390°C) was 2.1—2.0. The kinetics in the second decomposition step for AC and in the first decomposition step for ADC were studied, giving the values of the energy of activation of 24.2 and 22.4 kcal/mol, respectively.

In a preceding paper of this series,[2] it was reported that molybdenum(VI) oxide formed by thermal decomposition of ammonium paramolybdate oxidized ammonia evolved during the thermal decomposition. It is known that ammonia is oxidized more readily by oxyacids of chromium(VI) than those of molybdenum(VI).

Ammonium chromate decomposes slowly to form ammonium dichromate even at room temperature.[3] It is believed that the thermal decomposition of ammonium dichromate can be described by the following simple reaction:[4]

$$(NH_4)_2Cr_2O_7 \xrightarrow{\Delta} Cr_2O_3 + N_2 + 4H_2O$$

As the results of studies on isothermal decomposition of ADC, however, several authors noticed that ammonia and oxides of nitrogen were present in appreciable quantities amongst the decomposition products.[5-10] They examined the compositions of evolved gases and final solid products. Unfortunately, their results as to the composition of the final solid product were not in complete agreement with each other. All of them except Harbard investigated isothermal decomposition reactions, and Harbard carried out the decomposition experiment by heating ADC in a closed tube, the gas evolved being collected in a gas burette. Kinetics and mechanism of isothermal decomposition of ADC were studied by Taylor *et al.*[10,11] without using thermogravimetric analysis.

The present study has been undertaken to make clear the entire processes of thermal decomposition of AC and ADC by means of thermogravimetric analysis, to determine the composition and structure of each decomposition intermediate and the temperature range for the existence of each decomposition product, and to examine kinetics of the decomposition reactions.

Experimental

Thermogravimetric Analysis (TG). TG was carried out by using the quartz spring balance described in the preceding paper of this series.[2] AC and ADC (extra pure reagents of Nakarai Chemical Co.) were powdered to the size of 170—200 mesh prior to each measurement. A sample of 10 mg was heated at a rate of 2°C/min. The ambient pressure of the decomposition was 760 Torr.

Differential Thermal Analysis (DTA), Thermogravimetric Analysis (TG), and Derivative Thermogravimetry (DTG). By using the automatic recording thermobalance of Cho Balance Co., DTA, TG, and DTG were carried out simultaneously. A sample of 20 mg was heated at a rate of 3.7°C/min in the ambient pressure of 760 Torr, and α-Al_2O_3 was taken as a reference material for DTA.

Decomposition Rate Measurements. The experimental apparatus for decomposition rate measurements was similar to that used for TG under vacuum.[2] The kinetics of decomposition of AC and ADC were followed by use of the quartz spring balance. A sample of 20 mg was used for the determination of decomposition rates. The decomposition product in the first step of the thermal decomposition of AC was obtained by heating AC up to 120°C and annealing it for several hours under 760 Torr.

X-Ray Analysis. X-Ray patterns of the intermediates in each step of the decomposition reactions were obtained with an automatic recording diffractometer of Shimadzu Seisakusho, Ltd. using CuK_α radiation. Each decomposition intermediate for X-ray analysis was prepared by annealing the corresponding product at the respective temperatures for several hours.

Results

Thermogravimetric Analysis. The results for thermal decompositions of AC and ADC obtained under 760

* Present address: Department of Chemistry, College of Science & Engineering, Sung Kyun Kwan University, Seoul, Korea.

1) Part II: This Bulletin, **45**, 2739 (1972).

2) This Bulletin, **45**, 2745 (1972).

3) P. C. L. Thorne and E. R. Roberts, "Inorganic Chemistry," (Ephraims), 6th edition, Oliver & Boyd (1954), p. 507.

4) R. B. Heslop and P. L. Robinson, "Inorganic Chemistry," 3rd edition, Elsevier Publishing Company (1967), p. 666.

5) W. C. Ball, *J. Chem. Soc.*, **95**, 87 (1909).

6) W. M. Hooton, *Proc. Chem. Soc.*, **24**, 27 (1908).

7) E. Moles and A. Gonzalez, *Anal. Fis. Quim.*, **21**, 204 (1923).

8) E. H. Harbard and A. King, *J. Chem. Soc.*, **1938**, 955.

9) K. Fischbeck and H. Springler, *Z. Anorg. Chem.*, **235**, 183 (1938); *ibid.*, **241**, 209 (1939).

10) J. Simpson, D. Taylor, and D. M. W. Anderson, *J. Chem. Soc.*, **1958**, 2378.

11) D. Taylor, *ibid.*, **1955**, 1033.

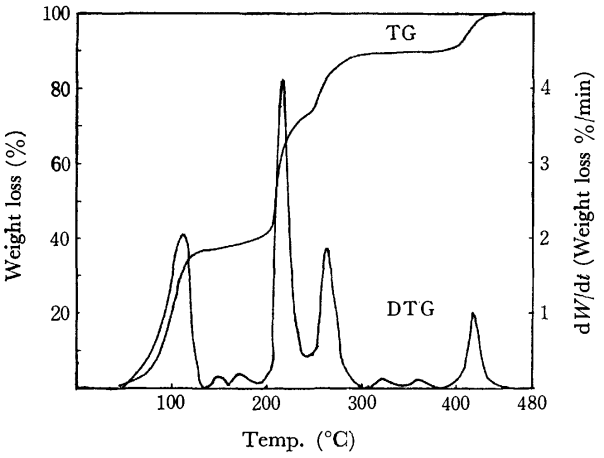

Fig. 1. Thermogravimetric and derivative thermogravimetric curves of AC (in 1 atm.).

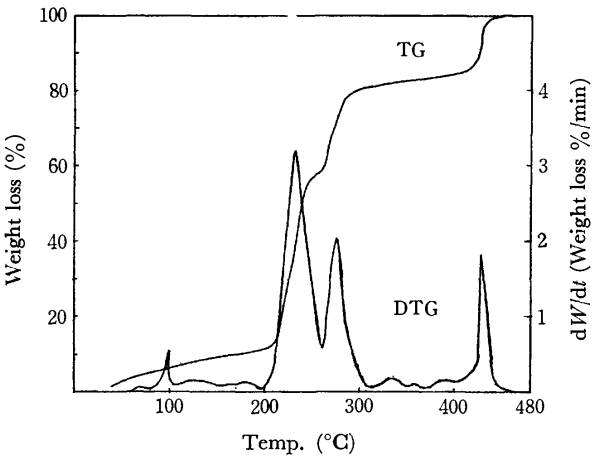

Fig. 2. Thermogravimetric and derivative thermogravimetric curves of ADC (in 1 atm.).

Torr are shown in Figs. 1 and 2, respectively. From these results it is seen that the decomposition of AC proceeds in four steps and that of ADC in three steps. The first step of the decomposition of AC produces an orange-colored ADC, and three succeeding steps of decomposition of AC are similar to the three steps of decomposition of ADC itself.

Differential Thermal Analysis, Thermogravimetric Analysis, and Derivative Thermogravimetry. The results of studies on thermal decomposition of AC and ADC obtained by simultaneous measurement of DTA, DTG, and TG are shown in Figs. 3 and 4. The TG and DTG curves obtained by this method are in good agreement with those obtained by the spring balance method (Figs. 1 and 2). It is seen that the first step of the decomposition of AC is endothermic, whereas the other three steps of the decomposition are exothermic. In this case again the decomposition after the first step of AC is similar to that of ADC itself.

Rate of Decomposition of AC and ADC. About 10—20 min were required for the reaction vessel and reactants to reach a desired constant temperature. The decomposition rates of AC in the second step and those of ADC in the first step were measured at constant temperatures from 180 to 200°C. The rate

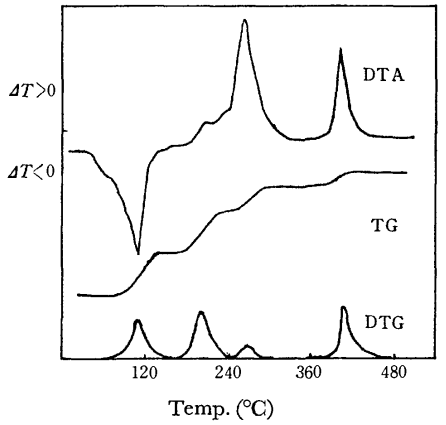

Fig. 3. DTA, TG, and DTG curves of AC.

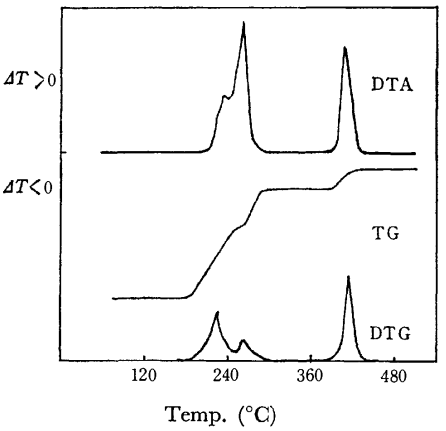

Fig. 4. DTA, TG, and DTG curves of ADC.

determination was followed until the plots of fraction decomposed (α) *vs.* time (t) reached to the end of sigmoid part.

X-Ray Analysis. A sample of AC was heated up to 120°C and annealed for several hours and its X-ray pattern was examined. Another sample of AC was heated up to 240°C and annealed for several hours and its X-ray pattern was examined. The first column-(a) and the third column(c) in Table 1 show the diffraction data of the intermediates prepared by heating AC at 120 and 240°C, respectively. These results are indicated to be almost in agreement with literature values, which are shown in the second (b) and fouth columns(d),[12] respectively. A sample of AC was heated up to 360°C and annealed for several hours, and its X-ray pattern was examined. The results are in the fifth column(e) in Table 1, which represents a pattern entirely different from that of CrO_2,[13] but indicates the presence of both CrO_3 and Cr_2O_3. A sample of AC was heated up to still higher temperature and annealed for several hours to form the final decomposition product, and its X-ray pattern was checked. The final product gave the diffraction data as shown in the sixth column(f), agreeing with those in the literature.[12]

12) S. Kato and K. Kubo, "Chemical Analysis by X-ray Diffraction," Nikkan Kogyo Shinbunsha (1955), pp. 134 and 159.

13) R. S. Schwartz, I. Fankunchen, and R. Ward, *J. Amer. Chem. Soc.*, **74**, 1676 (1952).

Table 1. X-Ray diffraction data for decomposition products of AC
(a) this study (sample heated in air for several hours at 120°C),
(c) this study (sample heated in air for several hours at 240°C),
(e) this study (sample heated in air for several hours at 360°C),
(f) this study (the final decomposition product of AC),
(b) ADC, (d) CrO_3, and (g) Cr_2O_3 data, Kato and Kubo.[12]

(a)		(b)		(c)		(d)		(e)		(f)		(g)	
d(Å)	I/I_0	d(Å)	I/I_0	d(Å)	I/I_0	d(Å)	I/I_0	d(Å)	I/I_0	d(Å)	I/I_0	d(Å)	I/I_0
6.61	0.12	6.60	0.58	4.53	0.16			4.23	0.24	3.63	0.25	3.63	0.45
5.13	1.00	5.10	1.00	4.31	0.25			4.17	0.32	2.67	0.67	2.67	0.70
4.61	0.17			4.19	0.41	4.20	0.75	3.72	0.21	2.48	0.90	2.47	0.70
4.11	0.50			3.74	0.14			3.65	0.44	2.17	0.33	2.17	0.30
												2.03	0.04
3.65	0.12	3.77	0.16	3.60	0.12			3.38	0.91	1.81	0.58	1.81	0.45
										1.67	1.00	1.67	1.00
3.44	0.37			3.39	1.00	3.40	1.00	2.67	0.76			1.58	0.06
												1.46	0.30
3.35	0.25	3.37	0.83	2.83	0.10	2.86	0.25	2.47	0.94	1.43	0.33	1.43	0.45
												1.29	0.16
3.30	0.37			2.47	0.08			2.27	0.12			1.23	0.06
												1.21	0.06
3.24	0.90			2.40	0.06	2.36	0.20	2.17	0.44			1.17	0.05
						2.25	0.20					1.15	0.06
3.16	0.29			2.15	0.04			1.81	0.29			1.12	0.06
		3.04	0.40									1.09	0.12
2.97	0.29			2.00	0.06	2.00	0.07	1.71	0.12			1.04	0.10
						1.96	0.10					1.02	0.02
2.77	0.20	2.77	0.27	1.82	0.10	1.84	0.05	1.67	1.00			0.95	0.06
		2.48	0.30			1.74	0.15						
2.32	0.25	2.33	0.18			1.71	0.03	1.58	0.15				
						1.68	0.01						
2.05	0.17	2.05	0.25			1.60	0.03	1.46	0.21				
		2.00	0.10			1.56	0.01						
1.82	0.13	1.92	0.10			1.54	0.01	1.43	0.38				
								1.33	0.09				
1.81	0.13	1.82	0.25										
		1.50	0.10										

Discussion

Thermal Analysis. The composition of each intermediate of the thermal decomposition was determined, and the temperature range where each intermediate existed was deduced from the TG and DTG curves. The decomposition processes are summarized as follows:

Ammonium chromate:

$$(NH_4)_2CrO_4 \xrightarrow{80\text{—}120^\circ C} (NH_4)_2Cr_2O_7\text{(orange)}\ 17.6\%(17.4\%)^{14)}$$

$$\xrightarrow{200\text{—}230^\circ C} CrO_3\text{(brown)}\ 34.7\%(34.2\%) \xrightarrow{260\text{—}275^\circ C} CrO_2\text{(black)}\ 44.5\%(44.6\%)$$

$$\xrightarrow{400\text{—}435^\circ C} Cr_2O_3\text{(dark green)}\ 49.1\%(50.0\%)$$

Ammonium dichromate:

$$(NH_4)_2Cr_2O_7 \xrightarrow{205\text{—}245^\circ C} CrO_3\text{(brown)}\ 22.0\%(20.6\%) \xrightarrow{260\text{—}285^\circ C}$$

$$CrO_2\text{(black)}\ 32.4\%(33.3\%) \xrightarrow{410\text{—}435^\circ C} Cr_2O_3\text{(dark green)}\ 38.5\%(39.7\%)$$

14) The values are weight loss percentages observed, the theoretical values being included in parentheses.

The values of weight loss percentage observed are consistent with the theoretical values within 1%. DTG curve shows a small weight decrease in ADC prior to the first decomposition step, as shown in Fig. 2. This is considered to be due to the removal of adsorbed water from the crystal surface. The percentage of the weight decrease amounts to about 3.5%.

According to the DTA curve of AC, the endothermic peak appears at $T_{max}=110^\circ C$ and the three exothermic peaks appear at $T_{max}=210$, 255, and 410°C, respectively. These temperatures are in good agreement with the temperatures at $dw/dt=$max. the on DTG curve determined by spring balance measurement.

It was confirmed by thermal analysis that AC decomposes in four steps, and the results of X-ray analysis for the intermediate of each step support the production of the above mentioned compounds. Namely, the first decomposition product from AC at about 120°C is ADC and the second decomposition product formed by heating AC up to 240°C is CrO_3. The product yielded by heating AC up to 360°C corresponds to one having formula of CrO_2 according to the result of weight loss determined by TG, and to the mixture of CrO_3 and Cr_2O_3 according to the X-ray analysis

(Table 1). Thus, the 3.38 Å line might be attributed to CrO_3 and the other strong lines (3.65, 2.67, 2.47, and 1.67 Å) are attributed to Cr_2O_3.

It can be said that an oxide which has the composition of Cr_5O_9 is formed in decomposition of CrO_3 to Cr_2O_3 and this oxide is generally regarded as a double compound of chromium(III) and chromium(VI) oxides, or chromium(III) chromate: $Cr_5O_9=2Cr_2O_3\cdot CrO_3$. The existence of Cr_5O_9 is, however, doubtful. King could not made Cr_5O_9, at least, in the thermal degradation of CrO_3, but he found two non-Daltonide compounds as the intermediates, one of which had 2.6—2.2 and the other 1.9—1.7 atoms of O per atom of Cr.[15] $2Cr_2O_3\cdot CrO_3$ is brown and paramagnetic, CrO_2 is black and both are insoluble in water.[3] On the other hand Taylor[16] has mentioned that CrO_3 melts at 193°C and forms brown chromic chromate ((CrO_2)-$CrO_4=Cr_3O_6$) and liberates oxygen at 250°C,

$$6CrO_3 = 2Cr_3O_6 + 3O_2$$

and on further heating yields chromium sesquioxide.

$$4CrO_3 = 2Cr_2O_3 + 3O_2$$

In the present work, the product obtained when AC was heated up to 360°C showed the composition of CrO_2 and had black color. However, it might be considered that during annealing at 360°C for several hours, some amounts of oxygen was lost by decomposition, a part of which oxidized residual nitrogen compounds or carbon impurity contained in sample, giving lower oxide, Cr_5O_9. Although it has been reported that there are oxides having the various compositions, *e.g.*, Cr_3O_8, Cr_2O_5 *etc.*,[17] none of these have been actually found in this work. The value of the ratio of O/Cr is calculated to be 2.1—2.0 at the temperature range of 300—390°C.

Reaction Kinetics. In order to examine the result of thermal analysis, the decomposition rate of the first step degradation product of AC was compared with that of ADC. Namely, the reaction rates of CrO_3 formation from these samples were measured in isothermal decomposition. The α *vs.* t curves were sigmoid in shape and were analyzed by use of the modified Prout-Tompkins equation:[18]

$$-\ln(1-\alpha) = kt$$

where α is the fraction decomposed in time t and k is the rate constant. The plots of $-\ln(1-\alpha)$ *vs.* t at various temperatures for the decomposition product in the first step of the thermal decomposition of AC and for ADC are shown in Figs. 5 and 6. The results clearly indicate that both reactions follow the unimolecular decay law. Arrhenius plots for the two reactions

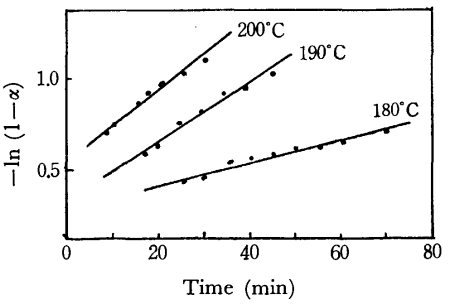

Fig. 5. The plot of $-\ln(1-\alpha)$ *vs.* t for ADC prepared by heating AC up to 120°C.

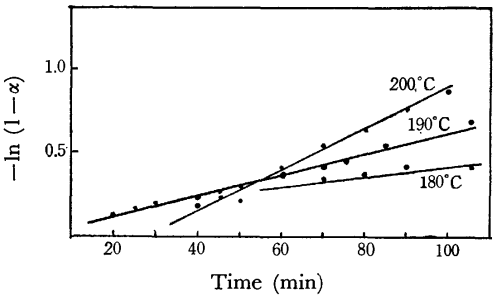

Fig. 6. The plot of $-\ln(1-\alpha)$ *vs.* t for ADC.

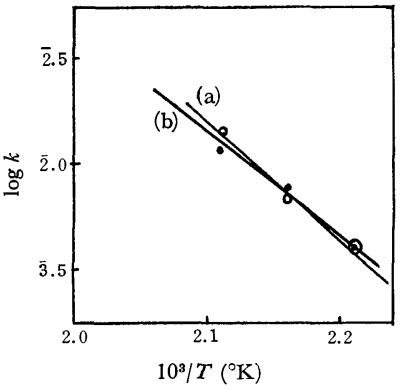

Fig. 7. Arrhenius plots of the rate constants.
(a) in 2nd decomposition step of AC
(b) in 1st decomposition step of ADC

are shown in Fig. 7. From the slopes of these lines, the activation energies of the two reactions are found to be 24.2 and 22.4 kcal/mol, respectively. From these results it may be said that the second step of AC decomposition corresponds to the first step of ADC decomposition, which is in agreement with the conclusion of X-ray analysis.

The author wishes to express his sincere thanks to Professor Kumasaburo Kodera of Kyoto University for his valuable advice and continuous encouragement throughout this work. Thanks are also to be expressed to Assistant Professor Norihiko Nakanishi of Kyoto University for his advice for X-ray analysis and to Assistant Professor Saburo Kako of Kyoto Univeristy for his valuable cooperation for DTA measurement.

15) H. Remy, "Treatises on Inorganic Chemistry," Vol. II, Elsevier (1956), p. 31.
16) F. Sherwood Taylor, "Inorganic and Theoretical Chemistry," 9th edition, Heinemann (1952), p. 672.
17) B. Kubota, *J. Amer. Ceram. Soc.*, **44**, (5), 239 (1961).
18) E. G. Prout and F. C. Tompkins, *Trans. Faraday Soc.*, **40**, 488 (1944); *ibid.*, **42**, 468 (1946).

Thermal Decompsition of Ammonium Salts of Transition Metal Oxyacids. IV.[1] Determination of Constituents of Gases Evolved in Decomposition of Ammonium Chromate

Il-Hyun PARK*

Department of Chemistry, Faculty of Science, Kyoto University, Sakyo-ku, Kyoto

(Received February 1, 1971)

Constituents of gases evolved in thermal decomposition of ammonium chromate and ammonium dichromate have been studied by an omegatron mass spectrometer. From the data of gas analysis, the following conclusions have been obtained. The decomposition of the first step started with proton transfer mechanism and the ratio of NH_3 to H_2O was not 2: 1 at the beginning. The second step corresponded to the formation of N_2, N_2O, and H_2O through oxidation of NH_3 by the chromate anion. The decomposition in the third step was accompanied by the evolution of oxygen molecules. The production of CrO_3 was confirmed by comparing the dissociation pressure of CrO_3 produced in AC decomposition with that of pure CrO_3. The decomposition in the last step corresponded to the process from CrO_2 to Cr_2O_3, with the evolution of O_2, CO_2, and CO.

In the preceding work,[1] the thermograms of ammonium chromate (AC) and ammonium dichromate (ADC) were obtained, and the composition and structure of each intermediate were determined from the results of weight decrease data and X-ray analysis.

The evolved gases in the decomposition of AC have not yet been analyzed but only the gases evolved in ADC decomposition near 200°C have been studied by some investigators. For instance, Simpson *et al.*[2] have reported that N_2, N_2O, and H_2O were the main products in the range of temperature from 180 to 215°C. However, the gas constituents reported by other workers differed from those mentioned above. In this study the evolved gases in the thermal decomposition of AC and ADC by heating them from room temperature up to 500°C were analysed by an omegatron mass spectrometer, in the hope of better interpretation of the thermogram and better understanding of the mechanism of decomposition in each step.

Experimental

Apparatus and procedure for gas analysis were similar to those used in the previous work,[3] except the use of dry ice to remove the hydrocarbon vapor from the stopcock grease. The total pressure was measured by a Pirani gauge. Extra pure reagents of AC and ADC from Nakarai Chemical Co. were used without further purification. Samples used were both powder and crystal grain. The gas analysis was carried out in closed and in evacuating systems up to 500°C, with the intervals of 50°C. The gaseous products were identified by the omegatron, comparing the mass spectrum observed with the standard pattern obtained from pure gases. In addition to the patterns for N_2, H_2O, CO, and CO_2 described in the previous paper,[3] the pattern coefficients for N_2O and O_2 are shown in Table 1.

Table 1. Pattern coefficients of oxygen and nitrous oxide

Gas	Mass No.						
	14	15	16	28	30	32	44
O_2			10—15			100	
N_2O	6	2—3	3	30—45	25—30		100

The decomposition pressure of CrO_3 was measured by similar method to that of Kodera *et al.*[4] Samples of CrO_3 used were either CrO_3 sample prepared in the laboratory or commercially available CrO_3 (extra pure reagent of Nakarai Chemical Co.). The former was prepared by heating AC up to 240°C and keeping it for 20 hr at this temperature during annealing. Color of the product was dark brown. The temperature range of measurement was from 225 to 400°C, and the decomposition of CrO_3 to CrO_2 proceeded at this temperature range.

Results

The Gases Evolved in the Closed System and in Evacuating System. The decomposed gases from AC at room temperature were studied in a closed system. The gases were collected for one hour and used for mass spectrum determination. After the measurement, the system was evacuated again and the same procedure was repeated at the interval of one hour. Percentages of NH_3 and H_2O were determined, as shown in Table 2. Similarly the constituents of decomposed gases from

Table 2. Percent molar fractions of the decomposed gases at 25°C (AC)

Run	1	2	3
Total pressure (Torr)	8.4×10^{-2}	6.7×10^{-2}	8.5×10^{-2}
H_2O	15	25	28
NH_3	84	74	72

ADC at 200°C were studied in the closed system at the interval of 30 min. The percentages of NH_3, oxidation products of NH_3 and H_2O, were determined, as shown in Table 3. Percent molar fractions of the evolved gases in the decomposition of AC and ADC at various temperatures are plotted in Figs. 1 and 2,

* Present address: Department of Chemistry, College of Science & Engineering, Sung Kyun Kwan University, Seoul, Korea.

1) Part III: I. H. Park, This Bulletin, **45**, 2749 (1972).

2) J. Simpson, D. Taylor, and D. M. W. Anderson, *J. Chem. Soc.*, **1958**, 2378.

3) I. H. Park, This Bulletin, **45**, 2739 (1972).

4) K. Kodera, I. Kusunoki, and S. Schimidzu, This Bulletin, **41**, 1039 (1968).

respectively. Similar measurements were carried out in an evacuating system using both crystal grain and powder. Evacuating system was constructed by placing the reaction tube near omegatron. The results obtained for AC under various conditions are shown in Figs. 3(a) and 3(b).

Measurement of Dissociation Pressure of CrO_3. The mass spectra were observed at various temperatures, starting from 225°C, for the CrO_3 sample prepared in

Table 3. Percent molar fractions of the decomposed gases at 200°C (ADC)

Run	1	2	3	4	5
Total pressure (Torr)	2.9×10^{-1}	1.4×10^{-1}	1.2×10^{-1}	1.3×10^{-1}	9.5×10^{-2}
N_2O	35.3	38.3	51.2	62.7	59.0
N_2	53.6	54.1	33.3	33.7	12.0
H_2O	7.6	5.9	9.3	3.6	17.0
NH_3	3.5	1.8	—	—	—

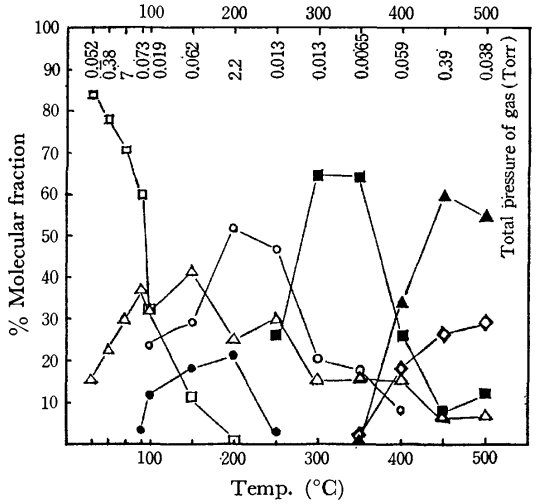

Fig. 1. Percent molecular fraction of the gases evolved by AC decomposition.
□ NH_3, △ H_2O, ● N_2, ○ N_2O, ■ CO_2, ◇ CO, ▲ O_2

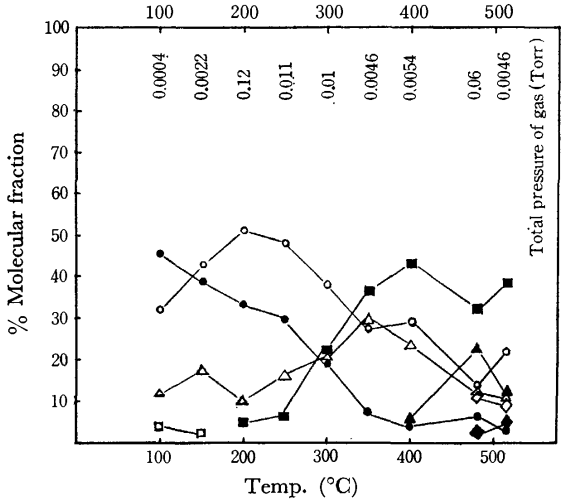

Fig. 2. Percent molecular fraction of the gases evolved by ADC decomposition.
□ NH_3, △ H_2O, ● N_2, ○ N_2O, ■ CO_2, ◇ CO, ▲ O_2, ◆ NO

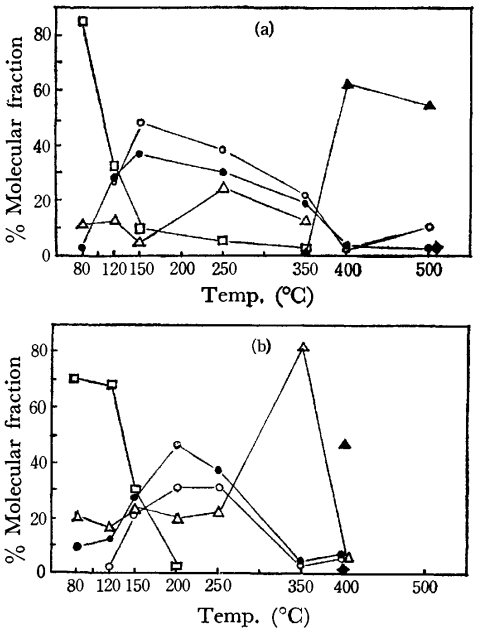

Fig. 3. Percent molecular fraction of the decomposed gases from AC in evacuating system.
(a) powder (b) whole crystal grain
□ NH_3, △ H_2O, ● N_2, ○ N_2O, ▲ O_2, ◆ NO

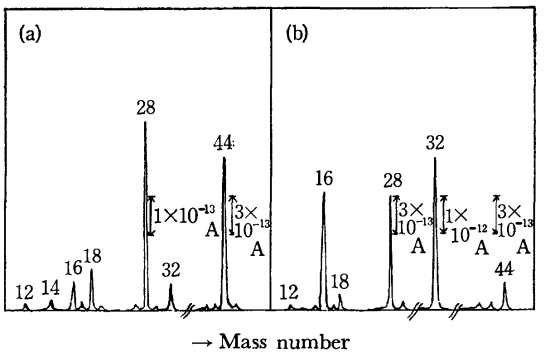

Fig. 4. Mass spectra of the gases which evolved from the prepared CrO_3.
(a): 300°C, $P_{total}=1.6\times10^{-7}$ Torr $P_{gas}=2.8\times10^{-3}$ Torr
(b): 375°C, $P_{total}=1.2\times10^{-6}$ Torr $P_{gas}=5.6\times10^{-2}$ Torr

Table 4. Total pressure and partial pressure of the gases evolved by pure CrO_3 decomposition

Temp., (°C)	Total press. at equil. (Torr)	$m/e=$ 44	$m/e=$ 32	$m/e=$ 28	Partial press. of O_2 (Torr)
325	1.6×10^{-3}	69.5	7.1	23.5	1.1×10^{-4}
350	1.6×10^{-3}	47.8	21.3	30.7	3.4×10^{-4}
375	3.0×10^{-3}	17.1	39.8	43.3	1.2×10^{-3}
400	8.5×10^{-3}	12.9	72.5	14.6	6.2×10^{-3}
425	1.4×10^{-2}	10.1	78.3	11.6	1.1×10^{-2}
450	1.9×10^{-2}	9.9	79.2	10.9	1.5×10^{-2}

the laboratory. Constituents of gas evolved were CO_2 with trace of nitrogen compounds. The mass spectrum of gas evolved at 300°C is shown in Fig. 4(a). The peak for $m/e=44$ is mainly due to CO_2^+ (95%) rather than N_2O^+ (5%). The peak for $m/e=28$ is assumed to be due to CO^+ or N_2^+, but from the pattern coefficient[3] it was decided that the peak is due to CO^+.

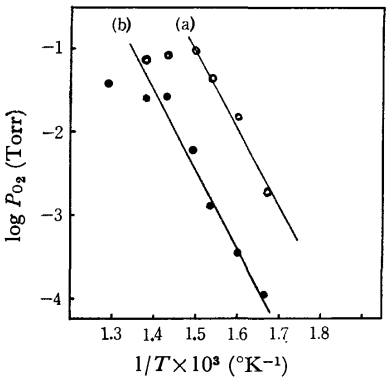

Fig. 5. Dissociation pressure of the prepared CrO_3 (a) and standard CrO_3 (b).

Oxygen is seen at $m/e=32$. The fact that CO_2 is formed is in agreement with the results of Kodera *et al.*[4] on the thermal decomposition of metal oxides *in vacuo*. Below 300°C, oxygen molecules produced might be consumed for the oxidation of nitrogen compounds or carbon impurities. The mass spectrum of gas evolved at 375°C is shown in Fig. 4(b). Main product is O_2 with some amounts of CO and a small amount of CO_2.

For comparison, similar experiments were carried out with the pure CrO_3[5] sample above 325°C. The results are shown in Table 4. The dissociation pressures of the prepared CrO_3 and pure CrO_3 were plotted against $1/T$ in Fig. 5.

Discussion

First Decomposition Step. From the results of thermogravimetric analysis,[1] it was supposed that AC was decomposed to ADC at the first step, two molecules of NH_3 and one molecule of H_2O being eliminated at this step. However, according to the gas analysis by omegatron, as seen in Fig. 1 and Table 2, the theoretical ratio 2: 1 ($=NH_3$: H_2O) in the gaseous phase does not appear until it is heated up to about 90°C, but this ratio is much larger than 2: 1 below 90°C. Namely, the evolution of NH_3 and H_2O does not take place in the form of $(NH_4)_2O$ as in the case of the decomposition of ammonium paramolybdate described in the previous paper,[3] where the ratio of NH_3 to H_2O was always 2: 1. Accordingly, it is considered that the elimination mechanisms of NH_3 and H_2O in the decomposition of ammonium chromate and ammonium paramolybdate differ with each other. Table 2 suggests that NH_3 is eliminated rapidly in the beginning whereas the amount of H_2O evolving gradually increases as the reaction proceeds. In other words, NH_3 is eliminated before H_2O is formed from the crystal in this step, and the following decomposition does not proceed: $2(NH_4)_2CrO_4 \longrightarrow (NH_4)_2Cr_2O_7+2NH_3+H_2O$.

5) This sample was sublimated at 200°C *in vacuo* and was condensed as dark red crystals at the upper part of the reaction cell, while CO_2 gas evolved. The dissociation pressure of CrO_3 at 650°C was 1.3×10^{-3} Torr and green Cr_2O_3 was condensed at the upper part of the reaction cell while the pressure decreases rapidly.

As described by Davies *et al.*[6] on the thermal decomposition of ammonium perchlorate, it is considered that only NH_3 is eliminated at the first step from the crystal by proton transfer mechanism. Thus, the mechanism may be expressed by

$$2(NH_4^+\text{-}CrO_4^{2-}) \rightleftharpoons 2(NH_3\text{-}H\text{-}CrO_4^-) \rightleftharpoons 2(NH_3\text{-}HCrO_4^-)$$
$$\quad\;\; | \qquad\qquad\quad | \qquad\qquad\quad |$$
$$\quad NH_4^+ \qquad\quad NH_4^+ \qquad\quad NH_4^+$$
$$\quad (I) \qquad\qquad (II) \qquad\qquad \Downarrow$$
$$2NH_3(g) \longleftarrow 2NH_3(a)+2NH_4^+HCrO_4^-$$
$$\qquad\qquad\qquad\qquad\qquad\quad \downarrow$$
$$H_2O(g) \longleftarrow H_2O(a)+(NH_4)_2Cr_2O_7$$
$$\qquad\qquad\qquad\qquad\qquad\quad \downarrow$$
$$(NH_4)_2Cr_2O_7,$$

where (a) and (g) indicate adsorbed and gaseous states, respectively.

The reaction begins with the transfer of a proton from NH_4^+ to CrO_4^-. After the proton transfer process is accomplished through a transition state (II), coulombic interaction between NH_3 and $H\text{-}CrO_4^-$ (NH^+) is lost, and NH_3 becomes free to migrate over the surface of the crystal as a mobile adsorbed phase. Then, NH_3(a) will be desorbed, followed by the desorption of H_2O(a). The total pressure showed 7 Torr at 70°C. Therefore the decomposition reaction of the first step takes place at this temperature, where the ratio of NH_3 to H_2O is approximately 2: 1.

Second Decomposition Step. It is seen from Fig. 1 that N_2 and N_2O begin to be evolved at 100°C and the fraction of NH_3 decreases rapidly with increasing temperature. Although the amount of H_2O is large at this temperature, it is less than that produced from oxidation of NH_3 into N_2 and N_2O. It is concluded from the total pressure measurements that the second decomposition step for AC begins at about 150°C. The total pressure increases greatly above this temperature, and amounts to 2.2 Torr at 200°C. At this temperature the evolved gases consist of about 52% N_2O, 21% N_2, 26% H_2O, and NH_3 of less than 1%. Nitrogen content decreases to about 3% at 250°C, while CO_2 begins to be evolved at this temperature. Amounts of CO_2 and N_2O were determined by comparing their pattern coefficients with the corresponding standard ones (Ref. 4 and Table 1). The production of CO_2 is considered to be due to the oxidation of carbon or carbon compounds as impurity in the sample.

The second step in AC decomposition corresponds to the first step for ADC. Many studies have been reported on the ADC decomposition at the temperature range of 180 to 230°C, but these results are not in agreement with each other. Simpson *et al.*[2] have reported that N_2, N_2O, and H_2O were evolved throughout the reaction but free ammonia (10%) was produced at the autocatalytic stage. In the present work, the evolution of NH_3 in the ADC decomposition at 200°C is observed in the beginning but the amount is very

6) J. V. Davies, P. W. M. Jacobs, and A. Russell-Jones, *Trans. Faraday Soc.*, **63**, 1737 (1967).

small as is shown in Table 3. The reason of the discrepancy may be explained by the difference of experimental condition: that is, Simpson used a single crystal as a starting material after evacuation at room temperature and temperature was raised rapidly to 195.5°C, while, in the present work, powdered sample was used and heating rate was rather slower than that adopted by Simpson. The evolution of NH_3 is small, as is shown in Fig. 2. Namely, most of NH_4^+ ions are oxidized from the beginning.

It was concluded from the thermal analysis that CrO_3 are produced by the decomposition of ADC. CrO_3 is a strong oxidizing agent and it is said that hydrogen itself, ammonia and hydrogen sulfide are oxidized by CrO_3.[7] Therefore, NH_3 produced in the crystal will be easily oxidized to form N_2 and N_2O, and consequently Cr(VI) is reduced to lower oxidation state. It is seen that nearly equal amounts of N_2 and N_2O are obtained in evacuating system when the powdered sample is used, as shown in Fig. 3(a), but the amount of N_2 exceeds slightly that of N_2O, when the crystal grain is used, as shown in Fig. 3(b), although the amounts of NH_3 in both cases are quite small as in the case of the closed system. This might be explained by the fact that most of NH_4^+ ions are oxidized as soon as the decomposition proceeds, and the amount of NH_3 which is oxidized after evolution is small. The formation of H_2O continues throughout the decomposition. This is in agreement with Simpson's results. It is expected that Cr(VI) ought to be reduced partly at this step because of the vigorous oxidation of NH_3. However, from the results of X-ray analysis[1] and the measurement of dissociation pressure of CrO_3, it is supported that the product formed in this decomposition step is mainly CrO_3.

Third Decomposition Step. The third step of the decomposition involves the formation of O_2 from the relatively unstable CrO_3. At the temperature near 250°C N_2O and H_2O are the main products and CO_2 is also found. Origin of N_2O and H_2O may be NH_3, NH_2, or N_2 remained in the crystal. The peak of oxygen does not appear at 300°C but appears at 350°C and the amount of CO_2 approaches to 64%. Accordingly the weight decrease at this decomposition step are related to the elimination of O_2, CO_2, H_2O, and N_2O. The evolution of oxygen begins after the production of CO_2 and N_2O are finished, as shown in Figs. 4(a) and 4(b). It seems that oxygen molecules produced by decomposition is consumed for the oxidation of nitrogen compounds and carbon impurities.

Fourth Decomposition Step. The constituents of gases evolved at 400°C are mainly O_2, CO_2, CO, H_2O, and the trace of N_2O. The decomposition takes place between 400 and 450°C as observed in the thermal analysis and the total pressure measurement. The gases evolved at 450°C are mainly O_2, CO, and CO_2 but N_2O is hardly seen. A small amount of NO was observed in this temperature range only when the decomposition was carried out in evacuating system.

Gases Evolved in ADC Decomposition. According to Fig. 2, it is seen that the total pressure at 100°C is very low and the amount of NH_3 is smaller than those of N_2 and N_2O. The first decomposition shows the maximum at about 200°C and the evolved gases are N_2 and N_2O. The formation of O_2 is observed at 400°C.

The author wishes to express his sincere thanks to Professor Kumasaburo Kodera of Kyoto University for his valuable advice and continuous encouragement throughout this work. He is also grateful to Assistant Professor Masaru Onchi of Kyoto University and Mr. Isao Kusunoki of Kyoto University for their helpful advice and discussion for omegatron measurement and to Mr. Tadasi Ito for the measurement by the omegatron.

7) P. C. L. Thorne and E. R. Roberts, "Inorganic Chemistry," (Ephraims), 6th edition, Oliver & Boyd (1954), p. 503.

Kinetics of Multidentate Ligand Substitution Reactions. XIII. Substitution Reactions of 1-(Hydroxy-4-methyl-2-phenylazo)-2-naphthol-4-sulfonic Acid (Calmagite) with Nickel(II)-Glutamate, -Aspartate, -Iminodiacetate, -Nitrilotriacetate and -Diethylenetriamine Complexes and That with the Cobalt(II)-Nitrilotriacetate Complex

Mutsuo KODAMA, Takami SATO, and Sadatsugu KARASAWA
Department of Chemistry, Ibaraki University, Bunkyo, Mito, Ibaraki
(Received January 27, 1972)

The substitution reactions of calmagite with nickel(II)-glutamate, -aspartate, -iminodiacetate, -nitrilotriacetate, and -diethylenetriamine complexes, and that with the cobalt(II)-nitrilotriacetate complex, were studied by employing the stopped-flow technique. In the calmagite reactions with the nickel(II)-glutamate, -aspartate, and -iminodiacetate complexes, the reaction products were found to be mixed-ligand complexes involving calmagite and glutamate, aspartate, or iminodiacetate anions. In these reactions, the 1:2 ratio complex dissociates rapidly into the 1:1 ratio complex first; then, the 1:1 ratio complex reacts slowly with the calmagite anion to form a mixed-ligand complex. From a comparison of the observed rate constant with that estimated on the basis of the proposed reaction intermediate, it was concluded that the latter step proceeds through the outer-sphere complex between the calmagite anion and a 1:1 ratio complex, and that the water-loss from the 1:1 ratio complex is the slowest step. In the cases of the reactions of calmagite with nickel(II)-nitrilotraicetate and -diethylenetriamine complexes, and that with the cobalt(II)-nitrilotriacetate complex, all the reaction invariably gave a metal(II)-calmagite complex with a 1:1 composition, MD^-. These reactions were found to proceed through the completely-deprotonated and divalent calmagite anions.

We have studied a series of substitution reactions of two *o,o'*-dihydroxyazo dyes, Eriochrome Black T (BT) and calmagite, with cobalt(II) and nickel(II)-aminopolycarboxylate complexes.[1,2] The reactions were invariably first-order in the metal(II)-aminopolycarboxylate complex, and gave a metal(II)-dye complex with a 1:1 composition, MD^-. In the present paper, the kinetics of the substitution reactions of calmagite with the nickel(II)-glutamate (Glut), -aspartate (Asp), -iminodiacetate (IDA), -nitrilotriacetate (NTA), and -diethylenetriamine (Dien) complexes, and that with the cobalt(II)-NTA complex, will be dealt with spectrophotometrically. From a comparison of the observed rate constant with that calculated on the basis of the reaction intermediate proposed, the detailed reaction mechanism and the structure of the reaction intermediate will also be discussed.

Experimental

Reagents. The preparation and the standardization of cobalt(II) and nickel(II) nitrate solutions were described in a previous paper.[3] Reagent-grade Glut, Asp, IDA, and NTA were recrystallized from their aqueous solutions by adding pure hydrochloric acid and ethanol. The Dien used in this study was purified by distilling it under reduced pressure. The calmagite was recrystallized from its ethanol solution by employing the Lindstrom-Isaac method.[4] The other reagents were of an analytical reagent grade and were used without further purification.

Apparatus and Experimental Procedures. All the absorption spectra were obtained with a Hitachi ESP-3 pen-recording spectrophotometer. For the measurement of the pH of the sample solution, a Hitachi-Horiba glass electrode pH meter F-5 was used. All the measurenmets were conducted in solutions of a constant ionic strength (0.30) ($NaClO_4$ or KNO_3). The reactions of calmagite with nickel(II)-IDA, -NTA, and -Dien complexes were followed spectrophotometrically at 620 mμ using a Hitachi ESP-3 pen-recording spectrophotometer. The kinetic investigation of the reactions of calmagite with nickel(II)-Glut and -Asp complexes and of that with the cobalt(II)-NTA complex were carried out by using a Hitachi Rapid Scanning Spectrophotometer RSP-2 with a stopped-flow mixing chamber. The experimental procedures were the same as those described previously.[3] In this study, no buffer reagent was used, because free Glut, Asp, IDA, NTA, and Dien have enough buffer capacity to maintain the pH values of sample solutions constant over the entire pH range covered. All the exchange reactions were studied in solutions containing large excesses of complexed and uncomplexed Glut, Asp, IDA, NTA, or Dien over calmagite. Therefore, all the exchange reactions could be treated as pseudo-first-order reactions. Thus, the apparent rate constant of the pseudo-first-order reaction, Kap^+, was obtained from the slope of the linear relation between $\log(A_0-A\infty)/(A-A\infty)$ and the time, t.[3] Here, A_0, A, and $A\infty$ indicate the absorbances of solutions at time $=0$, t, and ∞ respectively.

Results and Discussion

Equilibrium Study. In the cases of nickel(II)-glutamate, -aspartate and -iminodiacetate complexes, the absorbances of the equilibrium mixtures with calmagite were found to increase with an increase in the concentration of uncomplexed glutamate, aspartate or iminodiacetate. In considering that the calmagite anion and the aminopolycarboxylate anions used in this study can act as tridentate ligand in the complex-

1) M. Kodama, C. Sasaki, and T. Noda, This Bulletin, **41**, 2033 (1968).
2) M. Kodama, *Nippon Kagaku Zasshi*, **91**, 134 (1970).
3) a) M. Kodama, This Bulletin, **40**, 2575 (1967). b) M. Kodama, C. Sasaki, and M. Murata, *ibid.*, **41**, 1333 (1968).
4) F. Lindstrom and R. Isaac, *Talanta*, **13**, 1003 (1966).

formation reaction with the nickel(II) ion, this finiding suggests the possibility of the formation of a mixed-ligand calmagite complex involving the aminopolycarboxylate anion. From the thermodynamic point of view,[5] one can derive Eq. (2) for the following mixed-ligand-complex-formation equilibrium:

$$NiD^- + X^{2-} \overset{K^X_{NiD}}{\rightleftarrows} NiDX^{3-}$$

$$\log \frac{A-A_{NiD}}{A_{NiDX}-A} = \log \frac{K^X_{NiD}}{(\alpha_H)_X} + \log [X]_f \qquad (2)$$

where NiD^-, X^{2-}, and $NiDX^{3-}$ denote the nickel(II)-calmagite complex, the aminopolycarboxylate anion, and the mixed-ligand complex of the nickel(II) ion respectively, where $(\alpha_H)_X$ is the (α_H) value of aminopolycarboxylate, and where $[X]_f$ is the concentration of uncomplexed aminopolycarboxylate, where A_{NiD} is the absorbance of the solution in which all the nickel(II) complex ions are in the form of NiD^-, where A_{NiDX} is that of the solution in which all the nickel(II) complex ions exist in the form of $NiDX^{3-}$, and where A is that of the solution in which NiD^- and $NiDX^{3-}$ coexist. This relation was examined by using some typical experimental data. Typical results obtained for glutamate and aspartate systems are reproduced in Fig. 1. From the $\log [X]_f$ values at $\log (A-A_{NiD})/(A_{NiDX}-A)=0$, the $\log K^X_{NiD}$ values were determined to be 2.8_0 and 3.5_0 for the glutamate and aspartate systems respectively. In a similar way, the K^X_{NiD} value for the IDA system was determined to 4.3_0.

On the other hand, in the cases of the nickel(II)-NTA and Dien systems and of the cobalt(II)-NTA system, the concentrations of uncomplexed NTA and Dien had no effect on the absorption curve of the metal-(II)-calmagite complex, disproving the formation of a mixed-ligand complex involving the NTA anion or Dien.

Kinetic Study. In the kinetic study, although the results will not be shown here, the following facts were found in preliminary experiments:

i) In solutions of a given pH, a given concentration of a metal(II) complex of Glut, Asp, IDA, NTA, or Dien, and a given initial concentration of calmagite, k^+_{ap} is inversely proportional to the concentration of uncomplexed Glut, Asp, IDA, NTA, or Dien.

ii) In solutions of a given pH, a given concentration of uncomplexed Glut, Asp, IDA, NTA, or Dien, and a given initial concentration of calmagite, k^+_{ap} is exactly proportional to the total concentration of a metal(II)-Glut, -Asp, -IDA, -NTA, or -Dien complex.

iii) In solutions of a given pH and given concentrations of uncomplexed and complexed Glut, Asp, IDA, NTA, or Dien, k^+_{ap} is independent of the initial concentration of calmagite.

iv) As is shown in Figs. 2 and 3, in solutions of a given initial concentration of calmagite, and given concentrations of a free Glut, Asp, IDA, NTA, or Dien and its metal(II) complex, k^+_{ap} multiplied by $K_2\cdot[X]_f\cdot(\alpha_H)_D/(\alpha_H)_X$ is a linear function of the concentration of the hydrogen ion and is given by:

$$\frac{k^+_{ap}\cdot K_2[X]_f\cdot(\alpha_H)_D}{(\alpha_H)_X} = k_\alpha + k_\beta\cdot[H^+] \qquad (3)$$

where K_2 and $(\alpha_H)_D$ are the second successive formation constant of a metal(II)-Asp, -Glut, -IDA, -NTA, or -Dien complex and the (α_H) value of calmagite respec-

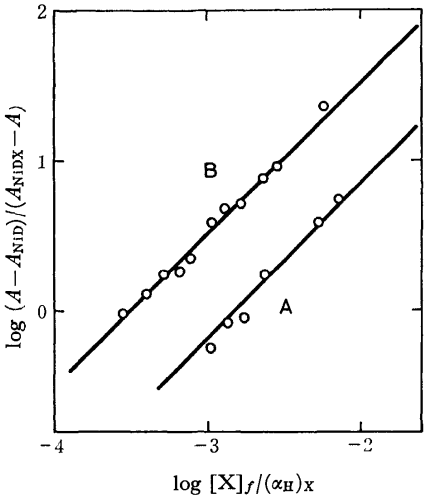

Fig. 1. The plot of $\log (A-A_{NiD})/(A_{NiDX}-A)$ against $\log [X]_f/(\alpha_H)_X$
The concentration of nickel(II) ion=4.0 mM
The concentration of calmagite=4.0×10^{-5} M
20°C, μ=0.30
A) Glutamate system
The concentration of glutamate ranged from 4.0 to 40.0 mM
pH ranged from 9.70 to 9.86
B) Aspartate system
The concentration of aspartate ranged from 8.0 to 30.0 mM
pH ranged from 9.76 to 9.92

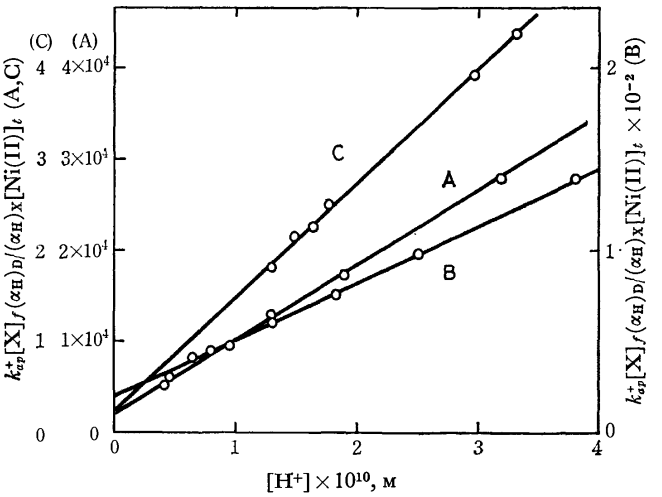

Fig. 2. The plot of $k^+_{ap}[X]_f(\alpha_H)_D/(\alpha_H)_X[Ni(II)]_t$ against the hydrogen ion concentration
The concentration of calmagite=4.0×10^{-5} M
μ=0.30, 20°C
A) Glutamate system
The concentration of nickel(II) ion=80.0 mM
The concentration of uncomplexed Glut=6.0 mM
B) Aspartate system
The concentration of nickel(II) ion=8.0 mM
The concentration of uncomplexed Asp=32 mM
C) Iminodiacetate system
The concentration of nickel(II) ion=8.0 mM
The concentration of uncomplexed IDA=6.0 mM

5) M. Kodama and K. Miyamoto, This Bulletin, **42**, 1596 (1969).

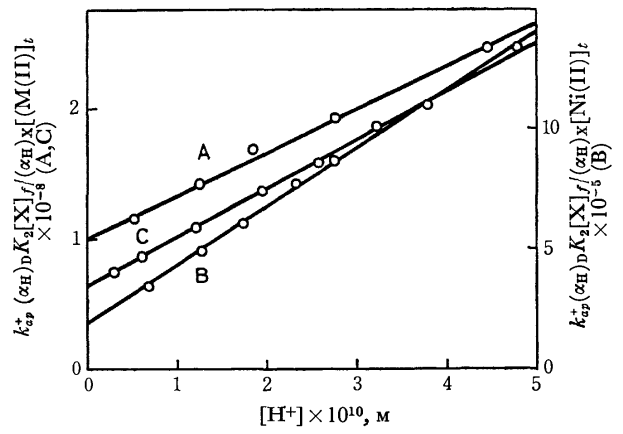

Fig. 3. The plot of $k_{ap}^{+}K_2\ [X]_f(\alpha_H)_D/(\alpha_H)_X\ [M(II)]_t$ against the hydrogen ion concentration
μ=0.30, 25°C
The concentration of calmagite=3.78×10^{-5} M
A) Ni(II)-Dien system
The concentration of nickel(II) ion=5.0 mM
The concentration of uncomplexed Dien=30.0 mM
B) Ni(II)-NTA system
The concentration of nickel(II) ion=5.0 mM
The concentration of uncomplexed NTA=30.0 mM
C) Co(II)-NTA system
The concentration of coblat(II) ion=2.0 mM
The concentration of uncomplexed NTA=40.0 mM

tively. In considering that, under the present experimental conditions, all the metal(II) ions are considered to exist in the form of MX_2^{2-2m}, the above experimental findings suggest that all the substitution reactions are first-order with respect to the concentration of a metal(II)-Glut, -Asp, -IDA, -NTA, or -Dien complex with a 1:1 composition, and first-order with respect to the concentration of calmagite, and also that the reactions invariably proceed through the completely-deprotonated and divalent calmagite anions, D^{3-} and HD^{2-}. The K_{NID}^{X} values obtained show that the reaction products in the substitution reactions of calmagite with the nickel(II)-Glut, -Asp, and -IDA complexes under the present experimental conditions are given by $NiDX^{3-}$. Therefore, the reaction mechanism for the exchange reactions of calmagite with nickel(II)-Glut, -Asp, and -IDA complexes can be depicted as:

$$NiX_2^{2-} \rightleftharpoons NiX^0 + X^{2-} \quad \text{in a rapid equilibrium}$$

$$NiX^0 + \begin{cases} HD^{2-} \overset{k_{HD}}{\rightleftharpoons} NiDX^{3-} + H^+ \\ D^{3-} \overset{k_D}{\rightleftharpoons} NiDX^{3-} \end{cases} \quad \text{r.d.s. I}$$

For the above reaction, Eq. (3) can be rewritten as:

$$k_{ap}^{+} = 2.303\times\text{log-plot slope} = \frac{[Ni(II)]_t}{(1+K_2'\cdot[X]_f)\cdot(\alpha_H)_D}\left(k_D+\frac{k_{HD}\cdot[H^+]}{K_3^D}\right) \quad (4)$$

From the slopes and intercepts of the straight lines in Fig. 2, the k_{HD} and k_D values for the substitution reactions of calmagite with the nickel(II)-Glut, -Asp, and -IDA complexes were determined; they are listed in Table 1. On the other hand, in the cases of the exchange reactions of calmagite with the nickel(II)-NTA and -Dien complexes, and that with the cobalt(II)-NTA complex, in connection with the experimental facts given above, it can be concluded that the reaction mechanism for these reactions can be formulated as:

$$MX_2^{2-2m} \rightleftharpoons MX^{2-m} + X^{m-} \quad \text{in a rapid equilibrium}$$

$$MX^{2-m} + \begin{cases} HD^{2-} \overset{k_{HD}}{\rightleftharpoons} MD^- + HX^{1-m} \\ D^{3-} \overset{k_D}{\rightleftharpoons} MD^- + X^{m-} \end{cases} \quad \text{r.d.s. II}$$

where X^{m-} means the tervalent NTA anion or completely-deprotonated Dien.

As in the cases of the nickel(II)-Glut, -Asp, and -IDA systems, the k_{HD} and k_D values for these reactions were determined from the slopes and intercepts of the straight lines in Fig. 3. The k_{HD} and k_D values determined are also listed in Table 1.

Table 1. Rate constants (μ=0.30, 25°C)

System	Rate constants, $M^{-1}\,sec^{-1}$	
	k_D	k_{HD}
Ni(II)-glutamate	4.9×10^7	$1.5_8\times10^6$
Ni(II)-aspartate	3.5×10^6	$4.0_5\times10^5$
Ni(II)-iminodiacetate	4.8×10^5	$1.5_2\times10^4$
Ni(II)-nitrilotriacetate	2.5×10^5	$1.6_7\times10^3$
Ni(II)-diethylenetriamine	9.8×10^7	$2.5_0\times10^5$
Co(II)-nitrilotriacetate	6.5×10^5	$2.6_4\times10^5$

We can propose the common water-loss mechanism for the substitution reactions of calmagite with nickel(II)-Glut, -Asp, and -IDA complexes. A nickel(II)-Glut, -Asp, or -IDA complex with a 1:2 composition diffuses first and dissociates rapidly to form an outer-sphere complex with the calmagite anion. Then, a coordinated water molecule dissociates from the nickel(II) complex, NiX^0, and a donor group of the calmagite anion coordinates with the nickel(II) ion at the vacated coordination site. In the above reaction mechanism, the water loss from the nickel(II) complex, NiX^0, is considered to be the rate-determining step. In the above water-loss mechanism, if, in the nickel(II)-Glut, -Asp, and -IDA complex segments of the outer-sphere complexes, the Glut, Asp, and IDA anions are bonded to the nickel(II) ion through two oxygen and one nitrogen atoms, all the rate constants (k_D or k_{HD} values) should be identical, because the difference in the electrostatic and steric effects among these three systems are considered to be negligible. On the other hand, if the outer-sphere complexes have the structure shown by I or II in Fig. 4, the rate constants, k_D and k_{HD},

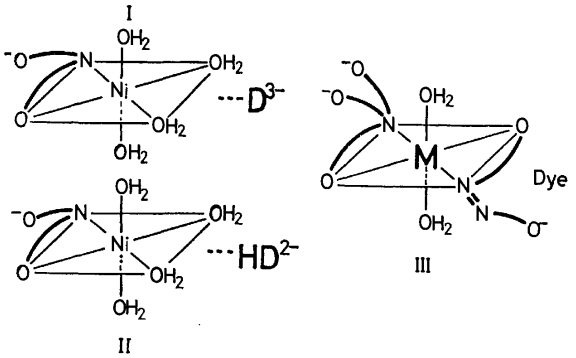

Fig. 4. Reaction intermediates

must be given by Eq. (5):

$$k^{6)} = k^{-H_2O}\frac{K_{Ni-gly}\cdot K_{as}\cdot K_{ele}\cdot K_{st}}{K_{NiX}} \quad (5)$$

where k^{-H_2O} is the rate constant of water-loss from the nickel(II) ion; K_{as}, the association constant of the outer-sphere complex, and K_{Ni-gly}, the stability constant of the nickel(II)-glycinate segment, and where K_{ele} and K_{st} are the electrostatic contribution to the stability of the reaction intermediate and the statistical factor respectively. This relation was examined experimentally. The k_D and k_{HD} values for the glutamate system were calculated to be 1.1×10^7 and $1.1\times10^6 M^{-1}sec^{-1}$ respectively by using $k^{-H_2O}=10^{5.30}$,[7] $K_{Ni-gly}=10^{4.71}$,[8] $K_{as}=10^{1.7}$ or $10^{0.7}$,[9] $K_{ele}=10^{0.5}$, and $K_{st}=1.0$. In consideration of the assumption made in the above calculation, the agreement between the calculated and observed rate constants can be regarded as satisfactory. Equation (5) also shows that k_D and k_{HD} values should be proportioanl to the reciprocal of the stability constant, K_{MX}^{-1}. In Table 2, the relative rate constants and the ratio of K_{MX} are compared. The K_{MX} values used in the estimation of the K_{MX}^{-1} ratio were calculated from the related stability constants in a solution with an ionic strength of 0.10 by using the activity coefficients calculated by means of the Davies equation.[10] Generally, the stability constants reported in the literature are of widely varying accuracy, differing from each other by several tenths of log K units. Considering this, and also the assumption made in the calculation of the activity coefficients, it can be said that the observed ratio agrees, at least semi-quantitatively, with the K_{MX}^{-1} ratio. These findings lend strong support to the above water-loss mechanism proposed for the substitution reactions of the nickel(II)-Glut, -Asp, and -IDA complexes with calmagite.

In the substitution reactions of calmagite with the nickel(II)-NTA and -Dien complexes, and that with the cobalt(II)-NTA complex, the fact that the rate constants are larger than the corresponding dissociation constants can be explained by assuming a reaction mechanism where the reaction proceeds through a mixed-ligand reaction intermediate involving leaving and attacking groups. Here, the dissociation of the leaving group from the reaction intermediate is the rate-determining step. As was discussed in connection with the substituion reaction of diethylenetriaminepentaacetic acid (DTPA) with the nickel(II)-NTA complex in the presence of ethylenediamine,[11] when the calmagite segments in the reaction intermediates of nickel(II)-NTA and -Dien complexes have the same structures, and when the leaving NTA anion and Dien are bonded to the nickel(II) ion through glycinate and ethylenediamine chelate rings respectively, the rate-constant ratio between the nickel(II)-NTA and -Dien complex systems should be 2.2×10^2. As is clear from the data in Table 1, the observed k_D and k_{HD} ratios are 3.9×10^2 and 1.5×10^2 respectively. The agreement between observed and calculated ratios can thus be regarded as satisfactory. Furthermore, if the calmagite reactions of both nickel(II)- and cobalt(II)-NTA complexes have as the reaction intermediate, (III), the rate constant ratio, k_{Co}/k_{Ni}, between the cobalt(II) and Nickel(II) systems should be given by:

$$\frac{k_{Co}}{k_{Ni}} = \frac{k_{Co}^{-gly}}{k_{Ni}^{-gly}}\times\frac{K_{Co-gly}}{K_{Ni-gly}}\times\frac{K_{NiX}}{K_{CoX}}\times\frac{K_{Co-D}}{K_{Ni-D}} \quad (6)$$

where k_M^{-gly}, K_{M-gly}, K_{M-D}, and K_{MX} are the dissociation rate constant of the metal(II)-glycinate complex of a 1:1 ratio, the stability constant of the metal(II)-glycinate complex, the stability constant of the metal(II)-calmagite segment, and the stability constant of the 1:1 ratio metal(II)-NTA complex respectively. From the above relation, the k_{Co}/k_{Ni} value was calculated to be 1.0×10^2, by using the $k_{Co}^{-gly}/k_{Ni}^{-gly}$ value reported by Hammes and Steinfeld[12] and the reported K values ($\mu=0.30$).[13] Here, the cobalt(II)- and nickel(II)-4-(*p*-arsonaphenylazo)-3-hydroxynaphthalene-2,7-disulfonic acid complexes were used as models of the metal(II)-calmagite segments of the mixed-ligand reaction intermediates.[13] The rate constant ratios for the k_D and k_{HD} were 2.5×10^2 and 1.6×10^2 respectively. The calculated ratio is in good agreement with the observed ratio. This agreement also supports the present authors' explanation that the calmagite reactions of cobalt(II)- and nickel(II)-NTA complexes proceed through the reaction intermediate III.

TABLE 2. RATE CONSTANT RATIOS

System	Rate constant ratio		K_{MX}^{-1} ratio
	k_D	k_{HD}	
Ni(II)-glutamate	1.04×10^2	1.04×10^2	5.9×10^2
Ni(II)-aspartate	7.3	26.6	14.1
Ni(II)-iminodiacetate	1.0	1.0	1.0

6) D. B. Rorabacher and D. W. Margerum, *Inorg. Chem.*, **3**, 382 (1964).
7) D. W. Margerum and H. M. Rosen, *J. Amer. Chem. Soc.*, **89**, 1088 (1967).
8) The nickel(II)-*N*-ethylglycinate complex was used as a model.
9) F. Basolo and R. G. Pearson, "Mechanisms of Inorganic Reactions," 2nd Ed., John Wiley and Sons (1967), p. 37.
10) J. N. Butler, "Ionic Equilibrium," Addison-Wesley Publishing Co., Reading, Massachusetts (1964), p. 437.
11) M. Kodama, S. Karasawa, and T. Watanabe, This Bulletin, **44**, 1815 (1971).
12) G. G. Hammes and J. I. Steinfeld, *J. Amer. Chem. Soc.*, **84**, 4639 (1962).
13) L. G. Sillen and A. E. Martell, "Stability Constants of Metal-Ion Complexes," 2nd Ed., The Chemical Society, London (1964).

Kinetics of Multidentate Ligand Substitution Reactions. XIV. Substitution Reactions of Ethylenediaminetetraacetic Acid (EDTA) and *N*-(2-Hydroxyethyl)ethylenediamine-*N*,*N*′,*N*′-triacetic Acid (EDTA-OH) with Nickel(II)-Ethylenediaminemonoacetate (EDMA) and -Diethylenetriamine (Dien) Complexes

Mutsuo KODAMA, Michinori HASHIMOTO, and Toshiyuki WATANABE
Department of Chemistry, Ibaraki University, Bunkyo, Mito, Ibaraki

(Received January 27, 1972)

The kinetics of the substitution reactions of EDTA and EDTA-OH with nickel(II)-EDMA and -Dien complexes were studied using the polarographic technique. The substitution reactions of EDTA and EDTA-OH with the nickel(II)-EDMA complex were found to have a common reaction mechanism. They were first-order with respect to EDTA or EDTA-OH, and also first-order with respect to the nickel(II)-EDMA complex with a 1:1 composition; their reaction mechanism could be formulated as:

$$NiX_2^0 \rightleftharpoons NiX^+ + X^- \quad \text{in a rapid equilibrium}$$

$$NiX^+ + \begin{cases} HY^{1-m} \overset{k_{HY}}{\rightleftharpoons} NiY^{2-m} + HX^0 \\ Y^{m-} \overset{k_Y}{\rightleftharpoons} NiY^{2-m} + X^- \end{cases} \quad \text{r.d.s.}$$

The substitution reactions of EDTA and EDTA-OH with the nickel(II)-Dien complex were also studied under experimental conditions where the reaction could be treated as a pseudo-first-order reaction. The reactions were first-order with respect to the concentration of EDTA or EDTA-OH. However, their reaction rate were independent of the concentrations of the nickel(II)-Dien complex and of uncomplexed Dien. This fact was ascribed to the formation of a stable outer-sphere complex between the nickel(II)-Dien complex with a 1:2 ratio and the EDTA or EDTA-OH anion, through which the substitution reaction proceeds.

Previous papers in this series[1-3] have dealt with substitution reactions involving nickel(II)-iminodiacetate (IDA), aspartate (Asp), -ethylenediaminemonoacetate (EDMA), and -nitrilotriacetate (NTA) complexes. Those reactions have been shown to proceed invariably through a nickel(II) complex of a 1:1 composition, a complex which is in a rapid equilibrium with a 1:2 ratio complex. The substitution reactions of the nickel(II)-EDMA complex with EDTA and EDTA-OH were also found to proceed with the 1:1 ratio nickel(II)-EDMA complex. However, in sharp contrast, the substitution reactions of the nickel(II)-diethylenetriamine (Dien) complex with EDTA and EDTA-OH are zero-order in concentrations of complexed and uncomplexed Dien. In this paper, the substitution reactions of nickel(II)-EDMA and Dien complexes with EDTA and EDTA-OH will be dealt with by employing the polarographic method. The reaction mechanism and the structure of the reaction intermediate also will be discussed in detail.

Experimental

Reagents. The ways of preparing EDMA dihydrochloride and of its purification were described previously.[4] The Dien used in this study was purified twice by distilling it under reduced pressure. The EDTA and EDTA-OH were recrystallized from their aqueous solutions by adding pure HCl and ethanol. The preparation of standard nickel(II) nitrate solution was also described previously.[5] The other reagents were of an analytical-reagent grade and were used without further purification.

Apparatus and Experimental Procedures. The apparatus and the experimental procedures were the same as those described previously.[3] In this study, all the measurements were conducted in solutions of an ionic strength of 0.30 ($NaClO_4$ for the EDMA system, KNO_3 for the Dien system). In the kinetic study of the substitution reaction of the nickel(II)-EDMA complex, no buffer reagent was used, because the free EDMA has enough buffer capacity to maintain the pH values of the solutions constant. In the substitution reactions of the nickel(II)-Dien complex, however, a phosphate buffer mixture was used over the entire pH range convered. All the sample solutions contained large excesses of complexed and uncomplexed Dien over EDTA or EDTA-OH. Therefore, all reactions could be treated as pseudo-first-order reactions.

Results and Discussion

Substitution Reactions of the Nickel(II)-EDMA Complex with EDTA or EDTA-OH. As in the case of the substitution reaction of the nickel(II)-EDMA complex with diethylenetriaminepentaacetic acid (DTPA),[2] provided that the other experimental conditions are kept constant, the apparent pseudo-first-order rate constants, k_{ap}^+s, as determined from the slope of the linear log (i_0/i_t) *vs.* t plot, were i) inversely proportional to the concentration of uncomplexed EDMA, ii) exactly proportional to the total concentration of the nickel(II) ion, and iii) independent of the initial concentration of EDTA or EDTA-OH. Furthermore, the k_{ap}^+ value

1) M. Kodama and T. Ueda, This Bulletin, **43**, 419 (1970).
2) M. Kodama, Y. Fujii, and T. Ueda, *ibid.*, **43**, 2085 (1970),
3) M. Kodama, *ibid.*, **42**, 2532 (1969).
4) Y. Fujii, E. Kyuno, and R. Tsuchiya, *ibid.*, **43**, 786 (1970).
5) M. Kodama, S. Karasawa, and T. Watanabe, *ibid.*, **44**, 1815 (1971).

multiplied by $K_2\cdot[X]_f\cdot(\alpha_H)_X/[Ni(II)]_t\cdot(\alpha_H)_Y$ was found to be a linear function of the hydrogen-ion concentration and to be given by Eq. (1) (Fig. 1):

$$k_{ap}^{+}\times\frac{K_2\cdot[X]_f\cdot(\alpha_H)_Y}{(\alpha_H)_X\cdot[Ni(II)]_t}=k_\alpha+k_\beta[H^+] \qquad (1)$$

where K_2 is the second successive formation constant of the nickel(II)-EDMA complex; $[X]_f$, the concentration of uncomplexed EDMA; $(\alpha_H)_Y$, the (α_H) value of EDTA or EDTA-OH, and $(\alpha_H)_X$, the (α_H) value of EDMA. As was discussed in connection with the substitution reaction of the nickel(II)-EDMA complex with DTPA,[2] these facts clearly indicate that the substitution reactions of the nickel(II)-EDMA complex with EDTA and EDTA-OH can be depicted as:

$$NiX_2^0 \rightleftharpoons NiX^+ + X^- \quad \text{in a rapid equilibrium}$$

$$NiX^+ + \begin{cases} HY^{1-m} \overset{k_{HY}}{\rightleftharpoons} NiY^{2-m} + HX^0 \\ Y^{m-} \overset{k_Y}{\rightleftharpoons} NiY^{2-m} + X^- \end{cases} \quad \text{r.d.s. I}$$

where Y^{m-} and X^- are completely-deprotonated EDTA or EDTA-OH and EDMA anions respectively. On the basis of the above reaction mechanism, k_{ap}^{+} can be written as:

$$k_{ap}^{+}=\frac{[Ni(II)]_t}{(1+K_2'\cdot[X]_f)\cdot(\alpha_H)_Y}\times\left(k_Y+k_{HY}\cdot\frac{[H^+]}{K_n}\right) \qquad (2)$$

where $[Ni(II)]_t$ and K_n denote the total concentration of the nickel(II) ion and the fourth dissociation constant of EDTA or the third dissociation constant of EDTA-OH respectively. The fact that, in the substitution reaction of EDTA-OH with the nickel(II)-EDMA complex, the $k_{ap}^{+}\cdot K'_2\cdot[X]_f\cdot(\alpha_H)_Y/[Ni(II)]_t$ value is almost constant under the present experimental conditions implies that the reaction proceeds only through its tervalent anion. From the slopes and intercepts of straight lines in Fig. 1, the k_{HY} and k_Y values were determined; they are listed in Table 1. The chloride ion was found to have no effect on the reaction.

Substitution Reactions of the Nickel(II)-Dien Complex with EDTA and EDTA-OH. The substitution reaction of the nickel(II)-Dien complex with EDTA was studied in the pH range from 7.10 to 9.00. At pH's lower than 8.00, a phosphate buffer mixture was used to keep the solution pH constant. However, it had no effect on the rate of the substitution reaction. As in the case of the substitution reaction of the EDMA complex, the k_{ap}^{+} value was independent of the initial concentration of EDTA or EDTA-OH. However, in striking contrast to the findings observed in the substitution reaction of the nickel(II)-EDMA complex, the k_{ap}^{+} value was independent of the concentrations of uncomplexed Dien and of the nickle(II) ions. Considering that, under the present experimental conditions, all the nickel(II) ions exist in the form of NiX_2^{2+},[2] the above findings clearly suggest that the EDTA and EDTA-OH anions form a stable outer-sphere complex with NiX_2^{2+}, only through which the reactions proceed. Furthermore, the k_{ap}^{+} value multiplied by $(\alpha_H)_Y$ was found to be a linear function of the hydrogen-ion concentration, corresponding to the following relation:

$$k_{ap}^{+}\cdot(\alpha_H)_Y=\text{constant}\times[H^+] \qquad (3)$$

Some typical results were reproduced in Fig. 2. From these experimental facts, we can conclude that the EDTA and EDTA-OH reactions with the nickel(II)-Dien complex under the present experimental conditions have the following reaction mechanism, IIa:

Table 1. Rate constants (μ=0.30,25°C)

System	k_Y, $M^{-1}\,sec^{-1}$	k_{HY}, $M^{-1}\,sec^{-1}$
EDTA—Ni(II)-EDMA	1.5×10^3	$3.9_0\times10^2$
EDTA-OH—Ni(II)-EDMA	2.8×10^2	—
EDTA—Ni(II)-Dien	—	$5.2_5\times10^{-2}$
EDTA-OH—Ni(II)-Dien	—	$1.1_8\times10^{-1}$

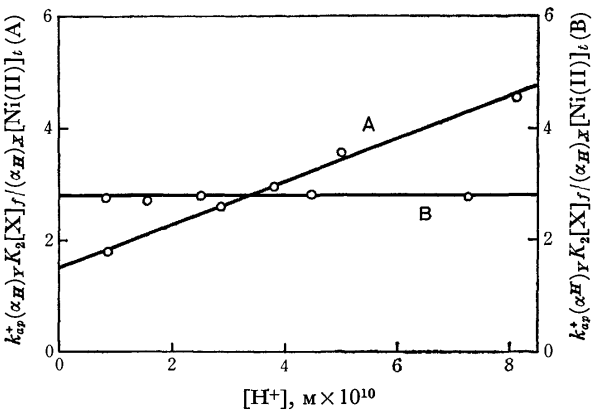

Fig. 1. The plot of $k_{ap}^{+}K_2[X]_f(\alpha_H)_Y/[Ni(II)]_t(\alpha_H)_X$ against the concentration of hydrogen ion.
Total concentration of nickel(II)-ion=10.0 mM
Initial concentration of EDTA or EDTA-OH=0.52 mM
μ=0.30, 25°C
A: EDTA system, $[X]_f$=20.0 mM
B: EDTA-OH system, $[X]_f$=15.0 mM

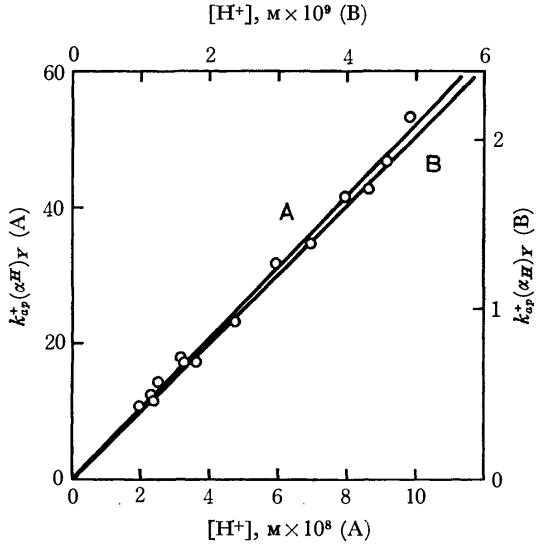

Fig. 2. The plot of k_{ap}^{+} $(\alpha_H)_Y$ against the concentration of hydrogen ion.
Total concentration of nickel(II)-ion=6.0 mM
Initial concentration of EDTA or EDTA-OH=0.52 mM
The concentration of uncomplexed Dien=18.0 mM
μ=0.30, 25°C
A: EDTA system B: EDTA-OH system

$$NiX_2^{2+} + HY^{1-m} \overset{K_{as}}{\rightleftharpoons} NiX_2^{2+} \cdots HY^{1-m} \quad \text{rapid}$$

$$NiX_2^{2+} \cdots HY^{1-m} \overset{k_{HY}}{\rightleftharpoons} NiY^{2-m} + HX^{+} + X^{0} \quad \text{r.d.s. IIa}$$

For the above reaction mechanism, if the formation of the outer-sphere complex, $NiX_2^{2+}\cdots HY^{1-m}$, is complete, k_{ap}^{+} can be written as:

$$k_{ap}^{+} = \frac{1}{(\alpha_H)_Y} \times \frac{k_{HY}\cdot[H^+]}{K_n} \qquad (4)$$

Therefore, from the slope of the linear relations in Fig. 2, the k_{HY} values for the EDTA and EDTA-OH reactions were determined. These values are also listed in Table 1.

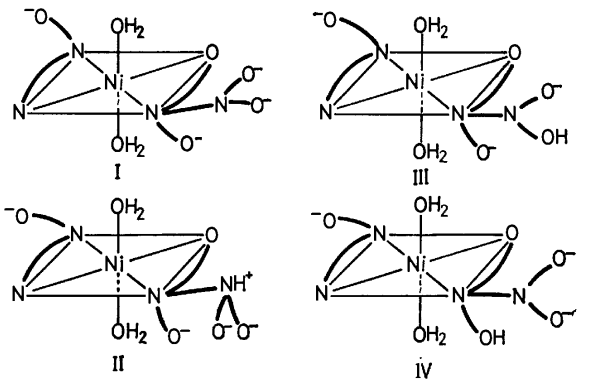

Fig. 3. Reaction intermediates.

As in the case of the substitution reaction of the nickel(II)-EDMA complex with DTPA, if the reaction of the nickel(II)-EDMA complex with EDTA proceeds through the two reaction intermediates (I and II) in Fig. 3, and if the dissociation of the EDMA anion from them is the rate-determining step, on the basis of these reaction intermediates the k_Y and k_{HY} values can be calculated from the $k_c = k_{Ni}^{en} K_{Ni-en} K_{Ni-gly}/K_{NiX}$ relation.[6] Here, k_{Ni}^{en} is the rate constant of the dissociation of the nickel(II)-ethylenediamine complex; K_{Ni-en}, the stability constant of the 1 : 1 nickel(II)-ethylenediamine complex; K_{Ni-gly}, the stability constant of the 1 : 1 nickel(II)-glycinate complex, and K_{NiX}, the stability constant of the 1 : 1 nickel(II)-EDMA complex. The calculated k_Y and k_{HY} values were 1.0×10^3 and 6.4×10^2 respectively. Of course, the electrostatic contribution to the stability of the reaction intermediate and the statistical factor were also taken into account. The nickel(II)-*N*-ethylglycinate complex was used as a glycinate model. The agreement of the observed k_Y and k_{HY} values with the calculated ones can be regarded as satisfactory. The rate constants calculated on the basis of every reaction intermediate other than I and II showed no good agreement with the observed values. Similarly, one of the following two reaction intermediates (III and IV in Fig. 3) would be possible for the substitution reaction of EDTA-OH with the nickel(II)-EDMA complex. The k_{HY} values calculated on the basis of III and IV were 1.6×10^2 and $8.1\times10\,M^{-1}sec^{-1}$ respectively. The former value agreed well with the observed value; this supports the reaction intermediate III.

In the substitution reactions of the nickel(II)-Dien complex, we previously assumed the formation of an outer-sphere complex between NiX_2^{2+} and HY^{1-m} in order to explain the reaction profile. However, it is very hard to believe that two Dien molecules dissociate simultaneously from the nickel(II) ion in the outer-sphere complex. For this reason, the experimental fact that the reaction rate is practically independent of the nickel(II)-Dien complex concentration indicates that the rate-determining step is the dissociation of the first Dien molecule from the nickel(II) ion, which is then followed by the rapid formation of a mixed 1 : 1 : 1 nickel(II), Dien, Y^{m-} complex and the rapid dissociation of the second Dien molecule from it. If the outer-sphere complex is depicted as V, the k_{HY} value can be given by $K_{Ni-L}\cdot K_{st}\times k_{rds}/K_2$. Here, K_2 denotes the second successive formation constant of the nickel(II)-Dien complex; K_{Ni-L}, the stability of the leaving Dien segment, and k_{rds}, the rate constant of the dissociation of the first Dien molecule from the reaction intermediate, V in Fig. 4. By approximating the k_{rds} value to the dissociation rate constant of a 1 : 2 ratio nickel(II)-ethylenediamine complex ($\log k = 0.72$[7]), and K_{Ni-L}, to the second successive formation constant of the nickel(II)-*N*-(2-hydroxyethyl)ethylenediamine complex,[8] the k_{HY} value was calculated to be 8.4×10^{-2} from the above relation. The k_{HY} value obtained experimentally agreed well with this value. To complete the substitution reaction, the above rate-determining step should be followed by the rapid dissociation of the second Dien molecule from the reaction intermediate. By analogy with the substitution reaction of the nickel(II)-Dien complex with DTPA, the latter step would proceed through the following mixed-ligand reaction intermediate (VI), where the dissociation of Dien from it is slow. Here, it must be noted that if

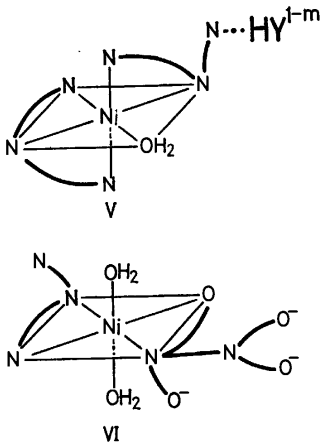

Fig. 4. Reaction intermediates.

6) D. B. Rorabacher and D. W. Margerum, *Inorg. Chem.*, **3**. 382 (1964).

7) R. Gould, ed., "Mechanisms of Inorganic Reactions," American Chemical Society, Washington D. C. (1965), p. 70.

8) L. G. Sillen and A. E. Martell, "Stability Constants of Metal-Ion Complexes," 2nd ed., The Chemical Society, London (1964).

the formation of the reaction intermediate VI is rapid enough, the rate constant calculated on the basis of the reaction intermediate VI should be much larger than the k_{HY} value obtained experimentally. By the common way of calculating the rate constant, the k_{HY} values for the EDTA and EDTA-OH systems were calculated to be 390. This rate constant, large compared with the observed k_{HY} value, shows that the IIa reaction mechanism can reasonably be rewritten as:

$$NiX_2^{2+} + HY^{1-m} \overset{K_{as}}{\rightleftharpoons} NiX_2^{2+} \cdots HY^{1-m} \quad \text{in a rapid equilibrium}$$

$$NiX_2^{2+} \cdots HY^{1-m} \overset{k_{HY}}{\rightleftharpoons} NiXY^{2-m} + HX^{+} \quad \text{r.d.s. IIa}$$

$$NiXY^{2-m} \rightleftharpoons NiY^{2-m} + X^{0} \quad \text{rapid}$$

The formation of a mixed-ligand complex of the nickel(II) ion involving both Dien and the EDTA or EDTA-OH anion as a reaction product could be disproved spectrophotometrically. In order to ascertain the formation of an outer-sphere complex between NiX_2^{2+} and the EDTA or EDTA-OH anion, a conductometric investigation was also carried out. However, it could provide no experimental evidence justifying the formation of an outer-sphere complex. Since the K_{as} value predicted from the Fuoss equation[9] is not large enough for the completion of the outer-sphere complex formation, it may be assumed that the internal hydrogen-bond formation between the HY^{1-m} anion and the free nitrogen atom of coordinated Dien plays an important role in the stabilization of the outer-sphere complex.

The substitution reaction of the cobalt(II)-Dien complex with EDTA was also studied. However, it proceeds so rapidly that we could not determine its rate or reaction mechanism by the present polarographic technique.

9) R. M. Fuoss, *J. Amer. Chem. Soc.*, **80**, 5059 (1958).

BULLETIN OF THE CHEMICAL SOCIETY OF JAPAN, VOL. 45, 2764—2767 (1972)

The Extraction and Spectrophotometric Determination of Titanium(IV) with Tiron[1]

Yoshinobu WAKAMATSU* and Makoto OTOMO**

*Department of Industrial Chemistry, Hachinohe Technical College, Hachinohe-shi, Aomori

**Department of Synthetic Chemistry, Nagoya Institute of Technology, Showa-ku, Nagoya-shi

(Received March 13, 1972)

A method has been described for the spectrophotometric determination of titanium(IV), which is based on the extraction of the titanium(IV)-Tiron chelate into *n*-butanol in the presence of 1,3-diphenylguanidinium salt. The extracted species containing titanium, Tiron, and diphenylguanidine in a molar ratio 1:2:4, has an absorption maximum at about 385 nm. The maximum extraction is obtained when the pH of the initial aqueous phase is controlled to about 3.0 to 4.0. Beer's law is obeyed up to 25 μg titanium per 10 m*l* of *n*-butanol. The molar absorptivity of the extracted species is 1.4×10^4 at 385 nm. Molybdenum(VI) and chelating agents interfere with the determination of titanium.

As is well known, Tiron, disodium salt of 1,2-dihydroxybenzene-3,5-disulfonic acid, forms water soluble chelates with many metal ions and has been used as a colorimetric reagent for several metal ions,[2-6] or as a masking agent[7] or a metallochromic indicator[8] in complexometric titrations. Recently, Busev *et al.*[9] applied the reagent to the selective extraction-spectrophotometric determination of molybdenum (VI), on the basis of the extraction of the ion-association complex formed between the molybdenum-Tiron chelate and 1,3-diphenylguanidinium cation. A similar method was also applied to the determination of iron(III).[10]

Because of its superior extraction efficiency, 1,3-diphenylguanidinium salt has recently been used in many analytical procedures with advantage. In our previous works, the anionic metal-chelates of Methylthymol Blue,[11,12] Xylenol Orange[13] or Indoferron[14-16] have been extracted into suitable organic solvents in

1) Presented at the 20th Annual Meeting of the Japan Society for Analytical Chemistry, Tokyo, October, 1971.

2) J. H. Yoe and A. L. Jones, *Ind. Eng. Chem. Anal. Ed.*, **16**, 111 (1944).

3) J. H. Yoe and A. R. Armstrong, *Anal. Chem.*, **19**, 100 (1947).

4) J. H. Yoe and F. Will, *Anal. Chim. Acta*, **8**, 546 (1953).

5) Y. Oka, N. Nakazawa, and H. Harada, *Nippon Kagaku Zasshi*, **86**, 1158 (1965).

6) T. Yotsuyanagi, K. Goto, and M. Nagayama, *ibid.*, **88**, 1282 (1967).

7) H. Flaschka and R. Puschel, *Z. Anal. Chem.*, **143**, 300 (1954).

8) Y. Sasaki, *Bunseki Kagaku*, **16**, 1199 (1967).

9) A. I. Busev and G. P. Rudzit, *Zh. Anal. Khim.*, **19**, 569 (1964).

10) A. I. Busev, G. P. Rudzit, and I. A. Tsurika, *ibid.*, **25**, 2151 (1970).

11) M. Otomo, *Nippon Kagaku Zasshi*, **89**, 503 (1968).

12) Y. Wakamatsu and M. Otomo, *ibid.*, **90**, 595 (1969).

13) M. Otomo and Y. Wakamatsu, *ibid.*, **89**, 1087 (1968).

14) Y. Wakamatsu and M. Otomo, *Bumseki Kagaku*, **19**, 537 (1970).

15) Y. Wakamatsu and M. Otomo, *Research Rep., Hachinohe Tech. Coll.*, **5**, 72 (1970).

16) Y. Wakamatsu and M. Otomo, *Bunseki Kagaku*, **20**, 862 (1971).

the presence of 1,3-diphenylguanidinium chloride. The extraction mechanisms of the ion-association complexes thus formed have also been investigated by a spectrophotometric method. The present paper will describe the spectrophotometric determination of titanium(IV), which is based on the extraction of the titanium-Tiron-1,3-diphenylguanidinium association complex into *n*-butanol. The extracted species, containing titanium, Tiron and diphenylguanidine in a molar ratio 1:2:4, has an absorption maximum at 385 nm and the molar absorptivity of about 1.4×10^4. By this method, up to 25 μg of titanium can be determined within the experimental error.

Experimental

Reagent. About 0.01 M titanium(IV) solution was prepared by dissolving the hydrolysis products of titanium tetrachloride in 6 N sulfuric acid and diluting with distilled water. The resultant solution was standardized by the complexometric titration.[17] A working standard solution was prepared by diluting the above solution with distilled water to a desired concentration.

A 5×10^{-2} M Tiron solution was prepared by dissolving the Dotite Tiron in distilled water without further purification.

A 0.5 M 1,3-diphenylguanidinium chloride (DPG-Cl) stock solution was prepared by dissolving 1,3-diphenylguanidine (Guaranteed Reagent, Tokyo Kasei Co., Ltd.) in calculated amounts of hydrochloric acid and diluting with distilled water.

All other chemicals used were of guaranteed reagent quality.

Apparatus. The absorbance measurements were made with a Hitachi Model 124 recording-spectrophotometer with 10-mm quartz cells and a Hitachi Model EPU-2A spectrophotometer with 10-mm glass cells. The shaking was done with an Iwaki Model V-D shaker with a time switch. The pH measurements were made with a Toa Denpa Model HM-5A glass electrode pH meter.

Standard Procedure. To a sample solution containing up to 25 μg of titanium in a 50 m*l* separating funnel were added 2 m*l* of a 5×10^{-2} M Tiron solution and 10 m*l* of a 0.1 M DPG-Cl solution which had been adjusted to pH 3.6 with monochloroacetic acid and sodium acetate solutions. The solution was diluted with water to 20.0 m*l* and shaken for 5 min. with 10.0 m*l* of *n*-butanol. The absorbance of the organic phase was then measured at 385 nm using a reagent blank as the reference.

Results and Discussion

Absorption Spectra. The absorption spectra of the association complex extracted into *n*-butanol are shown in Fig. 1, along with that of the reagent blank. At any pH values examined, the absorption maximum of the extracted species is found at about 385 nm. The extracted species was stable for at least several hours.

The Effect of pH. The effect of pH of the aqueous phase on the extraction was examined. The results are shown in Fig. 2. The maximum extraction is reached at pH 3.0 to 4.0 when the association complex is extracted into *n*-butanol from the aqueous solution containing 9.6 μg titanium, 5.0×10^{-3}M Tiron and 1.3×10^{-1}M DPG-Cl. This pH range is shifted to 3.3 to 4.0 for 19.2 μg titanium.

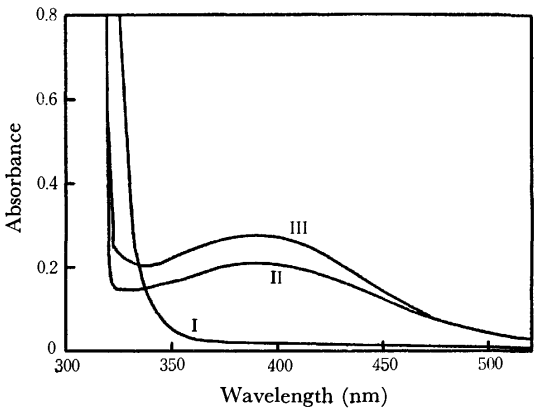

Fig. 1. Absorption spectra of the systems Tiron-DPG and Ti(IV)-Tiron-DPG in *n*-butanol.
Ti: 9.6 μg, Tiron: 5.0×10^{-3} M, DPG-Cl: 0.13 M, I: Tiron-DPG, pH 3.6, II: Ti-Tiron-DPG, pH 2.4; III: Ti-Tiron-DPG, pH 3.6

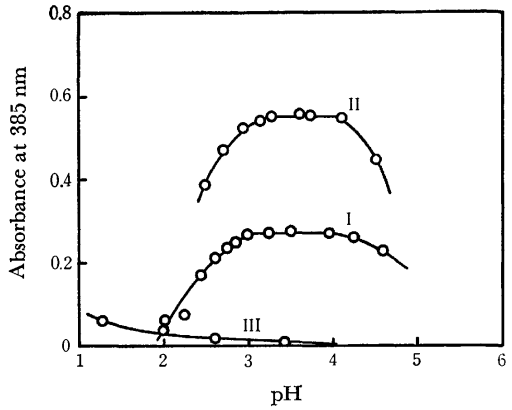

Fig. 2. Effect of pH on the extraction of Ti(IV)-Tiron-DPG.
Tiron: 5.0×10^{-3} M, DPG-Cl: 0.13 M, Ti: I; 9.6 μg, II; 19.2 μg, III; 0.

The Effect of the Tiron Concentration. The effect of the Tiron concentration on the extraction was investigated by varying the Tiron concentration, while other variables being held constant. The absorbance

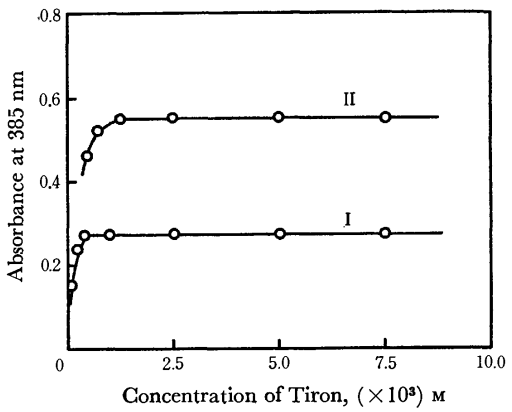

Fig. 3. Effect of Tiron concentration on the extraction of Ti(IV)-Tiron-DPG.
pH: 3.6, DPG-Cl: 0.13 M, Ti: I; 9.6 μg, II; 19.2 μg

17) K. Ueno, "Chelatometric Titration (In Japanese)", Nankodo, Tokyo (1965), p. 315.

of the organic phase was constant when the Tiron concentration in the initial aqueous phase was more than 2.0×10^{-3}M, as is shown in Fig. 3.

The Effect of the DPG-Cl Concentration. The absorbance of the organic phase remained essentially constant provided that the DPG-Cl concentration of the initial aqueous phase was more than about 9.0×10^{-2}M. The titanium-Tiron chelate could not be extracted into the organic phase in the absence of DPG-Cl. The absorbance of the organic phase was not affected by further addition of DPG-Cl at least up to 0.2M.

The Effect of the Shaking Time. The shaking time was varied from 0.5 to 30 min. It was found that shaking for 3 min sufficed; for safety, a shaking time of 5 min was selected. The aqueous phase after one extraction was colorless,indicating that only one extraction is needed for complete extraction of the association complex.

Choice of Solvent. The titanium-Tiron-DPG association complex can be extracted into such aliphatic alcohols as *n*-butanol, isobutyl alcohol and *n*-amyl alcohol, but not into hydrocarbons, halogenated hydrocarbons, esters and ketones. *n*-Butanol was chosen as the solvent which gave the highest absorbance.

Calibration Curve. A calibration curve for the determination of titanium was prepared under the optimum conditions. A good linear relationship was obtained over the concentration range 0 to 25 μg of titanium per 10 m*l* of *n*-butanol. The molar absorptivity of the extracted species was approximately 1.4×10^4 at 385 nm. This value is about 1.4 times as high as that obtained by the direct reaction in aqueous solution without DPG-Cl. The proposed method is comparable in sensitivity with the Xylenol Orange[18] or the chromotropic acid method.[19]

The Effect of Diverse Ions. Separate tests were made to elucidate the interference of various cations as well as that of anions on the determination of titanium. The results are summarized in Tables 1 and 2. Molybdenum(VI) interfered at all concentrations investigated, giving positive errors. Iron(III) up to about 10-fold excess did not interfere with the determination when nitrilotriacetic acid (NTA) (2×10^{-3}M) was added as a masking agent before extraction. The interference of the larger amounts of iron(III) may be prevented by addition of a suitable reducing agent. Of the anions tested, chloride, nitrate, sulfate, and phosphate ions, even at high concentrations, did not interfere with the determination. However, chelating agents such as ethylenediaminetetraacetic acid (EDTA) and cyclohexanediaminetetraacetic acid (CyDTA) interfered seriously, giving negative errors.

The Composition of the Extracted Species. The composition of the extracted species was studied by a graphical method, in which all the equilibrium concentrations and distribution ratios were estimated by measuring the absorbances of the organic or aqueous phases at suitable wavelengths.

18) M. Otomo, This Bulletin, **36**, 1577 (1963).
19) A. V. Endredy and F. Brugger, *Z. Anorg. Allgem. Chem.*, **249**, 263 (1942).

TABLE 1. EFFECT OF METAL IONS
Ti (IV): 1.5×10^{-5} M (14.4 g), Tiron: 5.0×10^{-3} M, DPG-Cl: 0.13M, pH: 3.6

Metal ion	Mole ratio to Ti	Ti found (μg)
Mg(II)	20	13.5
Zn(II)	20	14.1
Cu(II)	20	16.3
Cd(II)	20	14.2
Pb(II)	20	13.0
Ni(II)	20	14.3
Co(II)	20	14.4
Cr(III)	20	13.6
Al(III)	20	13.7
Fe(III)	2	14.5
	5	16.0
	10	14.8[a]
Th(IV)	20	14.9
V (IV)	10	17.7
	20	23.3
Zr(IV)	10	13.8
	20	8.5
U (VI)	20	16.9
W (VI)	5	16.8
	10	23.6
Mo(VI)	1	15.8
	5	21.2

a) NTA (2×10^{-3}M) was added as masikng agent.

TABLE 2. EFFECT OF ANIONS AND COMPLEXING AGENTS
(Conditions: the same as those in Table 1)

Anion or complexing agent	Mole ratio to Ti	Ti found (μg)
Cl^-	1000	14.4
NO_3^-	1000	14.2
SO_4^{2-}	500	13.9
	1000	12.7
$C_2O_4^{2-}$	10	12.8
	50	11.4
$C_2H_4O_6^{2-}$	50	12.1
	500	8.3
PO_4^{3-}	1000	14.2
NTA	30	14.4
	100	13.0
CyDTA	0.5	11.2
	1	9.2
EDTA	0.5	9.0

In Fig. 4, log (distribution ratio of Tiron, D_{Tiron}) is plotted against log (DPG-Cl concentration in the organic phase/chloride ion concentration in the aqueous phase, $[\text{DPG-Cl}]_0/[\text{Cl}^-]$), the Tiron and the hydrogen ion concentrations being kept constant. The slope of straight line portion shows that the ratio Tiron: DPG is 1: 2. Considering the acid dissociation constants ($K_{\text{OH},1}$ and $K_{\text{OH},2}$) of Tiron, it is reasonable to say that Tiron is combined with two DPG cations through its two sulfonate groups to give an extractable neutral species, $H_2R(DPG)_2$.

The number of moles of Tiron in the titanium-Tiron-DPG association complex was determined by plotting log (distribution ratio of titanium, D_{Ti}) against log

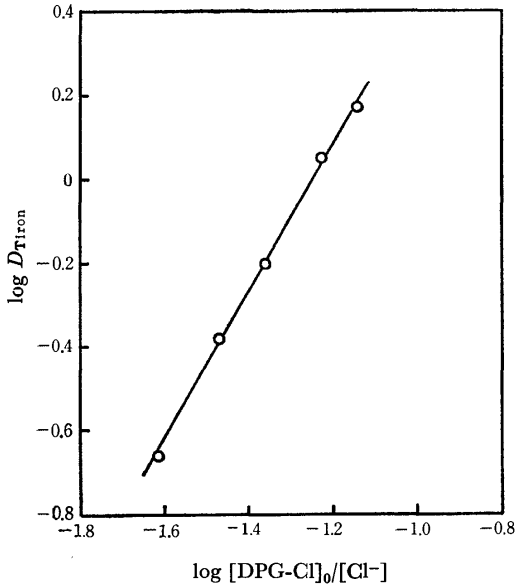

Fig. 4. Relationship between log D_{Tiron} and log [DPG-Cl]$_0$/[Cl$^-$] for the Tiron-DPG system.
Tiron: 5.0×10^{-4} M, pH: 3.6

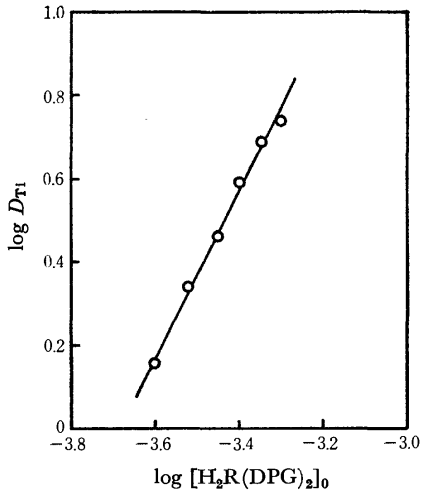

Fig. 5. Relationship between log D_{Ti} and log [$H_2R(DPG)_2$]$_0$ for the Ti(IV)-Tiron-DPG system.
Ti: 2.0×10^{-5} M, pH: 3.6

(Tiron-DPG concentration in the organic phase, [$H_2R(DPG)_2$]$_0$); all other variables were kept constant. The slope of 1.8 (Fig. 5) indicates that two molecules of Tiron combines with one atom of titanium. Evidently the composition of the extracted species is Ti: Tiron: DPG=1:2:4.

The pH dependence of the extraction was then examined by plotting log D_{Ti} against pH value of the aqueous phase. The curves shown in Fig. 6 indicates

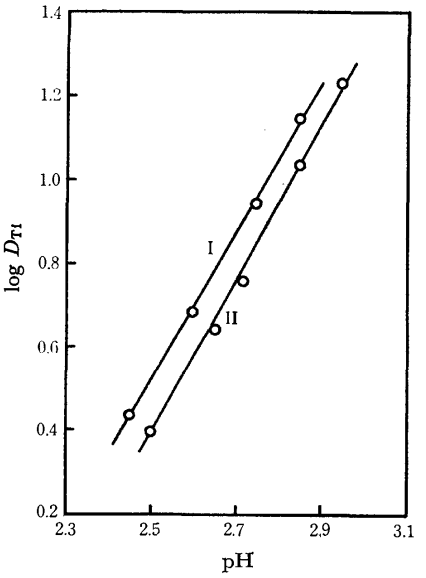

Fig. 6. Relationships between log D_{Ti} and pH for the Ti(IV)-Titon-DPG system.
Tiron: 5.0×10^{-3} M, DPG-Cl: 0.13 M, Ti: I; 1.0×10^{-5} M, II; 2.0×10^{-5} M

that two protons are concerned with the extraction process.

Since titanium(IV) exists predominantly as TiO^{2+} under the experimental conditions,[20] it may be assumed that the original complex is an anionic titanyl(IV)-Tiron species, $TiO(HR)_2^{4-}$, which combines with four DPG cations to form a neutral ion-association complex. From the foregoing observations, it seems natural that the extraction equilibrium expression is given in the simplest form

$$TiO^{2+} + 2[H_2R(DPG)_2]_0 \rightleftarrows [TiO(HR)_2(DPG)_4]_0 + 2H^+$$

and that the distribution ratio of titanium is therefore expressed by

$$\log D_{Ti} = \log [TiO(HR)_2(DPG)_4]_0/[TiO^{2+}] = \log K + 2\log [H_2R(DPG)_2]_0 + 2pH$$

where K is a constant including the acid dissociation constants of Tiron, the distribution coefficients of DPG-Cl, $H_2R(DPG)_2$, and $TiO(HR)_2(DPG)_4$, the formation constants of $H_2R(DPG)_2$ and $TiO(HR)_2(DPG)_4$, and the equilibrium constant of the reaction between titanium and Tiron.

The authors wish to thank Miss Tomiko Takebe for her laboratory work.

20) S. Musha and K. Ogawa, *Nippon Kagaku Zasshi*, **78**, 1686 (1957).

Cobalt(II) and -(III) Complexes of 1,5-Dialkylpentane-2,4-diones[1]

Isao YOSHIDA, Hiroshi KOBAYASHI, and Keihei UENO

Department of Organic Synthesis, Faculty of Engineering, Kyushu University, Fukuoka

(Received April 22, 1972)

Based on the spectral studies in visible, ultraviolet as well as in infrared regions, the dimeric octahedral structure was proposed for bis(heptane-3,5-dionato)cobalt(II) monohydrate, $[Co(DNPM)_2 \cdot H_2O]$, bis(nonane-4,6-dionato)cobalt(II) monohydrate, $[Co(DNBM)_2 \cdot H_2O]$, bis(2,8-dimethylnonane-4,6-dionato)cobalt(II) monomethanolate, $[Co(DIVM)_2 \cdot CH_3OH]$, and bis(tridecane-6,8-dionato)cobalt(II) monomethanolate, $[Co(DNCM)_2 \cdot CH_3OH]$. The dimeric chelates of the type $[CoL_2 \cdot B]$, where B represented water or methanol, were stable in solid state, however, they freed the base B to form a tetrahedral monomeric complex in non-donating solvents. A red-pink solution of the cobalt(II) chelates were oxidized spontaneously in the period of a few days to give a green solution of cobalt(III) chelates of type $[CoL_3]$. Cobalt(III) chelates of 2,6-dimethylheptane-3,5-dione (DIBM) and 2,2,6,6-tetramethylheptane-3,5-dione (DPVM) in addition to the above ligands were synthesized and their spectra were discussed in comparison with the corresponding cobalt(II) chelates.

It has been well established by X-ray crystallography that anhydrous bis(pentane-2,4-dionato)cobalt(II), $Co(AA)_2$, existed as a tetramer in solid state, in which four octaheral units attached face-to-face and edge-to-edge linearly.[2] However, molecular weight determinations in non-donating solvents such as carbon tetrachloride or benzene indicated that the degree of polymerization varied between 1.3 and 3.5, and that the depolymerization proceeded with decreasing concentration.[3] The spectral characteristics of $Co(AA)_2$ in such solvents also indicated the reversible interconversion between an octahedral oligomer and a tetrahedral monomer. The spectrum of the highly diluted solution of $Co(AA)_2$ in non-donating solvents, is quite similar to that of bis(2,2,6,6-tetramethylheptane-3,5-dionato)cobalt(II), $Co(DPVM)_2$, which is known as a mononuclear tetrahedral complex.[4]

A unique tetrahedral structure of $Co(DPVM)_2$ among the cobalt(II) β-diketone chelates, is understood to be due to the steric hindrance of the terminal *t*-butyl groups which are bulky enough to prevent the association of mononuclear species in solid state as well as in solution state.[3,4] The similar effect was also observed in the case of bis(2,2,6,6-tetramethylheptane-3,5-dionato)-nickel(II), $Ni(DPVM)_2$, which is known to be a square planar mononuclear complex.[5-7]

In this respect, it is of great interest to investigate the effect of alkyl substitution at 1- and 5-carbon of pentane-2,4-dione upon the property of resulting complexes. In the previous paper, we reported on the nickel chelates of some 1,5-dialkyl-pentane-2,4-diones with terminal alkyl groups of various bulkiness and proposed an octahedral dimeric structure based on the spectral studies.[8]

This paper is to report on the syntheses and the structural studies of cobalt(II) and -(III) chelates of the following six pentane-2,4-dione analogues: heptane-3,5-dione (or dipropionylmethane, DNPM), nonane-4 6-dione (or di-*n*-butyrylmethane, DNBM), 2,6-dimethylheptane-3,5-dione (or diisobutyrylmethane, DIBM), 2,8-dimethylnonane-4,6-dione (or diisovalerylmethane, DIVM), 2,2,6,6-tetramethylheptane-3,5-dione (or dipivaloylmethane, DPVM), and tridecane-6,8-dione (or di-*n*-caproylmethane, DNCM).

Experimental

Preparation of Compounds. Details of the syntheses and the properties of 1,5-dialkyl-pentane-2,4-diones were described in the previous paper.[8]

Cobalt(II) chelates were prepared by the following general procedure. To a solution containing 1.5 g (0.005 mol) of cobalt(II) nitrate hexahydrate in 20 m*l* of aqueous methanol, was added a solution of 0.01 mol of the ligand in 5 m*l* of methanol. Then, 6 m*l* of 1.5 M aqueous sodium hydroxide was added with vigorous stirring to the mixture, from which a red-pink complex precipitated immediately along with a small amount of green precipitate. The red-pink cobalt(II) chelate was much less soluble in cold methanol than the green cobalt(III) chelate, and was readily separated by fractional dissolution in cold methanol. The cobalt(II) chelate was recrystallized from methanol as fine blood-red needles. Of the ligands investigated in the present work, attempts to prepare the DIBM and DPVM chelates were unsuccessful. The results of elemental analysis and the composition of the chelates, which were successfully synthesized, are summarized in Table 1.

Cobalt(III) chelates were prepared by the following method.[9] A suspension of 1.72 g of cobalt(II) carbonate (0.003 mol) and 0.01 mol of a ligand in 50 m*l* of water was heated at about 95°C. Then, 24 m*l* of 10% hydrogen peroxide was added dropwise to the hot mixture under effective stirring over a period of 1 hr. At the end of the reaction, the mixture was cooled to the room temperature and the dark green reaction product was extracted with 100—200 m*l* of benzene. After evaporating the solvent from the clear extract until dryness under reduced pressure, the green solid residue was recrystallized from an appropriate solvent.

1) Contribution No. 266 from the Department of Organic Synthesis, Faculty of Engineering, Kyushu University.

2) F. A. Cotton and R. C. Elder, *Inorg. Chem.*, **4**, 1145 (1965).

3) F. A. Cotton and R. H. Soderberg, *ibid.*, **3**, 1 (1964).

4) F. A. Cotton and R. H. Soderberg, *J. Amer. Chem. Soc.*, **84**, 872 (1962).

5) F. A. Cotton and J. J. Wise, *Inorg. Chem.*, **5**, 1200 (1966).

6) G. S. Hammond, D. C. Nonhebel, and C. H. S. Wu *ibid.*, **2**, 73 (1963).

7) J. P. Fackler Jr. and F. A. Cotton, *J. Amer. Chem. Soc.*, **82**, 5005 (1960).

8) I. Yoshida, H. Kobayashi, and K. Ueno, This Bulletin, **45**, 1411 (1972).

9) B. E. Bryant and W. C. Fernelius, "Inorganic Synthesis", Vol. V, McGraw-Hill, Inc., New York, (1957), p. 188.

Table 1. Elemental analysis of cobalt(II) chelate investigated

Complex	Molecular formula	Elemental analysis C % Found	C % Calcd	H % Found	H % Calcd	Yield (%)
$Co(AA)_2 \cdot 2H_2O$	$C_{10}H_{18}O_6Co$	40.77	40.97	6.20	6.14	60
$Co(DNPM)_2 \cdot H_2O$	$C_{14}H_{24}O_5Co$	50.68	50.78	7.35	7.25	70
$Co(DNBM)_2 \cdot H_2O$	$C_{18}H_{32}O_5Co$	55.52	55.84	8.34	8.27	70
$Co(DIVM)_2 \cdot CH_3OH$	$C_{23}H_{42}O_5Co$	60.43	60.43	8.94	9.19	40
$Co(DNCM)_2 \cdot CH_3OH$	$C_{27}H_{50}O_5Co$	63.95	63.19	9.88	9.74	50

Table 2. Elemental analyses, appearance, recrystalyzation solvents, and percent yields of the tris(β-diketonato)cobalt(III)

Complex	Molecular formula	Elemental analyses C % Found	C % Calcd	H % Found	H % Calcd	Solvent for recrystallization	Appearance	Yield %
$Co(AA)_3$	$C_{15}H_{21}O_6Co$	50.94	50.59	6.02	5.90	benzene+pet. ether	dark green needles	59
$Co(DNPM)_3$	$C_{21}H_{33}O_6Co$	57.51	57.30	7.50	7.50	water+methanol	dark green needles	95
$Co(DNBM)_3$	$C_{27}H_{45}O_6Co$	62.23	61.86	8.70	8.58	—	dark green liq.	35
$Co(DIBM)_3$	$C_{27}H_{45}O_6Co$	60.99	61.86	8.56	8.58	water+methanol	dark green plates	86
$Co(DIVM)_3$	$C_{33}H_{57}O_6Co$	65.30	65.16	9.46	9.37	water+methanol	dark green plates	55
$Co(DPVM)_3$	$C_{33}H_{57}O_6Co$	65.22	65.16	9.40	9.37	methanol +ethylacetate	dark green grains	25
$Co(DNCM)_3$	$C_{39}H_{69}O_6Co$	67.89	67.66	10.01	9.97	—	dark green liq.	75

Most of the ligands afforded crystalline cobalt(III) chelates, while DNBM and DNCM gave green oily chelates, which eventually had to be purified by a column chromatography. The crude oil was dissolved in a mixture of methanol and ether, and was passed through alumina and silica gel columns, of both 10 cm length, successively. The pure oily chelates were obtained from the eluates by evaporating the solvent. The results of elemental analysis, compositions, solvents for recrystallization as well as appearances of the chelates are summarized in Table 2.

Measurements. All solvents used in the spectral studies were of reagent grade, and were dried and distilled by the standard method prior to use.

Solid reflectance spectra were measured on a Hitachi EPU-2A spectrophotometer with a diffuse reflectance attachment. Absorption spectra in visible and ultraviolet regions were measured with Hitachi EPS-2 and Hitachi 124 spectrophotometers respectively. Infrared absorption spectra were measured with a JASCO-DS-403G spectrophotometer.

Results and Discussion

Reflectance and Absorption Spectra in Visible Region. The result of elemental analyses of the cobalt(II) chelates, with an exception of pentane-2,4-dionate, agrees well with a molecular formula of $CoL_2 \cdot B$, where L and B represent β-diketonate anion and water or methanol respectively. Interestingly, DNPM and DNBM chelates were obtained as a monohydrate while DIVM and DNCM chelates as a monomethanolate. While the above compositions seem to suggest a pentacoordinate structure, the reflectance spectra on solid samples, which are shown in Fig. 1 and Table 3, are very similar to those of bis(pentane-2,4-dionato)-cobalt(II) dihydrate or tetrameric anhydrous bis-(pentane-2,4-dionato)cobalt(II), both being known to

Table 3. Characteristics of solid reflectance and absorption spectra of cobalt(II) chelates

Chelate	Peak in solid reflectance spectra (kK) ν_1	ν_2	Absorption peaks (kK) and molar absorptivities ($mol^{-1}\ l\ cm^{-1}$) in pyridine solution ν_1	ε	ν_2	ε	ν_3	ε
$Co(AA)_2 \cdot 2H_2O$	20.2	~ 8.3	21.3	(35.0)	19.6sh	(~22)	18.5sh	(~18)
$Co(DNPM)_2 \cdot H_2O$	20.8	~ 8.3	21.1	(39.5)	19.3sh	(~28)	18.2sh	(~21)
$Co(DNBM)_2 \cdot H_2O$	20.8	~ 8.3	20.7	(42.5)	19.3sh	(~32)	18.2sh	(~22)
$Co(DIVM)_2 \cdot CH_3OH$	20.8	~ 8.3	20.5sh	(~55)	19.2sh	(~39)	18.1sh	(~30)
$Co(DNCM)_2 \cdot CH_3OH$	20.5	~ 8.3	20.5sh	(~81)	19.2sh	(~55)	18.1sh	(~43)

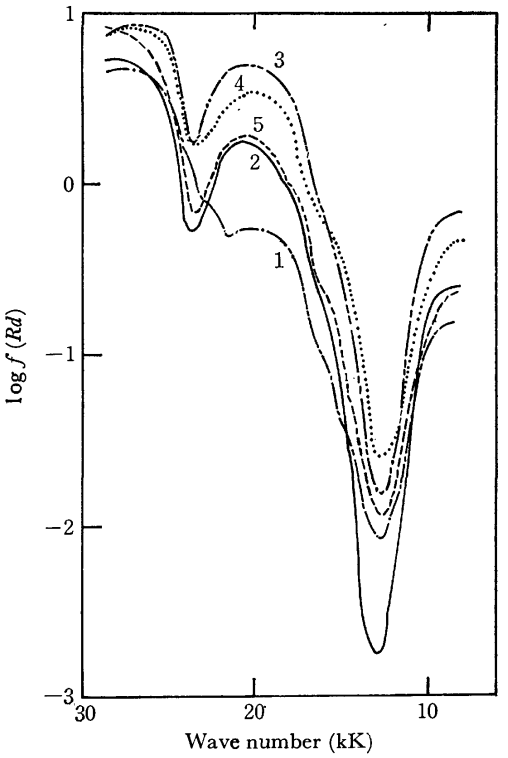

Fig. 1. The reflectance spectra of solid coblat(II) chelates: (1): $Co(AA)_2 \cdot 2H_2O$, (2): $Co(DNPM)_2 \cdot H_2O$, (3): $Co(NDBM)_2 \cdot H_2O$, (4): $Co(DIVM)_2 \cdot CH_3OH$, (5): $Co(DNCM)_2 \cdot CH_3OH$.

be octahedral hexacoordinate.[2,10] In the wave number range higher than 8.3 kK, two peaks can be observed at about 20 and 8.3 kK, which are assignable to the transitions of $^4T_{1g}(P) \leftarrow {}^4T_{1g}(F)$ and $^4T_{2g}(F) \leftarrow {}^4T_{1g}(F)$ respectively.[11]

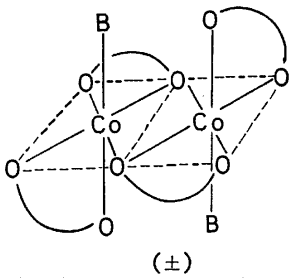

(±)

Proposed dimeric structure on the mono-base adduct complexes of bis(1,5-dialkyl-pentane-2,4-dionato)cobalt-(II).

Thus, in order to satisfy these requirements, it is reasonable to assume that the chelates are of dimeric structure, in which two octahedral CoL_2B units are jointed together by two bridging oxygens as shown in the structure (I). This structure may be indirectly supported by the similar dimeric structure which has been assigned to bis(pentane-2,4-dionato)cobalt(II) monohydrate by the X-ray diffraction study.[12] We have also proposed the similar structure for bis(1,5-dialkyl-pentane-2,4-dionato)nickel(II) monohydrate.[8]

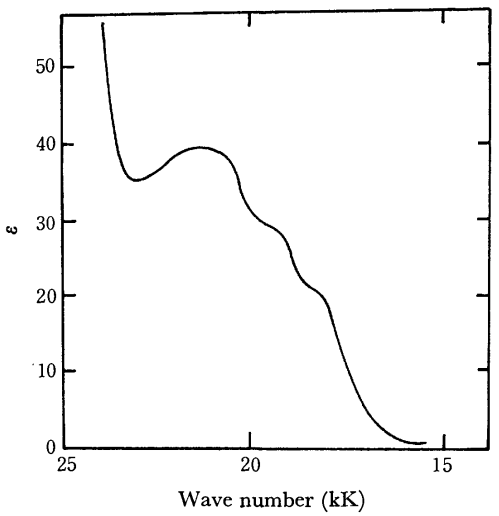

Fig. 2. The pyridine solution spectrum of the $Co(DNPM)_2 \cdot H_2O$ at room temperature.

The blood-red cobalt(II) chelates could dissolve easily into pyridine affording a pink solution. The absorption peaks of the cobalt(II) chelates in pyridine are summarized in Table 3. A typical example is shown in Fig. 2, in which three absorption peaks are observed at 21.1, 19.5, and 18.5 kK respectively, and the spectrum can be referred to an octahedral cobalt-(II) chelate.[10,11,13] Accordingly, the dimeric chelate must be cleaved therein to afford the monomeric octahedral *trans* bis-pyridine adducts.[13,14]

It has been known that the alkyl substitution on the 3-carbon of pentane-2,4-dione leads to the metal complex being a weaker Lewis acid,[15,16] and a similar effect may also be expected on the 1,5-dialkyl substitution on pentane-2,4-dione. The decrease in the acidity of CoL_2 unit may weaken the axial ligation by a base such as pyridine. Resulting elongation of the bond along z-axis leads to lowering the symmetry of octahedral pyridine adducts, and eventually to increase the absorption intensity. There may also operate the steric interaction between pyridine molecule and cobalt-(II) chelate. In our previous paper on the copper(II) complexes of 1,5-dialkyl-pentane-2,4-diones, we proposed that the terminal alkyl groups extended above or below of the xy-plane of copper(II) chelates.[17] If it is also true in this case, the elongation of the bond along z-axis may be more pronounced on the chelates with more bulky alkyl substituents. Thus, the combined inductive and steric effects of alkyl substituents may be responsible for the increase of the absorption intensity. The fact that the extent of increase in molar absorptivity is parallel to the bulkiness of alkyl substituents, positively favors our proposal.

On the other hand, absorption spectra of the present

10) J. T. Hashagen and J. P. Fackler, Jr., *J. Amer. Chem. Soc.*, **87**, 2821 (1965).
11) D. Sutton, "Electronic Spectra of Transition Metal Complexes", McGraw-Hill, Inc., New York, (1968), p. 147.
12) F. A. Cotton and R. C. Elder, *Inorg. Chem.*, **5**, 423 (1966).
13) J. P. Fackler, Jr., *ibid.*, **2**, 266 (1963).
14) D. P. Graddon, *Coordin. Chem. Rev.*, **4**, 1 (1969).
15) D. P. Graddon and K. B. Heng, *Aust. J. Chem.*, **24**, 1059 (1971).
16) D. P. Graddon and K. B. Heng, *ibid.*, **24**, 1781 (1971).
17) I. Yoshida, Y. Oono, H. Kobayashi, and K. Ueno, This Bulletin, **45**, 174 (1972).

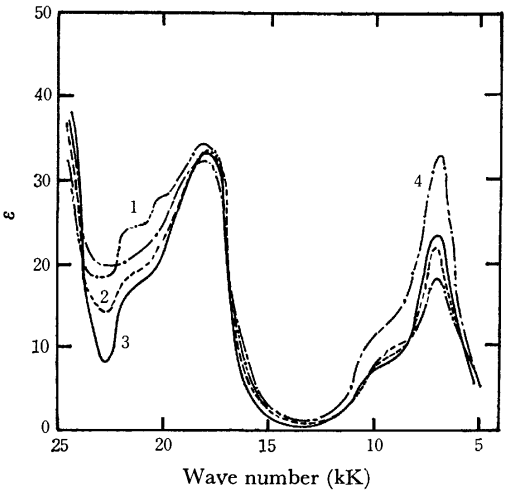

Fig. 3. The absorption spectra of $Co(DNPM)_2 \cdot H_2O$ in chloroform:
(1): 0.02 M, (2): 0.01 M, (3): 0.005 M (14°C), (4): 0.02 M (46°C).

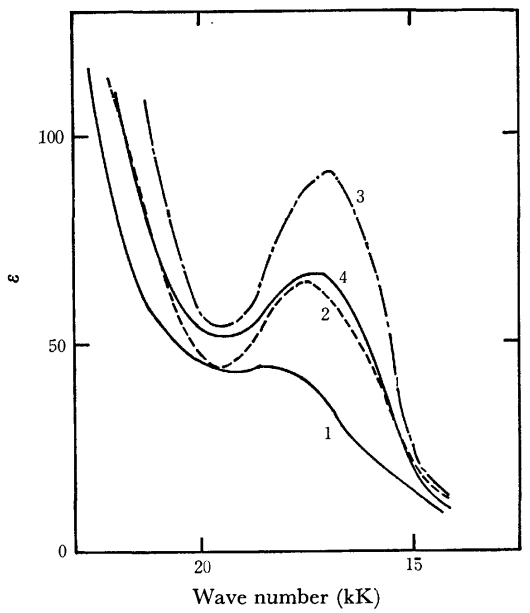

Fig. 4. The absorption spectra of coblat(II) chelates in toluene, measured at 24 hr after dissolution:
(1): $Co(DNPM)_2 \cdot H_2O$, (2): $Co(DNBM)_2 \cdot H_2O$, (3): $Co(DIVM)_2 \cdot CH_3OH$, (4): $Co(DNCM)_2 \cdot CH_3OH$. Absorption coefficient was evaluated from the above structures.

complexes in non-donating solvents are quite different from the reflectance spectra of solid samples or the absorption spectra of pyridine solutions. As an example, Fig. 3 shows the absorption spectra of $Co(DNPM)_2 \cdot H_2O$ in chloroform in a range of concentration and of temperature. The spectral characteristics in dilute solution are very much similar to that of $Co(DPVM)_2$, which is known as a monomeric tetrahedral complex.[4] Two absorption peaks at 18.0 and 7.0 kK may be assigned to $^4T_1(P) \leftarrow {}^4A_2$ and $^4T_1(F) \leftarrow {}^4A_2$ transitions, respectively.[18] These spectral features due to a tetrahedral structure are enhanced with decreasing the chelate concentration and with elevating temperature.

It is clear, therefore, that the dimeric 1:1 base adduct dissociates into a corresponding monomeric tetrahedral cobalt(II) complex and a free base in equilibrium in a chloroform solution as shown in Eq. (1).

$$[CoL_2 \cdot B]_2 \rightleftarrows 2[CoL_2] + 2B \qquad (1)$$

As expected, the bulkiness of the alkyl substituents on the ligands seems to favor the abundance of the monomeric form in the equilibria in solution phases. However, no quantitative study was undertaken owing to an undesirable oxidative side reaction, which will be described below.

Finally, the solutions of the present complexes in non-donating solvents gradually change their color from red-pink to green. Figure 4 shows the absorption spectra of such solutions measured at 24 hr after dissolution in toluene. It is interesting to note that the rate of the color change is parallel to the bulkiness of the alkyl substituents on the ligands. Thus, after 24 hr, the solution of $Co(DIVM)_2 \cdot CH_3OH$ is of an intense green color, while that of $Co(DNPM)_2 \cdot H_2O$ still remains in a pale-pink color. However, after one week standing at room temperature, the solution of cobalt(II) chelates changed to green color completely and their spectra were superimposable to those of the corresponding cobalt(III) chelates which were synthesized in separate routes. The spectral data of the cobalt(III) chelates are summarized in Table 4. Accordingly, these cobalt(II) chelates were oxidized spontaneously to cobalt(III) chelates, and the relative easiness of oxidation was again in parallel with the bulkiness of the alkyl substituents. As the oxidation proceeded even in the atmosphere of nitrogen, some redox reaction must have occurred in this system. However, further detailed investigation was not undertaken to elucidate the reaction mechanism.

Table 4. Spectral characteristics of cobalt(III) chelates in visible and ultraviolet regions

Chelate	Peak (kK) and molar absorptivity (mol^{-1} l cm^{-1}) in visible region (in carbon tetrachloride)		in ultraviolet region (in cyclohexane)			
$Co(AA)_3$	16.7	(144)	—	—	—	—
$Co(DNPM)_3$	16.8	(152)	38.4	(35500)	43.5	(40000)
$Co(DNBM)_3$	16.9	(157)	38.2	(35500)	43.2	(39500)
$Co(DIBM)_3$	16.9	(176)	38.0	(37500)	43.2	(43000)
$Co(DIVM)_3$	16.9	(153)	37.9	(37500)	43.1	(42000)
$Co(DPVM)_3$	17.0	(182)	37.9	(39000)	43.1	(43500)
$Co(DNCM)_3$	16.9	(158)	38.0	(36000)	43.1	(39000)

Absorption peaks of the cobalt(III) chelates, as shown in Table 4, shift slightly to higher energy side with increasing bulkiness of the alkyl substituents, probably due to the increased basicity of the ligands.

Ultraviolet Absorption Spectra. Tetrameric octahedral bis(pentane-2,4-dionato)cobalt(II) is known to dissociate to form a monomeric tetrahedral complex in non-donating solvents,[3] showing a single absorption peak at 292 nm in a diluted chloroform solution, for example.[19] On the other hand, the octahedral mono-

18) A. B. P. Lever, "Inorganic Electronic Spectroscopy", American Elsevier, Pub. Co., New York (1968), p. 323.

19) R. H. Holm and F. A. Cotton, *J. Amer. Chem. Soc.*, **80**, 5658 (1958).

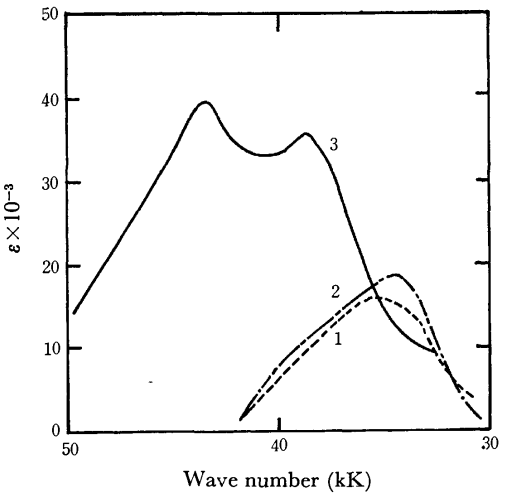

Fig. 5. Typical UV absorption spectra of cobalt(II) and -(III) chelates:
(1): $Co(DNPM)_2 \cdot H_2O$ in methanol, (2): $Co(DNPM)_2 \cdot H_2O$ in cyclohexane, (3): $Co(DNPM)_3$ in cyclohexane.

meric species of bis(pentane-2,4-dionato)cobalt(II), regardless of the kind of bases or donating solvents, always gave rise to an absorption peak at around 280 nm.

Concerning the present complexes also, as summarized in Fig. 5 and Table 5, the mono-solvent adducts shows a single absorption peak at 288—291 nm region upon dissolved in cyclohexane to a high dilution. Combined with the result of the visible spectral studies, these complexes are considered to exist as tetrahedral monomeric species in cyclohexane. On the other hand, the spectra of these complexes in methanol exhibit a single absorption peak at 282—283 nm region, which indicates the predominance of the solvent coordinated octahedral species, again being consistent with the visible spectral observations. Thus, in the ultraviolet absorption spectra of bis(pentane-2,4-dionato)cobalt-(II) and its analogues, such extent of difference in wave number may be utilized as a criterion in discriminating their coordination structures. The cobalt-(III) chelates, $Co(III)L_3$, show two UV absorption peaks in a much shorter wavelength region as shown in Table 4, and can be readily distinguished from those of the cobalt(II) chelates.

Infrared Absorption Spectra. A sharp, relatively strong ν_{OH} band is observed in a region of 3350—3360 cm^{-1} on each of the monohydrate complexes in nujol mull. The corresponding peak appears at a higher frequency region in non-donating solvents such as carbon tetrachloride or chloroform as summarized in Table 6. The ν_{OH} band shifts to a higher wave number region with the decreasing chelate concentration, approaching to that of free water molecule at 3710 cm^{-1}. This result suggests that the interaction between the coordinated water and the chelated cobalt(II) ion becomes weaker in non-donating solvents than in solid state, being in good agreement with the result of visible and ultraviolet spectral studies.

The monomethanol adducts show a ν_{OH} band at 3550—3540 cm^{-1}, appearing at a little lower wave number region than that of the free ν_{OH} band of primary alcohol (3640 cm^{-1}). The result again suggests the interaction between methanol and the chelated cobalt-(II) ion.

As stated previously, when the hydrated cobalt(II) chelates were recrystallized from methanol, DIVM and DNCM chelates came out as monomethanol adducts, while DNPM and DNBM chelates as monohydrates. Therefore, DIVM and DNCM chelates accept methanol as a second ligand in preference to

Table 5. Characteristics of ultraviolet absorption spectra of cobalt(II) chelates

Chelate	Absorption peak (kK and nm) and molar absorptivity ($mol^{-1}\ l\ cm^{-1}$)					
	in methanol[a)]			in cyclohexane[a)]		
	ν, kK	λ, nm	ε	ν, kK	λ, nm	ε
$Co(AA)_2 \cdot 2H_2O$	35.4	(282)	16000	34.2[c)]	(292)	16200
$Co(DNPM)_2 \cdot H_2O$	35.3	(283)	16000	34.7	(288)	18500
$Co(DNBM)_2 \cdot H_2O$	35.3	(283)	17500	34.4	(291)	19500
$Co(DIVM)_2 \cdot CH_3OH$	35.4[b)]	(282)	20500	34.4	(291)	19000
$Co(DNCM)_2 \cdot CH_3OH$	35.4[b)]	(282)	19500	34.6	(289)	21000

a) Measurements were carried out on $2—4 \times 10^{-5}$M solutions.
b) Observed in a methanol-cyclohexane (9:1) mixed solvent.
c) Reported value for $Co(AA)_2$ in chloroform.[18)]

Table 6. Infrared spectra of cobalt(II) chelates

Chelate	in Nujol mull		in Carbon tetrachloride	in Chloroform
	ν (C=O)	ν (O–H)	ν (O–H)	ν (O–H)
$Co(AA)_2 \cdot 2H_2O$	1605	3420	—	—
$Co(DNPM)_2 \cdot H_2O$	1592	3350	3530 (0.1M)	3420 (0.25M) 3430 (0.08M)
$Co(DNBM)_2 \cdot H_2O$	1589	3360	3520 (0.1M)	3420 (0.25M)
$Co(DIVM)_2 \cdot CH_3OH$	1585	3552	—	—
$Co(DNCM)_2 \cdot CH_3OH$	1586	3540	—	—

water. Although it seems contradictory that DIVM and DNCM chelates accepts a weaker base such as methanol in preference to a stronger base such as water, the result could be explained by the hydrophobic repulsion by non-polar alkyl substituents against polar water molecule, if one remind that DIVM and DNCM have more bulky alkyl substituents than those of DNPM and DNBM.

There is still remained to be elucidated a question why the alkyl substituents on the 1- and 5-positions of pentane-2,4-dione favors the formation of a dimeric form of the mono-solvent adduct in their cobalt(II) as well as nickel(II) complexes[8] rather than forming a mononuclear bis-adduct octahedral complex as observed in the parent pentane-2,4-dionates. However, this tendency may partly be ascribed to the mutual repulsion between solvent molecules and alkyl substituents, and partly to the increased basicity of coordinated carbonyl oxygen atoms which could eventually coordinate to the neighboring cobalt(II) or nickel(II) complex unit by forming the oxygen bridged binuclear complex.

BULLETIN OF THE CHEMICAL SOCIETY OF JAPAN, VOL. 45, 2773—2775 (1972)

Stable Paramagnetic Species in Natural Strontium Sulfate Crystals

Toshio MATSUZAKI, Morio SETAKA, V. V. GROMOV,* and Takao KWAN
Faculty of Pharmaceutical Sciences, The University of Tokyo, Bunkyo-ku, Tokyo
(Received November 22, 1971)

Natural strontium sulfate crystals were found to show complex ESR spectra without any special irradiation. The spectra were classified into three groups, A, B, and C; the thermal and photochemical behavior of each group was distinguished from that of the others. It was proposed that Group B originates from SO_3^- radicals, and Groups A and C were tentatively interpreted as due to lattice defects (F-center and V-center).

γ-Irradiated single crystals of potassium sulfate have been reported to give rise to stable paramagnetic species at room temperature,[1,2] and their physical and chemical nature was the object of interest with regard to the mechanism of electron transfer in the crystal.[3]

Recently we have found that some *natural* strontium sulfate crystals contain stable paramagnetic species even without any special irradiation. In the present paper we shall report the ESR characteristics of these paramagnetic species, with special attention paid to their assignments as well as to their thermal and photochemical behavior.

Experimental

Material. The strontium sulfate samples, produced in the USSR were subjected to ESR investigations, the numbering and the localities of production are shown below.

No	Localities	No	Localities
2	Fergana	5	Central Russia
3	North Caucasus	6	South Caucasus
4	North Fergana	7	Turkmenistan

These $SrSO_4$ samples were seemingly crystalline and transparent to a certain extent, and all gave rise to complex ESR spectra at room temperature. Only the No. 4 sample was subjected to detailed investigations because of its less irregular form. The X-Ray analysis of the No. 4 sample has, in fact, shown that it is a twin crystal. An emmission spectro-chemical analysis of the sample showed that it contains some alkali and alkaline earth metals as impurities: (Mg(+), Ca(###), Ba(##), Na(−), K(+), and Rb(−)), where (−) indicates the absence of metals and (+), (##) and (###) the relative abundance.

Apparatus and Procedure. The ESR measurements were made at room temperature with a JEOL-P-10-type spectrometer, using a microwave frequency of the X-band with 100kHz field modulation. The ESR spectra were taken at every 5° rotation around the three principal axes of an orthogonate (X,Y,Z) of the crystal. The g-values were calculated by using a standard signal of manganese dispersed in MgO powder, which had previously been calibrated with a DPPH signal.

The effects of annealing and photoirradiation on the paramagnetic species were monitored by means of an ESR spectrum observable at the fixed position of the sample crystal. The sample was heated in an electric furnace for 30 minutes at every 50°C from room temperature up to 350°C. Photoirradiations of the sample were carried out by means of a low-pressure mercury lamp (Ushio Denki Co., 200 W). γ-Irradiations (5×10^5 rad/hr from ^{60}Co) were also performed, and the results were compared qualitatively with the results of the photoirradiations.

The parallel surfaces of the sample used made it possible to measure the UV absorption spectra ranging from 210 to 700 mμ, and also the thermal effects on the UV spectra.

Results and Discussion

A typical ESR spectrum for the *virgin* $SrSO_4$ sample (No. 4) fixed at a certain position in the microwave cavity is shown in Fig. 1. The spectrum appeared to be characterized by a number of resonance lines,

* Visiting Scientist. Present address: Institute of Physical Chemistry of the Academy of Sciences of the USSR, Moscow.

1) V. V. Gromov and J. R. Morton, *Can. J. Chem.*, **44**, 527 (1966).
2) K. Aiki and K. Hukuda, *J. Phys. Soc. Japan*, **22**, 663 (1967).
3) V. V. Gromov and L. G. Karaseva, "Chemistry of High Energy (in Russian)", **1**, 51 (1967).

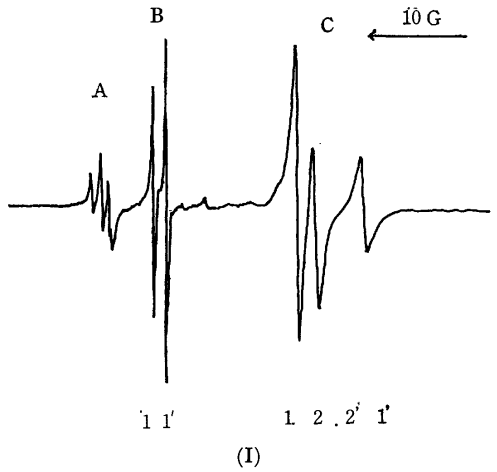

Fig. 1. A typical ESR spectrum of the natural $SrSO_4$ crystal.

probably due to different paramagnetic species. However, the lines may be classified for convenience into three groups, A, B, and C, from the higher to the lower magnetic field respectively as is illustrated in Fig. 1.

Group A was usually a minor one in the spectrum. Group B consisted of two resonance lines of a similar shape (designated as B-1 and B-1′ respectively), and Group C, probably of four lines (C-1 and C-1′, C-2 and C-2′). Figures 2a, b, and c show, respectively, the changes in the g-factors of these spectral lines when the sample crystal was rotated around its three axes (X, Y, Z). The principal g-values, calculated from the g-factor dependence, are shown in Table 1.

TABLE 1

Signal	g_1	g_2	g_3
A		1.9965—2.0018	
B-1	2.0041	2.0033	2.0021
B-1′	2.0041	2.0033	2.0021
C-1	2.0194	2.0094	2.0064
C-1′	2.0192	2.0091	2.0069
C-2	2.0167	2.0090	2.0082
C-2′	2.0166	2.0090	2.0082

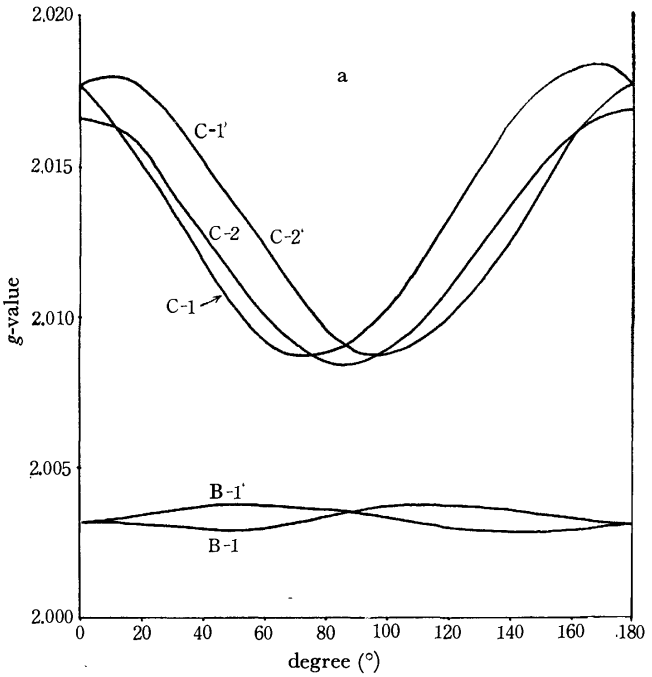

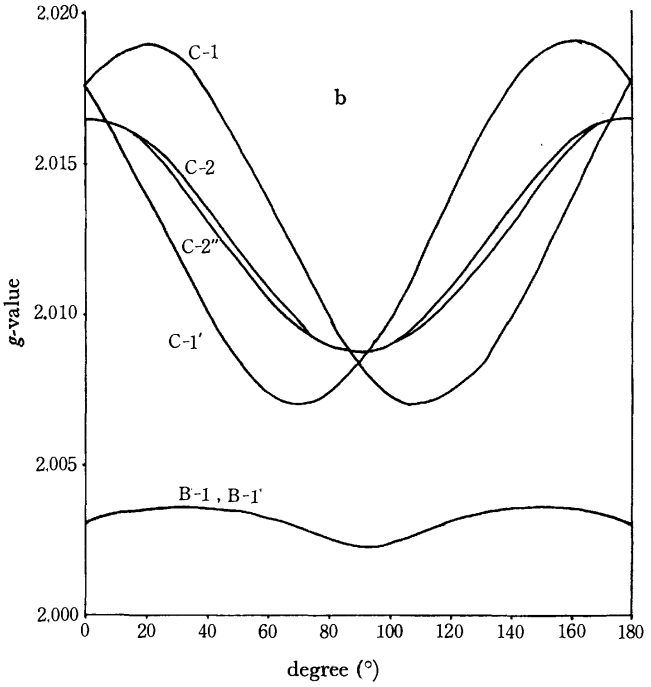

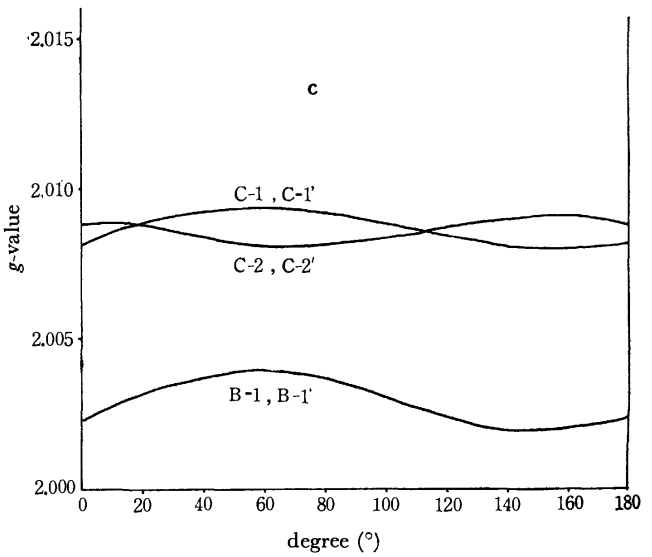

Fig. 2. a. b. c.
Angular dependence of g-factors of B and C signals around X, Y, and Z axes.

As is shown in Table 1, the principal g-values of the *paired* lines, such as B-1 and B-1′, C-1 and C-1′, and C-2 and C-2′, nearly coincided with each other, suggesting that the pair of signals is due to a common paramagnetic species and that the signals differ in their direction in the crystal in harmony with their twin characters, as revealed by X-ray analysis. The angular variation of the g-factor for Group A, consisting of several resonance lines, appeared to be rather complicated and did not permit us to derive any general trend. However, their g-values were all less than that

of a free spin (1.9965—2.0018).

We shall discuss the origin of each Group. First, the fact that the g-values of Group A were slightly less than that of a free spin suggests that Group A originates from electrons trapped at anion vacancies of F-centers rather than from hole defects in the $SrSO_4$ crystal; the g-values of F-centers in alkali halide crystals have been reported by many workers to be the results of negative g-shifts.[4] However, since g-values alone are not very informative, it is hard at present to identify the species corresponding to Group A without ambiguity.

The principal g-values of B-1 and B-1′ were isotropic and were close to that of a free spin (2.0041, 2.0033, 2.0021). It has already been reported by one of the present authors[1] that the γ-irradiated single crystals of K_2SO_4 give two kinds of ESR spectra; one is highly anisotropic, while the other is characterized by an almost isotropic g-tensor, with the principal g-values of 2.0033, 2.0033, and 2.0023. Accordingly, the two spectra were assigned to SO_4^- and SO_3^- respectively. Thus, on the basis of that report, the paramagnetic species corresponding to Group B are attributed to SO_3^- radicals rather than SO_4^- radicals.

The formation of O_3^- radicals has also been proposed for γ-irradiated single crystals of K_2SO_4.[5] The reported g-values (2.139, 2.0127, and 2.0102) for O_3^- radicals do not seem, however, to correspond to those of any Group. Also, the principal g-values for the SO_2^- produced in some ionic crystals have been reported to be 2.012, 2.0082, and 2.0037.[6] The g-values for our paramagnetic species are, again, distinguished from those of SO_2^-. Consequently, the origin of Group C seems to be associated with some lattice defects in the crystal rather than with sulfur- or oxygen-containing radicals.

The effects of thermal annealing on our paramagnetic species were investigated in order to support our assignments (Fig. 3). Group B was most stable on heating and did not decay until 350°C. Such a thermal stability has also been reported with SO_3^- in a γ-irradiated K_2SO_4 crystal;[3] this would support our assignment for the B signal.

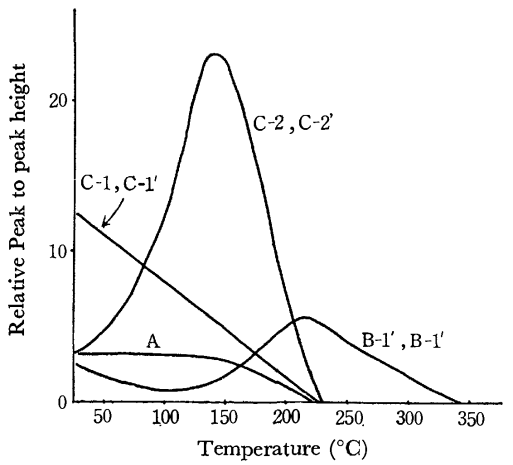

Fig. 3. Effects of thermal annealing on A, B, C signals.

Both the A and C groups were less stable on annealing; they nearly disappeared around the temperature of 200°C. However, it was rather surprising to note that the intensity of C-2 and C-2′ *increased* to a remarkable extent below 150°C, while the C-1 and C-1′ decreased monotonously within the temperature range studied. This phenomenon may suggest that the C-1 species can be distinguished from the C-2 species, even if the two species collapse at almost the same temperature. An inspection of the two annealing curves might lead one to presume that the C-1 paramagnetic center collapses upon heating by reaction with some other defects in the crystal, thus giving rise to another paramagnetic C-2 center.

As has already been mentioned, all the ESR signals (Fig. 1) disappeared completely when the crystal was heated to 350°C. However, some signals were restored upon UV irradiation. For example, when a highly-annealed sample, hence one showing no ESR signal, was irradiated with UV light at room temperature for less than 10 min, only the Group C signals were reproduced, while γ-irradiation for five hours showed a full recovery of all the signals, together with some additional signals. Thus, the C signal is considered to be quite sensitive to UV light as well as to heating as compared with the B singal.

UV absorption measurements of the sample crystal have shown that there exist two broad but distinct absorption bands around 250 and 550 mμ. In particular, the absorption band at 250 mμ was found to be unstable to heating; it disappeared completely at 200°C, quite in parallel with the ESR intensity of Group C upon annealing. All the results can be explained naturally if Group C is assumed to be associated with some labile crystal defects.

In recent years many types of color centers have been found, in particular in alkali halide crystals, and explained in terms of a variety of crystal defects. For example, the V- and F-centers in a potassium chloride crystal have been assumed to give two optical absorption bands[7] near the two wavelengths, 250 and 550 mμ, mentioned above with respect to our sample. Thus, the optical absorption at 250 mμ for the sample is likely to be associated with a color center such as a V-center, although further investigations will be required to confirm the assignments.

The authors are indebted to Professor Yoichi Iitaka for his X-ray analyses of the samples investigated in the present work. One of the authors (V.V.G) gratefully acknowledges the financial support from the Academy of Sciences of the USSR, which made it possbile for him to stay in Japan.

4) A. H. Kahn and C. Kittel, *Phys. Rev.*, **89**, 315 (1953). P. W. Atkins and M. C. R. Symons, "The Structure of Inorganic Radicals," Elsevier Pub. Co., (1967), p. 43.

5) N. Hariharan and J. Sobhanadri, *J. Mag. Resonance*, **1**, 639 (1969).

6) A. Reuveni, Z. Luz, and B. L. Silver, *J. Chem. Phys.*, **53**, 4619 (1970).

7) C. Kittel, "Introduction to Solid State Physics," John Wiley & Sons (1954), p. 315.

Chemical Behavior of Carbon in High-purity Silicon in the Dissolution and Fusion of the Matrix

Tadashi NOZAKI, Yoshihiro MAKIDE, Yoshifumi YATSURUGI,*
Yoshiyuki ENDO,* and Nobuyuki AKIYAMA*
The Institute of Physical and Chemical Research, Wako-shi, Saitama
**Komatsu Electronic Metals Co., Hiratsuka, Kanagawa*
(Received December 4, 1971)

The behavior of carbon in high-purity silicon in the dissolution and fusion of the matrix was studied by the ^{11}C-tracer technique. Silicon samples containing ^{11}C, either atomistically dispersed or mainly coagulated as SiC, were prepared. In alkali dissolution, no loss of ^{11}C was observed, and carbon originally dispersed in silicon was found to behave in a similar way to colloidal carbon under subsequent treatments. By $HF-HNO_3-KIO_4$ dissolution and succeeding $KMnO_4$ treatment, the dispersed carbon was oxidized almost quantitatively but the SiC coagulates were not completely decomposed. In alkali fusion a part of ^{11}C was lost. By fusion with $Pb_3O_4-B_2O_3$, carbon in both states was converted into CO_2. The results suggest a possible application of activation analysis to the measurement of the coagulation degree of carbon in high-purity silicon.

The behavior of a trace impurity element in the dissolution or fusion of a high-purity matrix has not yet been fully studied. We have examined the chemical behavior of carbon in semiconductor silicon in the decomposition of the matrix by means of radio-tracer technique. The results are given in this paper.

The following facts are known about carbon in silicon: (1) the solubility in solid silicon is slightly less than 3 ppm at the melting point, and carbon with a concentration above the solubility is coagulated as SiC;[1] (2) carbon is soluble up to 35 ppm in liquid silicon at the melting point, and in the solidification of carbon-saturated silicon slightly over 90% of the carbon coagulates into SiC;[1] (3) commercial semiconductor silicon usually contains from 30 ppb to 2 ppm of carbon;[1] and (4) carbon atoms dissolved in solid silicon occupy substitutionally the lattice points of the silicon crystal.[2]

As a radio-tracer, $^{11}C(\beta^+, T_{1/2}=20.3\text{ m})$ was used because it can be measured more easily and more precisely than ^{14}C by the scintillation counting of annihilation radiation. The excitation function and thick target yield for the $^{11}B(p,n)^{11}C$ reaction are known.[3,4] A sufficient activity of ^{11}C is easily produced by the proton bombardment of B_2O_3.

Experimental

Sample Preparation. The cyclotron at the Institute of Physical and Chemical Research was used for the proton bombardment, with the proton energy set at about 13 MeV. Three kinds of ^{11}C-containing samples were prepared by the following methods. (1) A silicon wafer doped with 50 to 100 ppm of boron was bombarded (a few μA beam, 20 min). After being left for 40 min for the ^{30}P formed by the $^{30}Si(p, n)^{30}P$ reaction to decay, the wafer was treated with a mixture of HF and HNO_3 to remove the surface contamination. (2) A B_2O_3 target was placed in a glass vessel with an aluminum foil window and bombarded with protons (about 10 μA beam, several minutes). A noticeable portion of the ^{11}C was evolved from the target as oxides and carried with a helium stream to the next room, where it was caught in a liquid-nitrogen trap after being passed through a dry-ice trap. About 50 mCi of carrier-free $^{11}CO_2$ was thus collected. A portion (about 1 g) of a semiconductor silicon rod, 1 cm in diameter and 5 cm long, sustained in an evacuated quartz tube was fused by radio-frequency heating, and the $^{11}CO_2$ was introduced into the tube. After being kept molten for a few minutes, the silicon was left to cool, and its surface layer was removed by etching. The silicon sample thus obtained contained a millicurie level of ^{11}C. (3) The process was similar to that in (2), but the silicon melt was brought into contact with a small amount of graphite powder or CO_2 gas.

The ^{11}C atoms in the sample prepared by Method (1) can occupy a higher-energy site in the silicon crystal since it has received the nuclear recoil energy in its nascent stage. Samples obtained from (1) and (2) contain the carbon homogeneously dispersed atomistically. The sample obtained from (3) contains coagulates of SiC. The carbon content of the samples prepared by each method was as follows: Method (1), 0.5—1 ppm; Method (2), 100—500 ppb; Method (3), 10—30 ppm of the coagulated carbon together with about 3 ppm of the dispersed carbon.

Dissolution and Fusion. The silicon matrix was decomposed by the following treatments: (a) dissolution in alkaline solutions, (b) dissolution in $HF-HNO_3$ solutions, (c) fusion with NaOH and $NaOH-NaNO_3$, and (d) fusion with $Pb_3O_4-B_2O_3$. About 0.5 g of the sample was used for each treatment. In most cases the products were treated with various reagents.

(a) The sample was pulverized and added to a NaOH solution (5 mol/*l*, 25 m*l*). When the dissolution reaction subsided, the mixture was gently heated to boil. Water was occasionally added to keep the volume of the solution almost constant. The sample was also subjected to a similar treatment with a NaOH solution (5 mol/*l*) containing $NaNO_3$ (2 mol/*l*), $KMnO_4$ (0.5 mol/*l*) or CrO_3 (0.5 mol/*l*) and with a Na_2O_2 solution (2.5 mol/*l*). In the absence of $KMnO_4$ or Na_2CrO_4, the silicon was dissolved within 30 min.

(b) The sample in small plates or blocks was added to a mixture of HF (46%, 15 m*l*) and HNO_3 (60%, 15 m*l*). The silicon was dissolved in 10 min with heat evolution. The $HF-HNO_3$ mixture containing KIO_4 (3 g) was also

1) T. Nozaki, Y. Yatsurugi, and N. Akiyama, *J. Electrochem. Soc.*, **117**, 1566 (1970).
2) R. C. Newman and J. B. Willis, *J. Phys. Chem. Solid*, **26**, 373 (1964).
3) M. Furukawa, Y. Ishizaki, Y. Nakano, T. Nozaki, Y. Saji, and S. Tanaka, *J. Phys. Soc. Japan*, **15**, 2167 (1960).
4) T. Nozaki, T. Okuo, H. Akutsu, and M. Furukawa, This Bulletin, **39**, 2685 (1966).

used to accelerate dissolution.

(c) The sample was coarsely pulverized and added in small portions to NaOH (15 g) or a mixture of NaOH (10 g) and $NaNO_3$ (5 g) kept just above their melting points. Since the reaction was highly exothermic, the rate could not be controlled.

(d) A mixture of the pulverized sample, Pb_3O_4 (30 g) and B_2O_3 (6 g) was put into a Vycor-glass tube, and heated under an oxygen stream by a town gas-oxygen flame, first gently and then violently. The fusion was completed within 5 min, leaving a pale yellow glassy matter with globules of metallic lead when cooled. The oxygen stream was led to an Ascarite column after being passed through an I_2O_5–H_2SO_4–SiO_2 column in order to confirm the quantitative recovery of the ^{11}C.

For acidification of the resulting alkaline solution, HCl (1:1), H_2SO_4 (1:2) or HNO_3 (1:1) was added, in about twice the stoichiometrical amount for the neutralization of the alkali used. The cake of the alkali fusion was treated with the acids diluted further twice. In some cases, $KMnO_4$ (3 g) or CrO_3 (3 g) was added to the mixture, which was then boiled for 5 min. For collection of the suspending colloidal particles in the solution, fine powder (50 mg) of quartz or charcoal was stirred into the solution and precipitated with the particles by centrifugation. For dissolution of the precipitated hydrated silicon oxide, HF (46%, 5 m*l*) was added to the mixture.

Radioactivity Measurement. Annihilation radiation from the sample was measured by a scintillation counter with a single channel analyzer. In order to confirm the radiochemical purity of the original samples, the γ-ray spectrum and decay curve were measured; no radio-nuclide other than ^{11}C was found. Before and after each treatment, the radioactivity of the sample was measured from outside the vessel. Care was taken to keep the counting efficiency constant.

Since the original silicon contained a high-level activity of ^{11}C, the sample was placed at least 30 cm apart from the scintillator, thus making the counting efficiency almost insensitive to a small variation in the sample position. When the sample lost most of its ^{11}C activity, it was placed close to the scintillator, and the efficiency was calibrated by a resin-covered ^{22}Na standard source inserted in the center of a non-radioactive replica of the sample. In order to stop the positrons completely and to make the self-absorption constant, the silicon sample before the dissolution or fusion was sandwiched between polystyrene or iron plates with such a thickness as to give almost the same absorption as the self-absorption in the sample after the treatment. The effect of volume change caused by the addition of acid was corrected by insertion of a polystyrene plate beneath the sample in the measurement before the addition.

Results and Discussion

The results for the silicon sample containing only the atomistically dispersed carbon are given in Fig. 1. No significant difference in the behavior of ^{11}C was observed between the samples prepared by Methods (1) and (2).

In the alkali dissolution, no loss of ^{11}C was observed and the behavior of ^{11}C was not affected by the addition of $NaNO_3$ or Na_2O_2. In the presence of $KMnO_4$ or K_2CrO_4 the dissolution did not proceed smoothly, probably because the silicon surface was covered with oxides of manganese or chromium. We see from

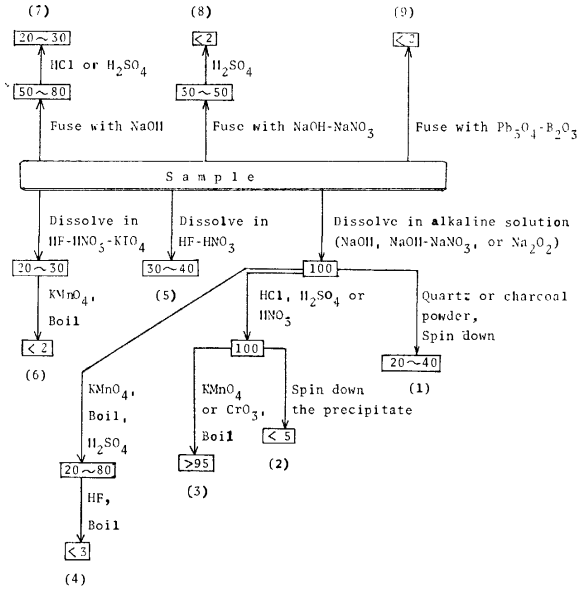

Fig. 1. Behavior of homogeneously dispersed carbon. Fraction of ^{11}C remaining in the reaction mixture (%). Figures in the parentheses are the treatment number in the text.

Treatments 1, 2, and 3 (Fig. 1) that the carbon in the alkaline solution was not dissolved as carbonate or any other soluble compound but turned into colloidal particles. The solution contained Na_2CO_3 in a quantity sufficient for a carrier of $^{11}CO_3^{2-}$. In order to examine whether CO_2 was evolved quantitatively by acidification of the solution, a solution containing $Na_2{}^{11}CO_3$ and Na_4SiO_4 was prepared and acidified; the evolution was almost quantitative, although a small fraction (less than 10%) of ^{11}C sometimes remained even after the solution was boiled. The results of Treatments 2 and 3 suggest that the carbon was held in the precipitate of hydrated silicon oxide formed by the acidification of the alkaline silicate solution. In Treatment 4 (Fig. 1), the fraction of ^{11}C remaining after the addition of H_2SO_4 varied remarkably depending mainly on the stirring efficiency and other conditions at the moment of addition. When the boiling in Treatment 4 before the acidification was prolonged, no noticeable difference in the remaining fraction of ^{11}C was found. It can thus be deduced that the oxidation of carbon by $KMnO_4$ was slow in the alkaline solution but made fast by the acidification, after which, however, hydrated silicon oxide soon precipitated embracing the carbon and thus preventing oxidation. When HF was added, the silicon oxide was dissolved and the carbon was rapidly oxidized. Treatment 6 (Fig. 1) also shows the effectiveness of the $KMnO_4$ oxidation in acid solution. The inefficiency of the oxidation in the alkaline solution might be due to the covering of the carbon suspension with hydroxides or carbonates of impurity elements in the reagents.

After the alkali fusion (Treatments 7 and 8, Fig. 1) the fraction of the ^{11}C remaining is found to depend markedly on the vigorousness of the fusion reaction—the more vigorous the reaction, the less the fraction remaining. The effect of $NaNO_3$ as oxidizing agent

was clearly observed in the alkali fusion.

Either by the dissolution in $HF-HNO_3-KIO_4$ and subsequent $KMnO_4$ treatment or by the $Pb_3O_4-B_2O_3$ fusion, the dispersed carbon was oxidized almost quantitatively. Thus either procedure could be used for the separation of ^{11}C in the activation analysis of carbon in silicon by means of the $^{12}C(^3He,\alpha)^{11}C$ reaction. A procedure for the activation analysis using Treatment 6 was given in detail.[5] In order to facilitate the complete oxidation of the carbon, however, it is recommended to use a larger quantity (10 g) of $KMnO_4$ than that given previously (1 g).[5] Treatment 9 (Fig. 1) was developed and has been used by Engelmann and co-workers.[6] From our experience in this treatment, a part of the carbon was likely to be incorporated in lead drops formed from Pb_3O_4 not being oxidized easily unless oxidation was completed rapidly. In our determination, we pulverize the sample, mix it with $Pb_3O_4-B_2O_3$ powder, and heat the mixture in a Vycor-glass tube with a town gas-oxygen flame.

The behavior of the coagulated carbon in the above two treatments are shown in Fig. 2. The sample contained also dispersed carbon. The entire carbon was decomposed by $Pb_3O_4-B_2O_3$ fusion. In the dissolution with $HF-HNO_3-KIO_4$ followed by treatment with $KMnO_4$, the decomposition of the coagulated carbon was incomplete. It is certain that the more perfect the crystal structure of the SiC coagulates, the less complete the decomposition into CO_2. In the activation analysis of carbon by the $^{12}C(^3He,\alpha)^{11}C$ reaction, a part of the ^{11}C formed in the coagulates is driven out of them by the nuclear recoil effect and converted into $^{11}CO_2$ by means of the $HF-HNO_3-KIO_4-KMnO_4$ treatment. Thus in this case, the fraction of ^{11}C converted depends also on the grain size of the coagulates.

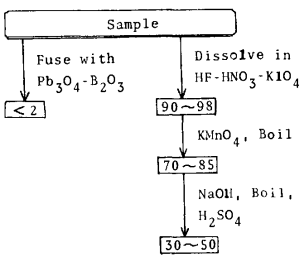

Fig. 2. Behavior of coagulated carbon.
Fraction of ^{11}C remaining in the reaction mixture (%).

TABLE 1. SENSIBILITY OF THE THREE METHODS FOR THE DIFFERENT PHYSICAL STATES OF CARBON IN SILICON

Method		Homogeneously dispersed carbon	Coagulated carbon
Activation analysis	$Pb_3O_4-B_2O_3$ fusion (or nondestructive)	+	+
	$HF-HNO_3-KIO_4-KMnO_4$ dissolution	+	±
Infrared spectrophotometry		+	−

The three methods for the determination of carbon in semiconductor silicon are given in Table 1. The nondestructive activation analysis (the first method) can be applied only to carbon-doped silicon. The fraction of the coagulated carbon determined as carbon by the second method is dependent on the state of the coagulates, namely, the grain size and the perfectness of the crystal structure. We have obtained the calibration curve for infrared spectrophotometry (the third method) using various semiconductor silicon samples analyzed for carbon by the activation analysis.

Therefore, by the use of all the three methods or two of them, it is now possible to get information on the physical state of carbon in silicon, though high accuracy is often needed in the determinations. Actually, when silicon samples of relatively high carbon contents were kept at 1300°C for many hours, the infrared-active carbon contents decreased gradually without any significant change in the results obtained by the second method.

We would like to express our thanks to members of the Cyclotron Operation Group of the Institute of Physical and Chemical Research for their help in the bombardment.

5) T. Nozaki, Y. Yatsurugi, and N. Akiyama, *J. Radioanal. Chem.*, **4**, 87 (1970).

6) Ch. Engelmann, J. Gosset, M. Loeuillet, A. Marschal, P. Ossart, and M. Boissier, "Modern Trends in Activation Analysis," Vol. 2, ed. by J. R. DeVoe, U. S. Dept. of Commerce, Washington D. C. (1969), p. 819.

Reactions of Diazoketones in the Presence of Metal Chelate. IV. Formation and Reaction of Carbonyl Ylides[1]

Kozaburo UEDA, Toshikazu IBATA, and Matsuji TAKEBAYASHI*

Department of Chemistry, College of General Education, Osaka University, Toyonaka, Osaka

(Received January 17, 1972)

The copper chelate-catalyzed decomposition of *o*-methoxycarbonyl-α-diazoacetophenone was carried out in benzene. The reaction gave a dimer of a carbonyl ylide intermediate. The intermediate was trapped with dipolarophiles such as *trans*-dibenzoylethylene, ethyl fumarate, isoprene and dimethyl acetylenedicarboxylate, yielding 1,3-dipolar adducts in a stereospecific and stereoselective manner. Similar results were obtained in the catalytic decomposition of *o*-(*n*-butoxycarbonyl)-α-diazoacetophenone. The configuration of adducts and the mechanism of the reaction are discussed.

Carbonyl ylide has been reported as an intermediate in the cycloaddition of some oxiranes having electron attracting group-s to olefinic and acetylenic dipolarophiles.[2] The formation of carbonyl ylide is also expected in the reaction of carbene with carbonyl compound. However, very few example-s were found in the literature.[3] In a previous paper,[1a] we showed that the copper chelate catalyzed reaction of α-diazoacetophenone (I) with aromatic carbonyl compounds such as benzaldehyde and acetophenone gave the corresponding tetrahydrofurans (V) and dioxolanes (VI) accompanied by some by-products derived from benzoylcarbenes, and that the mechanism of the reaction could be explained by assuming a carbonyl ylide intermediate (III), produced by the reaction of a ketocarbene-copper chelate complex, copper carbenoid (II) with carbonyl compounds (Scheme 1).

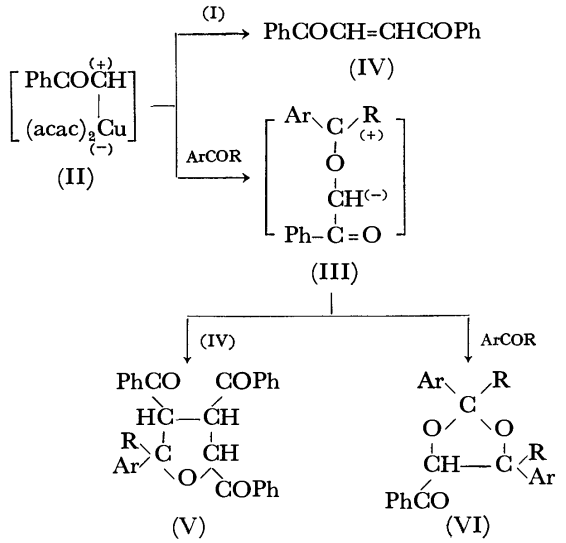

Scheme 1.

This paper deals with the copper chelate-catalyzed decomposition of substituted α-diazoacetophenones having methoxycarbonyl group at *ortho*-position.

Results and Discussion

Catalytic Decomposition of o-*Methoxycarbonyl-α-diazoacetophenone (VII) in Benzene.* The bis(acetylacetonato)-copper-catalyzed decomposition of VII was carried out in benzene at 80°C under nitrogen. The reaction gave X as the principal product, which had a similar structure to that obtained by Zimmerman and Simkin[4] in the photochemical reaction of 2,3-epoxy-2-methyl-3-phenylindanone. The IR spectrum of X showed a streching vibration band of carbonyl group at 1712 cm^{-1} and an absorption band of newly formed ring-ether linkages at 1285 and 1260 cm^{-1}, and showed no carbonyl streching vibration band of ester group of the starting diazo compound. Ullman and Milks[5] have obtained an another type of dimer yielded by the 1,3-dipolar cycloaddition of benzopyrilium oxide to carbonyl group of indenone oxide in the thermal reaction of 2,3-diphenylindenone oxide. Ullman-type structure of our reaction product (X) may be ruled out by the absence of characteristic IR absorption bands of dioxolane[1a] in the region of 1100—1000 cm^{-1}. The failure of the isolation of indenone oxide (IXd) may support the structure Xa because Xb is the adduct of IXd and IXb.

Since none of the Wolff rearrangement products and formal dimers of *o*-methoxycarbonyl-benzoylcarbene were obtained during the reaction, one reasonable mechanism involves forming of a ketocarbene-copper chelate complex (VIII), a copper carbenoid, followed by the formation of a carbonyl ylide intermediate (IX), and a head-to-tail dimerization (Scheme 2).

This intermediate (IX) seems to be produced intramolecularly by electrophilic attack of carbenoid-carbon on carbonyl oxygen at *ortho*-position, contrary to the case of intermolecular reaction of a copper-carbenoid with methyl benzoate.[1a] Facilities for the formation of carbonyl ylide (IX) may be attributed to that the carbonyl group of *o*-substituent is close to the carbenoid

* Present address: Department of Chemistry, Faculty of Science and Technology, Kinki University, Higashiosaka, Osaka.

1) a) Part III: M. Takebayashi, T. Ibata, and K. Ueda, This Bulletin, **43**, 1500 (1970). b) Presented in part at the 23rd International Congress of Pure and Applied Chemistry, Boston, Mass., U.S.A., July, 1971. Abstracts of paper, p. 124. (c) Preliminary Communication: M. Takebayashi, T. Ibata, K. Ueda, and T. Ohashi, This Bulletin, **43**, 3964 (1970).

2) a) H. Hamberger and R. Huisgen, *Chem. Commun.*, 1190 (1971). b) A. Dahmen, H. Hamberger, R. Huisgen, and V. Markowski, *Chem. Commun.*, 1192 (1971). c) References cited therein.

3) R. Huisgen, and R. Bermes, *Angew. Chem.*, **75**, 630 (1963).

4) H. E. Zimmerman and R. D. Simkin, *Tetrahedron Lett.*, 1847 (1964).

5) E. F. Ullman and J. E. Milks, *J. Amer. Chem. Soc.*, **84**, 1315 (1962); *ibid.*, **86**, 3814 (1964).

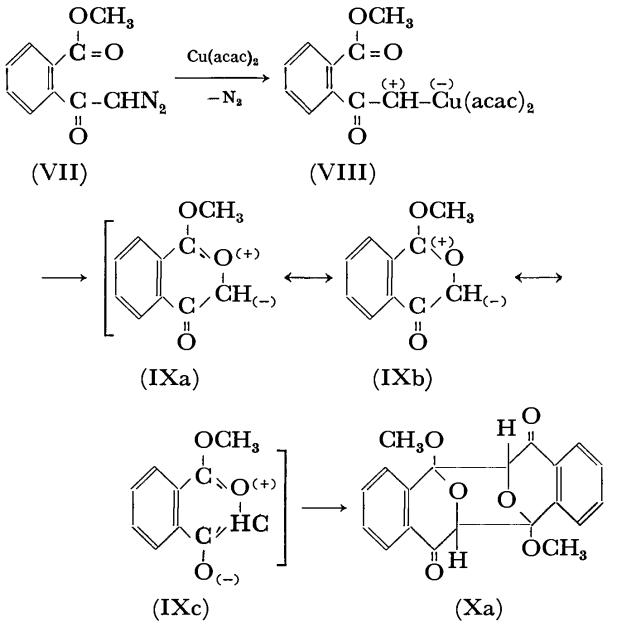

Scheme 2.

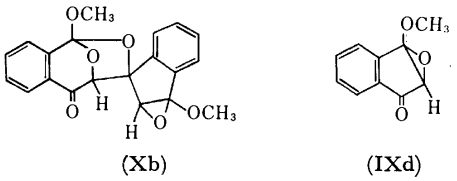

carbon atom (neighboring group participation), and that the newly created ring of IX is stabilized owing to the contribution of its canonical formula-e (IXa, IXb, and IXc). The contribution of IXc to the intermediate seems to be smaller than that of carbonyl ylide structure (IXa), because the color of the reaction mixture does not show the red color of benzopyrilium oxide,[5] but main-tain-s blue color of copper chelate during the reaction.

Reaction of o-Methoxycarbonyl-α-diazoacetophenone (VII) with Unsaturated Compounds. In order to investigate the reactivities of the carbonyl ylide toward dipolarophiles, the copper chelate-catalyzed decomposition of VII was carried out in the presence of unsaturated compounds. In the presence of *trans*-bis(*p*-methylbenzoyl)ethylene, the reaction gave an adduct (XI) in 75% yield. No cyclopropane derivatives, which would be formed by the reaction of the copper-carbenoid with the ethylenic compound, were recognized by the precise investigation of IR and NMR spectra of the reaction products. The coupling constants of NMR spectrum

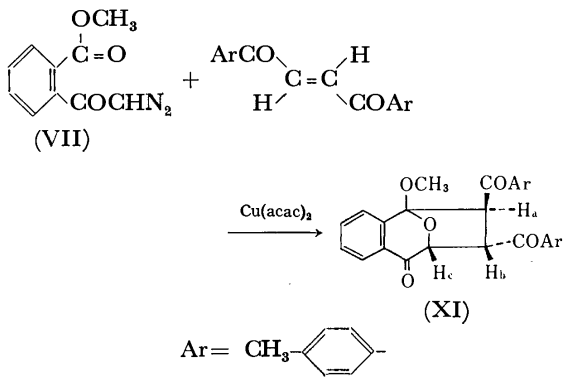

of XI show that H_a and H_b seems to be oriented in *trans*-configuration judging from its small value of $J_{a,b}=2.0$ Hz, whereas H_b and H_c to be in *cis*-configuration ($J_{b,c}=6.0$ Hz) from the analogy to the stereochemistry fo pyrrolidine system.[6]

The results indicate that the addition of IX to the ethylenic compound may be stereospecific, and that the reaction may proceed through a concerted ($_\pi 4_s + _\pi 2_s$) type of cycloaddition according to the Woodward-Hoffman rule.[7]

In a similar manner, the dipolar intermediate (IX) was trapped with diethyl and dimethyl fumarates to give adducts, XII and XIII, in yields of 59 and 70%, respectively.

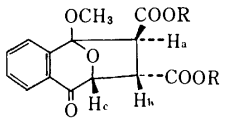

(XII) R: C_2H_5
(XIII) R: CH_3

The NMR spectra showed that the configurations concerning with H_a, H_b, and H_c of XII and XIII are quite same to that of XI.

Two kinds of transition states A and B, may be possible in the addition of IX to the ethylenic compounds (Scheme 3). The one (A) gives an adduct in which H_b and H_c are oriented in *cis*-configuration, whereas the other (B) leads to an adduct in which H_b and H_c are in *trans*-configuration. The fact that H_b and H_c of the adducts (XI, XII, and XIII) are oriented in *cis*-configuration indicates that the addition will take stereoselectively through A, owing to the overlapping of π-electrons of IX with those of acyl group of ethylenic compounds and/or to the repulsion of methoxy group of IX against acyl group of the ethylenic compounds.

The reaction of VII with dimethyl maleate seems to be remarkably slower than that with dimethyl fumarate,

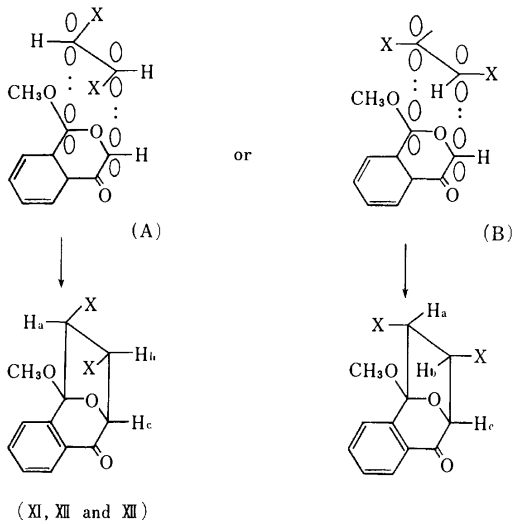

Scheme 3.

6) a) J. W. Lown and K. Matsumoto, *Can. J. Chem.*, **48**, 2215 (1970). b) R. Huisgen, W. Scheer, G. Szeimies, and H. Hube, *Tetrahedron Lett.*, 397 (1966).

7) R. B. Woodward and R. Hoffman, "The Conservation of Orbital Symmetry" Academic Press Inc, Weinheim (1970).

because the reaction of VII with a mixture of maleate and fumarate (99: 1), which contained almost equimolecular amount of dimethyl fumarate to VII, gave only an adduct (XIII) of IX to dimethyl fumarate in 70% yield. Dimethyl fumarate was found to be consumed completely during the reaction by the gas chromatographic analyses of recovered substrate.

In the presence of isoprene, two stereoisomeric adducts, XIV and XV, were obtained in yields of 34 and 43%, respectively. The NMR spectra show that the H_a of XV is deshielded by 0.14 ppm in comparison with that of XIV owing to π-electrons of the ethenyl group. The results indicate that the isoprene reacts with the carbonyl ylide (IX) by 1,2-addition to give XIV and XV. Cyclooctadiene-1,3 also reacted with IX to afford a 1: 1 adduct in a 18% yield, whose structure was assumed to be XVI by the similarity to the reaction with isoprene.

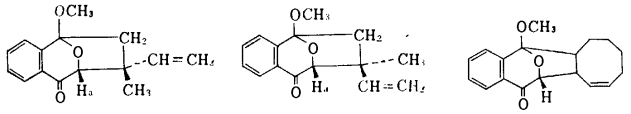

(XIV) (XV) (XVI)

Methyl acrylate, *trans*-methyl crotonate, crotonaldehyde, acrylonitrile, and crotononitrile gave also cycloaddition products in high yields (60—90%).[8]

However, *cis*- and *trans*-stilbenes, maleic anhydride, chalcone and norbornadiene gave no cycloaddition products, although the reason is not clear. In these cases, the dimer (X) was obtained in 40—50% yield.

In the presence of dimethyl acetylenedicarboxylate, the reaction gave XVII as an adduct in 70% yield.

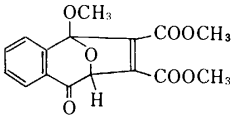

(XVII)

Similar results were obtained in the reaction of *o*-(*n*-butoxycarbonyl)-α-diazoacetophenone (VII′) as is shown in Table 1.

Table 1. Reaction of *o*-(*n*-butoxycarbonyl)-α-diazoacetophenone with dipolarophiles

Dipolarophile		Adduct Yield (%)	Adduct Mp (°C)
C_6H_5CO, H / C=C / H, COC_6H_5	(XI′)	92	91—92
$H_3COOC-C\equiv C-COOCH_3$	(XVII′)	80	oil

The Catalytic Decomposition of o-*Methoxycarbonyl-α-diazoacetophenone (VII) in Protic Solvents.* The copper chelate-catalyzed decompositions of VII were carried out in protic solvents such as ethyl alcohol and dioxane-water. The reaction gave isochromanedione-1,4 (XVIII) in yields of 40—50%, without any insertion products (XIX) of the ketocarbene to O–H bond of ethyl alcohol and water. The formation of XVIII

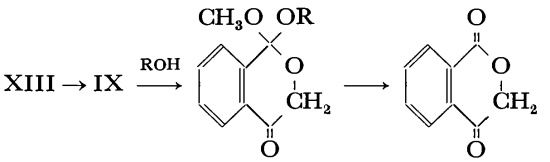

(XVIII)

Scheme 4.

gives another support to the intermediacy of carbonyl ylide (IX) as is shown in Scheme 4.

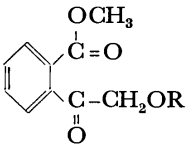

(XIX)

These results mentioned above suggest that the copper carbenoid (VIII) converts preferentially to give a carbonyl ylide intermediate (IX), followed by 1,3-dipolaraddition to unsaturated compounds.

Experimental

All melting and boiling points are uncorrected. The IR spectra were measured on a Hitachi Infrared Spectrometer, model EPI-S2. The NMR spectra were recorded at 60 Mc with a Varian Associates model A-60 Spectrometer, using tetramethylsilane as an internal standard.

Materials. o-*Alkoxycarbonyl-α-diazoacetophenones* were prepared starting from alkyl hydrogen phthalate according to the method of Hodson.[9]

o-*Methoxycarbonyl-α-diazoacetophenone*, mp 62.0—62.3°C. IR (KBr): 2200 (-N≡N), 1725 (ester C=O), 1605 (diazoketone C=O), 1370, and 740 cm^{-1} (Ph).

Found: C, 58.88; H, 3.89; N, 13.61%. Calcd for $C_{10}H_8O_3N_2$: C, 58.82; H, 3.95; N, 13.72%

o-(n-*Butoxycarbonyl*)-α-*diazoacetophenone*, oil, partially decomposes on standing at room temperature. IR (KBr); 2200 (-N≡N), 1725 (ester C=O), 1610 (diazoketone C=O), 1350, and 735 cm^{-1} (Ph).

Catalytic Decomposition of VII in Benzene. A solution of 2.0 g (0.01 mol) of VII and 0.05 g (1.9×10^{-4} mol) of $Cu(acac)_2$ in 50 m*l* of benzene was heated at 80°C under an atmosphere of nitrogen. The color of the reaction mixture turned dark-brown with an evolution of almost theoretical amount of nitrogen. After the reaction was over, the catalyst was separated by filtration and the solvent was removed by distillation. The residue was fractionated by silicagel chromatography (solvent: benzene) and a colorless crystalline product was obtained accompanied by a small amount of unknown solid. The structure of the crystalline product (X) was determined by elemental analyses and IR and NMR spectra after repeated crystallization from benzene-*n*-heptane, mp 233—235°C, yield 0.48 g (27%). IR (KBr): 1712 (ring C=O), 1285, 1260, 1237 (ring C=O and C–O–C), and 1052 cm^{-1} (C–O-CH_3)[10] NMR ($CDCl_3$): 1.7—2.7 (m, 8H, Ph), 5.08 (s, 1H, methyne-H), 5.62 (s, 1H, methyne-H), 6.30 (s, 3H, OCH_3), and 6.54 τ (s, 3H, OCH_3).

Found: C, 68.05; H, 4.32%. Calcd for $C_{20}H_{16}O_6$: C, 68.18; H, 4.58%.

8) The detail will be published elsewhere.

9) D. Hodson, G. Holt, and D. K. Wall, *J. Chem. Soc., C*, 971 (1970).

10) No absorption band of ester group was observed.

Reaction of VII and VII' with Ethylenic Compounds. A solution of VII or VII' (0.01 mol) in 50 ml of benzene was added dropwise to a solution of $Cu(acac)_2$ (1.9×10^{-4} mol) and an unsaturated compound (0.01 mol) in 100 ml of benzene on stirring at 80°C under the atmosphere of nitrogen. The reaction products were separated by silica gel chromatography and were identified by elemental analyses and IR and NMR spectroscopy.

In the reaction of VII with trans-*bis*(p-*methylbenzoyl*)*ethylene*, a white crystalline product (XI), mp 193.0—194.0°C, was obtained without any other detectable by-products, yield 3.50 g (83%). IR (KBr): 1710 (ring C=O), 1280, 1240 (ring C–O–C), 1065 (C–O-CH_3), 833, and 772 cm^{-1} (Ph). NMR ($CDCl_3$): 1.7—2.8 (m, 12H, Ph), 4.65 (d, 1H, Hc), 4.93 (d, 1H, Ha), 5.26 (dd, 1H, Hb), 6.32 (s, 3H, OCH_3), and 7.54 τ (s, 6H, CH_3). $J_{a,b}=2.0$ Hz, $J_{b,c}=6.0$ Hz.

Found: C, 76.53; H, 5.47%. Calcd for $C_{28}H_{24}O_5$: C, 76.35; H, 5.49%.

In the reaction of VII' with trans-*dibenzoylethylene*, a white crystalline adduct (XI'), mp 91.0—92.0°C, was isolated, yield 4.18 g (92%). IR (KBr): Nearly same to above concerning with characteristic bands. NMR ($CDCl_3$): 1.7—3.3 (m, 14H, Ph), 4.75 (d, 1H, Hc), 5.10 (d, 1H, Ha), 5.40 (dd, 1H, Hb), 6.0—6.25 (m, 2H, OCH_2), 8.0—9.0 (m, 4H, CH_2), and 9.10 τ (broad s, 3H, CH_3). $J_{a,b}=1.9$ Hz, $J_{b,c}=5.8$ Hz.

Found: C, 76.78; H, 5.76%. Calcd for $C_{29}H_{26}O_5$: C, 76.63; H, 5.77%.

In the reaction of VII with diethyl fumarate, an adduct (XII), mp 36.5—37.0°C, were obtained, yield 2.05 g (59%). NMR ($CDCl_3$): 1.7—3.0 (m, 4H, Ph), 5.20 (d, 1H, Hc), 5.73 (q, 2H, OCH_2), 6.02 (d, 1H, Ha), 6.12 (q, 2H, OCH_2), 6.40 (s, 3H, OCH_3), 6.52 (dd, 1H, Hb), 8.65 (t, 3H, CH_3), and 8.90 τ (t, 3H, CH_3). $J_{a,b}=1.8$ Hz, $J_{b,c}=5.8$ Hz. IR (KBr): 1735 (ester C=O), 1710 (ring C=O), 1288, 1232 (C–O–C), and 760 cm^{-1} (Ph).

Found: C, 61.76; H, 5.52%. Calcd for $C_{18}H_{20}O_7$: C, 62.06; H, 5.79%.

In the reaction of VII with dimethyl fumarate, a crystalline product (XIII), mp 110.5—111.0°C, was obtained, yield 2.25 g (70.3%). NMR ($CDCl_3$): 1.7—3.3 (m, 4H, Ph), 4.98 (d, 1H, Hc), 6.10 (d, 1H, Ha), 6.52 (dd, 1H, Hb), 6.20 (s, 3H, OCH_3), 6.40 (s, 3H, OCH_3), and 6.55 τ (s, 3H, OCH_3). $J_{a,b}=1.7$ Hz, $J_{b,c}=6.0$ Hz. IR (KBr): 1735 (ester C=O), 1710 (ring C=O), 1287, 1233 (ring C–O–C), 980, and 760 cm^{-1} (Ph).

Found: 59.86; H, 4.84%. Calcd for $C_{16}H_{18}O_7$: C, 60.00; H, 5.04%.

In the reaction of VII with isoprene, two kinds of liquid products (XIV and XV), were isolated in yields of 0.78 and 0.98 g (34 and 43%), respectively. IR (neat) of XIV: 1700 (C=O), 1635 (C=C), 1290 (ring C–O–C), 1050 (C–O-CH_3), and 765 cm^{-1} (Ph). NMR ($CDCl_3$) of XIV: 1.9—2.8 (m, 4H, Ph), 4.7—5.8 (m, 3H, CH=CH_2), 6.55 (s, 3H, OCH_3), 8.13 (s, 1H, methyne-H), 6.6—8.4 (m, 2H, CH_2), and 8.57 τ (s, 3H, CH_3).

Found: C, 73.41; H, 6.45%. Calcd for $C_{15}H_{16}O_3$: C, 73.75; H, 6.60%. IR (neat) of XV: The same above. NMR ($CDCl_3$) of XV: 1.9—2.8 (m, 4H, Ph), 4.7—5.8 (m, 3H, CH=CH_2), 6.55 (s, 3H, OCH_3), 8.32 (s, 1H, methyne-H), 6.6—8.4 (m, 2H, CH_2), and 8.55 τ (s, 3H, CH_3).

Found: C, 73.56; H, 6.35%. Calcd for $C_{15}H_{16}O_3$: C, 73.75; H, 6.60%.

In the reaction of VII with cyclooctadiene-1,3, a liquid product (XVI) and unidentified oil (XVI') were obtained in yields of 0.49 g (18.4%) and 0.16 g, respectively. IR (neat) of XVI: 1700 (ring C=O), 1300, 1250 (ring C–O–C), 1060 (C-OCH_3), and 770 cm^{-1} (Ph). NMR ($CDCl_3$) of XVI: 1.7—2.7 (m, 4H, Ph), 4.0—5.5 (m, 2H, CH=CH), 6.50 (s, 3H, OCH_3), and 6.6—9.3 τ (m, 11H, CH and CH_2).

Found: C, 75.87; H, 7.12%. Calcd for $C_{18}H_{20}O_3$: C, 76.03; H, 7.09%.

IR (neat) of XVI': 1700 (ring C=O), 1290, 1250 (ring C–O–C), 1060 (C-OCH_3), 770, and 740 cm^{-1} (Ph). NMR ($CDCl_3$) of XVI': 1.7—3.2 (m, 8H, Ph), 4.0—5.5 (m, contaminated with a trace of XVI), 6.55 (d, 6H, OCH_3), and 6.7—9.3 τ (m, 12H, CH and CH_2).

Reactions of VII and VII' with Acetylenic Compounds. The reactions were carried out in similar manner as described above.

In the reaction of VII with dimethyl acetylenedicarboxylate, a liquid product (XVII) was obtained, yield 2.11 g (70.3%). NMR ($CDCl_3$): 1.9—2.7 (m, 4H, Ph). 4.50 (s, 1H, methyne-H), singlets at 6.17, 6.30 and 6.47 τ (9H, OCH_3). IR (neat): 1725 (ester C=O), 1715 (ring C=O), 1660 (C=C), 1270 (ring C–O–C) and 760 cm^{-1} (Ph).

Found: C, 60.45; H, 4.31%. Calcd for $C_{16}H_{14}O_7$: C, 60.38; H, 4.43%.

In the reaction of VII' with dimethyl acetylenedicarboxylate, an oily product (XVII') was isolated, yield 2.99 g (80%). NMR ($CDCl_3$): 2.0—2.7 (m, 4H, Ph), 4.60 (s, 1H, methyne-H), 6.1—6.4 (q, 2H, OCH_2), 6.20 (s, 6H, OCH_3) and 8.1—9.15 τ (m, 7H, CH_2 and CH_3). IR (neat): 1725 (ester C=O), 1715 (ring C=O), 1660 (C=C), 1260 (ring C–O–C) and 760 cm^{-1} (Ph).

Catalytic Decomposition of VII in Protic Solvents. The catalytic decomposition of VII (2 g, 0.01 mol) in 150 ml of a mixed solvent of dioxane and water (5:1) was carried out as mentioned above. A white crystalline product (XVIII), 101.0—102.5°C, was obtained, yield 0.81 g (50%). IR (KBr): 1725 (ring C=O), 1280, 1140 (ring C–O–C) and 763 cm^{-1} (Ph). NMR ($CDCl_3$): 1.6—2.3 (m, 4H, Ph) and 4.90 τ (s, 2H, CH_2).

Found: C, 66.38; H, 3.51%. Calcd for $C_9H_6O_3$: C, 66.67; H, 3.73%.

The same product (XVIII) was isolated in the reaction in ethyl alcohol (yield; 0.72 g, 44%).

Anodic Reaction of 2-Furoic Acids. II. Electrolysis of Methyl 5-Acetyl-2-furoate and Its Homologous in Protic Solvents

Sigeru TORII, Hideo TANAKA, and Tsutomu OKAMOTO
Department of Industrial Chemistry, Okayama University, Okayama
(Received January 17, 1972)

Anodic oxidation of methyl 5-acetyl-2-furoate **4** in methanol leads to ring-opened diesters **8** and **9**, and lactone **10** in addition to methyl 5-acetyl-2,5-dimethoxy-2,5-dihydro-2-furoates **7**. Formation of **8**, **9**, and **10** can be rationalized as arising from **7**. On the other hand, oxidation of methyl 5-methoxy- and 5-bromo-2-furoates, **5** and **6**, also give **9** and **10**. The reactions involve initial production of cationic intermediates **13** and **15**, which are readily solvolized to give **8**, **9**, and **10**. A mechanism of the formation of the intermediates **13** from **5**, **6**, and **7** is discussed.

Recently a review[1] describing an anodic oxidation of 2-acetylfuran in methanol in the presence of sulfuric acid suggested that the corresponding 2,5-dimethoxy-2,5-dihydrofurans was isolated in low yield, but details on isolation and on structural assignment of the reaction products have not been described. Apparently little attention has been paid to the fate of the acetyl group attached to the furan ring under this oxidation conditions.

In the previous investigation on anodic oxidation of 5-alkyl-2-furoic acids in protic media,[2] we found that the oxidation of the furan ring and the carboxy group on the anode electrode proceeded stepwise as shown in the following scheme.

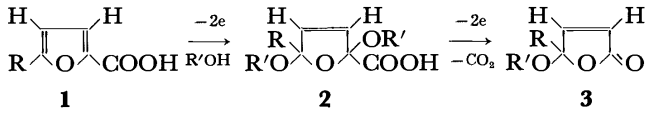

1 **2** **3**

R=Alkyl R′=Me, Ac

Our interest in the anodic reaction of more complex 2-furoic acids led us to investigate the oxidation of methyl 5-acetyl-2-furoate **4**[3] and the related compounds **5** and **6** on the electrode. We wish here to report on studies concerning anodic reaction of **4**, **5**, and **6** as well as detail structures of the products.

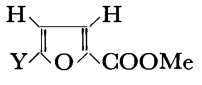

4 Y = MeCO
5 Y = MeO
6 Y = Br

Thus, **4** was electrolyzed in methanol containing concentrated sulfuric acid and lithium perchlorate under constant current using two platinium foil electrodes. Details of the experimental conditions together with results are shown in Table 1. The products were generally a mixture of **7a**, **7b**, **8**, **9a**, and **10**, however in runs 1 and 2 the major product was **9a**. In the experiment 3 an increase of the formation of ketoester **8** and lactone **10** was found to be caused by addition of a small amount of water. In the earlier stage of the reaction as shown in run 4, prominent proportion of **7a** and **7b** among the constituents of the

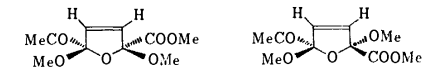

7a **7b**

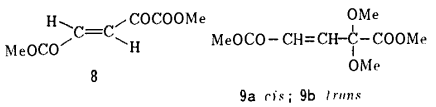

8 **9a** *cis*; **9b** *trans*

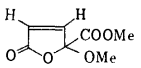

10

product was observed.

The results obtained in run 5 clearly showed that electrolysis of a mixture of **7a** and **7b** separated from the reaction products (run 4) gave **8**, **9**, and **10**, indicating that compounds **7a** and **7b** should be a precursor of the products.

Similar reaction fashions were observed (see Table 2) when methyl 5-bromo- and 5-methoxy-2-furoates, **5**[4] and **6**,[4] were electrolyzed in the almost same conditions as the cases of **4** and **7**, since oxidations of **5** and **6** gave principally **9** and **10**. Analytical specimen of these compounds were isolated by preparative vpc.

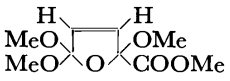

11

Electrolytic methoxydation of **6** has been attempted by several groups[5] and they assigned the incorrect structure **11** for the compounds **9**. They visualized the attack of methoxy group to the oxidized furan ring to yield trimethoxy derivative **11**, since anodic methoxydation of furan derivatives are known to afford 2,5-dimethoxy-2,5-dihydrofurans.[2,6] However, the

1) N. L. Weinberg and H. R. Weinberg, *Chem. Revs.*, **68**, 464 (1968).
2) S. Torii, H. Tanaka, H. Ogo, and S. Yamasita, This Bulletin, **44**, 1079 (1971).
3) R. Ercoli, E. Mantica, G. Claudia, S. Chiozzotto, and E. Santambrogio, *J. Org. Chem.*, **32**, 2917 (1967).
4) a) R. M. Whitlaker, *Rec. Trav. Chim. Pays-Bas*, **52**, 352 (1933); b) A. L. Mndzhoyan, *J. Gen. Chem. (USSR)*, **16**, 767 (1946); *Chem. Abstr.*, **41**, 2033 (1947); c) R. J. Ptfield and K. D. Amstutz, *J. Org. Chem.*, **19**, 1944 (1954); d) D. G. Manly and E. D. Amstutz, *ibid.*, **21**, 516 (1956).
5) a) G. P. Sokolov and S. Hillers, *Akad. Nauk Latv. SSR*, **1965**, 163; *Chem. Abstr.*, **63**, 6943 (1965); b) S. Hillers, G. P. Sokolov, and A. Ya, Karmilchik, *Konf. Po. Vysokomolekul. Soedin.*, **1962**, 170; *Chem. Abstr.*, **62**, 6449 (1965); c) Y. Hata, S. Senoo, and M. Murakami, *Nippon Kagaku Zasshi*, **79**, 1447 (1958).
6) a) A. J. Baggaley and R. Brettle, *J. Chem. Soc., C*, 969 (1968); b) S. D. Ross, M. Finkelstein, and J. J. Uebel, *J. Org. Chem.*, **34**, 1018 (1969).

Table 1. Reaction conditions and results in the cases of the compounds **4** and **7**

Experiment	1	2	3	4	5
Compound	**4**	**4**	**4**	**4**	**7**[a]
(g)	1	1	1	1	0.045
MeOH (*ml*)	130	130	130	130	130
H_2SO_4 (g)	0.3	0.3	0.3	0.3	0.3
$LiClO_4$ (g)	6	12	6	6	6
H_2O (*ml*)	—	—	13	—	—
Temp (°C)	27—28	20	27—28	20	22—25
Current (A)	0.5	0.5	0.5	0.5	0.5
Terminal voltage (V)	21—65	14—23	21—33	18—22	28—36
Time (hr)	5	5	5	1	1
Product (g)	0.99	0.87	0.70	0.97	0.045
Total conversion (%)	99	99	90	40	—
Products (mol %)					
7a	12	5	15	31	33
7b	6	1	7	12	10
8	—	4	20	—	4
9a	79	73	35	55	18
10	3	17	23	2	35

a) The ratio of **7a** to **7b** was 4 to 1.

Table 2. Reaction conditions and results in the cases of the compounds **5** and **6**

Experiment	6	7	8	9	10
Compound	**5**[a]	**5**[b]	**5**[b]	**6**	**6**
(g)	1	0.5	0.2	1	2.5
MeOH (*ml*)	30	20	20	30	9.2
H_2SO_4 (g)	0.1	—	0.03	0.1	0.1
H_2O (*ml*)	—	4	—	—	—
Temp (°C)	15	20	20	15	−13—−10
Current (A)	0.5	0.5	0.5	0.5	0.5
Terminal voltage (V)	11	7	25	6	4—6.5
Time (hr)	1.5	1.5	0.5	5	4
Products	0.97	0.16	0.2	0.91	2.2
Total conversion (%)	70	80	90	99	85
Products (mol %)					
8	—	—	—	—	—
9a	97	68	11	18	45
9b	3	22	4	82	55
10	—	10	85	trace	trace

a) The specimen was a mixture of **5** and **6** in a ratio 4/1. b) This specimen contains 2—3% of **6** elucidated by vpc.

Table 3. Comparison of NMR data of 2,5-dihydrofurans and their related compounds

	Compound	Functional group, τ							
		OMe		COOMe		COMe		>=<H	
19[2]**a**	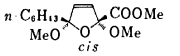 *cis*	6.55 (3H)	6.70 (3H)	6.17 (3H)					3.91 (2H)
19[2]**b**	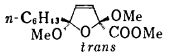 *trans*	6.61 (3H)	6.80 (3H)	6.17 (3H)					3.91 (2H)
7a	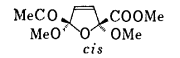 *cis*	6.55 (3H)	6.67 (3H)	6.21 (3H)		7.68 (3H)			3.87 (2H)
7b	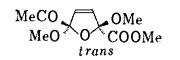 *trans*	6.76 (3H)	6.79 (3H)	6.17 (3H)		7.67 (3H)			3.77 (2H)
9a	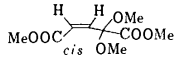 *cis*	6.73 (6H)		6.20 (3H)	6.29 (3H)				3.93 (2H)
9b	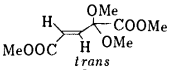 *trans*	6.68 (6H)		6.19 (3H)	6.22 (3H)			3.22 (1H) J_{AB}=15.7 Hz	3.62 (1H)
8	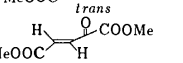 *trans*			6.07 (3H)	6.15 (3H)			2.37 (1H) J_{AB}=16.5 Hz	3.01 (1H)

ring opened structures of **8**, **9a**, and **9b** are now distinctly established by NMR spectra as shown in Table 3.

The NMR spectra of **9a** and **9b** had singlet bands at τ 6.73 (6H) and 6.68 (6H), respectively, ascribable to geminal methoxy groups and two bands at τ 6.19—6.29 regions due to the protons (6H) attached to carbomethoxy groups. The structure of **11** instead of **9** should be rejected, since NMR signals due to the methoxy groups of **11** would be expected to be magnetically nonequivalent by the influence of the carbonyl group, being observed upon **19**,[2] but the signals at τ 6.73 can account for the above assignment. The isomer **9b** had a typical AB type signals at τ 3.22 and 3.62 (J_{AB}=15.7 Hz) due to *trans* olefinic protons, in well agreement with the pattern observed in **8**, whereas the *cis* isomer **9a** had a singlet band appearing at τ 3.93 (2H, olefin), in agreement with values observed in 2,5-dihydrofuran derivatives **7** and **19** in Table 3. The carbonyl absorption bands of **9a** and **9b** assigned to the ester groups contiguous to dimethyl acetal carbon atoms were observed at 1762—1763 cm^{-1}.

The structure of butenolide **10** was confirmed by its infrared spectrum; 1810, 1785, and 1766 cm^{-1} (unsaturated lactone and ester carbonyls), by its NMR spectrum; τ 2.72 (d, 1H), 3.65 (d, 1H), 6.14 (s, 3H), and 6.54 (s, 3H), and by its microanalyses.

A plausible mechanism for the transformation of **5** and **6** by the anodic oxidation to **9** and **10** *via* intermediates **13** or **14** are shown in Schemes 1, 2, and 3. In fact, the same two electron oxidation, which is considered to involve cation radical or dication intermediates (path A and path B), has been shown by the results from electrolyses of furans and furoic acids.[1,2,6b,7] As shown in Scheme 2, it is possible that the intermediates **13a** and **13b** would be subjected to solvolysis to give **9** and **10** *via* **11** and **15**. However, it must be noted that **13** (X=Br) does not give any appreciable amount of **10** in vpc. This reveals that the intermediate **15b** derived from **13** (X=Br) should be generated more readily in contrast to **15a** (X=MeO).

Most of our endeavour to isolate the key intermediates **11** and **17** failed. On the other hand, it must be mentioned that relatively high terminal voltage and presence of water were effective in producing **10**. The precise mechanism of the formation of **10** is not

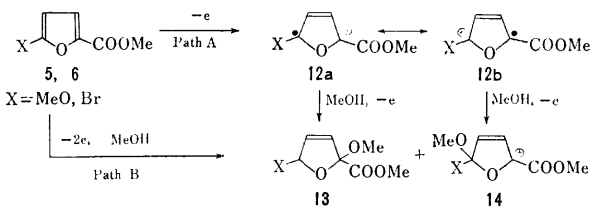

Scheme 1

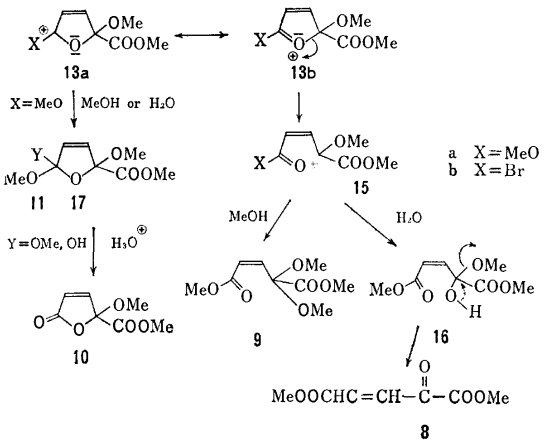

Scheme 2

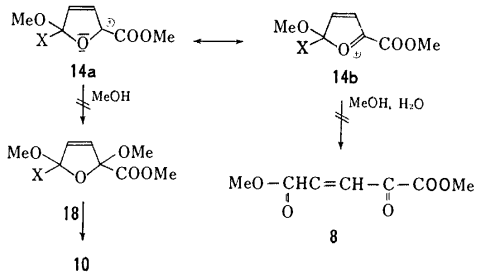

Scheme 3

certain, but the most likely explanation for the formation of **10** is that it results from methanolysis or hydrolysis of **13a** *via* **17**, probably in an acid-catalyzed hydrolysis *in situ* or during after treatment.

As illustrated in Scheme 3, the intermediates **14a** and **14b** (X=Br), if formed, would be expected to afford **8**, **18**, and **10** by the attack of the solvents. The results from the experiments 9 and 10 shown in Table 2 suggest that the absence of **8** and **18** reveals a probability of the presence of **13** rather than **14**.

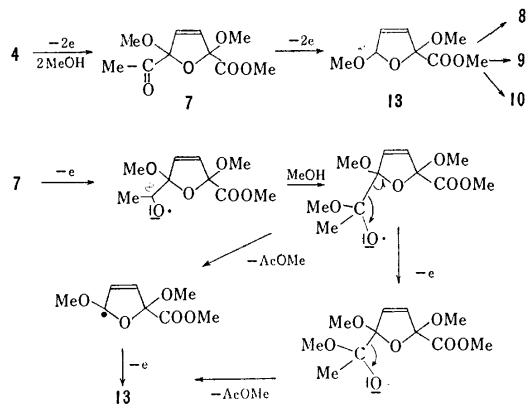

Scheme 4

In the course of the conversion of **7** to **8**, **9**, and **10**, the intermediate **13** is supposed to play an important role, but it is not easy to elucidate its behavior. A tentative mechanism of the conversion of **7** to **13** is depicted in Scheme 4. Any change could not be observed in its constituent on vpc, when a mixed solution of **7** in methanol in the presence of catalytic

7) S. Arita, Y. Takahashi, and K. Takeshita, *Kogyo Kagaku Zasshi*, **72**, 2289 (1969); K. Yoshida and T. Fueno, This Bulletin, **42**, 2411 (1969); C. K. Mann and K. K. Barnes, "Electrochemical Reactions in Nonaqueous Systems," Marcel Dekker, Inc., N. Y. (1970), p. 157.

amount of sulfuric acid was stirred for 5 hr without passing electric current. This demonstrates that removal of the acetyl group from **7** would be assisted by electrolysis, however, little is known of anodic oxidation on carbonyl function except for aroyl derivatives[8] and adduct of bisulfite.[9] Concerning the elimination of acetyl group from **7**, a further detailed mechanism could not be discussed on the basis of our present results.

The isomerization of the *cis* isomer **9a** to the *trans* **9b** occurred when the bromide **6** was electrolyzed. Addition of ammonium bromide to the runs 1 and 2 in Table 1 resulted in the production of **9b**. In both cases, liberation of bromine was encountered. This seems to implicate a catalyst of the **9a**→**9b** isomerization in the electrolytic media.

Experimental[10]

Ethyl 5-Acetyl-2-furoate **4**.[3] An improved method. To a solution of methyl 2-furoate (50.4 g, 0.4 mol) and acetic anhydride (20.4 g, 0.2 mol) in benzene (188 m*l*), anhydrous stannic chloride (104 g, 0.4 mol) was added at −5—0°C with stirring. The mixture was stirred for 7 hr at room temperature and then treated with 50 m*l* of 20% aqueous hydrochloric acid. The organic layer was extracted with benzene and the extract was shaken with aqueous sodium bicarbonate and aqueous sodium chloride. Distillation of the extract, after removal of the solvent, gave 13.3 g of oily material, bp 90—110°C (1 mmHg). The distillate was once dissolved in benzene and washed with aqueous sodium carbonate followed by aqueous sodium chloride. Evaporation of the solvent gave 10 g of crystalline **4** (yield 45%), mp 99—100°C from methanol (lit,[3] mp 101—102°C).

Anodic Oxidation of Methyl 5-Acetyl-2-furoate **4**. *Apparatus*: A cell used in this electrolysis is depicted in Fig. 1. The inside beaker (cathode compartment) fitted with a condenser, a cathode, a thermometer, a stirrer, and a drying tube was immersed in an anode vessel. The outside beaker (Anode compartment) fitted with an anode electrode, a thermometer, a stirrer, and a drying tube was immersed in a water bath. Electrodes were two platinium foils (1.5×2.0 cm^2). Current was controlled manually.

The reaction conditions and results are summarized in Table 1. A typical electrolysis procedure (Exp. 1) is indicated as follows: a solution of lithium perchlorate (6 g) in methanol (130 ml) containing 0.3 g of conc. sulfuric acid was poured into both the compartments. In the anode compartment, **4** (1.0 g) was charged and electrolyzed under a constant current of 0.5 A at 27—28°C for 5 hr with tirring. Then the electrolyzed solution in the anode compartment was

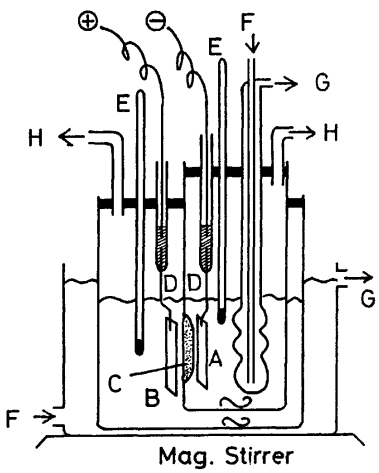

Fig. 1. Electrolysis cell. A: Cathode, B: Anode, C: Glass filter, D: Hg pool, E: Thermometer, F: Cooling water inlet, G: Cooling water outlet, H: $CaCl_2$ Tube

concentrated *in vacuo*. The residue was taken up in ether, and the solution was washed with aqueous sodium bicarbonate and sodium chloride, and dried over anhydrous sodium sulfate. Evaporation of the solvent gave 0.99 g of crude liquid product. The yield of the products was estimated by vpc and the results are listed in Tables 1 and 2. Isolation of main constituents was carried out by preparative vpc: **7a** (*cis*): n_D^{20} 1.4528, n_D^{25} 1.4511. IR (liq. film) 3100 (=C–H), 1755 (ester C=O), 1735 (ketone C=O), 1635, 1440, 1273, 1200, 1090, 1042, 856, and 796 cm^{-1}. NMR (see Table 3).

Found: C, 52.13; H, 6.02%. Calcd for $C_{10}H_{14}O_5$: C, 52.17; H, 6.13%.

7b (trans): n_D^{20} 1.4532, n_D^{25} 1.4514. IR (liq. film) 3100 (=C–H), 1755 (ester C=O), 1735 (ketone C=O), 1635, 1440, 1275, 1210, 1190, 1130, 1042, 1002, 953, 860, 812, and 790 cm^{-1}. NMR (see Table 3).

Found: C, 51.88; H, 5.88%. Calcd for $C_{10}H_{14}O_5$: C, 52.17; H, 6.13%.

8: IR (nujol) 3070 (=C–H), 1738, 1708 (ester, ketone C=O), 1640 (C=C), 1445, 1312, 1260, 1176, 1078, 996, 950, 928, 778, and 670 cm^{-1}. NMR (see Table 3).

Found: C, 48.68; H, 4.90%. Calcd for $C_7H_8O_5$: C, 48.84; H, 4.66%.

9a: n_D^{20} 1.4520, n_D^{25} 1.4579. IR (liq. film) 3000 (=C–H), 1763, 1735 (ester C=O), 1645 (C=C), 1440, 1392, 1280, 1220, 1190, 1138, 1100, 1050, 810, and 758 cm^{-1}. NMR (see Table 3).

Found: C, 49.28; H, 6.37%. Calcd for $C_9H_{14}O_6$: C, 49.54; H, 6.47%.

10: n_D^{20} 1.4597, n_D^{25} 1.4579. IR (liq. film) 3100 (=C–H), 1810, 1776, 1766 (lactone, ester C=O), 1618 (C=C), 1440, 1285, 1232, 1200, 1155, 1103, 1068, 1030, 997, 950, 824, 788, 759, and 690 cm^{-1}. NMR ($CDCl_3$) τ 2.72 (d, 1H, J=5.5 Hz, =C–H), 3.65 (d, 1H, J=5.5 Hz, =C–H), 6.14 (s, 3H, CO–O–CH_3), 6.54 (s, 3H, C–O–CH_3).

Found: C, 48.67; H, 4.63%. Calcd for $C_7H_8O_5$: C, 48.84; H, 4.68%.

Electrolysis of Methyl 5-Acetyl-2,5-dimethoxy-2,5-dihydro-2-furoate **7**. Compound **7** (*cis*/*trans* 4/1) isolated by preparative vpc from the product of the experiment 1 was electrolyzed

Table 4. Vpc data of the products

Rt (min)	3.6	3.9	4.3	4.7	5.4	6.3	7.5	8.6	8.8
Compound	**8**	**6**	**5**	**10**	**4**	**9a**	**7a**	**7b**	**9b**

8) A. Takeda, S. Torii, and H. Oka, *Tetrahedron Lett.*, **1968**, 1781; L. L. Miller, V. R. Koch, M. E. Larscheid, and J. F. Wolf, *ibid.*, **1971**, 1389.

9) M. Oyama and M. Ohno, *ibid.*, **1966**, 5201.

10) All melting and boiling points are uncorrected. Preparative gas chromatography was accomplished with a partially modified Yanagimoto GCG-550T unit, using a column (4ϕ, 3 m long) packed with 10% SE-30 on Celite 545, 80—100 mesh, and H_2 (20 m*l*/min) as a carrier gas at 140°C. The retention times of the products are shown in Table 4. Infrared spectra were determined by a Hitachi EPI-S2 spectrophotometer. NMR spectra were obtained on a Japan Electron Optics Laboratory spectrometer (JNM-C-60) in deuterochloroform with TMS as an internal reference. Microanalyses were carried out by Miss M. Harada of this Laboratory.

in the manner described previously. Vpc analysis of the product showed the presence of **7a**, **7b**, **8**, **9a**, and **10** (Table 1). Structural assignment of each constituents were performed by comparing their IR spectra with those of the corresponding authentic compounds.

Methyl 5-Bromo-2-furoate ***6***. Methyl 5-bromo-2-furoate **6** was prepared by the method of Amstutz *et al.*,[4d] mp 63—65°C from methanol (lit,[4c] mp 62.5—63.5°C).

Methyl 5-methoxy-2-furoate ***5***. To a solution of sodium (2 g, 0.087 atom) and sodium iodide (0.1 g) in 100 m*l* of absolute methanol, **6** (7.2 g, 0.035 mol) was added. After refluxing for 4 hr the solvent was removed under diminished pressure. The residue was dissolved in ether and washed with aqueous sodium chloride. Evaporation of the solvent followed by distillation gave 2.5 g of methyl 5-methoxy-2-furoate **5**: bp 78—79°C (1 mmHg) (yield 41%), mp 51—52°C from *n*-hexane (lit,[4c] mp 51—53°C).

Anodic oxidation of methyl 5-bromo-2-furoate ***6***. Electrolysis was carried out in the same manner described previously.[2] The reaction conditions along with the results are listed in Table 2. The reaction mixture was neutralyzed with methanolic sodium methoxide (Na 0.2 g/MeOH 20 m*l*). After evaporation of the solvent *in vacuo*, the residue was treated in the usual manner to give 0.9 g of crude oil whose constituents were analyzed by vpc and the results are shown in Tables 2 and 4. IR and NMR spectra of **9a** were identical with those of the specimen obtained by the above paragraph. Physical data of **9b** are as follows: n_D^{20} 1.4532, n_D^{25} 1.4513. IR (liq. film) 3000 (=C–H), 1762, 1732 (ester C=O), 1663 (C=C), 1440, 1310, 1260, 1170, 1090, 1050, 1013, 980, 942, 930, 910, 866, and 808 cm^{-1}. NMR (see Table 3).

Found: C, 49.80; H, 6.57%. Calcd for $C_9H_{14}O_6$: C, 49.54; H, 6.47%.

Electrolysis of Methyl 5-Methoxy-2-furoate ***5***. A solution of **5** (1.0 g) in methanol (30 m*l*) containing conc. sulfuric acid (0.1 g) was electrolyzed in the manner described in preceding paragraph (Table 2). Structural assignment of the products was carried out by vpc analyses and in comparison of their IR spectrum with that of the corresponding authentic specimen.

BULLETIN OF THE CHEMICAL SOCIETY OF JAPAN, VOL. 45, 2787—2790 (1972)

Reaction of Vinylic Radicals with Oxygen[1]

Naoto WADA and Katsumi TOKUMARU[2]

Department of Chemistry, Faculty of Science, The University of Tokyo, Bunkyo-ku, Tokyo, 113

(Received January 11, 1972)

Thermal decomposition of *trans*-α-phenylcinnamoyl peroxide and *t*-butyl *trans*- and *cis*-α-phenylperoxycinnamates and photolyses of 1,1-diphenyl-2-iodoethylene and 1,1,2-triphenyl-2-iodoethylene were carried out in benzene under oxygen and their products were determined. The intermediate vinylic radicals, on reaction with oxygen, undergo oxidative cleavage and dioxygenation of their unsaturated bonds. As an example, 1,2-diphenylvinyl radicals give benzaldehyde together with benzoin.

Much effort has been made to investigate the reaction of alkyl radicals with oxygen and to elucidate the products and reaction mechanism.[3] Aryl radicals have also been shown to react with oxygen giving phenolic products, though a detailed mechanism is not yet fully understood.[4] The reaction of vinylic radicals with oxygen has not been investigated much but one of us showed that *trans*-cinnamoyl peroxide and α-methylcinnamoyl peroxide, on thermal and photochemical decomposition in benzene or carbon tetrachloride under oxygen, gave benzaldehyde together with benzoic acid among the products through the oxidative cleavage of the intermediate styryl or 1-methyl-2-phenylvinyl radicals with oxygen as shown below.[5]

$$\mathrm{PhCH{=}\dot{C}R} + \mathrm{O_2} \longrightarrow \mathrm{PhCH{=}CR} \\ \quad\quad\quad\

TABLE 1. PRODUCTS FROM DECOMPOSITION OF VINYLIC RADICALS-GENERATORS IN BENZENE UNDER OXYGEN OR NITROGEN

Generators[a,b]	Reaction conditions[c]	Time (hr)	Oxidation products (%)[b]					Other products (%)[b]
			PhCHO	$PhCO_2H$	Ph_2CO	PhCHOHCOPh	PhCOCOPh	
(*t*-PhCH=CPhCO_2)$_2$ (I)	T, 64°, O_2	8	15	3		24		PhC≡CPh, 34 $PhCH_2COPh$, 3 *c*-PhCH=CHPh, 2 *t*-PhCH=CHPh, trace *t*-PhCH=CPhCO_2H, 6
t-PhCH=CPhCO_3*t*-Bu (II)	T, 75°, O_2	88	12	n.d.		3	15	PhC≡CPh, 15 *t*-PhCH=CPhCO_2H, n. d.
c-PhCH=CPhCO_3*t*-Bu (III)	T, 75°, O_2	64	19	n.d.			19	*c*-PhCH=CPhCO_2H, n. d.
Ph_2C=CHI (IV)	P, 25°, O_2	24			54			I_2, 78
Ph_2C=CHI (IV)	P, 25°, N_2	26						I_2, 25 Ph_2C=CHI (recovered), 68 $Ph_2C=CH_2$, 5 PhC≡CPh, trace $(Ph_2C=CH)_2$, 11
Ph_2C=CPhI (V)	P, 25°, O_2	24	trace	n.d.	34			I_2, n. d.

a) Initial concentration: 0.03—0.05M. b) *t*: *trans*; *c*: *cis*; n.d.: detected but not determined. c) Reaction conditions show method of decomposition, temperature and atmosphere. T: thermal decomposition; P: photolysis with a low pressure (160 W) mercury lamp.

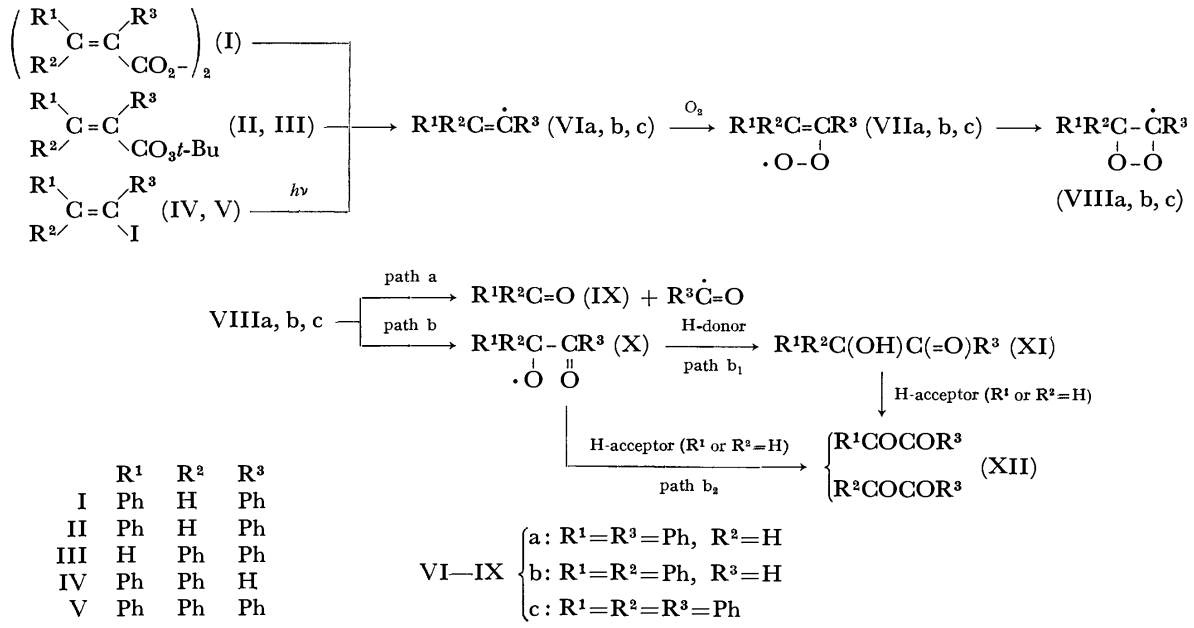

Scheme 1.

cis-α-phenylperoxycinnamate (III) carried out under oxygen in benzene afforded benzaldehyde (12% or 19% from II or III, respectively) and benzil (15% or 19% from II or III, respectively). Benzoin (3%) and benzoic acid along with diphenylacetylene (15%) were also found among the products from II.

Irradiation of 1,1-diphenyl-2-iodoethylene (IV) or 1,1,2-triphenyl-2-iodoethylene (V) in benzene in a stream of oxygen at room temperature with a low pressure mercury lamp afforded benzophenone (54% and 34% from IV and V, respectively).

The results are summarized in the table. In view of the generation of 1,2-diphenylvinyl radicals from the peroxidic sources, I, II, and III,[6] and the formation of 1-propyl-1-butenyl radicals from the photolysis of 4-iodo-3-heptene,[7] formation of the oxidation products can be attributed to the reaction of the intermediate vinylic radicals with oxygen. This might proceed as in the following scheme.

6) N. Wada, K. Tokumaru, and O. Simamura, This Bulletin, **44**, 1112 (1971).

7) R. C. Neuman, Jr. and G. D. Holmes, *J. Org. Chem.*, **33**, 4317 (1968).

Vinylic radicals (VI) generated from suitable sources react with oxygen to afford vinylperoxy radicals (VII), which subsequently cyclize to give 2,3-dioxetanyl radicals (VIII).[5] These radicals are either decomposed into carbonyl compound (IX) and acyl radicals (path a), or converted into α-ketoalkoxy radicals (X) (path b), which abstract hydrogen atoms from the reaction medium to give α-ketoalcohol (XI) (path b_1) or lose hydrogen atoms to give α-diketone (XII) (path b_2). Path a proposed previously[5] is supported by the formation of benzaldehyde, benzoic acid or benzophenone. Path b is proposed herewith on the basis of the production of benzoin and benzil from the decomposition of I, II, and III under oxygen.

Production of benzil at the expense of benzoin from the peroxyesters II and III might be due to the high reactivity of *t*-butoxy radicals to abstract hydrogen atom from benzoin or from the α-ketoalkoxy radical (X). A low yield of deoxybenzoin (3%) from I seems to occur with no participation of oxygen, on taking account of its formation from I decomposed under nitrogen,[6] although its path is ambiguous at the present time. The absence of α-ketoalcohol among the products from the irradiation is undoubtedly attributable to its further labile photolysis into aroyl and α-hydroxyaralkyl radicals[8] followed by their reaction with oxygen:

$$ArRC(OH)C(=O)Ar \xrightarrow{h\nu} ArC\dot{O} + ArR\dot{C}OH$$

Postulation of 2,3-dioxetanyl radicals as an intermediate undergoing facile cleavage is supported by the recent findings on 1,2-dioxetane (XIII), which was actually prepared and shown to decompose readily into two carbonyl components.[9]

$$R^1R^2C(-O-O-)CR^3R^4\ (XIII) \longrightarrow R^1R^2CO + R^3R^4CO$$

($R^1=R^2=R^3=Me$, $R^4=H$;[9a] $R^1=R^3=OEt$, $R^2=R^4=H$;[9b] $R^1=R^2=R^3=R^4=OMe$[9c])

1-Oxa-2-azacyclobutene-2 (XIV) was also proposed to be an intermediate during the course of the reaction of unsubstituted vinyl radicals with nitric oxide in gas phase and facilely decompose into formaldehyde and hydrogen cyanide.[10]

$$H_2C=\dot{C}H + NO \longrightarrow H_2C=CH(-O-N=) \longrightarrow$$

$$H_2C(-O-)CH(-N=)\ (XIV) \longrightarrow H_2CO + HCN$$

Irradiation of IV in benzene under nitrogen afforded 1,1,4,4-tetraphenyl-1,3-butadiene (11%), 1,1-diphenylethylene (5%) and diphenylacetylene (trace). A large amount of the starting material was recovered. In contrast, in the irradiation of the same iodide in a slow stream of oxygen under the same conditions as above, no starting iodide was recovered and iodine was liberated in 78% yield. The results suggest that the presence of oxygen, by capturing the vinylic radicals, prevents their reactions with iodine atoms or with molecular iodine returning to the starting iodide.

$$Ph_2C=CHI\ (IV) \longrightarrow Ph_2C=\dot{C}H\ (VIb) + I\cdot$$

$$Ph_2C=\dot{C}H + O_2 \longrightarrow Ph_2C=CHOO\cdot \longrightarrow \text{Products}$$

$$Ph_2C=\dot{C}H + I\cdot\ (\text{or } I_2) \longrightarrow Ph_2C=CHI\ (\text{or } +I\cdot)$$

Formation of 1,1,4,4-tetraphenyl-1,3-butadiene might be due to either dimerization of the intermediate vinylic radicals (VIb) or addition of the radical (VIb) to IV followed by elimination of an iodine atom.

$$2Ph_2C=\dot{C}H \longrightarrow Ph_2C=CH-CH=CPh_2$$

$$Ph_2C=\dot{C}H\ (VIb) + Ph_2C=CHI\ (IV) \longrightarrow$$

$$Ph_2C=CH-\dot{C}HI-CPh_2 \longrightarrow Ph_2C=CH-CH=CPh_2 + I\cdot$$

It should be pointed out that the absence of the products which would result from the substitution of the vinylic radicals on benzene, *viz.*, 1,1,2-triphenylethylene from I, II, III, or IV, or 1,1,2,2-tetraphenylethylene from V, indicates a low reactivity of the vinylic radicals towards aromatic substitution, in contrast to aryl radicals, which also belong to sp^2-hybridized σ-radicals and effectively undergo aromatic substitution.[11]

Experimental

Materials. *trans*-α-Phenylcinnamoyl peroxide (I), *t*-butyl *trans*- (II) and *cis*-α-phenylperoxycinnamate (III) were prepared as described before.[6] 1,1-Diphenyl-2-iodoethylene (IV) and 1,1,2-triphenyl-2-iodoethylene (V) were prepared according to literature.[12,13]

Thermal Decomposition of I, II, and III under Oxygen. One to three grammes of I, II, or III in 300 ml of benzene was placed in a 300—500 m*l* three-necked round-bottomed flask fitted with a gas inlet tube, a stopper and a reflux condenser. The mixture was kept in a slow stream of oxygen in a thermostat at a specified temperature for 8—70 hr until the peroxide was completely decomposed.

Photolyses of IV and V under Oxygen or Nitrogen. About 1 g of IV or V was irradiated in 100 m*l* of benzene for 20—24 hr with an immersion-type 160 W low pressure mercury lamp in a slow stream of oxygen or nitrogen.

8) P. de Mayo and A. Stoessl, *Can. J. Chem.*, **40**, 57 (1962); P. de Mayo, *Pure Appl. Chem.*, **9**, 597 (1964).

9) a) K. R. Kopeckey and C. Mumford, *Can. J. Chem.*, **47**, 709 (1969); E. H. White, J. Wiecko, and D. F. Roswell, *J. Amer. Chem. Soc.*, **91**, 5195 (1969); E. H. White, J. Wiecko, and C. C. Wei, *ibid.*, **92**, 2167 (1970). b) P. D. Bartlett and A. P. Schaap, *J. Amer. Chem. Soc.*, **92**, 3223 (1970). c) S. Mazur and C. S. Foote, *ibid.*, **92** 3226 (1970).

10) A. G. Sherwood and H. E. Gunning, *J. Amer. Chem. Soc.*, **85**, 3506 (1963); A. M. Tarr, O. P. Strausz, and H. E. Gunning, *Trans. Faraday Soc.*, **61**, 1946 (1965).

11) As general reference for homolytic aromatic substitution, see, for example, D. H. Hey, in G. H. Williams ed., "Advances in Free-radical Chemistry", Vol. II, Logos Press, London (1967), p. 47; G. H. Williams, "Homolytic Aromatic Substitution", Pergamon Press, Oxford (1960); O. Simamura, T. Migita, N. Inamoto, and K. Tokumaru, "Yuriki Hanno", Tokyo Kagaku Dozin, Tokyo (1969). Chapter 11; K. Tokumaru, *Yuki Gosei Kagaku Kyokai Shi* **28**, 773 (1970); K. Tokumaru, *Nippon Kagaku Zasshi* **92**, 886 (1971).

12) D. Y. Curtin and E. W. Flynn, *J. Amer. Chem. Soc.*, **81**, 4714 (1959).

13) L. L. Miller and D. A. Kaufman, *ibid.*, **90**, 7286 (1968).

Product Analysis. Determination of iodine liberated from the irradiation run was carried out by titration of an aliquot of the reaction mixture with a standard sodium thiosulphate solution.

For determination of the organic products the reaction mixture was shaken with 5% aqueous sodium carbonate. However, the reaction mixture from the photolysis was shaken with 5% aqueous sodium thiosulphate to remove iodine prior to the extraction with the carbonate. The alkaline layer was acidified with 5% hydrochloric acid, shaken with ether to remove acids and the extract was treated with diazomethane and the resulting methyl benzoate or α-phenylcinnamate was determined by vpc using Ucon Oil as a liquid phase. The benzene layer was dried over anhydrous sodium sulphate, and benzene was distilled off. The residue was subjected to chromatography on alumina and vpc using silicon oil or Ucon Oil as a liquid phase.

The authors' thanks are due to Professor O. Simamura for his encouragement throughout this work.

BULLETIN OF THE CHEMICAL SOCIETY OF JAPAN, VOL. 45, 2790—2793 (1972)

The Nuclear Magnetic Resonance Study of Several *o*-Disubstituted Benzenes

Michio KONDO

Central Research Laboratories, Sankyo Co., Ltd., Hiromachi 1-chome, Shinagawa-ku, Tokyo

(Received November 10, 1971)

The nuclear magnetic resonance spectra of six *o*-disubstituted benzenes containing a carbonyl group have been analyzed. The chemical shifts of the proton-6, adjacent to the carbonyl group, show a solvent dependence, indicating changes in the intramolecular interactions between the two *ortho* substituents.

It is known that the protons adjacent to the substituents in *o*-disubstituted benzenes often have chemical shifts differing by more than 0.1 ppm from the values estimated from a simple additive rule.[1] Interactions between the two substituents adjacent to each other must be responsible for these discrepancies. In some cases, the interactions fix the orientation of either one or both of the substituents. Fixing the substituent with a large magnetic anisotropy at one orientation markedly affects the chemical shifts of the *ortho* protons. In acetanilide, for example, the chemical shifts of the *ortho* protons depend to a great extent on whether the rotation about the bond connecting the amide nitrogen with the aromatic carbon atom is free or restricted.[2] Acetanilides, which have a substituent at the 2-position capable of forming intramolecular hydrogen bonds with the amide proton, exhibit deshielding, to a great extent, of the aromatic proton at C_6.[2]

The fixed orientation of some substituents into the plane of the ring often induces rather large long-range couplings between the substituents and particular ring protons.[3]

In this paper, the author will show that a difference in the carbonyl orientation through the intramolecular hydrogen bonding is responsible for the large difference between the chemical shifts of the proton-6 in *N*-methyl salicylamide and *N*-methyl-*o*-methoxy benzamide. Furthermore, the chemical shifts of the ring proton-6 in these compounds are very similar in dimethyl sulfoxide, which is known as a powerful solvent for disrupting the intramolecular and intermolecular hydrogen bonds of solute molecules.[4,5]

Experimental

The acids and esters used were commercial products. The amides were prepared by reacting the corresponding esters with an equimolar amount of methylamine (40% aqueous solution) in methanol at room temperature for a week. The solvent, the non-reacted ester, and the amine were distilled out under reduced pressures. The *N*-methyl salicylamide was purified by recrystallization from cyclohexane; mp 87.5—88.0°C. The *N*-methyl-*o*-methoxy benzamide was purified by distillation under reduced pressure; bp 148—150°C/4 mmHg.

The NMR spectra were obtained on a Varian A-60D spectrometer. Tetramethylsilane was used as the internal standard. A scale expansion of the recorder chart of 2 Hz/cm was used for determining the ring-proton resonances. The relative positions among the ring-proton signals were read with an accuracy of ± 0.05 Hz. The simulation of the NMR spectra was carried out by means of an electronic computer, CDC 3600, using an iterative computer program, LAOCON 3.[6] With very few exceptions, all the peaks observed were in accord with the calculated peaks within 0.1 Hz.

1) J. S. Martin and B. P. Dailey, *J. Chem. Phys.*, **39**, 1732 (1963).

2) a) M. Zanger, W. W. Simons, and A. R. Gannaro, *J. Org. Chem.*, **33**, 3672 (1968). b) R. Carter, *Acta Chem. Scand.*, **21**, 75 (1967). c) T. H. Siddall, III and W. E. Stewart, *J. Mol. Spectrosc.*, **24**, 290 (1967). d) R. F. C. Brown, L. Radom, S. Sternhell, and I. D. Rae, *Can. J. Chem.*, **46**, 2577 (1968).

3) J. G. Karabatsos and F. M. Vane, *J. Amer. Chem. Soc.*, **85**, 3886 (1963).

4) I. D. Rae, *Austr. J. Chem.*, **46**, 2588 (1968).

5) a) L. A. LaPlanche and M. T. Rogers, *J. Amer. Chem. Soc.*, **86**, 337 (1964). b) R. H. Barker and G. J. Boudreaux, *Spectrochim. Acta* **A23** 727 (1967).

6) S. Castellano and A. A. Bothner-By *J. Chem. Phys.* **41** 3863 (1964).

TABLE 1. THE CHEMICAL SHIFTS OF SOME *o*-DISUBSTITUTED BENZENES

		Solvent	Chemical shift			
			H(3)	H(4)	H(5)	H(6)
I	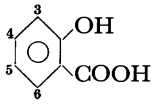	$CDCl_3$	423.18	453.52	418.32	478.20
		DMSO-d_6	419.02	451.95	417.05	470.98
II	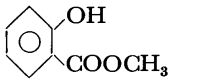	$CDCl_3$	420.92	448.56	414.35	471.83
		DMSO-d_6	420.65	452.64	417.85	468.64
		C_6D_6	418.51	425.77	395.65	463.52
III	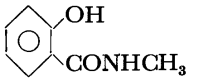	$CDCl_3$	419.22	443.30	410.33	444.73
		DMSO-d_6	415.95	444.68	414.17	470.57
		C_6D_6	421.24	425.70	394.11	411.79
IV	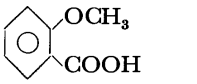	$CDCl_3$	424.27	454.01	426.95	488.62
		DMSO-d_6	429.39	452.09	422.67	461.92
		C_6D_6	383.61	424.56	404.42	494.11
V	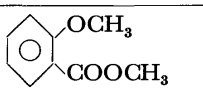	$CDCl_3$	419.19	448.02	419.04	468.07
		DMSO-d_6	429.62	452.71	421.97	459.92
		C_6D_6	392.38	426.71	404.50	470.18
VI	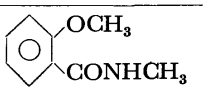	$CDCl_3$	418.32	445.65	424.03	492.97
		DMSO-d_6	427.87	447.67	422.21	468.10
		C_6D_6	390.67	426.36	412.27	514.37

Results and Discussion

The chemical shifts of the ring protons are summarized in Table 1. The chemical shifts reported for methyl salicylate in carbon tetrachloride[7] are almost uniformly located at fields higher by about 10 Hz than the present results. This is a general tendency when comparing the spectra of aromatic compounds dissolved in carbon tetrachloride and chloroform.

Dimethyl Sulfoxide Solutions. Interestingly, in dimethyl sulfoxide the chemical shifts of the ring protons at any given position are very similar for all the compounds studied. This is reasonable since, supposedly, the substituent variation in the present case has only a minor influence on the ring protons' electronic environment, provided that there are no special interactions between the two *ortho* substituents. In dimethyl sulfoxide, as is well known, the intermolecular interactions between solute and solvent molecules are preferred to intramolecular hydrogen bonds. Therefore, no special intramolecular interactions can be expected between the two substituents. Dimethyl sulfoxide molecules may interact with the hydroxyl or amide protons through the formation of intermolecular hydrogen bonds.[5] This kind of interaction shifts these resonances to lower fields. This expectation was actually realized (not listed in Table 1). The disruption of the intramolecular hydrogen bonds results in an increased freedom of movement of the substituents, probably a free rotation around the C_{ring}–CO bond, which would result in an averaing of the shielding effects of the carbonyl group on the ring proton-6. This may be the reason why the proton-6 chemical shift in all the compounds is nearly the same in dimethyl sulfoxide.

Consistent with this is the disruption of the intramolecular hydrogen bonds for methyl salicylate and other *ortho*-substituted phenols dissolved in dimethyl sulfoxide, as is suggested by the fact that the relative chemical shifts of OH in *ortho*-substituted phenols in dimethyl sulfoxide solutions are linearly-related to those for *para*-substituted phenols.[8]

Chloroform Solutions. In chloroform, on the other hand, the intramolecular interactions through hydrogen bonding may be expected to take place in some of the compounds studied, but not in others.

The proton chemical shifts of the compounds V, for which there is no possibility of intramolecular hydrogen bonding even in a chloroform solution, are very similar in both solvents, chloroform and dimethyl sulfoxide.

From the arguments given above, it appears that the chemical shift of the proton-6 is about 470 Hz from TMS when there are no special interactions between the two *ortho* substituents. From this point of view, the chemical shift of the ring proton-6 of *N*-methyl salicylamide in chloroform is considered to be strongly shielded. This suggests a certain interaction between the two substituents. The present author ascribes this remarkable shielding effect to the orientation fixing of the amide group through the intramolecular hydrogen bonding between phenolic hydroxyl proton and the carbonyl oxygen in the amide group, as is shown in A. A low-field resonance of the phenolic hydroxyl proton (744 Hz) is consistent with the argument described above. It is known that the resonance of phenolic hydroxyl protons is observed at about 270 Hz

7) R. Freeman and N. S. Bhacca, and C. A. Reilly, *J. Chem. Phys.*, **38**, 293 (1963).

8) M. T. Tribble and J. G. Traynham, *J. Amer. Chem. Soc.*, **91**, 379 (1969).

when they are free[9] and is shifted to lower fields when intramolecular hydrogen bonds are formed.[10,11] The phenolic hydroxyl protons of salicylaldehyde[11] and methyl salicylate[7] were observed at 665.5 and 641.7 Hz respectively. Unfortunately, however, no long-range coupling was observed between the phenolic hydroxyl proton and the ring proton-4 in *N*-methyl salicyalmide.

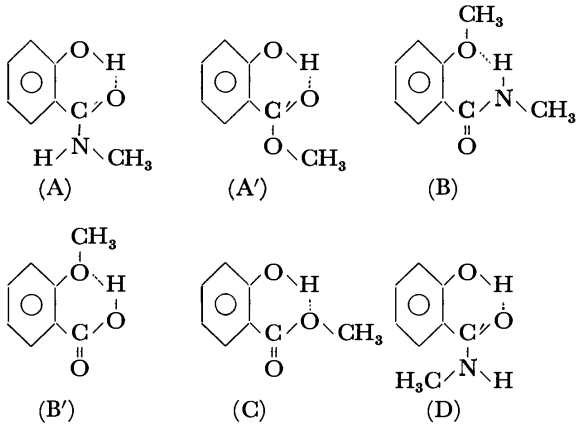

On the other hand, the ring proton-6 resonances of *o*-methoxy benzoic acid and *N*-methyl-*o*-methoxy benzamide were observed at very low fields, lower by about 20 Hz than the average value described in the preceding section. In these two compounds, the intramolecular hydrogen bonds give rise to planar molecules like B, where the carbonyl group is fixed in the molecular plane in quite a different way from that in A. In B, the proton-6 can be expected to be subjected to a strong electric field due to the carbonyl group and to resonate at lower fields. In the case of 2,5-dimethoxy acetanilide, where a strong effect of the carbonyl group could also be expected, the proton-6 resonance was found at 487 Hz.[2d] The amide proton resonance of *N*-methyl-*o*-methoxy benzamide was found at about 467 Hz, lower by about 60 Hz than that of *N*-methyl salicylamide, probably because of the intramolecular hydrogen bond.

Interestingly enough, the proton-6 resonates at about an average field in the case of methyl salicylate, although an intramolecular hydrogen-bond formation like A is expected to occur in this compound in chloroform; thus, the proton-6 could be expected to resonate at about the same field as that of *N*-methyl salicylamide. This unexpectedly low field resonance may be interpreted in terms of: (i) a considerable contribution by molecules of the C structure, or (ii) an electric-field deshielding exerted by the lone-pair electrons on the ester oxygen atom in A'. The IR study of methyl salicylate in carbon tetrachloride gave no evidence regarding any contribution of the C structure.[12] Therefore, the first interpretation can be ruled out.

The proton-6 of salicylaldehyde has been reported to resonate at 442.811 Hz from TMS.[11] This observation is consistent with the second explanation given above.

Ōki *et al.*[13] studied the conformations of several esters and concluded that the *s-trans* configuration is the exclusive one. Therefore, the A' structure is considered to be the most stable one for methyl salicylate. In this geometrical arrangement, the lone-pair electron cloud of the oxygen atom in the ester group exerts a strong electric field on the proton-6, inducing a pronounced deshielding effect.

Benzene Solutions. Benzene is known as a representative solvent which has a special effect on the proton chemical shifts of compounds with a carbonyl group.[14] A similar effect has been reported for some amides.[15]

According to these results, the ring proton-6 of *N*-methyl salicylamide would be expected to shift to higher fields when dissolved in benzene if the molecular structure assumed is A. This expectation is the case, as is shown in Table 1. By contrast, for *N*-methyl-*o*-methoxy benzamide the proton-6 resonance would be expected to remain unchanged or to shift to lower fields, provided that the molecular structure assumed is B. Actually, however, the resonance signal of the proton-6 was observed at a lower fields and that of the proton-3 shifted to higher fields. These observations prove the correctness of the structural assignments given above.

Furthermore, a consideration of van der Waals' repulsion for *N*-methyl salicylamide gives preference to the A structure over D, where the amide hydrogen lies *cis* to the carbonyl group with respect to the amide bond, N–CO, because of the strong repulsion expected between the methyl group and the proton-6 in the latter structure.

On the other hand, no remarkable benzene shift was observed for the proton-6 in the II and IV compounds. In the case of the latter, the flexibility of the carbomethoxy group, *i.e.*, the free rotation around the C_{ring}–CO bond, may be an important factor in interpreting this observation. In the former compound, the lone-pair electrons on the ester oxygen atom would prevent the benzene molecules from access to the proton-6.

Spin-spin Coupling. The results are presented in Table 2. None of the coupling constants varies significantly in changing the solvent. Furthermore, no appreciable variation in any of the coupling constants is observed from compound to compound. These observations are reasonable, because the change in the substituents of these compounds seems to cause only a weak perturbation in the ring moiety.

Previous empirical efforts to interpret substituent effects on proton-proton couplings have involved a

9) L. M. Jackman "Application of Nuclear Magnetic Resonance Spectroscopy in Organic Chemistry", Pergamon Press, London (1959), p. 69.
10) M. Kondo, This Bulletin, **38**, 1271 (1965).
11) D. G. de Kowalewski and S. Castellano, *Mol. Phys.*, **16**, 567 (1969).
12) N. Mori, Y. Asano, and Y. Tsuzuki, This Bulletin, **42**, 488 (1969).
13) M. Ōki and H. Nakanishi, This Bulletin, **43**, 2558 (1970).
14) a) J. D. Connolly and R. McCrindle, *Chem. Ind.* (London), **1965**, 379. b) D. H. Williams and N. S. Bhacca, *Tetrahedron* **21**, 2021 (1965). c) D. H. Williams and D. A. Wilson, *J. Chem. Soc., B.* **1966**, 144.
15) J. V. Hatton and R. E. Richards, *Mol. Phys.*, **3**, 253 (1960); *ibid.*, **5**, 139 (1962) and many other papers published later.

TABLE 2. COUPLING CONSTANTS

		J_{34}	J_{35}	J_{36}	J_{45}	J_{46}	J_{56}
I	$CDCl_3$	8.49	1.07	0.46	7.15	1.77	7.95
	DMSO-d_6	8.42	1.12	0.43	7.31	1.83	7.90
II	$CDCl_3$	8.31	1.08	0.42	7.17	1.78	7.83
	DMSO-d_6	8.39	1.17	0.41	7.35	1.73	8.08
	C_6D_6	8.51	1.14	0.45	7.25	1.75	7.98
III	$CDCl_3$	8.32	1.21	0.47	7.28	1.59	7.96
	DMSO-d_6	8.30	1.13	0.55	7.18	1.70	7.98
	C_6D_6	8.27	1.14	0.42	7.42	1.55	8.01
IV	$CDCl_3$	8.52	0.97	0.49	7.36	1.86	7.88
	DMSO-d_6	8.40	1.00	0.38	7.43	1.84	7.75
	C_6D_6	8.40	1.00	0.24	7.39	1.87	7.78
V	$CDCl_3$	8.38	1.02	0.35	7.45	1.83	7.69
	DMSO-d_6	8.46	0.98	0.36	7.45	1.86	7.67
	C_6D_6	8.51	1.08	0.34	7.41	1.84	7.59
VI	$CDCl_3$	8.31	1.01	0.34	7.36	1.90	7.79
	DMSO-d_6	8.24	1.05	0.34	7.35	1.85	7.69
	C_6D_6	8.33	1.00	0.23	7.33	1.92	7.67

correlation with the substituent electronegativity, E_x. Castellano and Sun[16] observed a definite trend of coupling values with E_x in a study of a number of monosubstituted benzenes. J_{23} and J_{26} were found to increase, and J_{24} and J_{25} to decrease, with E_x, and it was suggested that the inductive effect of the substituent was the principal factor involved. Fraser,[17] on the other hand, from a consideration of the J_{ortho} values in a series of monosubstituted derivatives, concluded that the π-contributions to J were at least as important as the inductive effect. Some other studies have been done in establishing a qualitative correlation between J and E_x for disubstituted benzenes.[18-22]

If a simple additivity rule can be applied to the H-H coupling constants, the following equations can give estimates for the coupling constants of *o*-disubstituted benzenes.

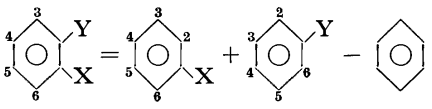

$$J_{34}(XY) = J_{34}(X) + J_{23}(Y) - J_o$$
$$J_{35}(XY) = J_{35}(X) + J_{24}(Y) - J_m$$
$$J_{36}(XY) = J_{36}(X) + J_{25}(Y) - J_p$$
$$J_{45}(XY) = J_{45}(X) + J_{34}(Y) - J_o$$
$$J_{46}(XY) = J_{46}(X) + J_{35}(Y) - J_m$$
$$J_{56}(XY) = J_{56}(X) + J_{45}(Y) - J_o$$

where J_o, J_m, and J_p stand for the *ortho*-, *meta*-, and *para*-coupling respectively between two ring protons of unsubstituted benzene.

From the above equations, one can calculate the 51 J_o's, 34 J_m's, and 17 J_p's, using the coupling constants of the present compounds and monosubstituted benzenes.[23,24] The averaged values are 7.46, 1.30, and 0.67 for J_o, J_m, and J_p respectively. These values are in good agreement with the experimental values.[25]

16) S. Castellano and C. Sun, *J. Amer. Chem. Soc.*, **88**, 4741 (1966).
17) R. R. Fraser, *Can. J. Chem.*, **44** 2737 (1966).
18) P. F. Cox, *J. Amer. Chem. Soc.*, **85**, 380 (1963).
19) J. E. Loemker, J. M. Read, Jr., and J. H. Goldstein, *J. Phys. Chem.*, **72**, 991 (1968).
20) A. R. Tarpley, H. B. Evans, and J. H. Goldstein, *Anal. Chem.*, **41**, 402 (1969).
21) H. B. Evans, Jr., A. R. Tarpley, and J. H. Goldstein, *J. Phys. Chem.*, **72**, 2552 (1968).
22) S. Castellano and R. Kostelnik, *Tetrahedron Lett.*, **1967**, 5211.
23) S. Castellano, C. Sun, and R. Kostelnik, *ibid.*, **1967**, 5205.
24) K. Hayamizu and O. Yamamoto, *J. Mol. Spectrosc.*, **25**, 422 (1968).
25) J. M. Read, Jr., R. E. Mayo, and J. H. Goldstein, *J. Mol. Spectrosc.*, **21**, 235 (1966).

Reaction of α-Halosulfoxides with Amines[1]

Tatsuo NUMATA and Shigeru OAE

Department of Applied Chemistry, Faculty of Engineering, Osaka City University, Sugimoto-cho, Sumiyoshiku, Osaka

(Received March 3, 1972)

When optically active bromomethyl *p*-tolyl sulfoxide was treated with sodium methylmercaptide or sodium ethoxide, optically active α-substituted methyl *p*-tolyl sulfoxides were obtained in good yields. By contrast, reaction with secondary amines produced achiral *p*-toluenesulfenamides, methylenediamines, and amine hydrobromides in nearly quantitative yields. The reaction with an amine is presumed to proceed through the initial nucleophilic substitution at α-carbon of the sulfoxide to form aminomethyl *p*-tolyl sulfoxide, followed by rearrangement to the corresponding sulfenate, and subsequent attack of the amine at the sulfur atom of the sulfenate to form the final product. Meanwhile, a facile interconversion of alkoxymethyl *p*-tolyl sulfoxide and corresponding sulfenate was also observed.

α-Halosulfoxides have become useful in the synthesis of various derivatives of sulfoxides. As a typical example,[2] α-epoxysulfoxide can be readily synthesized by the reaction of α-chlorosulfoxide with ketone in the presence of base. However, the nucleophilic substitution reactions of α-chloroalkyl sulfoxides are known to take place slowly.[3]

Recently, Ogura and Tsuchihashi[4] reported that this reaction proceeds through an S_N2 process with inversion of configuration at the α-carbon atom of an α-chloroalkyl sulfoxide.

For convenient synthesis of optically active α-substituted methyl aryl sulfoxides, however, this reaction is the shortest route, and hence we examined in detail the reaction of a more reactive and optically active bromomethyl *p*-tolyl sulfoxide with various nucleophiles.

Results and Discussion

When bromomethyl *p*-tolyl sulfoxide (**1**) was treated with CH_3S^-, $C_6H_5S^-$, CH_3O^-, and $C_2H_5O^-$, the corresponding α-substituted methyl *p*-tolyl sulfoxides were obtained in good yields (Eq. (1)).

$$\underset{\underset{\text{O}}{\downarrow}}{\text{Tol-S-CH}_2\text{Br}} + \text{X}^- \longrightarrow \underset{\underset{\text{O}}{\downarrow}}{\text{Tol-S-CH}_2\text{-X}} \qquad (1)$$

1

$X^-=CH_3S^-$, $C_6H_5S^-$, CH_3O^-, $C_2H_5O^-$
Tol=*p*-$CH_3C_6H_4$

Further, in the reaction of optically active bromomethyl *p*-tolyl sulfoxide with CH_3S^- and $C_2H_5O^-$, the corresponding optically active α-substituted methyl sulfoxides were obtained in good yields, and the starting optically active α-bromosulfoxide was also readily synthesized by bromination of optically active methyl *p*-tolyl sulfoxide with *N*-bromosuccinimide (NBS), bromine and pyridine in dichloromethane. The optical rotations of these sulfoxides are summarized in Table.

Table Optical rotation[a] of Tol-$\overset{*}{S}$(O)-CH_2-X

X	H	Br	SCH_3	OC_2H_5
$[\alpha]_D$	+201.0	+176.7	+193.3	+229.5
(*c*,*l*)	(1.00,1)	(1.05,1)	(1.04,1)	(0.83,1)

a) measured in benzene at 20°C

The data in this Table indicate that the configuration of the sulfoxide is little affected by α-bromination of the sulfoxide or by displacement reaction at the α-carbon atom of the sulfoxide.

However, in the reaction of optically active bromomethyl *p*-tolyl sulfoxide (**1**) with secondary amines (**2**), achiral *p*-toluenesulfenamides (**3**) were produced quantitatively, instead of forming optically active aminomethyl *p*-tolyl sulfoxides.

These reactions occurred when bromomethyl sulfoxide (**1**) was heated at 70°C for 1—2 hr with excess amine (**2a—c**) in benzene under nitrogen atmosphere, and *p*-toluenesulfenamide (**3a—c**), methylenediamine (**4a—c**) and amine hydrobromide (**5a—c**) were obtained in nearly quantitative yields (Eq. (2)).

$$\underset{\underset{\text{O}}{\downarrow}}{\text{Tol-S-CH}_2\text{-Br}} + 4\text{RR'NH} \xrightarrow{70^\circ} \text{Tol-S-N-RR'} + \text{RR'NCH}_2\text{NRR'} + \text{RR'NH}\cdot\text{HBr} + \text{H}_2\text{O} \qquad (2)$$

1 **2a—c** **3a—c** **4a—c** **5a—c**

a) R, R'=morpholino
b) R, R'=piperidino
c) R=R'=C_2H_5

This reaction was little affected by the solvent used, since the reaction in acetonitrile or ethanol proceeded smoothly in a similar fashion under the same condition in benzene to form the same products (**3**, **4**, **5**).

The physical and spectroscopic properties of sulfenamides (**3a—c**) are identical with those of authentic samples synthesized by the reaction of *p*-toluenesulfenyl chloride with the corresponding amines.

When chloromethyl *p*-tolyl sulfoxide (**6**) was allowed to react with morpholine (**2a**) in chlorobenzene, sulfenamide (**3a**), methylenediamine (**4a**), and amine hydrochloride were formed in nearly quantitative yields, as in the case of bromomethyl sulfoxide (**1**), though a somewhat more drastic condition was necessary. Similarly, chloromethyl methyl sulfoxide (**7**) was

1) Paper XLV on Sulfoxides. A preliminary accounts of this work was given in *Int. J. Sulfur Chem.*, *A*, **1**, 215 (1971).

2) a) D. F. Tavares, R. E. Estep, and M. Blezard, *Tetrahedron Lett.*, **1970**, 2373. b) T. Durst, *J. Amer. Chem. Soc.*, **91**, 1034 (1969). c) T. Durst and K.-C. Tin, *Tetrahedron Lett.*, **1970**, 2369.

3) a) F. G. Bordwell and W. T. Brannen, Jr., *J. Amer. Chem. Soc.*, **86**, 4645 (1964). b) M. Hojo and Z. Yoshida, *ibid.*, **90**. 4496 (1968).

4) K. Ogura and G. Tsuchihashi, *Chem, Commun.*, **1970**, 1689,

found to react with morpholine (**2a**) a little more readily, and methanesulfenomorpholide (*N*-methylthiomorpholine) was also obtained quantitatively (Eq. (3)).

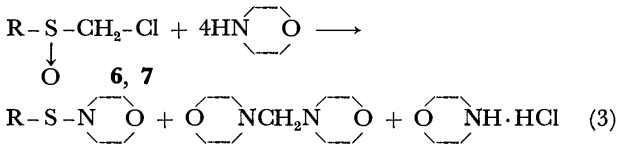

(3)

6) R=*p*-$CH_3C_6H_4$
7) R=CH_3

This reaction is influenced markedly by the steric requirement around the α-carbon atom of the sulfoxide, since when α-bromoethyl phenyl sulfoxide (**8**) with excess morpholine was heated in refluxing benzene for 50 hr, benzenesulfenomorpholide was produced in only 40% yield, accompanying with the formation of diphenyl disulfide (15%), while the starting sulfoxide was recovered in 40%. The formation of diphenyl disulfide is presumed to be due to the thermal decomposition of the sulfenamide produced *via* a homolytic pathway.

In the reaction of **1** or **7** with primary amine (*i.e.*, *n*-butylamine, cyclohexylamine, and aniline), *p,p'*-ditolyl disulfide or dimethyl disulfide was formed as main products in 50—80% yields. This appears to be related to the thermal instability of the sulfenamides formed.[5]

As for the stoichiometry, four molar equivalents of amine per one equimolar amount of the α-bromosulfoxide were necessary to complete the reaction according to Eq. (2).

When a solution of an equimolar mixture of the sulfoxide (**1**) and morpholine (**2a**) was heated at 70°C for 5 hr, **3a**, **4a**, and **5a** were formed in 21, 20, and 24% yields, respectively, and the starting sulfoxide (**1**) was recovered in 73%. This means that an intermediate of this reaction would be very reactive and cannot be isolated.

Based on the stoichiometry of the reaction, the following reaction scheme may be suggested:

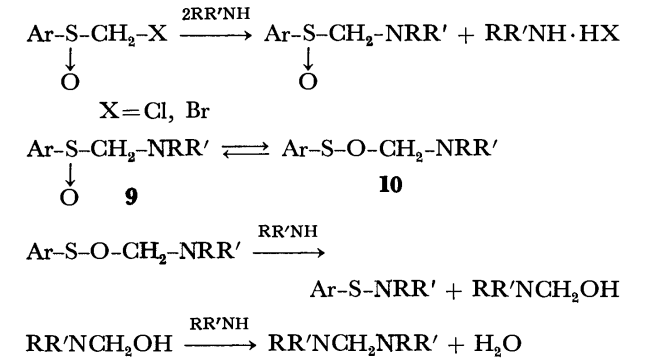

From the order of the reactivities of α-halosulfoxides (**1**, **6**, **7**, **8**) with morpholine, the reaction is presumed to proceed through the initial nucleophilic substitution at the α-carbon atom of the sulfoxide to form incipiently α-aminomethyl *p*-tolyl sulfoxide (**9**), followed by rearrangement to the sulfenate (**10**). Subsequent attack of an amine at the sulfur atom of the sulfenate (**10**) to afford the sulfenamide and aminomethanol would probably be very rapid. Aminomethanol thus formed would undergo condensation with the amine to afford methylenediamine and water.

Although the sulfenyl ester was not detected in this work, it may be reasonable to postulate that the conversion of the sulfoxide (**9**) to the sulfenyl ester (**10**) is facilitated because of the electron-releasing amino group at the α-carbon.

The reaction between the sulfenate (**10**) and an amine to form the sulfenamide would be very facile, though the reactions of the sulfenate with nucleophiles have little been studied.[6] While aminomethyl *p*-toluenesulfenate (**10**) is not available to test this pathway because of the difficulty in synthesis of this compound, a slightly more stable ethoxymethyl *p*-toluenesulfenate than aminomethyl sulfenate has been prepared and this was found to react readily with morpholine at room temperature to give *p*-toluenesulfenomorpholide quantitatively.

This interpretation for the α-halosulfoxides-amine reaction may also be supported by the observation that substituted ethoxymethyl (or methoxymethyl) *p*-toluenesulfenate is formed in the equilibrium when the corresponding ethoxymethyl (or methoxymethyl) *p*-tolylsulfoxide (which has another effective electron-releasing group at α-carbon) was heated under high vacuum. Meanwhile, the reverse conversion of this sulfenate to the sulfoxide is also found to occur readily by dissolving of the sulfenate in nonpolar aprotic solvents such as chloroform.[7]

Such a rearrangement is known in allyl aryl sulfoxides and aryl benzyl sulfoxides.[8]

A somewhat analogous formation of sulfenamides in the reaction of allyl or α-naphthylmethyl aryl sulfoxides with piperidine, apparently *via* the prior rearrangements of the sulfoxides to the sulfenates, was reported recently by Abbott and Stirling.[9]

Experimental

Materials. *Optically Active Methyl* p-*Tolyl Sulfoxide* was prepared by the method of Mislow[10] in which (−)menthyl (−)*p*-toluenesulfinate was reacted with methylmagnesium iodide in ether. mp 75°C, $[\alpha]_D$ +201.0° (*c*=1.00, benzene) Lit,[10] mp 73—74°C, $[\alpha]_D$ +145.5° (*c*=2, acetone).

Optically Active Bromomethyl p-*Tolyl Sulfoxide* (*1*) was prepared by bromination of optically active methyl *p*-tolyl sulfoxide with bromine, *N*-bromosuccinimide (NBS), and pyridine in dichloromethane in 80% yield, according to the procedure

5) N. E. Heimer and L. Field, *J. Org. Chem.*, **35**, 3012 (1970).

6) C. Brown and D. R. Hogg, *Chem. Commun.*, **1967**, 38.

7) Without solvent, the sulfenate is completely decomposed upon standing overnight at room temperature to form *p*-tolyl *p*-toluenethiolsulfinate quantitatively.

8) a) E. G. Miller, D. R. Rayner, H. T. Thomas, and K. Mislow, *J. Amer. Chem. Soc.*, **90**, 4861 (1968). b) P. Bickart, F. W. Carson, J. Jacobus, E. G. Miller, and K. Mislow, *ibid.*, **90**, 4869 (1968). c) R. Tang and K. Mislow, *ibid.*, **92**, 2100 (1970). d) S. Bravermann and Y. Stabinsky, *Chem. Commun.*, **1967**, 270.

9) D. J. Abbott and C. J. M. Stirling, *J. Chem. Soc., C*, **1969**, 818.

10) K. Mislow, M. Green, P. Laur, J. T. Mellio, T. Simmons, and A. L. Ternay, Jr., *J. Amer. Chem. Soc.*, **87**, 1958 (1965).

developed by Tsuchihashi.[11] The sulfoxide obtained was recrystallized from cyclohexane. mp 88—89°C, $[\alpha]_D$ +176.7° (c=1.05, benzene), ν_{SO} (KBr) 1044 cm^{-1}, NMR ($CDCl_3$) δ=2.53 (3H, s), 4.50 (2H, AB quartet, J=11 Hz, Δ_{AB}= 8.3 Hz), 7.74 (4H, m).

Optically Active Methylthiomethyl p-*Tolyl Sulfoxide* was prepared by the reaction of optically active bromomethyl *p*-tolyl sulfoxide with sodium mercaptide in 50% CH_3CN-H_2O at room temp. for 2 hr in 90% yield. The sulfoxide obtained was recrystallized from cyclohexane. mp 42—44°C, $[\alpha]_D$ +193.3° (c=1.04, benzene), ν_{SO} (KBr) 1038 cm^{-1}, NMR ($CDCl_3$) δ=2.35 (3H, s), 2.59 (3H, s), 3.96 (2H, s), 7.82 (4H, m) Found: C, 53.92; H, 5.72%. Calcd for $C_9H_{12}OS_2$: C, 53.96; H, 6.04%.

Optically Active Ethoxymethyl p-*Tolyl Sulfoxide* was prepared by the reaction of optically active bromomethyl *p*-tolyl sulfoxide with sodium ethoxide in ethanol at 70° for 5 hr in 85% yield. The sulfoxide obtained was purified by preparative TLC (silica gel) with chloroform as eluent. $[\alpha]_D$ +229.5° (c=0.83, benzene), ν_{SO} (neat) 1050 cm^{-1}, NMR ($CDCl_3$) δ=1.33 (3H, t, J=7 Hz), 2.56 (3H, s), 4.07 (2H, quartet J=7 Hz), 4.64 (2H, s), 7.80 (4H, m) Found: C, 60.72; H, 7.06%. Calcd for $C_{10}H_{14}O_2S$: C, 60.57; H, 7.12%.

Chloromethyl p-*Tolyl Sulfoxide* (**6**) was prepared by the chlorination of methyl *p*-tolyl sulfoxide, which was synthesized by bromine-oxidation of methyl *p*-tolyl sulfide in usual manner,[12] with *N*-chlorosuccinimide (NCS) and pyridine, according to the procedure developed by Tsuchihashi.[13] The sulfoxide obtained was recrystallized from ether-hexane. mp 60.0—61.0°C (lit:[14] mp 61.5—62°C).

Bromomethyl p-*Tolyl*, *Methylthiomethyl* p-*Tolyl*, *Methoxymethyl* p-*Tolyl*, *and Ethoxymethyl* p-*Tolyl Sulfoxides* were prepared by the same way used for synthesis of the corresponding optically active compounds as mentioned above.

Bromomethyl isomer, mp 63.0—64.0°C (lit,[11] mp 63°C); methylthiomethyl isomer, mp 61.0—61.5°C; methoxymethyl isomer, ν_{SO} (neat) 1049 cm^{-1}, NMR ($CDCl_3$) δ=2.40 (3H, s), 3.65 (3H, s), 4.38 (2H, s), 7.45 (4H, m).

Phenylthiomethyl p-*Tolyl Sulfoxide* was prepared by the reaction of bromomethyl *p*-tolyl sulfoxide with sodium thiophenoxide in ethanol at 70°C for 4 hr in 84% yield. The sulfoxide obtained was recrystallized from benzene-hexane. mp 51—52°C, ν_{SO} (KBr) 1042 cm^{-1}, NMR (CCl_4) δ=2.35 (3H, s), 4.12 (2H, s), 7.52 (9H, m) Found: C, 63.79; H, 5.08%. Calcd. for $C_{14}H_{14}OS_2$: C, 64.09; H, 5.38%.

α-Bromoethyl Phenyl Sulfoxide (**8**) was prepared by the bromination of ethyl phenyl sulfoxide with bromine, NBS and pyridine in 69% yield. bp 129—130°C/0.5 mmHg, ν_{SO} (neat) 1056 cm^{-1}, NMR ($CDCl_3$) δ=1.90 (3H, d, J=7 Hz), 4.87 (1H, quartet J=7 Hz), 7.69 (5H, m). Found: C, 41.35; H, 3.68%. Calcd for C_8H_9OSBr: C, 41.22; H, 3.89%.

Chloromethyl Methyl Sulfoxide (**7**) was prepared by the chlorination of dimethyl sulfoxide with NCS in the presence of K_2CO_3 according to the procedure of Tsuchihashi.[13] bp 66—68°C/1 mmHg, (lit,[13] 90°C/4 mmHg).

p-*Toluenesulfenamides* (**3**) were synthesized by the reaction of *p*-toluenesulfenyl chloride, which was synthesized by the method described in the text book,[15] with corresponding excess amines in dichloromethane.

p-Toluenesulfenodiethylamide, bp 67°C/1 mmHg; *p*-toluenesulfenomorpholide, bp 100°C/0.5 mmHg; *p*-toluenesulfenopiperidide bp 98°C/0.8 mmHg (Lit[9] 90°C/0.3 mmHg).

Methanesulfenomorpholide was prepared by the reaction of methanesulfenyl chloride, which was synthesized from the reaction of dimethyl disulfide with dry chlorine gas according to the procedure of Mislow,[8a] with excess morpholine in dichloromethane. bp 79°C/24 mmHg. (lit,[16] 48—49°C/ 5 mmHg).

Dimorpholino Methane (**4a**) was synthesized by condensation of morpholine and formaline according to the procedure of Harradence.[17] bp 120°C/23 mmHg (lit,[17] 139—140°C/29 mmHg).

Amines used were purified by twice distillation under nitrogen atmosphere.

Reaction of α-Haloalkyl Aryl Sulfoxides with Amines. *i*) *α-Bromosulfoxide with Secondary Amine*: α-Bromosulfoxide (0.5—1 g) was heated at 70°C for 1—2 hr with an excess amine (1—3 g) in dry benzene (5—10 cc) under nitrogen atmosphere until the spot of sulfoxide in thin layer chromatography (tlc) analysis disappeared and amine hydrobromide salt precipitated. After collecting the precipitated amine hydrobromide salt and evaporation of solvent and excess amine *in vacuo*, the oily residue was separated by preparative tlc (silica gel) to afford the sulfenamide and methylenediamine in 90—96% yields.

ii) *α-Chlorosulfoxide with Morpholine*: α-chlorosulfoxide (0.5 g) was heated at 120°C for 2.5 hr to complete the reaction with morpholine (1 g) in dry chlorobenzene (5 cc). Method of work up and product analysis are described above.

Reaction of Chloromethyl Methyl Sulfoxide with Morpholine. The sulfoxide (1 g) was heated at 70°C for 8 hr with morpholine (5 g) in benzene (20 cc). After collecting amine hydrochloride precipitated, fractional distillation of the reaction mixture under reduced pressure gave first benzene and unchanged morpholine, and subsequently the fraction of methanesulfenomorpholide (79°C/24 mmHg), and the final fraction of dimorpholino methane (120°C/23 mmHg).

Conversion of Ethoxymethyl p-*Tolyl Sulfoxide to Sulfenate* The sulfenate was produced as a distillate by rapid vacuum distillation of the sulfoxide using a micro-distillation apparatus in 70—80% yield. bp 100—110°C/1.5 mmHg, IR (neat) 1150, 1120, 920, 800 cm^{-1}.

11) S. Iriuchijima and G. Tsuchihashi, *Synthesis*, **1970**, 588.
12) S. Oae, Y. Ohnishi, S. Kozuka, and W. Tagaki, This Bulletin, **39**, 364 (1966).
13) G. Tsuchihashi and S. Iriuchijima, *ibid.*, **44**, 1726 (1971).
14) G. Tsuchihashi and S. Iriuchijima, *ibid.*, **43**, 2271 (1970).
15) F. Kurzer and J. Roy Powell, "Organic Synthesis," Coll. Vol. IV (1963), p. 934.
16) J. E. Dunbar and J. H. Rogers, *J. Org. Chem.*, **31**, 2842 (1966).
17) R. H. Harradence and F. Lions, *J. Proc. Roy. Soc. N. S. Wales*, **73**, 22 (1939).

The Photochemistry of 4,5-Disubstituted 1,3-Dioxolen-2-ones

Tamejiro HIYAMA, Shinsaku FUJITA, and Hitosi NOZAKI
Department of Industrial Chemistry, Kyoto University, Yoshida, Kyoto
(Received January 31, 1972)

The benzene-sensitized photoreaction of 4,5-dipropyl- (IIa) and 4,5-tetramethylene-1,3-dioxolen-2-one (IIb) in isopropyl alcohol gives two reduction products, *cis*- (V) and *trans*-4,5-disubstituted 1,3-dioxolan-2-one (VI). The irradiation of octa- (IId) and decamethylene-bridged vinylene carbonate (IIe) results in transannular hydrogen atom transfer from a methylene group to the olefinic bond and a subsequent recombination affording three tricyclic products, IX, X, and XIX. An examination of the stereochemistry of the products has indicated the participation of a diradical intermediate.

1,3-Dioxolen-2-ones (vinylene carbonates) are useful synthetic intermediates.[1] Recent reports have dealt with their photochemical dimerization[2] as well as with their cycloaddition reaction to olefins[3] and acetylenes.[4] We first wanted to obtain a general method for the preparation of 4,5-disubstituted derivatives, and then we proceeded to examine the photochemical behavior[5] of the derivatives.

Preparation of 4,5-Disubstituted 1,3-Dioxolen-2-ones. The known route to vinylene carbonates consisted of the chlorination of ethylene carbonates and a subsequent dehydrochlorination.[6] Vinylene carbonates are carbonic acid esters of ene-diols which are tautomeric with acyloins.[7] The treatment of an acyloin (I) with phosgene in the presence of pyridine afforded monochlorinated ethylene carbonate, III. The direct distillation of III caused a thermal dehydrochlorination, thus giving a crude vinylene carbonate, II (Scheme 1).

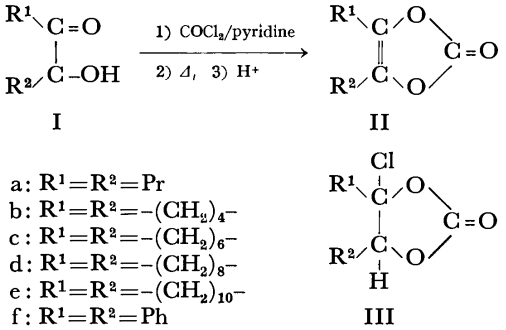

Scheme 1.

As the NMR spectrum showed contamination by exocyclic isomer(s), the crude carbonate, II, was converted to a pure form by heating a mixture dissolved in xylene with *p*-toluenesulfonic acid. The resulting II showed satisfactory NMR signals (no olefinic protons).

The carbonate, IId, was also prepared by the ethoxycarbonylation of sebacoin (Id) with ethyl chloroformate followed by treatment with *p*-toluenesulfonic acid in boiling xylene (Scheme 2).

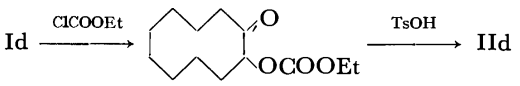

Scheme 2.

Photoreduction. The UV irradiation of IIa in isopropyl alcohol containing a benzene sensitizer afforded *cis*-4,5-dipropyl-1,3-dioxolan-2-one (Va) and its *trans* isomer (VIa), along with two dimers of IIa and acetone pinacol. The ratio of Va/VIa was determined by gas chromatography (GC) to be 8 : 92, (Scheme 3). The structures of the products were established by comparison with authentic samples prepared by the esterification of *meso*- and *dl*-4,5-octanediol[8] with phosgene.

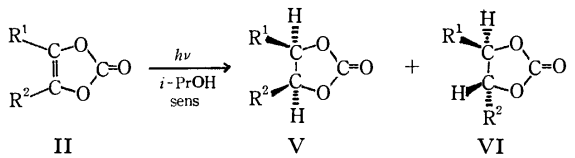

Scheme 3.

On the other hand, the UV irradiation of IIa in acetone gave only two kinds of dimers. The stereochemistry of the dimers was not examined.

The tetramethylene derivative, IIb, gave two saturated products, Vb and VIb (19% yield, 89: 11), upon irradiation in isopropyl alcohol–benzene. In the absence of hydrogen donors, IIb resisted the photoreaction.

The hexamethylene derivative, IIc, behaved differently and gave only a dimer upon irradiation both in acetone and in isopropyl alcohol–benzene.

Since the photoreaction of II required the presence

1) a) M. S. Newman and R. W. Addor, *J. Amer. Chem. Soc.*, **77**, 3789 (1955). b) M. S. Newman, *J. Org. Chem.*, **26**, 2630 (1961). c) J. C. Hinshaw, *Chem. Commun.*, **1971**, 630. d) H.-D. Scharf and H. Seidler, *Angew. Chem.*, **82**, 935 (1970). e) H.-D. Scharf and R. Klar, *Ann. Chem.*, **739**, 166 (1970). f) H.-D. Scharf and R. Klar, *Tetrahedron Lett.*, **1971**, 517. g) G. Hesse and P. Lechtken, *Angew. Chem.*, **83**, 143 (1971).

2) W. Hartmann and R. Steinmetz, *Chem. Ber.*, **100**, 217 (1967).

3) W. Hartmann, *ibid.*, **101**, 1643 (1968).

4) a) R. H. Grubbs, *J. Amer. Chem. Soc.*, **92**, 6693 (1970). b) J. Tancrede and M. Rosenblum, *Synthesis*, **1971**, 219.

5) A part of this work has previously been communicated: T. Hiyama, S. Fujita, and H. Nozaki, This Bulletin, **44**, 3222 (1971).

6) a) M. S. Newman, R. W. Addor, *J. Amer. Chem. Soc.*, **75**, 1263 (1953). b) N. D. Field and J. R. Schaefgen, *J. Polym. Sci.*, **58**, 533 (1962). c) J. R. Schaefgen and N. D. Field, *Macromol. Syn.*, **2**, 15 (1966). d) L. R. Morris, U. S. 3125582 (1964); *Chem. Abstr.*, **60**, 13248g (1964).

7) Schering Akt-Ges., Ger. 1044104 (1958); *Chem. Abstr.*, **55**, 4533h (1961).

8) The compound was obtained by sodium borohydride reduction of butyroin, followed by chromatographic separation. See J. Wiemann, G. Dana, Sa-Le-Thi-Thuan, and M. Brami, *Compt. Rend.*, **258**, 3724 (1964).

of triplet sensitizers,[2] such as acetone and benzene, the reaction must involve the triplet state of the olefinic functional group as a diradical. The photochemical behavior of the ene-diol carbonate moiety of II may be understood in the same way as the photoreduction of cyclopentenes.[9] The triplet state, VII, abstracts a hydrogen atom from isopropyl alcohol to produce the VIII radical stabilized by the adjacent oxygen atom. This then yields a mixture of ethylene carbonate isomer (V and VI), in which the thermodynamically more stable one predominates (Scheme 4).

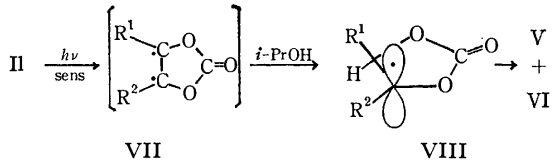

Scheme 4.

Intramolecular Hydrogen Abstraction. The irradiation of IId in acetone gave no dimers, but a mixture of novel tricyclic stereoisomers, IX and X, in a 71% yield. As the separation of the two isomers failed, the mixture was hydrolyzed to the *vicinal* diols, XI and XII (Scheme 5). The ratio of XI/XII was determined by GC as 85: 15. The separation of the two diols was accomplished by preparative thin-layer chromatography (plc).

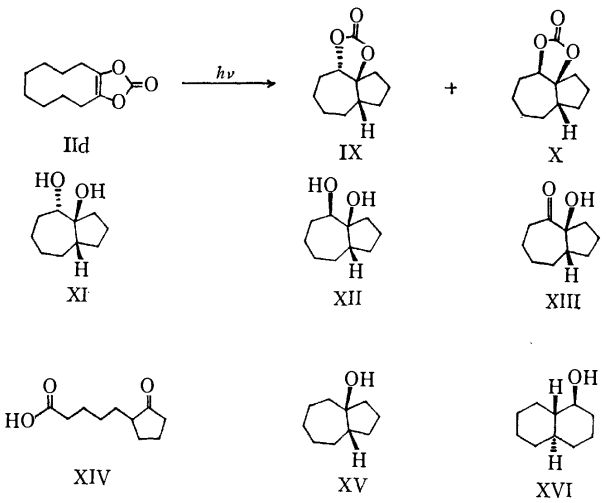

Scheme 5.

The structure and stereochemistry of XI and XII were established as follows. Since the oxidation of XI and XII by *N*-bromosuccinimide (NBS)[12] gave the same ketol, XIII, the diols should have the same ring system and ring fusion. The absorption of XIII at 1700 cm^{-1} implied that the ring including the carbonyl group was medium-sized. The glycol cleavage of XI and XII with periodate-permanganate[13] afforded ε-(2-ketocyclopentyl)valeric acid (XIV).[14] Hence, both XI and XII were established to have a bicyclo-[5.3.0]decane structure. The *cis*-ring fusion of the photoproducts was determined by the fact that the half-tosylation of a mixture of XI and XII, followed by reduction with lithium aluminum hydride or sodium borohydride, afforded *cis*-bicyclo[5.3.0]decane-1-ol (XV), along with *trans,trans*-α-decalol (XVI).[15] The formation of the latter can be ascribed to the base catalyzed rearrangement of the half-tosylate,[16] followed by the reduction of the resulting *trans*-α-decalone. In fact, the treatment of the half-tosylate of XI and XII with sodium methoxide in methanol afforded *trans*-α-decalone.

The reduction of XIII with sodium bis(2-methoxyethoxy)aluminum hydride (VSH) yielded XI almost exclusively. On the basis of Cram's rule,[17] the *trans*-configuration of the *vicinal* hydroxyl groups of XI was established, and consequently XII turned out to be its *cis*-diol isomer. Thus, XI and XII were concluded to be *cis*-bicyclo[5.3.0]decane-*trans*-1,2-diol and its *cis*-diol isomer respectively. The transannular photoreaction of IId proceeded even in isopropyl alcohol upon benzene sensitization, and neither reduction products nor dimers were detected among the products.

An inspection of the Dreiding models of IId suggests that the hydrogen atom on the C-6 in the excited state[18] resides closest to the C-1 (XVII) and that the abstraction of H_A by the C-1 radical probably occurs *via* seven-membered cyclic transition state. A subsequent recombination[19] of the resulting diradical, XVIII, may account for the preference for IX.

The decamethylene derivative, IIe, proved to be rather less reactive than IId. The irradiation of an

9) It has been well known that acyclic and large ring olefins undergo the *cis-trans* isomerization (Ref. 10) upon triplet sensitization, and that four- or five-membered cyclic olefins are reduced by hydrogen abstraction of the double bond (Ref. 11).

10) A. A. Lamola and N. J. Turro, "Energy Transfer and Organic Photochemistry", John Wiley and Sons, Inc., New York (1969), pp. 143, 153.

11) For four-membered ring, see a) R. L. Cargill, J. R. Damewood, M. M. Cooper, *J. Amer. Chem. Soc.*, **88**, 1330 (1966). For five-membered ring, see b) R. R. Sauers, W. Schinski, and M. M. Mason, *Tetrahedron Lett.*, **1967**, 4763. c) P. J. Kropp, *J. Amer. Chem. Soc.*, **89**, 3650 (1967). d) H.-D. Scharf, *Tetrahedron*, **23**, 3057 (1967). e) T. M. Gund, V. Z. Williams, Jr., E. Osawa. and P. von R. Schleyer, *Tetrahedron Lett.*, **1970**, 3877. f) L. Vollner, H. Parler, W. Klein, and F. Korte, *Tetrahedron*, **27**, 501 (1971).

12) L. F. Fieser and S. Rajagopalan, *J. Amer. Chem. Soc.*, **71**, 3938 (1949).

13) M. E. Wall and S. Serota, *J. Org. Chem.*, **24**, 741 (1959),

14) W. Herz, *ibid.*, **22**, 630 (1957).

15) W. G. Dauben, R. C. Tweit, and C. Mannerskantz, *J. Amer. Chem. Soc.*, **76**, 4420 (1954).

16) Similar rearrangements have been reported previously. For example, see a) G. Büchi, W. Hofheinz, and J. V. Paukstelis, *J. Amer. Chem. Soc.*, **91**, 6473 (1969). b) C. A. Grob, H. R. Kiefer, H. Lutz, and H. Wilkens, *Tetrahedron Lett.*, **1964**, 290. c) E. J. Corey, R. B. Mitra, and H. Uda, *J. Amer. Chem. Soc.*, **85**, 362 (1963).

17) D. J. Cram and K. R. Kopecky, *ibid.*, **81**, 2748 (1959).

18) A carbon-carbon double bond is well known to be twisted in its triplet state, see Ref. 10, p. 137.

19) Recombination of a diradical is known to occur with retention of the configuration at the radical centers separated by intervening one methylene, whereas it proceeds with partial inversion if the radical centers are separated by three or more methylenes. See C. G. Overberger and J. Anselme, *J. Amer. Chem. Soc.*, **84**, 869 (1962). The absence of *trans*-fused bicyclo[5.3.0]decanes in the photoproducts suggest that the recombination of the diradical XVIII precedes any conformational change. The reason is not clear yet, but may be explained by assuming fast spin-inversion at the radical center (C-10) adjacent to a hetero atom.

Table 1. Physical properties of 1,3-dioxolen-2-ones. II

Compound	Yield (%)	Bp (°C)/mmHg | Mp | (Solvent)	IR[a] (cm^{-1})	NMR[b] (δ)
IIa[c]	69	90—93/4	1830 1200 1030	1.97 (t, 6H, CH_3–), 1.62 (sextet, 4H, CH_2), 2.37 (t, 4H, CH_2C=)
IIb[d]	34	120—125/21	1820 1750 1200 940	1.0—2.1 (m, 4H), 2.1—2.7 (m, 4H)
IIc[e]	56	94—106/2	1820 1730 1710 1130 1040	1.0—2.3 (m, 12H, methylenes), 2.55 (t, 4H, CH_2C=)
IId[f]	80 67[h]	|44—45| (*n*-hexane)	1830 1730 1184[g] 1170 1130 1010	0.9—1.9 (m, 12H, methylenes), 2.45 (t, 4H, CH_2C=)
IIe[i]	50	|53.5—54| (*n*-hexane)	1825 1728 1215[g] 1142	1.1—2.0 (m, 16H, methylenes), 2.35 (t, 4H, CH_2C=)

a) Neat unless otherwise stated. b) Determined in CCl_4 at 24°C, 60 MHz. c) Found: C, 63.3; H, 8.3%. Calcd for $C_9H_{14}O_3$: C, 63.5; H, 8.3%. MS: *m/e* (relative abundance) 170 (M^+, 18), 141 (43), 83 (47), 71 (33), 69 (34), 55 (100) 44 (70). d) Found: C, 60.2; H, 6.0%. Calcd for $C_7H_8O_3$: C, 60.0; H, 5.8%. MS: *m/e* (relative abundance) 140 (M^+, 54), 112 (13), 95 (14), 68 (100), 67 (80), 55 (98). e) Found: C, 64.4; H, 7.2%. Calcd for $C_9H_{12}O_3$: C, 64.3; H, 7.2%. MS: *m/e* (relative abundance) 168 (M^+, 29), 95 (26), 81 (48), 68 (61), 67 (88), 55 (100). f) Found: C, 67.6; H, 8.2%. Calcd for $C_{11}H_{16}O_3$: C, 67.3; H, 8.2%. MS: *m/e* (relative abundance) 196 (M^+, 34), 137 (3), 123 (10), 109 (20), 97 (34), 95 (40), 81 (60), 67 (78), 55 (100), 41 (88). g) Nujol mull. h) Prepared by ethoxycarbonylation of sebacoin, followed by acid-treatment, *vide infra*. i) Found: C, 69.4; H, 9.0%. Calcd for $C_{13}H_{20}O_3$: C, 69.6; H, 9.0%. MS: *m/e* (relative abundance) 224 (M^+, 20), 151 (2), 137 (6), 123 (8), 111 (14), 109 (14), 98 (44), 95 (30), 81 (40), 67 (48), 55 (100).

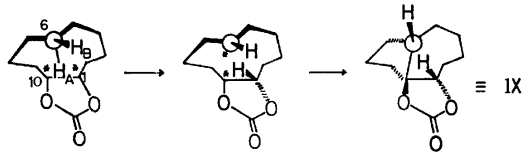

Scheme 6.

acetone solution of IIe yielded XIX in a 49% yield, along with a recovery of IIe (21%) (Scheme 7). The presence of the stereoisomers was not excluded, as no satisfactory separation of the isomers was accomplished. Alkaline hydrolysis gave the *vicinal* diol, XX, which was then subjected to Rudloff oxidation to afford 7-(2-ketocyclopentyl)heptanoic acid (XXI). IR bands of the keto acid appeared at 1737, and 1708 cm^{-1}, characteristic of a five-membered ketone and a carboxylic acid respectively. An authentic sample of XXI was obtained by the hydrogenation of the unsaturated derivative (XXII).[20] Consequently, the structure of XIX was established to be bicyclo[7.3.0]-dodecane-1,2-diol. The stereochemistry of the *vicinal* hydroxyl groups and the mode of the ring fusion were not examined.

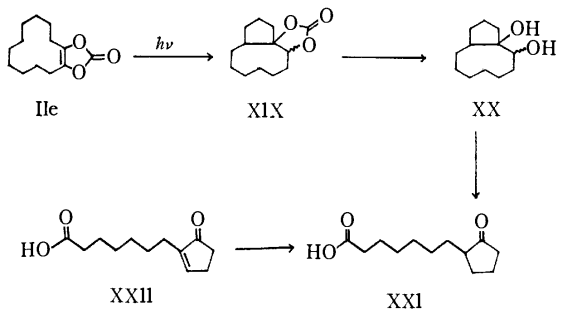

Scheme 7.

20) J. F. Bagli, T. Bogri, R. Deghenghi, and K. Wiesner, *Tetrahedron Lett.*, **1966**, 465. We are heartily grateful to Dr. Bagli for his kindness of sending us the sample of XXII.

The diphenylvinylene carbonate, IIf, was recovered unchanged upon irradiation in cyclohexane, whereas the photoreaction of IIf in the presence of iodine gave a phenanthrene derivative, XXIII, in a 77% yield.

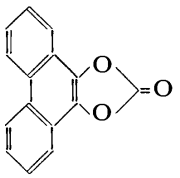

XXIII

Experimental

All the temperatures are uncorrected. The infrared spectra were recorded on a Shimadzu spectrophotometer IR-27-G; the ultraviolet spectra, on a Hitachi EPS-2 spectrometer; the nuclear magnetic resonance spectra, on a JEOL-60-H spectrometer, and the mass spectra, on a Hitachi RMU-6L spectrometer.

Preparation of I. *General Procedure*: To a solution of an acyloin (50 mmol) in benzene (60 m*l*) and pyridine (90 m*l*), a mixture of a 30% toluene solution (55 g) of phosgene (167 mmol) and benzene (80 m*l*) was added, drop by drop, at 0°C; the mixture was then stirred overnight. After dilution with *n*-hexane (300 m*l*), the precipitated pyridinium chloride was filtered off. The filtrate was washed twice with water (100 m*l*) and dried over anhydrous potassium carbonate. The evaporation of the solvent *in vacuo* and subsequent distillation gave a mixture of II and its isomer(s). The distillate was dissolved in a xylene mixture (*ca.* 80 m*l*), after which the solution was heated to reflux for 24 hr in the presence of *p*-toluenesulfonic acid (*ca.* 1 g). Neutralization with pyridine, filtration, and distillation gave II. The yields and physical properties are summarized in Table 1.

4,5-Diphenyl-1,3-dioxolen-2-one (IIf). This was prepared much as has been described above. Distillation at 140—150°C/0.15 mmHg gave IIf in a 61% yield; it then crystallized; mp 71—73°C (lit,[7] 74—76°C (*n*-hexane)). IR (KBr): 1820, 1695, 1208, 1068, 995, 727, 692 cm^{-1}. MS: *m/e* (relative abundance) 238 (M^+, 3), 165 (13), 152 (5), 105 (100), 77 (64).

4,5-Octamethylen-1,3-dioxolen-2-one (IId). An Alternate Procedure. Ethyl chloroformate (6 ml, 63 mmol) was added, drop by drop, to a solution of sebacoin (5.10 g, 30 mmol) in pyridine (30 ml) at room temperature, after which stirring was continued for 1 hr. The mixture was then diluted with *n*-hexane (100 ml), and the precipitated pyridinium chloride was filtered off. The solvents were evaporated *in vacuo* to yield ethyl 2-ketocyclodecyl carbonate quantitatively. IR (neat): 1750, 1728, 1260, 1010 cm^{-1}.

The unsymmetrical carbonate was directly mixed with *p*-toluenesulfonic acid (0.59 g, 3.4 mmol) in xylene (150 ml), and the whole was heated to reflux. After one day *p*-toluenesulfonic acid (1.18 g, 6.8 mmol) was added; the heating was then continued for another day. The acid was then neutralized with pyridine, and the precipitated salts were filtered off. Evaporation and distillation gave IId (3.97 g, 67%); bp 123—126°C/3 mmHg. The oil solidified and was recrystallized from *n*-hexane (see Table 1).

UV Irradiation of IIa in Acetone. A solution of IIa (1.14 g, 67 mmol) in acetone (50 ml) was placed in a quartz tube and irradiated with a 200-W high-pressure mercury lamp externally for 62 hr. The subsequent evaporation of the excess acetone *in vacuo* gave a crude solid (*ca.* 1.5 g), which was then recrystallized from *n*-hexane–ether–ethyl acetate to yield a dimer (0.05 g); mp 225—226°C. IR (Nujol): 1810, 1100, 1035 cm^{-1}. NMR ($CDCl_3$): δ 0.8—2.3 (m). MS: *m/e* (relative abundance) 171 (16), 170 ($M^+/2$, 100), 141 (30), 83 (18), 71 (25), 69 (8), 55 (22), 43 (66). Found: C, 63.6; H, 8.3%. Calcd for $C_{18}H_{28}O_6$: C, 63.5; H, 8.3%.

The mother liquid was subjected to chromatography on a silica gel column. Elution with benzene gave another crop of the crystalline dimer (0.18 g, totally, a 20% yield). Further elution gave an oily dimer (0.87 g, 76%); bp 100—110°C (bath temperature)/0.2 mmHg. IR (neat): 1810, 1212, 1131, 1032 cm^{-1}. NMR (CCl_4): δ 0.8—2.3 (m). MS: *m/e* (relative abundance) 170 ($M^+/2$, 28), 169 (11), 141 (21), 83 (20), 71 (59), 55 (43), 43 (100). Found: C, 63.5; H, 8.8%. Calcd for $C_{18}H_{28}O_6$: C, 63.5; H, 8.3%.

UV Irradiation of IIa in Isopropyl Alcohol–benzene. A mixture of IIa (1.12 g, 66 mmol), isopropyl alcohol (50 ml), and benzene (1 ml) was irradiated as has been described above for 5 days. Subsequent evaporation and distillation at 120—140°C/20 mmHg gave acetone pinacol (0.4 g). Further distillation (110°C/0.8 mmHg) gave a mixture of Va and VIa (0.22 g, 19%). The GC (High Vacuum Silicone Grease on Celite 545, 10%, 2 m) of the mixture revealed that the Va/VIa ratio was 8:92. Each component was separated by preparative GC (Silicone SE 30 on Chromosorb W, 30%, 1 m); the mass and infrared spectra and retention time on the GC were identical with those of the respective authentic samples (*vide infra*).

cis-*4,5-Dipropyl-1,3-dioxolan-2-one (Va).* Pyridine (2 ml) was added, drop by drop, at 0°C to a mixture of *meso*-4,5-octanediol (0.30 g, 2 mmol), benzene (10 ml), and a 30% phosgene solution in toluene (1.5 g). Stirring was continued overnight. A subsequent work-up gave Va quantitatively, bp 85—90°C (bath temperature)/3 mmHg. IR (neat): 1810, 1095, 1030 cm^{-1}. NMR (CCl_4): δ 0.8—2.1 (m, peak at δ 1.03 and 1.65, 14H, methyls and methylenes), 3.7—4.5 (m, 2H, CH–O). MS: *m/e* (relative abundance) 129 (M^+-43, 3), 128 (M^+-44, 1), 98 (4), 86 (9). 85 (11), 71 (16), 67 (26), 57 (68), 56 (61), 55 (53), 43 (84), 41 (100). Found: C, 62.9; H, 9.4%. Calcd for $C_9H_{16}O_3$: C, 62.8; H, 9.4%.

trans-*4,5-Dipropyl-1,3-dioxolan-2-one (VIa).* This was prepared much as above from *dl*-4,5-octanediol; it formed an oil; bp 105—110°C (bath temperature)/3 mmHg. IR (neat): 1802, 1180, 1030 cm^{-1}. NMR ($CDCl_3$): δ 0.8—2.2 (m, peak at δ 0.95 and 1.55, 14H, methyls and methylenes), 4.5—5.0 (m, 2H, CH–O). MS: *m/e* (relative abundance) 129 (4), 128 (3), 99 (5), 86 (10), 85 (12), 71 (28), 67 (36), 57 (78), 43 (100), 41 (98). Found: C, 62.9; H, 9.4%. Calcd for $C_9H_{16}O_3$: C, 62.8; H, 9.4%.

UV Irradiation of IIb in Isopropyl Alcohol–benzene. A mixture of IIb (0.42 g, 3 mmol), isopropyl alcohol (15 ml), and benzene (0.5 ml) was irradiated for 5 days. A subsequent GC of the mixture showed the presence of Vb and VIb, along with the recovered IIb. The separation of Vb and VIb was performed by preparative GC. The IR and mass spectra and retention times on the GC of both products were identical with those of the authentic samples. The yield of Vb and VIb was estimated by GC to be 13%, and the Vb/VIb ratio was determined to be 89:11.

cis- *and* trans-*4,5-Tetramethylene-1,3-dioxolan-2-one (Vb and VIb).*[21] These were prepared from *cis*- and *trans*-cyclohexane-1,2-diol much as has been described in the preparation of Va and VIa. The *cis* isomer, Vb, exhibited IR (neat): 1800, 1205, 1162, 1135, 1030 cm^{-1}. NMR ($CDCl_3$): δ 1.2—2.2 (m, 8H, methylenes), 4.5—5.0 (m, 2H, methines). The *trans* isomer, VIb, exhibited IR (Nujol): 1795, 1190, 1150, 1100, 1058, 1040 cm^{-1}. NMR ($CDCl_3$): δ 1.0—2.5 (m, 8H, methylenes), 3.8—4.3 (m, 2H, methines).

UV Irradiation of IIc. The irradiation of IIc (1.40 g, 8.3 mmol) in acetone for 6 days, and subsequent concentration and chromatography on a silica-gel column gave crystals (0.62 g, 44%); mp 268°C (acetonitrile-ethyl acetate (1:1)). IR (Nujol): 1805, 1190, 1050 cm^{-1}. NMR ($CDCl_3$): δ 0.8—2.8 (m, peak at δ 1.45, methylenes). MS: *m/e* (relative abundance) 168 ($M^+/2$, 61), 140 (9), 129 (14), 95 (35), 84 (62), 67 (48), 59 (76), 55 (89), 43 (100), 41 (73). Found: C, 64.1; H, 7.1%, MW (cryoscopic method) 325. Calcd for $C_{18}H_{24}O_6$: C, 64.3; H, 7.2%, MW 336.

The irradiation of IIc (1.01 g, 6 mmol) in isopropyl alcohol (18 ml) and benzene (1 ml) for 4 days, followed by the separation of the products by chromatography on a silica-gel column, gave the dimer in a 45% yield.

UV Irradiation of IId. An acetone solution (30 ml) of IId (1.00 g, 5.1 mmol) was irradiated for one day, then concentrated and subjected to chromatography on a silica-gel column. Elution with benzene gave the recovered IId (0.03 g) and an inseparable mixture of IX and X (0.71 g, 71%); bp 130—135°C/3 mmHg. IR (neat); 1800, 1175, 1160, 1028 cm^{-1}. NMR (CCl_4): δ 0.8—2.5 (m, peak at δ 1.80, 15H, methylenes and methine), 4.2—4.8 (m, 1H, CH–O). MS: *m/e* (relative abundance) 196 (M^+, 8), 152 (17), 124 (24), 110 (28), 109 (26), 97 (49), 95 (40), 84 (92), 81 (67), 67 (85), 55 (98), 41 (100). Found: C, 67.2; H, 8.0%. Calcd for $C_{11}H_{16}O_3$: C, 67.3; H, 8.2%.

Hydrolysis of IX and X. A mixture of IX and X (1.33 g, 6.8 mmol) was added to a solution of potassium hydroxide (1.5 g) dissolved in water (40 ml) and ethanol (40 ml). The whole was stirred for 6.5 hr at room temperature. The ethanol was then evaporated *in vacuo*, and residue was extracted with chloroform. The subsequent evaporation of the solvent and the purification of the residue by chromatography on a silica-gel column gave a mixture of XI and XII (0.83 g, 72%). The recrystallization of the mixture gave XI; mp 82—83°C (acetone). IR (Nujol): 3400, 1065, 1010, 910 cm^{-1}. NMR ($CDCl_3$): δ 0.8—2.3 (m, peak at δ 1.65, 15H, methylens and methine), 2.43 (s, 2H, OH), 3.2—3.8 (m, 1H, CH–O). MS: *m/e* (relative abundance) 170 (M^+, 6), 152 (9), 123 (15), 111 (17), 97 (100), 84 (66), 67 (29), 55 (41). Found:

21) P. Brown and C. Djerassi, *Tetrahedron*, **24**, 2949 (1968).

C, 70.5; H, 10.6%. Calcd for $C_{10}H_{18}O_2$: C, 70.5; H, 10.7%.

The plc of the mother liquid gave XII: bp 100—105°C/0.15 mmHg. IR (neat): 3480, 1085, 1035, 920 cm^{-1}. NMR ($CDCl_3$): δ 0.8—2.4 (m, 15H, methylenes and methine), 2.55 (s, 2H, OH), 3.0—3.7 (m, 1H, CH-O). MS: *m/e* (relative abundance) 170 (M^+, 12), 152 (12), 123 (15), 111 (34), 97 (100), 84 (70), 67 (33), 55 (50). Found: C, 70.5; H, 10.7%. Calcd for $C_{10}H_{18}O_2$: C, 70.5; H, 10.7%.

Oxidation of XI with NBS. A mixture of XI (0.14 g, 0.8 mmol), acetone (10 m*l*), water (1 m*l*), NBS (0.20 g, 1.1 mmol), and acetic acid (5 drops) was stirred overnight at room temperature. Subsequent work-up and purification by plc gave the ketol, XIII (0.07 g, 50%); bp 100°C (bath temperature)/3 mmHg. IR (neat): 3460, 1700, 1137 cm^{-1}. NMR ($CDCl_3$): δ 0.8—2.7 (m, peak at δ 1.75 and 2.25, methylenes and methine), 2.78 (s, 1H, OH). MS: *m/e* (relative abundance) 168 (M^+, 25), 150 (11), 124 (26), 111 (100), 98 (68), 97 (67), 83 (39), 78 (40), 55 (50). Found: C, 71.0; H, 9.6%. Calcd for $C_{10}H_{16}O_2$: C, 71.4; H, 9.6%.

Oxidation of XII with NBS. This was perfomed as has been described above. The IR and mass spectra and the retention time on GC were identical with those obtained by the oxidation of XI.

Reduction of XIII with VSH. A benzene solution of VSH (72 wt%, 0.5 m*l*) was added, drop by drop, to XIII (0.02 g, 0.12 mmol) in benzene (10 m*l*), and then the mixture was stirred overnight. A subsequent work-up gave diol (0.03 g, quantitative). The spectrum and retention time on the GC were identical with those of XI.

Periodate-permanganate Oxidation of XI and XII. To a mixture of XI and XII (0.36 g, 2.1 mmol), *t*-butyl alcohol (30 m*l*), potassium carbonate (0.10 g), and water (20 m*l*), we added an aqueous solution (50 m*l*) of sodium metaperiodate (2.60 g), potassium permanganate (0.05 g), and potassium carbonate (0.10 g) at room temperature; the mixture was then stirred for 3 hr. Extraction with chloroform and concentration gave the crude keto acid (XIV) (0.29 g, 78%). IR (neat): 3600—2400, 1735, 1710, 1200, 1155 cm^{-1}. MS: *m/e* (relative abundance) 184 (M^+, 4), 129 (14), 97 (16), 84 (100), 69 (24), 55 (50), 41 (58). The oxime melted at 121—124°C (lit,[14] 124—125.5°C). The semicarbazone melted at 192—193°C (lit,[14] 195—196°C).

Conversion of XI and XII to XV and XVI. A mixture of XI and XII (0.10 g, 0.6 mmol) and *p*-toluenesulfonyl chloride (0.12 g, 0.6 mmol) was treated with pyridine (5 m*l*) at room temperature, and stirring was continued overnight. A subsequent work-up gave the half-tosylate of XI and XII (0.15 g). IR (neat): 3420, 1170, 890 cm^{-1}.

The reduction of the half-tosylate with lithium aluminum hydride[22] or sodium borohydride[23] was performed according to the reported procedure. The GC of the mixture revealed the presence of XV as well as XVI, which was separated by preparative GC. The XVI alcohol showed IR (neat): 3380, 1140, 1035, 1015 cm^{-1}. MS: *m/e* (relative abundance) 154 (M^+, 7), 136 (100), 121 (35), 111 (33), 95 (55), 94 (58), 81 (50), 67 (83), 55 (60), 41 (73).

The attempted separation of XV was unsuccessful, but its formation was proven by comparing the retention times on two different GC columns (Dowfax 9N9, 10%, 2 m, and High Vacuum Silicone Grease, 10%, 2 m) with those of an authentic sample[24] which had been prepared by the hydroboration[25] of $\Delta^{1(7)}$-bicyclo[5.3.0]decene.[26] The XV alcohol thus obtained showed IR (neat): 3360, 1010 cm^{-1}. MS: *m/e* (relative abundance) 154 (M^+, 2), 136 (43), 121 (32), 97 (50), 95 (59), 81 (60), 67 (88), 55 (80), 41 (100).

UV Irradiation of IIe. The irradiation of IIe (4.29 g, 19 mmol) in acetone (60 m*l*) for 11 days and subsequent chromatography on a silica-gel column gave IIe (0.90 g, 21%) (elution with *n*-hexane–benzene (1:1)). Further elution with *n*-hexane–benzene (1:3) gave XIX (2.12 g, 49%). IR (neat): 1800, 1255, 1039 cm^{-1}. NMR (CCl_4): δ 1.2—2.8 (m, peak at δ 1.63, 19H, methylenes and methine), 4.0—4.7 (m, 1H, CH-O). MS: *m/e* (relative abundance) 224 (M^+, 9), 180 (3), 151 (6), 137 (6), 123 (14), 111 (24), 98 (66), 84 (52), 81 (49), 67 (63), 55 (100). Found: C, 69.5; H, 9.0%. Calcd for $C_{13}H_{20}O_3$: C, 69.6; H, 9.0%.

Hydrolysis of XIX. A mixture of XIX (2.12 g, 9.4 mmol), potassium hydroxide (2 g), water (40 m*l*), and ethanol (60 m*l*) was stirred overnight. A subsequent work-up gave crude XX (1.28 g, 69%). Recrystallization from *n*-hexane gave white needles; mp 90.4—91.6°C. IR (Nujol): 3360, 1094, 1015 cm^{-1}. NMR (CCl_4): δ 0.7—2.7 (m, 19H, methylenes and methine), 3.2—4.0 (m, 3H, CH-O and OH). MS: *m/e* (relative abundance) 198 (M^+, 10), 180 (4), 139 (12), 125 (27), 111 (19), 97 (93), 84 (100), 67 (57), 55 (90). Found: C, 72.7; H, 11.3%. Calcd for $C_{12}H_{22}O_2$: C, 72.7; H, 11.2%.

Oxidation of XX. This was performed much as has been described in the oxidation of XI and XII; it afforded XXI in an 86% yield. IR (neat): 3700—2300, 1737, 1708, 1410, 1250, 1200, 1155 cm^{-1}. MS: *m/e* (relative abundance 212 (M^+, 2), 163 (4), 123 (5), 109 (5), 97 (14), 84 (100), 83 (20), 69 (15), 55 (30). The semicarbazone melted at 169—171°C.

Hydrogenation of XXII. A mixture of XXII (0.13 g, 0.62 mmol) and Raney Nickel (*ca.* 0.1 g) in ethanol (10 m*l*) was stirred under a hydrogen atmosphere for a day. The subsequent filtration of the catalyst and concentration gave XXI quantitatively. The semicarbazone melted at 170—172°C.

UV Irradiation of IIf. A solution of IIf (2.5 g, 10.5 mmol) and iodine (0.2 g) in cyclohexane (75 m*l*) was irradiated for 7 days. The precipitates of XXIII (1.92 g, 77%) were collected by filtration and recrystallized from benzene to afford needles; mp 178—179°C. IR (KBr): 1840, 1805, 1622, 1605, 1120, 1045, 1024, 910, 740, 712 cm^{-1}. NMR ($CDCl_3$): δ 7.5—8.2 (m, 6H), 8.4—8.9 (m, 2H). MS: *m/e* (relative abundance) 236 (M^+, 80), 180 (44), 164 (100), 152 (28). UV (*n*-hexane): λ_{max} (log ε) 248 (5.72), 255 (5.82), 269 (4.95), 280 (4.67), 292 (4.86), 305 (5.12). Found: C, 76.1; H, 3.2%. Calcd for $C_{15}H_8O_3$: C, 76.3; H, 3.4%.

Financial support from the Ministry of Education, the Japanese Government, and from the Toray Science Foundation is acknowledged with pleasure.

22) W. W. Zorbach and C. O. Tio, *J. Org. Chem.*, **26**, 3543 (1961).

23) R. O. Hutchins, D. Hoke, J. Keogh, and D. Koharski, *Tetrahedron Lett.*, **1969**, 3495.

24) J.-M. Bessiere and H. Christol, *Bull. Soc. Chim. Fr.*, **1969**, 4063.

25) R. C. Fort, Jr., R. E. Hornish, and G. A. Liang, *J. Amer. Chem. Soc.*, **92**, 7558 (1970).

26) C. Arnal, J.-M. Bessiere, H. Christol, and R. Vanel, *Bull. Soc. Chim. Fr.*, **1967**, 2485.

The Phenolysis of Tetrahydrolinalyl and 2-Octyl Systems. The Rates, Steric Courses, and Product Distributions

Kunio OKAMOTO and Tomomi KINOSHITA

Department of Hydrocarbon Chemistry, Faculty of Engineering, Kyoto University, Sakyo-ku, Kyoto

(Received March 6, 1972)

As tertiary and secondary systems with optical activity, tetrahydrolinalyl (methylethylisohexylcarbinyl) chloride or *p*-nitrobenzoate and 2-octyl *p*-toluenesulfonate have been selected, and their titrimetric and polarimetric rate constants (k_t and k_p) for S_N1 phenolyses have been measured in the presence of triethylamine (or sodium phenoxide) in 50 wt% phenol-benzene. At higher amine (or phenoxide) concentrations, the k_t and k_p coincide with each other for tetrahydrolinalyl chloride (at 25.0°C) or *p*-nitrobenzoate (at 100.0°C), and also for 2-octyl tosylate (at 75.0°C), exhibiting the typical features of the S_N1 solvolysis rate constant. In the absence of the amine (or sodium phenoxide), the k_t diminishes to show a gap between the k_p and the k_t, indicating the occurrence of an ion-pair return in the phenolysis for both systems. Under the same reaction conditions as those of the rate measurement, tetrahydrolinalyl chloride and *p*-nitrobenzoate yield the phenyl ether, with a predominant racemization accompanied by some net inversion of the configuration, whereas 2-octyl tosylate gives 2-octyl phenyl ether, *o*-, and *p*-2-octylphenols, with a net inversion of the configuration accompanied by a slight racemization. These steric results indicate that phenol can be considered as a typical solvolytic solvent. The product distributions have been assessed for the reactions of 2-octyl chloride (200°C) and of tetrahydrolinalyl chloride (25.0°C) with the molecule of phenol under the S_N1 phenolysis conditions, by extrapolating the product composition curves to a zero concentration of the phenoxide. For both systems, the phenol molecule is predominantly *O*-alkylated (74 and 99% respectively), accompanied by minor amounts of *C*-alkylation. In contrast to the phenol reaction, the phenoxide ion undergoes more *C*-alkylation (42 and 50% respectively).

Our previous studies of the phenolytic reactivity with regard to optically-active substrates have concentrated upon the optically-active 1-phenylethyl system;[1] the phenolysis of this system proceeded to yield 1-phenylethyl phenyl ether with a partially-retained configuration. This is not a standard result for the steric course of the solvolysis, since the solvolyses of such simple *sec*- and *tert*-alkyl (or aralkyl) systems have generally been reported to give a product with a partially-inverted onfiguration.[2] Therefore, we considered it of interest to examine whether the solvolysis of simple optically-active systems other than the 1-phenylethyl system would proceed with a retention of the configuration in the phenolic solvent or not; we selected the 2-octyl and the tetrahydrolinalyl (methylethylisohexylcarbinyl) systems, which are readily available and which also have been reported to give partially-inverted products in common solvolytic solvents[3] other than phenol.

Our results show that, in contrast to the 1-phenylethyl system, the phenolysis for both systems proceeds with a net inversion of the configuration—a standard result expected of the typical S_N1 solvolysis of a simple optically-active system. We will also report on the distributions of the phenolysis products in both systems.

1) K. Okamoto, T. Kinoshita, and H. Shingu, This Bulletin, **43**, 1545 (1970), and the references cited therein.

2) A. Streitwieser, Jr., *Chem. Rev.*, **56**, 571 (1956); for the inversive solvolysis of the *tert*-alkyl system, see L. H. Sommer and F. A. Carey, *J. Org. Chem.*, **32**, 800, 2473 (1967).

3) For the 2-octyl system, see a) A. Streitwieser, Jr., T. D. Walsh, and J. R. Wolfe, Jr., *J. Amer. Chem. Soc.*, **87**, 3682 (1965); b) A. Streitwieser, Jr. and T. D. Walsh, *ibid.*, **87**, 3686 (1965); c) H. Weiner and R. A. Sneen, *ibid.*, **87**, 287 (1965); d) H. Weiner and R. A. Sneen, *ibid.*, **87**, 292 (1965). For tetrahydrolinalyl chloride, see e) E. D. Hughes, C. K. Ingold, R. J. L. Martin, and D. F. Meigh, *Nature*, **166**, 679 (1950).

Results and Discussion

The S_N1 *Characteristics of the Phenolyses of 2-Octyl and Tetrahydrolinalyl Systems.* The titrimetric and polarimetric rate constants (k_t and k_p) in a 50 wt% phenol-benzene solvent were measured in the presence of variable concentrations of triethylamine (or sodium phenoxide) on 2-octyl chloride at 175.0 and 200.0°C or on the *p*-toluenesulfonate at 75.0°C, and on tetrahydrolinalyl (methylethylisohexylcarbinyl) chloride at 25.0°C or on the *p*-nitrobenzoate at 100.0°C. Satisfactory first-order kinetic behavior, expected of a typical S_N1 reaction, was observed for each of the k_t's and k_p's; the results are tabulated in Table 1.

The effects of the triethylamine (or sodium phenoxide) concentrations upon the k_t and the k_p values in the phenolyses of 2-octyl tosylate and tetrahydrolinalyl *p*-nitrobenzoate are illustrated in Figs. 1 and 2 respectively. It is immediately obvious that the k_t's for the tetrahydrolinalyl *p*-nitrobenzoate (or chloride) are almost independent of the amine (or the phenoxide) concentrations; this is a typical kinetic feature of the S_N1 solvolysis (see also Table 1).

From Figs. 1 and 2 it is also evident that, at a zero concentration of the base, there exists a gap between the k_p and k_t values (*i.e.*, $k_p > k_t$) in the case of 2-octyl tosylate, and most probably in the case of tetrahydrolinalyl *p*-nitrobenzoate as well; these results indicate that the S_N1 phenolyses for these systems proceed with some "ion-pair" return.

The gap between the k_p and k_t values has already been observed in the phenolysis of 1-phenylethyl chloride.[4] However, in marked contrast to the 1-phenylethyl system, in which the gap actually widens as the

4) K. Okamoto, K. Takeuchi, and H. Shingu, This Bulletin, **35**, 525, (1962).

TABLE 1. THE RATE CONSTANTS FOR THE PHENOLYSIS OF 2-OCTYL AND TETRAHYDROLINALYL (THL) SYSTEMS IN 50 wt% PHENOL-BENZENE SOLVENT

	Temp °C	RX M	Et_3N (PhONa) M	$10^4 \times k_t$ sec^{-1}	$10^4 \times k_p$ sec^{-1}
2-Oct Cl	175 (±1)	0.0921	0.0930	0.713	—
	200 (±1)	0.0872	0.0968	3.12	—
		0.0490	0.0495	3.85	—
		0.0496	0.0996	4.55	—
2-Oct OTs	75.0 (±0.1)	0.100	0.000	1.69	2.00
		0.100	0.102	1.83	2.08
		0.103	0.301	1.93	2.17
		0.102	0.498	2.35	2.33
		0.101	0.703	2.51	2.55
THL Cl	25.0 (±0.1)	0.100	0.000	6.13	—
		0.010	0.012	16.5	—
		0.023	0.025	16.5	—
		0.049	0.051	16.6	—
		0.100	0.102	16.5	16.3
		0.100	0.201	16.7	—
		0.100	0.303	17.1	—
THL OPNB[b]	100.0 (±0.1)	0.101	0.0000	9.43	—
		0.0500	0.0509[a]	9.73	—
		0.0998	0.103[a]	9.93	—
		0.103	0.148[a]	10.1_5	—
		0.102	0.000	—	10.3
		0.0495	0.0503[a]	—	10.1
		0.0989	0.0993[a]	—	9.6^2
		0.102	0.146[a]	—	9.8_5

a) Sodium phenoxide was used instead of triethylamine. b) THL=Tetrahydrolinalyl; OPNB=*p*-Nitrobenzoate.

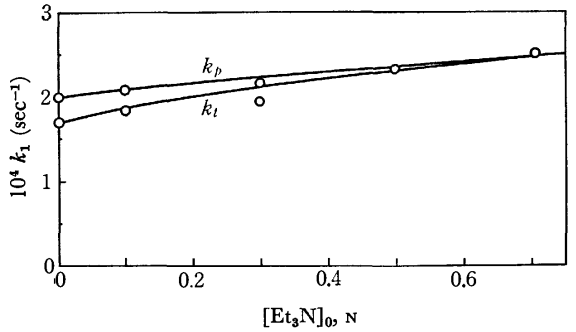

Fig. 1. Effect of the added triethylamine upon the first-order rate constants for the phenolysis of 2-octyl tosylate in 50 wt% phenol-benzene solvent at 75.0°C.

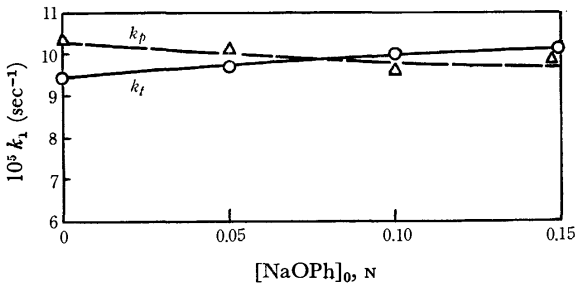

Fig. 2. Effect of the added sodium phenoxide upon the first-order rate constants for the phenolysis of tetrahydrolinalyl *p*-nitrobenzoate in 50 wt% phenol-benzene solvent at 100.0°C.

concentration of the base increases, in the 2-octyl and tetrahydrolinalyl systems the gap virtually disappears with an increase in the amine concentrations (see Figs. 1 and 2). The coincidence in the k_p and k_t values (within the limits of experimental error) suggests that the consumption rate (k_2[PhOH]+k_2'[PhO$^-$] in Eq. (1)) of the ion-pair intermediate becomes far greater than the return rate (k_{-1} in Eq. (1)) at higher amine or phenoxide concentrations, and that the return phenomena virtually disappear as the amine or the phenoxide concentration increases.

These kinetic features can be expressed by the following reaction scheme, which contains a single ion-pair intermediate; the observed rate constant can be expressed by Eq. (1):

$$RX \underset{k_{-1}}{\overset{k_1}{\rightleftharpoons}} [R^+ \cdots X^-] \xrightarrow{k_2[PhOH]+k_{2'}[PhO^\ominus]} \text{Phenolysis products}$$

$$k_{obs.} = \frac{k_1(k_2[PhOH]+k_{2'}[PhO^\ominus])}{k_{-1}+k_2[PhOH]+k_{2'}[PhO^\ominus]} \quad (1)$$

For the acetolysis of 2-octyl tosylate, a similar reaction scheme with a single ion-pair intermediate has already been proposed by Streitwieser *et al.*[3a,b] Thus, providing that the above scheme applies to these phenolyses, from the data illustrated in Figs. 1 and 2 and from Eq. (1) the k_{-1}/k_2 ratio can be estimated to be 0.925(M) for the phenolysis of 2-octyl tosylate at 75.0°C and 0.467(M) for that of the tetrahydrolinalyl system at 100.0°C.

The Steric Courses of the Phenolyses of 2-Octyl Tosylate and of Tetrahydrolinalyl Chloride and p-*Nitrobenzoate.* The phenolyses of optically-active 2-octyl tosylate were carried out at 75.0°C in 50 wt% phenol–benzene for one and for ten half-lives. By the chromatography on silica gel, from the reaction mixtures we isolated the

Table 2. The phenolysis products and their optical activities in the phenolyses of optically active 2-octyl tosylate or tetrahydrolinalyl chloride and *p*-nitrobenzoate[a)]

		2-Octyl tosylate		THL Cl	THL OPNB
RX,	M	0.100	0.100	0.100	0.0989
	$[\alpha]_D$	+6.97°[b)] (±0.02°)	+6.13°[b)] (±0.02°)	+0.50°[b)] (±0.02°)	−0.925° (±0.011°)
Et_3N,	M	0.0999	0.101	0.103	0.0993
Time,	hr	1.00[c)]	24.0	1.5	24
Temp,	°C	75.0	75.0	25.0	100
ROPh	α_D[b)]	−24.60° (±0.04°)	−20.11° (±0.03°)	+0.20° (±0.02°)	+1.27° (±0.01°)
	α%[d)]	91.0 Inv.	84.7 Inv.	Inv. + predominant Rac.[e)]	16.2 Inv.
	Yield %	14.6	27.9	13.6	12.5
o-RC_6H_4OH	$[\alpha]_D$	−3.80° (±0.28°)	−2.17° (±0.15°)		
	α%	101 Inv.	65.7 Inv.	—	—
	Yield %	3.64	9.30		
p-RC_6H_4OH	$[\alpha]_D$	−5.83° (±0.44°)	−4.69° (0.05°)		
	α%	108 Inv.	98.2 Inv.	—	—
	Yield %	1.89	6.11		

a) The maximum rotations for the relevant optically active compounds in this Table are shown in Table 3. b) The rotations for a neat sample at 21—25°C in a 1-dm tube. c) See text; ethy 2-octyl ether, which was obtained by the SN2 ethanolysis of the unchanged ROTs, possessed $[\alpha]_D$ −14.9°, and α% 91.2 (with respect to ROTs). d) A net steric course. e) See text; the calculated α% on the basis of the optical purity of tetrahydrolinalool, from which the starting chloride was prepared, amounts to 3.62%; the α%, calculated on the basis of the maximum rotation[11)] for tetrahydrolinalyl chloride, amounts to 3.21%.

elimination product in a 50—60% yield; this product was composed of 1-, *cis*-2-, and *trans*-2-octenes. From the subsequent eluents, the substitution products (2-octyl phenyl ether, *o*-, and *p*-2-octylphenols) were separated in a 40—60% yield. The configuration of each product was predominantly inverted, and the degree of racemization was quite small. The details of the results are tabulated in Table 2.

The inversion with some racemization is a standard result for the steric course of the solvolysis of a simple secondary alkyl system;[2)] similar stereochemical outcomes for the 2-octyl systems have been observed in acetic acid[3a,b)] and aqueous dioxane[3c,d)] solvents.

The phenolysis of tetrahydrolinalyl chloride, when conducted at 25.0°C in the 50 wt% phenol-benzene solvent for 10 half-lives, yielded a 86.2% yield of decenes (a mixture of 4 isomers), a 13.6% yield of tetrahydrolinalyl phenyl ether, and small amounts of *o*- and *p*-tetrahydrolinalylphenols (0.15 and 0.017% yields respectively); the configuration of the phenyl ether was inverted, with some racemization. Since we have no information about the extent of racemization during the retentive conversion of tetrahydrolinalool to tetrahydrolinalyl chloride, we can not estimate the optical purity of the starting chloride thus prepared nor, consequently, the exact degree of racemization for the phenyl ether in the course of the phenolysis. However, if we assume that the retentive chloride formation by thionyl chloride proceeds with a low degree of the racemization, as is observed in the case of optically-active 1-phenylethyl alcohol,[5)] we may expect that the tetrahydrolinalyl chloride phenolysis proceeds with a predominant racemization, with some net inversion.

Tetrahydrolinalyl *p*-nitrobenzoate, $[\alpha]_D^{21.0}$ −0.925°, was prepared from tetrahydrolinalool, $\alpha_D^{23.5}$ −0.43°, and *p*-nitrobenzoyl chloride in pyridine. The phenolysis of the *p*-nitrobenzoate was carried out at 100.0°C in the 50 wt% phenol-benzene solvent for 10 half-lives; it yielded a 85% yield of decenes (a mixture of 4 isomers), a 12.5% yield of tetrahydrolinalyl phenyl ether, and a small amount of *C*-alkylated phenols (less than a 0.5% yield). From the values of the maximum rotations of the *p*-nitrobenzoate and the phenyl ether (see Table 3), it was estimated that the phenolysis proceeded with a 83.8% racemization, accompanied by a net 16.2% inversion.

An inversion of the configuration with some racemization has been typically observed in the solvolyses of simple *tert*-alkyl systems, *e.g.*, in the solvolyses of tetrahydrolinalyl chloride in 80% aqueous acetone and methanol solvents,[3e)] in the methanolysis of methylethylisobutylcarbinyl hydrogen phthalate,[6)] and in solvolyses of methylethylphenylcarbinyl chloride,[7)]

5) See the experimental part of our previous report: K. Okamoto, M. Hayashi, K. Komatsu, and H. Shingu, This Bulletin, **40**, 624 (1967).

6) W. von E. Doering and H. H. Zeiss, *J. Amer. Chem. Soc.*, **75**, 4733 (1953).

7) L. H. Sommer and A. F. Carey, *J. Org. Chem.*, **32**, 2473 (1967).

TABLE 3. THE MAXIMUM ROTATIONS AND THE ABSOLUTE CONFIGURATIONS FOR THE PHENOLYSIS PRODUCTS AND RELEVANT SUBSTRATES

	$[\alpha]_D$ or α_D 22—25°	References
(*R*)-2-octyl phenyl ether	−38.7° (neat, 1 dm)	This work
(*R*)-*o*-2-octylphenol	−4.56° (in benzene)	This work
(*R*)-*p*-2-octylphenol	−6.57° (in benzene)	This work
(*R*)-tetrahydrolinalyl phenyl ether	+7.84° (neat, 1 dm)	This work
(*R*)-tetrahydrolinalyl *p*-nitrobenzoate	+1.67° (in benzene)	This work
(*R*)-2-octanol	+10.3° (neat, 1 dm)	Kornblum[a]
(*R*)-2-octyl *p*-toluenesulfonate	−9.96° (neat, 1 dm)	Streitwieser[b]
(*R*)-2-methyloctanoic acid	−16.4° (in *n*-heptane)	Ref. 11
(*S*)-tetrahydrolinalool	−0.76° (neat, 1 dm)	Ref. 12
(*R*)-tetrahydrolinalyl chloride	−0.63° (neat, 1 dm)	Ref. 12

a) Cited by N. Kornblum, L. Fishbein, and R. A. Smiley (*J. Amer. Chem. Soc.*, **77**, 6261 (1955)).
b) Calcd from the data reported by A. Streitwieser, Jr. *et al.* (Ref. 3a).

p-nitrobenzoate,[8] and hydrogen phthalate[8] in acetic acid,[8] methanol,[7,8] ethanol,[7] 80% aqueous ethanol,[7] and 75% aqueous dioxane.[7]

In conclusion, these steric results for both systems indicate that the phenolic solvent can be considered as a typical solvolytic solvent.

The Absolute Configurations and the Maximum Rotations for 2-Octyl Phenyl Ether, Tetrahydrolinalyl Phenyl Ether, and o- *and* p-*2-Octylphenols.* Optically-active compounds of the titled phenolysis products, the absolute configurations and maximum rotations of which are not yet known, were prepared from, or derived to, a known, optically-active compound by following the reaction schemes described below. The configurations and the rotations thus established are tabulated in Table 3, along with those of the relevant optically-active compounds. Using the values shown in Table 3, the net steric courses and extents of inversion (α%) in the course of the phenolyses have been estimated; they are tabulated in Table 2.

(*S*)-(+)-2-Octyl *p*-toluenesulfonate was treated with sodium phenoxide in dimethylformamide at 75.0°C for 20 hr. Since the reaction proceeds by means of the S_N2 mechanism, the (−)-2-octyl phenyl ether thus obtained was determined to possess the (*R*)-configuration.[9] The maximum rotation (Table 3) was calculated from the known rotation[3a] of 2-octyl tosylate:

$$(S)\text{-}(+)\text{-2-Oct-OTs} \xrightarrow[\text{in DMF}]{\text{NaOPh}} (R)\text{-}(-)\text{-2-Oct-OPh}$$

Optically-active *o*- and *p*-2-octylphenols, obtained by the acidic rearrangement of optically-active 2-octyl phenyl ether, were subjected to permanganate oxidation[10] in acetone. From the specific rotations of the optically-active 2-methyloctanoic acid[11] thus obtained, the maximum rotations of (*R*)-(−)-*o*-2-octylphenol and (*R*)-(−)-*p*-2-octylphenol were estimated (Table 3):

$$(R)\text{-}(-)\text{-}o\text{-2-Oct-C}_6\text{H}_4\text{OH} \xrightarrow[\text{in acetone}]{\text{KMnO}_4} (R)\text{-}(-)\text{-2-Me-Octanoic Acid}$$

$$(R)\text{-}(-)\text{-}p\text{-2-Oct-C}_6\text{H}_4\text{OH} \xrightarrow[\text{in acetone}]{\text{KMnO}_4} (R)\text{-}(-)\text{-2-Me-Octanoic Acid}$$

(*S*)-(−)-Methylethylisohexylcarbinol (Tetrahydrolinalool, THL-OH), with a somewhat lower rotation, was converted to potassium tetrahydrolinalate in benzene; then the potassium salt was treated with an excess of bromobenzene. The maximum rotation of the (*S*)-(−)-tetrahydrolinalyl phenyl ether thus obtained was calculated on the basis of the maximum rotation of tetrahydrolinalool[12] (Table 3):

$$(S)\text{-}(-)\text{-THL-OH} \xrightarrow[\text{in benzene}]{K} (S)\text{-THL-OK} \xrightarrow{\text{PhBr}} (S)\text{-}(-)\text{-THL-OPh}$$

The Product Distribution for the Phenolyses of 2-Octyl and Tetrahydrolinalyl Chlorides. The composition of the phenolysis product after ten half-lives was determined by gas chromatography, using diphenyl ether as the internal standard. Each phenolysis was conducted with a sodium phenoxide/substrate ratio higher than 10 in order to keep the base concentration approximately invariant during the phenolysis.

In Table 4 the effect of the sodium pheoxide concentration upon the product composition is presented for the phenolyses of 2-octyl and tetrahydrolinalyl chlorides in the 50 wt% phenol-benzene solvent at 200.0 and 25.0°C respectively; it is also illustrated in Figs. 3 and 4.

The product composition for the tetrahydrolinalyl system is approximately invariant, despite the wide variation in the concentration of the phenoxide ion. In contrast to this system, in the 2-octyl system the olefin % decreases with an increase in the phenoxide concentration.

Since, in the reaction media, there exist two species of nucleophiles, *viz.*, the phenol molecule and the

8) L. H. Sommer and A. F. Carey, *J. Org. Chem.*, **32**, 800 (1967).
9) The configuration of 2-octyl phenyl ether relative to the tosylate was assigned by J. Kenyon, H. Phillips, and V. P. Pittman, *J. Chem. Soc.*, **1935**, 1072.
10) H. Hart and H. S. Eleuterio, *J. Amer. Chem. Soc.*, **76**, 516 (1954).
11) A. Rothen and P. A. Levene, *J. Chem. Phys.*, **7**, 975 (1939).
12) P. E. Verkade, K. S. De Vries, and B. M. Wepster, *Rec. Trav. Chim. Pays-Bas*, **83**, 367 (1964).

Table 4. Effect of the added sodium phenoxide upon the product distribution for the phenolyses of 2-octyl and tetrahydrolinalyl chlorides in 50 wt% phenol–benzene solvent

RX M×10⁴	NaOPh M	Product distribution %			
		Olefin	ROPh	*o*-RC_6H_4OH	*p*-RC_6H_4OH
2-Octyl chloride, at 200°C					
8.8	0.0075	72.8[a]	19.2	4.94	3.06
8.4	0.0150	66.4	23.4	6.44	3.76
9.1	0.0300	63.4	24.8	7.50	4.32
9.5	0.0500	57.5	27.7	9.46	5.35
9.5	0.100	53.2	30.1	10.1	6.58
9.6	0.150	40.0	37.0	14.0	8.98
Tetrahydrolinalyl chloride, at 25.0°C					
9.0	0.0075	84.0[b]	16.0	0.0250	0.00500
9.1	0.0150	86.0	14.0	0.0408	0.00506
9.2	0.0300	85.7	14.3	0.0429	0.00760
9.8	0.0500	86.0	13.9	0.0655	0.0127
10.1	0.100	85.6	14.3	0.136	0.0173
10.0	0.150	86.4	13.4	0.175	0.0162

a) A mixture of 3 isomers. b) A mixture of 4 isomers.

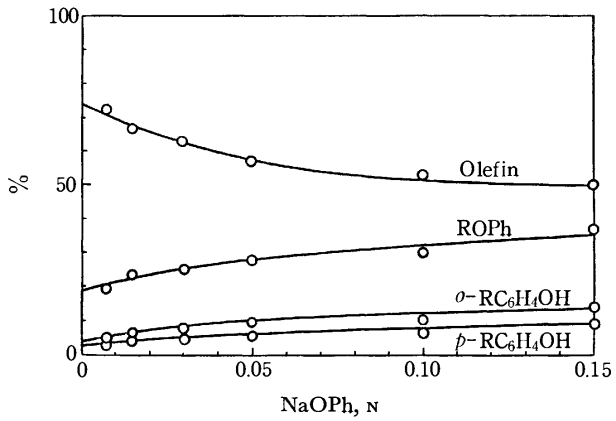

Fig. 3. Effect of the added sodium phenoxide upon the product distribution for the phenolysis of 2-octyl chloride in 50 wt% phenol–benzene solvent at 200.0°C.

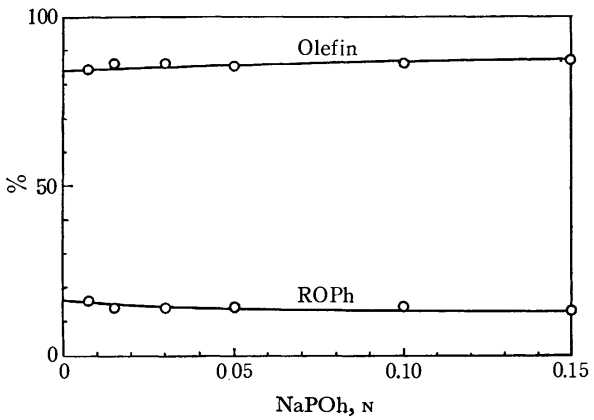

Fig. 4. Effect of the added sodium phenoxide upon the product distirbution for the phenolysis of tetrahydrolinalyl chloride in 50 wt% phenol–benzene solvent at 25.0°C.

Table 5. Product distribution for the reactions of phenol molecule and phenoxide ion

Substrate	Temp °C	Product distribution %			
		ROPh	*o*-RC_6H_4OH	*p*-RC_6H_4OH	Olefin
The reaction of phenol molecule					
2-Octyl Cl	200.0	19.3	4.2	2.85	73.65
		(73.2)[b]	(16.0)	(10.8)	—
1-Adamantyl Cl[a]	100.0	91.5	8.0	0.5	—
THL Cl	25.0	15.9	0.017	0.003	84.1
		(99.874)	(0.107)	(0.019)	—
The reaction of phenoxide ion					
2-Octyl Cl	200.0	52.5	27.1	9.98	12.4
		(58.6)	(30.3)	(11.1)	—
1-Adamantyl Cl[a]	100.0	70.0	23.0	9.0	—
THL Cl	25.0	10.6	8.3	2.1	82.4
		(50.5)	(39.5)	(10.0)	—
The values for k_2'/k_2					
2-Octyl Cl	200.0	35.0	26.6	41.5	33.9
1-Adamantyl Cl[a]	100.0	128	134	56	—
THL Cl	25.0	63.4	7810	4990	100

a) K. Okamoto, K. Matsubara, and T. Kinoshita, This Bulletin, **45**, 1191 (1972).
b) Distribution % for the substitution products.

phenoxide ion, it is of interest to assess the product distribution for each species.

We can, first, estimate the product distribution for the reaction of the phenol molecule with the ion-pair intermediate by extrapolating the composition lines in Figs. 3 and 4 to a zero concentration of the phenoxide ion. The results are tabulated in Table 5, along with the distribution % for the phenolysis of 1-adamantyl chloride, which has previously been estimated by the same procedure.[13]

Secondly, providing that the phenol molecule and the phenoxide ion competitively attack the ion-pair intermediate at the product-formation step, and that the concentrations of the phenol molecule and the phenoxide ion are actually invariant during the reaction, we can assess the product distribution ($r_{i,x}$, *vide infra*) for the phenoxide-ion reaction, by using Eq. (2), which expresses the relationships between the observed product composition (*viz.*, $r_{obs.,\ olefin}$, $r_{obs.,\ ether}$, $r_{obs.,\ ortho}$, and $r_{obs.,\ para}$) and the estimated product distributions for the phenol reaction (*viz.*, $r_{m,\ olefin}$, $r_{m,\ ether}$, $r_{m,\ ortho}$, and $r_{m,\ para}$) or for the phenoxide reaction (*viz.*, $r_{i,\ olefin}$, $r_{i,\ ether}$, $r_{i,\ ortho}$, and $r_{i,\ para}$). The details for the derivation of Eq. (2) have been reported previously.[13]

$$\mathrm{RX} \underset{k_{-1}}{\overset{k_1}{\rightleftharpoons}} \text{Ion-pair intermediate} \xrightarrow{k_2[\mathrm{PhOH}]} \underset{r_{m,ether}}{\mathrm{ROPh}} + \underset{r_{m,ortho}}{o\text{-}\mathrm{RC_6H_4OH}} + \underset{r_{m,para}}{p\text{-}\mathrm{RC_6H_4OH}} + \underset{r_{m,olefin}}{\text{Olefins}}$$

$$\text{Ion-pair intermediate} \xrightarrow{k_2'[\mathrm{PhO}^\ominus]} \underset{r_{i,ether}}{\mathrm{ROPh}} + \underset{r_{i,ortho}}{o\text{-}\mathrm{RC_6H_4OH}} + \underset{r_{i,para}}{p\text{-}\mathrm{RC_6H_4OH}} + \underset{r_{i,olefin}}{\text{Olefins}}$$

$$\frac{(r_{obs,x}-r_{m,x})}{([\mathrm{PhO}^\ominus]/[\mathrm{PhOH}])} = -\left(\frac{k_2'}{k_2}\right)r_{obs,x} + \left(\frac{k_2'}{k_2}\right)r_{i,x} \qquad (2)$$

In Eq. (2), x denotes olifin, ether, *ortho*, or *para*. Since we have already established the values for $r_{obs.,\ x}$, $r_{m,x}$, and ($[\mathrm{PhO}^\ominus]/[\mathrm{PhOH}]$), we can estimate the values for $r_{i,x}$ and k_2'/k_2 by a graphical method.[13] In Table 5 the results of the estimation of $r_{i,x}$ for 2-octyl chloride and tetrahydrolinalyl chloride are presented, along with the previously-reported values for 1-adamantyl chloride.[13]

From Table 5 it is immediately obvious that, for each substrate, the proportion of *O*-alkylation (the phenyl ether formation) is greater in the case of the phenol reaction than in the case of the phenoxide reaction. This indicates that the ambident phenol molecule reacts more selectively with the ion-pair intermediate than does the ambident phenoxide ion, which reacts more rapidly and, therefore, less selectively. The rapidness of the phenoxide reactions is reflected in the k_2'/k_2 rate ratio (27—7800), shown in Table 5.

It is also evident from Table 5 that the proportions of *O*-alkylation in the phenol-molecule reaction diminish in this sequence: tetrahydrolinalyl>1-adamantyl>2-octyl chlorides. It has been established in the case of 1-phenylethyl chloride[14] that the proportion of *O*-alkylation in the phenol-molecule reaction is virtually independent of the reaction temperature. If this is the case also in the phenolyses of these chlorides, the above-mentioned sequence of the proportions for *O*-alkylation on the phenol molecule will be independent of the temperature. Consequently, the sequence may indicate that the stabilization of the ion-pair intermediate in the tetrahydrolinalyl system contributes substantially to the enhanced tendency to undergo *O*-alkylation; this seems to be relevant, with the observation that the S_N1-like reaction of methyl iodide with silver nitrite predominantly yields the *O*-alkylation product, unlike the S_N2 reaction with sodium nitrite.[15]

For the phenoxide reaction there appears to be no simple correlation between the stability of the ion-pair intermediate and the structural sequence (*viz.*, 1-Ad>2-Oct>THL) for the *O*-alkylation proportions on the phenoxide ion; this sequence remains to be accounted for.

As has been mentioned above, the three substrates, 2-octyl, 1-adamantyl, and tetrahydrolinalyl chlorides, all undergo phenolysis to yield predominantly inversive, completely retentive, and substantially racemic phenyl ethers; it seems difficult to find a correlation between these steric outcomes and the sequence of the proportions of *O*-alkylation.

Rearrangement of the Phenyl Ether in the Medium of the Phenolysis. Since it is well known that the *sec*- and *tert*-alkyl phenyl ethers readily undergo a rearrangement to give *o*- and *p*-alkylphenols in the presence of an acidic catalyst,[16] the possibility of a rearrangement for 2-octyl phenyl ether and tetrahydrolinalyl phenyl ether even in the slightly acidic solvent phenol can not be eliminated. However, we detected no *o*- or *p*-alkylated phenols in the reaction mixtures when these phenyl ethers were subjected to a rearrangement in 50 wt% phenol–benzene for more than ten half-lives of the phenolysis at, respectively, 200 and 25°C. Consequently, all of the *o*- and *p*-alkylated phenols found in these phenolysis products are not produced as a result of the rearrangement of the phenyl ether, but are directly produced from the ion-pair intermediate in each phenolysis.

Experimental[17]

Materials. 2-Octyl chloride[18] and optically-active 2-octyl *p*-toluenesulfonate[19] were prepared in the usual

13) K. Okamoto, K. Matsubara, and T. Kinoshita, This Bulletin, **45**, 1191 (1972).

14) The *O*-alkylation %: 80—82% (25, 50, and 75°C) (K. Okamoto and Y. Ito, unpublished results).

15) N. Kornblum, R. A. Smiley, R. K. Blackwood, and D. C. Iffland, *J. Amer. Chem. Soc.*, **77**, 6269 (1955).

16) For a summary, see C. K. Ingold, "Structure and Mechanism in Organic Chemistry," 2nd ed., Cornell University Press, Ithaca and London (1969), pp. 904—906.

17) A Hitachi Model 023-6003 gas-chromatographic instrument, with a flame ionization detector, a Shimadzu Model IR-27 spectrophotometer, and a Japan Electronic Optics 60 MHz instrument were used for the analytical work. Microanalyses were performed by the Elemental Analysis Center, Kyoto University. For the measurement of the optical rotations, a JASCO DIP-SL polarimeter was used.

18) P. A. Levene and L. A. Mikeska, *J. Biol. Chem.*, **59**, 473 (1924).

19) A. Streitwieser, Jr. and A. C. Waiss, Jr., *J. Org. Chem.*, **27**, 290 (1962).

manners. The resolution of 2-octanol was perfomed according to the method of Kenyon.[20] Optically-active tetrahydrolinalyl *p*-nitrobenzoate (mp 39.5—40.1°C (cor.)) (see Tables 2 and 3) was prepared from tetrahydrolinalool[12] and *p*-nitrobenzoyl chloride in pyridine (*vide infra*) Optically-active tetrahydrolinalyl chloride[21] was prepared from tetrahydrolinalool.[12] Sodium phenoxide was prepared by refluxing a toluene solution of phenol with sodium metal. The other organic reagents employed were of an analytical reagent grade and were fractionated just prior to use. Titration with a Karl Fischer reagent indicated the water content of phenol to be less than 10^{-2} M.

Product Isolation. *The Phenolysis of 2-Octyl Tosylate (75°C)*: To 146 m*l* of a 1:1 (by wt.) mixture of phenol and benzene containing triethylamine (2.20 m*l*; 0.101 M), there was added optically-active 2-octyl *p*-toluenesulfonate (4.290 g, 0.01510 mol; $\alpha_D^{22.6}$ +5.195±0.015°, 1 dm, neat). The reaction mixture was kept at 75.0±0.1°C for 24 hr (about 10 half-lives). The mixture was then diluted with 300 m*l* of ether, and washed successively with 10% aqueous sodium hydroxide (100 m*l*×5) and 10% aqueous sodium chloride (100 m*l*×5) to make it neutral to pH indicator paper. The ethereal solution, dried with magnesium sulfate, was concentrated by distillation; a part (3.74 wt%) of the residual liquid was examined by gas chromatography. The remainder was evapolated, and then separated by column chromatography on silica gel (60 g). The column was eluted successively with *n*-hexane, *n*-hexane-benzene (1:1 by vol.), benzene, benzene-ether (97:3 by vol.), and ether. The fractions eluted with *n*-hexane–benzene gave 2-octyl phenyl ether (681 mg; bp 130—135°C/4.0 mmHg; 21.9% yield; the same infrared spectrum as in an authentic sample; $\alpha_D^{21.0}$ −10.05± 0.02°, 0.5 dm, neat). The fractions eluted with benzene gave *o*-2-octylphenol (99.8 mg; bp 138—145°C/4.0 mmHg; 3.21% yield; the same infrared spectrum as in an authentic sample; $[\alpha]_D^{21.4}$ −2.17±0.15° (*c* 12.9, benzene)). The fractions eluted with benzene-ether gave *p*-2-octylphenol (64.7 mg; bp 140—145°C/4.0 mmHg; 2.17% yield; the same infrared spectrum as in an authentic sample; $[\alpha]_D^{22.0}$ +4.69± 0.05° (*c* 72.3, benzene)).

The Phenolysis of Tetrahydrolinalyl Chloride (25°C). A 1:1 (by wt.) mixture (94.5 m*l*) of phenol and benzene, containing triethylamine (1.48 m*l*; 0.1030 M), was prepared and kept at 25.0±0.1°C for 1 hr. To the phenolic solvent, optically-active tetrahydrolinalyl chloride (2.000 m*l*, 1.703 g; 0.00965 mol; bp 55.0—59.5°C/4.0 mmHg; $\alpha_D^{25.8}$ +0.50± 0.02°, 1 dm, neat) was then added. The reaction mixture was maintained for 1.5 hr (about 11 half-lives). After the working-up described above, an oily material (0.3668 g) was chromatographed on alumina (30 g). The fractions eluted with *n*-hexane gave tetrahydrolinalyl phenyl ether (0.1693 g; bp 145—150°C/4.0 mmHg; 7.51% yield; $\alpha_D^{22.3}$ +0.20±0.02°, 1 dm, neat; IR (CCl_4) 2950, 1590, 1490, 1460, 1220, 1140, and 700 cm^{-1}; NMR (CCl_4) δ 2.85 (m, 5H) and 8.85 (m, 21H)).

Found: C, 81.96; H, 11.40%. Calcd for $C_{16}H_{26}O$: C, 82.00; H, 11.18%.

The Phenolysis of Tetrahydrolinalyl p-*Nitrobenzoate (100°C).* Optically-active tetrahydrolinalyl *p*-nitrobenzoate (3.0345 g; 0.00989 mol; mp 39.5—40.1°C (corr.); $[\alpha]_D^{16.0}$ −0.925± 0.011° (*c* 26.5, benzene)) was dissolved in 97 m*l* of a 1:1 (by wt.) mixture of phenol and benzene, containing sodium phenoxide (0.0993 M). After 24 hr (about 10 half-lives) at 100.0±0.1°C, the solution was treated in the usual way. A residual liquid (1.1055 g) was separated by thin-layer chromatography on silica gel to give tetrahydrolinalyl phenyl ether (0.2905 g; bp 145—150°C/4.0 mmHg; 12.5% yield; $\alpha_D^{16.5}$ +0.635±0.005°, 0.5 dm, neat).

Kinetic Measurements. *Titrimetric Rate Constant (k_t).* The previous procedure was followed.[22] For the runs of the tetrahydrolinalyl chloride phenolysis at 25°C, 1.000 m*l* aliquots were removed at intervals from 20 m*l* of the reaction mixture placed in a glass-stoppered flask. For the phenolyses of 2-octyl chloride, 2-octyl tosylate, and tetrahydrolinalyl *p*-nitrobenzoate at 200, 75, and 100°C respectively, the usual sealed-ampoule (1.000 m*l*) technique was employed. The diminution of the base concentrations was followed by titration with standard perchloric acid (0.05 N) in acetic acid, using crystal violet as the indicator. For the phenolysis of tetrahydrolinalyl chloride, carried out in the absence of a base, a 1 m*l* glass-stoppered flask was used. In this case, the free space was filled with liberated HCl in the course of the phenolysis. Therefore, after a specified length of time, the flask, filled with a 1 m*l* reaction mixture, was immersed and opened in a large quantity of cold acetic acid used as a stop-solvent. The increase in the HCl concentration was followed by titration with standard sodium acetate in acetic acid. All the rate data were treated graphically, plotting log $a/(a-x)$ against the time. In each case the reaction was followed to at least 70% completion; a smooth linear relationship was obtained. Infinity titers were determined after at least ten half-lives. The rate data are shown in Figs. 1 and 2 and in Table 1.

Polarimetric Rate Constant (k_p). For the phenolysis of 2-octyl tosylate, the usual sealed-ampoule (5 m*l*) technique was employed. Each ampoule, after having been kept at the reaction temperature for a specified time, was cooled and the reaction mixture was immediately transfered into a 2 dm polarimeter tube. The optical rotation was measured at room temperature. For the phenolysis of tetrahydrolinalyl *p*-nitrobenzoate, the observation of the optical rotation of a reaction mixture was impossible because of the low optical rotation of the reaction mixture. Therefore, the measurement was carried out by the use of another method as follows. After a specified reaction time, to 100 m*l* of the reaction mixture we added a large quantity of cold ether. The cold ethereal solution was promptly washed with cold 10% aqueous NaOH and then with cold 10% aqueous NaCl, and dried (Na_2SO_4); most of the solvent was subsequently removed by rotary-evaporation. To the residual liquid, benzene was added to make a 2.00 m*l* solution. The specific rotation of the benzene solution was determined. Thus, the rotations for two specified reaction times were treated graphically and a smooth first-order linear relationship was obtained. The data for the k_p's are shown in Figs. 1 and 2 and Table 1.

Product-distribution Analysis by Gas Chromatography. To several mg of 2-octyl chloride (or tetrahydrolinalyl chloride) with diphenyl ether (an internal standard), placed in a 12 m*l* ampoule, there was added 10 m*l* of a phenol-benzene (1:1 by wt.) solvent containing a specified amount of sodium phenoxide (or triethylamine). The sealed ampoule was kept at the reaction temperature for 10 half-lives. The reaction mixture was then diluted with 20 m*l* of ether, washed with 10% aqueous Na_2CO_3 and 10% aqueous NaCl, dried with $MgSO_4$, and distilled to leave 6—8 m*l* of the residual liquid, which was then analysed by glc using a 2 m×3 mm column with Apiezon Grease on Neopak 1A at 200°C.

20) "Organic Synthesis," Coll. Vol. I, (1967), p. 418.

21) P. G. Stevens and N. L. McNiven, *J. Amer. Chem. Soc.*, **61**, 1295 (1939).

22) K. Okamoto, H. Yamada, I. Nitta, and H. Shingu, This Bulletin, **39**, 299 (1966).

Rearrangement of the Phenyl Ethers. The usual sealed-ampoule technique was employed. To several mg of 2-octyl phenyl ether (or tetrahydrolinalyl phenyl ether), which contained diphenyl ether as an internal standard and which was placed in a 2 ml ampoule, we added 1 ml of a phenol–benzene (1:1 by wt.) mixture. The ampoule was kept at the same temperature as that of the chloride phenolysis for the 10 half-lives. The analysis was performed by glc using a 2 m×3 mm Apiezon Grease column at 200°C.

Syntheses of Optically-active Authentic Samples (cf. Table 3). *(R)-(−)-2-Octyl Phenyl Ether.* (*R*)-(−)-2-Octyl phenyl ether was prepared from (*S*)-(+)-2-octyl tosylate and sodium phenoxide under S_N2 reaction conditions. The reaction in DMF was determined to be a 2nd-order reaction, with k_2 3.58×10^{-3} (sec^{-1} M^{-1}) at 75.0°C. (*S*)-(+)-2-octyl tosylate (2.8467 g, 0.01001 mol; $\alpha_D^{22.6}$ +5.195±0.015°, 1 dm, neat), prepared from (*S*)-(+)-2-octanol $\alpha_D^{23.1}$ +7.27±0.02°, 1 dm, neat), was dissolved in 97.0 ml of DMF containing sodium phenoxide (2.44 g, 0.0210 mol). After 20 hr at 75°C, the mixture was treated as has been described above; the residual liquid was separated by column chromatography on basic alumina to give 2-octyl phenyl ether (1.461 g; bp 130—135°C/4.0 mmHg; 71.0% yield; $\alpha_D^{21.5}$ −22.95±0.01°, 1 dm, neat)

(S)-(−)-Tetrahydrolinalyl Phenyl Ether. A mixture of (*S*)-(−)-tetrahydrolinalool (3.160 g; 0.0200 mol; bp 54.0—59.5°C/5.0 mmHg; $\alpha_D^{23.5}$ −0.43±0.02°, 1 dm, neat) and potassium metal (0.78 g; 0.020 mol) in dry benzene (50 ml) was refluxed for 8 hr; the mixture then became homogeneous. To the mixture, bromobenzene (15.98 g; 0.200 mol) was added. The reaction mixture was then refluxed for an additional 14 hr. After the addition of ether (200ml), the mixture washed with 10% aqueous NaCl (100 ml×4) and dried with $MgSO_4$. The ethereal solutions was concentrated; the residual liquid was chromatographed on alumina. The fractions eluted with *n*-hexane and with benzene gave tetrahydrolinalyl phenyl ether (0.544 g, 0.00232 mol; bp 140—145°C/4.0 mmHg; 11.6% yield; $\alpha_D^{24.2}$ −5.53±0.03°, 1 dm, neat). The fractions eluted with ether and with ethanol gave unchanged tetrahydrolinalool (2.37 g; 75.0% recovery; $\alpha_D^{20.8}$ m0.42±0.02°, 1 dm, neat).

(S)-(−)-Tetrahydrolinalyl p-*Nitrobenzoate.* The usual method for the preparation of optically-active 1-phenylethyl *p*-nitrobenzoate[23] was modified for the preparation of tetrahydrolinalyl *p*-nitrobenzoate. A mixture of (*S*)-(−)-tetrahydrolinalool (4.07 g; 0.0257 mol; bp 54.0—59.5°C/5.0 mmHg; $\alpha_D^{23.5}$ −0.43±0.02°, 1 dm, neat) and *p*-nitrobenzoyl chloride (4.88 g; 0.0263 mol) in pyridine (12 ml) was stirred at 30.0—31.6°C for 5 hr in order to make it homogeneous. The mixture was then treated in the usual way to give (*S*)-(−)-tetrahydrolinalyl *p*-nitrobenzoate (6.55 g; 83.0% yield; mp 39.5—40.1°C (corr.); $[\alpha]_D^{21.0}$ −0.925±0.011° (*c* 26.5, benzene); IR (CCl_4) 3000, 1790, 1380, 1340, 1230, 1150, 1080, and 700 cm^{-1}; NMR (CCl_4) δ 1.3 (m, 21H) and 8.2 (d, 4H)).

Found: C, 66.43; H, 8.33%. Calcd for $C_{17}H_{25}NO_4$: C, 66.42; H, 8.20%.

Oxidation of 2-Octylphenols. Optically-active (−)-*o*- and (+)-*p*-2-octylphenols were prepared by the rearrangement (in the presence of *p*-toluenesulfonic acid, 100°C, 21 hr) of (*R*)-(−)-2-octyl phenyl ether ($\alpha_D^{20.5}$ −23.78±0.01°, 1 dm, neat) in phenol-benzene (1:1 by wt.). The optically-active *o*- and *p*-2-octylphenols thus were oxidized to 2-methyloctanoic acid according to the procedure of Hart and Eleuterio.[24] To a solution of *o*-2-octylphenol (1.94 g; 0.00943 mol; $[\alpha]_D^{24.1}$ −0.31±0.09° (*c* 56.5, benzene)) in acetone (200 ml), we added potassium permanganate (10.3 g, 0.0652 mol) in distilled water (750 ml) at 10—15°C. The mixture was then stirred for 2 hr and acidified with 6 N sulfuric acid, and the manganese dioxane thus precipitated was dissolved by the addition of sodium bisulfite. The mixture was extracted with 10% aqueous $NaHCO_3$ (100 ml×4), and the extracts were acidified with 6 N H_2SO_4 (100 ml) and then extracted with benzene (100 ml×4). The benzene solution was dried with $MgSO_4$. After the solvent had been removed by rotary-evaporation, the residual oil was distilled *in vacuo* to give 2-methyloctanoic acid (0.339 g, 22.8% yield; bp 98.4—111.5°C/2.0 mmHg; $[\alpha]_D^{16.8}$ −1.12±0.07° (*c* 28.5, *n*-heptane)). Since this conversion proceeds with the maintenance of the configuration of the assymmetric carbon atom, the configurations of 2-methyloctanoic acid and *o*-2-octylphenol should be identical. Thus, the specific rotation of optically-pure (*R*)-(−)-*o*-2-octylphenol may be estimated to be −4.56° (in benzene) on the basis of the value for optically-pure (*R*)-2-methyloctanoic acid, −16.4° (in *n*-heptane).[11] In the same manner, from (+)-*p*-2-octylphenol (2.64 g, 0.0128 mol; $[\alpha]_D^{24.1}$ +1.70±0.26° (*c* 26.5, benzene)) (+)-2-methyloctanoic acid (0.0477 g, 2.3% yield; bp 106.0—111.2°C/0.8 mmHg; $[\alpha]_D^{24.6}$ +4.25±0.19° (*c* 10.3, *n*-heptane)) was obtained. The specific rotation of optically-pure (*S*)-*p*-2-octylphenol can, therefore, be estimated to be +6.57° (in benzene).

The authors wish to express their thanks to Mr. Osamu Makino for his technical assistance.

23) H. L. Goering and J. P. Blanchard, *J. Amer. Chem. Soc.*, **76**, 5405 (1954).

24) H. Hart and H. F. Eleuterio, *ibid.*, **76**, 516 (1954).

Friedel-Crafts Aralkylation. II.[1] The $AlCl_3 \cdot CH_3NO_2$-catalyzed Phenethylation of Benzene and Toluene with 2-Arylethyl Chlorides in a Nitromethane Solution

Makoto Ichii

Institute for Chemical Research, Kyoto University, Gokasho, Uji, 611

(Received October 18, 1971)

The rates of $AlCl_3 \cdot CH_3NO_2$-catalyzed phenethylations of benzene (50°C) or toluene (25°C) with 2-arylethyl (ring-substituted phenethyl) chlorides were measured in homogeneous nitromethane solutions. The reactions are first-order in the aromatic component, first-order in the phenethyl chloride, and second-order in aluminum chloride. Substituent effects in the phenethyl chlorides give linear relationships with Hammett's σ constants. A displacement mechanism involving a nucleophilic attack by the aromatic substrate on the phenethyl chloride-catalyst system is proposed for the reactions. Competitive phenethylations of benzene and toluene were also carried out at 50°C. Both the isomer distribution and the relative reactivity of toluene to benzene are affected by the ring-substituents, the effects of which are correlated closer with the substrate selectivity. These results suggest that the transition state in the rate-determining step for the phenethylations is in nature an (oriented) π complex rather than a σ complex.

The Friedel-Crafts alkylation reaction of aromatics with primary alkyl halides continues to present various interesting problems. In particular, there are arguments as to the structure of the activated complex in the rate-determining step for the reaction.[2]

In the previous paper,[1] we reported the kinetics of the $AlCl_3 \cdot CH_3NO_2$-catalyzed phenethylation of benzene and toluene with 2-phenylethyl chloride and suggested the displacement mechanism for the reaction.

In this paper, we will describe a study of the aralkylations (phenethylations) of benzene and toluene with 2-arylethyl chlorides using the $AlCl_3 \cdot CH_3NO_2$ complex as the catalyst in nitromethane solutions; we will thus attempt to elucidate the nature of the transition state in the rate-determining step and the effect of ring-substituents on the reaction rates and the isomer distributions. Electron-donating substituents tend to decrease the electron deficiency of the reaction center in an aralkylating agent, while electron-withdrawing substituents tend to increase it. Thus, it is possible to correlate the electrophilicity of the substituting agent with the selectivity by changing its electrophilicity systematically, while keeping the other factors constant.

Results and Discussion

The phenethylation reactions in homogeneous nitromethane solutions can easily be followed kinetically, and they are considered to be free from consecutive isomerization. Proof of the non-isomerizing conditions is given clearly by the experimental fact that the phenethylation of benzene with 2-(*m*-tolyl)- or 2-(*p*-tolyl)-ethyl chloride yielded no isomer mixture of 1-phenyl-2-tolylethanes.

The rates of noncompetitive phenethylations of benzene (50°C) or toluene (25°C) with substituted phenethyl chlorides ($XC_6H_4CH_2CH_2Cl$) were measured under the same conditions. The mole ratio of benzene: $XC_6H_4CH_2CH_2Cl$: aluminum chloride in the solution was 5.6: 1: 1, and that of toluene: $XC_6H_4CH_2CH_2$-Cl: aluminum chloride was 4.7: 1: 1. Unfortunately, it was impossible to determine the reaction rates with 2-(*p*-nitrophenyl)ethyl chloride, since the reactions were too slow to be measured under the above conditions. It needed severe conditions (*e.g.*, using more than equimolar quantities of the catalyst to the chloride without nitromethane) to bring about *p*-nitrophenethylation, accompanied by side reactions.

During the course of the reactions, small amounts of by-products (di- or higher phenethylated and 1, 1-diarylethane-type rearranged products, and polymers resulting from the reactions between the aralkylating agents) were detected by gas chromatography and spectroscopic methods. In the early stages of the reactions, however, they are negligible and it is convenient to assume that only monoalkylation takes place under the present experimental conditions. Therefore, for all systems, pseudo-second-order plots were obtained, assuming that:

$$\frac{d[\text{product}]}{dt} = k_{obs}[\text{aromatic}][XC_6H_4CH_2CH_2Cl] \quad (1)$$

The obtained results are summarized in Table 1. A second-order dependence on the catalyst concentration was found (when the concentration of the catalyst was reduced to one half, the values of k_{obs} with benzene for X=*p*-CH_3O, *p*-CH_3, and *p*-Cl were 2.65×10^{-3}, 1.43×10^{-3}, and 2.73×10^{-4} respectively), as in the previous investigation with 2-phenylethyl chloride (X=H).[1] Thus, the reactions are second-order with respect to the catalyst; that is, $k_{obs}=k_4[AlCl_3]^2$, where k_4 is the overall fourth-order rate constant.

In order to clarify the mode in which a substituent group exerts its effect upon the reaction rate, the results in Table 1 are plotted against the substituent constants. Fairly good correlations with Hammett's σ constants were obtained (Fig. 1). The apparent reaction constants, ρ, calculated by the method of least squares,[3] are -1.71 ($r=0.940$) for the reaction with

1) Part I: M. Ichii, *Bull. Inst. Chem. Res., Kyoto Univ.*, **49**, 114 (1971).

2) For recent reviews see: a) G. A. Olah, "Friedel-Crafts and Related Reactions", Vol. I, Wiley-Interscience, New York, N. Y. 1963, p. 853; b) R. Nakane, *Nippon Kagaku Zasshi*, **90**, 17 (1969); c) G. A. Olah, *Accounts Chem. Res.*, **4**, 240 (1971).

3) H. H. Jaffé, *Chem. Revs.*, **53**, 191 (1953).

Table 1. The rates of $AlCl_3 \cdot CH_3NO_2$-catalyzed phenethylation of benzene or toluene with $XC_6H_4CH_2CH_2Cl$ in nitromethane solution[a)]

$XC_6H_4CH_2CH_2Cl$	Benzene at 50°C		Toluene at 25°C[b)]	
	k_{obs} (l mol^{-1}min^{-1})	Relative rate	k_{obs} (l mol^{-1} min^{-1})	Relative rate
p-CH_3O	1.04×10^{-2}	3.53	3.12×10^{-3}	12.9
p-CH_3	5.53×10^{-3}	1.87	1.36×10^{-3}	5.62
m-CH_3	3.90×10^{-3}	1.32	4.72×10^{-4}	1.95
H[c)]	2.95×10^{-3}	1.00	2.42×10^{-4}	1.00
p-Cl	1.23×10^{-3}	0.417	3.47×10^{-5}	0.143

a) Initial concentration, $[AlCl_3]=0.400$mol/*l*. b) The description of the isomer distributions of the products is omitted, because they are almost identical to those obtained in the competitive reactions described later. c) See Ref. 1.

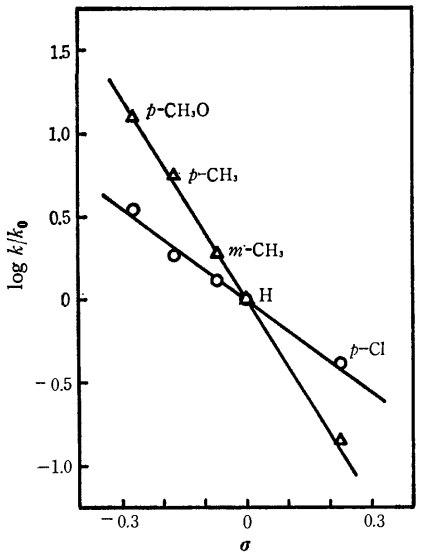

Fig. 1. Hammett plots for the $AlCl_3 \cdot CH_3NO_2$-catalyzed phenethylation of benzene (○) at 50°C or toluene (△) at 25°C with $XC_6H_4CH_2CH_2Cl$.

benzene and −3.72 (r=0.942) for toluene. The linear relationships with Hammett's σ, but not with Brown's σ^+ constants, suggest that the rate-determining step does not involve a phenonium ion-type intermediate (**1**) as an electrophile.[4] If any neighboring aryl

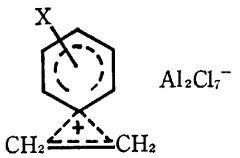

1

participation takes place, much larger substituent effects would be observed through a resonance interaction between the substituent and the reaction site, and then the reaction rates might be correlated with Brown's σ^+ constants. This is not true for the present phenethylation. Thus, the present results are more consistent with a displacement mechanism involving a rate-determining nucleophilic attack by the aromatic substrate on the phenethyl chloride-dimeric aluminum chloride system (Eq. (4)).[5] The transition state in

$$XC_6H_4CH_2CH_2Cl + AlCl_3\text{–}CH_3NO_2 \underset{k_{-1}}{\overset{k_1}{\rightleftharpoons}} XC_6H_4CH_2CH_2Cl\text{–}AlCl_3 + CH_3NO_2 \quad (2)$$

2

$$\mathbf{2} + AlCl_3\text{–}CH_3NO_2 \underset{k_{-2}}{\overset{k_2}{\rightleftharpoons}} XC_6H_4CH_2CH_2\overset{\delta+}{\text{—}}\overset{\delta-}{Cl}\cdots Al_2Cl_6 + CH_3NO_2 \quad (3)$$

3

$$\mathbf{3} + C_6H_6 \xrightarrow{k_3} \text{(arenium ion)}\ H,\ CH_2CH_2C_6H_4X\ \ Al_2Cl_7^- \quad (4)$$

4

$$\mathbf{4} \rightleftharpoons \text{(C}_6\text{H}_5\text{)}\text{–}CH_2CH_2C_6H_4X + HCl + Al_2Cl_6 \quad (5)$$

the rate-determining step may be represented as an oriented π-complex(**5**):[6,7]

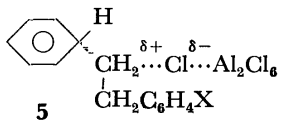

5

From the proposed mechanism, we can obtain the appropriate rate expression by using the steady-state approximation and by assuming that $k_{-1}, k_{-2} \gg k_1, k_2, k_3$:

$$\text{rate} = \frac{k_1k_2k_3}{k_{-1}k_{-2}}[XC_6H_4CH_2CH_2Cl][C_6H_6][AlCl_3\text{–}CH_3NO_2]^2 \quad (6)$$

This is in substantial agreement with Eq. (1).

The value of k_{obs} includes the k_1/k_{-1} and k_2/k_{-2} terms, the equilibrium constants for the formation of **3**. It seems reasonable to consider that the obtained ρ-value is determined largely by the preceding equilibria, especially by the k_1/k_{-1} term.[5] This explains the rather large negative ρ-values. Therefore, the substituent effects on the rate-determining step may be small. This means that the extent of the C–Cl bond cleavage has a great effect on the reactivity. In the case of the *p*-NO_2 group, little formation of **3** may take place. It appears that the group becomes much more electron-withdrawing than an ordinary one

4) M. A. McMahon and S. C. Bunce, *J. Org. Chem.*, **29**, 1515 (1964).

5) H. C. Brown and M. Grayson, *J. Amer. Chem. Soc.*, **75**, 6285 (1953).

6) G. A. Olah, S. J. Kuhn, and S. H. Flood, *ibid.*, **84**, 1688 (1962).

7) R. Nakane, O. Kurihara, and A. Natsubori, *ibid.*, **91**, 4528 (1969).

Table 2. Competitive phenethylation of benzene and toluene with $XC_6H_4CH_2CH_2Cl$ in nitromethane solution at 50°C

$XC_6H_4CH_2CH_2Cl$	k_T/k_B	Isomer distribution (%)			Partial rate factors			p_f/m_f
		ortho	*meta*	*para*	o_f	m_f	p_f	
p-CH_3O	4.61	54.0	14.2	31.8	7.47	1.96	8.80	4.48
o-CH_3	4.33	51.7	17.6	30.7	6.72	2.29	7.97	3.48
p-CH_3	4.06	51.1	17.9	31.0	6.22	2.18	7.55	3.46
m-CH_3	3.80	51.5	18.5	30.0	5.87	2.11	6.84	3.24
H[a)]	3.31	48.7	19.8	31.5	4.84	1.97	6.26	3.18
p-Cl	2.81	47.6	21.1	31.3	4.01	1.78	5.28	2.97
m-Cl	2.48	47.8	21.6	30.6	3.55	1.61	4.55	2.83
p-NO_2[a)]	2.85							

a) See Ref. 1. b) Mole ratio of reactants, aromatics: *p*-$NO_2C_6H_4CH_2CH_2Cl$:$AlCl_3$=37:1:2, without nitromethane. The k_T/k_B value seems to be influenced by the transalkylation of the products. The isomeric 1-(*p*-nitrophenyl)-2-tolylethanes were not separable by gas chromatography.

through complex formation with aluminum chloride.[8)]

Competitive phenethylations of benzene and toluene at 50°C were also carried out by treating equimolar amounts of aromatic components in nitromethane solutions. The mole ratio of aromatics: $XC_6H_4CH_2CH_2Cl$ catalyst was always 10:1:1 unless otherwise noted. In the course of the reaction, the isomer distribution and the rate of toluene relative to benzene were found to remain almost unchanged. The average values of the relative rates and isomer distributions, together with the partial rate factors for substitution, are summarized in Table 2. The competitive reaction with 2-(*p*-nitrophenyl)ethyl chloride was unsuccessful so long as it was conducted in a nitromethane solution.

The data of Table 2 reveal the most significant effects of substituents on the relative rates and the isomer distributions. That is, both substrate and positional selectivities are affected by changing the electrophilicity of the reagent. However, the effects are more remarkable in the former selectivity. The electron-donating substituents tend to increase the relative rate, k_T/k_B; at the same time they tend to decrease the amount of the *meta*-isomer, as reflected by the increasing ratio of the partial rate factors for the *para*- and *meta*-positions of toluene, p_f/m_f, shown at the last column in Table II. On the other hand, the electron-withdrawing substituents decrease both the k_T/k_B and p_f/m_f ratios. In other words, a more stable and, hence, weaker electrophile has higher substrate and positional selectivities. The formation of the nonionized intermediate (**3**) with a electron-withdrawing substituent is difficult. However, once it is formed, it is highly energetic and reacts with benzene or toluene, discriminating slightly between them and at the same time slightly between the *ortho*- or *para*- and the *meta*-positions in toluene. Hence, it is possible to correlate the electrophilicity of the substituting agent with its

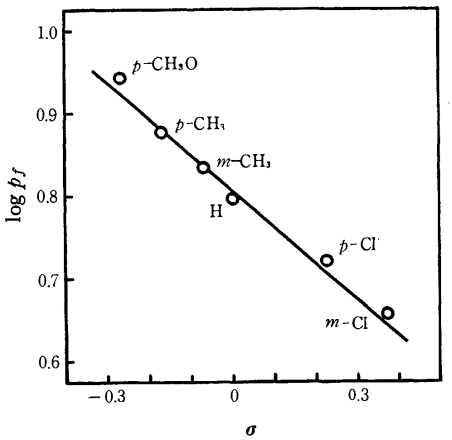

Fig. 2. Relationship between log p_f and Hammett's σ.

selectivity. In fact, as is shown in Fig. 2, a plot of the log p_f *versus* the substituent constant indicates a simple relationship between these quantities. The p_f-value is utilized as the measure of the substrate selectivity in order to eliminate any possible complications from steric factors. On the other hand, no simple relationship[9)] exists between the electrophilicity and the positional selectivity as reflected in the p_f/m_f ratio, although the latter actually depends on the former. These observations and the low k_T/k_B ratios suggest that the transition state in the displacement step should be regarded as an (oriented) π complex rather than as a σ complex.[2)]

Recently, Olah suggested that the position of the transition state in electrophilic aromatic substitutions is not a fixed one, but can be changed from a late one resembling the intermediate (σ complex) to an early one resembling the starting material (π complex).[2c)] According to this proposal, our present work provides good examples of early transition states. In substitutions where the rate-determining transition state is of a π-complex nature, the transition states of the subsequent σ-complex formation (leading to positional selectivity) appear relatively early on the reaction coordinate. In this case, the role of the methyl group in toluene in stabilizing the σ complex becomes less

8) In above discussions, little reference was made concerning the possibility of the aryl migration from β- to α-carbon atom. It was found that the ethylation with $^{14}CH_3CH_2Cl$ in excess benzene (R. M. Roberts, G. A. Ropp, and O. K. Neville, *J. Amer. Chem. Soc.*, **77**, 1764 (1955)) or with $^{14}CH_3CH_2F$ in nitromethane solution (A. Natsubori and R. Nakane, *J. Org. Chem.*, **35**, 3372 (1970)) gave practically no rearranged product. Rearrangement studies for the present phenethylations are in progress.

9) L. M. Stock and H. C. Brown, *Advan. Phys. Org. Chem.*, **1**, 35 (1963).

important with an increase in the electrophilicity of the reagent, and the higher proportion of *meta*-substitution is observed with a stronger electrophile. Consequently, the substrate selectivity is influenced directly by the electrophilicity of the substituting agent, which has relatively less effect on the positional selectivity.

Experimental

Materials.[10] The benzene, toluene, and 2-phenylethyl chloride (**6**) were commercial products of the highest available purity. They were further purified by distillation. The nitromethane was purified as has been described by Olah *et al.*[11] The preparation of 1,2-diphenylethane (**7**), 1-phenyl-2-tolylethanes (**8**), and 1,2-ditolylethanes (**9**) has been previously reported.[12] The 2-arylethanols were prepared as has been described in the literature.[13,14] They were converted to the corresponding chlorides by treatment with thionyl chloride. 2-(*p*-Anisyl)ethyl chloride (**15**); bp 98°C/4.5 mmHg (lit,[15] bp 90—92°C/2 mHg). 2-(*o*-Tolyl)ethyl chloride (**11**); bp 83—84°C/6 mmHg. 2-(*m*-Tolyl)ethyl chloride (**12**); bp 78—79°C/5 mmHg. 2-(*p*-Tolyl)ethyl chloride (**13**); bp 72—74°C/3 mmHg. 2-(*m*-Chlorophenyl)ethyl chloride (**14**); bp 91—92°C/3 mmHg. 2-(*p*-Chlorophenyl)ethyl chloride (**15**); bp 89—90°C/2 mmHg (lit,[16] bp 82—83°C/3 mmHg) 2-(*p*-Nitrophenyl)ethyl chloride (**16**) was obtained by the nitration of 2-phenylethyl chloride; mp 48.2—48.5°C (lit,[17] mp 48—49°C). Monosubstituted bibenzyls were prepared by treating the appropriate 2-arylethyl chloride with benzene in the presence of aluminum chloride. 4-Methoxybibenzyl (**17**); mp 54—56°C (lit,[18] mp 55—58°C). 3-Chlorobibenzyl (**18**); bp 130—131°C/2 mmHg (lit,[19] bp 148°C/3 mmHg). 4-Chlorobibenzyl (**19**); mp 47—48°C (lit,[19] mp 49°C). 4-Nitrobibenzyl (**20**); mp 68°C (lit,[20] mp 70—71°C). Non-contaminated isomer mixtures of 1-(*p*-anisyl)- (**21**), 1-(*m*-chlorophenyl)- (**22**), 1-(*p*-chlorophenyl)- (**23**), and 1-(*p*-nitrophenyl)-2-tolylethanes (**24**) were prepared by treating the appropriate 2-arylethyl chloride with toluene in the presence of aluminum chloride. Each isomer of **21**, **22**, and **23** was identified by a comparison of the infrared spectra (*o*-, 750—765 cm^{-1}, *m*-, 775—780 cm^{-1}; *p*-, 805—815 cm^{-1}) and gas chromatograms in a manner similar to that described previously.[21] Commercial aluminum chloride was sublimed before use.

Kinetic Measurements. Molar solutions in nitromethane of aluminum chloride and 2-arylethyl chloride were prepared. 20.0 m*l* of the catalyst solution and 10.0 m*l* of aromatic hydrocarbon (benzene or toluene) were placed in a 100 m*l*, three-necked flask equipped with a reflux condenser, a thermometer, and a stopcock. The flask was then placed in a constant-temperature bath (50 ± 0.1°C for benzene or 25 ± 0.1°C for toluene) and magnetically stirred. 20.0 m*l* of the 2-arylethyl chloride solution, maintained at the reaction temperature, was syringed through the stopcock into the flask. A small portion (2.0 m*l*) of the reaction mixture was drawn out from time to time with a calibrated syringe. Each sample was quenched with ice-water, washed with a small amount of water, dried over anhydrous sodium sulfate, and analyzed by gas chromatography. Each run consisted of at least 5 points, and the pseudo-second-order rate constant was determined graphically. The values obtained were corrected by blank experiments.

Competitive Phenethylations. A mixture (20.0 m*l*) of equimolar amounts of benzene and toluene was phenethylated in a nitromethane solution at 50°C in the same manner as has been described above. The samples were taken out periodically and analyzed by gas chromatography.

Analytical Procedure. The analyses were carried out with a Hitachi Perkin-Elmer model F6D gas chromatograph employing Golay-type capillary columns and a hydrogen flame ionization detector. For the determination of **6**, **7**, and **8**, a BDS-90 Golay column (length, 90 m; *i.d.*, 0.50 mm; coated with the butanediol succinate polyester) was used with a column temperature of 155°C and a nitrogen carrier-gas pressure of 1.0 kg/cm^2; for **8**, **9**, **11**, **12**, and **13**, 160°C and 1.2 kg/cm^2; for **10**, **17**, and **21**, 165°C and 1.5 kg/cm^2; for **14**, **15**, **18**, **19**, **22**, and **23**, 160°C and 1.5 kg/cm^2. Under these conditions, the isomer separation was complete. For the determination of **16**, **20**, and **24**, a Q-45 Golay column (length 45 m; *i.d.*, 0.50 mm, coated with Apiezon L) was with a column temperature of 170°C and a carrier-gas pressure of 1.5 kg/cm^2. In this case, however, the isomers of **24** were not separable. After the determination of the relative response data, the mol % were calculated from the areas of individual peaks by the internal standard method. The accuracy of measurements was found to be within the limit of a $\pm3.0\%$ relative error, based on analyses of mixtures of known composition.

The author is grateful to Professor S. Kunichika, Dr. S. Oka, Dr. J. Hayami, and Mr. T. Sugiyama for their helpful discussions.

10) All of the boiling and melting points are uncorrected. The structure of the authentic samples prepared was confirmed by infrared and NMR spectra. The infrared spectra were measured with a Hitachi EPI-S2 Spectrophotometer and the NMR spectra with a Varian T-60 Spectrometer.

11) G. A. Olah, S. J. Kuhn, S. H. Flood, and B. A. Hardie, *J. Amer. Chem. Soc.*, **86**, 1039 (1964).

12) S. Kunichika, S. Oka, T. Sugiyama, and M. Ichii, *Nippon Kagaku Zasshi*, **92**, 801 (1971).

13) C. H. DePuy and D. H. Froemsdorf, *J. Amer. Chem. Soc.*, **79**, 3710 (1957).

14) W. H. Saunders, Jr. and R. A. Williams, *ibid.*, **79**, 3712 (1957).

15) G. A. Olah, M. B. Comisarow, E. Namanworth, and B. Ramsey, *ibid.*, **89**, 5259 (1967).

16) C. H. DePuy and C. A. Bishop, *ibid.*, **82**, 2532 (1960).

17) A. Iliceto, A. Fava, and A. Simeone, *Gazz. Chim. Ital.*, **90**, 600 (1960); *Chem. Abstr.*, **55**, 14335i (1961).

18) R. L. Hinman and K. L. Hamm, *J. Amer. Chem. Soc.*, **81**, 3294 (1959).

19) F. Bergmann, J. Weizmann, and D. Shapiro, *J. Org. Chem.* **9**, 408 (1944).

20) L. M. Litvinenko and N. F. Levchenko, *Zh. Obshch. Khim.*, **29**, 3079 (1959); *Chem. Abstr.*, **54**, 13060e (1960).

21) S. Kunichika, S. Oka, T. Sugiyama, C. Inoue, and M. Ichii, *Nippon Kagaku Zasshi*, **92**, 539 (1971).

Aroyl Arenesulfonyl Peroxides IV. The Mechanism of Carboxy-inversion of Benzoyl *p*-Toluenesulfonyl Peroxide[1]

Ryuki HISADA, Hiroshi MINATO, and Michio KOBAYASHI

Department of Chemistry, Faculty of Science, Tokyo Metropolitan University, Fukazawa, Setagaya, Tokyo

(Received December 13, 1971)

Benzoyl *p*-toluenesulfonyl peroxide (BTP) with ^{18}O-labeled carbonyl oxygen and ^{18}O-labeled sulfonyl oxygen were prepared. They were decomposed in benzene in the presence or in the absence of trifluoroacetic acid,and the phenyl *p*-toluenesulfonyl carbonate (PTC)-^{18}O produced was isolated and analyzed. It was found that the carbonyl oxygen-18 of BTP was retained as the carbonyl oxygen of PTC, whereas the sulfonyl oxygen-18 of BTP was equilibrated with the peroxidic oxygen. The mechanism of the carboxy-inversion was discussed.

The thermal decompositions of symmetrical and asymmetrical acyl (aroyl) peroxides *via* the carboxy-inversion process are well documented.[2] It is known that the asymmetrical acyl (aroyl) peroxides rearrange to the corresponding anhydrides more readily than symmetrical peroxides. Therefore, the acyl sulfonyl

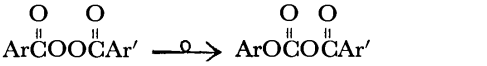

peroxides are expected to rearrange to the mixed anhydrides more easily than the diacyl peroxides. Razuvaev, Likhterov, and Etlis[3] reported that the decomposition of benzoyl alkanesulfonyl peroxides in benzene gave phenyl alkanesulfonyl carbonates in 83% yield. In the previous papers[4,5] from our laboratories, we have reported that benzoyl *p*-toluenesulfonyl peroxide (BTP) and *p*-chlorobenzoyl *p*-toluenesulfonyl peroxide rearrange to phenyl *p*-toluenesulfonyl carbonate (PTC) (48% yield), and *p*-chlorophenyl *p*-toluenesulfonyl carbonate (42% yield), respectively. Plausible mechanisms for this rearrangement are the followings.

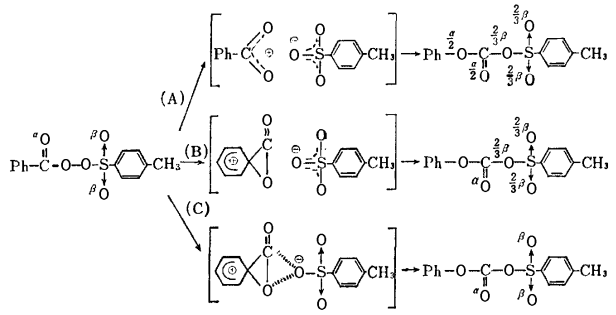

In order to establish the mechanism, the rearrangement of BTP to PTC has been investigated by the ^{18}O-labeling technique, and the results will be described in this paper.

Results and Discussion

BTP[carbonyl-^{18}O] and BTP[sulfonyl-^{18}O] were prepared and decomposed in benzene either in the presence or in the absence of trifluoroacetic acid. Yields of the carboxy-inversion product, PTC, were 43—48% in benzene and 67—71% in benzene-trifluoroacetic acid. The PTC produced from the decomposition of BTP-[carbonyl-^{18}O] was converted, by the reaction with aniline, to phenyl phenylcarbamate and *p*-toluenesulfonic acid. The phenyl phenylcarbamate obtained was hydrolyzed to phenol, which was then converted into 2,4,6-tribromophenol. The ^{18}O-contents of compounds I—VI in the following scheme were determined.

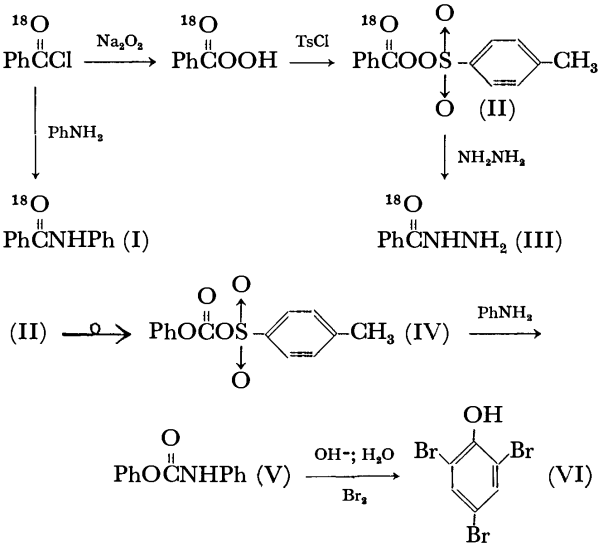

The results obtained are summarized in Table 1. Table 1 shows that practically all the carbonyl oxygen-18 of BTP is retained in the carbonyl oxygen of PTC, and that the rearrangement of BTP to PTC does not go through a state in which the carbonyl oxygen and the peroxidic oxygen of BTP are scrambled.

From *p*-toluenesulfonyl chloride-^{18}O the BTP[sulfonyl-^{18}O] was prepared, and the oxygen-18 contents of VII—XIII were determined.

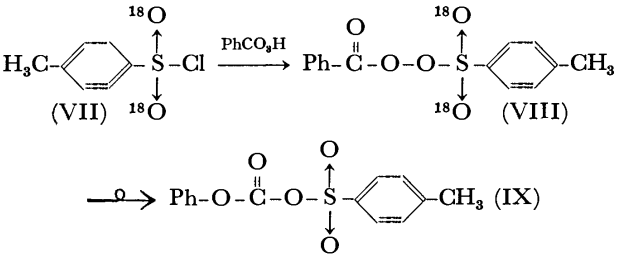

1) Organic Sulfur Compounds Part XXX.

2) L. S. Boguslavskaya, *Russian Chem. Rev.*, **34**, 501 (1965). A. G. Davies, "Organic Peroxides," Butterworths, London (1961). Chapter 10.

3) G. A. Razuvaev, V. R. Likhterov, and V. S. Etlis, *Zh, Obshch. Khim.*, **32**, 2033 (1962); *Tetrahedron Lett.*, **1961**, 527.

4) R. Hisada, H. Minato, and M. Kobayashi, This Bulletin, **44**, 2541 (1971).

5) R. Hisada, M. Kobayashi, and H. Minato, *ibid.*, **45**, 564 (1972).

Table 1. The ^{18}O-contents in BTP [carbonyl-^{18}O] and related compounds[a] (excess atom % oxygen-18)

Sample	Run 1			Run 2	
	Found[b]	Found[c]	Calcd[d]	Found[b]	Calcd[d]
$PhC(=^{18}O)NHPh$ (I)	1.20	1.20	(1.20)	1.26	(1.26)
$PhC(=^{18}O)OTs$ (II)	0.24	0.25	0.24	0.25	0.25
$PhC(=^{18}O)NHNH_2$ (III)	1.00	1.00	1.20	1.18	1.26
PhOC(=O)OTs (IV)	0.24	0.25	0.24	0.28	0.25
PhOC(=O)NHPh (V)	0.67	0.65	0.60	—	
$Br_3C_6H_2OH$ (VI)	0.07	0.01	0	0.06	0

a) Experimental error in two measurements for the same sample was ±0.02 excess atom %.
b) In benzene-trifluoroacetic acid. c) In benzene. d) Calculated on the assumption that the carbonyl oxygen is not equilibrated with the peroxidic oxygen.

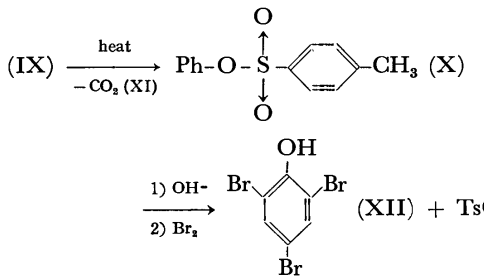

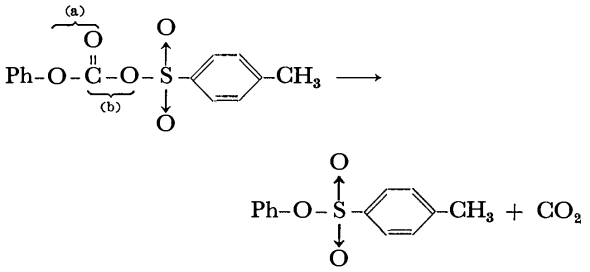

In order to determine the distribution of oxygen-18 in the sulfonyl oxygen and the ether oxygen in IX, one has to find some reactions with which these two kinds of oxygen can be distinguished. Reactions of IX with hydrazine or sodium methoxide were attempted, but they did not attack the sulfonyl sulfur atom. The method which met the requirements was the pyrolysis of neat IX at 230°C.

However, the mechanism of the pyrolysis of IX must be established. There are two possible modes of decarboxylation from IX. If the pyrolysis occurs according to process (a), the carbon dioxide evolved should contain no oxygen-18 regardless of whether or not the sulfonyl oxygen and the peroxidic oxygen of VIII were scrambled during the rearrangement.

The results of the ^{18}O analyses of VII—XIII are

Table 2. The ^{18}O-contents in BTP[sulfonyl-^{18}O] and related compounds[a] (excess atom % oxygen-18)

		Run 1		Run 2	
		Found	Calcd[b]	Found	Calcd[b]
TsCl-^{18}O	(VII)	0.81	(0.81)	0.76	(0.76)
$PhC(=O)O^{18}O-S(=^{18}O)-CH_3$	(VIII)	0.33	0.32	0.29	0.30
$PhOC(=O)O-S(=O)-CH_3$	(IX)	0.33	0.32	0.29	0.30
$PhO-S(=O)-CH_3$	(X)	0.37	0.36	0.32	0.34
CO_2	(XI)	0.32	0.27	0.27	0.25
$Br_3C_6H_2OH$	(XII)	0.03	0	0.04	0
$H_3C-C_6H_4-SO_3H$	(XIII)	0.36	0.36	0.35	0.34

a) Experimental error in two measurements for the same sample was ±0.02 excess atom %.
b) Calculated on the assumption that two sulfonyl oxygens are completely equilibrated with one peroxidic oxygen.

shown in Table 2. Since the carbon dioxide contains excess oxygen-18, process (a) is rejected, and thus it has been established that the thermal decarboxylation of arenesulfonyl aryl carbonates occurs according to process (b).

Since the hydrolysis of aryl arenesulfonates proceeds with S–O cleavage instead of C–O cleavage, no excess ^{18}O-incorporation in XII indicates that no excess ^{18}O in the phenoxy oxygen in IX and X. The ^{18}O-contents in IX, X, and XI show that during the rearrangement of VIII to IX two sulfonyl oxygens and one peroxidic oxygen of VIII are completely scrambled.

These findings reject mechanism (A), and probably mechanism (C) as well. It is possibe that the sulfonyl oxygen-18 atoms are completely retained during the carboxy-inversion process and then, prior to the decarboxylation, completely scrambled when the mixed anhydride was heated up to 230°C. However, the decarboxylation proceeds with the S–O bond cleavage, whereas the scrambling requires the C–O bond cleavage. It seems less likely that *both* the C–O bond and the S–O bond of the mixed anhydride are cleaved upon heating. Therefore, the rearrangement of aroyl arenesulfonyl peroxides to aryl arenesulfonyl carbonates probably proceeds through a state similar to that shown in mechanism (B). Mechanism (B) is similar to the mechanism proposed for the rearrangement of *p*-methoxybenzoyl *p'*-nitrobenzoyl peroxide.[6,7]

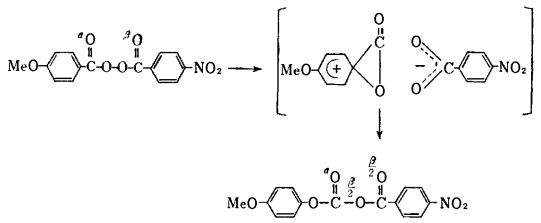

Experimental

Preparation of Peroxybenzoic Acid[carbonyl-^{18}O]. Benzoyl chloride [carbonyl-^{18}O] was prepared according to the method of Denney and Denney.[7] Peroxybenzoic acid[carbonyl-^{18}O] was prepared according to the procedure of Vilkas[8] by use of benzoyl chloride[carbonyl-^{18}O] and sodium peroxide with some modification. Peroxybenzoic acid[carbonyl-^{18}O] was extracted from the aqueous layer with dichloromethane, and the dichloromethane solution was used for preparation of BTP[carbonyl-^{18}O].

Preparation of BTP[carbonyl-^{18}O] or BTP[sulfonyl-^{18}O]. BTP[carbonyl-^{18}O] or BTP[sulfonyl-^{18}O] was prepared, according to the method used for the preparation of the unlabeled BTP,[3] by using peroxybenzoic acid[carbonyl-^{18}O] and *p*-toluenesulfonyl chloride, or peroxybenzoic acid and *p*-toluenesulfonyl chloride [sulfonyl-^{18}O], respectively.

Decomposition of BTP[carbonyl-^{18}O] or BTP[sulfonyl-^{18}O]. A solution of 4.39 g (15 mmol) of BTP[carbonyl-^{18}O] in 150 m*l* of benzene, or 2.64 g (9 mmol) of BTP[sulfonyl-^{18}O] in 120 m*l* of benzene in the presence of trifluoroacetic acid (5 mol/mol BTP) was decomposed under the conditions described previously.[4] Phenyl *p*-toluenesulfonyl carbonate (PTC) was isolated by elution chromatography on a silica gel column (Wako Gel Q 22), and then recrystallized from ether; mp 64—65°C.

Reaction of PTC with Aniline. To 1.33 g (4.6 mmol) of PTC dissolved in 30 m*l* of dichloromethane was added 0.93 g (10 mmol) of freshly distilled aniline. The reaction mixture was refluxed for 30 min, washed with water, dilute hydrochloric acid and water, successively, and dried over anhydrous magnesium sulfate. Solvent was evaporated under reduced pressure and phenyl phenylcarbamate obtained was recrystallized from carbon tetrachloride; yield, 850 mg (87%); recrystallized three times from carbon tetrachloride; mp 124—125°C (lit,[9] 126°C).

Hydrolysis of Phenyl Phenylcarbamate. A mixture of phenyl phenylcarbamate (626 mg), sodium (850 mg), water (15 m*l*) and ethanol (10 m*l*) was refluxed for 2 hr. The ethanol was evaporated under reduced pressure, and then water and ether were added to the residue. The aqueous layer was washed with ether twice, and neutrallized with hydrochloric acid. Phenol isolated was converted by bromine water into 2,4,6-tribromophenol; 850 mg (88%); purified by sublimation twice, mp 94—95°C (lit,[10] 95°C).

Pyrolysis of PTC. In a vessel connected with a gas buret, 1.00 g of PTC was placed. After the atmosphere was replaced with nitrogen, the vessel was heated gradually to 230°C and kept at this temperature until about 60 m*l* of carbon dioxide was evolved. The brownish reaction mixture obtained was dissolved in benzene, washed with water, and dried over anhydrous magnesium sulfate. After the benzene was removed under reduced pressure, the residue was chromatographed on a silica gel column. Phenyl *p*-toluenesulfonate isolated (223 mg, 26.5%) was twice recrystallized from *n*-hexane, mp 95°C (lit,[11] 95—96°C).

Hydrolysis of Phenyl p-*Toluenesulfonate.* A mixture of phenyl *p*-toluenesulfonate (172 mg), sodium hydroxide (276 mg), dioxane (3 m*l*) and water (4 m*l*) was sealed in an ampoule and heated at 94°C for 100 hr. After dioxane was removed under reduced pressure, water was added to the mixture. The aqueous layer was acidified with hydrochloric acid and the phenol formed was extracted with ether. *p*-Toluenesulfonic acid remaining in the aqueous layer was converted to its *S*-benzylisothiuronium salt (235 mg, 91%) which was recrystallized three times from water, mp 180—181°C (lit,[12] 181—182°C). Phenol obtained from the ether layer was converted to 2,4,6-tribromophenol; 171 mg (75%); purified by sublimation, mp 94—95°C.

Reaction of BTP[carbonyl-^{18}O] with Anhydrous Hydrazine. A solution of 0.90 g of BTP[carbonyl-^{18}O] in 25 m*l* of anhydrous benzene was added drop by drop to a mixture of 1.0 g of anhydrous hydrazine and 5 m*l* of benzene at 2°C with stirring. After the addition was over, benzene and unreacted hydrazine were removed under reduced pressure. Benzhydrazide produced (250 mg, 61%) was recrystallized three times from ether, mp 112.5—113°C (lit,[13] 112.5°C).

Determination of Oxygen-18 Contents. All the samples were converted to carbon dioxide according to the method of Rittenberg and Ponticorvo[14] for determination of the ^{18}O-contents. The ^{18}O-contents were determined by use of a Hitachi RMU-6E Type Mass Spectrometer.

6) D. B. Denney, *J. Amer. Chem. Soc.*, **78**, 590 (1956).
7) D. B. Denney and D. G. Denney, *ibid.*, **79**, 4806 (1957).
8) M. Vilkas, *Bull. Soc. Chim. France*, **1959**, 1401.
9) H. Eckenroth, *Ber.*, **18**, 516 (1885).
10) L. Coln and F. Schultze, *ibid.*, **38**, 3294 (1905).
11) F. Reverdin and P. Crepieux, *ibid.*, **35**, 1439 (1902).
12) E. Chambers and G. W. Watt, *J. Org. Chem.*, **6**, 376 (1941).
13) R. Stolle, *J. Prakt. Chem.*, **69**, 145 (1904).
14) D. Rittenberg and L. Ponticorvo, *Int. J. Appl. Radiat. Isotopes*, **1**, 208 (1956).

Photolyses of Alkyl Sulfinates and Sulfites[1)]

Michio KOBAYASHI, Hiroshi MINATO, Yoshiko MIYAJI, Takuji YOSHIOKA, Koji TANAKA, and Koichi HONDA*

Department of Chemistry, Faculty of Science, Tokyo Metropolitan University, Fukazawa, Setagaya, Tokyo

(Received February 15, 1972)

Methyl, ethyl, *n*-butyl, *n*-octyl, benzyl, and allyl *p*-toluenesulfinates were photolyzed in *n*-hexane or without solvent. The products analyses indicate that the photolyses of these esters involve the fission of ArSO–OR bond, producing a sulfinyl radical and an alkoxy radical. In the case of the allyl ester, isomerization to the corresponding sulfone took place to some extent. When optically active *l*-menthyl *l*-*p*-toluenesulfinate was irradiated, its optical activity decreased fairly quickly while very little photolysis was observed. This photo-racemization was ascribed to the reversible formation of sulfinyl radical and menthyloxy radical. When di-*n*-butyl sulfite was photolyzed, the products found were explained by assuming the initial formation of *n*-butoxysulfinyl radical and *n*-butoxy radical. When *n*-butyl chlorosulfite was photolyzed, the products found indicate the initial fission of the S–Cl bond instead of the S–O bond.

Concerning the photochemistry of organo-sulfur compounds, many reports have been published.[2)] However, no papers have been published concerning the photo-reactions of sulfinic acids and their esters. Since alkyl arenesulfinates show a fairly strong absorption at about 250 nm due to $n \rightarrow d\pi$ transition,[3)] they are expected to undergo photolyses.

In connection with our investigations on sulfinyl, sulfonyl, and sulfonyloxy radicals, photolyses of some sulfinic esters have been studied, and the results will be described in this paper.

Results and Discussion

A. Photolyses of Alkyl p-*Toluenesulfinates.* Methyl, ethyl, *n*-butyl, *n*-octyl, benzyl, and allyl *p*-toluenesulfinates without or with *n*-hexane as solvent were degassed in quartz vessels, and then photolyzed at room temperature. Gaseous products formed were identified and quantitatively determined by mass-spectrometry or gas chromatography. Low-boiling products were distilled together with the solvent. The compounds in the residue and the distillate were identified and quantitatively determined.

Table 1 shows the UV absorption maxima of various sulfinates.

Table 2 shows the results of photolysis of ethyl *p*-toluenesulfinate. When a degassed solution of ethyl *p*-toluenesulfinate in *n*-hexane (0.27 mol/*l*) was irradiated for 9 hr, the gaseous products obtained were found to be CO (50.6), CH_4 (22.2), H_2 (16.9), C_2H_4 (4.6), C_2H_6 (3.5), C_3H_8 (1.3), and C_3H_6 (1.0%).

The decomposition of ethyl *p*-toluenesulfinate can be ascribed to its absorption at 250 nm, because a) no decomposition was observed in dark in 120 hr at room temperature, and b) more than 95% of the ester was recovered after irradiation with a high pressure mercury lamp in a Pyrex vessel for 147 hr.

Table 3 shows the results of photolysis of methyl *p*-toluenesulfinate in *n*-hexane.

Formation of methyl *p*-toluenesulfonate is in contrast with the results in the ethyl ester. No contamination

TABLE 1. UV ABSORPTION MAXIMA OF SEVERAL *p*-TOLUENESULFINATES (p-$CH_3C_6H_4SO_2R$) IN HEXANE

R	CH_3	C_2H_5	n-C_4H_9	n-C_8H_{17}	CH_2CHCH_2	$PhCH_2$
λ_{max} (log ε)	224 (4.27)	224 (4.02)	224 (4.02)	224 (4.02)	225 (4.25)	
	254 (3.71)	256 (3.53)	256 (3.53)	254 (3.56)	258 (3.79)	257

TABLE 2. PRODUCTS OF PHOTOLYSIS OF ETHYL *p*-TOLUENESULFINATE IN HEXANE

$[C_7H_7SO_2C_2H_5]_0$ (mol/*l*)	Time (hr)	Unreacted ester (mol%)	Products (mol/100 mol ester)				
			$C_7H_7SO_2SC_7H_7$	$(C_7H_7S)_2$	TsOH	X[d)]	CH_3CHO
0.33	70.5[a)]	6.8	21.7	14.9	1.3	9.2	8.9
0.29	100	17.6	22.2	4.8	trace	19.8	e)
0.28	125	33.6	10.3	4.6	trace	18.1	e)
0.27	(120)[b)]	(100)	0	0	0	0	0
0.38	147[c)]	95	0	0	trace	0	0

a) With a low-pressure mercury lamp. All other experiments were carried out with a high-pressure mercury lamp. b) A blank experiment with no irradiation at room temperature. c) A Pyrex vessel was used. d) A sulfone of unknown structure, in weight %. e) Not determined.

* Department of Chemistry, Faculty of General Education, The University of Tokyo, Meguro, Tokyo

1) Organic Sulfur Compounds, Part XXXIII.

2) A recent review: E. Lock, *Quarterly Reports on Sulfur Chemistry*, **4**, No. 4 (1969). Intra-Science Research Foundation, Santa Monica, California.

3) M. Kobayashi and N. Koga, This Bulletin, **39**, 1788 (1966).

TABLE 3. PRODUCTS OF PHOTOLYSIS OF METHYL *p*-TOLUENESULFINATE IN *n*-HEXANE

$[C_7H_7SO_2CH_3]_0$ (mol/*l*)	Time (hr)	Products (mol/100 mol ester)			
		$C_7H_7SO_2SC_7H_7$	$(C_7H_7S)_2$	TsOH	$TsOCH_3$
0.34	66	16.5	12.0	2.8	8.4
0.41	130	19.8	8.2	3.9	7.6

TABLE 4. PRODUCTS OF PHOTOLYSIS OF *n*-BUTYL *p*-TOLUENESULFINATE IN *n*-HEXANE

$[C_7H_7SO_2C_4H_9]_0$ (mol/*l*)	Time (hr)	Unreacted ester (mol%)	Products (mol/100 mol ester)	
			$C_7H_7SO_2SC_7H_7$	$(C_7H_7S)_2$
0.23	107	35.6	12.5	+
neat	121	28.9	10.7	+

TABLE 5. PRODUCTS OF PHOTOLYSIS OF *n*-OCTYL *p*-TOLUENESULFINATE IN *n*-HEXANE

$[C_7H_7SO_2C_8H_{17}]_0$ (mol/*l*)	Time (hr)	Unreacted ester (mol%)	Products (mol/100 mol ester)		
			$C_7H_7SO_2SC_7H_7$	$(C_7H_7S)_2$	TsOH
0.29	45	100	0	0	0
0.40	117	100	0	0	0
neat	123	44.5	20.8	0.5	+

TABLE 6. PRODUCTS OF PHOTOLYSIS OF ALLYL *p*-TOLUENESULFINATE IN *n*-HEXANE

$[C_7H_7SO_2C_3H_5]_0$ (mol/*l*)	Time (hr)	Products (mol/100 mol ester)				
		$C_7H_7SO_2SC_7H_7$	$C_7H_7SO_2C_3H_5$ a sulfone[b]		polymer[c] sulfone	$(C_7H_7S)_2$
0.95	140	10.7	8.6	6.5	32.3	+
0.33	20	4.6	17.2	0	8.0	+
0.27	111	7.0	12.2	0	40.7	+
0.34	(192)[a]	0	0	0	0	0

a) A blank experiment with no irradiation at room temperature. No change was observed in its NMR spectrum. b) A sulfone of unknown structure, in weight %; mp 100—104.5°C: C, 66.28, 66.14%; H, 6.47, 6.52%. c) Polymeric sulfone of unknown structure, in weight %.

of the initial methyl sulfinate with *p*-toluenesulfonic acid or methyl *p*-toluenesulfonate was confirmed by the IR and NMR spectroscopy. When the solvent was removed from the reaction mixture under reduced pressure at room temperature, the NMR spectrum of the residue showed a signal ascribable to CH_3 of $TsOCH_3$ at 3.7 ppm (s), indicating that $TsOCH_3$ is present in the reaction mixture and is not produced during chromatography and other subsequent treatments.

Table 4 shows the results of photolysis of *n*-butyl *p*-toluenesulfinate in *n*-hexane. The reactivity of the butyl ester is much lower than that of the ethyl ester. The mass spectrum of the gaseous and low-boiling products shows peaks at *m/e* 92, 91, 79, 78(M), 77, 64, 56, 52, 51, 44, 39, 29, and 28, indicating the presence of some toluene.

Table 5 shows the results of photolysis of *n*-octyl *p*-toluenesulfinate in *n*-hexane.

These data show that alkyl *p*-toluenesulfinates with longer alkyl groups are less prone to undergo photolysis.

Table 6 shows the results of photolysis of allyl *p*-toluenesulfinate. When the mixture was irradiated longer, the yield of allyl *p*-tolyl sulfone decreased and that of polymeric sulfone increased. Cope, Morrison, and Field[4] reported thermal rearrangement of allyl benzenesulfinate to allyl phenyl sulfone upon heating at 100°C for 24 hr. No occurrence of such thermal rearrangement under our conditions was confirmed by a blank experiment in dark. It was also confirmed that allyl *p*-tolyl sulfone (0.02M in *n*-hexane, degassed) showed almost no change in its NMR spectrum upon irradiation for 113 hr with a high pressure mercury lamp.

When a degassed solution of benzyl *p*-toluenesulfinate (3.6 mmol) in *n*-hexane (30 m*l*) was irradiated for 192 hr with a high pressure mercury lamp, an absorption at 257 nm disappeared and a new absorption appeared at 243 nm. A weak absorption was observed at 290 nm. Analysis of the reaction mixture revealed the presence of 47 mol% of $C_7H_7SO_2SC_7H_7$, 27.4 mol% of benzaldehyde, and 2 mol% of dibenzyl. Thin layer chromatography showed the presence of some di-*p*-tolyl disulfide.

These results show that when alkyl *p*-toluenesulfinates are irradiated, the SO–O bonds are broken. The photolysis of the ethyl ester is shown as follows.

4) A. C. Cope, D. E. Morrison, and L. Field, *J. Amer. Chem, Soc.*, **72**, 59 (1950).

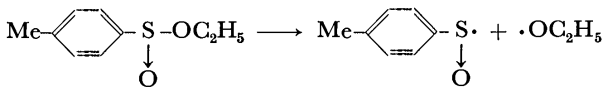

A part of the alkoxy radicals reacts with the sulfinyl radicals, yielding acetaldehyde, which undergoes further photolysis according to the scheme reported in the literature.[5]

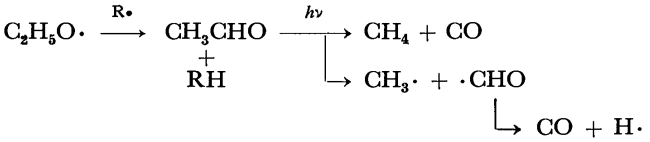

The products arising from the sulfinyl radicals are $C_7H_7SO_2SC_7H_7$, $C_7H_7SSC_7H_7$, and $C_7H_7SO_3H$. Formation of these products can be explained by the following scheme.

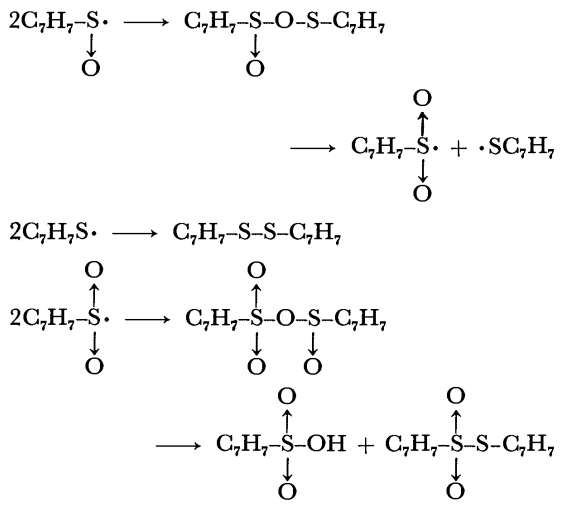

Formation of $ArSO_3H$, $ArSO_2SAr$, and ArSSAr from $ArSO_2$ have been reported by da Silva Correa and Waters.[6]

The mass-spectrometric analysis of the products of the photolysis of *n*-butyl *p*-toluenesulfinate showed the presence of toluene; this finding suggests the occurrence of the following process in cage.

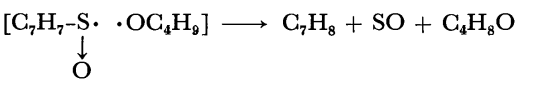

The following non-radical scheme is conceivable for the photolysis of alkyl *p*-toluenesulfinates.

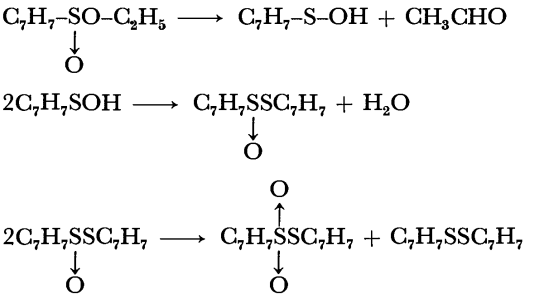

This scheme requires the formation of $ArSO_2SAr$ and ArSSAr in equal amounts. However, the yield of $ArSO_2SAr$ was much greater than that of ArSSAr in all the cases. The results of the photoracemization to be described later also favor the homolytic scheme.

When a degassed solution of ethyl *p*-toluenesulfinate-[sulfinyl-^{18}O] (excess ^{18}O, 0.37 atom%) in *n*-hexane (0.30M) was irradiated at room temperature for 114 hr and the ^{18}O content of the *p*-tolyl *p*-toluenethiolsulfonate isolated was analyzed, it was found to contain 0.54 excess ^{18}O atom%. If only the O–C bond is cleaved, the ^{18}O content of the thiolsulfonate must be equivalent to that of the sulfinate. The result of this experiment shows that the SO–O bond is cleaved by photolysis, though not exclusively.

In the case of the allyl ester, photo-isomerization to allyl *p*-tolyl sulfone took place to some extent. It requires the SO_2–C bond cleavage, which can be rationalized in terms of the stability of allyl radical.

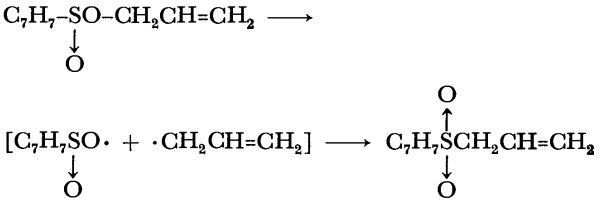

However, in the case of benzyl *p*-toluenesulfinate, no benzyl *p*-tolyl sulfone was detected and much benzaldehyde (a product of the SO–O bond cleavage) was found. Therefore, it is possible that the allyl ester is the only exceptional case and the photoisomerization proceeds by a cyclic process shown below.

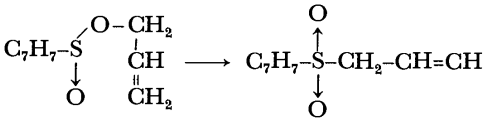

It has been reported that thermal isomerization of the allyl ester occurs *via* reversible dissociation to allyl cation and a sulfinate anion,[7] whereas benzyl *p*-toluenesulfinate does not isomerize thermally to the corresponding sulfone.[8]

In the case of methyl *p*-toluenesulfinate, photodisproportionation took place to some extent, yielding methyl *p*-toluenesulfonate.

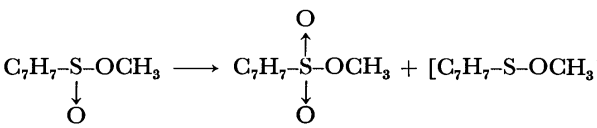

Photochemical oxygen transfer has been observed in the case of dimethyl sulfoxide,[9] but in sulfinate esters this is the only example.

In an attempt to determine whether a triplet or a singlet excited state is involved in photolyses of sulfinates, degassed solutions of ethyl *p*-toluenesulfinate (1.5 mmol) in *n*-hexane (30 m*l*) with or without a

5) J. G. Calvert and J. N. Pitts, Jr., "Photochemistry," John Wiley & Sons, New York, N. Y. (1967), p. 371.

6) C. M. M. da Silva Correa and W. A. Waters, *J. Chem. Soc., C*, **1968**, 1874.

7) D. Darwish and R. A. McLaren, *Tetrahedron Lett.*, **1962**, 1231; D. Darwish and E. A. Preston, *ibid.*, **1964**, 113.

8) A. H. Wragg, J. S. McFadyen, and T. S. Stevens, *J. Chem. Soc.*, **1958**, 3603.

9) Ref. 2, p. 315.

TABLE 7. CHANGE IN OPTICAL ACTIVITY OF *l*-MENTHYL *l*-*p*-TOLUENESULFINATE UPON IRRADIATION[a)]

Initial ester	Time (hr)	Recovered ester	Ph-SO-C_7H_7	% Retention of optical activity
$[\alpha]_D^{30}$ −222.0°	1	$[\alpha]_D^{30}$ −218.3°		98
$[\alpha]_D^{30}$ −210.5°	21	$[\alpha]_D^{34}$ −119.5°		57
$[\alpha]_D^{31.5}$ −263.3°	5	$[\alpha]_D^{31}$ −145.7°		55
$[\alpha]_D^{EtOH}$ −186.42°	4	—	$[\alpha]_D^{CH_2Cl_2}$ +16.87°	59
$[\alpha]_D^{EtOH}$ −186.42°	(4)[b)]	—	$[\alpha]_D^{CH_2Cl_2}$ +28.38°	(100)[b)]

a) Solvent is *n*-hexane, unless otherwise stated.
b) A blank experiment performed in dark without irradiation.

quencher (piperylene, 3.2 mmol) were irradiated by a high pressure mercury lamp in quartz vessels at room temperature for 105 hr. After the volatile components were removed under high vacuum at room temperature, the residues were dissolved in $CDCl_3$, and their NMR spectra were determined. It was found that in the presence of piperylene almost no thiolsulfonate was formed whereas in the absence of piperylene a considerable amount of thiolsulfonate was formed. However, since piperylene itself appeared to undergo some photopolymerization or addition in the presence of ethyl *p*-toluenesulfinate, no definite conclusion was obtained.

B. Photo-racemization of Sulfinate Esters. As shown in Table 1, λ_{max} and log ε of alkyl *p*-toluenesulfinates do not vary with the chain lengths of the alkyl groups, whereas the photolyses of these esters take place to much lesser extent when alkyl groups have longer chain lengths. A possible explanation for these phenomena is that internal return of the sulfinyl radicals and alkoxy radicals takes place in cage and this internal return takes place more easily when alkoxy groups are larger and less prone to diffuse away. If this is the case, irradiation of optically active sulfinate esters must result in photo-racemization.

$$\underset{\text{optically active}}{R-\overset{*}{S}(=O)-OR'} \xrightarrow{h\nu} [R-S(=O)\cdot \cdot OR'] \longrightarrow \underset{\text{racemic}}{R-S(=O)-OR'}$$

When a degassed solution of *l*-menthyl *l*-*p*-toluenesulfinate in *n*-hexane was irradiated with a high pressure mercury lamp at room temperature and then the solvent was removed under reduced pressure at room temperature, the optical activity of the residue was much smaller than that of the initial ester, as shown in Table 7. Very little photolysis is expected to take place during such a short time of irradiation. In order to exclude the possibility of apparent decrease of optical activity of the ester by the contamination of optically inactive decomposition products, the residual ester was converted to phenyl *p*-tolyl sulfoxide by reaction with phenylmagnesium bromide in ether and the optical activity of the sulfoxide was determined.

It is remarkable that considerable racemization took place by irradiation for a short time during which no appreciable photolysis was observed.

Photo-racemization of sulfoxides has been studied fairly extensively.[10)] Racemization of optically active benzhydryl *p*-toluenesulfinate has been studied in acetic acid, and ascribed to reversible dissociation to sulfinate anion and diphenylcarbonium ion. Rates of internal return of the ion pair to the sulfinate ester are approximately equal to those of isomerization to the sulfone.

$$(+)\text{-}C_7H_7\text{-}S(=O)\text{-}OCHPh_2 \rightleftharpoons [C_7H_7\text{-}S(=O)\text{-}O^{\ominus}\ {}^{\oplus}CHPh_2]$$

$$C_7H_7\text{-}S(=O)\text{-}CHPh_2 \qquad (-)\text{-}C_7H_7\text{-}S(=O)\text{-}OCHPh_2$$

Under our experimental conditions, extensive racemization took place while very little photolysis occurred and no sulfone was observed. Therefore, this photo-racemization should not be ascribed to the reversible dissociation to sulfinate anion and menthyl cation, but rather to the reversible formation of sulfinyl radical and menthyloxy radical.

C. Photolyses of Di-n-butyl Sulfite and n-Butyl Chlorosulfite. Since the photolyses of sulfinate esters were found to involve homolysis of the S-O bond, photolyses of di-*n*-butyl sulfite was investigated.

In contrast with alkyl *p*-toluenesulfinates, dialkyl sulfites show no absorption maxima in the ordinary ultraviolet region, and consequently photolysis proceeded rather slowly.

After neat liquid of di-*n*-butyl sulfite was degassed and irradiated by a high-pressure mercury lamp at room temperature for 31 hr, the gaseous portion of the products was analyzed by gas chromatography, and was found to be CO (26.5), H_2 (37.4), SO_2 (16.4), 1-butene (1.67), butane (0.086), propane (0.84), propene (0.24), ethylene (2.96), ethane (0.17), methane (0.65) (the sum of the hydrocarbons, 6.62), N_2 (14.9), and O_2 (4.32%).

Gas-chromatographic analysis of the liquid products showed that *n*-butanol (14 mol/100 mol ester) and *n*-butyraldehyde (1.7 mol%; confirmed by its 2,4-dinitrophenylhydrazone).

These results indicate that the SO-O bond of the sulfite is cleaved first. The products found can he rationalized by the scheme shown in the next page.

As another compound containing the sulfinyl group, *n*-butyl chlorosulfite was photolyzed. Since this compound has a UV absorption maximum at 230—235 nm, photolysis proceeds fairly rapidly. When neat liquid

10) R. S. Crooke and G. S. Hammond, *J. Amer. Chem. Soc.*, **90**, 2958 (1968); G. S. Hammond, H. Gotthardt, L. M. Coyne, M. Axelrod, D. R. Rayner, and K. Mislow, *ibid.*, **87**, 4959 (1965).

11) E. Ciuffarin, M. Isola, and A. Fava, *ibid.*, **90**, 3594 (1968).

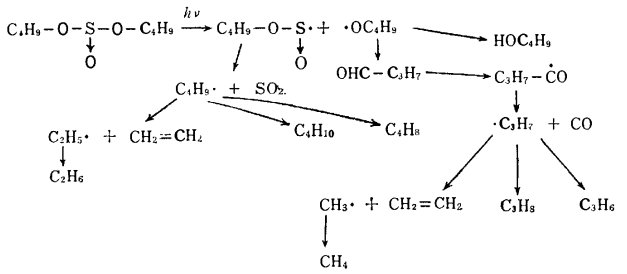

n-butyl chlorosulfite (75 mmol) was degassed and irradiated with a high-pressure mercury lamp at room temperature for 7.5 hr, n-C_4H_9Cl (2.0 mmol), HCl (0.5 mmol), SO_2 (0.35 mmol), and some $(n\text{-}C_4H_9O)_2SO$ were found as the products. These results indicate that the bond initially cleaved is not the SO–O bond but the S–Cl bond.

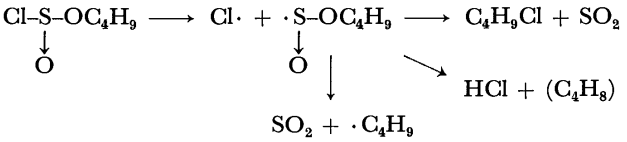

Experimental

Materials. Alkyl *p*-toluenesulfinates were prepared by condensation of *p*-toluenesulfinic acid and an alcohol in the presence of dicyclohexylcarbodiimide with or without solvent (dichloromethane).[12] Methyl ester, bp 78—79°C/1.5 mmHg; ethyl, 78°C/6×10^{-3} mmHg; butyl, 110—114°C/6×10^{-3} mmHg; octyl, 112°C/5×10^{-3} mmHg; allyl, 79—81°C/2×10^{-3} mmHg; benzyl, mp 48°C.

Photolyses of p-*Toluenesulfinates.* Neat ester or its solution in *n*-hexane (spectroscopic grade, 0.3—1.0 M) was placed in a quartz vessel and completely degassed. Then the vessel was irradiated with a 1 kW high-pressure or 30 W low-pressure mercury lamp. During the irradiation some solids began to appear on the wall. After the irradiation, the reaction mixture was frozen with liquid nitrogen, and the gaseous products were pumped out with a Töpler pump and analyzed by gas chromatography (molecular sieve column). In some cases these gaseous products were subjected to mass-spectrometric analysis. The remaining mixture was evaporated at room temperature under high vacuum, and the NMR spectrum of the residue was taken. Then the residue was analyzed by elution chromatography (Florisil, silca gel, or alumina column) and gas chromatography. *p*-Toluenesulfonic acid was extracted with water, and determined quantitatively as its *S*-benzylisothiuronium salt.

Photolysis of Ethyl p-*Toluenesulfinate-[sulfinyl-*^{18}*O]*. *p*-Toluenesulfinic acid was heated in $D_2{}^{18}O$ (^{18}O, 1.5 atom %) and converted to $C_7H_7S^{18}O_2D$, which was then allowed to react with ethanol and dicyclohexylcarbodiimide. Into 20 ml of *n*-hexane, 1.1 g (6.0 mmol) of the ethyl *p*-toluenesulfinate-[sulfinyl-^{18}O] thus produced was dissolved. The solution was degassed and then irradiated with a 1 kW high-pressure mercury lamp for 144 hr at room temperature. The reaction mixture was evaporated at room temperature under high vacuum, and the residue was chromatographed on a Florisil column, and the thiolsulfonate was isolated.

Photo-racemization of l-*Menthyl* l-p-*Toluenesulfinate.* *l*-Menthol and *p*-toluenesulfinic acid was allowed to react in the presence of dicyclohexylcarbodiimide in dichloromethane.[12] The diastereomeric menthyl ester mixture obtained was treated with hydrogen chloride in the presence of tetramethylammonium chloride, and the crystals of the *l-l* ester were obtained.

A solution of this *l-l* ester (1.0 g) in *n*-hexane (38 ml) was degassed and irradiated by a 1 kW high-pressure mercury lamp for 1—21 hr. After the optical activity of the solution irradiated was determined, the solvent was removed at room temperature under high vacuum. The residue was dissolved in ether, and converted to phenyl *p*-tolyl sulfoxide by reaction with ethereal phenylmagnesium bromide.

*Photolysis of Di-*n*-butyl Sulfite.* Di-*n*-butyl sulfite (bp 118—120°C/21 mmHg) (14.8 g; 76.2 mmol) was degassed in a quartz vessel, and irradiated with a 1 kW high-pressure mercuty lamp for 31 hr. The gaseous products collected with a Töpler pump was analyzed by gas chromatography.

Photolysis of n-*Butyl Chlorosulfite.* *n*-Butyl chlorosulfite (85—87°C/46 mmHg) (75 mmol) was degassed, and irradiated with a 1 kW high-pressure mercury lamp for 7.5 hr. The gaseous and low-boiling products were collected in a liquid-nitrogen trap by vacuum distillation, and dissolved in water. The amount of HCl was determined by titration, and that of SO_2 was determined after it was converted to sulfuric acid by H_2O_2. The amounts of *n*-butyl chloride and di-*n*-butyl sulfite were determined by gas chromatography.

12) Y. Miyaji, H. Minato, and M. Kobayashi, This Bulletin, **44**, 862 (1971).

β-(2,4,6-Cycloheptatrien-1-yl)ethylcarbene. The Synthesis of 9-Substituted Bicyclo[4.2.1]nona-2,4,7-trienes and 9-Substituted Barbaralanes[1]

Haruki TSURUTA, Katsuhiko KURABAYASHI, and Toshio MUKAI
Department of Chemistry, Faculty of Science, Tohoku University, Sendai
(Received December 22, 1971)

The thermal decomposition of sodium salt of (2,4,6-cycloheptatrien-1-yl)acetaldehydes tosylhydrazone (**4**, **6**, and **8**) afforded 9-substituted bicyclo[4.2.1]nona-2,4,7-triene (**9**, **11**, and **14**) and 9-substituted barbaralane (**10**, **12**, and **15**). In the case of **8**, products containing two nitrogen atoms (**17** and **18**) were isolated. The structure and the photochemical reaction of **17** provided strong support for the intermediacy of the tetracyclo[4.3.0.$0^{2,9}$.$0^{5,7}$]-nona-3-ene (**37**) derivative for the formation of the bicyclo[4.2.1]nona-2,4,7-triene derivatives. The difference in energy surface between C_9H_{10} and $C_{10}H_{10}$ hydrocarbons was discussed.

The intramolecular addition of carbene to an isolated double bond has been a useful tool in synthesizing strained compounds. Recently, the application of this reaction to compounds with conjugated double bonds has received considerable attention. However, these reactions tend to afford complicated products, because an originally-formed strained intermediate easily rearranges into more stable compounds under these reaction conditions. For example Jones[2] and Masamune[3] investigated the thermal and photochemical decomposition of bicyclo[6.1.0]nona-2,4,6-triene-9-carboxaldehyde tosylhydrazone and reported the formation of seven and six products respectively. Similarly, the thermal decomposition of bicyclo[5.1.0]octa-2,4-diene-8-carboxaldehyde tosylhydrazone afforded four products.[2,4] We chose to study the reaction of β-(2,4,6-cycloheptatrien-1-yl)ethylcarbene (**1**) in order to see how the terminal carbene reacts intramoleculary to a conjugated triene or to a conjugated diene of the norcaradiene valence isomer (**2**). It also seemed of

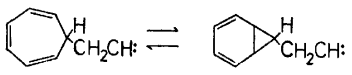

(**1**) (**2**)

interest to investigate the thermal stability of the expected highly strained intermediates.

Results

When sodium salt of (2,4,6-cycloheptatrien-1-yl)-acetaldehyde tosylhydrazone (**4**) was heated in dry dioxane at 90—95°C, two kinds of C_9H_{10} hydrocarbon were obtained. The major liquid product (yield= 16%) (M=118) was identified as bicyclo[4.2.1]nona-2,4,7-triene (**9**) by a comparison of its NMR and IR spectra with those of an authentic sample.[5] The catalytic reduction of **9** in ether afforded a known bicyclo[4.2.1]nonane (mp 95°C).[6]

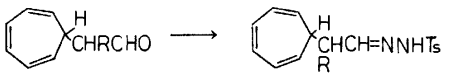

(**3**): R=H (**4**): R=H
(**5**): R=CH_3 (**6**): R=CH_3
(**7**): R=Ph (**8**): R=Ph

The minor crystalline compound (**10**; yield=4%) shows a very characteristic NMR spectrum containing four symmetrical groups of peaks with relative intensities of 2:4:2:2 (Table 1). This spectrum is in good agreement with that of tricyclo[3.3.1.$0^{2,8}$]nona-3,6-diene (barbaralane).[7,8] A comparison of the NMR data with those of known bridged homocycloheptatrienes shown in Table 1 indicate that H_a-absorption tends to shift to a lower field, while H_b and H_c tend to shift to a higher field, with an increase in the number of the bridged methylene. One of the reasons for this phenomenon may be a change in the anisotropic

TABLE 1. NMR SPECTRA OF BARBARALANE DERIVATIVES (τ).

	H_a	H_b	H_c	X	
Semibullvalene[10]	4.92	5.83	7.03		
10	4.45	6.10	7.72	$-(CH_2)-$	8.98
Dihydrobullvalene[11]	4.37	6.32	8.1	$-(CH_2)_2-$	8.1
12	4.46	6.13	7.98	$C\underline{H}CH_3$	8.78
15	4.34	6.00	7.58	$C\underline{H}Ph$	7.58

1) Preliminary reported: H. Tsuruta, K. Kurabayashi, and T. Mukai, *Tetrahedron Lett.*, **1967**, 3775; *J. Amer. Chem. Soc.*, **90**, 7167 (1968). Organic Thermal Reaction, XIV. Part XIII: H. Tsuruta, T. Sugiyama, and T. Mukai, *Chem. Lett.*, **1972**, 185.

2) a) M. Jones, Jr. and L. T. Scott, *J. Amer. Chem. Soc.*, **89**, 150 (1967). b) M. Jones, Jr., S. D. Reich, L. T. Scott, and L. E. Sullivan, *Angew. Chem. Internat. Edit.*, **7**, 644 (1968). c) M. Jones, Jr., S. D. Reich, and L. T. Scott, *J. Amer. Chem. Soc.*, **92**, 3118 (1970).

3) a) S. Masamune, C. G. Chin, K. Hojo, and R. T. Seidner, *ibid.*, **89**, 4804 (1967). b) S. Masamune, *Angew. Chem. Internat. Edit.*, **7**, 645 (1968).

4) M. Jones, Jr. and S. D. Reich, *J. Amer. Chem. Soc.*, **89**, 3935 (1967).

5) L. G. Cannell, *Tetrahedron Lett.*, **1967**, 5967. We thank Dr. Cannell for providing us a copy of the IR spectrum of **9**.

6) G. Sartori, U. Turba, A. Varvassori, and M. Riva, *ibid.*, **1966**, 4777.

7) W. von E. Doering, B. M. Ferrier, E. T. Fossel, J. H. Hartenstein, M. Jones, Jr., G. Klumpp, R. M. Rubin, and M. Saunders. *Tetrahedron*, **23**, 3943 (1967).

8) U. Biethan, H. Klusacek, and H. Musso, *Angew. Chem. Internat. Edit.*, **6**, 176 (1967); H. Musso, *ibid.*, **7**, 306 (1968).

effect[9] of the three-membered ring.

The heating of the sodium salt of α-(2,4,6-cycloheptatriene-1-yl)propionaldehyde tosylhydrazone (**6**) in dry dioxane at 75°C afforded two hydrocarbons. The major oil (yield=22%) was shown to be a mixture of **11a** and **11b** in a 2: 1 ratio, based on the area of the methylproton signal at τ 9.10 and 9.33 and of isolated olefinic-proton peaks at 4.85 and 4.97. Although the separation of the mixture was difficult, a reduced product which was obtained after the uptake of three equivalents of hydrogen could be separated into two sorts of $C_{10}H_{18}$. However, it remains uncertain which is the predominant product between **11a** and **11b**. The structure of the minor component (yield=5%) is consistent with 9-methylbarbaralane (**12**) judging from the NMR spectrum (Table 1).

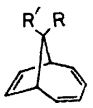

(**9**): R=R′=H
(**11a**): R=H, R′=CH_3
(**11b**): R=CH_3, R′=H

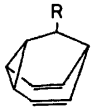

(**10**): R=H
(**12**): R=CH_3

The formation of barbaralane derivatives can be explained in terms of the intramolecular addition of the carbene to the C_4–C_5 bond in the cycloheptatriene nucleus, whereas that of bicyclo[4.2.1]nona-2,4,7-triene is rather surprising. One possible path is as follows. A highly-strained intermediate (**13**), formed by the addition of the carbene to the C_2–C_3 olefinic bond, rearranges to **9** and/or **11** by way of bond cleavage and migration, as is depicted in Scheme 1. As an alternative path, the rearrangement in barbaralane derivatives (**10** and **12**) shown by the arrow is pertinent, but the control experiment eliminated this possibility. The attempted thermolysis of barbaralane **10** under the same conditions as in the decomposition of **4** resulted in the complete recovery of **10**. Assuming the strained compound **13** to be an intermediate, the formation of *syn*- and *anti*-9-methyl bicyclo[4.2.1]nona-2,4,7-triene is understandable, because a small substituent such as hydrogen or methyl will not cause any significant difference in nonbonding interaction between **13a** and **13b**. However, when the substituent, R, is larger than hydrogen or methyl, the ratio of *syn*- and *anti*-**11** will change considerably because the nonbonding

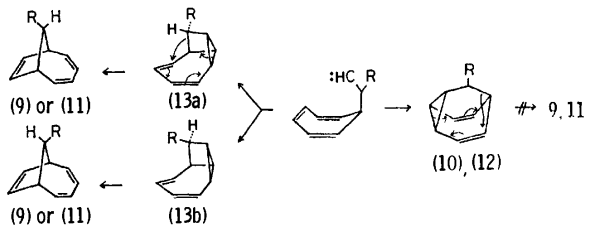

Scheme 1.

interaction of R with the rest of the molecule is heavier in **13b** than in **13a**. The phenyl derivative (R=Ph) was chosen for study next in order to confirm this point.

The thermolysis of the sodium salt of α-phenyl-α-(2,4,6-cycloheptatrien-1-yl)acetaldehyde tosylhydrazone (**8**) was carried out similarly; a three hydrocarbons (**14**, **15**, and **16**) in addition to two nitrogen-containing products (**17** and **18**) were thus formed. The structural elucidation of the main hydrocarbon (**14**, yield=33%) is based on a comparison of the spectral data with that of **9**. The geometry of the phenyl group at the C_9-position was determined in the following way. In the NMR spectrum of **14**, the signal ascribed to C_9-hydrogen appears as a singlet at τ 7.18, suggesting that the bond angle between the bridgehead proton and the C_9-proton is nearly 90°. An inspection of the model of **14** shows that the bond angles between *syn*-H_9 and H_1 and between *anti*-H_9 and H_1 are 90 and 30° respectively. The value calculated on the basis of the Karplus equation ($J_{syn\text{-}H_9,H_1}\approx 0$, $J_{anti\text{-}H_9,H_1}=6.0$ Hz) is in good agreement with the observed value for **14**, in which the phenyl group is located at the *anti*-position relative to the conjugated diene. Contrary to the case of methyl derivatives, it should be noted that only one stereoisomer **14** was selectively formed; this is in accord with the mechanistic discussion described in Scheme 1.

The NMR spectrum of (**15**, yield=3%) involves three groups of peaks, as is shown in Table 1, in addition to the peaks due to phenyl protons. Thus, compound **15** was identified as 9-phenylbarbaralane. The methin proton signal at the C_9-position bearing the phenyl group shifts downfield to overlap with the two protons at C_1 and C_5. The third crystalline hydrocarbon (**16**, yield=2%) was an aromatic compound; its structure was established to be 2-phenylindene by a comparison of its spectra and melting point with those of an authentic specimen.[12]

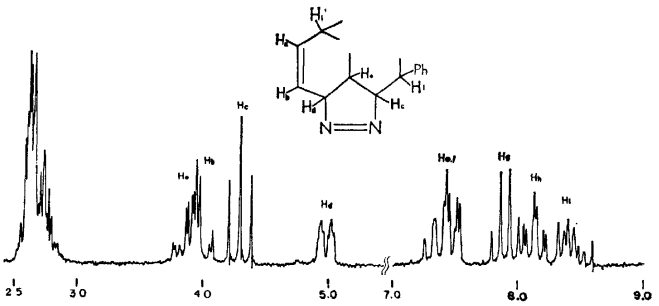

Fig. 1. NMR Spectrum of **17** in $CDCl_3$ (100 MHz).

Compound **17**, with a formula of $C_{15}H_{14}N_2$ (M=222), has no bands ascribable to NH and NH_2 groups in the IR spectrum, but the absorption band at 1534 cm^{-1} as well as the UV maximum (340 nm, ε 240) suggested the presence of an azo function. The NMR spectrum exhibits complex peaks (Fig. 1). All nine protons except the phenyl protons are in different circumstances; each proton is named alphabetically from downfield to upfield. It seems reasonable to assign H_c and H_d to

9) K. Tori and K. Kitahonoki, *J. Amer. Chem. Soc.*, **87**, 386 (1965).
10) H. E. Zimmerman and G. L. Grunewald, *ibid.*, **88**, 183 (1966).
11) R. Merényi, J. F. M. Oth, and G. Schröder, *Chem. Ber.*, **97**, 3150 (1964).
12) N. Campbell and E. Ciganek, *J. Chem. Soc.*, **1956**, 3834.

the protons adjacent to an azo group. Generally, under these circumstamces the methin proton appears in a fairly low field.[13-15] A decoupling experiment clarified the relationship between all the protons and led to the partial structure shown in Fig. 1. Irradiation on H_d affected the signals of three protons, H_a, H_b, and H_e. The signals due to H_a and H_b changed into a quartet (J=10.5, 4.5 Hz) and a doublet (J=10.5 Hz) respectively, while H_e, overlapped with H_f, turned into an apparent quartet (J=8.7, 7.0 Hz). Synchronous irradiation on both H_c and H_d made H_e a doublet (J=7.0 Hz), and H_f an apparent split doublet (J=2.0 Hz). Additional simultaneous irradiation on both H_e and H_f altered H_c to a sharp singlet and H_d to a finely-split singlet. Finally, H_i changed into a triplet upon irradiation on H_a. Three opened bonds of the partial structure in Fig. 1 are joined to build a three-membered ring and 7-phenyl-9,10-diazatetracyclo-[6.2.1.$0^{4,6}$.$0^{5,11}$]undeca-2,9-diene is assigned for **17**. The coupling constant (4.5 Hz) between H_a and H_i seems compatible with the reported values which were observed between a three-membered ring proton and an olefinic proton in bicyclo[4.2.1]heptene[16] and tricyclo[2.2.2.$0^{2,7}$]octene.[17] The chemical shifts and coupling constants of **17** are summarized in the Experimental section. Additional support for the structure was obtained from the photochemical behavior of **17** and from a mechanistic consideration of the reaction path which will be discussed later.

A nitrogen-containing product (**18**, yield=25%) (M=222) has the same formula as **17**. The NMR spectrum shows a very complicated multiplet between τ 2.4 and 3.9 containing two sets of doublets at 2.46 and 3.59 (J=2.0 Hz). The catalytic reduction of **18** over 10% Pd-C in ethanol afforded an oily product **19** after the uptake of three equivalents of hydrogen. In the NMR spectrum of **19**, the AB doublet still remains at τ 2.63 and 4.07 (J=2.0 Hz), whereas the complex signals of olefinic protons disappear and instead new two signals due to methylenic protons appear at τ 7.42 (4H, broad quartet) and 8.61 (multiplet, 8H). The signals at τ 7.42 can be ascribed to the methylene protons adjacent to the aromatic ring. The IR spectrum of **18** showed a strong hydrogen-bonded NH absorption at 3175—2883 cm^{-1}. In the NMR spectrum of monoacetate **20**, the AB doublet was observed at τ 3.53 and 1.83 (J=2.9 Hz), suggesting that the original peaks at τ 2.46 in **18** suffered from shielding by the acetyl group and shifted downfield such as to τ 1.83, whereas the other peaks remained unchanged in nearly the same field.[18] Another piece of evidence that **18** is a 3-substituted pyrazole derivative was given by oxidation with potassium permanganate, in which case pyrazole-3-carboxylic acid (**21**) was obtained.[19] When a solution of **18** in benzene containing iodine was heated under reflux, an isomer (**22**) was formed. In the IR spectrum of **22**, a strong peak appeared at 1005 cm^{-1} (*trans*-CH=CH), while the originally-observed peak at 746 cm^{-1} (*cis*-CH=CH) disappeared. Furthermore, the UV spectrum of **22** is very similar to that of *trans, trans, trans*-1,6-diphenyl-1,3,5-hexatriene,[20] suggesting the presence of the same triene system. On the basis of these data, compound **18** was identified as 1-phenyl-6-(3-pyrazolyl)-1,3,5-hexatriene, in which at least one double bond has a *cis*-configuration.

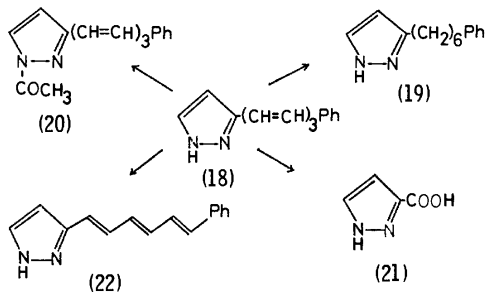

Discussion

A possible mechanistic pathway for the formation of all the products from the thermal decomposition of **8** is depicted in Scheme 2. Of the two nitrogen-containing products, the tetracyclic compound **17** is obviously produced from the norcaradiene valence isomer **24** by the 1,3-dipolar addition of a diazomethane counterpart to one of the double bonds. Another possible structure **17a** was ruled out on the basis of the decoupling experiment in the NMR spectrum. The formation of the pyrazole derivative **18** can be explained by assuming an intermediate of a tetracyclic azo compound **29**, which is derived by the 1,3-dipolar addition of a diazomethane counterpart to the C_2–C_3 bond in **23**, followed by the cleavage of the four-membered ring of **29** and by subsequent aromatization. The driving force for this reaction may be ascribed to release from the strain as well as to the stabilization arising from the formation of the full conjugated compound linked by two aromatic groups.

On the other hand, two pathways are possible for the formation of **14**. The divalent carbon in **25** may be added to the C_2–C_3 bond, giving a highly-strained intermediate **27**, which may then be immediately relieved from the strain in the manner described in Scheme 1 to afford **14**. An alternative route is that the carbene center in the norcaradiene isomer **26** is added to the C_2–C_3 bond[21,22] to form a tetracyclic intermediate **28**, which then easily gives rise to **14** by

13) R. M. Moriarty, *J. Org. Chem.*, **28**, 2385 (1963).
14) M. Schwarz, A. Besold, and E. R. Nelson, *ibid.*, **30**, 2425 (1965).
15) S. G. Cohen and R. Zand, *J. Amer. Chem. Soc.*, **84**, 586 (1962).
16) J. J. Sims, *ibid.*, **87**, 3511 (1965).
17) C. F. Huebner, E. Donoghue, L. Dorfman, F. A. Stuber, N. Danieli, and E. Wenkert, *Tetrahedron Lett.*, **1966**, 1185.
18) H. Dorn and H. Dilcher, *Ann. Chem.*, **707**, 141 (1967).
19) H. v. Pechmann and E. Burkard, *Chem. Ber.*, **33**, 3595 (1900).
20) K. Lunde and L. Zechmeister, *J. Amer. Chem. Soc.*, **76**, 2308 (1954).
21) M. J. Goldstein and B. G. Odell, *ibid.*, **89**, 6356 (1967).
22) J. Daub and P. von R. Schleyer, *Angew. Chem. Internat. Edit.*, **7**, 468 (1968).

the retro-Diels-Alder reaction.[23,24] In both routes the stereochemistry of the phenyl group in **14** can be satisfactorily explained by assuming that the phenyl group is on the less-crowded side to avoid a nonbonding repulsion. The fact that **14** was produced in a 43% yield by the irradiation of **17** with Pyrex-filtered light strongly supports the latter pathway (**26**→**28**→**14**).

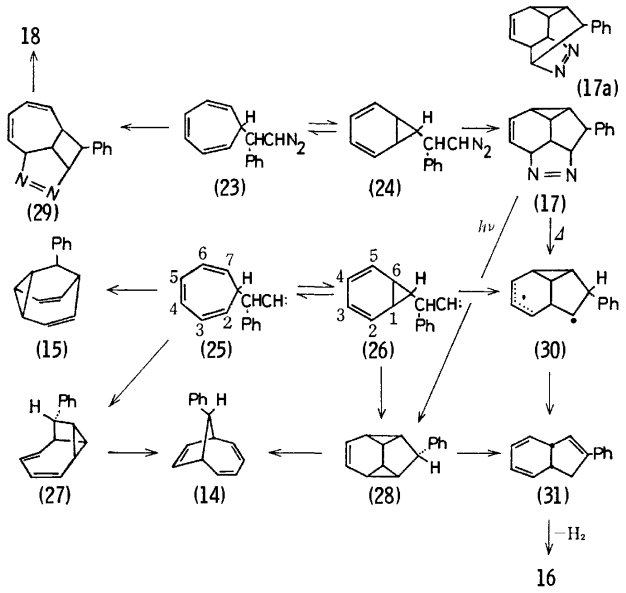

Scheme 2.

At this stage, it is of interest to compare the energy surface of C_9H_{10} hydrocarbons with that of $C_{10}H_{10}$ hydrocarbons. A part of the chemistry of the $C_{10}H_{10}$ hydrocarbons,[25] which have been extensively studied, is displayed in Scheme 3. The corresponding chemistry of the C_9H_{10} hydrocarbons, which are derived from the $C_{10}H_{10}$ hydrocarbons in Scheme 3 by the replacement of the etheno group with a methylene bridge, is depicted in Scheme 4.

A few years ago, Cannell[5] studied the photoreaction of **9** in acetone, in which case a (2+2)π cyclization of the conjugated diene moiety took place to give *exo*-(**38**) and *endo*-tricyclo[4.2.1.$0^{2,5}$]nona-3,7-diene (**39**). The repetition of the photolysis of **9** using a low-pressure

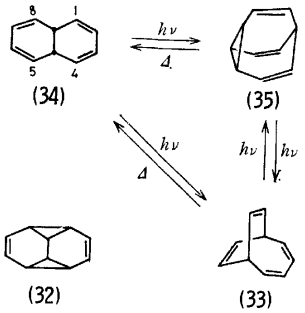

Scheme 3.

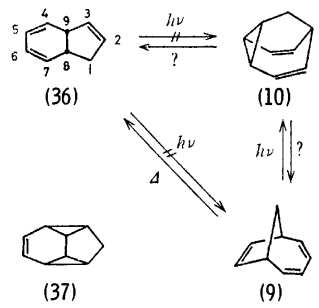

Scheme 4.

lamp without any sensitizer in dioxane resulted in the formation of four kinds of photoproducts and the recovery of a small amount of **9**. Although we confirmed two of the products to be **38** and **39** on the basis of their reported NMR spectra,[5] neither vpc nor NMR peaks due to **10** could be detected in the photoproducts.

The sensitized photoreaction of this system provided different results. When the photolysis of **14** was carried out in benzene using benzophenone as a sensitizer, **15** was formed as a single product. This transformation is in sharp contrast to the direct irradiation described above and may be characterized in terms of a di-π-methane cyclization, as is shown below. This reaction corresponds to the photoreaction of bicyclo[4.2.2]deca-2,4,7,9-tetraene (**33**) to bullvalene (**35**), as is shown in Scheme 3.[26]

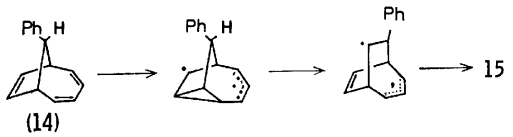

The thermal transformation of **9** to *cis*-8,9-dihydroindene (**36**) was recently found by Berson *et al.*[27] This is formally similar to the thermal conversion of **33** into 9,10-dihydronaphtalene (**34**), but the mechanism is different. The intermediate from **33** to **34** was proved to be tetracyclo[4.4.2.$0^{2,10}$.$0^{5,7}$]deca-3,8-diene (**32**) on the basis of a deuterium-labeling experiment,[28] while the conversion of **9** into **36** proceeds through an unsymmetric tricyclic intermediate (**40**). If a step-by-step mechanism is involved in the transformation of **33** to **34**, the cleavage of a three-memberd ring of **32** will afford a stable diallylradical, which will then force the subsequent fission of another three-membered ring and will be stabilized by the formation of two sets of conjugated diene **34**. On the other hand, the tetracyclic compound **28**, which is formed *via* the intramolecular Diels-Alder cyclization of **14**, can not afford such a stable radical; instead, it may give a rather unstable homoallyl or 1,3-diradical **30**. Moreover, it must be accompanied by a hydrogen shift to form a *cis*-8,9-dihydroindene derivative. Thus, **28**, even if formed, tends to return to **14** or, at a high temperatures,

23) S. Masamune, R. T. Seidner, H. Zenda, M. Wiesel, N. Nakatsuka, and G. Bigam, *J. Amer. Chem. Soc.*, **90**, 5286 (1968).
24) L. A. Paquette, R. E. Wingard, Jr., and R. H. Meisinger, *ibid.*, **93**, 1047 (1971).
25) T. L. Burkoth and E. E. van Tamelen, "Nonbenzenoid Aromatics" Ed. by J. P. Snyder, Academic Press (1969), Vol. 1, p. 115.
26) S. Masamune, H. Zenda, M. Wiesel, N. Nakatsuka, and G. Bigam, *J. Amer. Chem. Soc.*, **90**, 2727 (1968).
27) J. A. Berson, R. R. Boettcher, and J. J. Vollmer, *ibid.*, **93**, 1540 (1971).
28) a) M. Jones, Jr. and G. Fairless, *Tetrahedron Lett.*, **1968**, 4881. b) R. T. Seidner, N. Nakatsuka, and S. Masamune, *Canad. J. Chem.*, **48**, 187 (1970).

to follow the homodienyl hydrogen migration path to give dihydroindene (**31**).[27] The formation of **31** through a diradical, followed by a 1,2-hydrogen migration, or through a concerted 1,9-hydrogen shift ($_{\pi}2_s+_{\sigma}2_s+_{\sigma}2_s+_{\sigma}2_s+_{\sigma}2_s$), as is shown in **41**, was illustrated in the thermolysis of the diazo compound **17**. The refluxing of **17** in diglyme in air gave **16** in a 49% yield. The yield of **16**, however, dropped to 5% when the thermolysis was carried out in a nitrogen atmosphere, and instead 2-phenyl-8,9-dihydroindene **31** (mp 56—58°C) was formed in a 51% yield. The structure identity of **31** was based on the NMR spectrum, consisting of four groups of peaks at τ 2.72 (m, 5H), 4.00 (m, 1H), 4.36 (m, 4H), and 6.0—7.7 (m, 4H), and on its rapid interconversion into 2-phenylindene when left standing in air. Because of the existence of a thermally-labile diazo group, the heating of **17** easily releases nitrogen to give an energy-

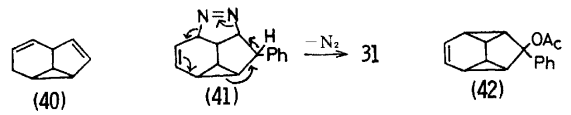

(40) (41) (42)

rich diradical intermediate **30**, which then affords **31** by 1,2-hydrogen migration (Scheme 2). The possibility that **31** was formed by the thermal rearrangement of initially-formed nonatriene **14**[27] could be precluded by control experiments. The nonatriene **14** was very stable and was recovered not only under the pyrolytic condition of **17** in refluxing diglyme, with or without an oxidizing reagent, but also upon pyrolysis in a flow system by passing it through a column containing glass helics preheated at 400°C. However, when **28** has a leaving group such as the acetyl group at the C_8-position such as **42**, the thermal conversion into 2-phenylindene becomes facile.[29]

The irradiation of **36** was performed by Vogel *et al.*[30] and by Schwartz,[31] in each case, *trans*-8,9-dihydroindene was obtained as the main product. This *trans*-formation was explained in terms of a disrotatory ring closure of the intermediate, *cis, cis, trans, cis-* or *cis, cis, cis, trans*-cyclononatetraene, formed from the dihydroindene **36** by a conrotatory ring opening. Neither **9** nor **10** was found in the photolysate. The bond formation between C_1 and C_8 and between C_4 and C_5 in **34** leads to tetracyclodecadiene **32** and takes place without a hydrogen shift (Scheme 3), whereas the hydrogen shift from the methylene group is essential to derive a tetracyclic intermediate such as **37** from **36** (Scheme 4). Therefore, in the photoreaction of **36**, a fission at the C_8–C_9 bond or $(2+2)\pi$ cycloaddition in the diene moiety is preferable to the cyclization leading to **37**. However, if *cis*-8,9-dihydroindene is highly substituted and if the ring opening to the corresponding cyclononatetraene causes steric hindrance, the bonding not only between C_3 and C_4, but also between other positions, becomes possible, depending on the nature of the sbustituents.[32] In these cases, no barbaralane or bicyclo[4.2.1]nona-2,4,7-triene derivatives were characterized. Although the photochemical and thermal reaction of **10** have not been well documented, Daub and Schleyer reported the acetone-sensitized conversion of tricyclo[3.2.2.$0^{2,4}$]nona-6,8-diene into **10**[22] and described that **10** is not stable under photolytic conditions.

In any event, these results add some information on the difference between the energy surfaces of C_9H_{10} and $C_{10}H_{10}$ hydrocarbons. Studies of the thermal and photochemical behavior of C_9H_{10} groups, especially that of barbaralane, are now in progress in this laboratory.

Experimental

All the melting points and boiling points are uncorrected. Vpc was carried out on Hitachi K-53 (analytical), Hitachi KGL-2B, and Willkins (A-700) (preparative) instruments. The IR and NMR spectra were taken on Shimadzu IR-27 and Varian 60A or 100A spectrometers respectively. The mass and UV spectra were recorded on Hitachi RUM-6D and Hitachi EPS-3 spectrometers respectively.

Preparation of (2,4,6-Cycloheptatrien-1-yl)acetaldehyde Tosylhydrazone (4). To a solution of tosylhydrazide (17.3 g, 0.93 mol) dissolved in a 3:1 mixture of ethanol and water, (**3**) (12.5 g, 0.93 mol) was added, drop-by-drop at room temperature, to produce white crystals (27.4 g, 98%). White needles from ethanol; bp 130°C (d).

Found: C, 63.61; H, 5.96; N, 9.05%. Calcd for $C_{16}H_{18}N_2O_2S$: C, 63.56; H, 6.00; N, 9.27%. IR (KBr): 3226, 1597, 1361, 1326, 1163, 747, 714 cm^{-1}. NMR ($CDCl_3$): τ 2.18 (m, 2H), 2.72 (m, 3H), 3.40 (m, 2H), 3.90 (m, 2H), 5.03 (m, 2H), 7.49 (m, 2H), 7.61 (s, 3H), 8.17 (m, 1H).

Thermal Decomposition of 4. Formation of Bicyclo[4.2.1]-nona-2,4,7-triene (9) and Tricyclo[3.3.1.$0^{2,8}$]nona-3,6-diene (10) (barbaralane). A suspension of 47% sodium hydride (5.1 g, 0.1 mol) in dry dioxane (5 ml) was added to a solution of **4** (20 g, 0.66 mol) in dioxane (130 ml). The suspension of the sodium salt was then heated at 90—95°C under a stream of nitrogen. The evolution of nitrogen ceased after one hour and left crystals of sodium *p*-toluenesulfinate (11 g). The filtrate was diluted with petroleum ether (bp 40—60°C) and washed well to remove the dioxane. The organic layer was extracted with a 40% aqueous silver nitrate solution, which was then decomposed by 28% aqueous ammonia (*ca.* 100 ml). It was extracted with petroleum ether, washed with water, dried (Na_2SO_4), and evaporated to give yellowish-orange oil (5 g), which was subsequently passed through a column containing alumina (B.G.I). Elution with petroleum ether (bp 40—60°C) afforded a colorless oil (1.0 g, 20%) which consisted of two components in a ratio of 4:1 and which was separated on a preparative vpc column (3 m × 1/4″ 10% Carbowax at 120°C). The oily product corresponding to the shorter retention time and to the main component was **9**.

Found: C, 91.34; H, 8.78%. Calcd for C_9H_{10}: C, 91.47; H, 8.53%. IR (neat): 3021, 1642, 732, 679 cm^{-1}. UV (cyclohexane nm ε) 259 (2710), 268 (2460), 278 (1360). NMR (CCl_4): τ 4.12 (m, 4H), 4.87 (m, 2H), 6.92 (bd, J=

29) T. S. Cantrell and H. Schechter, *J. Amer. Chem. Soc.*, **89**, 5868 (1967); A. S. Kende and T. L. Bogard, *Tetrahedron Lett.*, **1967**, 3383.

30) E. Vogel, W. Grimme, and E. Dinne, *ibid.*, **1965**, 391.

31) J. Schwartz, *Chem. Commun.*, **1969**, 833.

32) W. Eberbach and H. Prinzbach, *Helv. Chim. Acta*, **50**, 2490 (1967); R. Kitzing and H. Prinzbach, *ibid.*, **53**, 158 (1970), and references cited therein.

11.3 Hz, 1H), 8.07 (t×d, J=11.3, 6.2 Hz, 1H), 8.71 (d, J=11.3 Hz, 1H).

The second product was established to be **10**; mp 39—40°C.

Found: C, 91.08; H, 8.48%. Calcd for C_9H_{10}: C, 91.47; H, 8.53%. IR (CCl_4): 3030, 2915, 1678, 1616, 1381 cm^{-1}.

A solution of **10** (10 mg) in dioxane was heated under reflux and monitored by vpc. No other peaks except **10** appeared after heating for 116 min.

Catalytic Reduction of ***9***. A solution of **9** (118 mg, 1 mmol) dissolved in ether (10 m*l*) was catalytically reduced over an Adams catalyst (10 mg) at the temperature of ice water. It consumed three equivalents of hydrogen (72.3 m*l*, calcd 67.2 m*l*) after 138 min. The filtration of the catalyst and the evaporation of the ether left 117 mg of crystals; mp 90—93°C. Sublimation afforded bicyclo[4.2.1]nonane; mp 94—95°C.

Found: C, 86.96; H, 13.00%. Calcd for C_9H_{16}; C, 87.02; H, 12.98%. NMR (CCl_4): τ 7.8—9.3 (m).

*Preparation of α-(2,4,6-Cycloheptatrien-1-yl)propionaldehyde Tosylhydrazone (****6****).* Morphorinoenamine of propionaldehyde (27 g, 0.212 mol) was added, drop by drop and at room temperature, to a solution of tropyliumfluoroborate (41.5 g, 0.233 mol) in water (500 m*l*). The solution was stirred for two hours and then extracted with ether. The extracts were washed with water, dried (Na_2SO_4), and evaporated to leave 24.7 g (78.5%) of **5**: bp 86—87°C/0.8 mmHg.

Found: C, 80.94; H, 8.27%. Calcd for $C_{10}H_{12}O$: C, 81.04; H, 8.16%. IR (neat): 3012, 2817, 1724, 746, 709 cm^{-1}. NMR (CCl_4): τ 0.36 (d, J=2.0 Hz, 1H), 3.37 (m, 2H), 3.80 (m, 2H), 4.80 (m, 2H), 7.33 (d×q×d, J=7.5, 7.0, 2.0 Hz, 1H), 8.08 (m, 1H), 8.85 (d, J=7.0 Hz, 3H).

Into a solution of tosylhydrazide (11.2 g, 0.06 mol) in a mixture of ethanol and water (3:2) (260 m*l*), **5** (7.7 g, 0.052 mol) was stirred at room temperature. The filtration of the deposited white crystals yielded 15.5 g (94%) of the deposited white crystals yielded 15.5 g (94%) of the tosylhydrozone **6**. Needles from ethanol; mp 129—130°C.

Found: C, 64.56; H, 6.50; N, 8.89%. Calcd for $C_{17}H_{20}N_2O_2S$: C, 64.54; H, 6.37; N, 8.86%. IR (KBr): 3226, 1600, 1362, 1325, 1167, 751, 710 cm^{-1}. NMR ($CDCl_3$): τ 1.88 (bs, 1H), 2.14 (m, 2H), 2.68 (m, 2H), 2.87 (d, J=6.4 Hz, 1H), 3.38 (m, 2H), 3.92 (m, 2H), 4.98 (m, 2H), 7.33 (m, 1H), 7.57 (s, 3H), 8.50 (m, 1H), 8.89 (d, J=7 Hz, 3H).

Thermal Decomposition of ***6****. Formation of 9-Methylbicyclo[4.2.1]nona-2,4,7-triene (****11****) and 9-Methyltricyclo[3.3.1.0^{2,8}]nona-3,6-diene (****12****).* Sodium salt, prepared from 10 g of **6**, in dioxane (120 m*l*) was subjected to decomposition at 75—80°C. A subsequent workup similar to the decomposition of **4**, without extraction with a silver nitrate solution, produced 5 g of a crude oil, which was then passed through a column of alumina. Elution with petroleum ether (bp 40—60°C) yielded 1.35 g (27%) of a colorless oil, which was a mixture of **11** and **12** in a ratio of 9:2 (based on the area of the vpc peak). Preparative vpc (10 mm×1 m 20% DOP at 70°C) separated **11** (shorter retention time) and **12**. NMR of **11** (CCl_4): τ 4.10 (m, 8H), 4.85 and 4.97 (m, combined area 4H), 7.0—7.5 (4H), 7.6—8.5 (4H), 9.10 and 9.33 (d, J= 7.0 Hz, combined area 6H).

A solution of **11** (205 mg, 1.5 mmol) in ether (5 m*l*) was hydrogenated over 10% prereduced Pd-C (25 mg) at the temperature of ice-water. It absorbed three equivalents of hydrogen (104.8 m*l*, calcd 104.2 m*l*) after 170 min. The catalyst was removed, and the filtrate was evaporated to give 210 mg of a colorless oil, which was separated by preparative vpc (10 mm×1 m 20% DOP at 80°C). A colorless oil was eluted first.

Found: C, 87.09; H, 13.03%. Calcd for $C_{10}H_{18}$: C, 86.88; H, 13.12%. NMR (CCl_4): τ 7.8—8.9 (m, 15H), 9.12 (d, J=7.0 Hz, 3H). Then were eluted colorless, sublimable needles; mp 117—118°C.

Found: C, 86.79; H, 12.83%. Calcd for $C_{10}H_{18}$: C, 86.88; H, 13.12%. NMR (CCl_4): τ 7.7—8.6 (m, 15H), 8.95 (d, J=7.0 Hz, 3H).

*Preparation of α-Phenyl-α-(2,4,6-cycloheptatrien-1-yl)acetaldehyde Tosylhydrazone (****8****).* β-Ethoxystyrene (3.07 g, 0.021 mol) was dropped into a solution of tropyliumfluoroborate (7.3 g, 0.040 mol) in water (90 m*l*) at room temperature and stirred overnight. The separated oil was extracted with ether, and the extract was washed with water, dried (Na_2SO_4), and evaporated to give an orange oil. Distillation (bp 134—135°C/1.5 mmHg) yielded 4.1 g (95%) of the acetaldehyde **7**, which crystallized on standing. Colorless crystals from *n*-hexane; mp 55—57°C.

Found: C, 85.37; H, 6.78%. Calcd for $C_{15}H_{14}O$: C, 85.68; H, 6.71%. IR (neat): 3021, 2817, 1724, 760, 747, 701 cm^{-1}. NMR (CCl_4): τ 0.5 (d, J=2.6 Hz, 1H). 2.84 (m, 5H), 3.43 (m, 2H), 3.95 (m, 2H), 4.92 (m, 2H), 6.23 (d×d, J=11.0, 2.6 Hz, 1H), 7.47 (m, 1H).

To a solution of tosylhydrazide (10.2 g, 0.055 mole) dissolved in a mixture of ethanol and water (8:13) (210 m*l*), **7** (10 g, 0.048 mol) in ethanol (20 m*l*) was added, drop by drop and at room temperature, to form white crystals. Filtration afforded 15.5 g (87%) of **8**; mp 163—165°C. Needles from ethanol; mp 165.5—166°C.

Found: C, 69.69; H, 6.09; N, 7.58%. Calcd for $C_{22}H_{22}N_2O_2S$: C, 69.82; H, 5.86; N, 7.40%. IR (KBr): 3226, 1597, 1364, 1325, 1167, 747, 705 cm^{-1}. NMR ($CDCl_3$): τ 1.88 (bs, 1H), 2.20 (m, 2H), 2.80 (m, 8H), 3.36 (m, 2H), 3.87 (m, 2H), 5.01 (m, 2H), 6.24 (d×d, J=11.5, 7.0 Hz, 1H), 7.58 (s, 3H), 7.86 (m, 1H).

Thermal Decomposition of ***8****. Formation of* ***14****,* ***15****,* ***16****,* ***17****, and* ***18****.* A suspended sodium salt, prepared from 10 g of **8**, in dioxane (130 m*l*) was heated at 80—83°C and then treated as in the work-up described in connection with the formation of **11** and **12**. A crude red oil (4.7 g) was then separated using alumina-column chromatography. The product eluted first with petroleum ether (bp 40—60°C) was a colorless oil (1.7 g, 36%) whose vpc (20% DC-11 at 200°C) showed that it was a mixture of **14** and **15** in a ratio of 11:1. The petroleum ether solution of the mixture, upon cooling at −60°C, left erystals (mp 36—38°C), which, on sublimation, afforded **14** as colorless prisms; mp 39—41°C.

Found: C, 93.02; H, 7.38%. Calcd for $C_{15}H_{14}$: C, 92.74; H, 7.26%. IR (neat): 3030, 2933, 1605, 982, 794, 725, 699 cm^{-1}. UV (cyclohexane nm ε) 255 (2200) (sh), 261 (2480) (sh), 264 (2190). 271.5 (2370), 283 (1490) (sh), NMR (CCl_4): τ 2.93 (s, 5H), 3.65—4.35 (m, 4H), 4.83 (m, 2H), 6.90 (d, J=6.5 Hz, 2H), 7.18 (s, 1H).

The petroleum ether-benzene (2:1) mixture eluted yellow crystals (mp 150—156°C) (116 mg), which were subsequently recrystallized from ethanol to give **16** (95 mg, 2%) as colorless scales; mp 165—166°C.

Subsequent elution with ether afforded **17**; mp 91—93°C (410 mg). Colorless needles from cyclohexane-ethanol (10:1) (330 mg, 7%); mp 93—94°C.

Found: C, 80.84; H, 6.48; N, 12.66%. Calcd for $C_{15}H_{14}N_2$: C, 81.05; H, 6.35; N, 12.60%. IR (KBr): 3040, 2907, 1642, 1600, 1534, 1490, 1449, 930, 750, 725, 696 cm^{-1}. UV (MeOH nm ε) 260 (1080, sh), 269 (660, sh), 340 (240). NMR ($CDCl_3$) H_1 (split doublet, τ 4.97), H_2 (quartet, 4.01), H_3 (split quartet, 3.84), H_4 (octet, 8.42), H_5 (triplet of doublet, 7.90), H_6 (split quartet, 8.13), H_7 (split doublet, 7.48), H_8 (triplet, 4.29) and H_{11} (octet, 7.37); $J_{1,2}$=2.8, $J_{1,3}$=2.0,

$J_{1,11}$=8.0, $J_{2,3}$=10.5, $J_{3,4}$=4.5, $J_{4,5}$=7.5, $J_{4,6}$=8.0, $J_{5,6}$=7.0, $J_{5,11}$=7.0, $J_{6,7}$=2.0 and $J_{7,8}$=$J_{8,11}$=8.7 Hz.

Finally, an ether–ethanol mixture (9:1) eluted **18**; mp 125—130°C (1.3 g). Colorless needles from benzene; mp 133—134°C (1.18 g 25%).

Found: C, 81.25; H, 6.53; N, 12.52%. Calcd for $C_{15}H_{14}N_2$, C, 81.05; H, 6,35; N, 12.60%. IR (KBr): 3175—2888; 987, 746 cm^{-1}. UV (MeOH nm ε) 260 (7080), 340 (46710).

Reactions of 1-Phenyl-6-(3-pyrazolyl)-1,3,5-hexatriene ***18****. Acetate.* Acetylation was accomplished on the treatment of **18** with acetylchloride in pyridine. Pale yellow small scales from ethanol; mp 137—138°C (80%).

Found: C, 77.33; H, 6.31; N, 10.33%. Calcd for $C_{17}H_{16}N_2O$: C, 77.25; H, 6.10; N, 10.60%. IR (KBr): 3040, 1736, 986, 787, 751, 691 cm^{-1}. UV (MeOH nm ε) 235 (7150), 348 (63250), 364 (48870) (sh).

Catalytic Reduction. A solution of **18** (504 mg, 2.3 mmol) in ethanol (50 m*l*) was reduced over prereduced 10% Pd-C (50 mg). After the uptake of three equivalents of hydrogen (160 m*l*, calcd 152 m*l*), the filtration of the catalyst, followed by the evaporation of the filtrate, yielded a pale yellow oil (516 mg); bp 175—178°C/3 mmHg.

Found: C, 78.36; H, 8.81, N, 11.88%. Calcd for $C_{15}H_{20}N_2$: C, 78.90; H, 8.83, N, 12.27%. IR (neat): 3195, 3096, 2907, 2841, 1458, 936, 749, 700 cm^{-1}.

Oxidation with Potassium Permanganate. A solution of **18** (333 mg, 1.5 mmol) dissolved in acetone (50 m*l*) and water (200 m*l*) was refluxed for eight hours with potassium permanganate (10.7 g, 0.068 mol). The excess potassium permangnate was then decomposed by the addition of methanol and the manganese dioxide deposited was washed with hot water. The combined filtrate was concentrated to *ca.* 50 m*l*, neutralized with 6N HCl, and extracted with ether. The extract was washed with water, dried (Na_2SO_4), and evaporated to yield benzoic acid (84 mg, 63%). The acidic filtrate, from which the benzoic acid had been removed, was continuously extracted with ether, which was then evaporated to afford pyrazole-3-carboxylic acid (mp 208°C) (d) (96 mg, 78%). Colorless needles from water; mp 213°C; identified by a comparison of the IR spectra and by a mixed-melting-point determination with an authentic sample.[19]

IR (KBr): 3534, 3322, 3145, 1712, 1445, 770 cm^{-1}. NMR (D_2O): τ 2.13 (d, J=2.5 Hz, 1H), 3.03 (d, J=2.5 Hz, 1H).

Isomerization. A solution of **18** (222 mg, 1 mmol) in benzene (6 m*l*) was refluxed for five hours in the presence of iodine (22 mg). On cooling, yellow crystals (mp 186—191°C) (205 mg, 92%) were filtered. Pale yellow scales from benzene, mp 201—203°C.

Found: C, 80.60, H, 6.54; N, 12.27%. Calcd for $C_{15}H_{14}N_2$: C, 91.05; H, 6.35; N, 12.60%. IR (KBr): 3236, 3049, 2976, 1495, 1005, 933, 770, 751, 691 cm^{-1}. UV (MeOH nm ε) 240 (9550), 344 (74300), 361 (56500). NMR (DMSO-d_6): τ 2.38—3.98 (m).

Reactions of ***17****. Thermolysis. a)* An anhydrous diglyme (1 m*l*) solution of **17** (50 mg) was refluxed for six hours *in air*. The subsequent addition of ether, which has been washed with water and dried (Na_2SO_4), followed by the removal of the solvent, gave 46 mg of yellow crystals. The crude crystals were purified by alumina-column chromatography. Petroleum ether (bp 40—60°C)-benzene (2:1) eluted colorless **16**, mp 165—166°C (21 mg, 49%). *b)* The above reaction was carried out *in a nitrogen atmosphere* using 226 mg of **17** in diglyme (2 m*l*); it yielded a pale yellow oil (117 mg) which was then passed through a column of alumina. Colorless crystals (mp 49—55°C) (100 mg, 51%) were eluted with petroleum ether. Colorless needles from ethanol, mp 56—58°C; those needles were converted into **16** on standing in air and were assigned to **31**. IR (KBr): 3021, 2841, 1493, 1443, 754, 718, 686 cm^{-1}.

Petroleum ether–benzene (9:1) eluted colorless crystals (30 mg) (mp 161—164°C), which were recrystallized from ethanol to yield 10 mg (5%) of **16**. Finally we eluted 38 mg of colorless crystals; mp 173—182°C. Colorless needles from benzene; mp 185—186°C (29 mg, 15%); their structure was not identified.

Found: C, 92.32; H, 7.42%. Calcd for $C_{15}H_{14}$: C, 92.74; H, 7.26%. IR (KBr): 3021, 2882, 1597, 1493, 1443, 866, 753, 726, 687 cm^{-1}.

Photolysis. A solution of **17** (130 mg) dissolved in dioxane was irradiated for one hour through a Pyrex filter using a Toshiba H 400-p high-pressure lamp. The photolysate was diluted with ether, and then washed with water, dried (Na_2SO_4), and evaporated to yield a pale yellow oil (96 mg). Alumina-column chromatographic separation afforded 44 mg (43%) of **14** on elution with petroleum ether and 10 mg of **17** on elution with benzene ether (9:1).

Photolysis of ***9****.* A solution of **9** (3.5 g, 29.7 mmol) dissolved in anhydrous dioxane and placed in a quartz cell was irradiated for 72 hr using a 6 W low-presssure lamp (Ushio-UM6). Dilution with water was followed by the addition of petroleum ether (bp 40—60°C). The organic layer was washed well with water to remove the dioxane and then dried over Na_2SO_4. The evaporation of the solvent left a pale yellow oil (2.9 g), whose vpc (3 mm×1 m 5% DOP at 120°C) showed five peaks with a ratio of 4: 7.5: 5:1: 11.5 in the order of the retention time; it was submitted to preparative vpc (10 mm×3 m PEG 4000 at 100°C). The oil eluted first (area 4) involved five groups of peaks at τ 3.81 (s, 2H), 3.95 (bs, 2H), 7.66 (bs, 4H), 8.47 (bd, J=8.5 Hz, 1H), and 8.75 (bs, 1H), and was proved to **38** on the basis of the reported data.[5] Secondly, a colorless oil was obtained. Its NMR spectrum contained six groups of peaks, at τ 4.15 (s, 2H), 4.25 (t, J=2.0 Hz, 2H), 7.05 (bd, J=3.8 Hz, 2H), 7.43 (m, 2H), 8.13 (bd, J=8.5 Hz, 1H) and 8.50 (bd, J=8.5 Hz, 1H); it was identified as **39**. Besides **38**, **39**, and **9** (area 1), two kinds of oily products (area 5 and 11.5) were obtained, but their structures were not characterized.

Sensitized Photolysis of ***14****. Formation of 9-Phenylbarbaralane* ***15****.* A solution of **14** (58 mg, 0.3 mmol) and benzophenone (309 mg, 1.7 mmol) dissolved in benzene (5 m*l*) was irradiated through a Pyrex filter using Rayonet MGR-black light. The progress of the reaction was monitored on vpc (3 mm×1 m 5% SE-30 at 170°C), and the peak due to **14** disappeared after 5 hr of irradiation. The benzene was removed and the residue was subjected to preparative tlc separation and developed by a mixture of *n*-hexane–benzene (1:2) to afford **15** (27 mg) from R_f=0.91. IR (neat): 3030, 2940, 2875, 1618, 1602, 1492, 1450, 794, 735, and 694 cm^{-1}.

Heterocycles Structurally Influenced by a Side Chain. II.[1] 7-Phenacylxanthopterins and 6-Phenacylisoxanthopterins[2]

Yasuo IWANAMI and Taketsugu SEKI*
Sasaki Institute, Kanda-Surugadai, Tokyo
(Received November 11, 1971)

Phenacyl derivatives of two naturally-occurring pteridines and their 4-amino analogues (III and V) have been synthesized for their structural study. Since these compounds are obtained by the condensation of ethyl benzoylpyruvates (II) with tri- or tetraaminopyrimidine (I), a carbon-nitrogen double bond, which is adjacent to the phenyl group of the side chain, may be expected in the ring (-N=C-CH_2-CO-Ph). However, their NMR spectra show that the double bonds of all the products are displaced onto the side chain (-NH-C=CH-CO-Ph), the carbonyl of which is hydrogen-bonded with the secondary amino group thereby formed. This form of V makes striking contrast to alkyl isoxanthopterin-6-acetates (X), in which the corresponding double bond remains undisplaced. The intermediate products of V (IV) and V were hydrolyzed with acid or alkali into 6-methylisoxanthopterin (VI) and benzoic acids (VII).

When a side chain with a β-carbonyl group is introduced into nitrogen heterocycles at a position adjacent to the nitrogen atom, the carbon-nitrogen double bond of the ring is often displaced onto the side chain.[1] This displacement is likely to be facilitated by an intramolecular hydrogen bonding between the carbonyl and the secondary amino group of the ring thereby formed. One of our early reports[3] was the first presenting evidence for the fixation of the enamine form, which is illustrated below:

Imine form Enamine form

It is said that the imine form rather than the enamine form is predominant in imine-enamine tautomerism when hydrogen is present on the nitrogen atom.[4,5] However, the enamines reported[6] on by our laboratory are stable under ordinary conditions in spite of the presence of hydrogen.

During the course of further studies, many examples of similarly-fixed enamines in condensed[1,3,6,7] and noncondensed[3,6,7] heterocycles of five-,[7] six-,[1,3,6,7] and seven-membered[7] rings, and also in simpler alkyl β-aminoacrylates,[8] have been encountered. Interestingly, however, a structural resemblance is not always followed by such a fixation of the enamine form. Indeed, reverse is the case in alkyl isoxanthopterin-6-acetates and their 4-amino analogues (X), which exist in the imine form, as we recently reported.[9] It appears that the imine forms of these compounds are also fixed unless otherwise dissolved in a protic solvent.[9]

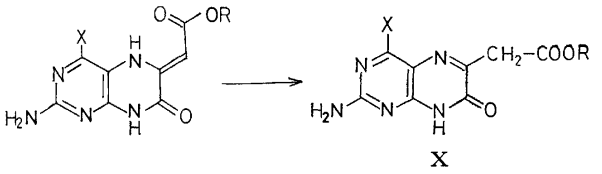

X

X=O or NH
R=CH_3 or C_2H_5

Consequently, we were particularly interested in whether or not the phenacyl derivatives of xanthopterin and isoxanthopterin exist in the enamine forms. We will now describe the synthesis and characterization of the phenacyl derivatives of these two naturally-occurring pteridines (originally found in butterfly wings), all of which are new compounds.

The condensation of 2,5,6-triamino-4-hydroxypyrimidine (Ia) with ethyl p-substituted benzoylpyruvate (or the corresponding acid in some cases) (II) under acidic conditions gave 7-(p-substituted phenacyl)xanthopterin (III), but in an ammoniacal solution it afforded an intermediate product (IV), which was then cyclized to 6-(p-substituted phenacyl)isoxanthopterin (V) in the presence of sulfuric acid. The 4-amino analogues of these three types of products (III, IV, V; X=NH_2) could be obtained by the reaction of 2,4,5,6-tetraaminopyrimidine (Ib) instead of Ia. The position of the phenacyl groups in V was confirmed by the fact that V was hydrolyzed into 6-methylisoxanthopterin (VI) and the corresponding benzoic acid (VII). A similar hydrolysis proceeded with the intermediate product (IV).

All these phenacylpteridines (III and V) were sparingly soluble or practically insoluble in the usual solvents, but could be dissolved into concentrated sulfuric acid. Thus, the NMR spectra of these com-

* Present address: Research Laboratories, Nikken Chemicals Co., Ltd., Ohmiya, Saitama.

1) Part I: Y. Iwanami, T. Seki, and T. Inagaki, This Bulletin, **44**, 1316 (1971).

2) Presented in part at the IVth International Symposium on Pteridines, Toba, July, 1969, and also partially described in the Symposium Proceedings, "Chemistry and Biology of Pteridines," distributed by Maruzen Co., Tokyo (1970), p. 129.

3) Y. Iwanami, *Nippon Kagaku Zasshi*, **82**, 778, 780 (1961).

4) J. March, "Advanced Organic Chemistry: Reactions, Mechanisms, and Structure," McGraw-Hill Book Co., New York (1968), p. 62.

5) J. D. Roberts and M. C. Caserio, "Basic Principles of Organic Chemistry," W. A. Benjamin, New York (1964), p. 486.

6) Y. Iwanami, This Bulletin, **44**, 1311 (1971); Y. Iwanami, Y. Kenjo, K. Nishibe, M. Kajiura, and S. Isoyama, *ibid.*, **37**, 1740 (1964); Y. Iwanami, S. Isoyama, and Y. Kenjo, *ibid.*, **37**, 1745 (1964)

7) Y. Iwanami, *Nippon Kagaku Zasshi*, **83**, 100, 161, 316, 593, 597 (1962); H. Sasaki, H. Sakata, and Y. Iwanami, *ibid.*, **85**, 704 (1964).

8) Y. Iwanami, *ibid.*, **82**, 632, 634 (1961); **83**, 600 (1962).

9) Y. Iwanami, This Bulletin, **44**, 1314 (1971).

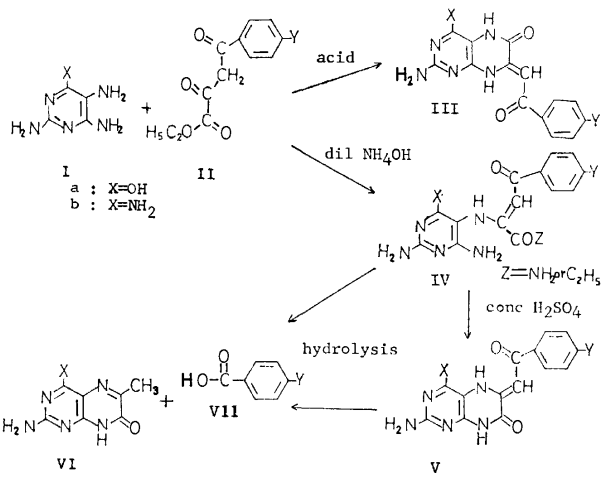

pounds were determined in sulfuric and deuteriosulfuric acid. 7-(*p*-Methylphenacyl)xanthopterin (IIIb), for example, exhibits no signal between 7.19 and 0 ppm (δ scale) except for a singlet at 2.60 ppm due to the methyl group which is attached to the benzene ring of IIIb. Therefore, IIIb does not involve methylene ($-CH_2-$) in its structure. Instead, it contains a methine (=CH-) group, which is revealed by a singlet at 7.19 ppm. The bands in the lowest field, *ca.* 8.3 ppm, must be due to the protons *ortho* to the electron-withdrawing carbonyl group. This, in turn, indicates that the carbonyl group does not exist as an enol in IIIb. Since the enol double bond is thus absent, the above methine can be assigned to another double bond, which is derived by the migration of the carbon-nitrogen double bond of the ring onto the side chain.

The NMR data obtained on the samples of the other analogues, III and V, are similar with those of this one, IIIb. It is, therefore, fitting to call them by the more practical expression "7-(*p*-methylphenecylidene)-7,8-dihydroxanthopterin" (IIIb) and so on. This type of partial structure of III and V is exactly the same as that of 3-phenacyl-2(1*H*)-quinoxalinones (VIII, X=NH) and 3-phenacyl-2*H*-1,4-benzoxazin-2-ones (VIII, X=O), which have been shown to exist in the "phenacylidene" structure (*i.e.*, the enamine form) both in solution and in crystalline states, as reported in a preceding paper.[1]

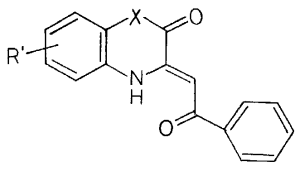

VIII

X=O or NH
R'=H, CH_3, Cl, or Benzo

In the case of VIII, an amino proton gave rise to a band in the lowest field (13.88—12.02 ppm), giving evidence of its participation in the intramolecular hydrogen bonding. In the present study, however, we could not observe the corresponding signal. The signal of the amino proton is probably overlapped with that of the solvent (11.38 ppm). Moreover, sulfuric acid is not a proper solvent for the NMR spectra of the intermediate (IV). Although IV exhibited an olefinic proton signal, this might be due to the methine of V, which could be derived from dehydration with sulfuric acid. Finally, we found that dimethyl sulfoxide-d_6 dissolved IV as well as III and V to a certain extent at a high temperature (175°C). In this solvent, the products, IIIb, IVb, and Vb, for example, gave methine proton signals at 6.54, 5.88, and 5.90 ppm respectively, in addition to the aromatic *ortho* protons around 8 ppm. This also supports the enamine structures of these three types of products.[10,11]

Returning to the NMR spectra in the sulfuric-acid solvent system, the profile of the spectrum of IIIb in sulfuric acid-d_2 was not the same as that in sulfuric acid. The methine proton signal disappeared in sulfuric acid-d_2. This accounts for the deuterium exchange. The exchange mechanism would be a concerted reaction,[9] similar to that proposed for VIII in trifluoroacetic acid-d[1] and to that for the compounds with the general formula of IX,[6] as is illustrated below:

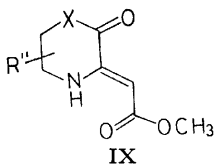

IX

X=O or NH
R''=Benzo or H

In trifluoroacetic acid, VIII exists in an equilibrium mixture of four forms, including not only the imine-enamine tautomers but also the keto-enol tautomers of a phenacyl moiety.[1] However, III, IV, and V, all possessing the same phenacyl group, gave no spectral indications of the keto-enol tautomers. There was thus a most impressive contrast between the products of this study and VIII, in spite of their structural resemblance. Therefore, the deuterium exchange mechanism of III, IV, and V is more closely related to that of IX,[6] which does not have a phenacyl substituent, and they must be essentially the same:

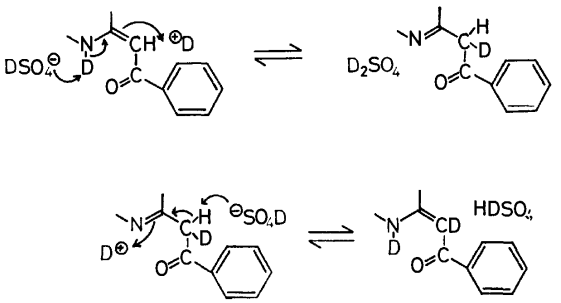

One of the possible exchange mechanisms

There is another striking contrast between V and alkyl isoxanthopterin-6-acetates (X).[9] Both of these compounds are 6-substituted derivatives of isoxan-

10) Since the spectra of VIII in this solvent are essentially the same (the enamine type) between 35 and 175°C, and since the spectra of X are also the same (the imine type), in this temperature range, we assume that the present products exist in the enamine form not only at 170° but also at lower temperatures.

11) The IR spectra of III, IV, and V are not so informative because of their complicated bands.

Table 1. Electronic absorption maxima of the products

Compound		Substituents X	Y	Z	λ_{max} nm ($\times 10^{-3}$) in 0.1N NaOH			
7-(*p*-Substitued phenacylidene)-7,8-dihydroxanthopterins	IIIa	OH	H		228 (34.5)		345 (11.0)	422 (11.5)
	IIIb	OH	CH_3		227 (31.9)	258 (18.8)	340 (9.4)	418 (14.7)
	IIIc	OH	Cl		225 (37.2)		335 (8.4)	433 (23.4)
	IIId	OH	Br		228 (33.9)		335 (8.8)	433 (20.7)
	IIIf	OH	CN		233 (34.6)			450 (21.1)
	IIIg	OH	COOH		231 (26.3)		340 (12.7)	446 (15.4)
	IIIa′	NH_2	H		242 (17.5)		325 (8.5)	470 (20.1)
	IIIb′	NH_2	CH_3		223 (37.0)	258 (26.0)	343 (15.1)	410 (3.2)
	IIIe′	NH_2	OH		223 (40.7)		339 (35.3)	
	IIIf′	NH_2	CN		227 (36.9)		343 (10.2)	441 (18.9)
2,6-Diamino-4-hydroxy-(or amino) pyrimid-5-ylamino (*p*-substituted phenacylidene) acetates	IVa	OH	H	NH_2	240 (23.1)		356 (9.8)	
	IVb	OH	CH_3	NH_2	251 (25.6)		360 (10.0)	
	IVe	OH	OH	NH_2	225 (32.0)		340 (23.6)	
	IVg′	OH	$CONH_2$	OH	232 (23.5)		350 (11.3)	440^{sh} (8.5)
	IVe′	NH_2	OH	OC_2H_5	223 (40.3)		339 (37.2)	
6-(*p*-Substituted phenacylidene)-5,6-dihydroisoxanthopterins	Va	OH	H			260 (——)	377 (——)	
	Vb	OH	CH_3			258 (20.8)	408 (17.5)	
	Vc	OH	Cl			252 (——)	374 (——)	
	Vd	OH	Br			271 (22.1)	377 (12.0)	
	Ve	OH	OH		243 (19.8)	283 (13.9)	322 (20.0)	440 (43.9)
	Vg	OH	COOH		233 (28.2)		343 (14.2)	438 (14.9)

Marks (——): Values undeterminable because of very limited solubility.
sh: Shoulder. All these compounds are sparingly soluble in dilute acids, and show melting points above 300°C.

thopterin, but they are different from each other in their existing forms; *i.e.*, V exists in the enamine form, and X in the imine form.

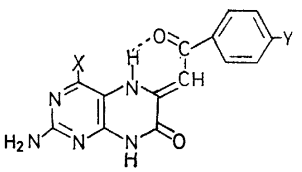

V

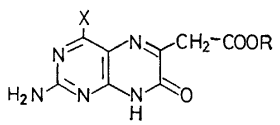

X

The replacement of an alkoxyl group in X by a phenyl group into V makes an extension of the conjugated system in the enamine form to include the benzene ring, so that the form is stabilized.[12]

None of the products, III, IV, or V, melt below 300°C. The maxima of the electronic absorption spectra of these products in 0.1N sodium hydroxide are listed in Table 1.

The NMR spectra show that the present products exist in the enamine form. The signals of the corresponding imine form do not appear in our results. The only indication of its existence was given when the spectra were measured in sulfuric acid-d_2. In other words, the fact that the methine proton signal disappeared upon deuterium exchange was interpreted to indicate the presence of the imine form[14] in a trace amount. The previous observations on VIII and IX indicated that the methine proton siganl of VIII in dimethyl sulfoxide-d_6 did not disappear when deuterium oxide was added (*i.e.*, exclusively in the enamine form), and that of IX in methanol-d_4 also remained unaffected; besides, the enamine structures of VIII and IX were fixed even in the crystalline state, as was proved by the IR spectroscopy. In a protic solvent like trifluoroacetic acid, however, VIII and IX have been shown to exist as an equilibrium mixture of imine and enamine tautomers,[15] because both methylene (imine) and methine (enamine) proton signals were observed, and were removed in trifluoroacetic acid-*d*. On the bases of these observations, we deduce that the present products, III, IV, and V, are fixed in the enamine structure unless dissolved in a protic solvent like sulfuric acid.

12) This is probably not the only factor in inducing the enamine form. The influence of phenyl substitution in the present comparison, however, would be similar to that of benzoylacetone (89.2% enolized) in contrast to ethyl acetoacetate (8.0% enolized).[13]

13) J. March, "Advanced Organic Chemistry: Reactions, Mechanisms, and Structure," McGraw-Hill Book Co., New York (1968), p. 60.

14) The other interpretation would be a similar migration and return of the double bond *via* its immonium ion, as was illustrated in a previous paper,[9] (this mechanism is at present indistinguishable from the concerted reaction already mentioned) or the direct ionization of the methine hydrogen (carbanion formation).

15) Many examples of NMR spectra which separately indicate both forms of keto-enol tautomers, and of imine-enamine tautomers[1,6,16] as well, are known. This suggests that, when either one of the forms is shown solely in the spectrum, the other form is improbable or exists in a very small amount, beneath the lebel of detection, rather than that the rapid interconversion (indistinguishable by a NMR spectrometer) of two (or more) forms gives rise to a spectrum of an appearently single form. In the latter case, it is most probable that all the signals of protons taking part in the interconversion fall into a single peak, together with that of solvent acid, at a moderate temperature, because hydroxyl or amino proton exchanging with the solvent proton rapidly constitutes one signal joined together.

16) L. Merlini, W. von Philipsborn, and M. Viscontini, *Helv. Chim. Acta*, **46**, 2592 (1963).

Even in this acid, the compounds mostly exist in the enamine form, as has already been mentioned.

Besides the physicochemical observations, we made a study of the biological effects of the products, III, IV, and V. Of these compounds, some of the IV compounds were shown to stimulate the cell growth of several microorganisms. The most active substance was 2,6-diamino-4-hydroxypyrimid-5-ylamino(*p*-hydroxyphenacylidene)acetamide (IVe). This compound remarkedly enriched the cell mass of *Escherichia coli*, *Clostridium butyricum*, *Candida utilis*, and *Rhodotorula glutinis* to two- or three-fold that of the control cultures.[17]

Experimental

The NMR spectra were determined on a Hitachi H-60 spectrometer, while the electronic absorption were taken on a Hitachi 124 spectrophotometer. All the melting points are uncorrected.

Ethyl (p-Substituted Benzoyl)pyruvates (IId, g, g').[18-20] Ethyl *p*-bromobenzoylpyruvate (IId) (yield 68%); colorless needles; mp 60.5—61.5°C.

Found: C, 48.50; H, 3.86%. Calcd for $C_{12}H_{11}O_4Br$: C, 48.19; H, 3.63%.

Ethyl *p*-carboxybenzoylpyruvate (IIg) (53%); colorless needles; mp 126—128°C.

Found: C, 58.97; H, 4.36%. Calcd for $C_{13}H_{12}O_6$: C, 59.09; H, 4.58%.

p-Ethoxycarbonylbenzoylpyruvic acid (IIg'). Ethyl *p*-ethoxycarbonylbenzoylpyruvate, prepared from *p*-ethoxycarbonylacetophenone and diethyl oxalate in a 45% yield, was hydrolyzed with a mixture of 10% sulfuric acid and acetic acid (2: 1) to give IIg' as colorless crystals (40%); mp 150—151°C.

Found: C, 55.68; H, 4.85%. Calcd for $C_{13}H_{12}O_6 \cdot H_2O$: C, 55.32; H, 5.00%.

7-Phenacylidene-7,8-dihydroxanthopterin (IIIa).[21] Into a warmed (*ca.* 50°C) suspension of 2,5,6-triamino-4-hydroxypyrimidine (IIa) sulfate (2.4 g) in water (50 m*l*), a solution of ethyl benzoylpyruvate (Ia) sodium salt (3.6 g) in 1N acetic acid (100 m*l*) was dropped with stirring, and then the temperature of the reaction mixture was gradually raised to 100°C. The mixture, which started to turn a deep orange with the formation of reddish precipitates, was refluxed for 1.5 hr, and then left to stand overnight at room temperature with continuous stirring. The crystals thus deposited were collected on a funnel, and washed well with water and ethanol. The crude product (2.4 g) was recrystallized from dimethyl sulfoxide to give IIIa as orange crystals; mp>300°C.

Found: C, 52.83; H, 4.65; N, 22.63%. Calcd for $C_{14}H_{11}O_3N_5 \cdot H_2O$: C, 53.33; H, 4.16; N, 22.22%.

7-(p-Methylphenacylidene)-7,8-dihydroxanthopterin (IIIb).[21] In to a warmed (*ca.* 50°C), a solution of IIb (1.9 g) in ethanol (50 m*l*) was dropped with stirring. The reaction mixture was gradually heated, and then refluxed for 1.5 hr to give an orange precipitate. After the mixture had been left to stand overnight at room temperature with stirring, the deposited crystals were collected on a funnel, and washed with water and ethanol. The crude product (1.4 g) was repeatedly recrystallized from dimethyl sulfoxide to give IIIb as orange-yellow crystals; mp>300°C.

Found: C, 54.47; H, 4.20; N, 21.36%. Calcd for $C_{15}H_{13}O_3N_5 \cdot H_2O$: C, 54.71; H, 4.59; N, 21.27%.

7-(p-Chlorophenacylidene)-7,8-dihydroxanthopterin (IIIc).[21] In a manner similar to that used in the preparation of IIIb, the crude product of IIIc (1.4 g) was obtained from Ia sulfate (1.2 g) and IIc (2.1 g). The product was recrystallized from dimethyl sulfoxide to afford IIIc as yellow prisms; mp>300°C.

Found: C, 50.46; H, 3.12; N, 20.95%. Calcd for $C_{14}H_{10}O_3N_5Cl$: C, 50.71; H, 3.02; N, 21.11%.

7-(p-Bromophenacylidene)-7,8-dihydroxanthopterin (IIId). The crude product of IIId (2.8 g) from Ia sulfate (1.2 g) and IId sodium salt (2.4 g) was recrystallized from dimethyl sulfoxide to give IIId as yellow prisms; mp>300°C.

Found: C, 44.42; H, 2.83; N, 18.33%. Calcd for $C_{14}H_{10}O_3N_5Br$: C, 44.71; H, 2.66; N, 18.61%.

7-(p-Cyanophenacylidene)-7,8-dihydroxanthopterin (IIIf). The crude product of IIIf (0.75 g) from Ia sulfate (0.96 g) and IIf sodium salt (1.2 g) was recrystallized from dimethyl sulfoxide to afford IIIf as brownish red crystals; mp>300°C.

Found: C, 51.10; H, 3.77; N, 23.76%. Calcd for $C_{15}H_{10}O_3N_6 \cdot 3/2H_2O$: C, 51.60; H, 3.72; N, 24.06%.

7-(p-Carboxyphenacylidene)-7,8-dihydroxanthopterin (IIIg). The crude product of IIIg (2.0 g) from Ia sulfate (1.8 g) and IIg (2.0 g) was recrystallized from dimethyl sulfoxide to give IIIg as brownish red crystals; mp>300°C.

Found: C, 48.49; H, 4.05; N, 18.63%. Calcd for $C_{15}H_{11}O_5N_5 \cdot 3/2H_2O$: C, 48.91; H, 3.83; N, 19.02%.

7-Phenacylidene-2,4-diamino-6(5H)-pteridinone (IIIa').[21] Into a suspension of 2,4,5,6-tetraaminopyrimidine (Ib) sulfate (1.4 g), a hot solution of IIa sodium salt (2.4 g) was dropped with stirring. The reaction mixture was then heated to 100°C for 2 hr, and thereafter maintained at pH 1—2. After the mixture had stood overnight, the precipitated crystals were collected by filtration. The crude product, IIIa' (0.8 g), was purified by reprecipitation. The crystalls were dissolved in a minimum amount of concentrated sulfuric acid, and then water was added into the solution chilled in an ice bath to give IIIa' as brownish red crystals; mp> 300°C.

Found: C, 50.65; H, 4.03; N, 24.74%. Calcd for $C_{14}H_{12}O_2N_6 \cdot 1/3H_2SO_4 \cdot 1/3H_2O$: C, 50.19; H, 4.01; N, 25.09%.

7-(p-Methylphenacylidene)-2,4-diamino-6(5H)-pteridinone (IIIb').[21] The crude product of IIIb' (1.4 g) from Ib sulfate (1.4 g) and IIb sodium salt (1.7 g) was recrystallized from dimethyl sulfoxide to give IIIb' as yellow crystals; mp>300°C.

Found: C, 56.41; H, 4.87; N, 26.68%. Calcd for $C_{15}H_{14}O_2N_6 \cdot 1/2H_2O$: C, 56.44; H, 4.70; N, 26.32%.

7-(p-Hydroxyphenacylidene)-2,4-diamino-6(5H)-pteridinone (IIIe'). The crude product of IIIe' (1.0 g) from Ib sulfate (1.4 g) and IIe sodium salt (3.2 g) was recrystallized from dimethyl sulfoxide to give IIIe' as orange crystals; mp>300°C.

Found: C, 50.63; H, 4.41; N, 25.42%. Calcd for $C_{14}H_{12}O_3N_6 \cdot H_2O$: C, 50.91; H, 4.27; N, 25.45%.

7-(p-Cyanophenacylidene)-2,4-diamino-6(5H)-pteridinone (IIIf'). The crude product of IIIf' (1.3 g) from Ib sulfate (1.4 g) and IIf sodium salt (1.8 g) was recrystallized from dimethy sulfoxide to give IIIf' as brownish red crystals; mp>300°C.

Found: C, 53.97; H, 4.09; N, 28.86%. Calcd for $C_{15}H_{11}O_2N_7 \cdot 3/4H_2O$: C, 53.81; H, 3.76; N, 29.29%.

2,6-Diamino-4-hydroxypyrimid-5-ylamino (phenacylidene) acet-

17) Details will be published elsewhere.
18) C. Beyer and L. Claisen, *Ber.*, **20**, 2181 (1887).
19) J. B. Wright, U.S. 3223703 (1965).
20) V. A. Zagorevskii and D. A. Zykov, *Zh. Obshch. Khim.*, **33**, 2426 (1963).
21) The mass spectral features of this compound will be reported elsewhere.

amide (IVa). Into a suspension of Ia sulfate (2.0 g) in water (50 ml), 1N ammonium hydroxide (50 ml) was added to alkalize it at about pH 8. A solution of IIa (1.7 g) in ethanol (20 ml) was then dropped with stirring into the suspension, the color of which had turned violet, during a course of about 30 min at room temperature; the pH was maintained by adding 1N ammonium hydroxide. The color of the reaction mixture then became gradually reddish-brown. After the IIa had all been dropped, the mixture was stirred more. In a little while, fine brown crystals began to deposit on the bottom of the reaction vessel. Stirring was continued overnight. The precipitated crystals were collected on a glass filter, and washed successively with 1N sulfuric acid, water, and ethanol. The crude product of IVa sulfate (1.0 g) was recrystallized from dimethy sulfoxide to give yellowish-brown crystals; mp>300°C.

Found: C, 49.66; H, 3.86; N, 24.62%. Calcd for $C_{14}H_{14}O_3N_6 \cdot 1/4H_2SO_4$: C, 49.63; H, 4.31; N, 24.81%.

2,6-Diamino-4-hydroxypyrimid-5-ylamino(p-methylphenacylidene)-acetamide (IVb). In a manner similar to that used in the preparation of IVa, the crude product of IVb (0.9 g) was obtained from Ia sulfate (2.0 g) and IIb (1.8 g). The IVb sulfate was recrystallized from dimethyl sulfoxide to afford IVb as dark yellow crystals; mp>300°C.

Found: C, 52.02; H, 4.47; N, 24.06%. Calcd for $C_{15}H_{16}O_3N_6 \cdot 1/5H_2SO_4$: C, 51.78; H, 4.75; N, 24.16%.

2,6-Diamino-4-hydroxypyrimid-5-ylamino(p-hydroxyphenacylidene)-acetamide (IVe). The crude product (1.6 g) from Ia sulfate (2.4 g) and IIe (2.4 g) was recrystallized from dimethyl sulfoxide to afford IVe as reddish-brown crystals; mp>300°C.

Found: C, 47.22; H, 4.13; N, 23.67%. Calcd for $C_{14}H_{14}O_4N_6 \cdot 3/2H_2O$: C, 47.05; H, 4.79; N, 23.52%.

2,6-Diamino-4-hydroxypyrimid-5-ylamino(p-carbamoylphenacylidene)acetic Acid (IVg'). The crude product (1.4 g) from Ia sulfate (1.8 g) and IIg (2.0 g) was dissolved in 1N sodium hydroxide, and the resulting solution was poured into warm 3N hydrochloric acid. The reprecipitation was repeated three times to give IVg' as dark red crystals; mp>300°C.

Found: C, 46.87; H, 3.93; N, 21.45%. Calcd for $C_{15}H_{12}O_5N_6 \cdot 3/2H_2O$: C, 47.00; H, 3.94; N, 21.93%.

Ethyl 2,4,6-Triaminopyrimid-5-ylamino(phenacylidene) acetate (IVe'). The crude product (0.3 g) obtained by the condensation of Ib sulfate (2.4 g) with IIa (2.2 g) in an ammoniacal solution of pH 7.7 was washed successively with a 1:1 mixture of dimethyl sulfoxide and 50% sulfuric acid, water, and ethanol on a glass filter, and was then recrystallized from dimethyl sulfoxide to give IVe' as reddish-brown crystals; mp>300°C.

Found: C, 45.92; H, 4.42; N, 20.05%. Calcd for $C_{16}H_{18}O_4N_6 \cdot 1/2H_2SO_4 \cdot 1/2H_2O$: C, 46.16; H, 4.84; N, 20.18%.

6-Phenacylidene-5,6-dihydroisoxanthopterin (Va).[21] The The crude product of IVa (1.0 g) was dissolved in a minimum amount of concentrated sulfuric acid. The dark-colored solution was gradually heated to 60°C. After it had been left to stand overnight at room temperature, water was added to the solution chilled in an ice bath; this step was then repeated to give Va(0.5 g) as yellowish-brown crystals; mp> 300°C.

Found: C, 46.46; H, 3.82; N, 18.89%. Calcd for $C_{14}H_{11}O_3N_5 \cdot 1/2H_2SO_4 \cdot H_2O$: C, 46.15; H, 3.87; N, 19.22%.

6-(p-Methylphenacylidene)-5,6-dihydroisoxanthopterin (Vb).[21] In a similar manner, the product, IVb (0.8 g), obtained from Ia sulfate (2.0 g) and IIb (1.8 g) was cyclized in the presence of concentrated sulfuric acid, and was then recrystallized from dimethyl sulfoxide to give Vb as dark orange crystals; mp>300°C.

Found: C, 54.89; H, 4.17; N, 21.15%. Calcd for $C_{15}H_{13}O_3N_5 \cdot H_2O$: C, 54.71; H, 4.59; N, 21.27%.

6-(p-Chlorophenacylidene)-5,6-dihydroisoxanthopterin (Vc).[21] The crude product (1.4 g) from Ia sulfate (2.0 g) and IIc (2.0 g) was recrystallized for hot dimethyl sulfoxide, in which cyclization probably took place, to give Vc as dark yellow crystals; mp>300°C.

Found: C, 50.28; H, 3.23; N, 20.57%. Calcd for $C_{14}H_{10}O_3N_5Cl \cdot 1/4H_2O$: C, 50.04; H, 3.15; N, 20.85%.

6-(p-Bromophenacylidene)-5,6-dihydroisoxanthopterin (Vd). The crude product (1.0 g) form Ia sulfate (2.4 g) and IId (3.0 g) was recrystallized from hot dimethyl sulfoxide to afford Vd as dark yellow crystals; mp>300°C.

Found: C, 44.97; H, 3.03; N, 18.87%. Calcd for $C_{14}H_{10}O_3N_5Br$: C, 44.71; H, 2.66; N, 18.61%.

6-(p-Hydroxyphenacylidene)-5,6-dihydroisoxanthopterin (Ve).[21] The crude product (2.1 g) from Ia sulfate (2.4 g) and IIe (2.3 g) was purified by reprecipitation from a cencentrated sulfuric acid solution to give Ve sulfate as yellow crystals; mp>300°C.

Found: C, 41.25; H, 3.50; N, 16.51%. Calcd for $C_{14}H_{11}O_4N_5 \cdot H_2SO_4$: C, 40.87; H, 3.18; N, 17.03%.

6-(p-Carboxyphenacylidene)-5,6-dihydroisoxanthopterin (Vg). The crude product (0.7 g) from Ia sulfate (0.8 g) and IIg (1.0 g) was reprecipitated from a dimethyl sulfoxide solution by adding water to give Vg as orange-red crystals; mp> 300°C.

Found: C, 48.30; H, 4.23; N, 18.41%. Calcd for $C_{15}H_{11}O_5N_5 \cdot 2H_2O$: C, 47.75; H, 4.01; N, 18.56%.

Hydrolysis of V and IV. A suspension of Ve (0.6 g) 2N sodium hydroxide (30 ml) was refluxed for 30 min, and then left standing to cool. The precipitate thereby formed was removed by filtration. The filtrate was acidified with 6N hydrochloric acid. The yellow crystals thus precipitated were collected on a funnel and washed repeatedly with ethanol. The crystals were dissolved into 1/2N sodium hydroxide, and then 2N hydrochloric acid was dropped into the solution to reprecipitate it. The purification step was repeated three times to afford 6-methylisoxanthopterin (VI) (0.2 g). The UV spectrum was identical with that previously reported.[22] Found: N, 36.69%.

From the combined ethanol extracts, the solvent was removed *in vacuo*; the residue was recrystallized from a mixture of ethanol and ether to give *p*-chlorobenzoic acid (VIIc); mp 243°C, undepressed on admixture with a commercial sample. The identity was also proved by UV spectroscopy.

Found: C, 53.67; H, 3.47%.

A suspension of Vc (0.5 g) in 6N hydrochloric acid (200 ml) was refluxed for 28 hr. The undissolved meterials were removed by filtration while the reaction mixture was still hot. The filtrate was then concentrated under reduced pressure, and the residue was repeatedly extracted with ether. The remaining crystals (0.2 g) were purified according to the above reprecipitation. The identity of the VI thereby formed with the corresponding product in the above alkaline hydrolysis and that of the VIIc obtained from the combined ether extracts with a commercial sample were proved by UV spectroscopy.

A suspension of VIe (0.5 g) in 2N sodium hydroxide (40 ml) was refluxed for 3 hr. After acidification followed by evaporation *in vacuo*, the residue was washed ethanol. The crystals were similarly purified to give VI, which was spectroscopically identical with the sample. The *p*-hydroxybenzoic acid (VIIe) obtained from the combined extracts

22) S. Matsuura, S. Nawa, H. Kakizawa, and Y. Hirata, *J. Amer. Chem. Soc.*, **75**, 4446 (1953).

was identified by a mixed-melting-point determination (mp 213—214°C) and UV spectroscopy.

The other compounds belonging to IV or V (both X=OH) behaved similarly under hydrolysis, as evidenced by the UV spectra of the hydrolysates.

Grateful acknowledgment is made to Miss Nobu Maruta for a part of the elementary analysis; to Mr. Takeshi Inagaki, Nitto Chemical Industry Co., for many NMR spectra; to Dr. Tetsuo Maruyama, JEOL Co., for NMR spectra at an elevated temperature, and to Mr. Jun-etsu Seo and Mr. Atsuo Norose for their valuable technical assistance.

BULLETIN OF THE CHEMICAL SOCIETY OF JAPAN, VOL. 45, 2834—2836 (1972)

1,2: 8,9-Dibenzo-3,10-bisdehydro[14]annulene-5,12-dione

Takashi KOJIMA, Yoshiteru SAKATA, and Soichi MISUMI*
The Institute of Scientific and Industrial Research, Osaka University, Suita, Osaka
(Received March 13, 1972)

An annelated[14]annulenedione (V) was prepared by the Castro reaction of cuprous salt of *o*-iodocinnamoylacetylene (IV) in order to examine the aromatic character of the inner fourteen membered ring. The NMR spectra of V in arsenic trichloride and deuterotrifluoroacetic acid suggest that significant downfield shift of the inner protons H_B is due to a paramagnetic ring current arising from polarization of two carbonyl groups in the inner ring, compared with the spectra of a reference compound VI.

A series of fully conjugated monocyclic monoketone, so-called annulenone, are predicted to be aromatic or non-aromatic owing to polarization of carbonyl group provided they contain $(4n+3)$ membered ring or $(4n+1)$ membered ring, respectively. Recently, several annulenones, *e.g.*, 4,9-methano[11],[1] [13],[2a] [15],[2b] and [17][2c] annulenone derivatives, have been synthesized in order to confirm this prediction. On the other hand, as in the case of annulenes, an effect of annelation on aromatic character of annulenone has been explored in a few annelated annulenones, dibenzo-[9],[3] 6,7-benzo-4,9-oxido[11],[4a] 4,7: 10,13-dioxido-[15],[4b] and 2,5: 8,11: 14,17-trioxido[17][4c] annulenones, indicating the delocalization of π-electrons through condensed benzene or furan nuclei.

For the purpose of comparison with the properties of the annelated annulenones, we attempted to examine the effect of annelation on conjugated cyclic diketone or annulenedione.[5] In this paper we wish to report the synthesis and properties of 1,2: 8,9-dibenzo-3,10-bisdehydro[14]annulene-5,12-dione (V). It is expected that this $(4n+2)$ membered ring compound is non-aromatic by virtue of polarization of two carbonyl groups and thereby represents a paramagnetic ring current.

Results and Discussion

Synthesis. *o*-Iodocinnamaldehyde (II) was obtained by the reaction of *o*-iodobenzaldehyde with acetaldehyde in anhydrous alcohol at room temperature in 40% yield.[6] The cinnamaldehyde II was treated with ethynyl magnesium bromide[7] in dry tetrahydrofuran to produce an ethynyl carbinol III in a yield of 74%. Oxidation of the carbinol III with active manganese dioxide[8] in carbon tetrachloride at 0°C yielded crude ethynyl *o*-iodostyryl ketone (IV) which gave red cuprous salt in 86% yield by treatment with Ilosvay reagent. Dry cuprous salt of IV was subjected

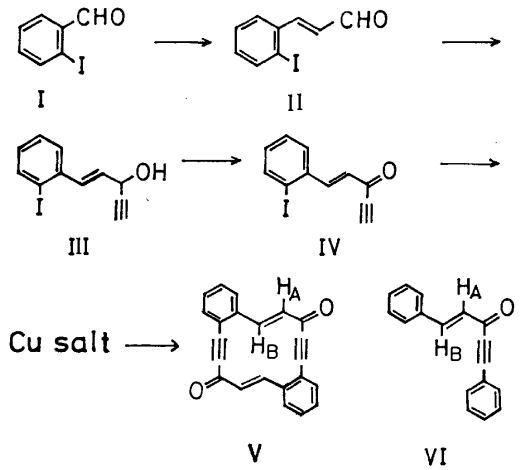

1) W. Grimme, J. Reisdorff, W. Jünemann, and E. Vogel, *J. Amer. Chem. Soc.*, **92**, 6335 (1970).

2) a) G. M. Pilling and F. Sondheimer, *ibid.*, **90**, 5610 (1968); G. M. Pilling, and F. Sondheimer, *ibid.*, **93**, 1977 (1971); b) G. P. Cotterrell, G. H. Mitchell, F. Sondheimer, and G. M. Pilling, *ibid.*, **93**, 259 (1971); c) G. W. Brown and F. Sondheimer, *ibid.*, **91**, 760 (1969).

3) M. Rabinovitz, F. D. Bergmann, and A. Gazit, *Tetrahedron Lett.*, **1971**, 2671.

4) a) H. Ogawa, H. Kato, and M. Yoshida, *ibid.*, **1971**, 1793; b) H. Ogawa, N. Shimojo, and M. Yoshida, *ibid.*, **1971**, 2013; c) T. M. Cresp and M. V. Sargent, *Chem. Commun.*, **1971**, 1458.

5) E. Vogel, E. Lohmar, W. A. Böll, B. Söhngen, K. Müllen, and H. Günther, *Angew. Chem. Inter. Edit.*, **10**, 398 (1971); E. Vogel, W. A. Böll and E. Lohmar, *ibid.*, **10**, 399 (1971).

6) W. S. Rapson and R. G. Shuttleworth, *J. Chem. Soc.*, **1941**, 487.

7) E. R. H. Jones, L. Skatteböl, and M. C. Whiting, *ibid.*, **1956**, 4765; "Organic Syntheses," Coll. Vol. IV, 792 (1963).

8) J. Attenburrow, A. F. B. Cameron, J. H. Chapman, R. M. Evans, B. A. Hems, A. B. A. Jansen, and T. Walker, *J. Chem. Soc.*, **1952**,1094; I. M. Goldmann *J. Org. Chem.*, **34**, 1979 (1969).

to the Castro reaction[9] in anhydrous *N,N*-dimethyl formamide at 120°C to give cyclic dimolecular product, 1,2 : 8,9-dibenzo-3,10-bisdehydro[14]annulene-5,12-dione (V), of fairly thermostable and lemon yellow needles in 1.2% yield. The structure of the annulene-dione V was confirmed by elemental analysis and IR, NMR, and Mass spectra. Styryl phenylethynyl ketone (VI) was obtained through the Castro reaction of cuprous salt of cinnamoyl acetylene with iodobenzene as a reference compound for the synthesis and NMR spectrum of V.

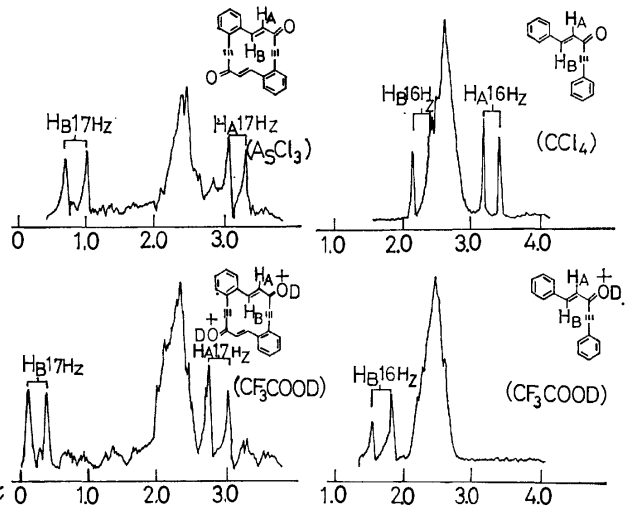

Fig. 1. The NMR spectra of V and VI (60 MHz, TMS)

Table 1. The chemical shifts (τ) of V and VI

	Solvent	H_B	BzH	H_A
V	$AsCl_3$	0.81	~2.4~	3.14
	CF_3COOD	0.22	~2.3~	2.88
VI	CCl_4	2.27	~2.6~	3.31
	CF_3COOD	1.68	~2.5~	~2.5~

NMR Spectra. The NMR spectra of V and VI are shown in Fig. 1 and Table 1. The spectrum of V was measured in arsenic trichloride and in deutero-trifluoroacetic acid because of poor solubility in the usual organic solvents, while VI gave no distinct spectrum owing to instability in the former medium. The chemical shift of inner protons H_B in V are at considerably lower field ($\Delta\delta$: *ca.* 1.5 ppm) than that of proton H_B in VI, in contrast to somewhat same position of both protons H_A in V and VI. A difference in the chemical shifts in different solvents is *ca.* 0.1 ppm between arsenic trichloride and carbon tetrachloride.[10] The extent to which the shift of the protons H_B in V is affected by shielding effects of the π-electron systems (-C≡C-, -C=C-, and >C=O) and electric field effect of carbonyl group other than a styryl phenylethynyl ketone moiety in V was estimated according to the McConnell equation (1)[11] and the Buckingham equation (2),[12] respectively, to be about −0.7 ppm at most. It is interesting that the protons H_B in V appear

$$\Delta\sigma = \Delta\chi \sum_{i=1} \frac{1}{3R^3}(1-3\cos^2\theta) \quad (1)$$

$$\Delta\sigma = -2\times 10^{-12}E_z - 10^{18}E^2 \quad (2)$$

at considerably lower field beyond the combined effect of both effects above-stated. The inner fourteen membered ring of V is considered as a twelve π-electron system, *i.e.*, a $4n\pi$ ring system of the Hückel rule, through the polarization of two carbonyl groups. So the inner ring system may reveal a paramagnetic ring current and thereby may show downfield shift of the inner protons. Accordingly, the marked downfield shift of the protons H_B in V described above can be accounted for by a total effect of the paramagnetic ring current and the other effects, mainly by the former.

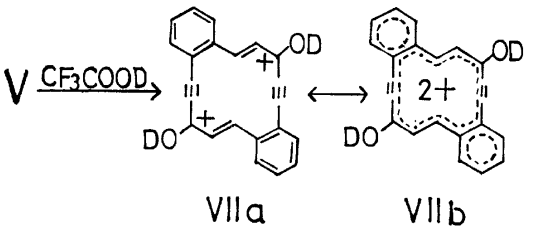

It is expected that when V is protonated, the inner protons H_B may indicate the signal at further lower field by way of additional paramagnetic ring current of the inner ring as depicted by VIIa and VIIb. This prediction was, in fact, realized with the chemical shift in deuterotrifluoroacetic acid as is shown in Table 1 and Fig. 1. In contrast to the chemical shift of the inner proton, the outer protons H_A and the benzenoid protons show little difference in the chemical shift, compared with ones in arsenic trichloride. It is most likely due to internal compensation of the paramagnetic ring current with an effect of positive charge. This postulate is possibly supported by marked down field shifts of both protons H_A and H_B of VI in deuterotrifluoroacetic acid by comparison with the chemical shifts in carbon tetrachloride.

Experimental

All melting points are uncorrected. The electronic, infrared, NMR, and mass spectra were measured on Hitachi ESP-3T, Jasco DS-402G, Hitachi R-20, and Hitachi RMU-7, respectively.

1-o-Iodophenyl-1-penten-4-yn-3-ol (III). To an ethynylmagnesium bromide[7] solution prepared by introduction of acetylene into ethylmagnesium bromide (from 6.9 g, 0.29 g-atom of magnesium and 30 g, 0.28 mol of ethyl bromide) in dry tetrahydrofuran added dropwise *o*-iodocinnamaldehyde[6] (II, 50 g, 0.19 mol) in dry tetrahydrofuran (100 ml) under ice cooling and stirring. After stirring at room temperature overnight, the reaction mixture was poured into a cooled aqueous solution saturated with ammonium chloride to decompose the Grignard complex. The aqueous layer was extracted with ether and the combined organic solution was washed with water and dried over magnesium sulfate.

9) R. D. Stephens and C. E. Castro, *ibid.*, **28**, 3313 (1963); C. E. Castro, E. J. Gaughan, and D. C. Owsley, *ibid.*, **31**, 4071 (1966); C. E. Castro, R. Havlin, V. K. Honwad, A. Malte, and S. Mojé, *J. Amer. Chem. Soc.*, **91**, 6464 (1969).

10) Cf. the protons of benzalacetophenone and dibenzalacetone, which show complicated patterns, in carbon tetrachloride are shifted to higher field by 0.05—0.15 ppm than in arsenic trichloride.

11) H. M. McConnell, *J. Chem. Phys.*, **27**, 226 (1957).

12) A. D. Buckingham, *Can. J. Chem.*, **38**, 300 (1960).

After evaporating organic solvent, the residue (57 g) was subjected to high vacuum distillation to give pale yellow oil (45 g, 83% yield) of the ethynyl carbinol III, bp 135—137°C/3×10^{-2} mmHg.

IR(neat): 3300 (s, ν_{OH}), 3250 (s, $\nu_{\equiv CH}$), 2200 (w, $\delta_{C\equiv C}$),960 (s, $\delta_{trans\ CH=CH}$), and 750 cm^{-1} (s, *o*-substituted benzene). NMR (CCl_4): τ 2.18—3.31 (m, 4H, aromatic), 3.04 (d, J= 15 Hz, 1H, olefin), 3.91 (dd, J=5, 15 Hz, 1H, olefin), 4.45 (m, 1H, methine), 6.52 (broad, 1H, OH), 7.45 (d, J=2 Hz, 1H, acetylene). Found: C, 46.29; H, 3.00; I, 45.02. Calcd for $C_{11}H_9OI$: C, 46.49; H, 3.19; I, 44.67.

o-Iodocinnamoylacetylene (IV). A suspension of active manganese dioxide[8] (100 g) in a carbon tetrachloride (500 m*l*) solution of above carbinol III (10 g, 36 mmol) was stirred under ice-cooling for 1.5 hr. After filtration and washing sufficiently with acetone, the combined filtrate and washings were evaporated in vacuum. Dark red residual solid (8.2 g) was used to prepare cuprous salt as it is because of difficult purification. A small amount of crude sample was extracted with ether and recrystallized from petroleum ether to give yellow plates of the ketone IV, mp 70—71°C.

IR (Nujol mull): 3210 (m, $\nu_{\equiv CH}$), 2100 (s, $\nu_{C\equiv C}$), 1630 (s, $\nu_{C=O}$), 979 (m, $\delta_{trans\ CH=CH}$), 765 cm^{-1} (m, *o*-substituted benzene). NMR (CCl_4): τ 1.92 (d, J=16 Hz, 1H, olefin.), 2.16—3.10 (m, 4H, arom.), 3.44 (d, J=16 Hz, 1H, olefin), 6.70 (s, 1H, acetylene). Found: C, 46.95; H, 2.33; I, 44.62. Calcd for $C_{11}H_7OI$: C, 46.83; H, 2.50; I, 44.98.

1,2:8,9-Dibenzo-3,10-bisdehydro[14]annulene-5,12-dione (V). To a solution of Ilosvay's reagent was added a solution of above-stated crude ketone IV (9 g, 31 mmol) in ethanol (100 m*l*) and acetone (50 m*l*) to give immediately red precipitate of cuprous salt. The cuprous salt was filtered, washed with water, ethanol, and ether, successively, and dried in vacuum at room temperature, 9.5 g (86% yield).

Dry cuprous salt (5.0 g, 15 mmol) in dry *N,N*-dimethyl formamide (150 ml) was heated with stirring at 120°C under nitrogen for 8 hr. After cooling the reaction mixture was poured into water and extracted with benzene. The organic layer was wahsed with water, dried over magnesium sulfate, and evaporated in vacuum. The residual solid dissolved in benzene was filtered through silica gel with benzene and ether–benzene (1: 99). After evaporating the solvent, crude solid was triturated with benzene and recrystallized from same solvent with active charcoal to give lemon yellow needles of the annulenedione V, mp>500°C, 27 mg (1.2% yield).

IR (Nujol mull): 2200 (s, $\nu_{C\equiv C}$), 1630 (s, $\nu_{C=O}$), 975 (m, $\delta_{trans\ CH=CH}$), 765 cm^{-1} (m, *o*-substituted benzene). UV (THF): λ_{max} (ε), 217 (35400), 304 nm (42200); Mass, *m/e* 308 (M^+). Found: C, 85.74; H, 3.77. Calcd for $C_{22}H_{12}O_2$: C, 85.70; H, 3.92; mol wt 308.

Styryl Phenylethynyl Ketone (VI). Styryl ethynyl carbinol[7] prepared by ethynylation of cinnamaldehyde was oxidized with active manganese dioxide in carbon tetrachloride to give cinnamoyl acetylene. Cuprous salt of this acetylenic ketone was subjected to the Castro reaction with iodobenzene in pyridine to yield a ketone VI, mp 72—73°C (lit,[13] 69—70°C).

13) D. V. Nightingale and F. Wadsworth, *J. Amer. Chem. Soc.*, **67**, 416 (1945).

BULLETIN OF THE CHEMICAL SOCIETY OF JAPAN, VOL. 45, 2836—2841 (1972)

Benzo- and Naphtho-derivatives of Triptycene: Synthesis and Properties

Makoto SUGIHASHI,* Ryosuke KAWAGITA, Tetsuo OTSUBO,
Yoshiteru SAKATA, and Soichi MISUMI**
The Institute of Scientific and Industrial Research, Osaka University, Suita, Osaka

(Received March 16, 1972)

Several benzo- and/or naphtho-derivatives of triptycene were prepared in a manner of addition reaction of dehydronaphthalene (XIII) or a new type of aryne, dehydroanthraquinone (XVI) generated from 3-amino-anthraquinone-2-carboxylic acid (XV), with a few acenes. The absorption bands in longer wavelength region of their UV spectra and the chemical shift of bridgehead protons in their NMR spectra led to a conclusion that the spectra of those annelated triptycenes are elucidated in terms of a superposition and a sum of magnetic effects of separated component chromophores, respectively, and thereby indicate a negligible existence of the across-space π-electron interactions, if any, among three aromatic nuclei.

Triptycene (II) is an interesting, rigid cage molecule having a higher order of symmetry (D_{3h}). Since the first synthesis by Bartlett and his co-workers,[1] this unique geometry of the molecule has attracted numerous investigators for studies of spectral properties. Thus an electronic interaction of three separated benzene nuclei in this molecule has early been considered to contribute significantly on the electronic spectrum, because σ-type overlap of $2p\pi$ orbitals was anticipated as in the case of parent compound, barrelene (I).[2] Many efforts have so far been done for examination of such σ-type interactions.[3] However, most of observed spectra of triptycene and its derivatives were

* Present address: Nippon Paint Co., Ōyodo-ku, Osaka.
** To whom inquiries should be addressed.

1) P. D. Bartlett, M. J. Ryan, and S. G. Cohen, *J. Amer. Chem. Soc.*, **64**, 2649 (1942).

2) C. F. Wilcox, Jr., S. Winstein, and W. McMillan, *ibid.*, **82**, 5450 (1960); J. Paldus and J. Koutecky, *Collect. Czech. Chem. Commun.*, **27**, 2139 (1962); *Tetrahedron*, **19**, Suppl. **2**, 201 (1963); R. Hoffmann, E. Heilbronner, and R. Gleiter, *J. Amer. Chem. Soc.*, **92**, 706 (1970). F. A. Van-Catledge, *ibid.*, **93**, 4365 (1971).

3) P. D. Bartlett and E. S. Lewis, *ibid.*, **72**, 1005 (1950); C. F. Wilcox, Jr., *J. Chem. Phys.*, **33**, 1874 (1960); C. F. Wilcox, Jr. and A. C. Craig, *J. Org. Chem.*, **26**, 2491 (1961).

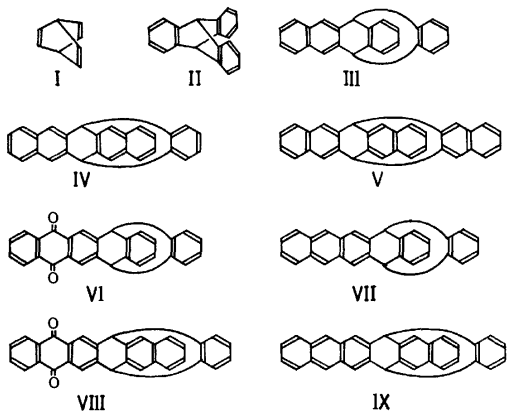

found to be explained in terms of a sum of three benzenoid chromophores and not of the interaction among those chromophores. Present authors also reported that the electronic spectra of several chloro-substituted triptycenes could be interpreted by a superposition of three benzenoid chromophores.[4]

On the other hand, there have been interesting investigations that CD spectra of a number of optically active triptycene derivatives were consistent with an explanation of interactions among electric transition moments of benzenoid chromophores[5] and that a triplet state arising from photoexcitation of tribenzotriptycene (V) was located in any one of naphthalene nuclei at 20°K, but delocalized among three naphthalene nuclei at 77°K.[6]

A stepwise annelation or condensation with additional aromatic nuclei to the triptycene molecule is of great interest in connection with the interaction in question. Since the spectral properties of condensed aromatic nuclei as naphthalene and anthracene have been well investigated, it is expected, from the examination of electronic absorption and emission spectra, that such annelated derivatives of triptycene may afford valuable informations about the intramolecular across-space interactions. In addition, it appears that they are appropriate systems for a study of magnetic anisotropies of containing aromatic nuclei because of their rigid structures.

Literature search revealed that there have been only two annelated derivatives (III[7] and V[6]) of triptycene containing naphthalene ring as condensed aromatic nucleus. In the present paper we wish to report the synthesis and spectral properties, electronic and NMR, of several triptycene derivatives (III—IX) including naphthalene, anthracene, and anthraquinone nuclei.

Results and Discussion

Synthesis. Since triptycene was prepared by the Diels-Alder reaction of anthracene with benzyne, various triptycene derivatives have generally been synthesized through the addition reaction of arynes. In the present investigation triptycene derivatives were

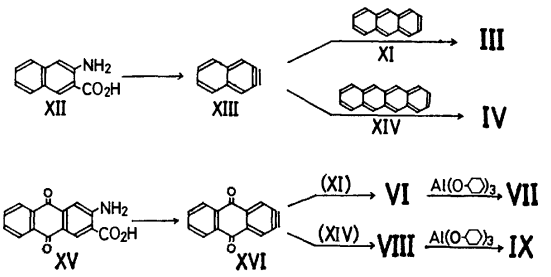

also prepared in a manner of aryne reaction except tribenzotriptycene (V) which was obtained by the addition reaction of 1,4-dihydronaphthalene-1,4-oxide with pentacene, followed by dehydration with acetic anhydride.[6] The synthesis of mono- and di-benzotriptycenes (III and IV) was carried out by the reaction of anthracene (XI) and tetracene (XIV) with an aryne, 2,3-dehydronaphthalene (XIII), generated from 3-amino-2-naphthoic acid (XII) according to Friedman,[7] in 11 and 25% yields, respectively. In order to obtain two triptycene derivatives (VII and IX) containing anthracene nucleus, a reaction path *via* reduction of phthaloyl derivatives, VI and VIII, was chosen in the present study because 2,3-dehydroanthracene corresponding to XIII might be difficult to generate for a reason of its self-condensation. The phthaloyl derivatives VI and VIII were obtained by the reaction of anthracene and tetracene with a new aryne, 2,3-dehydroanthraquinone (XVI), generated from 3-aminoanthraquinone-2-carboxylic acid (XV), in 24 and 29% yields, respectively. The aryne precursor XV was prepared *via* five steps from toluene in good yield according to the procedure of Hosoda.[8] The quinone derivatives VI and VIII were reduced by the Meerwein-Pondorf-Verley reaction using aluminum tri(cyclohexyl oxide)[9] to give two anthracene derivatives in 35% of VII and 29% yield of IX, respectively. All the triptycene derivatives (III—IX) are thermally stable and kept without any change for a long time. The addition reaction of tetracene was carried out in a nitrogen atmosphere and with degassed solvent, otherwise it would result in yielding mainly an oxidative product, tetracene quinone, instead of regular addition compounds IV and VIII.

Table 1. Chemical shifts of bridgehead protons (τ value)

Compound	Solvent	
	$AsCl_3$	$CDCl_3$
II	4.55	4.61
III	4.43	4.50
IV	4.29	4.37
V	4.17	4.25
VI	4.29	—
VII	4.40	4.47
VIII	4.18	—
IX	4.27	—

4) I. Mori, T. Kadosaka, Y. Sakata, and S. Misumi. This Bulletin, **44**, 1649 (1971).
5) F. Ogura and M. Nakagawa, *ibid.*, **38**, 155 (1965).
6) G. Wittig, H. Harle, E. Knauss, and K. Niethammer, *Chem. Ber.*, **93**, 951 (1960).
7) L. Friedman and F. M. Logullo, *J. Amer. Chem. Soc.*, **85**, 1549 (1963); *J. Org. Chem.*, **34**, 3089 (1969).
8) Y. Hosoda, "Senryo Kagaku," Gihodo, Tokyo (1957), p. 556.
9) S. Coffey and V. Boyd, *J. Chem. Soc.*, **1954**, 2468.

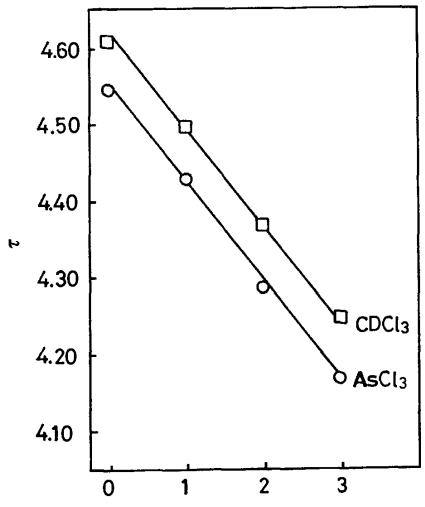

Fig. 1. Relation between the chemical Shifts of bridgehead protons of benzo-derivatives (III—V) and the number of naphthalene nuclei in deuterochloroform and arsenic trichloride.

Nuclear Magnetic Resonance Spectra. Table 1 shows the chemical shift of bridgehead protons of triptycene and some annelated triptycenes (III—IX) in arsenic trichloride and/or in deuterochloroform, because VI, VIII, and IX are sparingly soluble in the latter solvent. The chemical shifts of bridgehead protons in triptycene (II) and mono-, di-, and tri-benzotriptycenes (III, IV, and V) afford straight lines when plotted against number of naphthalene nuclei as is shown in Fig. 1. The figure reveals that the slope of the lines remains nearly constant even if the solvent is changed from deuterochloroform to arsenic trichloride and that the resonance positions of the bridgehead protons regularly shift to lower field by average 0.13 ppm along with the increase of the number of naphthalene nuclei. This finding seems to be accounted for in terms of additional ring current effect of naphthalene nuclei introduced stepwise into the triptycene molecule and therefore to substantiate the Schaefer's conclusion[10] about non-existence of "round-the-barrel" current in the triptycene molecules. In other words, the difference in the chemical shifts of bridgehead protons may be represented by a difference in the magnetic anisotropies of contained aromatic nuclei.

Thus, the chemical shifts $\Delta\sigma_1$ and $\Delta\sigma_2$ of the bridgehead protons in triptycene (II) and benzotriptycene (III) are expressed as follows:

$$\Delta\sigma_1 = 3\Delta\sigma_b + \Delta\sigma_0 \quad (1)$$

$$\Delta\sigma_2 = 2\Delta\sigma_b + \Delta\sigma_n + \Delta\sigma_0' \quad (2)$$

where $\Delta\sigma_b$ and $\Delta\sigma_n$ are chemical shifts due to ring current of a benzene nucleus and a naphthalene one, and $\Delta\sigma_0$ and $\Delta\sigma'_0$ are chemical shifts caused by various effects, *i.e.* the electric field, the van der Waals, the solvent, the electron density effects and so on, other than the ring current in II and III, respectively.

In a series of similarly constructed compounds the anisotropic effects of particular C–C and C–H bonds and the other effects are generally approximated to be equal, *i.e.* $\Delta\sigma_0=\Delta\sigma'_0$. From Eqs. (1) and (2):

$$\Delta\Delta\sigma = \Delta\sigma_1 - \Delta\sigma_2 = \Delta\sigma_b - \Delta\sigma_n \quad (3)$$

Eq. (3) implies that the difference ($\Delta\Delta\sigma$) in the chemical shifts of the bridgehead protons in triptycene and benzotriptycene can be represented as a difference in ring current effects of a benzene nucleus and a naphthalene one. Since $\Delta\sigma_b$ and $\Delta\sigma_n$ are the chemical shifts only due to magnetic anisotropy of ring current in each aromatic nucleus, they should be correlated with the McConnell equation[11] assuming that a center of the anisotropy is situated at the center of each benzene ring (Eqs. (4) and (5)). Thus, in the case of naphthalene nucleus two centers of the anisotropy are placed at the center of each benzene ring:

$$\Delta\sigma_b = -\frac{\Delta\chi(1-3\cos^2\theta_1)}{3R_1^3} \quad (4)$$

$$\Delta\sigma_n = -\left\{\frac{\Delta\chi'(1-3\cos^2\theta_2)}{3R_2^3} + \frac{\Delta\chi'(1-3\cos^2\theta_3)}{3R_3^3}\right\} \quad (5)$$

where R_n is a distance between a bridgehead proton and a center of each benzene ring, $\Delta\chi$ and $\Delta\chi'$ are the vectors which represent the anisotropies due to the ring currents of benzene ring and each benzene component in naphthalene nucleus, respectively, and θ is an angle between a line represented as R and $\Delta\chi$ or a main axis of each benzene, *i.e.* $\theta=90°$ in this case. Jonathan[12] calculated some ratios of ring current intensities of condensed aromatic nuclei to benzene ring as is shown in Table 2; *e.g.* for naphthalene nucleus, Eq. (6) are assumed.

$$\Delta\chi' = 1.1\Delta\chi \quad (6)$$

From Eqs. (3), (4), (5), and (6):

$$\Delta\Delta\sigma = -\frac{\Delta\chi(1-3\cos^2\theta_1)}{3R_1^3} + \frac{1.1\Delta\chi(1-3\cos^2\theta_2)}{3R_2^3} + \frac{1.1\Delta\chi(1-3\cos^2\theta_3)}{3R_3^3} \quad (7)$$

The observed value of $\Delta\Delta\sigma$ (-0.13×10^{-16}) and the values of the distances, $R_1=3.5$, $R_2=3.4$, and $R_3=5.5$ Å which are measured on the geometry drawn by reference to X-ray analysis,[13] are substituted in Eq.

Table 2.

Molecule	Ring	Current intensity
A	A	1.000
A A	A	1.093
A B A	A	1.085
	B	1.280

10) K. G. Kidd, G. Kotowycz, and T. Schaefer, *Can. J. Chem.*, **45**, 2155 (1967).

11) H. M. McConnell, *J. Chem. Phys.*, **27**, 226 (1957).

12) N. Jonathan, S. Gordon, and B. P. Dailey, *ibid.*, **36**, 2443 (1962).

13) K. J. Palmer and D. H. Templeton, *Acta Crystallogr.*, **B24**, 1048 (1968).

(7). A calculated value of the magnetic anisotropy of benzene, $\Delta\chi = -33 \times 10^{-30}$ cm^3/mol, is good agreement with the Craig's value[14] ($\Delta\chi = -31 \times 10^{-30}$ cm^3/mol) obtained by substracting a sum of Pascal's constants[15] from the observed value of magnetic susceptibility of benzene.

Using the value of $\Delta\chi$ calculated above and the ring current intensity of each benzene ring in Table 2, the chemical shifts of bridgehead protons in the triptycene derivatives containing anthracene nucleus, VII and IX, are calculated to be τ 4.39 and 4.30, respectively. Those values were found to be well compatible with the observed values of VII and IX, τ 4.40 and 4.27 in arsenic trichloride.

Consequently, it was found that the application of Jonathan's values and the assumption which the various effects other than ring current, $\Delta\sigma_0$ and $\Delta\sigma_0'$, are approximated to be equal were valid for study on magnetic anisotropies and relative intensities of ring currents in this system.

Electronic Spectra. The electronic absorption spectra of the annelated triptycenes above-stated are shown in Figs. 2, 3, and 4 and in Table 3.

It has been pointed out from the spectrum of triptycene that the electronic interaction among three separated benzene nuclei in the molecule would not be so large in spite of the presumption of significant overlaps among those π-electron systems.[3] If the strong interaction between naphthalene nuclei in benzo-derivatives of triptycene, III, IV, and V, is expected to occur, the spectra of dibenzo- and tribenzo-

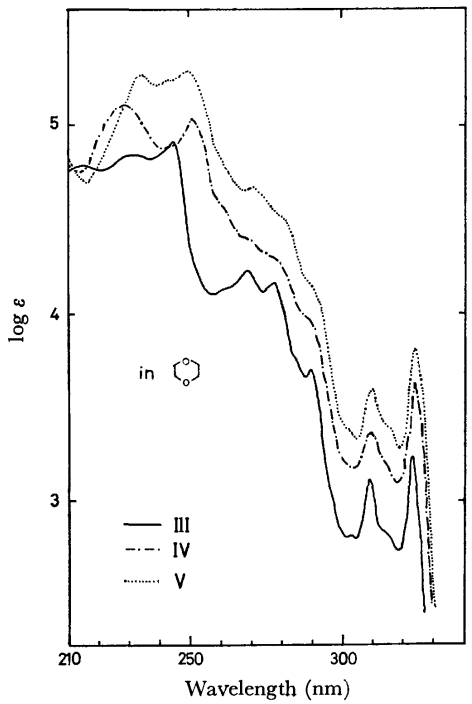

Fig. 2. The electronic spectra of benzo-(III), dibenzo-(IV), and tribenzo- (V) triptycenes in dioxane.

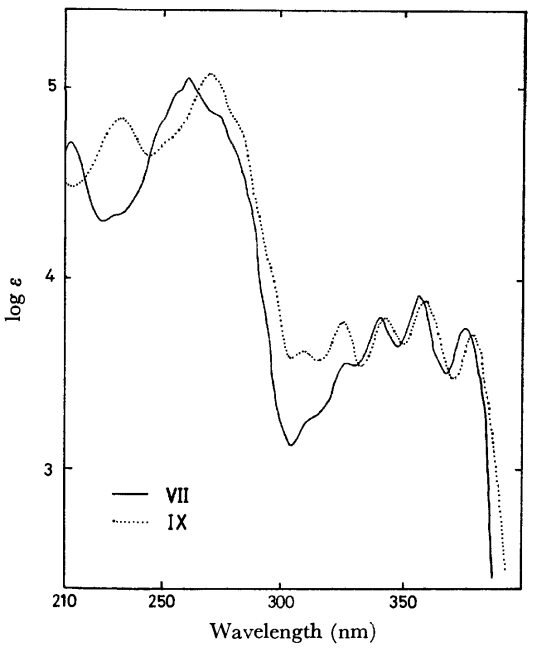

Fig. 3. The electronic spectra of phthaloyl- (VI) and benzophthaloyl- (VIII) triptycenes in dioxane.

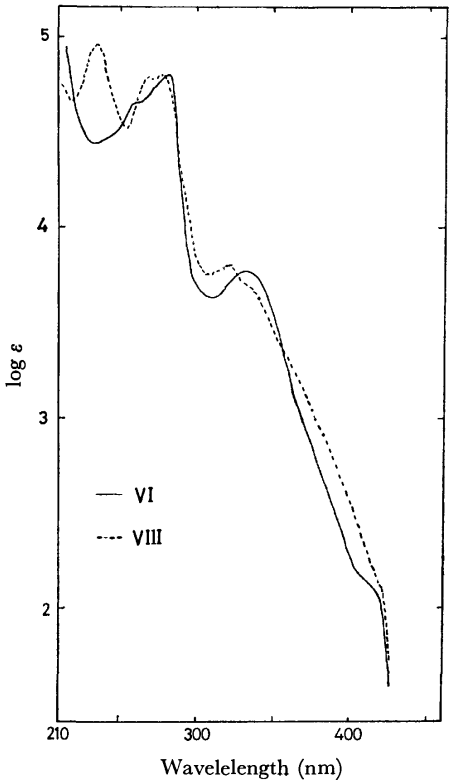

Fig. 4. The electronic spectra of naphtho- (VII) and benzonaphtho- (IX) triptycenes in dioxane.

triptycenes should reveal longer wavelength shifts of absorption maxima than that of monobenzotriptycene. However, Fig. 2 and Table 3 exhibit that the longest wavelength bands of these triptycene derivatives appear at nearly the same position. Similar phenomena are observed at longer wavelength region of VII and IX in Fig. 3 and of VI and VIII in Fig. 4. In addition, absorption bands of benzonaphtho-triptycene IX in

14) D. P. Craig, Aromaticity in "Non-benzenoid Aromatic Compounds," ed. by D. Ginsburg, Interscience, N. Y. (1959), p. 27.

15) C. K. Ingold, "Structure and Mechanism in Organic Chemistry," Cornell Univ. Press, Ithaca, N.Y. (1969), p. 224.

Table 3. The electronic spectrum data of triptycene derivatives (III—IX) in dioxane

Triptycene derivative		Absotption maximum (λ_{max}, nm) and intensity (ε)									
Benzo-(III)	λ	214	228	243	268	277	289	302	309	316[a]	323
	ε	59300	69800	83000	23800	15200	5400	800	1400	760	1800
Dibenzo-(IV)	λ		229.5	251	269[a]	278[a]	289[a]		310.5	314[a]	325
	ε		130000	111000	25300	20300	9800		2570	1600	4600
Tribenzo-(V)	λ		234	250	271	280[a]	290[a]		310.5	316[a]	325
	ε		186000	197000	47300	37000	2900		4140	2700	6950
Phthaloyl-(VI)	λ		257	282		334	412[a]				
	ε		37800	66200		66150	120				
Benzo-phthaloyl-(VIII)	λ	236	266	279	320	337[a]	412[a]				
	ε	142000	63700	66400	6620	5200	130				
Naphtho-(VII)	λ	213		255[a]	260	273[a]	310[a]	324	339	356	375
	ε	49400		99600	116000	80000	1900	3700	6400	8430	5900
Benzo-naphtho-(IX)	λ		233		269	283[a]	309	323.5	340.5	357.5	376
	ε		81200		130000	75000	4010	5100	6310	8040	5300

a) shoulder.

longer wavelength region more than 300 nm are compared with a sum of those of benzotriptycene III and naphthotriptycene VII in Table 3 as follows:

IX: λ_{max} nm (ε) 309(4010), 323.5(5100), 340.5(6310), 357.5(8040), and 376(5300)

III+VII: λ_{max} (ε) 310(3300), 324(5500), 339(6400), 356(8430), and 375(5900)

An excellent agreement between observed and calculated values of wavelength and intensity of absorption bands demonstrates additivity or superposition of component chromophores on the spectra of the annelated triptycenes.

On the other hand, absorption bands other than the longest wavelength bands of three benzo-derivatives, III, IV, and V, show a few features as follows: a) broadening of all the absorption bands with increasing number of naphthalene nuclei, especially of the bands at 270—290 nm (Fig. 2), b) differences in position of B_b bands (220—260 nm) in contrast to nearly the same position of L_a bands (260—300 nm) and L_b bands (300—330 nm) (Fig. 2), c) the intensity of L_b bands per naphthalene chromophore is in order of III<IV<V, but the intensity of L_a bands in order of III>V>IV (Table 3).

A **plausible elu**cidation may be put on these spectral changes. When two of the same chromophores, which are fixed closely with each other, interact slightly, the exciton theory[16] is applicable to this system just as molecular aggregate in crystal system which shows unambiguous shift and splitting of absorption bands due to interaction among the component chromophores. Thus, the phenomenon a) above-stated is explainable with the splitting of degenerated levels —Davydov splitting— due to exciton interaction as well as in the other phenomena b) and c).

The spectra of VII and IX, containing anthracene nucleus, in concentrated sulfuric acid were changed with time as shown in Fig. 5. The formation of cation radical of anthracene itself in that medium was demonstrated by ESR measurement[17] and by the fact that the position of the longest wavelength maximum of

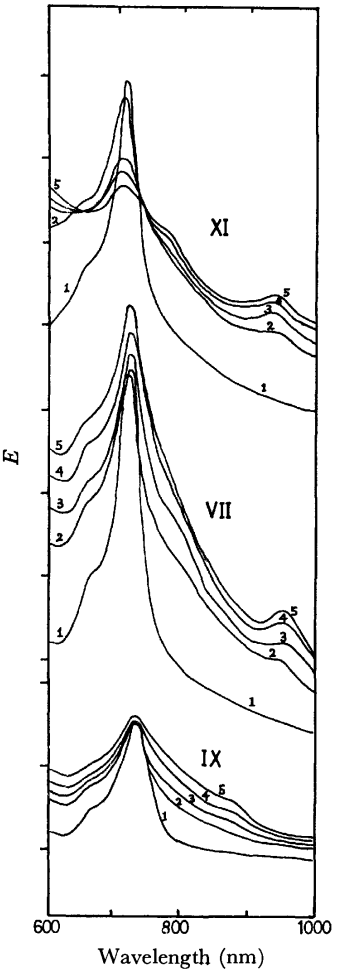

Fig. 5. The electronic spectra of cation radicals of anthracene (XI), naphthotriptycene (VII), and benzo-naphthotriptycene (IX) in conc. sulfuric acid at 15°C: curve 1, 45 min after dissolution; curve 2, 165 min; curve 3, 285 min; curve 4, 405 min; curve 5, 525 min.

16) M. Kasha, H. R. Rawls, and M. Ashraf El-Bayoumi, "Molecular Spectroscopy VIII," Butterworth, London, 1965 and references cited there on.

17) H. Kon and M. S. Blois, Jr., *J. Chem. Phys.*, **28**, 743 (1958); S. I. Weissman, E. de Boer, and J. J. Conradi, *ibid.*, **26**, 963 (1957).

the cation radical coincided with that of the anion radical of anthracene, an alternant hydrocarbon, in absorption spectra.

The cation radicals of the triptycene derivatives VII and IX show the longest wavelength absorption bands at longer wavelength region only by 10 and 20 nm, respectively, than that of anthracene itself. It indicates that there is weak interaction among the aromatic nuclei in triptycene radicals in contrast to an increase of interaction in the anion radical of [2.2]paracyclophane.[18] However, the maxima at 720—730 nm of the cation radicals of VII and IX remain unchanged with time, while the intensity of the maximum of anthracene radical decreases rapidly with time and falls to half after 10 hr. This phenomenon is possibly interpreted partly by stabilization due to delocalization of the cation radical in VII and IX, and mainly by stabilization due to protecting effect of bulky π-electron cloud in benzene and naphthalene nuclei.

Experimental

All melting points are uncorrected. The IR and UV spectra were obtained on a JASCO autorecording spectrometer DS-402G and on a Hitachi ESP-3T, respectively. The molecular weights were determined with a Hitachi mass spectrometer RMU-7 and/or with Knauer vapour pressure osmometer. The NMR spectra were measured on a Hitachi Perkin-Elmer R-20 spectrometer (60 M) using TMS as an internal standard. A frequency counter was used to measure the frequency separation between signals.

Materials. Tetracene was synthesized from tetralin and phthalic anhydride *via* 3 steps in 3.3% of over-all yield according to Fieser.[19] Pentacene was prepared by reduction of pentacene-6,13-dione, which was obtained from phthaldehyde and cyclohexane-1,4-dione in a 65% yield, with aluminum tri(cyclohexyl oxide).[20]

Triptycene (II). The synthesis of triptycene was carried out according to the procedure of Fieser[21] in a 42% yield, mp 262.0—262.5°C (lit, 255°C).

Benzotriptycene(III). III was prepared by the reaction of anthracene with 2,3-dehydronaphthalene (XIII), generated from 3-amino-2-naphthoic acid (XII) and isoamyl nitrite, in tetrahydrofuran according to the procedure of Friedman,[7] 11% yield, mp 263.5—265.0°C (lit, 257—258°C).

Dibenzotriptycene (IV). To a mixture of tetracene (1.0 g, 4.3 mmol) and 3-amino-2-naphthoic acid (2.1 g, 11 mmol) in dioxane (500 m*l*) was dropwise added a solution of isoamyl nitrite (10 m*l*, 75 mmol) in dioxane (50 m*l*) for 2 hr at 70°C with stirring in nitrogen atmosphere. After the addition, the reaction mixture was stirred for 30 min at 80°C. Colorless solid obtained by evaporating the solvent under reduced pressure was chromatographed on alumina (150 g). Early benzene fractions (200 m*l*) were collected and the solvent was removed *in vacuo*. The residue was re-chromatographed on silica gel (30 g) in each 100 m*l* fraction using the following solvents: petroleum ether (100 m*l*) and then petroleum ether–carbon tetrachloride (1: 1, 750 m*l*). From the third fraction was obtained 19 mg of white solid, which was recrystallized from acetone to give colorless needles, mp 213.5—214.5°C, of 5,12-dihydrotetracene (lit,[22] mp 212°C). NMR (in $CDCl_3$): τ 5.93 (s, 4H, methylene), 2.1—2.9 (m, 10H, aromatic).

The residue obtained from 4—9th fractions was recrystallized from ethanol to give 582 mg (37.5% based on tetracene) of pure IV, mp 277—280°C. Found: C, 94.98, H, 4.98%; mol wt, 354 (mass spectrometry). Calcd for $C_{28}H_{18}$: C, 94.88, H, 5.12%; mol wt 354. IR (KBr-disk): 890 (s), 882 (s), 739 (s), 562 (s), 477 (s) cm^{-1}.

Tribenzotriptycene (V). According to the procedure of Wittig,[6] the reaction of pentacene with 1,4-dihydronaphthalene-1,4-oxide, followed by treatment of the adduct with hydrochloric acid in acetic anhydride, afforded 28% yield of tribenzotriptycene (V), mp 386.5°C (lit,[6] 387—389°C). The IR spectrum of the compound is completely superimposable on the reported one.

Phthaloyltriptycene (VI). To a stirred mixture of 3-aminoanthraquinone-2-carboxylic acid (1.5 g, 6 mmol) and anthracene (3.2 g, 18 mmol) in dioxane (400 m*l*) was added dropwise a solution of isoamyl nitrite (34 m*l*) in dioxane (58 m*l*) over a period of two hours at 70°C and the mixture was stirred at 85°C for 30 min. After removal of the solvent the residue was chromatographed on alumina (250 g). From benzene fractions 555 mg (24.1%) of V was obtained. Recrystallized from ethyl acetate, mp 341—344°C. Found: C, 87.32; H, 4.23%; mol wt, 384 (mass spectrometry), 413 (vapour pressure osmometry). Calcd for $C_{28}H_{16}O_2$: C, 87.48; H, 4.20%; mol wt, 384. IR (KBr-disk): 1665 (s), 1352 (m), 1324 (s), 1300 (s), 951 (m), 734 (m), 709 (m) cm^{-1}.

Phthaloyl-benzotriptycene (VIII). Through the procedure described for VI, the synthesis of VIII was carried out with 3-aminoanthraquinone-2-carboxylic acid (XV) and tetracene (XIV), except the use of degassed dioxane as a solvent. Chromatography on alumina using benzene gave a 29% yield of VIII. Recrystallized from ethyl acetate, mp 352.0—352.5°C. Found: C, 88.20; H, 4.00; mol wt, 434 (mass spectrometry). Calcd for $C_{32}H_{18}O_2$: C, 88.46; H, 4.18%; mol wt, 434. IR (KBr-disk): 1670 (s), 1659 (s), 1592 (s), 1325 (s), 1300 (s), 954 (m), 742 (m), 714 (m) cm^{-1}.

Naphthotriptycene (VII). A mixture of VI (260 mg, 0.7 mmol) and aluminum tri(cyclohexyl oxide)[9] (3 m*l*) in cyclohexanol (1.5 m*l*) was refluxed for 48 hr. The mixture was poured into water and was stirred for one hour. It was extracted with benzene and the extract was washed with aqueous calcium chloride solution and then water and dried over calcium chloride. Removal of the solvent *in vacuo* gave 83 mg (35%) of VII, which was recrystallized from cyclohexane to give colorless leaflets, mp 287—288°C. Found: C, 94.78; H, 5.02%; mol wt, 354 (mass spectrometry), 349 (vapour pressure osmometry). Calcd for $C_{28}H_{18}$: C, 94.88; H, 5.02%; mol wt, 354. IR (KBr-disk): 907 (m), 733 (s), 625 (s) cm^{-1}.

Benzo-naphtho-triptycene (IX). The reduction of VIII was carried out in a manner similar to that described for VII. Recrystallization of the crude material (yield 33%) from ethyl acetate afforded pure IX as pale yellow columns, mp 295.5—296.0°C. Found: C, 94.98; H, 4.87%; mol wt, 405 (mass spectrometry), 403 (vapour pressure osmometry). Calcd for $C_{32}H_{20}$: C, 95.02; H, 4.98%; mol wt, 404.5. IR (KBr-disk): 902 (m), 887 (m), 882 (m), 736 (s), 629 (m), 572 (m), 511 (m), 473 (m), 459 (m) cm^{-1}.

18) S. I. Weissman, *J. Amer. Chem. Soc.*, **80**, 6462 (1958); F. Gerson and W. B. Martin, Jr., *ibid.*, **91**, 1883 (1969).
19) L. F. Fieser, *ibid.*, **53**, 2329 (1931).
20) W. Ried and F. Anthofer, *Angew. Chem.*, **65**, 601 (1953).
21) L. F. Fieser, "Organic Experiments," D. C. Heath and Co., Maruzen Asian Edi., Tokyo (1964), p. 315.
22) E. Clar, *Chem. Ber.*, **75**, 1271 (1942).

Studies on Aminosugars. XXIX. The Synthesis of 3′-*O*-Methylkanamycin[1,2]

Hamao UMEZAWA, Tsutomu TSUCHIYA, Ryujiro MUTO,* and Sumio UMEZAWA*

Institute of Microbial Chemistry, Shinagawa-ku, Tokyo

**Department of Applied Chemistry, Faculty of Engineering, Keio University, Koganei-shi, Tokyo*

(Received May 11, 1972)

6-*O*-(3-Amino-3-deoxy-α-D-glucopyranosyl)-2-deoxystreptamine, previously synthesized, was masked with ethoxycarbonyl, isopropylidene, and benzyl groups to give 6-*O*-(2-*O*-benzyl-3-deoxy-3-ethoxycarbonylamino-4,6-*O*-isopropylidene-α-D-glucopyranosyl)-*N*,*N*′-diethoxycarbonyl-2-deoxystreptamine, which was condensed with 6-azido-2,4-di-*O*-benzyl-6-deoxy-3-*O*-methyl-α-D-glucopyranosyl chloride by a modified Koenigs-Knorr reaction to give a mixture of α,α- and α,β-diglycoside compounds. Hydrogenation of the azido group and removal of the masking groups gave a mixture of 3′-*O*-methylkanamycin and its diastereomer. The 3′-*O*-methylkanamycin was devoid of antibacterial activity.

Recently, Umezawa and co-workers[3] have clarified the mechanism of the resistance of resistant bacteria in patients to kanamycins and streptomycin, and it was found that these resistant bacteria produce enzymes which inactivate these antibiotics. In the case of kanamycins, 3′-hydroxyl groups are phosphorylated (Fig. 1) by the enzymic reaction and, in the case of streptomycin, the 3-hydroxyl group of *N*-methyl-L-glucosamine moiety is adenylylated[4] by ATP or phosphorylated.[5] It was also proved that resistant *Pseudomonas aeruginosa* to kanamycin produces a similar enzyme[6] which phosphorylates kanamycin from ATP to give kanamycin-3′-phosphate. Furthermore, studies[6] on the substrate specificity of the phosphorylating enzyme using a variety of aminoglycosides showed that

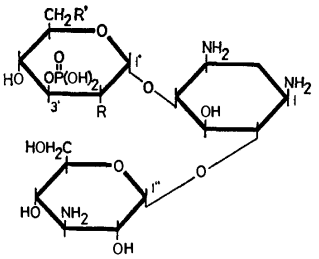

Kanamycin A 3′-phosphate: R=OH, R′=NH_2
Kanamycin B 3′-phosphate: R=NH_2, R′=NH_2
Kanamycin C 3′-phosphate: R=NH_2, R′=OH

Fig. 1.

the whole kanamycin structure is not required for the enzymic reaction and that only 4-*O*-glycosyl-2-deoxystreptamine is required for the enzymic reaction, whereas 3-amino-3-deoxy-D-glucose (3AG) moiety is not involved in binding of the antibiotics with the enzyme.

The above mentioned phosphorylation resistance mechanism suggested that variation of the surroundings of C-3 in the aminosugar moiety attached to C-4 of deoxystreptamine of kanamycins may lead to derivatives that are not susceptible to phosphorylation by the enzyme and active against the resistant bacteria. Our initial approach to such a derivative was the total synthesis of 3′-*O*-methylkanamycin and 3′-deoxykanamycin.

The synthesis has been accomplished by the condensation of 6-azido-2,4-di-*O*-benzyl-6-deoxy-3-*O*-methyl-α-D-glucopyranosyl chloride (**7**) with a masked derivative (**12**) of 6-*O*-(3-amino-3-deoxy-α-D-glucopyranosyl)-2-dexoystreptamine. In this synthesis, we tried to use an azido derivative of glucose for the condensation with an aglycone.

An anomeric mixture of methyl 3-*O*-methyl-D-glucopyranoside (**2**) was prepared by acidic methanolysis of 1,2: 5,6-di-*O*-isopropylidene-3-*O*-methyl-D-glucose[7] (**1**) and the anomers (**2a**, **2b**) were separated by resin column chromatography using Dowex 1×2. The procedure for the separation of the anomers was found to be more convenient than an alternative method[8] through a 4,6-*O*-benzylidene derivative. Preferential tosylation of **2a** and **2b** gave 6-*O*-tosylated product (**3a**, **3b**) in about 60% yields, respectively, and their structures were confirmed by NMR spectra. The tosyl group of **3a** and **3b** was displaced by an azido group with sodium azide in dimethyl formamide (DMF) to give 6-azido derivatives (**4a**, **4b**). Benzylation of **4a** with benzyl chloride and potassium hydroxide in DMF gave 2,4-di-*O*-benzylated derivative (**5a**) in a yield of 82%.

An anomeric mixture of **2** was led to an anomeric mixture of **5** in a yield of 50%, which was hydrolyzed

1) A part of this paper was read by S. Umezawa at Symposium of New Natural Product Syntheses, the 23rd International Congress of Pure and Applied Chemistry at Boston, U.S.A., July 28, 1971; A short communication was reported: S. Umezawa, T. Tsuchiya, R. Muto, Y. Nishimura, and H. Umezawa, *J. Antibiotics*, **24**(4), 274 (1971).

2) The numbering of the kanamycin structure was followed by that described in the following paper: T. Kobayashi, T. Tsuchiya, K. Tatsuta, and S. Umezawa, *ibid.*, **23**(5), 225 (1970).

3) H. Umezawa, *Progress in Antimicrobial And Anticancer Chemotherapy*, **2**, 567 (1970), University of Tokyo Press.; Related references are cited therein; H. Umezawa, M. Okanishi, S. Kondo, K. Hamana, R. Utahara, K. Maeda, and S. Mitsuhashi, *Science*, **157**, Sept. 29 (1967), 1559.

4) H. Umezawa, S. Takazawa, R. Utahara, M. Okanishi, and K. Maeda, *J. Antibiotics*, **21** (1), 81 (1968); *ibid.*, **21**(8), 477 (1968).

5) H. Naganawa, S. Kondo, K. Maeda, and H. Umezawa, *ibid.*, **24** (12), 823 (1971).

6) O. Doi, S. Kondo, N. Tanaka, and H. Umezawa, *ibid.*, **22**(6), 273 (1969).

7) "Methods in Carbohydrate Chemistry," Vol. II, edited by R. L. Whistler and M. L. Wolfrom, Academic Press Inc., New York (1963), p. 147.

8) R. W. Jeanloz and M. Gut, *J. Amer. Chem. Soc.*, **76**, 5793 (1954).

with hydrochloric acid and acetic acid in aqueous methanol to give 6-azido-2,4-di-*O*-benzyl-6-deoxy-3-*O*-methyl-D-glucopyranose (**6**), mp 112—113°C, $[\alpha]_D^{20}$ +108° (*c* 0.9, acetone). Expectedly,[9] in this reaction, the β-anomer (**5b**) was found to be more readily hydrolyzed than the α-anomer (**5a**). Chlorination of **6** with thionyl chloride gave the desired 6-azido-2,4-di-*O*-benzyl-6-deoxy-3-*O*-methyl-α-D-glucopyranosyl chloride (**7**), mp 33—35°C, $[\alpha]_D^{15}$ +184° (*c* 1.1, acetone). The α-anomeric configuration of the chlorine atom was confirmed by the NMR spectrum and optical rotation of **7**.

On the other hand, a partially masked derivative of 6-*O*-(3-amino-3-deoxy-α-D-glucopyranosyl)-2-deoxystreptamine was prepared. Previously in the total syntheses of kanamycins,[10] we prepared a suitably masked derivative of this glycoside and this derivative was expected to be usable again for the present synthesis, however, in the present synthesis, we turned hopefully to use an *N*-ethoxycarbonyl derivative instead of the carbobenzoxy derivative.

Treatment of 6-*O*-(3-amino-3-deoxy-α-D-glucopyranosyl)-2-deoxystreptamine with ethyl chloroformate in aqueous acetone in the presence of sodium carbonate gave tri-*N*-ethoxycarbonyl derivative (**8**) in a 82% yield. Isopropylidenation of **8** with 2,2-dimethoxypropane in the presence of *p*-toluenesulfonic acid at about 40°C afforded a di-*O*-isopropylidene derivative (**9**) in a 84% yield. Benzylation of **9** with benzyl chloride in the presence of barium oxide and barium hydroxide in DMF afforded the benzyl derivative (**10**), which, on deacetonation by treatment with 80% aqueous acetic acid, afforded 6-*O*-(2-*O*-benzyl-3-ethoxycarbonylamino-3-deoxy-α-D-glucopyranosyl)-*N*,*N*'-diethoxycarbonyl-2-deoxystreptamine (**11**), mp 149°C, $[\alpha]_D^{15}$ +77° (*c* 1, pyridine). Controlled isopropylidenation of **11** by treatment with 2,2-dimethoxypropane at 0°C for three hours successfully afforded the desired mono-*O*-isopropylidene derivative (**12**), mp 263°C, $[\alpha]_D^{20}$ +54° (*c* 1, pyridine), in a 60% yield. The orientation of the isopropylidene group in **12** was confirmed by the tritylation of **12** and **11**. When **11** which contains a primary hydroxyl group was tritylated with trityl chloride in pyridine, the product showed the characteristic color-reaction of a trityl derivative when sprayed with sulfuric acid on tlc, while **12** underwent no tritylation by the same procedure. In this connection, we would like to mention about the characteristic feature of the isopropylidene groups in the NMR spectra of the above mentioned compounds. When the NMR spectra of **10** and **12** were compared, it was found that methyl signals ascribable to the 4,5-*O*-isopropylidene group of deoxystreptamine moiety appeared at $\tau\sim8.6$, whereas those of 4,6-*O*-isopropylidene group of 3AG moiety appeared separately at $\tau\sim8.6$ and ~8.7. This clear-cut separation of signals was recognizable only in DMSO-d_6 and not in pyridine-d_5.

In the next place, the monoisopropylidene derivative (**12**) was condensed with the glycosyl chloride (**7**). In analogy to the previous studies on the total syntheses of kanamycins,[10] the condensation was effected by use of mercuric cyanide and Drierite in dioxane-benzene under an extremely anhydrous condition. The product was chromatographed on a silica gel column, affording the desired condensation product (**13**), mp 226°C $[\alpha]_D^{15}$ +92.6° (*c* 0.4, chloroform), in a 14% yield. Expectedly, **13** showed, in the NMR spectrum, the methyl signals of the isopropylidene group separated at τ 8.75 and 8.63, indicating that the group is attached at C-4,6 of the 3AG moiety in conformity with the above-mentioned observation.

Finally, **13** was treated with aqueous acetic acid to remove the isopropylidene group, hydrogenated over palladium black to remove the benzyl groups and treated with barium hydroxide to hydrolyze the *N*-ethoxycarbonylamino groups, affording an anomeric mixture of the 6-*O*-(3-amino-3-deoxy-α-D-glucopyranosyl)-4-*O*-(6-amino-6-deoxy-3-*O*-methyl-D-glucopyranosyl)-2-deoxystreptamine (**14**), mp 167—169°C, $[\alpha]_D^{15}$ +106° (*c* 0.5, water), in a 55% yield. Although paper chromatography of **14** with *n*-butanol–pyridine–water–acetic acid (6:4:3:1) showed a single spot by ninhydrin coloration, the NMR spectrum of **14** showed approximately 0.5 proton of the equatorial H-1 of 6-amino-6-deoxy-3-*O*-methyl-D-glucose moiety at τ 4.63 as doublet ($J\sim3$ Hz), indicating that **14** was an anomeric mixture of a ratio about 1:1.

The position of attachment of 6-amino-6-deoxy-3-*O*-methyl-D-glucosyl moiety to the 2-deoxystreptamine was demonstrated by the periodate oxidation of **14**. The survival of deoxystreptamine in the hydrolyzate of the oxidation mixture was shown by paper chromatography with ninhydrin indicating that the glycosidation did not occur at the C-5 of 2-deoxystreptamine, but at the C-4.

The 3'-*O*-methylkanamycin (**14**) showed no inhibition to *S. aureus*, *E. coli*, *Pseudomonas aeruginosa*, *Mycobacterium* 607 at 100 μg/ml in a nutrient agar, but inhibited *B. subtilis* PCI 219 at 25 μg/ml. It showed partial inhibition of *E. coli* carrying R factor at 100 μg/ml. As reported in the succeeding paper, 3'-deoxykanamycin exhibits a strong antibacterial activity in the similar strength as kanamycin. 3'-*O*-Methyl group was suggested to hinder the binding of 3'-*O*-methyl kanamycin with bacterial ribosomes, because it showed almost no inhibition of poly phenylalanine synthesis on poly U-ribosome system.

Experimental

Infrared spectra (IR) were recorded with a Perkin-Elmer Infrared Spectrophotometer. Nuclear magnetic resonance (NMR) spectra were obtained with a Varian A-60 spectrometer. Tetramethylsilane was used as the internal standard.

9) See, for examples, P. W. Austin, F. E. Hardy, J. G. Buchanan, and J. Baddiley, *J. Chem. Soc.*, **1965**, 1419; R. Gigg and C. D. Warren, *ibid.*, **1965**, 2205.

10) S. Umezawa, S. Koto, T. Tatsuta, and T. Tsumura, *J. Antibiotics*, **21**, 162 (1968); S. Umezawa, K. Tatsuta and S. Koto, *ibid.*, **21**, 367 (1968); S. Umezawa, S. Koto, K. Tatsuta, H. Hineno, Y. Nishimura, and T. Tsumura, *ibid.*, **21**, 424 (1968); S. Umezawa, S. Koto, K. Tatsuta, and T. Tsumura, This Bulletin, **42**, 529 (1969); S. Umezawa, K. Tatsuta, and S. Koto, *ibid.*, **42**, 533 (1969); S. Umezawa, S. Koto, K. Tatsuta, H. Hineno, Y. Nishimura, and T. Tsumura, *ibid.*, **42**, 537 (1969).

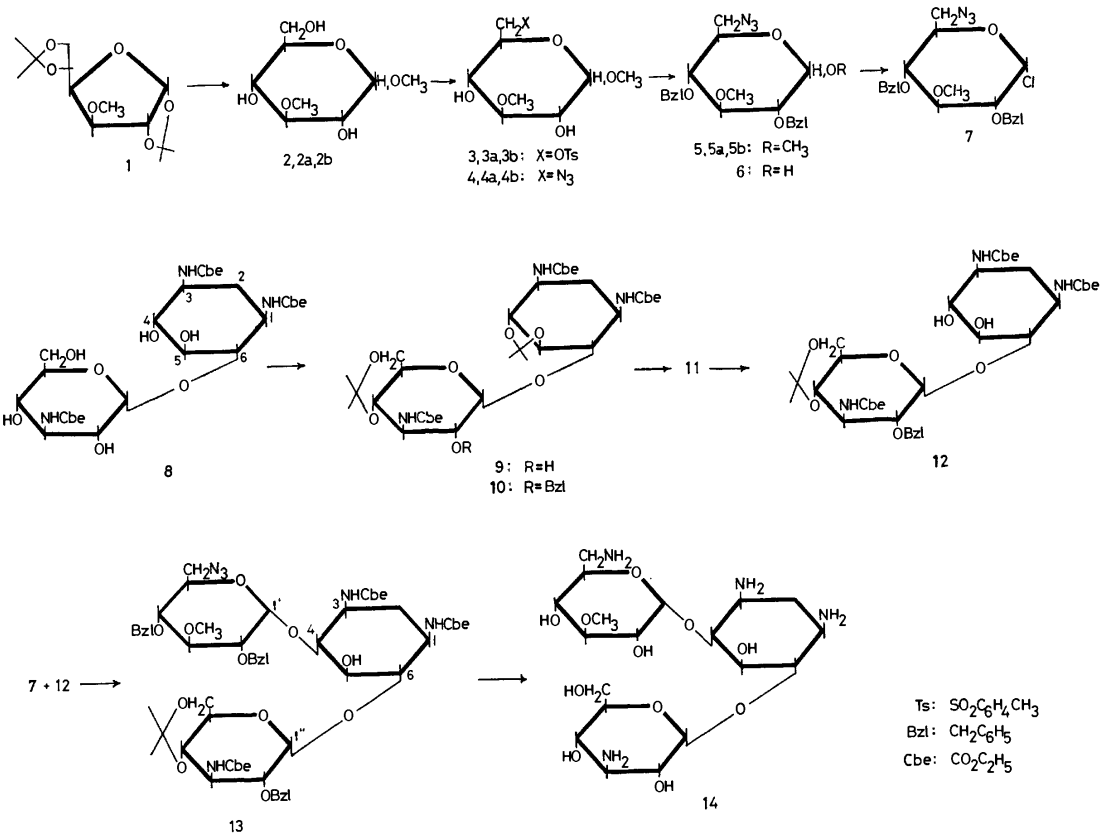

Chart 1.

Thin layer chromatography (tlc) was performed on silica gel and the spots were visualized with sulfuric acid. Paper chromatography was performed on Toyo-Roshi paper No. 50 and the spots were detected with 0.5% ninhydrin in pyridine and heating to 110°.

*Methyl 3-O-Methyl-α-D-glucopyranoside (**2a**) and its β-anomer (**2b**).* A solution of **1** (5.1 g) in methanolic 1% hydrochloric acid (120 m*l*) was refluxed for 7 hr and coevaporated with benzene. The residue was dissolved in methanol and the solution was neutralized with Amberlite IRA 400 (OH form), treated with charcoal and evaporated to give a syrup (3.51 g, 91%). On tlc (acetone–ethyl acetate 3:2), the product showed a single spot (*Rf* 0.6), indicating no contamination with the starting material (R_f 1.0). The syrup (2.76 g) was then chromatographed on a column of Dowex 1×2 (OH form, 400 m*l*) with water. After the first fraction (400 m*l*) was discarded, the eluate was cut into 10 g each. α-Anomer (**2a**) was eluted between tube Nos. 10—17 and β-anomer (**2b**) between Nos. 20—35. Evaporation of the former gave a syrup (1.42 g, 47%) which, on storage, crystallized in needles, mp 80—82°C (lit,[8] 80—81°C), $[\alpha]_D^{25}$ +161° (*c* 1.4, acetone) (lit, +164°); IR (KBr): 840 cm^{-1} (type 2a).

Found: C, 46.30; H, 8.02%. Calcd for $C_8H_{16}O_6$: C, 46.15; H, 7.75%.

Evaporation of the latter fraction gave a syrup (0.98 g, 32%), $[\alpha]_D^{25}$ −33° (*c* 0.8, acetone) (lit [8] −26°); IR 885 cm^{-1} (type 2b).

Found: C, 46.34; H, 7.80%.

*Mthyl 3-O-Methyl-6-O-tosyl-α-D-glucopyranoside (**3a**).* To an ice-cold solution of **2a** (1.42 g) in dry pyridine (28 m*l*, dried over fused sodium hydroxide), tosyl chloride (2 g) was added and the solution was allowed to stand in a refrigerater for 5 hr. After a few drops of water was added, the solution was concentrated. The residue was dissolved in chloroform (200 m*l*) and the solution was washed successively with 5% potassium bisulfate solution, water, saturated sodium bicarbonate solution and water, dried over sodium sulfate and evaporated, giving a syrup. Tlc (ethyl acetate) showed that the syrup contained three components of R_f 0.93 (ditosylated product), 0.61 (**3a**, major) and 0.17 (**2a**). The syrup was then chromatographed on silica gel column (70 g) with ethyl acetate. The ditosylated product was eluted between 160—190 m*l* and **3a** between 240—370 m*l*. The latter fraction was evaporated and the residue was dissolved in benzene. Addition of petroleum ether gave a solid (1.48 g, 60%), mp 100—103°C, $[\alpha]_D^{15}$ +107° (*c* 1, acetone); IR (KBr): 1360, 1170 cm^{-1} ($\nu_{a.s}$ and ν_s SO_2, respectively).

Found: C, 49.98; H, 6.37; S, 8.64%. Calcd for $C_{15}H_{22}O_8S$: C, 49.71; H, 6.12: S, 8.85%.

NMR (in $CDCl_3$): τ 7.54 (3H s, the methyl of a tosyl group), 6.61 (3H s, C(1)-OCH_3), 6.35 (3H s, 3(C)-OCH_3), 6.1—6.8 (4H, m H-2,3,4,5), 5.70 (2H d, H-6,6′; This shows that 6-OH was tosylated. Corresponding signals are not recognized in **2a** and **4a**), 5.33 (1H d, H-1), 2.05—2.75 (4H, AB quartet-like pattern, J~8 Hz, tosyl); $J_{1,2}$ 3 Hz, $J_{5,6}$′ ~$J_{5,6}$′ ~3 Hz.

*Methyl 3-O-Methyl-6-O-tosyl-β-D-glucopyranoside (**3b**).* Compound **2b** (0.98 g) was treated likewise as in the case of **2a** and the product (**3b**) was recrystallized from benzene-petroleum ether to give crystals (1.0 g, 59%), mp 132—133°C, $[\alpha]_D^{15}$ −13.6° (*c* 1.1, acetone).

Found: C, 49.91; H, 6.34; S, 8.99%. Calcd for $C_{15}H_{22}O_8S$: C, 49.71; H, 6.12; S, 8.85%.

*Methyl 6-Azido-6-deoxy-3-O-methyl-α-D-glucopyranoside (**4a**) and its β-Anomer (**4b**).* The anomeric mixture of methyl 3-*O*-methyl-D-glucopyranoside (**2**) was tosylated likewise as described in the case of **3a**, and the product (5.0 g) was dissolved in dry DMF (dried over calcium hydride and supernatant layer was used without distillation). After addition of sodium azide (1.8 g), the mixture was refluxed

for 1 hr. The resulting brown solution was filtered and the filtrate was evaporated with several additions of toluene to remove the remaining DMF. The syrupy residue was dissolved in ethyl acetate and the solution was passed through a short column of silica gel (15 g) with the same solvent; the fraction containing the products (**4a** and **4b**) was collected and evaporated to give a pale yellow syrup (3.14 g, 98%), which had the same R_f-value with that of **3a** or **3b** (R_f 0.61 with ethyl acetate, 0.6 with ethyl acetate–benzene 5: 1 and 0.8 with methyl ethyl ketone), however, the infrared spectrum of the syrup showed no absorption of sulfonyl group but showed that of an azide group (2100 cm^{-1}), indicating that the reaction was completed. Anomers (2.05 g) were separated by chromatography on a column of Dowex 1×2 (OH form, 33×450 mm) with water. After the first fraction (400 m*l*) had been discarded, the eluate was cut into 10 g each. The α-anomer was eluted between tube Nos. 22—28 and the β-anomer between Nos. 34—48. Evaporation of the former afforded a solid (0.56 g), which was recrystallized from benzene to give colorless crystals (0.51 g), mp 88—89°C, $[\alpha]_D^{20}$ +129° (*c* 1, acetone); IR (KBr): 2100 (N_3), 845 cm^{-1} (type 2a).

Found: C, 41.39; H, 6.61; N, 18.30%. Calcd for $C_8H_{15}O_5N_3$: C, 41.20; H, 6.48; N, 18.02%.

Evaporation of the latter fraction followed by recrystallization from benzene gave colorless crystals (0.56 g), mp 110—111°C, $[\alpha]_D^{20}$ −87° (*c* 1, acetone); IR (KBr): 2100 (N_3), 885 cm^{-1} (type 2b).

Found: C, 41.51; H, 6.73; N, 17.89%.

These α- and β-anomers (**4a** and **4b**) were identical with those prepared from the anomerically pure tosylated compounds (**3a** and **3b**), respectively.

*Methyl 6-Azido-2,4-di-*O*-benzyl-6-deoxy-3-*O*-methyl-α-*D*-glucopyranoside (5a) and its β-anomer (5b).* To an ice-cold solution of **4a** (207 mg) in dry DMF (4 m*l*), powdered potassium hydroxide (590 mg) and benzyl chloride (0.6 m*l*) were added in turn and the mixture was stirred for 30 min. at room temperature. Tlc (benzene–methyl ethyl ketone 25: 1) of the reaction mixture showed that the starting material (**4a**, R_f 0) disappeared and **5a** (R_f 0.55) appeared as a sole product. Filtration followed by evaporation gave a syrup, which was coevaporated with toluene several times. The resultant syrup was dissolved in chloroform and the solution was washed with water, dried over sodium sulfate, and evaporated to give a solid (302 mg, 82%), which gradually crystallized on storage, mp 59—61°C, $[\alpha]_D^{15}$ +111° (*c* 1, acetone); IR (KBr): 2100 (N_3), 840 (type 2a; 735, 690 cm^{-1} (phenyl).

Found: C, 64.20; H, 6.58; N, 10.07%. Calcd for $C_{22}H_{27}O_5N_3$: C, 63.90; H, 6.58; N, 10.16%.

Likewise, from the β-anomer (**4b**, 282 mg) **5b** was obtained as needles (392 mg, 79%), mp 62—65°C, $[\alpha]_D^{15}$ +1.7° (*c* 0.9, acetone); IR (KBr): 2100 (N_3), 885 (type 2b); 745, 695 cm^{-1} (phenyl).

Found: C, 64.11; H, 6.94; N, 10.06%.

*6-Azido-2,4-di-*O*-benzyl-6-deoxy-3-*O*-methyl-D-glucopyranose (6)* To an anomeric mixture of **5** (8.12 g) in acetic acid (46 m*l*), 2N hydrochloric acid in 50% aqueous-methanol (15.5 m*l*) was added and the solution was refluxed for 3 hr. Tlc (benzene–methyl ethyl ketone 15: 1) of the reaction mixture showed that the solution contained four components of R_f 0.76 (**5b**), 0.71 (**5a**), 0.5 (**6**), and 0. Evaporation *in vacuo* followed by coevaporation with toluene gave a syrup (2.86 g), which was then chromatographed on a column of silica gel (100 g) with benzene–methyl ethyl ketone (15: 1). After the first fraction (160 m*l*) was discarded, the eluate was cut into 5 g each. A mixture of **5a** and **5b** (rich in **5a**) was eluted between tube Nos. 3—10 and **6** between Nos. 16—35. Evaporation of the latter fraction gave a syrup (1.19 g), which was recrystallized from benzene–petroleum ether to give **6** (1.15 g), mp 112—113°C, $[\alpha]_D^{20}$ +108° (*c* 0.9, acetone; final value); IR (KBr): 3380, 2100; 750, 740, 697 cm^{-1}.

Found: C, 63.36; H, 6.52; N, 10.52%. Calcd for $C_{21}H_{25}O_5N_3$: C, 63.14; H, 6.31; N, 10.52%.

The former fraction was evaporated to give a syrup (1.18 g), which could again be used for hydrolysis to **6**.

When the reaction period exceeded the limit of 3 hr, the product was observed to increase in the undesirable product of R_f 0, decreasing the yield of **6**. NMR of **6** (in $CDCl_3$): τ 6.32 (3H, s, OCH_3), 5.26 (2H s, one of methylenes of benzyls), 5.13 and 5.37 (2H AB quartet; another methylene of benzyls; *J* 11 Hz).

*6-Azido-2,4-di-*O*-benzyl-6-deoxy-3-*O*-methyl-α-*D*-glucopyranosyl Chloride (7).* A solution of **6** (5.0 g) in thionyl chloride (55 m*l*) was allowed to stand for 1 hr at room temperature. Tlc (benzene–methyl ethyl ketone 30: 1) of the reaction mixture showed that the starting material (**6**, R_f 0.15) disappeared and **7** (R_f 0.82) appeared as a main product. Evaporation of the solution followed by coevaporation with toluene gave a syrup, which was then chromatographed on a column of silica gel (90 g) with benzene. The fraction containing **7** (500—800 m*l* portion) was evaporated and the resultant syrup (3.2 g, 61%) crystallized to needles after 2 weeks storage. Mp 33—35°C, $[\alpha]_D^{15}$ +184° (*c* 1.1, acetone).

Found: C, 60.18; H, 6.05; N, 9.85; Cl, 8.78%. Calcd for $C_{21}H_{24}O_4N_3Cl$: C, 60.36; H, 5.79; N, 10.06; Cl, 8.48%.

NMR (in $CDCl_3$): τ 6.20—6.62 (5H, m, H-2,3,4,6,6′), 6.30 (3H s, OCH_3), 5.90 (1H doublet of triplets, H-5), 5.28 (2H s, $C\underline{H}_2C_6H_5$), 5.12 and 5.36 (2H AB quartet, *J* 11 Hz, $C\underline{H}_2C_6H_5$), 3.98 (1H d, H-1), 2.64 and 2.60 (5H singlets, phenyl of benzyls); $J_{1,2}$ 3.2 Hz, $J_{4,5}$ 9.0 Hz, $J_{5,6}=J_{5,6'}\sim3$ Hz.

*N,N′-Diethoxycarbonyl-6-*O*-(3-deoxy-3-ethoxycarbonylamino-α-*D*-glucopyranosyl)-2-deoxysterptamine (8).* To a solution of 6-*O*-(3-amino-3-deoxy-α-D-glucopyranosyl)-2-deoxystreptamine (3AD) (5.52 g) and anhydrous sodium carbonate (5.30 g) in water (55 m*l*), acetone (55 m*l*) was added with vigorous stirring and to the suspension, ethyl chloroformate (5.8 g) was added all at once. An almost clear solution was soon formed with evolution of gas, after that precipitates appeared. Regardless of precipitation, agitation was continued for 18 hr at room temperature. Tlc (benzene–methyl ethyl ketone 4: 1) of the reaction mixture showed a single spot (R_f 0.4). After addition of 2N hydrochloric acid (22 m*l*), the reaction mixture was evaporated *in vacuo*. The residue was then suspended in DMF (200 m*l*), filtered from an insoluble matter and the filtrate was evaporated with several additions of toluene. The resultant residue was dissolved in DMF (40 m*l*) and worked up again as above. The desalted residue was boiled with ethanol (150 m*l*) for a while, cooled, and the insoluble product was taken by filtration; 7.50 g (82%), mp>250°C, $[\alpha]_D^{20}$ +64° (*c* 1, DMF); IR (KBr): 1695 (amide I), 1545 cm^{-1} (amide II).

Found: C, 47.01; H, 7.12; N, 7.83%. Calcd for $C_{12}H_{37}O_{13}N_3$: C, 46.75; H, 6.91; N, 7.79%.

*N,N′-Diethoxycarbonyl-6-*O*-(3-deoxy-3-ethoxycarbonylamino-4,6-*O*-isopropylidene-α-*D*-glucopyranosyl)-4,5-*O*-isopropylidene-2-deoxystreptamine (9).* To a solution of well dried **8** (973 mg) in dry DMF (dried over calcium hydride), dehydrated *p*-toluenesulfonic acid (30 mg, dried *in vacuo* at 100°C in the presence of P_2O_5) and 2,2-dimethoxypropane (1.4 m*l*) were added, and the mixture was allowed to stand for 5 hr at 40°C. Tlc (benzene–methanol 3: 1) of the reaction mixture showed that **8** (R_f 0.37) had completely been consumed and the main product (**9**, R_f 0.74) appeared, being accompanied

by a trace of mono-isopropylidene product (R_f 0.54). After treatment with Amberlite IRA-400 (OH form, 2 ml) resin, the mixture was filtered and the filtrate was evaporated with several additions of toluene to give a thick syrup (1.06 g). Purification was accomplished by dissolving the syrup in methanol–ethanol (1:1) with subsequent addition of petroleum ether; a colorless solid (940 mg, 84%), mp 237—238°C, $[\alpha]_D^{20}$ +41° (*c* 1, pyridine); IR (KBr): 1705, 1540, 1310 (isopropyl), 845 cm^{-1} (type 2a).

Found: C, 52.23; H, 7.55; N, 6.81%. Calcd for $C_{27}H_{45}O_{13}N_3$: C, 52.33: H, 7.32; N, 6.78%.

NMR (in DMSO-d_6): τ 8.85 (9H t, *J* 7 Hz, $CH_2C\underline{H}_3$), 8.70 (3H s, one of methyls of 4,6-*O*-isopropylidene group), 8.61—8.63 (9H singlet-like pattern, other methyls of isopropylidene groups).

*6-O-(2-O-Benzyl-3-deoxy-3-ethoxycarbonylamino-4,6-O-isopropylidene-α-D-glucopyranosyl)-N,N′-diethoxycarbonyl-4,5-O-isopropylidene-2-deoxystreptamine (**10**).* To a mixture of **9** (102 mg), powdered barium oxide (62 mg) and powdered barium hydroxide octahydrate (123 mg) in DMF (2 ml), benzyl chloride (0.14 ml) was added and the suspension was agitated vigorously for 1 hr at room temperature. Tlc (benzene–methanol 5: 1) of the reaction mixture showed that the starting material (R_f 0.52) disappeared and instead, a new spot (**9**, R_f 0.70) appeared. The suspension was filtered with the aid of chloroform (20 ml) and the filtrate was evaporated with several additions of toluene. The chloroform solution of the resultant residue was washed with saturated sodium bicarbonate solution, then with water, dried over sodium sulfate and concentrated. Addition of petroleum ether afforded a colorless solid (112 mg, 96%), which was recrystallized from methanol, mp 286°C, $[\alpha]_D^{20}$ +47° (*c* 1, pyridine); IR (KBr): 1695, 1545, 1375, 845; 735, 700 cm^{-1}.

Found: C, 57.20; H, 7.44; N, 5.81%. Calcd for $C_{34}H_{51}O_{13}N_3$: C, 57.53; H, 7.24; N, 5.92%.

NMR (in DMSO-d_6): τ 8.98 (3H t, *J* 7 Hz, $CH_2C\underline{H}_3$), 8.85 (6H t, *J* 7 Hz,$CH_2C\underline{H}_3$), 8.74 (3H s, isopropylidene), 8.63 (9H s, isopropylidene), 2.77 (5H s, phenyl).

*6-O-(2-O-Benzyl-3-deoxy-3-ethoxycarbonylamino-α-D-glucopyranosyl)-N,N′-diethoxycarbonyl-2-deoxystreptamine (**11**).* A suspension of **10** (3.36 g) in 80% aqueous acetic acid (100 ml) was heated for 10 min at 80°C. Tlc (benzene–methanol 5: 2) of the solution showed that the starting material (**10**, R_f 0.80) disappeared and instead, **11** (R_f 0.58) appeared as a sole product. The solution was evaporated with several additions of toluene-methanol. The resultant residue was dissolved in methanol, and the solution was treated with Amberlite IRA-400 (OH form), then with active charcoal. Concentration of the solution to about 100 ml followed by cooling gave a colorless crystals (2.58 g, 87%), mp 149°C, $[\alpha]_D^{15}$ +77° (*c* 1, pyridine); IR (KBr): 3340, 1690, 1545 cm^{-1}.

Found: C, 53.15; H, 6.93; N, 6.53%. Calcd for $C_{28}H_{43}O_{13}N_3$: C, 53.41; H, 6.88; N, 6.67%.

*6-O-(2-O-Benzyl-3-deoxy-3-ethoxycarbonylamino-4,6-O-isopropylidene-α-D-glucopyranosyl)-N,N′-diethoxycarbonyl-2-deoxystreptamine (**12**).* To an ice-cold solution of well dried **11** (1.76 g, 2.8 mmol) in dry DMF (35 ml, dried over calcium hydride), dehydrated *p*-toluenesulfonic acid (24 mg) and 2,2-dimethoxypropane (1.46 g, 14 mmol) were added and the mixture was allowed to stand for 3 hr at 0°C. Tlc (benzene–methanol 5: 1) of the reaction mixture showed that three components, namely, **10** (R_f 0.66), **11** (R_f 0.30) and **12** (R_f 0.54, major) were contained. After treatment with methanol-washed Amberlite IRA-400 (OH form), the mixture was filtered and the filtrate was evaporated with several additions of toluene to give a colorless powder (1.8 g). Since the powder had only very limited solubility against the solvent systems tested, several attempts to separate the components by column chromatography, however, were unsuccessful. The suspension of the powder (1.8 g) in benzene (60 ml) was refluxed for 15 min, cooled and filtered. Tlc showed that the benzene-insoluble material (1.50 g) contained **11** and **12**. The insoluble material was treated with warm chloroform and an insoluble part was removed. The chloroform-soluble portion (1.28 g) was then dissolved in dioxane (15 ml) and the solution was diluted with petroleum ether (100 ml) to give pure **12** (1.12 g, 60%), mp 263°C, $[\alpha]_D^{20}$ +54° (*c* 1, pyridine); IR (KBr): 3340, 1695, 1545, 1375; 750, 690 cm^{-1}.

Found: C, 55.12; H, 7.14; N, 6.15%. Calcd for $C_{31}H_{47}O_{13}N_3$: C, 55.60; H, 7.07; N, 6.27%.

NMR (in DMSO-d_6): τ 8.95 (3H, t, *J* 7 Hz, $CH_2C\underline{H}_3$), 8.84 (6H, t, *J* 7 Hz, $CH_2C\underline{H}_3$), 8.72 (3H s, isopropylidene), 8.61 (3H s, isopropylidene), 2.63 (5H, s, phenyl).

*Tritylation of **12** and **11**.* To a solution of **12** (one mol. equiv.) in pyridine, trityl chloride (2 mol. equiv.) was added and the solution was allowed to stand for 4 days at 27°C. Tlc (benzene–methanol 5: 1) of the reaction mixture showed that the starting material (**12**) was left unchanged throughout the reaction. On the other hand, by the same tritylation as mentioned above, the deacetonated compound **11** (R_f 0.30) was changed to a derivative which had R_f 0.56 and showed the characteristic yellow coloration on spraying sulfuric acid on tlc, indicating the presence of trityl group. These facts indicated that, in the compound **12**, the isopropylidene group is not attached to the deoxystreptamine moiety, but to C-4,6 positions of the 3-amino-3-deoxyglucose moiety.

*4-O-(6-Azido-2,4-di-O-benzyl-6-deoxy-3-O-methyl-D-glucopyranosyl)-6-O-(2-O-benzyl-3-deoxy-3-ethoxycarbonylamino-4,6-O-isopyropylidene-α-D-glucopranosyl)-N,N′-diethoxycarbonyl-2-deoxy streptamine (**13**).* Solvents used in this reaction were thoroughly dried as follows: purified dioxane was refluxed with sodium metal for 1 hr just before use and the supernatant layer was used; purified benzene was dried over $LiAlH_4$ overnight and the supernatant layer was used.

To a mixture of **12** (558 mg, 1 mol. equiv.), mercuric cyanide (836 mg) and freshly prepared Drierite (800 mg) in dry dioxane (6 ml), a solution of **7** (455 mg, 1.3 mol. equiv.) in dry benzene (6 ml) was added and the mixture was heated under vigorous stirring for 5 hr at 100—105°C in a pressure bottle. During the reaction period, absorption of the moisture from the air was avoided strictly, otherwise the yield of **13** become very poor with the formation of undesirable compound (R_f 0.58) mentioned below. The reaction mixture was poured into a saturated sodium bicarbonate solution with stirring and the product was extracted with chloroform. After dried over sodium sulfate, the chloroform solution was concentrated and diluted with petroleum ether to give a colorless powder (500 mg). Tlc (benzene–methanol 5: 1) of the product showed the presence of at least four components: The desired product (**13**, R_f 0.68, major), a deacetonated product (R_f 0.58) and the starring materials **12** (R_f 0.54) and **7** (R_f 1.0; **6** will also be included). The powder was chromatographed, without delay, on a column of silica gel (50 g) with benzene–methanol–ammonia saturated methanol[11] (5: 0.75: 0.25) and the fraction containing **13** (85—110 ml portion) was evaporated to dryness. The residue was treated with dioxane–petroleum ether to give a colorless solid (119 mg, 14%), mp 226°C, $[\alpha]_D^{15}$ +92.6° (*c* 0.4, $CHCl_3$); IR (KBr): 2100, 1700, 1535, 1370; 740, 695 cm^{-1}.

Found: C, 59.23; H, 6.78; N, 8.11%. Calcd for $C_{52}H_{70}$-

11) Since the silica gel is somewhat acidic and was found to cause the hydrolysis of the isopropylidene group, a small quantity of ammonia was added to the developer.

$O_{17}N_6$: C, 59.42; H, 6.71; N, 8.00%.

NMR (in DMSO-d_6): τ 8.94 (3H t, J 7 Hz, $CH_2C\underline{H}_3$), 8.86 (6H, t, J 7 Hz, $CH_2C\underline{H}_3$), 8.75 (3H s, isopropylidene), 8.63 (3H s, isopropylidene), 2.72, 2.73, 2.76 (5H, singlets, phenyl).

*6-O-(3-Amino-3-deoxy-α-D-glucopyranosyl)-4-O-(6-amino-6-deoxy-3-O-methyl-D-glucopyranosyl)-2-deoxystreptmine (**14**).*
A suspension of **13** (212 mg) in 80% aqueous acetic acid (4 m*l*) was heated at 80°C for 5 min. The resultant solution was evaporated with several additions of toluene to give a solid (200 mg), which had a R_f-value of 0.58 (by tlc with benzene–methanol 5: 1) and, in its NMR spectrum (in DMSO-d_6), showed no signals corresponding to an isopropylidene group. Other clear signals were: τ 8.95 (3H t, J 7 Hz, $CH_2C\underline{H}_3$), 8.83 (6H t, J 7 Hz, $CH_2C\underline{H}_3$), 2.61, 2.62, 2.65 (each 5-proton singlet, phenyl of benzyls). A methoxyl signal was not clear by being superimposed with other signals.

The solid was then suspended in a mixture of water (4.3 m*l*) and methanol (7 m*l*), and after the addition of a few drops of acetic acid, the mixture was hydrogenated with freshly prepared palladium black and hydrogen under pressure (30 lb/sq. inch) at 45°C for 2 hr. Water (5 m*l*) was added and the reaction was continued for additional 10 hr. The resultant solution was filtered and the filtrate was evaporated to give a solid (~100 mg), which had a R_f-value 0.26 on tlc with benzene–methanol (1: 2). Its infrared spectrum showed no absorption of azide (2100 cm^{-1}) and benzyl groups (~700 cm^{-1}) but showed the absorptions of amide groups (1700, 1550 cm^{-1}). By NMR spectroscopy (in D_2O), it showed also no aromatic peaks (τ 2—3). Other clear signals were: τ 8.78 (3H t, J 7 Hz), 8.74 (6H t, J 7 Hz), 4.84 (1H d, J ~3 Hz, H-1 of 3AG moiety), 4.62 (approximately 0.5 proton doublet, J ~ 3 Hz, H_{eq}-1 of 6-amino-6-deoxy-D-glucose moiety).

The solid (100 mg) was then heated with 10% solution of barium hydroxide octahydrate (5 m*l*) at 100°C for 7 hr, and then neutralized with sulfuric acid. The resultant precipitate was removed by filtration and the filtrate was concentrated. The residue was chromatographed on a column Dowex 1×2 (OH form, 10×100 mm) with water. Ninhydrin-positive fractions were collected and evaporated to give a crystalline product (**14**); 55 mg (55%), mp 167—169°C, $[\alpha]_D^{15}$ +106° (*c* 0.5, water). By paper chromatography with *n*-butanol–pyridine–water–acetic acid (6:4:3:1), it showed single spot of R_{fKM}[12] 2.2.

Found: C, 46.20; H, 7.47; N, 11.00%. Calcd for $C_{14}H_{38}O_{11}N_4$: C, 45.78; H, 7.68; N, 11.24%.

NMR (in D_2O): τ 6.37 (3H s, OCH_3); this singal is absent in the NMR of kanamycin; 4.95 (1H d, J ~3 Hz), 4.63 (~0.5 H d, J ~3 Hz). The whole pattern was closely resemble to that of kanamycin free base.

Bioassay. The anomeric mixture (approximately 1:1) of 3′-*O*-methylkanamycin (**14**) only inhibited the growth of *Bacillus subtilis* PCI 219 completely at a dilution 25 mcg/m*l*, but showed no inhibition against several kinds of strains such as *M. pyogenes* var. *aureus* 209P, *E. coli* K-12, *K. pneumoniae*, *Ps. aeruginosa*, *Mycobacterum* 607 and *M. phlei*, respectively, at 100 mcg/m*l* in nutrient agar.

The authors wish to thank Dr. Masa Hamada and members of the Institute of Microbial Chemistry for bioassay and Mr. Saburo Nakada for the elemental analysis. The authors also wish to thank Messrs. Hisamasa Abe and Kohei Watanabe for their techinical assistance.

12) R_f-value relative to kanamycin, which is taken as 1.

BULLETIN OF THE CHEMICAL SOCIETY OF JAPAN, VOL. 45, 2847—2851 (1972)

Studies on Aminosugars. XXX. The Synthesis of 3′-Deoxykanamycin[1,2]

Sumio UMEZAWA, Yoshio NISHIMURA, Hirokuni HINENO, Kohei WATANABE, Soichiro KOIKE, Tsutomu TSUCHIYA, and Hamao UMEZAWA*

Department of Applied Chemistry, Faculty of Engineering, Keio University, Hiyoshi-cho, Kohoku-ku, Yokohama

**Institute of Microbial Chemistry, Shinagawa-ku, Tokyo*

(Received May 11, 1972)

3′-Deoxykanamycin has been totally synthesized from 6-*O*-(2-*O*-benzyl-3-deoxy-3-ethoxycarbonylamino-4,6-*O*-isopropylidene-α-D-glucopyranosyl)-*N*,*N*′-diethoxycarbonyl-2-deoxystreptamine and 6-azido-2,4-di-*O*-benzyl-3,6-dideoxy-α-D-*ribo*-hexopyranosyl chloride. It has been found that the 3′-deoxykanamycin has strong antibacterial activity not only against common bacteria but also against kanamycin-resistant bacteria.

In a preceding paper[3] we described the synthesis of 3′-*O*-methylkanamycin as an initial approach to an active kanamycin derivative against resistant bacteria. However, the derivative was found to be inactive. The lack of activity is thought to be due to the presence of the *O*-methyl group at C-3′ hindering its binding to bacterial ribosome. Consequently, we undertook to replace the 3′-hydroxyl group by hydrogen, namely the synthesis of 3′-deoxykanamycin.

The synthesis has been accomplished by the condensation of 6-azido-2,4-di-*O*-benzyl-3,6-dideoxy-α-D-

1) A part of this paper was read by S. Umezawa at Symposium of New Natural Product Syntheses, the 23rd International Congress of Pure and Applied Chemistry at Boston, U.S.A., July 28, 1971.

2) Short communication: S. Umezawa, T. Tsuchiya, R. Muto, Y. Nishimura, and H. Umezawa, *J. Antibiotics*, **24**, 274 (1971).

3) H. Umezawa, T. Tsuchiya, R. Muto, and S. Umezawa, This Bulletin, **45**, 2842 (1972).

ribo-hexopyranosyl chloride (**10**) with masked derivative[3] (**11**) of 6-*O*-(3-amino-3-deoxy-α-D-glucopyranosyl)-2-deoxystreptamine (3AD).

The starting material, methyl 4,6-*O*-benzylidene-3-deoxy-α-D-*ribo*-hexopyranoside (**1**) was prepared from methyl 4,6-*O*-benzylidene-2,3-di-*O*-tosyl-α-D-glucopyranoside and lithium aluminium hydride according to a modified procedure[4] of the method of Vis and Karrer.[5] Debenzylidenation of **1** in aqueous acetic acid gave methyl 3-deoxy-α-D-*ribo*-hexopyranoside (**2**). Preferential tosylation of **2** followed by acetylation gave a 6-*O*-tosyl-2,4-di-*O*-acetyl derivative (**3**) in a yield of 39%. The tosyl group of **3** was then displaced by an azide group with sodium azide in DMF giving a 6-azide derivative (**4**) in a yield of 76%. Deacetylation of **4** followed by benzylation with benzyl bromide and barium oxide-barium hydroxide octahydrate in DMF gave a 6-azido-2,4-di-*O*-benzyl derivative (**6**) in a yield of 81%. The NMR spectrum of **6** showed the following coupling constants: $J_{2,3_{ax}}=J_{3_{ax},4}=J_{3_{eq},3_{ax}}$ ~11 Hz and these values indicated that **6** had a ribopyranoside structure. The retension of configuration in **6** showed that the displacement of the tosyl group of **3** by azide ion occured at C-6, indicating preferential tosylation occured at C-6 of 2. Hydrolysis of **6** by refluxing with hydrochloric acid in water-methanol-acetic acid gave 6-azido-2,4-di-*O*-benzyl-3,6-dideoxy-D-*ribo*-hexopyranose (**7**) in a yield of 75%. The high yield of the hydrolysis product (**7**) is noteworthy, since hydrolysis of glycosidic bond of a 2-*O*-benzylated glycoside is generally fairly slow[6] and the prolonged reaction causes the decomposition lowering the yield. The high yield of **7** may be ascribed to the absence of any substituents at C-3, causing an easy approach of hydrogen ion to the anomeric center. Chlorination of **7** with cold thionyl chloride gave a syrup of the desired 6-azido-2,4-di-*O*-benzyl-3,6-dideoxy-α-D-*ribo*-hexopyranosyl chloride (**10**) in a yield of 61%. The α-anomeric configuration of the chloride atom was confirmed by the NMR spectrum, in which H-1_{eq} resonated at τ 3.83 (J 3.5 Hz) and no other signals ascribable to H-1 were observed.

Since, as described above, the yield of the step of the preferential tosylation of **2** was low, an alternative method was searched. Treatment of **1** with *N*-bromosuccinimide according to the method of Hanessian[7] gave methyl 4-*O*-benzoyl-6-bromo-3,6-dideoxy-α-D-*ribo*-hexopyranoside (**8**) in a yield of 85%. Displacement of the bromine atom with an azide ion in DMF proceeded smoothly and the corresponding 6-azido derivative (**9**) was obtained in a yield of 81%. Removal of the benzoyl group gave a derivative identical with **5** (methyl 6-azido-3,6-dideoxy-α-D-*ribo*-hexopyranoside) prepared by the former route. Thus the new route was proved to be superior to the former.

The condensing partner, 6-*O*-(2-*O*-benzyl-3-deoxy-3-ethoxycarbonylamino-4,6-*O*-isopropylidene-α-D-glucopyranosyl)-*N*,*N*'-diethoxycarbonyl-2-deoxystreptamine (**11**) has been prepared by the method described in a preceding paper[3] starting from 3AD. Condensation of **10** with **11** was carried out in a strictly anhydrous condition as described in a preceding paper.[3] The solution of **10** and **11** in dry benzene-dioxane (3:1) was refluxed for 15 hr in the presence of mercuric cyanide and Drierite and the main condensation product, 4-*O*-(6-azido-2,4-di-*O*-benzyl-3,6-dideoxy-α-D-

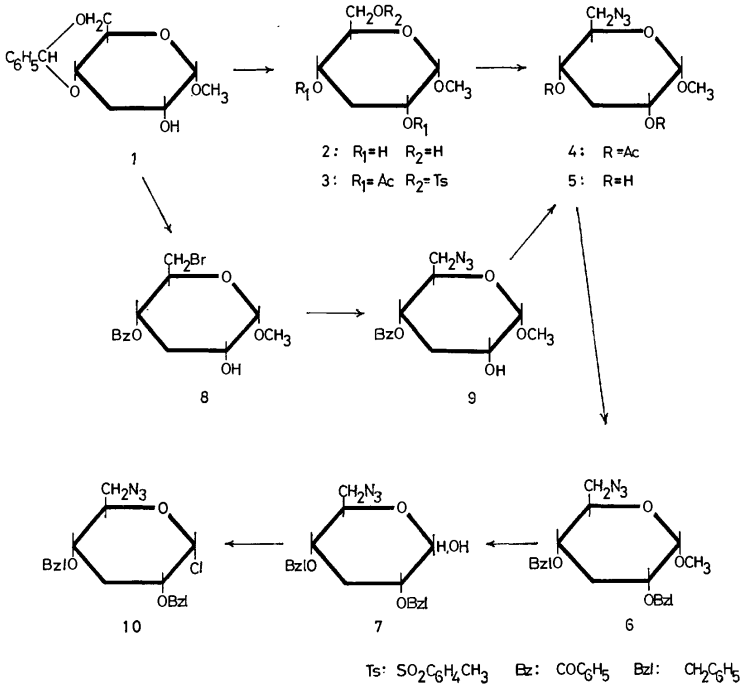

Chart 1.

4) S. Umezawa, T. Tsuchiya, and H. Hineno, This Bulletin, **43**, 1212 (1970).

5) E. Vis and P. Karrer, *Helv. Chim. Acta*, **37**, 378 (1954).

6) See, for example, P. W. Austin, F. E. Hardy, J. G. Buchanan, and J. Baddiley, *J. Chem. Soc.*, **1965**, 1419; R. Gigg and C. D. Warren, *ibid.*, **1965**, 2205.

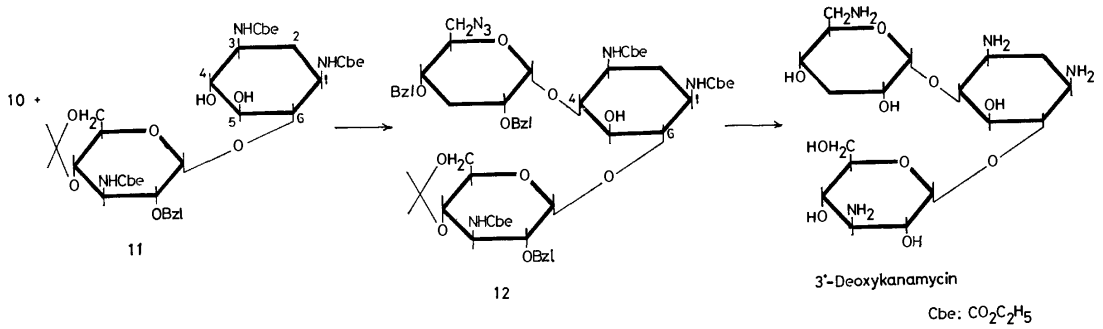

Chart 2.

ribo-hexopyranosyl)-6-*O*-(2-*O*-benzyl-3-deoxy-3-ethoxycarbonylamino-4,6-*O*-isopropylidene-α-D-glucopyranosyl)-*N*,*N*′-diethoxycarbonyl-2-deoxystreptamine (**12**) was isolated by column chromatography in a yield of 25%. The structural proof of the product was obtained by its elemental analysis, infrared and NMR spectra, confirming the presence of an azide, three *O*-ethyls, three benzyls, and an isopropylidene group. The sharp melting point, the chromatographycal homogeneity and the high positive rotation ($[\alpha]_D^{20}=+97°$, *c* 0.9, pyridine) indicated that the product was in a highly pure state and had 4-*O*-α-D-glycoside configuration. In the NMR spectrum, the signals assignable to the anomeric proton (H-1′) were not clear, overlapping with other signals.

The condensation product (**12**) was then deacetonated with 80% acetic acid and the azido group was reduced with Raney nickel and hydrogen to an amino group. The product was *N*-acylated with ethoxycarbonyl chloride and debenzylated with palladium black and hydrogen to give the tetra-*N*-ethoxycarbonyl derivative. Since the reduction of an azido group with consecutive removal of benzyl groups with palladium black sometimes[8] causes the damage[9] of the amino group liberated, the amino group was acylated in advance of the debenzylation. Finally, de-*N*-acylation followed by column chromatography with Amberlite CG50 and 0—0.3N ammonia yielded 3′-deoxykanamycin, manely, 6-*O*-(3-amino-3-deoxy-α-D-glucopyranosyl)-4-*O*-(6-amino-3,6-dideoxy-α-D-*ribo*-hexopyranosyl)-2-deoxystreptamine, $[\alpha]_D^{20}+146°$ (*c* 0.2, water).

3′-Deoxykanamycin thus synthesized showed[2] antibacterial activity in the similar strength as kanamycin and moreover, it showed inhibition against resistant *E. coli* carrying R factor, resistant *Staphylococci*, and *Pseudomonas aeruginosa*. This result is in accord with expectation based on the resistant mechanism.

Experimental

Infrared spectra (IR) were recorded with a Perkin-Elmer Infrared Spectrophotometer. Nuclear magnetic resonance (NMR) spectra were recorded with a Varian A-60D spectrometer. Tetramethylsilane was used as the internal standard. Thin layer chromatography (tlc) was performed on silica gel and the spots were visualized with sulfuric acid. Paper chromatography was performed on Toyo-Roshi paper No. 50 and the spots were detected with 0.5% ninhydrin in pyridine and heating to 110°C.

Methyl 3-Deoxy-α-D-ribo-hexopyranoside (2). A solution of **1** (1.59 g) in aqueous acetic acid (1:2, 50 m*l*) was heated at 100°C for 10 min. The solution was evaporated and the residue was treated with water and ether. After the ether layer was discarded, the aqueous solution was filtered, evaporated and coevaporated with toluene to give a syrup, 1.00 g, $[\alpha]_D^{20}+124°$ (*c* 1, water) (lit,[10] $+125.1°$ (*c* 2.3, water)).

Methyl 2,4-Di-O-acetyl-3-deoxy-6-O-tosyl-α-D-ribo-hexopyranoside (3). To a cold (−10°C) solution of **2** (1.61 g) in dry pyridine (75 m*l*), *p*-toluenesulfonyl chloride (1.81 g) was added and the mixture was stirred at the temperature for 3 hr and allowed to stand at 0°C overnight. Tlc (ethyl acetate) of the reaction mixture showed three spots corresponding to **2** (R_f 0.21), the monotosyl derivative (R_f 0.55, major) and the ditosyl derivative (R_f 0.93). Acetic anhydride (5.6 m*l*) was added and the mixture was allowed to stand at room temperature overnight. The solution was evaporated and the residue was extracted with chloroform. The solution was washed with water, dried over sodium sulfate and evaporated to give a syrup (3.47 g). Tlc (benzene–ethyl acetate 6:1) of the syrup showed three spots of R_f 0.34, 0.45 (major) and 0.57. The syrup was chromatographed on a column of silica gel (100 g) with benzene–ethyl acetate (5:1) and the fraction containing **3** (360—510 m*l*, R_f 0.45) was evaporated to give a syrup, 1.47 g (39%), $[\alpha]_D^{18}+108°$ (*c* 1, $CHCl_3$).

Found: C, 52.07; H, 5.92; S, 7.58%. Calcd for $C_{18}H_{24}O_9S$: C, 51.91; H, 5.81; S, 7.70%.

NMR (in $CDCl_3$): τ 8.00 and 7.94 (both 3H singlets, OAc), 8.3—7.7 (2H m, H-3,3′), 7.56 (3H s, CH_3Ph), 6.68 (3H s, OCH_3), 6.35—6.0 (1H m, H-5?), 6.0—5.7 (2H m, H-6,6′?), 5.6—5.15 (3H m; the signal pattern in this area was quite resemble with that of **4** at τ 5.5—5.0. Therefore these signals could be assigned to H-1,2 and 4.

Methyl 2,4-Di-O-acetyl-6-azido-3,6-dideoxy-α-D-ribo-hexopyranoside (4). A mixture of **3** (0.98 g) and sodium azide (1.6 g) in dry DMF (40 m*l*, dried over calcium hydride) was stirred at 145°C for 1.5 hr. The resulting yellow solution was filtered, evaporated, and coevaporated with toluene to give a syrup. Tlc (benzene–ethyl acetate 6:1) of the syrup showed two spots of R_f 0.55 (major, **4**) and 0.45 (**3**), the former being orange when sprayed with sulfuric acid. Chromatography with silica gel (100 g) and the same solvent system gave a pale yellow syrup, 0.51 g (76%), $[\alpha]_D^{18}+121°$C (*c* 1, $CHCl_3$); IR: 2100, 1745, 1445, 1370 cm^{-1}.

Found: C, 46.07; H, 6.03; N, 14.65%. Calcd for $C_{11}H_{17}N_3O_6$: C, 45.99; H, 5.97; N, 14.62%.

8) Y. Nishimura, T. Tsuchiya, and S. Umezawa, This Bulletin **44**, 2521 (1971).

9) Use of fresh palladium black prepared just before use also is of importance, as described in the preceding paper.[3]

10) E. J. Hedgley, W. G. Overend, and R. A. C. Rennie, *J. Chem. Soc.*, **1963**, 4701.

NMR (in $CDCl_3$): τ 8.00 and 7.97 (both 3H singlets, OAc), 8.4—7.5 (2H m, H-3.3′), 6.74 (2H d, J 5 Hz, H-6,6′), 6.58 (3H s, OCH_3), 6.16 (1H quintet, J 5,5 and ~10 Hz, H-5), 5.5—5.0 (3H m, H-1,2,4); $J_{4,5}$~10 Hz, $J_{5,6}=J_{5,6'}$ 5Hz. Comparison of the signal pattern of **3** and **4** showed that the H-6,6′ protons which appeared in **4**, as a doublet at τ 6.74, resonated at τ 5.85 in **3**, indicating the presence of a 6-*O*-tosyl group in **3**.

*Methyl 6-Azido-3,6-dideoxy-α-*D*-ribo-hexopyranoside (5).*

a) From 4: To a solution of **4** (0.51 g) in methanol (10 m*l*), a piece of sodium metal was added and subsequent procedures were carried out in a usual manner; a pale yellow syrup, 0.30 g (84%), $[\alpha]_D^{18}$ +142° (*c* 1, $CHCl_3$); IR: 3420 (s), 2960, 2100 (sharp), 1450, 1280, 1150, 1050, 1015, 970, 910, 840, 755 cm^{-1}.

Found: C, 41.45; H, 6.53; N, 20.49%. Calcd for $C_7H_{13}N_3O_4$: 41.37; H, 6.45; N, 20.68%.

NMR (in $CDCl_3$): τ 6.47 (3H s, OCH_3), 5.30 (1H d, J 3.5 Hz. H-1),

b) From 9: A solution of **9** in methanol was treated likewise as described above. Yield 97%.

*Methyl 6-Azido-2,4-di-O-benzyl-3,6-dideoxy-α-*D*-ribo-hexopyranoside (6).* To a solution of **5** (0.57 g) in DMF (12 m*l*), powdered barium oxide (2.2 g) and powdered barium hydroxide octahydrate (4.6 g) were added and to the suspension, benzyl bromide (5 m*l*) was stirred in dropwise under vigorous stirring at room temperature and the mixture was agitated overnight. Chloroform (80 m*l*) was added and the mixture was filtered through a layer of celite. The filtrate was evaporated and coevaporated with toluene to give a syrup, which showed four spots of R_f 0.80 (**6**, major), 0.20 (slight), 0.05 (slight) and 0 (slight) on tlc with benzene–ethyl acetate (10: 1). The syrup was chromatographed on a short column of silica gel (30 g) with the same solvent system and the fraction containing **6** was collected and evaporated to give a pale yellow syrup, 0.87 g (81%), $[\alpha]_D^{19}$ +90° (*c* 1, $CHCl_3$); IR: 2100, 735, 700 cm^{-1}.

Found: C, 65.84; H, 6.49; N, 10.99%. Calcd for $C_{21}H_{25}N_3O_4$: C, 65.78; H, 6.57; N, 10.96%.

NMR (in $CDCl_3$): τ 8.10 (1H q, J ~11 Hz, H_{ax}-3), 7.69 (1H sextet, J 4.5, 4.5, and 11 Hz, H_{eq}-3), 6.56 (3H s, OCH_3), 6.9—6.0 (5H m, H-2,4,5,6,6′), 5.58 and 5.38 (each 1H doublet (J 11.5 Hz) forming an AB quartet centered at 5.48, C(2?) $OC\underline{H}_2C_6H_5$), 5.40 (2H s, C(4?)$OC\underline{H}_2C_6H_5$), 5.28 (1H d, J 3.5 Hz, H-1), 2.65 and 2.62 (both 5H singlets, $OCH_2C_6\underline{H}_5$).

*6-Azido-2,4-di-O-benzyl-3,6-dideoxy-*D*-ribo-hexopyranose (7).* To a solution of **6** (0.51 g) in acetic acid (18 m*l*), 2N hydrochloric acid in 50% aqueous methanol (6 m*l*) was added and the solution was refluxed for 1.5 hr. After neutralization with sodium hydrogen carbonate, the solution was filtered, and the filtrate was evaporated to give a residue. The chloroform solution of the residue was washed with water, dried over sodium sulfate and evaporated to give a syrup, which, on tlc with benzene–ethyl acetate (10:1), showed three spots of R_f 0.80 (**6**, minor), 0.40 (**7**, major) and 0.0. The syrup was chromatographed on a short column of silica gel with the same solvent system and the fraction containing **7** was collected and evaporated to give a pale yellow syrup, 0.37 g (75%), $[\alpha]_D^{18}$ +75° (*c* 1, $CHCl_3$; the final value); IR: 2100, 740, 700 cm^{-1}.

NMR (in $CDCl_3$): The whole pattern of **7** was fairly resemble to that of **6**. However an anomeric proton appeared at τ 4.75 (J 3.5 Hz) in the strength of approximately 0.55 proton. Hence, **7** will be an anomeric mixture of approximately α:β-anomer 55: 45 at least in chloroform solution.

Found: C, 64.90; H, 6.61; N, 11.12%. Calcd for $C_{20}H_{23}N_3O_4$: C, 65.02; H, 6.28; N, 11.38%.

*Methyl 4-O-Benzoyl-6-bromo-3,6-dideoxy-α-*D*-ribo-hexopyranoside (8).* To a solution of **1** (19.6 g) in dry carbon tetrachloride (500 m*l*), *N*-bromosuccinimide (14.4 g) and barium carbonate (30 g) were added and the mixture was refluxed for 1.5 hr. The resulting yellow solution was filtered and the filtrate was washed with 2% sodium hydrogen carbonate solution and with water, dried over sodium sulfate, and evaporated to give a syrup, 21.7 g (85%), $[\alpha]_D^{18}$ +169° (*c* 1, $CHCl_3$); R_f 0.54 on tlc with benzene–ethyl acetate (1: 1) (**1**, R_f 0.45); IR (KBr): 3430, 1725, 710 cm^{-1}.

Found: C, 48.98; H, 4.92; Br, 23.47%. Calcd for $C_{14}H_{17}O_5Br$: C, 48.71; H, 4.97; Br, 23.15%.

NMR (in $CDCl_3$); τ 8.13 (1H, q, J 11.5 Hz, H_{ax}-3), 7.56 (1H sextet, J 5,5 and 11.5 Hz, H_{eq}-3), 6.45 (3H s, OCH_3), 6.8—5.8 (4H m), 5.22 (1H d, J 3.5 Hz, H-1), 5.03 (1H octet, J 5,10 and 11.5 Hz, H-4), 2.8—1.8 (5H m, typical for benzoyl protons).

*Methyl 6-Azido-4-O-benzoyl-3,6-dideoxy-α-*D*-ribo-hexopyranoside (9).* To a solution of **8** (9.5 g) in dry DMF (180 m*l*), sodium azide (9.0 g) was added and the mixture was stirred at 140°C for 1.5 hr. Tlc (benzene–ethyl acetate 1: 1) showed that **8** and **9** had an identical R_f value, but they were distinguished each other by the difference in coloration. After filtration, the solution was evaporated and the residue was dissolved in chloroform. The solution was washed with water, dried over sodium sulfate and evaporated to give a syrup. To remove color impurities, the solution of the syrup in benzene–ethyl acetate (1: 1) was passed through a short column of silica gel with the aid of the same solvent system and the fraction containing **9** was evaporated to give a pale yellow syrup, 6.90 g (81%), $[\alpha]_D^{18}$ +189° (*c* 1, $CHCl_3$); IR: 3440, 2100, 1725, 710 cm^{-1}.

Found: C, 54.95; H, 5.75; N, 14.01%. Calcd for $C_{14}H_{17}N_3O_5$: C, 54.71; H, 5.58; N, 13.68%.

*6-Azido-2,4-di-O-benzyl-3,6-dideoxy-α-*D*-ribo-hexopyranosyl Chloride (10).* To ice-cold thionyl chloride (5 m*l*), **7** (197 mg) was added gradually and the solution was allowed to stand in the cold for 1 hr and then at room temperature overnight. The solution was coevaporated with dry toluene *in vacuo* and the residue was dissolved in dry benzene. The solution was passed through a short column of silica gel (3 g), which was preactivated at 120°C *in vacuo* for 5 hr before use. The eluate containing **10** was collected and evaporated to give a pale yellow syrup, 125 mg (61%), $[\alpha]_D^{20}$ +170° (*c* 1, $CHCl_3$); R_f 0.5 on tlc with benzene (**7**, R_f 0); IR: 2930, 2870, 2100 (sharp, N_3), 1500, 1460, 1370, 1350, 1290, 1110 (s), 1000, 895, 740 (s), 700 cm^{-1}.

Found: C, 62.14; H, 5.98; N, 11.07; Cl, 9.61%. Calcd for $C_{20}H_{22}N_3O_3Cl$: C, 61.93; H, 5.72; N, 10.83; Cl, 9.14%.

NMR (in $CDCl_3$): τ 8.12 (1H q, J ~11.5 Hz, H_{ax}-3), 7.58 (1H sextet, J ~5, ~5, and ~12 Hz, H_{eq}-3), 6.8—5.8 (5H m, H-2,4,5,6,6′), 5.53 and 5.40 (both 1H doublets (J 11.5 Hz) forming an AB quartet centered at 5.46, C(2?) $OC\underline{H}_2C_6H_5$), 5.43 (2H s, C(4?) $OC\underline{H}_2C_6H_5$), 3.83 (1H d, J 3.5 Hz, H-1), 2.68 and 2.65 (both 5H singlets, $OCH_2C_6\underline{H}_5$).

*4-O-(6-Azido-2,4-O-di-O-benzyl-3,6-dideoxy-α-*D*-ribo-hexopyranosyl)-6-O-(2-O-benzyl-3-deoxy-3-ethoxycarbonylamino-4,6-O-isopropylidene-α-*D*-glucopyranosyl)-N,N′-diethoxycarbonyl-2-deoxystreptamine (12).* A mixture of **10** (400 mg, 1.6 mol and freshly prepared Drierite (1.5 g) in strictly dried[3] benzene–dioxane (3: 1, 16 m*l*) was refluxed for 30 min and to the mixture, **11**[3] (450 mg, 1 mol) and dried mercuric cyanide (0.57 g) were added. The mixture was refluxed for 6 hr. Mercuric cyanide (0.57 g) was added and the mixture was again refluxed for 6 hr. The procedure was repeated once again. The resulting reaction mixture was poured into a saturated sodium hydrogen carbonate

solution with stirring and the product was extracted with chloroform. After dried over sodium sulfate, the chloroform solution was evaporated to give a syrup (0.9 g). Tlc (chloroform–acetone 5: 1) of the syrup showed six spots of R_f 0.02 (**11**), 0.58, 0.49 (major, **12**), 0.47. 0.31, and 0.9 (**10** and **7**). The syrup was chromatographed on a column of alumina (E. Merck, neutral, 60 g) with chloroform–acetone (5: 1) initially, and after **10** and **7** (both, R_f 0.9) had been eluted (42—88 m*l*), with ethanol. The ethanol eluate was evaporated to give a solid (0.49 g), which contained all components cited above other than **10** and **7**. The solid was then chromatographed on a column of silica gel (Wako gel, 50 g) with chloroform–acetone (5: 1). Compound **12** (R_f 0.49, 250 mg, 36%), a mixture of **12** and the substance having R_f 0.47 (0.10 g), a mixture of the substance having R_f 0.47 and 0.3 (0.06 g) and the substance having R_f 0.31 (0.08 g) were eluted in this order in the fractions of 187—287, 287—400, 400—500, and 500—700 m*l*, respectively. Compound **12** was recrystallized from a mixture of ethanol–acetone (1:1) containing a small amount of ammonia: 170 mg (25%), mp 263—264°C, $[\alpha]_D^{20}$ +97° (*c* 0.9, pyridine); IR (KBr): 3360, 2940, 2110 (N_3), 1705 (amide I), 1545 (amide II); 1075, 1045, 860, 780, 745, 700 cm^{-1}.

Found: C, 59.79; H, 6.76; N, 7.91%. Calcd for $C_{51}H_{68}N_6O_{16}$: C, 59.98; H, 6.71; N, 8.28%.

NMR (in pyridine-d_5): τ 8.90, 8.87, and 8.85 (each 3H s, $CH_2C\underline{H}_3$), 8.57 and 8.54 (each 3H s, isopropylidene), 2.4—2.7 (15H m, phenyl).

*6-O-(3-Amino-3-deoxy-α-D-glucopyranosyl)-4-O-(6-amino-3,6-dideoxy-α-D-*ribo*-hexopyranosyl)-2-deoxystreptamine (3′-Deoxykanamycin).* A suspension of **12** (82 mg) in aqueous acetic acid (1: 4, 2 m*l*) was heated at 90°C for 5 min. Tlc (chloroform–acetone 5: 1) of the resulting solution showed that **12** (R_f 0.85) had disappeared and a deacetonation product (R_f 0.07) appeared. The solution was poured into water and the precipitates were filtered to give a solid (79 mg). The solid was dissolved in hot ethanol–dioxane (5: 1, 12 m*l*) and the solution was hydrogenated with Raney nickel (T-4) and hydrogen under pressure (50 *l*b/sq. inch) at 42°C for 3 hr. The reaction mixture was filtered and the filtrate was evaporated to give a solid (60 mg), which had an R_f value 0.22 on tlc with benzene–ethanol (5: 1) (the starting material, R_f 0.75). Its infrared spectrum showed no absorption corresponding to an azide (~2100 cm^{-1}).

To a suspension of the solid in aqueous acetone (1: 1, 3 m*l*), anhydrous sodium carbonate (70 mg) and ethoxycarbonyl chloride (36 mg) were added and the mixture was stirred at room temperature for 30 min, whereupon, on tlc with benzene–ethanol (5: 1), the starting material (R_f 0.22) disappeared and a product (R_f 0.71) appeared. The resulting solution was evaporated *in vacuo* and the residue was extracted with chloroform. The chloroform solution was washed with water, dried over sodium sulfate and evaporated to give a solid (53 mg).

The solid was dissolved in hot aqueous ethanol (1: 8, 9 m*l*) and, after addition of a few drops of acetic acid, the solution was hydrogenated with palladium black and hydrogen under pressure (50 *l*b/sq. inch) at 30°C for 12 hr. The reaction mixture was filtered and evaporated to give a solid (39 mg), which gave R_f 0 on tlc with benzene–ethanol (5:1). Its NMR spectrum showed no absorption peaks corresponding to benzyl protons.

The solid was then heated with 1N barium hydroxide solution at 90°C for 9 hr and the solution was neutralized with carbon dioxide. After filtration, the solution was evaporated *in vacuo*. The residue was dissolved in water to give a slightly turbid solution, which was filtered and evaporated. To remove barium carbonate thoroughly, the procedure was repeated untill a clear solution was obtained. Colorless solid, 24 mg. Paper chromatography (Toyo Roshi No. 50) of the solid with *n*-butanol–pyridine–water–acetic acid (6:4:3:1) showed that the solid was composed mainly of 3′-deoxykanamycin ($R_{f\text{kanamycin}}$ 2.2) being accompanied with a slight amount of 2-deoxystreptamine and by-products (R_f 0). The solid was then chromatographed with a column of Amberlite CG50 (NH_4^+ form, 5.5×55 mm); water (30 m*l*), 0.05N (70 m*l*) and 0.1N ammonia (100 m*l*) eluted impurities. Subsequent development with 0.3 N ammonia eluted 3′-deoxykanamycin in 99—135 m*l* fraction, colorless solid, 10 mg (27%). It was recrystallized from water–acetone, $[\alpha]_D^{20}$ +146° (*c* 0.2, H_2O).

Found: C, 46.10; H, 7.70%. Calcd for $C_{18}H_{16}H_4O_{10}$: C, 46.14; H, 7.75%.

Proofs for the Structure of 3′-Deoxykanamycin. *a) By Periodate Oxidation*: 3′-Deoxykanamycin (1.0 mg) was dissolved in 10% sodium periodate solution (0.09 m*l*) and the solution was allowed to stand at room temperature for 12 hr. After addition of ethylene glycol (0.09 m*l*), an equal volume of concentrated hydrochloric acid with that of the solution was added and the solution was heated at 90°C for 1 hr. Paper chromatography with *n*-butanol–pyridien–water–acetic acid (6:4:3:1) showed the presence of 2-deoxystreptamine. Parallel to this experiment, kanamycin and neomycin were treated likewise and it was shown that kanamycin gave 2-deoxystreptamine, whereas neomycin did not give it.

b) By Hydrolysis: A solution of 3′-deoxykanamycin in 6N hydrochloric acid was heated at 90°C for 40 min. Paper chromatography with the above-mentioned solvent-system of the resulting solution showed the presence of 2-deoxystreptamine and 3-amino-3-deoxy-D-glucose. Other products could not be clearly discerned because of diffusion of the spots.

The authors wish to thank Mr. Saburo Nakada for the elemental analysis and to Mr. Yasuhiro Ito for his technical assistance.

Improved Solid-Phase Synthesis of Tryptophan-Containing Peptides. I. Use of Hydrogen Chloride in Formic Acid as a Reagent for the Cleavage of *t*-Butyloxycarbonyl Group[1]

Motonori OHNO, Sadaji TSUKAMOTO, Satoru MAKISUMI, and Nobuo IZUMIYA

Department of Chemistry, Faculty of Science, Kyushu University, Fukuoka

(Received May 22, 1972)

An improved method has been described for the solid-phase synthesis of tryptophan-containing peptides. Hydrogen chloride in formic acid has been introduced as a reagent for the cleavage of the *t*-butyloxycarbonyl group owing to the stableness of tryptophan and N^{t}-formyltryptophan in this system. The effectiveness of the new reagent has been demonstrated in the synthesis of the tryptophan-containing heptapeptide, lysylalanylglycylleucylglycyltryptophylleucine.

The usefulness of the solid-phase synthesis of polypeptides has been documented in the syntheses of a number of biologically active peptides[2] and of proteins.[3] This quick technique has also been becoming a valuable tool in the syntheses of enzymic fragments involved in noncovalently bonded, active complexes and their analogs as an approach to understanding of protein structure and function relationships, as exemplified in bovine pancreatic ribonuclease A[3a,4] and staphylococcal nuclease.[5] It is well known, however, that tryptophan in the peptide chain growing on the polymer support undergoes oxidation during treatment with hydrogen chloride in acetic acid or dioxane for the cleavage of the *t*-butyloxycarbonyl (Boc) group[2,3] that is usually employed as an α-amino protecting group in the solid-phase peptide synthesis. In such cases, sulfhydryl reagent such as β-mercaptoethanol (EtSH)[6] or dithiothreitol[3b] has been used as a scavenger to protect tryptophan from oxidative destruction.

Bubbling of hydrogen chloride into a solution of tryptophan[7] or its derivatives (including even enzymes) in formic acid results in formylation of the indole nitrogen (N^{t}) and this formyl group can be removed in a weakly alkaline medium.[8]

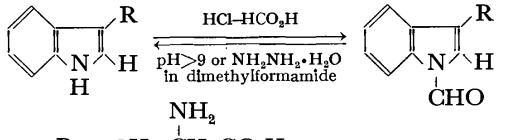

$R = -CH_2-CH(NH_2)-CO_2H$ etc.

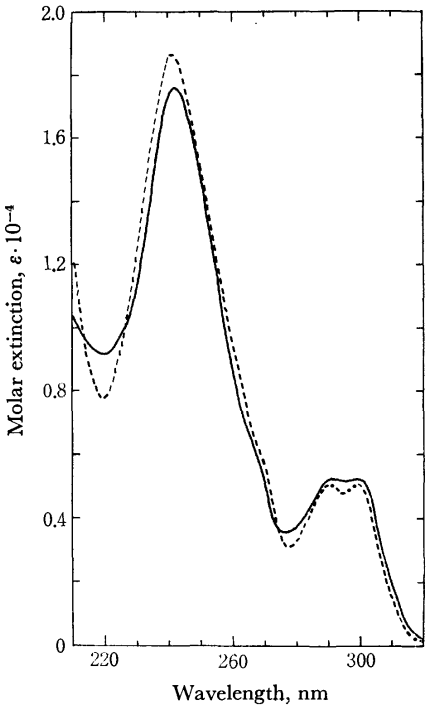

Fig. 1. Ultraviolet absorption spectra of N^{t}-formyltryptophan hydrochloride (——) in water and N^{α}-acetyl-N^{t}-formyltryptophan methyl ester (------) in methanol.

The UV absorption spectra characteristic of N^{t}-formyltryptophans are shown in Fig. 1. On the high-voltage paper electrophoresis (pH 2.08) of a solution of tryptophan dissolved in 0.1—1N hydrogen chlordie in formic acid, no band other than those of tryptophan and N^{t}-formyltryptophan has been detected even after a prolonged standing of the solution, showing the stability of the two indole derivatives in this system. The degree of transformation of tryptophan into N^{t}-formyltryptophan depends on concentration of hydrogen chloride and the time keeping in solution. No reaction occurred upon treatment of N^{t}-formyltryptophans with a large excess of anhydrous triethylamine in dimethylformamide. The formyl group, however, has been cleaved by dissolving N^{t}-formyltryptophans in dimethylformamide containing a 20—30 fold molar excess of hydrazine hydrate and standing for 48 hr. The thin-layer chromatographic studies using α-Boc-aspartic

1) A part of this work has been briefly communicated: M. Ohno, S. Tsukamoto, and N. Izumiya, *Chem. Commun.*, **1972**,, 663.

2) For example: R. B. Merrifield, *Biochemistry*, **3**, 1385 (1964); A. Marglin and R. B. Merrifield, *J. Amer. Chem. Soc.*, **88**, 5051 (1966).

3) For example: (a) B. Gutte and R. B. Merrifield, *J. Biol. Chem.*, **246**, 1922 (1971); (b) C. H. Li and D. Yamashiro, *J. Amer. Chem. Soc.* **92**, 7608 (1970).

4) M. C. Lin, B. Gutte, S. Moore, and R. B. Merrifield, *J. Biol. Chem.*, **245**, 5169 (1970).

5) D. A. Ontjes and C. B. Anfinsen, *ibid.*, **244**, 6316 (1969); I. M. Chaiken and C. B. Anfinsen, *ibid.*, **245**, 2337 (1970); *ibid.*, **245**, 4718 (1970); I. Parikh, L. Corley, and C. B. Anfinsen, *ibid.*, **246**, 7392 (1971).

6) J. Blake and C. H. Li, *J. Amer. Chem. Soc.*, **90**, 5882 (1968).

7) All amino acids in this report are of L-configuration except for glycine.

8) A. Previero, M. A. Coletti-Previero, and J.-C. Cavadore, *Biochim. Biophys. Acta*, **147**, 453 (1967).

acid β-benzyl ester showed that a 1.2—2.0 fold molar excess of hydrogen chloride (0.1N) in formic acid cleaves the Boc group as rapidly as with a 20-fold molar excess of hydrogen chloride (1N) in acetic acid. These observations led us to examine hydrogen chloride-formic acid as a reagent for cleavage of the Boc group in the solid-phase synthesis of tryptophan-containing peptides.

Since removability of the Boc group in the heterogeneous system such as solid-phase synthesis would not be expected to be the same level as in the homogeneous solution system and it is true, the more excess amount of hydrogen chloride than that required for complete cleavage in the solution system should be used.

In the preliminary experiments in which the syntheses of H-Lys-Ala-Gly-Trp-Leu-OH and H-Ala-Gly-Lys(ε-Tfa)-Gly-Trp-Leu-OH (Tfa: trifluoroacetyl) have been made by using hydrogen chloride-formic acid, it was clearly indicated through the UV absorption spectra and the electrophoretic behaviors of the products that the reagent was quite effective in protecting tryptophan from oxidative destruction. We report here, as a typical example, the details of the solid-phase synthesis of the heptapeptide, H-Lys-Ala-Gly-Leu-Gly-Trp-Leu-OH, using the new deblocking method.

The heptapeptide was built up by the usual manner[2,3] starting from Boc-leucyl resin and using a 6-fold molar excess of hydrogen chloride (0.1N) in formic acid. ε-Amino group of lysine was protected with benzyloxycarbonyl (Z) group. In parallel, two peptides with the same sequence were constructed on the resins using 1N hydrogen chloride in acetic acid in the presence and absence of EtSH (2%). Halves of the three protected peptidyl resins [**1a** (*via* HCl-HCOOH), **1b** (*via* HCl-AcOH-EtSH), and **1c** (*via* HCl-AcOH)] were cleaved by hydrazine hydrate in dimethylformamide as described.[9] In order to remove nonpeptide substances derived from the resin, the three products of Boc-Lys(ε-Z)-Ala-Gly-Leu-Gly-Trp*-Leu-$NHNH_2$[10] [**2a** (*via* HCl-HCOOH), **2b** (*via* HCl-AcOH-EtSH), and **2c** (*via* HCl-AcOH)] were reprecipitated from the methanolic solutions by addition of ethyl ether-petroleum ether (1:2 v/v). The other halves of **1a** and **1b** were treated with anhydrous hydrofluoric acid in the presence of anisole,[11,12] and the peptide produced *via* HCl-HCOOH was further treated with 0.1N aqueous piperidine to remove the N^{i}-formyl group attached to a part of tryptophyl residue since this group is resistant to anhydrous hydrofluoric acid (see Experimental section): the two completely deblocked heptapeptides [**3a** (*via* HCl-HCOOH) and **3b** (*via* HCl-AcOH-EtSH)] were obtained.

The UV absorption spectrum of **2a** (Fig. 2) was virtually identical with that of Z-tryptophan except that a trough in the 240—250 nm region showed somewhat greater absorption and was shifted to the red by 2 nm. This indicates that **2a** has been contaminated to only a minor extent by oxidized species. Extinction coefficients of **2b** and **2c** at 282 nm were respectively 1.34 and 1.45 times as large as that of **2a**. Such enhancement of the extinction at 282 nm should be ascribed to oxidation of the indole chromophore although what types of products formed has so far been unknown.

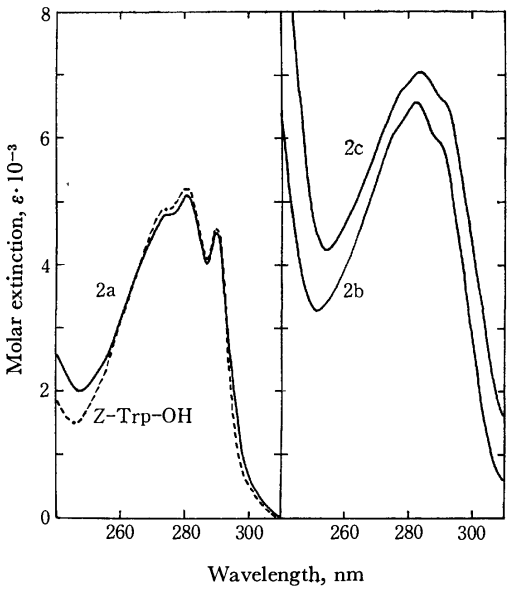

Fig. 2. Ultraviolet absorption spectra of the protected peptide hydrazides, **2a**, **2b**, and **2c**, and Z-tryptophan in methanol.

Figure 3 shows gel-chromatographic patterns of **3a** and **3b** on a Sephadex G-25 column. **3b** gave a complex profile owing to its heterogeneity. To ascertain whether the major peak from **3a** is due only to pure peptide, **3a** was treated with a 10-fold molar excess of 2-nitro-4-carboxyphenylsulfenyl chloride (NCPS-Cl)[13,14] in 80% formic acid and the modified peptide was chromatographed on the same column. Since the peptide containing 2-thio-(2-nitro-4-carboxyphenyl)-tryptophan[14] reveals an increased adsorptivity on the gel than the unmodified,[15] it is apparent from the delayed and shifted elution profile of the modified peptide that the original peptide in the major peak from **3a** involved only pure tryptophyl residue. This was further confirmed from the observation that the modified peptide from the major peak fractions gave exactly the same spectrum as that of 2-thio-(2-nitro-4-carboxyphenyl)-tryptophan and gave a single band upon thin-layer chromatography. Comparison of the two elution diagrams before and after reaction of **3b** with NCPS-Cl indicates that **3b** contains unchanged tryptophan to a small extent.

9) M. Ohno and C. B. Anfinsen, *J. Amer. Chem. Soc.*, **89**, 5994 (1967); M. Ohno, K. Kuromizu, H. Ogawa, and N. Izumiya, *ibid.*, **93**, 5251 (1971).

10) Asterisk signifies that the peptides may or may not involve pure tryptophyl residue.

11) S. Sakakibara, Y. Shimonishi, Y. Kishida, M. Okuda, and H. Sugihara, This Bulletin, **40**, 2164 (1967).

12) J. Leonard and A. B. Robinson, *J. Amer. Chem. Soc.*, **89**, 181 (1967).

13) A. J. Havlik and N. Kharasch, *ibid.*, **77**, 1150 (1955).

14) F. M. Veronese, E. Boccu, and A. Fontana, *Ann. Chim.*, **58**, 1309 (1968).

15) M. Ohno, T. F. Spande, and B. Witkop, Unpublished results.

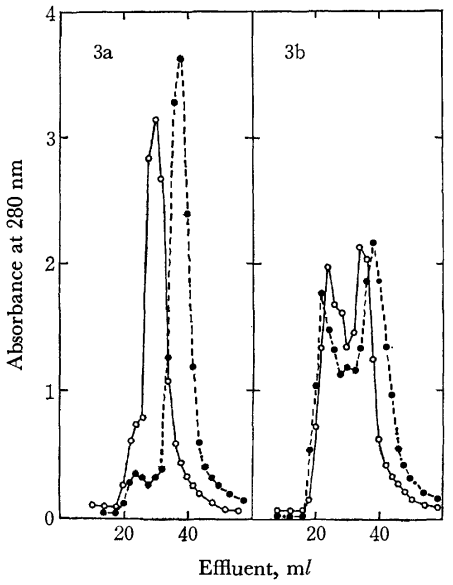

Fig. 3. Elution diagrams of the peptides, **3a** (6 mg) and **3b** (6 mg), on a Sephadex G-25 column (0.9×60 cm) before (○—○) and after (●·····●) modification with NCPS-Cl; solvent, 10% acetic acid. The details are described in the Experimental section.

Use of hydrogen chloride-formic acid for the cleavage of the Boc group in the solid-phase synthesis is worthy of attention in such a remarkable suppression of tryptophan oxidation. This merit of the reagent is due possibly to the reductive nature of formic acid. Since formylation of the indole nitrogen stabilizes the indole nucleus against oxidation, use of N^{α}-Boc-N^{i}-formyltryptophan in the solid-phase synthesis is under investigation and will be the subject of future publication.

Experimental

Melting points are uncorrected. UV spectra were taken with a Hitachi spectrophotometer EPS-3T or a Shimadzu UV-200 spectrophotometer equipped with a U-125MU recorder. Optical rotations were measured with a Yanagimoto polarimeter OR-20. Thin-layer chromatographies were performed on Merck silica gel G using either ethyl acetate–methanol (2:1 v/v) (solvent 1) or *n*-butanol–acetic acid–water (4:1:5 v/v, upper layer) (solvent 2) as the developing solvent. Paper electrophoreses were carried out under the following condition: paper, Whatman 3MM (57 cm length); solvent, 0.24N formic acid (pH 2.08); voltage gradient, 48 V/cm; period, 90 min. In this condition all amino acids and peptides in the present experiments moved to the cathode. Substances were detected by spraying ninhydrin (0.2% solution in 80% ethanol) or a modified Ehrlich reagent (0.5% solution of *p*-dimethylaminocinnamaldehyde in 0.5N hydrochloric acid). Amino acid analyses of peptides were carried out on samples that had been hydrolyzed with constant boiling hydrochloric acid for 24 hr in evacuated, sealed tubes at 110°C, and were recorded on a Hitachi amino acid analyzer KLA-3A.

Boc-Leucine, glycine, alanine, valine, and tryptophan were prepared by the reaction of each amino acid with Boc-azide[16] or purchased from the Protein Research Foundation (Osaka). α-Boc-ε-Z-Lysine and α-Boc-ε-Tfa-lysine (mp 101—102°C, lit,[17] 103°C) were prepared by the reaction of ε-Z-lysine[18] and ε-Tfa-lysine[19] with Boc-azide. Z-Tryptophan was prepared from Z-Cl[20] and tryptophan by the Schotten-Baumann procedure. 2-Thio-(2-nitro-4-carboxyphenyl)-tryptophan [λ_{max} in 10% acetic acid 260 (log ε 4.29), 282 (log ε 4.33), and 355 nm (log ε 3.65)] was prepared from 2-nitro-4-carboxyphenylsulfenyl chloride and tryptophan as reported.[14] Chloromethylated copolystylene-divinylbenzene (2%) resin (1.3 mmol/g, 100—200 mesh) was obtained from the Protein Research Foundation (Osaka). Formic acid (analytical grade, 98—100%) was purchased from the Merck Co. and used without purification. Acetic acid was refluxed over potassium permanganate and distilled. Concentration of hydrogen chloride in formic acid or acetic acid was based on the weight of hydrogen chloride absorbed per unit volume of the solvent, or determined by the Volhard titration. The other solvents for the solid-phase synthesis were purified by the appropriate procedures.

Formylation of Tryptophans. Dried hydrogen chloride was bubbled into a solution of tryptophan (7.0 g) in formic acid (100 ml) at room temperature. At suitable intervals aliquotes of the solution were diluted with water for recording UV spectra. After the absorbance at 298 nm reached maximum (about 3 hr), the solvent was removed *in vacuo* with slight warming. N^{i}-Formyltryptophan hydrochloride crystallized by addition of ethyl ether to the syrup. Crystals were collected and washed with ethyl ether, 9.20 g (100%), mp 218°—220°C, $[\alpha]_D^{23}$ −4.7° (*c* 1.91, water).

Found: C, 53.60; H, 4.99; N, 10.42. Calcd for $C_{12}H_{12}O_3N_2 \cdot HCl$: C, 53.64; H, 4.88; N, 10.43%.

α-Acetyltryptophan methyl ester (0.30 g) was treated by the same way as described above, and the syrup was taken into ethyl acetate that was washed with water, dried over sodium sulfate and evaporated. Crystallization of the residue by addition of petroleum ether gave 0.28 g (85%) of N^{α}-acetyl-N^{i}-formyltryptophan methyl ester; mp 102—104°C, $[\alpha]_D^{23}$ +21.0° (*c* 1.64, methanol).

Found: C, 62.10; H, 5.76; N, 9.68. Calcd for $C_{15}H_{16}O_4N_2$: C, 62.49; H, 5.59; N, 9.72%.

N^{i}-Formyltryptophans are nonfluorescent under UV lamp and negative to the modified Ehrlich reagent.

Paper Electrophoresis of a Solution of Tryptophan Dissolved in 0.1—1N Hydrogen Chloride in Formic Acid. As a typical experiment, 30 mg of tryptophan was dissolved in 5 ml of 0.4N hydrogen chloride in formic acid and the solution was allowed to stand at room temperature. At suitable intervals aliquotes of the solution were taken and subjected to paper electrophoresis. No band other than those of tryptophan and N^{i}-formyltryptophan has been detected even after 100 hr. The ratio of the latter to the former increased with time. Under the lower or higher concentration of hydrogen chloride than that of the example, transformation of tryptophan into N^{i}-formyltryptophan took place in slower or faster rate. It should be noted that the mobilities of tryptophan and N^{i}-formyltryptophan under the condition mentioned above are 15 and 12 cm, respectively.

Stability of N^{i}-Formyltryptophans. a) Anhydrous Triethylamine: N^{α}-Acetyl-N^{i}-formyltryptophan methyl ester (10 mg) was dissolved in 1 ml of dimethylformamide containing

16) R. Schwyzer, P. Sieber, and H. Kappeler, *Helv. Chim. Acta*, **42**, 2622 (1959).

17) C. B. Anfinsen, D. Ontjes, M. Ohno, L. Corley, and A. Eastlake, *Proc. Nat. Acad. Sci. U.S.A.*, **58**, 1806 (1967).

18) A. Neuberger and F. Sanger, *Biochem. J.*, **37**, 515 (1943).

19) E. E. Schallenberg and M. Calvin, *J. Amer. Chem. Soc.*, **77**, 2779 (1955).

20) M. Bergmann and L. Zervas, *Chem. Ber.*, **65**, 1192 (1932).

0.14 ml of anhydrous triethylamine. At suitable intervals aliquotes of the solution were taken and evaporated *in vacuo* to dryness. The residues were dissolved in ethanol and their UV spectra were recorded. No change has been observed in the starting spectrum even after standing for 24 hr.

b) Anhydrous Hydrofluoric Acid: In the reaction vessel of the type described by Sakakibara *et al.*,[11] N^i-formyltryptophan hydrochloride (10 mg) was treated with anhydrous hydrofluoric acid (2 ml) in the presence of anisole (0.1 ml) at 0°C for 1 hr.[11,12] After removal of anhydrous hydrofluoric acid *in vacuo* at room temperature, the residue was taken into 10% acetic acid. An aqueous solution was shaken with ethyl ether and lyophilized. The dried powder exhibited the typical N^i-formyltryptophan spectrum. On paper electrophoresis, mobility of a ninhydrin-positive but modified Ehrlich reagent-negative band was the same as that of the authentic N^i-formyltryptophan hydrochloride.

Hydrazinolytic Removal of Formyl Group from N^i-Formyltryptophans. N^α-Acetyl-N^i-formyltryptophan methyl ester (10 mg) was dissolved in 0.5 ml of dimethylformamide containing 0.05 ml of hydrazine hydrate and the solution was allowed to stand at room temperature. At suitable intervals aliquotes of the solution were diluted with ethanol for recording spectra. The complete indole spectrum was obtained after 48 hr.

Boc-Leucyl Resin. To 4.0 g of chloromethylated copolystylene-divinylbenzene (2%) resin (1.3 mmol of Cl/g), were added 34 ml of anhydrous ethanol containing 1.38 g (5.5 mmol) of Boc-leucine and 0.77 ml (5.5 mmol) of triethylamine. The mixture was refluxed for 72 hr with continuous stirring. The resin was filtered, rinsed repeatedly with ethanol and with methylene chloride, and dried *in vacuo*. Amino acid analysis of the resin indicated the leucine content to be approximately 0.20 mmol/g.

Boc-Lys(ε-Z)-Ala-Gly-Leu-Gly-Trp-Leu-resins (**1a**, **1b**, and **1c**).* Boc-leucyl resin (0.5 g) was placed in a reaction vessel of the type described by Merrifield for repeated deblocking, rinsing and coupling procedure. For the synthesis of **1a**, the following cycle was used for stepwise addition of the appropriate Boc-amino acid. The resin was rinsed with formic acid (three 6 ml portions), shaken for 30 min in 0.1N hydrogen chloride in formic acid (6 ml), rinsed with formic acid (three 6 ml portions), with anhydrous ethanol (three 6 ml portions) and with dimethylformamide (three 6 ml portions), shaken for 10 min in 10% triethylamine in dimethylformamide (two 6 ml portions), rinsed with dimethylformamide (three 6 ml portions) and with methylene chloride (three 6 ml portions). The resin was then suspended in 6 ml of methylene chloride containing a 4-fold molar excess of the appropriate Boc-amino acid and shaken for 15 min. Equimolar *N,N'*-dicyclohexylcarbodiimide was added in 1 ml of methylene chloride and shaking was continued overnight. The coupling steps were terminated by rinsing with methylene chloride (three 7 ml portions) and with anhydrous ethanol (three 6 ml portions). For the syntheses of **1b** and and **1c**, formic acid and 0.1N hydrogen chloride in formic acid were replaced by acetic acid and 1N hydrogen chloride in acetic acid, and EtSH (2% by volume) was added to the acid mixture in the case of **1b**.

Boc-Lys(ε-Z)-Ala-Gly-Leu-Gly-Trp-Leu-$NHNH_2$ (**2a**, **2b**, and **2c**).* To each suspension of **1a**, **1b**, and **1c** (0.40 g each) in 3.5 ml of dimethylformamide, were added 0.4 ml of 100% hydrazine hydrate and the mixture were shaken for 2 days at room temperature. The dimethyformamide solutions were separated by filtration and the resins were rinsed several times with dimethylformamide. The combined filtrates were evaporated *in vacuo* nearly to dryness. The hydrazides solidified upon the addition of water and were filtered and washed with water. The hydrazides were dissolved in methanol and the insoluble substances were filtered off. The filtrates were evaporated to a small volume and a mixture of ethyl ether and petroleum ether (1:2 v/v) was added. The crystalline products were filtered off: **2a**, 74 mg (86% yield of **2b**), mp 198—200°C, $[\alpha]_D^{20}$ −28° (*c* 0.165, methanol), $R_f(1)$ 0.91; **2b**, 86 mg, mp 189—191°C, $[\alpha]_D^{20}$ −22° (*c* 0.158, methanol), $R_f(1)$ 0.91;[21] and **2c**, 78 mg, mp 181—184°C, $[\alpha]_D^{20}$ −13° (*c* 0.205, methanol), $R_f(1)$ 0.91.[21] Amino acid analysis of **2a**: Lys, 0.97; Ala, 1.00; Gly, 1.85; Leu, 2.06. Amino acid analysis of **2b**: Lys, 1.00; Ala, 1.00; Gly, 2.09; Leu, 2.20. Amino acid analysis of **2c**: Lys, 1.12; Ala, 1.00; Gly, 2.14; Leu, 2.25. The UV absorption spectra were taken in the methanolic solutions (see Fig. 2). Elemental analysis was carried out only on **2a**.

Found: C, 57.98; H, 7.52; N, 15.13. Calcd for $C_{49}H_{73}N_{11}O_{11}\cdot H_2O$: C, 58.23; H, 7.29; N, 15.26%.

H-Lys-Ala-Gly-Leu-Gly-Trp-Leu-OH (**3a** and **3b**).* **1a** (0.2 g) was treated with 4—5 ml of anhydrous hydrofluoric acid for 1 hr at 0°C in the presence of anisole. After removal of anhydrous hydrofluoric acid *in vacuo*, the peptide cleaved was extracted with two 5 ml portions of 10% acetic acid. The aqueous solution was shaken with ethyl ether and lyophilized to afford 35 mg of a white powder. The UV spectrum of the product in 0.1N sodium hydroxide was virtually identical with that of tryptophan in the same solvent except for somewhat greater absorption in the 240—250 nm region. The above white powder was dissolved in 0.1N aqueous piperidine, and the solution was allowed to stand at room temperature for 10 min and lyophilized, to give **3a** as a white residue. **1b** (0.2 g) was treated by the same way as for **1a** except for treatment with 0.1N piperidine, to afford 49 mg of **3b** as a light brown powder. Its UV spectrum was similar to that of **2b** in Fig. 2. Amino acid analysis of **3a**: Lys, 0.98; Ala, 1.00; Gly, 1.90; Leu, 2.10. Amino acid analysis of **3b**: Lys, 0.96; Ala, 1.00; Gly, 2.10; Leu, 1.92.

Reaction of H-Lys-Ala-Gly-Leu-Gly-Trp-Leu-OH (**3a** and **3b**) with 2-Nitro-4-carboxyphenylsulfenyl Chloride (NCPS-Cl) and Sephadex G-25 Column Chromatographies of the Modified Peptides.* To a solution of 6 mg of **3a** in 2 ml of 80% formic acid, was added 16 mg of NCPS-Cl and the solution was stirred for 4 hr at room temperature and lyophilized. The dried residue was scratched with five 2 ml portions of acetone containing 2% concentrated hydrochloric acid in order to remove the excess reagent. The yellow peptide was separated by centrifugation from the acetone solution and dissolved in water, and the solution was lyophilized. The dried peptide was dissolved in 0.2 ml of 10% acetic acid and chromatographed on a Sephadex G-25 column (0.9×60 cm) equilibrated with the same solvent (Fig. 3). The elution was monitored by absorption at 280 nm. The spectra of the major peak fractions were exactly the same as that of 2-thio-(2-nitro-4-carboxyphenyl)-tryptophan. The unmodified peptide (**3a**) was chromatographed on the same column and its elution pattern was compared with that of the modified peptide (Fig. 3). The modified peptide recovered from the major peak fractions gave a single band on thin-layer chromatography, $R_f(2)$ 0.45, and on paper electrophoresis (mobility, 12.5 cm) and its amino acid analysis gave the ratio: Lys, 1.00; Ala, 1.00; Gly, 1.92; Leu, 1.98. **3b** (6 mg) was treated with 16 mg of NCPS-Cl and the modified peptide was chromatographed by the same manner as described above, and its elution diagram was compared with that of **3b** (Fig. 3).

21) When 47% hydrobromic acid was sprayed to cleave the Boc-group, the spot colored brown.

The Reaction of Elemental Sulfur with Organic Compounds. IV. The Reactions of *N*-Arenesulfonylsulfilimine and Sulfoximine with Sulfur and Diaryl Disulfide[1]

Shigeru OAE, Yoshiyuki TSUCHIDA, Kenji TSUJIHARA, and Naomichi FURUKAWA

Department of Applied Chemistry, Faculty of Engineering, Osaka City University, Sumiyoshiku, Osaka

(Received February 28, 1972)

The reactions of elemental sulfur and diaryl disulfide with the compounds bearing a semipolar S→N linkage were investigated. Elemental sulfur was found to react with *N*-arenesulfonylsulfilimine and sulfoximine affording the corresponding sulfide and the sulfoxide respectively. Diaryl disulfide also was found to undergo similar reactions with these compounds. In the reaction of diaryl disulfide with *N*-arenesulfonylsulfilimine, *N,N*-bis(arylthio)arenesulfonamide was obtained as a main product besides the corresponding sulfide. The mechanisms of these reactions are discussed.

In the course of our studies on the reactions of elemental sulfur and disulfide, we have shown that compounds bearing a semipolar linkage, such as sulfoxides,[2-4] sulfones,[2,4-6] and pyridine *N*-oxides,[7] are reduced to the corresponding sulfides or pyridines by treatment with either sulfur or diaryl disulfide. As an extension of these works we have investigated the reactions of *N*-arenesulfonylsulfilimine and sulfoximine, which are isoelectronic nitrogen analogs of sulfoxide and sulfone, respectively, with both elemental sulfur and diaryl disulfides. This paper will describe the reactions in detail.

Results and Discussion

Reactions of N-*arenesulfonylsulfilimine with Sulfur and Diaryl Disulfide.* When a mixture of one mole-equivalent diphenyl-*N*-*p*-tosylsulfilimine (I) and one atom-equivalent elemental sulfur was heated in refluxing chlorobenzene, diphenyl sulfide was obtained in *ca.* 50% yield. Similarly diphenyl disulfide also reduced I to afford diphenyl sulfide in an almost quantitative yield under a similar reaction condition. In the latter reaction, besides diphenyl sulfide, *N,N*-bis(phenylthio)-*p*-toluenesulfonamide (IIa) was isolated in 28% yield from the product mixture (Eq. (1)). The compound

$$\underset{\underset{\text{N-Ts}}{\downarrow}}{\text{PhSPh}} + \text{PhSSPh} \longrightarrow \text{PhSPh} + \underset{\underset{\text{Ts}}{|}}{\text{PhSNSPh}} \qquad (1)$$

I IIa

Ts=-$SO_2C_6H_4CH_3$-*p*

IIa gives the characteristic IR and NMR spectra and satisfactory analysis of carbon, hydrogen, and nitrogen. In Table 1 the results of the reactions of a few other sulfilimines with disulfides are shown. The relatively small yields of II were attributable to thermal instability of II. In fact, thermal decomposition of IIa took place readily at about 160°C to give diphenyl disulfide and dark colored substance (Eq. (2)).

$$\text{IIa} \longrightarrow \text{PhSSPh} + \text{dark colored substance} \qquad (2)$$

Reactions of Sulfoximine with Sulfur and Diaryl Disulfide. When a mixture of one mole-equivalent diphenyl sulfoximine (III) and one atom-equivalent elemental sulfur was heated at *ca.* 160°C, a dark red colored solution was obtained. From this solution diphenyl sulfoxide was separated in an almost quantitative yield through column chromatography. Diphenyl disulfide was found also to react with III to give diphenyl sulfoxide in *ca.* 86% yield. These results were tabulated in Table 2 together with the results of the reactions of methyl *p*-tolyl sulfoximine.

$$\underset{\underset{\text{NH}}{\downarrow}}{\overset{\overset{\text{O}}{\uparrow}}{\text{PhSPh}}} \xrightarrow[\text{PhSSPh}]{\text{S or}} \overset{\overset{\text{O}}{\uparrow}}{\text{PhSPh}} \qquad (3)$$

III

Mechanism of the Reactions of N-*arenesulfonylsulfilimine with Sulfur and Diaryl Disulfide.* *N*-Sulfonylsulfilimines are weak bases[8] and behave as effective nucleophiles,[9] while diaryl disulfide is susceptible to nucleophilic attack.[10] Therefore the initial step of the reaction (1) is considered to be the nucleophilic attack of the negatively charged nitrogen atom of the sulfilimine on the sulfur atom of the S-S bond, forming the sulfonium salt (IV). The subsequent step is presumed to be the homolytic cleavage of the N-S bond of IV to give radical cation of diphenyl sulfide and the amino radical (V) for the following two reasons, (A) and (B). (A) It is known that radical cations can be formed readily from such similar compounds as diaryl sulfide, thianthrene, and phenoxathiin.[11] Moreover, those sulfilimines which are presumed to give the stable radical cations such as thianthrene, phenoxathiin, and dibenzothiophene *N*-tosylsulfilimines actually were found to react with the disulfide very

1) Paper III; S. Oae and Y. Tsuchida, *Tetrahedron Lett.*, 1972, 1283.
2) S. Oae and S. Kawamura, This Bulletin, **36**, 163 (1963).
3) S. Kiso and S. Oae, *ibid.*, **40**, 1722 (1967).
4) S. Oae, Y. Tsuchida, and M. Nakai, *ibid.*, **44**, 451 (1971).
5) S. Oae, M. Nakai, Y. Tsuchida, and N. Furukawa, *ibid.*, **44**, 445 (1971).
6) F. Crafft and W. Vorster, *Ber.*, **26**, 2813 (1893).
7) K. Ikura and S. Oae, *Tetrahedron Lett.*, **1968**, 3791.
8) K. Tsujihara, N. Furukawa, and S. Oae, This Bulletin, **43**, 2153 (1970).
9) S. Oae, K. Tsujihara, and N. Furukawa, *Tetrahedron Lett.*, **1970**, 2663.
10) O. Foss, "Organic Sulfur Compounds," Vol. II, ed. by N. Kharasch, Pergamon Press, New York, N.Y. (1966), p. 8.
11) G. Vincow, "Radical Ions," ed. by E. T. Kaiser and L. Kavan, John Wiley & Sons, Inc., New York, N.Y. (1968). p. 151.

Table 1. Reactions of sulfilimines with sulfur and disulfide

Sulfilimine	Sulfur or Disulfide	Condition	Product
$Ph_2S(:NTs)$[a]	S_8	PhCl reflux, 24 hr	Ph_2S (50%)
$Ph_2S(:NTs)$	$(PhS)_2$	PhCl reflux, 35 min	Ph_2S (quantitative) $(PhS)_2NTs$ (IIa) (28%)
$Ph_2S(:NTs)$	$(p\text{-}CH_3C_6H_4S)_2$	PhCl reflux, 60 min	Ph_2S (20—30%) $(p\text{-}CH_3C_6H_4S)_2NTs$ (IIb) (14%)
$Ph_2S(:NTs)$	$(p\text{-}CH_3OC_6H_4S)_2$	PhCl reflux, 3 min	Ph_2S (quantitative) $(p\text{-}CH_3OC_6H_4S)_2NTs$ (IIc) (10%)
$Ph_2S(:NTs)$	$(p\text{-}ClC_6H_4S)_2$	PhCl reflux, 30 min	Ph_2S (quantitative) $(p\text{-}ClC_6H_4S)_2NTs$ (IId) (26%)
$Ph_2S(:NB)$[b]	$(PhS)_2$	PhCl reflux, 30 min	Ph_2S (quantitative) $(PhS)_2NB$ (IIe) (14%)
$Ph_2S(:NB)$	$(p\text{-}CH_3C_6H_4S)_2$	PhH reflux, 40 hr	Ph_2S (quantitative) $(p\text{-}CH_3C_6H_4S)_2NB$ (IIf) (21%)
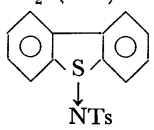	$(PhS)_2$	PhCl reflux, 20 min	IIa (16%)
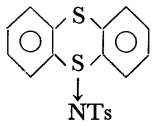	$(PhS)_2$	PhCl reflux, 15 min	IIa (21%)
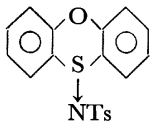	$(PhS)_2$	PhCl reflux, 13 min	IIa (36%)

a) Ts=$-SO_2C_6H_4CH_3$-*p* b) B=$-SO_2C_6H_5$

Table 2. Reactions of sulfoximines with sulfur and disulfide

Sulfoximine	Sulfur or disulfide	Condition	Product
$Ph_2S(:O)(:NH)$	S_8	neat 150—160°C, 15 min	$Ph_2S(:O)$ (quantitative)
$Ph_2S(:O)(:NH)$	$(PhS)_2$	*o*-$C_6H_4Cl_2$ reflux, 5 hr	$Ph_2S(:O)$ (86%)
p-$CH_3C_6H_4S(:O)(:NH)CH_3$	S_8	neat 150—160°C, 10 min	*p*-$CH_3C_6H_4S(:O)CH_3$ (quantitative)
p-$CH_3C_6H_4S(:O)(:NH)CH_3$	$(PhS)_2$	*o*-$C_6H_4Cl_2$ reflux, 17 hr	*p*-$CH_3C_6H_4S(:O)CH_3$ (82%)

readily (Table 1). However dialkyl or alkyl aryl sulfilimines, which would not give stable radical cation, did not react or reacted very little. These observations seem to suggest that a radical cation species is involved in the course of the reaction. (B) A strong ESR absorption was observed during the course of the reactions (1) and (2). The spectrum (Fig. 1) clearly indicates that the amino radical V was formed, and which may be considered to be a relatively stable radical species.

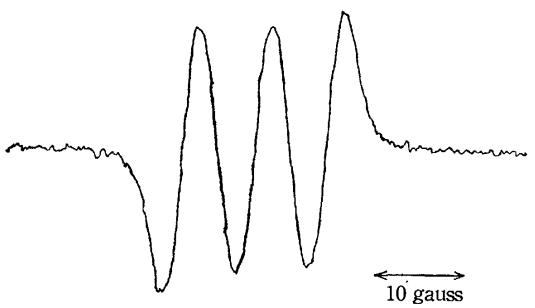

Fig. 1. ESR spectrum of $\cdot N(SPh)SO_2C_6H_4CH_3$-*p*.

In the following scheme the most likely reaction pathway is shown.

The reaction of the sulfilimine with elemental sulfur is considered to proceed through a similar route.

Mechanism of the Reactions of Sulfoximine with Sulfur and Diphenyl Disulfide. Sulfoximine is known to be basic,[12] therefore the following ionic pathway involving the nucleophilic attack of the sulfoximine on sulfur atom of diphenyl disulfide seems to be the most conceivable (Eq. (5)).

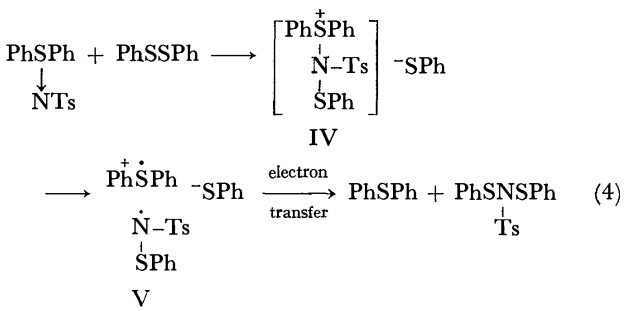

(4)

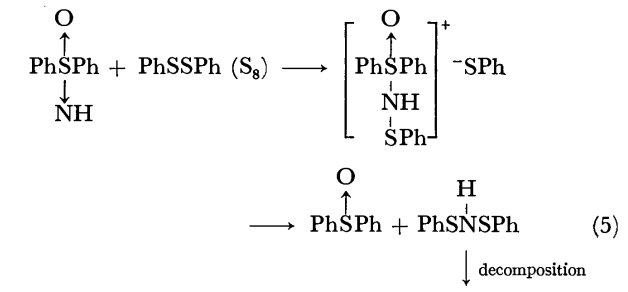

(5)

12) S. Oae, K. Tsujihara, and N. Furukawa, *Chem. Ind.* (London), **1969**, 1569.

Experimental

Materials. Diaryl disulfides were prepared from the corresponding aryl mercaptans by iodine or nitric acid ($(p\text{-}ClC_6H_4S)_2$) oxidation. $(C_6H_5S)_2$ mp 61°C (lit, 61.5°C[13]), $(p\text{-}CH_3C_6H_4S)_2$ mp 46°C (lit, 45.5°C[14]), $(p\text{-}CH_3OC_6H_4S)_2$ mp 43—44°C (lit, 44—45°C[15]), $(p\text{-}ClC_6H_4S)_2$ mp 70—71°C (lit, 73°C[16]).

N-p-Tosylsulfilimines were prepared from the corresponding sulfides and chloramine-T according to the usual procedure.[17] *N*-Benzenesulfonylsulfilimine was prepared similarly from the corresponding sulfide and chloramine-B. (Ts= $-SO_2C_6H_4CH_3$-*p*, B=$-SO_2C_6H_5$). $(CH_3)_2S(:NTs)$ mp 157°C (lit, 157—157.5°C,[17]) $PhS(:NTs)CH_3$ mp 129—130°C (lit, 129—130°C[17]), $Ph_2S(:NTs)$ mp 112°C (lit, 111—112°C[17]), $Ph_2S(:NB)$ mp 120°C, dibenzothiophene(:NTs) mp 169°C (Found: C, 64.06; H, 4.33; N, 3.81%. Calcd for $C_{19}H_{15}NO_2S_2$: C, 64.59; H, 4.25; N, 3.97%), thianthrene(:NTs) mp 166—167°C (Found: C, 59.58; H, 4.04; N, 3.46%. Calcd for $C_{19}H_{15}NO_2S_3$: C, 59.22; H, 3.90; N, 3.64%), phenoxathiin(:NTs) mp 169°C (Found: C, 61.38; H, 4.04; N, 3.74%. Calcd for $C_{19}H_{15}NO_3S_2$: C, 61.79; H, 4.06; N, 3.79%).

Sulfoximines were prepared by the hydrolysis of corresponding *N-p*-tosylsulfoximines with conc. sulfuric acid according to the method used by Bentley and Whitehead.[18] $Ph_2S(:O)(:NH)$ mp 102.5°C (lit, 102—102.5°C[12]), $p\text{-}CH_3C_6H_4S(:O)(:NH)CH_3$ mp 71°C (lit, 71—72°C[12]).

*The Reaction of Elemental Sulfur with Diphenyl-*N-p-*tosylsulfilimine.* Diphenyl-*N-p*-tosylsulfilimine (I), 0.71 g (0.002 mol) and 0.064 g (0.002 g atom) of sulfur was dissolved in 5 ml of chlorobenzene and the mixture was refluxed for about 24 hr. The product obtained was analyzed by thin layer and gas liquid chromatographies, and diphenyl sulfide was obtained as the main product. The yield of the sulfide was determined by gas liquid chromatography as *ca.* 50%.

The Reaction of Diaryl Disulfide with N-*Sulfonylsulfilimine.* Diphenyl disulfide, 0.436 g (0.002 mol) and 0.71 g (0.002 mol) of I was dissolved in 5 ml of chlorobenzene and refluxed for about 40 min until the color of the solution turned to dark red. After the solvent was evaporated a dark red tarry product mixture was obtained. The product was separated by column elusion chromatography through silica gel packed column, and diphenyl sulfide was obtained quantitatively with *n*-hexane as eluent, and subsequently *N,N*-bis(phenylthio)-*p*-toluenesulfonamide (IIa) was obtained with toluene as eluent. The crude IIa was recrystallized from absolute ethanol and colorless needles (mp 97.5—98°C) were obtained (0.276 g, 28%). This was the general procedure applied also for the other runs. The yields of II are shown in Table 1 while mp, IR, NMR, and CH analysis data are shown below. IIa mp 97.5—98°C. Found: C, 58.97; H, 4.49; N, 3.75%. Calcd for $C_{19}H_{17}NO_2S_3$: C, 58.91; H, 4.39; N, 3.62%. IR (cm^{-1}, KBr): ν_{SO_2} 1345 and 1160, ν_{S-N} 875. NMR ($CDCl_3$): 2.40 (s, 3H), 7.00—8.00 (m, 14H). IIb mp 94.5°C. Found: C, 60.43; H, 5.10; N, 3.33%. Calcd for $C_{21}H_{21}NO_2S_3$: C, 60.72; H, 5.06; N, 3.37%. IR (cm^{-1}, KBr): ν_{SO_2} 1345 and 1170, ν_{S-N} 835. NMR ($CDCl_3$): 2.52 (s, 6H), 2.59 (s, 3H), 7.30—8.30 (m, 12H). IIc mp 92.5°C. Found: C, 56.56; H, 4.63; N, 3.15%. Calcd for $C_{21}H_{21}NO_4S_3$: C, 56.38; H, 4.70; N, 3.13%. IR (cm^{-1}, KBr): ν_{SO_2} 1340 and 1160, ν_{S-N} 850. NMR ($CDCl_3$): 2.45 (s, 3H), 3.87 (s, 6H), 6.70—8.00 (m, 12H). IId mp 111—112°C. Found: C, 50.05; H, 3.38; N, 3.10%. Calcd for $C_{19}H_{15}Cl_2NO_2S_3$: C, 50.00; H, 3.29; N, 3.07%. IR (cm^{-1}, KBr): ν_{SO_2} 1350 and 1170, ν_{S-N} 850. NMR ($CDCl_3$): 2.55 (s, 3H), 7.20—8.10 (m, 12H), IIe mp 80.5°C. Found: C, 57.58; H, 4.05; N, 3.78%. Calcd for $C_{18}H_{15}NO_2S_3$: C, 57.91; H, 4.02; N, 3.75%. IR (cm^{-1}, KBr): ν_{SO_2} 1350 and 1170, ν_{S-N} 880. NMR ($CDCl_3$): 7.20—8.20 (m, 15H). IIf mp 92°C. Found: C, 59.51; H, 4.89; N, 3.37%. Calcd for $C_{20}H_{19}NO_2S_3$: C, 59.85; H, 4.74; N, 3.49%. IR (cm^{-1}, KBr): ν_{SO_2} 1350 and 1165, ν_{S-N} 880. NMR ($CDCl_3$): 2.31 (s, 6H), 7.00—8.00 (m, 13H).

The Reaction of Elemental Sulfur with Sulfoximine. Diphenyl sulfoximine (III), 0.217 g (0.001 mol) and 0.032 g (0.001 g atom) of sulfur was placed in a glass tube, and was heated in an oil bath maintained at *ca.* 160°C for 15 min. The red colored product was treated with column chromatography on silica gel. As a main product diphenyl sulfoxide (0.200 g) was obtained in an almost quantitative yield. The same procedure was found to be applied to the reactions of methyl *p*-tolyl sulfoximine with elemental sulfur.

The Reaction of Diphenyl Disulfide with Sulfoximine. Diphenyl disulfide, 0.218 g (0.001 mol), and diphenyl sulfoximine, 0.217 g (0.001 mol) was dissolved in 5 ml of *o*-dichlorobenzene and refluxed for about 5 hr. As a main product diphenyl sulfoxide was obtained in *ca.* 86% yield (0.174 g) by column elusion chromatography on silica gel. The same procedure could be applied to the reaction of methyl *p*-tolyl sulfoximine with diphenyl disulfide.

The Reaction of Diphenyl Disulfide with Dimethyl or Methyl Phenyl N-p-*Tosylsulfilimines.* The reaction of dimethyl-*N-p*-tosylsulfilimine with diphenyl disulfide did not proceed after 15 hr heating in refluxing chlorobenzene and the reactants were recovered. Methyl phenyl *N-p*-tosylsulfilimine was also treated with the disulfide under the same condition, however the reaction proceeded very little.

Thermal Decomposition of IIa. *o*-Dichlorobenzene solution of IIa was heated for *ca.* 1 hr at 160°C. From the dark colored product mixture diphenyl disulfide was obtained as a purely separable substance by chromatography through a silica gel column.

ESR Measurement. In a quartz sample tube 1 mm in diameter was placed the *o*-dichlorobenzene solution of IIa. The spectrum was recorded at 160°C with JES-ME-3X spectrometer. An identical spectrum was observed in the course of the reaction of I with diphenyl disulfide.

13) B. Holmberg, *Ann. Chem.*, **359**, 81 (1908).
14) L. Field and F. A. Grunwald, *J. Org. Chem.*, **16**, 946 (1951).
15) L. Gattermann, *Ber.*, **32**, 1136 (1899).
16) M. B. Sparke, J. L. Cameron, and N. Kharasch, *J. Amer. Chem. Soc.*, **75**, 4907 (1953).
17) K. Tsujihara, N. Furukawa, K. Oae, and S. Oae, This Bulletin, **42**, 2631 (1969).
18) H. R. Bentley and J. K. Whitehead, *J. Chem. Soc.*, **1950**, 2081.

Optical Resolution of Aspartic Acid by Using Copper Complexes of Optically Active Amino Acids*

Kaoru HARADA and Wung-wai Tso

Institute for Molecular and Cellular Evolution and Department of Chemistry, University of Miami, 521 Anastasia Avenue, Coral Gables, Florida 33134, U.S.A.

(Received September 28, 1971)

Optical resolution of DL-aspartic acid by using copper complexes of L-alanine, D-alanine, L-glutamic acid, D-glutamic acid, and L-proline in aqueous solution is described. In this investigation the effects of (1) the concentration of reactants and (2) the ratio of the optically active amino acid to racemic aspartic acid in the reaction mixture were studied.

Studies have been made[1,2] on the optical resolution of racemic aspartic acid by the use of enzymatic and also diastereomeric chemical methods. Several methods have been reported for the optical resolution of racemic aspartic acid or a racemic aspartic acid copper complex. Racemic aspartic acid was optically resolved by employing optically active amines[3] and by seeding a supersaturated solution of DL-aspartic acid with ammonium formate.[4,5] Racemic aspartic acid copper complex was resolved easily by seeding with either an L- or D-aspartic acid copper complex.[6] Racemic aspartic acid copper complex was partially resolved by using biopolymers such as cotton or wool.[7] It was found that a supersaturated solution of racemic aspartic acid copper complex was spontaneously resolved into partially optically active L-aspartic acid copper complex.[8] Several investigations of the utilization of metal chelate compounds for optical resolution of racemic amino acids have been reported.[9,10,11]

The optical resolution of DL-aspartic acid by adding a solution of DL-aspartic acid to solutions of the copper complexes of D- or L-alanine, D- or L-glutamic acid, or L-proline was reported.[12] The mixture was allowed to stand for 24 hr to crystallize the aspartic acid copper complex. The optically active aspartic acid copper complex that crystallized had a configuration opposite to the optically active amino acid used in the reaction. This simple procedure for the resolution of racemic aspartic acid yielded 90—100% optically active D- or L-aspartic acid. The phenomenon was explained as a stereoselective ligand exchange reaction.[12] This paper reports the effects of (1) the concentration of reactants and (2) the ratio of the optically active amino acid to racemic aspartic acid on the resolution of racemic aspartic acid.

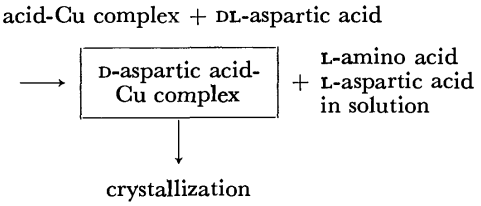

L-Alanine (0.01, 0.02, and 0.03 mol) was treated with copper carbonate for preparation of the solution (50 m*l*) of L-alanine copper complex. Racemic aspartic acid (0.01, 0.02, and 0.03 mol) in 100 m*l* of water was added to each of the solutions of L-alanine copper complex. Since the crystallization of the aspartic acid copper complex depended on the composition and concentration of the reaction mixture, the crystallization was carried out from several hours to 24 hr. The crystals were then collected by filtration (1st crop). The filtrate was allowed to stand longer (24—72 hr) for the 2nd crop of crystals of the aspartic acid copper complex to grow. The results of resolution of racemic aspartic acid by using L-alanine copper complex are summarized in Table 1.

We see that in reactions A-1, B-2, and C-3, the total amount of aspartic acid copper complex increased as the concentration of the reaction mixture was increased. Figure 1 shows the amount of crystalline aspartic acid copper complex normalized to 0.01 mole racemic aspartic acid. For the 1st crop of crystals, the maximum crystallization occurred when the molar ratio of L-alanine to DL-aspartic acid was about 1.5. The total amount of crystalline complex (1st and 2nd crops) was almost constant when the molar ratio of L-alanine to DL-aspartic acid exceeded 1.5. Figure 2 shows the optical purity of aspartic acid obtained from the 1st and 2nd crops as a function of the molar ratio of L-alanine to DL-aspartic acid. The aspartic acid from the 1st crop was always of the D-configuration; whereas, the configuration of aspartic acid from the 2nd crop depended upon the molar ratio of L-alanine to DL-aspartic acid. When the molar ratio was less than 1, the 2nd crop of crystals had a D-configuration as in the 1st crop. On the other hand, when the molar ratio was greater than 1, the 2nd crop of crystals had an L-configuration. The sharp inversion of configuration in the 2nd crop of

* Contribution No. 204 of the Institute for Molecular and Cellular Evolution, University of Miami.

1) T. Kaneko, "Optical Resolution and Racemization of Amino Acid," in Chemistry of Protein, ed. by S. Akabori and S. Mizushima, Kyoritsu Shuppan Co. Ltd., Tokyo (1954) I, p. 420.
2) J. P. Greenstein and M. Winitz, "Chemistry of the Amino Acids," John Wiley & Sons, Inc., New York (1961) I, II, III.
3) K. Harada, This Bulletin **37**, 1383 (1964).
4) K. Harada, *Nature*, **206**, 1354 (1965).
5) K. Harada, This Bulletin, **38**, 1552 (1965).
6) K. Harada and S. W. Fox, *Nature*, **194**, 768 (1962).
7) K. Harada, *ibid.*, **218**, 199 (1968).
8) K. Harada, *Naturwissenschaften*, **57**, 114 (1970).
9) B. D. Sarma and J. C. Bailar, Jr., *J. Amer. Chem. Soc.*, **78**, 895 (1956).
10) M. Shibata, Y. Fujita, M. Naito, and K. Hori, This Bulletin, **36**, 485 (1963).
11) M. Shibata, H. Nishikawa, and K. Hosaka, *ibid.*, **41**, 130 (1968).
12) K. Harada, *Nature*, **205**, 590 (1965).

TABLE 1. OPTICAL RESOLUTION OF DL-ASPARTIC ACID BY THE USE OF L-ALANINE COPPER COMPLEX

Reactions		L-Ala (mol) in 50 ml	DL-Asp (mol) in 100 ml	Optically active aspartic acid copper complex			Optically active aspartic acid	
				Crop	Weight (g)	Weight (g) normalized to 0.01 mol aspartic acid	Confign.	Optical purity (%)
A	1	0.01	0.01	1st	0.48	0.48	D	80
				2nd	0.51	0.51	L	33
				Total	0.99	0.99		
	2	0.01	0.02	1st	0.04	0.02	D	100
				2nd	0.62	0.31	D	96
				Total	0.66	0.33		
	3	0.01	0.03	1st	0.06	0.02	D	62
				2nd	0.60	0.20	D	31
				Total	0.66	0.22		
B	1	0.02	0.01	1st	0.87	0.87	D	84
				2nd	0.84	0.84	L	77
				Total	1.71	1.71		
	2	0.02	0.02	1st	1.06	0.53	D	80
				2nd	1.05	0.52	L	62
				Total	2.11	1.05		
	3	0.02	0.03	1st	0.24	0.12	D	74
				2nd	1.43	0.71	D	100
				Total	1.67	0.83		
C	1	0.03	0.01	1st	0.74	0.74	D	90
				2nd	1.13	1.13	L	40
				Total	1.87	1.87		
	2	0.03	0.02	1st	2.23	1.11	D	74
				2nd	1.11	0.56	L	97
				Total	3.34	1.67		
	3	0.03	0.03	1st	1.72	0.57	D	89
				2nd	1.40	0.47	L	98
				Total	3.12	1.04		

crystals is interesting and might be understood by taking into account the amount of DL-aspartic acid in the reaction mixture.

Figure 3 shows the results of a similar optical resolution of DL-aspartic acid by using L-proline copper complex. The amount of crystalline aspartic acid copper complex is normalized to 0.01 mole racemic aspartic acid. The curves are similar to those in Fig. 1. The 1st crop shows a maximum at a molar ratio of about 2. The total amount of crystalline complex reaches a plateau at a molar ratio of 2. Figure 4 shows the optical purity of aspartic acid obtained from the 1st and 2nd crops as a function of the molar ratio of L-proline to DL-aspartic acid. The aspartic acid from the 1st crop always had a D-configuration; whereas, the aspartic acid from the 2nd crop had a D-configura-

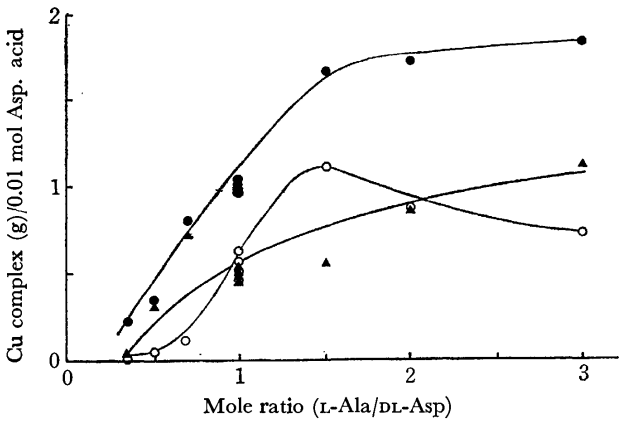

Fig. 1. Weight of crystallized aspartic acid copper complex *versus* molar ratio (L-Ala/DL-Asp).
▲ Aspartic acid copper complex (1st crop)
○ Aspartic acid copper complex (2nd crop)
● Total yield (1st+2nd)

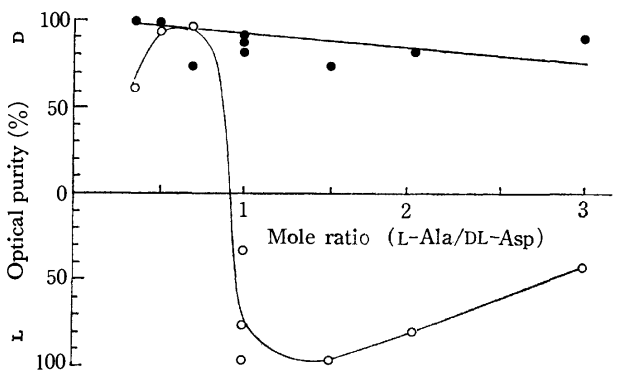

Fig. 2. Optical purity of aspartic acid *versus* molar ratio (L-Ala/DL-Asp).
●: Optical purity of aspartic acid (1st crop)
○: Optical purity of aspartic acid (2nd crop)

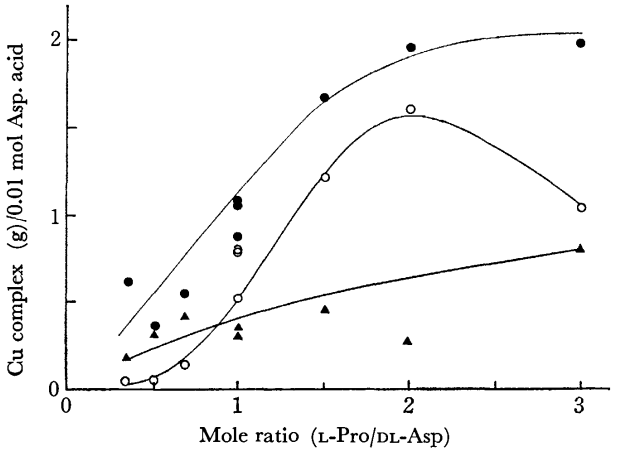

Fig. 3. Weight of crystallized aspartic acid copper complex *versus* molar ratio (L-Pro/DL-Asp).
▲: Aspartic acid copper complex (1st crop)
○: Aspartic acid copper complex (2nd crop)
●: Total yield (1st+2nd)

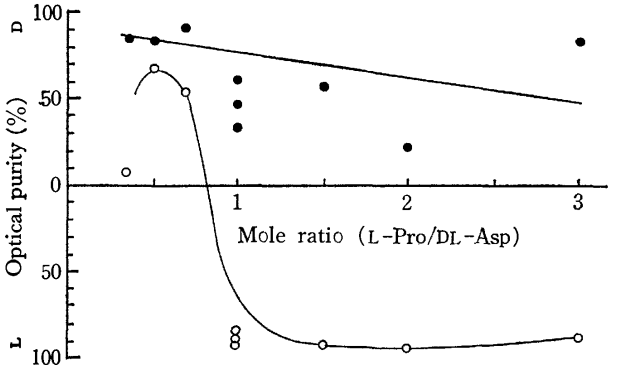

Fig. 4. Optical purity of aspartic acid *versus* molar ratio (L-Pro/DL-Asp).
●: Optical purity of aspartic acid (1st crop)
○: Optical purity of aspartic acid (2nd crop)

tion when the molar ratio of L-proline to DL-aspartic acid was less than 0.9. The aspartic acid had an L-configuration when the molar ratio was greater than 1. The curves are similar to those in Fig. 2. Figure 5 shows the amount of crystalline aspartic acid copper complex and optical purity of aspartic acid obtained by prolonged crystallization for up to 7 days. In this experiment, the molar ratio of L-proline to DL-aspartic acid was 1. As the degree of crystallization increased, the optical purity of the aspartic acid decreased rapidly.

Figure 6 shows the results of the optical resolution of DL-aspartic acid by using L- or D-glutamic acid copper complex. Optically active glutamic acid copper complex gave the highest stereospecific resolution of DL-aspartic acid. Figure 6a shows the optical purity of aspartic acid obtained from the 1st and 2nd crops as a function of the molar ratio of L-glutamic acid to DL-aspartic acid. The aspartic acid from the first crop shows a maximum optical purity when the molar ratio of L-glutamic acid to DL-aspartic acid was 1. In comparison, the optical purity of the aspartic acid from the 2nd crop is high throughout. Figure 6b shows almost the same results by using D-glutamic acid.

The optical resolution of racemic aspartic acid using several copper complexes of optically active amino acids was explained by a stereoselective ligand exchange mechanism and subsequent preferential crystallization.[9] However, attempts to observe the possible stereoselective ligand exchange by the absorption spectrum and the mutarotation of the reaction mixture were unsuccessful. These observations together with the rapid rate of ligand exchange in copper complexes suggest that the proposed stereoselective ligand exchange may not represent the mechanism of these reactions.

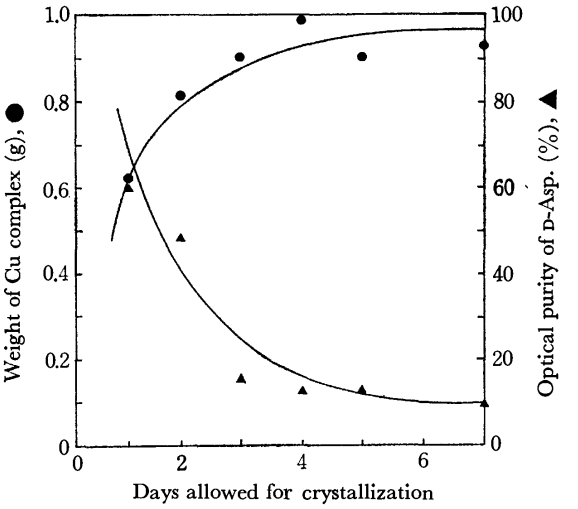

Fig. 5. Weight of aspartic acid copper complex and optical purity of aspartic acid *versus* days allowed for crystallization. (Cu complex prepared from 0.01 mol L-Pro and 0.01 mol DL-Asp in 150 m*l* H_2O)

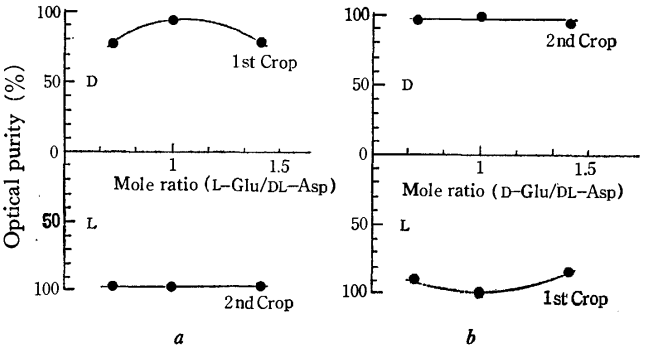

Fig. 6. Optical purity of aspartic acid *versus* mole ratio; a: L-glutamic acid copper complex was used; b: D-glutamic acid copper complex was used.

Experimental

Copper Complex of Optically Active Aspartic Acid (Reaction A-1). L-Alanine (0.89 g, 0.01 mol; Mann Research Laboratories, Inc.; $[\alpha]_D^{25} = +14.3°$ in 6N HCl) was boiled gently with 5.0 g of copper carbonate (Baker Analytical Grade) in 50 m*l* of water for five minutes. The excess of copper carbonate was removed by filtration under reduced pressure. DL-Aspartic acid (1.33 g, 0.01 mol; Mann assayed grade) in 100 m*l* of hot water was added through filter paper to the filtrate. The solution was kept at room temperature for 1 day without agitation. The crystallized D-aspartic acid copper complex, 0.48 g, was collected by filtration. The filtrate was allowed

to stand an additional two days for further crystallization. L-Rich aspartic acid copper complex, 0.51 g, was obtained.

Other amino acids used were L-proline ($[\alpha]_D^{20}=-51.8°$, 0.5N HCl), L-glutamic acid ($[\alpha]_D^{20}=+31.5°$, 6N HCl), and D-glutamic acid ($[\alpha]_{20}^{D}=-31.5°$, 6N HCl).

Preparation of Free Aspartic Acid. The optically active aspartic acid copper complexes were dissolved by heating in 30 to 50 m*l* of 7% acetic acid. The copper ion in each solution was removed by precipitation with hydrogen sulfide. After the precipitation was complete, a small amount of activated charcoal was added to the solution and the solution was cooled to room temperature. The mixture was then filtered and the filtrate was evaporated to dryness under reduced pressure. The aspartic acid was weighed and its specific rotation was measured without further purification.

Some of the optically active preparations of aspartic acid contained a trace to a small amount of the other optically active amino acid used in the resolution reaction (L-ala, L-pro, L- and D-glu). The impurities were detected by paper chromatography. The small amounts of impurities could be eliminated easily by one recrystallization from 25 volumes of water. The optical purity of aspartic acid was measured without recrystallization, since such a purification procedure would cause considerable fractionation of partially optically active aspartic acid. All the optical rotation measurements were carried out by the use of a Rudolph Model 80 polarimeter with a PEC-101 photometer at 25°C using a 10 cm cell.

This work was supported by Grant No. NGR 10-007-052 from the National Aeronautics and Space Administration. The authors wish to express their thanks to Dr. K. M. Wellman of the Department of Chemistry, University of Miami for valuable discussion. Thanks are extended also to Ajinomoto Co. Ltd. for supplying D-glutamic acid.

BULLETIN OF THE CHEMICAL SOCIETY OF JAPAN, VOL. 45, 2862—2866 (1972)

Polymerization of Vinyl Monomers in the Presence of Surface Active Agents. II. The Rate of Polymerization of Methyl Methacrylate

Teruzo ASAHARA, Manabu SENŌ, Shinsaku SHIRAISHI, and Yoshikazu ARITA

Institute of Industrial Science, University of Tokyo, Roppongi, Minato-ku, Tokyo

(Received January 22, 1972)

The polymerization of methyl methacrylate in the presence of sodium tetrapropylenebenzenesulfonate(ABS) in an aqueous system without any ordinary initiators was examined kinetically. The rate of polymerization of methyl methacrylate is dependent on the initial concentrations of methyl methacrylate and ABS, and expressed by the equation:

$$R_p \propto [\mathrm{ABS}]^{0.37}[\mathrm{MMA}]^{0.32}$$

The apparent activation energy of the polymerization is about 3 kcal/mol. It was confirmed by electron microscopic observation that the number of polymer molecules is in the same order as that of the micelle particles in the polymerization system.

We reported previously on the polymerization of methyl methacrylate (MMA) in the presence of anionic surface active agents such as alkylbenzenesulfonate (ABS) in an aqueous system without any ordinary initiators. This system gave a stable emulsion of poly(MMA) with an unusually high molecular weight in a good yield.[1)]

In this paper, the results of a kinetic study of the polymerization of MMA in the presence of ABS in an aqueous system will be described.

Experimental

Materials. Methyl methacrylate and sodium tetrapropylenebenzenesulfonate (ABS) were purified according to the method described previously.[1)] Diphenylpicrylhydrazyl (DPPH) of G.R. grade was used without further purification.

Determination of the Rate of Polymerization. 100 g of deionized water and a desired amount of ABS were placed in a four-necked, flat bottomed 100 m*l* flask equipped with a condenser, a dropping funnel, a nitrogen inlet tube and a rubber stopper. The mixture was then preheated at a prescribed reaction temperature for 40 min, a slow stream of nitrogen being introduced into the mixture. MMA was then added through the dropping funnel and allowed to polymerize. About 2 g of the reaction mixture was withdrawn by a syringe and accurately weighed at regular time intervals. The weighed sample was poured into 10 m*l* of methanol in order to precipitate the polymer formed, which was collected by filtration, washed with methanol, dried at 60°C under a vacuum and weighed. The rate of polymerization was determined from the weight of the precipitate.

Determination of Number of Particles. Particle size determination was carried out on a sample of about 1 g which was withdrawn from the reaction mixture and diluted with 10 times as much water containing 0.01% of hydroquinone which was used to minimize further change. The diluted sample was deposited onto the collodion substrates in the form of minute droplets of approximately 2 micron in radius. The specimen was shadow-cast with carbon, and the electron micrographs were taken with a JEM-5Y electron microscope of magnification 9800 at 80 kV. The surface average dia-

1) T. Asahara, M. Senō, S. Shiraishi, and Y. Arita, This Bulletin, **43**, 3895 (1970).

meters of particles were obtained on 50—100 particles in an enlarged (×2) photograph using a Scale Lupe of magnification 5. The number of particles was calculated from the volume average diameter and the density of particles which was approximated to be 1.0.

Measurement of the Generated Radicals. 50 m*l* of water or an organic solvent (THF or ethyl acetate), 0.3 g of ABS, and 1 m*l* of MMA or ethyl acetate, each containing 5.0 mg of DPPH, were placed in an apparatus as shown in Fig. 1. If the mixture was not a clear solution, a few drops of octaoxyethylene nonylphenyl ether were added as a solubilizer. The mixture was shaken well and subsequently frozen in a liquid nitrogen bath. It was then brought to a vacuum below 10^{-3} Torr in order to degas, and then allowed to melt. This freeze-thaw procedure was repeated three times to attain complete degassing. The degassed mixture was then heated in an oil bath at 80±0.2°C and the absorption of each sample at 530 mμ was measured at regular time intervals.

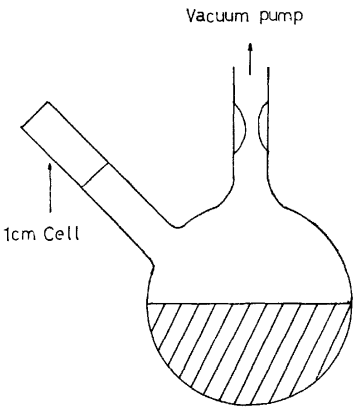

Fig. 1. Apparatus for measurement of generated radicals.

Results and Discussion

We found[1] that MMA polymerized readily in the presence of an anionic surface active agent in water without any ordinary initiators. The mechanism of the polymerization, however, has not been clarified yet. A kinetic approach to the polymerization was attempted and the relationship between the rate of polymerization and the initial monomer concentration or the ABS concentration was investigated. The quantity of the free radicals generated in the reaction system was also measured spectrometrically by using DPPH in order to obtain information on the initiation mechanism of the polymerization.

For a case of usual emulsion polymerization, Smith and Ewart presented the following equation for the rate of polymerization:[2]

$$R_p = k_p[\mathrm{M}]/N/2, \quad (1)$$

where k_p is the rate constant of the propagation reaction, [M] is the monomer concentration in the particles which is supposed to remain constant until the excess monomer droplets disappear in the system, and N is the number of particles. Thus R_p is dependent only on N. Smith and Ewart also pointed out that the relationship between N and the concentration of emulsifier was as follows:

$$N = k(\mathrm{CsAs})^{3/5}(\rho/\mu)^{2/5} \quad (2)$$

where As is the surface area of a particle, Cs is the concentration of the emulsifier present, ρ is the rate of generation of radicals, μ is the rate of volume increase of the particles and k is a constant with value 0.37—0.57.

Their theory, however, cannot be applied to our reaction system, in which R_p depends on the initial monomer concentration $[\mathrm{M}]_0$, which is defined as an apparent molarity calculated from the composition in the initial reaction mixture. A plot of log R_p against log $[\mathrm{M}]_0$ is found to be linear as shown in Fig. 2. The relationship can be expressed by the equation:

$$R_p \propto [\mathrm{M}]_0^{0.32}$$

The result may imply that the monomer concentration in the particles does not remain constant in the present reaction system.

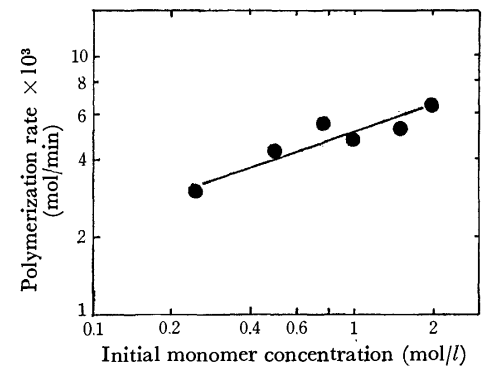

Fig. 2. Dependence of polymerization rate (mol/min) on initial monomer concentration (mol/*l*).
ABS 0.3 g/100 g of water, 80°C, under nitrogen atmosphere. Slope of line 0.32.

While Smith and Ewart also showed that the value of R_p was proportional to 0.6th power of the concentration of the emulsifier, Lee and Longbottom[3] have proposed the following equation:

$$R_p \propto [\mathrm{Cs}]^{0.18-0.55}$$

The rate of polymerization of our system depends on the concentration of ABS. As seen from Fig. 3, the relation between R_p and [Cs] is given by

$$R_p \propto [\mathrm{Cs}]^{0.37}$$

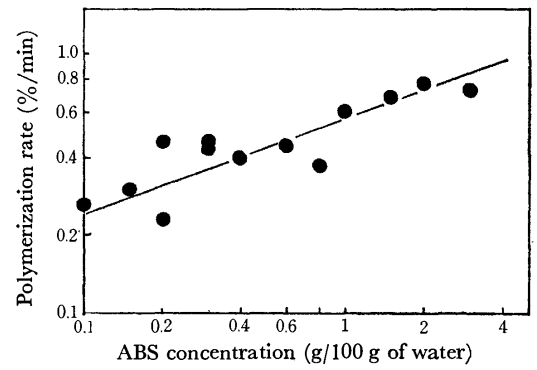

Fig. 3. Dependence of polymerization rate (%/min) on ABS concentration.
MMA 10 g, 80°C, under nitrogen atmosphere. Slope of line 0.37.

2) W. V. Smith and R. H. Ewart, *J. Chem. Phys.*, **16**, 592 (1948).

3) P. I. Lee and H. M. Longbottom, *J. Appl. Polym. Sci.*, **14**, 1377 (1970).

The rate of polymerization was measured at temperatures 70—100°C and the results are shown in Table 1. The activation energy of the overall polymerization reaction is about 3 kcal/mol. This value is very small compared to the values reported hitherto for the radical polymerization of MMA. The polymerization rate decreased at 100°C. This might be due to the increase of the rate of termination reaction or the reduced stability of particles caused by boiling of the reaction mixture. The induction period decreased with an increase of reaction temperature, but an estimation of the activation energy of the initiation reaction from the period was not successful.

The average degree of polymerization of the poly(MMA), DP, was obtained from the intrinsic viscosity measurement[1] and the result is plotted against the initial monomer concentration and the ABS concentration (Figs. 4 and 5). The DP is almost independent of both ABS and $[M]_0$. It tends to increase slightly with a rise in reaction temperature, presumably because the rate constant of the propagation increases with an increasing temperature (Table 1). In every case, DP is very high as we have emphasized.[1] It might be explained as follows: The number of generated radicals is very small, radicals rarely exist simultaneously in the same particle and the termination by radical coupling hardly takes place.

This is rationalised by a comparison of the number of polymer molecules formed with that of the polymer particles. The number of polymer molecules was calculated from polymer yields and molecular weight.

Table 1. Effect of reaction temperature on polymerization rate and DP

Reaction temperature (°C)	Polymerization rate (mol/min)	DP
70	4.42×10^{-3}	5.48×10^{-4}
80	4.59	5.90
85	4.39	5.50
90	6.05	6.80
100	5.38	6.31

MMA 10 g; water 100 g; ABS 0.3 g under nitrogen atmosphere.

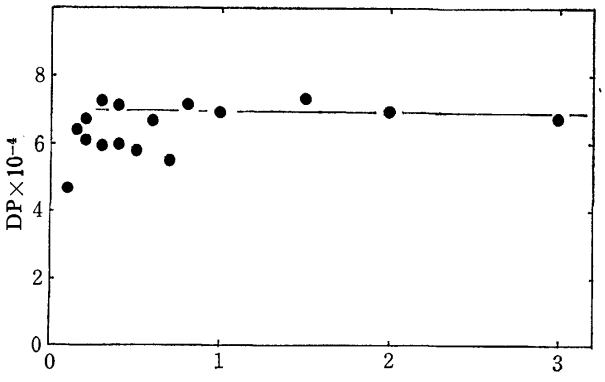

Fig. 4. Dependence of DP on ABS concentration.
MMA 10 g, 80°C, 2 hr, under nitrogen atmosphere.

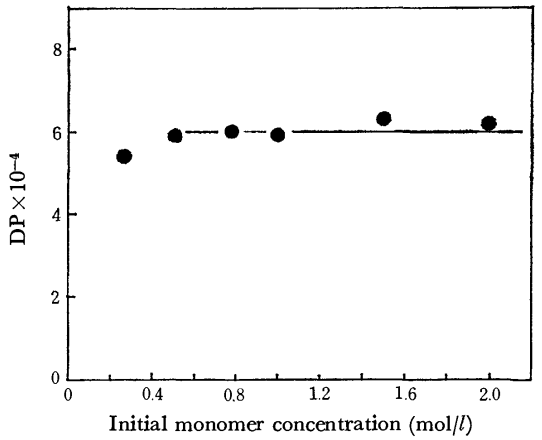

Fig. 5. Dependence of DP on initial monomer concentration.
ABS 0.3 g, water 100 g, 80°C, 2 hr, under nitrogen atmosphere.

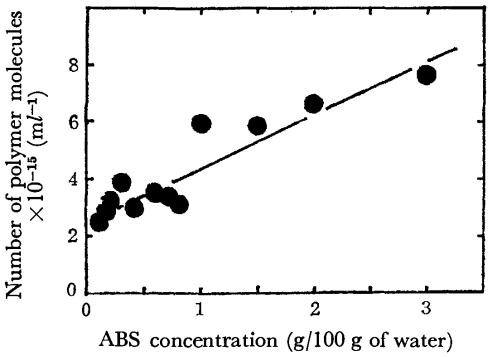

Fig. 6a. Dependence of number of polymer molecules on ABS concentration.
MMA 10 g, water 100 g, 80°C, 2 hr, under nitrogen atmosphere.

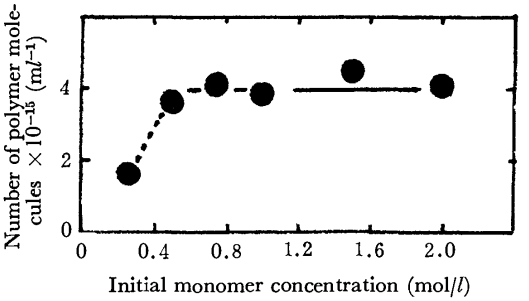

Fig. 6b. Dependence of number of polymer molecules on initial monomer concentration.
ABS 0.3 g, water 100 g, 80°C, 2 hr, under nitrogen atmosphere.

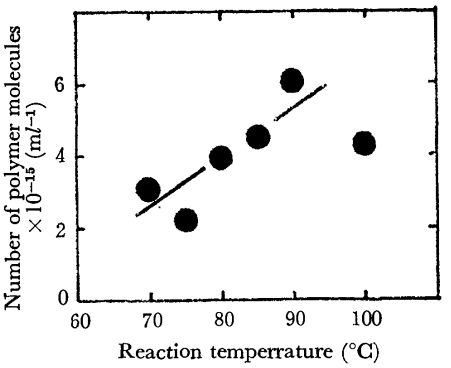

Fgi. 6c. Dependence of number of polymer molecules on reaction temperature.
ABS 0.3 g, MMA 10 g, water 100 g, 2 hr, under nitrogen atmosphere.

The effects of the concentrations of ABS and monomer and of the reaction temperature on the number of polymer molecules are shown in Figs. 6a, b, and c. The number of polymer molecules increased with the increasing concentration of ABS and increasing reaction temperature, but was not affected by the concentration of monomer in the concentration range above 0.5 mol/*l*. We see from the results that the generated radicals increased with the increasing concentration of ABS and temperature.

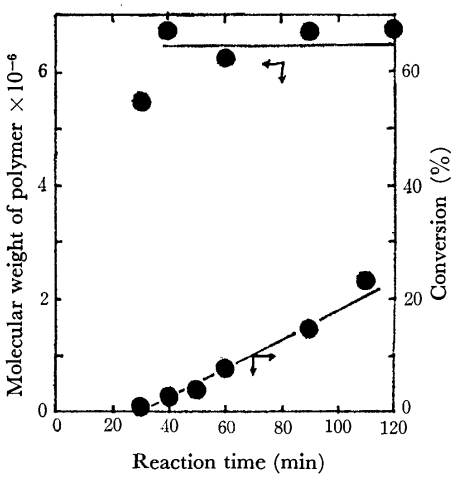

Fig. 7. Dependence of molecular weight of polymer on reaction time.
MMA 50 g, ABS 2.5 g, water 500 g, 80°C, under nitrogen atmosphere.

When a steady state was reached (Fig. 7), direct determination of particle size was attempted with an electron microscope. The samples were prepared under the conditions; reaction time 30, 60, and 120 min, the ABS concentration 1 g and 3 g per 100 g of water.

The results are shown in Fig. 8 and Table 2. The result in Table 2 shows that the particle size is in the relatively narrow range 300—400 Å independent of the concentration of ABS and the reaction time. The maximum particle size is 1000—1200 Å and the particles which are supposed to be generated newly were observed at every reaction time. The number of polymer particles per unit volume is about 1×10^{15}, which is in the same order as the number of polymer molecules calculated above. Since poly(MMA) scatter electrons poorly and give electron micrographs of a low contrast, we used the shadow-casting with carbon.

Table 2. Particle size of MMA latices

ABS (g)	Reaction time (min)	Average diameter (Å)	Number of polymer particles (ml^{-1})	Number of polymer molecules[a] (ml^{-1})
1	30	414		
1	60	462		
1	120	472	0.95×10^{15}	4.5×10^{15}
3	30	363		
3	60	411		
3	120	438	1.40×10^{15}	5.5×10^{15}

MMA 10 g; water 100 g; at 80°C under nitrogen atmosphere.
a) Calculated from molecular weight and yield of polymers.

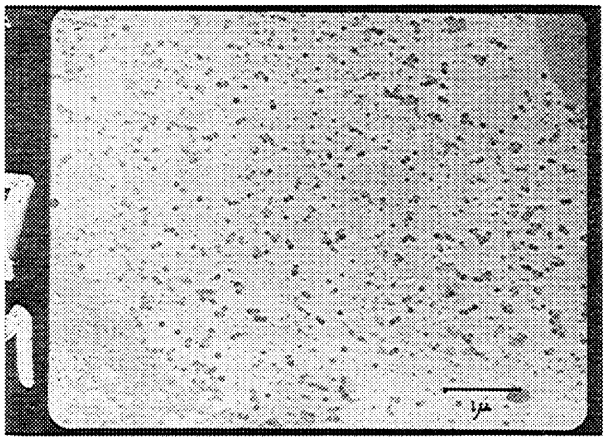

Fig. 8a

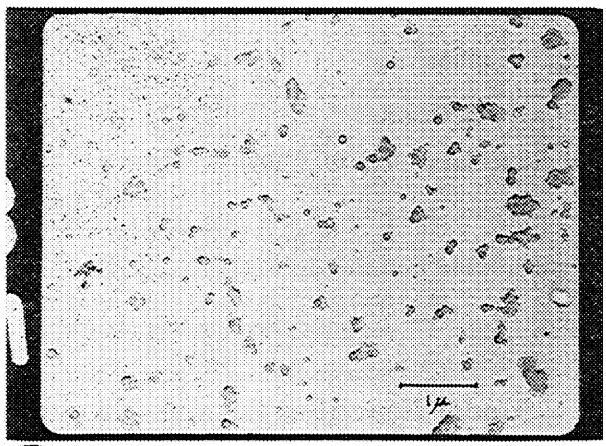

Fig. 8b

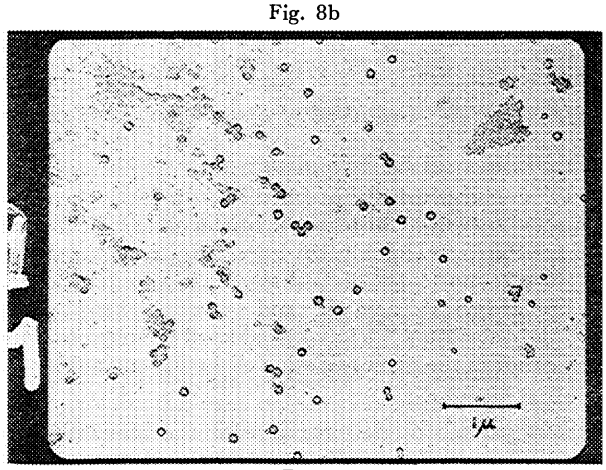

Fig. 8c

Fig. 8. Electron micrographs of MMA latices. The samples are at reaction time; 30 min (a), 60 min (b), 120 min (c). ABS 1 g/100 g water. (×19600).

It may be presumed that the polymerization in particles proceeds in a similar way to that in bulk polymerization. Thus the relation between the degree of polymerization and the initial monomer concentration can be represented by the equation:

$$DP = k_p/\{k_t[P\cdot]/[M]+k_{tr}\}$$

where k_p, k_t, and k_{tr} are rate constants of propagation, termination and chain transfer to monomer, respectively, and [P·] and [M] are concentration of growing radical and monomer in the particle, respectively.

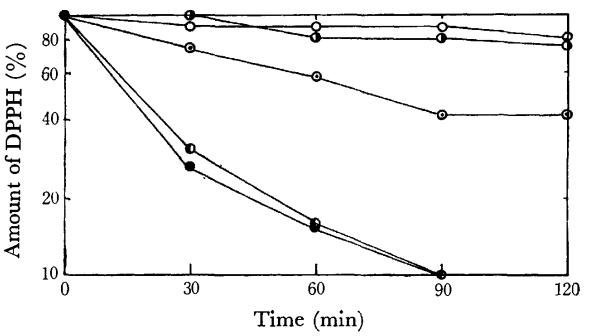

Fig. 9. Time changes of disappearance of DPPH in various system.
◐ H_2O 50 m*l*; ABS 0.3 g; MMA 1 m*l*; DPPH 5 mg
⊙ THF 50 m*l*; ABS 0.3 g; MMA 1 m*l*; DPPH 5 mg
◑ THF 50 m*l*; ABS none; MMA 1 m*l*; DPPH 5 mg
● H_2O 50 m*l*; ABS 0.3 g; ethyl acetate 1 m*l*; DPPH 5 mg
○ ethyl acetate 50 m*l*; ABS 0.3 g; ethyl acetate 1 m*l*; DPPH 5 mg

The ratio [P·]/[M] can be regarded as negligibly small from the results in Table 2. Thus $DP \simeq k_p/k_{tr}$ which is constant. In fact, DP is independent of monomer concentration as shown in Fig. 5, which gives $k_p/k_{tr}=6\times10^4$.

Measurement of the generated radicals was carried out by using DPPH as a radical scavenger in MMA or ethyl acetate. The absorption of DPPH in the presence of water or organic solvents was measured at 530 mμ with a spectrophotometer. As shown in Fig. 9, when an organic solvent such as THF or ethyl acetate was used instead of water, the amount of DPPH remained almost constant. In an aqueous system, in spite of the presence of MMA, the absorption of DPPH decreases markedly in intensity in the presence of ABS. These results are seen to reflect a specific role of the interface, and are consistent with the fact that a surfactant shows the surface activity only in an aqueous medium.

Thus, it is plausible that the polymerization is initiated at the surface of the micelle particles.

The authors are indebted to Mr. Shigeki Shiozawa for his technical assistance.

BULLETIN OF THE CHEMICAL SOCIETY OF JAPAN, VOL. 45, 2866—2871 (1972)

Model Reactions for the Biosynthesis of Thyroxine. XIX. The Formation of a Thyroxine Precursor by Photooxidation of 4-Hydroxy-3,5-diiodophenylpyruvic Acid in Organic Solvents[1-3]

Kanji OMURA, Akira NISHINAGA, and Teruo MATSUURA

Department of Synthetic Chemistry, Faculty of Engineering, Kyoto University, Sakyo-ku, Kyoto

(Received January 20, 1972)

Photooxidation of 4-hydroxy-3,5-diiodophenylpyruvic acid (I) in methanol was found to yield a hydroperoxide (IV). This hydroperoxide reacted anaerobically with 3,5-diiodotyrosine (II) to form thyroxine (III). A photoproduct, presumably IV, apparently accelerated the oxidation of I. Methanol, among several organic solvents, was found to be the best solvent for the photooxidation. Similar oxidations with 4-hydroxy-3-iodo-5-methoxyphenylpyruvic acid (V) and 4-hydroxyphenylpyruvic acid (VI) showed that the rate of oxidation decreased in the order I>V>VI. A product of the photooxidation of I, probably the hydroperoxide IV, also acts as an accelerator in the photooxidation of the desiodo analog VI of I.

A nonenzymic model reaction for the biosynthesis of thyroxine was reported by Meltzer and Stanaback,[4] who showed that autoxidation (pH 7.5) of 4-hydroxy-3,5-diiodophenylpyruvic acid (I) in the presence of 3,5-diiodotyrosine (II) yields thyroxine (III) in moderate yield. Nishinage *et al.*[5] have demonstrated that the reaction takes place in two distinct phases: the enolic form of I is first autoxidized to a hydroperoxide (IV), which then reacts with II to form III in an over-all yield of up to ~40%. Oxygen was found to be required only in the first step, but not in the second.[5]

Structural requirements for the autoxidation of I in aqueous media were found to be the existence of I in its enolic form and the dissociation of the phenolic proton. A solution of I in an organic solvent does not consume oxygen.[6] In organic solvents I exists in its enolic form,[5] but the phenolic hydroxyl is undissociated. This observation prompted us to investigate the photooxidation of I by oxygen in organic solvents. This paper also includes some results obtained in similar photooxidations (sensitized or unsensitized) of two analogs of I, *viz.* 4-hydroxy-3-iodo-5-methoxyphenyl-

1) Part XVIII: A. Nishinaga and H. J. Cahnmann, to be published.

2) Regarded as Part LV in the series of Photoinduced Reactions. Part LIV: T. Nagamachi, A. Nishinaga, and T. Matsuura, *Chem. Lett.*, **1972**, 111.

3) A preliminary communication was published in *Chem. Commun.*, **1969**, 366.

4) R. I. Meltzer and R. J. Stanaback, *J. Org. Chem.*, **26**, 1977 (1961).

5) A Nishinaga, H. J. Cahnmann, H. Kon, and T. Matsuura, *Biochemistry*, **7**, 388 (1968).

6) Unpublished data,

pyruvic acid (V) and 4-hydroxyphenylpyruvic acid (VI).

Results and Discussion

Photooxidation of I. A solution of I in methanol was irradiated at ~5°C with a 100 W high-pressure mercury lamp of Pyrex housing. Oxygen was bubbled through the solution during the irradiation until the absorption of oxygen was nearly quantitative (0.93 mol/mol of I). The solution contained the hydroperoxide IV as shown by the isolation of the diol acid VII after reduction of the photolysate with sodium borohydride. The yield of VII was 57% (based on I). The identity of VII was confirmed by direct comparison with the previously described diol acid VII.[5] Treatment of the photolysate with 3,5-diiodotyrosine (II), described previously,[5] gave thyroxine (III) in 18.6% yield (also based on I). Treatment of a methanolic solution of I with oxygen in the dark, followed by treatment with II yielded no thyroxine (III). It can therefore be concluded that dissociation of the phenolic proton of I, a prerequisite for the autoxidation in aqueous media (pH 7.5),[5] is not required for the photooxidation in methanol.

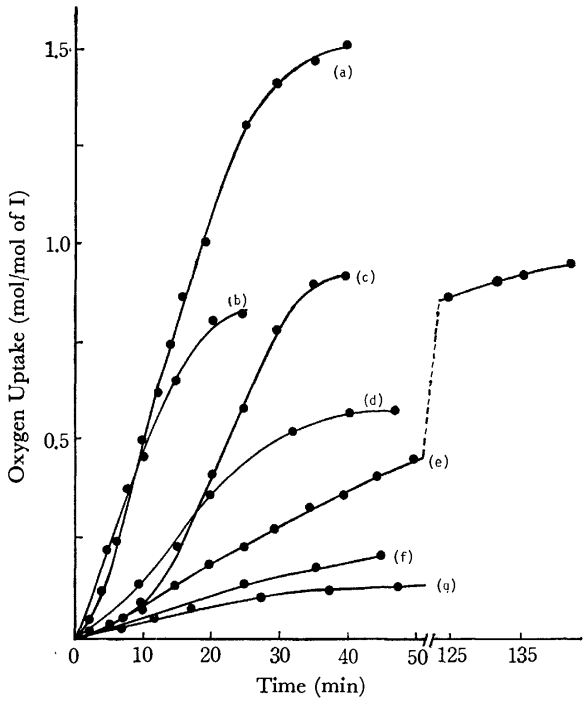

Fig. 1. Uptake of oxygen during photolysis (>2800 Å) of I in various solvents at ~5°C (see footnote a in Table 1). (a) Tetrahydrofuran, (b) acetone, (c) methanol, (d) acetonitrile–methanol (8:1), (e) pyridine, (f) 0.1 M boric acid and 1.1 mM rose bengal, (g) 0.2 M boric acid (pH 4.5).

Table 1. Photooxidation of I and formation of thyroxine (III)[a]

Exp. No.	Solvent	Irradiation time (min)	Oxygen uptake (mol/mol of I)	Yield of III (%)
1	MeOH	40	0.93	18.6
2	MeOH[b]	45	0.88	10.5
3	H_3BO_3 in MeOH (0.2M)	50	1.08	18.6
4	Acetone	25	0.84	11
5	CH_3CN–MeOH (8: 1)	47	0.59	11
6	Tetrahydrofuran	40	1.57	3
7	Pyridine	150	0.98	0
8	0.2M Borate buffer, pH 4.5	60	0.14	—[c]
9	Same+1.1 mM rose bengal	45	0.23	1.1

a) A solution of I (2.3 mmol) in a solvent (100 ml) was irradiated at ~5°C with light above 2800 Å under oxygen-bubbling.
b) Irradiated at 22°C.
c) Not determined.

The photochemical conversion of I to IV is an additional example of the resemblance betweeen certain photochemical and biological oxidations.[7] It is similar to the photooxidation of other enolic compounds.[7b,8] Moreover, it provides a new synthetic route to thyroxine.

Solvent Effect on the Photooxidation of I. The effect of solvents on the oxygen consumption of I under irradiation and on the formation of III after treatment of the photolysate with II are shown in Fig. 1 and Table 1. The best yield of III was obtained in methanol at ~5°C (Exp. 1). At room temperature the yield was decreased (Exp. 2). A similar decrease in yield with increased temperature had been observed previously in the autoxidation in an aqueous medium at pH 7.4.[6] It should be noted that the photooxidation in methanol is apparently an auto-catalytic reaction, since the maximam rate was reached only after about 10—15 min (Fig. 1). A similar phenomenon was also observed in the autoxidation of I in an aqueous medium,[5] where a radical chain reaction is believed to occur. In the case of the photooxidation, however, it probably can be attributed to an accelerating effect of the reaction product (IV) (see below). In acetone the rate of the reaction, without any induction period, was higher than with methanol. Acetone, however, seems to promote also the decomposition of the reaction product (IV), as suggested by the lower yield of III (Exp. 4). In tetrahydrofuran induced oxidation of the solvent appears to occur, since the yield of III was low in spite of the absorption of an excess of oxygen (Exp. 6). The slower rate of oxidation in pyridine can be attributed to the absorption of the incident light by the solvent (Exp. 7). It must be assumed that even in this case, the thermally[5] and presumably photochemically unstable hydroperoxide IV is formed, but then destroyed during the long period of irradiation. Consequently, no thyroxine (III) could be isolated in this case after treatment of the reaction mixture with

7) a) T. Matsuura, A. Nishinaga, N. Yoshimura, T. Arai, K. Omura, H. Matsushima, S. Kato, and I. Saito, *Tetrahedron Lett.*, **1969**, 1673; b) T. Matsuura, H. Matsushima, and H. Sakamoto, *J. Amer. Chem. Soc.*, **89**, 6370 (1967); c) T. Matsuura, H. Matsushima, and R. Nakashima, *Tetrahedron*, **26**, 435 (1970); d) T. Matsuura, and H. Matsushima, *ibid.*, **24**, 6615 (1968); e) A. C. Waiss, Jr., R. E. Lundin, A. Lee, and J. Corse, *J. Amer. Chem. Soc.*, **89**, 6213 (1967); f) J. E. Baldwin, H. H. Basson, and H. Krauss, Jr., *Chem. Commun.*, **1968**, 984; and references cited therein.

8) R. H. Young and H. Hart, *ibid.*, **1967**, 827.

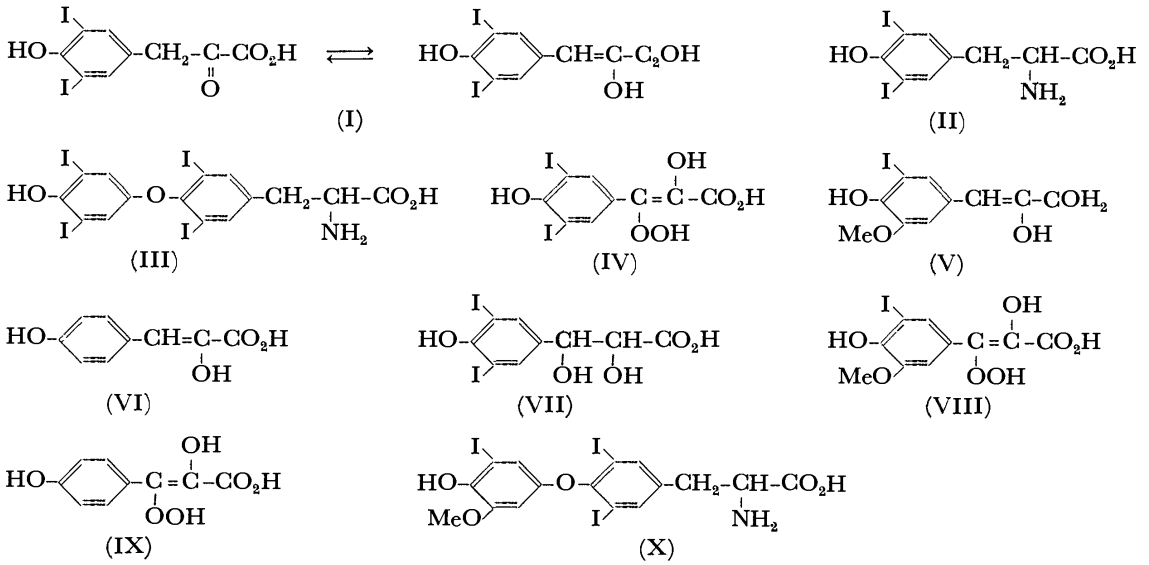

diiodotyrosine (II). Oxygen was hardly absorbed in boric acid solution (pH 4.5) on irradiation (Exp. 8), while facile absorption was observed in the autoxidation of I in boric acid–NaOH (pH 7.5).[5] The addition of boric acid to methanol did not alter the extent of oxygen uptake or the yield of thyroxine (III) (Exp. 3).

Accelerating Effect of the Hydroperoxide IV in Methanol. As mentioned above, the conversion of I into IV in methanol is slow at first, but becomes faster with time. A possible explanation for this is a photochemically initiated radical-chain reaction, since similar phenomena can often be found in many autoxidation reactions, including that of I itself,[5] which are believed to proceed *via* a radical-chain mechanism.

An intermittent irradiation experiment seemed, however, to exclude this possibility, since no oxygen uptake was observed during the interruption of irradiation (Fig. 2). Upon resumption of the irradiation the rate of oxygen uptake became the same value which had been reached prior to the interruption of the irradiation. An alternative explanation for the sigmoid shape of the oxygen uptake curve would be an accelerating effect exerted by the photoproduct, presumably the hydroperoxide IV or by one of its degradation products. This possibility was supported by a photooxidation experiment with I in the presence of the hydroperoxide IV which was supplied in the form of a freshly photooxygenated solution of I (Fig. 3). In

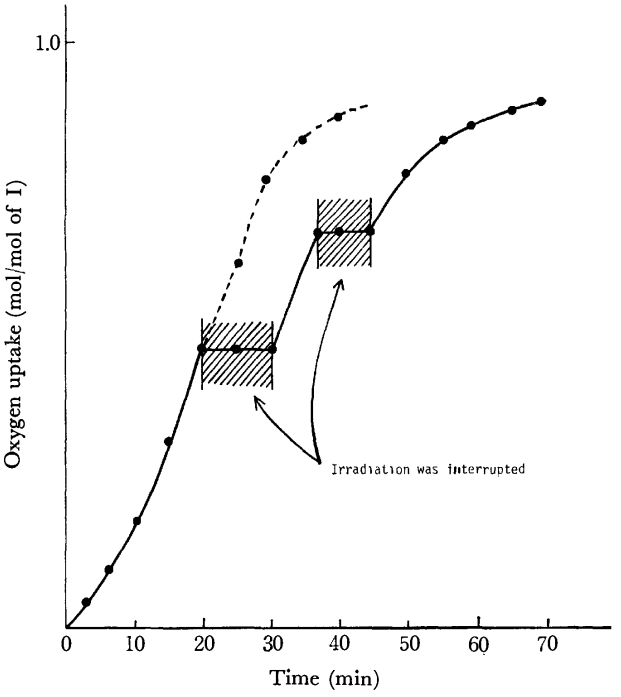

Fig. 2. Intermittent irradiation (>2800 Å) of I (2.3 mmol) in methanol (90 m*l*) at 25°C. ----Intermittent irradiation, ——uninterrupted irradiation.

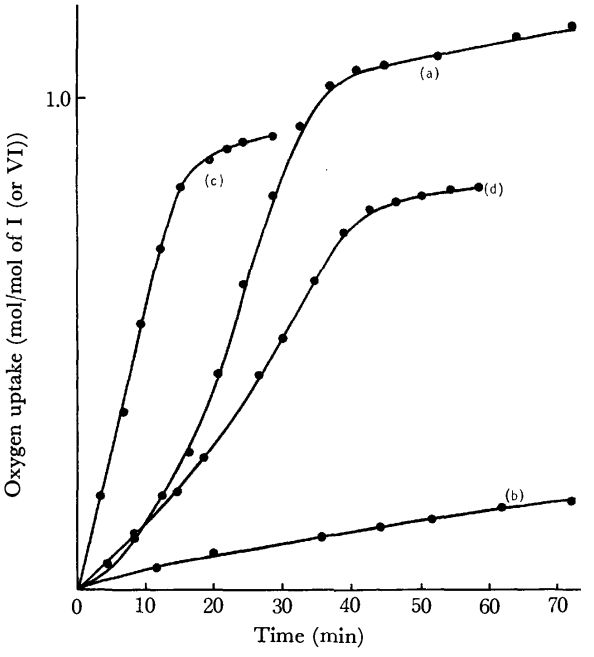

Fig. 3. Effect of the photooxidation product of I on the oxygen uptake of I (1.16 mmol) or VI (1.16 mmol) on irradiation (>2800 Å) in methanol (100 m*l*) at ~2°C. (a) I alone, (b) VI alone, (c) I added to a freshly photooxygenated solution (oxygen uptake 100%) of I (1.16 mmol), (d) VI added to a freshly photooxygenated solution (oxygen uptake 100%) of I (1.16 mmol).

this case the rate of oxygen uptake was maximal even at the initial stage of the reaction. The accelerating action of a photooxygenated solution of I is even more strikingly illustrated by the acceleration of the photooxidation of the desiodo analog of I, 4-hydroxyphenylpyruvic acid (VI), which by itself undergoes only very slow photooxidation (Fig. 3, see also below). The hydroperoxide IV is the main product (~60%) of the oxidation of I, and neither 4-hydroxy-3,5-diiodobenzaldehyde nor 2,6-diiodobenzoquinone, known as degradation products of IV,[5] had an appreciable accelerating effect.

The mechanism of the acceleration remains to be elucidated. The generation of singlet oxygen by the interaction of the excited IV with triplet oxygen[9] seems improbable since the photooxidation of 2,5-dimethylfuran was insufficiently sensitized by the hydroperoxide IV, and addition of a small amount of rose bengal, a typical sensitizer for generating singlet oxygen, had little effect on the photooxidation of I.

Sensitized and Unsensitized Photooxidation of V and VI. Photooxidations were also carried out with 4-hydroxy-3-iodo-5-methoxyphenylpyruvic acid (V) and 4-hydroxyphenylpyruvic acid (VI) in methanol in the presence or in the absence of a sensitizer. As shown in Fig. 4, the unsensitized oxygenation of V was slower than that of I. The slowest absorption of oxygen was observed in the case of the desiodo analog VI. The photooxidation of these acids was faster in acetone than in methanol, but the order of the reaction rates was again I>V>VI. Rose bengal was also found to accelerate the photooxidation of V and VI (Figs. 5 and 6). In each case the rate of oxygen consumption increased with increased sensitizer concentration. It should, however, be noted that the amount of rose bengal used was larger than that usually required for a typical photosensitized oxidation. Addition of a small amount of rose bengal, which is sufficient to sensitize the photooxidation of an olefinic compound, had only a weak sensitizing effect.

It may be therefore assumed that the mechanism of the rose bengal-sensitization of the photooxidations described in this respect is different from the usual

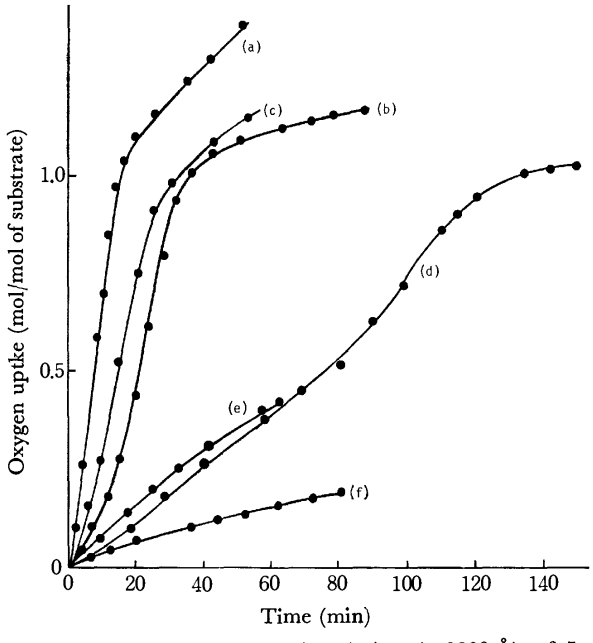

Fig. 4. Oxygen uptake by irradiation (>2800 Å) of I, V and VI (1.16 mmol, respectively) in methanol or acetone (90 m*l*) at ~2°C. (a) I in acetone, (b) I in methanol, (c) V in acetone, (d) V in methanol, (e) VI in acetone, (f) VI in methanol.

9) C. S. Foote, *Accounts Chem. Res.*, **1**, 104 (1968).

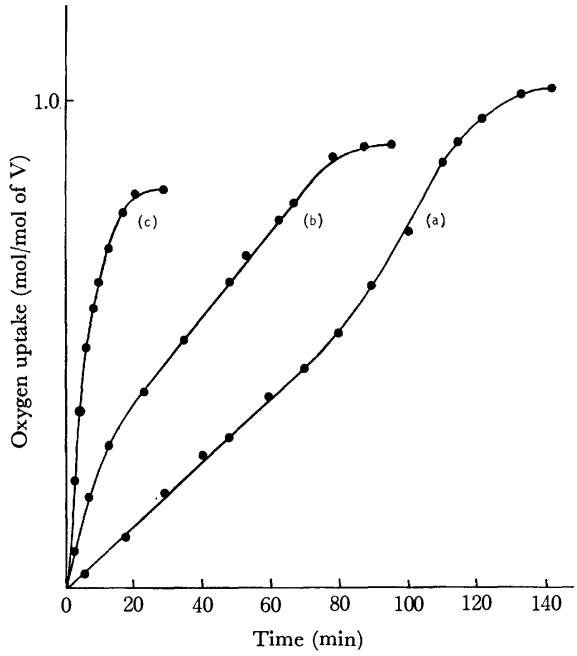

Fig. 5. Oxygen uptake by irradiation (>2800 Å) of V (1.16 mmol) in the presence of various amounts of rose bengal in methanol (90 m*l*) at ~2°C. (a) Without rose bengal, (b) with rose bengal (0.032 mmol), (c) with rose bengal (0.32 mmol).

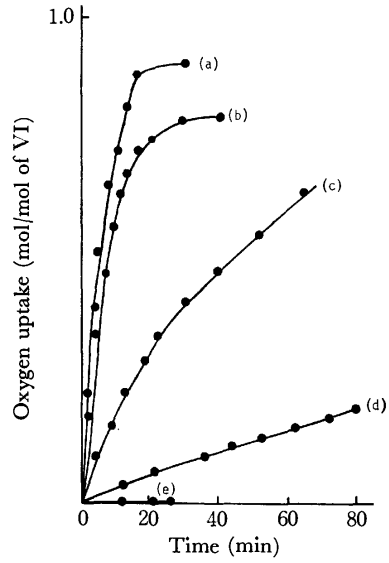

Fig. 6. Oxygen uptake by irradiation (>2800 Å) of VI (1.16 mmol) in the presence of various amounts of rose bengal in methanol (90 m*l*) at ~2°C. (a) Rose bengal (1.1 mmol), (b) rose bengal (0.32 mmol), (c) rose bengal (0.032 mmol), (d) without rose bengal, (e) rose bengal (1.1 mmol) alone (without VI).

Table 2. Photooxidation of V and VI in methanol[a)]

Exp No.	Compound	Rose bengal added (mmol)	Irradiation time (min)	Oxygen uptake (mol/mol of substrate)	Peroxide[b)] (%)	Thyroxine analogs[c)] (%)
10	V	—	120	0.90	—[d)]	X (trace)
11	V	0.12	35	0.57	—[d)]	X (1.3)
12	VI	—	60	0.12	—[d)]	—[d)]
13	VI	0.16	35	0.50	12	—[d)]
14	VI	1.1	35	0.80	40	—[d)]

a) A solution of V (2.3 mmol) or VI (4.6 mmol) in methanol (100 m*l* or 220 m*l*, respectively) was irradiated (>2800 Å) at ~2°C under oxygen-bubbling.
b) Estimated by iodometric titration.
c) Isolated after the photolysate was treated with II (see Experimental).
d) Not determined.

photosensitized oxidation, involving singlet oxygen and the triplet sensitizer, in which self-quenching occurs at higher concentrations of the sensitizer resulting in a slower reaction rate. Additional support for this assumption is provided by the finding that the rate of photosensitized oxidation of 2,6-di-*t*-butylphenol, where singlet oxygen is believed to be involved at least in part,[10] decreases with increased sensitizer concentration (Fig. 7).

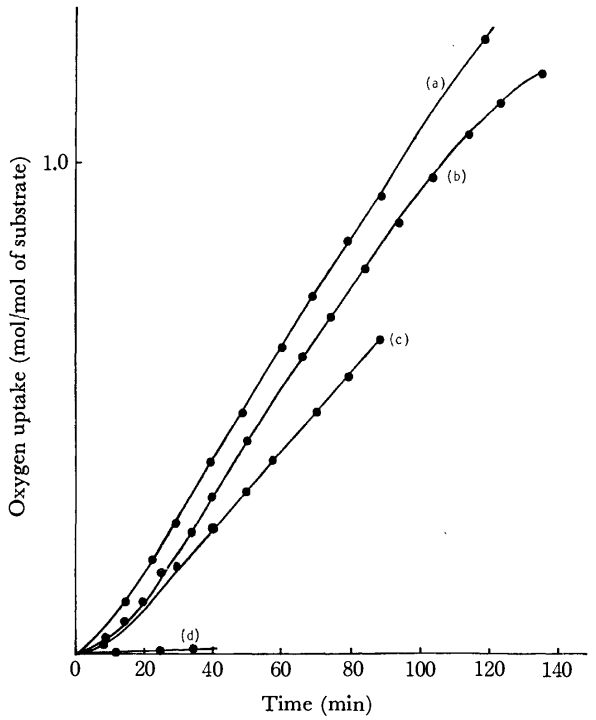

Fig. 7. Oxygen uptake by irradiation (>2800 Å) of 2,6-di-*t*-butylphenol (1.16 mmol) in the presence of various amounts of rose bengal in methanol (90 m*l*) at ~2°C. (a) Rose bengal (0.032 mmol), (b) rose bengal (0.32 mmol), (c) rose bengal (1.1 mmol), (d) without rose bengal.

The structure of the products of the photosensitized oxidation of V and VI has not yet been elucidated. The formation of a hydroperoxide (VIII or IX, analogs of IV) cannot be excluded, since irradiation of VI in the presence of rose bengal yielded a product capable of oxidizing iodide to iodine and the photolysate of V gave a thyroxine analog (X) on reaction with 3,5-diiodotyrosine (II), although in low yield (Table 2).

Experimental

Materials. 4-Hydroxy-3,5-diiodophenylpyruvic acid was purchased from Osaka Lanoratory of Synthetic Organic Chemicals. 4-Hydroxy-3-iodo-5-methoxyphenylpyruvic acid[11] and 4-hydroxyphenylpyruvic acid[12] were prepared according to the described methods. The solvents were freshly distilled before use.

Oxygen Uptake Experiments. A solution was irradiated using a 100W high-pressure mercury lamp with a Pyrex cooling jacket (ice-water). The reaction vessel was immersed in ice-water. During irradiation oxygen was bubbled through the solution in a closed circulating system equipped with a circulation pump and the consumption of oxygen was determined manometrically. In order to assure a constant irradiation level, the lamp was turned on at least 10 min before the start of the experiment while the solution was shielded from the light. The reaction was started by removal of the shield.

A. Photooxidation of 4-Hydroxy-3,5-diiodophenylpyruvic Acid (I) in Methanol. A solution of I (2.0 g) in methanol (200 m*l*) was irradiated at ~5°C for 70 min. During this period 97 m*l* of oxygen was absorbed. Iodometric titration of an aliquot (20 m*l*) of the light brown photolysate showed that liberated iodine was corresponding to 59% peroxide content. An aliquot (60 m*l*) was treated with sodium borohydride (3.0 g) at 0—36°C under nitrogen-bubbling. The mixture was acidified with dilute HCl and extracted with ether. The ether layer was dried over anhydrous Na_2SO_4 and evaporated to dryness. Vpc analysis of the residue after trimethylsilylation[13] (stationary phase, silicone DC on celite; temperature, 250°C; carrier gas, hydrogen) indicated the presence of 0.36 g of glycol VII (58%). The glycol was isolated as colorless needles by means of preparative tlc on silica gel (toluene-ethyl formate-formic acid, 5:4:1); 110°C with foaming. An authentic sample[5] had the same mp and identical mobility on tlc.

The remaining photolysate (120 m*l*) was deoxygenated by nitrogen-bubbling (10 min, ~2°C), then quickly added to a solution of 3,5-diiodotyrosine (II, 6.0 g) in 0.2M borate buffer (500 m*l*, pH 7.8, ~2°C) with nitrogen-bubbling, during

10) T. Matsuura, N. Yoshimura, A. Nishinaga, and I. Saito, *Tetrahedron Lett.*, **1969**, 1669.

11) T. Shiba, H. J. Cahnmann, T. Matsuura, A. Nishinaga, and H. Sakamoto, *J. Org. Chem.*, **29**, 3016 (1964). We thank Mr. Takeshi Kuri for the preparation of this compound.

12) H. D. Dakin, *J. Biol. Chem.*, **82**, 439 (1929). The corresponding azlactone was converted into the keto acid by treatment with 0.1M HCl under reflux.

13) K. Funakoshi and H. J. Cahnmann, *Anal. Biochem.*, **27**, 150 (1969).

which time the solution was permitted to warm up to room temperature. The reaction mixture was worked up as previously described.[5] A colorless precipitate (0.40 g) of thyroxine (III), identical with authentic sample, was obtained.

Other experiments with I are summarized in Table 1, Figs. 1, 2, 3, and 4.

B. Photooxidation of 4-Hydroxy-3-iodo-5-methoxyphenylpyruvic Acid (V) in Methanol (Table 2-Exp. 11). A solution of V (0.78 g) and rose bengal (0.1 g) in methanol (200 m*l*) was irradiated for 35 min at ~2°C. The oxygen-consumption was 33 m*l*. The photolysate was treated with II (6.0 g) in 0.2M borate buffer (500 m*l*, pH 7.7) under nitrogen and worked up. 3,5,3′-Triiodo-5′-methoxythyronine (X) (21 mg), identical with authentic sample,[11] was obtained.

Other experiments with V are summarized in Table 2, Figs. 4 and 5.

C. Photooxidation of 4-Hydroxyphenylpyruvic Acid (VI) in Methanol (Table 2-Exp. 12—14). A solution of VI (0.84 g) in methanol (200 m*l*) in the presence of various amounts of rose bengal was irradiated under oxygen at ~2°C. The photolysate, when added to a solution of KI in dilute acetic acid, liberated iodine, was iodometrically titrated for peroxide analysis.

Other experiments with VI are summarized in Figs. 3, 4, and 6.

This work was supported by U. S. Public Health Service Research Grant AM 07955 from the National Institute of Arthritis and Metabolic Diseases. The authors wish to thank Dr. H. J. Cahnmann, National Institute of Arthritis and Metabolic Diseases, Bethesda, Md., for his helpful discussion throughout this work.

BULLETIN OF THE CHEMICAL SOCIETY OF JAPAN, VOL. 45, 2871—2877 (1972)

The Structure and Synthesis of Rishitinol. A Sesquiterpene Alcohol from Diseased Potato Tubers[1]

Nobukatsu KATSUI, Akira MATSUNAGA, Kenji IMAIZUMI, and Tadashi MASAMUNE
Department of Chemistry, Faculty of Science, Hokkaido University, Sapporo
Kohei TOMIYAMA*
Hokkaido National Agricultural Experiment Station, Sapporo

(Received February 2, 1972)

The structure and configuration of rishitinol (**2**), isolated from tuber tissues of white potatoes (*Solanum tuberlosum*×*S. demissum*) infected by an incompatible race of *Phytophtora infestans*, were deduced from spectral and chemical data and confirmed by the synthesis of its recemate. 5,8-Dimethyl-1-tetralone-3-carboxylic acid (**13**) prepared from 2,5-dimethylbenzyl chloride was esterified, reduced, and then dehydrated to the dihydronaphthalene derivative (**20**), which was converted into the oxyisopropyl derivative (**21**). The hydroboration of **21** followed by hydrogen peroxide oxidation afforded a multi-component mixture, from which *dl*-rishitinol (**25**= *dl*-**2**) was isolated along with isomeric glycols (**22**—**24**).

A few years ago we reported on the isolation[2] and structure elucidation[3] of an antifungal norsesquiterpene alcohol, rishitin (**1**), from tuber tissues of white potatoes (*Solanum tuberlosum*×*S. demissum*) infected by an incompatible race of *Phytophtora infestans*. Since the isolation of rishitin qualified as "phytoalexin," efforts have been made to isolate the alcohol and its closely related compounds from diseased plants of various species of the *Solanum* family in search of its biological significance as well as the biogenetic route.[4-8]

Recently we isolated a new sesquiterpene alcohol (**2**), designated as rishitinol, from the diseased white potato tubers and reported on the structure as well as the total synthesis of its racemic form.[9] The details of the studies are given in this paper.

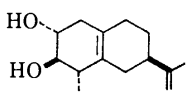

1

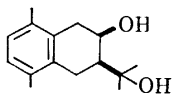

2

* Present address: Plant pathology Laboratory, Faculty of Agriculture, Nagoya University, Chikusa-ku, Nagoya.

1) Part VII of "Studies on the Phytoalexins"; Part VI, ref. 9.

2) K. Tomiyama, T. Sakuma, N. Ishizaka, N. Sato, N. Katsui, M. Takasugi, and T. Masamune, *Phytopathology*, **58**, 115 (1968).

3) a) N. Katsui, A. Murai, M. Takasugi, K. Imaizumi, T. Masamune, and K. Tomiyama, *Chem. Commun.*, **1968**, 43. b) For the absolute configurations of C_2, C_3, and C_4 of rishitin, see; N. Harada, and K. Nakanishi, *J. Amer. Chem. Soc.*, **91**, 3989 (1969); S. T. K. Bukhari and R. D. Guthrie, *J. Chem. Soc., C*, **1969**, 1073.

4) a) N. Sato, K. Tomiyama, N. Katsui, and T. Masamune, *Ann. Phytopathol. Soc. Japan*, **34**, 140 (1968). b) N. Sato, K. Tomiyama, N. Katsui, and T. Masamune, *Nippon Shokubutsu Byori Gakkaiho*, **34**, 344 (1969). c) N. Ishizaka, K. Tomiyama, N. Katsui, A. Murai, and T. Masamune, *Plant and Cell Physiology*, **10**, 183 (1969).

5) J. L. Varns, J. Kuc, and E. B. Williams, *Phytopathology*, **61**, 174 (1971); J. L. Varns and J. Kuc, *ibid.*, **61**, 178 (1971).

6) G. Van den Ende, *Phytopath., Z.* **64**, 68 (1969).

7) O.L. Ozeretskovskaya, N.I. Vasyukova, and L.V. Metlitsky, *Dokl. Acad. Sci.*, **5**, 189 (1969); L. V. Metlitsky, Yu. T. Djakov, O. L. Ozeretskovskaya, L. A. Yurganova, L. I. Chalova, and N. I. Vasyukova, *Izvestiya Acad. Nauk CCCD*, **3**, 399 (1971); N. I. Vasyukova, O. L. Ozeretskovskaya, and L. V. Metlitsky, *Pract. Biochem. Microbiol.*, **6**, 431 (1970); L. I. Chalova, N. I. Vasyukova, O. L. Ozeretskovskaya, and L. V. Metlitsky, *ibid.*, **7**, 55 (1971).

8) A. Stoessl, C. H. Unwin, and E. W. B. Ward, *Phytopath. Z.*, in the press.

9) N. Katsui, A. Mastunaga, K. Imaizumi, and T. Masamune, *Tetrahedron Lett.*, **1971**, 83.

The sesquiterpene alcohol **2** was isolated as follows. The tuber slices of diseased white potatoes (8.5 kg) were treated by the reported procedure[2] to yield "the hexane-soluble fraction" (24.5 g). This on column chromatography over silicic acid afforded two relevant fractions, one (10.5 g) eluted with hexane containing the compound in question and the other eluted with hexane–acetone (92: 8) being more polar and rishitin-rich. The former was chromatographed over silicic acid and celite, and the resulting ether eluate, after removal of acidic substances, was rechromatographed over alumina. A rishitinol-rich fraction (180 mg) eluted with ether–methanol was further purified by thin layer chromatography (tlc) on silica gel and recrystallized to yield rishitinol **2** (50 mg), mp 128—129°C and $[\alpha]_D$ +47° (chloroform), in pure state.

Compound **2** was analyzed for $C_{15}H_{22}O_2$, which was confirmed by the mass spectrum (*m/e* 234, M^+). The UV, IR, and NMR spectral data revealed the presence of the following structural units: one tetra-substituted benzene with two vicinal hydrogens [λ_{max} 263 mμ (ε 280); ν_{max} 3070, 1600, 810, and 804 cm^{-1}; τ 7.81 and 7.75 (each 3H, singlet), and 3.10 (2H, singlet)]; two *tertiary* methyl groups (τ 8.65 and 8.54 (each 3H, singlet)]; *secondary* and *tertiary* hydroxy groups [ν_{max} 3300 cm^{-1}; τ 7.25 (2H, broad singlet, disappeared on addition of deuterium oxide) and 5.30 (1H, broad singlet W_H=7 Hz)]. Compound **2** resisted acetylation under the usual conditions and oxidation with periodic acid. All the results together with the co-existence of rishitin in the same plant suggest that rishitinol would be represented either by (planar) structure **2a**, **2b**, or **2c**. Since these structures are regarded to be of hydroxyoccidol, we first intended to prepare *dl*-occidiol[10] (**3**) in anticipation of the effectiveness of the NMR spectrum of **3** for structural determination and the availability of the synthetic intermediates of **3** for the preparation of **2b**.

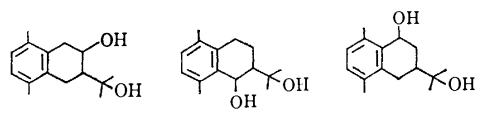

2a **2b** **2c**

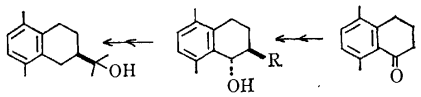

3 **5** R=$COOC_2H_5$ **4**
6 R=$C(OH)(CH_3)_2$

The synthesis of *dl*-occidol was carried out by a slight modification of the procedure by Hirose and Nakatsuka,[10a] starting with *p*-xylene and succinic anhydride *via* tetralone (**4**)[11] and oxyester (**5**). The resulting *dl*-occidol exhibited two six-proton singlets due to the gem-dimethyl and aromatic methyl protons, as shown in Table 1 in which the chemical shifts of relevant protons are summarized. In view of the large difference (0.11 ppm) in the chemical shift between two gem-dimethyl groups of **2**, this spectral pattern (*cf.*, Table 1) indicated that another hydroxyl group of **2** would hinder the presumed free rotation of the oxyisopropyl group and probably be located at one of the adjacent carbons. The possibility of structure **2c** would therefore be excluded. The synthetic intermediate **5** was then treated with methyl magnesium iodide to give glycol **6**. The relative configuration of the hydroxyl and oxyisopropyl groups in **6** was tentatively assigned to *trans*, because, in the NMR spectra of **5** and **6**, the proton on carbon bearing the hydroxyl group appeared as a doublet at τ 4.78 and 4.75 with coupling constants of 7 and 5 Hz, respectively. Glycol **6**, while it possessed the same molecular formula as **2**, differed definitely from **2**. On the basis of the large deshielding effect (0.24 ppm) caused by the hydroxyl group at the carbon adjacent to the benzene ring on the aromatic methyl protons, it was inferred that rishitinol would be formulated most favorably as **2a**.

As a synthetic approach to **2a**, 5,8-dimethyl-2-tetralone (**7**) was first prepared, starting from the corresponding 1-tetralone (**4**) and using a method analogous to that of the conversion of 1-tetralone into 2-tetralone.[12] However, the attempted formylation of **7** with methyl formate and sodium methoxide failed, forming a multi-component mixture. The one-step synthesis[13] of 5,8-dimethyl-2-tetralone-3-carboxylate was next undertaken but also failed; treatment of 2,5-dimethylphenylacetyl chloride with ethyl acrylate in the presence of aluminum chloride resulted in the formation of an intractable tarry material.

The synthesis of rishitinol was finally achieved as follows. 5,8-Dimethyl-4-oxo-1,2,3,4-tetrahydro-2-naphthoic acid (**13**) was first prepared in a manner analogous to the synthetic procedure of the corresponding 5,8-demethyl derivative by Haworth *et al.*[14] Alkylation of ethyl sodioacetoacetate with 2,5-dimethylbenzyl chloride[15] (**8**) produced the 2,5-dimethylbenzyl derivative (**9**), which was again treated with sodium in ethanol and then refluxed with ethyl chloroacetate to give acetylbenzylsuccinate (**10**) in 34% yield from **8**. In accordance with the structure **10**, the NMR spectrum exhibited signals due to an acetyl and two carbethoxy methyl protons. Further treatment of **10** with 2N sodium hydroxide under reflux effected both hydrolysis and removal of the acetyl group to yield 2,5-dimethylbenzylsuccinic acid (**11**) which on heating with acetic anhydride formed the corresponding anhydride (**12**) in 68% yield from **10**. The structure was supported by the IR absorption bands due to an acid anhydride group. The Friedel-Crafts cyclization of **12** led to the formation of a 2: 1 mixture of 5,8-dimethyl-1-tetralone-3-carboxylic acid (**13**) and its isomeric acid (**14**) containing a hydrindanone skeleton in 70% yield. They were separated by fractional recrystallization. While **13** showed an absorption maximum due to the carbonyl

10) a) Y. Hirose and T. Nakatsuka, *Bull. Agr. Chem. Soc. Jap.*, **23**, 143 (1959). b) M. Nakazaki, This Bulletin, **35**, 1387 (1962).

11) Bold and dotted lines described in some structural formulas except **1**, **2**, and **3** refer to only relative configurations.

12) F. Straus and A. Rohrbacker, *Ber.*, **54**, 40 (1921).

13) *Cf.*, J. H. Burckhalper and J. R. Campbell, *J. Org. Chem.*, **26**, 4232 (1961); A. Rosowsky, J. Battaglia, K. K. N. Chen, and E. J. Modest, *ibid.*, **33**, 4288 (1968).

14) R. Haworth, B. Jones, and M. Way, *J. Chem. Soc.*, **1943**, 10.

15) H. Stephen, W. F. Short, and G. Gladding, *ibid.*, **117**, 510 (1920).

Table 1. The NMR spectra of occidol **3** and its derivatives

Compound	Δ	Substitutents in formula **28** OH	Chemical Shift (τ) Methyl protons[a] at C_5	C_8	C_9		Protons[a] at C_6 and C_7
3	/	C_9	7.80	7.80	8.70	8.70	3.10
29[b]	Δ^1	C_9	7.78	7.70	8.58	8.58	3.14
21	Δ^3	C_9	7.77	7.80	8.80	8.80	3.20
6	/	C_9 and C_1 (α)	7.80	7.56	8.69	8.50	3.02
22	/	C_9 and C_4 (α)	7.60	7.82	8.72	8.75	3.05
24	/	C_9 and C_3 (α)	7.84	7.84	8.65	8.65	3.10
2	/	C_9 and C_3 (β)	7.75	7.81	8.65	8.54	3.10
30[b]	/	C_1 (α) and C_2 (α)	7.79	7.57	9.09[c]	8.99[c]	3.02

a) Singlet b) For preparation, see Experimental c) Doublet

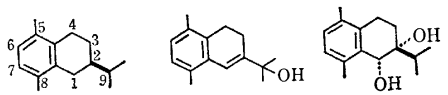

28 **29** **30**

group in a six-membered ring, **14** showed one due to the group in a five-membered ring. The UV and NMR spectra of both compounds also supported the assigned structures. In view of the fact that Haworth's cyclization with the demethyl derivative of **12** resulted in the isolation of only 1-tetralone-3-carboxylic acid,[14] it would be noticeable that compound **14** was formed in a considerable yield. Apparently the present result would be derived from large steric hindrance against the six-membered ring rather than the five-membered[16] caused by one of the aromatic methyl groups. Tetralone **13** was then converted with hydrogen chloride in ethanol into the corresponding ethyl ester (**15**) in 70% yield.

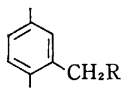

8 R=Cl
9 R=CH(COCH$_3$) COOC$_2$H$_5$
10 R=C(COCH$_3$)(COOC$_2$H$_5$) CH$_2$COOC$_2$H$_5$
11 R=CH(COOH) CH$_2$COOH
12 R=CH—CO
O
CH$_2$—CO

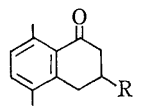

13 R=COOH
15 R=COOC$_2$H$_5$

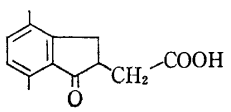

14

The reduction of the ketoester **15** with sodium borohydride in ethanol produced a mixture of hydroxy esters (**16**) and γ-lactone (**17**), which were isolated by column chromatography in 61 and 30% yields, respectively. Hydroxy esters (**16**) gave only one spot on tlc. However, on treatment with lithium aluminum hydride **16** formed a 1 : 1 mixture of two glycols, which were separated by preparative tlc to give a glycol (**18**), mp 125—127°C, and a glycol (**19**), mp 111—113°C, in 35 and 35% yields, respectively. The relative configuration of the hydroxyl and the carbethoxyl groups of these glycols was made by the formation of the *cis*-glycol **18** on reduction of the γ-lactone **17** with the *cis*-configuration at the carbons in question. **16** was thus, subjected to dehydration with phosphorus pentoxide. The reaction proceeded smoothly to give dihydronaphthalene derivate (**20**) in 70% yeild.

As a final step of the synthesis, an attempted hydration of dihydronaphthalenes by hydroboration followed by hydrogen peroxide oxidation[17] gave no fruitful result. Ester **20** was then converted into the oxyisopropyl derivative (**21**) in 53% yield by treatment with methylmagnesium iodide. Compound **21** showed the UV spectrum in good accord with the structure and also displayed an NMR spectrum resembling closely that of occidol **3** except for signals due to olefinic protons.

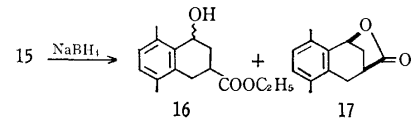

16 **17**

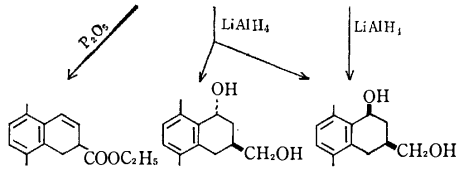

20 **19** **18**

Hydroboration of the olefin **21** folowed by oxidation with hydrogen peroxide afforded a multi-component mixture, which was separated roughly into three fractions by column chromatography over silica gel. The least mobile fraction obtained in 27% yield showed two spots on tlc. However, on purification by preparative

16) *Cf.*, R. T. Arnold and P. N. Craig, *J. Amer. Chem. Soc.*, **72**, 2728 (1950), and their previous papers.

17) G. Zweifel and H. C. Brown, "Organic Reactions," Vol. 13, John Wiley & Sons, Inc., London and New York (1963), p. 27.

tlc followed by recrystallization, it afforded only one 1-hydroxytetralin derivate (**22**) in 18% yield. However, the Jones oxidation[18] of both the pure alcohol **22** and the residue left on isolation of **22** produced the same 1-tetralone derivative (**26**) indicating the presence of an epimeric alcohol (**23**). The relative configurations of **22** and **23** were assigned to *trans* and *cis* on the basis of the appearance of the proton at C_1 of **22** as a triplet with J of 3 Hz at τ 5.10, since it is not probable that both the hydroxyl and oxyisopropyl groups would assume axial conformations. The middle fraction obtained in 26% yield was subjected to acetylation. The product was separated by preparative tlc to give monoacetate (**24a**) and the unreacted glycol (**25**) in 10 and 6% yields, respectively. **24a** on hydrolysis with alkali readily afforded glycol (**24**). As expected, both glycols **24** and **25** were oxidized with the Jones reagent to yield the same 2-tetralone derivative (**27**). The NMR spectra of these alcohols, consistent with the structures, made it possible to assign *trans* and *cis* configurations to the glycols **24** and **25**, respectively; the proton at C_2 of **24** appeared as a multiplet with W_H of 25 Hz centered at τ 6.50, while that of **25** as a broad singlet with W_H of 7 Hz at τ 5.24.

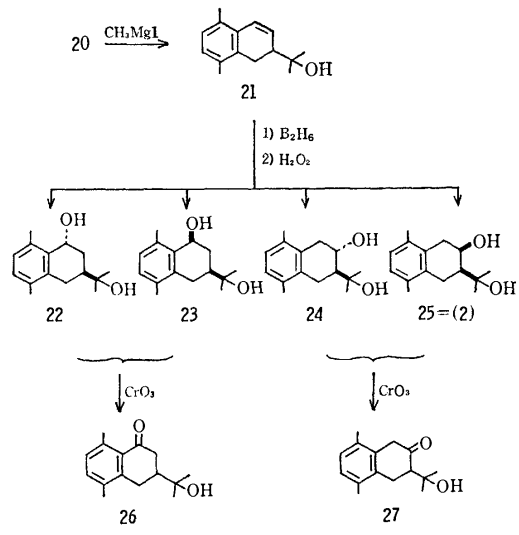

Compound **25** has now been identified as a racemate of rishitinol by comparison of the UV, IR, NMR, and mass spectra as well as tlc. In view of the absolute configuration of rishitin[3] and occidol,[10b] rishitinol would also possesses the β-oriented oxyisopropyl group. Hence rishitinol is represented most favorably by structure **2**.

Experimental

The melting points were measured in open capillaries and uncorrected. The optical rotations, UV and IR spectra were taken in chloroform, 99% ethanol and Nujol, respectively, unless otherwise stated. The NMR spectra were recorded in deuterochloroform at 60 and/or 100 MHz, tetramethylsilane being used as an internal standard. The following abbreviations were used in the NMR spectra. "s singlet, d doublet, t triplet, q quartet, b broad, and m multiplet." Thin layer chromatography (tlc) was carried out over silica gel of Merck G, and column chromatography over silica gel of Mallinckrodt A.R. 100 mesh or alumina of Merck Active I, neutral.

Isolation of Rishitinol (2). Tuber slices of the R_1 cultivar Rishiri (White potato, *Solanum tuberosum*×*S. demissum*) (60 kg), inoculated with an incompatible race of *Phytophthora infestans* (Mont.) d By, were dried (8.5 kg), homogenized, extracted, and separated in the same manner as that reported previously.[1] The resulting "hexane-soluble fraction"[1] (24.5 g) contained rishitin (**1**) and rishitinol (**2**). This fraction was chromatographed over silica gel (150 g) and celite (70 g), using hexane and hexane-acetone as eluents and separated roughly into two parts, one (10.5 g) eluted with hexane and the other eluted with hexane-acetone (92:8) and rishitin-rich (tlc). The former, less polar, was then rechromatographed over silica gel (100 g) and celite (30 g), using hexane, benzene, chloroform, ether, and ether–methanol as eluents. The yellow oil (5.9 g) obtained from the ether eluates was dissolved again in ether and shaken with 5% aqueous sodium carbonate to remove acidic components. The remaining ether solution was washed with water, dried, and evaporated to leave a neutral substance (3.1 g). This was again chromatographed over alumina (60 g), using hexane, hexane–benzene, benzene, benzene–ether, ether, and ether–methanol as eluents. The eluate from ether–methanol (99:1) gave a crystalline material (180 mg) on trituration with hexane, which showed a single spot on tlc (R_f=0.63, chloroform–ether, 1:1) and was collected by filtration. This was recrystallized twice from hexane to give pure rishitinol (**2**) (50 mg), mp 128—129°C, $[\alpha]_D$ +47°; mass, *m/e* 234 (M^+); IR, ν_{max} 3070, 1600, 810, and 804 cm^{-1}; UV. λ_{max} 263 mμ (ε 280); NMR, τ 8.65, 8.54, 7.81 and 7.75 (each 3H, s), 8.25 (1H, m), 7.25 (2H, br s, disappeared on addition of deuterium oxide), 7.05 (4H, m), 5.30 (1H, br s W_H= 7 Hz,) and 3.10 (2H, s).

Found: C, 76.88; H, 9.46%. Calcd for $C_{15}H_{22}O_2$: C, 76.37; H, 9.51%.

Rishitinol **2** was treated with acetic anhydride (0.3 m*l*) and pyridine (0.2 m*l*) at room temperature for 2 days. After the usual work-up, the starting material was recovered unchanged.

A solution of **2** (10 mg) in ethanol (10 m*l*) was added to a solution of sodium metaperiodate (15.6 mg) in water (18 m*l*) and acetic acid (2 m*l*), and the mixture was then diluted to 30 m*l* with water and allowed to stand at room temperature. A part (5 m*l*) of the solution was taken out three times at intervals of a day and titrated with a 0.0115 N sodium thiosulfate solution after addition of 2 m*l* of 0.1 N potassium iodide; 0.32, 0.29 and 0.25 moles of the metaperiodate were consumed in each run.

Ethyl 1-Hydroxy-5,8-dimethyl-1,2,3,4-tetrahydro-2-naphthoate (5). A solution of methyl 5,8-dimethyl-1-oxo-1,2,3,4-tetrahydro-2-naphthoate[10a] (10 g), mp 75—76°C, in ethanol (45 m*l*) was treated with a solution of sodium borohydride (2.2 g) in ethanol (75 m*l*) in the same manner as that of Hirose and Nakatsuka.[10a] The resulting oily product showed two spots and chromatographed over silica gel (120 g) and celite (40 g), using benzene, benzene–chloroform, and chloroform as eluents. Fractions eluted with benzene–chloroform gave a crude sample of **5** (3.7 g), which on trituration with hexane yielded a crystalline material, showing a single spot. Fractions eluted with chloroform afforded a brown oil (3.8 g), which was a mixture of **5** and, probably, its carbomethoxy

18) A. Bowers, T. G. Halsall, E. R. H. Jones, and A. J. Lemin, *J. Chem. Soc.*, **1953**, 2548.

homologue[19] (checked by tlc). The above crystalline substance was recrystallized from hexane for analysis to give **5** (2.1 g), mp 65—66°C; mass, *m/e* 248 (M^+); IR, ν_{max} 3360 and 1720 cm^{-1}; NMR, τ 8.68 (3H, t, J=7 Hz, $COOCH_2C\underline{H}_3$), 7.80 and 7.56 (each 3H, s, $C\underline{H}_3$ at C_5 and C_8), 5.75 (2H, q, J=7 Hz, $COOC\underline{H}_2CH_3$), 4.79 (1H, br s, $\underline{H}$ at C_1) and 3.03 (2H, s, $\underline{H}$ at C_6 and C_7).

Found: C, 72.48; H, 8.24%. Calcd for $C_{15}H_{20}O_3$: C, 72.55; H, 8.12%.

2-(1-Hydroxy-5,8-dimethyl-1,2,3,4-tetrahydro-2-naphthyl)propan-2-ol (6). A solution of the hydroxy ester **5** (200 mg) in dry ether (10 m*l*) was added to the Grignard solution prepared from magnesium (75 mg) and methyl iodide (450 mg) in dry ether (7 m*l*) at room temperature. After being left at the same temperature for 20 hr, the mixture was treated with a saturated ammonium chloride solution (20 m*l*) and extracted with ether. Evaporation of ether gave a brown residue (150 mg) which was separated into two portions by preparative tlc (solvent, ether). The more mobile portion (80 mg) was identified as the unreacted ester (**5**) by tlc and the mixed melting point method. The less mobile one, showing a single spot, was extracted with acetone–methanol from the plates and gave **6** (60 mg) which resisted crystallization and further purification. However, its NMR spectrum was in good accord with the structure; τ 8.69 and 8.50 (each 3H, s, $(C\underline{H}_3)_2COH$), 7.80 and 7.56 (each 3H, s, $C\underline{H}_3$ at C_5 and C_8), 4.75 (1H, d, J=5 Hz, $\underline{H}$ at C_1) and 3.02 (2H, s, *H* at C_6 and C_7).

dl-*Occidol (3).* Compound **19** (954 mg), dissolved in a 2:1 mixture (40 m*l*) of ethanol and acetic acid was hydrogenated over Adams platinum (500 mg as $PtO_2 \cdot H_2O$) at room temperature for 1 hr, when almost one mole of hydrogen was absorbed. The reaction was further continued for 7 hr. After removal of the catalyst and the solvent, the residue was dissolved in ether. The ethereal solution was washed with a sodium carbonate solution and water, dried, and evaporated to leave a crystalline material (800 mg), which was recrystallized from hexane to give **3**, mp 102—103°C; UV, λ_{max} 266 mμ (ε 200); NMR, 8.70 (6H, s), 7.80 (6H, s) and 3.10 (2H, s).

Found: C, 82.43; H, 9.97%. Calcd for $C_{15}H_{22}O$: C, 82.51; H, 10.16%.

2,5-Dimethylbenzyl Chloride (8). A mixture of *p*-xylene (500 m*l*), paraformaldehyde (32 g), and zinc chloride (40 g) was heated at 70°C for 15 min and then cooled to 50°C. Dry hydrogen chloride was passed into the mixture for 30 min at 50—60°C. After the whole mixture was washed with water, 5% sodium bicarbonate, and water successively, the xylene solution was separated, dried and distilled to give compound **8** (71 g), bp 88—90°C/5 mmHg (lit,[14] bp 105°C/15 mmHg).

Ethyl Aceto-2,5-dimethylbenzylacetate (9). The chloride **8** (140 g) was added slowly to an ethanol solution of ethyl sodioacetoacetate preparaed from sodium (20.8 g), ethanol (250 ml), and ethyl acetoacetate (234 g). The mixture was then refluxed for 6 hr, when sodium chloride precpitated was removed by filtration. The filtrate was concentrated and distilled *in vacuo* to yield a pale yellow oil (**9**) (167.4 g), bp 169—173°C/5 mmHg; IR, ν_{max} 1735 and 1720 cm^{-1}.

Ethyl α-Aceto-α-2,5-dimethylbenzylsuccinate (10). Compound **9** (167 g) was treated with sodium (15.4 g) dissolved in ethanol (200 m*l*), and mixed with ethyl chloroacetate (87.4 g). The whole mixture was worked up in the same manner as mentioned above. The product (**10**), oil, bp 185—198°C/5 mm Hg, showed spectra consistent with the assigned structure; IR, ν_{max} 1735 and 1705 cm^{-1}; NMR, τ 8.80 and 8.83 (each 3H, t, J=8 Hz, $COOCH_2C\underline{H}_3$), 7.77 (9H, s, CH_3CO and aromatic CH_3), and 5.90 and 5.93 (each 2H, q, J=8 Hz, $COOC\underline{H}_2CH_3$).

2,5-Dimethylbenzylsuccinic Acid (11). A suspension of the succinate **10** (261 g) in 2 N sodium hydroxide (1.2 *l*) was refluxed for 26 hr and poured onto a mixture of ice and hydrochloric acid. The resulting precipitates were collected, washed with water, and recrystallized from methanol to afford **11** (138 g); mass, *m/e* 236 (M^+); IR, ν_{max} 3300 and 1705 cm^{-1}. It turned gradually brown and then dark brown at 160—170°C, but did not melt below 240°C.

2,5-Dimethylbenzylsuccinic Anhydride (12). The acid **11** (80.5 g) was refluxed with acetic anhydride (161 g) for 30 min. The reaction mixture was worked up as usual and crude crystalline anhydride was recrystallized from carbon tetrachloride to afford **12** (69 g) mp 80—83°C; IR; ν_{max} 1865 and 1785 cm^{-1}.

5,8-Dimethyl-4-oxo-1,2,3,4-tetrahydro-2-naphthoic Acid(13) and 4,7-Dimethyl-1-indanone-2-acetic Acid (14). The anhydride **12** (7.4 g) was added slowly under stirring to aluminum chloride (10 g) suspended in nitrobenzene (35 m*l*) under cooling by an ice-bath. The cold mixture was stirred at the temperature for 1 hr and at room temperature overnight, and poured onto a mixture of ice and hydrochloric acid. The aqueous mixture was then subjected to steam distillation to remove nitrobenzene, and extracted with chloroform. On removal of the solvent the chloroform solution afforded a reddish residue (5.5 g), which was purified by column chromatography on silica gel (150 g) and celite (15 g). Fractions eluted with benzene–acetone (1:1—1:4) gave a crystalline mass, which was recrystallized from benzene to give **13** (4.9 g), fine needles, mp 127—131°C. This was recrystallized from the same solvent for analysis to give **13** (2.8 g), plates, mp 135—137°C; UV, λ_{max} 254 (log ε 4.07) and 305 mμ (log ε 3.34); IR, ν_{max} 3280, 1705, and 1665 cm^{-1}; NMR, τ 7.70 and 7.40 (each 3H, $C\underline{H}_3$ at C_5 and C_8), 7.00 (5H, m), 2.96 and 2.78 (each 1H, d, J=9 Hz, $\underline{H}$ at C_6 and C_7) and −0.80 (1H, s, $COO\underline{H}$).

Found: C, 71.71; H, 6.39%. Calcd for $C_{13}H_{14}O_3$: C, 71.54; H, 6.47%.

The mother liquors obtained on the above recrystallizations were combined and evaporated to leave a crystalline residue, which was recrystallized repeatedly from benzene to give **14** (1.1 g), mp 113—115°C; IR, ν_{max} 3150, 1705, and 1695 cm^{-1}; NMR, τ 7.70 and 7.40 (each 3H, s), *ca.* 7.0 (5H, m), 2.96 and 2.81 (each 1H, d, J=10 Hz) and −1.04 (1H, s).

Ethyl 5,8-Dimethyl-4-oxo-1,2,3,4-tetrahydro-2-naphthoate (15). The naphthoic acid **13** (20.5 g) was esterified with 5% ethanolic hydrogen chloride under reflux for 5 hr and gave a crystalline ester, which was recrystallized from hexane to yield **15** (16.2 g), mp 74—76°C; IR ν_{max} 1735 and 1670 cm^{-1}; NMR, τ 8.76 (3H, t, J=7 Hz, $COOCH_2C\underline{H}_3$), 5.85 (2H, q J=7 Hz, $COOC\underline{H}_2CH_3$), 7.71 and 7.41 (each 3H, s), *ca.* 7.0 (5H, m), and 2.98 and 2.86 (each 1H, AB q, J=10 Hz).

Ethyl 4-Hydroxy-5,8-dimethyl-1,2,3,4-tetrahydro-2-naphthoate (16) and 5,8-Dimethyl-1,2,3,4-tetrahydro-2,4-naphthalenecarbolactone (17). A solution of the naphtoate **15** (8 g), in ethanol (155 m*l*) was reduced with sodium borohydride (1.8 g) in ethanol (50 m*l*) under cooling in an ice-bath for 3 hr. The product consisted of two components (tlc), which were separated by column chromatography over silica gel (200 g), using benzene, benzene–ether and ether as eluents; one was eluted from benzene–chloroform (19:1—1:5) and the other

19) This substance, which had been reported to be methyl ester,[10a] was apparently a mixture of the methyl ester and ethyl ester **5**, since the result of elemental analysis did not agree with the calculated value for $C_{14}H_{18}O_3$.

from benzene–chloroform (1:6—1:1). The former was recrystallized from benzene to give lactone **17**, (2.4 g), mp 129—131°C; IR, ν_{max} 1765 cm^{-1}; NMR, τ 7.84 and 7.62 (each 3H, s), 4.30 (1H, d, J=6 Hz) and 3.00 (2H, s).

The latter was obtained as colorless oil which showed a single spot but proved to be a mixture of two C_4-epimers formulated as (planar) structure **16** from the NMR spectral data; τ 8.76 and 8.71 (total 3H, t, J=8 Hz, $COOCH_2C\underline{H}_3$) 7.80 and 7.60 (each 3H, s, $C\underline{H}_3$ at C_5 and C_8), 5.89 and 5.78 (total 2 H, q, J=8 Hz, $COOC\underline{H}_2CH_3$), and 3.03 (2H, s, $\underline{H}$ at C_6 and C_7).

cis-1-Hydroxy-3-hydroxymethylene-5,8-dimethyl-1,2,3,4-tetrahydronaphthalene (18) and its Isomer (19). To a solution of the hydroxy ester (**16**, 176 mg) in dry ether (20 m*l*) was added slowly an ether solution (5 m*l*) of lithium aluminum hydride (50 mg) under stirring at room temperature. After being left for 20 hr, the reaction mixture was worked up as usual to leave an amorphous product (143 mg) showing two spots on tlc. This was subjected to preparative tlc (ether) to give two crystalline glycols. The less polar glycol was recrystallized from hexane containing methanol to give the *cis* isomer (**18**, 51 mg), mp 125—127°C, and the more polar the *trans* isomer (**19**, 52 mg), mp 111—113°C (from ether). The *cis* isomer was also obtained in 70% yield from lactone **17** under the same conditions as above.

The *cis* glycol (**18**, 54 mg) was acetylated with acetic anhydride–pyridine (1:1, 1.2 m*l*) at room temperature for 24 hr. The reaction mixture was worked up as usual and gave the diacetate (41 mg), oil, showing a single spot on tlc; IR, ν_{max} 1730, 1240, and 810 cm^{-1}; NMR, τ 7.97 and 7.94 (each 3H, s, $OCOC\underline{H}_3$), 7.79 (6H, s, $C\underline{H}_3$ at C_5 and C_8), 5.88 (2H, d, J=7.5 Hz, $C\underline{H}_2OCOCH_3$), 3.99 (1H, double t, J=5, 5 and 0.5 Hz, $\underline{H}$ at C_1), and 3.02 (2H, s, $\underline{H}$ at C_6 and C_7).

The diacetate of *trans* isomer **19** was also obtained in 54% yield, oil; IR, ν_{max} 1727, 1240 and 810 cm^{-1}; NMR, τ 7.95 and 7.93 (each 3H, s), 7.79 (6H, s), 5.86 (2H, d, J=5 Hz), 3.88 (1H, t, J=3 Hz) and 2.95 (2H, s).

Ethyl 5,8-Dimethyl-1,2-dihydro-2-naphthoate (20). An epimeric mixture of the hydroxynaphthoates (**16**, 10.4 g) dissolved in dry benzene (25 m*l*) was dehydrated with phosphorus pentoxide (7.5 g) suspended in dry benzene (17 m*l*) in the manner described before. The reaction mixture was worked up as usual and purified by chromatography over silica gel (250 g) and celite (50 g) to give dihydronaphthoate **20** (6.8 g), oil, showing a single spot; IR ν_{max} 1735 cm^{-1}; UV, λ_{max} 260 mμ (log ε 3.90).

2-(5,8-Dimethyl-1,2-dihydro-2-naphthyl)propan-2-ol (21). A solution of the naphthoate (**20**, 2.9 g) in dry ether (15 m*l*) was subjected to the Grignard reaction by the same procedure as that for conversion of **5**, using the reagent prepared from magnesium (1.2 g) in ether (10 m*l*) and methyl iodide (9.0 g) in ether (20 m*l*). The reaction gave a crude alcohol (2.2 g) which was chromatographed over alumina (80 g). The eluate from benzene-chloroform (3:2—5:7) gave crystalline material on trituration with benzene. The crystals were recrystallized from benzene to yield **21** (1.6 g), needles, mp 46—48°C; UV, λ_{max} 260 mμ (log ε 4.04); IR, ν_{max} 3360 cm^{-1}; NMR, τ 8.80 (6H, s, $(C\underline{H}_3)_2COH$), 7.80 and 7.77 (each 3H, s), 4.01 (1H, double d, J=10 and 4 Hz, $\underline{H}$ at C_3), 3.37 (1H, double d, J=10 and 2 Hz, $\underline{H}$ at C_4) and 3.20 (2H, s).

Hydroboration of Compound 21. Into a stirred solution of the alcohol **21** (1.45 g) in dry tetrahydrofuran (35 m*l*) was passed diborane, prepared from sodium borohydride (1.0 g) dissolved in diglyme (5 m*l*) and boron trifluoride etherate (6 m*l*) dissolved in diglyme (4 m*l*), for 1 hr at room temperature under nitrogen. The mixture was then diluted with water and made alkaline with 3 N sodium hydroxide (5 m*l*). To the alkaline solution was added dropwise 30% hydrogen peroxide (6.5 m*l*), and the whole mixture was stirred at 35—50°C for 1 hr and then extracted with ether. The ether solution was washed with a saturated sodium chloride solution, dried, and evaporated to give a multi-component (1.35 g) which was separated into three fractions by chromatography over alumina (38 g). The most mobile fraction eluted with benzene–chloroform (4:1—3:2) gave the unreacted alcohol **21** (0.45 g). The niddle fraction eluted with benzene–chloroform (1:1) afforded a colorless oil (0.4 g), consisting meinly of two components and the least mobile eluted with benzene–chloroform (2:3) did a two other components mixture (0.43 g).

2-(trans-1-Hydroxy-5,8-dimethyl-1,2,3,4-tetrahydro-3-naphthyl)propan-2-ol (22) and its cis-*1-Hydroxy Isomer (23).* The least mobile fraction was further purified by preparative tlc using ether. A component showing a slightly smaller R_f value than that of rishitinol (**2**) was extracted with acetone–methanol. Removal of the solvent gave an amorphous substance which crystallized partially on trituration with benzene. The crystalline mass (**22**, 270 mg) was recrystallized from the same solvent and melted at 142—143°C; NMR, τ 8.72 and 8.75 (each 3H, s), 7.82 and 7.60 (each 3H, s), 5.10 (1H, t, J=3 Hz) and 3.05 (2H, s). The mother liquors obtained on removal of **22** were evaporated *in vacuo* to leave an amorphous residue (68 mg) showing almost the same IR spectrum as **22**. Examination of the residue by tlc indicated the presence of **22** and another component, the latter not being isolated in pure state even through its acetyl derivative. However, the component proved to be compound **23**, an epimer at C_4 of **22**, since both pure **22** and crude **23** on oxidation with the Jones' reagent afforded the same 1-tetralone derivative **26**, oil, in the same yield (70%); IR, ν_{max} 3420 and 1665 cm^{-1}.

2-(trans-2-Hydroxy-5,8-dimethyl-1,2,3,4-tetrahydro-3-naphthyl)-propan-2-ol (24) and its cis-*2-Hydroxy Isomer 25=dl 2).* The foregoing middle fraction, obtained from hydroboration products of **21**, was oxidized with the Jones' reagent to give 2-tetralone devative (**27**) (IR, ν_{max} 1705 cm^{-1}) as a single product, indicating the components to be 2-hydroxy tetralin derivatives. They were separated by acetylation; treatment of the fraction (390 mg) with acetic anhydride–pyridine (1:1, 4 m*l*) at room temperature for 24 hr afforded an oily mixture (353 mg). This was purified by preparative tlc using chloroform–ether (1:1) to yield an unacetylated, crude crystalline substance (90 mg), mp 127—129°C, and an oily acetate (**29a**, 180 mg); IR, ν_{max} 3360 and 1730 cm^{-1}; NMR, τ 8.75 (6H, s), 7.91 (3H, s, $OCOC\underline{H}_3$), 7.84 and 7.80 (each 3H, s), *ca.* 7.0 (6H, m), 4.80 (1H, m, W_H=25 Hz, $C\underline{H}OAc$) and 3.15 (2H, s). Hydrolysis of the acetate (**24a**) in refluxing 1 N methanolic potassium hydroxide afforded a glycol, which was crystallized from hexane to give compound **24** (39 mg), mp 127—128°C; IR, ν_{max} 3300 cm^{-1}; NMR, τ 8.65 (6H, s), 7.84 (6H, s), *ca.* 6.5 (1H, br m, W_H=25 Hz, $C\underline{H}OH$) and 3.10 (2H, s); R_f=0.60 (chloroform–ether, 1:1) and 0.32 (chloroform–ether, 4:1).

The crude crystalline glycol was recrystallized from hexane to afford compound **25** (25 mg), mp 127—129°C; mass, *m/e* 234 (M^+); UV, λ_{max} 265 mμ (ε 300); NMR, τ 8.65 and 8.54 (each 3H, s), 7.82 and 7.75 (each 3H, s), 5.30 (1H, br s, W_H=7 Hz) and 3.05 (2H, s); R_f=0.63 (chloroform–ether, 1:1) and 0.28 (chloroform–ether, 4:1). The compound was confirmed to be a racemic form of rishitinol (**2**) in all respects (NMR, IR, UV, and mass spectra and tlc).

2-(5,8-Dimethyl-3,4-dihydro-2-naphthyl)propan-2-ol (29). To a cooled and suspended mixture of phosphorus pentoxide

(1.6 g) in dry benzene (6 m*l*) was added a solution of compound **5** (3.7 g) in dry benzene (18 m*l*) under stirring, and the mixture was stirred at 0°C for 5 hr. The cold mixture was then poured into water and extracted with ether. After being washed with water and dried, the ether solution was evaporated to leave a crystalline material which, on recrystallization from ethanol, yielded ethyl 5,8-dimethyl-3,4-dihydro-2-naphthoate (3 g), mp 53—54°C; IR, ν_{max} 1695 and 1620 cm^{-1}; NMR, τ 8.64 (3H, t, J=7 Hz), 7.73 and 7.62 (each 3H, s), 5.74 (2H, q, J=7 Hz), 3.06 (2H, s) and 2.28 (1H, s).

Found: C, 78.05; H, 7.68%. Calcd for $C_{15}H_{18}O_2$: C, 78.23; H, 7.88%.

The naphthoate (2.3 g) was subjected to the Grignard reaction under the same conditions as for compound **6**. The reaction mixture was worked up as usual and gave an oily product (2.2 g), which was chromatographed over alumina (45 g) using hexane and benzene as eluents. Fractions eluted with benzene afforded a colorless oil (**29**) (2.0 g), showing a single spot; IR, ν_{max} 3360 cm^{-1}; NMR, τ 8.58 (6H, s), 7.78 and 7.70 (each 3H, s) and 3.33 (1H, s).

Found: C, 83.22; H, 9.42%. Calcd for $C_{15}H_{20}O$: C, 83.28; H, 9.32%.

*2-(1,2-Dihydroxy-5,8-dimethyl-1,2,3,4-tetrahydro-2-naphthyl)-propane (**30**).* *dl*-Occidol (**3**, 105 mg) was heated with 90% formic acid (1 g) on a water-bath for 1 hr, and the mixture was cooled and diluted with ether. The ether solution was washed with 5% sodium carbonate and water, dried, and evaporated to give an oily product. While this dehydratd product showed a single spot on tlc, it was found to consist of a few unsaturated compounds by examination of the NMR spectrum. This was therefore used for the subsequent reaction without further purification. Osmium tetroxide (80 mg) was added to a solution of oil (52 mg) in dry ether (3 m*l*) and pyridine (0.08 m*l*) under stirring at room temperatute. The mixture immediately turned dark violet and dark brown osmate esters deposited after 5 min. After being left for 2 days, the whole mixturs was evaporated under reduced pressure and the residual osmate ester was decomposed by reflux with a mixture of sodium sulfite (600 mg) and 50% aqueous ethanol (100 m*l*) for 2 hr. After filtration of black precipitates deposited, the filtrate was diluted with water and extracted with ether. Evaporation of the dried extract followed by trituration of the residue with hexane afforded a crystalline product, which was recrystallized from the same solvent to give pure **30** (18 mg), mp 85—86°C; NMR, τ 9.09 (3H, d, J=7 Hz), 8.09 (3H, J=7 Hz), 7.79 and 7.57 (each 3H, s), 5.25 (1H, br s, W_H=6 Hz) and 3.02 (2H, s).

Found: C, 76.63; H, 9.44%. Calcd for $C_{15}H_{22}O_2$: C, 76.88; H, 9.46%.

The authors are grateful to Mr. Norio Sato for the preparation of raw materials, to Mr. Shigezo Shimokawa for the measurement of NMR, to Miss Masako Takahashi for that of mass spectra, and to Misses Hiroko Kakizaki and Motoko Sato for microanalyses.

BULLETIN OF THE CHEMICAL SOCIETY OF JAPAN, VOL. 45, 2877—2882 (1972)

Studies of Acyl and Thioacyl Isocyanates. IX.[1] The Cycloaddition Reactions of Benzoyl and Thiobenzoyl Isocyanates with Anils

Otohiko TSUGE and Shuji KANEMASA

Research Institute of Industrial Science, Kyushu University, Higashi-ku, Hakozaki, Fukuoka 812

(Received March 17, 1972)

Thiobenzoyl isocyanates react with benzylidenanilines, benzylidenalkylamines and dianils to yield the corresponding mono- and bis(4+2) cycloadducts. Benzoyl isocyanates do not react with benzylidenanilines, but they are easily added to benzylidenebenzylamine to give the (4+2) cycloadducts in good yields. Cycloaddition of these isocyanates to anils is dependent upon the basicity of the nitrogen atom of C=N bond. Neither benzoyl isocyanates nor thiobenzoyl isocyanates are added to the C=C bond of cinnamylidenanilines, but they react with the C=N bond to afford the (4+2) cycloadducts.

The 1,4-dipolar contribution of benzoyl (I) and thiobenzoyl isocyanates (II) is manifest in cycloaddition reactions as evidenced by their dimerization[2] and reactions of carbodiimides.[3]

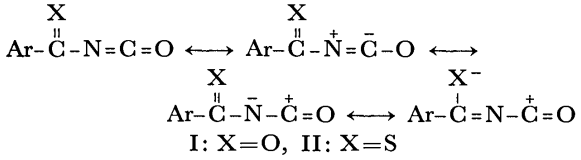

I: X=O, II: X=S

We have therefore undertaken to expand the cycloaddition reactions of these isocyanates with various compounds having a C=N bond. A preliminary report was given on the cycloaddition reaction of I and II with some benzylidenamines.[4]

Investigation was made to prepare new heterocycles, and obtain information on the differences between the reactivities of I and II in cycloaddition reactions. This paper deals with the cycloaddition to benzylidenamines, dianils and cinnamylidenanilines.

1) Part VIII of this series: O. Tsuge and K. Sakai, This Bulletin, **45**, 1534 (1972).

2) O. Tsuge and R. Mizuguchi, *Kogyo Kagaku Zasshi*, **69**, 939 (1966).

3) O. Tsuge and K. Sakai, This Bulletin, **45**, 1534 (1972).

4) O. Tsuge, M. Tashiro, R. Mizuguchi, and S. Kanemasa, *Chem. Pharm. Bull.* (Tokyo), **14**, 1055 (1966).

Table 1. 2,3,6-Triaryl-2*H*-1,3,5-thiadiazin-4(3*H*)-ones IV[a]

	IV			Yield	Mp[b]	Appearance (recryst. solvent)	IR, cm^{-1}		Microanalysis (%) Found (Calcd)		
	R^1	R^2	R^3	(%)	(°C)		$\nu_{C=O}$	$\nu_{C=N}$	C	H	N
a	H	H	H	100	193—194	colorless needles (benzene)	1675	1650	73.59 (73.24)	4.68 (4.68)	7.83 (8.14)
b	OMe	H	H	100	191.5—192	colorless needles (benzene)	1655	1640	70.79 (70.58)	4.78 (4.85)	7.09 (7.48)
c	Cl	H	H	100	185—186	pale yellow needles (benzene-petr. ether)	1680	1650	66.81 (66.60)	3.85 (3.97)	7.68 (7.40)
d[c]	H	OMe	H	88	185	colorless needles (benzene-petr. ether)	1685	1650	70.88 (70.58)	4.97 (4.85)	7.67 (7.48)
e[d]	H	H	OMe	94	168—169	colorless needles (benzene-petr. ether)	1670	1640	70.86 (70.58)	4.55 (4.85)	7.58 (7.48)
f	H	NO_2	H	89	184.5	pale yellow needles (benzene)	1685	1650	65.82 (65.83)	3.42 (3.77)	10.61 (10.47)
g	H	H	NO_2	70[e]	203—204	pale yellow needles (benzene)	1680 1660	1645	65.68 (65.83)	3.51 (3.77)	10.51 (10.47)

a) Reaction conditions: at room temperature for 5 min. b) All the compounds melted with decomposition. c) NMR ($CDCl_3$) δ ppm: 3.78 (3H, singlet, OCH_3), 6.18 (1H, singlet, >CH), 6.78—8.20 (14H, multiplet, aromatic protons). d) NMR ($CDCl_3$) δ ppm: 3.79 (3H, singlet, OCH_3), 6.16 (1H, singlet, >CH), 6.78—8.18 (14H, multiplet, aromatic protons). e) Reaction conditions: at room temperature for 5 hr.

Results and Discussion

Reactions with Benzylidenamines. No reaction of benzoyl isocyanates (I) with benzylidenanilines (III) took place even in xylene under reflux, but thiobenzoyl isocyanates (II) reacted easily with anils IIIa—IIIg at room temperature to afford the corresponding 1:1 adducts IVa—IVg in good yields.

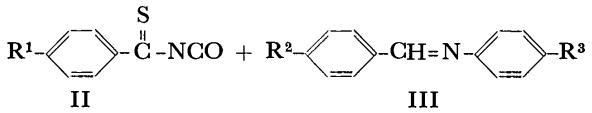

II III

a: R^1=H
b: R^1=OMe
c: R^1=Cl

a: R^2=R^3=H
b: R^2=OMe, R^3=H
c: R^2=H, R^3=OMe
d: R^2=NO_2, R^3=H
e: R^2=H, R^3=NO_2
f: R^2=R^3=NO_2

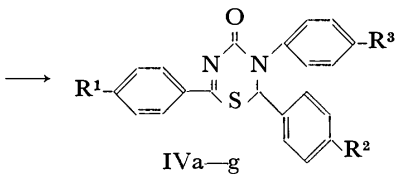

IVa—g

The structures of IV were deduced to be the (4+2) cycloadducts, 2*H*-1,3,5-thiadiazin-4(3*H*)-ones, on the basis of their spectral data. The yields, physical properties and results of elemental analyses of IV are given in Table 1.

IVe was easily hydrolyzed with hydrochloric acid to *N*-(*p*-methoxyphenyl)-*N'*-thiobenzoylurea (V), identical with an authentic sample prepared from IIa and *p*-anisidine. This supports the proposed structure for IV.[5]

V

As shown in Table 1, the yield of IV is affected by the nature of substituent R^3 but hardly at all by that of R^2, from the fact that IIa reacted easily with *p*-nitrobenzylidenaniline (IIId) to give IVf while it took 5 hr for IIa to disappear with benzylidene-*p*-nitroaniline (IIIe). Addition of IIa to *p*-nitrobenzylidene-*p*-nitroaniline (IIIf) did not take place even under forced conditions (90—100°C, 1 hr).

On the other hand, benzoyl isocyanates (I) as well as II reacted easily with benzylidenebenzylamine (VIa) at room temperature, forming (4+2) cycloadducts VII in excellent yields. Similarly, the (4+2) cycloadduct was obtained from IIa and benzylidene-*n*-propylamine (VIb) and -cyclohexylamine (VIc). The structures of VII were confirmed by their spectral data and elemental analyses. The yields, physical properties and results of elemental analyses of VII are given in Table 2.

I (X=O) VI
a: R^1=H, b: R^1=OMe a: R=CH_2Ph
c: R^1=Cl, d: R^1=NO_2 b: R=*n*-Pr
II (X=S) c: R=

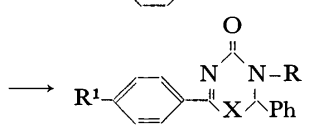

VIIa—i
X=O or S

Reactions with Dianils. Benzoyl isocyanate (Ia) reacted easily with dibenzylidenethylenediamine (VIIIa) at room temperature to afford colorless crystals, whose IR spectrum indicated that the product is a

5) After completion of this work, we learned that IVa, mp 185—190°C (decomp.), and IVb, mp 190°C (decomp.), were independently prepared by J. Goerdeler and H. Schenk (*Chem. Ber.*, **98**, 3831 (1965)).

TABLE 2. 3-ALKYL-2,6-DIARYL-2*H*-1,3,5-OXA(THIA)DIAZIN-4(3*H*)-ONES VII[a]

	VII[b] X	R′	R	Yield (%)	Mp[c] (°C)	IR, cm^{-1} $\nu_{C=O}$	IR, cm^{-1} $\nu_{C=N}$	Microanalysis (%) Found C	H	N	Calcd C	H	N
a	O	H	CH_2Ph	100	118	1680, 1660	1600	77.07	5.60	8.40	77.17	5.30	8.18
b	O	OMe	CH_2Ph	100	92	1660	1600	74.29	5.69	7.25	74.14	5.41	7.52
c	O	Cl	CH_2Ph	100	100	1660	1605	69.91	4.24	7.79	70.12	4.55	7.43
d	O	NO_2	CH_2Ph	100	102	1680	1620, 1600	68.32	4.75	10.63	68.21	4.42	10.85
e	S	H	CH_2Ph	88	180—181	1660	1640	73.75	5.13	8.17	73.73	5.06	7.82
f	S	OMe	CH_2Ph	80	155—157	1690, 1660	1645	70.89	5.06	6.92	71.12	5.19	7.21
g	S	Cl	CH_2Ph	100	167—168	1680, 1665	1640	67.25	4.37	6.84	67.26	4.33	7.13
h[d]	S	H	*n*-Pr	73	160—161	1660	1642	69.80	5.73	8.94	69.66	5.85	9.03
i[e]	S	H		74	216—216.5	1660	1637	72.05	6.48	8.10	71.98	6.33	8.00

a) Reaction conditions: at room temperature for 5 min. b) All the compounds are colorless needles. c) All the compounds melted with decomposition. d) NMR ($CDCl_3$) δ ppm: 0.92 (3H, triplet, $-(CH_2)_2-CH_3$), 1.4—2.0 (2H, multiplet, $-CH_2-CH_2-Me$), 3.11, 4.05 (each 1H, double triplet, $-CH_2-Et$), 5.85 (1H, singlet, >CH), 7.15—8.1 (10H, multiplet, aromatic protons). e) NMR ($CDCl_3$) δ ppm: 0.9—2.2 (10H, multiplet, CH_2), 4.4—5.0 (1H, broad signal, 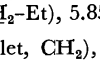), 5.97 (1H, singlet, >CH), 7.2—8.1 (10H, multiplet, aromatic protons).

mixture of bis(4+2) cycloadduct IXa and *N,N′*-dibenzoylcarbamoylethylenediamine X. As bis(4+2) cycloadduct IXa was rather unstable and decomposed during recrystallization to give X, the crystals were washed with benzene and then diethyl ether to obtain almost pure IXa, mp 131—132.5°C (decomp.), whose IR spectrum showed that the bands are due to $\nu_{C=O}$ and $\nu_{C=N}$ at 1680, 1665, and 1615 cm^{-1}. However, the NMR spectrum could not be determined because of decomposition of IXa in solution. Signals appeared at δ 3.78, 4.0 (each CH_2), 6.2 (NH), 6.9 (CH), 7.2—8.05 (aromatic protons), 8.32 (NH), and 10.05 ppm (CHO) in the NMR spectrum in deuteriochloroform ($CDCl_3$); this indicates that IXa was partially hydrolyzed to X and benzaldehyde. Hydrolysis of IXa with hydrochloric acid in ethanol afforded Xa, mp 270.5°C (decomp.), in a good yield.

The reactions of IIa with VIIIa and with hydrobenzamide (VIIIb) afforded the corresponding bis(4+2) cycloadducts IXb and IXc, even when equimolar amounts of IIa and VIII were used. The yields for the 2:1 molar ratio (Ia or IIa to VIII),

Ia or IIa + PhCH=N–R–N=CHPh

VIII

a: R=$(CH_2)_2$
b: R=PhCH

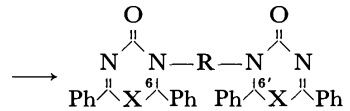

IX

a: X=O, R=$(CH_2)_2$
b: X=S, R=$(CH_2)_2$
c: X=S, R=PhCH

IXa $\xrightarrow[\text{in EtOH}]{\text{HCl}}$ $(PhCONHCONHCH_2)_2$ + PhCHO

X

physical properties and results of elemental analyses of IX are given in Table 3.

In the reaction with VIIIb, two isomers IXc-1 (high melting) and IXc-2 (low melting) were formed. Their IR spectra were very similar and the NMR spectra supported the (4+2) cycloadduct structures.[6]

TABLE 3. BIS-2*H*-1,3,5-THIA (OXA) DIAZIN-4(3*H*)-ONES IX[a]

	X	R	Yield (%)	Mp (°C)	IR, cm^{-1} $\nu_{C=O}$	IR, cm^{-1} $\nu_{C=N}$	Microanalysis (%) Found C	H	N	Calcd C	H	N
IXa	O	$(CH_2)_2$	82	131—132.5 (decomp.)	1680 1660	1615	72.02	5.00	10.63	72.44	4.94	10.56
IXb	S	$(CH_2)_2$	75	230—231 (decomp.)	1660	1640	68.32	4.66	9.95	68.27	4.40	9.58
IXc-1	S	PhCH	30	208—209 (decomp.)	1660	1636	71.32	4.25	8.59	71.14	4.52	8.97
IXc-2	S	PhCH	67	186	1660	1637	71.39	4.38	8.52	71.14	4.52	8.97

a) Reaction conditions: I or II/VIII (2/1 molar ratio), at room temperature for a few minutes. All the compounds are colorless needles.

6) Although it is conceivable that IXc-1 and IXc-2 are stereoisomers resulting from the configurations of 6- and 6′-phenyl groups in the 1,3,5-thiadiazine rings and from the conformation of the methine carbon atom between both rings, their stereochemistry is not clear.

Reaction with Cinnamylidenanilines. Very few investigations of cycloaddition to cinnamylidenaniline (XIa) have been reported. Pfleger and Jäger[7] proposed an addition reaction of phenylketene to XIa of the Diels-Alder type, but Sakamoto and Tomimatsu[8] analyzed the structure of the same reaction product and showed that it is the (2+2) cycloadduct, β-lactam. Recently,[9] we found that the reaction of benzoylsulfene with XIa gives an adduct of the Diels-Alder type. It thus seemed of interest to investigate the reaction of I or II with cinnamylidenanilines.

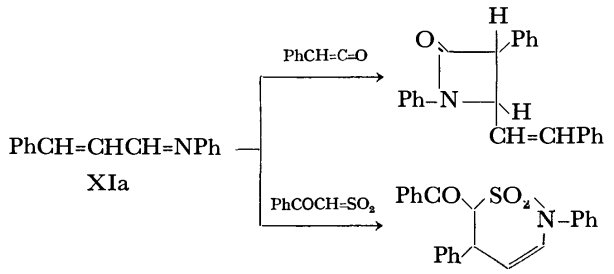

Under various conditions, the reaction of Ia with XIa gave resinous materials exclusively. However, IIa reacted easily with XIa at room temperature to afford a good yield of crystalline 1 : 1 adduct XIIa.

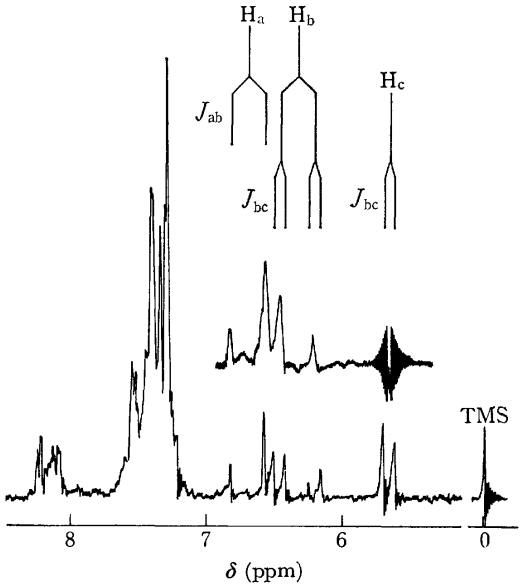

Fig. 1. NMR spectrum of XIIa.

The IR spectrum of XIIa was very similar to that of IVa and showed the characteristic band assignable to the CH=CH (*trans*) linkage at 976 cm^{-1}. The NMR spectrum (Fig. 1) exhibited two olefinic protons H_a and H_b, and methine proton H_c at δ 6.76 (1H, doublet with J_{ab}=15.8 Hz), 6.38 (1H, double doublet with J_{ab}=15.8 and J_{bc}=5.2 Hz, changed to a doublet with J_{ab}=15.8 Hz when irradiated at δ 5.70 ppm) and 5.70 ppm (1H, doublet with J_{bc}=5.2 Hz), besides aromatic protons.

The value of the ethylenic coupling constant of the β-lactam obtained from phenylketene and XIa has been reported to be 17 Hz,[8] and that of *trans*-cinnamaldehyde, the starting material of XIa, is 16.2 Hz.[10] Thus it is apparent that XIIa is the (4+2) cycloadduct of IIa to the C=N bond in XIa, 3,6-diphenyl-2-*trans*-styryl-2*H*-1,3,5-thiadiazin-4(3*H*)-one.

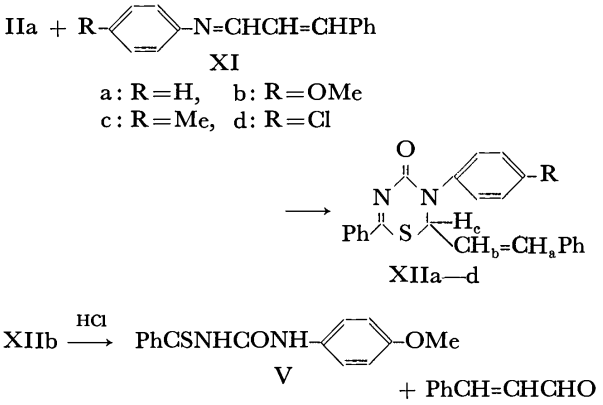

Similar reactions of IIa with cinnamylidenanilines XIb—XId gave the corresponding (4+2) cycloadducts XIIb—XIId. Finally, XIIb was easily hydrolyzed with hydrochloric acid to urea V and cinnamaldehyde, providing additional support for the proposed structure. The yields, physical properties, results of elemental analyses, and spectral data of XII are given in Tables 4 and 5, respectively.

Table 4. 3,6-Diaryl-2-*trans*-styryl-2*H*-1,3,5-thiadiazin-4(3H)-ones XII

XII	R	Yield (%)	Mp[a] (°C)	Appearance (recryst. solvent)	Microanalysis (%) Found C	Found H	Found N	Calcd C	Calcd H	Calcd N
a	H	88	175	pale yellow prisms (benzene-petr. ether)	74.98	5.01	7.36	74.58	4.90	7.56
b	OMe	86	147—148	colorless needles (benzene-petr. ether)	71.83	5.00	6.96	71.98	5.03	7.00
c	Me	73	169—170	yellow needles (benzene)	75.26	5.06	7.27	74.98	5.24	7.29
d	Cl	71	170—171	yellow needles (benzene-diethyl ether)	68.50	4.19	6.81	68.34	4.21	6.93

a) All the compounds melted with decomposition.

7) R. Pfleger and A. Jäger, *Chem. Ber.*, **90**, 2460 (1957).
8) M. Sakamoto and Y. Tomimatsu, *Yakugaku Zasshi*, **90**, 1386 (1970).
9) O. Tsuge and S. Iwanami, This Bulletin, **44**, 2750 (1971).
10) The olefinic coupling constant of XIa could not be measured as the olefinic protons appeared at the same position as the aromatic protons. The olefinic coupling constant of cinnamylidene-*n*-propylamine was 16 Hz.

Table 5. IR and NMR spectral data

	IR, cm^{-1}			NMR ($CDCl_3$) δ ppm				J (Hz)	
	$\nu_{C=O}$	$\nu_{C=N}$	$\delta_{CH=CH}$ (trans)	H_a	H_b	H_c	CH_3	J_{ab}	J_{bc}
XIIa	1680	1662	976	6.76	6.38	5.70		15.8	5.2
XIIb	1680	1645	975	6.70	6.33	5.60	3.77	15.8	5.3
XIIc	1670	1657	968	6.66	6.31	5.59	2.32	15.0	5.3
XIId	1670	1655	968	6.72	6.37	5.65		15.2	5.0

Experimental

All melting points are uncorrected. The IR spectra were measured as KBr pellets on a Nippon Bunko IR-S spectrophotometer; the NMR spectra were determined at 60 MHz on a Hitachi R-20 NMR spectrometer with TMS as an internal reference.

Materials. Benzoyl isocyanates (Ia—Id) were prepared by the method reported previously.[2] Thiobenzoyl isocyanates (IIa—IIc):[11] A solution of 1.0 g of 2-phenyl-,[12] 2-*p*-methoxyphenyl-[12] or 2-*p*-chlorophenylthiazoline-2,4-dione[12] in 10 m*l* of xylene was heated at 120°C, giving a reddish violet solution of II which was used *in situ*. This solution is referred to as the standard solution of II.

Anils were prepared from the corresponding aldehyde and amine. Benzylidenaniline (IIIa), mp 54°C (lit,[13] mp 53.5°C); *p*-methoxybenzylidenaniline (IIIb), mp 61°C (lit,[14] mp 58—59°C); benzylidene-*p*-anisidine (IIIc), mp 73—74°C (lit,[15] mp 72°C); *p*-nitrobenzylidenaniline (IIId), mp 93°C (lit,[16] mp 93°C); benzylidene-*p*-nitroaniline (IIIe), mp 118°C (lit,[17] mp 117—118°C); *p*-nitrobenzylidene-*p*-nitroaniline (IIIf), mp 199°C (lit,[18] mp 198.5°C); benzylidenebenzylamine (VIa), bp 200—201°C/18 mmHg (lit,[19] bp 205°C/20 mmHg); -*n*-propylamine (VIb), bp 101—102°C/16 mmHg (lit,[20] bp 208—210°C/744 mmHg); -cyclohexylamine (VIc), bp 154°C/18 mmHg (lit,[21] bp 136°C/16 mmHg). Dibenzylidenethylenediamine (VIIIa), mp 54°C (lit,[22] mp 53—54°C); hydrobenzamide (VIIIb), mp 110°C (lit,[23] mp 110°C). Cinnamylidenaniline (XIa), mp 109°C (lit,[22] mp 109°C); -*p*-anisidine (XIb), mp 118—119°C (lit,[24] mp 119°C); -*p*-toluidine (XIc), mp 82°C (lit,[25] mp 83°C); -*p*-chloroaniline (XId), mp 106—107°C (lit,[24] mp 107°C).

General Procedure for the Reaction of I or II with III and/or VI. A solution of equimolar amounts of I or II and III or IV in xylene was stirred at room temperature for a few minutes, during which time the reaction was completed. Filtration and recrystallization of crystals gave the corresponding (4+2) cycloadducts. The yields, physical properties, and results of elemental analyses of (4+2) cycloadducts IV and VII are given in Tables 1 and 2, respectively.

Hydrolysis of (4+2) Cycloadduct IVe. A solution of 0.3 g of IVe in 20 m*l* of methanol containing 2 m*l* of concentrated hydrochloric acid was stirred at 50°C for 5 min during which time it turned into a clear yellow solution. The solution was evaporated *in vacuo* to leave a residue which was washed with diethyl ether. Recrystallization of the ether-insoluble yellow crystals from ethanol gave 0.13 g (57%) of *N*-(*p*-methoxyphenyl)-*N'*-thiobenzoylurea (V), mp 178—179°C (decomp.) (lit,[26] mp 179°C (decomp.)), which was identical with the authentic sample prepared from IIa and *p*-anisidine. From the ether-washings, benzaldehyde was identified as its 2,4-dinitrophenylhydrazone.

Reaction of Ia with Dibenzylidenethylenediamine (VIIIa). A solution of 1.25 g of Ia and 1.0 g of VIIIa in 20 m*l* of dry benzene was stirred at room temperature for 10 min, and then filtered to give 1.85 g of solid whose IR spectrum indicated it to be a mixture of bis(4+2) cycloadduct IXa and *N,N'*-dibenzoylcarbamoylethylenediamine (X). The crystals were washed with benzene and then diethyl ether to leave colorless crystals, mp 131—132.5°C (decomp.), which were subjected to microanalysis without further purification.

The washings were evaporated *in vacuo* to leave X which corresponds to the hydrolyzed product of IXa.

A solution of 0.5 g of IXa in 20 m*l* of ethanol containing 2 m*l* of concentrated hydrochloric acid was stirred at 50°C for a few minutes, and the colorless crystals were filtered. Recrystallization from acetic acid afforded 0.28 g (84%) of X, mp 270.5°C (decomp.), as colorless prisms.

Found: C, 61.32; H, 4.96; N, 15.80%. Calcd for $C_{18}H_{18}N_4O_4$: C, 61.01; H, 5.12; N, 15.81%.

IR cm^{-1}: 3290 (NH), 1697, 1665 (C=O).

NMR (trifluoroacetic acid (CF_3COOH)) δ ppm: 3.88 (4H, broad signal, CH_2), 7.4—8.1 (10 H, multiplet, phenyl protons), 9.5, 10.0 (each 2H, broad signal, NH).

Reaction of IIa with Hydrobenzamide (VIIIb). When 0.8 g of VIIIb was added to the standard solution of IIa at room temperature, colorless crystals deposited immediately. Filtration gave 0.5 g (30%) of (4+2) cycloadduct IXc-l, which was washed with hot benzene and then subjected to microanalysis because of its insolubility in ordinary organic solvents.

NMR (CF_3COOH) δ ppm: 6.62 (1H, singlet, CH), 6.9—8.3 (22H, multiplet, two methine and 20 aromatic protons).

The xylene filtrate was evaporated *in vacuo* to leave a viscous oily substance, which solidified on trituration with petroleum ether. Recrystallization from benzene–petroleum ether (bp 45—65°C) gave 1.12 g (67%) of isomeric (4+2) cycloadduct IXc-2 as colorless needles.

NMR (carbon tetrachloride) δ ppm: 6.28 (1H, singlet, CH), 6.8—7.8 (22H, multiplet, two methine and 20 aromatic protons).

Similarly, the reaction of the standard solution of IIa with 0.62 g of VIIIa at room temperature for 5 min gave (4+2) cycloadduct IXb, which on recrystallization from

11) O. Tsuge, S. Kanemasa, and M. Tashiro, *Tetrahedron*, **24**, 5205 (1968).
12) J. Goerdeler and H. Schenk, *Chem. Ber.*, **98**, 2954 (1965).
13) G. Pyl, *Ber.*, **60**, 288 (1927).
14) A. Senier and R. B. Forster, *J. Chem. Soc.*, **107**, 1168 (1915).
15) F. G. Pope and G. R. Fleming, *ibid.*, **93**, 1915 (1908).
16) O. Fischer, *Ber.*, **14**, 2525 (1881).
17) W. von Miller and J. Plöchl, *ibid.*, **25**, 2020 (1892).
18) A. Lowy and C. G. King, *J. Amer. Chem. Soc.*, **43**, 625 (1921).
19) A. T. Mason and G. R. Winder, *J. Chem. Soc.*, **65**, 191 (1894).
20) H. Zauschirm, *Ann. Chem.*, **245**, 279 (1888).
21) A. Skita and C. Wulff, *Ber.*, **59**, 2691 (1926).
22) A. T. Mason, *ibid.*, **20**, 270 (1887).
23) F. Francis, *ibid.*, **42**, 2216 (1909).
24) A. Senier and P. H. Gallagher, *J. Chem. Soc.*, **113**, 28 (1918).
25) C. K. Tinkler, *ibid.*, **103**, 885 (1913).
26) J. Goerdeler and H. Schenk, *Chem. Ber.*, **99**, 782 (1966).

ethanol afforded 1.2 g (75%) of colorless needles.

NMR (CF_3COOH) δ ppm: 3.6—4.3 (4H, multiplet, CH_2), 6.63 (2H, singlet, CH), 7.5—8.2 (20H, multiplet, aromatic protons).

The physical properties and results of elemental analyses of IX are given in Table 3.

Reaction of IIa with Cinnamylidenanilines (XI). When an equimolar amount of XI was added to the standard solution of IIa, crystals were formed immediately. Filtration and recrystallization afforded the corresponding (4+2) cycloadduct XII.

Hydrolysis of (4+2) Cycloadduct XIIb. A solution of 0.3 g of XIIb in 20 m*l* of methanol containing 4 m*l* of concentrated hydrochloric acid was stirred at 50°C for 5 min during which time it turned into a clear yellow solution. The solution was evaporated *in vacuo* to leave a residue which was washed with diethyl ether and then ethanol. Recrystallization from ethanol afforded 0.11 g (52%) of urea V, mp 178—179°C (decomp.).

This research was supported financially in part by a grant from the Ministry of Education. The authors would like to express their thanks to Visiting Professor J.-P. Anselme, University of Massachusetts, Boston, for reading the manuscript.

BULLETIN OF THE CHEMICAL SOCIETY OF JAPAN, VOL. 45, 2882—2884 (1972)

Oxidative Coupling of Aminonaphthols

Yoshimori OMOTE, Yasuomi TAKIZAWA, and Noboru SUGIYAMA
Department of Chemistry, Tokyo Kyoiku University, Otsuka, Bunkyo-ku, Tokyo
(Received December 8, 1971)

The oxidative coupling of three aminonaphthols by manganese(III) tris(acetylacetonate) was examined. The products from 5-amino-2-naphthol were enol-acetylacetonylidene-1-(6-hydroxynaphthyl)-imine (**1**) and 2,2′-dihydroxy-5,5′-diamino-1,1′-binaphthyl (**2**); those from 8-amino-2-naphthol were 4-(acetylacetone-3″-yl)-7,7′-dihydroxy-1,1′-azonaphthalene (**3**) and enol-acetylacetonylidene-7-hydroxy-1-naphthylimine (**4**); the product from 5-amino-1-naphthol was enol-acetylacetonylidene-4-hydroxy-1-naphthylimine (**5**).

We reported on the synthesis of a DOPA dimer[1] and Swan and Chapman reported on that of other DOPA dimers.[2] The compounds are of interest with respect to possible intermediacy of DOPA melanogenesis. Piattelli *et al.*[3] isolated several dimers of catechol from its oxidation products. The melanin precursor is very susceptible to oxidation making it difficult to regulate its oxidation to afford a specific dimer.

It is known that 2,3-dihydroxynaphthalene is dimerized into 2,2′,3,3′-tetrahydroxy-1,1′-binaphthyl by oxidative coupling using iron(III) alum,[4] and that 2,2′-dihydroxy-1,1′-binaphthyl is prepared by the oxidative coupling of 2-naphthol with manganese(III) tris(acetylacetonate).[5]

This suggests the possibility of controlling oxidation of phenolic compounds by selecting proper substrate, oxidant, solvent, and temperature. The results of investigation of the oxidative coupling of aminonaphthols are given. They are interesting as models of melanin precursors and also of practical importance as modification of hair dyes.[6]

Results and Discussion

Three available aminonaphthols were chosen as substrates. Oxidation was carried out under conditions suitable for oxidative coupling to give specific dimers. In order to do so, several known methods[5,7] recommended for the oxidative coupling of phenols were compared with the use of 2-naphthol as a reference. Manganese(III) tris(acetylacetonate) (MTA) shows the best result (Table 1).

TABLE 1. OXIDATION PRODUCTS FROM 2-NAPHTHOL AND 5-AMINO-2-NAPHTHOL WITH SEVERAL OXIDANTS

Oxidant	Oxidation products			
	(2-Naphthol)		(5-Amino-2-naphthol)	
	Dimer	Polyer*	Dimer	Polymer[a]
O_2/OH^- [8]	+	+	−	++
$K_3Fe(CN)_6$[9,10]	+	+	−	++
$FeCl_2$[11]	+	+	−	++
$VOCl_3$[7]	++	−	−	+
MTA[5]	++	−	++	−

a) Polymer: The products were black tar and did not dissolve in any solvents.

1) Y. Omote, Y. Fujinuma, and N. Sugiyama, *Chem. Commun.*, **1968**, 190; This Bulletin, **42**, 1752 (1969).
2) R. F. Chapman, G. A. Swan, *J. Chem. Soc., C*, **1970**, 865.
3) M. Piattelli, E. Fattorusso, R. A. Nicolaus, and S. Magno, *Tetrahedron*, **21**, 3229 (1965).
4) H.-W. Wanzlick, M. Lehmann-Horchler, and S. Mohrmann, *Chem. Ber.*, **90**, 2529 (1957).
5) M. J. S. Dewar and T. Nakaya, *J. Amer. Chem. Soc.*, **90**, 7134 (1968).
6) a) H. H. Tucker, *J. Soc. Cosmetic Chem.*, **18**, 608 (1967); H. H. Tucker and I. Schwartz, *ibid.*, **22**, 139 (1971). b) E. Tsuchida, M. Kaneko, and Y. Kurimura, *Makromol. Chem.*, **132**, 209 (1970).
7) W. L. Carrick, G. L. Karapinka, and G. T. Kwiatkowski, *J. Org. Chem.*, **34**, 2388 (1969).
8) H. Musso and C. Rathjen, *Chem. Ber.*, **96**, 1563 (1963).
9) R. J. Molyneux, A. C. Waiss, Jr., and W. F. Haddon, *Tetrahedron*, **26**, 1409 (1970).
10) C. G. Haynes, A. H. Turner, and W. A. Waters, *J. Chem. Soc.*, **1956**, 2823.
11) D. R. Nelan and C. D. Robeson, *J. Amer. Chem. Soc.*, **84**, 2963 (1962).

Aminonaphthols were oxidized with MTA in acetonitrile at 80°C under nitrogen atmosphere. From 5-amino-2-naphthol two products were obtained. One product with R_f 0.39 and mp 185°C was proved to have the structure **1** because the NMR spectrum in $CDCl_3$ of the substance showed the peaks at δ 2.15 (s, methyl 3H), 5.3 (s, methine 1H), 7.1—7.9 (m, naphthalene 6H), 9.9 (broad, phenolic 1H, disappeared with D_2O), and 12.8 (s, enol 1H, disappeared with D_2O). Both elemental analyses and mass spectrum also fit the structure **1**. The other product with R_f 0.17 and mp 230°C showed the peaks at δ 3.0 (s, aromatic amine 4H), 5.05 (broad s, phenolic 2H) and 6.3—8.0 (m, naphthalene 10H) in the NMR spectrum in acetone-d_6. This revealed the structure **2**, which was also supported by elemental analyses and mass spectrum.

In case of the oxidative coupling of 6-amino-2-naphthol, binaphthyl-type dimer was not obtained, but a 1,1′-azonaphthalene-type dimer (**3**) was obtained accompanied by enol-acetylacetonylidene-hydroxynaphthylimine (**4**). The structure **3** is in accord with the NMR spectrum in $CDCl_3$ which showed the peaks at δ 1.75 (two s, two methyl 6H), 1.7 (broad, phenolic 2H, disappeared with D_2O), 3.2 (s, methine 1H), and 6.2—7.8 (m, naphthalene 11H).

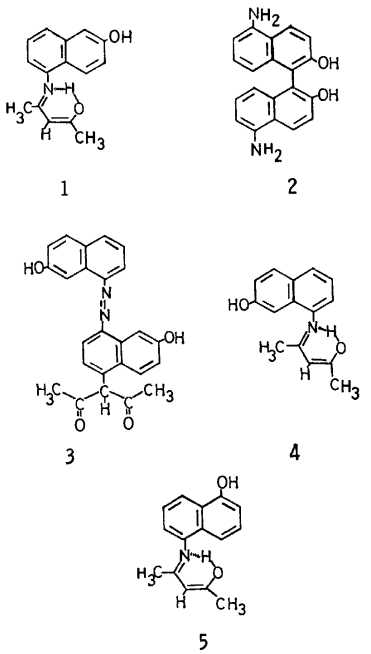

The UV spectrum of **3** also supports azonaphthalene structure showing λ_{max}(EtOH) at 255, 262 (sh), 315, 390, 409, and 514 nm. Recently Stead[12] reported on the formation of 2,8,8′-trihydroxy-1,1′-azonaphthalene-3,6,3′,6′-tetrasulfonic acid from the coupling of diazotized 1-amino-8-hydroxynaphthalene-3,6-disulfonic acid. It is interesting that a similar 1,1′-azonaphthalene is directly obtained by the oxidative coupling of an aminonaphthol.

The oxidative coupling of 5-amino-1-naphthol gave neither C–C coupling product like **2**, nor N–N coupling product like **3**, but afforded C–N coupling product between 5-amino-1-naphthol and acetylacetone from MTA. The structure of C–N coupling product is proposed as **5**. Spectral proofs of structure **4** and **5** are as follows. The NMR spectrum in $CDCl_3$ of **4** showed signals at δ 1.85 (s, 3H), 2.15 (s, 3H), 2.70 (broad, 1H), 5.30 (s, 1H), 7.10—7.90 (m, 6H), and 12.5 (s, 1H), and that of **5** showed signals at δ 1.9 (s, 3H), 2.2 (s, 3H), 5.3 (s, 1H), 6.9—7.5 (m, 6H), 9.1 (broad, 1H), and 12.6 (s, 1H).

Table 2. Linking of oxidative coupling of aminonaphthols

Coupling	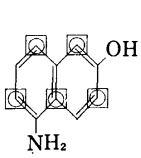	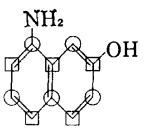	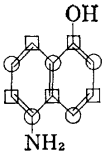
C–C	+ (**2**)	—	—
N–N	—	+ (**3**)	—
C–N	+ (**1**)	+ (**4**)	+ (**5**)

The mark (○) shows a position which will be radical rich by resonance when naphthoxy radical is formed. The mark (□) shows a position where electron density is large because of the electron releasing effect of amino group. The mark (+) means positive reaction and the product is shown by a number in ( ).

The results of the oxidative coupling of three aminonaphthols are summarized in Table 2. In the case of 5-amino-2-naphthol, the C–C coupling is possible because the inductive effect of amino group will increase radical density at *ortho* position to hydroxyl group. In the case of 8-amino-2-naphthol, however, the C–C coupling at *ortho* position is prevented by steric hindrance of amino group, affording the N–N coupling product. In the case of 5-amino-1-naphthol, *ortho* position to hydroxyl group is not active enough to dimerize, only the C–N coupling product being obtained. The C–N coupling product between amino group and acetylacetone of MTA is formed in every case.[13]

Experimental

Enol-acetylacetonylidene-1-(6-hydroxynaphthyl)imine (1). 5-Amino-2-naphthol (0.79 g) was added to a solution of acetonitrile (30 ml) containing manganese(III) tris(acetylacetonate) (MTA) (2.11 g) under atmosphere of nitrogen. The mixture was stirred and kept under reflux at 80°C overnight. The solvent was then evaporated under reduced pressure. The concentrated product was examined by tlc (silica gel, benzene–ethyl acetate, 2: 1, v/v), two spots being observed at R_f 0.39 and 0.17. A portion (0.5 g) of the crude product was purified by silica gel column chromatography using the mixture of benzene and ethyl acetate (2: 1, v/v). The first fraction having R_f 0.39 gave a pale yellow solid which was recrystallized from benzene–ethyl acetate as pale yellow needles, mp 185°C (0.16 g). IR (KBr): 3100, 2900, 1630, 1600, 1500, 1430, 1420, 1300, and 900 cm^{-1}. MS (*m/e*): 241 (M^+).

12) C. V. Stead, *J. Chem. Soc., C*, **1970**, 693.

13) K. Kaeriyama, This Bulletin, **43**, 1511 (1970).

Found: C, 74.71; H, 6.23; N, 5.84%. Calcd for $C_{15}H_{15}O_2N$: C, 74.66; H, 6.27; N, 5.81%.

2,2'-Dihydroxy-5,5'-diamino-1,1'-binaphthyl (2). Evaporation of the second chromatographic fraction of the preceding experiment gave a gray solid which was reprecipitated from benzene–ethyl acetate to give grayish powder (0.2 g), mp 230°C (decomp.).

IR: (KBr) 3370, 3300, 1620, 1590, 1510, 1429, 930, and 810 cm^{-1}. MS (*m/e*): 316 (M^+).

Found: C, 75.73; H, 5.36; N, 8.88%. Calcd for $C_{20}H_{16}O_2N_2$: C, 75.93; H, 5.10; N, 8.86%.

4-(Acetylacetone-3"-yl)-7,7'-dihydroxy-1,1'-azonaphthalene (3). A mixture of 8-amino-2-naphthol (0.8 g), acetonitrile (40 m*l*) and MTA (2.1 g) was treated in the same way as described above. The first elution of column chromatography gave red powder (0.21 g) which was reprecipitated from benzene, mp 251—252°C (decomp.). IR (KBr): 3400, 2900, 1705, 1685, 1655, 1625, 1590, 1320, and 830 cm^{-1}.

Found: C, 73.20; H, 4.94; N, 6.88%. Calcd for $C_{25}H_{20}O_4N_2$: C, 72.80; H, 4.89; N, 6.79%.

Enol-acetylacetonylidene-7-hydroxy-1-naphthylimine (4). The second fraction of the preceding chromatography gave a pale yellow solid which was recrystallized from benzene–ethyl acetate as pale yellow needles (0.04 g), mp 179—180°C. IR (KBr): 3400, 3100, 2900, 1620, 1600, 1550, 1320, 1250, and 1220 cm^{-1}.

Enol-acetylacetonylidene-4-hydroxy-1-naphthylimine (5). A mixture of 5-amino-1-naphthol (0.8 g), acetonitrile (40 m*l*) and MTA (2.5 g) was treated in the same way as described above. Only one product could be obtained. It was purified by column chromatography and recrystallization from ethyl acetate to give pale yellow needles (0.14 g), mp 187—188°C. IR (KBr): 3000, 2800, 1625, 1600, 1550, 1420, 1380, and 820 cm^{-1}. MS (*m/e*): 241 (M^+).

Calculation of S_R of 7,7'-Dihydroxyazonaphthalene. In order to determine the position of acetylacetonyl group in compound **3**, it was assumed that **3** was formed by the reaction of 7,7'-dihydroxyazonaphthalene radical and MTA. Parameters and superdelocalizability (radical) were as follows.

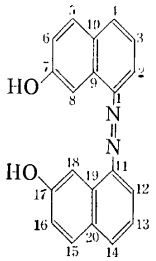

$$\alpha_{\dot{N}} = \alpha + 0.5\beta$$

$$\alpha_{\dot{O}} = \alpha + 2.0\beta$$

$$\beta_{NC} = 0.8\beta$$

$$\beta_{OC} = 0.8\beta$$

$$\beta_{NN} = 1.0\beta$$

Position No.	S_R(R)	Position No.	S_R(R)
1	0.9087	6	0.8887
2	1.0925	7	0.8859
3	0.8684	8	1.0129
4	1.1790	9	0.7690
5	1.0282	10	0.7129

The value of S_R(R) shows that position No. 4 will be most active in radical reaction.

The authors wish to thank Dr. Osamu Kikuchi, Department of Chemistry, Tokyo Kyoiku University, for HMO calculations.

BULLETIN OF THE CHEMICAL SOCIETY OF JAPAN, VOL. 45, 2884—2887 (1972)

The Synthesis and Stereochemistry of 2,3-Ferrocenocyclopentenone

Tamio SHIRAFUJI, Akio ODAIRA, Yasusi YAMAMOTO, and Hitosi NOZAKI

Department of Industrial Chemistry, Kyoto University, Yosida, Kyoto

(Received February 29, 1972)

An optical isomer of 2,3-ferrocenocyclopentenone (X) has been synthesized from methyl (1*S*) (−)-2-hydroxymethylferrocenecarboxylate *via* a six-step synthesis. The absolute configuration of (−)-X has been confirmed by a comparison of its CD and ORD curves with those of the corresponding ferrocene homologs previously recorded. The mass spectrum of X is also discussed.

The asymmetric induction achieved in the lithiation of (*S*)(+)-(*N*-α-pipecolylmethyl)ferrocene (I)[1] has opened a synthetic route to chiral 1,2-disubstituted ferrocene derivatives, such as methyl (1*S*)(−)-2-hydroxymethylferrocenecarboxylate (III). Schlögl and his co-workers have established the absolute configuration of ferrocene derivatives in their study of ferrocene chirality.[2] They prepared 2,3-ferrocenocyclohexenone and several substituted 2,3-ferrocenocyclopentenones, but not the parent compound (X). The conventional

1) T. Aratani, T. Gonda, and H. Nozaki, *Tetrahedron* **26**, 5453 (1970).

2) a) H. Lehner and K. Schlögl, *Monatsh. Chem.*, **102**, 277 (1971); b) H. Falk and K. Schlögl, *ibid.*, **102**, 33 (1971); c) H. Falk, H. Lehner, and K. Schlögl, *ibid.*, **101**, 967 (1970); d) H. Falk and O. Hofer, *ibid.*, **100**, 1540 (1969); e) H. Falk, O. Hofer, and K. Schlögl, *ibid.*, **100**, 624 (1969); f) H. Falk and K. Schlögl, *ibid.*, **96**, 266, 1065 (1965); g) K. Schlögl, M. Fried, and H. Falk, *ibid.*, **95**, 576 (1964).

cyclization of ferrocenylpropionic acid preferentially gives the heteroannularly-bridged ketone.[3,4] We now wish to report on a successful synthetic approach to this ketone (X) in its optically-active form (*cf.* Scheme 1).

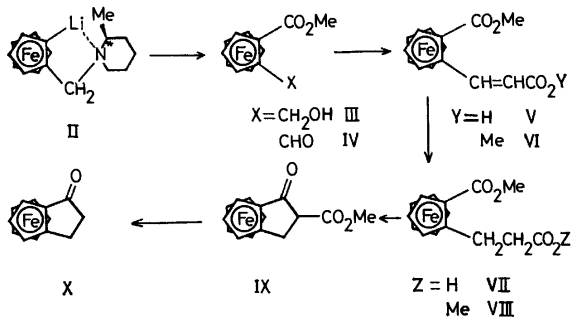

Scheme 1

The oxidation of (1*S*)(−)-III with MnO_2 gave methyl (−)-2-formylferrocenecarboxylate (IV). The subsequent Knoevenagel-Doebner condensation of the aldehyde (−)-(IV) with malonic acid gave the acid (−)-V. The catalytic hydrogenation of (−)-V with PtO_2, followed by esterification with diazomethane, afforded the diester (−)-VIII. The Dieckmann-type cyclization of the diester (−)-VIII with NaH in tetrahydrofuran gave the *β*-ketoester (IX),[5] which was then treated with dilute KOH to furnish the ketone (−)-X.

The ORD and CD curves of (−)-VI, (−)-VIII, and (−)-X were very similar to those of (1*S*)(−)-III of a known configuration,[1] as is shown in Figs. 1 and 2. Thus, every product obtained in each step of this synthetic route possesses the (1*S*,2*R*)-configuration.

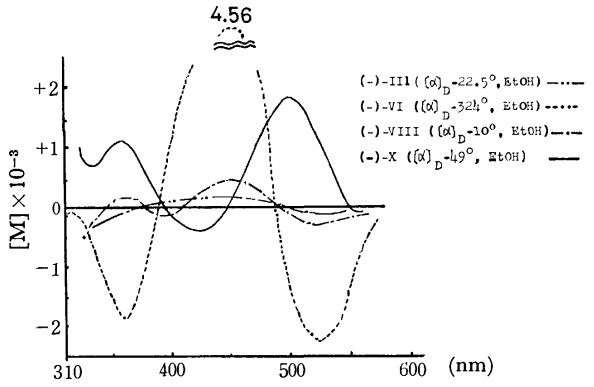

Fig. 1. ORD of III, VI, VIII, and X.

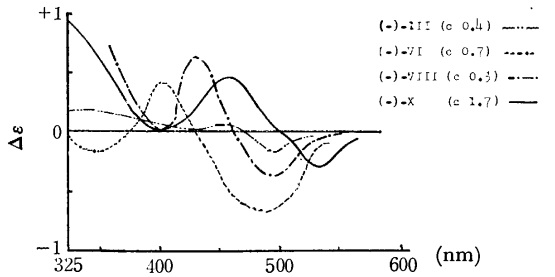

Fig. 2. CD of III, VI, VIII, and X (EtOH).

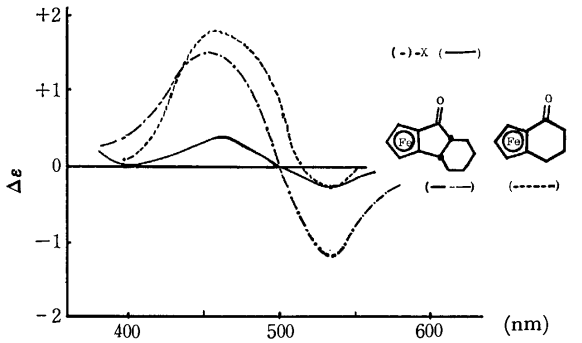

Fig. 3. CD of (−)-X and its homologs so far reported.

Furthermore, the CD curve of (−)-X in the region of the 300—600 nm ferrocene band area was similar to that of the ferrocenocyclohexenone of the (1*S*)-configuration[2g] and had the opposite sign of those of the substituted ferrocenocyclopentenones of the (1*R*)-configuration[2a,d,e] (see the following Scheme and Fig. 3).

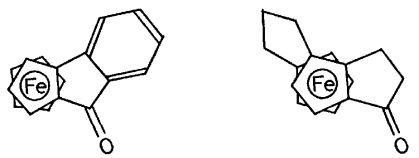

CD value:
Δε −3.50 (485 nm, EtOH)

CD value:
Δε −1.30 (490 nm, EtOH)

On the basis of these facts, it was confirmed that the absolute configuration of (−)-X is (1*S*,2*R*).[6]

Finally, it should be added that the mass spectrum of the ketone (X) now synthesized exhibited an intense peak at *m/e* 212. The exact mass of this peak (212.027) showed that decarbonylation had occurred instead of the loss of ethylene.[8] The cleavage accounts for the metastable peak at *m/e* 187 (see Fig. 4).

3) a) B. Gantheron and J. C. LeBlanc, *Bull. Soc. Chim. France*, **1971**, 3629; b) B. Gantheron, J. C. LeBlanc, and C. Moise, *C. R. Acad. Sci., Ser. C*, **271**, 1394 (1970); c) M. Rosenblum, A. K. Banerjee, N. Danieli, R. W. Fish, and V. Schlatter, *J. Amer, Chem. Soc.*, **85**, 316 (1963); d) K. L. Rinehart, Jr., R. J. Curby, Jr., D. H. Gustafson, K. G. Harbison, R. E. Bozak, and D. E. Bublitz, *ibid.*, **84**, 3263 (1962); e) E. A. Hill and J. H. Richards, *ibid.*, **83**, 4216 (1961); f) J. W. Huffman and D. J. Raff, *J. Org. Chem.*, **26**, 3588 (1961).

4) In the cyclization of substituted ferrocenylpropionic acids, the homoannularly-bridged ketones have occasionally been obtained as minor products. See Refs. 3a and 3b.

5) a) J. D. Hobson, J. Raines, and R. J. Whiteoak, *J. Chem, Soc.*, **1963**, 3495; b) W. Mock and J. H. Richards, *J. Org. Chem.*, **27**, 4050 (1962).

6) The thermolysis of the tosylhydrazone sodium salt of (−)-X in pyridine,[7] and the dehydration of the corresponding alcohol of (−)-X with acidic Al_2O_3,[2] were attempted, but neither gave any of the expected cyclopentadiene.

7) a) A. Sonoda and I. Moritani, *J. Organometal. Chem.*, **26**, 133 (1971); b) A. Sonoda, I. Moritani, S. Yasuda, and T. Wada, *Tetrahedron*, **26**, 3075 (1970); c) A. Sonoda and I. Moritani, This Bulletin, **43**, 3522 (1970).

8) This result is coincident with the fragmentation of 1-indanone (90% decarbonylation, 10% loss of ethylene). See: J. H. Bowie, *Aust. J. Chem.*, **19**, 1619 (1966).

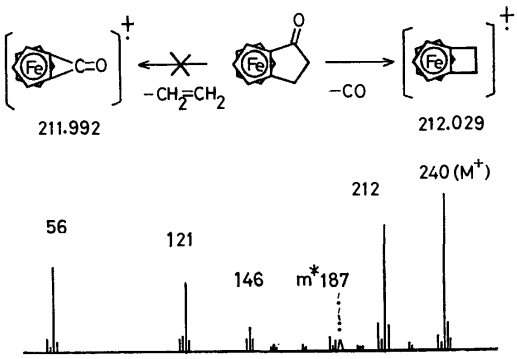

Fig. 4. Mass spectrum of ketone X.

Experimental

All the melting points and the boiling points are uncorrected. The microanalyses were performed at the Elemental Analyses Center of Kyoto University. The IR spectra were recorded on a Shimadzu IR-27-G spectrophotometer, and the mass spectra, on a Hitachi RMU-6L spectrometer. The NMR spectra were taken in a $CDCl_3$ or CCl_4 solution at 60 MHz on a JEOL C-60-H spectrometer; the chemical shifts are given in ppm from a TMS internal standard. The NMR signals are designated as *s* for a singlet, *d* as a doublet, *t* as a triplet, and *m* as a multiplet. The optical rotations were measured using a cell 1 or 5 cm in length at room temperature (20°C), and *c* is given in g/100 m*l*. The ORD and CD spectra were recorded on a JASCO ORD-5 spectropolarimeter in a EtOH solution (*c* in mg/m*l*), with a cell 1 cm long. The UV spectra were taken in EtOH on a Hitachi EPS-2 recording spectrophotometer. Column chromatography was carried out on Sumitomo activated alumina unless otherwise stated. The purity of every product was checked on tlc (Merck Aluminiumoxid G).

(S) (+)-(N-α-Pipecolylmethyl)ferrocene (I). The optical resolution of α-pipecoline was performed by fractional recrystallizations of its hydrogen tartrate from water.[9] A mixture of (*S*) (+)-α-pipecoline ($[\alpha]_D$ +32.0° (neat) (*i.e.*, 89% optical purity based on the reported value 36.0°), 96.9 g, 980 mmol) and (dimethylaminomethyl)ferrocene methiodide (74.8 g, 200 mmol) in water (70 m*l*) was stirred under refluxing (120°C) for 65 hr. Work-up, followed by distillation, gave (*S*) (+)-I as a dark red oil (61.3 g, 96%); bp 147—150°C/0.3 mmHg; $[\alpha]_D$ +69.1° (*c* 2.1, EtOH). The IR and NMR spectra were superimposable on those of an authentic sample.[1]

Methyl (1S) (−)-2-Hydroxymethylferrocenecarboxylate (III). The lithiation of the amine (+)-I ($[\alpha]_D$ +69.1° (EtOH), 36.3 g, 130 mmol) with *n*-BuLi, followed by carbonation, gave a lithium salt of the amino acid.[1] The treatment of the lithium salt with an excess of methyl iodide in methanol gave a crude methiodide (124 g), which was subsequently heated under reflux for 25 hr with aqueous KOH (10%, 600 m*l*). The resulting product was esterified with diazomethane to afford (*1S*) (−)-III ($[\alpha]_D$ −22.5° (*c* 5.5, $CHCl_3$), 8.0 g, 23%). This alcohol was identified by comparison with an authentic sample (IR, NMR).[1]

Preparation of Methyl (1S) (−)-2-(β-Methoxycarbonylvinyl)-ferrocenecarboxylate (VI). A mixture of the alcohol (1*S*) (−)-III ($[\alpha]_D$ −22.5°, 8.0 g, 29 mmol) and dry, active MnO_2 (35 g, 400 mmol) in chloroform was stirred under reflux in a nitrogen atmosphere for 2 hr. The subsequent filtration from an inorganic solid and the evaporation of the filtrate gave the aldehyde (*1S*) (−)-IV ($[\alpha]_D$ −384° (*c* 0.60, EtOH), 7.9 g 99%). IR (neat): 1710, 1670, 1290, 1275, 1220, 1190, 1160, 1150, 1080, 1035, 1005, 825, 805, and 750 cm^{-1}. NMR ($CDCl_3$, 10%); δ 10.68 (s, 1H, -CHO), 5.15 (m, 2H), 4.78 (m, 1H), 4.33 (s, 5H, cyclopentadienyl ring protons), and 3.88 (s, 3H, $-CO_2Me$). The semicarbazone was prepared as usual and was recrystallized from chloroform; mp 210°C (decomp.).

Found: C, 50.6; H, 4.6; N, 12.5%. Calcd for $C_{14}H_{15}FeO_3N_3$: C, 51.1; H, 4.6; N, 12.8%.

A mixture of the aldehyde ($[\alpha]_D$ −384°, 7.9 g, 29 mmol), malonic acid (5.4 g, 52 mmol), and piperidine (20 drops) dissolved in pyridine (130 m*l*) was heated under reflux (90—100°C) in a nitrogen atmosphere for 1.5 hr. The reaction mixture was evaporated *in vacuo*, and the residue was dissolved in chloroform. After the solution had been washed with aqueous phosphoric acid, the acidic product was extracted with excess aqueous NaOH. The aqueous layer was acidified with aqueous phosphoric acid and extracted with ether–chloroform to give the (1*S*) (−)-acid, V ($[\alpha]_D$ −520° (*c* 0.10, acetone), 2.0 g, 22% based on the starting amount of III), which was sufficiently pure for a further reaction. The esterifcation of V with diazomethane, followed by column chromatography (benzene elution), gave VI as dark red needles; ($[\alpha]_D$ −324° (*c* 0.56, EtOH), mp 92.5—94°C (from EtOH). IR (KBr): 1710, 1695, 1627, 1273, 1250, 1220, 1190, 1155, 1083, 1030, 1015, 992, 940, 850, and 812 cm^{-1}. NMR ($CDCl_3$, 5%): δ 8.37 (*d*, 1H, -CH=), 6.15 (*d*, 1H, -CH=), 5.00, 4.80, 4.60 (m, 3H) and 4.20 (s, 5H, cyclopentadienyl ring protons), and 3.80, 3.85 (s, 6H, $-CO_2Me$). ORD (*c* 0.7): $[M]_{520}$ −2280°, $[M]_{490}$ 0°, $[M]_{446}$ +4560°, $[M]_{384}$ 0°, $[M]_{368}$ −1930°, $[M]_{324}$ 0°, $[M]_{300}$ −300°.

Found: C, 58.9; H, 5.1%. Calcd for $C_{16}H_{16}FeO_4$: C, 58.6; H, 4.9%.

Preparation of Methyl (1S) (−)-2-(β-Methoxycarbonylethyl)-ferrocenecarboxylate (VIII). A mixture of the acid V ($[\alpha]_D$ −520°, 0.30 g, 1.0 mmol), PtO_2 (0.03 g), and ethanol was stirred under a hydrogen atmosphere at room temperature for 12 hr. A usual work-up, followed by column chromatography (ethanol elution), gave VII as fine, yellow-orange crystals; ($[\alpha]_D$ 0°, $[\alpha]_{545}$ −25.0° (*c* 4.5, EtOH), 0.27 g, 90%). The saturated acid, VII, was esterified with diazomethane in water–benzene–ether (1 : 1 : 1 ratio). Column chromatography (benzene elution) gave fine, yellow-orange crystals; diester VIII ($[\alpha]_D$ −10° (*c* 0.56, EtOH), 0.25 g, 90%), mp 66.5—68°C (from EtOH). IR (Nujol): 1730, 1715, 1305, 1290, 1257, 1215, 1193, 1175, 1138, 1105, 1030, 818, and 780 cm^{-1}. NMR ($CDCl_3$, 10%): δ 4.73 (m, 1H), 4.28 (m, 2H), 4.13 (s, 5H, cyclopentadienyl ring protons), 3.79, 3.15 (s, 6H, $-CO_2Me$), and 3.30—2.85, 2.65—2.35 (m, 4H, methylenes). ORD (*c* 0.3): $[M]_{524}$ −270°, $[M]_{494}$ 0°, $[M]_{454}$ +540°, $[M]_{418}$ 0°, $[M]_{400}$ −216°, $[M]_{384}$ 0°, $[M]_{364}$ +270°, $[M]_{350}$ 0°, $[M]_{296}$ −620° and $[M]_{260}$ 0°.

Found: C, 58.4; H, 5.6%. Calcd for $C_{16}H_{18}FeO_4$: C, 58.2; H, 5.5%.

Cyclization of VIII to (1S) (−)-2,3-ferrocenocyclopentenone (X). A mixture of VIII ($[\alpha]_D$ −10°, 0.33 g, 1.0 mmol) and NaH (50%) (0.20 g, 4.0 mmol) in dry tetrahydrofuran (25 m*l*) was stirred under reflux in a nitrogen atmosphere for 7 hr.[5] After cooling, methanol (10 m*l*) was added to the reaction mixture. Acidification with aqueous hydrochloric acid, followed by ether extraction, gave the crude β-ketoester, IX (0.20 g, 70%).

The product, IX (0.20 g, 0.7 mmol), dissolved in tetra-

9) W. Marckwald, *Ber.* **29**, 43 (1896); b) W. Leithe, *Monatsh. Chem.*, **50**, 40 (1932).

hydrofuran-benzene (1:2) (15 m*l*), was heated with aqueous NaOH (4%, 5 m*l*) for 5 hr under reflux in a nitrogen atmosphere. After cooling, the dark red benzene layer was separated from the aqueous tetrahydrofuran layer, and then benzene (10 m*l*) was added to the aqueous tetrahydrofuran layer in the reaction vessel. The mixture was again refluxed. This operation was repeated until no dark red color appeared in the new benzene layer. The combined benzene layers were then washed with water, and dried (Na_2SO_4). Column chromatography (benzene elution) gave X as dark red crystals; ($[\alpha]_D$ −49° (*c* 0.32, EtOH), 0.10 g, 60%), mp 82—83°C (from MeOH). IR (KBr): 1685, 1300, 1255, 1230, 1194, 1100, 1082, 1039, 999, 838, 827, and 815 cm^{-1}. NMR ($CDCl_3$, 7%): δ 4.57 (m, 3H), 4.12 (s, 5H, cyclopentadienyl ring protons), and 2.83 (*m*, 4H, methylenes). MS (relative abundance): *m/e* 240 (100), 212 (80), 186 (9), 184 (9), 146 (14), 121 (41), and 56 (60). ORD (*c* 1.7): $[M]_{580}$ −16°, $[M]_{564}$ −83°, $[M]_{550}$ 0°, $[M]_{494}$ +1849°, $[M]_{448}$ 0°, $[M]_{428}$ −414°, $[M]_{398}$ 0°, $[M]_{362}$ +1242°, $[M]_{341}$ +662°, $[M]_{305}$ +2070°, $[M]_{284}$ +1242°, $[M]_{230}$ +2484°. λ_{max} (EtOH): 465 nm (log, ε 2.39), 328 nm (log ε 2.84).

Found: C, 65.1; H, 5.1%. Calcd for $C_{13}H_{12}FeO$: C, 65.0; H, 5.0%.

The authors are indebted to the staffs of the Sankyo Co. for the measurement of the high-resolution mass spectra. This work was initiated by the valuable suggestions of Dr. Tadatosi Aratani. Financial support from the Ministry of Education, the Japanese Government, and from the Toray Science Foundation is acknowledged with pleasure.

BULLETIN OF THE CHEMICAL SOCIETY OF JAPAN, VOL. 45, 2887—2891 (1972)

The Constituents of Hops (*Humulus lupulus* L.). VII.[1] The Rapid Analysis of Volatile Components

Yoko NAYA and Munio KOTAKE
The Institute of Food Chemistry, Dojimanaka, Kita-ku, Osaka

(Received February 5, 1972)

The volatile constituents from several varieties of Hops have been investigated by the direct loading of fresh plant tissue through GC-MS. The Saaz variety was distinguished among the examined varieties by its high content of β-farnesene. Hallertau was characterized by a low content of myrcene and a high content of humulenes. Shinshu-wase differed in its high content of myrcene and its low content of humulenes. Northern Brewer was rather close to Hallertau, whereas Yakima appeared to be closely related to Shinshu-wase. The myrcene content of hop oil was observed to correlate competitively with the total amount of humulenes, caryophyllene, and farnesene. 2-Methylbutyl isobutyrate accumulates in company with myrcene. The biosynthetic implication of these relationships have been briefly discussed.

Hop oil is conventionally obtained by the steam distillation of hops involving solvent extraction. The analytical results of the volatiles have, therefore, usually been affected by various treatments after the picking of the cones. Recently, Hautke *et al.*[2] reported a headspace analysis useful for the discrimination of hop varieties, but the identification of the volatile compounds has generally been limited to the major constituents. The technique[3] to release the volatile constituents from fresh plant tissue seemed to demand a simple and rapid analysis of the hop aroma by combined gas chromatography-mass spectrometry (GC-MS), as has been previously described.[1] The present work will report the analytical results by GC-MS from several varieties of hops, using a solid-sampler for direct volatilization from fresh plant tissue "lupulin". The correlation between the characteristic volatile constituents and the varieties of hops has also been attempted in order to connect this experiment with phylogeny.

1) Previous paper of this series: Y. Naya and M. Kotake, This Bulletin, **44**, 3116 (1971).
2) P. Hautke and D. Petříček, *Wallerstein Commun.*, **33**, 89(1970); *Monatsschrift für Brauerei*, **23**, 241 (1970).
3) E. von Rudloff, *J. Gas. Chromatog.*, **3**, 390 (1965).

Experimental

Commercial hop samples harvested in 1971 were used for the experiment (Table 1). Lupulin, glands of hop oil, were sifted from hop cones after manual grinding under freezing with liquid nitrogen or dry ice. For the quantitative glc analysis, a Hitachi Model K-53 apparatus equipped with an inlet-arrangement "solid-sampler" (an optional part of the JEOL SS-801) and a flame ionization detector was used in connection with a digital integrator (Takedariken TR-2213). The capillary column used for the analysis was 45 m × 0.25 mm; it was made of stainless steel and was coated with HB 2000. A precolumn trap system was provided for the condensation of the volatiles. The trapped volatiles were then evaporated at once; the temperature was programmed so

TABLE 1. SAMPLES FROM SEVERAL VARIETIES OF HOPS HARVESTED IN 1971

Variety	Origin	Oil yield (%)
Saaz	Czechoslovakia	2.2
Hallertau	Germany	1.8
Northern Brewer	Germany	2.2
Yakima	U.S.A.	2.2
Shinshu-wase	Japan	1.7

TABLE 2. PERCENTAGE ABUNDANCE OF THE CONSTITUENTS DRIVED FROM THE FIVE VARIETIES OF HOPS BY DIRECT LOADING GC–MS AND SUBSEQUENT PEAK AREA MEASURMENT

Peak No	Constituent	Saaz	Hallertau	Northern brewer	Yakima	Shinshu-wase
1	Acetone		○		○	○
2	Methyl isopropyl ketone		○			○
3	Methyl isobutyl ketone	0.33	0.80	0.05	○	0.08
4	Dimethylvinylcarbinol	0.40	0.97	0.64	0.71	0.27
5	α-Pinene	0.03	0.04	0.13	0.38	0.06
6	67 (B) 124[a)]		0.08		0.19	
7	Isobutyl isobutyrate		0.06	0.29	0.13	0.39
9	β-Pinene	0.36	0.46	0.71	1.09	0.86
10	2-Methyl-1-butanol					0.67
10	Methyl hexanoate			0.15		
11	Myrcene	29.44	24.09	42.67	52.03	73.41
12	2-Methylbutyl isobutyrate		0.26	1.85	2.13	3.15
13	Limonene	0.05	0.16	0.29	0.49	0.38
14	β-Phellandrene[a)]	0.05	0.12	0.30	0.45	0.41
15	Methyl 5-methylhexanoate				0.61	
15	3-Methyl-2-buten-1-ol	0.06	○	0.29		0.09
16	105 (B) 120[a)]	○	○	0.06	0.13	
17	2,2,7,7-Tetramethyl-1,6-dioxaspiro-[4.4]-nona-3,8-diene	0.11	0.08	0.92		
17	β-Ocimene[a)]				0.61	0.17
18	Methyl heptanoate	0.13	0.14	0.30	0.18	0.07
19	Furfural				○	
20	Methyl 4-methyl-2-hexenoate	0.19	0.26	0.39	0.44	
20	2-Methylbutyl 2-methylbutyrate					0.22
21	2-Methylbutyl isovalerate			0.12	0.15	0.05
22	Methyl 6-methylheptanoate	0.16	0.05	0.18	0.36	0.18
23	2-Nonanone	0.18	0.18	0.08	○	○
24	Methyl octanoate	0.11	0.18	0.14	0.35	0.02
24	Perillene					
26	4,4-Dimethylcrotonolactone	0.09	0.37	0.05	0.05	0.07
27	Methyl 7-methyloctanoate				0.12	
28	Hexyl isobutyrate			0.02		
29	2-Decanone	0.15	○		○	○
30	Linalool	0.40	0.51	0.30	0.23	0.55
31	Methyl nonanoate	0.17		0.09	0.10	
32	α-Cubebene[a)]	○	0.05	0.03		0.03
33	9-Methyldecanone-2	0.29	0.04	0.07	○	0.06
34	α-Ylangene	0.27	0.20	0.17	0.24	0.09
35	Methyl 8-methylnonanoate	0.39		0.43	0.32	0.20
35	α-Copaene		0.59			
36	2-Undecanone	0.67	0.60	0.52	0.20	0.07
37	Methyl decanoate				0.23	
38	Methyl 4-decenoate	0.81	0.25	0.33	0.86	0.09
39	Myrtenol[a)]	0.24				
39–1	Isocaryophyllene[a)]	0.22				
40	Caryophyllene	8.73	13.08	10.44	9.68	3.68
41	85 (B) 182[a)]		○			0.20
42	Humulene	28.84	41.72	29.38	20.47	5.29
43	β-Farnesene	16.19				
43	Nerol					0.10
44	γ-Muurolene	1.10	1.89	1.04	0.61	0.49
46	Germacrene-D[a)]	0.53	1.01	0.74	0.79	
46	β-Selinene					1.73
47	α-Muurolene[a)]	0.68	0.93			
47	α-Selinene	○		0.62	0.87	1.98
48	Geraniol					○
48	β-Bisabolene[a)]	0.29				
49	δ-Cadinene	2.03	3.68	2.35	1.53	1.29

Peak No	Constituent	Saaz	Hallertau	Northern brewer	Yakima	Shinshu-wase
51	δ_2-Cadinene[a)]	0.16	0.22	0.16	0.08	0.06
52	α-Cadinene	0.32		0.16		0.46
53	2-Tridecanone	0.24	0.36	0.23	0.34	
53	Geranyl isobutyrate					○
54	Calamenene	0.05	0.12	0.07	○	0.02
55	79 (B) 210[a)]	0.24	○	0.02	○	0.02
56	γ-Calacorene		○			
57	α-Calacorene	0.03	0.11	0.06	0.06	0.02
60	Caryophyllene oxide	0.16	0.29	0.07	0.04	○
61	Humulene epoxide-I	0.11	0.42	0.05		
62	Humulene epoxide-II	0.62	1.72	0.29	0.11	0.05
64	epi-Cubenol	○	0.07	0.03	○	○
65	43 (B) 224[a)]	0.22	0.04	0.08	○	
66	79 (B) 222[a)]	0.51	0.03	0.16	○	0.02
67	Humulol	0.09	0.06	0.02		
68	γ-Eudesmol	0.03				
69	T-cadinol	0.15	0.17	0.11		0.08
70	T-muurolol	0.04		0.02		
71	δ-Cadinol	○	0.04	0.05		
71	Cadalene	○				
72	α-Eudesmol	0.22		0.07		
73	α-Cadinol	0.10	0.17	0.09		0.19
74	Junipercamphor					
75	Humulenol-II	0.18	1.46	0.11		
76	Humulene dioxide	○	0.21			
	Total	97.16	98.34	97.99	97.37	97.30

a) Tentatively identified.

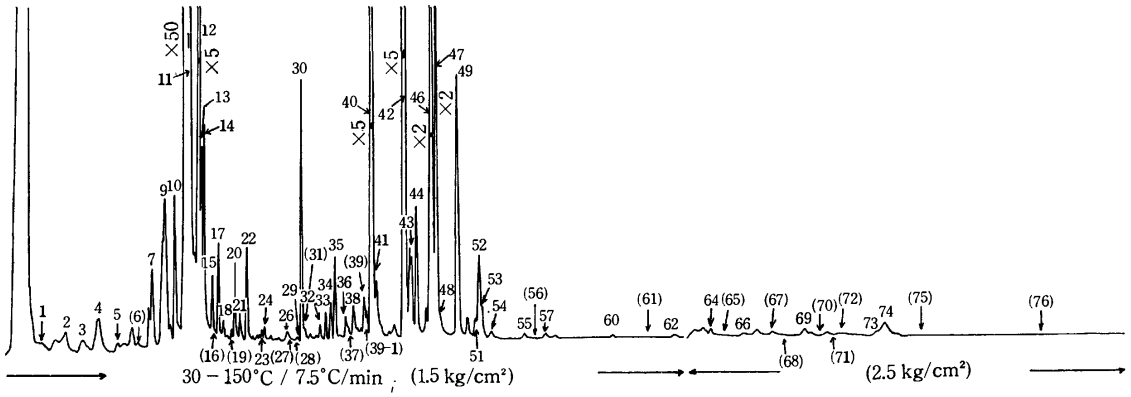

Fig. 1. Gas chromatographic record obtained from 5 mg of lupulin from Shinshu-wase, through capillary column (HB 2000, 45 m × 0.25 mm) with the vapor splitting assembly (1:70). The peak numbers correspond to those of Table 2. Those in parentheses were found in the different varieties.

that the volatiles could be detected as very sharp bands. 5 mg of lupulin was placed in the solid-sampler, and then the solid-sampler placed inside the injection block heated at 180°C for 1.5 min under a nitrogen-carrier gas-inlet pressure of 1.5 kg/cm², which swept the volatilized constituents onto the trapping column cooled by dry ice–isopropanol. After the cooling jacket had been taken off, the whole column system was heated by temperature programming from 30° to 150°C at the rate of 7.5°C/min. It was necessary to heat the injection block at around 180°C and to withdraw the plunger within 2 min in order to obtain a sufficient volatility of the volatiles without any thermal decomposition.

For the GC-MS analysis, a capillary column (45 m × 0.5 mm) coated with HB 2000 was used. The sample amount was about 10 mg for each analysis, which was done by the technique described above (hellium-carrier gas-inlet pressure, 0.7 kg/cm²; temperature programming, 30—150°C at 5°C/min. The mass spectrometer was a Hitachi Model RMU-6 apparatus, and the operating conditions were as follows: ionization energy, 80 eV; acceleration voltage, 2000 V. The compounds were identified by the agreement of the mass spectra, as well as by that of the retention time on glc, with those of authentic samples or of published standard references.

Results and Discussion

In our study, 10 mg of lupulin were sufficient for the identification of about fifty constituents, amounting to more than 97% of the total oil (Table 2). 5 mg of

lupulin were required for a satisfactory gas chromatogram, obtained through a capillary column equipped with a vapor-splitting assembly (1: 70). The gas chromatogram (Fig. 1) obtained for 5 mg of lupulin from Shinshu-wase is shown as an example. The chromatogram obtained using 1 mg of the sample without the splitting assembly was still sufficient for the purpose of comparison. A chromatogram using an essential oil from the same variety, obtained by the conventional method, was compared with the above chromatogram; it was found that low-boiling constituents were inevitably lost to a certain extent in the course of steam distillation and solvent extraction.

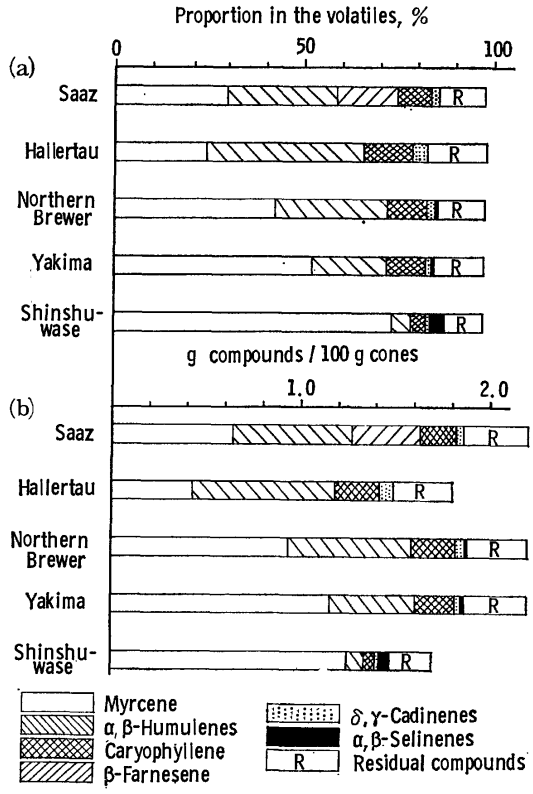

Fig. 2. Variation in the varieties and correlation among the contents of some hydrocarbons: (a) Proportion in the volatiles. (b) amounts calculated for the yield of essential oil.

The results (Fig. 2) indicate the differences among the varieties. A substantial amount of β-farnesene is contained only in the lupulin from Saaz. This fact is in agreement with the report of Šorm *et al.*[4] though not with that of Haward *et al.*[5] In this point, Saaz can be clearly distinguished from Hallertau, Northern Brewer, Yakima, and Shinshu-wase. The major hydrocarbons of Shinshu-wase, caryophyllene, and a mixture of α- and β-humulenes have been shown[1] to be characteristic constituents throughout the whole plant and to be no concern in ripening, while the amount of myrcene increases greatly in the course of ripening. Thus, Shinshu-wase is characterized by a high content of myrcene and a low content of humulenes. On the contrary, Hallertau is characterized by a low content of myrcene and a high content of humulenes. Furthermore, the composition of the hydrocarbons from Northern Brewer was similar to that of Hallertau, whereas Yakima appeared to be closely related to Shinshu-wase. The myrcene content of hop oil is observed to correlate competitively with the total amount of humulenes, caryophyllene, and farnesene. The biosyntheses of myrcene, humulenes, caryophyllene, and farnesene possibly proceed through enzymic transformations in the limited supply of the common intermediate. Accordingly, an increase in the amount of the one must cause a corresponding decrease in the amount of the rest. It is also observed that the selinene group competes with cadinenes from the common intermediate, the germacrenium ion.[6] The myrcene-rich varieties show a high content of selinenes, whereas the humulene-rich varieties are characterized by a high content of cadinenes. We can not explain readily the correlation in the contents between myrcene and selinenes as well as between humulene and cadinenes.

The oxygenated compounds can be divided into the two groups based on the difference in development. The one formed by the deterioration of the hop consists of oxidized volatiles (caryophyllene-oxide, humulene-epoxide-I and -II, humulenol-II, *etc.*) and the decomposed bitter principles[7] (dimethylvinylcarbinol, dimethylcrotonolactone *etc.*) (Fig. 3). The other group, in the course of the maturing of the cones, probably contains some monoterpenic alcohols, methyl ketones, and methyl esters and higher esters of various fatty acids. 2-Methylbutyl isobutyrate, which was the most rich component among the esters, can be correlated with myrcene. The myrcene-rich varieties show high contents of this esters (Fig. 4). Therefore, 2-methylbutyl isobutyrate must correspond to the Peak II-substance,[5] which accumulates in company with myrcene according to Haward *et al.* In fact, the amount of

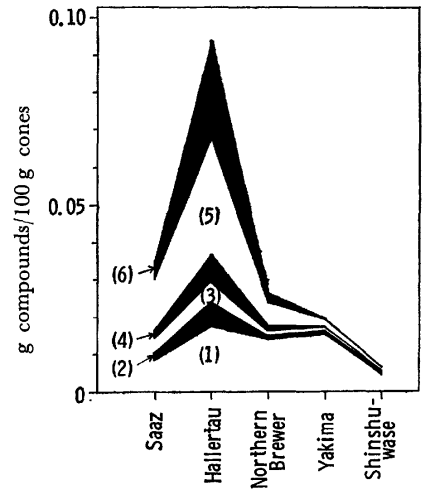

Fig. 3. Proportion of some oxygenated compounds caused from deterioration of hop. (1): dimethylvinylcarbinol, (2): 4,4-dimethylcrotonolactone, (3): caryophyllene-oxide, (4): humulene-epoxide-I, (5): humulene-epoxide-II, (6): humulenol-II.

4) F. Sǒrm, J. Mleziva, Z. Arnold, and J. Pliva, *Coll. Czech. Chem. Commun.*, **14**, 699 (1949).
5) G.A. Haward and C.A. Slater, *J. Inst. Brew.*, **63**, 491 (1957).
6) K. Morikawa and Y. Hirose, *Tetrahedron Lett.*, **1969**, 1799.
7) J. P. Regan and J. A. Elvidge, *J. Inst. Brew.*, **75**, 10 (1969).

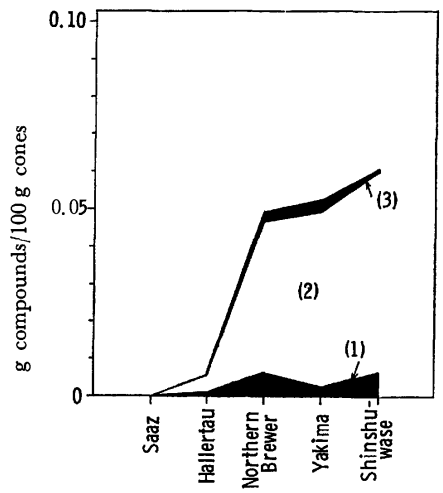

Fig. 4. Proprotion of some higher esters in the volatiles. (1): isobutyl isobutyrate, (2): 2-methylbutyl isobutyrate, (3): 2-methylbutyl isovalerate.

2-methylbutyl isobutyrate increases in the course of ripening in proportion to the formation of myrcene.[1] It has been shown that[8] a representative group of bitter principles, alpha-acid (I), and essential oil do not all reach a maximum at the same time. That is, the volatiles are accumulated later than alpha-acid. The various pieces of evidence above suggest that the formation of 2-methylbutyl isobutyrate is possibly connected with the biosynthesis of the acyl side-chains[9] of bitter principles, while myrcene is connected with isoprenyl units of them. Further study is now under way.

In spite of the short history of hop cultivation in Japan (since 1915),[10] the phylogeny of Japanese hops is uncertain. In order to elucidate the phylogeny of these hops, investigation[11] has been done on the basis of cytology. It is said that the sex chromosome types of wild and garden male hops are the same and are characteristic of their geographical groups namely, those of European origin are of the XY^w type, those of American origin are of the XY^h and XY^{nw} types, and those of Japanese origin are of the XA^vAY^a type. Only a few simple XY^h and XY^{nw} types were found in Japanese garden hops. This shows that intercrossings between the cultivated and wild hops have actually occurred. Thus, when the hops were introduced to a new region, acclimated new varieties have grown in the new habitat. From the viewpoint of phylogeny, our study lends support to the assumption that the local varieties in Europe named Saaz and Hallertau went over to America and then came to Japan, where they developed into a new local variety.

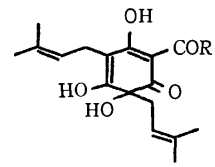

(I)	Humulone	R: *i*-Bu
alpha-Acid	Cohumulone	*i*-Pr
	Adhumulone	*sec*-Bu
	Posthumulone	*i*-Val
	Prehumulone	Et

The authors are deeply indepted to Dr. Junichi Kumada of Suntory, Ltd., for kindly supplying hop samples.

8) D. E. Bullis and S. T. Likens, *Brewers Digest.*, **1962**, 54.
9) S.C. Fang and D.E. Bullis, *Wallerstein Commun.*, **21**, 107 (1958).
10) T. Ono, *Bull. Brew. Sci.*, **5**, 1 (1959).
11) T. Ono, *Jap. J. Gen.*, **29**, 170 (1954).

Syntheses and Reactions of Ferrocene-Containing Polymers. VI. Polarography and Electron Transfer Equilibria of Some Ferrocene-Containing Polymers[1]

Toshihide NAKASHIMA and Toyoki KUNITAKE*

Department of Organic Synthesis, Faculty of Engineering, Kyushu Universtiy, Fukuoka

(Received February 17, 1972)

Polarography and electron transfer equilibria of some ferrocene-containing polymers were studied in comparison with small-molecule analogs. The oxidation half-wave potentials of polyvinylferrocene and polydivinylferrocene (almost completely cyclized) in CH_2Cl_2 were close to those of ferrocene and [3]ferrocenophane, respectively. This is in line with structural similarity. Only one oxidation step was observed in the polarogram of triferrocenylbenzene and polyethynylferrocene, suggesting that the electronic interactions between ferrocene units are small in these compounds. Electron transfer equilibrium was observed between ferrocene units in polymer and iodine. Equilibrium constants of the [3]ferrocenophane unit were greater than those of the unbridged ferrocene unit. The ferrocene unit in polymer showed greater equilibrium constants than those of their small-molecule analogs.

Ferrocene-containing polymers are expected to show interesting physical properties,[2] and the electrical property of the polymers prepared by polycondensation and polyrecombination has been studied.[3] However, detailed structural studies were often difficult, since many of these polymers were infusible and insoluble, and it was not possible to clarify the correlation between structure and property.

We have synthesized some ferrocene-containing polymers through addition polymerization of vinylferrocene, 1,1'-divinylferrocene and ethynylferrocene, and determined their structures by spectroscopic and other means.[4-7] Since the structures are rather simple, it was thought that the structure-property relationship would be comparatively straightforward. In this paper we describe the results of polarographic study and electron-transfer equilibria of these polymers in solutions.

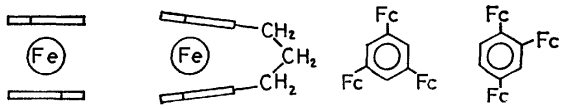

Ferrocene [3] Ferrocenophane 1,3,5- and 1,2,4-Triferrocenylbenzene

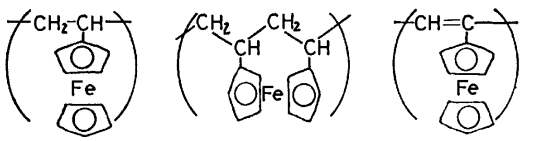

Poly(vinylferrocene) Cyclized poly(divinylferrocene) Poly(ethynylferrocene)

Fc: Ferrocenyl group

Experimental

Materials. Polymerizations of vinylferrocene, 1,1'-divinylferrocene and ethynylferrocene have been described.[4-7] The polymerization conditions are given in each case. Triferrocenylbenzene (mixture of 1,3,5- and 1,2,4-isomers) was prepared by the trimerization of ethynylferrocene.[7] [3]-Ferrocenophane(1,1'-trimethyleneferrocene) was prepared from formylferrocene according to the method of Rinehart *et al.*,[8] mp 97.3—99.0°C (lit, mp 107.5—108°C). The NMR spectrum showed sharp singlets in line with that in literature. Minor impurity (<4%) peaks observed might be ascribed to *n*-propylferrocene and/or to 1,2-trimethyleneferrocene. Found: C, 69.05; H, 6.08%. Calcd for $C_{13}H_{14}Fe$: C, 69.05; H, 6.25%.

Methyltriethylammonium triiodide was prepared from triethylamine, methyl iodide, and iodine, according to the method of Buckles *et al.*,[9] mp 65.0—65.6°C; λ_{max} ($CHCl_3$) 365 nm ($\varepsilon=2.4\times10^4$) (lit,[9] $(CH_3)_4NI_3$ λ_{max} ($ClCH_2CH_2Cl$) 365 nm ($\varepsilon=2.53\times10^4$)).

Instruments. Polarographic study was carried out with a Yanagimoto Polarograph PA 102 using rotating platinum electrode as a cathode and mercury pool as an anode. Electronic spectra were obtained with a Shimadzu UV 200 spectrophotometer.

Results and Discussion

Polarography. It is well-known that ferrocene compounds undergo one-electron oxidation to ferricenium ions electrolytically, photolytically, and by organic and inorganic oxidants. Thus polarographic studies have been made for many ferrocene derivatives

* To whom correspondence should be addressed.

1) Contribution No. 267 from this department.

2) *E.g.*, E.W. Neuse and H. Rosenberg, "Metallocene Polymers (Reviews in Macromolecular Chemistry, Vol. 5, Part 1)" Marcel Dekker, New York, N. Y. (1970).

3) Ya. M. Paushkin, L. S. Polak, T. P. Vishnyakova, I. I. Patalakh, F. F. Machus, and T. A. Sokolinskaya, *J. Polym. Sci., Part C*, **4**, 1481 (1963).

4) C. Aso, T. Kunitake, and T. Nakashima, *Makromol. Chem.*, **124**, 232 (1969).

5) T. Kunitake, T. Nakashima, and C. Aso, *J. Polym. Sci., Part A-1*, **8**, 2853 (1970).

6) T. Kunitake, T. Nakashima, and C. Aso, *Makromol. Chem.*, **146**, 79 (1971).

7) T. Nakashima, T. Kunitake, and C. Aso, *ibid.*, **146**, 79 (1971).

8) K. L. Rinehart, Jr., R. J. Curby, Jr., D. H. Gustafson, K. G. Harrison, R. E. Bozak, and D. E. Bublitz, *J. Amer. Chem. Soc.*, **84**, 3263 (1962).

9) R. E. Buckles, J. P. Yuk, and A. I. Popov, *ibid.*, **74**, 4379 (1952).

Table 1. Oxidation half-wave potential of polymers and related compounds

Rotating platinum electrode *vs.* mercury pool.
Solvent: methylene chloride.
Supporting electrolyte: n-Bu_4NBF_4, 0.1M.

Sample (concn. of ferrocene unit)	(mM)	Half-wave potential ($E_{1/2}$) (V)
Ferrocene	(0.1)	0.55±0.01
	(1)	0.50±0.01
[3] Ferrocenophane	(0.1)	0.47±0.01
	(1)	0.44±0.01
Triferrocenylbenzene[a)]	(0.1)	0.57±0.02
	(1)	0.60±0.03
Poly(vinylferrocene)[b)]	(1)	0.54±0.01
Cyclized poly(divinylferrocene)[c)]	(1)	0.43±0.02
Poly (ethynylferrocene)[d)]	(1)	0.60±0.01
Poly (ethynylferrocene)[e)]	(1)	0.58±0.01

a) Approximately 1: 1 mixture of the 1,3,5- and 1,2,4-isomers.
b) Polymerization condition: Et_2AlCl/t-BuCl (1/1), CH_2Cl_2, 0°C (Ref. 4).
c) Polymerization condition: AIBN, benzene, 60°C (Ref. 5).
d) Polymerization condition: $Al(i\text{-}Bu)_3/Ti(OBu)_4$(5/1), toluene, 80°C (Ref. 7).
e) Polymerization condition: $Al(i\text{-}Bu)_3/Ti(OBu)_4$(10/1), toluene, 80°C (Ref. 7).

(small molecules).[10-13] On the other hand, ferrocene-containing polymers have seldom been investigated polarographically, because of the limited solubility in solvents used for the polarographic study.[14,15]

Polarographic measurements were made in CH_2Cl_2 solution with tetra-n-butylammonium fluoroborate (n-Bu_4NBF_4) as supporting electrolyte. The system was selected beacuse of better solubility and conductivity than the following combinations: $LiClO_4$/tetrahydrofuran, $LiClO_4$/benzene-dioxane, and n-Bu_4NBF_4/benzene-dioxane. The oxidation half-wave potentials ($E_{1/2}$) of the ferrocene-containing polymers and their low-molecular-weight analogs are given in Table 1. The potentials are given relative to that of the mercury pool. Sample concentrations were 0.1 and 1 mM. Reproducibility of $E_{1/2}$ was good, being almost independent of concentration. However, lower concentrations seem to be favorable for removing the maxima on the polarogram which seem to be due to the adsorption of the product on the electrode. The $E_{1/2}$ values of polyvinylferrocene and cyclized polydivinylferrocene were close to those of ferrocene and [3]ferrocenophane, respectively. This supports the fact that the repeat unit of cyclized polydivinylferrocene is a [3]ferrocenophane derivative.[5] The polymer main chain does not seem to exert a great influence upon the oxidation potential of the pendent ferrocene ring.

It is established that two cyclopentadienyl rings of ferrocene are parallel with each other with 3.3 Å separation.[16] However, the two rings cannot be parallel in some heteroannularly-bridged ferrocenes such as [m]ferrocenophane with $m \leq 3$, owing to geometrical limitation.[17,18] Ferrocene derivatives of this type (hot-dog structure) are known to possess unique electronic properties.[19-21]

A polarographic study of bridged ferrocenes has been reported by Gorton *et al.*[13] They found that the half-wave potential of [2]ferrocenophane was appreciably lower than that of its unbridged counterpart, but the half-wave potential of [3]ferrocenophane was close to that of 1,1′-diethylferrocene. The difference in $E_{1/2}$ we observed between ferrocene and [3]ferrocenophane ($\Delta E_{1/2} = -0.07$ V) coincides with their data. Thus, the influence of bridging on the electronic property does not seem to be great in [3]ferrocenophane compared with that in [2]ferrocenophane. On the other hand, the difference in $E_{1/2}$ between polyvinylferrocene and cyclized polydivinylferrocene ($\Delta E_{1/2} = -0.11$ V) is greater than that found between 1-alkyl and 1,1′-dialkylferrocenes (small molecule).[11] Thus bridging seems to lower the oxidation potential.

Only one-step oxidation was observed in the polarogram of triferrocenylbenzene. It is known that two-step oxidation is involved with some binuclear ferrocene derivatives such as [1.1]ferrocenophane[13] and biferrocenyl.[22] This is interpreted as follows. A ferricenium group formed in the initial oxidation enhances the oxidation potential of the second ferrocene nucleus by interactions operating through the carbon skeleton of the ligands or directly between the iron atoms. The one-step oxidation polarogram indicates that there is no appreciable interaction among ferrocene nuclei in triferrocenylbenzene.

The electronic spectral data similarly indicate that there is no strong interaction between the ferrocene nuclei. The absorption coefficient of triferrocenylbenzene at 450 nm region (d-d^* transition of ferrocene nucleus) was approximately three times as large as that of phenylferrocene.[23]

The $E_{1/2}$ value of polyethynylferrocene agreed with that of triferrocenylbenzene within experimental error (0.59 and 0.58 V, respectively), which also shows that there is not much interaction between ferrocene nuclei directly or through the polyene chain.

10) J. Tirouflet, E. Laviron, R. Dabard, and J. Komenda, *Bull. Soc. Chim. Fr*, **1963**, 857.
11) G. L. K. Hoh, W. E. McEwen, and J. Kleinberg, *J. Amer. Chem. Soc.*, **83**, 3949 (1961).
12) H. Hennig and O. Gürtler, *J. Organometal. Chem.*, **11**, 307 (1968).
13) J. E. Gorton, H. L. Lentzner, and W. E. Watts, *Tetrahedron*, **27**, 4353 (1971).
14) K. Sonogashira and N. Hagiwara, *Kogyo Kagaku Zasshi*, **66**, 1090 (1063).
15) Y.-H. Chen, M. Fernandez-Refojo, and H. G. Cassidy, *J. Polym. Sci.*, **40**, 433 (1959).
16) M. Rosenblum, "Chemistry of the Iron Group Metallocenes, Part I," John Wiley, New York, N. Y. (1965), p. 31.
17) N. D. Jones, R. E. Marsh, and J. H. Richards, *Acta Crystallogr.* **19**, 330 (1965).
18) M. B. Laing and K. N. Trueblood, *ibid.*, **19**, 373 (1965).
19) T. H. Barr and W. E. Watts, *J. Organometal. Chem.*, **15**, 177 (1968).
20) T. H. Barr and W. E. Watts, *Tetrahedron*, **24**, 6111 (1968).
21) H. L. Lentzner and W. E. Watts, *ibid.*, **27**, 4343 (1971).
22) T. Matsumoto, M. Sato, and A. Ichimura, This Bulletin, **44**, 1720 (1971).
23) M. Rosenblum, J. O. Santer, and W. G. Howells, *J. Amer. Chem. Soc.*, **85**, 1450 (1963).

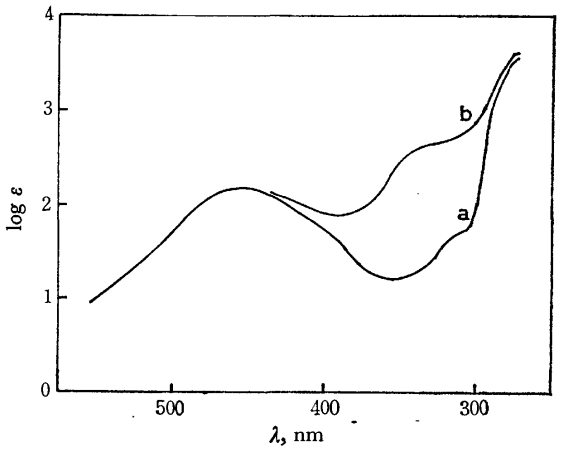

Fig. 1. Electronic spectra of poly(vinylferrocene). Solvent a: cyclohexane, b: CCl_4.

Electron Transfer Equilibria. Although ferrocene-containing polymers have been shown to react with appropriate acceptors to give corresponding ferricenium ions,[24] no quantitative studies have been made on electron transfer.

The electronic spectrum of ferrocene shows a peculiar solvent effect at around 300 nm in some halogenated hydrocarbon solvents. This was attributed to the dissociative charge transfer between ferrocene and a solvent molecule.[25] A similar solvent effect was observed in polyvinylferrocene as shown in Fig. 1. The extinction coefficient in the 300—400 nm region is greater in CCl_4 than in cyclohexane.

It has been reported that electron transfer equilibria hold between ferrocene and iodine in appropriate solvents.[25,26]

$$\text{Fe} + \frac{3}{2}I_2 \underset{}{\overset{K}{\rightleftharpoons}} \text{Fe}^+I_3^- \qquad (1)$$

The equilibrium was studied in chloroform with ferrocene-containing polymers. The equilibrium constant K was determined from the absorption of the triiodide anion at 365 nm.

$$K = \frac{[Fc^+I_3^-]}{[Fc][I_2]^{3/2}} = \frac{[Fc^+I_3^-]}{([Fc]_0-[Fc^+I_3^-])([I_2]_0-3/2[Fc^+I_3^-])^{3/2}} \qquad (2)$$

Fc: ferrocene unit

It was confirmed by using $CH_3(C_2H_5)_3N^+I_3^-$ that Beer's law holds. Formation of the triiodide anion by dissociation of iodine was negligible under the experimental conditions. The absorption at 365 nm was measured by the continuous variation method. The variation of absorption intensity with composition is given in Fig. 2.

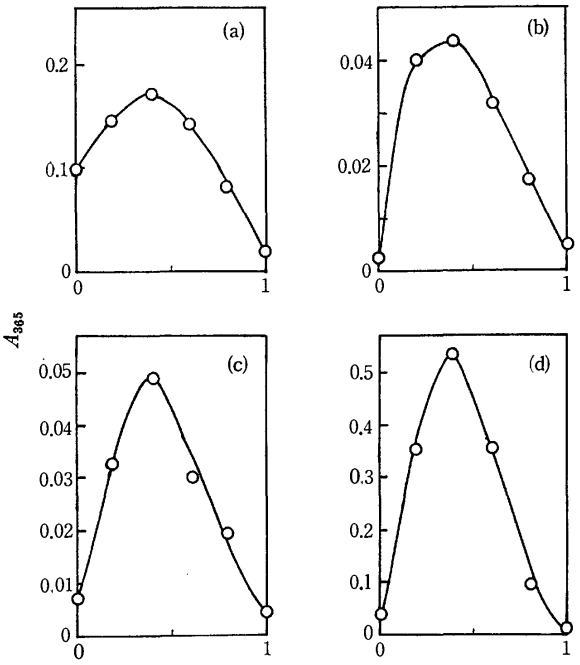

Fig. 2. Determination of the equilbrium constant of electron transfer by the continuous variation method. Solvent: chloroform. 1 cm silica cell. A_{365}: absorption intensity of I_3^- at 365 nm.
a: Ferrocene/I_2 (total concentration, 10^{-3} M), b: [3]Ferrocenophane/I_2 (total concentration, 10^{-4} M), c: Poly(vinylferrocene)/I_2 (total concentration, 10^{-4} M), d: Poly(divinylferrocene)/I_2, (total concentration, 10^{-4} M)

The maximum of A_{365} (absorption intensity at 365 nm) observed for ferrocene–iodine, mole fraction of ferrocene *ca.* 0.4, was in line with the stoichiometry of Eq. (1). Similar results were obtained for [3]ferrocenophane and ferrocene-containing polymers. The total concentration was set at 10^{-4}M in the case of ferrocene-containing polymers in order to avoid precipitation of oxidized polymers. Since polyethynylferrocene possesses a broad absorption in this region, determination of the equilibrium constant was impossible.

TABLE 2. EQUILIBRIUM CONSTANT OF THE ELECTRON TRANSFER REACTION FROM POLYMERS AND RELATED COMPOUNDS TO IODINE
28±2°C, Total concentration 10^{-4}M.

Sample	log K				
	Mole fraction of ferrocene unit				Average
	0.2	0.4	0.6	0.8	
Ferrocene[a]	3.0	3.0	3.1	3.2	3.1
[3]Ferrocenophane	5.4	5.3	5.3	5.5	5.4
Poly(vinylferrocene)	5.4	5.3	5.4	5.6	5.4
Poly(vinylferrocene)	5.4	5.3	5.3	5.5	5.4
Cyclized poly(divinylferrocene)	7.2	7.1	7.0		7.1
Cyclized poly(divinylferrocene)	6.5	6.5	6.2	7.2	6.6

a) Total concentration 10^{-3}M.

24) C. U. Pittman, Jr., J. C. Lai, D. P. Vanderpool, M. Good, and R. Prado, *Macromolecules*, **3**, 746 (1970).
25) J. C. D. Brand and W. Snedden, *Trans. Faraday Soc.*, **53**, 894 (1957).
26) A. V. Savitskii and Ya. M. Syrkin, *Dokl. Akad. Nauk SSSR*, **120**, 119 (1958).

The equilibrium constants were calculated for each run (Table 2). It is of interest that the bridged ferrocene units show greater K values than the unbridged units ([3]ferrocenophane *vs.* ferrocene, and cyclized polydivinylferrocene *vs.* polyvinylferrocene). Thus, electron transfer occurs more readily with the ferrocenophane structure, in line with the polarographic data. On the other hand, the polymers possess greater equilibrium constants than the low-molecular-weight analogs, in contrast with the polarographic results. Accumulation of the ferrocene unit along the polymer chain may make electron transfer favorable, probably through interactions of neighboring cyclopentadienyl rings with iodine molecule and/or through the change of polymer conformation associated with the reaction with iodine.

The authors are grateful to Professor W. Sakai for use of the polarographic apparatus. They also appreciate the helpful advice and encouragement of Dr. C. Aso during the course of investigation.

BULLETIN OF THE CHEMICAL SOCIETY OF JAPAN, VOL. 45, 2895—2898 (1972)

Studies on Tritylated Sucrose. II. Di-*O*-Tritylsucroses

Toshiki OTAKE

Nippon Electric Varian, Ltd., Azabu, Iigura-machi, Minato-ku, Tokyo

(Received January 31, 1972)

Three isomeric di-*O*-tritylsucrose were isolated from a mixture of tritylated sucrose by the reaction of sucrose and trityl chloride in mole ratio 1: 2. Structures of isomeric diethers were established by application of NMR to the hexa acetyl derivatives. They are recognized as 6,6′-, 1′,6-, and 1′,6′-di-*O*-tritylsucrose. The former two substances were crystallized as colorless prisms.

In the preceding paper,[1] the isolation and structure of mono-*O*-tritylsucroses through the reaction of sucrose with trityl chloride in mole ratio 1: 1.2 were described. The content of monoether in the reaction product was 53% for total tritylated sucrose. The trityl groups on monoethers obtained were at 6- and 6′-position of sucrose. No other positional isomer such as 1′-mono-*O*-tritylether was detected. However, by thin-layer chromatography, at least three kinds of di-*O*-tritylsucroses and one triether were recognized in the reaction mixture. Formation of the three diethers suggests that at least one reactive hydroxyl group against trityl chloride should be present on sucrose in addition to the hydroxyl groups of 6- and 6′-position. The structures of diethers were established by NMR spectra. The structure of the triether was confirmed by McKeown *et al.*[2] McKeown and Hayward[3] and Bredereck *et al.*[4] to be 1′,6′,6-tri-*O*-trityl sucrose from the analysis according to the complex chemical procedures. In both works, one mole of sucrose was tritylated with 3 mol of trityl chloride, followed by acetylation in the same vessel, no description being given on mono- and di-*O*-tritylethers.

Results and Discussions

After removal of mono-*O*-tritylsucrose from the product obtained by the reaction of sucrose and trityl chloride in 1: 2 mole ratio, the residue was chromatographed on silica gel to divide it into fractions of di-*O*-tritylsucroses, tri-*O*-tritylsucroses, and non-sugar trityl compounds. On the total solid recovered by chromatography, the yields of mono-*O*-tritylsucroses, di-*O*-tritylsucroses, tri-*O*-tritylsucrose, and non-sugar trityl-compounds were accounted for in 27, 37, 17, and 19% weight, respectively. The thin-layer chromatogram of diethers showed that the diethers fraction consisted of at least three isomers and the order of amount of each isomer was IIa (R_f value 0.62)>IIb (R_f value 0.67)>IIc (R_f value 0.72).

Diethers IIa and IIc were crystallized, and melted at 124.5—126.5 and 133°C (corr), respectively, while IIb was obtained as colorless amorphous powder, softening at 129°C. The yield for crystalline IIa was 74%, as compared with 14% for IIb and 12% for IIc, on the total weight of the di-*O*-tritylsucroses. The IR spectra of all the diethers exhibited the O–H stretching absorption near 3500 cm^{-1} and the characteristic phenyl absorption at 1600, 1495, and 1450 cm^{-1}. On the UV spectra, the diethers and trityl chloride showed almost the same absorption pattern (λ_{max} = 260 mμ) and the molar extinction coefficient of the diethers (ε_{max}: IIa 1440, IIb 1415, and IIc 1460) gave twice the value of trityl chloride (ε_{max} 720). Thus, it is confirmed that IIa, IIb, and IIc are all di-*O*-tritylsucroses. The peracetyl derivative of III was crystallized in 70% yield against the total acetyl product of III-fraction. Its melting point (mp 234.4°C corr) was equal to that of 1′,6′,6-tri-*O*-trityl penta-*O*-acetylsucrose which had been reported by McKeown and Bredereck.

Diethers IIa, IIb, and IIc were acetylated with

1) T. Otake, This Bulletin, **43**, 3199 (1970).
2) G. G. McKeown, R. S. E. Serenius, and L. D. Hayward, *Can. J. Chem.*, **35**, 28 (1957).
3) G. G. McKeown, and L. D. Hayward, *ibid.*, **35**, 992 (1957).
4) H. Bredereck, H. Zinner, A. Wagner, G. Faber, W. Greiner, and W. Huber, *Chem. Ber.*, **91**, 2824 (1958).

acetic anhydride in a pyridine solution. The residues on evaporation were chromatographed on silica gel to obtain di-*O*-trityl-hexa-*O*-acetylsucroses (IVa, IVb, and IVc) in good yield. The product IVa was crystallized as colorless prisms (mp 102°C), while the others remained as amorphous solid by the same treatment. IR data of each product showed no absorption corresponding to the O–H stretching vibration, and the thin-layer chromatogram showed the products to be homogeneous. It was thus revealed that acetylation of the diether was completed.

In the NMR spectra of the acetyl derivatives, the integrated intensities of acetyl, trityl, and other protons agreed with the theoretical values calculated as di-*O*-trityl-hexa-*O*-acetylsucrose. The chemical shifts of the acetyl-group protons were in the δ value 1.5—2.0, showing certain differences between them: IVa; δ 1.57 (3H), 1 88 (3H), 1.92 (3H), 1.98 (3H), 2.00 (6H), IVb; δ 1.78 (3H), 1.91 (3H), 1.95 (3H), 1.96 (3H), 1.98 (3H), 2.03 (3H), IVc; δ 1.66 (3H), 1.88 (3H), 1.97 (3H), 2.00 (9H).

In each case, signals arising from the methine and the methylene protons fell into the region between δ 2.5 and δ 5.9, which could be subdivided into the three non-overlapping regions; A (δ 2.5—3.5 (4H)), B (δ 3.6—4.5 (4H)), and C (δ 4.5—5.9 (6H)).

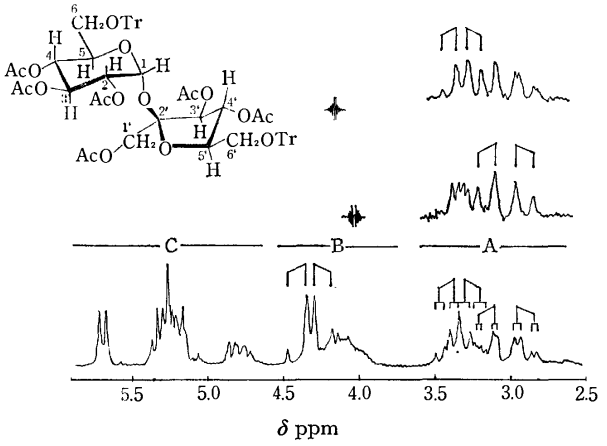

Fig. 1. Partial NMR spectrum of 100 MHz of IVa in $CDCl_3$.

The signals in region A may be assigned to the protons of the methylene groups to which *O*-trityl group is directly attached.[1] For IVa, the signals in A are considered to consist of the two independent AB parts in each ABX system (Fig. 1). This was confirmed for IVa by carrying out irradiation near δ 4.0 and observing the perturbation of the signals, as it gives the two groups of signals with each four transitions. The following simulation spectrum was obtained by a computer, confirming the proposed ABX system defined by δ (1) 2.91, δ (2) 3.15, and δ (3) 4.15, with J (1, 2) −10.8, J (1, 3) 4.0, and J (2, 3) 2.0 Hz, δ (1′) 3.28, δ (2′) 3.41, and δ (3′) 4.15 with J (1′, 2′) −10.0, J (1′, 3′) 6.8, J (2′, 3′) 6.3 Hz,

	1	2	3	4	5	6	7	8
Observed (δ)	2.83	2.88	2.94	2.98	3.10	3.12	3.21	3.23
Generated (δ)	2.83	2.86	2.93	2.97	3.10	3.12	3.21	3.23

	1′	2′	3′	4′	5′	6′	7′	8′
Observed (δ)	3.17	3.24	3.27	2.34×2		3.40	3.44	3.50
Generated (δ)	3.17	3.24	3.27	3.34×2		3.41	3.44	3.51

On the basis of these observations, the signals in region A can be assigned to the methylene protons of H-6 and H-6′, and the original diether IIa should be 6,6′-di-*O*-tritylsucrose. By comparison with the chemical shifts of H-6 or H-6′ on mono-*O*-trityl-sucrose,[1] it is concluded that the signals of lower field in region A is ascribed to H-6′, and those of high field to H-6. The AB quartet observed in the lower field of region B is assigned to protons of C-1′methylene-group to which an *O*-acetyl group is directly attached, giving further confirmation of the structure.

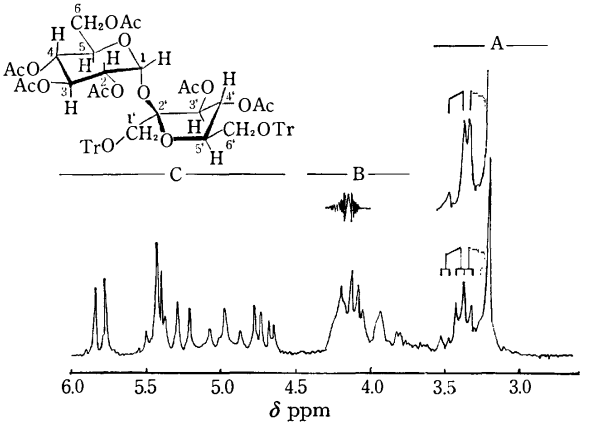

Fig. 2. Partial NMR spectrum at 100 NHz of IVb in $CDCl_3$.

In the spectrum of IVb (Fig. 2) a broad singlet at δ 3.30 is considered to be due to protons of C-1′ methylene. The other signals in region A (δ 3.3—3.6) are assumed to be AB part of an ABX system which is turned to four-transition signals by irradiation near 4 ppm. The generated spectra in NMR spin simulation defined by δ (1) 3.31, δ (2) 3.43, and δ (3) 4.10, with J (1, 2) −10.5, J (1, 3) 4.5, and J (2, 3) 5.0 Hz, agreed with the observed spectrum of region A:

	1	2	3	4	5	6	7	8
Observed (δ)	—*	3.29	3.32	3.37×2		3.42	3.46	3.52
Generated (δ)	3.21	3.26	3.32	3.36	3.37	3.42	3.48	3.53

* overlapped with the protons of H-1′.

This system is almost consistent with that formed with the protons of C-6′methylene and H-5′ on 6′-mono-*O*-trityl-hepta-*O*-acetylsucrose. Thus the original diether IIb is perceived to be 1′,6′-di-*O*-tritylsucrose.

Signals in region A of IVc (Fig. 3) are considered to be overlapping signals of part AB in system ABX and system AB. The latter is assigned to the protons of C-1′methylene to which a trityl group is directly attached. Irradiation near 4 ppm gave rise to the collapse of signals other than those of C-1′methylene in region A and the appearance of four-transition signals. Comparison of the observed and the generated spectra in region A which is defined by δ (1) 2.85, δ (2) 3.3, and δ (3) 4.15 with J (1, 2) −10.7, J (1, 3)

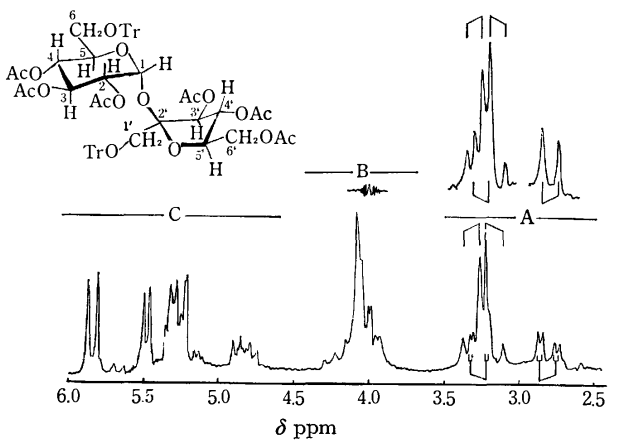

Fig. 3. Partial NMR spectrum at 100 NHz of IVc in $CDCl_3$.

3.2, and J (2, 3) 2 Hz, and δ (1') 3.22, δ (2') 3.33 with J (1', 2') −10.2 Hz, is as follows.

	1	2	3	4	5	6	7	8
Observed (δ)	2.78	2.81	2.88	2.91	3.23	3.25	3.34	3.36
Generated (δ)	2.77	2.81	2.88	2.91	3.24	3.26	3.34	3.37

	1'	2'	3'	4'
Observed (δ)	3.16	3.26	3.30	3.40
Generated (δ)	3.15	3.25	3.30	3.40

The above approximate three-spin system agreed well with that consisting of the proton of C-6 methylene and H-5 on 6-mono-trityl-hepta-*O*-acetylsucrose. Thus, the original diether should be 1,6-di-*O*-trityl-hepta-*O*-acetylsucrose.

The three possible isomeric diethers through the tritylation at two of the three primary alcohol (1'-, 6'-, and 6-position) are all recognized in the reaction mixture. The trityl group at the 1'-position was not observed in mono-*O*-tritylsucroses.[1] It should be noted that the tritylation at 1'-position is only observed in the ethers of higher trityl content.

Inactivity of 1'-hydroxyl group has also been observed in the *trans*-esterification of sucrose.[5] Formation of 1',6-, and 1',6'-di-*O*-tritylsucrose may take place through 6-, or 6'-mono-*O*-tritylsucrose gradually.

Experimental

General Methods. Thin-layer chromatography was carried out using Merck silica gel G as an adsorbent in a thickness of 0.25 mm and with the solvent systems: (A) methanol–water–acetone–chloroform (20: 4: 2: 56) for tritylated sucrose, (B) methyl ethyl ketone (MEK)–toluene for the *O*-acetyl derivatives of sucrose. The developed plates were sprayed with 50% sulfuric acid and heated at 120°C. Column chromatography was carried out using silica gel, 60—80 mesh (Kanto Chemical Co.). IR and UV spectra were measured with a Hitachi EPI-II RI spectrometer and a Cary Model 14R recording spectrophotometer, respectively. The NMR spectra were recorded with a Varian HA-100D (100 MHz) spectrometer using chloroform-*d* with tetramethylsilane as an internal lock, the signal positions being expressed in δ values. The NMR simulations were accomplished by a Varian Spectro. System SS-100 equipped with a Varian 620/i computer.

Tritylation of Sucrose. Commercial granulated sucrose (6.84 g) was reacted with recrystallized trityl chloride (11.4 g) in dry pyridine (100 m*l*) at room temperature. The reaction was accelerated by agitation of the reaction solution for 96 hr. At the end of the reaction period, the solution was dried *in vacuo* on a rotary evaporator. The residue was dissolved in 1-butanol (200 m*l*) and then washed with a Mckirrvin buffer (pH 7.0) and water in order to remove the free sucrose. Evaporation of the butanol solution under reduced pressure left 15.25 g of tritylated sucrose as colorless glass.

Separation of di-O-tritylsucroses. The mixture of tritylated sucrose was then subjected to counter currentgraphy for separation into mono-*O*-tritylsucroses and a mixture of ethers of higher trityl content. Evaporation of non-polar layer yielded the mixture (11.25 g) as colorless glass, which was subsequently chromatographed on 50 g of silica gel. After washing the column with chloroform (1 *l*) and with 2% methanol/chloroform (1 *l*), the diethers were eluted with 6% methanol/chloroform (1 *l*). Evaporation of the last solution left 5.319 g of a mixture of diethers.

6,6'-di-O-tritylsucrose (IIa). The mixture of diethers was resolved in an admixture of *n*-hexane and trichloroethylene (1: 1 vol/vol) (50 m*l*) at 55°C. The solution was then left at room temperature to precipitate an admixture of IIa and IIb. The residue of the filtration was dissolved in 80% methanol (30 m*l*) to crystallize IIa. By crystallization twice, 1.893 g of IIa was obtained as colorless prisms, melting at 125—126°C. Further 0.941 g of crystalline IIa was obtained from the mother liquid of recrystallization by recycling column chromatography.

Found: C, 70.78; H, 6.39%. Calcd for $C_{50}H_{58}O_{11}\cdot H_2O$: C, 71.09; H, 6.16%.

1',6'-di-O-tritylsucrose (IIb). Evaporation residue (0.9 g) from the mother liquid of the recrystallization of IIa from 80% methanol was added to silica gel (10 g) column as a chloroform solution; the column was then gradually washed with 4, 5, 6, and 7% methanol/chloroform (200 m*l* each). The eluent was divided into sixteen 50 m*l*-fractions after all the solvent passed through the column, each fraction was returned gradually to the column. After repeating the recycling procedure, each fraction was examined by thin-layer chromatography to find out the fractions consisting of IIb. Evaporation of the fractions yielded 0.602 g of IIb as amorphous colorless powder melting at 129°C.

Found: C, 72.72; H, 6.37%. Calcd for $C_{50}H_{58}O_{11}$: C, 72.63; H, 6.09%.

1',6-di-O-tritylsucrose (IIc). The evaporation residue of the mother liquid of the crystallization of IIa with an admixture of *n*-hexane and trichloroethylene was chromatographed in the same manner as in the separation of IIb. The residue of IIc fraction (0.536 g) was crystallized twice from 5 m*l* of 80% methanol solution to yeild about 0.4 g of crystalline IIc melting at 133°C.

Found: C, 71.37; H, 6.22%. Calcd for $C_{50}H_{58}O_{11}\cdot H_2O$: C, 71.09; H, 6.16%.

Di-O-trityl-hexa-O-acetylsucroses (IVa, IVb, and IVc). Acetylation of di-*O*-tritylsucroses was caried out as reported.[1] Each residue of reaction solution was chromatographed on a silica gel (10 g) column. After washing the column with 200 m*l* of toluene, each hexa-*O*-acetyl derivative (IVa, IVb, and IVc) was eluted with 7% methyl ethyl ketone (MEK)/toluene (200 m*l*) in an almost theoretical yield. IVa was

5) T. Otake, *Nippon Kagaku Zasshi*, **90**, 393 (1969).

obtained in a crystalline form, melting at 102°C, by recrystallization with 10 m*l* of 80% methanol, in about 85% yield against the evaporation residue; attempts to crystallize the other hexa-*O*-acetyl derivatives were unsuccessful. Each acetyl derivative was found to be homogeneous on the thin-layer chromatogram developed with MEK-toluene (1; 1 vol/vol); every compound had the same R_f value of 0.89.

Found, IVa: C, 69.28; H, 5.72%. Calcd for $C_{62}H_{62}O_{17}$: C, 69.01; H, 5.79%.

The author wishes to thank Professor Tetsuo Suami, Keio University, for his helpful advice and Mr. Iwao Miura for determination of NMR spectra.

BULLETIN OF THE CHEMICAL SOCIETY OF JAPAN, VOL. 45, 2898—2902 (1972)

Electrocatalytic Chemistry of the Transition Metal Complexes. II. Dehydrogenation of Cyclohexene Catalyzed by the Electroreduced Cobalt Complex of α,β,γ,δ-Tetraphenylporphine

Hironori KAGEYAMA, Masanobu HIDAI, and Yasuzo UCHIDA

Department of Industrial Chemistry, Faculty of Engineering, The University of Tokyo, Hongo, Tokyo

(Received December 17, 1971)

The metal complexes of α,β,γ,δ-tetraphenylporphine (M(TPP), M=Co(II), Ni(II), FeCl(III), Pd(II), Pt(II), Cu(II), MnCl(III), and V(IV)O) were electrolyzed at −2.0 V *vs.* Ag wire in the presence of cyclohexene under nitrogen atmosphere. The cobalt complex only had the catalytic activity of dehydrogenating cyclohexene to 1,3- and 1,4-cyclohexadiene and benzene. With the use of dimethylformamide, dioxane, and hexamethylphosphoric triamide as solvent, cyclohexadienes were produced, and with that of benzonitrile, and dimethyl sulfoxide, benzene was produced and cyclohexadienes were scarcely produced at all. In all cases, the current efficiency of the products was much higher than 100%, indicating that the dehydrogenation reaction is catalytic. The composition of the products also varied with the reaction temperature. When ethanol was added to the reaction solution, the amount of cyclohexadienes increased with benzonitrile used as solvent. The ESR spectrum observed at $g=2.003$ under electrolysis at the second wave potential is due to the anion radical of cobalt(I) tetraphenylporphine. From polarographic data and other experiments, the species is considered to be an intermediate for dehydrogenation of cyclohexene. The active sites for dehydrogenation are considered to be both the central metal atom and the conjugated ring.

The chemistry of metal complexes of α,β,γ,δ-tetraphenylporphine has currently received much interest with respect to their catalysis. Some works have been carried out in which these complexes were used as catalysts such as synthesis of ammonia from hydrogen and nitrogen,[1] isomerization from quadricyclene to norbornadiene,[2] oxidation of olefins,[3] syntheses of aniline and benzene from 1,4-cyclohexadiene and nitrobenzene.[4]

While there are many reports on the electrochemical studies of the transition metal complexes, only a few have appeared in which electroreduced metal complexes were used as catalysts such as oligomerization of butadiene and polymerization of acrylonitrile catalyzed by the electroreduced tetrakis(pyridine)dichloronickel(II),[5] oligomerization of butadiene catalyzed by the electroreduced nickel acetylacetonate.[6]

The electroreduced species in the above two cases were very stable after the current was cut off. It is well-known that an analogous species is produced by the reduction of nickel acetylacetonate with chemical reagents such as $AlEt_3$, $LiAlH_4$.[7]

In a previous paper,[8] the authors briefly reported that the electroreduced cobalt complex of α,β,γ,δ-tetraphenylporphine had the catalytic activity of dehydrogenating cyclohexene to cyclohexadienes and benzene, and the electroreduced species was unstable. In this paper a detailed study of the catalytic reaction is given.

Experimental

Materials. All solvents were purified by refluxing over dehydrating agents and distilled several times. Cyclohexene was purified by refluxing over $CaSO_4$ and fractionally distilled twice. Tetra-*n*-butylammonium perchlorate (TBAP) used as a supporting electrolyte was obtained by adding hydroperchloric acid to aqueous tetra-*n*-butylammonium bromide and was recrystallized from ethanol three times after washing with water.

α,β,γ,δ-Tetraphenylporphine free base (H_2(TPP)) was prepared from benzaldehyde and pyrrole according to the method of Ball *et al.*[9]

1) M. Ichikawa, *Kagaku no Ryoiki*, **24**, 863 (1970).
2) J. Manassen, *J. Catal.*, **18**, 38 (1970).
3) US 2950237, Aug. 23 (1960).
4) J. Manassen and A. Bar-Ilan, *J. Catal.*, **17**, 86 (1970).
5) N. Yamazaki and S. Murai, *Chem. Commun.*, **1968**, 147.
6) H. Lehmkuhl and W. Leuchte, *J. Organometal. Chem.*, **23**, C30 (1970).
7) G. Wilke, *Angew. Chem.*, **69**, 397 (1957).
8) H. Kageyama, M. Hidai, and Y. Uchida, *Chem. Lett.*, **1972**, 139.
9) R. H. Ball, G. D. Dorough, and M. Calvin, *J. Amer. Chem. Soc.*, **68**, 2278 (1946).

The cobalt complex of TPP (Co(TPP)) was prepared from cobalt acetate and H_2(TPP).[10] Ni(TPP), Cu(TPP), and MnCl(TPP) were obtained by a similar method.[10] Pd(TPP), Pt(TPP), and VO(TPP) were prepared by using $PdCl_2$, K_2PtCl_4, and vanadyl acetylacetonate, respectively.[11,12]

Reaction Apparatus. The reaction apparatus is an H type cell with an arm to enable the insertion of the reference electrode. The platinum coil, platinum plate (electrode area, 2.7 cm^2), and silver coil were used as cathode, anode, and reference electrode, respectively.

Procedure. M(TPP), 1.0×10^{-4} mol and TBAP, 2.0×10^{-3} mol were dissolved in 10.0 m*l* of the solvent under nitrogen atmosphere, and 2.0 m*l* (*ca* 2×10^{-2} mol) of cyclohexene was added to the solution. After stirring for 30 min at room temperature, the solution was introduced into the electrolytic cell. The cathode potential was set up and controlled *vs.* silver wire using a Yanagimoto Controlled Potential Electrolyzer Model VE-3.

Electrolysis was carried out for 6—24 hr at room temperature. After the reaction the solution was analyzed by gas chromatography. The current was measured by a copper coulometer.

Analysis. The polarograph used was a Yanagimoto Model PB-105. Polarography was carried out by using an H type cell. The cathode and anode were a dropping mercury electrode and a mercury pool, respectively. The concentration of the metal complexes and TBAP were 5.0×10^{-3} mol/*l* and 2.0×10^{-1} mol/*l*, respectively.

Quantitative analysis of the dehydrogented products was carried out by gas chromatography. Column, Carbowax 1500 (10%) on Diasolid M (60—80 mesh) 2 m; Column temperature, 40°C; Carrier gas, H_2 30 cc/min; Detector, Thermal conductivity cell.

Detection of hydrogen evolved was carried out by gas chromatography. Column, Molecular sieve 5A 2 m; Column temperature, 20 °C; Carrier gas. N_2 5 cc/min.

ESR Measurement. The ESR spectra were recorded using a JEOL JS-3BS-X Spectrometer. The cathode, anode and reference electrode were a mercury pool, platinum wire and silver wire, respectively. The ESR spectra were measured under controlled potential electrolysis under nitrogen atomosphere.

Visible Spectra. The visible spectra of the complexes were measured using a Shimadzu MPS-50L Spectrophotometer. All operations were carried out under nitrogen atmosphere.

Results and Discussion

Electrolysis of the Metal Complexes in the Presence of Cyclohexene. The half wave potentials of Co(TPP), Ni(TPP), Pd(TPP), Pt(TPP), Cu(TPP), FeCl(TPP), and MnCl(TPP) used as the metal complexes are shown in Table 1. The electrolysis of the above-mentioned complexes and VO(TPP) were carried out at −2.0 V *vs.* Ag wire which was more negative than the second wave potential of all complexes, in a dimethylformamide(DMF) solution of cyclohexene for 6 hr at room temperature.

Table 1. The half wave potentials of the metal complexes

Complex	Prewave	$E_{1/2}$ (1)	$E_{1/2}$ (2)	Δ[b]
H_2 (TPP)[a]	−0.70	−1.05	−1.47	0.42
Co (TPP)[a]	—	−0.82	−1.87	1.05
Ni (TPP)[a]	—	−1.18	−1.75	0.57
Pd (TPP)	—	−1.00	−1.53	0.53
Pt (TPP)	—	−1.18	−1.71	0.53
Cu (TPP)[a]	−0.72	−1.20	−1.68	0.48
MnCl (TPP)	−0.09	−1.52	−1.91	0.39
FeCl (TPP)	−0.18, −0.82	−1.07	−1.68	0.61

conditions: concentration of the metal complex, 5.0×10^{-3} mol/*l*; supporting electrolyte, TBAP, 2.0×10^{-1} mol/*l*; solvent, DMF; potential *vs.* Hg pool.
a) Ref. 9. b) $\Delta=E_{1/2}(1)-E_{1/2}(2)$.

Only when the cobalt complex was electrolyzed in the presence of cyclohexene, cyclohexene was dehydrogenated to 1,3- and 1,4-cyclohexadiene with evolution of hydrogen, no cyclohexane being observed in the reaction mixture. The subsequent experiments were carried out by using the cobalt complex as the metal complex.

Dehydrogenation of Cyclohexene Catalyzed by the Electroreduced Co(TPP) in a Variety of Solvents. The current efficiency for the formation of 1,3-cyclohexadiene(1,3-CHD) and 1,4-cyclohexadiene(1,4-CHD), benzene(Bz) was defined as follows:

$$\eta_{CHD} = (\text{Amount of CHD(mol)} \times 2/\text{Current passage(Faraday)}) \times 100$$

Table 2. Dehydrogenation of cyclohexene catalyzed by the electroreduced Co(TPP) in various solvents

Solvent	cC_6'/Co mole ratio	Yield (%) CHD[a]	Yield (%) Bz[b]	CHD/Co mole ratio	Bz/Co mole ratio	η_{CHD}[c] (%)	η_{Bz}[d] (%)	Dielectric constant
Dioxane	195	6.88	0	14.3	0	277	0	2.28
Pyridine	204	trace	trace	~0	~0	~0	~0	12.3
PhCN	212	trace	11.0	~0	23.3	~0	872	25.2
HMPT	204	2.02	0	4.11	0	180	0	30
DMF	202	4.73	0	9.52	0	160	0	36.7
DMSO	204	trace	3.23	~0	6.58	~0	274	49

Conditions: anode, Pt coil; cathode, Pt plate; reference electrode, Ag coil; supporting electrolyte, TBAP, 2.0×10^{-1} mol/*l*; concentration of Co(TPP), 1.0×10^{-2} mol/*l*; electrolysis at −2.0 V *vs.* Ag wire for 24 hr at room temperature (19—23°C).
a) total amount of 1,3- and 1,4-cyclohexadiene. b) benzene
d) current efficiency for formation of CHD. c) current efficiency for formation of Bz.

10) P. Rothermund and A. R. Menotti, *ibid.*, **70**, 1808 (1948).
11) D. W. Thomas and A. E. Martel, *ibid.*, **81**, 5111 (1959).
12) J. T. Horeczy, B. N. Hill, A. E. Walters, H. G. Shutze, and W. H. Bonner, *Anal. Chem.*, **27**, 1899 (1955).

$$\eta_{Bz} = (\text{Amount of Bz(mol)} \times 4/\text{Current passage(Faraday)}) \times 100$$

We see from Table 2 that 1,3-CHD and 1,4-CHD were formed when DMF, dioxane, and hexamethylphosphoric triamide(HMPT) were used as solvent. When dimethyl sulfoxide(DMSO) and benzonitrile (PhCN) were used as solvent, benzene and only a little cyclohexadienes were obtained. When pyridine was used as solvent, only a little of the dehydrogenated products were obtained. This may be ascribed to the strong coordination of pyridine to cobalt atom thus preventing the coordination of cyclohexene.

When DMF, dioxane, DMSO, HMPT, and PhCN were used as solvent, the current efficiency of the dehydrogenated products was much higher than 100%, indicating that the dehydrogenation reaction is catalytic.

No direct relation was found between the dielectric constants of the solvents and the current efficiency of the products.

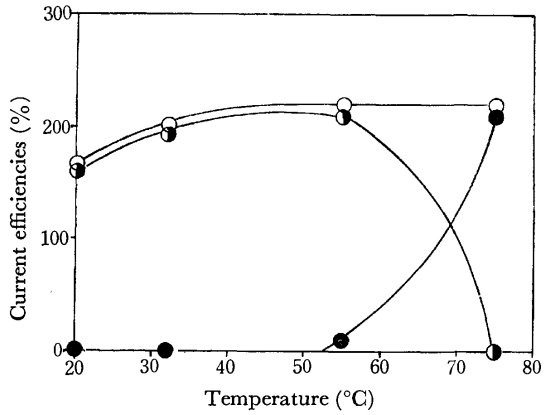

Fig. 1. Effects of the reaction temperature in DMF.
-○- $\eta_{Bz}+\eta_{CHD}$ -●- η_{Bz} -◑- η_{CHD}
η_{Bz}: current efficiency for the formation of benzene
η_{CHD}: current efficiency for the formation of cyclohexadienes

Effects of the Reaction Temperature. The current efficiency of CHD and Bz varied with the reaction temperature when DMF was used as solvent. The results are shown in Fig. 1. Only cyclohexadienes were obtained at 20 and 32°C, cyclohexadienes and benzene at 55°C and only benzene at 75°C. The maximum value of η_{CHD} was 220% at 50°C.

TABLE 3. EFFECTS OF ADDITION OF ETHANOL

Solvent	cC_6'/Co mole ratio	Yield (%) CHD[a]	Yield (%) Bz	η_{CHD}[b] (%)	η_{Bz}[c] (%)	η[d] (%)
PhCN	226	2.2	24.0	8.6	188	197
HMPT	199	trace	trace	~0	~0	~0

Conditions: concentration of Co (TPP), 1.0×10^{-2} mol/*l*; TBAP, 2.0×10^{-1} mol/*l*; EtOH, 1.0 m*l*; potential, −2.0 V *vs.* Ag wire; time, 24 hr; temp., room temp.; solvent, 10.0 m*l*.
a) total amount of 1,3- and 1,4-cyclohexadiene
b) current efficiency for formation of cyclohexadienes
c) current efficiency for formation of benzene
d) $\eta=\eta_{CHD}+\eta_{Bz}$

Effects of the Addition of Ethanol to the Reaction Solution. η_{CHD} and η_{Bz} varied with the addition of 1.0 m*l* of dry ethanol to the reaction solution of HMPT and PhCN. The results are given in Table 3.

When ethanol was added to the HMPT solution, η_{CHD} was about 0%, and by adding ethanol to the PhCN solution, η_{Bz} was much lower than that when ethanol was not added. Addition of ethanol thus prevented the formation of CHD in the case of HMPT solution, and that of benzene in the case of PhCN solution.

The ESR Spectra of the Reaction Solution. When the ESR spectra of the DMF solution of Co(TPP) were measured during electrolysis at the first wave potential, no signal was observed in any of the cases. However, at the second wave potential a signal (g= 2.003, peak-to-peak width 5.7 gauss, total width 12 gauss) was observed.

In general, the reduction steps of the metalloporphyrins(MP) are described as follows:

$$MP \xrightarrow{e^-} MP^- \xrightarrow{e^-} MP^{2-} \xrightarrow{e^-} MP^{3-} \xrightarrow{e^-} MP^{4-}$$

The paramagnetic species are the metalloporphyrin monoanion(MP^-) and trinegative ion(MP^{3-}).

Felton and Linschitz reported[13] that in the case of Co(TPP), one electron was transferred into the central metal atom to geve $[Co^I(TPP)]^-$ under electrolysis at the first wave potential, while in other metal complexes of TPP, the electron was transferred into the conjugated ring of TPP at the first wave potential, because there is a big difference between the first wave potential ($E_{1/2}$ (1)) and the second ($E_{1/2}$ (2)), *viz.*, Δ was 1.05 V as shown in Table 1, and the visible spectra of the Co(TPP) electroreduced at the first wave potential differed a great deal from the typical spectra of the monoanion of M(TPP), *viz.*, $M(TPP)^-$ (M=Zn, Cd, Mg, and H_2)[13] whose electrons were delocalized on the conjugated ring of TPP.

The signal observed when the Co(TPP) was electrolyzed at the second wave potential was similar to that of $M(TPP)^-$ as shown in Table 4. On the trinegative ion, Hush and Rowland reported[14] that the ESR spectra of the metal porphyrins such as zinc tetrabenzporphine, zinc etioporphyrin I reduced with sodium in tetrahydrofuran showed hyper fine structure,

TABLE 4. ESR SPECTRAL CHARACTERISTICS OF $M(TPP)^-$

Compound	g value	Peak-to-peak width(gauss)	Total width (gauss)
$Zn(TPP)^{-}$[a]	2.0000	20	100
$Cd(TPP)^{-}$[a]	2.0025	7	22
$Mg(TPP)^{-}$[a]	2.0024	4.7	15
$H_2(TPP)^{-}$[a]	2.0027	3.8	15
$[Co(TPP)^{2-}]^-$	2.003	5.7	12

Conditions: concentration of Co (TPP), 5.0×10^{-3} mol/*l*; supporting electrolyte, TBAP, 2.0×10^{-1} mol/*l*; solvent, DMF; cathode, Hg pool; anode, Pt wire; reference electrode, Ag wire; potential −2.0 V *vs.* Ag wire.
a) Ref. 9

13) R. H. Felton and H. Linschitz, *J. Amer. Chem. Soc.*, **88**, 1113 (1966).
14) N. S. Hush and J. R. Rowlands, *ibid.*, **89**, 2976 (1967).

and the paramagnetic species was considered to be either a trinegative ion of the porphyrin or a phlorin dianion in which hydrogen atom was attached to a methine carbon atom of the porphyrin skelton. (*cf.* Fig. 2)

The signal observed at the second wave potential was singlet and no hyper fine structure was observed. The ESR characteristics of the signal observed at the second wave potential indicates that electron is delocalized on the conjugated ring of porphyrin. Thus it is reasonable to conclude that the signal observed at the second wave potential is due to the anion radical of Co(I), *viz.*, $[Co^{I}(TPP)^{\cdot-}]^{-}$.

It is assumed that the reaction steps in the electroreduction of Co(TPP) dissolved in DMF are described as follows:

$$\text{1st step}\quad Co^{II}(TPP) \xrightarrow{e^-} [Co^{I}(TPP)]^{-} \quad E_{1/2} = -0.82\ \text{V}$$

$$\text{2nd step}\quad [Co^{I}(TPP)]^{-} \xrightarrow{e^-} [Co^{I}(TPP)^{\cdot-}]^{-} \quad E_{1/2} = -1.87\ \text{V}$$

The color of $[Co^{I}(TPP)]^{-}$ dissolved in tetrahydrofuran[15] and also that of $[Co^{I}(TPP)^{\cdot-}]^{-}$ is green.

The Intermediate for Dehydrogenation of Cyclohexene. The dehydrogenated products were not considered to be derived from the decomposition of the metal complex, since the molar ratio of the products to the metal complex was over 4. The products were obtained only when the reaction solution was electrolyzed at −2.0 V *vs.* Ag wire. No products were formed when the reaction solution was not electrolyzed and kept at room temperature under nitrogen or oxygen, or when the electrolysis was performed at −1.5 V *vs.* Ag wire (the first wave potetential) under nitrogen atmosphere. The results indicate that the dehydrogenation reaction was not catalyzed by $Co^{II}(TPP)$ or $[Co^{I}(TPP)]^{-}$.

When a cell with diaphragm (glass filter) was used and the electrolysis was carried out in DMF at −2.0 V *vs.* Ag wire, the dehydrogenated products were detected only in catholyte, and none in anolyte. On the other hand, when the electrolysis was carried out at −2.0 V *vs.* Ag wire under oxygen atmosphere, no products were obtained.

Thus the products were not formed by the electrooxidation of cyclohexene. It is reasonable to conclude that the species electroreduced at the second wave potential had catalytic activity for dehydrogenating cyclohexene to cyclohexadienes and benzene, $[Co^{I}(TPP)^{\cdot-}]^{-}$ being reaction intermediate.

Felton *et al.* reported that in the cases of metal complexes (M=Ni, Cu, Pb, Mg *etc.*) except for the cobalt complex, the difference between the first wave potential and the second, Δ was constant 0.44±0.04 V. Thus one electron was transferred to the ring of porphyrin rather than the central metal atom to give the monoanion of M(TPP) at the first wave potential and the dianion of M(TPP) at the second wave potential.

In the cases of Pd(TPP), Pt(TPP), FeCl(TPP), and MnCl(TPP), Δ was much lower than Δ in the case of Co(TPP) (1.05 V) as shown in Table 1. Thus it is considered that the dianion of these complexes was produced under electrolysis at the second wave potential.

It should be noted that the metal complexes except for the cobalt complex in which electrons were transferred to the conjugated ring of TPP under electrolysis had no activity for the dehydrogenation of cyclohexene.

The Active Sites of the Reaction Intermediate for the Dehydrogenation of Cyclohexene. No products were detected when the electrolysis was carried out in pyridine solution. This might be ascribed to the strong coordination of pyridine to the cobalt atom preventing the coordination of cyclohexene. One of the active sites is therefore considered to be the central metal atom.

No products were detected when the electrolysis of H_2TPP in HMPT solution was carried out at the first wave potential (−1.2 V *vs.* Ag wire). Thus the dehydrogenation reaction of cyclohexene was not catalyzed by H_2TPP^{-} which had only the conjugated ring of TPP.

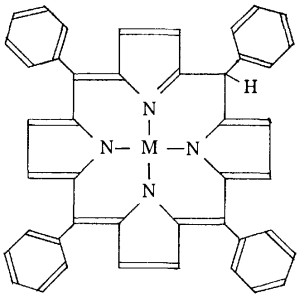

Fig. 2. The structure of tetraphenylphlorin.

Closs and Closs reported[16] that $[Zn(TPP)]^{2-}$ obtained by the reduction of Zn(TPP) with anthracene negative ion was reacted with equimolecular methanol to give the monoanion of zinc tetraphenylphlorin as shown in Fig. 2. When $[Zn(TPP)]^{2-}$ is reacted with excess methanol, the monoanion of zinc tetraphenylchlorin in which two hydrogen atoms are attached to a pyrrole fragment of porphyrin skeleton is produced.[16] Thus it may be reasonable to assume that added alcohol

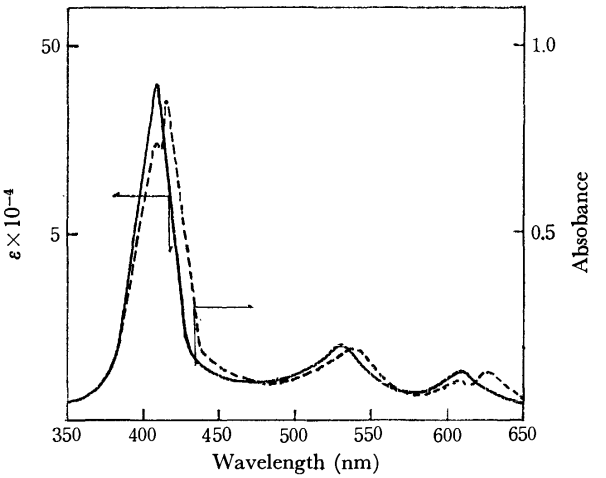

Fig. 3. The visible spectrum of the reaction solution after electrolysis.
solid line: Co(TPP) in dioxane solution
dashed line: the dioxane solution after electrolysis

15) H. W. Whitlock, Jr., and B. K. Bower, *Tetrahedron Lett.*, **52**, 4827 (1965).

16) G. L. Closs and L. E. Closs, *J. Amer. Chem. Soc.*, **85**, 818 (1963).

reacts with the conjugated ring of the porphyrin skeleton to cleave or weaken the conjugated ring, and the composition of the dehydrogenated products changes with the addition of ethanol.

On the other hand, Ichikawa *et al.* reported[17] that the active site for the exchanging reaction of H_2 and D_2 catalyzed by the Na-phthalocyanine electron donor-acceptor complexes may be the conjugated ring of the phthalocyanines[17]. Thus the active sites for the dehydrogenation of cyclohexene are considered to be both the central metal atom and the conjugated ring of $[Co^{I}(TPP)^{\cdot-}]^{-}$.

The visible spectrum of the reaction solution after electrolysis is shown in Fig. 3. The band at 620 nm assigned to that of the cobalt complex of tetraphenylchlorin,[18,19] and free hydrogen molecule was detected by gas chromatography. It might be considered that the hydrogen molecule extracted from cyclohexene hydrogenated the conjugated ring of porphyrin giving rise to the evolution of hydrogen molecule.

17) M. Ichikawa, M. Soma, T. Onishi, and K. Tamaru, *J. Amer. Chem. Soc.*, **91**, 1538 (1969).

18) G. D. Dorough and F. M. Huennekens, *ibid.*, **74**, 3974 (1952).

19) T. Araki, K. Yamamoto, and S. Sotomura, *Rikagaku Kenkyu-jo Hokoku*, **39**, 156 (1963).

BULLETIN OF THE CHEMICAL SOCIETY OF JAPAN, VOL. 45, 2902—2906 (1972)

Aroyl Arenesulfonyl Peroxides. VI. Benzoyloxylation and *p*-Toluenesulfonyloxylation of Aromatic Compounds with Benzoyl *p*-Toluenesulfonyl Peroxide[1]

Ryuki HISADA, Michio KOBAYASHI, and Hiroshi MINATO

Department of Chemistry, Faculty of Science, Tokyo Metropolitan University, Fukazawa, Setagaya, Tokyo

(Received March 18, 1972)

Benzoyl *p*-toluenesulfonyl peroxide (BTP) was decomposed in benzene, toluene, chlorobenzene, nitrobenzene, or anisole in a nitrogen or oxygen atmosphere. Yields of aryl benzoates and *p*-toluenesulfonates were always greater in an oxygen atmosphere than those in a nitrogen atmosphere, except those with nitrobenzene. The isomer distributions of these aryl benzoates and *p*-toluenesulfonates were determined. The rate of decomposition in anisole was considerably greater than those in other arenes. When BTP[carbonyl-^{18}O] was decomposed in anisole, the *o*- or *p*-anisyl benzoate formed was found to contain about equal amounts of oxygen-18 at both the carbonyl and phenoxy oxygens. On the basis of these findings the mechanisms of benzoyloxylation and *p*-toluenesulfonyloxylation were discussed.

A previous paper from our laboratories described that decomposition of benzoyl *p*-toluenesulfonyl peroxide (BTP) in benzene with suspended magnesium oxide under nitrogen yielded 44% diphenyl, 8% phenyl benzoate, and 1% phenyl *p*-toluenesulfonate.[2] It was proposed that under these conditions BTP decomposes homolytically, yielding phenyl radical and benzoyloxy radical, and *p*-toluenesulfonyloxy radical functions as an efficient hydrogen-abstractor.[3]

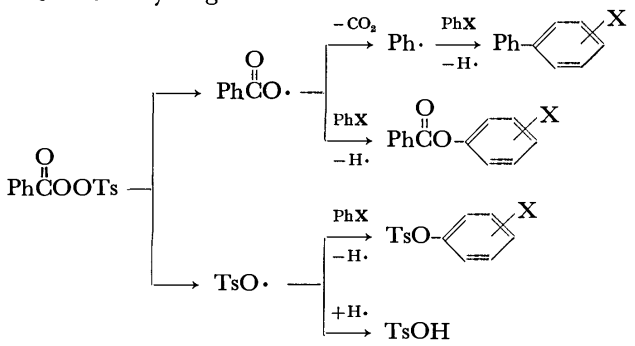

Benzoyloxylation of arenes with benzoyl peroxide (BPO) was studied by various groups.[4-7] Nakata, Tokumaru, and Simamura investigated the thermolysis and photolysis of BPO in arenes, and reported that the yields of aryl benzoates under oxygen are considerably greater than those under nitrogen.[4]

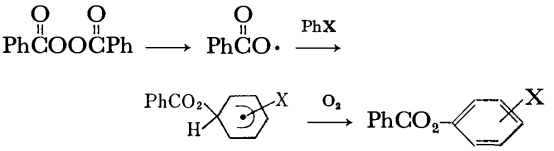

An investigation on the photolysis by use of BPO-[carbonyl-^{18}O] ascertained that this benzoyloxylation involves benzoyloxy free radical.[8]

BTP is a new reagent for benzoyloxylation, and a detailed investigation seems desirable. The decom-

1) Organic Sulfur Compounds. XXXIV.

2) R. Hisada, H. Minato, and M. Kobayashi, This Bulletin, **44**, 2541 (1971).

3) R. Hisada, N. Kamigata, H. Minato, and M. Kobayashi, *ibid.*, **44**, 3475 (1971).

4) T. Nakata, K. Tokumaru, and O. Simamura, *Tetrahedron Lett.*, **1967**, 3303.

5) P. Kovacic and his co-workers, *ibid.*, **1966**, 2689; *J. Org. Chem.*, **33**, 1950 (1968); *ibid.*, **35**, 2152 (1970).

6) S. Hashimoto, W. Koike, and M. Yamamoto, This Bulletin, **42**, 2733 (1969).

7) J. Bargon, *J. Amer. Chem. Soc.*, **93**, 4630 (1971).

8) M. Kobayashi, H. Minato, and Y. Ogi, This Bulletin, **42**, 2737 (1969).

Table 1. Yields and isomer distributions of the products of phenylation, benzoyloxylation, and *p*-toluenesulfonyloxylation of PhX with BTP under nitrogen or oxygen[a)]

X	N_2 or O_2	PhC_6H_4–X				$PhCO_2C_6H_4$–X				$TsOC_6H_4$–X			
		Yield (mol %)	Isomer distribution (%) *o*-	*m*-	*p*-	Yield (mol %)	Isomer distribution (%) *o*-	*m*-	*p*-	Yield (mol %)	Isomer distribution (%) *o*-	*m*-	*p*-
OMe[b)]	N_2	4.2	Not detnd.			50.8	48	<1	52	1.3	36	<1	64
	O_2	4.2	Not detnd.			63.1	40	<1	60	2.4	37	<1	63
Me[c)]	N_2	24.1	52	18	30	3.1	Not detnd.			3.5	53	21	26
	O_2	0.3	Not detnd.			34.5	55	32	13	5.3	54	18	28
H[c)]	N_2	45.6				7.6				1.3			
	O_2	1.4				33.7				3.5			
Cl[c)]	N_2	63.0	65	20	15	1.6	Not detnd.			0.9	12	32	56
	O_2	6.2	64	21	15	8.9	16	43	41	2.4	13	23	64
NO_2[c)]	N_2	15.2	80	4	16	0				0			
	O_2	18.5	79	5	16	0				0			

a) These are the average values of two experiments. Errors in the isomer distributions are ±2%.
b) 25°C, 10 hr. c) 45°C, 15 hr.

position of BTP and BTP[carbonyl-^{18}O] in arenes with suspended magnesium oxide in oxygen atmosphere has been investigated under various conditions, and the results will be described in this paper.

Results and Discussion

In an oxygen atmosphere, BTP was decomposed in benzene, toluene, chlorobenzene, or nitrobenzene with suspended magnesium oxide for 15 hr at 45°C. Since BTP decomposes very rapidly in anisole, a dichloromethane solution of BTP was stirred into anisole containing suspended magnesium oxide under oxygen. Yields and isomer distributions of the products are shown in Table 1.

The yields of the products are much affected by the kinds of the atmosphere with the exceptions of the decompositions in nitrobenzene and anisole. Under nitrogen, the yields of phenylated products are greater than those of benzoyloxylated products, whereas under oxygen the yields of benzoyloxylated products are greater than those of phenylated products. Since the isomer distributions of aryl benzoates are similar in both atmospheres, the mechanism must be the same. The yields of aryl benzoates decrease in the order of anisole, toluene, benzene, chlorobenzene, and nitrobenzene, and the yield in nitrobenzene is zero. These results are in agreement with those of Nakata *et al.*[4)] The increases in the yields of the esters are more extensive in toluene, benzene, and chlorobenzene than those in anisole.

In nitrobenzene, BTP gave no nitrophenyl benzoate, and phenyl *p*-toluenesulfonyl carbonate was formed in 52—60% yield. This suggests that the main reaction in nitrobenzene is the carboxy-inversion even though magnesium oxide was suspended in the medium. A previous paper described that, when magnesium oxide was absent, the main reaction of BTP in benzene was the carboxy inversion.[2)] It is reasonable that the ionic carboxy inversion process takes place more easily in polar solvents such as nitrobenzene. Even when BTP undergoes homolysis to some extent, both radicals produced ($PhCO_2\cdot$ and $TsO\cdot$) are strongly electrophilic and not likely to attack the electron-deficient nitrobenzene.

It is possible that aryl benzoates are produced by the attack of benzoyloxy cation. However, this possibility is rejected by the findings that 1) much substituted diphenyls are produced, 2) in nitrobenzene the main products are *ortho* and *para* nitrodiphenyls which must be formed by the attack of phenyl free radical, not by phenyl cation, and 3) the yields of aryl benzoates are much greater under oxygen because of abstraction of hydrogen from the substituted cyclohexadienyl radicals by oxygen.

Except nitrobenzene, all the arenes are *p*-toluenesulfonyloxylated although the yields are not so great. The yields under oxygen are greater than those under nitrogen (1.5—2.7 times), but the mechanism must be similar since the isomer distributions do not differ.

Dannley and his co-workers reported that the reactions between *m*-nitrobenzenesulfonyl peroxide and arenes are ionic, and electrophilic attack of the peroxidic oxygen on arenes results in the formation of aryl *m*-nitrobenzenesulfonates.[9,10)] In the reactions of BTP with toluene and chlorobenzene, considerable amounts of *meta* substituted products were found. It is concluded that these aryl *p*-toluenesulfonates arise, not from electrophilic attack of the *p*-toluenesulfonyloxy oxygen, but from attack of *p*-toluenesulfonyloxy radical, on the basis of the findings that 1) free radical phenylation and benzoyloxylation take place simultaneously, 2) yields of aryl benzoates and *p*-toluenesulfonates are greater under oxygen, and 3) considerable *meta*-substitution takes place with toluene and chlorobenzene. The decomposition of BTP in arenes is the first example which clearly indicates the attack of a sulfonyloxy radical on an aromatic ring.

The mechanism of the substitutions of an arene is expressed as follows.

9) R. L. Dannley and G. E. Corbett, *J. Org. Chem.*, **31**, 153 (1966).
10) R. L. Dannley, J. E. Gagen, and O. J. Stewart, *ibid.*, **35**, 3076 (1970).

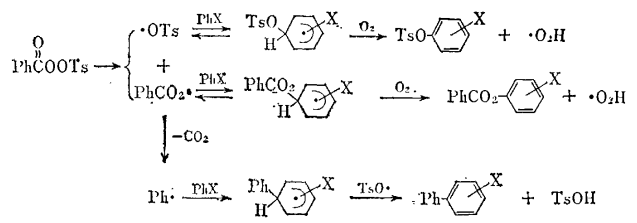

Additions of *p*-toluenesulfonyloxy and benzoyloxy radicals on an arene are reversible. When abstraction of a hydrogen atom from the cyclohexadienyl radicals is slow (under nitrogen), *p*-toluenesulfonyloxy and benzoyloxy radicals are reformed; the latter further decomposes to carbon dioxide and phenyl radical.

The decomposition of BTP in anisole is quite different from the decompositions in other solvents; 1) the rate of decomposition was much faster, 2) even under nitrogen the yields of benzoates were very large (that is, very little decarboxylation of benzoyloxy radical occurs) and the yields under oxygen are only slightly greater, and 3) no carboxy inversion product (phenyl *p*-toluenesulfonyl carbonate, PTC) was found. Therefore, attack of free benzoyloxy radical on anisole does not appear to be the reaction which is taking place in an anisole solution of BTP.

It is conceivable that the electron-rich anisole nucleus attacks the electron-deficient O–O bond of BTP, and thus the rate is faster and the yields of benzoates are greater. In order to check this possibility, BTP-[carbonyl-^{18}O] was synthesized and decomposed in anisole in the presence and absence of suspended magnesium oxide. Even in the absence of magnesium oxide, anisyl benzoates were formed in 40 mol% yield ($o:m:p$ =41:<1: 59%) and PTC was formed only in 10 mol% yield. The compounds I—VII shown in the following scheme were converted to carbon dioxide,[11] which was then analyzed by use of a mass spectrometer. The results are shown in Table 2.

It is clear that within experimental error the carbonyl

Table 2. ^{18}O Analyses in the benzoyloxylation of anisole with BTP [carbonyl-^{18}O] in the presence and absence of magnesium oxide[a]

Compound	Excess atom %		
	Found (with MgO)	Found (without MgO)	Calcd[b]
BzNHPh (I)	1.20	1.20	(1.20)
BzOOTs (II)	0.23	0.24	0.24
BzN_2H_3 (III)	1.00	1.00	1.20
$BzOC_6H_4OMe$-*o* (IV)	0.42	0.41	0.40
$BzOC_6H_4OMe$-*p* (V)	0.39	0.37	0.40
BzN_2H_3 (VI)	0.53	0.61	0.60
BzN_2H_3 (VII)	0.51	0.71	0.60

a) Experimental error in two measurements with the same sample was ±0.02 excess atom %.
b) Calculated on the assumption that the carbonyl oxygen is completely equilibrated with the ester oxygen.

11) D. Rittenberg and L. Ponticorvo, *Int. J. Appl. Radiat. Isotopes*, **1**, 208 (1956).

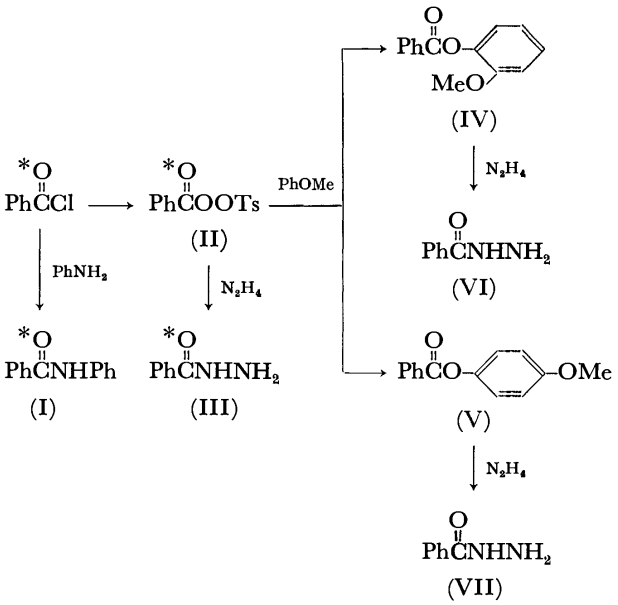

oxygen of BTP is completely equilibrated between the carbonyl and phenoxy oxygens in anisyl benzoates (IV) and (V). These results are similar to those of the photochemical benzoyloxylation of benzene with BPO[8] and $CuCl_2$-catalyzed benzoyloxylation of *p*-xylene with BPO.[12] The results of the ^{18}O study reject the possibility of the electrophilic (S_N2 type) attack of the benzoyloxy oxygen on anisole.

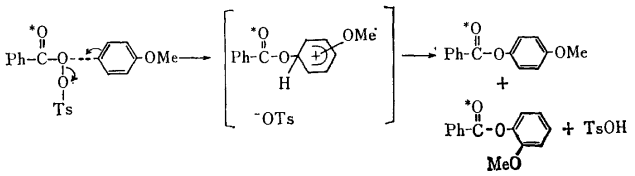

Since the rate of decomposition of BTP in anisole is much greater than those in other solvents, some sort of interaction between BTP and anisole must exist. On the basis of all the results obtained so far, the following scheme seems to represent what is taking place in an anisole solution of BTP.

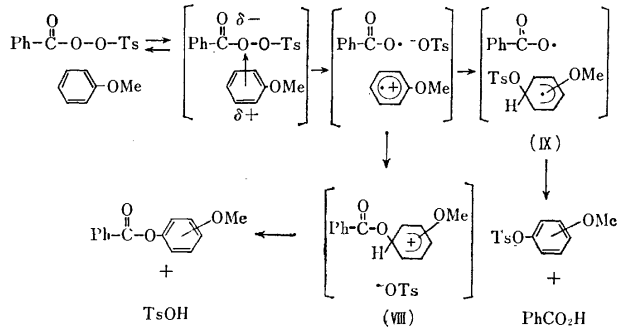

A charge-transfer complex is formed by donation of π-electrons of anisole to the antibonding orbital of the O–O bond of BTP, and the O–O bond scission is much accelerated by this electron donation. A related example is the enhancement of the homolysis rates of

12) C. G. Reid and P. Kovacic, *J. Org. Chem.*, **34**, 3308 (1969).

ortho substituted perbenzoates.[13]

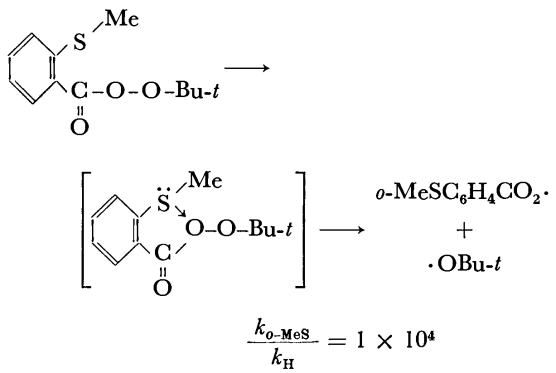

$$\frac{k_{o\text{-MeS}}}{k_H} = 1 \times 10^4$$

The C. T. complex formed from BTP and anisole dissociates to give a trio of benzoyloxy radical, *p*-toluenesulfonate anion and anisole radical cation in cage. A one-electron transfer reaction of this kind is observed in the reaction of BPO with dimethylaniline.[14] Two processes are possible from the trio of benzoyloxy radical, *p*-toluenesulfonate anion and anisole radical cation; benzoyloxy radical and anisole radical cation may combine to form a benzenium ion (VIII), or *p*-toluenesulfonate anion and anisole radical cation may combine to form a cyclohexadienyl radical (IX).

When BTP was photolyzed in benzene under oxygen or nitrogen with a high pressure mercury lamp at 9°C for 5 hr, the results were similar to those shown in Table 1; under oxygen the yield of diphenyl is lower and the yields of phenyl benzoate and *p*-toluenesulfonate are greater. The results of the photolyses also support the hypothesis that benzoyloxylation and *p*-toluenesulfonyloxylation of arenes proceed by the free radical mechanism.

Experimental

Materials. Benzene and substituted benzenes were purified by the procedures described previously.[15] BTP and BTP[carbonyl-^{18}O] were prepared by the method described in the previous papers.[2,16]

Decomposition of BTP in Benzene, Toluene, Chlorobenzene, or Nitrobenzene with Suspended Magnesium Oxide under Nitrogen or Oxygen. A solution of BTP (4 mmol) in benzene, toluene, chlorobenzene, or nitrobenzene (50 m*l*) with suspended magnesium oxide (40 mmol) was stirred with a mechanical stirrer for 15 hr at 45°C. Throughout the reaction nitrogen or oxygen was bubbled in the reaction mixture. After the completion of the decomposition the internal standard samples for gas chromatographic analyses of the products were added to the mixture. After the magnesium oxide was filtered off, the filtrate was washed successively with a sodium hydrogen carbonate solution and water, and dried over anhydrous magnesium sulfate. It was concentrated under reduced pressure, and subjected to gas chromatographic analyses.

Decomposition of BTP in Anisole with Suspended Magnesium Oxide under Nitrogen or Oxygen. Nitrogen (or oxygen) was bubbled through a solution of BTP (4 mmol) in dichloromethane (10 m*l*) for 15 min. Nitrogen (or oxygen) was also bubbled through anisole (50 m*l*) with suspended magnesium oxide (40 mmol). Then, the BTP solution was added drop by drop with stirring into the anisole, and the mixture was stirred for 10 hr at 25°C with bubbling of nitrogen (or oxygen). The work-up procedure was the same as described above.

Gas Chromatography. The amounts of substituted diphenyls, aryl benzoates, and aryl *p*-toluenesulfonates produced were determined by a Hitachi Gas Chromatograph K-53, on the basis of the comparison with authentic samples. The columns and the internal standard samples used are described in Table 3.

Table 3. Conditions used for gas chromatographic analyses

Products (*o*, *m*, and *p* isomers)	Internal standards	Column[a]	Column length (m)	Temp (°C)
Ph_2	$(PhCH_2)_2$	(A)	1	190
$PhCO_2Ph$; TsOPh	*p*-$ClC_6H_4CO_2Ph$	(A)	1	210
PhC_6H_4OMe; $PhCO_2C_6H_4OMe$	*m*-$NO_2C_6H_4Ph$	(A)	3	210
$TsOC_6H_4OMe$	*p*-$MeOC_6H_4O_2CPh$	(B)	2	220
$PhC_6H_4CH_3$; $PhCO_2C_6H_4CH_3$	*β*-MeO-Naphthalene $PhCO_2Ph$	(A)	3	190
$TsOC_6H_4CH_3$	*p*-$ClC_6H_4O_2CPh$	(B)	2	220
PhC_6H_4Cl	$(PhCH_2)_2$	(A)	5	190
$PhCO_2C_6H_4Cl$	*m*-$CH_3C_6H_4O_2CPh$	(A)	2	230
		(B)	5	225
$TsOC_6H_4Cl$	*p*-$MeOC_6H_4OTs$	(A)	2	230
		(B)	3	235
$PhC_6H_4NO_2$	$(PhCH_2)_2$	(A)	2	190
$PhCO_2C_6H_4NO_2$	*m*-$MeOC_6H_4OTs$	(C)	3	200
$TsOC_6H_4NO_2$	*m*-$MeOC_6H_4OTs$	(C)	3	220

a) Column: (A), 10% Apiezon L on Chromosorb W. (B), 10% Silicone DC 550 on Chromosorb W. (C), 10% Silicone SE 30 on Chromosorb W.

13) W. G. Bentrude and J. C. Martin, *J. Amer. Chem. Soc.*, **84**, 1561 (1962).

14) C. Walling, "Free Radicals in Solution," John Wiley & Sons, Inc., New York, N. Y. (1957), pp. 590—595, and the references cited therein.

15) M. Kobayashi, H. Minato, E. Yamada, and N. Kobori, This Bulletin, **43**, 215 (1970).

16) R. Hisada, H. Minato, and M. Kobayashi, *ibid.*, **45**, 2814 (1972).

Decomposition of BTP[carbonyl-^{18}O] in Anisole in the Presence or Absence of Suspended Magnesium Oxide under Nitrogen. A solution of BTP[carbonyl-^{18}O] (12 mmol) in anisole (150 m*l*) was decomposed in the presence or absence of magnesium oxide (120 mmol), and the reaction mixture was washed successively with a sodium hydrogen carbonate solution and water, and dried over anhydrous magnesium sulfate. After the anisole was evaporated under reduced pressure, the residue was chromatographed on silica gel (Wako Gel Q 22). Phenyl *p*-toluenesulfonyl carbonate (in the absence of magnesium oxide), *o*- and *p*-anisyl benzoates and *o*- and *p*-anisyl *p*-toluenesulfonates were isolated, and identified by comparison of their infrared spectra with those of authentic samples. *o*-Anisyl and *p*-anisyl benzoates were recrystallized three times from *n*-hexane; mp 57—58°C (lit,[17] 58—59°C) and mp 86—87°C (lit,[18] 87.5—88.5°C), respectively.

Reaction of o-*Anisyl or* p-*Anisyl Benzoate with Anhydrous Hydrazine.* A mixture of *o*- or *p*-anisyl benzoate (*ca.* 300 mg) and anhydrous hydrazine (300 mg) in benzene (10 m*l*) was refluxed for 3 hr. After the benzene and unchanged hydrazine were evaporated under reduced pressure, the benzhydrazide produced were recrystallized three times from ether; mp 111—112°C (from *o*-anisyl benzoate) and mp 112°C (from *p*-anisyl benzoate) (lit,[19] 112.5°C).

17) G. Cilento, *J. Org. Chem.*, **24**, 413 (1959).
18) G. Cilento, *J. Amer. Chem. Soc.*, **75**, 3748 (1953).
19) R. Stolle, *J. Prakt. Chem.*, **69**, 145 (1904).

BULLETIN OF THE CHEMICAL SOCIETY OF JAPAN, VOL. 45, 2906—2909 (1972)

Photolyses of Diaryl α-Disulfones[1)]

Michio KOBAYASHI, Koji TANAKA, and Hiroshi MINATO

Department of Chemistry, Faculty of Science, Tokyo Metropolitan University, Setagaya-ku, Tokyo

(Received April 15, 1972)

Di-*p*-tolyl disulfone and diphenyl disulfone were decomposed in various arenes by irradiation of UV light. The products found were arenesulfonic acids, arenesulfonic anhydrides, thiolsulfonates, diaryl sulfones, biaryls, and sulfur dioxide. All the findings indicate that photolyses of α-disulfones yield a pair of arenesulfonyl radicals.

In comparison with the thiyl radicals, the sulfonyl radicals have been investigated to a much lesser extent. Some of the methods described in the literature for generation of sulfonyl radicals are thermolyses[2)] and photolyses[3)] of azosulfones, oxidation of sulfinic acids in water,[4)] and thermolyses and photolyses of arenesulfonyl iodides.[5)] It was reported that no substitution occurs from the reaction of arenes with the sulfonyl radicals formed by addition of phenyl radical to sulfur dioxide,[6)] photolyses of diaryl sulfones,[7)] or oxidation of *N,N'*-diarenesulfonylhydrazines.[8)] Kice and Favstritsky studied the thermolysis of di-*p*-tolyl disulfone in bromobenzene, and the formation of phenyl *p*-tolyl sulfone was ascribed to the attack of *p*-toluenesulfonyl radical to bromobenzene.[9)]

In an attempt to understand the chemistry of arenesulfonyl radicals, di-*p*-tolyl disulfone (I) and diphenyl disulfone (II) have been photolyzed in various arenes, and the products formed have been investigated. The results will be described in this paper.

Results and Discussion

Diaryl α-disulfones are very stable at room temperature, but were found to decompose fairly rapidly upon irradiation of UV light. After 30 min of irradiation, a thin layer chromatographic analysis showed the presence of diaryls, and more than 50% of disulfones were found to decompose in 2—3 hr.

Diaryl α-disulfones have an absorption maximum near 250 nm, which matches with the wavelength of the light at 253.7 nm from a mercury lamp. The recently reported value[10)] for S-S bond length (2.193 Å) in diphenyl disulfone is 0.16 Å longer than the average bond length of the ordinary disulfides. The elongation of the bond length means the weakning of the S-S bond in α-disulfones, which may explain the easy splitting of these compounds by photolyses.

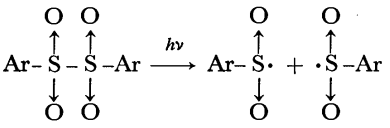

The results of the photolyses of di-*p*-tolyl disulfone (I) and diphenyl disulfone (II) in aromatic solvents are shown in Table 1 and 2. It should be noted that

1) Organic Sulfur Compounds. XXXVI.

2) C. G. Overberger and A. J. Rosenthal, *J. Amer. Chem. Soc.*, **82**, 117 (1960); M. Kobayashi, H. Minato, M. Kojima, and N. Kamigata, This Bulletin, **44**, 2501 (1971).

3) M. Kobayashi, S. Fujii, and H. Minato, *ibid.*, **45**, 2039 (1972).

4) J. McMillan and W. A. Waters, *J. Chem. Soc., B*, **1966**, 422.

5) C. M. M. da Silva Correa and W. A. Waters, *J. Chem. Soc., C*, **1968**, 1872.

6) J. M. Squire and W. A. Waters, *J. Chem. Soc.*, **1962**, 2068; C. M. M. da Silva Correa, A. S. Lindsay, and W. A. Waters, *J. Chem. Soc., C*, **1968**, 1874.

7) N. Kharasch and A. I. A. Khodair, *Chem. Commun.*, **1967**, 98.

8) Y. Kohara, M. Kobayashi, and H. Minato, This Bulletin, **43**, 2933 (1970).

9) J. L. Kice and N. A. Favstritsky, *J. Org. Chem.*, **35**, 116 (1970).

10) C. Th. Kiers and A. Vos, *Rec. Trav. Chim. Pays-Bas*, **91**, 126 (1972).

TABLE 1. PRODUCTS OF PHOTOLYSIS OF DI-*p*-TOLUENESULFONYL (I) IN BENZENE[a]

(I) (mmol)	Time irradiated hr	Extent of reaction[b] %	Products (mol/100 mol disulfone photolyzed)						
			$C_7H_7SO_3H$	$C_7H_7SO_2$-SC_7H_7	C_7H_7Ph	$C_7H_7\overset{\overset{O}{\uparrow}}{\underset{\underset{O}{\downarrow}}{S}}Ph$	$(C_7H_7)_2SO_2$	$(C_7H_7\overset{\overset{O}{\uparrow}}{\underset{\underset{O}{\downarrow}}{S}})_2O$	$(C_7H_7S)_2$
4.06	7	84.9	113	14.2	15.1	d	d	3.3[c]	4.1
4.26	8	85.7	91.2	9.0	13.4	0.5	0.5	11.1	3.3

a) Irradiated in 500 m*l* of benzene with a high pressure mercury lamp.
b) On the basis of the unchanged disulfone.
c) The amount of the anhydride which was not hydrolyzed upon treatment with water.
d) Not determined.

TABLE 2. PRODUCTS OF PHOTOLYSIS OF $(PhSO_2)_2$ (II) IN TOLUENE

(II) (mmol)	PhMe (m*l*)	Time irradiated hr	Products (mol/100 mol disulfone used[a])							
			$PhSO_3H$	$PhSO_2SPh$	PhC_7H_7	$PhSO_2C_7H_7$	$PhSO_2$-CH_2Ph	Ph_2SO_2	$(PhS)_2$	$(PhCH_2)_2$
10.74	500	7	75.3	9.7	2.5	0.6	1.7	0.7	1.0	3.0
10.66	500	14	83.8	15.1	2.9	0.7	1.8	0.8	b)	3.0
4.05	300	7	94.9	b)	12.4	1.2	4.4	1.2	b)	3.0

a) Extent of photolysis was estimated to be 70—80%, but exact determination was not possible. Yields are based on the amount of disulfone initially added.
b) Not determined.

the yields of sulfones are very small. Addition of arenesulfonyl radicals to benzene is considered as a reversible step and hydrogen abstraction from an arenesulfonylcyclohexadienyl radical must be a very slow step in comparison with the dissociation of the cyclohexadienyl radicals.

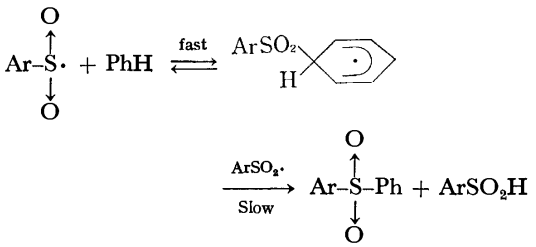

Formation of methylbiphenyls shows that the following desulfonylation takes place to some extent. This reaction is known to be a reversible process.[11]

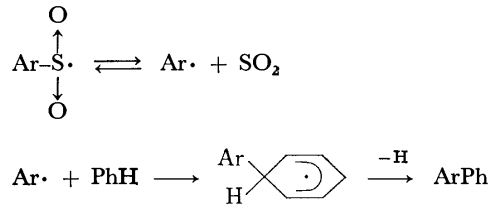

Bond dissociation energy $D(C\text{–}SO_2\cdot)$ of the related methanesulfonyl radical is estimated to be 23 kcal/mol.[12] This rather high value suggests that the cleavage of sulfur dioxide from the sulfonyl radical must be much slower than that of carbon dioxide from the corresponding aroyl radicals. In order to ascertain that arenesulfonyl radicals lose sulfur dioxide under these conditions, a benzene solution of (I) was degassed and irradiated in a quartz tube. Sulfur dioxide was found as a product; yield, 0.26 mol per mol of (I). Other products found were *p*-toluenesulfonic acid (86 mol%), *p*-tolyl *p'*-toluenethiolsulfonate (50 mol%), and *p*-methylbiphenyl (10 mol%).

Di-*p*-tolyl sulfone among the decomposition products of (I) in benzene is probably the product of combination of radicals in cage.

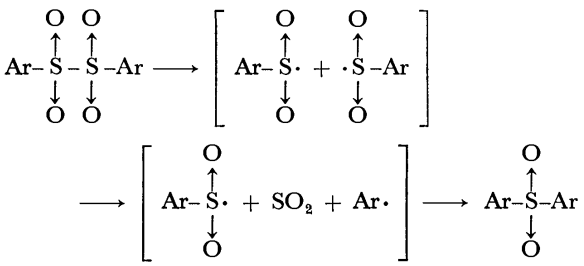

Di-*p*-tolyl disulfide is the product of dimerization of ArS· radical, which is probably formed by photolysis of thiolsulfonates.

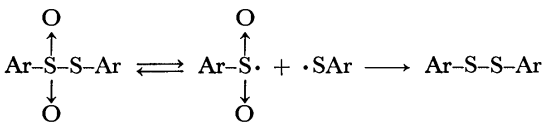

Formation of *p*-toluenesulfonic anhydride and *p*-tolyl *p*-toluenethiolsulfonate can be explained as the result of disproportionation of sulfonyl radicals as suggested by da Silva Correa and Waters.[5]

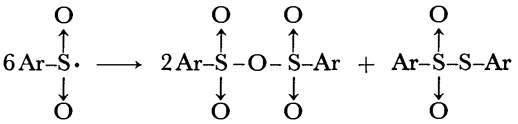

The above equation is the summary of the following

11) H. Goldwhite, M. S. Gibson, and C. Harris, *Tetrahedron*, **20**, 1613 (1964).
12) W. K. Busfield, K. J. Ivin, H. Mackle, and P. A. G. O'Hare, *Trans. Faraday Soc.*, **57**, 1064 (1961); A. Good and J. C. J. Thynne, *ibid.*, **63**, 2708 (1967).

multi-step reactions.

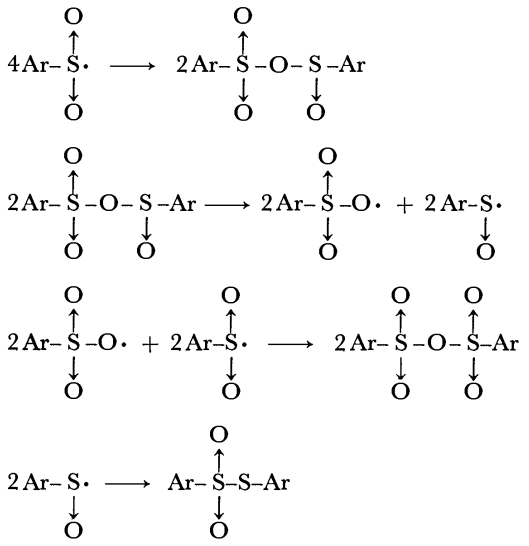

The results shown in Table 2 are generally in agreement with those in Table 1 except the formation of benzyl phenyl sulfone and bibenzyl, which can be explained as the products of combination of two radicals.

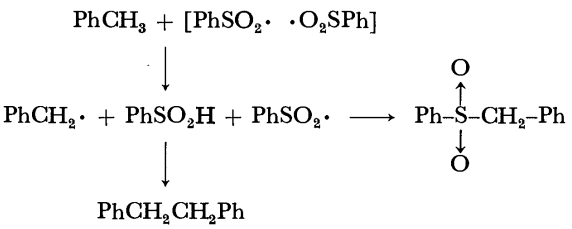

The higher yields of these products than those of phenyl *p*-tolyl sulfones suggest that abstraction of a benzyl hydrogen from toluene is faster than substitution on the aromatic ring.

Although it has been reported that substitution of arenes with arenesulfonyl radicals does not occur,[6,7] formation of phenyl *p*-tolyl sulfone in this investigation clearly shows that an arenesulfonyl radical reacts with an arene ring to some extent. In order to study the aromatic substitution with benzenesulfonyl radical in detail, the isomer distribution of aryl phenyl sulfones were determined in toluene, anisole, and chlorobenzene. The results of benzenesulfonylation and phenylation are summarized in Table 3.

Table 3. Isomer distribution of substituted biphenyls and phenyl aryl sulfones produced from photolysis of diphenyl disulfone (II) in arenes

Arene	Isomer distributions %					
	PhC_6H_4X			$PhSO_2C_6H_4X$		
	o-	*m*-	*p*-	*o*-	*m*-	*p*-
PhMe	32.7	40.0	27.3	31.6	35.8	32.6
PhOMe	46.6	19.9	33.5			
PhCl	33.4	35.1	31.5			

The isomer distributions of substituted biphenyls in Table 3 are different from what is expected for phenylation with phenyl cation,[13,14] and are similar to those observed for phenylation with phenyl radical produced from thermolyses of benzoyl peroxide or *N*-nitrosoacetanilide. However, the amounts of *ortho*-substituted products are much less than those usually observed for phenylation with the phenyl radical produced by thermolyses. It is possible that the behavior of thermally produced phenyl radicals and that of photolytically produced phenyl radicals are somewhat different due to the difference of the extent of the solvation. The isomer distributions of substituted biphenyls in Table 3 are in agreement with those reported for phenylation with the phenyl radical produced from the photolysis of diphenyl sulfone (Me; *o*-, 30.4, *m*-, 43.5, *p*-, 26.1; MeO; *o*-, 32.3, *m*-, 13.5, *p*-, 55.2; Cl; *o*-, 41.8, *m*-, 28.6, *p*-, 29.6),[15] and those with the phenyl radical produced from the photolysis of phenylazo *p*-tolyl sulfone.[3]

In the photolysis of diphenyl disulfone in chlorobenzene, 176 mol chlorobiphenyls and 15.2 mol biphenyl were formed from 100 mol disulfone. These results show that chlorobenzene itself was photolyzed under these conditions.

When diphenyl disulfone was irradiated in nitrobenzene with a low pressure mercury lamp for 22 hr, almost no reaction took place. It appears that nitrobenzene absorbs light but does not transfer the energy to the disulfone.

In order to estimate the electrophilicity of sulfonyl radicals, di-*p*-tolyl disulfone was photolyzed in anisole, and the amounts of isomeric anisyl phenyl sulfones were determined. From 6.5 mmol of the disulfone, 0.031 mmol of the *p*-anisyl sulfone and 0.180 mmol of the *o*- and *m*-anisyl sulfones were formed (separation of the *o*- and *m*-isomers was not possible). Therefore, the isomer distribution is *o*+*m*, 85.3% and *p*-, 14.7%.

The isomer distribution of substituted diphenyl sulfones shown in Table 3 indicate that this benzenesulfonylation involves not benzenesulfonyl cation, but benzenesulfonyl radical. Electrophilic arenesulfonylation of arenes is known as a highly selective reaction. Cationic *p*-toluenesulfonylation of toluene gave the *o*- and *p*-(main product) sulfones exclusively, and no *m*-substituted product was found.[16]

The result of the present investigation clearly shows the occurrence of free radical arenesulfonylation of aromatic rings, whereas it was stated in the literature[6,7] that the sulfonyl radical generated in an aromatic solvent is not reactive enough to give a sulfone. This contradiction can be ascribed to the difference of the hydrogen abstracting agent from the sulfonylcyclohexadienyl radical. In the photolyses of the sulfonyl iodide, the hydrogen must be abstracted by iodine

13) M. Kobayashi, H. Minato, E. Yamada, and N. Kobori, This Bulletin, **43**, 215 (1970).
14) M. Kobayashi, H. Minato, and N. Kobori, *ibid.*, **43**, 219 (1970).
15) T. Nakabayashi, Y. Nagata, and J. Tsurugi, III Abstracts of 23th Annual Meeting of the Chemical Society of Japan, p. 1270.
16) M. Kobayashi, H. Minato, and Y. Kohara, This Bulletin, **43**, 234 (1970); Y. Kohara, M. Kobayashi, and H. Minato, *ibid.*, **43**, 520 (1970).

atoms which have very low reactivity for this role. In the thermolyses or photolyses of azosulfones, the sulfonyl radicals mainly act as the hydrogen abstractor from the arylcyclohexadienyls formed by the attack of aryl radicals on arene. In the photolyses of diaryl disulfones, sulfonyl radicals abstract hydrogen atom from the sulfonylcyclohexadienyl radicals produced by the attack of sulfonyl radicals on arene, and therefore, considerable amounts of diaryl sulfones are isolated.

Experimental

Materials. Benzene, toluene, anisole, and chlorobenzene were purified according to the methods described in the literature.[17] Di-*p*-tolyl disulfone was prepared by $KMnO_4$-oxidation of *p*-toluenesulfinic acid in acetic acid;[18] yield, 28%; recrystallized from acetone, and then three times from benzene; mp (decomp.) 217—219°C (lit, 211°C,[18] 218—220°C,[19] 220°C[20]). Diphenyl disulfone (II) was synthesized by $KMnO_4$-oxidation of benzenesulfinic acid in acetic acid; yield, 22%; recrystallized from acetone and then twice from benzene; mp 190—192°C (lit, 193—194°C,[18] 193°C[20]).

Photolysis of I in Benzene under Nitrogen. A benzene solution (500 m*l*) of (I) (3—5 mmol) was stirred and irradiated with a 100 W high pressure mercury lamp at 16—22°C under nitrogen. Then the reaction mixture was washed with water, and the amount of *p*-toluenesulfonic acid in the aqueous layer was determined by converting it into *S*-benzylisothiuronium *p*-toluenesulfonate. The organic layer was dried over anhydrous magnesium sulfate, concentrated under reduced pressure, and the residue was separated to its components by column chromatography (Florisil, 100—200 mesh). *p*-Methylbiphenyl (eluted with hexane), di-*p*-tolyl disulfide (hexane–benzene) and *p*-tolyl *p'*-toluenethiolsulfonate (benzene) were identified by comparison with authentic samples. Compounds containing a sulfone group (eluted with diethyl ether) were identified by use of an Ohkura Gas Chromatograph 1100 on an SE-30 column. The amount of *p*-toluenesulfonic anhydride was determined by converting it to *N*-phenyl-*p*-toluenesulfonamide and anilinium *p*-toluenesulfonate by the reaction with aniline.

Photolysis of I in Degassed Benzene. A benzene solution (60 m*l*) of (I) (0.32 mmol) in a quartz vessel was degassed by the freeze-thaw technique, and then irradiated with a 1 kW high pressure mercury lamp for 2 hr at 16—17°C. Then, the mixture was distilled at room temperature in high vacuum. Sulfur dioxide contained in the distillate was extracted with a 5% sodium hydroxide solution, and its amount was determined by iodometry. From the higher boiling fraction the unchanged (I) was filtered off, and then the rest was separated by column chromatography.

Photolysis of II in Toluene under Nitrogen. The photolysis was carried out according to the procedure described for (I). Diphenyl disulfide (eluted with hexane–benzene), phenyl benzenethiolsulfonate (benzene), diphenyl sulfone (benzene), and benzyl phenyl sulfone (benzene) were identified by comparison with authentic samples. A mixture of phenyl *o*-, *m*-, *p*-tolyl sulfones and a mixture of *o*-, *m*-, *p*-methylbiphenyls and bibenzyl (eluted with hexane) were analyzed by use of a Hitachi Gas Chromatograph K53.

Photolysis of II in Anisole under Nitrogen. An anisole solution of (II) (4.05 mmol) was stirred and irradiated with a 6 W low pressure mercury lamp under nitrogen at 16—19°C for 21.5 hr. The reaction mixture was analyzed in a manner similar to that described above.

17) A. Weissberger, "Organic Solvents," Interscience Publishers, Inc., New York, (1955).
18) T. P. Hilditch, *J. Chem. Soc.*, **93**, 1526 (1908).
19) P. Allen, Jr. and J. W. Brook, *J. Org. Chem.*, **27**, 1019 (1962).
20) J. M. Damson, A. M. Mathieson, and J. M. Robertson, *J. Chem. Soc.*, **1948**, 322.

BULLETIN OF THE CHEMICAL SOCIETY OF JAPAN, VOL. 45, 2909—2914 (1972)

Diazotization of Tetrafluoroanthranilic Acid and Several Reactions of Related Compounds

Sei-ichi HAYASHI and Nobuo ISHIKAWA

Department of Synthetic Chemistry, Faculty of Engineering, Tokyo Institute of Technology, Ookayama, Meguro-ku, Tokyo

(Received February 8, 1972)

Diazotization of tetrafluoroanthranilic acid with nitrosylsulfuric acid in acetic acid gave a ring-hydroxylated, stable diazonium salt **4**, which was isolated in high yield. Several reactions on this diazo compound were carried out. Replacement of the diazonium group with hydrogen, chlorine, or bromine was accomplished with the usual reagents. The reaction of diazo compound with diazomethane afforded a benzoxadiazine compound **13**. Other related polyfluoroaromatic compounds were prepared.

Tetrafluoroanthranilic acid (**1**) is a valuable precursor of tetrafluorobenzyne through the diazotized intermediate, tetrafluorobenzenediazonium-2-carboxylate (**2**).[1] Since an unsubstituted benzenediazonium-2-carboxylate is known as a stable, isolable compound,[2] we intended to isolate the analogous stable diazonium compound from **1**. When **1** was diazotized with sodium nitrite in dilute hydrochloric acid in the usual

1) S. Hayashi and N. Ishikawa, *Nippon Kagaku Zasshi*, **91**, 1000 (1971).

2) M. Stiles, R. G. Miller, and U. Burckhardt, *J. Amer. Chem. Soc.*, **85**, 1792 (1963).

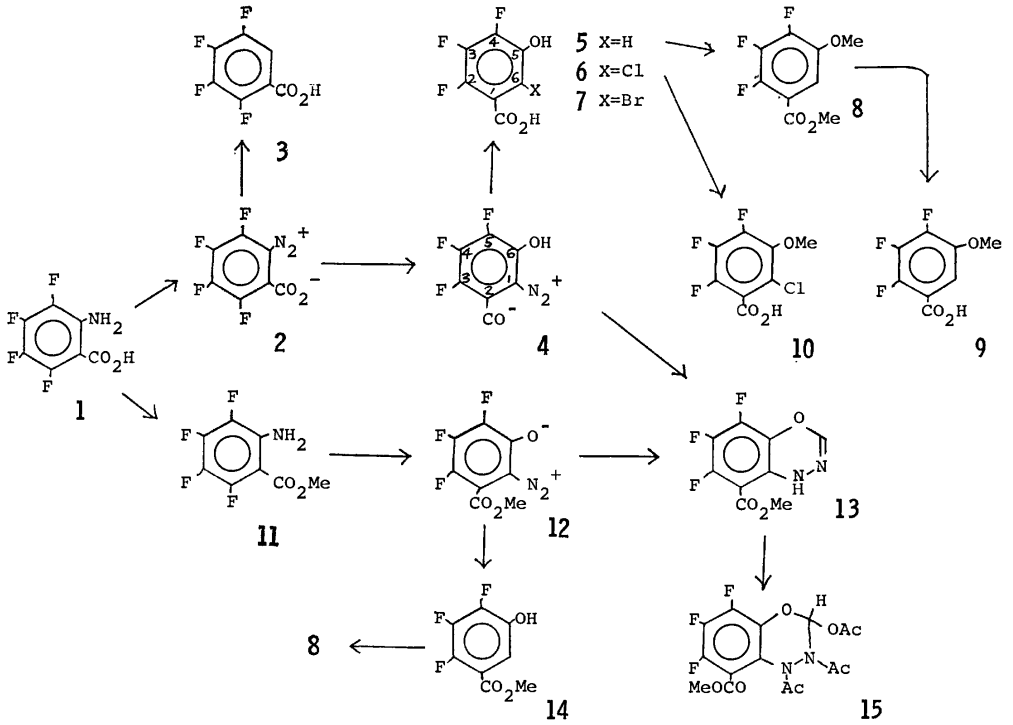

Chart A

manner, only a clear diazo solution was obtained, from which any attempted isolation of the diazonium compound was unsuccessful.

When the reaction was carried out with nitrosylsulfuric acid in acetic acid, however, a very stable diazonium compound of mp 187°C (decomp.) was obtained in good yield, and the structure of this compound was proved to be 3,4,5-trifluoro-6-hydroxybenzenediazonium-2-carboxylate (**4**) by ^{1}H and ^{19}F NMR and mass spectra. In this case, it was evident that the fluorine atom *ortho* to diazo group had been nucleophilically replaced with hydroxyl group during the course of the diazotization. This is not peculiar since a halogen substituent in *para* or *ortho*, especially the latter, to diazonium group is known readily replaceable by nucleophile.[3,4] As for polyfluoroaromatic compounds, it was reported that pentafluoroaniline gave *p*-hydroxytetrafluorobenzenediazonium salt exclusively when it was diazotized with sodium nitrite in hydrochloric acid or in 70% sulfuric acid.[5]

For the purpose of clarifying the structure and reactivity of a exceptionally stable diazonium compound **4**, we examined several reactions on this material. On heating with aqueous hypophosphorous acid it was reduced into 2,3,4-trifluoro-5-hydroxybenzoic acid (**5**) with evolution of nitrogen gas. The same reaction occurred when the diazonium compound was warmed with copper powder in either water, or ethanol, or dimethylformamide.

The diazonium group was also readily replaced with halogens affording 2,3,4-trifluoro-6-halogeno-5-hydroxybenzoic acid, **6** and **7**, in good yields when **4** was treated with the corresponding cuprous halides in aqueous hydrogen halides. However, the replacement of the diazonium group with iodine was unsuccessful. With aqueous potassium iodide alone there was no reaction, whereas in the presence of copper powder diazonium group was split off to give 2,3,4-trifluoro-5-hydroxybenzoic acid (**5**). This might be attributed to the steric effect on the attack of the bulky iodide ion. The NMR spectra of the compound **5**—**10** served for the determination for the positions of substituents (*loc. cit.*).

When diazomethane was allowed to react with 3,4,5-trifluoro-6-hydroxybenzenediazonium-2-carboxylate, an interesting heterocyclic compound, 6,7,8-trifluoro-5-methoxycarbonyl-4H-1,3,4-benzoxadiazine (**13**), was obtained. The yield was rather good (83%), and the structure was derived from its mass, NMR, and IR spectra. In the course of this reaction diazomethane should have attacked 3,4,5-trifluoro-2-methoxycarbonylbenzenediazonium-6-oxide (**12**), and this was confirmed preparatively.

Thus, the diazo oxide **12**, obtained from tetrafluoroanthranilic acid by methylation with methanol-sulfuric acid and subsequent diazotization of the resulting ester **11** with nitrosylsulfuric acid, was similarly converted to the oxadiazine **13** on treating with diazomethane. An analogous reaction between a diazo oxide and a substituted diazomethane was reported by R. Huisgen *et al.*[6] who observed the formation of 5,6,7,8-tetrachloro-2-phenyl-4*H*-1,3,4-benzoxadiazine from 3,4,5,6-tetrachlorobenzenediazonium-2-oxide and phenyldiazomethane.

The structure of the trifluoromethoxycarbonylben-

3) K. H. Saunders, "The Aromatic Diazo Compounds", Edward Arnold & Co., London (1964), p. 117.

4) J. F. Bunnett and R. E. Zahler, *Chem. Rev.*, **49**, 273 (1951).

5) G. M. Brooke, E. J. Forbes, R. D. Richardson, M. Stacey, and J. C. Tatlow, *J. Chem. Soc.*, **1965**, 2088.

6) R. Huisgen and R. Fleischman, *Ann.*, **623**, 47 (1959).

TABLE 1. NMR SPECTRA OF **5**—**10**

Compd	^{1}H (τ)			^{19}F					
				δ ppm[a]			J (Hz)		
	R	X	R′	2-F	3-F	4-F	2-3	3-4	4-2
5	H	H 2.63[b]	H	66.2	82.1	72.5	21.8	21.8	4.8
6	H	Cl	H	71.3	83.3	75.0	22.1	19.6	~0
7	H	Br	H	70.8	82.2	74.8	22.0	19.6	~0
8	Me 6.17 (s)	H 2.90[c]	Me 6.17 (s)	60.4	78.2	67.7	16.8	16.8	
9	H	H 2.57[d]	Me 6.00 (s)	64.7	89.7	78.1	20.0	20.0	
10	H	Cl	Me 6.02 (d) J_{F-OMe} 1.5Hz	65.3	85.4	71.1	20.0	20.0	

a) From ext. CF_3CO_2H in Me_2CO or CCl_4.
b) J^m_{HF} 6.5, 9.0, J^p_{HF} 2.8 Hz.
c) J^m_{HF} 7.5, 7.8, J^p_{HF} 2.5 Hz.
d) J^m_{HF} 7.2, 8.1, J^p_{HF} 2.6 Hz.

zenediazonium oxide (**12**) was easily deduced by converting it to methyl 2,3,4-trifluoro-5-methoxybenzoate (**8**). Thus, treatment of **12** with 50% hypophosphorous acid afforded the phenol **14**, which gave **8** with diazomethane, indicating the validity of the assignment of structure **12** to the diazo oxide.

Benzoxadiazine **13** reacted with acetic anhydride to give 2-acetoxy-3,4-diacetyl-6,7,8-trifluoro-5-methoxycarbonyl-2*H*-3,4-dihydro-1,3,4-benzoxadiazine (**15**). The structure was confirmed by ^{1}H NMR spectrum.

For the generation of tetrafluorobenzyne, tetrafluoroanthranilic acid was diazotized with *n*-butyl nitrite in organic solvent.[1] No hydroxylation or other nucleophilic reaction seemed to occur in this case. To confirm this we carried out the above diazotization in the presence of copper powder. As a result 2,3,4,5-tetrafluorobenzoic acid (**3**) was obtained in 62% and no other product was detected. Formation of **3** could be rationalized by the reductive decomposition of tetrafluorobenzenediazonium-2-carboxylate, which had not been hydroxylated in the absence of water.

NMR Spectra. In NMR spectra of polyfluoroaromatic compounds, it is generally known that the hydrogen nucleus in XCH_3 (X=O, N, S *etc.*) couple with both fluorine nuclei in *ortho* positions,[7] but if one *ortho* position is unsubstituted such a coupling is not observed.[8] This rule played an important role in the determination of positions of substituents in our compounds. Thus, in trifluoromethoxybenzoic acid **9** which was derived from **4**, *via* **5** and **8**, the signal of OCH_3 appeared as a sharp singlet. This means that the methoxyl group has one *ortho* fluorine atom and the other *ortho* position is unsubstituted. Among four trifluoromethoxybenzoic acids which can be considered in this case, only 2,3,4-trifluoro-5-methoxybenzoic acid is suited for this limitation (Table 1).

As for chlorotrifluoromethoxybenzoic acid (**10**), the NMR signal of OCH_3 protons appeared as a doublet (J=1.5 Hz). This also supports the assignment of structure of **10** as 6-chloro-2,3,4-trifluoro-5-methoxybenzoic acid, because it means one *ortho* position to methoxyl group is occupied with fluorine and the other with chlorine.

The structure of the methyl trifluoromethoxybenzoate (**8**) was deduced from the ^{19}F NMR spectrum. Utilizing Bruce's substituent shielding parameter,[9] the chemical shifts of the various fluorine atoms for two possible structures, methyl 2,3,4-trifluoro-5-methoxybenzoate (**8**) and methyl 2,4,5-trifluoro-3-methoxybenzoate (**8a**) were calculated. The observed fluorine chemical shifts are in agreement with those expected for the former (**8**) (Fig. 1).

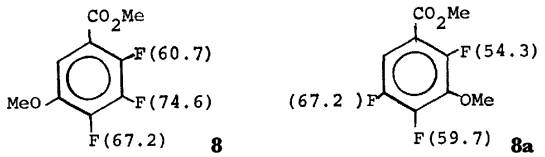

Fig. 1. Calculated ^{19}F NMR chemical shift for **8** and **8a**.

Regarding ^{19}F NMR spectra of polyfluoroaromatic compounds it is also known that the signal of fluorine atom lying between two *ortho* fluorine atoms shift considerably to the upper field.[10] In the spectra of the polyfluorodiazo compounds **4** and **12**, however, a shift to lower field of the 4-F signal was observed. This was probably caused by the strong electron-withdrawing effect of diazo group. A similar observation in the case of 3,4,5,6-tetrafluorobenzenediazonium-2-oxide was reported recently.[11]

The structure for the acetoxy compound **15** was

7) J. Burdon, *Tetrahedron*, **21**, 1101 (1965).
8) J. Burdon and W. B. Hollyhead, *J. Chem. Soc.*, **1965**, 6326.
9) M. I. Bruce, *J. Chem. Soc.*, *A*, **1968**, 1459.
10) J. W. Emsley, J. Feeney, and L. H. Sutchliffe, "High Resolution Nuclear Magnetic Resonance Spectroscopy", Pergamon Press (1966), Vol. 2, p. 905.
11) J. B. Birchall, R. N. Haszeldine, J. Nikokavouras, and E. S. Wilks, *J. Chem. Soc.*, *C*, **1971**, 562.

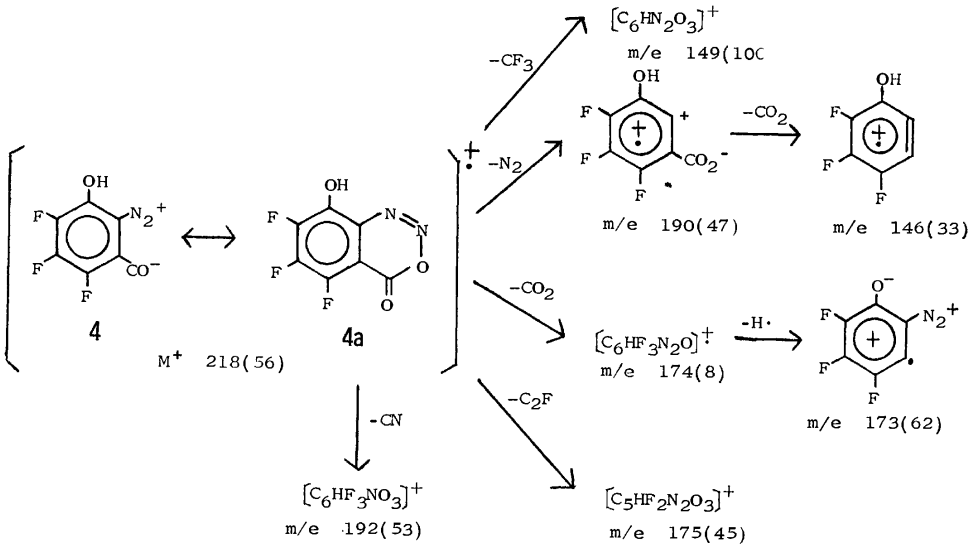

Fig. 2. MS fragmentation of **4**.

deduced from a consideration of the ^1H NMR spectrum. It showed five singlet signals, namely 7.88, 7.74, 7.65, 6.07, and 1.77 at τ-value. Signals, each integrating for three protons, at 7.88 and 7.74 were assigned to $=N-COCH_3$, while those at 7.65 and 6.07 were attributed to $COCH_3$ and CO_2Me respectively. Since it is well-known that methyl shift of acetamide is 7.85—8.25, usual acetic compounds 7.65—8.05 and methyl ester 5.8—6.6,[12] a signal at 1.77 was assigned to a methine proton.

Mass Spectra. The spectrum of 3,4,5-trifluoro-6-hydroxybenzenediazonium-2-carboxylate (**4**) was explained by the various fragments shown in Fig. 2. The intensity of the molecular ion (*m/e* 218) was unexpectedly strong. As anticipated, loss of N_2 (*m/e* 190) and then of CO_2 gave the ion of mass number 146, which was ascribed to ionized trifluorohydroxybenzyne. The ions of *m/e* 149 (base peak) and 175 could be rationalized by elimination of CF_3 and C_2F respectively, since such fragmentations are characteristic of polyfluorinated aromatic compounds.[13] Aside from the expected fragmentations, loss of CN (*m/e* 192) is interesting, as this ion could be considered to have been derived only from the structure (**4a**).

In the spectrum of 2,3,4-trifluoro-5-hydroxybenzoic acid (**5**), a strong molecular ion, also the base peak, was observed at *m/e* 192. Besides the expected decompositions, namely loss of OH, CO_2H, and (CO_2H+CO), peaks corresponding to *m/e* 149 and 69 were also observed. These could similarly be rationalized, as in the case of **4**, by eliminations of C_2F or CF_3 ion itself.

For 6,7,8-trifluoro-5-methoxycarbonyl-4*H*-1,3,4-benzoxadiazine (**13**), the spectrum showed a peak *m/e* 214 which corresponded to an ion formed by elimination of CH_3OH from the molecular ion (*m/e* 246), thus suggesting the presence of a H-containing group located on an *ortho* position to the methoxycarbonyl group[14] (Fig. 3). Other significant decompositions observed were loss of OMe (*m/e* 215), followed by eliminations of CO and HCN to give ions of *m/e* 187 and 160 respectively, the last process being charac-

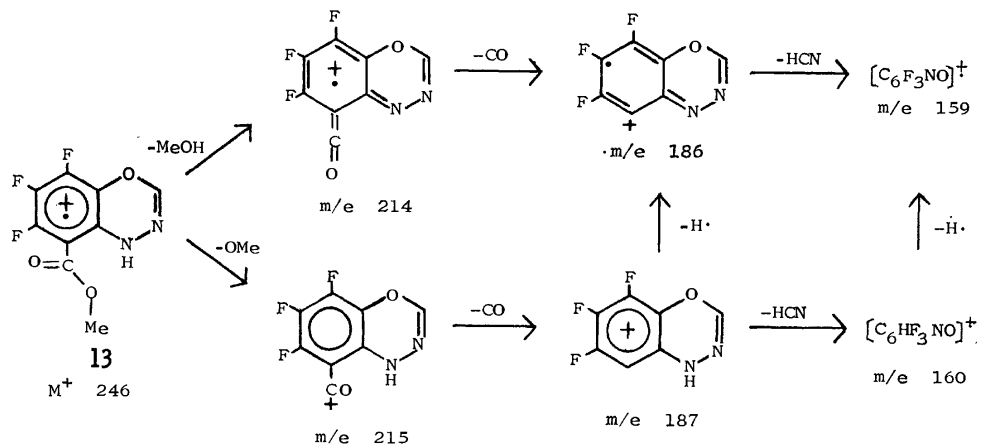

Fig. 3. MS fragmentation of **13**.

12) N. Nakagawa, "Interpretation of NMR Spectra" Kyoritsu, (1966), pp. 30—31.
13) H. Budzikiewicz, C. Djerassi, and D. H. Williams, "Mass Spectrometry of Organic Compounds", Holden-Day, Inc. (1967), p. 441.
14) *Ibid.*, pp. 199—200, 220.

teristic of nitrogen heterocycles.[15]

Experimental

3,4,5-Trifluoro-6-hydroxybenzenediazonium-2-carboxylate (4). Nitrosylsulfuric acid, prepared from sodium nitrite (7.6 g; 110 mmol) and concentrated sulfuric acid (60 ml), was added to a vigorously stirred solution of tetrafluoroanthranilic acid (20.9 g; 100 mmol) in glacial acetic acid (100 ml) during 15 min, the temperature of the reaction mixture being maintained below 40°C. The mixture was further stirred for 2 hr at room temperature and then poured onto crushed ice. After stirring for a further 1 hr, the mixture was left overnight in a refrigerator. The orange precipitate (15.4 g) was filtered, washed successively with cold water, cold ethanol-ether (1: 1 v/v) and dried. The filtrate was saturated with sodium chloride and extracted with ethyl ether. The ether extract was washed with saturated aqueous sodium chloride, dried and the solvent was removed under reduced pressure. After rinsing with a small amount of ether, the residue (2.4 g) was combined with the initial crop to give 3,4,5-trifluoro-6-hydroxybenzenediazonium-2-carboxylate (17.8 g, 81.5%), which crystallized from dioxane as orange crystals, mp 187°C (decomp.).

Found: C, 38.5; H, 0.40; F, 26.2; N, 13.2%. Calcd for $C_7HF_3N_2O_3$: C, 38.6; H, 0.46; F, 26.1; N, 12.8%. IR (KBr): 2800 (OH), 2180 ($-N_2^+$), 1710 (CO), 1630, 1474 (Ar). 1550, 1415 (CO_2^-) cm^{-1}. ^{19}F NMR: (δ ppm from ext. CF_3CO_2H in DMF) +61.8 (5-F, dd, J_{54} 21.3, J_{53} 4.2 Hz), +68.2 (4-F, dd, J_{43} 15.4 Hz), +71.0 (3-F, dd).

2,3,4-Trifluoro-5-hydroxybenzoic Acid (5). *a) With Hypophosphorous Acid*: A mixture of 3,4,5-trifluoro-6-hydroxybenzenediazonium-2-carboxylate (5.0 g; 22.9 mmol) and 50% hypophosphorous acidd (50 ml) was refluxed for 1 hr. After cooling to room temperature, the reaction mixture was extracted with ethyl ether. The ether extract was washed with water, dried and evaporated to give 2,3,4-trifluoro-5-hydroxybenzoic acid (3.0 g, 68%), which crystal lized from chlorobenzene, mp 163—165°C.

Found: F, 30.2%. Calcd for $C_7H_3F_3O_3$: F, 29.7%. IR (KBr): 3208 (OH), 1681 (CO), 1618, 1489 (Ar) cm^{-1}.

b) With Copper in Ethanol: A mixture of copper powder (0.5 g) and diazoniumcarboxylate **4** (0.5 g; 2.29 mmol) in ethanol (5 ml) was heated on a steam-bath for 1 hr. After cooling to room temperature, the copper was filtered and the filtrate was evaporated to dryness. The solid was treated with 2% aqueous sodium hydroxide and insoluble matter was removed by filtration. The filtrate was acidified and then extracted with ethyl ether. Evaporation of the dried ether extract afforded a residue (0.18 g, 41%) which was recrystallized from toluene to give **5**, mp 163—165°C, undepressed on admixture with a sample from *a*).

c) With Copper in Water: Diazoniumcarboxylate **4** (1.0 g; 4.58 mmol) was added in small portions to a mixture of copper powder (1.0 g) and water (10 ml) at 60°C. After the evolution of gas had subsided the mixture was refluxed for 10 min. The reaction mixture was treated as described in *b*) to give **5** (0.73 g, 83%), mp 163—165°C.

d) With Copper in Dimethylformamide: A solution of diazoniumcarboxylate **4** (1.0 g; 4.58 mmol) in dimethylformamide (5 ml) was added dropwise to a mixture of copper powder (1.0 g) and dimethylformamide (5 ml) at room temperature during 20 min. The reaction mixture was stirred for 40 min, then heated on the steam-bath for 30 min, and similarly treated as in *b*) to give **5** (0.31 g; 35%), mp 163—165°C.

5-Acetoxy-2,3,4-trifluorobenzoic acid. 2,3,4-Trifluoro-5-hydroxybenzoic acid (**5**) (1.0 g; 5.21 mmol) was heated with acetic anhydride (92 ml) and a trace of concentrated sulfuric acid at 60—65°C for 10 min. The mixture was poured onto ice and stirred. The acetoxyl compound was collected (0.98 g; 80%) and recrystallized from cyclohexane. mp 154°C.

Found: F, 24.2%. Calcd for $C_9H_5F_3O_4$: F, 24.3%. IR: 3080 (Ar-H), 2840 (OH), 1782, 1682 (CO), 1616, 1476 (Ar) 1190, 1110 (C-F) cm^{-1}.

Methyl 2,3,4-Trifluoro-5-methoxybenzoate (8). An ethereal solution of diazomethane was added dropwise to hydroxybenzoic acid **5** (1.0 g; 5.21 mmol) in ether (10 ml) and then stirred for 2—3 hr at room temperature. Evaporation of the ether, followed by recrystallization from *n*-hexane gave **8** (1.06 g, 92%), mp 60—62°C.

Found: F, 25.5%. Calcd for $C_9H_7F_3O_3$: F, 25.9%.

2,3,4-Trifluoro-5-methoxybenzoic Acid (9). Methyl ester **8** was refluxed with 5% sodium hydroxide solution for 0.5 hr to give **9** (86%), mp 161—162°C (from benzene).

Found: F, 27.6%. Calcd for $C_8H_5F_3O_3$: F, 27.7%.

6-Chloro-2,3,4-trifluoro-5-hydroxybenzoic Acid (6). 3,4,5-Trifluoro-6-hydroxybenzenediazonium-2-carboxylate (**4**) (2.0 g; 9.16 mmol) was added in small portions to a stirred solution of cuprous chloride (5.0 g) in concentrated hydrochloric acid (20 ml) at 60—70°C during 10 min. The mixture was refluxed for 0.5 hr and worked up as described for the compound **5** (Method *b*) to give chlorotrifluorohydroxybenzoic acid **6** (2.09 g; quantitatively). The acid has mp 131—132°C after sublimation followed by recrystallization from dichloroethane.

Found: Cl, 15.6; F, 25.5%. Calcd for $C_7H_2ClF_3O_3$: Cl, 15.6; F, 25.2%. IR: 3227 (OH), 1720 (CO), 1611, 1485 (Ar), 1119, 1049 (C-F), 858 (C-Cl) cm^{-1}.

6-Chloro-2,3,4-trifluoro-5-methoxybenzoic Acid (10). Excess ethereal diazomethane was added dropwise to a stirred solution of the acid **6** (0.77 g; 3.40 mmol) in ether and the reaction mixture was stirred for 2 hr at room temperature. After the solvent was evaporated the residual solid was refluxed with 5% aqueous sodium hydroxide (20 ml) for 40 min, then acidified with hydrochloric acid. The precipitate (0.53 g; 65%) was recrystallized from cyclohexane, and after sublimation the pure product showed mp 99—100°C.

Found: F, 23.2%. Calcd for $C_8H_4ClF_3O_3$: F, 23.7%.

6-Bromo-2,3,4-trifluoro-5-hydroxybenzoic Acid (7). Diazoniumcarboxylate (**4**) (2.0 g; 9.16 mmol) was treated similarly with cuprous bromide (5.0 g) in 47% hydrobromic acid (20 ml) as described for **6** gave bromotrifluorohydroxybenzoic acid **7** (1.18 g; 73%) which was purified by crystallization from cyclohexane-benzene followed by sublimation, mp 146—147°C.

Found: Br, 29.8; F, 20.7%. Calcd for $C_7H_2BrF_3O_3$: Br, 29.5; F, 21.0%. IR: 3240 (OH), 1718 (CO), 1620, 1475 (Ar), 1194, 1038 (C-F) cm^{-1}.

5-Acetoxy-6-bromo-2,3,4-trifluorobenzoic Acid. The acid **7** (0.50 g; 1.84 mmol) heated with acetic anhydride (1 ml) and concentrated sulfuric acid (2 drops) at 60—80°C for 10 min gave the acetate (0.50 g, 87%), mp 192—194°C (from 1,2-dichloroethane).

Found: F, 18.8%. Calcd for $C_9H_4BrF_3O_4$: F, 18.2%.

2,3,4,5-Tetrafluorobenzoic Acid (3). A solution of tetrafluoroanthranilic acid (4.2 g; 20 mmol) in dioxane (15 ml) was added dropwise to a mixture of *n*-butyl nitrite (2.6 g; 25 mmol), copper powder (6.8 g) and dioxane (20 ml) during 1 hr at 50°C. Stirring was continued for a further 5 hr at 90—93°C, the mixture was then cooled, filtered and the

15) Q. N. Porter and J. Baldas, "Mass Spectrometry of Heterocyclic Compounds", Wiley-Interscience, (1971), Chap. 11—14.

filtrate was made alkaline by adding 2% aqueous sodium hydroxide solution. The aqueous layer was then acidified with hydrochloric acid, and the separated matter extracted with ether. The ether extract was washed with water, dried and then evaporated to give 2,3,4,5-tetrafluorobenzoic acid (**3**) (2.4 g; 62%), which was purified by sublimation followed by recrystallization from *n*-hexane, mp 90—92°C (lit,[16] mp 92—92.5°C).

Found: F, 39.2%. Calcd for $C_7H_2F_4O_2$: F, 39.2%. NMR (CCl_4): ^1H: τ −0.43 (s, CO_2H), 2.15—2.65 (m, Ar–H), ^{19}F (δ ppm from ext. CF_3CO_2H) +59.2 (2-F), +59.6 (5-F), +72.8 (4-F), +74.9 (3-F).

*6,7,8-Trifluoro-5-methoxycarbonyl-4H-1,3-benzoxazine (**13**).* *a) From 3,4,5-trifluoro-6-hydroxybenzenediazonium-2-carboxylate (**4**)*: An excess of ethereal diazomethane was added dropwise to the diazoniumcarboxylate **4** (1.00 g; 4.58 mmol) in ether (20 m*l*) with stirring. Evolution of gas was observed immediately and the reaction mixture changed to a reddish solution. After further stirring for 2 hr at room temperature the solvent was evaporated, 2% aqueous solution of sodium hydroxide was added and the mixture kept overnight in a refrigerator. The yellowish green solid (0.94 g, 83%) was filtered, washed successively with dilute hydrochloric acid and water then recrystallized from cyclohexane to give the benzoxadiazine **13**, mp 153—154°C.

Found: C, 44.3; H, 1.99; F, 22.8; N, 11.0%. Calcd for $C_9H_5F_3N_2O_3$: C, 43.9; H, 2.05; F, 23.2; N, 11.4%. IR: 3289 (NH), 1695 (CO), 1650 (C=N), 1603, 1470 (Ar), 1218 (–O–), 1110, 1073 (C–F) cm^{-1}. NMR (in acetone at 50—60°C): ^1H, τ 1.63 (br, =NH), 3.55 (s, CH), 6.10 (s, CO_2Me). ^{19}F (δ from ext. CF_3CO_2H), +60.6 (6-F), +71.4 (8-F), +89.9 (7-F).

*b) From 3,4,5-trifluoro-2-methoxycarbonylbenzenediazonium-6-oxide (**12**)*: Instead of the diazoniumcarboxylate **4** in the above reaction, diazo oxide **12** (1.00 g) in acetone (10 m*l*) was used. The reaction was run similarly and the solid (0.91 g, 86%) obtained was recrystallized to give **13**, mp 151—152°C, which was identified with that prepared in *a*) by IR and mixed mp.

*2-Acetoxy-3,4-diacetyl-6,7,8-trifluoro-5-methoxycarbonyl-2H-3,4-dihydro-1,3,4-benzoxadiazine (**15**).* A mixture of the benzoxadiazine **14** (0.50 g; 2.03 mmol), acetic anhydride (5 m*l*) and concentrated sulfuric acid (3 drops) was refluxed for 5 min, then cooled and poured onto ice-water. The precipitate (0.60 g, 76%) was recrystallized from ethanol to give the triacetate **15**, mp 152—153.5°C.

Found: C, 46.2; H, 3.29; N, 6.88%. Calcd for $C_{15}H_{13}F_3N_2O_7$: C, 46.2; H, 3.36; N, 7.18%. NMR ($CDCl_3$): ^1H τ 7.88 (s), 7.74 (s), 7.65 (s), 6.07 (s), 1.77 (s), relative intensity, 3:3:3:3:1.

*Methyl Tetrafluoroanthranilate (**11**).* A mixture of tetrafluoroanthranilic acid (20.9 g; 100 mmol), methanol (200 m*l*) and concentrated sulfuric acid (50 m*l*) was refluxed for 5 hr. The excess methanol was evaporated under reduced pressure, and the mixture poured onto ice-water. The precipitate (17.4 g, 73%) was filtered, washed with water, dried, and recrystallized from methanol to give the methyl ester **11**, mp 104—105°C.

Found: F, 33.9; N, 6.28%. Calcd for $C_8H_5F_4NO_2$: F, 34.1; N, 6.28%.

*3,4,5-Trifluoro-2-methoxycarbonylbenzenediazonium-6-oxide (**12**).* Methyl tetrafluoroanthranilate (**11**) (16.25 g; 73 mmol in glacial acetic acid (70 m*l*) was treated similarly with nitrosylsulfuric acid [prepared from sodium nitrite (5.54 g; 80 mmol) and concentrated sulfuric acid (50 m*l*)] as described for the compound **4** to give the diazonium oxide **12** (11.85 g, 70%), mp 117—117.5°C.

Found: C, 41.3; H, 1.22; N, 12.4%. Calcd for $C_8H_3F_3N_2O_3$: C, 41.4; H, 1.30; N, 12.1%. IR: 2144 ($-N_2^+$), 1720 (CO), 1656, 1477 (Ar), 1141, 1078 (C–F) cm^{-1}. NMR ($CDCl_3$): ^1H; τ 6.00 (s, CO_2Me). ^{19}F; δ +58.6 (4-F), +67.9 (5-F), +68.3 (3-F).

*Methyl 2,3,4-Trifluoro-5-hydroxybenzoate (**14**).* A mixture of the diazo oxide **12** (2.0 g; 8.62 mmol) and 50% hypophosphorous acid (20 m*l*) was refluxed for 2 hr, then cooled to room temperature, and the precipitate (0.90 g) was filtered. The filtrate was extracted with ether which was then evaporated, and the solid residue (0.57 g) was crystallized from chlorobenzene. The purified product (0.43 g) was combined with the precipitate obtained earlier to give the hydroxybenzoate **14** (1.33 g, 77%), mp 154—156°C after recrystallization from chlorobenzene.

Found: F, 27.3%. Calcd for $C_8H_5F_3O_3$: F, 27.6%.

The hydroxy benzoate **14** (0.88 g; 4.27 mmol) was methylated with ethereal diazomethane to give methyl 2,3,4-trifluoro-5-methoxy benzoate, **8** (0.91 g, 97%), mp 61—62°C.

16) R. J. Harper, E. J. Solosky, and C. Tamborski, *J. Org. Chem.*, **29**, 2385 (1964).

Constituents and Properties of Ammoniated Slurry From Wet-process Phosphoric Acid

Takashi AKIYAMA and Jumpei ANDO

Faculty of Science and Engineering, Chuo University, Kasuga Bunkyo-ku, Tokyo

(Received October 20, 1971)

A large amount of gel-like substance is formed during the ammoniation of wet-process phosphoric acid and affects the production of phosphate fertilizers. The authors have found that the main constituent of the gel-like substance is a compound "S" whose composition has been determined to be $(Al,Fe)NH_4HF_2PO_4$. Several other compounds, $Fe_3NH_4H_8(PO_4)_6\cdot 6H_2O$, $(Fe,Al)NH_4H_2(PO_4)_2\cdot 1/2H_2O$, $Fe(NH_4)_2H_2F(PO_4)_2\cdot xH_2O$, $(NH_4)_3AlF_6$, gelatinous silica, *etc.*, are also formed during the ammoniation and curing of the ammoniated slurry, depending upon pH, atomic ratio of F/(Al+Fe) and temperature. Tests also were made on the properties of the ammoniated slurry; solubility, viscosity, filterability, and the rate of sedimentation. It has been found that the properties vary with the formation of the above compounds. A high-temperature modification of $(NH_4)_2HPO_4$ which is stable above 155°C has been newly found during the tests.

Wet-process phosphoric acid has been produced in large amounts in many countries. Most of the acid is ammoniated to pH 4—8 to give a slurry which is used for the production of granular, slurry, and liquid fertilizers.

Gel-like substance is formed in a large amount during the ammoniation and affects the properties of the slurry and consequently the production of the fertilizers. The constitution of the gel-like substance, however, was not clear. It sometimes happens in commercial scale plants that the properties of the slurry change seriously for some unknown reason causing much trouble in the operation of the plants. In the present study, tests were made on the constitution and the properties of the ammoniated slurry.

Acids Used for the Tests. The chemical compositions of the acids used for the tests are shown in Table 1.

The acids W-1 and W-2 were produced from Florida phosphate ore by the hemihydrate-dihydrate process with the addition of silica to promote the hydration of hemihydrate. Their atomic ratios F/Si are close to 6 illustrating that most of the fluorine is present in the form of SiF_6^{2-}. The acid W-3 was produced from Florida ore by the dihydrate process. The ratio of the acid is larger than 6 indicating that a considerable portion of the fluorine is not combined to silica. Other acids are composite acids prepared with chemical reagents.

Ammoniation and Measurement of pH. For most tests, 100 m*l* each of the acids was put in a polyethylene bottle and ammoniated with gaseous ammonia at a rate of about 2 g NH_3 per minute at about 100°C.

The pH of the ammoniated slurry was tested with a glass electrode pH meter after being diluted with 100 times as much water. The composition of the liquid phase corresponds to $NH_4H_2PO_4$ with $(NH_4)_2SO_4$ at pH 4.5 and $(NH_4)_2HPO_4$ with $(NH_4)_2SO_4$ at pH about 8.

Major Water-insoluble Compounds Formed During the Ammoniation. After the ammoniation to various

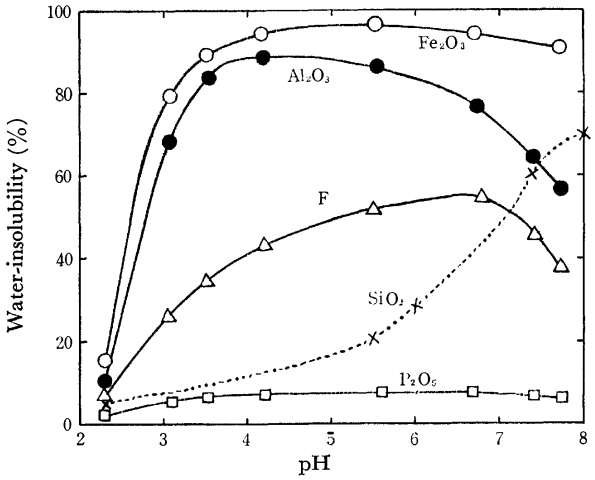

Fig. 1. Change of water-insolubility of each component of W-1 during the ammoniation at 100°C.

TABLE 1. ACIDS TESTED

Marks	Composition (%)						Atomic ratio	
	P_2O_5	SO_3	Fe_2O_3	Al_2O_3	SiO_2	F	F/(Al+Fe)	F/Si
W-1	26.2	4.5	0.7	1.0	1.1	2.4	4.5	6.9
W-2	25.1	5.1	1.0	1.3	1.1	2.1	2.9	6.0
W-3	30.0	2.4	0.7	0.8	1.0	2.5	5.5	7.9
R-1	25.0	4.1	0.7	1.0	0	0	0	—
RF-1	25.0	4.1	0.7	1.0	0	2.5	4.6	—
RSF-1	25.0	4.1	0.7	1.0	1.3	2.5	4.6	6.0
R-2	26.0	5.1	1.3	1.0	0	0	0	—
RF-3	25.0	4.1	2.3	0	0	2.5	4.5	—
R-4	25.0	4.1	0	1.5	0	0	0	—
RF-4	25.0	4.1	0	1.5	0	2.5	4.6	—

pH, the slurries were kept at 95°C for 30 min, filtered, washed with water and acetone, dried at 50°C and tested by chemical and X-ray analyses. Some of the samples were tested by electron microscope.

The change of water-insolubility of each component of W-1 during the ammoniation at about 100°C is shown in Fig. 1. Insoluble compounds started to form around pH 2.3. The amount of insoluble Fe_2O_3 and F reached maximum at pH about 6, and that of insoluble Al_2O_3 at pH 4.5. The amount of insoluble silica increased markedly above pH 6 indicating the decomposition of SiF_6^{2-} ions. Tests with W-2 and W-3 gave similar results.

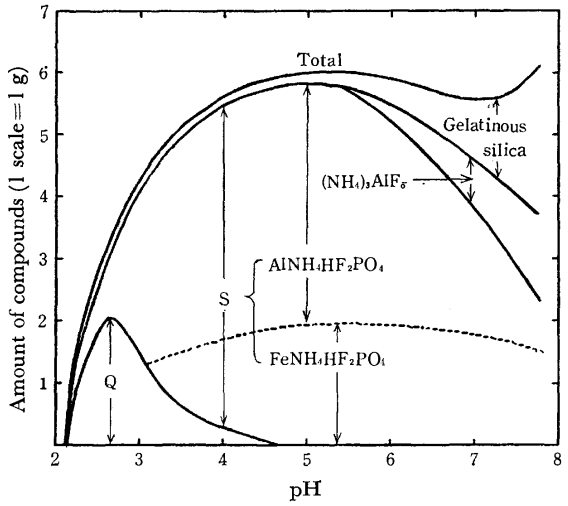

Fig. 2. Water-insoluble compounds formed from 100 g of W-1 during the ammoniation at 100°C.
(Amount of each compound is shown by the scale between 2 curves)
S: (Al, Fe)$NH_4HF_2PO_4$
Q: (Fe, Al)$NH_4H_2(PO_4)_2 \cdot 1/2\ H_2O$

The relation between pH and the amount of water-insoluble compounds formed during the ammoniation of W-1 at 100°C is shown in Fig. 2. The amounts are approximate values estimated by X-ray and chemical analyses. The water-insoluble phosphate first formed at pH 2.3 was gelatinous immediately after the ammoniation and crystallized gradually to form a compound (Fe,Al)$NH_4H_2(PO_4)_2 \cdot 1/2H_2O$[2] which will be referred to as "Q".

On further ammoniation "Q" decreased and a large amount of other gel-like phosphate formed. Tests with X-ray diffraction, electron microscope, and chemical analysis have shown that the main constituent of this gel-like substance is not (Fe,Al)$PO_4 \cdot nH_2O$ as was generally assumed but a compound "S" which has been determined as (Al,Fe)$NH_4HF_2PO_4$.[1] "S" is a solid solution of $AlNH_4HF_2PO_4$ and $FeNH_4HF_2PO_4$. "S" consists of very small round shaped particles about 20 millimicrons in diameter as shown in Fig. 3.

Above pH 5, $AlNH_4HF_2PO_4$ decreased with the formation of $(NH_4)_3AlF_6$; "S" became richer in $FeNH_4HF_2PO_4$. Gelatinous silica increased substantially above pH 6. When a small amount of Na^+ ion was added to W-1 and ammoniated, $(NH_4)_2NaAlF_6$ formed above pH 5.

Tests were made to study the effect of fluorine on the

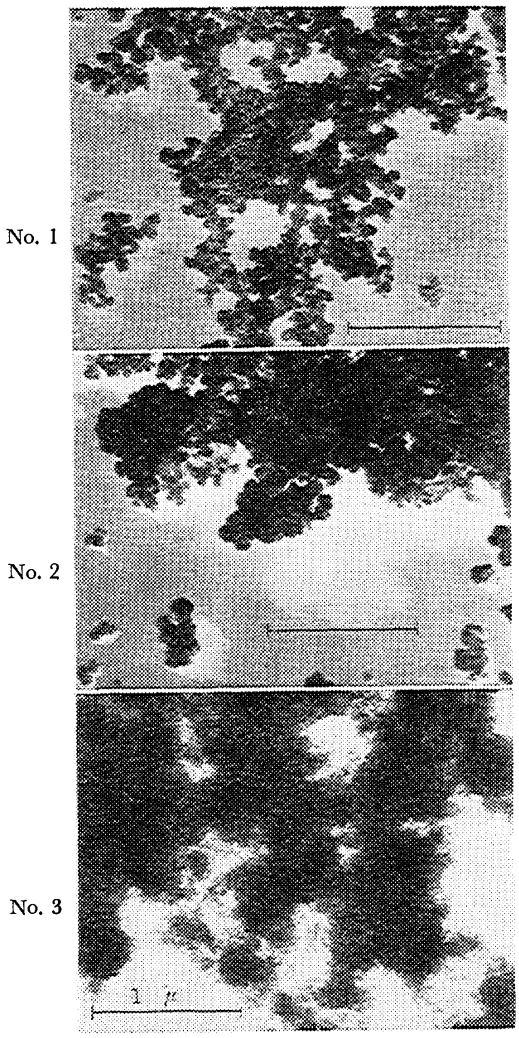

Fig. 3. Electron microscopic photographs of water-insoluble gel-like compounds formed during ammoniation at 100°C.
No. 1: RF-1 at pH 3.5, (Al, Fe)$NH_4HF_2PO_4$
No. 2: W-1 at pH 3.5, mainly (Al, Fe)$NH_4HF_2PO_4$
No. 2: R-1 at pH 6.5, gelatinous ferric aluminium phosphate

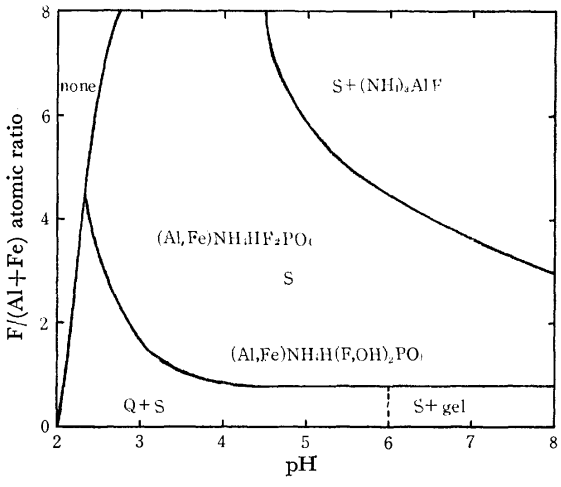

Fig. 4. Water-insoluble ferric and aluminium compounds formed at various F/(Al+Fe) ratio and pH (from W-1).

1) T. Akiyama, M. Hashimoto, H. Muraoka, and J. Ando, *Kogyo Kagaku Zasshi*, **74**, 1774 (1971).

formation of these compounds. Acids with large F/(Al+Fe) ratios were prepared by adding H_2SiF_6 to W-1. Those with small ratios were prepared by adding small amount of K_2CO_3 to W-1 to precipitate and separate K_2SiF_6. The relation between the ratio of the acid and the compounds formed at various pH is shown in Fig. 4.

Only "S" was detected in a wide range above pH3 with the acids whose ratios were larger than 1. The stoichiometric F/(Al+Fe) ratio of "S" is 2. When the ratio of the acid was smaller than 1, "Q" and "S" were present between pH 2 and 6 while gelatinous ferric aluminium phosphate hydrate and "S" were present above pH 6. $(NH_4)_3AlF_6$ formed at pH 4.5 when the ratio was 8 and at higher pH as the ratio decreased.

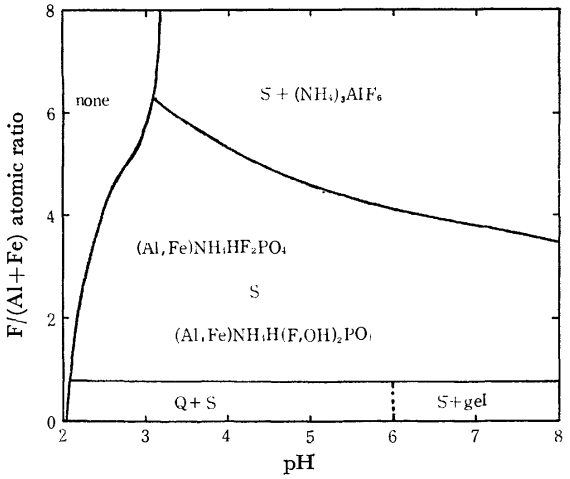

Fig. 5. Water-insoluble ferric and aluminium compounds formed at various F/(Al+Fe) ratio and pH (R-1 and HF, without silica).

The results of similar tests with the acid R-1 to which various amounts of HF were added are shown in Fig. 5. Silica was absent in the system. In this case, "Q" did not form when the ratio was larger than 1 even at pH 2.3. $(NH_4)_3AlF_6$ formed at pH 3.5 when the ratio was larger than 6.

These results illustrate that F^- ions favor the formation of "S" to depress the formation of "Q" and that silica combines with fluorine at lower pH to favor the formation of "Q" depressing the formation of $(NH_4)_3AlF_6$.

X-Ray Diffraction Patterns and Data. X-Ray powder diffraction patterns of the water-insoluble residues of the six samples of the ammoniated slurries are shown in Fig. 6. Each acid was ammoniated to pH 3.5 or 6.5 at 100°C, filtered, washed with water, dried and tested by means of X-ray diffraction. Nos. 1 and 3 of Fig. 6 show the diffraction patterns of "S". Nos. 2 and 4 show those of $AlNH_4HF_2PO_4$ and $FeNH_4HF_2PO_4$, respectively. The diffraction peaks are very broad illustrating the low crystallinity of the compounds. X-ray tests on crystal size have indicated that the single crystals are much smaller than 20 mμ.

No. 5 indicates the pattern of $(Fe,Al)NH_4H_2(PO_4)_2 \cdot 1/2H_2O$ ("Q") formed on ammoniating the acid R-1 to pH 3.5 and No. 6 gelatinous ferric aluminium phsophate hydrate formed on ammoniating the acid to pH 6.5.

The crystallinity of "S" was found to vary widely with the conditions of the formation, particularly with the temperature. The diffraction patterns of $AlNH_4$-

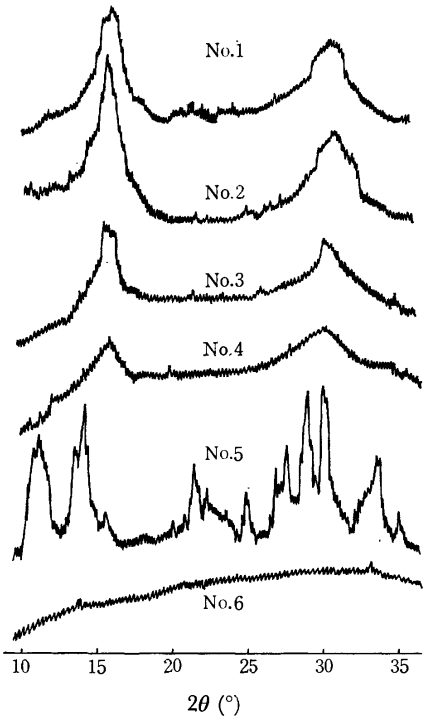

Fig. 6. X-Ray diffraction patterns of water-insoluble compounds formed during the ammoniation at 100°C (Cu, K_α).
No. 1: W-1 at pH 3.5, mainly (Al, Fe)$NH_4HF_2PO_4$
No. 2: RF-4 at pH 3.5, $AlNH_4HF_2PO_4$
No. 3: RF-1 at pH 3.5, (Al, Fe)$NH_4HF_2PO_4$
No. 4: RF-3 at 3.5, $FeNH_4HF_2PO_4$
No. 5: R-1 at pH 3.5, (Fe, Al)$NH_4H_2(PO_4)_2 \cdot 1/2H_2O$
No. 6: R-1 at pH 6.5, gelatinous ferric aluminium phosphate

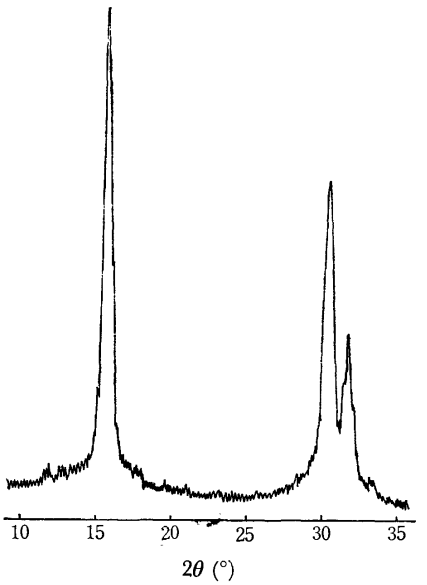

Fig. 7. X-Ray diffraction pattern of $AlNH_4HF_2PO_4$ prepared at 210°C (Cu, K_α).

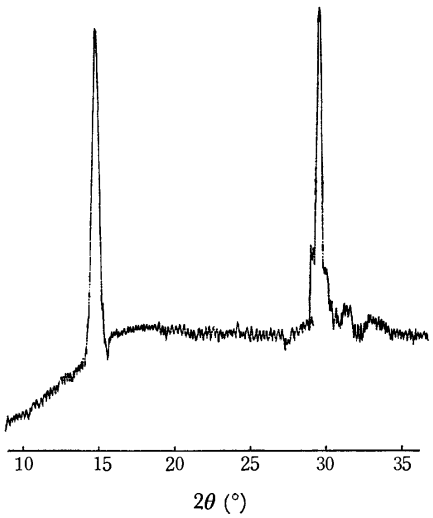

Fig. 8. X-Ray diffraction pattern of $FeNH_4HF_2PO_4$ prepared at 170°C (Cu, K_α).

HF_2PO_4 and $FeNH_4HF_2PO_4$ with high crystallinity prepared in an autoclave at 210 and 170°C respectively are shown in Figs. 7 and 8. The data of these compounds are shown in Table 2. The data indicate that the crystals belong to tetragonal system.

Table 2. X-Ray diffraction data of the compounds prepared at elevated temperature

$AlNH_4HF_2PO_4$ tetragonal (a=5.64, c=4.34)				$FeNH_4HF_2PO_4$ tetragonal (a=6.05, c=4.35)		
I/I_{100}	$d_{obs.}$, Å	$d_{calc.}$, Å	$h\ k\ l$	I/I_{100}	$d_{obs.}$, Å	$d_{calc.}$, Å
100	5.64	5.64	1 0 0	100	6.05	6.05
70	2.94	2.94	1 1 1	60	3.05	3.05
35	2.82	2.82	2 0 0	90	3.025	3.025
4	1.99	1.99	2 2 0			
11	1.88	1.88	3 0 0			
17	1.72	1.72	2 0 2	10	1.765	1.765
5	1.65	1.65	2 1 2			
3	1.469	1.469	2 2 2			
4	1.270	1.269	2 1 3			

Other Minor Water-insoluble Compounds. A very small amount of compound "R", $Fe_3NH_4H_8(PO_4)_6 \cdot 6H_2O$[2] was found to form when the ammoniated slurry of W-1 at pH 2 was kept at 100°C for 2 hr. Another compound "T"[3] formed in a small amount when the slurry of W-1 at pH 6 was kept at 100°C for several hours. Similar results were obtained with a composite acid RSF-1. The composition of "T" has been determined to be nearly $Fe(NH_4)_2H_2F(PO_4)_2$; "T" might contain some water of crystallization.

A very small amount of "R" formed when the acid R-1 was ammoniated at pH 2, but disappeared above pH 2 to form "Q". On further ammoniation of R-1, "Q" disappeared above pH 6 to form gelatinous ferric aluminium phosphate hydrate whose electron microscopic photograph is shown in Fig. 3.

During the concentration of the slurry at pH 7 containing the gelatinous phosphate by evaporation at 110°C, another compound "U" formed in a small amount. The X-ray diffraction pattern of "U" resembles that of $KFe_2(PO_4)_2(OH) \cdot 2H_2O$.[4] When ammonium fluoride was added at 100°C to the ammoniated slurry of R-4 at pH 6 to give the F/Al ratio of 1, another compound formed in a very small amount. The X-ray pattern of this compound is similar to that of $K_2O \cdot 2Al_2O_3 \cdot 2P_2O_5 \cdot 1.6HF \cdot 6.2H_2O$.[2]

Change of Solubility. The change of citric solubility of P_2O_5 during the ammoniation of three acids is shown in Fig. 9. With R-2 which does not contain fluorine only "Q" formed in a large amount above pH 2 and the citric solubility decreased. "Q" is soluble in alkaline citrate but less soluble in citric acid, while "S" is soluble in both citrate and citric acid. "Q" also formed with W-2, but the amount was much less than with R-2. Only a small amount of "Q" formed with W-3 containing fluorine which was not combined with silica.

Tests also were made on the solubility of other phosphates. Like "Q", "R" is soluble in alkaline citrate but less soluble in citric acid. "T" is less soluble in alkaline citrate but soluble in citric acid, contrary to "Q" and "R". "U" is less soluble in both citrate and citric acid.

The change of water-solubility of P_2O_5 during the ammoniation is shown in Fig. 10. The solubility was much lower with R-2 than with W-2 and W-3 although all these acids contain nearly equal amounts of Fe_2O_3+Al_2O_3. The difference in solubility is caused by the difference of compounds formed. "Q" containing 2 mol P_2O_5 per 1 mol Fe_2O_3 or Al_2O_3 formed in a large amount with R-2, while "S" containing 1 mol P_2O_5 per 1 mol Fe_2O_3 or Al_2O_3 formed in similar amount with W-2 and W-3.

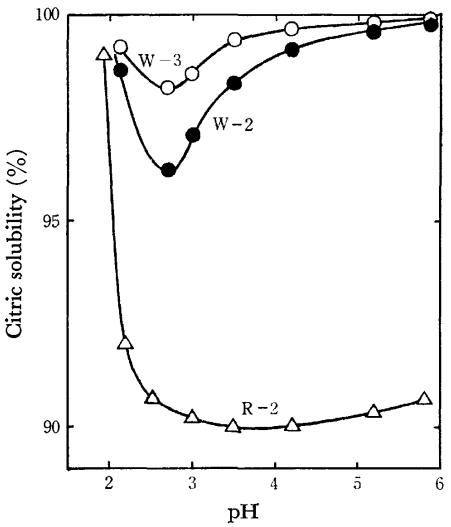

Fig. 9. Change of citric solubility of P_2O_5 during ammoniation at 100°C.

2) J. F. Haseman, J. R. Lehr, and J. P. Smith, *Soil Science Soc. Proceeding*, **15**, 76 (1950).

3) J. Ando and T. Akiyama, *Kogyo Kagaku Zasshi*, **68**, 1056 (1965).

4) A. S. T. M. card No. 9—446.

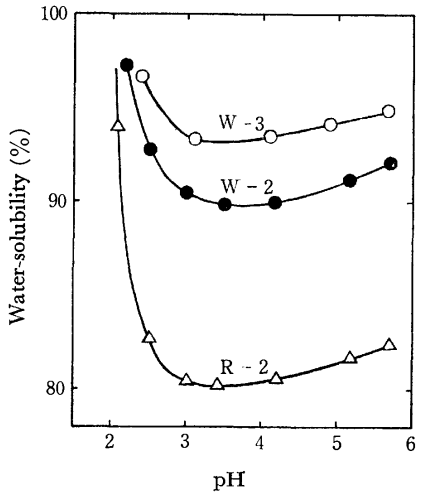

Fig. 10. Change of water-solubility of P_2O_5 during ammoniation at 100°C.

Viscosity of the Ammoniated Slurry. The viscosity of the ammoniated slurry of W-1 is shown in Fig. 11. For the tests about 500 m*l* of W-1 was first ammoniated to pH 8. The ammoniated slurry was then acidified to pH 2.5 by adding the acid W-1. The viscosity was tested after the slurry was kept for about 5 min at various pH during the ammoniation and acidification. The temperature of the slurries was 90—100°C.

Relatively high viscosity was obtained around pH 2.7. Immediately after ammoniation to this pH the water-insoluble substance formed was gelatinous and the viscosity was as high as 100 cp. The viscosity decreased to about 20 cp by curing for 5 min as "Q" crystallized with the decrease of the gel. On further ammoniation "S" formed and the viscosity decreased to 10 cp. The viscosity increased above pH 6, presumably because of the increase of gelatinous silica. The viscosity during the acidification was higher than that during the ammoniation when the pH was above 5 and lower below pH 5.

The change of viscosity on the ammoniation of W-1

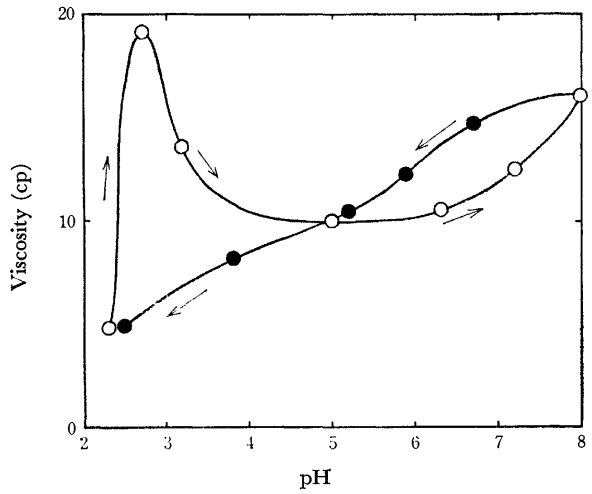

Fig. 11. Change of viscosity of ammoniated slurry of W-1 during ammoniation and acidification at 100°C.
○: in case of increasing pH on ammoniation
●: in case of decreasing pH on acidification

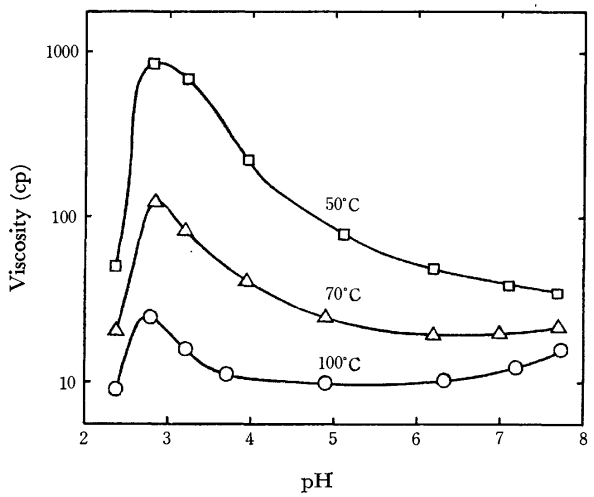

Fig. 12. Change of viscosity of ammoniated slurry during ammoniation at different temperatures.

at different temperatures is shown in Fig. 12. The viscosity was much higher when ammoniated at lower temperature due to the poor crystallinity of the insoluble substance and was as high as 800 cp when ammoniated to pH 2.7 at 50°C. Such low-temperature ammoniation occurs in commercial scale plants where dilute ammonia gas such as coke-oven gas is used.

Rate of Sedimentation. W-1 was ammoniated to various pH at 100°C and diluted with an equal amount of water to prevent the crystallization of ammonium phosphate on cooling. About 50 m*l* of the diluted slurry was put in a glass cylinder to a depth of 140 mm and kept at room temperature. The depth of the clear solution layer which formed on the surface of the slurry due to the sedimentation of the insoluble substance was measured several times in 150 hr. The results are shown in Fig. 13.

The rate of sedimentation was larger for the slurries at pH 4.0 and 5.9 which had lower viscosity than for the slurries at pH 2.8 and 7.2. The slurry ammoniated to pH 8 and then acidified to pH 5.4 showed the smallest rate.

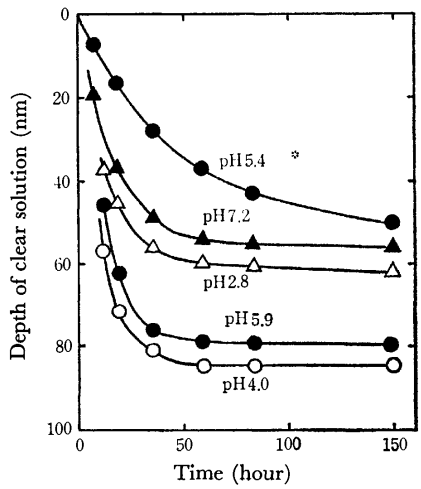

Fig. 13. Rate of Sedimentation of gel-like substance in ammoniated slurry of W-1 (Ammoniated and then diluted. *The sample ammoniated and then acidulated to pH 5.4).

In other series of tests, W-1 was first diluted with an equal amount of water and then ammoniated to various pH for measurement of the rate of sedimentation. The results are shown in Fig. 14. The rate was considerably smaller than that shown in Fig. 13, possibly because of the lower crystallinity of "S" formed at lower temperature.

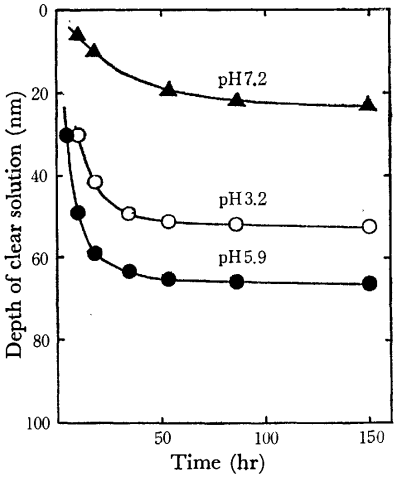

Fig. 14. Rate of sedimentation of gel-like substance in ammoniated slurry of W-1 (Diluted and then ammoniated).

Filterability. For the tests of filterability, 100 m*l* each of the acids was ammoniated to various pH at 100°C in most tests and at 50°C in some tests. The slurry was filtered with a filter paper (diameter 11 cm) in a Buechner funnel (diameter 12 cm) applying a vacuum of 100 mmHg below atmospheric pressure. The amount of the filtrate was recorded every 30 sec.

The best filterability obtained with the slurry at pH about 4 is shown in Fig. 15. The poor filterability with slurry ammoniated at lower temperature is in good agreement with the results shown in Figs. 12 and 13.

High Temperature Modification of $(NH_4)_2HPO_4$. X-Ray tests of a commercial product of diammonium phosphate manufactured by ammoniation of wet-process phosphoric acid in a spray tower showed that the major phase of the product was a previously unknown compound while the product contained small amounts of ammonium sulfate and the compound "S". The

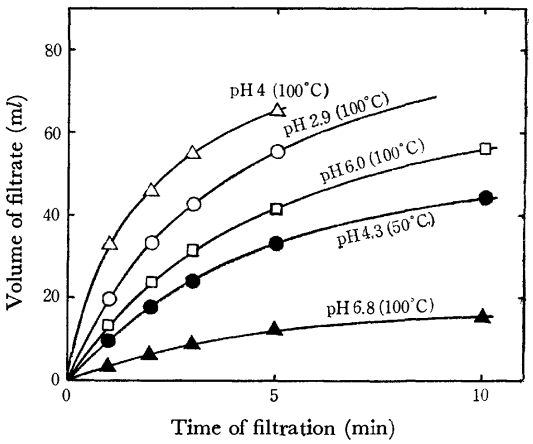

Fig. 15. Effect of pH and temperature on the filterability of ammoniated slurry of W-1.

unknown compound has been identified as a high temperature modification of $(NH_4)_2HPO_4$. This modification can be prepared in a laboratory by heating the usual form of $(NH_4)_2HPO_4$ at 160°C in a sealed tube to prevent the loss of ammonia during the heating. The inversion occurred above 155°C indicating that the ammoniation reaction in the spray tower occurred above this temperature. The presence of ammonium sulfate and "S" did not appreciably affect the inversion temperature. X-Ray diffraction data of the modification are shown in Table 3. This modification can stay at room temperature as long as it is dry. Addition of moisture at room temperature resulted in an instantaneous conversion into the usual form of $(NH_4)_2HPO_4$.

TABLE 3. X-RAY DIFFRACTION DATA OF HIGH TEMPERATURE MODIFICATION OF $(NH_4)HPO_4$

d, Å	I/I_{100}	d, Å	I/I_{100}
6.27	3	2.71	3
5.46	53	2.64	10
4.54	100	2.50	15
3.85	30	2.485	10
3.32	20	2.320	3
3.29	23	2.267	12
3.02	11	2.165	5
2.93	52	2.092	9
2.79	15		

NOTES

BULLETIN OF THE CHEMICAL SOCIETY OF JAPAN, VOL. 45, 2921—2923 (1972)

Spectrophotofluorometric Determination of Terbium with α,α'-Ethylenediiminodi(o-hydroxyphenylacetic acid)

Tomitsugu TAKETATSU and Setsuko YOSHIDA
College of General Education, Kyushu University, Fukuoka

(Received December 11, 1971)

Spectrophotofluorometric methods for the determination of terbium have been described using 1,10-phenanthroline-salicylic acid,[1] potassium carbonate,[2] ethylenediaminetetraacetic acid-sulfosalicylic acid,[3] 2-thenoyltrifluoroacetone,[4] and hexafluoroacetylacetone–trioctylphosphine oxide.[5] These methods are based on the measurement of luminescence, which is characteristic of the metal ion and shows the line-like spectrum, enhanced by the formation of the metal complexes. Recently we have found that the intensity of the fluorescence spectrum of terbium was remarkably enhanced by the formation of α,α'-ethylenediiminodi-(*o*-hydroxyphenylacetic acid), (EDDHA), chelate. In the present paper, the fundamental conditions for the spectrophotofluorometric determination of terbium with EDDHA will be described.

Experimental

Reagents. Standard solutions of metal ions were prepared by dissolving the 99.9% pure oxides (scandium, yttrium, and the rare earths except for cerium), chlorides (cerium-[III] and thorium), and nitrate (uranyl) in dilute hydrochloric acid. The concentration of scandium, yttrium, rare earth, and thorium ions were determined titrimetrically with EDTA using Xylenol Orange as an indicator. The titration of uranyl ion with EDTA was made using PAN as an indicator.

Standard solution of EDDHA was prepared by dissolving the known amount of the reagent obtained from the Dojindo Co., Ltd. Research laboratories in dilute sodium hydroxide solution.

All other chemicals used were analytical reagent grade.

Apparatus. Fluorometric measurement was carried out using a Hitachi fluorescence spectrophotometer Model 203 with a medium pressure mercury lamp. 1 cm × 1 cm quartz cell was used.

Procedure. A dilute hydrochloric acid solution containing less than about 50 μg was transferred into a beaker. Then, 5 *ml* of 2.5×10^{-3} M EDDHA solution and 2 *ml* of 5% triethanolamine solution were added to the solution. After the pH of the solution was adjusted to 7.6—7.8 with dilute hydrochloric acid and sodium hydroxide solutions, the solution was transferred into a 25 *ml* volumetric flask and made up to volume with water. The intensity of the fluorescence of the solution was measured on the spectrophotofluorometer. The apparent excitation and fluorescence wavelengths used were 295 and 545 nm, respectively. The content of terbium was calculated by using the calibration curve obtained from the standard. A solution of quinine sulfate was used to a constant reading for measurement made at 545 nm.

Results and Discussion

Fluorescence Spectrum. The apparent fluorescence spectrum of the solution (pH 7.7), containing the terbium-EDDHA chelate, excited with radiation at a wavelength of 295 nm is shown in Fig. 1. The apparent wavelengths of the prominent maxima of the fluorescence spectrum are 487, 545, and 585 nm and the most intense wavelength is 545 nm.

Effect of pH. Figure 2 shows the variation of the fluorescence at 545 nm as a function of pH. The apparent fluorescence gives almost constant over pH range 7.5—7.8. In this case, triethanolamine was used as the buffer reagent because it gave an effective buffer action in the pH region from 6.5 to 8 and the intensity of fluorescence was not influenced by an addition of excessive amounts of the reagent.

Effect of EDDHA Concentration. The variation of intensity of the fluorescence was investigated as a function of mole ratio (EDDHA/Tb^{3+}) plots. The intensity of the fluorescence gives almost constant over

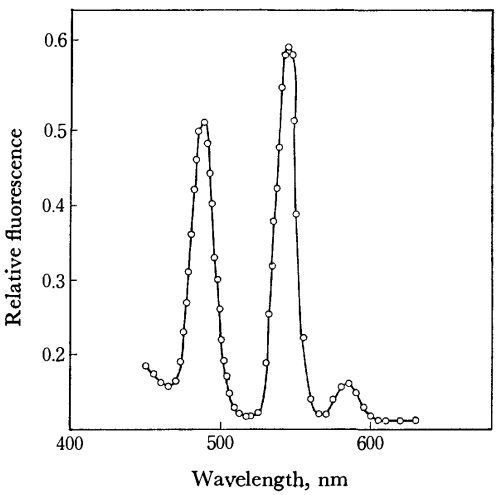

Fig. 1. Apparent fluorescence spectrum of terbium-EDDHA complex.
1.0×10^{-5} M Tb^{3+}, 5.0×10^{-4} M EDDHA, pH 7.7, excitation wavelength 295 nm.

1) L. I. Kononenko, R. S. Lauer, and N. S. Pouektov, *Zh. Anal. Khim.*, **18**, 1468 (1963).
2) T. Taketatsu, M. A. Carey, and C. V. Banks, *Talanta*, **13**, 1081 (1966).
3) R. M. Dagnall, R. Smith, and T. S. West, *Analyst* (London), **92**, 358 (1967).
4) R. Belcher, R. Perry, and W. I. Stephen, *ibid.*, **94**, 26 (1969).
5) R. P. Fisher and J. D. Winefordner, *Anal. Chem.*, **43**, 454 (1971).

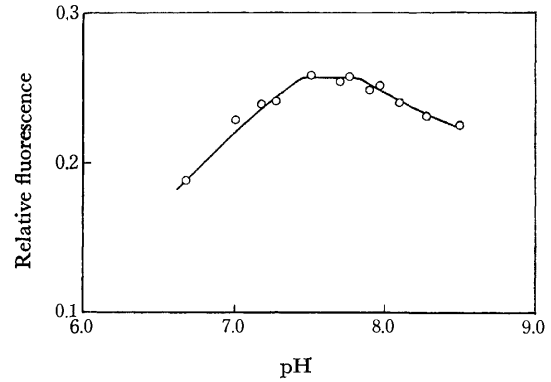

Fig. 2. Variation of intensity of the fluorescence as a function of pH.
1.0×10^{-6} M Tb^{3+}, 1.0×10^{-4} M EDDHA, excitation wavelength 295 nm, fluorescence wavelength 545 nm.

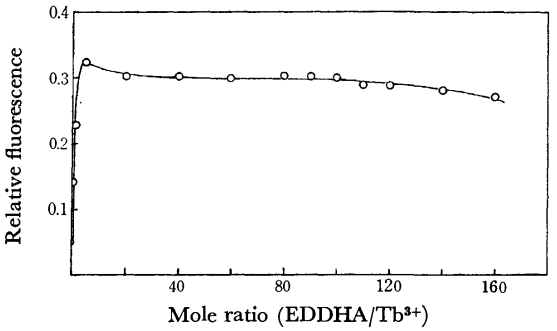

Fig. 3. Variation of intensity of the fluorescence as a function of concentration of EDDHA.
5.0×10^{-6} M Tb^{3+}, pH 7.7, excitation wavelength 295 nm, fluorescence wavelength 545 nm.

the mole ratio range 20—100 as shown in Fig. 3.

Stability of Fluorescence with Time. The intensity of the fluorescence remained sensibly constant for 7 hr after a few minutes.

Calibration Experiments. It is found that the fluorescence is a linear function of the concentration in the range from 0.03 to 1.5 μg/ml of terbium as shown in Fig. 4. Also, by amplifying the sensitivity of the instrument, the linear relationship is obtained for solutions containing from 0.0015 to 0.015 μg/ml.

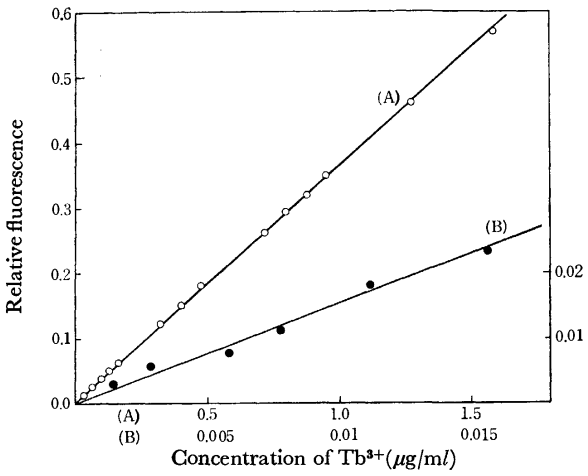

Fig. 4. Calibration curve.
(A) 1.0×10^{-4} M EDDHA: (B) 1.0×10^{-5} M EDDHA, pH 7.7 excitation wavelength 295 nm, fluorescence wavelength 545 nm. Relative fluorescence between (A) and (B) does not represent the correlative intensity.

TABLE 1. DETERMINATION OF TERBIUM IN SYNTHETIC SAMPLES CONTAINING DIVERSE METAL IONS

Metal ions added, μg		Tb[a] found, μg	Metal ions added, μg		Tb[a] found, μg
La	50.0	19.3	Ho	32.9	18.7
Ce	22.7	17.9	Ho	61.4	19.3
Ce	45.2	17.4	Er	32.9	19.1
Pr	22.1	19.0	Er	61.5	19.9
Pr	44.4	18.6	Tm	25.3	19.7
Nd	24.2	18.5	Tm	50.7	21.0
Nd	48.5	18.3	Yb	28.3	19.3
Sm	23.9	18.6	Yb	59.7	20.1
Sm	47.7	18.4	Lu	27.3	19.9
Eu	24.9	18.8	Y	32.2	19.6
Eu	49.8	18.8	Sc	7.8	19.4
Gd	23.6	19.0	UO_2	42.8	19.4
Gd	47.2	19.2	Th	33.7	13.6
Dy	47.9	19.9	Th	67.3	11.3

a) *Tb taken, 19.9 μg

Effect of Other Substances. The effect of other rare earth, scandium, yttrium, thorium, and uranyl ions was studied under the optimum conditions. The results are shown in Table 1. Lanthanum, gadolinium, dysprosium, holmium, erbium, thulium, ytterbium, lutetium, scandium, yttrium, and uranyl ions do not interfere. Cerium, praseodymium, neodymium, samarium, and europium give a slight interference. Thorium gives a serious interference.

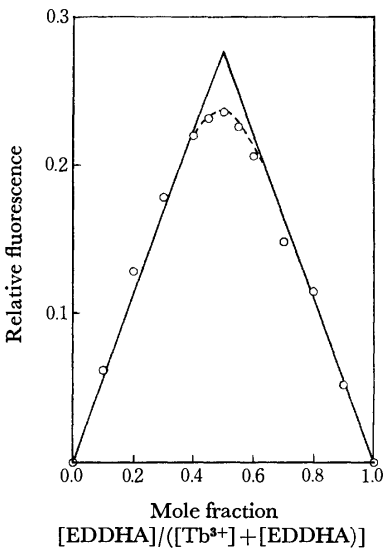

Fig. 5. Continuous variation plot.
$[Tb^{3+}]+[EDDHA]=1.0\times10^{-5}$ M, pH 7.7, excitation wavelength 295 nm, fluorescence wavelength 545 nm.

Composition of the Terbium-EDDHA Chelate. The continuous variation method was used to investigate the ratio in which EDDHA combines with terbium. The total concentration of EDDHA and terbium was maintained at 1.0×10^{-5}M. The continuous variation plot is illustrated in Fig. 5. The peak at mole fraction

Table 2. A comparison amoung data found in various literatures.

Reagents	Range of linearity or limit of detection	Condition of experiment	Literatures
1,10-Phenanthroline-salicylic acid	0.05 μg/ml	in benzene (solvent extraction)	1)
Potassium carbonate	0.3—70 μg/ml	in 1.5 M K_2CO_3 solution	2)
Ethylenediaminetetraacetic acid-sulfosalicylic acid	0.0064—3.2 μg/ml	in alkaline solution at pH 11.6—11.9	3)
2-Thenolytrifluoroacetone	10^{-3} to 10 M 0.15—15 μg/ml	in dimethylformamide	4)
Hexafluoroacetylacetone-trioctylphosphine oxide	10^{-7} to 10^{-4} M 0.015—15 μg/ml	in methylcyclohexane (solvent extraction)	5)
EDDHA	0.03—1.5 g/ml and 0.0015—0.015 μg/ml	in weak alkaline solution at pH 7.5—7.8	This paper

[EDDHA]/([EDDHA]+[Tb^{3+}]) of 0.5 indicates combining ratio of one EDDHA molecule per one terbium ion.

Comparison with Other Methods. Table 2 shows a comparison amoung the data reported by several investigators. The EDDHA method can be carried out more easily and rapidly in comparison with the methods[1,5] which are in need of solvent extraction procedure. Also it is known that the present method is almost similar to or superior to the other methods concerning the range of linearity and the degree of limit of detection though the comparison is not always appropriate because the data depend upon the performance of instruments used.

BULLETIN OF THE CHEMICAL SOCIETY OF JAPAN, VOL. 45, 2923—2924 (1972)

Mono- and Bi-photonic Ionization of Aromatic Molecules in Liquid Solutions by the 347 nm Light Pulse

Yoshio TANIGUCHI, Yasuzo NISHINA, and Noboru MATAGA*

Department of Chemistry, Faculty of Engineering Science, Osaka Universtiy, Toyonaka, Osaka

(Received February 21, 1972)

The photoionization of aromatic molecules constitutes a primary step of growing importance in photochemical processes. Richards *et al.* observed the absorption spectra of the pyrene cation radical which was produced by the biphotonic absorption of the 347 nm light pulse.[1] The ionization of perylene was found to occur by a biphotonic process.[2] Recently, a monophotonic ionization of perylene has been suggested when the excitation is below 230 nm.[3] However, the monophotonic ionization of aromatic molecules in liquid solutions by the excitation with the 347 nm light pulse has not been reported.

We have confirmed by means of the laser photolysis and transient photoconductivity measurements that the ionization of *N,N*-diphenyl-*p*-phenylenediamine (DPPD) and phenothiazine in an acetonitrile solution occurs by monophotonic excitation at 347 nm.

The second harmonics of a Q-switched ruby laser (Japan Electron Optics, JLR-02A) was used as an exciting light pulse. The produced ion radicals were observed by measuring the photocurrent induced by laser excitation. Details of the measurement are given elsewhere.[4] For examining the effect of the excitation light intensity on the photocurrent, the intensity of the laser pulse was reduced by using neutral filters composed of wire gauzes. Relative values of the exciting intensity were monitored by measuring the intensity of light partially reflected by means of a beam splitter with a photomultiplier. The absolute value was determined by a ballistic thermopile TRG model 100 (Hadron).

The samples were purified in the usual way. All the solutions for the measurment were deaerated completely by repeated freeze-pump-thaw cycles.

The effects of the exciting light intensity on the peak photocurrent of the acetonitrile as well as the tetrahydrofuran (THF) solutions of the aromatic molecules at room temperature are shown in Figs. 1 and 2, respectively.

One can see from Fig. 1 that the ionization process of phenothiazine as well as that of DPPD in acetonitrile are monophotonic. Since the curves of the photocurrent consist of the exponential rise curve and the hyperbolic decay curve which varies with the initial

* To whom the correspondence should be addressed.

1) J. T. Richards, G. West, and J. K. Thomas, *J. Phys. Chem.*, **74**, 4137 (1970).

2) K. Kawai, N. Yamamoto, and H. Tsubomura, This Bulletin, **43**, 2266 (1970).

3) K. H. Grellmann and A. R. Watkins, *Chem. Phys. Lett.*, **9**, 439 (1971).

4) Y. Taniguchi, Y. Nishina, and N. Mataga, This Bulletin, **45**, 764 (1971).

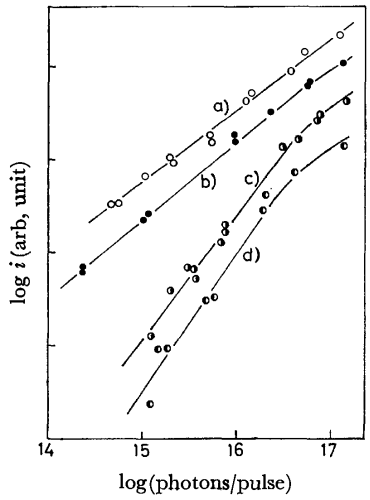

Fig. 1. The effects of the exciting light intensity on the peak photocurrent in acetonitrile solutions. (a) phenothiazine (10^{-3} M), (b) DPPD (10^{-3} M), (c) pyrene (10^{-3} M), (d) perylene (saturated).

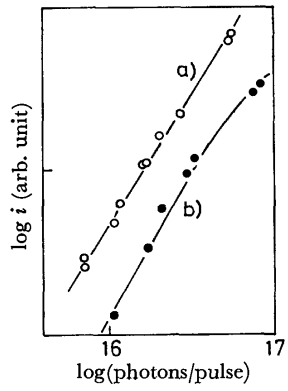

Fig. 2. The effects of the exciting light intensity on the peak photocurrent in THF solutions. (a) phenothiazine (10^{-3} M), (b) DPPD (10^{-3} M).

concentration of ions, *i.e.*, the decay is more remarkable at higher exciting light intensity, the observed value of the peak photocurrent appears to be somewhat smaller than the true value at high light intensity. Therefore, the slopes of the straight lines in Figs. 1 and 2 seem to give slightly smaller values than the real ones. Contrary to this, both ionization processes of the phenothiazine–THF and the DPPD–THF systems are not monophotonic but biphotonic as indicated in Fig. 2. We have confirmed also that the photoionization process of DPPD by the 347 nm pulse is biphotonic in nonpolar solvents.

It has been suggested from a detailed kinetic study that the photo-oxidation of DPPD originates from the upper excited singlet state.[5] Then, the photoionization of DPPD may occur from the upper excited singlet state, since it seems to be certain that the intermediate of the photo-oxidation is a DPPD cation radical.[5] In relation to the above statement, we have observed the laser-induced photocurrent with the rise and decay curves quite similar to the laser pulse in the case of the DPPD-nonpolar as well as moderately polar solvent systems.[6] Although the details of the result will be given elsewhere, the laser-induced photocurrent with very short lifetime might be ascribed to the electrons with a quite large mobility produced by the ionization from the excited Franck-Condon state.

Now, the photoionization process in a considerably polar solvent such as acetonitrile is monophotonic as described above, although the ionization potential of DPPD in the gas phase may be much larger than the energy of 347 nm excitation. However, the energy required for the separation of cation and electron may be compensated by the solvation energies for them. The circumstance in the case of the monophotonic ionization of phenothiazine may be quite similar to that of DPPD. One might suppose that acetonitrile forms a molecular complex with the solute in the ground state and the complex ionizes in the excited state. We have, however, confirmed that there is no indication of such a complex formation in the absorption spectra of these molecules in acetonitrile. Since the solvation energy of THF for the cation and an electron may be much smaller than that of acetonitrile, the monophotonic ionization cannot take place in a THF solution.

We have confirmed that both of the photoionization processes of pyrene and perylene in acetonitrile by the 347 nm pulse are biphotonic as shown in Fig. 1. Of course, the photoionization processes of these molecules in a THF solution are biphotonic. However, it seems to be rather difficult at the present stage of investigation to determine whether the biphotonic ionization process involves excited singlet or triplet state as photoactive intermediate. It might be possible also that both of excited singlet and triplet states are involved in the process as the intermediates.

5) H. Shizuka, Y. Sawaguri, and T. Morita, This Bulletin, **45**, 24 (1972).

6) Y. Taniguchi, A. Miyoshi, and N. Mataga, to be published.

BULLETIN OF THE CHEMICAL SOCIETY OF JAPAN, VOL. 45, 2925—2926 (1972)

Mechanism of Chromic Acid Oxidation of Aldehydes

C. GOSWAMI and Kalyan K. BANERJI*
Department of Chemistry, University of Jodhpur, Jodhpur, India

(Received August 23, 1971)

In a previous communication[1] we showed that the oxidation of acetaldehyde by Cr(VI) involves an attack on the keto-form of the aldehyde and suggested that the reaction proceeds through the transfer of a hydride ion. The present study of the oxidation of chloroacetaldehydes and formaldehyde by chromic acid was undertaken to substantiate the mechanism proposed earlier.

Results

Product Analysis. Oxidation of monochloro-, dichloro-, trichloro-acetaldehydes and formaldehyde by aqueous chromic acid yielded the corresponding carboxylic acid as characterized by the spot tests.[2]

It was observed that for every mole of Cr(VI) consumed, nearly 1.5 mol of the carboxylic acid was formed. The overall reaction may be written as follows.

$$3RCHO + 2CrO_4^{2-} + 10H^+ \longrightarrow 3RCOOH + 5H_2O + 2Cr^{3+} \quad (1)$$

Rate Laws. When the concentrations of the aldehyde and hydrogen ion are in excess, the rate of disappearance of Cr(VI) follows first order rate laws, but the values of rate constants decrease with increase in the concentration of Cr(VI). The results show that the reaction is strictly of first order with respect to acid chromate ion $HCrO_4^-$. Since the results in all aldehydes are similar, only results of reaction with monochloroacetaldehyde (MCA) are reproduced (Table 1).

Table 1. Dependence of reaction rate on the concentration of chromic acid
[MCA] 5.0×10^{-2}M, [H$^+$] 1.0M, temp. 30°C

10^3[Cr(VI)] mol·l^{-1}	10^4[$HCrO_4^-$] mol·l^{-1}	10^5k_1 sec^{-1}	$\frac{10^5k_1[Cr(VI)]}{[HCrO_4^-]}$
1.0	9.24	6.5	7.0
2.5	21.2	5.9	7.0
4.0	31.7	5.6	7.1
5.0	38.0	5.3	7.0
10.0	64.9	4.5	6.9

The concentrations of $HCrO_4^-$ were calculated assuming a value of 2.3×10^{-2} for association constant for dichromate formation ($K=[HCrO_4^-]^2/[Cr_2O_7^{2-}]$) at 30°C.[3]

Table 2. Dependence of the reaction rate on the concentration of aldehyde
[Cr(VI)] 1×10^{-3}M, [H$^+$] 1.0M, temp. 30°C

10^2[MCA]mol·l^{-1}	1.0	2.0	3.0	4.0	5.0
10^4k_1(sec^{-1})	1.3	2.6	4.0	5.4	6.5
10^2k_1/[MCA]	1.30	1.30	1.33	1.35	1.30

The reactions are also of first order with respect to aldehyde (Table 2).

Under the conditions of constant ionic strength the rate is proportional to the square of hydrogen ion concentration (Table 3). There is also a marked positive ionic salt effect.

Table 3. Acidity dependence of the reaction rate
[MCA] 2×10^{-2}M, [Cr(VI)] 1×10^{-3}M, temp. 30°C
Ionic strength (μ)=2.0M

[H$^+$] mol·l^{-1}	0.50	0.75	1.00	1.25	1.50	2.0
10^4k_1 (sec^{-1})	1.2	2.8	5.0	8.1	11.5	20.0
10^4k_1/[H$^+$]^2	6.0	5.0	5.0	5.2	5.1	5.0

Effect of Solvent Composition. Increase in the proportion of acetic acid in the solvent mixture increases the rate of oxidation (Table 4), probably because of the lowering of dielectric constant of the medium,[4] which favours reactions involving protonation. Moreover, in acetic acid, chromic acid exists as acetochromic acid which is assumed to be a stronger acid and a much more powerful oxidizing agent.[5] This also contributes to the increase in the reaction rate.

Effect of Temperature. Data on the effect of temperature on the oxidation rate are summerized in Table 5. A plot of log k against the inverse of temperature gives a straight line. The Arrhenius equation is, therefore, valid for these reactions. The specific rate constant k is obtained from the relation $k=k_1/[\text{Aldehyde}]\,[H^+]^2$.

The activation parameters were also evaluated (Table 6).

Discussion

It has been proposed that aliphatic aldehydes are oxidized *via* their hydrates.[6,7] The aldehydes we studied exist mostly as hydrates in solution, and hence either the aldehyde hydrate or its simple derivative is the most likely intermediate. Since the aldehyde hydrates so closely resemble the alcohols in structure

* Present address: Dyson Perrins Laboratory, South Parks Road, Oxford, OX1 3QY England.

1) C. Goswami and K. K. Banerji, This Bulletin, **43**, 2643 (1970).
2) F. Feigl, "Spot Tests in Organic Analysis," Elsevier Publishing Co., Amsterdam, (1956), p. 382.
3) F. H. Westheimer and A. Novick, *J. Chem. Phys.*, **11**, 506 (1943).
4) M. Cohen and F. H. Westheimer, *J. Amer. Chem. Soc.*, **74**, 4387 (1952).
5) K. B. Wiberg and H. Schafer, *ibid.*, **91**, 927 (1969).
6) T. J. Kemp and W.A. Waters, *Proc. Roy. Soc., Ser. A*, **274**, 480 (1963).
7) J. Rocek, *Tetrahedron Lett.*, **5**, 1 (1959)

Table 4. Solvent composition dependence of reaction rate $10^3k(l^3mol^{-3}sec^{-1})$

Compound	Acetic acid, %					
	20	40	50	60	70	80
HCHO[a)]	47	105	150	230	360	510
$ClCH_2CHO$[a)]	13	26.5	38.5	50	80	110
Cl_2CHCHO[b)]	1.4	2.7	3.8	4.7	6.3	10
CCl_3CHO[b)]	0.23	0.37	0.50	0.66	0.93	1.10

Temp.: a) 30°C, b) 35°C.

Table 5. Effect of temperature on oxidation rate $10^3k(l^3mol^{-3}sec^{-1})$

Compound	Temp. (°C)			
	25	30	35	40
HCHO	34	47	64	87
$ClCH_2CHO$	9.5	13.0	17.3	23
Cl_2CHCHO	0.76	1.05	1.42	1.90
CCl_3CHO	0.12	0.17	0.23	0.32

Table 6. Activation parameters

Compound	ΔE^* kcal mol^{-1}	ΔS^* e.u.	ΔF^* 298°K kcal mol^{-1}
HCHO	11.6	−27	19.6
$ClCH_2CHO$	10.9	−32	20.4
Cl_2CHCHO	11.4	−35	21.8
CCl_3CHO	12.0	−37	23.8

as well as in practically all aspects of oxidation, it is reasonable to expect a similarity in the mode of their oxidation as well.

Recently, Wiberg and Schafer[8)] established that oxidation of alcohols by chromic acid proceeds *via* the chromate esters. We have shown[1)] that oxidation of aldehydes is also best represented by assuming the formation of a similar intermediate which then decomposes in the rate-determining step.

The activation parameters suggest that C–H bond is ruptured in the rate-determining step.[9,10)] This was confirmed by the fact that formaldehyde shows a primary isotope effect.[6)] It is, however, far less clear whether hydrogen leaves as a proton, an atom or an anion. Wiberg and Mill,[11)] and Graham and Westheimer[12)] preferred the abstraction of proton whereas Rocek[7)] favoured the transfer of hydride ion from the substrate to the oxidant. When the rate constants of the aldehydes studied here are plotted against Taft's σ* values,[13)] a straight line is obtained with a value of ρ* approximately −1.1 (Fig. 1).

This result indicates that oxidation is facilitated by

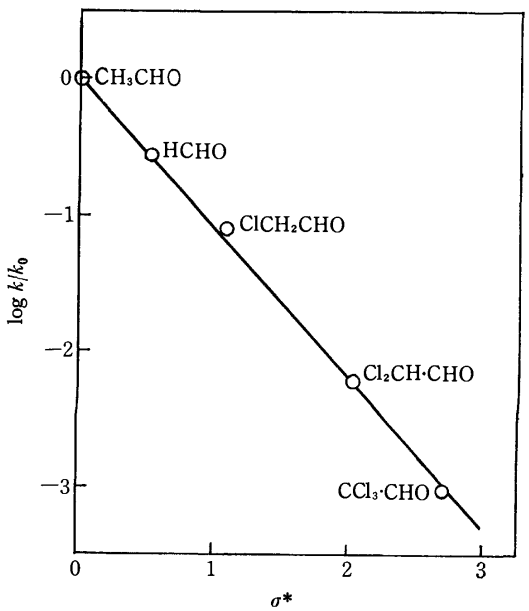

Fig. 1. Dependence of rate constants on Taft's σ* values (Rate data of MeCHO are taken from Ref. 1).

a high electron density at the C–H bond and strongly suggests that the oxidation of aldehydes by chromic acid involves a hydride transfer as follows:

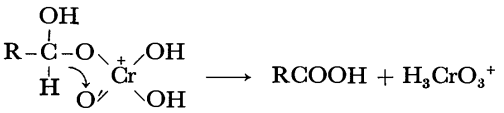

Experimental

Materials. Aldehydes were purified by the usual methods. Perchloric acid (60%, E. Merck) was used as a source of hydrogen ions. Acetic acid (B. D. H., AnalR) was distilled over chromic acid before use. All other chemicals used were chemically pure.

Product Analysis. For a quantitative estimation of carboxylic acid, the completely reduced reaction mixture was shaken with ether, and the amount of the acid present in the ether solution was determined colorimetrically by ferric hydroximate method.[14)]

Kinetic Measurements. The reactions were carried out at constant temperature (±0.05°C). Unless otherwise stated the solvent was 20% acetic acid (v/v). The aldehydes were always kept in excess. Reactions were followed iodometrically.

8) K. B. Wiberg and H. Schafer, *J. Amer. Chem. Soc.*, **91**, 933 (1969).
9) G. V. Bakore and S. Narain, *J. Chem. Soc.*, **1963**, 3419.
10) G. V. Bakore and S. Narain, *Z. Phys. Chem.*, **227**, 8 (1964).
11) K. B. Wiberg and T. Mill, *J. Amer. Chem. Soc.*, **80**, 3022 (1958).
12) G. T. E. Graham and F. H. Westheimer, *ibid.*, **80**, 3030 (1958).
13) R. W. Taft, "Steric Effect in Organic Chemistry," ed. by M. S. Newman, John Wiley & Sons Inc., New York (1956), p. 598.
14) J. Mitchell, Jr., "Organic Analysis," Vol. III, Interscience Publishers Inc., New York (1956), p. 63.

BULLETIN OF THE CHEMICAL SOCIETY OF JAPAN, VOL. 45, 2927—2928 (1972)

The Influence of Off-axial Ligands on the Crystal-field Energies of the Copper(II) Ion

R. J. FEREDAY
University Malaya, Kuala Lumpur, Malaysia

(Received August 30, 1971)

The assignment of the electronic spectra of various complexes of the copper(II) ion has been put on a sounder basis recently by the polarised single-crystal measurements of several workers.[1-10] This has resulted in the reassessment[11-13] of the various theoretical methods used to calculate the *d*-electron energy levels in the copper(II) ion. Both crystal-field[12,13] and orbital overlap[11] methods have been used and found to be in general agreement.[14] The crystal-field approach being the simpler approach, while perhaps not giving as good a physical picture as the orbital overlap method, has been adopted here, as virtually similar results are obtained by both procedures.

One of the problems highlighted by this reinvestigation was the role played by the off-axial ligands in determining the energy of the one-electron *d*-orbitals, especially in the case of the complex $CaCu(CH_3CO_2)_4 \cdot 6H_2O$, which has D_{2d} symmetry, where several reports have been published.[15,16] Off-axial coordination is also found in basically axial copper(II) systems, *e.g.* $Cu(NH_3)_2(CH_3CO_2)_2$ (Ref. 17). This note reports the effect on the *d*-electron orbitals of the inclusion of off-axial coordination and discusses the importance of their contribution in determining the energy-level sequences.

Crystal-field Calculations. These calculations were based on a point charge model described by Krishnamurthy and Schaap[18] and Garner and Mabbs.[13] The same approximations as in Refs. 12 and 13 are made, that is, Dq and Cp of the long bonded ligand have been taken to be:

$$(Dq)' = Dq \times a^5$$

$$\text{and } (Cp)' = Cp \times a^3$$

where $a = R_E/R_A$ (where R_E and R_A are the lengths of the equatorially and axially bonded ligands respectively) and θ is the angle between the axial ligand and the z-axis. The eigenvalues and eigenfunctions resulting from the perturbation by the crystal fields have been evaluated for various values of a and θ.

Results and Discussion

The values chosen for the parameters Dq, Cp, θ, and a were in line with those of other workers,[13,20] and correspond to known physical situations in order that the sensitivity of the energy-levels to the variation of the parameters may be meaningful. The results are presented graphically and are conveniently split into two types, the first representing the variation of the energies of the *d*-orbitals with a (at several values of θ) and the second the variation with θ (at different values of a).

(a) The Effect of Varying a. The effect of the variation of a on the *d*-orbital energy-levels, while maintaining a fixed value of Dq ($=1000\ cm^{-1}$) and Cp ($=4000\ cm^{-1}$) is shown in Fig. 1 which represents several values of θ.

Figure 1 represents the changes in energy of the one electron orbitals, when a is varied, and the angle between the z-axis and the long bonded ligands is 5, 15, and 25° respectively. From these figures it can be

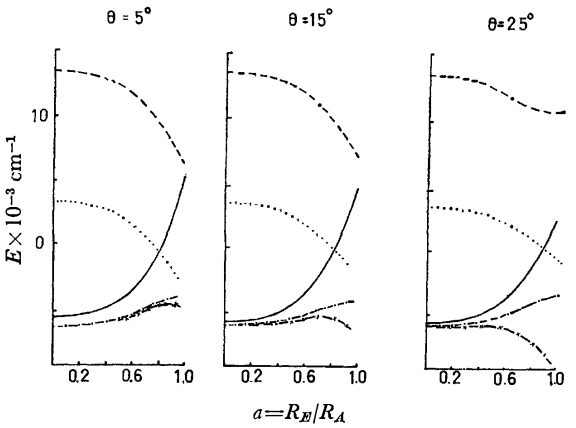

Fig. 1. The variation of the *d* orbital energies with a, when θ=5, 15, and 25°.
——: d_{z^2}, ----: $d_{x^2-y^2}$, ·····: d_{xy}, -·-·: d_{xz} ×-×-: d_{yz}

1) D. E. Billing and B. J. Hathaway, *J. Chem. Soc., A*, **1968**, 1516.
2) D. E. Billing, B. J. Hathaway, and P. Nicholls, *ibid.*, **1969**, 316.
3) D. E. Billing, R. J. Dudley, B. J. Hathaway, P. Nicholls, and I. M. Proctor, *ibid.*, **1969**, 312.
4) B. J. Hathaway, D. E. Billing, and R. J. Dudley, *ibid.*, **1970**, 1420.
5) I. M. Proctor, B. J. Hathaway, D. E. Billing, R. J. Dudley, and P. Nicholls, *ibid.*, **1969**, 1192.
6) B. J. Hathaway, D. E. Billing, R. J. Dudley, R. J. Fereday, and A. A. G. Tomlinson, *ibid.*, **1970**, 806.
7) M. J. Bew, R. J. Dudley, R. J. Fereday, B. J. Hathaway, and R. C. Slade, *ibid.*, **1971**, 1437.
8) J. Fergusen, *J. Chem. Phys.*, **34**, 1609 (1961).
9) T. S. Piper and R. L. Belford, *Mol. Phys.*, **5**, 169 (1962).
10) Y. Nishida and S. Kida, This Bulletin, **43**, 3814 (1970).
11) D. W. Smith, *J. Chem. Soc.*, **1971**, 3035.
12) R. J. Fereday, *ibid., A*, **1969**, 1708.
13) C. D. Garner and F. E. Mabbs, *ibid.*, **1970**, 1711.
14) D. W. Smith, *ibid.*, **1971**, 1024.
15) F. E. Mabbs and W. R. Smail, *ibid.*, **1970**, 1716.
16) D. W. Smith, *ibid.*, **1971**, 1209.
17) Y. A. Simonoo, A. U. Abloo, and T. I. Molmoski, *Kristallografiya*, **8**, 205 (1963).
18) R. Krishnamurthy and W. B. Schaap, *J. Chem. Educ.*, **46**, 799 (1969).
19) R. Krishnamurthy and W. B. Schaap, *ibid.*, **47**, 433 (1970).
20) C. J. Ballhausen and E. M. Ancon, *Kgl. Danske Videnskab Selskab, Mat.-fys. Medd.*, **31**, 3 (1958).

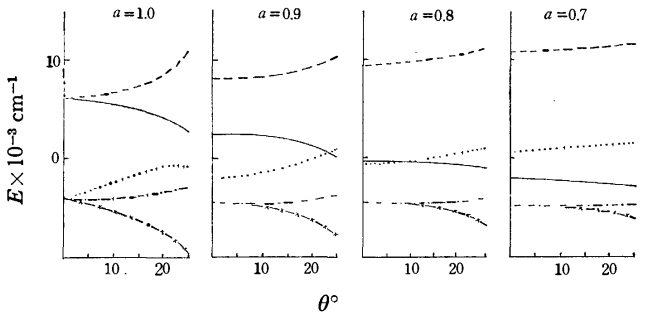

Fig. 2. The variation of the d orbital energies with $\theta°$, when a=1.0, 0.9, 0.8, and 0.7.
——: d_{z^2}, – – –: $d_{x^2-y^2}$, ·····: d_{xy}, –·–·: d_{xz}, ×–×–: d_{yz}

seen that, although the ligands are not directed along the z-axis, they still have a profound effect upon the d-orbital energies. The first obvious difference in these diagrams is the easily intuitively predictable stabilization of the d_{z^2} orbital as θ increases, at least at larger values of a. This effect is still small at θ=5°, but when θ=15 and 25° the d_{z^2} orbital is stabilized by approximately 1500 and 2000 cm^{-1} respectively at $a\approx1.0$. Similarly the $d_{x^2-y^2}$ and d_{xy} orbitals are increased in energy by a corresponding amount. The other obvious feature is the lifting of the degeneracy of the d_{xz} and d_{yz} orbitals, the d_{xz} orbital being destabilized due to the larger potential of the off-axial ligands as they become closer, while the d_{yz} orbital is lowered in energy. The energy-level sequences show little variation with change in the angle θ and are essentially similar to the tetragonal-octahedral case; we might therefore expect similar experimental data. The experimental data available for the complex Cu(ethoxyacetate)$_2\cdot2H_2O$ (Ref. 21) (a=0.84; θ=15°) gives the energy level sequence of the one-electron orbitals as $d_{x^2-y^2} > d_{z^2} > d_{xy} > d_{yz} > d_{xz}$, with the d_{xy} orbital lying close to the d_{z^2} orbital. This is in reasonable agreement with Fig. 1 (θ=15°) with, in fact, the d_{xy} orbital as suggested in Ref. 21, lying very close in energy to the d_{z^2} orbital. However, the relative ordering of the d_{xz} and d_{yz} orbitals are reversed. This may be a result of π-bonding or any covalency effects which are totally ignored in the crystal-field approach.

(b) Variation with θ. A significant feature of all these diagrams is that at values of $a\approx0.7$, the energy-levels obtained for the one-electron orbitals vary very little with the angle θ. This suggests that, although the off-axial ligands have a significant effect on the crystal-field potential as the metal-ligand distance alters (just as in the tetragonal-octahedral case), the variation of θ has little significance and, therefore, the actual position of the ligands (be it axial or off-axial) is of little importance compared with the metal-ligand distance. Thus only when $a\approx1.0$ do the d-orbital energy-levels vary significantly with the angle θ and this is shown most clearly in Fig. 2 which plots the energy of the d-orbitals as θ varies (for several values of a). When $a\approx0.8$, a variation of θ produces little change in the one-electron energy-levels, but at a=1.0, the d-orbital energies have been altered by approximately $\pm$4000 cm^{-1}, a not insignificant change.

In short then, when attempting the assignment of the electronic spectra of copper(II) complexes, which contain off-axial ligands, we may in essence treat the problem as being that of assigning a tetragonal-octahedral complex, as the most important contribution in determining the energy of the one-electron d-orbitals is the metal-ligand distances and the actual value of θ is, at best, only a secondary consideration. Notwithstanding this, when $a\approx1.0$, then the value of θ does become significant and may cause a change in transition energy by as much as 4000 cm^{-1}.

Nevertheless, it must be noted that the crystal-field approach will tend to overestimate the contribution due to the long-bonded ligands,[14] much smaller effects being predicted when using the orbital overlap procedure and a certain amount of care must be employed in the assignment of these spectra.

21) R. J. Fereday and B. J. Hathaway, *J. Chem. Soc., A*, **1971**, 2760.

BULLETIN OF THE CHEMICAL SOCIETY OF JAPAN, VOL. 45, 2929—2930 (1972)

ESR Study of V_2O_5, MoO_3, and V_2O_5–MoO_3 Catalysts

R. S. MANN and K. C. KHULBE
Faculty of Science and Engineering, University of Ottawa, Ottawa, Canada

(Received October 8, 1971)

Tarama and co-workers[1] and other investigators[2,3] have demonstrated the usefulness of electron spin resonance (ESR) in obtaining information about the local structure surrounding V^{4+} ion in V_2O_5 catalyst. Petcherskaya *et al.*[4] and Kazanskii and co-workers[5] could not observe any ESR signal in pure vanadium pentoxide, while Tarama *et al.*[1,5] reported a single broad ESR signal. This contrast may be due to the different methods employed for the preparation of the catalysts. In this note the results of ESR studies of the catalysts V_2O_5, MoO_3, and V_2O_5–MoO_3 system, have been compared with the results of the other investigators.

The mixed oxide catalyst was prepared by weighing ammonium molybdate (B. D. H., A. R. Grade) and ammonium metavanadate (Fisher) according to a desired ratio of the MoO_3 and V_2O_5. Ammonium molybdate dissolved in distilled water was mixed with ammonium metavanadate to make a paste. The paste was dried for 12 hr at 40°C and for 6 hr at 150°C. The temperature was increased stepwise and maintained successively for 2 hr at 200, 300, and 400°C. The catalyst was calcined at 500°C for 6 hr and activated at 600°C for 2 hr. Pure MoO_3 and V_2O_5 were obtained by thermal decomposition of ammonium molybdate and purified ammonium metavanadate. The catalysts were calcined at same temperature similar to their mixtures.

Recently Dosi[6] studied the oxidation of methanol over these catalysts and observed that 20: 80 vanadium pentoxide and molybdenum trioxide catalyst proved to be highly active and selective for the formaldehyde formation and gave nearly 99% conversion of methanol to formaldehyde for a feed ratio, (W/F), of 31.7 gm·hr/mol and 8 mol percent methanol in air.

The ESR measurements were carried out by a Varian E9, ESR spectrometer, in which the microwave frequency was in the X band and a 2G modulation was adopted. All measurements were made at room temperature unless otherwise noted.

Pure V_2O_5 showed an asymmetric broad ESR signal (Fig. 1) for which g value was 1.972. Pure MoO_3 gave no ESR signal. On addition of 10% V_2O_5 to MoO_3, strong signals were obtained (Fig. 2). Similar

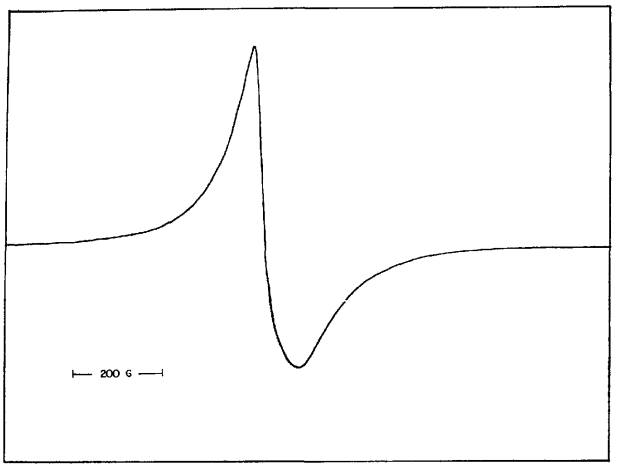

Fig. 1. 100% V_2O_5.

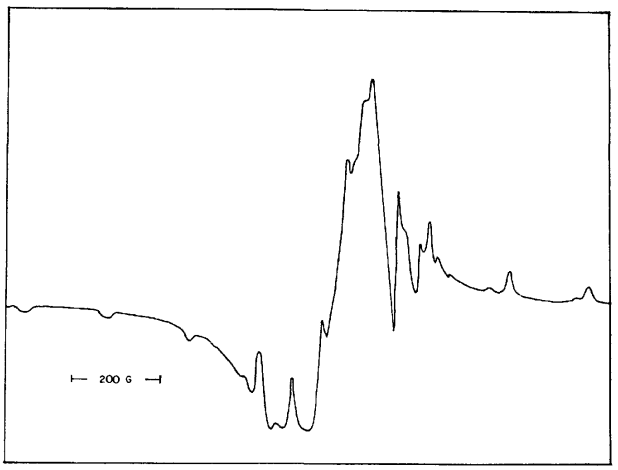

Fig. 2. 10% V_2O_5-90% MoO_3.

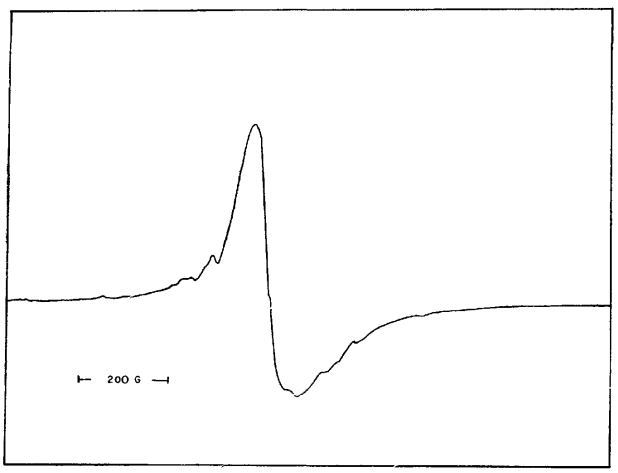

Fig. 3. 50% V_2O_5–50% MoO_3.

1) K. Tarama, S. Teranishi, S. Yoshida, and N. Tamura, Proc. Intern. Congr. Cat. 3rd Amsterdam, (1964), p. 202, North America Publ. Co. 1965.
2) V. B. Kazanskii, Z. I. Ezhkova, A. G. Lyubarskii, V. V. Voevodskii, and I. I. Ioffe, *Kinet. Katal.* **2**, 862 (1961).
3) K. Hirota and K. Kuwata, This Bulletin, **36**, 229 (1963).
4) V. I. Petcherskaya, V. B. Kazanskii, and V. V. Voevodskii, Proc. Intern. Cong. Cat. 2nd Paris, 1961, Edition Technip 2121.
5) K. Tarama, S. Teranishi, S. Yoshida, and H. Yoshida, This Bulletin, **34**, 1195 (1961).
6) M. K. Dosi, M. A. Sc. Thesis, University of Ottawa, Ottawa, 1971.

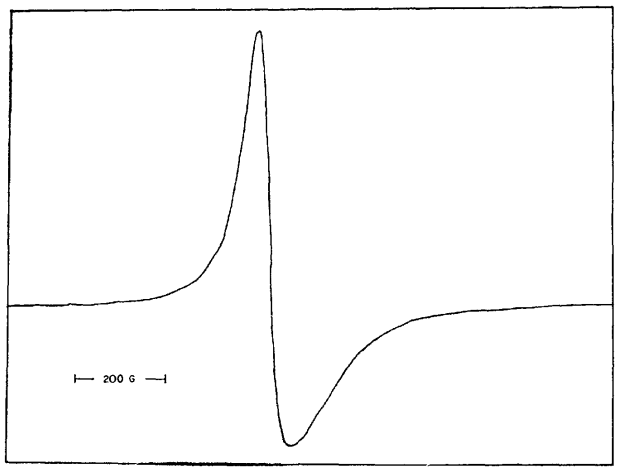

Fig. 4. 75% V_2O_5–25% MoO_3.

results were obtained by Tarama *et al.*[5] for the sample containing 15 mol% V_2O_5 and 8.5 mol% $K_2S_2O_7$. Tarama *et al.*[1] observed that every sample of the V_2O_5–MoO_3 system (5, 25, 50, 75, 95, and 100% V_2O_5) gave a single broad ESR spectrum and their shapes were similar to the pattern of the pure V_2O_5 sample. In the present study 10% V_2O_5–90% MoO_3 showed more than eleven components (Fig. 2). However, these components disappeared on further addition of V_2O_5 to MoO_3 (Figs. 3 and 4). Catalyst containing 75% V_2O_5 and pure V_2O_5 gave one broad signal. The intensity of ESR signal was highest for 10% V_2O_5–75% MoO_3 catalyst and decreased with increasing concentration of V_2O_5 in the system. The disparity between the shape of spectra observed by Tarama *et al.*[1] and in the present study in MoO_3–V_2O_5 system are atrributed to the dissimilarity in the methods of preparation of the two catalysts. The present work supports the views of Tarama *et al.*,[1] who suggested that the ESR spectrum of the system is not due to Mo^{5+} as proposed by Petcherskaya *et al.*,[4] but due to V^{4+}.

Kazanskii *et al.*,[2] found that pure MoO_3 and V_2O_5 do not give any ESR signals (at room temperature and at −196°C), but in freshly prepared mixed catalysts which have not been used in a reaction an ESR signal was observed whose width and intensity depended on the molybdenum content. With a molybdenum content less than 5% the signal has hyperfine structure (HFS) consisting of two groups of lines with a split between the 50 and 140G components in each group. But in the present study no such spectra were observed. It seems that the method for the preparation of the catalyst plays an important role to give ESR spectra.

For the purpose of comparison, the ESR spectrum of Analar Grade V_2O_5 (Fisher certified) was taken. The signal intensity observed with the sample (Fisher) was approximately 6 times less than the intensity of V_2O_5 catalyst prepared in our laboratory, confirming the dependence of the ESR spectrum on the method of the preparation and activation of the catalyst.

On raising the temperature of the catalyst, (upto 400°C) the intensity of ESR signals of V_2O_5 and V_2O_5–MoO_3 decreased.

The authors wish to thank Dr. I. C. P. Smith, National Research Council, Canada for allowing us the use of the ESR apparatus and NRC, Canada for grant.

BULLETIN OF THE CHEMICAL SOCIETY OF JAPAN, VOL. 45, 2930—2932 (1972)

The Preparation of Acyl Alkoxycarbonyl Sulfides and the Related Compounds

Shinichi MOTOKI and Hikaru SATSUMABAYASHI

Department of Chemistry, Faculty of Science, Science University of Tokyo, Kagurazaka, Shinjuku-ku, Tokyo

(Received November 19, 1971)

A number of mixed carboxylic carbonic anhydrides (**1**) were prepared by the reaction of carboxylic acid and chloroformate in a series of studies by Tarbell.[1] *p*-Nitrobenzoic thiolcarbonic anhydrides (**3**), the sulfur analogue of the mixed anhydride, were prepared from *p*-nitrobenzoic acid and thiolchloroformate more recently.[2] In the present paper, the preparation of another types of sulfur analogues of the mixed anhydride such as acyl alkoxycarbonyl sulfides (**2**) and acyl alkylthiocarbonyl sulfides (**4**) is described.[3]

$$RCOXH + ClCOYR' \longrightarrow R\text{-}\overset{\overset{O}{\|}}{C}\text{-}X\text{-}\overset{\overset{O}{\|}}{C}\text{-}Y\text{-}R'$$

1: X=O, Y=O **3**: X=O, Y=S
2: X=S, Y=O **4**: X=S, Y=S

First, acyl alkoxycarbonyl sulfides (**2a**—**f**) were pre-

1) D. S. Tarbell and J. A. Price, *J. Org. Chem.*, **21**, 144 (1956), and the later papers.

2) D. S. Tarbell and T. Parasaran, *ibid.*, **29**, 2471 (1964); L. Wei and D. S. Tarbell, *ibid.*, **33**, 1884 (1968).

3) During the course of the present work, H. Yoshida, T. Ogata, and S. Inokawa reported the synthesis of **4** starting from tetramethylammonium dithiolcarbonate [This Bulletin, **44**, 1949 (1971)] and H. Böhme and H. P. Steudel reported the synthesis of **2** starting from potassium *O*-alkyl thiolcarbonate [*Ann.*, **730**, 121 (1969)].

Table 1. Acyl alkoxycarbonyl sulfides; RCOSCOOR′

Compound	R	R′	Bp (°C/mmHg)	Yield (%)	Found (%) C	H	S	Calcd (%) C	H	S
2a	CH_3	CH_3	60—61/6	23	35.37	4.50	23.44	35.81	4.51	23.90
2b	CH_3	C_2H_5	63—65/5	23	41.07	5.55	21.20	40.53	5.44	21.64
2c	CH_3	n-C_3H_7	52—53/1	26	44.95	6.23	20.11	44.43	6.21	19.77
2d	CH_3	i-C_4H_9	66.5—67/1.5	24	47.81	6.81	18.03	47.71	6.86	18.19
2e	C_2H_5	n-C_3H_7	63.5—64.5/1.5	30	47.95	6.79	17.92	47.71	6.86	18.19
2f	C_2H_5	i-C_4H_9	65—66/1	13	50.90	7.41	16.68	50.50	7.42	16.85

Table 2. Diacyl sulfides and bis(alkoxycarbonyl)sulfides

Diacyl sulfides, $(RCO)_2S$ Compound	R	Bp (°C/mmHg)	Yield[a] (%)	Bis(alkoxycarbonyl)sulfides, $(R'OCO)_2S$ Compound	R′	Bp (°C/mmHg)	Yield[a] (%)	Found (Calcd) C(%)	H(%)	S(%)
5a	CH_3	38—39.5/5 (lit, 63/20)	45	**6a**	CH_3	79.5/7 (mp 34—35)	35	31.72 (32.00)	4.29 (4.03)	21.10 (21.35)
5b			45	**6b**	C_2H_5	87—88/4.5 (lit, 118/22)	47	40.75 (40.44)	5.71 (5.66)	18.01 (17.99)
5c			27	**6c**	n-C_3H_7	87—88/1.5	22	46.64 (46.59)	6.60 (6.84)	15.68 (15.55)
5d			39	**6d**	i-C_4H_9		21			
5e	C_2H_5	54—55/3	36	**6e**	n-C_3H_7		23			
5f			66	**6f**	i-C_4H_9	87—93/1	52	51.48 (51.26)	7.49 (7.74)	13.72 (13.68)

a) Calculated based on the assumption that these compounds were formed by the decomposition of **2** according to the following reaction; 2 RCOSCOOR′ ⟶ $(RCO)_2S+(R'OCO)_2S$, [*Ann.*,**730**, 121 (1969)].

pared from thiocarboxylic acid and alkyl chloroformate in THF at −50°C in the presence of triethylenediamine (Table 1). In the preparation, diacyl sulfides (**5a**—**f**) and bis(alkoxycarbonyl)sulfides (**6a**—**f**) were isolated as by-products (Table 2). The NMR spectra and the analytical values were in accord with the expected structure for **2a**—**f** and **6a**—**f** (Tables 1 and 2) and the IR spectra of **2a**—**f** showed the double peaks (about 1780 and 1720 cm^{-1}) in the carbonyl region which resemble closely the typical anhydride absorption. Butyryl methoxycarbonyl sulfide (**2g**) and butyryl ethoxycarbonyl sulfide (**2h**) were not isolated because the boiling point was very close to those of the by-products. When triethylamine was used in the reaction instead of triethylenediamine, **2** was not obtained but **5** and **6** were formed. *p*-Nitrobenzoyl benzyloxycarbonyl sulfide (**2i**) was obtained as pale yellow crystals by a similar procedure, accompanied by no bis(*p*-nitrobenzoyl)sulfide (**5i**) or bis(benzyloxycarbonyl)sulfide (**6i**) as by-products.

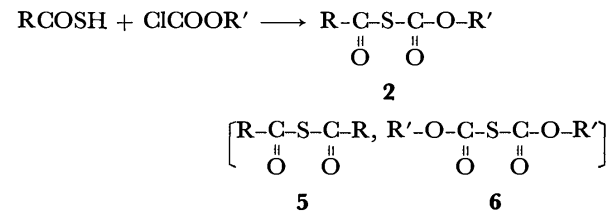

2

5 **6**

a: R=CH_3, R′=CH_3 **e**: R=C_2H_5, R′=n-C_3H_7
b: R=CH_3, R′=C_2H_5 **f**: R=C_2H_5, R′=i-C_4H_9
c: R=CH_3, R′=n-C_3H_7 **i**: R=p-$O_2NC_6H_4$,
d: R=CH_3, R′=i-C_4H_9 R′=$C_6H_5CH_2$

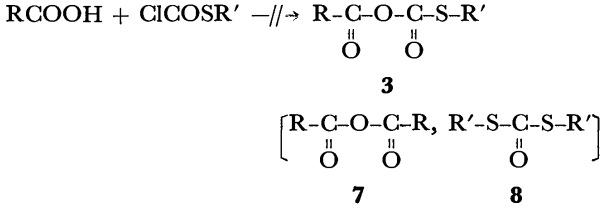

3

7 **8**

a: R=CH_3, R′=C_2H_5

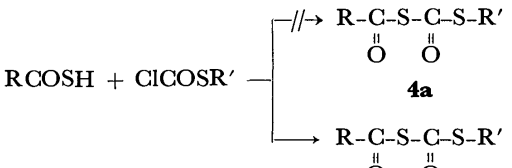

4a

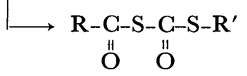

4b

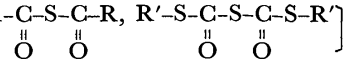

9a **10a**

a: R=CH_3, R′=C_2H_5
b: R=p-$O_2NC_6H_4$, R′=$C_6H_5CH_2$

Although *p*-nitrobenzoic thiolcarbonic anhydrides (**3**) were already prepared by Tarbell,[2] preparation of acetic ethylthiolcarbonic anhydride (**3a**) was unsuccessful in the present study, and the reaction in the presence of triethylamine afforded acetic anhydride (**7a**) and diethyl dithiolcarbonate (**8a**).

Similarly, *p*-nitrobenzoyl benzylthiocarbonyl sulfide (**4b**) was obtained from *p*-nitrothiobenzoic acid and benzyl thiolchloroformate but acetyl ethylthiocarbonyl

sulfide (**4a**) was not obtained from thioacetic acid and ethyl thiolchloroformate. Diacetyl sulfide (**9a**) and bis(ethylthiocarbonyl)sulfide (**10a**)[4] were formed as by-products.

Experimental

Materials. Thioacetic acid was obtained commercially. Thiopropionic acid was prepared by the method of Kitamura.[5] *p*-Nitrothiobenzoic acid prepared by the method of Khaletskii and Yanovitskaya[6] was recrystallized from *n*-hexane, mp 94—95°C (lit,[7] mp 94°C).

Methyl, ethyl, isobutyl, and benzyl chloroformates obtained commercially were purified by distillation. *n*-Propyl chloroformate and benzyl thiolchloroformate were prepared by the method of Tarbell and Longosz.[8]

Commercially available triethylenediamine was used after sublimation.

Acyl Alkoxycarbonyl Sulfides (2a—f). To a cooled solution of 0.1 mol of triethylenediamine in 500 m*l* of anhydrous THF, 0.2 mol of thiocarboxylic acid was added slowly. After cooling the mixture to −50°C, 0.2 mol of alkyl chloroformate was added dropwise over a period of 1 hr with vigorous stirring. The stirring was continued for additional 2 hr and then the temperature of the mixture was allowed to rise to −10°C. The amine hydrochloride was removed by filtration, and the THF was evaporated under reduced pressure. Fractional distillation of the residue gave acyl alkoxycarbonyl sulfide (**2a—f**), diacyl sulfide (**5a—f**) and bis(alkoxycarbonyl)sulfide (**6a—f**). The results are shown in Tables 1 and 2.

p-*Nitrobenzoyl Benzyloxycarbonyl Sulfide (2i).* To a solution of 3.66 g (0.02 mol) of *p*-nitrothiobenzoic acid and 3.41 g (0.02 mol) of benzyl chloroformate in 200 m*l* of anhydrous ether, 1.12 g (0.01 mol) of triethylenediamine in a mixture of 20 m*l* of ether and 10 m*l* of THF was added dropwise over a period of 1 hr with vigorous stirring at −60°C. The stirring was continued for additional 3 hr and then the temperature of the mixture was allowed to rise to 10°C. The amine hydrochloride was filtered, and the solvent was evaporated at room temperature. Recrystallization of the solid residue from chloroform-petroleum ether yielded 2.83 g (45%) of **2i** as pale yellow needles, mp 92—94°C.

Found: C, 56.92; H, 3.57; N, 4.50; S, 10.11%. Calcd for $C_{15}H_{11}O_5NS$: C, 56.78; H, 3.49; N, 4.41; S, 10.10%. IR ($CHCl_3$) cm^{-1}: 1766, 1694 (>C=O).

p-*Nitrobenzoyl Benzylthiocarbonyl Sulfide (4b).* This sulfide was prepared from 3.66 g (0.02 mol) of *p*-nitrothiobenzoic acid, 3.73 g (0.02 mol) of benzyl thiolchloroformate and 1.12 g (0.01 mol) of triethylenediamine in 200 m*l* of THF in a similar way to the preparation of **2i**. After removing the THF, the residue was filtered to yield 2.83 g of solid material which melted at 60—130°C. Petroleum ether (500 m*l*) was added to the solid. The mixture was refluxed for short time, and filtered to remove insoluble material. Cooling the filtrate gave 0.65 g (10%) of **4b** as pale yellow needles, mp 72—73°C with decomposition.

Found: C, 54.04; H, 3.32; N, 4.19; S, 19.27%. Calcd for $C_{15}H_{11}O_4NS_2$: C, 54.04; H, 3.33; N, 4.20; S, 19.24%. IR ($CHCl_3$) cm^{-1}: 1731, 1690, 1646 (>C=O).

Recrystallization of the insoluble material from toluene gave 0.70 g (21%) of bis(*p*-nitrobenzoyl)sulfide (**9b**) as yellow needles, mp 135.5—137°C.

Found: C, 50.63; H, 2.42; N, 8.36; S, 9.52%. Calcd for $C_{14}H_8O_6N_2S$: C, 50.60; H, 2.43; N, 8.43; S, 9.65%.

4) Bp 108—109°C/1 mmHg, Found: C, 34.62; H, 4.85; S, 45.30%. Calcd for $C_6H_{10}O_2S_3$: C, 34.25; H, 4.79; S, 45.75%.

5) R. Kitamura, *Yakugaku Zasshi*, **57**, 31 (1937).

6) A. M. Khaletskii and A. M. Yanovitskaya, *Zh. Obshch. Khim.*, **19**, 1193 (1949).

7) F. J. Ritter, Rubber-Stichting, Delft, Commun., No. **324**, (1956) 130 pp.; *Chem. Abstr.*, **50**, 16168 (1956).

8) D. S. Tarbell and E. J. Longosz, *J. Org. Chem.*, **24**, 774 (1959).

BULLETIN OF THE CHEMICAL SOCIETY OF JAPAN, VOL. 45, 2932—2934 (1972)

Reactions between Acyl Halides and Silver Hyponitrite

Masatsugu SEKIGUCHI, Michio KOBAYASHI, and Hiroshi MINATO

Department of Chemistry, Faculty of Science, Tokyo Metropolitan University, Fukazawa, Setagaya, Tokyo

(Received March 31, 1972)

Organic esters of hyponitrous acid (HON=NOH) have not been studied extensively, the only examples reported being ethyl,[1] benzyl,[2] and *t*-butyl[3] esters. In connection with the generation of sulfonyloxy radicals, disulfonyl hyponitrites appear to be of interest as a possible source of sulfonyloxy radicals. The reaction between silver hyponitrite and *p*-toluenesulfonyl bromide and that between silver hyponitrite and benzoyl chloride have been investigated, and the results are given in this paper.

Results and Discussion

Since silver hyponitrite decomposes slowly upon irradiation of light, the reactions were carried out in its absence. Silver hyponitrite is hardly soluble in any organic solvent (including DMF, HMPA, and DMSO), and the reactions were carried out in heterogeneous media in the presence of excess hyponitrite.

When *p*-toluenesulfonyl bromide was let to react with silver hyponitrite in various solvents at room temperature or lower temperatures (0 to −30°C), di-*p*-toluenesulfonyl hyponitrite was not formed and nitrous oxide and nitrogen evolved. The results of the products analyses are given in Table 1.

1) J. R. Partington and C. C. Shah, *J. Chem. Soc.*, **1932**, 2589.
2) J. B. Sousa and S. K. Ho, *ibid.*, **1961**, 1788; *Nature*, **186**, 776 (1960); N. H. Ray, *J. Chem. Soc.*, **1960**, 4023.
3) H. Kiefer and T. G. Traylor, *Tetrahedron Lett.*, **1966**, 6163; R. L. Huang, T. W. Lee, and S. H. Ong, *J. Chem. Soc., C*, **1969**, 40; R. C. Neuman and R. J. Bussey, *J. Amer. Chem. Soc.*, **92**, 2440 (1970).

Table 1. Products of reactions between *p*-toluenesulfonyl bromide (TsBr) and silver hyponitrite

Reactants (mmol)		Solvent	Time[a] (hr)	Products (mol/mol TsBr Used)				Ts% Accounted For	(N_2+N_2O) mol/200 molTsBr
TsBr	$Ag_2N_2O_2$			TsOTs	TsOAg	N_2O	N_2		
2.00	5.0	$C_2H_4Cl_2$	3 (3)	0.391	trace	0.156	1.114	78.2	54
2.00	4.0	$C_2H_4Cl_2$	15 (3)	0.431	0.153	0.086	0.035	100	24
16.00	40.0	$C_2H_4Cl_2$	48 (48)	0.388	0.234	(b)	(b)	100	80[b]
12.00	11.1	$C_2H_4Cl_2$	20 (20)	0.239	0.447	0.096	0.159	92.5	54
2.00	3.4	CH_2Cl_2	15 (3)	0.401	0.156	0.146	0.042	95.8	38
2.00	5.0	C_6H_6	15 (2)	0.350	0.135	0.125	9.004	83.5	26
2.00	2.5	CH_3CN	15 (0.5)	—	0.840	0.304	0.002	84.0	62

a) Products were analyzed after the time shown, except for gaseous products which were analyzed when the reaction appeared essentially complete; the time which elapsed before the analyses of gas is shown in parentheses.
b) The amount of total gas was determined with a gas buret.

No *p*-toluenesulfonic anhydride was found in acetonitrile. Silver *p*-toluenesulfonate is soluble in acetonitrile, but not in other solvents in which it covers the surface of silver hyponitrite hindering the reaction between silver hyponitrite and *p*-toluenesulfonic anhydride in solution. Silver *p*-toluenesulfonate does not behave thus in acetonitrile, and *p*-toluenesulfonic anhydride is smoothly converted into silver *p*-toluenesulfonate by the reaction with silver hyponitrite. By a separate experiment, it was confirmed that *p*-toluenesulfonic anhydride reacts with silver hyponitrite, forming silver *p*-toluenesulfonate.

Since the reaction took place between the solid salt and *p*-tosyl bromide in solution and the solubility of the salt differed with the solvent, the results of the reaction varied with solvent. In 1,2-dichloroethane, considerable amounts of nitrogen were evolved. This indicates that the following homolysis takes place to some extent in 1,2-dichloroethane.

$$\mathrm{AgON{=}NOAg + 2TsBr \xrightarrow{-2AgBr}}$$
$$\mathrm{TsON{=}NOTs \longrightarrow 2TsO\cdot + N_2} \quad (1)$$

In order to obtain further evidence for the formation of *p*-tosyloxy radicals, the reaction was carried out in benzene, which is expected to be substituted by *p*-tosyloxy radical. However, it was found that in benzene almost all the gas evolved was not nitrogen but nitrous oxide, and thus the homolysis shown above must be a very minor reaction in benzene.

As for the reaction responsible for evolution of nitrous oxide, the following two processes are possible.

$$\mathrm{AgON{=}NOAg + 2TsBr \xrightarrow{-2AgBr}}$$
$$\mathrm{TsON{=}NOTs \longrightarrow TsOTs + N_2O} \quad (2)$$
$$\mathrm{AgON{=}ONAg + TsBr \xrightarrow{-AgBr}}$$
$$\mathrm{TsON{=}NOAg \longrightarrow TsOAg + N_2O} \quad (3)$$

Silver *p*-tosylate can be converted into *p*-toluenesulfonic anhydride, and *vice versa*, depending upon the reaction conditions; the reaction between silver *p*-tosylate and *p*-tosyl bromide yields *p*-toluenesulfonic anhydride, and that between *p*-toluenesulfonic anhydride and silver hyponitrite yields silver *p*-tosylate.

$$\mathrm{TsOAg + TsBr \xrightarrow{-AgBr} TsOTs}$$
$$\mathrm{\uparrow \xleftarrow[-N_2O]{+AgON{=}NOAg} \downarrow}$$

It was reported that a mixture of benzoyl halides and silver hyponitrite initiates polymerization of ethylene.[4] However, products and the mechanism of the reaction were not described. In order to ascertain whether or not free radicals are produced from these reactants, the reaction was studied in some detail. The results are given in Table 2.

The major component of the gas evolved was nitrous oxide. Thus homolysis (4) should be a minor reaction, Nitrous oxide was evolved either by reaction (5) or (6).

$$\mathrm{AgON{=}NOAg + 2BzCl \xrightarrow{-2AgCl}}$$
$$\mathrm{BzON{=}NOBz \longrightarrow 2BzO\cdot + N_2} \quad (4)$$
$$\mathrm{AgON{=}NOAg + 2BzCl \xrightarrow{-2AgCl}}$$
$$\mathrm{BzON{=}NOBz \longrightarrow BzOBz + N_2O} \quad (5)$$
$$\mathrm{AgON{=}NOAg + BzCl \xrightarrow{-AgCl}}$$
$$\mathrm{BzON{=}NOAg \longrightarrow BzOAg + N_2O} \quad (6)$$

Chlorodiphenyls and nitrodiphenyls were formed in small yields from the reactions in chlorobenzene and nitrobenzene, respectively. In order to clarify the nature of this phenylation, the isomer distributions of the substituted diphenyls were studied by gas chromatography. The isomer distribution of chlorodiphenyls is *o*- 59.8, *m*- 23.3, and *p*- 16.9%; that of nitrodiphenyls is *o*- 53.5, *m*- 12.5, and *p*- 33.9%. They are similar to the isomer distributions found in free radical phenylation with benzoyl peroxide or *N*-nitrosoacetanilide. This also supports the idea that homolysis (4) takes place to a small extent.

In summary, the reactions between *p*-tosyl bromide and silver hyponitrite yield both nitrogen and nitrous oxide, the former probably being a product of the homolysis of di-*p*-tosyl hyponitrite formed as an intermediate, and the latter a product of ionic reactions.

4) G. Scott and L. Seed, Brit. 839884 (1960); U. S. 2946776 (1960); A Mercer and D. A. Scott, Brit. 848492 (1960); *Chem. Abstr.*, **55**, 5346 (1961).

TABLE 2. PRODUCTS OF REACTIONS BETWEEN BENZOYL CHLORIDE AND SILVER HYPONITRITE

Reactants (mmol)		Solvent	Products (mol/mol BzCl Used)					Ph % Accounted For	(N_2+N_2O) mol/200 mol BzCl
BzCl	$Ag_2N_2O_2$		Bz_2O	BzOH	Substituted Diphenyls	N_2O	N_2		
4.00	4.00	PhCl	0.416	0.072	0.0088	0.290	0.02	91.3	61.0
4.00	4.00	$PhNO_2$	0.335	0.135	0.0085	(a)	(a)	95.4	59.6

a) not determined.

The reactions between benzoyl chloride and silver hyponitrite were essentially similar.

Experimental

Materials. Silver hyponitrite was prepared by the reduction of silver nitrate with sodium amalgam.[5] *p*-Toluenesulfonyl bromide was synthesized by the reaction of sodium *p*-toluenesulfinate and bromine.[6] Solvents were purified by conventional procedures.[7]

Reactions between Silver Hyponitrite and p-*Toluenesulfonyl Bromide.* In a helium atmosphere, well-dried powder of silver hyponitrite (1.380 g, 5 mmol) was slowly added for about 1 hr to a stirred solution of *p*-toluenesulfonyl bromide (0.470 g, 2 mmol) in 1,2-dichloroethane (6 m*l*) at room temperature. After stirring was continued for 3 hr, the gas evolved was collected in a sampling tube and subjected to gas-chromatographic analysis (a Shimadzu Gas Chromatograph GC3AH, helium 60 m*l*/min, 35°C, a 1 m silica gel column; retention time, O_2 and N_2, 0.30 min, N_2O, 4.2 min). The possibility of contamination of nitrogen from air was checked by observing the amount of oxygen in the gas (a 1 m molecular sieve 5A column, helium 120 m*l*/min, 35°C; retention time, O_2, 0.45 min, N_2, 0.55 min). The identity of nitrous oxide and nitrogen was further confirmed by use of a mass spectrometer. The mass spectrum of the gas evolved showed peaks at 44 (N_2O), 30 (NO), and 28 (N_2). By comparison with the mass spectra of pure N_2O (at 70 eV, N_2O 100, NO 25.6, N_2 11.0) and pure N_2, the presence and the amounts of N_2O and N_2 in the gas evolved were determined.

The reaction mixture was filtered, and the residue was washed with 1,2-dichloroethane. When the filtrate and washings were combined and evaporated under reduced pressure, white solids of *p*-toluenesulfonic anhydride (0.309 g) were obtained (IR, 1400, 1200, and 1180 cm^{-1}). The identity of *p*-toluenesulfonic anhydride was further checked by the reaction with aniline; from 100 mg of the anhydride, 67 mg of $PhNH_3^+OTs^-$ and 88 mg of PhNHTs were obtained. When a similar reaction mixture was allowed to stand overnight at room temperature, the amount of the anhydride decreased (0.281 g, 0.862 mmol) and a considerable amount of silver *p*-tosylate was found (0.085 g, 0.305 mmol). The amount of silver *p*-tosylate was determined by converting it into *S*-benzylisothiuronium *p*-tosylate by the reaction with *S*-benzylisothiourea hydrochloride.

Reactions in dichloromethane, benzene, and acetonitrile were carried out in a similar manner.

Reactions between Silver Hyponitrite and Benzoyl Chloride. In a helium atmosphere, well-dried powder of silver hyponitrite (1.104 g, 4.0 mmol) was slowly added for about 1 hr to a stirred solution of benzoyl chloride (0.560 g, 4.0 mmol) in chlorobenzene (11.26 g). After 3.5 hr, the gas collected was analyzed as described above.

The reaction mixture was filtered, the filtrate and washings were combined and extracted with a saturated $NaHCO_3$ solution. From the alkaline extracts, 35 mg (0.287 mmol) of benzoic acid was obtained. Benzoic anhydride contained in the organic layer was converted into PhCONHPh by the reaction with aniline; 0.337 g (1.71 mmol).

For determination of the amounts of chlorodiphenyls, a similar reaction mixture was prepared by a separate experiment, and concentrated. Benzoic anhydride was decomposed by refluxing with a 10% NaOH solution (10 m*l*) and ethanol (10 m*l*). The mixture was extracted with ether, the ethereal extracts were dried over anhydrous magnesium sulfate, and then concentrated. The amounts of *o*-, *m*-, and *p*-chlorodiphenyl in the residue were determined by gas chromatography (a Hitachi K-53 Gas Chromatograph, a 5 m Apiezon grease L column, 190°C; internal standard, dibenzyl).

Grateful acknowledgment is made to the donors of the Petroleum Research Fund, administered by the American Chemical Society, for support of this research.

5) A. Hantzsch and L. Kaufmann, *Ann.*, **292**, 320, 323 (1896); G. Brauer, "Handbook of Preparative Inorganic Chemistry," Vol. 1, Academic Press Inc., New York (1963), p. 493; R. C. Newman and R. J. Bussey, Ref. 3.

6) F. C. Whitmore and F. H. Hamilton, "Organic Syntheses," Coll. Vol. I, p. 492 (1941).

7) W. Weissberger, "Organic Solvents," Interscience Publishers, Inc., New York (1955).

BULLETIN OF THE CHEMICAL SOCIETY OF JAPAN, VOL. 45, 2935 (1972)

Preparation of Rhodium Acrolein Complexes

Masanobu HIDAI, Kazuo ISHIMI, Masa-aki IWASE, and Yasuzo UCHIDA
Department of Industrial Chemistry, The University of Tokyo, Hongo, Tokyo

(Received May 18, 1972)

Several acrolein complexes of nickel,[1] iron,[2] molybdenum,[3] and copper[4] have been known. We have now prepared rhodium acrolein complexes from acrolein and the rhodium(I) cyclooctene complex $[RhCl(C_8H_{14})_2]_2$.

Acrolein reacts smoothly with $[RhCl(C_8H_{14})_2]_2$ in toluene at $-10°C$ under nitrogen and a brown complex formulated as $RhCl(CH_2{=}CHCHO)_2$ (I) was obtained in a high yield. Infrared spectroscopic evidence indicates the manner of attachment of acrolein to the metal atom. The C=C stretching frequency of acrolein is shifted about 13 cm^{-1} to the lower frequency side by the ligation. Two strong C=O stretching bands are observed at 1670 and 1545 cm^{-1}. The former band is very close to the aldehydic carbonyl absorption for the free ligand in the liquid state (1675 cm^{-1}). The latter band is 130 cm^{-1} lower than that of free acrolein. These indicate the presence of two types of coordinated acrolein ligands: One coordinates to the rhodium metal with both C=O and C=C groups, while the other coordinates with only the C=C bond.

The reaction of acrolein with $[RhCl(C_8H_{14})_2]_2$ at 30°C also yields a brown complex with the same empirical formula as the above complex in a high yield. However, the IR spectrum of the complex exhibites a sharp band at 2000 cm^{-1} and a weak band at 1740 cm^{-1} in addition to two bands at 1670 and 1545 cm^{-1} described above. The reaction of this complex with excess of triphenylphosphine yields a mixture of $RhCl(CO)(PPh_3)_2$ and $RhCl(PPh_3)_3$ in a ratio of about 4:1 with evolution of ethylene. The band at 2000 cm^{-1} is, therefore, assigned to C≡O stretching vibration. Furthermore, the intensity of the band at 1670 cm^{-1} is weak compared with that of the complex obtained at $-10°C$, indicating that some of acrolein ligands coordinating to the metal *via* the C=C bond are converted into ethylene and carbon monoxide ligands and $RhCl(CO)(CH_2{=}CH_2)(CH_2{=}CHCHO)$ (II) is formed. On the other hand, the weak band at 1740 cm^{-1} in the keto-region may indicate the presence of a small amount of an acyl complex. From these results, it may be reasonable to conclude that the acrolein complex obtained at 30°C is a mixture of I, II, and an acyl complex.

$$[RhCl(C_8H_{14})_2]_2 + CH_2{=}CHCHO \longrightarrow \underset{(I)}{RhCl(CH_2{=}CHCHO)_2} + \underset{(II)}{RhCl(CO)(CH_2{=}CH_2)(CH_2{=}CHCHO)} + \text{Acyl complex}$$

These rhodium acrolein complexes are fairly air-stable. They are slightly soluble in tetrahydrofuran and scarcely soluble in benzene and ether. The thermal decomposition of the complexes occurs *in vacuo* above about 145° with evolution of ethylene and carbon monoxide, yielding $[RhCl(CO)_2]_2$. Numerous fruitless attempts were made to isolate the complex II and the acyl complex in a pure state.

Experimental

All reactions were carried out under a nitrogen atmosphere. The rhodium(I) cyclooctene complex $[RhCl(C_8H_{14})_2]_2$ was prepared by the published procedure.[5]

Reaction of Acrolein with $[RhCl(C_8H_{14})_2]_2$ at $-10°C$. To a stirred solution of $[RhCl(C_8H_{14})_2]_2$ (1.0 g) and toluene (80 m*l*) was added 2 m*l* of acrolein at 0°C. After stirring for 3 hr, a brown complex precipitated was washed with toluene and petroleum ether several times (0.38 g, 54% yield).

Found: C, 28.55; H, 3.40; O, 12.86; Cl, 14.46%. Calcd for $C_6H_8O_2ClRh$: C, 28.77; H, 3.22; O, 12.78; Cl, 14.15%.

Reaction of Acrolein with $[RhCl(C_8H_{14})_2]_2$ at 30°C. The procedure was the same as above, except that the reaction temperature was 30°C and the reaction time was 0.5 hr (0.40 g, 57% yield).

Found: C, 28.97; H, 3.38; O, 11.52; Cl, 14.60%. Calcd for $C_6H_8O_2ClRh$: C, 28.77; H, 3.22; O, 12.78; Cl, 14.15%.

1) G. N. Schrauzer, *J. Amer. Chem. Soc.*, **81**, 5310 (1959); *Chem. Ber.*, **94**, 642 (1961).
2) E. Weiss, K. Stark, J. E. Lancaster, and H. D. Murdoch, *Helv. Chim. Acta*, **46**, 288 (1963).
3) D. P. Tate, A. A. Buss, J. M. Augl, B. L. Ross, J. G. Grasselli, W. M. Ritchey, and F. J. Knoll, *Inorg. Chem.*, **4**, 1323 (1965).
4) S. Kawaguchi and T. Ogura, *ibid.*, **5**, 844 (1966).
5) L. Porri, A. Lionetti, G. Allegra, and A. Immirzi, *Chem. Commun.*, 336 (1965).

BULLETIN OF THE CHEMICAL SOCIETY OF JAPAN, VOL. 45, 2936—2937 (1972)

Ultraviolet Luminescence of Ternary Compounds (La, Al, Ce)F_3[1)]

Kazuo NARITA and Akira TAYA

Toshiba Research and Development Center, Tokyo Shibaura Electric Co., Ltd. Komukai Toshiba-cho, Kawasaki

(Received May 11, 1972)

Luminescence of trivalent metal fluorides activated by Ce^{3+} ion has been reported by several authors.[2-4)] Emission due to the Ce^{3+} center was found in the ultraviolet and/or the blue region. In these papers, however, descriptions were made only on pure CeF_3 and on binary fluorides containing CeF_3. Relations between the preparing conditions of the phosphors and their luminescence efficiency were not mentioned.

We prepared ternary (La, Al, Ce)F_3 phosphors by solid state reaction at high temperatures and found the best composition and firing conditions for these phosphors. Reflection, excitation and emission spectra were also measured.

Experimental

LaF_3 (99.999%), CeF_3 (99.99%) and other rare earth fluorides were obtained from Shin-etsu Chemical Company. AlF_3 was a C.P. reagent of Amend Drug and Chemical Co. The weighed materials were dry-mixed, placed in ceramic crucibles and fired in air for 30 min at 800°C. Firing above or below 800°C resulted in much poorer efficiency. The chemical composition of the finished phosphors was approximately the same as that before firing. X-ray diffraction data showed that the phosphors consist of two tysonite phases, one having a lattice constant slightly smaller than LaF_3, the other having a lattice constant slightly larger than CeF_3. AlF_3 diffraction lines were very weak. Thus, under the preparing conditions mentioned above, LaF_3 and CeF_3 seem to react poorly, whereas AlF_3 appears to be dissolved almost completely into two tysonite phases.

Spectroscopic measurements were made with a Perkin-Elmer Model E-1 spectrometer. A deuterium discharge lamp was used as a light source for reflection and excitation measurements. Photoluminescence was excited by 2537 Å Hg line from a low pressure mercury lamp.

Results and Discussion

Figure 1 shows the emission spectra of $(La_{0.5}Al_{0.3}Ce_{0.2})F_3$ at 300 and 77°K. In the former, the peak is located at 2860 Å. In the latter, two well-separated peaks are observed with an energy separation of about 2000 cm^{-1}, which is close to the splitting of the ground state in a Ce^{3+} free ion, 2253 cm^{-1}. In the (La, Al, Ce)F_3 system, the feature of the emission spectrum does not depend on the chemical composition, but it shifts to the longer wavelength region when La is replaced by Y. For example, $(Y_{0.5}Al_{0.2}Ce_{0.3})F_3$ has its emission peak at 2933 Å at 300°K.

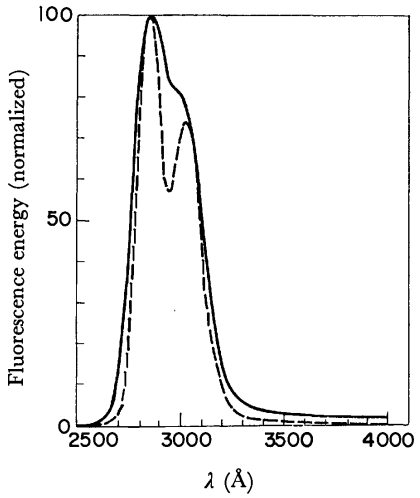

Fig. 1. Emission spectra of $(La_{0.5}Al_{0.3}Ce_{0.2})F_3$ phosphor under 2537 Å excitation.
———: 300°K, - - - - - -: 77°K

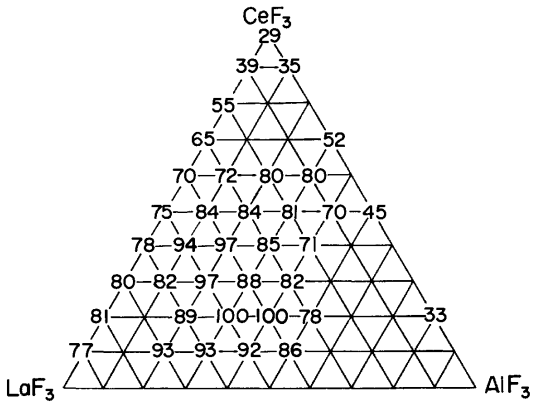

Fig. 2. Relative fluorescence efficiency of (La, Al, Ce)F_3 system.

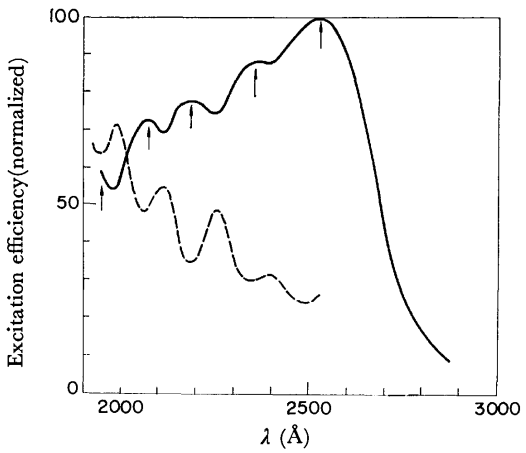

Fig. 3. Excitation and reflection spectra of $(La_{0.5}Al_{0.3}Ce_{0.2})F_3$.
———: Excitation, ———: Reflection

1) Paper presented at the 26th Annual Meeting of the Chemical Society of Japan, Phosphor Section, 1972.
2) F. A. Kroeger and J. Bakker, *Physica*, **8**, 628 (1941).
3) J. H. Gisolf, F. A. Kroeger, and J. Bakker, U. S. 2450548 (1948).
4) G. Blasse and A. Bril, *J. Chem. Phys.*, **51**, 3252 (1969).

Figure 2 shows the fluorescence efficiency of (La, Al, Ce)F_3 as related to phosphor compositions. The maximum efficiency is obtained for $(La_{0.5}Al_{0.3}Ce_{0.2})F_3$ and $(La_{0.4}Al_{0.4}Ce_{0.2})F_3$, which have 20% more output than the best binary solid solution $(La_{0.8}Ce_{0.2})F_3$.

Figure 3 shows the excitation as well as the diffuse reflection spectrum at 300°K. The excitation spectrum is similar to that reported by Blasse and Bril.[4] In the present spectrum, however, five bands are identified with the peaks at 1950 (51280 cm^{-1}), 2070 (48300 cm^{-1}), 2190 (45660 cm^{-1}), 2350 (42540 cm^{-1}), and 2535 (39520 cm^{-1})Å, the energy splittings between the sequent peaks being 2980, 2640, 3120, and 3020 cm^{-1}, respectively.

In the treatment of the $5d$ excited state of Ce^{3+}, the spin-orbit interaction is usually neglected and only the crystal field splitting is considered.[5,6] This approximation seems to be justified also in the case of (La, Al, Ce)F_3, since the spin-orbit coupling energy, which is 2489 cm^{-1} with the coupling constant $\zeta_{5d}=995.6$ cm^{-1} [7] in a free Ce^{3+} ion and is expected to become smaller by several tens of per cent in the crystal,[8] is too small to account for the splitting observed in the excitation and reflection spectra. The space group of tysonite structure is D_{3d}, in which the cation occupies the site with C_2 symmetry.[9] Hence, the $5d(^2D)$ state splits into five Kramer's doublets. This is in agreement with the observation.

5) E. Loh, *Phys. Rev.*, **154**, 270 (1967).
6) G. Blasse and A. Bril, *J. Chem. Phys.*, **47**, 5139 (1967).
7) B. G. Wybourne, "Spectroscopic Properties of Rare Earths," Interscience Publishers, New York (1965), p. 41.
8) C. J. Ballhausen, "Introduction to Ligand Field Theory," McGraw-Hill, New York (1962), p. 115.
9) M. Mansmann, *Z. Anorg. Allgem. Chem.*, **331**, 98 (1964).

BULLETIN OF THE CHEMICAL SOCIETY OF JAPAN, VOL. 45, 2937—2938 (1972)

Synthesis of Aliphatic Isoselenocyanates by the Reaction of Aliphatic Isocyanides with Selenium in the Presence of Triethylamine

Noboru SONODA, Goro YAMAMOTO, and Shigeru TSUTSUMI

Department of Petroleum Chemistry, Faculty of Engineering, Osaka University, Suita, Osaka

(Received November 19, 1971)

Bulka and co-workers[1] have reported that the reaction of selenium with aryl isocyanide produces aryl-isoselenocyanate. However, the reaction of selenium with aliphatic isocyanide has not been reported yet. We tried the reaction of aliphatic isocyanide under the same conditions to those employed in the reaction of aryl isocyanide.[1] However, the corresponding isoselenocyanate was not obtained. Recently we confirmed that amine catalyzed the reaction between carbon monoxide and selenium to give carbonyl selenide[2] and this fact prompted us to try to use of strongly basic tertiary amine as catalyst in the present reaction, because of similarity of electronical structure between isocyanide and carbon monoxide. Now, we found that the addition of triethylamine promoted the reaction effectively, and aliphatic isoselenocyanate was obtained in a high yield. The results obtained from representative isocyanides were shown in Table 1. The aliphatic isoselenocyanates isolated were identified by IR, NMR, mass spectroscopy, and elemental analyses. These isoselenocyanates were somewhat unstable and gradually decomposed at room temperature.

$$\text{R-NC} + \text{Se} \xrightarrow{\text{Et}_3\text{N}} \text{R-N=C=Se}$$

R: -, *n*-C_4H_9-, *tert*-C_4H_9-

Some characteristic reactions of the isoselenocyanates were carried out. The reaction of aliphatic isoselenocyanates with *n*-butylamine produced corresponding selenoureas in excellent yields, which were fairly stable

TABLE 1. THE REACTION OF ALIPHATIC ISOCYANIDE WITH SELENIUM IN THE PRESENCE OF TRIETHYLAMINE

Isocyanide (R-NC) R	(mmol)	Se (mmol)	Et_3N (mmol)	React. time (hr)	React. temp. (°C)	Product	Yield[a] (%)
Cyclohexyl	59	38	38	4	66	Cyclohexyl isoselenocyanate	96
n-Butyl	21	15	15	1.5	66	*n*-Butyl isoselenocyanate	83
tert-Butyl	21	15	15	6	66	*tert*-Butyl isoselenocyanate	97

a) Based on selenium used.

1) E. Bulka, K. D. Ahlers, and E. Tucek, *Chem. Ber.*, **100**, 1376 (1967).

2) N. Sonoda, T. Yasuhara, T. Ikeda, K. Kondo, and S. Tsutsumi, *J. Amer. Chem. Soc.*, **93**, 6344 (1971).

Table 2. The reaction of aliphatic isoselenocyanate with *n*-butylamine or ethanol

Isoselenocyanate (R-N=C=Se) R	(mmol)	*n*-$BuNH_2$ (mmol)	EtOH (mmol)	React. time (hr)	React. temp. (°C)	Product	Yield[a] (%)
Cyclohexyl	3	3	—	48	r.t.	*N*-*n*-Butyl-*N'*-cyclohexylselenourea	90
n-Butyl	5	5	—	0.5	66	*N,N'*-Di-*n*-butylse enourea	98
tert-Butyl	5.5	5.5	—	0.5	66	*N*-*n*-Butyl-*N'*-*tert*-butylselenourea	89
Cyclohexyl	22	—	740	24	78	*N*-Cyclohexylselenocarbamate	49

a) Based on selenium used.

at room temperature. Selenocarbamate was easily obtained by the reaction of isoselenocyanate with ethanol. These results were summarized in Table 2.

$$R\text{-}N{=}C{=}Se + R'\text{-}NH_2 \longrightarrow R\text{-}NH\text{-}\underset{\underset{Se}{\|}}{C}\text{-}NH\text{-}R'$$

$$R\text{-}N{=}C{=}Se + R'\text{-}OH \longrightarrow R\text{-}NH\text{-}\underset{\underset{Se}{\|}}{C}\text{-}OR'$$

Furthermore, it was confirmed that the reaction of isocyanide with selenium and *n*-butylamine yielded the corresponding selenourea directly. In this case *n*-butylamine might catalyze the reaction of isocyanide with selenium to give isoselenocyanate as an intermediate.

Experimental

Cyclohexyl Isoselenocyanate. To a solution of 5.79 g (53 mmol) of cyclohexyl isocyanide in 45 m*l* of THF were added 3.00 g (38 mg atom) of selenium and 3.85 g (38 mmol) of triethylamine. The mixture was stirred under reflux for 4 hr, and at this stage selenium was completely dissolved. The mixture was concentrated, and distillation of the residual liquid gave 6.90 g (96%) of colorless product: bp 90—92°C (3.0 mm); IR 2130 cm^{-1} (N=C=Se); NMR (CCl_4) τ 7.7—8.9 (10H), 6.2 (1H); Mass *m/e* 189 (parent ion containing ^{80}Se), 83 ($C_6H_{11}^+$).

Found: N, 7.32%. Calcd for $C_7H_{11}NSe$: N, 7.45%.

n-*Butyl Isoselenocyanate.* To a solution of 1.74 g (21 mmol) of *n*-butyl isocyanide were added 1.18 g (15 mg atom) of selenium and 1.52 g (15 mmol) of triethylamine. The mixture was stirred under reflux for 1.5 hr. Selenium was dissolved completely and the solution became dark brown. The mixture was concentrated and distillation of the residue gave 2.02 g (83%) of colorless liquid: bp 56—58°C (3 mm); IR 2160 (N=C=Se); NMR (CCl_4) τ 8.8—9.2 (3H), 7.9—8.8 (4H), 6.2—6.4 (2H); Mass *m/e* 163 (parent ion containing ^{80}Se), 57 ($C_4H_9^+$).

Found: N, 8.52%. Calcd for C_5H_9NSe: N, 8.60%.

tert-*Butyl Isoselenocyanate.* To a solution of 1.74 g (21 mmol) of *tert*-butyl isocyanide were added 1.18 g (15 mg atom) of selenium and 1.52 g (15 mmol) of triethylamine. The mixture was concentrated *in vacuo* to give 2.37 g (97%) of colorless solid. This solid was fairly unstable and decomposed on recrystallization or on standing overnight: mp 51—52°C; IR 2050 cm^{-1} (N=C=Se); NMR (CCl_4) τ 8.5 (s); Mass *m/e* 163 (parent ion containing ^{80}Se), 57 ($C_4H_9^+$).

Found: N, 8.43%. Calcd for C_5H_9NSe: N, 8.60%.

N-n-*Butyl*-N'-*cyclohexylselenourea.* *A*: To a solution of 0.55 g (3 mmol) of cyclohexyl isoselenocyanate in 5 m*l* of THF was added 0.24 g (3 mmol) of *n*-butylamine. The solution was allowed to stand for 48 hr at room temperature, then was concentrated *in vacuo* to dryness, and the yellow solid deposited was filtered and recrystallized from ethanol to yield 0.67 g (90%) of colorless crystal: mp 107.5—108.5°C; IR 3210 cm^{-1} (NH); NMR (CCl_4) τ 7.8—9.1 (17H), 6.6 (2H), 5.9 (1H), 3.0 (2H); Mass *m/e* 262 (parent ion containing ^{80}Se), 83 ($C_6H_{11}^+$), 99 ($C_6H_{11}NH_2^+$), 57 ($C_4H_9^+$).

Found: N, 10.68%. Calcd for $C_{11}H_{22}N_2Se$: N, 10.72%.

B: To a solution of 3.85 g (35 mmol) of cyclohexyl isocyanide in 20 m*l* of THF were added 2.37 g (30 mmol) of selenium and 2.20 g (30 mmol) of *n*-butylamine. The mixture was stirred under reflux for 4 hr, and at this stage selenium was dissolved. The mixture was concentrated and the yellow solid deposited was filtered and recrystallized from ethanol to yield 7.60 g (97%) of colorless crystal which was identical with *N*-*n*-butyl-*N'*-cyclohexylselenourea obtained by the procedure *A*.

N,N'-*Di*-n-*butylselenourea.* To a solution of 0.73 g (5 mmol) of *n*-butyl isoselenocyanate in 9 m*l* of THF was added dropwise 0.37 g (5 mmol) of *n*-butylamine. After complete addition of *n*-butylamine, the reaction mixture was stirred under reflux for 0.5 hr to complete the reaction. The solution was concentrated *in vacuo* and the residual solid was recrystallized from benzene–petroleum ether mixture to give 1.05 g (98%) of colorless plates: mp 72—73°C; IR 3220 cm^{-1} (NH); NMR τ 8.8—9.2 (6H), 8.0—8.8 (8H), 6.2—6.8 (4H), 2.5—3.0 (2H); Mass *m/e* 236 (parent ion containing ^{80}Se), 57 ($C_4H_9^+$).

Found: N, 12.13%. Calcd for $C_9H_{10}N_2Se$: N, 11.91%.

N-n-*Butyl*-N'-tert-*butylselenourea.* To a solution of 0.89 g (5.5 mmol) of *tert*-butyl isoselenocyanate in 15 m*l* of THF was added dropwise 0.46 g (5.5 mmol) of *n*-butylamine. After addition of *n*-butylamine, the reaction mixture was stirred under reflux for 0.5 hr to complete the reaction. The reaction mixture was concentrated and the yellow solid deposited was recrystallized from benzene to yield 1.15 g (89%) of colorless plates: mp 76—77°C; IR 3220 cm^{-1} (NH); NMR τ 8.2—9.2 (16H), 6.2—6.7 (2H), 3.1—3.4 (2H); Mass *m/e* 236 (parent ion containing ^{80}Se), 57 ($C_4H_9^+$).

Found: N, 11.68%. Calcd for $C_9H_{10}N_2Se$: N, 11.91%.

N-*Cyclohexylselenocarbamate.* Cyclohexyl isoselenocyanate, 4.19 g (22.3 mmol), was added to 43 m*l* of ethanol. The mixture was refluxed for 24 hr. The resulting solution was concentrated to give yellow solid, which was recrystallized from ethanol to yield 2.57 g (49%) of colorless plates: mp 77—78°C; IR 3210 cm^{-1} (NH); NMR τ 7.7—9.1 (13H), 6.3 (1H), 5.4 (2H), 1.8 (1H); Mass *m/e* 235 (parent ion containing ^{80}Se), 83 ($C_6H_{11}^+$).

Found: N, 5.82%. Calcd for $C_9H_{17}NOSe$: N, 5.98%.

BULLETIN OF THE CHEMICAL SOCIETY OF JAPAN, VOL. 45, 2939—2940 (1972)

Heat Capacity Changes of Some Sodium Alkylsulfates in Aqueous Solutions

Kunio TAMAKI, Yoshio ISOMURA, and Yōko ŌHARA

Department of Chemistry, Yokohama City University, Kanazawa-ku, Yokohama

(Received January 31, 1972)

Recently, the physical properties of aqueous electrolyte solutions have mainly been discussed in terms of the resultant change in the water structure upon the introduction of ions into water.[1] Small ions, such as lithium, sodium, and fluoride ions, have a net structure-making effect on the water structure, while large ions, such as potassium, chloride, and bromide ions, have a net structure-breaking effect.[1] On the other hand, nonpolar solutes such as hydrocarbons and amphiphilic compounds, such as alkyl alcohols or fatty acids, act as water-structure-making solutes in water; that is, the water molecules form an "iceberg" around nonpolar groups of the molecules.[2] This type of hydration is called "hydrophobic hydration" or "hydration of the second kind."[1]

It seems that it would be interesting to study the strength of hydrophobic hydration for amphiphilic electrolytes, that is, the molecules with both nonpolar and ionized groups. The solute-solvent interaction of this kind of compound is determined from the balance of the two different modes of hydration (ionic hydration and hydrophobic hydration). The object of this paper is to consider the role of alkyl groups in the change in the water structure, in the case of a series of sodium alkylsulfates; this work is based on the experimentally-determined values of the change in the partial molal heat capacity. The method has been applied to tetraalkylammonium salts,[3] sodium tetraphenylboron,[4] aliphatic alcohol,[5] and poly(ethylene glycol) and related compounds.[6]

At a constant pressure, the following relation is derived between the heat of solution at an infinite dilution, ΔH_s^0, and the temperature, T:[7]

$$d\Delta H_s^0/dT = \Delta C_p^0 = \bar{C}_p^0 - C_p^s$$

where ΔC_p^0 is the change in the heat capacity for dissolution, $\bar{C}_p^0$ is the partial molal heat capacity of the solute at an infinite dilution, and C_p^s is the heat capacity of the pure solute. As the C_p^s values of the sulfates are unavailable at present, discussion will be limited to the ΔC_p^0 values in this paper.

Experimental

Materials. The sodium methylsulfate used in this work was prepared from the precipitation by the addition of petroleum benzine to an ethanol solution of commercial sodium methylsulfate monohydrate. Analysis showed the obtained sample was anhydrous. The other sodium alkylsulfates were synthesized by the esterification of the corresponding alcohols by concentrated sulfuric acid, and were neutralized with a concentrated solution of sodium hydroxide. The reaction mixtures were dried in air and extracted with ethanol, and then the products were recrystallized twice from ethanol and dried in a vacuum desiccator. The water was obtained by redistillation from an alkaline permanganate solution.

Apparatus. Heat-of-solution measurements at 10, 25, and 45°C were made with an Ōyodenki Kenkyujo (Tokyo) Model CM-204D1 twin conduction calorimeter. An ampoule containing an apropriate amount of a sample was mechanically broken into 50 cc of water at a constant temperature. Because of the hygroscopic property of the sodium alkylsulfates used, the samples introduced into ampoules were dried in a vacuum before final weighing. The calorimeter was checked by measuring the heats of solution of potassium chloride. The values thus obtained were within 2% of those reported in the literature.[8]

Results and Discussion

The heat of solution at an infinite dilution is generally obtained by extrapolating the plot of the heat of solution as a function of the concentration (or the square root of the concentration in the case of electrolytes). However, it was found that the results obtained at concentrations below 0.01 M showed some scattered values. Thus, the heats of solution at 0.01 M, ΔH_s, are presented in Table 1. A correction for the heats of dilution must be made to obtain ΔH_s^0. With sodium chloride, a typical uni-univalent electrolyte, the heat of dilution from a solution at 0.01 M to one at an

Table 1. Heats of solution of sodium alkylsulfates at 0.01 M

$ROSO_3Na$	10°C kcal/mol	25°C kcal/mol	45°C kcal/mol	ΔC_p° cal/deg·mol
Methyl	2.30±0.03	2.01±0.02	1.70±0.01	−17
Ethyl	1.20±0.04	1.14±0.02	1.15±0.02	≒0
Propyl	1.23±0.01	1.38±0.02	1.63±0.05	+11
Butyl	1.44±0.02	1.74±0.04	2.20±0.04	+21
Pentyl	1.00±0.05	1.55±0.02	2.33±0.06	+38
Hexyl	1.20±0.04	1.98±0.04	3.08±0.08	+54

1) H. S. Frank and W-Y. Wen, *Discuss. Faraday Soc.*, **24**, 133 (1957); B. E. Conway, *Ann. Rev. Phys. Chem.*, **17**, 481 (1966); E. Wicke, *Angew. Chem. Int. Ed. Engl.*, **5**, 106 (1966); M. J. Blandamer, *Quart. Rev.*, **24**, 169 (1970).

2) H. S. Frank and M. J. Evans, *J. Chem. Phys.*, **13**, 507 (1945).

3) T. S. Sarma, R. K. Kohanty, and J. C. Ahluwalia, *Trans. Faraday Soc.*, **65**, 2333 (1969).

4) S. Subramanian and J. C. Ahluwalia, *J. Phys. Chem.*, **72**, 2525 (1968).

5) E. M. Arnett, W. B. Kover, and J. V. Carter, *J. Amer. Chem. Soc.*, **91**, 4028 (1969).

6) H. Nakayama, This Bulletin, **43**, 1683 (1970).

7) C. M. Criss and J. W. Cobble, *J. Amer. Chem. Soc.*, **83**, 3223 (1961).

8) G. Somsen, J. Coops, and M. W. Tolk, *Rec. Trav. Chim. Pays-Bas*, **82**, 231 (1963).

infinite dilution is −0.039 kcal/mol;[9] this value is sometimes comparable with the range of error of this work. The average values of ΔC_p^0 between 10 and 45°C are calculated by assuming that the change in the partial molal heat capacity at 0.01 M is equal to that at an infinite dilution. The ΔC_p^0 values obtained on the basis of this assumption are also listed in Table 1. A procedure similar to this was employed by Greyson and Snell.[10]

As will be seen in Table 1, sodium methylsulfate shows only negative ΔC_p^0 values in the homologous series. Though the ΔC_p^0 or $\bar{C}_p^0$ value of an electrolyte naturally consists of the sum of the contributions of both cation and anion, so far no reliable procedure for assigning a value to the individual ions has been established. The $\bar{C}_p^0$ values, and thus the ΔC_p^0 values, of most simple electrolytes are negative;[11] *e.g.*, the $\bar{C}_p^0$ value of sodium chloride is −22.1 cal/deg·mol at 25°C.[11] As the ΔC_p^0 value of methyl alcohol is 23.1 cal/deg·mol,[5] the methyl group must cause a positive change in the ΔC_p^0 value. The overall change in the partial molal heat capacity of sodium methylsulfate is as low as −17 cal/deg·mol as is shown in Table 1; this means that the methyl salt displays behavior rather similar to that of simple salt in the water phase. In this sense, sodium methylsulfate may be considered to behave as a net structure-breaking salt.

The ΔH_s values of sodium ethylsulfate are virtually independent of the temperature. With this salt, the contributions of the two types of hydration (ionic and hydrophobic) seem to cancel each other out.

The ΔC_p^0 values of sodium propylsulfate and higher homologues are positive; these salts exhibit an excellent water-structure-making effect. The positive ΔC_p^0 values in Table 1 indicate that the promotion of the water structure ("iceberg" formation[2]) around the nonpolar groups of these salts increases with the number of carbon atoms of alkyl chain.

9) T. F. Young and O. G. Vogel, *J. Amer. Chem. Soc.*, **54**, 3030 (1932).
10) J. Greyson and H. Snell, *J. Phys. Chem.*, **73**, 3208 (1969).
11) K. S. Pitzer and L. Brewer, "Thermodynamics," McGraw-Hill, New York, N. Y. (1961), p. 652.

BULLETIN OF THE CHEMICAL SOCIETY OF JAPAN, VOL. 45, 2940—2941 (1972)

Nuclear Quadrupole Resonance of the 1:1 Molecular Complex between Antimony Trichloride and Ethylbenzene

Tsutomu OKUDA, Yoshihiro FURUKAWA, and Hisao NEGITA
Department of Chemistry, Faculty of Science, Hiroshima University, Hiroshima

(Received February 7, 1972)

We have already reported on the antimony-halogen bond character and the molecular shape of antimony trihalide in its 2:1 molecular complex with an aromatic compound, as determined by means of the nuclear quadrupole resonance (NQR).[1-3] As for the 1:1 molecular complex, NQR studies have been performed by several authors.[4] All of them, however, used polycrystalline samples, and their crystal structures are still unknown except for $SbCl_3 \cdot C_6H_5NH_2$,[5] in which the NQR has not yet been observed.

In the present experiment, we observed the Zeeman effect of NQR in $SbCl_3 \cdot C_6H_5C_2H_5$ in order to obtain information on the Sb-Cl bond character and the molecular structure of antimony trichloride in its molecular complex.

The molecular complex was prepared by the method of Shinomiya and Asahina,[6] and the single crystal was obtained by the Bridgman-Stockbarger method. A Weber-Todd type[7] super-regenerative oscillator was used for the detection of the resonance line. The magnetic field used for the Zeeman study was provided by a Helmholtz coil[8] with a field strength of about 200 gauss.

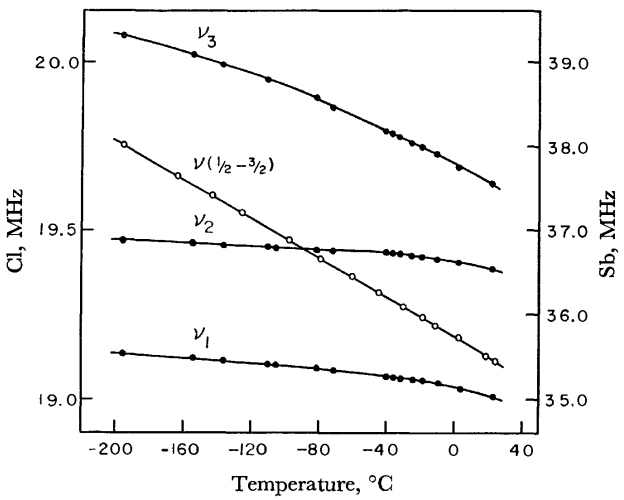

Fig. 1. Temperature dependence of ^{35}Cl and ^{123}Sb NQR frequencies in $SbCl_3 \cdot C_6H_5C_2H_5$.

1) T. Okuda, A. Nakao, M. Shiroyama, and H. Negita, This Bulletin, **41**, 61 (1968).
2) T. Okuda, H. Terao, O. Ege, and H. Negita, *ibid.*, **43**, 2398 (1970).
3) T. Okuda, *J. Sci. Hiroshima Univ., Ser. A*, **35**, 213 (1971).
4) I. P. Biryukov, M. G. Voronkov, and I. A. Safin, "Frequency Tables of Nuclear Quadrupole Resonance," Israel Program for Scientific Translations, Jerusalem (1969).
5) R. Hulme and J. C. Scruton, *J. Chem. Soc., A*, **1968**, 2448.
6) S. Shinomiya and T. Asahina, *Nippon Kwagaku Kwaishi*, **59**, 1165 (1938).
7) K. E. Weber and J. E. Todd, *Rev. Sci. Instr.*, **33**, 390 (1962).
8) K. Shimomura, *J. Phys. Soc. Jap.*, **12**, 657 (1957).

TABLE 1. NUCLEAR QUADRUPOLE RESONANCE FREQUENCIES, ν, ASYMMETRY PARAMETERS, η, AND QUADRUPOLE COUPLING CONSTANTS, eQq_{zz}, IN ANTIMONY TRICHLORIDE AND ITS COMPLEX WITH ETHYLBENZENE AT ROOM TEMPERATURE (20°C)

Compound	Resonance line	ν, MHz	η, %	eQq_{zz}, MHz
$SbCl_3 \cdot C_6H_5C_2H_5$	^{35}Cl ν_1	19.010	5.5±1.4	38.001
	^{35}Cl ν_2	19.388	13.5±1.7	38.426
	^{35}Cl ν_3	19.641	9.0±1.5	39.126
	^{123}Sb ν (1/2—3/2)	35.478	13.3±0.3	467.698
$SbCl_3$	^{35}Cl ν'_1	19.180	15.3	38.211
	^{35}Cl ν'_2	20.422	5.7	40.822
	^{123}Sb ν' (1/2—3/2)	37.431	15.9	481.560

The NQR frequencies of ^{35}Cl and ^{123}Sb were observed between the temperature of liquid nitrogen and room temperature, as is shown in Fig. 1. The present molecular complex gave three ^{35}Cl resonance lines (designated as ν_1, ν_2, and ν_3) and one ^{123}Sb ($1/2 \leftrightarrow 3/2$) resonance line (designated as $\nu(1/2—3/2)$), as Table 1 shows.

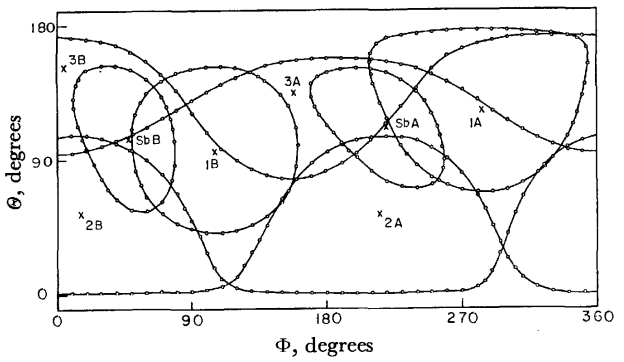

Fig. 2. Zero-splitting patterns of ^{35}Cl and ^{123}Sb Zeeman lines in $SbCl_3 \cdot C_6H_5C_2H_5$. Θ and Φ are polar and azimuthal angles, respectively, in the coordinate fixed to the sample.

The patterns of the zero-splitting were obtained by measuring the Zeeman effect on the resonance line as is shown in Fig. 2. Two patterns were obtained for each resonance line, indicating that the molecular complex is monoclinic. The angles between any two Sb–Cl bonds can be calculated by assuming that the z axis of the field gradient of chlorine is parallel to the Sb–Cl bond. The bond angles, ∠Cl–Sb–Cl, thus obtained are 90°26′, 93°8′, and 96°1′. These angles are almost the same as those of pure antimony trichloride[9] and $2SbCl_3 \cdot C_{10}H_8$,[10] indicating that the molecular shape of antimony trichloride hardly changes upon complex-formation with ethylbenzene. On the other hand, it is considerably different from that of $SbCl_3 \cdot C_6H_5NH_2$, though both crystals are 1:1 molecular complexes. This discrepancy may be attributed to the difference in the strength of the intermolecular bond, which may deform the molecular shape to various degrees.

The values of the asymmetry parameter were determined from the distortion of the zero-splitting loci. Once the asymmetry parameter was obtained, the quadrupole coupling constant could be calculated from the observed resonance frequency. The results are listed in Table 1, along with those for pure antimony trichloride. In pure antimony trichloride, the quadrupole coupling constant and the temperature gradient of the lower ^{35}Cl resonance line (ν'_1) is considerably smaller than those of the higher (ν'_2), so the former is assigned to the chlorine atom, which forms the stronger Sb···Cl intermolecular bond.[9,11] In the present complex, since the quadrupole coupling constants and the temperature gradients of ν_1 and ν_2 are smaller than those of ν_3 and all comparable to those of ν'_1 in pure antimony trichloride, ν_1 and ν_2 may be assigned to the chlorine atoms (Cl_1 and Cl_2) in the stronger Sb···Cl intermolecular bonds, and ν_3, to that (Cl_3) in the weaker bonds. However, the asymmetry parameter of ν_1 is too small to be attributed to that in the stronger Sb···Cl intermolecular bond. This suggests the presence of another effect such as the *trans* effect, which is considered to exist in $2SbCl_3 \cdot C_{10}H_8$.[10] That is, if the configuration of the antimony atom in the present complex is a distorted sp^3d or sp^3d^2 environment and if the Cl_1 atom occupies the position opposite to the intermolecular bond between ethylbenzene and antimony trichloride, a part of the charge from ethylbenzene may transfer to the Cl_1 atom through the antimony atom. Such an effect will cause the quadrupole coupling constant to decrease without any increase in the asymmetry parameter because the electron populations of the p_z orbital increase. As the temperature increases, the degree of the charge transfer to the Cl_1 atom decreases since the intermolecular bond becomes weaker, resulting in the smaller change of ν_1 in comparison with that of ν_3.

9) G. E. Peterson, Thesis, Pittsburgh, 1962.
10) R. Hulme and J. T. Szymanski, *Acta Crystallogr.*, **B 25**, 753 (1969).
11) H. Chihara, N. Nakamura, and H. Okuma, *J. Phys. Soc. Jap.*, **24**, 306 (1968).

BULLETIN OF THE CHEMICAL SOCIETY OF JAPAN, VOL. 45, 2942—2943 (1972)

The Syntheses and Properties of Some 2-Methyl-4-phenyl-1,5-benzodiazepinium Chlorometalates

Akiko FURUHASHI, Sumio KOMATSU, and Akira OUCHI*

Department of Chemistry, College of Science and Engineering, Aoyama Gakuin University, Chitosedai, Setagaya-ku, Tokyo

**Department of Chemistry, College of General Education, The University of Tokyo, Komaba, Meguro-ku, Tokyo*

(Received March 22, 1972)

In a previous paper,[1] the present authors reported on the syntheses of 2,4-dimethyl-1,5-benzodiazepinium halogenometalates. However, similar compounds with different substituent on the 2 and/or the 4 position of the 1,5-benzodiazepinium ring have not yet been studied. It seemed that it would be of interst to study the influence of the substituents on the stability of the complex. In this way, some new compounds, 2-methyl-4-phenyl-1,5-benzodiazepinium chlorometalates, were obtained by the same synthetic technique as was used for the 2,4-dimethyl derivatives.

Experimental

The Syntheses of the 2-Methyl-4-phenyl-1,5-benzodiazepinium Chlorometalates. The chloride was synthesized from *o*-phenylenediamine and benzoylacetone by Thiele's method.[2] The chloride and the anhydrous metal chloride were separately dissolved in ethyl alcohol and then mixed. The mixture was kept in a refrigerator overnight, thus yielding crystalline products.

Instruments. The IR spectra were obtained by means of a JASCO model IR-G IR as well as model 403G spectrophotometer. The electronic spectra were obtained with a Hitachi EPS-3T-type automatic recording spectrophotometer.

Results and Discussion

The analytical results of the 2-methyl-4-phenyl-1,5-benzodiazepinium salts are shown in Table 1.

The magnetic moment of the tetrachlorocobaltate(II), as measured by a Gouy balance at room temperature, was 4.44 B.M (per mole of cobalt(II)); this fact shows the cobalt(II) ion is coordinated and is in the tetrahedral configuration.[3]

In the far IR region, the spectra of all of these chlorometalates have the characteristic bands, as is shown in Table 2; these bands are not observed in the spectrum of the simple chloride. They were identified as ν(M-Cl) bands by reference to Nakamoto's[4] and Ferraro's[5] data. This proves the existence of the tetrahedral chlorometalate ion in these compounds. As the wave numbers of the bands of 2-methyl-4-phenyl derivatives are lower than those of the corresponding 2,4-dimethyl-1,5-benzodiazepinium salts, the chlorometalate ions of the former compounds can be said to be less stable.

The IR spectra in the 400—4000 cm^{-1} region of these chlorometalates and of the simple chloride with the same 1,5-benzodiazepinium ion were almost identical. Consequently, in these compounds the 2,4-disubstituted 1,5-benzodiazepinium ion does not seem to coordinate to the metal ion, but seems to work as a counter cation, although some kind of interaction between the cation and the anion may exist as in the case of dithiolium halogenometalates.[6,7]

Table 1. Elemental analyses (%)

		C	H	N	Cl	M
$[C_{16}H_{15}N_2]_2[CoCl_4]\cdot H_2O$	C	55.73	4.64	8.13	20.61	8.56
	F	55.91	4.65	8.20	21.10	8.60
$[C_{16}H_{15}N_2]_2[ZnCl_4]$	C	56.72	4.43	8.27	20.98	9.60
	F	56.55	4.31	8.21	21.59	9.65
$[C_{16}H_{15}N_2]_2[CdCl_4]$	C	53.04	4.15	7.73	19.61	15.47
	F	53.00	4.08	7.68	20.67	15.42
$[C_{16}H_{15}N_2]_2[HgCl_4]$	C	47.23	3.69	6.89	17.47	24.72
	F	47.20	3.66	6.78	17.39	a)

a) The usual EDTA titration gave always a little too low analysis (about 23%), due to the interference of the coexistent components.

Table 2. ν (M-Cl) band of the chlorometalates (cm^{-1})

$[C_{16}H_{15}N_2]_2[CoCl_4]\cdot H_2O$	275
$[C_{16}H_{15}N_2]_2[ZnCl_4]$	255
$[C_{16}H_{15}N_2]_2[CdCl_4]$	245
$[C_{16}H_{15}N_2]_2[HgCl_4]$	280
$[C_{16}H_{13}N_2]_2[CoCl_4]\cdot H_2O$	291
$[C_{11}H_{13}N_2]_2[ZnCl_4]$	297
$[C_{11}H_{13}N_2]_2[CdCl_4]$	266

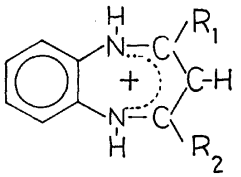

Fig. 1. The 2,4-disubstituted 1,5-benzodiazepinium ion.
1 $R_1=R_2=CH_3$: 2,4-dimethyl-1,5-benzodiazepinium ion $C_{11}H_{13}N_2$
2 $R_1=CH_3$, $R_2=C_6H_5$: 2-methyl-4-phenyl-1,5-benzodiazepinium ion $C_{16}H_{15}N_2$

1) A. Ouchi, T. Takeuchi, M. Nakatani, and Y, Takahashi, This Bulletin, **44**, 434 (1971).
2) J. Thiele and G. Steimmig, *Chem. Ber.*, **40**, 955 (1907).
3) F. A. Cotton and G. Wilkinson, "Advanced Inorganic Chemistry," 2nd ed., Interscience, New York, N. Y. (1967), p. 872.
4) K. Nakamoto, "Infrared Spectra of Inorganic and Coordination Compounds," 2nd ed., Wiley & Sons., New York, N. Y., (1969), p. 214.
5) J. R. Ferraro, "Far Infrared Properties of Solid," edited by S. Mitra and S. Nudelman, Plenum, New York, N. Y. (1970), p. 475.
6) A. Furuhashi, T. Takeuchi, and A. Ouchi, This Bulletin, **41**, 2049 (1968).
7) A. Ouchi, H. Eguchi, T. Takeuchi, and A. Furuhashi, *ibid*, **42**, 2259 (1969). G. A. Heath, R. L. Martin, and I. M. Stewart, *Aust. J. Chem*, **22**, 83 (1969).

Table 3. Some infrared absorption bands of the salts of 1,5-benzodiazepinium derivatives

	$[C_{11}H_{13}N_2]Cl\cdot 2H_2O$	$[C_{11}H_{13}N_2][CoCl_4]\cdot H_2O$	$[C_{16}H_{15}N_2]Cl\cdot 3H_2O$	$[C_{16}H_{15}N_2][CoCl_4]\cdot H_2O$
ν(N–H)	3275(m) 3200(m)	3275(m) 3200(m)	3250(m) 3175(m)	3270(m) 3200(m)
ν(C=C), ν(C=N) or the mixture of them	1639(s) 1595(s)	1625(m) 1598(s)	1610(s) 1590(s)	1615(s) 1590(s)
δ(C–H) of benzene ring	760(s)	760(s)	760(s)	760(s)

It is of interest to compare some wave numbers of the infrared absorption bands of the 2-methyl-4-phenyl-1,5-benzodiazepinium salts with those of 2,4-dimethyl derivatives. The results are shown in Table 3. The assignments of the band were obtained by reference to those of 2,4-dimethyl derivatives presented in the previous paper[1] as well as in Bellamy's books.[8,9]

The bands caused by the benzene ring of the cation are almost identical in the two types of salts, as in the case of the δ(C–H) (760 cm^{-1}) of the benzene ring shown in the table.

The ν(C=C), ν(C=N), or mixed bands appear in the 1400—1600 cm^{-1} region of both derivatives are not very different from each other. In the spectra of both derivatives, two ν(N–H) bands at about 3200—3270 cm^{-1} were observed, on the other hand, no characteristic bands appeared in the 2550—2800 cm^{-1} region (ν(N–H) of $-NH_3^+$).

From these results, the seven-membered rings of both ions seem to have pseudo aromaticity and to be stabilized. The ring of the 2-methyl-4-phenyl derivative is, however, likely to be less stable; consequently, the cation cannot stabilize the tetrabromometalate anion and solid tetrabromometalates were not obtained, although those of the 1,4-dimethyl derivatives had already been synthesized.[1]

Table 4. Electronic spectra of the 1,5-benzodiazepinium salts in ethyl alcohol solution

Figures are given in kK and logε (calculated about the cation) in parentheses

$[C_{11}H_{13}N_2]_2[CoCl_4]\cdot H_2O$	$[C_{16}H_{15}N_2]_2[CoCl_4]\cdot H_2O$
44.5 (4.09)	44.1 (4.10)
38.2 (4.35)	37.6 (3.80)
37.2 (3.32)	36.6 (4.40)
30.1 (2.90)	29.7 (3.20)
28.4 (3.00)	
19.6 (2.90)	19.4 (3.01)

These 2-methyl-4-phenyl-1,5-benzodiazepinium chlorometalates as well as the chloride are all deep violet in color, and the electronic absorption spectra of their ethyl alcohol solutions are almost identical. The data of the main peaks of the chlorometalates, together with those of the 2,4-dimethyl derivative, are shown in Table 4. The *d-d* band was covered by stronger bands and was not identified. The patterns of the spectra of the salts containing the same cation are almost the same; moreover, the spectra of the 2,4-dimethyl and 2-methyl-4-phenyl derivatives resemble each other. These spectral patterns and their intensities seem to be characteristic of the 1,5-benzodiazepinium seven-membered ring of the cation; therefore, both the rings seem to have a considerable pseudo-aromatic character.

The chlorides of the 2,4-dimethyl-, 2-methyl-4-trifluoromethyl-, and 2,4-bis(trifluoromethyl)-1,5-benzodiazepinium were synthesized by almost the same method, but they were much less stable than those of the 2,4-dimethyl or the 2-methyl-4-phenyl derivatives. The solid chlorides obtained were pale in color and were crystallized out only from concentrated hydrochloric acid media. They were easily decomposed even by a dilute acid solution or when kept in the open air for several days. Their solid halogenometalates were not separated when the metal chloride was added to a concentrated hydrochloric acid solution of the chloride.

A ν(N–H) band of these chlorides appeared at 2550 cm^{-1}, as in usual amine hydrochlorides. Consequently, it may be concluded that the seven-membered ring cation with delocalized π-electrons is stabilized by the electron-donating property of the methyl groups on the 2 and/or 4 position of the ring; on the other hand, if such an electron-withdrawing group as a phenyl or trifluoromethyl group is bonded to the position, the ring is destabilized. The halogenometalate anion seems to be stabilized by such a stable, large-size cation. Therefore, if the cation is not stable, the halogenometalate anion is not stabilized and the salts are not obtained in the solid state.

8) L. J. Bellamy, "The Infrared Spectra of Complex Molecules," 2nd ed., Methuen, New York, N. Y. (1958), pp. 64, 277.

9) L. J. Bellamy, "Advances in Infrared Group Frequencies," Methuen, New York, N. Y. (1918), pp. 29, 37.

BULLETIN OF THE CHEMICAL SOCIETY OF JAPAN, VOL. 45, 2944—2945 (1972)

Acylation of Sydnones

Hsien-Ju TIEN and Masaki OHTA

Department of Chemistry, Faculty of Science, Tokyo Institute of Technology, Ookayama, Meguro-ku, Tokyo

(Received March 31, 1972)

4-Acetyl-3-phenylsydnone was prepared by the reaction of the Grignard reagent obtained from 4-bromo-3-phenylsydnone, with acetic anhydride.[1] Acylation of sydnone is an electrophilic reaction which shows the aromaticity of sydnone ring. Successful results were obtained by using aliphatic carboxylic acid in the presence of phosphorus pentoxide[2] (method A) and acetic anhydride in the presence of boron trifluoride etherate[3] (method B). Formylation of sydnone by the Vilsmeier reaction was also reported.[4] However, only a few 4-acylsydnones were obtained by these methods.

In this note we report on some attempts at acylation by methods A and B, and present a new mode of acylation of sydnones with acid anhydride and perchloric acid (method C).

Acylation of 3-phenylsydnone with phenylacetic acid, cyclohexanecarboxylic acid, or *trans*-cinnamic acid in the presence of phosphorus pentoxide afforded the corresponding 4-acyl derivatives. However, acylation with chloroacetic acid, α-bromopropionic acid or crotonic acid was unsuccessful, resulting in the recovery of 3-phenylsydnone or the formation of benzene-insoluble tarry product. 3-Phenylsydnone also was not acylated by either the action of carboxylic acid in the presence of dicyclohexylcarbodiimide in benzene solution or that of acid anhydride in the presence of sulfuric acid. Benzoylation of 3-phenylsydnone by benzoyl perchlorate in benzene was also unsuccessful. Acylation of 3-benzylsydnone by method A or B afforded 4-acetyl-3-benzylsydnone.

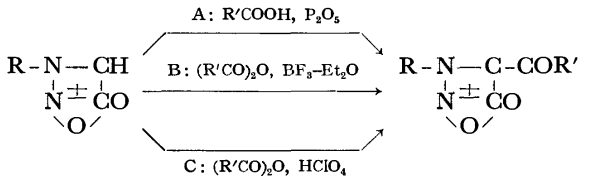

We found that acylation of sydnones with acid anhydrides in the presence of perchloric acid took place easily at room temperature with good yields. However, there is a limit in the effectiveness of acid anhydride, and acylation with acid anhydrides having electron-withdrawing groups such as monochloroacetic anhydride, trichloroacetic anhydride, trifluoroacetic anhydride, or benzoic anhydride was unsuccessful.

The 4-acyl derivatives obtained are given in the following Table.

Experimental

4-Acetyl-3-phenylsydnone (1). A typical procedure for the preparation of 4-acyl-3-substituted sydnones is as follows. To a suspension of 3-phenylsydnone (3.2 g) in 15 m*l* of acetic anhydride, 1 m*l* of perchloric acid (60%) was added drop by drop with stirring in an ice-salt bath. After stirring and cooling for 0.5 hr, the cooling bath was removed and stirring was continued for 12 hr at room temperature. The reaction mixture was poured into cold water, stirred to decompose the excess acetic anhydride and neutralized with sodium carbonate. The product, a viscous oil at first, solidified gradually on standing overnight. Recrystallization from ethanol gave 2.5 g (61%) of **1**, colorless plates, mp 143°C. IR: 1795, 1778, 1667 cm^{-1}.

3-Phenyl-4-propionylsydnone (2). The reaction of 3-phenylsydnone (1.6 g) with propionic anhydride (15 g) in the presence of perchloric acid (0.5 m*l*) afforded 1.5 g of crude product (mp 87—88°C), which was recrystallized from ethanol to give 1.1 g (50%) of **2**, colorless thin needles, mp 90—91°C. IR: 1798, 1666 cm^{-1}.

4-Acetyl-3-cyclohexylsydnone (3). The reaction of 3-cyclohexylsydnone (0.42 g) with acetic anhydride (5 m*l*) in the

Table 1.

Comp no.	Comp R	Comp R'	Method	Mp °C	Yield%	Found (Calcd) C%	Found (Calcd) H%	Found (Calcd) N%
1	C_6H_5	CH_3	C	143[a]	61	—	—	—
2	C_6H_5	C_2H_5	C	90—91[b]	50	—	—	—
3	C_6H_{11}	CH_3	C	42—43	74	57.25 (57.13)	6.60 (6.71)	13.16 (13.33)
4	$C_6H_5CH_2$	CH_3	A	61—62	29	—	—	—
			B	62—63	45	—	—	—
			C	60—62	73	60.40 (60.54)	4.63 (4.62)	13.04 (12.84)
5	C_6H_5	C_6H_{11}	A	101—102	59	66.42 (66.16)	6.03 (5.92)	10.56 (10.29)
6	C_6H_5	$C_6H_5CH_2$	A	96—97	19	68.38 (68.56)	4.35 (4.32)	10.08 (10.00)
7	C_6H_5	$C_6H_5CH=CH$	A	142	34	69.67 (69.85)	4.00 (4.14)	9.81 (9.59)

a) Lit,[2] 141.5—142.5°C. b) Lit,[2] 92.5—94°C.

1) H. Kato and M. Ohta, *Nippon Kagaku Zasshi*, **78**, 1653 (1957).

2) C. V. Greco, J. Tobias, and L. B. Kier, *J. Heterocyclic Chem.* **4**, 160 (1967).

3) V. G. Yashunskii and V. F. Vasil'eva, *Dokl. Akad. Nauk SSSR*, **130**, 350 (1960).

4) C. J. Thoman, D. J. Voaden, and I. M. Hunsberger, *J. Org. Chem.*, **29**, 2044 (1964).

presence of perchloric acid (3 drops) afforded 0.49 g of crude product (mp 38°C), which was recrystallized from ethanol to give 0.39 g (74%) of **3**, colorless plates, mp 42—43°C. IR: 1771, 1658 cm^{-1}.

4-Acetyl-3-benzylsydnone (4). Method A. 4.4 g of 3-benzylsydnone, 2 m*l* of glacial acetic acid and 12 g of phosphorus pentoxide afforded 1.6 g (29%) of **4**, colorless needles, mp 61—62°C.

Method B. 0.88 g of 3-benzylsydnone, 2.0 g of acetic anhydride and three drops of boron trifluoride-etherate afforded 0.49 g (45%) of **4**, mp 62—63°C (from ether–petroleum ether).

Method C. 3.52 g of 3-benzylsydnone, 15 m*l* of acetic anhydride and 1 m*l* of perchloric acid afforded 4 g of the crude product (mp 56—59°C) which was recrystallized from ether–petroleum ether to give 3.2 g (73%) of **4**, colorless needles, mp 60—62°C. IR: 1780, 1662 cm^{-1}. The IR spectra of the three product obtained above are superimposable.

4-Cychohexylcarbonyl-3-phenylsydnone (5). Method A. 4 g of 3-phenylsydnone, 3.5 g of cyclohexanecarboxylic acid and 12 g of phosphorus pentoxide afforded 4 g (59%) of **5**, mp 101—102°C (from ethanol). IR: 1785, 1665 cm^{-1}.

3-Phenyl-4-phenylacetylsydnone (6). Method A. 4 g of 3-phenylsydnone, 4.3 g of phenylacetic acid and 12 g of phosphorus pentoxide afforded 1.34 g (19%) of **6**, colorless needles, mp 96—97°C. IR: 1790, 1655 cm^{-1}.

4-Cinnamoyl-3-phenylsydnone (7). Method A. 4 g of 3-phenylsydnone, 4.5 g of cinnamic acid (*trans*) and 12 g of phosphorus pentoxide afforded the crude product containing cinnamic acid anhydride and was recrystallized from methanol to give 2.5 g (34%) of **7**, colorless needles, mp 142°C. IR: 1786, 1650 cm^{-1}.

BULLETIN OF THE CHEMICAL SOCIETY OF JAPAN, VOL. 45, 2945—2947 (1972)

Linear Relationships between CN Stretching Frequencies and Polar Substituent Constants of L in $Co(CN)_5L^{3-}$ Complexes

Takuzo FUNABIKI and Kimio TARAMA

Department of Hydrocarbon Chemistry, Faculty of Engineering, Kyoto University, Sakyo-ku, Kyoto

(Received November 26, 1971)

In the chemistry of pentacyanocobaltate(II), ultraviolet and visible spectroscopies have usually been used to establish the structures of the complexes and to clarify the reaction mechanisms kinetically, but they have scarcely been used to distinguish the organocobalt complexes. In the study to elucidate the reaction mechanism and the novel solvent effect on the selectivity in the hydrogenation of butadiene by pentacyanocobaltate(II),[1] infrared spectroscopy was expected to be useful to observe directly the variation of the intermediates under the reaction condition. In this paper, CN stretching frequencies of various substituted pentacyanocobaltates and some tetracyanocobaltates measured in the aqueous reaction solutions are reported. Also presented here linear relationships between the CN stretching frequencies and polar substituent constants.

Results and Discussion

CN stretching frequencies of substituted pentacyanocobaltate are given in the Table 1 together with other published data. The complexes in aqueous solutions exhibit single bands in the CN stretching region probably on account of the broadening effect. As shown in Fig. 1, a linear relationship is found between $\Delta\nu_{CN}$ and Taft's σ_I function of substituent L. With regard to the organic and hydridic substituents, a much better linear relationship is found with Taft's σ^* function as shown in Fig. 2. Similar correlations have been found in substituted metal carbonyls between ν_{CO} and substituent constants,[2] but the linear relationships reported here are the first for the metal cyano complexes and are noteworthy because L is bound directly to the cobalt atom and the linearity holds in the wide range of L.

In metal cyano complexes, the variation of the CN stretching frequency has been interpreted in terms of the following resonance structures; *i.e.* the larger the contribution of II, the lower the CN stretching frequency.[3,4]

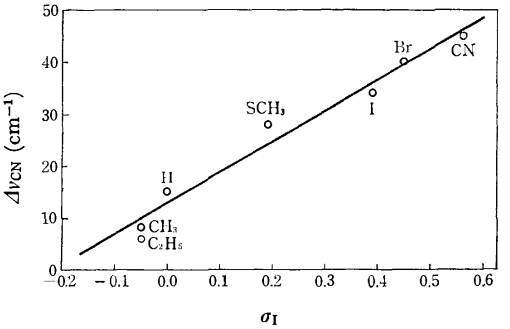

Fig. 1. Plot of $\Delta\nu_{CN}$ *versus* Taft's σ_I
(σ_I: R. W. Taft, Jr., *et al.*, *J. Amer. Chem. Soc.*, **85**, 709 (1963)).

1) K. Tarama and T. Funabiki, This Bulletin, **41**, 1744 (1968); T. Funabiki and K. Tarama, *ibid.*, **44**, 945 (1971); *Tetrahedron Lett.*, **1971**, 1111.

2) M. Bigorgne, *J. Inorg. Nucl. Chem.*, **26**, 107 (1964); R. Ugo, S. Cenini, and F. Bonati, *Inorg. Chim. Acta*, **1**, 451 (1967); A. A. Ioganson, A. B. Antonova, B. V. Lokshin, N. E. Kolobova, K. N. Anisimov, and A. N. Nesmeyanov, *Izv. Akad. Nauk SSSR, Ser Khim.*, **1969**, 1957 (*Chem. Abstr.*, **72** 26649e (1970)); A. N. Nesmeyanov, K. N. Anisimov, B. V. Lokshin, N. E. Kolobova, and Yu. V. Makarov, *Dokl. Akad. Nauk SSSR*, **176**, 1082 (1967) (*Chem. Abstr.*, **68**, 44365j (1968)); N. Herberhold and H. Brabetz, *Chem. Ber.*, **103**, 3909 (1970).

3) M. F. A. El-Sayed and R. K. Sheline, *J. Inorg. Nucl. Chem.*, **6**, 187 (1958).

4) K. Nakamoto, "Infrared Spectra of Inorganic and Coordination Compounds," Wiley-Interscience, New York, (1969).

TABLE 1. CN STRETCHING FREQUENCIES OF SUBSTITUTED PENTACYANOCOBALTATE $Co(CN)_5L^{3-}$

$Co(CN)_5L^{3-}$ L	ν_{CN}(obs.) cm^{-1}	$\Delta\nu_{CN}$ cm^{-1}	ν_{CN}(in literatures) cm^{-1}
None or H_2O	2082	0	2095, 2136;[a] 2083;[b] 2093, 2127;[c] 2080;[d]
$(CH_3)_2CH-$	2087	5	
$CH_3CH_2CH_2-$	2088	6	2084;[e]
CH_3CH_2-	2088	6	2085;[e] 2094±3;[f]
CH_3-	2090	8	2087;[e] 2094±3;[f]
$(CH_3)_2C=CH-CH_2-$	2090	8	2092;[e]
$CH_3-CH=CH-CH_2-$	2091	9	2092;[e]
$CH_2=CH-CH_2-$	2094	12	2092;[e]
$C_6H_5CH_2-$	2094	12	2092;[e] 2093±3;[f]
H-	2097	15	2113;[g] 2098;[b] 2090, 2115, 2127, 2145;[c]
RS- ($R=CH_3$, C_2H_5, $C_6H_5CH_2$)	2110	28	
I-	2116	34	2117;[h]
Br-	2122	40	2125;[h]
CN-	2127	45	2126, 2129, 2143;[i] 2134;[h] 2128;[j] 2120;[d]

a), i) W. P. Griffith and G. Wilkinson, *J. Chem. Soc.*, **1959**, 2757, b), h) J. Halpern and J. P. Maher, *J. Amer. Chem. Soc.*, **87**, 5361 (1965); c) G. Pregaglia *et al.*, *Discuss. Faraday Soc.*, **46**, 110 (1968); d) J. Halpern and M. Pribanic, *J. Amer. Chem. Soc.*, **93**, 96 (1971); e) J. Kwiatek and J. K. Seyler, *J. Organometal. Chem.*, **3**, 421 (1965); f) J. Halpern and J.P. Maher, *J. Amer. Chem. Soc.*, **86**, 2311 (1965); g) R. S. G. Banks and J. M. Pratt, *Chem. Commun.* **1965**, 776; j) L. H. Jones, *Inorg. Chem.*, **2**, 277 (1963); [(a), (b), (d), and (j) were observed in aqueous solution.]

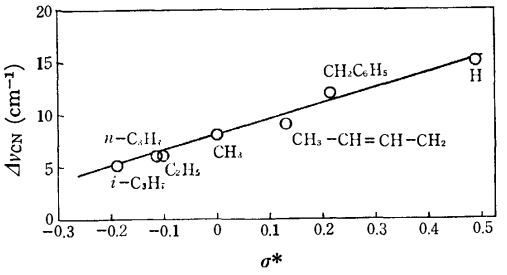

Fig. 2. Plot of $\Delta\nu_{CN}$ *versus* Taft's σ^*.
(σ^*: R. W. Taft, Jr., in M. S. Newman: "Steric Effects in Organic Chemistry," John Wiley & Sons, Inc., New York (1956)).

$$\underset{\text{I}}{M-C\equiv N:} \longleftrightarrow \underset{\text{II}}{\overset{+}{M}=C=\overset{-}{\underset{\cdot\cdot}{N}}:} \qquad (1)$$

According to El-Sayed and Sheline,[3] the CN stretching frequencies of cyano complexes depend on: (i) the electronegativity, (ii) the oxidation state, and (iii) the coordination number of the metal. The variation of the CN stretching frequency in the substituted pentacyanocobaltates is related to (ii), but the concept of the oxidation state of the metal atom does not seem to be enough to explain the linear variation of the CN stretching frequency with polar substituent constants. The results are explained as follows. From the correlation of σ_I or σ^* value with the inductive electron-withdrawing power of the substituent L, it is reasonable to suppose that the net charge density on the substituent L increases with the increasing σ_I or σ^* value, which, consequently, decreases the contribution of structure II in Eq. (1). Thus, in the case of the complexes such as $Co(CN)_6^{3-}$ and $Co(CN)_5X^{3-}$ (X=halogen), the net charge density on the substituents must be large, and the contribution of the structure II must be small. This is supported by the fact that the linearity holds for $Co(CN)_6^{3-}$, because the linear relationship in Fig. 1 holds when there is little back donating of electron from the cobalt atom to the substituent L. In these complexes the oxidation state of Co(III) seems appropriate as proposed. On the other hand, in the case of alkyl complexes, the net charge density on the alkyl groups must be small or nil. The small $\Delta\nu_{CN}$ values suggest that Co(II) may be preferable to Co(III) although Co(III) has been proposed for these complexes. This difference in the net charge density on the substituent may be connected with the difference in the type of fission of the Co–L bond. In the former complexes, the Co–L bond is split heterolytically[5] and in the latter homolytically. From this point of view, it would be interesting to study the type of fission of the Co–SR bond in $Co(CN)_5SR^{3-}$, because it is assumed from the CN stretching frequency in Table 1 that the net charge density on SR and the contribution of structure II in Eq. (1) are intermediate between the above two groups of complexes.

With regard to $Co(CN)_5H^{3-}$, which is the active complex in the hydrogenation reactions, the oxidation state of Co(I),[6] Co(II),[7] and Co(III)[8] have been proposed. Figure 1 indicates that the net charge density on the hydrogen atom may be only slightly larger than that on the alkyl substituents. This is consistent with the low basicity of the complex[9] and the homolytic fission of the Co–H bond in the catalytic hydrogenation. Thus, Co(II) seems most preferable for this complex. The linear relationships in Figs. 1 and 2 may be used to estimate the approximate sub-

5) R. Grassi, A. Haim, and W. K. Wilmarth, *Inorg. Chem.*, **6**, 237 (1967).

6) G. A. Mills, S. Weller, and A. Wheeler, *J. Phys. Chem.*, **63**, 403 (1959).

7) L. Simandi and F. Nagy, *Acta Chim. Acad. Sci. Hung.*, **46**, 101 (1965); M. G. Burnett, P. J. Connolly, and C. Kemball, *J. Chem. Soc., A*, **1967**, 800.

8) N. K. King and M. E. Winfield, *J. Amer. Chem. Soc.*, **83**, 3366 (1961).

9) J. Halpern and L-Y. Wong, *ibid.*, **90**, 6665 (1968).

stituent constant: $\sigma^*(-CH_2CH=CH_2)=0.26$, $\sigma^*(-CH_2-CHC=(CH_3)_2)=0.0$.

The CN stretching frequencies of π-allyl- and *syn*-π-(1-methylallyl)-tetracyanocobaltates were observed at 2102 and 2098 cm^{-1}, respectively.[10] They are higher than those of σ-allyl- and σ-but-2-enyl-pentacyanocobaltates, which is consistent with the postulate that an increase in the coordination number results in the decrease in the CN stretching frequency.[11]

Experimental

Aqueous solutions of the complexes with a cobalt concentration of 0.2M were prepared at 0°C. In all experiments, the $CoCl_2$ solution was added to the KCN solution, and organic substances were added to the KCN solution before the addition of the $CoCl_2$ solution. The complexes were prepared either by the reaction of $Co(CN)_5^{3-}$ with alkyl halides and mercaptans, or by the reaction of $Co(CN)_5H^{3-}$ with conjugated dienes. In the reaction with alkyl halide, rapid transformation of $Co(CN)_5X^{3-}$ to $Co(CN)_5OH_2^{2-}$ was observed.[5] In the reaction with mercaptans, two distinct bands corresponding to $Co(CN)_5SR^{3-}$ and $Co(CN)_5H^{3-}$ were observed, demonstrating the proposed mechanism for this reaction,[12] and that was confirmed by the observation of the single band of $Co(CN)_5SR^{3-}$ in the reaction with dialkyldisulfides. $Co(CN)_6^{3-}$ was prepared by the method described by Benedetti-Pichler.[13]

Formations and structures of the organocobalt complexes were confirmed by the NMR spectra of the reaction solution as reported earlier in the case of σ-but-2-enyl and *syn*-π-(1-methylallyl) complexes.[10]

Samples in small polyethylene envelopes were placed between two plates of rock salt, and the infrared spectra were recorded on a JASCO DS-403G spectrophotometer in the 2000—2200 cm^{-1} region. Frequencies were accurate to within ± 1 cm^{-1}.

10) T. Funabiki and K. Tarama, *Chem. Commun.*, **1971**, 1177. Values of ν_{CN} are corrected in this paper.

11) L. H. Jones and R. A. Penneman, *J. Chem. Phys.*, **22**, 965 (1954); R. A. Penneman and L. H. Jones, *ibid.*, **24**, 293 (1956); *J. Inorg. Nucl. Chem.*, **20**, 19 (1961).

12) T. Mizuta and T. Kwan, *Nippon Kagaku Zasshi*, **87**, 825 (1966).

13) Benedetti-Pichler, *Z. Anal. Chem.*, **70**, 258 (1927).

BULLETIN OF THE CHEMICAL SOCIETY OF JAPAN, VOL. 45, 2947—2949 (1972)

Effect of Transition Metal Chlorides in the Coupling of Allyl Chloride and *n*-Butylmagnesium Bromide[1]

Yoshihiro OHBE and Tsutomu MATSUDA

Department of Organic Synthesis, Faculty of Engineering, Kyushu University, Hakozaki, Higashi-ku, Fukuoka, 812

(Received June 5, 1972)

Coupling reaction of allylic halides with Grignard and other organometallic reagents has been a subject of investigations[2] and used as synthetic procedure. Contrary to the Kharasch reaction which involves the coupling of alkyl halides in a Grignard reagent solution in the presence of transition metal salts, the allylic coupling does not usually require any added catalysts. Probably because of this reason which certainly is attributable to the enhanced reactivity of the halides, there are few works which threw attention into a catalytic effect of added metal salts in the latter reaction.

In the previous paper[3] we showed a considerable difference in their catalytic features among various metallic chlorides in the Kharasch coupling. This paper concerns with another example of a pronounced difference in activity among iron(III), copper(II), cobalt(II), and nickel(II) chlorides in the coupling reaction of allyl chloride with *n*-butylmagnesium bromide. To a solution of anhydrous metallic chloride suspended in anhydrous ether, a filtered ethereal *n*-butylmagnesium bromide (0.2 mol) was added and stirred under reflux until the evolution of gas ceased (reaction A) for 0.5 to 1 hr. To the resultant dark solution, an equivalent amount of allyl chloride in ether was added in a period of 10 min and again stirred under reflux for 3 to 5 hr (reaction B) until concurrent evolution of larger amount of gas stopped. After the reaction mixture was hydrolyzed and treated in a usual manner, distillation of the ethereal solution gave a mixture of liquid products. The compositions of gaseous products in reaction A and B, and the liquid products were analyzed by gas chromatography.

The effects of four metal salts in varying concentrations on the amounts of gas in reaction A and B, and the yields of the liquid products were illustrated in Figs. 1 to 4. The quantities of gas evolved in reaction A, indicative of the amount of the Grignard reagent utilized in the reduction of the metallic salts to lower valence states, were rather small and nearly independent on the kind of the metal salts when the relative concentration of the salts to the Grignard reagent are less than 10^{-2}. A pronounced difference, however, was observed in reaction B. When cobalt(II) and nickel(II) salts were used, a large amount of gas which were

1) Reaction of Grignard Reagent Catalyzed by Transition Metal Salts. III.

2) a) S. Czernecki, C. Georgoulis, B. Gross, and C. Prevost, *Bull. Soc. Chim. Fr.*, **1968** 3713. b) R. M. Magid, E. C. Nieh, and R. D. Gandour, *J. Org. Chem.*, **36**, 2099 (1971) and references cited there. c) R. G. Gough and J. A. Dixon, *ibid.*, **33**, 2148 (1968).

3) Y. Ohbe and T. Matsuda, *Nippon Kagaku Zasshi*, **89**, 298 (1968).

Table 1. Comparison of the composition of the gas in reaction A and B for the four metal salts[a)]

		Co (II)		Ni (II)		Cu (II)		Fe (III)	
		1×10^{-4}	7×10^{-3}	1×10^{-4}	1×10^{-3}	1×10^{-3}	2×10^{-2}	3.3×10^{-3}	5×10^{-2}
A	Butane	81	121	178	233	140	177	164	321
	1-Butene	126	131	82	37	81	76	96	419
B	Butane	42	306	46	77	429	1523	425	900
	1-Butene	3510	3907	3180	3653	546	3420	765	2970
	Propylene	3740	3387	3130	3120	165	155	510	1080

a) 1 ML at 25 °C under atmospheric pressure.

consisted mainly of 1-butene and propylene resulted, but the yields of liquid products stayed at a low level throughout the catalyst concentrations adopted in this study. On the other hand, iron(III) and copper(II) salts showed an enhanced promoting effect in the coupling between allyl chloride and *n*-butylmagnesium bromide to afford 1-heptene as a major product with optimal concentrations of 5×10^{-3} equivalent for iron(III) and 1×10^{-3} for copper(II) salts. However, the reaction of allyl chloride with itself to give 1,5-hexadiene was little affected by the presence of any metal salt, and the yields remained at a low level irrespective of the nature of the added catalysts. Another information of interest was obtained by inspection of the compositions of gas in reaction B illustrated in Table 1 for the representative concentrations of each salts.

The major role of Grignard reagent in alkyl halide coupling under similar condition has been inferred[3)] to be regeneration of active catalytic species by reduction of the transition metal salts oxidized in the course of the coupling reaction, on the basis that the composition of the gas in reaction B was closely analogous to that of reaction A, which was consisted of alkane and alkene derived from the alkyl group of the Grignard reagent utilized. The striking contrast between the previous observation and the results in Table 1 could be rationalized as follows: (1) all four metallic chlorides are taking part in the reaction between allyl chloride and the Grignard reagent in their reduced forms, (2) cobalt(II) and nickel(II) chlorides promote exclusively the transfer of hydrogen from the alkyl group of the Grignard reagent to allyl chloride, thus, giving a nearly equal amount of propylene and 1-butene, and (3) substitution of the alkyl group is more favored in the presence of iron(III) and copper(II) chlorides (1a and 1b).

$$CH_2{=}CH{-}CH_2{-}Cl + CH_3(CH_2)_2CH_2MgBr$$

$$\text{1a: } \overset{Co(II)}{Ni(II)} \swarrow \qquad \searrow \text{1b: } \overset{Fe(III)}{Cu(II)}$$

$$CH_2{=}CH{-}CH_3 + CH_2{=}CH{-}C_2H_5 + MgBrCl \qquad CH_2{=}CH{-}(CH_2)_4{-}CH_3 + MgBrCl$$

Although the amount of gas in reaction B markedly increased with iron(III) and copper(II) salts in the concentrations around 10^{-2}—10^{-1} equivalent, the results in Table 1 seems to suggest that the difference among two pairs of the salts is retained, especially in the case of copper(II) salt even in this concentration range. Alkyl metals have been recently proposed to be the active species in Kharasch coupling[4a)] and related reaction[4b)]. The present results could be accounted by assuming that these unstable species react with allyl chloride to form either ion-pair[2a)] or radical-pair[2c)] intermediate and the nature of carbon-metal bond of the alkyl metals determines which route favors 1a or 1b. However, a possibility of the intermediate

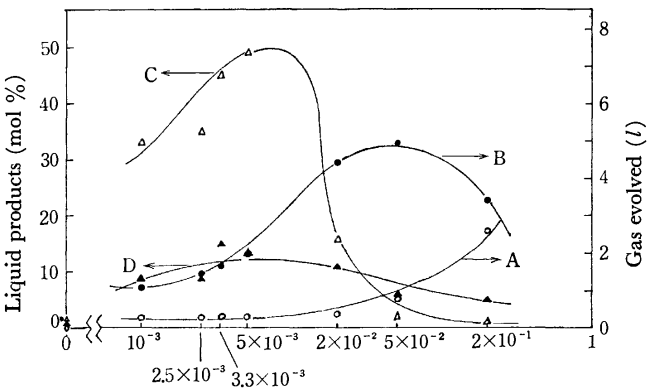

Fig. 1. Amounts of gaseous product in reaction A and B, and yields of liquid product.
A: A reaction gas, B: B reaction gas
C: 1-Heptene, D: 1,5-Hexadiene

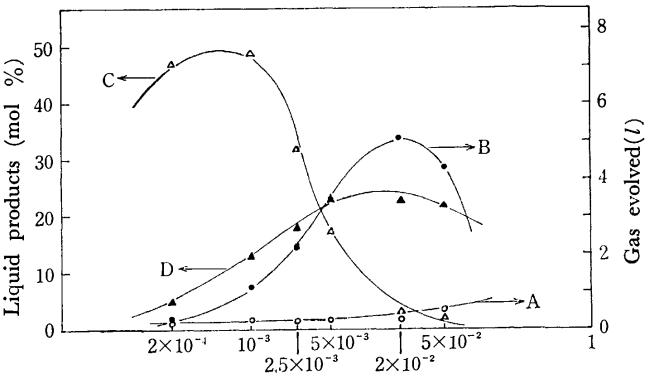

Fig. 2. Amounts of gaseous product in reaction A and B, and yields of liquid product.
A: A reaction gas B: B reaction gas
C: 1-Heptene D: 1,5-Hexadiene

4) a) T. Tamura and J. K. Kochi, *J. Amer. Chem. Soc.*, **92**, 6656 (1970). *ibid.*, **93**, 1483, 1485 (1971). *J. Organometal. Chem.*, **29**, 111 (1971). *ibid.*, **31**, 289 (1971). b) T. Tamura and J. K. Kochi, *J. Amer. Chem. Soc.*, **93**, 1487 (1971).

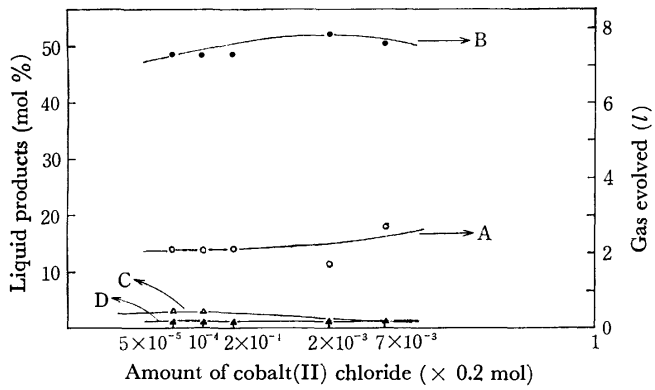

Fig. 3. Amounts of gaseous product in reaction A and B, and yields of liquid product.
A: A reaction gas B: B reaction gas
C: 1-Heptene D: 1,5-Hexadiene

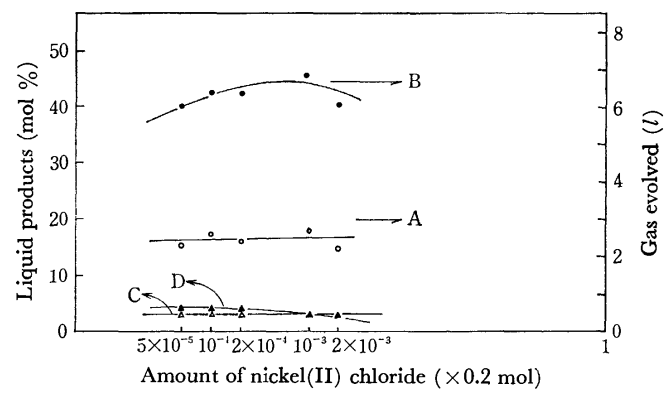

Fig. 4. Amounts of gaseous product in reaction A and B, and yields of liquid product.
A: A reaction gas B: B reaction gas
C: 1-Heptene D: 1,5-Hexadiene

formation of π-allylmetal species could not be entirely excluded in view of our preliminary observation that the reaction of crotyl halides with ethylmagnesium bromide afforded a mixture of three kinds of dienes which produced by coupling of the halide itself as principal product but little of hexenes, irrespective of the metallic chlorides utilized, and the chemical behavior[5] of π-allylnickel complexes which react rapidly with allylic halides and tosylates to give nonspecific cross coupling products.

Further studies are in progress to disclose the reason of the marked difference between allyl and crotyl halides and also a plausible structure of active intermediate.

5) E. J. Corey and M. F. Semmelhack, *J. Amer. Chem. Soc.*, **89**, 2755 (1967), E. J. Corey, M. F. Semmelhack, and L. S. Hegedus, *ibid.*, **90**, 2416 (1968).

BULLETIN OF THE CHEMICAL SOCIETY OF JAPAN, VOL. 45, 2949—2951 (1972)

Sensitized Delayed Fluorescence in Frozen Aqueous Solutions of Dinucleotide- and Polyadenylic Acid-Proflavine Systems

Yukio KUBOTA

Department of Chemistry, Yamaguchi University, Yamaguchi

(Received December 24, 1971)

We have previously shown that the sensitized delayed fluorescence (SDF) in frozen aqueous solutions of DNA- and mononucleotide-acridine dye systems arises from the triplet-singlet energy transfer, in which excitation energy is transferred from the triplet state of the DNA base to the singlet state of the dye.[1] This phenomenon has also been observed in frozen aqueous solutions of dinucleotide- and polynucleotide-acridine systems. This paper will present the results on adenosine dinucleotide- and polyadenylic acid-proflavine systems.

Experimental

Adenosine monophosphate (AMP) and cytidine monophosphate (CMP) were purchased from the Sigma Chemical Co. Thymidine monophosphate (TMP), adenyl-3′: 5′-adenosine (ApA), adenyl-3′: 5′-cytidine (ApC), and polyadenylic acid (poly A) were purchased from Miles Laboratories, Inc. Proflavine (PF) was the same sample as has been described previously.[2]

The emission spectra were measured at 77°K in the same way as has been described previously.[2] The solvents used were a 0.01M phosphate buffer (pH 7.0) and an ethylene glycol-buffer mixture.[3] The concentration of nucleotide was 5×10^{-3}M (in base units); it was spectrophotometrically determined.[4,5] The concentration of PF was changed from 5×10^{-6} to 2×10^{-4}M. Unless otherwise stated, all the luminescence data presented in this paper were obtained by an excitation at 280 nm.

Results and Discussion

ApA- and Poly A-PF Systems. Figures 1 and 2 show the total and delayed emission spectra of the ApA- and poly A-PF systems respectively. In the

1) Y. Kubota, This Bulletin, **43**, 3126 (1970).

2) Y. Kubota, *ibid.*, **43**, 3121 (1970).

3) This solvent contains 1% of ethylene glycol by volume and will hereinafter be abbreviated as EGW.

4) M. M. Warshaw and I. Tinoco, Jr., *J. Mol. Biol.*, **13**, 54 (1965).

5) D. N. Holcomb and I. Tinoco, Jr., *Biopolymers*, **3**, 121 (1965).

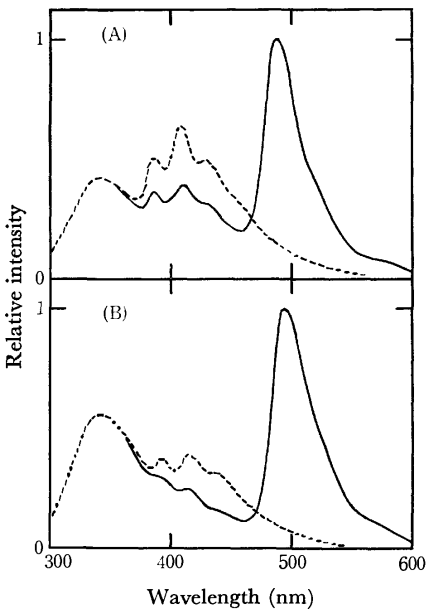

Fig. 1. Total emission spectra of (A) ApA-PF and (B) poly A-PF systems in frozen EGW solutions.
----: in the absence of PF
——: in the presence of PF
Nucleotide: 5×10^{-3}M in adenine residue. PF: 5×10^{-5}M.

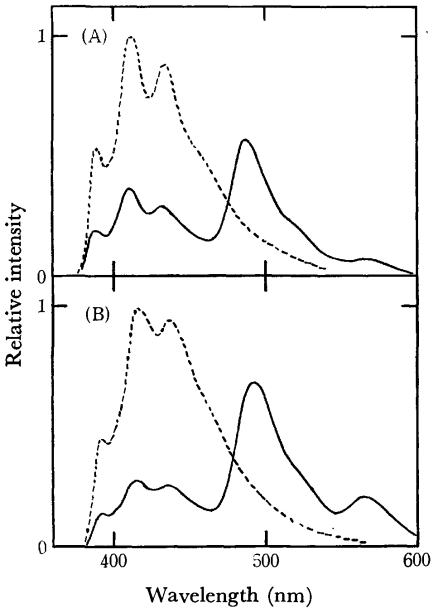

Fig. 2. Delayed emission spectra of (A) ApA-PF and (B) poly A-PF systems in frozen EGW solutions.
----: in the absence of PF
——: in the presence of PF
Nucleotide: 5×10^{-3}M in adenine residue. PF: 5×10^{-5}M.

absence of PF, the band centered at 340 nm is ascribed to the adenine fluorescence, and the emission at 390—500 nm, to the adenine phosphorescence.[6] In the presence of PF, the delayed emissions are composed of adenine phosphorescence, SDF (490 nm), and the phosphorescence (570 nm) of PF. It may be seen from Fig. 1 that the adenine phosphorescence is selectively quenched in the presence of PF. Further, the excitation spectrum of SDF is the same as that of the adenine phosphorescence. As has been interpreted previously in connection with mononucleotide-PF systems,[1] it may be concluded that this SDF is caused by the energy transfer from the triplet state of the adenine residue to the singlet state of PF.

Next, the phosphorescence efficiency of the adenine residue, ϕ_P^D, can be estimated from the energy-transfer data. ϕ_P^D is given by the following equation:[7,8]

$$\phi_P^D = \frac{\Phi_P}{\Phi_{SDF}} \cdot \frac{\phi_{TR}}{1-\phi_{TR}} \Phi_F^A$$

where Φ_P is the quantum yield of the adenine phosphorescence in the presence of PF; Φ_{SDF}, the quantum yield of SDF; ϕ_{TR}, the efficiency of energy transfer,[9] and Φ_F^A, the quantum yield of the PF fluorescence.[10] From our data, the ϕ_P^D values of AMP, ApA, and poly A were estimated to be 0.28, 0.22, and 0.16 respectively. These values are not extremely accurate because of some sources of error;[7] however, the value of AMP can be compared with the value of 0.3 calculated from the data of Guéron *et al.*[12] It may be considered, therefore, that the values presented here are reasonable and that the ϕ_P^D value of poly A is somewhat smaller than that of AMP.

ApC-PF Systems. Recently, triplet-triplet energy transfer between nucleotide molecules has been found to occur in dinucleotides or in mixtures of nucleotide molecules.[13–15] In order to obtain some information on the relation between this energy transfer and SDF, we also examined the ApC-PF, (AMP+CMP)-PF, and (AMP+TMP)-PF systems. In the case of ApC or mixtures of mononucleotides, the phosphorescence intensity of adenine lowers remarkably compared with that of AMP alone, while the phosphorescence intensity of cytosine or thymine increases; this phenomenon may be ascribed to the occurrence of the triplet-triplet energy transfer. In parallel with this phenomenon, the decay of SDF in the case of ApC or mixtures becomes faster than that in the case of AMP alone (Fig. 3). As may be seen from Fig. 3, all the decays of SDF deviate from single exponentials. It is, therefore, impossible to determine meaningful rate constants as reciprocals of the decay times of SDF. For convenience,

6) T. Montenay-Garestier, C. Hélene, and A. M. Michelson, *Biochim. Biophys. Acta*, **182**, 342 (1969).

7) R. G. Bennett, R. P. Schwenker, and R. E. Kellogg, *J. Chem. Phys.*, **41**, 3040 (1964).

8) W. C. Galley and L. Stryer, *Biochemistry*, **8**, 1831 (1969).

9) ϕ_{TR} can be estimated from the measurements of the ratio of the phosphorescence to the fluorescence of adenine in the presence of PF, (I_P/I_F), and in the absence of PF, $(I_P/I_F)_0$:

$$\phi_{TR} = 1 - \frac{(I_P/I_F)}{(I_P/I_F)_0}$$

10) Φ_F^A in nucleotide solutions was determined to be 0.37 by using 9-aminoacridine as the standard of the quantum yield.[11]

11) G. Weber and F. W. J. Teale, *Trans. Faraday Soc.*, **53**, 646 (1957).

12) M. Guéron, J. Eisinger, and R. G. Shulman, *J. Chem. Phys.*, **47**, 4077 (1967).

13) C. Hélene, *Biochem. Biophys. Res. Commun.*, **22**, 237 (1966).

14) C. Hélene, P. Douzou, and A. M. Michelson, *Proc. Natl. Acad. Sci. U. S.*, **55**, 376 (1916).

15) M. Guéron, R. G. Shulman, and J. Eisinger, *ibid.*, **56**, 814 (1966).

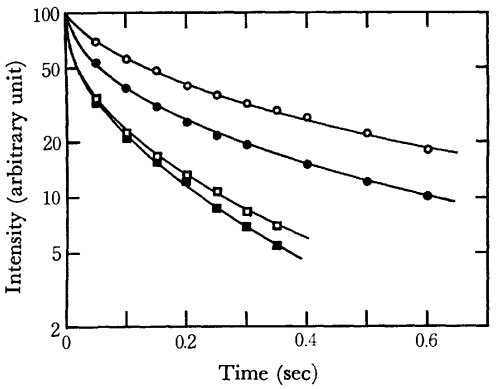

Fig. 3. Decay curves of SDF.
○: AMP-PF ■: CMP-PF ●: (AMP+CMP)-PF
□: ApC-PF Total nucleotide: 5×10^{-3}M in base unit
PF: 5×10^{-5}M

we adopt the half-life, $\tau_{1/2}$, as a qualitative measure of rate constants. As may be noticed from Table 1, the $\tau_{1/2}$ values in the cases of the mononucleotide-PF systems depend on the phosphorescence lifetimes of nucleotides, τ_P, and are about one tenth of τ_P. Consequently, the $\tau_{1/2}$ values will tell us which nucleotide is important as the energy donor in the case of ApC or mixtures. The $\tau_{1/2}$ value in the case of ApC or mixtures is comparable to that in the case of CMP or TMP (Table 1). This indicates that the triplet state of CMP or TMP plays an important role; that is, first, a base-to-base energy transfer produces the triplet state of CMP or TMP, and next, the triplet energy is transferred to the singlet state of PF. This

Table 1. Decays of nucleotide phosphorescence (τ_P) and SDF ($\tau_{1/2}$) in frozen aqueous solutions

Nucleotide	τ_P (sec)		$\tau_{1/2}$ (msec)
AMP	2.32		135[a]
CMP	0.40		30[a]
TMP	0.20		20[a]
AMP+CMP (1:1)	non-exponential		
	fast (0.4)	60%	60
	slow (2.2)	40%	
AMP+TMP (1:1)	non-exponential		
	fast (0.2)	90%	24
	slow (1.8)	10%	
ApC	non-exponential		
	fast (0.4)	85%	35
	slow (2.3)	15%	
ApA	2.28		42
Poly A	non-exponential		
	fast (0.5)	25%	38
	slow (2.2)	75%	

Total nucleotide: 5×10^{-3} M in base units. PF: 5×10^{-5} M.
a) Ref. 1.

conclusion confirms our previous interpretation of SDF in DNA-acridine complexes.[1] On the other hand, the $\tau_{1/2}$ values in the cases of ApA and poly A are much smaller than that in the case of AMP; this phenomenon probably results from the difference in conformation between the monomer and the polymers of adenylic acid.[4,5]

This work was supported in part by a Grant for Scientific Research from the Ministry of Education.

BULLETIN OF THE CHEMICAL SOCIETY OF JAPAN, VOL. 45, 2951—2953 (1972)

The Photosensitized Reduction of 4-Nitropyridine *N*-Oxides

Isao ONO and Norisuke HATA

Department of Chemistry, College of Science and Engineering, Aoyama Gakuin University
Chitosedai, Setagaya-ku, Tokyo

(Received March 2, 1972)

4-Nitropyridine *N*-oxides are photochemically reduced to afford 4-hydroxylaminopyridine *N*-oxides in ethanol under nitrogen atmosphere.[1] From the measurements of the quantum yields and the flash-spectrophotometric experiments, such a photochemical reduction has been considered to proceed through an intermediate species originating from the excited singlet state of 4-nitropyridine *N*-oxide.[2,3] However, the photochemical reduction of aromatic nitro compounds are generally thought to proceed through the lowest n,π^* triplet state;[4] detailed investigations have been performed on the nitrobenzene,[5] 1-nitronaphthalene,[6] and 4-nitropyridine.[7] Therefore, it seems to be of importance, in elucidating the reaction mechanism, to clarify whether or not the reduction of 4-nitropyridine *N*-oxide can occur from the lowest triplet state. In the present investigation, the biacetyl-sensitized reac-

1) C. Kaneko, S. Yamada, I. Yokoe, N. Hata, and Y. Ubukata, *Tetrahedron Lett.*, **1966**, 4729.

2) N. Hata, E. Okutsu, and I. Tanaka, This Bulletin, **41**, 1769 (1968).

3) N. Hata, I. Ono, and T. Tsuchiya, *ibid.*, **45**, 2386 (1972).

4) H. A. Morrison, "The Chemistry of the Nitro and Nitroso Groups," Part 1, ed. by H. Feuer, Interscience Publishers, New York, (1969), Chapter 4.

5) R. Hurley and A. C. Testa, *J. Amer. Chem. Soc.*, **88**, 4330 (1966), *ibid.*, **89**, 6917 (1967).

6) S. Hashimoto and K. Kano, *Kogyo Kagaku Zasshi*, **72**, 188 (1969).

7) S. Hashimoto, K. Kano, and K. Ueda, *Tetrahedron Lett.*, **1969**, 2733. This Bulletin, **44**, 1102 (1971).

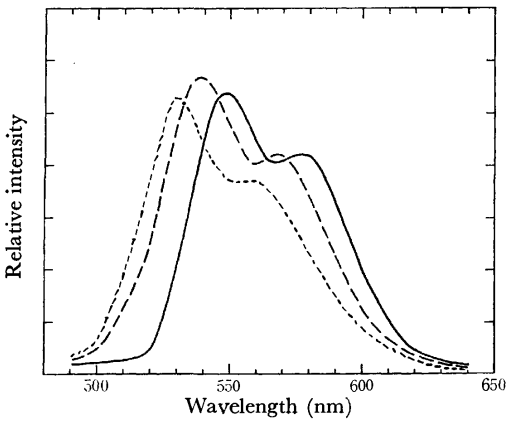

Fig. 1. The phosphorescence spectra of 4-nitropyridine *N*-oxide (——), 3-methyl-4-nitropyridine *N*-oxide (----) and 3,5-dimethyl-4-nitropyridine *N*-oxide (-·-·-) in 2-propanol at 77°K.

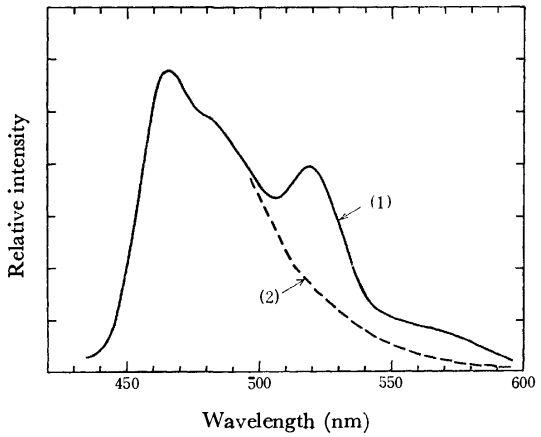

Fig. 2. Quenching of the biacetyl phosphorescence by an addition of 4-nitropyridine *N*-oxide in deaerated 2-propanol at room temperature.
(1) biacetyl alone (5×10^{-2}M)
(2) biacetyl (5×10^{-2}M) and 4-nitropyridine *N*-oxide (1×10^{-3}M)

tions of 4-nitropyridine *N*-oxide (I), 3-methyl-4-nitropyridine *N*-oxide (II), and 3,5-dimethyl-4-nitropyridine *N*-oxide (III) were carried out in deaerated 2-propanol or ethanol.

The lowest triplet state of 4-nitropyridine *N*-oxide has been studied by Kubota *et al.*[8] by means of both its phosphorescence and S-T absorption spectroscopy. As a result, the lowest triplet state of 4-nitropyridine *N*-oxide has been concluded to be a π,π^* state with an excitation energy of about 52 kcal·mol^{-1}. Figure 1 shows the phosphorescence spectra of (I), (II), and (III) in 2-propanol glass at 77°K. Consequently, the biacetyl (E_T=56.3 kcal·mol^{-1}) is expected to be usable as a triplet sensitizer for these *N*-oxides, (I), (II), and (III). As is shown in Fig. 2, the biacetyl phosphorescence in deaerated 2-propanol (5×10^{-2}M) at room temperature was observed to be completely quenched by the addition of the 4-nitropyridine *N*-oxide (1×10^{-3}M). Similar results were also obtained when (II) or (III) was used as a triplet quencher instead of (I). In addition, Fig. 3 shows the progressive spectral change in 4-nitropyridine *N*-oxide in deaerated 2-propanol containing biacetyl when the solution was irradiated with the visible light longer than 400 nm which is absorbed by biacetyl alone; there, it was observed that the absorption spectrum of 4-nitropyridine *N*-oxide decreased progressively in intensity and a new absorption band with its maximum at about 290 nm appeared.

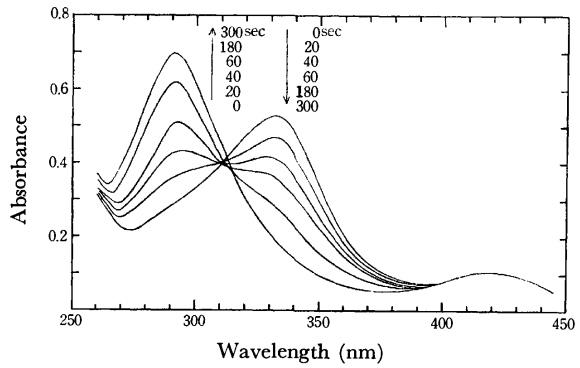

Fig. 3. The progressive spectral change of 4-nitropyridine *N*-oxide (5×10^{-5}M) in deaerated 2-propanol containing 5×10^{-3}M biacetyl on visible light irradiation (>400 nm). Numbers refer to the irradiation time.

Next, the separation and identification of the photoproducts formed in the photosensitized reactions of (I), (II), and (III) were carried out; the procedures will be described below.

An 2-propanol or ethanol solution containing 100 mg of (I) and 200 mg of biacetyl in a quartz cylindrical reaction vessel (5.0 cm in length and 4.5 cm in diameter) was irradiated with a high-pressure mercury lamp (Toshiba H-400 P) equipped with a Hoya L-42 filter for 14 hr while nitrogen was bubbled in. After the removal of the solvent under reduced pressure in an atmosphere of nitrogen, benzene was added to the residue. Then, the undissolved product was collected and washed with a mixture of ethanol and diethyl ether (1 : 1). The mp of the photoproduct (Ia) thus obtained was 213—215°C (decomp.), and that of its hydrochlorate, 157—159°C (decomp.). In the same way, the photoproduct (IIa) was also isolated from the irradiated solution of (II): mp 210—213°C (decomp.), and its hydrochlorate, 175—176°C (decomp.). The UV and IR spectra of the two photoproducts, (Ia) and (IIa), were superimposable upon those of 4-hydroxylaminopyridine *N*-oxide or 3-methyl-4-hydroxylaminopyridine *N*-oxide.[9]

In the case of 3,5-dimethyl 4-nitropyridine *N*-oxide (III), white crystals (IIIa) were isolated by the same procedures as those used for (I) and (II): recrystallized from ethanol in a nitrogen atmosphere, mp 151°C (decomp.), yield 35%, UV λ_{max}^{EtOH} 296 nm (log ε 4.24), NMR (CF_3COOH, TMS) δ 2.45 ppm (s, 6H, $(CH_3)_2$), 7.94 ppm (s, 2H, aromatic), molecular weight (meas-

8) M. Yamakawa, Y. Mizuno, and T. Kubota, Annual meeting of the Chemical Society of Japan, Tokyo, April, 1970, M. Yamakawa, T. Kubota, and Y. Mizuno, Symposium on the Molecular Structures, Kyoto, October, 1971.

9) E. Ochiai and H. Mitarashi, *Ann. Rept. ITSUU. Lab.*, **14**, 17 (1965).

ured by freezing-point depression of benzoic acid) 160, Found: C, 54.00; H, 6.48; N, 18.08%. Calcd for $C_7H_{10}N_2O_2$: C, 54.56; H, 6.49; N, 18.18%. On the basis of these analytical data, the photoproduct (IIIa) was assumed to be a 3,5-dimethyl-4-hydroxylaminopyridine *N*-oxide. Further confirmation of the structure (IIIa) was provided by its conversion into 4,4'-azoxy or 4-nitroso derivative in the following way. The treatment of 100 mg of (IIIa) with 5m*l* of 10% aqueous ammonia resulted in a red coloration, which then gradually faded to yellow. After the solution has been allowed to stand for 20 min, extraction with chloroform gave *ca.* 40 mg of yellow crystals (IIIb). The (IIIb) thus obtained was purified by recrystallization from ethanol: mp 265°C (decomp.), UV λ_{max}^{EtOH} 275 nm (log ε 4.21), NMR ($CDCl_3$, TMS) δ 2.22 ppm (s, 6H, $(CH_3)_2$), 2.40 ppm (s, 6H, $(CH_3)_2$), 8.08 ppm (s, 4H, aromatic), Mass (M^+)=288, Found: C, 58.20; H, 5.66; N, 19.25%. Calcd for $C_{14}H_{16}N_4O_3$: C, 58.33; H, 5.56; N, 19.44%. Thus, the product (IIIb) was identified as 4,4'-azoxy-3 5-lutidine 1,1'-dioxide. Similarly, a 100-mg portion of (IIIa) was treated with 5 m*l* of a 10% $FeCl_3$ solution, then, extraction with chloroform gave 70 mg of greenish-yellow crystals (IIIc): mp 203—205°C (decomp.), UV λ_{max}^{EtOH} 253 nm (log ε 3.80), 363 nm (log ε 4.10), NMR ($CDCl_3$, TMS) δ 2.63 ppm (s, 6H, $(CH_3)_2$), 8.05 ppm (s, 2H, aromatic), Mass (M^+)=152, Found: C, 54.54; H, 5.21; N, 17.78%. Calcd for $C_7H_8N_2O_2$: C, 55.26; H, 5.26; N, 18.42%. These analytical data indicate that the product (IIIc) is 3,5-dimethyl-4-nitrosopyridine *N*-oxide

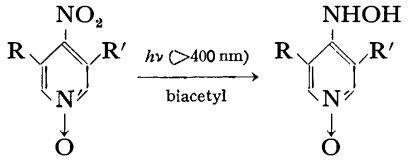

R and R'=H or CH_3

It was revealed by the present experiments that the 4-nitropyridine *N*-oxide and its methyl-substituted derivatives were reduced by a biacetyl sensitization to the corresponding 4-hydroxylamino derivatives; this suggests that the hydrogen abstraction from a solvent molecule can occur from the lowest π,π^* triplet state of 4-nitropyridine *N*-oxide. This is of particular interest because Rosenberg and Servé's mechanism of the hydrogen abstraction by a π,π^* triplet molecule[10] appears to be operative in the photosensitized reduction of 4-nitropyridine *N*-oxide. For this reason, further studies are necessary in order to elucidate the nature of the lowest lying triplet state of 4-nitropyridine *N*-oxide.

10) H. M. Rosenberg and P. Servé, *J. Amer. Chem. Soc.*, **92**, 4746 (1970).

BULLETIN OF THE CHEMICAL SOCIETY OF JAPAN, VOL. 45, 2953—2955 (1972)

The Second CMC of the Aqueous Solution of Sodium Dodecyl Sulfate. III. Light-scattering

Michiko KODAMA, Yukio KUBOTA,* and Masaji MIURA

Department of Chemistry, Faculty of Science, Hiroshima University, Higashisenda-machi, Hiroshima

(Received January 24, 1972)

In our previous papers, the micelle structure of the aqueous solution of sodium dodecyl sulfate (SDS) has been investigated, mainly in the concentration region above the 1st critical micelle concentration (CMC), through the measurements of the conductivity,[1] the viscosity, and the density.[2] In the present study, the light-scattering measurements were carried out in order to obtain further information about the micelle structure of the aqueous solution of SDS.

Experimental

Dust-free water was obtained by the distillation method.[3] The SDS solutions were prepared in the same way as has previously been described[1] and then repeatedly filtered through a Graba-type filtering apparatus (membrane ultrafilter, No. 8) under a pressure of 5—10 cmHg until the solutions became completely clear. The light scattering was measured with a Brice-type light-scattering photometer (Shimadzu Seisakusho) using a semioctagonal cell. The reduced scattering intensities (R_θ) at $\theta=45$, 90, and 135° were calculated by the following equation:

$$R_\theta = \phi_\theta \cdot G_\theta / G_0 \qquad (1)$$

where G_θ and G_0 are the intensities of the scattered light at $\theta°$ and 0° respectively, and where ϕ_θ is the apparatus constant, which was determined by using the Rayleigh ratio (R_{90}) of benzene.[4] The refractive index increments (dn/dC) were measured with a Debye-type differential refractometer (Shimadzu Seisakusho). All the measurements were made at 25°C and at the wavelengths of 436 and 546 mμ.

Results and Discussion

Figure 1 shows a plot of R_{90} against the concentration of SDS in the neighborhood of the 1st CMC. R_{90}

* Present address: Department of Chemistry, Yamaguchi University, Yamaguchi.

1) M. Miura and M. Kodama, This Bulletin, **45**, 428 (1972).

2) M. Kodama and M. Miura, *ibid.*, **45**, 2265 (1972).

3) M. Nakagaki and H. Inagaki, "Hikari Sanran Zikken Hou," Nankodo, Tokyo (1965), p. 108.

4) C. I. Carr and B. H. Zimm, *J. Chem. Phys.*, **18**, 1616 (1950).

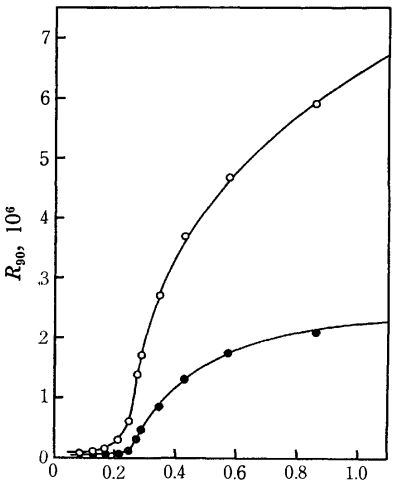

Fig. 1. Light-scattering of SDS solution in the neighborhood of the 1st CMC.
—○—: R_{90} at 436 mμ, —●—: R_{90} at 546 mμ.

remains small until the 1st CMC is reached, and then it increases with the concentration of the SDS solution. As is well-known, the Debye Eq. (2) is used to calculate the micellar molecular weight; the reciprocal of the micellar molecular weight is obtained by plotting $K(C-C_0)/(R_{90}-R_{90,0})$ against $(C-C_0)$:

$$K(C-C_0)/(R_{90}-R_{90,0}) = 1/M + 2B(C-C_0), \qquad (2)$$

where $R_{90,0}$ is the Rayleigh ratio at the 1st CMC, M is the micellar molecular weight, B is a constant, C is the concentration of the solution (g/ml), C_0 is the 1st CMC, $K=2\pi^2 n_0^2(\partial n/\partial C)^2/N_A\lambda^4$, n and n_0 are the refractive indices of solution and solvent respectively, N_A is the Avogadro number, and λ is the wavelength of the light.

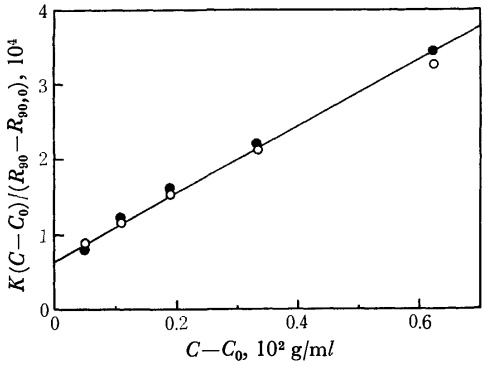

Fig. 2. Debye plot of SDS solution.
—○—: 436 mμ, —●—: 546 mμ.

As can be seen in Fig. 2, the Debye plot for the SDS solutions shows a linear nature at low micellar concentrations. Since the Debye equation is strictly valid only for the uncharged colloidal particles, it is necessary to take into account the effect of the charge of the micelles on the light-scattering properties. Therefore, the aggregation number and also the micellar molecular weight were calculated by using the equation[5] corrected for the effect of the charge of the micelles. The values thus obtained were 60 and 17200

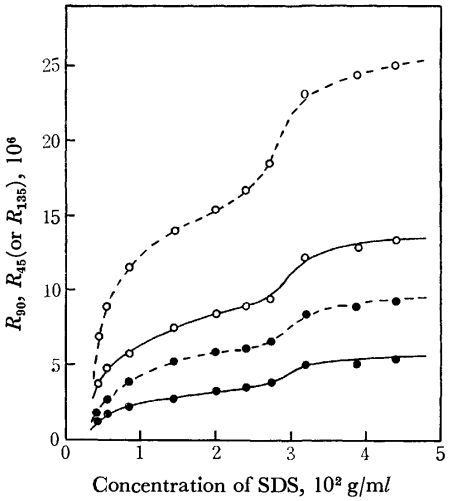

Fig. 3. Light-scattering of SDS solution in the neighborhood of the 2nd CMC.
—○—: R_{90} at 436 mμ, —●—: R_{90} at 546 mμ, --○--: R_{45}(or R_{135}) at 436 mμ, —●--: R_{45} (or R_{135}) at 546 mμ.

Table 1. The 1st and 2nd CMC's of SDS solution

1st CMC (mmol/l)	2nd CMC (mmol/l)	Method
8.3	70	Light-scattering
8.3	65	Conductivity[1]
8.0—8.5	65—70	Viscosity[2]
8.5	65	Density[2]

respectively, in fairly good agreement with those obtained by Mysels and Princen.[5]

The values of R_{90} and R_{45} (or R_{135}) in the high-concentration region of the SDS solution are plotted against the concentration in Fig. 3. It may be noted from this figure that R_{90} shows a marked rise at the concentration corresponding to the 2nd CMC,[1,2] as it does at the 1st CMC in Fig. 1, and that the behavior of R_{45} (or R_{135}) is quite similar to that of R_{90}. The 1st and 2nd CMC's obtained in the present study are listed in Table 1 along with those reported in previous works.[1,2] Ekwall and his co-workers[6] measured the light-scattering of the aqueous solution of cetyl trimethylammonium bromide and found that there is an extremely marked rise in the intensity of the scattered light in the high-concentration region above the 1st CMC. Robins and Thomas[7] also observed similar light-scattering behavior in aqueous solutions of 2-dodecylaminoethanol salts. In our previous paper, the viscosity and density studies of the aqueous solution of SDS revealed that, below the 2nd CMC, only one type of micelle, with an almost constant size and shape, spherical or nearly so, may exist but that at the 2nd CMC there occurs a change in the micelle structure caused by a variation in the type of aggregation of SDS molecules and by a decrease in the counter-ion

5) K. J. Mysels and L. H. Princen, *J. Phys. Chem.*, **63**, 1696 (1959).
6) P. Ekwall, L. Mandell, and P. Solyom, *J. Colloid Interface Sci.*, **35**, 519 (1971).
7) D. C. Robins and I. L. Thomas, *ibid.*, **26**, 415 (1968).

binding by the micelle. Very recently, we found, from our measurements of the fluorescence depolarization of acridine dye solubilized in the SDS micelle, that the micellar volume at the 2nd CMC increases by *ca.* 30% more than that below the 2nd CMC.[8]

It can be concluded, therefore, that the marked rise of R_{45}, R_{90}, and R_{135} at about the 2nd CMC is to be attributed to a certain change in the micelle structure, probably an increase in the size of the micelle. On the other hand, the dissymmetry (Z_{45}), expressed as the ratio of R_{45} to R_{135}, will provide available information regarding the shape of micelle. The values of Z_{45}, however, were in the region of 1.00—1.02 over the whole range of SDS concentrations investigated. Therefore, even in the high-concentration region, the size of the SDS micelle may be too small to cause any appreciable dissymmetry in the scattered light.[9]

8) Y. Kubota, M. Kodama, and M. Miura, to be published.

9) P. Debye and E. W. Anacher, *J. Phys. Colloid Chem.*, **55**, 644 (1951).

BULLETIN OF THE CHEMICAL SOCIETY OF JAPAN, VOL. 45, 2955—2956 (1972)

Aromatic Nitration. III.[1] Competitive Nitration of Toluene and Benzene in Carbon Tetrachloride

Akiko HIROSE, Kohji MATSUI, and Shizen SEKIGUCHI*

Department of Synthetic Chemistry, Gunma University, Tenjincho, Kiryu, Gunma

(Received February 22, 1972)

In the previous paper[2] we reported competitive nitration of toluene and benzene with nitric acid in several organic solvents, such as carbon tetrachloride, *n*-hexane, cyclohexane, methylene dichloride, and nitromethane. The rate ratios (k_T/k_B) were in the range of 2.0 to 3.2 in the first three solvents and in the range of 15.8 to 19.7 in the latter solvents. The reaction showed the high positional selectivities in all above solvents. In nitromethane at 30°C the ratio and the selectivity factor were 19.7 and 1.219, respectively. The results were similar to those obtained by Ingold *et al.*[3]

The results in the non-polar solvents (carbon tetrachloride, *n*-hexane, and cyclohexane) are contrary to the expectation that nitric acid in non-polar solvents is a weak electrophile. Therefore, in the present paper we have investigated the effects of concentrations of nitric acid, the polarity of mediums on the substrate (k_T/k_B) and positional selectivities (o/p) in the competitive nitration of toluene and benzene in carbon tetrachloride.

The results are shown in Table 1. With increasing amount of nitric acid, the positional selectivities (o/p) increased. The selectivity factors were comparatively low in comparing with those (about 1.2 to 1.3) obtained in the previous works.[4] The result, obtained when 0.12 mol of 75% nitric acid was used, is much similar to that of Olah *et al.*[3] This suggests that the system of nitric acid–carbon tetrachloride may become a strong electrophile.

Next, the results of the competitive nitration in a mixed solvent of carbon tetrachloride and nitromethane (1 : 1 by volume) are shown in Table 2. These results are comparatively similar to that of Ingold *et al.*,[3]

Table 1. Effects of concentrations of nitric acid[a]

HNO_3 Concn (%) (mol)	$\frac{k_T}{k_B}$	Isomer ratio (%)			Partial rate factor			S_f[b]	$\frac{o}{p}$
		o-	*m*-	*p*-	o_f^T	m_f^T	p_f^T		
100 (0.02)	2.0	57.0	4.6	68.4	3.4	0.3	4.5	1.224	1.48
(0.06)	2.1	59.3	4.9	35.8	3.8	0.3	4.6	1.164	1.65
85 (0.03)	3.4	60.4	5.0	34.6	6.1	0.5	7.0	1.142	1.74
(0.06)	2.5	61.7	4.7	33.6	4.7	0.4	5.1	1.154	1.83
(0.12)	2.6	62.7	4.6	32.6	4.9	0.4	5.1	1.152	1.92
75 (0.03)	3.5	60.5	6.5	33.0	6.4	0.7	7.0	1.011	1.83
(0.06)	2.5	60.3	6.6	33.1	4.6	0.5	5.0	1.005	1.82
(0.12)	1.9	61.9	5.4	32.6	3.5	0.3	3.6	1.079	1.89

a) Toluene, 0.01 mol; benzene, 0.02 mol; CCl_4, 40 ml; reaction temperature, 20°C; reaction time, 24 hr.
b) S_f; selectivity factor.

* Adress correspondence to this author.

1) Part II, S. Kato, A. Hirose, K. Matsui, and S. Sekiguchi, This Bulletin, submitted for.

2) G. A. Olah, S. J. Kuhn, and S. H. Flood, *J. Amer. Chem. Soc.*, **83**, 4571 (1961).

3) C. K. Ingold, A. Lapworth, E. Rothstein, and D. Ward, *J. Chem. Soc.*, **1931**, 1959.

4) L. M. Stock and H. C. Brown, *Advan. Phys. Org. Chem.*, **1**, 35 (1963).

TABLE 2. COMPETITIVE NITRATION OF TOLUENE AND BENZENE WITH NITRIC ACID IN CARBON TETRACHLORIDE–NITROMETHANE (1:1 BY VOLUME)

Temperature (°C)	$\frac{k_T}{k_B}$	Isomer ratio (%)			Partial rate factor			S_f	$\frac{o}{p}$
		o-	*m*-	*p*-	o_f^T	m_f^T	p_f^T		
30	17.4	61.1	3.3	35.6	31.9	1.7	37.2	1.341	1.71
40	15.0	58.6	3.8	37.6	26.3	1.7	26.3	1.292	1.55
50	14.9	58.1	4.2	37.7	14.9	1.9	33.6	1.256	1.54

a) Toluene, 0.01 mol; benzene, 0.02 mol; mixed solvent,40 m*l*; nitric acid (99.67%), 0.03 mol; reaction time, 24 hr.

TABLE 3. EFFECT OF NITROMETHANE AND ACETIC ACID[a)]

Solvent (1 vol %)	$\frac{k_T}{k_B}$	Isomer ratio (%)			Partial rate factor			S_f	$\frac{o}{p}$
		o-	*m*-	*p*-	o_f^T	m_f^T	p_f^T		
CCl_4 (—)	2.0	57.0	4.6	38.4	3.4	0.3	4.5	1.224	1.48
CCl_4 (CH_3NO_2)	6.4	59.4	5.4	35.2	11.5	1.1	13.6	1.112	1.68
CCl_4 (CH_3COOH)	8.0	58.8	4.6	36.6	14.1	1.1	17.5	1.204	1.60

a) Toluene, 0.01 mol; benzene, 0.02 mol; mixed solvent, 40 m*l*; nitric acid (99.67%), 0.03 mol; reaction temperature, 20°C; reaction time, 24 hr.

indicating that the polarity of mediums has a large effect on the substrate selectivities.

Further, the results of the competitive nitration in carbon tetrachloride with one volume percentage of other solvent are shown in Table 3. The rate ratios are intermediate between those in Table 1 and 2, indicating that even the addition of a small amount of a polar solvent has a large effect on the rate ratios.

Experimental

Materials. Benzene, toluene, nitrobenzene, and *o*-, *m*-, and *p*-nitrotoluene were commercial materials of the highest available purity. Their purities were examined by vapor phase chromatography on a column containing 10% polypropylene glycol in Diasolid M at 170°C.

Competitive Nitration. The competitive nitration and product analysis were carried out by the method described in the previous paper.[1)]

BULLETIN OF THE CHEMICAL SOCIETY OF JAPAN, VOL. 45, 2956—2957 (1972)

^{119}Sn Mössbauer Quadrupole Splittings in Compounds with Sn-Mn Bonds

B. V. LIENGME, J. R. SAMS*†, and J. C. SCOTT*

Department of Chemistry, St. Francis Xavier University, Antigonish, N.S., Canada

**Department of Chemistry, University of British Columbia, Vancouver, B.C., Canada*

(Received October 12, 1971)

Onaka, Sasaki, and Sano[1] have recently reported ^{119}Sn Mössbauer data for the four series of compounds $(CO)_5MnSnR_{3-n}X_n$, where R=Me, Ph, and X=Cl, Br. The quadrupole splitting values (Δ) for n=1, 2 are always higher than those for n=0, 3, rather than showing a monotonic change as n increases, but no explanation was offered for this unexpected order. We have recently suggested[2] that a similar trend in Δ for the compounds $(\pi\text{-}C_5H_5)Fe(CO)_2SnPh_{3-n}Cl_n$ is due to a change in sign of the quadrupole coupling constant, which can be explained on the basis of point-charge calculation. We wish to show that the results of Onaka, *et al.*[1] are susceptible to a like explanation.

The point-charge model assumes that the electric field gradient (EFG) is an additive quantity,[3] so that the quadrupole splitting can be evaluated from partial quadrupole splitting (PQS) values, [L], for the various ligands. Since the EFG at tin is largely due to an imbalance in the polarity of the tin-ligand σ-bonds, [L] values are related to this polarity and can be correlated with the Taft inductive constants for the ligands.[4] The model has been discussed in detail by Parish and Platt,[4] who also derived a number of PQS values from data for pentacoordinate tin compounds. It has been suggested that these PQS values should not be applied to compounds in which the tin atom has a different coordination number.[5] For the

† To whom correspondence should be addressed.

1) S. Onaka, Y. Sasaki, and H. Sano, This Bulletin, **44**, 726 (1971).

2) B. V. Liengme, M. J. Newlands, and J. R. Sams, *Inorg. Nucl. Chem. Lett.*, **7**, 1223 (1971).

3) M. G. Clark, *Mol. Phys.*, **20**, 257 (1971).

4) R. V. Parish and R. H. Platt, *Inorg. Chim. Acta*, **4**, 65 (1970).

5) A. G. Maddock and R. H. Platt, *J. Chem. Soc.*, *A*, **1971**, 1191.

present tetracoordinate derivatives we have therefore derived a self-consistent set of PQS values. If we assume an arbitrary value for [Cl], then point-charge expressions for molecules of the types $SnAB_3$ and SnA_2B_2[4] with experimental Δ values[2] for $(CO)_5Mn$-$SnCl_3$, $(CO)_5MnSnMe_3$, and $[(CO)_5Mn]_2SnPh_2$ yields PQS values for $(CO)_5Mn$, Me, and Ph, respectively.[2] A value for [Br] is obtained from the measured[1] splitting in $(CO)_5MnSnBr_3$. These [L] values are given in footnote (a) to Table 1. It should be noted that our results are independent of the value chosen for [Cl].[2] These PQS values are used to compute the EFG tensor elements, assuming tetrahedral bond angles.[6] After diagonalising the tensor, the nonvanishing elements are ordered such that $|V_{zz}| \geq |V_{yy}| \geq |V_{xx}|$, then the asymmetry parameter $\eta = (V_{yy} - V_{xx})/V_{zz}$ and

$$\Delta = \frac{1}{2} eQV_{zz}\left(1 + \frac{\eta^2}{3}\right)^{1/2}$$

are calculated. The results for a number of compounds with Sn–Mn bonds are presented in Table 1, along with experimental Δ values.

Table 1. Measured and predicted quadrupole splittings for some compounds with Sn–Mn bonds[a]

Compound	Δ_{obs}[b] (mm sec^{-1})	Δ_{pred} (mm sec^{-1})	η_{pred}
$(CO)_5MnSnCl_3$	1.57	+	0
$(CO)_5MnSnMeCl_2$	2.62	+2.37	0.85
$(CO)_5MnSnMe_2Cl$	2.66	−2.24	0.48
$(CO)_5MnSnMe_3$	0.61	−	0
$(CO)_5MnSnPhCl_2$	2.36	+2.13	0.93
$(CO)_5MnSnPh_2Cl$	2.49	−1.95	0.34
$(CO)_5MnSnPh_3$	0[c]	−0.50	0
$(CO)_5MnSnBr_3$	1.41	+	0
$(CO)_5MnSnMeBr_2$	2.51	+2.22	0.83
$(CO)_5MnSnMe_2Br$	2.54	−2.11	0.51
$(CO)_5MnSnPhBr_2$	2.63	+1.97	0.92
$(CO)_5MnSnPh_2Br$	2.28	−1.82	0.36
$[(CO)_5Mn]_3SnCl$	1.55[d]	−1.56	0
$(CO)_5MnSn(Cl)[(\pi\text{-}C_5H_5)Fe(CO)_2]_2$	2.02[e]	−1.73	0.18

a) PQS values used in the calculations are (in mm sec^{-1}): [Cl] = +0.63, [Br] = +0.56, [Me] = −0.56, [Ph] = −0.40, $[(CO)_5Mn]$ = −0.15.
b) Experimental values from Ref. 1) except as noted.
c) Splitting not resolved.
d) Reference 15.
e) Reference 16.

The calculated Δ values are in only moderately good numerical agreement with the measured[1] ones. The lack of better agreement between Δ_{pred} and Δ_{obs} may be due largely to distortions from tetrahedral symmetry. Although insufficient structural data are available to allow a quantitative estimate of such effects, X-ray data for related compounds[7-11] suggest that the distortions are likely to be such as to increase the calculated $|V_{zz}|$ values.[6,12] Another possible source of discrepancy is a variation in the σ-character of the tin-halogen bonds as the number of halogens bonded to tin changes. Such an effect has been suggested[13] for the compounds $RSnCl_3$ and R_2SnCl_2 (R = *n*-Bu, Ph) on the basis of ^{35}Cl NQR data.

More important than the actual numerical agreement is the fact that in all four series $(CO)_5MnSnR_{3-n}X_n$ the magnitude of Δ is predicted to be greater for $n=1$ and 2 than for $n=0$ and 3, as observed experimentally. The sign of Δ_{pred} is the sign of the quadrupole coupling constant, eQV_{zz}. This sign has recently been shown to be positive for both $(CO)_5MnSnCl_3$ and $(CO)_5Mn$-$SnCl_2Me$,[14] but the signs of eQV_{zz} for the remaining derivatives in Table 1 have not yet been reported. The positive eQV_{zz} for $(CO)_5MnSnCl_3$ shows that the charge distribution about tin is prolate, *i.e.*, there is greater electron density near the tin atom along the *z*-(Sn–Mn bond) direction than in the *xy*-plane, as expected from the greater electronegativity of Cl. The increase in Δ upon replacing one halogen by an organic group is due in part to the non-zero η, but the largest contribution comes from a reorientation of the *z*-axis of the EFG and a concomitant increase in $|V_{zz}|$. When there are two or three organic groups attached to tin, our calculations predict a negative eQV_{zz} (oblate charge distribution). We hope to verify these predictions in the near future. It is relevant to note that eQV_{zz} for tin is positive in $YSnCl_3$ and negative in $YSnBu_3$ ($Y = (\pi\text{-}C_5H_5)Fe(CO)_2$[14] as predicted by the point-charge model.[2]

The small (or zero) observed splittings for $(CO)_5Mn$-SnR_3[1] and $[(CO)_5Mn]_2SnPh_2$[2] suggest that the σ-bonding characteistics of the $(CO)_5Mn$ group and Me or Ph are quite similar. This presumably accounts for the fact that the predicted value of η is less than ~0.5 for the cases $(CO)_5MnSnR_2X$, and greater than ~0.8 for $(CO)_5MnSnRX_2$. The former molecules approximate to the stoichiometry SnA_3B (for which $\eta=0$), whilst the latter approximate to SnA_2B_2 (for which $\eta=1$ if tetrahedral bond angles are assumed).

Finally, it should be noted that our calculations give an adequate estimate of $|\Delta|$ for $(CO)_5MnSn(Cl)$-$[(\pi\text{-}C_5H_5)Fe(CO)_2]_2$, in which the tin atom is bonded to two different transition metals.

We wish to thank the National Research Council of Canada for financial support, and Dr. G. M. Bancroft for a preprint of his paper.

6) G. N. Bancroft, K. D. Butler, and A. T. Rake, *J. Organometal. Chem.*, **34**, 137 (1972).
7) R. F. Bryan, *J. Chem. Soc., A*, **1967**, 172, 192.
8) J. E. O'Connor and E. R. Corey, *Inorg. Chem.*, **6**, 968 (1967).
9) P. T. Greene and R. F. Bryan, *J. Chem. Soc., A*, **1970**, 1696, 2261.
10) H. P. Weber and R. F. Bryan, *Acta Crystallogr.*, **22**, 822 (1967).
11) R. F. Bryan, *J. Chem. Soc., A*, **1968**, 696.
12) J. R. Sams and J. C. Scott, unpublished results.
13) E. D. Swiger and J. D. Graybeal, *J. Amer. Chem. Soc.*, **87**, 1464 (1965).
14) B. A. Goodman, R. Greatrex, and N. N. Greenwood, *J. Chem. Soc., A*, **1971**, 1868.
15) A. N. Karasev, N. E. Kolobova, L. S. Polak, V. S. Shpinel, and K. A. Anisimov, *Teor. Eksp. Khim.*, **2**, 126 (1966).
16) V. I. Gol'danskii, B. V. Borshagovskii, E. F. Makarov, R. A. Stukan, K. A. Anisimov, N. E. Kolobova, and V. V. Skripkin, *Teor. Eksp. Khim.*, **3**, 478 (1967).

SHORT COMMUNICATION

Synthesis and Thermal Decomposition of 2,2′-Diazido-2,2′-azoadamantane

Masuo FUNABASHI,[1] Akira TANAKA,[2] and J. Pierre ANSELME*

Department of Chemistry, University of Massachusetts at Boston, Boston, Massachusetts, 02116 USA

During the couse of our investigation of the reaction of 1,1-chloronitrosocyclohexane (IVa) with azide ion,[3] we have identified 1,1′-diazido-1,1′-azocyclohexane (VIa) as one product of a very complex reaction mixture. The reported explosive nature of the corresponding isopropyl analogue (VIc)[4] and our hope to reduce the number of products formed led us to utilize 2-chloro-2-nitrosoadamantane (IVb)[5] as a substrate with azide

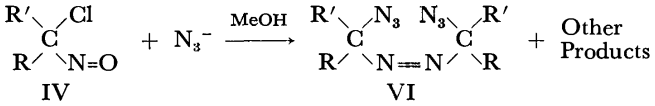

IV VI

a) R, R′ = $-(CH_2)_5-$
b) R, R′ = 2-adamantyl
c) R, R′ = CH_3

ion. As expected, the number of products decreased drastically[6] and 2,2′-diazido-2,2′-azoadamantane (VIb), mp 164°C (decomp.), was isolated as yellow crystals. It exhibited a strong azide absorption at 2080 cm^{-1} and was conclusively identified by its elemental analysis and by comparison with an authentic sample prepared from 2,2′-dichloro-2,2′-azoadamantane (Vb).[7]

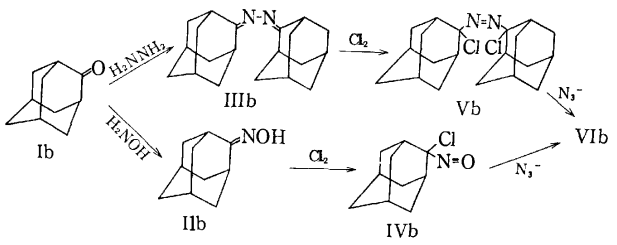

The presence of two functional groups capable of eliminating nitrogen prompted us to investigate the behavior of VIb on pyrolysis.[4] A solution of VIb in 1,2-dichlorobenzene at reflux smoothly evolved nitrogen as it gradually changed from yellow to colorless. Evaporation of the solution gave an 88% yield of a colorless solid, mp >300°C, which was identified as adamantanone azine (IIIb). Since α,α′-diazidoazoalkanes (VI) can be regarded as "formal" dimerization products of α-azidonitrenes, it is interesting to contrast our results with the fact that in all the decompositions of *gem*-diazides studied so far,[8] only in one case was azine reported as a minor product; an α,α′-diazidoazoalkane (VI) was suggested as a possible precursor to the azine.[9] Although mechanistic studies have yet to be carried out, one may speculate that rupture of the azo linkage would yield radical VIII which can eliminate to the ketimino radical (IX) or couple to give the hexazatetraene (X), both of which could lead to the azine by coupling or further loss of nitrogen respectively. Alternatively, internal "displacement" a nitrene intermediate (VII) on the neighbouring azide could lead to the cyclic bis azo compound XI, thence to IIIb.

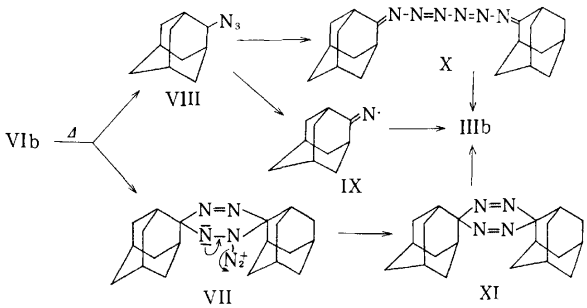

We are presently investigating the scope and the mechanism of the decomposition of α,α′-diazidoazoalkanes.

Support for this work was provided by the Alfred P. Sloan Foundation to whom the senior author is deeply grateful for the award of a Fellowship.

* Fellow of the Alfred P. Sloan Foundation; Visiting Professor, Research Institute of Industrial Science, Kyushu University; Fellow of the Japan Society for the Promotion of Science; to whom inquiries should be addressed.

1) Present address: Tokyo Institute of Technology, Tokyo, Japan.

2) Present address: Meijo University, Nagoya, Japan.

3) The origin of the α,α′-diazidoazoalkanes is still not completely clear. One possible reaction path might involve the *dimeric* nitroso compounds; this will be discussed as part of the report of our investigation of *gem*-chloronitroso compounds with azide ion.

4) Authentic VIa was prepared by the reaction of azobis(1-chlorocyclohexane) with azido ion; E. Benzing, *Ann.*, **631**, 1 (1960).

5) Mp 161—163°, prepared in 95% yield as shown in the equation. Since the completion of this work, the preparation and photolysis of IVb has been reported by A. H. M. Kayen, L. R. Subramanian and Th, J. DeBoer, *Rec. Trav. Chim. Pays-Bas*, **90**, 866 (1971). We wish to thank Prof. DeBoer and Dr. Kayen for informative correspondence.

6) Glc examination of the product mixture of the reaction of *gem*-chloronitrosocyclohexane with azide ion revealed the presence of at least thirteen components. The presumption was that the presence of α-hydrogens was in large part responsible for the complexity of the reaction. This presumption was confirmed by the fact that in addition to nitrous oxide (formed as a major product), only five solid products were formed. They were identified as 2,2′-diazidoadamantane, 2,2′-dichloroadamantane, 2-chloro-2-nitroadamantane, adamantanone and VIb.

7) 2,2′-Diazido-2,2′-azoadamantane (VIb) was obtained in 70% yield (from ethanol). So far as we have been able to determine, it dose not display the explosive properties reported for VIc; a correct elemental analysis was obtained routinely. However, we *urge all due caution* because no detailed study of its properties has been performed.

8) F. D. Lewis and W. H. Saunders in "Nitrens", ed. by W. Lwowski, Interscience Publisher, New York, N. Y. (1970), p. 47.

9) G. Ege and G. Joos, *Chem. Zeitung*, **94**, 215 (1970). These investigators have isolated benzophenone azine in 4% yield from the photolysis of diphenylazidomethane in acetone.

The Crystal Structure of Cupric Complex with Succinimide I. Cesium Tetrakis(succinimidato)copper(II) Dihydrate

Tomitake TSUKIHARA, Yukiteru KATSUBE, Kumiko FUJIMORI, and Toshiaki ITO

Faculty of Engineering, Tottori University, Koyama-cho, Tottori

(Received February 23, 1972)

The crystal structure of cesium tetrakis(succinimidato) copper(II) dihydrate, $Cs_2(Cu(sucim)_4).2H_2O$, has been determined by means of X-ray analysis. The crystals are violet rhombic plates. Dimensions of the triclinic unit cell are $a=9.19$, $b=15.32$, $c=8.39$ Å, $\alpha=88.7°$, $\beta=92.0°$, $\gamma=93.8°$, and $z=2$. The space group is $C\bar{1}$. The structure has been determined by the Patterson synthesis, a series of Fourier syntheses and the least-squares method. The coordination around the copper atom is a square planar. Two independent cesium ions have a quite different environment. Complex anions, $(Cu(sucim)_4)^{2-}$, are linked with each other through the hydrogen bonds between water and carboxyl oxygen atoms.

Succinimide forms complexes with various metallic ions. A number of cupric compounds with succinimide having the general formula $M_2^+[Cu(sucim)_4]^{2-}\cdot nH_2O$ and a red or violet color in solid state have been reported.

A structural investigation of compounds of this type is thought to be of interest from the viewpoint of the coordination chemistry of cupric complexes. Some of these complexes have been studied spectroscopically.[1]

As a part of studies of the crystal structure of such complexes, a detailed description of the crystal structure of cesium tetrakis(succinimidato)copper(II) dihydrate is given in this paper.

Experimental

The crystals are violet rhombic plates. Preliminary Weissenberg and oscillation photographs established that the crystal was triclinic with axis *a* along an edge of the plate and axes *b* and *c* along the diagonals of the rhombic plane (Fig. 1). By the systematic extinction of *hkl* for odd $h+k$ the space group was restricted to $C1$ or $C\bar{1}$. The cell dimensions were obtained by means of the least-squares method. The crystal data were collected on a Rigaku Denki Computer-controlled four-circle diffractometer, using Ni-filtered Cu$K\alpha$ radiation. All the intensities were obtained from a crystal with dimensions $0.25\times0.25\times0.08$ mm³. Reflections with 2θ values up to 120° in octants of *(hkl)*, *($\bar{h}$kl)*, *(h$\bar{k}$l)*, and *($\bar{h}\bar{k}$l)* were measured by ω-2θ scanning technique at a scan rate of 2° per minute. The scan range of ω for each reflection was calculated by the formula $\omega=0.90°+0.15°\tan\theta$, and the backgrounds were measured at both ends of the scan range for 10.0 seconds. Attenuators were inserted automatically when the maximum counting rate exceeded 8000 cps. Reflections whose counts at mid point of the scan range were less than 10 cps were not measured. The intensities of two reference reflections $I(006)$ and $I(008)$ were measured after every fifty reflections. Owing to sublimation of the crystal, the intensities of these two reflections decreased gradually during the course of measurement. Correction was made for a decay of the crystal by multiplying each reflection by a factor found from the normalized plot of the intensities of the reference reflections. Application of Lotrentz-polarization factors was made but no correction for absorption.

TABLE 1. CRYSTAL DATA

$Cs_2CuC_{16}H_{20}N_4O_{10}$	Mw=748.71	
Triclinic:	$C\bar{1}$	
a=9.189 Å	$b=15.315$ Å	$c=8.387$ Å
$\alpha=88.7°$	$\beta=92.0°$	$\gamma=93.8°$
$D_{cal}=2.11$ g/cm³		
$D_{obs}=2.13$ g/cm³ (by flotation)		

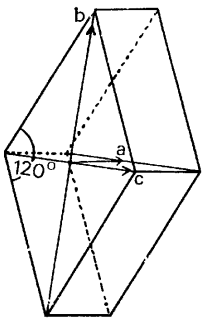

Fig. 1. The crystal shape and the orientation of the axes.

Structure Determination and Refinement

A sharpened three-dimensional Patterson function showed that a copper atom and two cesium ions should be located on the special positions (0,0,0), (1/4,1/4,0) and (1/4,1/4,1/2), respectively. The space group was restricted to $C\bar{1}$ by an interpretation of the Patterson function.

The remaining light atoms were located by successive cycles of structure factor calculations and difference Fourier synthesis. The trial structure was refined by a diagonal least-squares procedure with the positional and isotropic thermal parameters. The isotropic refinement converged the reliability index ($R=\Sigma||F_o|-|F_c||/\Sigma|F_o|$) to 0.19. Further refinement was carried out by the least-squares of block-diagonal matrix approximation with the positional parameters for all the non-hydrogen atoms, the anisotropic thermal parameters for three metal atoms and the isotropic thermal parameters for the other atoms. The final value of R was 0.11. The atomic scattering factors were taken from the literature.[2] Those of copper and cesium atoms were corrected for real and

1) S. Yamada and S. Miki, This Bulletin, **36**, 680 (1963).

2) "International Tables for X-Ray Crystallography," Vol. III, Kynoch Press, Birmingham (1962), p. 202 and p. 211.

Table 2. Final atomic parameters

Atom	x	y	z	Atom	x	y	z
Cs1	0.2500	0.2500	0.0000	CB3	0.2199	−0.0130	−0.4505
Cs2	0.2500	0.2500	0.5000	CB4	0.1722	0.0291	−0.2924
Cu	0.0000	0.0000	0.0000	OA1	0.0693	−0.1990	0.1219
CA1	0.1712	−0.1410	0.1304	OA2	0.3311	0.0648	0.1220
CA2	0.3272	−0.1685	0.1995	OB1	−0.0426	−0.1617	−0.2507
CA3	0.4127	−0.0788	0.1989	OB2	0.2178	0.1033	−0.2548
CA4	0.3047	−0.0139	0.1363	OW1	0.0076	−0.3368	0.3282
CB1	0.0410	−0.0980	−0.2906	NA1	0.1708	−0.0570	0.1019
CB2	0.1306	−0.1033	−0.4481	NB1	0.0746	−0.0258	−0.2136

Atom	B_{11} or B	B_{22}	B_{33}	B_{12}	B_{13}	B_{23}
Cs1	0.0068	0.0017	0.0130	−0.0011	0.0028	0.0000
Cs2	0.0192	0.0043	0.0183	−0.0080	−0.0122	0.0050
Cu	0.0045	0.0013	0.0089	0.0001	0.0025	0.0006
CA1	7.12					
CA2	7.76					
CA3	7.08					
CA4	6.56					
CB1	6.47					
CB2	7.44					
CB3	6.94					
CB4	5.89					
OA1	3.91					
OA2	3.55					
OB1	3.07					
OB2	3.04					
OW1	6.33					
NA1	1.44					
NB1	1.29					

Temperature Factor

$$=\exp[-(B_{11}\times h^2+B_{22}\times k^2+B_{33}\times l^2+B_{12}\times hk+B_{13}\times hl+B_{23}\times kl)]$$

or

$$=\exp[-B(\sin\theta/\lambda)^2]$$

Table 4. Bond distances and angles with their e.s.d.

Bond	Length	e.s.d.	Bond	Length	e.s.d.
Cu-NA1	2.00 Å	0.02 Å	Cu-NB1	2.00 Å	0.02 Å
CA1-CA2	1.61	0.04	CB1-CB2	1.59	0.03
CA1-NA1	1.31	0.03	CB1-NB1	1.31	0.03
CA2-CA3	1.54	0.03	CB2-CB3	1.56	0.04
CA3-CA4	1.52	0.03	CB3-CB4	1.58	0.03
CA1-OA1	1.25	0.03	CB1-OB1	1.26	0.03
CA4-OA2	1.22	0.03	CB4-OB2	1.22	0.03
CA4-NA1	1.38	0.03	CB4-NB1	1.38	0.03
	Angle	e.s.d.		Angle	e.s.d.
CA2-CA1-OA1	118°	2°	CB2-CB1-OB1	119°	2°
CA2-CA1-NA1	112	2	CB2-CB1-NB1	112	2
OA1-CA1-NA1	130	2	OB1-CB1-NB1	128	2
CA1-CA2-CA3	100	2	CB1-CB2-CB3	102	2
CA2-CA3-CA4	105	2	CB2-CB3-CB4	102	2
CA3-CA4-OA2	125	2	CB3-CB4-OB2	121	2
CA3-CA4-NA1	110	2	CB3-CB4-NB1	111	2
OA2-CA4-NA1	125	2	OB2-CB4-NB1	128	2
Cu-NA1-CA1	123	1	Cu-NB1-CB1	124	1
Cu-NA1-CA4	124	1	Cu-NB1-CB4	123	1
NA1-Cu-NB1	89	1	NA1-Cu-NB1	89	1
CA1-NA1-CA4	112	2	CB1-NB1-CB4	112	2

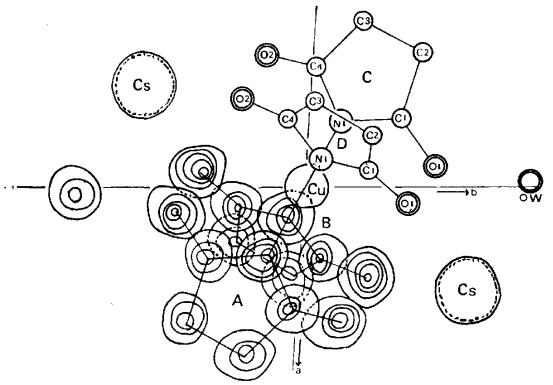

Fig. 2. The composite electron density map of $Cs_2(Cu(sucim)_4)\cdot 2H_2O$, contours are drawn at intervals of 1.0 e/Å^3 starting at 2.0 e/Å.

imaginary parts of anomalous dispersion: $\Delta f_{Cu}'=-2.1$, $\Delta f_{Cu}''=0.7$, $\Delta f_{Cs}'=-1.8$, and $\Delta f_{Cs}''=8.0$. The composite electron density map is given in Fig. 2, and the final atomic parameters in Table 2. The standard deviations of the positional parameters are 0.02 Å for oxygen, nitrogen, and carbon atoms. Table 3 containing the observed and calculated structure factors is kept as Document No. 7208 at the Chemical Society of Japan.

Description and Discussion of the Structure

The bond distances and angles are given in Table 4. The structure of the complex anion $(Cu(sucim)_4)^{2-}$ is centrosymmetric about the copper atom. Four nitrogen atoms of four succinimides take a square planar arrangement around the copper atom with a mean Cu–N distance of 2.00 Å. The distance is in good agreement with that generally found in the planar part of other Cu(II)-complexes: 1.963 Å in ethyl-

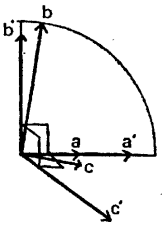

Fig. 3—1. The orientation of the orthogonal axes, a', b', and c' related to the crystal axes, a, b, and c.

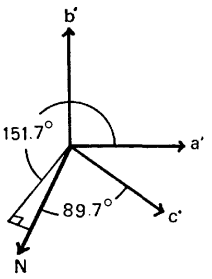

Fig. 3—2. The orientation of the coordination-plane related to the orthogonal axes. Symbol N represents the normal line of the plane.

TABLE 5. EQUATIONS OF THE LEAST-SQUARES PLANE THROUGH ATOMS

Equation	Atom	Deviation
Succinimide group of A		
$0.3037x'-0.1584y'-0.9395z'+0.2122=0$	NA1	0.0303 Å
	CA1	0.0332
	CA2	−0.0093
	CA3	−0.0106
	CA4	0.0110
	OA1	−0.0259
	OA2	−0.0151
	*Cu	0.2122
Succinimide group of B		
$0.7564x'-0.3965y'+0.5202z'+0.2095=0$	NB1	0.0353
	CB1	−0.0181
	CB2	0.0001
	CB3	−0.0057
	CB4	0.0183
	OB1	−0.0024
	OB2	−0.0179
	*Cu	0.2095
Succinimide group of C		
$-0.3037x'+0.1584y'+0.9395z'+0.2122=0$		
Succinimide group of D		
$-0.7564x'+0.3965y'-0.5202z'+0.2095=0$		
The plane of the coordination square		
$-0.4744x'-0.8803y'+0.0061z'+0.0000=0$		

where $x'=ax+by\cos\gamma+cz\cos\beta$, $y'=by\sin\gamma-cz\sin\beta\cos\alpha^*$, $z'=cz\sin\beta$

* Atom not included in the least-squares calculations.

enebidiguanide copper(II) chloride monohydrate,[3] 2.01 Å in Bis(pyridine-2-acetamide)copper(II) perchlorate[4] and 2.003 Å in copper(II) complex with *o*-hydroxyacetophenone isobutylimine.[5] Since the copper atom is located at the center of symmetry, it is exactly on a coordination-plane defined by the four nitrogen atoms. An orientation of the coordination-plane is given in Fig. 3.

The dimensions of the succinimides in the complex anion are consistent with those of the free molecule.[6] Each succinimide ring is planar within a limit of error. The best planes determined by the least-squares calculation are given in Table 5. The dihedral angle between the coordination-plane and the A-ring of succinimide is 90.6° and that for the B-ring 90.4°. Four succinimide rings are therefore almost perpendicular to the coordination-plane. Thus, the complex anion has approximate symmetry of D_{4h}. This configuration agrees with that proposed spectroscopically for $K_2(Cu(II)(sucim)_4)\cdot 6H_2O$ by Yamada and Miki.[1] The structure of the complex anion is given in Fig. 4.

Two independent cesium ions exist in the structure. That at (1/4,1/4,0), Cs1, has eight oxygen atoms situated at the corners of an almost perfect tetragonal prism with dimensions $3.32\times3.34\times4.09$ Å^3. These atoms belong to the carbonyl groups. This arrangement may be compared to the CsCl-type structure of eight-coordination. The cesium ion at (1/4,1/4,1/2), Cs2, fits into a cavity in the crystal, and is surrounded by six oxygen atoms which form a somewhat distorted octahedron. Two of these belong to water molecules and the other four are carbonyl oxygen atoms. The Cs2 ion is also at the center of symmetry with respect to the six oxygen atoms. The mean value 3.04 Å

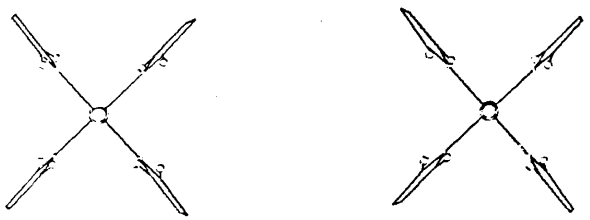

Fig. 4. The complex anion of $(Cu(sucim)_4)^{2-}$ shown by a stereo pair.

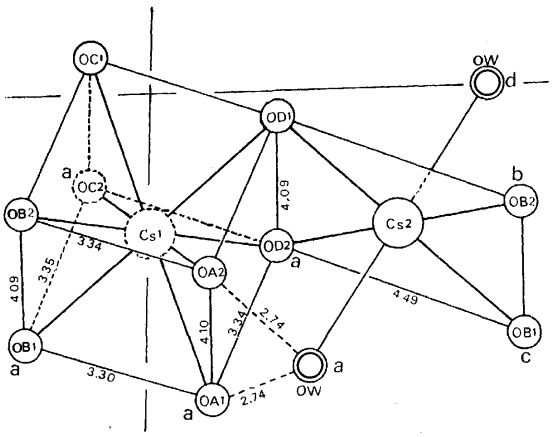

Fig. 5—1. The arrangement of oxygen atoms around two independent cesium ions. Small letters, *a*, *b*, and *c* indicate the symmetry operations in Table 6.

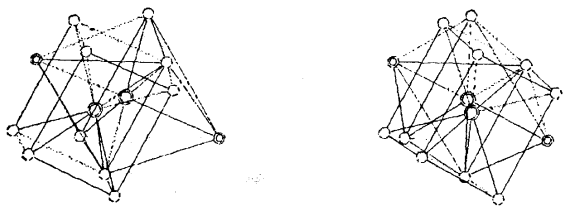

Fig. 5—2. The arrangement of oxygen atoms around two cesium ions shown by a stereo pair.

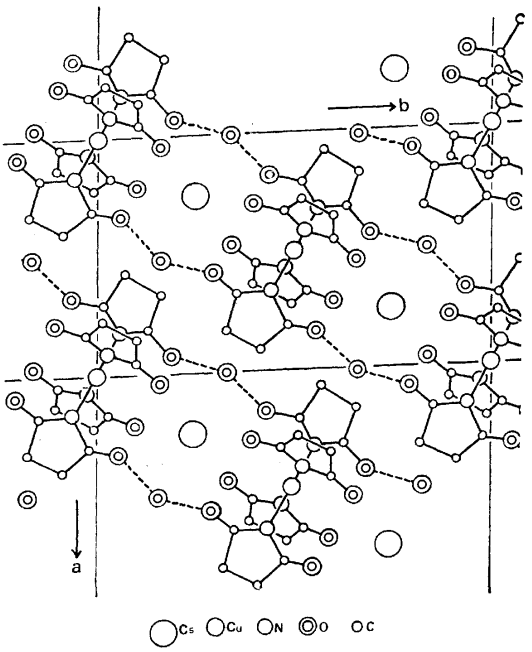

Fig. 6—1. The crystal structure of $Cs_2(Cu(sucim)_4)\cdot 2H_2O$ projected along the *c* axis. Hydrogen bonds are indicated by broken lines.

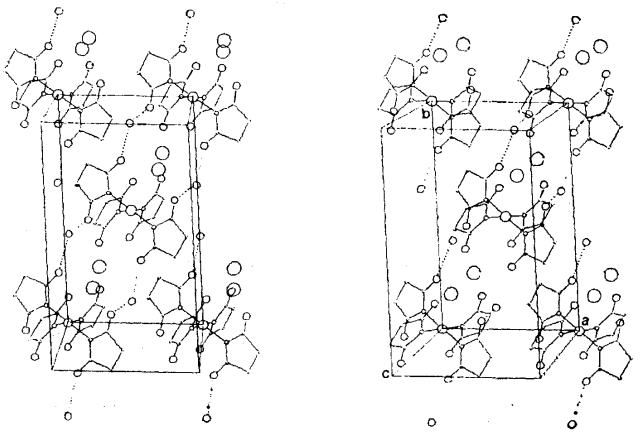

Fig. 6—2. The crystal structure of $Cs_2(Cu(sucim)_4)\cdot 2H_2O$ shown by a stereo pair.

3) M. Matthew and N. R. Kunchur, *Acta Crystallogr.*, **B26**, 2054 (1970).
4) M. Sekizaki, F. Marumo, K. Yamasaki, and Y. Saito, This Bulletin, **44**, 1731 (1971).
5) C. A. Ghilardi and E. C. Lingafelter, *Acta Crystallogr.*, **B26**, 1807 (1970)
6) R. Mason, *ibid.*, **9**, 405 (1956).

TABLE 6. ENVIRONMENT OF CESIUM IONS AND WATER MOLECULES

Atom	Neighbor atom		Distance	Atom	Neighbor atom		Distance
Cs1	OA2	or OC2(a)	3.12 Å	Cs1	OB2	or OD2(a)	3.13 Å
Cs1	OC1	OA1(a)	3.13	Cs1	OD1	OB1(a)	3.12
Cs2	OD1	OB1(c)	3.06	Cs2	OD2 (a)	OB2(b)	3.02
Cs2	OW1(a)	OW1(d)	3.19	Cs1	Cs2		4.19

Hydrogen bonds

OA2···OW1(a)	2.74 Å	OA1···OW1	2.74 Å

Angles

OA2-Cs1-OB2		or OC2(a)-Cs1-OD2(a)	65°
OB2-Cs1-OC1		OD2(a)-Cs1-OA1(a)	65
OC1-Cs1-OD1		OA1(a)-Cs1-OB1(a)	64
OA2-Cs1-OD1		OC2(a)-Cs1-OB1(a)	65
OA2-Cs1-OA1(a)		OC2(a)-Cs1-OC1	82
OB2-Cs1-OB1(a)		OD2(a)-Cs1-OD1	82
OB2-Cs1-OD1		OD2(a)-Cs1-OB1(a)	98
OA2-Cs1-OC1		OC2(a)-Cs1-OA1(a)	98
OD1-Cs2-OD2(a)		OB1(c)-Cs2-OB2(b)	85
OD1-Cs2-OB2(b)		OB1(c)-Cs2-OD2(a)	95
OD1-Cs2-OW1(a)		OB1(c)-Cs2-OW1(d)	87
OD2(a)-Cs2-OW1(a)		OB2(b)-Cs2-OW1(d)	87
OD1-Cs2-OW1(d)		OB1(c)-Cs2-OW1(a)	93
OD2(a)-Cs2-OW1(d)		OB2(b)-Cs2-OW1(a)	93
OB2-OA2-OD1	90°	OA2-OD1-OC1	90°
OD1-OC1-OB2	90	OC1-OB2-OA2	90
OB2-OB1(a)-OA1(a)	91	OB1(a)-OA1(a)-OA2	90
OA1(a)-OA2-OB2	90	OA2-OB2-OB1(a)	90
OD1-OA2-OA1(a)	90	OA2-OA1(a)-OD2(a)	90
OA1(a)-OD2(a)-OD1	90	OA2-OD1-OD2(a)	90
OD1-OD2(a)-OB1(c)	91	OB2(b)-OD1-OC1	175

Key for molecular position

a: $(0.5+x, 0.5+y, z)$ b: $(x, y, 1.0+z)$ c: $(0.5+x, 0.5+y, 1.0+z)$, d: $(-x, -y, 1.0-z)$

of the Cs2-O(carbonyl) is slightly less than 3.12 Å of Cs1-O(carbonyl). The arrangement around the Cs2 ion may be compared to the six-coordination NaCl-type structure. The Cs-O distances are in fairly good agreement with the sum of ionic radii, 3.09 Å. Thus all the oxygen atoms gather around the cesium ions whose positive charges are probably neutralized by negative charges of the oxygen atoms. The environment is illustrated in Fig. 5 and Table 6.

The complex anions are linked to the neighbouring anions in the [110] direction through the hydrogen bonds between the water molecules and carbonyl oxygen atoms and through the ionic contacts between the cation of Cs1 and carbonyl oxygen atoms. The complex anions are also linked together by Cs2-O(carbonyl) contacts in the direction of axis *c*.

The crystal structure is shown in Fig. 6.

The authors express their thanks to Dr. S. Komorita for valuable discussions and the kind supply of crystals, and to Dr. T. Ashida for permission to use his program.

Study on Reverse Osmosis. The Permeation Behavior of Amino Acid Solutions through Cellulose Acetate Membranes

Chiyoshi KAMIZAWA, Hitoshi MASUDA, and Seiichi ISHIZAKA
National Chemical Laboratory for Industry, Hon-machi, Shibuya-ku, Tokyo

(Received November 2, 1971)

Transport phenomena of some aliphatic amino acids and aminobenzoic acids were investigated with Loeb type membranes annealed at 60—80°C.

The quantitative relation between permeability through the membrane and dissociation of amino acid was examined. The charged species are rich in the solutions of amino acids such as L-leucine, L-alanine, and L-glutamic acid, regardless of the pH of solution, thus making the rejection by membranes large; the rejection of L-leucine which had a rejection of 35% for NaCl, was 63.2% even for the membrane cured at 60°C. On the other hand, for aminobenzoic acids, the number of uncharged species in solution varied with the change in pH, and the rejection varied with pH. The fluxes of aminobenzoic acids were in linear relation to the calculated amount of uncharged species. The results of adsorption experiments indicate that the amounts of adsorbed aminobenzoic acid to cellulose acetate were in logarithmic relation to calculated amounts of undissociated species. The results support the view that dissociated species are more difficult to be distributed in membrane than undissociated ones.

It is known that electrolytes such as NaCl, $MgSO_4$, and CH_3COONa[1] can hardly pass through the Loeb type skinned membranes annealed at or above 80°C, but non-electrolytes such as phenol,[2] acetic acid[3] can do so easily. However, the relation between the ionic dissociation of the molecules in solution and the amount of transport in reverse osmosis processes has not been sufficiently discussed. Aliphatic amino acids and aminobenzoic acids were chosen to clarify the relation, since they are amphoteric and the charged state of molecules can easily be controlled by changing the pH of the solution.[4]

Experimental

The modified cellulose acetate (E-398-3) membranes were prepared by the method reported by Loeb and Manjikian.[5] DDS-880 membranes (Loeb type, De Danske Sukkerfabrikker, Denmark) were also used. Annealing temperatures of the Loeb type membranes were 60, 70, 75, and 80°C. Evaporation temperature was 18±1°C and evaporation time was 1 minute for all Loeb type membranes. The effective membrane area in the desalination cell[3] was 12.6 cm^2. The pressurized (40 atm) solution was circulated along the surface of the membrane at 250 ml/min to reduce concentration polarization. For aminobenzoic acids, a batched type apparatus[6] with 28.3 cm^2 effective membrane area was used in order to obtain more precise values. The impeller was rotated over the membrane at 300 r.p.m. by magnetic induced force. Solutions of 0.1 N NaCl, 0.01 N L-leucine, L-alanine, L-glutamic acid, 0.001 N *p*-aminobenzoic acid, and *m*-aminobenzoic acid were tested. Their pH was controlled by adding 0.1 N HCl to the solution. In all the experiments the permeated water was collected one hour after the beginning of the operation. Analysis of the components was performed by the method of Yemm and Cocking[7] for amino acids and by photo-absorption at 254 mμ and 214 mμ for *p*- and *m*-aminobenzoic acid, respectively, with a spectrophotometer (Simazu MPS 50L). The properties of the membrane were shown by water flux (g/cm^2·sec), salt flux (mol/cm^2.sec) and salt rejection. Salt rejection is given by

$$Re = (1 - C_p/C_f) \times 100 \quad (1)$$

where C_p and C_f are solute concentration of product and feed solutions, respectively. The membrane is known to be degradated by hydrolysis[8] in strong alkaline solutions. Thus no base was added to the feed solution, although it was desirable to test the pH effect on transport phenomena.

To avoid marked pH change, experiments were carried out as rapidly as possible.

Results

Rejection of Amino Acids. The rejection of amino acids was larger than that of NaCl as shown in Fig. 1. For instance, the rejection of L-leucine was 63.2% and 99.6% for the membrane annealed at 60°C and 80°C, respectively. There was a difference in the rejection of amino acids, the rejection of L-glutamic acid being somewhat larger than that of L-leucine, especially of the membrane annealed at low temperature (Fig. 1).

Effect of pH on the Transport of Amino Acids. To find the relation between the dissociation of the acids and their transport behavior, the permeation of *p*- and *m*-aminobenzoic acids was examined. Since it was required to analyze data more precisely, a DDS-880 membrane reheated at as high a temperature as 85°C was used in order to reduce membrane defects through which the feed solution would permeate at its concentration.

The rejection of NaCl by this membrane was 98.4% at 40 atm. As shown in Fig. 3, the rejection of *p*- and *m*-aminobenzoic acid changed with the pH of feed solution, the rejection of *m*-aminobenzoic acid being 57.0% and 95.7% at pH 3.88 and 1.77, respectively.

1) S. Kimura and S. Sourirajan, *Am. Inst. Chem. Engrs., Journal*, **13**, 497 (1967).
2) U. Merten and H. K. Lonsdale, "Office of Saline Water Report," No. 265, (1967), p. 150.
3) C. Kamizawa and S. Ishizaka, *Kogyo Kagaku Zasshi*, **72**, 1227 (1969).
4) J. P. Greenstein and M. Winitz, "Chemistry of the Amino-acids" Vol. 1, Wiley, New York (1961), p. 435.
5) S. Manjikian, S. Loeb, and J. W. McCutchan, First Symposium on Water Desalination Washington, D. C., (1965), SWD/12.
6) T. Nakane and S. Ishizaka, *Bull. Soc. Sea Water Sci. Japan*, **26**, 11 (1972).
7) E. W. Yemm and E. C. Cooking, *Analyst*, **80**, 209 (1955).
8) K. D. Vos, F. Burris, and R. L. Riley, *J. Appl. Polym. Sci.*, **10**, 825 (1966).

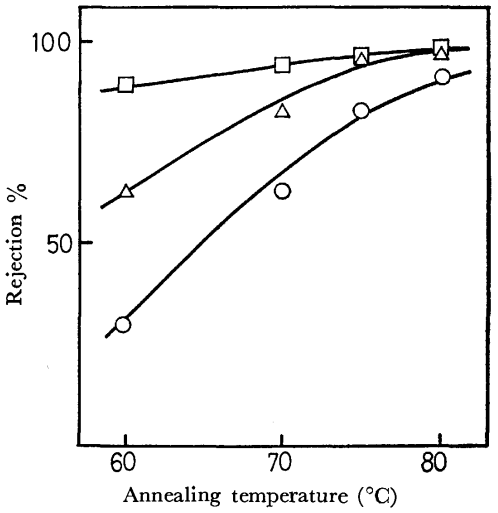

Fig. 1. Rejections of amino acids.
○: NaCl 0.1 M, △: L-leucine 0.01 M (pH 3.60), □: L-glutamic acid 0.01 M (pH 3.80)

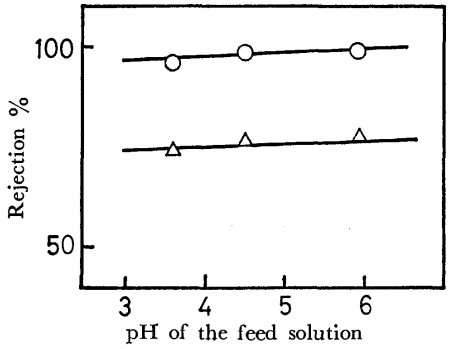

Fig. 2. The effect of pH on the transport of L-leucine.
○: Membrane annealed at 80°C, △: Membrane annealed at 70°C.

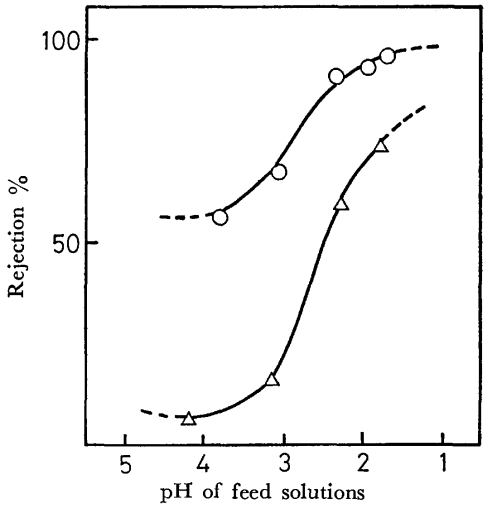

Fig. 3. Rejections of aminobenzoic acids.
○: *m*-Aminobenzoic acid 10^{-3} M, △: *p*-Aminobenzoic acid 10^{-3} M, Membrane: Annealed at 85°C.

Discussion

Rejection of Amino Acids. An evidence for the zwitter-ion structure of amino acids has been presented.[4] Amino acids dissociate as follows.

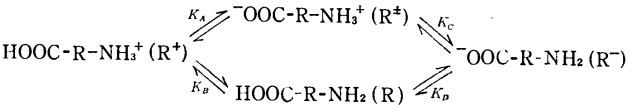

The equilibrium can be represented by the equations

$$K_1 = \frac{(H^+)[(R\pm)+(R)]}{(R^+)} = K_A + K_B \qquad (2)$$

$$K_2 = \frac{(H^+)(R^-)}{(R\pm)+(R)} \quad ; \quad \frac{1}{K_2} = \frac{1}{K_C} + \frac{1}{K_D} \qquad (3)$$

where K_A, K_B, K_C, and K_D are equilibrium constants for R^+ and $R^\pm$, R^+ and R, $R^\pm$ and R^-, and R and R^-, respectively. We obtain the relation

$$K_Z = \frac{(R\pm)}{(R)} = \frac{K_A}{K_B} = \frac{K_D}{K_C} = \frac{K_1}{K_E} - 1 \qquad (4)$$

where K_E, the dissociation constant of the amino acid ester, was assumed to be almost equal to K_B and is used in place of K_B. As K_1 is much larger than K_E, for aliphatic amino acids[9] Eq. (4) is reduced to

$$K_Z = \frac{K_1}{K_E} \quad ; \quad -\log K_Z = pK_Z \qquad (5)$$

K_Z is of the order of 10^5 for most amino acids, and the quantity of uncharged species normally present in their solutions is insignificant. If the pH of the solution is changed, the composed ratio of R^+, $R^\pm$, R, and R^- changes, but the quantity of uncharged species remains insignificant. This seems to be the cause of the large rejection of amino acids regardless of the change of pH in the solution. The $R^\pm$; NH_3^+-R-COO^- species of the amino acid are of a dissociated form, but the apparent effective charge is zero. Thus in electrophoresis, ions do not move as if they had no charge but seem to act as charged species in reverse osmosis experiments.

Rejections of Aminobenzoic Acids. Only in the case of aminobenzoic acids, where -pK_Z are −0.70, +0.36, and −0.87, for *o*-, *m*-, and *p*-compounds, respectively, the uncharged species assumes comparable concentration (Fig. 4). The behaviors of *m*- and *p*-compounds whose values of $R^\pm$/R are 2.29 and 0.135, respecitively, were examined with values of K_A, K_B, K_C, K_D, K_1, and K_2 taken from a table.[10] The quantities of $R^\pm$, R^+, R, and R^-, were calculated from Eqs. (2), (3), (4), and (5). The calculated values of R in the *m*- and *p*-aminobenzoic solutions at various pHs are shown in Fig. 4. The relation between the concentration of R, uncharged species in equilibrium at pH of the feed and the permeated fluxes of *m*-aminobenzoic acid is shown in Fig. 5. The solute fluxes of *m*-aminobenzoic acid are proportional to the amounts of the uncharged species in the feed solutions. In the same manner, the relation holds for *p*-aminobenzoic acid. It can thus be said that the dissociation of the molecule plays an important role in the transport phenomena through the Loeb type membrane. Some differences were seen between the pH of feed and permeated solu-

9) E. J. Cohn and J. T. Edsall, "Proteins, Amino Acids and Peptide as Ions and Dipolar Ions" (1943), p. 99.
10) Greenstein and Winiz, "Chemistry of the Aminoacids" Vol. 1 (1952), p. 447.

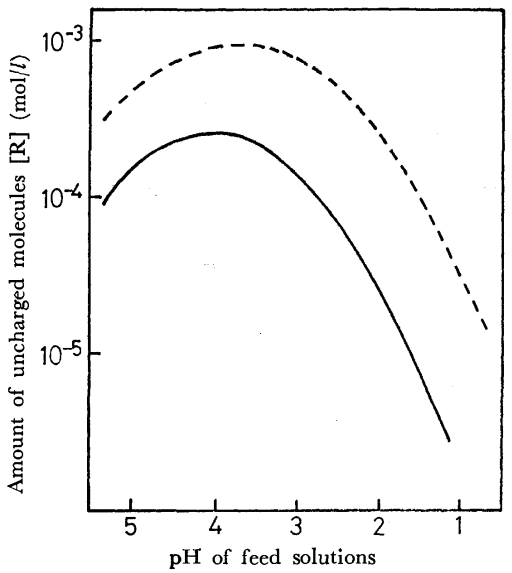

Fig. 4. Calculated amount foruncharged molecules.
——: *m*-Aminobenzoic acid 10^{-3} M, ----: *p*-Aminobenzoic acid 10^{-3} M.

tions, as 3.86 and 4.19, respectively, in the case of *m*-aminobenzoic acid. Thus a gradient of pH exists in the membrane.

However, in spite of the pH gradient, the interface between the membrane and the feed solution seems to be more effective for the transport of the solute than the charged molecules in the membrane, as is indicated by the result shown in Fig. 5.

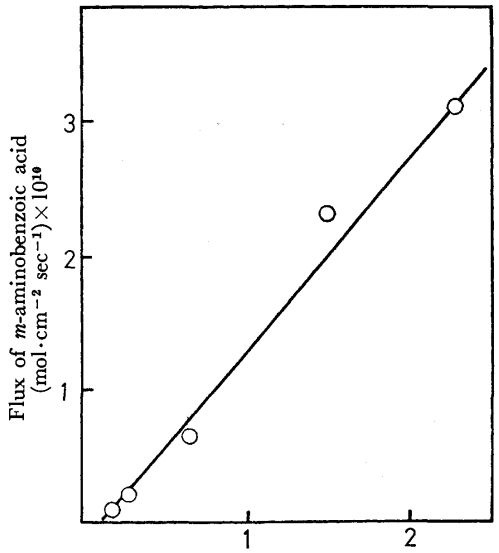

Fig. 5. The relation between the quantity of uncharged molecules and the flux.

Adsorption of m-*Aminobenzoic Acid to Cellulose Acetate Powder.* To understand the relation between the permeation and the dissociation of the solute more precisely, the adsorption of *m*-aminobenzoic acid to cellulose acetate powder was measured.

A definite amount of each of the *m*-aminobenzoic solutions (0.001 N) containing various amounts of HCl, was mixed with 3 g of dry cellulose acetate powder in a 200 m*l* conical flask. It was left at ambient temperature and shaken vigorously from time to time, The apparent adsorbed amount was determined from the difference between the solute concentrations before and after the adsorption. Adsorption of water to cellulose acetate was not taken into consideration.

The adsorbed amounts of *m*-aminobenzoic acid were proportional to the logarithm of calculated amounts of uncharged species (R) in the form of Freundlich type adsorption isotherm (Fig. 6).

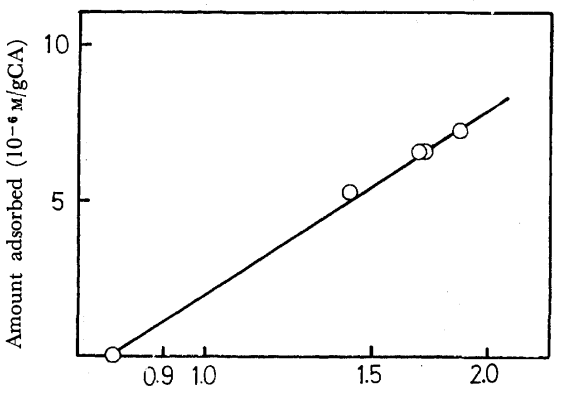

Fig. 6. Amounts adsorbed of *m*-aminobenzoic acid to cellulose acetate powder.

This seems to indicate that undissociated species have greater affinity to cellulose acetate. If affinity of solute to cellulose acetate is considered to be an important factor for determining the distribution coefficient, our result would support the fact that the dissociated species are more difficult to be distributed in the membrane than the undissociated ones. On the rejection of electrolytes, Glueckauf described[11] the potential wall by dielectric constant of cellulose acetate, but this is not satisfactory for explaining the behavior of most electrolytes.[12]

The authors wish to thank Mr. Ryozo Hiraoka for his help in the experiment.

11) E. Glueckauf, First Symposium on Water Desalination, Washington, D. C., (1965), SWD/1.
12) T. S. Govindan and S. Sourirajan, *Ind. Eng. Chem. Proc. Des. Develop.* **5**, 422 (1966).

Study on Reverse Osmosis. The Permeation Behavior of Surfactant Solutions through Cellulose Acetate Membranes

Chiyoshi KAMIZAWA and Seiichi ISHIZAKA

National Chemical Laboratory for Industry, Hon-machi, Shibuya-ku, Tokyo

(Received November 2, 1971)

Transport phenomena of some surfactants were investigated with Loeb-type skinned membranes annealed at 60, 70, 75, and 80°C, with the following results. (1) The rejection of cationic and anionic surfactants is larger than that of nonionic surfactants, especially at concentrations below CMC. (2) In the case of nonionic surfactants, their fluxes decrease with the increase of molecular weight. (3) The effect of CMC on the transport of surfactants is great, particulary in the case of nonionic surfactants. (4) Concentration polarization on the surface of the membrane can be predicted by taking into account the difference between surfactant fluxes below and above CMC.

Waste water contains various solutes of which surfactant is one of the most troublesome because of its harmfulness to human bodies. In this work, the behavior of anionic, cationic and nonionic surfactants was examined with Loeb-type skinned membranes. We intended to clarify the transport phenomena of various solutes with the membranes. However, in order to make the problem simpler a solution containing only one solute was examined in each case.

Expermental

Modified cellulose acetate (E-398-3) membranes were prepared by the method reported by Loeb and Manjikian[1] at annealing temperatures 60, 70, 75, and 80°C. The evaporation temperature was 18°±1°C, and evaporation time one minute. The membranes were placed in a stainless desalination cell described previously.[2] The pressurized (40 atm) solution was circulated along the surface of the membrane at 250 ml/min to reduce concentration polarization.

Solutions of sodium dodecylbenzenesulfonate (ABS) as anionics, tetradecylbenzylammonium chloride (TDBNC) as cationics and polyoxyethylene nonylphenyl ether (NP) as nonionics were tested at their various concentrations, since the surfactants have their critical micelle concentration (CMC). In the case of NP, NP-10 (C_9H_{19}- 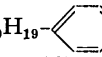 -O-(CH_2-CH_2O)$_n$ H; $n=10$), NP-16 (where : $n=16$) and NP-27 (where : $n=27$) were used to test the effects of the molecular weight on the permeation of surfactants. Analysis of surfactants was performed by photo-absorbance at 224 mμ for ABS, at 214 mμ for TDBNC and NP. The critical micelle concentrations were estimated from the plots of surface tension *vs.* surfactant concentration and from those of photo-absorption *vs.* surfactant concentration. Surface tensions were measured by the ring method.[3] Properties of the membrane were shown by water flux, salt flux, and salt rejection.[2,4]

Results

Rejection of Surfactants. The rejection of ABS was larger than that of the other two surfactants. The rejection of ABS was 88.9% even for the membrane annealed at 60°C and 99.8% for that annealed at 80°C (Table 1-1). The rejection was so large that no significant difference was observed between the solute fluxes below and above CMC. TDBNC also has a large rejection, *e.g.*, 86.5% and 93.4% for the membranes annealed at 60°C and 75°C, respectively. The rejection of NP-27 was the smallest, *e.g.*, 26% for the membrane annealed at 60°C (Fig. 1) and 86% for the membrane annealed at 80°C. The rejection of NP was almost the same as that of NaCl. The results obtained below CMC are given in Fig. 1.

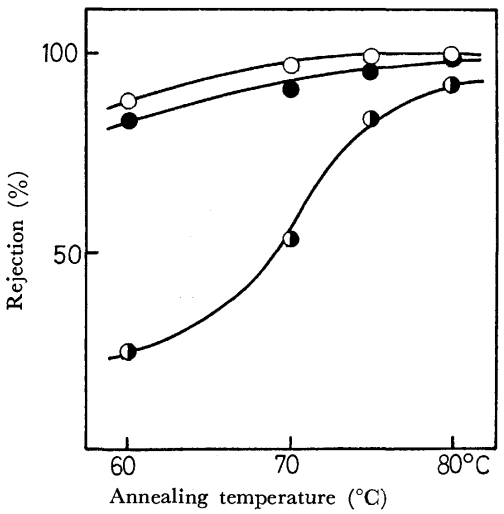

Fig. 1. Rejections of surfactants.
○: ABS 6.00×10^{-4} M
●: TDBNC 2.67×10^{-4} M
◑: NP-27 5.08×10^{-5} M

Effect of CMC. The effect of CMC on permeability through the membrane was measured. No detectable difference was found in the cases of ABS and TDBNC. The influence was remarkable in the case of NP, since its rejection was small below CMC, *e.g.*, the rejection of NP-10 was 42.1% below, and 83.9% above CMC for the membrane cured at 75°C (Table 1-2).

Effect of Molecular Weight. The influence of molecular weight on permeability through the membrane was examined for NP by changing the mole number of oxyetheylene unit. The flux of NP decreases with the increase of molecular weight of NP and

1) S. Manjikian, S. Loeb, and J. W. McCutchan, First Symposium on Water Desalination, Washington, D. C., 1965, SWD/12.
2) C. Kamizawa and S. Ishizaka, *Kogyo Kagaku Zasshi*, **72** 1227 (1969).
3) A. W. Adamson, "Physical Chemistry of Surfaces," Interscience Publishers (1963), p. 29.
4) C. Kamizawa, H. Masuda, and S. Ishizaka, This Bulletin, **45**, 2964 (1972).

TABLE 1-1 RESULTS OF REVERSE OSMOSIS EXPERIMENTS

Solute	Membrane	Concn of feed 10^{-4} mol/l	Water flux 10^{-3} g/cm^2·sec	Solute flux 10^{-10} m mol/cm^2·sec	Rejection %
ABS	60—1*[a]	6.0	2.04	17.8	85.5
	60—2	6.0	2.75	18.8	88.9
	70—1	6.0	1.74	3.53	96.7
	70—2	6.0	2.24	4.52	96.7
	75—1	6.0	1.61	0.65	99.3
	80—1	6.0	0.43	0.06	99.8
ABS	60—2	21.8	2.46	53.8	89.6
	70—2	21.8	2.01	13.4	97.0
	75—1	21.8	1.16	2.75	98.9
	75—2	21.8	1.43	2.02	99.4
	80—2	21.8	0.53	0.53	99.6
TDBNC	60—3	2.67	1.74	6.29	86.9
	60—4	2.67	2.53	14.2	78.9
	70—4	2.67	1.86	4.56	90.9
	75—3	2.67	1.44	2.54	93.4
	75—4	2.67	1.61	2.72	93.7

a) 60—1 (60: Annealing Temperature; 1: Identification Number of the Membrane)
CMC; ABS: 1.40×10^{-3} mol/l, TDBNC: 4.20×10^{-3} mol/l

TABLE 1-2 RESULTS OF REVERSE OSMOSIS EXPERIMENTS

Solute	Membrane	Concn of feed 10^{-5} mol/l	Water flux 10^{-3} g/cm^2·sec	Solute flux 10^{-10} mol/cm^2·sec	Rejection %
NP-10	60—3	2.54	1.40	3.42	5.0
	60—4	2.54	1.82	4.42	5.0
	70—4	2.54	1.43	2.87	21.4
	75—3	2.54	1.10	1.62	42.1
NP-10	60—2	7.85	1.41	6.97	37.3
	60—3	7.85	1.89	10.1	31.3
	70—2	7.85	1.52	4.33	63.6
	70—5	7.85	1.38	3.93	63.6
	75—3	7.85	1.23	1.57	83.9
	75—6	7.85	1.48	2.20	80.9
NP-16	60—3	3.75	1.40	4.98	5.4
	60—4	3.75	1.82	6.37	5.4
	70—4	3.75	1.43	4.07	24.3
	75—3	3.75	1.10	1.68	59.5
NP-16	60—4	10.8	2.33	14.2	33.0
	70—4	10.8	1.92	6.17	70.0
	75—3	10.8	1.47	1.56	90.1
	80—1	10.8	0.47	0.22	96.0
NP-27	60—5	5.08	1.93	6.38	26.0
	70—4	5.08	1.56	3.33	54.8
	75—3	5.08	1.26	1.08	83.1
	80—1	5.08	0.36	0.27	86.0
NP-27	60—5	16.9	1.74	13.24	55.0
	70—4	16.9	1.40	6.19	73.9
	75—3	16.9	1.15	1.52	92.0

CMC; NP-10: 5.27×10^{-5} mol/l, NP-16: 6.80×10^{-5} mol/l, NP-27: 1.44×10^{-4} mol/l.

that of NP-27 is approximately one-third of that of NP-10 (Fig. 3). The concentration of feed solution is below CMC; in the solution above CMC, the tendency is almost the same (Fig. 2).

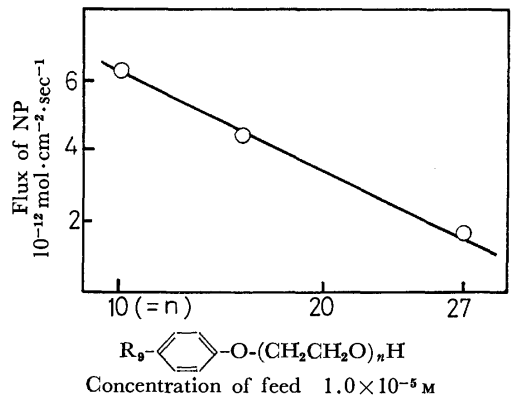

Fig. 2. Effect of molecular weight on the permeation of NP.

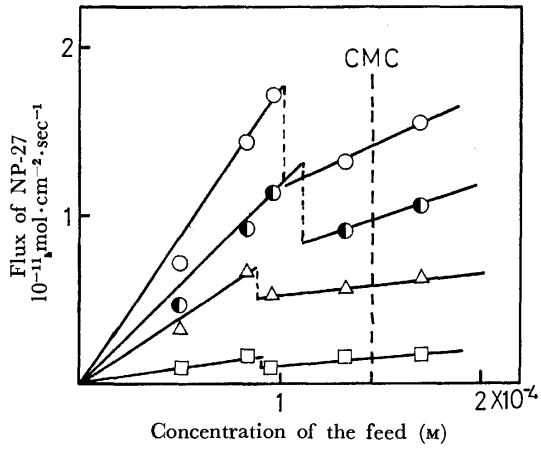

Fig. 3. Effect of CMC on the permeation of NP-27.
○: Membrane annealed at 60°C.
◐: Membrane annealed at 60°C.
△: Membrane annealed at 70°C.
□: Membrane annealed at 75°C.

Discussion

Rejections of Surfactants. The rejection of ABS and TDBNC is approximately the same and greater than that of NP-27 (Fig. 1). It was observed that the dissociated species can hardly pass through the membrane.[4] The present results seem to support this. The size of the molecule should be closely related to its permeability, but to explain molecular permeability through the membrane by ascribing it mainly to the molecule is not satisfactory since the molecular weights of ABS, TDBNC, and NP-27 are 348, 327, and 1408, respectively.

Effect of Molecular Weight. The permeation of NP changes with its molecular weight, but it cannot be said whether this is due to the molecular size or to hydrophilic property by increasing ethylene oxide units. No difference was found between the decreasing tendencies of NP flux with increasing molecular weight below and above CMC. Most of the permeated NP is supposed to be a monomer in equilibrium with micelle. According to Kesting *et al.*,[5] water flux increases with the increase of hydrophilic property of the surfactant, but in the present work, the change of water flux with chemical property of surfactant was within experimental error.

Effect of CMC. It is generally recognized that in the case of inorganic salts, their fluxes are in linear proportion to the concentrations of the feed solution.[6,7] In the case of NP the rejection of the solute below CMC differs remarkably from that above CMC for each membrane (Table 1-2). In other words the solute fluxes are not in proportion to the feed concentration for a determined membrane. To make this effect clearer, the relation between concentration of the feed and the solute flux was investigated in detail with NP-27. The fluxes of NP-27 were in linear proportion to the concentration of the feed before it reached a certain concentration, at which an abrupt decrease occurred (Fig. 3). It might be considered that the concentration of NP-27 at the surface of the membrane reached CMC. The concentration polarization can be given by[8]

$$\frac{C_2-C_3}{C_1-C_3}=e^{J_v/K}$$

where C_1, C_2, and C_3 are the bulk concentration of the feed, the concentration at the membrane surface and the concentration of the product, respectively. J_v is water flux (cm/sec), and K is mass-transfer coefficient (cm/sec). If we know the critical feed concentration which would cause the concentration at the membrane surface to amount to CMC, the ratio of the concentration at bulk solution to that at boundary layer ($=C_2/C_1$) could be estimated.

Under the assumption that the value of K remains constant below and above CMC, the value of K was calculated by the above equation with the values of C_2 ($=1.45\times10^{-4}$ mol/l=CMC), C_3 ($=0.30\times10^{-4}$ mol/l), and J_v ($=1.62\times10^{-3}$ cm/sec), the data for the membrane annealed at 70°C. The value of C_1 was assumed to be the average 0.89×10^{-4} mol/l of the concentrations which lie on both sides of inflection (see Fig. 3). The critical values ($=C_1$) for the other membranes were then calculated with $K(=2.40\times10^{-3}$ cm/sec) estimated above. The concentrations shown by dotted lines indicate calculated values (Fig. 3). A micelle is supposed to be composed of 20—30 monomers, making it large enough to be rejected by the membrane.

From the results (Fig. 3) the ratio of the concentration at bulk solution to that at boundary layer ($=C_2/C_1$) is found to be between 1.32—1.61 depending on the membrane under conditions described in the experimental section.

The authors wish to thank Dr. Hiroshi Suzuki for his kind advice and the supply of materials, and Mr. Masato Moroishi for his help in the experiments.

5) R. E. Kesting, W. J. Subcasky, and J. D. Patch, *J. Colloid Interfac. Sci.*, **28**, 156 (1968).
6) W. Banks and A. Shaples, *J. Appl. Chem.*, **16**, 153 (1966).
7) R. L. Riley, H. K. Lonsdale, C. R. Lyons, and U. Merten, *J. Appl. Polym. Sci.*, **11**, 2143 (1967).
8) U. Merten, "Desalination by Reverse Osmosis," The M. I. T. Press., (1967), p. 181.

Shapes of Fundamental Bands of Liquid Carbon Disulfide. Vibrational and Reorientational Relaxations

Masao KAKIMOTO and Tsunetake FUJIYAMA

Department of Chemistry, Faculty of Science, The University of Tokyo, Hongo, Bunkyo-ku, Tokyo

(Received March 27, 1972)

The shapes and intensities of the fundamental bands, ν_2 (the CSC bending) and ν_3 (the C–S antisymmetric stretching), were measured for liquid carbon disulfide and its chloroform solutions. The intensity data were corrected for the effect of the dielectric field at each frequency. The analyses of the ν_2 and ν_3 bands indicate that the band-widths of liquid carbon disulfide can not be explained only in terms of reorientational relaxation. It is also shown that the vibrational relaxation of the resonance type can well explain the concentration dependence of the observed band-widths. The magnitudes of the vibrational and reorientational relaxations obtained from the band-shape analyses are given. It is emphasized that the measurement of the absolute intensity is indispensable for the analyses of the infrared-band shapes of condensed phases.

In recent years it has been realized that the band shapes of infrared absorption spectra of liquid should yield much information about molecular motion. The descriptions of Shimizu[1] and Gordon[2] have encouraged infrared spectroscopists interested in the rotational motions of molecules in the liquid phase. However, progress has been rather disappointing because of many problems, both experimental[3–5] and theoretical. A question has arisen about the analyses of band shapes by the use of reorientational-relaxation theories, that is, it has been questioned whether or not the half band-widths of the infrared absorption spectra of liquids can be completely explained in terms of the reorientational relaxations. One of the criteria is whether or not the half-widths associated with the same symmetry species of a molecule have the same value. In fact, the fundamental bands of methyl cyanide or carbon disulfide have been found to be too strange to be explained only in terms of the reorientational relaxations.[6,7]

The present report will be concerned with observations of the band shapes for liquid carbon disulfide and with the introduction of vibrational relaxation to explanations of the band-widths. The theoretical and experimental evaluation of vibrational relaxation in liquids is under active discussion.[8–13] We will tentatively follow the idea of Valiev[13] in the present work.

Theoretical

The intensity distribution of an infrared absorption band, $I(\omega)$, has been shown to be a Fourier transform of a dipole correlation function, $\Phi(t)$:[1,2]

$$I(\omega) = \frac{1}{2\pi}\int_{-\infty}^{\infty}\Phi(t)e^{-i\omega t}\mathrm{d}t \tag{1}$$

and:

$$\Phi(t) = \int_{-\infty}^{\infty} I(\omega)e^{i\omega t}\mathrm{d}\omega = <\boldsymbol{M}(0)\boldsymbol{M}(t)>_{av} \tag{2}$$

where ω is the angular frequency displacement from a band origin, $\boldsymbol{M}(t)$ is the Heisenberg operator of the transition dipole moment of the vibration concerned, and $\langle\ \rangle_{av}$ means an ensemble average over the equilibrium distribution. If we assume that the mechanisms of the vibrational and reorientational relaxation processes are not correlated, then the ensemble average can be taken separately with respect to the two processes:[14]

$$\Phi(t) = \Phi_v(t)\Phi_r(t) \tag{3}$$

where $\Phi_v(t)$ and $\Phi_r(t)$ refer to the vibrational and reorientational correlation functions respectively.

If both $\Phi_v(t)$ and $\Phi_r(t)$ are assumed to be exponential functions, $\Phi(t)$ is expressed as:

$$\Phi(t) = e^{-|t|/\tau} \tag{4}$$

Therefore:

$$(1/\tau) = (1/\tau_v) + (1/\tau_r) \tag{5}$$

where τ_v and τ_r are the vibrational and reorientational relaxation times respectively. The intensity distribution function, $I(\omega)$, is calculated from Eqs. (1) and (4):

$$I(\omega) = \frac{1}{\pi}\frac{(1/\tau)}{(1/\tau)^2+\omega^2} \tag{6}$$

Thus, the half band-width of the absorption band, $\Delta\nu_{1/2}$, is given by:

$$\frac{1}{2}\Delta\nu_{1/2} = (1/\tau_v) + (1/\tau_r) \tag{7}$$

Equation (7) means that a total half-width of an absorption band is a sum of the vibrational and reorientational widths. In some cases the assumption of an exponential function for $\Phi_v(t)$ or $\Phi_r(t)$ may not be appropriate. This can be checked by seeing whether

1) H. Shimizu, *J. Chem. Phys.*, **43**, 2453 (1965).
2) R. G. Gordon, *ibid.*, **43**, 1307 (1965).
3) T. Fujiyama, J. Herrin, and B. L. Crawford, Jr., *Appl. Spectrosc.*, **24**, 9 (1970).
4) B. L. Crawford, Jr., A. C. Gilby, A. A. Clifford, and T. Fujiyama, *Pure and Applied Chemistry*, **18**, 373 (1969).
5) R. P. Young and R. N. Jones, *Chem. Rev.*, **71**, 219 (1971).
6) C. Alliot, M. Cameo, and J. Vincent-Geisse, *C. R. Acad. Sci., Paris, Ser. B*, **266**, 391 (1968).
7) T. Fujiyama and B. L. Crawford, Jr., The lecture presented in Gordon Conference (1969).
8) L. Landau and E. Teller, *Physik. Z. Sowjetunion*, **10**, 34 (1938).
9) A. Litoviz, *J. Chem. Phys.*, **26**, 469 (1957).
10) M. Fixman, *ibid.*, **34**, 369 (1961).
11) R. Zwanzig, *ibid.*, **34**, 1931 (1961).
12) B. J. Berne, J. Jortner, and R. G. Gordon, *ibid.*, **52**, 439 (1970).
13) K. A. Valiev, *Opt. Spectrosc.*, **11**, 253 (1961).
14) S. Bratoz, J. Rios, and Y. Guissani, *J. Chem. Phys.*, **52**, 439 (1970).

or not the observed band shapes are of the Lorentzian type of Eq. (6).

If we assume that the contribution of the vibrational relaxation to a band shape is much smaller than that of the reorientational relaxation, $\Phi(t)$ may be set equal to a reorientational relaxation function, $\Phi_r(t)$. Then the observed half-width, $\Delta\nu_{1/2}$, of the band can be simply related to τ_r by:

$$\frac{1}{2}\Delta\nu_{1/2} = 1/\tau_r \tag{8}$$

If we designate the molecular fixed axes by i (where $i=x$, y, and z), the physical meaning of $(1/\tau_r)^i$ is the rate of reorientation of a molecule around the i-th axis. For example, consider the parallel and perpendicular bands of a linear or symmetric-top molecule. For a parallel band,

$$\frac{1}{2}\Delta\nu_{1/2}^{(p)} = 2(1/\tau_r)^x \tag{9a}$$

and for a perpendicular band,

$$\frac{1}{2}\Delta\nu_{1/2}^{(s)} = (1/\tau_r)^x + (1/\tau_r)^z \tag{9b}$$

If absorption-band shapes of both parallel and perpendicular types are observed, we can determine τ_r^x and τ_r^z from Eq. (9) provided that the contributions of the vibrational relaxation are negligibly small.

On the other hand, when the contribution of the vibrational relaxation is predominant, an observed half-width, $\Delta\nu_{1/2}$, is directly related to the vibrational relaxation time, τ_v. At first, let us confine ourselves to one type of vibrational relaxation—the transfer of vibrational energy from a vibrationally-excited molecule to its surroundings by resonance between oscillators of the same type. For this particular case, Valiev[13] evaluated the probability per unit time that an excited molecule undergoes a transition $n\rightarrow n-1$. Some further modification of Eq. (24) of the reference leads to, for a fundamental band:

$$W_{1-0} = \frac{c}{2\pi}\sqrt{\rho\frac{c_m}{3W_m}}S\cdot\Gamma \tag{10}$$

where c is the velocity of light (cm/sec); ρ, the density of a solute itself (g/cm^3); W_m, the molar weight of a solute (g/mol); c_m, the molar concentration of a solution (mol/cm^3), and Γ, the absolute intensity of a vibration band (cm^2/mol). It is found that n_i' of Eq. (24) of the reference should be replaced by a factor, S, defined by:

$$S = \frac{1}{2}\left(1 + \frac{1}{\tanh(\hbar\omega_i/2kT)}\right) \tag{11}$$

This arises from the fact that, in the derivation of Eq. (24) of the reference,[13] only one transition, $n'-1\rightarrow n'$, is taken into account for the surrounding molecules. Actually, all the transitions, $0\rightarrow1$, $1\rightarrow2$, $2\rightarrow3$, $\cdots$ *etc.*, should be considered. Moreover, Valiev multiplies Eq. (10) by the probability of a molecule being in a n-th vibrational state, or by the Boltzmann factor. However, as the quantity we need is not a joint probability but a condition probability that the vibrational energy of a molecule relaxes if it is in a state n at time zero, multiplication by the Boltzmann factor is not necessary. A little observation of Eq. (10) leads to the conclusion that the vibrational width depends on both the vibrational intensity and the molar concentration of a solute. In the case of liquid carbon disulfide, where $W_m=76.14$, $\rho=1.2634$, and $c_m=\rho/W_m$, an absolute intensity of 4×10^3 cm^2/mol corresponds to 1 cm^{-1} of the W_{1-0} of Eq. (10) if S is put equal to 1.

In case where the contributions of vibrational and reorientational relaxations to the band shapes are comparable, the explanation of a half-width is not straightforward. However, it is very probable that the rate of reorientation depends little upon the molar concentration. If so, observations of half-widths for various concentrations can be useful in identifying vibrational and reorientational widths, because a vibrational width is concentration-dependent.

Experimental

The carbon disulfide and chloroform used in the present work were commercial products. Prior to each observation, samples were purified following the procedures described in a reference.[15]

The infrared spectra were recorded by the use of a Perkin-Elmer 112G single-beam infrared spectrometer and a Perkin-Elmer 12C single-beam infrared spectrometer mounted with a CsBr prism. These spectrometers had been carefully modified to eliminate the effect of stray light or thermal emission originating from the spectrometers themselves. The spectrometers were operated with a resolution of about 2 cm^{-1} and at room temperature (23°C). The thicknesses of the sample cell were determined by means of the interference fringes. The observed spectra of ν_2 (the CSC bending vibration) of liquid carbon disulfide are shown in Fig. 1. The spectra were corrected for the dielectric field using the method described in the Appendix. Measurements were also made for ν_2 of carbon disulfide in chloroform solutions (80, 60, 40, 20, and 0.6 mol%).

The spectra for the ν_3 (the C–S antisymmetric stretching) of carbon disulfide were recorded only for dilute solutions because of its very strong intensity. For higher concentrations, the ATR data observed by William Krueger of the University of Minnesota were used.[16] In Fig. 2, the observed

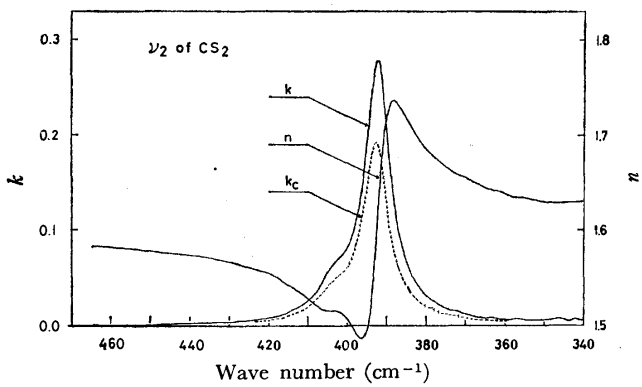

Fig. 1. Absorption and refractive indices for ν_2 band of liquid carbon disulfide. k: absorption index, n: refractive index, k_c: corrected absorption index.

15) "Organic Solvents" Clarendon Press, Oxford, (1935).
16) W. C. Krueger, Thesis submitted to the University of Minnesota (1966).

spectra for dilute solutions are illustrated. In this case, the dielectric-field correction was rather straightforward, because the refractive indices are also available from the ATR data. The effect of the slit function on the observed band shapes was ascertained to be small for both ν_2 and ν_3.

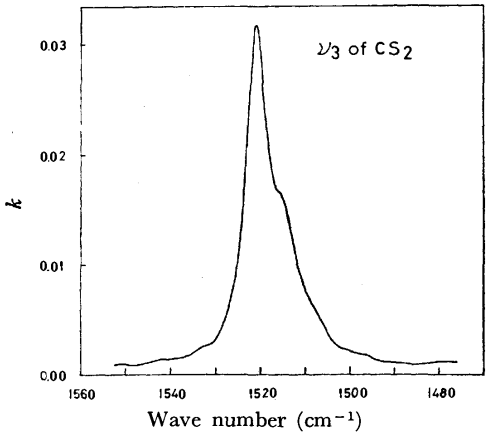

Fig. 2. Absorption index for ν_3 band of carbon disulfide in chloroform solution (0.6 mol%).

Discussion

Band Shape and Evaluation of Half-band-width. As both ν_2 and ν_3 suffer considerably from the effect of overlapping with other bands, especially in chloroform solutions, too detailed discussions of the band shapes might be misleading, especially for the wing parts of the bands. It may be concluded, however, that the band shape of the ν_2 of liquid carbon disulfide follows a good Lorentzian-type function. Figure 3 shows the logarithmic time-correlation function calculated from the observed $I(\omega)$ through Eq. (2). It may be seen that the logarithmic plot of the time-correlation function of ν_2 falls beautifully on a straight line. This justifies the assumption used in the derivation of Eq. (4) and, at the same time, indicates that free rotational reorientation does not play an important role in the relaxation process of liquid carbon disulfide.

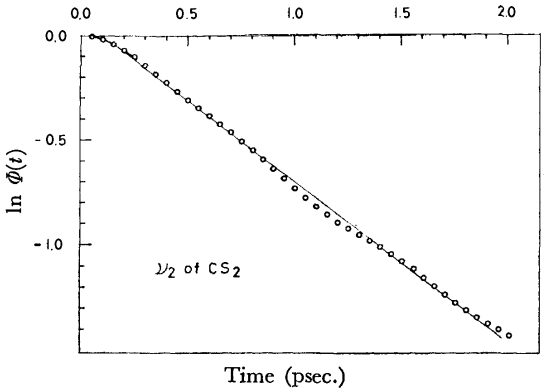

Fig. 3. Logarithmic time-correlation function for ν_2 band of liquid carbon disulfide.

It is known that the ν_3 band of carbon disulfide is overlapped with the hot band, $\nu_2+\nu_3-\nu_2$.[17] It may be seen from Fig. 2 that the separation of these two bands is not large enough for us to evaluate the half-band-width directly from the observed spectra. The situation is even more serious for higher concentrations. Therefore, we resolved the bands into two Lorentzian-type bands by means of numerical calculations. It seems reasonable to assume that the shapes of these bands are of a Lorentzian type because of the conclusion obtained from the ν_2 band.

The evaluated half-band-widths for ν_2 and ν_3 are listed in Table 1, together with the observed absolute intensity values.

Analysis of Half-band-width. It may be seen from Table 1 that the half-width of the ν_3 band changes its magnitude approximately from 5 to 20 cm^{-1} as the concentration of the chloroform solution increases, while that of ν_2 takes a constant value of about 7 cm^{-1}.

If the band-widths are treated as being completely determined by the reorientational motions of the solute, then the reorientational relaxation times around the principal axes can be evaluated from Eqs. (8) and (9):

TABLE 1. CONCENTRATION DEPENDENCE OF BAND SHAPE PARAMETERS.
(Numbers in parentheses indicate standard errors.)

	Γ 10^3 cm²/mol	mol%	$W_{obs}=\frac{1}{2}\Delta\nu_{1/2}$ cm^{-1}	W_v cm^{-1}	$W_{obs}-W_v$ cm^{-1}
ν_2	1.74 (0.06)	100	3.95 (0.04)	0.48 (0.00)	3.47 (0.04)
		80	3.69 (0.05)	0.42 (0.00)	3.27 (0.05)
		60	3.79 (0.04)	0.37 (0.00)	3.42 (0.04)
		40	3.58 (0.04)	0.27 (0.00)	3.31 (0.04)
		20	3.62 (0.08)	0.21 (0.00)	3.41 (0.08)
		0.6	0.42 (0.09)	0.03 (0.00)	3.39 (0.09)
ν_3	33.32 (1.37)	100	10.3 (0.5)	8.07 (0.32)	2.23 (0.82)
		80	9.67 (0.47)	7.01 (0.27)	2.66 (0.74)
		60	8.74 (0.42)	5.89 (0.21)	2.85 (0.63)
		40	7.50 (0.36)	4.67 (0.16)	2.83 (0.52)
		20	5.73 (0.28)	3.24 (0.11)	2.49 (0.39)
		0.6	3.20 (0.08)	0.35 (0.02)	2.67 (0.10)

17) D. F. Smith, Jr. and J. Overend, *Spectrochim. Acta*, **26A**, 2269 (1970).

$$(1/\tau_r)^x = \frac{1}{4}\Delta\nu_{1/2}^{(\nu_3)}$$

and:

$$(1/\tau_r)^z = \frac{1}{4}\left(2\Delta\nu_{1/2}^{(\nu_2)} - \Delta\nu_{1/2}^{(\nu_3)}\right) \quad (12)$$

where $\Delta\nu_{1/2}^{(\nu_2)}$ and $\Delta\nu_{1/2}^{(\nu_3)}$ are the half-widths of ν_2 and ν_3 respectively. The reciprocal relaxation times thus obtained are shown in Fig. 4 (designated as "apparent $(1/\tau_r)$").

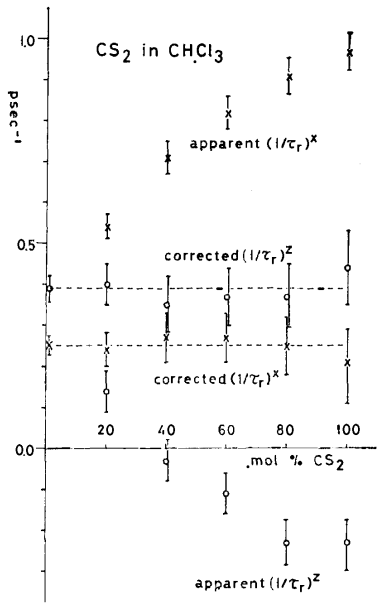

Fig. 4. Reciprocal reorientational relaxation times for carbon disulfide in chloroform solutions. Vertical lines indicate limit of experimental errors.

The results are peculiar in showing that:

(1) The $(1/\tau_r)^x$'s are larger than the $(1/\tau_r)^z$'s for all the concentrations, which means that carbon disulfide rotates around the molecular axis much slower than it does around the axis perpendicular to the molecular axis, and

(2) $(1/\tau_r)^z$ becomes negative for the higher concentrations. Thus, it may be concluded that the band-widths are not determined only by the reorientational relaxation.

Let us consider next the effect of the vibrational relaxation of the resonance type. The vibrational relaxation width, W_v, is calculated from Eq. (10) and the relation:

$$W_v = (1/\tau_v) = W_{1-0} \quad (13)$$

The results thus calculated are summarized in Table 1. It may be seen from the table that the calculated W_v's are smaller than the observed half-widths. If we assume that the contributions of vibrational and reorientational relaxations to the band-widths are comparable and that the difference between the observed band-width and the calculated W_v value originates from the reorientational relaxation, then the reciprocal reorientational relaxation time can be calculated from Eq. (12). The results are visualized in Fig. 4 (designated as "corrected $(1/\tau_r)$").

Now we can see from Fig. 4 that the corrected $(1/\tau_r)$ does not vary over the entire concentration range, $(1/\tau_r)^z$ being always greater than $(1/\tau_r)^x$. The results seem reasonable in the sense that the molecule rotates around the molecular axis more rapidly than it does around the axis perpendicular to the molecular axis. We are not going to assert too strongly that the difference between the observed band-width and W_v is due to the reorientational relaxation only. However, the constancy of the reciprocal relaxation times for all the concentrations seems to support this idea, for the reorientational relaxation time is expected to be rather independent of the concentration.

Table 2. Concentration dependence of reciprocal reorientational relaxation times.
(Numbers in parentheses indicate standard errors.)

mol%	$(1/\tau_r)^x$ psec^{-1}	$(1/\tau_r)^z$ psec^{-1}
100	0.21 (0.08)	0.44 (0.09)
80	0.25 (0.07)	0.37 (0.08)
60	0.27 (0·06)	0.37 (0.07)
40	0.27 (0.06)	0.35 (0.07)
20	0.24 (0.04)	0.40 (0.05)
0.6	0.25 (0.01)	0.39.0.03)

Conclusion

The mechanism of reorientation is mainly governed by the diffusional reorientation, rather than by the free rotation of the carbon disulfide molecule. This can be concluded from the band shape of ν_2.

It is evident from the analyses of the ν_2 and ν_3 bands that the band-widths of liquid carbon disulfide can not be explained only in terms of the reorientational relaxation. It can also be concluded that the vibrational relaxation of the resonance type can well explain the concentration dependence of the band-widths. The differences between the observed band-widths and W_v's may be ascribed to the reorientational relaxation.

The reciprocal reorientational relaxation times are calculated to be:

$$(1/\tau_r)^x \simeq 0.25 \text{ (psec}^{-1}\text{)}$$

and: $$(1/\tau_r)^z \simeq 0.39 \text{ (psec}^{-1}\text{)}$$

This means that carbon disulfide rotates by these rates around the molecular axis (z-axis) and the perpendicular axis (x,y-axes) respectively.

Appendix Dielectric-field Correction for Transmittance Data

It has previously been pointed out that dielectric-field correction is indispensable for band-shape analyses of condensed phases.[4,18,19] For this correction, a formula has been presented expressing the corrected absorption index, k_c, in terms of the observed absorption index, k, and the refractive index, n, assuming the Lorentz field for the internal field.[18] When k and n are measured simultaneously (*e. g.*, by the ATR method), k can be corrected at

18) A. A. Clifford and B. L. Crawford, *J. Phys. Chem.*, **70**, 1536 (1965).

19) T. Fujiyama and B. L. Crawford, Jr., *ibid.*, **72**, 2174 (1968).

each frequency. On the other hand, when the measurement of an absorption band is carried out by the use of the transmittance method, the correction can not be made straightforwardly. In this case, however, the following method may be conveniently used.

As is well known, n and k are related by the Kramers-Kronig dispersion formula:

$$n(\nu) = n_0 + \frac{2}{\pi}\int_0^\infty \frac{k(\nu')\nu'}{\nu'^2-\nu^2}d\nu'$$

Therefore, when reliable data of $k(\nu)$ are available, $n(\nu)$ can be calculated by this formula, and then $k(\nu)$ can be corrected at each frequency. In doing so, the most difficult problem is to determine the constant n_0. Generally, n_0 is not equal to the refractive index in the visible region or to the square root of the static dielectric constant. Furthermore, n_0 may take different values for different absorption bands. There is, in fact, no general way to estimate n_0. The only way to override this difficulty is to observe $n(\nu)$ experimentally for at least one point near the absorption band. Once n_0 is determined for an absorption band, the n_0 corresponding to the next lower-frequency band can be estimated as follows: Let ν of Kramers-Kronig's formula go to infinity; then

$$n(\nu) \to n_0 \quad (\nu\to\infty)$$

and if ν goes zero,

$$n(\nu) \to n_0 + \frac{2}{\pi}\int_0^\infty \frac{k(\nu')}{\nu'}d\nu' \quad (\nu\to 0)$$
$$\simeq n_0 + (c_m\Gamma/2\pi^2\nu_0)$$

where ν_0 is the resonance frequency in cm^{-1}, and Γ, the absolute intensity in cm^2/mol. Thus, the increment in n_0 by this absorption band, Δn, is $c_m\Gamma/2\pi^2\nu_0$. $n_0+\Delta n$ may be considered to be the n_0 for the next-lower-frequency band. In Fig. 1, the $n(\nu)$ curve is calculated using $n_0=1.6000\pm 0.0046$, which is estimated in this way from the $n(\nu)$ and $k(\nu)$ curves of ν_3 as observed by the ATR method.

The authors are indebted to all the members of Shimanouchi Laboratory for their helpful correspondence about this work. They are particularly grateful to Professor Takehiko Shimanouchi of the University of Tokyo for giving them the opportunity of publishing this work.

BULLETIN OF THE CHEMICAL SOCIETY OF JAPAN, VOL. 45, 2974—2976 (1972)

Vibronic Bands of Phosphorescence Spectra of Quinoxaline in Host Crystals

Kasumi IKEGAMI and Mitsuo ITO

Department of Chemistry, Faculty of Science, Tohoku University, Sendai

(Received January 11, 1972)

The polarized phosphorescence spectra of quinoxaline in durene and *p*-dimethoxybenzene host crystals were observed at 4.2°K, and the vibronic bands of the phosphorescence spectrum were assigned. It was found that the intensity of vibronic bands polarized along long molecular axis arises from the vibronic spin-orbit coupling routes

$$^1A_2(\pi, \pi^*) \begin{cases} \xrightarrow{b_1} {}^1B_1 \\ \xrightarrow{R_z} {}^3A_2 \end{cases} \begin{cases} \xrightarrow{R_z} \\ \xrightarrow{b_1} \end{cases} {}^3B_2(\pi, \pi^*)$$

and the intensity of vibronic bands polarized along short molecular axis from the routes

$$^1B_2(\pi, \pi^*) \begin{cases} \xrightarrow{R_z} {}^3B_1 \\ \xrightarrow{a_2} {}^1B_1 \end{cases} \begin{cases} \xrightarrow{a_2} \\ \xrightarrow{R_z} \end{cases} {}^3B_2(\pi, \pi^*)$$

It was concluded that all the vibronic phosphorescence bands of quinoxaline originate from the Tz zero-field sublevel. This is in line with the results of El-Sayed and Brewer deduced from the magnetic field effect on the phosphorescence spectrum.

Effects of vibronic coupling or vibronic spin-orbit coupling on the phosphorescence spectrum of quinoxaline have been studied by several investigators using the method of photoselection[1,2] or with mixed crystal.[3,4] However, discussion is limited because of the ambiguity in the assignment of the fundamental vibrational frequencies. In this work the ploarized phosphorescence spectra of quinoxaline in several host crystals have been observed at liquid helium temperature, the orgin in vibronic bands being discussed.

1) M. A. El-Sayed and R. G. Brewer, *J. Chem. Phys.*, **39**, 1623 (1963).
2) E. C. Lim and J. M. H. Yu, *ibid.*, **49**, 3878 (1968).
3) N. K. Chaudhuri and M. A. El-Sayed, *ibid.*, **44**, 3728 (1966).
4) S. M. Ziegler and M. A. El-Sayed, *ibid.*, **52**, 3257 (1970).

Experimental

The polarized phosphorescence spectra were measured photographically with a Shimadzu GE-100 grating spectrograph (of reciprocal linear dispersion of 8.4 A/mm in the first order) equipped with a Wollaston prism behind entrance slit. A 500 W Hg lamp was used as an exciting source. A quarter-wave plate was placed behind the slit of the spectrograph for correction of the polarization characteristic of the spectrograph. Photoelectric recording of the spectra was also carried out with a Narumi 750Z—1200 grating double monochromator having a reciprocal linear dispersion of 11 A/mm in the first order.

Quinoxaline (Tokyo Kasei Co.) was purified by repeated recrystallization and distillation under several times reduced pressure. Durene and *p*-dimethoxybenzene used as host

crystals were purified by recrystallization and zone refining.

The single crystals were obtained by cutting large crystals grown by the Bridgeman method. The crystallographic axes were determined by observation of isogyric pattern under a polarizing microscope and by X-ray diffraction. The crystal was fixed on the copper plate of a helium cryostat and immersed directly into liquid helium.

Results and Discussion

The *p*-dimethoxybenzene crystal belong to a space group $V_h^{15}(P_{bca})$ with four molecules in a unit cell.[5] Projection of the molecule on plane *ab* of the crystal is shown in Fig. 1. The durene crystal belongs to a space group $C_{2h}^5(P_{2_1/a})$ with two molecules in a unit cell.[6,7] Rrojection of the molecules on plane *bc** of the crystal is shown in Fig. 2. In the mixed crystals of quinoxaline, we assumed that quinoxaline molecule occupies substitutional positions in the host crystals with the molecular orientation in which the *L,M,N* axes of quinoxaline molecule coincide with the *L,M,N* axes of the host molecules, respectively.

We see from Fig. 1 that when the polarized spectra of the guest molecule are observed on plane *ab* of *p*-dimethoxybenzene crystal, it is possible to distinguish the in-plane and out-of-plane polarized transitions of the guest molecule. The polarized phosphorescence spectra of quinoxaline on plane *ab* of *p*-dimethoxybenzene crystal at 4.2°K is shown in Fig. 3. It is clear that the bands 0-0, 0-527, and 0-603 cm^{-1} are out-of-plane polarized ones and the 0-466, 0-490, 0-635, and 0-872 cm^{-1} in-plane polarized ones. The vibrational frequency 527 cm^{-1} forms a long progression starting from band 0-0 and corresponds to the strong Raman line of 535 cm^{-1}.[8] Band 0-603 cm^{-1} is also the origin of a short progression of 527 cm^{-1}. Since bands 0-527 and 0-603 cm^{-1} behave in a similar way to band 0-0, the frequencies of 527 and 603 cm^{-1} are assigned to vibrational mode a_1.

On the other hand, when the polarized spectra are measured on plane *bc** of durene crystal, the short axis polarized transition can be distinguished from the long axis and out-of-plane plarized transitions (Fig. 2). The polarized phosphorescence spectra on plane *bc** of durene crystal is shown in Fig. 4. We see that bands

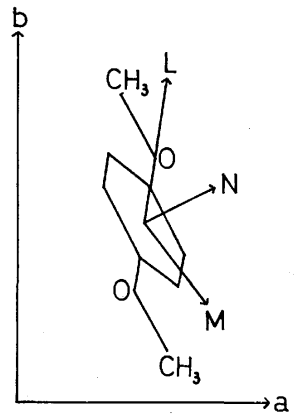

Fig. 1. Molecular projection on *ab* plane of *p*-dimethoxybenzene crystal.

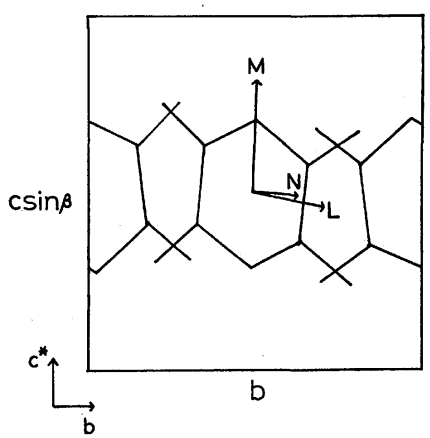

Fig. 2. Molecular projection on *bc** plane of durene crystal.

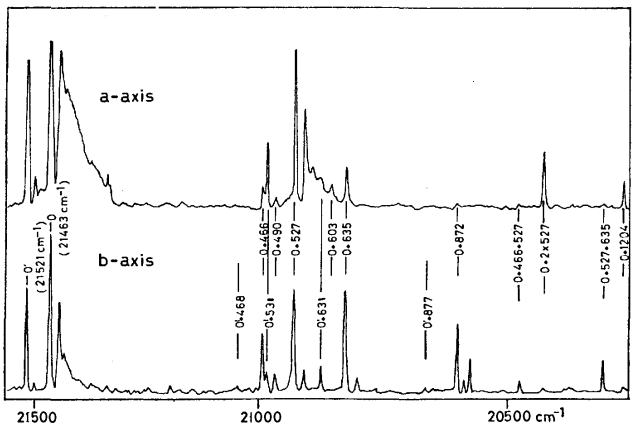

Fig. 3. The microphotometer tracing of the polarized phosphorescence spectra of quinoxaline in *p*-dimethoxybenzene host crystal at 4.2°K.

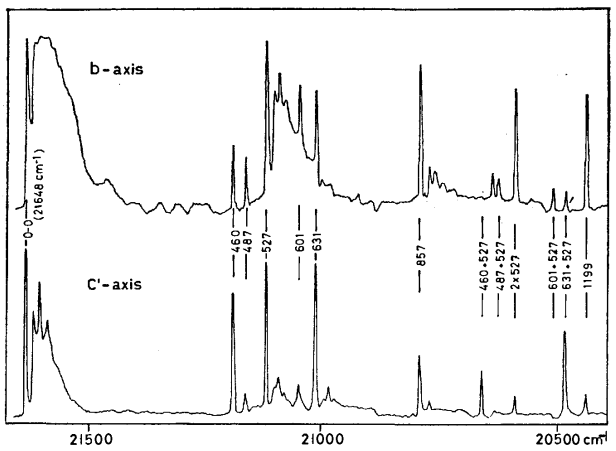

Fig. 4. The microphotometer tracing of the polarized phosphorescence spectra of quinoxaline in durene host crystal at 4.2°K.

5) T. H. Goodwin, M. Przybylska, and J. M. Robertson, *Acta Crystallogr.*, **3**, 279 (1950).
6) J. M. Robertson, *Proc. Roy. Soc. Ser. A*, **141**, 594 (1933).
7) J. M. Robertson, *ibid.*, **142**, 659 (1933).
8) R. W. Mitchell, R. W. Glass, and J. A. Meritt, *J. Mol. Spectrosc.*, **36**, 310 (1970).

TABLE 1. THE MAIN VIBRONIC BANDS OF QUINOXALINE PHOSPHORESCENCE IN *p*-DIMETHOXYBENZENE HOST CRYSTAL AT 4.2°K AND THEIR POLARIZATIONS

Vibronic bands of quinoxaline in *p*-dimethoxybenzene host crystal (cm^{-1})	Polarization direction of the vibronic band	Assignment of fundamental vibration involved
0-466	*Y*	a_2
0-490	*Z*	b_1
0-527	*X*	a_1
0-603	*X*	a_1
0-635	*Y*	a_2
0-872	*Z*	b_1
0-1204	*X*	a_1

0-466 and 0-635 cm^{-1} are the short polarized along axis. The remaining bands of 0-490 and 0-872 cm^{-1} are necessarily assigned to be polarized along the long axis. The polarization direction of the individual vibronic bands are given in Table 1.

Let us consider the symmetry species of the vibrations involved in the vibronic bands. In their study of the vapor absorption spectrum of quinoxaline, Glass *et al.* reported a hot band involving the vibration of 454 cm^{-1} which assigned to mode a_2 from the rotational contour of the band.[9] On the other hand, the 0-635 cm^{-1} band behaves in a similar way to the 0-466 cm^{-1} bands in the various polarization spectra, and thus the frequencies of 466 and 635 cm^{-1} are assigned to mode a_2. The vibrational frequencies of 490 and 872 cm^{-1} are assigned to mode b_1 based on the assignment by Mitchel *et al.*[8] The assignments are given in Table 1. It was found that the vibronic bands involving fundamental vibrations a_1, a_2, and b_1 are out-of-plane (*X*), short-axis (*Y*) and long-axis (*Z*) polarized, respectively.

The low-lying electronic states of quinoxaline are shown schematically in Fig. 5. The lowest singlet excited state of quinoxaline molecule is $^1B_1(n,\pi^*)$. The two higher states are $^1A_1(\pi,\pi^*)$ and $^1B_2(\pi,\pi^*)$ which correspond to $^1B_{1u}$ and $^1B_{2u}$ of naphthalene, respectively. For the triplet states, the lowest is established to be $^3B_2(\pi,\pi^*)$. $^3B_1(n,\pi^*)$ seems to lie at a slightly higher energy than $^3B_2(\pi,\pi^*)$ although its existence is not yet confirmed experimentally. Since the spin-orbit coupling between n,π^* and π,π^* is generally much greater than that between $\pi,\pi^*,^1B_1(n,\pi^*)$ is expected to be the intensity source of band 0-0 and the vibronic bands involving fundamental vibration a_1.

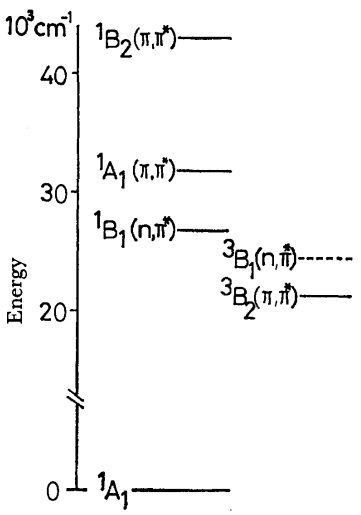

Fig. 5. The low-lying electronic states of quinoxaline.

The expectation is confirmed by our observation that they are out-of-plane polarized bands. Thus for band 0-0 and the vibronic bands involving fundamental vibration a_1, the route $^1B_1(n,\pi^*) \overset{R_z}{\text{----}} {}^3B_2(\pi,\pi^*)$ is given,[10] where R_z is rotation operator of the spin-orbit coupling. For occurrence of the vibronic bands involving nontotally symmetric vibrations, we must consider the spin-orbit interaction as well as the vibronic interaction. For the long-axis polarized vibronic bands involving vibration b_1(0-490, 0-872) the following vibronic spin-orbit coupling routes are most probable.

$$^1A_1(\pi,\pi^*) \begin{cases} \xrightarrow{b_1} {}^1B_1(n,\pi^*) \xrightarrow{R_z} \\ \xrightarrow{R_z} {}^3A_2(n,\pi^*) \xrightarrow{b_1} \end{cases} {}^3B_2(\pi,\pi^*)$$

For the short-axis polarized bands involving vibtation a_2(0-466, 0-635), the following routes are given.

$$^1B_2(\pi,\pi^*) \begin{cases} \xrightarrow{R_z} {}^3B_1(n,\pi^*) \xrightarrow{a_2} \\ \xrightarrow{a_2} {}^1B_1(n,\pi^*) \xrightarrow{R_z} \end{cases} {}^3B_2(\pi,\pi^*)$$

It is seen that all the routes commonly involve the spin-orbit coupling through R_z. This means that the phosphorescence of all the vibronic bands originates from Tz sublevel of state $^3B_2$. This supports the results given by Zigler and El-Sayed that band 0-0 and all the vibronic bands occur from Tz sublevel in study of the magnetic field effect.[11]

The authors wish to thank Dr. N. Mikami for helpful discussions and advice.

9) R. W. Glass, L. C. Robertson, and J. A. Meritt, *J. Chem. Phys.* **53**, 3877 (1970).

10) M. A. El-Sayed and R. G. Brewer, *ibid.*, **39**, 1623 (1963).

11) S. M. Ziegler and M. A. El-Sayed, *ibid.*, **52**, 3257 (1970).

Rate-controlling Processes in the Phosphidation of Copper by Phosphorus Vapor

Yoshinori SASAKI and Shiro UEDA

Department of Synthetic Chemistry, Faculty of Engineering, Chiba University, Yayoi-cho, Chiba

(Received October 12, 1971)

The phosphidation kinetics of a copper exposed to a phosphorus atmosphere from 1 to 10 Torr absolute pressure in the temperature range of 150—250°C have been determined with a closed system. The reaction rate in the earlier periods of time was linear and, subsequently, parabolic; therefore, it can be considered that the rate-determining process changes from adsorption to diffusion. The linear rate constants were expressed as a function of the phosphorus pressure on the basis of the Langmuir adsorption isotherm. The P_4 molecule is chemically adsorbed as two $-P=P-$, whereas at higher temperatures and pressures the solubility process appears to be predominant. From the phosphorus distribution in cross sections of scaling films, it has been revealed that, in the adsorptoin-controlled regions, the phosphorus content is maintained at a constant concentration, corresponding to Cu_3P, and that, in the diffusion-controlled regions, solid solutions more rich in phosphorus than Cu_3P are formed at the outer layers. The faceted crystals of Cu_3P have sometimes developed with an orientation of the (300) plane, depending on the reaction conditions.

In the nineteenth century, the existence of copper phosphides with various compositions, namely, Cu_3P, Cu_5P_2, Cu_2P, Cu_3P_2, CuP, and CuP_2, was reported. In 1907, Heyn and Bauer[1] determined the equilibrium diagram of copper-phosphorus systems up to 15 wt% phosphorus. The rate of the combination of copper and phosphorus was first investigated by Edwards and Murphy.[2] Haraldsen[3] pointed out, on the basis of the thermal analysis and the X-ray diffraction, that the CuP_3 and Cu_2P_5 compounds are solid solutions, in which a phosphorus dissolves in any CuP_2-matrix, and concluded that no compounds other than Cu_3P and CuP_2 exist as copper phosphides. The crystal structures of Cu_3P[3] and CuP_2[4], the magnetic[3] and electrical[5] properties of these two phosphides, and the heats of formation[6] of the two have been investigated.

The present authors reported previously[7] the rate of the reaction of copper with gaseous phosphorus, as determined by gravimetric means, using a spring-helix method, in a flow system in the temperature range of 400—650°C and under the partial pressures of 0.8 to 110 Torr. According to those results, the copper was linearly phosphidized in the early stages of reaction, and when the phosphide layers reached a certain thickness, a transition from linear to parabolic behavior took place.

The present paper will deal with the behavior of copper at comparatively lower temperatures (150—250°C) in a gaseous phosphorus at pressures of 1 to 10 Torr, as determined by means of a sealed-tube method.[8]

Experimental Details

Materials. A copper sheet 0.5 mm thick was cut in the form of rectangles of approximately 7 by 25 mm. The purity was about 99.95 wt%; this sheet contains as much as 0.05 wt% phosphorus as an impurity. The copper coupons were abraded lightly with emery paper, defatted with trichloroethylene, and polished chemically for 120 sec at 70°C in a solution consisting of 200 parts (by volume) of 85% H_3PO_4, 100 parts of 60% HNO_3 and 120 parts of glacial acetic acid. The coupon specimens thus cleaned were then weighed, and their apparent geometric surface areas were determined.

Red phosphorus was treated with a boiling 10% aqueous solution of sodium hydroxide for about 5 hr, and then with dilute hydrochloric acid. After being washed with distilled water, the refined red phosphorus was stored in a desiccator with phosphorus pentoxide.

Methods. A closed reaction system was used for the phosphidation. Figure 1 represents schematically the apparatus employed; it consists of a tube placed over two temperature zones and controlled within variations of less than 3°C, the first zone being used to heat the sample copper sheet in the sealed tube, and the second zone, to control the vapor pressure of phosphorus. The vapor pressure of phosphorus is governed by the minimum temperature in the closed system.

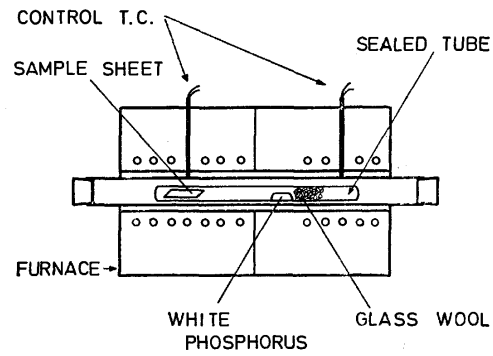

Fig. 1. Schematic drawing of the phosphidation apparatus.

The vapor pressure, P_{Torr}, of white phosphorus is given as a function of the absolute temperature, T, as follows:[9]

$$\log P_{Torr} = 7.808 - 2.729 \times 10^3/T,$$

$$349.6° \text{ (1 Torr)} \leq T \leq 553°K \text{ (760 Torr)}$$

This equation was used to obtain the desired pressure.

1) E. Heyn and O. Bauer, *Z. Anorg. Allgem. Chem.*, **52**, 129 (1907).
2) C. A. Edwards and A. J. Murphy, *J. Inst. Metals* (London), **27**, 183 (1922).
3) H. Haraldsen, *Z. Anorg. Allgem. Chem.*, **240**, 337 (1939).
4) O. Olofsson, *Acta Chem. Scand.*, **19**, 229 (1965).
5) R. Juza and K. Bär, *Z. Anorg. Allgem. Chem.*, **283**, 230 (1956).
6) F. Weibke and G. Schrag, *Z. Elektrochem.*, **47**, 222 (1941).
7) S. Ueda, Y. Sasaki, M. Matsuura, and S. Nishimura, *J. Electrochem. Soc.*, **117**, 84 (1970).
8) Y. Sasaki, A. Kato, and S. Ueda, *ibid.*, **118**, 101 (1971).
9) D. R. Stull, *Ind. Eng. Chem.*, **39**, 540 (1947).

The gaseous phosphorus molecule in the form of symmetrical P_4 tetrahedra dissociates into P_2 molecules according to the following equation[10]:

$$\log K_{atm} = \log (P_d^2/P_t) = 7.5787 - 11489/T°K$$

where P_d and P_t denote the pressures, in atmospheres, of the diatomic and tetratomic molecules respectively. Therefore, for the temperature region of 150—250°C employed in this study, the phosphorus vapor can be regarded as being made up of P_4 molecules.

The sealed tube containing the copper specimen and white phosphorus was prepared as follows. A moderate amount of the refined red phosphorus was introduced into a one-side-closed Pyrex tube (inside diameter: 7 mm). Some clean glass wool was packed in, and then the copper specimen was put in this tube. This tube was evacuated to 10^{-2} Torr, then filled to 1 atm with argon gas purified by having been passed through phosphorus pentoxide and heated active copper, and finally reevacuated. The evacuating and the filling were repeated five times at 200°C in order to remove any moisture, oxygen, and other gaseous impurities adsorbed on the red phosphorus, the glass wool, and the inner wall of the tube. In this case, only the copper specimen placed near the entrance end of the tube was not heated. After these operations, this tube was sealed under a vacuum.

Although red phosphorus is generally amorphous, it can also have various crystal structures; hence, a conversion from red to white phosphorus is necessary to secure stable pressures of phosphorus vapor. In this study, the phosphorus vapor which evolved when the red phosphorus was heated in the sealed tube was condensed into white phosphorus by water cooling in the neighborhood of the packed glass wool.

After selected periods of time of the phosphidation, the tube was taken out of the furnace; the end of the tube opposite the specimen was immediately quenched in order to avoid the condensation of the phosphorus vapor on the phosphidized specimen. Then, this was removed from the sealed tube and weighed. No appreciable attack on the Pyrex tube was detected.

The constituents of the corrosion products were identified by X-ray analyses. Information about the diffusion profiles of the phosphorus across the scale was obtained by means of a scanning electron microscope (JSM-U3, Japan Electron Optics Laboratory Co., Ltd.).

Experimental Results

Kinetics. The results are based on the experimental observations of copper coupons from 150° to 250°C at absolute phosphorus pressures of 1 to 10 Torr. These are plotted in Figs. 2 and 3 as the log of the weight gain per unit area *vs.* the log of the reaction time. The points represented are scattered. It should be noted that each point was obtained by phosphidizing an individual specimen.

The rate of phosphidation obviously increases with an increase in the temperature and with an increase in the phosphorus pressure. Generally, at the temperatures and pressures investigated, copper was found to phosphidize according to the linear mechanism during the first periods of time, showing a phase-boundary-control mechanism. However, when the thickness of the phosphide layers reached a certain

10) J. R. Van Wazer, "Phosphorus and Its Compounds," Vol. 1, Interscience Publishers, New York, N. Y. (1958).

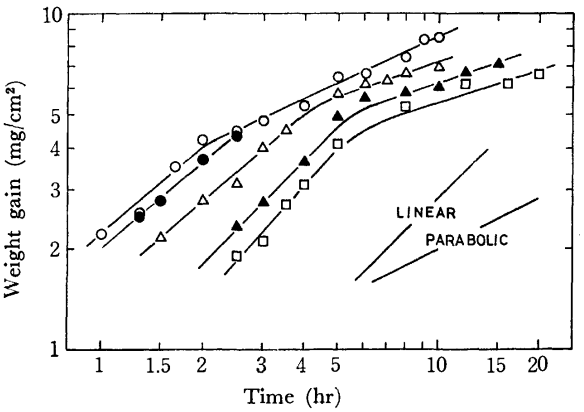

Fig. 2. Phosphidation of copper under various phosphorus pressures at 150°C; ○: 10; ●: 7; △: 4; ▲: 2; □: 1 Torr.

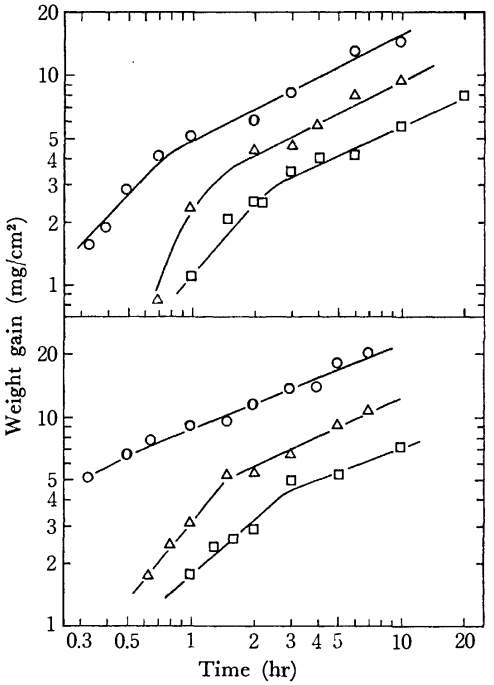

Fig. 3. Phosphidation of copper at 200° (top) and 250°C (bottom): The same symbols as in Fig. 2.

TABLE 1. LINEAR AND PARABOLIC RATE CONSTANTS FOR THE PHOSPHIDATION OF COPPER

Temp (°C)	Pressure (Torr)	$K_l \times 10^5$ (g/cm²-min)	$K_p \times 10^8$ (g²/cm⁴-min)
150	1	1.28±0.08	2.58±0.42
	2	1.57±0.07	4.08±0.58
	4	2.20±0.13	4.67±0.67
	7	3.06±0.15	—
	10	3.62±0.12	11.8 ±1.2
200	1	2.01±0.24	5.42±0.41
	4	3.75±0.33	17.0 ±1.7
	10	8.75±0.92	38.7 ±3.6
250	1	2.71±0.29	7.15±0.85
	4	5.17±0.67	26.0 ±1.0
	10	—	95.0 ±7.7

$w = K_l t$, $w^2 = K_p t + C$; w: weight gain, t: time, C: constant.

TABLE 2. COMPARISON OF INTERPLANAR SPACINGS OF THE PHOSPHIDES FORMED ON COPPER METAL (d-values, Å)

(I) Powder

D as typical in A-E	Cu_3P (Ref. 3)		CuP_2 (Ref. 4)	
		Plane		Plane
2.50 M	2.49 VS	(112)	2.89 VS	(111), ($11\bar{2}$)
2.31 M	2.29 S	(202)	2.68 W	($20\bar{2}$)
2.18 M	2.16 S	(211)	2.48 W	($21\bar{1}$)
2.01 VS	2.01 VS	(300)	2.22 M	($11\bar{3}$)
1.97 S	1.95 VS	(113)	1.85 W	($22\bar{1}$)
1.93 W	1.92 W	(212)	1.81 M	($20\bar{4}$), (202)
	1.74 W	(302)	1.79 M	($22\bar{2}$)
	1.70 M	(104)	1.78 W	($31\bar{1}$)
	1.62 W	(311)	1.73 W	(122)
	1.56 M	(222)		

A: 250°, 4 Torr, 1 hr (l); B: 250°, 4 Torr, 5 hr (p); C: 250°, 10 Torr, 3 hr (p); D: 150°, 10 Torr, 9 hr (p); E: 150°, 1 Torr, 3.5 hr (l).
(l): Linear rate portion, (p): Parabolic rate portion.
VS: Very strong, S, Strong, M: Medium, W: Weak, VW: Very weak.

(II) Surface (s) and Reverse side (r) of films

F		G		H		I		J	
s	r	s	r	s	r	s	r	s (porous, black)	s (flat, silver)
2.52 W	2.52 W			2.51 VW	2.52 W		2.51 M	2.52 W	
2.32 W	2.33 W			2.31 VW	2.33 W		2.32 W	2.32 VW	
2.19 W	2.19 W	2.18 W	2.19 W	2.19 M	2.19 M	2.18 VW	2.18 M	2.18 W	2.18 VW
		2.09 W						2.10 VW	
2.02 VS	2.03 VS	2.02 VS	2.02 VS	2.02 VS	2.02 VS	2.02 VS	2.02 VS	2.02 VS	2.01 VS
1.98 W	1.98 M	1.97 VW		1.97 VW	1.98 M		1.98 M	1.98 M	
1.93 VW	1.93 VW			1.93 VW	1.93 W		1.93 W	1.93 VW	1.89 VW
		1.82 W						1.82 W	
		1.64 VW	1.64 VW	1.63 VW	1.64 VW	1.63 VW	1.63 VW	1.64 VW	1.63 VW
					1.57 VW		1.57 W	1.57 VW	1.60 VW

F: 150°, 1 Torr, 2.5 hr (l); G: 200°, 10 Torr, 0.7 hr (l); H: 200°, 1 Torr, 6 hr (p); I: 250°, 10 Torr, 3 hr (p); J: 250°, 1 Torr, 1.6 hr (l).

Using a nickel-filtered copper radiation. The employed range of diffraction angle: $15° \leq \theta \leq 30°$.

value, the kinetics undergo a gradual transition from the linear to the parabolic law; the rate-controlling process changes from adsorption to diffusion. This fact is constituent with the previous conclusion reached under the experimental conditions of a 400—650°C temperature range and a pressure range of 0.8—110 Torr in a flow system.[7]

The values of the linear rate constant, K_l, and the parabolic one, K_p, are listed in Table 1.

Phase Identification and Scale Morphology. The phosphidation commenced with the growth of many phosphide crystallites. The coupon specimens have been phosphidized more rapidly at the edges and corners than at the centers of the flat faces. The scaling layers formed on the unchanged copper beneath were examined on a X-ray spectrometer, using nickel-filtered copper radiation. The d values, the interplanar spacings, of the phosphides obtained under various reaction conditions are summarized in Table 2. A division was made between the results obtained for pulverized phosphides and those obtained for the phosphide films. The diffraction pattern of the powder reflects the bulk of the scaling layers.

The known d values of Cu_3P[3] and CuP_2[4] are given in the same table. The d values obtained from the powder patterns revealed that all the scaling films are essentially Cu_3P. No special dependence of the X-ray patterns on the phosphorus pressure was observed.

According to Haraldsen,[3] the Cu_3P compound is silver grey, while CuP_2 is black. In the linear-rate portions, regardless of the reaction conditions, the phosphide surfaces are mostly silver; black products are rare. The silver surfaces are very flat, and the black, apparently porous. The silver products were almost completely Cu_3P. The black products were composed of the Cu_3P phase containing slight amounts of CuP_2 (Table 2-J). Otherwise, in the parabolic-rate portions, the surface products were almost all dark silver grey and were chiefly composed of Cu_3P, X-ray-spectrographically speaking.

The reverse sides of the phosphide films were obviously composed of Cu_3P; it is noteworthy that, at the phosphide/copper interface, the formation of Cu_3P takes place.

As examples, electron micrographs of the silver surfaces of the specimen phosphidized at 150°C for 2 hr in 7 Torr phosphorus are given in Fig. 4. The crystal features are clear; the upper micrograph shows many small pillars; the second, faceted grains which are the largest in faceted crystals grown under the reaction conditions employed and which have the orientation of the (300) plane; and the lower, a chain of mountains composed of numerous crystallites.

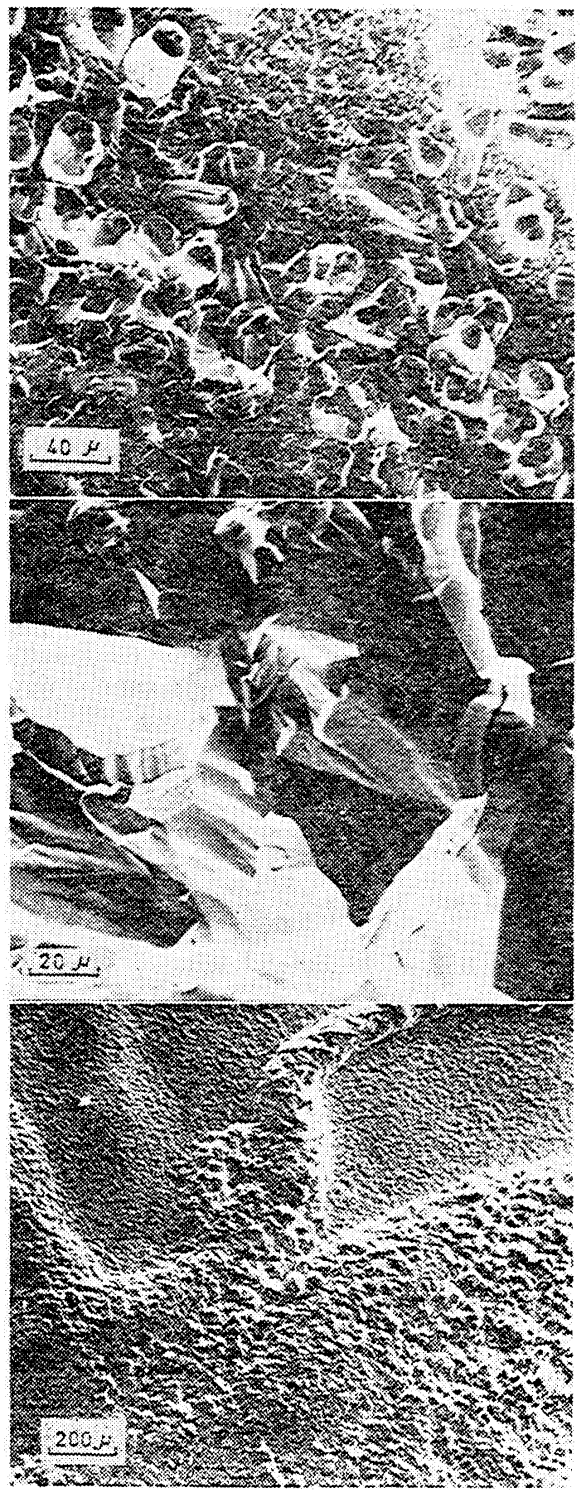

Fig. 4. Electron micrographs of the silver surface of the specimen phosphidized at 150°C for 2 hr in 7 Torr. Upper micrograph, showing many pillars; the second, the faceted crystals; and the lower, a chain of mountains.

These three micrographs were obtained from the different positions of the same phosphidized specimen. As has been indicated just above, all these products are made up of Cu_3P. Localized phosphidation leads to the growth of the porous black products containing CuP_2 as a higher phosphide, such as is exemplified in Fig. 5, in polarized light, showing tablet-like crystals.

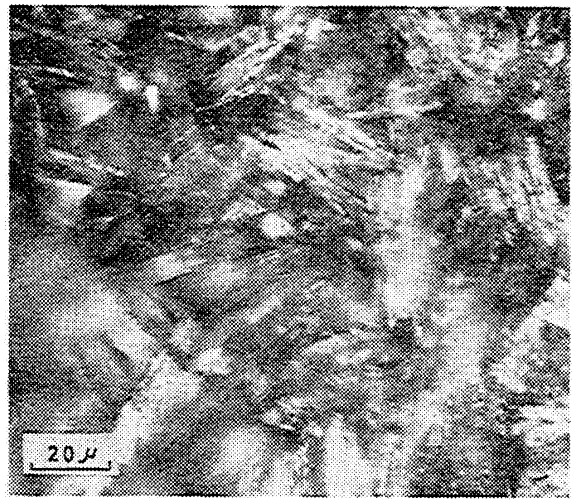

Fig. 5. Optical micrograph showing tablet-like crystals formed for 1.5 hr at 200°C in phosphorus vapor at 1 Torr, in polarized light.

Figure 6 represents a typical cross section of the scale, showing approximatly the formation of two scaling layers. Almost all the scaling films formed in the present study were similar to that shown in Fig. 6. In general, the scales are laminar; the generation of fissures was also faintly observed. This is apparently due to the tensile stresses produced in the outer layers of the scale by the outward pressure of the newly-forming phosphide.

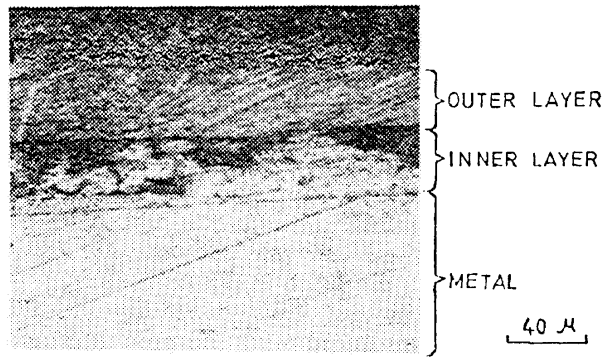

Fig. 6. The cross section of the specimen phosphidized at 150°C for 2.5 hr in 7 Torr, showing the scale to consist of two phosphide layers.

The distributions of phosphorus in phosphide films, obtained with the electron microprobe, suggest that, in the linear-rate portion (Fig. 7A), the phosphorus concentration is held constant, corresponding to Cu_3P, while in the parabolic-rate portion (Fig. 7C) the solid solutions that phosphorus dissolves in the Cu_3P-matrix are formed; the outer layers of the scale are more phos-

phorus-rich than the inner. It is reasonable that some phosphorus-activity gradient exists across the adherent layer, thus providing the driving force for the phosphorus flux required by the reactions at the inner interface. However, at the linear rate, since an adsorption process is slower than a diffusion process, it can be concluded that the content of phosphorus was maintained at the constant concentration. The reaction conditions of Fig. 7B exactly correspond to that of the neighborhood of a transition point from a linear to a parabolic rate (Fig. 2); this pattern may be due to the rate-determining diffusion.

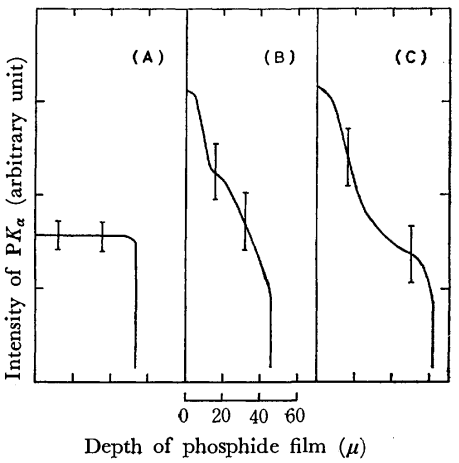

Fig. 7. The profiles of distribution of phosphorus in the phosphide films, obtained with electron microprobe facilities: (A) 250°C, 4 Torr, 1 hr; (B): 150°C, 7 Torr, 2.5 hr; (C): 150°C, 4 Torr, 5 hr.

Discussion

During the earlier stages of the reaction, the observed rates of phosphidation are linear; hence, the rate-determining step is presumably a surface reaction, that is, a phase-boundary reaction or an adsorption process. The generalized mechanism for such a heterogeneous surface reaction involves the following consecutive steps: (a) the diffusion of gas molecules to the surface, (b) the adsorption of gas on the surface, (c) a reaction on the surface, (d) the desorption of the products, and (e) the diffusion of the products away from the reacting surface.

The general form of the linear equation in terms of the weight gained, $w=K_l t$, is not suitable to account for the effect of the pressure at a constant temperature. It is possible to explain the pressure dependence of the reaction by assuming that (I) the phosphorus concentration at some interface is determined by an equilibrium adsorption process, and (II) the rate of the rate-determining process is a function of the phosphorus concentration at this interface. On this model, the interface concentration is given by a Langmuir isotherm. If an adsorbed molecule dissociates into n phosphorus atoms, the fractional coverage of the adsorption interface, θ, is given by:

$$\theta = \alpha P^{1/n}/(1+\alpha P^{1/n}) \qquad (1)$$

where P is the pressure of the vapor composed of P_4 molecules and where α is the chemisorption equilibrium constant, and where an interaction between the adsorbed matters is neglected completely. At low pressures, $\alpha P^{1/n} \ll 1$ and $\theta = \alpha P^{1/n}$.

Assuming that the chemical adsorption of the phosphidation obeys a Langmuir isotherm and that the rate of nucleation and the growth of phosphide nuclei are proportional to the number of chemisorbed phosphorus atoms, the linear rate may be rewritten as:

$$rate = dw/dt = k'\theta = k'\alpha P^{1/n}/(1+\alpha P^{1/n}) \qquad (2)$$

where k' is a specific rate constant.

As Fig. 8 demonstrates, plots of K_l against the pressure on a log-log scale give about 0.5 as a slope, namely, $n=2$ under the experimental conditions of "150°C, 1—10 Torr," "200°C, 1—4 Torr," and "250°C, 1—4 Torr." It should be emphasized that the adsorption takes place with the dissociation of the P_4 molecule into two –P=P– or P≡P. This can be explained in terms of the facility of the dissociation of P_4 into two P_2 molecules at high temperatures in the gas phase. For the pressure range of 1—2 Torr at 150°C, however, the slope appears to become somewhat smaller (the broken line in Fig. 8), showing $n=ca.$ 4; this suggests that the P_4 molecule probably adsorbs as four phosphorus atoms.

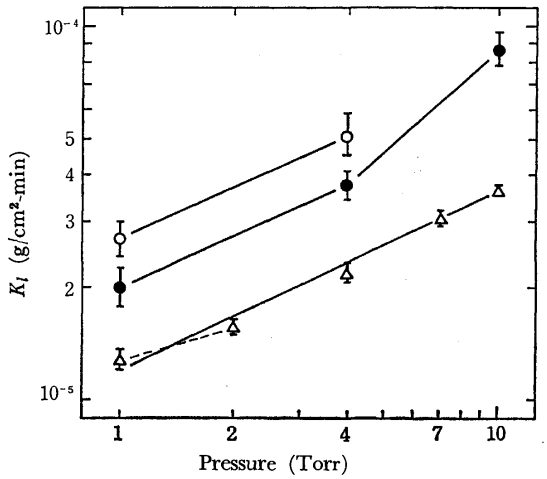

Fig. 8. Influence of the phosphorus pressure on the rate of phosphide formation on copper: ○ 250°; ● 200°; △ 150°C.

On the other hand, for 4—10 Torr at 200°C, the solubility process seems to govern the reaction, because n is approximately equal to unity. This process appears to be predominant at higher temperatures and pressures.

From the above, the processes of the phosphidation can be described as:

$$1/2\ P_4(g) + 2\ \text{Site(Cu or Phosphide)} \rightleftarrows \underset{\underset{\text{P-Site}}{\|}}{\text{P-Site}}\ (\text{Chemisorbed})$$

or; $1/4\ P_4(g) + \text{Site} \rightleftarrows \text{P-Site}$

$$\text{Site-P=P-Site or P-Site} + \text{Cu} \underset{\text{dissolution}}{\overset{\text{diffusion}}{\longrightarrow}} \text{Cu-P solid solution} \underset{\text{growth}}{\overset{\text{nucleation}}{\longrightarrow}} \text{Cu}_3\text{P and CuP}_2$$

In Table 3, the values of n, k', and α in Eq. (2), calculated from the observed values of K_l, are summarized.

The empirical equations obtained from Table 3 are based on a reaction mechanism in which the rate-controlling process is linearly dependent on the concentration of the phosphorus adsorbed as P_2 or P_4. Figure 9 indicates the curves of these equations. Since the original kinetic data are scattered, these calculated curves are of a low precision. The fractional coverages were found to be, for instance, 0.18 at 150°C–10 Torr, 0.12 at 200°C–10 Torr, and 0.05 at 250°C–1 Torr, on calculation.

Table 3. Values of n, k', and α

Temp (°C)	Pressure range (Torr)	n	$k' \times 10^4$ (g/cm²-min)	α
150	1—10	2	1.9	0.068
200	1—4	2	2.9	0.075
250	1—4	2	5.2	0.055
200	4—10	1	7.7	0.013

$K_l = k'\alpha P^{1/n}/(1+\alpha P^{1/n})$

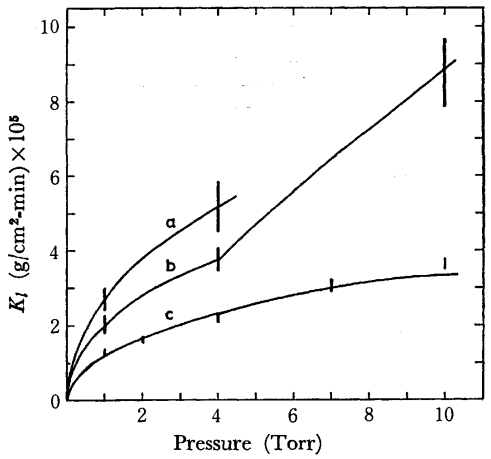

Fig. 9. The relations between K_l and the pressure of phosphorus vapor composed of P_4 molecule: a, 250°; b, 200°; c, 150°C. Curve: calculated, Rod: observed.

From Eq. (2) and the Clausius-Clapeyron equation, $q = RT^2(\mathrm{d}\ln P/\mathrm{d}T)$, the following relation can be derived;

$$q = -RT^2 n(\partial \ln \alpha/\partial T)_\theta \qquad (3)$$

Accordingly, $\alpha = \alpha_0 \exp(q/RTn)$, where α_0 is a constant and where q is the heat of adsorption. From the $\log \alpha$ —$1/T$ plots at $n=2$, it has become apparent that q falls into the category of approximately 2—6 kcal/mol.

Table 4. Activation energies of phosphidation of copper

Pressure (Torr)	Temp range (°C)	E_l (kcal/mol)	E_p (kcal/mol)
1	150—250	3.3±0.7	—
	150—200	—	6.2±1.9
	200—250	—	2.6±1.7
4	150—250	3.9±0.7	—
	150—200	—	10.7±1.8
	200—250	—	3.9±1.2
10	150—200	7.3±1.1	—
	150—250	—	9.3±0.8

E_l: derived from K_l, E_p: derived from K_p.

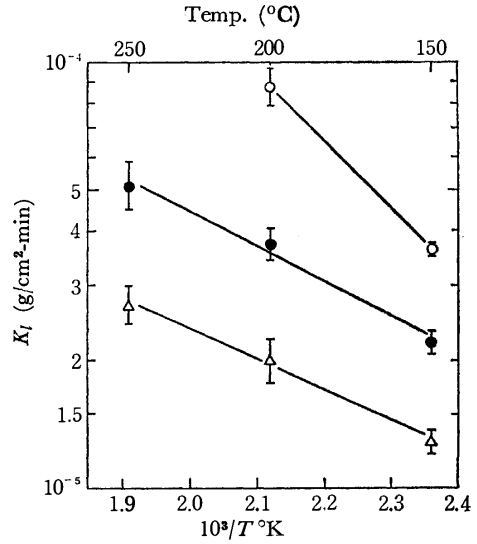

Fig. 10. Arrhenius plot for the linear phosphidation rate of copper: ○: 10; ●: 4; △: 1 Torr.

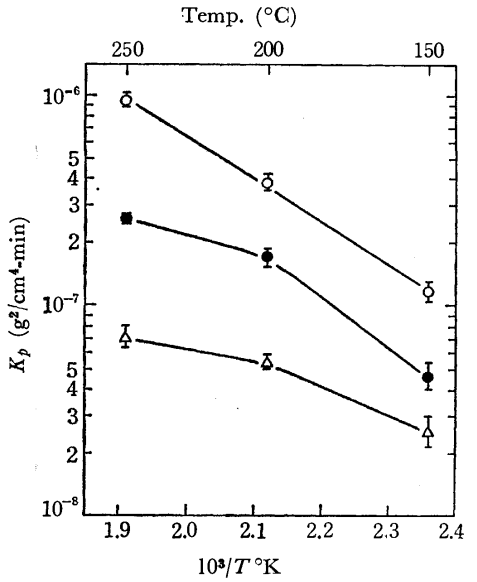

Fig. 11. Temperature dependence of the parabolic rate of phosphidation of copper: The same symbols as in Fig. 10.

The temperature dependence of K_l and K_p is plotted in Figs. 10 and 11. The apparent activation energies, E, evaluated from them are represented in Table 4.

The Eyring absolute-rate theory[11] was used here for a further discussion of the linear behavior. From the θ and the specific rate constant expressed as $\kappa(kT/h)\exp(-\Delta G^{\ddagger}/RT)$, the linear rate constant may be written as follows:

$$K_l = k_0\theta\kappa(kT/h)\exp(-\Delta G^{\ddagger}/RT)$$
$$= k_0\{\alpha P^{1/n}/(1+\alpha P^{1/n})\}\kappa(kT/h)\exp(\Delta S^{\ddagger}/R - \Delta H^{\ddagger}/RT) \qquad (4)$$

where k_0 is a proportionality constant; κ, the transmission coefficient; k, Boltzmann's constant; h, Planck's constant, and T and R, the usual significance.

11) S. Glasstone, K. J. Laidler, and H. Eyring, "The Theory of Rate Processes," McGraw-Hill Book Co., New York, N. Y. (1941).

In the case of the present phosphidation, the enthalpy of activation is expressed as $\Delta H^{0\neq}=E-RT$. Therefore,

$$K_l = k_0\theta\kappa e(kT/h)\exp(\Delta S^{0\neq}/R)exp(-E/RT) \quad (5)$$

In Eq. (5), the usual assumption is made that the κ is unity. By the division of the experimental values of K_l on the Arrhenius plot in Fig. 10 by θ, the relation can be obtained as independent of the change in the surface concentration of phosphorus. Figure 12 shows the $\log(K_l h/\theta kT)-1/T$ relationship, which gives about 3.6 kcal/mol as the free energy of activation, $\Delta G^{0\neq}$, for the 150—250°C range. Hence, since E_l is, for example, at 4 Torr and 200°C, 3.9 kcal/mol, the value of $\Delta H^{0\neq}$ is approximately 3 kcal/mol, and the entropy of activation, $\Delta S^{0\neq}$, is about —1.3 e. u. The negative value in $\Delta S^{0\neq}$ is thus reasonable.

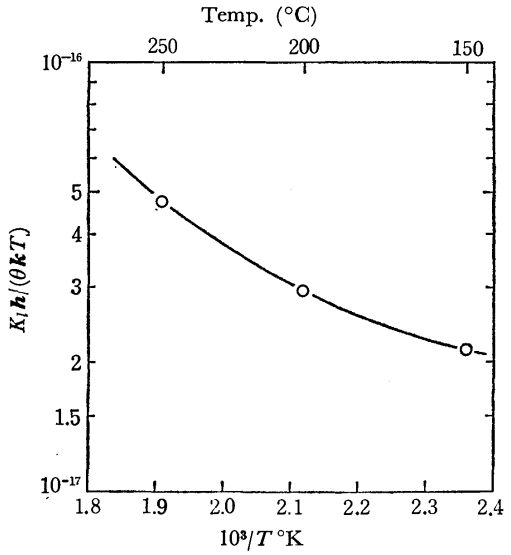

Fig. 12. Absolute rate of reaction of copper in phosphorus vapor *vs.* reciprocal temperature.

The decomposition of CuP_2 has been found to be as follows[3,10]:

$$12/5\ CuP_2(s) \rightleftarrows 4/5\ Cu_3P(s) + P_4(g)$$

$$\log P_{atm} = -11370/T°K + 10.946$$

where P_{atm} stands for the pressure of the P_4 vapor. In Fig. 13, the chemical potential diagram of the copper-phosphorus system reveals that the phase structure becames (P_4 vapor)/CuP_2/Cu_3P/Cu under the present experimental conditions, because the CuP_2 and Cu_3P compounds alone exist in the phosphorus-copper system. The formation of CuP_2 mentioned before can be explained on these thermodynamic grounds.

The pressure dependence of K_p is shown in Fig. 14, which yields following relations: $K_p \propto P^{0.6}$ at 150°, $K_p \propto P^{0.9}$ at 200°, and $K_p \propto P^{1.1}$ at 250°C. The Cu_3P compound was formed at the scale/metal interface. Even if the mass action law is applied as a *p*-type scale to the lattice-defect equation:

$$1/4\ P_4(g) \rightleftarrows Cu_3P + 3\ Cu\square' + 3\oplus,$$

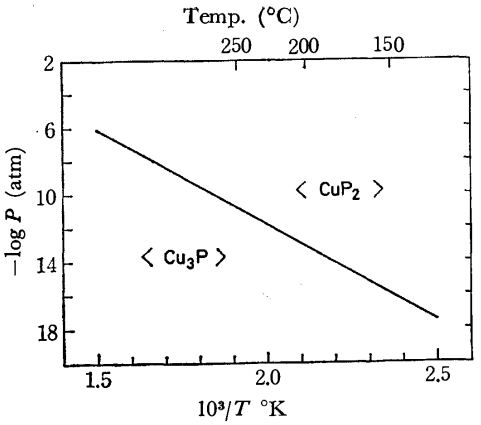

Fig. 13. Chemical potential diagram of the copper-phosphorus system.

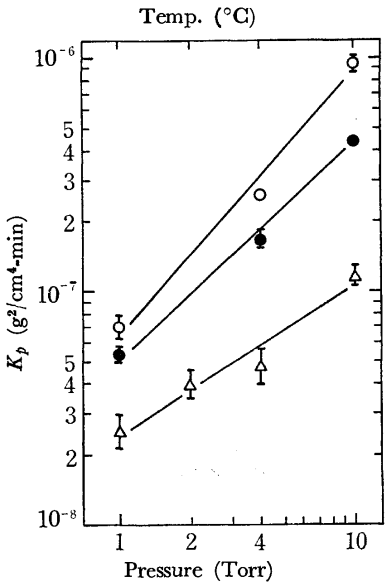

Fig. 14. Phosphorus-pressure dependence for the parabolic rate of phosphidation of copper: The same symbols as in Fig. 8.

the pressure dependence of the parabolic rate is only 1/24 power of the pressure. According to the phase diagram,[1,10] the solubility of phosphorus in metallic copper is about 0.5 wt% *viz.* 1 at% around 200°C. The higher pressure-dependence of K_p, shown above, can probably be attributed to the phosphorus-solubility process. The temperature dependence of K_p at 1 and 4 Torr (Fig. 11) gives two apparent activation energies; this fact may result from differences in the nucleation and growth of copper phosphides and in the solubility of phosphorus in metallic copper.

Although several explanations have been proposed, the fundamental mechanism underlying the phosphidation phenomena has hardly been clarified yet.

This study was supported in part by a Grant from the Ministry of Education.

Ternary Diffusion in the ^{20}Ne–^{22}Ne–CO_2 System

Yasumichi OISHI, Masayasu SUGISAKI, Yoshinobu KAMEI, and Yasuyuki SHONO

Department of Nuclear Engineering, Faculty of Engineering, Kyushu University, Fukuoka

(Received January 13, 1972)

Self-diffusion coefficients of CO_2 of the binary system of Ne and CO_2 were measured for the whole composition range at 25°C under 760 mmHg. The system was also analysed as a ternary system of ^{20}Ne, ^{22}Ne, and CO_2. The isotope separation of ^{20}Ne and ^{22}Ne during the course of diffusion was measured and analyzed by means of the ternary diffusion equations obtained by an extension of Darken's binary diffusion equation. The experimentally observed $^{22}Ne/^{20}Ne$ ratios agreed well with the values calculated by the equations. The results show that the concept of the intrinsic diffusion flux density, introduced by Darken for binary diffusion, is valid and applicable to ternary diffusion in the gaseous system.

Darken derived the following equation for the binary diffusion in a thermodynamically ideal system[1] in order to explain the Kirkendall effect which takes place in interdiffusion of a binary metallic alloy:

$$J_i = -D_i\frac{\partial C_i}{\partial x} + C_i v \tag{1}$$

where J is the diffusion flux density, D the intrinsic diffusion coefficient, C molar concentration, v the velocity of mass flow, and subscript i refers to component i. Eq. (1) is defined with respect to the volume center reference frame. It also holds with respect to the cell-fixed reference frame in the case where partial molar volumes of the respective components remain constant, *viz.*,

$$\sum C_i = C_0 = \text{constant} \tag{2}$$

The first term in Eq. (1) is the diffusion flux density relative to the mass flow velocity and is called intrinsic diffusion flux density. The magnitude of v is equal to the sum of intrinsic diffusion flux densities of both components, *i. e.* the difference of their absolute values, and can be represented by

$$v = \frac{1}{C_0}\left(D_1\frac{\partial C_1}{\partial x} + D_2\frac{\partial C_2}{\partial x}\right) \tag{3}$$

Substituting Eq. (3) in Eq. (1), Darken obtained

$$J_i = -(N_2D_1 + N_1D_2)\frac{\partial C_i}{\partial x} \tag{4}$$

where N_i is the mole fraction of the ith component. He also derived the following binary diffusion equation for a nonideal system:

$$J_i = -(N_2D_1 + N_1D_2)\frac{\partial C_i}{\partial x}\left(1+\frac{\mathrm{d}\ln\gamma_i}{\mathrm{d}\ln N_i}\right) \tag{5}$$

where γ_i is the activity coefficient of the ith component on the mole fraction basis.

Darken's binary diffusion equations have been tested with many metallic alloy systems, but the lack of thermodynamical information on metallic alloys has made quantitative validity of the equations ambiguous. Some binary organic liquid systems showed the validity of Darken's equation quantitatively[2] but not others.[3]

If Darken's analysis is sound for binary diffusion, it could be extended to ternary diffusion and also to general multicomponent diffusion. The purpose of present work is to confirm experimentally the validity of ternary diffusion equation obtained by extending Darken's binary diffusion equation.

In order to avoid a complex effect of thermodynamical nonideality, gaseous systems are utilized. The Kirkendall effect also was experimentally demonstrated for binary diffusion of gaseous system.[4]

We have employed the ^{20}Ne–^{22}Ne–CO_2 system. Validity of the derived ternary diffusion equations was confirmed by comparing the experimental gaseous compositions with the calculated ones for interdiffusion between CO_2 and mixture of ^{20}Ne and ^{22}Ne by a diaphragm-cell method.

Theoretical

A. Ternary Diffusion Equations in Terms of Intrinsic Diffusion Coefficients. If the system is thermodynamically ideal, Eq. (1) can also be applied to ternary diffusion. In this case, Eq. (3) should be replaced by the following equation.

$$v = \frac{1}{C_0}\left(D_1\frac{\partial C_1}{\partial x} + D_2\frac{\partial C_2}{\partial x} + D_3\frac{\partial C_3}{\partial x}\right) \tag{6}$$

If Eq. (2) also holds in a ternary system, we obtain

$$\sum\frac{\partial C_i}{\partial x} = 0 \tag{7}$$

Substitution of Eq. (6) in Eq. (1) with the use of Eq. (7) leads to

$$\left.\begin{aligned} J_1 &= -D_1\frac{\partial C_1}{\partial x} - N_1\left[(D_1-D_2)\frac{\partial C_2}{\partial x} + (D_1-D_3)\frac{\partial C_3}{\partial x}\right] \\ J_2 &= -D_2\frac{\partial C_2}{\partial x} - N_2\left[(D_2-D_3)\frac{\partial C_3}{\partial x} + (D_2-D_1)\frac{\partial C_1}{\partial x}\right] \\ J_3 &= -D_3\frac{\partial C_3}{\partial x} - N_3\left[(D_3-D_1)\frac{\partial C_1}{\partial x} + (D_3-D_2)\frac{\partial C_2}{\partial x}\right] \end{aligned}\right\} \tag{8}$$

A similar derivation is also applicable to the general multicomponent diffusion, giving

$$J_i = -D_i\frac{\partial C_i}{\partial x} - N_i\sum_{j}^{i\neq j}(D_i-D_j)\frac{\partial C_j}{\partial x} \tag{9}$$

1) L. S. Darken, *Trans. Met. Soc., AIME*, **175**, 184 (1948).

2) R. Mills, *J. Phys. Chem.*, **67**, 600 (1963). L. Miller and P. C. Carman, *Trans. Faraday Soc.*, **55**, 1831 (1959). J. E. Reynolds, B. L. Averbach, and M. Cohen, *Acta Metal.*, **5**, 29 (1957).

3) A. P. Hardt, D. K. Anderson, R. Rathbun, B. W. Mar, and A. L. Babb, *J. Phys. Chem.*, **63**, 2059 (1959). R. R. Irani and R. W. Adamson, *ibid.*, **64**, 199 (1960).

4) E. J. Hellund, *Phys. Rev.*, **57**, 737 (1940). L. Miller and P. C. Carman, *Nature*, **186**, 594 (1960). K. P. McCarty and E. A. Mason, *Phys. Fluids*, **3**, 908 (1960).

Ternary diffusion described by Eqs. (8) is characterized by the curved diffusion path on the ternary composition diagram. In special cases the diffusion path becomes linear on the ternary diagram, the following equations being satisfied.

$$J_1 : J_2 : J_3 = \frac{\partial C_1}{\partial x} : \frac{\partial C_2}{\partial x} : \frac{\partial C_3}{\partial x} \tag{10}$$

The conditions which lead Eqs. (8) to Eq. (10) are as follows:

(i) $D_1=D_2=D_3$.
(ii) $D_1=D_2$ for the diffusion with no concentration gradient for component 3.
(iii) $D_1=D_2$ for the diffusion between two compositions with an equal ratio of concentrations 1 and 2.

If D_1 is greater than D_2 in the diffusion between two compositions with an equal ratio of two concentrations, the diffusion path is curved in an S shape on the ternary diagram as shown schematically in Fig. 1. If D_1 is smaller than D_2, the diffusion path should be in a reversed S shape.

The greater the difference between the two diffusion coefficients or the smaller the value of D_3 than of the other two, the more curved the diffusion path on the diagram. Detailed characteristics of ternary diffusion have been discussed elsewhere.[5]

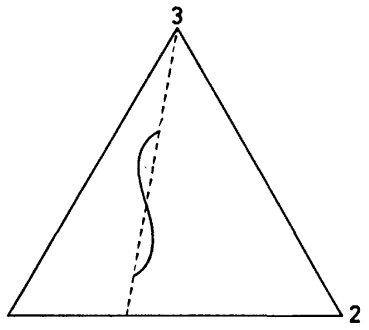

Fig. 1. Schematic diagram of diffusion path for ternary diffusion.

In a ternary diffusion given by Eqs. (8), a linear combination of two of the three concentrations given by Eq. (11) obeys Fick's law as is given by Eq. (12), in which the diffusion coefficient is $1/\mu^2$.

$$C = rC_2 + sC_1 \tag{11}$$

$$\frac{\partial C}{\partial t} = \frac{1}{\mu^2}\frac{\partial^2 C}{\partial x^2} \tag{12}$$

The μ and the ratio of r and s are defined as follows:

$$\mu_1 = \left\{\frac{D_1+D_2+N_1\,{}_3D_1+N_2\,{}_3D_2+[{}_2D_1{}^2+2{}_2D_1(N_2\,{}_3D_2-N_1\,{}_3D_1)+(N_1\,{}_3D_1+N_2\,{}_3D_2)^2]^{1/2}}{2(D_1D_2+N_1D_2\,{}_3D_1+N_2D_1\,{}_3D_2)}\right\}^{1/2},$$
$$\mu_2 = \left\{\frac{D_1+D_2+N_1\,{}_3D_1+N_2\,{}_3D_2-[{}_2D_1{}^2+2{}_2D_1(N_2\,{}_3D_2-N_1\,{}_3D_1)+(N_1\,{}_3D_1+N_2\,{}_3D_2)^2]^{1/2}}{2(D_1D_2+N_1D_2\,{}_3D_1+N_2D_1\,{}_3D_2)}\right\}^{1/2}, \tag{13}$$

$$R_1 = 1/S_1 = (r/s)_1 = \frac{{}_2D_1-N_1\,{}_3D_1+N_2\,{}_3D_2-[{}_2D_1{}^2+2{}_2D_1(N_2\,{}_3D_2-N_1\,{}_3D_1)+(N_1\,{}_3D_1+N_2\,{}_3D_2)^2]^{1/2}}{2N_2\,{}_3D_1},$$
$$R_2 = 1/S_2 = (r/s)_2 = \frac{{}_2D_1-N_1\,{}_3D_1+N_2\,{}_3D_2+[{}_2D_1{}^2+2{}_2D_1(N_2\,{}_3D_2-N_1\,{}_3D_1)+(N_1\,{}_3D_1+N_2\,{}_3D_2)^2]^{1/2}}{2N_2\,{}_3D_1}, \tag{14}$$

where ${}_iD_j=D_i-D_j$,
D is the intrinsic diffusion coefficient regarded as equal to the self-diffusion coefficient, N is the mole fraction, and subscript numbers refer to components.

B. Diaphragm-Cell Diffusion of Ternary System. When diffusion takes place through a diaphragm between two well-stirred cells, the concentration difference between the two cells varying with time is given by

$$\Delta c' = \Delta c \exp(-DKt) \tag{15}$$

where Δc is the concentration difference between two cells at time zero, $\Delta c'$ that at time t, D the diffusion coefficient, and K the cell constant.[6]

Similarly for a diaphragm-cell diffusion in a ternary system, the difference of linear combinations of the two concentrations between two cells is given by

$$\Delta C' = \Delta C \exp\left(-\frac{Kt}{\mu^2}\right) \tag{16}$$

where ΔC is the difference of linear combinations of two concentrations between two cells at time zero and $\Delta C'$ is that at time t, which are given by the following equations derived respectively from Eq. (11).

$$\Delta C = r\Delta C_2 + s\Delta C_1, \tag{17}$$

$$\Delta C' = r\Delta C_2' + s\Delta C_1', \tag{18}$$

where ΔC_i and $\Delta C_i'$ are the concentration differences of component i between two cells at times zero and t, respectively. It should be noted that Eq. (16) is quadratic, since μ and r/s are given in two pairs as in Eqs. (13) and Eqs. (14). Substituting Eqs. (17) and (18) in Eq. (16) we obtain

$$\left(\frac{r}{s}\right)_1\Delta C_2' + \Delta C_1' = \left[\left(\frac{r}{s}\right)_1\Delta C_2+\Delta C_1\right]\exp\left(-\frac{Kt}{\mu_1{}^2}\right) \tag{19a}$$

$$\left(\frac{r}{s}\right)_2\Delta C_2' + \Delta C_1' = \left[\left(\frac{r}{s}\right)_2\Delta C_2+\Delta C_1\right]\exp\left(-\frac{Kt}{\mu_2{}^2}\right) \tag{19b}$$

By solving the simultaneous equations for $\Delta C_1'$ and $\Delta C_2'$, we obtain the following equations.

$$\Delta C_1' = \frac{(\Delta C_2+S_1\Delta C_1)\exp\left(-\frac{Kt}{\mu_1{}^2}\right)-(\Delta C_2+S_2\Delta C_1)\exp\left(-\frac{Kt}{\mu_2{}^2}\right)}{S_1-S_2} \tag{20a}$$

5) Y. Oishi, *J. Chem. Phys.*, **43**, 1611 (1965).
6) J. H. Northrop and M. L. Anson, *J. Gen. Physiol.*, **12**, 543 (1929).

$$\Delta C_2' = \frac{(R_1\Delta C_2+\Delta C_1)\exp\left(-\frac{Kt}{\mu_1^2}\right)-(R_2\Delta C_2+\Delta C_1)\exp\left(-\frac{Kt}{\mu_2^2}\right)}{R_1-R_2} \tag{20b}$$

where

$$R_1=\frac{1}{S_1}=\left(\frac{r}{s}\right)_1, \qquad R_2=\frac{1}{S_2}=\left(\frac{r}{s}\right)_2.$$

Eqs. (20a) and (20b) give the differential concentrations between two cells for two of three components varying with time for the diaphragm-cell diffusion of a ternary system. The concentrations of the three components in the two cells are given by combining Eqs. (20a) and (20b) with the conditions of mass conservation for the respective components as follows.

$$C'_{1a}=\frac{\alpha C_{1a}+C_{1b}+\Delta C_1'}{1+\alpha} \tag{21a}$$

$$C'_{2a}=\frac{\alpha C_{2a}+C_{2b}+\Delta C_2'}{1+\alpha} \tag{21b}$$

$$C'_{3a}=(C_{1a}+C_{2a}+C_{3a})-(C'_{1a}+C'_{2a}) \tag{21c}$$

$$C'_{1b}=\frac{\alpha C_{1a}+C_{1b}-\alpha\Delta C_1'}{1+\alpha} \tag{22a}$$

$$C'_{2b}=\frac{\alpha C_{2a}+C_{2b}-\alpha\Delta C_2'}{1+\alpha} \tag{22b}$$

$$C'_{3b}=(C_{1b}+C_{2b}+C_{3b})-(C'_{1b}+C'_{2b}) \tag{22c}$$

where C_{ia} and C_{ib} are the initial concentrations of component i in cell a and cell b, respectively, C_{ia}' and C_{ib}' the concentrations of component i at time t in cell a and cell b, respectively, and α the ratio of the volumes of cell a and cell b. The concentrations of the three components in the two cells can be calculated for an arbitrary time by using Eqs. (21a), (21b), (21c), (22a), (22b), and (22c).

Experimental

Apparatus. Experiments were carried out by means of the diaphragm-cell technique of Ney-Armistead type[7] (Fig. 2). Cell 1 is movable along the ground glass plate relative to cell 2. Balance of pressures of cells 1 and 2 was ascertained by using an oil-manometer. Pressure was measured with a mercury manometer. The cell constant of the apparatus, K, was determined by using the self-diffusion coefficient of carbon dioxide by Winn[8] as a standard.

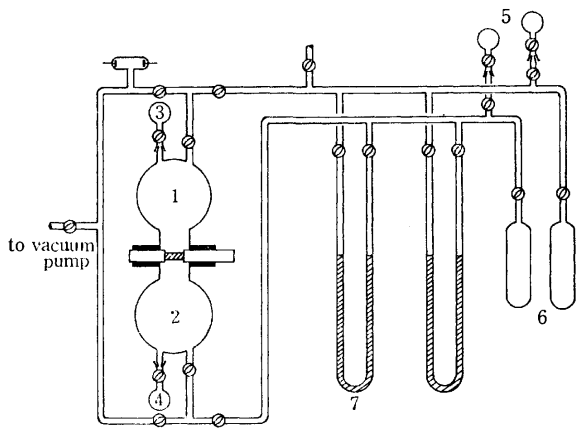

Fig. 2. Diffusion Apparatus:
1: upper cell, 2: lower cell, 3: upper sample holder, 4: lower sample holder, 5: sample holder, 6: gas holder, and 7: manometer.

Samples. Commercial neon gas of 99.99% purity (Mathison Co., U.S.A.) and commercial carbon dioxide gas of 99.95% purity (Nihon Tansan, Japan) were used without further purification. The isotope ratios of these gases are of natural abundance ratios. CO_2 gas was ^{18}O-enriched with the use of exchange reaction between $C^{16}O^{16}O$ and ^{18}O-enriched oxygen of 5% enrichment on the surface of a red-heated iron wire. The ^{18}O-enriched oxygen gas was obtained from commercial ^{18}O-enriched water by electrolysis.

Procedures. For measurement of the cell constant, the ^{18}O-enriched CO_2 gas was placed in cell 2 and natural CO_2 gas in cell 1 with the diffusion path between the two cells shut off by a glass plate. After the pressure of cell 1 was balanced to that of cell 2, cell 1 was shifted relative to cell 2 to open the diffusion path through the glass filter. A similar procedure was taken for the measurements of self-diffusion coefficients of CO_2 in a binary mixture of Ne and CO_2. All the experiments were carried out at 25°C under 760 mmHg. The diffusion apparatus was set in a vinyl sheet case installed in a temperature controlled room within 25±0.5°C. The diffusion time was about 100 minutes so that the ratio of M_t/M_∞ came up to one third. M_t and M_∞ stand for the amounts of diffusion at time t and infinity, respectively.

The composition of binary mixture of Ne–CO_2 system and the isotope ratio of ^{20}Ne and ^{22}Ne were determined by a mass spectrometer (Hitachi RM-60R). Accurate measurement of the isotope ratio of ^{20}Ne and ^{22}Ne in the mixture of Ne and CO_2 gases is disturbed by the coexisting CO_2, since the mass spectrometer does not distinguish $^{22}Ne^+$ ion from $^{44}CO_2^{2+}$ ion. To get rid of the disturbance it was necessary to remove CO_2 from the gas mixture with a cold trap of liquid nitrogen.

Results

The self-diffusion coefficients[9] of CO_2 for the binary system of Ne and CO_2 were measured for various compositions. The results are summarized in Table 1. The reciprocals of the self-diffusion coefficients of CO_2 are plotted in Fig. 3 as a function of the mole fraction of CO_2.

The variation of the isotope ratio of $^{22}Ne/^{20}Ne$ during interdiffusion of Ne and CO_2 was examined by considering the system as a ternary system of ^{22}Ne, ^{20}Ne, and $^{44}CO_2$. The results are given in Table 2 and plotted in Fig. 4, where M_t and M_∞ stand for the amounts of Ne diffusing into the CO_2 cell after time t, and infinite time, respectively, and R_i and R_t are the $^{22}Ne/^{20}Ne$ ratios at times zero and t, respectively. In Fig. 4 the circles show experimental results and the

7) E. P. Ney and F. C. Armistead, *Phys. Rev.*, **71**, 14 (1947).

8) E. B. Winn, *ibid.*, **80**, 1024 (1950).

9) "Self-diffusion coefficient" referred to in this paper is defined as the diffusion coefficient for diffusion in a homogeneous system where no chemical concentration gradient exists. The term is used for the diffusion coefficient not only in a pure system of a single component but also in a homogeneous multicomponent system. Thus, the intradiffusion coefficient defined by Albright and Mills (*J. Phys. Chem.*, **69**, 3120 (1965)) and McCarty and Mason (*Phys. Fluids*, **3**, 908 (1960)) is included in the definition of self-diffusion coefficient given above.

Table 1. Self-diffusion coefficient of CO_2 in the system of Ne and CO_2 at 25°C and 760 mmHg

Mole fraction of CO_2	D (cm²/sec)
1.000	0.113
0.796	0.123
0.624	0.131
0.500	0.137
0.356	0.153
0.189	0.179

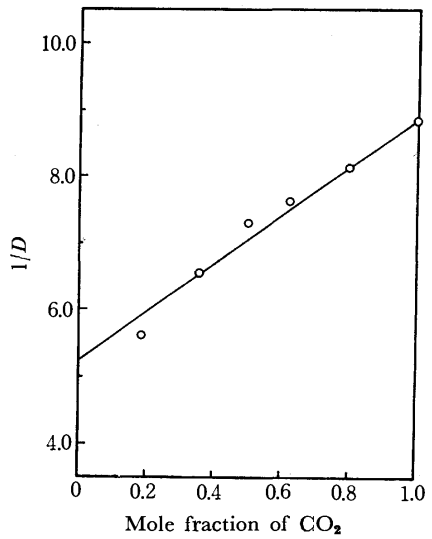

Fig. 3. Self-diffusion coefficient of CO_2 in the system of CO_2 and Ne at 25°C and 760 mmHg.

Table 2. Variation of isotope ratio $^{22}Ne/^{20}Ne$ during diffusion of a ternary system ^{20}Ne-^{22}Ne-CO_2 at 25°C and 760 mmHg

Diffusion time (min)	M_t/M_∞	$(R_t-R_t)/R_t$ Cell 1	$(R_t-R_t)/R_t$ Cell 2
20	0.225	4.83×10^{-3}	-4.15×10^{-2}
20	0.226	4.83	−3.47
30	0.292	6.80	−3.79
30	0.299	6.76	−3.57
45	0.450	10.61	−3.38
60	0.537	10.68	−3.01
75	0.619	9.65	−2.22
90	0.690	11.65	−2.14
90	0.704	12.62	−2.14
120	0.804	10.68	−1.55

soild lines represent the theoretical values calculated by Eqs. (20a) and (20b) with the values of the self-diffusion coefficients of ^{20}Ne,^{22}Ne, and $^{44}CO_2$.

For calculation of the theoretical values, the self-diffusion coefficients of the respective components for the composition of 0.5 mole fraction of CO_2 were taken as average values. The self-diffusion coefficients of ^{20}Ne for the composition of 0.5 mole fraction of CO_2 was estimated by making use of Darken's relation

$$D = N_2D_1^* + N_1D_2^*$$

where D denotes the binary diffusion coefficient of

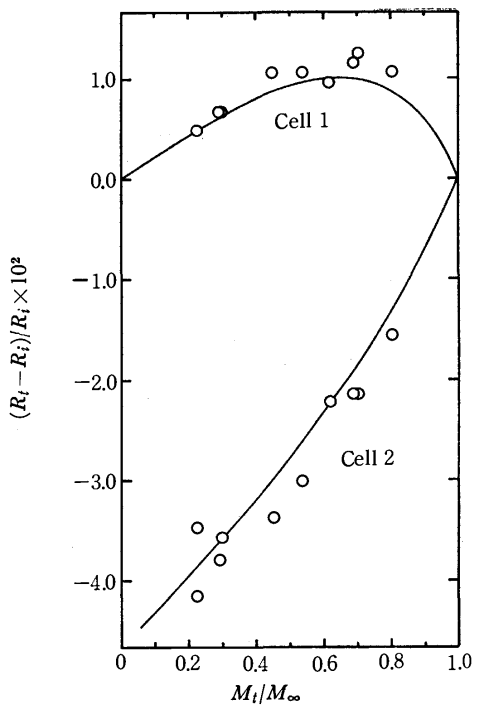

Fig. 4. Variation of isotope ratio $^{22}Ne/^{20}Ne$ during diffusion of a ternary system ^{20}Ne-^{22}Ne-CO_2 at 25°C and 760 mmHg.

the system of Ne and CO_2, D_1^* and D_2^* repersent the self-diffusion coefficients of Ne and CO_2, and N_1 and N_2 mole fractions of the components, respectively. Thus the self-diffusion coefficient of ^{20}Ne can be calculated since we have measured the self-diffusion coefficient of CO_2 and the interdiffusion coefficient of the binary system are known.[10] Estimation of the self-diffusion coefficient of ^{22}Ne was made by means of the mass correction

$$D(^{22}Ne) = \left(\frac{M_2+M_1}{M_2+M_3}\times\frac{M_3}{M_1}\right)^{1/2} D(^{20}Ne) \qquad (23)$$

where $D(^{22}Ne)$ denotes the self-diffusion coefficient of ^{22}Ne in the binary system of ^{22}Ne and $^{44}CO_2$, $D(^{20}Ne)$ the self-diffusion coefficient of ^{20}Ne in the binary system of ^{20}Ne and $^{44}CO_2$, and M_1,M_2, and M_3, the masses of ^{22}Ne, $^{44}CO_2$, and ^{20}Ne, respectively.

Discussion

A. Self-diffusion Coefficients. A kinetic theory gives the following relations between three kinds of diffusion coefficients:

$$\frac{1}{D_1^*} = \frac{N_1}{D_{11}} + \frac{N_2}{D_{12}}$$
$$\frac{1}{D_2^*} = \frac{N_2}{D_{22}} + \frac{N_1}{D_{12}} \qquad (24)$$

where D_1^* and D_2^* denote self-diffusion coefficients of species 1 and 2 for a binary mixture, D_{11} and D_{22} self-diffusion coefficients for the respective pure system, D_{12} an interdiffusion coefficient for the binary system,

10) B. K. Annis, A. E. Humphreys, and E. A. Mason, *Phys. Fluids*, **12**, 78 (1969).

and N_1 and N_2 mole fractions of the respective components. The equations show that the reciprocal of the self-diffusion coefficient of one component in a binary system are dependent linearly upon its mole fraction if the interdiffusion coefficient is independent of composition. The experimental results for CO_2 support the relation (Fig. 3). The data for the smaller mole fractions of CO_2 deviate from the straight line. This is probably due to the experimental error tending to be larger than that for the larger mole fraction of CO_2 because of the fact that the CO_2 content in the binary system is insufficient for accurate measurement of isotope ratios of $C^{16}O^{18}O/C^{16}O^{16}O$.

B. Isotope Separation in Ternary Diffusion. The agreement of the theoretically calculated variation of the isotope ratio $(R_t-R_i)/R_i$ with the experimental results indicates the validity of Eqs. (8).

Consequence of Eqs. (8), (20a), and (20b) with respect to the present isotope separation of neon shows that the greater the difference of self-diffusion coefficients of ^{22}Ne and ^{20}Ne, the higher the degree of isotope separation of neon, and that the smaller the self-diffusion coefficient of CO_2 that those of ^{22}Ne and ^{20}Ne, the greater the mass flow toward the neon side and the higher the degree of isotope separation of neon.

Kinetic theory predicts the mass dependency of the ratio of the self-diffusion coefficients:

$$\frac{D_1^*}{D_2^*} \propto \frac{(1/M_1+1/M_3)^{1/2}}{(1/M_2+1/M_3)^{1/2}} = \left(\frac{M_2}{M_1} \times \frac{1+M_1/M_3}{1+M_2/M_3}\right)^{1/2} \quad (25)$$

where M_i is the mass of i species.

Therefore, when M_3 is much larger than M_1 and M_2, the D_1^*/D_2^* ratio tends to approach the maximum value $(M_2/M_1)^{1/2}$, if M_2 is greater than M_1. Moreover, the large mass of the third component relative to ^{20}Ne and ^{22}Ne gives rise to its small self-diffusion coefficient and subsequently to the large mass flow, which is more effective for the purpose of the isotope separation of ^{20}Ne from ^{22}Ne. Consequently the larger separation factor can be obtained when the mass of the third component is larger than that of CO_2.

BULLETIN OF THE CHEMICAL SOCIETY OF JAPAN, VOL. 45, 2988—2992 (1972)

Photochemistry of Acridines. XVIII. Photoreduction by Nonpolar H-donors and the Disproportionation of C-Radicals

Mikio HOSHINO, Shigeya NIIZUMA, and Masao KOIZUMI

Department of Chemistry, Faculty of Science, Tohoku University, Katahira, Sendai

(Received February 18, 1972)

It was found that the photoreduction of acridine in cyclohexane and toluene occurs *via* molecular and radical mechanisms. The T-energy transfer experiments using biacetyl as an energy acceptor have revealed that the molecular mechanism occurs in the $T(n-\pi^*)$ state, and the radical in the singlet excited state. The effect of the addition of piperylene on the quantum yield of photoreduction was investigated in cyclohexane, methanol, ethanol and isopropanol. The results have been interpreted on the following assumptions. 1) Complete T-energy transfer from acridine to piperylene. 2) No quenching action of piperylene on the singlet excited acridine. 3) Complete transformation of C-radicals of acridine to stable products by piperylene. The results have led to the conclusion that the C-radical undergoes disproportionation in cyclohexane, methanol and ethanol, while it is completely transformed to an acridan-type compound in isopropanol.

Studies on the photoreduction of acridines have been made extensively,[1,4] but most of them dealt with photoreduction in various alcohols. We have investigated the kinetics of photoreduction in nonpolar H-donors such as cyclohexane and toluene. It has been established that both radical and molecular mechanisms occur in these solvents just as in alcoholic solvents.[4l] However, energy transfer experiments with the use of biacetyl have revealed that the radical mechanism occurs mainly in the singlet state while molecular mechanism, in the $T(n-\pi^*)$ state, in contrast to the case with alcoholic solvents.

We have tried using piperylene as a T-energy ac-

1) a) V. Zanker and G. Prell, *Ber. Bunsenges. Physik. Chem.*, **73**, 791 (1969). b) V. Zanker and E. Erhardt, *ibid.*, **72**, 267 (1968). c) V. Zanker, E. Erhardt and H. H. Mantsch, *Z. physik. Chem. N. F.*, **58**, 1 (1968).

2) E. Vander Donckt and G. Porter, *J. Chem. Phys.*, **46**, 1173 (1967).

3) a) A. Kellmann and L. Lindqvist, "The Triplet State," ed by A. B. Zahlan, Cambridge University Press, (1967), p. 439. b) A. Kellmann and J. T. Dubois, *J. Chem. Phys.*, **42**, 2518 (1965).

4) Our previous paper will be numbered as follows from now on. a) I, S. Kato, S. Minagawa, and M. Koizumi, This Bulletin, **34**, 1026 (1961). b) II, S. Niizuma and M. Koizumi, *ibid.*, **36**, 1629 (1963). c) III, A. Kira, S. Kato, and M. Koizumi, *ibid.*, **39**, 1221 (1966). d) IV, A. Kira, Y. Ikeda, and M. Koizumi, *ibid.*, **39**, 1673 (1966). e) V, S. Niizuma, Y. Ikeda, and M. Koizumi, *ibid.*, **40**, 2249 (1967). f) VI, A. Kira, *Sci. Rep. of Tohoku Univ. Ser.* I, **69**, No. 3—4, 129 (1966). g) VII, A. Kira and M. Koizumi, This Bulletin, **40**, 2486 (1967). h) VIII, M. Koizumi, Y. Ikeda, and T. Iwaoka, *J. Chem. Phys.*, **48**, 1869 (1968). i) IX, M. Koizumi, Y. Ikeda, and H. Yamashita, This Bulletin, **41**, 1056 (1968). j) X, K. Nakamaru, S. Niizuma, and M. Koizumi, *ibid.*, **42**, 255 (1969). k) XI, A. Kira and M. Koizumi, This Bulletin, **42**, 625 (1969). l) XII, M. Koizumi, S. Niizuma, and Y. Miyashita, *Z. Phys. Chem. N. F.*, **71**, 165 (1970). m) XIII, Y. Miyashita, S. Niizuma, and M. Koizumi, This Bulletin, **43**, 3435 (1970). n) XIV, K. Nakamaru, S. Niizuma, and M. Koizumi, *Z. Phys. Chem. N. F.*, **73**, 113 (1970). o) XV, K. Nakamaru, S. Niizuma, and M. Koizumi, This Bulletin, **44**, 1256 (1971). p) XVI, S. Niizuma, K. Nakamaru, and M. Koizumi, *Chem. Lett.*, **1972**, 59. q) XVII, K. Nakamaru, S. Niizuma, and M. Koizumi, This Bulletin, **45**, 2445 (1972).

ceptor to confirm the above result. We found that the compound acts as a radical scavenger as well as T-energy acceptor which indicates that the C-radical in cyclohexane, ethanol and mehtanol undergoes disproportionation. The results with the latter two solvents are in complete agreement with our previous conclusion.[4m] In the case of isopropanol it was found that semiquinone is most likely reduced further to acridan by isopropanol or by the isopropyl radical.

In view of the present results and another unpublished one concerning φ_{ST}, the values of Φ_M^S, Φ_R^S, Φ_M^T, and Φ_R^T previtusly published[4i] have been criticized and corrected to some extent.

Experimental

Acridine was recrystallized twice from aqueous ethanol. Biacetyl was purified by distillation immediately before use. Piperylene used was a mixture of *cis*- and *trans*-forms, and was subjected only to distillation. Ethanol, cyclohexane, and isopropanol were purified by the usual method. Methanol, G. R. grade of Wako Junyaku was used without further purification. The apparatus and procedures were described previously.[4d,m]

Results and Discussion

Photoreduction of Acridine in Cyclohexane and Toluene.

Photoreduction of acridine in cyclohexane which occurs upon irradiation at 365 nm is distinct. In the couse of the reduction, gradual decrease of acridine peak at 356 nm and a well-defined isosbestic point at 320 nm were observed. The feature of the reaction is similar to that in alcohols, occurring both in the deaerated and aerated solutions. The product has an absorption peak at 278—279 nm which differs slightly from that of acridan dissolved in cyclohexane (a peak at 282~283 nm). It is likely that the product is a mixture of acridan and an acridan-type compound.

The kinetic runs, *i. e.*, the plots $\ln(10^D-1)$ *vs.* t always give good straight lines. From the slopes the quantum yields in the deaerated and aerated solutions were obtained as $\Phi_{dea}=0.14_4$—0.14_9 and $\Phi_{aer}=0.05_1$, respectively. These values are a little larger than those in methanol and ethanol. The contributions of the molecular and radical mechanisms are 35 and 65%, respectively, of the entire reaction.

To determine the contribution of singlet excited state and triplet n-π^* state to the molecular and radical mechanisms, the effect of the addition of biacetyl as a T-energy acceptor was examined. Experiments were carried out in the same way as in alcohols[4i] for both the aerated and deaerated solutions. They are given in Fig. 1. It is seen that the quantum yeild in the aerated solution Φ_M decreases remarkably with the increase in biacetyl concentration. Judging from the concentration of biacetyl, this quenching is mostly related to T(n-π^*). This is in sharp contrast to alcohol systems in which the molecular mechanism scarcely occurs or not at all in T(n-π^*).

It has been found that the radical mechanism is scarcely affected by the adition of biacetyl in this concentration region. As shown in Fig. 1, the calculated values for $(\Phi/\Phi_0)_{dea}$ fit fairly well the experimental ones on the assumption that only Φ_M is decreased by the above amount. It is thus concluded that the radical mechanism occurs mainly in the singlet excited state. This is also remarkable in view of our previous results where T(n-π^*) contributes to radical mechanism to some extent in the case of methanol and ethanol.[4i]

The photoreduction of acridine in cyclohexane occurs mainly according to the following scheme,

$$A \xrightarrow{h\nu} A^*(S) \xrightarrow{RH_2} AH\cdot + RH\cdot \rightsquigarrow \text{acridan or acridan-like compound}$$
$$A^*(S) \rightarrow A(T n\text{-}\pi^*) \xrightarrow{HR_2} \text{acridan-like compound}$$

The reason for such a difference between alcohols and cyclohexane is unknown at the present stage but it might possibly be related to the presence or absence of the OH group which interacts specifically with N of acridine. We thus carried out similar experiments to those above, replacing cyclohexane with toluene. The relative quantum yields for the aerated and deaerated solutions obtained as a function

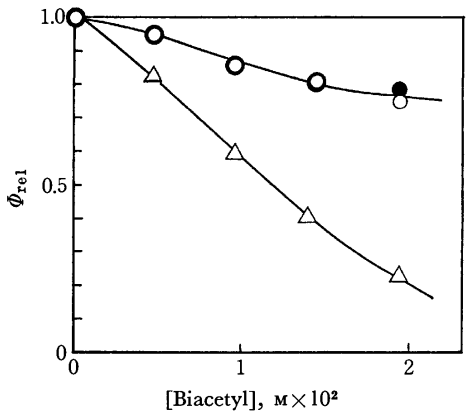

Fig. 1. Dependence of Φ_{rel} on biacetyl concentration for the aerated (Φ_M) and the deaerated ($\Phi_M+\Phi_R$) cyclohexane solutions.
△: Φ_M, ○: $\Phi_M+\Phi_R$, ●: ($\Phi_M+\Phi_R$)-values calculated on the assumption that Φ_R is not affected by biacetyl.

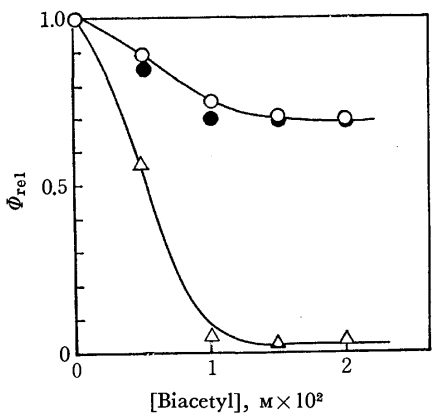

Fig. 2. Dependence of Φ_{rel} on biacetyl concentration for the aerated (Φ_M) and the deaerated ($\Phi_M+\Phi_R$) toluene solutions.
△: Φ_M, ○: $\Phi_M+\Phi_R$, ●: ($\Phi_M+\Phi_R$)-values calculated on the assumption that Φ_R is not affected by biacetyl.

of biacetyl concentration are given in Fig. 2. It is seen that biacetyl acts as a more effective quencher in aerated toluene than in aerated cyclohexane. This might be due to the difference in viscosity. All other results were much the same as those with cyclohexane. Thus we might say that in nonpolar solvents having no such group as OH, molecular mechanism does not occur in the singlet state but occurs in the T(n-π^*) state and that radical mechanism occurs mainly in the singlet state.

Reevaluation of the Values of Φ_M^S, Φ_R^S, Φ_M^T *and* Φ_R^T. Since these values were reported,[41] the values of $\Phi_R=\Phi_R^S+\Phi_R^T$ for ethanol and methanol were found to agree respectively with the quantum yeilds of oxygen consumption during the photoreduction of acridine in the aerated ethanol and methanol solutions,a reasonable interpretation being given. This confirmed the reliability of our values for $\Phi_R^S+\Phi_R^T$,[4m] but not of our individual values of Φ_R^S and Φ_R^T.

From recent measurements of the values of intersystem crossing probabilities of acridine in methanol, ethanol and isopropanol, our Φ_R^S and Φ_R^T values for ethanol appeared to be somewhat unreliable[5] and we reinvestigated our previous method. Taking ethanol as an example, the values of Φ_R^T,Φ_R^S and Φ_M^S (Φ_M^T is zero for ethanol) were determined in the following way from the plots given in Fig. 3. Φ_M^S was determined from the quantum yield of photoreduction in the areated solution. The value of $\Phi_M^S+\Phi_R^S$ was evaluated from the intercept of part b of the plot for the dearated solution. However, the slopes of part b of the Φ_0/Φ *vs.* [Biacetyl] plots (k_q) for the deaerated solutions in methanol, ethanol and isopropanol were always larger than the corresponding slopes of the aerated solutions. The latter agreed very well with the quenching constants of acridine fluorescence by biacetyl. We mentioned that somewhat larger values for the deaerated solutions might be due to participation of the T(n-π^*) state. From this viewpoint it would be more reliable to use the slopes of the aerated solutions and to calculate the $\Phi_M^S+\Phi_R^S$ value from the intercept of the dotted line shown in Fig. 3.[6] The recalculated values of Φ_M^S, Φ_R^S, Φ_M^T and Φ_R^T (italicized) are listed in Table 1 along with the old values.

The new values of Φ_M^S,Φ_R^S, and Φ_R^T for n-propanol and ethanol are about the same percentage of the Φ_{total}-value. Although the difference between the new and old values is not so great, except in the case of ethanol, and could be considered within experimental accuracy, most of the results, particularly for ethanol, might be well comprehended on the basis of the new data.

Effect of the Addition of Piperylene on the Photoreduction Quantum Yield in Cyclohexane. It is well-known that piperylene ($CH_3-CH=CH-CH=CH_2$) acts as a good T-energy acceptor.[7] Therefore in order to reconfirm the results obtained

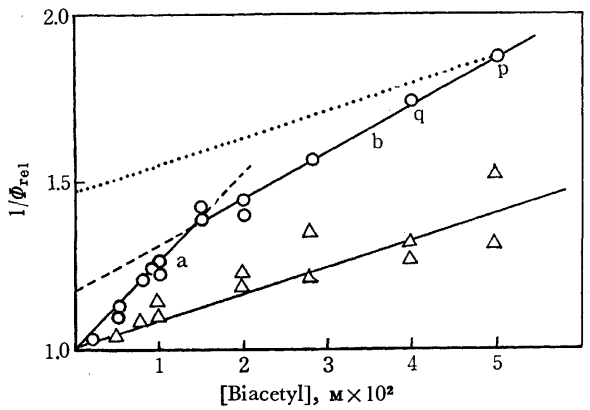

Fig. 3. Plot of $1/\Phi_{rel}$ *vs.* [Biacetyl] for the aerated and deaerated ethanol solution of acridine.
○: deaerated, △: aerated.

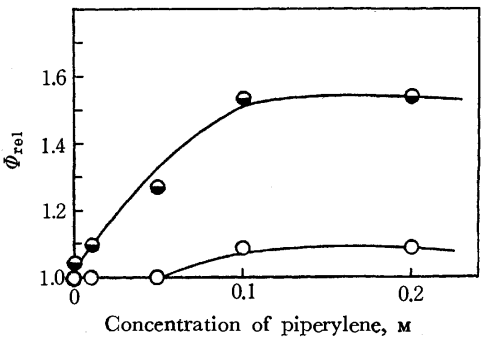

Fig. 4. Plot of Φ_{rel} *vs.* piperylene concentration in the aerated and deaerated solution of acridine in cyclohexane.
○: aerated, ◒: deaerated.

Table 1. Separate quantum yields due to different mechanism

	Φ_M^S	Φ_R^S	Φ_M^T	Φ_R^T	Φ_{total}
Methanol	0.027 (21%)	*0.032* (24%)	0.006 (5%)	*0.063* (50%)	0.128
	0.027 (21%)	0.039 (30%)	0.006 (5%)	0.057 (45%)	
Ethanol	0.043 (33%)	*0.043* (33%)	0	*0.043* (33%)	0.129
	0.043 (33%)	0.067 (52%)	0	0.019 (15%)	
1-Propanol	0.030 (34%)	0.030 (34%)	0	*0.028* (31%)	0.088
	0.030 (34%)	0.030 (40%)	0	0.022 (25%)	
Isopropanol	0.03 (35%)	0.058 (65%)	0	0	0.088
	0.03 (35%)	0.058 (65%)	0	0	

5) It has been found that the apparent inconsistence is also due to another quite different fact.

6) From the Φ *vs.* [Biacetyl] plot, it seems appropriate to draw the dotted line from a point located in a p~q region. If it is drawn from the neighborhood of q, the Φ_R^T and Φ_R^S-values become about 10% smaller and greater, respectively.

7) G. H. Hammond, J. Salticel, A. A. Lamola, N. J. Turro, I. S. Bradshaw, D. O. Cowan, R. C. Counsell, V. Vogt and C. Datton, *J. Amer. Chem. Soc.*, **86**, 3197 (1964).

from the effect of the addition of biacetyl, we have made similar experiments using piperylene. It was confirmed that the spectral change and the $\ln(10^D-1)$ *vs.* t plots run just as in the absence of piperylene.

The effect, however, was found to be contrary to expectation. Thus the quantum yield does not decrease but increases with addition of piperylene both in the aerated and deaerated solutions (Fig. 4). The increase is especially remarkable for the deaerated solution, the Φ-value reaching 10^{-1} M piperylene about one and a half times the value in the absence of piperylene. The increase for the aerated solution is about 10%. Thus

Φ_{dea}(in the presence of piperylene)$=0.22$
Φ_{aer}(in the presence of piperylene)$=0.05_6$

as compared with

Φ_{dea}(in the absence of piperylene)$=0.146$
Φ_{aer}(in the absence of piperylene)$=0.051$

from which $\Phi_R=0.095$, $\Phi_M=0.051$

The above result for the deaerated solution may be interpreted in the following way. The concentration of piperylene is so high that the T-energy transfer from acridine to piperylene is considered to be practically complete. However, piperylene acts as a radical scavenger and the intermediate produced is stabilized most likely as follows,

$$AH\cdot + P \rightarrow AH-P\cdot \quad (1)$$

$$2AH-P\cdot \rightarrow (AH-P)_2$$

$$\text{or } AH-P\cdot + AH\cdot \rightarrow AH-P-AH \quad (2)$$

The essential point is that all the intermediates are stabilized without reconverting to acridine. If we assume that acridine semiquinone undergoes the following disproportionation as in the case of ethanol and methanol,[4m]

$$2AH \rightarrow A + AH_2\ , \quad (3)$$

then the addition of piperylene is expected to double the value of Φ_R^S. Hence the expected value of

Φ_{dea}(in the presence of piperylene)$=0.19$.

Taking the experimental error into account, the agreement is fairly satisfactory.

It is to be noted that two assumptions have been made:

1) the complete quenching of $T(n\text{-}\pi^*)$
2) no quenching action of piperylene on the singlet excited acridine.

The result for the aerated solution is difficult to explain, because the features of reaction seem to be very complicated. Firstly, much higher concentrations of piperylene than that of oxygen make the deactivation of $T(n\text{-}\pi^*)$ by piperylene predominant. Whether oxygen or piperylene acts as a deactivator does not matter as long as both act as simple deactivators. The complication may be caused by various types of reaction involving semiquinone. It is expected that competition occurs between reaction (1) and the following reaction

$$AH\cdot + O_2 \rightarrow A + HO_2\cdot \quad (4)$$

High concentrations of piperylene make reaction (1) more favorable. The intermediate produced by this reaction may also be attacked in part by oxygen;

$$AH-P\cdot + O_2 \rightarrow AH-P-O_2\cdot \quad (5)$$

and the product is expected to act as an oxidizing agent toward acridine semiquinone. Moreover radicals produced from cyclohexane will be oxidized to peroxy-radical which again acts as an oxidizing agent. Thus the eventual reactions consist of the recovery of acridine and the formation of an acridan-like compound. Quantitative treatment is far outside our scope. What we can say is only that the result is reasonable at least qualitatively on the basis of the above reasoning.

The value of $\Phi_{aer}=0.056$ is only about 30% of $\Phi_R\times 2=0.19$ which is expected if all the intermediates produced by reaction (1) undergo reaction (2).

Effect of the Addition of Piperylene on the Quantum Yield of the Photoreduction of Acridine in Methanol. In order to make clearer the reactions in the presence of piperylene and to confirm the assumptions made above, photoreduction in methanol has been investigated. The experiments and the analysis of the reuslts were made in the same way as in the case of cyclohexane.

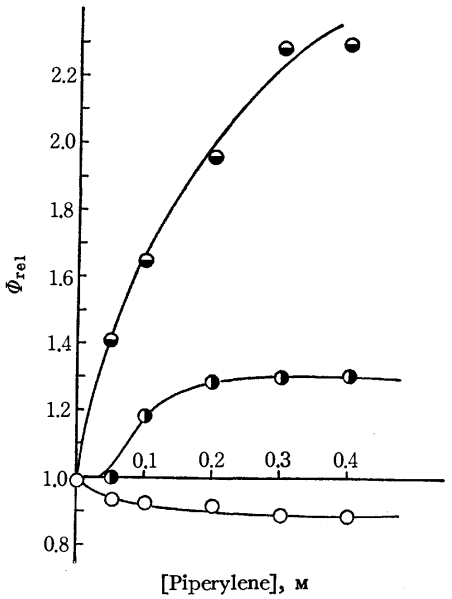

Fig. 5. Plot of Φ_{rel} *vs.* piperylene concentration in the aerated and deaerated solution of acridine in methanol.
◒: for the first stage, ◑: for the later stage } aerated.
○: deaerated.

For the aerated solutions, the plots $\ln(10^{+D}-1)$ *vs.* t consist of two steps, the slopes in the later stage being about 1/2 of those in the early one. This suggests the complicated nature of the entire reaction. It is more suitable to adopt the slopes in the early stage (up to about 15% decrease of acridine) because of the anticipated participation of the reaction products in the later stage. The results are shown in Fig. 5. It is seen that in contradistinction to the result for cyclohexane, a remarkable increase of Φ_{aer} occurs, *i. e.*, the Φ_{aer} value reaches 2.3 times that in the absence of piperylene. The value of Φ_{dea} decreases by about

10%. Thus

Φ_{dea}(in the presence of piperylene)$=0.115$
Φ_{aer}(in the presence of piperylene)$=0.07_6$

The value of Φ_{dea} is discussed as follows. According to our previous result,[4m] acridine semiquinone undergoes mainly disproportionation in methanol. It is likely as in cyclohexane that in the presence of piperylene, all the acridine semiquinone is stabilized to an acridan-like compound. If we further assume, as before, the complete quenching of $T(n\text{-}\pi^*)$ and no quenching action of piperylene on the singlet excited state of acridine, the values calculated using the data in Table 1 are

$\Phi_{dea}=0.32\times2+0.027=0.091$...with the new data
$\Phi_{dea}=0.039\times2+0.027=0.105$...with the old data

Both values agree with the experimental one within about twenty percent.

On the other hand, Φ_{aer}(in the presence of piperylene is 75—80% of the value expected on the assumption that reaction (2) overwhelms reaction (4) or other types of reaction recovering acridine.

Effect of the Addition of Piperylene on the Photoreduction of Acridine in Ethanol and Isopropanol. The results for ethanol are shown in Fig. 6. Thus

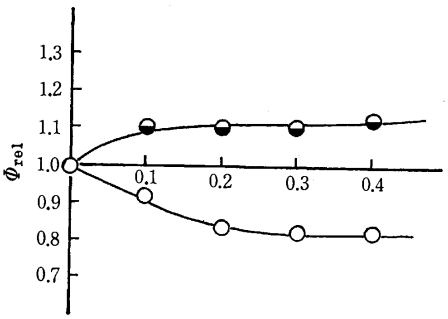

Fig. 6. Plot of Φ_{rel} *vs.* piperylene concentration in the aerated and deaerated solution of acridine in ethanol.
◒: aerated, ○: deaerated.

Φ_{dea}(in the presence of piperylene)$=0.10_7$
Φ_{aer}(in the presence of piperylene)$=0.04_7$

If we make the same assumptions as in the case of cyclohexane and methanol. Φ_{dea} is expected to be 0.129 with the new data but 0.177 with the old one. Thus the experimental value is about 20% less for the former.

The value of Φ_{aer} is about 30% of the value expected if reaction (2) overwhelms reaction (4) or similar oxidizing reactions.

The results for isopropanol are given in Figure 7. This system is considered to be simple in one sense because only singlet excited state participates in the reaction. From the plots given in Fig. 6.

Φ_{dea}(in the presence of piperylene)$=0.08_0$

But a reliable value of Φ_{aer} can not be obtained from the plot. In our previous paper,[4m] we could not make any conclusion about the behavior of acridine semiquinone in isopropanol. Hence it is quite unknown

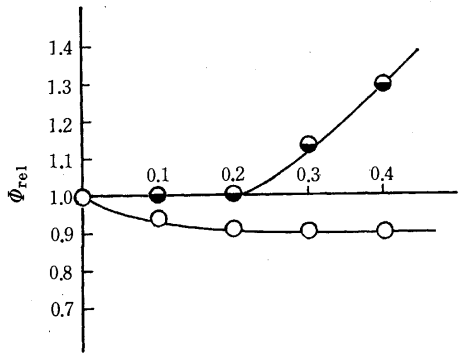

Fig. 7. Plot of Φ_{rel} *vs.* piperylene concentration in the aerated and deaerated solution of acridine in *iso*-propanol.
◒: aerated, ○: deaerated.

whether $2AH\rightarrow A+AH_2$ or $AH+RH\rightarrow AH_2+R$ or $AH+RH_2\rightarrow AH_2+RH$ occurs predominantly. If we assume that disproportionation is predominant, Φ_{dea} should reach $0.058\times2+0.03=0.15$ which exceedes very much the experimental value of Φ_{dea}. If one considers that for other alcohols and for cyclohexane the calculated values of Φ_{dea} (on the assumption of disproportionation of semiquinone) agree with the experimental Φ_{dea}-value within *ca.* 20%, the disagreement in the present case is too large to attribute it to the experimental error. It seems therefore more likely to consider that the reaction

$$AH + \text{isopropanol} \rightarrow AH_2 + (CH_3)_2C - OH$$
$$\text{or } AH + RH \rightarrow AH_2 + R \qquad (6)$$

mainly occurs in isopropanol. This is not unreasonable in view of the high reactivity of isopropanol. If we assume reaction (6), the experimental value of Φ_{dea} is about 10% less than the calculated one, $0.058+0.03=0.088$. This may be within experimental error, but one can safely say that even if piperylene deactivates singlet excited state the amount does not exceed 10% or so of Φ^S in isopropanol. The results for other solvents are consistent with this conclusion. Thus the second assumption made at the start has been substantiated to some extent.

In conclusion, we can say firstly that in nonpolar solvents with a hydrogen atom easily detachable, radical mechanism mainly occurs in the singlet excited state and molecular mechanism in $T(n\text{-}\pi^*)$. This may be due to the non-existence of a specific interaction between acridine and H-donor. Under such conditions, a two site reaction like molecular mechnaism may not be able to occur during the lifetime of singlet excited state. A little longer lifetime of $T(n\text{-}\pi^*)$ may be favorable for the occurrence of this mechanism in $T(n\text{-}\pi^*)$.

Secondly, the results obtained from the experiments concerning piperylene effects have led to the conclusion that in the case of methanol, ethanol and cyclohexane, the half-reduced radical of acridine mainly undergoes disproportionation while in the case of isopropanol it is highly probable that semiquinone is further reduced by isopropanol or by isopropyl radical.

Statistical Thermodynamics and Adsorption

Ralph J. TYKODI

Department of Chemistry, Southeastern Massachusetts University, North Dartmouth, Massachusetts 02747, U.S.A.

(Received November 12, 1971)

The proper correlation of thermodynamic quantities derived from experimental gas-solid adsorption systems with those derived from statistical mechanical models is discussed; the usual method of making the correlation is found to be unsatisfactory, and a new method is proposed.

The considerations of this paper apply to systems involving the physical adsorption of gases on solids.

In some treatments of the thermodynamics of gas-solid adsorption[1,2] the change of pertinent bulk (not merely surface) properties of the solid component with amount adsorbed is an important feature of the development. It is not customary, however, in the usual statistical mechanical treatments of gas-solid adsorption explicitly to allow for changes in the bulk properties of the solid component.[3] Given that the macrothermodynamic considerations of references 1 and 2 are correct, should not the usual statistical mechanical procedure be mended so as to allow for, at least implicitly, changes in the bulk properties of the solid component?

A Special Case

In order to show clearly the issues involved, let us first examine the special case of an ideal localized monolayer.[4] Consider an enclosure containing a solid component and a gas component, with N_A of the gas molecules adsorbed on the surface of the solid. For purposes of discussion attribute to the solid surface a site structure and consider the ideal localized monolayer adsorption of the N_A molecules on N_S sites.

Represent the (Helmholtz) free energy of the solid component *in vacuo* as

$$F^{\circ}_{sol(id)} = F^{\circ}_{b(ulk)} + F^{\circ}_{sur(face)}, \tag{1}$$

and with N_A molecules adsorbed on its surface as

$$F_{sol} = F_b + F_{sur}. \tag{2}$$

We can then write for the total free energy of the enclosure

$$F_{tot(al)} = F_b + F_{gas} + F_{mix}, \tag{3}$$

where F_{gas} is the free energy contribution of the unadsorbed gas molecules and F_{mix} is the contribution of the "mixture" of N_A adsorbed molecules and N_S sites. We can now define an excess free energy F_f by

$$F_f \equiv F_{tot} - F_{gas} - F^{\circ}_{sol} = F_{mix} - F^{\circ}_{sur} + F_b - F^{\circ}_b. \tag{4}$$

We find[2,3] that F_f is expressible as

$$F_f = \mu N_A - \phi A, \tag{5}$$

where $\mu \equiv (\partial F_f/\partial N_A)_{T,A}$ is the chemical potential of an adsorbed molecule, A is the surface area of the solid, and $\phi \equiv -(\partial F_f/\partial A)_{T,N_A}$ is commonly called the spreading pressure.

Now the statistical mechanical free energy F of the assembly of N_A molecules adsorbed on N_S sites in just[3]

$$F = -kT \ln Q_{ads}, \tag{6}$$

$$Q_{ads} = \frac{N_S!}{(N_S - N_A)!\,N_A!} e^{N_A\chi/kT} j^S(T)^{N_{Ac}}, \tag{7}$$

where Q_{ads} is the partition function for the adsorbed monolayer, $j^S(T)$ is the partition function for the internal degrees of freedom of an adsorbed molecule (including vibrations relative to its mean position on a site), and $(\pm)N_A\chi$ may be viewed either $(+)$ as a minimum energy required to desorb the N_A molecules and carry them to the gas state at infinite separation or $(-)$ as the potential energy of the N_A asdorbed molecules relative to the gas state at infinite separation.[3,5]

The very crux of the matter is that investigators dealing with the statistical mechanics of gas-solid adsorption customarily assert that

$$F^{(1)} \equiv F_{mix} - F^{\circ}_{sur} = F_f, \tag{8}$$

$$F_b - F^{\circ}_b = 0, \tag{9}$$

$$\phi A \equiv F^{\circ}_{sol} - F_{sol} = F^{\circ}_{sur} - F_{sur}; \tag{10}$$

and consequently also that

$$(\partial F^{(1)}/\partial N_A)_{T,A} = \mu, \tag{11}$$

$$-(\partial F^{(1)}/\partial A)_{T,N_A} = \phi. \tag{12}$$

(The index on F merely shows that this is the first of several assertions about the relationship of F to F_f.)

At this point a brief digression concerning the structure of Eq. (5) will prove instructive. Although Eq. (5) is a thermodynamic identity, it is nevertheless possible to produce equations of the same general form, also identities, but subject to different interpretation. For any equation of the form

$$F_*{}^{(k)} \equiv F_f + Af_*{}^{(k)}(T, N_A/A), \tag{13}$$

where $f_*{}^{(k)}(T, N_A/A)$ is an arbitrary function of the indicated arguments, it follows that

$$F_*{}^{(k)} = N_A(\partial F_*{}^{(k)}/\partial N_A)_{T,A} + A(\partial F_*{}^{(k)}/\partial A)_{T,N_A} \tag{14}$$

holds identically. Since Eq. (14) has the same general form as Eq. (5), we may, if we wish, write it as

$$F_*{}^{(k)} = \mu^{(k)} N_A - \phi^{(k)} A, \tag{15}$$

with $\mu^{(k)} \equiv (\partial F_*{}^{(k)}/\partial N_A)_{T,A}$ and $\phi^{(k)} \equiv -(\partial F_*{}^{(k)}/\partial A)_{T,N_A}$. Equations (13)—(15) point up a possible pitfall in the sort of work that we are discussing: we might find ourselves in possession of a free energy such as $F_*{}^{(k)}$

1) T. L. Hill, *J. Chem. Phys.*, **18**, 246 (1950).
2) R. J. Tykodi, *ibid.*, **22**, 1647 (1954).
3) R. H. Fowler and E. A. Guggenheim, "Statistical Thermodynamics" Cambridge University Press, Cambridge, (1939) Chap. X, for example.
4) *ibid.*, pp. 426 and 427.
5) T. L. Hill, *J. Chem. Phys.*, **17**, 762 (1949).

and, having determined that the functional relationship (14) holds, we might be tempted to conclude that we are dealing with Eq. (5)—clearly such need not be the case, and in general $\mu^{(k)} \neq \mu$ and $\phi^{(k)} \neq \phi$.

Returning now to the case of the ideal localized monolayer, note that the assertions (8)—(10) are not simple deductions from Eqs. (4), (6), and (7). In order to investigate the matter more closely, let us express F as $F=E-TS$ and $F^{(i)}$ as $F^{(i)}=E^{(i)}-TS^{(i)}$; then it follows from Eq. (6) that

$$F = -N_A\chi + E_{int} - TS_{config} - TS_{int}, \tag{16}$$

where S_{config} is the configurational entropy deducible from the factorial part of Q_{ads} and E_{int} and S_{int} are, respectively, those parts of E and S deducible from the $j^s(T)^{N_A}$ portion of Q_{ads}.

Suppose first that $-N_A\chi$ represents a change in energy for the process

N_A gas molecules at infinite separation + bare solid component → N_A molecules adsorbed on the solid component;

i.e., suppose that

$$-N_A\chi = E_{mix} + E_b - E^0_{sol} - E^0_{gas}, \tag{17}$$

where E^0_{gas} is the energy (potential energy plus that due to internal degrees of freedom) of N_A gas molecules at infinite separation. In addition let the zero of (potential) energy be chosen in such a way that the potential energy of N_A gas molecules at infinite separation is zero. Under the assumptions operative in the case of ideal localized monolayer adsorption[3,5] it then follows that $E^0_{gas}=E_{int}$.

From Eqs. (16) and (17) we see that

$$F^{(2)} = E_{mix} + E_b - E^0_{sol} - TS_{config} - TS_{int}. \tag{18}$$

Since $S_{mix} \equiv S_{config}+S_{int}+S_{sur}$, we may express Eq. (18) as

$$F^{(2)} = F_{mix} + TS_{sur} - E^0_{sol} + E_b; \tag{19}$$

and, with some further manipulation, we may reduce it to the form

$$F^{(2)} = F_{mix} - F^0_{sur} + F_b - F^0_b + T(S_{sol}-S^0_{sol}). \tag{20}$$

Referring back to Eq. (4) we see that under the present assumptions

$$F^{(2)} = F_f + T(S_{sol}-S^0_{sol}); \tag{21}$$

i.e., the statistical mechanical free energy $F^{(2)}$ fails to take into account possible changes in the entropy content of the solid component with varying amounts adsorbed.

Suppose next, in Eq. (16), that a different interpretation is given to the term $-N_A\chi$. Let $-N_A\chi$ now be considered as representing a form of (potential) energy associated (merely by convention) with the adsorbed molecules alone; *i.e.* suppose that

$$-N_A\chi = E_{mix} - E_{int} - E_{sur}. \tag{22}$$

Substituting from Eq. (22) into Eq. (16), we obtain

$$\begin{aligned} F^{(3)} &= E_{mix} - E_{sur} - TS_{config} - TS_{int} \\ &= F_{mix} - F_{sur}. \end{aligned} \tag{23}$$

Referring back to Eq. (4), we note that Eq. (23) can be written as

$$F^{(3)} = F_f - (F_{sol}-F^0_{sol}) = F_f + \phi A. \tag{24}$$

Thus the statistical mechanical free energy $F^{(3)}$ fails to take into account possible changes in the free energy content of the solid component with varying amounts adsorbed.

(The preceding material relating to $F^{(2)}$ and $F^{(3)}$, shows that *contrary to expectation* $F^{(i)} \neq F_f$ $(i=2,3)$ and that the reason for $F^{(i)} \neq F_f$ is the indicated one in each case.)

Since we usually assume the $\phi=\phi(T,N_A/A)$, we see that Eq. (24) is of the general form of Eq. (13); consequently the relation

$$\begin{aligned} F^{(3)} &= N_A(\partial F^{(3)}/\partial N_A)_{T,A} + A(\partial F^{(3)}/\partial A)_{T,N_A} \\ &= \mu^{(3)}N_A - \phi^{(3)}A, \end{aligned} \tag{25}$$

where $\mu^{(3)} \equiv (\partial F^{(3)}/\partial N_A)_{T,A}$ and $\phi^{(3)} \equiv -(\partial F^{(3)}/\partial A)_{T,N_A}$, holds identically.

A relation similar to (25) would hold in the case of $F^{(2)}$ also, provided we could show that $T(S_{sol}-S^0_{sol}) = Af_*^{(2)}(T,N_A/A)$.

General Considerations

The foregoing considerations pose a serious problem for the comparison of statistical mechanical models with experimental adsorption systems. In the experimental case we deal with quantities such as μ, ϕ, F_f, S_f, *etc.* and with relations between such quantities —hereafter called *proper quantities* and *proper relations*—; whereas in the statistical mechanical case we produce quantities such as $\mu^{(i)}$, $\phi^{(i)}$, $F^{(i)}$, $S^{(i)}$, *etc.* and relations between such quantities—hereafter called *eikonic quantities* and *eikonic relations*. There would be no problem if we found that the assertions of Eqs. (8)—(12) hold true; however, in view of the considerations advanced in references 1 and 2 and in view of experimental results such as those of Yates[6,7] (*e.g.*), the assertions of Eqs. (8)—(12) appear to be untenable.

It appears then that the usual statistical mechanical treatment of the physical adsorption of gases on solids (whether couched in terms of ordinary or grand partition functions) always produces eikonic quantities and relations rather than proper ones, the exact nature of the eikonic quantities depending upon how the various parts of $E^{(i)}$ are interpreted. The notation $F^{(i)}$ in this section is used to denote the free energy derived from *any statistical mechanical model whatsoever* in which —speaking somewhat loosely— the "energy of the adsorbed molecules" is interpreted in the same manner as the term $-N_A\chi$ was interpreted in the discussion of the ideal localized monolayer. The conventional statistical mechanical treatments of gas-solid adsorption, therefore, fail to consider either (a) changes in the entropy content or (b) changes in the free energy content of the solid component with varying amounts adsorbed; and so, unwittingly, in the past, we have been led to compare theoretical eikonic quantities with experimental proper ones —the correct procedure is to make a comparison either on an eikonic-eikonic or on a proper-proper basis *via* suitable equations of transformation.

6) D. J. C. Yates, *Proc. Roy. Soc., Ser. A*, **224**, 526 (1954).
7) D. J. C. Yates, *J. Phys. Chem.*, **60**, 543 (1956).

It appears that the statistical mechanical work to date has produced statistical free energies $F^{(3)}$ and associated eikonic quantities and variables, in that most treatments of gas-solid adsorption take the quantity analogous to $-N_A\chi$ as being the potential energy of interaction of the adsorbed molecules with the solid component, this potential energy of interaction being conventionally treated as a property of the assembly of adsorbed molecules. As we saw previously, such a treatment leads to free energies of the type $F^{(3)}$.

In the remainder of this paper we will therefore limit our attention to $F^{(3)}$ and related eikonic quantities, with no further mention of $F^{(2)}$.

The comparison of statistical mechanical models with experimental gas-solid adsorption systems may proceed along either of two different lines: (a) we may transform the proper quantities and relations derived from the experimental data to appropriate eikonic quantities and relations by means of suitable equations of transformation and so compare them to the eikonic quantities and relations generated from $F^{(3)}$ by standard methods; or (b) we may attempt to win from the statistical mechanical model proper quantities and relations and compare these directly with the proper quantities and relations derived from experiment. Procedure (a) is a relatively easy and mechanical procedure; whereas procedure (b) can be exceedingly difficult to put into practice.

At this point let us drop the uncomfortable formalism (bulk properties, surface properties, *etc.*) thus far developed, and carry on the remainder of the discussion in terms of the molar macroscopic thermodynamic formalism established in reference 2.

For purposes of orientation note that the Gibbs adsorption is written as

$$\mu_f = -\boldsymbol{R}T\int_0^P X d\ln P, \tag{26}$$

where μ_f is the change in the chemical potential of the solid component due to the adsorption process and $X \equiv \Gamma/n_s$ is the adsorption excess (in terms of moles of gas component) per mole of solid. Integral molar excess properties are indicated by a superior bar and differential molar excess properties by a superscript partial differential operator; thus

$$Z_f^{\partial} \equiv (\partial Z_f/\partial\Gamma)_{T,n_s} = \bar{Z}_f + X(\partial\bar{Z}_f/\partial X)_T. \tag{27}$$

The change in a molar property for an adsorption process

$$i(\text{gas}) \rightarrow i(\text{adsorbed})$$

is written as $\Delta\bar{Z} \equiv \bar{Z}_f - \bar{Z}_g$; thus, the integral molar heat of adsorption $Q \equiv \bar{H}_f - \bar{H}_g$, according to this convention, is normally a *negative* quantity. For convenience functions appropriate to processes at constant μ_f —*isomunal* processes— are defined; in reference 2, script capital letters were used to designate these special functions; in this paper they are designated by means of square brackets, which thus correspond to the script capital symbols in reference 2. As an example, note that the ordinary integral molar heat of adsorption is related to the isomunal integral molar heat of adsorption by the equation

$$\Delta[H] \equiv \Delta\bar{H} - (\mu_f/X). \tag{28}$$

Eikonic Relations

In terms of the present notation[8] we would write relation (13) as

$$F_*^{(k)} \equiv F_f + n_s f_*^{(k)}(T, X); \tag{29}$$

correspondingly, the identity (14) would appear as

$$F_*^{(k)} \equiv \Gamma(\partial F_*^{(k)}/\partial\Gamma)_{T,n_s} + n_s(\partial F_*^{(k)}/\partial n_s)_{T,\Gamma} \tag{30}$$

and the form (15) as

$$F_*^{(k)} = \Gamma\mu_g^{(k)} + n_s\mu_f^{(k)}, \tag{31}$$

with $\mu_g^{(k)} \equiv (\partial F_*^{(k)}/\partial\Gamma)_{T,n_s}$ and $\mu_f^{(k)} \equiv (\partial F_*^{(k)}/\partial n_s)_{T,\Gamma}$.

For convenience let us write $\mu_g^{(k)}$ as

$$\mu_g^{(k)} = \mu^{\dagger}(T) + \boldsymbol{R}T\ln P^{(k)} \tag{32}$$

and refer to $P^{(k)}$ as the eikonic pressure; we may call a relation such as $P^{(k)} = P^{(k)}(T,X)$ an eikonic isotherm relation. Of course eikonic quantities and variables are merely mathematical constructs and are related to the proper experimental quantities and variables by suitable equations of transformation.

The proper equilibrium condition for gas-solid adsorption systems is[2]

$$\mu_g = G_f^{\partial} \equiv [G_f]. \tag{33}$$

The corresponding eikonic relations are

$$F^{(3)} = G_f - n_s\mu_f, \tag{34}$$

$$\mu_g^{(3)} = (G_f - n_s\mu_f)^{\partial}. \tag{35}$$

The following transformation relations hold between proper variables and the corresponding eikonic variables:

$$X^{(3)} = X, \tag{36}$$

$$T^{(3)} = T, \tag{37}$$

$$\mu_g^{(3)} = \mu_g - (\partial\mu_f/\partial X)_T, \tag{38}$$

$$\mu_f^{(3)} = X(\partial\mu_f/\partial X)_T. \tag{39}$$

Equations (26), (32), (38), and the perfect gas assumption lead to the relations

$$\ln(P^{(3)}/P) = (\partial\ln P/\partial\ln X)_T, \tag{40}$$

$$q_{st}^{(3)} = q_{st} - (\partial\mu_f/\partial X)_T + T(\partial^2\mu_f/\partial T\partial X), \tag{41}$$

$$Q^{(3)} = Q - (\mu_f/X) + TX^{-1}(\partial\mu_f/\partial T)_X = q_{st}, \tag{42}$$

where q_{st} is the proper isosteric heat of adsorption, Q is the proper integral molar heat of adsorption, and

$$q_{st}^{(3)} = -\boldsymbol{R}T^2(\partial\ln P^{(3)}/\partial T)_X,$$

$$Q^{(3)} = X^{-1}\int_0^X q_{st}^{(3)} dX(\text{constant } T).$$

Let us here introduce molar eikonic integral and differential quantities which are related to the proper quantities of the adsorption system in the following way:

$$\bar{G}_f^{(3)} = [G_f], \tag{43}$$

$$\bar{H}_f^{(3)} = [H_f] + TX^{-1}(\partial\mu_f/\partial T)_X, \tag{44}$$

$$\bar{S}_f^{(3)} = \bar{S}_f + X^{-1}(\partial\mu_f/\partial T)_X, \tag{45}$$

and

$$\{Z_f^{(3)}\}^{\partial} \equiv (\partial Z_f^{(3)}/\partial\Gamma)_{T,n_s} = \bar{Z}_f^{(3)} + X(\partial\bar{Z}_f^{(3)}/\partial X)_T \tag{46}$$

for any extensive property Z. The additional relations

8) In passing, note that $E_f \equiv H_f$ and $F_f \equiv G_f$ because of the way in which the adsorption excesses are defined (see Ref. 2).

$$\bar{H}_g^{(3)} = \bar{H}_g, \tag{47}$$

$$\bar{S}_g^{(3)} = \bar{S}_g + T^{-1}(\partial\mu_f/\partial X)_T, \tag{48}$$

follow from Eq. (38) and the perfect gas assumption. Now a little calculation will show that

$$q_{st}^{(3)} = \{H_f^{(3)}\}^\partial - \bar{H}_g^{(3)}, \tag{49}$$

$$q_{st}^{(3)}/T = \{S_f^{(3)}\}^\partial - \bar{S}_g^{(3)}, \tag{50}$$

$$Q^{(3)} = \bar{H}_f^{(3)} - \bar{H}_g^{(3)}, \tag{51}$$

$$Q^{(3)}/T = \bar{S}_f^{(3)} - \bar{S}_g^{(3)} + (\mu_f^{(3)}/TX). \tag{52}$$

A consequence of Eqs. (36)—(39), (43)—(48), and the definitions

$$[H_f^{(3)}] \equiv \bar{H}_f^{(3)} - (\mu_f^{(3)}/X), \tag{53}$$

$$[G_f^{(3)}] \equiv [H_f^{(3)}] - T\bar{S}_f^{(3)}, \tag{54}$$

is that *all the thermodynamic identities of reference 2 remain valid when the proper quantities and variables in each equation are replaced by the corresponding eikonic quantities and variables.*

Isotherm Relations

Let us investigate some of the simpler relations between proper and eikonic isotherm equations, basing our considerations chiefly on Eq. (40). Consider the twin problems (a) Given the form of the proper isotherm deduce from it the eikonic isotherm and (b) Given the form of the eikonic isotherm deduce from it the proper isotherm.

From the proper isotherm relations

$$P = kX^\nu \text{ (Freundlich)}, \tag{55}$$

$$bP = X/(X_m - X) = \theta/(1-\theta) \quad \text{(Langmuir)}, \tag{56}$$

with $\theta \equiv X/X_m$, we obtain by means of Eq. (40) the relations

$$P^{(3)} = Pe^\nu = k^{(3)}X^\nu, \tag{57}$$

$$bP^{(3)} = bP\exp\{1/(1-\theta)\} = \{\theta/(1-\theta)\}\exp\{1/(1-\theta)\}. \tag{58}$$

Thus Freundlich-type isotherms (of which Henry's law isotherms are a special case) remain formally invariant under the transformation; whereas Langmuir isotherms become changed somewhat in form.

The inverse case for the Langmuir isotherm is a good deal more peculiar. From the relation

$$bP^{(3)} = \theta/1-\theta \tag{59}$$

and Eq. (40) it follows that

$$bP = \{\theta/(1-\theta)\}(1-\theta)^{1/\theta}\exp(-K/\theta), \tag{60}$$

where K is an arbitrary constant. The rather bizarre relation (60), which implies a finite pressure for $\theta=1$, is simply a consequence of the fact that $F^{(3)} \neq F_f$.

First Order Phase Changes

Statistical mechanical considerations[3] indicate that first order phase changes should be possible in theoretical gas-solid adsorption systems. In some previous work[2,9] it was argued that first order phase changes in experimental gas-solid adsorption systems are thermodynamically unlikely. We can reconcile the apparent discrepancy between the preceding two conclusions if we consider that the statistical mechanical deductions pertain to *eikonic* relations rather than to *proper* relations.

In experimental adsorption systems we assume that a first order phase change occurs when $(\partial X/\partial P)_T=\infty$ or, equivalently, when $(\partial P/\partial X)_T=0$ or $(\partial \ln P/\partial X)_T=0$. Now these statistical mechanical considerations[3] merely imply that $(\partial \ln P^{(3)}/\partial X)_T=0$ and not that $(\partial \ln P/\partial X)_T=0$ (eikonic interpretation of statistical mechanical procedures).

We see from Eq. (40) that

$$\left(\frac{\partial \ln P^{(3)}}{\partial X}\right)_T = \frac{1}{X}\frac{\partial}{\partial X}\{X^2(\partial \ln P/\partial X)_T\}. \tag{61}$$

The condition $(\partial \ln P^{(3)}/\partial X)_T=0$ then leads to the relation

$$\ln P = -L_m(T)X^{-1} + M_m(T), \tag{62}$$

where L_m and M_m are constants of integration and the subscript m allows for the possibility that the condition $(\partial \ln P^{(3)}/\partial X)_T=0$ may be satisfied at several different points on the adsorption isotherm.

In the case of the eikonic interpretation of $F^{(3)}$ the condensation type phenomena predicted by theory will probably produce smooth, rolling bumps in the *proper* adsorption isotherm;[10,11] in the regions where the theoretically predicted "phase changes" take place the proper isotherm relation will satisfy Eq. (62).

In statistical mechanical discussions of first order phase changes in gas-solid adsorption systems we may retain all those thermodynamic relations developed for such changes[2] provided we understand that they deal in the statistical mechanical case with *eikonic* quantities and variables; *e.g.* during the "phase change" $\delta\mu_f^{(3)}=0$ (and not $\delta\mu_f=0$).

Eikonic Programming

The foregoing considerations indicate that in the construction of partition functions for various statistical mechanical models of gas-solid adsorption systems we must have clearly in mind the type of statistical free energy —Eq. (8), (21), or (24)— that we expect to generate. Whereas in the past free energies $F^{(3)}$ were produced by ignoring possible variations in the properties of the solid component with changing amounts adsorbed, we can make such a procedure a well-defined technical operation, an operation to which the name *eikonic programming* will be attached. Under the eikonic programming procedure we would concern ourselves only with the energetic behavior of the gas component, treating the solid component as merely the source of the requisite potential field, and we would *deliberately* ignore the changes in the properties of the solid concomitant with the adsorption process. We would then derive eikonic quantities and variables from the eikonic programming free energy $F^{(3)}$ by the usual methods, and we would either (a) convert such eikonic quantities and variables into proper ones by means of Eqs. (34), (36)—(39), (43)—(48), (53), and (54) (also see below) in order to compare them to the proper quantities and variables of experimental adsorption systems or (b)

9) R. J. Tykodi, *J. Phys. Chem.*, **59**, 383 (1955).

10) R. A. Beebe and D. M. Young, *ibid.*, **58**, 93 (1954).

11) J. H. Singleton and G. D. Halsey, Jr., *ibid.*, **58**, 1011 (1954).

convert the proper quantities and variables of experimental adsorption systems into eikonic ones by means of the appropriate equations of transformation and compare the experimental eikonic quantities to those derived from the statistical mechanical model.

Under an eikonic programming procedure the comparison of theory with experiment is relatively easy. From Eq. (34) and section 2 of reference 2 it follows that

$$F^{(3)} = \Gamma\mu_g; \tag{63}$$

so in order to establish the *proper* isotherm appropriate to the theoretical model we need merely set $F^{(3)}/\Gamma$ equal to the chemical potential in the gas phase. Of course if we wish, we may derive the *eikonic* isotherm from the relation $(\partial F^{(3)}/\partial\Gamma)_{T,n_s} = \mu_g^{(3)}$. *Another attractive feature of the eikonic programming procedure is that eikonic integral molar quantities are identical with proper differential molar quantities,*[12] *i.e.* $\bar{Z}_f^{(3)} \equiv Z_f^{\ominus}$. *Thus in discussing the entropy or the heat capacity of the adsorbed molecules we should compare the appropriate integral molar (eikonic) properties of the theoretical model with the differential molar (proper) properties of experimental adsorption systems.*

12) See Eqs. (43)—(45) and Ref. 2.

BULLETIN OF THE CHEMICAL SOCIETY OF JAPAN, VOL. 45, 2997—3002 (1972)

The Catalytic Exchange of Hydrogen-Deuterium on Copper-Nickel Alloy Plates after Various Surface Treatments

Yoshio TAKASU and Toshiro YAMASHINA

Department of Nuclear Engineering, Hokkaido University, Sapporo

(Received October 13, 1971)

The catalytic activities of nine copper-nickel alloys (5 cm^2 in area) in hydrogen-deuterium exchange were examined at 1.5 Torr partial pressures of hydrogen and deuterium, using an ultra-high vacuum apparatus incorporated with an omegatron mass spectrometer for continuous gas analysis. Without any surface treatment, the activity was greatest on pure nickel, decreased gradually as the content of copper in the alloys increased and virturally vanished in the alloys containing copper more than 70%. The activity of each alloy sample was observed to be extremely enhanced by a slight surface treatment of oxidation-reduction (P_{O_2}=2.3 Torr at 500°C for 1 min, P_{H_2}=16 Torr at 300°C for 2 hr). The activity of the 85% copper alloy after the oxidation-reduction treatment was greatest, one hundred times that of pure nickel. Annealing for a short time in an ultra-high vacuum subsequent to the oxidation-reduction treatment caused the catalytic activity to decrease abruptly at a critical temperature (425°C). On the bases of the electron microscopic observations and the measurement of the surface roughness changed by the pre-treatments, the nature of active sites on copper-nickel alloys was discussed.

A number of investigations have been undertaken in order to confirm the influence of the electronic structure of alloys, particularly the copper-nickel system, on catalytic activity since the proposal of the *d*-band theory by Dowden and Reynolds.[1,2] In recent investigations of this subject, vacuum evaporated alloy films have frequently been used because they are capable of producing clean surfaces by adaptation to ultra-high vacuum conditions. However, there have been pronounced discrepancies of the catalytic activity patterns in the experimental results reported for copper-nickel alloy catalysts.

A series of papers by Sachtler and his co-workers[3-5] have reported that the activity pattern for benzene hydrogenation showed a constant activity in overall compostion; this is in agreement with the expectation from the work function measurement and also from the thermodynamical fact that the surface compositions of the copper-nickel system should be the same in most of the overall alloy composition region due to the miscibility gap of the system at 200°C. In contrast to these results, many investigators, including Russell,[6] Emmett,[7] and Takeuchi[8] have reported, in similar studies of copper-nickel film catalysts, that the maximum of catalytic activity for the hydrogenation reaction is found in the alloy region, and that it is approximately ten times as active as pure nickel. Particularly, Campbell and Emmett,[7] in their X-ray measurement of film structure, found only one alloy phase containing 60% copper in any case after heating to 500°C in hydrogen; nevertheless they also observed the maximum activity in the alloy region.

These facts suggest that the catalytic activity does not always correspond to the composition of the alloy film. Several possible reasons for the discrepancies in the experimental results for alloy-film catalysts can be considered, as has, for example, been pointed out by Plank and Sachtler.[5]

Many findings have shown that the catalytic activity of film, foil, or metal plate and alloy plate can be greatly influenced by the treatment of their surfaces.

1) D. A. Dowden, *J. Chem. Soc.*, **1950**, 242.
2) D. A. Dowden and P. Reynolds, *Disc. Faraday Soc.*, **8**, 184 (1950).
3) W. M. H. Sachtler and G. J. H. Dorgelo, *J. Catal.*, **4**, 654 (1965).
4) W. M. H. Sachtler and R. Jongepier, *ibid.*, **4**, 665, (1965).
5) P. van der Plank and W. M. H. Sachlter, *ibid.*, **7**, 300, (1967) **12**, 35 (1968).
6) E. G. Alexander and W. W. Russell, *ibid.*, **4**, 184 (1965).
7) J. S. Campbell and P. H. Emmett, *ibid.*, **7**, 252 (1967).
8) T. Takeuchi, Y. Tezuka, and O. Takayasu, *ibid.*, **14**, 126 (1969).

In the study of catalysis by metals and alloys, increased in activity due to deformation with cold-rolling and ion-bombardment have been found. Results have been obtained for nickel[9-12] and silver[13] by plastic deformation, and for nickel,[14,15] platinum,[14] silver,[16] palladium[17] and copper-nickel alloys,[15,18] by ion-bombardment. In these studies, most of the authors have considered that increases in activity may be attributed to the introduction of lattice imperfections by the treatments. In the cases of the catalytic behaviour of alloy films, as reviewed above, lattice imperfections as active sites should be taken into consideration, since it is well known that various imperfections can be produced in films during evaporation.

We have previously studied[18] the catalysis for the clean surfaces of copper-nickel alloy plates after argon-ion bombardment in the reaction of ethylene hydrogenation, and found that the maximum activity of the 60% copper alloy was the greatest, fifteen times greater than that of pure nickel; we explained the activity increases in association with the formation of the lattice defects due to the removal of copper atoms, which are nearest neighbors of the nickel atoms.

The purpose of the present study was to obtain more detailed information on the nature of active sites of the copper-nickel alloy surface by means of various experimental techniques, and to compare these information with the results described above.

By using an ultra-high vacuum apparatus, the surfaces of copper-nickel alloy plates have been treated by oxidation-reduction, hydrogen reduction, annealing and so on, and the catalytic activity for hydrogen-deuterium exchange at low pressures has been measured as a function of the copper-nickel alloy composition.

Experimental

Materials. High-purity nickel (>99.9%) and copper (>99.99%), and nine copper-nickel alloys with compositions of 95,90, 85, 80, 60, 40, 30, 20, and 10 weight per cent copper have been investigated. Each sample was about 0.6 mm in thick and 4.8 cm^2 in total surface area. These samples were polished with metallographic emery paper, an aqueous suspension of alumina, and then with fine cloth in streaming water, and rinsed in distilled water and acetone. Gaseous reactant hydrogen and deuterium of a high purity in a glass cylinder from the Takachiho Chemical CO. were used without further purification. The oxygen and argon gases were prepared by bulb-to-bulb distillation from commerical cylinders at the temperature of liquid nitrogen.

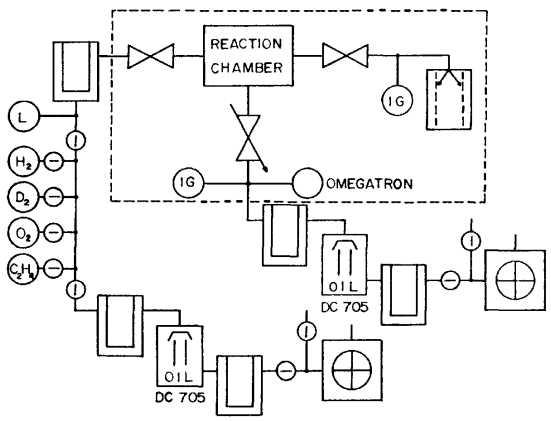

Fig. 1. Ultra-high vacuum apparatus for catalytic measurement (The inside part of dotted line is bakable).

Catalytic Activity. The main features of the vacuum apparatus for catalytic activity measurements are shown schematically in Fig. 1, which has a configuration similar to that used by Farnsworth *et al.*[14,15] The vacuum apparatus consisted of three separate systems—a reaction-chamber, a mass spectrometer, and a gas handling system. These systems could be connected with each other through metal stop cocks and valves. The reaction chamber was a vessel approximately 300 cc in volume, capable of being evacuated to 1×10^{-8} Torr or less by means of a sputter ion pump (8 *l*/sec). The progress of the reaction at low pressures was observed with an omegatron rf. mass spectrometer, which could be evacuated and baked to obtain a residual pressure of 5×10^{-8} Torr or less. The sensitivity and resolution of the omegatron were very satisfactory for tracing the course of the reaction. All the reactant gases were admitted to the reaction chamber through cold traps at the temperature of liquid nitrogen. These gases were mixed at a pressure of 1.5 Torr before they were admitted into the reaction chamber. The pressure in the mass spectrometer was kept at precisely 2×10^{-7} Torr by adjusting the variable leak valve. The reaction rate was determined by using the following equation;[19]

$$k_m = n\cdot\frac{1}{t}\ln\frac{x_e-x_o}{x_e-x_t}\left(\frac{1}{60\cdot A}\right)\ \text{molecules/cm}^2\cdot\text{sec.}$$

where n is the number of molecules in the reaction space and where x_o, x_t, and x_e are the fractions of hydrogen deuteride present at time zero, t, and at equilibrium. A is the geometrical surface area of the samples. The k_m rate is termed the catalytic activity in the present paper.

Surface Area. Changes in the surface area (roughness factor of sample plates with various treatments could be detected precisely by the rapid measurement method for a small surface area.[20]

Results

Catalytic Activity of Copper-Nickel Alloys after Oxidation-reduction Treatments. Figures 2 and 3 show the catalytic activity curves after various surface treatments for the hydrogen-deuterium exchange reaction as a function of the alloy composition. In all the cases shown in the figures, the reaction temperature was 100°C and the initial pressures of both hydrogen and

9) J. Eckell, *Z. Elektrochem.*, **46**, 433 (1933).
10) G. Rienäcker, *ibid.*, **46**, 369 (1940).
11) I. Uhara, T. Hikino, Y. Numata, H. Hamada, and Y. Kageyama, *J. Phys. Chem.*, **66**, 1374 (1962) and their many papers.
12) E. Miyazaki, T. Fukushima, K. Kawasaki, and K. Nakada, This Bulletin **44**, 291 (1971).
13) I. Uhara, S. Kishimoto, Y. Yoshida, and T. Hikino, *J. Phys. Chem.*, **69**, 880 (1965).
14) H. E. Farnsworth and R. E. Woodcock, *Advan. Catal.*, **9**, 123 (1957), *Ind. Eng. Chem.*, **49**, 258 (1957).
15) J. Tuul and H. E. Farnsworth, *J. Amer. Chem. Soc.*, **83**, 2247 (1961).
16) H. M. C. Sosnovsky, *J. Phys. Chem. Soilds*, **10**, 304 (1959),
17) Y. Inoue and I. Yasumori, *J. Phys. Chem.*, **73**, 1618 (1969).
18) T. Yamashina and H. E. Farnsworth, *Ind. Eng. Chem. Prod. Res. Develop.*, **2**, 34 (1963).
19) D.D. Eley and P.R. Norton, *Dis. Faraday Soc.*, **41**, 135 (1966).
20) K. Watanabe and T. Yamashina, *J. Catal.*, **17**, 257 (1970).

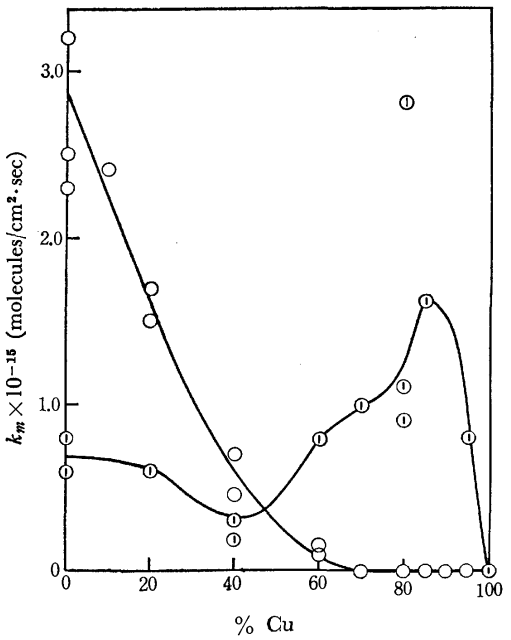

Fig. 2. Catalytic activity pattern for hydrogen-deuterium exchange reaction at 100°C.
○: Treatment (1) (Non-treatment)
◑: Treatment (2) (Hydrogen-treatment)

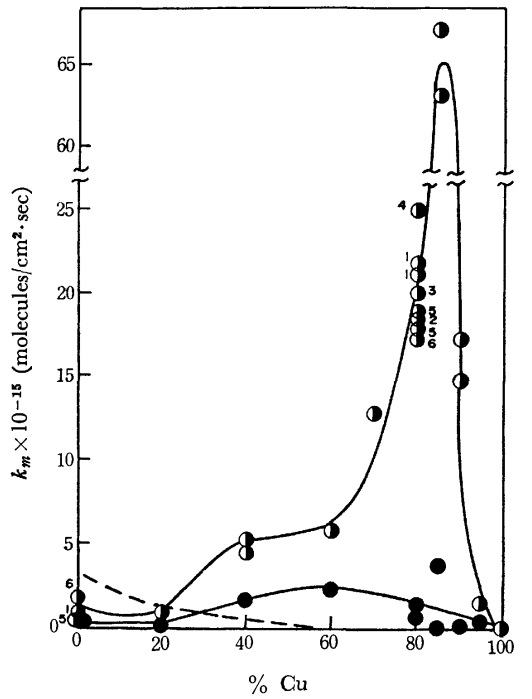

Fig. 3. Catalytic activity pattern for hydrogen-deuterium Exchange reaction at 100°C.
◑: Treatment (3) (Oxidation-reduction treatment)
●: Treatment (4) (Annealing-treatment)
Dotted line: Treatment (1)
Number of each activity point of 80% copper alloy signifies different oxidation condition as follows;

Number	O-R treatment	
	Oxidation (1 min)	Reduction (2 hr)
1	P_{O_2}=2.3 Torr	P_{H_2}=16 Torr
2	0.175	16
3	0.135	16
4	0.068	16
5	0.024	16
6	0.017 (2 min)	16

deuterium were 1.5 Torr. The number of each curve on the figures indicates the order of surface treatment procedure as follows:

(1) Non-treatment: Mechanically-polished with metallographic emery paper and alumina powder, and then with fine cloth in a stream of water.

(2) Hydrogen-treatment: Heated in hydrogen (16 Torr) at 300°C for 1 hr subsequent to the (1) treatment.

(3) Oxidation-reduction Treatment: Deoxidized by hydrogen (16 Torr) at 300°C for 2 hr after oxidation with oxygen (2.3 Torr) at 500°C for 1 min subsequent to the (1) and (2) treatments (in that order) (hereinafter referred to as the O-R treatment).

(4) Annealing-treatment: Vacuum-annealed under below 5×10^{-8} Torr at 500°C for 0.5 hr subsequent to the (1), (2), and (3) treatments (in that order).

In the case of the (1) treatment, the activity was observed to be greatest on pure nickel, to decrease gradually as the content of copper in the alloys increases, and virtually to vanish in the alloys containing more than 70% copper. After the (2) treatment, however, the activity of pure nickel decreased while catalytic activity appeared in the range of copper-rich compositions.[21] Besides, after the O-R treatment, the activity curve appeared to be quite different from the others, as may be seen in Fig. 3, in which the catalytic activity of copper-nickel alloys may be seen to be much greater than that of pure nickel; in particular, the activity of the 85% copper alloy was found to be greater than that of pure nickel, after the same treatment, by a factor of one hundred. Of particular interest in Fig. 3 is the very narrow range of composition around the 85% copper alloy. Such a high activity was found to remain unchanged even after several days and several reaction runs. When the catalysts activated by the O-R treatment were annealed, the catalytic activity was decreased drastically, as is shown in Fig. 3(4); the activity values were nearly the same regardless of the alloy composition.

Effect of Vacuum Annealing. In order to examine the nature of the active sites produced by the O-R treatment, the deactivation process of the catalytic activity due to thermal annealing *in vacuo* was examined.

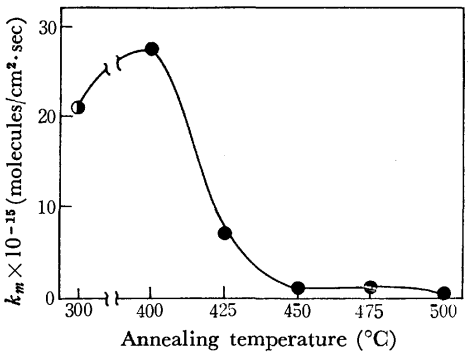

Fig. 4. Effect of annealing on catalytic activity of 80% copper alloy for hydrogen-deuterium exchange reaction at 100°C (Annealing time, 10 min).

21) It should be noted that the fluctuation in the activity data was found to be quite large after the (2) treatment.

Figure 4 shows the effect of the annealing temperature on the catalytic activity of the 80% copper alloy after the O-R treatment, where each sample was annealed under below 5×10^{-8} Torr for 10 min at various temperatures. The reaction temperature for the hydrogen-deuterium exchange was 100°C.

The catalytic activity is found not to be changed after annealing at 300°C and to increase slightly after annealing at 400°C, while it decreases abruptly at temperatures above 425°C. Figure 5 shows the effect of the annealing time on the catalytic activity. It is seen that, at 300°C, the activity remained nearly the same even after 8 hrs' annealing, and that at 400°C, the maximum activity was found to be twice that before annealing, but at 500°C a rapid decrease of activity for the initial few minutes was observed. It should be noted that there was a critical temperature at which the activity decreased drastically.

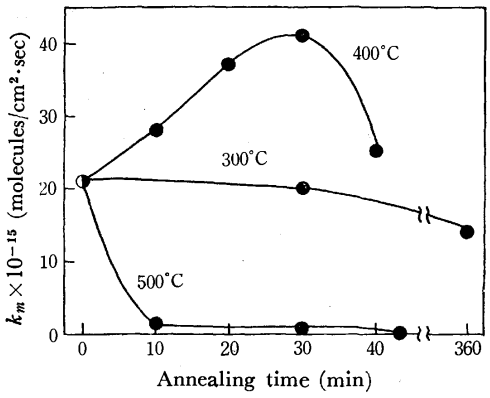

Fig. 5. Effect of annealing time on catalytic activity of 80% copper alloy for hydrogen-deuterium exchange reaction at 100°C.

Observation of the Surface State. Figure 6 represents the results of the electron-microscopic observation of the surface of the 80% copper alloy after each treatment, (1) to (4), as is shown above. As may be seen in the figure, the surface became smooth after the hydrogen treatment (2), many pits on the surface appeared after the O-R treatment (3), and the surface was invisibly changed by the annealing treatment (4). The values of the roughness factor (the ratio of the true surface area to the geometric surface area), as estimated by means of the above method,[20] are also shown in Fig. 6. The roughness factor of the surface was increased about twice by the O-R treatment, but no change was found in the values between those after the O-R treatment and the subsequent annealing treatment. It should also be emphasized that changes in the roughness factor with the surface treatment were not related to changes in the catalytic activity shown in Fig. 3.

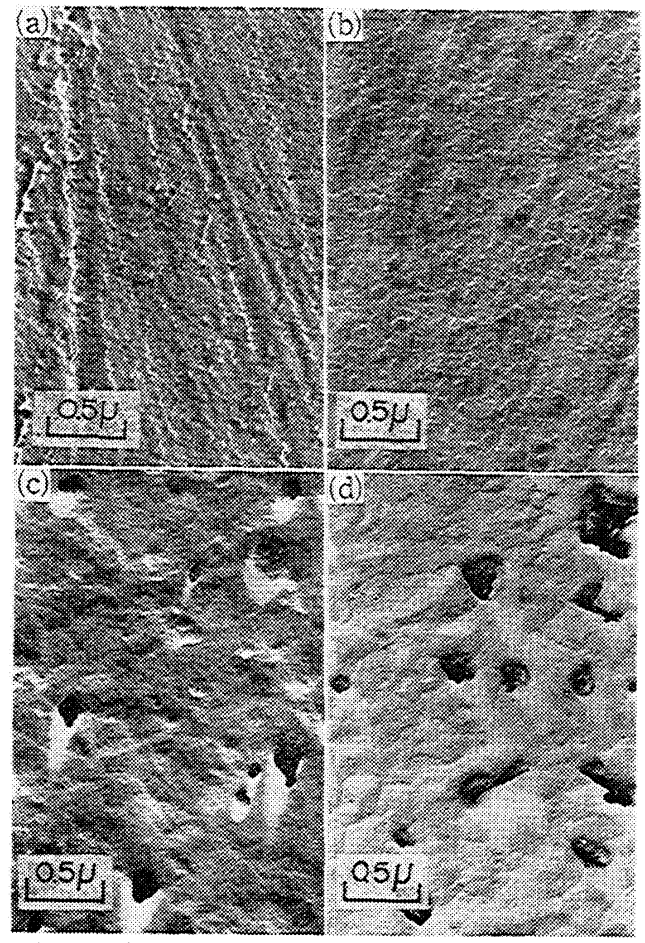

Fig. 6. Electron micrographs and roughness factor of 80% copper alloy surface after various treatments.
(a): Non-treatment (1), Roughness factor 3.1
(b): Hydrogen-treatment (2), Roughness factor 3.1
(c): Oxidation-reduction treatment (3), Roughness factor 5.7
(d): Annealing-treatment (4), Roughness factor 5.6

Discussion

As has descrived above, the catalytic activities of copper-nickel alloy plates were extremely enhanced by the O-R treatment; the activity was greatest after the O-R treatment in the very narrow range of alloy composition lying around 85% copper. On the contrary, pure metals, copper, and nickel were not activated by the treatment.

The thickness of the surface layer which was oxidized and deoxidized by the O-R treatment was estimated by means of a tortional microbalance with high sensibility. The results from this experiment, after treatment under different oxidation conditions, are shown in Table 1. In each case, the oxide layer was observed to be completely deoxidized by the reduction treatment. From these results, it should be pointed out that the very thin layer (a few monolayers) on the alloy surface is possibly closely related to the catalytic phenomena.

Two possible reasons for the enhancement in catalytic activity after the treatment may be considered to be : (a) an increase in the surface area (the roughness factor) of the catalyst, and (b) a production of new active sites after the O-R treatment. Measurement of the changes in the surface area indicated that the roughness factor was increased only about twice after the O-R treatment; it did not correspond to the catalytic activity. Consequently, it is possible to conclude that the origin of the remarkable enhancement of activity is the production of new active sites by the

TABLE 1. RESULTS OF GRAVIMETRIC MEASUREMENT WITH SURFACE TREATMENT

Treatment		Mass Gain after Oxidation	Thickness of oxide layer	Roughness factor after reduction	Catalytic activity ($H_2+D_2=2HD$)
Oxidation	Reduction				
$P_{O_2}=0.017$ Torr 2 min, 500°C	$P_{H_2}=16$ Torr 2 hr, 300°C	9.7×10^{-8} g/cm²	15—20 Å	5.5	1.6×10^{16} molecules/cm²·sec
$P_{O_2}=2.3$ Torr 1 min, 500°C	$P_{H_2}=16$ Torr 2 hr, 300°C	1.9×10^{-6} g/cm²	300 Å	5.7	2.1×10^{16} molecules/cm²·sec

treatment.

In our previous study[18] of the effect of ion bombardment on the catalytic activity of copper-nickel alloys, a result similar to that of the present work was obtained; we found the composition of the copper-nickel alloy which gives the maximum activity, fifteen times that of pure nickel. Measurement of the annealing effect of alloy catalysts after ion bombardment also showed that, for the copper-nickel alloys, the critical temperatures at which the activity began suddenly to decrease were observed to be between 300 and 500°C. When we compare the activity pattern and deactivation process after the ion bombardment with those after the O-R treatment, many similar general tendencies can be found.

To account for the enhancement of activity after the treatments, it is assumed that lattice defects resulting from the O-R treatment or the ion bombardment contribute to the greatly-enhanced catalytic activity. According to the study of the effect of ion bombardment on the surface of silver by Sosnovsky,[16] the catalytic activity of silver is increased in the order of several tens of times by the treatment; it was concluded on the basis of the evidence by Ogilvie[22] that ion bombardment produces disoriented regions bounded by stable arrays of dislocations, that the reaction occurs at sites where dislocation lines intersect the surface. Takeuchi *et al.*[8] also concluded that the activity of copper-nickel alloy films can be explained by taking the unstable lattice imperfactions into considerations. Similarly, large numbers of structural defects of various kinds were found in thin oxide films on copper, nickel, and alloys.[23] It seems likely that same structural defects in oxide films, especially dislocation, remain even after the hydrogen reduction of the oxide in the temperature range below 300°C. Uhara and his co-workers[11] pointed out that the catalytic activity of cold-worked metals was decreased in two temperature ranges during annealing; those ranges correspond to the disappearance of vacancies (>200°C) and dislocations (>400°C).

Considering these results, it can be concluded that the active sites produced by the O-R treatment may be related to surface dislocations of a particular type on copper-nickel alloys. Otherwise after the O-R treatment the active sites seem to be associated with a heterogeneous surface in alloy composition. Kubaschewsky and his co-workers[24] have shown that the miscibility gap forms a phase separation in copper-nickel alloys at temperatures lower than 322°C. On the other hand, Hall and Emmett[25] in their study of powder catalysts of copper-nickel alloys, found activity pattern in the effect of hydrogen pre-adsorption quite similar to that of the O-R treatment (Fig. 3) in the present study. The effect of pre-adsorbed hydrogen by alloy surfaces is probably important in accounting for the remarkable enhancement of the catalytic activity.

As has been described in the Introduction, a number of papers on the catalysis of copper-nickel alloy films have been published. Sachtler *et al.*[3-5] have shown that particular copper-nickel alloys in copper-rich appear to be formed preferentially after heating at 200°C; they also revealed, by calculations, that the free energy of the formation of an alloy containing 80% copper at 200°C appears to be favored as a result of a wide miscibility gap of the alloy system, and suggested on the basis of experiments on the CO adsorption, that the 80% copper alloy must exist in the surface layer. In similar experiments, Campbell and Emmett[7] found that when alloy films were homogenized by heating to 500°C in hydrogen from an alloy containing about 60% copper (bulk composition), the excess of

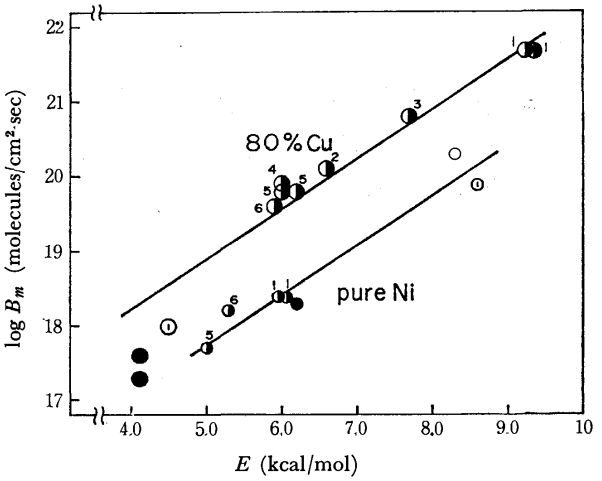

Fig. 7. Plot of the activation energy against the log B_m for nickel and 80% copper alloy, for hydrogen-deuterium exchange reaction.
Smaller circle: pure nickel
Larger circle: 80% copper alloy
○: Treatment (1), ◑: Treatment (3),
◐: Treatment (2), ●: Treatment (4).
Number of each activity point of 80% copper alloy signifies different oxidation condition as same as in Fig. 3.

22) G. J. Ogilvie, *J. Phys. Chem. Soilds*, **10**, 222 (1959).
23) J. V. Cathcart, G. F. Petersen, and C. J. Spanks, *Proc. Cagamore Army Master Res. Confer.*, **13**, 333 (1967).
24) L. Elford, F. Müller and O. Kubaschewski, *Ber. Bunsenges.*, **73**, 601 (1969).
25) W. K. Hall and P. H. Emmett, *J. Phys. Chem.*, **63**, 1102 (1959).

nickel or copper present gives the X-ray diffraction pattern of the pure metals. The activity patterns obtained by Sachtler *et al.*[3-5] showed a constant value over these films with an equal surface composition, while that obtained by Campbell and Emmett[7] showed a promoting effect, increasing to a value of from five to fifteen times as great as for pure nickel in spite of the wide miscibility gap. The structure and surface phenomena of alloy films might be very complicated in comparison with the plates of the alloys used in the present work.

Finally, plots of the logarithm of the pre-exponential B_m factor against the energy of activation are shown in Fig. 7. It appears that the tendency for increased energies of activation to be compensated for by an increase in the pre-exponential factor was found to be separable in pure nickel and in the copper-nickel alloy.

BULLETIN OF THE CHEMICAL SOCIETY OF JAPAN, VOL. 45, 3002—3005 (1972)

ESR Studies of the Conformation and Restricted Rotation of 4-Phenyl-1,3-dioxane Anion

Masamoto IWAIZUMI, Takashi MATSUZAKI, and Taro ISOBE

The Chemical Research Institute of Non-Aqueous Solutions, Tohoku University, Katahira, Sendai

(Received January 5, 1972)

The ESR of the 4-phenyl-1,3-dioxane anion shows a line-width alternation effect which can be attributed to the restricted rotation between the 1,3-dioxane and benzene rings. From the temperature dependence of the line-width alternation effect, the activation energy was determined to be 180 ± 110 cal·mol^{-1}. The preferential conformation between the two rings was estimated from the hyperfine splitting constant of the proton at the 4 position in the 1,3-dioxane ring, to be that where the two rings have some angle close to 90° rather than the structure where they are parallel. It was also found that an odd electron, which mainly occupies a vacant π orbital in the benzene ring, delocalizes appreciably into a part of the 1,3-dioxane ring.

Studies of hindered intramolecular motion have attracted much interest. In some cases, ESR has been a very effective technique for this kind of study. In this paper we wish to report an investigation of the restricted rotation and the preferential conformation between the benzene and 1,3-dioxane rings in the anion of 4-phenyl-1,3-dioxane (I) by means of ESR.

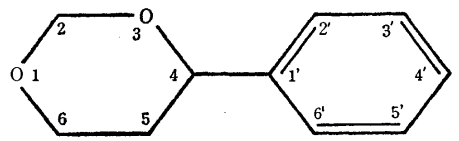

[I]

The ESR of this anion shows a line-width alternation effect, which can be connected to the restricted rotation between the benzene and 1,3-dioxane rings. Since β-proton hyperfine splitting constants are sensitive functions of molecular geometry,[1] the hyperfine splitting constants of the proton at the 4 position of the 1,3-dioxane ring are also an effective source of information about the conformation and restricted rotation between the two rings. Although the conformational analysis of saturated heterocyclic rings is one of the most interesting problems in organic stereochemistry, no information about the structure of the 1,3-dioxane ring of this anion can be obtained by ESR. It can be seen, however, from a NMR study of the neutral molecule of 4-phenyl-1,3-dioxane that the phenyl group is in an equatorial position of the 1,3-dioxane ring. The details of the NMR study of this material, however, will not be discussed here.

1) a) C. Heller and H. M. McConnell, *J. Chem. Phys.*, **32**, 1535 (1960). b) E. W. Stone and A. H. Maki, *ibid.*, **37**, 1326 (1962).

Experimental

The anion of 4-phenyl-1,3-dioxane was prepared by the reduction of 4-phenyl-1,3-dioxane with sodium-potassium alloy using a mixed solvent of tetrahydrofuran (THF) and 1,2-dimethoxyethane (DME) in a 1 : 1 volume ratio. The 4-pheyl-1,3-dioxane used was obtained commercially (Tokyo Kasei's product) and was purified by distillation. The distilled 4-phenyl-1,3-dioxane was stored over a potassium metal in a bottle connected to a vacuum line. For the preparation of the anion, the compound was taken by distillation from the bottle through the vacuum line into a reaction vessel. The reduction reaction did not proceed in THF or when sodium or potassium was used separately.

The ESR spectra were obtained on a Hitachi Model 771 X-band ESR spectrometer. Variable temperature experiments were performed using a Hitachi gas-flow-temperature control unit. The calculation for the simulation of the spectra was carried out using the NEAC 700 computer at the Tohoku University Computer Center.

Results and Discussion

Reaction of 4-phenyl-1,3-dioxane with Sodium-potassium Alloy. A colorless solution of 4-phenyl-1,3-dioxane turns orange upon contact with sodium-potassium alloy and then changes to green in a few hours. This reaction rate is prompted by an increase

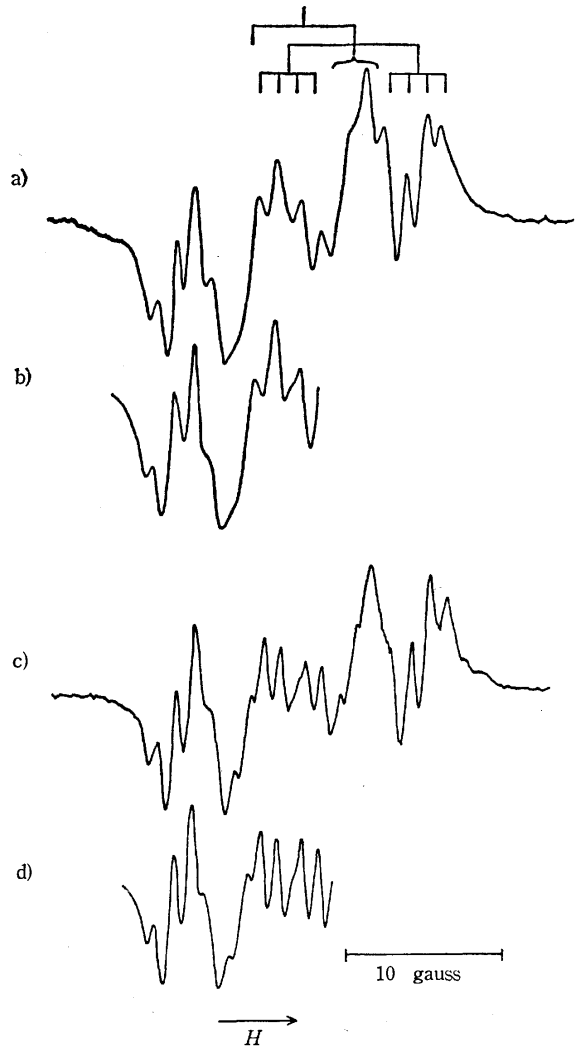

Fig. 1. ESR spectra of the 4-phenyl-1,3-dioxane anion.
a) Spectrum at −8°C. b) Computer-simulated spectrum for (a) using the hyperfine splitting constants listed in Table 1 and the parameters, $\Delta a=1.30$ gauss, $\tau=1.6\times10^{-7}$ sec, and $T_2^{-1}=2.43$ MHz. c) Spectrum at −100°C. d) Computer-simulated spectrum for (c) using the hyperfine splitting constants listed in Table 1 and the parameters, $\Delta a=1.30$ gauss, $\tau=2.0\times10^{-7}$ sec, and $T_2^{-1}=1.80$ MHz.

in the quantity of DME in the mixed solvent. Both the orange and green solutions show ESR spectra. Figure 1 shows the spectra which were taken from the orange solution. This spectra can be attributed to the 4-phenyl-1,3-dioxane anion, while the spectrum taken from the green solution consists of $25(=5\times5)$ hyperfine lines and fits perfectly with the hyperfine pattern of the naphthalene anion.[2] The change in color from orange to green, therefore, may be attributed to the formation of the naphthalene anion from the 4-phenyl-1,3-dioxane anion. The reaction mechanism will be discussed elsewhere.

The Line-width Alternation Effect in ESR and the Restricted Rotation between the Benzene and 1,3-dioxane Rings. Figure 1 shows that the spectra of the 4-phenyl-1,3-dioxane anion are temperature-dependent, although the change with the temperature is not very drastic. The spectra at room temperature can be analyzed in terms of two sets of doublet splittings due to hyperfine interaction with single protons, a triplet splitting which is due to two protons and which shows a line-width alternation effect, and a quartet splitting due to the interaction with three protons. It is seen, through the computer simulation of the spectra, that the quartet splitting splits to a doublet and a triplet splitting at lower temperatures. The hyperfine splitting constants, as determined by the computer simulation of the spectra, are listed in Table 1. The assignment of the hyperfine splitting constants to the proton positions was reasonably made by comparison with the hyperfine splitting constants for the acetophenone or benzaldehyde anion previously reported by Steinberger and Fraenkel.[3] The hyperfine splitting constants for the 4-phenyl-1,3-dioxane and benzaldehyde anions are compared in Table 1. Apparently the protons which show the line-width alternation effect can be assigned to the protons at the 2′ and 6′ positions of the benzene ring. In the cases of the acetophenone and benzaldehyde anions, the carbonyl groups are locked into the plane of the aromatic ring, and the two ortho protons as well as the two meta protons show different hyperfine splitting constants. It seems likely that, as in the case of the acetophenone or benzaldehyde anion, the hyperfine splitting constants of two protons at the 2′ and 6′ positions of the 4-phenyl-1,3-dioxane anion have different splitting constants because of the presence of the oxygen atom at the 3 position in the

Table 1. Hyperfine splitting constants of the 4-phenyl-1,3-dioxane and benzaldehyde anions (in gauss)

4-Phenyl-1,3-dioxane anion			Benzaldehyde anion[b]	
Positions	Splitting constants −100°C	−8°C	Positions[c]	Splitting constants
2′, 6′	4.186[a]	4.285[a]	2	4.685
			6	3.393
3′, 5′	1.035	1.209	3	1.307
			5	0.750
4′	6.712	6.703	4	6.471
4	1.166	1.209	CHO	8.507

a) These protons show the line-width alternation effect and the hyperfine splitting constant listed is the average value for the two potons.
b) Taken from reference 3.
c) Numbering for the proton positions is as follows.

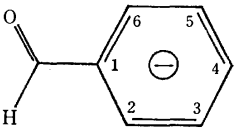

2) a) B. H. J. Bielski and J. M. Gebicki," Atlas of Electron Spin Resonance", Academic Press, New York, N. Y. (1967), p. 351.
b) M. Iwaizumi, M. Suzuki, T. Isobe, and H. Azumi, This Bulletin, **41**, 732 (1968).

3) N. Steinberger and G. K. Fraenkel, *J. Chem. Phys.*, **40**, 723 (1964).

1,3-dioxane ring. The line-width alternation effect, therefore, can be attributed to the modulation effect of the 2′ and 6′ proton hyperfine splittings caused by the restricted rotation between the benzene and 1,3-dioxane rings, the modulation of the hyperfine splittings having an out-of-phase correlation for the two protons.

By using Bloch's two-jump model,[4] the spectra at various temperatures were analyzed in order to estimate the activation energy for the rotation. According to the theory of the line-width alternation effect,[4d,5] the line-width broadening is proportional to the square of the magnitude of fluctuation in the hyperfine splitting, Δa, and to the correlation time for the fluctuation, τ, *i. e.*, proportional to $\Delta a^2 \cdot \tau$. Since the hyperfine splitting constants for the static conformation of the molecule were not available, we assumed the magnitude of the fluctuation for the 2′ and 6′ proton hyperfine splittings to be 1.30 gauss by reference to the case for the hyperfine splitting constants of the benzaldehyde anion. By neglecting the temperature dependence of the value for Δa, the τ values were evaluated for the spectra at various temperatures by computer simulation of the spectra. Of course, the absolute magnitude for the τ thus obtained contains some error, because of the use of an assumed value for Δa. However, the error in the τ will not lead to a large error in the calculation of the activaiton energy for the rotation, since a large part of the error in τ can be compensated for the procedure for obatining the activation energy by the Arrhenius relation. In Fig. 2, the plot of $\log_{10}(1/\tau)$ *vs.* $1/T$ is shown. The activation energy is obtained as 180 ± 110 cal·mol^{-1} from the slope by the Arrhenius relation. Here the $1/\tau = k$ relation was assumed, where k is a rate constant for rotation.

In the cases of the acetophenone and benzaldehyde anions, the meta protons also have different hyperfine splitting constants, just as they have different ortho

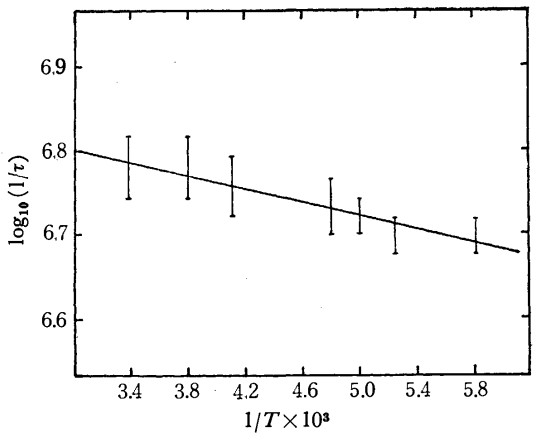

Fig. 2. Plot of $\log_{10}(1/\tau)$ against $1/T \times 10^3$.

proton hyperfine splittings. In the present case, however, it was not obvious from the computer simulation of the spectra whether or not the hyperfine splitting of the 3′ and 5′ protons also shows a line-width alternation effect.

It should be noticed here that the evaluated activation energy is small compared to kT. In such a situation, the two-jump model, which assumes a "jump" between the two conformations, may not be strictly correct for treating the system. However, it may not be unreasonable to consider that the activation energy thus estimated still has meaning as an approximate value.

Electron-spin Delocalization in the Molecule. It is well known that the hyperfine splitting constant of the aromatic ring proton, a_i^H, can be related to the spin density, ρ_i^H, on the carbon atom to which the proton is attached by McConnell's relation, $a_i^H = Q^H \rho_i^H$, or a modification of it.[6] Here, Q is an empirical constant and has a value of $-22.5 \sim -30$ gauss. In Table 2 the spin densities evaluated by McConnell's relation using $Q = -22.5$ guass are listed. From a comparison with the calculated spin densities for the acetophenone or benzaldehyed anion,[3] a negative sign

Table 2. Spin densities for the 4-phenyl-1,3-dioxane and benzaldehyde anions

4-Phenyl-1,3-dioxane anion		Benzaldehyde anion	
Positions	Spin densities[a]	Positions	Spin densities[b]
2′, 6′	0.186	2	0.1748
		6	0.1196
3′, 5′	(−)0.046[c]	3	−0.0567
		5	−0.0226
4′	0.299	4	0.2492

a) Calculated by the relation, $|\rho_i| = |a_i^H|/22.5$ using the hyperfine splitting constants obtained at −100°C.
b) Taken from reference 3. Calculated values.
c) See text.

was assigned to that for the 3′ and 5′ positions. As Table 1 shows, the hyperfine splitting constant for the protons at the 3′ and 5′ positions has a positive temperature coefficient, showing a contrast to the other ring-proton hyperfine splittings. On a basis of a consideration of the vibrational effects on the proton hyperfine splitting constants,[7] the assignment of the negative sign to the spin density at the 3′ and 5′ positions may also be justified by this positive temperature coefficient of the hyperfine splitting constant.

Interstingly, it is shown that the spin density on the benzene ring is far less from unity. That is, the algebraic sum of the spin densities for the carbon positions from 2′ to 6′ is only 0.6; in order for the sum of the spin densities on the benzene ring to be unity, one must consider the spin density of the 1′ position

4) a) H. S. Gutowski and C. H. Holm, *J. Chem. Phys.*, **25**, 1288 (1956). b) H. S. Gutowski, D. W. McCall and C. P. Slichter, *ibid.*, **21**, 279 (1953). c) H. M. McConnell, *ibid.*, **28**, 430 (1958). d) P. Sullivan and J. R. Bolton," Advances in Magnetic Resonance" Vol. 4 ed J. S. Waugh, Academic Press, New York, N. Y., (1970) p. 39.

5) a) J. H. Freed and G. K. Fraenkel, *J. Chem. Phys.*, **39**, 326 (1963). b) G. K. Fraenkel, *J. Phys. Chem.*, **71**, 139 (1967).

6) a) H. M. McConnell and D. B. Chesnut, *J. Chem. Phys.*, **28**, 107 (1958). b) J. P. Colpa and J. R. Bolotn, *Mol. Phys.*, **6**, 273 (1963). c) G. Giacometti, P. L. Nordio, and M. V. Pavan, *Theoret. Chim. Acta* (Berlin) **1**, 404 (1963).

7) a) M. Iwaizumi and G. K. Fraenkel, unpublished data. b) A. H. Reddoch, C. L. Dodson and D. H. Paskovich, *J. Chem. Phys.*, **52**, 2318 (1970).

to be 0.4. One can see from the comparison with the spin densities for the acetophenone or benzaldehyde anion that this estimated spin density for the 1 position is unreasonably large; about 0.1 seems to be suitable for this position. The spin density on the benzene ring is, therefore, apparently far from a full unit. This decrease in the spin densities on the benzene ring from unity indicates that the electron spin delocalizes into a part of the 1,3-dioxane ring.

In studies of the conformation of organic π radicals with a cyclopropyl substituent, it has been shown that the cyclopropyl ring preferentially adopts a bisected conformation to the aromatic ring except in sterically-crowded environments, and that the electron-donative hyperconjugation effect of the cyclopropyl ring has an important role in the adoption of the conformation.[8] This hyperconjugation effect of the cyclopropyl ring has been explained by Walsh's model,[9] which considerd the sp^2 hybridization for the carbon valency to hydrogen and the $2p$ atomic orbital for carbon valencies to carbon. Walsh points out, in his theoretical study of cyclopropane and related compounds, that even cyclohexane appears to have a greater tendency towards a $2p$ character in the carbon valencies to carbon. In view of the fact that the 1,3-dioxane ring prefers a conformation at right angles to rather than planar with the benzene ring, as will be discussed later, the electron-spin delocalization may take place by means of the hyperconjugation effect of the 1,3-dioxane ring. On the other hand, the charge-transfer effect of a lone-pair electron on the oxygen atom at the 3 position may be considered as another possible mechanism for the electron-spin delocalization into the 1,3-dioxane part. In both cases, an electron with a β spin will transfer from the 1,3-dioxane ring or the lone-pair electron of the oxygen into the vacant π orbital of the benzene ring, leaving a α spin on the 1,3-dioxane part. However, there is not definite experimental proof on which mechanism is dominant.

Conformation Preference of the 1,3-*dioxane Ring in Relation to the Benzene Ring.* The β proton hyperfine splitting constants are sensitive to the conformation of the C-H$_\beta$ bond. When the alkyl group is undergoing torsional oscillation about a particular equilibrium conformation of a restricted rotation, the β proton hyperfine splitting constants are temperature-dependent and are generally expressed by the equation;[1a]

$$a_\beta^{\mathrm{H}} = B\langle\cos^2\theta\rangle_{\mathrm{av}}\rho_i \qquad (1)$$

Here, B is an empirical constant and in the range of of 45 ± 6 gauss, ρ_i, is the spin density at the trigonal carbon (i) of the attachment, and θ is the dihedral angle between the C-H$_\beta$ bond and the $2p$ orbital on the i-th carbon. The average $\langle\mathrm{con}^2\theta\rangle$ depends upon the nature of the rotation and is expressed by the following equation:

$$\langle\cos^2\theta\rangle_{\mathrm{av}} = \frac{\sum_{j=0}^{\infty} g_j\langle\cos^2\theta\rangle_j \exp(-E_j/kT)}{\sum_{j=0}^{\infty} g_j \exp(-E_j/kT)} \qquad (2)$$

with:

$$\langle\cos^2\theta\rangle_j = \langle\phi_j(\alpha)\,|\cos^2(\alpha+\theta_0)|\,\phi_j(\alpha)\rangle \qquad (3)$$

in which ϕ_j and E_j designate the wave function and the energy eigenvalue respectively for the torsional quantum state or rotational state j, in which g shows the degeneracies of the state, and in which θ_0 is the equilibrium angle of the θ. The ϕ_j and E_j values used for these equations are obtained by solving the Schrödinger equation for the torsional oscillation or restricted rotation of the system. In the present case, as Table 1 shows, the proton at the 4 position shows a temperature-dependent hyperfine splitting with a positive temperature coefficient. However, it is not quantitatively treated here, and only the equilibrium conformation of the 1,3-dioxane ring against the benzene ring is qualitativaly considered.

Stone and Maki[1] calculated the values of $\langle\cos^2\theta\rangle$ for some typical cases as a function of the activation energy for four possible values of θ_0 and $T=298$°K. We refer to his calculation for estimating θ_0 for the case of the 4-phenyl-1,3-dioxane anion. In the present case, if it is assumed that the spin density at the 1′ position is 0.1, and if we use $B=45$ guass, $\langle\cos^2\theta\rangle$ is obtained as 0.25, corresponding to $\langle\theta\rangle=60°$. The value of $\langle\theta\rangle$ for the free rotation is 45°, and as the potential barrier for rotation increases, the value of $\langle\theta\rangle$ approaches the value for the equilibrium conformation. Taking into consideration the fact that

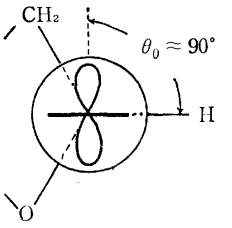

[II]

the activation energy for the rotation of the 4-phenyl-1,3-dioxane anion is 180 cal·mol^{-1}, the equilibrium angle of the C-H bond must be larger than 60°, and rather close to 90° (II). The positive temperature coefficient of the hyperfine splitting constant for this proton will support such a bisected conformation of the 1,3-dioxane ring against the benzene, ring. Such a conformation seems plausible from the point of view of the steric effect between the two rings, and also in view of the conjugative electronic interaction discussed above, although the contribution of both interactions are small, as is shown by the small activation energy obtained.

8) a) G. A. Russell and H. Malkus, *J. Amer. Chem. Soc.*, **89**, 160 (1967). b) N. L. Bauld, R. Gordon and J. Zoeller, Jr., *ibid.*, **89**, 3948 (1967). C) N. L. Bauld, J. D. McDermed, C. E. Hudson, Y. S. Rim, J. Zoeller, Jr., R. D. Gordon and J. S. Hyde, *ibid.*, **91**, 6666 (1969).

9) A. D. Walsh, *Trans. Faraday Soc.*, **45**, 179 (1949).

Computer Simulations of the ESR Spectra of the Triplet Dimers of Bis-(*N*-Salicylidenemethylaminato)copper(II) in Toluene

Makoto CHIKIRA and Taro ISOBE

Chemical Reserach Institute of Non-aqueous Solutions, Tohoku University, Katahira, Sendai

(Received January 31, 1972)

It has been concluded, from computer simulations of the observed ESR line shapes, that the dimeric structure of bis-(*N*-salicylidenemethylaminato)copper(II) in a frozen toluene solution is similar to that in its γ-form crystals. Furthermore, the difference between the hyperfine splittings observed at both edges of the triplet spectra for $\Delta M=1$, the large frequency dependence of the fine-structure splitting, and the additional hyperfine structures observed in the field range between the so-called low-field parallel and perpendicular lines have been found to be due to the noncoincidence of the principal axes of the g tensor with those of the fine-structure tensor.

The ESR spectra of the triplet dimers of copper complexes in frozen solutions have been studied by many authors.[1-7] Although there are a variety of dimeric structures, it has always been assumed that the spin Hamiltonian applied to the dimers is axially symmetric and that the principal axes of the g tensor are coincident with those of the fine-structure tensor, $\boldsymbol{D}$. Recently, Yokoi and Isobe[7] found that triplet dimers are formed at considerably high concentrations in the toluene solutions of some 1 : 2 β-diketone chelate complexes of copper(II) and that the dimers are in equilibrium with the monomers. We established that such a equilibrium exists in the toluene solution of bis-(*N*-salicylidenemethylaminato)copper(II) (abbreviated as Cu(Mesal)$_2$). Furthermore, its ESR line shapes at 77°K could not be explained in terms of the spin Hamiltonian usually applied.

The dimeric structure shown in Fig. 1 is found in the γ-form crystals of Cu(Mesal)$_2$.[8] It can naturally be supposed that the complex in toluene has the same dimeric structure as in the γ-form crystals. The axes of the fine-structure tensor due to magnetic dipole interactions in such a dimer do not coincide with those of the g tensor. The purpose of this paper, therefore, is to estimate the dimeric structure of the complex in toluene on the basis of computer simulations of the ESR line shapes of randomly-oriented triplet dimers, using a more general spin Hamiltonian.

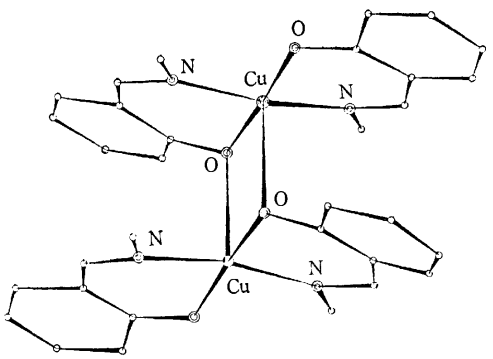

Fig. 1. Structure of the dimer in the γ-form crystals of Cu(Mesal)$_2$.[8]

Experimental

The ESR spectra of Cu(Mesal)$_2$ in toluene were recorded at 77°K with two HITACHI ESR spectrometers, Model 771 (*X*-band) and Model MES 4001 (*K*-band). The field was calibrated with an NMR probe and then with a benzen solution of vanadyl acetylacetonate. Cu(Mesal)$_2$ was prepared according to the method in the literature[9] and was recrystallized from methanol several times.

Results and Discussion

ESR Spectra of the Triplet Dimers. The *X*-band and *K*-band ESR spectra of Cu(Mesal)$_2$ in toluene measured at 77°K are shown in Figs. 2, 3, and 4. The spectra in Figs. 2 and 4 consist of two kinds of spectra; one is due to monomer species ($S=1/2$), and the other, to triplet dimer species ($S=1$). Various magnetic parameters are defined in these figures; A_3 is the hyperfine splitting constant of the so-called[4] minimum-field lines of $\Delta M=2$ transitions, A_L and A_H are those of the low-field and high-field parallel lines of $\Delta M=1$

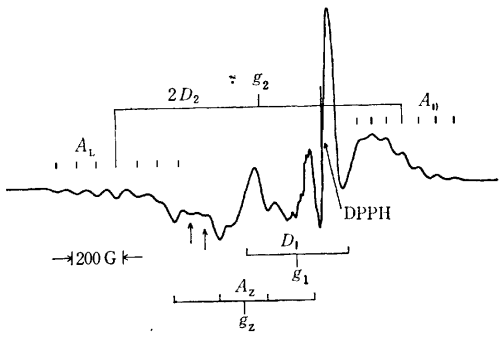

Fig. 2. The *X*-band ESR spectrum of Cu(Mesal)$_2$ in toluene at 77°K (0.01 M).

1) R. H. Dunhill, J. R. Pilbrow, and T. D. Smith, *J. Chem. Phys.*, **45**, 1474 (1961).
2) J. F. Boas, R. H. Dunhill, and J. R. Pilbrow, *J. Chem. Soc., A*, **1969**, 94.; J. F. Boas, J. H. Price, J. R. Pilbrow, K. S. Murray, and T. D. Smith, *ibid., A*, **1970**, 968.
3) G. F. Kokoszka, M. Linzer, and G. Gordon, *Inorg. Chem.*, **7**, 1730 (1968).
4) N. D. Chasteen and R. L. Belford, *ibid.*, **9**, 169 (1970).
5) W. E. Hatfield, J. A. Barnes, D. Y. Jeter, R. Whymann, and E. R. Jones, Jr., *J. Amer. Chem. Soc.*, **92**, 4982 (1970).
6) G. O. Carlisle and W. E. Hatfield, *Inorg. Nucl. Chem. Lett.*, **6**, 633 (1970).; J. F. Villa and W. E. Hatfield, *Inorg. Chim. Acta*, **5**, 145 (1971).
7) H. Yokoi and T. Isobe, This Buletin, 44, 1446 (1971); *ibid.*, to be published.
8) D. Hall, S. V. Sheat, and T. N. Water, *J. Chem. Soc., A*, **1968**. 460.
9) P. Peifer and H. Glaser, *J. Prakt. Chem.*, **153**, 265 (1939).

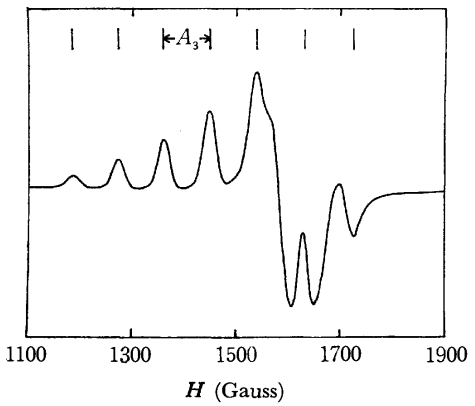

Fig. 3. "Half-field" $\Delta M=2$, ESR spectrum of $Cu(Mesal)_2$ in toluene at 77°K (0.1 M).

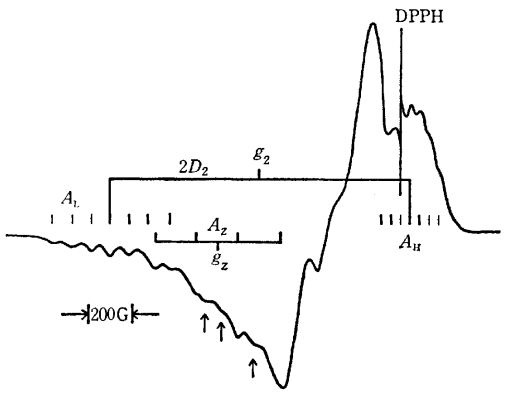

Fig. 4. The K-band ESR spectrum of $Cu(Mesal)_2$ in toluene at 77°K (0.05 M).

transitions, respectively. D_2 is one half of the splitting between the full-field parallel lines, and D_1 is a splitting between the full-field perpendicular lines. The values of g_1 and g_2 were determined from the centers of the full-field perpendicular and parallel lines respectively. These results are listed in Table 1.

The ESR spectra of the triplet dimers of copper complexes show seven-line hyperfine patterns upon the coupled nuclear spin ($I=3$) of two copper ions ($I=3/2$), and the separations of the hyperfine components can be expected to be about one half of those observed for the monomer.[10] It should be noted that the A_3, A_L, and A_H at the X-band spectra are all different, and that they decrease in this order. In the K-band spectrum, A_L becomes a little larger, but the A_H is considerably smaller than that in the X-band spectrum. It is also evident that the D_2 in the X-band differs both from the D_1 in the same band and from the D_2 in the K-band. In addition, the g_2 is considerably smaller than the g_z of the monomers. If the dimers were axially symmetric and if the axes of the g, D, and hyperfine tensors were all coincident with each other, A_L and D_2 would have to be almost equal to A_H and D_1 respectively.[3,4] In this case, therefore, the small difference between A_L and A_H must be attributed to the second-order effect of hyperfine interactions. However, this difference cannot be explained only by this effect, because the second-order effect weakens as the resonance frequency increases. This fact contradicts the experimental result that the difference between A_L and A_H in the K-band becomes quite a bit larger than that in the X-band. Moreover, we must point out that additional hyperfine structures, which are indicated by arrows in Figs. 2 and 4, were found in the field range between the so-called low-field parallel and perpendicular lines; it is clear that the hyperfine structures are due not to the monomers, but to the dimers. Similar hyperfine structures had been found more clearly in the spectra of the aqueous solutions of copper tartrates at 77°K.[4] However, these structures have not yet been explained theoretically.

Table 1. Magnetic parameters

	Observed values		Case A		Case B	
	X-band	K-band	X-band	K-band	X-band	K-band
A_3	87 G					
A_L	79	82 G	75 G	81 G	80 G	85 G
A_H	65	46	60	51	64	52
g_1	2.069				2.116	2.094
g_2	2.170	2.169	2.126	2.127	2.164	2.186
D_1	394 G				475 G	430 G
D_2	563	657 G	753 G	830 G	560	679

Magnetic parameters of the monomer; $g_z=2.220$, $A_z=0.0192\,cm^{-1}$, $g_0=2.112$, $A_0=0.0079\,cm^{-1}$, where g_0 and A_0 were determined from the X-band spectra at room temperature. (X-band: 9.2202 GHz, K-band: 23.816 GHz).

The resonance conditions of triplet dimers for the $\Delta M=1$ transitions can be expressed by this first-order approximation:[11]

$$\hbar\omega = g(z,\varphi)\beta H \pm D(z,\varphi) + A(z,\varphi)M_I;\ z=\cos\theta \quad (1)$$

where θ and φ are the polar co-ordinates of the direction of the static magnetic field, where M_I is the quantum number of the hyperfine component of the coupled nuclear spin, and where ω is the angular frequency of the oscillating magnetic field. Then, the resonance magnetic field can be calculated from Eq. (1) as:

$$H(z,\varphi) = \frac{\hbar\omega \mp D(z,\varphi) - A(z,\varphi)M_I}{g(z,\varphi)\beta} \quad (2)$$

It was indicated by Kottis and Lefebvre[12] that the ESR spectrum of a paramagnetic powder or a glassy solution show characteristic peaks in the fields where the stationary conditions (3) are satisfied:

$$dH = \frac{\partial H}{\partial z}dz + \frac{\partial H}{\partial \varphi}d\varphi = 0 \quad (3)$$

From Eqs. (2) and (3), two stationary conditions for the $\Delta M=1$ transitions can be obtained according to the plus and minus signs in Eq. (2). If the principal axes of the g, D and A tensors are coincident with each other, the two conditions will be simultaneously satisfied in the directions of the tensor axes, because both $\partial H/\partial z$ and $\partial H/\partial\varphi$ always vanish in those directions. If these axes do not coincide with each other, the ori-

10) C. P. Slichter, *Phil. Mag.*, **42**, 441, (1951).

11) B. Bleaney, *Phil. Mag.*, **42**, 441, (1951).

12) P. Kottis and R. Lefebvre, *J. Chem. Phys.*, **39**, 393 (1963); *ibid.*, **41**, 379 (1964).

entations which satisfy Eq. (3) will differ according to the plus or minus sign in Eq. (2), and they will not generally agree with the orientation of the principal axes. In that case, the observed parameters are not the principal values of these tensors. These facts suggest that the unusual behavior of the observed hyperfine and fine-structure splittings is due to the noncoincidence of the principal axes of the g tensor with those of the D tensor. In order to confirm this speculation more quantitatively, computer simulations of the ESR line shapes of the randomly-oriented triplet dimers were performed in this investigation. All the calculations were carried out at the Computer Center of Tohoku University.

Simulations of the ESR Line Shapes. The appropriate spin Hamiltonian for the triplet dimers can be expressed as:

$$\mathscr{H} = \boldsymbol{H}\cdot\boldsymbol{g}\cdot\boldsymbol{S} + \boldsymbol{H}_d + \boldsymbol{S}\cdot\boldsymbol{A}\cdot\boldsymbol{I} + J\boldsymbol{S}_1\cdot\boldsymbol{S}_2 \qquad (4)$$

where $\boldsymbol{S} = \boldsymbol{S}_1 + \boldsymbol{S}_2$, $\boldsymbol{I} = \boldsymbol{I}_1 + \boldsymbol{I}_2$

and:

$$\boldsymbol{H}_d = \left(\frac{\beta^2}{r^3}\right)\left\{(\boldsymbol{g}\boldsymbol{S}_1\cdot\boldsymbol{g}\boldsymbol{S}_2) - \frac{3}{r^2}(\boldsymbol{g}\boldsymbol{S}_1\cdot\boldsymbol{r})(\boldsymbol{g}\boldsymbol{S}_2\cdot\boldsymbol{r})\right\} \qquad (4a)$$

where $\boldsymbol{S}_1$, $\boldsymbol{S}_2$, $\boldsymbol{I}_1$, and $\boldsymbol{I}_2$ are the electron and nuclear spin operators of the copper ions, $\boldsymbol{H}_d$ is the operator of the spin dipole interaction, $\boldsymbol{r}$ is the distance between the two ions, and the other symbols have their usual meanings. We assumed here that (a) the g tensors of the two molecules are identical, (b) the spin-exchange interaction parameter, J, is large enough for the coupled electronic and nuclear spin quantum numbers ($S=1$, $I=3$) to be good ones, although the contribution of J to the fine-structure splitting is negligibly small as compared with that of $\boldsymbol{H}_d$, (c) the principal axes of the g and the A tensors are coincident with each other, and (d) $\boldsymbol{H}_d$ can be estimated from a point-dipole approximation.

Our method of calculating the line shapes is essentially the same as that used by many other authors.[12-16] We first calculated the resonance magnetic fields as a function of the orientation with respect to the static magnetic field, integrated it into the powder pattern, and convoluted it with the derivatives of Gaussian or Lorenzian line shapes. We chose the spin eigenfunctions of the Zeeman and exchange interaction terms for a basis set, and regarded $\boldsymbol{H}_d$ and $\boldsymbol{SAI}$ as small perturbations. The line shapes of the $\Delta M=2$ transitions in the X-band will not be discussed here. In the case of the $\Delta M=2$ transitions, the amount of Zeeman splitting is not large enough, as compared with the fine-structure or hyperfine splittings, for the perturbation calculations to give proper energy levels. Since the angular dependence of the transition probability cannot be neglected, it is necessary to solve the higher-order secular equations in order to obtain the exact energy levels and matrix elements of the transition moments. The perturbation calculations were made to the seconds order for $\boldsymbol{H}_d$ and to the first order for $\boldsymbol{SAI}$. As Fig. 5 shows, the x, y, and z axes of the Cartesian co-ordinates were chosen as the principal axes of the g and A tensors. The directions of the static magnetic field and of the copper-copper axes are expressed by the polar co-ordinates, (θ, φ) and (ξ, η) respectively.

Figure 6 shows the angular dependence of the resonance magnetic field for the $\Delta M=1$ transitions for the $M_I=0$ hyperfine component. The parameters used in these calculations were estimated from the parameters of the monomer species and from the structure of the γ-form crystals. These adopted parameters

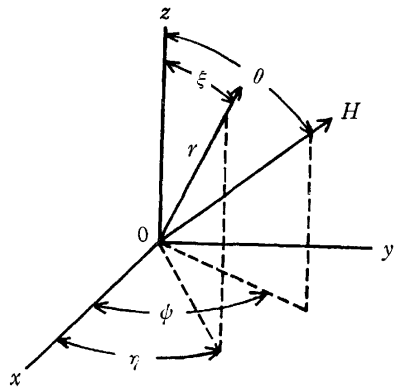

Fig. 5. The directions of the external magnetic field and copper axis with respect to the principal axes of g and A tensors.

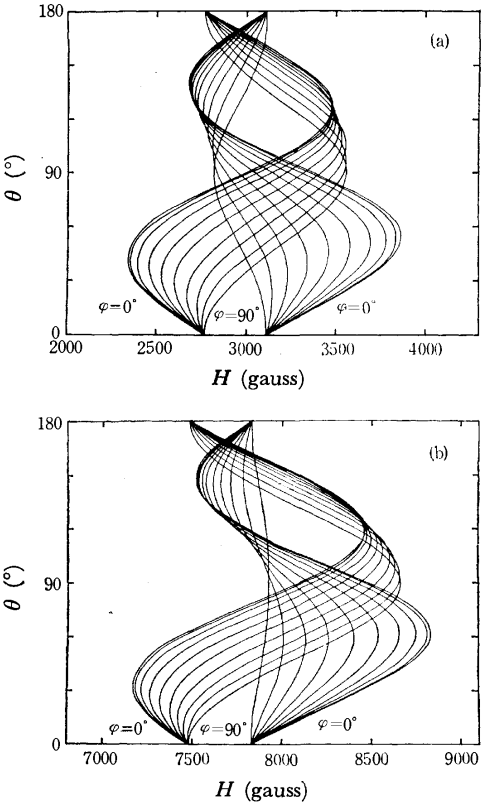

Fig. 6. The angular dependence of the resonance magnetic field of the $\Delta M=1$ transitions for the $M_I=0$ hyperfine component. (a) For X-band, (b) for K-band; $g_{//}=2.22$, $g_{\perp}=2.04$, $\xi=45°48'$, $\eta=0°$, $r=3.4$ Å.

13) E. Wasserman, L. C. Snyder, and W. A. Yager, *J. Chem. Phys.*, **41**, 1736 (1964).
14) F. K. Kneubuhl, *ibid.*, **35**, 156 (1961).
15) R. Neiman and D. Kivelson, *ibid.*, **35**, 156 (1961).
16) P. C. Taylor and P. J. Bary, *J. Mag. Res.*, **2**, 305 (1970); Line Shape Program Manual, 1968, unpublished.

may not be accurate. It is considered, however, that they do not differ from the exact ones greatly enough for the essential features of the line shapes to disappear, because the electronic states of this complex are not changed very much by the weak dimerization force. As is clearly shown in these figures, the dimers which are resonating at both edges of the $\Delta M=1$ spectra are differently oriented; their θ values are different. The approximate values of A_L, A_H, D_2, and g_2, which are defined in Figs. 2 and 4, can be estimated from these figures. If we put $A_{//}=0.0095$ cm^{-1} and $A_{\perp}=0.0010$ cm^{-1}, values which are about one half of those observed for the monomers, A_L and A_H can be calculated from Eq. (5),[11] as is shown in Case A of Table 1:

$$gA=\sqrt{A_{//}^2g_{//}^2\cos^2\theta+A_{\perp}^2g_{\perp}^2\sin^2\theta} \tag{5}$$

These values agree satisfactorily with the observed values. D_2 and g_2 values similarly obtained from the figures are also tabulated there. These values do not agree with the experimentally-obtained values quantitatively, as the A values do, but they do agree qualitatively. For instance, in both the calculations and the experiment, the D_2 in the X-band is smaller than that in the K-band, and the g_2 is significantly smaller than the g_z usually observed for various five-co-ordinated copper complexes. These facts suggest that the structures of the dimers in toluene are very similar to those in the γ-form crystals. In order to determine the parameters more precisely, A_L, A_H, g_2, and D_2 were estimated graphically at different values of r and ξ. First of all, we will discuss the behaviors of g_2 and D_2. From Eq. (1), g_2 and D_2 can be expressed to the first-order approximation:

$$g_2=\frac{2g_Lg_H}{g_L+g_H} \tag{6}$$

and:

$$2D_2=\frac{\hbar\omega}{\beta}\left(\frac{1}{g_H}-\frac{1}{g_L}\right)+\frac{1}{\beta}\left(\frac{D_H}{g_H}-\frac{D_L}{g_L}\right) \tag{7}$$

where g_L, g_H, D_L, and D_H are the g factors and the fine-structure splittings of the dimers, whose orientations can be determined graphically from the minimum and maximum resonance fields of the $\Delta M=1$ transitions. Practically, g_2 is almost equal to $g(\xi, \eta)$. The difference between g_L and g_H becomes larger as the anisotropy of the g tensor, the frequency of the oscillating magnetic field, and the gaps between the copper-copper axis and g tensor axes increase. Accordingly, the first term of Eq. (7) varies greatly with the microwave frequency. On the other hand, the values of the second term changes only a little with the frequency. If the fine-splittings are due only to the magnetic dipole interactions, the value of the second term will be approximately determined by the distance between the two cupric ions and, therefore, somewhat affected by a change in the ξ value. In the X-band spectra, the first term of Eq. (7) is negligibly small as compared with the second one. In this case, the D_2 in the X-band almost agrees with one of the principal values of the zero-field splitting tensor, which is usually represented as Eq. (8) for a point-dipole interaction:

$$D_{d-d}=\frac{3}{4}g^2\beta^2\left\{\frac{1-3\cos^2\theta}{r^3}\right\}_{\max} \tag{8}$$

Accordingly, the distance between the two cupric ions in the dimers can be calculated from Eq. (8) to be 3.39 Å, using the value of g_2 and D_2 obtained from Fig. 6. It is almost the same as the value of r (3.4 Å) used for the calculations in Fig. 6. The ξ and r dependence of D_2 is shown in Fig. 7. As is evident from Fig. 7, the ξ dependence of D_2 in the K-band is larger than that in the X-band. When ξ is closer to 0° or 90°, the difference between the D_2 values in the X-band and the K-band becomes very small. In other words, if the difference is large and the second-order effect of the fine-structure tensor is negligible, there will be a large gap between the copper-copper and g tensor axes.

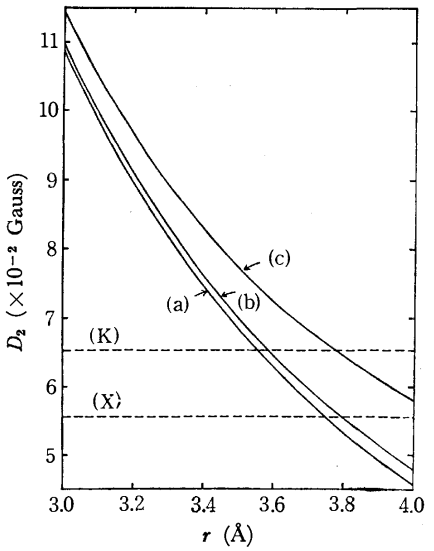

Fig. 7. The relation between D_2 and r. $g_{//}=2.22$, $g_{\perp}=2.04$; As ξ changes $0°\rightarrow 90°$, D_2 changes (a)→(b)→(a) at X-band, and (a)→(c)→(a) at K-band. The broken lines, (K) and (X), indicate the observed values of D_2 at K-band and X-band, respectively.

Next, we will discuss the hyperfine structures of the so-called full-field parallel lines. The dependence of A_L and A_H on r for different values of ξ in the X-band is shown in Fig. 8. This figure indicates that the calculated values of A_L and A_H depend sharply on ξ, but that they do not change greatly with r at any of the ξ values. In these figures, the observed values of A_L and A_H are also indicated. The approximate values of ξ could be estimated from these figures to be between 30° and 40°. The difference between A_L and A_H increases with the increase in the anisotropy of the g tensor. The relations between ΔA and Δg can be understood well from Fig. 9, where $\Delta A=A_L-A_H$ is plotted against ξ for different values of $\Delta g=g_L-g_H$. As is evident from these figures, the change in ΔA with Δg depends on the ξ angle and on the frequency of the oscillating magnetic field. It also depends naturally on the anisotropy of the A tensor. When the shift of the spectral lines due to the anisotropy of the g tensor is smaller than that due to the fine-structure tensor, ΔA becomes zero at $\xi=0°$ and 90°. This condition is not satisfied in the case of (5) in the K-band in Fig. (9). In this case, the $(-1\rightarrow 0)$ transition at the minimum resonance field or the $(0\rightarrow 1)$ transition at the maximum does not occur in the directions of these principal axes. The angular

dependence of the resonance magnetic field, however, becomes so small that the lines of the various hyperfine splitting constants overlap with each other in the corresponding narrow range of the magnetic field. Consequently, the hyperfine splittings are completely smoothed out and the calculated A values are of no practical use.

Finally, we calculated the total line shapes according to the method by Taylor and Bray.[16] For the sake of simplicity we neglected the angular dependence of the transition probabilities. The patterns which were made up by neglecting the linewidths of all the transitions were convoluted with the Gaussian line shapes, and then numerically differentiated. As the absorption lines of the monomers overlap greatly with those of the dimers, it is impossible to fit the total line shapes of the calculated spectra to those of the observed ones. Therefore, we adjusted the magnetic parameters so that the parameters defined in Figs. 2 and 4 became consistent with those experimentally determined. Figures 7—11 suggest the ranges of the more exact parameters of the triplet dimers. Since the behavior of the hyperfine structures can be adequately explained by the parameters used for the calculations in Fig. 6, the true values will not deviate too much from them. We made them change gradually by the trial-and-error method, and finally obtained the spectra

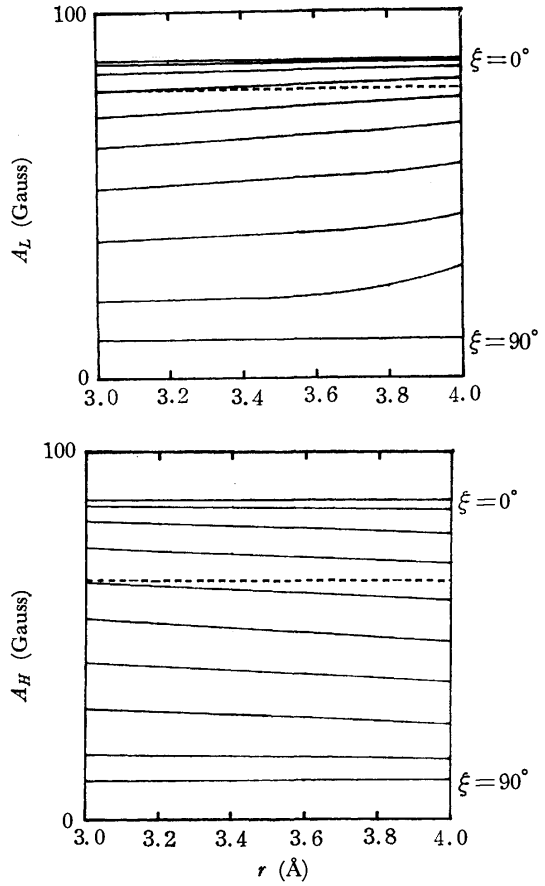

Fig. 8. The r and ξ dependence of A_L and A_H at X-band. $A_{//}=0.0090\,cm^{-1}$, $A_\perp=0.0010\,cm^{-1}$, $g_{//}=3.22$, $g_\perp=2.04$; Broken lines in the figure indicate the observed values of A_L and A_H; A_L and A_H were calculated changing ξ at intervals of 10°.

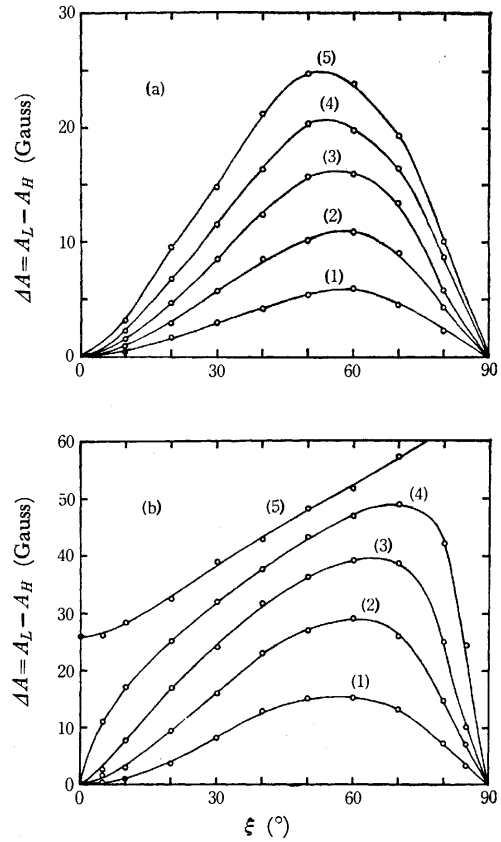

Fig. 9. The relation between $\Delta A=A_L-A_H$ and $\Delta g=g_L-g_H$ at different values of ξ. (a) X-band, (b) K-band; $A_{//}=0.0090\,cm^{-1}$, $A_\perp=0.0010\,cm^{-1}$, $g_\perp=2.05$, $g_{//}=$, (1), 2.10, (2), 2.15, (3), 2.20, (4), 2.25, (5), 2.30.

shown in Fig. 10. The parameters determined from Fig. 10 are tabulated in Case B of Table 1; the magnetic parameters for the triplet dimer are shown below, with a rough estimation of the maximum errors:

$$g_{//}=2.23\begin{cases}+0.08\\-0.03\end{cases} \qquad g_\perp=2.05\pm0.02$$

$$A_{//}=90\pm5 \qquad A_\perp=10\pm5 \quad (\times10^{-4}\,cm^{-1})$$

$$r=3.75\begin{cases}+0.05\\-0.35\end{cases}\ (Å) \qquad \xi=35°\pm5° \qquad \eta=0°$$

The agreement of the calculated spectra with the observed spectra is good in the low-field range. In the high-field range, however, the calculated intensity of the perpendicular component becomes larger and the calculated linewidth becomes smaller than those of the observed spectra. As a result, it seems that the hyperfine structures in this region appear only indistinctly.

The calculated spectra clearly show unusual hyperfine structures in the field range between the low-field parallel and perpendicular lines. The structures became more distinct in the K-band spectra. The perpendicular transitions occur when the static magnetic field is oriented along the direction perpendicular to the copper-copper axis. If the symmetrical axes of the g and D tensors are not coincident with each other, the perpendicular transition will split as a result of the anisotropy of the g tensor. Hence, the $\Delta M=1$ transitions do not show the typical pattern due to the axially symmetric tensors, and the stationary resonant field conditions for the low-field perpendicular transitions

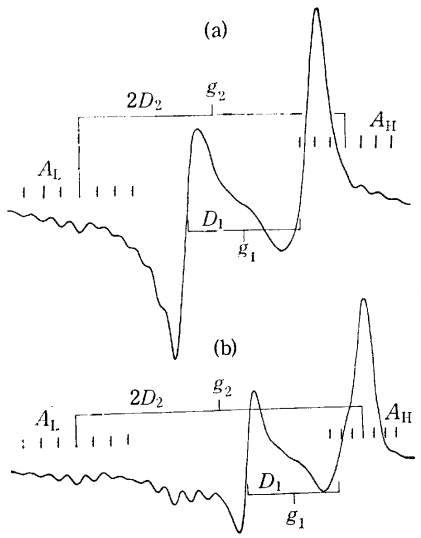

Fig. 10. The calculated ESR spectra of the triplet dimers of $Cu(Mesal)_2$. (a) *X*-band, (b) *K*-band; $g_{//}=2.23$, $g_{\perp}=2.05$, $A_{//}=0.0090\,cm^{-1}$, $A_{\perp}=0.0010\,cm^{-1}$, $r=3.75$ Å, $\xi=35°$; These spectra were convoluted by Gaussian line shapes, ($\Delta H=25$ Gauss).

are satisfied at the angle of a considerably large hyperfine coupling constant.

Estimation of the Copper-Copper Distance. In the above calculations, we neglected the effect due to the distributions of electron spins in their orbitals and the effect of pseudo-dipolar interaction. Taking this distribution effect into account will bring about a decrease in the estimated value of r, as was indicated by Chasteen and Belford.[4] Moreover, if a super-exchange interaction through the oxygen atoms operates anti-ferromagnetically, the sign of the pseudo-dipolar interaction will become positive[17] and opposit to that of the real spin dipolar interaction. This effect may reduce the estimated value of r. However, the principal axes of the pseudo-dipolar interaction are directed along the direction parallel or perpendicular to the two co-ordination planes, rather than to the copper-copper axis.[17] If the total fine-structure tensor, $\boldsymbol{D}$, results mainly from the psudo-dipolar interaction, the principal axes of the $\boldsymbol{D}$ will be close to those of the g tensor. The calculated value of $\xi=35°\pm5°$ suggests that the D value originates mostly from the real dipolar interactions. At any rate, the estimated value of r (3.75 Å) will be the upper limit of the distance and the real value may possibly be smaller than this estimated value.

The authors would like to express their grateful acknowledgement to Dr. H. Yokoi for many helpful discussions and suggestions throughout this work.

17) B. Bleaney and K. D. Bowers, *Proc. Roy. Soc., Ser. A*, **214**, 451 (1952).

BULLETIN OF THE CHEMICAL SOCIETY OF JAPAN, VOL. 45, 3011—3016 (1972)

Infrared Absorption Intensities of Out-of-plane CH Bending Vibrations of Substituted Benzenes. IV. Solvent Effect on the Intensities of the Bands of Aniline

Seiichiro HIGUCHI, Eisaku KUNO, Shigeyuki TANAKA, and Hitoshi KAMADA

Department of Industrial Chemistry, Faculty of Engineering, The University of Tokyo; Bunkyo-ku, Tokyo

(Received February 3, 1972)

The infrared absorption intensities of out-of-plane CH bending and ring out-of-plane deformation vibrations of aniline have been measured in an acetone solvent mixed with various quantities of acetic acid. When such solvents are used, new peaks attributable to aniline interacting with the acid appear as shoulders of each of the original bands. A marked decrease in the sums of the intensities of the above two modes (A_0) has been observed for the bands of aniline interacting with the acid. It is demonstrated that the degree of such a decrease in intensity depends on the molar ratios of aniline and the acid. When there exists enough the acid in comparison with aniline, the values of A_0 become minimum. On the other hand, when the numbers of the exsiting acetic acid molecules are much smaller than those of aniline, the values of A_0 are considerably greater than those in the former case. In this case, a farily long time is needed until the interaction reaches an equilibrium state. Finally, when a very large amount of the acid is added, the bands attributable to aniline interacting with the acid are no longer observed. An attempt has been made to interpret these phenomena in terms of the state of the aggregation of aniline, acid and acetone molecules in the solutions.

In our previous studies, we examined the infrared absorption intensities of the out-of-plane CH bending and ring out-of-plane deformation vibration bands of various monosubstituted (PhX-, Ph_2X-, and Ph_3X-type molecules) and meta disubstituted benzenes and discussed the intensities of those bands in terms of several basic factors, *i. e.*, the forms of group vibrations, the C–H bond dipole moment, and the structural factors, including the angles of rotation of benzene rings (in case of Ph_n X-type molecules) and the conformational isomerism.[1-3] Several conclusions have been drawn from these studies. Those of them essential to the

1. S. Higuchi, K. Nakamori, S. Tanaka, and H. Kamada, *Nippon Kagaku Zasshi*, **89**, 565 (1968).
2. Y. Gōda, S. Higuchi, S. Tanaka, and H. Kamada, *ibid.*, **92**, 21 (1971).
3. S. Higuchi, Y. Gōda, S. Tanaka, and H. Kamada, *ibid.*, **92**, 670 (1971).

present problem are enumerated below.

1) The forms of group vibrations corresponding to the two strong bands in the 800—670 cm^{-1} region are determined by strong coupling of the two vibrational modes, *i.e.*, out-of-plane CH bending and ring out-of-plane deformation vibrations. As a result of this, there occurs an intensity borrowing between these two vibrational modes.

2) The degree of coupling of the above two modes is sensitive to slight changes in the structure of substituents attached to the benzene ring. Thus, the forms of the group vibrations corresponding to each of the bands are not characteristic of the series of related compounds.

3) Considering that the moment induced by the ring out-of-plane deformation mode is much smaller than that by the out-of-plane CH bending mode (in the case of monosubstituted benzenes, we can estimate the former to be about one-fifth of the latter, thus, in intensity, it is about 4 percent of the latter.), the sums of the intensities of the two bands in question can be regarded as approximately corresponding to an out-of-plane CH bending vibrational mode similar to that of benzene, which is the in-phase vibration of all the hydrogen atoms attached to the benzene ring.

4) The vibrational coordinates corresponding to these sums of intensities can be considered characteristic of the series of the related compounds.[1] Consequently, the differences in the intensity sums among the compounds can be discussed in terms of the alterations in the C–H bond moment, the electric factor of the intensities of the vibrations in question. From the correlations between the intensity sums and the wavelength of the benzenoid bands in the UV spectra, it was pointed out that, when there is n-π conjugation between substituents and the benzene ring, the intensity sums (hence, the C–H bond moment) increase considerably with the effect, while, otherwise, they stay approximately constant.

On the basis of these results, we have examined this time the effect of solvents on the intensity sums, which we will hereafter call the group characteristic intensities, A_0. As the solute molecule, we have selected aniline. In this molecule, the effect of n-π conjugation, which has been found to be the major factor in determining the magnitude of the C–H bond moment, is considerably pronounced; it is interesting to examine the solvent dependences of A_0 in relation to the effect of solvents on the n-π conjugation between the substituent and the benzene ring. Thus, in this study, we have tried to consider from this viewpoint the factors attributable to the media and responsible for the changes in A_0.

Experimental

A Japan Spectroscopic Company Model DS-403G Infrared Spectrophotometer was used for the measurement of the intensities. The spectra were recorded in absorbance with a frequency scale in cm^{-1}, and the integrated areas were obtained directly from the instrumental charts. The concentration range was about 0.3—1.0 mol/l, and the cell thickness, 33 and 38 μm. The solvents used were cyclohexane, dioxane, carbon disulfide, acetone, nitromethane, acetonitrile, and mixed solvents of acetone and various carboxylic acids (acetic acid, n-propionic acid, n-butyric acid, and p-hydroxybenzoic acid). The slit width, $S/\Delta\nu_{1/2}$, was kept between 0.2 and 0.1. The scanning speed was about 10 cm^{-1}/min.

As will be shown later, two bands overlap for each of out-of-plane CH bending and ring out-of-plane deformation vibration modes, and it becomes necessary to divide these overlapping bands into components. In this study, such curve resolution was made by the use of a Du Pont 310 Curve Resolver, assuming the Lorentzian band contour for each component. The bands of aniline in the acetone solvent have shapes relatively close to those of Lorentzian curves. However, it should be noted that, strictly speaking, the asymmetric character of the band shapes is slightly more pronounced in the case of the acetone solvent than in the case of nonpolar solvents; moreover, the wings of the bands do not fit so well with the Lorentzian contours. Taking these facts into consideration, it may be necessary to make allowance for errors of 10—15 percent in the measured areas through the use of this procedure of curve resolution.

The root-mean-square difference between the individual intensity values and their mean was found to be less than 10 percent.

Results and Discussion

1. *The Behaviour of A_0 of Aniline in Usual Polar and Nonpolar Solvents.* Table 1 lists the observed intensities of the out-of-plane CH bending (A_1) and ring out-of-plane deformation vibration bands (A_2), and their sums (A_0) of aniline in six different solvents. These values of A_0 are plotted in Fig. 1 against the corresponding "reaction-field constant" $(\varepsilon-1)/(2\varepsilon+1)$, which is used here as a quantitative measure of the polarity of the solvents. These plots show distinctly that A_0 is little influenced by the polarity of solvents in the usual sense of the word. Such a situation has also been observed in the cases of other monosubstituted benzenes. Figure 1 shows the plots for toluene for the sake of comparison. Although the absolute magnitudes of A_0 are different between aniline and toluene, a difference which is attributable to the difference in the substituent effect between NH_2 and CH_3 groups, the behaviour of the A_0 according to the polarity of the solvents is always similar. This may be due to the facts that the major factor in determining the values of A_0 is the conjugation effect between the substituent and the benzene ring and that the solvents used here can not be expected to affect this very much.

Table 1. The observed intensities A_1, A_2 and their sum A_0 of aniline in various solvents

Solvent	A_1	A_2	A_0
Cyclohexane	4270	1790	6060
Dioxane	4350	1950	6300
Carbon disulfide	4190	1860	6060
Acetone	4070	1950	6020
Nitromethane	4330	1800	6130
Acetonitrile	4320	1890	6210

Unit of intensities: [$cm^{-2}\cdot l\cdot mol^{-1}$]

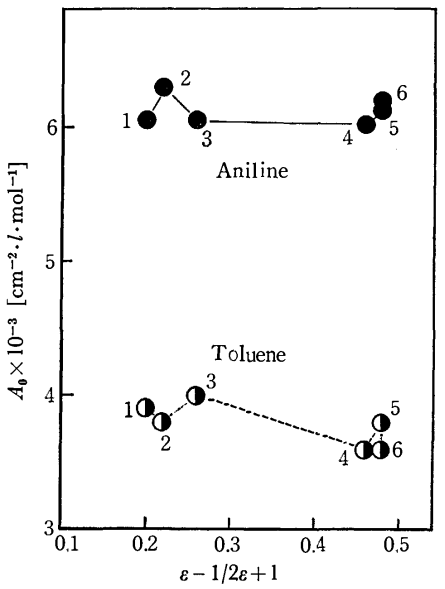

Fig. 1. The behaviors of A_0 of samples in polar and nonpolar solvents, 1: cyclohexane, 2: dioxane, 3: carbon disulfide, 4: acetone, 5: nitromethane, 6: acetonitrile.

2. *The Behavior of A_0 of Aniline in Acetone Mixed with Various Quantities of Acetic Acid.* From above experimental results, the marked changes in A_0, if any, may be expected when the solvent contains some chemical species which have a strong interaction with the *n*-electrons on the NH_2 group. Thus, we next examined the behaviour of A_0 of aniline in a mixed solvent consisting of acetone and organic acids.

Figures 2 and 3 show the spectra of aniline in acetone and in an acetone-acetic acid mixed solvent. As is shown in Fig. 3, two new bands, 1′ and 2′, appear as shoulders of the original peaks, 1 and 2, when the mixed solvent is used. These four bands can be interpreted as follows. The 1 and 2 bands are assigned, respectively, to out-of-plane CH bending and ring out-of-plane deformation vibrations of aniline not interacting with the acid, and the 1′ and 2′ bands, to the corresponding vibrations of aniline interacting with the acid. As has already been mentioned, these overlapping bands have been divided into components with a Lorentzian band contour, using a Du Pont 310 Curve Resolver. An example of such curve resolving is shown in Fig. 3.

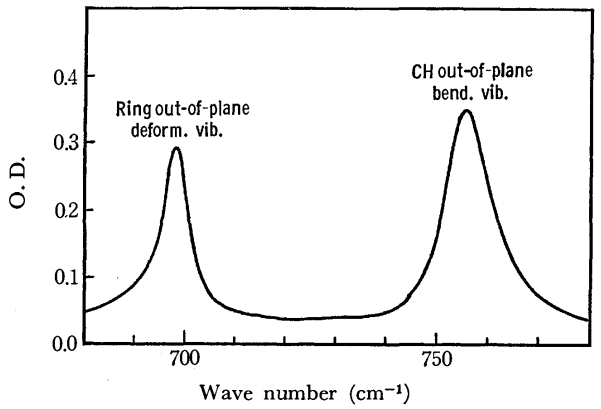

Fig. 2. The spectrum of aniline in acetone solvent.

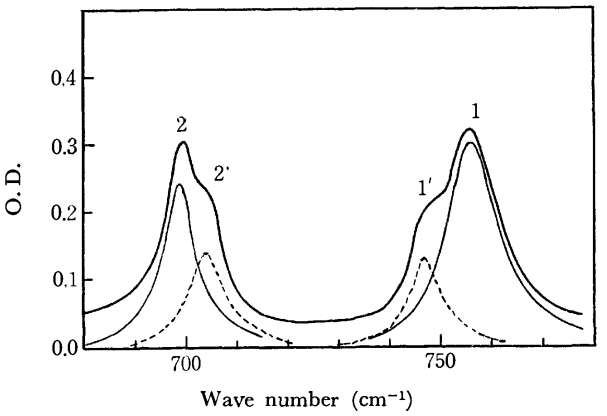

Fig. 3. The spectrum of aniline in the mixed solvent.

Table 2. The kinds of added acids and A_0 of aniline interacting with the acid

Acid	pK_a	A_0
Acetic acid	4.76	3500
n-Propionic acid	4.85	2900
n-Butyrlic acid	4.82	3400
p-Hydroxybenzoic acid	4.54	3300

Unit of intensities [cm^{-2}·l·mol^{-1}]

In order to calculate the intensities of each of the four bands, it is necessary to estimate the concentrations of aniline interacting and not interacting with the acid. For this purpose, the concentrations of aniline not interacting with the acid have been obtained from the areas of each of the two bands attributed to this kind of chemical species. In doing this, it was assumed that the concentration of not-interacting aniline corresponding to a certain area of a band is equal to that corresponding to the same area of the band of aniline in an acetone solvent. From the results of this procedure, the concentration of aniline interacting with the acid has been determined. It may be worth mentioning that the concentrations determined from the two different bands agree with each other within the limits of experimental error.

Figure 4 shows the plots of the intensity sums, A_0, of aniline interacting with the acid against the cor-

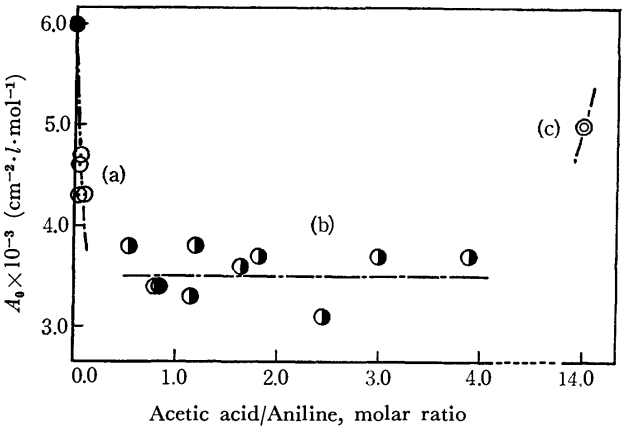

Fig. 4. The dependence of A_0 on the concentrations of the acid.

responding molar ratios of aniline and acetic acid. It can be seen from this figure that the intensity behavior can be classified into at least three categories, (a), (b) and (c). We will now consider these types of intensity behavior individually.

First, we will discuss the molar ratio range, (b), where the magnitude of A_0 becomes lower than in the case of the acetone solvent. In this case, the intensity value, 3500 ± 200 cm$^{-2}\cdot l\cdot$mol^{-1}, has been obtained as the A_0 value of aniline interacting with the acid; this value is remarkably lower than that of 6000 ± 100cm$^{-2}\cdot l\cdot$mol^{-1} when no acetic acid is added. This lowering of the intensity is considered to be due to a decrease in the interaction of n-electrons on the NH_2 group with π-electrons of the benzene ring as a result of a strong interaction of the acid with n-electrons of the substituent.

The validity of the above discussion of the physicochemical mechanism of the decrease in intensity can be inferred from the correlations of A_0 with the wavelengths of the benzenoid bands in the UV spectra. Fig. 5 shows the correlations for several monosubstituted benzenes. It is known that the maximum absorption of aniline occurs at 288 nm in the case of a neutral solution, while, in the case of an acidic solution, it appears at 254 nm.[4] It can be seen that the values of A_0 for aniline in acetone-acetic acid mixed solvents are well on the correlation curve in Fig. 5 when plotted against the data for the wavelength quoted above. The shift to the shorter wavelength in the case of an acidic solution is said to be due to the decrease in the conjugation between the NH_2 group and the benzene ring, resulting from the interaction of the substituent with the acid. Thus, this result supports the first assumption that such an effect of acidic substances will cause a marked change in the C–H bond moment and, therefore, in the magnitude of A_0.

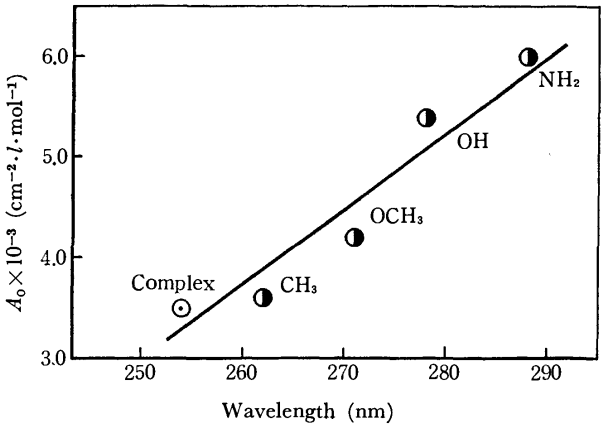

Fig. 5. The comparison of A_0 of aniline with that of its complex in terms of the correlation with UV spectra.

A similar decrease in intensity has been observed when different acidic substances are added to acetone. Table 2 lists the data for A_0 of aniline interacting with various carboxylic acids having similar pK_a values. These results show that there is no wide difference among these acids in their effects on the aniline molecule, regardless of the substituents attached to the COOH group.

Quite different phenomena have been observed in the molar ratio range (a), where the existing acetic acid molecules are much fewer than the aniline molecules. First, a considerable amount of time is required until the interaction reaches the equilibrium state (about two hours after sampling). The change of the spectra with the time is demonstrated in Fig. 6. Second, the group characteristic intensity, A_0, is 4500 ± 200 cm$^{-2}\cdot l\cdot$mol^{-1}, considerably larger than that in the (b) range. Third, the molar concentration of aniline molecules interacting with the acid is much greater than that of the added acid molecules. From these experimental facts, it can be guessed that the state of the aggregation of aniline, acid, and acetone molecules is different from that in the case of (b).

In the molar ratio range (c), where a very large quantity of the acid is added to acetone, the following phenomena can be observed, although, in this case, the observed spectra are not clear enough for a precise estimation of the intensities. The new bands attributable to aniline interacting with the acid can no longer be observed in this case, and the intensity sum, A_0, estimated roughly from the observed bands becomes near to that of aniline not interacting with the acid. These experimental results show clearly that, in this concentration range, the acid becomes almost inactive to the aniline molecule.

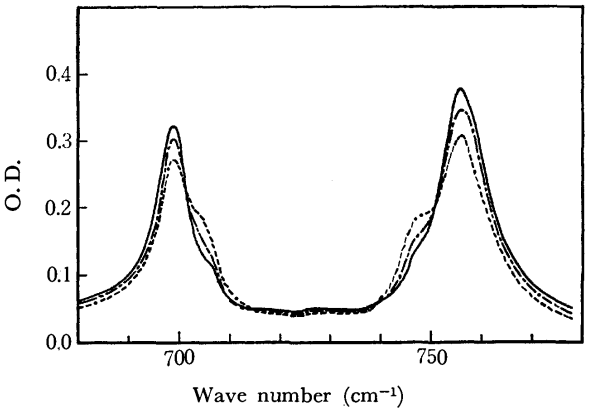

Fig. 6. The change of spectra with time, ——: immediately after sampling, – – – –: 30 min. after sampling, ……: 120 min. after sampling.

3. *The Relation between the Behavior of A_0 and the State of Aggregation for the Molecular Systems in Question.* The above-mentioned experimental results clearly suggest that the factor determining the behaviour of A_0 is the state of aggregation for the molecular systems in question. Therefore, in this paragraph, we will try to present some details on the state of molecules in the solutions, expressed so far in the rather ambiguous term "interacting", and will discuss the changes in A_0 from that viewpoint. The molecular systems treated here are very complex, and there are several kinds of possible molecular associations. That is, the following five kinds of combinations of the molecules are considered to be possible in this case; (1)

4) H. H. Jaffé and M. Orchin, "Theory and Applications of Ultraviolet Spectroscopy", John Wiley and Sons, Inc., New York London (1962), p. 257.

aniline-aniline, (2) aniline-acetone, (3) aniline-acid, (4) acid-acid, and (5) acid-acetone. Since, in general, primary amines are very weak proton donors, the (1) and (2) associations are, if present at all, weak. On the other hand, the (3), (4) and (5) associations may be inferred to be considerably stronger. In the solutions, these molecular associations are considered to be in certain equilibrium states, resulting from complicated mutual interferences among them.

First, we will consider the state of aggregation when no acetic acid is added; here the only possible molecular associations are (1) and (2). The information on the formation of such a state of aggregation will be given by the spectra in the wavenumber region of NH_2 stretching vibrations. Those spectra are shown in Fig. 7. It can be seen that the NH_2 stretching bands of aniline in the acetone solvent show no shift of wavenumbers, even when the concentrations of the solute are made about twenty five times smaller than those used in the measurements of the intensities of the out-of-plane bending vibrations in question. This fact proves that there is no self-association (1) among aniline molecules. However, it is also observed that the wavenumbers in the case of the acetone solvent are about 20 cm^{-1} lower than those in the case of carbon tetrachloride, suggesting that there occurs a weak association (2) by hydrogen bonding between the aniline and the acetone molecules. In fact, it has been reported in the literature that amines associate with carbonyl compounds by weak hydrogen bonding.[5,6] Thus, it can be concluded that the state of aggregation in this case is the associated complex of a certain number of aniline molecules with carbonyl groups between them. Since, in the formation of this type of complex, the hydrogen atoms of the NH_2 group act the principal role, while the *n*-electrons on the group do not, this interaction has no effect on the intensity sum, A_0, resulting in no marked changes in A_0 among the different solvents, as is demonstrated in Table 1 and Fig. 1.

When acetic acid is added to the acetone solvent,

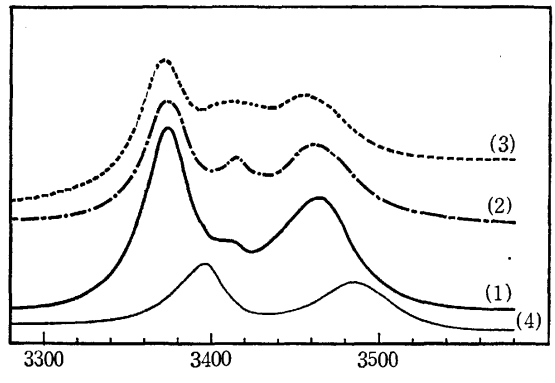

Fig. 7. The spectra of aniline in NH_2 stretching region, (1), (2), (3): in acetone, (4): in carbon tetrachloride, rough concentrations: (1) 0.5 mol/*l*, (2) 0.1 mol/*l*, (3) 0.02 mol/*l*.

three molecular associations, (3), (4), and (5), may all be realized. In this case, it is natural to consider that the acid added to the solvent interacts with the NH_2 groups involved in the complex originally formed between the aniline and the acetone molecules, and that, in this interaction, *n*-electrons on the NH_2 group act the principal role, resulting in the great changes in A_0 described in the foregoing paragraph. At the same time, the added acid molecules will associate with themselves (4) and with acetone molecules (5). These three associations, (3), (4), and (5), will reach some equilibrium state determined by the relative concentration of each of the component molecules. Since the A_0 values of the aniline interacting with the acid change with the concentration of the acid, as is demonstrated in Fig. 4, the strength of the (3) interaction can be thought to change with the alterations in the equilibrium relations among the (3), (4), and (5) associations. In a very simple picture, however, it may safely be said that the degree of the interaction, which has appeared as the change in the A_0 of aniline, is regulated by the degree of the competing associations, (4) and (5), in the equilibrium state at each concentration of the acid. On the basis of this simple model, the following qualitative interpretations of the behaviours of A_0 shown in Fig. 4 are possible, though no quantitative discussion of the chemical equilibria in question here are possible at present. As has already been mentioned, the interaction determining the behaviour of A_0 is between the acid and the associated complex of a certain number of aniline molecules with carbonyl groups between them. In the molar ratio range (b), where there is enough of the acid, each of the NH_2 groups in the complex undergoes sufficient interaction with the acid, resulting in the lowest magnitude of A_0. The experimental results demonstrated in Fig. 5 and Table 2 suggest that, in this case, aniline molecules interacting with the acid exist in the solutions as anilinium ions or a similar state of molecular aggregation. As the concentrations of the acid become higher, the dimerization of the acid (4) gradually becomes pronounced. However, at least in the concentration range (b) examined in the present study, the effect of this dimerization does not appear in the values of A_0; A_0 keeps approximately constant within the limits of experimental error. This suggests that, in this range of concentration of the acid, the dimerization of the acid molecules competes only with the association between the acid and acetone molecules (5), and that the association (3) is not much influenced until the concentration of the acid becomes much higher, though no quantitative and decisive discussion of this phenomenon can be given here.

In relation to the above discussions, the phenomenon observed in the molar ratio range (c), where a very large amount of the acid is added to acetone, can be interpreted easily. That is, in this concentration range, the effect of the dimerization of the acid is extremely pronounced; as a result, the acid molecules become inactive not only to acetone, but also to aniline molecules, resulting in the disappearance of the bands attributable to aniline interacting with the acid.

As has already been mentioned, the results for the

5. E. A. Cutmore and H. E. Hallam, *Trans. Faraday Soc.*, **58**, 40 (1962).

6. J. Lauransan, P. Pineau, and M. L. Josien, *Ann. Chim.* (Paris), **9**, 213 (1964).

molar ratio range (a) suggest that the state of aggregation of the molecules in this case is different from that in the case of (b). Also, in this case, the interaction in question is considered to occur between the associated complex [aniline-acetone] and the acid molecules. However, there is a difference in this case in that there does not exist enough of the acid as compared with aniline. From the experimental results, it may be supposed that, in the (a) range, NH_2 groups in the complex exist not as a state similar to anilinium ions (1 : 1 association), as in the case of (b), but as a state such as when one acid molecule interacts with several NH_2 groups simultaneously. On the basis of this model, the relatively greater values of A_0 observed in this concentration range can be understood easily, for, under such circumstances, the action of the acid which the *n*-electrons of each of the NH_2 groups in the complex receive in the equilibrium state becomes weaker on the average. Although a more detailed microscopic image of the molecular associations in this case cannot be given at present, the assumption of the possibility of the above-mentioned state of aggregations is consistent with all the phenomena observed in the (a) range. Be that as it may, it can at least be said that the experimental facts presented here are very suggestive as to the elucidation of the state of molecules in solutions similar to those in question here.

Conclusion

It has been demonstrated that the present experimental results are all consistent with the concept that the n-π conjugation between the substituent and benzene ring is the major factor in determining the magnitude of the C–H bond moment. The conclusion was drawn originally from the studies of the substituent effect; this time, it has been confirmed by discussion of the state of aggregation of the solute and solvent molecules. The authors realize that more detailed experimental and theoretical research over a wide range of related compounds is required before a more general rule as to the influences of media on the intensities in question can be set up. We realize also that there remain considerable ambiguities concerning the explanations of the state of molecules in the solutions in question. However, we believe that the experimental results demonstrated in this paper will be of value in stimulating the advancement of more detailed and exact studies of this subject.

The authors would like to thank Mr. K. Yamamoto of Tokyo Research Center, Bridgestone Tire Co., Ltd. for giving us permission to use a Du Pont 310 Curve Resolver belonging to his laboratory.

BULLETIN OF THE CHEMICAL SOCIETY OF JAPAN, VOL. 45, 3016—3020 (1972)

Vibration Spectra and Molecular Structures of *n*-Butyl Chloride and *n*-Butyl Bromide in Relation to Parallel (1 : 3) Interactions

Tsunetake FUJIYAMA

Department of Chemistry, Faculty of Science, The University af Tokyo, Bunkyo-ku, Hongo, Tokyo

(Received February 15, 1972)

The vibration spectra of liquid *n*-butyl chloride and *n*-butyl bromide are observed in the region of 1500—100 cm^{-1}. From the analyses of spectra corresponding to the skeletal deformation vibrations, the molecular configurations are determined for both molecules. All the possible rotational isomers, the TT, GT, TG, GG, and GG′ forms, are observed for *n*-butyl chloride, while four isomers, the TT, GT, TG, and GG forms, are observed for *n*-butyl bromide. The results are compared with those of the electron-diffraction methods. It is shown that unfamiliar interactions must be considered for the parallel (1 : 3) interaction between methyl and chlorine substituents.

Ukaji and Bonham[1] studied the structures of *n*-butyl chloride by an electron-diffraction method and found that the concentration of the GG′ form is twenty-four percent in the gas phase at room temperature. This result is very important because the GG′ form is the most highly coiled among the five possible rotational isomers. Figure 1 shows the possible rotational isomers for $CH_3CH_2CH_2CH_2X$ type molecules. It can naturally be assumed from the figure that the GG′ form is the most unstable because of methyl/chlorine interactions.

The infrared spectra of this molecule have been studied by Snyder[2] for the crystalline state from the point of view of the molecular force field. Snyder concluded that the stable form in the crystalline state is the TT form.

The present work will be concerned with the confirmation of the electron-diffraction results through analyses of the vibration spectra of liquid *n*-butyl chloride and *n*-butyl bromide. The skeletal deformation vibrations will be discussed mainly, because they are characteristic in molecular geometry and are sensitive to any change in molecular configuration.[3]

Experimental

The samples used in the present work were commercial products. After fractional distillation, the purity was checked

1) T. Ukaji and R. A. Bonham, *J. Amer. Chem. Soc.*, **84**. 3627 (1962).

2) R. G. Snyder and J. H. Sachtschneider, *J. Mol. Spectry.*, **30**, 290 (1969).

3) T. Fujiyama, This Bulletin, **44**, 1194 (1971).

by gas chromatography.

The Raman spectra were recorded using a laser Raman spectrometer which was designed and constructed in our laboratory.[4] Figures 2 and 3 show the Raman spectra of *n*-butyl chloride and *n*-butyl bromide in the region of 100—1000 cm^{-1}. The Raman spectra of crystalline samples observed at the temperature of liquid nitrogen are illustrated in Figs. 4 and 5. The spectrometer was operated under a resolution of 5—10 cm^{-1}. The temperature dependence of the Raman spectra of *n*-butyl chloride was observed at low temperatures; the results are shown in Fig. 8. The temperature was observed by means of a thermocouple directly inserted in the sample.

The infrared spectra of liquid *n*-butyl chloride and *n*-butyl bromide in the region of 200—600 cm^{-1} are illustrated in Figs. 6 and 7. A Hitachi EPI-GII infrared spectrometer was used for the measurements. The observation of the infrared spectra at low temperatures reproduced the results of a previous author[2] quite well; therefore, those results are not illustrated here.

Normal Coordinate Treatment

In confirming the vibrational assignment, normal frequencies of *n*-butyl chloride and *n*-butyl bromide were calculated for all the possible rotational isomers by using the force constants obtained for a series of alkanohalides.[5] The method of calculation may be found described in the references.[6] In the present report, the results of the calculation will not be discussed in detail, but they are available upon request from the author.

Vibrations Spectra and Molecular Configuration

A molecule of the $CH_3CH_2CH_2CH_2X$ type can have the five rotational isomers of Fig. 1, because it

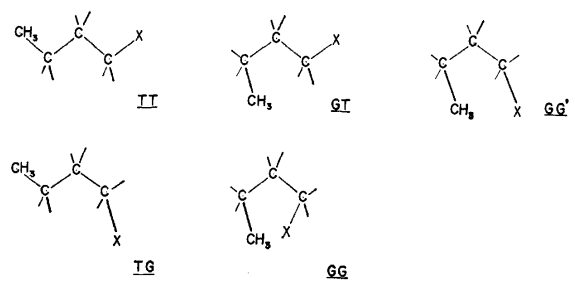

Fig. 1. Possible rotational isomers for the $CH_3CH_3CH_2CH_2X$ type molecules.

has two axes of internal rotation. We define the two axes as:

$$CH_3CH_2\text{-(I)-}CH_2\text{(II)-}CH_2X$$

and call them the I axis and the II axis. In the case of *n*-butyl chloride or *n*-butyl bromide, configurations about the II axis can easily be determined by referring to the well known empirical rule of a stretching-vibration frequency of a carbon-halogen bond.[7] An empirical rule was previously proposed by the present author for the relationship between skeletal deformation vibrations and the molecular configurations of rotational isomers.[3] Based upon this rule, the molecular configuration will be discussed below.

n-Butyl Chloride. Among the three skeletal deformation vibrations of *n*-butyl chloride, the so-called A type vibration is expected to occur in the region of about 350—500 cm^{-1} in this frequency order:[3]

$$\nu(GG') > \nu(GG) > \nu(TG) > \nu(GT) > \nu(TT),$$

where ν(TG) refers to, for example, a frequency of the A type vibration corresponding to a rotational isomer whose configurations is *trans* and *gauche* about the I axis and the II axis respectively.

In Figs. 2 and 5, we can see five Raman lines, at 529, 476, 465, 438, and 382 cm^{-1}, and seven infrared counterparts, namely, the 525, 472, 456, 435, 399, 388, and 375 cm^{-1} bands. The Raman shift at 382 cm^{-1} can be explained as an unresolved band which corresponds to the infrared bands at 399, 388, and 375 cm^{-1}. The observed bands may be assigned to molecular configurations of *n*-butyl chloride if the location of the TT form band is determined, because it occurs at the lowest frequency of all the five bands.

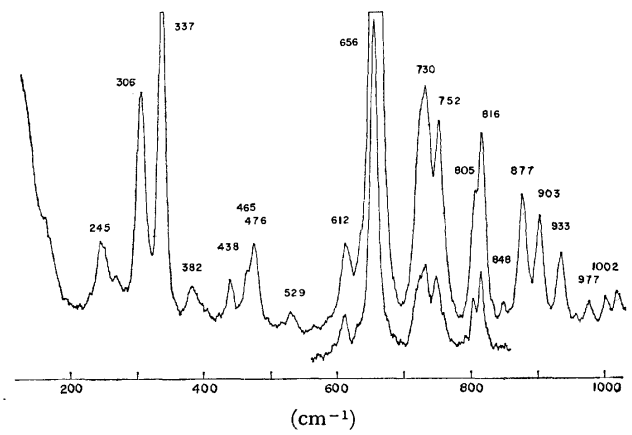

Fig. 2. Raman spectra of liquid *n*-butyl chloride at 25°C.

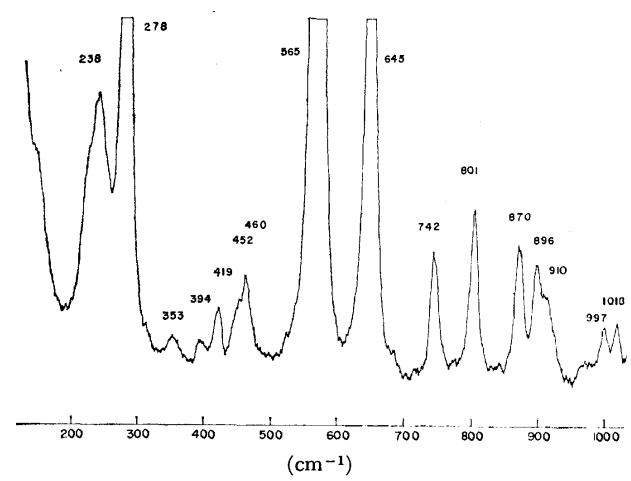

Fig. 3. Raman spectra of liquid *n*-butyl bromide at 25°C.

4) T. Fujiyama and M. Tasumi, *Bunko Kenkyu*, **20**, 28 (1971).
5) M. Tasumi and T. Shimanouchi, *Polymer J.*, **2**, 66 (1971).
6) T. Shimanouchi, *J. Chem. Phys.*, **17**, 245, 734, 848 (1949).
7) S. Mizushima, T. Shimanouchi, K. Nakamura, M. Hayashi, and T. Tsuchiya, *ibid.*, **26**, 970 (1957).

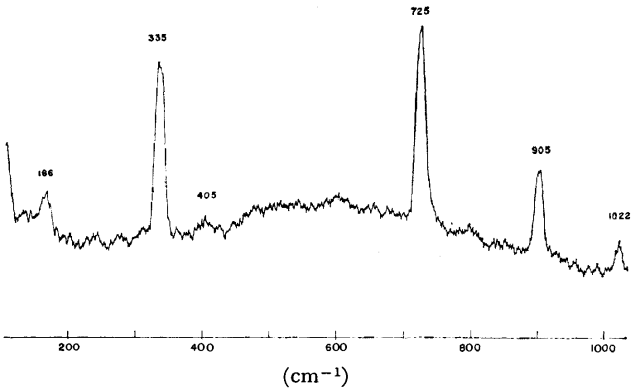

Fig. 4. Raman spectra of crystalline *n*-butyl chloride at −160°C.

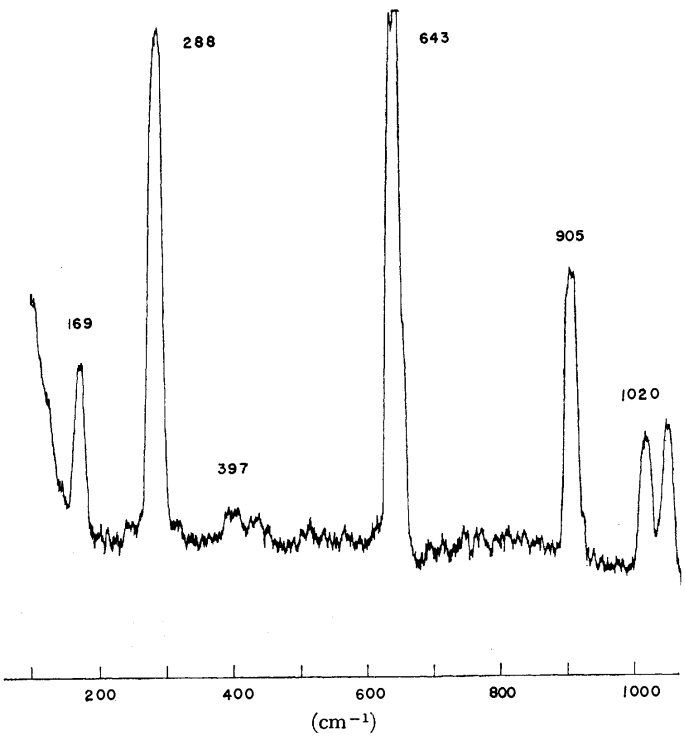

Fig. 5. Raman spectra of crystalline *n*-butyl bromide at −162°C.

Snyder[2] reports a band at 411 cm^{-1} observed in the infrared spectra of crystalline *n*-butyl chloride. The band corresponds clearly to the Raman line at 405 cm^{-1} of Fig. 6. The results of the normal coordinate treatment of Snyder and of the present work show that the Raman shifts at 405, 355, and 166 cm^{-1} of Fig. 6 can be definitely assigned to the skeletal deformation vibrations of the TT form in the crystalline state.

A little observation of Figs. 2 and 6 leads to the conclusion that the remaining four bands can be assigned to the remaining four rotational isomers. The band at 405 cm^{-1} of Fig. 6 is assumed to be buried in the wing part of the Raman shift at 382 cm^{-1} of Fig. 2. By referring to the frequency order of the empirical rule, the four bands at 438, 465, 476, and 529 cm^{-1} of Fig. 2 can be assigned to the GT, TG, GG, and GG′ forms respectively.

n-*Butyl Bromide.* The vibration spectra of *n*-butyl bromide may be analyzed in a manner similar to that used for *n*-butyl chloride. The frequencies of the A type skeletal deformation vibrations of this molecule can be expected to be slightly lower than those of *n*-butyl chloride. In Figs. 3 and 7, we see four Raman lines, at 460, 452, 419, and 394 cm^{-1}, and four infrared counterparts, at 460, 448, 417, and 394 cm^{-1}.

The Raman lines at 169, 288, and 397 cm^{-1} of Fig. 5 can be expected to correspond to the three skeletal deformation vibrations of the TT form from analogy with the results obtained for *n*-butyl chloride. Actually, the normal frequencies of these vibrations are calculated to be 155, 267, and 381 cm^{-1}. Thus, *n*-butyl bromide takes the TT form in the crystalline state and the band at 394 cm^{-1} of Fig. 5 can definitely be assigned to the A type skeletal deformation vibration of the TT form. The remaining three bands, at 460, 452, and 419 cm^{-1}, can reasonably be assigned to the GG, TG, and GT forms of *n*-butyl bromide respectively. The close similarity of the spectral patterns observed for *n*-butyl chloride and *n*-butyl bromide in the region of 350—500 cm^{-1} probably support the validity of the above-described assignments (see Figs. 2 and 3).

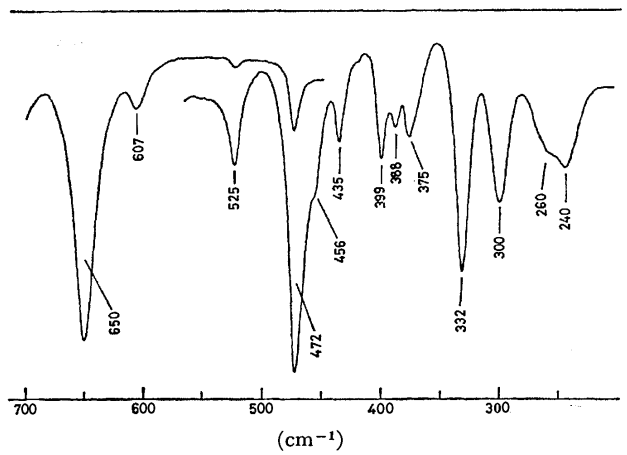

Fig. 6. Infrared spectra of liquid *n*-butyl chloride at 25°C.

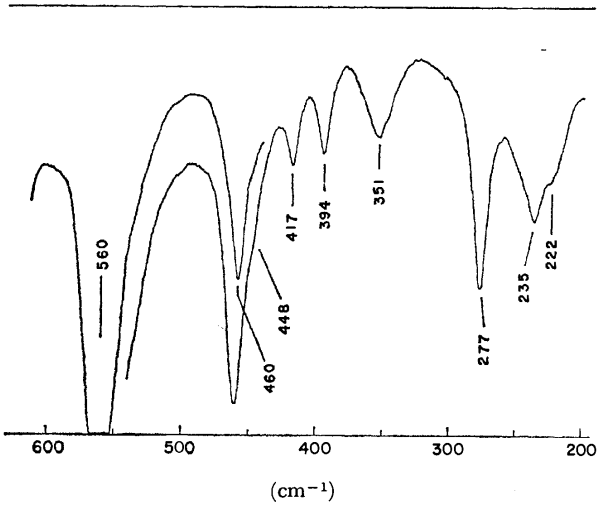

Fig. 7. Infrared spectra of liquid *n*-butyl bromide at 25°C.

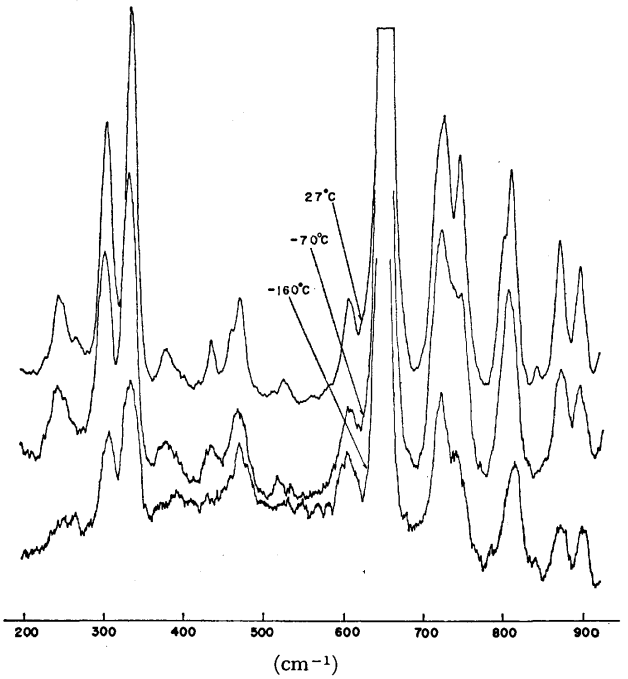

Fig. 8. Raman spectra of liquid *n*-butyl chloride at low temperature.

Discussion

The GG' Form and the Parallel (1 : 3) Interaction. It may be concluded from the spectral analyses that the numbers of rotational isomers observed in the vibration spectra of liquid *n*-butyl chloride and *n*-butyl bromide are five and four respectively. Only the TT form remains in the crystalline state of both molecules. The most remarkable finding is the existence of the GG' form of *n*-butyl chloride in the liquid state. In the GG' form, strong methyl/chlorine interactions are assumed to occur, because substituents on the carbon atoms, 1 and 3, give rise to parallel C–Cl and C–CH_3 bonds on the same side of the carbon skeleton. Actually, it has been widely agreed to reject the possibility of the existence of molecular configurations in which parallel (1 : 3) interactions are involved. We call those interaction by the term "parallel (1 : 3) interactions" following the suggestion of Sheppard.[8]

Table 1 shows the isomer percentage of the $CH_3CH_2CH_2CH_2X$-type molecules (X–CH_3, Cl, and Br) observed by the gas electron diffraction methods.[1,9,10] It may be seen from the table that these good agreement between the electron diffraction data and the present results in the senses that the GG' form of *n*-butyl chloride is present in a considerable concentration and that the GG' form of *n*-butyl bromide is not present in a readily measurable concentration. The qualitative agreement between the two sets of experimental results, namely, for the gas and liquid phases, is naturally accepted because the change in a dipole moment due to the change in molecular configuration is very small for the $CH_3CH_2CH_2CH_2X$ type molecules; therefore, the relative stabilities of the rotational isomers change little on passing from the vapour to the liquid phase. This only emphasizes that parallel (1 : 3) interactions between methyl and chlorine groups do not satisfy the criterion for rejecting the presence of a certain rotational isomer.

Table 1. Isomer percentages for the $CH_3CH_2CH_2CH_2X$ type molecules (After Bonham *et al.* (1, 9, 10))

Isomer	Concentration (per cent)		
	n-Pentane	*n*-Butyl chloride	*n*-Butyl bromide
TT	43	11	36
GT	25	11	24
TG	25	37	24
GG	7	17	16
GG'	—	24	—

Relative Stabilities of Rotational Isomers. All attempts to obtain the energy differences between rotational isomers were unsuccessful because of the poor S/N ratios of the spectra. From the temperature dependence of the Raman spectra of Fig. 8, however, a few conclusions may be drawn. The relative Raman intensities do not change remarkably; this indicates that the energy differences between the rotational isomers of *n*-butyl chloride are rather small. The relative intensity of the 438 cm^{-1} line of Fig. 2 decreases rapidly as the temperature goes down. This result supports the conclusion of the gas-phase data that GT form is the most unstable form. Two Raman lines are seen at 405 and 476 cm^{-1} in the spectra observed at about −160°C; they may correspond to an unannealed glassy solid. This indicates that both TT and GG forms coexist in the glassy solid. The most important conclusion may be drawn from the relative intensity change in the Raman line at 529 cm^{-1}. Although the temperature changes from 27°C to 70°C, its relative intensity changes little. Thus, we can conclude that the GG' form is as stable as the other rotational isomers. It is of some interest to add that the relative stability of the five rotational isomers of vapour *n*-butyl chloride is calculated from the percentage concentrations of Table 1 to be in this order:

$$TG > TT > GG' > GG > GT\text{-form},$$

where the contribution of the entropy term to the concentrations is taken into account in the calculation.

In order to emphasize the anomalous feature of the present results (or those of Ref. 1.) for *n*-butyl chloride, a rough estimation of internal energies of rotational isomers will be made for $CH_3CH_2CH_2CH_2X$-type molecules. If we assume that the magnitude of the internal-energy difference between *trans* and *gauche* isomers of *n*-butane or *n*-propyl chloride can be transferred to *n*-butyl chloride, the internal-energy difference between the TT isomers and others may be estimated to a zero-th order approximation;

$$\Delta E(\text{TT-TT}) = 0,$$

8) A. B. Dempster, K. Price, and N. Sheppard, *Spectrochim. Acta*, **25A**, 1381 (1969).
9) F. A. Monany, R. A. Bonham, and W. H. McCoy, *J. Amer. Chem. Soc.* **85**, 3077 (1963).
10) R. A. Bonham, L. S. Bartell and D. A. Kohl, *ibid.*, **81**, 3491 (1959).

$$\Delta E(\text{GT-TT}) \simeq 0,$$

$$\Delta E(\text{TG-TT}) \simeq 0.75,$$

$$\Delta E(\text{GG-TT}) \simeq 0.75,$$

and $\Delta E(\text{GG'-TT}) \simeq 0.75 + E$ (parallel (1 : 3) interactions)

in units of kcal/mol, as the internal-energy differences of *n*-butane[11] and *n*-propyl chloride[12,13] are

$$\Delta E(C_4H_{10}) \simeq 0.75$$

and $$\Delta E(C_3H_7Cl) \simeq 0,$$

where $\Delta E = E(gauche) - E(trans)$. In other words, the relative stability of the rotational isomers may be in this order:

$$\text{TT} \simeq \text{GT} > \text{TG} \simeq \text{GG} > \text{GG'-form.}$$

These results are quite different from those obtained from Table 1 (see the preceding paragraph).

Similar calculations can be performed for *n*-butyl bromide using $\Delta E(C_4H_{10}) = 0.75$ kcal/mol and $\Delta E(C_3H_7Br) \simeq 0$[12-14], or for *n*-pentane using $\Delta E(C_4H_{10}) = 0.75$; the results agree well with those obtained from Table 1. In the cases of *n*-pentane and *n*-butyl bromide, the absence of the GG' form can be accounted for if we consider large enough parallel (1 : 3) interactions between two methyl groups or between methyl and bromine substituents. In order to stabilize the GG' form of *n*-butyl chloride, however, we have to consider some unfamiliar parallel (1 : 3) interactions whose interaction energy is negative, that is, attractive rather than repulsive.

Conclusion

It was ascertained that liquid *n*-butyl chloride is a mixture of the TT, GT, TG, GG, and GG' isomers, while liquid *n*-butyl bromide is a mixture of the TT, GT, TG, and GG isomers. Only the TT isomer remains in the crystalline state of *n*-butyl chloride or *n*-butyl bromide. These conclusions confirm the results obtained by means of the electron-diffraction method by Ukaji and Bonham.

The existence of the GG' form in a redily measurable concentration leads to the conclusion that we cannot deny the possibility of the presence of certain rotational isomers by the reason that there are expected parallel (1 : 3) interactions between methyl and chlorine substituents in the configurations. The results also indicate that the parallel (1 : 3) interactions between methyl and chlorine substituents might be attractive rather than repulsive in nature.

11) G. J. Szasz, N. Sheppard, and D. H. Rank, *J. Chem. Phys.*, **16**, 704 (1948).
12) C. Komaki, I. Ichishima, K. Kuratani, T. Miyagawa, T. Shimanouchi, and S. Mizushima, This Bulletin, **28**, 330 (1955).
13) Y. A. Pentin and V. M. Tatevskii, *Dokl. Akad. Nauk. SSSR*, **108**, 290 (1956).
14) T. Yoshino and H. J. Bernstein, *Can. J. Chem.* **35**, 339 (1957).

Absorption Band Shapes and Molecular Reorientation of Liquid Methyl Cyanide

Masao KAKIMOTO and Tsunetake FUJIYAMA

Department of Chemistry, Faculty of Science, The University of Tokyo, Hongo, Bunkyo-ku, Tokyo

(Received March 27, 1972)

The shapes and intensities of the fundamental bands of liquid methyl cyanide were observed by conventional transmittance method. Using the refractive indices observed by the ATR method, the observed absorption indices were corrected for the dielectric-field effect. The band shapes were analyzed from the point of view of moment analysis or correlation-function analysis. The results indicate that the shapes of a_1-type vibrations are good Lorentzian shapes, while those of the *e*-type can be explained as superpositions of Lorentzian and Gaussian functions. It is also found that the band-widths of the *e*-type vibrations were quite different from each other. Taking into account the effect of vibration-rotation interaction on the band-widths, the disagreement could be explained well. From the analyses of the band shapes of ν_7 and ν_8, the life-time function, $\phi(t)$, was obtained; it represents the decay of the fraction of freely-rotating molecules.

It has been widely accepted that an infrared absorption band shape of a liquid molecule is the Fourier transform of a dipole-correlation function, as was first pointed out theoretically by Shimizu[1] and Gordon.[2] Since a dipole-correlation function describes the time correlation of a transition-dipole moment related to the vibrational transition concerned, precise measurements of band shapes are expected to afford information about the anisotropic rotational motion of molecules in liquids. Based upon this principle, a number of experimental studies have been undertaken in order to elucidate the nature of molecular motions in liquids. Some of them have achieved fairly successful results,[3] but various difficulties have confronted spectroscopists at the same time. One of the most striking of them is seen in the spectra of liquid carbon disulfide; that is, an apparent reorientational relaxation time has a negative value if we follow the theory literally. It has been shown that this peculiarity can be resaonably explained by taking into account the contribution of vibrational relaxation to the observed band-widths.[4]

Another difficulty is found in the spectra of liquid methyl cyanide; that is, the shapes or half-widths of absorption bands belonging to the same symmetry species do not agree with each other, as was first pointed out by Vincent *et al.*[5] Vibrational transitions of particular symmetry species have their transition moments in the same direction in the molecular-fixed coordinate system; therefore, the corresponding correlation functions must be the same. No theoretical explanation of these experimental results had been found until Yamashita and Shimizu recently emphasized the effect of vibration-rotation interaction on the band-widths.[6] They calculated the change in a correlation function on varying a Coriolis constant, ζ, and showed that a correlation function decays more rapidly with an increase in $(1-\zeta)$. They also presented algebraic expressions of the second and fourth moments of vibrational bands for symmetric-top molecules, where a Coriolis coupling constant is explicitly included.

In the present work, an attempt is made to interpret the peculiarity observed for the band shapes of liquid methyl cyanide using the idea of Yamashita and Shimizu. An attempt is also made to describe the details of molecular reorientation quantitatively and to establish a general procedure for obtaining rotational diffusion constants from observed spectral information.

Experimental

The methyl cyanide used in the present work was a commercial product and was used after fractional distillation. No trace of any impurity was found in the infrared spectra covering the range of 400—4000 cm^{-1}.

All the infrared absorption spectra except for that of ν_8 were recorded by the use of a Perkin-Elmer 112G single-beam infrared spectrometer. A Perkin-Elmer 12C sinlge-beam infrared spectrometer mounted with a CsBr prism was used for the measurement of ν_8. These spectrometers had been carefully modified to eliminate the effect of stray light or thermal emission originating from the spectrometers themselves. The photometric effects and the nature of the noise spectra have also been thoroughly studied for these particular spectrometers.[7] The spectrometers were operated under a resolution of about 2 cm^{-1} and at room temperature (25°C). The effect of the finite slit-width on the observed band shapes was ascertained to be very small.

It has been recognized that an ATR method has many advantages for the precise measurements of the optical constants of liquid samples.[8] At the same time, the method is not particularly powerful for the study of absorption bands with weak intensities. Though the absorption bands of methyl cyanide were measured by the use of the transmittance method in this work, the agreement of the present data and those of the ATR method[9] was found to be excellent, probably because the absorption intensities of methyl cyanide are rather weak.

The observed light-energy distribution curve, $I(\nu)$ and $I_0(\nu)$, were reduced to the absorption index curve, $k(\nu)$, through the relation:

1) H. Shimizu, *J. Chem. Phys.*, **43**, 2453 (1965).
2) R. G. Gordon, *ibid.*, **43**, 1307 (1965).
3) C. F. Favelukes, A. A. Clifford, and B. L. Crawford, Jr., *J. Phys. Chem.*, **72**, 962 (1968); T. Fujiyama and B. L. Crawford, Jr., *ibid.*, **73**, 4040 (1969).
4) M. Kakimoto and T. Fujiyama, This Bulletin **45**, 2970 (1972).
5) C. Alliot, M. Cameo, and J. Vincent-Geisse, *C. R. Acad. Sci. Paris, Ser. B*, **266**, 391 (1968).
6) T. Yamashita and H. Shimizu, Lecture in Symposium on Molecular Structure, Tokyo (1970).
7) T. Fujiyama, Ph-D thesis submitted to the University of Tokyo (1966).
8) B. L. Crawford, Jr., A. C. Gilby, A. A. Clifford, and T. Fujiyama, *Pure Appl. Chem.*, **18**, 373 (1969).
9) T. Fujiyama and B. L. Crawford, Jr., The Lecture presented in Gordon Conference (1969).

$$k(\nu) = \frac{1}{4\pi l\nu} \ln(I_0(\nu)/I(\nu)) \quad (1)$$

where ν is the wave number in cm^{-1} and l is the thickness of the sample cell in cm. The thickness of the sample cell was determined by the interference-fringe method.

The observed $k(\nu)$ curves were corrected for the dielectric-field effect[10] using the observed $k(\nu)$ curve and the refractive index data obtained by the ATR method.[9] The observed $k(\nu)$ and/or the corrected $k_c(\nu)$ curves are shown in Figs. 1 through 4, 7, and 8. As may be seen from Fig. 1, for example, the effects of the dielectric field on the band shape are very small for these weak absorption bands. Throughout the following sections, the intensity distribution function, $I(\omega)$, should be understood as a normalized function of $k(\nu)$ and/or $k_c(\nu)$.

It is ascertained that the effects of the vibrational relaxation of the resonance type[4] are negligibly small for all the observed bands of methyl cyanide because of their weak intensities. The experimental fact that the shapes of ν_4 and ν_7 do not change essentially in a carbon tetrachloride solution (4 wt%) is another piece of evidence for this point of view.

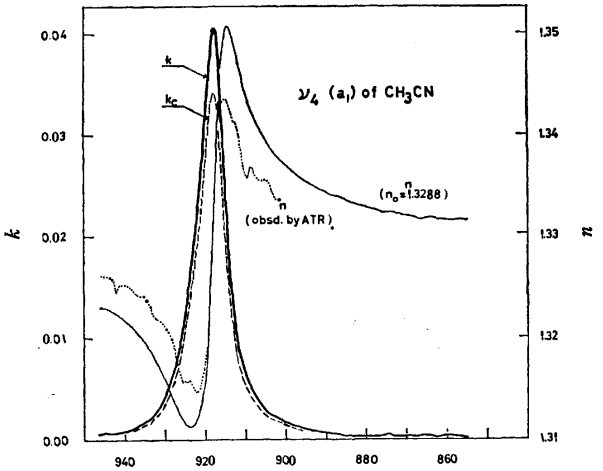

Fig. 1. $\nu_4(a_1)$ of liquid methyl cyanide. k: observed absorption index, n(solid line): refractive index calculated from k through Kramers-Kronig's formula, n(dotted line): refractive index observed by ATR method, k_c: corrected absorption index.

Discussion

Half-band-width. The half-band-widths, $\Delta\nu_{1/2}$'s, estimated from the observed $k_c(\nu)$ curves are summarized in Table 1. There is a relatively large uncertainty as to the $\Delta\nu_{1/2}$-values of ν_5 and ν_6 because they overlapped other bands considerably. It may clearly be seen from the table that the $\Delta\nu_{1/2}$'s of absorption bands

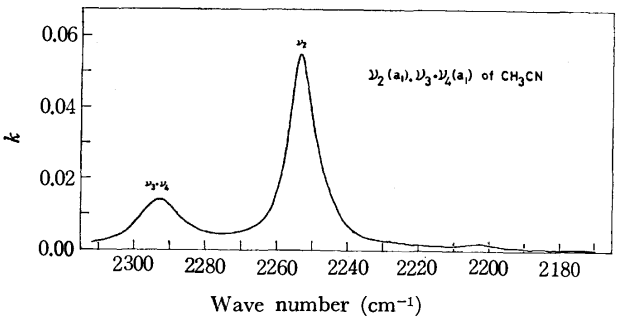

Fig. 2. Absorption index curve for $\nu_2(a_1)$ and $\nu_3+\nu_4(a_1)$ of liquid methyl cyanide.

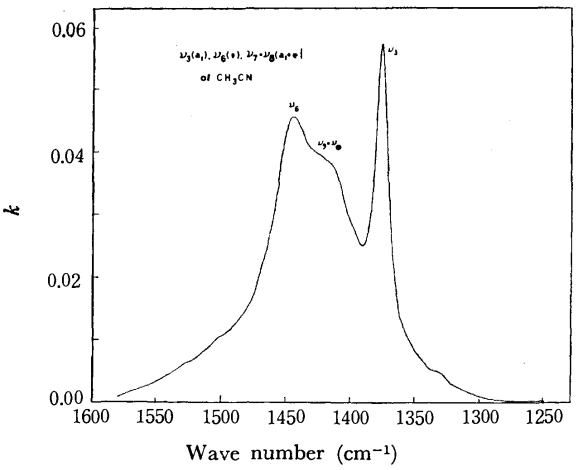

Fig. 3. Absorption index curve for $\nu_3(a_1)$ and $\nu_6(e)$ of liquid methyl cyanide.

Table 1. Spectral parameters of liquid methyl cyanide.

Γ is observed intensity. Γ_c is the intensity corrected for dielectric-field. Γ_{PW} is obtained from Γ through Polo-Wilson's formula.[19] Numbers in parentheses indicate the limits of experimental error.

	$\Delta\nu_{1/2}$ cm^{-1}	ν_0 cm^{-1}	Γ cm^2/mole	Γ_c cm^2/mole	Γ_{PW} cm^2/mole	ζ	$(1-\zeta)$
$\nu_1(a_1)$	15	2943.6	77(35)				
$\nu_2(a_1)$	8	2253.0	517(34)				
$\nu_3(a_1)$	12	1376.0	580(92)				
$\nu_4(a_1)$	8	918.4	329(24)	277(18)	277		
$\nu_2+\nu_4(a_1)$	13	3164	70(34)				
$\nu_3+\nu_4(a_1)$	14	2293.1	185(57)				
$\nu_5(e)$	40	3006	486(95)			0.062	0.938
$\nu_6(e)$	40	1443	2411(477)			−0.305	1.305
$\nu_7(e)$	23	1039.1	955(43)	806(35)	807	0.422	0.578
$\nu_8(e)$	10	379.0	699(49)	618(42)	606	0.88	0.12
$2\nu_8(a_1+e)$	18	748.8	315(13)	265(11)	266		

10) A. A. Clifford and B. L. Crawford, Jr., *J. Phys. Chem.*, **70**, 1536 (1966).

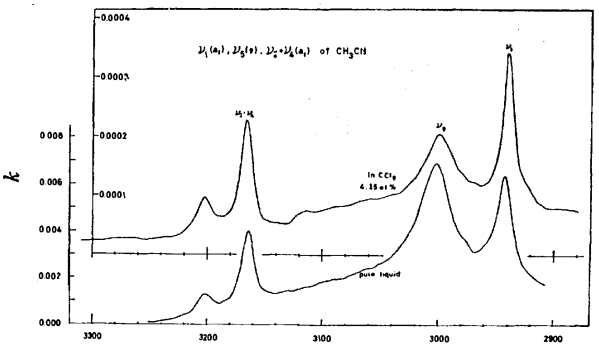

Fig. 4. Absorption index curves for $\nu_1(a_1)$ and $\nu_5(e)$ of methyl cyanide in pure liquid and carbon tetrachloride solution (4 wt%).

belonging to the same symmetry species do not agree with each other, especially for those of the *e*-type.

The observed values of Coriolis constants, ζ's, reported in the references[11,12] are also included in Table 1. It can quickly be observed in the table that there is apparent correlation between the $\Delta\nu_{1/2}$'s and the ζ's; this qualitatively coincides with the conclusion of Yamashita and Shimizu[6] that $\Delta\nu_{1/2}$ becomes larger with an increase in $(1-\zeta)$.

Moment Analysis and Mechanism of Molecular Reorientation. Corresponding to an absorption band's shape, $I(\omega)$, its n-th moment, M_n, is defined as [2,13]:

$$M_n = \int_{-\infty}^{\infty} I(\omega)\omega^n d\omega \qquad (2)$$

where ω is the angular frequency displacement from a band origin and where $I(\omega)$ is normalized to unity. Among the moments, the second moment, M_2, is the most important in the present discussion. As has been emphasized by Jones *et al.*,[14] the plotting of a second moment of an absorption band against its integration range is a useful tool in seeing if the band shape is a Lorentzian or a Gaussian function. This arises from the fact that a second moment plotted against the integration range diverges if $I(\omega)$ is a Lorentzian function, while it converges to a definite value if $I(\omega)$ is a Gaussian function. From the viewpoint of molecular rotation, a Gaussian band shape corresponds to a free-rotor model, while a Lorentzian band shape corresponds to a model of diffusional reorientation.[15]

The second-moment plottings for the bands of the a_1-type (ν_2 and ν_4) and of the *e*-type (ν_7 and ν_8) are shown in Figs. 5 and 6 respectively. It may be seen from the figures that the second moments of a_1-type bands go to infinity as the integration range increases, while those of *e*-type bands seem to converage to certain values. These facts indicate that the bands of the a_1-type have Lorentzian shapes, while those of *e*-type do not have simple Lorentzian shapes, but are presumably superpositions of Lorentzian and Gaussian curves. In other words, the molecular reorientational motion around an *x*- or *y*- axis may be described by diffusional reorientation, while molecular reorientation around a *z*-axis must be explained by a mechanism such as one in which both free and diffusional rotations take place simultaneously. The molecular symmetry axis coincides with the *z*-axis in the discussion.

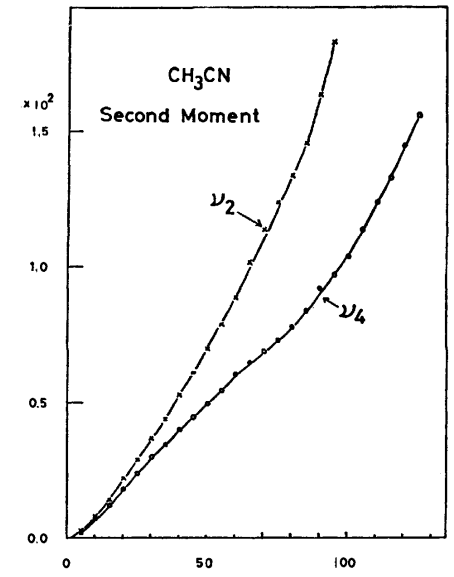

Fig. 5. Second moment plottings *vs.* integration range for ν_2 and $\nu_4(a_1)$ of liquid methyl cyanide.

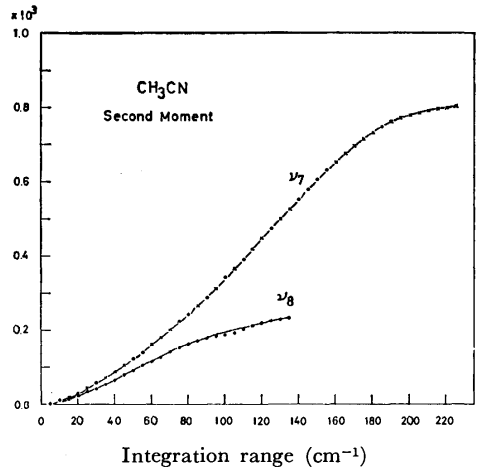

Fig. 6. Second moment plottings *vs.* integration range for ν_7 and $\nu_8(e)$ of liquid methyl cyanide.

Based upon a free-rotor model, Yamashita and Shimizu[6] proposed this algebraic expression of a second moment for a symmetric-top molecule:

$$M_2 = \begin{cases} kT\dfrac{2}{I_x}(\text{sec}^{-2}), \text{ for } a_1\text{-type} & (3a) \\ kT\left(\dfrac{1}{I_x}+\dfrac{1}{I_z}(1-\zeta)^2\right)(\text{sec}^{-2}), \text{ for } e\text{-type} & (3b) \end{cases}$$

where k is the Boltzmann constant; T, the absolute temperature, and I_i, the moment of inertia around the i-th axis. Equation(3) is essentially the same as the second-moment expression proposed by Gordon[13]

11) I. Nakagawa and T. Shimanouchi, *Spectrochim. Acta*, **18**, 513 (1962).
12) H. Matsuura, This Bulletin, **44**, 2379 (1971).
13) R. G. Gordon, *J. Chem. Phys.*, **39**, 2788 (1963); **41**, 1819 (1964).
14) R. P. Young and R. N. Jones, *Chem. Rev.*, **71**, 219 (1971).
15) L. D. Favro, *Phys. Rev.*, **119**, 53 (1960).

TABLE 2. CALCULATED AND OBSERVED SECOND MOMENTS OF LIQUID METHYL CYANIDE IN 10^2 cm^{-2}

	Gordon[13]	Yamashita[6] Shimizu	Obsd
$\nu_2, \nu_4(a_1)$	2.53	2.53	diverge
$\nu_7(e)$	23.0	4.32	8.1
$\nu_8(e)$		0.80	2.5

if we put ζ equal to zero. In Table 2, the observed and the calculated M_2's are compared for a few fundamental bands of methyl cyanide. Since the calculations of Gordon and Yamashita-Shimizu are clearly based upon free-rotor models, it is rather natural that the magnitude of M_2 calculated from Eq.(3) does not agree with the observed values.

Band-shape Analysis and Life-time Function, $\psi(t)$.
It was concluded in the preceding section that molecular reorientational motion around the z-axis of methyl cyanide may be interpreted as an intermediate state of free-rotation and rotational diffusion. The next problem is to analyze the observed band-shape data in a more quantitative way.

Theoretical expressions for a time-correlation function corresponding to the intermediate state may be found in the reports of Bratoz *et al.*[16] and of Shimizu.[1] Bratoz's formula is:

$$\Phi(t) = (1-\xi)\Phi_F(t) + \xi\Phi_D(t) \tag{4}$$

where $\Phi_F(t)$ and $\Phi_D(t)$ refer to time-correlation functions corresponding to free-rotation and rotational diffusion respectively, and where ξ is a constant which represents the fraction of molecules whose reorientational motion is diffusional. Shimizu expresses a time-correlation function as:

$$\Phi(t) = \psi(t)\Phi_F(t) + (1-\psi(t))\Phi_D(t) \tag{5}$$

Eqs.(4) and (5) differ only in whether the coefficients of $\Phi_F(t)$ and $\Phi_D(t)$ are time-dependent or not. In Eq.(5), $\psi(t)$ is a function of time and represents the decay of the fraction of freely-rotating molecules. We will call it a "life-time function" hereafter.

If we grant Eq.(4), then a band shape can be expressed as:

$$I(\omega) = (1-\xi)I_F(\omega) + \xi I_D(\omega) \tag{6}$$

where:

$$I_F(\omega) = \frac{1}{2\pi}\int_{-\infty}^{\infty}\Phi_F(t)e^{-i\omega t}dt \tag{7}$$

and:

$$I_D(\omega) = \frac{1}{2\pi}\int_{-\infty}^{\infty}\Phi_D(t)e^{-i\omega t}dt \tag{8}$$

$I_F(\omega)$ is a Gaussian function, and its half-width may be different for different vibrational transitions, while $I_D(\omega)$ is a Lorentzian function whose half-width is considered to be the same for all the bands belonging to the same symmetry species. Therefore, the decomposition of an observed band shape, $I(\omega)$, into Lorentzian and Gaussian functions can be expected to confirm the validity of the theory of Bratoz. Two e-type

16) S. Bratoz, J. Rios, and Y. Guissani, *J. Chem. Phys.*, **52**, 439 (1970).

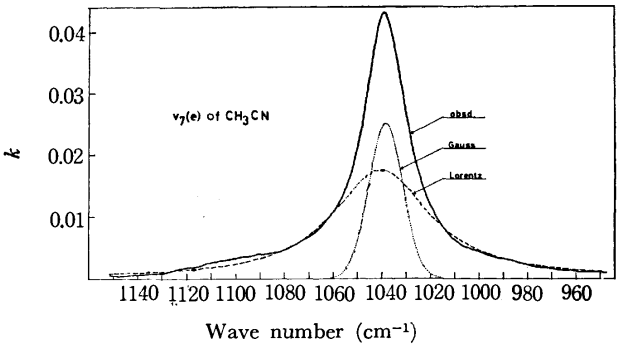

Fig. 7. Result of least-squares decomposition of $\nu_7(e)$ of liquid methyl cyanide into Lorentzian and Gaussian curves. Resultant Lorentzian and Gaussian components are shown by broken line and dotted line, respectively.

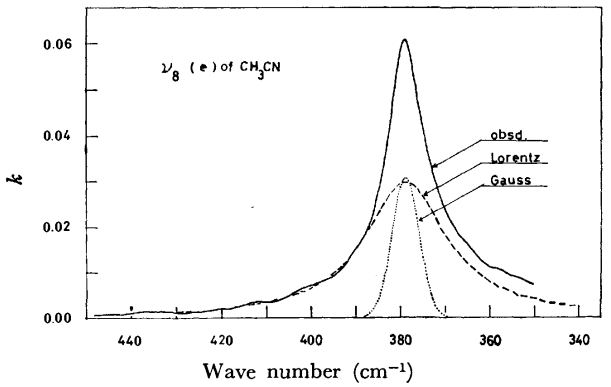

Fig. 8. Result of least-squares decomposition of $\nu_8(e)$ of liquid methyl cyanide into Lorentzian and Gaussian curves. Resultant Lorentzian and Gaussian components are shown by broken line and dotted line, respectively.

bands, ν_7 and ν_8, were decomposed into Lorentzian and Gaussian functions by the method of least-squares; the results are illustrated in Figs. 7 and 8 respectively. Unfortunately, the attempt was unsuccessful, because the shapes of the resultant Lorentzian components of ν_7 and ν_8 did not agree with each other. Therefore, Bratoz's model must be discarded.[17]

As the Fourier transform of Shimizu's formula of Eq. (5) is rather complicated to deal with, an attempt was made to analyze the correlation function obtained through the Fourier transformation of the observed band shapes of ν_7 and ν_8.

Let $\Phi_F(t)$ be a Gaussian function that will give a second moment of Yamashita and Shimizu (cf. Eq. (3b)):

$$\Phi_F(t) = \exp[-(M_2/2)t^2] \tag{9}$$

$\Phi_D(t)$ takes, as usual, an exponential form of the diffusion type:[14]

$$\Phi_D(t) = \exp[-D_e|t|] \tag{10}$$

where D_e is a rotational diffusion constant related to the e-type vibrations. Both $\Phi_D(t)$ and $\psi(t)$ are considered to be the same for all the vibrations of the e-type. Now that two sets of data, correlation functions for ν_7 and ν_8, are available, the form of $\psi(t)$ can be readily

17) The least-squares fitting did not result in a unique solution. However, the conclusion drawn here was the same for all sets of converged parameters.

estimated. A preliminary calculation showed that $\psi(t)$ is somewhat like an exponential function initiating from 1 at time zero. This fact may support the treatment of Shimizu,[1] who assumed the life-time function to be:

$$\psi(t) = \exp[-(1/\tau_L)|t|] \tag{11}$$

By employing the same form for $\psi(t)$, Eq.(5) is reduced to the form:

$$\Phi(t) = \exp[-(1/\tau_L)|t|]\cdot\exp[-(M_2/2)t^2] + (1-\exp[-(1/\tau_L)|t|])\cdot\exp[-D_e|t|] \tag{12}$$

Finally, the least-squares fitting of the correlation function of Eq.(12) to the observed correlation functions for ν_7 and ν_8 leads to the values of:

$$1/\tau_L = 1.8 \pm 0.7\ \text{psec}^{-1}$$

and:
$$D_e = 1.34 \pm 0.15\ \text{psec}^{-1} \tag{13}$$

In Figs. 9 and 10, the observed correlation functions for ν_7 and ν_8 are compared with those reproduced by Eq.(12) and the D_e and $1/\tau_L$ values thus obtained. The agreement of the two sets of correlation functions is fairly good. The standard errors attached to the parameters of Eq.(13) are estimated from the deviations between the observed and the calculated correlation functions. A rotational diffusion constant related

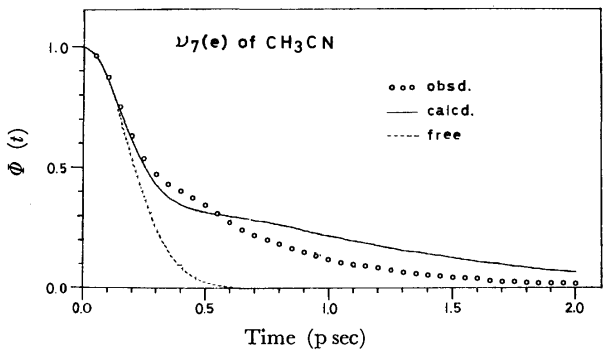

Fig. 9. Time-correlation function for $\nu_7(e)$ of liquid methyl cyanide. Open circles: Fourier transform of observed absorption index, solid line: calculated by Eq. (12), broken line: time-correlation function for a free-rotor of the form of Eq. (9).

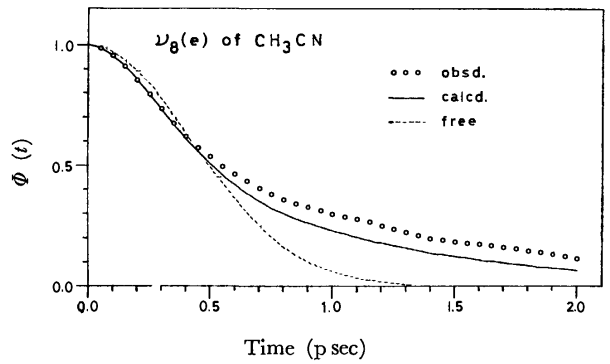

Fig. 10. Time-correlation function for $\nu_8(e)$ of liquid methyl cyanide. Open circles: Fourier transform of observed absorption index, solid line: calculated by Eq. (12), broken line: time-correlation function for a free-rotor of the form of Eq. (9).

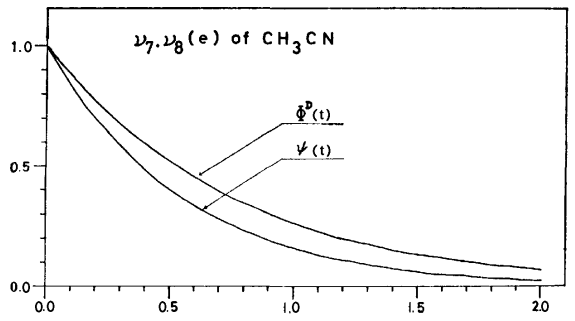

Fig. 11. Time-correlation function for diffusional reorientation, $\Phi_D(t)$, and life-time function, $\psi(t)$, obtained from time-correlation functions for ν_7 and $\nu_8(e)$ of liquid methyl cyanide.

with vibrations of the a_1-type, D_{a_1}, is directly obtained from the half-width of ν_2 or ν_4, namely:

$$D_{a_1} = 0.76 \pm 0.02\ \text{psec}^{-1} \tag{14}$$

because the shapes of a_1-type bands are good Lorentzian shapes. Using the values of D_e and D_{a_1}, the rotational diffusion constants about the x-and z-axes (D_x and D_z respectively) are calculated to be:

$$D_x = 0.38 \pm 0.01\ \text{psec}^{-1}$$

and:
$$D_z = 0.96 \pm 0.16\ \text{psec}^{-1}.$$

The correlation function related to the rotational diffusion, $\Phi_D(t)$, and life-time function, $\psi(t)$, are illustrated in Fig. 11. A comparison of Fig. 11 and Fig. 9 or 10 shows that $\Phi_D(t)$ and $\Phi(t)$ are essentially the same after about 1.0 psec; this corresponds to the situation in which $\psi(t)\Phi_F(t)$ decays very rapidly. In other words, almost all the molecules in the system follow diffusional reorientation at long times even if they behave like free-rotors at $t=0$. This result is consistent with that of a general theory of stochastic processes,[18]—that is, the finding that a correlation function of a random variable approaches a Markoffian exponential form at long times if the distribution of the variable is Gaussain.

Conclusion

The preceding discussion may be summarized as follows.

(1) The molecular reorientational motion of liquid methyl cyanide is diffusional around the x- and y-axes. The rotation around the z-axis must be understood as an intermediate state between free and diffusional ones.

(2) The vibration-rotation interaction affects the apparent correlation time.

(3) The intermediate state between free rotation and rotational diffusion may be described by the correlation function of Eq.(5).

(4) Rotational diffusion constants can safely be obtained if we can calculate a time-correlation function over a long period from the observed absorption spectra.

18) R. Kubo, *Lectures Theoret. Phys.* (Boulder), **1**, 120 (1958).
19) S. R. Polo and M. K. Wilson, *J. Chem. Phys.*, **23**, 2376 (1955).

This conclusion supports the description of a reference.[3)]
(5) Incidentally, a life-time function can be calculated if we have enough absorption data, which conversely describes the details of the molecular reorientation process.

The authors are indebted to all the members of the Shimanouchi Laboratory for their helpful correspondence about this work. They are particularly grateful to Professor Takehiko Shimanouchi of the University of Tokyo for giving them the opportunity of publishing this work. They are also indebted to Professor Hiroshi Shimizu and Miss Teruyo Yamashita of Kyushu University for their discussions of the effects of vibration-rotation interaction on band-widths.

BULLETIN OF THE CHEMICAL SOCIETY OF JAPAN, VOL. 45, 3026—3030 (1972)

CNDO Calculations on the Electronic Spectra of Several Saturated Compounds

Naoto OHMICHI, Akio TAJIRI,* and Takeshi NAKAJIMA
Department of Chemistry, Faculty of Science, Tohoku University, Sendai

(Received April 10, 1972)

CNDO calculations of the excited states were performed on the first three members of paraffinic hydrocarbons —methane, ethane, and propane, and on three compounds of saturated three-membered rings—cyclopropane, ethylenimine, and ethylene oxide. The method gives a reasonable interpretation of the electronic spectra of both kinds of compounds.

Most of the molecular orbital calculations on excited electronic states of organic compounds have so far been confined to π-electronic systems. There have been very few systematic and quantitative studies of electronic spectra on saturated compounds either theoretically or experimentally. One reason for this has been that the energy range of the electronic transitions in saturated compounds lies in the vacuum ultraviolet region, so that we had to wait until the spectroscopes of this energy range became avialabe for chemists.

Recently many experimental results on the electronic excitations in this energy region have been reported. Raymonda and Simpson[1] observed the vacuum ultraviolet absorption spectra of alkanes, while Lassettre *et al.*[2] and Brongersma *et al.*[3] reported the results of their electron-impact experiments on methane, ethane, and cycloalkanes. Particularly, the low-energy electron-impact excitation spectra observed by Brongersma *et al.* provide information about the singlet-triplet transitions in saturated hydrocarbons.[3] Moreover, Basch *et al.* reported very important experimental results in which they distinguished Rydberg transitions from valence-shell absorptions by making a condensed-phase vacuum ultraviolet experiment.[4]

As for theoretical treatments, several new molecular orbital methods, in which all valence electrons are treated and which can be applied to saturated molecules, have been proposed, one after another. Particularly, the CNDO method first proposed by Pople, Santry and Segal[5-7] has recently been used by many authors for MO calculations, mainly of the ground states of molecules. On the other hand, Del Bene and Jaffé[8-10] succeeded in reproducing experimental results on the electronic spectra of π-electronic systems including heteroatoms by using a modified version of this method. There have been however, few studies of the electronic spectra of σ-systems within the framework of the CNDO method.[11,12]

In view of these circumstances, we previously proposed[13] an approximate method with a new parametrization for the bonding parameter, β_A^0, and the two-center electron repulsion integral, γ_{AB}, within the framework of the CNDO/2 method; this method can be applied to the calculation of the electronic spectra of both saturated and unsaturated molecules.

In the present paper, we will apply this method to a series of paraffinic hydrocarbons and to a series of saturated three-membered ring compounds. We will compare the calculated electronic spectra of these molecules with those of Katagiri and Sandorfy,[14] who used the Pariser-Parr-Pople-type method on paraffinic hydrocarbons, and with those of Clark, obtained using the Pople-Segal CNDO/2 method[11] on ring compounds.

Method of Calculation

As we mentioned in the previous paper, our method is a compromise between the methods of Bene-Jaffé[8]

* Present address: Chemical Research Institute of Non-Aqueous Solutions, Tohoku University, Katahira, Sendai.

1) J. W. Raymonda and W. T. Simpson, *J. Chem. Phys.*, **47**, 430 (1967).
2) E. N. Lassettre, A. Skerbele, and M. A. Dillon, *ibid.*, **49**, 2382 (1968).
3) H. H. Brongersma and L. J. Oosterhoff, *Chem. Phys. Lett.*, **3**, 437 (1969).
4) H. Basch, M. B. Robin, N. A. Kuebler, C. Baker, and D. W. Turner, *J. Chem. Phys.*, **51**, 52 (1969).
5) J. A. Pople, P. P. Santry, and G. A. Segal, *ibid.*, **43**, 129 (1965).
6) J. A. Pople and G. A. Segal, *ibid.*, **43**, 136 (1965).
7) J. A. Pople and G. A. Segal, *ibid.*, **44**, 3289 (1966).
8) J. Del Bene and H. H. Jaffé, *ibid.*, **48**, 1807 (1968).
9) J. Del Bene and H. H. Jaffé, *ibid.*, **48**, 4050 (1968).
10) J. Del Bene and H. H. Jaffé, *ibid.*, **49**, 1221 (1968).
11) D. T. Clark, *Theor. Chim. Acta*, **10**, 111 (1968).
12) D. R. Salahub and C. Sandorfy, *ibid.*, **20**, 227 (1971).
13) A. Tajiri, N. Ohmichi, and T. Nakajima, This Bulletin, **44**, 2347 (1971).
14) S. Katagiri and C. Sandorfy, *Theor. Chim. Acta*, **4**, 203 (1966).

Table 1. Parameter values (eV)

		H	C	N	O
U_{ss}	CNDO/2	−17.38	−70.3	−106.03	−149.07
	Sichel and Whitehead[a] / This work	−13.60	−50.69	−70.09	−101.31
U_{pp}	CNDO/2	—	−61.8	−93.99	−132.80
	Sichel and Whitehead[a] / This work	—	−41.53	−57.85	−84.28
γ_{AA}	CNDO/2	20.40	16.06	19.27	22.49
	Clark[b]	12.85	11.11	12.02	13.00
	Sichel and Whitehead[a] / This work	12.85	10.21	11.05	13.63
γ_{AA}^*	Sichel and Whitehead[a] / This work	12.85	10.33	11.31	13.91
β_A^0	CNDO/2	9	21	25	31
	Clark[b]	12	17	26	45
	Sichel and Whitehead[a]	5.4	8.2	8.8	12.8
	This work	8.0	15.0	23.0	41.0

a) Ref. 15. b) Ref. 11.

and of Sichel-Whitehead.[15] The F matrix elements are given in this method as:

$$F_{\mu\mu} = U_{\mu\mu} + \left(P_{AA} - \frac{1}{2}P_{\mu\mu}\right)\gamma_{AA} + \sum_{B \neq A}(P_{BB} - Z_B)\gamma_{AB}, \quad (1)$$

$$F_{\mu\nu} = \kappa/2(\beta_A^0 + \beta_B^0)S_{\mu\nu} - \frac{1}{2}P_{\mu\nu}\gamma_{AB}, \quad (2)$$

where μ and ν denote atomic orbitals centered on the A atom and the B atom respectively. The empirical parameter, κ, is taken as 0.75 for the π-bonds and as 1.0 otherwise. $U_{\mu\mu}$ is the diagonal matrix element of the atomic orbital, ϕ_μ, for the core Hamiltonian of the A atom. $P_{\mu\nu}$ is the charge density and bond-order matrix. P_{AA} is the total charge on the A atom. γ_{AB} is an average interaction energy between an electron in any valence atomic orbital of the A atom with another in an orbital of the B atom. β_A^0 is the bonding parameter, which depends only on the nature of the A atom.

For $U_{\mu\mu}$ and γ_{AA}, we used the values of Sichel and Whitehead.[15] In evaluating the interatomic electron repulsion integral, γ_{AB}, we employed Mataga-Nishimoto's formula;

$$\gamma_{AB} = 1/(R_{AB} + a), \qquad a = 2/(\gamma_{AA}^* + \gamma_{BB}^*), \quad (3)$$

where γ_{AA}^* is the "extrapolated" one-center electron repulsion integral.[15] The empirical parameter, κ, and the bonding parameters, β_H^0 and β_C^0 were so reparametrized that they reproduce the experimental spectra of the reference molecules—methane, ethylene, and benzene.[13] The values of β_N^0 and β_O^0 needed for calculating ethylenimine and ethylene oxide were determined using pyrole and furan as reference molecules. In Table 1, the parameter values used in this work are compared with those used in other methods.

The geometries of methane, cyclopropane, ethylenimine, and ethylene oxide were taken from Sutton's tables.[16] For ethane and propane, all the angles are assumed to be tetrahedral, and the bond lengths of C-C and C-H are assumed to be 1.54 Å and 1.09 Å respectively; this is done for convenience in calculation and in comparison of the results. For ethane, we adopted two thermally-probable conformers, staggered (D_{3d}) and eclipsed (D_{3h}).

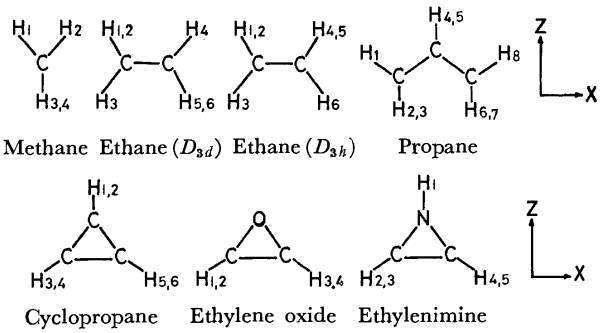

Fig. 1. Co-ordinate systems for calculated molecules.

The calculations were carried out on the NEAC 2200 Model 500 computer of Tohoku University, using the program of our modified CNDO method including configuration interactions restricted to 30 lowest singly-excited configurations.

Results and Discussion

Electronic Spectra of Paraffinic Hydrocarbons.

Methane: Table 2 shows the calculated and observed energies of excited states of methane. The calculated $T_2 \leftarrow A_1$ transition at 10.64 eV was used, together with some transitions in ethylene and benzene, for the parametrization of κ, β_H^0 and β_C^0.[13] The next higher allowed transition is calculated to be 13.42 eV($T_2 \leftarrow A_1$). This value is too high to be associated with the observed second transition at 11.7 eV.[3] We may, therefore, reasonably assign this observed band to one of the quintuply-degenerate forbidden transitions, $E \leftarrow A_1$ and $T_1 \leftarrow A_1$, at 12.27 eV. These forbidden transitions may be perturbed by vibrations belonging to the T_2 symmetry and may become vibronically-allowed by borrowing intensity from the $T_2 \leftarrow A_1$ transition at 13.42 eV, which is very intense.

15) J. M. Sichel and M. A. Whitehead, *Theor. Chim. Acta*, **7**, 32 (1967).
16) L. E. Sutton, "Tables of Interatomic Distances," The Chemical Society, London (1958), p. M113, M132, M134, M149.

Table 2. Excitation energies (in eV) and intensities of methane

	Obs. (Ref. 3)	This work		Katagiri and Sandorfy (Ref. 14)	
Singlet	9.7—10.2	T_2	10.64 (0.22)	T_2	10.26
	11.7	$E+T_1$	12.27 (0)	$A_1+E+T_1+T_2$	10.48
		T_2	13.42 (1.77)		
Triplet	8.8	T_2	9.39	T_2	9.31
	11.0	A_1	10.74	$A_1+E+T_1+T_2$	10.11
		T_2	11.57		

Table 3. Excitation energies (in eV) and intensities of ethane

		Obs.		This work		Katagiri and Sandorfy (Ref. 14)	
		Light absorption (Ref. 2)	Electron impact (Ref. 3)				
C_2H_6 (D_{3d})	Singlet	8.5		E_u	8.81 (0.26)	E_u	7.81
						E_g	8.78
		9.4	9.3	A_{2u}	9.55 (0.32)	$A_{1u}+A_{2u}+E_u$	8.84
				E_g	9.77 (0)		
				A_{1g}	10.22 (0)		
				A_{1u}	10.70 (0)		
		10.68		E_u	11.02 (0.15)		
				E_u	11.43 (0.57)	A_{2u}	10.15
	Triplet		7.1 (onset)	E_u	7.88	E_u	7.37
			⟩	E_g	8.66	$A_{1u}+A_{2u}+E_u$	8.01
			9.3	A_{2u}	8.83	E_g	8.05
C_2H_6 (D_{3h})	Singlet			E'	8.80 (0.29)	E''	7.84
				A_2''	9.58 (0.32)	E'	8.51
				E''	9.64 (0)	$A_1''+A_2''+E''$	8.56
				A_1'	10.20 (0)	A_2''	10.12
				A_1''	10.63 (0)		
				E''	11.02 (0)		
				E'	11.24 (0.02)		
	Triplet			E'	7.83	E''	7.25
				E''	8.54	E'	7.87
				A_2''	8.83	$A_1''+A_2''+E''$	7.89
				A_1'	9.72	A_2''	9.27

Using the low-energy electron impact as a spectroscopic tool, Brongersma *et al.*[3] observed excitation spectra for saturated hydrocarbons considerably different from the optical ones. The difference arises from the fact that the selection rules for electronic excitation by electron impact differ fundamentally from those encountered in light-absorption spectroscopy. In the case of low-energy electron impact, in particular, as it is thought that the exchange between the incident electron and a molecular electron is possible, the difference between the two types of spectra may mainly be a result of singlet-triplet transitions. For methane, Brongersma *et al.* reported a low-energy electron impact excitation spectrum—a trapped electron (TE) spectrum—showing singlet-triplet transitions at 8.8 and 11.0 eV.[3] Our results on the triplet states of methane are in good agreement with their experimental data.

Ethane: Table 3 shows the calculated and observed excited states of ethane. The difference in predicted spectrum between the conformational isomers of ethane, staggered and eclipsed, turned out to be very small. We assign the observed values to the predicted values for the staggered ethane, thermally-most-probable conformer. According to Lassettre *et al.*, [2] three transitions are observed, at 8.5, 9.4, and 10.68 eV (third column). They may be assigned to the $E_u \leftarrow A_{1g}$ transition predicted at 8.81 eV (0.26), the $A_{2u} \leftarrow A_{1g}$ transition at 9.55 eV (0.32), and the $E_u \leftarrow A_{1g}$ transitions at 11.02 eV (0.15) and 11.43 (0.57) respectively. Thus, a good agreement between theory and experiment is obtained.

For triplet states, the present calculation predicted the first transition at 7.88 eV with a transition type of $E_u \leftarrow A_{1g}$. Brongersma *et al.*[3] observed the first peak at 9.3 eV, one with an onset at 7.1 eV, by using the low-energy electron-impact technique. In the optical[1] and high-energy electron-impact[2] spectra, the onset is at 8.1 eV. According to Brongersma *et al.*, the difference between these two types of spectra suggests that the contribution of singlet-triplet transitions is important. It is likely that the absorption between 7.1 eV and 8.1 eV observed in the TE spectrum is due mainly to the singlet-triplet transition, which is predicted at 7.88 eV by our method.

Propane: The results of the calculation of the elec-

Table 4. Excitation energies (in eV) and intensities of propane

	Obs. (Ref. 1 and 2)	This work		Katagiri and Sandorfy (Ref. 14)	
Singlet	8.1 (Shoulder)	B_1	8.40 (0.16)	B_1	7.53
		B_2	8.37 (0.35)	A_2	8.22
	8.9	A_1	8.63 (0.24)	B_1	8.28
		A_1	9.16 (0.01)	A_1	8.31
		B_2	9.18 (0.04)	A_1	8.49
		A_2	9.24 (0)	B_2	8.91
		B_2	9.65 (0.02)	A_1	8.98
	9.6	B_1	9.72 (0.00)		
		A_1	9.93 (0.05)		
		A_2	10.24 (0)		
Triplet		B_1	7.55	B_1	7.00
		B_2	7.73	A_1	7.77
		A_1	7.86	B_1	7.79
		A_2	8.51	A_1	7.79

tronic-transition energies of propane are given in Table 4, together with the experimental results. We calculated the excited states of propane, assuming an all-*trans* C_{2v} conformation. Actually, however, the propane molecule is not fully in an all-*trans* conformation; rather, it takes various *gauche*-type forms. Although each conformer will have excitation energies different from those of other conformers, the difference, may be guessed from the results concerning ethane conformers, may be very small. Thus, we may tentatively give the assignments shown in Table 4.

The lowest singlet-singlet transition ($B_2 \leftarrow A_1$) was calculated to be at 8.37 eV, with the very large oscillator strength of 0.35. From the experimental data given by Raymonda *et al.*[1] and by Lassettre *et al.*,[2] however, we can read the weak absorption at 8.1 eV as the first band. According to Salahub *et al.*[12] and Katagiri *et al.*,[14] the symmetry of the predicted first transition for propane is B_1. Our method, on the other hand, predicts the lowest $B_1 \leftarrow A_1$ transition at 8.40 eV (0.16), higher by 0.03 eV than the lowest calculated transition. This energy difference is so small that the order of these two predicted transitions is not essential for this type of calculation. We may thus assign the weak band observed at 8.1 eV as a shoulder to the $B_1 \leftarrow A_1$ transition predicted at 8.40 eV and the next strong absorption band observed at 8.9 eV to the group transitions including the $B_2 \leftarrow A_1$ transition calculated at 8.37 eV.

The transitions predicted by Katagiri and Sandorfy[14] seem, in general, to be too low to be assigned to the observed spectrum.

Electronic Spectra of the Saturated Three-membered Rings. Several discussions of the electronic structures of saturated three-membered rings have been reported; the earlier works focussed on the bonding nature,[17,18] and the more recent works, on their spectral properties.[4,11,19-22] Walsh has discussed the olefin-like structures of cyclopropane and ethylene oxide.[18] The results of our calculations of the electronic spectra of these molecules seem to support the study of Walsh,[18] since all the first singlet-singlet transitions of these molecules are predicted to be in about the 7 eV energy region, considerably lower than in the case of ususal saturated molecules and rather close to those met with in the case of olifins.

Cyclopropane: The calculated excited states of cyclopropane are shown in Table 5, alobg with the experimental values. Our calculations provide results very close to those predicted by Clark.[11] He associated the calculated transitions with the experimental ones obtained by Wagner and Duncan, including Rydberg transitions.[20] Recently Basch *et al.*[4] have reported new spectral data on cyclopropane: they proposed the values of 7.4, 8.6, and 10.3 eV for the N→V transitions. These values were obtained by comparing the gas-phase and condensed-phase spectra.

Table 5. Excitation energies (in eV) and intencities of cyclopropane

	Obs.				This work		Clark (Ref. 11)		Brown and Krishna (Ref. 21)	
	Light absorption			Electron impact						
	Ref. 20	Ref. 1	Ref. 4	Ref. 3						
Singlet					A_2'	6.76 (0)	A_2'	6.68 (0)		
	6.79						E'	6.93 (0.04)		
		7.0 (onset)								
			7.4 (N→V)	7.4	E'	7.39 (0.06)				
	7.78	7.8	7.67 (Ryd.)				A_1'	7.77 (0)	A_2'	7.23
					A_1'	8.34 (0)				
	8.55	8.6	8.6 (N→V)	9.7	E'	8.87 (0.17)	E'	8.46 (1.10)	E'	7.72
					E''	9.14 (0)	E''	8.48 (0)	A_1'	8.71
					E''	9.71 (0)	E''	8.79 (0)		
	10.32		10.3 (N→V)		A_2''	9.73 (0.67)	A_2''	9.72 (0.44)	E'	11.66
Triplet				5.9 (onset)	A_2'	6.76	E'	5.95	A_2'	6.79
					E'	7.10	A_2'	6.68	E'	6.95
				7.4	A_1'	7.85	E'	7.19	E'	8.07

17) A. D. Walsh, *Nature*, **159**, 165, 712 (1947).
18) A. D. Walsh, *Trans. Faraday Soc.*, **45**, 179 (1949).
19) A. Lawrey and K. Watanabe, *J. Chem. Phys.*, **28**, 208 (1958).
20) P. Wagner and A. B. F. Duncan, *ibid.*, **21**, 516 (1953).
21) R. D. Brown and V. G. Krishna, *ibid.*, **45**, 1482 (1966).
22) G. Herzberg, "Electronic Spectra and Electronic Structure of Polyatomic Molecules," D. Van Nostrand Co. Inc., New York (1966), p. 548, 651.

Table 6. Excitation energies (in eV) and intensities of ethylene oxide

	Obs.		This work		Clark (Ref. 11)	
	Ref. 22	Ref. 4				
Singlet					A_2	5.61 (0)
					B_2	6.30 (0.06)
	5.83~7.23 (tail)		A_2	7.26 (0)	B_1	6.34 (0.03)
					A_1	6.53 (0.00)
	7.23	7.24 (Ryd.)			B_2	6.99 (0.05)
					A_2	8.27 (0)
		7.7 (N→V)	B_2	7.74 (0.11)		
	7.89	7.89 (Ryd.)			B_1	8.39 (0.00)
					B_1	8.40 (0.01)
		8.6 (N→V)	B_1	8.15 (0.17)		
			A_1	8.46 (0.00)		
	8.64	8.64 (Ryd.)			B_2	8.49 (0.43)
			A_2	8.75 (0.00)		
	8.96	8.97 (Ryd.)			A_1	8.68 (0.12)
	9.56	10.54 (N→V)	B_1	9.28 (0.24)	A_1	9.39 (0.05)
			A_1	10.06 (0.04)		
Triplet			A_2	6.43	B_2	5.16
			B_1	6.80	A_2	5.59
			B_2	7.23	B_1	6.19

This is based on the fact that Rydberg bands do not appear in condensed phases. We may assign these observed transitions to the predicted 7.39 eV (E'←A_1' (0.06), 8.87 ev(E'←A_1') (0.17), and 9.73 eV (A_2''←A_1') (0.67) transitions respectively.

The TE spectrum of cyclopropane reported by Brongersma *et al.*[3] is quite different from the optical spectrum in the region of about 6—7.5 eV, suggesting that there is an important contribution of the singlet-triplet transition in the TE spectrum. In addition, Wagner *et al.*[20] observed a weak absorption centered around 6.79 eV for cyclopropane. The calculation by Brown *et al.*[21] suggests that this absorption is due to a singlet-triplet transition. In accordance with these peices of evidence, our calcualtion gives the A_2'←A_1' transition at 6.76 eV as the first singlet-triplet transition. The corresponding value calculated by Clark[11] is 5.95 eV (E'—A_1').

Table 7. Excitation energies (in eV) and intensities of ethylenimine

	Obs. (Ref. 4)	This work		Clark (Ref. 11)	
Singlet	6 (Ryd.)			A''	5.98 (0.04)
	6.9 (Ryd.)			A'	6.50 (0.01)
	7.4 (N→V)	A''	7.13 (0.03)	A'	6.81 (0.01)
		A'	7.91 (0.02)	A''	7.22 (0.03)
	8.4 (Ryd.)			A'	7.87 (0.04)
		A''	8.76 (0.01)	A'	8.19 (0.02)
		A'	9.01 (0.09)		
		A'	9.07 (0.02)		
		A''	9.07 (0.05)		
		A'	9.40 (0.37)		
	9.0 (N→V)	A''	9.72 (0.09)		
	≀	A'	9.77 (0.00)		
	10.5 (N→V)	A'	10.20 (0.08)		
		A''	10.30 (0.03)		
		A''	10.43 (0.00)		
		A''	10.94 (0.00)		
		A'	11.09 (0.04)		
		A'	11.29 (0.04)		
		A''	11.33 (0.78)		
Triplet		A''	6.83	A''	5.22
		A'	7.37	A'	6.27
		A''	7.80	A''	6.62
		A'	8.00	A'	6.70

Ethylene Oxide: The calculated and observed excited states of ethylene oxide are listed in Table 6. Our method and Clark's method[11] give quite different results. Moreover, his assignments seem to be inadequate, for, according to Bash *et al.*,[4] some experimental values to which Clark assigned his calculated values come from Rydberg transitions. For example, the observed values of 7.23, 7.89, 8.64, and 8.96 eV[22] with which Clark associated his calculated values turned out to be due to Rydberg transitions.[4] The results of our calculation of ethylene oxide agree fairly well with the new experimental results.

Our calculation predicts three low-lying triplet states at 6.43 eV (A_2←A_1), 6.80 eV (B_1←A_1), and 7.23 eV (B_2←A_1); they are higher than Clark's results by ca. 1 eV.

Ethylenimine: In Table 7 we show the calculated and observed excited states of ethylenimine. Here again our method gives results quite different from those obtained usnig Clark's method.[11] This molecule belongs to the point group C_s, so that all singlet-singlet transitions are allowed. According to Basch *et al.*,[4] the lowest N→V transition is observed at 7.4 eV, so Clark's values[11] seem to be too low. The two rather close transitions predicted using our method, the A''←A' transition at 7.13 eV (0.03) and the A'←A' transition at 7.91 eV (0.02), may be associated with the observed first transition at 7.4 eV. In the energy region above 8 eV, our method predicts a large number of transitions very close to each other. We may associate these predicted transitions with the two bands observed at 9.0 and 10.5 eV, which are very broad, probably because of the overlapping of transitions.

The authors are greatly indebted to Professor S. Katagiri of Hirosaki University for many helpful discussions.

Properties of Water in Macromolecular Gels. IV. Proton Magnetic Resonance Studies of Water iu Macromolecular Gels

Masuo AIZAWA, Jun MIZUGUCHI, Shuichi SUZUKI, Shoichi HAYASHI*, Teruo SUZUKI*, Noriko MITOMO*, and Hiroshi TOYAMA*

Research Laboratory of Resources Utilization, Tokyo Institute of Technology, Meguro-ku, Tokyo

**Japan Electron Optics Co., Akishima, Tokyo*

(Received November 11, 1971)

Electrochemical and dilatometric studies have indicated that at least three states of water exist in macromolecular gels. The properties of each state of water in gels such as agarose gels were investigated by high-resolution and broadline PMR over the temperature range from +50 to −60°C. The linewidth of water protons in gels was found to depend markedly on the water content of gels, and the linewidth *vs.* water content curve gave two inflection points. One of the inflection points can be attributed to the so-called bound water, but the other cannot be explained unless three states of water are assumed in gels. Three kinds of transition temperatures were confirmed by anomalous changes in the PMR linewidth below 0°C. The so-called bound water exhibited no transition temperature between 0 and −20°C, and free water gave the transition temperature at 0°C. Moreover, the transition temperature of a quantity of water was distributed in the range from 0 to −20°C. On the basis of the transition temperature, the properties of water in macromolecular gels are discussed.

A solid-like state of a biopolymer adsorbing a small amount of water and an aqueous solution of biopolymer have been taken as the samples in most of the investigations of the properties of water in biopolymers, such as proteins, starch, and cellulose.[1] These two states of biopolymers investigated, however, seem to be somewhat different from that of native biotissues, which include a large quantity of water in their network. Macromolecular gels, such as polysaccharide and protein, have been used as the samples during the present investigation. Especially the results on agarose gels will be described in this report.

Two states of water, a so-called bound water and free water, are accepted to be present in macromolecular gels. Electrochemical[2,3] and dilatometric studies of the properties of water in macromolecular gels[4] have made it clear that free water in macromolecular gels should be classified into at least two groups. Furthermore, the properties and states of water in agarose gels were investigated by PMR in this investigation.

The nuclear magnetic resonance linewidth is known to be related with the spin-spin relaxation time, T_2, indicating the motional state of a nuclear spin.[5] Therefore, the motional state of water can be estimated by means of the PMR linewidth of water protons. In recent years, the technique of nuclear magnetic resonance has been used with some success to characterize distinct types of the molecular motion of water adsorbed on biopolymers.[6-10] Several PMR studies of water in agar have been carried out. Woessner[11] used pulse PMR to study the temperature hysteresis in agar sol-gel transitions of both the agar macromolecules and water in the agar–water system; his results indicate that the major portion of the water molecules (in the agar–water system) is not in an "ice-like" or modified state. These applications of PMR, however, have been limited to investigations on the state of water adsorbed by macromolecules containing either small amounts of water or a large quantity of water. In order to obtain additional information concerning molecular motions of water in macromolecular gels, the high-resolution and broad-line PMR spectra of water in agarose gels were measured over the full range of water content from 0 to 100% by weight. Additionally, the solid-liquid transition of water in gels was investigated by studying the temperature dependence on the PMR linewidth of the water proton in the agarose–water system to clarify the properties and the states of water in gels.

Experimental

Materials. The agarose for immuno-electrophoresis use was purchased from the Nakarai Chemicals Co., Ltd., and was assayed for its ash content by the atomic-absorption analysis method. The agarose contained Mg 0.04, Ca 1.01, K 0.09, and Na 1.75 mg/g dry agarose.

A series of samples was obtained by varying the mixing ratio of water and agarose; they were sealed in a standard PMR sample tube (5 mm O.D.). The water content of the sample was determined by drying it at 105°C for 24 hr and by then weighing the dried matter.,

PMR-spectra Analysis. The proton NMR spectra were obtained using a JNM-C-60HL high-resolution NMR spectrometer and a MW-40 broad-line NMR spectrometer operating at 60 MHz and 40 MHz respectively, with an external NMR lock system. Since the signals were wider than those normally seen in high-resolution work, it was necessary to operate at optimum rf power levels, just below signal saturation. The spectrometer was equipped with a variable-temperature controller which maintained the sample within ±0.5°C of the desired temperature. The temperature

1) L. P. Kayushin, ed. "Water in Biological Systems" Consultants Bureau, New York (1969), p. 28.
2) J. Mizuguchi, M. Takahashi, and M. Aizawa, *Nippon Kagaku Zasshi* **91**, 723 (1970).
3) J. Mizuguchi, M. Takahashi, and M. Aizawa, *ibid.*, **91**, 961 (1970).
4) M. Aizawa and S. Suzuki, This Bulletin, **44**, 2967 (1971).
5) H. S. Gutowsky and G. E. Pake, *J. Chem. Phys.*, **18**, 162 (1950).
6) A. Odajima, J. Sohma, and S. Watanabe, *ibid.*, **31**, 276 (1959).
7) J. Clifford and B. Sheard, *Biopolymers*, **4**, 1057 (1968).
8) W. S. Brey, T. E. Evans, and L. H. Hitzrot, *J. Colloid Interface Sci.* **26**, 306 (1968).
9) D. J. Blears, and S. S. Danyluk, *Biochim. Biophys. Acta* **154**, 17 (1968).
10) Y. Ogiwara, H. Kubota, S. Hayashi, and N. Mitomo, *J. Appl. Polymer Sci.* **13**, 1689 (1969); **14**, 303 (1970).
11) D. E. Woessner, B. S. Snoeden, Jr. and Y. C. Chiu, *J. Colloid Interface Sci.* **34**, 283 (1970).

of a sample was calibrated by means of a copper-constantan thermocouple placed inside the sample tube. The linewidth of the spectra was expressed in terms of half linewidth, *i.e.*, the linewidth at half of the maximum peak height.

Results

Broad-line PMR Spectra of Agarose Gels. The broad-line PMR spectra of agarose gels were measured in order to distinguish the signal of the water proton from that of the agarose protons. For the agarose-water system containing 10% of water by weight, the spectra are shown in Fig. 1, with the abscissa expressed

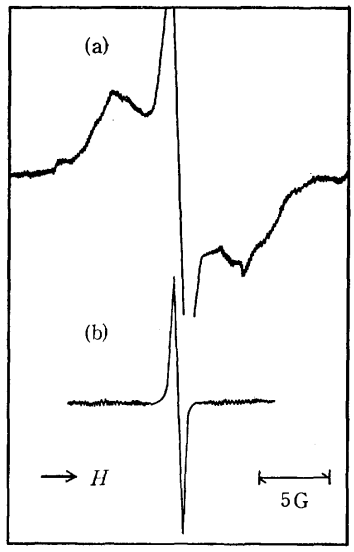

Fig. 1. Broad line PMR spectra of agarose containing 10% of water.
(a): Gain 1.0×100, Response 2, Mod. width 1G; (b): Gain 1.0×10, Response 1, Mod. width 1G, (25±0.5°C).

in Gauss units. Two components, namely, a broad one which can be attributed to the agarose proton and a narrow one attributable to the water proton, were detected, though the broad component disappeared in the (b) spectrum. The linewidth for the agarose proton in the (a) spectrum is evaluated as approximately 9 gauss. Therefore, it is reasonable to assign the signal in high-resolution PMR spectra to the water proton.

PMR Linewidth of water in Various Water Contents of Agarose Gel. PMR measurements showed that the line shape and width of the water proton are independent of the orientation of the gels in the magnetic field; this means that there is no preferential orientation of water molecules with respect to the gel structure when this technique is used.

The PMR spectra for agarose gels containing 98 and 80% water at room temperature are illustrated in Fig. 2; the spectra are attributed to protons of water in agarose gels.

The PMR linewidth of water in agarose gels was measured for the full range of water content from 0 to 100%. The results are presented in Fig. 3, where the linewidth is given as the linewidth at half of the maximum peak height. In the water-content range from 100 to 60% and from 30 to 0%, the linewidth was found to increase with a decrease in the water content.

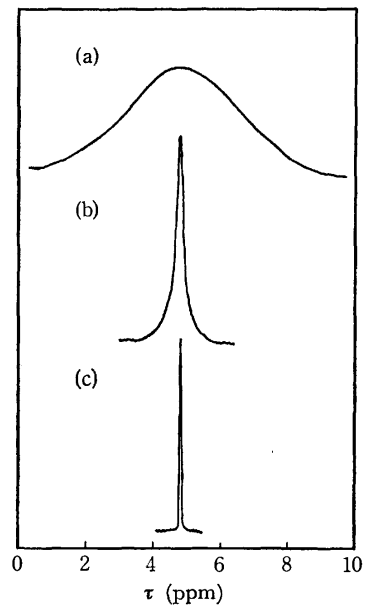

Fig. 2. PMR spectra of water in agarose gels; water content.
(a): 80%, (b): 98%, (c): pure water (H_2O), (25±0.5°C).

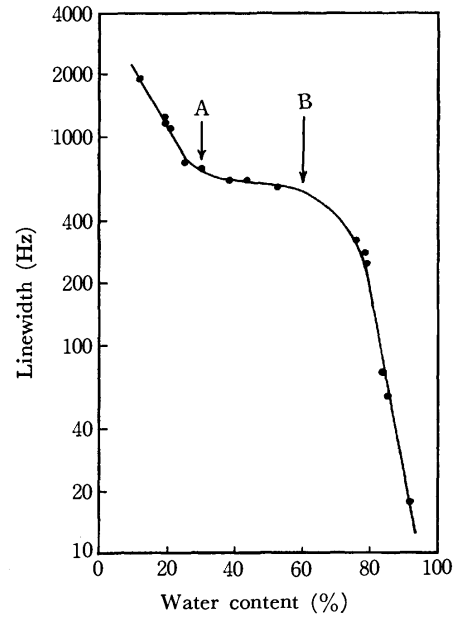

Fig. 3. Water content dependence of the linewidth of water proton in an agarose gel (25±0.5°C).

On the other hand, the linewidth of water protons is seen to be independent of the water content in the water-content range approximately from 60 to 30%.

Temperature Dependence of the PMR Linewidth of Water at Lower Temperatures. It has been known that ordinary water exhibits a transition at 0°C, which is accompanied with a marked change in the NMR linewidth of its proton. On the other hand, the water in gels is considered to give a transition temperature different from that of the ordinary water.

The transition temperature at lower temperatures was determined in accordance with the relationship between the temperature and the NMR linewidth of the water proton.

Agarose gels with various amounts of water were classified into three groups, A, B, and C. Group A

contains less than approximately 30% of water, most of which may be dominantly contributed to a motional state of the so-called bound water. The water content of Group B ranges from approximately 30 to 60%, while that of Group C is above about 60%.

The PMR spectrum for each sample was at first measured with an elevation of temperature in the range from 0 to 50°C, and then in the range from −60 to 0°C after a sufficient precooling of the sample in liquid nitrogen.

The PMR spectra of a sample containing 78.5% of water (by weight) at various temperatures are shown in Fig. 4. Each linewidth increases markedly with a decrease in the temperature.

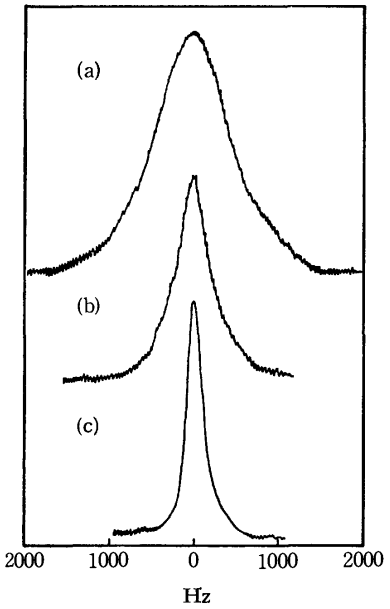

Fig. 4. PMR spectra of agarose gel (water content 78.5%); (a): −50°C, (b): −14°C, (c): 25°C.

The temperature dependence of the linewidth for Group A is shown in Fig. 5, where the abscissa represents the reciprocal of the absolute temperature (1/°K) and where the coordinate represents the half-linewidth (Hz). The PMR linewidth for Group A increases linearly with a decrease in the temperature up to approximately −20°C ($1/T=3.95\times10^{-3}$); the increase in the rate is found to change slightly at this temperature. In other words, an inflection point (T_γ) is found in Fig. 5.

The temperature dependence of the linewidth for Group B is presented in Fig. 6, and that for Group C, in Fig. 7. In contrast with Group A, the linewidth for Group B decreases with a decrease in the temperature up to approximately −20°C ($1/T=3.95\times10^{-3}$), though the inclination is changed in the range approximately from 0°C to −20°C ($1/T=3.66$ to 3.95×10^{-3}). On the other hand, the linewidth for Group C was found to change markedly at 0°C ($1/T=3.66\times10^{-3}$) in addition to the marked change at −20°C ($1/T=3.95\times10^{-3}$).

Discussion

We expected to detect one inflection point in the linewidth-water content curve, because two states of

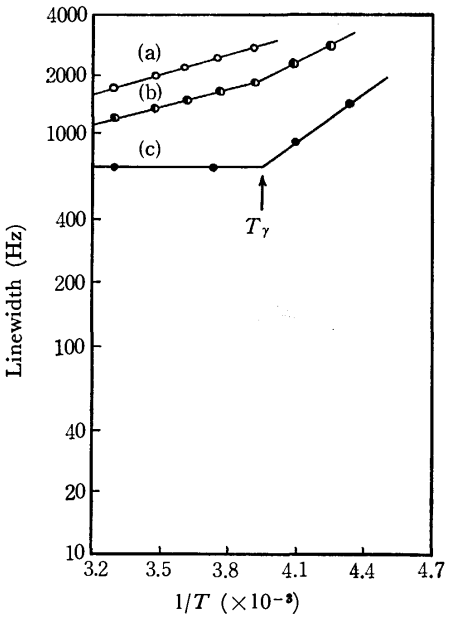

Fig. 5. PMR linewidth of water in agarose gels (Sample belonging to Group A) as a function of temperature. Water content; (a): 12%, (b): 19%, (c): 26%.

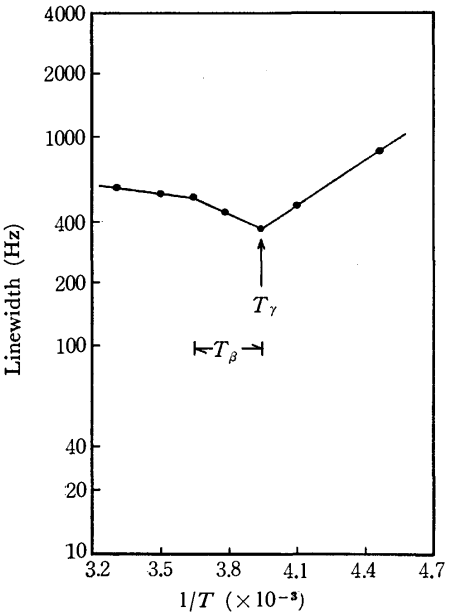

Fig. 6. PMR linewidth of water in agarose gel containing 48% of water (Sample belonging to Group B) as a function of temperature.

water are generally considered to exist in gels. We found, however, two inflection points, A and B, on the curve, as is shown in Fig. 3. The water content at the A inflection point can be attributed to the amount of so-called bound water in an agarose gel. Whereas the B inflection point is a new finding. From the independence of the linewidth of the water content, it seems reasonable to suppose that the water molecules in agarose gels containing 30 to 60% of water are in comparable motional states, for the curve is flat in the water-content range from 30 to 60% shown in Fig. 3.

On the other hand, the results obtained in previous electrochemical and dilatometric studies[2-4] can not be explained without supposing three states of water

in gels.

Therefore, it can be concluded that there are at least three states of water molecules in macromolecular gels. These states of water may be named W_1, W_2, and W_3, of which W_1 and W_2 are comparable to conventional free water, and W_3 to the so-called bound water.

The transition of water is expected to be accompanied by a marked change in the PMR linewidth. Each agarose gel was found to exhibit marked changes in PMR linewidth at lower temperatures, as is shown in Figs. 5, 6 and 7. In addition, these changes depend on the water content of agarose gel, as is presented in Fig. 8. Therefore, the marked changes in Figs. 5, 6 and 7 may be presumed to be caused by the transition of water in gels.

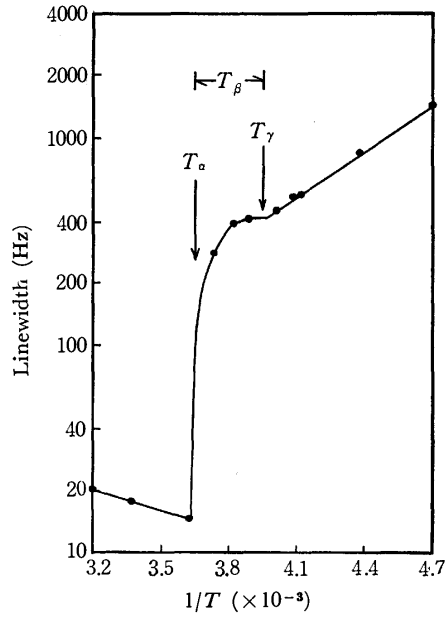

Fig. 7. PMR line width of water in agarose gel containing 92% of water (Sample belonging to Group C) as a function of temperature.

When these inflection points for Group C are named T_α, T_β, and T_γ respectively, as is presented in Fig. 7, the two in Fig. 6 may be T_β and T_γ, and the one in Fig. 5 may be T_γ, because the corresponding temperatures at the inflection points agree with each other.

The electrochemical studies have shown that the transition temperature of water in a gel was distributed from 0°C to approximately −20°C, but no transition temperature for a gel containing a small amount of water was confirmed at lower temperatures. Those results agree with those of nuclear magnetic resonance studies. As is shown in Fig. 7, the transition temperature is distributed from T_α to T_γ, *i.e.*, in the range of T_β. On the other hand, an agarose gel containing a very small amount of water exhibits no transition temperature.

On the basis of these results, the properties of W_1, W_2, and W_3 in gels can be presumed to be as follows.

As is shown in Fig. 7, the linewidth changes abruptly at T_α; W_1 may exhibit a transition between the liquid and the solid states corresponding to ordinary water at 0°C ($1/T=3.66\times10^{-3}$), *i.e.*, free water, though W_1 in gels is hindered from flowing out.

W_3, corresponding to the so-called bound water, may be oriented on agarose by the interaction between the H_2O molecule and the OH group of agarose, since the W_3 content almost agree with the OH-group content of agarose, which is calculated according to the proposed structure[12] of agarose shown in Fig. 9. Therefore, W_3 should exhibit solid-like behavior if such interaction is strong. Since the linewidth of W_3 is of the order of 1000 Hz, W_3 is supposed to be in a solid-like state, even at room temperature, due to the strong interaction between the H_2O molecule and the OH group of agarose. On this supposition, it is reasonable that the transition temperature for W_3 cannot be confirmed in the range of temperature investigated here.

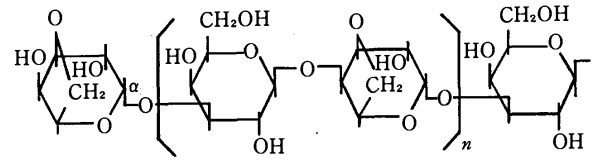

Fig. 8. Structural formula of agarose[12]

The properties of W_2 have not yet been clarified except that the linewidth of W_2 is several hundred Hz, and except that the transition temperature of W_2 may be distributed from 0°C to approximately −20°C. As one would expect, the molecules of water in gels are hydrogen-bonded; W_1, W_2 and W_3 cannot be sufficiently discriminated, but each of them shows dominant properies related to the restriction of water in the potential fields which exist in cavities of the gel. The properties of W_2 described above, however, indicate that W_2 is more fixed than W_1, but more mobile than W_3. It should be emphasized that W_2 is presumed to play an important role in the structure and properties of macromolecular gels because its properties are intermediate compared to those of W_3 and W_1. The detailed properties and the states of W_2 are under the investigation.

Conclusion

The properties of three states of water in agarose gels were investigated by high-resolution PMR over the temperature range from +50 to −60°C.

The transition temperature for water in agarose gels was confirmed to be distributed from 0°C to approximately −20°C by the anomalous temperature-dependence of the PMR linewidth. The transition temperature at 0°C is attributed to that of W_1, and the transition temperature of W_2 may be distributed from 0°C to approximately −20°C. On the other hand, W_3 may give no transition tempersture in this temperature range. Therefore, W_1 may be ordinary water, though it is prevented from flowing out. W_2 may be more fixed than W_1, but more mobile than W_3, and W_3 may be in a solid-like state even at room temperature due to a strong interaction with the OH group of agarose.

12) C. Araki, This Bulletin, **29**, 543 (1956).

Molecular Vibrations, Conformational Analyses, and Force Fields of Normal and Monodeuterated (Methylthio)methanethiol

Masaru OHSAKU, Yuji SHIRO,* and Hiromu MURATA

Department of Chemistry, Faculty of Science, Hiroshima University, Higashisenda-machi, Hiroshima

**Shinonome Branch School, Faculty of Education, Hiroshima University, Shinonome-3-chome, Hiroshima*

(Received December 6, 1971)

(Methylthio)methanethiol, CH_3SCH_2SH, and (methylthio)methanethiol-d_1, CH_3SCH_2SD, were prepared, and their infrared spectra were obtained in the gaseous, liquid, and solid states. The obtained spectra have been assigned. The frequency shifts by D-substitution, gaseous-liquid transition. and liquid-solid transition have also been discussed. The normal coordinates of these thiols have been treated by a modified Urey-Bradley force field. The force constants used in the computation have been transferred from those previously reported, but we adjusted them to produce the experimental wave numbers. The calculated wave numbers correspond well with those observed. The stable molecular conformations of the normal and deuterated species have been determined by the aid of the normal coordinate treatment. In the gaseous and liquid states, at least three to four forms from among TT, TG, GT, GG, and GG′ have been confirmed to exist. In the solid state, though, CH_3SCH_2SH or CH_3SCH_2SD exists in only one form: GG.

Recently, the molecular vibrations and conformations of alkanethiols have been extensively studied.[1-6] At present, however, we can find no report on the vibrational and structural analysis of (methylthio)methanethiol. In this paper we will discuss the vibrational assignments; we prepared CH_3SCH_2SH and CH_3SCH_2SD and recorded their infrared spectra. From the vibrational data thus obtained, we will first treat the molecular vibrations of these molecular species in detail. (Methylthio)methanethiol, CH_3SCH_2SH has a molecular unit in common with CH_3SCH_2–D and CH_3SCH_2–SCH_3. We previously reported the existence of rotational isomers on the CH_3SCH_2D species.[7] As for the $CH_3SCH_2SCH_3$ species, we also postulated the existence of rotational isomers around the C–S bond.[8] Therefore, we will now try to establish the existence of rotational isomers on the CH_3SCH_2SH and CH_3SCH_2SD species. In order to determine the molecular conformation and confirm the vibrational assignment, the normal coordinate treatment has also been carried out for normal and monodeuterated (methylthio)methanethiol. For the organo-sulfur compounds without the SCS skeleton, Scott and El-Sabban carried out[5] the normal coordinate treatment by the use of the valence force field; they thus obtained a set of valence force constants. In the present study, the molecular vibrations were treated with a modified Urey-Bradley-type potential function, and the force constants were determined on a part of the SCS skeleton. The obtained force constants were then compared with Scott and El-Sabban's force constants.

Experimental

(Methylthio)methanethiol, CH_3SCH_2SH, was prepared by the method of Fehér and Vogelbruch.[9]

Bp 61°C/47 mmHg, (reported[9] bp 60°C/47 mmHg). The purity of the sample was above 98%, as estimated by gas chromatography. The deuterated species, CH_3SCH_2SD, was prepared from normal (methylthio)methanethiol by the direct exchange of thiol-hydrogen with D_2O in the presence of a small amount of catalytic potassium carbonate. The gaseous spectra (4000—550 cm^{-1}) were recorded by means of a 10-cm gas cell equipped with KBr windows under an appropriate vapour pressure. The liquid spectra (4000—200 cm^{-1}) were recorded by means of a liquid cell equipped with CsI windows. The solution spectra (4000—550 cm^{-1}) were recorded in carbon disulfide. The solid spectra (4000—200 cm^{-1}) were recorded near the temperature of liquid nitrogen with a low-temperature cell. The instrument used for the infrared measurement was a Perkin-Elmer Model 621 Spectrophotometer.

Vibrational Assignment

Tables 1 and 2 show the vibrational data obtained for CH_3SCH_2SH and CH_3SCH_2SD respectively. In the obtained spectra of the 3000—1000 cm^{-1} region,

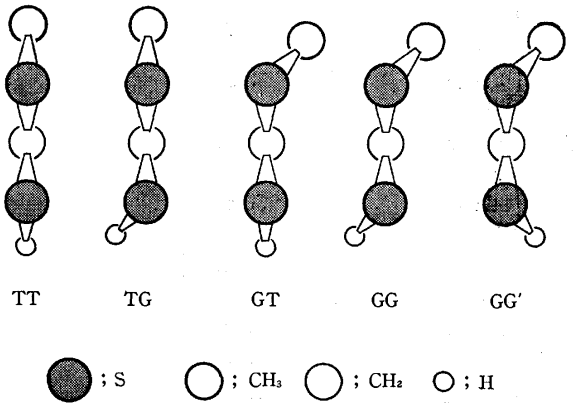

Fig. 1. Structures and conformations of (methylthio)-methanethiol.
T = *trans*, G = *gauche*.

1) I. W. May and E. L. Pace, *Spectrochim. Acta*, **24A**, 1605 (1968).
2) D. Smith, J. P. Devlin, and D. W. Scott, *J. Mol. Spectrosc.*, **25**, 174 (1968).
3) D. W. Scott and G. A. Crowder, *ibid.*, **26**, 477 (1968).
4) I. W. May and E. L. Pace, *Spectrochim. Acta*, **25A**, 1903 (1969).
5) D. W. Scott and M. Z. El-Sabban, *J. Mol. Spectrosc.*, **30**, 317 (1969).
6) P. J. Krueger, J. Jan, and H. Wieser, *J. Mol. Structure*, **5**, 375 (1970).
7) Y. Shiro, M. Ohsaku, M. Hayashi, and H. Murata, This Bulletin, **43**, 609 (1970).
8) M. Ohsaku, Y. Shiro, and H. Murata, *ibid.*, **45**, 113 (1972).
9) F. Fehér and K. Volgebruch, *Chem. Ber.*, **91**, 996 (1958).

Table 1. Infrared frequencies (cm^{-1}) and assignments of (methylthio)methanethiol[a)]

Gaseous	Liquid	CS_2 soln	Solid[b)]	Assignment[c)]
3010 sh, vw 3003 w 2996 sh, vw		2985 sh, s	2985 sh, w	ν_{C-H}
2987 w 2980 w	2975 s	2974 s	2971 m	ν_{C-H}
2951 w 2941 w				
2937 2932 vs 2927	2915 vs	2913 vs	2914 s	ν_{C-H}
2918 sh, w 2913 sh, w				
2905 sh, vw 2902 sh, vw				
~2850 w	2854 w	2852 w	2853 vw	over or combi
~2835 sh, vw	2829 w	2827 w	2825 vw	over or combi
	2605 sh, vw, br	2610 sh, vw, br	—	
	2545 s, vvbr	2550 m, vbr	2515 s, vbr	ν_{S-H}
	2500 sh, w	2500 sh, w	—	
	2430 sh, vw		—	
1461 w	1437 sh, vw		1438 sh, w	
1451 m 1447 m 1445 m 1441 m 1435 m	1435 vs		1433 s	$\delta^{d}_{CH_3}$
1428 1426 m 1423	1422 vs		1418 s	$\delta^{d}_{CH_3}$
1415 w 1405 w	1415 sh, vw		—	over or combi
1395 vw	1393 m	1393 m	1383 w	$\delta^{b}_{CH_2}$
1323 vvw	1318 w	1317 w	1313 vw	$\delta^{s}_{CH_3}$
	1220 sh, m	1220 sh, m	—	$\delta^{w}_{CH_2}$
1224 1219 s 1211	1214 vs	1212 vs	1217 vs	$\delta^{w}_{CH_2}$
	1200 sh, m	1201 sh, m	—	$\delta^{w}_{CH_2}$
	1164 w	1162 w	1169 w	$\delta^{t}_{CH_2}$
	1137 sh, w	1135 sh, w	—	over or combi
1000 sh, vw	994 sh, vw	992 sh, vw	—	$\delta^{r}_{CH_3}$
995 989 w 983	988 s	985 s	992 vs	$\delta^{r}_{CH_3}$
980 w	977 sh, vw	975 sh, vw	—	$\delta^{r}_{CH_3}$
970 962 w 955	960 s	959 s	961 m	$\delta^{r}_{CH_3}$
935 vw	934 sh, vw	933 sh, vw	—	δ^{b}_{CSH}
928 vw	927 m	926 m	925 w	δ^{b}_{CSH}
917 vw	917 sh, vw	916 sh, vw	—	δ^{b}_{CSH}
	805 vw	805 vvw	807 vw	$\delta^{r}_{CH_2}$
765 m 758 m	755 sh, s	756 s	—	ν_{C-S}
753 sh, m 751 sh, m 747 sh, m	745 vs	746 vs	745 vs	ν_{C-S}
740 sh, m	740 sh, w	740 sh, w	—	ν_{C-S}

TABLE 1. Continued

Gaseous	Liquid	CS_2 soln	Solid[b]	Assignment[c]
712 w 705 w	705 sh, m	705 sh, s	—	ν_{C-S}
698 w 694 w 687 sh, w	697 vs	700 vs	697 vs	ν_{C-S}
	693 sh, vw	696 sh, vw	—	ν_{C-S}
670 vvw	669 sh, vw	669 vw	—	ν_{C-S}
639 vw	639 w	638 w	643 w	ν_{C-S}
	345 sh, vvw		—	
	335 vw		338 vw	
	~295 sh, vvw		—	
	~285 vvw		—	
	272 sh, vvw		—	δ_{skel}
	~260 vw		—	
	237 vw		235 vvw	
	220 sh, vvw		—	

s, -strong; m, -medium; w, -weak; v, -very; sh, -shoulder; br, -broad; and ~, poorly estimated bands.
a) Above 3100 cm^{-1}, 2800—2650 cm^{-1}, and 2400—1500 cm^{-1} regions are omitted.
b) —, bands disappeared in the solid state.
c) ν, -stretching; δ^d, -degenerate deformation; δ^b, -bending; δ^s, -symmetrical deformation; δ^w, -wagging; δ^t, -twisting; δ^r, -rocking; and δ_{skel}, -skeletal deformation.

there appeared nearly the same number of bands as we expected for one conformation. In the 1000—200 cm^{-1} region, however, a fairly larger number of bands appeared than that expected for one form. Therefore the question of the existence of rotational isomers comes to mind.

Now we can see five possible molecular conformations of (methylthio)methanethiol: TT (C_s), TG (C_1), GT (C_1), GG (C_1), and GG′ (C_1), all of which are shown in Fig. 1. All of the fundamental vibrations of each conformation are infrared-active.

Liquid-state Spectra. The liquid-state spectra of CH_3SCH_2SH and CH_3SCH_2SD are shown in Figs. 2 and 3 respectively. The obtained spectra of normal (methylthio)methanethiol are similar to those of bis-(methylthio)methane.[8]

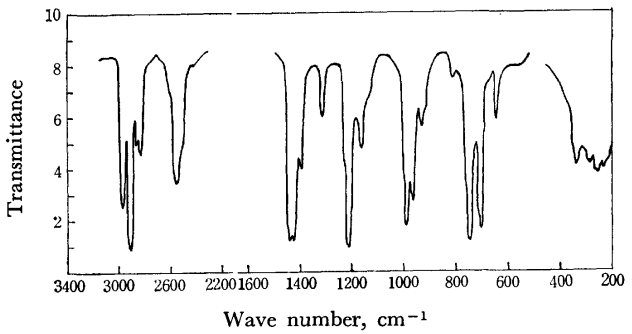

Fig. 2. Infrared spectra of (methylthio)methanethiol in the liquid state.

Five C-H stretching vibrations are expected for one conformation. In this region, we observed five bands. The bands at 2854 and 2829 cm^{-1} (2828 cm^{-1} in D-species), however, may not be due to the fundamentals. The characteristic bands of normal thiols (or deuterated thiols) are expected in the 2600—2500 cm^{-1} (or 1900—1800 cm^{-1}) region. The very broad bands around 2540 and 1860 cm^{-1} are assigned to the S-H

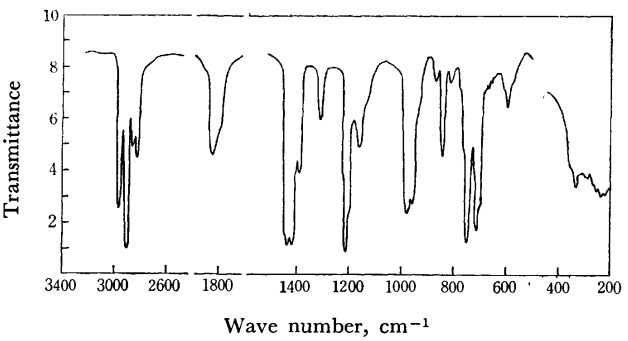

Fig. 3. Infrared spectra of (methylthio)methanethiol-d_1 in the liquid state.

and S-D stretching vibrations respectively. From the assignments of dimethylsulfide and $CH_3S(CH_2S)$-CH_3 (n=1—3),[8] the bands appearing around 1430 cm^{-1} are assigned to the CH_3 degenerate deformation, and a band around 1390 cm^{-1} is assigned to the CH_2 bending vibrations, although, these vibrations are not independent of each other. For the CH_3 symmetrical deformation, the band at 1318 cm^{-1} of the normal species and the band at 1317 cm^{-1} of the deuterated species are assigned. The band maxima at 1214 and 1164 cm^{-1} of the normal species, and at 1210 and 1158 cm^{-1} of the deuterated species, are assigned to the CH_2 wagging and twisting vibrations respectively. The CH_2 wagging and twisting bands are shifted in *ca.* 5 cm^{-1} to the lower-frequency region by D-substitution. The two shoulder bands around 1210 cm^{-1} of both the normal and deuterated species may be due to the rotational isomerism. The strong bands accompanied by weak shoulder bands at 988 and 960 cm^{-1} of the normal species and at 974 and 961 cm^{-1} of the deuterated species are assigned to the CH_3 rocking vibrations. The CSH bending vibration is expected around 900—800 cm^{-1}. Nothing appears in this region. Although the medium bands with weak

Table 2. Infrared frequencies (cm^{-1}) and assignments of (methylthio)methanethiol-d_1[a)]

Gaseous	Liquid	CS_2 soln	Solid[b)]	Assignment[c)]
3010 sh, vw 3005 w 2996 sh, vw		2985 sh, s	2985 sh, w	ν_{C-H}
2990 2980 w 2965	2975 s	2974 s	2971 m	ν_{C-H}
2946 sh, w 2942 sh, w				
2937 2932 vs 2927	2915 vs	2914 vs	2913 s	ν_{C-H}
2915 sh, w 2905 sh, w				
2894 sh, w 2880 sh, w				
2864 sh, vw 2853 w 2844 sh, vw	2854 w	2852 w	2853 vw	over or combi
2835 sh, vw	2828 w	2827 w	2824 vw	over or combi
	1900 vw, vvbr	1900 vw, vvbr	—	
	1850 s, vvbr	1850 s, vvbr	1830 s, vvbr	ν_{S-D}
	1810 sh, w	1810 sh, w	—	
1460 w	1437 sh, w		1438 sh, w	
1451 m 1447 m 1443 m 1440 m 1437 m	1435 vs		1433 s	$\delta^d_{CH_3}$
1428 m 1426 m 1425 m 1423 m	1421 vs		1418 s	$\delta^d_{CH_3}$
1415 w 1405 w	1418 sh, w		—	over or combi
1395 vw	1393 m	1393 m	1383 w	$\delta^b_{CH_2}$
1322 vvw	1317 w	1317 w	1314 vw	$\delta^s_{CH_3}$
	1217 sh, m	1214 sh, m	—	$\delta^w_{CH_2}$
1219 1213 s 1207	1210 vs	1207 vs	1210 vs	$\delta^w_{CH_2}$
	1200 sh, m	1200 sh, m	—	$\delta^w_{CH_2}$
	1158 w	1156 w	1162 w	$\delta^t_{CH_2}$
	1137 sh, vw	1135 sh, vvw	—	over or combi
988 981 w 978	974 s	973 s	977 vs	$\delta^r_{CH_3}$
970 w	970 sh, vw	969 sh, vw	—	$\delta^r_{CH_3}$
967 sh, w 962 w 954 w	961 s	959 s	961 s	$\delta^r_{CH_3}$
	870 vw		—	over or combi ?
	840 m		842 m	$\delta^r_{CH_2}$
	808 vw	807 vw	—	$\delta^r_{CH_2}$
774 w	774 sh, vw	774 sh, vw	—	ν_{C-S}
765 m 759 m	758 sh, m	757 m	—	ν_{C-S}
754 m 749 sh, m 746 sh, m	746 vs	747 vs	747 vs	ν_{C-S}

TABLE 2. Continued

Gaseous	Liquid	CS_2 soln	Solid[b]	Assignment[c]
724 sh, vw 720 vw	725 sh, vw	728 sh, w	—	ν_{C-S}
711 705 w 700	707 vs	708 vs	707 vs	ν_{C-S}
695 w	695 s	695 s	—	ν_{C-S}
670 vvw	670 vw	670 vw	—	ν_{C-S}
~660 vvw	661 vw	661 vw	663 w	ν_{C-S}
	658 sh, vw		—	ν_{C-S}
600 vvw	600 sh, vw	600 sh, vw	—	δ^b_{CSD}
594 vvw	594 w	593 w	597 w	δ^b_{CSD}
587 vvw	587 sh, vw	587 sh, vw	—	δ^b_{CSD}
	338 sh, vvw		—	
	330 vw		330 vw	
	~295 vvw		—	
	~285 vvw		—	
	272 sh, vvw		—	δ_{skel}
	~260 vw		—	
	235 vw		225 vvw	
	219 vvw		—	

s, -strong; m, -medium; w, -weak; v, -very; sh, -shoulder; br, -broad; and ~, poorly estimated bands.
a) Above 3100 cm^{-1}, 2800—1950 cm^{-1}, and 1800—1500 cm^{-1} regions are omitted.
b), c) See b), c) of Table 1.

shoulders around 930 cm^{-1} are fairly higher than those expected, these bands may be assigned to the CSH bending vibrations. In the deuterated species, a band accompanied by two shoulders around 600 cm^{-1} is assigned to its also. The bands appearing in this region are many more than those expected for one conformation. The obtained band at 805 cm^{-1} of the normal species, and the 840 and 808 cm^{-1} bands of the deuterated species may be assigned to the CH_2 rocking vibrations. The C–S stretching vibrations may appear in the 800—600 cm^{-1} region. Three bands are expected for each conformation. In the infrared measurements, eight bands were observed—at 755, 745, 740, 705, 697, 693, 669, and 639 cm^{-1}—for the normal species, and nine bands—at 774, 758, 746, 725, 707, 695, 670, 661, and 658 cm^{-1}—for the deuterated species. The numbers of observed bands show the possibility of rotational isomerism. In this region, the bands of the normal species are shifted to a higher-frequency region by D-substitution. In the 400—200 cm^{-1} region, we observed eight bands, including very weak shoulder bands, for both the normal and deuterated species. In this region, the bands obtained are also many more than those expected for one form.

Gaseous-state Spectra. The gaseous-state spectra of CH_3SCH_2SH and CH_3SCH_2SD are shown in Figs. 4 and 5 respectively. We could not observe the S–H stretching, S–D stretching, CH_2 twisting, or CH_2 rocking vibrations. In the C–H stretching region, the resolution was fairly good. In both species, very strong and sharp PQR bands were obtained around 2930 cm^{-1}. Those bands are shifted by *ca.* 20 cm^{-1} to a higher frequency region than that in the liquid state. In the CH_3 degenerate deformation and the CH_2 bending region, rotational bands of the water vapor in the atmosphere are overlapped. Therefore,

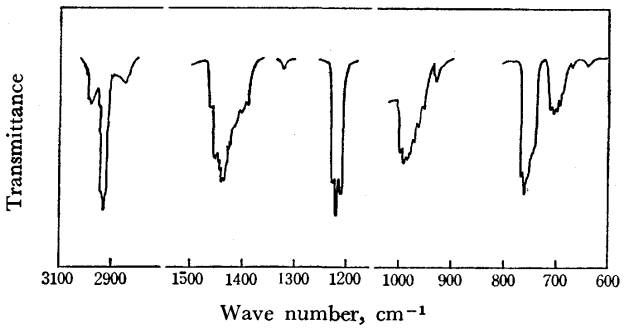

Fig. 4. Infrared spectra of (methylthio)methanethiol in the gaseous state.

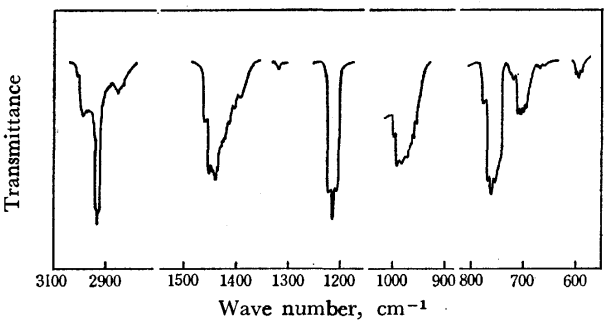

Fig. 5. Infrared spectra of (methylthio)methanethiol-d_1 in the gaseous state.

the band assignments are very difficult. In the CH_2 wagging region around 1200 cm^{-1}, very strong RQP peaks appeared at 1224, 1219, and 1211 cm^{-1} for the normal species, and at 1219, 1213, and 1207 cm^{-1} for the deuterated species. The Q-branch of the D-species shifts lower 6 cm^{-1} than that of the normal species. In the CH_3 rocking region, a lower-frequency

shift upon D-substitution is also observed. In the C-S stretching region, fairly complex spectra were obtained. The bands in this region may be mutually overlapped. In this region, a higher-frequency shift upon D-substitution was observed. In order to confirm the existence of the rotational isomers on CH_3SCH_2SH species, we attempted to investigate the temperature dependence of the intensity of the gaseous bands in the 850—600 cm^{-1} region (33—124°C). However, we could not obtain intensity changes sufficient to decide the energy differences because of the rotational isomerism in this temperature region.

Solid-state Spectra. Near the temperature of liquid nitrogen, we obtained the solid-state spectra of CH_3SCH_2SH and CH_3SCH_2SD shown in Figs. 6 and 7 respectively. Although we repeated annealing above and below their melting points, the samples were not completely crystallized. In the C-H stretching region, the difference between the liquid and solid spectra was not observed. In the S-H or S-D stretching region, a large lower-frequency shift due to the liquid-solid transition was observed. The reason for this lower frequency shift is not clear. In the solid state, however, it is supposed that the intermolecular hydrogen bonding is formed more strongly than the liquid, and that the S-H (S-D) stretching band is shifted lower on a weakening of the S-H or S-D bond. In the CH_3 degenerate deformation, CH_3 symmetrical deformation, CH_2 wagging, CH_2 twisting, CH_3 rocking, CSH or CSD bending, CH_2 rocking, and the skeletal deformation regions, the liquid-solid transition shifts stay within *ca.* 10 cm^{-1}. In the C-S stretching region, the frequency shift due to the liquid-solid transition was not so clear.

From the infrared spectra we have obtained, the following questions arise. The first concerns the extraordinary breadth of the S-H and S-D stretching bands. The second concerns the very large lower-frequency shift (*ca.* 330 cm^{-1}) of the CSH bending vibration upon D-substitution. The third concerns the large higher-frequency shift (*ca.* 35 cm^{-1}) of the CH_2 rocking vibration upon D-substitution. The first can be explained as the result of the rotational isomerism; it may also be due to the hydrogen bond just as in the alcohols. As for the second and third problems, these large frequency shifts will be explained in the following section.

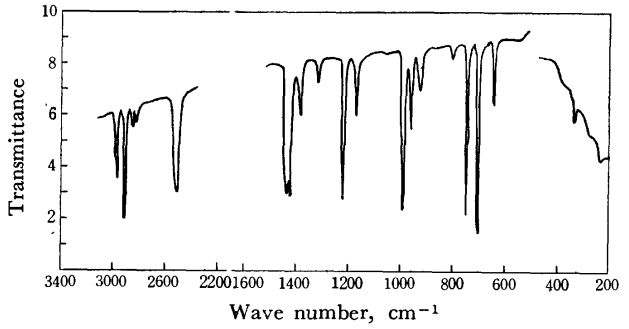

Fig. 6. Infrared spectra of (methylthio)methanethiol in the solid state.

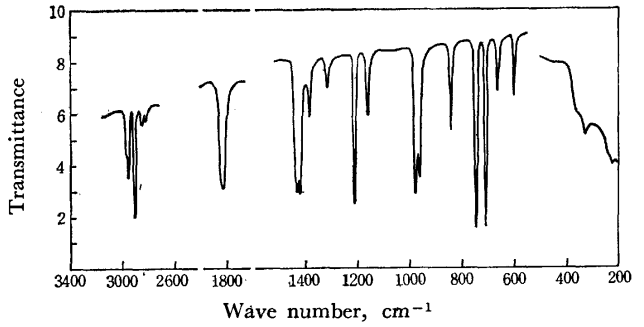

Fig. 7. Infrared spectra of (methylthio)methanethiol-d_1 in the solid state.

Normal Coordinate Treatment

We made the normal coordinate treatment for the five most probable forms: TT, TG, GT, GG, and GG'. The molecular parameters used in the computations were as follows:

r(C-H)=1.09Å, ϕ(CSC)=99°,
r(C-S)=1.81Å, ϕ(CSH)=96.5°,
r(S-H)=1.335Å.

Table 3. Modified Urey-Bradley force constants[a] of (methylthio)methanethiol

K(C-H)	4.286	CH_3 and CH_2 groups
K(C-S)	1.691	CH_3-S, S-CH_2, and CH_2-SH bonds or CH_2-SD bond
K(S-H)	3.500	S-H bond
K(S-D)	3.591	S-D bond
H(HCS)	0.030	CH_3 group
H(HCH)	0.366	CH_3 group
H(CSC)	0.244	CH_3-S-CH_2 angle
H(SCS)	0.150	S-CH_2-S angle
H(SCH)	0.170	CH_2 group
H(HCH)	0.335	CH_2 group
H(CSH)	0.060	CH_2-S-H or CH_2-S-D angle
F(HCS)	0.763	
F(HCH)	0.200	
F(CSC)	0.210	
F(SCS)	0.500	
F(SCH)	0.390	
F(HCH)	0.200	
F(CSH)	0.580	
κ	0.060	CH_3 group
	−0.005	CH_2 group
Y	0.054	CH_3-S and S-CH_2 bonds
	0.035	CH_2-SH or CH_2-SD bond
p	−0.115	CH_3 and CH_2 groups
p'	−0.189	CH_3-S, S-CH_2, and CH_2-SH bonds or CH_2-SD bond
n	0.033	CH_3 group ($\angle$HCS and $\angle$HCH)
t	0.070	CH_3 group ($\angle$HCS and $\angle$CSC, *trans*)
g	−0.050	CH_3 group ($\angle$HCS and $\angle$CSC, *gauche*)
l	0.005	S-CH_2-S

a) K, stretching (mdyn/Å); H, bending (mdyn/Å); F, repulsion (mdyn/Å); $F'=-0.1F$; κ, intramolecular tension (mdyn·Å); Y, internal rotation (mdyn·Å); p and p', stretching interaction (mdyn/Å); n, angle interaction (mdyn·Å); t and g, *trans*- and *gauche* couplings (mdyn·Å); and l, angle interaction (mdyn·Å).

TABLE 4. OBSERVED AND CALCULATED FREQUENCIES (cm^{-1}), AND POTENTIAL ENERGY DISTRIBUTION, PED, (%) OF (METHYLTHIO)METHANETHIOL

Obsd[a]	Calcd TT	PED[b]	Calcd TG	PED[b]	Calcd GT	PED[b]	Calcd GG	PED[b]	Calcd GG'	PED[b]
2985	2999	ν_{C-H}(100)	2999	ν_{C-H}(100)	2999	ν_{C-H}(110)	2999	ν_{C-H}(100)	2999	ν_{C-H}(100)
2985	2999	ν_{C-H}(100)	2999	ν_{C-H}(100)	2999	ν_{C-H}(100)	2999	ν_{C-H}(100)	2999	ν_{C-H}(100)
2975	2963	ν_{C-H}(100)	2964	ν_{C-H}(100)	2964	ν_{C-H}(100)	2964	ν_{C-H}(100)	2964	ν_{C-H}(100)
2915	2910	ν_{C-H}(100)	2910	ν_{C-H}(100)	2910	ν_{C-H}(100)	2910	ν_{C-H}(100)	2910	ν_{C-H}(100)
2915	2901	ν_{C-H}(100)	2901	ν_{C-H}(100)	2901	ν_{C-H}(100)	2901	ν_{C-H}(100)	2901	ν_{C-H}(100)
2545	2542	ν_{S-H}(100)	2542	ν_{S-H}(100)	2542	ν_{S-H}(100)	2542	ν_{S-H}(100)	2542	ν_{S-H}(100)
1435	1441	$\delta^{d}_{CH_3}$(100)	1441	$\delta^{d}_{CH_3}$(100)	1441	$\delta^{d}_{CH_3}$(100)	1441	$\delta^{d}_{CH_3}$(100)	1441	$\delta^{d}_{CH_3}$(100)
1422	1441	$\delta^{d}_{CH_3}$(100)	1441	$\delta^{d}_{CH_3}$(100)	1441	$\delta^{d}_{CH_3}$(100)	1441	$\delta^{d}_{CH_3}$(100)	1441	$\delta^{d}_{CH_3}$(100)
1393	1396	$\delta^{b}_{CH_2}$(100)	1397	$\delta^{b}_{CH_2}$(100)	1396	$\delta^{b}_{CH_2}$(100)	1397	$\delta^{b}_{CH_2}$(100)	1397	$\delta^{b}_{CH_2}$(100)
1318	1317	$\delta^{s}_{CH_3}$(100)	1317	$\delta^{s}_{CH_3}$(100)	1317	$\delta^{s}_{CH_3}$(100)	1317	$\delta^{s}_{CH_3}$(100)	1317	$\delta^{s}_{CH_3}$(100)
1220[c]	1224	$\delta^{w}_{CH_2}$(100)			1221	$\delta^{w}_{CH_2}$(100)				
1214							1211	$\delta^{w}_{CH_2}$(100)		
1200[c]			1214	$\delta^{w}_{CH_2}$(100)					1211	$\delta^{w}_{CH_2}$(100)
1164	1158	$\delta^{t}_{CH_2}$(100)	1158	$\delta^{t}_{CH_2}$(100)	1158	$\delta^{t}_{CH_2}$(100)	1158	$\delta^{t}_{CH_2}$(100)	1158	$\delta^{t}_{CH_2}$(100)
994[c]									991	$\delta^{r}_{CH_3}$(100)
988	989	$\delta^{r}_{CH_3}$(100)	990	$\delta^{r}_{CH_3}$(100)	990	$\delta^{r}_{CH_3}$(100)	990	$\delta^{r}_{CH_3}$(100)		
977[c]	968	$\delta^{r}_{CH_3}$(100)								
960			968	$\delta^{r}_{CH_3}$(100)	967	$\delta^{r}_{CH_3}$(100)	967	$\delta^{r}_{CH_3}$(100)	967	$\delta^{r}_{CH_3}$(100)
934[c]			932	δ^{b}_{CSH}(75)					933	δ^{b}_{CSH}(74)
				$\delta^{r}_{CH_2}$(10)						$\delta^{r}_{CH_2}$(11)
927							931	δ^{b}_{CSH}(78)		
								$\delta^{r}_{CH_2}$(11)		
917[c]	928	δ^{b}_{CSH}(73)			926	δ^{b}_{CSH}(74)				
		ν_{C-S}(13)				ν_{C-S}(11)				
805	805	$\delta^{r}_{CH_2}$(96)	791	$\delta^{r}_{CH_2}$(86)	814	$\delta^{r}_{CH_2}$(90)	801	$\delta^{r}_{CH_2}$(78)	797	$\delta^{r}_{CH_2}$(76)
								ν_{C-S}(11)		ν_{C-S}(14)
755[c]			746	ν_{C-S}(100)						
745							745	ν_{C-S}(100)		
740[c]	740	ν_{C-S}(100)			733	ν_{C-S}(100)			742	ν_{C-S}(100)
705[c]			714	ν_{C-S}(100)					702	ν_{C-S}(100)
				δ^{b}_{CSH}(12)						δ^{b}_{CSH}(12)
697							698	ν_{C-S}(100)		
								δ^{b}_{CSH}(13)		
693[c]	698	ν_{C-S}(100)								
		δ^{b}_{CSH}(30)								
669[c]					687	ν_{C-S}(100)				
						δ^{b}_{CSH}(30)				
639	633	ν_{C-S}(90)	630	ν_{C-S}(86)	620	ν_{C-S}(98)	616	ν_{C-S}(95)	615	ν_{C-S}(96)
		δ^{b}_{SCS}(20)		δ^{b}_{SCS}(21)		δ^{b}_{SCS}(19)		δ^{b}_{SCS}(20)		δ^{b}_{SCS}(20)
				δ^{b}_{CSH}(13)				δ^{b}_{CSH}(14)		δ^{b}_{CSH}(14)
				δ^{b}_{CSC}(10)						
345[c]					335	δ^{b}_{CSC}(50)				
						δ^{b}_{SCS}(29)				
						ν_{C-S}(11)				
335							336	δ^{b}_{CSC}(50)	332	δ^{b}_{CSC}(50)
								δ^{b}_{SCS}(28)		δ^{b}_{SCS}(30)
								ν_{C-S}(10)		ν_{C-S}(10)
295[c]	289	δ^{b}_{SCS}(40)								
		δ^{b}_{CSC}(22)								
		ν_{C-S}(21)								
285[c]			289	δ^{b}_{SCS}(40)						
				δ^{b}_{CSC}(21)						
				ν_{C-S}(20)						
272[c]									245	δ^{b}_{SCS}(31)
										δ^{b}_{CSC}(35)
										τ_{C-S}(25)

Table 4. Continued

Obsd[a]	Calcd TT	PED[b]	Calcd TG	PED[b]	Calcd GT	PED[b]	Calcd GG	PED[b]	Calcd GG'	PED[b]
260[c]					239	δ^{b}_{SCS} (34) δ^{b}_{CSC} (37) τ_{C-S} (19)				
237							235	δ^{b}_{SCS} (37) δ^{b}_{CSC} (38) τ_{C-S} (15)		
220[c]	220	δ^{b}_{CSC} (67) δ^{b}_{SCS} (31)	223	δ^{b}_{CSC} (66) δ^{b}_{SCS} (28)						
	192	τ_{C-S} (99)	193	τ_{C-S} (93)			187	τ_{C-S} (91)		
					183	τ_{C-S} (90)			181	τ_{C-S} (88)
	174	τ_{C-S} (99)	174	τ_{C-S} (99)	169	τ_{C-S} (92)	169	τ_{C-S} (93)	168	τ_{C-S} (88)
	73	τ_{C-S} (98)	71	τ_{C-S} (97)	70	τ_{C-S} (94)	69	τ_{C-S} (95)	69	τ_{C-S} (94)

a) From Table 1.
b) ν, -stretching; δ^{d}, -degenerate deformation; δ^{b}, -bending; δ^{s}, -symmetrical deformation; δ^{w}, -wagging; δ^{t}, -twisting; δ^{r}, -rocking; and τ, -torsion.
c) Bands disappeared in the solid state.

The other bond angles were tetrahedral. The force field used was one in which we added some correction terms to the simple Urey-Bradley force field. The correction terms are: the bond-interaction constant of C–H bonds (p), the bond-interaction constant of C–S bonds (p'), the angle-interaction constant between ∠HCS and ∠HCH in the CH_3 group (n), the *trans* and *gauche* coupling constants between ∠HCS and ∠CSC in the CH_3 group (t and g), and the angle-interaction constant between SCH angles in the CH_2 group (l). Most of the force constants relating to the CH_3 group were transferred from those of dimethyl sulfide.[7] Some of the force constants relating to the CH_3 group were used by being changed within their dispersion.[10] The other force constants were referred to those of 1,2-ethanedithiol,[11] *n*-propanethiol,[12] polymethylene disulfide,[13] and bis(methylthio)-methane.[14] It has been supposed that the potential constants of CH_3SCH_2SH and CH_3SCH_2SD are common except for the S–H or S–D stretching constant.

The force constants of (methylthio)methanethiol obtained in the present study are listed in Table 3. The calculated wavenumbers are listed in Tables 4 and 5, together with the observed wavenumbers. Figs. 8 and 9 show the observed and calculated frequencies (1250—200 cm^{-1}), together with the observed band intensities. The calculated frequencies, in general, reproduced the observed frequencies well. The problems described in the previous section, that is, the very large lower-frequency shift of the CSH (CSD) bending and the large higher-frequency shift of the CH_2 rocking upon D-substitution, can also be well explained in the calculated wavenumbers.

C–H Stretching Region. The calculated C–H stretching frequencies did not reproduce the observed frequencies so well. The reason may be that we assumed the values of all the C–H stretching constants to be equal. This poor agreement might be overcome by distinguishing between two K(C–H) force constants in relation to the CH_3 and CH_2 groups.

S–H and S–D Stretching Regions. The S–H or S–D stretching vibration mainly depended on the S–H or S–D stretching constant, K(S–H) or K(S–D), and the CSH or CSD repulsion constant, on F(CSH) or F(CSD). We at first used the common value

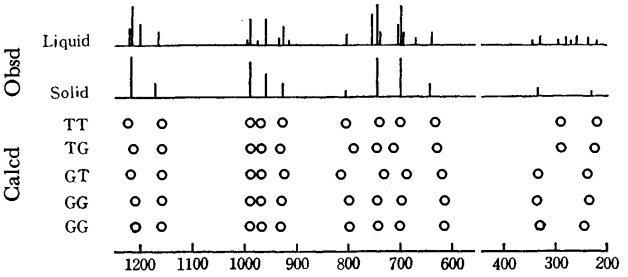

Fig. 8. Observed frequencies and relative intensities, and calculated frequencies of (methylthio)methanethiol (1250—200 cm^{-1}).

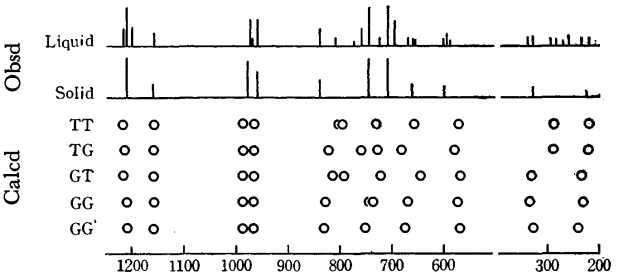

Fig. 9. Observed frequencies and relative intensities, and calculated frequencies of (methylthio)methanethiol-d_1 (1250—200 cm^{-1}).
The sets of the calculated wave numbers with close together are shown by the complete open circle which attached to the incomplete open circle.

10) T. Ogawa and T. Miyazawa, *Spectrochim. Acta*, **20**, 557 (1964).
11) M. Hayashi, Y. Shiro, T. Oshima, and H. Murata, This Bulletin, **38**, 1734 (1965).
12) M. Hayashi, Y. Shiro, and H. Mruata, *ibid.*, **39**, 112 (1966).
13) M. Hayashi, Y. Shiro, and H. Murata, *ibid.*, **39**, 1857 (1966).
14) M. Ohsaku, unpublished work.

TABLE 5. OBSERVED AND CALCULATED FREQUENCIES (cm^{-1}), AND POTENTIAL ENERGY DISTRIBUTION, PED, (%) OF (METHYLTHIO)METHANETHIOL-d_1

Obsd[a]	Calcd TT	PED[b]	Calcd TG	PED[b]	Calcd GT	PED[b]	Calcd GG	PED[b]	Calcd GG'	PED[b]
2985	2999	ν_{C-H}(100)	2999	ν_{C-H}(100)	2999	ν_{C-H}(100)	2999	ν_{C-H}(100)	2999	ν_{C-H}(100)
2985	2999	ν_{C-H}(100)	2999	ν_{C-H}(100)	2999	ν_{C-H}(100)	2999	ν_{C-H}(100)	2999	ν_{C-H}(100)
2975	2963	ν_{C-H}(100)	2964	ν_{C-H}(100)	2964	ν_{C-H}(100)	2964	ν_{C-H}(100)	2964	ν_{C-H}(100)
2915	2910	ν_{C-H}(100)	2910	ν_{C-H}(100)	2910	ν_{C-H}(100)	2910	ν_{C-H}(100)	2910	ν_{C-H}(100)
2915	2901	ν_{C-H}(100)	2901	ν_{C-H}(100)	2901	ν_{C-H}(100)	2901	ν_{C-H}(100)	2901	ν_{C-H}(100)
1850	1845	ν_{S-D}(100)	1845	ν_{S-D}(100)	1845	ν_{S-D}(100)	1845	ν_{S-D}(100)	1845	ν_{S-D}(100)
1435	1441	$\delta^{d}_{CH_3}$(100)	1441	$\delta^{d}_{CH_3}$(100)	1441	$\delta^{d}_{CH_3}$(100)	1441	$\delta^{d}_{CH_3}$(100)	1441	$\delta^{d}_{CH_3}$(100)
1421	1441	$\delta^{d}_{CH_3}$(100)	1441	$\delta^{d}_{CH_3}$(100)	1441	$\delta^{d}_{CH_3}$(100)	1441	$\delta^{d}_{CH_3}$(100)	1441	$\delta^{d}_{CH_3}$(100)
1393	1396	$\delta^{b}_{CH_2}$(100)	1396	$\delta^{b}_{CH_2}$(100)	1396	$\delta^{b}_{CH_2}$(100)	1396	$\delta^{b}_{CH_2}$(100)	1396	$\delta^{b}_{CH_2}$(100)
1317	1317	$\delta^{s}_{CH_3}$(100)	1317	$\delta^{s}_{CH_3}$(100)	1317	$\delta^{s}_{CH_3}$(100)	1317	$\delta^{s}_{CH_3}$(100)	1317	$\delta^{s}_{CH_3}$(100)
1217[c]	1220	$\delta^{w}_{CH_2}$(100)			1217	$\delta^{w}_{CH_2}$(100)				
1210							1211	$\delta^{w}_{CH_2}$(100)		
1200[c]			1214	$\delta^{w}_{CH_2}$(100)					1211	$\delta^{w}_{CH_2}$(100)
1158	1158	$\delta^{t}_{CH_2}$(100)	1158	$\delta^{t}_{CH_2}$(100)	1158	$\delta^{t}_{CH_2}$(100)	1158	$\delta^{t}_{CH_2}$(100)	1158	$\delta^{t}_{CH_2}$(100)
974					990	$\delta^{r}_{CH_3}$(100)	990	$\delta^{r}_{CH_3}$(100)	990	$\delta^{r}_{CH_3}$(100)
970[c]	989	$\delta^{r}_{CH_3}$(100)	989	$\delta^{r}_{CH_3}$(100)						
961	968	$\delta^{r}_{CH_3}$(100)	968	$\delta^{r}_{CH_3}$(100)	967	$\delta^{r}_{CH_3}$(100)	967	$\delta^{r}_{CH_3}$(100)	967	$\delta^{r}_{CH_3}$(100)
840			823	$\delta^{r}_{CH_2}$(78) δ^{b}_{CSD}(11)			828	$\delta^{r}_{CH_2}$(80)	832	$\delta^{r}_{CH_2}$(75) δ^{b}_{CSD}(11)
808[c]	804	$\delta^{r}_{CH_2}$(96)			815	$\delta^{r}_{CH_2}$(85) ν_{C-S}(10)				
774[c]	797	ν_{C-S}(72) δ^{b}_{CSD}(16)			793	ν_{C-S}(68) δ^{b}_{CSD}(17)				
758[c]			760	ν_{C-S}(90) $\delta^{r}_{CH_2}$(10)					753	ν_{C-S}(100)
746							746	ν_{C-S}(100)		
725[c]	733	ν_{C-S}(100)	730	ν_{C-S}(100)	722	ν_{C-S}(100)			722	ν_{C-S}(82) $\delta^{r}_{CH_2}$(16)
707							738	ν_{C-S}(83) δ^{b}_{CSD}(12)		
695[c]			683	ν_{C-S}(75) δ^{b}_{CSD}(27) δ^{b}_{SCS}(11)						
670[c]	660	ν_{C-S}(81) δ^{b}_{CSD}(30) δ^{b}_{SCS}(20)							676	ν_{C-S}(82) δ^{b}_{CSD}(30)
661							670	ν_{C-S}(84) δ^{b}_{CSD}(25)		
658[c]					644	ν_{C-S}(88) δ^{b}_{CSD}(35) δ^{b}_{SCS}(19)				
600[c]			581	δ^{b}_{CSD}(71) ν_{C-S}(50)						
594							574	δ^{b}_{CSD}(66) ν_{C-S}(60)		
587[c]	572	δ^{b}_{CSD}(62) ν_{C-S}(52)			569	δ^{b}_{CSD}(55) ν_{C-S}(56)			571	δ^{b}_{CSD}(66) ν_{C-S}(63)
338[c]					333	δ^{b}_{CSC}(50) δ^{b}_{SCS}(28) ν_{C-S}(11)				
330							335	δ^{b}_{CSC}(51) δ^{b}_{SCS}(28) ν_{C-S}(10)	328	δ^{b}_{CSC}(50) δ^{b}_{SCS}(30)
295[c]	289	δ^{b}_{SCS}(39) δ^{b}_{CSC}(23) ν_{C-S}(21)								

TABLE 5. Continued

Obsd[a]	Calcd TT	PED[b]	Calcd TG	PED[b]	Calcd GT	PED[b]	Calcd GG	PEG[b]	Calcd GG'	PED[b]
285[c]			287	δ^{b}_{SCS}(40) δ^{b}_{CSC}(23) ν_{C-S}(19)						
272[c]									241	δ^{b}_{SCS}(34) δ^{b}_{CSC}(39) τ_{C-S}(17)
260[c]					237	δ^{b}_{SCS}(36) δ^{b}_{CSC}(39) τ_{C-S}(14)				
235							231	δ^{b}_{SCS}(38) δ^{b}_{CSC}(39) τ_{C-S}(12)		
219[c]	218	δ^{b}_{CSC}(66) δ^{b}_{SCS}(31)	222	δ^{b}_{CSC}(66) δ^{b}_{SCS}(31)						
	178	τ_{C-S}(100)	178	τ_{C-S}(100)	169	τ_{C-S}(92)	169	τ_{C-S}(91)	169	τ_{C-S}(94)
	138	τ_{C-S}(98)	140	τ_{C-S}(97)	134	τ_{C-S}(95)	139	τ_{C-S}(96)	133	τ_{C-S}(89)
	73	τ_{C-S}(98)	69	τ_{C-S}(98)	70	τ_{C-S}(94)	67	τ_{C-S}(95)	67	τ_{C-S}(95)

a) From Table 2. b), c) See b), c) of Table 4.

for the S-H and S-D stretching constants, which gave higher S-H and lower S-D stretching frequencies than the observed ones. This phenomenon is known[15] to be common when the stretching constants of K(X-H) and K(X-D) are used. Therefore, we assumed that the K(S-D) to be 1.026 times[16,17] the K(S-H) constant, that is, K(S-H)=3.500 and K(S-D)=3.591 mdyn/Å; we thus obtained adequate calculated results.

1500—550 *cm*$^{-1}$ *Region.* Two calculated CH_3 degenerate deformation frequencies were fairly higher (5—20 cm^{-1}) than the observed values; also the spacing of the calculated wavenumbers did not explain the observed spacing. The CH_3 degenerate deformation vibrations depend mainly on the potential constants, H(HCS), F(HCH), and $\kappa(CH_3)$, and on the angle interaction constant, n. Each of these four constants relates almost equally to both frequencies. The observed CH_2 wagging vibration in the liquid spectra is shifted 4 cm^{-1} by the D-substitution. In the calculated frequency, this tendency is also seen. The calculated CH_3 rocking vibrations are mainly due to the potential constants, H(HCS), H(HCH), and $\kappa(CH_2)$. They depend on the two rocking bands nearly equally. The CH_3 rocking vibration of normal and monodeuterated band maxima were obtained in the liquid spectra at 988 and 960 cm^{-1}, and at 974 and 961 cm^{-1}, respectively. The spacings of the observed spectra are 28 and 13 cm^{-1} for the normal and deuterated species. In the calculated wavenumbers, however, these spacings were not reasonably explained. The potential field of the CH_3 group of the molecule may not have a C_3 symmetry. The similar spacing of dimethyl sulfide was explained[7] in terms of the non-bonded interaction between two CH_3 groups. In this treatment, however, such interactions were not taken into consideration, since the constants could not be directly transferred. The calculated wavenumbers of the CH_2 rocking and the C-S stretching changed fairly much according to their molecular conformations.

Skeletal Deformation Region. The skeletal bending vibrations are mainly affected by the force constants, H(CSC), H(SCS), F(CSC), and F(SCS). The calculated frequencies fairly well reproduced the observed ones.

Molecular Forms

From the results of the calculated frequencies, we have seen that the CH_2 wagging, CH_3 rocking, CSH (CSD) bending, CH_2 rocking, C-S stretching, and skeletal deformation vibrations are fairly much affected by the internal rotation angles. In the observed spectra, there appeared three bands for the CH_2 wagging, four bands for the CH_3 rocking, three bands for the CSH bending, eight bands for the C-S stretching, and eight bands for the skeletal deformation regions on the normal species. On the deuterated species, we have seen three bands for the CH_2 wagging, three bands for the CH_3 rocking, two bands for the CH_2 rocking, nine bands for the C-S stretching, three bands for the CSD bending, and eight bands for the skeletal deformation regions. One CH_2 wagging, two CH_3 rocking, one CSH or CSD bending, three C-S stretching, and two to three bands for the skeletal deformation can be expected for each conformation. Therefore, if all of the observed bands are fundamentals, we can expect at least three or four conformations to coexist in the liquid and gaseous states.

The numbers of the bands appearing in the solid state suggest that only one form stays in the solid state. It was seen from the calculated results for the various molecular conformations that, in the region below

15) G. Herzberg, "Spectra of Diatomic Molecules," D. Van Nostrand Co., Inc., Princeton, N. J. (1950), pp. 519, 537, and 561.
16) T. Shimanouchi and I. Suzuki, *J. Chem. Phys.*, **42**, 296 (1965).
17) T. Shimanouchi, I. Nakagawa, J. Hiraishi, and M. Ishii, *J. Mol. Spectrosc.*, **19**, 78 (1966).

TABLE 6. OBSERVED AND CALCULATED FREQUENCY SHIFTS, Δ (cm^{-1}),[a] OF (METHYLTHIO)METHANETHIOL BY D-SUBSTITUTION

Mode	Obsd[b]			Calcd				
	H[c]	D[d]	Δ	TT, Δ	TG, Δ	GT, Δ	GG, Δ	GG', Δ
$\delta^{w}_{CH_2}$	1217	1210	7	4	0	4	0	0
$\delta^{t}_{CH_2}$	1169	1162	7	0	0	0	0	0
$\delta^{r}_{CH_3}$	992	977	15	0	1	0	0	1
δ^{b}_{CSH}	925	597	328	356	351	357	357	362
$\delta^{r}_{CH_2}$	807	842	−35	1	−32	−1	−27	−35
ν_{C-S}	745	747	−2	−57	−14	−60	−1	−11
ν_{C-S}	697	707	−10	−35	−16	−35	−40	−20
ν_{C-S}	643	663	−20	−27	−53	−24	−54	−61
δ_{skel}	338	330	8	0	2	2	1	4
δ_{skel}	235	225	10	2	1	2	4	4

a) $\Delta=\nu_H-\nu_D$. b) Solid bands. c) H, CH_3SCH_2SH. d) D, CH_3SCH_2SD.

1500 cm^{-1}, their rotational angles affect the wave numbers. The calculated wave numbers themselves, however, are not definite enough for us to decide the molecular conformation, since the force constant has an arbitrary value. The isotopic frequency shifts, however, give us more information about the molecular conformations if we compare the calculated results with the observed results, because the isotopic shifts of the calculated frequencies are, in general, little affected by the ambiguity of the force field.

In the obtained spectra, we observed frequency shifts in the S-H (S-D) stretching, CH_2 wagging, CH_2 twisting, CH_3 rocking, CSH (CSD) bending, CH_2 rocking, C-S stretching, and skeletal deformation regions. The calculated results have also shown shifts. Table 6 shows the observed results in the solid spectra and the calculated frequency shifts upon deuteration. In Table 6, the plus signs of Δ show the lower frequency shifts, while the minus signs show the higher ones, upon D-substitution. In the wagging region, the observed frequency shift is 7 cm^{-1}; the calculated frequency shifts are: TT (4 cm^{-1}), TG (0 cm^{-1}), GT (4 cm^{-1}), GG (0 cm^{-1}), GG' (0 cm^{-1}). The observed frequency shift of the CH_2 twisting vibration is 7 cm^{-1}. On the other hand, the shift is not seen in the calculated frequencies. In the CH_3 rocking region, one of the observed shifts is 15 cm^{-1}; we can see the calculated frequency shift in the TG and GG' conformations—1 cm^{-1}. In the CSH (CSD) bending region, we observed a frequency shift of 328 cm^{-1} upon deuteration. The calculated shifts of the TT, TG, GT, GG, and GG' conformations are 356, 351, 357, 357, and 362 cm^{-1} respectively. In the CH_2 rocking region, the observed frequency shift is −35 cm^{-1}; the calculated frequency shifts are: TG (−32 cm^{-1}), GT (−1 cm^{-1}), GG (−27 cm^{-1}), and GG' (−35 cm^{-1}). The shift of the TT form is in the reverse direction—1 cm^{-1}. The higher frequency shifts of the observed results in the C-S stretching bands become wide, ——2, −10, and −20 cm^{-1}, from short to long wavelengths. The conformations of TG, GG, and GG' show the above-mentioned tendency. In the skeletal deformation region, the shifts of the five forms of the calculated results show nearly the same behavior. Above all, the calculated frequency shifts of the TG, GG, and GG' conformations explain well the observed frequency shifts due to D-substitution. On the other hand, in the skeletal deformation region, the calculated wave numbers of the GT, GG, and GG' conformations correspond well to the observed wave numbers in the solid state. The calculated wave numbers of the TG form do not explain the observed wave numbers of the skeletal vibrations. In the case of the GT form, the isotopic shifts are not reasonably explained either. Therefore, we excluded the TG and GT forms from the stable form in the solid state. There, the possibility of the GG and GG' forms remains. In the cases of the GG and GG' forms, the repulsion forces between the S-H (S-D) and CH_3 groups may be stronger in the GG' form than in the GG form, so long as a strong hydrogen bond is not formed between S-H (S-D) and CH_3 groups. We, therefore, postulated the stable conformation in the solid state to be the GG form.

The molecular conformations existing in the liquid and gaseous states were also taken into consideration among the five conformation. Since the distance between S-H (S-D) and CH_3 groups is not so close in the GG' conformation, we did not neglect the GG' form, unlike the case of bis(methylthio)methane.[8] The molecular form in the solid state, GG, also exists in the gaseous and liquid states. Therefore, we will discuss mainly the liquid and gaseous band which disappear in the solid state. In the CH_2 wagging region of the liquid and gaseous spectra, we observed three bands of the normal species and also of the deuterated species. Among these three bands, two shoulder bands disappeared in the solid state. According to the calculated results of the normal species, the band at 1220 cm^{-1} corresponds to the TT and/or GT conformation, and the band at 1200 cm^{-1} corresponds to the TG and/or GG' conformation. In the deuterated species, the band at 1217 cm^{-1} corresponds to the TT and/or GT form, and the band at 1200 cm^{-1} corresponds to the TG and/or GG' conformation. In the CH_3 rocking region, two very weak shoulders and one very weak shoulder band are observed in the normal and deuterated species respectively. These shoulder bands correspond to the TT, TG, and/or GG' conformations.

Table 7. *F*-matrices of the modified Urey-Bradley and valence force fields[a)]

A[b)]

	R_1	R_2	R_3	R_4	R_5	R_6	R_7	R_8	R_9
R_1	4.879 4.663								
R_2	0.509 0.	3.633 3.213							
R_3	0.025 0.026	0.509 0.	4.879 4.663						
R_4	0.025 0.026	0.509 0.	0.025 0.026	4.879 4.663					
R_5	0. 0.	−0.059 0.	0. 0.	0. 0.	2.744 3.213				
R_6	0. 0.	0. 0.	0. 0.	0. 0.	0.161 0.	3.011 3.213			
R_7	0. 0.	0. 0.	0. 0.	0. 0.	0.260 0.	0.260 0.	4.760 4.663		
R_8	0. 0.	0. 0.	0. 0.	0. 0.	0.260 0.	0.260 0.	0.025 0.026	4.760 4.663	
R_9	0. 0.	0. 0.	0. 0.	0. 0.	0. 0.	0.337 0.	0. 0.	0. 0.	3.712 3.800

B[b)]

	R_{10}	R_{11}	R_{12}	R_{13}	R_{14}	R_{15}	R_{16}
R_{10}	0.675 0.615						
R_{11}	0.042 −0.015	0.675 0.615					
R_{12}	0.075 0.	0.075 0.	0.594 0.536				
R_{13}	0.042 −0.015	0.042 −0.015	0. 0.	0.675 0.615			
R_{14}	0.075 0.	0. 0.	0.042 0.	0.075 0.	0.594 0.536		
R_{15}	0. 0.	0.075 0.	0.042 0.	0.075 0.	0.042 0.	0.594 0.536	
R_{16}	0.070 0.150	−0.050 −0.150	0. 0.	−0.050 −0.150	0. 0.	0. 0.	1.129 1.422

C[b)]

	R_{16}	R_{17}	R_{18}	R_{19}	R_{20}	R_{21}	R_{22}	R_{23}
R_{17}	0. —	1.141 —						
R_{18}	0. 0.	−0.004 —	0.613 0.615					
R_{19}	0. −0.150	−0.004 —	0.002 0.	0.613 0.615				
R_{20}	0. 0.	−0.004 —	−0.009 −0.015	0. 0.	0.613 0.615			
R_{21}	0. −0.150	−0.004 —	0. 0.	−0.009 −0.015	0.002 0.	0.613 0.615		
R_{22}	0. 0.	0. —	−0.004 0.	−0.004 0.	−0.004 0.	−0.004 0.	0.479 0.536	
R_{23}	0. 0.	0. —	0. 0.184	0. 0.	0. 0.184	0. 0.	0. 0.	0.817 0.814

D[b)]

	R_{24}	R_{25}	R_{26}
R_{24}	0.054 0.054		
R_{25}	0. 0.	0.054 0.054	
R_{26}	0. 0.	0. 0.	0.035 0.035

TABLE 7. Continued

$E^{b)}$

	R_1	R_2	R_3	R_4	R_5	R_6	R_7	R_8
R_{10}	0.327	0.509						
	0.	0.349						
R_{11}	0.	0.509	0.327					
	0.	0.349	0.					
R_{12}	0.093	0.	0.093	0.				
	0.	0.	0.	0.				
R_{13}	0.	0.509	0.	0.327	0.			
	0.	0.349	0.	0.	0.			
R_{14}	0.093	0.	0.	0.093	0.	0.		
	0.	0.	0.	0.	0.	0.		
R_{15}	0.	0.	0.093	0.093	0.	0.	0.	
	0.	0.	0.	0.	0.	0.	0.	
R_{16}	0.	0.169	0.	0.	0.169	0.	0.	0.
	0.	0.251	0.	0.	0.251	0.	0.	0.

$F^{b)}$

	R_5	R_6	R_7	R_8	R_9	R_{10}	R_{11}	R_{12}
R_{17}	0.384	0.384						
	—	—						
R_{18}	0.	0.260	0.167					
	0.	0.349	0.					
R_{19}	0.260	0.	0.167	0.				
	0.349	0.	0.	0.				
R_{20}	0.	0.260	0.	0.167	0.			
	0.	0.349	0.	0.	0.			
R_{21}	0.260	0.	0.	0.167	0.	0.		
	0.349	0.	0.	0.	0.	0.		
R_{22}	0.	0.	0.093	0.093	0.	0.	0.	
	0.	0.	0.	0.	0.	0.	0.	
R_{23}	0.	0.459	0.	0.	0.317	0.	0.	0.
	0.	0.322	0.	0.	0.	0.	0.	0.

a) Figures are listed in order: Urey-Bradley, valence; matrices are symmetrical; and the non-listed parts are all zero; valence constants from Ref. 5.
b) See an appended map.

In the CSH or CSD bending region, two shoulders of three bands disappeared in the solid state. On the normal species, the weak shoulder band at 934 cm^{-1} may be due to the TG and/or GG′ form, and the band at 917 cm^{-1}, to the TT and/or GT form. The bands at 600 and 587 cm^{-1} of the deuterated species correspond to the TG, and to the TT, GT, and/or GG′ form, respectively. In the CH_2 rocking region, we can expect more than one band in view of the calculated frequencies. We obtained one band for the normal species and two for the deuterated species. The band at 808 cm^{-1} of the deuterated species corresponds well to the TT and/or GT conformation. In the C–S stretching region, we observed that five (or six) bands of the normal (or deuterated) disappeared in the solid state. The calculated frequencies of the TT, TG, GT, and GG′ forms correspond well to the bands which disappeared in the solid state. In the skeletal deformation region, eight bands were observed in both the normal and deuterated species. If all of these eight bands are due to the fundamentals, more than four conformations coexist in the gaseous and liquid states. Since the most stable GG form in the solid state has two bands in both the normal and deuterated species, the remaining six bands may due to the other conformations: TT, TG, GT, and GG′.

We have discussed the conformations coexisting in the liquid and gaseous states. In the liquid and gaseous spectra, the isotopic frequency shift cannot be used for the conformational analysis, since the selection of the corresponding pairs from among many bands is difficult. We can postulate that at least three to four conformations, including the GG form, coexist in the liquid and gaseous states. However, we cannot decide, from the results we have obtained, how many conformations, and which conformations among the TT, TG, GT, and GG′ forms, persist, except for the GG form, which exists in all three states. The existence of the GG′ form cannot now be denied.

Force Constants

In order to confirm the reasonableness of our obtained Urey-Bradley force constants, we attempted to compare these Urey-Bradley constants and Scott and El-Sabban's force constants.[5] Scott and El-Sabban reported valence force constants for various organosulfur compounds which did not have the SCS skeleton. Table 7 shows the non-zero parts of both types of ***F***-matrix elements. The coordinate numbering is shown

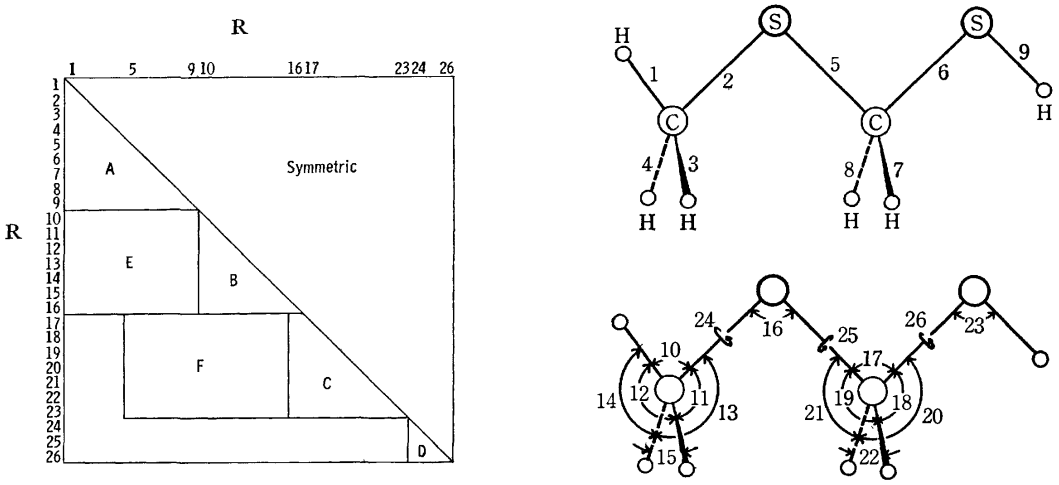

Fig. 10. Coordinates numbering for (methylthio)methanethiol.

in Fig. 10. The figures are listed in this order: Urey-Bradley, and valence force constants. No angle constant of ϕ(SCS) in the valence force field was obtained. In the diagonal elements, f_{ii} (i=1—26), our values agree well with Scott and El-Sabban's. Even for the off-diagonal parts, f_{ij} ($i \neq j$), the modified Urey-Bradley force elements and valence elements are in fairly good agreement. This shows that there is a good transferability of the obtained force constants for a wide range of organo-sulfur compounds. The newly-determined values for the SCS angle may be used on the valence force-type potential, *e.g.*, $f_{\mathrm{scs,scs}}$=1.141 and $f_{\mathrm{cs,scs}}$=0.384 mdyn/Å.

The authors wish to express their gratitude to Assistant Professor Michiro Hayashi of our University for his encouragement throughout this work. One of the authors (M. O.) is also greatly indebted to the foundation of the Kumura Syogakukai (Teijin Co., Tokyo).

BULLETIN OF THE CHEMICAL SOCIETY OF JAPAN, VOL. 45, 3048—3053 (1972)

Electrochemical Behaviour of the Lithiated Nickel Oxide Crystal

Hiroshi YONEYAMA and Hideo TAMURA

Department of Applied Chemistry, Faculty of Engineering, Osaka University, Yamadakami, Suita, Osaka

(Received November 26, 1971)

The electrochemical properties of lithiated nickel oxide were studied using a single-crystal (100) face and a sintered body. The I–V curves of the Fe^{2+}/Fe^{3+} system on the single-crystal electrode were almost the same as those on the sintered-body electrode when the electric resistivities of the crystals were equal. However, a high amount of charge was obtained at the sintered-body electrode compared with the single-crystal electrode when the crystals were oxidized anodically. The effect on these reaction rates of the space charge depletion layer formed on the electrode surface will be discussed. The dependence of the reaction rates on the electric resistivity of the crystal can be understood to a certain extent through this discussion.

Charge transfer reactions of some redox systems on sintered-body lithiated nickel oxide electrodes were studied previously[1], and it was concluded that the electric resistivity of the crystal influences the charge-transfer reaction rates. It was also found[2] that the resistivity of the crystal affects the quantity of higher-valency nickel oxides formed by anodic oxidation. It is often pointed out that the grain boundaries of the crystal act as peculiar defect sites, such as charge-trapping or -generating centers. According to Morin,[3] sintered-body nickel oxide contains cation vacancies, the number of which is influenced by the preparation conditions. Taking account of this information, the electrochemical behaviour of the crystal may be said to be influenced by the grain boundaries. One purpose of this paper is to present the difference in the electrochemical behaviour of lithiated nickel oxide between the single crystal and the sintered body. Another purpose is to discuss the electrochemical behaviour of the material from the semiconductor's point of view.

1) H. Yoneyama and H. Tamura, This Bulletin, **43**, 1603 (1970).

2) H. Yoneyama and H. Tamura, *ibid.*, **42**, 1795 (1969).

3) F. J. Morin, *Phys. Rev.*, **93**, 1199 (1954).

Experimental

Electrodes. The single-crystal lithiated nickel oxide was prepared by the method of Rouse and Weininger,[4] using commercial lithiated nickel oxide (Nakazumi Crystal Co. Ltd.). Electroless plating nickel was chosen as the electrical contact. The contact prepared by this method showed good ohmic behaviour. The electrode surface was the (100) face. The sintered-body lithiated nickel oxide electrode was prepared by a method described in a previous paper.[1] It was prepared by firing at 1350°C in the air. The distribution of the grain size of nickel oxide powder as a raw material is shown in Fig. 1; it was determined by the Andreasen pipet method. The electric resistivity of the electrode was estimated by means of the voltage drop between the end faces of the crystal.

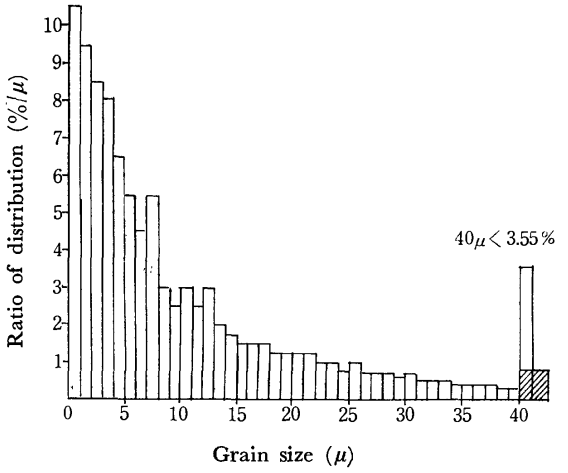

Fig. 1. Distribution of grain of NiO powder as a raw material.

Effective Surface Area of the Electorde. The effective surface area of the sintered-body electrode was determined by comparing the space charge capacitance of the depletion layer of the electrode with that of the single-crystal eleetrode in the following way.

Electrode surfaces of various single crystals and sintered bodies were polished with No. 2000 emery paper, followed by immersion in a mixed solution of conc. H_2SO_4 and conc. HNO_3 (1 : 1); then it was pretreated with a conc. HCl solution. After the electrode had been thoroughly washed with de-ionized water, the electric capacitance of the electrodes was measured in a 1N H_2SO_4 solution as a function of the electrode potential by means of the bridge arrangement shown in Fig. 2. Then the nominal carrier densities of various single-crystal electrodes were estimated usnig the relationship which can be applied for the depletion layer of the semiconductor:[5,6]

$$d(1/C^2)/dV = 2/(q\varepsilon\varepsilon_0 N) \quad (1)$$

In this equation, $q,\varepsilon,\varepsilon_0,N$, and C represent the elementary charge of the electron, the dielectric constant of the semiconductor, that of the vacuum, the carrier density of the semiconductor, and the capacitance of the depletion layer per unit of surface area of the semiconductor electrode. Typical examples are shown in Fig. 3. In the estimation of the nominal carrier densities of the various single crystals, the apparent geometric dimension was adopted as the effective surface area and the dielectric constant of the semiconductor was assumed to be 12.[7] Figure 4 shows the nominal carrier densities of the single-crystal electrodes as a function of their

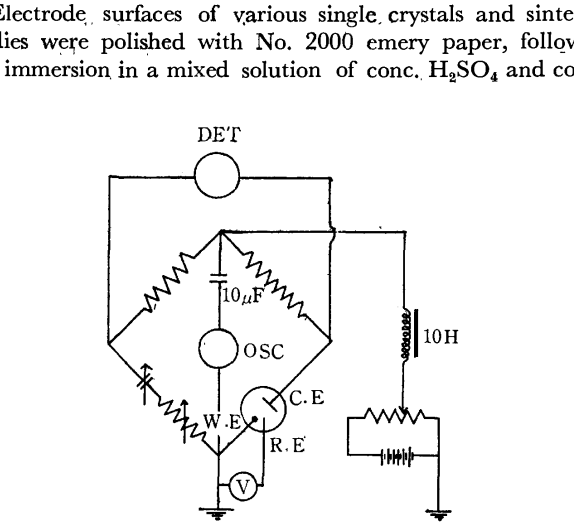

Fig. 2. Bridge arrangement for measurement of differential capacitance of electrode.

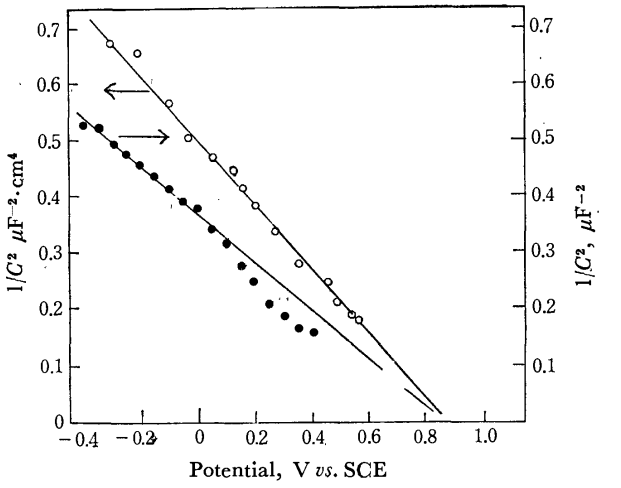

Fig. 3. Typical example of $1/C^2$ *vs.* V plot for two electrodes.
—●—: 580 Ω·cm sintered body, —○—: 580 Ω·cm single crystal.
solution: 1 N H_2SO_4

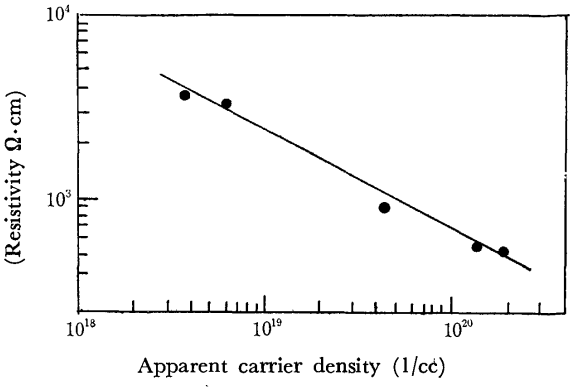

Fig. 4. Nominal carrier density as a function of resistivity of single crystal lithiated NiO.

4) T. O. Rouse and J. L. Weininger, *J. Electrochem. Soc.*, **113**, 184 (1966).

5) J. F. Dewald, *Bell System Tech. J.*, **39**, 615 (1960).

6) P. J. Boddy, *J. Electrochem. Soc.*, **115**, 199 (1968).

7) R. Newman and R. M. Chrenko, *Phys. Rev.*, **114**, 1507 (1959).

resistivities.[8]

Let it be assumed that the carrier density of the sintered body is eventually equal to that of the single crystal of the same resistivity. Then, the slope of the plots of $1/C^2$ *vs.* V should be equal to each other for the electrodes of the same resistivity when the effective areas of the electrodes are equal. The effective surface area of the sintered-body electrode was determined by correcting the area of the measured capacitance so as to have the same slope of $1/C^2$ *vs.* V plot as that of the single-crystal of the corresponding resistivity.

Measurement of I–V Curves and V–t Curves. *I–V* curves of the redox system were obtained potentiostatically. *V–t* curves during the anodic oxidation and cathodic reduction of the electrode were obtained by means of an electrometer connecting to a voltage recorder. Measurements were made for current densities in which the ohmic drop across the electrode could be almost negligible. Commercial dry nitrogen gas was bubbled into the electrolyte thermostated at 25±0.5°C during the measurements. Electrolytes were prepared by the use of reagent-grade chemicals and deionized water. The electrolytic cell was a conventional H-type cell.

Results

Redox Reaction of the Fe^{2+}/Fe^{3+} System. Figure 5 shows the anodic portions of the *I–V* curves of the Fe^{2+}/Fe^{3+} system (5×10^{-3} M Fe^{2+}, 5×10^{-3} M Fe^{3+}, in 1 N H_2SO_4) on single-crystal and sintered-body electrodes of the same resistivity. It is evident from this figure that no difference in the *I–V* curves can be observed between these two electrodes. The *I–V* curves of this system on various single-crystal electrodes are shown in Fig. 6.[9] The apparent exchange current

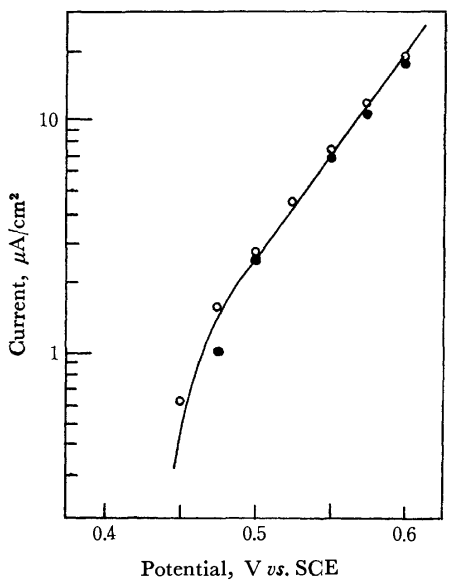

Fig. 5. Anodic portion of *I–V* curves of Fe^{2+}/Fe^{3+} system on sigle crystal and sintered body electrode having the same resistivity of 580 Ω·cm.
—●— sinterd body, —○— single crystal, solution: 5×10^{-3} M Fe^{2+}, 5×10^{-3} M Fe^{3+}/1 N H_2SO_4.

8) As has previously been observed by Rouse and Weininger, the nominal carrier density, as estimated from the $1/C^2$ *vs.* V plot, does not accord with the lithium content in the crystal. However, the use of this nominal carrier density in the estimation of the effective surface area of the sintered-body electrode will not introduce any trouble.

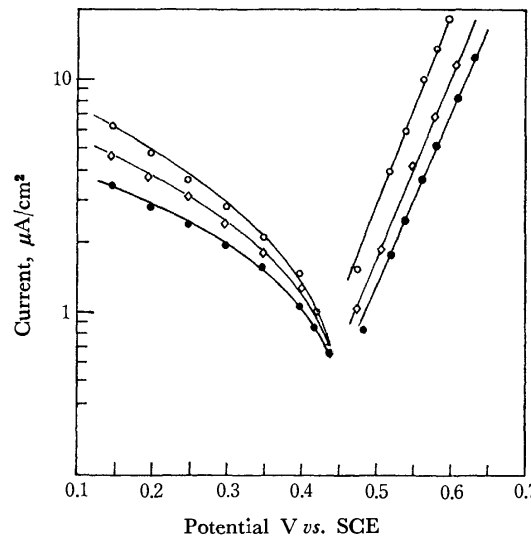

Fig. 6. *I–V* curves of Fe^{2+}/Fe^{3+} system on various single crystal electrodes.
—○— 580 Ω-cm, —◇— 1.6 kΩ-cm, —●— 3.8 kΩ-cm, solution: the same as in Fig. 5.

TABLE 1. APPARENT EXCHANGE CURRENT DENSITIES OF Fe^{2+}/Fe^{3+} SYSTEM ON VARIOUS SINGLE CRYSTAL ELECTRODES

Resistivity of electrode (Ω-cm)	580	1600	3800
Apparaent exchange current (A/cm²)	2.2×10^{-6}	1.1×10^{-6}	8.5×10^{-7}

Solution: 5×10^{-3} M Fe^{2+}, 5×10^{-3} M Fe^{3+} in 1 N H_2SO_4

densities of the system were estimated by the extrapolation of the anodic portion of the *I–V* curves in Fig. 6 to a redox potential of the system; they are shown in Table 1. According to Fig. 6, a linear slope was observed in the log I *vs.* V plot of the *I–V* curves of the anodic process, while the current showed a tendency to become saturated with the cathodic polarization. On the other hand, it can be seen in Table 1 that the exchange current densities of the system are influenced by the resistivity of the electrode. Such observations have previously been reported[1] for sintered-body electrodes. Therefore, they seems to be connected with the genuine properties of the lithiated nickel oxide.

Anodic Oxidation. Figure 7 shows the electrode potential behaviour of various electrodes during the 1st oxidation and reduction cycle. 10 μA/cm² and 1 μA/cm² were chosen as the anodic and cathodic current densities respectively. In this figure, the effective area of the 25 Ω·cm sintered-body electrode was estimated by a different method.[1] The cathodic *I–V* curves obtained in the electrolyte into which oxygen gas was bubbling are also shown in Fig. 7 for two kinds of electrodes, that is, the 180 Ω·cm sintered body and the 64 Ω·cm single crystal. A plateau of the potential was observed in the cathodic *V–t* curves. This poten-

9) Judging from the *I–V* curves in a system of Ni–NiO–Ni, where V is the applied voltage between nickel contacts and where I is the current, the voltage drops across the crystal per 1 μA/cm² were as follows: 580 Ω·cm: 0.075 mV, 1.6 kΩ·cm: 0.34 mV 3.8 kΩ·cm: 0.36 mV. *I–V* curves which have been corrected on the basis of thse voltage drops are presented in Fig. 6.

tial which appeared in the oxygen-bubbling electrolyte was by far more noble than that in the nitrogen-bubbling electrolyte. Figure 7 shows that the oxygen gas pressure has no influence on the V–t curves in the reduction process before the plateau of the potential due to oxygen reduction appears. From a comparison of the V–t curves under oxygen-bubbling conditions with those under nitrogen-bubbling conditions, it may be expected that V–t curves during the reduction in the noble potential region, more noble, say, than 0V, are mainly the result of the charge retained by anodic oxidation.[10] Hence, it follows from Fig. 7 that the

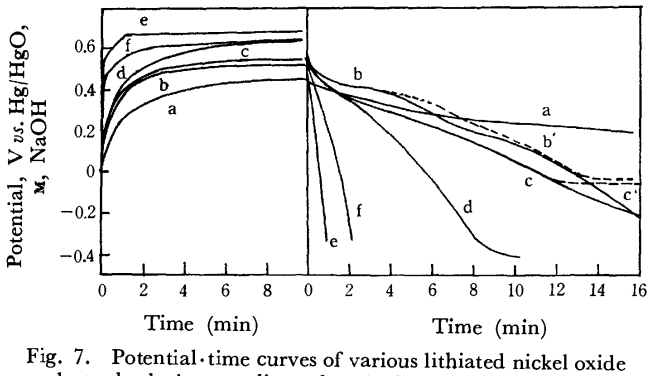

Fig. 7. Potential-time curves of various lithiated nickel oxide electrode during anodic and cathodic polarization.
anodic current density: 10 μA/cm^2, cathodic current density: 1μA/cm^2. solid line: in N_2 gas bubbling, dotted line: in O_2 gas bubbling, a: 25 Ω·cm, b: 64 Ω·cm single crystal, c: 180 Ω·cm. d: 580 Ω·cm, e: 580 Ω·cm single crystal, f: 2300 Ω·cm, b': 64 Ω·cm single crystal, c': 180 Ω·cm. solution: 1 M NaOH.

charge retained by anodic oxidation is high for an electrode of low resistivity. This conclusion is supported by the previous report[2] as well. Figure 7 suggests that the single crystal is less active in the anodic oxidation than the sintered body.

Discussion

Charge-transfer Reaction on the Lithiated Nickel Oxide Electrode. The rate equation of the charge-transfer reaction on the lithiated nickel oxide electrode will be presented first.

As only the positive hole participates in the charge-transfer process, the electrode reaction of the redox couple of Fe^{2+}/Fe^{3+} can be represented as[1];

$$Fe^{2+} + p \rightleftarrows Fe^{3+}$$

The positive hole concentration at the electrode surface, P_s, is related to the bulk concentration, P_b, according to the formulation by Myamlin and Pleskov[11]:

$$P_s = P_b \exp(F\phi_{sc}/\boldsymbol{R}T) \quad (2)$$

where ϕ_{sc} is the potential drop in the surface of the semiconductor and has a negative value when the space charge depletion layer is formed. The anodic current, J_a, and the cathodic current, J_c, can be expressed as:

$$J_a = kC_{Fe^{2+}}P_s \exp(\alpha F\phi_e/\boldsymbol{R}T) = kC_{Fe^{2+}}P_b \times \exp(F\phi_{sc}/\boldsymbol{R}T)\exp(\alpha F\phi_e/\boldsymbol{R}T) \quad (3)$$

$$J_c = k'C_{Fe^{3+}}\exp(-\beta F\phi_e/\boldsymbol{R}T) \quad (4)$$

where ϕ_e is the potential drop in the Helmholtz double layer. The exchange current density, J_o, is:

$$J_o = kC_{Fe^{2+}}P_b \exp(F\phi_{sc}^\circ/\boldsymbol{R}T)\exp(\alpha F\phi_e^\circ/\boldsymbol{R}T) = k'C_{Fe^{3+}}\exp(-\beta F\phi_e^\circ/\boldsymbol{R}T) \quad (5)$$

where ϕ_{sc}° and ϕ_e° are, respectively, the potential drop in the space charge layer of the electrode surface and that in the Helmholtz double layer when the electrode is in equilibrium with the redox couple. By substituting Eq. (5) into Eq. (3) and Eq. (4), we obtain:

$$J_a = J_o \exp[\{F(\phi_{sc}-\phi_{sc}^\circ) + \alpha F(\phi_e-\phi_e^\circ)\}/\boldsymbol{R}T] \quad (6)$$

$$J_c = J_o \exp\{-\beta F(\phi_e-\phi_e^\circ)/\boldsymbol{R}T\} \quad (7)$$

The potential drop in the Helmholtz double layer may be neglected when a distinct space-charge layer exists on the surface of the electrode. Then, ϕ_{sc}° and ϕ_{sc} relate to the flat-band potential, E_{fb}, the redox potential of the redox couple, E_{redox}, and the electrode potential, E, all of which are measurable values:

$$\phi_{sc}^\circ = E_{redox} - E_{fb} \quad (8)$$

$$\phi_{sc} = E - E_{fb} \quad (9)$$

In this case, the total current, J, is formulated as:

$$J = J_a - J_c = J_0 \exp\{(E-E_{redox})/\boldsymbol{R}T - 1\} \quad (10)$$

In the above formulation, $C\mathrm{Fe}^{2+}$ and $C\mathrm{Fe}^{3+}$ are used as the concentrations of the ferrous and ferric ions in the electrolyte. The concentration of the redox couple at the energy level of the positive hole of the electrode surface is truly determined by the product of the concentration of the redox couple and the distribution function of the couple, which is approximately a function of the energy difference between the positive hole level at the electrode surface and the Fermi energy of the redox couple.[12] The effect of the distribution function on the charge-transfer reaction rate is contained in the rate constants, k and k' in Eq. (3) and Eq. (4) respectively.

Figure 3 suggests that the flat-band potential of the electrode in 1 N H_2SO_4 is 0.85 V *vs.* SCE, while Fig. 6 shows that the equilibrium potential of the redox couple and the electrode is by far less noble. Judging from these pieces of information, there must be a space-charge depletion layer on the surface of the electrode. Figure 8 shows an energy diagram[13] of the electrolyte/electrode interface; the potential drop in the Helm-

10) The difference in the charge value between this and the previous paper is due to the anodic oxidation conditions. In the previous experiments, the electrode had been exposed to a high anodic current density in the first oxidation cycle, while in the subsequent cycles the total charge supplied during the oxidation as well as the oxidation current density had not exceeded the value of the first cycle. For this reason, an almost constant charge was obtained regardless of the anodic oxidation conditions. In this sence, the previous description that the charge corresponding to the higher-valency nickel oxides formed by anodic oxidation is constant, regardless of the anodic oxidation current density, is inadequate. Hence, all the data presented previously should be understood to those for electrodes which had been exposed to the first oxidation conditions (10 mA/cm^2 × 5 min).

11) V. A. Myamlin and Yu. V. Pleskov, "Electrochemistry of Semiconductors," Plenum Press, New York (1967), p. 159.

12) H. Gerischer, *Surface Sci.*, **18**, 97 (1969).

13) The energy diagram presented in a previous paper (Ref. 1) contains a fault.

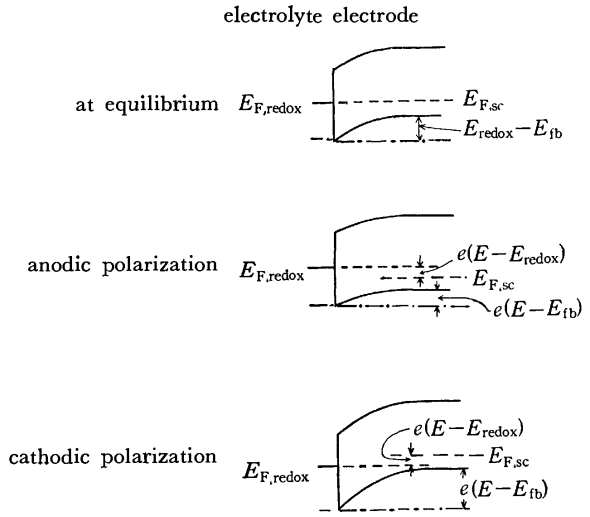

Fig. 8. Energy diagram of the electrode/electrolyte interface when the electrode contacts with a redox solution of Fe^{2+}/Fe^{3+} system.

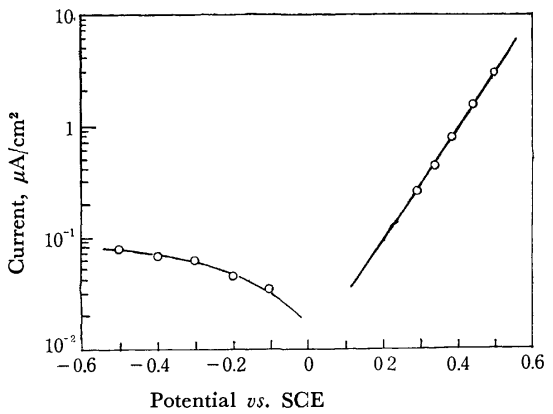

Fig. 9. *I-V* curves of Ti^{3+}/Ti^{4+} system in 1 N HCl solution on 580 Ω·cm single crystal electrode. Solution: 0.9 M Ti^{3+}, 0.1 M Ti^{4+} 1 N HCl.

holtz double layer is neglected. The solid lines of the energy diagram of the semiconductor shown in Fig. 8 denote the energy level of the positive hole and the electron respectively.[14,15] The experimental results which are shown in Fig. 6 for the Fe^{2+}/Fe^{3+} and in Fig. 9 for the Ti^{3+}/Ti^{4+} suggest that the ideal case, which is illustrated in Fig. 8, was not realized, for the anodic Tafel slope was not 59 mV/decade. However, the dependence of the exchange-current density on the resistivity of the electrode and the appearence of the Tafel slope in the anodic process can be understood by means of Eq. (5) and Eq. (6).

Anodic Oxidation. The charge retained by the anodic oxidation is possibly due to the formation of higher-valency nickel oxides. The phenomenon that the resistivity of the crystal affects this charge can not be explained on the basis of the atom arrangement of the crystal, since the dimensions of the unit cell decrease with increase in the lithium content.[16]

14) D. Adler, *Phys. Rev.* B, **2**, 3112 (1970).
15) S. van Houten, *J. Phys. Chem. Solid*, **17**, 7 (1960).
16) E. J. W. Verway, P. W. Haaijman, F. C. Romeijn, and G. W. van Osterhout, *Philips Res. Rept.*, **5**, 173 (1950).

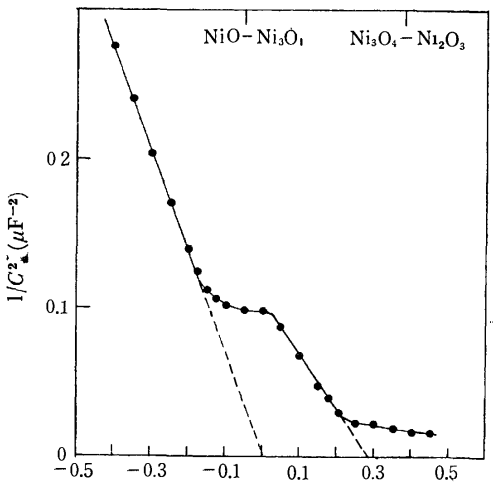

Fig. 10. $1/C^2$ *vs.* V plot for the sintered body of 580 Ω·cm. solution: 1 M NaOH, electrode area: 0.183 cm².

According to the above discussion, a potential drop in the space-charge depletion layer influences the electrochemical behaviour of the lithiated nickel oxide. Figure 10 shows the $1/C^2$ *vs.* V plot for the 580 Ω·cm sintered-body electrode in a 1 M NaOH solution. The thermodynamically-calculated equilibrium potentials of various nickel oxides[17] are also shown in this figure. Figure 10 clearly shows that the inflection of the $1/C^2$ vs. V plot occurs around the potential at which surface oxidation begins to occur, and that the flat-band potential shifts towards a more noble potential after beginning of surface oxidation. The shift of the flat-band potential towards a more noble potential may be brought about by the formation of the surface state, which is due to oxide formation. At any rate, Fig. 10 implies that there is a space-charge depletion layer on the electrode surface in the less noble potentials below 0.3 V (*vs.* Hg/HgO, M NaOH). According to Fig. 7, anodic oxidation proceeds to a certain extent in the potentials below 0.3 V. Therefore, the anodic oxidation mechanism below the flat-band potential will be discussed first.

When the space-charge layer exists on the electrode surface, the field strength across the space-charge layer will be different according to various resistivities of the electrode at the same polarization potential. The electric capacitance in Eq. (1) is related to the depth of the space-charge layer, d:

$$C = \varepsilon\varepsilon_0/d \qquad (9)$$

The potential drop in the space-charge layer corresponds ideally to the electrode potential as measured from the flat-band potential, $E-E_{fb}$. By replacing V in Eq. (1) with $(E-E_{fb})$ and by combining Eq. (1) with Eq. (9), we finally obtain the electric-field strength across the space-charge layer, which is shown in Eq. (10):

$$F = (E-E_{fb})/d = \{qN(E-E_{fb})/2\varepsilon\varepsilon_0\}^{1/2} \qquad (10)$$

Figure 11 shows the calculated field strength across

17) M. Pourbaix, "Atlas of Electrochemical Equilibria in Aqueous Solutions," Pergamon Press, Oxford (1966), p. 330.

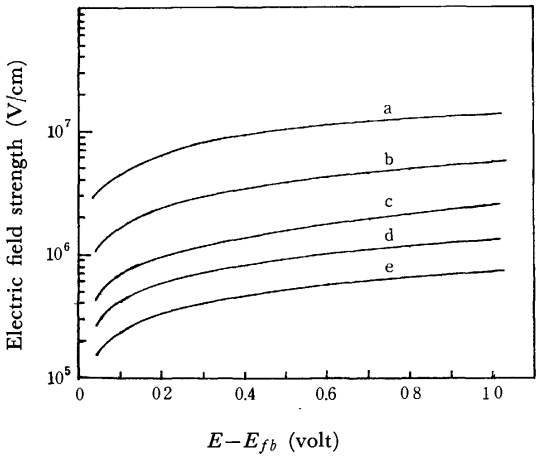

Fig. 11. Calculated electric field strength across the space charge in the electrode surface as a function of $E-E_{fb}$ a: 5.6 Ω·cm, b: 25 Ω·cm, c: 180 Ω·cm, d: 560 Ω·cm, e: 2300 Ω·cm.

the space-charge layer of the various electrodes as a function of $E-E_{fb}$. In the calculation, the value of N was estimated from the relationship between the lithium content and the resistivity of the crystal.[2] Figure 11 shows that the electric-field strength across the space-charge layer is high for the electrode of low resistivity.

The ionic current, I, in the anodic film formation process is generally expressed as:[18]

$$I = A \exp(\beta F) \tag{11}$$

where A and β are constants and where F is the electric-field strength. During the film formation process, an order of 10^6 V/cm is required for the value of F. According to Dewald's theoretical treatment of the mechanism of the formation of anodic oxide film at a high field,[19] there is a case where the contribution of the space charge layer to the F is predominate and where the rate of oxidation is determined almost entirely by the bulk properties of the film. If it is accepted that Dewald's theory is suitable for the anodic oxidation of the lithiated nickel oxide, it can be seen that the electrode of low-bulk resistivity suffers anodic oxidation more easily, although, in a strict sense, the precise estimation of various parameters in Dewald's theory is necessary in order to determine the applicability of the theory to this case.

The above mechanism of the anodic oxidation is probably restricted in the potential region below the flat-band potential, because the polarization potential is almost entirely concentrated in the Helmholtz double layer in the potential region above the flat-band potential of the electrode. The anodic oxidation above the flat-band potential will be influenced by the properties of the oxides formed by that time. Unfortunately, the properties of the oxides formed can not be elucidated at present becaue of its thinness.

Difference in Quantity of Higher-valency Oxides between Single Crystal and the Sintered Body. According to Fig. 7, the charge retained by the anodic oxidation seems to be different between the single crystal and the sintered body of the same resistivity. If the anodic oxidation mechanism ascribed above is valid, the difference should not be observed. The fact that the difference does appear suggests that other factors control the formation of the higher-valency oxides as well.

The following factors may influence the formation of the higher-valency oxides: 1) The sintered body prepared in the air presumably contained many cation vacancies.[3] The existence of vacancies is favorable for the ion movement in the crystal. 2) The gain in crystal-field stabilization energy on the chemisorption of oxygen on nickel oxide is high for the (110) face rather than the (100) face of the crystal.[20] This suggests that the (110) face is more active than the (100) face in the anodic oxidation. In the case of the sintered-body electrode, various crystal faces came in contact with the electrolyte. 3) Grain boundaries are considered to be high in surface free energy.[21] It has been pointed out that the surface free energy of a solid influences the rate of the anodic film formation process[22] as well as crystal growth.[23,24] Further study is necessary to elucidate which factor is most effective for the anodic oxidation of the nickel oxide crystal.

18) D. A. Vermilyea, "Advance in Electrochemistry and Electrochemical Engineering," Vol. 3, ed. by P. Delahay and C. W. Tobias, Interscience, New York (1963), p. 248.
19) J. F. Dewald, *J. Electrochem. Soc.*, **102**, 1 (1955).
20) J. Harber and F. S. Stone, *Trans. Farady Soc.*, **59**, 192 (1963).
21) E. Fujita, *Ōyō Butsuri*, **36**, 129 (1967).
22) D. A. Vermilyea, "Advance in Electrochemistry and Electrochemical Engineering," Vol. 3, ed. by P. Delahay and C.W. Tobias, Interscience, New York (1963), p. 223.
23) M. Fleishmann and H. R. Thirk, *Electrochim. Acta*, **2**, 22 (1960).
24) D. A. Vermilyea, *J. Chem. Phys.*, **25**, 1254 (1956).

The Preparation of Divalent Cation Non-permselective Cation Exchange Membrane by Coating with Vinylon Film[1]

Reizo DOHNO, Takatugu AZUMI, and Shiro TAKASHIMA
Himeji Institute of Technology, Shosha, Himeji

(Received December 16, 1971)

The preparation of non-permselective membrane for the divalent cation was attempted by coating it with thin vinylon film on one side of a commercial cation-exchange membrane. When the coating surface of the cation-exchange membrane was set on the concentration-compartment side (cathode side), the permselectivity coefficient of the calcium ion to the sodium ion was equal to that of untreated cation-exchange membrane and no effect of the selective treatment was recognized. However, when the coating sufrace was directed to the desalting-compartment side (anode side), an effect of the selective treatment was observed; in this case, the permeability of the calcium ion was more depressed, corresponding with the formalation degree of the selective-treatment membrane; for example, the permselectivity of the calcium ion for the membrane which was formalated for 180 min at 30°C decreased about one half compared with the untreated membrane. The electric resistance of the cation-exchange membrane increased upon the coating with the vinylon film, and especially the resistance of the calcium ionic-form membrane indicated a remarkable increase.

In the concentration of sea-water by electrodialysis through an ion-exchange membrane, the preparation of a non-permselectivity membrane for the divalent cation is one of the important subjects in connection with the increase in the current efficiency of sodium chloride and the prevention of scaling. At present, with regard to the procedure of increasing the non-permselectivity for the divalent cation, several papers have been published as to either the synthesis of new kinds of base membranes[2] or the addition of surfactants as selective improvement agents to sea water during electrodialysis.[3]

The present authors[4–6] studied the mechanism of the permselectivity between same-charge ions across the cation-exchange membrane and recognized that the divalent cation show a large permselectivity in spite of their small mobility in a cation-exchange membrane because they have a much larger separation factor than the sodium ion in the ion-exchange equilibria. Also, as has been described in a previous paper,[7] the permselectivity between ions of the same charge across a vinylon membrane is predominantly effected by the mobility ratio of both ions in the membrane, regardless of the total concentration or of the composition ratio in the original solution. On the other hand, the ion-transport numbers for membranes with a very low ion-exchange capacity approximate to a neutral membrane have been reported by Kumins and London,[8] and other workers,[9] but these membranes can not be used as practical as diaphrams in an electrodialysis concentration because the transport number decreases remarkably in a highly concentrated solution.

In this paper, vinylon-coated ion-exchange membranes were prepared by the following method. A thin film of polyvinyl alcohol (PVA) was smeared on the surface of one side of a commercial cation-exchange membrane, and then it was formalated under various conditions. Then the permselectivities of the calcium ion to the sodium ion across these selective-treatment membranes were measured, and the mechanism was discussed.

Experimental

Selective Treatment of Cation-exchange Membrane. A commercial cation-exchange membrane (exchange capacity, 1.79 meq/g dry; water content, 33.5%; membrane thickness, 0.16 mm) was used as the base membrane; a 10% aqueous solution of polyvinyl alcohol (polymerization degree 2400—2500) was smeared on one side of this membrane and it was dried in an air bath at room temperature for 24 hours. The dried membrane was then formalated under various conditions of time and temperature in a solution composed of concentrated H_2SO_4 200 g/*l*, Na_2SO_4 200 g/*l* and 135 g/*l* of 37% formalin, and it was washed in deionized water. These formalated membranes were used for the experiments.

The symbols of all the selective-treatment membranes and the formalation conditions are listed in Table 1.

Apparatus and Procedure of Electrodialysis. The cation-exchange membrane and anion-exchange membrane used in this experiment were strongly acidic and basic membranes. The electrodialysis apparatus was a cell with eight compartments separated by a cation-exchange membrane and an anion-exchange membrane, each with an area of 13×4 cm^2; the selective-treatment membrane was placed between the 5th compartment and the 6th compartment (Fig. 1).

In this cell, a mixed solution of a 0.35N-NaCl solution and a 0.03 N-$CaCl_2$ solution, as the original solution (20 *l*), was circulated in order from the 4th through the 6th to 2nd compartment at about 500 ml/min. at 30 ± 1°C, and the 3rd, 5th, and 7th compartments were filled with a 0.1N-$NaNO_3$ solution. The left- and the right-side compartments, separated by a cation-exchange membrane, were cathode and anode compartments respectively, and in both electrode compartments a 0.3 N-Na_2SO_4 solution was circulated. The electrodialysis was carried out at a constant quantity of elec-

1) Presented at the Local Meeting of the Chemical Society of Japan, Nagoya, October, 1970.

2) For example, R. Yamane, Y. Mizutani, H. Motomura, and R. Izuno, *Denki Kagaku*, **32**, 277 (1964).

3) For example, T. Sata, *Kolloid-Z. Polym.*, **243**, 157 (1971); A. Kuzuyama, S. Nagata, and S. Saito, the 20th Annual Meeting of the Science of Sea Water Society of Japan, Abstract, p. 3 (1969).

4) R. Dohno, T. Azumi, and S. Takashima, *Nippon Kagaku Zasshi*, **89**, 245 (1968).

5) R. Dohno, T. Azumi, and S. Takashima, *ibid.*, **91**, 131 (1970).

6) R. Dohno, T. Azumi, and S. Takashima, *ibid.*, **92**, 136 (1971).

7) R. Dohno, T. Azumi, and S. Takashima, *ibid.*, **91**, 1133 (1970).

8) C. A. Kumins and A. London, *J. Polym. Sci.*, **46**, 395 (1960).

9) T. M. Ellison and H. G. Spencer, *Polym. Lett.* **1**, 707 (1963).

Table 1. Formalation condition and membrane symbol

Symbol of membrane		A-60	A-120	A-180	B-50	B-70	D-60	D-120	C-M
Formalation condition	Temp. (°C)	30	30	30	50	70	40	40	untreatment membrane
	Time (min)	60	120	180	120	120	60	120	

Table 2. T_{Na}^{Ca} for treatment and untreatment membranes

Current density (A/dm²)		0.42	0.83	1.67	2.50	3.33
Untreatment membrane (Cation membrane)		2.88	2.04	1.60	1.42	1.33
Treatment membrane[a)]	Cathode side	2.86	1.98	1.58	1.37	1.30
	Anode side	2.32	1.62	1.23	0.95	0.95

a) A-60

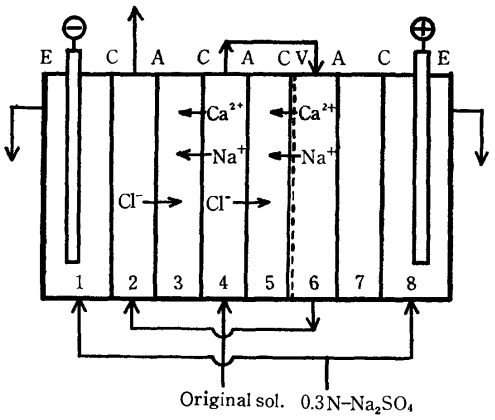

Fig. 1. Schematic diagram of electrodialysis cell.
C: cation exchange membrane
A: anion exchange membrane
CV: selective treatment membrane
E: carbon electrode

tricity by alternating the current density and the time respectively, and then the transfer eqivalents of the calcium ion and the sodium ion were determined from the concentrations of these ions in the 3rd and 5th compartments respectively. From these values, the permselectivity coefficients of the calcium ion to the sodium ion were calculated by means of Eq. (1):

$$T_{Na}^{Ca} = (E_{Ca}/E_{Na})/(C_{Ca}/C_{Na}) \quad (1)$$

where E is the transfer equivalent and where C is the concentrantion in the original solution. The analysis of the chloride ion and the calcium ion was done by Mohr's method and the EDTA method, while the sodium ion was determined by calculation.

Membrane Resistance. The untreated membrane (*i. e.*, the cation-exchange membrane) and the selective-treatment membranes were equilibrated with a 0.5N-NaCl or 0.5N-$CaCl_2$ solution for 50-hr. A cell with two compartments equipped with platinized platinum electrodes was used for the measurement, and the resistances were measured by means of a 1000-cycle AC bridge (Yokogawa Electric Works Ltd. BV-Z-103 B) at 30±0.5°C. The membrane resistance was obtained as the difference between the reading with the membrane and without the membrane.

Results and Discussion

Direction of Treatment Surface. The permselectivity coefficients in each case of the treatment surface of a cation-exchange membrane placed in the direction of the concentration-compartment side and in that of the desalting-compartment side are shown in Table 2.

When the selective-treatment surface was directed at the concentration-compartment side, the permselectivity coefficients were equal to that of the untreated membrane; that is, no effect of selective treatment was recognized. However, when it was directed to the desalting-compartment side, the values of the permselectivity coefficients decreased in comparison with

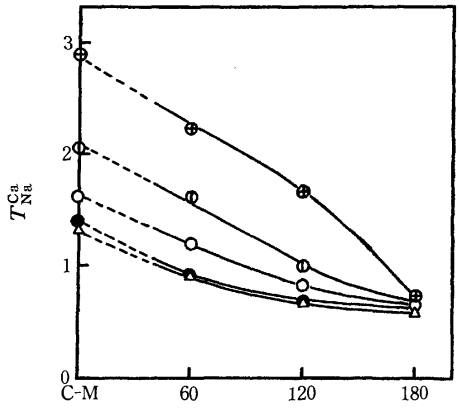

Fig. 2. Effect of formalation time on permselectivity coefficient.
Current density (A/dm²);
⊕: 0.42, ⓘ: 0.83, ○: 1.67, ●: 2.50, △: 3.33

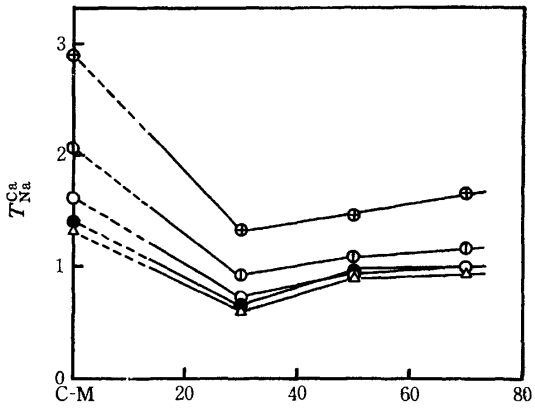

Fig. 3. Effect of formalation temperature on permselectivity coefficient.
Current density (A/dm²);
⊕: 0.42, ⓘ: 0.83, ○: 1.67, ●: 2.50, △: 3.33

that of the untreated membrane. From these results, it can be concluded that the permselectivity of the calcium ion varies with the direction of the treated surface. Therefore, in the subsequent experiments, the permselectivities were measured for the treated surface directed to the desalting-compartment side.

Change of Permselectivity with the Formalation Conditions. Figures 2 and 3 show the change in the permselectivity coefficients due to the formalation conditions at each current density.

The permselectivity coefficients of the treated membrane decrease with an increase in the formalation time. It is presumed that the transfer of the calcium ion, which possesses a larger hydration radius,[10] was more depressed than that of the sodium ion because the vinylon phase came to have a fine structure upon formalation.[11] However, when the formalation time is over a certain length, the permselectivity coefficient does not decrease, because the transfer of the sodium ion is depressed as well as that of the calcium ion. For example, the permselectivity of the calcium ion to the sodium ion across the A-180 membrane is nearly equal to that of the A-120 membrane, but these values were about half that of the untreated membrane. On the other hand, at a constant formalation time, the permselectivity coefficient appears to have a tendency to increase somewhat with a rise in the formalation temperature (Fig. 3).

Membrane Resistance. The effective resistance of the treatment membrane in a calcium ionic form and in a sodium ionic form *vs.* the formalation time and the temperature are shown in Figs. 4 and 5 respectively.

In all cases, the resistance of the calcium ionic-form membrane was larger than that of the sodium ionic-form membrane. The resistance of both ionic-form membranes increased with an increase in the formalation time and temperature; the resistance of the calcium ionic-form membrane indicated an especially remarkable increase. This suggests that the transfer of the calcium ion is depressed by the vinylon-film coat on the cation-exchange membrane. Also, the degree of the increase in resistance due to the formalation conditions is greater with the formalation temperature than with the formalation time.

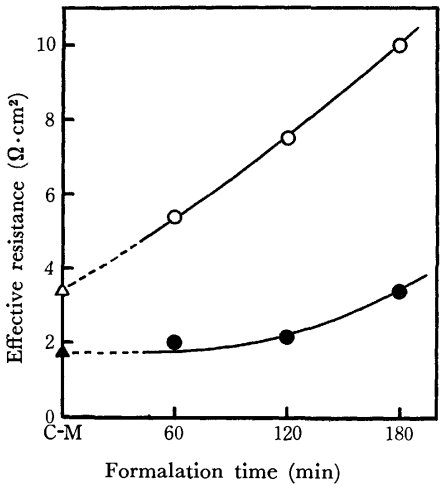

Fig. 4. Change of resistance by formalation time.
(Formalation temperature: 30°C)
○: 0.50 N-$CaCl_2$ ●: 0.50 N-NaCl, △▲: C-M

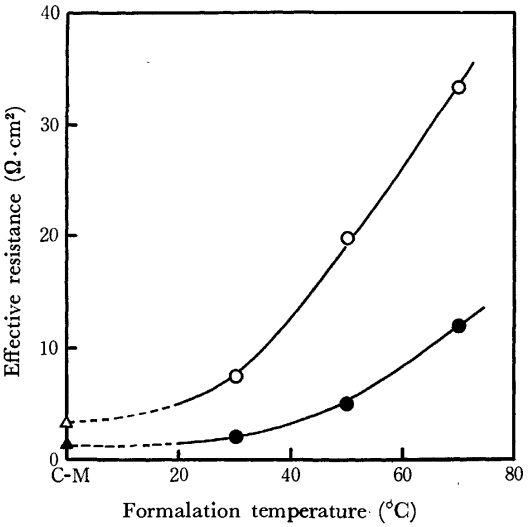

Fig. 5. Change of resistance by formalation temperature.
(Formalation time: 120 min.)
○: 0.50 N-$CaCl_2$, ●: 0.50 N-NaCl, △▲: C-M

It can be considered that, at low temperatures, the formalation proceeds with the increase of time until the PVA phase, because the formalation reaction does not proceed very fast; a fine structure will thus be formed. However, at high temperatures, a layer of a higher formalation degree will be formed on the surface of the PVA phase in even a short reaction time and the formalation can not succeed until within this phase.

Mechanism of Permselectivity for Treatment Membrane. The permselectivity between the same-charge ions across an ion-exchange membrane is split into two terms, the mobility term and the concentration term, as is shown by Eq.(2);

$$T_A^B = (\bar{U}_B/\bar{U}_A)S_A^B \qquad (2)$$

where $\bar{U}$ is the mobility in the ion-exchange membrane and S_A^B is the separation factor of the B ion to the A ion the cation-exchange membrane which is defined by Eq. (3);

$$S_A^B = (\bar{C}_B/\bar{C}_A)/(C_B/C_A) \qquad (3)$$

where $\bar{C}$ is the concentration in the ion-exchange membrane and C is the concentration in the solution.

Usually, the mobility ratio and the separation factor of the calcium ion to the sodium ion for the cation-exchange membrane are established experimentally as follows:

$$(\bar{U}_{Ca}/\bar{U}_{Na})<1,\ S_{Na}^{Ca}>1$$

The permeability of the calcium ion is larger than the sodium ion because the effect of S_{Na}^{Ca} is larger than the $(\bar{U}_{Ca}/\bar{U}_{Na})$ term. *i. e.*, $T_{Na}^{Ca}>1$. Thus, it is possible that the permselectivity of the calcium ion de-

10) T. Yamabe and M. Seno, "Ion Kokan Jushimaku," Gihodo, Tokyo, Japan (1964), p. 47.
11) N. Takahashi and K. Onozata, *Kogyo Kagaku Zasshi*, **63**, 1540 (1960).

pressed by a decrease in the concentration of the calcium ion in the cation-exchange membrane, *i. e.* $S^{Ca}_{Na}<1$.

On the other hand, the permselectivity for the vinylon membrane is given by Eq. (4) as well as for the cation-exchange membrane:

$$V^{Ca}_{Na} = (\overline{U}'_{Ca}/\overline{U}'_{Na})S'^{Ca}_{Na} \quad (4)$$

where $\overline{U}'$ is the mobility in the vinylon membrane and where S'^{Ca}_{Na} indicates the selective adsorption of the calcium ion to the sodium ion for the vinylon membrane, as defined by Eq. (5):

$$S'^{Ca}_{Na} = (\overline{C}'_{Ca}/\overline{C}'_{Na})/(C_{Ca}/C_{Na}) \quad (5)$$

where $\overline{C}'$ is the concentration in the vinylon membrane and where C is in accordance with that in Eq.(3).

Table 3 shows the values of S'^{Ca}_{Na} measured for the vinylon membrane formalated under various conditions. These values indicate that $S'^{Ca}_{Na}\fallingdotseq 1$ within the experimental error; that is, the concentartion ratio of the calcium ion to the sodium ion in the vinylon membrane is equal to that of the original solution. Also, $(\overline{U}'_{Ca}/\overline{U}'_{Na})<1$ is deduced from Figs. 4 and 5. Accordingly, $V^{Ca}_{Na}<1$. That is to say, the permselectivity for the vinylon membrane is primarily ruled by the mobility ratio of both ions in the vinylon phase, and this ratio is closely related to the fine structure of vinylon.

Table 3. S'^{Ca}_{Na} of vinylon membrane

Symbol of membrane	A-60	A-120	D-60	D-120
S'^{Ca}_{Na}	1.3	1.0	0.8	1.0

Now, in the case of the treatment membrane obtained by combining a cation-exchange membrane and vinylon film, the value of V^{Ca}_{Na} indicates the ratio of the transfer equivalent of the calcium ion to the sodium ion which is supplied to the cation-exchange membrane across the vinylon film coated on the desalting-compartment side. Since V^{Ca}_{Na} is smaller than that of the original solution, the concentration ratio of the calcium ion to the sodium ion in the cation-exchange membrane phase will decrease compared with the untreated membrane. Consequently, the permselectivity of the calcium ion across the treatment membrane decreases. However, when the treatment surface was directed to the concentration-compartment side, the concentration ratio of the two ions in the cation-exchange membrane phase become the same value as that of the untreated membrane because the cation exchange membrane directly contacts the original solution. Accordingly, no change in the permselectivity of the treatment membrane was observed.

On the other hand, the transport number of cations in the vinylon phase will be nearly equal to that in the original solution because the vinylon has no ion-exchange group, and the concentration polarization on the interface between the vinylon film and the original solution is negligibly small. Thus the deficiency of calcium ions and the accumulation of sodium ions will occur at the interface between the

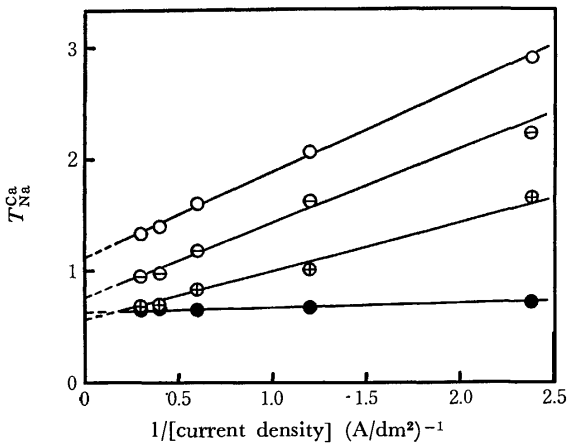

Fig. 6. Relationship between permselectivity and reciprocal of current density.
(Effect of formalation time)
○: C-M, ⊖: A-60, ⊕: A-120, ●: A-180

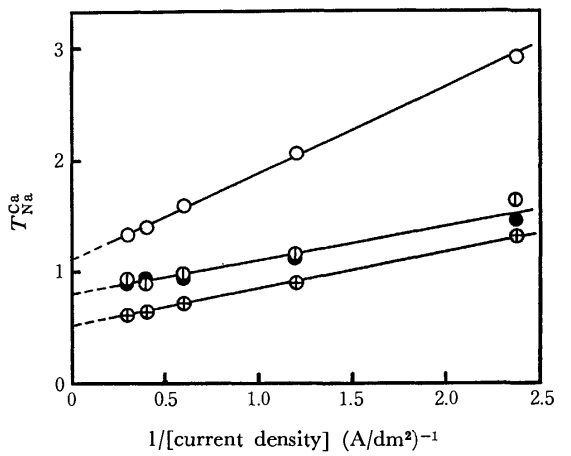

Fig. 7. Relationship between permselectivity and reciprocal of current density.
(Effect of formalation temperature)
○: C-M, ⊕: A-120, ●: B-50, ⊕: B-70

Table 4. Mobility ratio in vinylon phase

Symbol of membrane	A-60	A-120	A-180	B-50	B-70
$\overline{U}'_{Ca}/\overline{U}'_{Na}$	0.77	0.52	0.66	0.80	0.80

cation-exchange membrane and the vinylon film because $T^{Ca}_{Na}>1$ and $V^{Ca}_{Na}<1$. The value of $\overline{C}_{Ca}/\overline{C}_{Na}$ in the cation-exchange membrane decreases with an increase in the current density, and approaches $(\overline{U}'_{Ca}/\overline{U}'_{Na})S^{Ca}_{Na}$. That is, the permselectivity coefficient at infinity of a current density for the treatment membrane is equal to the mobility ratio $(\overline{U}'_{Ca}/\overline{U}'_{Na})$ of both ions in the vinylon phase by reason of $S'^{Ca}_{Na}\fallingdotseq 1$.

The relationship between the permselectivity and the reciprocal of the current density is shown in Figs. 6 and 7, while Table 4 shows the value of the permselectivity coefficient (*i. e.*, $\overline{U}'_{Ca}/\overline{U}'_{Na}$) obtained by an extrapolation to infinity of the current density in these figures.

For the untreated membrane the extrapolating value is 1.15; this value is consistent with the mobility ratio of both ions in a free solution, but for the other mem-

branes, which are formalated under various conditions, the values of $\bar{U}'_{Ca}/\bar{U}'_{Na}$ are smaller than that in solution; these results indicate that the mobility of the calcium ion to the sodium ion in the vinylon phase is depressed, as can be expected from Figs. 4 and 5.

From the above experimental results, it can be considered that the permeability of the divalent cation can be depressed by coating the desalting side of the cation-exchange membrane with vinylon film. However, in this case the electric resistance of the membrane increases; this problem may be resolved to a certain extent by making the vinylon-phase coat as thin as possible.

BULLETIN OF THE CHEMICAL SOCIETY OF JAPAN, VOL. 45, 3058—3064 (1972)

Normal Vibrations and Far-infrared Spectra of Ammonium Chloride and Ammonium Chloride-d_4 Crystals

Kunio FUKUSHIMA and Hiroko YAMAMOTO

Department of Chemistry, Faculty of Science, Shizuoka University, Oya, Shizuoka

(Received March 8, 1972)

The normal coordinate treatment of optically active lattice vibrations of ammonium chloride and ammonium chloride-d_4 at low temperature was made in order to elucidate the nature of the vibrations and obtain force constants in the potential in the crystals by the method of least squares. Using the constants, the optically active lattice vibrations of a crystal model for ammonium chloride and ammonium chloride-d_4 at room temperature were calculated. The far-infrared spectra obtained and the Raman and infrared spectra in literature were discussed.

Investigations of spectral change due to the phase transition in ammonium halides have been made by means of Raman and infrared spectroscopy.[1-11] Recently, by laser Raman spectroscopy, several weak Raman lines of the halides not detected in the Raman spectra obtained by use of mercury-vapor lamps as light sources, were observed. Assignments of some Raman lines to lattice vibrations were made, giving information on the lattice vibrations.[12,13] Neutron scattering expriments have given vibrational frequency data which Raman and infrared spectroscopy could not afford.[14-17] Studies on crystal structures of ammonium halides by means of X-ray, electron diffraction and neutron diffraction indicated an ordered structure for the low temperature phase.[18,19] However, no decisive conclusion has been obtained as regards the structure of the higher temperature phase.[18-21] We carried out a normal coordinate treatment of the optically active lattice vibrations of ammonium chloride and ammonium chloride-d_4 crystals in the low temperature phase in order to determine the force field in the crystals. The optically active lattice vibrations of a crystal model proposed as a model of ammonium chloride crystal at room temperature,[18] were calculated for interpretation of the infrared and Raman spectra of ammonium chloride and ammonium chloride-d_4 at room temperature.

Experimental

Ammonium chloride of the Wako Chemical Industries, Ltd. (JIS Special Grade) was recrystallized from its aqueous

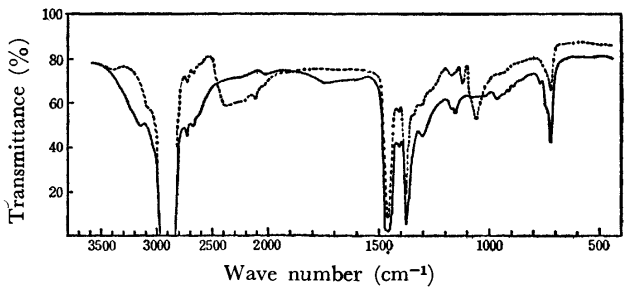

Fig. 1. Infrared spectra of ammonium chloride and ammonium chloride-d_4 in Nujol mulls.
Solid line: ammonium chloride, Dotted line: ammonium chloride-d_4.

1) R. S. Krishnan, *Nature* **160**, 711 (1947).
2) L. Couture and J. P. Mathieu, *C. R. Acad. Sci., Paris*, **266**, 1261 (1948).
3) E. L. Wagner and D. F. Hornig, *J. Chem. Phys.*, **17**, 105(1948).
4) E. L. Wagner and D. F. Hornig, *ibid.*, **18**, 296 (1950).
5) D. F. Hornig, *Discuss. Farad. Soc.*, **1950**, 115.
6) L. F. H. Bovey, *J. Chem. Phys.*, **18**, 1684 (1950).
7) J. P. Mathieu, R. M. Aguirre, and L. Couture-Mathieu, *C. R. Acad. Sci., Paris*, **232**, 318 (1951).
8) J. P. Mathieu and L. Couture-Mathieu, *ibid.*, **233**, 1595(1951).
9) L. F. H. Bovey, *J. Opt. Soc. Am.*, **41**, 836 (1951).
10) T. C. Waddington, *J. Chem. Soc.*, **1958**, 4340.
11) C. W. Garland and N. E. Schumaker, *J. Phys. Chem. Solids*, **28**, 799 (1966).
12) C. H. Perry and R. P. Lowndes, *J. Chem. Phys.*, **51**, 3648(1969).
13) L. Rimai, J. Cole, and J. Parsons, "Proceedings of the Conference on Light Scattering Spectra of Solids," G. B. Wright Ed., Springer-Verlag, New York, (1969).
14) J. J. Rush, T. I. Taylor, and W. W. Havens, Jr., *Phys. Rev. Lett.*, **5**, 507 (1960).
15) K. Mikke and A. Kroh, Proceedings of the Symposium on Inelastic Scattering of Neutrons in Solids and Liquids (Chalk River, Canada, 10—14 September 1962); Inelastic Scattering of Neutrons in Solids and Liquids II, p. 237 (1963) (International Atomic Energy Agency, Vienna, 1963).
16) P. S. Leung, T. I. Taylor, and W. W. Havens, Jr., *J. Chem. Phys.*, **48**, 4912 (1968).
17) H. G. Smith, J. G. Taylor, and W. Reichard, *Phys. Rev.*, 181, 1218 (1969).
18) G. H. Goldschmidt and D. G. Hurst, *ibid.*, **83**, 88 (1951).
19) S. Kuwabara, *J. Phys. Soc. Jap.*, **14**, 1205 (1959).
20) G. H. Goldschmidt and D. G. Hurst, *Phys. Rev.*, **86**, 797(1952).
21) H. A. Levy and S. W. Petersen, *ibid.*, **86**, 766 (1952).

TABLE 1. INTERACTIONS TAKEN INTO ACCOUNT IN THE POTENTIAL AND INTERNAL COORDINATES (R_i)

Cell	Atom (ion)	Cell	Atom (ion)		bond length (Å)
R_1 (i,j,k)	1	(i,j,k)	2	N-H	1.032
R_2 (i,j,k)	1	(i,j,k)	3	N-H	
R_3 (i,j,k)	1	(i,j,k)	4	N-H	
R_4 (i,j,k)	1	(i,j,k)	5	N-H	
R_5 (i,j,k)	1	(i,j,k)	6	$N^+ \cdot Cl^-$	3.308
R_6 (i,j,k)	1	$(i+1,j+1,k)$	6	$N^+ \cdot Cl^-$	
R_7 (i,j,k)	1	$(i,j+1,k-1)$	6	$N^+ \cdot Cl^-$	
R_8 (i,j,k)	1	$(i+1,j,k-1)$	6	$N^+ \cdot Cl^-$	
R_9 (i,j,k)	1	$(i,j,k-1)$	6	$N^+ \cdot Cl^-$	
R_{10} (i,j,k)	1	$(i+1,j+1,k-1)$	6	$N^+ \cdot Cl^-$	
R_{11} (i,j,k)	1	$(i,j+1,k)$	6	$N^+ \cdot Cl^-$	
R_{12} (i,j,k)	1	$(i+1,j,k)$	6	$N^+ \cdot Cl^-$	
R_{13} (i,j,k)	2	(i,j,k)	6	$H \cdot Cl^-$	2.276
R_{14} (i,j,k)	3	$(i+1,j+1,k)$	6	$H \cdot Cl^-$	
R_{15} (i,j,k)	4	$(i,j+1,k-1)$	6	$H \cdot Cl^-$	
R_{16} (i,j,k)	5	$(i+1,j,k-1)$	6	$H \cdot Cl^-$	
R_{17} (i,j,k)	6	$(i+1,j,k)$	6	$Cl^- \cdot Cl^-$	3.820
R_{18} (i,j,k)	6	$(i,j+1,k)$	6	$Cl^- \cdot Cl^-$	
R_{19} (i,j,k)	6	$(i,j,k-1)$	6	$Cl^- \cdot Cl^-$	
R_{20} (i,j,k)	6	$(i+1,j+1,k)$	6	$Cl^- \cdot Cl^-$	
R_{21} $(i,j+1,k)$	6	$(i+1,j,k)$	6	$Cl^- \cdot Cl^-$	
R_{22} $(i,j,k-1)$	6	$(i,j+1,k)$	6	$Cl^- \cdot Cl^-$	
R_{23} (i,j,k)	6	$(i,j+1,k-1)$	6	$Cl^- \cdot Cl^-$	
R_{24} $(i,j,k-1)$	6	$(i+1,j,k)$	6	$Cl^- \cdot Cl^-$	
R_{25} $(i+1,j,k-1)$	6	(i,j,k)	6	$Cl^- \cdot Cl^-$	
R_{26} (i,j,k)	1	$(i+1,j,k)$	1	$N^+ \cdot N^+$	3.820
R_{27} (i,j,k)	1	$(i,j+1,k)$	1	$N^+ \cdot N^+$	
R_{28} (i,j,k)	1	$(i,j,k+1)$	1	$N^+ \cdot N^+$	
R_{29} (i,j,k)	1	$(i+1,j+1,k)$	1	$N^+ \cdot N^+$	
R_{30} $(i,j+1,k)$	1	$(i+1,j,k)$	1	$N^+ \cdot N^+$	
R_{31} $(i,j,k-1)$	1	$(i,j,k+1)$	1	$N^+ \cdot N^+$	
R_{32} (i,j,k)	1	$(i,j+1,k-1)$	1	$N^+ \cdot N^+$	
R_{33} $(i,j,k-1)$	1	$(i+1,j,k)$	1	$N^+ \cdot N^+$	
R_{34} $(i+1,j,k-1)$	1	(i,j,k)	1	$N^+ \cdot N^+$	
R_{35} (i,j,k)	3	$(i+1,j,k)$	2	H·H	2.886
R_{36} (i,j,k)	3	$(i+1,j,k)$	4	H·H	
R_{37} (i,j,k)	5	$(i+1,j,k)$	2	H·H	
R_{38} (i,j,k)	5	$(i+1,i,k)$	4	H·H	
R_{39} (i,j,k)	3	$(i,j+1,k)$	2	H·H	
R_{40} (i,j,k)	3	$(i,j+1,k)$	5	H·H	
R_{41} (i,j,k)	4	$(i,j+1,k)$	2	H·H	
R_{42} (i,j,k)	4	$(i,j+1,k)$	5	H·H	
R_{43} (i,j,k)	2	$(i,j,k+1)$	4	H·H	
R_{44} (i,j,k)	2	$(i,j,k+1)$	5	H·H	
R_{45} (i,j,k)	3	$(i,j,k+1)$	4	H·H	
R_{46} (i,j,k)	3	$(i,j,k+1)$	5	H·H	
R_{47} (i,j,k)	5	$(i+1,j-1,k)$	4	H·H	3.717
R_{48} (i,j,k)	3	$(i+1,j+1,k)$	2	H·H	
R_{49} (i,j,k)	3	$(i,j+1,k+1)$	5	H·H	
R_{50} (i,j,k)	2	$(i,j-1,k+1)$	4	H·H	
R_{51} (i,j,k)	3	$(i+1,j,k+1)$	4	H·H	
R_{52} (i,j,k)	2	$(i-1,j,k+1)$	5	H·H	
R_{53} $\Delta\alpha_{213}$					
R_{54} $\Delta\alpha_{214}$					
R_{55} $\Delta\alpha_{215}$					
R_{56} $\Delta\alpha_{415}$					
R_{57} $\Delta\alpha_{314}$					
R_{58} $\Delta\alpha_{315}$					
R_{59} $\Delta\theta_1$					
R_{60} $\Delta\theta_2$					
R_{61} $\Delta\theta_3$					

R_1-R_{52} represent change of the corresponding atom(ion)-atom(ion) distances, respectively.

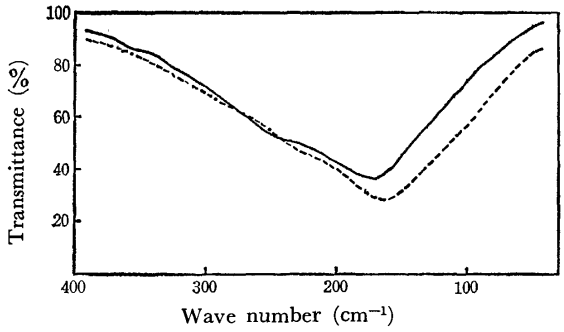

Fig. 2. Far-infrared spectra of ammonium chloride and ammonium chloride-d_4 in Nujol mulls.
Solid line: ammonium chloride, Dotted line: ammonium chloride-d_4.

solution. The deuterate was obtained by recrystallization of the ammonium chloride from its heavy water solution. Infrared spectra of Nujol mulls of the samples were measured in the region 4000—400 cm^{-1} with a Hitachi EPI-G3 spectrophotometer and in the region 400—30 cm^{-1} with a Hitachi FIS-3 Far-infrared spectrometer. The obtained spectra are shown in Figs. 1 and 2. The spectra in the region 4000—400 cm^{-1} are given in order to show the degree of deuteration by the relative intensities of N-H and N-D stretching bands.

Normal Coordinate Treatment

Normal coordinate treatments were carried out for the crystal structure of ammonium chloride at low temperature, which was confirmed by Goldschmidt and Hurst[18] (lattice parameter, a=3.820 Å; N-H=1.03 Å; space group, T_d^1; see Fig. 3) and for a crystal model[18] which might be related to the dominant structure in ammonium chloride crystal at room temperature (lattice parameter, a=7.73 Å; space group, O_h^5; see Fig. 4). Bravais lattice for the former structure is the cubic P lattice, to each lattice point of which a Bravais cell containing one NH_4Cl chemical unit belongs. That for the latter is a cubic F lattice, and the Bravais cell belonging to each lattice point contains two NH_4Cl

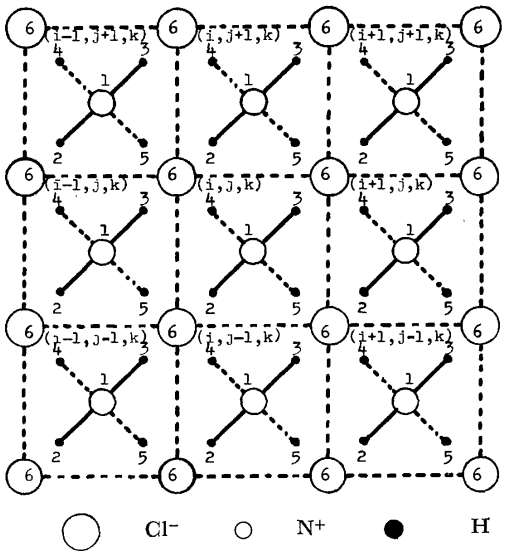

Fig. 3. A part of the structure of ammonium chloride and ammonium chloride-d_4 at low temperature (Cubic P lattice, number of chemical units per Bravais cell is one).

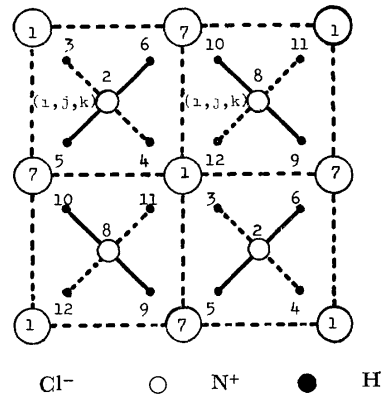

Fig. 4. A part of the unit lattice for a model of ammonium chloride and ammonium chloride-d_4 at room temperature.

chemical units as shown in Fig. 4. Cell repeating unit vectors are $(a_1+a_2)/2$, $(a_2+a_3)/2$, $(a_3+a_1)/2$, where a_1, a_2 and a_3 are the unit lattice vectors.

Calculation of optically acitve lattice vibrations was made according to the GF matrix method developed by Shimanouchi *et al.*[22] Optically active Cartesian and internal symmetry coordinate vectors, X_{op} and R^s_{op}, are expressed as follows:

$$X_{op} = \lim_{n_1,n_2,n_3\to\infty}(n_1n_2n_3)^{-1/2}\sum_{i=0}^{n_1}\sum_{j=0}^{n_2}\sum_{k=0}^{n_3}(X)^{i,j,k}_{\text{Bravais}}$$

$$R^s_{op} = \lim_{n_1,n_2,n_3\to\infty}(n_1n_2n_3)^{-1/2}\sum_{i=0}^{n_1}\sum_{j=0}^{n_2}\sum_{k=0}^{n_3}(R^s)^{i,j,k}_{\text{Bravais}}$$

Here, $(X)^{i,j,k}_{\text{Bravais}}$ and $(R^s)^{i,j,k}_{\text{Bravais}}$ represent, respectively, the Cartesian displacement coordinate vector and the internal symmetry coordinate vector, which belong to the Bravais cell (i,j,k). The internal coordinate vector belonging to the Bravais cell, (i,j,k), $(R)^{i,j,k}_{\text{Bravais}}$, and $(R^s)^{i,j,k}_{\text{Bravais}}$, are shown in Tables 1 and 2, respectively. In Table 1, R_1—R_{52}, R_{53}—R_{58}, R_{59}—R_{61} are coordinate of bond stretching, angle bending and NH_4^+ rotational motions, respectively. R^s_{op} and X_{op} are related by the optically active B matrix, B^s_{op} by

$$R^s_{op} = B^s_{op}X_{op}$$

Optically active F matrix, F_{op}, is expressed by F matrix associated with the Bravais cell, (i,j,k), F_{000}, and interaction matrices between the cell and the other cells surrounding it, F_{100},F_{010},F_{001}···

$$F_{op} = F_{000} + F_{100} + \tilde{F}_{100} + F_{010} + \tilde{F}_{010} + F_{001} + \tilde{F}_{001} + \cdots$$

Using X_{op}, R^s_{op} and F_{op}, optically acitve lattice vibrational frequencies were calculated by the equation

$$|M^{-1}F_{xs} - \lambda E| = 0, \quad F_{xs} = \tilde{B}^s_{op}F_{op}B^s_{op}$$

where M^{-1} is a matrix whose diagonal elements are constructed from the inverse of masses of atoms or ions in a Bravais cell.

The following potential was assumed for a Bravais cell.

$$V = V_{NH_4^+} + (1/2)\sum K(N^+\cdot Cl^-)(\Delta r_{N^+\cdot Cl^-})^2$$

22) T. Shimanouchi, M. Tsuboi, and T. Miyazawa, *J. Chem. Phys.*, **35**, 1597 (1961).

$$+ (1/2)\sum K(\mathrm{H\cdot Cl^-})(\Delta r_{\mathrm{H\cdot Cl^-}})^2$$
$$+ (1/2)\sum K_1(\mathrm{Cl^-\cdot Cl^-})(\Delta r_{\mathrm{Cl^-\cdot Cl^-}})_1^2$$
$$+ (1/2)\sum K_2(\mathrm{Cl^-\cdot Cl^-})(\Delta r_{\mathrm{Cl^-\cdot Cl^-}})_2^2$$
$$+ (1/2)\sum K_1(\mathrm{N^+\cdot N^+})(\Delta r_{\mathrm{N^+\cdot N^+}})_1^2$$
$$+ (1/2)\sum K_2(\mathrm{N^+\cdot N^+})(\Delta r_{\mathrm{N^+\cdot N^+}})_2^2$$
$$+ (1/2)\sum\sum_i K_i(\mathrm{H\cdot H})(\Delta r_{(\mathrm{H\cdot H})_i})^2$$
$$+ (1/2)\sum_{i=1}^{3} K_\theta \Delta(\theta_i)^2$$

where $V_{NH_4^+}$ represents the Urey-Bradley force field[23] for NH_4^+ ion, and the summation was taken over all atom(or ion)-atom(or ion) pairs of the same kind.

Table 2. Internal symmetry coordinates

A_1
$$S_i = (\sum_{j=1}^{4} R_{4(i-1)+j})/2 \quad (i=1,2,3,4)$$
$$S_5 = (\sum_{j=53}^{58} R_j)/\sqrt{6}$$
$$S_6 = (\sum_{j=35}^{46} R_j)/2\sqrt{3}$$
$$S_7 = (\sum_{j=1}^{3} R_{17+2(j-1)})/\sqrt{3}$$

E
$$S_1 = (\sum_{j=1}^{2} 2R_{53+3(j-1)} - R_{54+3(j-1)} - R_{55+3(j-1)})/2\sqrt{3}$$
$$S_2 = (\sum_{j=1}^{2} R_{54+3(j-1)} - R_{55+3(j-1)})/2$$
$$S_3 = (2(\sum_{j=35}^{38} R_j) - (\sum_{j=39}^{42} R_j) - (\sum_{j=43}^{46} R_j))/2\sqrt{6}$$
$$S_4 = ((\sum_{j=39}^{42} R_j) - (\sum_{j=43}^{46} R_j))/2\sqrt{2}$$
$$S_5 = (R_{15+4i} - R_{16+4i} - R_{17+4i} - R_{18+4i})/2 \quad (i = 5,6,7)$$
$$S_8 = (2R_{47} - R_{49} - R_{51})/\sqrt{6}$$
$$S_9 = (R_{49} - R_{51})/\sqrt{2}$$

F_1
$$S_1 = (R_{35} - R_{38} - R_{39} + R_{42})/2$$
$$S_2 = (R_{36} - R_{37} + R_{44} - R_{45})/2$$
$$S_3 = (R_{40} - R_{41} + R_{43} - R_{46})/2$$
$$S_4 = R_{59}$$
$$S_5 = R_{60}$$
$$S_6 = R_{61}$$

F_2
$$S_{3i-2} = (3R_{4(i-1)+1} - R_{4(i-1)+2} + R_{4(i-1)+3} - R_{4(i-1)+4})/2\sqrt{3}$$
$$S_{3i-1} = (2R_{4(i-1)+2} - R_{4(i-1)+3} - R_{4(i-1)+4})/\sqrt{6}$$
$$S_{3i} = (R_{4(i-1)+3} - R_{4(i-1)+4})/\sqrt{2} \quad (i = 1,2,3,4)$$
$$S_i = R_{i+4} \quad (i = 13,14,15,22,23,24)$$
$$S_i = (R_{i+4} + R_{i+5})/\sqrt{2}$$
$$S_{i+1} = (R_{i+4} - R_{i+5})/\sqrt{2} \quad (i = 16,18,20,25,27,29)$$
$$S_{31} = (R_{35} - R_{38} + R_{39} - R_{42})/2$$
$$S_{32} = (R_{36} - R_{37} - R_{44} + R_{45})/2$$
$$S_{33} = (R_{40} - R_{41} - R_{43} + R_{46})/2$$
$$S_{34} = R_{48}$$
$$S_{35} = R_{50}$$
$$S_{36} = R_{52}$$
$$S_{37} = (2R_{53} - R_{54} - R_{55} - 2R_{56} + R_{57} + R_{58})/2\sqrt{3}$$
$$S_{38} = (R_{54} - R_{55} - R_{57} + R_{58})/2$$
$$S_{39} = (R_{53} + R_{54} + R_{55} - R_{56} - R_{57} - R_{58})/\sqrt{6}$$

23) T. Shimanouchi, *ibid.*, **17**, 245 (1949).

Computations were carried out at the Computer Center, the University of Tokyo, using programs BGLZ and LSMB set up in the Shimanouchi laboratory, Dept. of Chem., Faculty of Science, the University of Tokyo, and also a program made by one of the authors (K. F.).

Optically active lattice vibrations of low temperature structure were calculated for the set I force constants in Table 3. The $Cl^-\cdot Cl^-$ or $N^+\cdot N^+$ interaction potential change due to displacement Δr of a Cl^- or N^+ ion in the crystal along $Cl^-\cdot Cl^-$ or $N^+\cdot N^+$ line consists primarily of that between the ion and the nearest neighbor ions at both sides. As the interaction is electronic and proportional to r^{-1}, the potential change is expected to be proportional to $r^{-3}\cdot\Delta r^2$. Thus, $K_2(Cl^-\cdot Cl^-)$ and $K_2(N^+\cdot N^+)$ were calculated from $K_1(Cl^-\cdot Cl^-)$ and $K_1(N^+\cdot N^+)$, assuming that the $Cl^-\cdot Cl^-$ and the $N^+\cdot N^+$ force constants are proportional to r^{-3}. Using the observed frequencies in Table 4, the set of force constants were revised to set II force constants by the method of least squares.[24] Of the force constants, $K_1(Cl^-\cdot Cl^-)$, $K_2(Cl^-\cdot Cl^-)$, $K_1(N^+\cdot N^+)$ and $K_2(N^+\cdot N^+)$ were not adjusted since the optically active lattice vibrations do not change by them. By use of the set II force constants except for $K_i(H\cdot H)$ and K_θ, optically active lattice vibrations of the model for the structure of ammonium chloride at room temperature were calculated. The atom(or ion)-atom(or ion) interactions taken into account in the calculation are shown in Table 5. $K_i(H\cdot H)$ force constants for H.H length greater than 3 Å were assumed to be zero and that for 2.67$_6$ Å was set to 0.008 on the basis of the $K_i(H\cdot H)$ values in the set II and the H·H force constant values.[25] It was found by obtaining

Table 3. Force constants (in mdyn/Å)

	Set I	Set II	
K(N-H)	5.260[a]	5.193	
H(H-N-H)	0.533[a]	0.502	
F(H-N-H)	0.057[a]	0.085	
$\kappa(NH_4^+)$	−0.057[a]	−0.070	mdyn Å
$K(N^+\cdot Cl^-)$	0.067[b]	0.068	
$K(H\cdot Cl^-)$	0.067[c]	0.049	
$K_1(Cl^-\cdot Cl^-)$	0.068[c]	0.068	
$K_2(Cl^-\cdot Cl^-)$	0.024[d]	0.024	
$K_1(N^+\cdot N^+)$	0.044[e]	0.044	
$K_2(N^+\cdot N^+)$	0.016[d]	0.016	
$K_1(H\cdot H)$	0.005[f]	0.005	
$K_2(H\cdot H)$	0.000[f]	0.000	
K_θ	0.013[d]	0.013	mdyn Å

a) Ref. 29. b) These were determined to fit the observed frequencies, fixing other force constants. c) Ref. 26. d) These force constants were determined from $K_1(Cl^-\cdot Cl^-)$ and $K_1(N^+\cdot N^+)$, assuming that they are proportional to r^{-3}, where r represents interatomic distance. e) Ref. 22. f) Ref. 25.

24) D. E. Mann, T. Shimanouchi, J. H. Meal, and L. Fano, *ibid.*, **27**, 43 (1957).
25) I. Harada and T. Shimanouchi, *ibid.*, **46**, 2708 (1967).
26) K. Fukushima and H. Kataiwa, This Bulletin, **43**, 690 (1970).

TABLE 4. CALCULATED AND OBSERVED FREQUENCIES AND DOMINANT POTENTIAL ENERGY DISTRIBUTION TERMS

		Species	$\nu_{obs.}$	$\nu_{calc.}$	δ	p. e. d.
	ν_1	A_1	3038[a]	3068	+1.0	s_1(99)
	ν_2	E	1720[a]	1724	+0.2	s_1, s_2(98)
	ν_3	F_1	390[b]	390	0.0	s_1, s_2, s_3(20); s_4, s_5, s_6(80)
NH_4Cl						
	ν_4		3126[c]	3138	+0.4	s_1, s_2, s_3(100)
	ν_5	F_2	1403[c]	1410	+0.5	s_{37}, s_{38}, s_{39}(100)
	ν_6		185[d]	187	+1.1	s_4, s_5, s_6(37); s_7, s_8, s_9(37) s_{10}, s_{11}, s_{12}(26)
	ν_1	A_1	2215[a]	2170	−2.0	s_1(99)
	ν_2	E	1225[a]	1220	−0.4	s_1, s_2(98)
	ν_3	F_1		276		s_1, s_2, s_3(20); s_4, s_5, s_6(80)
ND_4Cl						
	ν_4		2336[c]	2320	−0.7	s_1, s_2, s_3(98)
	ν_5	F_2	1067[c]	1057	−0.9	s_{37}, s_{38}, s_{39}(98)
	ν_6		177[d]	175	−1.1	s_4, s_5, s_6(37); s_7, s_8, s_9(37) s_{10}, s_{11}, s_{12}(26)

$\delta=100(\nu_{calc}-\nu_{obs})/\nu_{obs}$ a) Ref. 13. b) Ref. 9. c) Ref. 4. d) Ref. 12. p. e. d.: potential energy distributions (%)

TABLE 5. THE INTERACTIONS BETWEEN m-TH ATOM (OR ION) OF (i,j,k) CELL AND n-TH ATOM (OR ION) OF (i',j',k') CELL

m	(i',j',k')	n
2(N^+)	(i,j,k)	3(H), 4(H), 5(H), 6(H), 1(Cl^-), 7(Cl^-), 8(N^+)
3(H)		1(C^-)
1(Cl^-)		7(Cl^-)
6(H)		10(H), 12(H)
2(N^+)	$(i+1,j-1,k)$	1(Cl^-), 2(N^+)
4(H)		1(Cl^-), 3(H)
1(Cl^-)		1(Cl^-)
2(N^+)	$(i,j-1,k)$	2(N^+), 7(Cl^-)
1(Cl^-)		7(Cl^-)
7(Cl^-)		7(Cl^-)
4(H)		10(H), 11(H)
5(H)		6(H)
2(N^+)	$(i,j,k-1)$	7(Cl^-)
1(Cl^-)		7(Cl^-)
7(Cl^-)		7(Cl^-)
5(H)		11(H), 12(H)
2(N^+)	$(i+1,j,k-1)$	1(Cl^-)
6(H)		1(Cl^-)
1(Cl^-)		1(Cl^-)
2(N^+)	$(i+1,j-1,k-1)$	7(Cl^-), 1(Cl^-)
5(H)		1(Cl^-)
1(Cl^-)		1(Cl^-)
2(N^+)	$(i-1,j+1,k)$	8(N^+), 2(N^+)
3(H)		4(H), 9(H), 12(H)
2(N^+)	$(i,j+1,k)$	2(N^+)
6(H)		5(H)
2(N^+)	$(i-1,j,k+1)$	8(N^+), 2(N^+)
3(H)		9(H), 10(H)
5(H)	$(i-1,j,k)$	9(H), 11(H)
2(N^+)	$(i-1,j+1,k+1)$	2(N^+)
2(N^+)	$(i,j-1,k+1)$	2(N^+)
7(Cl^-)		7(Cl^-)
2(N^+)	$(i,j,k+1)$	2(N^+)

bond length (Å)
N–H 1.032, $N^+\cdot Cl^-$ 3.350, H·Cl^- 2.318, 1(Cl^-)·7(Cl^-) 3.868, 1(Cl^-)·1(Cl^-), 7(Cl^-)·7(Cl^-) 5.470, 2(N^+)·8(N^+) 3.868, 2(N^+)·2(N^+), 8(N^+)·8(N^+) 5.470, 6(H)·10(H), 4(H)·11(H), 3(H)·12(H), 5(H)·9(H), 3(H)·10(H), 5(H)·12(H) 2.676, 6(H)·12(H), 4(H)·10(H), 5(H)·11(H), 3(H)·9(H) 3.163, 4(H)·3(H), 5(H)·6(H) 3.785

Cell indices are expressed *on the basis of the basic vectors*, a_1, $(a_1+a_2)/2$, $(a_1+a_3)/2$, for convenience, and the other necessary atom(or ion)-atom(or ion) sets, which can be produced from the corresponding ones in this table by either or both of the following operations, are omitted: 1) inversion with respect to the center of 2(N^+)-8(N^+) line in (i,j,k) cell; 2) C_2 operation around any one of axes passing through both 2(N^+) in (i,j,k) cell and any of 8(N^+)'s.

calculated frequencies for various values of K_θ that only the frequencies of F_{1g} and F_{2u} vibrations (NH_4^+ rotational vibrations) change by K_θ. Therefore, K_θ value of 0.0063 mdyn. Å giving the calculated frequencies of F_{1g} vibrations fitting the observed frequencies, 345 cm^{-1}($NH_4^+Cl^-$) and 220 cm^{-1}($ND_4^+Cl^-$), was used. Calculated frequencies of low temperature structure for the set II force constants and the dominant terms of potential energy distributions, $(F_{op})_{ii}(l_{ij})^2/\lambda_j(l_{ij}$; i-th element of eigenvector for eigen value of λ_j) are shown in Table 4. The calculated frequencies of the model of room temperature phase are shown in Table 6.

Discussion

For the crystal structures of ammonium chloride and ammonium chloride-d_4 at low temperature, which belong to the space group T_d^1, the optically active lattice vibrations are classified into nine internal vibrational modes ($1A_1+1E+2F_2$) and six external modes ($1F_2$(translational vibrations)$+1F_1$(rotational vibrations)) by factor group analysis. Fundamental frequencies of these vibrations were selected (Table 4) on the basis of the assignments.[4,6,12,13] The F_1 vibration is both Raman and infrared inactive. The frequency value in the table is determined from combination bands by Bovey.[9] The frequency is considered to be reliable by the fact that it is in line with neutron scattering data.[14,16,17] We see from Table 4 that ν_1 is almost pure N-H(or N-D) stretching vibtations, and ν_2 and ν_5 are almost pure H-N-H(or D-N-D) bending vibrations. ν_6 vibrations of F_2 species (185 cm^{-1}, NH_4Cl; 177 cm^{-1}, ND_4Cl) are the translational lattice vibrations, in which NH_4^+ and Cl^- vibrate each other as shown in the large potential energy distribution values in Table 4, which are associated with the coordinates, s_4-s_{12}($N^+\cdot Cl^-$ stretching coordinates and $H\cdot Cl^-$ stretching coordinates). The assignment is also confirmed by the fact that shift of frequency, 185 cm^{-1}, to 177 cm^{-1} on deuteration corresponds well to the calculated shift, 187 cm^{-1} to 175 cm^{-1}. In the infrared and Raman inactive vibration ν_3, the potential energy is concentrated largely in the coordinates s_4,s_5,s_6(rotational motion coordinate of NH_4^+) and also in H·H stretching coordinates s_1,s_2,s_3. This suggests that the vibration may change its frequency on order-disorder transition. Actually, it has been found that the frequency of ν_3 vibration decreases during phase change caused by elevation of temperature.[14,16]

The set II force constants (Table 3) obtained by the method of least squares can explain the observed frequencies. The force constants except for K_i(H·H)'s and K_θ are considered to be applicable to calculations of the optically active lattice vibrations of the structure model in the room temperature phase, in which the atom(or ion)-atom(or ion) distances (Table 5) except for H·H distances are very close to those of the low temperature structure.

It has been concluded by laser Raman spectroscopic investigation[13] that among the Raman lines having frequency shifts 171 cm^{-1}, 345 cm^{-1} (NH_4Cl); 176 cm^{-1}, 220 cm^{-1} (ND_4Cl), those having frequency shifts 171 cm^{-1} and 176 cm^{-1} are due to the translational lattice vibrations corresponding to the optically active lattice vibrations (185 cm^{-1}, NH_4Cl; 177 cm^{-1}, ND_4Cl) of the low temperature phase. The Raman line with frequency shift of 345 cm^{-1} changes the shift to 220 cm^{-1} on deuteration.[13] This is clearly assigned to NH_4^+ rotational vibration. On the other hand, the infrared bands of the translational vibrations have been observed at 172 cm^{-1} (NH_4Cl) and at 166 cm^{-1} (ND_4Cl).[12] However, the bands are very broad and asymmetrical. Each band might be composed of two or more overlapped bands. Precise measurement of the purified sample of ammonium chloride in the present investigation revealed that there are at least two bands at about 240 cm^{-1} and at 170 cm^{-1}. The corresponding bands of ammonium chloride-d_4 are at about 230 cm^{-1} and at 160 cm^{-1} (Fig. 2). The results

Table 6. Comparison of the observed vibrational frequencies of NH_4Cl and ND_4Cl at room temperature with the calculated frequencies for a model having O_h^5 symmetry

Observed frequencies				Calculated frequencies		Species
NH_4Cl		ND_4Cl		NH_4Cl	ND_4Cl	
IR	R	IR	R			
	3040[a]		2215[a]	3070	2172	A_{1g}
				1616	1143	E_g
	3165[a]		2350[a]	3139	2320	F_{2g}
	1400[a]		1065[a]	1358	1017	F_{2g}
	345[a]		220[a]	351	248	F_{1g}
	171[a]			171	155	F_{2g}
				3066	2169	A_{2u}
				1607	1137	E_u
3138[b]		2350[b]		3141	2322	F_{1u}
1403[b]		1066[b]		1359	1022	F_{1u}
				388	274	F_{2u}
240[c]		230[c]		255	237	F_{1u}
170[c]	171[a]	160[c]	176[a]	166	161	F_{1u}

IR: infrared absorption R: Raman scattering, a) Ref. 13. b) Ref. 4. c) Present investigation.

conclude that there are one Raman line due to translational lattice mode and two infrared bands of the corresponding modes in the Raman and infrared spectra of both ammonium chloride and ammonium chloride-d_4 at room temperature.

For the structure of ammonium chloride at room temperature three models have been proposed: (a) the free rotation model by Pauling[27] (b) the disordered model by Frenkel[28] (c) a model having the space group symmetry of O_h^5.[18,20] The possibility of (a) has been denied on experimental results. Goldschmidt and Hurst examined the validity of the models, and denied either of the models,[18] but revised their conclusion,[20] and (b) and (c) still remain as possible models. Levy and Petersen have deduced a disordered structure from their experimental results.[21] In (c), each NH_4^+ is either of two locations corresponding to its potential minima, and the nearest neighbor NH_4^+ ions surrounding one NH_4^+ are all in the same structural relation with respect to the NH_4^+. It is likely that the structural units of the model might exist as the dominant structure in (b) at higher temperature. 33 optically active lattice vibrations of (c) are classified into one A_{1g}, one A_{2u}, one E_g, one E_u, one F_{1g}, four F_{1u}, three F_{2g} and one vibrations. Among these, there are translational vibrations $(2F_{1u}+1F_{2g})$, rotational vibrations $(1F_{1g}+1F_{2u})$ and internal vibrations $(1A_{1g}+1A_{2u}+1E_g+1E_u+2F_{1u}+2F_{2g})$. The translational vibrations of F_{1u} species are infrared active and the translational vibration of F_{2g} species is Raman active. If fraction of these structural units becomes dominant in the disordered crystal, at least two infrared bands and one Raman line are expected to appear for translational vibrations. In the observed spectra, two bands which can be assigned to translational vibrations appear at 240 cm^{-1} and 170 cm^{-1} in the case of ammonium chloride, and two corresponding bands appear at 230 cm^{-1} and 160 cm^{-1} for ammonium chloride-d_4. In the Raman spectra observed by Rimai *et al.*[13] one Raman line having frequency shift of 171 cm^{-1} appears and has been assigned to a translational vibration. The rotational vibrations of NH_4^+ are both Raman and infrared inactive for the model itself. However, the corresponding vibrations of the structure in the disordered crystal, in which fraction of the structural units of the model is large, may become both Raman and infrared active because of the absence of O_h^5 symmetry in the crystal as a whole. In this case, one infrared band and one Raman line due to rotational lattice vibrations are expected to appear. Rimai *et al.* observed a Raman line having frequency shift of 345 cm^{-1}. This is reduced to 220 cm^{-1} for ammonium chloride-d_4.[13] In the infrared spectra of ammonium chloride (Fig. 2), a very weak band appears at about 360 cm^{-1} which shifts to a lower frequency on deuteration.

The calculated frequencies of the vibrations 255 cm^{-1}, 166 cm^{-1} (NH_4Cl), 237 cm^{-1}, 161 cm^{-1} (ND_4Cl) (infrared active translational vibrations) correspond to the observed frequencies of the above mentioned infrared bands (Table 6). The frequency shift expected from calculation on deuteration also corresponds to the observed shift. The calculated frequency of F_{2g} translational vibration of the model also corresponds to the observed Raman shift frequency of 171 cm^{-1} (Table 6). The results suggest that in the disordered structure of ammonium chloride in the room temperature phase, its dominant structure consists of the model units of (c).

27) L. Pauling, *Phys. Rev.*, **36**, 430 (1930).
28) J. Frenkel, *Acta Physicochimica*, **3**, 23 (1935).
29) I. Nakagawa and S. Mizushima, This Bulletin, **28**, 589 (1955).

Cotton Effect Induced in Optically Inactive Molecules and Molecular Complexes by Optically Active Environment. I. Pyrene, TCNNQ, and Their Molecular Complex in Acetylcellulose Film

Yasumasa J. I'HAYA and Toru YUNOKI*

Department of Materials Science, The University of Electro-Communications, Chofu-shi, Tokyo

(Received April 6, 1972)

Ultraviolet absorption spectra, induced optical rotatory dispersion and circular dichroism of pyrene, TCNNQ, and their molecular complex were measured in acetylcellulose film and solution. The Cotton effect corresponding to each absorption maximum of these systems appeared. A perturbation of excited states of these molecules and their complex due to an asymmetric environment of acetylcellulose might be of paramount importance in producing a non-zero rotational strength in the corresponding molecular absorption region. The second charge-transfer band was clearly detected in the differential optical rotatory dispersion spectrum of the TCNNQ-pyrene molecular complex embedded in an acetylcellulose film. The method was shown to be promising in detecting very weak and closely overlapped transitions in various molecules.

Several works have appeared demonstrating the Cotton effect induced in various optically inactive molecules by optically active solvents.[1-5] Racemic or symmetric metal complexes were found to exhibit pronounced circlular dichroism (CD) sepctra in the region of their *d-d* absorptions when they were dissolved in optically active alcohols, usually diols.[1,2] In similar solvents, ketones, both aliphatic and aromatic, were also investigated in detail and confirmed to have a single (sometimes a double or more) CD spectrum induced around their $n\rightarrow\pi^*$ transition region.[3-5]

The precise mechanism of the phenomenon is still unkown but certain inferences have been made. One is that CD may be induced by a dissymmetric potential due to a solvent. Originally, hydrogen bonding was supposed to be the main origin,[1-3] but later it was found that such associative forces including hydrogen bonding are not a prerequisite since induced CD is observed also in the $n\rightarrow\pi^*$ absorption region of some nitrite or nitrate dissolved in optically active solvents.[4,5] The other explanation was that molecules like ketones are probably solvated into some dissymmetric configurations making themselves optically active.[3]

In this paper, we show that aromatic hydrocarbons in acetylcellulose film and solution also exhibit induced Cotton effect in their $\pi\rightarrow\pi^*$ absorption region. To the best of our knowledge no work has been reported on the induced optical activity for $\pi\rightarrow\pi^*$ transitions of aromatic molecules. Furthermore, we show that similar effects can be observed for a donor-acceptor type molecular complex in their charge-transfer absorption region.

Experimental

Pyrene, commercial reagent grade, was purified by recrystallization and sublimation. TCNNQ (11,11,12,12-tetracyano-1,4-naphthaquinodimethane) was synthesized by the method reported by Chantterjee[6] and purified by repeated recrystallization from methanol and methylenechloride, followed by vacuum sublimation. The pyrene-TCNNQ molecular complex was prepared from the purified pyrene and TCNNQ by simultaneous sublimation onto a heated glass plate.

The materials were first added to an acetone solution of acetylcellulose of commercial grade used as a matrix without further purification. The viscous solution was then drawn onto a fused quartz plate and baked in an oven to remove actone. Films approximately 5—15 μ in thickness with excellent transparency were obtained. The sample concentration in a film state was estimated from the measured density of acetylcellulose and was held in the range 10^{-2}–10^{-3} M. The film thickness was roughly estimated from birefringence and retardation using a polarizing microscope.

A Jasco ORD/UV/CD-5 spectrophotometer was used for the measurement of electronic absorption, ORD, and CD spectra of the samples. In each measurement, the ORD datum was calibrated with reference to the base line of the pure acetylcellulose film whose thickness was identical with that of the sample film. This was because acetylcellulose itself has a large negative rotatory dispersion. Similar measurements were carried out for the samples dissolved in an acetone solution of acetylcellulose.

Results and Discussion

The ultraviolet absorption (UV), ORD, and CD spectra of pyrene in an acetylcellylose film are shown in Fig. 1. The sample film used was 5μ in thickness and estimated to contain 5.3×10^{-2} M pyrene. The scales of the ordinate are the optical density(a vertical bar shown in the figure), the angle of rotation in degree (ϕ) and the circular dichroic optical density (ΔD), respectively, for the UV, ORD, and CD spectra. These quantities were not converted into the corresponding molecular characteristics, *i. e.*, molecular extinction coefficient, molecular rotation, and molecular ellipticity, since the concentration and thickness of each sample film could not be determined accurately.

The over-all UV spectrum shown in Fig. 1 is displaced to the red approximately by 300 cm^{-1}, compared to that observed in an ethanol solution. This suggests that the pyrene molecule embedded in an acetylcellulose film is in the same and/or the like surroundings as that in solution. Corresponding to each absorption maximum, namely to each vibrational

* Present address: ULVAC Corporation, Chigasaki, Kanagawa.

1) S. F. Mason and B. J. Norman, *Chem. Commun.*, **1965**, 335.
2) B. Bosnich, *J. Amer. Chem. Soc.*, **88**. 2606 (1966).
3) B. Bosnich, *ibid.*, **89**, 6143 (1967).
4) E. Axelrod, G. Barth, and E. Bunnenberg, *Tetrahedron Lett.*, **1969**, 5031.
5) L. D. Hayward and R. N. Totty, *Can. J. Chem.*, **49**, 624 (1971).
6) S. Chatterjee, *J. Chem. Soc., B*, **1967**, 1170.

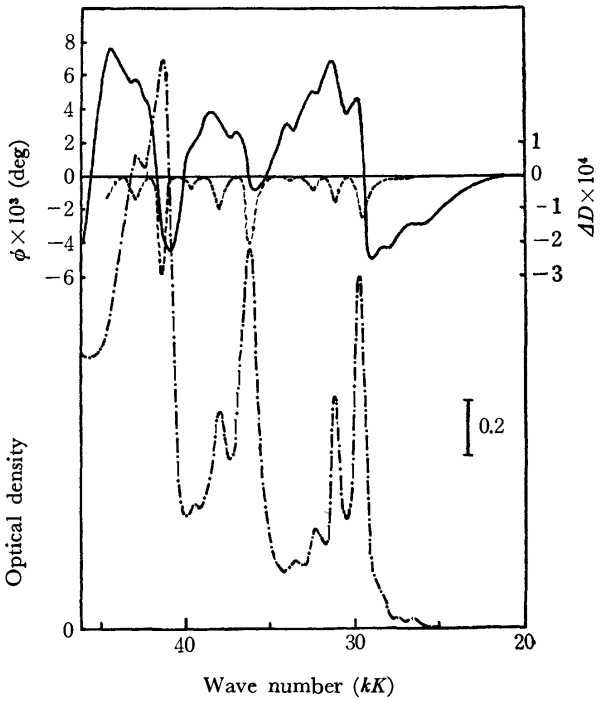

Fig. 1. UV (—·—·), ORD (——), and CD (·····) spectra of pyrene in acetylcellulose film. Film thickness: 5 μ; concentration of pyrene: 5.3×10^{-2} M. A vertical bar indicates the scale of optical density.

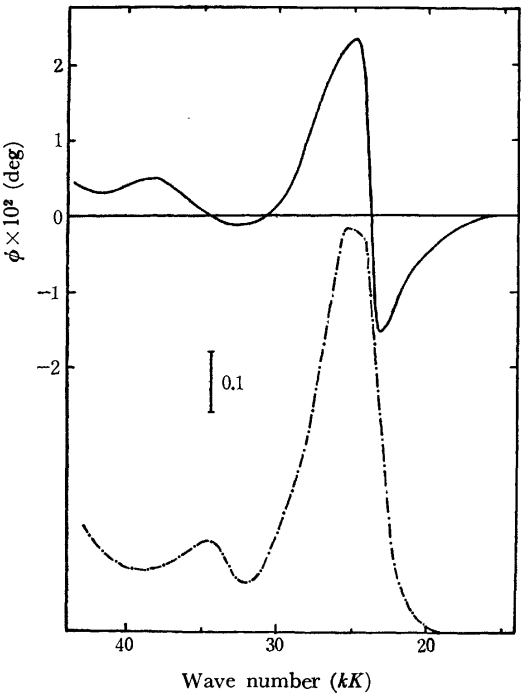

Fig. 2. UV (—·—·) and ORD (——) spectra of TCNNQ in acetylcellulose film. Film thickness: 14μ; concentration of TCNNQ: 1.5×10^{-2} M. A vertical bar indicates the scale of optical density.

spectrum of the ^1L_b, ^1L_a, ^1B_b, and ^1B_a bands of pyrene, a negative CD Cotton effect appears, the circular dichroic optical density of each minimum being roughly proportional to the intensity of the corresponding vibrational absorption maximum.

We have confirmed that the experimental ORD spectrum, though appearing somewhat complicated, can be well reproduced from the experimental CD spectrum, or *vice versa*, by the use of the Kronig-Kramers transform.[7] Only exception for this is the frequency region 26—29 kK where no CD spectral detail was detected as seen in Fig. 1. However, if more concentrated film of pyrene could be obtained, the respective vibrational transitions in this spectral region would show single negative CD absorptions.[8]

Fig. 2 shows the UV and ORD spectra of TCNNQ embedded in the acetylcellulose film of 14 μ thickness. The sample film contains approximatley 1.5×10^{-2} M TCNNQ. The UV absorption spectrum in this frequency region is in line with that observed in methylenechloride solution.[9] We have shown that the 25.3 kK absorption band corresponds to the lowest $\pi \rightarrow \pi^*$ B_2 transition polarized along the molecular longer axis (axis joining the carbon atoms of the 1- and 4-positions) and the weak 34.7 kK band to the next to the lowest $\pi \rightarrow \pi^*$ A_1 transition polarized along the molecular short axis.[9] As can be seen in Fig. 2, the respective $\pi \rightarrow \pi^*$ transitions show a sinlge negative Cotton effect, its rotational strength being roughly proportional to the corresponding dipole strength. A negative CD spectrum for each transition, which was originally expected to appear, was not detected under the present experimental conditions due to the low TCNNQ concentration. When the concentration of TCNNQ was increased, an induced CD spectrum, not a single negative but a double, was observed corresponding to each transition. It is thus found that the shape and intensity of the induced Cotton effect is markedly dependent on concentration. The situation is quite similar to that produced, for example, by nucleic acid-dye interactions in solution.[10,11] A monomer-dimer equilibrium of TCNNQ in sample films seems to play an important part.

The UV and ORD spectra of the pyrene-TCNNQ molecular complex in an acetylcellulose film are shown in Fig. 3. The thickness of the film was 10μ. In the lower frequency region beyond the strong 25.3 kK band of TCNNQ, the UV spectrum has one weak and broad band whose maximum is located at 15.3 kK and can be assigned to a charge-transfer band.[12] The ORD spectrum demonstrates the existence of some other bands at around 20 kK.

If we subtract the component ORD spectra of pyerne and TCNNQ from the ORD spectrum of the pyrene-TCNNQ complex, we obtain the plot in Fig. 4 (*differential* ORD spectrum), in which there remain two negative and one strong positive Cotton effect. This suggests that the first charge-transfer band is located at 15.5 kK, the second at around 23 kK, and the other strong band whose maximum is approximately at 27 kK is ascribed to an interaction between the component molecules.

7) W. Moffitt and A. Moscowitz, *J. Chem. Phys.*, **30**, 648 (1959).
8) This is shown to be the case in the succeeding paper.
9) N. Suzuki and Y. J. I'Haya, *Tetrahedron*, **26**, 5379 (1970).
10) Y. J. I'Haya and T. Nakamura, This Bulletin, **44**, 951 (1971).
11) Y. J. I'Haya, T. Nakamura, Y. Yagi, T. Sano, and H. Ito, *Intern. J. Quantum. Chem.*, Symposium **5**, 361 (1971).
12) Y. J. I'Haya, T. Yunoki, and N. Suzuki, This Bulletin, **43**, 3636 (1970).

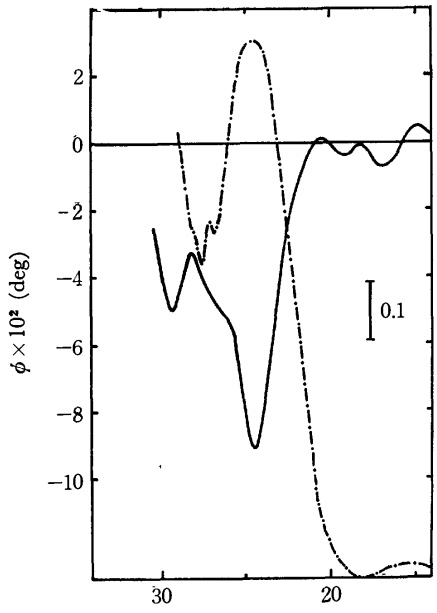

Fig. 3. UV (—·—·) and ORD spectra of the TCNNQ-pyrene molecular complex in acetylcellulose film. Film thickness: 10μ. A vertical bar indicates the scale of optical density.

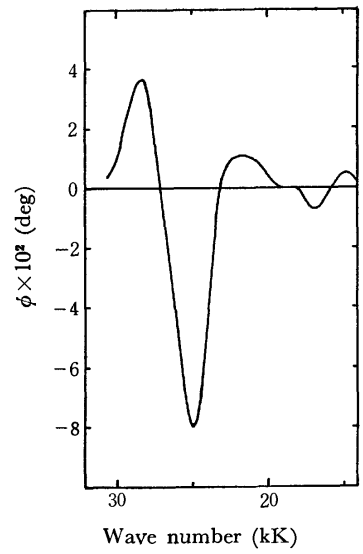

Fig. 4. The differential ORD curve for the TCNNQ-pyrene molecular complex.

According to our recent work on the polarized absorption spectrum of a pyrene-TCNNQ molecular complex crystal, the first charge-transfer band is found at 14.6 kK and the second charge-transfer band at 21.9 kK at room temperature.[13] The agreement is thus fairly good as to the location of the two charge-transfer bands, considering possible band shifts in solution and crystal. Though the 27 kK band can be seen as a tiny peak in Fig. 3, its origin is hard to guess. Even supposing that the peak is directly connected with the higher frequency side large Cotton component (negative and the absorption center is 27 kK) of the differential ORD spectrum (Fig. 4) and that this is induced from an inter-molecular interaction, it is inexplicable why such a large Cotton component is revealed.

The ORD and CD spectra of pyrene measured in an acetone solution of acetylcellulose were almost exactly the same as those in film, though whole spectral features were extremely obscure. It was confirmed that such optical activity is not induced for pyrene embedded in films of optically inactive polymers such as polyethylene and polystyrene. The situation is the same for the ORD spectra of TCNNQ and of the pyrene-TCNNQ molecular complex. These facts suggest that the induced optical activity is acribed *not* to distortion of molecular frames of the sample molecule and/or arrangement of the molecule in a crystalline state, but to dissymmetric potentials exerted by an optically active matrix.

Besides the fact that not only the intensity but also the shape of these induced ORD and CD spectra are strongly dependent on concentration, all their features remind us of the nucleic acid-dye interactions in solution.[10,11] If the induced Cotton effect in both cases is a general phenomenon caused by the same origin, the following interpretation might be right. A perturbation of molecular excited states (and possibly a ground state) due to an asymmetric environment of a matrix material may be of paramount imoprtance in producing non-zero matrix elements of electric and magnetic transition dipole moments for the molecule. The non-zero matrix elements yield a non-zero rotational strength at the molecular vibrational absorption region. Such an interaction more or less occurs whenever dissymmetric potentials exist, regardless of molecular species and molecular arrangement in matrix materials.[14] However, such problems as why the signs of all the CD bands of pyrene are negative, or why there is a sign reversal in the CD spectrum of TCNNQ, cannot be understood without consideration of the relative orientation of interacting units.[10]

The advantage of the present method is that many absorption bands in large molecules, even very weak and/or closely overlapped vibrational bands unresolved by the usual solution spectroscopy, may be observed in the corresponding induced CD and ORD spectra. In particular, very weak charge-transfer bands in donor-acceptor type charge-transfer complexes are detected with high probability and accuracy. A good example is the second charge-transfer band of the TCNNQ-pyrene molecular complex mentioned above, which was observed with difficulty in the single crystalline state of the complex.[12,13] The present method is thus considered superior to the usual microspectrophotometry, the technique for which is troublesome and a clear-cut spectrum rarely obtained.

The present work was supported in part by a grant from the Ministry of Education.

13) Y. J. I'Haya, T. Yunoki, and N. Suzuki, *ibid.*, **45**, 1004 (1972).

14) A rough estimate of molecular rotation of pyrene embedded in an acetylcellulose film gives an roder of 10^4 deg·mol.$^{-1}$ which is the same order of magnitude as met in the system of nucleic acid and dyes.

Activity Coefficients for the System Glycylglycine–Urea–Water

Hatsuho UEDAIRA

Research Institute for Polymeres and Textiles, Sawatari 4, Kanagawa-ku, Yokohama

(Received November 22, 1971)

Activity coefficients for the ternary system glycylglycine–urea–water were measured by the isopiestic vapor pressure method at 25°C. The activity coefficients of glycylglycine were lowered by urea. The lowering increased with increasing concentration of urea and with decreasing concentration of the amino acid. It was dependent on amino acid concentration to a greater extent than in the system α-amino-*n*-butyric acid–urea–water. The activity coefficients of urea were also decreased by glycylglycine. The free energy of the transfer of glycylglycine from water to urea solutions in various concentrations was calculated. The values obtained were combined with enthalpy data to yield −3.9 e. u. as the entropy value for the transfer from water to 6 M urea solution. Results have been interpreted to support the existence of interaction between urea and glycylglycine.

The interaction of urea on amino acids or oligopeptides in aqueous solutions has been investigated for the purpose of elucidating the denaturing action of urea on globular protein.

The solubility of amino acids and peptides in water and aqueous urea solutions was measured by Whitney and Tanford,[1] and Nozaki and Tanford.[2] They showed that aqueous urea solutions are able to accomodate nonpolar amino acid side chains better than water and that urea also interacts favorably with peptide groups, so that urea stabilizes both nonpolar groups and peptide groups.

Robinson and Jencks[3] examined the effect of a series of denaturing agents on the solubility of acetyltetraglycine ethyl ester and three carbobenzoxyglycine derivatives. They suggested that a nonhydrophobic effect of urea makes a major contribution to its denaturing action on some proteins.

Heat of transfer of amino acids from water to 6 M urea solution was measured by Kresheck and Benjamin.[4] It was shown that the ordering of water molecules around a solute molecule is increased due to the presence of the nonpolar part of the solute molecules and that part of this ordering is removed by urea. It was also shown that there is evidence for the existence of specific interactions between urea and polar parts of the solute molecules including the peptide bond.

The change in interaction as a continuous function of urea and amino acid concentrations can be obtained from the activity coefficients measured by the isopiestic vapor pressure method. Cussler[5] measured activity coefficients for the system α-amino-*n*-butyric acid–urea–water by the isopiestic method. In this system, the activity coefficient of the amino acid decreased with increasing urea concentration and increased with amino acid concentration.

The activity coefficients for the system glycylglycine—urea—water were measured by the isopiestic method to examine their dependence on concentrations of both amino acid and urea. Hydrophobic interaction need not be taken into consideration, as the peptide has no hydrophobic side chain.

Experimental

Materials. Glycylglycine (G. R.) was decolorized and recrystallized twice from a water-ethanol solution. Urea (G. R.) was recrystallized twice from water, without being heated above 60°C. The peptide and urea were dried *in vacuo* over phosphorus pentoxide at room temperature. Potassium chloride of analytical grade (Merck Co.) was not purified further and was dried in vacuo over phosphorus pentoxide at 110°C. Solutions were prepared with deionized water freed of air by boiling.

Measurements and calculation of the activity coefficients for the ternary solutions. Osmotic and activity coefficients were determined with an apparatus[6] similar to that used by Robinson and Stokes.[7] Four or five ternary peptide–urea solutions with varying compositions were put in silver dishes. Reference potassium cholride solutions were present in triplicate or quadruplicate. The dishes were placed on a flat copper block in a glass vacuum desiccator set in a thermostat bath at 25°C and controlled within 0.01°C. All the solutions were prepared afresh for each measurement. The intial concentrations in the solutions were adjusted to be sufficiently close to their equilibrium concentrations by the method reported previously.[8] The time required for attainment of equilibrium was 4—7 days. Equilibrium concentration was measured by weighing, all weights being corrected to those in vacuum.

An experimental quantity Δ is defined[7] by

$$\Delta = 2m_R\phi_R - m_1\phi_1 - m_2\phi_2 \quad (1)$$

where m_1 and m_2 are the molalities of glycylglycine (solute 1) and urea (solute 2), respectively, in aqueous ternary solutions. ϕ_1 and ϕ_2 are the osmotic coefficients of binary aqueous glycylglycine and urea solutions at a molality of m_1 and m_2, respectively. m_R and ϕ_R are the molality and osmotic coefficient, respectively, of reference potassium chloride solution which is in vapor pressure equilibrium with a ternary solution containing glycylglycine and urea at molalities m_1 and m_2.

The value of Δ is thus obtained experimentally from the concentrations m_R, m_1, and m_2, provided that the osmotic coefficients of reference solution and binary solutions of glycylglycine and urea are known.

The value of Δ/m_1m_2 is given by the equation

$$\Delta/m_1m_2 = A + Bm_1 + Cm_2 + Dm_1^2 + Em_1m_2 + Fm_1m_2^2 + Gm_1^3 + Hm_1^2m_2 + Im_1m_2^2 + Jm_2^3 \quad (2)$$

1) P. L. Whitney and C. Tanford, *J. Biol. Chem.*, **237**, PC1735 (1962).
2) Y. Nozaki and C. Tanford, *ibid.*, **238**, 4074 (1963).
3) D. R. Robinson and W. P. Jencks, *J. Amer. Chem. Soc.*, **87**, 2462 (1965).
4) G. C. Kresheck and L. Benjamin, *J. Phys. Chem.*, **68**, 2476 (1964).
5) E. L. Cussler, Jr., *ibid.*, **71**, 901 (1967).
6) H. Uedaira and H. Uedaira, This Bulletin, **42**, 2137 (1969).
7) R. A. Robinson and R. H. Stokes, *J. Amer. Chem. Soc.*, **65**, 1954 (1961).
8) H. Uedaira and H. Uedaira, *J. Phys. Chem.*, **74**, 1931 (1970).

TABLE 1. TERNARY ISOPIESTIC DATA AT 25°C FOR THE SYSTEM GLYCYLGLYCINE–UREA–WATER

m_R	m_1	m_2	Δ/m_1m_2		
			Exptl	Calcd	Diff. %
0.59422	0.30393	0.82598	-0.070_{52}	-0.067_{25}	0.08
	0.45138	0.69074	-0.062_{61}	-0.059_{86}	0.08
	0.61061	0.54705	-0.055_{52}	-0.052_{89}	0.08
0.81451	0.63366	0.95362	-0.045_{67}	-0.049_{78}	−0.17
	1.0306	0.59809	-0.035_{41}	-0.038_{99}	−0.15
	1.2386	0.41251	-0.031_{94}	-0.035_{03}	−0.11
0.95786	1.5529	0.41159	-0.035_{18}	-0.031_{58}	0.13
1.0731	0.39843	1.6926	-0.052_{29}	-0.053_{27}	−0.03
	0.71011	1.3975	-0.036_{03}	-0.044_{12}	−0.42
	0.92038	1.2157	-0.038_{57}	-0.039_{57}	−0.06
	1.2219	0.93663	-0.030_{43}	-0.035_{07}	−0.28
1.2522	0.30117	2.1531	-0.048_{38}	-0.052_{22}	−0.11
	0.61438	1.8642	-0.041_{74}	-0.043_{24}	−0.08
	0.91965	1.5867	-0.037_{06}	-0.037_{45}	−0.03
	1.2086	1.3210	-0.033_{01}	-0.034_{07}	−0.08
	1.5161	1.0381	-0.032_{68}	-0.031_{96}	0.05
1.4119	0.93465	1.9066	-0.032_{77}	-0.034_{96}	−0.15
	1.2077	1.6855	-0.043_{12}	-0.032_{34}	0.86
1.4549	1.3471	1.6164	-0.029_{23}	-0.031_{30}	−0.17
1.4964	0.85004	2.2067	-0.051_{71}	-0.034_{22}	1.21
	0.99471	2.0532	-0.044_{21}	-0.032_{79}	0.87
	1.1709	1.8832	-0.035_{23}	-0.031_{61}	0.30
1.7651	0.49254	3.0884	-0.033_{78}	-0.034_{10}	−0.02
	0.72814	2.8648	-0.029_{06}	-0.030_{73}	−0.11
	0.95557	2.6500	-0.025_{75}	-0.028_{72}	−0.23
	1.1841	2.4365	-0.024_{37}	-0.027_{63}	−0.29
1.9521	0.21485	3.7775	-0.033_{38}	-0.035_{10}	−0.04
	0.67882	3.3300	-0.025_{58}	-0.027_{32}	−0.11
	0.93178	3.0880	-0.022_{23}	-0.025_{34}	−0.25
	1.1929	2.8392	-0.020_{33}	-0.024_{44}	−0.39
2.0182	1.5386	2.6560	-0.018_{73}	-0.023_{13}	−0.49
2.1249	0.15800	4.2375	-0.031_{28}	-0.032_{12}	−0.01
	0.64568	3.7717	-0.027_{33}	-0.024_{00}	0.21
	0.90599	3.5115	-0.021_{08}	-0.022_{16}	−0.09
	1.1643	3.2603	-0.018_{57}	-0.021_{36}	−0.27
2.4102	0.47371	4.6065	-0.022_{35}	-0.021_{06}	0.06
	0.65589	4.4279	-0.020_{35}	-0.019_{01}	0.09
	0.83587	4.2494	-0.018_{00}	-0.017_{66}	0.03
	1.0141	4.0763	-0.016_{86}	-0.016_{78}	0.01
	1.2086	3.8855	-0.015_{85}	-0.016_{23}	−0.04
2.6062	0.31875	5.2391	-0.019_{89}	-0.021_{30}	−0.05
	0.62787	4.9292	-0.017_{19}	-0.017_{00}	0.01
	0.95470	4.6020	-0.014_{23}	-0.014_{41}	−0.02
	1.2895	4.2645	-0.012_{11}	-0.012_{96}	−0.10
	1.6230	3.9288	-0.011_{42}	-0.011_{81}	−0.05
2.6519	0.30391	5.3890	-0.029_{48}	-0.021_{26}	0.27
	0.52501	5.1472	-0.017_{25}	-0.017_{86}	−0.03
	0.75794	4.9153	-0.013_{27}	-0.015_{35}	−0.16
	0.98926	4.6885	-0.015_{06}	-0.013_{67}	0.13
	1.2086	4.4617	-0.012_{73}	-0.012_{60}	0.01
2.8825	0.30271	5.9615	-0.018_{87}	-0.021_{59}	−0.09
	0.52619	5.7316	-0.016_{20}	-0.017_{59}	−0.08
	0.75920	5.4942	-0.013_{92}	-0.014_{45}	−0.04
	0.99162	5.2676	-0.013_{54}	-0.012_{04}	0.15
	1.2107	5.0338	-0.010_{98}	-0.010_{18}	0.09
3.0133	0.29538	6.3277	-0.025_{10}	-0.023_{44}	0.06
	0.61972	5.9654	-0.012_{22}	-0.017_{07}	−0.32
	0.92474	5.6789	-0.014_{18}	-0.012_{85}	0.12
	1.2332	5.3342	-0.008_{86}	-0.009_{29}	−0.05
	1.5479	5.0076	-0.008_{24}	-0.005_{80}	0.33

By means of Eqs. (1) and (2), the activity coefficient for glycylglycine in the ternary solution is given[9,10] by

$$\ln \gamma_1 = \ln \gamma_{10} + Am_2 + Bm_1m_2 + \frac{C}{2}m_2^2 + Dm_1^2m_2 + \frac{2E}{3}m_1m_2^2 + \frac{F}{3}m_2^3 + Gm_1^3m_2 + \frac{3H}{4}m_1^2m_2^2 + \frac{I}{2}m_1m_2^3 + \frac{J}{4}m_2^4 \quad (3)$$

and that of urea by

$$\ln \gamma_2 = \ln \gamma_{20} + Am_1 + \frac{B}{2}m_1^2 + Cm_1m_2 + \frac{D}{3}m_1^3 + \frac{2E}{3}m_1^2m_2 + Fm_1m_2^2 + \frac{G}{4}m_1^4 + \frac{H}{2}m_1^3m_2 + \frac{3I}{4}m_1^2m_2^2 + Jm_1m_2^3 \quad (4)$$

where γ_1, and γ_2 are the molal activity coefficients of solutes 1 and 2 in a ternary solution containing solute 1 and 2 with molalities m_1 and m_2, respectively. γ_{10} and γ_{20} are the molal activity coefficients, respectivley, of binary solutions containing only solute 1 at molality m_1 or solute 2 at molality m_2. The values of osmotic and activity coefficients for reference potassium chloride solutions were taken from the values given by Robinson and Stokes.[11] The values of osmotic and activity coefficients for glycylglycine solutions were taken from the data of Ellerton *et al.*,[12] and the values for urea solutions, from Ellerton and Dunlop.[10]

Results and Discussion

The isopiestic data for the system glycylglycine—urea—water are given in Table 1. The values of Δ/m_1m_2 (calcd) were calculated by the least-squares treatment of Eq. (2) and Table 2. The percentage

TABLE 2. COEFFICIENTS IN EQ. (2) FOR TERNARY SOLUTIONS GLYCYLGLYCINE–UREA–WATER AT 25°C

Coefficients		Coefficients	
A	−0.099457	F	0.002963
B	0.099905	G	0.007619
C	0.009731	H	0.004752
D	−0.047333	I	0.000847
E	−0.017318	J	−0.000434

error in the molality of the reference solution is defined by[7,13]

$$\text{diff. } \% = \frac{m_R(\text{calcd}) - m_R(\text{exptl})}{m_R(\text{exptl})} \times 100 \quad (5)$$

where

$$m_R(\text{calcd}) = \frac{m_1\phi_1 + m_2\phi_2 + \Delta(\text{calcd})}{2\phi_R} \quad (6)$$

The coefficients of Eq. (2) were calculated from the experimental values of Δ/m_1m_2 by the method of least-squares with a HITAC 8400 computer, and are given in Table 2.

Substituting the numerical values into Eqs. (3) and (4), we have for glycylglycine

$$\ln \gamma_1 = \ln \gamma_{10} - 0.099457m_2 + 0.099905m_1m_2 + 0.004865m_2^2 - 0.047333m_1^2m_2 - 0.011546m_1m_2^2 - 0.000988m_2^3 + 0.007619m_1^3m_2 + 0.003564m_1^2m_2^2 + 0.000424m_1m_2^3 - 0.000109m_2^4 \quad (7)$$

and for urea

$$\ln \gamma_2 = \ln \gamma_{20} - 0.099457m_1 + 0.049952m_1^2 + 0.009731m_1m_2 - 0.015778m_1^3 - 0.011546m_1^2m_2 + 0.002963m_1m_2^2 + 0.001905m_1^4 + 0.002376m_1^3m_2 + 0.000636m_1^2m_2^2 - 0.000434m_1m_2^3 \quad (8)$$

The activity coefficients of glycylglycine at various concentrations of urea in ternary solutions are shown in Fig. 1. The solid line shows the activity coefficients in binary solutions. The activity coefficients of glycylglycine decreased with the increase in concentration of urea. The lowering effect of urea was more marked at smaller concentrations of glycylglycine.

The activity coefficients of urea at various concentrations of glycylglycine are shown in Fig. 2. The activity coefficients of urea also decreased with the increase in concentration of glycylglycine.

Unlike the activity coefficients of glycylglycine, those of α-amino-*n*-butyric acid in aqueous solution are greater than unity and increase with concentration.[5] Addition of urea to aqueous solution of α-amino-*n*-butyric acid, however, also decreases the activity coefficients of the amino acid.[5] Urea decreases hydrophobic bonding of amino acids having larger hydrocarbon residues, resulting in an increase in

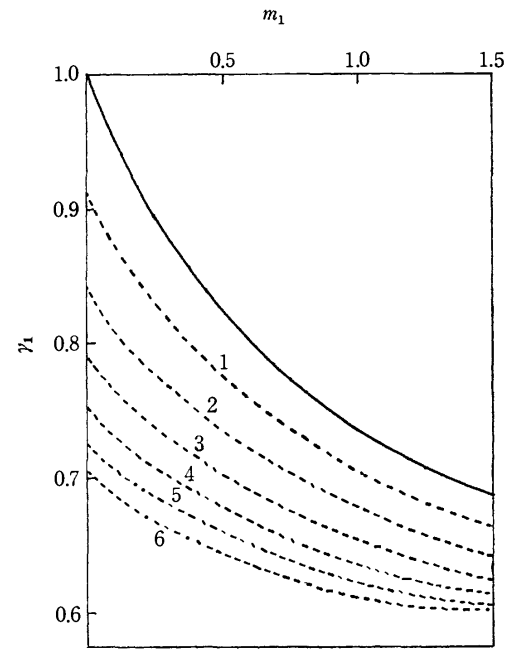

Fig. 1. Activity coefficients of glycylglycine in urea solutions: ——, in water; ----, in urea solution of various concentrations. The concentrations of urea: 1 1.0 m; 2, 2.0 m; 3, 3.0 m; 4, 4.0 m; 5, 5.0 m; 6, 6.0 m.

9) V. E. Bower and R. A. Robinson, *J. Phys. Chem.*, **67**, 1524 (1963).
10) H. D. Ellerton and P. J. Dunlop, *ibid.*, **70**, 1831 (1966).
11) R. A. Robinson and R. H. Stokes, "Electrolyte Solutions," 2nd ed., Butterworths, London (1959).
12) H. D. Ellerton, G. Reinfelds, D. E. Mulcahy, and P. J. Dunlop, *J. Phys. Chem.*, **68**, 398 (1964).
13) F. J. Kelly, R. A. Robinson, and R. H. Stokes, *ibid.*, **65**, 1958 (1961).

Table 3. Free energy of transfer (in cal/mol) of glycylglycine from water to urea solutions

m_1	m_2 1.0	2.0	3.0	4.0	5.0	6.0
0	−55.5	−103	−140	−169	−190	−207
0.5	−36.0	− 68.4	− 95.2	−116	−133	−147
1.0	−25.3	− 49.8	− 70.8	− 87.5	− 99.7	−109
1.5	−20.4	− 40.7	− 57.8	− 68.5	− 72.7	−. 70.4

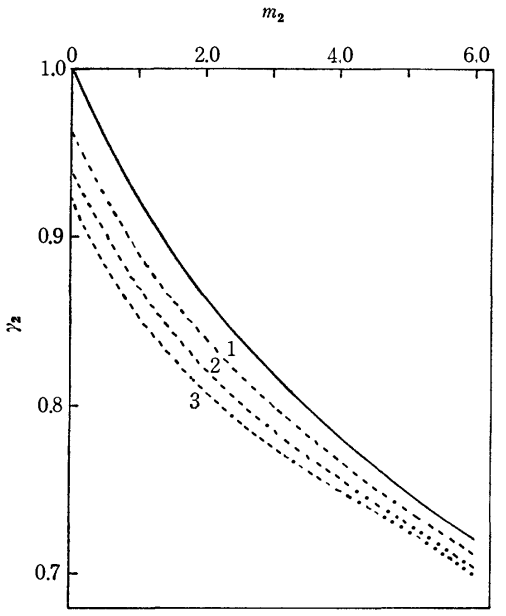

Fig. 2. Activity coefficients of urea in glycylglycine solutions: ——, in water; ----, in glycylglycine solutions at several concentrations of glycylglycine. The concentrations of glycylglycine: 1, 0.5 m; 2, 1.0 m; 3, 1.5 m.

solubility.[2] The decrease in activity coefficient of α-amino-*n*-butyric acid is caused by the decrease in hydrophobic bonding.[5]

On the contraty, as there is no hydrophobic part in glycylglycine, the decrease in activity coefficient is due to some factor other than hydrophobic interaction.

Robinson and Jencks[3] showed that the increase in solubility of acetyltetraglycine ethyl ester by urea is not caused by hydrophobic interaction.

At lower concentrations of amino acids, urea decreases the activity coefficient of glycylglycine to a greater extent than that of α-amino-*n*-butyric acid, the degree of decreases being reversed at relatively high concentrations ($\gtrsim 1.2\ m$). The decrease in activity coefficients of glycylglycine in urea solutions is due to the factor which is more dependent on the concentration of amino acid than hydrophobic interaction.

The activity coefficients of solute i in urea solutions are all relative to unity in the standard state in water and do not refer to the standard state in a water-urea solvent,[14] because of the method of calculation adopted in isopiestic measurements.[9,10] Thus, the free energy of transfer ΔG_t of solute i at constant concentration of the solute, from water to urea solution, is given by an equation containing only the term of the change in activity coefficients. When urea is treated as a component of solvent, the appropriate concentration scale for solute i is the mole fraction. The free energy of transfer ΔG_t for solute i is given by

$$\Delta G_t = RT \ln(f_i/f_{i0}) \tag{9}$$

where f_{i0} and f_i are the activity coefficients in mole fraction scale of solute in binary and ternary solutions, respectively, both at mole fraction N_{i0}. The activity coefficient in the molality scale was calculated at a certain molality in a binary solution from the data referred to before. The activity coefficients of the solute were calculated at the same concentration in mole fraction scale in a ternary solution, by Eq. (7). The activity coefficients in the molality scale were then converted into the rational activity coefficients by the equation[11]

$$f = \gamma(1 + 0.001 m_i W_A) \tag{10}$$

where W_A is the molecular weight of solvent. In a binary solution, W_A is equal to the molecular weight of water. In a ternary solution, W_A is the molecular weight of mixed solvent (water-urea) defined by

$$W_A = \frac{55.51 W_{A0} + W_u m_u}{55.51 + m_u} \tag{11}$$

where W_{A0} is the molecular weight of water, and W_u and m_u are the molecular weight and molality of urea, respectively, in the mixed solvent.

The free energy of transfer of glycylglycine from water to urea solutions at various concentrations is shown in Table 3. At comparatively small concentrations of glycylglycine, the free energy of transfer becomes more negative with increasing concentration of urea, and at higher concentrations, the value changes a little with urea concentration and rather tends to approach zero at higher concentrations of urea. In addition, at the same concentration of urea, the values of ΔG_t approach zero with increasing concentrations of glycylglycine. The values of ΔG_t for glycylglycine (Table 3) have neither maximum not minimum as observed by Nozaki and Tanford[2] from measurement of solubility.[15]

The values of ΔG_t at $m_1=0$ are the free energy change when a mole of glycylglycine is transferred from water with a given mole fraction to the mixture urea-water of the same mole fraction in the limit $m_1=0$. Consequently, they can be compared with the enthalpy of transfer of the solute from water to aqueous urea at infinite dilution ΔH_t which is the difference between partial molal enthalpy of the solute at infinite dilution

14) H. S. Harned and R. A. Robinson, "Multicomponent Electrolyte Solutions," Pergamon Press Inc., London (1968), p. 94.

15) The values of transfer free energy for glycylglycine from water to various urea solution were: −5, to 2 M urea; −12, to 4 M urea; −1, to 6 M urea; and −4 (cal/mol), to 8 M urea.[2]

in ternary and binary solutions.

The enthalpy of transfer of the solute from water to aqueous 6 M (molarity scale) urea solution at infinite dilution was obtained by Kresheck and Benjamin.[4] The value obtained was −1425 cal/mol. Concentration of urea in the molality scale was converted into that in the molality scale by means of density of solution,[16] *i. e.* 6 molarity urea solution is 8.2402 molality. The corresponding values of ΔG_t of glycylglycine at infinite dilution is obtained by extrapolating Eq. (7). The extrapolated value for activity coefficient gives $\Delta G_t = -259$ cal/mol.[17] The entropy of transfer ΔS_t was thus calculated to be −3.9 e. u. Kresheck and Benjamin[4] calculated it with the ΔG_t of Nozaki and Tanford,[2] giving −4.8 e. u. Though the two values are not the same, their signs are negative in both calculations. The transfer of glycylglycine from water to urea solution is accompanied by negative free energy change, negative enthalpy change and negative entropy change. The negative value of free energy of transfer is caused by the large negative value of enthalpy of transfer which surpasses the unfavorable entropy decrease.

It is known that urea destroys the ordered structure of water in aqueous solution.[18] The self diffusion coefficients of water in aqueous glycylglycine solution were measured at 25—50°C by Altunina *et al.*[19] Glycylglycine decreases the activation energy of self diffusion of water. The peptide molecule shifts the equilibrium between ordered and free structures of water to the disordered structure by decreasing activation energy of self diffusion of water. Glycylglycine is ranked thus as a sturcture breaker (negative hydration), that is, water molecules move more easily in glycylglycine solution than in pure water.

In the case of a ternary system containing two sturcture breaking solutes, their activity coefficients are lowered by each other as a result of sturcture salting in,[20,21] occuring in the system, *e. g.*, sodium benzenesulfonate-urea-water.[8] The proportion of free water thus should increase and entropy of transfer should be positive. The data of partial molar heat capacity, obtained with dipeptides by Kresheck and Benjamin,[4] show that the peptide unit has no conspicuous effect on the solvent structure in water, but the negative value of partial molar heat capacities at infinite dilution, associated with transfer of glycylglycine from water to 6 M urea, suggests a peptide-urea interaction resulting in less ordered water structure. The explanations are in line with the lowering of activity coefficients in ternary systems, and with the negative free energy of transfer. However, the entropy of tansfer of glycylglycine from water to urea solutions is negative.

Thus, the interaction between glycylglycine and urea might be the main cause of decreasing activity coefficient and negative free energy of transfer. In order to confirm interaction such as complex formation between glycylglycine and urea, X-ray refraction intensity curves were obtained for the crystalline complex crystallized from aqueous glycylglycine and urea solution (mole ratio, 1 : 4), and soild mixture of glycylglycine and urea of the same mole ratio as crystallized from solution. A difference was found between the curves for the crystalline and solid mixture of glycylglycine and urea.[22] Thus, even in aqueous solution, glycylglycine and urea may form a certain complex aggregation.

Swenson and Koob[23] found by NMR study that rates of exchange for the peptide proton of glycylglycine and triglycine were smaller in aqueous urea than in water. They stated that urea might decrease the base-catalyzed rate by specifically interacting with the peptide hydrogen bond. Their data suggest an interaction between glycylglycine and urea in aqueous solution.

Robinson and Jencks[3] showed that an increase in the number of amide bonds in carbobenzoxyglycine derivatives has no appreciable influence on the effect of urea on the solubility of peptides and that solubility of acetyltetraglycine ethyl ester increases linearly with urea concentration. They pointed out that the evidence is more easily explained in terms of complex formation.

The interaction between urea and glycylglycine increases with urea concentratoin and decreases with glycylglycine concentration. In a relatively small concentration (at about 0.1 M amino acid residue) at which the usual investigations on denaturation of protein by urea are carried out, the decrease in the activity coefficient of glycylglycine is greater than that of α-amino-*n*-butyric acid. These results suggest that urea interacts with polar parts of amino acids, and the effect is important at relatively small concentrations of amino acids. The denaturation of globular protein by urea may thus be caused by the interaction of polar parts of amino acids and urea besides the weakening of hydrophobic bonding between hydrophobic side chains of constituent amino acid residues.

The author thanks Dr. Hisashi Uedaira for discussions. She is also indebted to Mr. Mitsuhiro Kikuchi for his assistance in measurements, and to Mr. Toshio Kurita for his help with the measurements of X-ray refraction.

16) E. P. Eagen, Jr. and B. B. Luff. *J. Chem. Eng. Data*, **11**, 192 (1966).

17) The values of ΔG_t differ from those of Nozaki and Tanford.[2] The results in this paper show that activity coefficients of glycylglycine in urea solutions are a function of the concentrations of both urea and glycylglycine, containing their cross terms. It is therefore thought that the main cause of difference is that Nozaki and Tanford assumed the activity coefficients of glycylglycine in aqueous urea solutions to be dependent on the concentration of glycylglycine only and independent of the concentration of urea.

18) H. S. Frank, *Fed. Proc.*, **S24**, 1 (1965).

19) L. K. Altunina, O. F. Bezrikov, N. A. Smirnova, I. A. Moskbicheva, and V. P. Fokanov, *Struktura i Rol' Vodui v Zhivom Organizme*, **2**, 57 (1968).

20) O. Ya. Samoilov, V. I. Tikhomirov, V. P. Ionov, and A. A. Kuznetzova, *Radiokhimiya*, **1**, 14 (1961); O. Ya. Samoilov, *Stukt. Khim.*, **7**, 15, 175 (1966); O. Ya. Samoilov, "Sostoyanie i Rol' Vodui v Biologicheskiv Obiektov," Nauka, Moskow (1967), p. 31.

21) H. S. Frank, *J. Phys. Chem.*, **67**, 1554 (1963).

22) The samples were rotated vertically to the X-ray beam and the refraction intensity was measured by a Geiger counter in the angle range $2\theta = 10°—50°$. The crystalline complex showed two new peaks at face distances of 4.85—5.0 Å and 3.25—3.30 Å, and the peak at 5.85—5.90 Å existing in the solid mixture was absent from the complex.

23) C. A. Swenson and L. Koob, *J. Phys. Chem.*, **74**, 3376 (1963).

Formation Constants of Some Bivalent Metal Chelates of *N*-Phenylbutyrohydroxamic Acid

J. P. SHUKLA* and S. G. TANDON

Department of Chemistry, Government College of Science, Raipur, M.P., India

(Received December 25, 1970)

The formation constants for the metal chelates of Mn(II), Ni(II), Zn(II), and Cu(II) with *N*-phenylbutyrohydroxamic acid have been determined in 50 volume per cent dioxane–water mixture following the Bjerrum-Calvin pH titration technique and maintaining the titration medium at a constant salt background (0.1 M $KClO_4$) and a temperature 25±0.1°C. The formation constants found are log K_1=9.68(Cu), 6.85(Zn), 6.67(Ni), 5.25(Mn), and log K_2=8.58(Cu), 5.52(Zn), 5.21(Ni), and 4.09(Mn), the stability order being Mn<Ni<Cu>Zn.

Substitution of different groups at different positions of aryl nuclei of the parent compound influences the stabilities of the resulting metal complexes. A more or less quantitative survey of the effects of substitution in the aryl nuclei on the stability constants of metal chelates of the ligand was first carried out by Calvin and Wilson.[1] Such studies are important in as much as they help predict what type of substituents in the molecule might enhance its use for a particular purpose. Several *N*-arylhydroxamic acids represented by the general formula have been synthesised during the last

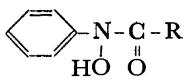

few years and their possible analytical applications examined. Recently, the stabilities of metal chelates of some aryl substituted *N*-arylhydroxamic acids (R= aryl), mainly of *N*-phenylbenzohydroxamic acid (PBHA) have been reported.[2,3] But so far no attempt seems to have been made except for a few instances[2,4] to elucidate the stability of metal chelates of alkyl substituted *N*-arylhydroxamic acids (R=alkyl). The present paper deals with the determination of formation constant of Cu(II), Ni(II), Zn(II), and Mn(II) chelates with *N*-phenylbutyrohydroxamic acid, P(n)BHA, by employing Calvin and Melchior's method,[5] commonly referred to as Bjerrum-Calvin pH titration technique. Titrations were carried out in duplicate in a medium of salt background 0.1 M adjusted with $KClO_4$, at 25± 0.1°C. A ratio 10: 1 of the ligand to metal ion concentration was used in order to satisfy the highest possible coordination number namely, 6, of the metal ions under study. Since evaluation of the formation constant required knowledge of the acid dissociation constant not found in literature, it was also determined under similar experimental conditions. As both the ligand and its complexes are fairly insoluble in water, 1: 1 dioxane–water was used as the solvent medium.

Experimental

B.D.H. *p*-dioxane was purified by the procedure of Weissberger and Proskauer.[6] Carbonate free KOH was prepared following the method of Vogel[7] and diluted to 0.1 M; the proportion of dioxane and water in the final solution was 1: 1. It was standardized against analytical grade potassium hydrogen phthalate.

Measurements of pH were made with a Radiometer pHM-4c pH meter, saturated calomel reference electrode and a glass electrode. Buffer solutions of pH 4.01 (at 25°C) and 9.18 (at 25°C), prepared from potassium hydrogen phthalate and borax respectively, were used for standardization of the pH meter, which was done at the beginning of each titration and checked after completion.

Chelating Agent. P(n)BHA was synthesised by the method of Priyadarshini and Tandon.[8] This was recrystallised before use from a mixture of benzene and petroleum ether and dried in a vacuum over P_2O_5. Purity of the compound was checked by elemental analyses, mp, UV and IR spectra.

Metal Perchlorates. Metal salt solutions were prepared by dissolving the respective metal carbonates or oxides in a known volume of perchloric acid. The concentration of the metal ion in each of the metal perchlorates was determined by EDTA titration.[9] Finally, these solutions were suitably diluted before use. In the case of copper perchlorate, however, no further dilution of the stock solution was made since the pH of hydrolysis for Cu(II) is rather low, *i.e.* 5.3.[10]

Determination of Acid Dissociation Constant (pK_a). The titration procedure for determination of pK_a was essentially the same as that given by Albert and Serjeant.[11] A half millimoles of the compound was transferred to a four-necked, flat bottomed titration cell and dissolved in known volumes of dioxane and water. Five milliliters of 1 M $KClO_4$ was added to maintain a constant salt background of 0.1 M. The total volume of the contents was made to 47.5 m*l* by adding dioxane and water in such proportion that it finally became 1: 1 dioxane–water mixture. Before performing the titration

* Present address: Radiochemistry Division, Bhabha Atomic Research Centre, Trombay, Bombay-85, India.

1) M. Calvin and K. W. Wilson, *J. Amer. Chem. Soc.*, **67**, 2203 (1945)

2) N. K. Dutt and T. Seshadri, *J. Inorg. Nucl. Chem.*, **31**, 2153 (1969).

3) G. A. Brydon and D. E. Ryan, *Anal. Chim. Acta*, **35**, 190 (1966).

4) J. P. C. Jaimini and N. C. Sogani, *J. Indian Chem. Soc.*, **45**, 59 (1968).

5) M. Calvin and N. C. Melchior, *J. Amer. Chem. Soc.*, **70**, 3270 (1948).

6) A. Weissberger and E. S. Proskauer, "Organic Solvents," Interscience Publishers, New York, Vol. 7, p. 139 (1955).

7) A. I. Vogal, "A Text Book of Quantitative Inorganic Analysis," 3 rd ed., Longmans (1961), p. 240.

8) U. Priyadarshini and S. G. Tandon, *J. Chem. and Eng. Data*, **12**, 143 (1967).

9) F. J. Welcher, "The Analytical Uses of Ethylenediamine tetraacetic Acid," D. Van Nostrand Co., Princeton (1961), p. 234.

10) H. T. S. Britton, "Hydrogen Ions," Vol. II, Chapman & Hall Ltd., London (1956), p. 102

11) A. Albert and E. P. Serjeant, "Ionization Constants of Acids and Bases," Methuen and Co. Ltd., London (1962), p. 28.

TABLE 1. DETERMINATION OF THE ACID DISSOCIATION CONSTANT
Concentration of P(n)BHA=0.01M at 50 ml level
Salt background=0.1M $KClO_4$
Medium=1:1 Dioxane-water
Temperature=25±0.1°C

Titrant 0.1M KOH (ml)	pH	Stoichiometric concentrations (10^{-3}) [HA]	[A^-]	[OH^-] (10^{-6})	$\frac{[HA]+[OH^-]}{[A^-]-[OH^-]}$	log of column 6	pK_a= (pH+column 7)
0.05	10.200	9	1	1	9001/999	+0.955	11.155
1.00	10.570	8	2	3	8003/1997	+0.603	11.173
1.50	10.770	7	3	5	7005/2995	+0.369	11.139
2.00	10.970	6	4	8	6008/3992	+0.178	11.148
2.50	11.145	5	5	10	501/499	+0.002	11.147
3.00	11.335	4	6	20	402/598	−0.173	11.162
3.50	11.505	3	7	30	303/697	−0.362	11.143
4.00	11.740	2	8	40	204/796	−0.591	11.149
4.50	12.070	1	9	80	108/892	−0.917	11.153

pK_a=11.15±0.02 (using all nine values of the set)

the contents of the titration vessel were thermostated at 25±0.1°C. Pre-saturated nitrogen (with 50 volume per cent aqueous dioxane) was continuously bubbled through the solution. After about 15 min, the titration was started by adding 0.5 ml increments of 0.1M KOH each time and noting the highest pH-meter reading which remained steady. Titrations carried out in duplicate were reproducible within±0.01 pH unit. The results of the titration are recorded in Table 1.

Determination of Formation Constants. A weighed quantity of P(n)BHA, corresponding to 0.01M in the final solution of 50 ml was transferred to the titration cell and 25 ml of dioxane was added to it. Next, 10 ml of about 0.005M solution of the metal perchlorate, 5 ml of 1M $KClO_4$ and 10 ml of water were added to yield a 1:1 dioxane-water mixture. The titration procedure followed was exactly the same as that described above except that KOH was added in small aliquots of 0.25 ml until the pH of the titre solution crossed the hydrolysis point. The results of the copper(II)-ligand titration are summarized in Table 2. For the sake of brevity, results of titrations of Ni(II), Zn(II), and Mn(II) are not given here. The first and second stepwise stability constants, K_1 and K_2, were evaluated by the method of least squares as illustrated by Albert and Serjeant.[12]

TABLE 2. DETERMINATION OF THE FORMATION CONSTANTS OF Cu(II) COMPLEX WITH *N*-PHENYL-BUTYROHYDROXAMIC ACID
Salt background=0.1M $KClO_4$
Medium=1:1 Dioxane-water
Temperature=25±0.1°C

KOH (0.1M) ml	pH	log [L^-]	$\bar{n}$	log K_1	log K_2	log K_1K_2
0.00	3.10	—	—	—	—	—
0.50	3.26	$\bar{10}$.060	0.20	a)	a)	a)
1.00	3.47	$\bar{10}$.215	0.41	a)	a)	a)
1.25	3.59	$\bar{10}$.304	0.53	9.66	8.54	18.20
1.50	3.71	$\bar{10}$.392	0.60	9.67	8.56	18.23
1.75	3.84	$\bar{10}$.488	0.72	9.79	8.64	18.43
2.00	4.00	$\bar{10}$.611	0.80	9.77	8.55	18.32
3.00	4.70	$\bar{9}$.127	1.20	9.60	8.63	18.23
3.25	4.90	$\bar{9}$.267	1.31	9.62	8.60	18.22
3.50	5.11	$\bar{9}$.408	1.44	9.59	8.67	18.26
3.75	5.36	$\bar{9}$.577	1.52	9.68	8.51	18.19
4.00	5.66	$\bar{9}$.778	1.64	9.69	8.48	18.17
4.25	6.02c)	$\bar{8}$.011	1.70	b)	b)	b)
			Average	9.68	8.58	18.26

a) Discarded.
b) Not calculated as pH crossed the hydrolysis point.
c) No precipitation took place up to this stage of titration.
Result: log K_1=9.68±0.07, log K_2=8.58±0.06
log K_1K_2=18.26±0.08

Results and Discussion

Log K_1, log K_2, and log (K_1/K_2) of the complexes of Cu(II), Ni(II), Zn(II), and Mn(II) are given below. All the constants reported here including pK_a may be termed concentration (or stoichiometric) constants because they were obtained without applying activity corrections. It is quite evident from Table 3 that all the metal chelates are fairly stable. P(n)BHA is believed to react with these metal ions as leading to the formation of a five membered ring in the chelate. On the basis of published data, it has been assumed that P(n)BHA yields 1:2 complex with the aforesaid metal ions. In the present experiments $\bar{n}$ (average number

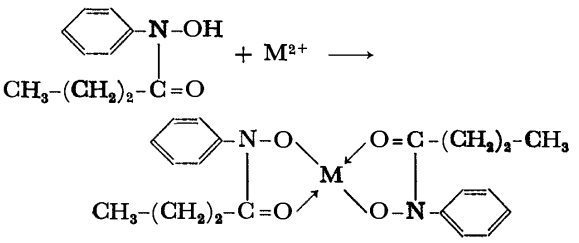

TABLE 3. FORMATION CONSTANTS OF METAL CHELATES

Metal ion	log K_1	log K_2	log (K_1/K_2)
Cu	9.68	8.58	1.10
Zn	6.85	5.52	1.33
Ni	6.67	5.21	1.46
Mn	5.25	4.09	1.16

12) Ref. 11, p. 165.

of ligand molecules attached per metal ion) gradually reached a value of nearly 2 before precipitation. So our assumption of 1 : 2 complex formation in solution seems to be valid.

Order of Stability Constants or log K Values. From Table 3 it can be seen that the order Mn<Ni<Cu>Zn is in agreement with that of Irving and Williams.[13] In all the cases $K_1 > K_2$. The values of $\log(K_1/K_2)$ is the highest for the nickel complex. Furthermore, it is observed that the values of log K_2 are lower than log K_1 by approximately 1.1—1.5 units. This suggests that in these systems not only the statistical effect (which gives the value of log K_1—log K_2=0.60 units) should be considered but the electrostatic effect also becomes important.[14]

Values of log K for copper differs considerably from those for other metals and values for Zn are greater than Ni. The enormously higher log K value for copper chelate may be due to its possible square planar structure. The order Zn>Ni has been observed earlier,[15] where the relatively low value of Ni is attributed to steric hindrance preventing the formation of a square planar structure. Again the hydrolysis constant for Zn is greater than that of Ni indicating a greater affinity of Zn(II) for OH ions. These factors seem to account for the order Zn>Ni.

Financial assistance from the Chemical Society, London and Van't Hoff Fund, Amsterdam is gratefully acknowledged. One of the authors (J.P.S) is indebted to CSIR, New Delhi, for the award of Junior Research Fellowship.

13) H. Irving and R. J. P. Williams, *J. Chem. Soc.*, **1953**, 3192.
14) N. Bjerrum, *Z. Phys. Chem.*, **106**, 238 (1932).
15) W. D. Johnston and H. Freiser, *Anal. Chim. Acta*, **11**, 201, 301 (1954).

BULLETIN OF THE CHEMICAL SOCIETY OF JAPAN, VOL. 45, 3075—3077 (1972)

Order of Quencher Participation in Photochemistry. II. Quenching Action of Ethanol on the Photoreduction of *p*-Aminobenzophenones

Mikio HOSHINO and Masao KOIZUMI

Department of Chemistry, Faculty of Science, Tohoku University, Aramaki, Aoba, Sendai

(Received March 21, 1972)

The effect of the addition of ethanol (quencher of the reaction) on the photoreduction of *p*-aminobenzophenone (NH_2BP) and dimethyl-*p*-aminobenzophenone in cyclohexane and in ether has been studied. The order of quencher participation for ethanol has been found to be two for the former and one for the latter. The results were interpreted to be due to the formation of intramolecular C–T state during excitation, promoted by the attachment of one ethanol (or ether) molecule to the NH_2-group and one ethanol molecule to O=C of NH_2BP.

We previously reconfirmed[1] the view that proton transfer is a cause of the quenching action of ethanol on the photoreduction of *p*-hydroxybenzophenone (HOBP). This was in line with the work of Porter *et al.*[2] It was found, however, from the measurement of relative quantum yields in the mixed solvents of cyclohexane and alcohols, that the participation of several alcohol molecules is required for the eventual proton transfer to occur from HOBP in cyclohexane. An approach of the same type will enable us to attain a dynamic aspect of the quenching action not obtained with pure solvents. We have extended similar sutdies to the quenching action of alcohols on the photoreduction of *p*-aminobenzophenone (H_2NBP) and dimethyl-*p*-aminobenzophenone ($(CH_3)_2NBP$).

H_2NBP is photoreduced in cyclohexane with a quantum yield of 0.2 but not at all in ethanol.[3] The difference was explained to be due to the different character of the lowest triplet state. Thus in cyclohexane, the lowest triplet is $T(n\text{–}\pi^*)$ whereas in ethanol it is an intramolecular C–T state. However, from analogy of HOBP, the quenching action of ethanol in the case of H_2NBP is also expected to be dynamic in nature, and studies in the mixed solvents should give more detailed information. In particular, we thought it possible that in cyclohexane containing a suitable amount of ethanol, intramolecular C–T state of H_2NBP might be stabilized during the lifetime of the excited state by a suitable reorientation of alcohol molecules around $^+NH_2$ and $C{=}O^-$ group, notwithstanding the lack of C–T type absorption spectrum. Our results indicate that this is actually the case.

Experimental

H_2NBP was prepared by the reduction of 4-nitrobenzophenone with zinc powder and glacial acetic acid. $(CH_3)_2NBP$ was obtained by the hydrolysis of 4-dimethylaminobenzophenone anil. These aminobenzophenones were recrystallized twice from ethanol. Mp=97—98°C (lit,98°C) for $(CH_3)_2NBP$ and 123°C (lit, 123~124°C) for H_2NBP. Cyclohexane and ethanol were purified by the usual method. Ether was refluxed on sodium metal for 24 hrs before dis-

1) M. Hoshino and M. Koizumi, *Chem. Lett.*, **1972**, 189. M. Hoshino and M. Koizumi, This Bulletin, **45**, 2731 (1972).

2) G. Porter and P. Suppan, *Trans. Faraday Soc.*, **61**, 1164 (1965). T. S. Godfrey, G. Porter, and P. Suppan, *Discuss. Faraday Soc.*, **39**, 194 (1965).

3) A. Beckett and G. Porter, *Trans. Faraday Soc.*, **59**, 2038, 2051 (1963). J. N. Pitts, Jr., H. W. Johnson, Jr., and T. Kuwana, *J. Phys. Chem.*, **66**, 2456 (1962).

tillation. The spectral change was followed with a Hitachi EPS-3T spectrophotometer. A 6W germicidal lamp was used as a light source of 2537 Å.

Results and Discussion

p-Aminobenzophenone (H_2NBP). The peak of the absorption at 303 nm in cyclohexane shifts to 335 nm in ethanol. The spectral change with the increase in ethanol concentration is shown in Fig. 1.

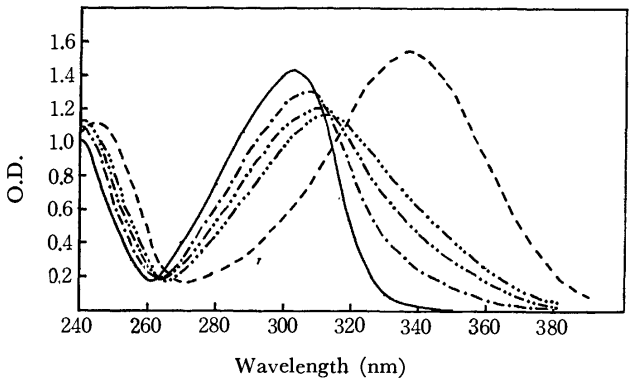

Fig. 1. Spectral change of H_2NBP (8.0×10^{-5} M) in cyclohexane with the addition of ethanol.
—— in cyclohexane
concentration of ethanol:
—·— 1.72×10^{-1} M, —··— 3.44×10^{-1} M, —···— 5.16×10^{-1} M, ---- in pure ethanol

A gradual *red* shift with no isosbestic point suggests that the interaction between NH_2-group and ethanol is hydrogen bonding of the type

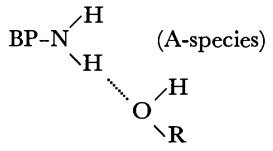

(A-species) (1)

which the general solvent effect is superposed. By analogy with a similar H-bonding species in the case of HOBP the photoreactivity of A-species was not expected to be reduced remarkably as compared with free H_2NBP.

It was found on the contrary that the relative quantum yield Φ_{rel} of the photoreduction decreases with the addition of ethanol much more rapidly than the spectral change.

The spectral change of H_2NBP in cyclohexane upon irradiation by 2357 Å is shown in Fig. 2. The change is due to the reaction

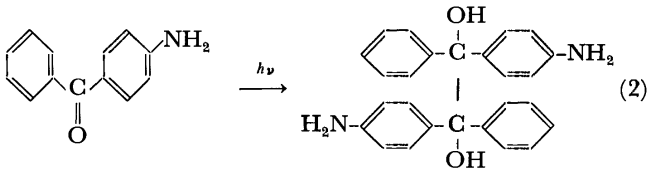

(2)

The analysis was made by the equation

$$-\frac{dC_A}{dt} = \Phi I_0(1-10^{-D})\frac{D_A}{D} \quad (3)$$

where D and D_A are the optical density of the irradiated solution and that due to H_2NBP at 2537 Å, respectively.

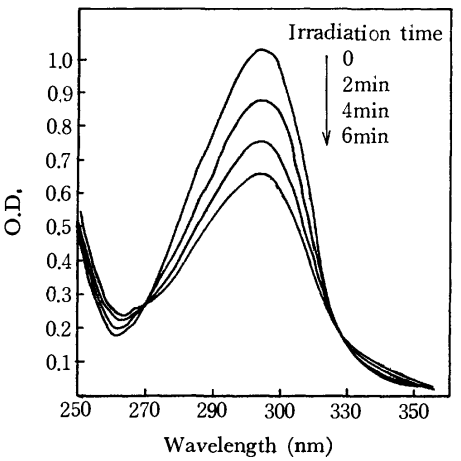

Fig. 2. Spectral change of H_2NBP containing ethanol (5.16×10^{-2} M) upon UV irradiation.

The other notations are the usual ones. Integrating we have

$$-\frac{1}{\varepsilon}\ln C_A = \Phi I_0 \int \frac{(1-10^{-D})}{D}dt \quad (4)$$

Because of a small change in optical density at 2537 Å, C_A was determined from the change at ~303 nm. The values of Φ_{rel} thus obtained at various ethanol concentrations [S] can be reproduced by the equation

$$\Phi_{rel} = \frac{1}{1+K[S]^n} \quad (5)$$

where $n=2$ and $K=3.03\times10^2$ M^{-2}. The plot of $1/\Phi_{rel}$ against $[S]^2$ gives a very good straight line as shown by curve a in Fig. 3. The value of 2 as the order of quencher participation suggests that another ethanol molecule is attached to C=O by H-bonding thus stabilizing the C-T state.

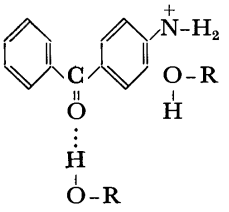

(6)

This is reasonable since the electron donating power of amino-group is much greater than that of the hydroxy

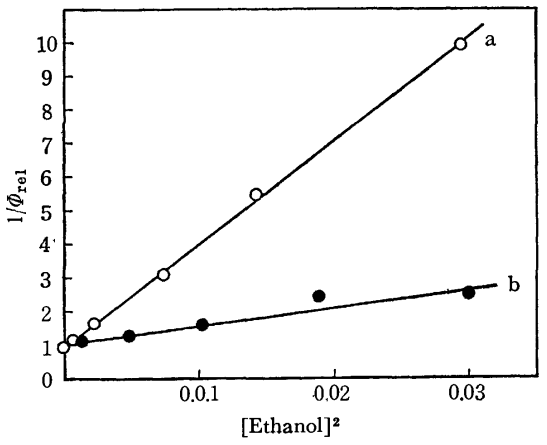

Fig. 3. Plots of $1/\Phi_{rel}$ *vs.* [ethanol]^2, ○: H_2NBP, ●: $(CH_3)_2NBP$.

group, for which such an electronic configuration is not so prominent. The interaction between $^{+}NH_2$ and ethanol in this state would be mainly due to a dipole-dipole one instead of H-bonding.

p-Dimethylaminobenzophenone ($(CH_3)_2$NBP). The absorption spectrum of $(CH_3)_2$NBP has a peak at 332 nm in cyclohexane and at 358 nm in ethanol, but it scarcely changes upon addition of ethanol up to about 1.7×10^{-1}M. However, the relative quantum yield of photoreduction obtained by the above analysis decreased to 40% at this ehtanol concentration.

$(CH_3)_2$NBP with no amino-hydrogen cannot form a H-bonded species as in the case of H_2NBP and it is quite natural that no spectral change occurs. Thus it is concluded that the decrease in Φ_{rel} in H_2NBP as well as in $(CH_3)_2$NBP is not related to the spectral change and accordingly the hydrogen bonding between NH_2 and alcohol.

The polt of $1/\Phi_{rel}$ against $[S]^2$ ($S=C_2H_5OH$) is linear as shown by curve b in Fig. 3 and the value of K was evaluated as 0.61×10^2 M^{-2}. All the results are similar to those of H_2NBP at least qualitatively and the mechanism of quenching is considered to be the same.

It is interesting that the K-value of $(CH_3)_2$NBP is much smaller than that of H_2NBP. Judging from a larger electron releasing power of dimethyl-group than hydrogen, structure (6) is expected to be more stable for $(CH_3)_2$NBP than for H_2NBP. The opposite result might be due to the kinetics of the phenomenon. Thus for H_2NBP, an ethanol molecule is in intimate interaction with H_2NBP molecule by H-bonding already in the ground state while no such an interaction takes place in $(CH_3)_2$NBP. However, there is a possibility that the structure itself is more stabilized by H-bonding in H_2NBP than in $(CH_3)_2$NBP.

The order of quencher participation of two could be interpreted by structure (6). It is conceivable that the quenching is caused by a dimeric ethanol molecule although this is less likely. The following experiment was carried out to clarify the mechanism.

Effect of the Addition of Ethanol on the Quantum Yield of the Photoreduction of H_2NBP in Ether. Ether is expected to interact with the amino group of H_2NBP in a similar way to ethanol, acting as a H-acceptor of H-bonding, but differing from ethanol in that no hydrogen bond formation occurs with carbonyl of H_2NBP. If by analogy to HOBP, a hydrogen bonded species of the type $\overset{R}{R}\!>\!O\cdots\overset{H}{H}\!>\!N$-BP and $\overset{H}{R}\!>\!O\cdots\overset{H}{H}\!>\!N$-BP (A-species (1)) is reactive, then the photoreduction of H_2NBP is expected to occur in pure ether as in HOBP. But when a small amount of ethanol is added, formation of species (6) becomes possible and the reaction may be suppressed. If this is the actual mechanism for the quenching of reaction, the order of quencher participation is now expected to become one. On the other hand, the mechanism due to ethanol dimer should result in the order of quencher participation of two. Thus it will be easy to discriminate the two mechanisms experimentally. From such a viewpoint, we have investigated the photoreduction of H_2NBP in ether.

The absorption peak of H_2NBP in ether lies at 320 nm compared with 303 nm in cyclohexane and 337 nm in alcohol. It was established that the photoreduction occurs in pure ether with a quantum yield about the same as or a little larger than in cyclohexane. This indicates that A-species (1) itself is reactive. The plot of Φ_{rel} and $1/\Phi_{rel}$ aganist the concentation of ethanol is shown in Fig. 4. It is evident that the quenching action of ethanol occurs according to the equation

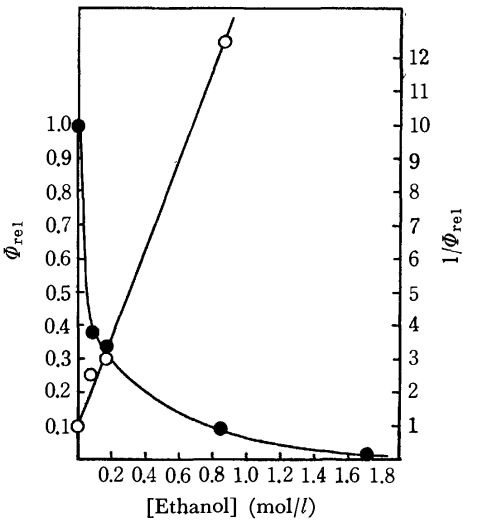

Fig. 4. Plots of Φ_{rel} *vs.* [ethanol] (●) and $1/\Phi_{rel}$ *vs.* ethanol (○) in ether.

$$\Phi_{rel}=\frac{1}{1+K[S]} \tag{7}$$

where [S] is the concentration of ethanol. The value of K evaluated from the solpe of $1/\Phi_{rel}$ *vs.* [S] plot is 13.2 M^{-1}. The absorption spectrum of H_2NBP in ether changes gradually to longer wavelength with the addition of ethanol, but the magnitude of change is very small at the ethanol concentration where the value of Φ_{rel} becomes about 1/10. This is reasonable in view of the fact that the effect of the hydrogen bond of this type on the π–π absorption spectra is rather small.[4]

It is thus concluded that the formation of intramolecular C-T state during the excitation by a solvent interaction as written in (6) is a cause for the quenching of reaction.

4) M. Ito, M. Inuzuka, and S. Imanishi, *J. Amer. Chem. Soc.*, **82**, 1317 (1960).

Heat Capacities of Antimony Trichloride and Tribromide

Kuniko TAKEYAMA and Tetsuzo ATODA
The Institute of Physical and Chemical Research, Hirosawa, Wako-shi, Saitama

(Received March 24, 1972)

Heat capacities of liquid antimony trichloride and tribromide saturated with their respective vapors were determined with an adiabatic calorimeter as follows: 35.2 cal K^{-1} mol^{-1} in the range, 90—210°C, for trichloride, and 34.6 cal $K^{-1}mol^{-1}$ in the range, 130—270°C, for tribromide.

For thermodynamic consideration on vaporization of antimony trichloride ($SbCl_3$) and tribromide ($SbBr_3$) at moderately high temperature, heat capacities of both halides in liquid state, which have never been determined, were required to be known, and the present authors measured them with an adiabatic calorimeter. Measurements were carried out for $SbCl_3$ in the range, 90—210°C, and for $SbBr_3$, 130—270°C, respectively.

Experimental

Apparatus and Procedure of Measurement. The calorimetric apparatus is shown schematically in Fig. 1. A capsule made of fused quartz, 5—6 cm^3 in volume, 0.8 mm in wall thickness, 5—6 g in weight, and provided with a well for an internal heater at its center was used as a sample container. Two alumel-chromel thermocouples, one for measuring the temperature of a capsule and another for adiabatic control, were fastened tightly with fine alumel wire at the middle part of the outside wall of the capsule to make a junction point of each couple touch surely to the wall surface. For measurements on $SbCl_3$, a thermocouple of 0.3 mm in diameter, and on $SbBr_3$, another of 0.2 mm in diameter were used. Calibration of each thermocouple was made by measuring the ice-point and melting points of In,[1] Sn,[2] and Pb[2] metals, the nominal purities of these metals being higher than 99.99%.

On heat capacity measurements, the pressure of argon gas filled in a nickel ball enveloping a capsule was kept at about 50 mmHg. Each sample was heated at a rate of 1°C/min with an internal heater to which practically constant wattage, the fluctuation being within ±0.5%, was supplied by a watt-stabilizer. Adiabatic control was made to make the temperature of the nickel ball equal to the temperature of the outer surface of the capsule with a heater equipped outside of the nickel ball. The heater was controlled by a proportional, integral, and differential heating device. The control fluctuation indicated by thermal emf of the alumel-chromel thermocouple was within ±1μV. Time required to elevate the temperature of a capsule containing a sample by 10°C was measured by a stop watch or a timer in error of less than 0.2%.

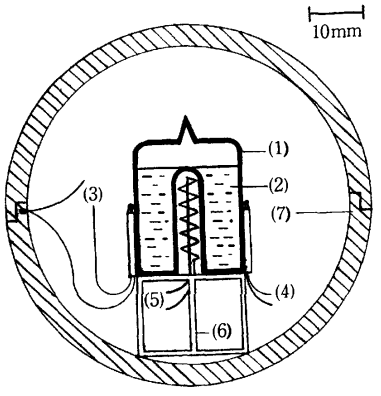

Fig. 1. The calorimetric apparatus
(1): Quartz capsule, (2): Sample, (3): Thermocouple for adiabatic control, (4): Thermocouple for measuring temperature of a capsule, (5): Internal heater, (6): Quartz stand, (7): Nickel ball.

Each sample in a reservoir was heated at a temperature between 100 and 150°C for several tens of minutes in reduced pressure (10^{-2}–10^{-3} mmHg) to remove any dissolved gas and volatile impurities prior to a distillation of the sample into a capsule through a vacuum line connecting the reservoir and the top of the capsule. The amount of the sample in the capsule was 4—5 cm^3. When the distillation was finished, the vacuum line was disconnected from the capsule by fusion. After heat capacity measurements were over, the top of the capsule was cut off to make the sample evaporate out of the capsule. After washed and dried, the empty capsule together with the cut tip was weighed. By subtracting the weight from that of the capsule containing the sample, a net weight of the sample was obtained. Buoyancy correction, less than 0.1% of total weight, was made for that purpose.

Materials. *$SbCl_3$*: $SbCl_3$,[3] the nominal purity being, higher than 99%, was purified with five times' vacuum distillation. $SbCl_3$ thus prepared was analyzed chemically; obsd. Sb, 53.36; Cl, 46.55 wt% calcd. Sb, 53.37; Cl, 46.63 wt%. Any impurities were not found by the emission spectrophotometric analysis. Mp 73.4°C.

$SbBr_3$: $SbBr_3$ was prepared at 250°C by direct reaction of metallic Sb,[1] the nominal purity six nines, with bromine,[4] the nominal purity higher than 99.5%. The reaction product thus prepared was then distilled five times in vacuum. The chemical composition of the purified $SbBr_3$ is: obsd. Sb, 33.70; Br, 66.19 wt% calcd. Sb, 33.68; Br, 66.32 wt%. The emission spectrophotometric analysis indicated very weak spectrum lines of Cu and Si on the purified $SbBr_3$. Mp 96.4°C. Liquid densities observed in the range, 100—250°C, by the pycnometric method were estimated to be: $3.95-2.67\times10^{-3}t$ (g/cm^3), where t is °C.

Hg: Hg,[5] the nominal purity being higher than 99.9%, was washed with dilute aqueous HNO_3, and then distilled five times in vacuum. Any impurities were not found by the emission spectrophotometric analysis on Hg thus purified.

Phenylether: Phenylether of special grade[6] was once distilled in reduced pressure of 7 mmHg, and then purified with five times' fractional recrystallization and two times' vacuum distillation. Any impurities were not found on phenylether thus prepared by the gaschromatographic technique. Mp 26.9°C.

Heat Capacity Determination. Heat capacity is deter-

1) Osaka Asahi metal.
2) Nihon Kinzoku.
3) Yotsuhata Kagaku, GR.
4) Merck, GR.
5) Junsei Kagaku, EP.
6) Tokyo Kasei, GR.

mined according to the following equation:

$$P = (m_c/M_c)C_c + (m_s/M_s)C_s + E \quad (1)$$

where P is the input energy required to elevate the temperature of a calorimeter by 1°C, m weight in gram, M molecular weight in gram, C heat capacity per mole and E the sum of energies for thermocouples, protective tubes, an internal heater, a stand for a capsule and small heat exchange between the capsule containing a sample and the surroundings. c refers to a capsule and s to a sample. The amount of heat exchange varies depending on the stray emf of a thermocouple used for adiabatic control, on the heating rate, on the amount of a sample and on its thermal properties defining the extent of heat transfer. Except for thermal properties of a sample used, it is possible to keep all experimental conditions almost invariable in every heat capacity measurement. Therefore, when E, which is determined by measuring known heat capacity of a material chosen as a standard in strictly the same condition as in measurements on a sample, heat capacity of which is unknown, is used for determining heat capacity of the sample, the systematic error of heat capacity thus determined is caused principally by the difference in thermal properties between the standard and the sample.

The authors determined E on Hg, heat capacity of which is well-established,[7] for heat capacity calculation on antimony halides. To estimate the accuracy of heat capacity thus determined, heat capacity of phenylether determined by Furukawa *et al.*[8] with the probable error of ±0.25% was chosen as a relative standard, and was compared with that measured by the present authors in the same way as described above. Difference between the two would indicate the upper limit of accuracy of heat capacity on halides; thermal conductivity of a molten salt is, in general, smaller than that of Hg and larger than that of phenylether, hence, its heat capacity can be measured more accurately than that of phenylether by the adiabatic calorimetric technique.

In each work, heat capacity of two-phase system (C'), *i. e.* heat capacity of saturated vapor plus heat capacity of liquid in equilibrium with saturated vapor (C_{sat}), was observed, and C_{sat}/mol was obtained by calculation according to the following equation[9]:

$$C_{sat} = C' - \{(\Delta Hv_2 \cdot x_2 - \Delta Hv_1 \cdot x_1)/\Delta\theta - (\Delta Hv \cdot x/T)_m\} \quad (2)$$

where $\Delta\theta$ is the difference between initial and final temperature of a capsule containing a sample, T the absolute temperature, ΔH_v the latent heat of vaporization per mole, x the mass ratio of vapor to the total sample. 1, 2, and m refer to initial, final, and intermediate stages upon rise of temperature. In Eq. (2), values of ΔH_v and x were quoted from the following references: Ref. 10 and Ref. 11 on Hg; Ref. 12 on phenylether; Ref. 11 and Ref. 13 on $SbCl_3$; ΔH_v from Ref. 14 and x from liquid densities measured here and Ref. 14 on $SbBr_3$. The vapor correction was made to be: less than 0.1% of C_{sat} at 265°C on Hg; less than 0.2% of C_{sat} at 245°C on phenylether; less than 0.3% of C_{sat} at 205°C on $SbCl_3$; less than 0.2% of C_{sat} at 265°C on $SbBr_3$.

Heat capacities[7] of Hg and quartz at constant pressure (C_p) are:

$$C_p = 6.44 + 0.19\times10^5 T^{-2} \text{ (cal K}^{-1}\text{ mol}^{-1}\text{)(Hg)}:$$

$$C_p = 13.38 + 3.68\times10^{-3}T - 3.45\times10^5 T^{-2} \text{ (cal K}^{-1}\text{ mol}^{-1}\text{)(quartz)}.$$

These values were used here without conversion into C_{sat}, because the difference between the two is very small on both materials in the range of temperature in which the present work was carried out.

Results

Heat capacity measurements were made three to five times on one sample at each temperature, and values of P observed were within ±1% at each temperature. In every case, P was around 3 cal K^{-1} and its 60—70% was for heat capacity of a sample.

$SbCl_3$. Heat capacity measurements were made on Hg and $SbCl_3$ alternately, then on Hg and phenylether alternately in the range, 90—210°C, at each interval of 10°C. The value of E in every case is about 1% of P in the vicinity of 100°C and about 4% of P in that of 200°C. Seven samples of $SbCl_3$ were used for measurements. Mean heat capacity obtained at each temperature is shown in Table 1 and Fig. 2. Mean error of each value, about 1% of C_{sat}, is also given in Table 1. As shown in Fig. 2, the temperature dependency of heat capacity seems to be negative. When one, however, takes mean error on the measurements into account, the dependency should be disregarded. Therefore, averaging mean heat capacity obtained at each temperature in the range, 90—210°C, 35.2 cal $K^{-1}mol^{-1}$ is determined as the heat capacity of saturated liquid $SbCl_3$.

Mean heat capacities obtained on two samples of phenylether in the range, 90—210°C, are shown in Fig. 3 and compared with those determined by Furu-

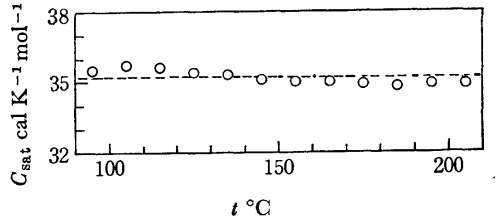

Fig. 2. Heat capacity *vs.* temperature on $SbCl_3$.

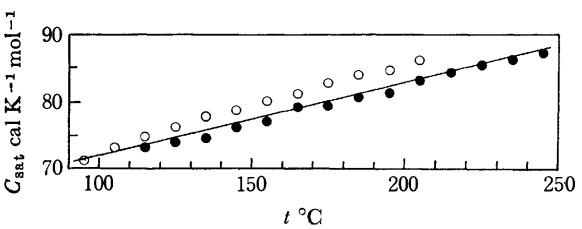

Fig. 3. Heat capacity *vs.* temperature on phenylether.
Solid line: by Furukawa *et al.*
○ and ●: by the present authors in experimental series on $SbCl_3$ and $SbBr_3$, respectively.

7) K. K. Kelley, *Bull. U. S. Bur. Mines*, No. 584 (1960).
8) G. T. Furukawa, D. C. Ginning, R. E. McCoskey, and R. A. Nelson, *J. Res. Nat. Bur. Stand.*, **46**, 195 (1951).
9) B. H. Sage and W. N. Lacey, *Ind. Eng. Chem.*, **27**, 484 (1935),
10) "Gmelins Handbuch der anorg. Chem.", 34, Quecksilber 1, S. 34, (1960).
11) O. Kubaschewski, E. LL. Evans, and C. B. Alcock, "Metallurgical Thermochemistry", 4ed. The Pergamon Press Ltd., England (1967) (Japanese translation, Sangyotosho Co., (1968), p. 338 (Table D.)).
12) "Landolt-Börnstein Phys.-Chem. Tab.", 6 Aufl., II-2-a, (1960) S. 125 and 206.
13) "Gmelins Handbuch der anorg. Chem.", **18**, Antimon B (1949).
14) R. J. Sime, *J. Phys. Chem.*, **67**, 501 (1963).

TABLE 1. HEAT CAPACITIES OF $SbCl_3$ AND $SbBr_3$ (cal K^{-1} mol^{-1})

t°C	$SbCl_3$		$SbBr_3$	
	C_{sat}[a]	ε%[b]	C_{sat}[a]	ε%[b]
95	35.5	1.1		
105	35.7	1.1	—	—
115	35.6	0.9	36.3	1.0
125	35.4	1.1	35.7	0.9
135	35.3	1.2	35.1	0.9
145	35.1	1.0	35.0	1.0
155	35.0	1.1	34.7	0.9
165	35.0	1.0	34.6	0.9
175	34.9	1.1	34.4	0.8
185	34.8	1.3	34.4	1.0
195	34.9	1.2	34.4	0.8
205	34.9	1.3	34.4	1.1
215	—	—	34.4	0.8
225	—	—	34.6	0.9
235	—	—	34.8	1.0
245	—	—	34.6	0.9
255	—	—	34.7	1.1
265	—	—	34.8	0.9

a) Mean value obtained in the range $t \pm 5$°C.
b) Mean error $(\sqrt{\sum(C_{sat\ mean}-C_{sat\ obsd})^2/n(n-1)})/C_{sat}$ (%).

kawa *et al.* The present authors' are higher than Furukawa *et al.*'s, the discrepancy within 3% of C_{sat} in overall temperature range. As mentioned before, 3% is regarded as the accuracy of heat capacity on $SbCl_3$.

$SbBr_3$. Heat capacities of Hg, $SbBr_3$, and phenylether were measured alternately in the range, 110—270°C. For the measurements on $SbBr_3$, finer thermocouples, 0.2 mm in diameter, and protective tubes were used, resulting easier and more reproducible setting of the capsule and thermocouples. The value of E in every case is about −5% of P in the vicinity of 110°C and −2% of P in that of 250°C. Five samples of $SbBr_3$ were used for measurements. Mean heat capacity obtained at each temperature is shown in Table 1 and Fig. 4. Mean error of each value, about 1% of C_{sat}, is also shown in Table 1. As shown in Fig. 4, heat capacities which practically do not vary with temperature are obtained in the range, 130—270°C, however, higher values below 130°C; the reason remains unexplained. Except for those obtained below 130°C, mean heat capacity obtained at each temperature in the range, 130—270°C, was averaged, and 34.6 cal $K^{-1}mol^{-1}$ is determined as the heat capacity of saturated liquid $SbBr_3$.

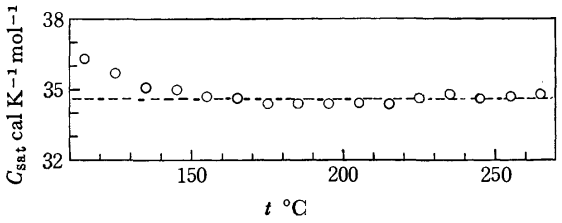

Fig. 4. Heat capacity *vs.* temperature on $SbBr_3$.

Mean heat capacities obtained in this run on three samples of phenylether in the range, 110—250°C, are also shown in Fig. 3. The present authors' agreed with Furukawa *et al.*'s within 1%, indicating that the accuracy of heat capacity on $SbBr_3$ is 1%.

Conclusion

Heat capacities of $SbCl_3$ and $SbBr_3$ saturated with their respective vapors are determined as follows:

$SbCl_3$: 35.2 cal $K^{-1}mol^{-1}$ in the range, 90—210°C. Accuracy is 3%, mean error 1%.

$SbBr_3$: 34.6 cal $K^{-1}mol^{-1}$ in the range, 130—270°C. Accuracy is 1%, mean error 1%.

Studies of Ruthenium Complexes. III. Kinetics of Isotopic Ligand-Exchange Reactions of Halogenopentaammineruthenium(III) Complexes in Aqueous Solution

Tetsuo SHINOHARA, Takato YAMADA, Noriyuki TAKEBAYASHI, Shun-ichi HIRAKI and Akira OHYOSHI

Department of Industrial Chemistry, Faculty of Engineering, Kumamoto University, Kumamoto

(Received January 24, 1972)

Kinetic studies of isotopic ligand-exchange reactions, $[Ru(NH_3)_5X]^{2+}+X^{*-}=[Ru(NH_3)_5X^*]^{2+}+X^-$, where X=Cl, Br, and I, have been made in aqueous solutions. The effects of the hydrogen- and halide-ion concentrations, and of the ionic strength of the aqueous solution on the exchange rate had not been observed under certain definite experimental conditions. The rate constants were determined to be 3.15×10^{-4} sec^{-1} for the chloropentaammine 3.63×10^{-4} sec^{-1} for the bromopentaammine, and 1.1×10^{-4} sec^{-1} for the iodopentaammine at 80°C. The energies of activation were 20 kcal/mol (chloropentaammine), 23 kcal/mol (bromopentaamine), and 30 kcal/mol (iodopentaammine). The reactions proceed through the following two steps:

$$[Ru(NH_3)_5X]^{2+} + H_2O \longrightarrow [Ru(NH_3)_5H_2O]^{3+} + X^-$$

$$[Ru(NH_3)_5H_2O]^{3+} + X^{*-} \longrightarrow [Ru(NH_3)_5X^*]^{2+} + H_2O$$

The first step is regarded as the rate-determining one.

There have been several investigations of the direct replacement of a halide ligand by a free halide ion in solutions of metal halides[1,2] and halogenoammine complexes[3,4]. In most instances of this type of isotopic replacement, especially with octahedral complexes, the rate of exchange has been found to be controlled by the rate of aquation of the complex. For halogenopentaammineruthenium(III) complexes, however, no research has been done, as far as we know.

The results of the present kinetic study were compared with the results for d^6-metal halogenopentaammines, and the mechanism of the isotopic exchange reaction was explained on the basis of the kinetic data.

Expermental

Reagents. All the chemicals used were of a reagent grade. The radio-isotopes, ^{36}Cl(HCl), ^{82}Br(NH_4Br), and ^{131}I(NaI), were obtained from the Japan Radioisotope Association, Tokyo, and were used as radioactive tracers. Distilled water was used in all the kinetic runs. The ionic strength and the acidity of the reaction mixture were adjusted with p-toluenesulfonic acid and its sodium salt. The sodium salt was prepared by the neuralization of the acid with sodium hydroxide.

Halogenopentaammineruthenium(III) Complexes. The $[Ru(NH_3)_5X]X_2$ (X=Cl, Br, I) complexes were prepared by the method described by Allen.[5] One gram of ruthenium trichloride mono-hydrate was dissolved in distilled water (6 ml), and then hydrazine (85%, 10 ml) was added. The mixture was stirred for 17 hr at room temperature, and then filtered several times. To this filtrate, concentrated hydrohalogenic acid was added to make the solution strongly acidic. After this solution had been refluxed for three hours, the respective complexes were obtained. The complex was collected by filtration and washed with ethanol and ether. The final product was obtained by three recrystallizations from the distilled water.

Found: H, 5.08; N, 23.75%. Calcd for $[Ru(NH_3)_5Cl]Cl_2$: H, 5.13; N, 23.93%.

Found: H, 3.30; N, 16.48%. Calcd for $[Ru(NH_3)_5Br]Br_2$: H, 3.52; N, 16.44%.

Found: H, 2.50; N, 12.11%. Calcd for $[Ru(NH_3)_5I]I_2$: H, 2.65; N, 12.35%.

Kinetic Runs. A reaction vessel containing a solution of p-toluenesulfonic acid, sodium halide, and the respective halogenopentaammine complex was kept in a water bath at a constant temperature. A small amount of a solution of radioactive halide was added, and the exchange reaction was initiated. For the cases of the chloro- and the bromocomplex, aliquots of the reaction mixture were pipetted out at appropriate intervals and added to the ice-cooled silver nitrate solution. The free halide ion was precipitated as the silver halide. In the case of the iodocomplex, however, the decomposition of the complex was observed when the reaction mixture was added to the silver nitrate solution; therefore, we used an anion-exchange resin (Amberlite IR-4B) to collect free iodide ions.

In all cases, the supernatant containing the redioactive halogenopentaammine complex was separated and the radioactivity was measured.

The beta-activity of ^{36}Cl was measured by means of a G.M. counter while the gamma-activities of ^{83}Br and ^{131}I were measured by means of a well-type NaI(Tl) scintillation counter.

Results and Discussion

The recovery yields of the free halide ion in reaction solutions were determined, by a series of preliminary experiments, to be: Cl^-: 100%, Br^-: 98.5%, and I^-: 99.5%. Therefore, the exchange rates were calculated using these corrected values.

The reactions have been carried out for a period 8—10 times half-time, and the exchange rates were calculated by McKay's equations,[6] (1) and (2):

$$\ln(1-X/X_\infty) = -[(a+b)/ab]Rt \quad (1)$$

$$R = 0.693\,ab/[(a+b)\cdot T_{1/2}] \quad (2)$$

where R, exchange rate; t, time; a and b, the initial concentrations of the complex and the halide ion and X and X_∞, the radioactivity of the halogenopentaam-

1) D. R. Stranks and R. G. Wilkins, *Chem. Rev.*, **57**, 789 (1955).
2) M. G. Adamson, *J. Chem. Soc., A*, **1968**, 1370.
3) G. B. Schmidt, *Z. Physik. Chem. (N. F.)*, **41**, 26 (1964).
4) G. B. Schmidt, *ibid.*, **50**, 222 (1966).
5) A. D. Allen and C. V. Senoff, *Can. J. Chem.*, **45**, 1337 (1967).
6) H. A. C. McKay, *J. Amer. Chem. Soc.*, **65**, 702 (1943).

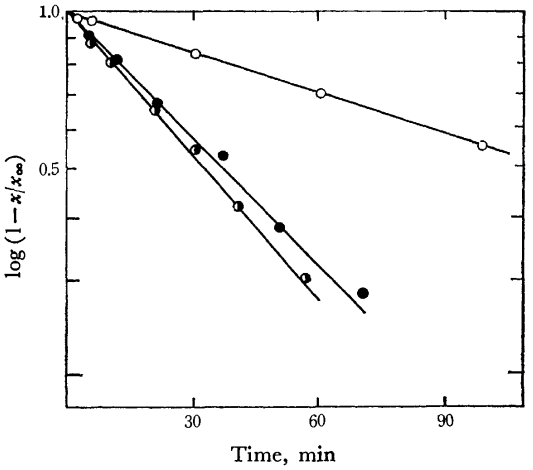

Fig. 1. Plots of $\log(1-x/x_\infty)$ *vs.* reaction time at 80°C.
●: Chloro-, ◑: Bromo-, ○: Iodocomplex.

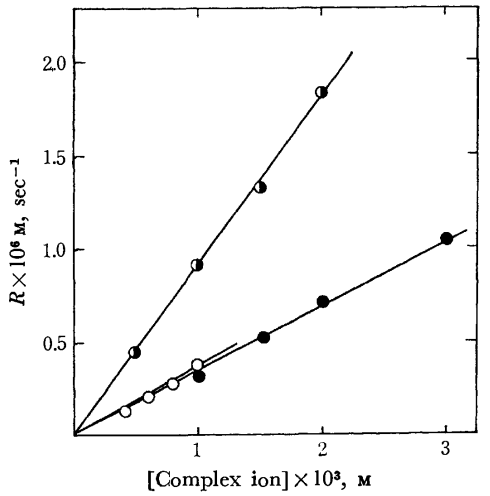

Fig. 2. Relationship between reaction rate (R) and complex-ion concentration.
●: Chlorocomplex, $[H^+]=1\times10^{-3}$ M, 80°C.
◑: Bromocomplex, $[H^+]=4\times10^{-3}$ M, 90°C.
○: Iodocomplex, $[H^+]=8\times10^{-3}$ M, 90°C.

mine complex at time t and at an infinite time. From Eq. (1), it can be expected that the plot of $\ln(1-X/X_\infty)$ *vs.* the reaction time will give a straight line with a slope of $-(a+b)R/ab$. From the plots in Fig. 1, the half-time of the exchange reaction was determined.

As is shown in Fig. 2, it is found that the exchange reaction is first-order with respect to the concentration of the complex.

As is shown in Fig. 3, there is no influence of the initial concentration of the halide ion on the reaction rate. This suggests that the bond formation between the halide and complex ion is not connected with rate-determining step in the exchange reaction.

No influence of the hydrogen ion on the reaction rate was observed under the present experimental conditions, as is shown in Fig. 4. Thus, the reaction rate, R, and rate constant, k_{ex}, can be expressed as follows:

$$R = k_{ex}[\text{complex}] \quad (3)$$

$$k_{ex} = 0.693\, b/[(a+b)\cdot T_{1/2}] \quad (4)$$

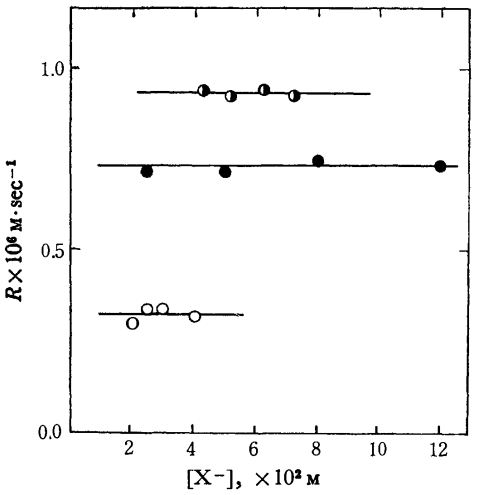

Fig. 3. Effects of halide-ion concentration on the rate
●: Chlorocomplex, $[H^+]=1\times10^{-3}$ M, 80°C.
◑: Bromocomplex, $[H^+]=4\times10^{-3}$ M, 90°C.
○: Iodocomplex, $[H^+]=8\times10^{-3}$ M, 90°C.

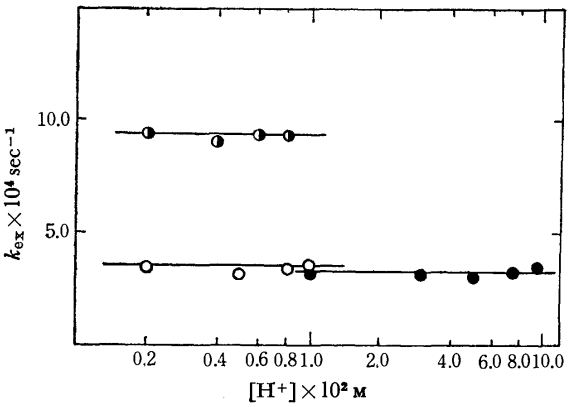

Fig. 4. Effects of hydrogen-ion concentration on the rate constants.
●: Chlorocomplex, ◑: Bromocomplex, ○: Iodocomplex

To know the dependence of the rate on the ionic strength, experiments were carried out while varying the ionic strength of the aqueous solution from 0.04 to 0.4 using sodium *p*-toluenesulfonate. The results are shown in Fig. 5. No practical effect of the ionic strength on the rate is found, this fact suggests that the charged species do not participate in the rate-determining process.

Figure 6 shows the Arrhenius plots, while the activation energies are listed, along with those of analogous and reference reactions, in Table 1.

The values of the rate constants of the exchange reactions are nearly the same as those of the acid-hydrolysis reactions. The values of both activation energies are also the same in the two kinds of the reactions except in the case of the iodopentaammine. From these facts, it may be concluded that the exchange reaction proceeds through the aquation process (5), and that the anation reaction (6) follows. The former step is presumably the rate-determining one.

$$[Ru(NH_3)_5X]^{2+} + H_2O = [Ru(NH_3)_5H_2O]^{3+} + X^- \quad (5)$$

$$[Ru(NH_3)_5H_2O]^{3+} + X^{*-} = [Ru(NH_3)_5X^*]^{2+} + H_2O \quad (6)$$

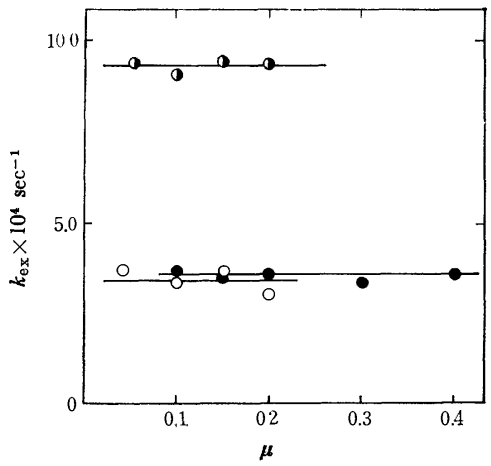

Fig. 5. Dependence of ionic strength on the rate constant.
●: Chloro-, ◑: Bromo-, ○: Iodocomplex

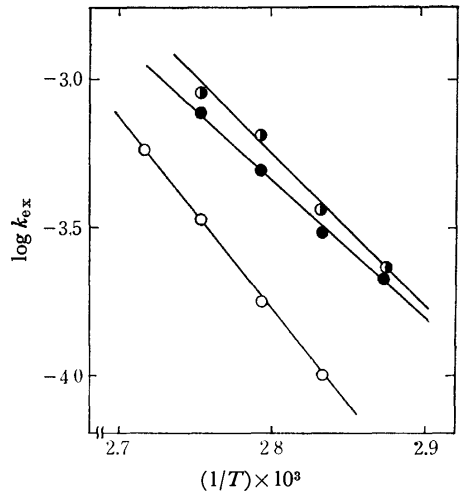

Fig. 6. Arrhenius plots for isotopic ligand exchange reactions.
●: Chloro-, ◑: Bromo-, ○: Iodocomplex

As the exchanging group is varied from chloride to bromide or iodide, the exchange rates are found to be in the order; Br>Cl>I for the halogenopentaammineruthenium(III) complexes. Similar trends have been found by Schmidt[4] for the halide-ion exchange rates of rhodium(III) and iridium(III) pentaammines.

If the mechansim for the aquation reaction (5) were of the dissociative (S_N1 lim) type, then the iodocomplex would be expected to be faster than the others. The present slower rate may be attributed to the higher activation energy term (Table 1) and indicates that bond breaking alone is not of major importance in Reaction (5).

A soft base such as an iodide ion tends to make a covalent bond, and the effective charge of the central metal may be decreased. If Reaction (5) proceeds through an S_N2 path, the exchange rate increases with an increase in the effective charge of the central metal ion.

Table 1. Rates and activation energies of isotopic ligand exchange reactions of $[M(NH_3)_5X]$ complexes

Complex	k_{ex}[a] 10^{-4} sec^{-1}	E_a kcal mol^{-1}	k[b] 10^{-4} sec^{-1}
$[Ru(NH_3)_5Cl]^{2+}$	3.15	20.0±0.5	3.28[c]
$[Ru(NH_3)_5Br]^{2+}$	3.63	23.2±0.9	3.99[f]
$[Ru(NH_3)_5I]^{2+}$	1.1	30 ±1	1.64[f]
$[Rh(NH_3)_5Cl]^{2+}$	0.32[c]	21	
$[Rh(NH_3)_5Br]^{2+}$	0.278[d]	24	
$[Rh(NH_3)_5I]^{2+}$	0.070[e]	26	
$[Ir(NH_3)_5Cl]^{2+}$	0.0048[e]	23	
$[Ir(NH_3)_5Br]^{2+}$	0.0047[d]	23	
$[Ir(NH_3)_5I]^{2+}$	0.0017[e]	26	

a) Temperature 80°C, ionic strength μ=0.1.
b) Rate constants for acid hydrolyses at 80.1°C.
c) from Ref. 4.
d) from Ref. 3.
e) from Ref. 7.
f) from Ref. 8.

Broomhead and Maguire[8] cited the ideas of Pearson and Songstad[9] to interpret their experimental results on the hydrolysis of analogous complexes. The replacement of the hard base, H_2O, by bases such as Cl^-, Br^-, or I^-, where the hardness is decreasing, should lead to a destabilization of the transition state in an S_N2 process and, consequently, to a slower reaction with a high E_a value. The slower rate and the higher activation energy for the iodocomplex are in good agreement with the predictions, assuming the presence of an S_N2 mechanism.

As is shown in Table 1, the exchange rate constants, k_{ex}, are generally smaller than those of acid hydrolyses. This would seem to suggest that Reaction (6) may be partly concerned with the over-all reaction rate; however, these differences are too small for another reaction mechanism to be considered.

Table 1 shows the isotopic exchange reaction rates of the three metal complexes for comparative purposes. It can be seen that the relative rate constants for the isotopic ligand exchange at 80°C are Ru(III)> Rh(III)>Ir(III) for all the halogenopentaammine complexes. This order is also in agreement with that predicted from the crystal-field consideration by Broomhead *et al.*,[7] assuming a seven-coordinated intermediate in an acid hydrolysis reaction corresponding to Eq. (5).

7) J. A. Broomhead, F. Basolo, and R. G. Pearson, *Inorg. Chem.*, **3**, 826 (1964).
8) J. A. Broomhead and L. Kane-Maguire, *ibid.*, **7**, 2519 (1968).
9) R. G. Pearson and J. Songstad, *J. Amer. Chem. Soc.*, **89**, 1827 (1967).

An NMR Study of Metal Complexes Containing Acetylacetone and Related Compounds. IV. The NMR Spectra and the Ligand-exchange Reaction of Cobalt(III) Complexes Containing *N,N'*-Ethylenebis(acetylacetonimine) and Amino Acid

Yuki Fujii

Department of Chemistry, Ibaraki University, Bunkyo-cho, Mito, Ibaraki

(Received January 26, 1972)

A series of mixed cobalt(III) complexes with the general formula of K[Co(baen)(amino acid anion)$_2$]·nH$_2$O (baen=dianion of *N,N'*-ethylenebis(acetylacetonimine); amino acid =glycine, β-alanine, L-alanine, D-alanine, D,L-alanine, L-valine, D-valine D,L-valine, L-leucine, L-isoleucine, and L-phenylalanine) were newly prepared from a reaction mixture of *trans*-*N,N'*-ethylenebis(acetylacetoniminato)diaquocobalt(II), [Co(baen)(H$_2$O)$_2$], and the amino acids. Also prepared were mixed cobalt(III) complexes having the general formula of [Co(baen)(X)$_2$]-ClO$_4$(X=glycine ethyl ester, L-alanine ethyl ester, L-leucine ethyl ester, L-phenylethylamine, D-phenylethylamine, and D,L-phenylethylamine). From the elemental analyses, and the IR and NMR spectra, the amino acid anions were found to coordinate as a unidentate ligand, and the structures of all the complexes were determined to be *trans* with respect to the two nitrogen atoms of the coordinated amino groups. The NMR spectral behavior of the complexes containing D,L-amino acid anions and D,L-phenylethylamine was well interpreted in terms of the existence of the following three species in a relative ratio of 1 : 2 : 1; [Co(baen)(L-form ligand)$_2$]$^{\pm n}$, [Co(baen)(L-form ligand)(D-form ligand)]$^{\pm n}$, and [Co(baen)(D-form ligand)$_2$]$^{\pm n}$. A rapid intermolecular exchange reaction of the apical amino acid anion groups was newly found in water: [Co(baen)(A)$_2$]$^-$+[Co(baen)-(B)$_2$]$^-$⇌2[Co(baen (A)(B)]$^-$ (where A and B indicate the apical amino acid anions). Also found was a rapid exchange reaction of the apical amino acid anion groups between the complex and free amino acid anion. Strong support for the rapid inter molecular exchange reaction was obtained in a CD spectral study of them.

It has been well established that the cobalamine ($V_{B_{12}}$) and its related compounds are labile for the apical ligand substitution reactions, even though the cobalt(III) complexes are generally inert.[1-3] Many anomalous properties of the cobalamines, as compared with the usual cobalt(III) complexes, have been reported by many investigators, and these anomalous properties have been explained in terms of the coordination of the macrocyclic unsaturated corrin to the cobalt(III) ion.[4]

Costa *et al.* found that the cobalt(III) complexes containing *N,N'*-ethylenebis(acetylacetonimine) (baen) and *N,N'*-bis(salicylidene)ethylenediamine (salen) had chemical properties similar to those of the cobalamines.[5-9] Cobalt(III)-baen,-salen complexes make cobalt-carbon bonds, and they show unusual stability in the lower valence state.[10]

In these circumstances, it seemed that it would be very interesting to study the lability of the apical ligands of the cobalt(III)-baen complexes. In this series of studies,[11,12] we found that the cobalt(III)-bean complexes show a rapid intermolecular exchange reaction of the apical ligands. In this paper, we will report the preparation, the NMR spectra, and the rapid intermolecular exchange reaction of the cobalt-(III)-baen complexes containing amino acid anions.

Experimental

Preparation of the Complexes. 1) *Complexes with the General Formula of K[Co(baen)(amino acid anion)$_2$]·nH$_2$O.* *N,N'*-Ethylenebis(acetylacetoniminato)diaquocobalt(II), *trans*-[Co-(baen)(H$_2$O)$_2$][13] (6.3 g, 0.02 mol), was dissolved in 200 m*l* of methanol. Amino acid (0.04 mol) neutralized with an equimolar amount of potassium hydroxide in 100 m*l* of water was then added. After air had been sucked through the solution for three hours, the solution was concentrated to a volume of about 100 m*l*. Acetone (100—200 m*l*) was added, and the mixture was allowed to stand for two days in a refrigerator. Brown crystals separated out; they were subsequently recrystallized from water and acetone. The yield was about 60—80%. The formulas and the elemental analyses data are listed in Table 1.

Complexes with the General Formula of [Co(baen)(amino acid ethyl ester)$_2$]ClO$_4$. Amino acid ethyl ester hydrochloride (0.022 mol), neutralized with an equimolar amount of potassium hydroxide in 50 m*l* of water, was added to a methanol solution (200m*l*) of *N,N'*-ethylenebis(acetylacetoniminato)-diaquocobalt(II) (3.1 g, 0.01 mol). Then, a hydrogen peroxide solution (5%, 5 m*l*) and sodium perchlorate monohydrate (5 g, 0.36 mol) were added to the solution, and the resulting solution was concentrated to about 100—150 m*l*.

1) J. M. Pratt, *J. Chem. Soc.*, **1964**, 5154.
2) G. C. Hayward, H. A. O. Hill, J. M. Pratt, N. J. Vanston, and R. J. P. Williams, *ibid.*, 6485 (1965).
3) J. M. Pratt and R. G. Thorp, *ibid.*, 188 (1966).
4) S. Fukui and R. Yamaka, Special numbers of "Kagaku no Ryoiki," No. 79, p. 240 (1967), No. 91, p. 1 (1970), Nankodo, Tokyo.
5) G. Costa, G. Mestroni, G. Tauzher, and L. Stefani, *J. Organometal. Chem.*, **6**, 181 (1966), **7**, 493 (1967).
6) G. Costa and G. Mestroni, *Tetrahedron Lett.*, 1783 (1967).
7) G. Costa and G. Mestroni, *J. Organometal. Chem.*, **11**, 325, 333, (1968).
8) G. Costa, A. Puxeddu, and G. Tauzher, *Inorg. Nucl. Chem. Lett.*, **4**, 319 (1968
9) G. Costa, G. Mestroni, and G. Pellizer, *J. Organometal. Chem.*, **15**, 187 (1968).
10) M. Kodama, Y. Fujii, and M. Sakurai, This Bulletin, **45**, 1729 (1972).
11) Y. Fujii, *ibid.*, **43**, 1722 (1970).
12) Y. Fujii, A. Osawa, Y. Furukawa, F. Ebina, and S. Takahashi, *ibid.*, **45**, 2459 (1972).
13) G. T. Morgan and J. D. Smith, *J. Chem. Soc.*, **127**, 2030 (1925).

Table 1. Elemental analyses of the complexes

	Complex	C (%) Found (Calcd)	H (%) Found (Calcd)	N (%) Found (Calcd)
(I)	K[Co(baen)(gly)$_2$]·2H$_2$O	38.40 (38.09)	5.78 (5.98)	11.19 (11.12)
(II)	K[Co(baen((L-ala)$_2$]·7H$_2$O	34.53 (34.72)	6.88 (7.14)	8.74 (8.94)
(III)	K[Co(baen)(D-ala)$_2$]·7H$_2$O	34.74 (34.72)	7.03 (7.14)	9.04 (8.94)
(IV)	K[Co(baen)(DL-ala)$_2$]·3H$_2$O	38.92 (39.27)	6.63 (6.60)	10.11 (10.19)
(V)	K[Co(baen)(β-ala)$_2$]·3H$_2$O	39.34 (39.27)	6.80 (6.60)	10.33 (10.19)
(VI)	K[Co(baen)(L-val)$_2$]·8H$_2$O	38.16 (37.92)	7.81 (7.83)	7.73 (8.05)
(VII)	K[Co(baen)(D-val)$_2$]·8H$_2$O	37.98 (37.92)	7.95 (7.83)	7.94 (8.05)
(VIII)	K[Co(baen)(DL-val)$_2$]·8H$_2$O	37.68 (37.92)	7.69 (7.83)	7.79 (8.05)
(IX)	K[Co(baen)(L-leu)$_2$]·8H$_2$O	40.00 (39.77)	8.16 (8.10)	7.76 (7.87)
(X)	K[Co(baen)(L-isoleu)$_2$]·8H$_2$O	39.51 (39.77)	7.92 (8.10)	7.58 (7.87)
(XI)	K[Co(baen)(L-phe)$_2$]·6H$_2$O	47.97 (47.61)	6.01 (6.17)	7.47 (7.41)
(XII)	[Co(baen)(glyOEt)$_2$]ClO$_4$	40.82 (40.92)	6.33 (6.19)	9.76 (9.55)
(XIII)	[Co(baen)(L-alaOEt)$_2$]ClO$_4$	42.96 (42.96)	6.73 (6.57)	9.02 (9.11)
(XIV)	[Co(baen)(L-leuOEt)$_2$]ClO$_4$	48.05 (48.09)	7.58 (7.51)	8.17 (8.01)
(XV)	[Co(baen)(L-phenylethylamine)$_2$]ClO$_4$	53.78 (53.97)	6.42 (6.48)	8.86 (8.99)
(XVI)	[Co(baen)(D-phenylethylamine)$_2$]ClO$_4$	53.92 (53.97)	6.54 (6.48)	8.86 (8.99)
(XVII)	[Co(baen)(DL-phenylethylamine)$_2$]ClO$_4$	53.87 (53.97)	6.54 (6.48)	8.88 (8.99)

When the solution was cooled to 0°C, brown crystals separated out; they were subsequently recrystallized from methanol-water. The yield was about 80%. The formulas and the elemental analyses data are summarized in Table 1.

3) *Cobalt(III)-baen Complexes Containing* D-, L-, *and* D,L-*phenylethylamine.* These complexes were prepared by the method employed for the preparation of the complexes containing the amino acid ethyl ester. The yeild was about 80—90%. The phenylethylamine was prepared by a known method[14] and was resolved with acetyl-L-leucine.[15] The (+)-amine had $[\alpha]_D^{25}$+39.1°(without solvent), lit. +39.2°, and the (−)-amine had $[\alpha]_D^{25}$−33.4°, lit. −33.6°. The formulas and the elemental analyses data are listed in Table 1.

Measurements. All the NMR spectra were recorded with a Hitachi R-20 spectrometer (60 MHz) at 35°C. The NMR spectra were measured in D_2O or deuterated DMSO, with NaTMS as the internal reference. The IR spectra were measured with a Hitachi EPI-S2 spectrometer, using a potassium bromide disk. The CD spectra were recorded with a Jasco Optical Rotatory Dispersion Recorder, Model ORD/UV-5. All the visible and ultraviolet absorption spectra were recorded with a Hitachi EPS-3 spectrometer.

Results and Discussion

Amino Acid in Unidentate Coordination. It is well known that an amino acid coordinates to a metal ion as a chelate ligand. In some particular complexes, however, the amimo acid acts as a unidentate ligand.[16-18] In the present study, the analytical values of the complexes (in Table 1) suggest that the amino acid in these complexes coordinates to the cobalt(III) ion as a unidentate ligand. Amino acid can coordinate to the cobalt(III) ion as a unidentate ligand in two ways; one is with the oxygen atom of the carboxylate group, and the other, with the nitrogen atom of the amino group. In the present case, the IR spectra suggest that the amino acid anions coordinate in the latter way. All the complexes with the general formula of K[Co(baen)(amino acid anion)$_2$] show the C-O stretching band of the free carboxylate group at about 1600 cm^{-1}, as is shown in Table 2. The carboxylate group of the amino acid anion coordinated to the cobalt(III) ion shows asym. ν_{COO-Co} band at about 1650 cm^{-1},[19] and the amino acid anions in these complexes obtained here seem to coordinate to the cobalt(III) ion, with their amino groups. Their absorption and CD spectra give further evidence for the cobalt(III)-nitrogen linkage in the complexes. The absorption and CD spectra of the K[Co(baen)-(amino acid anion)$_2$] complexes are very similar to

Table 2. The infrared absorption spectra (in cm^{-1})

Complex	*asym.* ν_{COO}	*asym.* $\nu_{C=C}$	*asym.* $\nu_{C=N}$ and $\nu_{C=O}$
I	1603	1580	1510
II, III, IV	1603	1560	1510
V	1603	1560	1510
VI, VII, VIII	1603	1603	1515
IX	1603	1603	1511
X	1603	1603	1514
XI	1623	1595	1510
XII	1732 (COOEt)	1595	1512
XIII	1732 (COOEt)	1602	1510
XIV	1740 (COOEt)	1602	1510
XV, XVI, XVII		1590	1510

14) A. W. Ingersoll, "Organic Synthesis," Coll. Vol. II (1950), p. 503.
15) H. D. Dewitt and A. W. Ingersoll, *J. Amer. Chem. Soc.*, **73**, 5782 (1951).
16) J. Fujita, T. Yasui, and Y. Shimura, This Bulletin, **38**, 654 (1965).
17) T. Yasui, J. Hidaka, and Y. Shimura, *ibid.*, **39**, 2417 (1966).
18) M. D. Alexander and D. H. Busch, *Inorg. Chem.*, **5**, 1590 (1966).
19) K. Nakamoto, Y. Morimoto, and A. E. Martell, *J. Amer. Chem. Soc.*, **83**, 4528 (1961).

Table 3. The NMR spectra of the complexes in D_2O (in δ, ppm)

Complex	C=CH	CH_2-CH_2	CH(R) (amino acid)	CH_3 (C=O)	CH_3 (C=N)	R (amino acid)
I	5.18	3.69	2.51	2.27	2.11	
II, III	5.17	3.69	2.90 2.78 2.66 2.54	2.25	2.11	1.14, 1.02 (CH_3)
IV	5.20 5.17 5.13	3.69	2.90 2.78 2.66 2.54	2.28 2.25 2.22	2.12 2.11 2.08	1.14, 1.02 (CH_3)
V	5.18	3.69	2.19	2.27	2.11	
VI, VII	5.17	3.72	2.48 2.40	2.25	2.12	1.80 (center of $-CH(Me)_2$ peaks) 0.84, 0.72 (CH_3), 0.80, 0.68 (CH_3)
VIII	5.21 5.17 5.14	3.73	2.48 2.40	2.28 2.25 2.22	2.13 2.12 2.11	1.80 (center of $-CH(Me)_2$ peaks) 0.84, 0.72 (CH_3), 0.80, 0.68 (CH_3)
IX	5.17	3.69	2.70 2.60 2.50	2.25	2.12	1.35 (center of $-CH_2-CH(Me)_2$ peaks) 0.89, 0.80 (CH_3)
X	5.17	3.69	2.51 2.44	2.25	2.12	2.15 (center of $-CH(Me)-CH_2(Me)$ peaks) 0.99, 0.90, 0.79 (CH_3), 0.93, 0.90 (CH_3)
XI	4.82	3.36	2.96 2.57 2.82 2.50 2.71 2.36 2.63 2.22	2.08	1.86	7.46 7.29 7.39 7.19 7.36 7.13 7.32 7.07 (C_6H_5)

Table 4. The NMR spectra of the complexes (in δ, ppm)

Complex	Solvent	Baen				Axial ligand
		C=CH	CH_2-CH_2	CH_3 (C=O)	CH_3 (C=N)	
XII	D_2O	5.02	3.69	2.25	2.08	2.76 (CH_2 of gly) 3.95, 4.08, 4.20, 4.32 (CH_2-Me of OEt), 1.30, 1.18, 1.06 (CH_3 of OEt)
XIII	D_2O	4.98	3.69	2.23	2.04	1.17, 1.05 (CH_3 of ala) 3.96, 4.08, 4.20, 4.32 (CH_2-Me of OEt), 1.29, 1.17, 1.05 (CH_3 of OEt)
XIV	DMSO	5.02	3.69	2.17	1.94	2.94 (center of CH(R) of leu) 1.26 (center of CH_2-$CH(Me)_2$ of leu) 0.81, 0.76 (CH_3 of leu) 4.33, 4.11, 3.99, 3.87 (CH_2-Me of OEt), 1.26, 1.14, 1.02 (CH_3 of OEt)
XV, XVI	DMSO	4.99	3.47	2.13	2.03	7.31 (C_6H_5), 1.18, 1.08 (CH_3)
XVII	DMSO	5.14 4.99 4.81	3.47	2.21 2.13 2.03	2.13 2.03 1.92	7.31 (C_6H_5), 1.18, 1.08 (CH_3)

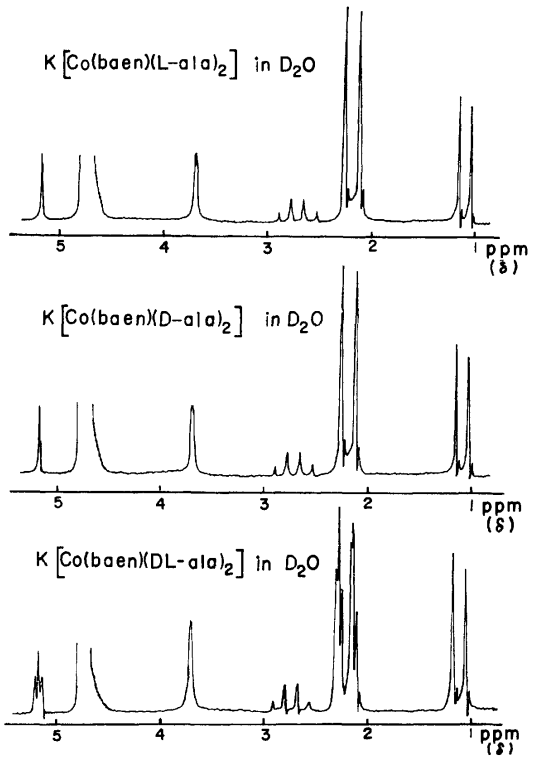

Fig. 1. The NMR Spectra of K[Co(baen)(L-ala)$_2$], K[Co(baen)(D-ala)$_2$], and K[Co(baen)(DL-ala)$_2$] complexes in D_2O.

those of the [Co(baen)(amino acid ethyl ester)$_2$]ClO_4, in which the amino acid ethyl ester coordinated to the cobalt(III) ion, with its amino group.

An attempt to prepare a cobalt(III)-baen complex in which unidentate amino acid coordinates to the cobalt(III) ion with its carboxylate group was not successful. It is well known that the amino acid in a unidentate coordination generally prefers the formation of a bond to the cobalt(III) ion with its carboxylate group than one with its amino group.[20] Therefore, this unusual chemical property of the cobalt(III)-baen complex that the cobalt(III)-baen complex prefers the coordination-bond formation with an amino group of the amino acid anion, may be thought to be due to the anomalous chemical properties of the cobalt(III) complexes containing an unsaturated planar quadridentate ligand.

NMR Spectra of Complexes I, II, III, V, VI, VII, IX, X, XI, XII, XIII, XIV, XV, and XVI. The NMR spectral data of all the complexes are summarized in Tables 3 and 4, while some typical NMR spectra are shown in Fig. 1.

All the complexes except IV, VIII, and XVII show NMR spectral patterns with one C=CH and two CH_3 signals in a relative ratio of 1 : 3 : 3. Although there are three possible geometrical structures, *trans*-planar, *cis*-α, and *cis*-β, these spectral patterns clearly correspond to the *trans*-planar or *cis*-α structures. Since the cobalt(III)-baen complexes containing such unidentate ligands as ammonia, pyridine, and nitro group take the *trans*-planar structure,[12] we can safely assign the *trans*-planar structure to the complexes synthesized in this study.

NMR Spectra of Complexes IV, VIII, and XVII. The NMR spectra of the complexes IV, VIII, and XVII, however, show split patterns for the C=CH and two CH_3 signals of baen. The C=CH signal splits into three peaks with a relative intensities of 1 : 2 : 1, and, the two CH_3 signals, into a pair of three peaks with relative intensities of 3 : 6 : 3 respectively. Since these complexes were prepared by using D,L-racemic amino acid or amine as the starting materials, if the reaction between [Co(baen)$(H_2O)_2$] and the D,L-racemic ligand proceeded statistically it can be thought that Complexes IV, VIII, and XVII are obtained as a 1 : 2 : 1 mixture product of the following three species: [Co(baen)(L-form ligand)$_2$]$^{\pm n}$, [Co(baen)(L-form ligand)(D-form ligand)]$^{\pm n}$, and [Co(baen)(D-form ligand)$_2$]$^{\pm n}$. Complexes II and III, Complexes VI and VII, and Complexes XV and XVI show the same NMR spectra with one another, and the central peak of the C=CH signal and the two central peaks of two CH_3 signals of Complexes IV, VIII, of and XVII coincide with the corresponding peaks Complexes II, VI, and XV respectively. Therefore, we can assign these signals to those based on the [Co(baen)(L-form ligand)$_2$]$^{\pm n}$ and [Co(baen)(D-form ligand)$_2$]$^{\pm n}$ complexes. Thus, we can conclude that the split of two C=CH peaks and the split of four CH_3 peaks of Complexes IV, VIII, and XVII are based on the [Co(baen)(L-form ligand)(D-form ligand)]$^{\pm n}$ complex. The relative ratio between the central C=CH peak and the split of the two C=CH peaks of these complexes is estimated to be 1 : 1. Therefore, we can determine the relative ratio of the three species, [Co(baen)(L-form ligand)$_2$]$^{\pm n}$, [Co(baen)(L-form ligand)(D-form ligand)]$^{\pm n}$, and [Co(baen)(D-form ligand)$_2$]$^{\pm n}$, to be 1 : 2 : 1, which is in agreement with the above statistical considerations. The origin of the peak splitting is thought to be based on the asymmetric

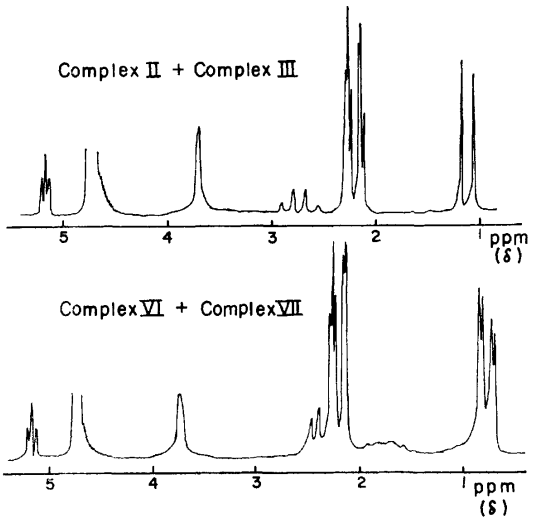

Fig. 2. The NMR spectra of 1 : 1 mixtures of complexes II and III, and VI and VII in D_2O. The pH of the solutions is about 11. The compounds are referred to Table 1.

20) A. Nakahara and M. Shibata, ed. A special number of "Kagaku no Ryoiki," **90**, Nankodo, Tokyo (1970), p. 9.

Table 5. The NMR spectra of the 1 : 1 mixtures (in δ, ppm)

Mixture of complexes	C=CH	CH_2-CH_2	CH_3(C=O)	CH_3(C=N)
II+III	5.20 5.17 5.13	3.69	2.28 2.25 2.22	2.12 2.11 2.08
II+V	5.18 5.17	3.69	2.27 2.25	2.11
II+VI	5.17	3.71	2.25	2.11
II+VII	5.20 5.17 5.14	3.71	2.27 2.25 2.22	2.11
II+IX	5.17	3.69	2.25	2.11
II+X	5.17	3.69	2.25	2.11
II+XI	5.17 5.04 4.96 4.82	3.69 3.55 3.36	2.25, 2.22, 2.08, 2.02,	2.18, 2.11 1.95, 1.86

Table 6. The NMR spectra of the 1 : 1 mixtures (in δ, ppm)

Mixture of complexes	C=CH	CH_2-CH_2	CH_3(C=O)	CH_3(C=N)
III+V	5.18 5.17	3.69	2.27 2.25	2.11
III+VI	5.20 5.17 5.14	3.71	2.27 2.25 2.22	2.11
III+VII	5.17	3.71	2.25	2.11
III+IX	5.20 5.17 5.14	3.69	2.27 2.25 2.22	2.11
III+X	5.20 5.17 5.14	3.69	2.27 2.25 2.22	2.11
III+XI	5.17 5.02 4.99 4.82	3.69 3.52 3.36	2.25, 2.20, 2.11, 2.01,	2.15, 2.13 1.86

nature of these complexes, as will be mentioned latter.

Exchange Reaction of the Apical Amino Acid Anions in Cobalt(III)-baen Complexes. The NMR spectra of 1 : 1 mixtures of Complexes II and III and of Complexes VI and VII are shown in Fig. 2, while their numerical values are tabulated in Tables 5 and 6. Both NMR spectra show peak splitting for C=CH and two CH_3 signals respectively, and the NMR spectra are the same as those of Complexes IV and VIII respectively. If there were no intermolecular interaction between the complexes, the NMR spectrum of the 1 : 1 mixture should be a superposition of the spectra of their original complexes. Therefore, some kind of intermolecular interaction is thought to occur in these complexes in water.

Since the split peaks of the C=CH and CH_3 signals are based on the [Co(baen)(L-form ligand)(D-form ligand)]$^{\pm n}$ complex, as mentioned above, we can interpret the NMR spectral behavior of the 1 : 1 mixtures of Complexes II and III and of Complexes VI and VIII by assuming that the following intermolecular exchange reaction of the apical amino acid anions occurs rapidly and that the corresponding three species exist as a 1 : 1 : 2 equilibrium mixture:

$$[\text{Co(baen)(L-from amino acid anion)}_2]^- + [\text{Co(baen)(D-form amino acid anion)}_2]^- \rightleftharpoons 2[\text{Co(baen)(L-form amino acid anion)-(D-form amino acid anion)}]^- \quad (1)$$

NMR Spectra of 1 : 1 Mixtures of the Complexes. In order to confirm the above assumption in detail, we measured the NMR spectra of 1 : 1 mixtures of the complexes. The NMR spectral data are summarized in Tables 5, 6, 7, and 8, while some representative NMR spectra are shown in Fig. 3.

The NMR spectra of the 1 : 1 mixtures of [Co(baen)$(A)_2]^-$ and[Co(baen)$(B)_2]^-$ complexes (where A and B indicate the apical amino acid anions) show peaks based on the two original complexes. Furthermore, when the optical forms of A and B are different, the peaks of the [Co(baen)(A)(B)]$^-$ complex also appear. Therefore, these experimental facts strongly support the above assumption. When the optical forms of A and B are identical, however, the peaks of the [Co(baen)(A)(B)]$^-$ complex can not be clearly distinguished except in the cases of the complexes containing the phenylalanine anion. In phenylalanine complexes, [Co(baen)-

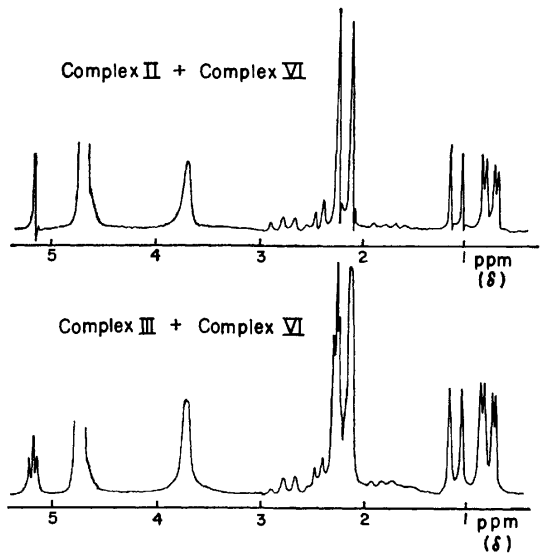

Fig. 3. The NMR spectra of 1 : 1 mixtures of complexes II and VI, and III and VI in D_2O. The solution pH is about 11. The compounds are referred to Table 1.

Table 7. The NMR spectra of the 1 : 1 mixtures (in δ, ppm)

Mixture of complexes	C=CH	CH_2-CH_2	CH_3(C=O)	CH_3(C=N)
I+II I+III	5.18 5.17	3.69	2.27 2.25	2.11
I+VI I+VII	5.18 5.17	3.70	2.27 2.25	2.11
I+IX	5.17	3.69	2.27 2.25	2.11
I+XI	5.18 5.00 4.82	3.69 3.51 3.36	2.27, 2.19, 2.01, 1.98,	2.11, 2.08 1.86

(phenylalanine anion)(A)]$^-$, a large peak splitting resulting from the large magnetic anisotropy effect of a phenyl group is observed regardless of the optical form of A. Therefore, when the optical forms of A and B are identical, the formation of the [Co(baen)-(A)(B)]$^-$-type complexes can also be assumed.

Table 8. The NMR spectra of 1 : 1 mixtures (in δ, ppm)

Mixture of complexes	C=CH	CH_2-CH_2	CH_3(C=O)	CH_3(C=N)
VI+VII	5.21 5.17 5.14	3.72	2.28 2.25 2.22	2.13 2.12 2.11
VI+IX	5.17	3.70	2.25	2.11
VI+X	5.17	3.70	2.25	2.11
VI+XI	5.17 5.03 4.93 4.82	3.70 3.56 3.36	2.25, 2.17, 2.08, 2.01,	2.15, 2.12 1.92, 1.86
VII+IX	5.20 5.17 5.14	3.70	2.27 2.25 2.22	2.11
VII+X	5.20 5.17 5.14	3.70	2.27 2.25 2.22	2.11
VII+XI	5.17 5.02 4.98 4.82	3.70 3.56 3.36	2.25, 2.17, 2.01, 1.92,	2.12, 2.08, 1.86
IX+XI	5.17 5.02 4.94 4.82	3.69 3.53 3.36	2.25, 2.18, 2.08, 2.03,	2.14, 2.12 1.96, 1.86

NMR Spectra of the Mixtures of the Complexes and the Free Amino Acid Anion. If the exchange reaction of the apical amino acid anions occur rapidly and if all the possible products exist as equilibrium mixtures, we can expect that the following reactions between the complex and the free amino acid anion also occur rapidly, and that the corresponding products exist as equilibrium mixtures:

$$[Co(baen)(A)_2]^- + B^- \rightleftharpoons [Co(baen)(A)(B)]^- + A^- \quad (2)$$

$$[Co(baen)(A)(B)]^- + B^- \rightleftharpoons [Co(baen))B)_2]^- + A^- \quad (3)$$

We can confirm the above assumption by observing the peaks of the free amino acid anion A^-.

In order to confirm this again, we measured the NMR spectra of mixtures of the complex and the free amino acid anion. The NMR spectral data of 1 : 2 mixtures are listed in Tables 9 and 10, while some typical NMR spectra are shown in Fig. 4.

Through these measurements, we can clearly observe the peaks corresponding to A^-. The following facts are also observed. When the ratio between the complex and the free amino acid anion is kept at 1 : 2, the observed NMR spectra for these mixtures coincide with the corresponding NMR spectra of the 1 : 1 mixtures of the complexes, except for the additional peaks of the free amino acid anions. In these cases, the NMR spectra correspond to those of the possible species in the relative ratio of 1 : 2 : 1 : 4 : 4; [Co-

Table 9. The NMR spectra of the 1 : 2 mixtures of complex and free amino acid anion at pH 13 (in δ, ppm)

1 : 2 mixture of complex and free amino acid anion	C=CH	CH_2-CH_2	CH_3(C=O)	CH_3(C=N)	Peaks of axial amino acid anion	Peaks of free amino acid anion
I+L-ala$^-$ I+D-ala$^-$ II+gly$^-$ III+gly$^-$	5.18 5.17	3.69	2.27 2.25	2.11	2.51 (CH_2 of gly) 2.90, 2.78, 2.66, 2.54 (CHMe of ala) 1.14, 1.02 (CH_3 of ala)	3.23 (CH_2 of gly) 3.27, 3.38, 3.49, 3.60 (CHMe of ala) 1.20, 1.31 (CH_3 of ala)
I+L-val$^-$ I+D-val$^-$ VI+gly$^-$ VII+gly$^-$	5.18 5.17	3.70	2.27 2.25	2.11	2.51 (CH_2 of gly) 2.48, 2.40 (CHR of val) 1.80 (center of $-CH(Me)_2$ of val) 0.84, 0.72 (CH_3 of val) 0.80, 0.68 (CH_3 of val)	3.23 (CH_2 of gly) 3.08, 3.17 (CHMe of val) 0.99, 0.88 (CH_3 of val) 0.92, 0.81 (CH_3 of val)
I+L-leu$^-$ IX+gly$^-$	5.17	3.60	2.27 2.25	2.11	2.51 (CH_2 of gly) 2.70, 2.60, 2.50 (CHR of leu) 1.35 (center of $CH_2CH(Me)_2$ of leu) 0.89, 0.80 (CH_3 of leu)	3.23 (CH_3 of gly) 3.45, 3.33, 3.21 (CH(R) of leu) 0.93, 0.84 (CH_3 of leu)
I+L-phe$^-$ XI+gly$^-$	5.18 5.01 4.98 4.82	3.69 3.50 3.35	2.27, 2.19, 2.01, 1.98,	2.11, 2.08 1.86	2.51 (CH_2 of gly) 2.39 (CH_2 of gly) 7.46—7.07 (C_6H_5 of phe)	3.23 (CH_2 of gly) 7.48 (C_6H_5 of phe)

Table 10. The NMR spectra of the 1 : 2 mixtures of complex and free amino acid anion at pH 13 (in δ, ppm)

1 : 2 mixture of complex and free amino acid anion	C=CH	CH_2-CH_2	CH_3(C=O)	CH_3(C=N)	Peaks of axial amino acid anion	Peaks of free amino acid anion
II+D-ala$^-$ / III+L-ala$^-$	5.20 5.17 5.13	3.69	2.28 2.25 2.22	2.12 2.11 2.08	2.90, 2.78, 2.66, 2.54 (CHMe of ala) 1.14, 1.02 (CH_3 of ala)	3.27, 3.38, 3.49, 3.60 (CHMe of ala) 1.32, 1.20 (CH_3 of ala)
II+L-val$^-$ / VI+L-ala$^-$	5.17	3.71	2.25	2.11	2.90, 2.78, 2.66, 2.54 (CHMe of ala) 1.14, 1.02 (CH_3 of ala) 2.48, 2.40 (CHR of val)	3.27, 3.38, 3.49, 3.60 (CHMe of ala) 1.32, 1.20 (CH_3 of ala) 3.08, 3.17 (CHR of val)
II+D-val$^-$ / VI+D-ala$^-$	5.20 5.17 5.14	3.71	2.27 2.25 2.22	2.11	1.80 (center of $-CH(Me)_2$ of val) 0.84, 0.72 (CH_3 of val) 0.80, 0.68 (CH_3 of val)	0.99, 0.88 (CH_3 of val) 0.92, 0.82 (CH_3 of val)
II+L-leu$^-$ / XI+L-ala$^-$	5.17	3.69	2.25	2.11	2.90, 2.78, 2.66, 2.54 (CHMe of ala) 1.14, 1.02 (CH_3 of ala) 2.70, 2.60, 2.50 (CHR of leu) 1.35 (center of CH_2-$CH(Me)_2$ of leu) 0.89, 0.80 (CH_3 of leu)	3.27, 3.38, 3.49, 3.60 (CHMe of ala) 1.32, 1.20 (CH_3 of ala) 3.45, 3.33, 3.21 (CHR of leu) 0.93, 0.84 (CH_3 of leu)
II+L-phe$^-$ / XI+L-ala$^-$	5.17 5.04 4.96 4.82	3.69 3.55 3.36	2.25, 2.25, 2.22, 2.18, 2.11, 2.11, 2.08, 2.02, 1.95, 1.95		2.90, 2.78, 2.66, 2.54 (CHMe of ala) 1.14, 1.02 (CH_3 of ala) 1.22, 1.12 (CH_3 of ala) 2.57 (center of CHR of phe) 7.46 7.07 (C_6H_5 of phe)	3.27, 3.38, 3.49, 3.60 (CHMe of ala) 1.32, 1.20 (CH_3 of ala) 7.48 (C_6H_5 of phe)

(baen)$(A)_2]^-$, $[Co(baen)(A)(B)]^-$, $[Co(baen)(B)_2]^-$, A^-, and B^-. When the ratio is kept at 1 : 20, the observed NMR spectra are the same as those of the complexes corresponding to $[Co(baen)(B)_2]^-$, except for the additional peaks of the free amino acid anions. These facts indicate that Reactions 1, 2, and 3 occur and that the corresponding equilibria are made up at the same time; the equilibrium constants in Reactions 1, 2, and 3 are all estimated to be about 1 for all the cases.

Peak Splitting and the Conformation of the Apical Amino Acid Anions. The fact that the NMR spectra of the complexes containing L-form amino acid anions are the same as those of the corresponding complexes containing D-form amino acid anions indicates that both complexes have the same symmetrical nature (C_2) and that both complexes have the same conformation for the apical ligand groups, although they are in the relation of an optical isomer. From the molecular-model test, it is found that the mobility of the apical ligand groups is somewhat restricted by the steric hindrance between the apical ligand groups and the coordinated baen. Although, in the cases of Complexes II, III, VI, VII, XV, and XVI, the symmetry of these complexes belongs to C_2, in the cases of Complexes IV, VIII, and XVII, in which both D- and L-form ligands are present, as the configurational effect of the optically-different forms of the apical ligands are not averaged because of the restriction of the mobility of the apical ligand groups, the symmetry of these complexes belongs to C_1. Perhaps this lowering of the symmetry from C_2 to C_1 may make

TABLE 11. THE CD SPECTRA OF THE COMPLEXES (in c/s$\times 10^{-13}$)

Complex	Solvent	ν ($\Delta\varepsilon_{max}$)	ν ($\Delta\varepsilon_{max}$)	ν ($\Delta\varepsilon_{max}$)	ν ($\Delta\varepsilon_{max}$)
II	H_2O	49.2 (+0.20)	55.6 (−0.63)	62.5 (+2.42)	71.0 (−1.87)
	MeOH	49.2 (−0.45)	55.6 (−2.28)	62.5 (+2.05)	71.0 (−1.34)
III	H_2O	49.2 (−0.21)	55.6 (+0.64)	62.5 (−2.43)	71.0 (+1.88)
	MeOH	49.2 (+0.45)	55.6 (+2.28)	62.5 (−2.05)	71.0 (+1.34)
VI	H_2O	49.2 (+0.80)	55.6 (0.00)	62.5 (+4.87)	71.0 (−3.51)
	MeOH	49.2 (+0.43)	55.6 (−1.75)	62.5 (+4.33)	71.0 (−3.33)
VII	H_2O	49.2 (−0.80)	55.6 (0.00)	62.5 (−4.88)	71.0 (+3.51)
	MeOH	49.2 (−0.44)	55.6 (+1.75)	62.5 (−4.33)	71.0 (+3.32)
IX	H_2O	49.0 (−0.73)	55.6 (−0.72)	62.5 (+4.80)	71.0 (−3.40)
	MeOH	49.0 (+0.31)	55.6 (−2.26)	62.5 (+4.36)	71.0 (−2.80)
X	H_2O	49.0 (+1.20)	55.6 (−1.25)	62.5 (+4.54)	71.0 (−3.55)
	MeOH	49.0 (+0.41)	55.6 (−2.28)	62.5 (+4.94)	71.0 (−3.69)
XI	H_2O	49.0 (+0.73)	55.6 (−0.27)	62.5 (+2.92)	71.0 (−2.25)
	MeOH	49.0 (+0.69)	55.6 (−0.68)	62.5 (+2.17)	71.0 (−1.95)
XIIII	MeOH	49.0 (+0.31)	55.6 (−0.16)	62.5 (+1.81)	71.4 (−1.79)
XIV	MeOH	49.0 (+0.97)	55.6 (+0.76)	62.5 (+3.70)	71.4 (−2.92)
XV	MeOH	49.0 (+0.76)	55.6 (+2.02)	66.6 (−0.31)	74.0 (+0.82)
XVI	MeOH	49.0 (−0.65)	55.6 (−1.73)	66.6 (+0.25)	74.0 (−0.70)

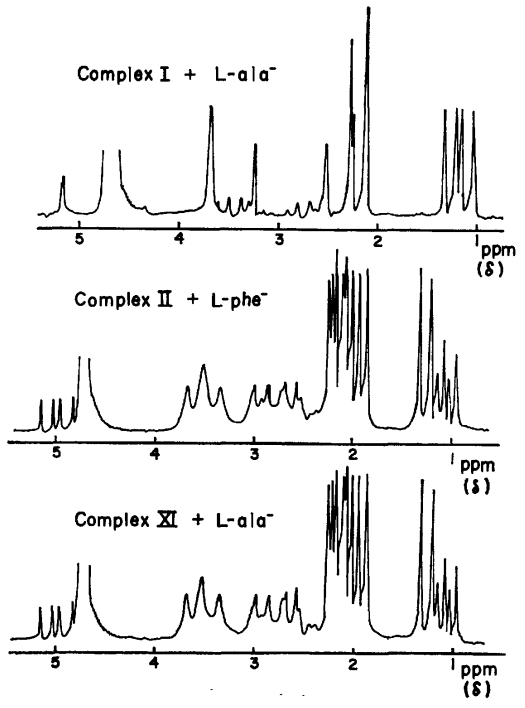

Fig. 4. The NMR spectra of 1 : 2 mixture of complex and potassium salt of amino acid in D_2O. The solution pH is adjusted to about 13 by adding NaOD solution. The compounds are referred to Table 1.

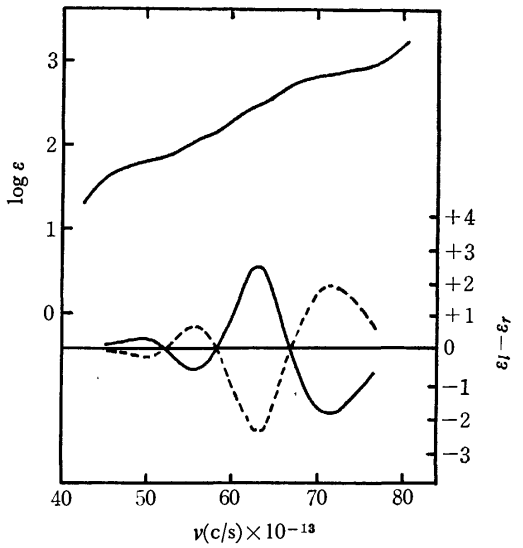

Fig. 5. The AB and CD spectra of K[Co(baen)(L-ala)$_2$] (——) and) K[Co(baen)(D-ala)$_2$] (----) in water.

the main contribution to the peak splitting for the NMR spectra of the complexes containing both D- and L-form ligands. The [Co(baen)(A)(B)]$^-$ complexes (where A and B have the same optical form) show no distinctive peak splitting in their NMR spectra, except when A or B is a phenylalanine anion. These facts indicate that the contribution of the conformation of the apical ligand groups for the peak splitting is bigger than that of the variation in the alkyl group of the amino acid groups. When the complexes contain phenylalanine and the other amino acid anions, because of the big magnetic shielding effect of the phenyl group, the peak splitting is observed in their complexes regardless of the optical forms of the apical ligands. For these complexes, the peak splitting is observed not only in the C=CH and CH_3 signals, but also in the CH_2-CH_2 signal.

On the other hand, when the complexes contain gylcine and β-alanine anions, there is no optically-active form in them. Therefore, no peak splitting is observed for the NMR spectra concerning those of glycine and β-alanine anions.

Table 12. The electronic absorption spectra of the complexes (in $c/s \times 10^{-13}$)

Complex	ν_{sh}	(log ε)	ν_{sh}	(log ε)	ν_{sh}	(log ε)	ν_{sh}	(log ε)	ν_{sh}	(log ε)	ν_{max}	(log ε)
I	49.0	(1.70)	55.0	(1.96)	62.0	(2.45)	71.4	(2.90)	83.0	(3.63)	89.2	(3.86)
II, III, IV	49.2	(1.80)	55.6	(2.05)	62.5	(2.52)	71.4	(2.90)	85.2	(3.76)	89.6	(3.92)
V	49.0	(1.74)	55.5	(2.04)	62.3	(2.48)	71.4	(2.90)	85.2	(3.75)	89.5	(3.89)
VI, VII, VIII	49.0	(1.74)	55.5	(2.06)	62.5	(2.52)	71.0	(2.90)	85.6	(3.79)	89.3	(3.91)
IX	49.6	(1.74)	55.6	(2.04)	62.5	(2.49)	71.0	(2.90)	85.5	(3.74)	89.3	(3.89)
X	49.6	(1.76)	55.6	(2.04)	62.5	(2.48)	71.0	(2.89)	85.2	(3.70)	89.3	(3.88)
XI	49.2	(1.70)	55.6	(2.05)	62.5	(2.50)	71.5	(2.90)	85.2	(3.70)	89.2	(3.88)
XII	49.0	(1.62)	55.5	(1.98)	62.5	(2.56)	71.0	(2.89)	83.3	(3.70)	88.2	(3.86)
XIII	49.0	(1.64)	55.5	(2.00)	62.5	(2.58)	71.0	(2.90)	83.3	(3.72)	88.2	(3.86)
XIV	49.0	(1.62)	55.5	(2.00)	62.5	(2.57)	71.0	(2.90)	83.3	(3.71)	88.2	(3.87)
XV, XVI, XVII	48.0	(1.67)	55.0	(2.08)	64.0	(2.67)	71.0	(2.90)	84.0	(3.60)	88.2	(3.70)

The data of complexes I, II, III, IV, V, VI, VII, VIII, IX, X, and XI are those in water.
The data of complexes XII, XIII, XIV, XV, XVI, and XVII are those in methanol.

CD Spectra of the Complexes. Some typical AB and CD spectra of the complexes are shown in Figs. 5 and 6, while their numerical data are listed in Tables 11 and 12.

The absorption and CD spectra of all the complexes are very complicated because of the π-π^* transition of the baen and charge-transfer transitions,[21-23] and so we can not make band assignemnts at this stage. However, since the CD spectra of the complexes containing L-form ligands are symmetric with those of the corresponding complexes containing D-form ligand, and since the two CD spectra differ only in their signs, by using this CD spectral behavior, we can obtain evidence for the rapid intermolecular exchange reaction of the apical amino acid groups. The CD spectra of mixtures of the complexes containing the L-alanine anion and the free D-alanine anion were measured. When the ratio between the L-alanine complex and the free D-alanine anion was kept at 1 : 1, the observed CD spectrum is that of one-half of the L-alanine complex only. When it was 1 : 2, no CD peaks were observed. When it was 1 : 20, the observed CD spectrum corresponded to that of the D-alanine complex only. These CD spectral changes are found to occur within a few sec. Therefore, it can be concluded that the exchange reactions are very rapid for the cobalt(III) complex, but it is sufficiently slow for all the species in the equilibrium condition to be distinguished separately in the NMR spectra.

These exchange reactions are observed in water, but not in dimethylformamide and dimethylsulfoxide;

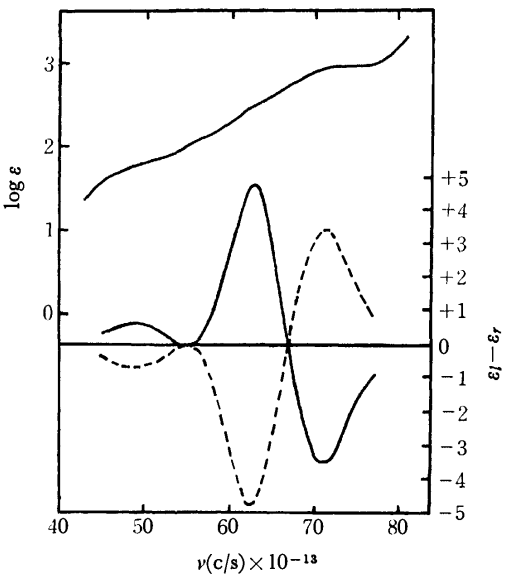

Fig. 6. The AB and CD spectra of K[Co(baen)(L-val)$_2$] (——) and K[Co(baen)(D-val)$_2$] (----) in water.

this is in agreement with the results of the polarographic study.[10] These exchange reactions are thought to be based on the unusual chemical properites of the cobalt(III) complexes containing an unsaturated planar quadridentate ligand.

The author wishes to express his deep thanks to Professor M. Shibata and Mr. K. Kawasaki of Kanazawa University and Professor M. Hatano of Tohoku University for their kind help in the CD spectral measurements. The author also wishes to express his deep thanks to Dr. M. Kodama of Ibaraki University for his encouragement.

21) B. Bosnich, *J. Amer. Chem. Soc.*, **90**, 627 (1968).
22) R. S. Dowing and F. L. Urbach, *ibid.*, **91**, 5977 (1969).
23) R. L. Farmer and F. L. Urbach, *Inorg. Chem.*, **9**, 2562 (1970).

The Kinetics of Electron-transfer Reactions between Oxalato-Cobalt(III) Complexes and Iron(II) in Acid Aqueous Solutions

Kousaburo Ohashi

Department of Chemistry, Ibaraki University, Mito

(Received February 18, 1972)

An investigation of the Fe^{2+} reductions of $Co(ox)(NH_3)_4^+$, $Co(ox)(en)_2^+$, $Co(ox)(trien)^+$, $Co(ox)(dip)_2^+$, $Co(ox)_2(en)^-$, and *cis*-$Co(ox)_2(NH_3)_2^-$ has been carried out spectrophotometrically. The rate constants of $Co(ox)N_4^+$-type complexes increase in this order: $Co(ox)(phen)_2^+ > Co(ox)(dip)_2^+ > Co(ox)(NH_3)_4^+ > Co(ox)(en)_2^+ > Co(ox)(trien)^+$, and these of $Co(ox)_2N_2^-$-type complexes, *cis*-$Co(ox)_2(NH_3)_2^- > Co(ox)_2(en)^-$. The variation in reactivity is mainly ascribed to a change in the enthalpy of activation. The rate constants of $Co(ox)(NH_3)_4^+$, $Co(ox)(en)_2^+$, *cis*-$Co(ox)_2(NH_3)_2^-$, and $Co(ox)_3^{3-}$ increase with the values of the half-wave potential of the polarographic reduction ($Co^{III} \rightarrow Co^{II}$) and with the decrease in the wave number of the maxima of the absorption spectra of the complexes.

The effect of a variation in the nonbridging ligand on the Fe^{2+} reductions of Co(III) complexes containing chloride, bromide, and azide ions as the bridging ligands has been investigated extensively[1-8] It has been demonstrated that the reactivities of *trans*-$CoN_3X(en)_2^{n+}$ ($X=H_2O$, Cl^-, N_3^-) with Fe^{2+} are affected by the free energy of activations required to stretch the *trans*-ligand of X away from the Co(III) center before electron-transfer occurs.[2]

Link found that a change in the nonbridging ligands has the same effect on the reaction of *cis*- and *trans*-$CoClY(en)_2^{2+}$ ($X=H_2O$, NH_3) with Fe^{2+} as it does on the reactions with *cis*- and *trans*-$CoBrY(en)_2^{2+}$.[8]

Recently, the kinetics of the Fe^{2+} reductions of *trans*-(O,Cl)-CoCl(am)(dien)$^+$ (am=amino acid ion and dien=diethylenetriamine) and *trans*(N)-$Co(am)_2(ox)^-$ (ox=oxalate ion) were studied. The effect of amino acids as the nonbridging ligands on the reduction rate of the former is not essentially different from that observed in the reductions of the latter.

In this connection the kinetics of the Fe^{2+} reductions of *cis*-$Co(ox)_2(NH_3)_2^-$, $Co(ox)_2(en)^-$, $Co(ox)(NH_3)_4^+$, $Co(ox)(en)_2^+$, $Co(ox)(trien)^+$, $Co(ox)(dip)_2^+$, and $Co(ox)(phen)_2^+$, (trien=triethylenetetramine, dip=2,2′-dipyridyl, phen=1,10-phenanthroline) were studied. The correlation between the reactivity and the activation parameters, and also the half-wave potential of the polarographic reduction ($Co^{III} \rightarrow Co^{II}$) will be reported here. The effect of an unsaturated nonbridging ligand, such as 2,2′-dipyridyl or 1,10-phenanthroline, on the Fe^{2+} reduction rate of Co(III) complexes will also be discussed.

Experimental

Preparations of Co(III) Complexes. $[Co(ox)NH_3)_4]Cl$,[9] $[Co(ox)(en)_2]Cl \cdot H_2O$,[10] $[Co(ox)(trien)]Cl$,[11] $NH_4[Co(ox)_2(NH_3)_2]H_2O$,[12] $Na[Co(ox)_2(en)]$,[13] and $[Co(ox)(phen)_2]Cl \cdot 4H_2O$ were prepared by methods similar to those described in the references cited. Found: C, 9.11; H, 4.62; N, 21.94%; Calcd for $[Co(ox)(NH_3)_4]Cl$: C, 9.58; H, 4.83; N, 22.36%. Found: C, 22.55; H, 5.65; N, 16.92%; Calcd for $[Co(ox)(en)_2]Cl \cdot H_2O$: C, 22.47; H, 5.65; N, 17.47%. Found: C, 28.18; H, 5.99; N, 16.55%; Calcd for $[Co(ox)(trein)]Cl$: C, 28.89; H, 5.47; N, 16.85%. Found: C, 15.69; H, 4.01; N, 13.20%; Calcd for $NH_4[Co(ox)_2(NH_3)_2] \cdot H_2O$: C, 15.75; H, 3.97; N, 13.78%. Found: C, 22.44 H, 2.31; N, 8.79%: Calcd for $Na[Co(ox)_2(en)]$: C, 22.66; H, 2.54; N, 8.81%. Found: C, 50.84; H, 3.72; N, 9.42%: Calcd for $[Co(ox)(phen)_2]Cl \cdot 4H_2O$: C, 50.80: H, 3.90; N, 9.10%.

Preparation of $[Co(ox)(dip)_2]ClO_4$.[15] To a hot water solution (100 *ml*) containing 2.1 g of *cis*-$[CoCl_2(dip)_2]Cl$, we added 2.0 g of sodium oxalate dissolved in 50 *ml* of hot water; the mixture was then heated on a water bath (60~70°C) for 30 min. The solution was filtered, and the sodium perchlorate was added to the filtrate. The orange crystals which precipitated were filtered. The crude complex was recrystallized from hot 5 N sulfuric acid by the addition of sodium perchlorate. Found: C, 47.93; H, 2.78; N, 10.08%: Calcd for $[Co(ox)(dip)_2]ClO_4$: C, 47.29; H, 2.89; N, 10.21%.

Materials. The preparation of the iron(II) solution and the determinations of the iron(II), the sulfate ion, and the hydrogen ion were carried out by a method similar to that described in a previous paper.[3] The concentration of the sulfate ions of all the reaction mixtures except for *cis*-$Co(ox)_2(NH_3)_2^-$ and $Co(ox)_2(en)^-$ was adjusted to 1.5 M by the addition of sulfuric acid. The reductions of *cis*-$Co(ox_2)(NH_3)_2^-$ and $Co(ox)_2(en)^-$ were carried out in perchloric acid media. All the other reagents used for the preparation of the stock solutions were of a guaranteed reagent quality.

Kinetic Measurements. The cobalt(III) and the iron(II) solutions, both of which contained the necessary amount of sulfuric acid, were kept in a thermostat. The desired volume of the iron(II) solution was added to the cobalt(III) solution. The solution was then transferred into a 1-cm cell compartment of a Hitachi Model EPS-3 type recording

1) A. Haim and P. Benson, *J. Amer. Chem. Soc.*, **87**, 3826 (1965).
2) K. Ohashi, K. Yamamoto, K. Yokouchi, and Y. Kurimura, *Nippon Kagaku Kaishi*, **1972**, 740.
3) Y. Kurimura, K. Ohashi, T. Otsuki, and K. Yamamoto, This Bulletin, **44**, 1239 (1971).
4) Y. Kurimura and K. Ohashi, *ibid.*, **44**, 1797 (1971).
5) K. Ohashi, *ibid.*, **45**, 947 (1972).
6) Y. Kurimura, I. Meguro, and K. Ohashi, *ibid.*, **44**, 3367 (1971).
7) K. Ohashi, K. Yamamoto. I. Hirako, and Y. Kurimura, *ibid.*, **45**. 1712 (1972).
8) R. G. Link, *Inorg. Chem.*, **9**, 252 (1970).
9) W. Schramm, *Z. Anorg. Chem.*, **167**, 177 (1929).
10) A. Werner and A. Vilmos, *ibid.*, **21**, 150 (1899).
11) E. Kyuno, L. J. Boucher, and J. C. Bailar, Jr., *J. Amer. Chem. Soc.*, **87**, 4458 (1965).
12) E. H. Riesenfeld and R. Klement, *Z. Anorg. Chem.*, **124**, 11 (1922).
13) F. R. Dwyer, I. K. Reid, and F. L. Garvan, *J. Amer. Chem. Soc.*, **83**, 1285 (1961).
14) J. A. Broomhead, M. Dwyer, and N. Kane-Maguire, *Inorg. Chem.*, **7**, 1390 (1968).
15) Independent of this work, another method of preparation has already appeared; *cf.* Ref. **14**.

Table 1. Rate constants, activation parameters, and the spectral data for the oxalato-cobalt(III) complexes

Complex	Rate constant M^{-1} sec^{-1}	$\Delta H^{\neq}$ kcal mol^{-1}	$\Delta S^{\neq}$ eu	λ_1[c], nm	λ_2[d], nm
$Co(ox)(NH_3)_4^+$	7.45×10^{-4} [a]	16.7±0.3	−16.7±1.0	512	360
$Co(ox)(en)_2^+$	2.28×10^{-5} [a]	19.1±0.3	−15.6±1.0	500	358
$Co(ox)(trien)^+$	1.67×10^{-5} [a]	19.6±0.7	−14.8±2.3	496	360
$Co(ox)(dip)_2^+$	1.24 [a]	10.8±0.5	−19.1±1.7	500	—
$Co(ox)(phen)_2^+$	3.55 [a]	9.5±0.4	−24.0±1.3	508	—
$Co(ox)_2(NH_3)_2^-$	4.78×10^{-2} [b]	14.3±0.5	−16.5±1.7	555	386
$Co(ox)_2(en)^-$	3.67×10^{-3} [b]	16.1±0.3	−15.6±1.0	544	358

a) $\Sigma[SO_4^{2-}]=1.5$ M, $[H_2SO_4]=0.55$ M, 25±0.1°C. b) $\Sigma[ClO_4^-]=1.0$ M, $[HClO_4]=0.20$ M, 25±0.1°C, $[Fe^{2+}]=0.271$ M.
c) Wavelength for the first absorption maxima. d) Wavelength for the second absorption maxima.

spectrophotometer.[16] The absorbance at the wavelengths corresponding to the first absorption maxima for the complexes was measured automatically. All the kinetic experiments except for that of $Co(ox)(dip)_2^+$ were run under pseudo-first order conditions with respect to $[Fe^{2+}]$. For $Co(ox)(dip)_2^+$, the rate constants were obtained under second-order conditions. The second-order rate constants were obtained by the usual method.

Results

Reductions of Co(III) Complexes. The reduction rates of all the Co(III) complexes except for *cis*-$Co(ox)_2(NH_3)_2^-$ and $Co(ox)_2(en)^-$ were first-order with respect to both the Fe^{2+} and Co(III) concentrations. Therefore, the rate equation may be represented as follows: $-d[Co(III)]/dt=k[Co(III)]\,[Fe^{2+}]$. The rate constants and the activation parameters are summarized in Table 1.

As may be seen from the kinetic data of $Co(ox)_2(en)^-$ listed in Table 2, the second-order constants increase slightly with the Fe^{2+} concentration under the conditions of constant perchlorate-ion and hydrogen-ion concentrations. Similar results were obtained in the reaction of *cis*-$Co(ox)_2(NH_3)_2^-$. The ionic strength increases with the Fe^{2+} concentration, though the perchlorate-ion concentration remains constant (Table 2). The increase in the ionic strength must be one of the reasons for the increase in the second-order rate constant with the Fe^{2+} concentration. No further experiments were carried out in order to investigate the effect of the Fe^{2+} concentration on the reduction rate.

Table 2. The kinetic data for the Fe^{2+} reductions of $Coox_2(en)^-$ under the conditions of $[H^+]=0.50$ M, 25±0.1°C and $\Sigma[ClO_4^-]=2.0$ M.[a]

Fe(II), M	Ionic-strength	Rate constant, M^{-1} sec^{-1}
0.136	2.14	3.60×10^{-3}
0.271	2.27	4.08×10^{-3}
0.407	2.41	4.58×10^{-3}
0.541	2.54	4.83×10^{-3}
0.679	2.69	5.50×10^{-3}

a) The perchlorate ion concentration was adjusted by the addition of lithium perchlorate.

16) A 10-cm cell was used for the reaction of $Co(ox)(phen)_2^+$, because the solubility of this complex into sulfuric acid is small.

The activation parameters for *cis*-$Co(ox)_2(NH_3)_2^-$ and $Co(ox)_2(en)^-$ were obtained from the temperature dependence of the rates, which were obtained under the conditions of a constant Fe^{2+} concentration (Table 1).

Discussion

An oxalate-bridged mechanism was demonstrated for the Fe^{2+} reductions of $Co(ox)_3^{3-}$ and $Coox(H_2O)(NH_3)_3^{+}$[17] by observing the spectrum of the Fe(III) product and by determining its rate of formation. Therefore, the present author thinks that all the reactions occur *via* similar mechanisms.

The relative reactivity for the Fe^{2+} reductions of $Co(ox)(NH_3)_4^+$ and *cis*-$Co(ox)_2(NH_3)_2^-$ decreased upon the replacement of the ammonia molecules with ethylenediamine and triethylenetetramine molecules (Table 1). A similar chelate effect was also observed in Fe^{2+} reductions of $CoCl_2N_4^+$ and $CoCl(H_2O)N_4^{2+}$ (N=$(NH_3)_4$, $(en)_2$ and trien).[3] It was demonstrated that the reactivity of chloro-cobalt(III) with Fe^{2+} is affected by the effects of a) and b) : a) the ligand-field strength of the *trans*-ligand,[1,18,19] and b) the energy required to stretch the *trans*-ligand away from the Co(III) center. The rate constants of $Co(ox)N_4^+$-type complexes (N=saturated ligand) increase with a decrease in the wavenumber of the first absorption band of the complexes.

It is of interest to note here that the reactivities of $Co(ox)N_4^+$-type complexes (N=$(NH_3)_4$, $(en)_2$, trien, $(dip)_2$, $(phen)_2$) and $Co(ox)_2N_2^-$-type complexes (N=$(NH_3)_2$, and (en)) decreases remarkably with an increase in the enthalpy of activation, and that there is a certain degree of compensation effect between $\Delta H^{\neq}$ and $T\Delta S^{\neq}$ for the Fe^{2+} reductions of these complexes (Table 1). Figure 1 shows the good linearity between the logarithm of the rate constant and the enthalpy of activation of $Co(ox)N_4^+$-type complexes. This illustrates that the variation in reactivity is mainly due to the change in the enthalpy of activation.

The reactivity of $Co(ox)(dip)_2^+$ and $Co(ox)(phen)_2^+$ is

17) A. Haim and N. Sutin, *J. Amer. Chem. Soc.*, **88**, 5343 (1966).
18) L. Orgel, Report of the Tenth Solvay Conference, Brussels, p. 289 (1956).
19) H. Taube, *Adv. Inorg. Chem. Radiochem.*, **1**, 1 (1959).

Table 3. The rate constants, spectral data and the half-wave potentials of the polarographic reduction ($Co^{III} \rightarrow Co^{II}$) for the oxalato-Co(III) complexes

Complex	Rate constant $M^{-1}\,sec^{-1}$	λ_1[d], nm	λ_2[e], nm	Half-wave potential[f] (V *vs.* S.C.E.)
$Coox(en)_2^+$	2.28×10^{-5} [a]	500	358	−0.32
$Coox(NH_3)_4^+$	7.45×10^{-4} [b]	512	360	−0.21
$Coox_2(NH_3)_2^-$	7.24×10^{-2} [b]	555	375	−0.03
$Co(ox)_3^{3-}$	$(3.3\pm0.1)\times10^{0}$ [c]	600	424	+

a) Present work, $\Sigma[SO_4^{2-}]=1.5$ M, $[H_2SO_4]=0.55$ M, 25±0.1°C, $[Fe^{2+}]=0.35$ M. b) $\Sigma[SO_4^{2-}]=1.5$ M, $[H_2SO_4]=0.55$ M, 25±0.1°C, $[Fe^{2+}]=0.35$ M. c) Ref. 16, $\Sigma[ClO_4^-]=1.0$ M, 25±0.1°C. d) Wavelength for the first absorption maxima. e) Wavelength for the second absorption maxima. f) From Ref. 20.

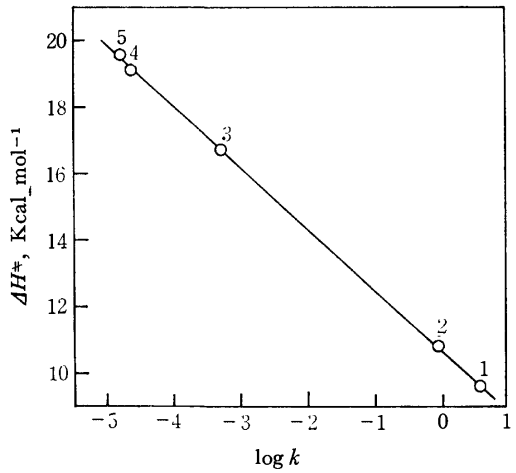

Fig. 1. Relation between the enthalpy of activation and logarithm of the rate constant for the Fe^{2+} reductions of $Co(ox)N_4^+$-type complexes.
1): $Co(ox)(phen)_2^+$, 2): $Co(ox)(dip)_2^+$, 3): $Co(ox)(NH_3)_4^+$, 4): $Co(ox)(en)_2^+$, 5): $Co(ox)(trien)^+$.
$\Sigma[SO_4^{2-}]=1.5$ M, $[H_2SO_4]=0.55$ M, 25±0.1°C.

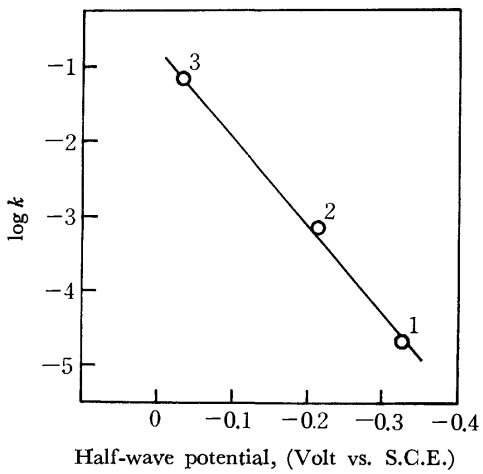

Fig. 2. Relation between the logarithm of the rate constant for the Fe^{2+} reductions of oxalato-Co(III) complexes and the half-wave potential of the polarographic reduction wave ($Co^{III}\rightarrow Co^{II}$).
1): $Co(ox)(en)_2^+$, 2): $Co(ox)(NH_3)_4^+$, 3): *cis*-$Co(ox)_2(NH_3)_2^-$, $\Sigma[SO_4^{2-}]=1.5$ M, $[H_2SO_4]=0.55$ M, 25±0.1°C.

very much larger than that of $Co(ox)(en)_2^+$. The larger reactivity of the former must result from the following factors: a) the efficiency of the mediators for the electron-transfer increases by the coordination of 2,2'-dipyridyl and 1,10-phenanthroline to the Co(III) ion, b) the oxidation-reduction potentials of $Co(ox)(dip)_2^+$, and $Co(ox)(phen)_2^+$ are very different from that of $Co(ox)(en)_2^+$, and c) the free energy of activation required to remove 2,2'-dipyridyl and 1,10-phenanthroline from the Co(III) center is smaller than that of ethylenediamine. However, no further, more detailed discussion could be made on the basis of the present limited kinetic data.

The rate constants of $Co(ox)_{3-n}(NH_3)_{2n}^{(3-2n)+}$ (n= 0, 1, 2) shown in Table 3 increase with the number of oxatate ion coordinated to Co(III). It is also of interest that the reactivity of $Co(ox)_{3-n}(NH_3)_2^{(3-2n)+}$ with Fe^{2+} increases with the decrease in the wavenumber of the first absorption band of the complexes.

It can be seen from Table 3 that the reactivities of $Co(ox)(NH_3)_4^+$, $Co(ox)(en)_2^+$, *cis*-$Co(ox)_2(NH_3)_2^-$, and $Co(ox)_3^{3-}$ with Fe^{2+} increases with the values of the half-wave potential of the polarographic reduction ($Co^{III}\rightarrow Co^{II}$). It has already been demonstrated that there is a relation between the half-wave potentials of polarographic reduction waves and the wavenumbers of the maxima of the absorption spectra of Co(III)-oxalato complexes.[20] The relation between the values of the half-wave potential and the logarithm of the rate constants is shown in Fig. 2. This linear behavior suggests that the reduction potential ($Co^{III}\rightarrow Co^{II}$) affects the reactivity of complexes with Fe^{2+}. No attempt was made to explain quantitatively the relation between the reactivity of complexes and the half-wave potential because of the present lack of much kinetic data.

The author wishes to thank Professor Katsumi Yamamoto and Professor Yoshimi Kurimura for their helpful advice and encouragement.

20) N. Maki, Y. Shimura, and R. Tsuchida, This Bulletin, **30**, 909 (1957).

A Kinetic Study of the Monomer-dimer Reaction in Propionic Acid by Means of Ultrasonic Absorption Measurements

Nobuhide TATSUMOTO, Takayuki SANO, and Tatsuya YASUNAGA

Department of Chemistry, Faculty of Science, Hiroshima University, Higashisenda-machi, Hiroshima

(Received September 16, 1971)

Second ultrasonic absorptions with relaxation frequencies of 26, 36, 53, and 70 MHz could be observed in 0.27, 0.47, 1.0, and 2.0 M cyclohexane solutions respectively of propionic acid at 20°C. The consideration of the variations in the sound absorption, the sound velocity, and the chemical shift with the concentration leads us to the conclusion that the relaxation is attributable to the perturbation of the equilibrium between the open dimer and the monomer of propionic acid. The backward rate constant in this reaction is estimated to be about 10^9 sec^{-1} M^{-1}.

The present authors[1,2] have previously reported that the cyclic and open dimers of propionic acid in several solvents are formed by an intermoleuclar hydrogen bond between carboxylic groups over the concentration range from 4 to 13.4 M(100%). In other ultrasonic studies[3] it has been discussed how the mechanism is associated with the equilibrium between the cyclic dimer and monomer. On the other hand, it has been reported by investigations of NMR,[4] the dielectric constant, and the sound velocity[5] that the monomer is scarcely detected at all in 100% carboxylic acid, but is detected in dilute solutions. The purpose of this paper is to study the kinetics of the reaction system containing the monomer. The ultrasonic absorption was measured in cyclohexane solutions of propionic acid over the concentration range from 0.27 to 13.4 M.

Experimental

The measurement of the ultrasonic absorption in a cyclohexane solution of propionic acid was made over the frequency range from 2.5 to 95 MHz at 20°C by the pulse method, while the sound velocity was measured at 3.00 MHz 20°C by using an ultrasonic interferometer. The chemical shift of the carboxylic proton in propionic acid was measured relative to protons in tetramethylsilane at 34°C. The propionic acid and cyclohexane were of a guaranteed grade. The propionic acid was purified once by fractional distillation at reduced pressure, while the cyclohexane was used without further purification.

Results

The ultrasonic absorptions in 3.9, 7.0, 10.1, and 13.4 M solutions are expressed by the equation for a single relaxation in the experimental frequency range, and the relaxation frequencies are 1.8, 2.4, 3.3, and 4.5 MHz respectively, as can be seen in Fig. 1a. On the other hand, in the 0.27, 0.47, 1.0, and 2.0 M solutions the absorptions are expressed by the equation for a double relaxation, in which the higher relaxation frequencies are 26, 36, 53, and 79 MHz respectively, as can be seen in Fig. 1b. These relaxations are represented by Eqs. (1) and (2):

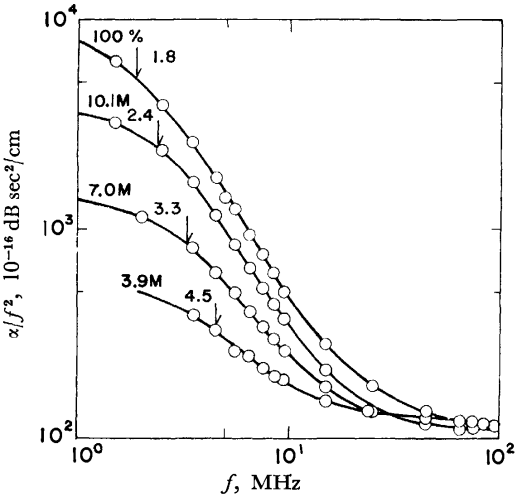

Fig. 1a. Ultrasonic absorptions in cyclohexane solution of propionic acid at 20°C.

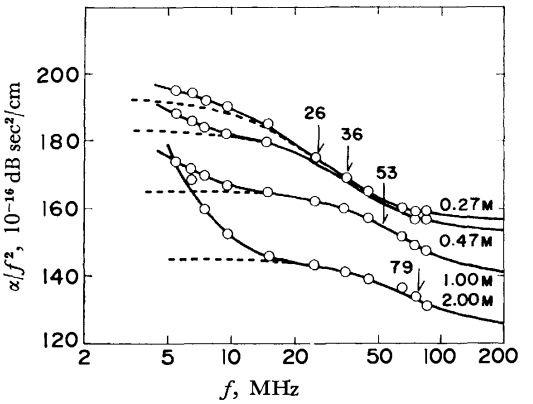

Fig. 1b. Ultrasonic absorptions in cyclohexane solution of propionic acid at 20°C.

$$\alpha/f^2 = \frac{A_1}{1+(f/f_{m_1})^2} + B, \quad (1)$$

$$\alpha/f^2 = \frac{A_1}{1+(f/f_{m_1})^2} + \frac{A_2}{1+(f/f_{m_2})^2} + B, \quad (2)$$

where α is the absorption coefficient of sound, f is the frequency, A_1, A_2, and B are the first and second chemical absorptions and the classical absorption respec-

1) N. Tatsumoto, *J. Chem. Phys.*, **47**, 4561 (1967).
2) N. Tatsumoto, T. Sano, T. Yasunaga, N. Matsunaga and E. Tochigi, This Bulltein, **45**, 2083 (1972).
3) E. Freedman, *J. Chem. Phys.*, **21**, 1784 (1953).
4) L. W. Reeves and W. G. Schneider, *Trans. Faraday Soc.*, **54**, 314 (1958), F. Conti and C. Franconi, *Ber. Bunsenges. Physik. Chem.*, **71**, 146 (1967).
5) M. Blinc and R. Blinc, *J. Polymer Sci.*, **32**, 506 (1958).

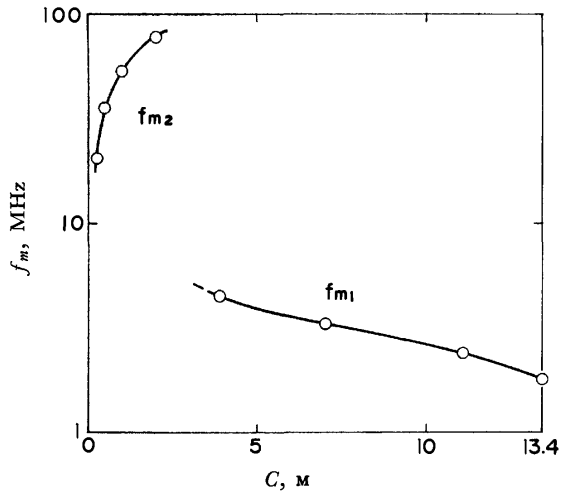

Fig. 2. Variations of f_{m_1} and f_{m_2} with concentration of propionic acid in cyclohexane at 20°C.

tively, and f_{m_1} and f_{m_2} are the first and second relaxation frequencies respectively. The variation in the relaxation frequency with the concentration of propionic acid is shown in Fig. 2.

The variation in the sound velocity with the conecntration is expressed in the next equation for an ideal solution[6]:

$$V = \{V_1 p + V_2(100-p)\}/100, \quad (3)$$

where V is the sound velocity of the solution, V_1 and V_2 are those in the solute and the solvent respectively, and p is weight percentage of the solute. The experimental values of the sound velocity, as plotted against p in Fig. 3, however, deviate from the straight line. In Fig. 4, the values of $\Delta V/p$ are plotted against the molarity, where ΔV represents the deviation from the straight line in Fig. 3; the dependence of the proton shift on the concentration is also shown in Fig. 4.

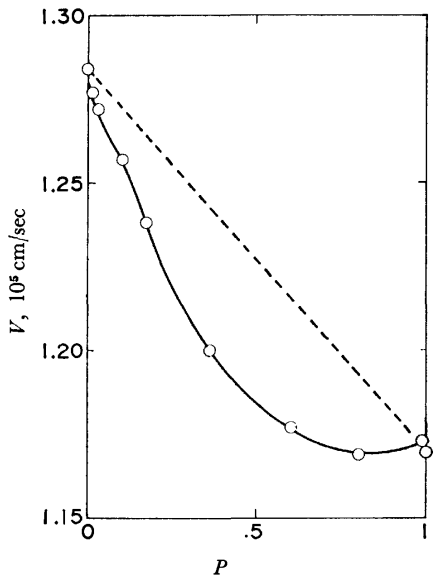

Fig. 3. Variation of sound velocity with concentration of propionic acid in cyclohexane at 20°C.

6) W. Schaaffs, *Z. Phys.*, **105**, 658 (1937).

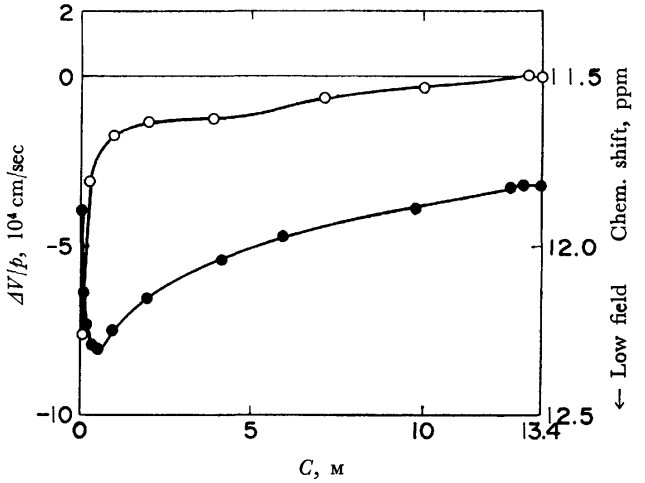

Fig. 4. Variations $\Delta V/p$ and chemical shift of carboxylic acid proton with concentration of propionic acid in cyclohexane at 20 and 34°C, respectively.
○: $\Delta V/p$; ●: chemical shift

Discussion

The first relaxation frequencies in the concentration range from 0.27 to 2.0 M, as estimated roughly from the absorption data in the frequency range from 5.5 to 15 MHz, are less than 10 MHz. The mechanism of the first relaxation in the dilute solutions, therefore, seems to be the same as that in the concentration range from 4 to 13.5 M, the mechanism of which is due to the perturbation of the equilibrium between cyclic and open dimers of propionic acid.[2] On the other hand, the second relaxation mechanism can be assigned to the perturbation of the equilibrium which might exist in the dilute solutions, provided the relaxation is chemical.

This behavior, the fact that $\Delta V/p$ decreases gradually first and then rapidly below 1 M with a decrease in the concentration, indicates the existence of a monomer in the dilute solution of propionic acid, because the decrease in the molecular weight is one of the factors lowering the sound velocity. The absorption in NMR, moreover, shifts to a lower magnetic field at first, and then to a higher field below 0.7 M, with a decrease in the concentration. This indicates that two equilibria exist between cyclic and open dimers and the polymer in a concentrated solution of propionic acid[4] and that the proportion of the number of cyclic dimers to that of open dimers or polymers increases with a

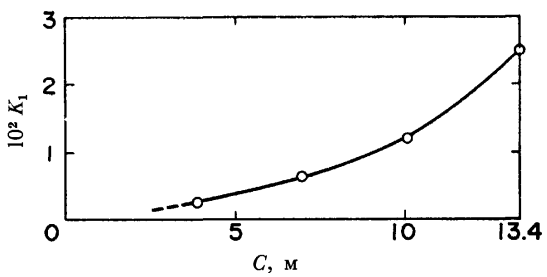

Fig. 5. Variation of equilibrium constant for the reaction between cyclic dimer and open dimer with concentration of propionic acid in cyclohexane at 20°C.

decrease in the concentration. This can also be understood by the change in the equilibrium constant for the reaction between open and cyclic dimers, as calculated from ultrasonic and other data,[2] with the concentration as shown in Fig. 5. That is, the decrease in the equilibrium constant means a relative decrease in the number of the open dimer. Below 0.7 M, the number of the hydrogen bond decreases rapidly, that is, the monomer becomes predominant in the solution. Hence, over the concentration range from 0.27 to 2 M there exist two equilibria between cyclic and open dimers and the monomer:

$$\text{cyclic dimer} \underset{k_2}{\overset{k_1}{\rightleftarrows}} \text{open dimer} \underset{k_4}{\overset{k_3}{\rightleftarrows}} \text{monomer}$$

$$\bar{C}_c \qquad\qquad \bar{C}_o \qquad\qquad \bar{C}_M$$

where k_1, k_2, k_3, and k_4 are the forward and backward rate constants for the reactions between the cyclic and open dimers and between the open dimer and the monomer, and where $\bar{C}_C$, $\bar{C}_O$, and $\bar{C}_M$ are the equilibrium concentrations of cyclic and open dimers and the monomer respectively. The above considerations lead us to the conclusion that the second relaxation is due to the perturbation of the equilibrium between the open dimer and the monomer.

Davies *et al.*[7] have obtained the equilibrium constant between the monomer and the dimer of propionic acid in light petroleum, carbon tetrachloride, and benzene below 1 M by the measurement of the distribution, although they have not separated the open dimer from the cyclic dimer. In this case, the expression of the equilibrium constant is as follows:

$$K = \frac{[\text{monomer}]^2}{[\text{dimer}]} = \frac{(\bar{C}_M)^2}{\bar{C}_c + \bar{C}_o}. \tag{4}$$

From the literature values,[7] the value of K would be expected to be about 10^{-2} M in cyclohexane. On the other hand, the equilibrium constant between open and cyclic dimers is given by:

$$K_1 = \frac{k_1}{k_2} = \frac{\bar{C}_o}{\bar{C}_c}. \tag{5}$$

Equation (4) can, then, be rewritten as in the following equation:

$$K = \frac{(\bar{C}_M)^2}{\bar{C}_c(1+K_1)}. \tag{6}$$

The rough extrapolation of the previous data[2] of K_1 to 1 M gives about 10^{-3}; then:

$$K = \frac{(\bar{C}_M)^2}{\bar{C}_c}. \tag{7}$$

The total concentration of the acid in the monomer unit is expressed as:

$$C = 2\bar{C}_c + 2\bar{C}_o + \bar{C}_M, \tag{8}$$

and Eq. (8) is rewritten as Eq. (9) when K and K_1 are much smaller than unity:

$$C \simeq 2\bar{C}_c, \tag{9}$$

and K_1 is given by:

$$K_1 = \frac{2\bar{C}_o}{C}. \tag{10}$$

The values of $\bar{C}_M$ and $\bar{C}_O$ at C=0.27—2 M are listed in Table 1.

TABLE 1. THE EQUILIBRIUM CONCENTRATIONS OF MONOMER AND OPEN DIMER

C, M	2	1	0.49	0.27
$\bar{C}_M$, 10^{-2} M	10	7.1	5.0	3.7
$\bar{C}_o$, 10^{-4} M	10	5.0	2.5	1.4

The second relaxation frequency is given by:

$$2\pi f_{m_2} = 1/\tau_2 = 4k_4\bar{C}_M - k_2, \tag{11}$$

for $k_1 \ll (k_2 \text{ and } k_3) \ll 4k_4\bar{C}_M$,

and $$2\pi f_{m_2} = 1/\tau_2 = k_2 + k_3, \tag{12}$$

for $4k_4\bar{C}_M \ll k_1 \ll k_2$ and k_3, where τ_2 is the second relaxation time. The variation in $1/\tau_2$ with $\bar{C}_M$ is described in Fig. 6 (see Appendix). The variation in $1/\tau_2$ with $\bar{C}_M$ in this experiment is shown in Fig. 7,

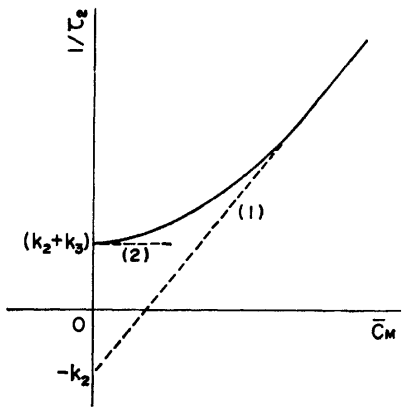

Fig. 6. Theoretical curve of variation of $1/\tau_2$ with equilibrium concentration of monomer, (1) according to Eq. 11; (2) to Eq, 12.

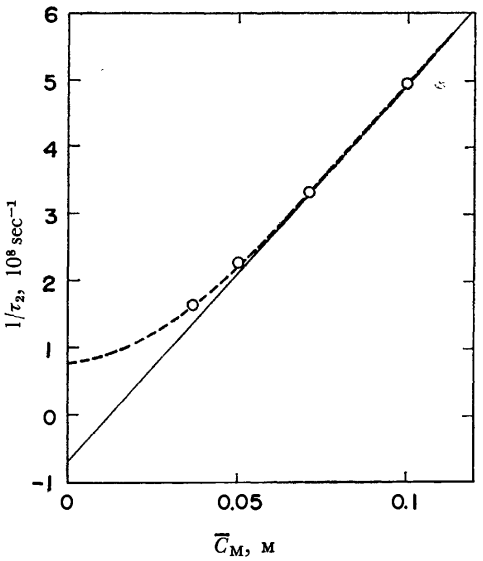

Fig. 7. Variation of $1/\tau_2$ with equilibrium concentration of monomer at 20°C.

7) M. M. Davies, P. Jones, D. Patinaki and E. A. Molelwyn-Hughes, *J. Chem. Soc.*, **1951**, 1249.

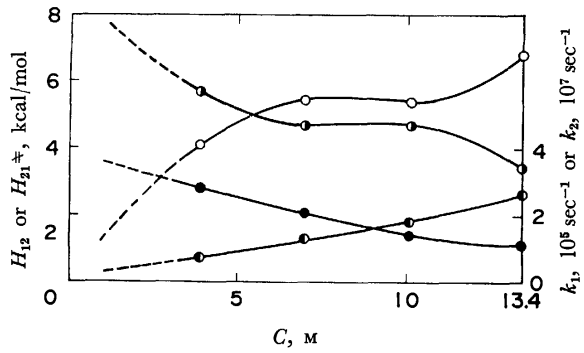

Fig. 8. Variations of $H_{21}^{\neq}$, H_{12}, k_1 and k_2 with concentration of propionic acid in cyclohexane at 20°C.
○: $H_{21}^{\neq}$; ◑: H_{12}; ◐: k_1; ●: k_2

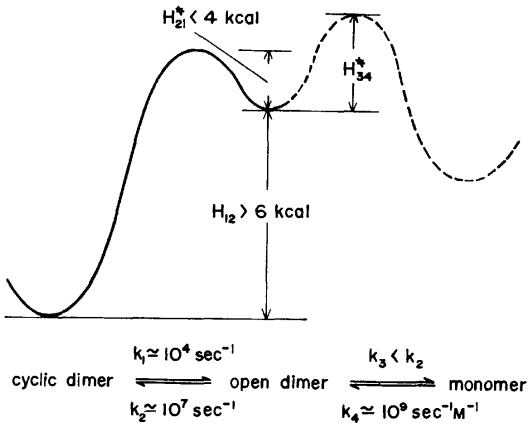

Fig. 9. Energy diagram for propionic acid in cyclohexane in the concentration range of 0.27 to 2 M at 20°C.

and an intercept of the tangent to the curve gives a value of k_2 which is about 7×10^7 sec^{-1}. This is in fair agreement with the value, 10^7 sec^{-1}, estimated approximately from the previous experimental values,[2] which are plotted against the concentration in Fig. 8. If the value of $1/\tau_2$ changes with the concentration, as in Fig. 7, k_2+k_3 can be estimated by the extrapolation of the curve to the intercept. The value of k_2+k_3 is nearly equal to that of k_2; therefore, k_3 is less than k_2. The value of k_4, moreover, is determined to be approximately 10^9 sec^{-1}M^{-1} by the slope of the curve. In order to illustrate the approximate energy diagram for propionic acid in the concentration range from 0.27 to 2.0 M, the values of the activation enthalpy of the backward reaction, $H_{21}^{\neq}$, and the enthalpy change of the reaction, H_{12}, in the reaction between the cyclic dimer and the open dimer, were estimated, along with those of k_1 and k_2, by the extrapolation of the curved $H_{21}^{\neq}$, H_{12}, k_1, and k_2 *vs.* C plots (Fig. 8) to approximately 1 M; the estimated values are listed in Table 2. The comparison between the magnitude of the equilibrium concentrations of the monomer and the open dimer informs us that the monomer is probably more stable than the open dimer. The fact that the activation enthalpy of the forward reaction between the open dimer and the monomer, $H_{34}^{\neq}$, is greater than $H_{21}^{\neq}$ is revealed by taking account of the magnitude of the corresponding rate constant. The energy diagram, consequently, may be described as in Fig. 9. More

Table 2. The kinetic parameters for the first reaction at $C\simeq1$ M and at 20°C

k_1 sec^{-1}	k_2 sec^{-1}	$H_{21}^{\neq}$ kcal / mole of dimer	H_{12} kcal / mole of dimer
$\sim10^4$	$\sim10^7$	<4	>6

detailed kinetic values of the reaction between the open dimer and the monomer can be determined by the change in the ultrasonic absorption with the temperature, but the relaxation strength is too small to determine f_{m_2} and $(\alpha\lambda)_{m_2}$ with accuracy, where λ is the wavelength of sound.

In liquid acetic acid and solutions of acetic acid, a second relaxation similar to that in the solution of propionic acid has been observed,[8] and the perturbation of the equilibrium between the open dimer and the monomer has been proposed as one of the mechanisms. There is no direct evidence for the existence of monomeric acid in liquid acetic acid, but the fact that the second relaxation could be detected in these monocarboxylic acids is very interesting. Finally, it can be expected that the second relaxation will be observed in other monocarboxylic acids and that the mechanism can be assigned more precisely and in more detail in the near future.

Appendix

Variation in $1/\tau_2$ with the Equilibrium Concentration. In the case of the coupled mechanism, the reciprocal relaxation times, $1/\tau_i$, are the eigenvalues, λ_{ii}, of the characteristic equation, which, in the determinant form, reads:

$$\begin{vmatrix} (k_1-\lambda) & -k_2 & 0 \\ -k_1 & (k_2+k_3-\lambda) & -4k_4\bar{C}_M \\ 0 & -k_3 & (4k_4\bar{C}_M-\lambda) \end{vmatrix} = 0 \qquad \text{(A1)}$$

The relaxation times then reduce to:

$$\text{I)}\quad \lambda_1 = 1/\tau_1 = 2\pi f_{m_1} = k_1 + k_2 \simeq k_2, \qquad \text{(A2)}$$

and:

$$\lambda_2 = 1/\tau_2 = 2\pi f_{m_2} = 4k_4\bar{C}_M - (k_2+k_1) \simeq 4k_4\bar{C}_M - k_2, \qquad \text{(A3)}$$

for $k_1 \ll (k_2 \text{ and } k_3) \ll 4k_4\bar{C}_M$ (here, if $k_4/k_2 \leqq 10^3$, $\bar{C}_M$ is relatively large), and to

$$\text{II)}\quad \lambda_1 = 1/\tau_1 = 2\pi f_{m_1} \simeq \frac{k_1k_3}{k_2+k_3}, \qquad \text{(A4)}$$

and:

$$\lambda_2 = 1/\tau_2 = 2\pi f_{m_2} = k_2 + k_3, \qquad \text{(A5)}$$

for $4k_4\bar{C}_M \ll k_1 \ll k_2$ and k_3 (here, if $k_4 \gg k_1$, $\bar{C}_M$ is very small). This consideration holds only in the extremely high or low concentration ranges of $\bar{C}_M$. One, accordingly, should examine whether or not the function, $\lambda_2(\bar{C}_M)$, is represented by a continuous and monotonous increase in the middle concentration range. From Eq. (A1), $\bar{C}_M$ is given by:

$$\bar{C}_M = \frac{\lambda_2{}^2 - (k_1+k_2+k_3)\lambda_2 + k_1k_3}{4k_4\{\lambda_2-(k_1+k_2)\}}, \qquad \text{(A6)}$$

8) J. E. Piercy and J. Lamb, *Trans. Faraday Soc.*, **52**, 930 (1956), F. Bader and K. G. Plass, *Ber. Bunsenges. Physik. Chem.*, **75**, 553 (1971).

where $\lambda_2 \neq k_1+k_2$.

1) The derivative of $\overline{C}_M$ with respect to λ_2 is:

$$\frac{\partial \overline{C}_M}{\partial \lambda_2} = \frac{1}{4k_4} \cdot \frac{\{\lambda_2^2 - 2\lambda_2(k_1+k_2) + (k_1+k_2)(k_1+k_2+k_3) - k_1k_3\}}{(\lambda_2-k_1-k_2)^2}. \tag{A7}$$

A discriminant for a numerator in Eq. (A7) is negative, so that the tangent of a plot of $\partial \overline{C}_M/\partial \lambda_2$ *vs.* λ_2 is always positive.

2) The second derivative of $\overline{C}_M$ with respect to λ_2 is:

$$\frac{\partial^2 \overline{C}_M}{\partial \lambda_2^2} = \frac{-1}{2k_4} \cdot \frac{k_2k_3}{(\lambda_2-k_1-k_2)^3}. \tag{A8}$$

Considerable simplification is possible for two conditions:

i) $$\frac{\partial^2 \overline{C}_M}{\partial \lambda_2^2} < 0, \quad \text{for} \quad \lambda_2 > k_1 + k_2, \tag{A9}$$

and:

ii) $$\frac{\partial^2 \overline{C}_M}{\partial \lambda_2^2} > 0, \quad \text{for} \quad \lambda_2 < k_1 + k_2. \tag{A10}$$

From the definitions of τ_1 and τ_2, $f_{m_1} < f_{m_2}$, and hence $\lambda_2 > k_1+k_2$. Consequently, the $\overline{C}_M(\lambda_2)$ function can be represented by a continuous and monotounous increase, as is shown in Fig. 10.

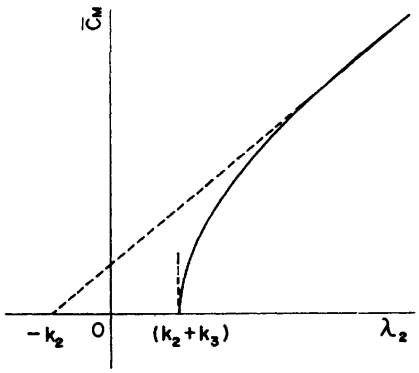

Fig. 10. Theoretical curve of variation of $\overline{C}_M$ with λ_2.

BULLETIN OF THE CHEMICAL SOCIETY OF JAPAN, VOL. 45, 3100—3104 (1972)

Stereoselectivity in Mixed Tris-type Complexes of Cobalt(III) with Glycine and L-Glutamic Acid[1]

Kiyoshi KAWASAKI and Muraji SHIBATA

Department of Chemistry, Faculty of Science, Kanazawa University, Kanazawa

(Received February 19, 1972)

The following ten complexes have been isolated from a reaction mixture of the $[CoCO_3(gly)_2]^-$ ion and L-glutamate in the presence of active charcoal: *mer*-[Co(gly)$_2$L-glutH] (two isomers), *mer*-Cogly(L-glutH)$_2$], *mer*-*Λ*-[Co(L-glutH)$_3$], *fac*-*Λ* and *Δ*-[Co(gly)$_2$(L-glutH], *fac*-*Λ* and *Δ*-[Cogly(L-glutH)$_2$], and *fac*-*Λ* and *Δ*-[Co(L-glutH)$_3$]. These complexes have been characterized by various spectral data. The *Δ*/*Λ* ratios in the *fac* isomers have been estimated to be ca. 60/40, 68/32, and 75/25 for the bis(glycinato), bis(L-glutamato) and tris(L-glutamato) complexes respectively, while no appreciable stereoselectivity has been found in the corresponding *mer* isomers.

Several works on the stereoselectivity in mixed-ligand complexes of cobalt(III) containing L-aspartic acid as a ligand have been made in our laboratory; the complexes studied were of the tris(glycinato-L-aspartato),[2] tris(L-or D-alaninato-L-aspartato),[3] tris-(l-propylenediamine-L-aspartato)[4] and tris(ethylene-diamine-L-aspartato)[5] series. Through these works, it has been found that the stereoselectivity observed can be explained in terms of the favorable interaction of the dangling *β*-carboxylate group in the chelated L-aspartate ion with the amino group in the adjacent chelated ligand.

In the present work, L-glutamic acid (L-glutH_2), with a *γ*-carboxyl group, was taken in order to make a comparison with previous works. That is, a series of tris(glycinato-L-glutamato) complexes, $[Co(gly)_{3-n}(L\text{-glut})_n]^{n-}$ ($n=1, 2, 3$), have been prepared and their diastereoisomers have been isolated. On the basis of the absorption, the circular dichroism, and the proton magnetic resonance spectral data, the isolated isomers have been characterized; then the degree of the stereoselectivity has been evaluated on the basis of the spectral data of the characterized isomers.

By the way, Gillard et al. have recently reported a more detailed study[6] than the previous one[7] on the reaction of L-glutamic acid with the $[CoCO_3(en)_2]^+$ ion.

Experimental

Preparations. The preparative reaction and the chromatographic separation were done similarly to the ways

1) Presented at the 21st Symposium on Coordination Chemistry, Nagoya, October, 1971.

2) K. Kawasaki, J. Yoshi, and M, Shibata, This Bulletin, 43, 3819 (1970).

3) T. Matsuda, T. Okumoto, and M. Shibata, *ibid.*, accepted for publication.

4) Y. Kojima and M. Shibata, *Inorg. Chem.*, **10**, 2382 (1971).

5) Y. Kojima and M. Shibata, presented at the 21st Symposium on Coordination Chemistry, Nagoya, October, 1971.

6) R. D. Gillard, R. Maskill, and A. Pasini, *J. Chem. Soc.*, *A*, **1971**, 2268.

7) J. H. Dunlop, R. D. Gillard, and N. C. Payne, *ibid.*, **1967**, 1469.

described in the previous work[2]; potassium carbonatobis(glycinato)cobaltate(III) (6.4 g, 0.02 mol) was used as the starting material. The L-glutamic acid (5.9 g, 0.04 mol) and sodium hydroxide (1.6 g, 0.04 mol) used were of a reagent grade. Dowex 1-X8 resin in the chloride form was used for the chromatographic separation, and an aqueous solution of calcium chloride (0.05 M) was used as the eluting solution.

When chromatographed on a column of the resin, the reaction mixture finally gave six bands colored alternatively violet and red. These bands were separately collected in fractions labelled from E-1 to E-6 according to the elution order. By careful elution, the first band was further separated into two bands, which were then collected in fractions labelled Nos. 1 and 2. Each fraction, stored up to a certain amount, was concentrated under reduced pressure; ethanol was then added to the concentrate to precipitate the desired complex as its calcium salt. This crude salt was dissolved in a minimum amount of water, and then the solution was acidified with 6 *N* hydrochloric acid in order to convert the calcium salt into the less soluble hydrogen compound. From each fraction corresponding to the red bands (E-2, E-4, E-6), a pair of diastereoisomers (Δ and Λ) was obtained by means of the solubility difference. As for the other fractions, those corresponding to the violet bands (E-1, E-3, E-5), only the E-5 fraction gave one isomer of the diastereomeric pair in the course of crystallization, while the other fractions gave mixtures of the diastereoisomers. The compounds were purified by dissolving them in slightly alkalined water and by then acidifying the solutions with diluted hydrochloric acid. However, one isomer of the pair in E-4 was purified from a large amount of hot water, because it was sparingly soluble in water. For all of the optically-pure compounds, the purification procedure was repeated until the main CD peak of the compound showed a constant intensity ($\Delta\varepsilon$ value).

The results of the elemental analyses of the isolated compounds will be shown below (Table 1).

Formation Ratios. A similar but smaller-scale reaction was carried out; the starting complex (1.71 g, 0.005 mol), L-glutamic acid (1.47 g, 0.01 mol), sodium hydroxide (0.40 g, 0.01 mol), and active charcoal (0.5 g) were used. The temperature in the reaction was kept at *ca.* 60°C, but the reaction time was varied—0.5, 1 and 3 hr. Each reaction mixture, under different conditions, was chromatographed on a small column in a way similar to that described above. From the spectral data of the fractions, the percent compositions among the six bands were evaluated. Moreover, the percent compositions of the Δ isomers in the red bands were calculated on the basis of the spectral data of the isolated diastereomers.

Similar experiments were also carried out with the reaction times of 2 and 5 hr without sodium hydroxide.

Measurements. The absorption spectra were measured with a Hitachi Perkin-Elmer Model 139 UV-VIS spectrophotometer. The circular dichroism spectra were recorded on a JASCO Model ORD/UV-5 spectropolarimeter. The proton magnetic resonance spectra were all measured in deuterium oxide containing an equivalent Na_2CO_3, with a JEOL Model C-60H spectrometer using sodium 3-(trimethylsilyl)-1-propanesulfonate as the internal reference.

Results and Discussion

Characterization of the Isomers. It was apparent, from the absorption spectra and the elution order, that both types of bands, those colored violet and those colored red, consisted of *mer* and *fac* isomers in the *tris*(glycinato-L-glutamato) series, $[Co(gly)_{3-n}(L\text{-glut})_n]^{n-}$ $(n=1, 2, 3)$; A total of ten compounds were crystallized from the fraction. The six compounds obtained from the E-2, E-4, and E-6 fractions were pairs of diastereoisomers of the *fac* complexes. The compound obtained from E-5 was the Λ isomer of *mer*-$[Co(L\text{-glut})_3]^{3-}$, while the corresponding Δ isomer was not isolated, although the existence of the species

Table 1. Elemental analysis and absorption spectral data[a] of the isolated complexes

Label	Complex	Elemental Anal. %[b] C	N	H	Band I ν[c]	Band I ε	Band II ν[c]	Band II ε
E-1	*mer*-$[Co(gly)_2L\text{-glutH}]\cdot H_2O$ (No. 1)	29.23 (29.12)	11.60 (11.32)	4.78 (4.90)	55.6	111	80.7	156
	mer-$[Co(gly)_2L\text{-glutH}]\cdot 2H_2O$ (No. 2)	27.79 (27.77)	10.80 (10.80)	5.00 (5.19)	56.1	110	80.7	168
E-2	*fac*-Λ-$[Co(gly)_2L\text{-glutH}]$	30.44 (30.60)	11.90 (11.90)	4.95 (4.58)	57.4	163	80.0	146
	fac-Δ-$[Co(gly)_2L\text{-glutH}]$	30.38 (30.60)	11.87 (11.90)	4.70 (4.58)	57.6	158	80.0	134
E-3	*mer*-$[Cogly(L\text{-glutH})_2]\cdot 2H_2O$	31.70 (31.24)	9.10 (9.11)	5.37 (5.25)	56.7	106	80.4	153
E-4	*fac*-Λ-$Ca[Cogly(L\text{-glut})_2]\cdot 4H_2O$	26.92 (26.91)	10.03 (10.07)	4.81 (4.80)	57.6	176	80.0	160
	fac-Δ-$[Cogly(L\text{-glutH})_2]$	33.64 (33.89)	9.85 (9.88)	4.84 (4.51)	57.8	170	80.0	139
E-5	*mer*-Λ-$[Co(L\text{-glutH})_3]$	36.51 (36.22)	8.58 (8.45)	4.99 (4.87)	56.4	107	80.4	169
E-6	*fac*-Λ-$[Co(L\text{-glutH})_3]$	35.92 (36.22)	8.49 (8.45)	5.26 (4.83)	57.6	185	80.0	169
	fac-Δ-$[Co(L\text{-glutH})_3]\cdot 0.5H_2O$	35.92 (35.57)	8.49 (8.30)	5.26 (4.99)	57.8	185	80.0	146

a) Measured in 60% perchloric acid. b) ( ): calcd. c) All ν: 10^{13} sec^{-1}.

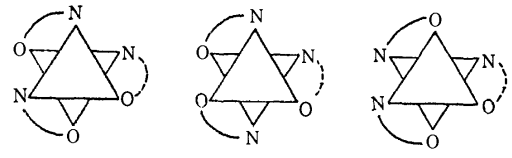

cis(N) *cis*(O) *trans*(N) *cis*(O) *cis*(N) *trans*(O)

Fig. 1. Possible geometrical isomers.

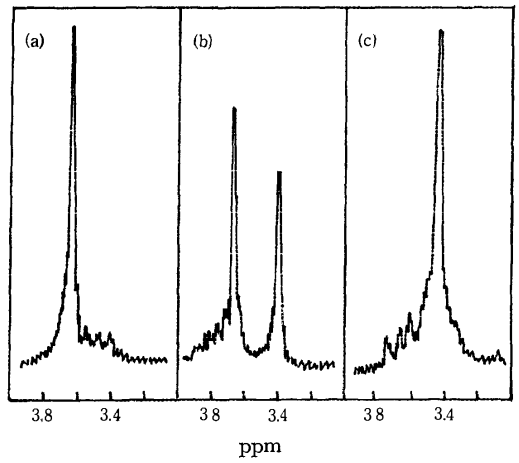

Fig. 2. PMR spectra of $[Co(gly)_2L\text{-glut}]^-$ (3~4 ppm region).
a) *mer* (No. 1) b) *mer* (No. 2) c) *fac*

had been evidenced by the CD spectral change in the process of crystallization. The compound obtained from the No. 1 fraction of E-1 was a mixture of the *Λ* and *Δ* isomers of the *mer*-$[Co(gly)_2L\text{-glut}]^-$ complex, while the compound obtained from No. 2 was the *Λ* isomer contaminated with a small amount of the *Δ* isomer. The compound obtained from the E-3 fraction was also a mixture of the paired isomers of *mer*-$[Cogly(L\text{-glut})_2]^{2-}$. The results of the elemental analyses and the absorption spectral data in 60% perchloric acid are summarized in Table 1.

Structure of mer *Isomers.* In general, the *mer* form of a tris-chelated complex with two kinds of α-aminoacidates has three possible geometrical isomers concerned with the arrangement of two identical ligands (Fig. 1). In the previous works, at least two isomers have been found to exist in the *mer*-$[Cogly(L\text{-asp})_2]^{2-}$[2] amd *mer*-$[CoL\text{-ala}(L\text{-asp})_2]^{2-}$[3] complexes. The spectra of the present *mer*-$[Co(gly)_2\text{-}L\text{-glut}]^-$ complexes are shown in Fig. 2. The CH_2 resonance of the glycinate rings is observed in the 3.3~3.7 ppm region as a single line for the compound obtained from the No. 1 fraction, while it is observed as two lines of the compound obtained from No. 2. The weak lines near the CH_2 resonance are due to the CH resonance of the glutamate ring.

Denning and Piper[8] have reported the PMR spectra of the *mer*-$[Co(L\text{-ala})_3]$ and *mer*-$[Co(L\text{-leu})_3]$ complexes; these spectra show only two sets of doublets, with the ratio of 1 : 2, in the CH_3 resonance region; this fact can be related to the near equivalence of the two chelated rings with respect to the pseudo-three fold axis compared to the third ring. If analogous consideration is made of the present *mer* mixed complexes by disregarding the side group ($-CH_2CH_2COOH$) of the chelated glutamate, the two glycinate rings in the *cis*(N)*cis*(O) isomer seem to be near equivalent and can be expected to show a single CH_2 resonance line. For the remaining two isomers, two resonance lines would be expected. Thus, the complex isolated from the No. 1 fraction can tentatively be identified as the *cis*(N)*cis*(O) isomer, and the other one, obtained from No. 2, as either the *trans*(N)*cis*(O) or the *cis*(N)-*trans*(O) isomer. The above supposition seems to be realistic judging from the evidence that the CH_2 resonance of the *Λ* and *Δ* mixture of *fac*-$[Co(gly)_2L\text{-glut}]^-$ exhibited only one peak, indicating little influence of the side group of the chelated glutamate (Fig. 2, (c)).

CD Spectra. The additivity rule of the vicinal effects on the CD spectra has been reported for several cobalt(III) complexes.[9] Figure 3 shows the CD

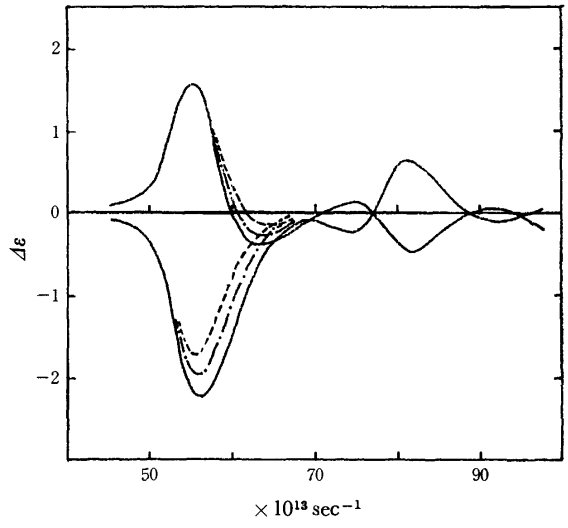

Fig. 3. CD spectra of *fac*-$[Co(gly)_{3-n}(L\text{-glut H})_n]$ in 60% $HClO_4$.
----: $n=1$, —·—: $n=2$, ——: $n=3$

spectra of the six *fac* compounds in 60% perchloric acid. The spectra for the *Λ* and *Δ* isomers are not mirror images of each other and change in a regular way with the number of the chelated L-glutamate because of the vicinal effect of the ligand. Figure 4 shows the vicinal curves of the three *fac* complexes and also the configurational curve of the tris-(L-glutamato) complex, all of which were calculated from the observed spectra of the pairs of *Λ* and *Δ* isomers. The configurational curves of the bis(glycinato) and bis(L-glutamato) complexes accord with that of the tris(L-glutamato) complex. The magnitude of the vicinal effects obtained for each complex is estimated to be 1 : 2 : 3 in proportion to the number fo the chelated glutamato ligand. This proves not only the additivity between the vicinal and configurational effects, but also the additivity within the vicinal effects themselves.

8) R. G. Denning and T. S. Piper, *Inorg. Chem.*, **5**, 1056 (1966).

9) For example, B. E. Douglas and S. Yamada, *ibid.*, **4**, 1561 (1965).

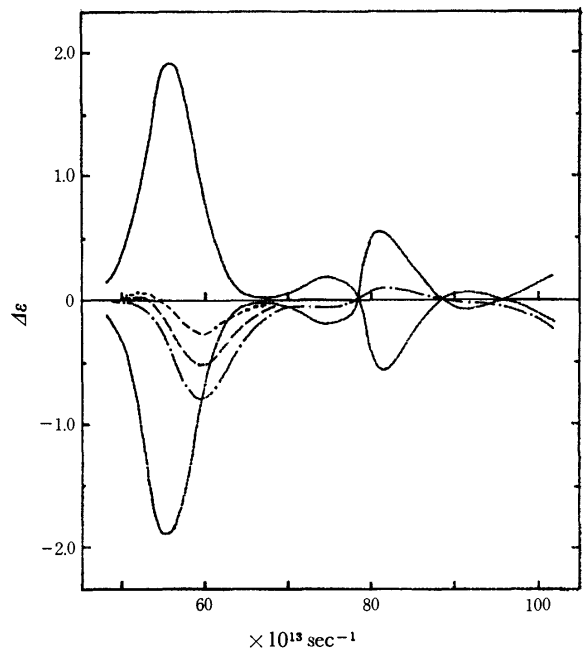

Fig. 4. Vicinal and configurational curves for CD spectra of *fac*-[Co(gly)$_{3-n}$(L-glutH)$_n$].
Vicinal curve; ----: $n=1$, ——: $n=2$, —·—: $n=3$
Configurational curve; ——: $n=3$

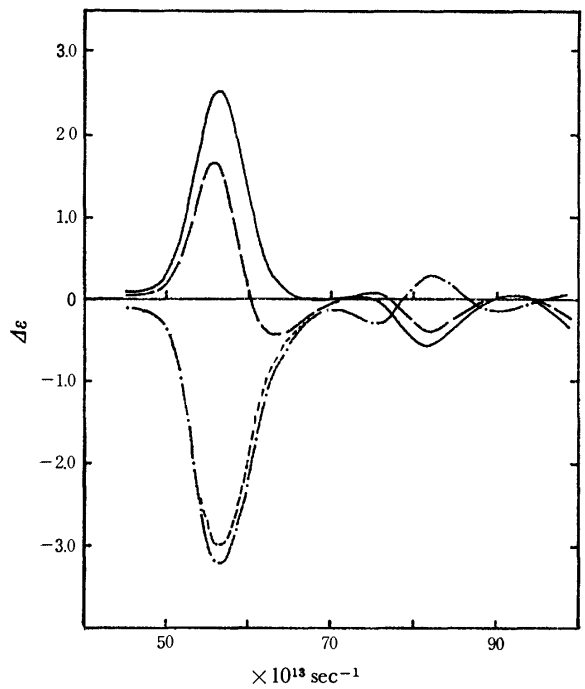

Fig. 5. CD spectra of *fac*-[Co(L-glutH)$_3$].
——, —·—: in 0.1 N NaOH aq. soln.
----, ---: in 0.5 N Na_3PO_4 aq. soln.

Figure 5 shows the CD spectra of *fac*-[Co(L-glut)$_3$]$^{3-}$ measured in 0.1 N sodium hydroxide and 0.5 N trisodium phosphate solutions. The spectrum of the *Λ* isomer in the sodium hydroxide solution shows a single peak with a positive sign in the first absorption band region. When the same sample is measured in a trisodium phosphate solution, the small negative peak appears on the shorter wavelength side and the positive peak decreases in its intensity to a large extent. The spectra of the *Δ* isomer, however, do not show such a large difference between the above two solvents. A similar effect on the CD spectrum by the phosphate ion was observed for *Λ*-[Co(en)$_3$]$^{3+}$ and *Λ*-[Co(*l*-pn)$_3$]$^{3+}$ and was studied in detail by Mason *et al.*[10] The reason for such an effect on the CD spectrum in our case seems to be that it is hard for the phosphate ion to interact with the amino groups in the *Δ* isomer by the repulsion with the *γ*-carboxylate groups, since the chelated glutamate ring seems to be near-planar in the isomers concerned. The spectrum of the *Λ* isomer measured in the trisodium phosphate solution very similar to that in 60% perchloric acid, implying that the latter medium interacts with the complex as the phosphate ion.

Figure 6 shows the CD spectra of the *mer*-*Λ*-[Co(L-glut)$_3$]$^{3-}$ in 60% perchloric acid, 0.1 N sodium hydroxide, and 0.5 N trisodium phosphate solutions. The spectra in an alkaline solution are not influenced very much by the presence of the phosphate ion. The similarity of the spectra in the perchloric acid and trisodium phosphate solutions was not observed for this isomer. The *mer* arrangement of the amino groups seems to inhibit the outer-sphere complexation.

Stereoselectivity. Figure 7 shows the CD spectra in the first absorption band region for the E-1, E-3, and E-5 fractions. Each spectrum exhibits a rather weak Cotton effect curve similar to the vicinal curve for such a complex as *mer*-[Co(L-ala)$_3$].[9] This indicates that the stereoselective formation of one diastereoisomer has scarcely occurred for the *mer* isomers. (By the way, the corresponding spectra for the *mer* fractions of the L-aspartato complexes showed strong Cotton effect curves, indicating the stereoselective formation of the *Λ* isomers.)[2]

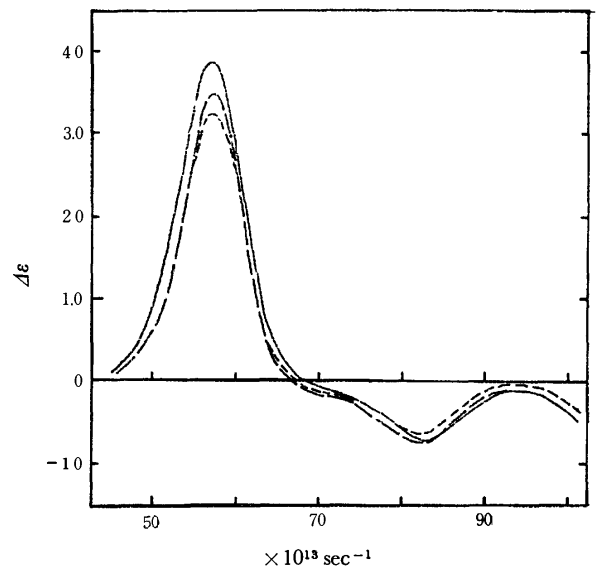

Fig. 6. CD spectra of *mer*-*Λ*-[Co(L-glutH)$_3$].
——: in 60% $HClO_4$
——: in 0.1 N NaOH aq. soln.
----: in 0.5 N Na_3PO_4 aq. soln.

10) R. Larsson, S. F. Mason, and B. J. Norman, *J. Chem. Soc.*, *A*, **1966**, 301; S. F. Mason and B. J. Norman, *ibid.*, **1966**, 307.

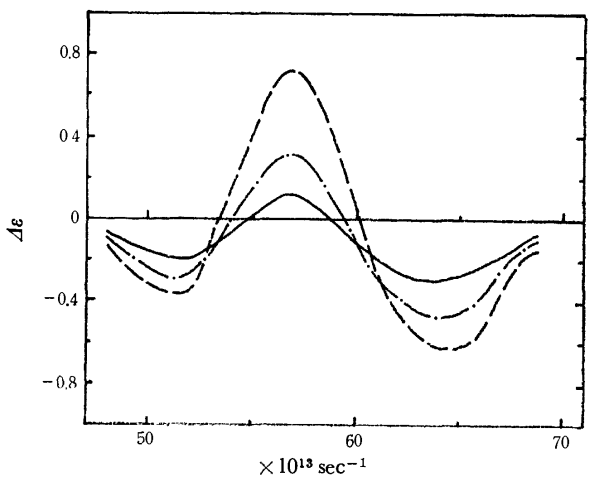

Fig. 7. CD spectra of *mer* fractions.
——: E-1, —·—: E-3, ----: E-5

The percent compositions of the *Λ* isomers in the E-2, E-4, and E-6 fractions are given in Table 2, together with the data on the corresponding fractions of the L-aspartato complexes.[2] The results in both sets of data show the preferential formation of the *Λ* isomers, but the degree of the selectivity in the L-glutamato complexes is considerably less than that in the L-aspartato complexes.

TABLE 2. PERCENT COMPOSITIONS OF *Λ* ISOMERS FOR *fac* FORMS

Reaction time (hr)	Complexes		
	E-2 $[Co(gly)_2$L-glut$]^-$	E-4 $[Cogly($L-glut$)_2]^{2-}$	E-6 $[Co($L-glut$)_3]^{3-}$
0.5	60%	67%	74%
1	60	68	75
3	60	68	75
2[a]	59	66	69
5[a]	50	50	50
	$[Co(gly)_2$L-asp$]^-$	$[Cogly($L-asp$)_2]^{2-}$	$[Co($L-asp$)_3]^{3-}$
1	89	95	95

a) These two reactions were performed at acidic condition (pH *ca.* 6). The others were all performed at pH *ca.* 10.

The stereoselectivity in the L-aspartato complexes has been interpreted in terms of an enhanced stability through hydrogen-bonding between the *β*-carboxylate group of the coordinated L-aspartate ion and the amino group in the adjacent ligand.[2] By the same interpretation, the weaker stereoselectivity in the L-glutamato complexes may be said to be due to the lower ability of the *γ*-carboxylate group of the coordinated L-glutamato ion to interact with the adjacent group. Indeed, there are some cobalt(III) complexes containing the L-aspartate ion as a terdentate ligand,[11] but no such glutamato complexes have yet been found. All of several attempts to make bis(L-glutamato)cobaltate-(III) were unsuccessful.

The percent compositions of the *mer* and *fac* isomers in the reaction mixture are given in Table 3. Similar data[2] on the related complexes are also cited in the table.

TABLE 3. PERCENT COMPOSITIONS OF THE REACTION MIXTURE

Reaction time (hr)	Complexes					
	$[Co(gly)_2$L-glut$]^-$		$[Cogly($L-glut$)_2]^{2-}$		$[Co($L-glut$)_3]^{3-}$	
	mer	*fac*	*mer*	*fac*	*mer*	*fac*
1	22%	16%	26%	20%	10%	5%
	Complexes					
	$[Co(gly)_2$L-asp$]^-$		$[Cogly($L-asp$)_2]^{2-}$		$[Co($L-asp$)_3]^{3-}$	
	mer	*fac*	*mer*	*fac*	*mer*	*fac*
1	17%	15%	22%	30%	6%	10%

In the present complexes, more of the *mer* isomers are formed than the *fac* isomers, whereas more *fac* isomers are formed than the *mer* isomers in the *tris*- and bis(L-aspartato) complexes. The larger formation of the *fac* isomer in the *tris*(L-aspartato) complex can be attributed to the possible hydrogen bonding. That is, the amounts formed increased in the order of *fac-Λ*<*mer-Λ*<*mer-Δ*<*fac-Δ*; this order agrees with the order of the number of the possible hydrogen bonding for for these isomers (their numbers are 0, 1, 2 and 3). This is not true for the isomers of the tris(L-glutamato) complexes, because their amounts increased in the order of *fac-Λ*<*fac-Δ*<*mer-Δ*≃*mer-Λ*. The formation ratio of each *fac-Δ* isomer against the *Λ* isomer was kept constant at various reaction times when the reaction mixture had been prepared as an alkaline solution with sodium hydroxide (pH∼10). On the other hand, with the reaction mixture without sodium hydroxide (pH∼6), the formation ratio was estimated to be nearly 1.0 for the 5-hour reaction. That is, the stereoselectivity disappeared when the reaction was prolonged under such acidic conditions. This fact seems to suggest that the *γ*-carboxylate groups of the chelated glutamates protonate partially in an acidic medium and are less able to form hydrogen bonds with the adjacent groups. Thus, it may be concluded that the polar interaction of the dangling (*β*- or *γ*-) carboxylate groups with adjacent coordinated groups plays an important part in the stereoselectivity in complexes containing optically-active aspartic or glutamic acid. The lower selectivity in the L-glutamato complexes may be responsible for the longer side group ($-CH_2CH_2COO^-$).

11) J. I. Legg and D. W. Cooke, *J. Amer. Chem. Soc.*, **89**, 6854 (1967); K. Hosaka, H. Nishikawa, and M. Shibata, This Bulletin, **42**, 277 (1969); S. Yamaka, J. Hidaka, and B. E. Douglas, *Inorg. Chem.*, **10**, 2187 (1971).

Derivatographic Studies on Transition Metal Complexes. VIII.[1] Thermal Deaquation-Anation Reaction of *cis*-$[CoX(H_2O)N_4]Y_2$ Type Complexes in Solid Phase

Ryokichi Tsuchiya, Masatatsu Suzuki,* and Eishin Kyuno

Department of Chemistry, Faculty of Science, Kanazawa University, Kanazawa
**Department of Chemistry, Faculty of Science, Kyushu University, Fukuoka*

(Received May 15, 1972)

The deaquation-anation reaction of *cis*-$[CoX(H_2O)N_4]Y_2$ type complexes, where X is chloride or bromide ion, N_4 is tetraammine or bis(ethylenediamine), and Y is chloride, bromide or nitrate ion, was investigated by means of both derivatographic and isothermal methods. Some of these reactions were found to include the stereochemical changes, the structure of reaction products formed by deaquation-anation reaction being considerably affected by the counter ionic species: the chloride complexes, where Y=Cl, were deaquated with retention of *cis*-structure, whereas the bromide complexes, where Y=Br, underwent *cis*-to-*trans* stereochemical change. According to the isothermal measurement in the isomerization of *cis*-$[CoCl(H_2O)en_2]Br_2\cdot H_2O$, *cis*-$[CoCl(H_2O)en_2]Br(NO_3)$ and *cis*-$[CoBr(H_2O)en_2]Br_2\cdot H_2O$, these rates were found to obey the first-order rate law and the activation energies, E_a, were obtained to be 38 ± 5, 68 ± 6 and 37 ± 5 kcal mol^{-1} and the enthalpy changes, ΔH, 13.5 ± 2.0, 7.5 ± 2.0 and 13.3 ± 2.0 kcal mol^{-1} for the respective complexes.

Several studies on the thermal deaquation-anation reactions containing the exchange between coordinated water and a counter ion without the displacement of the other ligands in the solid phase are known for $[Co(H_2O)(NH_3)_5]X_3$,[2] $[Cr(H_2O)(NH_3)_5]X_3$,[3] where X is halide, nitrate or sulfate ion, and for *cis*-$[CoX(H_2O)en_2]Y_2$ type complexes,[4] where X and Y are both halide ions.

In the thermal isomerization reaction, *cis,trans*-$[CoCl_2(NH_3)_2en]Br\cdot H_2O \rightarrow$ *trans,cis*-$[CoCl_2(NH_3)_2en]Br$,[5] *cis*-$[CoCl(H_2O)(NH_3)_2en]ClBr$ was presumed to present as an intermediate on the basis of the "aquation-anation" mechanism, the following reaction pathway being deduced,

$$\begin{aligned} &\textit{cis, trans}\text{-}[CoCl_2(NH_3)_2en]Br\cdot H_2O \longrightarrow \\ &\quad \textit{cis}\text{-}[CoCl(H_2O)(NH_3)_2en]ClBr \longrightarrow \\ &\quad \textit{trans, cis}\text{-}[CoCl_2(NH_3)_2en]Br + H_2O. \end{aligned} \quad (1)$$

Since the stereochemical change is considered to occur in the deaquation-anation of *cis*-$[CoCl(H_2O)(NH_3)_2en]ClBr$ in the above pathway (1), it is very interesting to investigate the thermal behavior of halogenoaquo complexes as an intermediate in the isomerization reaction. The aim of this study will be placed on attempting the elucidation of nature for these thermal deaquation-anation reaction involving the stereochemical change and investigating the reaction mechanism thermochemically and kinetically. Such studies on the thermochemical change in the deaquation-anation step will indirectly support the rationality of the reaction pathway (1).

Experimental

Preparation of Complexes. cis-$[CoCl(H_2O)en_2]Br\cdot H_2O$: This complex was prepared by the known method,[6] being purified by the recrystallization from a small amount of concentrated hydrobromic acid.

cis-$[CoCl(H_2O)en_2]Br(NO_3)$. A cold solution of *cis*-$[CoCl(H_2O)en_2]Br_2\cdot H_2O$ obtained above was treated with saturated solution of lithium nitrate to precipitate the desired reddish violet crystals.

cis-$[CoClBren_2]Br\cdot H_2O$ *and* trans-$[CoClBren_2]NO_3$. These compounds were synthesized according to the same method as described in Ref. 6.

cis-$[CoBr_2en_2]Br\cdot H_2O$. $[Co(CO_3)en_2]Br$ was treated with alcoholic hydrogen bromide according to the method of Werner[7] to obtain the desired complex.

cis-$[CoBr(H_2O)en_2]Br_2\cdot H_2O$. This compound was prepared by the method of Werner.[7]

cis-$[CoCl(H_2O)(NH_3)_4]Cl_2$, cis-$[CoCl(H_2O)(NH_3)_4]Br_2$, cis-$[CoBr(H_2O)(NH_3)_4]Br_2$ *and* cis-$[CoBr(H_2O)(NH_3)_4]Cl_2$: These compounds were synthesized according to the literature.[8]

Derivatographic Measurement. The apparatus and techniques for derivatography used in this work were the same as described in the earlier paper.[3] The heating rate was 1°C min^{-1}.

Isothermal Measurement. A Shimadzu TM-1A Thermanobalance and Abderhalden apparatus were used for the isothermal measurement. The procedure of measurement and analytical method for the experiments are similar to those already described.[9] In order to determine the change of the conversion ratios in the thermal reactions of *cis*-$[CoBr(H_2O)en_2]Br\cdot H_2O$, the visible and UV absorption spectra of the complexes were measured consecutively with a Hitachi R-3 Spectrophotometer with 1.0 cm cell: the ratio of *cis*-$[CoBr(H_2O)en_2]Br\cdot H_2O$, *cis*-$[CoBr_2en_2]Br\cdot H_2O$ and *trans*-$[CoBr_2en_2]Br$ were estimated by using the following three simultaneous equations,

$$\begin{aligned} 9.5X + 37.0Y + 55.1Z &= D_{530} \\ 85.0X + 111.1Y + 13.4Z &= D_{554} \\ 102.6X + 101.0Y + 14.2Z &= D_{655}, \end{aligned}$$

1) Presented at the 21st Symposium on Coordination Chemistry, Nagoya, October, 1971.
2) M. Mori, R. Tsuchiya, and Y. Okano, This Bulletin **32**, 1029 (1959).
3) R. Tsuchiya, Y. Kaji, A. Uehara, and E. Kyuno, *ibid.*, **42**, 1881 (1969).
4) F. C. Chang and W. W. Wendlandt, *Thermochim. Acta*, **1**, 495 (1970).
5) R. Tsuchiya, M. Suzuki, and E. Kyuno, This Bulletin, **45**, 1065 (1972).
6) J. W. Vaughn and R. D. Lindholm in S. Y. Tyree, Jr., (ed.) Inorganic Syntheses Vol. IX, McGraw-Hill, New York, 1967, p. 163.
7) A. Werner, *Ann.*, **386**, 111 (1912).
8) S. M. Jørgensen, *Z. Anorg. Chem.*, **2**, 294 (1892).
9) R. Tsuchiya, M. Suzuki, and E. Kyuno, This Bulletin, **44**, 709 (1971).

Table 1. Temperature range of deaquation-anation and the reaction products

Complex	Temperature range of reaction (°C)	Reaction product
cis-$[CoCl(H_2O)en_2]Br_2 \cdot H_2O$	65—130	*cis*- + *trans*-$[CoClBren_2]Br$
cis-$[CoCl(H_2O)en_2]Br(NO_3)$	110—140	*trans*-$[CoClBren_2]NO_3$
cis-$[CoBr(H_2O)en_2]Br_2 \cdot H_2O$	70—130	*cis*- + *trans*-$[CoBr_2en_2]Br$
cis-$[CoCl(H_2O)(NH_3)_4]Cl_2$	135—170	*cis*-$[CoCl_2(NH_3)_4]Cl$
cis-$[CoCl(H_2O)(NH_3)_4]Br_2$	100—130	*trans*-$[CoClBr(NH_3)_4]Br$
cis-$[CoBr(H_2O)(NH_3)_4]Br_2$	100—135	*trans*-$[CoBr_2(NH_3)_4]Br$

where X, Y and Z are the respective concentrations (mol l^{-1}) of the above three complexes, and D_{530}, D_{554} and D_{655} are the observed absorbancies at 530 nm, 554 nm and 655 nm, respectively.

Results and Discussion

When a number of aquo complexes of *cis*-$[CoX(H_2O)N_4]Y_2 \cdot nH_2O$ type are heated, the following reaction takes place,

cis-$[CoX(H_2O)N_4]Y_2 \cdot nH_2O$

$\longrightarrow$ *cis*- or *trans*-$[CoXYN_4]Y + (n+1)H_2O$.

The aquo complexes prepared in the present work listed in Table 1, together with their reaction products and the range of the reaction temperatures.

Derivatography. *(a)* cis-$[CoBr(H_2O)en_2]Br_2 \cdot H_2O$: The complex undergoes the following reaction upon heating,

cis-$[CoBr(H_2O)en_2]Br_2 \cdot H_2O$

$\longrightarrow$ *cis*- + *trans*-$[CoBr_2en_2]Br + 2H_2O$.

The derivatogram for this reaction is shown in Fig. 1, together with those of the other two complexes, *cis*-$[CoCl(H_2O)en_2]Br_2 \cdot H_2O$ and *cis*-$[CoCl(H_2O)en_2]Br(NO_3)$, which will be described in the following sections. The TG curve indicates that the liberation of one mole of lattice water and one mole of coordinated water simultaneously begins to appear at about 70°C and ceases completely at 130°C, where the color change from violet to grayish green was observed, and no further mass loss is detected until about 210°C. The DTA curve shows one endothermic peak centered at 80°C, corresponding to the deaquation-anation process, and one more sharp exothermic peak centered at 170°C: in the latter peak region, no change of weight is detected in TG curve.

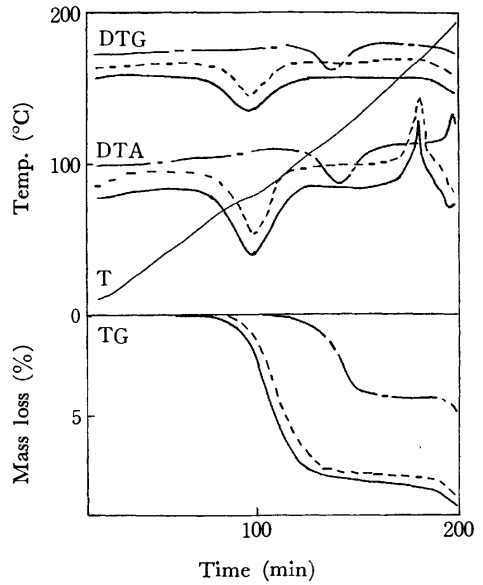

Fig. 1. Derivatograms of *cis*-$[CoCl(H_2O)en_2]Br_2 \cdot H_2O$ (——), *cis*-$[CoCl(H_2O)en_2]Br(NO_3)$ (– – –) and *cis*-$[CoBr(H_2O)en_2]Br_2 \cdot H_2O$ (----).

In order to compare the thermal behavior of halogenoaquo complexes with that of dihalogeno complexes, derivatograms of dihalogeno complexes, *cis*-$[CoBr_2en_2]Br \cdot H_2O$, *cis*-$[CoClBren_2]Br \cdot H_2O$ and *trans*-$[CoBr_2en_2]Br$, are shown in Fig. 2.

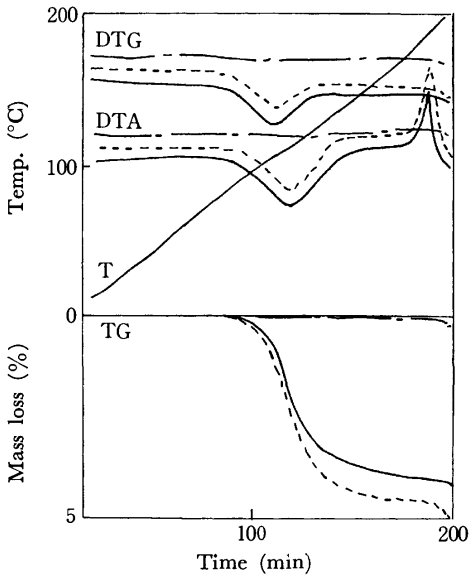

Fig. 2. Derivatograms of *cis*-$[CoBr_2en_2]Br \cdot H_2O$ (——), *cis*-$[CoClBren_2]Br \cdot H_2O$ (– – –) and *trans*-$[CoBr_2en_2]Br$ (— — —).

When *cis*-$[CoBr_2en_2]Br \cdot H_2O$ was heated, the dehydration reaction began to take place at about 90°C. The TG curve exhibits the mass loss of lattice water in the temperature range of 90 to 160°C and no further mass loss was detected until 210°C. The DTA curve exhibits a large endothermic peak at 120°C and a sharp exothermic peak at 185°C. This curve is approximately the same as that for *cis*-$[CoBr(H_2O)en_2]Br_2 \cdot H_2O$ in the temperature range of 160 to 210°C. During the dehydration process, the color change from blue to grayish green was observed. This change may be attributed to the *cis*-to-*trans* isomerization,

cis-$[CoBr_2en_2]Br \cdot H_2O \rightarrow$ *trans*-$[CoBr_2en_2]Br + H_2O$.

The isomerization could be also interpreted in terms of "aquation-anation" mechanism.[9]

When the trans-complex obtained in the above thermal reaction was cooled to room temperature, the reverse *trans*-to-*cis* isomerization occurred; *i.e.*, the *trans*-complex absorbed one mole of water as shown in the following reaction,

trans-[$CoBr_2en_2$]Br + H_2O → *cis*-[$CoBr_2en_2$]Br·H_2O,

the color change from grayish green to blue being observed.

In the derivatogram of *trans*-[$CoBr_2en_2$]Br shown in Fig. 2, differing from the corresponding *cis*-complex, no change was found in the DTA curve until the genuine decomposition began to appear at about 210°C. And even when the *trans*-complex was cooled to room temperature after heating, no *trans*-to-*cis* isomerization was observed.

(b) cis-[*CoCl*(H_2O)*en*$_2$]*Br*$_2$·H_2O: The complex undergoes the following reaction upon heating,

cis-[CoCl(H_2O)en_2]Br_2·H_2O
⟶ *cis*- + *trans*-[CoClBren_2]Br + H_2O.

The derivatogram for this change is very similar to that for the corresponding bromoaquo-bromide (a) as shown in Fig. 1. The TG curve indicates that the mass loss of lattice water begins to appear at approximately 65°C. An endothermic peak is observed at 85°C in the DTA. The deaquation-anation was completed at 130°C, and the mass was kept constant until 180°C, whereupon the genuine decomposition began to occur as shown in the TG curve. The DTA curve exhibits a sharp exothermic peak at a similar temperature, 175°C, to that seen in the corresponding bromoaquo-bromide complex.

The sharp exothermic peak is also found or *cis*-[CoClBren_2]Br·H_2O at the same temperature as shown in Fig. 2. The thermochromism was also observed in the dehydration process,

cis-[CoClBren_2]Br·H_2O → *trans*-[CoClBren_2]Br + H_2O,

in the temperature range of 95 to 155°C. The *trans*-complex obtained above was hygroscopic and completely turned back to *cis*-complex again under cooling.

(c) cis-[*CoCl*(H_2O)*en*$_2$]*Br*(*NO*$_3$): The complex undergoes the following reaction upon heating at 110—140°C, *cis*-[CoCl(H_2O)en_2]Br(NO_3) → *trans*-[CoClBren_2]NO_3+H_2O, as shown in Fig. 1, the color change from violet to green being found. The DTA curve exhibits an endothermic peak at 130°C and an exothermic peak at 200°C, which correspond to the deaquation-anation and the genuine decomposition reactions respectively.

(d) cis-[*CoCl*(H_2O)(*NH*$_3$)$_4$]*Cl*$_2$: The derivatogram of *cis*-[CoCl(H_2O)(NH_3)$_4$]Cl_2 is shown in Fig. 3, together with those of *cis*-[CoCl(H_2O)(NH_3)$_4$]Br_2 and *cis*-[CoBr(H_2O)(NH_3)$_4$]Br_2. The TG curve indicates that the deaquation-anation reaction proceeds in the temperature range of 135 to 170°C, and the DTA curve exhibits an endothermic peak corresponding to the deaquation-anation at 150°C. During the dehydration process, the color change from violet to bluish violet was first observed and then the bluish violet was gradually converted to green by heating for a long time, suggesting the formation of *trans*-complexes. From these results, the following stepwise reactions occur,

cis-[CoCl(H_2O)(NH_3)$_4$]Cl_2 → *cis*-[$CoCl_2$(NH_3)$_4$]Cl
→ *trans*-[$CoCl_2$(NH_3)$_4$]Cl.

The thermal behavior of *cis*-[CoBr(H_2O)(NH_3)$_4$]-Cl_2 was analogous to that of *cis*-[CoCl(H_2O(NH_3)$_4$]-Cl_2, so far as the initiation temperature and the reaction product of the deaquation-anation reaction are concerned.

(e) cis-[*CoCl*(H_2O)(*NH*$_3$)$_4$]*Br*$_2$ *and* cis-[*CoBr*-(H_2O)(*NH*$_3$)$_4$]*Br*$_2$: When these were heated, the following reactions were considered to occur,

cis-[CoCl(H_2O)(NH_3)$_4$]Br_2 → [CoClBr(NH_3)$_4$]Br (green)

cis-[CoBr(H_2O)(NH_3)$_4$]Br_2 → [$CoBr_2$(NH_3)$_4$]Br (green).

The color change from violet to green was found in both cases. The TG curves in Fig. 3 indicate that

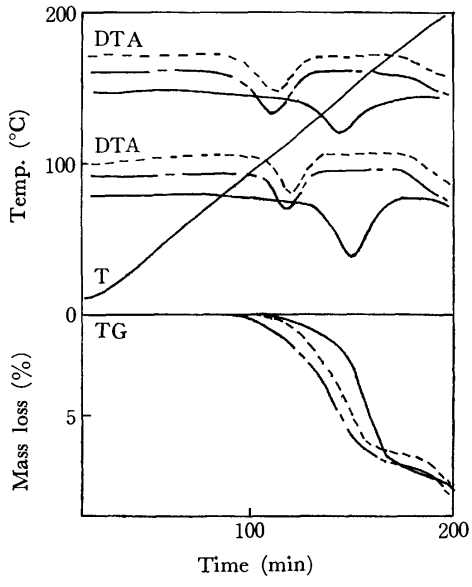

Fig. 3. Derivatograms of *cis*-[CoCl(H_2O)(NH_3)$_4$]Cl_2 (——), *cis*-[CoCl(H_2O)(NH_3)$_4$]Br_2 (– – –) and *cis*-[CoBr(H_2O)-(NH_3)$_4$]Br_2 (----).

the mass loss of the bromoaquo-bromide and of the chloroaquo-bromide was completed at 130 and 135°C, respectively, whereupon the produced *trans*-complexes were decomposed. A single endothermic peak was observed at 120°C in both DTA curves, where the deaquation-anation reaction occurred.

Electronic Spectra. Deaquation-anation reactions of the complexes were followed and the reaction products were identified by measuring the electronic spectra. The electronic spectra of *cis*-[CoBr(H_2O)en_2]-Br_2·H_2O and of the related complexes are shown in Fig. 4.

When *cis*-[CoBr(H_2O)en_2]Br_2·H_2O is heated, the first absorption maximum is gradually shifted from 530 nm (ε=102.0) to considerably lower frequency side. After the deaquation-anation was completed, the reaction product gave the broad absorption band at 554 nm with less intense shoulder at 630—650 nm. This suggests the superposition of spectra of *cis*-[$CoBr_2$-

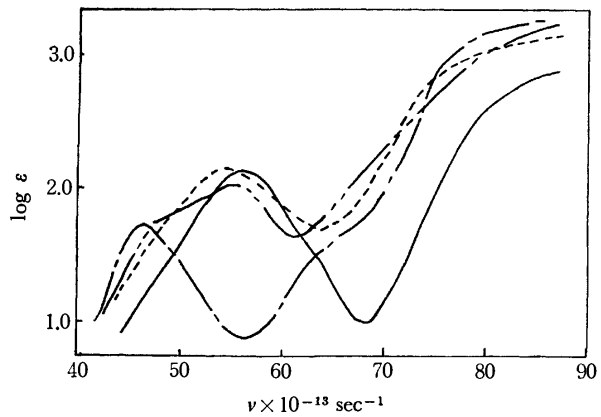

Fig. 4. Electronic spectra of *cis*-[CoBr(H_2O)en_2]$Br_2\cdot H_2O$ (——), *cis*-[$CoBr_2en_2$]$Br\cdot H_2O$ (----), *trans*-$CoBr_2en_2$]Br (———) and of thermal reaction product of *cis*-[CoBr(H_2O)en_2]$Br_2\cdot H_2O$ (—·—·—).

$en_2]^+$ and *trans*-[$CoBr_2en_2]^+$, which showed the first absorption maxima at 554 nm (ε=101.0) and at 655 nm (ε=55.1), respectively, as shown in Fig. 4. In the present work, no attempt was made to isolate the two isomers from the mixture.

The absorption spectra of *cis*-[CoCl(H_2O)en_2]-$Br_2\cdot H_2O$ and of the related complexes are shown in Fig. 5, which displays that the heating of *cis*-[CoCl-(H_2O)en_2]$Br\cdot H_2O$ also gives the formation of the mixture of *trans*-[CoClBren_2]Br and *cis*-[CoClBren_2]-Br as similar as that of *cis*-[CoBr(H_2O)en_2]$Br_2\cdot H_2O$.

When the bromide-nitrate complex, *cis*-[CoCl(H_2O)-en_2]$Br(NO_3)$, was heated, the first absorption peak of *cis*-complex disappeared and the same absorption spectrum as found for *trans*-[CoClBren_2]NO_3 was obtained.

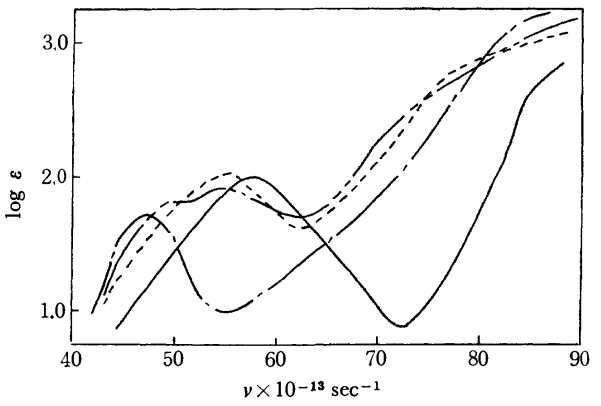

Fig. 5. Electronic spectra of *cis*-[CoCl(H_2O)en_2]$Br_2\cdot H_2O$ (——), *cis*-[CoClBren_2]$Br\cdot H_2O$ (----), *trans*-[CoClBren_2]Br (———) and of thermal reaction product of *cis*-[CoCl(H_2O)-en_2]$Br_2\cdot H_2O$ (—·—·—).

The deaquation-anation reactions for the ammine-complexes, (d) and (e), were only followed by the observation of their color change.

Rate Studies. Isothermal dehydration of *cis*-[CoBr(H_2O)en_2]$Br_2\cdot H_2O$ was followed by using a thermobalance at several constant temperatures in the range of 92 to 120°C and the conversion ratios this complex to *cis*-[$CoBr_2en_2$]Br and to the corresponding *trans*-complex were determined spectrophotometrically by the method described in the experimental section.

The dehydration reactions of all the monoacidoaquo-complexes treated in the present work were found to proceed in the first order. For example, the rate constant for the deaquation-anation reaction of *cis*-[CoBr(H_2O)en_2]$Br_2\cdot H_2O$ is expressed by,

$$k_a = \frac{1}{t}\ln\frac{a}{a-x}$$

the rate constant concerning the formation of *cis*-[$CoBr_2en_2$]Br by,

$$k_b = \frac{1}{t}\cdot\frac{y}{x}\ln\frac{a}{a-x}$$

and that concerning the formation of *trans*-[$CoBr_2en_2$]-Br by

$$k_c = \frac{1}{t}\cdot\frac{z}{x}\ln\frac{a}{a-x}$$

where a denotes the initial amount of the starting complex, *cis*-[CoBr(H_2O)en_2]$Br_2\cdot H_2O$, x is the amount of the complex that has disappeared, y is the amount of *cis*-[$CoBr_2en_2$]Br formed, and z is the amount of *trans*-[$CoBr_2en_2$]Br formed in the time t. Since the plots, $\log a/(a-x)\sim t$, $(y/x)\log a/(a-x)\sim t$ and $(z/x)\log a/(a-x)\sim t$, give straight lines at each temperature as shown in Fig. 6, the above three reactions are considered to proceed in parallel with each other and in the first order respectively.

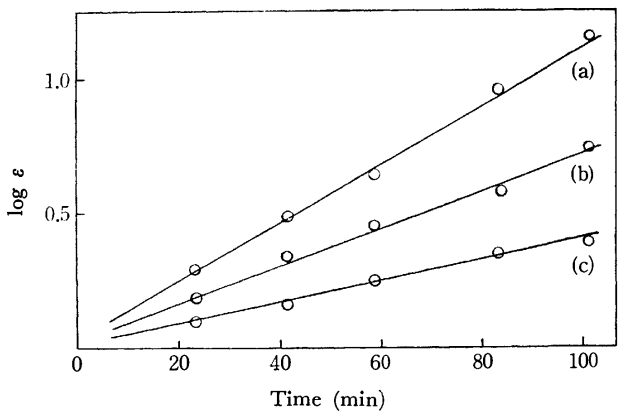

Fig. 6. The relationships of $\log a/(a-x)$ (a), $y/x\cdot\log a/(a-x)$ (b) and $z/x\log a/(a-x)$ (c) against t for deaquation-anation of *cis*-[CoBr(H_2O)en_2]$Br_2\cdot H_2O$.

Rate constants calculated for *cis*-[CoBr(H_2O)en_2]-$Br_2\cdot H_2O$ are listed in Table 2, together with those for only the dehydration of *cis*-[CoCl(H_2O)en_2]$Br_2\cdot H_2O$. The activation energies (E_a) were obtained from the temperature dependency of the rate constant, and entropies of activation (ΔS_a) were calculated by using "absolute rate theory", which are given in Table 3.

Taking into account for the data of the initiation temperatures of deaquation-anation reaction in Table 1 and those of the activation energies in Table 3, the order of the thermal stability is deduced to be, *cis*-[CoCl(H_2O)en_2]$Br(NO_3)$ > *cis*-[CoBr(H_2O)en_2]$Br_2\cdot H_2O$ ≈ *cis*-[CoCl(H_2O)en_2]$Br_2\cdot H_2O$ for halogenoaquo ethylenediamine complexes, and *cis*-[CoCl(H_2O)$(NH_3)_4$]Cl_2 > *cis*-[CoCl(H_2O)$(NH_3)_4$]Br_2 ≈ *cis*-[CoBr(H_2O)$(NH_3)_4$]-

TABLE 2. RATE CONSTANTS OF DFAQUATION-ANATION OF *cis*-$[CoBr(H_2O)en_2]Br_2 \cdot H_2O$ AND DEHYDRATION OF *cis*-$[CoCl(H_2O)en_2]Br_2 \cdot H_2O$

Temp. (°C)	k_a (sec^{-1})	k_b (sec^{-1})	k_c (sec^{-1})	k_d [a] (sec^{-1})
92	$(1.9\pm0.3)\times10^{-4}$	$(1.2\pm0.3)\times10^{-4}$	$(7.2\pm0.3)\times10^{-5}$	$(2.4\pm0.3)\times10^{-4}$
100	$(2.3\pm0.3)\times10^{-4}$	$(1.4\pm0.3)\times10^{-4}$	$(8.5\pm0.3)\times10^{-5}$	$(2.8\pm0.3)\times10^{-4}$
110	$(1.3\pm0.2)\times10^{-3}$	$(7.5\pm0.3)\times10^{-4}$	$(4.8\pm0.3)\times10^{-4}$	$(1.7\pm0.2)\times10^{-3}$
120	$(3.5\pm0.4)\times10^{-3}$	$(2.2\pm0.4)\times10^{-3}$	$(1.2\pm0.4)\times10^{-3}$	$(4.0\pm0.3)\times10^{-3}$

a) k_d: rate constant for dehydration of *cis*-$[CoCl(H_2O)en_2]Br_2 \cdot H_2O$

TABLE 3. THE THERMOCHEMICAL FUNCTIONS FOR DEAQUATION-ANATION REACTIONS

Complex	E_a (kcal/mol)	ΔH (kcal/mol)	ΔS_a^a (e. u.)	ΔS_a^b (e. u.)	ΔS_a^c (e. u.)
cis-$[CoCl(H_2O)en_2]Br_2 \cdot H_2O$	38±5	13.5±2.0			
cis-$[CoCl(H_2O)en_2]Br(NO_3)$	68±6	7.5±2.0			
cis-$[CoBr(H_2O)en_2]Br_2 \cdot H_2O$	37±5	13.3±2.0	16±5	15±5	15±5

ΔS_a^a: the disappearance for *cis*-$[CoBr(H_2O)en_2]Br_2 \cdot H_2O$, ΔS_a^b: the formation of *cis*-$[CoBr_2en_2]Br$, ΔS_a^c: the formation of *trans*-$[CoBr_2en_2]Br$.

Br_2 for halogenoaquoammine complexes.

The ratios of *cis*-$[CoBr_2en_2]Br$ to *trans*-$[CoBr_2en_2]Br$ in the products at all temperatures investigated were found to be 62 : 38 at the end of deaquation-anation.

The reaction products produced by the deaquation-anation reactions are considerably affected by the entering groups: *i.e.*, *cis*-$[CoCl(H_2O)en_2]Br_2 \cdot H_2O$, *cis*-$[CoBr(H_2O)en_2]Br_2 \cdot H_2O$ and *cis*-$[Co(H_2O)_2en_2]Br_3 \cdot 2H_2O$ gave the mixture of *cis*- and *trans*-complexes, while *cis*-$[CoCl(H_2O)en_2]Cl_2$ and *cis*-$[Co(H_2O)_2en_2]Cl_3 \cdot 2H_2O$ gave *cis*-$[CoCl_2en_2]Cl$ with retention of structure.

As for the ammine-complexes, the reactions proceeded in the same manner as found for ethylenediamine-complexes: *i. e.*, *cis*-$[CoCl(H_2O)(NH_3)_4]Cl_2$ and *cis*-$[CoBr(H_2O)(NH_3)_4]Cl_2$ were deaquated with retention of structure to give the corresponding *cis*-complexes as reaction products, whereas *cis*-$[CoCl(H_2O)(NH_3)_4]Br_2$ and *cis*-$[CoBr(H_2O)(NH_3)_4]Br_2$ underwent *cis*-to-*trans* stereochemical change to give the corresponding *trans*-complexes as reaction products.

From these facts, it is concluded that, when the entering group is chloride ion, deaquation-anation reaction proceeds with the retention of structure, while, when it is bromide ion, the stereochemical change occurs during the deaquation-anation process. In addition, *cis*-$[CoCl(H_2O)en_2]Br(NO_3)$ was found to undergo the complete conversion into *trans* form. As seen in these complexes, the kind of counter ions in the outer coordination sphere affects the geometrical structure of deaquation-anation reaction products, though the kind of acidic ligands coordinated does not so much affect it.

Kinetics and Stoichiometry of Nitrogen Fixation with $TiCl_3$-Mg and VCl_3-Mg in Tetrahydrofuran

Akio YAMAMOTO, Shigeo GO,* Masaharu OOKAWA, Mitsuaki TAKAHASHI, Sakuji IKEDA, and Tominaga KEII*

Research Laboratory of Resources Utilization, Tokyo Institute of Technology, Meguro, Tokyo
**Department of Chemical Engineering, Tokyo Institute of Technology, Meguro, Tokyo*

(Received May 15, 1972)

The kinetics and stoichiometry of nitrogen fixation with $TiCl_3$–Mg and VCl_3–Mg in tetrahydrofuran (THF) systems were studied. The systems react with molecular nitrogen at room temperature and normal pressure giving magnesium dichloride and nitrogen-containing complexes of compositions $[MNMg_2Cl_2(THF)]$, where M= Ti and V, according to the stoichiometry: $MCl_3(THF)_3 + \frac{5}{2}Mg + \frac{1}{2}N_2 \rightarrow [MNMg_2Cl_2(THF)] + \frac{1}{2}MgCl_2(THF)_2$. Properties of the isolated nitrogen-containing complexes were examined. Reactions under argon and hydrogen gave hydride-containing complexes. The initial rate of nitrogen fixation was first order with respect to the amounts of MCl_3, Mg, and nitrogen pressure. A mechanism involving the complexation of N_2 with dimeric M(II) species followed by rate-determining process to react with magnesium is proposed and discussed.

Since the discovery of Vol'pin and Shur that molecular nitrogen can be fixed under mild conditions by mixed systems of transition metal compounds and reducing agents,[1] there have been reported a number of systems which react with molecular nitrogen.[2] Among these systems, early transition metal compounds in combination with reducing agents contrast in their ability to fix molecular nitrogen with later transition metal compounds which often form stable dinitrogen complexes but the coordinated N_2 ligand can not be readily reduced. A variety of N_2-fixing systems based mostly on titanium compounds have been reported and the mechanism of nitrogen fixation has been studied to some extent. As the apparently simplest N_2-fixing systems we have selected the $TiCl_3$–Mg[3] and VCl_3–Mg systems in tetrahydrofuran (THF) and studied the mechanism of nitrogen fixation by kinetic as well as preparative methods.

Results

Stoichiometry and Kinetics of Nitrogen Fixation. $TiCl_3(THF)_3$ and $VCl_3(THF)_3$ in the presence of magneiusm in tetrahydrofuran react at room temperature and normal pressure with molecular nitrogen. The amounts of molecular nitrogen absorbed by the $TiCl_3$–Mg and VCl_3–Mg systems were equivalent to the amounts of ammonia formed after the hydrolysis of the system. Figure 1 shows typical kinetic runs of N_2 fixation with $TiCl_3$–Mg system; the VCl_3–Mg system behaves similarly but with much slower absorption. In no case the amount of ammonia formed per mole of $TiCl_3$ or VCl_3 exceeded one mole at ambient temperature and pressure. Figure 1 also indicates that the N_2 absorption starts after an induction period. This induction period can be shortened to some extent by using fine powder of magnesium or by pretreatment of magensium with iodine but can not be removed completely. As will be described later this induction period can be ascribed to the period of reduction of Ti(III) to Ti(II) or V(III) to V(II).

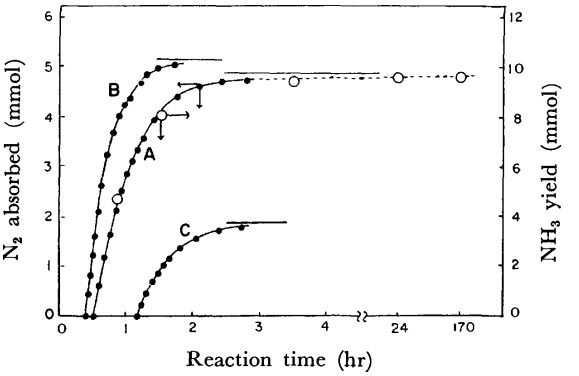

Fig. 1. N_2 absorption and ammonia formation by $TiCl_3$–Mg system at 20°C. ●: Amount of N_2 absorbed in mmol; ○: Amount of ammonia formed after hydrolysis. Curve A: $TiCl_3$, 1.50 g, reduced with 2.0 g of Mg. B: $TiCl_3$, 1.58 g; Mg, 4.0 g. C: $TiCl_3$, 0.57 g; Mg, 3.0 g. Horizontal lines for the curves indicate the calculated values for absorption of 0.5 mol of N_2 per titanium.

The kinetic experiment were carried out mostly with the $TiCl_3$–Mg system which absorbs nitrogen more rapidly than the VCl_3–Mg system. The kinetic curves shown in Fig. 1 have been replotted in Fig. 2 to indicate that the rate of N_2 absorption is first-order with respect to the concentration of a titanium species which is able to combine with molecular nitrogen.

$$r = d[NH_3]/dt = k[Ti] \quad (1)$$

Figure 3 illustrates the kinetic curves of magnesium consumption by the $TiCl_3$–Mg sytem under nitrogen and under argon. Evidently the rate of magnesium consumption under nitrogen is much faster than that under argon after the first 0.5 g-atom of magnesium per titanium was consumed, although the ultimate

1) M. E. Vol'pin and V. B. Shur, *Nature*, **209**, 1236 (1966).

2) For recent reviews, see a) R. Murray and D. C. Smith, *Coord. Chem. Rev.*, **3**, 429 (1968); b) K. Kuchynka, *Catal. Rev.*, **3**, 111 (1969); c) G. Henrici Olivé and S. Olivé, *Angew. Chem.*, **81**, 679 (1969); d) T. Ito and A. Yamamoto, *Yuki Gosei Kagaku Kyokai Shi*, **28**, 598 (1970); e) Yu. G. Borod'ko and A. E. Shilov, *Usp. Khim.*, **38**, 761 (1969); f) M. E. Vol'pin and V. B. Shur, *Organometal. Reactions*, **1**, 55 (1970); g) R. F. Gould, Ed., "Bioinorganic Chemistry, Adv. Chem. Series 100, Am. Chem. Soc., (1971); h) E. E. van Tamlen, *Accounts Chem. Res.*, **3**, 361 (1970); i) J. Chatt, *Platinum Metals Rev.*, **13**, 9 (1969); *Proc. Roy. Soc., Ser. B*, **172**, 327 (1969); j) M. Ichikawa, *Kagaku no Ryoiki*, **24**, 863 (1970).

3) For a preliminary communication, see A. Yamamoto, M. Ookawa, and S. Ikeda, *Chem. Commun.*, **1969**, 841.

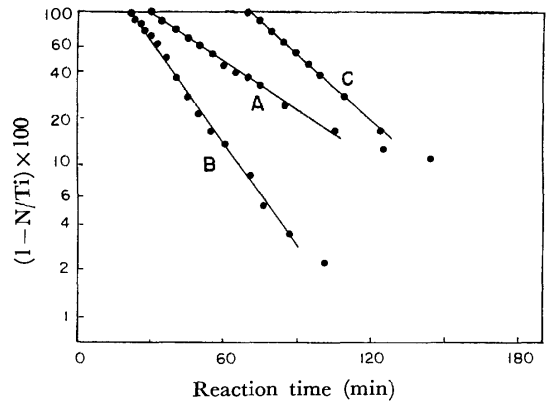

Fig. 2. First order plots of Fig. 1. Legends are the same with Fig. 1. N/Ti in the ordinate represents the number of moles of NH_3 produced per mol of $TiCl_3$ added.

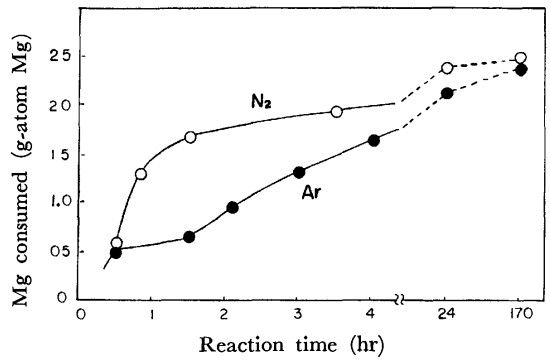

Fig. 3. Consumption of magnesium with time by $TiCl_3$-Mg system. $TiCl_3$, 1.50 g; Mg, 2.0 g, 20°C.
○, under nitrogen; ●, under argon.

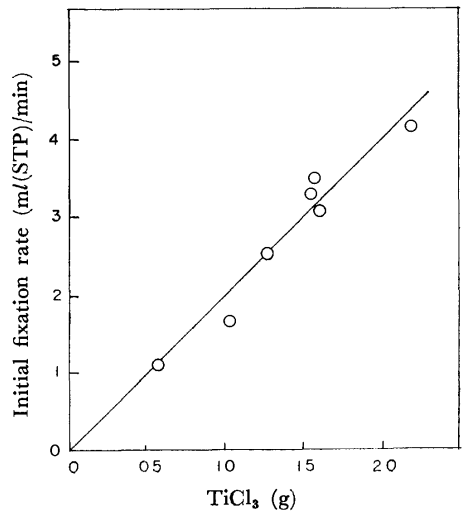

Fig. 4. Relationship between the initial rate of nitrogen fixation and the amount of $TiCl_3$ used.

amount of magnesium consumed is almost the same in either case. (2.5 g-atoms Mg per Ti or V.)

Figures 4, 5, and 6 show the dependences of the initial rate of N_2 fixation on the amount of $TiCl_3$ used, the amount of Mg consumed in the nitrogen fixation (the amount consumed in the induction period is excluded) and on the nitrogen pressure. It can be seen that the initial rate of N_2 fixation is first order with respect to these quantities. From the result

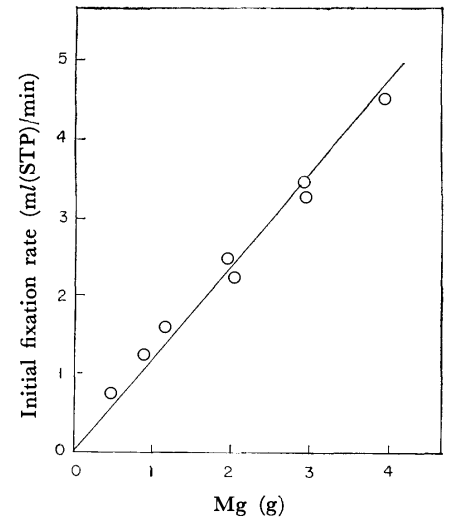

Fig. 5. The dependence of the initial rate of nitrogen fixation on the amount of Mg. The amount of Mg in the abssisae indicates the amount of Mg used for nitrogen fixation, *i.e.*, the amount of Mg consumed in the induction period is substracted from the total amount of Mg used. $TiCl_3$, 1.50 g; P_{N_2}, 62 cmHg; temperature, 20°C.

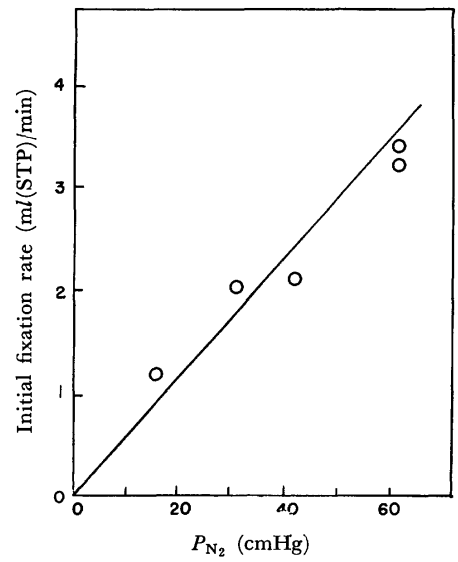

Fig. 6. The dependence of the initial rate of nitrogen fixation on nitrogen pressure at 20°C. $TiCl_3$, 1.50 g; Mg, 3.0 g; total pressure, 76 cmHg with argon as diluent.

of the temperature dependence of the initial rate, the activation energy for this process was estimated as 5 kcal/mol.

In both cases of $TiCl_3$-Mg and VCl_3-Mg the total amounts of magnesium consumed per mole of $TiCl_3$ or VCl_3 did not exceed 2.5 g-atoms but there was some difference observed between the $TiCl_3$-Mg and VCl_3-Mg systems in the relationships between the amount of N_2 fixed and the amount of Mg consumed. As Fig. 7 shows, in both cases with $TiCl_3$ and VCl_3, no N_2 absorption takes place until 1/2 g-atom of magnesium is consumed, and beyond this stage the amount of N_2 fixed increases linearly with the Mg consumption. In the case with $TiCl_3$-Mg system, 1 mol of NH_3 is produced by consumption of 2 g-atoms of Mg, and the system consumes further 0.5 g-atom of Mg without

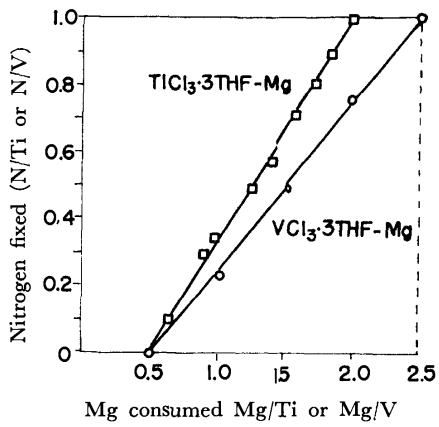

Fig. 7. The relationships between the amount of Mg consumed and the amount of nitrogen fixed by $TiCl_3(THF)_3$-Mg (□) and $VCl_3(THF)_3$-Mg system (○).

N_2 absorption. On the other hand, for VCl_3-Mg system the production of 1 mol of NH_3 is performed by consumption of 2.5 g-atoms of magnesium.

Taking into account the amounts of magnesium chloride formed and of nitrogen-containing titanium and vanadium complexes isolated from the reaction systems *(vide infra)*, the stoichiometries of the overall reactions for $TiCl_3$-Mg and VCl_3-Mg systems can be expressed by:

$$TiCl_3(THF)_3 + \frac{5}{2}Mg + \frac{1}{2}N_2 \rightarrow \underset{\mathbf{1}}{[TiNMg_2Cl_2(THF)]} + \frac{1}{2}MgCl_2(THF)_2 \quad (2)$$

$$VCl_3(THF)_3 + \frac{5}{2}Mg + \frac{1}{2}N_2 \rightarrow \underset{\mathbf{3}}{[VNMg_2Cl_2(THF)]} + \frac{1}{2}MgCl_2(THF)_2 \quad (3)$$

When these N_2 fixing systems are reduced with magnesium prior to contact with N_2 under argon beyond the oxidation state of Ti(II) and V(II), the ability of the systems to fix nitrogen is reduced as illustrated in Fig. 8. When $VCl_3(THF)_3$ is reduced with magnesium until 0.5 g-atom of Mg is consumed, no loss in the N_2 fixing ability is observed. Further usage of magnesium reduces the ability of the system to fix nitrogen and after consumption of 2.5 g-atoms of Mg the system does not show any more reactivity toward nitrogen. Similarly the titanium system which has been reduced with 2.5 g-atoms of magnesium does not react with nitrogen any more. The presence of other ligands such as triphenylphosphine and 2,2'-dipyridyl hinders the nitrogen fixation. The system containing $TiCl_2(acac)(THF)_2$[4] and magnesium in THF did not react with nitrogen.

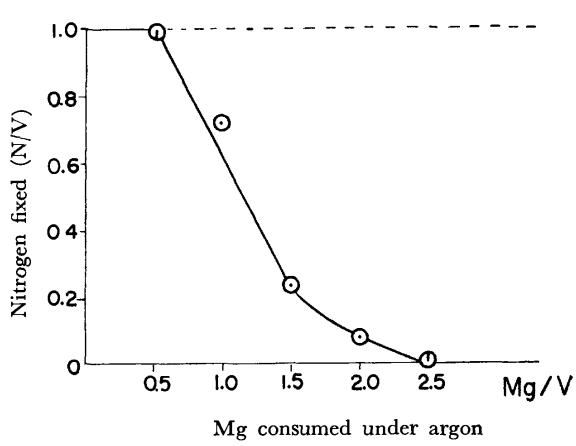

Fig. 8. Residual N_2-fixing capability of $VCl_3(THF)$-Mg system after controlled reduction of $VCl_3(THF)_3$ with limited amount of Mg under argon.

$TiCl_3(THF)_3$-Mg and $VCl_3(THF)_3$-Mg systems react with molecular hydrogen with the similar color change of the systems to the reduction under nitrogen or argon. The reactivity of the $TiCl_3(THF)_3$-Mg system was higher than that of the $VCl_3(THF)_3$-Mg system: The $TiCl_3(THF)_3$-Mg system absorbed 2.7 mol of H_2 per titanium in 18 hr whereas the latter system absorbed the same amount of hydrogen per vanadium in 3 weeks. The addition of hydrogen gas to the nitrogen gas competitively inhibits the nitrogen fixation: in an experiment with a 1 : 1 mixture of N_2 and H_2 2.6 mol of the gas was absorbed but only 0.25 mol of N_2 was fixed per titanium without formation of NH_3 in the gas phase.

The $TiCl_3(THF)_3$-Mg system reacted with propylene, absorbing 1.6 mol of propylene per titanium in 40 hr at room temperature and atmospheric pressure. Formation of propylene dimers including 2-methylpentane, 1-hexene and 2-hexene in a ratio of 4 : 2 : 1 was confirmed by gas chromatography. Under similar conditions the system absorbed 4 mol of ethylene in 15 hr yielding mainly ethane along with 1-butene, *n*-butane, and other hydrocarbons.

Separations of Low Valent Titanium and Vanadium Complexes. (i) Titanium Complexes: From the reaction system containing $TiCl_3(THF)_3$, magnesium and molecular nitrogen, a titanium complex containing nitrogen was isolated. After the system absorbed 0.5 mol of N_2 per titanium consuming 2.5 g-atoms of magnesium with the color change from blue through green to black, unreacted magnesium was removed and black benzene soluble diamagnetic powder of a composition $[TiNMg_2Cl_2(THF)]$ (**1**) was separated from benzene-insoluble crystals of $MgCl_2(THF)_2$. Complex **1** and other titanium or vanadium complexes to be described later were not obtained as crystals and we can not claim that they are unequivocally pure. However, they were homogeneous as far as one can judge from column chromatography of the THF solutions using sucrose, $MgCO_3$ or Na_2CO_3 and from the analytical data which always gave the same compositions. The titanium complex **1** contained a small amount of titanium hydride as detected by evolution of hydrogen on reaction of **1** with iodine. Complexes **1** gave one mole of ammonia per titanium on reactions with water and ethanol. The reaction of **1** with dry hydrogen chloride proceeded as follows:

$$[TiNMg_2Cl_2(THF)] + 6HCl \xrightarrow[THF]{} NH_4Cl + TiCl_3(THF)_3 + 2MgCl_2(THF)_2 + H_2$$

4) A. Yamamoto, M. Murai, N. Oshima, and S. Ikeda, unpublished.

The nitrogen bound in complex **1** can not be removed readily except by treatment with protic reagents. On heating the complex at 200°C no dinitrogen was released. The gas evolved by the thermal decomposition of the complex contained THF as the main decomposition product together with 1-butene, 2-butene, ethylene, propylene, ethane, butane and hydrogen which may be generated by decomposition of THF bound in complex **1**. The pyrolysis residue contained still 1 atom of nitrogen per titanium and some THF.

In order to find how nitrogen is bound in the complex, the following reactions of **1** were carried out. A part of magnesium contained in **1** was removed on reaction of **1** with pyridine yielding $MgCl_2(Py)_2$ and a black complex with a composition of $[TiNMgCl_{0.5}(THF)]$. The complex obtained by the reaction of **1** with pyridine released one mole of ammonia per titanium on hydrolysis.

A part of magnesium in **1** was removed also as a zerovalent complex with addition of 2,2′-dipyridyl. On reaction of **1** with 2,2′-dipyridyl in THF, reddish purple crystals which are soluble in THF were obtained and identified as $Mg(dipy)_3$ by elemental analysis. After the removal of $Mg(dipy)_3$, a THF-insoluble residue with a composition of $[TiNMg_{1.5}Cl_2(dipy)_{1.5}(THF)]$ remained. Further removal of magnesium from this residue by reaction with pyridine gave $MgCl_2(Py)_2$ and a black powder with a composition of $[TiNMgCl(Py)_2]$. THF in **1** was not replaced by a soft base such as triphenylphosphine.

Complete removal of magnesium component from **1** was achieved by using benzoyl chloride in THF. The reaction yielded $MgCl_2(THF)_2$, some polymer of THF and a dark green substance with an approximate composition of $[TiNCl(C_6H_5CO)_{1.5}]$. The polymer of THF is considered to be formed by cationic polymerization. The mode of combination of benzoyl chloride component with titanium was not clear. In none of the complexes which were obtained by various treatments of **1** the decrease of the nitrogen to titanium ratio was observed.

Complex **1** dissolved in THF showed no reactivity toward nitrogen but still reacted with hydrogen in the presence of magnesium. The system slowly absorbed hydrogen and the reaction continued as long as excess magnesium was present. From the system excess magnesium and a gray powder which are insoluble in THF were separated. The gray powder released hydrogen on reaction with iodine and probably contains magnesium hydride beside unreacted magnesium. As described in the preparation of **1**, $MgCl_2(THF)_2$ was separated from the system and a black powder of a composition of $[TiH_2NMg_3Cl_{1.5}(THF)_2]$ (**2**) was isolated. The reaction of iodine with **2** released one mole of H_2 per titanium. The nitrogen in **2** is still bonded with titanium after the reaction of **1** with hydrogen as revealed by the formation of 1 mol of ammonia and of ammonium chloride respectively on reactions of **2** with water and hydrogen chloride.

(ii) Vanadium Complexes. *a. Under Nitrogen:* In a similar manner to the $TiCl_3$–Mg system, $VCl_3(THF)_3$ was reduced in THF with magnesium under nitrogen. The color of the THF solution changed from red through green to black. $MgCl_2(THF)_2$ and a vanadium complex of a composition $[VNMg_2Cl_2(THF)]$ (**3**), were separated from the system. Complex **3**, diamagnetic ($\chi = 0.0113 \times 10^{-6}\ g^{-1}$) and very sensitive to air, gave 1 mol of ammonia per vanadium on hydrolysis. On iodolysis **3** released 0.026 mol of H_2 per vanadium thus showing the presence of a small amount of hydride ingredient as in titanium complex **1**. Thermal decomposition of **3** over 200°C for 10 hr released no nitrogen but hydrogen together with THF, 1-butene, *n*-butane, *trans*- and *cis*-2-butenes, propylene, ethylene, ethane, and methane were detected in the gas evolved. These products may be formed by decomposition of THF in **3**. The pyrolysis residue still contained nitrogen as proved by the formation of 1 mol of ammonia per vanadium on hydrolysis of the residue.

b. Under Argon: From the $VCl_3(THF)_3$–Mg system reacted under argon a diamagnetic vanadium complex of composition $[VHMg_2Cl_{1.5}(THF)]$ (**4**) and $MgCl_2(THF)_2$ were separated. The presence of hydride was deduced from the amount of H_2 produced on iodolysis of **4**. The IR spectrum of **4** was very similar to that of **3** and no band ascribable to ν(V–H) was detected.

c. Under Hydrogen: When $VCl_3(THF)_3$ was reduced with magnesium in THF under hydrogen at ambient temperature and pressure, the system absorbed hydrogen slowly but steadily over a long period; 3.5mol of H_2 was absorbed per mol of the vanadium complex in 35 days. The diamagnetic vanadium complex separated from the system has the composition of $[VH_2MgCl(THF)_2]$ (**5**). The amount of hydridic hydrogen in the complex was deduced from the amount of hydrogen produced on iodolysis.

Chemical Properties of $[VNMg_2Cl_2(THF)]$ ***3***. In order to examine the properties of **3**, the following reactions of **3** were carried out. Complex **3** dissolved in THF reacted in the presence of magnesium with hydrogen at room temperature and atmospheric pressure. The reaction proceeded slowly but steadily as long excess magnesium was present. More than 10 mol of H_2 per the vanadium complex was absorbed in a month. From the system black powder with a composition of $[VN(H)_2Mg_5Cl_2(THF)_2]$ (**6**) and magnesium hydride were separated.

Complex **3** as well as other vanadium complexes prepared under argon and hydrogen reacts with ethylene forming ethane. In the presence of hydrogen complex **3** catalyzes the hydrogenation of ethylene. The formation of amine was not detected.

Complex **3** reacted with various organic halides. The reaction of benzyl chloride with **3** took place with evolution of heat, and $MgCl_2(THF)_2$, dibenzyl, and a vanadium complex with a composition of $[VNMgCl_{1.5}(THF)]$ were formed. By the reaction of **3** with chlorotriphenylmethane, a part of magnesium in **3** was removed as $MgCl_2(THF)_2$ and a black complex of a composition $[VNMgCl_2(THF)]$ was obtained. A similar reaction with methyl iodide released 0.5 mol of methane per vanadium with partial removal of

magnesium chloride from **3**. A part of magnesium in **3** was also removed as magnesium chloride on reaction with benzoyl chloride accompanied by the formation of a polymer of THF.

Discussion

Comparison of the reductions of $TiCl_3(THF)_3$ and $VCl_3(THF)_3$ with magnesium under nitrogen, argon, and hydrogen clearly indicates the striking similarity of the two systems belonging to the IVth and Vth groups in the periodic table. The stoichiometries of the N_2-fixation reactions given by Eqs. (2) and (3) are satisfactorily substantiated from the analyses of the products as well as from kinetic studies. Clearly the induction periods observed in the nitrogen fixation with these systems are due to the one electron reductions of $TiCl_3(THF)_3$ and $VCl_3(THF)_3$ with 0.5 g-atom of Mg accompanied by the formation of 0.5 mol of $MgCl_2$. Similar induction period has been reported in the nitrogen fixation by $VCl_3(THF)_3$–lithium naphthalide system.[5] Examination of the visible spectrum of the $VCl_3(THF)_3$–Mg system after the one electron reduction revealed the formation of a divalent vanadium species as shown by the presence of absorption maxima at 410 and 650 nm which can be compared with the spectrum of known $VCl_2(THF)_2$ at 407 and 643 nm.[6] Similarly the absorption band at 380 nm observed in the induction period of the N_2-fixing $TiCl_3$–Mg system may be due to the divalent titanium species. Accompanying the change of the electronic spectrum the ESR spectrum of the $VCl_3(THF)_3$–Mg system changed with increasing amount of magnesium added to the system. Vanadium having the nuclear spin of 7/2 gives 8 hyperfine splittings but the shape of the ESR spectrum changed depending on the amount of Mg consumed. The ultimate reduction products of VCl_3–Mg system which consumed 2.5 g-atoms of magnesium per vanadium were diamagnetic and showed no ESR absorption. The ESR spectra of the intermediate reduction products prepared under nitrogen and argon were identical. The ultimate oxidation states of titanium and vanadium complexes after absorption of 2.5 g-atoms of Mg (**1** and **3**) are difficult to assign, since the magnesium contained in the complexes can be removed by reactions with organic nitrogen bases as Mg(II) in one case and as Mg(0) in the other, although the diamagnetism of **1** and **3** suggests Ti(0) and V(I) as the formal oxidation states. Some ESR studies on VCl_3–alkali naphthalide system have been reported.[5,7]

From the kinetics of nitrogen fixation by $TiCl_3$–Mg system, the initial rate of nitrogen absorption after the induction period was shown to be first order with respect to the amounts of $TiCl_3$, of Mg and the pressure of nitrogen, whereas the stoichiometry of the nitrogen fixation (Eq. 2) shows that half a molecule of nitrogen combines with mole of titanium and vanadium. As a reasonable explanation compatible with these results we assume a dimeric titanium or vanadium species which combines with molecular nitrogen and the N_2 complex thus formed is further reduced reacting with magnesium in the succeeding rate determining step:

$$[M]_2 + N_2 \rightleftarrows [MN_2M] \quad (4)$$
$$M = Ti, V$$

$$[MN_2M] \xrightarrow{Mg} [MN_2M] \xrightarrow{3Mg} M_2N_2Mg_4Cl_4(THF)_2$$
$$\vdots$$
$$Mg$$

$$\text{or } MNMg_2Cl_2(THF) \quad (5)$$

As the N_2-binding species, divalent and univalent transition metal may be considered but the latter appears to be less probable. The experiment shown in Fig. 8 indicates that VCl_3–Mg which reacted with 1.0 g-atom of Mg per vanadium under argon has the N_2-fixing ability of about 70%. This system would be expected to show the full N_2-fixing ability if V(I) formed by stepwise reduction of V(III) should be responsible as the N_2-binding species.

Therefore we propose the divalent vanadium and titanium compounds as the N_2 binding species. Negligible absorption of nitrogen in the divalent state of vanadium and titanium at room temperature and normal pressure may be understood if the equilibrium (4) is on the side of dissociation. Recent isolations of titanium[8–10] and molybdenum[11] complexes with N_2, as the bridging ligand between two metal atoms, lend support to the assumption. We are presently investigating the possibility of identifying the species with a composition $[Ti(II)\cdot N_2\cdot Ti(II)]$ or $[V(II)\cdot N_2\cdot V(II)]$. We do not have at present any information about the state of aggregation of the divalent titanium and vanadium species to combine with nitrogen but $TiCl_3(THF)_3$ is reported to be dimeric.[12]

Alternative pathway to the above mechanism is that a monomeric species combines with N_2 followed by a rapid combination with another monomeric species forming a bridged N_2 complex. Van Tamelen presented evidence to indicate the formation of TiN_2 type complex.[2h,13]

The linear relationship between the amount of magnesium consumed and the amount of N_2 fixed (Fig. 7) suggests that stepwise change of the oxidation states of titanium and vanadium is not involved during the consumption of Mg between 0.5 and 2.0 g-atoms in the titanium system and between 0.5 and 2.5 g-atom in the vanadium system. Probably the reaction of

5) T. P. M. Beelen and W. Van Erk, *Rec. Trav. Chim. Pays-Bas*, **90**, 1197 (1971).

6) H. J. Seifert and T. Auel. *J. Inorg. Nucl. Chem.*, **30**, 2081 (1968).

7) G. Henrici-Olivé and S. Olivé, *J. Organometal. Chem.*, **9**, 325 (1967).

8) J. H. Teuben and H. J. de Liefde Meijer, *Rec. Trav. Chim. Pays-Bas*, **90**, 360 (1971).

9) A. E. Shilov, A. K. Shilova, and E. F. Krashina, *Kinet. Katal.*, **10**, 1402 (1969).

10) J. E. Bercaw and H. H. Brintzinger, *J. Amer. Chem. Soc.*, **93**, 2045 (1971); R. H. Marvich and H. H. Brintzinger, **93**, *ibid.*, 2046 (1971).

11) M. L. H. Green and W. E. Silverthorn, *Chem. Commun.*, **1971**, 557.

12) R. J. H. Clark, J. Lewis, D. Machin, and R. S. Nyholm, *J. Chem. Soc.*, **1963**, 379.

13) E. E. van Tamelen, R. B. Fechter, S. W. Schneller, G. Boche, R. H. Greeley, and B. Akermark, *J. Amer. Chem. Soc.*, **91**, 1551 (1969).

magnesium with the previously assumed N_2-bridged species (Eq. 5) is irreversible and once the nitrogen is partially reduced in the titanium or vanadium complex, further reaction with magnesium would take place preferentially with the nitrogen bound, partially reduced species, leaving the other species the full capacity to combine with molecular nitrogen. This assumption is supported by Fig. 3 which shows much faster rate of Mg consumption under nitrogen than under argon and by Fig. 8 which demonstrates that the system reacted with 1.5 g-atoms of Mg under argon still shows considerable capacity to combine with nitrogen.

When $TiCl_3(THF)_3$ was reduced with sodium amalgam under nitrogen, the system became heterogeneous when 2.7 equivalents of Na was consumed with the N_2 fixation of 0.35 mol per titanium. In a similar experiment with $VCl_3(THF)_3$ using 5 equivalents of sodium amalgam per vanadium the fixation of nitrogen after 1 day was almost negligible. These results show the suitability of magnesium in the N_2 fixation and suggest its particular role in the reduction of the combined nitrogen.

The mode of combination of magnesium with titanium or vanadium presents a difficult problem to explain. The magnesium content in the benzene-soluble vanadium complexes **3**—**6** varies depending on the preparative conditions and magnesium in $[TiNMg_2Cl_2(THF)]$ **1** can be removed either in zerovalent or in divalent state as described earlier. Magnesium is supposed in these complexes to be present in the vicinity of titanium or vanadium and of chlorine, and can be driven in different ways depending on the reagent to attack magnesium. It is clear that the nitrogen in these complexes is not present in the form of magnesium nitride since the removal of magnesium takes place leaving the nitrogen in the complexes intact.

Evidently the nitrogen in the complexes is bound with titanium or vanadium but we can not conclude from the available data whether it is in the form of nitride or exists as the bridging ligand. The absence of the N_2 stretch band in the IR spectrum above 1600 cm^{-1} excludes the possibility of the presence of N_2 ligand as in later transition metal-N_2 complexes.[2] No distinct band assignable to metal-nitride stretch was observed above 400 cm^{-1} and the possibility of N_2-bridged binuclear structure with low N-N bond order can not be excluded, although the failure of detection of hydrazine after hydrolysis of the nitrogen-containing complexes favors the nitride structure.

Tetrahydrofuran in complexes **1**—**6** appears to be bonded with titanium or vanadium. Symmetric and antisymmetric stretching bands of C-O-C bond of THF were observed at 860 and 1015 cm^{-1} for titanium complex **1** and at 875 and 1026 cm^{-1} for vanadium complex **3** in comparison with those of free THF at 910 and 1075 cm^{-1} and of $MgCl_2(THF)_2$ at 890 and 1040 cm^{-1}. The tetrahydrofuran is bonded with titanium very strongly in complex **1** and thermal decomposition of **1** at 200°C could not remove all THF in the complex and the decomposition was accompanied by partial decomposition of the THF ligand whereas THF in $MgCl_2(THF)_2$ was easily removed.

The presence of a small amount of hydridic hydrogen in complexes **1** and **3** and of one hydridic hydrogen in complex **4** prepared under argon should be explained by hydrogen abstraction from THF by titanium or vanadium. This result may be understood as the indication of the reactivity of the low valent vanadium and titanium complexes toward hydrogen in the absence of nitrogen.

The high reactivities of the low valent titanium and vanadium complexes are reflected in their reactions with various reagents. The reactions with organic halides may probably proceed through oxidative addition reactions which yield unstable transition metal-alkyl complexes. The formations of dibenzyl in the reaction of benzyl chloride and of methane in the reaction of methyl iodide with **3** support the above assumption.

The catalytic activities of the low valent complexes in the dimerization and hydrogenation of olefins may be understood by assuming titanium and vanadium hydrides as the active species which can be formed by the reaction with molecular hydrogen and also by hydrogen abstraction from THF.

The $TiCl_3$-Mg and VCl_3-Mg systems described here react with molecular nitrogen and hydrogen respectively but no ammonia was formed in the presence of both reactants except after hydrolysis. Previously we considered necessary conditions for ammonia synthesis from N_2 and H_2 by a transition metal complex to proceed including the activation of N_2 and H_2 and transfer of hydrogen from the activated hydrogen to nitrogen.[14] The present systems are capable to activate both N_2 and H_2 but apparently the conditions for hydrogen transfer to occur are not fulfilled. Interestingly complexes **1** and **3** containing nitrogen catalyze the hydrogenation of magnesium to magnesium hydride. Complex **1** or **3** containing reduced nitrogen reacts with hydrogen forming a titanium hydride or vanadium hydride complex but the hydride formed is passed to magnesium, not to nitrogen, giving magnesium hydride despite the high reactivity of the bound nitrogen toward protonic reagents. Apparently the bound nitrogen in the complex has anionic nature and so does the hydride formed by the reactions of titanium or vanadium complex with molecular hydrogen, thus the hydrogen transfer of the hydride to the bound nitrogen may be hindered. Finding a proper method to make this hydrogen transfer possible seems a key problem for the catalytic formation of NH_3 from N_2 and H_2 to proceed under mild conditions.

Experimental

Materials. Titanium trichloride was used by dissolving in THF or after conversion to $TiCl_3(THF)_3$ by refluxing in THF for several hours and then purifying by recrystallization from THF.

Found: C, 39.2; H, 6.6; Cl, 28.0; Ti, 13.2% μ_{eff} 1.91 B. M. Calcd for $C_{12}H_{24}O_3Cl_3Ti$: C, 38.9; H, 6.5; Cl, 28.7; Ti, 12.9%.

14) A. Yamamoto, S. Kitazume, L. S. Pu, and S. Ikeda, *ibid.*, **93**, 371 (1971).

Vanadium trichloride was always used as $VCl_3(THF)_3$. VCl_3 which was prepared by the reaction of V_2O_5 with S_2Cl_2[15] was converted to the THF adduct which was purified by recrystallization from THF.

Found: C, 37.7; H, 6.2; Cl, 28.0; V, 13.9% μ_{eff}, 2.95. B. M. Calcd for $C_{12}H_{24}O_3Cl_3V$: C, 38.6; H, 6.5; Cl, 28.5; V, 13.9%.

Nitrogen, hydrogen, and argon gases were dried and deoxygenated by passing through columns of $CaCl_2$, P_2O_5, and activated copper. Solvents were dried by usual methods and deoxygenated by distillation under nitrogen or argon. Granular or powder magnesium was used; in some experiments granular magnesium was pretreated with iodine and washed with THF. Sodium amalgam was prepared by the reaction of sodium with mercury in Nujol; the sodium content was 0.2%.

Analytical Methods. Analysis of Ti, V, Mg, and Cl was carried out after hydrolysis of a sample (0.1—0.6 g) with 20% sulfuric acid. Titanium was precipitated by Cupferron (nitrosophenylhydroxylamine) and determined as TiO_2 by gravimetric method. Vanadium was determined in a similar method as V_2O_5. Magnesium was analyzed after removal of titanium or vanadium component from the sample by titration with ethylenediaminetetracetic acid. Chlorine content was determined by Mohr method with silver nitrate. The amount of nitrogen fixed by the complex was determined by Kjeldahl method and referred to as N* in analytical data to distinguish when necessary from the amount of total nitrogen content N obtained by microanalysis. The microanalysis was performed by Mr. T. Saito of our laboratory.

The amount of coordinated THF in complexes was determined by displacing the coordinated THF with 2,2'-dipyridyl and by analyzing the liberated THF by gas chromatography. This method is not quite quantitative but can be used as a measure to estimate the number of the coordinated THF approximately. In the case of $TiCl_2(acac)(THF)_2$[4] we have confirmed that 85% of THF for the theoretical value was released.

Because the complexes obtained are very air-sensitive, considerable difficulties were encountered in analysis. Furthermore, since the amount of THF contained in complexes varied, the absolute percentage of the analytical data can not be regarded as the criteria for purity. Therefore the empirical composition based on the ratio of atoms and THF in the complexes will be given below in most places.

IR spectra were recorded in KBr discs with Hitachi EPI-G3 and Shimadzu IR 27C spectrophotometers. Electronic spectrum was measured with a Shimadzu SV-50 spectrophotometer and ESR spectra was recorded on a Jeolco JES 3B-X.

Kinetic Studies. Kinetics studies were carried out using a 1-liter glass flask with a magnetic stirrer in a thermostatted bath regulated within 0.1°C. $TiCl_3$ was added to 100 m*l* of THF containing Mg and the time was measured from the point of addition. Previous dissolution of $TiCl_3$ somewhat shortened the induction period but no change in the essential feature of the N_2 absorption rate was observed. The absorption rate was followed by a gas flow meter, keeping the pressure constant by an oil seal and removing the moisture of the flowing gas by passing through a P_2O_5 column. The reaction with argon diluent was carried out as follows; after all the reagents were introduced into the reactor under argon, the pressure of argon was adjusted to a given pressure and N_2 was introduced. The reaction was terminated by removing the gas and solvent *in vacuo*. The amount of nitrogen fixed was determined as ammonia after hydrolysis with sulfuric acid and the amount of magnesium consumed was measured by weighing the unreacted magnesium which was separated from the solution, washed with THF and dried *in vacuo*.

Isolation and Reactions of Complexes. Since the complexes were isolated in a similar way some typical examples will be given.

1. [*$TiNMg_2Cl_2(THF)$*] **1**: $TiCl_3(THF)_3$ (18 g, 50 mmol) was dissolved in 150 m*l* of THF under nitrogen and the solution was added to 12 g of magnesium. The color of the solution changed slowly from blue through green to black with evolution of heat and absorption of N_2 which was measured by a gas burette. The absorption of N_2 stopped after several hours but the contact of the solution with nitrogen was continued for 24 hr to complete the reaction. The total amount of nitrogen absorbed was 0.5 mol per titanium. Unreacted magnesium was separated by filtration and the black THF solution was evaporated to dryness at room temperature. The residue was extracted with benzene *in vacuo* until no benzene-soluble dark substance remained. The white residue (5.7 g) was recrystallized from THF-hexane mixture as white needles. The benzene soluble fraction was dissolved again in THF and precipitated by addition of a controlled amount of hexane. The dark precipitate thus obtained was dried *in vacuo* to yield black very air-sensitive powder (11.2 g).

The white needles readily lose THF on drying and the amount of THF varied depending on the extent of drying. The ratio of magnesium to chlorine of the powder obtained on drying the crystals was 1 : 1.94, thus indicating the compound as $MgCl_2$ probably coordinated with 2 mol of THF in the crystalline state.

The benzene soluble fraction obtained as black powder analyzed as follows: Ti, 18.3; Mg, 17.6; Cl, 23.8; N, 4.7; THF, 24.5; C, 21.6; H, 4.5%. The empirical composition based on the ratio of atoms and THF: $TiMg_{1.9}Cl_{1.8}N_{0.94}(THF)_{0.89}$.

Reactions of **1** *a. Iodolysis* of this complex (0.32 g) released 1.89 m*l* at STP of H_2 which was measured by a Toepler pump and identified by mass spectrometry. The amount of H_2 evolved corresponded to 6.34% per titanium.

b. With HCl: **1** dissolved in THF (0.439 g, 1.67 mmol as calculated from the Ti content) reacted with dry hydrogen chloride consuming 10.07 mmol (6.02 mmol/Ti) and evolved 1.26 mmol (0.76 mol/Ti) of H_2.

c. With Pyridine: The reaction of **1** (2.3 g) in 100 m*l* of THF with pyridine (13.2 g) caused the precipitation of a black substance. Extraction of the system with THF and recrystallization from THF gave colorless crystals.

Found: C, 47.4; H, 4.0; N, 10.8; Cl, 28.3; Mg, 9.65%. Calcd for $MgCl_2(C_5H_5N)_2$: C, 47.4; H, 4.0; N, 11.1; Cl, 28.1; Mg. 9.60%.

Analysis of the black precipitate purified by repeated reprecipitation from pyridine-THF-hexane mixture: Ti, 22.7; Mg, 13.6; Cl, 8.62; N*, 6.31. Empirical composition: $TiMg_{1.2}CI_{0.5}N^*_{0.95}$

d. With 2,2'-Dipyridyl: Addition of THF solution of dipyridyl (20 g) to the black THF solution containing 5.2 g of **1** caused the color change to reddish violet and a precipitate was formed. Extraction of a THF soluble fraction from the system gave dark reddish violet crystals which are very sensitive to air.

Found: Mg, 4.6; C, 69.5; H, 5.7; N, 15.9%; Atomic ratio: Mg, 1.0; C, 30; H, 26; N, 6.0.

The THF insoluble fraction could not be purified because of the lack of appropriate solvent.

15) H. Funk and C. Muller, *Z. Anorg. Allg. Chem.*, **244**, 94 (1940).

Found: Ti, 9.9; Mg, 7.2; Cl, 13.9; N*, 2.9; C, 46.7; H, 4.8; N, 10.4%. Empirical formula: $TiMg_{1.4}Cl_{1.9}M^*_{1.0}C_{19}H_{23}(N\text{-}N^*)_{2.6}$.

Reaction of the THF-insoluble fraction with pyridine gave homogeneous black solutiom. Addition of THF formed the black precipitate which was separated from the solution and analyzed after reprecipitation from pyridine-THF mixture.

Found: Ti, 17.6; Mg, 0.87; Cl, 10.1; N*, 4.4; C, 36.4; H, 3.7; (N-N*), 9.2%. Empirical formula: $TiMg_{0.87}Cl_{0.78}N^*_{0.86}C_{8.3}H_{10}(N\text{-}N^*)_{1.8}$. From the solution white crystals of $MgCl_2(C_2H_5N)_2$ were isolated.

e. With Benzoyl Chloride: $[TiNMg_2Cl_2(THF)]$ **1** (2.1 g, 8.2 mmol) was dissolved in 50 m*l* of THF and a THF solution containing 3.5 g of benzoyl chloride was added at room temperature. The black solution turned dark green with addition of benzoyl chloride. On cooling the mixture with addition of *n*-hexane colorless plates of $MgCl_2(THF)_2$ separated out. After removal of the white crystals, all the titanium complex was precipitated with addition of *n*-hexane and the precipitate was washed to remove excess benzoyl chloride. The precipitate was extracted with benzene, purified and analyzed as usual.

Found: Ti, 17.6; Cl, 10.9; N*, 4.89; C, 48.5; H, 4.0%. Empirical formula: $TiCl_{0.84}N_{0.95}C_{11}H_4$.

f. With Hydrogen and Magnesium: Complex **1** (2.35 g, 9.2 mmol) dissolved in THF (50 m*l*) was put in contact with 2.3 g of magnesium under hydrogen at room temperature. The system absorbed 3.33 mol of H_2/Ti in 90 hr and still showed ability to react with hydrogen. From the system black powder was separated as the benzene-soluble fraction.

Found: Ti, 13.0; N*, 3.4; Mg, 26.6; Cl, 14.6; C, 25.0 H, 5.0; N, 3.8%. Iodolysis of the powder 0.1164 g (0.318 mmol based on Ti content) in benzene gave 0.318 mmol of H_2 (98.5% based on Ti content). Empirical formula: $TiN_{1.0}(H)_2Mg_{4.0}Cl_{1.5}C_{7.7}H_{16}$(**2**).

2. Preparation of Vanadium Complexes. 2.1 Under Nitrogen: Complex **3** was prepared in a similar way to titanium complex **1** from 28.7 g (75.9 mmol) of $VCl_3(THF)_3$ in 200 m*l* of THF and 18.7 g (0.77 mol) of Mg under nitrogen. The absorption of nitrogen took 15—20 hr at room temperature and the color of the solution turned from red through green to black.

Found: V, 17.5; Mg, 15.9; Cl, 25.5; N, 4.9; C, 21.5; H, 3.8%. Empirical formula: $VMg_{2.1}Cl_{2.1}N_{1.0}C_{5.2}H_{11.0}$. Iodolysis of the complex, 0.311 g, released 0.615 m*l* of H_2 which corresponded to 2.75 mol% of vanadium.

2.2 Under Argon: $VCl_3(THF)_3$ (17.3 g, 46.3 mmol) in 150 m*l* of THF was reduced under argon with 11.4 g (0.47 mol) of magnesium at room temperature. After the reaction for 3 days with the color change of the solution as observed in the reaction under nitrogen, the argon was replaced with nitrogen but no absorption was observed. $MgCl_2(THF)_2$ and benzene-soluble black powder were separated.

Found: V, 20.4; Mg, 18.5; Cl, 21.3; C, 25.6; H, 4.4%. Empirical formula: $VH_{0.6}Mg_{1.9}Cl_{1.5}C_{5.3}H_{10.0}$. Iodolysis of the complex 0.258 g (1.03 mmol) gave 0.303 mol of hydrogen per vanadium.

2.3 Under Hydrogen: $VCl_3(THF)_3$ (22.6 g, 60.4 mmol) dissolved in 200 m*l* of THF was stirred with 29.2 g of Mg under hydrogen at room temperature for 1 month and the system absorbed 3.5 mol of hydrogen per vanaduim. Magnesium chloride and benzene soluble black powder were separated.

Found: V, 19.6; Mg, 17.8; Cl, 11.6; C, 32.8; H, 6.2%. Empirical formula: $V(H)_{1.8}Mg_{1.9}Cl_{0.81}C_{7.1}H_{14.2}$. Hydride content was determined by iodolysis which relaesed 0.90 mol of H_2 per vanadium.

Reaction of **3**. *a. With Hydrogen and Magnesium*: Complex **3** (2.8 g, 9.7 mmol) was dissolved in 80 m*l* of THF and stirred with 4.7 g (0.19 mol) of magnesium at room temperature under hydrogen. The solution absorbed 10 mol of H_2 per vanadium in 40 days. Black powder was recovered from the solution.

Found: V, 11.6; Mg, 28.6; Cl, 16.8; N, 3.0; C, 21.6; H, 4.2%. Empirical formula: $V(H)_{1.9}Mg_{5.2}Cl_{2.1}N_{0.94}C_{7.9}H_{18.5}$. Hydride content was determined by iodolysis which released 0.95 mol of H_2 per vanadium.

b. With Benzyl Chloride: Benzyl chloride 4.8 g (38 mmol) in THF (80 m*l*) was added to **3**(3.7 g, 12.7 mmol) and the reaction took place with evolution of heat. The solution was evaporated to dryness, washed with *n*-hexane and ether, and extracted with benzene. In the ether washing the presence of dibenzyl, mp 51—53.5°C, was detected and identified by comparison of the IR spectrum with authentic sample. As the benzene insoluble residue magnesium dichloride remained and from the benzene extract a nitrogen containing vanadium complex was recovered.

Found: V, 23.2; Mg, 8.8; Cl, 19.3; N, 5.9; C, 27.8; H, 4.6%. Empirical formula: $VMg_{0.79}Cl_{1.2}N_{0.92}C_{5.1}H_{10.1}$. The IR spectrum of this complex was similar to that of **3**.

c. With Chlorotriphenylmethane: Reaction of **3** (4.2 g, 14.4 mmol) with chlorotriphenylmethane (9.4 g, 33.6 mmol) in 60 m*l* of THF took place with evolution of heat and a black benzene soluble powder with a similar IR spectrum to **3** was obtained.

Found: V, 18.4; Mg, 10.3; Cl, 24.6; N, 4.7; C, 22.3; H, 4.1%. Empirical formula: $VMg_{1.1}Cl_{1.9}N_{0.93}C_{5.1}H_{11.4}$. White benzene insoluble crystals were identified as magnesium chloride.

d. With Methyl Iodide: A THF solution containing 8.6 g (60.5 mmol) of methyl iodide was added to 4.5 g (15.5 mmol) of **3**. Reaction took place with evolution of gas. As the benzene soluble powder a vanadium complex was obtained.

Found: V, 18.1; Mg, 15.7; Cl, 23.6; N, 4.8; C, 21.6; H, 3.9%. Empirical Formulas: $VMg_{1.8}Cl_{1.9}N_{0.96}C_{5.2}H_{10.9}$. The IR spectrum of the complex was similar to **3**. By an independent experiment the gas evolved was identified as methane (0.5 mol/V) and traces of ethane and ethylene by mass spectroscopy and gas chromatography.

The authors are grateful for the grant support of this work from the Ministry of Eduction.

Kinetics of Liquid-phase Hydrogenation of Aliphatic α,β-Unsaturated Aldehyde over Raney Cobalt Catalyst Modified with Co-, Mn-, Ni-, and $PdCl_2$

Kazuhiko HOTTA and Teruo KUBOMATSU

The Osaka Municipal Technical Research Institute, Kita-ku, Osaka

(Received May 4, 1971)

Kinetic studies were carried out on the hydrogenation of the α,β-unsaturated aldehyde, 2-methyl-2-pentenal (UD), over the Raney cobalt catalyst modified with various amounts of Co-, Mn-, Ni- and $PdCl_2$ in *n*-hexane under atmospheric pressure at 40 and 20°C. Initial rates of formation of the saturated aldehyde (r_{SD}), saturated alcohol(r_{SA}) and unsaturated alcohol(r_{UA}) were determined in the concentration range of UD(C_{UD}) 0.018—0.263 mol/*l*. It was found that ($r_{SD}+r_{SA}$) obeyed a Langmuir-type rate equation and r_{UA} a different one. The rate equations are as follows.

$$r_{SD} + r_{SA} = \frac{k_1 \cdot b_1 \cdot C_{UD}}{(1+b_1 \cdot C_{UD})^2}, \qquad r_{UA} = \frac{k_2 \cdot b_2 \cdot C_{UD}}{(1+b_2 \cdot C_{UD})^2}$$

where k and b denote the rate constant of the surface reaction and parameter for the adsorption of UD and hydrogen, respectively, the subscripts 1 and 2 representing the formation of SA and SD and that of UA, respectively. Kinetic parameters k_1, k_2, b_1 and b_2 were found to vary with the amount and kind of modifier. The variation of b_1 and b_2 was irregular. The rate constant k_1 decreased with increasing amount of Co-, Mn- and $NiCl_2$ added; it increased remarkably with the addition of $PdCl_2$. The variation of k_2 was more complicated. Addition of a small amount of the modifiers did not decrease k_2. Further addition of Co- and $MnCl_2$ made k_2 decrease, while that of $NiCl_2$ made it increase. Mechanism of the modification with these metal chlorides is discussed on the basis of the active site hypothesis.

In the course of studies on selectivities of Raney-type catalysts modified with various compounds in the liquid phase hydrogenation of the α,β-unstaturated aldehyde, we have found that the formation of the saturated aldehyde and alcohol over the Raney cobalt catalyst was inhibited by the addition of $FeCl_2$ and that of the unsaturated alcohol was retarded only slightly.[1]

Kishida *et al.* have studied the modifier effect of some organic compounds in the liquid phase hydrogenation of acetone over the Raney nickel catalyst and found that the addition of tripropylamine decreased the rate of hydrogenation at low concentrations of acetone but increased at high concentrations.[2] The effect of the modifier depends on the concentration of the reactant at which the rate measurement was carried out.

Thus in studying the modifier effect on a solid catalyst, it is advisable to determine the kinetic parameters for the adsorption of reactants and for surface reaction, both being independent of the concentration of reactants, and to examine the variation of the two parameters. Such a treatment has seldom been performed on the modifier effect of metal chlorides. In the present paper, kinetics of the liquid phase hydrogenation of the α,β-unsaturated aldehyde, 2-methyl-2-pentenal, over the Raney cobalt catalyst modified with manganese(II)-, cobalt(II)-, nickel(II)- and palladium(II) chlorides are described. Variation of the rate constant and adsorption coefficient with the amount and kind of modifier is examined. Mechanism of uneven poisoning of the catalyst observed when Co- and $MnCl_2$ were added, is discussed on the basis of the active site hypothesis. The promoter effect of $PdCl_2$ on the reaction of the carbon-carbon double bond is also discussed.

Experimental Methods

Catalyst. A Raney cobalt-aluminum alloy(50 wt% Co) was developed with a sodium hydroxide solution and washed with distilled water and then with 2-propanol.[3] The catalyst thus obtained was stirred with specified amounts of anhydrous metal chlorides in 2-propanol for 1 hr in a hydrogen atmosphere. The amount of metal chlorides adsorbed was determined by measuring polarographically the amount of metal ions remaining in 2-propanol solution. It was found that these ions were completely adsorbed on the catalyst when the amount of metal chlorides added was less than 0.10 mmol/g-Co. When metal chloride of 0.15 mmol/g-Co was used, the amount of adsorbed ion was 0.14 mmol/g-Co.

It was observed that the brown color of $PdCl_2$ solution faded by stirring for a few minutes. Absorption of hydrogen was observed, and the blue color of Co(II) ion appeared and then disappeared completely by stirring for 5 min. This indicates that $PdCl_2$ is adsorbed on the catalyst and reduced to the metal according to the following equations

$$PdCl_2 + Co \longrightarrow Pd + CoCl_2$$

$$PdCl_2 + H_2 \longrightarrow Pd + 2HCl$$

and HCl formed reacts with cobalt atom to give $CoCl_2$ and $CoCl_2$ formed is also adsorbed on the catalyst surface.

The modified catalyst thus obtained was washed twice with 2-propanol and 10 times with *n*-hexane and then dried in a hydrogen atmosphere. The resulting catalyst was weighed and stored in the portion containing *ca.* 500 mg of cobalt.[3]

Apparatus, Procedure, and Materials. Hydrogenation was carried out as described previously.[3] Over the catalyst modified with $PdCl_2$, however, it was carried out at 20°C since a too rapid reaction took place at 40°C. Reaction products were analyzed by glc. Adsorbed metal chlorides were not removed during the reaction. Substrate: 2-methyl-2-pentenal, cylinder hydrogen, 2-propanol, and

1) K. Hotta and T. Kubomatsu, This Bulletin, **42**, 1447 (1969).

2) S. Kishida, C. Ko and S. Teranishi, *Shokubai*, **11**, 146 (1969).

3) K. Hotta and T. Kubomatsu, This Bulletin, **44**, 1348 (1971).

Table 1. Initial rates of the formation of SD, SA, and UA over Raney cobalt catalyst modified with $CoCl_2$ at 40°C

$CoCl_2$ (mmol/g-Co)		C_{UD} (10^{-2} mol/l)						
		3.5	7.0	10.5	14.0	19.3	26.3	
0.0	r_{SD}	12.3	15.8	13.4	12.1	11.1	8.8	
	r_{SA}	9.7	8.2	5.5	5.3	4.6	2.4	
	r_{UA}	7.2	8.7	10.0	9.7	8.4	6.9	
0.025	r_{SD}	6.1	6.7	5.7	5.5	5.5	4.9	
	r_{SA}	8.5	6.7	5.0	3.6	2.8	2.0	
	r_{UA}	6.9	9.5	10.5	11.3	10.7	9.5	
0.05	r_{SD}	2.3	2.9	3.3	3.1	2.8	2.3	
	r_{SA}	5.3	3.8	2.5	2.2	1.8	1.2	
	r_{UA}	7.9	9.5	9.4	9.3	8.7	7.2	
	C_{UD}	1.8	3.5	7.0	10.5	14.0	17.5	22.8
0.10	r_{SD}		1.0	1.3	1.5	1.4	1.2	0.92
	r_{SA}		1.2	1.1	0.65	0.38	0.36	0.33
	r_{UA}		4.0	4.1	3.8	3.7	3.6	3.0
0.15	r_{SD}	0.36	0.49	0.66	0.58	0.49		
	r_{SA}	0.53	0.43	0.31	0.24	0.17		
	r_{UA}	1.7	2.3	2.4	2.6	2.5		

Unit of initial rate: 10^{-2} mmol/min·g-Co, C_{UD}: concentration of UD.

n-hexane were the same as those described previouly. Commercial anhydrous metal chlorides of extra pure grade were used without further purification.

Determination of Initial Rate of Formation of Product. The initial rate of formation was determined by extrapolating the plot, rate of formation *vs.* reaction time, to zero.[3]

Results

Initial Rate of Formation of Product. Products of the reaction were found to be the saturated aldehyde 2-methylpentanal(SD), saturated alcohol 2-methylpentan-1-ol(SA) and unsaturated alcohol 2-methyl-2-penten-1-ol(UA). Isomerization of UA to SD, and dehydrogenation of UA to UD and of SA to SD and/or UA were not observed under the conditions studied.

Initial rates of the formation of SD(r_{SD}), SA(r_{SA}), and UA(r_{UA}) are given in Tables 1 and 2 for the catalyst modified with $CoCl_2$, abbreviated as R-Co-(Co), the one with $PdCl_2$ as R-Co(Pd), respectively. R_{UA} decreased by the addition of 0.025 mmol/g-Co of $CoCl_2$ at low concentrations of UD and increased at high concentrations. r_{UA} decreased by the further addition of the modifier. On the other hand, r_{SD} and r_{SA} decreased with increasing amount of $CoCl_2$. A similar behavior was observed for the catalyst modified with Ni- and $MnCl_2$. The behavior of the initial rates mentioned above is not contradictory to that reported by other workers.[4,5]

r_{UA} increased by the addition of 0.025 mmol/g-Co of $PdCl_2$ at low concentrations of UD and decreased at high concentrations, and decreased by the further addition of the modifier. r_{SD} increased by the addition of $PdCl_2$ more remarkably than r_{SA}.

Table 2. Initial rates of the formation of SD, SA and UA over Raney cobalt catalyst modified with $PdCl_2$ at 20°C

$PdCl_2$ (mmol/g-Co)		C_{UD} (10^{-2} mol/l)				
		3.5	7.0	10.5	15.8	21.0
0.0	r_{SD}	5.7	8.0	8.0	7.5	7.0
	r_{SA}	3.7	3.2	2.7	2.2	2.0
	r_{UA}	2.2	3.1	4.3	4.4	4.3
	C_{UD}	5.3	8.8	14.0	19.3	26.3
0.025	r_{SD}	35	38	29	26	21
	r_{SA}	6.0	3.6	3.3	3.0	1.9
	r_{UA}	3.7	3.8	4.0	4.5	3.9
0.050	r_{SD}	44	50	52	55	54
	r_{SA}	5.9	4.4	3.2	2.4	1.1
	r_{UA}	2.8	3.6	2.8	2.5	2.3
0.10	r_{SD}	60	68	70	79	80
	r_{SA}	5.3	3.8	3.2	2.6	1.5
	r_{UA}	+	+	+	+	1.9

Rate Equation and Kinetic Parameters. The data in Table 1 were analyzed by means of the equation

$$r = \frac{k \cdot b \cdot C_{UD}}{(1 + b \cdot C_{UD})^2} \quad (1)$$

where k denotes the rate constant, C_{UD} the concentration of UD, and b is the ratio of the adsorption equilibrium constant of UD to that of hydrogen, divided by the liquid phase concentration of hydrogen *i.e.* $b = K_{UD}/$

4) Z. Csuros and J. Petro, *Acta Chem. Acad. Sci. Hung.*, **20**, 129 (1959).

5) Y. Takagi and T. Yamanaka, *Sci. Papers Inst. Phys. Chem. Res.*, **55**, 105 (1961).

TABLE 3. KINETIC PARAMETERS

		With respect to the formation of SA+SD		UA	
	(mmol/g-Co)	k_1 (mmol/min·g-Co)	b_1 (l/mol)	k_2	b_2
$CoCl_2$	0.0	1.0	25	0.38	11
	0.025	0.25	21	0.43	7.5
	0.050	0.28	22	0.39	11
	0.10	0.094	20	0.20	16
	0.15	0.040	25	0.11	13
$MnCl_2$	0.025	0.44	18	0.39	7.2
	0.050	0.26	24	0.33	8.4
	0.10	0.091	20	0.17	14
	0.15	0.032	22	0.13	13
$NiCl_2$	0.025	0.54	15	0.38	12
	0.050	0.53	23	0.39	12
	0.10	0.44	27	0.40	12
$PdCl_2$	0.0	0.44	11	0.17	6.1
	0.025	1.4	17	0.17	20

$K_H \cdot C_H$ and called adsorption coefficient. As the rate measurement was carried out under the constant pressure of hydrogen, and the solubility of hydrogen is assumed to be independent of the composition of reaction mixture, C_H is constant at a given temperature, and b depends only on the adsorption equilibrium constants of UD and hydrogen.

Rearranging Eq. (1), we obtain: $(C_{UD}/r)^{1/2}=1/(k\cdot b)^{1/2}+(b/k)^{1/2}\cdot C_{UD}$. This gives a linear relation between $(C_{UD}/r)^{1/2}$ and C_{UD} when $(C_{UD}/(r_{SD}+r_{SD}))^{1/2}$ *vs.* C_{UD} for R-Co(Co) are plotted (Fig. 1), and $(C_{UD}/r_{UA})^{1/2}$ *vs.* C_{UD} (Fig. 2). From these plots, the values of kinetic parameters k and b were determined (Table 3). The values of the kinetic parameters for R-Co-(Mn), R-Co(Ni) and R-Co(Pd-0.025) determined similarly are also given.

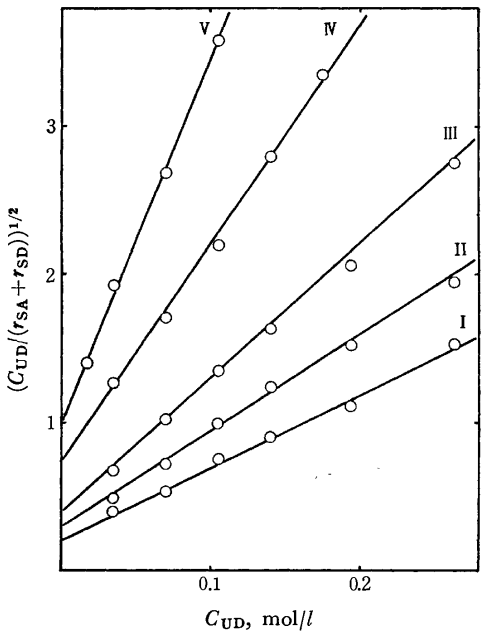

Fig. 1. $(C_{UD}/(r_{SA}+r_{SD}))^{1/2}$ *vs.* C_{UD} plots for R-Co catalyst modified with $CoCl_2$ of 0.0 mmol/g-Co, I; 0.025, II; 0.050, III; 0.10, IV; 0.15, V.

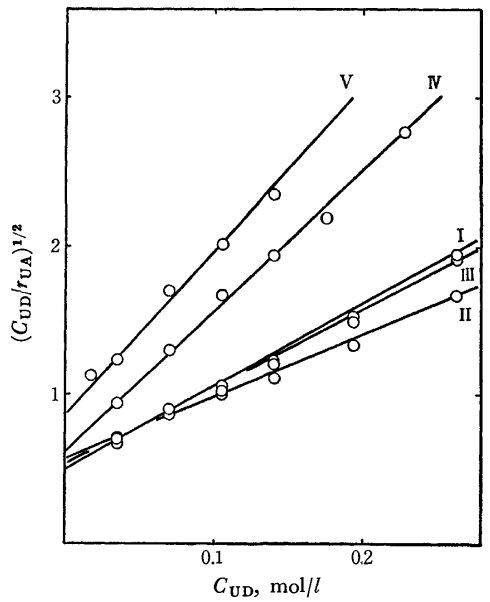

Fig. 2. $(C_{UD}/r_{UA})^{1/2}$ *vs.* C_{UD} plots.

The rate data over R-Co(Pd-0.050 and 0.10) were not analyzed by the same method since SA was supposed to be formed through both SD and UA. Variation of the values of b_1 and b_2 is irregular (Table 3). Variation of the rate constant with the amount of metal chlorides is shown in Fig. 3. The rate constant for the formation of SA and SD (k_1) decreases with increasing amount of Co-, Mn- and $NiCl_2$, but it increases with the addition of $PdCl_2$.

Addition of a small amount of these modifiers does not decrease the rate constant for the formation of UA (k_2). Further addition of Co- and $MnCl_2$ decreases k_2, while that of $NiCl_2$ makes it increase.

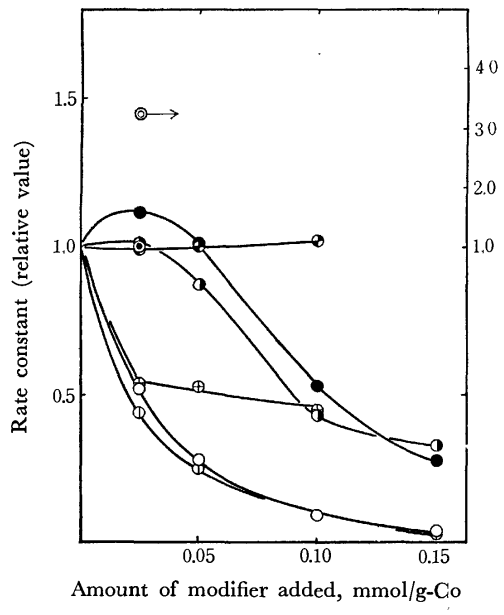

Fig. 3. Variation of rate constant with amount of modifier added, for k_1 with $CoCl_2$, ○; $MnCl_2$, ◑; $NiCl_2$, ⊕; $PdCl_2$, ◎; k_2 with $CoCl_2$, ●; $MnCl_2$, ◑; $NiCl_2$, ◒; $PdCl_2$, ⊙

Discussion

It has been reported[1] that, in the hydrogenation of a mixture of SD and UA (mole ratio 1 : 1) over the Raney cobalt catalyst in the absence and in the presence of $FeCl_2$, SD was preferentially hydrogenated. Since the initial rates of formation of the three products varied with the addition of Co-, Mn- and $NiCl_2$ in a similar way to that observed when $FeCl_2$ was added, it can be considered that the hydrogenation of UA to SA does not occur over the catalyst modified with Co-, Mn-, and $NiCl_2$ in the period in which the concentrations of SD and UA are comparable. Thus, the reaction scheme,[3] in which the formation of UA and that of SA and SD were separately treated, can also be valid for the present systems over the catalyst modified with Co-, Mn-, and $NiCl_2$.

When the mixture of UA and SD was hydrogenated over the Raney cobalt catalyst modified with $PdCl_2$ (0.050 and 0.10 mmol/g-Co), both SD and UA were hydrogenated simultaneously. Thus in the hydrogenation of UD over the $PdCl_2$-modified catalyst the reaction path of the hydrogenation of UA to SA has to be considered, and the formation of SD and SA and that of UA can not be treated separately. This is considered to be due to the formation of metallic palladium which is active for the hydrogenation of the carbon-carbon double bond. This is supported by the result where r_{SD} over the $PdCl_2$-modified catalyst increased remarkably. Promotion in the activities of the Raney nickel and cobalt catalysts by the addition of platinum-metal compounds was reported by several workers.[6-8]

The decrease of k_1 over R-Co(Co) and R-Co(Mn) (Fig. 3), can be explained as being due to the poisoning of active sites. The variation of k_2 over R-Co(Mn) might indicate that the formation of UA, SA and SD takes place on different sites of catalyst surface and the site responsible for the formation of UA is not occupied with $MnCl_2$ when 0.025 mmol/g-Co of the modifier was used.

Modification of the catalyst with $CoCl_2$ of 0.025 mmol/g-Co caused the increase of k_2. Promotion in the rate constant can not be explained by a simple active site hypothesis. As the number of active sites responsible for the formation of UA can not be considered to increase with the addition of 0.025 mmol/g-Co of $CoCl_2$ although k_2 was found to increase, the specific rate constant defined as the rate constant per unit active site must increase. This suggests a promoting effect which is induced onto a site by the modifier adsorbed on another site. The fact that k_2 begins to decrease can be explained by considering that further addition of the modifier causes the adsorption of $CoCl_2$ even on the site responsible for the formation of UA and, hence, the increase in the number of sites covered by the modifier overcomes an increase in the specific rate constant. A similar behavior of rates has also been observed in acetone hydrogenation over the Raney nickel catalyst by the addition of a small amount of triethylamine.[2]

The ratio k_2/k_1 increased with the amount of Co- and $MnCl_2$, and decreased with the addition of $PdCl_2$. Although behaviors of k_1 and k_2 over R-Co(Ni) differ somewhat from those over R-Co(Co) and R-Co(Mn), the ratio k_2/k_1 over R-Co(Ni) increased with the amount of $NiCl_2$ added, as found for the modification with Co- and $MnCl_2$. It can therefore be considered that $NiCl_2$ acts as the modifier in the original form and is not reduced to the metal on the catalyst surface.

6) D. R. Levering, F. L. Morritz, and E. Lieber, *J. Amer. Chem. Soc.*, **72**, 1190 (1950).
7) M. Delepine and A. Horeau, *C. R. Acad. Sci. Paris*, **201**, 1301 (1935), *ibid.*, **202**, 995 (1936).
8) B. V. Aller, *J. Appl. Chem.*, **8**, 492 (1958).

The Photolysis of Ethoxycarbonylmethyltriphenylphosphonium Salts[1]

Yoshihiro NAGAO, Kensuke SHIMA, and Hiroshi SAKURAI
The Institute of Scientific and Industrial Research, Osaka University, Suita, Osaka
(Received October 28, 1971)

Irradiation of ethoxycarbonylmethyltriphenylphosphonium salts (IV) gave products expected to be derived from the homolytic fission of the P-CH_2CO_2Et or P-Ph bond. The rate of the product formation was dependent strongly on the anion species and on the solvent polarity; an oxidizable anion was effective for the photolysis and the less polar the solvent the faster the rate became. It was found through the measurement of the electrical conductance that the degree of electrolytic dissociation of IV was very low at the concentration employed in the photolysis. On the basis of these results, the photolysis of IV was confirmed to proceed through a direct charge transfer from an anion to a cation.

A fair number of works have been reported on the photochemistry of the compounds containing nitrogen or sulfur atoms.[2] However, little attention has been paid to the photochemical behavior of organophosphorus compounds.[3]

We found previously that the P-Ph bond was broken at the primary step of the photolysis of the phosphonium ylids,[4] I and II, and that the mode of the bond fission of III depended on the wavelength of exciting light used.[5] Now, we studied the photolysis of ethoxycarbonylmethyltriphenylphosphonium salts (IV).[6] Although it has been reported that phosphonium salts are decomposed by ultraviolet irradiation.[7] the mechanism is not yet established. In the present paper the effect of the anion species and solvent polarity on the rate of the product formation were examined in detail and the possibility of four different paths leading to the decomposition of IV was discussed. Further, we discussed briefly on the differences of the modes of the bond fission in the photolysis of I,[4] IV, and ammonium[8] and sulfonium salts.[9]

$Ph_3P{=}CHCO_2Et$ (I), $Ph_3P{=}CHCOR$ R=Me or Ph (II),
$Ph_3P{=}CPh_2$ (III),
$Ph_3P^+CH_2CO_2Et\ X^-$
X=Cl, Br, I, BF_4, ClO_4, or NO_3 (IV).

Results

Acetonitrile solutions of IV (X=Cl, Br, or I) (3.5 mmol in 10 m*l*) in quartz tubes were degassed by three cycles of the freeze-pump-thaw method and irradiated with a high pressure mercury lamp for 150 hr. Triphenylphosphine (TPP), ethoxycarbonylmethyldiphenylphosphine (EDP), diphenyl, halobenzenes, diethyl succinate, ethyl phenylacetate, benzene, and ethyl acetate were detected by gas chromatographic analysis. The yields of the products are shown in Table 1.

$$Ph_3P^+CH_2CO_2Et\ X^- \xrightarrow{h\nu} Ph_3P + Ph_2PCH_2CO_2Et + Ph\text{-}Ph + PhX + EtO_2CCH_2CH_2CO_2Et + PhCH_2CO_2Et + PhH + CH_3CO_2Et$$
X=Cl, Br, or I

In order to see the effect of the nature of the anion species on the rate of the formation of the product, the quantum yields for the formation of TPP, EDP, benzene, and ethyl acetate (ϕ_{TPP}, ϕ_{EDP}, ϕ_{PhH}, and $\phi_{CH_3CO_2Et}$) from the phosphonium halides and tetrafluoroborate were determined at 253.7 nm using ferrioxalate actinometry.[10] As shown in Table 2, ϕ_{TPP} and $\phi_{CH_3CO_2Et}$, or ϕ_{EDP} and ϕ_{PhH} were approximately

Table 1. Photolysis of IV in acetonitrile[a]

X	Product yield (%)							
	TPP	EDP	PhX	$(EtO_2CCH_2-)_2$	Ph-Ph	PhH	CH_3CO_2Et	$PhCH_2CO_2Et$
Cl	2.0	2.6	5.7	5.7	0.5	13.1	18	1.0
Br	10.6	2.6	0	7.1	2.4	6.3	35	0.5
I	6.9	0.9	6.0	0.1	0.2	6.0	49	0.1

a) IV (3.5 mmol) in 10 m*l* of acetonitrile.

1) A preliminary report of this work has been published: Y. Nagao, K. Shima, and H. Sakurai, *Tetrahedron Lett.*, **1971**, 1101.
2) A. Schönberg, G. O. Schenck, and O-A. Neumller, "Preparative Organic Photochemistry," Springer-Verlag, Berlin (1968), pp. 48, 105, 242, 434.
3) R. S. Davidson, "Organophosphorus Chemistry," S. Trippett (Senior Reporter), The Chemical Society, London, Vol. 1, (1970) p. 246 and Vol. 2, (1971) p. 221.
4) Y. Nagao, K. Shima, and H. Sakurai, *Kogyo Kagaku Zasshi*, **72**, 236 (1969).
5) Y. Nagao, K. Shima, and H. Sakurai, *Tetrahedron Lett.*, **1970**, 2221.
6) H. J. Bestmann, "Newer Methods of Preparative Organic Chemistry," Vol. 5, ed. by W. Foerst, Academic Press, New York (1968), p. 2.
7) C. E. Griffin and M. L. Kaufman, *Tetrahedron Lett.*, **1965**, 773.
8) a) J. W. Knapczyk and W. E. MacEwen, *J. Org. Chem.*, **35**, 2539 (1970). b) A. L. Maycock and G. A. Berchtold, *ibid.*, 2532 (1970). c) T. Laird and H. Williams, *Chem. Commun.*, **1969**, 561 and *J. Chem. Soc., C*, **1971**, 1863.
9) T. D. Walsh and R. C. Long, *J. Amer. Chem. Soc.*, **89**, 3943 (1967). b) C. Pac and H. Sakurai, *Chem. Commun.*, **1969**, 20.
10) The yields of these four products were increased linearly with the irradiation time and the determination was done within such irradiation time as the linearlity was held.

Table 2. Quantum yields for the formation of the products[a)]

X	TPP	EDP	CH_3CO_2Et	PhH
Cl	0.04	0.005	0.008	0.005
Br	0.04	0.001	0.03	0.001
BF_4	0.05	0.002	0.04	0.002
I	0.0004	0	0.13	0.02

a) Acetonitrile solution (0.5 M). Low pressure mercury lamp.

equal for each salt except in the case of the iodide, where ϕ_{TPP} and ϕ_{EDP} were extremely low. It is noteworthy that both ϕ_{PhH} and $\phi_{CH_3CO_2Et}$ were increased in the order, chloride<bromide<tetrafluoroborate<iodide.

The photochemical stability of IV (X=NO_3, Cl, Br, BF_4, or I) was estimated from the amount of the recovered salt after the photolysis. The results are shown in Table 3. The rate of the photodecomposition of IV was increased with the change of the anion in the order, $NO_3^-<Cl^-<Br^-<BF_3^-<I^-$. This order was essentially the same as obtained in the quantum yields measurements. Thus, the photolysis of IV in acetonitrile solution was found to be very sensitive to the nature of the anion species.

The effect of the solvent polarity on the rate of the product formation was examined in the photolysis of the bromide. The data shown in Table 4 indicate that with decreasing solvent polarity the yields of TPP and EDP were increased and the yield ratio TPP/EDP was decreased. These tendencies might suggest that a direct relation exists between solvent polarity and the rate of the product formation. More definitive evidence indicating the relation was obtained when the photolysis was carried out in benzene–ethanol mixed solvent in quartz tube. As shown in Fig. 1, the yields of TPP and EDP were increased linearly

Table 3. The relative reactivity of the salts

X	NO_3	Cl	Br	BF_4	I
Conversion[a)] (%)	12	18	24	33	45
Relative reactivity	1.0	1.5	2.0	2.8	3.7

a) Calculated from the amount of the recovered salts.

Table 4. Photolysis of IV (X=Br) in various solvents[a)]

Solvent	Yield (%) TPP	Yield (%) EDP	TPP/EDP	Relative rate	E_T value[b)] (kcal/mol)
MeOH	0.4	0	—	0.2	55.5
EtOH	6.1	0.38	16	1.2	51.9
i-PrOH	6.3	0.38	18	1.2	48.6
MeCN	4.9	0.38	14	1.0	46.0
DMF	10.3	0.94	11	2.1	43.8
EtOH-PhH (1 : 4)	7.8	1.25	7	1.7	—

a) IV (1.6 mmol) in 4 ml of appropriate solvent.
b) This value represents the polarity of the solvent; K. Dimroth, C. Reichardt, T. Siepmann, and F. Bohlmann, *Ann. Chem.*, **661**, 1 (1963).

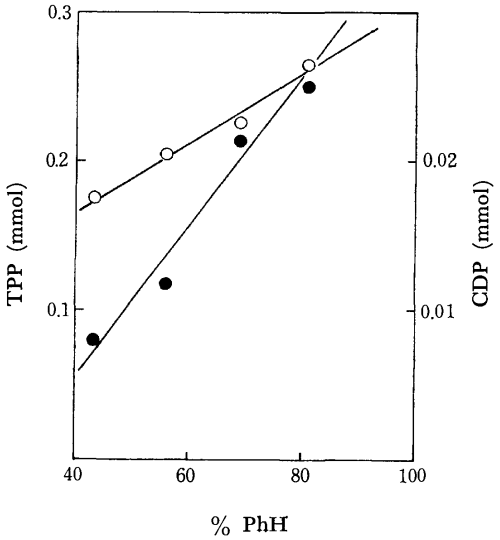

Fig. 1. Photolysis of IV in PhH-EtOH mixed solvent. IV (1.6 mmol) in 4 ml of solvent.
○: TPP, ●: EDP

with the increase in the ratio of benzene to ethanol. Similar results as shown in Fig. 1 were also obtained when the photolysis was done in Pyrex tube.[11)] This result indicates that the absorption of the light by benzene does not contribute to the acceleration of the rate of the formation of phosphines (that is, benzene does not sensitize the photodecomposition of IV). Thus, it was found that the rate of the product formation was sensitive to the solvent polarity and less polar solvents were effective for the photolysis.

As it was suggested through the examination of the solvent effect that the degree of the interaction between an anion and a cation in a solution may be an important factor in the photolysis of IV, the degree of the electrolytic dissociation of IV were determined through the measurements of electrical conductances of the acetonitrile solutions of IV. The degree of dissociation ($\alpha=\Lambda/\Lambda_\infty$) at 0.32 M (this concentration is close to that at which the photolysis was done; 0.37 M) was calculated to be 0.24 for the bromide and 0.26 for the iodide. Under such circumstances an appreciable interaction between an anion and a cation may be possible.

Table 5 shows the effects of the additives on the yields of the products in the photolysis of the bromide. The addition of iodine strongly inhibited the formation of all the products. Lithium nitrate also showed the inhibition. Oxygen and phenyl iodide enhanced the rate of the photodecomposition of IV.

Discussion

Four different paths are possible for the photochemical decomposition of the ionic compounds, RY^+X^-.

$$X^- \xrightarrow{h\nu} X\cdot + e^-$$
$$RY^+ + e^- \longrightarrow R\cdot + Y \qquad (A)$$

11) Since a Pyrex tube eliminates wavelengths below 280 nm, benzene does not absorb the light energy in this case.

TABLE 5. PHOTOLYSIS OF IV IN THE PRESENCE OF THE ADDITIVES[a)]

X	Additive	Product yield (%)					
		PhH	CH_3CO_2Et	$(EtO_2CCH_2-)_2$	$PhCH_2CO_2Et$	Ph–Ph	H^+
NO_3	none	0.25	0.38	0	0	0	nd[b)]
ClO_4	none	0	0.12	0	0	0	3.1
Br	none	0.9	17.2	2.3	0.2	0.1	33.8
Br	$LiNO_3$	0.9	10.4	4.1	0.3	0	2.5
Br	PhI	4.6	44.1	1.4	0.1	0.1	32.5
Br	O_2	2.1	38.4	3.3	0.3	0.1	50.6
Br	I_2	0.1	3.3	0	0	0	nd[b)]

a) IV (1.6 mmol) in 4 m*l* of acetonitrile. b) Not determined.

$$RY^+ \xrightarrow{h\nu} R\cdot + Y^+\cdot \quad (B)$$

$$RY^+ \xrightarrow{h\nu} R^+ + Y \quad (C)$$

$$RY^+X^- \xrightarrow{h\nu} R\cdot + Y + X\cdot \quad (D)$$

A solvated electron is involved in Path A. Path B involves a homolytic cleavage of a bond to produce a cation radical. Path C involves a heterolytic bond cleavage to produce a carbonium ion. Both Path B and Path C predict no anion dependency. Path D represents a direct charge transfer reaction under the interaction between an anion and a cation.

All the products shown in Table 1 can be expected to be derived from radical reactions because the rates of their formation were retarded markedly by the addition of iodine, a radical scavenger (Table 5). Path C (a heterolytic bond cleavage) can be ruled out on the basis that phenetole could not be detected at all when the photolysis was carried out in ethanol.

Tables 2, 3, and 5 show that the photochemical reactivity of IV depends strongly on the anion species. The quantum yields of the products (Table 2) and the rate of the photodecomposition of IV (Table 3) were increased with the change of the anion in the order, ClO_4^-, $NO_3^-<Cl^-<Br^-<BF_4^-<I^-$. An oxidizable anion was shown to be more effective except for BF_4^-.[12] This result indicates that Path A and/or Path D may be operative in the photolysis. However, Path A can be safely ruled out on the basis that any anion does not absorb the light above 250 nm,[13] and that a Brønsted acid which is a good scavenger of the solvated electron[14] is generated during each overall reaction (Table 5). Consequently, Path D may be most likely among the four paths.

The observation that no more than 30% of IV is ionized in solution at the concentration employed in the photolysis may be a further support for the direct charge transfer mechanism (Path D) because at such a low degree of dissociation the electron transfer from an anion to a cation should be easy. Further, as shown in Table 6, an absorption band which may be due to the charge transfer was observed at 245 nm in the UV spectrum of the iodide.[15]

The solvent effect on the rates of the formation of the phosphines can also be explained well by the charge transfer mechanism. That is, the degree of dissociation of IV in benzene–ethanol mixed solvent may be decreased with increasing proportion of benzene to ethanol. As a result, an anion may transfer an electron to a cation more easily at high concentration of benzene. TPP and EDP may be obtained in better yields under these conditions. It may be reasonable to explain the solvent effect in this way since the degree of dissociation of $Ph_4P^+I^-$ in solution has been reported to be increased with increasing solvent polarity in the order, $MeCN<MeOH<H_2O$.[16] It is not yet clarified why the ratio TPP/EDP was decreased with solvent polarity in this experiment.

As shown in Table 5, the addition of lithium nitrate retarded the photodecomposition. This may be due to that the charge transfer became difficult as a result of an increase in ionic strength of the medium. The acceleration of the reaction by the addition of oxygen may be accounted for by the oxidative decomposition of the phosphonium salts. Such accelerative effect of oxygen has been observed also in the pyrolysis of I in cyclohexene, producing triphenylphosphine oxide instead of TPP.[17] Formation of neither TPP nor EDP could be detected in the photolysis of the nitrate or perchlorate. This may be due to the interaction of oxygen atoms in a nitrate or perchlorate anion with the resulting phosphines. Further, the observation that ϕ_{TPP} and ϕ_{EDP} were very low for the iodide may be attributable to the formation of the diiodophosphorane (Ph_2PRI_2) by the reaction of TPP or EDP with an iodine molecule, which is formed by the dimerization of iodine atoms.

$$2I\cdot \rightarrow I_2$$

$$Ph_2PR + I_2 \rightarrow Ph_2PRI_2, \quad R=Ph \text{ or } CH_2CO_2Et$$

12) J. G. Calvert and J. N. Pitts, Jr., "Photochemistry," John Wiley & Sons, Inc., New York (1966), p. 268.

13) a) Ref. 9, p. 269. b) H. L. Friedman, *J. Chem. Phys.*, **21**, 319 (1953).

14) L. E. Orgel, *Quart. Rev.*, **8**, 422 (1954).

15) The assignment of the band should be reasonable since it has been reported that the absorption bands at 233 nm in the UV spectra of tris-*p*-tolylalkylphosphonium iodides are attributable to the charge transfer: M. A. A. Beg and Samiuzzaman, *Tetrahedron*, **24**, 191 (1968).

16) A. Honiger and H. Schindlbauer, *Ber. Bunsenges. Phys. Chem.*, **69**, 138 (1965).

17) Y. Nagao, K. Shima, and H. Sakurai, This Bulletin, **43**, 1885 (1970).

On the basis of the above discussion, we can conclude that the photolysis of IV proceeds through the charge transfer from an anion to a cation. The processes shown in Scheme 1 may account for the observations in the photolysis of IV.

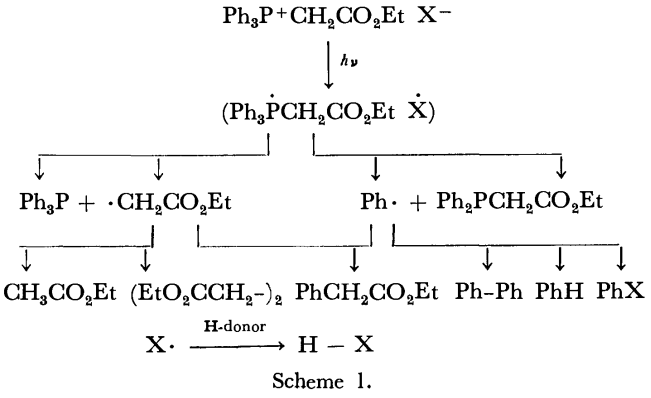

Scheme 1.

In this scheme, the phosphoranyl radical ($Ph_3\dot{P}CH_2CO_2Et$)[18] formed by one electron transfer decomposes mainly to TPP and an ethoxycarbonylmethyl radical, and partly to EDP and a phenyl radical. Radicals such as Cl· or Br· may abstract hydrogen atoms from solvent molecules, yielding hydrogen halides.

The photolysis of the tetrafluoroborate is the only one case where the charge transfer mechanism may not be operative. That is, the tetrafluoroborate was photolyzed more easily than the bromide although a tetrafluoroborate ion is less oxidizable than a bromide ion. Probably Path B, a direct cation excitation mechanism, may be important in this case.

Now, as the photolysis of IV has been confirmed to proceed through the charge transfer mechanism, we have compared the results with those of the photolysis of I and sulfonium and ammonium salts.

Owing to the important contribution of the ylid structure,[19] the compound I would have a positively charged phosphorus atom in its ground state. However, the mode of the photodecomposition of I differs significantly from that of IV. In the photolysis of I, a homolytic fission of a P-Ph bond may take place in the first stage by the direct absorption of light at a triphenylphosphinyl moiety. The charge transfer mechanism may not be important in this case.[20] On the other hand, a homolytic fission of a $P-CH_2CO_2$-Et bond took place preferentially through the electron transfer from the counter-anion to the associated acceptor cation in the photolysis of IV.

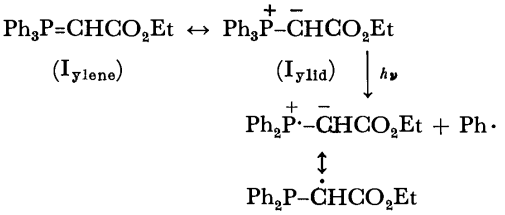

The charge transfer mechanism has also been proposed to take place in the direct[8a] and acetone sensitized photolysis[8b] of trimethylphenylammonium salts. However, a less stable radical (a phenyl radical) has been formed exclusively in these photolyses. In contrast, a more stable radical (an ethoxycarbonylmethyl radical) was produced preferentially in the photolysis of IV. Such a difference may arise from whether the *d* orbitals of the phosphorus or the nitrogen atom can participate or not in the photodecomposition. In the photolysis of IV, the phosphoranyl radical may be formed as an intermediate by the participation of the *d* orbitals of the phosphorus atom after the charge transfer. It is, thus, reasonable that a more stable ethoxycarbonylmethyl radical is produced preferentially from this intermediate. On the other hand, the energy level of the *d* orbitals of the nitrogen atom is so high that the *d* orbitals cannot participate in the photolysis of the ammonium salts. Possibly the direct electron transfer from an anion to the lowest antibonding orbital of the phenyl group of the cation might result in the exclusive cleavage of the N-Ph bond.

The photolysis of triarylsulfonium salts in alcohol[9] has been reported to involve both a charge transfer

Table 6. Preparation and properties of phosphonium salts

X	Cl[a]	Br	I	NO_3	ClO_4	BF_4
Mp (°C)	87—88	158	161—163	137	160—162	139—140
(lit, mp)	(87—88)	(158)	—	—	—	—
Literature	21	22	—	—	—	—
Method	A	A	A	B	B	B
UV λ_{max}^{EtOH} (nm)	267	267	245 268	267	268	267
$\varepsilon \times 10^{-3}$	3.85	3.38	9.78 3.96	3.29	3.23	3.40
			C H	C H	C H	C H
Anal. Found	—	—	55.82 4.70	64.29 5.60	58.68 5.05	68.65 5.87
Calcd	—	—	55.48 4.66	64.22 5.39	58.87 4.94	69.68 5.85

a) This compound was obtained as a dihydrate, and dehydrated with phosphorus pentoxide.

18) J. I. G. Cadogan, "Advances in Free Radical Chemistry," Vol. 2, ed. by G. H. Williams, Academic Press, New York (1967), p. 220.

19) Z. Yoshida, "Quantum Organic Chemistry," ed. by S. Nagakura, K. Fukui, and Z. Yoshida, Kagaku Dojin, Kyoto (1966), p. 231.

20) In the UV spectrum of III, an absorption band, being attributable to the charge transfer, has been observed at 432 nm. The photolysis of III using light above 320 nm may proceed through the charge transfer.[5]

21) W. J. Considine, *J. Org. Chem.*, **27**, 647 (1962).

22) O. Isler, H. Gutmann, M. Montavon, R. Ruegg, G. Ryser and P. Zeller, *Helv. Chim. Acta*, **40**, 1242 (1957).

(Path D) and a direct excitation of a cation yielding an aryl radical and a sulfinium cation radical (Path B). It has been considered that triarylsulfur radicals (sulfur analogs of phosphoranyl radicals) are formed by the participation of the *d* orbitals of the sulfur atom as the intermediate in the charge transfer process. Although the photolysis of dimethylphenacylsulfonium salts[9b,c] has been found to form a phenacyl radical (more stable than a methyl radical), the *d* orbitals may not participate in this system since this reaction proceeds through the direct cation excitation mechanism (Path B) only.

Experimental

All melting points are uncorrected. UV spectra were recorded on a Hitachi 124 Spectrophotometer. Gas chromatographic analysis were performed on a Shimadzu Gas Chromatograph, GC-3AF (carrier gas; N_2).

Preparation of Phosphonium Salts. Phosphonium salts were prepared by the following two methods, A and B.

Method A: A solution of 0.06 mol of TPP in 30 m*l* of benzene was treated with a solution containing an equivalent amount of ethyl α-haloacetate in 30 m*l* of benzene. The salt was filtered, washed with benzene, dried, and recrystallized from methylene chloride–ether.

Method B: A solution of 0.01 mol of AgX (X=ClO_4, NO_3 or BF_4) in water was added dropwise with stirring to a solution containing an equivalent amount of phosphonium bromide in methanol and the mixture was washed with methanol, and the filtrate and washing were combined and concentrated to a residue that was recrystallized from methylene chloride–ether.

Melting points and the UV spectral data of the salts are shown in Table 6.

Ethoxycarbonylmethyldiphenylphosphine (EDP). This compound was prepared by the method of Issleib and Thomas.[23] Hydrolysis of this compound gave carboxymethyldiphenylphosphine, mp 121—122°C (lit,[23] mp 120—121°C).

Photochemical Studies. A solution of 3.5 mmol of IV (X=Cl, Br, or I) in 10 m*l* of acetonitrile was placed in a quartz tube and degassed by three cycles of the freeze-pump-thaw method. The solution was irradiated with a quartz Eikosha PIH 350-W water-cooled, high pressure mercury lamp for 150 hr. After the irradiation the tube was opened and the contents were analyzed directly by gas chromatography. Four different columns were used in order to separate the peaks of the products: (1) a 1-m 15% SE-30 column for TPP and EDP, (2) a 3-m 25% DEGS column for most of the volatile components, (3) a 3-m 25% Silicone-DC column for halobenzenes, and (4) a 3-m 25% PEG column for benzene and ethyl acetate. Cyclohexane, α-methyl naphthalene and ethyl succinate were used as the internal standards in determining product yields.

Kinetic Experiments. Solutions containing 1.6 mmol of IV and equimolar amounts of the appropriate additives in the appropriate anhydrous solvents (4 m*l*) were degassed in quartz or Pyrex tubes and irradiated with the same high pressure mercury lamp as used above. Samples in quartz tubes were irradiated for 45 min. Within such irradiation time the yields of the products increased linearly. Samples in Pyrex tubes needed longer irradiation. The amounts of unreacted salts were found by adding ether to the reaction mixture slowly. The crystals formed were filtered, washed with ether, dried, and weighed. The concentrations of Brønsted acids were determined by titrating the reaction mixture with 0.1 N potassium hydroxide solution.

Quantum yields were measured by use of a 4 m*l* of quartz spectrophotometric cell. Acetonitrile solutions of IV (0.5 M) were degassed and irradiated at 253.7 nm. Potassium ferrioxalate was used as an actinometer. The yields of the products were determined by gas chromatography.

The Measurement of the Electrical Conductance. Resistances were measured with a Yokokawa On-Ichi-Go Impedencemeter at a frequency of 1000 Hz. An oscilloscope, Yokokawa OL-51C, and an oscillator, Matsushita VP-706 were used. The cell constant was 0.393 cm^{-1}.

23) K. Issleib and G. Thomas, *Chem. Ber.*, **93**, 803 (1960).

Brominations of Aliphatic Ketones by Copper(II) Bromide in Organic Solvents. II. The Reaction of Acetone with Copper(II) Bromide in *N,N*-Dimethylformamide

Yoshitane KOJIMA, Kimiko USUI, and Shinichi KAWAGUCHI

Department of Chemistry, Faculty of Science, Osaka City University, Sumiyoshi-ku, Osaka 558

(Received November 25, 1971)

Because of a long induction period, the reaction between acetone and copper(II) bromide does not occur readily in pure DMF. However, in the presence of an acid, it proceeds readily. The initial rate is proportional to the product of the concentration of acetone and perchloric acid, but independent of the concentration of copper-(II) bromide. The acid-catalyzed bromination of acetone by bromine has also been studied in DMF and found to obey the same second-order rate law as that in water. Both bromination reactions of acetone in DMF by copper(II) bromide and bromine were interpreted to be controlled by the enolization process of acetone.

In a previous paper[1] we reported on the reaction of copper(II) bromide with acetone in methanol. In the presence of copper(II) bromide, the reaction of acetone with methanol to form acetone dimethylacetal attained equilibrium quickly even at 0°C, making the reaction system complicated. Water produced in the acetal formation made the acid-catalyzed reaction so complicated that the observed dependence of the rate upon the acetone concentration could not be explained quantitatively.

To avoid such troubles the reaction between copper-(II) bromide and acetone has been studied in *N,N*-dimethylformamide (DMF) and found not to proceed at room temperature unless assisted by an acid catalyst. The acid-catalyzed reaction is reported in this paper.

Experimental

Materials. DMF was boiled with benzene (5 vol%) to eliminate water as an azeotrope and distilled twice under reduced pressure (bp 27—29°C/5mmHg). Contamination with the free amine was examined by means of a saturated ethanol solution of 2,4-dinitrofluorobenzene.[2] Bromine was washed with water repeatedly to eliminate chlorine and iodine, and then dissolved in a solution of pure potassium bromide and distilled over zinc oxide. The distillate was again distilled over calcium oxide and finally dried with phosphorus pentoxide. Acetone was purified by a standard method.[3] Purity of organic solvents was checked by vapor phase chromatography.

Identification and Determination of Reaction Products. After the reaction mixture was kept standing at room temperature for a few days, volatile substances were distilled under reduced pressure. In one experiment to determine the amount of copper(I) bromide, the residue was dissolved in a sulfuric acid solution containing iron(III) ammonium sulfate, and iron(II) produced was titrated with an aqueous solution of cerium(IV) ammonium sulfate.[4] In another experiment, the residue was dissolved in aqueous ammonia, and total copper was determined by electrolysis, and bromine gravimetrically as silver bromide.

Monobromoacetone in the distillate was identified by comparing the infrared spectrum and gas-chromatogram with those of the authentic specimen. A 3 m column (4 mm in diameter) containing Diglycerol (5%) and Silicone Grease (5%) on Neosorb NCS was used at 63°C with hydrogen as a carrier gas at a flow rate of 20 cc/min. Content of monobromoacetone in the distillate was determined by iodometry, and that of hydrogen bromide by titration with an aqueous solution of sodium hydroxide.

Kinetics. Acetone and perchloric acid were added to a DMF solution of copper(II) bromide in a three-necked flask equipped with a stirrer, a nitrogen gas inlet tube and an outlet tube containing calcium chloride. At appropriate time intervals, aliquots were withdrawn from the flask and quenched in cold sulfuric acid solutions of iron(III) ammonium sulfate and titrated with cerium(IV) solutions as described above.

The reaction of acetone with bromine in DMF was also followed in a similar fashion without the nitrogen flow. Each aliquot was quenched in a potassium bromide solution buffered with acetic acid and sodium acetate, and the liberated iodine was titrated with a thiosulfate solution.[5] Monobromoacetone does not liberate iodine under these conditions.

In spite of careful purification of DMF, fluctuation in the reaction rate with the change of solvent was inevitable. Hence the dependence of the reaction rate on concentration was examined with DMF in the same bottle.

Results

Stoichiometry of the Reaction. Acetone was allowed to react with copper(II) bromide at room temperature for several days, and then the mixture was analyzed by the methods described in the Experimental Section. As shown in Table 1, the mole ratio of copper(I) bromide to monobromoacetone in the first experiment was close to 2 : 1 in conformity with the following equation.

$$CH_3COCH_3 + 2CuBr_2 = CH_3COCH_2Br + 2CuBr + HBr \quad (1)$$

The very low acid content in the distillate is due to the formation of a non-volatile adduct $(CH_3)_2NCHO \cdot HBr$.[6] This was proved by the second set of data in Table 1 which shows that sum of bromine gram-atoms in the residue and in the distillate is colse to twice moles of copper(II) bromide employed.

Kinetics. When acetone was mixed with a DMF solution of copper(II) bromide at 30°C, an in-

1) Y. Kojima and S. Kawaguchi, This Bulletin, **45**, 1293 (1972).
2) S. Buffagni and T. M. Dunn, *J. Chem. Soc.*, **1961**, 5105
3) J. A. Riddick and E. E. Toops, Jr., "Organic Solvents," Vol. 7 of "Technique of Organic Chemistry" ed. by A. Weissberger, 2nd ed., Interscience Publishers, New York (1955).
4) J. K. Kochi, *J. Amer. Chem. Soc.*, **77**, 5274 (1955).
5) R. P. Bell and K. Yates, *J. Chem. Soc.*, **1962**, 1927.
6) S. J. Kuhn and J. S. McIntyre, *Can. J. Chem.*, **43**, 995 (1965).

TABLE 1. PRODUCTS OF THE REACTION BETWEEN ACETONE AND COPPER(II) BROMIDE IN DMF AT ROOM TEMPERATURE FOR SEVERAL DAYS

$CuBr_2$ used mmol	Residue			Distillate	
	Total Cu mg·atom	Total Br mg·atom	Cu(I) mg·atom	H^+ mmol	CH_3COCH_2Br mmol
			10.87	0.35	4.92
10.13	10.00	15.17		0.41	4.18

duction period longer than 100 min was observed before the reaction started (curve 1, Fig. 1). This result suggests that copper(II) bromide does not react with acetone in pure DMF and the reaction after the induction period might be caused by the catalytic effect of hydrogen bromide produced by side reactions. In fact when perchloric acid was added to the system, the reaction started without the induction period (curve 2, Fig. 1). However, the disturbing influences of reaction products made the kinetic run too difficult to analyze, and the effects of various factors were investigated by the initial rate method.

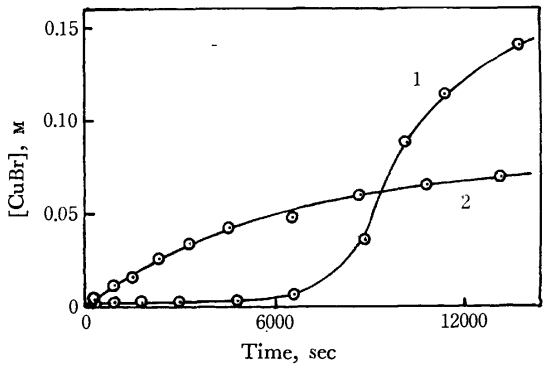

Fig. 1. Rates of reactions between acetone and copper (II) bromide in the absence (Curve 1) and presence (Curve 2) of perchloric acid. Curve 1: $[CuBr_2]=0.310$ M, [acetone] $=3.45$ M, 30°C. Curve 2: $[CuBr_2]=0.227$ M, [acetone] $=1.73$ M, $[HClO_4]=0.115$ M, 25°C.

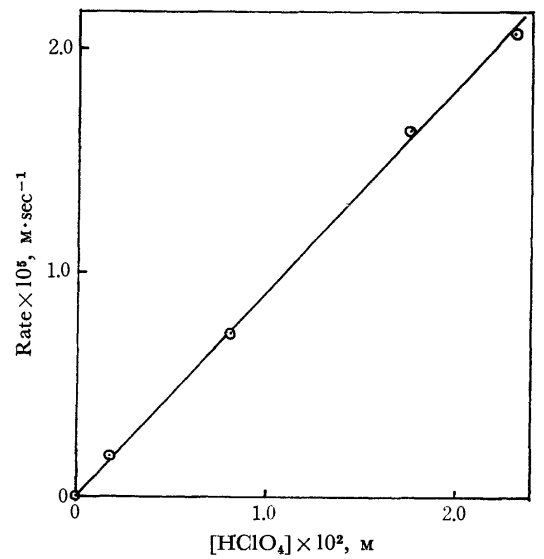

Fig. 2. The dependence of the reaction rate on the perchloric acid concentration at 23.2°C. $[CuBr_2]=0.284$ M, [acetone] $=1.73$ M.

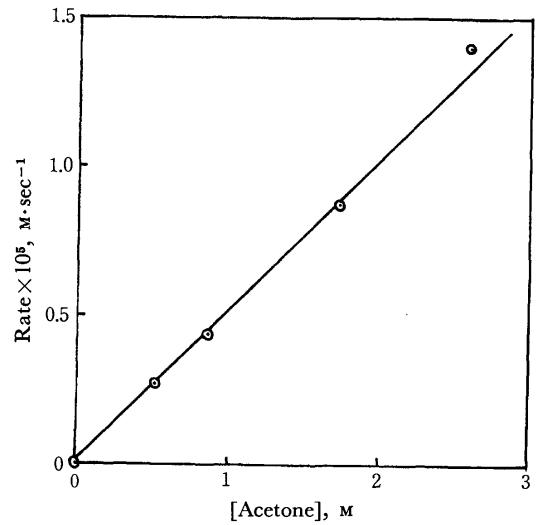

Fig. 3. The dependence of the reaction rate on the acetone concentration at 23.2°C. $[CuBr_2]=0.284$ M, $[HClO_4]=0.0115$ M.

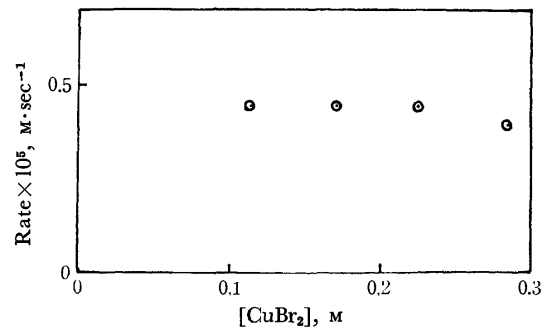

Fig. 4. The independence of the reaction rate from the copper(II) bromide concentration at 23.2°C. [acetone] $=0.875$ M, $[HClO_4]=0.0115$ M.

As shown in Figs. 2, 3, and 4 the initial rates of the reaction of acetone with copper(II) bromide in DMF at 23.2°C are proportional to the products of perchloric acid and acetone concentrations and independent of the copper(II) bromide concentration, providing the following equation.

$$d[CuBr]/dt = k[\text{acetone}][HClO_4] \quad (2)$$

The second order rate constant was obtained as $k=4.60\times10^{-4}M^{-1}sec^{-1}$ at 23.2°C. In these experiments perchloric acid was added as a 60% aqueous solution. The effect of water on the reaction rate was confirmed in advance to be negligible.

At 0°C, however, the rate of the acid-catalyzed reaction of acetone with copper(II) bromide was not independent of the latter concentration. As shown in Table 2 the pseudo second-order rate constant k in-

Table 2. Rate data of the acid-catalyzed reaction between acetone and copper(II) bromide in DMF at 0°C

$[CuBr_2]$, M	[acetone], M	$[HClO_4]$, M	Initial rate $\times 10^6$ M·sec^{-1}	Pseudo 2nd-order rate const. $\times 10^5$ M^{-1} sec^{-1}
0.038	1.75	0.046	0.88	1.1
0.075	1.75	0.046	1.18	1.5
0.113	1.75	0.046	1.75	2.2
0.200	1.75	0.046	2.27	2.8
0.225	0.87	0.023	0.52	2.9

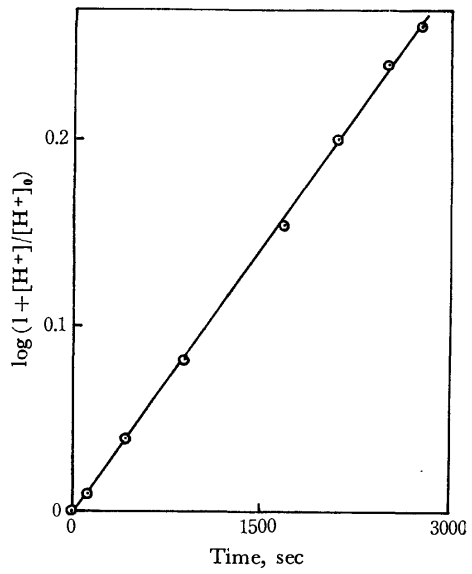

Fig. 5. The pseudo first-order plot of a kinetic run of the reaction of acetone with bromine in DMF at 23.2°C. [acetone]=1.144 M, $[Br_2]$=0.189 M, $[HClO_4]$=0.096 M.

creased with the concentration of copper(II) bromide, but no simple relationship between them could be found.

The Acid-catalyzed Bromination of Acetone by Bromine. For the sake of comparison, the acid-catalyzed bromination of acetone by bromine was followed in DMF solutions. With a large excess of acetone the reaction proceeded according to the pseudo first-order rate law as evidenced by the linear plot of $\log(1+[H^+]/[H^+]_0)$ *vs.* time in Fig. 5. Values of the second-order rate constant k_{Br} in the equation

$$-d[Br_2]/dt = d[H^+]/dt = k_{Br}[\text{acetone}]([H^+]_0 + [H^+]) \quad (3)$$

were 2.2×10^{-5}, 6.1×10^{-5}, and 19.0×10^{-5} M^{-1}sec^{-1} at 0.0, 11.0, and 23.2°C, respectively. From these data kinetic parameters were calculated as E_a=14.8 kcal·mol^{-1} and A=1.65×10^7 M^{-1}sec^{-1}.

Although the reaction of acetone with copper(II) bromide was followed by measuring the copper(I) bromide concentration according to Eq. (1), that with elemental bromine was followed by measuring the bromine concentration according to the following equation.

$$CH_3COCH_3 + Br_2 \rightarrow CH_3COCH_2Br + HBr$$

Thus k_{Br} defined by Eq. (3) should be compared with one half of k in Eq. (2). The value of k_{Br}, 19.0×10^{-5} M^{-1}sec^{-1} at 23.2°C is close to one half of k at the same temperature.

Discussion

Kosower *et al.*[7] reported reactions of various ketones with copper(II) chloride or copper(II) bromide at temperatures higher than 80°C. However, the present investigation revealed that copper(II) bromide does not react readily with acetone in pure DMF at room temperature, a long induction period being observed before the reaction starts. Dissolution of copper(II) bromide in DMF is very exothermic and the solutions were usually prepared with cooling in an ice-bath. If a copper(II) bromide solution in DMF prepared without cooling and heated spontaneously is allowed to react with acetone, the induction period almost disappears. On heating, DMF tends to decompose to dimethylamine and carbon monoxide,[8] and dialkylamine is known to react with copper(II) halides.[9] In fact it was confirmed that copper(II) bromide reacts with dimethylamine much faster than with acetone in DMF. Thus the following reactions may occur during the induction period of the reaction between copper(II) bromide and acetone in DMF, and hydrogen bromide produced may catalyze the latter reaction.

$$(CH_3)_2NCHO \rightarrow (CH_3)_2NH + CO \quad (4)$$

$$CuBr_2 + (CH_3)_2NH \rightarrow CuBr + HBr + \text{oxidation products of the amine} \quad (5)$$

Ichikawa *et al.*[10] noticed that about 20% of copper(II) chloride was consumed when heated with DMF at 80—90°C for 10 hr. These results are also interpreted to be caused by reactions similar to (4) and (5).

Copper(II) bromide reacts with acetone in methanol, playing dual roles as the catalyst which activates acetone and also as the brominating agent.[1] On the contrary the same reaction does not occur in DMF possibly because DMF is a stronger ligand to copper(II) than acetone, and the following ligand substitution equilibrium is very unfavorable to the latter.

7) E. M. Kosower, W. J. Cole, G.-S. Wu, D. E. Cardy, and G. Meisters, *J. Org. Chem.*, **28**, 630 (1963); E. M. Kosower and G.-S. Wu, *ibid.*, **28**, 633 (1963).

8) A. B. Thomas and E. G. Rochow, *J. Amer. Chem. Soc.*, **79**, 1843 (1957).

9) For instance, J. R. Clifton and J. T. Yoke, III, *Inorg. Chem.*, **7**, 39 (1968).

10) K. Ichikawa, S. Uemura, T. Hiramoto, and Y. Takagaki, *Kogyo Kagaku Zasshi*, **71**, 1657 (1968).

$$CuBr_2(DMF)_n + n \text{ acetone} \rightleftharpoons CuBr_2(\text{acetone})_n + n \text{ DMF} \quad (6)$$

However, copper(II) bromide still retains brominating ability and reacts with acetone even in DMF if an acid is added to catalyze the enolization of acetone.

It has been well established that the rate of acid-catalyzed halogenation of acetone by elemental halogen in an aqueous solution is controlled by the enolization step.[5] The bromination of acetone in DMF proceeds according to the same rate law (3) as that in water, and is represented by the following steps.

$$HA + DMF \rightarrow DMFH^+ + A^- \quad (7)$$

$$(CH_3)_2CO + DMFH^+ \rightleftharpoons (CH_3)_2COH^+ + DMF \quad (8)$$

$$(CH_3)_2COH^+ + DMF \xrightarrow{\text{slow}} CH_3C(OH)=CH + DMFH^+ \quad (9)$$

$$CH_3C(OH)=CH_2 + Br_2 \xrightarrow{\text{fast}} CH_3COCH_2Br + HBr \quad (10)$$

The second order rate constant k_{Br} at 25°C obtained by extrapolation of data at three temperatures is 2.2×10^{-4} M^{-1}sec^{-1} which is several times larger than 2.8×10^{-5} M^{-1}sec^{-1} in water.[5] This seems to reflect the higher basicity of DMF than that of water which functions as the proton acceptor in the rate-determining step (9).

By analogy the reaction of acetone with copper(II) bromide at around room temperature is also considered to be controlled by the enolization step (9). It is not certain, however, whether copper(II) bromide or bromine liberated therefrom brominates enolic molecules of acetone in the succeeding step (10). Castro *et al.*[11] found the formula rate$=k[CuBr_2]^2$ for the reaction between allyl alcohol and copper(II) bromide at 64°C and attributed the rate law to the rate determining dissociation of the latter followed by bromination of the unsaturated alcohol by bromine. Barnes and Hume[12] also reported that elemental bromine was distilled from a boiling solution of copper(II) bromide in acetonitrile. On the other hand, Koyano[13] has recently reported that the bromination of olefins with copper(II) bromide in methanol at 40°C may be represented by the following polar mechanism.

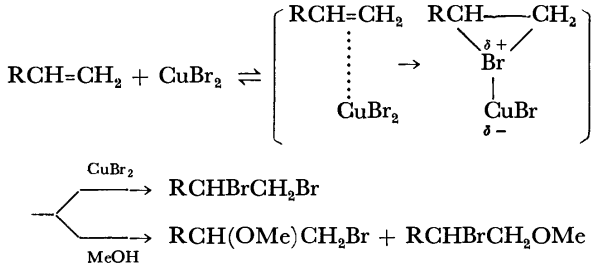

At such lower temperatures as employed in the present investigation, the following equilibrium concentration of elemental bromine produced by the dissociation of copper(II) bromide may not be enough to explain the observed overall rates.

$$2CuBr_2 \rightleftharpoons 2CuBr + Br_2 \quad (11)$$

It might be preferable to consider that copper(II) bromide plays a role of the brominating agent.

At 0°C the initial rate shows some dependence on the copper(II) bromide concentration. This may indicate that the brominating step is slower than the preceding enolization steps (7)—(9) at 0°C. The detailed mechansim is not clear.

11) C. E. Castro, E. J. Gaugham, and O. C. Owsley, *J. Org. Chem.*, **30**, 587 (1965).

12) J. C. Barnes and D. N. Hume, *Inorg. Chem.*, **2**, 444 (1963).

13) T. Koyano, This Bulletin, **44**, 1158 (1971).

BULLETIN OF THE CHEMICAL SOCIETY OF JAPAN, VOL. 45, 3130—3132 (1972)

Reactions of Cuprous Acetate with Organic Halides

Takao KAWAKI and Harukichi HASHIMOTO*

Department of Synthetic Chemistry, The University of Tokyo, Bunkyo-ku, Tokyo
**Department of Applied Chemistry, Faculty of Engineering, Tohoku University, Sendai*

(Received December 18, 1971)

Cuprous acetate was prepared from phenylcopper and acetic acid, and its reactivity for organic halides was investigated. The mixed anhydrides containing an acetyl group are formed easily from cuprous acetate and acyl halides. The reaction of cuprous acetate with CH_3I, C_2H_5I, CH_2=$CHCH_2Br$, and $PhCH_2Cl$ in acetonitrile gives the corresponding ester. The addition of ethylenediamine converts the above reaction to a reductive coupling reaction, resulting in bibenzyl (50% yield) from benzyl chloride and 1,5-hexadiene (95—98% yield) from allyl chloride or bromide. The reaction of cuprous acetate-ethylenediamine with aryl bromide or iodide in DMF gives a reductively dehalogenated product, *i.e.*, the corresponding hydrocarbon, in a small yield.

Although numerous copper salts have been utilized in organic syntheses, little has been investigated about cuprous acetate. Cuprous acetate was first prepared from cuprous oxide and acetic anhydride by Calvin.[1] Recently, Sheppard[2] reported to obtain this compound quantitatively from *m*-(trifluoromethyl)phenylcopper octamer and acetic acid. It has also been reported that cuprous acetate activates the molecular hydrogen in quinoline,[1,3] and that cuprous acetate executes

1) M. Calvin, *J. Amer. Chem. Soc.*, **61**, 2230 (1939).

2) A. Cairncross, J. R. Foland, R. M. Henderson, and W. A. Sheppard, *ibid.*, **92**, 3187 (1970).

3) S. Weller and G. A. Mills, *ibid.*, **75**, 770 (1953).

a reductive dehalogenation on aryl halides in nitrogen heterocyclic solvents.[4] However, the reaction of cuprous acetate with organic halides has not yet been fully investigated. Therefore, we prepared cuprous acetate from phenylcopper and acetic acid, and examined its reactions with acyl halides and some aliphatic and aromatic halides.

Results and Discussion

Although Sheppard used *m*-(trifluoromethyl)phenylcopper as an organocopper, we found that cuprous acetate can be synthesized quantitatively from phenylcopper and acetic acid;

$$PhCu + CH_3COOH \rightarrow Cu(OCOCH_3) + PhH$$

As cuprous acetate was easily decomposed by both oxygen and moisture, it was isolated and characterized as a complex with triphenylphosphine according to the usual procedures for Cu(I) complexes.[5,6] It is a white crystalline oxygen-stable compound, is soluble in an organic solvent and has the composition of $CuOAc\text{-}(PPh_3)_2$.

Reactions of Cuprous Acetate with Acyl Halides. Cuprous acetate similar to cuprous alkoxides reacted with acyl halides to produce the corresponding anhydrides in fairly good yields, as is shown in Table 1. The yield of anhydride diminishes with the increase in the carbon chain in the acyl group. This fact may be attributable to the increase in the electron-releasing ability in the order of $-CH_3 < -C_2H_5 < -C_3H_7$. Mixed anhydrides have been synthesized from carboxylic acid or its metal salts[7] and acyl halide. Recently, Taylor[8] reported that mixed anhydrides could be prepared in high yields by utilizing Tl(OCOR). Considering that thallium salts are very toxic, the above reaction seems to be a useful method of synthesizing mixed anhydrides containing acetyl group.

Table 1. Reactions of CuOAc with acyl halides in ether[a]

Acyl halide	Product	Yield (%)
CH_3COCl	$CH_3COOCOCH_3$	76.5
C_2H_5COCl	$CH_3COOCOC_2H_5$	39.4
$n\text{-}C_3H_7COCl$	$CH_3COOCOC_3H_7$	26.5

a) CuOAc, 0.01 mol; acyl halide, 0.01 mol; in refluxing ether for 5 hr.

Reactions of Cuprous Acetate with Aliphatic Halides. The halogen-exchange reactions of copper salts with organic halides have been studied by many investigators. Therefore, the reactions of cuprous acetate with organic halides were examined, as is shown in Table 2.

It is clear from Table 2 that all alkyl halides except bromobenzene and iodobenzene are converted to the corresponding esters in acetonitrile. Cohen[9] reported that cuprous benzoate reacts with aryl halides in diglyme to produce aryl benzoate in good yields and that organocopper ArCuOCOPh is an intermediate in the reaction. Cuprous phenoxide[10] also reacted with aryl halides in diglyme to produce aryl phenyl

Table 2. Reaction of CuOAc with halides in acetonitrile[a]

Halide	Solvent	Temp. (°C)	Product	Yield (%)
CH_3I	CH_3CN	60	CH_3OAc	46.2
C_2H_5I	CH_3CN	80	C_2H_5OAc	50.8
$CH_2{=}CHCH_2Br$	CH_3CN	60	$CH_2{=}CHCH_2OAc$	68.3
$PhCH_2Cl$	Diglyme	87	$PhCH_2OAc$	63.5
	CH_3CN	150	$PhCH_2OAc$	42.7
PhBr, PhI	Diglyme	87	—	
		150	—	

a) CuOAc, 0.01 mol; halides, 0.01 mol; reaction time, 5 hr.

Table 3. Effects of the addition of ligands in acetonitrile[a]

Halide	Ligand	Temp (°C)	Product and Yields (%)	
$PhCH_2Cl$	en[b]	87	$PhCH_2CH_2Ph$ (40.2)	$PhCH_2OAc$ (18.2)
$PhCH_2Cl$	2en	87	$PhCH_2CH_2Ph$ (50.1)	$PhCH_2OAc$ (19.8)
$PhCH_2Cl$	dipy[c]	87	$PhCH_2CH_2Ph$ (1.8)	$PhCH_2OAc$ (18.8)
$CH_2{=}CHCH_2Br$	en	80	1,5-hexadiene (97.8)	
$CH_2{=}CHCH_2Cl$	en	65	1,5-hexadiene (95.3)	
PhBr, PhI	en	87	—	

a) CuOAc, 0.01 mol; halides, 0.01 mol; reaction time, 5 hr. b) en=ethylenediamine. c) dipy=dipyridyl.

4) R. G. R. Bacon and H. A. O. Hill, *Quart. Rev.*, **19**, 95 (1965).
5) G. Costa, E. Reisenhofer, and L. Stefani, *J. Inorg. Nucl. Chem.*, **27**, 2581 (1965).
6) F. H. Jardine, L. Ruleand, and A. G. Voha, *J. Chem. Soc., A*, **1970**, 238.
7) R. Schijf and W. Stevens, *Rec. Trav. Chim., Pays-Bas* **85**, 627 (1966).
8) E. C. Taylor, G. W. Mclay, and A. McKillop, *J. Amer. Chem. Soc.*, **90**, 2422 (1968).
9) T. Cohen and A. H. Lewin, *ibid.*, **88**, 4521 (1966).
10) T. Kawaki and H. Hashimoto, This Bulletin, **45**, 1499 (1972).

ether. However, cuprous acetate did not react with aryl halides under similar experimental conditions. As toluene has not been detected in the reaction of cuprous acetate with benzyl chloride, the reaction of cuprous acetate with organic halide seems not to proceed through an organocopper intermediate of the RCuOAc type, but seems to proceed through the four-centered mechanism proposed by Bacon.

The Effect of Ligands on the Reactions with Aliphatic Halides. Although cuprous acetate was expected to have more reducing power than the other cuprous salts, it could not dehalogenate organic halides. It has been reported that the reducing power of cuprous chloride is remarkably enhanced by the addition of ethylenediamine in acetonitrile[11] and that the resulting complex dehalogenates benzyl chloride. Table 3 shows the effects of the addition of ligands on the reactions of the cuprous acetate with halides in acetonitrile. In the reaction with benzyl chloride, the addition of 1 mol of ethylene diamine enhanced the reducing power of cuprous acetate, resulting in a higher yield of bibenzyl. Dipyridyl would stabilize cuprous acetate too strongly resulting in a much smaller yield of bibenzyl. Allyl chloride and bromide were converted to 1,5-hexadiene quantitatively without any formation of the ester. Cuprous acetate–ethylenediamine is expected to have more reducing power in DMF because ethylenediamine stabilizes the higher valent state of copper. However, even under these conditions, the reductive coupling product of iodo- and bromobenzene could not be prepared, although the reductively dehalogenated products were obtained in low yields, as is shown in Table 4.

Because the coupling products were not detected when oxygen was bubbled into the reaction mixture prior to hydrolysis, it seems that organocopper is not an intermediate in this reaction. Bacon and his coworkers[4] proposed the following mechanism in the reaction of cuprous acetate with aryl halides in pyridine or quinoline;

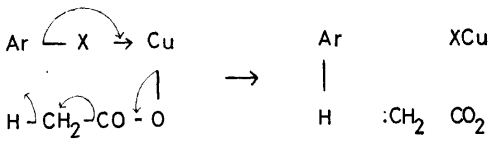

Fig. 1

The reaction of cuprous acetate–ethylenediamine with aryl halides in DMF may also proceed through a similar process.

TABLE 4. REACTIONS OF CuOAc-ETHYLENEDIAMINE WITH ARYL HALIDES IN DMF[a]

Aryl halide	Product	Yield (%)
PhI	benzene	6.8
PhBr	benzene	5.4
p-$CH_3C_6H_4Br$	toluene	23.0
p-BrC_6H_4Br	bromobenzene	10.9
p-$NO_2C_6H_4Br$	nitrobenzene	8.2

a) CuOAc, 0.01 mol; aryl halide, 0.01 mol; reaction time, 2 hr; reaction temperature, 150°C.

11) K. Wada and H. Hashimoto, This Bulletin, **41**, 3601 (1968).

Experimental

Preparation of Cupous Acetate and its Characterization as the Triphenylphosphine Complex. Phenylcopper was prepared according to the direction of Costa.[12] To the phenylcopper (0.1 mol) suspended in fresh ether under nitrogen was added a slight excess of acetic acid at 0—20°C, after which the mixture was stirred for 4 hr. The resulting white solid of CuOAc was washed several times with ether and dried under nitrogen. CuOAc is so air-sensitive that we failed in elemental analysis under the usual conditions.

Triphenylphosphine (0.02 mol) was added to CuOAc (0.01 mol) suspended in benzene under nitrogen, and the mixture was refluxed for 5 hr. The reaction mixture was then decanted, and the supernatant solution was concentrated to deposit $CuOAc(PPh_3)_2$.

Found: C, 70.81; H, 5.20; Cu, 10.06%. Calcd for $CuOAc(PPh_3)_2$: C, 70.53; H, 5.13; Cu, 9.80%.

Reactions of Cuprous Acatate with Oraganic Halides. Organic halide or acyl halide (0.01 mol) was added to CuOAc (0.01 mol) suspended in acetonitrile or ether under nitrogen, and the mixture was heated under the conditions shown in Tables 1 and 2. The yields of the products were determined by gas chromatography.

The Effect of Addition of Ethylenediamine. Ethylenediamine (0.01 mol) was added to CuOAc (0.01 mol) suspended in acetonitrile under nitrogen, and the mixture was refluxed for 0.5 hr, after which organic halide (0.01 mol) was dropped in. Then, the mixture was stirred under the conditions shown in Table 3. The reactions in DMF were also conducted in a manner similar to the experiment described above.

12) G. Costa, A. Camus and L. Gatti, *J. Organometal. Chem.*, **5**, 568 (1966).

Effects of Substituents on the Smiles Rearrangement of *O-s*-Triazinyl-2-aminophenols

Norio MAENO, Takeshi ITAGAKI, Seiichi UNO, and Kohji MATSUI
Department of Chemistry, Faculty of Engineering, Gunma University, Tenjincho, Kiryu, Gunma
(Received December 22, 1971)

Several 4- or 5-substituted *O*-(*s*-triazinyl)-2-aminophenols were synthesized, and the kinetics of the Smiles rearrangement of these compounds have been studied spectrophotometrically in methanol, ethanol, and 2-propanol in order to make clear the effects of substituents on the rearrangement. Substituents in the *s*-triazine nucleus were found to affect the progress of the reaction to a great extent by changing the positive character of the triazine-ring carbon. On the other hand, a substituent in the aminophenol moiety affects both the nucleophilic reactivity of the attacking amino group and the stability of the leaving phenoxide anion or the reactivity of the *s*-triazinyl group, but the effect on the amino group was found to be predominant, the effect of a substituent in the aminophenol moiety was smaller than that of the substituents in the *s*-triazine nucleus.

In previous papers[1] we reported that *O-s*-triazinyl-2-aminophenols rearrange under various conditions, especially readily in the presence of acid, to give *N-s*-triazinyl-2-aminophenols. The migration of the triazinyl group was thought to proceed through an intramolecular nucleophilic attack by the amino group on the ring carbon of an *s*-triazinyl group, and substituents in *O-s*-triazinyl-2-aminophenol were found to affect the progress of the reaction to a great extent. The electronic effects of substituents on the Smiles rearrangement have already been studied, especially with the derivatives of *O*-nitrophenyl-2-aminophenols.[2] However, these studies have been limited to qualitative discussions and the details of the substituent effects have not been made clear. Therefore, it was of interest to study quantitatively the electronic effects of substituents upon the Smiles rearrangement with *O-s*-triazinyl-2-aminophenols.

In preliminary experiments, it was found that solvents affect the progress of the rearrangement. *O-s*-Triazinyl-2-aminophenols are stable in aprotic solvents, such as cyclohexane, benzene, carbon tetrachloride, butyl ether, and acetone, but most of the *O-s*-triazinyl-2-aminophenols were found to rearrange readily to give *N-s*-triazinyl-2-aminophenols in protic solvents, such as water and lower alcohols. This paper will report the effects of substituents on the rearrangement with *O-s*-triazinyl-2-aminophenols in methanol, ethanol, and 2-propanol.

Results and Discussion

Syntheses of O-s-*triazinyl-2-aminophenols and* N-s-*triazinyl-2-aminophenols.* *O-s*-Triazinyl-2-aminophenols and *N-s*-triazinyl-2-aminophenols of the following general formulas—(I), (II), (III), and (IV)—were prepared according to Schemes 1 and 2:

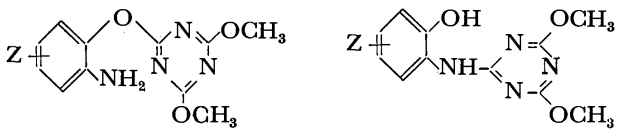

(I) (III)

Z=H, 4-CH_3, 4-Cl, 4-OCH_3, 4-$COCH_3$, 5-CH_3, 5-Cl, 5-OCH_3

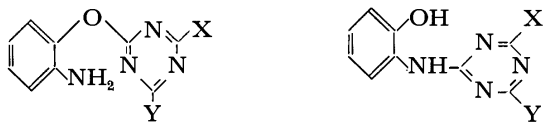

(II) (IV)

(II-1), (IV-1), X=OCH_3, Y=$N(CH_3)_2$
(II-2), (IV-2), X=Y=$N(CH_3)_2$
(II-3), (IV-3), X=C_6H_5, Y=$N(CH_3)_2$
(II-4), (IV-4), X=NH_2, Y=OCH_3

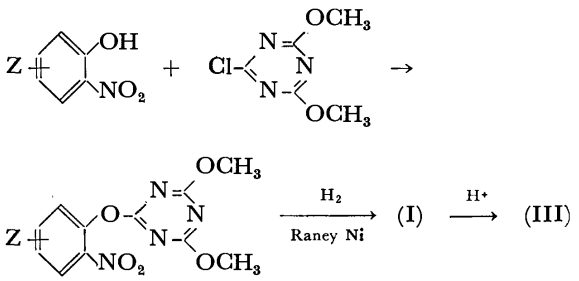

Scheme 1.

The compounds (I) were prepared by the condensation of *o*-nitrophenol or substituted *o*-nitrophenols with chloro-dimethoxy-*s*-triazine, followed by catalytic hydrogenation in the presence of Raney nickel. On the other hand, *o*-nitrophenol was converted with 2,4-dichloro-6-methoxy-*s*-triazine or cyanuric chloride into 2-chloro-4-methoxy-6-(2-nitrophenoxy)-*s*-trizine or 2,4-dichloro-6-(2-nitrophenoxy)-*s*-triazine, which, with dimethylamine or ammonia, gave 2-dimethylamino-4-methoxy-6-(2-nitrophenoxy)-*s*-triazine, 2-amino-4-methoxy-6-(2-nitrophenoxy)-*s*-triazine, or 2,4-bis(dimethylamino)-6-(2-nitrophenoxy)-*s*-triazine. Compounds (II-1), (II-4), and (II-2) were obtained by the hydrogenation of 2-dimethylamino-4-methoxy-6-(2-ni-

1) T. Harayama, K. Okada, S. Sekiguchi, and K. Matsui, *J. Heterocycl. Chem.*, **7**, 981 (1970); K. Matsui, N. Maeno, S. Suzuki, H. Shizuka and T. Morita, *Tetrahedron Lett.*, **1970**, 1467.

2) W. E. Truce, E. M. Kreider and W. W. Brand, "The Smiles and Related Rearrangements of Aromatic Systems," Organic Reactions Vol. 18, p. 117 John Wiley & Sons, Inc. (1970); J. Bunnett, R. E. Zahler, *Chem. Rev.*, **49**, 362 (1951). A. A. Levi and S. Smiles, *J. Chem. Soc.*, **1932**, 1488; F. Galbraith and S. Smiles, *ibid.*, **1935**, 1234, B. A. Kent and S. Smiles, *ibid.*, **1934**, 422; W. J. Evans and S. Smiles, *ibid.*, **1935**, 181; K. C. Roberts et al., *ibid.*, **1935**, 196, K. C. Roberts and C. G. M. DeWorms, *ibid.*, **1935**, 1309; K. C. Roberts, J. A. Phys., *ibid.*, **1937**, 39; G. Pappalardo, *Gazz. Chim. Ital.*, **90**, 645 (1960).

trophenoxy)-*s*-triazine, 2-amino-4-methoxy-6-(2-nitrophenoxy)-*s*-triazine, and 2,4-bis(dimethylamino)-6-(2-nitrophenoxy)-*s*-triazine using Raney nickel as the catalyst. Compound (II–3) was obtained in a similar manner from *o*-nitrophenol and 2,4-dichloro-6-phenyl-*s*-triazine. The rearranged products of the general formulas of (III) and (IV) were obtained by treating the corresponding *O*-*s*-triazinyl-2-aminophenols with diluted hydrochloric acid. The intermediates, *O*-*s*-triazinyl-2-aminophenols and *N*-*s*-triazinyl-2-aminophenols, thus obtained are listed in Tables 1, 2, and 3.

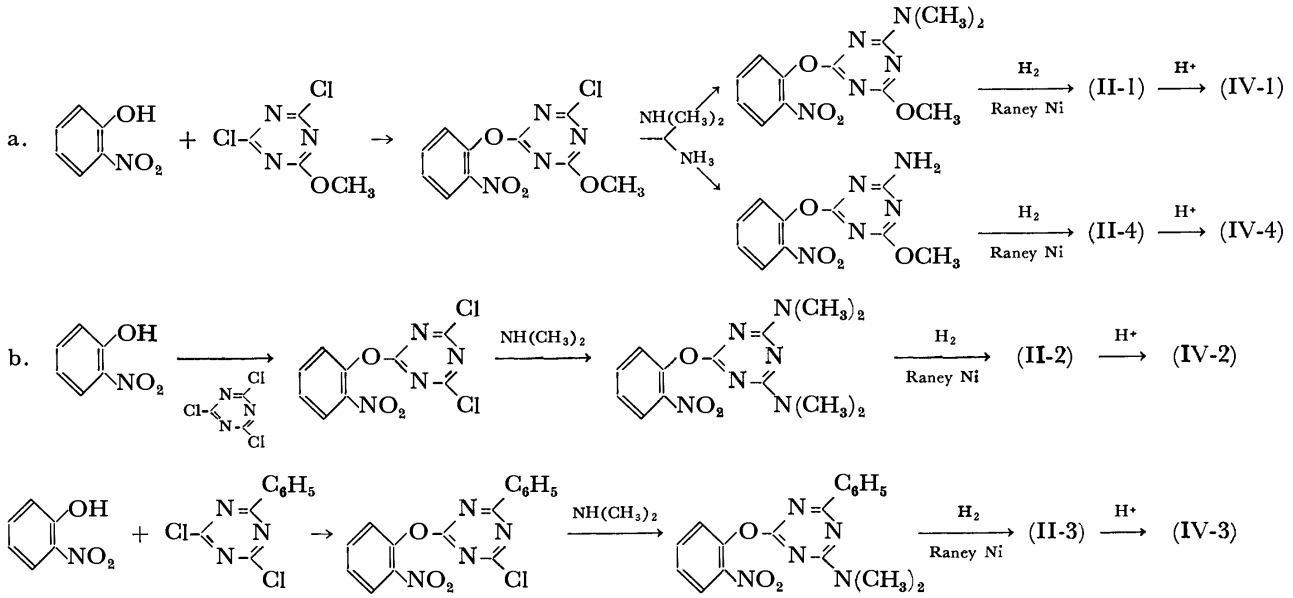

Scheme 2.

Table 1. Aryloxy-*s*-triazines, 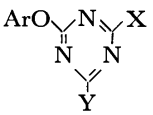

Ar	X	Y	Yield, %	Mp, °C	Solvent for recrystallization		Analysis, % Found	Calcd
2-Nitrophenyl	$-OCH_3$	$-OCH_3$	88	137.5—138.5[a)]	Benzene-Ligroin		—	—
4-Methyl-2-nitrophenyl	$-OCH_3$	$-OCH_3$	88	114.5[a)]	Benzene-Ligroin		—	—
4-Methoxy-2-nitrophenyl	$-OCH_3$	$-OCH_3$	Quant.	120	Benzene-Ligroin	C	47.18	46.76
						H	4.23	3.92
						N	17.91	18.17
4-Chloro-2-nitrophenyl	$-OCH_3$	$-OCH_3$	77	119—120[a)]	Benzene-Ligroin		—	—
4-Acetyl-2-nitrophenyl	$-OCH_3$	$-OCH_3$	50	122	Benzene-Ligroin	C	49.27	48.76
						H	4.02	3.78
						N	17.41	17.33
5-Methyl-2-nitrophenyl	$-OCH_3$	$-OCH_3$	Quant.	127—128	Benzene-Ligroin	C	50.00	49.32
						H	4.50	4.14
						N	19.17	19.23
5-Methoxy-2-nitrophenyl	$-OCH_3$	$-OCH_3$	Quant.	129	Benzene-Ligroin	C	47.22	46.76
						H	4.18	3.92
						N	18.07	18.17
5-Chloro-2-nitrophenyl	$-OCH_3$	$-OCH_3$	Quant.	123—124	Benzene-Ligroin	C	42.12	42.26
						H	3.22	2.90
						N	18.10	17.92
2-Nitrophenyl	$-OCH_3$	$-N(CH_3)_2$	Quant.	119.5—120.5	Benzene-Ligroin	C	49.67	49.48
						H	4.65	4.49
2-Nitrophenyl	$-N(CH_3)_2$	$-N(CH_3)_2$	88	169—170	Benzene-Ligroin	C	51.30	51.31
						H	5.20	5.29
2-Nitrophenyl	$-C_6H_5$	$-N(CH_3)_2$	Quant.	193—195	Benzene-Ligroin	C	60.55	60.53
						H	4.61	4.48
2-Nitrophenyl	$-OCH_3$	$-NH_2$	72	179—181	Benzene	C	45.88	45.63
						H	3.62	3.45

a) T. Harayama, K. Okada, S. Sekiguchi, and K. Matsui, *J. Heterocycl. Chem.*, **7**, 981 (1970).

TABLE 2. *O*-*s*-TRIAZINYL-2-AMINOPHENOLS

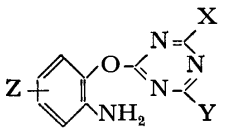

Compound	X	Y	Z	Yield, %	Mp, °C	Solvent for recrystallization		Analysis, % Found	Calcd
I-1	$-OCH_3$	$-OCH_3$	-H	60	91—92[a]	Petroleum ether		—	—
I-2	$-OCH_3$	$-OCH_3$	4-CH_3	89	123—124[a]	Benzene		—	—
I-3	$-OCH_3$	$-OCH_3$	4-OCH_3	69	121—122	Benzene	C	51.32	51.79
							H	5.29	5.71
							N	20.24	20.13
I-4	$-OCH_3$	$-OCH_3$	4-Cl	94	154—155[b]	Benzene		—	—
I-5	$-OCH_3$	$-OCH_3$	4-$COCH_3$	70	155	Benzene	C	53.75	53.79
							H	5.10	4.86
							N	19.44	19.30
I-6	$-OCH_3$	$-OCH_3$	5-CH_3	78	136—137	Benzene-Ligroin	C	54.88	54.96
							H	5.22	5.38
							N	20.84	21.36
I-7	$-OCH_3$	$-OCH_3$	5-OCH_3	43	137	Benzene-Ligroin	C	52.31	51.79
							H	5.20	5.71
							N	20.40	20.13
I-8	$-OCH_3$	$-OCH_3$	5-Cl	75	132	Benzene-Ligroin	C	46.41	46.74
							H	4.08	3.92
							N	20.17	19.81
II-1	$-OCH_3$	$-N(CH_3)_2$	-H	54	104—105	Benzene-Ligroin	C	55.24	55.16
							H	5.92	5.78
II-2	$-N(CH_3)_2$	$-N(CH_3)_2$	-H	75	134—135	Petroleum-ether-Benzene	C	56.60	56.92
							H	6.58	6.61
II-3	$-C_6H_5$	$-N(CH_3)_2$	-H	88	149—150	Benzene-Ligroin	C	66.25	66.43
							H	5.74	5.57
II-4	$-NH_2$	$-OCH_3$	-H	53	185—186	Benzene	C	51.77	51.50
							H	5.15	4.75

a) T. Harayama, S. Sekiguchi, and K. Matsui, *J. Heterocycl. Chem.*, **7**, 975 (1970).
b) T. Harayama, K. Okada, S. Sekiguchi, and K. Matsui, *ibid.*, **7**, 981 (1970).

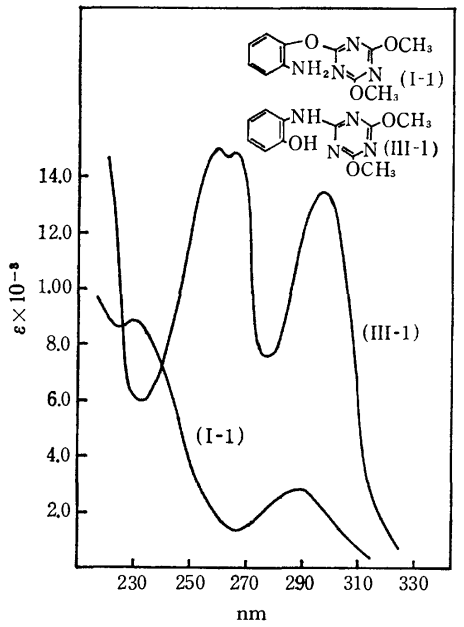

Fig. 1. Absorption spectra of *O*-(4,6-dimethoxy-*s*-triazin-2-yl)-2-aminophenol (I-1) and *N*-(4,6-dimethoxy-*s*-triazin-2-yl)-2-aminophenol (III-1) in methanol

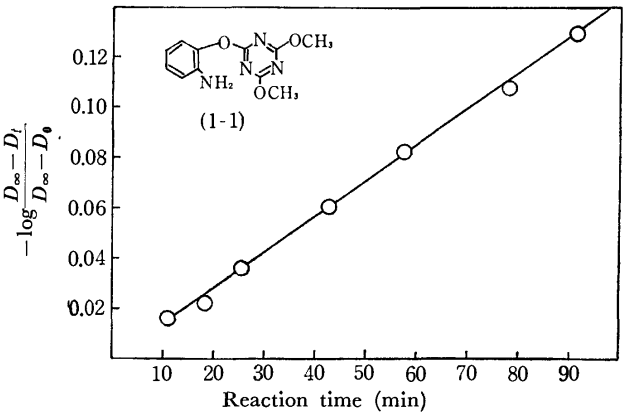

Fig. 2. The first order plot for the rearrangement of *O*-(4,6-dimethoxy-*s*-triazin-2-yl)-2-aminophenol (I-1) in methanol at 30°C.

Rates of the Rearrangement of O-s-*triazinyl-2-aminophenols.* Both *O*-*s*-triazinyl-2-aminophenols and *N*-*s*-triazinyl-2-aminophenols have absorption maxima in the region from 290 to 310 nm, but in every case the molar extinction coefficient of the original compound is much smaller than that of the rearranged product, as is shown in Table 4 and Fig. 1. Therefore, the absorption in this region increases with the progress

Table 3. *N-s*-triazinyl-2-aminophenols,

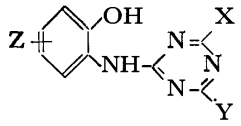

Compound	X	Y	Z	Mp, °C	Solvent for crystallization		Analysis % Found	Calcd
III-1	$-OCH_3$	$-OCH_3$	-H	172—173[a]	Benzene		—	—
III-2	$-OCH_3$	$-OCH_3$	4-CH_3	179—180[b]	Methanol		—	—
III-3	$-OCH_3$	$-OCH_3$	4-OCH_3	205	Methanol	C	52.04	51.79
						H	5.56	5.71
						N	20.46	20.13
III-4	$-OCH_3$	$-OCH_3$	4-Cl	211—212[b] (decomp.)	Methanol		—	—
III-5	$-OCH_3$	$-OCH_3$	4-$COCH_3$	178	Methanol	C	53.25	53.79
						H	5.30	4.86
III-6	$-OCH_3$	$-OCH_3$	5-CH_3	182—183	Methanol	C	55.28	54.96
						H	5.66	5.38
III-7	$-OCH_3$	$-OCH_3$	5-OCH_3	189	Methanol	C	51.79	51.79
						H	5.64	5.71
						N	20.23	20.13
III-8	$-OCH_3$	$-OCH_3$	5-Cl	210	Methanol	C	47.16	46.74
						H	4.18	3.92
						N	20.03	19.81
IV-1	$-OCH_3$	$-N(CH_3)_2$	-H	213—214	Ethanol	C	55.27	55.16
						H	5.89	5.78
IV-2	$-N(CH_3)_2$	$-N(CH_3)_2$	-H	185—186	Ethanol	C	56.83	56.92
						H	6.69	6.61
IV-3	$-C_6H_5$	$-N(CH_3)_2$	-H	159—160	Benzene–Ligroin	C	66.56	66.43
						H	5.66	5.57
IV-4	$-NH_2$	$-OCH_3$	-H	204—205	2-Propanol	C	50.95	51.50
						H	4.63	4.75

a) T. Harayama, S. Sekiguchi, and K. Matsui, *J. Heterocycl. Chem.*, **7**, 975 (1970).
b) T. Harayama, K. Okada, S. Sekiguchi and K. Matsui, *ibid.* **7**, 981 (1970).

Table 4. Molar extinction coefficients of *O-s*-triazinyl-2-aminophenols and *N-s*-triazinyl-2-aminophenols in ethanol

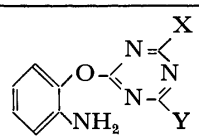

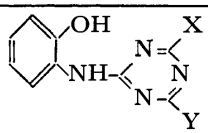

X	Y	λ_{max} (nm)	ε	X	Y	λ_{max} (nm)	ε
$-OCH_3$	$-OCH_3$	287	2400	$-OCH_3$	$-OCH_3$	295	13400
$-OCH_3$	$-N(CH_3)_2$	287	2800	$-OCH_3$	$-N(CH_3)_2$	292	12600
$-N(CH_3)_2$	$-N(CH_3)_2$	286	2900	$-N(CH_3)_2$	$-N(CH_3)_2$	290	11900

Table 5. Rate constants for the rearrangement of *O-s*-triazinyl-2-aminophenols in methanol

Compound	k_1 (min^{-1})					
	10°C	20°C	30°C	40°C	50°C	60°C
I-1	6.03×10^{-4}	1.43×10^{-3}	3.30×10^{-3}	6.50×10^{-3}	—	—
I-2	1.91×10^{-4}	5.24×10^{-4}	1.27×10^{-3}	2.72×10^{-3}	—	—
I-4	6.92×10^{-5}	1.83×10^{-4}	5.62×10^{-4}	1.26×10^{-3}	—	—
II-1	—	—	2.33×10^{-5}	5.85×10^{-5}	1.33×10^{-4}	2.91×10^{-4}
II-2*	—	—	—	—	—	—
II-3	—	—	1.08×10^{-5}	—	—	—
II-4	—	—	1.17×10^{-4}	—	—	—

* Rate constant was too slow to measure.

Table 6. Rate constants for the rearrangement of *O*-*s*-triazinyl-2-aminophenols in 2-propanol

Compound	k_1 (min^{-1})					
	10°C	20°C	30°C	40°C	50°C	60°C
I-1	1.85×10^{-4}	5.21×10^{-4}	1.18×10^{-3}	2.36×10^{-3}	—	—
I-2	—	1.53×10^{-4}	3.85×10^{-4}	9.06×10^{-4}	1.89×10^{-3}	—
I-4	—	9.06×10^{-5}	2.29×10^{-4}	5.53×10^{-4}	1.31×10^{-3}	—
II-1	—	—	5.67×10^{-6}	1.38×10^{-5}	3.59×10^{-5}	9.66×10^{-5}

Table 7. Activation parameters for the rearrangement of *O*-*s*-triazinyl-2-aminophenols

Compound	2-PrOH		MeOH	
	E (kcal/mol)	$\Delta S^{\neq}$ (e.u.) (40°C)	E (kcal/mol)	$\Delta S^{\neq}$ (e.u.) (40°C)
I-1	15.4	−31.6	14.0	−34.0
I-2	16.5	−29.9	15.5	−31.0
1-4	17.4	−28.0	16.7	−28.7
II-1	19.0	−30.3	16.8	−34.4

of the rearrangement, and the rates of the rearrangement of *O*-*s*-triazinyl-2-aminophenols can be measured spectrophotometrically. For example, a plot of $-\log(D_\infty-D_t)/(D_\infty-D_0)$ against the reaction time, t, for the rearrangement of (I-1) in methanol gave a straight line, as is shown in Fig. 2.

Accordingly, the first-order rate constant for the rearrangement can be calculated using Eq. (1):

$$k_1 = -2.303\cdot\frac{1}{t}\cdot\log\frac{D_\infty-D_t}{D_\infty-D_0} \quad (1)$$

where D_0=initial optical density of a solution of *O*-*s*-triazinyl-2-aminophenol.
D_t=optical density of a solution at time t.
D_∞=optical density of a solution at an infinite time.

In Table 5 are listed the first-order rate constants for the rearrangements of (I-1), (I-2), (I-4), (II-1), (II-2), (II-3), and (II-4) at 10, 20, 40, 50, and 60°C in methanol, while in Table 6 are listed those in 2-propanol; the energies and entropies of activation thus obtained are listed in Table 7. Table 8 compares the rate constants of these compounds in methanol, ethanol, and 2-propanol.

As is shown in Table 8, the rate of the rearrangement varied with the dielectric constant of the alcohol used, and in methanol the rearrangement took place most rapidly. However, no simple relation between the dielectric constant of the solvent and the rate constant has been observed. On the other hand, from a comparison of the rate constants, activation energies, and activation entropies in methanol and 2-propanol, it is apparent that, in the rearrangement of *O*-*s*-triazinyl-2-aminophenols, in spite of the counteracting change in the entropy of activation, the change in the activation energy dominates the rate change. These results can be explained as follows:[3] because the transition state of the reaction may be assumed to be more polar than the initial state, in a more polar solvent the rearrangement can be expected to proceed more rapidly by lowering activation energy under the formation of a stronger solvated transition state than in a less polar solvent.

Effects of Substituents on the Rearrangement. In Table 9, the rate constants for the rearrangement of 4- or 5-substituted *O*-(4,6-dimethoxy-*s*-triazin-2-yl)-2-aminophenols in methanol at 20°C are listed. From Tables 5 and 9, it is apparent that the substituents in *O*-*s*-triazinyl-2-aminophenol affect the rate of the rearrangement to a great extent, and that the effects

Table 8. Effect of solvent on the rate constant at 30°C

Compound	k_1(min^{-1})		
	MeOH	EtOH	2-PrOH
I-1	3.30×10^{-3}	2.22×10^{-3}	1.18×10^{-3}
I-2	1.27×10^{-3}	7.22×10^{-4}	3.85×10^{-4}
I-4	5.62×10^{-4}	3.91×10^{-4}	2.29×10^{-4}
II-1	2.33×10^{-5}	1.49×10^{-5}	5.67×10^{-6}

Table 9. Rate constants for the rearrangement of substituted *O*-(4,6-dimethoxy-*s*-triazin-2-yl)-2-aminophenols in methanol at 20°C

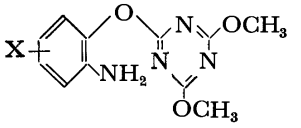

Compound	Substituent X	k_1 (min^{-1})
I-1	H	1.43×10^{-3}
I-2	4-CH_3	5.24×10^{-4}
I-3	4-OCH_3	1.02×10^{-4}
I-4	4-Cl	1.83×10^{-4}
I-5	4-$COCH_3$	1.05×10^{-2}
I-6	5-CH_3	3.23×10^{-3}
I-7	5-OCH_3	2.43×10^{-2}
I-8	5-Cl	2.69×10^{-3}

3) C. K. Ingold, "Structure and Mechanism in Organic Chemistry," Cornell University Press. Itaca and London 2nd ed (1969) p. 457.

of substituents differ according to the nature and the position of substituents. The effect of the substituents in the triazine nucleus may become clear from a comparison of the rate constants of (I-1), (II-1), (II-2), (II-3), and (II-4). Although the rate of the rearrangement of (II-2) in methanol was too slow to measure, the facility of the rearrangement was found to vary in the following order:

$$\text{II-2} \ll \text{II-3} < \text{II-1} < \text{II-4} < \text{I-1}$$

In *s*-triazine compounds, it was found that the Hammett σ_m values of the benzene series are applicable in studying the effects of substituents and that the total effect of two substituents in the *s*-triazine ring on the reaction center is given by the summation of the two substituent constants, $\sum\sigma_m$.[4] Therefore, the sensitivity of the rearrangement towards the substituents in a triazine ring can be evaluated by a reaction constant which is calculated from the rate constants of (I-1), (II-1), (II-3), and (II-4) using the respective $\sum\sigma_m$ values. In the case studied, the reaction constant (ρ) thus obtained was 6.43, with a correlation coefficient of 0.987. As will be described later, this ρ value is considerably larger than those of the reactions attributable to the substituent in the aminophenol moiety.

Although it is yet uncertain whether this migration proceeds by the S_N2 mechanism or by the intermediate-complex mechanism, the effect of a substituent in the aminophenol moiety may reasonably be considered in view of the following two points: the influence of the substituent upon the nucleophilic reactivity of the attacking amino group, and the influence upon the reactivity of the migrating *s*-triazinyl group towards the amino group (the positive character of the ring carbon of the *s*-triazine nucleus) or the stability of the leaving phenoxide anion. In the former, an electron-releasing effect of a substituent favors the rearrangement, while an electron-attracting effect is favored in the latter. Therefore, the Hammett equation for reactions like this rearrangement may be expressed by Eq. 2, which consists of a sum of two terms.[5]

$$\log k/k_0 = \sigma\rho' + \sigma\rho'' \qquad (2)$$

where the reaction constants, ρ' and ρ'', are attributable to the effect of a substituent on the reactivity of the migrating triazine nucleus through the -O- bridge or the stability of the leaving phenoxide anion and the effect of a substituent on the nucleophilicity of the amino group respectively.

Using the rate constants (in the case of 4-$COCH_3$, the σ^- value was used), the ρ' and ρ'' values calculated by the method of least squares were:

$$\rho' = 2.86; \qquad \rho'' = -4.15$$

respectively, and the ρ''/ρ' ratio was -1.45. A Hammett plot of $\log k_1$ against $\sigma_m - 1.45\sigma_p$ when a substituent is in the 5-position or $\sigma_p - 1.45\sigma_m$ when a substituent is in the 4-position gave a straight line, with a correlation coefficient of 0.990, as is shown in Fig. 3.

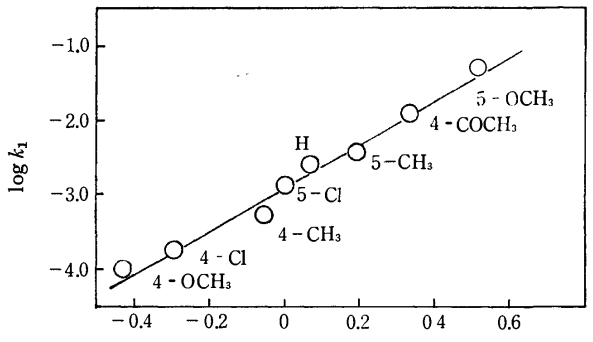

Fig. 3. Hammett plot for the rearrangement of 4- or 5-substituted *O*-(4,6-dimethoxy-*s*-triazin-2-yl)-2-aminophenols in methanol (20°C).

However, a linear relation between the substituent constants and log k_1 was not obtained by using a usual Hammett equation, involving only one term.

Therefore, a substituent in the 5-position affects the nucleophilic reactivity of the attacking amino group as a *para*-substituent and, simultaneously, the reactivity of the migrating *O*-*s*-triazinyl group as a *meta*-substituent. Such a situation holds for a substituent in the 4-position. As a result, the logarithm of the rate constants apparently depends upon a composite effect of these two. These results indicate that, in 4- or 5-substituted *O*-*s*-triazinyl-2-aminophenols, a substituent in the aminophenol moiety affects the nucleophilic reactivity of the free amino group more effectively than the reactivity of the *s*-triazinyl group or to stability of the leaving phenoxide anion. Moreover, as has been described previously, it has become apparent from a comparison of the value of ρ with those of ρ' and ρ'' that, in the Smiles rearrangement of *O*-*s*-triazinyl-2-aminophenols, the effect of the substituents in the *s*-triazine nucleus is larger than that of a substituent in the aminophenol moiety.

Experimental

All the melting points are uncorrected. The ultraviolet spectra were recorded on a Hitachi-124 UV-VIS spectrophotometer. The elemental analyses were performed in the Micro-analytical Center of the Gunma University.

Materials. *Aryloxy-4,6-dimethoxy-s-triazines*: A typical preparation is the case of 2,4-dimethoxy-6-(4-methoxy-2-nitrophenoxy)-*s*-triazine. Into a solution of 4.1 g (0.024 mol) of 2-nitro-4-methoxyphenol and 1.2 g(0.03 mol) of sodium hydroxide in 40 m*l* of acetone, we stirred, drop by drop, a solution of 5.0 g (0.028 mol) of 2-chloro-4,6-dimethoxy-*s*-triazine in 50 m*l* of acetone. After an additional 24 hrs' stirring at 40°C, the mixture was poured into 500 m*l* of ice water, filtered, and dried.

4- or 5-Substituted O-(4,6-dimethoxy-s-triazin-2-yl)-2-aminophenols (I). A typical run is shown in the case of *O*-(4,6-dimethoxy-*s*-triazin-2-yl)-4-methoxy-2-aminophenol. A mixture containing 50 m*l* of dioxane, 5.0 g (0.016 mol) of 2,4-dimethoxy-6-(4-methoxy-2-nitrophenoxy)-*s*-triazine, and 3 g of Raney nickel was stirred for 2 hr at room temperature under a pressure of 60 kg/cm² of hydrogen. After the

4) Y. Fukushima, N. Nohara, Y. Hashida, S. Sekiguchi, and K. Matsui, This Bulletin, **44**, 794 (1971).

5) J. Tirouflet, *Bull. Soc. Chem. Fr.*, **1954**, 769.

catalyst had then been removed by filtration, the solution was poured into 500 m*l* of ice water containing a small amount of sodium hydroxide. The precipitate was filtered, washed with water, and dried.

O-(4-Dimethylamino-6-methoxy-s-triazin-2-yl)-2-aminophenol (II-1). i) 2-Chloro-4-methoxy-6-(2-nitrophenoxy)-s-triazine: A solution of 139 g (1.0 mol) of *o*-nitrophenol and 45 g (1.1 mol) of sodium hydroxide in 500 m*l* of water was stirred, drop by drop, over 3-hr period and at 0—5°C, into a solution of 180 g (1.0 mol) of 2,4-dichloro-6-methoxy-*s*-triazine in 1 *l* of acetone. After an additional 2 hrs' stirring at room temperature, the mixture was poured into 2 *l* of ice water. The precipitate was then filtered and dried to give 270 g (quantitative) of crude 2-chloro-4-methoxy-6-(2-nitrophenoxy)-*s*-triazine (mp 116—120°C). Recrystallization from benzene-ligroin gave an analytical sample; mp 122—123°C.

Found: C, 42.29; H, 2.47%; Calcd for $C_{10}H_7ClN_4O_4$: C, 42.49; H, 2.47%.

ii) 2-Dimethylamino-4-methoxy-6-(2-nitrophenoxy)-s-triazine: Into a solution of 230 g (0.84 mol) of 2-chloro-4-methoxy-6-(2-nitrophenoxy)-*s*-triazine in 1 *l* of acetone, we stirred 190 m*l* of a 40% dimethylamine solution (1.7 mol) drop by drop over a 2-hr period at 10°C. Stirring was continued for 5 hr at 40°C; then the mixture was refluxed for 3 hr and poured into 2 *l* of ice water. The precipitate was filtered and dried to give 226 g (quantitative) of crude 2-dimethylamino-4-methoxy-6-(2-nitrophenoxy)-*s*-triazine; mp (116—120°C). Recrystallization from benzene–ligroin gave an analytical sample.

iii) O-(4-Dimethylamino-6-methoxy-s-triazin-2-yl)-2-aminophenol (II-1): This was obtained in a 54% yield by the hydrogenation of 2-dimethylamino-4-methoxy-6-(2-nitrophenoxy)-*s*-triazine in dioxane in the presence of Raney nickel. Recrystallization from benzene–ligroin gave an analytical sample; mp 104—105°C.

O-[4,6-Bis(dimethylamino)-s-triazin-2-yl]-2-aminophenol (II-1). i) 2,4-Dichloro-6-(2-nitrophenoxy)-s-triazine: This compound was obtained in a 94% yield by the condensation of *o*-nitrophenol with cyanuric chloride in the presence of sodium hydroxide in acetone at 0—5°C. Recrystallization from benzene–ligroin gave an analytical sample; mp 136—137°C.

Found: C, 37.93; H, 1.51%; Calcd for $C_9H_4Cl_2N_4O_3$: C, 37.65; H, 1.40%.

ii) 2,4-Bis(dimethylamino)-6-(2-nitrophenoxy)-s-triazine: Into a solution of 75 g (0.26 mol) of 2,4-dichloro-6-(2-nitrophenoxy)-*s*-triazine in 300 ml of acetone, we stirred 130 ml of a 40% dimethylamine solution drop by drop over a 2-hr period at 10°C. The mixture was then processed according to the procedure used for 2-dimethylamino-4-methoxy-6-(2-nitrophenoxy)-*s*-triazine. Yield, 99%. Recrystallization from benzene–ligroin gave an analytical sample; mp 169—170°C.

iii) O-[4,6-Bis(dimethylamino)-s-triazin-2-yl]-2-aminophenol (II-2): The compound (II-2) was obtained in a 75% yield by the catalytic reduction of 2,4-bis(dimethylamino)-6-(2-nitrophenoxy)-*s*-triazine, using Raney nickel as the catalyst in dioxane. Recrystallization from benzene gave an analytical sample of (II-2); mp 134—135°C.

O-(4-Dimethylamino-6-phenyl-s-triazin-2-yl)-2-aminophenol (II-3). 2-Chloro-4-phenyl-6-(2-nitrophenoxy)-*s*-triazine was obtained by treating *o*-nitrophenol with 2,4-dichloro-6-phenyl-*s*-triazine in acetone in the presence of sodium hydroxide; mp 152—153°C (benzene-ligroin)

Found: C, 54.75; H, 3.07%; Calcd for $C_{15}H_9ClN_4O_3$; C, 54.81; H, 2.76%.

it was then condensed with dimethylamine in acetone to give 2-dimethylamino-4-phenyl-6-(2-nitrophenoxy)-*s*-triazine; mp 193—195°C (benzene-ligroin). The compound (II-3) was obtained in an 88% yield by the catalytic hydrogenation of 2-dimethylamino-4-phenyl-6-(2-nitrophenoxy)-*s*-triazine in dioxane, using Raney nickel as the catalyst. Mp 149—150°C (benzene-ligroin).

O-(4-Amino-6-methoxy-s-triazin-2-yl-2-aminophenol (II-4). 2-Amino-4-methoxy-6-(2-nitrophenoxy)-*s*-triazine obtained by treating 2-chloro-4-methoxy-6-(2-nitrophenoxy)-*s*-triazine with ammonia in acetone [mp 179—181°C (benzene)] was hydrogenated using Raney nickel as the catalyst in dioxane. Recrystallization from benzene then gave an analytical sample of (II-4); mp 185—186°C.

N-(s-Triazinyl)-2-aminophenols (III, IV). A typical run is the case of (IV-1). To a solution of 1.0 g (II-1) in 50 m*l* of acetone we added one drop of concentrated hydrochloric acid at room temperature, and then the mixture was stirred for 12 hr. After the mixture had been poured into 200 m*l* of ice water, the precipitate was filtered and dried to give 0.9 g of crude (IV-1) (mp 213—214°C).

Kinetic Measurements. Kinetic measurements were carried out spectrophotometrically by measuring the increase in the absorbance at 280—310 nm of an alcoholic solution of *O-s*-triazinyl-2-aminophenol at 10, 20, 30, 40, 50, and 60°C; the first-order rate constant for the rearrangement was calculated using Eq. 1.

The $N^1 \rightarrow N^2$ Migration of the *s*-Triazinyl Group of 4-Substituted N^1,N^1-Bis-(*s*-triazinyl)-*o*-phenylenediamines

Kenji NAKAMURA, Noboru NOHARA, and Kohji MATSUI

Department of Chemistry, Faculty of Engineering, Gunma University, Tenjincho, Kiryu, Gunma

(Received December 22, 1971)

Several 4-substituted N^1-[bis-(diethylamino)-*s*-triazinyl]-N^1-(dimethoxy-*s*-triazinyl)-*o*-phenylenediamines were synthesized, and the migrations of the *s*-triazinyl group were investigated in these compounds. In methanol, every 4-substituted N^1,N^1-bis(*s*-triazinyl)-*o*-phenylenediamine gave only 4-substituted N^1-[bis-(diethylamino)-*s*-triazinyl]-N^2-(dimethoxy-*s*-triazinyl)-*o*-phenylenediamine by the migration of the dimethoxy-*s*-triazinyl group; the rearrangement was assumed to proceed through an intramolecular nucleophilic attack by the *ortho* amino group upon the ring carbon of the dimethoxy-*s*-triazinyl group. However, in the presence of a small amount of acid, the $N^1 \rightarrow N^2$ migration of the bis(diethylamino)-*s*-triazinyl group occurred preferentially, and two kinds of rearranged products were obtained. The kinetics of the rearrangement have also been studied spectrophotometrically in methanol, and the effects of the substituents on the rearrangement have been discussed.

Rearrangements involving intramolecular nucleophilic substitutions as are shown in Eq (1) are well known as Smiles rearrangements:[1]

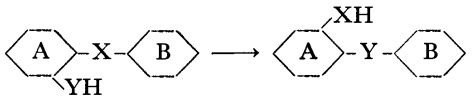

(1)

(I) (II)

where X=O, S, CO_2, SO_2, *etc.*

YH=-OH, $-NH_2$, $-CONH_2$, -NH-Acyl, and -SH

A=substituted phenyl or other aromatic group

B=substituted phenyl or nitrogen heteroaromatic group

As for the Smiles rearrangement involving aryl migrations between two functional groups of the same kind, several examples of an oxygen-oxygen displacement have been reported.[2]

Recently, $N^1 \rightarrow N^2$ migrations of the aryl group have been observed in the reactions of *N*-phenyl derivatives of *o*-phenylenediamine or hydrazine[3] with alkyllithium and α-bromoacetanilides with amines.[4] However, little is known about the Smiles rearrangement of the nitrogen-nitrogen type. It was, therefore, of interest to study the $N^1 \rightarrow N^2$ migration of an aromatic system with *s*-triazinyl derivatives of *o*-phenylenediamine or other diamines in which the *s*-triazinyl group migrates as an aromatic system. For this purpose, 4-substituted N^1,N^1-bis(*s*-triazinyl)-*o*-phenylenediamines were found to be suitable substrates; the present work will report the $N^1 \rightarrow N^2$ migration of the *s*-triazinyl group and the effect of substituents on the rearrangement with these compounds.

1) For example, W. E. Truce, E. M. Kreider, and W. W. Brand, "The Smiles and Related Rearrangements of Aromatic Systems," Organic Reactions Vol. 18, John Wiley & Sons, Inc. (1970), p. 99; T. Harayama, K. Okada, S. Sekiguchi, and K. Matsui *J. Heterocycl. Chem.*, **7**, 981 (1970).

2) J. D. Loudon, J. R. Robertson, J. N. Watson, and S. D. Aiton, *J. Chem. Soc.*, **1950**, 55; J. D. Loudon and J. A. Scott, *ibid.*, **1953**, 265; W. Mayer and H. Csheuermann, *Angew. Chem.*, **71**, 382 (1959).

3) R. West and H. F. Stewart, *J. Amer. Chem. Soc.*, **92**, 853 (1970).

4) N. W. Gilman, P. Levitan, and L. H. Sternbach, *Tetrahedron Lett.*, **1970**, 4121.

Results and Discussion

Syntheses of 4-substituted N^1,N^1-bis-(*s*-triazinyl)-*o*-phenylenediamines of the following general formula (III) were synthesized from 4-substituted 2-nitroanilines as follows:

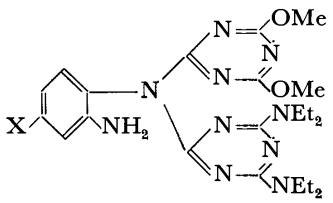

(III) X=-H, $-CH_3$, $-OCH_3$, -Cl

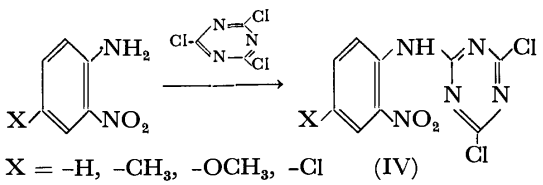

X = -H, $-CH_3$, $-OCH_3$, -Cl (IV)

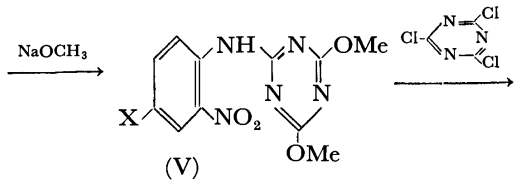

(V)

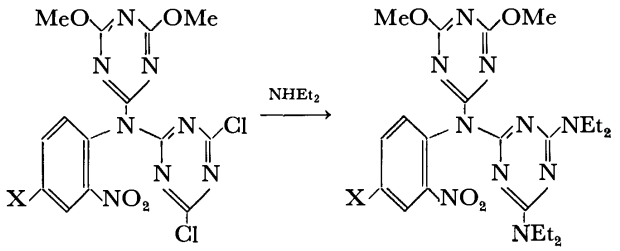

(VI) (VII)

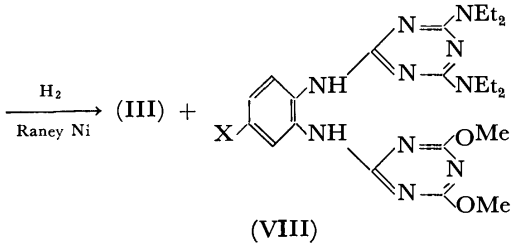

(VIII)

TABLE 1. 2-ARYLAMINO-4,6-DICHLORO-*s*-TRIAZINES (IV)

No.	Aryl	Yield (%)	Mp (°C)	Recrystn. solvent	Anal. (%) Found C	Found H	Calcd C	Calcd H
IV-1	2-Nitrophenyl-	70	196.5—197[a)]	Benzene	——		——	
IV-2	4-Methyl-2-nitrophenyl-	71	173—174	Benzene	40.35	2.46	39.98	2.33
IV-3	4-Methoxy-2-nitrophenyl-	95	168—168.5	Benzene	38.45	2.41	37.99	2.23
IV-4	4-Chloro-2-nitrophenyl-	88	144.5—146	Beuzene	33.65	1.39	33.72	1.25

a) N. Nohara, S. Sekiguchi, and K. Matsui, *J. Heterocycl. Chem.*, **7**, 519 (1970).

TABLE 2. 2-ARYLAMINO-4,6-DIMETHOXY-*s*-TRIAZINES (V)

No.	Aryl	Yield (%)	Mp (°C)	Recrystn. solvent	Anal. (%) Found C	Found H	Calcd C	Calcd H
V-1	2-Nitrophenyl-	Quant.	174—176[a)]	Benzene	——		——	
V-2	4-Methyl-2-nitrophenyl-	Quant.	188—188.5	Benzene	49.29	4.27	49.46	4.46
V-3	4-Methoxy-2-nitrophenyl-	Quant.	192—193	Benzene	47.35	4.57	46.91	4.26
V-4	4-Chloro-2-nitrophenyl-	Quant.	207—207.5	Benzene	41.87	3.20	42.38	3.23

a) N. Nohara, S. Sekiguchi, and K. Matsui, *J. Heterocycl. Chem.*, **7**, 519 (1970).

TABLE 3. *N*-(4,6-DICHLORO-*s*-TRIAZIN-2-YL)-*N*-(4,6-DIMETHOXY-*s*-TRIAZIN-2-YL)-ARYLAMINES (VI)

No.	Aryl	Yield (%)	Mp (°C)	Recrystn. Solvent		Anal. (%) Found	Calcd
VI-1	2-Nitrophenyl-	94	164.5—166.5[a)]	Chloroform		—	—
VI-2	4-Methyl-2-nitrophenyl-	74	155—156	Ligroin–Benzene	C	40.80	41.01
					H	2.90	2.75
VI-3	4-Methoxy-2-nitrophenyl-	70	158—159	Ligroin–Benzene	C	39.98	39.57
					H	2.93	2.65
					N	24.57	24.61
VI-4	4-Chloro-2-nitrophenyl-	76	165.5—166.5	Ligroin–Benzene	C	37.01	36.58
					H	2.02	1.97

a) N. Nohara, S. Sekiguchi, and K. Matsui, *J. Heterocycl. Chem.*, **7**, 519 (1970).

TABLE 4. *N*-[4,6-BIS(DIETHYLAMINO)-*s*-TRIAZIN-2-YL]-*N*-(4,6-DIMETHOXY-*s*-TRIAZIN-2-YL)-ARYLAMINES (VII)

No.	Aryl	Yield (%)	Mp (°C)	Recrystn. solvent		Anal. (%) Found	Calcd
VII-1	2-Nitrophenyl-	—	115—116	Methanol	C	53.25	53.00
					H	6.47	6.07
					N	28.35	28.15
VII-2	4-Methyl-2-nitrophenyl-	71	104—105	Methanol	C	53.65	53.89
					H	6.23	6.29
VII-3	4-Methoxy-2-nitrophenyl-	85	115.5—116.5	Methanol	C	52.47	52.26
					H	6.07	6.10
VII-4	4-Chloro-2-nitrophenyl-	76	89— 91	Methanol	C	49.13	49.58
					H	5.69	5.48
					N	26.27	26.19

4-Substituted 2-nitroanilines were converted with cyanuric chloride into 2,4-dichloro-6-(4-substituted 2-nitrophenylamino)-*s*-triazines (IV), which, with sodium methoxide, then gave 2,4-dimethoxy-6-(4-substituted 2-nitrophenylamino)-*s*-triazines (V). The substances (V) were converted with cyanuric chloride into 4-substituted *N*-(4,6-dichloro-*s*-triazin-2-yl)-*N*-(4,6-dimethoxy-*s*-triazin-2-yl)-2-nitroanilines(VI), which, with diethylamine, then gave 4-substituted *N*-[4,6-bis(diethylamino)-*s*-triazin-2-yl]-*N*-(4,6-dimethoxy-*s*-triazin-2-yl)-2-nitroanilines (VII); 4-substituted N^1-[4,6-bis(diethylamino)-*s*-triazin-2-yl]-N^1-(4,6-dimethoxy-*s*-triazin-2-yl)-*o*-phenylenediamines (III) were obtained by the hydrogenation of VII, using

Table 5. 4-Substituted N^1-[4,6-bis(diethylamino)-*s*-triazin-2-yl]-N^1-(4,6-dimethoxy-*s*-triazin-2-yl)-*o*-phenylenediamines (III)

No.	Substituent	Yield (%)	Mp (°C)	Recrystn. Solvent	Anal. (%) Found C	Found H	Calcd C	Calcd H
III-1	H	98	141.5—142.5	Ligroin	56.60	6.98	56.51	6.68
III-2	CH_3-	85	100—101	Petroleum ether	57.31	7.22	57.24	7.10
III-3	CH_3O-	94	124—125	Ligroin	54.99	6.86	55.40	6.87
III-4	Cl-	88	113—114	Petroleum ether	51.94	6.12	52.53	6.21

Raney nickel as the catalyst. However, in the case of every hydrogenated product, the presence of N^1,N^2-bis(*s*-triazinyl)-*o*-phenylenediamine (VIII), which is assumed to be produced by a rearrangement of preformed N^1,N^1-bis(*s*-triazinyl)-*o*-phenylenediamine (III), was observed. The formation of N^1,N^2-bis(*s*-triazinyl)-*o*-phenylenediamine (VIII) during the hydrogenation shows that the rearrangement of N^1,N^1-bis(*s*-triazinyl)-*o*-phenylenediamine (III) occurred fairly readily.

The intermediates IV, V, VI, VII, and N^1,N^1-bis(*s*-triazinyl)-*o*-phenylenediamines (III) thus obtained are listed in Tables 1, 2, 3, 4, and 5.

Rearrangement of N¹,N¹-*Bis(*s*-triazinyl)-*o*-phenylenediamines.* Because of the presence of two different *s*-triazinyl groups in these 4-substituted N^1,N^1-bis(*s*-triazinyl)-*o*-phenylenediamines (III), it is assumed that each compound may rearrange to give two kinds of 4-substituted N^1,N^2-bis(*s*-triazinyl)-*o*-phenylenediamines, depending upon whether the migrating group is the dimethoxy-*s*-triazinyl or bis(diethylamino)-*s*-triazinyl group. Authentic samples of these rearranged compounds were synthesized from IV or V as follows:

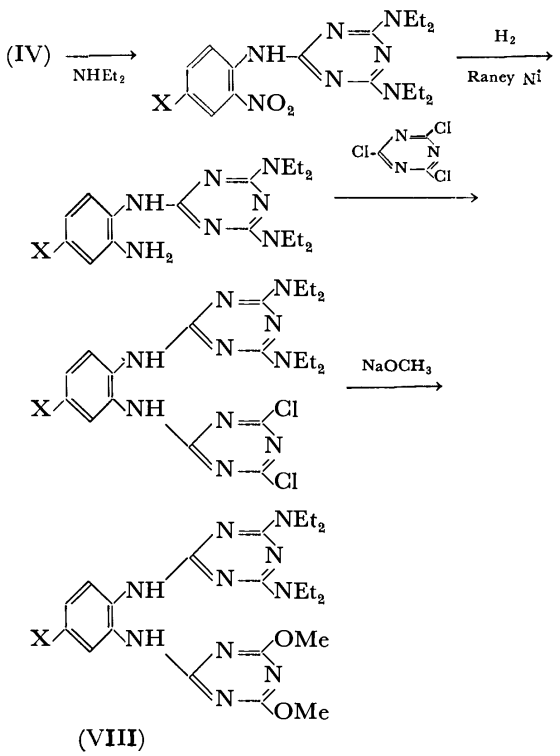

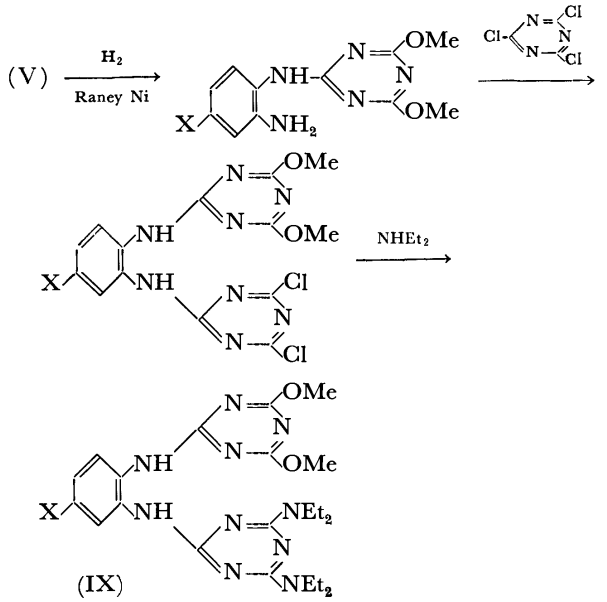

The N^1,N^2-bis(*s*-triazinyl)-*o*-phenylenediamines (VIII and IX) thus obtained are listed in Tables 6 and 7.

In preliminary experiments, it was found that the compounds III are stable in such aprotic solvents as benzene, cyclohexane, carbon tetrachloride, and acetone, but that they rearrange to give N^1,N^2-bis(*s*-triazinyl)-*o*-phenylenediamines (VIII) in methanol and ethanol, and somewhat more readily in the presence of sodium hydroxide in these protic solvents, as will be described kinetically later. However, an intermolecular reaction between III-1 and aniline to give 2,4-dimethoxy-6-anilino-*s*-triazine or 2,4-bis(diethylamino)-6-anilino-*s*-triazine did not take place. Moreover, *N*-[bis(diethylamino)-*s*-triazinyl]-*N*-(dimethoxy-*s*-triazinyl)-2-nitroaniline (VII-1), whose *s*-triazinyl groups are expected to be more reactive towards a nucleophilic reagent than those of III-1 because of the presence of a nitro group, did not react with aniline or *p*-anisidine under similar reaction conditions. From these results, it is obvious that the rearrangement of N^1,N^1-bis(*s*-triazinyl)-*o*-phenylenediamine (III) is intramolecular.

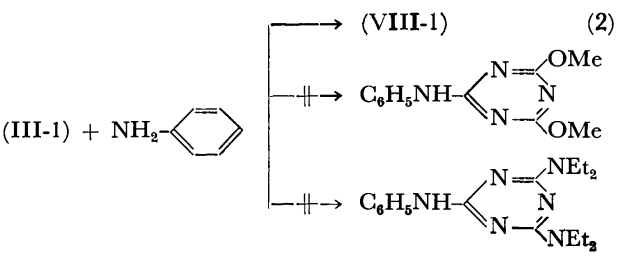

TABLE 6. 4-SUBSTITUTED N^1-[4,6-BIS(DIETHYLAMINO)-*s*-TRIAZIN-2-YL]-N^2-(4,6-DIMETHOXY-*s*-TRIAZIN-2-YL)-*o*-PHENYLENEDIAMINES (VIII)

No.	Substituent	Mp (°C)	Recrystn. Solvent	Anal. (%) Found C	Found H	Calcd C	Calcd H
VIII-1	H	127.5—128.5	Methanol	56.43	7.05	56.51	6.68
VIII-2	CH_3-	155—155.5	Methanol	57.45	7.13	57.24	7.10
VIII-3	CH_3O-	106—107	Methanol	55.19	7.04	55.40	6.87
VIII-4	Cl-	161—162	Methanol	52.76	6.11	52.53	6.21

TABLE 7. 4-SUBSTITUTED N^1-(4,6-DIMETHOXY-*s*-TRIAZIN-2-YL)-N^2-[4,6-BIS(DIETHYLAMINO)-*s*-TRIAZIN-2-YL]-*o*-PHENYLENEDIAMINES (IX)

No.	Substituent	Mp (°C)	Recrystn. Solvent	Anal. (%)	Found	Calcd
IX-2	CH_3-	130—131	Methanol	C	57.03	57.24
				H	7.22	7.10
				N	29.13	29.02
IX-3	CH_3O-	103.5—104.5	Methanol	C	54.99	55.40
				H	6.97	6.87
				N	28.01	28.09
IX-4	Cl-	140—141	Methanol	C	53.00	52.53
				H	6.71	6.21
				N	27.54	27.85

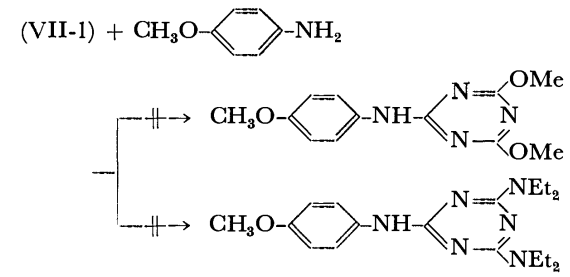

When 4-substituted N^1,N^1-bis(*s*-triazinyl)-*o*-phenylenediamine was heated in methanol in either the presence or absence of sodium hydroxide, only one kind

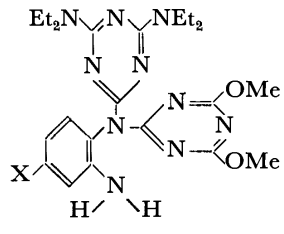

(III)

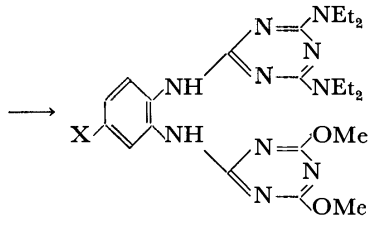

(3)

(VIII)

X = -H, $-CH_3$, $-OCH_3$, -Cl

of 4-substituted N^1,N^2-bis(*s*-triazinyl)-*o*-phenylenediamine was obtained, regardless of the substituent in the 4-position; in every case the rearranged product was proved to be 4-substituted N^1-[bis(diethylamino)-*s*-triazinyl]-N^2-(dimethoxy-*s*-triazinyl)-*o*-phenylenediamine (VIII) by a mixed-melting-point test with an authentic sample. These results show that, in these 4-substituted N^1,N^1-bis(*s*-triazinyl)-*o*-phenylenediamines, a migration of the dimethoxy-*s*-triazinyl group occurs under these reaction conditions.

Effects of Substituents on the Rearrangement of 4-Substituted N^1,N^1-*bis(s-triazinyl)-o-phenylenediamines.* Table 8 lists the yields of the rearranged products of several 4-substituted N^1,N^1-bis(*s*-triazinyl)-*o*-phenylenediamines when they are heated at 50°C for 50 hrs in methanol in the presence of a small amount of sodium hydroxide. From these figures, it is apparent that the facility of the rearrangement varies with the substituent according to the following order:

$$H > CH_3 > Cl > OCH_3$$

TABLE 8. YIELDS OF REARRANGED PRODUCTS OF 4-SUBSTITUTED N^1-[4,6-BIS(DIETHYLAMINO)-*s*-TRIAZIN-2-YL]-N^1-(4,6-DIMETHOXY-*s*-TRIAZIN-2-YL)-*o*-PHENYLENEDIAMINES (III) IN METHANOL IN THE PRESENCE OF SODIUM HYDROXIDE (50°C)

Substituent	H	CH_3	Cl	CH_3O
Yield (%)	53	48	25	21

As has been described above, the compounds III gave 4-substituted N^1,N^2-bis(*s*-triazinyl)-*o*-phenylenediamines in alcohols. In methanol, both N^1,N^1-bis(*s*-triazinyl)- and N^1,N^2-bis(*s*-triazinyl)-*o*-phenylenediamines have absorption maxima at about 270 nm, but in every case the molar extinction coefficient of the original substance is much smaller than that of the rearranged product, as Table 9 shows. Therefore, the absorption in this region increases with the progress of the rearrangement, and the rate of the rearrangement can be measured spectrophotometrically. Since a plot of $-\log (D_\infty - D_t)/(D_\infty - D_0)$ against the reaction time, t, was found to give a straight line, as is shown in Fig. 1, the first-order rate constant for the rearrangement can be calculated using Eq. 6. (See Experimental section). Table 10 lists the first-order rate constants

TABLE 9. MOLAR EXTINCTION COEFFICIENTS OF 4-SUBSTITUTED N^1-[BIS-(DIETHYLAMINO)-*s*-TRIAZINYL]-N^1-(DIMETHOXY-*s*-TRIAZINYL)-*o*-PHENYLENEDIAMINES (III) AND 4-SUBSTITUTED N^1-[BIS(DIETHYLAMINO)-*s*-TRIAZINYL]-N^2-(DIMETHOXY-*s*-TRIAZINYL)-*o*-PHENYLENEDIAMINES (VIII) AT 270 nm

III			VIII		
No.	Substituent	ε at 270 nm	No.	Substituent	ε at 270 nm
III-1	H-	7340	VIII-1	H-	23700
III-2	CH_3-	7160	VIII-2	CH_3-	22400
III-3	CH_3O	7120	VIII-3	CH_3O-	21000
III-4	Cl-	8200	VIII-4	Cl-	18700

Solvent; methanol

TABLE 10. RATE CONSTANTS AND ACTIVATION PARAMETERS FOR THE REARRANGEMENT OF 4-SUBSTITUTED N^1,N^1-BIS(*s*-TRIAZINYL)-*o*-PHENYLENEDIAMINES (III) IN METHANOL

No.	Substituent	Rate constant (min^{-1})			Activation parameter	
		40°C	45°C	50°C	E (kcal/mol)	$\Delta S^{\neq}$ (e. u.)
III-1	H-	1.36×10^{-4}	2.08×10^{-4}	2.78×10^{-4}	15.0	−38.4 (40°C)
III-2	CH_3-	9.08×10^{-5}	1.41×10^{-4}	1.88×10^{-4}	15.0	−39.2 (40°C)
III-3	CH_3O-	1.49×10^{-5}	——	——	——	——
III-4	Cl-	2.36×10^{-5}	——	——	——	——

The rate constants and activation parameters for the rearrangement of 4-substituted *O*-(dimethoxy-*s*-triazinyl)-2-aminophenols in methanol are as follows.[a)]

Substituent	Rate constant (min^{-1})			Activation parameters	
	20°C	30°C	40°C	E (kcal/mol)	$\Delta S^{\neq}$ (e. u.)
H	1.43×10^{-3}	3.30×10^{-3}	6.50×10^{-3}	14.0	−34.0 (40°C)
4-CH_3	5.24×10^{-4}	1.27×10^{-3}	2.72×10^{-3}	15.5	−31.0 (40°C)

a) See Ref. 5.

TABLE 11. EFFECT OF SODIUM METHOXIDE ON THE RATE OF THE REARRANGEMENT OF N^1-[BIS(DIETHYLAMINO)-*s*-TRIAZINYL]-N^1-(DIMETHOXY-*s*-TRIAZINYL)-*o*-PHENYLENEDIAMINE IN METHANOL (40°C)

Solvent	Rate constant (min^{-1})
Methanol	1.36×10^{-4}
Methanol–water (96.2 : 3.8 by volume)	1.34×10^{-4}
CH_3ONa methanolic solution (1.5×10^{-3} mol/*l*)	2.42×10^{-4}

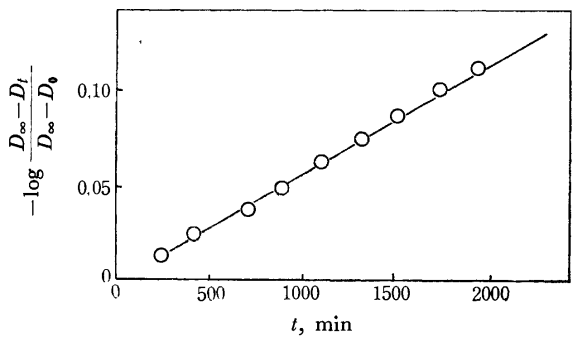

Fig. 1. First-order rate plot for the rearrangement of N^1-[4,6-bis(diethylamino)-*s*-triazin-2-yl]-N^1-(4,6-dimethoxy-*s*-triazin-2-yl)-*o*-phenylenediamine (III-1) in methanol at 40°C.

and activation parameters for the rearrangements of III in methanol. From a comparison of these figures with those of the rearrangement of 4-substituted *O*-(dimethoxy-*s*-triazinyl)-2-aminophenols,[5)] it is apparent that these reactions proceed somewhat more slowly than those of the corresponding 4-substituted *O*-(dimethoxy-*s*-triazinyl)-2-aminophenols in methanol. However, *O*-(*s*-triazinyl)-2-aminophenols are also stable in aprotic solvents and rearrange readily in protic solvents, and the rearrangement is catalyzed by bases[6)] in a manner similar to that in the case of III. As an example, a catalytic effect of sodium methoxide on the rearrangement of III-1 in methanol is shown in Table 11. Moreover, both these reactions are intramolecular, and the activation energies and activation entropies of the rearrangements of III in methanol are close in magnitude to those of the rearrangement of *O*-(*s*-triazinyl)-2-aminophenols. Therefore, it may be assumed that the process of the rearrangement of N^1,N^1-bis(*s*-triazinyl)-*o*-phenylenedi-

5) N. Maeno, T. Itagaki, S. Uno, and K. Matsui, submitted to This Bulletin.

6) T. Shiojima, Y. Hashida, and K. Matsui, details will be published elsewhere.

amines is very similar to that of *O*-(*s*-triazinyl)-2-aminophenols, involving an intramolecular nucleophilic attack by the *ortho* amino group upon the ring carbon of one of the *N*-*s*-triazinyl groups.

It can be seen from Table 10 that the substituents in N^1,N^1-(bis-*s*-triazinyl)-*o*-phenylenediamines affect the progress of the rearrangement to a great extent, but the effect of substituents differs according to the nature and the position of substituents. With respect to the substituents in the triazine nucleus, it is expected that an electron-withdrawing substituent will favor the nucleophilic attack by the amino group by lowering the electron density of triazine carbon atoms. In the cases studied, the dimethoxy-*s*-triazinyl group is anticipated to be more reactive towards nucleophiles than the bis(diethylamino)-*s*-triazinyl group. In fact, the formation of VIII from III indicates that, under the reaction conditions described above, the nucleophilic attack by the *ortho* amino group takes place preferentially upon the more electron-deficient ring carbon of the dimethoxy-*s*-triazinyl group.

Although it is still uncertain whether this migration proceeds by the S_N2 mechanism or by the intermediate-complex mechanism, the effect of a substituent in the *o*-phenylenediamine moiety may be considered from two points of view. One is the influence of the substituent upon the nucleophilic reactivity of the attacking amino group, and the other is the influence upon the reactivity of the migrating triazine nucleus through the nitrogen atom or the stability of the leaving amide anion. In the former, an electron-releasing effect of a substituent favors the rearrangement, while an electron-attracting effect favors the latter. In the cases studied, the position of the substituent was *meta* to the free amino and *para* to the bis-*s*-triazinylamino group, and it can be assumed that the more the σ_m value of a substituent becomes negative, and the more the σ_p value becomes positive, the more readily does the rearrangement occur. Therefore, the Hammett equation for reactions like this rearrangement may be expressed by Eq. (4), which consists of a sum of two terms:[7]

$$\log k/k_0 = \sigma_p\rho + \sigma_m\rho' \qquad (\rho \mp \rho') \tag{4}$$

where the reaction constants ρ and ρ' are attributable to the effect of a substituent on the reactivity of the migrating triazine ring or on the stability of the leaving amide anion, and to the effect of a substituent on the nucleophilicity of the amino group, respectively. Using the rate constants at 40°C and the Hammett substituent constants, the ρ and ρ' values calculated by the method of least squares were found to be:

$$\rho = 2.20, \qquad \rho' = -3.35$$

respectively; the ratio ρ'/ρ was -1.52, and a Hammett plot of log k_1 against $\sigma_p - 1.52\ \sigma_m$ gave a straight line, with a correlation coefficient of 0.993, as is shown in Fig. 2.

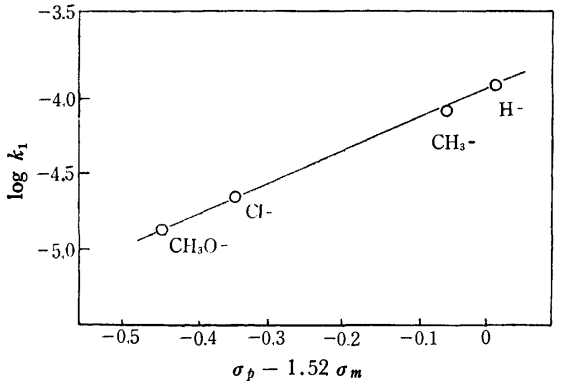

Fig. 2. Plot of log k_1 against $(\sigma_p - 1.52\ \sigma_m)$ for the rearrangement of 4-substituted N^1,N^1-Bis-(*s*-triazinyl)-*o*-phenylenediamines (III) in methanol. (40°C).

Thus, in this reaction, it became clear that, by using Eq. (4) instead of the usual Hammett equation, involving only one term, a good linear relationship is obtained between the substituent constants and the logarithm of the rate constants. These figures show that, in the rearrangement of 4-substituted N^1,N^1-bis(*s*-triazinyl)-*o*-phenylenediamines (III), the substituent affects the nucleophilic reactivity of the the free amino group more than the stability of the leaving amide anion or the reactivity of the triazinyl group.

Rearrangement of N¹,N¹-*Bis(s-triazinyl)-o-phenylenediamines in the Presence of Acid.* As has been mentioned in the preceding paragraph, 4-substituted N^1 - [bis(diethylamino) - *s* - triazinyl] - N^1 - (dimethoxy-*s*-triazinyl)-*o*-phenylenediamines (III) gave, in methanol, only 4-substituted N^1-[bis(diethylamino)-*s*-triazinyl]-N^2-(dimethoxy-*s*-triazinyl)-*o*-phenylenediamines (VIII). In the presence of sodium hydroxide, the rearrangement was found to proceed more readily, as has been described above, but the compound VIII was the only product obtained in this case. However, in methanol in the presence of a small amount of hydrochloric acid (5×10^{-3} mol/*l*), 4-substituted N^1,N^1-bis(*s*-triazinyl)-*o*-phenylenediamine (III) (7×10^{-3} mol/*l*) gave two kinds of rearranged products, regardless of the substituent in the 4-position. One was 4-substituted N^1-[bis(diethylamino)-*s*-triazinyl]-N^2-(dimethoxy-*s*-triazinyl)-*o*-phenylenediamine (VIII), while the other was proved to be 4-substituted N^1-(dimethoxy-*s*-triazinyl)-N^2-[bis(diethylamino)-*s*-triazinyl]-*o*-phenylenediamine (IX), which is obviously produced by the migration of the bis(diethylamino)-triazinyl group. Under the present reaction conditions, the ratios of the yields of the two isomers (IX/VIII) were found to vary depending upon the substituentt in the 4-position; they were 1.1 when the substituent was the methoxyl group and 1.7 when the substituent was chlorine. Thus, in every case the major product was a compound of the IX type. These results indicate that the presence of acid accelerates the migration of the bis(diethylamino)-*s*-triazinyl group, and it can be assumed that the predominant rearrangement of the bis(diethylamino)-*s*-triazinyl group proceeds as follows. The initial stage of this reaction is a preferential lowering of the electron density of ring carbon atoms of the bis-diethylamino-*s*-triazinyl group by a protonation at the ring nitrogen atom[8] of this

7) J. Tirouflet, *Bull. Soc. Chim. Fr.*, **1954**, 769.

8) G. Morimoto, *Nippon Kagaku Zasshi*, **87**, 790 (1966), T. Tashiro and M. Yasuda, *Kobunshi Kagaku*, **26**, 853 (1969).

more basic *s*-triazine nucleus; the next step of the reaction is a nucleophilic attack by the *ortho* amino group upon the ring carbon of the activated triazine nucleus by protonation. A compound of the VIII type is anticipated to be produced by a non-catalytic process under the reaction conditions described above.

A study concerning the influences of solvents and bases on the rearrangement is in progress; it will be reported in the near future.

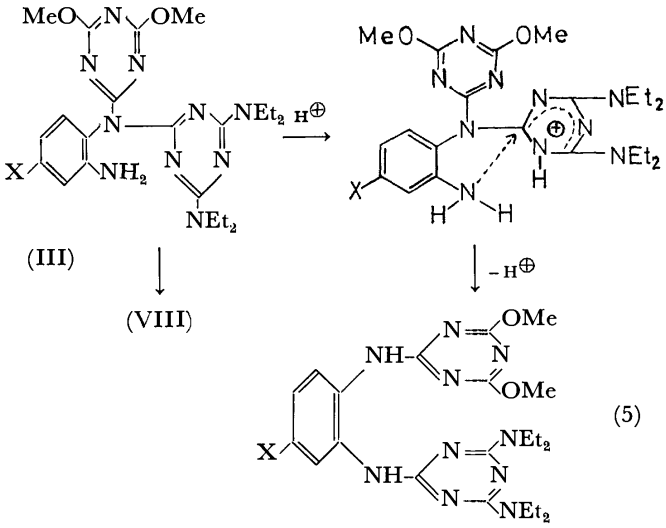

Experimental

All the melting points are uncorrected.

The ultraviolet spectra were recorded on a Hitachi-124 UV-VIS spectrophotometer. The NMR spectra were recorded on a Varian A-60D spectrometer. The elemental analyses were performed in the Micro-analytical Center of Gunma University.

Materials. *2-Arylamino-4,6-dichloro-s-triazines (IV)*: 2-Arylamino-4,6-dichloro-*s*-triazines were prepared by treating 4-substituted 2-nitroanilines with cyanuric chloride, as has been described in the case of 2-(*o*-carbomethoxyanilino)-4,6-dichloro-*s*-triazine.[9]

2-Arylamino-4,6-dimethoxy-s-triazines (V): 2-Arylamino-4,6-dimethoxy-*s*-triazines were prepared by treating 2-arylamino-4,6-dichloro-*s*-triazines with sodium methoxide in methanol, as has been described in the case of 2,4-dimethoxy-6-(2-nitroanilino)-*s*-triazine (V-1).[9]

N-(4,6-Dichloro-s-triazin-2-yl)-N-(4,6-dimethoxy-s-triazin-2-yl)-arylamines (VI): These compounds were prepared by treating 2-arylamino-4,6-dimethoxy-*s*-triazines (V) with cyanuric chloride under conditions similar to those used in the preparation of *N,N*-bis(4,6-dichloro-*s*-triazin-2-yl)-arylamines[9] from IV.

N-[4,6-Bis(diethylamino)-s-triazin-2-yl]-N-(4,6-dimethoxy-2-s-triazin-2-yl)-arylamines (VII): A typical preparation is shown below in the case of *N*-[4,6-bis(diethylamino)-*s*-triazin-2-yl]-*N*-(4,6-dimethoxy-*s*-triazin-2-yl)-4-methoxy-2-nitroaniline (VII-3). A solution of 8.8 g (0.12 mol) of diethylamine in 50 m*l* of acetone was stirred drop by drop into a solution of 13.7 g (0.03 mol) of *N*-(4,6-dichloro-*s*-triazin-2-yl)-*N*-(4,6-dimethoxy-*s*-triazin-2-yl)-4-methoxynitroaniline (VI-3) in 200 m*l* of acetone at 0—5°C. Stirring was continued for 8 hr at 35—40°C, and then the mixture was refluxed for 2 hr and poured into 500 m*l* of ice-water. The oily precipitate was extracted with chloroform and the chloroform layer was dried and evaporated and the residue was collected (VII-3).

4-Substituted N¹-[4,6-bis(diethylamino)-s-triazin-2-yl]-N¹-(4,6-dimethoxy-s-triazin-2-yl)-o-phenylenediamines (III): A typical run is noted in the case of *N*¹-[4,6-bis(diethylamino)-*s*-triazin-2-yl]-*N*¹-(4,6-dimethoxy-*s*-triazin-2-yl)-4-chloro-*o*-phenylenediamine (III-4). A mixture containing 30 m*l* of dioxane, 5.4 g (0.01 mol) of VII-4, and 3 g of Raney nickel was stirred for 5 hr at room temperature under a pressure of 100 kg/cm² of hydrogen. After the catalyst had then been removed by filtration, the solution was poured into 500 m*l* of ice water. The precipitate was then filtered and dried. The recrystallization of the product from benzene–ligroin gave 3.5 g (88%) of III-4. NMR (DMSO-d_6) δ 1.10 (t, 12H), 3.48 (q, 8H), 3.80 (s, 6H), 5.24 (s, 2H), 6.84 (m, 3H).

4-Substituted N¹-[4,6-bis(diethylamino)-s-triazin-2-yl]-N²-(4,6-dimethoxy-s-triazin-2-yl)-o-phenylenediamines (VIII). *i)* *N¹-[4,6-Bis(diethylamino)-s-triazin-2-yl]-N²-(4,6-dimethoxy-s-triazin-2-yl)-o-phenylenediamine (VIII-1).* A mixture containing 5.6 g (0.02 mol) of V-1, 40 m*l* of dioxane, and 3 g of Raney nickel was stirred for 7 hr at 50°C under a pressure of 60 kg/cm² of hydrogen. The mixture was processed according to the procedure for III-4 to give 4.8 g (97%) of crude *N*-(4,6-dimethoxy-*s*-triazin-2-yl)-*o*-phenylenediamine. Recrystallization from benzene gave an analytical sample. Mp 150—151°C. Found: C, 53.72; H, 5.20%. Calcd for $C_{11}H_{13}N_5O_2$: C, 53.43; H, 5.30%.

Compound VIII-1 was prepared by treating the *N*-(4,6-dimethoxy-*s*-triazin-2-yl)-*o*-phenylenediamine thus obtained with cyanuric chloride, followed by treatment with diethylamine according to the procedures used in the preparation of VII-3. Recrystallization from methanol gave an analytical sample. Mp 127.5—128.5°C. NMR (DMSO-d_6) δ 1.09 (t, 12H), 3.51 (q, 8H), 3.83 (s, 6H), 7.48 (m, 4H), 8.31 (s, 1H), 9.66 (s, 1H).

ii) *N¹-[4,6-Bis(diethylamino)-s-triazin-2-yl]-N²-(4,6-dimethoxy-s-triazin-2-yl)-4-methyl-o-phenylenediamine (VIII-2).* Compound VIII-2 was prepared in a manner similar to that to be described below, the preparation of VIII-3 from IV-2 without any purification of the intermediates. Mp 155—155.5°C. NMR (DMSO-d_6), δ 1.10 (t, 12H), 2.31 (s, 3H), 3.52 (q, 8H), 3.87 (s, 6H), 7.29 (m, 3H), 8.31 (s, 1H), 9.60 (s, 1H).

iii) *N¹-[4,6-Bis(diethylamino)-s-triazin-2-yl]-N²-(4,6-dimethoxy-s-triazin-2-yl)-4-methoxy-o-phenylenediamine (VIII-3).* 2,4-Bis(diethylamino)-6-(4-methoxy-2-nitroanilino)-*s*-triazine obtained by treating IV-3 with an excess of diethylamine [mp 95.5—96°C (ethanol), Found: C, 55.54; H, 7.32%. Calcd for $C_{18}H_{27}N_7O_3$: C, 55.51; H, 6.98%] was hydrogenated in dioxane in the presence of Raney nickel. The resulting oily product [crude 2,4-bis(diethylamino)-6-(2-amino-4-methoxyanilino)-*s*-triazine] was treated with cyanuric chloride and then with sodium methoxide in methanol. Recrystallization from methanol gave an analytical sample of VIII-3. Mp 106—107°C, NMR (DMSO-d_6) δ 1.08 (t, 12H), 3.50 (q, 8H), 3.76 (s, 3H), 3.87 (s, 6H), 7.15 (m, 3H), 8.32 (s, 1H), 9.58 (s, 1H).

iv) *N¹-[4,6-Bis(diethylamino)-s-triazin-2-yl]-N²-(4,6-dimethoxy-s-triazin-2-yl)-4-chloro-o-phenylenediamine (VIII-4).* 2,4-Bis(diethylamino)-6-(4-chloro-2-nitroanilino)-*s*-triazine obtained by treating IV-4 with an excess of diethylamine in acetone [mp 128—129°C (benzene) Found: C, 51.50; H, 5.80%, Calcd for $C_{17}H_{24}ClN_7O_2$: C, 51.84: H, 6.14%] was hydrogenated in dioxane in the presence of Raney nickel to give 2,4-bis(diethylamino)-6-(2-amino-4-chloroanilino)-

9) N. Nohara, S. Sekiguchi, and K. Matsui, *J. Heterocycl. Chem.*, **7**, 519 (1970).

s-triazine [mp 122—122.5°C (methanol)]. Found: C, 55.80; H, 7.02%. Calcd for $C_{17}H_{26}ClN_7$: C, 56.11; H, 7.20%.

The 2,4-bis(diethylamino)-6-(2-amino-4-chloroanilino)-*s*-triazine thus obtained was treated with cyanuric chloride and then with sodium methoxide in methanol. The recrystallization of the reaction product from methanol gave an analytical sample of VIII-4; mp 161—162°C. NMR (DMSO-d_6)δ 1.09 (t, 12H), 3.51 (q, 8H), 3.86 (s, 6H), 7.33 (m, 3H), 8.41 (s, 1H), 9.70 (S, 1H).

4-Substituted N¹-*(4,6-Dimethoxy-*s*-triazin-2-yl)*-N²-*[4,6-bis-(diethylamino)-*s*-triazin-2-yl]-o-phenlyenediamines (IX).* A typical run, that in the case of N^1-(4,6-dimethoxy-*s*-triazin-2-yl)-N^2-[4,6-bis(diethylamino)-*s*-triazin-2-yl]-4-methyl-*o*-phenylenediamine (IX-2), will be described. A mixture containing 3.5 g (0.012 mol) of V-2, 30 m*l* of dioxane, and 3 g of Raney nickel was stirred for 5hr at 60—70°C under a pressure of 100 kg/cm² of hydrogen. After the catalyst had then been removed by filtration, the solution was evaporated *in vacuo*. The residue was, without purification, treated with cyanuric chloride and then with diethylamine. The subsequent recrystallization of the product from methanol gave an analytical sample of IX-2. Mp 130—131°C. NMR (DMSO-d_6),δ 1.12 (t, 12H), 2.30 (s, 3H), 3.49 (q, 8H), 3.85 (s, 6H), 7.29 (m, 3H), 8.18 (s, 1H), 9.56 (s, 1H).

Identification and Quantitative Determination of Rearranged Products. A typical example is shown below in the case of III-3. A solution of III-3 in methanol (0.1009 g/30 m*l* $=2\times10^{-4}$ mol/30 m*l*) containing a small amount of sodium hydroxide (1×10^{-4} mol/30 m*l*) was warmed for 20 hr at 50°C. To the mixture, 0.0498 g (2.89×10^{-4} mol) of 4-chloro-2-nitroaniline was added as an internal standard, after which the mixture was developed on a silica-gel layer, using a mixture of benzene and acetone (40 : 3 by volume) as the developing solvent. From the thin-layer chromatogram thus obtained, the original substance, a rearranged product, and the internal standard were eluted with ethanol separately and afterward diluted to a constant volume, the concentration of each solution being determined by measuring the absorbance at 280 nm (original substance), 270 nm (rearranged product), and 410 nm (4-chloro-2-nitroaniline). The rearranged product was identified by a mixed-melting-point test with an authenitc sample after the rearranged product had been separated from the original and other substances by tlc and purified by recrystallization.

Kinetic Measurements. The kinetic measurements were carried out spectrophotometrically by measuring the increase in the absorbance at 270 nm of a methanolic solution of III (*ca.* 10^{-4} mol/l) at 40, 45, and 50°C; the first-order rate constant for the rearrangement was calculated using Eq. 6:

$$k_1 = -2.303\frac{1}{t}\log\frac{D_\infty - D_t}{D_\infty - D_0} \qquad (6)$$

where D_0=initial optical density of a solution of N^1,N^1-bis(*s*-triazinyl)-*o*-phenylenediamine (III) in methanol.

D_t=optical density of a solution at time t.

D_∞=optical density of a solution at an infinite time.

BULLETIN OF THE CHEMICAL SOCIETY OF JAPAN, VOL. 45, 3147—3149 (1972)

Syntheses of Isoprenoids from Isoprene. III. The Dimerizations of Dimethylcyclopropanes[1]

Juntaro TANAKA, Takao KATAGIRI, Kunihiko TAKABE, and Tadashi SAKAMOTO

Department of Synthetic Chemistry, Faculty of Engineering, Shizuoka University, Hamamatsu

(Received December 27, 1971)

1,1-Dimethylcyclopropane(I) was found to dimerize selectively by the action of boron trifluoride etherate. In the products, compound (III), which had been presumed, and the reaction intermediates (VII and VIII) were identified. The reaction mechanism was discussed. 1,2-Dimethylcyclopropane(VI) gave the same products.

1,1-Dimethylcyclopropane(I) has been reported to polymerize.[2-4] However, the oligomers have not been studied in detail. We will reported here, however, that I is dimerized selectively by the action of boron trifluoride etherate to give 3,4,5,5-tetramethyl-2-hexene(II), 2,3,4,4-tetramethyl-1-hexene(III), 3,5,5-trimethyl-2-heptene(IV), and 3,4,4,5-tetramethyl-2-hexene(V). Furthermore, the reaction intermediates were confirmed, and the reaction mechanism was discussed. 1,2-Dimethylcyclopropane(VI) was also reacted by the same catalyst.

Experimental

Materials. 1,1-Dimethylcyclopropane(I) was synthesized from isoprene by our method.[5] Bp 21°C, NMR(τ); 8.97(6H, s), 9.80(4H, s). 1,2-Dimethylcyclopropane(VI) was prepared from 2-butene by a modification of Doering and Hoffmann's method.[6] Bp 28—37°C, NMR(τ); 9.00(d), 9.01(d), 9.20—9.91(m).

Measurements. The products were analyzed after glc fractionation (15% Apiezon grease L/Celite 545, 4 mmϕ $\times$2.5 m, H_2: 45ml/min, 90°C). The IR spectra were recorded on a Perkin Elmer Model 337 infrared spectrophotometer. The NMR spectra were run on a Hitachi-Perkin Elmer Model R-20 (60 MHz) spectrometer, using tetramethyl-

1) Part II: J. Tanaka, T. Katagiri, and T. Hirabayashi, *Nippon Kagaku Zasshi*, **88**, 1106 (1967).

2) H. Pines, W. D. Huntsman, and V. N. Ipatieff, *J. Amer. Chem. Soc.*, **75**, 2315 (1953).

3) A. D. Ketley, *J. Polym. Sci., Part B*, **1**, 313 (1963).

4) S. Aoki, Y. Harita, T. Otsu, and M. Imoto, This Bulletin, **39**, 889 (1966).

5) J. Tanaka, T. Katagiri, and K. Takabe, *Yuki Gosei Kagaku Kyokai Shi*, **28**, 763, 764 (1970).

6) W. von E. Doering and A. K. Hoffmann, *J. Amer. Chem. Soc.*, **76**, 6162 (1954).

TABLE 1. THE REACTIONS OF 1,1-DIMETHYLCYCLOPROPANE (I) AT THE DIFFERENT TEMPERATURES[a]
(I: 2 g, $BF_3 \cdot O(C_2H_5)_2$: 1 g, one hour)

Temp. (°C)	Yield (%)	Dimer (%)	Products (%)				
			II	III	IV	V	Others
−17	10	94	4	65	trace	22	9
−7	22	94	4	55	7	23	11
0	40	92	7	27	9	46	11
5	52	91	12	21	9	43	15
14	70	88	34	7	9	33	17

a) In the NMR spectra of the volatile fraction of the reaction mixtures, the signals at τ 8.30—8.50(m), τ 5.40(s), and τ 4.86(q) were noted. The first signal came from methyl groups, the second came from VII, and the third came from VIII.

TABLE 2. THE REACTIONS OF 1,1-DIMETHYLCYCLOPROPANE(I) FOR THE VARIOUS PERIODS
(I: 2 g, $BF_3 \cdot O(C_2H_5)_2$: 1 g, 0°C)

Period (hr)	Yield (%)	Dimer (%)	Products (%)				
			II	III	IV	V	Others
0.5	30	93	6	31	10	40	13
1	40	92	7	27	9	46	11
3	55	83	17	13	16	36	18

TABLE 3. THE REACTIONS OF 2-METHYLBUTENES(VII/VIII=6/1) AND 1,2-DIMETHYLCYCLOPROPANE(VI)
(Reactant: 2 g, $BF_3 \cdot O(C_2H_5)_2$: 1 g)

Reactant	Temp. (°C)	Period (hr)	Yield (%)	Dimer (%)	Products (%)				
					II	III	IV	V	Others
VII and VIII	−17	0.15	74	99	0	72	11	12	5
VII and VIII	−17	0.5	81	95	0	68	10	18	4
VII and VIII	−17	1	90	93	2	54	10	27	8
VII and VIII	−7	1	90	93	38	5	13	29	15
VII and VIII	0	1	91	87	48	3	21	9	19
VII and VIII	20	1	90	70	52	3	21	6	18
VI	22	1	17	93	6	56	10	20	8
VI	22	3	28	89	43	8	13	22	14

silane as the internal reference and carbon tetrachloride as the solvent, at an ordinary temperature. The mass spectra were recorded on a Hitachi RMU-7U mass spectrometer.

Procedure. In a 30-ml flask, which was controlled at a fixed temperature, we placed 2 g of I, and then 1 g of boron trifluoride etherate was stirred on, drop by drop. After the reaction, the catalyst was deactivated with water and the reaction mixture was extracted with ether. The ether layer was washed with a saturated NaCl aqueous solution and dried over K_2CO_3. VI was reacted in the same manner.

3,4,5,5-Tetramethyl-2-hexene(II). RT: 10.5 min. IR(cm^{-1}): 1670, 820. Mass(*m/e*): 140(M^+, 22%), 84 ($M^+-C_4H_9$, 100%), IR(cm^{-1}): Mass(*m/e*): 140($M^+-C_4H_9$, 1670, 820. 100%), 57($C_4H_9^+$, 60%). NMR(τ): 4.89(1H, q, J=6.0 Hz), 8.09(1H, q, J=6.8 Hz), 8.45(3H, s), 8.49 (3H, d, J=6.0 Hz), 9.04(3H, d, J=6.8 Hz), 9.16(9H, s). n_D^{20} 1.4377(lit,[7] n_D^{20} 1.4360).

2,3,4,4-Tetramethyl-1-hexene(III). RT: 12.5 min. IR(cm^{-1}): 1650, 890. Mass(*m/e*): 140(M^+, 2%), 70($C_5H_{10}^+$, 100%), 43($C_3H_7^+$, 77%). NMR(τ): 5.23(1H, s), 5.39(1H, s), 7.94(1H, q, J=7.0 Hz), 8.30(3H, s), 8.81(2H, q, J=7.0 Hz), 9.03(3H, d, J=7.0 Hz), 9.19(3H, t, J=7.0 Hz). n^{20} 1.4389.

3,5,5-Trimethyl-2-heptene(IV) and 3,4,4,5,-Tetramethyl-2-hexene(V). IV and V had the same RT (14.0 min) and could not be identified. Therefore, these two compounds were confirmed after an ozonolysis of the glc fraction (RT: 14.0 min) carried out in chloroform. *3,3,4-Tetramethyl-2-pentanone*[8] (which was derived from V). RT: 12.9 min. IR(cm^{-1}): 1710. NMR(τ): 7.79(3H, s), 7.75—8.50(1H, m), 9.02(6H, s), 9.18(6H, d, J=6.8 Hz). *4,4-Dimethyl-2-hexanone* (which was derived from IV). RT: 11.7 min. IR(cm^{-1}): 1710. NMR(τ): 7.77(2H, s), 7.99(3H, s), 8.75(2H, q, J=6.8 Hz), 9.07(6H, s), 9.07(3H, t, J=6.8 Hz).

Results and Discussion

The yields of IV were not seriously affected by the reaction periods or times, as is shown in Tables 1 and 2. Therefore, the reaction path to produce IV seems to

7) F. C. Whitmore and A. Mosher. *J. Amer. Chem. Soc.*, **63**, 1120 (1941).

8) This compound was identical with the authentic sample synthesized by the method of the literature (J. W. Baker, *J. Chem. Soc.*, **1950**, 1302.

be different from the path to give other dimers, such as II, III, and V. Furthermore, the components in the volatile fraction of the reaction mixture were confirmed to be 2-methyl-2-butene(VII) and 2-methyl-1-butene (VIII). Since these seemed to be the reaction intermediates, mixtures of these compounds obtained from *t*-amyl alcohol by dehydration (VII: VIII=6 : 1) were reacted by the same catalyst. The results (Table 3) were very similar to those for I, while the reactivity to the dimers was superior to that of I.

From these results, the mechanism to produce II, III, V, and IV may be as follows. The cation(IX) formed from I was deprotonated to give VII and VIII, and then coupled with VII to give the cation(X). From this cation, III was obtained by deprotonation. The formation of II and V from the cation(X) can be explained by the mechanism of the carbonium-ion rearrangements:[9-11] these rearrangements were clarified by the reaction of III.[12] That is, the confirmation of III clarified the existence of X predicted by Whitmore and Mosher.[9] The other dimer, IV, was formed through the cation(XI), which was formed by the coupling of the above-mentioned cation (IX) and VIII.

Since scarcely VII and VIII could be obtained in the reaction of III,[12] the two reaction paths seem to be largely independent. The reaction scheme is illustrated in Fig. 1.

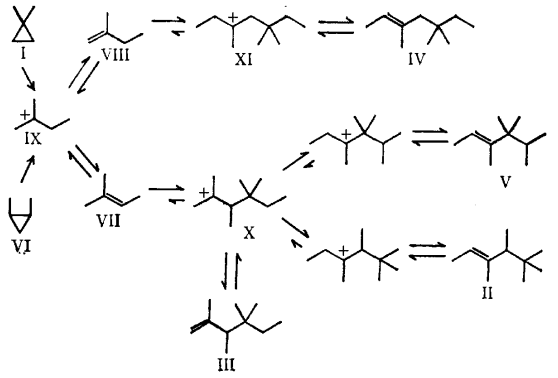

Fig. 1. The reaction scheme.

When 1,2-dimethylcyclopropane(VI) was reacted by the same catalyst (Table 3), the results were very similar to those for I, but the reactivity was inferior to that of I. The difference in the reactivities may be due to the relative difficulties of the cleavage of the cyclopropanes.[13,14]

9) F. C. Whitmore and W. A. Mosher, *J. Amer. Chem. Soc.*, **68**, 281 (1946).
10) A. Schneider and R. M. Kennedy, *ibid.*, **73**, 5017 (1951).
11) G. J. Karabatsos, F. M. Vane, and S. Mayerson, *ibid.*, **85**, 733 (1963).
12) When III was reacted by boron trifluoride etherate at 37°C for one hour, the C_{10} fraction was obtained in a 95% yield; its composition was II (37%), III (15%), and V (35%).
13) O. E. Nesmeyanova, M. Yu. Lukina, and B. A. Kazanskii, *Dokl. Akad. Nauk SSSR*, **153**, 357 (1963).
14) M. Yu. Lukina, O. A. Nesmeyanova, G. A. Khotimskaya, V. A. Ovodova, and B. A. Kazanskii, *ibid.* **158**, 652 (1964).

BULLETIN OF THE CHEMICAL SOCIETY OF JAPAN, VOL. 45, 3149—3155 (1972)

Syntheses and Reactions of Functional Polymers. LXVI. Activation of Carboxylic Acid by Means of Polymers Containing Hydroxamic Acid Residue and *N*-Hydroxysuccinimide Residue

Mitsuaki NARITA,* Takero TERAMOTO, and Makoto OKAWARA

Research Laboratory of Resources Utilization, Tokyo Institute of Technology, Ookayama, Meguroku, Tokyo

(Received January 20, 1972)

In order to achieve solid-phase acyl activation of carboxylic acid, the syntheses and reactions of polymers containing hydroxamic acid and *N*-hydroxysuccinimide residues were investigated. A polymer containing hydroxamic acid residue was obtained by the modification of cross-linked copolymer of *p*-nitrophenyl acrylate with styrene, and one containing *N*-hydroxysuccinimide residue was prepared by copolymerization of *N*-acetoxymaleimide with styrene followed by hydrolysis. These *N*-hydroxy polymers were allowed to react with *N*-protected amino acids by means of the dicyclohexylcarbodiimide method giving the activated polymer ester. While the polymer containing hydroxamic acid residue was inferior to that containing *N*-hydroxysuccinimide residue in activation of carboxylic acid, amino acid esters of the latter were active enough to react with another amino acid to yield dipeptides almost quantitatively without racemization.

Activation of carboxylic acid under mild conditions is a useful method for selective acylation in peptide syntheses. The utilization of polymers carrying the active ester group in stepwise syntheses of peptides has been described for the polymers containing *o*-nitrophenol,[1] *p,p'*-dihydroxydiphenyl sulfone[2] and *N*-hydroxysuccinimide[3] moieties.

In a study on polymeric reagents, we reported on

* Present address: Department of Industrial Chemistry, Tokyo University of Agriculture and Technology, Koganei, Tokyo.

1) M. Fridkin, A. Patchornik, and E. Katchalski, *J. Amer. Chem. Soc.*, **90**, 2953 (1968); G. T. Panse, D. A. Laufer, *Tetrahedron Lett.*, **1970**, 4181.

2) Th. Wieland and Ch. Birr, *Angew. Chem.*, **78**, 303 (1966).

3) D. A. Laufer, D. I. Marborough, T. M. Chapman, V. M. Vaidya, and E. R. Blout, *J. Amer. Chem. Soc.*, **90**, 2696 (1968).

TABLE 1. IR DATA OF POLYMERS(I)—(VI) AND MODEL COMPOUNDS (KBr Disk)

Compound	Characteristic absorption (cm^{-1})			
	OH, NH	Ester	Amide	Other[assignment]
Polymer(I)		1760		1525, 1345[NO_2]
				1210[-C-O-]
Polymer(II)	3200		1670—1620	
Polymer(III)	3400—3200		1620	
AcNHOH	—3200, —3100		1620	
Polymer(IV)	3400—3200	1790	1680, 1620	1180[-C-O-]
AcONHAc	3350, 3150	1790	1655	1175[-C-O-]
Polymer(VI)	3350	1790	1620	1520 1500
		1720—1690		
Z-GlyONHAc	3300	1790	1650	1520
		1720—1680		

the preparation and use of polymers having *N*-hydroxysuccinimide unit in the chain.[4] Use of such polymers would facilitate synthetic procedure, *i.e.*, separation of reaction mixture, purification of product, and recovery of the original polymer. In this article, preparation of hydroxamic acid polymer and activation of carboxylic acid by means of polymers containing hydroxamic acid and *N*-hydroxysuccinimide residues are described.

Results and Discussion

Preparation of Polymer Containing Hydroxamic Acid Residue. A series of polymer modifications was carried out as shown in scheme 1. Copolymerization of *p*-nitrophenyl acrylate with styrene (St) in the presence of divinylbenzene (DVB) was carried out to obtain cross-linked copolymer (I). Polymer (I) was reacted with benzyloxyamine and debenzylated by treatment with hydrogen bromide in acetic acid to give insoluble polymer(III). Polymer(III) was acetylated with acetic anhydride to give polymer(IV). Nitrogen analysis of polymer(I) showed that the total molar fraction of the ester was 38%. The reaction of I with benzyloxyamine proceeded almost quantitatively at 130°C for 25 hr. A characteristic feature in its IR spectrum was the presence of bands of ester at 1760 cm^{-1} and of the nitro group at 1525 cm^{-1} and

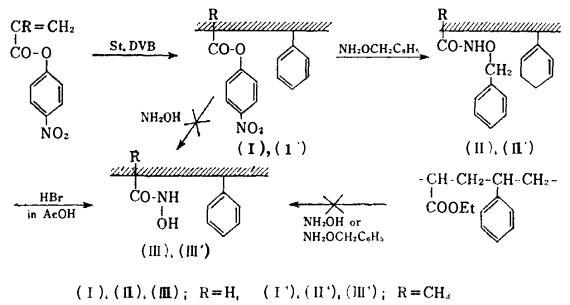

(I), (II), (III); R=H, (I'), (II'), (III'); R=CH_3

Scheme 1.

4) a) M. Akiyama, M. Narita, and M. Okawara, *J. Polym. Sci., Part A-I*, **7**, 1299 (1969). b) M. Akiyama, Y. Yanagisawa, and M. Okawara, *ibid.*, **7**, 1905 (1969). c) M. Narita, T. Teramoto, and M. Okawara, This Bulletin, **44**, 1084 (1971).

1345 cm^{-1}. In the IR spectrum of polymer(II), these absorptions disappeared and characteristic absorptions of amide appeared at 1650 cm^{-1}.

The IR absorptions of polymers(I)—(IV) and those of model compounds are shown in Table 1. The acyl content in polymer(IV) was determined from the yield of *N*-cyclohexylacetamide obtained in the reaction with excess cyclohexylamine.

Similarly, copolymerization of *p*-nitrophenyl methacrylate with styrene in the presence of DVB yielded cross-linked polymer(I'). A series of polymer modifications (scheme 1) was carried out. Polymer(I') was less reactive than polymer(I). It was transformed into amide polymer(II') almost quantitatively by treatment with benzyloxyamine in DMF at 120—140°C for 100 hr. Polymer(II'), however, was not debenzylated by treatment with hydrogen bromide in acetic acid at 80°C for 10 hr.

In general, amino acid *p*-nitrophenyl esters are remarkably reactive, and have been used frequently for peptide bond formation.[5] In the case of polymers(I) and (I'), however, their reactivities are so reduced as to need high temperature and long reaction time probably due to their insolubility and steric hindrance of main chain.

The direct reaction of polymer(I) with hydroxylamine was also attempted. A DMF solution containing hydroxylamine was prepared by mixing hydroxylamine hydrochloride with equimolar anhydrous triethylamine in DMF. Polymer(I), which was swelled enough in DMF, was then combined with the above solution and kept at room temperature overnight. The IR spectrum of polymer(III") thus obtained, however, showed that it contained carboxylic acid residue in addition to hydroxamic acid residue[broad absorptions at 3400—2300 cm^{-1} and 1730—1600 cm^{-1}].

On the other hand, the reaction of ethylacrylate–styrene copolymer with hydroxylamine or benzyloxyamine was carried out under various conditions. However, the starting polymer was recovered in all cases.

In order to prepare polymers(III) and (III'), pre-

5) B. Iselin, W. Rittel, and R. Schwyzer, *Helv. Chim. Acta*, **40**, 373 (1957); W. Kern, and R. C. Schulz, *Angew. Chem.*, **69**, 153 (1957).

Table 2. The crude products of the reaction of polymers(IV) and (VI) with cyclohexylamine[a]

Polymer	IV	VIa	VIb	VIc
Yield of Amide (mg)	156	296	366	235
Mp (°C)	100—103	86—102	114—121	131—159
(Lit.)	(104)[7a]	(110)[8]	(129—131)[b]	(179—179.5)[c]
Acyl Content of Polymer(meq/g)[d]	1.1	1.02	1.06	0.68
Acyl Content of Polymer(meq/g)[e]		1.08	1.06	0.74

a) Polymer(1.0 g) was reacted with 1.0 g of cyclohexylamine in 30 m*l* of methylene chloride at room temperature for 20 hr. b) Recrystallized from *n*-hexane-ethyl acetate. c) Recrystallized from ethyl acetate. d) Determined from the yield of *N*-cyclohexylacylamide. e) Determined from the increase in weight of the insoluble polymer as a result of the coupling reaction.

Table 3. The yields of dipeptides by the acylation of ethyl esters of amino acids with polymers(VIa) and (VIb)

Polymer	HGlyOEt Yield of dipeptide (%)	H-L-LeuOEt Yield of dipeptide (%)
VIa	86	73
VIb	47	39

paration and polymerization of monomers having hydroxamic acid residue were attempted (scheme 2). Methacryloylhydroxamic acid was prepared by Smith's method,[6] but its copolymerization with styrene in the presence of DVB was not successful under various conditions. An attempt to prepare monomer(V') having protected hydroxy group was also carried out. However, the reaction of *p*-nitrophenyl acrylate with benzyloxyamine produced only the Michael type addition product, *p*-nitrophenyl ester of γ-(*N*-benzyloxyamino)-propionic acid(V).

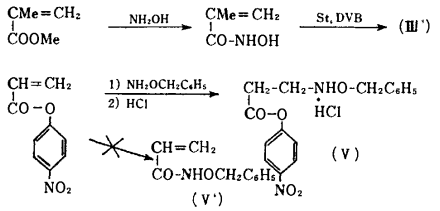

Scheme 2.

Activation of Carboxylic Acid by Means of Polymer(III) Containing Hydroxamic Acid Residue. The acyl activation of amino acids with polymer(III) was investigated. Acylated polymers(VIa—c) were obtained (scheme 3) by the coupling reaction of polymer(III) with *N*-carbobenzoxy glycine(Z-GlyOH), -L-leucine(Z-LeuOH) or -glycylglycine(Z-GlyGlyOH) by

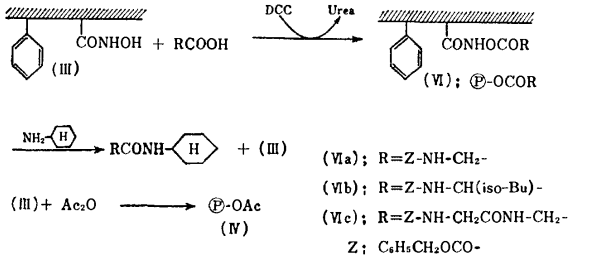

Scheme 3.

6) H. Smith, Brit. 852176 (1960); *Chem. Abstr.*, **55**, 9284[i] (1961).

use of dicyclohexylcarbodiimide(DCC) as a dehydration reagent in DMF at room temperature for 40 hr. The IR spectra of polymers(VI) exhibited characteristic absorptions similar to those of a model compound ($Z\text{-GlyONHCOCH}_3$) as shown in Table 1.

Determination of acyl contents of polymers(VIa—c) was made: (1) base on the yields of *N*-cyclohexylacylamides obtained by the reaction with excess of cyclohexylamine and (2) from the increase in weight of the polymer obtained. The results of the two methods agreed well, as shown in Table 2.

Acylation of ethyl esters of amino acids with acylated polymer (VIa, b) was carried out as shown in scheme 4.

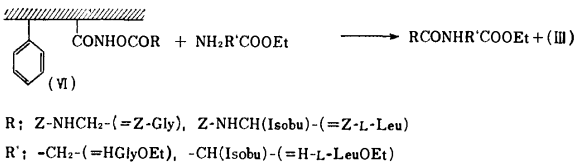

Scheme 4.

The reaction was carried out by use of a slight molar excess of polymer(VI) in DMF at room temperature for 40 hr. The yield of acylation products was not always good as shown in Table 3. In particular, the yield of acylation with polymer(VIb) [Z-L-LeuO-Ⓟ] was low. This seems to be due to the fact that the steric hindrance reduced its reactivity as well as polymer(I) carrying active ester group adjacent to the polymer chain. This shows that the polymer used for activation of carboxylic acid should have the active ester group detached from the polymer backbone.

Although activation of carboxylic acid by means of a polymer containing hydroxamic acid residue was slightly inferior to reported polymer,[1-3] it was observed

7) J. R. A. Pollock, Ed. "Dictionary of Organic Compounds," 4th Ed., Eyre and Spottiswoode, London (1965) a) p. 790; b) p. 21.

8) D. W. Clayton, J. A. Farrington, G. W. Kenner, and J. M. Turner, *J. Chem. Soc.*, **1957**, 1398; *ibid.*, **1956**, 375.

TABLE 4. THE COUPLING REACTION OF POLYMER(IXb) WITH Z-L-LeuOH IN VARIOUS SOLVENTS[a]

Solvent	Methylene chloride	Chloroform	Dioxane	Ethyl acetate	DMF
Yield of polymer(g)	4.05	2.60	2.50	2.75	4.08
Acyl content of polymer(meq/g)[b]	1.54	0.15	0	0.37	1.56
Acyl content of polymer(meq/g)[c]	1.53				1.56

a) The coupling reaction of polymer(IXb) (2.50 g) with 3.98 g of Z-L-LeuOH by use of 4.10 g of DCC as a dehydration reagent was performed in 20 m*l* of various solvents at room temperature for 40 hr.
b) Determined from the increase in weight of the insoluble polymer as a result of the coupling reaction.
c) Determined from the yield of *N*-cyclohexylacetamide.

TABLE 5. THE CRUDE PRODUCTS OF THE REACTION OF POLYMER(X) WITH CYCLOHEXYLAMINE[a]

Polymer	Xa	Xb	Xc
Yield of Amide(mg)	450	518	620
Mp (°C)	101—103	81—97	107—118
(Lit.)	(104)[7a]	(110)[8]	[129—131][b]
Acyl content of polymer(meq/g)[c]	3.19	1.78	1.78

a) Polymer(1.0 g) was reacted with 1.0 g of cyclohexylamine in 20 m*l* of DMF at room temperature for 24 hr.
b) Recrystallized from *n*-hexane-ethyl acetate.
c) Determined from the yield of *N*-cyclohexylacylamide.

TABLE 6. IR DATA OF POLYMERS(VIII)—(XI). (KBr Disks)

Polymer	Characteristic absorption[a] (cm^{-1})		
	OH[NH]	C=O	Other
(IXa), (IXb)	3500(m)	1780(m)	1210(s), 1050(m)
	2700(w)	1710(s), 1650(sh)	
(IXc)	3500(s)	1780 50(m)	1240(s), 1070(m)
	2500(m)	1700(sh), 1650(s)	
(VIII), (Xa)		1820(m), 1790(m)	1370(m), 1220(s)
		1740(s)	1160(s), 1050(m)
(X), (XI)	[3400](m)	1820(m), 1785(m)	1510(m), 1340(m)
		1740(s)	1250(sh), 1220(s), 1050(s)

a) Absorption intensity; s=strong, m=medium, w=weak, sh=shoulder

that insoluble polymeric reagents were useful for simplifying the procedures and making the separation of product easier.

Activation of Carboxylic Acid by Means of Polymer(IX) Containing N-*Hydroxysuccinimide Structure.* Several methods to prepare *N*-acyloxymaleimides were reported.[4c] *N*-Benzyloxymaleimide thus obtained was copolymerized with styrene(St) in the presence of DVB to afford cross-linked copolymer(VII), which contained 47 mol% of imide moiety according to nitrogen analysis.

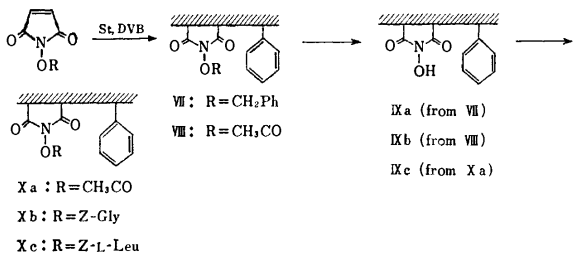

Scheme 5.

Polymer(VII) was debenzylated by treatment with hydrogen bromide in acetic acid to give the intended polymer(IXa) containing *N*-hydroxysuccinimide structure as shown in scheme 5. Polymer(IX) was acylated with acetic anhydride to give *N*-acetoxy polymer (Xa) whose acyl content (3.19 meq/g) was determined by the cyclohexylamine method. The content shows that the debenzylation of polymer(VII) to (IXa) about 90%. Similarly, cross-linked copolymer(VIII) of *N*-acetoxymaleimide and styrene was prepared and hydrolyzed with 6 N-hydrochloric acid at 100°C for 10 hr in dioxane to give cross-linked polymer(IXb) with 3.12 meq/g of *N*-hydroxyimide moiety.

The coupling reaction of polymer(IXb) with Z-L-LeuOH by means of DCC was examined in various solvents. The amino acid content in the acylated polymer was determined from the yield of cyclohexylamide and the weight increase. Both results agreed well as shown in Table 4. Polymer(IXb) was swelled well in DMF and methylene chloride, but not in chloroform, dioxane and ethyl acetate. Thus, the acylation reaction proceeded effectively in good swelling solvents. Similarly, the coupling reactions of polymer(IXa) with Z-GlyOH and Z-L-LeuOH were performed in DMF by means of DCC method. The acyl contents of polymer(Xb, Xc) thus obtained were

Table 7. The coupling reaction of polymer(IXb) with peptide derivative[a]

No.	Polymer (IXb) (g)	Z-Amino acid or Z-Peptide (g)		DCC (g)	Yield of polymer (XI) (g)	Acyl content of polymer[b] (meq/g)	A fraction of reacted OH group[c] (%)
1	5.00	Z-GlyOH	6.40	8.2	7.44 (XIa)	1.71 (1.69)[d]	69
2	5.00	Z-LeuOH	8.0	8.2	8.15 (XIb)	1.56 (1.69)[d]	69
3	1.00	Z-GlyOH	1.55	0.61[e]	1.29	1.18	42
4	2.00	$Z\text{-}Gly_2OH$	2.96	3.10	3.36 (XIc)	1.63 (1.53)[d]	74
5	2.00	$Z\text{-}Gly_3OH$	3.56	3.10	2.79	0.93	41
6	2.00	$Z\text{-}Leu_2OH$	4.30	3.10	3.22 (XId)	1.05 (1.02)[d]	56
7	0.50	$Z\text{-}Leu_3OH$	1.37	0.77	0.71	0.63	24
8	1.00	$Z\text{-}Leu_4OH$	3.36	1.53	1.51	0.58	23

a) The reaction was carried out in DMF at room temperature for 40 hr. DMF was used 10 ml/polymer 1.0 g. In the case of Nos. 1 and 2, acyl contents of polymer were the same when the reaction time was 15 hr.
b) Determined from the increase in weight of the insoluble polymer obtained.
c) Calculated by use of acyl content of polymer determined based on b).
d) Determined from the yield of *N*-cyclohexylacylamide.
e) Ethyl chloroformate was used instead of DCC.

Table 8. The acylation of ethyl esters of amino acids with polymers(X)[a]

Ester of amino acid	Dipeptide obtained	Polymer		
		IX	Xa	Xb
HGlyOEt	Yield (%)	92	100	94
	Mp (°C)	38—42	54—67	73—91
	(Lit.)	(48)[7b]	(82)[9]	(102—103)[10]
H-L-LeuOEt	Yield (%)	100	98	86
	Mp (°C)	oil	oil	
	(Lit.)	oil	oil	

a) Polymer(1.0 g) was reacted with 1.3 mmol of ester of amino acid in 20 ml of DMF at room temperature for 12 hr.
b) Recrystallized from *n*-hexane.

Table 9. Optical rotation of dipeptide $[\alpha]_D^{18}$ ($c=0.2$, in ethanol)

Dipeptide	Prepared by using polymer(Xc)	Prepared by using the DCC method	Lit.
Z-L-LeuGlyOEt	−27.5	−25	−27.2
Z-L-Leu-L-LeuOEt	−37	−40.5	

determined by use of cyclohexylamine and the results are shown in Table 5 together with those of polymer (Xa). The regenerated *N*-hydroxyimide polymer(IXc) from X combined with cyclohexylamine (from IR data) as discussed in the preceding paper.[4c] The characteristic IR absorption data on these polymers are shown in Table 6.

For the sake of confirmation, polymer(IXc) was allowed to react with excess acetic anhydride. The acyl content in the polymer obtained was 3.19 meq/g, the same as in the above polymer(Xa).

The coupling of polymer(IXb) with various chain length acids was investigated. The acyl contents of polymer(XI) obtained are shown in Table 7. The DCC method was superior to the mixed anhydride method. The acyl content did not increase with prolonged reaction time. The fraction of reacted *N*-hydroxy group decreased with the increase of the number of amino acids in peptide. On the other hand, the fraction was higher in the case of glycine derivatives than in leucine derivatives for the same number of amino acids.

The acylation of ethyl esters of amino acids with polymer(X) was carried out. The reaction was carried out by using a slight excess of the acylated polymer in DMF at room temperature. The melting points and yields of the crude dipeptide derivatives obtained are shown in Table 8. The acylation with polymers (Xa—c) proceeded almost quantitatively. Crude products gave pure dipeptide derivatives by recrystallization. The optical rotations of Z-L-LeuGlyOEt and Z-L-Leu-L-LeuOEt obtained by the reaction of polymer (Xc) are shown in Table 9. The values agree with those in literature and those of the product obtained by the usual DCC method. Thus, acylation with polymer(Xc) seems to proceed without racemization.

In conclusion, the *N*-hydroxyimide polymer(IX) is superior to the hydroxamic acid polymer(III) in its

9) St. Goldschmidt, and M. Wick, *Ann.*, **575**, 217 (1952).
10) G. W. Anderson, J. Bloninger, and A. D. Welcher, *J. Amer. Chem. Soc.*, **74**, 5309 (1952).

effectiveness for acyl activation, probably because the former has a reactive site detached from the polymer backbone. The bulkiness of the amino acid derivative would also affect the reactivities of polymers both in their acylation and coupling processes.

Experimental

The melting points were uncorrected. The IR spectra were obtained as potassium bromide disks with a Hitachi Infrared Photometer Model EPI-S2. Solvents used for reactions were purified by the usual method.

Preparation of Polymer(I). *p*-Nitrophenyl acrylate (17.0 g, 0.088 mol), prepared by Morawetz's method,[11] 9.15 g(0.088 mol) of styrene, 5.72 g (0.044 mol) of DVB and 0.90 g(0.0055 mol) of AIBN were dissolved in 150 m*l* of dioxane. The polymerization tube was sealed off in a vacuum, and heated in a bath thermostatted at 80°C for 20 hr. The separated polymer(I) was washed with ether, and crashed to small species, and dried in a vacuum. The total yield was 26.5 g. Polymer(I) was pale yellow. Elemental analyses; Found; C 71.21, H 5.86, N 3.68%. Nitrogen analysis showed that total molar fraction of the ester was 38%.

Preparation of Polymer(II). Polymer(I) thus obtained (25.0 g) was swelled in 200 ml of DMF and 18.5 g(0.15 mol) of benzyloxyamine was added. The mixture was heated at 120—140°C for 25 hr. Polymer(II) thus obtained was filtered off, and washed with ether, DMF and ether. It was collected and dried in a vacuum. The yield was 16.6 g.

Preparation of Polymer(III). Polymer(II)(16.0 g) was suspended in 100 m*l* of 28% HBr-AcOH solution and heated at 80—85°C for 6 hr. Polymer(III) thus obtained was separated by decantation, and washed with ether and methanol several times. Soluble parts of polymer(III) was extracted with methanol by use of a Soxhlet extractor. The yield of polymer(III) was 12.4 g. Polymer(III) was light brown.

Polymers(I′) and (II′) were prepared in similar ways. Preparation of polymer(II′) was carried out in DMF at 120—140°C for 100 hr. The reaction of polymer(II′) with hydrogen bromide in acetic acid at 80—85°C for 10 hr recovered the starting polymer(II′).

Reaction of Polymer(I) with Hydroxylamine. Ten m*l* of DMF solution containing hydroxylamine was prepared by mixing 0.7 g (0.01 mol) of hydroxylamine hydrochloride (dried at 140°C/0.1 mmHg for 3 hr) with 1.0 g (0.01 mol) of triethylamine (free from water) in 10 m*l* of DMF. Polymer(I) was swelled in 10 m*l* of DMF, and then these were combined, and kept at room temperature for 24 hr. Polymer (III″), thus obtained, was filtered off, and washed by swelling in methanol, and dried in a vacuum. The yield was 0.71 g.

Polymerization of Methacryloyl Hydroxamic Acid. Copolymerization of methacryloyl hydroxamic acid (0.51 g) prepared by Smith's method,[6] with DVB (0.65 g) in 15 m*l* of dioxane with AIBN (0.08 g) in polymerization tube sealed in a vacuum at 80°C for 12 hr gave no polymer.

Reaction of p-*Nitrophenyl Acrylate with Benzyloxyamine.* *p*-Nitrophenyl acrylate (18.5 g, 0.096 mol) and 12.0 g (0.098 mol) of benzyloxyamine were dissolved in 100 m*l* of ether, and kept at room temperature for 12 hr. The ether solution was washed with water, 1 N hydroxy ammonium solution and water by means of a separation funnel, and then washed with 1 N hydrochloric acid solution to precipitate crystalline needles. This product was filtered off. The filtrate was washed with water and dried over sodium sulfate. Although the filtrate was evaporated in a vacuum, the desired *N*-benzyloxyacrylamide was not obtained. The yield of the crystalline was 17.3 g. The product was confirmed to be *p*-nitrophenyl ester hydrochloride of γ-(*N*-benzyloxyamino)-propionic acid by elemental analysis and IR data. The yield was 17.3 g (51%), Mp 132—134°C(recrystallized from acetonitrile). Found: C, 54.28; H, 4.79; N, 7.93; Cl, 10.08%. Calcd for $C_{16}H_{17}N_2O_5Cl$: C, 54.7; H, 8.43 N, 7.97; Cl, 10.1%.

Preparation of Acetylated Polymer(IV). Polymer(III) (2.0 g) was swelled in 25 m*l* of DMF and 1.0 g of acetic anhydride was added. The mixture was kept at room temperature for 40 hr. Polymer(IV) thus obtained was filtered off and washed sith methanol. Polymer(IV) was further washed with methanol by use of a Soxhlet extractor and dried in a vacuum. The yield was 2.18 g.

Preparation of Acylated Polymer(VI). Polymer(III) (2.5 g) was swelled in 25 m*l* of DMF and 3.14 g (15 mmol) of Z-GlyOH was added. DCC (4.2 g, 20 mmol) was added to the mixture with stirring under cooling with ice-cold water, and kept at room temperature for 40 hr. The reaction mixture was diluted with methanol and precipitated *N,N′*-dicyclohexylurea was separated by decantation, and then polymer(VIa) was filtered off and washed with methanol. Polymer(VIa) was further washed with methanol by use of of a Soxhlet extractor and dried in a vacuum. Similar reaction were carried out with the use of 3.98 g (15 mmol) of Z-L-LeuOH and 3.74 g (15 mmol) of Z-GlyGlyOH. The yields of polymers(VIa), (VIb,) and (VIc) were 3.16 g, 3.38 g, and 3.07 g, respectively.

Preparation of N-*Acetyl*-O-*(*N-*carbobenzoxy)-glycyl Hydroxylamine[The Model Compound for Polymer(VI)].* Acetohydroxamic acid (4.50 g, 0.051 mol) and 10.45 g (0.05 mol) of Z-GlyOH were dissolved in 100 m*l* of DMF. DCC (10.3 g) was added to the solution with stirring under cooling with ice-cold water. The reaction mixture was kept for 2 hr with stirring under cooling with ice-cold water, and then at room temperature for 12 hr. *N,N′*-Dicyclohexylurea precipitated was filtered off and the filtrate was concentrated in a vacuum to give *N*-acetyl-*O*-(*N*-carbobenzoxy)-glycyl hydroxylamine. It was recrystallized from the mixture of hexane and ethyl acetate (1 : 1). The yield was 5.71 g (43%). Mp 137—139°C. Found: C, 53.87; H, 5.38; N, 10.44%. Calcd for $C_{12}H_{14}N_2O_5$: C, 54.13; H, 5.30; N, 10.52%.

Acylation of Cyclohexylamine with Polymers(IV) and (VI). One gram of polymer(IV) or (VI) was swelled in 30 m*l* of methylene chloride and 1.0 g of cyclohexylamine was added. The reaction mixtrue was kept at room temperature for 20 hr. The polymer recovered was filtered off and washed with ethyl acetate and methanol. The filtrate and the washing were combined and concentrated in a vacuum to obtain *N*-cyclohexylacylamide. The results are shown in Table 2. The crude products gave pure products by recrystallization.

Acylation of Ethyl Ester of Amino Acid with Polymer(VI). Glycine ethyl ester hydrochloride (0.112 g, 0.8 mmol) or 0.156 g (0.8 mmol) of L-leucine ethyl ester hydrochloride and 0.081 g (0.8 mmol) of triethylamine were dissolved in 10 m*l* of DMF. Polymer(VIa) or (VIb) (1.0 g) was swelled in 15 m*l* of DMF. Both were mixed and kept at room temperature for 40 hr. The consumed polymer was filtered off and washed with methanol. The filtrate and washings were combined and concentrated in a vacuum. The residue was dissolved in ethyl acetate, and insoluble triethylamine

11) E. Gaetjens, H. Morawetz, *J. Amer. Chem. Soc.*, **83**, 1738 (1961); H. Morawetz, and P. E. Zimmering, *J. Phys. Chem.*, **58**, 753 (1954).

hydrochloride was filtered off. Ethyl acetate was evaporated in a vacuum, and the residue was worked up by the same procedure to obtain the crude products. The results are shown in Table 3.

Preparation of Polymer(VII). A mixture of 10.0 g (0.049 mol) of *N*-benzyloxymaleimide prepared by means of the method given previously,[4c] 10.0 g (0.096 mol) of styrene, 0.12 g (0.6 mol% contrary to all monomers) of DVB and 0.10 g of AIBN in 100 m*l* of benzene was heated at 40°C for 5 hr under a stream of nitrogen. The separated polymer (VII) was washed with benzene and methanol, and crashed to small species, and dried in a vacuum. The yield was 16.4 g. Found: C, 73.59; H, 5.18; N, 4.35%.

Preparation of Polymer(VIII). A mixture of 35.6 g (0.23 mol) of *N*-acetoxymaleimide prepared by means of the method given previously,[4c] 36.0 g (0.345 mol) of styrene, 1.5 g (0.0115 mol, 2 mol% toward all monomers) of DVB and 0.73 g (0.003 mol) of benzoyl peroxide in 150 m*l* of benzene was heated at 75°C for 6 hr under a stream of nitrogen. Separated polymer(VIII) was crashed to small species, and washed with methylene chloride by use of a Soxhlet extractor, and dried in a vacuum. The yield was 70.2 g.

Preparation of Polymer(IXa), A mixture of 15.0 g of polymer(VII) in 100 m*l* of 20% hydrogen bromide acetic acid solution was heated at 65—70°C for 15 hr. The reaction mixture was poured into ether. Polymer(IXa) was filtered off and washed with acetic acid, DMF, ether, and methanol. It was collected and dried in a vacuum. The yield was 10.95 g.

Preparation of Polymer(IXb). Polymer(VIII) was hydrolized with 6 N hydrochloric acid solution in dioxane to give polymer (IXb), and then subjected to the usual work-up.

Preparation of Polymer(Xa). Polymer(IXa) (5.0 g) was swelled in 50 m*l* of DMF and 20 m*l* of acetic anhydride was added. The mixture was kept at room temperature for 12 hr. Polymer(Xa) thus obtained was filtered off and with ether, tetrahydrofuran and ether. It was collected and under vacuum. The yield was 5.35 g.

Preparation of Peptide Derivatives. Z-GlyOH and Z-L-LeuOH were prepared according to the methods reported.[8,9] Z-GlyGlyOH and Z-GlyGlyGlyOH were prepared from Z-GlyOH and GlyOEt by the DCC method. Z-GlyGlyOH; mp 177—178°C (lit,[14] 175—176°C). Z-GlyGlyGlyOH; mp 197—198°C (lit,[15] 198°C). Z-L-Leu-L-LeuOH and Z-L-Leu-L-Leu-L-LeuOH were prepared from Z-L-LeuOH and L-LeuOEt by the DCC method. Z-L-Leu-L-LeuOEt; mp 86—88°C (recrystallized from *n*-hexane)., Found: C, 64.69; H, 8.43; N, 7.02%. Calcd for $C_{22}H_{34}N_2O_5$: C, 65.00; H, 8.43; N, 6.89%. Z-L-Leu-L-LeuOH; mp 117—119°C(recrystallized from *n*-hexane) (lit,[16] 99—99.5°C). Found: C, 63.16; H, 8.12; N, 7.38%. Calcd for $C_{20}H_{30}N_2O_5$: C, 63.47; H, 7.99; N, 7.40%. Z-L-Leu-L-Leu-L-LeuOEt; mp 137—139°C (recrystallized from carbon tetra chloride-ethyl acetate. Z-L-Leu-L-Leu-L-LeuOH; mp 150—152°C (recrystallized from carbon tetrachloride-ethyl acetate). Found: C, 63.28; H, 8.71; N, 8.49%. Calcd for $C_{26}H_{41}N_3O_6$: C, 63.52; H, 8.41; N, 8.55%.

Preparation of Polymers(X) and (XI). Polymers(Xb) and (Xc) were prepared by using polymer(IXa) as well as polymer(VI) [reaction time; 30 hr]. Polymer(X) washed with mathanol, DMF and methanol, and then dried in a vacuum. Polymer(Xb), 3.45 g, was obtained from 2.5 g polymer(IXa). Polymer(Xc), 3.84 g, was obtained from 2.4 g of polymer(IXa).

Polymer(XI) was prepared similarly in the reaction conditions shown in Table 9.

Acylation of Cyclohexylamine with Polymer(VIII), (X) and (XI). These reactions were performed as well as the reactions of cyclohexylamine with polymers(IV) and (VI). DMF was used as a solvent instead of methylene chloride. The results are shown in Table 5. In the case of polymer (XI), 1.0 g polymers(XIa—d) gave the corresponding acyl amides 490 mg, 540 mg, 530 mg, and 470 mg, respectively. These crude products offered pure products by recrystallization. Z-GlyNH-⟨H⟩; mp 108—109°C(lit,[8] 110°C). Z-GlyGlyNH-⟨H⟩; mp 179—179.5°C(lit,[8] 173°C). Z-L-LeuNH-⟨H⟩; mp 129—131°C(recrystallized from *n*-hexane-ethyl acetate). Found: C, 68.96; H, 8.92; N, 7.93%. Calcd for $C_{20}H_{30}N_2O_3$: C, 69.33; H, 8.73; N, 8.09%. Z-L-Leu-L-LeuNH-⟨H⟩; mp 194—195°C(recrystallized from ethyl acetate). Found: C, 67.36; H, 8.95; N, 8.93%. Calcd for $C_{26}H_{41}N_3O_4$: C, 67.94; H, 8.99; N, 9.14%.

Acylation of Ethyl Ester of Amino Acid with Polymer(X).

Glycine ethyl ester hydrochloride(0.182 g, 1.3 mmol) or 0.245 g (1.3 mmol) of L-leucine ethyl ester hydrochloride and 0.132 g (1.3 mmol) of triethylamine were dissolved in 10 m*l* of DMF. Polymer(X)(1.0 g) was swelled in 10 ml of DMF. Both of them were mixed and kept at room temperature for 12 hr, and then treated as above. The results are shown in Table 8. The optical rotations of products were measured in ethanol(c=0.2) at 18°C using a Japan Spectroscopic Co., Model ORD/UV-5 spectropolarimeter. The results are shown in Table 9.

12) Th. Wieland, and B. Heinke, *Ann.*, **599**, 70 (1956).
13) W. Grassmann, and E. Wünsch, *Ber.*, **91**, 449 (1958).
14) F. Weygand, W. Steglich, and J. Kaelicke, Ger. 1114200 (1962); *Chem. Abstr.*, **57**, 950 (1962).
15) G. Losse, and H. Weddige, *Ann.*, **678**, 148 (1964).
16) E. L. Smith, D. H. Spackmann, and W. J. Polglass, *J. Biol. Chem.*, **199**, 801 (1952).

The Stereochemistry of Nucleophilic Addition. V.[1] The Reformatsky Reaction of 2-Phenylpropanal with Methyl α-Bromopropionate

Takashi MATSUMOTO, Yūkei HOSODA, Kiyomi MŌRI, and Kenji FUKUI

Department of Chemistry, Faculty of Science, Hiroshima University, Higashisenda-machi, Hiroshima

(Received January 24, 1972)

The Reformatsky reaction of 2-phenylpropanal (I) with methyl α-bromopropionate gave the diastereomeric methyl 3-hydroxy-2-methyl-4-phenylvalerates, IIa, IIb, IIc, and IId, in a 5 : 24 : 16 : 55 ratio. The configurations of these β-hydroxy esters were assigned by the following experiments. The reduction of IIa—IId with $LiAlH_4$ gave the corresponding diols, IIIa—IIId, which were then converted to the monotosylates, IVa—IVd. The further reduction of IVa or IVc and IVb or IVd with $LiAlH_4$ gave the epimeric 2-methyl-4-phenyl-3-pentanols, V and VI respectively. Since V and VI were also obtained as minor and major products (20 : 80 ratio) of the Grignard reaction of I with isopropylmagnesium iodide, the configurations of the C-3 and C-4 positions in IIa—IId were assigned. The Wittig reaction of I with carbomethoxyethylidenetriphenylphosphorane gave methyl 2-methyl-4-phenyl-2-*cis*-pentenoate (VII) and its *trans*-isomer (VIII), which were then reduced to the corresponding alcohols, IX and X respectively. The *cis*-hydration of IX gave IIIc and IIId, while a similar treatment of X gave IIIa and IIIb. From this experiments, the relative configurations from the C-2 position to the C-3 position in IIa—IId were also assigned. These configurational assignments of IIa—IId were further confirmed by the ozonization of IIa—IId.

In previous papers,[2-4] we reported on the stereochemistry of the Reformatsky reaction of carbonyl compounds possessing an asymmetric α-carbon atom with methyl (or ethyl) bromoacetate. In these reactions the products had two vicinally-situated asymmetric carbon atoms, which led to two epimeric racemates. On the other hand, if methyl α-bromopropionate is used as a nucleophilic reagent in place of the bromoacetate, the product can be expected to have three asymmetric carbon atoms; therefore, four racemic isomers will be present. The present paper will describe the stereochemistry of the Reformatsky reaction of 2-phenylpropanal (I) with methyl α-bromopropionate.

The condensation of I with methyl α-bromopropionate in dry benzene in the presence of zinc gave a mixture of diastereomeric methyl 3-hydroxy-2-methyl-4-phenylvalerates in a 75% yield. The separation of these esters was subsequently carried out by means of column chromatography on silica gel to give, in the order of elution, the IIa, IIb, IIc, and IId esters in a 5 : 24 : 16 : 55 ratio. The configurations of these β-hydroxy esters (IIa—IId) were assigned in the following manner. The reduction of IIa, IIb, IIc, and IId with $LiAlH_4$ in ether afforded the corresponding 2-methyl-4-phenylpentane-1,3-diols, IIIa, IIIb, IIIc, and IIId respectively. Subsequently, the IIIa—IIId diols were subjected to tosylation with *p*-toluenesulfonyl chloride in pyridine to give the corresponding monotosylates, IVa, IVb, IVc, and IVd respectively. The reduction of IVa and IVc in dry tetrahydrofuran with $LiAlH_4$ gave the same alcohol, 2-methyl-4-phenyl-3-pentanol (V). Therefore, it is clear that IIa and IIc possess the same configuration at the C-3 and C-4 positions. On the other hand, the tosylates, IVb and IVd, were also reduced to another alcohol (VI). These findings mean that the configurations of IIb and IId at the C-3 and C-4 positions are the same. Furthermore, the Grignard reaction of I with isopropylmagnesium iodide gave the epimeric alcohols in a 20 : 80 ratio; these minor and major alcohols were shown to be identical with the above V and VI respectively by a comparison of their IR spectra.

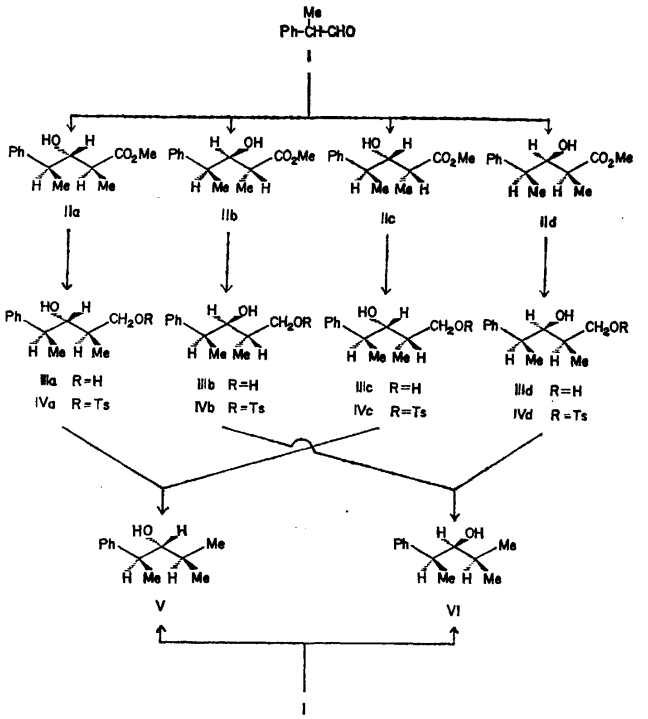

Since the stereochemistry of the Grignard reaction is well known as Cram's rule[5,6] of asymmetric induction, the configurations of the C-3 and C-4 positions in

1) Part IV. T. Matsumoto, G. Sakata, Y. Tachibana, and K. Fukui, This Bulletin, **45**, 1147 (1972). Although the formula depicted represent only one enantiomer, they are taken to indicate a racemate.

2) T. Matsumoto and K. Fukui, *ibid.* **44**, 1090 (1971).

3) T. Matsumoto, I. Tanaka, and K. Fukui, *ibid.*, **44**, 3378 (1971).

4) T. Matsumoto, Y. Tachibana, T. Ohno, and K. Fukui, *J. Sci. Hiroshima Univ. Ser. A*, **35**, 231 (1971).

5) D. J. Cram and F. A. Abd Elhafez, *J. Amer. Chem. Soc.*, **74**, 5828 (1952).

6) G. J. Karabatsos, *ibid.*, **89**, 1367 (1967).

the β-hydroxy esters were assigned to as is shown in IIa—IId. To obtain the data on the configuration of the C-2 position relative to the C-3 position in IIa–IId, the following experiments were carried out.

The Wittig reaction of I with carbomethoxyethylidene triphenylphosphorane in dry benzene gave an 87% yield of a mixture of geometric isomers, which were then successfully separated by means of column chromatography on silica gel into two oily esters in a 3 : 97 ratio. It is well known[7,8] that the ylids stabillized by an adjacent carbonyl function yield, as the predominant product, an isomer in which the carbonyl function is *trans* to the larger group at the beta carbon atom. In the NMR spectra it is also known that the signal of a *cis*-vinyl proton to the methoxycarbonyl group appeares in a field lower than that of the corresponding *trans*-vinyl proton.

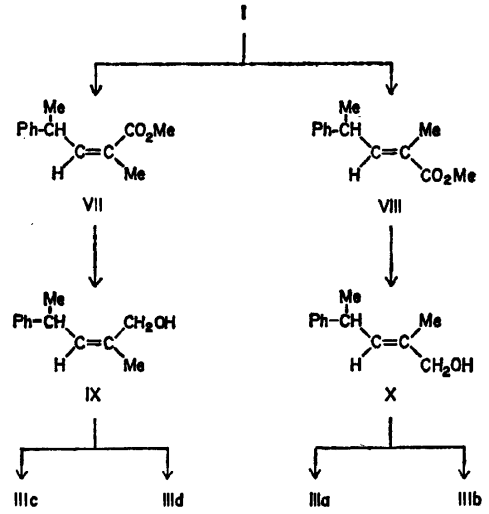

The chemical shifts of the vinyl protons in the above minor and major esters were observed at δ 5.88 ppm and at δ 6.78 ppm respectively. Therefore, the structures of the minor and major esters were identified as methyl 2-methyl-4-phenyl-2-*cis*-pentenoate (VII) and its *trans*-isomer (VIII) respectively. These assignments were further supported by the chemical shifts of the methine protons at the C-4 position in VII and VIII. That is, VII showed the signal of the methine proton at δ *ca.* 4.5 ppm, suggesting the presence of a *cis*-methoxycarbonyl group relative to the methine proton, because VIII showed the corresponding signal at δ *ca.* 3.7 ppm. The VII and VIII esters were then reduced with $LiAlH_4$ in ether to give the corresponding alcohols, IX and X respectively. The hydroboration of the *cis*-alcohol (IX), followed by oxidation with alkaline hydrogen peroxide, gave the diols (IIIc and IIId). This result means that the configurations of the IIIc and IIId diols differ only at the C-4 position. On the other hand, a similar treatment of the *trans*-alcohol (X) gave the IIIa and IIIb diols. Therefore, the difference between the configurations of the IIIa and IIIb diols is also at the C-4 position. Further, it is well known[9] that the hydration of the carbon-carbon double bond by the hydroboration-oxidation procedure proceeds in a *cis* manner.

On the basis of the above experiments, the configurations of all the asymmetric carbon atoms in the β-hydroxy esters were assigned as is shown in IIa—IId. These configurational assignments of IIa—IId were further confirmed by the following experiments. If the phenyl group in IIa—IId could be converted to the methoxycarbonyl group, it might be expected that IIa and IId would afford, respectively, two meso isomers, XIa and XId, while IIb or IIc would afford a racemate, XIb. Therefore, the ozonization of IIb and IIc in acetic acid, followed by the methylation of the resulting acids with diazomethane, was carried out; as would be expected, the same diester, XIb, was obtained. However, a similar treatment of IIa and IId afforded the corresponding diesters, XIa and XId.

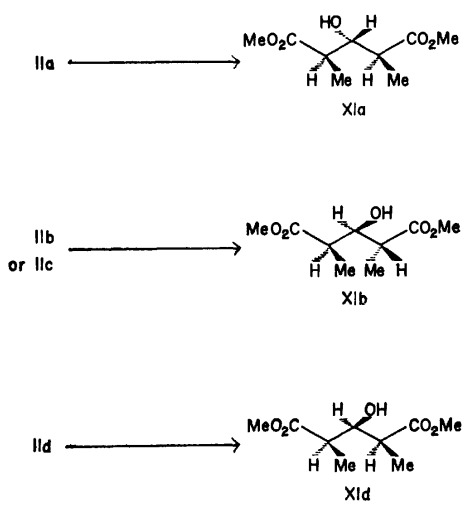

An attempt will now be made to explain the ratio of IIa–IId. It is known[3] that the stereochemistry of the Reformatsky reaction of the carbonyl compound possessing an asymmetric α-carbon atom has been explained by Cram's rule of asymmetric induction. Further, the stereochemistry of this reaction has also been explained on the hypothesis of an enolate-anion mechanism[10] involving a cyclic transition state, as in the case of the Ivanov reaction.[11] Therefore, the four models (A, B, C, and D) of transition states for the Reformatsky reaction of I with methyl α-bromopropionate in the presence of zinc are as is shown in Fig. 1. The conformation of I in A and B is more stable than that in C and D, as has been reported by Karabatsos.[6] For the steric interaction between the methyl group at the C-2 position and the hydrogen at the C-3 position, the B and D transition states should be less stable than the corresponding A and C transition states. Thus, the stability of these transition states decreases in the order of A, B, C, and D, leading to the IId, IIb, IIc, and IIa esters respectively.

7) A. Maercker, "Organic Reactions," Vol. 14, Wiley, New York (1965), p. 270.

8) T. Matsumoto, K. Hidaka, T. Nakayama, and K. Fukui, *Chem. Lett.*, **1972**, 1.

9) G. Zweifel and H. C. Brown, "Organic Reactions," Vol. 13, Wiley, New York (1963), p. 1.

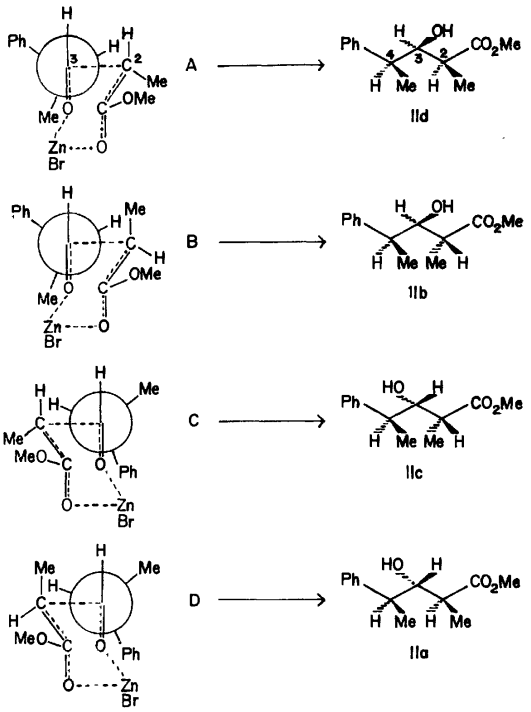

Fig. 1

Experimental

All the melting and boiling points are uncorrected. The NMR spectra were taken on a Hitachi Model R-20 NMR spectrometer (60 MHz), using tetramethylsilane as the internal standard. The chemical shifts are presented in terms of δ values; s: singlet, bs: broad singlet, d: doublet, bd: broad doublet, dd: double doublet, t: triplet, dqa: double quartet, qi: quintet, m: multiplet. The column chromatography was performed on Merck silica gel (0.08 mm).

Methyl 3-Hydroxy-2-methyl-4-phenylvalerates (IIa, IIb, IIc, and IId). A solution of methyl α-bromopropionate (6.01 g) and 2-phenylpropanal (I: 3.22 g) in dry benzene (10 ml) was added, drop by drop at 80°C and over a period of 20 min, to a stirred suspension of purified zinc powder[12] (2.35 g) in dry benzene (3.0 ml); the temperature was kept at 80—85°C during the addition. After the addition was complete, the mixture was refluxed for 70 min, cooled, decomposed with dilute hydrochloric acid, and then extracted with benzene. The extract was successively washed with aqueous sodium hydrogen carbonate and water, dried over sodium sulfate, and then evaporated. The residue was distilled to give a mixture of methyl 3-hydroxy-2-methyl-4-phenylvalerates (IIa—IId) as an oil; bp 115—125°C/1 mmHg; yield, 4.80 g. The above oil was purified by means of column chromatography on silica gel (500 g), using benzene containing 1% ether and then 7% ether as the eluents. The first fraction gave IIa as a solid (199 mg) which was recrystallized from petroleum ether to give colorless crystals; mp 59—59.6°C. NMR in CCl_4: 1.13(d, J=6.5 Hz, $-CH(C\underline{H}_3)CO_2CH_3$), 1.31 (d, J=7 Hz, $-CH(C\underline{H}_3)C_6H_5$), 2.32(qi, J=6.5 Hz, $-C\underline{H}CO_2CH_3$), 2.75 (s, $-O\underline{H}$), *ca.* 2.8 (m, overlap, $-C\underline{H}-C_6H_5$), 3.53 (s, $-CO_2C\underline{H}_3$), *ca.* 3.6 (m, overlap, $-C\underline{H}OH$), 7.18 (s, $-C_6\underline{H}_5$).

Found: C, 70.32; H, 8.17%. Calcd for $C_{13}H_{18}O_3$: C, 70.24; H, 8.16%.

The second fraction gave IIb as an oil; yield, 954 mg. NMR in CCl_4: 1.15 (d, J=7 Hz, $-CH(C\underline{H}_3)CO_2CH_3$), 1.32 (d, J=7 Hz, $-CH(C\underline{H}_3)C_6H_5$), *ca.* 2.3 (m, $-C\underline{H}CO_2CH_3$), *ca.* 2.75 (m, overlap, $-C\underline{H}C_6H_5$), 2.85 (s, $-O\underline{H}$), *ca.* 3.4 (m, overlap, $-C\underline{H}OH$), 3.60 (s, $-CO_2C\underline{H}_3$), 7.16 (s, $-C_6\underline{H}_5$).

Found: C, 70.22; H, 8.16%. Calcd for $C_{13}H_{18}O_3$: C, 70.24; H, 8.16%.

The third fraction gave IIc as an oil; yield, 636 mg. NMR in CCl_4: 1.12 (d, J=7 Hz, $-CH(C\underline{H}_3)CO_2CH_3$), 1.24 (d, J=5 Hz, $-CH(C\underline{H}_3)C_6H_5$), 1.83 (d, J=5 Hz, $-C\underline{H}CO_2CH_3$), *ca.* 2.2—3.0 (m, $-C\underline{H}C_6H_5$), *ca.* 2.7 (overlap, $-O\underline{H}$), 3.60 (s, $-CO_2C\underline{H}_3$), *ca.* 3.9 (m, $-C\underline{H}OH$), 7.17(s, $-C_6\underline{H}_5$).

Found: C, 70.22; H, 8.17%. Calcd for $C_3H_{18}O_3$: C, 70.24; H, 8.16%.

The fourth fraction gave IId as an oil; yield, 2185 mg. NMR in CCl_4: 1.09 (d, J=7 Hz, $-CH(C\underline{H}_3)CO_2CH_3$, 1.32 (d, J=6.5 Hz, $-C\underline{H}(C\underline{H}_3)C_6H_5$), 2.22 (m, $-C\underline{H}CO_2CH_3$), *ca.* 2.7 (m, overlap, $-O\underline{H}$ and $-C\underline{H}C_6H_5$), 3.58 (s, $-CO_2C\underline{H}_3$), 3.95 (m, $-C\underline{H}OH$), 7.12 (s, $-C_6\underline{H}_5$).

Found: C, 70.31; H, 8.18%. Calcd for $C_{13}H_{18}O_3$: C, 70.24; H, 8.16%.

The total yield of IIa—IId was 3.974 g (75% from I).

Reduction of IIa, IIb, IIc, and IId with $LiAlH_4$. *a)*: A solution of IIa (523 mg) in dry ether (5.0 ml) was added, drop by drop over a period of 30 min, to a suspension of $LiAlH_4$(200 mg) in dry ether (15 ml) at room temperature, and then the mixture was refluxed for 2.5 hr. After cooling, the mixture was decomposed with dilute hydrochloric acid and extracted with ether. The extract was washed with an aqueous sodium chloride solution, dried over sodium sulfate, and then evaporated. The residue was chromatographed on silica gel (30 g), using benzene containing 20% ether as the eluent, to give 2-methyl-4-phenylpentane-1,3-diol (IIIa) as an oil; yield, 245 mg. NMR in $CDCl_3$: 0.90 (d, J=6.5 Hz, $-CH(C\underline{H}_3)CH_2OH$), 1.24 (d. J=7 Hz, $-CH(C\underline{H}_3)C_6H_5$), 1.55 (m, $-C\underline{H}CH_2OH$), 2.86 (qi, J=6.5 Hz, $-C\underline{H}C_6H_5$), 3.41 (s, $-O\underline{H}$), *ca.* 3.55 (m, overlap, $-C\underline{H}OH$ and $-CH_2\underline{O}H$), 7.23 (s, $-C_6\underline{H}_5$).

Found: C, 74.28; H, 9.57%. Calcd for $C_{12}H_{18}O_2$: C, 74.19; H, 9.34%).

b): The IIb ester (400 mg) was reduced with $LiAlH_4$ by a method similar to that used for IIIa. The crude product was recrystallized from petroleum ether to give IIIb as colorless crystals; mp 52—53°C; yield, 275 mg. NMR in $CDCl_3$: 0.95 (d, J=7 Hz, $-CH(C\underline{H}_3)CH_2OH$), 1.29 (d, J=7 Hz, $-CH(C\underline{H}_3)C_6H_5$), 1.75 (m, $-C\underline{H}CH_2OH$), 2.90 (s, $-O\underline{H}$), 3.0 (m, overlap, $-C\underline{H}C_6H_5$), *ca.* 3.7 (m, overlap, $-C\underline{H}OH$ and $-CH_2\underline{O}H$), 7.28 (s, $-C_6\underline{H}_5$).

Found: C, 74.36; H, 9.47%. Calcd for $C_{12}H_{18}O_2$: C, 74.19; H, 9.34%.

c): The IIc ester (749 mg) was also reduced with $LiAlH_4$ to give IIIc as colorless crystals (from petroleum ether); mp 70.5—71°C; yield, 452 mg. NMR in $CDCl_3$: 1.02 (d, J=7 Hz, $-CH(C\underline{H}_3)CH_2OH$), 1.19(d, J=7 Hz, $-CH(C\underline{H}_3)C_6H_5$), *ca.* 2.0 (m, overlap, $-C\underline{H}CH_2OH$), 2.02 (s, $-OH$), 2.84 (m, $-C\underline{H}C_6H_5$), 3.73 (d, J=5 Hz, $-CH_2\underline{O}H$),

10) Ref. 3 and the references cited therein.

11) H. E. Zimmerman and M. D. Traxler, *J. Amer. Chem. Soc.*, **79**, 1920 (1957).

12) R. L. Shriner, "Organic Reactions," Vol. 1, Wiley, New York (1942), p. 16.

3.88 (dd, overlap, J=9.5 and 2 Hz, -CHOH), 7.30 (s, -C_6H_5).

Found: C, 74.29; H, 9.48%. Calcd for $C_{12}H_{18}O_2$: C, 74.19; H, 9.34%.

d): Similarly, the IId ester (2.20 g) was reduced to IIId; colorless crystals (1.30 g); mp 98—98.5°C (from *n*-hexane containing ether). NMR in $CDCl_3$: 0.92 (d, J=6.5 Hz, -CH(CH_3)CH_2OH), 1.34 (d, J=6.5 Hz, -CH(CH_3)C_6H_5), *ca.* 1.4 (m, overlap, -CHCH$_2$OH), 2.39 (s, -OH), 2.8 (m, -CHC$_6$H$_5$), 3.62 (d, J=4 Hz, -CH_2OH), 3.97 (dd, J=9.5 and 2 Hz, -CHOH), 7.24 (s, -C_6H_5).

Found: C, 74.28; H, 9.53%. Calcd for $C_{12}H_{18}O_2$: C, 74.19; H, 9.34%.

The Tosylates (IVa, IVb, IVc, and IVd). a): A mixture of the IIIa diol (189 mg) and *p*-toluenesulfonyl chloride (186 mg) in dry pyridine (3.0 m*l*) was allowed to stand at room temperature for 72 hr. After a usual work-up, the crude product was chromatographed on silica gel (15 g). Elution with benzene containing 5% ether was then carried out to give IVa as an oil; yield, 133 mg.

Found: C, 65.72; H, 7.08%. Calcd for $C_{19}H_{24}O_4S$: C, 65.50; H, 6.94%.

b): The other tosylates (IVb, IVc, and IVd) were also prepared from the corresponding diols (IIIb, IIIc, and IIId) by a method similar to that used for IVa.

IVb; Found: C, 65.70; H, 7.04%. Calcd for $C_{19}H_{24}O_4S$: C, 65.50; H, 6.94%.

IVc; Found: C, 65.48; H, 6.95%. Calcd for $C_{19}H_{24}O_4S$: C, 65.50; H, 6.94%.

IVd; Found: C, 65.80; H, 7.15%. Calcd for $C_{19}H_{24}O_4S$: C, 65.50; H, 6.94%.

2-Methyl-4-phenyl-3-pentanols (V and VI). a) By the Grignard Reaction: A solution of I (1.960 g) in dry ether (5.0 m*l*) was added, drop by drop over a period of 30 min, to a Grignard reagent, prepared from magnesium (0.660 g) and isopropyl iodide (3.950 g) in dry ether (20 m*l*). The mixture was refluxed for 90 min, cooled, decomposed with a mixture of ice and dilute hydrochloric acid, and then extracted with ether. The extract was successively washed with aqueous sodium thiosulfate and water. After drying over sodium sulfate, the solvent was evaporated; the residue (2.032 g) was then chromatographed on silica gel (200 g), using benzene containing 3% ether as the eluent. The first fraction gave a minor alcohol (V) as an oil (327 mg).

Found: C, 80.64; H, 10.21%. Calcd for $C_{12}H_{18}O$: C, 80.85; H, 10.18%.

The second fraction gave a major alcohol (VI) as an oil (1142 mg).

Found: C, 80.81; H, 10.14%. Calcd for $C_{12}H_{18}O$: C, 80.85; H, 10.18%.

b) From the Tosylates (IVa and IVc): The tosylate (IVa: 133 mg) was reduced with $LiAlH_4$ (50 mg) in dry tetrahydrofuran (3.0 m*l*) by a method similar to that used for IIIa. The crude product was purified by column chromatography on silica gel (30 g), using benzene containing 2% ether as the eluent, to give an oil (36 mg); this oil was shown to be identical with the above minor alcohol (V) of the Grignard reaction by an IR spectral comparison.

By a similar reduction, IVc was converted to V; its identity was also confirmed by an IR spectral comparison.

c) From the Tosylates (IVb and IVd): The tosylates (IVb and IVd) were treated with $LiAlH_4$ by a method similar to that used in *b*). After chromatographic purification, the two products were shown by a spectral comparison to be identical with the major alcohol (VI) of the Grignard reaction.

*Methyl 2-Methyl-4-phenyl-2-*cis*-pentenoate (VII) and Its* trans*-Isomer (VIII).* A mixture of I (2.68 g), carbomethoxyethylidene triphenylphosphorane (6.96 g), and dry benzene (50 m*l*) was refluxed for 2 hr under a stream of nitrogen; the solvent was then evaporated under a vacuum. The residue was extracted with ether. The extract, after the removal of the ether, was chromatographed on silica gel (500 g), using benzene containing 1% ether as the eluent. The first fraction gave methyl 2-methyl-4-phenyl-2-*cis*-pentenoate (VII) as an oil (0.12 g). NMR in CCl_4: 1.31 (d, J=7 Hz, -CHCH_3), 1.83 (d, J=1.5 Hz, =CCH_3), 3.66 (s, -CO_2CH_3), *ca.* 4.5 (m, -CHCH_3), 5.88 (dqa, J=10 and 1.5 Hz, =CH), 7.15 (s, -C_6H_5).

Found: C, 76.66; H, 7.96%. Calcd for $C_{13}H_{16}O_2$: C, 76.44; H, 7.90%.

The second fraction gave methyl 2-methyl-4-phenyl-2-*trans*-pentenoate (VIII) as an oil (3.41 g), NMR in CCl_4: 1.36 (d, J=7 Hz, -CHCH_3), 1.83 (d, J=1.5 Hz, =CCH_3), 3.65 (s, -CO_2CH_3), *ca.* 3.65 (m, overlap, -CHCH_3), 6.78 (dqa, J=9 and 1.5 Hz, =CH), 7.18 (s, -C_6H_5).

Found: C, 76.35; H, 7.87%. Calcd for $C_{13}H_{16}O_2$: C, 76.44; H, 7.90%.

*2-Methyl-4-phenyl-2-*cis*-pentenol (IX) and Its* trans*-Isomer (X). a)*: A solution of VII (225 mg) in dry ether (5.0 m*l*) was added, drop by drop over a period of 10 min at —10—0°C, to a stirred suspension of $LiAlH_4$ (100 mg) in dry ether (4.0 m*l*). The mixture was further stirred for 1.5 hr at this temperature and then decomposed with a mixture of ice and dilute hydrochloric acid. The mixture was extracted with ether. The extract was washed with an aqueous sodium chloride solution, dried over sodium sulfate, and then evaporated. The residual oil was purified by column chromatography on silica gel (30 g). Elution with benzene containing 15% ether gave IX as an oil (118 mg). NMR in CCl_4: 1.24 (d, J=7 Hz, -CHCH_3), 1.71 (d, J=1.5 Hz, =CCH_3), 2.33 (s, -OH), 3.66 (m, -CHCH_3), 3.99 (s, -CH_2-), 5.31 (bd, J=9 Hz, =CH), 7.10 (s, -C_6H_5).

Found: C, 81.79; H, 9.21%. Calcd for $C_{12}H_{16}O$: C, 81.77; H, 9.15%.

b): By a method similar to that used for IX, the ester (VIII: 1.36 g) was also reduced with $LiAlH_4$ to give X as an oil (0.97 g). NMR in CCl_4: 1.26 (d, J=7 Hz, -CHCH_3), 1.58 (d, J=1.5 Hz, =CCH_3), 3.00 (bs, -OH), *ca.* 3.6 (m, overlap, -CHCH_3), 3.78 (s, -CH_2-), 5.44 (bd, J=9 Hz, =CH), 7.12 (s, -C_6H_5).

Found: C, 81.98; H, 9.27%. Calcd for $C_{12}H_{16}O$: C, 81.77; H, 9.15%.

*Hydroboration of 2-Methyl-4-phenyl-2-*cis*-pentenol (IX) and 2-Methyl-4-phenyl-2-*trans*-pentenol (X). a)*: A solution of the *cis*-alcohol (IX: 380 mg) in dry tetrahydrofuran (5.0 m*l*) was added to a solution of sodium borohydride (150 mg) in dry tetrahydrofuran (3.0 m*l*) at 0—5°C over a 10-min period. To the stirred and cooled solution, a solution of freshly-distilled boron trifluoride etherate (0.7 m*l*) in dry tetrahydrofuran (3.0 m*l*) was added at this temperature over a period of 5 min. After the sitrring had been continued for 3 hr at 0—10°C, a few drops of water, aqueous sodium hydroxide (12%: 3.0 m*l*), and then hydrogen peroxide (30%: 0.7 m*l*) were added successively. The mixture was stirred for 30 min, poured into an aqueous sodium hy-

droxide solution, and then extracted with ether. The extract was washed successively with aqueous sodium hydroxide and water. After the removal of the dried ether, the residue (368 mg) was chromatographed on silica gel (35 g), using benzene containing 15% ether as the eluent. The first fraction gave the recovered IX (150 mg). The second fraction gave colorless crystals (50 mg), which were shown to be identical with the above IIIc by a comparison of their IR spectra. The third fraction gave colorless crystals (88 mg), which were also shown to be identical with the above IIId by a comparison of their IR spectra.

b): The *trans*-alcohol (X: 3.75 g) was treated by a method similar to that used in *a)*. The crude product was purified by means of column chromatography on silica gel to give IIIa (256 mg) and IIIb (1787 mg), which were shown to be identical with the authentic samples by a comparison of their IR spectra.

Ozonolyses of IIa—IId. *a)* The ozone gas stream from a laboratory ozonator (Nihon Ozon Co.) was passed through a solution of IId (1.755 g) in acetic acid (40 m*l*) for 40 hr at room temperature. The mixture was allowed to stand at room temperature with hydrogen peroxide (30%: 10 m*l*). After the decomposition of the excess reagent with aqueous sodium hydrogen sulfite (25%: 40 m*l*), the solution was evaporated under a vacuum. The residue was extracted with ether, after which the extract was methylated with diazomethane. The crude ester, after the removal of the ether, was purified by means of column chromatography on silica gel (200 g). Elution with benzene containing 3% ether gave the recovered IId (574 mg). Further elution with benzene containing 7% ether gave XId (221 mg) as an oil. NMR in CCl_4: 1.19 (d, J=7 Hz, 2-$\underset{|}{C}HC\underline{H}_3$), 2.48 (qi, J=7 Hz, 2-$C\underline{H}CH_3$), 3.0 (bs, -O$\underline{H}$), 3.67 (s, 2-$CO_2C\underline{H}_3$), 3.98 (t, J=7 Hz, -$\underset{|}{C}\underline{H}OH$).

Found: C, 52.78; H, 8.07%. Calcd for $C_9H_{16}O_5$: C, 52.93; H, 7.90%,

b) The ozonization of the IIa ester (215 mg) was carried out, by a method similar to that used for XId, to give XIa (15 mg) as an oil. NMR in CCl_4: 1.18 (d, J=7 Hz, 2-$\underset{|}{C}HC\underline{H}_3$), 2.58 (qi, J=7 Hz, 2-$\underset{|}{C}\underline{H}CH_3$), 3.03 (bs, -O$\underline{H}$), *ca.* 3.6 (m, overlap, -$\underset{|}{C}\underline{H}OH$), 3.65 (s, 2-$CO_2C\underline{H}_3$).

Found: C, 52.91; H, 7.98%. Calcd for $C_9H_{16}O_5$: C, 52.93; H, 7.90%.

c) The IIb ester (497 mg) was treated, by a method similar to that used for XId, to give XIb (56 mg) as an oil. NMR in CCl_4: 1.18 (d, J=7 Hz 2-$\underset{|}{C}HC\underline{H}_3$), 2.48 (qi, J=7 Hz, 2-$\underset{|}{C}\underline{H}CH_3$), 2.81 (bs, -O$\underline{H}$), 3.67 (s, 2-$CO_2C\underline{H}_3$), 3.78 (m, overlap, -$\underset{|}{C}\underline{H}OH$).

Found: C, 52.81; H, 7.96%. Calcd for $C_9H_{16}O_5$: C, 52.93; H, 7.90%.

Similarly, the IIc ester (290 mg) was also treated by a method similar to that used for XId, thus giving an oil (43 mg) which was shown to be identical with XIb by a comparison of their IR spectra.

BULLETIN OF THE CHEMICAL SOCIETY OF JAPAN, VOL. 45, 3160—3164 (1972)

Oxidative Dimerization of Pyrrole Derivatives. II. The Formation and Structure of Dimers of 3-Alkoxycarbonyl-substituted Pyrryls[1,2]

Kuniyuki TOMITA and Norio YOSHIDA

Central Research Laboratories, Sankyo Co., Ltd., Shinagawa-ku, Tokyo

(Received January 31, 1972)

Oxidation of 3-alkoxycarbonyl-substituted pyrrolic compounds with aqueous potassium ferricyanide in the presence of potassium hydroxide afforded 2,2′- and 5,5′-bispyrrolenine derivatives, which were in equilibrium with each other in solution *via* radical intermediates. The substituent effects on the dimer formation will also be discussed in connection with the characters of the intermediate pyrryl radicals.

Several *N*-heteroaromatic compounds have been known to form dimers *via* oxidation, and some of these exist in equilibrium with dissociated radicals.[3a–h] However, the structures of such dimers have not been elucidated except in the case of bis-triarylimidazolyl radicals.[4a,b]

In the previous paper, we reported that some 3-acyl-substituted pyrrole derivatives (I) gave dimers (II) which were in equilibrium with stable pyrryl radicals (III) in solution, on oxidation with potassium ferricyanide.[5a,b]

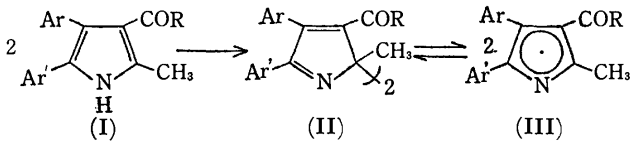

The formation of such dimers seems to raise discussion connected with the characters of the radicals, since the intermediacy of the heteroaromatic radicals has been suggested for the oxidative dimerization of *N*-

1) Part I of this series: Ref. 5a.

2) Presented at the 24th Meeting of the Chemical Society of Japan, Tokyo, October, 1971.

3) a) K. Maeda and T. Hayashi, This Bulletin, **43**, 429, 1431 (1970) and references therein. b) K. Shillfarth and H. Zimmerman, *Chem. Ber.*, **98**, 3124 (1965). c) R. Kuhn and H. Kainer, *Biochim. Biophys. Acta*, **12**, 325 (1953). d) H. Zimmerman, H. Baumgärtel, and F. Bakke, *Angew. Chem.*, **73**, 808 (1961). e) S. M. Blinder, M. L. Peller, N. W. Lord, L. C. Aamodt, and N. S. Ivanchukov, *J. Chem. Phys.*, **36**, 540 (1962). f) Y. Nagai and Y. Sakaino, *Nippon Kagaku Zasshi*, **90**, 309 (1969). g) H. Baumgärtel and H. Zimmerman, *Chem. Ber.*, **99**, 843 (1966). h) H. J. Teuber, G. Schutz, and H. J. Gross, *Angew. Chem.*, **82**, 522 (1970).

4) a) D. M. White and J. Sonnenberg, *J. Amer. Chem. Soc.*, **88**, 3825 (1966). b) H. Tanino, T, Kondo, K. Okada, and T, Goto, Preprints p. 146, for the 9th NMR Symposium, Kanazawa. August 1970.

5) a) K. Tomita and N. Yoshida, *Tetrahedron Lett.*, **1971**, 1169. b) K. Tomita and N. Yoshida, Preprints p. 449, for the Third International Congress of Heterocyclic Chemistry, Sendai, August, 1971.

heteroaromatic compounds with potassium ferricyanide.[3a])

This paper will discuss the formation and structure of the dimers of 3-alkoxycarbonyl-substituted pyrryl radicals obtained from the corresponding pyrrole derivatives. We will also discuss briefly the characters of these radicals on the basis of the substituent effects on the dimer formation.

Results and Discussion

Formation of Dimers. Oxidation of ethyl 4,5-bis(*p*-methoxyphenyl)-2-methylpyrrole-3-carboxylate (IV) with potassium ferricyanide under alkaline conditions afforded a crystalline precipitate (D-IV)[6] quantitatively. The results of an elemental analysis and the molecular weight of D-IV, listed in Table 1, support the formation of a pyrryl-radical dimer. The reduction of D-IV with hydroquinone affords the pyrrole derivatives IV quantitatively, which shows that the dimer still contains the intact pyrrole ring. The IR spectrum of D-IV is characterized by strong imine absorptions at 1610 cm^{-1} and carbonyl at 1720 cm^{-1} (appearing at 1675 cm^{-1} in IV) and an absence of NH absorptions.

The Occurrence of Equilibrium in D-IV. The NMR spectra of D-IV showed characteristic features, as is shown in Fig. 1.

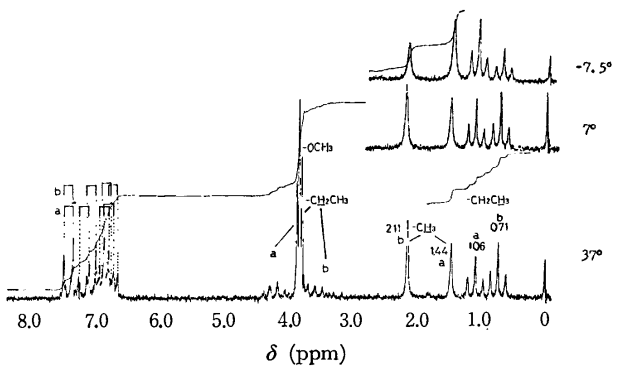

Fig. 1. NMR spectra of D-IV in $CDCl_3$.

Since it shows the presence of the two ester, four *p*-methoxyphenyl, and two methyl groups in a ratio dependent on the temperature, D-IV seems to be a mixture of two dimers, (D-IVa) and (D-IVb) (assigned as *a* and *b* in Fig. 1), which are in equilibrium with each other in solution. In fact, as expected, one of the dimers D-IVa was isolated on the recrystallization of D-IV from acetone.[7] Its NMR spectrum, measured at −7.5°C immediately after D-IVa was dissolved in cold $CDCl_3$, showed only the signals, *a* in Fig. 1, corresponding to a single compound. With the passage of time, the spectrum showed the gradual appearance of the other isomer, D-IVb, from D-IVa, and after a long time afforded the same pattern of spectrum of a mixture of D-IVa and D-IVb, as is shown in Fig. 1. Those phenomena were also observed on a thin layer chromatogram (tlc); a tlc of D-IV showed two spots (R_f; 0.6 and 0.2, developed in a mixture of benzene and acetone (20 : 1) on a silicagel plate), while that of D-IVa showed one spot (R_f; 0.6) when it was developed immediately, and an additional spot (R_f; 0.2), developed after the solution of D-IVa was allowed to stand for a long time at room temperature.

These results strongly indicate the presence of the equilibrium, though attempt at the isolation and characterization of the other isomer, D-IVb, have thus far been unsuccessful.

The Structures of D-IVa and D-IVb. The structures of D-IVa and D-IVb were determined to be 2,2′- and 5,5′-bispyrrolenine derivatives respectively, as is shown in Scheme 1, on the basis of the following results.

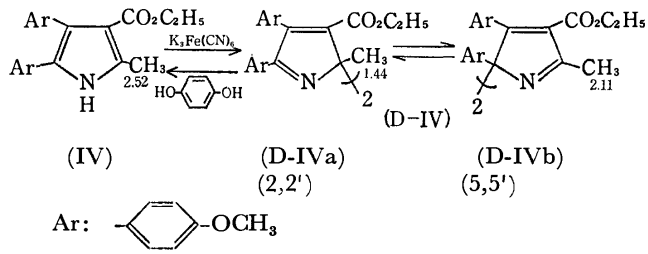

Scheme 1.

The single 2-methyl signal at 1.44 ppm in the NMR spectrum of D-IVa supported a symmetrical dimer structure, while the two overlapping A_2B_2-type signals in the aromatic region indicate that the phenyl rings were not involved in the dimerization-bond formation, as they are in the dimer of the triphenylmethyl radical.[8a–d] The IR spectrum of D-IVa shows the same absorptions as D-IV, and the strong imine absorptions at 1610 cm^{-1} indicate the pyrrolenine structure, eliminating the possibility of the formation of a 1,1′ (N,N′) bond. The absorptions at 1720 cm^{-1} show the presence of an α,β-unsaturated ester group, which also suggests that the formation of a 3,3′ bond is unlikely.

The 2-methyl proton signal in the NMR spectrum of tetramethylpyrrole (V) is markedly shifted upfield with further substitution at the 2-position,[9] as is shown in Compound (VI) in Scheme 2.

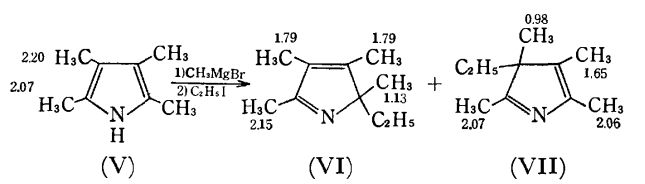

Scheme 2.

In the case of the dimer D-IVa, the methyl signal which appeared at 2.52 ppm in the pyrrolic compound, IV, underwent a remarkable upfield shift to

6) The dimer of compound (Y) is noted (D-Y) symbolically.

7) See Experimental.

8) a) H. Lankamp, W. Th. Nauta, and C. MacLean, *Tetrahedron Lett.*, **1968**, 249. b) H. A. Staab, H. Brettschneider, and H. Brunner, *Chem. Ber.*, **103**, 1101 (1970). d) R. D. Guthrie and G. R. Weisman, *Chem. Commun.*, **1969**, 1316. d) H. Takeuchi, T. Nagai, and N, Tokura, This Bulletin, **44**, 753 (1971).

9) J. L. Wong and M. H. Ritchie, *Chem. Commun.*, **1970**, 142.

Table 1.

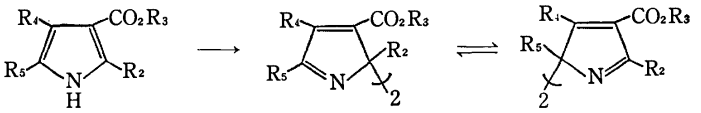

(IV, VIII—XV) (D-IVa, D-VIIIa—XVa) (2,2′) (D-IVb, D-VIIIb—XVb) (5,5′)

	R_2	R_3	R_4	R_5	Mp °C (decomp.)	IR (CO) (cm^{-1})	NMR 2-CH_3 ($CDCl_3$, 37.0°C) ppm a	b	a : b
D-IV	CH_3	C_2H_5	*p*-$CH_3OC_6H_4$	*p*-$CH_3OC_6H_4$	132—135	1725	1.44	2.11	41 : 59
D-IVa					141—143	1725			
D-VIII	CH_3	C_2H_5	CH_3	*p*-ClC_6H_4	125—128	1715	1.35 2.24[a]	1.92 2.08[a]	61 : 39
D-VIIIa					130—133	1715			
D-IX	C_2H_5	C_2H_5	CH_3	*p*-ClC_6H_4	117—120	1720	2.05[b] 2.25[a]	2.90[b] 2.10[a]	55 : 45
D-IXa					124—126	1720			
D-X	CH_3	CH_3	*p*-$CH_3OC_6H_4$	*p*-$CH_3OC_6H_4$	—125[c]	1730	1.44	2.10	49 : 51
D-XI	CH_3	C_2H_5	C_6H_5	*p*-$CH_3OC_6H_4$	140—142	1720	1.44	2.15	42 : 58
D-XII	CH_3	C_2H_5	*p*-$CH_3OC_6H_4$	C_6H_5	130—135	1720	1.46	2.13	50 : 50
D-XIII	CH_3	C_2H_5	C_6H_5	C_6H_5	140—142	1725	1.50	2.15	49 : 51
D-XIIIa					157—159	1725			
D-XIV	CH_3	C_2H_5	*p*-ClC_6H_4	*p*-ClC_6H_4	—150[c]	1720	1.44	2.10	51 : 49
D-XV	CH_3	$CH_2C_6H_5$	CH_3	*p*-$CH_3OC_6H_4$	125—128	1715	1.30	1.90	58 : 42

	Formula	Anal. Found % C	H	N	Cl	Calcd % C	H	N	Cl	Mass (M^+)
D-IV	$C_{44}H_{44}O_8N_2$ (728.81)	72.37	5.97	3.88		72.51	6.09	3.84		728
D-IVa		72.61	6.03	3.97						
D-VIII	$C_{30}H_{30}O_4N_2Cl_2$ (553.47)	65.11	5.48	4.82	12.85	65.10	5.46	5.06	12.81	552
D-IX	$C_{32}H_{34}O_4N_2Cl_2$ (581.56)	66.02	5.94	4.68	12.28	66.08	5.89	4.82	12.19	580
D-IXa		66.05	5.80	4.60	12.21					
D-X	$C_{42}H_{40}O_8N_2$ (700.76)	72.26	5.48	4.02		71.98	5.75	4.00		700
D-XI	$C_{42}H_{40}O_6N_2$ (668.76)	75.15	5.94	4.18		75.43	6.03	4.19		668
D-XII	$C_{42}H_{40}O_6N_2$ (668.76)	75.15	6.05	4.18		75.43	6.03	4.19		668
D-XIII	$C_{40}H_{36}O_4N_2$ (608.70)	78.76	5.95	4.75		78.92	5.96	4.60		608
D-XIIIa		78.88	5.72	4.65						
D-XIV	$C_{40}H_{32}O_4N_2Cl_4$ (746.52)	64.21	4.47	3.67	18.78	64.36	4.32	3.75	19.00	744
D-XV	$C_{42}H_{40}O_6N_2$ (668.76)	74.84	6.08	4.15		75.43	6.03	4.19		668

a) 4-C<u>H</u>$_3$. b) 2-C<u>H</u>$_2$CH$_3$. c) obscure.

1.44 ppm. The 2,2′ bond formation was thus assigned for the dimer D-IVa; which was analogous to the dimers II of 3-acylpyrryls III.[5]

Although the other isomer, D-IVb, was not isolated, its NMR and IR spectra, deduced from a comparison of the spectra of D-IVa with those of the mixture D-IV, also support the symmetrical bispyrrolenine structure in which 1,1′ or 3,3′ bond formation is excluded. In this isomer, the methyl signal (2.11 ppm), which is not shifted upfield as in the case of D-IVa, allows for the possibility of two dimers, 4,4′ or 5,5′, by comparison with the results described by Wong *et al.* (Scheme 2); however the 5,5′ structure, as is shown in Scheme 1, seems reasonable on the basis of the following facts. When the oxidation of the 4-methyl-substituted analogue (VIII) was undertaken, a mixture of two dimers, (D-VIIIa) and (D-VIIIb), also resulted; the isomer isolated on the recrystallization from acetone, D-VIIIa, was identified as a 2,2′-dimer from the same consideration of NMR spectral data, postulated in Scheme 3, as in the case of D-IVa. The 4-methyl proton signal of the other isomer, D-VIIIb, was observed at 2.08 ppm;[10] this fact strongly supports the 5,5′ structure, since a much larger upfield shift would be expected if the carbon at the 4,4′-position is involved

10) Assigned on comparison with that of IXb, as shown in Table 1.

TABLE 2.

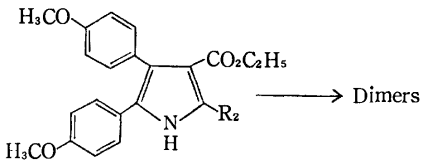

(XVI—XIX) (D-XVI—XVIII)

	R_2	Yield %	Mp °C (decomp.)	IR (CO) cm^{-1}	Formula	Anal. Found % C	H	N	Calcd % C	H	N	Mass (M^+)
D-XVI	C_2H_5	45	130—133	1725	$C_{46}H_{48}O_8N_2$ (756.86)	72.84	6.29	3.66	73.00	6.39	3.70	756
D-XVII	*i*-C_3H_7	10	—65[a]	1725	$C_{48}H_{52}O_8N_2$ (784.91)	73.28	7.43	3.77	73.45	6.68	3.57	—[b]
D-XVIII	*t*-C_4H_9	10	—75[a]	1725	$C_{50}H_{56}O_8N_2$ (812.96)	73.06	6.81	3.26	73.87	6.89	3.45	812
D-XIX	H	0(recovery)										
(D-IV	CH_3	quant.										

a) obscure. b) not detected.

in the bonding, as is shown by the 4-methyl proton signal of (VII).

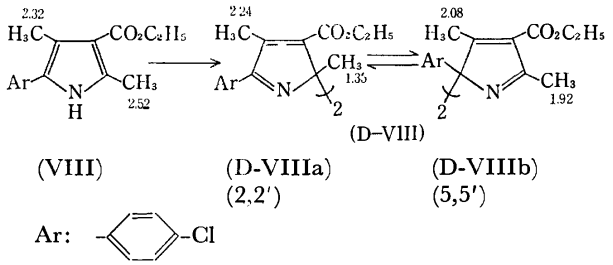

Scheme 3.

It was found that analogous reactions of some other derivatives (IX—XV) gave the corresponding dimers (D-IX—XV) quantitatively, and that each of them consisted of 2,2'- and 5,5'-bispyrrolenines. Their physical properties, spectral data, and occurrence ratio in equilibrium are summarized in Table 1. It is not clear why the 3-alkoxycarbonyl-substituted derivatives give a mixture of the dimers, while the 3-acyl analogues I afforded only 2,2' dimers II. It seems, however, that the steric effect of this difference is not important, since the 3-methoxycarbonyl-substituted compound (X) gives two dimers, while the sterically-not-so-unequivalent 3-propionyl derivative (I, Ar=Ar'=*p*-$CH_3OC_6H_4$-, R=C_2H_5) forms a single dimer.

The Mechanism of the Interconversion between the 2,2'- and 5,5'-Dimers. We consider that the interconversion of the 2,2'-dimers to 5,5'-isomers proceeds *via* a pyrryl radical as an intermediate, from the reasons described below.

Firstly, the conversion of 2,2'-dimers to 5,5'-dimers is inhibited by hydroquinone. A second reason is based on the substituent effects. Kinetic studies by means of NMR showed that the interconversion obeyed first-order kinetics, and the rate constants, $k_{a\to b}$ and $k_{b\to a}$, for the dimers D-IV and D-XIII were estimated to be 2.7×10^{-3}, 1.9×10^{-3} (D-IV) and 0.75×10^{-3}, 0.71×10^{-3} (D-XIII), both at 37.0°C. Thus, a significant increase in the rate constant was observed for the former; this was explainable from the radical stabilizing ability of the *p*-methoxy substituent, as was suggested by Zimmerman *et al.*[3g]

The Effect of Substituents on the Dimerization Reactions. In order to estimate the effect of 2-alkyl substituents on the dimerization reactions, Compounds (XVI—XIX) were examined; the results are listed in Table 2.

Table 2 indicates that the 2-alkyl groups have a direct influence on the yield of the dimers. It is likely that the oxidation of these compounds proceeds *via* pyrryl radicals, as was mentioned before; therefore, it seems reasonable to consider that the yield of the dimers depends mainly upon the reactivity of the intermediate pyrryl radicals. As is shown in Table 2, the order of the yields is as follows; $CH_3>C_2H_5>i$-C_3H_7, *t*-$C_4H_9\gg$H. This order is in accord with that of the stabilizing ability of the radicals by a hyperconjugation effect caused by the 2-alkyl substituents. Thus, in this series, the largest increase in resonance energy can be obtained when R_2 is CH_3 (IV), as is shown below;

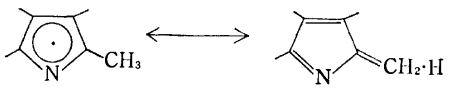

On the other hand, in the case of XIX (R_2=H), which gave no dimer, the intermediate pyrryl radical is less stabilized. When R_2 is isopropyl (XVII) and *t*-butyl (XVIII), however, the remarkable decrease in the yield of the dimers can not be fully explained by a decrease in the hyperconjugation effect. These facts suggest that the dimerization is also markedly subject to steric hindrance by the bulky 2-substituents in the approach of two pyrryl radicals. An analogous steric effect was observed in the case of the acid-catalysed dimerization of 2-alkyl-indole and -benzofuran derivatives.[11,12]

The experimental results, which suggest the effects of substituents at other positions (4 and 5), are shown below.

11) G. F. Smith and A. E. Walters, *J. Chem. Soc.*, **1961**, 940.
12) T. Abe and R. Shimizu, *Nippon Kagaku Zasshi*, **91**, 753 (1970).

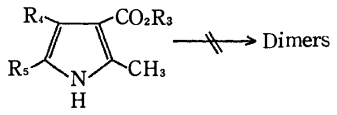

(XX—XXII)

	R_3	R_4	R_5
XX	$CH_2C_6H_5$	p-$CH_3OC_6H_4$	CH_3
XXI	C_2H_5	H	C_6H_5
XXII	C_2H_5	CH_3	CH_3

These results indicate that the 5-aryl substituent is more essential for the dimer formation than that of the 4-position, since 4-alkyl-5-aryl derivatives (VIII, IX and XV) afford the corresponding dimers in good yields, whereas the 4-aryl-5-alkyl compound (XX) gives no dimer and the starting material is recovered. (However, the effect of the 4-alkyl substituent is not entirely negligible, as is shown by the lack of dimerization of Compound XXI (R_4=H).) From this point of view, the fact that the 4,5-dimethyl-substituted compound (XXII) gives no dimer is very understandable.

Finally, these substituent effects show that the 2- and and 5-substituents play an important role in the stabilization of the pyrryl radicals. Similar substituent effects have been suggested in the case of tetraarylpyrryl radicals.[13a,b]

The Properties of the Dimers. Some of the dimers, for example, D-IV and D-XI, exhibit thermochromism in solution due to the reversible dissociation of the dimers into pyrryl radicals; this will be shown in detail in the following paper.

Experimental

All the melting points are uncorrected. The IR spectra were determined by means of Nujol mulls with a Hitachi EPI-S2 spectrophotometer; the mass spectra, with a JEOL-JMS-OIS mass spectrometer, and the NMR spectra, with a Varian A-60 NMR spectrometer, using tetramethylsilane as the internal standard.

Materials. The pyrrolic compounds were synthesized by the methods of Davidson[14] and Knorr[15),16]

Preparation of D-IV. To a stirred solution of IV (1.0 g) in 100 m*l* of ethanol was added gradually an aqueous solution (100 m*l*) of potassium ferricyanide (1.7 g) and potassium hydroxide (0.3 g) at room temperature. The precipitate which was thus formed was filtered and washed with water repeatedly and then dried at room temperature under reduced pressure. This precipitate of D-IV (0.95 g) was pure enough as to require no further purification. The recrystallization of D-IV from acetone gave D-IVa, while from the other solvents, ethanol or benzene-petroleum ether, a mixture of D-IVa and D-IVb was formed.

The oxidation reactions of other pyrrolic compounds were carried out in a similar way.

The Reaction of D-IV with Hydroquinone. To a solution of D-IV (174 mg) in 20 m*l* of benzene, hydroquinone (50 mg) was added, and then the mixture was heated at 80°C for 15 min under a stream of nitrogen. The solution was placed on an alumina column and eluted with benzene. The residue obtained by the evaporation of the solvent was recrystallized from benzene-petroleum ether, yielding 158 mg of colorless needles, mp 138°C, which were found to be identical with IV on a mixed melting point determination and by a comparison of their IR and UV spectra.

D-XIII and D-XIV also afforded the corresponding pyrrolic compounds, XIII and XIV respectively, both in quantitative yields.

The authors wish to thank Dr. G. Sunagawa, the Director of these Laboratories, and Dr. K. Tanabe for encouragement through the course of this work.

13) a) B. S. Tanaseichuk, S. L. Vlasova, A. N. Sunin, and V. E. Gavrilov, *Zh. Org. Khim.*, **5**, 144 (1969). b) B. S. Tanaseichuk, S. L. Vlasova, and E. N. Morozov, *ibid.*, **7**, 1264 (1971).

14) D. Davidson, *J. Org. Chem.*, **3**, 361 (1938).

15) L. Knorr and H. Lange, *Chem. Ber.*, **35**, 2998 (1902).

16) N. Yoshida, K. Tomita, K. Wachi, K. Tanaka, and Y. Iizuka, *Yakugaku Zasshi*, submitted.

Studies of the Synthesis of Furan Compounds. XXVIII.[1] Syntheses and Steric Configurations of 3-(5-Nitro-2-furyl)-2-(2-furyl)acrylonitrile and Its Bromine Derivatives[2]

Yasuhiko KATO, Takashi KUBOYAMA, and Ichiro HIRAO

Laboratory of Organic Synthesis, Department of Chemical Engineering, Kyushu Institute of Technology, Tobata-ku, Kita-kyushu

(Received February 2, 1972)

In continuing a previous report[3] concerning the syntheses and steric configurations of 3-(5-nitro-2-furyl)-2-(2-furyl)acrylic acid derivatives, *trans* and *cis* 3-(5-nitro-2-furyl)-2-(2-furyl)acrylonitrile and their related compounds have been synthesized. The isomerization was involved in the conversion of *cis*-3-(5-nitro-2-furyl)-2-(2-furyl)acrylamide (I) to *trans*-3-(5-nitro-2-furyl)-2-(2-furyl)acrylonitrile (II) upon the treatment of phosphoryl chloride. II was converted to its *cis* isomer (III) by treating it with hydroxylamine, hydrazine hydrate, or hydrochloric acid. II and III were treated with bromine at 5—10°C in carbon tetrachloride to afford dibromo compounds, (3*S* : 5*S* and 3*R* : 5*R*)-(IV) and (3*S* : 5*R* and 3*R* : 5*S*)-3-(5-nitro-2-furyl)-3-bromo-2-(5-bromo-2,5-dihydro-2-furylidene)propionitrile (V) respectively. When the bromination was carried out at a higher temperature (70—73°C), a monobromo compound, *cis*-3-(5-nitro-2-furyl)-2-(5-bromo-2-furyl)acrylonitrile (VI), was obtained from both II and III. VI was also produced by heating IV or V in refluxing acetone. The structures and configurations of these compounds were discussed on the basis of their experimental and spectral data.

3-(5-Nitro-2-furyl)acrylonitrile has been prepared by various methods,[1,4-6] and it gives an amidoxime derivatives upon treatment with hydroxylamine.[1,7] In a similar treatment of 3-(5-nitro-2-furyl)-2-(2-furyl)acrylonitrile with hydroxylamine, the corresponding amidoxime-type compound was not obtained, but a configurational interconversion was observed. In this report, the systheses and steric configurations of *trans* and *cis* 3-(5-nitro-2-furyl)-2-(2-furyl)acrylonitrile and their bromine derivatives will be described.

Results and Discussion

3-(5-Nitro-2-furyl)-2-(2-furyl)acrylonitrile (II) was easily obtained in a good yield from 3-(5-nitro-2-furyl)-2-(2-furyl)acrylamide[8] (I) by treatment with phosphoryl chloride at 50—60°C according to the method described in a previous report.[1] When treated with hydroxylamine at 60—70°C, II was converted to its isomer (III); the results of an elemental analysis of this isomer agreed with the value calculated for II. In this isomerization, the hydroxylamine seems to serve as an isomerization catalyst, much like the hydrazine.[3] In fact, the same isomerization also occurred when II was treated with hydrazine hydrate. Further, the isomerization by a hydroxylamine or hydrazine catalyst was confirmed to be irreversible. In order to compare the structures of II and III with those of the corresponding mother acids and identify them, II and III were both heated with hydrochloric acid. The desired acids, however, were not obtained; II was converted to III, while III remained unchanged.

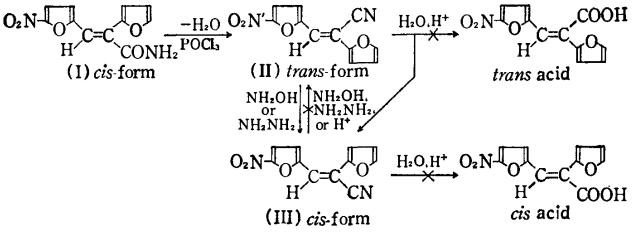

Scheme 1. Preparation and isomerization of II and III.

The IR spectra of II and III showed a C≡N stretching absorption band at about 2240 cm^{-1}. In the UV spectra, as is shown in Fig. 1, two absorption maxima of II, one near 300 mμ and the other near 400 mμ, were observed; the former one showed a hypsochromic shift upon comparison with the corresponding one of III. The extinction coefficient of the former was larger and that of the latter was smaller than in III. The NMR spectra (Fig. 2) indicate precisely that the olefinic proton and the CN group are on the same side of the ethylene double bond in the molecule of III, since the olefinic proton of III reveals a signal in a lower magnetic field than that of II (Δ_{tc} 0.44 ppm), as a result of the magnetic anisotropy of the C≡N bond. Thus, the configuration of III was determined to be *cis*, and that of II, to be *trans*, necessarily.[9] Saikachi *et al.*[8] gave a *trans* symbolism in the configurational nomenclature to the general 3-(5-nitro-2-furyl)-2-(2-furyl)acrylic acid and its amide, I, even though their two furan rings are on the same side of the ethylene bond. In a recent experiment, Kato prepared two isomeric 5-[2-(5-nitro-2-furyl)-1-(2-furyl)-vinyl]-2-amino-1,3,4-thiadiazoles from 3-(5-nitro-2-furyl)-2-(2-furyl)acrylic acid and determined the steric configurations of the 1,3,4-thiadiazoles, the starting acids, and their esters,[3] according to the nomenclature[8] mentioned above; it was necessary to correlate and/or compare the starting acids and esters with those described by Saikachi *et al.* We consider

1) Part XXVII of this series: I. Hirao and Y. Kato, This Bulletin, **45**, 2055 (1972).
2) Presented at the 25th Annual Meeting of the Chemical Society of Japan, Tokyo, October, 1971.
3) Y. Kato, This Bulletin, **44**, 489 (1971).
4) M. Ikeda, *Ann. Rept, Fac. Pharm. Kanazawa Univ.*, No **3**, 25 (1953).
5) A. Sugihara, *Yakugaku Zasshi*, **86**, 525 (1966).
6) H. Saikachi and S. Nakamura, *ibid.*, **88**, 110 (1968).
7) I. Saikawa and A. Takai, *ibid.*, **85**, 948 (1965).
8) H. Saikachi and A. Tanaka, *ibid.* **83**, 147 (1963).
9) If we use the nomenclature presented by Saikachi and Tanaka,[8] II is *cis*, and III, *trans*.

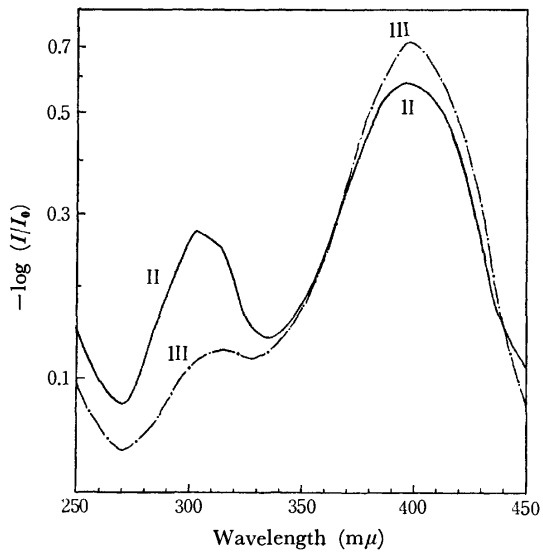

Fig. 1. UV spectra of II and III (in ethanol).
II: 9.3 μg/ml, III: 7.6 μg/ml.

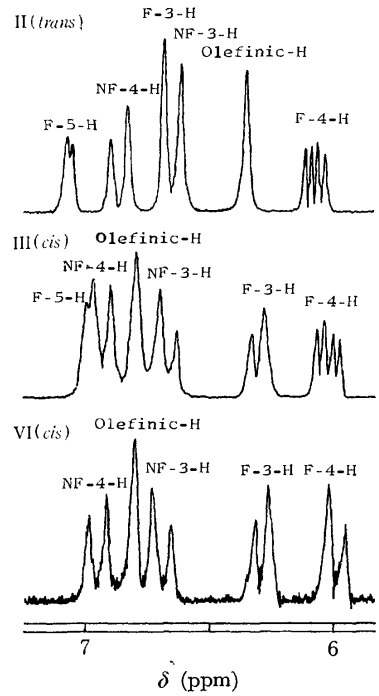

Fig. 2. NMR spectra of II, III, and VI (in CCl_3COOH).

F-5-H: C_5-H of furan ring 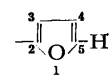

NF-4-H: C_4-H of 5-nitrofuran ring 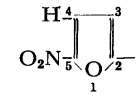

that it is most reasonable and suitable to conclude that the configurations of such an acid and I are *cis*. Furthermore, the symbolism of the compounds previously presented by Kato should also be corrected, changing *cis* to *trans*, and *trans*, to *cis*.

In the above dehydration reaction, it was found that a particularly facile isomerization[3,10] was involved in the conversion of I (*cis*) to II (*trans*) by the action of phosphoryl chloride.

The mass spectral data exhibited no difference between II and III. As is shown in Scheme 2, the molecular ion (M^+, *m/e* 230) is the most prominent (the base peak) and forms a distinct ion peak at mass 200 upon the elimination of NO. The M−NO ion successively loses three carbon monoxides to give the *m/e* 172, 144, and 116 ions. The ion with mass 89 results from the *m/e* 116 ion by the loss of HCN. On the other hand, the molecular ion loses NO_2 and CO fragments by a one-step process to give an ion at mass 156. This ion undergoes the elimination of CO and the subsequent loss of HCN to form *m/e* 128 and 101 ions successively.

On the treatment of II and III with bromine at 5—10°C in carbon tetrachloride, two dibromo compounds, IV and V respectively, were obtained, while in the bromination carried out at 70—73°C a monobromo compound (VI) was produced from both II and III. Moreover, IV and V were found to be unstable both in air and in solvents, and they gave only VI, with the release of hydrogen bromide. For example, this elimination reaction occurred satisfactorily

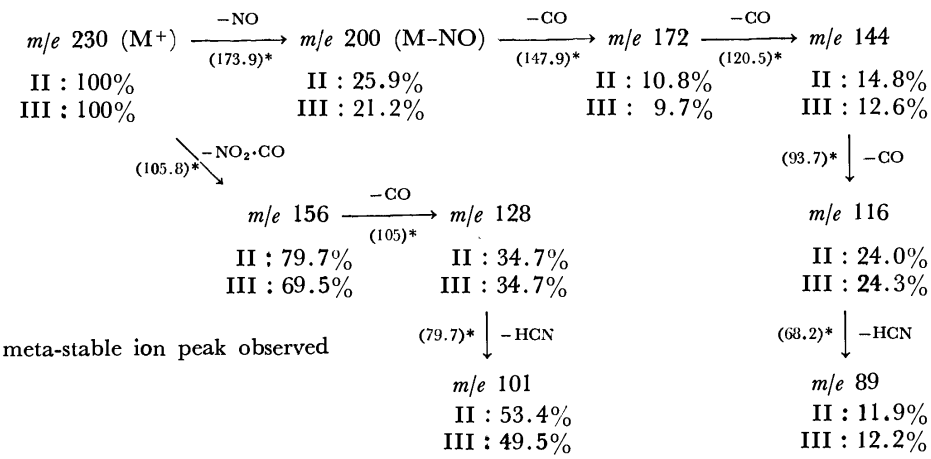

Scheme 2. The fragmentation of II and III.

10) S. M. Kupchan and A. Afonso, *J. Org. Chem.*, **25**, 2217 (1960); see also R. E. Buckles, G. V. Mock, and L. Locatell, *Chem. Rev.*, **55**, 659 (1955).

when a dioxane solution of IV or V was left standing at room temperature or heated in refluxing acetone. The monobromo compound VI was stable, and it was recovered unchanged when heated with hydroxylamine in aqueous ethanol for 2 hr or with 36% hydrochloric acid for 12 hr.

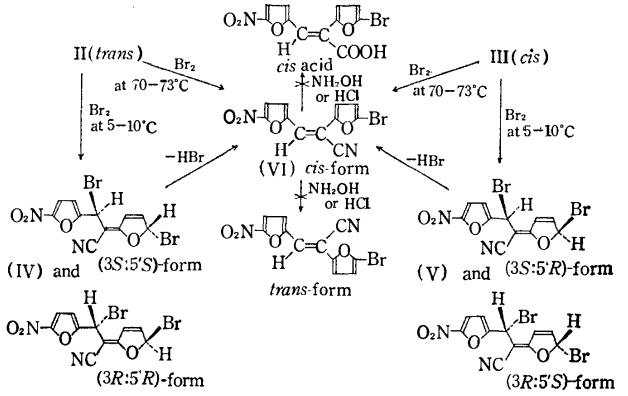

Scheme 3. Preparation of bromo compounds from II and III.

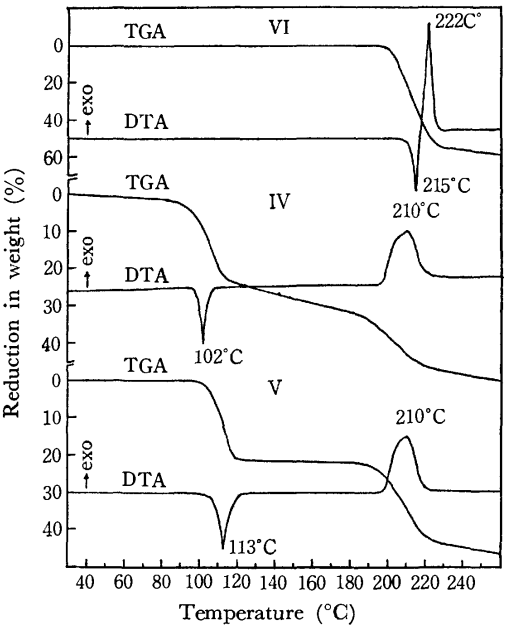

Fig. 3. The thermal analyses of IV, V, and VI at the heating rate of 3°C/min in a nitrogen stream.

The thermostability of IV, V, and VI was investigated by thermogravimetric analysis (TGA) and differential thermal analysis (DTA) under a nitrogen atmosphere. As is shown in Fig. 3, the DTA curve of VI shows an endothermic peak and an exothermic peak at 215°C and 222°C respectively; these peaks coincide with the melting and decomposition points of VI. On the other hand, in the DTA curves of IV and V, the endothermic peak at 102°C for IV and that at 113°C for V, and the exothermic one (210°C for IV and V) are in agreement with the initial and the second stages (80—114°C and 180—220°C for IV, 100—120°C and 185—220°C for V) of the reduction in weight of the corresponding TGA curves. About 23% and 21% of the loss of weight occur for IV and V respectively in the initial stage; this corresponds to the loss of a hydrogen bromide molecule from both IV and V (theoretical: 20.8%). The second stage of the reduction in weight agrees with the decomposition point of VI during the pyrolysis.

The IR spectrum of VI showed two C–H stretching absorption bands and a weak C≡N stretching absorption band at 3150, 3063, and 2240 cm^{-1} respectively. In the spectra of IV and V, the absorbances of the C–H and C≡N stretching bands were more intense than those of VI, and the C–H absorption bands were observed at 3135 and 2985 cm^{-1} for IV, and at 3175, 3085, and 3025 cm^{-1} for V. The C≡N absorption bands appeared at 2220 cm^{-1}. The NMR spectra of IV and V were unsatisfactory because of their lower solubility and greater instability in solvents. On the other hand, VI was clearly determined to be *cis*-3-(5-nitro-2-furyl)-2-(5-bromo-2-furyl)acrylonitrile by a comparison of its NMR spectrum with those of II and III (Fig. 2). The mass spectrum also supported the above structure. In Scheme 4, the molecular ion (M^+, *m/e* 310/308) peak is strong; this undergoes two modes of cleavage. One path is the loss of NO_2 and CO fragments by a one-step process to give an ion at mass 236/234, and the other is the loss of NO, giving rise to the *m/e* 280/278 ion. The following fragmentations are virtually identical with that of II or III, but the substituted position of bromine is demonstrated by the elimination porcess of a bromine atom previous to the loss of the last CO.

Considering the above experimental data and the

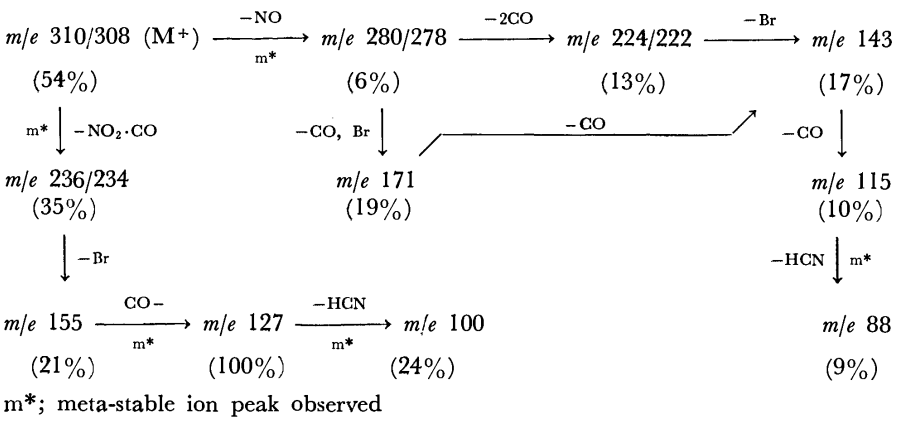

m*; meta-stable ion peak observed

Scheme 4. The fragmentation of VI.

rule of *trans*-addition in the usual bromination, IV and V can be presumed to be (3*S* : 5*S* and 3*R* : 5*R*)- and (3*S* : 5*R* and 3*R* : 5*S*)-3-(5-nitro-2-furyl)-3-bromo-2-(5-bromo-2,5-dihydro-2-furylidene)propionitrile respectively, though more precise data as to the confirmation of the configuration of IV and V could not be obtained. In conclusion, by the elimination of hydrogen bromide, as has been mentioned above, only a sort of monobromo compound, VI, was obtained from both IV and V. It can be suggested that the elimination is not a simple *trans*-one, but that the configurational interconversion is involved in the releasing process of a bromine anion after a proton has been pulled off.

Experimental

The melting and decomposition points are uncorrected. The elemental analyses were carried out with a Yanagimoto CHN Corder, MT-2 type. The ultraviolet absorption spectra (UV) were performed on a Perkin-Elmer Model 202 spectrophotometer. The infrared absorption spectra (IR) were measured with a JASCO Model IRA-2 grating infrared spectrophotometer. The nuclear magnetic resonance spectra (NMR) were determined with a Japan Electron Optics Lab. JNM-C-60HL spectrometer. All the spectra were measured in trichloroacetic acid at 60 MHz, with hexamethyldisiloxane as the internal reference; the chemical shifts are expressed in δ-values. The mass spectra were taken on a Hitachi RMU-6L mass spectrometer by means of a direct insertion (at 70 eV, 3.2 kV). The thermal analyses were carried out with a Chyo Balance and with a Rigaku Denki Thermoflex in a nitrogen stream.

trans-*3-(5-Nitro-2-furyl)-2-(2-furyl)acrylonitrile (II).* A mixture of *cis*-3-(5-nitro-2-furyl)-2-(2-furyl)acrylamide (10 g, 40 mmol), 40 m*l* of phosphoryl chloride, and 2 drops of *N,N*-dimethylaniline was heated at 50—60°C for 45 min, cooled, and then poured into crushed ice with agitation. The solidified crude product was collected and purified by recrystallization from methanol to afford 7.8 g (84.4%) of ochreous needles; mp 132—133°C. UV λ_{max}^{EtOH} mμ (ε): 302 (6800) and 396 (15000). IR (KBr) cm,$^{-1}$: 3143, 3050 (C–H), and 2232 (C≡N). NMR (CCl_3COOH) δ: 6.07 (q, 1H, J=1.7 Hz, furan ring C_4–H), 6.36 (s, 1H, olefinic proton), 6.66 (d, 1H, J=*ca.* 3.5 Hz, furan ring C_3–H; overlapped with nitrofuran ring C_3–H), 6.66 (d, 1H, J=4.0 Hz, nitrofuran ring C_3–H), 6.85 (d, 1H, J=4.0 Hz, nitrofuran ring C_4–H), and 7.07 (d, 1H, J=2.1 Hz, furan ring C_5–H). Mass: the spectral fragmentation is indicated in Scheme 2.

Found: C, 57.40; H, 2.57; N, 12.28%. Calcd for $C_{11}H_6N_2O_4$: C, 57.39; H, 2.61; N, 12.17%.

cis-*3-(5-Nitro-2-furyl)-2-(2-furyl)acrylonitrile (III).*

From the Conversion of II to III with Hydroxylamine: To a stirred, warmed (70—75°C) mixture of II (2 g, 8.7 mmol) and 2 drops of *N,N*-dimethylaniline in 50 m*l* of ethanol, we gradually added an aqueous solution of free hydroxylamine (16 mmol in 10 m*l* of water) during a period of 15—20 min. After the addition, the reaction mixture was heated under reflux for 5 hr. Cooling provided a crude product, and then recrystallization was carried out from methanol. Orange-yellow needles; mp 186—187°C. The yield was 1.96 g (98%). UV λ_{max}^{EtOH} mμ (ε): 316 (5900) and 398 (21800). IR (KBr) cm^{-1}: 3138, 3065 (C–H), and 2240 (C≡N). NMR (CCl_3COOH) δ: 6.03 (q, 1H, J=1.7 Hz, furan ring C_4–H), 6.31 (d, 1H, J=3.4 Hz, furan ring C_3–H), 6.66 (d, 1H, J=4.0 Hz, nitrofuran ring C_3–H), 6.80 (s, 1H, olefinic proton), 6.93 (d, 1H, J=4.0 Hz, nitrofuran ring C_4–H), and 6.98 (d, 1H, J=*ca.* 2 Hz, furan ring C_5–H; overlapped with nitrofuran ring C_4–H). Mass: shown in Scheme 2.

Found: C, 57.75; H, 2.61; N, 12.55%. Calcd for $C_{11}H_6N_2O_4$: C, 57.39; H, 2.61; N, 12.17%.

On the other hand, III was not converted to II under the above conditions.

From the Conversion of II to III with Hydrazine Hydrate: A mixture of II (0.6 g, 2.6 mmol), 80% hydrazine hydrate (0.63 g, 10 mmol), and methanol (100 m*l*) was stirred at 0—5°C for 1 hr, at room temperature for 3 hr, and then at 50—60°C for 3 hr. Cooling subsequently provided 0.5 g (83.3%) of a product which melted at 186—187°C. Recrystallization from methanol gave orange-yellow needles; mp 187—188°C. This product was identified as III by an admixture-test and by a comparison of its IR spectrum with that of the sample prepared by the above procedure. Compound III was not converted to II under the above conditions.

From the Conversion of II to III with Hydrochloric Acid: A mixture of II (1 g, 4.4 mmol) and 36% hydrochloric acid (50 m*l*) was heated under reflux for 50 min. Work-up as above gave 0.98 g (98%) of orange-yellow needles. Mp 186°C; undepressed upon admixture with a sample prepared by the above two methods. In a similar manner, III was recovered without any conversion.

(*3S* : *5S and 3R* : *5R*)-*3-(5-Nitro-2-furyl)-3-bromo-2-(5-bromo-2,5-dihydro-2-furylidene)propionitrile (IV).* To a stirred, cooled (5—10°C) mixture of II (5 g, 21.7 mmol) and carbon tetrachloride (250 m*l*) was added dropwise a solution of bromine (4 g, 22.3 mmol) in 50 m*l* of carbon tetrachloride. The mixture was stirred below 10°C until the bromine had been absorbed completely. The solid product was collected by filtration, washed with cooled dry petroleum ether, and dried on paraffin wax in a cold box. In this way, a 8.4-g portion (quantitative yield) of a pale yellow powder was obtained; it melted, with decomposition, at 102°C. However, the recrystallization of this product could not be achieved from the solvents or solvent mixtures, and the product could not be stored over 3 days; nevertheless, the freshly-prepared product was pure enough for elemental analysis and was used in the following experiments without further purification. IR (KBr) cm^{-1}: 3135, 2985 (C–H), and 2220 (C≡N).

Found: C, 34.27; H, 1.83; N, 6.82%. Calcd for $C_{11}H_6N_2O_4Br_2$: C, 33.86; H, 1.54; N, 7.18%.

(*3S* : *5R and 3R* : *5S*)-*3-(5-Nitro-2-furyl)-3-bromo-2-(5-bromo-2,5-dihydro-2-furylidene)propionitrile (V).* This was prepared by the method used for IV, using 5 g (21.7 mmol) of III. Work-up as above afforded 8.3 g (quantitative) of V as a pale yellow powder; mp 113°C (decomp.). This product was also unstable and gradually decomposed during storage. IR (KBr) cm^{-1}: 3175, 3085, 3025 (C–H), and 2220 (C≡N).

Found: C, 33.53; H, 1.53; N, 6.83%. Calcd: the same value as IV above.

cis-*3-(5-Nitro-2-furyl)-2-(5-bromo-2-furyl)acrylonitrile (VI).* *Procedure A*: A solution of bromine (0.8 g, 5 mmol) in 20 m*l* of carbon tetrachloride was stirred into a warmed (70°C) mixture of 1 g (4.4 mmol) of II (or III) and carbon tetrachloride (50 m*l*) and then the mixture was refluxed for 2 hr. After cooling, the precipitated product was collected, washed with carbon tetrachloride, and then dried. Recrystallization from acetone–dioxane gave 1.2 g (63%) of VI as an orange-red powder, which melted at 218—220°C with decomposition. IR (KBr) cm^{-1}: 3150, 3063 (C–H), and 2240 (C≡N). NMR (CCl_3COOH) δ: 6.00 (d, 1H, J=3.4 Hz, bromofuran ring C_4–H), 6.29 (d, 1H, J=3.4 Hz, bromofuran ring C_3–H), 6.71 (d, 1H, J=4.0 Hz, nitrofuran

ring C_3–H), 6.81 (s, 1H, olefinic proton), and 6.95 (d, 1H, J =4.0 Hz, nitrofuran ring C_4–H). Mass: shown in Scheme 4.

Found: C, 43.17; H, 1.63; N, 8.73%. Calcd for $C_{11}H_5N_2O_4Br$: C, 42.72; H, 1.62; N, 9.06%.

Procedure B: IV or V (each 1 g, 5 mmol) was heated in acetone under reflux for 1 hr, or was dissolved in dioxane and allowed to stand at room temperature for 2 hr. A work-up as above afforded 0.8 g (quantitative) of an orange-red powder; mp 218—220°C (decomp.). This product was identical in its infrared spectrum with an authentic sample of VI.

Found: C, 42.91; H, 1.63; N, 8.81%. Calcd: the same value as VI by *Procedure A*.

This compound, VI, could not be converted to its *trans*-isomer or carboxylic derivative by treatment with hydroxylamine at 70—80°C in aqueous ethanol for 2 hr or by refluxing with 36% hydrochloric acid for 12 hr.

The authors are indebted to Mr. A. Yamamoto and Mr. S. Iwasaki for their experimental assistance.

BULLETIN OF THE CHEMICAL SOCIETY OF JAPAN, VOL. 45, 3169—3171 (1972)

Solvent Shifts of Methyl Proton Resonances of Pinanols and Related Compounds[1]

Toshifumi HIRATA

Department of Chemistry, Faculty of Science, Hiroshima University, Higashisenda-machi, Hiroshima

(Received February 14, 1972)

The chemical shifts of methyl protons of a number of bicyclo[3.1.1]heptanols and their acetates were measured on carbon tetrachloride and benzene in order to examine the correlation between the benzene-induced shifts and the spatial arrangements of the functional groups concerned. Thus, the shifts induced by benzene were found to be useful in establishing both the location and the stereochemistry of methyl protons situated in the vicinity of the hydroxyl or the acetoxyl function in a pinane skeleton.

It has been reported[3-10] that solvent shifts (Δ) of proton resonances can be used in the elucidation of stereochemical problems. Particularly, the empirical rule[3-6] for ketones has been useful in considering these problems. However, attempts to extend the rule to alcohols and their acetates and to find a generalization in these fields have not been successful. In connection with our studies of the stereochemistry and the reaction of pinane derivatives, significant solvent effects were found for the methyl protons of pinanols and their acetates. The author now wishes to report his findings regarding the benzene-induced shifts and to correlate the shifts with the stereochemistry of the functional groups concerned.

Results and Discussion

The benzene-induced shifts ($\Delta=\delta_{CCl_4}-\delta_{C_6H_6}$) were measured for three methyl protons in pinanols

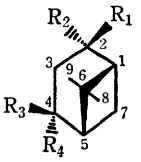

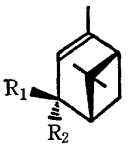

1: R_1=OH, R_2=CH_3, R_3=R_4=H
2: R_1=CH_3, R_2=OH, R_3=R_4=H
3: R_1=OH, R_2=R_3=R_4=H
4: R_1=R_3=R_4=H, R_2=OH
5: R_1=CH_3, R_2=R_4=H, R_3=OH
6: R_1=CH_3, R_2=R_3=H, R_4=OH
15: R_1=OAc, R_2=R_3=R_4=H
16: R_1=R_3=R_4=H, R_2=OAc
17: R_1=CH_3, R_2=R_4=H, R_3=OAc
18: R_1=CH_3, R_2=R_3=H, R_4=OAc

7: R_1=OH, R_2=H
8: R_1=H, R_2=OH
19: R_1=OAc, R_2=H
20: R_1=H, R_2=OAc

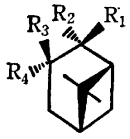

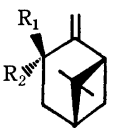

9: R_1=CH_3, R_2=R_4=H, R_3=OH
10: R_1=CH_3, R_2=R_3=H, R_4=OH
11: R_1=R_4=H, R_2=CH_3, R_3=OH
12: R_1=R_3=H, R_2=CH_3, R_4=OH
21: R_1=CH_3, R_2=R_4=H, R_3=OAc
22: R_1=CH_3, R_2=R_3=H, R_4=OAc
23: R_1=R_4=H, R_2=CH_3, R_3=OAc
24: R_1=R_3=H, R_2=CH_3, R_4=OAc

13: R_1=OH, R_2=H
14: R_1=H, R_2=OH
25: R_1=OAc, R_2=H
26: R_1=H, R_2=OAc

and their acetates, which have a known configuration, as is depicted. The results indicated that, in all the cases examined, the 8-methyl protons suffered increased shielding to a considerably large extent, as is shown in Table 1. On the other hand, the methyl

1) This paper forms Part XIX[2] in the Hiroshima University series on "Stereochemical Studies of Monoterpene Compounds."
2) Part XVIII of this series: T. Suga and K. Imamura, This Bulletin, **45**, 2060 (1972).
3) G. Agami and J. -L. Pierre, *Bull. Soc. Chim. Fr.*, **1969**, 1963.
4) D. H. Williams and N. S. Bhacca, *Tetrahedron*, **21**, 2021 (1965).
5) J. D. Connolly and R. McCrindle, *Chem. Ind.* (London), **1965**, 2066.
6) G. J. Karabatsos, G. C. Sonnichsen, N. Hsi, and D. J. Fenoglio, *J. Amer. Chem. Soc.*, **89**, 5068 (1967).
7) J. Ronayne and D. H. Williams, *J. Chem. Soc., B*, **1967**, 540.
8) T. Ledaal, *Tetrahedron Lett.*, **1968**, 1683.
9) P. V. Demarco and L. A. Spangle, *J. Org. Chem.*, **34**, 3205 (1969).
10) E. M. Engler and P. Laszlo, *J. Amer. Chem. Soc.*, **93**, 1317 (1971).

TABLE 1. VALUES (δ_{CCl_4}-$\delta_{C_6H_6}$ ppm) FOR METHYL PROTON RESONANCES AT THE 8-, 9-, AND 10-POSITIONS IN HYDROXYPINANES AND THEIR ACETATES

Compd	$\Delta\delta_{CCl_4-C_6H_6}$ (ppm)		
	C-8	C-9	C-10
2β-hydroxy-10α-pinane (**1**)	+0.09	−0.03	+0.07
2α-hydroxy-10β-pinane (**2**)	+0.09	+0.11	+0.04
2β-hydroxyapopinane (**3**)	+0.05	−0.04	—
2α-hydroxyapopinane (**4**)	+0.10	+0.14	—
4β-hydroxy-10β-pinane (**5**)	+0.02	−0.02	+0.05
4α-hydoxy-10β-pinane (**6**)	+0.10	+0.11	+0.07
4β-hydroxy-pin-2-ene (**7**)	+0.08	−0.07	+0.12
4α-hydroxy-pin-2-ene (**8**)	+0.13	+0.07	+0.13
3β-hydroxy-10β-pinane (**9**)	+0.06	−0.06	0.00
3α-hydroxy-10β-pinane (**10**)	+0.07	+0.11	+0.01
3β-hydroxy-10α-pinane (**11**)	+0.07	0.00	+0.01
3α-hydroxy-10α-pinane (**12**)	+0.08	+0.10	0.00
3β-hydroxy-pin-2(10)-ene (**13**)	+0.13	−0.01	—
3α-hydroxy-pin-2(10)-ene (**14**)	+0.12	+0.06	—
2β-acetoxyapopinane (**15**)	+0.12	+0.04	—
2α-acetoxyapopinane (**16**)	+0.16	+0.18	—
4β-acetoxy-10β-pinane (**17**)	+0.10	−0.01	+0.11
4α-acetoxy-10β-pinane (**18**)	+0.18	+0.25	+0.15
4β-acetoxy-pin-2-ene (**19**)	+0.12	−0.12	+0.19
4α-acetoxy-pin-2-ene (**20**)	+0.21	+0.14	+0.20
3β-acetoxy-10β-pinane (**21**)	+0.10	−0.01	−0.01
3α-acetoxy-10β-pinane (**22**)	+0.14	+0.19	+0.01
3β-acetoxy-10α-pinane (**23**)	+0.14	+0.05	+0.02
3α-acetoxy-10α-pinane (**24**)	+0.09	+0.17	−0.03
3β-acetoxy-pin-2(10)-ene (**25**)	+0.17	−0.02	—
3α-acetoxy-pin-2(10)-ene (**26**)	+0.15	+0.13	—

protons at the 9-position showed a different value of shifts, in dependence on the spatial arrangements between the functional group and the *gem*-dimethyl bridge. Shifts to a lower field were noted for a *cis*-form, and to a higher one, for a *trans*-form. The downfield shifts have been observed[9] for monohydroxy-steroids in which the hydroxyl and the methyl groups are 1,3-diaxial. We observed the same phenomena for 2- or 4-hydroxypinanes and their acetates respectively. For *cis*-3-hydroxypinanes and their acetates, also, downfield shifts or very small upfield shifts were observed, although the 9-methyl and the hydroxyl groups are not perfectly 1,3-diaxial but, rather, those are situated in a nearly diaxial arrangement, as is shown in **9a**. Therefore, it is very likely that the 9-methyl

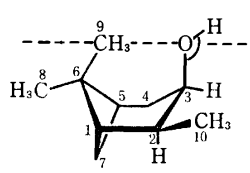

9a

protons of *cis*-3-hydroxypinanes and their acetates suffer decreased shielding by benzene. These observations suggest that the unknown configuration of a hydroxyl or acetoxyl group of pinane derivatives can probably be determined by measuring the benzene-induced shifts of the methyl protons at the 9-position.

On the modification of the rule[3-6] established for ketones, an empirical rule can thus be proposed on the bases of the above observations and the data reported for hydroxy-steroids.[9] As an aid for predicting the benzene-induced shifts, a reference plane is imagined through the hydroxyl oxygen atom at right angles to the carbon-oxygen bond of the hydroxyl group. The Δ values are negative for protons lying on the reference plane; they become positive as they leave the plane. The bonzene-induced shifts of the hydroxylated or the acetoxylated pinane derivatives may be useful in establishing both the location and the stereochemical relationship of protons situated in the vicinity of the hydroxyl or the acetoxyl function.

Experimental

The NMR spectra were measured with a Varian Associates HA-100 spectrometer and a Hitachi Perkin-Elmer R-20 high-resolution spectrometer on the carbon tetrachloride and the benzene solution in a 5% (w/v) concentration at normal probe temperatures (*ca.* 30°C), using tetramethylsilane as the internal standard. The chemical shifts of the proton resonances of the 8-, 9-, and 10-methyl protons of pinanols and their acetates are shown in Table 2, expressed in δ-values (accuracies, $\pm$0.02 ppm). The purity of the samples used was checked by a combination of thin-layer chromatography with silica gel and vapor-phase chromatography using a Hitachi Perkin-Elmer F6-D Gas Chromatagraph with a stainless-steel column (3 mm$\times$1 m) packed with 20% PEG-6000 on Celite (60—80 mesh) at 120—150°C. All the spectral data (IR, NMR and MS) and physical properties of each sample coincided with those of the data reported in the literature and completely supported the structure depicted above.

The 2-hydroxypinanes, (**1**) and (**2**), were generously donated by Ohloff,[11] while the hydroxypinanes, (**5**), (**9**), (**10**), (**11**) and (**12**), had been previously synthesized in our laboratory by the reduction of the appropriate ketones.[12-14] Most of the acetates were prepared from the corresponding alcohols by treating them with acetic anhydride in pyridine, followed by purification with preparative thin-layer chromatography on silica gel, using a mixture of *n*-hexane and ethyl acetate as solvent.

*2-Hydroxyapopinanes (**3**) and (**4**).* A mixture of 1.0 g of (+)-nopinone ($[\alpha]_D^{25}$+20.3°, prepared from (−)-β-pinene by ozonization), 2.6 g of aluminum isopropoxide, and 20 m*l* of isopropyl alcohol was refluxed for 4 hr, and then worked-up following the method in the literature.[15] The oily product (910 mg) thus obtained was subjected to column chromatography on silica gel with a mixture of ethyl acetate and *n*-hexane to give 334 mg of 2β-hydroxyapopinane (**3**) (mp 103.5—104.0°C, lit,[15] mp 101.5—102.0°C; $[\alpha]_D^{25}$−12.0° (*c* 0.75, MeOH); the phthalate, mp 131.0—131.5°C, lit,[15] mp 131.0—131.5°C) and 175 mg of the 2α-epimer (**4**) (mp 35—36°C, lit,[15] mp 37.0—37.5°C; $[\alpha]_D^{25}$−15.2° (*c* 0.67,

11) G. Ohloff and E. Klein, *Tetrahedron*, **18**, 37 (1962).
12) A. F. Regan, *ibid.*, **25**, 3801 (1969).
13) T. Hirata, This Bulletin, **45**, 599 (1972).
14) T. Suga, T. Shishibori, T. Hirata, and T. Matsuura, *ibid.*, **41**, 1180 (1968).
15) S. Winstein and N. J. Holness, *J. Amer. Chem. Soc.*, **77**, 3054 (1955).

TABLE 2. CHEMICAL SHIFTS (δ_{ppm}) OF METHYL PROTON RESONANCES OF HYDROXYPINANES AND THEIR ACETATES IN CARBON TETRACHLORIDE AND BENZENE

Compd	CCl_4			C_6H_6		
	C-8	C-9	C-10	C-8	C-9	C-10
1	1.23	1.10	1.25	1.14	1.13	1.18
2	1.27	0.94	1.46	1.18	0.83	1.23
3	1.23	1.10	—	1.18	1.14	—
4	1.26	0.84	—	1.16	0.70	—
5	1.26	1.19	1.07	1.24	1.21	1.02
6	1.26	0.99	1.00	1.16	0.88	0.93
7	1.34	1.04	1.71	1.26	1.11	1.59
8	1.33	0.87	1.72	1.20	0.80	1.59
9	1.17	1.05	1.05	1.11	1.11	1.05
10	1.24	0.95	1.11	1.17	0.84	1.10
11	1.23	0.92	1.00	1.16	0.92	0.99
12	1.22	0.77	0.94	1.16	0.67	0.94
13	1.28	0.76	—	1.15	0.77	—
14	1.30	0.66	—	1.18	0.60	—
15	1.24	1.06	—	1.12	1.02	—
16	1.22	0.87	—	1.06	0.69	—
17	1.23	1.11	1.06	1.13	1.12	0.95
18	1.28	1.07	1.05	1.10	0.84	0.90
19	1.34	0.98	1.72	1.22	1.12	1.53
20	1.36	0.94	1.74	1.15	0.80	1.54
21	1.18	1.01	0.94	1.08	1.02	0.95
22	1.22	0.99	1.08	1.08	0.80	1.07
23	1.21	0.90	0.96	1.07	0.85	0.94
24	1.20	0.80	0.82	1.11	0.63	0.85
25	1.27	0.78	—	1.10	0.80	—
26	1.29	0.72	—	1.14	0.59	—

MeOH); the phthalate, mp 154—155°C, lit,[15] mp 155.8—156.2°C).

*4β-Hydroxy-pin-2-ene(**7**).* The reduction of 680 mg of (−)-verbenone ($[\alpha]_D^{25}$−208.6°, prepared from (−)-α-pinene by *t*-butyl chromate oxidation) with 200 mg of sodium borohydride gave 600 mg of a crude sample of Compound **7**; this sample was purified by recrystallization followed by preparative gas chromatography with a PEG-6000 column; mp 67—68°C (lit,[16] mp 68—70°C); $[\alpha]_D^{25}$−17.3° (*c* 0.75, MeOH) (lit,[16] $[\alpha]_D^{22}$−16.0°).

*4α-Hydroxy-pin-2-ene (**8**) and Its Acetate (**20**).* Following the procedure previously reported,[17] (−)-α-pinene (3.0 g; $[\alpha]_D^{25}$−39.9°) was oxidized with lead tetraacetate in dry benzene. The oxidation product (2.95 g) was isomerized with glacial acetic acid to give an oily product (2.90 g). Purification by column chromatography on silica gel gave the acetate (**20**) (1.55 g) ($[\alpha]_D^{25}$−128.1° (*c* 1.00, MeOH), lit,[16] $[\alpha]_D^{22}$−135.6°; IR (liq.) 1735 ($OCOCH_3$) and 1650 cm^{-1} (C=C)). The saponification of the acetate (**20**) (0.7 g) with methanolic sodium hydroxide gave the alcohol (**8**) (0.45 g) ($[\alpha]_D^{25}$−107.2° (*c* 0.78, MeOH), lit,[16] $[\alpha]_D^{22}$−112.7°; the *p*-nitrobenzoate; mp 98—99°C, lit,[16] mp 98—98.5°C).

*4α-Hydroxy-10β-pinane (**6**).* The hydrogenation of 4α-hydroxy-pin-2-ene (**8**) (250 mg) in the presence of the Adams catalyst (10 mg) in cyclohexane gave the pinanol (**6**) (249 mg); mp 85—86°C (lit,[12] mp 87°C).

*3β-Hydroxy-pin-2(10)-ene (**13**).* Following the procedure previously reported,[18] pinocarvone (7.0 g; bp 69.0—70.0°C (6.5 mmHg), $[\alpha]_D^{25}$+55.1°, n_D^{25} 1.4959, d_4^{25} 0.9952), which had been prepared from (−)-β-pinene by selenium dioxide oxidation,[18] was treated with bromine and then zinc powder in acetic acid to yield 3β-hydroxy-pin-2(10)-ene (**13**) (3.4 g); mp 49—50°C (lit,[18] mp 50—50.5°C), $[\alpha]_D^{25}$−37.4° (*c* 3.6, MeOH) (lit,[18] $[\alpha]_D$−41°).

*3α-Hydroxy-pin-2(10)-ene (**14**) and Its Acetate (**26**).* Lead tetraacetate (10 g) was added, over 10-min periods, to a stirred suspension of calcium carbonate (1.0 g) in dry benzene (50 m*l*) containing (−)-β-pinene (5.0 g; $[\alpha]_D^{25}$−20.0°); the mixture was then stirred at 60°C for a further 30 min. The reaction mixture was worked up as usual to afford an oily product, which was then subjected to column chromatography on silica gel with a mixture of *n*-hexane and ethyl acetate to give 3α-acetoxy-pin-2(10)-ene (**26**) (3.2 g) ($[\alpha]_D^{25}$−15.9° (*c* 12.8, MeOH), n_D^{25} 1.4739, d_4^{25} 0.9894). The saponification of the acetate (**26**) (0.6 g) with methanolic potassium hydroxide gave the alcohol (**14**) (0.4 g) ($[\alpha]_D^{25}$+60.7° (*c* 1.61, MeOH), lit,[18] $[\alpha]_D$+60°).

The author is thankful to Dr. Takayuki Suga of Hiroshima University for his guidance and encouragement, to Dr. E. von Rudloff of the National Research Council of Canada for measuring the NMR spectra with a Varian Associates HA-100 Spectrometer, and to Dr. G. Ohloff of the Max-Planck Institut for the gift of the samples of pinan-2-ols (**1**) and (**2**).

16) M. A. Cooper, J. R. Salmon, and D. Whittaker, *J. Chem. Soc., B*, **1967**, 1259.
17) G. H. Whithan, *J. Chem. Soc.*, **1960**, 2864.
18) M. P. Hartshorn and A. F. A. Wallis, *ibid.*, **1964**, 5254.

Syntheses and Reactions of Metal Organics. VII. Reactions of *n*-Butoxytitanium Chlorides with Saturated Cyclic Ethers

Norio Yoshino and Takeshi Yoshino

Department of Industrial and Engineering Chemistry, Science University of Tokyo, Kagurazaka, Shinjuku-ku, Tokyo

(Received March 7, 1972)

The reactions of *n*-butoxytitanium chloride, $TiCl_n(O^nBu)_{4-n}$ (n=0,1,2,3,4), with 1,4-dioxane, tetrahydrofuran, and tetrahydropyran have been studied. No adducts have been isolated when n=0,1,but the compounds $TiCl_2(O^nBu)_2\cdot O(CH_2CH_2)_2O$, $TiCl_2(O^nBu)_2\cdot C_4H_8O$, $TiCl_2(O^nBu)_2\cdot C_5H_{10}O$, $TiCl_3(O^nBu)\cdot O(CH_2CH_2)_2O$, $TiCl_3(O^nBu)\cdot 2C_4H_8O$, $TiCl_3(O^nBu)\cdot 2C_5H_{10}O$, $TiCl_4\cdot O(CH_2CH_2)_2O$, $TiCl_4\cdot 2C_4H_8O$ and $TiCl_4\cdot 2C_5H_{10}O$ have been isolated when n=2,3,4. Possible structures for these adducts were discussed on the basis of elemental analysis, IR spectra, NMR spectra, and molecular weights. The adducts undergo hydrolysis very quickly with moisture.

Tin and titanium tetrachlorides have been shown to readily form stable, solid adducts with various ethers, but not silicon and germanium tetrachlorides.[1-4] Formation of tin tetrachloride adducts was understood to result from Lewis acid-base reactions in which the metal atom expanded its valence shell by accepting a pair of electrons from an oxygen atom of each of two molecules of ether to form compounds of the type $MCl_4\cdot 2R_2O$. Failure of silicon and germanium tetrachlorides to form such compounds was attributed to the fact that the size of the chlorine atom causes four of these atoms to fill the coordination sphere of the silicon and germanium atoms so completely as to prevent any reaction with the ether. The effect of the replacement of the chlorine atoms in titanium tetrachloride by larger halogens was studied as regards the tendency for titanium tetrahalides to react with 1,4-dioxane, tetrahydrofuran, and tetrahydropyran. It was shown that the adducts $TiBr_4\cdot O(CH_2CH_2)_2O$, $TiBr_4\cdot 2C_4H_8O$, and $TiBr_4\cdot 2C_5H_{10}O$ have been isolated, but not the pure adduct of titanium tetraiodide with any ether.[4] The formulas were proposed only on the basis of elemental analysis.

It was shown that the reactions of alkoxy- and phenoxy-titanium chlorides with amides and other compounds involve the carbonyl group. The present investigation revealed that the effect of the alkoxy groups replaced the chlorine atoms of titanium tetrachloride in the reaction with ethers. We used saturated cyclic ethers which are more basic than aliphatic ethers.[5] Possible structures for these adducts were discussed on the basis of elemental analysis, IR spectra, NMR spectra, and molecular weights.

Experimental

All the experiments were carried out in a dry atmosphere or nitrogen.

Materials. Titanium tetrachloride (I) was purified by the method of Clabaugh *et al.*[6] Mono-*n*-butoxytitanium trichloride (II), di-*n*-butoxytitanium dichloride (III), tri-*n*-butoxytitanium monochloride (IV), and tetra-*n*-butyltitanate (V) were prepared by the methods of Bradley *et al.*[7,8] and Jennings *et al.*[9]).

1,4-Dioxane (DO) was purified by the method of Fieser.[10] Tetrahydrofuran (THF) and tetrahydropyran (THP) were dried over calcium chloride, and fractionated from over sodium in a dry nitrogen atmosphere using a 30 cm Widmer distilling column. A constant boiling middle fraction was retained. Boiling point data: DO, 100.3—100.5°C; THF, 65.2—65.5°C; THP, 87.5—88.0°C. To avoid the presence of peroxides, the ethers were purified immediately before use.

Apparatus. All-glass apparatus fitted with standard interchangeable joints was used and special precautions were taken to exclude moisture.

Instruments. The IR spectra were measured in a nujol or a liquid film with a Japan Spectroscopic Co. DS-403G Spectrophotometer. The NMR spectra were measured with a Varian A-60 Spectrometer in a solution of carbon tetrachloride with tetramethylsilane as an internal standard. The molecular weights were determined by the cryoscopic method in benzene.

Preparation of $TiCl_4\cdot O(CH_2CH_2)_2O$ (VI). To a stirred solution of I (3.5 g, 0.018 mol) in 30 m*l* of *n*-hexane was added dropwise a solution of DO (4.9 g, 0.054 mol) in 10 m*l* of *n*-hexane, under cooling at 0—5°C. The reaction, highly exothermic, rapidly yielded a yellow solid. After stirring for 1 hr at room temperature for completion of the reaction, the resulting precipitation of VI (5.1 g) was collected by filtration and washed with *n*-hexane and dried in a vacuum at room temperature, decompn. >200°C.

Found: Ti, 17.25; Cl, 50.82; C, 16.81; H, 2.88%. Calcd for $TiCl_4C_4H_8O_2$: Ti, 17.24; Cl, 51.04; C, 17.29; H, 2.90%. IR (nujol) 1044 (ν_{C-O-C}) cm^{-1}.

Preparation of $TiCl_4\cdot 2C_4H_8O$ (VII) and $TiCl_4\cdot 2C_5H_{10}O$ (VIII). The procedure for the preparation of VI was adopted. Yellow powder (8.2 g) of VII was collected by the reaction of I (4.7 g, 0.025 mol) with THF (5.4 g, 0.075 mol), mp 118—120°C.

Found: Ti, 14.53; Cl, 42.71; C, 28.59; H, 4.61%. Calcd for $TiCl_4C_8H_{16}O_2$: Ti, 14.34; Cl, 42.47; C, 28.78; H, 4.83%. IR (nujol) 990 (ν_{C-O-C}) cm^{-1}.

Yellow powder (2.9 g) of VIII was collected by the reaction of I (2.0 g, 0.010 mol) with THP (2.8 g, 0.030 mol), mp

1) H. H. Sisler, W. J. Wilson, B. J. Gibbins, H. H. Betey, B. Pfahler, and R. Mattair, *J. Amer. Chem. Soc.*, **70**, 3818 (1948).
2) H. H. Sisler, H. H. Betey, B. Pfahler, and R. Mattair, *ibid.*, **70**, 3821 (1948).
3) H. H. Sisler, P. M. Hamilton, R. McBeth, and W. Bekebrede, *ibid.*, **75**, 2881 (1953).
4) H. H. Sisler and R. F. Rolsten, *ibid.*, **79**, 1068 (1957).
5) H. E. Wirth, P. I. Slick, *J. Phys. Chem.*, **66**, 2277 (1962).
6) N. S. Clabaugh, R. T. Leslie, and R. Gilchrist, *J. Res. Nat. Bur. Stand.*, **55**, 261 (1955).
7) D. C. Bradley, D. C. Hancock, and W. Wardlaw, *J. Chem. Soc.*, **1952**, 2773.
8) D. C. Bradley, F. M. El-Halim, R. C. Mehrotra, and W. Wardlaw, *ibid.*, **1952**, 4609.
9) J. S. Jennings, W. Wardlaw, and W. J. Way, *ibid.*, **1936**, 637.
10) L. Fieser, "Experiments in Organic Chemistry," D. C. Heath and Co., Boston (1941), Pt. II, p. 368.

TABLE 1. 60MHz-NMR-SPECTRA OF THE ADDUCTS

Adducts	τ[a]	Intensity	Proton number	Attribution
$Cl_2Ti(OCH_2^1CH_2^2CH_2^3CH_3^4)_2\cdot$	4.86—5.52(m)	2	4	H^1
	5.78(*t*, *J*=6.2Hz)	2	4	H^5
	7.80—8.75(m)	6	12	$H^{2,3,6}$
	9.01(*t*, *J*=6.2Hz)	3	6	H^4
$Cl_2Ti(OCH_2^1CH_2^2CH_2^3CH_3^4)_2\cdot$	4.95—5.67(m)	2	4	H^1
	5.73—6.10(m)	2	4	H^5
	7.75—8.83(m)	7	14	$H^{2,3,6,7}$
	9.01(*t*, *J*=6.4Hz)	3	6	H^4
$Cl_2Ti(OCH_2^1CH_2^2CH_2^3CH_3^4)_2\cdot$	5.10—5.50(m)	2	4	H^1
	6.22(s)	4	8	$H^{5,6}$
	7.84—8.76(m)	4	8	$H^{2,3}$
	9.01(*t*, *J*=6.0Hz)	3	6	H^4
$Cl_3Ti(OCH_2^1CH_2^2CH_2^3CH_3^4)\cdot 2$	4.80—5.17(m)	2	2	H^1
	5.71(*t*, *J*=6.9Hz)	8	8	H^5
	7.60—8.80(m)	12	12	$H^{2,3,6}$
	9.01(*t*, *J*=6.2Hz)	3	3	H^4
$Cl_3Ti(OCH_2^1CH_2^2CH_2^3CH_3^4)\cdot 2$	4.75—5.25(m)	2	2	H^1
	5.48—6.07(m)	8	8	H^5
	7.80—8.80(m)	16	16	$H^{2,3,6,7}$
	9.01(*t*, *J*=6.5Hz)	3	3	H^4

a) s, singlet; *t*, triplet; m, multiplet. Internal standard TMS in *ca.* 20% CCl_4 solution.

130—132°C.

Found: Ti, 13.42; Cl, 38.99; C, 33.23; H, 5.61%. Calcd for $TiCl_4C_{10}H_{20}O_2$: Ti, 13.23; Cl, 39.18; C, 33.18; H, 5.57%. IR (nujol) 991 (ν_{C-O-C}) cm^{-1}.

Preparation of $TiCl_3(O^nBu)\cdot O(CH_2CH_2)_2O$ (IX). To a solution of II (4.7 g, 0.020 mol) in 30 m*l* of benzene was added dropwise a solution of DO (7.3 g, 0.080 mol) in 10 m*l* of benzene with stirring at 5—10°C. The reaction was slightly exothermic. A white precipitate was obtained after 25 hr of agitation at room temperature. After filtration, the precipitate was washed with benzene and dried in a vacuum at room temperature, mp 159—160°C.

Found: Ti, 15.28; Cl, 33.50; C, 30.33; H, 5.24%. Calcd for $TiCl_3C_8H_{17}O_3$: Ti, 15.18; Cl, 33.71; C, 30.46; H, 5.43%.

Preparation of $TiCl_3(O^nBu)\cdot 2C_4H_8O$ (X) and $TiCl_3(O^nBu)\cdot 2C_5H_{10}O$ (XI). Excess THF (1.9 g, 0.027 mol) in 10 m*l* of benzene was added to II (2.0 g, 0.009 mol) in 30 m*l* of benzene at 15—20°C. The reaction was not exothermic. No solid was obtained after 25 hr of agitation at room temperature. A brown viscous liquid (3.2 g) of X was obtained after the removal of THF and benzene in the mixture in a vacuum at room temperature. The drying in a vacuum was continued 48 hr, at the end of which time the unit was pressurized to one atmosphere with dry nitrogen.

Found: Ti, 12.99; Cl, 28.46; C, 38.77; H, 6.72%, mol wt, 348±20. Calcd for $TiCl_3C_{12}H_{25}O_3$: Ti, 12.89; Cl, 28.62; C, 38.79; H, 6.78%, mol wt, 371.6. IR (liquid film) 1012 (ν_{C-O-C}) cm^{-1}. NMR (Table 1).

Similarly, brown viscous liquid (7.5 g) of XI was obtained by the reaction of II (4.3 g, 0.019 mol) with THP (4.9 g, 0.057 mol) in benzene.

Found: Ti, 11.94; Cl, 26.49; C, 42.05; H, 7.12%, mol wt, 377±21. Calcd for $TiCl_3C_{14}H_{29}O_3$: Ti, 11.99; Cl, 26.61; C, 42.08; H, 7.31%, mol wt, 399.6. IR (liquid film) 1015 (ν_{C-O-C}) cm^{-1}. NMR (Table 1).

Preparation of $TiCl_2(O^nBu)_2\cdot O(CH_2CH_2)_2O$ (XII), $TiCl_2(O^nBu)_2\cdot C_4H_8O$ (XIII) and $TiCl_2(O^nBu)_2\cdot C_5H_{10}O$ (XIV). The procedure was the same as that for preparation of X. A brown jelly adduct (6.6 g) of XII was obtained from III (5 g, 0.019 mol) and DO (6.6 g, 0.075 mol) in benzene.

Found: Ti, 13.34; Cl, 19.94; C, 40.73; H, 7.44%, mol wt, 361±22. Calcd for $TiCl_2C_{12}H_{26}O_4$: Ti, 13.56; Cl, 20.08; C, 40.81; H, 7.42%, mol wt, 353.1. NMR (Table 1).

A brown viscous liquid (2.6 g) of XIII was prepared from III (2.0 g, 0.008 mol) with THF (4.4 g, 0.060 mol) in benzene.

Found: Ti, 14.36; Cl, 21.12; C, 42.66; H, 7.68%, mol wt, 318±25. Calcd for $TiCl_2C_{12}H_{26}O_3$: Ti, 14.21; Cl, 21.03; C, 42.75; H, 7.68%, mol wt, 337.1. IR (liquid film) 1020 (ν_{C-O-C})cm^{-1}. NMR (Table 1).

A brown viscous liquid (2.8 g) of XIV was obtained from III(2.1 g, 0.008 mol) and THP (2.0 g, 0.024 mol) in benzene.

Found: Ti, 13.63; Cl, 20.49; C, 44.19; H, 8.00%, mol wt, 342±30. Calcd for $TiCl_2C_{13}H_{28}O_3$: Ti, 13.46; Cl, 20.19; C, 44.46; H, 8.04%, mol wt, 351.2. IR (liquid film) 1020(ν_{C-O-C}) cm^{-1}. NMR (Table 1).

IV and V did not react with ethers.

Results and Discussion

The reactivity of I—V with acetanilide (Lewis base) and the IR measurement of the adducts of I—IV with the amide showed that the activity of Lewis acid decreased as reported.[11] I>II>III>IV>V. From this fact, it seems probable that no adducts have been isolated from the reaction of ethers with IV and V, which are less active Lewis acids.

The IR spectra of VII, X, and XIII indicated that the ν_{C-O-C} of THF (1068 cm^{-1}) indicate the shift toward the lower wave numbers, 990, 1012, and 1020 cm^{-1} respectively. The negative shifts of the ν_{C-O-C} of THF (1093 cm^{-1}) for VIII, XI, and XIV were observed at 991, 1015, and 1020 cm^{-1} respectively. The shifts indicate the order of the activity of the Lewis acids (I—III). The shifts of the ν_{C-O-C} of DO (1119 cm^{-1}) in IX and XII were not confirmed because of the mixing of their frequencies with that of the alkoxy group ν_{C-O} in alkoxytitanium chlorides, but we found adduct VI at 1044 cm^{-1}.

NMR spectra of adduct XIII indicate that, for ex-

11) N. Yoshino and T. Yoshino, *Kogyo Kagaku Zasshi*, **71**, 1025 (1968).

ample, the chemical shift of the proton H^5 (τ 5.78) should be lower than that of THF (τ 6.37).[12] Similar lower chemical shifts of the adducts of THF and THP were measured. Thus we conclude that the oxygen atom of THF or THP is coordinated to the titanium atom of each of the alkoxytitanium chlorides.

In the case of the adducts of DO, either two oxygen atoms of DO are coordinated to a titanium atom to form a five-membered-ring chelate, or only one oxygen atom of DO coordinated to a titanium atom, and otherwise two oxygen atoms of DO coordinate to two titanium atoms such as 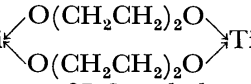 . A comparison of the IR spectrum of DO with that of its adduct VI indicates that the ν_{C-O-C} of the latter is shifted to lower values; this indicates that the oxygen atom of DO is involved in coordination. Observation of the NMR spectra of XII indicates that, the intensity of H^1, $H^{2,3}$, $H^{5,6}$, and H^4 is 2 : 4 : 4 : 3, respectively the results indicate that the two oxygen of DO are on even conditions. Since the molecular weight determination of adduct XII gives a monomeric value, one can believe that two oxygen atoms of DO are coordinated to a titanium atom of III to form a chlate ring.

Sisler[3] and his co-workers have shown the molecular weight of the adduct VIII to be monomeric in benzene.

Molecular weight determination of all the liquid adducts and a jelly adduct indicate them to be monomeric in benzene. X and XI filled the coordination number of titanium 6, but XIII and XIV did not. Thus it seems reasonable to assume that the adducts in non-solution state are dimeric, but monomeric in solution.

The adducts undergo rapid hydrolysis with moisture.

12) F. A. Bovey, "NMR Data Tables for Organic Compounds," Vol. 1, John Wiley & Sons, New York, London, Sydney, p. 73.

BULLETIN OF THE CHEMICAL SOCIETY OF JAPAN, VOL. 45, 3174—3178 (1972)

The Reaction of Troponoid with Ylide. III.[1,2] The Reaction of Tropone with Pyridinium Compounds

Yukio SUGIMURA, Nobuo SOMA, and Yukichi KISHIDA

Central Research Laboratories, Sankyo Co., Ltd., Hiromachi, Shinagawa-ku, Tokyo

(Received March 13, 1972)

Phenacylpyridinium ylide (**2**) reacted with tropone (**1**) to afford 2-hydroxy-2-phenyl-3-phenacyl-2*H*-cyclohepta[*b*]furan (**3**) which was converted into 2-(1′,2′-dibenzoylethyl)tropone (**4**). The reactions of tropone with several kinds of pyridinium bromides (**7**) yielded 2-substituted tropones in the presence of amine, and 1-azaazulene derivatives (**9, 10, 11**) in a one-step formation in the presence of ammonium acetate.

Many reactions of tropone with nucleophiles have been reported since its unique conjugated cyclic trienone system is thought to exert a contribution of the 6π cation system. We earlier reported[3] on the reaction of troponoids with sulfur ylides. In this paper we describe the reactions of tropone with pyridinium salts and pyridinium ylides under various conditions giving 2-substituted tropones and resulting in some one-step azaazulene formations. The chemistry of pyridinium salts and the corresponding ylides has been extensively studied by Krohnke and his collaborator.[4] For example, pyridinium ylide reacted with conjugated carbonyl compounds giving stable pyridinium ylides by Michael addition. The newly formed ylides were utilized to synthesize some heterocyclic systems. Since tropone generally reacts with a nucleophile at 2-position, we at first presumed that the reaction of tropone with pyridinium ylide would give an ylide having tropone moiety or, in the presence of ammonium ion, 1-azaazulene derivatives.

Results

The Reactions of Tropone with Phenacylpyridinium Ylides. When tropone (**1a**) was treated in benzene with phenacylpyridinium ylide prepared by Krohnke's method, red crystals were obtained. Recrystallization gave a pure substance of cycloheptafuran derivative (**3**), mp 134.5—135.5°C in 58.4% yield. The IR showed absorption maxima at 3450 cm^{-1} (OH stretching) and 1680 cm^{-1} (C=O stretching) and the UV exhibited $\lambda_{max}^{ethanol}$ at 240, 320, 335, and 350 nm. The patterns of the spectra closely resembled those of heptafulvene. The elemental analysis and high resolution mass spectrum agreed with the formula $C_{23}H_{18}O_3$ for **3**. **3** was converted into 2-(1′,2′-dibenzoylethyl)tropone (**4a**) on silica gel column chromatography and into a tropylium salt (**5**), $C_{46}H_{34}O_4Cl_6Pt$, by treatment with platinic chloride. The IR of **4a** showed maxima at 1690, 1635, and 1585 but lacked the OH band at 3450 cm^{-1} originally observed in **3**, while the UV highly resembled that of tropone. The elemental analysis and mass spectra agreed with

1) Studies on Seven Membered Ring Compounds XXXVIII. Part II: Y. Sugimura, N. Soma, and Y. Kishida, *Tetrahedron Lett.*, **1971**, 91.

2) A part of this work was reported at the 22nd Annual Meeting of The Chemical Society of Japan (April, 1969, Tokyo): Y. Sugimura and N. Soma, Abstract of papers, p. 1465.

3) Y. Sugimura and N. Soma, *Tetrahedron Lett.*, **1970**, 1721.

4) F. Krohnke, *Angew. Chem.*, **65**, 605 (1953). F. Krohnke and W. Zecher, *Angew. Chem. Int. Ed. Engl.*,, **1**, 626 (1962). F. Krohnke, *ibid.* **2**, 225 (1963), *ibid.* **2**, 380 (1963).

the formula for **4a** (equal to **3**). Analogously, *p*-bromophenacylpyridinium ylide reacted with tropone or 2-phenyltropone (**1b**) giving compounds of mp 195—197°C; $C_{23}H_{16}O_3Br_2$ (**4b**) in 44.5% and mp 191—193°C; $C_{29}H_{20}O_3Br_2$ (**4c**) in 54.5%, respectively. The molecular formulas were obtained by elemental analyses and mass spectra. The NMR (δ ppm, in $CDCl_3$) of **4b** exhibited ABX pattern at 3.20, 3.89, and 5.83 ($J_{AB}=18$, $J_{AX}=4$, and $J_{BX}=10$ Hz), and 6.8—7.4 (5H, protons of tropone ring), 7.5—8.0 (8H, phenyl protons). The spectroscopic data of **4c** were analogous to those of **4b**, except for the presence of one more phenyl group in the tropone system. **4c** was chosen as a representative for further hydrolysis to determine the structure; refluxing in an aqueous sodium hydroxide-methanol solution gave an oily compound (**6**), $C_{22}H_{17}O_2Br$ and *p*-bromobenzoic acid. The UV absorption maxima of **6** at 230, 255, and 330 nm in ethanol strongly suggested the presence of phenyltropone moiety in **6**. Its IR absorption maxima at 1690 (benzoyl C=O) and 1585 cm^{-1} (tropone C=O) and the NMR [in CCl_4: 2.8—3.5 (4H, A_2B_2; $-CH_2-CH_2-$), 6.8—7.0 (2H), and 7.2—7.4 (7H) ascribed to the phenyltroponyl protons, 7.48 (2H) and 7.77 (2H), ascribed to the benzoyl phenyl protons] suggested that **6** should have the structure of 2-(2′-*p*-bromobenzoylethyl)-7-phenyltropone. Mechanistic consideration together with all the evidence enabled us to assign the structure of 2-(1′,2′-di-*p*-bromobenzoylethyl)-7-phenyltropone for **4c**. Thus the structures of **4a** and **4b** were assigned to be 2-(1′,2′-dibenzoylethyl)tropone and 2-(1′,2′-di-*p*-bromobenzoylethyl)tropone, respectively. The assignments led to determination of the structures of **3** and **5** to be 2-hydroxy-2-phenyl-3-phenacyl-2*H*-cyclohepta[*b*]furan and 2-phenyl-3-phenacylcyclohepta[*b*]furanium hexachloroplatinate.[5] Analogously, tropone reacted with *p*-bromophenacylpyridinium bromide in the presence of K_2CO_3 in DMSO to give **4b** in 30% yield.

The Reactions of Pyridinium Salts with Tropone in the Presence of Amines. Application of the forementioned reactions was limited, since phenacylpyridinium ylides are so stable as to be isolated among pyridinium ylides. The use of pyridinium salts in the presence of amine was then attempted in order to extend the applicability of the reactions.

Tropone was added to a suspension of phenacylpyridinium bromide in tetrahydrofuran (THF) containing triethylamine. The reaction product obtained as a partially crystallized syrup was chromatographed to give 2-phenacyltropone (**8a**) in 61% yield. Identification was carried out by mixed melting point and spectroscopy with an authentic sample. Analogous treatments of tropone with *p*-bromophenacylpyridinium bromide (**7b**), ethoxycarbonylmethylpyridinium bromide (**7c**) and acetonylpyridinium

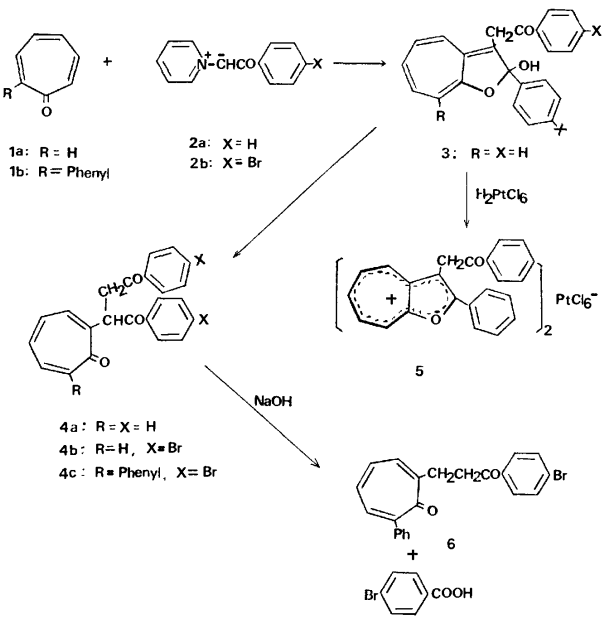

Chart 1.

bromide (**7d**) in the presence of triethylamine gave the corresponding 2-substituted tropones (**8b**, **8c**, and **8d**). Tropone did not react with *o*-cyanobenzylpyridinium bromide (**7e**) in THF–triethylamine, but reacted in ethanol–piperidine giving 2-(*o*-cyanobenzyl)tropone (**8e**) in 45.5% yield. The structure of **8e** was determined by physicochemical data (see Experimental). It is noteworthy that the reaction of tropone with *p*-bromophenacylpyridinium bromide (**7b**) gave only **8b** and not **4b** even when pyridinium bromide and amine were present in excess.

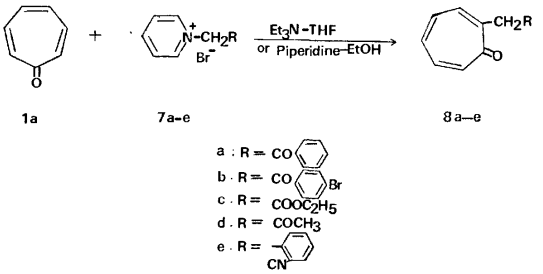

Chart 2.

Synthesis of 1-Azaazulenes. From the fact that the pyridinium ylides attack 2-position of tropone giving 2-substituted tropone, 1-azaazulene derivatives would be formed in the presence of ammonium ion. In fact 2-phenacyltropone (**8a**) was converted into 2-phenyl-1-azaazulene (**9a**) by treatment with ammonium acetate in acetic acid. **9a** was directly obtained by refluxing a mixture of tropone, phenacylpyridinium bromide (**7a**) and ammonium acetate in acetic acid. The principle of the procedure was exactly the same as in the pyridine synthesis by Krohnke.[6] Purple crystals of **9a** were obtained in 21% yield, mp 157—159°C. The structural confirmation was made by physicochemical data, especially the characteristic

5) 2-Phenylcycolhepta[*b*]furanium fluorosulfonate was isolated and the structure was determined (unpublished work). The UV absorption closely resembles that of **5** (see Experimental) and NMR suggests the hybridization of the charge in 10π system. UV: $\lambda_{max}^{ethanol}$ 255, 300, 425 nm. NMR (in DMSO): 7.94 (2H, A_2B_2), 8.25 (2H, A_2B_2), 8.33 (1H, s), 8.8—9.2 (3H. m), 9.3—9.5 (2H, m).

6) W. Zecher and F. Krohnke, *Chem. Ber.*, **94**, 690 (1961).

UV: $\lambda_{max}^{ethanol}$ 237.5 (log ε=4.20), 287.5 (4.58), 312 (4.45), 357 (4.08), and 373 (4.03) nm (the other data are given in Experimental). Analogously, tropone reacted with acetonylpyridinium bromide (**7d**) giving a blue oil of 2-methyl-1-azaazulene (**9b**), which was converted into its picrate, mp 196—198°C. A similar treatment of tropone with cyanomethylpyridinium chloride (**7f**) gave 2-imino-1,2-dihydrocyclohepta-[*b*]pyrrole (**10**), mp 177°C, in 14% yield. Identification of the structure was made by comparison of the spectroscopic data with those of an authentic sample.[7] Tropone also reacted with 2-oxo-3,4-benzocyclohexylpyridinium bromide (**7g**) in the presence of triethylenediamine (DABCO) and ammonium acetate in ethanol to give 12-aza-5,6-dihydronaphth[2,1-*a*]-azulene (**11**) as purple oil. This was dehydrogenated to 12-azanaphth[2,1-*a*]-azulene (**12**), mp 195—197°C, by refluxing with DDQ in benzene. The UV and visible light spectra of $\lambda_{max}^{ethanol}$ 337, 374, and 537 nm indicate characteristics of the structure.

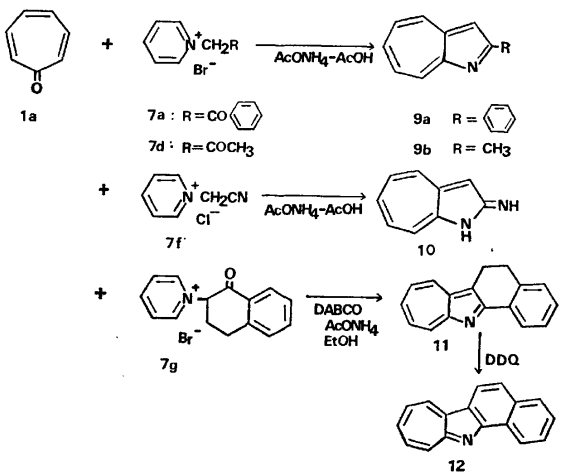

Chart 3.

Discussions

Plausible mechanisms for the formation of **3**, **4**, and **8** are shown in Fig. 1. For **3**, two moles of pyridinium ylide participate in the reaction, such a mode of reaction being very rare.[8] Pyridinium betaine (**13**) formed at first is further attacked by the second ylide to give **14** with concomitant liberation of pyridine, subsequent cyclization affording **15**. By an alternative route, betaine **13** would first cyclize to give **16** which is succeedingly attacked by the second ylide to afford **15** *via* **17**. On the other hand, for the formation of **8**, *viz.*, in the reaction of tropone with a phenacylpyridinium bromide in the presence of amine, the ylide is not present in excess so as to be able to attack **13**, since an equilibrium between the ylide (**2**) and its conjugate acid (**7**) should exist under such reaction conditions and the ylide formed is immediately consumed by tropone to give betaine (**13**). Elimination of pyridine from **13** to give heptafulvene (**18**) would be reasonable because of the stability of **18**. Phenacyltropone (**8b**) thus obtained did not give **4b** by the reaction with ylide (**2b**). Thus a proton exchange between **8** and **2** would not be feasible. Recently Sasaki *et al.*[9] reported that the reaction of tropone with ethoxycarbonylaminopyridinium ylide gave 2-ethoxycarbonylaminotropone and they obtained no 1 : 2-adduct such as **4**. It is not certain whether the difference in reaction pattern is derived from the nucleophilicity of ylide or other factors.

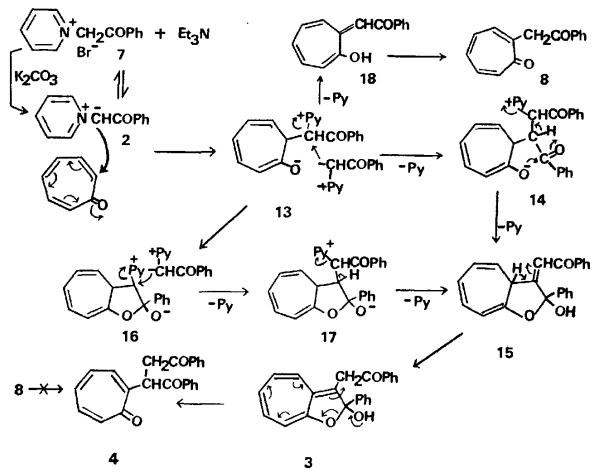

Py: Pyridine Ph: Phenyl

Fig. 1.

The reaction mentioned in the second paragraph is valuable for the preparation of 2-substituted tropones which have hitherto been synthesized from oxaazulanone in lower yields.

Experimental

All melting points are uncorrected. The NMR spectra were taken on Varian A-60 (60 MHz) and HA-100 (100 MHz) spectrometers, and indicated in δ ppm using TMS as an internal standard.

2-Hydroxy-2-phenyl-3-phenacyl-2H-cyclohepta[b]*furan* (**3**). Tropone (2.05 g) was added dropwise under cooling with an ice-water bath to a suspension of phenacylpyridinium ylide (**2a**) in dry benzene (80 m*l*), obtained from phenacylpyridinium bromide (7 g) and potassium carbonate (23 g) by the method of Krohnke. The reaction mixture turned red when the orange crystals of ylide were dissolved. The precipitated white crystals were separated and washed with benzene. The filtrate and washing were combined and evaporated to dryness to give reddish yellow crystals. The crystals were washed with a small amount of benzene and recrystallized from benzene-chloroform to give 1.56 g of the compound, mp 134.5—135.5°C, in 58.6% yield. The mother liquor was chromatographed and the starting tropone (1.22 g) was recovered. Found: C, 80.77; H, 5.40%. Calcd for $C_{23}H_{18}O_3$: C, 80.68; H, 5.30%. IR: ν (Nujol) 3450, 1680 cm^{-1}. UV: $\lambda_{max}^{ethanol}$ 240, 320, 335, 350 nm; $\lambda_{max}^{0.1N\,HCl}$ 250 (log ε=4.51), 292 (4.36), 423 (4.27) nm. High

7) H. Nakao, N. Soma and G. Sunagawa, *Chem. Pharm. Bull.* (Tokyo), **13**, 828 (1965).

8) For the sulfur ylide, some reactions were reported: T. Kunieda and B. Witcop, *J. Org. Chem.*, **35**, 3981 (1970).

9) T. Sasaki, K. Kanematsu, and S. Kakei, Abstract papers of The Annual Meeting of the Organic Synthetic Society of Japan (Nov. 1971, Tokyo) p. 71.

resolution mass spectrum: *m/e* M^+ 342.123. Calcd for $C_{23}H_{18}O_3$: 342.125.

*2-(1',2'-Dibenzoylethyl)tropone (**4a**).* Chromatography of **3** (1.2 g) on silica gel (100 g) with chloroform-benzene gave the compound (100 mg), mp 128—129°C. Found: C, 80.82; H, 5.40%. Calcd for $C_{23}H_{18}O_3$: C, 80.68; H, 5.30%. IR: *ν* (nujol) 1690, 1635, 1585 cm^{-1}. UV: $\lambda_{max}^{ethanol}$ 242 (log ε=4.55), 313 (3.94) nm.

2-Phenyl-3-phenacyclohepta [b] *furanium Hexachloroplatinate (**5**).* An aqueous solution of platinic chloride was added to an ethereal solution of **3** to give precipitates of yellow powder, mp above 300°C. Found: C, 51.89; H, 3.35; Cl, 19.61%. Calcd for $C_{46}H_{34}Cl_6Pt$: C, 52.28; H, 3.24; Cl, 20.1%. IR: *ν* (Nujol) 1690, 1600 cm^{-1}: UV: $\lambda_{max}^{ethanol}$ 252.5, 290, 412 nm.

*2-(1',2'-Di-*p*-bromobenzoylethyl)tropone (**4b**).* Tropone (1 g) was added under cooling with ice-water to a suspension of *p*-bromophenacylpyridinium ylide (**2b**) in dry benzene (40 m*l*) prepared from *p*-bromophenacylpyridinium bromide (5 g) in dry benzene. The reaction mixture was stirred for 2 hr at 0—10°C and the precipitated crystals were separated by filtration and washed with benzene. The filtrate and the washing were combined and evaporated to dryness to give colorless crystals. The crystals were recrystallized from benzene to give 1.87 g of the compound (**4b**), mp 195—197°C, in 44.5% yield. Found: C, 54.95; H, 3.30; Br, 31.94%. Calcd for $C_{23}H_{16}O_3Br_2$: C, 55.21; H, 3.22; Br, 31.95%. IR *ν* (Nujol) 1672, 1575 cm^{-1}. UV: $\lambda_{max}^{0.1N\,HCl}$ 258 (log ε=4.58), 314 (3.92) nm. NMR (in $CDCl_3$): 3.20 (1H, d of d, *J*=18 and 4 Hz), 3.89 (1H, d of d, *J*=18 and 10), 5.83 (1H, d of d, *J*=10 and 4), 6.8—7.4 (5H, m), 7.5—8.0 (8H, m, aromatic). Mass spectrum (*m/e*) 498 ($^{79}Br_2$, M^+), 480 ($^{79}Br_2$) 452 ($^{79}Br_2$), 315 (^{79}Br), 298 (^{79}Br), 183 (^{79}Br), 155 (^{79}Br).

*2-(1',2'-Di-*p*-bromobenzoylethyl)-7-phenyltropone (**4c**)* The compound (1.57 g) was obtained from *p*-bromophenacylpyridinium bromide (5 g) and 2-phenyltropone (910 mg) in 54.5% yield by a similar method to that for the preparation of **4b**, mp 191—193°C. Found: C, 60.34; H, 3.68; Br, 27.43%. Calcd for $C_{29}H_{20}O_3Br_2$: C, 60.44; H, 3.50; Br, 27.74%. IR $\nu_{C=O}$ (Nujol) 1685, 1585 cm^{-1}. UV: $\lambda_{max}^{ethanol}$ 259 (log ε=4.65), 312 (3.98) nm. NMR (in $CDCl_3$): 3.28 (1H, d of d, *J*=17.6 and 4 Hz), 3.93 (1H, d of d, *J*=17.6 and 9.4), 5.84 (1H, d of d, *J*=9.4 and 4), 6.75—7.05 (2H, m), 7.3—8.0 (15 H).

*2-(1',2'-Di-*p*-bromobenzoylethyl)tropone (**4b**) from the Pyridinium Salt.* A suspension of *p*-bromophenacylpyridinium bromide (3.5 g) and K_2CO_3 (0.7 g) in DMSO (30 m*l*) was stirred for 50 min at room temperature and then cooled to 0°C. Tropone (530 mg) was added to the suspension and the reaction mixture was stirred for two hours at 0°C. The reaction mixture was then poured onto ice-water and extracted with chloroform. The extract was washed with water, dried over magnesium sulfate and condensed to give oily residue (1.68 g) which partially crystallized. The crystals were collected by filtration and washed with benzene to give 120 mg of **4b**. The filtrate and washing were combined and subjected to silica gel column chromatography. The benzene-chloroform (1 : 1) eluate gave 190 mg of **4b**. Yield 30%.

*2-(2'-*p*-Bromobenzoylethyl)-7-phenyltropone (**6**).* **4c** (1 g) was added to a solution of sodium hydroxide (524 mg) in 50% aqueous methanol (50 m*l*) and the reaction mixture was refluxed for five hours. After removal of the solvents, the residual oil was extracted with chloroform. The extract was washed with water, dried over magnesium sulfate and condensed to give a partially crystallized syrup. The crystals were collected by filtration to recover the starting **4c** (350 mg). The filtrate was purified by silica gel column chromatography to afford 170 mg of compound (**6**) as syrup. Found: C, 66.70; H, 4.59; Br, 20.04%. Calcd for $C_{22}H_{17}O_2Br$: C, 67.17; H, 4.36; Br, 20.32%. IR $\nu_{C=O}$ (liquid) 1685, 1585 cm^{-1}. UV: $\lambda_{max}^{ethanol}$ 230, 255, 330 nm. NMR (in $CDCl_3$): 2.9—3.4 (4H, A_2B_2 pattern), 6.8—7.0 (2H, m), 7.2—7.4 (7H), 7.48 and 7.77 (each 2H, A_2B_2).

*2-Phenacyltropone (**8a**).* Triethylamine (1 m*l*) was added to a suspension of phenacylpyridinium bromide (**7a**, 2.78 g) in tetrahydrofuran (14 m*l*) and the reaction mixture was stirred for fifteen minutes at room temperature. To this was added a tetrahydrofuran solution of tropone (1.06 g/10 m*l*) and the whole mixture was stirred overnight at room temperature. The precipitated crystals were separated by filtration and the filtrate was condensed to give a syrup, which was purified by silica gel dry column chromatography to afford 2-phenacyltropone (**8a**, 1.43 g) in 61% yield. **8a**, mp 113—113.5°C, was identified with an authentic sample by spectrometry.

2-p-*Bromophenacyltropone (**8b**).* The compound (**8b**, 1.21 g) was obtained from *p*-bromophenacylpyridinium bromide (1.8 g), triethylamine (0.6 m*l*), and tropone (0.5 g) in 80% yield by a similar method to that for the preparation of **8a**, mp 102—104°C. Found: C, 59.45; H, 3.78; Br, 26.16%. Calcd for $C_{15}H_{11}O_2Br$: C, 59.40; H, 3.66; Br, 26.35%. IR: $\nu_{C=O}$ (nujol) 1685, 1585 cm^{-1}. NMR (in $CDCl_3$): 4.23 (2H, s), 6.9—7.3 (4H, m), 7.3—7.55 (1H, m), 7.67 (2H, A_2B_2), 8.00 (2H, A_2B_2).

*2-Ethoxycarbonylmethyltropone (**8c**).* The compound (**8c**, 0.95 g) was obtained from ethoxycarbonylmethylpyridinium bromide (**7c**, 2.46 g), triethylamine (1 m*l*), and tropone (1.0 g) in 63% yield (considering the recovery of the starting tropone, 0.42 g) by a similar method to that for the preparation of **8a**, mp 66°C (recrystallized from isopropyl ether). Found: C, 66.42; H, 6.93%. Calcd for $C_{11}H_{12}O_3$: C, 66.65; H, 6.71%. IR$\nu_{C=O}$ (Nujol) 1740, 1585 cm^{-1}. NMR (in $CDCl_3$): 1.27 (3H, t, *J*=7 Hz), 3.62 (2H, s) 4.20 (2H, q, *J*=7), 6.85—7.50 (5H, m).

*2-Acetonyltropone (**8d**).* The compound (**8d**, 1.47 g) was obtained from acetonylpyridinium bromide (**7d**, 2.16 g), triethylamine (1 m*l*), and tropone (1.06 g) in 95% yield by a similar method to that for the preparation of **8a**. **8d** was a yellow oil whose purity was checked by vpc. (PEG 10% column). Found: C, 71.54; H, 6.83%. Calcd for $C_9H_{10}O_2$: C, 71.98; H, 6.71%. IR: $\nu_{C=O}$ (liquid) 1715, 1585 cm^{-1}. NMR (in $CDCl_3$): 2.30 (3H, s), 3.68 (2H, s), 6.85—7.40 (5H, m).

2-o-*Cyanobenzyltropone (**8e**).* Piperidine (1 m*l*) was added to a solution of *o*-cyanotolylpyridinium bromide (**7e**, 2.77 g) in ethanol (10 m*l*) and the reaction mixture was stirred for ten minutes. Tropone (1.06 g) was then added. After being left to stand overnight at room temperature, the reaction mixture was poured onto ice-water and extracted with chloroform. The extract was washed with water, dried over magnesium sulfate, and condensed to give a syrup. The residual syrup was purified by silica gel dry column chromatography to afford 503 mg of the compound **8e** as colorless crystals which were recrystallized from chloroform-isopropyl ether, mp 110—112°C. Found: C, 81.40; H, 5.13; N, 6.18%. Calcd for $C_{15}H_{11}ON$: C, 81.43; H, 5.01; N, 6.33%. IR $\nu_{C=O}$ (Nujol) 1575, $\nu_{C\equiv N}$ 2220 cm^{-1}. NMR (in $CDCl_3$) 4.22 (2H, s), 6.9—7.8 (11H, m).

*2-Phenyl-1-azaazulene (**9a**).* Tropone (2.12 g) was added at room temperature to a solution of phenacylpyridinium bromide (**7a**, 5.6 g) and ammonium acetate (8 g) in acetic acid (40 m*l*) and the reaction mixture was stirred

and heated to refluxing. The reaction mixture turned dark red at about 80°C and black at refluxing temperature. After refluxing for two hours, the solvent was evaporated and the residual syrup was poured onto ice-water and allowed to stand overnight at room temperature. The precipitates were filtered off with the aid of celite and washed with chloroform. The filtrate and washing were combined and extracted with chloroform. The chloroform extract was washed with water, dried over magnesium sulfate and condensed to give reddish purple crystals of the compound (**9a**, 850 mg) in 21% yield, mp 157—159°C (recrystallized from benzene-cyclohexane). Found: C, 87.71; H, 5.61; N, 6.78%. Calcd for $C_{15}H_{11}N$: C, 87.77; H, 5.40; N, 6.82%. UV: $\lambda_{max}^{ethanol}$ 237.5 (log ε=4.20), 287.5 (4.58), 312 (4.45), 357 (4.08), 373 (4.03) nm. NMR (in $CDCl_3$): 7.3—7.9 (7H, m), 8.3—8.9 (4H, m). Mass spectrum (*m/e*): 205 (M^+), 190, 178, 176, 151, 127, 102.

*2-Methyl-1-azaazulene (**9b**).* Tropone (3.18 g) was added at room temperature to a solution of acetonylpyridinium bromide (**7b**, 6.48 g) and ammonium acetate (12 g) acetic acid (60 m*l*). The reaction mixture was stirred and heated to refluxing. The mixture then turned dark brown. After refluxing for one hour, the solvent was evaporated and the residual syrup was poured onto ice-water. The precipitate was filtered off with the aid of celite and washed with chloroform. The combined filtrate and washing were neutralized with 10% aqueous sodium hydroxide solution and extracted with chloroform. The extract was washed with water, dried over magnesium sulfate and condensed to give a dark green syrup which was subjected to alumina column chromatography. From the benzene eluate 970 mg of the compound (**9b**) was obtained as a blue syrup (23%). **9b** was converted into its picrate of green crystal, mp 196—198°C, by treatment with an ethanol solution of picric acid. Picrate of **9b**: Found: C, 51.54; H, 3.75; N, 14.61%. Calcd for $C_{16}H_{12}N_4O_7$: C, 51.62; H, 3.25; N, 15.05%.

2-Imino-1,2-dihydrocyclohepta[b]*pyrrole (**10**).* Tropone (2.12 g) was added at room temperature to a solution of cyanomethylpyridinium chloride (**7g**, 3.09 g) and ammonium acetate (8 g) in acetic acid (30 m*l*) and the reaction mixture was stirred and refluxed for seven hours. After evaporation of the solvent, the residue was poured onto ice-water and allowed to stand overnight at room temperature. The precipitates were filtered off with the aid of celite, and washed with water. The combined filtrate and washing were washed with chloroform, neutralized with 10%-aqueous sodium hydroxide solution and extracted with chloroform. The chloroform extract was washed with water, dried over magnesium sulfate and condensed to give the compound as brown crystals, mp 175—177°C (recrystallized from benzene), 0.4 g (yield 14%). Found: C, 74.80; H, 5.63; N, 19.36%. Calcd for $C_9H_8N_2$: C, 74.97; H, 5.59; N, 19.43%.

12-Aza-5,6-dihydronaphth[*2,1*-a]*azulene (**11**).* 2-Oxo-3,4-benzocyclohexylpyridinium bromide (3.04 g) was added to a solution of triethylenediamine (1.12 g) and ammonium acetate (1 g) in ethanol (20 m*l*) and the reaction mixture was stirred at 50°C for ten minutes. Tropone (1.06 g) was added and the whole mixture was refluxed for five hours. The precipitated crystals were then filtered off and the filtrate was condensed to give a partially crystallized syrup. The crystals were filtered off and washed with benzene. The combined filtrate and washing were subjected to silica gel dry column chromatography. After development with benzene-ethyl acetate (4 : 1), each fraction of R_f 0.2 and 0.1 was collected and extracted with chloroform. The starting tropone (0.7 g) was recovered from the former the compound **11** (170 mg) as a purple syrup from the latter. Mass spectrum (*m/e*): 231 (M^+, base peak), 230, 202, 121, 93. UV: $\lambda_{max}^{ethanol}$ 244, 292, 324, 502 nm. NMR (in $CDCl_3$): 3.13 (4H, s), 6.7—7.3 (6H, m), 8.1—9.0 (3H, m).

12-Azanaphth[*2,1*-a]*azulene (**12**).* A solution of **11** (140 mg) and DDQ (300 mg) in benzene (20 m*l*) was refluxed for two hours. The reaction mixture was then poured onto 10%-aqueous sodium hydroxide solution and extracted with chloroform. The chloroform extract was washed with water, dried over magnesium sulfate and condensed to give violet crystals of the compound (**12**) which were recrystallized from benzene-*n*-hexane, mp 195—197°C, 60 mg. Found: C, 89.13; H, 4.76; N, 6.02%. Calcd for $C_{17}H_{11}N$: C, 89.05; H, 4.84; N, 6.11%. Mass spectrum (*m/e*): 229 (M^+, base peak), 205, 203, 202, 200, 178, 177, 176, 175, 174. UV: $\lambda_{max}^{ethanol}$ 337, 374, 537 nm. NMR (in $CDCl_3$) 7.6—8.3 (8H, m), 8.7—9.2 (3H, m).

We are grateful to Professor T. Nozoe for his helpful discussion.

The Kinetic Study on the Reaction of Oxaziridine with Tri-*n*-Butylphosphine

Seizo TAMAGAKI, Keishi SAKAKI, and Shigeru OAE

Department of Applied Chemistry, Faculty of Engineering, Osaka City University, Sugimoto-cho, Sumiyoshiku, Osaka

(Received March 24, 1972)

The mechanism of deoxygenation reaction of oxaziridine with trivalent phosphine was kinetically examined by changing substituents, solvents, and temperatures. The reaction proceeds through an attack of phosphine on oxgen in a concerted manner rather than on nitrogen or carbon, eventually producing the corresponding imine and phosphine oxide. The mechanism of the title reaction was compared with those of similar deoxygenations of epoxide and thioepoxide.

Oxaziridines are three-membered ring compounds bearing an active oxygen like organic peroxides and can be assayed iodometrically with potassium iodide in acetic acid. Generally, oxaziridine ring is cleavaged slowly by treatment with strong acids, but fairly stable to weakly basic reagents. The stability of the heterocycle varies sharply with the nature and number of substituents.[1] However, the reactions of oxaziridines with various nucleophiles have not been extensively explored.[2]

The present paper describes a detailed kinetic study on the reaction of oxaziridine with tervalent phosphorous compound in order to clarify the mechanism of the reaction in comparison with those of the epoxides and thioepoxides.[3]

Experimental

Materials. *Oxaziridines*: Oxaziridines were prepared by per-acid oxidation of Shiff's bases according to the method described previously.[4] The physical properties of Schiff's bases and oxaziridines are listed in Table 1 together with the NMR spectral data in Table 2.

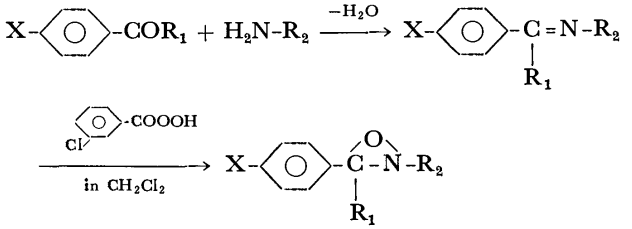

Tri-n-butylphosphine: Commercial phosphine was purified by repeated distillation, bp 128—130°/27 mmHg (lit, 149.5°/50 mmHg).

Solvent: Commercial acetonitrile and special analytical grade *n*-hexane were dried over phosphorous pentoxide and distilled just before use.

Product Analysis. The reaction of 2-alkyl-3-aryloxaziridines with triphenylphosphine or tri-*n*-butylphosphine at room temperature quantitatively afforded the corresponding imines and the phosphine oxides. The product analysis was readily performed by measuring the NMR signals of the methyne protons of both oxaziridines and imines.

Kinetics. A typical procedure is as follows: 2-*t*-butyl-3-(*p*-chlorophenyl)oxaziridine (74.03 mg, 3.5×10^{-4} mol) was dissolved in 50 m*l* acetonitrile. Tri-*n*-butylphosphine (141.4 mg, 7×10^{-4} mol) was also dissolved in 50 m*l* of the same solvent. Five m*l* of each solution was mixed in a reaction vessel which was kept at 50.0°C in a thermostat. Accordingly, the concentrations of the oxaziridine and the phosphine at the initial reaction stage were 3.5×10^{-3} mol/*l* and 7×10^{-3} mol/*l*, respectively. Every ten minute an aliquot (1 m*l*) was withdrawn and poured into 50 m*l* of acetonitrile in order to stop the reaction. The rate was followed by measuring the concentration of the imine produced by means of UV spectrometer. The second-order rate constants were calculated by the integral form (2) of the differential equation (1), where a and b signify the initial concentrations of the oxaziridine and the phosphine, respectively,

$$dx/dt = k_2(a-x)(b-x) \quad (1)$$

$$1/(b-a)\ln(b-x)a/(a-x)b = k_2t \quad (2)$$

while, x is the amount of the imine formed at the given time (t) from the start and k_2 is the second-order rate constant. A typical run is shown in Fig. 2.

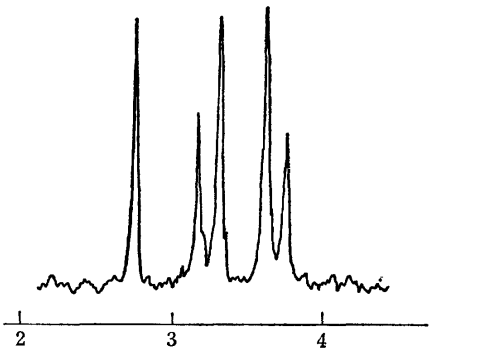

Fig. 1. NMR spectrum of reaction product of *p*-chlorophenyl-*t*-butyl-oxaziridine with phosphine.

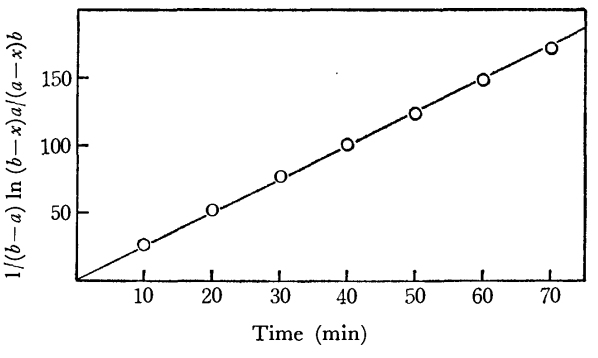

Fig. 2. Deoxygenation of 2-*t*-butyl-3-(*p*-chlorophenyl)oxaziridine with tri-*n*-butylphosphine in acetonitrile at 50°C.

1) W. D. Emmons, *J. Amer. Chem. Soc.*, **79**, 5739 (1957). E. Schmitz and D. Murawski, *Chem. Ber.*, **98**, 2525 (1965).
2) D. St. C. Black and K. G. Watson, *Angew. Chem.*, **83**, 355 (1971).
3) L. Horner and E. Jurgens, *Chem. Ber.*, **90**, 2184 (1957).
4) W. D. Emmons, *J. Amer. Chem. Soc.*, **78**, 6208 (1956); *ibid.*, **79**, 5739 (1957). R. G. Pews, *J. Org. Chem.*, **32**, 1629 (1967).

Table 1. Physical properties of oxaziridines and Schiff's bases

R_1	R_2	X	Mp or bp	Mp or bp
H	*t*-Bu	NO_2	63—63.5°C (lit, 65—66°C)	74—74.5°C (lit, 73—75°C)
H	*n*-Pr	NO_2	a)	50.5—51.5°C (lit, 53.5°C)
CH_3	*n*-Pr	NO_2	a)	b)
H	*t*-Bu	Cl	62—64°C	33—35°C
H	*t*-Bu	H	27—28°C (lit, 61—63°C/0.3 mmHg)	89—91°C/11 mmHg
H	*t*-Bu	CH_3	65—70°C	97°C/5 mmHg

a) Purified by tlc and used without further purification.
b) Used for subsequent oxidation without any purification.

Table 2. Spectral data of some oxaziridines

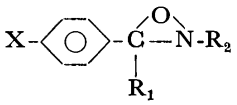

R_1	R_2	X	NMR (τ) in $CDCl_3$
H	*t*-Bu	NO_2	1.95 q ; 5.12 s ; 8.75 s ;
H	*n*-Pr	NO_2	2.06 q ; 5.37 s ; 7.10 m; 8.20 m; 8.91 t
CH_3	*n*-Pr	NO_2	1.96 q ; 7.65 t ; 8.11 s ; 8.36 m; 9.01 t
H	*t*-Bu	Cl	2.52 s ; 5.25 s ; 8.75 s ;
H	*t*-Bu	H	2.53 s ; 5.28 s ; 8.80 s ;
H	*t*-Bu	H	2.73 q ; 5.35 s ; 7.65 s ; 8.82 s

Table 3. Second-order rate constants for deoxygenation reaction at 50.1°C in various solvents

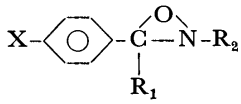

R_1	R_2	X	k_2, *l*/mol·sec in *n*-hexane	k_2, *l*/mol·sec in CH_3CN	k_2, *l*/mol·sec in EtOH
H	*t*-Bu	NO_2	1.087×10^{-1}	1.46×10^{-1}	
H	*n*-Pr	NO_2	1.61×10^{-1}		
CH_3	*n*-Pr	NO_2	4.44×10^{-2}		
H	*t*-Bu	Cl	3.55×10^{-2}	4.28×10^{-2}	6.81×10^{-2}
H	*t*-Bu	H	1.69×10^{-2}	1.61×10^{-2}	
H	*t*-Bu	CH_3	1.07×10^{-2}	1.44×10^{-2}	

Results and Discussion

The second-order rate constants obtained in the deoxygenation reaction of a few substituted oxaziridines with tri-*n*-butylphosphine are given in Table 3 and the activation parameters are represented in Table 4.

A straight Hammett line was obtained by plotting log k values against sigma values as shown in Fig. 3 and a rho values of +1.12 in acetonitrile and +1.06 in *n*-hexane were obtained. Accordingly, the reactivity increases with an electron-withdrawing *para*-substituent in phenyl ring. This observation, together with the lack of reactivity of the poorly nucleophilic tri-

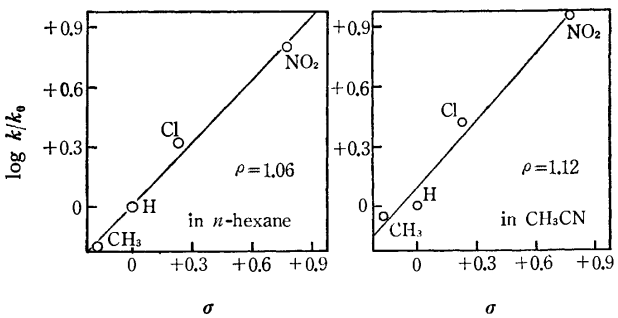

Fig. 3. Correlation of second-order rate constants with Hammett sigma values.

TABLE 4. SECOND-ORDER RATE CONSTANT FOR DEOXYGENATION OF 2-*tert*-BUTYL-3-(*p*-CHLOROPHENYL)OXAZIRIDINE WITH TRI-*n*-BUTYLPHOSPHINE AT VARIOUS TEMPERATURE

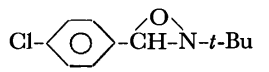

React. temp.	k_2 in CH_3CN, l/mol·sec	React. temp.	k_2 in *n*-hexane, l/mol·sec
40.3°C	2.28×10^{-2}	39.9°C	1.82×10^{-2}
50.1°C	4.28×10^{-2}	50.1°C	3.55×10^{-2}
59.0°C	7.27×10^{-2}	55.2°C	4.22×10^{-2}
		59.9°C	5.76×10^{-2}
E_a=12.1 kcal/mol		E_a=11.7 kcal/mol	
$\Delta S^{\neq}$=−29.2 e. u.		$\Delta S^{\neq}$=−33.4 e. u.	

phenylphosphite in the deoxygenation, suggests that the reaction involves the nucleophilic attack of the trivalent phosphine on the oxaziridine ring.

In general, from these data we may conclude that the rate of reaction is not much affected by the change in the dielectric constants of the reaction media. Even in ethanol which is known to act as protonating solvent, the rate increase was only less than two fold as compared with that in acetonitrile, although the values of k_2 are not very accurate due to the decomposition of phosphine itself in ethanol.

In the reaction of the oxaziridine with a trivalent phosphorous compound which is usually a softer nucleophile and a good deoxygenating or desulfurizing reagent, the deoxygenation reaction takes place instantaneously even at room temperature in benzene, *n*-hexane, and actonitrile.

It has been well known that epoxides were also readily deoxygenated by trivalent phosphines to afford the corresponding phosphine oxides and olefins.[5] The mechanism of this reaction has been investigated extensively and is known to involve the nucleophilic attack of the phosphine on the carbon of the epoxide to form the betaine as an intermediate, as shown below.

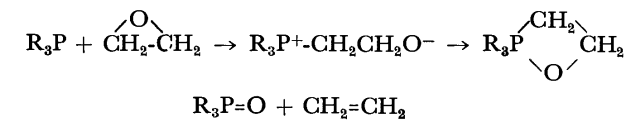

$$R_3P=O + CH_2=CH_2$$

However, this mechanism can explain only one side of the reaction. Other stereochemical studies indicate that the reaction is better explained by the scheme involving the direct attack of the phosphine on the oxygen atom of the epoxide.[5]

As for analogous reaction of episulfide, Neureiter *et al.*[6a] and Denney[6b] have concluded that both the direct attack of the phosphine on the sulfur atom and the subsequent desulfurization are completely stereospecific.[6]

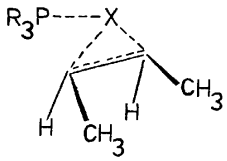

X = O or S

The results in Table 3 indicate that in the deoxygenation reaction of oxaziridines the effect of the change of the solvent from nonpolar to polar solvent on rate of the reaction is found insignificant like in the desulfurization reaction of the thioepoxide.[6] This fact is in a marked contrast to the results by Bartlett in the desulfurization reaction of elemental sulfur with trialkyl phosphine in which the increase in polarity of solvent resulted in a sharp increase in reaction rate by over several hundred fold.[7]

Therefore, based on these observations and considerations we may conclude that the structure of the transition state for the deoxygenation is assumed not to be like (A) which has a large charge separation, but like that (B) which is essentially non-polar. This is essentially a concerted process and dose not require any appreciable charge separation in the transition state.

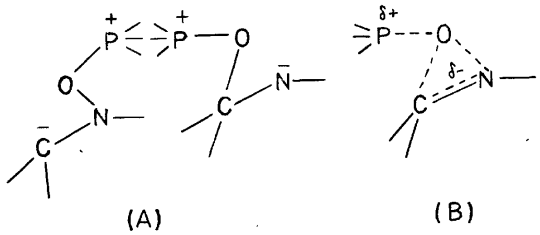

(A) (B)

However, it should be open to question whether the phosphine exclusively attacks the oxygen atom rather than the carbon or nitrogen atom, because there are three possible attacking sites by a nucleophile in the oxaziridine ring at the initial step of the reaction, *i.e.*, either carbon (a) or nitrogen (b) or oxygen atom (c).

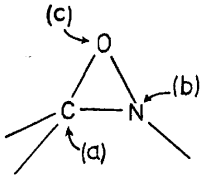

The following observation may be taken as evidence to confirm the attacking on oxygen. Substitution of *t*-butyl group on the nitrogen atom by the less sterically hindered *n*-propyl group results in the rate-increase of only 1.5. In a normal nucleophilic substitution reaction the difference in steric effects by changing the group from *n*-propyl to *tert*-butyl may be estimated as at least over ten.[8] Thus the attacking site can not be the nitrogen atom.

5) G. Witting and W. Haag, *Ber. Deut. Chem. Ges.*, **88**, 1654 (1955). C. B. Soctt, *J. Org. Chem.*, **22**, 1118 (1957).

6) a) M. J. Boskin and D. B. Denney, *Chem. Ind.* (London), **1959**, 330. b) N. P. Neureiter and F. G. Bordwell, *J. Amer. Chem. Soc.* **81**, 578 (1959). D. B. Denney and M. J. Boskin, *ibid.*, **82**, 4736 (1960).

7) P. D. Bartlett and G. Megnerian, *ibid.*, **78**, 3710 (1956).

8) M. S. Newman, "Steric Effects in Organic Chemistry" John Wiley & Sons (1955), p. 205.

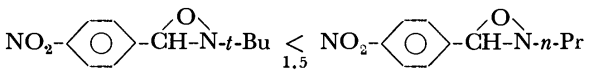

As for another alternative possibility involving the nucleophilic attack of the phosphine on the carbon atom, Pearson reported that in methanol various nucleophiles reacted with methyl iodide in the following decreasing rate-order:

$$PhS^- > (n\text{-}Bu)_3P > Ph_3P > CN^- > P(OCH_3)_3$$
$$(17) \quad (1) \quad (2\times10^{-2}) \quad (1\times10^{-2}) \quad (3\times10^{-4})$$

where the numbers denote the relative rates.[9] Accordingly, if the initial nucleophilic attack would take place at the carbon atom, the reactivities of the nucleophiles in this reaction would fall in the same order as that found with methyl iodide. Contrary to the expectation, in the reaction of oxaziridine, PhS^-, I^-, and CN^- did not react at all even in dimethylformamide in which nucleophiles are known to be markedly activated. Meanwhile, triphenyl- and tri-*n*-butylphosphines can readily reduce the oxaziridine ring to the imine in a good yield. This cannot be account for by assuming the attack of the phosphine on the carbon atom. Moreover, the possibility of the carbon attack could not be compatible with the very small solvent dependency on the rate, because the carbon attack by phosphine must require a charge-separated structure for the transition state (C) due to C–O bond fission as shown below:

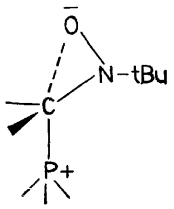

(C)

As Table 3 indicates, further striking negative evidences against nucleophilic carbon attack may be the very small influence on the rate produced by the replacement of methyne hydrogen attacked to the carbon by methyl group (D).

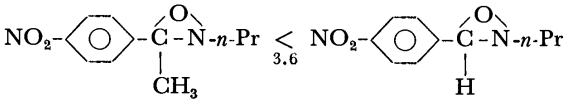

(D)

In usual S_N2 reaction retardation in rate caused by the change of steric crowdness from hydrogen to methyl groups has been reported to be larger than 10^2.[8] The lack of difference is markedly contrast to what one normally expects when hydrogen is replaced by methyl group in the S_N2 reaction on the carbon atom.

Such a small decrease in rate may better be explained in terms of the electron-donating nature of methyl group rather than the steric origin, since Fig. 3 indicates that the electron-donating substituents in the three-membered ring decrease the rate quite significantly. Consequently in view of these considerations, the posibility of either carbon or nitrogen attack by the trivalent phosphine seems unlikely. The remaining posibility, which is in harmony with the experimental results, is the rate-determining nucleophilic attack of the phosphine on the oxygen atom of the oxaziridine. Thus, we may conclude that deoxygenation reaction proceeds through nonpolar transition state, with subsequent synchronous deoxygenation.

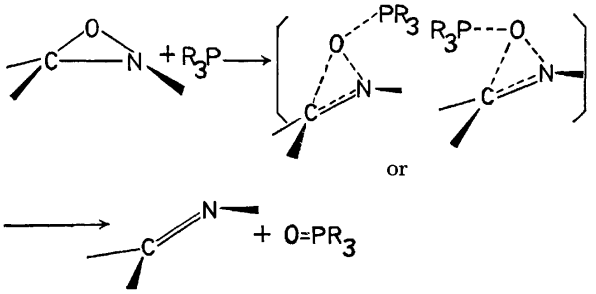

The large negative entropies of the reaction in both *n*-hexane and acetonitrile can be also rationalized in terms of such a rigid and highly oriented transition state. The priority for attack on oxygen would be attributed to the large driving force of forming a strong P=O and a C=N double bond.

9) R. G. Pearson, H. Sobel, and J. Songstad, *J. Amer. Chem. Soc.*, **90**, 319 (1968).

Linear Conjugated Systems Bearing Aromatic Terminal Groups. IX. Syntheses and Elctronic Spectra of α,ω-Di-1-anthrylpolyenes*

Yasuhira TAKEUCHI, Shuzo AKIYAMA, and Masazumi NAKAGAWA

Department of Chemistry, Faculty of Science, Osaka University Toyonaka, Osaka 560

(Received May 12, 1972)

Syntheses of α,ω-di-1-anthrylpolyenes have been carried out by the Wittig reaction for information on the role of aromatic terminal groups on the electronic spectral regularity of α,ω-diarylpolyenes. The reaction of phosphoranes derived from 1-anthrylmethyl-, 3-(1-anthryl)propenyl-, and 5-(1-anthryl)-pentadienyltriphenylphosphonium bromides with 1-formylanthracene, 3-(1-anthyrl)propenal, 5-(1-anthryl)pentadienal, and muconic aldehyde afforded a series of di-1-anthrylpolyenes (I_{1-6}) by a proper combination of the phosphorane and the aldehyde moiety. Owing to the broading of absorption bands in the long wavelength region, no discussion could be made on the electronic spectral regularity.

It has been generally accepted that the square of wavelength of the longest wavelength absorption maxima (λ^2_{max}) of a series of all-*trans* linear polyenes varies linearly with the number of double bond (n) [$\lambda^2_{max} \propto n$].[1] However, the linear relationship between the longest wavelength absorption maxima (λ_{max}) and the xth power of the number of acetylenic bond (n) [$\lambda_{max} \propto n^x$, $1 \leqq x \leqq 2$] observed in various kinds of diarylpoly-ynes[2-13] clearly indicates the marked influence of terminal groups on the electronic excitation of polyacetylene chromophore. This suggests that the aromatic terminal groups in α,ω-diarylpolyenes also exert a similar effect on the spectral regularity of linear polyenes. In order to clarify the effect, we have carried out the synthesis of α,ω-di-1-anthrylpolyenes (I_n) first, because anthryl groups have

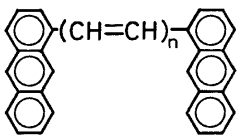

I_n

been found to exert the most prominent effect in polyyne series.[2,4]

Syntheses. The reaction sequence of the syntheses of α,ω-di-1-anthrylpolyenes (I_n) is outlined in the Scheme. The starting material of syntheses of I_n is 1-hydroxymethylanthracene (II).[14] 1-Anthrylmethyltriphenylphosphonium bromide (III) was prepared

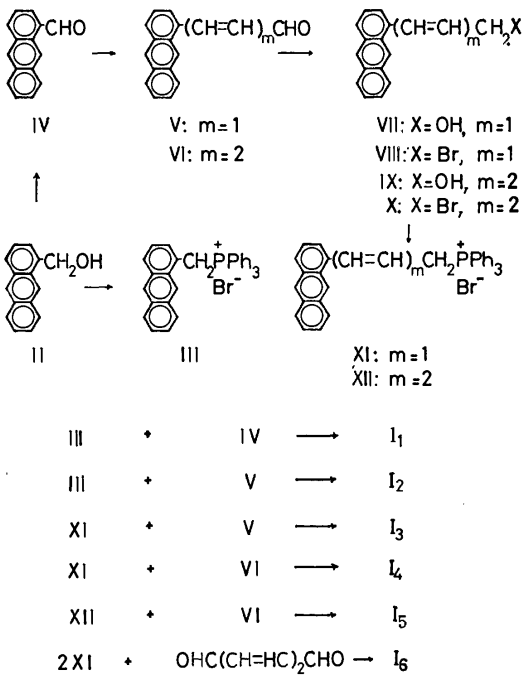

Scheme. Syntheses of Di(1-anthryl)polyenes (I_n)

from II *via* 1-bromomethylanthracene.[8] 1-Formylanthracene (IV) which was obtained from II was converted into 3-(1-anthryl)-2-propen-1-al (V) according to a modified J. F. Arens and van Dorp method.[15] 5-(1-Anthryl)-2,4-pentadien-1-al (VI) was synthesized from IV by the reaction of Grignard derivative of methoxybutenyne.[16] Reduction of V and VI with sodium borohydride afforded allyl alcohol derivatives, VII and IX, respectively. The bromides (VIII and X) obtained from VII and IX were treated with triphenylphosphine to give phosphonium bromides (IX and XII). The reaction of aldehyde (IV, V, or VI) with phosphorane derived from phosphonium bromide (III, XI, or XII) according to the combination shown in the Scheme afforded α,ω-di-1-anthrylpolyenes

* For Part VIII of this series, see Ref. 13.

1) L. N. Ferguson, *Chem. Rev.*, **43**, 408 (1948) and references cited therein; F. Sondheimer, D. A. Ben-Efraim, and R. Wolovsky, *J. Amer. Chem. Soc.*, **83**, 1675 (1961).
2) S. Akiyama and M. Nakagawa, *Tetrahedron Lett.*, **1964**, 719.
3) K. Nishimoto, R. Fujishiro, S. Akiyama, and M. Nakagawa, This Bulletin, **39**, 2320 (1966).
5) S. Akiyama, K. Nakasuji, K. Akashi, and M. Nakagawa, *Tetrahedron Lett.*, **1968**, 1121.
6) S. Akiyama and M. Nakagawa, This Bulletin, **43**, 3561 (1970).
7) K. Nakasuji, S. Akiyama, K. Akashi, and M. Nakagawa, *ibid.*, **43**, 3567 (1970).
8) S. Akiyama, K. Nakasuji, and M. Nakagawa, *ibid.*, **44**, 2231 (1971).
9) S. Akiyama and M. Nakagawa, *ibid.*, **44**, 2237 (1971).
10) S. Akiyama and M. Nakagawa, *ibid.*, **45**, 259 (1972).
11) M. Nakagawa, S. Akiyama, K. Nakasuji, and K. Nishimoto, *Tetrahedron*, **27**, 5401 (1971).
12) K. Nakasuji, S. Akiyama, and M. Nakagawa, This Bulletin, **45**, 875 (1972).
13) K. Nakasuji, S. Akiyama, and M. Nakagawa, *ibid.*, **45**, 883 (1972).
14) S. Akiyama, S. Misumi, and M. Nakagawa, This Bulletin, **35**, 1826 (1962).
15) O. Isler, M. Montavon, R. Rüegg, and P. Zeller, *Helv. Chim. Acta*, **39**, 259 (1956).
16) Marshall and M. C. Whiting, *J. Chem. Soc.*, **1956**, 4082.

(I_{1-5}). 1,12-Di-1-anthryldodecahexene (I_6) was obtained by the reaction of XI with muconic aldehyde.[17] The Wittig reaction was performed under shielding from light in anhydrous benzene or xylene. An ethereal solution of phenyllithium was used as a base for the conversion of phosphonium bromides to phosphoranes. The reaction product was extracted with hot benzene or toluene and percolated through a column of alumina. The first crop of crystals obtained from the concentrated filtrate was recrystallized from benzene or toluene. The pure specimen of I_n thus prepared was subjected to measurement of the electronic spectrum. 1,4-Di-1-anthryl-1,3-butadiene (I_2) was also prepared from di-1-anthryldiacetylene[18] by reduction with sodium in liquid ammonia and proved to be identical with I_2 obtained by the Wittig reaction.

The color of the crystals, melting points, and wave numbers of IR absorption due to CH out-of-plane deformation (δ) of *trans*-double bonds of I_n are summarized in Table 1. The polyenes (I_n) were found to be stable and exhibited definite melting points in contrast to the fact that almost all diarylpoly-ynes showed decomposition points. Regular increase in melting point with the increase in the number of ethylenic bonds reported in α,ω-diphenylpolyenes[19] could not be observed in I_n. The solubility of I_n in organic solvents decreases markedly with the increase of n. Shift of δ due to C–H out-of-plane deformation of the *trans*-double bond to a higher wave number and an increase in the absorption intensity with the increase of n were observed (Table 1).

Electronic Spectra. Absorption curves and numerical data of the electronic spectra of I_n are shown in Fig. 1 and Table 2. The intense and broad bands in the long wavelength region which presumably arise from an interaction of L_a band of anthracene nucleus with the polyene chromophore shift to a longer wavelength with the increase in the length of polyene chain. On the other hand, the length of polyene chain exerts no effect on the location of short wavelength bands. The bands with moderate intensity at medium wavelength region shift to longer wavelength with an increase in n. Owing to disappearance of the vibrational fine structure, exact estimation of wavelength of the maxima of long wavelength bands was difficult. However, the plots of the square of approximate wavelength of long wavelength absorption maxima (λ^2) against the number of double bonds (n) gave no straight line (Fig. 2). The fact that the widely accepted linear relationship ($\lambda^2 \propto n$) does not hold for di-1-anthrylpolyenes (I_n) indicates an appreciable effect of terminal groups on polyene chromophore. Disappearance of

Table 1. Physical properties of α,ω-di(1-anthryl)polyenes (I_n)

n	Color of crystals	Mp (°C)	δ (cm^{-1})
1	greenish yellow	277—279	967
2	yellow	273—275	990
3	yellowish orange	304—305	1001
4	bright yellow	289.5—290	1004
5	orange	290—292	975, 1010
6	orange red	279—280	995, 1010

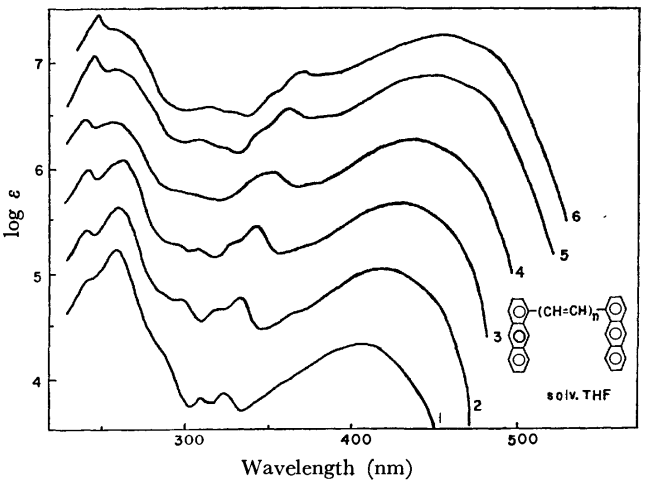

Fig. 1. The absorption curves of di(1-anthryl)polyenes (I_n). The curves, with the exception of I_1 at the bottom have been displaced upward on the ordinate axis by 0.5 log ε unit increments from the curve immediately below.

Table 2. Electronic spectral data of I_n

n	λ_{max} nm (log ε)					
1			259.5 (5.20)	310.5 (3.81)	324.5 (3.87)	406 (4.31)
2	241.5 (4.79)	261.5 (5.15)	299.5 (4.26)	321.5 (4.16)	334 (4.27)	423 (4.51)
3	243 (4.66)	265 (4.85)	3.3 (4.23)		344.5 (4.44)	433 (4.65)
4*					352 (4.43)	440 (4.73)
5	246.5 (5.08)	259 (4.95)			364 (4.56)	452 (4.87)
6*				314 (4.16)	374 (4.41)	456 (4.76)

Solvent: tetrahydrofuran. * Measured in glass cells.

17) F. G. Fischer and K. Löwenberg, *Ber.*, **66**, 665 (1933).
18) S. Asiyama and M. Nakagawa, This Bulletin, **33**, 1291 (1960).
19) R. Kuhn and A. Winterstein, *Helv. Chim. Acta*, **11**, 87 (1928).

the vibrational fine structure is attributed to a steric interference between hydrogen atoms at ethylenic linkage and those at *peri*- and *o*-positions of anthracene nuclei.

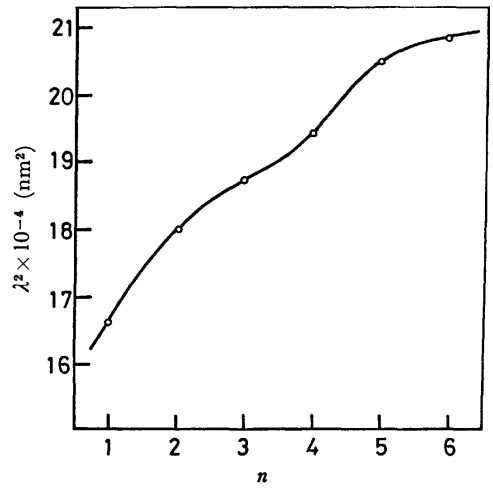

Fig. 2. Plot of λ^2_{max} against n for I_n

Experimental

All the melting points are uncorrected. The electronic spectra were obtained on a Hitachi EPS-3T spectrophotometer at room temperature using a well-matched pair of 1-cm cells, unless otherwise stated. The IR spectra were determined with a Hitachi EPI-2 infrared spectrophotometer by KBr-disk method.

3-(1-Anthryl)-2-propen-1-al (V). To a solution of lithium salt of ethoxyacetylene (prepared from 2-chlorovinyl ethyl ether (35.3 g, 0.33 mol) and lithium amide (lithium, 4.55 g, 0.66 g-atom)) in liquid ammonia (500 m*l*) was added a solution of 1-formylanthracene (IV, 13.6 g, 0.066 mol) in tetrahydrofuran (120 m*l*) over a period of 15 min. After the mixture had been stirred for 12 hr at the boiling point of liquid ammonia, a saturated solution of ammonium chloride (50 g) was added and the ammonia was allowed to evaporate. The organic layer was separated and combined with the benzene extract of aqueous layer. After washing and drying, the solvent was removed under reduced pressure. A benzene solution of the residue was passed through a thin layer of alumina. Dark red liquid (IR: 2260 (C≡CH), 3400 cm^{-1} (OH)) obtained by concentration of the filtrate *in vacuo* was dissolved in ether (110 m*l*). The ethereal solution was added under stirring to a suspension of lithium aluminum hydride (5.7 g, 0.15 mol) in ether (200 m*l*). After 4 hr, ethyl acetate (20 m*l*) and then 4 N sulfuric acid were added to the stirred mixture. After 30 min, the mixture was extracted with ether and the extract was washed with water and dried. The residue obtained by evaporating the solvent under reduced pressure was dissolved in benzene. The solution was percolated through a short column of alumina. The dark brown liquid obtained from the filtrate was triturated with a small amount of benzene-cyclohexane to yield yellow crystals (4.95 g). The crystals were recrystallized from cyclohexane to give pure V, yellow plates. V showed double melting point, mp 98—99°C and mp 119—120°C, IR: 2815 (CHO), 1690 (C=O), 965 (C=CH) cm^{-1}.

Found: C, 87.73; H, 5.22%. Calcd for $C_{17}H_{12}O$: C, 87.90; H, 5.21%.

5-(1-Anthryl)-2,4-pentadien-1-al (VI). A solution of 1-methoxy-1-buten-3-yne (12.5 g, 0.152 mol) in tetrahydrofuran (20 m*l*) was added to a stirred solution of ethylmagnesium bromide (prepared from ethyl bromide, 8.8 g and magnesium, 1.5 g) in the same solvent (38 m*l*) at 40°C. The mixture was stirred under nitrogen atmosphere for 30 min at 40°C and then 1 hr at room temperature. A solution of 1-formylanthracene (8.2 g, 0.04 mol) in tetrahydrofuran (90 m*l*) was added to the ice-cooled solution of Grignard derivative of methoxybutenyne over a period of 1 hr. After the mixture had been stirred overnight at room temperature, a saturated solution of ammonium chloride (90 m*l*) was added. The organic layer was separated, washed with water and dried. Brown liquid obtained by evaporation of the solvent *in vacuo* was dissolved in ether (100 m*l*) and added to a suspension of lithium aluminum hydride (4.5 g, 0.12 mol) in ether (65 m*l*). The mixture was stirred at room temperature for 2 hr and then ethyl acetate (18 m*l*), water (5 m*l*) and 4 N sulfuric acid (135 m*l*) were added successively. After the mixture had been stirred for 30 min at room temperature, the organic layer was separated and washed with water and dried. Fine orange crystals obtained by evaporation of the solvent under reduced pressure were dissolved in methanol and mixed with a saturated solution of sodium hydrogen sulfite. The adduct precipitated was filtered, washed successively with methanol and hot benzene. The adduct was decomposed with a solution of sodium carbonate, and the mixture was extracted with benzene. The extract was worked up according to the usual manner to yield orange yellow fine crystals (6.4 g, 63%). This material was recrystallized from cyclohexane to give pure VI as yellow plates, mp 147.5—149°C, IR: 1685 (C=O), 985 (C=CH) cm^{-1}.

Found: C, 87.90; H, 5.43%. Calcd for $C_{19}H_{14}O$: C, 88.34; H, 5.46%.

3-(1-Anthryl)-2-propen-1-ol (VII). A solution of sodium borohydride (0.23 g, 6.0 mmol) in methanol (22 m*l*) was added to a stirred solution of anthrylpropenal (V, 0.23 g, 1.0 mmol) in tetrahydrofuran (10 m*l*) and methanol (40 m*l*). Stirring was continued for 1.5 hr at room temperature. Dilute hydrochloric acid was then added to the reaction mixture. Pale yellow crystals (0.22 g, 92%, mp 138—140°C) obtained from the organic layer were recrystallized from benzene to afford pure VII as yellow needles, mp 141.0—141.5°C, IR: 3300 (OH), 995 (C–O), 980, 970 (C=CH) cm^{-1}.

Found: C, 87.38; H, 6.16%. Calcd for $C_{17}H_{14}O$: C, 87.15; H, 6.02%.

5-(1-Anthryl)-2,4-pentadien-1-ol (IX). A solution of sodium borohydride (0.40 g, 10 mmol) in methanol (20 m*l*) was added at room temperature to a stirred solution of anthrylpentadienal (VI, 0.90 g, 3.5 mmol) in tetrahydrofuran (13 m*l*) and methanol (20 m*l*). After 2 hr, dilute hydrochloric acid was added to the reaction mixture and the organic solvent was removed under reduced pressure. The solid deposited was filtered, washed and dried to give yellow fine crystals (1.0 g, mp 140—147°C). The crude alcohol (IX) thus obtained was recrystallized from benzene-cyclohexane, yielding pure IX as yellow plates, mp 159—160.5°C, IR: 3350 (OH), 1015 (C–O), 995, 980, 972 (C=CH) cm^{-1}.

Found: C, 87.44; H, 6.12%. Calcd for $C_{19}H_{16}O$: C, 87.66; H, 6.19%.

3-(1-Anthryl)-2-propen-1-yltriphenylphosphonium Bromide (XI). To a solution of anthrylpropenol (VII, 1.5 g, 6.4 mmol) in chloroform (60 m*l*) containing 2 drops of pyridine which was chilled on an ice-salt bath was added a solution of phosphorus tribromide (1.7 g, 6.5 mmol) in the same solvent (10 m*l*) and the mixture was stirred for 1 hr at room temperature. The reaction mixture was poured onto ice-water

and the organic layer was separated, washed and dried. Crude bromide (VIII) obtained as yellow fine crystals by evaporation of the solvent under reduced pressure was mixed with triphenylphosphine (1.9 g, 7.2 mmol) in benzene (26 ml). The mixture was refluxed overnight, and the crystals deposited were filtered and washed with benzene, yielding pale yellow crude phosphonium bromide (XI, 3.2 g, 89.5%, mp 256—260°C). Recrystallization of crude XI from ethanol afforded pure XI as yellow crystals, mp 260—262°C.

Found: C, 73.14; H, 5.45%. Calcd for $C_{35}H_{28}PBr \cdot C_2H_5OH$: C, 73.40; H, 5.62%.

5-(1-Anthryl)-2,4-pentadien-1-yltriphenylphosphonium Bromide (XII). A solution of phosphorus tribromide (0.97 g, 3.8 mmol) in chloroform (20 ml) was added to a strongly chilled (ice-salt bath) solution of anthrylpentadienol (IX, 0.465 g, 1.8 mmol) in chloroform (70 ml) containing 2 drops of pyridine. After stirring for 30 min at the same temperature, the reaction mixture was poured onto ice-water and the organic layer was separated. After washing and drying the organic layer was treated with active charcoal. Greenish yellow crystals obtained by evaporation of the solvent under reduced pressure were mixed with benzene (40 ml) and triphenylphosphine (0.54 g, 2.2 mmol) and the mixture was allowed to stand overnight at room temperature. Evaporation of the solvent under reduced pressure gave fine greenish yellow crystals. The crystals were washed with a small amount of benzene–cyclohexane (1 : 1) to give slightly crude XII, mp 140—143°C, 0.45 g (44%). The crude XII was used in the subsequent reaction without further purification.

1,2-Di(1-anthryl)ethylene (I_1). To a suspension of 1-anthrylmethyltriphenylphosphonium bromide[8] (III, 0.533 g, 1.0 mmol) in benzene (15 ml) was added 0.22 N ethereal solution of phenyllithium (4.6 ml) under nitrogen atmosphere. After stirring for 15 min, a solution of 1-formylanthracene[14] (IV, 0.206 g, 1 mmol) in benzene (10 ml) was added to the resulting red solution of phosphorane and the mixture was stirred overnight at room temperature. The crystals deposited were filtered and digested with boiling benzene. Yellow crystals (0.108 g, 28.5%, mp 267—279°C) obtained by concentration of the extract were recrystallized from benzene, yielding pure I_1 as greenish yellow crystals, mp 277—279°C, IR: 1615, 1540, 1455, 1430, 1325, 975, 967, 875, 795, 734 cm^{-1}.

Found: C, 94.38; H, 5.29%. Calcd for $C_{30}H_{20}$: C, 94.70; H, 5.30%.

1,4-Di(1-anthryl)-1,3-butadiene (I_2). (a) By the Wittig Reaction: An ethereal solution of phenyllithium (0.84 N, 1.6 ml) was added to a suspension of 1-anthrylmethyltriphenylphosphonium bromide (III, 0.69 g, 1.3 mmol) in xylene (70 ml) under nitrogen atmosphere and the mixture was stirred for 30 min at 50—60°C resulting in a dark red solution of phosphorane. To this was added under shielding from light a solution of 3-(1-anthryl)-2-propen-1-al (V, 0.30 g, 1.3 mmol) in xylene (50 ml) and the mixture was stirred for 19 hr at room temperature. The crystals deposited were filtered and digested with hot toluene. The yellow crystals (0.256 g, 48%, mp 266—270°C) obtained by concentration of the extract were recrystallized from toluene to yield pure I_2 as yellow leaflets, mp 273—275°C, IR: 1613, 1538, 1455, 1300, 990, 874, 784, 728 cm^{-1}.

Found: C, 94.41; H, 5.46%. Calcd for $C_{32}H_{22}$: C, 94.54; H, 5.46%.

(b) Reduction of Di-(1-anthryl)diacetylene: Sodium (0.4 g) was added to a solution of di-(1-anthryl)diacetylene[18] (0.603 g) in liquid ammonia (120 ml). After the mixture had been stirred for 5 hr, ammonium nitrate and then water were added. The insoluble material was collected by filtration, washed successively with water and ethanol and dried. The crude material was dissolved in benzene (90 ml). The crystals obtained by concentration of the solution up to 70 ml were recrystallized from benzene, yielding yellow leaflets, mp 273—275°C.

Found: C, 94.10; H, 5.65%. Calcd for $C_{32}H_{22}$: C, 94.54; H, 5.46%.

The butadiene (I_2) thus prepared was found to be identical with that prepared by the Wittig reaction.

1,6-Di(1-anthryl)-1,3,5-hexatriene (I_3). 3-(1-Anthryl)-2-propen-1-yltriphenylphosphonium bromide (XI, 0.839 g, 1.5 mmol) in xylene (80 ml) was mixed with phenyllithium (0.5 N ether solution, 3 ml) under nitrogen atmosphere and the mixture was stirred at 50—60°C for 30 min. A solution of 3-(1-anthryl)-2-propen-1-al (V, 0.348 g, 1.5 mmol) in xylene (50 ml) was added to the dark violet solution of phosphorane under shielding from light. Stirring was continued for 5 days at room temperature, and the yellow crystalline powder deposited (0.214 g, 33%) was digested with hot toluene and the hot extract was passed through a short column of alumina. Concentration of the filtrate under reduced pressure yielded pure I_3 as orange yellow plates, mp 304—305°C, IR: 1610, 1454, 1297, 1001, 877, 788, 728 cm^{-1}.

Found: C, 94.33; H, 5.64%. Calcd for $C_{34}H_{24}$: C, 94.41; H, 5.59%.

1,8-Di(1-anthryl)-1,3,5,7-octatetraene (I_4). A solution of 5-(1-anthryl)-2,4-pentadien-1-al (VI, 0.260 g, 1.0 mmol) in xylene (20 ml) was added under shielding from light to a dark violet solution of phosphorane [prepared by stirring a mixture of 3-(1-anthryl)-2-propen-1-yltriphenylphosphonium bromide (XI, 0.560 g, 1.0 mmol) in xylene (22 ml) and phenyllithium (0.06 N, ether solution, 16.6 ml) for 1 hr under nitrogen atmosphere]. After the reaction mixture had been stirred overnight at room temperature, the solvent was removed under diminished pressure. The residue was digested with hot toluene and the hot extract was percolated through a thin layer of alumina. Concentration of the filtrate yielded fine orange crystals (0.065 g, 14%), mp 286—290°C which were recrystallized from toluene to give pure I_4, bright yellow plates, mp 289.5—290.0°C, IR: 1610, 1537, 1428, 1010, 880, 787, 732 cm^{-1}.

Found: C, 93.79; H, 5.69%. Calcd for $C_{36}H_{26}$: C, 94.28; H, 5.72%.

1,10-Di(1-anthryl)-1,3,5,7,9-decapentaene (I_5). A solution of 5-(1-anthryl)-2,4-pentadien-1-al (VI, 0.130 g, 0.5 mmol) in benzene (20 ml) was added to a solution of phosphorane prepared from 5-(1-anthryl)-2,4-pentadien-1-yltriphenylphosphonium bromide (XII, 0.290 g, 0.5 mmol) in benzene (20 ml) and an ethereal solution of phenyllithium (0.12 N, 8.3 ml). After stirring overnight at room temperature, the solvent was removed under reduced pressure. The residue was extracted with hot toluene and the hot extract was passed through a short column of alumina. Orange crystalline powder (0.044 g, 18%, mp 282—292°C) deposited on cooling the filtrate was recrystallized from toluene to give pure I_5 as orange plates, mp 290—292°C, IR: 1610, 1535, 1428, 1010, 990, 975, 878, 865, 790, 730 cm^{-1}.

Found: C, 93.85; H, 5.87%. Calcd for $C_{38}H_{28}$: C, 94.18; H, 5.82%.

1,12-Di(1-anthryl)-1,3,5,7,9,11-dodecahexaene (I_6). To a suspension of 3-(1-anthryl)-2-propen-1-yltriphenylphosphonium bromide (XI, 0.670 g, 1.2 mmol) in benzene (20 ml) was added an ethereal solution of phenyllithium (0.33 N, 3.6 ml) under nitrogen atmosphere. After the mixture had been stirred for 20 min at room temperature, a solution

of muconic aldehyde[17] (0.044 g, 0.4 mmol) in benzene (3 m*l*) was added and the mixture was stirred for 23 hr at room temperature. Crystalline orange powder deposited was digested with hot toluene. The extract was concentrated under reduced pressure to yield fine orange red crystals, 0.084 g, (41%), mp 273—280°C. The crude crystals were dissolved in hot toluene and the hot solution was passed through a short column of alumina, yielding pure I_6 as orange red plates, mp 279—280°C, IR: 1612, 1535, 1455, 1428, 1010, 995, 876, 868, 788, 730 cm^{-1}.

Found: C, 93.71; H, 5.87%. Calcd for $C_{40}H_{30}$: C, 94.08; H, 5.92%.

BULLETIN OF THE CHEMICAL SOCIETY OF JAPAN, VOL. 45, 3187—3191 (1972)

Compounds Related to Acridine. VIII.[1] Reaction of 9-Vinylacridine with *p*-Substituted Nitrosobenzenes

Otohiko Tsuge[2] and Akiyoshi Torii[3]

Research Institute of Industrial Science, Kyushu University, Hakozaki, Higashi-ku, Fukuoka, 812

(Received May 17, 1972)

In the presence of hydrochloric acid, 9-vinylacridine reacts with nitrosobenzenes having electron-donating groups such as *p*-nitroso-*N*,*N*-dialkylaminoaniline and *p*-methylnitrosobenzene to yield a four-membered oxazetidine, as the first example of a non-fluorinated oxazetidine ring system. A new 2 : 2 adduct, to which the perhydro-1,2,7-oxadiazepine structure is assigned tentatively, is formed in the reaction of 9-vinylacridine with nitrosobenzene or *p*-chloronitrosobenzene under similar conditions.

So far no report has been given on non-fluorinated oxazetidines.[4,5] Hepfinger *et al.*[6] have shown that the oxazetidines reported by Ingold and Weaver[7] from the reaction of nitrosobenzene with diethyl methylenemalonate and 1,1-diphenylethylene are diethyl *β*-*N*-hydroxy-*N*-phenylmethylenemalonate and triphenylnitrone as proposed by Lapworth *et al.*[8]

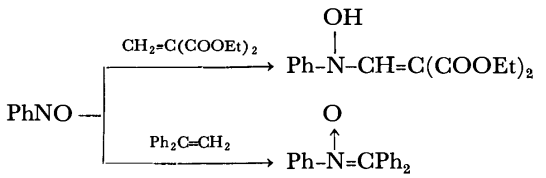

We reported[9,10] that hydrochloric acid (HCl) is an extremely effective catalyst for the condensation of *p*-substituted nitrosobenzenes with 9-methyl- and 9-ethylacridine. Furthermore, even 9-ethynylacridine undergoes condensation with two moles of *p*-nitroso-*N*,*N*-dialkylaniline in the presence of HCl to yield 1-(9-acridinyl)-1,2-bis(*p*-dialkylaminophenylimino)-ethane *N*,*N*-dioxide.[11]

We report herewith that in the presence of HCl, 9-vinylacridine reacts with nitrosobenzenes having electron-donating groups to give oxazetidine compounds as the first example of a non-fluorinated oxazetidine ring system. With nitrosbenzene or *p*-chloronitrosobenzene, a new 2 : 2 adduct was obtained.

Results and Discussion

From previous results,[9-11] *cis*- or *trans*-1-(9-acridinyl)-2-methylethylene (**1**) might be expected to react with *p*-nitroso-*N*,*N*-dialkylaniline to give the *α*,*β*-unsaturated anil and/or nitrone. Contrary to expectation, the reaction of **1** with *p*-nitroso-*N*,*N*-dimethylaniline (**2a**) in the presence of HCl in refluxing ethanol afforded acridine-9-carboxaldehyde-*N*-(*p*-*N*,*N*-dimethylaminophenyl)anil (**3a**), whose structure was confirmed by comparison with the authentic sample.[9] Olefin **1** did not react with **2a** in the presence of HCl at room temperature nor in the presence (or absence) of a basic catalyst such as potassium carbonate in ethanol.[12]

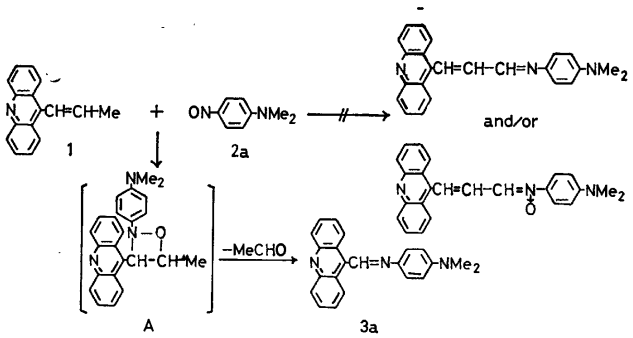

Scheme 1.

1) Part VII of this series: O. Tsuge and A. Torii, This Bulletin, **43**, 2920 (1970).

2) To whom inquiries should be directed.

3) Present address: Department of Industrial Chemistry, Kurume Technical College, Komorino, Kurume, 830.

4) D. A. Barr and K. N. Haszeldine, *J. Chem. Soc.*, **1955**, 1881.

5) V. A. Cinsburg, S. S. Dubov, A. N. Medvedev, L. L. Martynova, B. I. Tetel'baum, M. N. Vasil'eva, and A. Ya. Yakubovich, *Dokl. Akad. Nauk SSSR*, **152** (5), 1104 (1963).

6) N. F. Hepfinger, C. E. Griffin, and B. L. Shapiro, *Tetrahedron Lett.*, **1963**, 1365.

7) C. K. Ingold and S. D. Weaver, *J. Chem. Soc.*, **125**, 1146 (1924).

8) G. N. Burkhardt and A. Lapworth, *ibid.*, **127**, 1748 (1925); G. N. Burkhard, A. Lapworth, and J. Walkden, *ibid.*, **127**, 2458 (1925).

9) O. Tsuge, M. Nishinohara, and M. Tashiro, This Bulletin, **36**, 1477 (1963).

10) O. Tsuge, M. Nishinohara, and K. Sadano, K. Sadano, *ibid.*, **37**, 436 (1964); O. Tsuge, M. Nishinohara, and K. Sadano, *ibid.*, **38**, 2037 (1965).

11) O. Tsuge and A. Torii, *ibid.*, **43**, 2920 (1970).

It is conceivable that **3a** might have been formed *via* the oxazetidine intermediate **A** with the elimination of acetaldehyde, although an attempt at isolation of **A** was unsuccessful (Scheme 1).

On the other hand, 9-vinylacridine (**4**) reacted easily with **2a** in the presence of HCl at room temperature to afford a 1 : 1 adduct **5a**, mp 156—157°C (decomp.), as violet prisms, while under reflux in ethanol **3a** was obtained.

The structure of the 1 : 1 adduct was established to be 3-(9-acridinyl)-2-(*p*-*N*,*N*-dimethylaminophenyl)-oxazetidine (**5a**) on the basis of spectra data and chemical conversions. The IR spectrum of **5a** showed a characteristic band ascribable to ν_{C-O-N} at 1050 cm^{-1}. The mass spectrum exhibited a parent peak (M^+) at *m/e* 355 together with major fragment peaks at *m/e* 341 (M^+-CH_2), 339 (M^+-O), 337 (M^+-H_2O), 325 (M^+-CH_2O), 324 (325^+-H), 221 (341^+- $-NMe_2$), 217 (337^+- $-NMe_2$), and 204 (324^+- $-NMe_2$). However, the NMR spectrum could not be obtained owing to the insolubility of organic solvents.

When a solution of **5a** in ethanol was refluxed, anil **3a**, a new compound **6** and formaldehyde were formed. This indicates that **3a** was formed from **5a** by the elimination of formaldehyde.[13] Reduction of **5a** with sodium borohydride gave 1-(9-acridinyl)-2-(*p*-*N*,*N*-dimethylanilino)ethane (**7**), whose structure was confirmed by spectral data as well as by microanalysis. Although the exact pathway for the formation of **7** is not clear, it seems to have been caused by the initial reductive cleavage of oxazetidine, followed by the formation of an aziridine by the loss of water and subsequent ring opening as shown in Scheme 2.

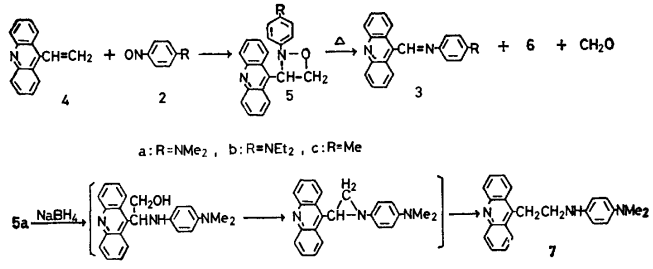

Scheme 2.

Similarly, the reaction of **4** with *p*-nitroso-*N*,*N*-diethylaniline (**2b**) or *p*-methylnitrosobenzene (**2c**) in the presence of HCl at 0°C afforded the corresponding oxazetidine compound **5b** or **5c**. Refluxing of an ethanol solution of **5b** or **5c** gave the corresponding anils **3b** and **3c**, and **6b**. In the case of **5c**, however, the compound of type **6** could not be isolated.

The results of microanalyses and mass spectra of **6a** and **6b** agreed with the molecular formulas of the corresponding 1 : 1 adduct of **4** and **3**. The IR spectra of **6a** and **6b** were very similar to each other, and showed no bands ascribable to ν_{NH}. The NMR spectrum of **6a** exhibited signals at δ 2.85 (2H, multiplet, CH_2), 2.95 (6H, singlet, $N(CH_3)_2$), and 6.7—8.7 ppm (22H, complicated, aromatic (20H) and two methine protons). It was thus deduced that the most reasonable structure for **6** is 2,4-di(9-acridinyl)-1-(*p*-*N*,*N*-dialkylaminophenyl)azetidine rather than the 2,3-di(9-acridinyl)azetidine compound **6'**.

The reaction of **4** with **3a** did not occur and starting materials were recovered. It is thus conceivable that the formation of **6** might have taken place from a secondary reaction of **5** with **3** by the elimination of nitroso compound **2**. Although no increase in the yield of **6a** was observed in the thermolysis of **5a** in the presence of **3a**, the formation of **6** can be viewed as proceeding by the initial formation of the perhydro-1,2,4-oxadiazine intermediate from the reaction of **5** with **3**, followed by the elimination of nitroso compound **2** as illustrated in Scheme 3.

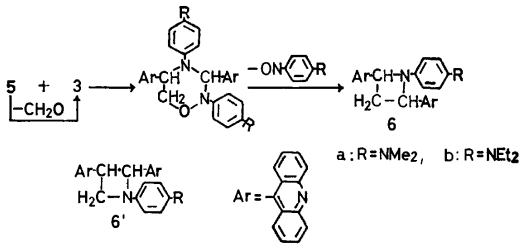

Scheme 3.

4 reacted with nitrosobenzene (**2d**) in the presence of HCl to afford a 2 : 2 adduct **8d** as pale yellow prisms, accompanied by a large amount of tarry material. In a similar reaction of **4** with *p*-chloronitrosobenzene (**2e**), a 2 : 2 adduct **8e** was isolated together with a small amount of oxazetidine **5e**. However, *p*-nitronitrosobenzene did not react with **4** but was converted into *p*,*p'*-dinitroazobenzene.

Although the formation of 1 : 2 adduct of styrene and trifluoronitrosomethane[5] and 1 : 2 adduct of styrene and nitrosobenzene[14] was observed in the reaction of styrene with the respective nitroso compound, formation of 2 : 2 adducts from olefin and nitroso compound has not been reported.

Although **8d** was stable against reduction with sodium borohydride and lithium aluminum hydride, its treatment with sodium ethoxide in ethanol afforded 1-anilino-1,3-di(9-acridinyl)propane (**9**) and 2,4-di-(9-acridinyl) butyraldehyde-*N*-phenylanil (**10**), accompanied by a trace amount of azobenzene. Structures of **9** and **10** were confirmed by their spectral data as well as by the results of microanalyses. **10** was hydrolyzed with aqueous potassium hydroxide to give 1,3-di(9-acridinyl)propane (**11**) *via* the carboxylic acid, which could not be isolated in a pure form; **11** was identified by comparison with an authentic sample prepared from the Mannich reaction of 9-methylacridine with paraformaldehyde (Scheme 4).

12) The reaction of *trans*-9-styryl- and *trans*-9-(*p*-nitrostyryl)-acridine with **2a** did not take place under various conditions.

13) Formaldehyde in exhaust gas was identified by means of the fuchsin-sulfuric acid color test. It was reported that perfluoroxazetidine obtained from trifluoronitrosomethane and tetrafluoroethylene decomposed thermally to form perfluoromethylenemethylamine and carbonylfluoride.[4]

14) N. F. Hepfinger and C. E. Griffin, *Tetrahedron Lett.*, **1963**, 1361.

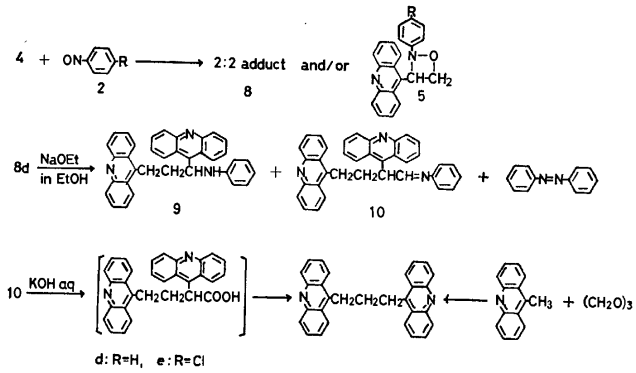

Scheme 4.

Contrary to oxazetidine **5**, 2 : 2 adducts **8d** and **8e** were stable in refluxing ethanol. Heating of **8d** in triethylphosphite for 10 hr afforded a new compound **12d**, mp 276—277°C, and azobenzene. On the basis of its spectral data and reaction with triethylphosphite, compound **12d** was assumed to be either 2,3-di(9-acridinyl)-1-phenyl-Δ^2- or -Δ^4-pyrroline. On heating with triethylphosphite, **12d** was converted into 2,3-di(9-acridinyl)-1-phenylpyrrole (**13d**), mp 280—281°C, whose structure was established by its spectral data. Similarly, treatment of **8e** with triethylphosphite gave the corresponding pyrroline **12e** and *p,p'*-dichloroazobenzene (Scheme 5).

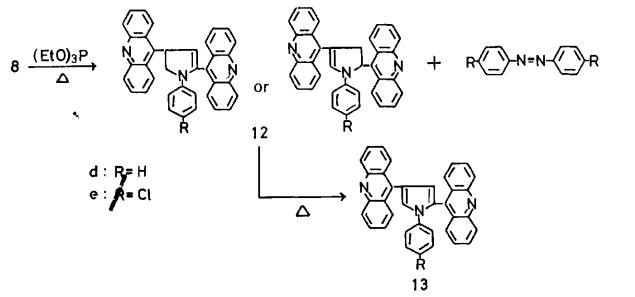

Scheme 5.

The NMR spectrum of **8d** exhibited multiplets at δ 2.5 (2H, CH_2), 4.0 (2H, CH_2), 6.2 (2H, $\rightarrow$CH), and 6.7—9.5 ppm (26H, aromatic protons).

From the above NMR spectra and chemical conversions it is evident that the 2 : 2 adducts **8** have the moiety **B** in the molecule, while three types of arrangements **C**, **D**, and **E** are possible for the remainder of the adduct (Fig. 1). 1,2,3-Oxadiazolidin 3-oxide **F** and 1,2,5-oxadiazolidin 2-oxide **G** were proposed, respectively, for the 1 : 2 adducts of styrene with trifluoronitrosomethane[5] and with nitrosobenzene.[14] Structures **F** and **G** correspond to **E** and **C**, respectively.

The results of reduction and deoxygenation of **8** eliminate the possibility of a structure incorporating **E**. Thus, perhydro-1,2,7-oxadiazepin 1-oxide **8-1**, 7-oxide **8-2** (from **B** and **C**), and perhydropyridazine 1,2-dioxide **8-3** (from **B** and **D**) are possible structures for adducts **8**. From the spectral data it could not be decided which type of structure **8-1**—**8-3** would be most reasonable for **8**. However, perhydro-1,2,7-oxadiazepine structure **8-1** or **8-2** was assumed to be

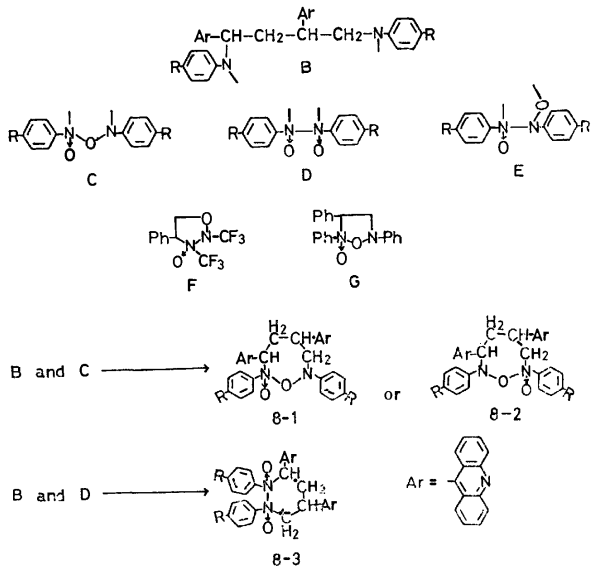

Fig. 1.

more reasonable than perhydropyridazine structure **8-3**, because pyrrole **13** was obtained on deoxygenation of **8** but no pyridazine. Furthermore, hydrolysis of **8d** with hydrochloric acid afforded the 1-(*p*-chlorophenyl)pyrroline compound **12e**; formation of **12e** seems to take place by the hydrolytic cleavage of -N-O- bond in the ring, followed by the Orton rearrangement. This seems to support the proposed structure **8-1** or **8-2** for **8**.

Experimental

All melting points are uncorrected. The IR spectra were measured as KBr pellets and the UV spectra were determined in ethanol solutions. The mass spectra were obtained on a Hitachi RMS-4 mass spectrometer with a direct inlet and an ionization energy of 70 eV. The NMR spectra were determined at 60 MHz with a Hitachi R-20 NMR spectrometer, with TMS as an internal reference. The microanalyses were carried out by Miss M. Akita.

Materials. 1-(9-Acridinyl)-2-methylethylene (**1**)[15] (*cis*: mp 56—58°C; *trans*: mp 98—99°C); *trans*-9-styrylacridine,[16] mp 184—185°C; *trans*-9-(*p*-nitrostyryl)acridine,[16] mp 291—292°C, and 9-vinylacridine (**4**),[15] mp 87—88°C, were prepared by our previous methods.

Nitrosobenzenes were prepared by methods described in literature: *p*-nitroso-*N,N*-dimethylaniline (**2a**), mp 93—94 °C (lit,[17] mp 92—95°C); *p*-nitroso-*N,N*-diethylaniline (**2b**), mp 84—85°C (lit,[17] mp 84°C); *p*-methylnitrosobenzene (**2c**), mp 49°C (lit,[18] mp 48.5°C); nitrosobenzene (**2d**), mp 65—66°C (lit,[19] mp 64—67°C); *p*-chloronitrosobenzene (**2e**), mp 90—91°C (lit,[18] mp 89.5°C); *p*-nitronitrosobenzene, mp 118°C (lit,[20] mp 118°C).

15) O. Tsuge, A. Torii, and T. Tomita, *Nippon Kagaku Zasshi*, **90**, 1263 (1969).
16) O. Tsuge, T. Tomita, and A. Torii, *ibid.*, **89**, 1104 (1968).
17) H. E. Fiez-David and L. Blangey, "Grundlegends Operationen der Farbenchemie," Springer-Verlag (1943), p. 292.
18) E. Bamberger, *Ber.*, **28**, 247 (1895).
19) G.H. Coleman, C. M. McClosky, and F. A. Stuart, "Organic Syntheses," Coll. Vol. III, p. 668 (1961).
20) E. Bamberger and E. Huebner, *Ber.*, **36**, 3803 (1903).
21) HCl used in this paper: d^{27} 1.1748.

*Reaction of **1** with **2a**.* A typical reaction is as follows. To a solution of 1.0 g of **1** (*trans*) and 0.8 g of **2a** in 20 m*l* of ethanol was added 0.05 m*l* of HCl[21] at room temperature, and the reaction mixture was heated under reflux for 8 hr. After it was allowed to stand overnight, filtration gave reddish crystals which on recrystallization from ethanol afforded 0.16 g (15%) of acridine-9-carboxaldehyde-*N*-(*p*-*N*,*N*-dimethylaminophenyl)anil (**3a**), mp 249—250°C (lit.,[9] mp 248°C). The structure of **3a** was established by identification with an authentic sample.[9]

*Reaction of **4** with **2a**.* To a solution of 1.0 g of **4** and 0.8 g of **2a** in 20 m*l* of ethanol was added 0.1 m*l* of HCl. The reaction mixture was then stirred at room temperature for 1 hr. Filtration gave 0.6 g (35%) of 3-(9-acridinyl)-2-(*p*-*N*,*N*-dimethylaminophenyl)oxazetidine (**5a**), mp 156—157°C (decomp.), as violet prisms, which was subjected to microanalysis without further purification.

Found: C, 77.31; H, 5.93; N, 11.75%. Calcd for $C_{23}H_{21}N_3O$: C, 77.72; H, 5.96; N, 11.82%.

UV λ_{max} nm (log ε): 253 (4.5), 537 (4.4).

The reaction of **4** with **2a** in refluxing ethanol gave anil **3a**. The effects of reaction conditions on yields of products are given in Table 1.

Table 1. Reaction of **4** with **2a**[a]

Run	Reaction conditions			Product, Yield (%)	
	2a/**4** (mol/mol)	Time (hr)	HCl (m*l*)	**3a**	**5a**
1	1	1	0.1	—	35
2	2	1	0.1	—	64
3	3	1	0.1	—	65
4	1	8	0.05	11	—
5	1	8	0.1	9	—
6	1	8	0.2	8	—
7	2	8	0.1	15	—
8	3	8	0.1	22	—

a) A mixture of 1.0 g of **4**, the specified amounts of **2a** and HCl in 20 m*l* of ethanol was stirred at room temperature (Runs 1-3) or under reflux (Runs 4-8).

*Reaction of **4** with **2b**.* One gram of **4** was reacted with 1.8 g of **2b** in the presence of 0.1 m*l* of HCl in 20 m*l* of ethanol at 0°C for 15 min to give 1.35 g (69%) of 3-(9-acridinyl)-2-(*p*-*N*,*N*-diethylaminophenyl)oxazetidine (**5b**) monohydrate, mp 112—113°C (decomp.), as violet prisms.

Found: C, 74.81; H, 6.73; N, 10.47%. Calcd for $C_{25}H_{25}N_3O \cdot H_2O$: C, 74.95; H, 7.07; N, 10.54%.

IR cm^{-1}: ν_{C-O-N} 1045. UV λ_{max} nm (log ε): 253 (4.8), 539 (4.2). Mass spectrum *m/e*: 383 (M^+), 369 ($M^+ - CH_2$), 367 ($M^+ - O$), 365 ($M^+ - H_2O$), 353 ($M^+ - CH_2O$), 205 ($M^+ - $**2b**).

Similarly, the reaction of 0.5 g of **4** with 0.6 g of **2c** in the presence of 0.05 m*l* of HCl in 10 m*l* of ethanol at 0°C for 2.5 hr gave 0.25 g (31%) of 3-(9-acridinyl)-2-(*p*-tolyl)oxazetidine (**5c**), mp 192—193°C (decomp.), as violet prisms.

Found: C, 80.60; H, 5.46; N, 8.54%. Calcd for $C_{22}H_{18}N_2O$: C, 80.98; H, 5.52; N, 8.59%.

IR cm^{-1}: ν_{C-N-O} 1045. UV λ_{max} nm (log ε): 253 (4.8), 524 (4.4). Mass spectrum *m/e*: 326 (M^+), 312 ($M^+ - CH_2$), 310 ($M^+ - O$), 308 ($M^+ - H_2O$), 296 ($M^+ - CH_2O$), 205 ($M^+ - $**2c**).

*Thermolysis of Oxazetidine **5**.* A solution of 2.0 g of **5b** in 20 m*l* of ethanol was refluxed for 8 hr, during which time evolution of formaldehyde was confirmed by means of fuchsin-sulfurous acid color test. The reaction mixture was concentrated *in vacuo* to leave a residue, which was then chromatographed on alumina using benzene as an eluent to obtain 0.42 g (23%) of anil **3b**, mp 168°C (lit,[9] mp 168—169 °C) and 0.4 g (15%) of 2,4-di(9-acridinyl)-1-(*p*-*N*,*N*-diethylaminophenyl)azetidine (**6b**), mp 295—296°C, as pale yellow prisms.

Found: C, 83.71; H, 5.94; N, 9.90%. Calcd for $C_{39}H_{34}N_4$: C, 83.84; H, 6.13; N, 10.03%.

UV λ_{max} nm (log ε): 247 (4.8), 365 (3.9).

NMR (in $CDCl_3$) δ ppm: 1.15 (6H, triplet, $-CH_2-CH_3$), 3.0—3.6 (6H, multiplet, CH_2), 6.7—8.55 (22H, complicated, aromatic (20H) and two methine protons).

Mass spectrum *m/e*: 558 (M^+).

Similarly, heating of **5a** or **5c** in ethanol afforded anil **3a** (22%) and azetidine **6a** (32%), or anil **3c** (22%), mp 180—181°C (lit,[22] mp 182—183°C), respectively.

Azetidine **6a**: mp 294—295°C, yellow needles.

Found: C, 84.02; H, 5.51; N, 10.63%. Calcd for $C_{37}H_{30}N_4$: C, 83.74; H, 5.70; N, 10.56%.

UV λ_{max} nm (log ε): 247 (4.7), 362 (3.7). Mass spectrum *m/e*: 530 (M^+).

*Reduction of **5a** with Sodium Borohydride.* A solution of 1.3 g of **5a** in 16 m*l* of ethanol-dioxane mixture (1 : 1) was stirred with 0.5 g of sodium borohydride at room temperature for 1.5 hr. To the reaction mixture was added 50 m*l* of water. The resulting solution was then extracted with 100 m*l* of diethyl ether. The extract was dried over anhydrous sodium sulfate and then evaporated to leave a reddish oily residue. The residue was chromatographed on alumina using benzene as an eluent to obtain 0.56 g (58%) of 1-(9-acridinyl)-2-(*p*-*N*,*N*-dimethylanilino)ethane (**7**), which on recrystallization from petroleum ether (bp 45—60°C) gave orange prisms, mp 131—132°C.

Found: C, 80.79; H, 6.81; N, 12.03%. Calcd for $C_{22}H_{23}N_3$: C, 80.90; H, 6.79; N, 12.31%. IR cm^{-1}: ν_{NH} 3280.

NMR (in $CDCl_3$) δ ppm: 2.8 (6H, singlet, $N(CH_3)_2$), 3.5 (2H, triplet, CH_2, J=6 Hz), 3.8 (2H, triplet, CH_2, J= 6 Hz), 3.55 (1H, singlet, NH), 6.6—8.4 (21H, multiplet, aromatic protons).

Mass spectrum *m/e*: 341 (M^+).

*Reaction of **4** with **2e**.* A solution of 1.0 g of **4** and 1.4 g of **2e** in 20 m*l* of ethanol containing 0.1 m*l* of HCl was stirred at room temperature for 24 hr. Filtration gave 0.31 g (18%) of 2 : 2 adduct **8e**, which on recrystallization from chloroform afforded pale yellow prisms, mp 212—213°C (decomp.).

Found: C, 72.80; H, 4.18; N, 7.93%. Calcd for $C_{42}H_{30}N_4O_2Cl_2$: C, 72.54; H, 4.32; N, 8.08%.

UV λ_{max} nm (log ε): 253 (4.2), 520 (4.1).

The mass spectrum of **8e** did not show a parent peak (M^+), but major fragment peaks at *m/e* 656, 658, 660 (9 : 6 : 1, $M^+ - 2H_2O$), 531, 533 ($M^+ - 2H_2O$ — Cl- -N), 316, 318 (3 : 1, 9-acridinyl-CH=N- -Cl^+), 315, 317, and other peaks appeared in the spectrum.

The filtrate was evaporated *in vacuo* to leave a residue, which was chromatographed on alumina using chloroform as an eluent to give 10 mg of oxazetidine **5e**, mp 191°C (decomp.), as violet prisms, together with a large amount of tar.

Found: C, 72.66; H, 4.33; N, 8.00%. Calcd for $C_{21}H_{15}N_2OCl$: C, 72.54; H, 4.32; N, 8.08%.

Mass spectrum *m/e*: 346, 348 (3 : 1, M^+), 330, 332 ($M^+ - O$), 316, 318 ($M^+ - CH_2O$).

22) N. S. Drozdov and E. V. Yavorskaya, *Zh. Obshch. Khim.*, **30**, 3421 (1960).

Similarly, the reaction of 1.0 g of **4** with 1.2 g of **2d** in 20 ml of ethanol containing 0.1 ml of HCl afforded 0.3 g (20%) of 2 : 2 adduct **8d**, mp 172—173°C, as pale yellow prisms.

Found: C, 81.03; H, 5.09; N, 8.90%. Calcd for $C_{42}H_{32}N_4O_2$: C, 80.76; H, 5.12; N, 8.97%.

Mass spectrum *m/e*: 588 (M^+-2H_2O), 497 (M^+-2H_2O-PhN), 282 (9-acridinyl-CH=N-Ph^+), 281.

Reduction of ***8d*** *with Sodium Ethoxide.* A solution of 3.0 g of **8d** in 20 ml of ethanol was stirred with 0.5 g of sodium at room temperature for 12 hr. Filtration afforded 0.4 g (23%) of 2,4-di(9-acridinyl)butyraldehyde-*N*-phenylanil (**10**), which on recrystallization from pyridine gave yellow prisms, mp 296—297°C.

Found: C, 85.66; H, 5.27; N, 9.13%. Calcd for $C_{36}H_{27}N_3\cdot 1/2C_5H_5N$: C, 85.55; H, 5.48; N, 8.95%. IR cm^{-1}: $\nu_{C=N}$ 1660.

NMR (in CF_3COOH) δ ppm: 3.5, 5.6 (each 2H, multiplet, CH_2), 7.3—8.8 (23H, multiplet, aromatic (21H) and two methine protons).

Mass spectrum *m/e*: 501 (M^+), 309 (M^+—9-acridinylmethyl, base peak), 295 (9-acridinyl-$\overset{+}{C}$HCH=NPh), 206 (9-acridinyl-$CH_2CH_2^+$).

The filtrate was concentrated *in vacuo* to leave a residue, which was chromatographed on alumina using benzene as an eluent to give 10 mg of azobenzene and 0.25 g (11%) of 1-anilino-1,3-di(9-acridinyl)propane (**9**). Recrystallization of **9** from pyridine afforded yellow prisms, mp 214—215°C.

Found: C, 85.79; H, 5.28; N, 8.76%. Calcd for $C_{35}H_{27}N_3$: C, 85.86; H, 5.56; N, 8.58%. IR cm^{-1}: ν_{NH} 3280.

NMR (in $CDCl_3$) δ ppm: 2.9, 3.5 (each 2H, multiplet, CH_2), 4.5 (1H, multiplet, NH), 6.0 (1H, multiplet, >CH), 6.5—8.7 (21H, multiplet, aromatic protons).

Mass spectrum *m/e*: 489 (M^+), 397 (M^+—PhNH), 297 (M^+—9-acridinyl-CH_2^+), 283 (9-acridinyl-CH=$\overset{+}{N}$HPh, base peak), 206 (9-acridinyl-$CH_2CH_2^+$).

Hydrolysis of ***10***. After 0.1 g of **10** in 4 ml of ethanol-concentrated potassium oxide aqueous solution (1 : 1) was stirred at 90°C for 30 min, filtration afforded 70 mg of crystals. The crystals were washed with diethyl ether to leave 60 mg (75%) of yellow crystals, which on recrystallization from benzene gave 1,3-di(9-acridinyl)propane (**11**), mp 201—202°C, as yellow prisms.

Found: C, 87.70; H, 5.53; N, 7.03%. Calcd for $C_{29}H_{22}N_2$: C, 87.40; H, 5.57; N, 7.03%. Mass spectrum *m/e* 398 (M^+).

NMR spectrum (in CF_3COOH) δ ppm: 2.7 (2H, multiplet, CH_2), 4.5 (4H, multiplet, CH_2), 7.9—8.9 (16H, multiplet, aromatic protons).

The ether-washings were concentrated to give a trace amount of pale yellow crystals, whose IR spectrum showed the bands ascribable to ν_{OH} and $\nu_{C=O}$ at 3400 and 1700 cm^{-1}, respectively. However, the carboxylic acid could not be isolated in pure state.

Preparation of ***11***. A mixture of 3.0 g of 9-methylacridine, 0.5 g of paraformaldehyde and 1.5 g of dimethylamine hydrochloride in 25 ml of ethanol was refluxed for 2 hr. The reaction mixture was neutralized with aqueous sodium hydroxide to give brown oily substance, which solidified on trituration with diethyl ether. The solid was recrystallized from benzene to afford 0.75 g (72%) of **11**. mp 201—202°C.

Reaction of ***8d*** *with Triethylphosphite.* A solution of 1.0 g of **8d** in 5 ml of triethylphosphite was refluxed for 10 hr. The reaction mixture was concentrated *in vacuo* and the residue was allowed to stand overnight to give 0.25 g (32%) of 2,3-di(9-acridinyl)-1-phenylpyrroline (**12d**), which on recrystallization from benzene afforded orange prisms, mp 276—277°C.

Found: C, 86.79; H, 4.91; N, 8.08%. Calcd for $C_{36}H_{25}N_3$: C, 86.54; H, 5.04; N, 8.41%.

NMR (in CF_3COOH) δ ppm: 4.7 (2H, multiplet, CH_2), 7.0—9.3 (23H, multiplet, aromatic (21H), >CH and =CH).

Mass spectrum *m/e*: 499 (M^+), 497 (M^+-H_2, base peak), 422 (M^+—Ph), 420, 406 (497^+—PhN), 393 (497^+—PhN=CH), 312 (M^+—9-acridinyl), 295 (M^+—9-acridinyl-CH=CH), 281 (9-acridinyl-C≡$\overset{+}{N}$Ph), 205 (9-acridinyl-CH=CH_2^+), 204.

The filtrate was further concentrated to leave a residue, which was chromatographed on alumina using chloroform as an eluent to give 0.1 g of azobenzene and tar.

Similarly, treatment of 0.5 g of **8e** with 3 ml of triethylphosphite yielded 0.12 g (38.5%) of pyrroline **12e**, mp 292—293°C, as orange prisms and a small amount of *p,p'*-dichloroazobenzene, mp 189°C (lit,[23] mp 187°C).

Found: C, 81.07; H, 4.19; N, 7.65%. Calcd for $C_{36}H_{24}N_3Cl$: C, 80.79; H, 4.49; N, 7.87%.

Mass spectrum *m/e*: 533, 535 (3 : 1, M^+).

Hydrolysis of ***8d***. A solution of 0.5 g of **8d** in 10 ml of 20% aqueous hydrochloric acid was stirred at 90°C for 10 min. The reaction mixture had been cooled and neutralized with ammonium hydroxide to precipitate crystals. Recrystallization from benzene afforded 0.17 g (40%) of **12e**, mp 292—293°C.

*2,3-Di(9-acridinyl)-1-phenylpyrrole (****13d****).* A solution of 0.5 g of pyrroline **12d** in 3 ml of triethylphosphite was refluxed for 15 hr. The reaction mixture was concentrated *in vacuo* to give 0.3 g (60%) of crystals. Recrystallization from benzene afforded **13d**, mp 280—281°C, as orange yellow prisms. The pine reaction color test of **13d** was positive.

Found: C, 86.90; H, 4.46; N, 8.26%. Calcd for $C_{36}H_{23}N_3$: C, 86.92; H, 4.62; N, 8.45%. Mass spectrum *m/e*: 497 (M^+). NMR (in CF_3COOH) δ ppm: 7.3—9.1 (multiplet, aromatic protons).

23) E. Bamberger, *Ann. Chem.*, **382**, 95 (1911).

Thiocyanoacetate. IV. The Reaction of Ethyl Thiocyanoacetate with Aromatic Aldehydes in the Presence of Thioureas[1]

Satoshi KAMBE and Toshio HAYASHI*
Oyama Technical College, Oyamashi, Tochigi
**The Institute of Physical and Chemical Research, Wako-shi, Saitama*
(Received January, 31, 1972)

Ethyl thiocyanoacetate (**1**) reacts with anomatic aldehydes in the presence of *N,N'*-dialkylthiourea to give arylidene *N,N'*-dialkyl-*N*-thiocarbamoyl thiocyanoacetamides (**3**). On the other hand, the treatment of the ester (**1**) with benzaldehyde in the presence of thiourea or *N*-methylthiourea under the same conditions affords 5-benzylidene-2-imino-4-thiazolidinone (**5a**) or 5-benzylidene-3-methylthiazolidine-2,4-dione (**6a**).

In the first paper of this series[2] it was shown that, in the presence of potassium carbonate or fluoride, thiocyanoacetic acid esters (**1**) and aldehydes undergo an Aldol-type condensation, followed by ring closure, to give *N*-carbamoyl-2-imino-1,3-oxathiolanes and α,β-unsaturated esters. However, we have found that *N,N'*-dialkyl-*N*-thiocarbamoyl thiocyanoacetamide (**2**) and aromatic aldehydes lead to a Knoevenagel-type condensation giving arylidene *N,N'*-dialkyl-*N*-thiocarbamoyl thiocyanoacetamides (**3**) in a good yield. This means that, in the case of the amide **2**, the dehydration rate of the intermediate **4** is larger than the rate of ring closure, whereas with the ester **1**, the reverse is true. It seems interesting that the modification of the ester group by the *N*-carbamoyl amide group causes a drastic change in the reaction course.

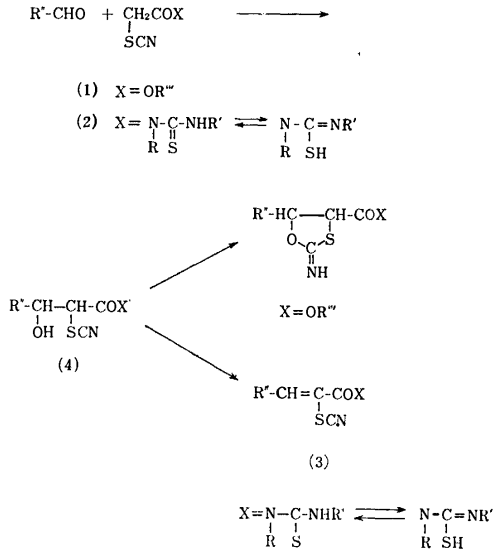

Scheme 1.

Results and Discussion

The reaction of the ester **1** with aromatic aldehydes in the presence of *N,N'*-dialkylthioureas gave arylidene *N,N'*-dialkyl-*N*-thiocarbamoyl thiocyanoacetamides (**3**), whose structures were confirmed on the basis of elemental analyses and spectral studies.

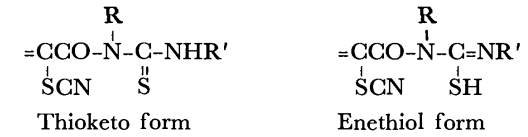

Thioketo form Enethiol form

Compounds **2** and **3** can exist in two tautomeric forms, the thioketo and enthiol forms, as is shown above. Product **3a**, for example, consisted of pale yellow needles with the structural formula $C_{13}H_{13}ON_3S_2$; mp 185—186°C. The IR spectrum of **3a** (KBr pellet) revealed the existence of the SH (near 2550 cm^{-1}), SCN (2050 cm^{-1}), C=O (1740 cm^{-1}), C=N (1640 cm^{-1}), and C=C (1600 cm^{-1}) groups. The NMR spectrum of **3a** (DMSO-d_6) showed the CH_3 proton signal δ at 3.25 and 3.30, =C<u>H</u> at 7.90, $C_6\underline{H}_5$ at 7.60, and a broad line with intensity of one proton at 8.85 ppm, a line which might be attributed to the SH proton. These facts suggest that **3** exists predominantly in the enethiol form.

The products (**3b—n**) could be obtained similarly from the reaction of substituted benzaldehyde with the ester **1** in the presence of *N,N'*-dialkylthiourea (see Table 1). However, the substituent effect was obscure in this case.

A plausible reaction sequence is illustrated in Scheme 2. Presumably, the reaction proceeds through the intermediacy of *N,N'*-dialkyl-*N*-thiocarbamoyl thio-

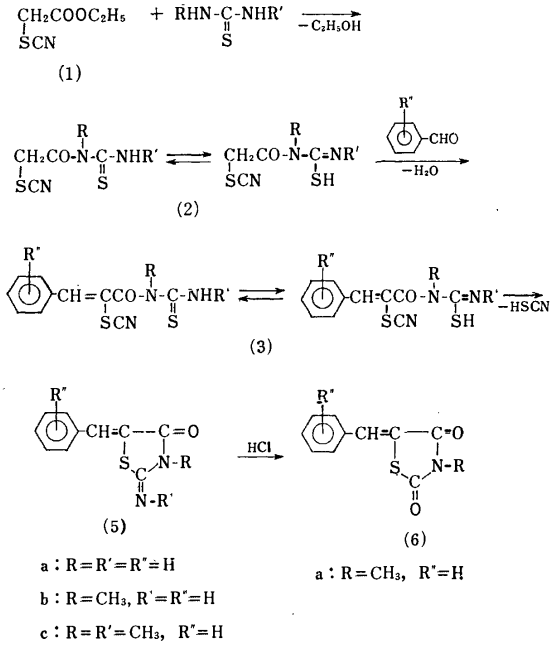

a : R=R'=R"=H
b : R=CH₃, R'=R"=H
c : R=R'=CH₃, R"=H

a : R=CH₃, R"=H

Scheme 2.

1) Part III of this series: S. Kambe and T. Hayashi, This Bulletin, **45**, 952 (1972).
2) S. Kambe, T. Hayashi, H. Yasuda, and H. Midorikawa, *ibid.*, **44**, 1357 (1971).

Table 1. Properties of arylidene *N,N*-dialkyl-*N*-thiocarbamoyl thiocyanoacetamides (**3**)

Product	R=R′	R″	Reaction time (hr)	Mp (°C)	Yield (%)	Formula	Analysis (%) Found (Calcd) C	H	N	S	SH str. (cm^{-1})	SCN str. (cm^{-1})	C=O str. (cm^{-1})	C=N str. (cm^{-1})	C=C str. (cm^{-1})
a	CH_3	H	2	185—186	65	$C_{13}H_{13}ON_3S$	53.48 (53.61)	4.44 (4.50)	14.35 (14.43)	21.90 (21.90)	2550 w	2050 s	1740 s	1640 s	1600 s
b	CH_3	*p*-CH_3	1.5	172—173	53	$C_{14}H_{15}ON_3S_2$	55.24 (55.08)	4.90 (4.95)	13.89 (13.77)	21.00 (20.96)	2550 w	2050 s	1750 s	1640 a	1610 sh
c	CH_3	*o*-OCH_3	1.5	196—197	47	$C_{14}H_{15}O_2N_3S_2$	52.38 (52.33)	4.76 (4.71)	13.10 (13.08)	19.28 (19.22)	2600 w	2050 s	1740 a	1640 s	1600 s
d	CH_3	*p*-OCH_3	2	180—181	43	$C_{14}H_{15}O_2N_3S_2$	52.42 (52.33)	4.55 (4.71)	13.50 (13.08)	19.34 (19.22)	2600 w	2050 s	1740 s	1640 s	1600 s
e	CH_3	*p*-$N(CH_3)_2$	2	236—237	56	$C_{15}H_{18}ON_4S_2$	53.90 (53.88)	5.48 (5.43)	16.72 (16.76)	19.18 (19.14)	2550 w	2050 s	1730 s	1630 a	1600 s
f	CH_3	*o*-OH	2	210—211	46	$C_{13}H_{13}O_2N_3S_2$	51.00 (50.81)	4.52 (4.26)	13.71 (13.68)	21.01 (20.82)	2600 w	2050 s	1730 s	1620 m	1590 s
g	CH_3	*p*-OH	2	219—221[a]	39	$C_{13}H_{13}O_2N_3S_2$	51.16 (50.81)	4.30 (4.26)	13.74 (13.68)	20.89 (20.82)	2600 sh	2050 s	1730 s	1640 s	1600 s
h	C_2H_5	H	2	169—170	62	$C_{15}H_{17}ON_3S_2$	56.82 (56.42)	5.40 (5.37)	13.20 (13.16)	20.10 (20.04)	2600 w	2050 s	1720 s	1620 sh	1600 s
i	C_2H_5	*p*-CH_3	2	157—158	65	$C_{16}H_{19}ON_3S_2$	57.67 (57.65)	5.78 (5.75)	12.64 (12.61)	19.15 (19.19)	2600 w	2050 s	1720 s	1640 s	1590 s
j	C_2H_5	*o*-OCH_3	1.5	164—165	59	$C_{16}H_{19}O_2N_3S_2$	55.09 (55.01)	5.50 (5.48)	12.10 (12.03)	18.45 (18.32)	2600 w	2050 s	1720 s	1640 s	1590 s
k	C_2H_5	*p*-OCH_3	1.5	174—175	45	$C_{16}H_{19}O_2N_3S_2$	55.29 (55.01)	5.48 (5.48)	12.22 (12.03)	18.49 (18.32)	2600 w	2050 s	1740 s	1650 s	1610 m
l	C_2H_5	*p*-$N(CH_3)_2$	2	201—202	45	$C_{17}H_{22}ON_4S_2$	56.39 (56.34)	6.18 (6.12)	15.41 (15.46)	17.61 (17.66)	2600 w	2050 s	1720 s	1640 s	1590 s
m	C_2H_5	*o*-OH	2	137—138	48	$C_{15}H_{17}O_2N_3S_2$	53.61 (53.73)	5.23 (5.11)	12.86 (12.53)	19.15 (19.08)	2550 w	2050 s	1730 s	1620 s	1590 s
n	C_2H_5	*p*-OH	2	98— 99	49	$C_{15}H_{17}O_2N_3S_2$	53.78 (53.73)	5.32 (5.11)	12.49 (12.53)	19.28 (19.08)	2550 w	2050 s	1730 s	1630 s	1590 s

a) Decomp. All IR spectra were measured in KBr pellets.

cyanoacetamide (**2**), which subsequently condenses with aromatic aldehyde to give **3**.

Support for this may be supplied by the fact that the ester **1** reacted easily with *N,N'*-dialkylthiourea to give the amide **2**, and that the amide **2** thus isolated condensed with an aromatic aldehyde in the presence of *N,N'*-dialkylthiourea as a basic catalyst to give the product **3**. In contrast with the above reaction, when thiourea was used instead of *N,N'*-dialkylthiourea, the reaction of the ester **1** with benzaldehyde led to the formation of 5-benzylidene-2-imino-4-thiazolidinone (**5a**).[3]

The reaction of ester **1** with benzaldehyde in the presence of *N*-methylthiourea afforded 5-benzylidene-3-methylthiazolidine-2,4-dione (**6a**).[3] This compound is considered to be produced by the hydrolysis of 5-benzylidene-2-imino-3-methylthiazolidin-4-one (**5b**), which may be formed as an intermediate. Compound **6a** was obtained by the hydrolysis of the **3a** product with hydrochloric acid–ethanol. In addition, the reaction of the ester **1** with *N*-methylthiourea gave the corresponding amide (**2a**) (R=CH_3, R=H), but not 2-imino- or oxothiazolidinone. On the other hand, the treatment of **3a** with potassium carbonate or fluoride gave 5-benzylidene-2-methylimino-3-methyl-4-thiazolidinone (**5c**), which was identical with the authentic sample prepared by the alternative synthesis from benzaldehyde and 2-methylimino-3-methyl-4-thiazolidinone.[4] Furthermore, this compound (**5c**) was also obtained by the reaction of the amide **2b** (R=R'=CH_3) with benzaldehyde in the presence of potassium carbonate or fluoride. These facts suggest that, in the reaction of the amide **2** with aromatic aldehyde, the formation of a 4-thiazolidinone ring occurs after the condensation between the amide **2** and aromatic aldehyde has taken place. It is interesting that the ring closure of **3** might occur with the elimination of hydrogen thiocyanide, as is shown in Scheme 2.

Experimental

All the melting points are uncorrected. The IR spectra were recorded with a Shimadzu IR-27G spectrometer. The NMR spectra obtained on a Nihondenshi JNM-C-60 high-resolution NMR spectrometer (60 MHz). Tetramethylsilane was used as the internal standard. The chemical shifts of the protons are presented in terms of δ values.

General Procedure for the Reaction of Ethyl Thiocyanoacetate. (1) With Aromatic Aldehyde in the Presence of N,N'-*Dialkylthiourea*: A mixture of the ester **1** (0.02 mol), an aldehyde (0.02 mol), and an *N,N'*-dialkylthiourea (0.02 mol) in ethanol (20 m*l*) was refluxed for a suitable period. After the reaction mixture had then been cooled, the resulting precipitates were filtered and washed with water. They were recrystallized from ethanol to give arylidene *N,N'*-dialkyl-*N*-thiocarbamoyl thiocyanoacetamide (**3**). The results are summarized in Table 1.

The Reaction of Ethyl Thiocyanoacetate (1) with Benzaldehyde in the Presence of N-*Methylthiourea.* A mixture of the ester **1** (0.02 mol), benzaldehyde (0.02 mol), and *N*-methylthiourea (0.02 mol) in ethanol (20 m*l*) was refluxed for 5 hr. After cooling, the resulting precipitate was filtered and washed with water. Recrystallization from ethanol gave 5-benzylidene-3-methylthiazolidine-2,4-dione (**6a**); yield, 48%; mp 133—134°C (lit,[3] 134—135°C).

The Reaction of Ethyl Thiocyanoacetate (1) with Benzaldehyde in the Presence of Thiourea. A mixture of the ester **1** (0.02 mol), benzaldehyde (0.02 mol), and thiourea (0.02 mol) in ethanol (20 m*l*) was refluxed for 3 hr. A crystalline precipitate was deposited during the reaction; this was collected on a filter and washed with ethanol. Recrystallization from dimethyl sulfoxide gave 5-benzylidene-2-imino-4-thiazolidinone (**5a**); yield, 37%; decomp. 282—284°C (lit,[3] decomp. 282—284°C).

The Reaction of Ethyl Thiocyanoacetate (1) with N-*Methylthiourea.* The ester **1** (0.02 mol) was added, drop by drop at approximately 60°C, to a mechanically-stirred solution of *N*-methylthiourea (0.02 mol) in 20 m*l* of ethanol. Stirring was continued for 3 hr. After the solvent had then been removed with a vacuum evaporater, the residue was allowed to stand overnight. The precipitate which thus formed was separated by filtration, washed with water, and recrystallized to give *N*-methyl-*N*-thiocarbamoyl thiocyanoacetamide (**2a**); yield, 25%; decomp. 175—178°C.

IR (KBr): near 3300 (NH), near 2500 (SH), 2050 (SCN), 1670 (C=O), 1650 (C=N) cm^{-1}.

Found: C, 31.71; H, 3.69; N, 21.43; S, 33.81%. Calcd for $C_5H_7ON_3S_2$: C, 31.75; H, 3.73; N, 22.22; S, 33.83%.

The Reaction of Ethyl Thiocyanoacetate (1) with N,N-*Dimethylthiourea.* A mixture of the ester **1** (0.02 mol) and *N,N'*-dimethylthiourea (0.02 mol) in ethanol (20 m*l*) was refluxed for 2 hr. The resulting precipitate was collected on a filter and washed with water. Recrystallization from ethanol gave *N,N'*-dimethyl-*N*-thiocarbamoyl thiocyanoacetamide (**2b**); yield, 68%; mp 174—175°C.

IR (KBr): near 2550 (SH), 2050 (SCN), 1750 (C=O, 1640 (C=N) cm^{-1}.

Found: C, 35.51; H, 4.50; N, 20.89; S, 31.67%. Calcd for $C_6H_9ON_3S_2$: C, 35.47; H, 4.47; N, 20.69; S, 31.50%.

The Reaction of Ethyl Thiocyanoacetate (1) with N,N'-*Diethylthiourea.* A solution which contained the ester **1** (0.02 mol) and *N,N'*-diethylthiourea (0.02 mol) in ethanol (20 m*l*) was refluxed for 4 hr. After the solvent had then been removed with a vacuum evaporator, the residue was allowed to stand for several days. The crystalline matter thus formed was collected, washed with water, and air-dried. Recrystallization from ethanol–water gave *N,N'*-diethyl-*N*-thiocarbamoyl thiocyanoacetamide (**2c**); yield, 21%; mp 96—97°C.

Found: C, 41.52; H, 5.66; N, 18.31; S, 27.73%. Calcd for $C_8H_{13}ON_3S_2$: C, 41.56; H, 5.67; N, 18.18; S, 27.73%.

The Reaction of Ethyl Thiocyanoacetate (1) with Thiourea. Thiourea (0.02 mol) was stirred in ethanol (20 m*l*) at approximately 60°C; the stirring was then continued until the thiourea was completely dissolved. To a stirred alcoholic solution there was then added, drop by drop, the ester **1** (0.02 mol) over a 0.5-hr period. After this addition, stirring was continued for an additional 4 hr, and then the reaction mixture was allowed to stand for several hours. The crystalline matter thus formed was collected and washed with ethanol. Recrystallization from acetic acid gave 2-imino-4-thiazolidinone; yield, 19%; decomp. 232—235°C (lit,[5] 233—238°C).

3) S. Kambe, T. Hayashi, H. Yasuda, and A. Sakurai, *Nippon Kagaku Zasshi*, **92**, 867 (1971).

4) R. Andreasch, *Monatsh. Chem.*, **39**, 417 (1918).

5) H. R. Snyder and E. X. Werber, "Organic Syntheses" Vol. 27, p. 71 (1947).

The Reaction of N,N'-*Dimethyl*-N-*thiocarbamoyl Thiocyanoacetamide (***2b***) with Benzaldehyde in the Presence of* N,N'-*Dimethylthiourea.* A solution of the amide **2b** (0.01 mol) benzaldehyde (0.01 mol), and *N,N'*-dimethylthiourea (0.0025 mol) in ethanol (30 m*l*) was refluxed for 4 hr. After cooling, a crystalline matter separated; this was recrystallized from ethanol to afford benzylidene *N,N'*-dimethyl-*N*-thiocarbamoyl thiocyanoacetamide (**3a**); yield, 65%.

The Reaction of N,N'-*Dimethyl*-N-*thiocarbamoyl Thiocyanoacetamide (***2b***) with Benzaldehyde in the Presence of Potassium Carbonate or Fluoride.* To a solution of the (**2b**) amide (0.01 mol) and benzaldehyde (0.01 mol) in ethanol (20 m*l*), potassium carbonate or fluoride (0.01 mol) was added, after which the mixture was refluxed for a suitable period. After standing overnight, the resulting precipitate was collected on a filter and washed with water. Recrystallization from ethanol gave 5-benzylidene-2-methylimino-3-methyl-4-thiazolidinone (**5c**); mp 109—110°C.

When potassium carbonate was used as the catalyst, the reaction time was 2 hr and the yield was 54%.

When potassium was used as the catalyst, the reaction time was 7 hr and the yield was 58%.

IR (Nujol): 1750 (C=O), 1660 (C=N), 1620 (C=C) cm^{-1}.

NMR (DMSO-d_6): δ 3.20, 3.40 (CH_3), 6.05 (C_6H_5), 6.15 (=CH) ppm.

Found: C, 61.89; H, 5.20; N, 12.04; S, 13.74%. Calcd for $C_{12}H_{12}ON_2S$: C, 62.06; H, 5.21; N, 12.06; S, 13.77%.

The Reaction of Benzylidene N,N'-*Dimethyl*-N-*thiocarbamoyl Thiocyanoacetamide (***3a***) in the Presence of Potassium Carbonate or Fluoride.* A mixture of the amide **3a** (0.01 mol) in ethanol (20 m*l*) containing potassium carbonate or fluoride (0.01 mol) was refluxed for a suitable period. After the mixture had then stood overnight, the precipitate formed was separated by filtration, washed with water, and recrystallized from ethanol to afford 5-benzylidene-2-methylimino-3-methyl-4-thiazolidinone (**5c**).

When potassium carbonate was used as the catalyst, the reaction time was 2 hr and the yield was 56%.

When potassium fluoride was used as the catalyst, the reaction time was 6 hr and the yield was 58%.

The Hydrolysis of Benzylidene N,N'-*Dimethyl*-N-*thiocarbamoyl Thiocyanoacetamide (***3a***).* To a solution containing concentrated hydrochloric acid (10 m*l*) and ethanol (10 m*l*), we added the amide **3a** (0.01 mol), and then the mixture was refluxed for 6 hr. After cooling, the reaction mixture was poured onto cracked ice. The crystalline matter thus formed was collected, washed with water, and air-dried. Recrystallization from ethanol gave 5-benzylidene-3-methylthiazolidin-2,4-dione (**6a**); yield, 52%; mp 133—134°C (lit,[3] 134—135°C).

The Hydrolysis of 5-Benzylidene-2-methylimino-3-methyl-4-thiazolidinone. The procedure used was essentially the same as that described above; yield, 53%; mp 133—134°C.

The Reaction of 2-Methylimino-3-methyl-4-thiazolidinonew ith Benzaldehyde. 2-Methylimino-3-methyl-4-thiazolidinone was prepared according to the procedure described in the literature.[4]

A mixture of 2-methylimino-3-methyl-4-thiazolidinone (0.01 mol) and benzaldehyde (0.01 mol) in ethanol (10 m*l*) containing potassium acetate (0.01 mol) was refluxed for 4 hr. After the solvent had been removed, the residue was allowed to stand overnight. The resulting crystals were collected on a filter. Recrystallization from ethanol gave 5-benzylidene-2-methylimino-3-methyl-4-thiazolidinone (**5c**); yield, 56%; mp 109—110°C.

The authors wish to express their hearty thanks to Dr. Hiroshi Midorikawa and Heinosuke Yasuda for their kind advice and encouragement, and Dr. Haruo Homma and his staff for their microanalyses.

The Michael Reactions of Substituted 9,9′-Bifluorenylidenes with 2-Iodo- and 2,7-Diiodofluorene, and Some Other Reactions of Iodofluorenes[1,2]

Masahiro MINABE and Kazuo SUZUKI

Department of Industrial Chemistry, Faculty of Technology, Utsunomiya University, Ishii-cho, Utsunomiya

(Received September 28, 1971)

The Michael-addition reaction between 2-iodofluorene and 9,9′-bifluorenylidene gave exclusively the normal addition product. The same reaction of fluorene with 2,2′-diiodo-9,9′-bifluorenylidene, of 2,7-diiodofluorene with 9,9′-bifluorenylidene, and of fluorene with 2,7,2′,7′-tetraiodo-9,9′-bifluorenylidene afforded not only the normal adducts, but also some abnormal compounds. Some new iodo-substituted fluorenes, -9,9′-bifluorenylidenes, -9,9-bifluorenyls, and -1,4-bis(2,2′-biphenylylene)-1,3-butadienes, were synthesized. The hydrogenolyses of 2- or 2,7-di-iodofluorene with lithium aluminum hydride, Raney nickel, and hydriodic acid were performed relatively smoothly to give fluorene. The Grignard and the Ullmann reactions of 2- or 2,7-di-iodofluorene gave the usual, expected compounds, accompanied by some unusual products. The cyano-substituted fluorenes were prepared by the reaction of 2- or 2,7-diiodofluorene with potassium cyanide-cupric cyanide in *N,N*-dimethylformamide.

The Michael reaction[3] of 9,9′-bifluorenylidene (**7**) with 2,7-dibromofluorene gave an abnormal product, 2,7,2″,7″-tetrabromo-9,9′,9′,9″-terfluorenyl, as the main product, and the normal addition product, 2,7-dibromo-9,9′,9′,9″-terfluorenyl, as a by-product. The similar addition of fluorene (**1**) to 2,7,2′,7′-tetrabromo-9,9′-bifluorenylidene afforded three abnormal products, 2,7-dibromo-9,9′,9′,9″-terfluorenyl and 2,7,2″,7″-tetrabromo-9,9′,9′,9″-terfluorenyl, as the main products, and 9,9′,9′,9″-terfluorenyl (**22**), and the normal addition product, 2,7,2′,7′-tetrabromo-9,9′,9′,9″-terfluorenyl, as by-products.

An analogous reaction[2] of 2-fluorofluorene with **7** in the presence of a sodium hydroxide–pyridine solution or sodium ethoxide in ethanol gave exclusively the normal addition product, 2-fluoro-9,9′,9′,9″-terfluorenyl. Also, 2,2′-difluoro-9,9′,9′,9″-terfluorenyl, 2,7-difluoro-9,9′,9′,9″-terfluorenyl, and 2,7,2′,7′-tetrafluoro-9,9′,9′,9″-terfluorenyl were obtained as normal main products by similar reactions of **1** with 2,2′-difluoro-9,9′-bifluorenylidene, of 2,7-difluorofluorene with **7**, and of **1** with 2,7,2′,7′-tetrafluoro-9,9′-bifluo-renylidene respectively.

The present paper will deal with the Michael reaction of iodo-substituted 9,9′-bifluorenylidenes with fluorenes and will attempt to elucidate some effects due to the difference between iodo-substitutions. It will also compare a few reactions in 2-iodofluorene (**2**)[4] or 2,7-diiodofluorene (**3**)[4b,4c,4e,5] with other, corresponding halogeno derivatives.

The Michael reaction of **7** with **2** in the presence of potassium hydroxide–pyridine gave 2-iodo-9,9′,9′,9″-terfluorenyl (**15**), 2-iodofluorenone (**5**)[4a,4d,4e,4f] and fluorenone (**4**). The yield of **15** increased with the increase in the base concentration, as is shown in Table 1.

The same reaction of 2,2′-diiodo-9,9′-bifluorenylidene (**8**)[6] with **1** afforded 2,2′-diiodo-9,9′,9′,9″-terfluorenyl (**16**), 2,2″-diiodo-9,9′,9′,9″-terfluorenyl (**17**), **4**, and **5**. The yield of **17** increased as the base concentration increased, while, on the contrary, the yield of **16** decreased, as is shown in Table 2. Compounds **16** and **17** are isomeric, and their structures were estimated by comparing the fragmentation peaks in the mass spectra.

An analogous reaction between **7** and **3** yielded 2,7-diiodo-9,9′,9′,9″-terfluorenyl (**19**), 2,7,2″,7″-tetraiodo-9,9′,9′,9″-terfluorenyl (**21**), and **22** as both normal and abnormal addition products, and 2,7-diiodofluorenone (**6**)[4e,5] and **4** as elimination products, as is shown in Table 3. The yields of these reaction products are closely related with the base concentration and with the molar ratio of the reactants.

2,2′,2″-Triiodo-9,9′,9′,9″-terfluorenyl (**18**) and 2,7,2′,7′,2″,7″-hexaiodo-9,9′,9′,9″-terfluorenyl (**23**) were obtained by the reactions of **2** with **8**, and of **3** with 2,7,2′,7′-tetraiodo-9,9′-bifluorenylidene (**9**). These products could be obtained as normal products, but the stereoisomeric 9,9′,9′,9″-terfluorenyls[7] were not isolated.

In the reaction of **9** with **1**, 2,7,2′,7′-tetraiodo-9,9′,9′,9″-terfluorenyl (**20**), **19**, **21**, **22**, **3**, **4**, and **6** were separated.

The sequences for the formation of the compounds in these Michael reactions can be represented by the typical reaction of **9** with **1** as is illustrated in Scheme 1. A transitory carbanion (D) is formed by the nucleophilic attack of the fluorenyl carbanion (**1′**) generated from **1** on the highly-polarized ethylenic carbons of **9** in the presence of the base. Subsequently, D may be transformed to the normal addition product, **20**, by protonation, but then, the D dis-

1) Studies on Fluorene Derivatives. XXVIII. A part of this paper was presented at the 23rd Meeting of the Chemical Society of Japan, Tokyo, April, 1970; Preprints, III, p. 1739.

2) Part XXVII of this series: M. Minabe, A. Tanaka, M. Wakui, and K. Suzuki, This Bulletin, **44**, 1614 (1971).

3) K. Suzuki, M. Minabe, M. Fujimoto, and N. Nohara, *ibid.*, **42**, 1609 (1969).

4) a) L. Chardonnens and L. Avar, *Helv. Chim. Acta*, **52**, 1091 (1969). b) Y. Ogata and I. Urasaki, *J. Chem. Soc., C*, **1970**, 1689. c) P. S. Varma and V. S. Rao, *J. Indian Chem. Soc.*, **15**, 72 (1938). d) M. D. Barnett, G. H. Daub, F. N. Hayes, and D. G. Ott, *J. Amer. Chem. Soc.*, **81**, 4583 (1959). e) F. Dewhurst and P. K. J. Shak, *J. Chem. Soc., C*, **1969**, 1503. f) Ch. Courtot, *Ann. Chem.*, **14**, 5 (1930).

5) T. Stauner, L. Avar, and L. Chardonnens, *Helv. Chim. Acta*, **53**, 1311 (1970).

6) This compound is not clear in respect to *cis-trans* isomerism.

7) K. Suzuki, *Nippon Kagaku Zasshi*, **70**, 189 (1949); *ibid.*, **75**, 795 (1954); K. Suzuki, *Technol. Repts. Tohoku Univ.*, **19**, 63 (1955).

sociates into **3'** and the intermediate 2,7-diiodo-9,9'-bifluorenylidene (E)[8] by the fission of the 9-9' carbon-carbon bond, with the elimination of the 9''-proton. Therefore, the anomalous formation of **21** can be explained by a secondary Michael reaction of **3'** with (E), followed by protonation.

The reaction of E with **1'** gives the carbanion (C), which then yields an abnormal product, **19**. Further, the complete process of formation to the iodine-free compound, **22**, involves three additions and two eliminations through the two intermediates, (D and C), under consideration. Moreover, **3**, **4**, and **6** were also isolated by elimination or oxidation reactions in the process.[9]

Meanwhile, the 9-methylene hydrogen in 2-halo- or 2,7-dihalo-fluorenes are more reactive in forming fluorenyl carbanions than that in the parent fluorene in the Michael reaction. For this reason, the electron-withdrawing effect[10] of these substituents may operate on the 9-carbon atom in fluorenes. Moreover, the base concentration seems to be an important factor in the 9-methylene hydrogen.

In view of this effect, the ethylenic 9-carbon in E, for example, is more electronegative than the 9'-carbon,

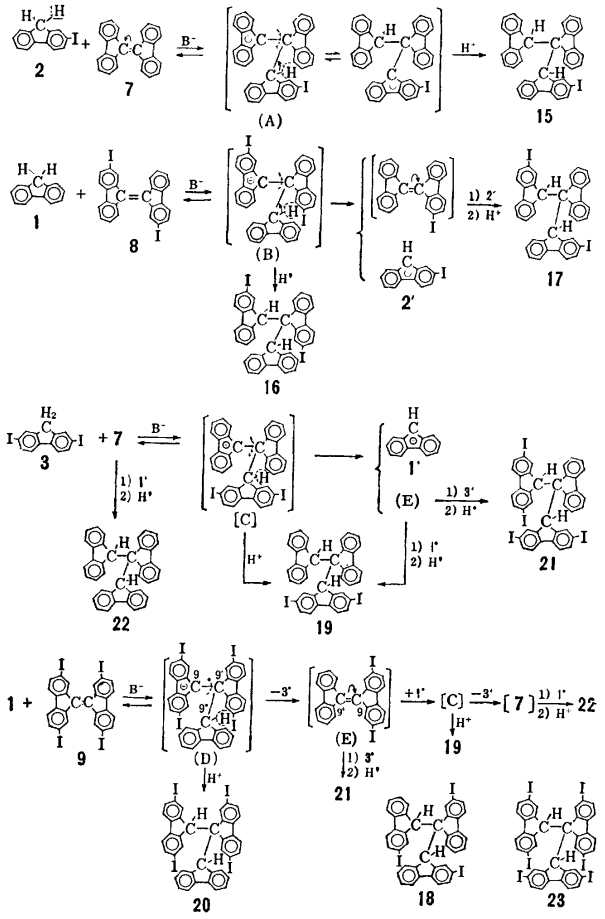

Scheme 1.

8) The Michael reaction of **7** with 2-bromofluorene afforded a trace amount of 2-bromo-9,9'-bifluorenylidene. And therefore, (E) or 2-iodo-9,9'-bifluorenylidene can be regarded as intermediates in this series. See K. Suzuki and M. Fujimoto, This Bulletin, **37**, 1833 (1964).

and the addition of **3'** is preferential in forming the 9'-carbon leading to **21** than the other possible way. These effects were supported experimentally by the corresponding bromo derivatives[3] in the analogous Michael reaction. The crowded carbanions, for example, C and D, which contain bulky iodine atoms, might be reactive because of the steric compression. Therefore, under reasonably mild reaction conditions, the addition products are chiefly normal compounds. However, the reaction is accelerated toward elimination upon an increase in the alkali concentration.

Because there is more active iodine than any other halogen on the 2- or 2,7-positions of fluorene, attempts at the step-by-step syntheses of iodine-substituted 9,9',9',9''-terfluorenyls were unsuccessful. However, we are able to estimate the positions of iodine by comparing the melting points and the mass and IR spectra of iodo-9,9',9',9''-terfluorenyls with those of the bromo-[3] and chloro-[11] analogues.

Barnett and others[4d] reported that 2,2'-bifluorenyl-9,9'-dione (**14**) was obtained by the Ullmann reaction of **5**, even though no 2,2'-bifluorenyl (**13**) was formed from **2**. The syntheses of these compounds were re-investigated by the Ullmann reaction; 42% of **14** was obtained from **5**, and 9% of **13** from **2**. In addition, a considerable amount of **1** was formed from **2**. The same reaction of **3** gave 15% of **1** instead of a polymeric substance upon dehalogenation.

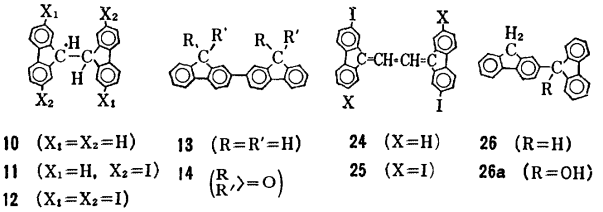

10 ($X_1=X_2=H$) **13** ($R=R'=H$) **24** ($X=H$) **26** ($R=H$)
11 ($X_1=H$, $X_2=I$) **14** ($R,R'>C=O$) **25** ($X=I$) **26a** ($R=OH$)
12 ($X_1=X_2=I$)

Scheme 2.

The iodine atoms in **2** and **3** were completely removed by reaction with Raney nickel, lithium aluminum hydride, or hydriodic acid. However, no reaction occurred at all for 2-bromofluorene and 2,7-dibromofluorene[12] under the same conditions.

The reaction of **2** with ethylmagnesium bromide afforded **1**, 2-ethylfluorene, and **13**. The yield of the anticipated compound, 2-ethylfluorene, was, however, very low, and **1** and **13** were unexpectedly ob-

9) A small amount of **3** can be oxidized to **6** under these reaction conditions.

10) The high reactivity of fluorene is due to the coplanarity enforced by the 9-methylene bridge. And the activation of 9-methylene group is attributable to enhanced hyperconjugation between the aromatic rings. See for example, P. B. D. de la Mare, D. M. Hall, M. M. Harris, and M. Hassan, *Chem. Ind.* (London), **1958**, 1086; H. C. Brown, M. Bubeck, and G. Goldman, *J. Amer. Chem. Soc.*, **84**, 1229 (1962).

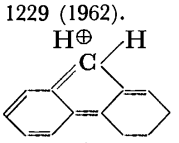

11) K. Suzuki and M. Minabe, unpublished.

12) 2,7-Dibromofluorene, however, was reduced to **1** by refluxing with Raney nickel in xylene; see A. Schoenberg, K. H. Brosowski, and E. Singer, *Chem. Ber.*, **95**, 2984 (1962).

Table 1. The Michael reaction of **7** with **2**

Reactants g			Reaction conditions			Products g(%)			Recovered g(%)	
7	**2**	Mole ratio	Pyridine(ml)	KOH(%)	Time(hr)	**15**	**5**	**4**	**7**	**2**
2.19	1.95	1/1	30	0.1	22	0.96(23)	0.03 (2)	0.24(10)	1.03(53)	1.26(65)
2.19	1.95	1/1	30	1	11	2.06(50)	0.02 (2)			
2.19	1.95	1/1	30	10	7	3.06(74)	0.10 (5)	0.08 (3)		
2.19	2.92	1/1.5	30	1	9	3.31(79)	0.43(14)			0.93(32)
3.28	1.95	1.5/1	30	1	11	2.92(71)	0.04 (2)	0.15 (8)	0.36(11)	

Table 2. The Michael reaction of **8** with **1**

Reactants g			Reaction conditions			Products g(%)				Recovered g(%)	
8	**1**	Mole ratio	Pyridine(ml)	KOH(%)	Time(hr)	**16**	**17**	**5**	**4**	**8**	**1**
2.32	0.83	4/5	30	0.1	40	1.19(40)	0.56(19)	0.10(4)	0.02(2)	0.49(21)	0.37(45)
2.32	0.83	4/5	30	10	8	0.90(30)	1.10(37)	0.15(6)			0.08(10)
2.90	0.50	5/3	30	10	8	0.30(13)	0.84(37)	0.05(2)	0.02(4)	0.45(16)	

Table 3. The Michael reaction of **7** with **3**

Reactants g			Reaction conditions			Products g(%)						Recovered g(%)	
7	**3**	Mole ratio	Pyridine(ml)	KOH(%)	Time(hr)	**19**	**21**	**22**	**6**	**4**	**1**	**7**	**3**
2.2	2.8	1/1	30	0.05	24	0.48(10)			0.05			1.58	2.29
2.2	2.8	1/1	30	0.1	18.5	1.28(26)						0.004	0.98
2.2	2.8	1/1	30	1	2.5	3.69(74)	0.10 (3)		0.12	0.01		0.13	0.08
2.2	2.8	1/1	30	5	2.5	3.55(71)	0.36(11)		0.13	0.015		0.01	0.02
2.2	2.8	1/1	30	10	2.5	3.72(75)	0.38(11)		0.01	0.01	0.02	0.03	0.02
1.1	2.8	1/2	30	5	2.5	1.67(67)	0.53(16)		0.04	0.01	0.19		0.69
3.3	2.8	3/2	30	5	2.5	4.08(82)		0.002	0.04	trace	0.005	1.01	

tained in relatively high yields. The formation of **1** and **13** can be regarded as occurring by means of the reaction between **2** and magnesium, which was activated by ethyl bromide, followed by hydrolysis or alkylation. **1** was obtained in a 60% yield from **2** following the procedure of Morrison.[13]

The synthesis of 2,9′-bifluorenyl (**26**)[14] was examined by interaction between 2-fluorenylmagnesium iodide and 9-bromofluorene, but 9,9′-bifluorenyl (**10**), **13**, and **1** were afforded. These results can be explained in terms of the reactions of 9-fluorenylmagnesium bromide with 9-bromofluorene and of 2-fluorenylmagnesium iodide with **2** respectively. The reaction of 2-fluorenylmagnesium iodide with **4** afforded **26**, but not 9′-hydroxy-2,9′-bifluorenyl (**26a**). The interpretation of the unusual formation is not yet clear.

The synthesis of α-cyanonaphthalene, as has been reported by House and Fischer,[15] was adapted to the syntheses of 2-cyanofluorene derivatives. The reaction of **2** with potassium cyanide–cupric cyanide gave 2-cyanofluorene[16] and a small amount of 2-cyanofluorenone. Similarly, 2,7-dicyanofluorene and 2,7-dicyanofluorenone were obtained from **3**. The melting point of 2-cyanofluorene was 91—92°C,[16a] slightly different from that of the literature;[16b,16c] the structure of this compound was assigned by elemental analysis and by means of the IR and mass spectra. If 2-cyanofluorene is contaminated by a small amount of impurities, **1** and/or **2**, the mass spectra can be expected to be 166 and 292 *m/e*. However, neither fragmentation was observed.

Experimental[17]

The IR spectra were recorded on KBr pellets using a JASCO model IR-G spectrophotometer (Japan Spectroscopic Co., Ltd.). The gas chromatograms were obtained by means of GCG-550T gas chromatograph (Yanagimoto Mfg. Co., Ltd.), using a column containing 5% of Silicone SE-30 on Celite 545-AW. The mass spectra were measured with a model RMU-6E apparatus (Hitachi, Ltd.) by means of the direct inlet system. The sample evaporating temper-

13) D. C. Morrison, *J. Amer. Chem. Soc.*, **74**, 3430 (1952).
14) K. Suzuki, *J. Org. Chem.*, **27**, 2224 (1962).
15) H. O. House and W. F. Fischer, *ibid.*, **34**, 3626 (1969).
16) a) M. Fortner, *Monatsh. Chem.*, **25**, 443 (1904). b) N. Ishikawa and T. Ozawa, *Yuki Gosei Kagaku Kyokai Shi*, **17**, 553 (1959). c) F. E. Ray and P. Quinlin, *J. Org. Chem.*, **13**, 652 (1948). d) J. V. Braun and H. Engel, *Ber.*, **57**, 191 (1923).
17) All the melting points are uncorrected. The identities of the compounds in this series were confirmed by mixed-melting-point determinations and by comparison of IR absorption spectra with those of authentic samples.

ature, chamber volt, total emission, and target current were maintained at 200°C, 80 V, 80 μA, and 50 μA respectively.

3 (mp 215—216.5°C) was synthesized in a 75% yield from **2** in a manner similar to that used for **2**[4a]; it was then converted to the corresponding ketone, **6** (80%); mp 207—208°C; IR (>C=O): 1716 cm^{-1}.

2-Iodofluorenol. A mixture of 5.2 g of **5**, 53 g of zinc dust, 220 m*l* of ethanol, and 5 g of calcium chloride in 10 m*l* of water was refluxed for 1 hr. The reaction mixture was then filtered, and the filtrate was poured into water. The precipitate was recrystallized from benzene-cyclohexane (1 : 1). Colorless needles; mp 121—123°C; yield 1.22 g (23%). IR (>OH): 3190 cm^{-1}. Found: C, 50.95; H, 2.88%. Calcd for $C_{13}H_9OI$: C, 50.68; H, 2.94%.

2,7-Diiodofluorenol. A 1.3-g portion of **6** was treated under the conditions described above to yield 1.02 g (78%) of 2,7-diiodofluorenol as fine, colorless needles; mp 201.5—203°C (decomp. to yellow). IR (-OH): 3270 cm^{-1}. Found: C, 36.13; H, 1.74%. Calcd for $C_{13}H_8OI_2$: C, 35.98; H, 1.86%.

2-Iodo-9-bromofluorene. a): A mixture of 8.76 g (0.03 mol) of **2**, 5.60 g of *N*-bromosuccinimide (NBS), and 50 m*l* of dry benzene was refluxed for 3 hr to afford 7.10 g (64%) of 2-iodo-9-bromofluorene; mp 126—127°C (from cyclohexane). Found: C, 42.36; H, 1.96%. Calcd for $C_{13}H_8BrI$: C, 42.09; H, 2.17%.

b): 2-Iodofluorenol (1.03 g) was brominated by hydrogen bromide in acetic acid to yield 0.75 g (53%) of the product; mp 126—127°C.

2,7-Diiodo-9-bromofluorene: a): A 2.1-g portion of **3** was worked up with NBS (1.0 g) to yield 1.6 g (64%) of 2,7-diiodo-9-bromofluorene; mp 204—205°C (from benzene and cyclohexane). Found: C, 31.43; H, 1.22%. Calcd for $C_{13}H_7BrI_2$: C, 31.42; H, 1.42%.

b): **3** (8.4 g; 0.02 mol) was dissolved in 150 m*l* of benzene, and then a trace amount of benzoyl peroxide was added. Into this boiling mixture there was stirred a solution of benzene containing 3.5 g (0.022 mol) of bromine under the irradiation with UV light for 15 min. After the mixture had been left standing to cool, 4.0 g of 2,7-diiodo-9-bromofluorene (mp 204—205°C) were collected by filtration. The mother solution was then treated as usual to afford an additional 2.3 g (total 6.3 g; 63%) of the product.

Furthermore, a small amount of 2,7-diiodo-9,9-dibromofluorene (mp 230—232°C) was isolated. Found: C, 27.30; H, 0.93%. Calcd for $C_{13}H_6Br_2I_2$: C, 27.56; H, 1.06%.

c): The bromination of 2,7-diiodofluorenol (15 g in 1 *l* of acetic acid) with hydrogen bromide yielded 7.7 g (45%) of the same compound; mp 204—205°C.

*1,4-Bis(4-iodo-2,2'-biphenylylene)-1,3-butadiene (**24**)*: A mixture of 1.46 g (0.005 mol) of **2**, 55 m*l* of ethanol, and 2.5 g of potassium hydroxide in 5 m*l* of water was refluxed under a gentle stream of air for 20 hr. The deposited product was then recrystallized from pyridine to yield 1.01 g (67%) of **24** (mp 405—405°C (decomp.)) as orange-red needles. Found: C, 55.50; H, 2.48%. Calcd for $C_{28}H_{16}I_2$: C, 55.47; H, 2.66%.

*1,4-Bis(4,4'-diiodo-2,2'-biphenylylene)-1,3-butadiene (**25**)*: The compound was prepared in a 54% yield by the same procedure; red needles; mp 455°C (decomp.). Found: C, 39.17; H, 1.25%. Calcd for $C_{28}H_{14}I_4$: C, 39.20; H, 1.64%.

*2,2'-Diiodo-9,9'-bifluorenylidene (**8**)*: An acetone solution (110 m*l*) containing 3.71 g (0.01 mol) of 2-iodo-9-bromofluorene was refluxed for 5 hr with potassium hydroxide-methanol (0.56 g/20 m*l*) to afford 1.91 g (66%) of red **8**; 262—263°C. Found: C, 53.48; H, 2.17%. Calcd for $C_{26}H_{14}I_2$: C, 53.82; H, 2.43%.

*2,7,2',7'-Tetraiodo-9,9'-bifluorenylidene (**9**)*: To a mixture of 10.0 g (0.02 mol) of 2,7-diiodo-9-bromofluorene and 3 *l* of methyl ethyl ketone, was added 30 m*l* of methanol containing equimolar sodium hydroxide at 5—8°C over a period of 15 min. Thereupon, the reaction mixture was worked up by the two following methods.

a) After stirring for 2 hr, the precipitate was filtered off, washed with water, dried, and washed with 50 m*l* of boiling benzene to afford 5.6 g (67%) of **9** (mp 425°C (decomp.)). Found: C, 37.51; H, 1.69%. Calcd for $C_{26}H_{12}I_4$: C, 37.54; H, 1.45%.

b) The other reaction mixture, which was prepared from 4.0 g of 2,7-diiodo-9-bromofluorene, was refluxed for 20 hr to yield 2.01 g (60%) of **9** (mp 423°C (decomp.)), 0.98 g (28%) of **6** (mp 206—207°C), and 0.01 g (0.3%) of **23** (mp 316—318°C (decomp.)).

*Reduction of **8**.* A mixture of 0.58 g (0.001 mol) of **8**, 700 m*l* of acetic acid, 10 g of zinc granule and 100 m*l* of concentrated hydrochloric acid was refluxed for 1.5 hr. The reaction mixture was evaporated to dryness, and the residue was recrystallized from ethyl acetate to afford 0.12 g (21%) of **8** (mp 260—262°C) and 0.18 g (31%) of 2,2'-diiodo-9,9'-bifluorenyl (**11**) (mp 287—288°C (decomp.) (from benzene)). Found: C, 53.77; H, 2.64%. Calcd for $C_{26}H_{16}I_2$: C, 53.64; H, 2.77%.

*The Michael Reaction of 9,9'-Bifluorenylidene (**7**) with 2-Iodofluorene (**2**).* A mixture of 2.19 g (1/150 mol) of **7**, 1.95 g (1/150 mol) of **2**, 28 m*l* of pyridine, and 3.0 g (10% for the solvent) of potassium hydroxide in 2 m*l* of water was placed in a sealed tube and heated at 97—100°C for 7 hr. The reaction mixture was then poured into 500 m*l* of water, and the precipitate was recrystallized from cyclohexane and then from benzene to give 3.02 g of **15** (mp 272—274°C (decomp.)). The analytical sample was recrystallized from *N,N*-dimethylformamide (DMF) and then from benzene. Found: C, 75.75; H, 3.90%. Calcd for $C_{39}H_{25}I$: C, 75.49; H, 4.06%.

The subsequent evaporation of the mother liquor *in vacuo* and chromatography on alumina in benzene gave an additional 0.04 g (total 3.06 g; 74%) of **15** (mp 271—274°C (decomp.)), 0.08 g (3%) of **4** (mp 81—82°C), and 0.10 g (5%) of **5** (mp 148—150°C).

*The Michael Reaction of 2,2'-Diiodo-9,9'-bifluorenylidene (**8**) with Fluorene (**1**).* A mixture of 2.32 g (0.004 mol) of **8**, 0.83 g (0.005 mol) of **1**, 28 m*l* of pyridine, and 3.0 g of potassium hydroxide in 2 m*l* of water was heated at 98—100°C for 8 hr in a sealed tube. The reaction mixture was then treated in a manner analogous to that described above to yield 0.90 g (30%) of **16** (mp 261—262°C (decomp.)) and 1.10 g (37%) of **17** (mp 281—282°C (decomp.)) from benzene and ethyl acetate. Anal for **16**. Found: C, 62.60; H, 3.07%. Calcd for $C_{39}H_{24}I_2$: C, 62.76; H, 3.24%. Mass (M^+): 746 *m/e*. For **17**. Found: C, 62.75; H, 3.47%. Calcd for $C_{39}H_{24}I_2$: C, 62.76; H, 3.24%. Mass (M^+): 746 *m/e*.

Although the compounds **16** and **17** are isomeric to each other, we have speculated on these structures by comparing the IR spectra, melting points, and relative intensities of the fragment ions in the mass spectra.

In addition, 0.08 g (10%) of **1** (mp 111—112.5°C) and 0.15 g (6%) of **5** (mp 149—150.5°C) were isolated by alumina column chromatography.

*The Michael Reaction of 2,2'-Diiodo-9,9'-bifluorenylidene (**8**) with 2-Iodofluorene (**2**).* A mixture of 2.32 g (0.004 mol) of **8**, 1.46 g (0.005 mol) of **2**, 28 m*l* of pyridine, and 1.5 g of potassium hydroxide in 2 m*l* of water was placed in a

sealed tube; then the mixture was heated in boiling water for 10 hr. The precipitate formed upon dilution with 400 ml of water was sublimed at 160°C. The sublimate afforded 0.15 g of **2** (mp 126—128°C) and 0.03 g of **5** (mp 146—147°C) by alumina-column chromatagraphy. The sublimation residue was recrystallized from ethyl acetate and then from benzene to afford 1.49 g (43%) of **18** (mp 281—282°C (decomp.)). Found: C, 54.06; H, 2.41%. Calcd for $C_{39}H_{23}I_3$: C, 53.70; H, 2.66%.

Further, 0.07 g of **8** (mp 258—261°C) was recovered from the mother solution.

*The Michael Reaction of 9,9'-Bifluorenylidene (**7**) with 2,7-Diiodofluorene (**3**).* A mixture of 2.2 g (1/150 mol) of **7**, 2.8 g (1/150 mol) of **3**, 28 ml of pyridine, and 0.3 g of potassium hydroxide in 2 ml of water was heated at 95—100°C for 2.5 hr. During this period, the reaction mixture turned dark and colorless crystals were deposited.

The crude product was recrystallized from benzene to afford 2.69 g of **19** (mp 286—288°C (decomp.)). The pyridine mother liquor was then poured into water, and the deposited product was separated by a combination of recrystallization, alumina-column chromatography, and vacuum sublimation to yield 1.00 g (total 3.69 g; 74%) of **19** (mp 287—288°C (decomp.)), 0.10 g (3%) of **21** (mp 307—307.5°C (decomp.)), 0.12 g of **6** (mp 205—207°C), 0.01 g of **4** (mp 81—82°C), 0.08 g of **3** (mp 213—214°C), and 0.13 g of **7** (mp 180—182°C). Anal for **19**. Found: C, 62.75; H, 3.15%. Calcd for $C_{39}H_{24}I_2$: C, 62.76; H, 3.24%. For **21**. Found: C, 46.86; H, 1.95%. Calcd for $C_{39}H_{22}I_4$: C, 46.93; H, 2.22%.

*The Michael Reaction of 2,7,2',7'-Tetraiodo-9,9'-bifluorenylidene (**9**) with Fluorene (**1**).* **1** (4.2 g, 0.025 mol) also underwent a similar reaction with **9** (4.2 g, 0.005 mol) in 112 ml of pyridine in the presence of potassium hydroxide (1.2 g; 1% for the solvent) in 8 ml of water at 95—100°C for 20 hr.

The following compounds were thus obtained; 0.47 g of **19** (mp 286—287°C (decomp.)), 0.09 g of **20** (mp 299—300°C (decomp.)), 0.17 g of **21** (mp 312—314°C (decomp.)), 0.02 g of **22** (mp 290—292°C (decomp.)), 0.89 g of **3** (mp 213—215°C), 0.23 g of **6** (mp 205—207°C), and 0.04 g of **4** (mp 83—84°C). In addition, 1.73 g of **1** (mp 113—114°C) and 0.03 g of **9** (mp 423—424°C (decomp.)) were recovered. Anal for **20**. Found: C, 46.84; H, 2.03%. Calcd for $C_{39}H_{22}I_4$: C, 46.93; H, 2.22%. For **21**. Found: C, 46.89; H, 2.31%. Calcd for $C_{39}H_{22}I_4$: C, 46.93; H, 2.22%. For **19**. Found: C, 63.11; H, 3.29%. Calcd for $C_{39}H_{24}I_2$: C, 62.76; H, 3.24%.

The **20** and **21** compounds are isomeric, and we estimated their structures by comparing the mass and IR spectra and melting points.

*The Michael Reaction of 2,7,2',7'-Tetraiodo-9,9'-bifluorenylidene (**9**) with 2,7-Diiodofluorene (**3**).* A 2.9-g portion of **3** was allowed to react with 1.11 g of **9** (mol. ratio 5/1), using 0.3 g of potassium hydroxide as a catalyst in 30 ml of pyridine for 55 hr. The reaction mixture was then worked up as usual. Thus, 0.14 g (9%) of **23** (mp 318—319°C (decomp.) and 1.00 g (90%) of recovered **9** (mp 424°C (decomp.)) were isolated. Also, 0.31 g (10%) of **6** (mp 207—207.5°C) and 2.20 g (76%) of **3** (mp 216—217°C) were obtained from the mother solution by alumina-column chromatography. Found for **23**: C, 37.70; H, 1.50%. Calcd for $C_{39}H_{20}I_6$: C, 37.47; H, 1.61%.

Under other conditions, **3** (1.67 g) was allowed to react with **9** (1.11 g) (mole ratio 3/1), using sodium ethoxide (10% for the solvent) in absolute ethanol (30 ml) for 40 hr; 0.66 g of **9** (mp 424°C (decomp.)) and a compound (mp 323—324°C (decomp.) (0.23 g)) were thus isolated. Found for compound with mp 323—324°C (decomp.): C, 37.63; H, 1.45%. Calcd for $C_{26}H_{14}I_4$: C, 37.44; H, 1.69%.

The IR spectrum of this compound resembles that of halogen-substituted 9,9'-bifluorenyl; hence, the compound is presumably a reduction product, 2,7,2',7'-tetraiodo-9,9'-bifluorenyl (**12**).

*The Ullmann Reaction of 2-Iodofluorene (**2**) and 2,7-Diiodofluorene (**3**).* *a)*: A mixture of 3.0 g of **2** and 6.0 g of activated copper bronze[18] was heated in a sealed tube at 150°C for 20 hr to give 0.15 g (9%) of **13** (mp 316°C (lit,[4d] mp 316.5—318°C)) and 0.36 g (22%) of **1** (mp 110—112°C).

In another reaction, in which a mixture of 1.5 g of **2**, 10 g of zinc-copper couple,[19] and 30 ml of dry xylene was refluxed for 19 hr, 0.225 g (27%) of **1** (mp 111—112.5°C) was isolated.

b): A mixture of 4.0 g of **3** and 8.0 g of a zinc-copper couple was treated in a sealed tube at 230°C for 20 hr to afford 0.25 g (15%) of **1** (mp 113—114.5°C).

*Hydrogenolyses of 2-Iodofluorene (**2**) and 2,7-Diiodofluorene (**3**).* *a)*: A suspension of 5.0 g of Raney nickel (W-7)[20] in 150 ml of ethanol containing 1.46 g of **2** was shaken under an atmospheric pressure of hydrogen at room temperature for 2 hr. The reaction mixture was then filtered from Raney nickel, and the nickel was washed with 100 ml of ethanol. The combined filtrate was concentrated to dryness under reduced pressure, and the residue was washed with water, dried, and recrystallized from ethanol to yield 0.73 g (88%) of **1** (mp 112—113°C).

b) A mixture of 2.09 g of **3**, 50 ml of tetrahydrofuran, and 10 g of Raney nickel was worked up in a manner similar to Method a) to give 0.70 g (84%) of **1** (mp 111—113°C).

*Reduction of 2-Iodofluorene (**2**) and 2,7-Diiodofluorene (**3**) with Lithium Aluminum Hydride.* *a)* To the stirring mixture of 0.38 g of lithium aluminum hydride and 40 ml of dry dioxane, was added, drop by drop, 2.92 g (0.01 mol) of **2** in 60 ml of dry dioxane at room temperature; the resulting solution was then refluxed for 4 hr. Upon concentration, the precipitate was decomposed with 100 ml of 10% hydrochloric acid, washed with water, dried, and recrystallized from ethanol; 1.36 g (47%) of recovered **2** (mp 124—125°C) and 0.84 g (51%) of **1** (mp 110—112°C (no halogen)) were thus obtained.

b) A 4.18-g portion (0.01 mol) of **3** was treated with 0.76 g of lithium aluminum hydride in 160 ml of dry tetrahydrofuran by the same procedure as in Method a); this afforded 0.48 g (29%) of **1** (mp 111—112°C), 1.43 g (49%) of **2** (mp 123—125°C), and 0.64 g (15%) of recovered **3** (mp 215—216°C).

*Reduction of 2-Iodofluorene (**2**) and 2,7-Diiodofluorene (**3**) with Hydriodic Acid.* *a)*: A mixture of 2.92 g (0.01 mol) of **2**, 5 ml of hydriodic acid, 2 g of red phosphorus, and 50 ml of acetic acid was refluxed for 22 hr. The resulting mixture was filtered, the filtrate was poured into 500 ml of water, and the precipitate was recrystallized from cyclohexane. This compound was confirmed to be **1** (mp 112—114°C; 1.61 g 97%).

b) A 2.09-g portion (0.005 mol) of **3** in 150 ml of acetic acid was allowed to react with 5 ml of hydriodic acid and 2 g of red phosphorus for 22 hr to yield 0.41 g (49%) of **1** (mp 111—113°C), 0.15 g (10%) of **2** (mp 123—125°C), and 0.57 g (27%) of recovered **3** (mp 213—215°C).

18) R. C. Fuson and E. A. Cleveland, "Organic Syntheses", Coll. Vol. III, p. 339 (1955).
19) E. Legoff, *J. Org. Chem.*, **29**, 2048 (1964).
20) H. Adkins and A. A. Pavlic, *J. Amer. Chem. Soc.*, **68**, 1471 (1946).

A 3.24-g portion (0.01 mol) of 2,7-dibromofluorene was worked up as in the case of **3**, but only 3.16 g (98%) of the starting material was recovered.

*Reaction of 2-Iodofluorene (**2**) with Ethylmagnesium Bromide.* A solution of ethylmagnesium bromide (from 0.02 mol of ethyl bromide and 0.04 g atom of magnesium) in ether (40 m*l*) was added to a solution of 2.92 g (0.01 mol) of **2** in 25 m*l* of dry tetrahydrofuran, and the mixture was gently refluxed for 5 hr. The reaction mixture was then worked up as usual, and the crude product was recrystallized from ethanol to yield 0.09 g (6%) of **13** (mp 316—318°C (from benzene)) and 1.03 g of recovered **2** (mp 124—126°C). The ethanol mother liquor was analyzed by means of gas chromatography; 0.16 g (10%) of **1**, 0.04 g (2%) of 2-ethylfluorene, and 0.25 g (total 1.28 g; 44%) of **2** were confirmed.

Reaction of 2-Fluorenylmagnesium Iodide. a) With 9-bromofluorene: To magnesium, which had been activated by ethylmagnesium iodide, in dry tetrahydrofuran (25 m*l*) was added a solution of 25 m*l* of dry tetrahydrofuran containing 2.92 g of **2**; this mixture was refluxed by stirring for 23 hr. Then, a mixture of 2.45 g (0.01 mol) of 9-bromofluorene and 25 m*l* of dry tetrahydrofuran was added, drop by drop, to the foregoing Grignard solution, and the mixture was refluxed for 3 hr.

The reaction mixture was worked up as usual; consequently, 0.52 g (32%) of **10** (mp 242—243°C), 0.46 g (28%) of **13** (mp 312—314°C), and 0.25 g of **1** (mp 113—115°C) were isolated. Found for **13**: C, 94.34; H, 5.41%. Calcd for $C_{26}H_{18}$: C, 94.55; H, 5.45%.

The sodium bichromate oxidation of **13** gave **14** (mp 290—291°C; IR (>C=O): 1710 cm^{-1}; lit,[4d] mp 295—297°C); this compound was identical in all respects with the product obtained by the Ullmann reaction of **5**.

*b) With **4***: 2-Fluorenylmagnesium iodide was prepared in the same manner as has been described above. A 1.80-g portion of **4** in 20 m*l* of tetrahydrofuran was added to the resulting Grignard solution, and the mixture was refluxed for 2 hr to afford 0.13 g (8%) of **26** (mp 224—225°C). In addition, a trace amount of a compound (mp 252—254°C (decomp.)) was isolated, but its structure is not clear at present.

*Reaction of 2-Iodofluorene (**2**) and 2,7-Diiodofluorene (**3**) with Potassium Cyanide-Cupric Cyanide in DMF. a)*: A mixture of 2.92 g of **2**, 1.30 g of potassium cyanide, and 1.79 g of cupric cyanide in 40 m*l* of freshly-distilled DMF was refluxed for 25 hr. During the period, the reaction mixture turned from brown to dark green.

The mixture was then cooled and poured into 500 m*l* of cold water, and 50 m*l* of hydrochloric acid was added. The precipitate was collected and sublimed *in vacuo* at 120°C. The sublimate was recrystallized from 20 m*l* of cyclohexane to yield 1.15 g (60%) of pure 2-cyanofluorene (mp 91—92°C) as colorless needles. (Lit, mp 88°C,[16a] 100.5—101.5°C,[16b] 105°C[16c]). Found: C, 87.82; H, 4.65; N, 7.49%. Calcd for $C_{14}H_9N$: C, 87.93; H, 4.74; N, 7.33%. IR (-CN): 2245 cm^{-1}. Mass: 191 (M^+); 186; 149 *m/e*.

The residual part was further sublimed at 170°C; the sublimate yielded 0.03 g (1%) of 2-cyanofluorenone (mp 175—177°C) as yellow needles (from benzene). Found: C, 82.13; H, 3.38; N, 6.47%. Calcd for $C_{14}H_7NO$: C, 81.94; H, 3.44; N, 6.83%. IR: (-CN) 2245; (>C=O) 1715 cm^{-1}. Mass (M^+): 205 *m/e*.

b): A mixture of 2.09 g of **3**, 1.30 g of potassium cyanide, and 1.79 g of cupric cyanide in 50 m*l* of DMF was refluxed for 25 hr. When the reaction products were sublimed *in vacuo* at 200°C, the sublimate afforded 0.11 g of 2,7-dicyanofluorene (mp 285°C), upon recrystallization from benzene. Found: C, 83.07; H, 4.05; N, 12.70%. Calcd for $C_{15}H_8N_2$: C, 83.32; H, 3.73; N, 12.95%. IR (-CN): 2245 cm^{-1}. Mass (M^+): 216 *m/e*.

The residue of the sublimation was extracted with four 40-m*l* portions of benzene, and 0.12 g of 2,7-dicyanofluorenone (mp 340°C (decomp.)) was obtained from the benzene extract. Found: C, 78.36; H, 2.87%. Calcd for $C_{15}H_6N_2O$: C, 78.26; H, 2.63%. IR: (-CN) 2245; (>C=O) 1715 cm^{-1}.

Photochemical Reactions of 3-Alkyl-4-phenylsydnones[1)]

Yoshiharu HUSEYA, Akiko CHINONE, and Masaki OHTA

Department of Chemistry, Faculty of Science, Tokyo Institute of Technology, Ookayama, Meguro-ku, Tokyo

(Received March 28, 1972)

Photochemical reaction of 3-cyclohexyl-4-phenylsydnone (**4**) in nitrogen atmosphere afforded 2-cyclohexyl-4,5-diphenyl-1,2,3-triazole (**5**), 1,2-biscyclohexylazo-1,2-diphenylethylene (**6**) and 4-cyclohexyl-2-phenyl-Δ^2-1,3,4-oxadiazoline-5-one (**7**). The results showed that the reaction of **4** in the presence of carbon dioxide, carbon disulfide and dimethyl acetylenedicarboxylate proceeded *via* nitrile imine intermediate. Irradiation of 3-*t*-butyl-4-phenylsydnone (**11**) afforded 1-benzoyl-2-*t*-butyl-4-phenyl-1,2-diazetidine-3-one (**12**). Variation of the absorbance of **4** at the longest wavelength with irradiation was affected by 1,3-pentadiene, but not that of **11**. This shows that the excited triplet state is responsible for the photochemical reaction of **4**.

We reported[2)] that photolysis of 3,4-diarylsydnones afforded 2,4,5-triaryltriazoles *via* bicyclic intermediate (**2**) and nitrile imine (**3**). In this report, we give details on the photolysis of 3,4-diphenylsydnone (**1**) and 3-alkyl-4-phenylsydnones.

From the consideration that the stability of the nitrile imine (**3**) controls the reaction, we investigated the photolysis of 3-alkyl-4-phenylsydnone. 3-Cyclohexyl-4-phenylsydnone (**4**) was prepared by treating α-(*N*-cyclohexyl-*N*-nitrosamino)phenylacetic acid with acetic anhydride. Irradiation of **4** in a dilute benzene solution was carried out with high pressure mercury lamp through a Pyrex filter under nitrogen atmosphere. The reaction was followed by withdrawal of a small aliquot at various time intervals and examination by means of UV spectroscopy. The products were separated by column chromatography and identified as 2-cyclohexyl-4,5-diphenyl-1,2,3-triazole (**5**), 1,2-biscyclohexylazo-1,2-diphenylethylene (**6**) and 4-cyclohexyl-2-phenyl-Δ^2-1,3,4-oxadiazoline-5-one (**7**). The structure of **5** was confirmed on its elementary analysis and spectral data, which were closely similar to those of 2,4,5-triphenyl-1,2,3-triazole. The structure of **6** was deduced from elementary analysis, spectral data and its characteristic red color, but the configuration was not defined unambiguously. The structure of **7** was deduced from its elementary analysis and spectral data. The IR spectrum of **7** exhibited a peak at 1780 cm^{-1} which was attributed to the CO group of 1,3,4-oxadiazoline-5-one. It is noteworthy that the yields of **5** and **6** showed correlation with the period of irradiation. The yield of **5** increased with the increase of the period of irradiation, and that of **6** decreased with the increase of the yield of **5**. The results are in line with the reaction mechanism postulated,[2-5)] in which triazole was originated from bisazoethylene formed by "head to head" interaction of nitrile imine. Additional support for this mechanism was obtained by following examination. In contrast to the photochemical reaction of **1** which did not afford the corresponding oxadiazoline, **7** was obtained predominantly by irradiation of a benzene solution of **4** under carbon dioxide atmosphere. Similarly, when a benzene solution of **4** was irradiated in the presence of carbon disulfide, 4-cyclohexyl-2-phenyl-Δ^2-1,3,4-thiadiazoline-5-thione (**8**) was obtained. Formation of **7** and **8** is explained by the reaction of *N*-cyclohexyl-*C*-phenylnitrile imine with carbon dioxide and carbon disulfide, respectively. It is evident that *N*-cyclohexyl-*C*-phenylnitrile imine is more reactive than *N,C*-diphenylnitrile imine toward dipolarophiles such as carbon dioxide and carbon disulfide. It seems that *N*-phenylnitrile imine, which is an intermediate of the photolysis of 3-phenylsydnone,[6)] reacted preferentially with carbon dioxide, giving no corresponding triazole. 1,3-Dipolar cycloaddition of **4** under irradiation was carried out in the presence of dimethyl acetylenedicarboxylate to give dimethyl 1-cyclohexyl-3-phenylpyrazole-4,5-dicarboxylate (**9**), whose structure was deduced from its composition ($C_{19}H_{22}O_4N_2$) and IR spectrum. Treatment of **4**

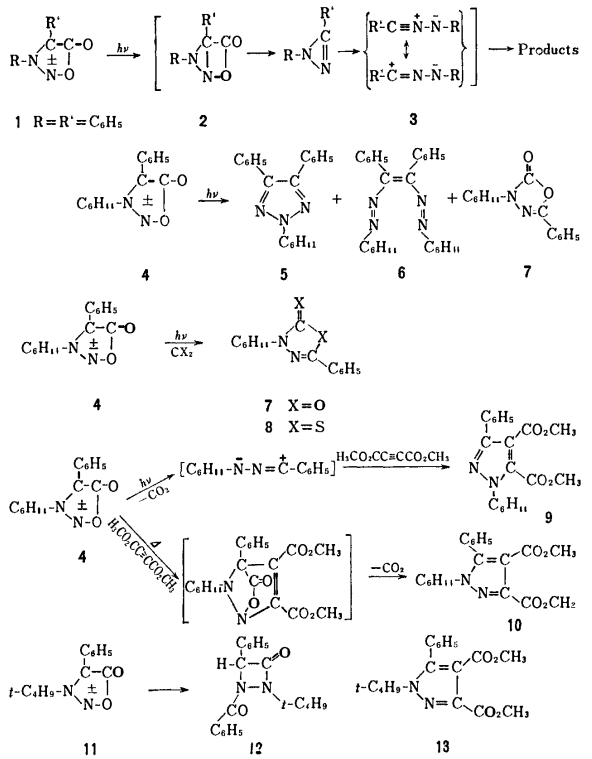

1) Studies of mesoionic compounds. XXXVII. Part XXXVI: A. Chinone, K. Inouye, and M. Ohta, This Bulletin, **45**, 213 (1972).

2) Y. Huseya, A. Chinone, and M. Ohta, *ibid.*, **44**, 1667 (1971).

3) P. Scheiner and J. F. Dinda, *Tetrahedron*, **26**, 2619 (1970).

4) G. S. Angadiyavar and M. V. George, *J. Org. Chem.*, **36**, 1589 (1971).

5) M. Marky, H. —J. Hansen, and H. Schmid, *Helv. Chim. Acta*, **54**, 1275 (1971).

6) C. H. Krauch, J. Kuhls, and H. J. Piek, *Tetrahedron Lett.*, **34**, 4043 (1966).

with dimethyl acetylenedicarboxylate at 120—140°C afforded a product **A** whose elementary analysis gave the same formula $C_{19}H_{22}O_4N_2$ as that of **9**. A mixed melting point measurement of **A** with **9** showed a depression, and the structure of **A** was assigned to dimethyl 1-cyclohexyl-5-phenylpyrazole-3,4-dicarboxylate (**10**).

The different course of the over-all photoreaction was observed in 3-*t*-butyl-4-phenylsydnone (**11**), prepared by treating α-(*N*-*t*-butyl-*N*-nitrosamino)phenylacetic acid with acetic anhydride. Exposure of a dilute solution of **11** in benzene to a high pressure mercury lamp gave 1-benzoyl-2-*t*-butyl-4-phenyl-1,2-diazetidine-3-one (**12**). Satisfactory analytical data were obtained for **12** whose mass spectral fragmentation pattern was consistent with that of the assigned structure. Compound **12** was obtained even in toluene under the same conditions. It is known that diazetidinones are prepared photochemically by the reaction of azo compounds with ketones.[7] Formation of **12** by the irradiation of **11** may be explained by the intermolecular addition of an excited >N-N- grouping to C=C=O grouping of sydnone, followed by an introduction of benzoyl group through ambiguous mechanism. Dipolar addition of **11** to carbon dioxide, carbon disulfide and dimethyl acetylenedicarboxylate was not successful under irradiation. However, **11** reacted with dimethyl acetylenedicarboxylate in refluxing toluene to give addition product **13**.

The absorption spectra of **1**,**4** and **11** in cyclohexane showed bands at 345 mμ (ε 9750), 325 mμ (ε 10890) and 312 mμ (ε 7090), respectively. A hypsochromic shift in a more polar solvent was observed as shown in Table 1. The absorptions might be assigned to *n*-π*

Table 1. UV spectra

Compound		1	4	11
λ_{max}(cyclohexene)	mμ(ε)	345(9750)	325(10890)	312(7090)
λ_{max}(methanol)	mμ(ε)	330(9140)	310(9490)	297(7800)

transition, though relatively high extinction coefficient are observed. Under irradiation, the variation of absorbances of **1**, **4** and **11** at the longest wavelength corresponded to their concentrations, since their photoreaction products showed no absorptions in these regions. The variations of absorbances at the longest wavelength of **4** and **11** in the absence or presence of 1,3-pentadiene, which is known as a quencher of triplet state, are plotted against irradiation time (Fig. 1 and 2). This shows that a sydnone (**4**) excited state transferred its energy to 1,3-pentadiene. Irradiation of a benzene solution of **4** in the presence of 1,3-pentadiene gave **5** in a low yield (6%). Colorless crystals whose structure was not determined were obtained with a mp of 201—202°C. On the other hand, variation of the absorbance of **11** was not appreciably affected by 1,3-pentadiene. The yield of **12** did not decrease even in the presence of 1,3-pentadiene.

From the results a mechanism is postulated which rationalizes the experimental observations. It seems

7) J. H. Hall and R. Kellogg, *J. Org. Chem.*, **31**, 1079 (1966).

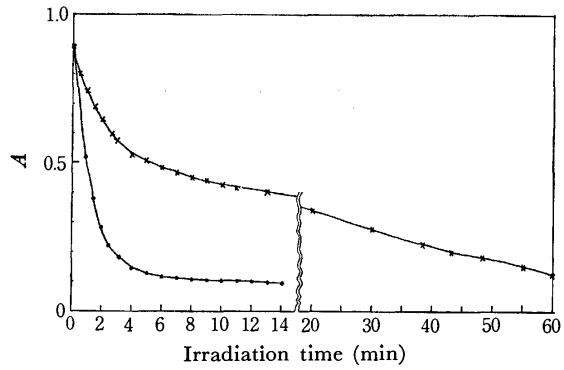

Fig. 1. Variation of absorbance of **4** at the longest wavelength, $\lambda_{max}^{benzene}$ 322 mμ.
—●— in the absence of 1,3-pentadiene
—×— in the presence of 1,3-pentadiene

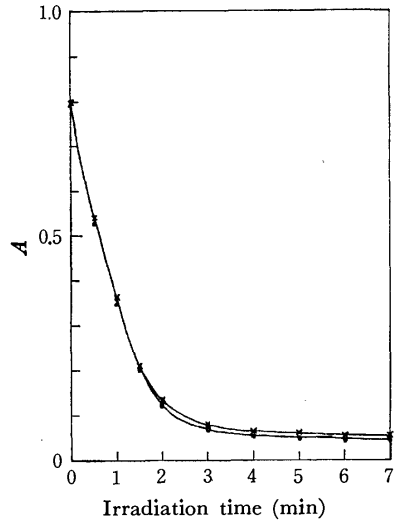

Fig. 2. Variation of absorbance of **11** at the longest wavelength, $\lambda_{max}^{benzene}$ 310 mμ.
—●— in the absence of 1,3-pentadiene
—×— in the presence of 1,3-pentadiene

that the photochemical reaction of **4** is derived from the lowest triplet state, which has an *n*-π* configuration. The reaction proceeds from the triplet state *via* bicyclic intermediate, from which diazirine is formed by the extrusion of carbon dioxide as in the case of the photochemical reactions of 3,4-diarylsydnones. It is suggested that either the excited triplet state of **11** is not responsible for the conversion into **12**, or the triplet state has too low energy to be affected by 1,3-pentadiene. It seems that the photochemical reaction of **11** proceeds through an intermediate other than nitrile imine.

Experimental

3-Cyclohexyl-4-phenylsydnone (4). Mandelonitrile prepared from 30 ml of benzaldehyde was added dropwise to a mixture of cyclohexylamine (25 g), sodium acetate (0.5 g) and ethanol (25 ml) and the reaction mixture was heated at 60—70°C for a few minutes. After being stirred at room temperature for 2 hr, α-cyclohexylaminophenylacetonitrile precipitated, mp 57.5—58.5°C, 28.6 g (52%).

α-Cyclohexylaminophenylacetonitrile (5 g) was stirred in

15 ml of concentrated sulfuric acid for 2 days at room temperature. The reaction mixture was added to 75 ml of water, and concentrated aqueous ammonia was added until the pH became about 9, and α-cyclohexylaminophenylacetamide precipitated was collected, mp 115—117°C, 5.3 g (98%).

After refluxing a 10% hydrochloric acid solution (43 ml) of α-cyclohexylaminophenylacetamide (5.3 g) for 6 hr, the reaction mixture was cooled to room temperature, and concentrated aqueous ammonia was added until the pH became about 4. α-Cyclohexylaminophenylacetic acid precipitated as white crystals, mp (decomp.) 280°C, 4.5 g (85%).

An aqueous solution of sodium nitrite (1.5 g/10 ml) was added dropwise below 0°C to a solution of α-cyclohexylaminophenylacetic acid (4.7 g) in 10% hydrochloric acid (86 ml). The reaction mixture was kept below 0°C for 1 hr and allowed to stand overnight at room temperature. α-(*N*-Cyclohexyl-*N*-nitrosamino)phenylacetic acid precipitated as yellow crystals, mp 133—136°C, 3.5 g (66%). After being dried the acid was dissolved in 30 ml of acetic anhydride and kept at 60—70°C for 20 min. After cooling, the reaction mixture was poured into 100 ml of water and stirred vigorously. Precipitates were collected and recrystallized from ethanol to give colorless prisms with a mp of 161—162°C, 3 g (91%).

Found: C, 68.98; H, 6.58; N, 11.76%. Calcd for $C_{14}H_{16}O_2N_2$: C, 68.83; H, 6.60; N, 11.47%. IR: $\nu_{C=O}$ 1730 cm^{-1}.

Irradiation of **4**. *i) Under Nitrogen Atmosphere*: A solution of 1.0 g of **4** in 300 ml of benzene was irradiated with a 100 W high pressure mercury lamp using a Pyrex filter under nitrogen atmosphere. The reaction was followed by withdrawal of small aliquots at various time intervals and measurement of their UV spectra. After irradiation for 3 hr, the solvent was removed *in vacuo* and the resulting residue was placed on a silica gel column. A petroleum ether solution was used to elute the column. The first elute contained an oil whose structure was not determined. The next petroleum ether-benzene (2 : 1) solution contained a white solid, which was recrystallized from ethanol to give colorless needles, mp 131—132°C, 0.08 g (12%). This was identified as **5**.

Found: C, 79.46; H, 7.12; N, 14.15%. Calcd for $C_{20}H_{21}N_3$: C, 79.17; H, 6.89; N, 13.85%. IR: 3050; 2920, 1460, 1440, 1350, 1260, 1080, 990, 770, 700 cm^{-1}. UV: λ_{max}^{MeOH} 255 mμ (ε 9170).

The next petroleum ether-benzene (1 : 1) solution afforded a crude solid, which was recrystallized from methanol to give red needles, mp 100—101°C, 0.13 g (15%), and identified as **6**.

Found: C, 77.63; H, 7.77; N, 14.21%. Calcd for $C_{26}H_{32}N_4$: C, 77.96; H, 8.05; N, 13.99%. IR: 3030, 2910, 1490, 1440, 760, 710, 700 cm^{-1}. UV: λ_{max}^{MeOH} mμ(ε) 310 (6440), 253 (10900). NMR: τ_{Me_4Si} ($CDCl_3$) 2.6—2.9 (10H), 6.2—6.7 (2H), 8.1—9.1 (20H).

The next benzene solution contained a crude solid, which was recrystallized from methanol to give colorless prisms, mp 78—80°C, 0.15 g (15%), and identified as **7**.

Found: C, 68.78; H, 6.47; N, 11.64%. Calcd for $C_{14}H_{16}O_2N_2$: C, 68.83; H, 6.60; N, 11.47%. IR: 3060, 2920, 1780, 1450, 1350, 1020, 740, 700 cm^{-1}. UV: λ_{max}^{MeOH} 268 mμ (ε 7350).

ii) Under Carbon Dioxide Atmosphere: A solution of **4** (1.0 g) in benzene (300 ml) was irradiated under carbon dioxide atmosphere for 3 hr, and treated as mentioned above to give **7**, 0.47 g (47%).

iii) In the Presence of Carbon Disulfide: Compound **4** (1.0 g) was dissolved and irradiated in a mixture of 200 ml of benzene and 100 ml of carbon disulfide. After removal of the solvent in a vacuum, the residue was placed on a silica gel column and eluted with a petroleum ether-benzene (1 : 1) solution. The elute contained a crude solid, which was recrystallized from ethanol to give colorless silky crystals, mp 136—137°C, 0.19 g (20%), and identified as **8**.

Found: C, 60.61; H, 5.65; N, 10.03; S, 22.93%. Calcd for $C_{14}H_{16}N_2S_2$: C, 60.86; H, 5.84; N, 10.14; S, 23.16%. IR: 3050, 2910, 1490, 1450, 1350, 1280, 1210, 1060, 760, 690 cm^{-1}.

The starting material (0.15 g) was eluted with benzene-ethyl acetate (3 : 1).

iv) In the Presence of Dimethyl Acetylenedicarboxylate: A solution of **4** (1.0 g) and dimethyl acetylenedicarboxylate (1.2 g) in benzene (300 ml) was irradiated for 2.3 hr. The reaction mixture was treated as mentioned above and the resulting residue was eluted first with petroleum ether to give 0.7 g starting material and next with benzene to give a crude solid, which was recrystallized from methanol to give colorless needles, mp 92—93°C, 0.6 g (43%), and identified as **9**.

Found: C, 66.40; H, 6.32; N, 8.15%. Calcd for $C_{19}H_{22}O_4N_2$: C, 66.65; H, 6.48; N, 8.18%. IR: 3050, 2920, 1730, 1530, 1450, 1250, 1160, 790, 700 cm^{-1}.

Reaction of **4** *with Dimethyl Acetylenedicarboxylate*. A mixture of **4** (1.0 g) and dimethyl acetylenedicarbaxylate (2.0 g) was heated at 120—140°C for 4 hr, during which time evolution of carbon dioxide was observed. Excess dimethyl acetylenedicarboxylate was removed, and a small amount of methanol was added to the residue and the reaction mixture was kept in a refrigerator. Precipitates were collected and recrystallized from methanol to give colorless prisms, mp 98—99°C, 0.3 g (21%), identified as **10**.

Found: C, 66.60; H, 6.67; N, 8.32%. Calcd for $C_{19}H_{22}O_4N_2$: C, 66.65; H, 6.48; N, 8.18%. IR: 2940, 1730, 1550, 1500, 1440, 1220, 1170, 1080, 760, 700 cm^{-1}.

*3-t-Butyl-4-phenylsydnone (***11***)*. Mandelonitrile prepared from 75 ml of benzaldehyde was added to a mixture of *t*-butylamine (52 g), sodium acetate (1.3 g) and ethanol (60 ml) under ice cooling. The reaction mixture was kept at 50—60°C for 5 min, and allowed to stand overnight with stirring at room temperature. Unreacted *t*-butylamine and ethanol were removed *in vacuo*. To the residue was added 500 ml of 5% hydrochloric acid and the mixture was vigorously stirred, and the precipitates were filtered off. Filtrate was neutralized with aqueous potassium hydroxide and oily layer was extracted with ether. After drying the ether layer over sodium sulfate, ether was evaporated off and crude α-*t*-butylaminophenylacetonitrile (100 g) was obtained, which was added dropwise to 300 ml of concentrated sulfuric acid under ice cooling. After the solution was stirred for 2 days at room temperature, the reaction mixture was diluted with sixford amount of water and treated with activated charcoal and neutralized with concentrated aqueous ammonia until the pH became 8. Precipetates were collected and refluxed in 800 ml of 10% hydrochloric acid for 14 hr. The solution was treated with activated charcoal and hydrochloric acid solution of α-*t*-butylaminophenylacetic acid was subjected to subsequent reaction.

An aqueous solution of sodium nitrite (18 g/100 ml) was added dropwise below 0°C with vigorous stirring to a hydrochloric acid solution of α-*t*-butylaminophenylacetic acid. The reaction mixture was kept below 0°C for one hour, and stirred at room temperature for 24 hr. α-(*N*-*t*-Butyl-*N*-nitrosamino)phenylacetic acid precipitated as pale yellow crystals, mp 179—180°C.

To this was added 250 ml of acetic anhydride and the mixture was stirred at room temperature for 3 days in the dark. The resulting yellow solution was concentrated in a vacuum

to one-third of the total volume, and poured into 1 *l* of water with vigorous stirring to give colorless crystals. Recrystallization from ethanol afforded colorless prisms, mp 124—125.5°C, 23 g (19%).

Found: C, 65.82; H, 6.49; N, 13.10%. Calcd for $C_{12}H_{14}O_2N_2$: C, 66.03; H, 6.47; N, 12.84%. IR: $\nu_{C=O}$ 1750 cm^{-1}.

Irradiation of ***11****. i) Under Nitrogen Atmosphere*: After irradiation of a solution of **11** (1.0 g) in 300 m*l* of benzene for 1.5 hr, the solvent was removed *in vacuo* and the resulting residue was analyzed by column chromatography. A benzene-ethyl acetate (4 : 1) elute contained a solid, which was recrystallized from ethanol to give colorless needles, mp 114—115°C, 0.42 g (59%) and identified as **12**.

Found: C, 73.57; H, 6.52; N, 9.05%. Calcd for $C_{19}H_{20}O_2N_2$: C, 74.00; H, 6.54; N, 9.09%. IR: 2960, 1780, 1680, 1280, 750, 730, 700 cm^{-1}. NMR τ_{Me_4Si} ($CDCl_3$) 2.3—2.9 (m, 10H), 4.6 (s, 1H), 8.4 (s, 9H). Mass spectra M^+ *m/e* 308, C_6H_5CO *m/e* 105 (base peak), $C_6H_5CHNCOC_6H_5$ *m/e* 209 (70% of the base peak), C_6H_5CHCO *m/e* 118 (90%), $C_6H_5CH_2$ *m/e* 91 (84%).

Compound **12** was also obtained by irradiation of a solution of **11** in toluene with a yield of 68%.

ii) Under Carbon Dioxide Atmosphere: Irradiation of a solution of **11** under carbon dioxide atmosphere for 1.5 hr afforded **12** in a yield of 62%.

iii) In the Presence of Carbon Disulfide: A solution of **11** (0.8 g) in 200 m*l* of benzene and 100 m*l* of carbon disulfide was irradiated under the same conditions for 1.5 hr to give 0.08 g (14%) of **12**.

Reaction of ***11*** *with Dimethyl Acetylenedicarboxylate.* A solution of 0.75 g of **11** and 0.9 g of dimethyl acetylenedicarboxylate in 5 m*l* of toluene was refluxed for 1.5 hr. Analysis by column chromatography afforded **13**, which was recrystallized from methanol, mp 117—119°C, 0.84 g (77%).

Found: C, 64.09; H, 6.17; N, 8.41%. Calcd for $C_{17}H_{20}O_4N_2$: C, 64.54; H, 6.37; N, 8.86%. IR: 2980, 1730, 1240, 1200, 1080, 760, 710 cm^{-1}.

NOTES

BULLETIN OF THE CHEMICAL SOCIETY OF JAPAN, VOL. 45, 3206—3207 (1972)

The Chlorine Nuclear Quadrupole Resonance of *o*-, *m*-, and *p*-Chlorobenzamide

Seiichi KONDO, Hiroyuki INOUE, Akemi SAKAMOTO, and Haruo KATSUMATA
Laboratory of Physical Chemistry, Osaka Kyoiku University, Tennoji-ku, Osaka-shi

(Received November 6, 1971)

The nuclear quadrupole resonance of *o*-, *m*-, and *p*-chlorobenzamide has been studied in this laboratory; the results and their relation to the crystal structures of these materials, the various polymorphic modifications of which have been extensively studied by Sakurai, Takaki, and others,[1] will be reported in this paper.

The materials were synthesized by the reaction of monochlorobenzoic acid with thionyl chloride and then with ammonia. No impurity was seen in the X-ray powder diffraction patterns or in the infrared spectra of the materials purified by repeated recrystallization from the various solvents mentioned below. The melting points of the final samples are shown in Table 1. These samples were sealed *in vacuo* in glass ampules for the NQR measurement. We were not successful in growing a single crystal for the Zeeman measurement.

The NQR signal was searched for in the range from 28 to 40 MHz using a super-regenerative oscillator-detector of the Dean type with a frequency-modulation and phase-sensitive detection system. The S/N ratio of the signal of *p*-dichlorobenzene was better than 200 with this system. The frequency was determined with an eight-figure digital counter. For the visual detection, a Braun tube with a long decay time was employed, and the random noise was fairly well smoothed out with the S/N ratio—about five times better than that of an ordinary tube. The resonance frequencies observed are shown in Table 1 and Fig. 1.

TABLE 1.

	Mp, °C	Space group	NQR frequency at 77K, MHz	S/N
o-chlorobenzamide	142.3	$P2_1/a$	35.593	3
m-chlorobenzamide	132.0	$P2_1/a$	34.876	3
p-chlorobenzamide	177.6	$P\bar{1}$	35.130	3
			34.944	2.5
			34.731	2.5

The thermal behavior of these materials between −100°C and their melting points was studied by means of a differential scanning calorimeter of the Rigakudenki Co., 8001 SC, with a heating and cooling rate of 10°C/min and with a sensitivity of 0.5 mcal/sec in full scale. About 10 mg of each sample was placed in a shallow aluminum dish, covered with an aluminum plate or packed with pressure, and then used for the DSC measurement.

1) o-*Chlorobenzamide.* One NQR signal was observed with the crystal grown from the melt, bu

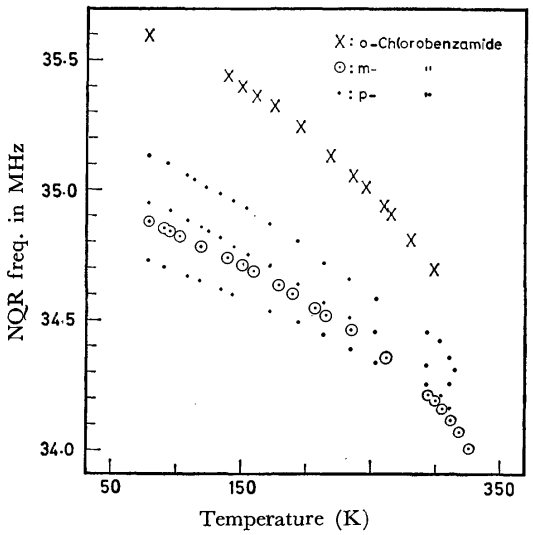

Fig. 1. Frequency *versus* temperature curves of the NQR frequencies of *o*-, *m*-, and *p*-chlorobenzamide.

no signal was detected with the crystals grown from water, ethanol, or acetone. The X-ray study[1] showed that the former crystal belonged to the space group $P2_1/a$ with $Z=4$ and had an ordered structure, while the latter ones seemed to be mixtures of three modifications, one with the space group $P2_12_12_1$ and two with some disordered structures. The crystallographically-equivalent chlorine atom in the unit cell is expected to be one in the former case; this agrees with our findings. The reason for the absence of the NQR signal in the latter case may be that the sample was a mixture of different crystal modifications, two of which have disordered structures. No thermal anomaly was detected with any of these crystals.

2) m-*Chlorobenzamide.* The crystals grown from the melt and from water or ethanol possess the same space group, $P2_1/a$, with $Z=4$ according to the X-ray study.[1] These crystals showed only one signal each, all of the same frequency. The crystallographic consideration of this structure described in section 1 agrees with those NQR results. No anomalous thermal behavior was observed in this study with these crystals.

3) p-*Chlorobenzamide.* Three signals were observed with the crystal grown from the melt in the temperature range from 77 K to about 316 K. This finding agrees well with the crystallographic consi-

1) Y. Harada, T. Taniguchi, Y. Takaki, and K. Sakurai, *Mem. Osaka Kyoiku University*, **18**, *Ser.* III, 1 (1969); Y. Kato, Y. Takaki, and K. Sakurai, Symposium on the Molecular Structure, Chem. Soc. Japan, 1970.

derations that the crystal at room temperature possesses the space group $P\bar{1}$ with $Z=6$[1] and the three different electric fields are supposed to surround the chlorine atoms in this unit cell. A phase transition from the room-temperature phase to the phase with the same space group and $Z=2$ was found at about 43°C by the X-ray study[1]; this was confirmed by DTA measurements.[2] The six molecules in the unit cell of the low-temperature phase displace a small amount at the phase transition, and the crystal assumes a disordered structure. The periodicity or the length of the *a*-axis of the unit cell of the high-temperature phase decreases to one third of that of the low-temperature phase, while the lengths of the *b*- and *c*-axes are kept the same, with a small entropy of transition (about 0.40 e. u., according to the present DSC measurement). The temperature coefficient of the curves of the NQR frequencies of this material against the temperature in Fig. 1 increases gradually near the transition point; these signals fade out at the transition point, 43°C. This result suggests that the thermal motion of the molecule in the low-temperature phase begins to increase near the transition temperature and that this thermal motion and the disorder of the structure of the upper phase[1] make it impossible to observe the signal above the phase transition. The signal frequencies of these three compounds have values similar to those of other monochlorobenzene derivatives. The frequency of *o*-chlorobenzamide has the highest value and, therefore, the largest covalent character of the C–Cl bond.

This research was partly supported by the Science Research Fund of the Ministry of Education of Japan.

2) T. Koide, private communication.

BULLETIN OF THE CHEMICAL SOCIETY OF JAPAN, VOL. 45, 3207—3208 (1972)

Hydrogen-transfer Reaction between Ketones and Alcohols over Metal Oxide Catalysts

Yasuaki OKAMOTO, Toshinobu IMANAKA, and Shiichiro TERANISHI

Department of Chemical Engineering, Faculty of Engineering Science, Osaka University, Osaka

(Received December 17, 1971)

Intermolecular hydrogen-transfer reactions have been studied by many workers. According to Schächter and Pines,[1] when a mixture of isopropyl alcohol and 2-butanone was passed over calcium oxide at about 320°C, both acetone and butanol were produced. Niiyama *et al.*[2] have reported the hydrogen-transfer reaction between alcohol and ketone over silica-magnesia catalysts and proposed a mechanism similar to that of the Meerwein-Ponndorf reduction. In our preceding papers,[3] it was found that the reactions between allyl alcohol and propionaldehyde or propylene oxide are accelerated by silica-magnesia and metal oxide catalysts. In this paper, the mechanism of the hydrogen-transfer reaction on metal oxides was studied using a conventional pulse reactor (carrier gas: He) at 260°C.

Materials. The metal oxides used were MgO, CaO, SrO, and BaO of a commercial grade. The properties of the metal oxides used are given in Table 1.

TABLE 1. THE PROPERTIES OF METAL OXIDE CATALYSTS AND THE REACTIVITIES OF THE HYDROGEN TRANSFER REACTION BETWEEN METHYL ETHYL KETONE AND 2-PROPANOL OVER THESE OXIDES AT 260°C

Catalyst	Surface area (m^2/g)	Basicity[a] (mmol/g)	Activity/g[b] (arbitrary unit)
MgO	55.6	0.288	65.5
CaO	13.3	0.014	62.6
SrO	5.3	0.004_5	1.6
BaO	1.9	0.005_3	3.4

a) Measured at $H_0 = +7.2$.
b) Obtained from the formation of *sec*-butyl alcohol.

Results and Discussion

The hydrogen-transfer reaction was carried out over metal oxides using an equimolar mixture of alcohol and ketone. Under our reaction conditions, the reactivity of the dehydrogenation of alcohol was very small. In all cases, the dehydrogenated product of alcohol and the hydrogenated product of ketone were obtained. Table 1 shows the reactivities of the reaction between 2-propanol and methyl ethyl ketone (MEK) over several metal oxides. The reactivities were calculated from the formation of 2-butanol. The reactions are poisoned by dichloroacetic acid. Though the basicity[4] (measured at $H_0 = +7.2$) of magnesium oxide is much larger than that of calcium oxide, the activities of these metal oxides are almost the same. According to Take *et al.*[5] these metal oxides have the same amount of a strong base, which is stronger than $H_0 = +24$, but strontium oxide has only a small amount of the strong base. Therefore, it is considered that the strong base is favorable for the reaction.

Table 2 gives the reactivities of the reaction between

1) Y. Schächter and H. Pines, *J. Catal.*, **11**, 147 (1968).
2) H. Niiyama and E. Echigoya, The 23rd Annual Meating of Chemical Society of Japan, Preprints of papers, No. 1 p. 51 (1970).
3) Y. Okamoto, T. Imanaka, and S. Teranishi, This Bulletin, in press.
4) K. Tanabe and T. Yamaguchi, *J. Res. Inst. Catal., Hokkaido Univ.*, **11**, 179 (1964).
5) J. Take, N. Kikuchi, and Y. Yoneda, *J. Catal.*, **21**, 164 (1971).

Table 2. The reactivities of hydrogen transfer reactions between methyl ethyl ketone and several alcohols on MgO at 260°C

Alcohol	Reactivity/g[a] (arbitrary unit)	$D_r^{(R)}$ [b]
Methanol	9.94	1.0523
Ethanol	32.9	1.0699
2-propanol	68.1	1.0896
n-Butanol	37.5	——
t-Butanol	8.44	——

a) Obtained from the formation of *sec*-butyl alcohol.
b) The delocalizability for radical reaction of α-hydrogen of alcohol.

Table 3. Kinetic isotope effect of hydrogen transfer reactions between methyl ethyl ketone and deuterated alcohols over MgO at 260°C

Alcohol	k_D/k_H [a]
C_2H_5OD	1.04
CD_3OD	0.722

a) The ratio of reactivity of deuterated alcohol to non-deuterated one.

MEK and several alcohols, while Table 3 shows the kinetic isotope effects on the reaction. Fig. 1 shows the relation between the reactivity and the delocalizability, $D_r^{(R)}$, of the hydrogen attached to the α-carbon of alcohol.[6] On the basis of these fact, it may be concluded that the rate-determining step is the hydrogen-abstraction process from the α-carbon, not from the hydroxyl group. When intermolecular hydrogen-tansfer reactions between 2-propanol and several ketones were carried out, a good parallel relation between the reactivity and the electron-donating power of ketone ($\Delta\nu_D$; cm^{-1}) was found, as was revealed in a preceding paper.[3] The electron-donating power of a compound is defined[7] as the relative difference (countered as wave numbers) of the O–D adsorption band of methanol-*d* observed in the compound from that in benzene.

The poisoning effect of pyridine on the reaction was

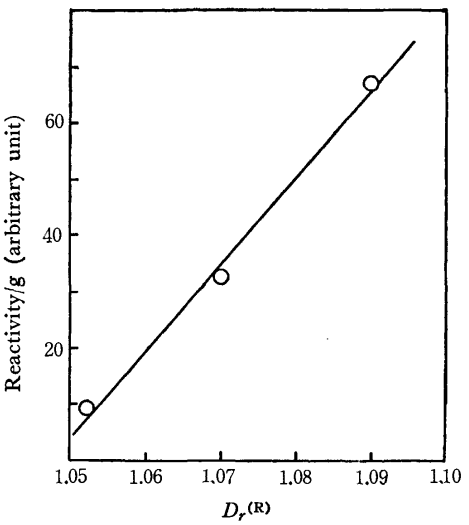

Fig. 1. Correlation between the reactivity of the hydrogen transfer reaction and $D_r^{(R)}$ of α-hydrogen of alcohol.

studied over a magnesium-oxide catalyst in order to make it clear which were the active centeres, but pyridine has no effect on the reaction, whereas magnesium oxide is considered to have a very weak acid site.[3,8] It is considered that alcohol is adsorbed on a strong basic site, thus dissociating the hydroxyl group, and that the basic strength of the anion formed is stronger than that of pyridine. As the electron-donating power of pyridine ($\Delta\nu_D$; 128 cm^{-1}) is much larger than those of the ketones used, the reaction must be poisoned, if the weak acid site also favorable for the adsorption of ketones. Therefore, it is considered that ketone is not adsorbed and not activated by the acid site on metal oxide. Taking these facts into consideration, the reaction mechansim on metal oxides is deduced to be as follows:

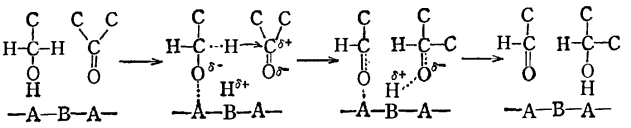

A: Weak acid site
B: Strong basic site

6) K. Morokuma "Organic Quantum Chemistry" Kagakudozin, Kyoto (1966), p. 90.
7) T. Kagiya, Y. Sumida, and T. Inoue, This Bulletin, **41**, 767 (1968).
8) St. Malinowski, S. Szczepaniska, A. Bielanski, and J Sloczynski, *J. Catal.*, **4**, 324 (1965).

BULLETIN OF THE CHEMICAL SOCIETY OF JAPAN, VOL. 45, 3207 (1972)

Polymorphic Transformation in Copper Ferrite and Manganite by Grinding

Yasuhiko UEHARA

Electron Tube Division, Hitachi Ltd., Hayano, Mobara, Chiba, 297

(Received January 25, 1972)

Many spinels such as $CuFe_2O_4$ and Mn_3O_4 have a tetragonally-distorted structure. The origin of the tetragonal distortion is the cooperative Jahn-Teller ordering of Cu^{2+} or Mn^{3+} at octahedral sites of the spinel structure. The tetragonality $\sigma=(c-a)/a$ is about 6% for $CuFe_2O_4$ and about 16% for Mn_3O_4 at room temperature. The variation of the tetragonality, σ, with the temperature has been studied by Ohnishi and his co-workers[1] for $CuFe_2O_4$ and by McMurdie and his co-worders[2] for Mn_3O_4. The transformation from the tetragonal to the cubic structure occurs at 360°C for $CuFe_2O_4$[1] and at 1170°C for Mn_3O_4.[2] The observation to be described here is that $CuFe_2O_4$ can be transformed from the tetragonal to the cubic structure by mechanical grinding at room temperature, while Mn_3O_4 can not be transformed by the same procedure.

$CuFe_2O_4$ was prepared from powders of CuO and Fe_2O_3 by heating at 930°C for 3 hr and by subsequent cooling to room temperature. Mn_3O_4 was prepared from powder of MnO_2 by heating at 1000°C for 3 hr and by subsequent quenching in water. These samples were ground in a ball mill with water for intervals up to 190 hr. The ground samples were examined by means of an electron microscope and by the X-ray diffraction method, using Mn-filtered Fe$K\alpha$ radiation.

The electron micrographs of the tetragonal $CuFe_2O_4$ particles before and after grinding are shown in Fig. 1. Before grinding, each particle is fairly rounded in shape and has a size between 0.5 and 1.0 μ. As the grinding progresses, the particles became smaller and irregular and the amount of small-size chipping increases.

X-Ray diffraction diagrams of the tetragonal $CuFe_2O_4$ at various stages of grinding are given in Fig. 2. As the grinding increases, the (311) peak of the cubic structure appears, in the intermediate-time grinding it is seen that both tetragonal and cubic structures existing, while in long-time grinding the tetragonal structure is almost entirely transformed into the cubic one. Such changes in diffraction lines by grinding are similar to those caused by heating.[3]

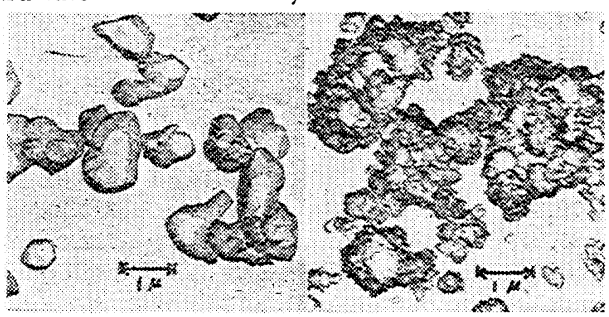

Original Ground for 190 hr

Fig. 1. Electron micrographs of $CuFe_2O_4$ particles before and after grinding.

X-Ray diffraction lines gradually broaden with grinding, as is shown in Fig. 2. Such a fact was more clearly seen in the experiment of grinding cubic $CuFe_2O_4$ (quenched from 930°C). The analysis of line-broadening using Hall's method[4] revealed that the strain increased and the crystallite size decreased with grinding. The increased strain might be described in terms of large dislocation density, whereas the small crystallite might be due to multiple twinning.[5] Therefore, it can be presumed as the main effect of polymorphic transformation that the cooperative Jahn-Teller ordering is destroyed by lattice imperfections, such as dislocation and stacking fault generated by grinding. As the another factor in the transformation, the change in the surface energy should also be considered. However, since there are no suitable methods for the measurement and theoretical calculation of the surface energy, it is beyond the scope of this discussion to consider the contribution of surface energy to the transformation.

On the other hand, Mn_3O_4 could not be transformed by grinding, even after 100 hrs' grinding. In the case of the transformation of Mn_3O_4, a greater amount of energy will be required, because Mn_3O_4 has a much higher transition temperature than $CuFe_2O_4$.

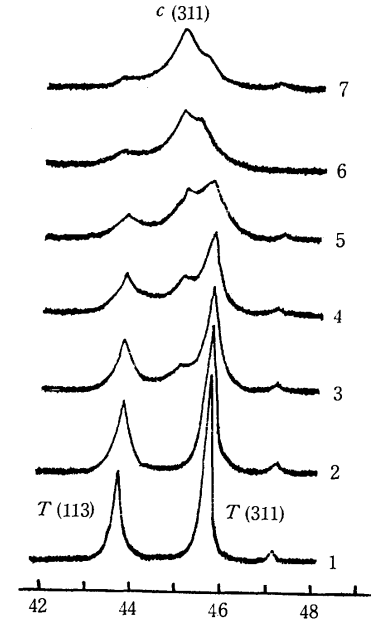

Fig. 2. X-ray diffraction diagrams of tetragonal $CuFe_2O_4$ after grinding.
Time of grinding 1: 0 hr, 2: 5 hr, 3: 20 hr, 4: 40 hr, 5: 70 hr, 6: 110 hr, 7: 190 hr.

1) H. Ohnishi, T. Teranishi, and S. Miyahara, *J. Phys. Soc. Jap.*, **14**, 106 (1959).
2) H. F. McMurdie, B. M. Sullivan, and F. A. Mauer, *J. Res. Nat. Bur. Stand.*, **45**, 35 (1950).
3) S. Miyahara, *J. Phys. Soc. Jap.*, **17**, Suppl. B-1, 181 (1962).
4) W. H. Hall, *Proc. Phys. Soc., Ser. A*, **62**, 741 (1949).
5) I. Bergman, J. Cartwright, and C. Casswell, *Brit. J. Appl. Phys.*, **14**, 399 (1963).

BULLETIN OF THE CHEMICAL SOCIETY OF JAPAN, VOL. 45, 3210—3211 (1972)

Vapor Pressure of Acetylacetone below Normal Boiling Point

Koichiro NAKANISHI* and Osamu TŌYAMA

Department of Industrial Chemistry, Shinshu University, Wakasato, Nagano-shi

(Received May 8, 1972)

Acetylacetone(2,4-pentanedione) has been used frequently in studies on keto-enol tautomerism and complex formation with metals, but no vapor pressure data are available in literature. This note describes new vapor pressure data for acetylacetone from room temperature up to the normal boiling point.

Experimental

Acetylacetone was purified by distillations under reduced nitrogen pressure. Since the affinity of acetylacetone to metals is fairly large, final distillation was carried out in a column with glass packing.

The vapor pressure was measured by means of the following apparatus:

(a) Vapor pressure apparatus (16—50°C)

(b) Isoteniscope[1] (40—70°C)

(c) A modified Swietoslawski-type ebulliometer[1] (60—138°C)

A sketch of (a) is given in Fig. 1. Purified liquid was confined in a mercury-sealed cell and degassed in a vacuum at liquid nitrogen temperature. Mercury was then introduced to form a manometer in a U-tube on the left-hand side of the cell which was immersed in a thermostat maintained on a laboratory jack. After temperature equilibrium was reached, the pressure was read both on the manometer and an open manometer with a travelling microscope and a Shimadzu Model HV-100 cathetometer.

The apparatus (b) and (c) were connected to a vacuum system and operated by conventional methods.[1] Reduced pressures required were obtained by introducing dry nitrogen into the system. A porous-disk type manostat was used to keep the whole system at a constant pressure of ±0.2 mmHg. The isoteniscope was immersed in a glycerine thermostat controlled within ±0.05°C during the course of measurement.

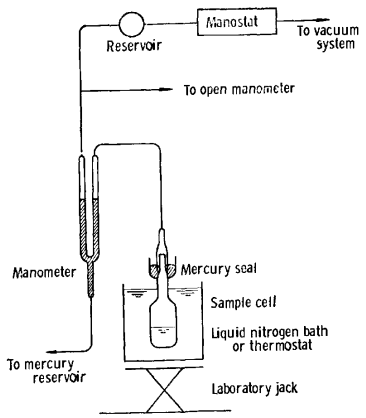

Fig. 1. Schematic diagram of vapor pressure apparatus.

The temperature was measured by a thermistor calibrated against a standard thermometer. The overall average error of the vapor pressure measurement was believed to be less than ±0.2 Torr at lower temperatures, but larger at temperatures above 100°C.

In order to confirm the validity of the data, the vapor pressure of toluene was measured between 92° and 107°C with our ebulliometer and the results were compared with the accepted values.[2] No systematic deviation from literature values was observed, and the average deviation was less than ±0.6 Torr or ±1.2%.

Results and Discussion

Vapor Pressure Data. The vapor pressure of acetylacetone from 16° to 137°C is given in Table 1. The mean value of the barometric pressure during the measurements was 733 mmHg, where acetylacetone boiled at 137.3°C. Extrapolation of the data to 1 atmosphere yields 138.3°C as the normal boiling point. This is between the two literature values, 137.7 and 140.2°C.[3] Mutual consistency among the

Table 1. Vapor pressure of acetylacetone

t (°C)	P (Torr)	t (°C)	P (Torr)
16.48	5.93 a	83.84	142.2 c
22.76	8.62 a	88.95	171.3 c
24.92	9.77 a	91.25	188.0 c'
29.69	11.88 a	91.49	188.3 c
33.50	14.22 a	94.20	210.1 c
38.08	18.34 a	97.09	231.3 c
40.02	19.93 a	102.38	270.4 c
41.03	20.80 b	103.68	284.8 c
48.28	30.54 a	105.25	305.2 c'
51.90	34.60 a	105.44	308.7 c
52.08	37.70 b	110.48	360.4 c
61.16	54.80 b	110.68	362.2 c'
63.65	63.30 c	115.90	424.2 c'
65.75	65.95 b	120.20	476.1 c
68.38	76.75 b	123.97	526.9 c
70.18	81.05 b	127.00	570.2 c'
74.11	94.75 c	129.08	599.9 c
76.91	108.2 c	131.19	630.0 c
79.37	121.0 c	136.45	728.2 c'
81.94	133.3 c	137.25	732.8 c

a) Vapor pressure apparatus.
b) Isoteniscope.
c) Ebulliometer.
c') Ebulliometer (data obtained by K. Sato).

* To whom correspondence should be sent: Department of Industrial Chemistry, Kyoto University, Kyoto 606.

1) E. Hala, J. Pick, V. Fried, and O. Vilim, "Vapour-Liquid Equilibrium," 2nd Ed., Pergamon, London (1967).

2) API Research Project 44, Data Sheets, Table 21k, Carnegie Inst. Tech., Pittsburgh, Pa., 1954.

3) C. H. Horsley, "Azeotropic Data," Adv. in Chem. Ser. Nos. 6 and 35, Amer. Chem. Soc., (1952 and 1962).

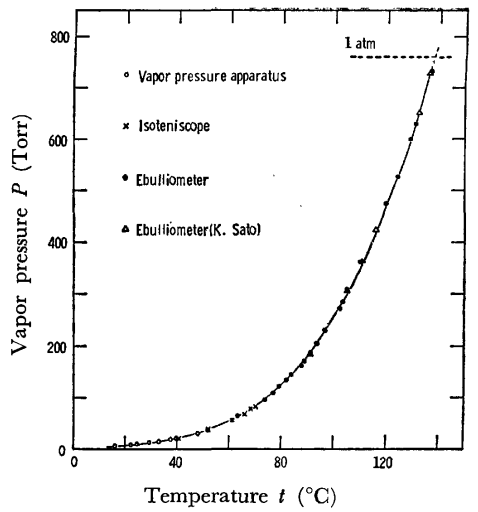

Fig. 2. Vapor pressure curve of acetylacetone.

data obtained with different apparatus may be confirmed by the P *vs.* t plot in Fig. 2, where the ranges of the applicability of each apparatus are seen to overlap.

Correlation with Empirical Equations. An attempt to correlate the data for the whole range of the measurement by means of the Antoine equation was not successful. We assigned two set of constants of the Antoine and Clapeyron-Clausius equations for different temperature ranges. They were evaluated by the method of least squares. The resulting vapor pressure equations are as follows.

$$\log P(\text{Torr}) = A - \frac{B}{C+t(^\circ\text{C})}$$

$A = 6.86495$, $B = 1377.34$, $C = 208.35$
for $t = 15$—105°C

$A = 7.3522$, $B = 1840$, $C = 273.16$
for $t = 105$—138°C

The experimental points scattered nearly at random from the values obtained by these equations, overall average deviation being ± 1.2 Torr or $\pm 2.3\%$ in P.

In order to express the whole data by one single equation, the following Antoine-type equation is suggested.

$$\log P(\text{Torr}) = 6.86495 - \frac{1377.34}{207.35+t(^\circ\text{C})}$$

Heat and Entropy of Vaporization. The heat and entropy of vaporization at normal boiling point have been estimated from the log P *vs.* $1/T$ plot. They are 8.42 kcal/mol and 20.5 cal/deg·mol, respectively.

Discussion. The Antoine equation has been widely used and proved satisfactory for correlating the vapor pressure curve of organic liquids. In view of the relatively narrow pressure range covered by the present measurement, it was expected that any three-constant equation would correlate the data. It is tempting to ascribe this failure to the fact that the keto-enol equilibrium in acetylacetone molecule also changes with temperature.[4,5] However, acetylacetone is rather unstable at higher temperatures and, unless the atmosphere is completely inert, it undergoes partial decomposition as the temperature approaches normal boiling point. In fact, prolonged boiling has led to a pronounced brown coloration. Thus we might assume that there would be a slight boiling point elevation under such conditions. In practical distillation processes, it is possible that an even higher boiling point than that reported might be observed. We thank Mr. K. Sato and Mrs. H. Shirai-Tsujimoto for their assistance in the experiments.

4) E. Funk and R. Mecke, in D. Hadzi ed. "Hydrogen Bond," Pergamon, New York, N. Y. (1959), p. 433.

5) G. Allen and R. A. Dwek, *J. Chem. Soc.*, *B*, **1960**, 161.

BULLETIN OF THE CHEMICAL SOCIETY OF JAPAN, VOL. 45, 3211—3213 (1972)

Thin-layer Chromatographic Behavior of Transition Metals on a Weakly Basic Cellulosic Ion-Exchanger in Hydrazoic Acid Medium

Rokuro KURODA and Nobuo KOJIMA

Laboratory for Analytical Chemistry, Faculty of Engineering, Chiba University, Yayoi-cho, Chiba

(Received February 9, 1972)

Metal complexes containing azide ions have received considerable attention recently; the preparation and physical properties of azido complexes of the transition metals have been investigated extensively.[1,2] However, little information is available so far on the ion-exchange behavior of metals in hydrazoic acid media. We have examined the anion-exchange behavior of transition metals in aqueous hydrazoic acid solution. Because of its simplicity and rapidity, the thin-layer chromatographic technique using diethylaminoethyl-cellulose as an adsorbent was employed to study the adsorbability of metals from the aqueous hydrazioc acid solution.

1) L. G. Sillén and A. E. Martell, "Stability Constants of Metal Ion Complexes," Spec. Publ. No. 17, Sect. 1, The Chemical Society, London, (1964), p. 160.

2) For example, R. G. Clem and E. H. Huffman, *J. Inorg. Nucl. Chem.*, **27**, 365 (1965); W. Beck, W. P. Fehlhammer, P. Pöllmann, E. Schuierer, and K. Feldl, *Chem. Ber.*, **100**, 2335 (1967); H. -H. Schmidtke and D. Garthoff, *J. Amer. Chem. Soc.*, **89**, 1317 (1967); P. Senise and O. E. S. Godinho, *J. Inorg. Nucl. Chem.*, **32**, 3641 (1970); P. Senise and E. F. de A. Neves, *ibid.*, **33**, 351 (1971); K. Bowman and Z. Dori, *Inorg. Chem.*, **9**, 395 (1970).

TABLE 1. R_f VALUES OF THE TRANSITION METALS ON DEAE-CELLULOSE AND AVICEL SF IN 0.1 M HN_3 (pH, 2.8)

Metal	R_f		Metal	R_f	
	DEAE	Avicel SF		DEAE	Avicel SF
Sc(III)	0—0.57	0.79—0.87	Ag(I)	0—0.01	0—0.02
Ti(IV)	0.07—0.12	0—0.91	Cd(II)	0.67—0.77	0.53..0.83
V(IV)	0—0.54	0.57..0.85			—0.87
		—0.89	La(III)	0.72—0.81	0.79—0.89
Cr(III)	0—0.90	0.86—0.94	Sm(III)	0.68—0.79	0.77—0.89
Mn(II)	0.65—0.75	0.69..0.86	Yb(III)	0.68—0.77	0.81—0.89
		—0.91	Hf(IV)	0.03—0.15	0..0.78
Fe(III)	0.08—0.17	0.83—0.91			—0.86
	..0.73		W(VI)	0—0.02	0.14—0.71
Co(II)	0.70—0.77	0.50—0.88			..0.97
Ni(II)	0.70—0.77	0.45—0.87	Re(VII)	0—0.04	0.76—0.87
Cu(II)	0.09—0.13	0.50—0.83	Ir(IV)	0—0.04	0.84—0.98
	..0.23		Pt(IV)	0—0.04	0.81—0.97
Zn(II)	0.61—0.72	0.55..0.84	Au(III)	0—0.03	0.31..0.67
		—0.89			—0.73
Y(III)	0.69—0.80	0.81—0.89	Hg(II)	0.03—0.35	0.56—0.66
Zr(IV)	0—0.14	0—0.42	Th(IV)	0—0.39	0..0.76
Nb(V)	0—0.18	0—0.83			—0.86
Mo(VI)	0—0.02	0.15—0.64	U(VI)	0.11—0.29	0.80—0.88
Pd(II)	0—0.02	0—0.70			

"..." Denotes a weak streak.

Experimental

About 12 g of diethylaminoethylcellulose(abbreviated as DEAE), Serva, was treated batchwise by 0.1 M sodium hydroxide and washed with deionized water. DEAE was then converted to the azide form by treating with 0.5 M sodium azide solution acidified with hydrazoic acid to pH 5. In order to obtain hydrazoic acid, a 0.5 M sodium azide solution was passed through a column of cation-exchange resin in the hydrogen form. After washing with deionized water by centrifugation, DEAE was slurried with 35 ml of deionized water and spread 250 μ thick on five 20×20 cm glass plates. The 250 μ thick thin-layer plates of microcrystalline cellulose, Avicel SF(Avicel Sales Division, FMC Corp.), were also prepared.[3] All the plates were dried at 40°C for 3 hr and stored in a desiccator containing a saturated potassium bromide solution. For most metals the test solutions were 0.1 M metal chlorides of varying hydrochloric acid concentration. The test solutions of Nb(V), Mo(VI), Ag(I), W(VI), and Re(VII) were prepared as reported previously.[3]

A 0.5 μl portion of the test solutions was applied to the plate at 2 cm from the edge. After drying the plate in the desiccator for 30 min, it was developed in a tank(23×11×22 cm) equilibrated with 0.1 M hydrazoic acid solution for 1 hr. After developing (solvent front 15 cm high) and drying the plate, metals were detected.[3] Mn(II) and V(IV) were detected by spraying 0.1% alkaline PAR solution, and Ti(IV) by 0.1% tannic acid solution.

Results and Discussion

In Table 1 the R_f values are given for 29 metals on DEAE together with those on a plain cellulose Avicel SF as a reference, both in 0.10 M hydrazoic acid solution. We see that almost none of the metals are adsorbed on Avicel SF from 0.1 M hydrazoic acid. Ag(I) forms an insoluble precipitate with azide, giving the R_f value of approximately zero. In contrast to Avicel SF, enhanced adsorption can be observed for most metals on DEAE in hydrazoic acid solution. Within the group of the first transition metals, Mn(II), Co(II), Ni(II), and Zn(II) are not adsorbed on DEAE while the other metals including Sc(III), Ti(IV), V(IV), Cr(III), Fe(III), and Cu(II) exhibited increased adsorption on DEAE relative to Avicel SF, although marked streaks were often found for some of them.

It is of interest to note that the hydrazoic acid allows the strongest adsorption on DEAE of Mo(VI), W(VI), Re(VII), and the platinum group of metals including Pd(II), Ir(IV), and Pt(IV). All the metals except for Ir(IV) have been reported to be adsorbed strongly on DEAE from thiocyanic acid,[4,5] which resembles hydrazoic acid in many aspects, both being grouped to pseudohalogenic acid.

Considerable differences in the adsorbability between DEAE and Avicel SF are also observed for Zr(IV), Nb(V), Hf(IV), Au(III), Hg(II), Th(IV), and U(VI). This is also the case for Y(III) and the rare earth metals, the difference being less remarkable. Cd(II) behaves like Zn(II). Diethylaminoethyl group does not seem to be responsible for the R_f value of Cd(II) on DEAE, even though a weak azido complex formation takes place.[6] The R_f value is rather high for Hg(II).

3) K. Oguma and R. Kuroda, *J. Chromatogr.*, **52**, 339 (1970).

4) K. Ishida and R. Kuroda, *Anal. Chem.*, **39**, 212 (1967).

5) K. Ishida, T. Kiriyama, and R. Kuroda, *Anal. Chim. Acta*, **41**, 537 (1968).

6) P. Senise and E. F. de A. Neves, *J. Amer. Chem. Soc.*, **83**, 4146 (1961).

This might not allow the uptake of Hg(II) on a DEAE column from 0.1 M hydrazoic acid. This is in contrast to its behavior in thiocyanate media, where the pronouced adsorption of Hg(II) takes place, permitting a very specific column separation of Hg(II) from about 40 metals.[7]

The absorption of the transition metals on DEAE from the hydrazoic acid solution may be mostly accounted for, by assuming azido complex formation and the subsequent anion-exchange. However, it might be possible for some metals that adsorption is caused merely through the anion-exchange of their oxyanions.

7) R. Kuroda, T. Kiriyama, and K. Ishida, *Anal. Chim. Acta*, **40**, 305 (1968).

BULLETIN OF THE CHEMICAL SOCIETY OF JAPAN, VOL. 45, 3213—3214 (1972)

The Effects of Additives on the Chemical Behavior of ^{60}Co Recoil Species in Neutron-irradiated Benzene Solutions of Tris(acetylacetonato)cobalt(III)

Takeshi TOMINAGA and Yasuo NISHI

Department of Chemistry, Faculty of Science, The University of Tokyo, Hongo, Tokyo

(Received March 24, 1972)

In the course of our investigation of the behavior of recoil species in organic solutions of metal chelate complexes, we found that some metal salts could work as effective scavengers to suppress thermal reactions and thus minimize the apparent retention in the irradiated solutions as well as in solutions of the irradiated solids.[1-4] While the use of such metal salts as scavengers has proved to be a very useful technique for studying recoil reactions in solutions or solids, the detailed mechanism of the scavenging reactions has not yet been fully clarified. Accordingly, we have further investigated the effects of additives other than metal salts on the reactions of recoil species in irradiated organic solutions of metal complexes.

In the present article, a probable mechansim of the scavenging effect by metal salts is proposed on the basis of our recently obtained data concerning the change in the ^{60}Co retention with the time in irradiated $Co(acac)_3$ benzene solutions containing metal acetylacetonates as additives.

Experimental

The 0.2 M solutions of $Co(acac)_3$ in benzene containing 10% (by volume) of ethanol and small quantities of additives, such as metal acetylacetonates, metal chlorides and acetylacetone, were prepared by procedures similar to those described previously.[2] About 1-m*l* portions of $Co(acac)_3$ benzene solutions containing various additives were irradiated with slow neutrons for 5 min at room temperature in the rotary specimen rack of a TRIGA Mark II reactor at Rikkyo University (thermal neutron flux: 5×10^{11} n/cm^2·sec; γ dose: 7×10^4 R for 5 min). After the irradiated solutions had been kept standing for a desired length of time at room temperature, chemical separation was performed by means of a solvent-extraction method described previously.[2] The ^{60}Co retention, or the radiochemical yield of the parent chemical form, $^{60}Co(acac)_3$, was obtained as the percentage of the total ^{60}Co activity found in the organic phase after the solvent extraction.

Results and Discussion

Figure 1 illustrates the change in the apparent ^{60}Co retention with the time after the irradiation of the $Co(acac)_3$ benzene solutions containing metal acetylacetonates and other additives. The ^{60}Co retention remains unchanged even after a solution has stood 7 days in the presence of ferric chloride as an additive, while it increases appreciably when the solution stands in the presence of magnesium chloride. It is worth mentioning that as additives both $Ni(acac)_2\cdot2H_2O$ and $Mg(acac)_2$ (3×10^{-3} M) enhance the increase in the ^{60}Co retention remarkably, as compared with the retention curve in the absence of an additive, whereas $Fe(acac)_3$ has practically no effect as an additive. It appears that the transfer of the ligand acetylacetonate ion from the less stable metal acetyl-

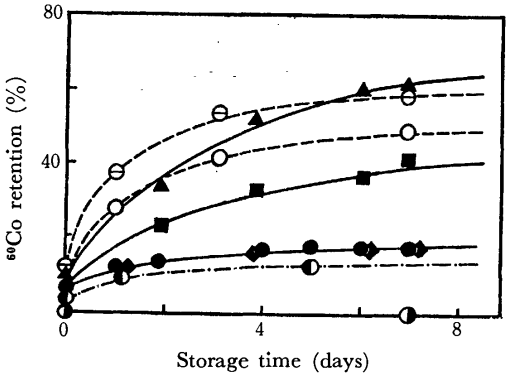

Fig. 1. ^{60}Co retention in the irradiated 0.2 M solutions of $Co(acac)_3$ in benzene containing 10% of ethanol and various additives.
—●—: No additive; —◑—: 2×10^{-3} M $FeCl_3\cdot6H_2O$; ···◐···: 2×10^{-3} M $MgCl_2\cdot6H_2O$; —◆—: 3×10^{-3} M $Fe(acac)_3$; —■—: 3×10^{-3} M $Ni(acac)_2\cdot2H_2O$; —▲—: 3×10^{-3} M $Mg(acac)_2$; --⊖--: 10^{-2} M acetylacetone; --○--: 2×10^{-3} M acetylacetone.

1) T. Tominaga and K. Fujiwara, This Bulletin, **43**, 2279 (1970).
2) T. Tominaga, T. Sakai, and K. Fujiwara, *ibid.*, **44**, 3036 (1971).
3) T. Tominaga and Y. Nishi, *Radiochem. Radioanal. Lett.*, **8**, 151 (1971).
4) T. Tominaga and T. Sakai, This Bulletin, **45**, 1237 (1972).

acetonates (*i. e.*, $Mg(acac)_2$ and $Ni(acac)_2 \cdot 2H_2O$) to the ligand-deficient ^{60}Co recoil species mainly contributes to the increase in the ^{60}Co retention in the presence of such metal acetylacetonates as additives. Similar effects were observed when the irradiated solid $Co(acac)_3$ was dissolved in benzene containing such additives and the mixture was then kept standing.

As is shown in Fig. 2, the scavenging power (percentage of the thermal reactions scavenged by an equal

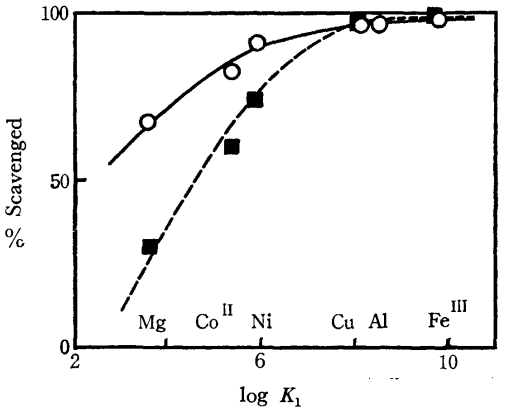

Fig. 2. Correlation of scavenging powers of various metal salts (2×10^{-3} M) with the thermodynamic stability constants of their acetylacetonates.
—○—: Separated within a few hours after irradiation;
--■--: Separated after 7 days.

molar concentration of a scavenger) of metal salts measured within a few hours after irradiation[2] and after 7 days' standing apparently correlates well with the thermodynamic stability constants[5] of their acetylacetonates. Based on the present results, the mechanism of the overall phenomenon (apparent scavenger effect) may be explained in terms of the following reactions:

(1) Recombination. $[^{60}Co(acac)_{3-x}] + acac^- \longrightarrow {}^{60}Co(acac)_3$

(2) Scavenging reaction. $MX_n + acac^- \longrightarrow M(acac)_n$

(3) Ligand transfer. $[^{60}Co(acac)_{3-x}] + M(acac)_n \longrightarrow {}^{60}Co(acac)_3 + M(acac)_m \quad (n>m)$

where $[^{60}Co(acac)_{3-x}]$ denotes the ligand-deficient ^{60}Co recoil species ($x=1$, 2, or 3; cationic) and MX_n, scavenger salt. In the period immediately after irradiation, the competition between (1) and (2) is important, whereas the (3) reaction may still be relatively unimportant. The competition between (1) and (2) predominantly favors (2), and the correlation curve in Fig. 2 should closely approach the 100%-scavenged level for most of the metal salts investigated if the irradiation and storage periods become as brief as possible. If the (3) reaction gradually proceeds between the unreacted ligand-deficient ^{60}Co recoil species and $M(acac)_n$ remaining in the system,[6] the ^{60}Co retention increases, and the apparent scavenging power decreases, on standing. Hence, the corresponding plot-point on the correlation curve may be lowered from the 100%-scavenged level by a magnitude equivalent to the contribution of (3). Accordingly, the correlation between the apparent scavenging power and the stability constant may be explained by presuming that the extent of the (3) reaction reached after a solution has stood for a sufficiently long time depends mainly upon the stability of the metal acetylacetonate relative to $Co(acac)_3$. The present results on the effect of acetylacetonates of Fe, Ni, and Mg (Fig. 1) indicate that the extent of such a reaction actually increases with the decreasing stability of the acetylacetonates. Very similar results were obtained with irradiated $Cr(acac)_3$ benzene solutions.[7]

In conclusion, the scavenging effect of the salts of metals which can form more stable acetylacetonates may be ascribed mainly to the competition between the recombination (1) and the scavenging reactoin (2) to capture acetylacetone. For the salts of metals which form less stable acetylacetonates, however, the ligand transfer (3) may proceed appreciably on standing and may apparently diminish the overall scavenging effect.

The present authors wish to express their thanks to Professor Nobufusa Saito, The University of Tokyo, for his encouragement.

5) R. M. Izatt, C. G. Haas, Jr., B. P. Block, and W. C. Fernelius, *J. Phys. Chem.*, **58**, 1133 (1954); R. M. Izatt, W. C. Fernelius, and R. P. Block, *ibid.*, **59**, 80 (1955); R. M. Izatt, W. C. Fernelius, C. G. Haas, Jr., and B. P. Block, *ibid.*, **59**, 170 (1955).

6) Although the decomposition of the parent complex was spectrophotometrically found to be almost negligible even after standing, the irradiated solutions might contain very small amounts (10^{-4}—10^{-3} M) of free acetylacetone (as radiolytic product or impurity), from which resulted $M(acac)_n$.

7) T. Tominaga and Y. Nishi, *Radiochem. Radioanal. Lett.*, in press.

BULLETIN OF THE CHEMICAL SOCIETY OF JAPAN, VOL. 45, 3215—3216 (1972)

The Effect of Intramolecular Hydrogen Bonding on Benzoylation of 2-(*N*,*N*-Dialkylamino)ethanols

Kunihiro ICHIMURA and Junko YOSHIDA*

Research Institute for Polymers and Textiles, Sawatari 4, Kanagawa-ku, Yokohama

** Department of Chemistry, Faculty of Science, Toho University, Narashino, Chiba*

(Received December 4, 1971)

We have synthesized some *O*-acylated 2-(*N*,*N*-dialkylamino)ethanols by the action of acyl chloride on aminoalcohols. When an equimolar amount of acyl chloride was used, the yields of the hydrochloride of *O*-acylated aminoalcohol were found to be relatively low, the hydrochloride of aminoalcohol also being formed. Although various *O*-acylated 2-(*N*,*N*-dialkylamino)ethanols have been synthesized, the mechanism does not seem to be fully understood. We have examined the reaction mechanism of some 2-(*N*,*N*-dialkylamino)ethanols with benzoyl chloride by means of IR-spectrometry. It was found that the reaction rate is affected by the intramolecular hydrogen bonding of the aminoalcohols.

Results and Discussion

It was observed that the reaction of acyl chloride with equimolar 2-(*N*,*N*-dialkylamino)ethanol at room temperature gives a mixture of the hydrochloride of *O*-acylated aminoalcohol and of the parent aminoalcohol. The yields of acylated amines were thus reduced, although the reaction was expected to proceed smoothly through the intramolecular base-catalysed mechanism. Because of the good solubility of the hydrochloride of products in dichloromethane, benzoylation of aminoalcohols was followed by means of infrared spectrometry.

As soon as an equimolar amount of *N*,*N*-diethylaminoethanol (Ia) was mixed with benzoyl chloride (3.30×10^{-2} M) in dichloromethane at room temperature, the ester C=O band of diethylaminoethyl benzoate (IIa) at 1717 cm^{-1} and OH stretching vibration of diethylaminoethanol hydrochloride (Ia-HCl) at 3280 cm^{-1} began to develop. After 24 hr, the C=O ester band was found to shift to 1727 cm^{-1} due to formation of the hydrochloride of diethylaminoethyl benzoate (IIa-HCl), as the OH band at 3280 cm^{-1} weakened. About 42% benzoyl chloride remained. The products were identified with the authentic samples.

However, the IR-spectrum of a reaction mixture of benzoyl chloride and twofold molecular amount of aminoalcohol differs from the above result. The ester carbonyl band of IIa-HCl at 1727 cm^{-1} and OH band of Ia-HCl at 3280 cm^{-1} increase monotonously and isoabsorptive points at 3400 cm^{-1} are observed. This indicates that a twofold molecular amount of aminoalcohol is neccessary to complete the reaction to afford diethylaminoethyl benzoate and hydrochloride of diethylaminoethanol. The spectral change during the course of the reaction of equimolar amount of

$$C_6H_5COCl + \underset{\text{I}}{R^1_2NCHR^2CHR^3OH} \xrightarrow{k_1} \underset{\text{II-HCl}}{C_6H_5COOCHR^3CH\overset{+}{R}^2NHR^1_2\cdot Cl^-} \quad (1)$$

$$\text{II-HCl} + \text{I} \xrightarrow{k_2} \underset{\text{II}}{C_6H_5COOCHR^3CHR^2NR^1_2} + \underset{\text{I-HCl}}{R^1_2\overset{+}{N}HCHR^2CHR^3OH\cdot Cl^-} \quad (2)$$

$$C_6H_5COCl + \text{II} + \text{I-HCl} \xrightarrow{k_3} 2\ \text{II-HCl} \quad (3)$$

Scheme 1. Benzoylation of 2-(*N*,*N*-dialkylamino)ethanols (Ia: $R^1=CH_3CH_2$, $R^2=R^3=H$; Ib (*threo*), Ic (*erythro*): $R^1=R^2=CH_3$, $R^3=C_6H_5$).

aminoalcohol is then interpreted by the following scheme (scheme 1). Aminoalcohol (Ia) is at first benzoylated to give ester hydrochloride (IIa-HCl) according to reaction (1), which, in turn, is readily deprotonated by aminoalcohol (Ia) to form Ia-HCl and free ester (IIa)(reaction (2)). Reaction (2) was confirmed by the fact that the infrared spectrum of an equimolar mixture of IIa-HCl and Ia is essentially the same as that of IIa and Ia-HCl.[1] Twofold molar aminoalcohol is thus consumed according to reactions (1) and (2). Remaining benzoyl chloride reacts then more slowly with the hydrochloride of aminoalcohol (Ia-HCl), free ester (IIa) acting as the scavenger of hydrogen chloride formed (reaction (3)). From observation of the infrared spectral change we assume that the rate constants are qualitatively in the order; $k_2 \gg k_1 > k_3$, where k_1, k_2, and k_3 are the rate constants of reactions (1), (2), and (3), respectively.

Using the stationary state approximation, we obtain the kinetic equation

$$dx/dt = k_1(a-x)(b-2x) \quad (4)$$

$$\text{if } a = b,\ k_1t = 2.303\log((a-x)/(a-2x)) \quad (5)$$

$$\text{if } 2a = b,\ k_1t = x/(2a(a-x)) \quad (6)$$

where a and b are the initial concentrations of benzoyl chloride and aminoalcohol, respectively, and x is the concentration of the product or benzoyl chloride consumed at time t. The rate at 24°C was thus calculated by estimating the disappearance of carbonyl band of benzoyl chloride at 1775 cm^{-1}. The second order kinetic plots according to Eq. (6) gave a straight line

1) It is reported that aminoethanol (pK_a=9.50) is more basic than the *O*-acetylated derivative (9.10).[2]

2) D. D. Perrin, "Dissociation Constants of Organic Bases in Aqueous Solution," Butterworths, (1965).

Table 1. Physical properties of 2-(*N*,*N*-dialkylamino)ethanols

	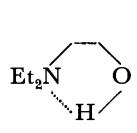	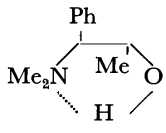	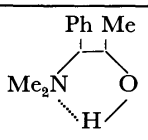	Cinchonidine
rate const. (k_1)[a] (l mol^{-1} sec^{-1})	2.64×10^{-2}	3.94×10^{-3}	1.01	too rapidly
pK_a (26°C)[2]	9.74[b]	10.00	9.26	8.40[c]
ν_{OH} (cm^{-1})[d]	3420	3300	3400	3280
ν_{OH} of HCl salt[d]	3280	3280	3240	3280

a) Although the rate constants may be lacking accuracy with respect to constancy and homogeneity of temperature of the reaction mixture during the kinetic measurement, the present method (see Experimental) is sufficient for a discussion of the difference in rate under the same conditions. b) Corrected to 26°C.[5] c) In 80% Methyl Cellosolve at 15°C.[4] d) The wave numbers did not change in the range 0.12—0.024 M in dichloromethane.

when twofold molecular amount of aminoalcohol was used. In the case of equimolar aminoalcohol a straight line was also obtained only up to 40% consumption of benzoyl chloride according to Eq. (5). The second order rate constants in both cases are identical within experimental error. It is therefore noteworthy that the concerted push-pull mechanism is excluded, in contrast to the alcoholysis of some acyl chloride which have been found to be second order in alcohol.[3] In order to obtain further information with regard to the acylation, benzoylation of *threo*-1-phenyl-2-dimethylaminopropanol-1 (Ib) and the diastereomeric *erythro* compound (Ic) was carried out in the same manner. A remarkable difference in reaction rate between these diastereomers was observed (Table 1). If the rate determining step of reaction (1) is the attack of benzoyl chloride upon hydroxy group of aminoalcohol, then the stronger the intramolecular hydrogen bonding, the faster the reaction. Although the hydrogen bonding of *threo* compound (Ib) is stronger than that of *erythro* isomer (Ic) as a result of the steric requirement (see ν_{OH} in Table 1), the benzoylation of *erythro* isomer (Ic) is about 250 times faster than that of *threo* isomer (Ib). The effects of molecular structure of these diastereomers on the rate should predominantly arise from the intramolecular hydrogen bonding. We can thus conclude that the intramolecular hydrogen bonding reduces the nucleophilicity of nitrogen atom to form *N*-acylammonium cation (III). In view of failure to detect the intermediate and from observation of isoabsorptive points during the course of reaction by means of IR-spectroscopy, we propose that the intermediate (III) undergoes immediately the *N-O* acyl rearrangement to yield hydrochloride of *O*-acylated aminoalcohol.

The rate of benzoylation (k_1) increases apparently with decrease in pK_a of aminoalcohol. Cinchonidine whose pK_a is 8.40 was in fact found to be benzoylated so rapidly that measurement of the rate by the present method failed. The correlation could be caused by the effect of intramolecular hydrogen bonding which gives rise to depression of the nucleophilicity of nitrogen atom as mentioned above and contrariwise to enlargement of pK_a value. It is seen that the geometrical isomer of β-aminoalcohol with a stronger intramolecular hydrogen bonding is more basic than that with a weaker one.[4]

Such acyl chlorides as phenylacetyl- or phthaloylaminoacyl chloride also react too rapidly with 2-(*N*,*N*-dialkylamino)ethanols to make observation of the infrared spectral change of the reaction mixture possible. This suggests another mechanism where hydrogen at the α-position of acyl chloride could readily be eliminated to give ketene as Pracejus has proposed from the results of the asymmetric esterification of acyl chloride in the presence of alkaloids.[5]

Experimental

Materials: Benzoyl chloride was distilled before use. Diethylaminoethanol was fractionally distilled and used immediately. *erythro*- and *threo*-1-Phenyl-2-dimethylaminopropanol-1 were obtained by the Leuckardt reaction of ephedrine and ψ-ephedrine and purified by distillation or sublimation. Cinchonidine was recrystallized from aqueous propanol-2 and dried *in vacuo*. 2-*N*,*N*-Diethylaminoethyl benzoate (bp$_7$ 140—141°C), hydrochloride of the ester (mp 124—125°C) and 2-(*N*,*N*-diethylamino)ethanol hydrochloride (mp 134—135°C) were synthesized in the usual way. Dichloromethane was purified and dried.

Kinetic Measurement: The absorbance of benzoyl chloride at 1775 cm^{-1} in dichloromethane was found to be proportional to concentration in the range 0.8×10^{-2}—3.5×10^{-2} M. A solution of benzoyl chloride of 3.30×10^{-2} M(1 m*l*) in dichloromethane was mixed rapidly with shaking with equi- or twofold molecular amount of aminoalcohol solution (1 m*l*) in a test tube immersed in a water bath, the temperature of which was equilibriated with room temperature controlled at 24°C. This instant was taken as the origin of time. The KBr cell (0.5 mm thick) was then filled with the combined solution. These operations required at least 30 sec. The IR-spectrum was recorded at intervals with a JASCO DC-402 Type IR-Spectrometer. We could observe no other band than that due to aromatic ring system within the range 2400—1800 cm^{-1}. The concentration of benzoyl chloride in the reaction mixture was calculated by the estimation of absorbance of carbonyl band at 1775 cm^{-1}. The second order kinetic plots of Ia, Ib, and Ic according to Eq. (5) or (6) deviated from a straight line within 4%, 10%, and 5% error, respectively.

3) E. S. Gould, "Mechanism and Structure in Organic Chemistry," Henry Holt and Company, (1959), p. 332.

4) V. Prelog and O. Häfliger, *Helv. Chim. Acta*, **33**, 2021 (1950).

5) G. Pracejus, *Liebigs Ann. Chem.*, **622**, 10 (1959).

6) A. Albert and E. P. Serjeant, "Ionization Constants of Acids and Bases," Methuen (1962).

BULLETIN OF THE CHEMICAL SOCIETY OF JAPAN, VOL. 45, 3217—3218 (1972)

Synthesis of the New 1,4,2-Dithiazine 1,1-Dioxides[1)]

Kazuaki NAKAHASHI, Syuzi HIROOKA, and Kiyoshi HASEGAWA

Department of Industrial Chemistry, Faculty of Engineering, Toyama University, Takaoka-shi

(Received January 10, 1972)

Previously, the synthesis of *N*-(2-phenylethene-1-sulfonyl)-*N'*-alkylthioureas and their intramolecular cycloadducts, 3-alkylamino-5-phenyl-1,1-dioxo-5,6-dihydro-1,4,2-dithiazines, from 2-phenylethene-1-sulfonamides was reported.[2)]

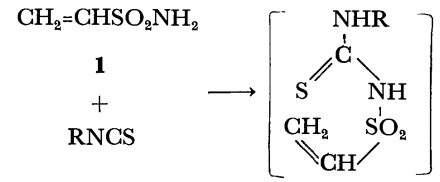

2

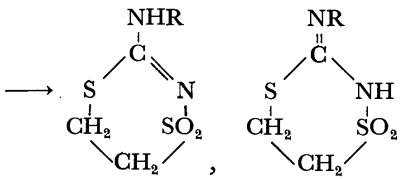

3 **4**

The present paper will describe the reaction of vinylsulfonamide (**1**) with isothiocyanates to give new heterocyclic compounds, 3-alkylamino-1,1-dioxo-5,6-dihydro-1,4,2-dithiazines (**3**) and 3-phenylimino-1,1-dioxo-2,3,5,6-tetrahydro-1,4,2-dithiazines (**4**), which are the intramolecular Michael cycloadducts of the probable intermediates, vinylsulfonyl thioureas (**2**).

The reaction of **1** with carbon disulfide and dimethyl sulfate in DMF in the presence of sodium hydroxide yielded 3-methylthio-1,1-dioxo-5,6-dihydro-1,4,2-dithiazine (**5**). The treatment of **5** with chlorine in chloroform gave the 3-chloro derivative (**6**), and the reaction of **6** with alcohol or amines afforded 3-alkoxy (**7**) or 3-amino derivatives (**8**), respectively.

Analogous syntheses starting from 2-phenylethene-1-sulfonamides were reported in a previous work,[3)] but the ethylenic bond in vinylsulfonamide is very reactive and we failed to secure the vinylsulfonylated thioureas **2** and dithiocarbamate, which are the noncyclic intermediates between **1** and **3**, and between **1** and **5**, respectively.

Experimental

3-Methylamino-1,1-dioxo-5,6-dihydro-1,4,2-dithiazine (***3a***). To vinylsulfonamide (2.6 g, 0.025 mol) in acetone (15 *ml*), we added methyl isothiocyanate (2.2 g, 0.03 mol) and anhydrous potassium carbonate (4.2 g, 0.03 mol); the reaction mixture was then refluxed for 10—15 hr with stirring and subsequently filtered. The acetone layer was concentrated *in vacuo*, and the crude residue was cooled to give 3.0 g of a solid. Recrystallization from methanol gave colorless crystals. IR (KBr): 3260 (ν_{NH}), 1550—1570 ($\nu_{C=N}$), 1200—1300, 1120—1160 (ν_{SO_2}) cm^{-1}. NMR (DMSO-d_6): δ 2.710 (s, $=NCH_3$), 2.713 (d, J_{NHCH_3}=4.6 Hz), 3.16—3.56 (m, 4H, CH_2CH_2), 8.56 (broad, 0.53H, NH). Ms: *m/e* 45 (CHS), 180.061 (calculated molecular weight, 180.059).

3-Phenylimino-1,1-dioxo-2,3,5,6-tetrahydro-1,4,2-dithiazine (***4c***). To vinylsulfonamide (1.0 g, 0.009 mol) in acetone (10 *ml*), we added phenyl isothiocyanate (1.4 g, 0.010 mol) and anhydrous potassium carbonate (1.4 g, 0.010 mol); the reaction mixture was then refluxed for 10—15 hr with stirring and subsequently filtered; the potassium salt of **4c** thus obtained was dissolved in water, and the resulting solution was acidified to give 2.2 g of **4c**. Although crude **3c** was obtained by concentrating the acetone layer *in vacuo*, it was converted to **4c**

TABLE 1. 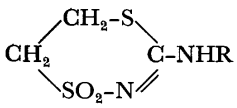 **3** or 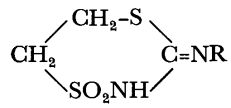 **4**

Compd	R	Yield (%)	Ratio[a)] (%)	Mp (°C)	Found (%) C	H	N	S	Calcd (%) C	H	N	S	Solvent of recrystn
3a / **4a**	CH_3	68	100 / 0	146—147	26.69	4.52	15.31	35.01	26.65	4.47	15.54	35.57	methanol
3b / **4b**	C_6H_{11}	73	94 / 6[b)]	186—187	43.24	6.66	11.15	25.62	43.52	6.49	11.28	25.82	methanol
3c / **4c**	C_6H_5	91	45[c)] / 55	161—163	44.31	4.14	11.48	26.30	44.61	4.16	11.56	26.48	methanol
3d / **4d**	*p*-$CH_3C_6H_4$	90	0 / 100	170—171	47.15	4.81	11.05	24.87	46.85	4.72	10.93	25.01	methanol
3e / **4e**	*p*-ClC_6H_4	79	100 / 0	233—235	39.16	3.23	10.17	22.96	39.06	3.28	10.12	23.17	ethanol

a) Ratio of **3** *vs.* **4** before recrystallization. b) **4b** could not be recrystallized. c) **4c** was given by recrystallization from methanol.

1) Presented at the 25th Annual Meeting of the Chemical Society of Japan, Tokyo, October, 1971.

2) K. Hasegawa and S. Hirooka, This Bulletin, **45**, 525 (1972).

3) K. Hasegawa and S. Hirooka, *ibid.*, **45**, 1567 (1972).

TABLE 2.

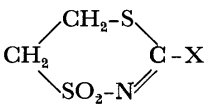

Compd	X	Yield (%)	Mp (°C)	Found (%)					Calcd (%)				
				C	H	N	S	Cl	C	H	N	S	Cl
5	SCH_3	84	126—127	24.30	3.62	7.08	48.43	—	24.35	3.58	7.10	48·75	—
6	Cl	80	131—132	19.24	2.29	7.44	34.28	19.64	19.41	2.17	7.55	34.54	19.10
7	OCH_3	51[a)]	139—140	26.47	3.84	7.81	35.07	—	26.51	3.89	7.73	35.38	—
8a	$N(CH_3)_2$	68[a)]	171—172	30.89	4.98	14.38	32.60	—	30.91	5.19	14.42	33.01	—
8b	NH_2	97	196—197	21.96	3.64	16.64		—	21.68	3.64	16.86	38.58	—

a) Yield after recrystallization.

when recrystallized from methanol.
IR (KBr): 3240 (ν_{NH}), 1590 (ν_{phenyl}), 1540 ($\nu_{C=N}$), 1300—1310, 1260—1270 (ν_{SO_2}) cm^{-1}. NMR (acetone-d_6): δ 3.17—3.80 (m, 4H, CH_2CH_2), 7.00—7.73 (m, 5H, phenyl CH), 9.25 (broad, 0.63H, NH). Ms: *m/e* 46 (CH_2S), 242 (M).

The **5**, **6**, **7**, **8a**, and **8b** compounds were prepared and confirmed in an analogous manner,[3)] starting from vinylsulfonamide.

3-Methylthio-1,1-dioxo-5,6-dihydro-1,4,2-dithiazine (***5***). IR (KBr): 1505 ($\nu_{C=N}$), 1260—1310 and 1110—1170 (ν_{SO_2}) cm^{-1}. NMR ($CDCl_3$): δ 2.52 (s, 3H, SCH_3). Ms: *m/e* 197 (M).

3-Chloro-1,1-dioxo-5,6-dihydro-1,4,2-dithiazine (***6***). IR (KBr): 1570 and 1550 ($\nu_{C=N}$), 1270—1325 and 1140—1180 (ν_{SO_2}) cm^{-1}. Ms: *m/e* 185 (M).

3-Methoxy-1,1-dioxo-5,6-dihydro-1,4,2-dithiazine (***7***). IR (KBr): 1560 ($\nu_{C=N}$), 1250—1320 and 1110—1170 (ν_{SO_2}) cm^{-1}. Ms: *m/e* 181 (M). NMR ($CDCl_3$): δ 3.95 (s, 3H, OCH_3).

3-Dimethylamino-1,1-dioxo-5,6-dihydro-1,4,2-dithiazine (***8a***). IR (KBr): 1545 ($\nu_{C=N}$), 1310, 1270, and 1110—1140 (ν_{SO_2}) cm^{-1}. NMR ($CDCl_3$): δ 3.12 (s, 6H, $N(CH_3)_2$). Ms: *m/e* 194 (M).

3-Amino-1,1-dioxo-5,6-dihydro-1,4,2-dithiazine (***8b***). IR (KBr): 3330, 3250, and 3160 (ν_{NH}), 1610 (ν_{NH}), 1515 ($\nu_{C=N}$), 1140, 1110, and 1100 (ν_{SO_2}) cm^{-1}.

BULLETIN OF THE CHEMICAL SOCIETY OF JAPAN, VOL. 45, 3218—3220 (1972)

Studies of Dithiobiurets. I. Some New Cyclization Reactions of 1,1-Dimethyl-2,4-dithiobiuret

Isao IWATAKI

Chemical Research Laboratory, Nippon Soda Co., Ltd., Khozu, Odawara

(Received March 2, 1972)

Several cyclization reactions of dithiobiurets have been known hitherto. For instance, alkyl or aryldithiobiurets (**1**) react with aldehydes or ketones in the presence of hydrogen chloride to give hexahydrotriazine derivative (**2**).[1] Another example is their oxidation. They are easily oxidized with bromine or iodine to yield 1,2,4-dithiazole derivatives (**3**), which are known as thiurets.[2] Dixit obtained the same compounds by the oxidative debenzylation of the *S*-benzylisodithiobiurets, (**4**) and (**5**).[3] He also obtained benzothiazole and 1,2,4-thiadiazole derivatives, (**6**) and (**7**),[3] which were formed as by-products when a large quantity of nonpolar solvents were used at the time of the oxidation.

We wish to report here some cyclization reactions of 1,1-dimethyldithiobiuret (**8**). Like thiourea, it reacted with α,β-dichloroethyl acetate to form a thiazole derivative (**9**) in a 27% yield. Fromm and Philippe[4] reacted phenyldithiobiuret with monochloroacetone and obtained a product which melted at 163°C. They considered that the structure was **10** or **11**. Compound **10** can easily be obtained by the reaction of 4-methylthiazole and phenylisothiocyanate (mp 174—175°C)[5] or 4-methyl-2-thiazolylisothiocyanate and aniline (mp 168—169°C).[6] We tried Fromm's method and confirmed that the product had not an **11** but a **10** structure; the structure was identified by the undepressed mixed melting points and by comparing the infrared spectrum with that of an authentic sample. Choubey and Singh[7] obtained 2-arylimino-3-arylthiazolidin-4-ones when arylthioureas were

1) E. Fromm, *Ann.*, **275**, 20 (1893); A. E. S. Fairfull and D. A. Peak, *J. Chem. Soc.*, **1955**, 803.

2) E. Fromm, *Ber.*, **28**, 1096 (1895); S. N. Dixit, *J. Indian Chem. Soc.*, **38**, 44 (1961).

3) S. N. Dixit, *ibid.*, **38**, 988 (1961); **39**, 407 (1962); **40**, 153 (1963).

4) E. Fromm and E. Philippe, *Ber.*, **32**, 835 (1899).

5) F. Fromm and R. Kapeller-Alder, *Ann.*, **467**, 259 (1928); T. Uno and S. Akihama, *Yakugaku Zasshi*, **80**, 1015 (1960); A. Silberg, D. Tefas, and D. Bedeleanu, *Acad. rep. populare Romane*, **3**, 70 (1952), *Chem. Abstr.*, **50**, 12043f (1956).

6) O. E. Schultz and K. K. Gauri, *Arch. Pharm.*, **295**, 146 (1962).

7) V. N. Choubey and H. Singh, This Bulletin, **43**, 2233 (1970).

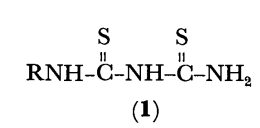

(1)

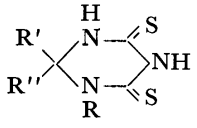

(2)

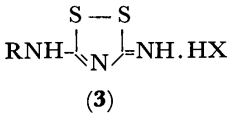

(3)

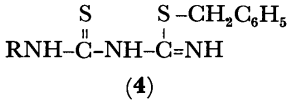

(4)

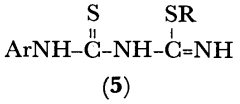

(5)

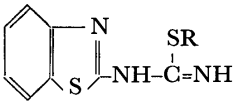

(6)

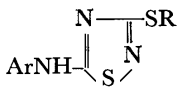

(7)

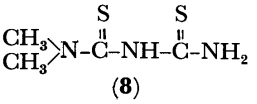

(8)

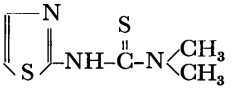

(9)

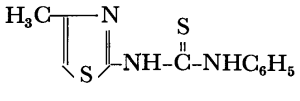

(10)

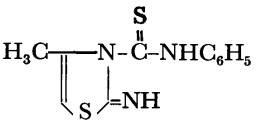

(11)

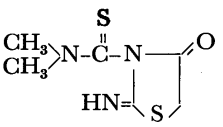

(12)

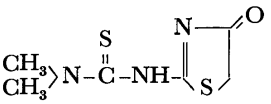

(13)

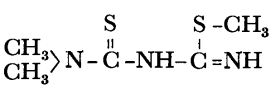

(14)

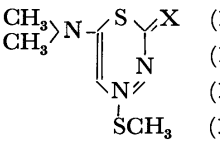

(15) X=O
(16) X=S
(17) X=$NSO_2C_6H_5$-*p*-CH
(18) X=NSO_2CH_3

treated with monochloroacetyl chloride in the presence of sodium acetate. Compound **8** also reacted with the chloride to give a thiazolin-4-one derivative (**13**). When an equimolar pyridine was used instead of sodium acetate, monochloroacetylation occurred at the 3-position and **12** was obtained as a by-product. It was converted to the thiazoline derivative **13** by acid treatment. 1,1-Dimethyl-4-*S*-methylisodithiobiuret (**14**) reacted with phosgene and thiophosgene to yield 1,3,5-thiadiazine derivatives, (**15**) and (**16**). Imidoyl dichlorides also reacted with **14** to give 2-substituted imino-1,3,5-thiadiazine derivatives, (**17**) and (**18**).

Experimental

*2-(3,3-Dimethylthioureido)thiazole (**9**).* A suspended solution of 1,1-dimethyldithiobiuret **8** (16.3 g) in 100 m*l* of water was heated at 70°C, and then 19 g of α,β-dichloroethyl acetate were added with stirring. The solution gradually become homogeneous. The reaction mixture was then stirred for 1 hr and cooled at 0°C. The crystals thus precipitated were filtered and recrystallized from methanol; 6 g of white plates (hydrochloride) were thus obtained. Mp 175—176°C with decomposition.

Found: C, 32.43; H, 4.57; N, 18.85; S, 28.30; Cl, 16.05%. Required for $C_6H_{10}ClN_3S_2$: C, 32.14; H, 4.47; N, 18.75; S, 28.57; Cl, 16.07%. This was converted to the free base by treatment with aqueous sodium hydroxide. Mp 122—123°C.

Found: C, 38.55; H, 4.82; N, 22.25; S, 34.30%. Required for $C_6H_9N_3S_2$: C, 38.50; H, 4.81; N, 22.46; S, 34.22%.

*4-Methyl-2-(3-phenylthioureido)thiazole (**10**).* A mixture of phenyldithiobiuret (3 g) and monochloroacetone (2.7 g) was heated at 85°C for 10 min, and then 50 m*l* of acetone were added. The precipitate was filtered and recrystallized from ethanol. Then 2.8 g of the hydrochloride, melting at 162—163°C (Ref. 4: mp 163°C), were obtained. The hydrochloride (2.8 g) was dissolved in 15 m*l*) of pyridine, a 50-m*l* portion of ice water was added, and then the precipitate was collected. Recrystallization from ethanol gave 2.2 g of white prisms; mp 173—174°C. No depression of the melting points was observed when this substance was mixed with an authentic sample, obtained from 2-amino-4-methylthiazole and phenylisothiocyanate.

*2-(3,3-Dimethylthioureido)thiazolin-4-one (**13**).* A mixture of 1,1-dimethyldithiobiuret **8** (5 g), anhydrous sodium acetate (2.5 g), and monochloroacetyl chloride (3.4 g) in 50 m*l* of absolute ethanol was refluxed for 1.5 hr. After the sodium chloride had been filtered off, the solvent was evaporated *in vacuo*. The residue was washed with 30 m*l* of 1 N-hydrochloric acid and recrystallized from ethanol as yellow scalies (3.5 g); mp 208—209°C with decomposition. IR: 1700 cm^{-1} (C=O), 1580, 1550, NMR: δ 3.27 ppm (s, 6H, NMe_2), 4.50 (s, 2H, CH_2). UV: λ_{max} (in alc) 224 mμ (log ε 4.26), 241 (4.23), 287 (4.15). Found: C, 35.21; H, 4.43; N, 20.50; S, 31.74%. Required for $C_6H_9N_3OS_2$: C, 35.47; H, 4.43; N, 20.69; S, 31.53%.

*3-(N,N-Dimethylthiocarbamoyl)-2-iminothiazolin-4-one (**12**).* Into a solution of 1,1-dimethyldithiobiuret **8** (2 g) and pyridine (1 g) in 10 m*l* of acetone, monochloroacetyl chloride (1.5 g) was added at 0°C, after which the mixture was allowed to stand for 10 hr at room temperature. The precipitated plates were filtered and dissolved in 50 m*l* of water. After the solution had then been neutralized with sodium carbonate, the yellow powder was separated and recrystallized from ethanol to give 0.3 g of yellow prisms; mp 138—139°C with decomposition.

IR: 3400 cm^{-1} (NH), 1720 (C=O), 1605, 1530. UV: λ_{max} (in alc) 283 mμ (log ε 4.48). NMR: δ 3.45 ppm (s, 2H, CH_2), 3.30 and 3.18 (s, NMe_2). Found: C, 35.58; H, 4.58; N, 20.63; S, 31.74%. Required for $C_6H_9N_3OS_2$: C, 35.47; H, 4.43; N, 20.69; S, 31.53%.

From the reaction mixture, 1.3 g of **13** were obtained.

*Isomerization of 3-(*N,N-*dimethylthiocarbamoyl)-2-iminothiazolidin-4-one (**12**).* The sample (0.1 g) was dissolved in 10 m*l* of 1N-hydrochloric acid, and the mixture was allowed to stand overnight. The precipitated yellow scalies were collected. This substance was identified with **13** by means of IR, tlc, and a mixed mp determination.

*6-Dimethylamino-4-methylthio-2*H-*1,3,5-thiadiazin-2-one (**15**).* 1,1-Dimethyl-4-*S*-methylisodithiobiuret **14** (2.5 g) was dissolved in 50 m*l* of tetrahydrofuran, and then phosgene (5 g) in 20 m*l* of tetrahydrofuran was added at 0°C. An insoluble white powder was filtered off and dried. Recrystallization from ethanol afforded 2 g of white crystals (hydrochloride); mp 170—172°C with decomposition. Found: C, 29.89; H, 4.17; N, 17.28; S, 26.47; Cl, 14.78%. Required for $C_6H_{10}ClN_3OS_2$: C, 30.06; H, 4.18; N, 17.54; S, 26.72; Cl, 14.82%. IR: 1690 cm^{-1}(C=O), 1600, 1530. The neutralization of this hydrochloride with potassium carbonate gave the base **15**; it was then recrystallized from ethanol as white plates. Mp 157—158°C. IR: 1650 cm^{-1} (C=O), 1560. UV: λ_{max} (in alc) 224 mμ (log ε 3.66), 283 (4.08), 302^{sh} (4.01). Found: C, 35.23; H, 4.33; N, 20.52; S, 31.65%. Required for $C_6H_9N_3OS_2$: C, 35.47; H, 4.43; N, 20.69; S, 31.53%.

*6-Dimethylamino-4-methylthio-2*H-*1,3,5-thiadiazin-2-thione(**16**).* The isodithiobiuret **14** (1 g) was dissolved in 50 m*l* of tetrahydrofuran, and then thiophosgene (0.7 g) in 5 m*l* of the same solvent was added at 0°C. After the reaction mixture had been stirred for 1 hr, a yellow precipitate was filtered off. The solid (0.8 g) was recrystallized from ethanol as yellow crystals. Mp 192—193°C. UV: λ_{max} (in alc) 238 mμ (log ε 4.18), 297 (4.36), 379 (4.14). Found: C, 32.93; H, 4.15; N, 19.01; S, 43.78%. Required for $C_6H_9N_3S_3$: C, 32.88; H, 4.11; N, 19.18; S, 43.84%.

*6-Dimethylamino-4-methylthio-2-tosylimino-2*H-*1,3,5-thiadiazine (**17**).* To a mixture of the isodithiobiuret (3.2 g) and tosylcarbonimidoyl dichloride (5 g) in 50 m*l* of dry benzene, triethylamine (2 g) was added. The solution was warmed at 50°C for 1 hr and then poured into ice water. The benzene layer was washed with 1N-hydrochloric acid and dried over sodium sulfate. After the solvent had been evaporated, the residue was washed with methanol and recrystallized from acetone. White scalies (1.5 g) were thus obtained. Mp 159—160°C. UV: λ_{max} (in alc) 228 mμ (log ε 4.39), 301 (4.35), 333 (4.28). NMR: (in $CDCl_3$) δ 2.41 ppm (s, 3H, Me), 2.50 (s, 3H, SMe), 3.18, 3.35 (s, s, NMe_2), 7.28 (d, 2H, arom), 7.95 (d, 2H, arom). Found: C, 43.71; H, 4.63; N, 15.72; S, 26.84%. Required for $C_{13}H_{16}N_4O_2S_3$: C, 43.82; H, 4.50; N, 15.73; S, 26.96%.

*6-Dimethylamino-4-methylthio-2-methylsulfonylimino-2*H-*1,3,5-thiadiazine (**18**).* This was prepared by the same method from 3.2 g of the isodithiobiuret, 3.5 g of methylsulfonylcarbonimidoyl dichloride, and 2 g of triethylamine. The yield was 2 g. It was recrystallized from acetone as white scalies. Mp 174—175°C. UV: λ_{max} (in alc) 226 mμ (log ε 4.33), 298 (4.40), 327 (4.29). NMR: (in $CDCl_3$) δ 2.58 ppm (s, 3H, SMe), 3.13 (s, 3H, SO_2Me), 3.22 and 3.39 (s, s, 6H, NMe_2). Found: C, 29.84; H, 4.33; N, 19.95; S, 34.37%. Required for $C_7H_{12}N_4O_2S_3$: C, 30.00; H, 4.29; N, 20.00; S, 34.29%.

BULLETIN OF THE CHEMICAL SOCIETY OF JAPAN, VOL. 45, 3220—3222 (1972)

Studies of Dithiobiurets. II. The Thermal Decomposition of 1,1-Dimethyl-5-acetyl-2,4-dithiobiuret

Isao IWATAKI and Akiyoshi UEDA

Chemical Research Laboratory, Nippon Soda Co., Ltd., Khozu, Odawara

(Received March 2, 1972)

1,1-Dimethyl-5-acetyl-2,4-dithiobiuret (**2**), which is obtained by ordinary acetylation from 1,1-dimethyl-2,4-dithiobiuret (**1**), is thermally unstable and decomposes with a strong acidic odor, even at room temperature, upon standing more than 10 days.

We carried out the decomposition under various conditions and confirmed that a crystalline substance (**3**) was obtained in a 10% yield when **2** was heated at 100°C without a solvent or was refluxed in alcohol or acetone. Compound **3** shows a strong absorption band at 2030 cm^{-1} which corresponds to a SCN or NCS group and a carbonyl band at 1680 cm^{-1} in the infrared spectrum. It is soluble in water or diluted mineral acid and reacts with heavy metal ions, especially the Fe^{3+} ion, showing a pink color. An aqueous solution of it is acidic ($pK_a'=4.5$) and, upon neutralization with potassium carbonate, affords a crystalline substance (**4**) which gives analytical results corresponding to the molecular formula of $C_6H_9N_3OS_2$. Compound **4** is only two hydrogen atoms less than the starting acetyldithiobiuret **2** and still contains a singlet methyl proton at δ 2.35 ppm in addition to the *N,N*-dimethyl peaks in the NMR spectrum, but no absorption band appears in the carbonyl region of the infrared spectrum except for two sharp bands at 1580 and 1600 cm^{-1}. The high-resolution mass spectrum of **3** gave useful information for the structural elucidation of **3**. The molecular ion peak appeared at *m/e* 203; it consisted of $C_6H_9N_3OS_2$. The base peak was *m/e* 161, and the loss of the element of ketene (42 molecular units) was observed.

N,N-Dimethylthiocarbamoyl fragment was absent in **3** and **4**; the fragment peak at *m/e* 88, $Me_2N^+=C=S$, which was prominent in the mass spectrum of **2**, could not be observed in the spectra of **3** and **4**. Meanwhile, **4** was reconverted quantitatively to **3** by the addition of aqueous potassium thiocyanate to an acidic solution of **4**.

From the above results, it is clear that **3** is the hydrothiocyanate of **4**. When **4** was treated with methanolic sodium hydroxide, a yellow crystalline substance **5** was obtained; its molecular formula was identified with that of **4**. Compound **5** shows a carbonyl absorption band at 1710 cm^{-1} in the infrared spectrum, and a new singlet methylene signal appears at δ 4.50 ppm instead of the singlet methyl peak at δ 2.35 ppm

in the NMR spectrum.

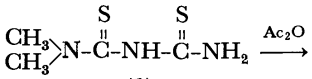

(1)

(2)

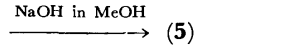

(5)

It showed the same molecular ion peak (*m/e* 203) as those of **3** and **4**, and the presence of the prominent ion peak at *m/e* 88 suggested that the acetylimino-dithiazole system of **3** was rearranged to the *N,N*-dimethylthiocarbamoylthiazoline system. The structure of **5** was confirmed synthetically by the reaction of **1** and monochloroacetyl chloride described previously.[1] The acetyl methyl group in **2** was effected to be very active, and the dithiazole skeleton isomerized to the thiazoline one under alkaline conditions.

Since the starting substance **2** was presumed to be oxidized to yield **4**, **2** was oxidized under various conditions. When **2** was oxidized with iodine in alcohol or acetic acid, deacetylation occurred at the same time and gave the product **6**, which was stable; however, its free base could not be isolated. As for other non-acidic conditions, the potassium-permanganate oxidation of **5** in acetone affords **4** in a 20% yield. When **6** was treated with acetic anhydride in the presence of an equimolar triethylamine, a crystalline substance which was identified with **4** was obtained.

From the above results, the thermal decomposition product **3** from **2** was confirmed to be the hydrothiocyanate of 3-acetylimino-5-dimethylamino-3*H*-1,2,4-dithiazole (**4**).

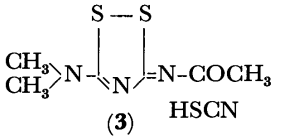

(3) HSCN

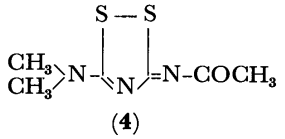

(4)

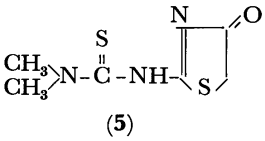

(5)

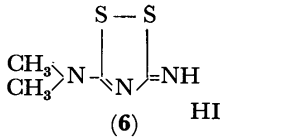

(6) HI

Generally, alkyldithiobiurets were obtained by the reaction of perthiocyanic acid and alkylamines at an ordinary temperature. When perthiocyanic acid was treated with amines at a higher temperature, alkyldithiobiurets were once formed and then decomposed further to yield sulfur, aminothiocyanate, H_2S, *etc.*[2] In the case of **2**, it is presumed that the acetyldithiobiuret **2** is oxidized by oxygen (from air) or isolated sulfur, as is shown in Scheme 1, and that then its salt is formed with the thiocyanic acid which is derived from the decomposition of **2**, as is shown in Scheme 2.

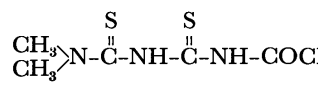

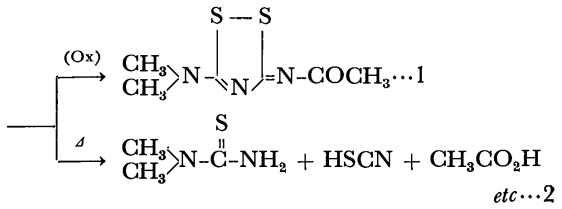

An analogous reaction was observed by Fairfull *et al*, in the preparation of 1-(2-pyridyl)dithiobiuret.[3] They reacted perthiocyanic acid with 2-aminopyridine and thus obtained 2-aminopyridine hydrothiocyanate.

The reaction mechanism from **4** to **5** was considered to be as in the following scheme:

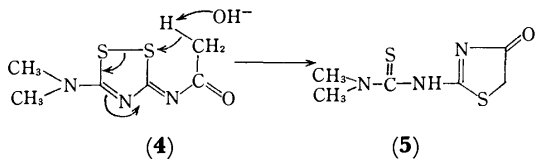

(4) (5)

Experimental

Preparation of Starting Products. 1,1-Dimethyl-2,4-dithiobiuret **1** was prepared from aqueous dimethylamine and perthiocyanic acid by the method of Dixit.[2] 1,1-Dimethyl-5-acetyldithiobiuret **2** was obtained by the standard acetic anhydride-pyridine method.

*The Thermal Decomposition of **2**, the Preparation of 3-Acetylimino-5-dimethylamino-3H-1,2,4-dithiazole **3**.* *Procedure 1*: 1,1-Dimethyl-5-acetyldithiobiuret **2** (10 g) was heated for 1 hr at 100°C in a round-bottomed flask; then a 100 m*l* portion of acetone was added, and the insoluble crystalline substance was filtered off and washed with acetone. Recrystallization from methanol gave 1 g of white needles melting at 183—184°C with decomposition. IR: 2020 cm^{-1} (S-CN), 1690 (C=O), 1610 (C=N). NMR: δ 3.45 ppm (broad s, 6H, NMe_2), 2.18 (s, 3H, Ac). Mass: *m/e* 205, 204, 203, 188, 163, 162, 161, 146, 128, 116, 102, 97. UV: λ_{max} (in alc) 274, 302 mμ. Found: C, 31.65; H, 3.92; N, 21.46; S, 36.20%. Calcd for $C_7H_{10}N_4OS_3$: C, 32.06; H, 3.81; N, 21.37; S, 36.64%.

Procedure 2: A suspended solution of 1,1-dimethyl-5-acetyldithiobiuret **2** (10 g) in 20 m*l* of ethanol was refluxed for 4 hr and then cooled. The solution turned dark red at that time. The precipitated white needles were collected and washed with cold ethanol. The yield was 1.2 g.

Procedure 3: A mixture of the dithiobiuret (10 g) in 50 m*l* of acetone and 5 m*l* of picoline was refluxed for 5 hr, when the precipitate was then collected, 1.2 g of white or pale pink needles were obtained.

*3-Acetylimino-5-dimethylamino-3H-1,2,4-dithiazole **4**. As Obtained from the Hydrothiocyanate **3***: The hydrothiocyanate (2 g) was dissolved in 20 m*l* of 3.5 N-hydrochloric acid and made alkaline with an excess of aqueous potassium carbonate. The white precipitate was filtered and recrystallized from isopropyl alcohol to give 1.4 g of white needles, melting at 160—161°C. IR: 1600, 1570 cm^{-1}. NMR: δ 2.38 ppm (s, 3H, Ac), 3.28, 3.47 (s,s, 6H, NMe_2). UV: λ_{max} (in alc) 298 mμ (log *e* 4.3). Mass: *m/e* 203 (M^+), 161, 141, 97, 82. Found: C, 35.27; H, 4.67; N, 20.68; S, 31.46%. Calcd for $C_6H_9N_3OS_2$: C, 35.47; H, 4.43; N, 20.69; S, 31.53%.

*As Obtained from the Potassium-permanganate Oxidation of **2**.* 1,1-Dimethyl-5-acetyldithiobiuret (1 g) was dissolved in

1) I. Iwataki, This Bulletin, **45**, 3218 (1972).
2) S. N. Dixit, *J. Indian Chem. Soc.*, **38**, 44 (1961).
3) A. E. S. Fairfull and D. A. Peak, *J. Chem. Soc.*, **1955**, 796.

40 ml of acetone, and then 3 g of potassium permanganate in 60 ml of acetone were stirred in, drop by drop, at room temperature. After the manganese dioxide had been filtered off, the solvent was distilled off and the residue was dissolved in water and made alkaline with potassium carbonate. The precipitate was filtered and dried to give 0.2 g of **4**.

As Obtained from the Acetylation of 5-Dimethylamino-3-imino-3H-1,2,4-dithiazole hydroiodide ***6***: The hydroiodide **6** which was prepared by Dixit's method[2] (5 g) was suspended in 20 ml of acetone, and then 5 ml of acetic anhydride and 2 g of triethylamine were stirred in. After 30 minutes, the solution was poured into ice water and neutralized with potassium carbonate to give 3 g of **4**.

The Preparation of the Dithiazole Hydrothiocyanate ***3*** *from* ***4*** *with Thiocyanic Acid.* 3-Acetylimino-5-dimethylamino-3*H*-1,2,4-dithiazole **4** (0.1 g) was dissolved in 3.5 N-hydrochloric acid (3 ml), and then 1 g of potassium thiocyanate in 1 ml of water was added. The white needles thus precipitated were collected. The mp, IR, and NMR coincided with those of **3**.

The Isomerization of ***4*** *to* ***5***, *the Preparation of 2-(3,3-Dimethylthioureido)thiazolin-4-one.* A solution of the dithiazole **4** (0.3 g) in 8 ml of ethanol and 2 ml of 5N-KOH was kept at room temperature for 15 hr, and then poured into ice water and acidified with hydrochloric acid. The precipitate was extracted with chloroform, dried over magnesium sulfate, and evaporated *in vacuo*. Recrystallization from methanol gave 0.1 g of yellow scalies melting at 208—209°C Ref. 1: mp 208—209°C).

BULLETIN OF THE CHEMICAL SOCIETY OF JAPAN, VOL. 45, 3222—3223 (1972)

Studies on the Derivatives of Thiiranes. II.[1] Ring-opening of 2-Alkoxymethylthiiranes and Their Derivatives[2]

Eiichi KAMEYAMA, Motoki NAKAJIMA,* and Tsunehiko KUWAMURA

Department of Synthetic Chemistry, Faculty of Engineering, Gunma University, Tenjincho, Kiryu

(Received May 20, 1972)

2-Chloromethylthiirane (**1**)[3,4] and many other thiiranes[5-7] predominantly yield their corresponding abnormal ring-opening products. We found, however, that **1** predominantly yields a normal ring-opening product by the reaction with hydrogen chloride and chloroxidation.[8] Schwartz[9] later reported a similar results. The reaction of 2-alkoxymethylthiiranes (**2**) with some nucleophilic reagents has been found to yield a normal product.[10]

The present work was undertaken to clarify the ring-opening direction of **2** on chloroxidation and to establish a synthetic route to some alkoxylated sulfonyl compounds from **2**. The reaction of **2** with hydrogen chloride at low temperature exclusively gave a normal product, 1-alkoxy-3-chloropropane-2-thiol (**3**). On chloroxidation in water, **2** and **3** gave the same product, 1-alkoxy-3-chloropropane-2-sulfonyl chloride (**4**).

These results are similar to those for **1**. Dominance of the normal ring-opening on these reactions of **1** and **2** is seemingly due to both polar and steric effects of the substituents on the site of attack on an episulfonium ion intermediate by the nucleophile.[9]

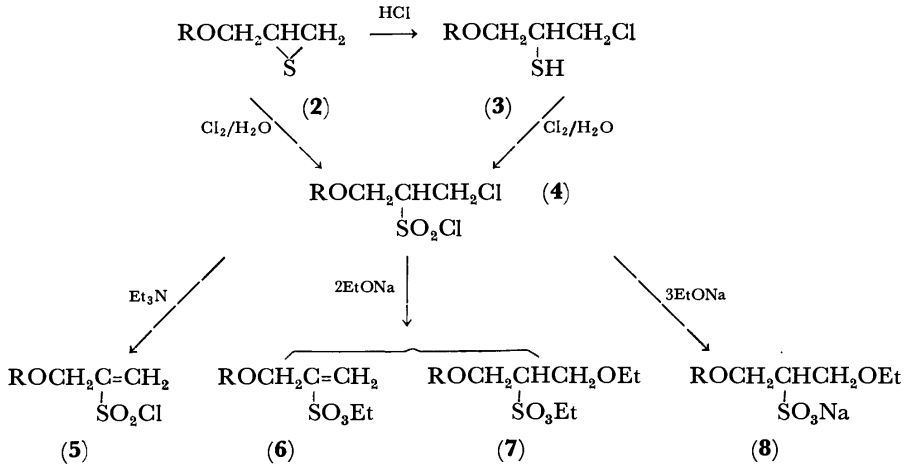

* Present address: Kao Soap Co. Ltd., Sumidaku, Tokyo.

1) Part I of this series: T. Kuwamura, E. Kameyama, and M. Nakajima, This Bulletin, **45**, 1244 (1972).

2) Presented at the 21st Annual Meeting of the Chemical Society of Japan, Osaka, April, 1968.

3) W. Davies and W. E. Savige, *J. Chem. Soc.*, **1951**, 774.

4) J. M. Stewart, *J. Org. Chem.*, **29**, 1655 (1964).

5) W. Davies and W. E. Savige, *J. Chem. Soc.*, **1950**, 317.

6) J. M. Stewart, *J. Org. Chem.*, **28**, 596 (1963).

7) G. Y. Epshtein, I. A. Uson, and S. Z. Ivin, *Zh. Obshch. Khim.*, **33**, 3638 (1963) and *ibid.*, **34**, 1948 (1964).

8) T. Kuwamura, E. Kameyama, M. Nakajima, S. Mishiba, and Y. Onoguchi, presented at the 20th Annual Meeting of the Chemical Society of Japan, Tokyo, March, 1967, Lect. No. 4S111.

9) N. V. Schwartz, *J. Org. Chem.*, **33**, 2895 (1968).

10) R. L. Jacobs and R. D. Schuetz, *ibid.*, **26**, 3472 (1961).

Table 1. The yields, properties and analytical data of the prepared sulfonyl compounds

No.	Compd. R	Yield (%)	Bp (°C/mmHg)	n_D^{25}	Elementary analysis (calcd) C%	H%	S%	Cl%
3	Me	67	67/16	1.4827	34.57 (34.16)	6.43 (6.45)	—	—
3	Et	67	74—76/2	1.4733	39.33 (38.83)	7.17 (7.27)	—	—
4	Me	63	77—78/1	1.4870	23.10 (23.20)	4.04 (3.89)	15.03 (15.48)	34.55 (34.24)
4	Et	64	80/0.5	1.4768	26.81 (27.16)	4.46 (4.56)	14.49 (14.50)	32.13 (32.07)
5	Me	36	53/1	1.4725	28.67 (28.16)	4.23 (4.14)	18.07 (18.79)	21.10 (20.78)
5	Et	50	63/0.5	1.4670	32.27 (32.52)	4.91 (4.90)	16.67 (17.37)	—
6	Et	19	80/1	1.4426	42.88 (43.28)	8.33 (8.26)	16.07 (16.51)	—
7	Et	51	107/1	1.4375	44.52 (44.98)	8.24 (8.39)	13.54 (13.34)	— Na%
8	Et	54	—	—	34.72 (35.89)	6.59 (6.45)	13.71 (13.69)	9.82 (9.82)

On the reaction with a tertially amine and metal alkoxide at low temperature, **4** gave new olefinic sulfonyl compounds and bisalkoxy derivatives, in good yields.

The reactions are summarized in the following scheme. The yields and other data are listed in Table 1.

Although **7** and **8** could also be derived from 2-chloromethylthiirane,[1] the present route is much more advantageous with respect to the yield. Some higher homologues of **8** have been prepared by the same method and found to be highly surface active.[11]

Experimental[12]

Materials. Alkoxymethylthiiranes were prepared from the corresponding glycidylethers by the method of Bordwell and Andersen.[13] The methyl homologue, bp 54—55°C/20 mmHg, n_D^{25} 1.4775. The ethyl homologue, bp 56.5°C/20 mmHg, n_D^{25} 1.4705.

Addition of Hydrogen Chloride to ***2****.* The reactions with anhydrous hydrogen chloride were carried out by the same method as that for the addition to **1**.[1] Spectra of **3**(R: CH_3); IR(neat), 2580(SH), 1118 (C-O-C) cm^{-1}; NMR(in CCl_4), 1.95 (d, 1H, *sec.* SH), 3.30 (s, 3H, CH_3), 3.48—3.69 m, 5H, CH_2 and CH), no triplet band at 1.5—2.0 ppm assignable to a prim. thiol proton[1] could be found.

Chloroxidation of ***2*** *and* ***3****.* The thiirane **2** was added dropwise at −10—5°C to an aqueous solution saturated with chlorine. Concurrently chlorine was bubbled through the mixture at such a rate that an excess was always present. After addition of **2**, chlorine was further bubbled for 1 hr. The heavy oil layer was separated, diluted with ether and then washed successively with water, 5% bisulfite solution and water. The ether solution was distilled in a stream of nitrogen to give **4** in a good yield. Spectra of **4**(R : CH_3); IR(neat), 1380(SO_2), 1170(SO_2), 1120(C-O-C), 757(C-S) cm^{-1}; NMR (in benzene), 3.18(s, 3H, CH_3), 3.75—3.90 (m, 5H, CH_2 and CH).

Chloroxidation of **3** was similarly carried out, giving **4** in 60—70% yield.

*3-Alkoxypropene-2-sulfonyl Chloride (****5****).* An equimolar solution of triethylamine at −50—−40°C was added dropwise to an ether solution of **4**. After being stirred for 1 hr, the mixture was filtered and then distilled to give **5** in 40—50% yield. Spectra of **5**(R : CH_3); IR(neat), 3110 (=CH_2), 1630(C=C), 1370(SO_2), 1183(SO_2), 1105(C-O-C) cm^{-1}; NMR(in CCl_4), A 3.40(s, 3H, CH_3), B 4.30(t, 2H, J_{BC}=1.5, J_{BD}=1.5 Hz, $CH_3OC\underline{H}_2$-), C 6.18(q, 1H, J_{CD} =3.0 Hz, CH_2=C *trans* proton against $-SO_2Cl$), D 6.43 (q, 1H, CH_2=C *cis*).

Reaction of ***4****(R : Et) with Sodium Ethoxide.* When **4** was treated in ethanol with an equimolar solution of ethoxide, **4** remained mostly unreacted and gave a small amount of three unknown products difficult to isolate. A solution of ethoxide(0.1 mol) at −5°C was added dropwise over a period of 30 min with stirring to a solution of **4**(11 g, 0.05 mol) in ethanol(18 m*l*). After the addition, the mixture was centrifuged from the salt and distilled to give two fractions, **6** (1.8 g) and **7**(5.4 g). Spectra of **6**; IR(neat), 3120(=CH_2), 1650(C=C), 1350(SO_2), 1160(SO_2), 1105(C-O-C-), 800(C-S) cm^{-1}; NMR(in CCl_4), A 1.23(t, 3H, $C\underline{H}_3CH_2OCH_2$), B 1.38(t, 3H, $C\underline{H}_3CH_2O_3S$), C 3.57(q, 2H, J_{AC}=7.0 Hz, $CH_3C\underline{H}_2OCH_2$), D 4.14(q, 2H, J_{BD}=7.0 Hz, $CH_3C\underline{H}_2O_3S$), E 4.18(t, 2H, $EtOC\underline{H}_2$), F 6.09(t, 1H, J_{EF}=1.0, J_{FG}=1.0 Hz, CH_2=C *trans* proton against $-SO_3Et$), G 6.25(t, 1H, J_{EG} =1.0 Hz, CH_2=C *cis*).

A 3-fold molar quantity of ethoxide relative to **4** was added in the same manner. The mixture was stirred for 10 hr at 25—30°C, neutrallized, centrifuged and evaporated. The residue was recrystallized three times from acetone to yield the pure product **8**. The IR and NMR spectra of **7** and **8** agreed with those of the same products[1] derived from **1**.

11) E. Kameyama, M. Nakajima, A. Ozaki, and T. Kuwamura, *Yukagaku*, **20**, 32 (1971).

12) Boiling points are uncorrected. Measurements of 60 MHz NMR and glc analysis were carried out in the same manner as given in the previous report.[1] Chemical shifts are presented by δ from TMS.

13) F. G. Bordwell and H. M. Andersen, *J. Amer. Chem. Soc.*, **75**, 4959 (1953).

BULLETIN OF THE CHEMICAL SOCIETY OF JAPAN, VOL. 45, 3224—3225 (1972)

Free-Radical Chlorination of Alkylsilanes. VII.* The Hydrogen Abstraction from 1-Silabicyclo[2.2.1]heptane by the Trichloromethyl Radical

Yoichiro NAGAI, Shin-ichi INABA, Hideyuki MATSUMOTO, and Hamao WATANABE

Department of Chemistry, Gunma University, Kiryu, Gunma

(Received May 22, 1972)

In general, carbon free radicals are assumed to have either the pyramidal configurations undergoing rapid inversion, or the planar structures, so that the bridgehead carbon radicals are formed only with difficulty.[1] For example, the homolytic chlorination of norbornane results in the formation of 2-chloronorbornane exclusively, the 1-chloro isomer being not formed in any appreciable amount.[2] In harmony with this fact, Applequist and Kaplan[3] reached a conclusion that the 1-bicyclo[2.2.1]heptyl radical is less stable than simple alkyl radicals from their results of the decarbonylation of aliphatic and bridgehead aldehydes. In constrast, simple silyl radicals tend to maintain the original tetrahedral geometry without turning itself inside out, and some spectroscopic evidence supporting this point has recently been obtained by several workers.[4–6] Also, two groups of workers[7,8] have reported that silyl radicals, consistent with their tetrahedral structures, abstract a chlorine atom from carbon tetrachloride with high retention of configuration. These preceding evidences might lead to an assumption that the 1-silabicyclo[2.2.1]hept-1-yl radical would readily be formed by the hydrogen abstraction from the corresponding bridgehead hydrosilane, but confirmation of this hypothesis must provide a desirable research objective. The present paper describes the homolytic hydrogen-chlorine exchange reaction between 1-silabicyclo[2.2.1]heptane and carbon tetrachloride which involves the hydrogen abstraction by the trichloromethyl radical from the bridgehead silicon hydride, the silicon analogue of norbornane.

Experimental

All the boiling and melting points are uncorrected. Spectral data of the bicyclic silicon hydride and chloride are presented in Table 1.

1-Silabicyclo[2.2.1]heptane. This compound was prepared by the method of Sommer and Bennett.[9] The pure product was a white crystalline solid which sublimed very readily and had mp 75°C in a sealed tube (lit.[9] mp 63°C)[10]

Chlorination of 1-Silabicyclo[2.2.1]heptane with Carbon Tetrachloride. Chlorination procedures were essentially the same as described previously.[11–13] Results obtained are summarized in Tables 2 and 3.

Results and Discussion

1-Silabicyclo[2.2.1]heptane was heated with carbon tetrachloride at 80°C in the presence or absence of benzoyl peroxide. As is seen from Table 2, the hydrogen-chlorine exchange reaction between the bridgehead hydrosilane and carbon tetrachloride readily occurs under homolytic conditions, giving a pair of the expected products, the corresponding chlorosilane and chloroform. The reaction can most pro-

TABLE 1. NMR, IR AND MASS SPECTRA OF THE BICYCLIC SILICON COMPOUNDS

Compound	NMR, δ, ppm	IR, cm^{-1} (intensity)	MS, *m/e* (rel. intensity)
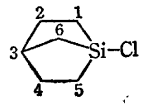	0.73 (H^1, H^5 and H^6; 6H), 1.87 (H^2 and H^4; 4H), 2.26 (H^3; 1H)	2955(s), 2920(s), 2150(s), 1445(w), 1406(w), 1250(w), 1154(m), 1142(w), 1134(w), 1100(w), 1055(m), 987(w), 928(w), 898(w), 882(w), 854(s)	114(8), 113(23), 112(54), 111(34), 85(40), 84(100), 83(77), 82(58), 56(92), 55(62), 43(60)
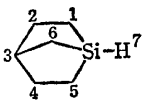	0.50 (H^1, H^5 and H^6; 6H), 1.63 (H^2 and H^4; 4H), 2.33 (H^3; 1H), 4.51 (H^7; 1H), $J(^{29}Si\text{-}H) = -205.8$ Hz	2940(s), 2900(s), 1435(w), 1393(m), 1143(m), 1135(w), 1127(w), 1093(w), 1046(s), 972(w), 920(w), 888(w), 826(s), 813(s), 780(m), 743(w), 701(m)	148(19), 146(52), 120(36), 119(44), 118(100), 117(94), 92(15), 90(33), 82(28), 65(26), 63(45)

* For Part VI, see Ref. 16.

1) W. A. Pryor, "Free Radicals," McGraw-Hill, New York (1966), p. 28.
2) J. D. Roberts, L. Urbanek, and R. Armstrong, *J. Amer. Chem. Soc.*, **71**, 3049 (1949).
3) D. P. Applequist and L. Kaplan, *ibid.*, **87**, 2194 (1965).
4) P. J. Krusic and J. K. Kochi, *ibid.*, **91**, 3938 6161 (1969).
5) A. Hudson and H. A. Hussain, *Mol. Phys.*, **16**, 199 (1969); Idem, *J. Chem. Soc., B*, **1969**, 793.
6) S. W. Bennett, C, Eaborn, R. A. Jackson, and K. D. J. Root, *J. Chem. Soc., A*, **1970**, 348.
7) H. Sakurai, M. Murakami, and M. Kumada, *J. Amer. Chem. Soc.*, **91**, 519 (1969).
8) A. G. Brook and J. M. Duff, *ibid.*, **91**, 2118 (1969).
9) L. H. Sommer and O. F. Bennett, *ibid.*, **79**, 1008 (1957).
10) Our value of mp is some 12°C higher than that of Sommer and Bennett, but the purity of our sample was confirmed by glpc to be not less than 99%.
11) Y. Nagai, K. Yamazaki, N. Kobori, and M. Kosugi, *Nippon Kagaku Zasshi*, **88**, 793 (1967).
12) Y. Nagai, K. Yamazaki, I. Shiojima, and M. Hayashi, *J. Organometal. Chem.*, **9**, p. 21 (1967).
13) Y. Nagai, K. Yamazaki, I. Shiojima, H. Matsumoto, and S. Nakaido, *Yuki Gosei Kagaku Kyokai Shi*, **26**, 884 (1968).

Table 2. The reaction of 1-silabicyclo[2.2.1]heptane with carbon tetrachloride at 80°C for 10 hr

Without BPO		With BPO	
Reactants	(mmol)	Reactants	(mmol)
$C_6H_{12}Si$	(1.42)	$C_6H_{12}Si$	(1.51)
CCl_4	(2.73)	CCl_4	(3.33)
BPO	(none)	BPO	(0.02)
Products	(mmol)	Products	(mmol)
$C_6H_{12}Si$	(1.32)	$C_6H_{12}Si$	(0.44)
CCl_4	(2.54)	CCl_4	(2.04)
$C_6H_{11}SiCl$	(trace)	$C_6H_{11}SiCl$	(0.97)
$CHCl_3$	(trace)	$CHCl_3$	(1.09)

Table 3. Competitive chlorinations of 1-silabicyclo [2.2.1]heptane (A) and triethylsilane (B) with carbon tetrachloride (80°C)[a)]

$[A]_{i'}$ mmol	$[A]_{f'}$ mmol	$[B]_{i'}$ mmol	$[B]_{f'}$ mmol	$[CCl_4]_{i'}$ mmol	k_A/k_B
1.13	0.681	1.20	0.382	12.19	0.442
1.12	0.665	1.23	0.353	12.43	0.452
				Av.	0.447

a) $[A]_{i'}$ $[B]_{i'}$ represent the initial concentrations of two hydrosilanes, $[A]_{f'}$ $[B]_{f'}$ the final concentrations and k_A/k_B the ratio of rate constants for the attack of the abstracting reagent on the two species.

bably be explained in terms of the following chain carrying processes and thus confirms an anticipation previously raised that the SiH hydrogen atom at the bridgehead position can be abstracted by carbon radicals with ease.

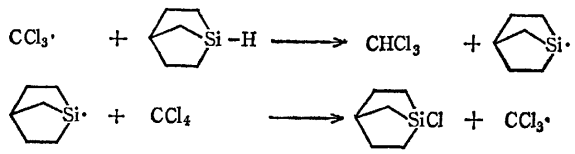

The reactivity of the bicyclic silicon hydride toward the trichloromethyl radical was next determined by competition experiments. A mixture of 1-silabicyclo-[2.2.1]heptane and triethylsilane was allowed to react with carbon tetrachloride at 80°C in the presence of benzoyl peroxide. The relative rate was calculated with the equation of Ingold and Shaw[14] from concentrations of the reactants or products as determined by glpc (Table 3). Results show that 1-silabicyclo-[2.2.1]heptane reacts with carbon tetrachloride 0.45 times as fast as triethylsilane. The hydrogen abstraction rate from the bridgehead silicon hydride was thus found to be comparable to that from its open chain analogue, triethylsilane.* However, it is noteworthy that the bridgehead hydride reacts distinctly slower than triethylsilane. This trend cannot be explained

14) C. K. Ingold and F. R. Shaw, *J. Chem. Soc.*, **1927**, 2918.

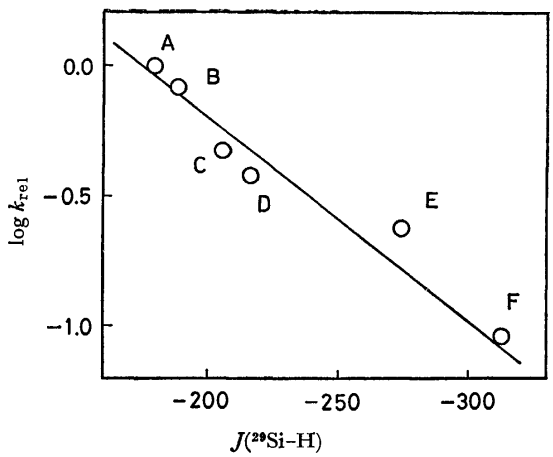

Fig. 1. A plot of relative rates for reactions of hydrosilanes toward the trichloromethyl radical (80°C) *versus* $J(^{29}Si-H)$. (A): Et_3SiH, (B): $PhMe_2SiH$, (C): 1-silabicyclo[2.2.1]-heptane, (D): Et_2ClSiH, (E): $EtCl_2SiH$, (F): Cl_3SiH.

on the basis of electronic effects of substituents alone, since there is by no means expected any appreciable difference in the magnitude of the electronic effect between the bridgehead and open chain structures. An attractive explanation for the observed reactivity of the bicyclic system can be advanced, however, by taking into consideration the change in bond hybridization at the bridgehead silicon atom. The fraction of *s* character employed by the silicon in its bond to hydrogen[15] would be forced to increase by special geometrical situation which exists. This was found to be the case as indicated by the large value (in the absolute sence) of $J(^{29}Si-H)$ for 1-silabicyclo-[2.2.1]heptane, −205.8 Hz, compared to that for triethylsilane, −179.6 Hz. It should be noted at this point that the relative reactivities of a variety of Si-H bonds toward the trichloromethyl radical are linearly correlated with values of $J(^{29}Si-H)$ which reflect the magnitude of *s* character employed by silicon in the Si-H bonds.[16] In view of this relationship, data for the bridgehead silicon hydride were treated in a similar fashion (Fig. 1). Obviously, the point for 1-silabicyclo[2.2.1]heptane falls on the straight line with a reasonable precision and this fact again indicates that the trichloromethyl radical preferentially attacks a Si-H bond of smaller *s* character. More significant is that the special conformation modifies the electronic structure and hence the reactivity of the molecule to some appreciable extent.

15) Y. Nagai, M. Ohtsuki, T. Nakano, and H. Watanabe, *J. Organometal. Chem.*, **35**, 81 (1972).

16) Y. Nagai, H. Matsumoto, M. Hayashi, E. Tajima, and H. Watanabe, This Bulletin, **44**, 3113 (1971).

* **Note added in proof.** After this paper was accepted for publication, we were informed that Sommer and Ulland reported similar kinetic measurements of the bicyclic silicon hydride under very nealy the same conditions: see *J. Amer. Chem. Soc.*, **94**, 3803 (1972). Their figures are in almost complete agreement with ours.

BULLETIN OF THE CHEMICAL SOCIETY OF JAPAN, VOL. 45, 3226—3227 (1972)

Inositol Derivatives. VI. Convenient Synthesis of DL-*proto*-Quercitol from *myo*-Inositol

Tetsuo SUAMI, Seiichiro OGAWA, Tsunehisa UEDA, and Hayashi UCHINO

Department af Applied Chemistry, Faculty of Engineering, Keio University, Hiyoshi, Yokohama

(Received June 8, 1972)

(+)-*proto*-Quercitol was discovered in acorns in 1849,[1] and its configuration was established in 1932,[2] whereas, levorotatory isomer remained unknown until 1961.[3] Plouvier[3] prepared a racemic form of *proto*-quercitol by mixing an equal weight of the two enantiomers, and it was shown to exist as a solid solution.

The total synthesis of (−)-*proto*-quercitol was first accomplished in 1966 by McCasland and his coworkers[4] starting from quebracitol or, somewhat less conveniently from (−)-*chiro*-inositol. Their identical procedure applied to (+)-*chiro*-inositol should lead to (+)-*proto*-quercitol, and, similarly, DL-*proto*-quercitol should be synthesized from DL-*chiro*-inositol.

Since we require large quantities of DL-*proto*-quercitol in order to synthesize deoxyinosadiamines and pseudo sugars of biological interest, we have been studying its alternative and facile preparation from *myo*-inositol. In the present paper, we wish to report the convenient synthesis of DL-*proto*-quercitol from readily avairable DL-1,2-anhydro-5,6-*O*-cyclohexylidene-*chiro*-inositol (**2**).[5]

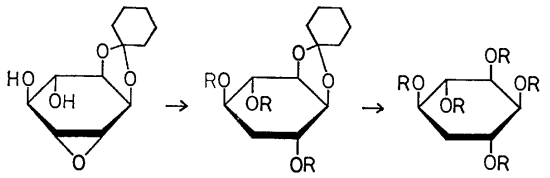

2 **3a** R=H **b** R=Ac **4a** R=H **b** R=Ac

Treatment of DL-1,2-*O*-cyclohexylidene-3-*O*-*p*-tolylsulfonyl-*myo*-inositol (**1**)[6] in methanol with a slight excess of sodium methoxide gave **2** almost exclusively in 86% yield. Reduction of **2** with lithium aluminum hydride in tetrahydrofuran at refluxing temperature for 4 hr gave DL-1,2-*O*-cyclohexylidene-4-deoxy-*muco*-inositol (**3a**) predominantly in 87% yield, which was converted into the tri-*O*-acetyl derivative (**3b**) in the usual way. Hydrolysis of **3a** with boiling 6N hydrochloric acid gave crystals of DL-*proto*-quercitol (**4a**) in 80% yield. The crystalline pentaacetate (**4b**) was also prepared from **4a**.

Assuming that an epoxide-migration occurred under the reduction condition, two stereoisomers of deoxyinositols should be formed from **2**; namely, DL-*proto*- and DL-*vibo*-quercitols. In the proton magnetic resonance (PMR) spectrum of **4b** in deuteriochloroform ($CDCl_3$), the signals of five acetyl methyl protons appeared as three singlets at τ 7.86, 7.97, and 7.99 in the relative intensities of 2 : 2 : 1, which could be assigned to the signals of two axial, two equatorial and one equatorial acetoxy groups, respectively.[7] Therefore, the spectrum was not compatible with the *vibo*-configuration, since it has only one axial acetoxy group. Moreover, an authentic sample of the pentaacetate of DL-*vibo*-quercitol[8] was proved to be different from **4b** in all respect.

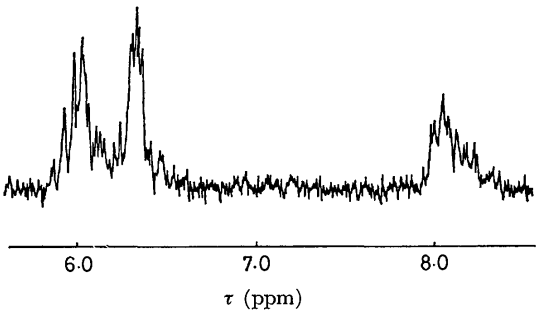

Fig. 1. PMR spectrum of DL-*proto*-quercitol (**4a**) in D_2O at 60 MHz,

The PMR spectrum of **4a** in deuterium oxide (D_2O) was shown to be identical with that of (−)-*proto*-quercitol reported by McCasland[9] (Fig. 1). Consequently, the structure of **4a** was established unequivocally, and it was found that the reduction of **2** with lithium aluminum hydride proceeded almost stereospecifically to afford **3a**. The overall yield of **4a** from **1** was 60%.

Experimental

Melting points were determined on a Mitamura Riken micro hot stage and are uncorrected. PMR spectra were measured on a Varian Associates A-60D (60 MHz) spectrometer with tetramethylsilane as an internal standard. Chemical shifts are expressed in τ-values. Thin layer chromatography (tlc) was done with silica gel (Wakogel B-10, Wako pure chemical industries Ltd.) and the compounds were detected by heating after spraying 50% sulfuric acid.

DL-*1,2-Anhydro-5,6-O-cyclohexylidene*-chiro-*inositol* (*2*). This compound was prepared from DL-1,2-*O*-cyclohexylidene-3-*O*-*p*-tolylsulfonyl-*myo*-inositol (**1**)[6] in 86% yield, following the procedure previously mentioned.[5]

1) H. Braconnot, *Ann. Chem. et Phys.*, **27**, 392 (1849).
2) T. Posternak, *Helv. Chim. Acta*, **15**, 948 (1932).
3) V. Plouvier, *C. R. Acad. Sci. Paris*, **253**, 3047 (1961).
4) G. E. McCasland, M. O. Naumann, and L. J. Durham, *Carbohyd. Res.*, **4**, 516 (1967); *J. Org. Chem.*, **33**, 4220 (1968).
5) T. Suami, S. Ogawa, S. Oki, and K. Ohashi, This Bulletin, **45**, 2597 (1972).
6) T. Suami, S. Ogawa, T. Tanaka, and T. Otake, *ibid.*, **44**, 835 (1971).
7) F. W. Lichtenthaler and P. Emig, *Carbohyd. Res.*, **7**, 121 (1968).
8) G. E. McCasland and E. C. Horswill, *J. Amer. Chem. Soc.*, **75**, 4020 (1953).
9) G. E. McCasland, "Deoxy Sugars," ed. by P. F. Gould, American Chemical Society (1968), p. 51.

DL-*1,2*-O-*Cyclohexylidene-4-deoxy*-muco-*inositol* (**3a**). To a solution of **2** (7.5 g) in dry tetrahydrofuran (350 m*l*) was added lithium aluminum hydride (5.0 g) in dry tetrahydrofuran (50 m*l*) and the mixture was refluxed for 4 hr. After cooling, water (30 m*l*) was added dropwise to destroy the excess of metal hydride. The solution was allowed to stand overnight at room temperature, and then the white precipitates were collected by filtration. The filtrate was evaporated to give a crystalline residue which was digested with ethanol and filtered to afford practically pure **3a** (5.2 g, 71%), mp 164—166°C. An additional crop (1.2 g, 87%) was recovered by extraction from dried white precipitates using Soxhlet extractor with tetrahydrofuran. An analytical sample was obtained by recrystallization from ethanol, mp 165—167°C. Tlc indicated a single spot (methyl ethyl ketone-toluene=1 : 1 volume).

Found: C, 58.97; H, 8.11%. Calcd for $C_{12}H_{20}O_5$: C, 59.00; H, 8.25%.

The tri-*O*-acetyl derivative (**3b**) was prepared by treatment of **3a** with acetic anhydride and pyridine at room temperature in a quantitative yield. Recrystallization from ethanol gave a pure sample, mp 103—104°C. Tlc indicated a single spot (methyl ethyl ketone-toluene=1 : 10 volume). PMR ($CDCl_3$): τ 4.57 (1, quartet, H-3, J=3.0 Hz), 7.89, 7.92, 7.98 (3, singlet, OAc).

Found: C, 58.71; H, 7.03%. Calcd for $C_{18}H_{26}O_8$: C, 58.37; H, 7.08%.

DL-proto-*Quercitol* (**4a**). Compound **3a** (1.0 g) was treated with boiling 6N hydrochloric acid (20 m*l*) for 2 hr. Then the mixture was evaporated to dryness to give an oily product which was crystallized from ethanol-water to give crystals (540 mg, 80%) of **4a**, mp 208—215°C (decomp.). Recrystallization from the same solvent afforded an analytically pure sample, mp 236.5—238°C (lit,[4] mp 238—239°C). The PMR spectrum in D_2O was superimposable with that of an authentic sample of (−)-*proto*-quercitol reported by McCasland.[9]

Found: C, 44.01; H, 7.12%. Calcd for $C_6H_{12}O_5$: C, 43.90; H, 7.37%.

DL-proto-*Quercitol Pentaacetate* (**4b**). Compound **4a** (50 mg) was acetylated with acetic anhydride (5 m*l*) and pyridine (5 m*l*) overnight at room temperature. The mixture was evaporated to give an oily product which was crystallized from ethanol to give pure crystals (73 mg, 63%) of **4b**, mp 114—116.5°C. Tlc indicated a single spot (methyl ethyl ketone-toluene=1 : 10 volume).

Found: C, 51.63; H, 5.81%. Calcd for $C_{16}H_{22}O_{10}$: C, 51.33; H, 5.92%.

The authors are grateful to Professor Sumio Umezawa for his kind advice, and to Mr. Saburo Nakada for his elementary analyses. The authors thank Professor G. E. McCasland for an identification of DL-*proto*-quercitol by mixed melting point determination. The financial support from the Ministry of Education for this work is gratefully acknowledged.

SHORT COMMUNICATIONS

Three Crystalline Phases of Octachloropropane as Evidenced by Chlorine NQR

Masao HASHIMOTO and Koichi MANO*

Department of Chemistry, Faculty of Science, Kobe University, Nada-ku, Kobe

** Research Institute for Atomic Energy, Osaka City University, Sumiyoshi-ku, Osaka*

(Received July 3, 1972)

In this communication, we wish to report the existence of three crystalline phases of octachloropropane (OCP), found by means of the NQR technique.

The experimental procedures of NQR measurements have been reported previously.[1] For the NQR experiments, a purified sample was used.[2] The sample was fused and packed in an ampoule.

The experimental results are given in Table 1, in which we can see that OCP posesses three crystalline phases (α, β, and γ). The phases were prepared by the following procedures:

The α phase. OCP was once sufficiently cooled at 77°K in the ampoule; next, it was left to stand at about 245°K and finally at 196°K for twenty minutes each. The last two procedures were repeated several times. Subsequent cooling in liquid nitrogen yielded the α spectrum.

The β phase. After the sample tube has been left to stand at room temperature for two days, it was immersed in a dry ice-petroleum ether bath (196°K) and then left to stand at the same temperature for two hours. Subsequent cooling in liquid nitrogen yielded the β spectrum.

The γ phase. After the sample has been once completely fused, the sample tube was immediately thrown into a dry ice-petroleum ether bath and left to stand at the same temperature for fifteen minutes. Subsequent cooling in liquid nitrogen yielded the γ spectrum.

The NQR spectrum of OCP has already been reported by Zeil and Haas.[3] Their results are also shown in Table 1. It can be seen in Table 1 that none of the three spectra, α, β, or γ, coincide with the Zeil's results. After certain annealings, we frequently observed an NQR spectrum corresponding to a mixture of the α and γ phases.[4] In this connection, it should be noted that Zeil's results are in rather good agreement with a superposition of the lower-frequency parts of the α and γ spectra.

Our DSC experiments showed that OCP posesses a plastic crystalline phase at room temperature (mp: *ca.* 433°K, ΔH_{mp}: *ca.* 560 cal/mol, and ΔS_{mp}: *ca.* 1.3 e. u.).[5] This is consistent with the apparent plasticity of OCP at room temperature and with the fact that the NQR signals were not observed at room temperature.[6,7]

Details of the NQR and DSC studies will be reported in a later publication.

TABLE 1. ^{35}Cl NQR FREQUENCIES OF OCTACHLOROPROPANE AT LIQUID NITROGEN TEMPERATURE

	No.	Frequency (MHz)	Relative Intensity
α Spectrum[a]	ν_1	41.457	4
	ν_2	41.322	4
	ν_3	41.261	4
	ν_4	41.183	10
	ν_5	41.089	2
	ν_6	40.991[b]	6
	ν_7	40.991[b]	6
	ν_8	40.764	4
β Spectrum	ν_1	41.454	10
	ν_2	41.270	3
	ν_3	41.173	8
	ν_4	41.112	8
	ν_5	40.994	4
	ν_6	40.890	6
	ν_7	40.845	10
	ν_8	40.795	6
γ Spectrum	ν_1	41.570	10
	ν_2	41.445	8
	ν_3	41.069	7
	ν_4	41.060	7
	ν_5	40.932	6
	ν_6	40.857	6
	ν_7	40.760	6
	ν_8	40.643	6
Zeil's result[c]		41.180	
		41.056	
		41.046	
		40.932	
		40.850	
		40.765	
		40.750	
		40.637	

a) The intensity of the α spectrum is so much stronger than those of the β and γ spectra that all the resonance lines were observable on an oscilloscope screen. b) This degeneracy was confirmed by the temperature dependence of the resonance frequencies. c) Ref. 3.

1) M. Hashimoto and K. Mano, This Bulletin, **45**, 706 (1972).

2) The gas chromatographic analysis of the sample showed a purity of approx. 99.5%.

3) W. Zeil and B. Haas, *Z. Naturforsch.*, **23a**, 1225 (1968).

4) After certain annealings the DSC curves on heating (from 113 to 253°K) showed four thermal anomalies, one of which was observed as an exothermic peak. The results of the DSC experiments, however, are rather complicated and depend strongly on the thermal conditions. This may be correlated to the observations of the superpositions of the NQR spectra.

5) J. Timmermans, *J. Chim. Phys.*, **35**, 331 (1938).

6) H. S. Gutowsky and D. W. McCall, *J. Chem. Phys.*, **32**, 548 (1960).

7) S. Kondo, This Bulletin, **39**, 249 (1966).

Complexes of Copper(II) with Cyclodextrins

Yoshihisa MATSUI, Toyoaki KURITA, and Yoshio DATE

Department of Agricultural Chemistry, Faculty of Agriculture, Shimane University, Nishikawazu, Matsue

(Received June 22, 1972)

It is known that a number of organic and inorganic substances are enclosed and fixed within the void spaces of cyclodextrins, thus forming inclusion compounds.[1] However, the inclusion of metal cations in the dextrins has never been studied. We wish here to report that copper(II) reacts with cyclodextrins in alkaline solutions to form soluble complexes.

When two aqueous solutions, 0.2 N NaOH and 0.02 M $CuSO_4$, of an equal volume were mixed, the precipitate of $Cu(OH)_2$ formed immediately. The supernatant was virtually colorless and contained no appreciable amount of Cu(II) (below 10^{-5} M). However, upon the addition of β-cyclodextrin (I) to the mixture, a part of the precipitate was dissolved and the supernatant became blue. The concentration of the dissolved Cu(II) was titrimetrically determined by the use of EDTA and murexide, as a titrant and an indicator respectively, after the neutralization of the supernatant by an aqueous HCl. The Cu(II) concentration determined was then plotted against the concentration of I added (Fig. 1, Plot a). It is obvious that

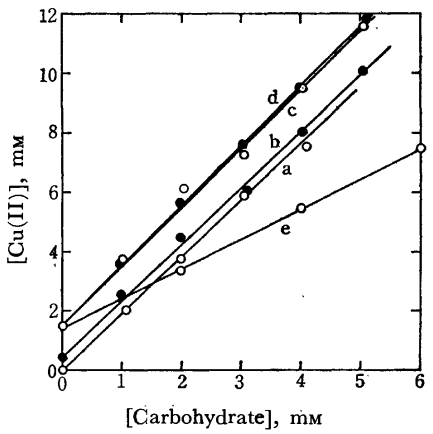

Fig. 1. Plots of the concentration of the dissolved Cu(II) *vs.* those of carbohydrates added.
a, I in 0.1 N NaOH; b, I in 0.5 N NaOH; c, I in 1 N NaOH; d, II in 1 N NaOH; e, III in 1 N NaOH

the plot is linear with the slope of *ca.* 1.9. Similar plots were obtained in solutions more basic than 0.1 N NaOH (Fig. 1, Plots b and c), although a small amount of Cu(II) had been dissolved before the addition of I. The results indicate that Cu(II) forms a complex with I in which two Cu(II) ions are bound to a molecule of I (2 : 1 complex).

The Cu(II)-I complex was isolated from a solution. When 10 m*l* of ethanol was added to 12 m*l* of 2 N NaOH containing 0.01 M I and 0.02 M $CuSO_4$, blue crystal were precipitated; they were then filtered off, washed with aqueous ethanol, and dried *in vacuo*. The content of Cu(II) in the crystals was titrimetrically determined to be 0.59 mmol/g. The content of I was estimated to be 0.29 mmol/g by the measurement of the optical rotation of an aqueous solution of the crystals buffered at pH *ca.* 7, where the complex dissociates into I and Cu(II). In this estimation, the specific rotation of I was taken to be 162.5°.[1] The results also show the formation of the 2 : 1 Cu(II)-I complex.

The dissolution of $Cu(OH)_2$ in an alkaline solution also took place on the addition of α-cyclodextrin(II) or of methyl-α-D-glucopyranoside(III). In each case, the plot of the concentration of the dissolved Cu(II) *vs.* that of the carbohydrate added is linear (Fig. 1, Plots d and e). The slope of the plot for II was 2.0, while it was 1.0 for III. This shows that Cu(II) forms 2 : 1 and 1 : 1 complexes with II and III respectively.

The structures of the Cu(II)-I and -II complexes are presumed to be as is shown schematically in Fig. 2.

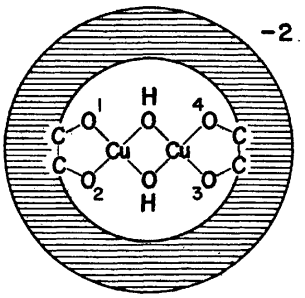

Fig. 2. Schematic structure of the Cu(II)-cyclodextrin complex.

The two pairs of C-2 and C-3 secondary hydroxyl groups of I and II may be ionized and cross-linked by the $Cu(OH)_2Cu$ ion bridge. Such a coordination of 1,2-diols to Cu(II) has often been reported to occur in alkaline solutions.[2] Since each bond length of Cu–O may be about 2 Å,[3] the distance between the oxygen atoms numbered 1 and 3 may be about 6.3 Å; this agrees well with the internal diameter (6 Å[4]) of the void of II. Thus, it seems that the $Cu(OH)_2Cu$ bridge is tightly fixed within the void of II. In the Cu(II)-I complex, the length of the $Cu(OH)_2Cu$ bridge may be somewhat shorter than the internal diameter (7.5 Å[4]) of the void of I. Hence, the direction of the bridge may not coincide with that of the internal diameter. In the Cu(II)-III complex, two molecules of III may be coordinated to both ends of the $Cu(OH)_2Cu$ bridge to form the 2 : 2 Cu(II)-III complex. The structures of the complexes will be discussed further in a subsequent communication.

The spectra of the Cu(II)-I and -II in 0.1 N NaOH at 25°C are characterized by maxima at 668 mμ ($\varepsilon=128\pm1$) and 666 mμ ($\varepsilon=118\pm1$) respectively.

1) D. French, *Advan. Carbohyd. Chem.*, **12**, 189 (1957).

2) R. E. Reeves and P. Bragg, *J. Amer. Chem. Soc.*, **84**, 2491 (1962).

3) H. Koyama, Y. Saito, and H. Kuroya, *J. Inst. Polytech., Osaka City Univ.*, **4**, Ser. C, 43 (1953).

4) F. Cramer, W. Saenger, and H.-Ch. Spatz, *J. Amer. Chem. Soc.*, **89**, 14 (1967).

Novel Radical Salts Polymer Catalyst Carrying Enhanced Para-Ortho-Hydrogen Conversion

Kentaro MURANO, Hiroshi KAWAZURA,* Hiroo INOKUCHI, and Toshio OHMORI*

The Institute for Solid State Physics, The University of Tokyo, Roppongi, Tokyo

** Research Laboratory, Japan Synthetic Rubber Co., 7569, Ikuta, Kawasaki*

(Received July 12, 1972)

The catalytic behaviour of aromatics-alkali metal ion radical salts has been extensively studied since the disclosure of the catalytic activity of the tetracyanopyrene-cesium complex in the hydrogen-deuterium exchange reaction.[1] In this paper, we will establish that novel polymeric radical salts obtained by alkali metal insertion into poly(tetrahalophenylene sulphide)s and into semiconducting materials derived therefrom exhibit a strongly enhanced catalytic activity in para-ortho-hydrogen conversion.

The poly(tetrahalophenylene sulphide)s were prepared by the careful polycondensation of sodium pentahalothiophenoxide, while the semiconducting materials were obtained by dehalogenating poly(tetrahalophenylene sulphide)s in the presence of polar solvent such as pyridine at about 200°C. A possible structure of these semiconducting materials as likely to consist of a dibenzothiophene nucleus was suggested in a preceding paper,[2] along with the details of their preparations.

The radical salts complexes were easily obtained by placing the poly(tetrahalophenylene sulphide)s or the semiconducting materials in contact with alkali metal vapour in vacuum at the evaporation temperature of the alkali metal.

Table 1 shows the characteristics of the resulting complexes, which were obtained by inserting the Cs metal into the acceptor polymers to approximately saturation amounts. In spite of much occlusion of the Cs metal, the resulting complexes were stable in air—*i.e.*, they were not inflammable and did not show a rapid decomposition, though they absorbed much gaseous oxygen and humidity,—contrary to the generally-accepted idea of the unstable character of the organic-alkali metal ion salts. It is apparent that the stability of the complexes does not depend on the fact that the acceptor is simply polymeric, since we have confirmed that the complexes[3] of alkali metal poly(phenylene oxide) and alkali metal poly(phenylene sulphide), which constitute the basic skeleton of the poly(tetrahalophenylene sulphide)s, cause a rapid decomposition when in contact with air. The stability may be due to some specific structure of the semiconducting materials formed by the dehalogenation of the poly(tetrahalophenylene sulphide)s.

The para-ortho-hydrogen conversion on these complexes as catalysts was conducted in a manner analogous with that preported previously.[4] The same table, Table 1, summarizes the rate constants of the hydrogen conversion obtained by assuming a first-order reaction and the activation energies of the conversion. As is seen from Table 1, the rate constants in the range of 10^{-1}—10^{0} min^{-1} are obviously extraordinarily high, since the rate constants of the radical-salt catalysts so far studied have lain in the range of 10^{-2}—10^{-4} min^{-1}.[5]

At any rate, the high rate constants indicate enhanced catalytic activities of the present complexes in hydrogen-participating reactions. Applications of the present new catalysts to these reactions are in progress, along with the more precise elucidation of the relation between the para-ortho-hydrogen conversion and their structures.

TABLE 1. THE ELECTRICAL RESISTIVITY, THE SPIN CONCENTRATION, THE RATE CONSTANT (k), AND ITS ACTIVATION ENERGY (E) OF THE PARA-ORTHO-HYDROGEN CONVERSION OF POLY(TETRAHALOPHENYLENE SULPHIDE)-Cs AND THE SEMICONDUCTIVE POLYMER-Cs COMPLEX

Complex[a]	Elemental analysis of acceptor polymer (%)			Cs inserted (wt%)	Resistivity at 20°C ($\Omega \cdot cm$)	Concentration of free spin per g	k at 20°C (min^{-1})	E (kcal/mol)
	C	Halogen	S					
PTF-Cs	40.2	—	19.0	57.2	2.0×10^{2}	2.7×10^{17}	1.9×10^{-1}	—
PTCl-Cs	29.3	57.4	12.8	68.8	1.8×10^{4}	1.8×10^{18}	3.7×10^{-1}	—
PTBr-Cs	18.9	73.0	8.0	70.2	—	4.0×10^{19}	1.2×10^{-1}	—
SMF-Cs	44.8	—	18.0	70.0	—	1.1×10^{18}	1.2×10^{0}	—
SMCl-Cs	40.8	38.9	12.5	77.6	4.0×10^{2}	9.6×10^{19}	2.3×10^{-1}	4.0
SMBr-Cs	26.6	61.0	8.5	79.5	3.0×10^{-1}	1.1×10^{19}	2.0×10^{-1}	5.7

a) PTF, PTCl, and PTBr are abbreviations for the poly(tetrahalophenylene sulphide) in which the halogens are fluorine, chlorine, and bromine respectively. SMF, SMCl, and SMBr are abbreviations for the semiconductive polymers, mentioned in this paper, derived from PTF, PTCl, and PTBr respectively.

1) T. Kondow, H. Inokuchi, and N. Wakayama, *J. Chem. Phys.*, **43**, 3776 (1965).

2) H. Kawazura and T. Taketomi, *Polym. Lett.*, **B10**, 265 (1972).

3) These were obtained by a procedure analogous with that of the preparation of the complexes of poly(tetrahalophenylene sulphide)s.

4) H. Inokuchi, N. Wakayama, T. Kondow, and Y. Mori, *J. Chem. Phys.*, **46**, 837 (1967).

5) See, for example, Y. Mori, N. Wakayama, and H. Inokuchi, *J. Catal.* **14**, 1 (1969).

An MO Approach to the Interpretation of Organic Mass Spectra. I. Relative Bond Energy of the Molecule Ion by the Extended Hückel Method

Michihiko OGATA and Hiroshi ICHIKAWA
Hoshi College of Pharmacy, Ebara, Shinagawa-ku, Tokyo
(Received August 6, 1971)

A method of comparing the relative bond energies is applied to the interpretation of the simple cleavage and the McLafferty rearrangement reactions in organic mass spectrometry. A qualitative correlation between the relative bond energy and the charge density at the highest occupied orbital is found. The behavior of the highest occupied and some lower vacant orbitals is discussed.

In the molecular orbital approaches to the interpretation of organic mass spectra, many papers have appeared[1-6] discussing only the relationship between the scission probability and the charge density at the highest occupied (HO) orbital of the molecule ion. Some[2,3,6] of these studies explain well the experimental data. However, some explanation is needed for the correlation between the bond energy and the charge distribution at the HO orbital, since apparently the bond energy is governed not only by the electron(s) of the HO orbital, but by all the electrons included. Besides, it has been shown that σ-π interactions play a significant role in the organic reactions.[7,8] The characteristic allylic cleavage and the McLafferty rearrangement reactions give evidence of direct and/or spacial σ-π interactions in the fragmentation processes of the electron-impact state. Some authors[9,10] have pointed out the significance of the excitation of electrons to some vacant orbitals.

Our object is to solve those problems by using a simple expression for the correlation between the electronic state and the bond energies, including all the valence electrons. In this paper we will adopt the extended Hückel (EH) MO theory,[11] which has the simplest form as an MO for valence electrons.

Method

The bond energies may vary according to the electronic state. Though the electronic state for the molecule ion remains an unsolved problem,[9,10] for the sake of simplification, we will consider the states in which a single electron occupies the HO orbital and will consider that only one electron is excited in a vacant orbital from the HO orbital. (The extension to multi-excited states may be straightforward.)

The total energy (E^j) is expressed by using the LCAO wave functions to give the Coulomb (H_{pp}) and the exchange (B^j_{AB}) terms. If the unpaired electron occupies the jth orbital, E^j is calculated by means of the following equations:

$$E^j = \sum_p [\sum_i^{occ-1} 2(C_p^i)^2 + (C_p^j)^2] H_{pp} + \sum_{A>B} B^j_{AB} \quad (1)$$

$$B^j_{AB} = \sum_p^{onA} \sum_q^{onB} K(H_{pp}, H_{qq})(4 \sum_i^{occ-1} C_p^i C_q^i + 2C_p^j C_q^j) \quad (A \neq B) \quad (2)$$

where H_{pp} is the Coulomb integral and where C_p^i is the coefficient for the atomic orbital (ϕ_p) of the ith wave function. *occ* is the number of the occupied orbitals in the ground state of the molecule. $\sum_p^{onA}$ indicates the summation on the atom, A. $K(H_{pp}, H_{qq})$ represents the function which gives the approximate exchange integral; *e.g.*, in the present calculation, we adopted the Wolfsberg-Helmholtz's approximation,[12] $0.5K(H_{pp}+H_{qq})S_{pq}$, where S_{pq} is the overlap integral between ϕ_p and ϕ_q and where the value of K is 1.75, according to Hoffmann's result.[11]

The exchange term (B^j_{AB}) is considered to express the relative bond energy[13] between two atoms, A and B. The Coulomb integrals are usually approximated by the negative values of the valence-state ionization potentials (VSIP) in terms of eV. Therefore, B^j_{AB} has the unit of eV, where a negative value indicates a bonding character and a positive value, an antibonding character.

A neglect of the explicit consideration of electron-electron repulsions causes, in some cases, an inversion of the orbitals which may play an important role in the chemical reaction.[14,15] The iterative extended Hückel (IEH) method for the self-consistent charge distribution has been reported[14-18] to improve the

1) N. D. Coggeshall, *J. Chem. Phys.*, **30**, 593 (1959).
2) K. Fueki and K. Hirota, *Nippon Kagaku Zasshi*, **81**, 212 (1960).
3) K. Hirota and Y. Niwa, *J. Phys. Chem.*, **72**, 5 (1968).
4) J. C. Lorquet, *Mol. Phys.*, **9**, 101 (1965).
5) J. C. Lorquet, *J. Phys. Chem.*, **73**, 463 (1969).
6) K. Hirota, I. Fujita, M. Yamamoto, and Y. Niwa, *ibid.*, **74**, 410 (1970).
7) S. L. Altmann, *Proc. Roy. Soc. Ser., A*, **210**, 327 (1952).
8) R. B. Woodward and R. Hoffmann, *J. Amer. Chem. Soc.*, **87**, 395 (1965); *ibid.*, **87**, 2045 (1965).
9) R. C. Dougherty, *ibid.*, **90**, 5780 (1968).
10) R. A. W. Jonstone and S. D. Ward, *J. Chem. Soc., C*, **1968**, 1805.
11) R. Hoffmann, *J. Chem. Phys.*, **39**, 1397 (1963).
12) M. Wolfsberg and L. Helmholtz, *ibid.*, **20**, 837 (1952).
13) K. Shimizu, K. Miyamichi, H. Kato, and T. Yonezawa, *Nippon Kagaku Zasshi*, **90**, 1206 (1969).
14) T. Yonezawa, K. Shimizu, H. Morimoto, and H. Kato, *ibid.*, **90**, 1196 (1969).
15) O. Yamamoto, H. Kato, and T. Yonezawa, *ibid.*, **91**, 23 (1970).
16) L. C. Cusachs and J. W. Reynolds, *J. Chem. Phys.*, **43**, S160 (1965).
17) D. G. Carroll, A. T. Armstrong, and S. P. McGlynn, *ibid.*, **44**, 1865 (1966).
18) R. Rein, N. Fukuda, H. Win, and G. A. Clarke, *ibid.*, **45**, 4743 (1966).

faults of the original EH method. Besides, the converged Coulomb integrals which are obtained from the calculation of the IEH method for small molecules are shown[14] to be successfully applicable, as parameters, to large molecules. This enables self-consistent calculations for such large molecules as steroids by medium-sized computers.

The iteration was carried out according to the following equation:

$$H_{rr}(n+1) = H_{rr}(0) - (Z_X - M_X(n))(I_{pr} - A_r) \quad (3)$$

Here, $H_{rr}(n+1)$ is the Coulomb integral at the $(n+1)$-th turn. X indicates the atom to which the atomic orbital (ϕ_r) belongs, Z_X is the number of the valence electrons, and $M_X(n)$ is the atomic population of the nth turn. A_r is the electron affinity of ϕ_r.

Results and Discussion

Energetic Consideration on Simple Cleavage. It has been established[19] that, under electron-impact, amines and unsaturated hydrocarbons go mainly through the paths which are shown by a "fishhook" as below:

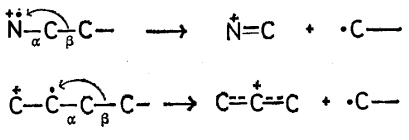

For convenience, we call this type of simple cleavage "β-bond cleavage." It has been reported[6] for alkylamines that there is a quantitative correlation between the scission probability and the charge density at the HO orbital of the molecule ion. Our first purpose is to find out the relationship between the relative bond energy and such a charge density. If we can determine this relationship for these simple compounds, it can probably be adapted to discussions of the fragmentation mechanisms of their derivatives.

The relative bond energies of ethylamine, *n*-propylamine (by the IEH method), and 1-butene (by the EH method) are calculated. The input parameters are as follows:

Atom	H	C		N	
ϕ	1*s*	2*s*	2*p*	2*s*	2*p*
$H_{rr}(0) = -I_{pr}$(eV)[20]	−13.60	−21.43	−11.42	−27.50	−14.49
A_r(eV)[20]	0.75	9.26	0.58	13.79	1.58

and the bond lengths are, C-H 1.09, N-H 1.02, C=C 1.35, =C-C 1.50, C-C 1.54, and C-N 1.50 (in Ångstroms).

In Tables 1, 2, and 3, we set the conformation of the amines so that the lone pair is *trans* (Conformation *A*), perpendicular (Conformation *B*), and *cis* (Conformation *C*) to the β bond respectively. For each electronic state of the electron-impact ion, the difference in energy from its closed-shell ground state (which is referred to as the normal state), that is, $B'_{AB} - B^{normal}_{AB}$, is listed. In all the conformations, the

TABLE 1. THE ELECTRONIC STATE OF MOLECULE IONS AND RELATIVE BOND ENERGIES (eV) OF AMINES (CONFORMATION *A*)

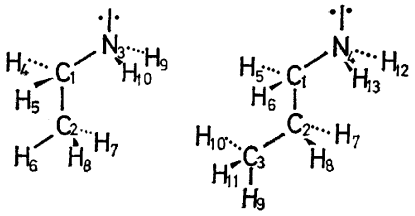

Ethylamine

Bond	normal state	$j=10$ (HO)	$j=11$ (LV)	$j=12$
C_1-C_2	−17.23	0.75	1.88	19.55
C_1-N_3	−15.70	−0.80	15.87	−1.12
C_1-H_4	−21.18	0.05	0.23	1.62
C_2-H_6	−19.82	0.02	0.33	0.29
C_2-H_7	−19.79	0.01	0.05	1.38
N_3-H_9	−20.27	−0.01	0.71	0.34

n-Propylamine

Bond	normal state	$j=13$ (HO)	$j=14$ (LV)	$j=15$
C_1-C_2	−18.07	0.87	1.11	14.49
C_1-N_4	−15.63	−0.85	13.08	−0.29
C_1-H_5	−21.14	0.05	0.19	1.32
C_2-C_3	−16.38	0.06	2.07	4.40
C_2-H_7	−20.57	0.00	0.08	0.32
C_3-H_9	−19.88	0.05	0.11	1.73
C_3-H_{10}	−19.87	0.01	0.06	0.01
N_4-H_{12}	−20.28	0.00	0.55	0.51

TABLE 2. THE ELECTRONIC STATE OF MOLECULE IONS AND RELATIVE BOND ENERGIES (eV) OF AMINES (CONFORMATION *B*)

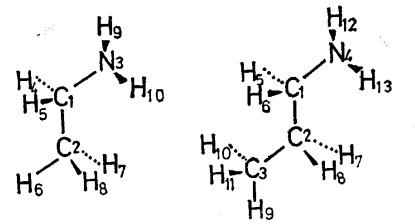

Ethylamine

Bond	normal state	$j=10$ (HO)	$j=11$ (LV)	$j=12$
C_1-C_2	−17.15	−0.06	0.94	12.59
C_1-N_3	−15.93	−0.76	14.00	−2.72
C_1-H_4	−21.12	0.37	0.99	2.17
C_1-H_5	−21.24	0.44	0.87	2.57
C_2-H_6	−19.82	0.02	0.37	0.14
C_2-H_7	−19.81	0.04	0.08	0.87
C_2-H_8	−19.79	0.01	0.03	1.86
N_3-H_9	−19.14	−0.02	0.93	0.88
N_3-H_{10}	−19.17	−0.03	0.86	3.41

19) H. Budzikiewicz, C. Djerassi, and D. H. Williams, "Mass Spectrometry of Organic Compounds," Holden-Day, Inc., San Fransisco, California.

20) H. O. Pritchard and H. A. Skinner, *Trans. Faraday Soc.*, **49**, 1254 (1953).

n-Propylamine

Bond	normal state	$j=13$ (HO)	$j=14$ (LV)	$j=15$
C_1-C_2	−17.99	−0.03	−0.08	11.69
C_1-N_4	−15.87	−0.75	13.06	1.63
C_1-H_5	−21.07	0.36	0.91	2.38
C_1-H_6	−21.19	0.43	0.85	2.40
C_2-C_3	−16.39	0.02	2.17	0.59
C_2-H_7	−20.59	0.01	0.03	0.44
C_2-H_8	−20.57	0.01	0.07	1.25
C_3-H_9	−19.88	0.00	0.02	1.05
C_3-H_{10}	−19.87	0.01	0.05	0.05
C_3-H_{11}	−19.87	0.00	0.06	0.10
N_4-H_{12}	−19.13	−0.03	0.68	0.26
N_4-H_{13}	−19.19	−0.02	0.64	3.24

TABLE 3. THE ELECTRONIC STATE OF MOLECULE IONS AND RELATIVE BOND ENERGIES (eV) OF AMINES (CONFORMATION *C*)

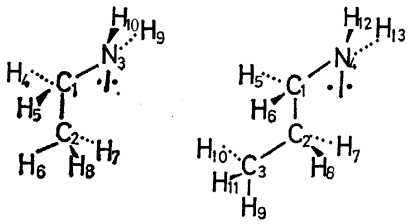

Ethylamine

Bond	normal state	$j=10$ (HO)	$j=11$ (LV)	$j=12$
C_1-C_2	−17.04	0.63	3.06	17.64
C_1-N_3	−15.35	−0.83	13.56	1.81
C_1-H_4	−21.28	0.07	0.11	2.15
C_2-H_6	−19.81	−0.02	0.28	0.04
C_2-H_7	−19.80	−0.01	−0.03	1.24
N_3-H_9	−20.29	0.01	0.69	−0.07

n-Propylamine

Bond	normal state	$j=13$ (HO)	$j=14$ (LV)	$j=15$
C_1-C_2	−17.90	0.73	2.13	13.44
C_1-N_4	−15.30	−0.90	11.75	3.37
C_1-H_5	−21.22	0.06	0.09	1.39
C_2-C_3	−16.38	0.01	1.96	4.91
C_2-H_7	−20.58	−0.01	−0.02	0.12
C_3-H_9	−19.88	0.02	0.05	1.90
C_3-H_{10}	−19.87	0.00	0.02	0.00
N_4-H_{12}	−20.29	0.01	0.53	0.02

relative bond energies of the C–C bonds are lower than those of C–N in the closed-shell ground state. These are qualitatively in the same inclination as the experimental values. (They are not directly comparable to the experimental values, since the energies of the electronic and internuclear interaction among all non-bonding atoms are not taken into account in determining the relative bond energy.) On the other hand, in the *A* and *C* conformations, the removal of one electron from the HO orbital ($j=10$ and 13 respectively for ethylamine and *n*-propylamine) causes the energy of the β C–C bond to be higher than that in the closed-shell ground state, while the α C–N bond is strengthened. In the *B* conformation, however, this inclination is not clearly observed. Instead, the β C–H bond is weakened. It should be pointed out that the β C–H bond *trans* to the lone pair is more weakened than that of *cis*. These results indicate that the conformation of the nitrogen atom plays an important role in the strength of the β bond. This will be discussed in the next section.

TABLE 4. THE ELECTRONIC STATE OF MOLECULE ION AND RELATIVE BOND ENERGIES (eV) OF 1-BUTENE

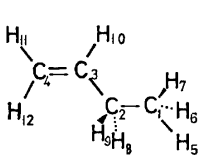

Conformation *D*

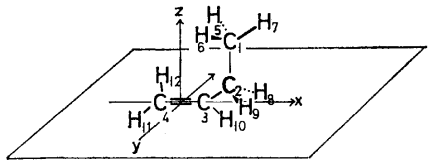

Conformation *E*

Conformation *D*

Bond	normal state	$j=12$ (HO)	$j=13$ (LV)	$j=14$
C_1-C_2	−17.71	−0.34	−0.69	18.09
C_1-H_5	−19.92	0.00	0.00	0.66
C_1-H_6	−20.01	0.26	0.52	1.43
C_2-C_3	−20.39	−1.25	−1.89	−2.74
C_2-H_8	−20.08	1.21	2.22	2.99
C_3-C_4	−32.50	3.34	14.13	6.97
C_3-H_{10}	−21.05	0.00	0.00	0.88
C_4-H_{11}	−20.37	0.00	0.00	0.05
C_4-H_{12}	−20.32	0.00	0.00	0.07

Conformation *E*

Bond	normal state	$j=12$ (HO)	$j=13$ (LV)	$j=14$
C_1-C_2	−17.26	1.33	2.51	18.23
C_1-H_5	−19.97	0.08	0.15	0.91
C_1-H_6	−19.92	−0.02	−0.08	0.34
C_1-H_7	−19.94	0.16	0.33	1.64
C_2-C_3	−20.30	−0.66	−0.96	4.10
C_2-H_8	−20.42	0.24	0.47	0.44
C_2-H_9	−20.31	0.00	−0.06	0.19
C_3-C_4	−32.58	3.24	13.89	5.72
C_3-H_{10}	−20.97	0.02	0.04	0.82
C_4-H_{11}	−20.31	0.06	0.12	0.40
C_4-H_{12}	−20.37	0.09	0.19	1.18

Though it is well known that the Hückel method is not well adapted to the study of excited states, the general behavior of the excited molecule ion is considered to be significant. In all conformations, the excitation to the lowest vacant (LV) orbital weakens the α C–N bond. Usually, however, the M-NH_2 peaks are not intensely observed in alkylamines. It should also be pointed out that the positive charge remains not on the fragment of NH_2 but on the alkyl site, judging from Stevenson's rule.[21] That is, the

21) D. P. Stevenson, *Discussions Faraday Soc.*, **10**, 35 (1951).

TABLE 5. COEFFICIENTS OF HO AND SOME LV ORBITALS OF ETHYLAMINE

Conformation	Wave function	C_1				C_2			
		$2s$	$2p_x$	$2p_y$	$2p_z$	$2s$	$2p_x$	$2p_y$	$2p_z$
A	$j=10$(HO)	−0.003	−0.030	−0.180	0.000	0.070	0.058	0.235	0.000
	$j=11$(LV)	0.144	0.910	0.421	0.000	0.050	0.070	0.249	0.000
	$j=12$	−0.174	−0.364	0.969	0.000	0.094	−0.094	1.018	0.000
B	$j=10$(HO)	0.027	0.090	0.041	−0.163	−0.006	−0.030	−0.041	0.028
	$j=11$(LV)	0.130	0.883	0.474	0.044	0.049	0.050	0.321	0.030
	$j=12$	−0.140	−0.388	0.820	0.020	0.070	−0.121	0.881	−0.075
C	$j=10$(HO)	0.035	0.099	−0.131	0.000	0.062	0.016	0.177	0.000
	$j=11$(LV)	0.137	0.849	0.541	0.000	0.052	0.030	0.391	0.000
	$j=12$	−0.186	−0.547	0.895	0.000	0.098	−0.105	0.962	0.000

Conformation	Wave function	N_3				Hydrogens	
		$2s$	$2p_x$	$2p_y$	$2p_z$	H_4	H_5
A	$j=10$(HO)	0.156	0.013	0.939	0.000	−0.048	−0.048
	$j=11$(LV)	−0.143	0.934	0.060	0.000	0.146	0.146
	$j=12$	−0.072	−0.140	−0.097	0.000	−0.371	−0.371
B	$j=10$(HO)	−0.186	−0.341	−0.118	0.868	0.119	−0.182
	$j=11$(LV)	−0.163	0.858	0.290	0.254	0.165	0.078
	$j=12$	0.002	−0.296	0.271	−0.070	−0.344	−0.350
C	$j=10$(HO)	−0.167	−0.556	0.766	0.000	−0.102	−0.102
	$j=11$(LV)	−0.127	0.772	0.466	0.000	0.088	0.088
	$j=12$	0.121	−0.191	−0.224	0.000	−0.407	−0.407

ionization potential (I_p) of NH_2 might almost be equal to that of the $2p$ orbital of the nitrogen atom in the valence state.[22] The I_p's of alkyl radicals are considered to be lower than that of the $2p$ orbital of the carbon atom because of hyperconjugation (*e.g.*, 8.64, 8.35, 7.93, and 7.42 eV for *n*-, *iso*-, *sec*-, and *t*-butyl radicals respectively.[23] The I_p's of the $2p$ orbitals of nitrogen and carbon atoms have been shown[20] to be 14.49 and 11.42 respectively. Therefore, the positive charge is located predominantly on the fragment of the alkyl group.

This consideration raises a question concerning the role of the electronic excitation. As for higher excitation, it is significant that excitation to the second level (LV+1; $j=12$ and 15 respectively for ethylamine and *n*-propylamine) makes the β bond sharply antibonding. Thus, interestingly, electronic excitation to a vacant orbital makes a certain bond extraordinarily loose. Similar results are obtained for 1-butene. In this case, π electrons play a role similar to that of the lone pair in amines. On calculations, two kinds of conformations were chosen. Conformation *D* shows that all the carbon atoms are on the *x*-*y* plane, while Conformation *E* shows only the bond of C_1–C_2 as perpendicular to the *x*-*y* plane (Table 4).

Characteristics of the HO and Some LV Orbitals.
As has already been shown, the bond energy of β C–C varies according to the conformation of the nitrogen atom. This indicates that the lone pair which occupies the HO orbital of amine plays an important role in determining the strength of the

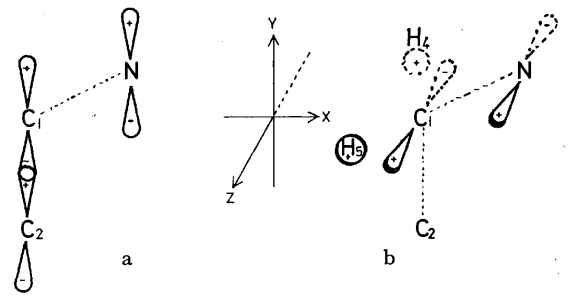

Fig. 1. Coordinate-dependent atomic orbitals of ethylamine.

β bond. In Table 5, the coefficients of the HO and some lower vacant orbitals are listed. In the *A* and *C* conformations, the electron of the HO orbital is predominantly distributed on the $2p_y$ atomic orbitals of N_3, C_1, and C_2. The sign of the coefficient for N_3 is positive, and that for C_1 is negative. The π-overlap integral ($S_{\pi\pi}$) between these atomic orbitals has a positive value (Fig. 1-a). Therefore, the HO orbital has an antibonding effect on the C_1–N_3 bond, since the interaction energy (e^j_{pq}) between atomic orbitals, ϕ_p and ϕ_q, given by singly-occupied jth orbital is expressed by Eq. (4), where H_{pp} is negative:

$$e^j_{pq} = C_p{}^j C_q{}^j K(H_{pp}+H_{qq})S_{pq} \qquad (4)$$

The sign of the coefficient for the $2p_y$ of C_2 is positive, while the σ-overlap integral ($S_{\sigma\sigma}$) between the $2p_y$ atomic orbitals of C_1 and C_2 is negative. Hence, the HO orbital is bonding in this bond. On the other hand, in the *B* conformation it is shown in Fig. 1-b and Table 5 that the HO orbital is antibonding in N_3–C_1, while it is bonding in both the C_1–H_4 and

22) The configurations of those radicals are assumed to be sp^2.
23) F. P. Lossing and J. B. de Sousa, *J. Amer. Chem. Soc.*, **81**, 281 (1959).

C_1–H_5 bonds. Likewise, it will be shown below that the LV and LV+1 orbitals are sharply antibonding in the C_1–N_3 and C_1–C_2 bonds respectively.

From the above considerations, it can be understood that the removal of one electron from the HO orbital makes the α C–N bond stronger (because the HO orbital is antibonding on this bond), while the β bond especially *trans* to the lone pair of the nitrogen atom becomes weaker. The behavior of the HO orbitals in other homologous amines is found to be analogous to that of ethylamine.

It may be evident that the positive charge is not distributed on the position where the HO orbital is antibonding, but where the HO orbital is bonding. We now recognize a correlation between the bond scission and the net positive-charge density. It is, however, not observed that the bond energy of the α C–N is lower than that of β C–C. The actual difference in energy becomes almost zero. There are two probable reasons for this. One might be the rough application of the MO theory, in which the molecule ions are calculated on the basis of the parameters for the closed-shell ground state. The electron distribution of the HO orbital is concentrated on the nitrogen atom under the electron-impact state; the values of the Coulomb integrals for the atomic orbitals belonging to the nitrogn atom should be lowered compared to those in the normal state. The other is that there may be other factors that regulate the reaction path, *e.g.*, the stability of the ions produced.

The McLafferty Rearrangement Reaction. Boer *et al.*[24] have already treated the McLafferty rearrangement reaction on 2-pentanone by means of Mulliken's population analysis. The following results, therefore, may serve to reconfirm the reaction processes proposed by them.

It has been established[25–26] that the γ-hydrogen

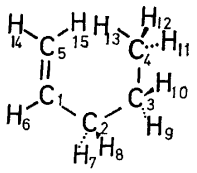

1-Pentene

atom is transferred in the rearrangement. Hence, it can be expected that, as the molecule ion takes a conformation favorable for the rearrangement, the bonding interaction between γ-hydrogen and the hydrogen-accepting atoms increases, while that between γ-hydrogen and the hydrogen-leaving atoms decreases.

The values of B^j_{AB} between those atoms when the distances between γ-H(H_{13}) and C_4 are 2.4 Å (Conformation *F*) and 1.7 Å (Conformation *G*) were calculated for 1-pentene; they are listed in Tables 6 and 7 respectively. On the *F* conformation, it is shown in all the electronic states of the molecule ion (j=15—17)

Table 6. The values of B^j_{AB} of 1-pentene (Conformation *F*)

A–B	normal state	j=15 (HO)	j=16 (LV)	j=17
C_1–C_2	−20.87	−0.95	1.58	−1.08
C_1–C_5	−32.56	3.05	13.41	6.20
C_1–H_6	−20.99	0.07	0.14	0.14
C_2–C_3	−16.47	0.79	1.42	9.23
C_2–H_7	−20.40	0.67	1.31	2.12
C_2–H_8	−20.43	0.01	−0.02	0.92
C_3–C_4	−17.93	−0.06	−0.17	9.57
C_3–H_9	−20.82	0.35	0.71	0.73
C_3–H_{10}	−20.80	0.35	0.70	0.76
C_4–H_{11}	−19.80	0.00	0.00	0.97
C_4–H_{12}	−20.06	0.02	0.00	0.31
C_4–H_{13}	−20.21	0.80	1.64	1.73
C_5–H_{14}	−20.38	0.00	0.00	0.00
C_5–H_{15}	−20.32	0.00	−0.01	0.05
C_5–H_{11}	−0.02	0.01	0.02	0.02
C_5–H_{12}	0.15	0.04	0.06	0.10
C_5–H_{13}	0.15	−0.46	−1.10	−0.89

Table 7. The values of B^j_{AB} of 1-pentene (Conformation *G*)

A–B	normal state	j=15 (HO)	j=16 (LV)	j=17
C_1–C_2	−20.80	0.07	0.66	0.13
C_1–C_5	−32.88	0.75	8.59	1.49
C_1–H_6	−20.90	0.22	0.44	1.10
C_2–C_3	−16.68	−0.04	−0.22	0.00
C_2–H_7	−20.37	0.00	−0.06	1.19
C_2–H_8	−20.10	0.12	0.07	0.64
C_3–C_4	−18.56	−0.18	−0.15	6.42
C_3–H_9	−20.78	0.24	0.46	0.47
C_3–H_{10}	−20.73	0.00	−0.03	0.00
C_4–H_{11}	−19.57	0.33	0.65	1.42
C_4–H_{12}	−20.63	0.06	0.12	0.25
C_4–H_{13}	−19.16	3.72	7.15	7.64
C_5–H_{14}	−20.51	0.18	0.36	0.40
C_5–H_{15}	−20.17	3.05	6.00	6.52
C_5–H_{11}	0.06	0.12	0.20	0.30
C_5–H_{12}	0.70	−0.06	0.08	−0.08
C_5–H_{13}	1.33	−1.98	−3.61	−3.69

that: (1) C_5 has a strong bonding interaction with H_{13} and (2) the relative bond energy between C_4 and H_{13} becomes quite small, indicating cleavage at this bond. This inclination becomes more apparent when the molecule ion takes the *G* conformation. The relative bond energy between C_2 and C_3, however, is not weakened by changing the conformation from *F* to *G*. As for the electronic gound state (j=15), those observed are quite analogous to Boer's results. It may be worth considering that the excited molecule ion has a similar reaction tendency.

Conclusion

(1) There is a clear correlation between the bond energy and the charge density at the HO orbital of the molecule ion, which might support Hirota's assumption.[2,3,6] However, there also seem to be other

24) F. P. Boer, T. W. Shannon, and F. W. McLafferty, *J. Amer. Chem. Soc.*, **90**, 7239 (1968).
25) R. Srinivasan, *ibid.*, **81**, 5061 (1959).
26) J. Seibl and T. Gaumann, *Helv. Chim. Acta*, **46**, 2867 (1963).

factors that regulate the reaction path. (2) The conformation of the nitrogen atom plays an significant role in connection with the strength of the β-bond. The β bond *trans* to the lone pair is more weakened than that of *cis*. (3) Electronic excitation from the HO orbital to a vacant orbital makes a certain bond extraordinarily loose. (4) As for the simple β cleavage of amines, electronic excitation to a vacant orbital is in doubt. (5) A method of comparing the relative bond energies is useful in the interpretation of rearrangement reactions.

The calculations were carried out on a HITAC 5020E computer at the computation center of the University of Tokyo. The authors wish to thank Dr. C. Kaneko (Tokyo Medical and Dental University) and Dr. S. Nakajima and Miss Y. Miyaji (Hoshi College of Pharmacy) for their helpful discussions. The research described in this paper was supported by a grant-in-aid for Scientific Research from the Ministry of Education of Japan.

BULLETIN OF THE CHEMICAL SOCIETY OF JAPAN, VOL. 45, 3236—3240 (1972)

Adsorption of *N*-Vinyl-2-pyrrolidone at the Mercury/Solution Interface

Tadashi YOSHIDA, Tetsuya OHSAKA, and Hajime YAMAMOTO
Applied Electrochemical Laboratory, Graduate School of Science and Engineering, Waseda University, Nishi-Okubo, Shinjuku-ku, Tokyo 160

(Received October 4, 1971)

The adsorption of *N*-vinyl-2-pyrrolidone (NV2P) or the monomer of polyvinylpyrrolidone (PVP) at the mercury/solution interface was examined by means of differential capacity *vs.* potential relations (*C-E* curves). The usual *C-E* curve obtained in 1N sulfuric acid was similar to that of the saturated aliphatic compounds. However, in 1N sodium sulfate or sodium hydroxide potential dependence of C_{min} (minimum differential capacity) was observed as a result of π-electron interaction of adsorbed molecules. The adsorption behavior in 1N sulfuric acid followed the Langmuir isotherm. The peculiar behavior in 1N sodium sulfate or sodium hydroxide was explained by means of the Frumkin isotherm with the potential dependence of interaction constant (g), which varied linearly with potential in a range more negative than *ca.* -0.6 V (SCE) in contrast to nearly constant values in a more positive range. At a relatively high bulk concentration, there was a slight deviation from the Frumkin isotherm and the standard free energy of adsorption (ΔG^0) *vs.* $\theta^{3/2}$ plot revealed a sharp break in the same way as pointed out by Conway and his co-worker. The C_{min} value of NV2P coincided approximately with that of its polymer of PVP in aqueous sulfuric acid, sodium sulfate or sodium hydroxide, respectively. The results are utilized for the discussion on the configuration of adsorbed PVP at the interface.

For *N*-vinyl-2-pyrrolidone (NV2P)[1] with pyrrolidone and vinyl radicals, π-electron seems to have a strong influence upon its adsorption behavior.

The role of π-electron interaction on adsorption was first pointed out by Gerovich[2] and further has been discussed by several authors.[3-6] Klyukina and Damaskin[7] investigated the Frumkin adsorption isotherm considering the potential dependence of interaction constant (g) among adsorbed molecules, while Conway[5] discussed the molecular orientation due to the π-electron interaction in connection with the coverage (θ) dependence of standard electrochemical free energy of adsorption (ΔG^0) obtained by means of the Langmuir adsorption isotherm.

We have investigated the adsorption of NV2P as regards the results[8,9] obtained for its polymer or polyvinylpyrrolidone (PVP) by measurement of the differential capacity at the mercury/solution interface.

Experimental

Electrodes. A dropping mercury electrode (DME) with a flow rate of *ca.* 4.5×10^{-4} g/sec was used, with a ring-like platinum wire of sufficiently large suface area as the counter electrode. The electrode potentials were measured with reference to a 3.3N calomel or mercury/mercuric oxide electrode, and the results are given against the saturated calomel electrode (SCE).

Apparatus and Materials. The differential capacity at the mercury/solution interface was determined at 22°C by

1) Molecular structural formula:

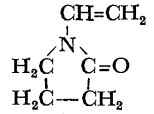

2) M. Gerovich, *Dokl. Akad. Nauk. SSSR*, **96**, 543 (1954).
3) A. Frumkin, R. Kaganovich, and E. Bit-Popova, *ibid.*, **141**, 670 (1961).
4) E. Blomgren, J. O'M. Bockris, and C. Jesh, *J. Phys. Chem.*, **65**, 2000 (1961).
5) B. Conway and R. Barradas, *Electrochim. Acta*, **5**, 319 (1961).
6) H. Nürnberg and G. Wolff, *Collect. Czech. Chem. Commun.*, **30**, 3997 (1965).
7) L. Klyukina and B. Damaskin, *Izv. Akad. Nauk SSSR Ser., Khim.* **1963**, 1022; B. Damaskin, *Electrochim. Acta*, **9**, 231 (1964).
8) T. Yoshida, T. Ohsaka, and S. Tanaka, This Bulletin, **45**, 326 (1972).
9) T. Yoshida, T. Ohsaka, and S. Nomoto, *ibid.*, **45**, 1585 (1972).

the universal bridge (Yokogawa BV-Z13A) equipped with an oscilloscope as a detector and d.c. polarization circuit. The balance time (*i.e.*, time, elapsed from the beginning of a drop growth) was set at 8 sec with a sinusoidal wave of 1 kHz adjusted to a input voltage of *ca.* 10 mV_{p-p} or less. Interfacial impedance was assumed as series equivalent circuit of capacitance and resistance. NV2P of pure chemical grade prepared by Tokyo Kasei Co. was used without further purification. All the solutions were prepared from triply-distilled water and pure chemicals. Observation was carried out in the atmosphere of purified nitrogen.

Results and Discussion

Variation of Differential Capacity with Potential. The relations between differential capacity and potential (*C-E* curves) caused by the addition of NV2P were observed in 1N sulfuric acid, 1N sodium sulfate and 1N sodium hydroxide. The results are shown in Figs. 1—3.

The *C-E* curves in Figs. 1—3 can be regarded as the results of the adsorption equilibrium except for peak regions, since the capacity data per unit area are independent of the balance time exceeding 8 sec in the solution containing 1 mmol/*l* NV2P.

In the case of low bulk concentration of NV2P in 1N sulfuric acid the peak caused by ad- or desorption appears on the positive side, but none on the negative owing to hydrogen evolution. In 1N sulfuric acid with a relatively high content of NV2P, the differential capacity (*C*) attains almost a constant value in the range more negative than *ca.* −0.5 V(SCE).

In 1N sodium sulfate, the peak appears both on the positive and negative sides (Fig. 2) and the differential capacity is depressed in the adsorption range as the potential becomes negative. However, it is well-known that the potential dependence of capacity is hardly observed for the adsorption range in usual cases. Both peaks are asymmetric and the cathodic peak becomes somewhat negative and sharp with the increase of bulk concentration of NV2P (Fig. 2). This tendency might be due to the attractive interaction among the adsorbed molecules. The peculiar adsorption is also found in 1N sodium hydroxide (Fig. 3). Similar behavior was discussed for pyridine in potassium chloride by Damaskin.[7] The anodic peak seems to be due to reorientation of adsorbed pyridine molecules and not to ad- or desorption. Nearly the

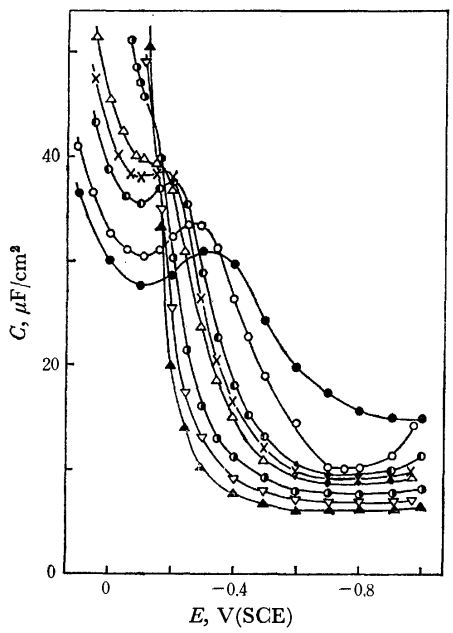

Fig. 1. Differential capacity *vs.* potential curves.
22°C, 1 kHz, 1N sulfuric acid +NV2P (●: 0 mol/*l*, ○: 1.0×10^{-2}, ◐: 5.0×10^{-2}, ×: 7.5×10^{-2}, △: 1.0×10^{-1}, ◑: 2.0×10^{-1}, ▽: 3.0×10^{-1}, ▲: 4.7×10^{-1}).

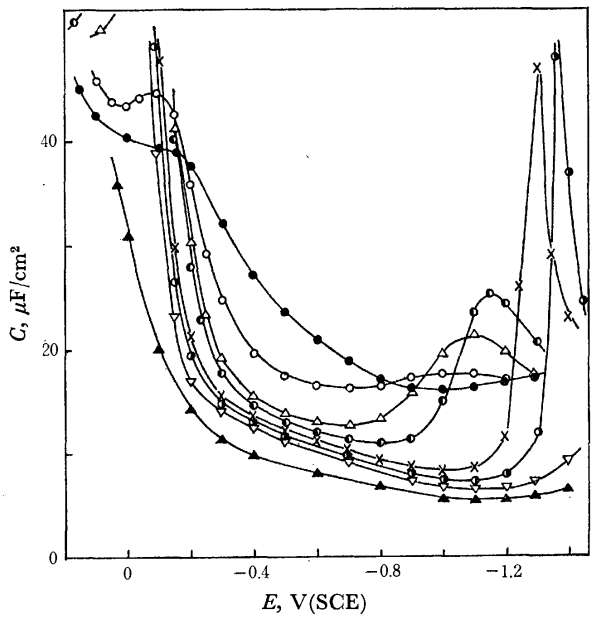

Fig. 2. Differential capacity *vs.* potential curves.
22°C, 1 kHz, 1N sodium sulfate +NV2P (●: 0 mol/*l*, ○: 1.0×10^{-3}, △: 5.0×10^{-3}, ◐: 1.0×10^{-2}, ×: 3.0×10^{-2}, ◑: 5.0×10^{-2}, ▽: 1.0×10^{-1}, ▲: 4.0×10^{-1}).

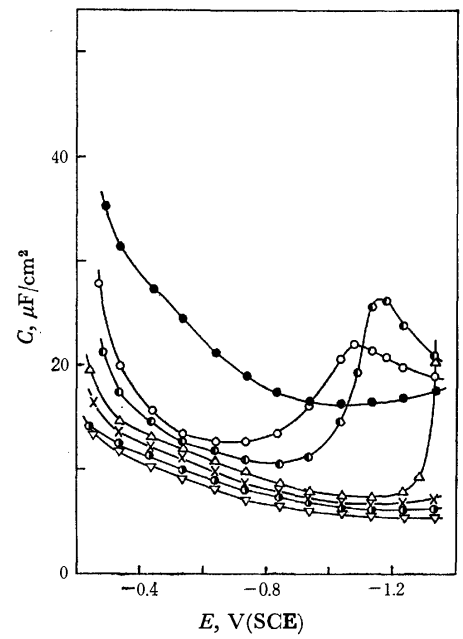

Fig. 3. Differential capacity *vs.* potential curves.
22°C, 1 kHz, 1N sodium hydroxide +NV2P (●: 0 mol/*l*, ○: 5.0×10^{-3}, ◐: 1.0×10^{-2}, △: 4.1×10^{-2}, ×: 8.4×10^{-2}, ◑: 1.7×10^{-1}, ▽: 3.4×10^{-1}, 5.0×10^{-1}).

same values of capacity obtained by the solutions with and without pyridine in the more positive range than the anodic peak may result from the interfacial structure, not from the adsorbed layer because of the strong interaction between the π-electron and the electrode. The anodic peak in Figs. 1 and 2 might be assumed as the above. For the unusual adsorption of NV2P in 1N sodium sulfate or 1N sodium hydroxide, π-electron interaction seems to play an important role.

Potential Dependence of Coverage (θ-E Curves). The θ-E relations in sulfuric acid (Fig. 4) were given from the C-E curves (Fig. 1) by means of Frumkin's parallel condenser model. The computation was carried out for the region with a slight potential dependence of C. The θ-E curves (Fig. 4) reveal an usual bell-type form, their maximum adsorption being attained at *ca.* −0.7 V (SCE).

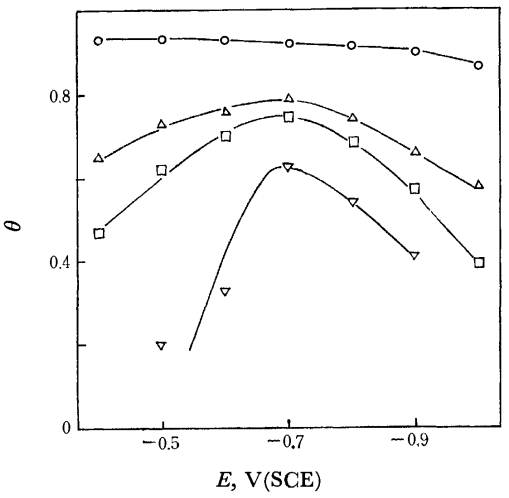

Fig. 4. Coverage *vs.* potential curves.
22°C, 1N sulfuric acid +NV2P (▽: 1.0×10^{-2} mol/*l*, □: 5.0×10^{-2}, △: 1.0×10^{-1}, ○: 3.1×10^{-1}).

It is necessary to find the minimum differential capacity (C_{min}) for determination of coverage by Frumkin's model. In the case of 1N sodium sulfate or 1N sodium hydroxide, however, no definite value can be found for C_{min} owing to its potential dependence (Figs. 2 or 3). In these cases, the lowest value within the adsorption range may be taken, while the lowest value at each potential may be used respectively for the determination of coverage in consideration of the potential dependence of capacity due to the gradual reorientation of adsorbate. The θ-E curves in sodium sulfate solution (Fig. 5) were derived from C_{min} at each potential. At a relatively low bulk concentration (Fig. 5), the bell-type θ-E curves were obtained. The maximum coverage at *ca.* −0.45 V (SCE) increased with bulk concentration. In the case of high bulk concentration, the tendency was reversed and minimum coverage was observed contrary to the usual cases. This tendency was also shown by another θ-E plot where θ was evaluated by the lowest common capacity instead of respective C_{min} at each potential.

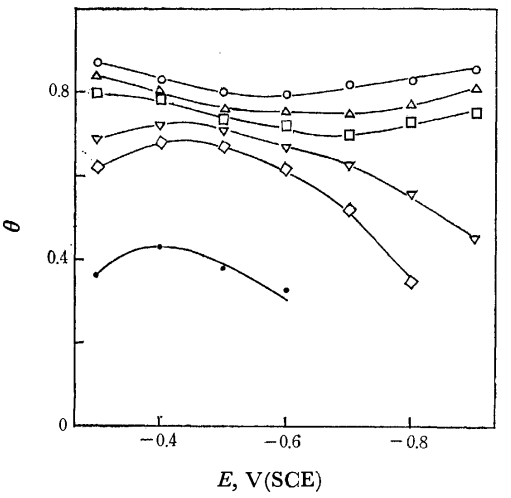

Fig. 5. Coverage *vs.* potential curves.
22°C, 1N sodium sulfate +NV2P (●: 1.0×10^{-3} mol/*l*, ◇: 5.0×10^{-3}, ▽: 1.0×10^{-2}, □: 3.0×10^{-2}, △: 5.0×10^{-2}, ○: 1.0×10^{-1}).

Adsorption Isotherm. The Langmuir adsorption isotherm was always applied to the adsorption of NV2P in 1N sulfuric acid, while the Frumkin adsorption isotherm was applied to that in 1N sodium sulfate or 1N sodium hydroxide in view of the potential dependence of interaction constant (g). The adsorption isotherm in 1N sodium sulfate is shown in Fig. 6, where the coverage is calculated with the respective C_{min} at each potential. The curve becomes somewhat S-type at the negative potential (Fig. 6), which might indicate the change from repulsive to attractive interaction. In the adsorption isotherm of pyridine given by the potential dependence of interfacial tension, almost the same tendency as above was also pointed out by Gierst,[10] Conway and Barradas,[5] and Nürnberg and Wolff.[6] The adsorption isotherm of NV2P in sodium sulfate or sodium hydroxide solution is similar to that of pyridine to some extent.

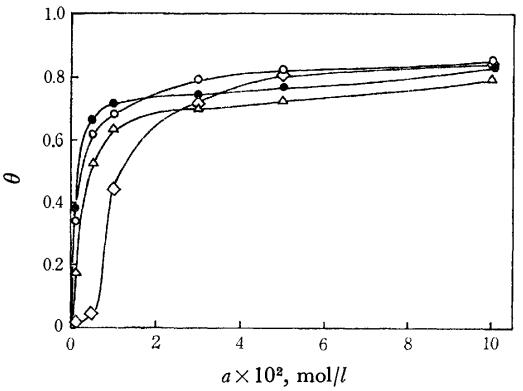

Fig. 6. Adsorption isotherms.
22°C, 1N sodium sulfate +NV2P [○: −0.3 V(SCE), ●: −0.5 V, △: −0.7 V, ◇: −0.9 V].

Potential Dependence of Interaction Constant. The coverage of NV2P in 1N sodium sulfate or 1N sodium hydroxide solution was evaluated by Frumkin's condenser model with minimum capacity at each potential on the assumption of full coverage at each C_{min}. The

10) L. Gierst, "Transactions of the Symposium on Electrode Processes," ed. by E. Yeager, John Wiley and Sons Inc., New York, (1961), p. 294.

interaction constant (g) is given by the Frumkin isotherm

$$\beta a = \frac{\theta}{1-\theta}\exp(-2g\theta) \quad (1)$$

where β, a, θ, and g are the adsorption coefficient, the bulk concentration, the coverage, and the interaction constant, respectively. According to Frumkin and Damaskin,[11] the interaction constant (g) might be obtained by means of the adsorption isotherm.

Substituting the relative concentration $y=a/a_{\theta=0.5}$ into Eq. (1), we have

$$y = \frac{\theta}{1-\theta}\exp[g(1-2\theta)] \quad (2)$$

and

$$(dy/d\theta) = \frac{(1-2g\theta+2g\theta^2)}{(1-\theta)}\exp[g(1-2\theta)] \quad (3)$$

At $\theta=0.5$:

$$(dy/d\theta)_{\theta=0.5} = 4-2g \quad (4)$$

Thus, g can be determined graphically. The results are shown in Fig. 7.

The g value gives a constant of *ca.* -1.3 in the range from -0.3 to nearly -0.6 V (SCE). This might indicate a certain repulsive interaction between the molecules. In the range from -0.6 to about -0.9 V

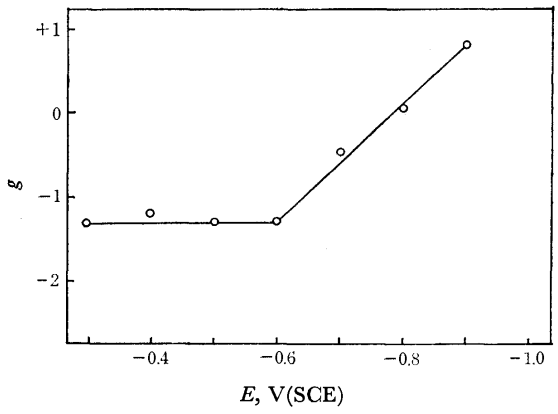

Fig. 7. Potential dependence of interaction constant.
22°C, 1N sodium sulfate +NV2P.

(SCE), the g value varies almost linearly with a slope of *ca.* 6.7 (V^{-1}) as the potential becomes negative, and the g value turns positive at *ca.* -0.8 V (SCE). This indicates the attractive interaction between the adsorbed molecules.

Coverage Dependence of Standard Free Energy of Adsorption ($\Delta\bar{G}^0$). For the purpose of investivating some deviations from the Frumkin isotherm in Fig. 5 or 6 (*i.e.*, the unusual shape of θ-E in Fig. 5 and the slight rise of isotherm at a relatively high concentration in Fig. 6), the results were examined in terms of the coverage dependence of $\Delta\bar{G}^0$ [12] after Conway.[5]

If no interaction is assumed for the adsorbed molecules at the interface, $\Delta\bar{G}^0$ is given by the Langmuir isotherm.[5]

$$\ln\left(\frac{55.5}{a}\frac{\theta}{1-\theta}\right) = -\frac{\Delta\bar{G}^0}{RT} \quad (5)$$

When the surface interaction of the adsorbates is taken into account, Eq. (5) can be written as follows:[5]

$$\ln\left(\frac{55.5}{a}\frac{\theta}{1-\theta}\right) - \ln f_\theta = -\frac{\Delta\bar{G}^0}{RT} \quad (6)$$

where the surface activity coefficient (f_θ) at a coverage θ consists of an electrostatic dipole-dipole interaction term ($\theta^{3/2}$) and van der Waals-London interaction term (θ^3).[5]

Equation (6), then, becomes:

$$\ln\left(\frac{55.5}{a}\frac{\theta}{1-\theta}\right) + \frac{P_a\theta^{3/2}-Q_a\theta^3}{RT} = -\frac{\Delta\bar{G}^0}{RT} \quad (7)$$

where P_a and Q_a are constants dependent on the characteristics of adsorbed layer. If θ is not too close to unity, the term $Q_a\theta^3$ is almost negligible and the relation between $\Delta\bar{G}^0$ and $\theta^{3/2}$ becomes approximately linear. $\Delta\bar{G}^0$ varies with $\theta^{3/2}$ as expected, although a remarkable break is revealed on each curve as shown in Fig. 8. Such a sharp inflection may be attributed to onset of extensive orientation with the increase of coverage.[5]

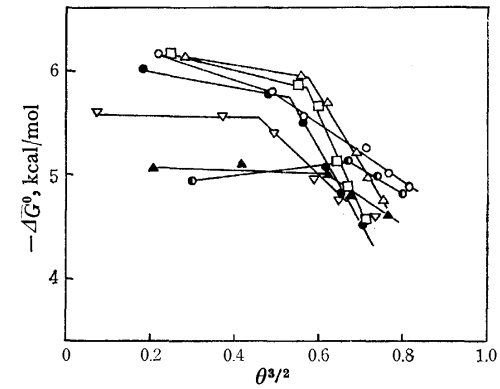

Fig. 8. Coverage dependence of $\Delta\bar{G}^0$.
22°C, 1N sodium sulfate +NV2P [○: −0.3 V(SCE), △: −0.4 V, □: −0.5 V, ●: −0.6 V, ▽: −0.7 V, ▲: −0.8 V, ◐: −0.9 V].

The Frumkin isotherm can be written as follows, where the value of 55.5 is taken for a comparison with Conway's treatment and $\beta=(1/55.5)\exp(-\Delta\bar{G}^0/RT)$ in Eq. (1)

$$\ln\left(\frac{55.5}{a}\frac{\theta}{1-\theta}\right) - 2g\theta = -\frac{\Delta\bar{G}^0}{RT} \quad (8)$$

The correction term for surface interaction on the adsorbed layer is assumed to be $-2g\theta$ instead of $(P_a/RT)\theta^{3/2}$ term in Eq. (7). $\Delta\bar{G}^0$ is expected to vary linearly with θ. This relation was verified for the adsorption of phenol by Blomgren[4] except for the case where θ is close to unity. In the case of NV2P, a sharp break was also shown in $\Delta\bar{G}^0$-θ plot. The result does not seem to be in line with the Frumkin isotherm. The Frumkin isotherm, however, is approximately applicable to the adsorption of NV2P at a relatively low coverage ($0<\theta<$*ca.* 0.7), because the g values at $\theta=0.5$ derived from Eq. (8) with $\Delta\bar{G}^0$ of

11) A. Frumkin and B. Damaskin, "Modern Aspects of Electrochemistry," No. 3, eds. by J.O'M. Bockris and B. Conway, Butterworth, London, (1964), p. 182.

12) Refer to Refs. 13 and 5 for the definition of ΔG^0.

13) P. Delahay, "Double Layer and Electrode Kinetics," John Wiley and Sons Inc., New York (1965), p. 81.

14) Molar concentration of H_2O per liter given by Conway *et al.*

the Langmuir isotherm nearly coincided with the values in Fig. 7, where the g values at $\theta=0.5$ were chosen for convenience as the typical data in the range of low coverage before the appearance of the sharp break. The sharp variation of $\Delta\bar{G}^0$ with θ at relatively high coverage is considered to be mainly caused by reorientation of adsorbed molecules, although the variation might be explained by the Frumkin isotherm modified with the association number of adsorbed water molecules.[15]

Orientation of NV2P at the Interface. For NV2P in aqueous sodium sulfate or sodium hydroxide, the variation of differential capacity within the adsorption range seems to be due to π-electron interaction. The reorientation of adsorbed molecules may take place gradually in the above range, as discussed by Damaskin for the adsorption of pyridine[7] or aniline,[16] where results analogous to Figs. 2 and 3 are obtained.

g values of NV2P in Fig. 7 change with the potential in the range more negative than *ca.* −0.6 V (SCE) but they are nearly constant in the range more positive than the above. The tendency might be related to surface charge, since the point of zero charge for mercury in the solution with no adsorbates is about—0.43V (SCE).[17] In the negative range, a nearly perpendicular form of the adsorbed molecules may be expected because of the repulsion between the electrode surface and π-electron while the attractive force between adsorbed molecules is considered to increase as the potential becomes negative. In the range more positive than *ca.* −0.6 V (SCE), the repulsive force between adsorbed molecules is considered to become nearly constant because the gradual reorientation of the adsorbed molecule may be expected as the potential becomes positive, or the attraction between the electrode surface and π-electron increases. The reorientation might take place gradually as the electrode potential changes, since the differential capacity varies gradually with the potential in the adsorption range.

Examination of Minimum Differential Capacity. The relation between the minimum differential capacity (C_{min}) and the thickness (δ) of adsorbed layer is as follows:

$$C_{min} = \varepsilon/(4\pi\delta) \quad (9)$$

where ε is the dielectric constant of adsorbed layer. The values of C_{min} of NV2P in several solutions are shown in Table 1, where almost the same values of C_{min} are given for both cases of sodium sulfate and sodium hydroxide solutions, while C_{min} value in sulfuric acid is about 1.1 times those in the above solutions. This difference of C_{min} is considered to result from the difference of δ on the assumption that ε hardly varies with supporting electrolyte.

The perpendicular/planar ratio of orientation for NV2P is about 2.5 from the approximate calculation with the molecular model. It appears from the C_{min} ratio 1.1 that the variation of orientation with electrolytes does not take place completely from perpendicular to planar. In the adsorption range of NV2P in sulfuric acid, the nearly constant C_{min} may be due to the alleviation of π-electron interaction by the highly concentrated hydrogen ion, but the conclusion from only C-E relations is somewhat doutful as pointed out by Damaskin[16] for the adsorption of aniline.

Table 1. C_{min} of NV2P and PVP (μF/cm^2)

Electrolyte	C_{min} of NV2P (Monomer)	PVP (Polymer) $\bar{M}$	PVP (Polymer) C_{min}
1N H_2SO_4	6.4	10000	6.5
		26000	6.3
		37000	6.15
		750000	6.05
1N Na_2SO_4	5.6	10000	5.8
1N NaOH	5.7	10000	5.7
		750000	5.9

Adsorption Behavior of PVP Expected from That of NV2P. The adsorption behavior of PVP at the mercury interface may be discussed in reference to that of NV2P or the monomer of PVP. In Table 1 of the C_{min} values of PVP depending a little upon $\bar{M}$ (mean molucular weight), the values of C_{min} for $\bar{M}$ of 10000 are used for the discussion in view of the lieast difference between the values of PVP and its monomer.

In aqueous solutions of sulfuric acid, sodium sulfate and sodium hydroxide, C_{min} of NV2P hardly differs from that of PVP in each solution as shown in Table 1. Thus, it may be considered that the thickness of adsorbed NV2P layer is similar to that of its polymer layer adsorbed in each solution, if ε remains nearly constant.

It is interesting that C_{min} value of the polymer or PVP varies with a supporting electrolyte similarly to the case of its monomer or NV2P. However, the variation of C_{min} due to reorientation of the adsorbed polymer is almost impossible. Therefoe, the dependence of C_{min} value on the supporting electrolyte may be connected with the compactness of adsorbed layer in the case of polymer.

The dependence of inhibition effect by PVP upon the supporting electrolyte is observed[18] from the comparison of inhibition effect for some electrodeposition processes. It is considered to be also related to the compactness of adsorbed layer to a certain extent.

It appears from C_{min} value of PVP in accordance with that of its monomer that the configuration of adsorbed PVP at the interface is spread or flattened as assumed previously.[8] Strictly speading, however, the above assumption is a mere approximation in consideration of the fact that C_{min} of PVP depends slightly on $\bar{M}$.

Financial aid from the Ministry of Education is gratefully acknowledged.

15) B. Damaskin, *J. Electroanal. Chem.*, **23**, 431 (1969); L. Pospišil and J. Kůta, *Collect. Czech. Chem. Commun.*, **34**, 3047 (1969).

16) B. Damaskin, I. Mishutushkina, V. Gerovich, and R. Kaganovich, *Zhur. Fiz. Khim.*, **38**, 1797 (1964).

17) P. Delahay, "Double Layer and Electrode Kinetics," John Wiley and Sons Inc. (1965), p. 23; B. Conway, "Electrochemical Data," Elsevier (1952), p. 221.

18) T. Yoshida and T. Ohsaka, *Bull. Sci. Eng. Res. Lab. Waseda Univ.*, **58**, 34 (1972).

Competitive Adsorption of Polyvinylpyrrolidone with *n*-Alkyl Alcohols at the Mercury/Solution Interface

Tadashi Yoshida, Tetsuya Ohsaka, and Yasuo Iida

Applied Electrochemical Laboratory, Graduate School of Science and Engineering, Waseda University, Nishi-Okubo, Shinjuku-ku, Tokyo, 160

(Received October 12, 1971)

Competitive adsorption of polyvinylpyrrolidone (PVP, $\bar{M}=10000$) with *n*-hexanol, *n*-pentanol, or *n*-butanol was examined by observation of the differential capacity at the mercury interface in 1 N sulfuric acid. Adsorption of PVP coexistent with alcohol hardly differed from the single adsorption[1] controlled by its diffusion. The competitive adsorption curve of *C* (differential capacity) *vs.* $t^{1/2}$ (adsorption time) was expected from the sum of the individual capacity depressions by the single adsorption at −0.5 or −0.6 V (SCE) and the expected curve of *C vs.* $t^{1/2}$ was compared with the curve observed. The competitive behavior of alcohol coexistent with PVP was examined by the relation "θ_{Alc}^{com} (coverage of coexistent alcohol) *vs.* $t^{1/2}$" at −0.5 or −0.6 V (SCE), where θ_{Alc}^{com} was estimated from the difference between the differential capacities with and without PVP, in view of the fact that behavior of PVP is nearly independent of the coexistent alcohol. The results are discussed in terms of four types of models assumed for the competitive behavior of coexistent alcohols with different adsorbability. It is considered that the alcohol is replaced with PVP as soon as the latter reaches the interface by diffusion, the adsorption equilibrium of an alcohol being achieved immediately. The relation $\theta_{Alc}^{com}=(1-\theta_{PVP})\theta_{Alc}$ holds in the case of *n*-butanol coxistent with PVP, where θ_{PVP}, θ_{Alc}, and θ_{Alc}^{com} are the coverages due to the single adsorption of PVP and butanol and to the competitive adsorption of butanol, respectively. The tendency of alcohol to be replaced with PVP is inversely proportional to its adsorption coefficient. *n*-Butanol was most sensitive to the coexistence of PVP.

The adsorption of PVP(polyvinylpyrrolidone) at the mercury/solution interface was previously discussed[2] in terms of the process controlled by diffusion. We have investigated the competitive adsorption of PVP with *n*-alkyl alcohol of low molecular weight at the mercury interface with the alcohol attaining its adsorption equilibrium immediately.

Not many electrochemical studies on competitive adsorption have been published. Only the tensammetry wave for competitive adsorption has been shown by Jehring.[3] The treatment of the Flory-Huggins adsorption isotherm[4] and analyses of the reorientation of the adsorbed molecules at equilibrium[5,6] may be applied to the equilibrium of the competitive adsorption. The analyses, however, are useless for the competitive process influenced by the diffusion of PVP.

The results of competitive adsorption of PVP with an alcohol will, therefore, be discussed with respect to the behavior of the single adsorption of each compoent.

Experimental

The test electrode and counter electrode were a dropping mercury electrode (DME) with a drop time *ca.* 11 sec and a cylindrical platinum net. The potentials were referred to the saturated calomel electrode (SCE). The differential capacity was observed by a transformer impedance bridge[2] with an input of 1 kHz wave adjusted to below 10 mV_{p-p}. PVP ($\bar{M}=10000$) prepared by BASF was used without further purification. Observation was always conducted with 1 N sulfuric acid at 22°C in the atmosphere of purified nitrogen. The DME[2] was composed of Pyrex parts and a molybdenum glass capillary with a ground glass joint, the other conditions being the same as described previously.[2]

Results and Discussion

Differential Capacity vs. Potential Curves (C-E Curves) for Competitive Adsorption. An example of *C-E* curves at the adsorption time (t_B) of 8 sec for the competitive adsorption of PVP with *n*-butanol is given in Fig. 1. 1 N sulfuric acid containing 0.1 mol/*l* *n*-butanol and various amounts of PVP ($\bar{M}=10000$) were employed. The *C-E* relation for the single adsorption of *n*-butanol is also shown. The adsorption process of PVP revealed at $t_B=8$ sec is expected to be controlled by diffusion. In the case of the single adsorption of PVP, an ad- or desorption peak is revealed at *ca.* 75 mV (SCE) and the peak height increases with bulk concentration. The differential capacity is depressed by the adsorption of PVP in the more cathodic potential than the above peak. The inhibitive action of PVP on the adsorption of *n*-butanol can be seen in Fig. 1, since the adsorption or desorption peak due to *n*-butanol is depressed and the peak due to PVP grows with PVP concentration. In the competitive adsorption of PVP with *n*-pentanol or *n*-hexanol, the tendency of the *C-E* relation was similar to that for *n*-butanol.

Time-Dependence of Differential Capacity for Competitive Adsorption (C-t Curves). For the purpose of examining competitive adsorption accompanied by the process controlled by the diffusion of PVP, the time-dependence of differential capacity was observed at *ca.* −0.5 V (SCE), where the saturated adsorption of

1) "Single adsorption" is used in contrast to "competitive adsorption" and means the adsorption of an organic substance contained solely in a supporting electrolyte.

2) T. Yoshida, T. Ohsaka, and S. Tanaka, This Bulletin, **45**, 326 (1972).

3) H. Jehring, *J. Electroanal. Chem.*, **21**, 77 (1969).

4) L. Pospišil and J. Kůta, *Collect. Czech. Chem. Commun.*, **34**, 3047 (1969).

5) J. M. Parry and R. Parsons, *J. Electrochem. Soc.*, **113**, 992 (1966).

6) B. B. Damaskin, *J. Electroanal. Chem.*, **21**, 149 (1969).

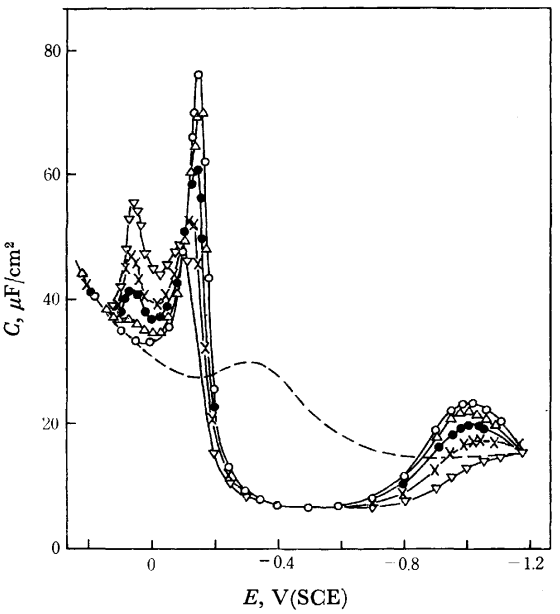

Fig. 1. Potential-dependence of differential capacity in 1N sulfuric acid solution containing 0.1M/*l* *n*-butanol and several amount of PVP.
1 kHz, 22°C, t_B=8 sec, $\bar{M}$ of PVP=10000, dashed line: 1N sulfuric acid solution, ○: PVP content 0 mg/*l*, △: PVP 2.0 mg/*l*, ●: PVP 5.0 mg/*l*, ×: PVP 10.0 mg/*l*, ▽: PVP 15.0 mg/*l*.

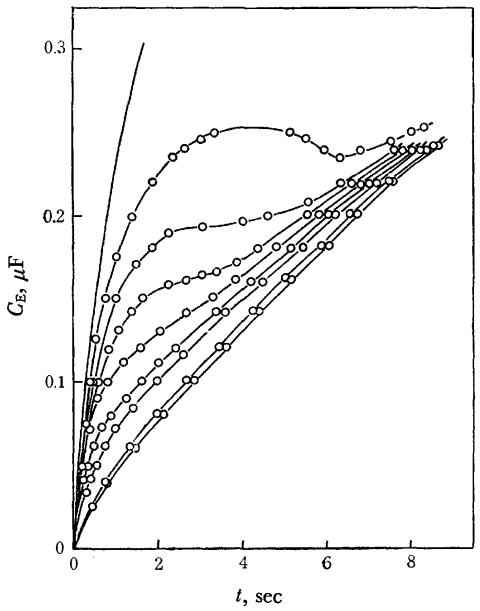

Fig. 2. Time-dependence of observed capacity at −0.5 V (SCE) in 1N sulfuric acid solution containing 30 mg/*l* PVP and several amount of *n*-hexanol.
1 kHz, 22°C, solid line: 1N sulfuric acid solution, *n*-hexanol content mM/*l* from top to the bottom: 0, 0.25, 0.50, 0.75, 1.00, 1.25, 5.00, 30.0.

PVP is always attainable.[2] Figure 2 shows typical plots of time-dependence of the observed capacity (C_E) for competitive adsorption in 1N sulfuric acid containing PVP (30 mg/*l*) and various amounts of *n*-hexanol, where the adsorption of PVP is controlled by diffusion.[2]

Single adsorption of PVP was found to approach saturation after the appearance of maximum value of C_E (Fig. 2). The transient range from diffusion-controlled to saturated adsorption becomes gradually ambiguous as *n*-hexanol content increases. It appears that the individual adsorption equilibrium is attained in the case of relatively high hexanol content. The C–$t^{1/2}$ plot obtained from the C_E–t relation is shown in Fig. 3, where (a) and (b) refer to the competitive adsorption of PVP with *n*-hexanol and *n*-butanol, respectively.

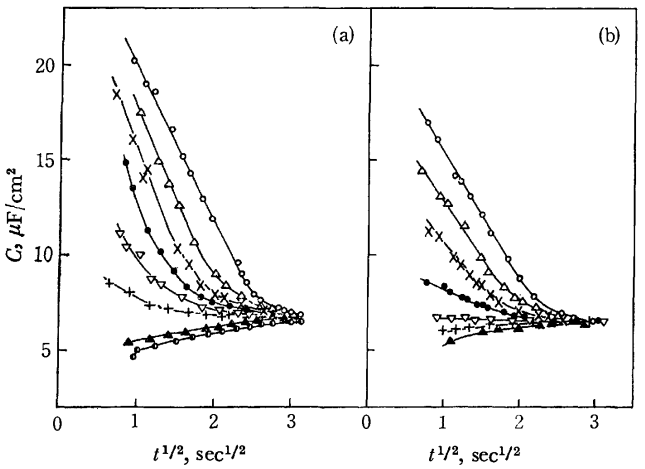

Fig. 3. Relation between differential capacity and square root of time at the competitive adsorption.
1N sulfuric acid solution, 1 kHz, 22°C, (a) PVP ($\bar{M}$=10000) +*n*-hexanol at −0.5 V(SCE): (30 mg/*l* PVP +*n*-hexanol mM/*l*, ○: 0, △: 0.25, ×: 0.5, ●: 0.75, ▽: 1.00, +: 1.25, ▲: 5.00, ◐: 30.0). (b) PVP ($\bar{M}$=10000)+*n*-butanol at −0.6 V(SCE): (35 mg/*l* PVP +*n*-butanol mM/*l*, ○: 0, △: 0.01, ×: 0.02, ●: 0.04, ▽: 0.08, +: 0.15, ▲: 0.50).

In the case of adsorption controlled by the diffusion of adsorbates, the behavior on a DME is approximately explained in terms of the Koryta equation.[7] The following equation[8] can be derived by substitution of the Koryta equation into the relation for the Frumkin parallel condenser model:

$$C = C_0 - 0.736(C_0 - C_1)D^{1/2}\Gamma_m^{-1}at^{1/2} \quad (1)$$

where C_0 and C_1 are the differential capacities at θ=0 and θ=1, respectively, and D, Γ_m, and a are diffusion coefficient (cm²/sec), maximum surface concentration (mol/cm²) and bulk concentration (mol/cm³). Equation (1) holds for $t<t_m$, where t_m is the time required to attain the saturated adsorption. When $t \geq t_m$, we have

$$C = C_1 \quad (2)$$

In Fig. 3, the linear portion of C–$t^{1/2}$ plot decreases and the transient range from diffusion-controlled to saturated adsorption increases with the content of *n*-hexanol or *n*-butanol. In each single adsorption, the minimum differential capacities of PVP ($\bar{M}$= 10000), *n*-hexanol and *n*-butanol were found to be 6.5, 4.7, and 5.2 μF/cm², respectively. It is expected that the hexanol molecules are replaced gradually

7) J. Koryta, *Collect. Czech. Chem. Commun.*, **18**, 206 (1953).
8) P. W. Board, D. Britz, and R. V. Holland, *Electrochim. Acta*, **13**, 1633 (1968).

by the PVP molecules which reach the interface by diffusion.

In the case of competitive adsorption of PVP with *n*-butanol shown in Fig. 3-(b), or with *n*-pentanol, a similar tendency to that in the case of hexanol was also observed in the relation C-$t^{1/2}$.

Competitive Adsorption Curves (C-$t^{1/2}$) Observed and Expected. The C-$t^{1/2}$ relation of competitive adsorption was expected from the sum of individual capacity depression[9] for PVP and alcohol. The expected behavior was compared with the result obtained from competitive adsorption in the same electrolyte. Typical cases[10] of competitive adsorption of PVP with *n*-hexanol and *n*-butanol are shown in Fig. 4-(a) and (b). The capacity due to the adsorption of hexanol

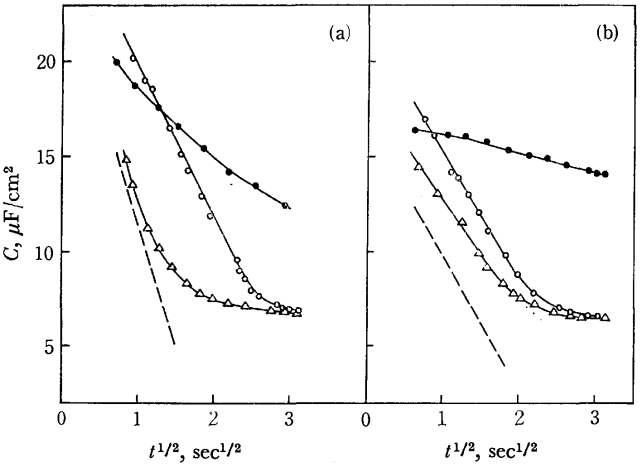

Fig. 4. Relation between differential capacity and square root of time at the competitive adsorption.
1N sulfuric acid solution, 1 kHz, 22°C, (a) PVP+*n*-hexanol at −0.5 V(SCE), ○: 30 mg/*l* PVP at the single adsorption, ●: 0.75 mM/*l* *n*-hexanol at the single adsorption, △: 30 mg/*l* PVP+0.75 mM/*l* *n*-hexanol at the competitive adsorption, dashed line: the curve of the competitive adsorption expected from the individual behaviour of the single adsorption. (b) PVP+*n*-butanol at −0.6 V(SCE), ○: 35 mg/*l* PVP at the single adsorption, ●: 0.01 mM/*l* *n*-butanol at the single adsorption, △: 35 mg/*l* PVP+0.01 mM/*l* *n*-butanol at the competitive adsorption, dashed line: the curve of the competitive adsorption expected from the individual behaviour of the single adsorption.

decreases with time. The adsorption equilibrium is not attained but influenced somewhat by the diffusion process under such hexanol content. The expected curve of C-$t^{1/2}$ agrees approximately with that observed for competitive adsorption in the initial stage of the linear portion. The observed curve, however, approaches the minimum differential capacity due to the saturated adsorption of PVP. Results nearly analogous to the above were obtained for the competitive adsorption of PVP with *n*-pentanol. With *n*-butanol, however, the expected curve is relatively isolated from the observed one [Fig. 4-(b)].

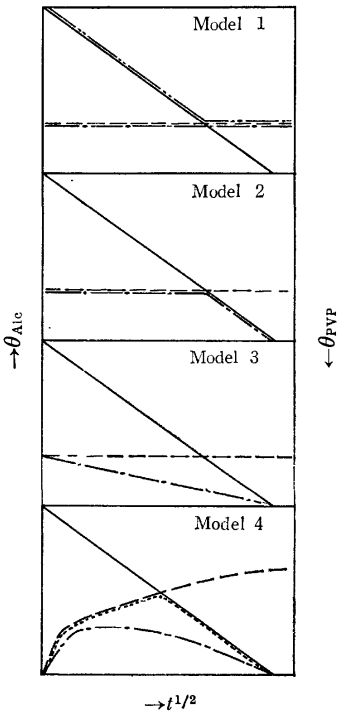

Fig. 5. Models assumed for the competitive adsorption of *n*-aliphatic alcohol with PVP.
solid line: the behaviour of diffusion-controlled adsorption of PVP at the single adsorption whose coverage is shown by θ_{PVP}, dashed line: the behaviour of adsorption equilibrium of *n*-aliphatic alcohol at the single adsorption whose coverage is shown by θ_{Alc}, dashed-two-dotted line in Model 1: the behavior of PVP at the competitive adsorption (*cf.* In the other models, the behavior of PVP at the competitive adsorption is nearly the same as that at the single adsorption.), dotted and dashed-dotted lines: the behavior of alcohol at the competitive adsorption with PVP, where the coverage of alcohol coexistent with PVP is shown by $\theta_{Acl}^{com.}$.

Behavior of Alcohols during Competitive Adsorption. Some models of competitive adsorption are shown in Fig. 5. One of the adsorbates (PVP) undergoes diffusion-controlled adsorption and the other (alcohol) easily attains adsorption equilibrium. In each single adsorption, the coverage of PVP and alcohol are expressed by θ_{PVP} (solid line) and θ_{Alc} (dashed line), respectively. The coverage of alcohol during competitive adsorption is expressed by θ_{Alc}^{com} and plotted with dashed-dotted lines. The coverage of PVP coexistent with alcohol is assumed to be nearly analogous to θ_{PVP}.

Model 1 (Fig. 5) is the case in which interaction or replacement between alcohol and PVP hardly takes place, and θ_{Alc}^{com} remains constant after the full coverage of ($\theta_{PVP}+\theta_{Alc}=1$) is established. The behavior of PVP in single adsorption, expressed by the dashed-two-dotted line, differs only for this case from that in competitive adsorption. Since the behavior of PVP in single and competitive adsorption is considered to be the same in the other models, it is always shown by a solid line. Model 1 is impractical because PVP has a higher adsorbability than that of the saturated alcohol.

9) The individual capacity depression is the difference between the capacity of the individual adsorbate for the single adsorption and that in the solution without adsorbates at a certain potential and adsorption time.

10) Extrapolation of the three solid lines in Fig. 4 should coincide at $t=0$. The results of differential capacity at t less than 1 sec are not shown, an accurate estimation of the mercury drop surface being difficult.

Model 2 is the case in which the adsorbed alcohol in its equilibrium begins to be replaced by PVP arriving after the full coverage of ($\theta_{PVP}+\theta_{Alc}=1$) is achieved. In this case, the space in the electrode is preferentially covered by PVP until the time ($\theta_{PVP}+\theta_{Alc}=1$), the rate of the replacement being controlled by the diffusion of PVP.

Model 3 is the case in which replacement of the adsorbed alcohol with PVP takes place as soon as PVP reaches the interface by diffusion. The amount of alcohol replaced by PVP is proportional to that of the adsorbed PVP. Thus the coverage of θ_{Alc}^{com} (dashed-dotted line) is given by $\theta_{Alc}^{com}=(1-\theta_{PVP})\theta_{Alc}$.

It is necessary to assumed another model in consideration of practical cases in which the adsorption of saturated alcohol is somewhat controlled by its diffusion dependent on the adsorption isotherm. This diffusion process was discussed by Delahay[11] by means of Henry's law, by Reinmuth[12] by means of the Langmuir isotherm and by Rampazzo[13] by means of the Frumkin isotherm. In view of these discussions, Model 4 is shown qualitatively as a practical case. The dashed-dotted line corresponds to that in Model 3. The plot is also expressed by the relation $\theta_{Alc}^{com}=(1-\theta_{PVP})\theta_{Alc}$, and the dotted line corresponds to the dashed-dotted line in Model 2.

θ_{Alc}^{com} was expected from the difference between the capacity depressions for the competitive and single adsorption of PVP by means of the relation "$\theta=(C_0-C)/(C_0-C_1)$" on the assumption that the adsorption behavior of PVP coexistent with alcohol is analogous to that of the single adsorption in view of the results in Figs. 1, 2, and 3. The θ_{Alc}^{com}-$t^{1/2}$ relations

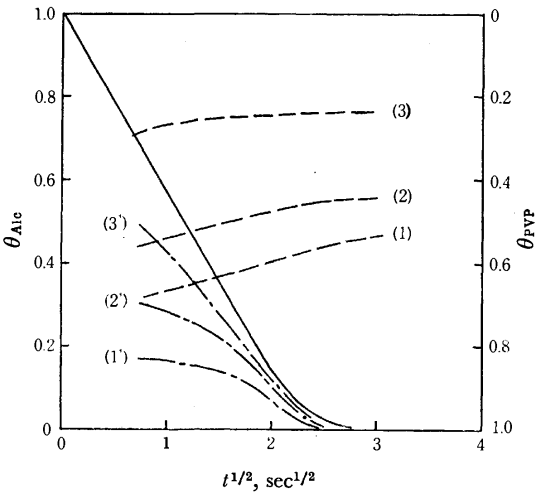

Fig. 6. Relation between coverage and square root of time in the case of hexanol.
1N sulfuric acid solution, −0.5 V(SCE), solid line: the single adsorption of PVP 30 mg/l, dashed lines; the single adsorption of n-hexanol mM/l: [(1): 0.25, (2): 0.50, (3) :0.75], dashed-dotted lines: the competitive adsorption of n-hexanol expected from the capacity depression, PVP 30 mg/l +n-hexanol mM/l: [(1)′: 0.25, (2)′: 0.50, (3)′: 0.75].

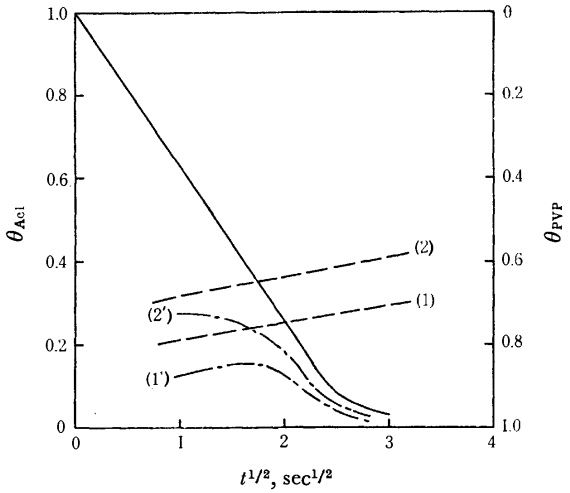

Fig. 7. Relation between coverage and square root of time in the case of pentanol.
1N sulfuric acid solution, −0.5 V(SCE), solide line: the single adsorption of PVP 30 mg/l, dashed lines: the single adsorption of n-pentanol mM/l: [(1): 2.0, (2) : 3.0], dashed-dotted lines: the competitive adsorption of n-pentanol expected from the capacity depression, PVP 30 mg/l +n-pentanol mM/l: [(1)′: 2.0, (2)′: 3.0].

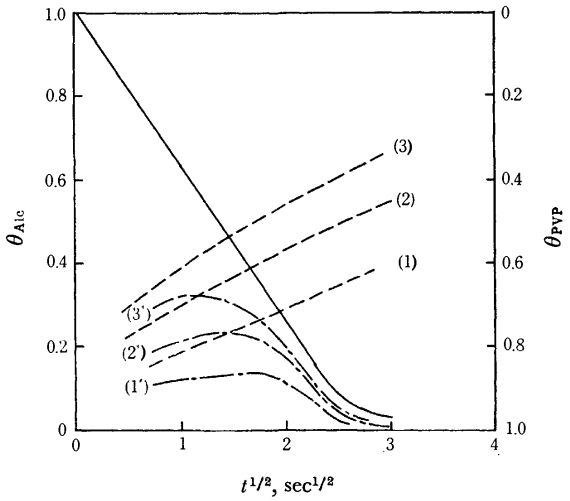

Fig. 8. Relation between coverage and square root of time in the case of butanol.
1N sulfuric acid solution, −0.6 V(SCE), solid lines: the single adsorption of PVP 35 mg/l, dashed lines: the single adsorption of n-butanol M/l: [(1): 0.01, (2): 0.02. (3): 0.04], dashed-dotted lines: the competitive adsorption of n-butanol expected from the capacity depression, PVP 35 mg/l+n-butanol M/l: [(1)′: 0.01, (2)′: 0.02, (3)′: 0.04].

expected for the competitive adsorption of PVP with n-hexanol, n-pentanol, and n-butanol are shown by the dashed-dotted lines in Figs. 6, 7, and 8, respectively. θ_{Alc} given by the dashed lines is obtained from the capacity depression observed for the single adsorption.

The values of θ_{Alc}^{com} somewhat deviates from θ_{Alc} in the early stage of the adsorption for n-hexanol (Fig. 6), the deviation becoming greater at lower bulk concentration. The θ_{Alc}^{com} plots come closer to the θ_{PVP} curve with increasing adsorption time. The

11) P. Delahay and I. Trachtenberg, *J. Amer. Chem. Soc.*, **79**, 2355 (1957); P. Delahay and C. T. Fike, *ibid.*, **80**, 2628 (1958).
12) W. H. Reinmuth, *J. Phys. Chem.*, **65**, 473 (1961).
13) L. Rampazzo, *Electrochim. Acta*, **14**, 733 (1969).

tendency shows the gradual replacement of the adsorbed alcohol with PVP which reaches the interface. This behavior of *n*-hexanol coexistent with PVP is explained in terms of the intermediate type between the dashed-dotted and dotted lines in Model 4, *viz.*, between Models 2 and 3.

The value of θ_{Alc} for *n*-pentanol (Fig. 7) shows a relatively smaller dependence on t than that for *n*-hexanol. The adsorption behavior of *n*-pentanol, coexistent with PVP is similar to that of *n*-hexanol.

The plot of θ_{Alc}^{com} for butanol (Fig. 8) approaches the θ_{PVP} curve in a relatively early stage and the effect of the coexistence of PVP is remarkable as compared with the other cases. This behavior might correspond to that shown by the dashed-dotted line in Model 4 or 3, since the values agree approximately with those of θ_{Alc}^{com} derived from the relation $\theta_{Alc}^{com}=(1-\theta_{PVP})\theta_{Alc}$.

The adsorption behavior of alcohol coexistent with PVP is considered to be dependent on its adsorbability. The adsorption coefficients of *n*-butanol, *n*-pentanol, and *n*-hexanol were found to be 1.25×10^2, 5.00×10^2, and 2.20×10^3 (l/mol), respectively, assuming the Langmuir isotherm. These are approximately in agreement with those published by Delahay,[11] Lorenz,[14] and Kalvoda,[15] and the order of the magnitude of the adsorbability is as *n*-hexanol>*n*-pentanol>*n*-butanol. Thus, it is considered that the influence of coexistent PVP with high adsorbability is the largest for *n*-butanol and relatively small for *n*-hexanol during the course of competitive adsorption.

Models 1—3 (Fig. 5) are shown in the order of magnitude of the adsorbability of alcohol. It is natural that the relation $\theta_{Alc}^{com}=(1-\theta_{PVP})\theta_{Alc}$ holds in the case of *n*-butanol because of its low adsorbability. In conclusion, the behavior during competitive adsorption of *n*-butanol is explained by Model 3, and that of *n*-hexanol and *n*-pentanol by an intermediate type between Models 2 and 3 due to their somewhat higher adsorbability.

14) W. Lorenz and F. Möckel, *Z. Electrochem.*, **60**, 507 (1956).
15) R. Kalvoda and A. Vaškelis, *Collect. Czech. Chem. Commun.* **32**, 2206 (1967).

BULLETIN OF THE CHEMICAL SOCIETY OF JAPAN, VOL. 45, 3245—3250 (1972)

Adsorption of Polyethyleneglycol at the Mercury/Solution Interface

Tadashi YOSHIDA, Tetsuya OHSAKA, and Masayuki SUZUKI

Applied Electrochemical Laboratory, Graduate School of Science and Engineering, Waseda University, Nishi-Okubo, Shinjuku-ku, Tokyo, 160

(Received December 8, 1971)

The adsorption of polyethyleneglycol (PEG) was investigated at the mercury/solution interface by the observation of the differential capacity and the inhibitive action on the deposition of cadmium or copper. From the differential capacity measurements, the adsorption of PEG was found to be controlled by the diffusion of the adsorbate to the dropping mercury electrode under the present experimental conditions. The relation between the time required to attain the saturated adsorption and the bulk concentration (a) was explained approximately by the Koryta equation, though its deviation from the Koryta equation was somewhat larger than that for polyvinylpyrrolidone. When the maximum surface concentration and the mean molecular weight of PEG were expressed by Γ_m and $\bar{M}$ respectively, the plot of $\log \Gamma_m$-$\log \bar{M}$ revealed two linear parts crossing each other at $\bar{M}=ca.$ 600. The slope for $\bar{M}\geq 600$ was *ca.* -1, which implied the relation of "$\bar{M}\cdot\Gamma_m=$const.", *i.e.*, the segment numbers of PEG molecules adsorbed per unit area were constant, independently of $\bar{M}$, in the region of $\bar{M}\geq 600$. The configuration of PEG of $\bar{M}<600$ at the interface was considered to be different from that of PEG of $\bar{M}\geq 600$ because the slope for $\bar{M}<600$ was different from that for $\bar{M}\geq 600$. From the polarographic current measurements (*i.e.*, the inhibitive effect on the reduction of Cd^{2+} or Cu^{2+}), the time (t_{ml}) needed to achieve the maximum inhibition was obtained; it was then compared with that obtained from the capacity data. The relation of "$\log a=(-1/2)\log t_{mi}+$const." based on the Koryta equation was approximately applicable to the cases with a relatively large $\bar{M}$ value.

In many cases, organic high polymers are adsorbed so strongly at the electrode/solution interface, that the adsorption from its dilute solution is mainly controlled by the diffusion. Such a diffusion process was discussed for PVP (polyvinylpyrrolidone)[1] and the Koryta equation[2] was approximately applicable to the adsorption of PVP. Electrochemical studies on the adsorption of polyethyleneglycol (PEG) have been scarcely published, though Jehring and Horn[3] computed the maximum surface concentration (Γ_m) at the mercury interface by means of AC polarography. In this paper, the adsorption of PEG[4] at the mercury inter-

1) T. Yoshida, T. Ohsaka, and S. Tanaka, This Bulletin, **45**, 326 (1972).

2) J. Koryta, *Collect. Czech. Chem. Commun.*, **18**, 206 (1953).

3) H. Jehring and E. Horn, *Deut. Akad. Wiss. Berlin*, **10**, 295 (1968).

4) Molecular formula: $H(OCH_2CH_2)_nOH$.

face was investigated by the observations of differential capacity and of inhibitive effect on the electrodeposition. The time (t_{me}) needed to attain the saturated adsorption was observed by the capacity measurement and it was compared with that (t_{mi}) obtained from the inhibitive effect of PEG on the electrodeposition of cadmium or copper.

Experimental

Electrodes. For the measurements of the differential capacity and the instantaneous current, a DME (dropping mercury electrode) and a counter electrode of cylindrical platinum net were used. The drop time of DME was about 12 sec, while it was nearly 5 sec for the polarography. All the potentials were referred to the saturated calomel electrode (SCE).

Differential Capacity Measurements. The impedance bridge used for the capacity measurements was a condenser-connected type with both arms composed of 1 μF mica condensers; the input of 1 kHz sinusoidal wave was adjusted to be less than *ca.* 10 mV_{p-p}. The balance of the bridge was detected with a selective amplifier and a cathode-ray oscilloscope. The series-equivalent circuit with resistance and capacitance was assumed in balancing the bridge.

Instantaneous Current vs. Time Curves (i-t Curves). The instantaneous *i-t* curves were observed by connecting a recorder or oscilloscope in parallel with 2 kΩ resistance equipped in series with the polarizing circuit of DME.

Polarograph and Others. The polarograph was the PA102 type of Yanagimoto. The test cell and DME were the same as have been described previously;[1] all the experiments were conducted in an atmosphere of purified hydrogen at 25°C.

Materials. Seven kinds of chemical-grade PEG by the Sanyo Chemical Industry Co. were used without further purification. The mean molecular weights ($\bar{M}$) were calculated from those OH values obtained by end-group determination; they were 200, 300, 400, 600, 1000, 3100, and 8400 respectively. Mercury was distilled twice *in vacuo*, and all the solutions were prepared from chemical-grade reagents and triply-distilled water.

Results and Discussion

I) Differential Capacity Measurements. Differential Capacity vs. Potential Curves (C-E Curves): Some typical *C-E* curves of PEG $\bar{M}$=600 and 8400 in 1N potassium chloride are shown in Fig. 1, where t_B is the duration from the beginning of a drop growth to the balancing the bridge. In Fig. 1-(a) with PEG $\bar{M}$=600, ad- or desorption peaks are observed at *ca.* −0.2 and *ca.* −0.6 V (SCE). Figure 1-(b) with $\bar{M}$=8400 is similar to the case of $\bar{M}$=600, though the anodic peak shows only a steep slope on the right side. The potential of the ad- or desorption peak for PVP[1] or PMA[5] has been reported to be almost independent of the bulk concentration; for PEG however, the peak potential is dependent to some extent on the bulk concentration. The peak becomes steeper with the increase in $\bar{M}$; this tendency suggests that the interaction among the adsorbed molecules

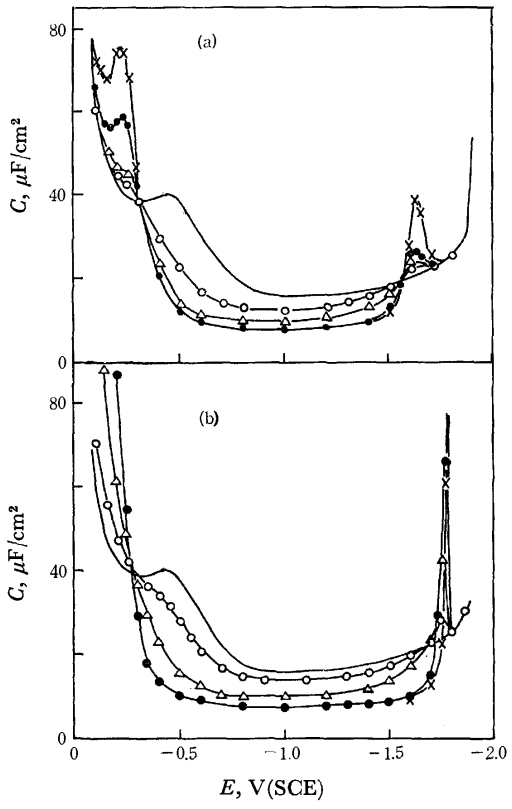

Fig. 1. Differential capacity *vs.* potential curves.
1 kHz, t_B=8 sec, (a) 1N potassium chloride+PEG $\bar{M}$=600, −: 0 mg/*l* PEG, ○: 5 mg/*l*, △: 10 mg/*l*, ●: 50 mg/*l*, ×: 200 mg/*l*, (b) 1N potassium chloride+PEG $\bar{M}$=8400, −: 0 mg/*l* PEG, ○: 6 mg/*l*, △: 15 mg/*l*, ●: 30 mg/*l*, ×: 100 mg/*l*.

becomes stronger with the increase in $\bar{M}$. The differential capacity is depressed as the concentration increases in the adsorption range of PEG between the two peaks. The increase in the adsorbability of PEG with $\bar{M}$ may be expected from the extension of the adsorption range by the increase in $\bar{M}$ under a constant *a*. When the saturated adsorption of PEG was attainable, the differential capacity became approximately constant at −0.9——1.2 V, where the time-dependence of the capacity and of the instantaneous current were examined. The *C-E* curves for the adsorption of PEG in 1N solutions of hydrochloric acid, sulfuric acid, and sodium sulfate were similar to Fig. 1; however, the cathodic peak in the acid solution was not revealed because of the hydrogen evolution.

Observed Capacity vs. Time Curves (C_E-t Curves): The C_E-*t* curves at −1.2 V in 1N potassium chloride are shown in Fig. 2, where (a) and (b) are concerned with $\bar{M}$=600 and 8400. In the solution without adsorbates, the observed capacity (C_E) increases with $t^{2/3}$ or with the growth of a mercury drop;[6] further, the same tendency is also shown after the attainment of the adsorption equlibrium in a relatively concentrated PEG solution. In a relatively concentrated PEG solution the curve for the process controlled

5) PMA (polymethacric acid); I. R. Miller and D. C. Grahame, *J. Amer. Chem. Soc.*, **78**, 3577 (1956).

6) $C_E=0.85\,C_0 m^{2/3} t^{2/3}$, where C_0 and m are the differential capacity (μF/cm²) in the solution without adsorbates and the flow rate of mercury (g/sec).

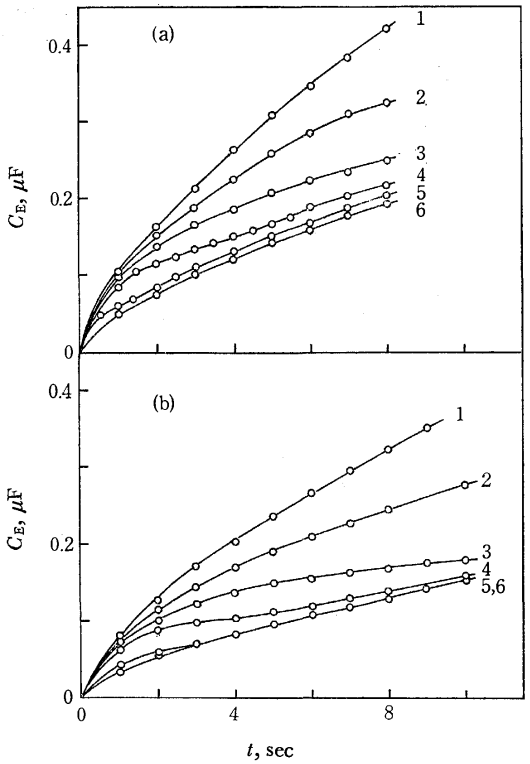

Fig. 2. Observed differential capacity *vs.* time curves.
1 kHz, at $E=-1.2$ V, (a) 1N potassium chloride+PEG $\bar{M}=600$, 1: 0 mg/*l*, 2: 4.3 mg/*l*, 3: 8.6 mg/*l*, 4: 14.0 mg/*l*, 5: 33.2 mg/*l*, 6: 864 mg/*l*, (b) 1N potassium chloride+PEG $\bar{M}=8400$, 1: 0 mg/*l* PEG, 2: 10.0 mg/*l*, 3: 20.0 mg/*l*, 4: 30.0 mg/*l*, 5: 70.0 mg/*l*, 6: 200 mg/*l*.

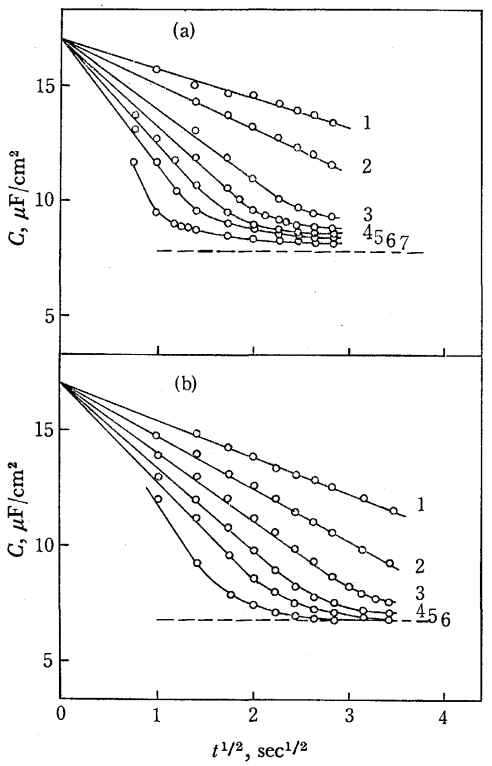

Fig. 3. Differential capacity *vs.* square root of time curves.
1 kHz, at $E=-1.2$ V, (a) 1N potassium chloride+PEG $\bar{M}=600$, 1: 4.3 mg/*l*, 2: 8.6 mg/*l*, 3: 10.8 mg/*l*, 4: 14.0 mg/*l*, 5: 17.3 mg/*l*, 6: 21.6 mg/*l*, 7: 33.2 mg/*l*, ----: C_{min} (minimum differential capacity), (b) 1N potassium chloride+PEG $\bar{M}=8400$, 1: 10.0 mg/*l*, 2: 15.0 mg/*l*, 3: 20.0 mg/*l*, 4: 25.0 mg/*l*, 5: 30.0 mg/*l*, 6: 40.0 mg/*l*, ——: C_{min}.

mainly by the diffusion seems to approach that of the adsorption equilibrium with the increase in time. Such a transition from a diffusion-controlled adsorption to an equilibrium one is clearly revealed in the adsorption of PVP,[1] whereas the transition range for PEG is not so clear.

Differential Capacity vs. Square Root of the Time Curves (C-$t^{1/2}$ Curves): For the adsorption controlled by the diffusion of adsorbates, the surface concentration (Γ_t) on a DME at the time (t) was introduced by Koryta;[2]

$$\Gamma_t = 0.736 D^{1/2} a t^{1/2} \qquad (1)$$

where Γ_t, D, a, and t are the surface concentration of adsorbates at time t in mol/cm², the diffusion coefficient in cm²/sec, the bulk concentration in mol/cm³, and the time from the beginning of its adsorption in sec. For the sake of convenience, the bulk concentration in mg/*l* was used for the experiments instead of that in mol/cm³. By replacing Eq. (1) in the relation of Frumkin's parallel condencer model with $\theta=\Gamma_t/\Gamma_m$, the time-dependence of C on the diffusion-controlled adsorption is obtained as follows:

$$C = C_0 - 0.736(C_0 - C_1) D^{1/2} \Gamma_m^{-1} a t^{1/2} \qquad (2)$$

where C is the differential capacity in μF/cm², θ, the coverage; C_0 or C_1, the differential capacity at $\theta=0$ or $\theta=1$, and Γ_m, the maximum surface concentration. When t_{mc} is the time required to attain the saturated adsorption, Eq. (2) holds for $t \leq t_{mc}$. For $t > t_{mc}$,

$$C = C_1 \qquad (2)'$$

Figure 3 is obtained from C_E-t curves with Eqs. (2) and (2)', where (a) and (b) are concerned with $\bar{M}=600$ and 8400. The linear decrease in C with $t^{1/2}$ is due to the diffusion-controlled adsorption, while a nearly constant C is revealed, independently of t,

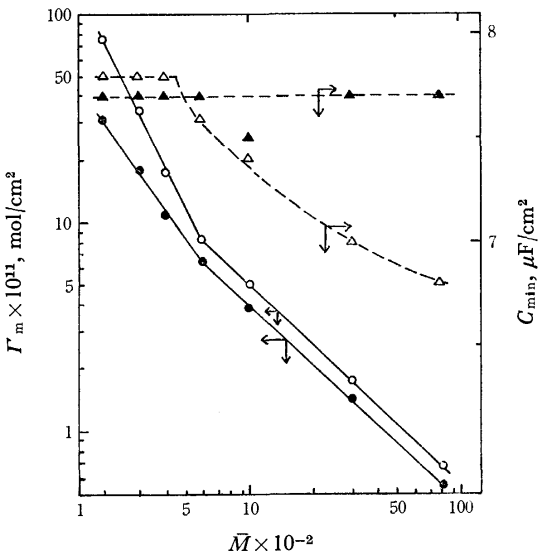

Fig. 4. Relation between mean molecular weight and maximum surface concentration (solid lines) or minimum differential capacity (broken lines).
solid lines: Γ_m—$\bar{M}$ curves (○: 1N potassium chloride+PEG, ●: 1N hydrochloric acid+PEG), broken lines: C_{min}—$\bar{M}$ curves (△: 1N potassium chloride+PEG, ▲: 1N hydrochloride acid+PEG).

with the adsorption equilibrium. The behavior of PEG deviated somewhat from Eqs. (2) and (2)', unlike that of PVP,[1] which was approximately consistent with the Koryta equation based on pure diffusion except for the transient range from the diffusion-controlled to the saturated adsorption. Such a deviation is obviously revealed by the curves for PEG of an especially low $\bar{M}$, as is shown in Fig. 3-(a), where each curve seems to attain an individual capacity at the adsorption equilibrium dependent on the concentration. This tendency is due to the lower adsorbability of PEG as compared with that of PVP. The time (t_{mc}) needed to attain Γ_m can be estimated by extrapolating the linear relation of C-$t^{1/2}$ to the minimum differential capacity; then, Γ_m is obtainable from the Koryta equation [Eq. (1)] on the assumption of its diffusion coefficient.

Relation between the Maximum Surface Concentration and the Mean Molecular Weight (Γ_m-$\bar{M}$ Curves): It is necessary to assume the diffusion coefficient (D) of adsorbates in order to evaluate Γ_m from the Koryta equation. Scholtan's relation[7] between D and $\bar{M}$, which is used for the assumption of D, is as follows:

$$D^2\bar{M} = 10^{-8} \quad (3)$$

In Fig. 4, the Γ_m obtained from Eq. (1) is plotted against $\bar{M}$ by the solid line; the values of Γ_m in 1N potassium chloride are larger than those in 1N hydrochloric acid by *ca.* 20%. Both plots of log Γ_m *vs.* log $\bar{M}$ reveal linear relations with the slope of *ca.* -1 in the range of $\bar{M}\geq 600$. The relation of the $\bar{M}\cdot\Gamma_m =$ const. may be found from the above slope. From this relation, obtained also for PVP,[1] the total segment numbers of PEG molecules adsorbed per unit area at the interface can be considered to be constant, regardless of $\bar{M}$. In the range of $\bar{M}<600$, each slope of logΓ_m *vs.* log$\bar{M}$ plots is different from that for $M\geq 600$; therefore, the configuration for $\bar{M}<600$ at the interface can be considered to be different from that for $M\geq 600$. The Γ_m values dependent on the electolyte may result from a small change in the adsorbed layer influenced by the pH value of the solution.

Relation between the Minimum Differential Capacity and the Mean Molecular Weight (C_{min}-$\bar{M}$ Curves): The thickness of the adsorbed layer can be examined by means of the following well-known relation:

$$C_{min} = \varepsilon/(4\pi\delta) \quad (4)$$

where C_{min}, ε, and δ are the minimum differential capacity, the dielectric constant, and the thickness of the adsorbed layer. In the case of $\bar{M}\geq 600$, the $\bar{M}$-dependence of C_{min} may be negligible because of nearly constant segment numbers adsorbed per unit area, as found previously from the Γ_m-$\bar{M}$ relation, and the C_{min} observed in 1N hydrochloric acid is independent of $\bar{M}$, whereas the C_{min} in 1N potassium chloride depends on $\bar{M}$ in the range of $\bar{M}\geq 600$, as is shown by the broken line in Fig. 4. The maximum difference between C_{min}'s in 1N solutions of potassium chloride and hydrochloric acid is about 1 μF/cm^2; it may be caused by the variation in the thickness or in the dielectric constant of adsorbed layer. From such a difference as about 10% of C_{min}, however, hardly no basic variation in the adsorbed structure is considered to take place. In this connection, it may be considered, with a constant segment numbers per unit area, that the decrease in C_{min} in aqueous potassium chloride is mainly due to the change in the compactness of the adsorbed layer, which is itself related to the inhibitive action of PEG.

Consequently, for PEG of $\bar{M}\geq 600$, the configuration at the interface may be a spread or flat form consisting of a chain, as may be expected from the Γ_m-$\bar{M}$ relation, and the compactness of the adsorbed layer somewhat depends on $\bar{M}$ in some cases, while in relation to the PEG of $\bar{M}<600$, the configuration at the interface may be quite different from that for PEG of $\bar{M}\geq 600$, in view of the results shown in Fig. 4.

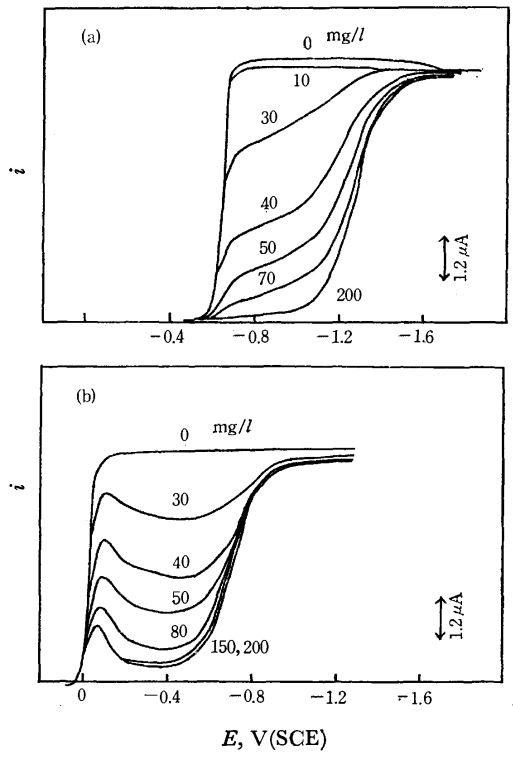

Fig. 5. Polarograms inhibited by PEG.
1N sodium sulfate+PEG $\bar{M}$=8400, (a) depolarizer: 1 mM Cd^{2+}, (b) depolarizer: 1 mM Cu^{2+}.

II) Inhibitive Effect of Adsorbed PEG. Polarograms: Figure 5 consists of typical polarograms which show the inhibitive effect of the PEG of $\bar{M}$=8400 on the reduction of Cd^{2+} or Cu^{2+} in 1N sodium sulfate. In Fig. 5-(a) for Cd^{2+}, the reaction current is depressed as the bulk concentration of PEG is increased, and the depression becomes less with the negative potential. The maximum depression of the reaction current is revealed at nearly -0.9 V, where the instantaneous *i-t* relations are observed, as will be shown later. Judging from the results shown in Fig. 1-(b), it is difficult to consider the current rise at *ca.* -1.2 V to be due to the desorption of PEG, but it may be ascribed to the inhibition weakened at a sufficiently negative potential.

7) W. Scholtan, *Makromol. Chem.*, **7**, 209 (1951).

In Fig. 5-(b) for Cu^{2+}, a current peak appears at *ca.* -0.1 V; it seems to be due to the desorption of PEG because of the increase in capacity at *ca.* -0.1 V in Fig. 1-(b), though the formation of an intermediate product[8] should also be taken into account. For the copper deposition, instantaneous *i-t* curves were observed at -0.4 V.

In 1N solutions of potassium chloride and hydrochloric acid, no inhibitive effect of adsorbed PEG was revealed because of the effect of the chloride ion, as has been discussed by Delahay.[9] Therefore, the inhibitive effect of PEG was examined in 1N solution of sodium sulfate or sulfuric acid.

Instantaneous Current vs. Time Curves (i-t Curves): The instantaneous *i-t* curves for the inhibitive effect of PEG on the reduction of Cu^{2+} revealed a tendency similar to that for Cd^{2+}; therefore, only the latter will be discussed here as an example. Figure 6 shows the *i-t* curves for the reduction of Cd^{2+} in 1N sodium sulfate with several concentrations of PEG, where (a) and (b) are related to the PEG of $\bar{M}=600$ and 8400 These curves are nearly analogous to the results by Schmid and Reilley[10] obtained for the adsorption of Triton X, which is controlled by the diffusion. The time t_{mi} (or t_{mc}) needed to complete a monolayer or the full coverage may be computed from Eq. (1) or (5)[11] modified as follows on the assumption that the complete inhibition takes place under full coverage by the adsorbates, whose process is controlled by the diffusion.

$$t_{mi} = t_{mc} = 1.82\Gamma_m^2/a^2D \qquad (5)$$

Therefore, t_{mi} should be in accordance with the t_{mc} obtained from the C-$t^{1/2}$ relation in Fig. 3.

In the adsorption of PVP,[12] t_{mi} was in good agreement with t_{mc}; in this case, t_{mi} was estimated by extrapolating the steeply depressed part to the time of zero current in the *i-t* relation.

In the case of PEG, the adsorption behavior somewhat deviates from that of the process simply controlled by the diffusion as has been stated previously, and a complete inhibition can not always be expected, even for the full coverage. Therefore, the value of t_{mi} for PEG was determined from the intersection obtained by extrapolating the steeply depressed part of the current to the extremely inhibited current in a considerably concentrated solution of PEG, on the assumption that the extremely inhibited current corresponded to the minimum current in the case of the maximum inhibition.

Comparison of t_{mc} with t_{mi}: The relations of log *a* *vs.* log t_{mi} are shown in Fig. 7. Further, the values of $at_{mc}^{1/2}$ and $at_{mi}^{1/2}$ are listed in Table 1, where $at_{mi}^{1/2}$ and $at_{mi}^{1/2}$ are shown instead of Γ_m since they are the values obtained directly without assuming the diffusion coefficient. The result for $at_{mc}^{1/2}$ shown in Table 1 was evaluated by extrapolating the C in the C-a relation to the minimum differential capacity at a constant t on the basis of Eq. (2). The value of $at_{mc}^{1/2}$ or $at_{mi}^{1/2}$ should be equal to a at $t_{mi}=1$ in Fig. 7.

Equation (5) can be rewritten as follows:

$$\log a = (-1/2)\log t_{mi} + \text{const.}$$

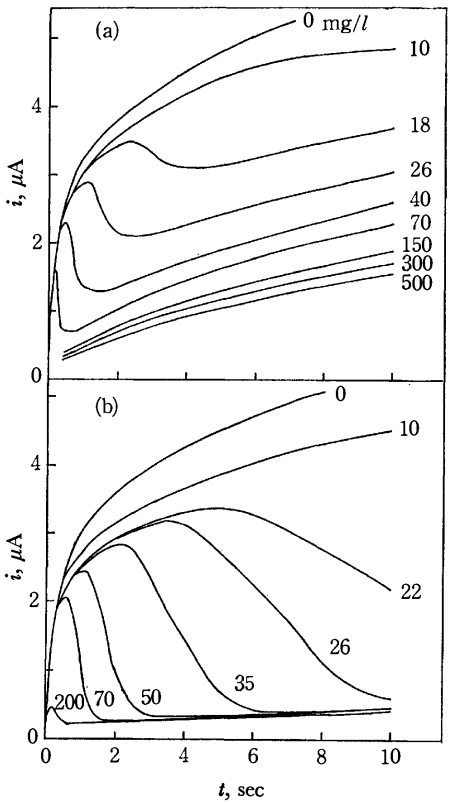

Fig. 6. Instantaneous current *vs.* time curves.
1N sodium sulfate+1 mM Cd^{2+}+PEG, at $E=-0.9$ V, (a) PEG of $\bar{M}=600$, (b) PEG of $\bar{M}=8400$.

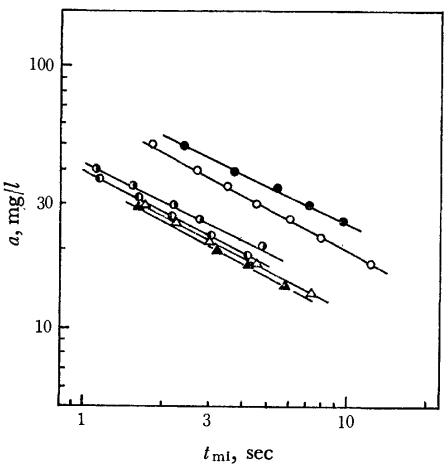

Fig. 7. Relation between saturation time (t_{mi}) and bulk concentration.
1N sodium sulfate+PEG (◑: $\bar{M}=600$, ▲: $M=1000$, ●: $\bar{M}=8400$), 1N sulfuric acid+PEG (◐: $\bar{M}=600$, △: $\bar{M}=1000$, ○: $\bar{M}=8400$).

8) I. M. Kolthoff and Y. Okinaka, *J. Amer. Chem. Soc.*, **81**, 2296 (1959).
9) P. Delahay and I. Trachtenberg, *ibid.*, **80**, 2094 (1958).
10) R. W. Schmid and C. N. Reilley, *ibid.* **80**, 2087 (1958).
11) t_{mi} and t_{mc} are the times needed to attain the maximum inhibition and the minimum differential capacity respectively, when $\Gamma_t=\Gamma_m$, $t=t_{mi}=t_{mc}$. Then, Eq. (5) can be given by Eq. (1).
12) T. Yoshida and T. Ohsaka, *Bull. Sci. Eng. Res. Lab, Waseda Univ.*, **58**, 34 (1972).

Table 1. Comparison of $at_{mc}^{1/2}$ with $at_{mi}^{1/2}$

PEG $\bar{M}$	$at_{mc}^{1/2}$ (mg·sec$^{1/2}$·l^{-1})$^{a)}$		$at_{mi}^{1/2}$ for Cd^{2+} $^{b)}$	
	1N KCl	1N HCl	1N Na_2SO_4	1N H_2SO_4
200	76.2 (−0.9 V)	89.2 (−0.9 V)		
300	60.5 (−1.2 V)	34.7 (−0.9 V)		
400	40.3 (−1.2 V)	29.1 (−1.0 V)		
600	32.8 (−1.2 V)	25.1 (−1.0 V)	43.6 (−0.9 V)	40.9 (−0.9 V)
1000	35.5 (−1.2 V)	27.8 (−1.0 V)	36.0 (−0.9 V)	38.7 (−0.9 V)
3100	55.3 (−1.2 V)	45.8 (−1.0 V)		
8400	71.8 (−1.2 V)	59.2 (−1.0 V)	79.4 (−0.9 V)	79.4 (−0.9 V)

a) The mean values of $at_{mc}^{1/2}$ at t of 3, 5, and 7 sec from *C-a* curves.
b) The mean values of $at_{mi}^{1/2}$ at several concentrations from *i-t* curves.

As can be expected from this relation, the log t_{mi} *vs.* log a plot in Fig. 7 reveals a nearly linear relation with the slope of *ca.* −1/2, regardlesss of $\bar{M}$, and so the adsorption process of PEG is controlled by the diffusion under the present experimental conditions.

The data in Table 1 are markedly scattered. In the case of $\bar{M}$=1000, however, the result of $at_{mc}^{1/2}$ in aqueous potassium chloride is approximately accordance with that of $at_{mi}^{1/2}$ in aqueous sodium sulfate or sulfuric acid. The results of t_{mi} for PEG of $\bar{M}$=1000 and 8400 are considered to be approximately reliable.

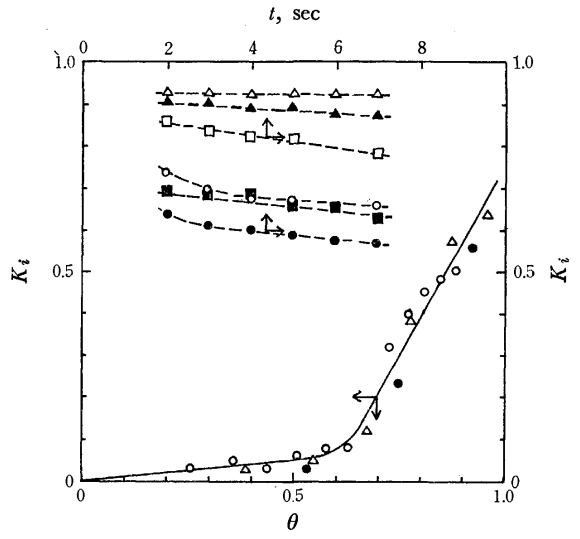

Fig. 8. Dependence of inhibitive efficiency on coverage, or on time after the attainment of saturated adsorption.
at E=−0.9 V, depolarizer: 1 mM Cd^{2+}, solid line: K_i—θ ($t \leq t_{mi}$) curve, 1N sodium sulfate+PEG of $\bar{M}$=1000 (○: 10 mg/l PEG, △: 15 mg/l, ●: 20 mg/l), broken lines: K_i—t ($t > t_{mi}$) curves, 1N sodium sulfate+PEG (○: PEG of $\bar{M}$=600, □: $\bar{M}$=1000, △: $\bar{M}$=8400), 1N sulfuric acid+PEG (●: PEG of $\bar{M}$=600, ■: $\bar{M}$=1000, ▲: $\bar{M}$=8400).

For $\bar{M}$=600,, the data are too scattered, perhaps because the behavior deviates somewhat from that of the adsorption simply controlled by the diffusion, as is revealed in Fig. 3-(a). The result in aqueous hydrochloric acid differs considerably from those in other solutions, though the dependence on the supporting electrolyte remains to be explained.

Relation between the Inhibitive Efficiency and the Coverage (K_i-θ Curve): The inhibitive efficiency (K_i) is given by $(i_b-i)/i_b$, where i and i_b are the instantaneous currents in the solution with and without PEG. At the time $t \leq t_{mi}$ during the diffusion-controlled adsorption, the coverage can be written by means of the Koryta equation as follows: $\theta = \Gamma_t/\Gamma_m = (t/t_{mi})^{1/2}$. The solid line in Fig. 8 is a typical plot of the K_i-θ relation, where the inhibition is hardly shown until θ=0.6; then, the sharp increase in K_i is revealed. When the inhibitor and the depolarizer are adsorbed by the process controlled the diffusion, the inhibitive effect on the reaction current is hardly revealed soon compared with t_{mi}; this tendency is clearly shown in Fig. 8. The tendency is revealed by the adsorption of the PEG or PVP of several $\bar{M}$, regardlesss of a. If a blocking effect of adsorbates is solely considered, K_i should be proportional to θ, however, this relation hardly holds usually and other effects must be taken into account in order to explain the behavior of the solid line in Fig. 8. The behavior of the K_i-θ plot may be explained by the geometrical relation between the effective radius of the congregated molecules adsorbed at the interface and the thickness of diffusion paths of the depolarizer. Matsuda[13] derived a theoretical *i-t* relation similar to the above case from the fundamental model assumed for the adsorbed layer; recently he has introduced a relation even more useful for analysis.

In the case of $t > t_m$, the K_i-t relations after the attainment of the saturated adsorption are plotted by the broken lines in Fig. 8. For the purpose of making the inhibitive condition uniform, regardless of $\bar{M}$, the value of K_i for any $\bar{M}$ is always determined in a solution containing PEG of 100 mg/l, because the segment numbers of the PEG adsorbed per unit area are nearly constant, independent of $\bar{M} \geq 600$, and the concentration in mg/l may be approximately proportional to that in segment numbers/l.

The variation in K_i after the completion of the saturated adsorption is shown somewhat in the figure, and it may be discussed from the viewpoint of the rehomogeneity proposed by Kastening.[14] The broken lines also reveal some dependence of K_i on $\bar{M}$ or on the supporting electrolyte. The inhibitive efficiency, K_i, after the attainment of the saturated adsorption increases with $\bar{M}$, which can be expected from the $\bar{M}$-dependence of adsorbability, as is revealed in Figs. 1—3. In the reduction of Cd^{2+}, the observed K_i in 1N sodium sulfate is always higher than that in 1N sulfuric acid; however, the reverse is the case in the reduction of Cu^{2+}, though the cause remains to be explained.

13) H. Matsuda, *Rev. Polaro.* (Japan), **14**, 87 (1969).
14) B. Kastening, *J. Electroanal. Chem.*, **9**, 41 (1965).

The Isomerization of Propylene Oxide on Zeolite Catalysts

Toshinobu IMANAKA, Yasuaki OKAMOTO, and Shiichiro TERANISHI

Department of Chemical Engineering, Faculty of Engineering Science, Osaka University, Osaka

(Received October 9, 1971)

The selectivity and activity of propylene oxide isomerization have been investigated over zeolite catalysts at 100°C. It has been found that the acid strength of a catalyst is a dominant factor in the selectivity and activity. The stronger the acid strength, the larger the ratio of acetone to propionaldehyde. The reaction intermediates are deduced to be a propylene oxide protonated or that adsorbed on a Lewis-acid site. It has also been found that, in the cases of HY, Silnex (SiO_2), and HY treated with pyridine, the selectivity and activity correlate with the strength of the interaction between the propylene oxide and the surface hydroxyl group. Moreover, it has been clarified that the H_0 value of the surface hydroxyl group observed at 3660 cm^{-1} on HY is -8.2——5.6, while that found at 3540 cm^{-1} is $+4.0$—$+4.8$.

The activities and selectivities for reactions catalyzed by solid acid are determined by means of the acid properties of catalysts. The relations between activities for reactions catalyzed by acid and the observed acidities of catalysts have already been reported by many investigators,[1-7] but there have been few studies of the relations between the selectivity and the acid properties. Misono and his coworkers[8,9] have shown that the selectivities for the isomerization of *n*-butenes over metal sulfates are controlled by the acid strength of the catalysts or by the electronegativities of the metal ions. The acid strength determines the electron distributions of the reaction intermediates and consequently controls their stabilities and reactivities. Therefore, it is considered that the acid strength elucidates the selectivity of an acid-catalyzed reaction. In this investigation, the isomerization of propylene oxide on zeolite catalysts was studied in order to clarify the reactions between the selectivity and the acid strength.

Venuto and Landis[10] have reported that propylene oxide is isomerized to propionaldehyde, acetone, and allyl alcohol on NaX and REX catalysts at 100—200°C. Matsumoto and his coworkers[11] have studied the selectivity for propylene oxide isomerization over metals supported on silica, metal oxides, and metal sulfates. Mathieu *et al.*[12,13] have reported that propylene oxide is isomerized to allyl alcohol on the basic sites of lithium phosphates and to propionaldehyde on acid sites of the 3.9 $Cr_2O_3 \cdot 1.1\ WO_3 \cdot 1.8\ H_2O$ catalyst.

In this report, the isomerization of propylene oxide will be studied and the relation between the selectivity (acetone/propionaldehyde) and the acid strength will be discussed. Moreover, the relation between the selectivity for isomerization and the strength of the interaction of the surface hydroxyl group with the reactant will be studied.

Experimental

Materials. The NaY and 10X zeolites were commercial grade. The HY was prepared by conventional ion-exchange procedures using analytical-grade NH_4Cl. The exchange degree of the sodium ion in NaY was found to be 75% according to flame-photometric analysis. The PtY, PdY, and PdHY were prepared from NaY and NH_4Y by the ion-exchange method using chloroplatinic acid and palladiumtetramine dichloride respectively. The degrees of ion exchange were 3.8% for PtY and PdY, and 6.9% for PdHY. PyHY represents the catalyst which was exposed to pyridine vapor of 5 mmHg at 150°C for 30 min and then evacuated at the same temperature for 1 hr under a vacuum of 10^{-4} mmHg. The Silnex (P-526N); SiO_2 was supplied by the Mizusawa Chemical Company.

Procedures. The isomerization of propylene oxide was carried out in a batch reactor at 100°C for 1 hr after treating the catalysts at 400°C for 4 hr under a vacuum of 10^{-4} mmHg. The total pressure was maintained at 10 cmHg by adding propylene oxide to the system in order to compensate for the pressure drop due to adsorption on the catalyst. The weight of the catalyst used was 0.5 g in all cases. The mixture was trapped in a glass ampoule at the temperature of liquid nitrogen, and the liquid components were analyzed by means of gas chromatography.

The infrared spectra of pyridine and propylene oxide adsorbed on catalysts were observed in a IR cell by means of a Hitachi infrared spectrometer. The disks of zeolites and Silnex were prepared by pressing them between polished stainless steel plates to a pressure of about 10 ton/cm^2. After the disks had been treated at 400°C for 4 hr in the IR cell under a vacuum, adsorption experiments were carried out at room temperature.

The acid strength of the catalysts, which had been evacuated at 400°C for 4 hr, were measured by a conventional indicator method using Hammett indicators.

Results and Discussion

The main products arising from the isomerization of propylene oxide on zeolite catalysts were propional-

1) M. W. Tamele, *Discuss. Faraday Soc.*, **8**, 270 (1950).
2) Y. Matsumoto and Y. Morita, *Nenryo Kyokai Shi*, **46**, 168 (1967).
3) V. Z. Drisko, Proc. Intern, Catalysis, 3rd, Amsterdam I, No. 19 (1964).
4) K. Tarama, S. Teranishi, K. Hattori, and T. Ishibashi, *Shokubai*, **4**, No. 1, 69 (1962).
5) Y. Ogino, *ibid.*, **4**, No. 1, 73 (1962).
6) T. Kawakami and Y. Ogino, *ibid.*, **10**, 136 (1968).
7) T. Kagiya, T. Sano, T. Shimidzu, and K. Fukui, *Kogyo Kagaku Zasshi*, **66**, 1893 (1963).
8) M. Misono, Y. Saito, and Y. Yoneda, *J. Catal.*, **9**, 135 (1967).
9) M. Misono, Y. Saito, and Y. Yoneda, *ibid.*, **10**, 88 (1968).
10) P. B. Venuto and P. S. Landis, *Adv. Catal.*, **18**, 259 (1968).
11) H. Matsumoto, Y. Saito, and Y. Yoneda, *Shokubai*, **11**, No. 4, 202 (1969).
12) M. Coudurier, M. V. Mathieu, M. Prettre, B. Imelik, and M. E. Degeorges, *Bull. Soc. Chim. Fr.*, **1968**, 1921.
13) G. France and M. V. Mathieu, *ibid.*, **1971**, 2891.

TABLE 1. CONVERSION AND SELECTIVITY OF THE PROPYLENE OXIDE ISOMERIZATION AND ACID STRENGTH OF THE CATALYSTS

Catalyst	Conversion (%)		Acetone/ Propion-aldehyde	Acid strength H_0
	Acetone	Propion-aldehyde		
HY	7.2	12.8	0.63	−8.2——5.6
PdHY	4.7	9.3	0.51	−5.6—0.8
PdY	2.9	10.1	0.29	0.8—2.0
PtY	5.1	9.9	0.51	0.8—2.0
10X	7.0	13.0	0.54	0.8—2.0
NaY	0.0_{02}	0.0_1	0.20	4.0—4.8
PyHY	0.07	0.23	0.37	4.0—4.8
Silnex	0.27	6.2	0.043	4.0—4.8

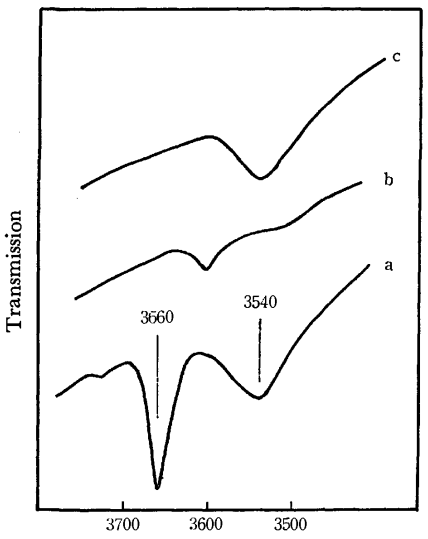

Fig. 1. IR spectra of HY and PyHY catalysts. a: HY, b: HY treated with pyridine vapor of 5 mmHg at 150°C for 30 min c: PyHY —— after treatment with pyridine vapor, evacuation was carried out at 150°C for 1 hr.

dehyde and acetone. Traces of allyl alcohol, acrolein, water, and condensed products were observed. Table 1 shows the conversions of propylene oxide to propionaldehyde and acetone and the selectivities (acetone/propionaldehyde) for each catalyst. The observed acid strength of each catalyst is presented in the last column of Table 1. The acid strength of PyHY (H_0=+4.0—+4.8) is as weak as those of NaY and Silnex. The IR spectra of PyHY and HY are shown in Fig. 1. HY zeolite has two species of surface hydroxyl groups, which are observed at 3660 cm^{-1} and 3540 cm^{-1}. However, the PyHY catalyst has only one kind of surface hydroxyl group, observed at 3540 cm^{-1}. Therefore, it is considered that the H_0 value of the surface hydroxyl group observed at 3660 cm^{-1} is −8.2——5.6, while the one found at 3540 cm^{-1} is +4.0—+4.8. The acid strength of each surface hydroxyl group has been measured by Hair and Hertl[14] by comparing the frequency shifts observed during the adsorption of basic compounds on surface hydroxyl

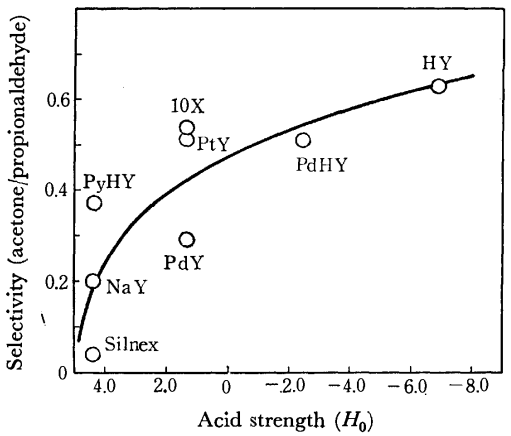

Fig. 2. Correlation between the selectivity (at 100°C) and the acid strength of the zeolite catalyst.

groups of several oxides with those of alcohols. However, no measurements have been reported using the indicator method.

Figure 2 shows the relation between the selectivities for propylene oxide isomerization and the acid strengths of the catalysts used. It is surprising that the stronger the acid strength, the larger the ratio of acetone to propionaldehyde. The only product may be propionaldehyde when the acid strength of the catalyst becomes weaker.

The IR spectra of the HY and Silnex catalysts exposed to propylene oxide are shown in Fig. 2. In the case of Silnex catalyst, the surface hydroxyl group observed at 3740 cm^{-1} interacts with propylene oxide and produces a new broad absorption band at 3370 cm^{-1}, but the surface hydroxyl group found at 3650 cm^{-1} has no interaction with the reactant. The difference between these two hydroxyl groups has been reported by Basila[15] for several compounds adsorbed on silica gel. The adsorption band due to CH_2 in the epoxide ring of propylene oxide exists at 3040 cm^{-1}, and there is no absorption band due to a carbonyl group. These

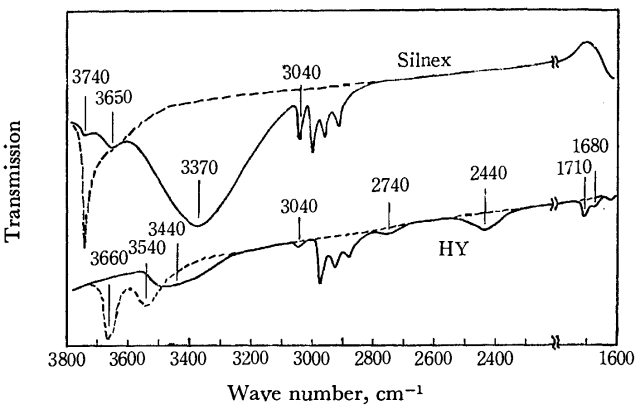

Fig. 3. IR spectra of HY and Silnex after exposure to propylene oxide. Dotted line: before exposure, Solid line: after exposure. Introduction of propylene oxide (pressure; HY: 8 mmHg, Silnex: 18 mmHg), subsequent evacuation for 1 hr, and measurements of IR spectra were carried out at room temperature.

14) M. L. Hair and W. Hertl, *J. Phys. Chem.*, **74**, 91 (1970).

15) M. R. Basila, *J. Chem. Phys.*, **35**, 1151 (1961).

facts show that the epoxide ring is not open, and that propylene oxide adsorbs on Silnex to form a protonated propylene oxide. In the case of the HY catalyst, however, a weak absorption band of CH_2 is observed and new bands appear immediately after exposure to propylene oxide at room temperature; these bands are 1710 cm^{-1} (due to carbonyl groups of physisorbed acetone and propionaldehyde), 1680 cm^{-1} (carbonyl groups of chemisorbed acetone and propionaldehyde), 1380 cm^{-1} (CH bending of acetone), and 2740 cm^{-1} (CHO of propionaldehyde). These facts show that acetone and propionaldehyde are produced. Both of the surface hydroxyl groups on HY catalysts observed at 3660 cm^{-1} and 3540 cm^{-1} are considered to interact with propylene oxide to form broad new bands at 3440 cm^{-1} and 2440 cm^{-1}. The reason for this is that when a small amount of acetone or propionaldehyde is adsorbed on the HY catalyst, strong absorption bands due to carbonyl group are observed, but the strength of the band due to surface hydroxyl group is not particularly reduced. The weak absorption bands due to carbonyl groups are observed only in the case of propylene oxide adsorption. Therefore, it is considered that the shifts of the hydroxyl groups can be ascribed to the interaction with propylene oxide. The surface hydroxyl group observed at 3540 cm^{-1} on the PyHY catalyst interacts with propylene oxide to produce a new band at 3440 cm^{-1}, but no bands at about 1700 cm^{-1} and 2440 cm^{-1}. Consequently, the surface hydroxyl group observed at 3660 cm^{-1} interacts with the oxygen atom of the propylene oxide to form a new band at 2440 cm^{-1} and produces two isomerized products, acetone and propionaldehyde, immediately after exposure, while that observed at 3540 cm^{-1} gives a new band at 3440 cm^{-1} because of the interaction with propylene oxide. In the cases of the other catalysts, the propylene oxide interacting with a proton of adsorbed water and the propylene oxide adsorbed on a Lewis-acid site may be reaction intermediates.

The strength of interaction between the surface hydroxyl group and the propylene oxide is measured in terms of $\Delta\nu_{OH}$ that is, the difference between the wave number of the perturbed hydroxyl group and that of the unperturbed hydroxyl group. The values of $\Delta\nu_{OH}$ are 1220 cm^{-1}, 370 cm^{-1}, and 100 cm^{-1} for

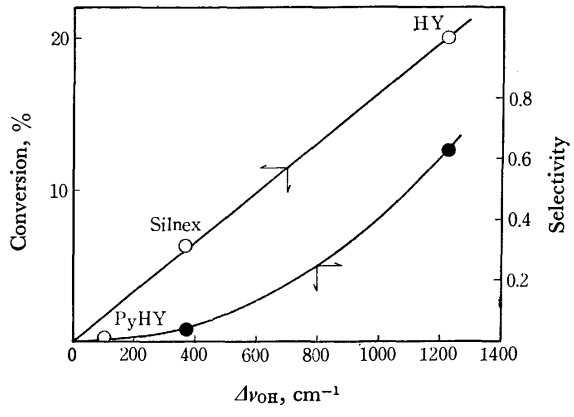

Fig. 4. Correlation between $\Delta\nu_{OH}$ and the reactivity of propylene oxide isomerization.

3660 cm^{-1} on HY; 3740 cm^{-1} on Silnex, and 3540 cm^{-1} on the HY and PyHY catalysts. The total conversions of propylene oxide to acetone and propionaldehyde are 20.0, 6.47, and 0.30% for the HY, Silnex, and PyHY catalysts, as is shown in Table 1. Fig. 4 shows the relation between the strength of the interaction and the conversion. The relation between the selectivity and $\Delta\nu_{OH}$ is also shown in Fig. 4. It has been reported[16,17] that the acidities of the HY catalyst are about 1 mmol/g in the regions of $-8.2 \leqq H_0 \leqq -5.6$ and $-5.6 \leqq H_0 \leqq +4.8$, and that the acid content of silica gel is also about 1 mmol/g. Therefore, it can be deduced that Fig. 4 shows the approximate effect of the acid strength. The selectivity of isomerization to acetone on the PyHY catalyst in Table 1 is higher than the value estimated from Fig. 4. It is considered, from the IR studies, that the pyridine interacting with the 3660 cm^{-1} hydroxyl group is desorbed partially by the adsorption of propylene oxide during the reaction, and that consequently the isomerized products on PyHY contain some products arising from the HY catalyst. These facts support the idea that the protonated propylene oxide is a reaction intermediate on the HY, PyHY, and Silnex catalysts, and that the acid strength of catalyst controls the selectivity. Therefore, the reaction path may be as follows:

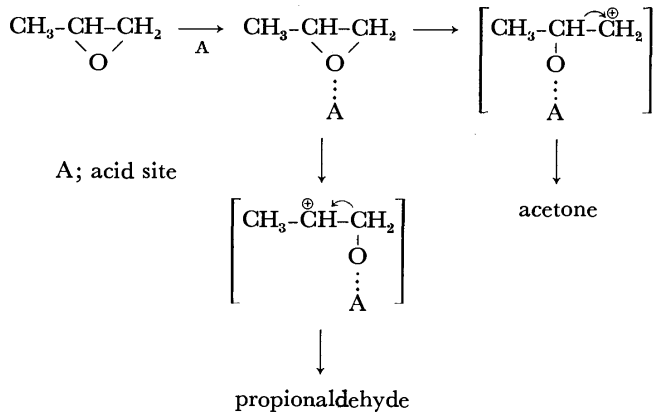

The selectivity for this reaction is determined by the acid strength of the catalyst, as is shown in Fig. 2 and 4. This fact can be explained as follows. It is generally considered that the stronger the acid strength of the catalyst, the more strongly is the electron drawn from carbon-oxygen bonds in the epoxide ring by the acid site. In the case of strong acid, the bond strengths of O-CH(α-bond) and O-CH_2(β-bond) are consequently weakened, but the methyl group releases electrons and strengthens the α-bond. Therefore, the ratio of the probability of β-bond opening to that of α-that is, the selectivity of acetone to propionaldehyde-is large. However, in the case of weak acid, since the acid site draws the electron mildly, the electron released by the methyl group enters the antibonding

16) S. Otoma, Y. Arai, and H. Ukihashi, Preprints for the 20th Annual Meeting of the Chemical Society of Japan (April 1967), No. 11209.

17) W. K. Hall, H. P. Leftin, F. J. Cheselske, and D. E. O'Reilly, *J. Catal.*, **2**, 506 (1963).

level[18] of the α-bond and the strength of the α-bond is weakened. Hence, the α-bond opening becomes more easily than the β-bond opening; that is, the selectivity of acetone to propionaldehyde becomes lower.

In this reaction, the deactivation for HY and PdHY is caused by the formation of coke and polymerized products which have an absorption band at 1570 cm^{-1}. Propylene oxide is dehydrated by sulfuric acid and forms cokes, but no coke is formed by hydrochloric acid, which has no dehydration ability. Therefore, the deactivation may be due to the large dehydration ability of the surface hydroxyl groups on HY and PdHY, mainly the 3660 cm^{-1} hydroxyl groups.

The selectivity of isomerization at 200°C becomes lower than that at 100°C except for PtY; (selectivity at 200°C; 0.53) and PdY (0.99). Matsumoto and his co-workers[11] have reported that the selectivity of acetone to propionaldehyde is high on platinum (0.42 at 350°C) and palladium metals (1.89 at 256°C). It is considered that the activity of metal ions becomes comparable at 200°C with that of acid sites. The metal ions on zeolites are deduced to be active as metals supported on silica, metal sulfates, and metal oxides.

18) K. Simizu, H. Kato, and T. Yonezawa, Preprints for the 20th Annual Meeting of the Chemical Society of Japan (April, 1967), No. 1, 92.

Conclusions

The activity and selectivity of the propylene oxide isomerization of a zeolite catalyst are found to be controlled by the acid strength of the catalyst. It is considered that the reaction intermediates are the protonated propylene oxide and propylene oxide adsorbed on the Lewis-acid site. The electron distributions of intermediates may be determined by the acid strength of the catalyst, and, consequently, the selectivity and activity may be controlled by the acid strength.

Interestingly, it is found that, in the cases of the HY, PyHY, and Silnex catalysts, the activity and selectivity are related to the strength of the interaction, which is represented by $\Delta\nu_{OH}$.

Moreover, it is clarified that the H_0 value of the surface hydroxyl group observed at 3660 cm^{-1} on HY zeolite is -8.2——5.6 while that found at 3540 cm^{-1} is $+4.0$—$+4.8$.

BULLETIN OF THE CHEMICAL SOCIETY OF JAPAN, VOL. 45, 3254—3261 (1972)

Studies on Intermolecular Complex Formation. II. Crystal Structure of Cytosine-*N*-Benzoylglycine Complx Monohydrate

Chihiro TAMURA, Tadashi HATA, Sadao SATO, and Noriko SAKURAI

The Central Research Laboratories of Sankyo Co., Ltd., Hiromachi, Shinagawa-ku, Tokyo

(Received December 28, 1971)

Many intermolecular complexes between *N*-acylamino acids and nucleotide bases have been found by means of X-ray powder diffractometry. Among these, the crystal structure of *N*-benzoylglycine cytosine complex monohydrate has been determined by the direct method. The crystal data are: $a=18.71$, $b=7.11$, $c=18.37$ Å, and $\beta=144.0°$. The space group is $P2_1/c$; $D_{obsd}=1.37$; $D_{calcd}=1.35$ g/cm^3. The final R factor was 0.131. In the crystal, a cytosinyl cation and a *N*-benzoylglycyl anion are joined by two NH···O hydrogen bonds, of which the shorter one is 2.652 Å long. Such a complex formation may exist *in vivo*.

Complementary hydrogen bonding between purine and pyrimidine bases in the Watson-Crick model of DNA is widely known, and several crystals of model complexes of nucleotide bases have been studied by single-crystal analysis.[1-7] Such base pairs are also assumed in explaining the structure of the stem in the clover model of *t*-RNA and the codon-anticodon interaction between *t*- and *m*-RNA. In biological systems, similar hydrogen bonding may exist not only between these bases, but also between nucleotides and peptides. However, no structural studies of the latter hydrogen bonding have yet been published. As we have previously reported,[8] a survey of the complex formation ability by means of X-ray diffractometry showed that none of the amino acids binds with any bases in spite of the fact that the carboxylic acid could give rise to an affinity for adenine and/or cytosine. It was assumed that the inertness of amino acids was due to their zwitterion structure. Subsequently, we have continued the survey using some modified amino acids which were presumed to suppress the zwitterion

1) F. S. Mathews and A. Rich, *J. Mol. Biol.*, **8**, 89 (1964).
2) L. Katz, K. Tomita, and A. Rich, *ibid.*, **13**, 340 (1969).
3) A. E. V. Hashemeyer and H. M. Sobell, *Acta Crystallogr.*, **18**, 525 (1965).
4) E. J. O'Brien, *ibid.*, **23**, 92 (1967).
5) H. M. Sobell, K. Tomita, and A. Rich, *Proc. Natl. Acad. Sci. U. S.*, **40**, 885 (1963).
6) A. E. Hashemeyer and H. M. Sobell, *Nature*, **202**, 969 (1964).
7) K. Hoogsteen, *Acta Crystallogr.*, **12**, 822 (1959); *ibid.*, **16**, 907 (1963).
8) C. Tamura, N. Sakurai, and S. Sato, This Bulletin, **44**, 1473 (1971).

formation; we found that many *N*-acylamino acids combine with adenine and/or cytosine. Herein we will describe the formation of the complexes of N-acylamino acids with nucleotide bases[9] and the crystal structure of one such complex: *N*-benzoylglycine-cytosine complex monohydrate.

Experimental

The ability of complex formation for nucleotide bases was examined in a similar manner, as has already been reported[8]

The procedure may be described briefly as follows: equivalent moles of the *N*-acylamino acid derivative and the base were dissolved in hot 70% aqueous ethanol, and the mixture was allowed to stand for several days in a refrigerator. X-ray diffractions of the materials obtained were measured up to $2\theta=50°$ (for CuK_α) with a Rigaku Denki model D6C diffractometer. These materials were generally fine crystalline powders which were not suitable for X-ray single-crystal analysis. The formation of new crystalline species was verified by comparing their diffraction patterns with those of the components. The only complex obtained as a single crystal at this stage was *N*-benzoylglycine-cytosine.

Because of the coexistence of the component crystals, single crystals of the complex were separated under a stereomicroscope; two components, cytosine and *N*-benzoylglycine, were detected by means of a mass spectrogram. The unit-cell dimensions and the space group were determined from Weissenberg photographs, and the density of the crystals was measured by the floatation technique. The crystal and physical data obtained are as follows: Monoclinic, $a=18.71$, $b=7.11$, $c=18.37$ Å, $\beta=144°$, Volume$=1436.4$ Å^3, $Z=4$, $D_{obsd}=1.37$, $D_{calcd}=1.35$ g/cm^3. Space group $P2_1/c$. Three-dimensional intensity data were collected from the equi-inclination Weissenberg photographs along the *b* axis through the layers of *h*0*l*—*h*6*l*. The intensities of 1993 independent reflections were measured by means of visual comparison with a standard scale. Lorentz-polarization corrections were made in the usual way, and the structure factors on an absolute scale were derived by Wilson's plot.

Structure Analysis

The phases of the structure factors were determined directly by the symbolic addition procedure for a centrosymmetric case. All the structure factors were converted to $|E|$'s. For the reflections with $E\geqq1.50$, triple-product sign relationships and the associated probabilities were listed by the use of the $\sum$ 2 list program. As a starting set, three linearly independent reflections which had large $|E|$ magnitudes and a large number of interactions (9,1,-6; 5,1,9; 7,6,-3) were assigned to +, and four other reflections were given symbols (2.2,8;A: 6,0,-4;B: 12,3,1;C: 0,1,13;D). After the symbolic addition procedure using $|E|$'s greater than 1.50, the B,C, and D symbols were uniquely assigned to −, +, and − respectively. For two possible signs of A, the E-maps were synthesized, and a satisfactory molecular structure was obtained when A is +; the structure factor calculation on the basis of this approximate structure gave an *R* factor of 0.55. After three cycles of a full-matrix least-squares refinement with isotropic thermal parameters, the *R* factor decreased to 0.45. Since the temperature factors of some of the atoms became large, the Fourier synthesis was carried out. In the resulting map, the water molecule was found, and it was revealed that two of the atomic positions had been incorrectly assigned. Starting from the new set of atomic coordinates, six cycles of the full-matrix least-squares refinement with isotropic thermal parameters were carried out; the *R*-factor was thus reduced to 0.17. The hydrogen coordinates were given by the optimum positional calculation, assuming the distances of 1.05 Å for C–H and N–H bonds, since only a few hydrogen atoms were revealed on the difference map. Final cycles of the full-matrix least-squares, with anisotropic thermal parameters except for hydrogen atoms, dropped the *R* to 0.131. The structure factor amplitudes are listed in Table 1, while the final positional and thermal parameters are listed in Table 2(a) and (b).

Results and Discussion

General Ability of Complex Formation of N-*Acylamino acids for Nucleotide Bases.* Table 3 shows the ability of complex formation of *N*-acylamino acid with the nucleotide bases. A + sign denotes the formation of a new crystalline species, and a − shows that no change in diffraction patterns was observed under these conditions. It is remarkable that many *N*-acylamino acids produce complex crystals, contrary to the case of free amino acids. In a previous paper, the inertness of free amino acids for nucleotide bases was assumed to be due to their zwitterion form, which has been established in the crystal structures of many amino acids.[10-15] On the other hand, the crystal analysis of 2-amino-3-methyl-benzoic acid,[16] which can bind with adenine, shows that proton transfer from the carboxylic acid to the amino group does not occur, probably because the amino group is stabilized by π electrons in the benzene ring. Similarly, the *N*-acylation of the amino acids gives rise to a decrease in the proton-accepting ability of the amino group because of the formation of the peptide bond. Consequently, the carboxylic group can donate a proton to any proton-accepting group other than the amino group.

About 88 and 78% of the acidic and neutral *N*-acylamino acids form complex with adenine and/or cytosine under the present experimental conditions, while neither of the basic *N*-acyl derivatives, histidine or arginine, produces any complexes. Therefore, it can be assumed that the acidity of *N*-acylamino acid strongly affects the complex formation with nucleotide bases. How-

9) C. Tamura, N. Sakurai, and S. Sato, The proceeding of the Conference of Pharmaceutical Society of Japan, p. IV-131 (1970).

10) G. A. Jeffrey and Y. Kinoshita, *Acta Crystallogr.*, **16**, 20 (1963).
11) G. S. Parry, *ibid.*, **7**, 313 (1954).
12) R. Gerdil, *ibid.*, **14**, 333 (1961).
13) B. D. Sharman and J. F. McConnell, *ibid.*, **19**, 797 (1965).
14) P. J. Wheatley, *ibid.*, **13**, 80 (1960).
15) Y. Iitaka, *ibid.*, **13**, 35 (1960).
16) G. M. Brown and R. E. March, *ibid.*, **16**, 191 (1963).

TABLE 1. OBSERVED AND CALCULATED STRUCTURE FACTORS

H	FO	FC
L= 0, K= 0		
1	266	383
2	216	241
3	1152	1246
4	172	206
5	95	109
6	265	256
7	493	493
8	120	112
9	72	67
10	111	99
11	32	33
12	44	27
14	32	30
L= 2, K= 0		
0	217	206
1	33	36
2	623	682
3	422	457
4	86	73
5	77	74
6	496	491
7	70	71
8	81	63
9	56	45
10	55	42
11	46	30
-1	256	254
-2	303	240
-3	901	560
-4	1056	974
-5	301	298
-6	220	164
-7	360	327
-8	252	250
-10	55	62
-11	161	148
-12	219	179
-13	45	37
-14	66	27
L= 4, K= 0		
0	372	367
1	539	559
2	216	209
3	232	172
4	66	48
5	112	105
6	45	35
9	112	89
10	30	18
-1	347	359
-2	753	842
-3	266	337
-4	371	442
-5	1756	1717
-6	2215	2274
-7	673	735
-8	260	278
-9	310	369
-10	265	242
-11	117	123
-12	295	297
-13	129	111
L= 6, K= 0		
0	252	264
1	265	310
3	117	84
4	94	96
6	85	80
9	57	38
-1	205	196
-2	314	358
-3	420	460
-4	1161	1047
-6	469	513
-7	403	321
-8	430	349
-9	328	326
-10	246	237
-11	42	45
-12	56	44
-13	134	144
-14	110	117
-15	216	166
-16	32	32
-17	89	71
-18	87	49
L= 8, K= 0		
3	31	26
4	45	22
5	41	31
-1	53	71
-2	191	157
-3	311	283
-4	199	187
-5	267	262
-6	455	485
-7	297	299
-8	334	316
-9	334	302
-10	401	376
-11	514	521
-12	793	774
-13	444	352
-14	75	62
-15	390	383
-17	69	54
-19	66	36
L= 10, K= 0		
1	89	44
-1	146	89
-2	20	9
-3	67	43
-4	130	141
-5	100	127
-6	292	283
-7	36	23
-8	274	277
-9	613	626
-10	235	215
-11	153	110
-12	83	53
-13	94	87
-14	104	101
-15	292	263
-16	156	151
-17	108	81
-18	210	174
-19	72	51
-20	44	44
-21	34	34
L= 12, K= 0		
0	43	21
2	18	6

H	FO	FC
-1	115	62
-2	125	76
-3	51	35
-5	20	24
-6	130	101
-7	66	66
-8	254	184
-9	184	163
-10	35	16
-11	129	129
-12	406	370
-14	66	79
-15	166	148
-16	126	95
-17	218	189
-18	241	224
-19	169	145
-20	79	59
-21	96	83
L= 14, K= 0		
-1	39	12
-2	123	46
-3	67	30
-4	45	18
-5	70	39
-6	159	116
-7	62	36
-9	156	134
-10	70	48
-11	116	124
-12	60	91
-14	81	65
-15	105	78
-16	62	67
-17	32	33
-20	122	101
L= 16, K= 0		
-3	48	16
-5	46	15
-7	89	46
-9	91	49
-10	59	43
-12	89	86
-13	58	36
-14	126	103
-15	59	43
-17	112	78
-19	106	78
-19	64	43
-20	71	66
-21	125	80
-23	72	67
L= 18, K= 0		
-7	63	18
-9	39	8
-10	114	43
-12	45	23
-13	32	4
-16	88	65
-17	55	51
-19	83	52
-20	32	19
-24	25	23
L= 20, K= 0		
-3	54	22
-10	63	27
-11	83	11
-12	67	25
-13	42	22
-14	31	19
-15	44	9
-16	54	21
-17	94	46
-18	54	26
-19	43	26
-20	29	28
-22	43	31
-24	30	35
L= 22, K= 0		
-16	52	14
-17	42	14
-18	50	23
-19	25	15
-20	34	8
-21	50	36
L= 0, K= 1		
1	378	364
2	405	366
3	774	784
4	231	202
5	161	156
6	265	222
7	258	267
11	33	46
12	49	48
14	24	3
L= 1, K= 1		
0	701	725
1	171	173
2	321	365
3	334	357
4	35	45
6	119	123
7	23	22
8	17	6
9	30	37
10	33	29
-1	20	51
-2	61	106
-3	217	246
-4	402	401
-5	37	22
-6	237	251
-7	46	47
-8	192	176
-9	164	143
-10	86	127
-11	233	235
-12	68	72
-13	95	93
-15	78	86
-16	22	26
L= 2, K= 1		
0	655	649
1	467	493
2	507	551
4	53	50
5	167	161
6	106	98
7	17	13
8	56	66
9	77	73
10	19	23
11	63	46
-1	405	447
-2	74	32

H	FO	FC
-3	920	903
-4	566	513
-5	357	350
-6	199	201
-7	314	260
-9	51	56
-10	24	34
-12	62	66
L= 3, K= 1		
0	216	271
1	242	234
2	452	415
3	170	197
5	61	55
6	65	55
7	30	33
8	19	22
9	63	55
11	17	2
-1	552	510
-2	651	579
-3	46	66
-4	321	321
-5	707	681
-6	165	149
-7	212	211
-8	61	82
-10	35	34
-11	76	88
-12	25	35
-13	46	47
-16	26	27
L= 4, K= 1		
0	475	453
1	546	559
2	57	74
3	51	54
4	145	131
5	23	29
6	71	70
7	27	26
8	19	20
9	29	24
10	16	14
-1	93	130
-2	977	933
-3	437	409
-4	299	271
-5	320	317
-6	53	37
-7	475	397
-8	56	71
-9	369	357
-10	61	63
-11	46	59
-12	101	117
-13	106	123
-14	44	41
-15	103	86
L= 5, K= 1		
0	44	56
1	267	253
3	22	22
4	42	42
5	39	30
7	61	61
9	16	15
-1	35	41
-2	503	500
-3	350	372
-4	171	208
-6	22	6
-7	420	435
-8	176	176
-9	54	81
-10	243	226
-11	104	124
-12	70	77
-14	16	25
-15	66	65
-17	42	44
L= 6, K= 1		
0	27	32
1	131	123
2	23	22
4	47	32
6	27	32
7	24	26
9	16	16
-1	195	202
-2	196	219
-3	546	627
-4	14	32
-6	433	423
-7	348	345
-8	171	125
-9	796	762
-10	73	75
-11	116	118
-12	99	102
-13	92	96
-14	80	64
-15	81	76
-16	133	125
L= 7, K= 1		
0	173	165
1	32	32
2	24	9
3	99	104
-1	20	51
-2	61	106
-3	217	246
-4	402	401
-5	37	22
-6	237	251
-7	46	47
-8	192	176
-9	164	143
-10	86	127
-11	233	235
-12	68	72
-13	95	93
-15	78	86
-16	22	26
L= 8, K= 1		
1	57	91
2	35	33
3	51	31
5	36	24
-1	100	104
-2	63	59
-3	19	42
-4	16	38
-5	137	155

H	FO	FC
-5	115	113
-6	79	76
-9	123	93
-10	234	225
-11	223	211
-12	26	57
-13	72	67
-14	96	97
-15	25	26
-16	19	23
-17	33	45
L= 9, K= 1		
0	35	23
1	61	63
2	42	26
5	71	50
-1	56	56
-2	77	72
-3	63	84
-4	164	166
-5	119	113
-6	42	39
-7	16	23
-8	61	76
-9	121	112
-11	150	125
-12	166	200
-13	83	108
-15	135	140
-17	49	47
-20	26	28
L= 10, K= 1		
0	61	39
1	85	59
-2	89	94
-4	181	163
-5	183	189
-6	79	73
-7	215	212
-8	166	179
-9	75	83
-10	176	166
-11	176	130
-12	177	183
-13	60	77
-15	333	315
L= 11, K= 1		
0	53	41
1	26	21
2	16	9
-3	134	129
-5	85	82
-6	79	81
-7	39	74
-8	48	75
-9	237	241
-10	130	134
-11	50	40
-13	45	57
-14	130	133
-15	40	57
-16	122	122
-17	104	99
-18	36	36
L= 12, K= 1		
0	44	26
-3	16	18
-5	47	50
-7	156	136
-8	15	7
-9	93	121
-11	87	91
-12	111	115
-13	147	158
-14	16	36
-17	44	42
-18	82	80
L= 13, K= 1		
3	73	36
5	15	22
-1	58	27
-3	19	11
-5	39	55
-6	24	35
-7	91	64
-8	20	29
-10	104	93
-11	32	33
-12	26	33
-13	98	101
-15	30	37
-17	48	52
-19	74	80
-20	41	46
L= 14, K= 1		
-1	34	18
-3	35	36
-11	33	38
-12	66	83
-13	34	33
-15	94	93
-16	16	36
-17	71	81
-18	54	44
-20	47	46
-21	51	63
L= 15, K= 1		
-3	46	28
-4	25	19
-5	47	35
-7	42	46
-9	51	61
-10	65	63
-11	52	86
-13	59	64
-14	25	47
-15	73	84
-16	16	28
-17	31	43
-21	24	31
L= 16, K= 1		
-4	36	23
-7	53	31
-10	52	34
-13	30	27
-17	37	41
-19	64	61
L= 17, K= 1		
-7	63	37
-11	27	21
-13	67	40

H	FO	FC
-19	76	66
-15	16	14
-17	42	36
-19	53	40
L= 18, K= 1		
-13	27	22
-14	54	44
-15	33	32
-17	71	65
-22	27	27
L= 19, K= 1		
-5	49	25
-12	77	51
-13	33	27
-15	73	43
-17	47	34
-19	33	34
-20	16	25
-22	21	26
L= 20, K= 1		
-7	15	9
-10	52	22
-11	36	26
-12	45	22
-15	37	17
-17	26	16
-21	26	33
L= 21, K= 1		
-11	13	17
-12	54	25
-13	14	11
L= 22, K= 1		
-19	18	14
-17	32	27
-19	14	2
-13	14	14
-20	19	20
L= 23, K= 1		
-17	22	16
-23	16	14
L= 0, K= 2		
1	303	267
2	47	53
3	190	205
5	150	161
6	57	59
7	12	17
8	26	33
9	30	33
10	20	37
12	52	53
13	42	44
L= 1, K= 2		
0	296	315
1	150	141
2	440	429
3	125	119
4	191	175
5	113	129
6	62	69
7	22	23
8	13	40
9	123	127
10	43	46
11	23	30
12	60	61
-2	240	192
-3	537	453
-4	286	218
-6	39	58
-9	27	34
-13	64	87
-12	112	110
-13	27	33
-14	49	44
L= 2, K= 2		
0	35	52
1	350	382
2	220	229
3	69	102
4	78	86
5	151	153
6	104	118
7	23	30
8	24	37
10	14	25
11	16	18
-1	260	263
-2	110	101
-3	45	44
-4	72	78
-5	393	383
-6	547	463
-7	33	28
-8	23	25
-9	69	67
-10	19	33
-11	115	133
-12	67	65
-13	50	66
-14	16	26
L= 3, K= 2		
0	117	126
1	35	54
2	25	30
3	40	72
4	61	60
5	49	49
6	40	46
8	117	115
9	49	45
10	17	19
11	8	10
-1	159	208
-2	563	523
-3	380	339
-4	291	251
-5	555	438
-6	39	44
-9	249	211
-11	57	61
-12	63	73
-13	25	26
-14	32	33
-15	12	1
-15	39	38
L= 4, K= 2		
0	309	314
1	55	35

H	FO	FC
2	47	50
3	61	65
4	72	73
5	30	32
7	148	127
9	76	73
10	25	28
-1	21	14
-3	178	150
-4	124	132
-5	71	68
-6	374	297
-7	313	225
-9	261	215
-11	46	44
-11	70	95
-12	13	26
-14	49	57
-15	14	17
-16	34	34
L= 5, K= 2		
0	478	455
1	112	292
2	26	40
3	53	62
4	89	91
5	47	63
6	21	33
7	20	38
9	26	33
-1	160	209
-2	112	174
-3	461	461
-4	50	71
-5	53	61
-7	122	115
-8	109	96
-9	127	116
-10	176	111
-11	17	8
-13	62	72
-14	32	40
-15	77	76
-17	37	45
L= 6, K= 2		
0	46	52
1	50	56
2	42	44
3	35	43
6	32	29
-1	425	344
-2	126	158
-3	24	24
-4	499	498
-5	43	67
-6	50	37
-7	55	56
-8	160	174
-9	203	242
-10	27	38
-11	51	54
-15	25	20
-17	50	51
L= 7, K= 2		
0	12	27
1	54	54
2	143	141
3	115	105
5	57	53
6	61	45
-1	88	91
-2	151	131
-3	244	244
-4	273	284
-5	107	103
-6	160	131
-7	265	257
-8	194	153
-9	37	29
-10	93	84
-11	85	102
-12	46	68
-13	65	74
-15	51	54
-17	33	32
L= 8, K= 2		
1	126	96
2	211	177
5	66	66
-1	101	97
-2	27	23
-3	167	198
-4	47	63
-5	313	295
-7	19	35
-8	48	46
-9	20	31
-10	145	146
-11	11	5
-12	105	84
-13	46	52
-14	27	46
-15	57	73
-17	14	17
-19	13	23
L= 9, K= 2		
0	125	123
1	14	32
2	54	30
3	60	39
-1	114	117
-2	66	57
-3	100	177
-5	44	78
-6	27	46
-7	133	153
-8	55	61
-11	46	36
-13	57	56
-14	27	24
-13	93	92
-15	20	35
-17	11	21
L= 10, K= 2		
4	34	25
-1	57	61
-2	13	16
-3	13	21
-5	34	52
-6	24	35
-7	150	134
-9	30	41
-13	63	83
-19	126	132

H	FO	FC
-11	11	17
-15	46	55
-16	26	37
L= 11, K= 2		
3	21	15
5	41	33
-1	48	25
-3	81	86
-4	137	145
-5	24	29
-6	61	53
-7	134	145
-9	66	83
-10	35	31
-10	112	100
-12	60	69
-13	70	86
-14	41	47
-17	46	50
-18	36	59
-21	23	33
L= 12, K= 2		
0	46	37
1	29	8
-2	29	31
-3	35	36
-4	104	96
-5	142	136
-6	102	101
-9	60	67
-10	45	49
-11	51	57
-14	40	56
-15	122	125
-17	68	71
L= 13, K= 2		
-1	33	16
-5	43	47
-6	56	105
-7	84	100
-8	18	11
-9	26	26
-10	40	46
-11	25	13
-13	156	144
-14	72	69
-15	103	113
-17	47	44
-18	62	83
-20	42	35
L= 14, K= 2		
-2	69	29
-4	15	25
-5	15	13
-6	14	12
-7	56	55
-8	23	24
-9	47	53
-11	67	75
-12	32	37
-13	26	30
-15	27	43
-19	15	16
L= 15, K= 2		
-3	46	23
-4	58	32
-5	29	25
-6	32	40
-8	160	135
-12	52	53
-14	51	50
-15	36	33
-17	51	53
-18	103	103
-19	25	29
-22	10	1
L= 16, K= 2		
-4	42	2
-5	46	4
-7	41	36
-10	114	93
-11	84	75
-12	41	36
-13	74	73
-14	47	44
-16	32	35
-17	44	44
-19	36	42
-20	20	32
L= 17, K= 2		
-6	26	18
-7	13	11
-9	20	15
-10	15	7
-12	155	131
-13	25	11
-15	29	26
-16	32	41
-17	33	35
-19	29	30
-20	20	25
L= 18, K= 2		
-4	30	17
-11	32	28
-13	26	42
-15	36	31
-16	45	43
-17	25	24
-20	18	19
L= 19, K= 2		
-10	63	49
-16	43	34
L= 20, K= 2		
-11	22	13
-15	27	23
-16	19	20
-17	47	41
L= 21, K= 2		
-18	43	35
-22	12	14
L= 22, K= 2		
-15	22	13
L= 0, K= 3		
1	321	266
2	322	275
3	165	145
4	342	321

H	FO	FC
5	120	124
6	61	104
7	62	68
9	106	111
10	12	15
11	52	84
12	48	46
13	21	23
L= 1, K= 3		
0	144	133
1	317	297
2	14	31
3	25	38
4	34	37
5	165	177
6	144	150
7	22	34
8	119	124
10	43	46
11	43	40
12	66	70
-2	67	57
-3	36	34
-5	145	115
-6	402	367
-7	33	36
-8	25	32
-9	35	36
-10	18	20
-12	34	37
-13	75	57
L= 2, K= 3		
0	0	14
1	79	76
2	146	151
3	81	67
4	205	221
5	103	106
6	53	59
7	18	15
8	30	43
11	17	13
-1	346	344
-2	326	351
-3	356	331
-5	33	33
-6	171	165
-7	31	46
-8	47	44
-9	141	146
-13	50	77
-11	27	27
L= 3, K= 3		
0	359	357
1	56	54
2	140	123
4	60	91
5	75	82
6	103	114
9	49	43
-1	94	85
-2	156	168
-4	126	126
-5	96	95
-6	154	135
-7	66	66
-8	84	85
-10	51	59
-11	169	178
-13	17	22
-15	15	18
L= 4, K= 3		
0	231	233
1	23	31
2	244	244
3	23	26
5	206	195
6	32	31
7	46	55
8	55	47
-1	143	167
-2	275	265
-3	232	231
-4	163	185
-5	250	224
-6	32	27
-7	154	125
-8	127	132
-9	211	181
-11	21	37
-11	64	80
-12	98	95
-14	29	42
-16	23	26
L= 5, K= 3		
0	171	165
1	80	60
2	115	124
3	42	57
6	128	135
7	20	11
8	35	22
1	6	10
-1	262	289
-3	372	367
-4	464	443
-5	78	87
-6	118	118
-7	139	127
-8	83	110
-9	49	44
-10	29	41
-11	116	114
-12	157	169
-14	33	49
-15	17	25
L= 6, K= 3		
0	72	79
2	36	46
3	93	94
4	36	49
5	43	43
6	81	94
7	9	12
8	8	11
-1	37	50
-2	132	141
-3	224	233
-4	154	159
-5	21	49
-6	224	249
-7	134	121
-8	231	227
-10	20	34
-11	24	36

Table 1. (Continue)

H	FO	FC
-12	25	30
-14	54	61
-15	32	43
-16	22	31
-17	33	33
L= 7, K= 3		
0	173	131
1	119	123
2	139	131
3	124	119
4	35	39
5	23	23
7	14	19
-1	38	47
-3	116	126
-4	222	221
-5	145	154
-6	220	193
-7	396	315
-8	76	60
-9	152	151
-10	9	20
-11	36	33
-12	82	84
-16	21	29
L= 8, K= 3		
0	159	188
1	46	50
3	54	58
-1	89	91
-3	89	94
-4	162	165
-6	179	169
-7	89	118
-8	186	193
-9	45	52
-10	117	117
-11	126	127
-13	41	55
-14	96	106
-17	54	52
L= 9, K= 3		
0	91	92
2	51	42
-1	130	119
-2	121	119
-3	132	142
-5	84	88
-6	68	74
-7	59	57
-9	180	188
-10	208	181
-11	37	55
-12	53	63
-14	42	57
-15	23	29
-16	12	26
-17	63	67
-13	16	28
L= 10, K= 3		
0	33	32
2	21	19
-1	41	40
-4	24	33
-5	33	37
-7	18	17
-8	119	133
-9	115	128
-10	51	60
-11	105	104
-12	37	53
-13	31	44
-15	11	17
L= 11, K= 3		
0	46	43
1	14	13
-1	35	36
-2	24	23
-3	53	61
-5	34	33
-6	157	156
-7	93	103
-8	79	87
-9	117	124
-10	53	65
-11	29	30
-12	96	98
-13	89	104
-15	43	51
-16	42	55
-13	26	41
L= 12, K= 3		
-2	17	16
-5	117	113
-6	96	94
-7	112	112
-9	61	69
-10	105	105
-12	59	131
-13	24	24
-14	33	44
-15	83	75
-17	32	42
-19	36	46
L= 13, K= 3		
0	27	17
-1	48	25
-2	42	31
-3	21	18
-5	59	53
-6	52	49
-7	84	74
-8	16	23
-9	37	45
-10	95	96
-11	32	44
-12	25	40
-13	46	43
-14	34	39
-16	46	48
-19	16	21
L= 14, K= 3		
-4	34	23
-6	34	36
-7	42	41
-8	52	57
-9	43	57
-10	58	61
-12	52	51
-13	42	54
-14	55	66
-15	98	92

H	FO	FC
-17	27	39
-16	27	38
-11	24	32
L= 15, K= 3		
-6	36	32
-7	25	22
-8	17	19
-9	32	41
-6	72	76
-7	23	21
-12	162	163
-13	51	52
-15	27	33
-19	58	48
L= 16, K= 3		
-9	30	27
-10	27	29
-12	117	99
-13	58	45
-15	57	79
-16	43	51
-17	25	19
-11	12	12
-20	22	24
L= 17, K= 3		
-6	40	23
-9	26	19
-11	36	30
-12	21	22
-13	73	63
-14	33	35
-15	17	21
-16	53	60
-17	53	53
-13	17	16
L= 18, K= 3		
-7	14	14
-13	30	27
-14	12	9
-16	12	16
-23	25	31
-21	16	28
L= 19, K= 3		
-11	14	13
-15	16	14
-16	42	35
-14	66	56
-21	9	15
L= 20, K= 3		
-15	14	15
-17	15	24
-15	34	36
-13	19	23
-20	25	27
-22	17	23
L= 21, K= 3		
-17	15	13
-19	31	26
L= 22, K= 3		
-13	15	13
-23	6	14

H	FO	FC
-17	23	25
-15	9	9
-11	3	13
L= 10, K= 4		
0	31	27
1	37	28
2	26	24
3	14	11
-1	37	41
-3	49	50
-4	121	126
-5	62	62
-6	8	11
-12	103	120
-6	13	18
-9	24	37
-10	87	92
-11	118	122
-13	44	37
-14	31	48
-16	16	23
-17	12	14
L= 11, K= 4		
0	31	28
1	37	26
-1	49	50
-3	146	148
-4	69	98
-5	44	56
-6	64	64
-10	43	39
-11	37	35
-12	26	34
-13	9	11
-10	87	84
-11	62	62
-12	103	136
-13	47	46
-17	20	19
-15	34	30
-16	19	19
-17	16	19
-18	33	35
L= 12, K= 4		
-2	33	23
-3	14	5
-4	32	27
-5	94	96
-7	15	15
-8	105	103
-9	47	60
-10	37	46
-11	33	38
L= 13, K= 4		
-1	16	14
-2	44	54
-3	56	62
-4	7	6
-5	43	48
-6	27	29
-7	43	48
-8	25	20
-9	45	47
-10	18	16
-11	24	19
L= 3, K= 5		
-7	25	30
-6	6	6
-5	21	25
-4	30	26
-3	30	29
-2	8	12
L= 4, K= 5		
-8	12	22
-9	30	29
L= 5, K= 5		
-16	24	26
-17	23	22
L= 6, K= 5		
-10	63	59
-12	27	26
-13	7	11
-14	24	20
L= 8, K= 5		
1	75	62
2	112	101
3	149	134
-1	33	29
-2	7	3
-3	71	76
-4	37	40
-5	9	11
-6	16	21
-7	43	45
-8	39	39
-9	11	15
-10	62	128
-11	65	60
-13	7	8
-14	70	62
-15	12	12
-17	13	13
L= 9, K= 5		
-4	47	59
-5	9	13
-6	13	8
-7	11	13
-8	57	58
-9	27	35
-10	81	89
-11	82	81
-12	37	38
-13	36	35
-14	21	22
-15	6	12
-10	68	97
-11	82	88
-12	65	67
-13	33	36
-14	20	20
-15	53	47
-16	24	24
-13	9	3
L= 11, K= 5		
0	23	14
1	9	6
-1	17	11
-2	17	11
-3	7	5
-4	33	33
-5	20	30
-6	21	25
-7	10	10
-8	12	22
-9	11	11
-10	13	12
-11	9	11
-12	7	12
L= 12, K= 5		
-1	6	5
-2	14	14
-3	9	11
-4	32	30
-5	18	15
-6	18	10
-7	9	10
-8	21	19
-9	7	6
-10	14	20
-11	13	11
-12	36	24
-13	7	9
-11	25	22
-12	32	26
-13	6	15
L= 13, K= 5		
-2	27	13
-3	25	15
-5	7	9
-6	40	36
-7	13	10
-8	23	21
-9	18	22
-10	7	13
-11	7	9
-12	25	33
-13	10	10
-14	25	25
-15	13	13
-17	50	41
L= 14, K= 5		
-3	4	6
-5	24	12
-6	13	4
-7	16	14
-8	12	12
-9	10	10
-10	37	38
-11	15	14
-12	27	27
-13	16	19
-14	13	13
-15	8	12
-16	28	25
-17	5	6
-18	8	8
-19	18	13
L= 19, K= 5		
-4	4	3
-5	7	8
-6	9	5
-7	4	4
-8	16	17
-9	27	20
-10	16	19
-11	44	75
-12	64	61
-13	42	43
-14	7	4
L= 8, K= 6		
0	6	11
2	24	16
-1	16	15
-3	22	20
-4	41	41
-5	9	7
-6	9	12
-7	7	6
-8	6	6
-9	12	10
-10	13	13
-11	19	19
-12	47	43
-13	23	23
-14	40	42
-15	8	6
-16	9	5
L= 9, K= 6		
1	20	21
-1	41	35
-2	10	9
-3	26	31
-4	16	13
-5	51	58
-6	61	78
-7	19	19
-10	13	13
-11	32	32
-12	47	43
-13	46	43
-14	22	23
-15	29	32
L= 10, K= 6		
-1	10	8
-2	16	16
-3	7	7
-4	30	40
-5	10	9
-10	34	29
-11	25	26
-12	74	78
-13	42	37
-14	14	14
-15	9	8
-17	14	18
L= 11, K= 6		
-2	14	14
-3	8	8
-6	17	15
-7	8	6
-8	28	21
-9	14	15
-10	16	12
-11	16	14
-12	14	16
-13	14	16
-14	30	29
-15	27	26
-16	23	27
-17	26	30
L= 12, K= 6		
-4	7	7
-5	13	8
-6	9	12
-7	27	23
-10	34	27
-12	16	15
-13	38	29
-14	34	33
-15	23	27
-16	7	6
-17	12	12
L= 13, K= 6		
-4	4	7
-5	23	20
-6	11	11
-7	35	35
-8	16	15
-9	12	10
-10	23	22
-11	36	35
-12	47	41
-13	9	10
-14	4	7
-15	7	6
-17	11	13
L= 14, K= 6		
-5	3	4
-7	17	11
-9	6	9
-12	14	14
-14	15	18
-15	16	26
-16	19	19
-17	12	14
-14	23	26
L= 15, K= 6		
-7	0	9
-9	6	5
-10	4	6
-11	11	5
-14	6	7
-16	3	6
-17	12	12
L= 16, K= 6		
-10	9	6
-13	5	3
-14	3	6
-16	5	9
-17	3	4
-18	3	7
L= 17, K= 6		
-13	27	20
-15	9	10
-16	18	17
-17	11	13
L= 18, K= 6		
-14	3	6
-15	3	3

TABLE 2(a). POSITIONAL AND THERMAL PARAMETERS OF NON-HYDROGEN ATOMS AT THE END OF THE LEAST-SQUARES REFINEMENT

Thermal parameters are in the form $\exp[-(\beta_{11}h^2+\beta_{22}k^2+\beta_{33}l^2+\beta_{12}hk+\beta_{13}hl+\beta_{23}kl)]$

	x	y	z	β_{11}	β_{22}	β_{33}	β_{12}	β_{13}	β_{23}
C 1	0.0298	0.2223	0.4229	0.009440	0.041027	0.012760	−0.001028	0.009408	−0.001358
N 2	0.0599	0.4026	0.4665	0.008729	0.032611	0.012819	−0.000650	0.008456	−0.001447
C 3	0.0115	0.5566	0.3960	0.009027	0.034110	0.014488	0.000088	0.009703	−0.000135
N 4	−0.0663	0.5264	0.2769	0.008621	0.041154	0.011100	0.000678	0.007539	0.001027
C 5	−0.0993	0.3508	0.2300	0.011079	0.042139	0.013539	0.000406	0.009612	−0.000921
C 6	−0.0549	0.2008	0.2968	0.010665	0.036418	0.014486	−0.001966	0.009988	−0.004521
N 7	0.0840	0.0865	0.5045	0.013986	0.035738	0.016550	0.000783	0.012416	0.001230
O 8	0.0404	0.7116	0.4400	0.012334	0.029898	0.018218	−0.000672	0.011098	−0.001541
C 9	0.2659	0.3198	0.7750	0.008003	0.040756	0.012200	0.000808	0.007993	0.001240
O10	0.2388	0.1521	0.7397	0.012562	0.036416	0.013705	0.000753	0.009682	0.000685
O11	0.2255	0.4562	0.7092	0.011351	0.038137	0.012554	0.000657	0.009121	0.001800
C12	0.3544	0.3598	0.9087	0.009957	0.036054	0.013597	−0.001510	0.008842	−0.000132
N13	0.3900	0.2042	0.9827	0.008718	0.039390	0.012153	−0.000378	0.007793	0.000097
C14	0.3119	0.1251	0.9643	0.008587	0.037040	0.011234	−0.000049	0.007280	−0.000335
O15	0.2107	0.1879	0.8930	0.008629	0.040653	0.014995	0.001273	0.008615	0.002498
C16	0.3530	−0.0454	1.0360	0.008204	0.040764	0.008935	−0.000543	0.006457	−0.000031
C17	0.4419	−0.1654	1.0806	0.011505	0.044265	0.012424	0.002275	0.009952	0.002192
C18	0.4717	−0.3277	1.1402	0.014799	0.044156	0.015478	0.004897	0.012590	0.004688
C19	0.4179	−0.3732	1.1584	0.013295	0.049619	0.012459	0.000169	0.009706	0.004184
C20	0.3324	−0.2569	1.1188	0.010457	0.057842	0.013718	−0.001265	0.009233	0.003567
C21	0.3022	−0.0920	1.0596	0.009271	0.052496	0.011961	0.001616	0.008100	0.001508
C22	0.3568	−0.3050	1.3331	0.009346	0.043034	0.014898	−0.001109	0.009199	−0.000518

TABLE 2 (b). POSITIONAL AND THERMAL PARAMETERS OF SOME HYDROGEN ATOMS WHICH ARE OBTAINED FROM D-SYNTHESIS

	x	y	z	B		x	y	z	B
H 1	0.136	0.420	0.579	3.12	H10	0.456	−0.148	1.042	5.57
H 3	−0.112	0.599	0.215	7.47	H11	0.525	−0.426	1.160	9.85
H 4	−0.161	0.344	0.132	6.72	H12	0.464	−0.479	1.123	9.37
H 5	−0.060	0.098	0.282	9.59	H13	0.277	−0.286	1.129	8.89
H 7	0.316	0.470	0.907	7.17	H14	0.221	0.017	1.015	9.98
H 8	0.427	0.423	0.945	5.25					

TABLE 3. INTERMOLECULAR COMPLEX FORMATION BETWEEN NUCLEOTIDE BASES AND *N*-ACYLAMINOACIDS

		Free amino acids		*N*-Formyl-		*N*-Acetyl-		*N*-Benzoyl-		*N*-Carbobenzoxy-	
		A	C	A	C	A	C	A	C	A	C
Neutral Amino acid	Glycine	−	−	+	+	+	−	+	+	+	+
	α-Alanine	−	−	+	+	+	−	+	/	+	+
	β-Alanine	−	−	/	/	−	−	+	+	−	−
	Valine	−	−	+	+	+	+	−	+	−	+
	Leucine	−	−	+	+	+	+	+	+	/	/
	Isoleucine	−	−	−	+	−	+	−	+	/	/
	Phenylalanine	−	−	+	+	+	−	+	+	−	/
	Tyrosine	−	−	+	+	+	+	+	?	+	/
	Serine	−	−	/	/	/	/	/	/	+	+
	Threonin	−	−	/	/	−	?	/	/	+	+
	Methionine	−	−	+	+	+	+	+	+	−	/
	Cysteine	−	−	/	/	+	+	/	/	/	/
	Proline	−	−	?	?	+	+	/	/	−	?
	Tryptophane	−	−	/	/	+	+	−	+	/	/
Acidic Amino acid	Glutamic acid	−	−	/	/	+	+	+	+	+	/
	Aspartic acid	−	−	/	/	/	/	+	?	+	−
Basic Amino acid	Arginine	−	−	/	/	−	−	−	−	/	/
	Histidine	−	−	−	−	−	−	−	−	/	/

A: adenine, C: cytosine, for thymine and uracil all are —.
? : For this combination, the only gel-like material is obtained.
\: No *N*-Acylation is available.

Table 4. Bond lengths and angles

Bond lengths (Å)				Bond angles (°)			
C 1–N 2	1.368	C12–N13	1.430	C 2–C1–C 6	116.8	C 9–C12–N13	117.0
C 1–C 6	1.399	N13–C14	1.331	N 2–C1–N 7	116.5	C14–N13–C12	120.9
C 1–N 7	1.322	C14–O15	1.220	C 6–C1–N 7	126.8	N13–C14–O15	123.3
N 2–C 3	1.341	C14–C16	1.469	C 1–N2–C 3	124.3	C16–C14–O15	119.8
C 3–N 4	1.341	C16–C17	1.401	N 2–C3–N 4	116.0	C16–C14–N13	116.9
N 4–C 5	1.350	C17–C18	1.361	N 2–C3–O 8	120.9	C17–C16–C14	122.6
C 5–C 6	1.298	C18–C19	1.332	N 4–C3–O 8	123.2	C14–C16–C21	119.4
O 8–C 3	1.206	C19–C20	1.374	C 3–N4–C 5	121.5	C17–C16–C21	118.0
C 9–O10	1.252	C20–C21	1.372	N 4–C5–C 6	123.0	C16–C17–C18	120.4
C 9–O11	1.223	C16–C21	1.366	C 1–C6–C 5	118.5	C17–C18–C19	120.4
C 9–C12	1.508	C12–H 8	1.01	O10–C9–O11	125.2	C18–C19–C20	120.9
N 2–H 1	1.24	C17–H10	0.95	O10–C9–C12	118.3	C19–C20–C21	119.4
N 4–H 3	0.85	C18–H11	1.01	O10–C9–C12	116.5	C16–C21–C20	120.8
C 5–H 4	1.10	C19–H12	1.08				
C 6–H 5	0.80	C20–H13	1.21				
C12–H 7	1.05	C21–H14	1.25				

ever, it should be noticed that, in some cases, a small structural differece in neutral *N*-acylamino acids may play a major role in forming a complex; for instance, *N*-acetylleucine and *N*-acetylisoleucine have a similar acidities, but the former binds only with adenine, and the latter, with cytosine.

The Geometry of the Complex. From the structure determination of the present crystal, it is established that the complex is formed by two hydrogen bonds between cytosine and *N*-benzoylglycine. The interatomic distances and angles in the complex between cytosine and *N*-benzoyl glycine were calculated from the parameters in Table 1, as is shown in Fig. 1(a) and (b), and in Table 4. The maximum standard deviation was 0.017 Å for the bond length in cytosine and the carboxyl group and 0.033 Å for that in the benzoyl group.

The bond lengths and angles of the cytosine moiety of the complex do not agree well with those found in the crystal of cytosine hydrate. Table 5 shows a comparison with related structures. The significantly large bond angle of 124.3° for C1–N2–C3 implies that the hydrogen atom might be attached to N2, since the mean bond angles of C–NH–C and C=N–C are 125° and 116° respectively.[17] In the pyrimidine ring, the rather short distance, 1.298 Å might indicate that the C5–C6 bond is a double bond. The short bond distance, 1.322 Å, for C1–N7 might be attributed to the double-bond character. The C–O bond lengths of 1.223 and 1.252 Å, and the O10–C9–O11 angle of 125° are close to those observed in many amino acids and suggest the formation of a carboxyl anion. Although the difference electron density map is not good enough

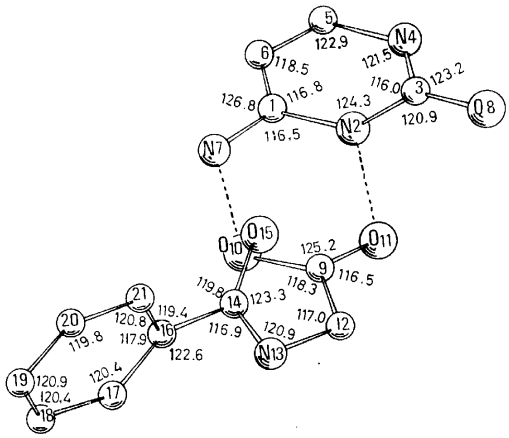

Fig. 1. (b) Bond angles of the complex.

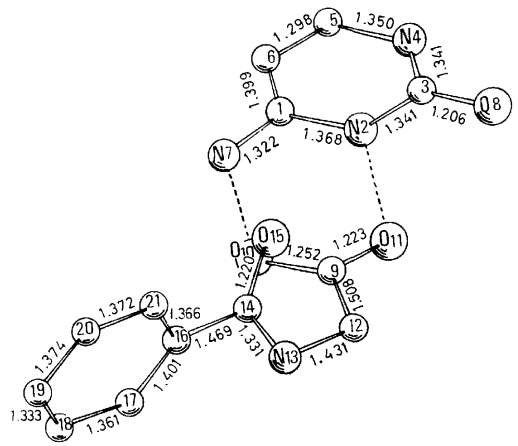

Fig. 1. (a) Bond distances of the complex.

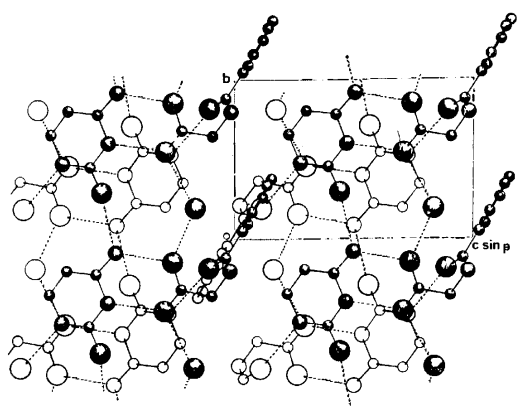

Fig. 1. (c) A view through two adjacent molecular layers, showing the stacking arrangement of the cytosine and carboxyl group viewed down the *c*-axis.

17) C. Singh, *Acta Crystallogr.*, **19**, 861 (1965).

TABLE 5. BOND LENGTHS AND ANGLES OF PYRIMIDINE DERIVATIVES

	This work	Cytosine[10]	Uracil[25]	Thymine[26]	Isocytosine[27]		Pyrimidine[28]
C1-N2	1.368Å	1.351	1.371	1.391	1.363	1.375	1.332
N2-C3	1.341	1.354	1.384	1.361	1.333	1.369	1.317
C3-N4	1.341	1.376	1.344	1.355	1.357	1.330	1.313
N4-C5	1.350	1.361	1.341	1.382	1.358	1.350	1.343
C5-C6	1.298	1.348	1.408	1.349	1.331	1.356	1.358
C6-C1	1.399	1.432	1.417	1.447	1.438	1.442	1.387
C6-C1-N2	116.8°	122.0	118.1	115.6	118.7	114.8	122.5
C1-N2-C3	*124.3	118.9	*124.7	*126.3	119.7	*123.3	115.1
N2-C3-N4	116.0	120.1	115.6	115.2	121.8	121.9	128.2
C3-N4-C5	*121.5	*121.3	*123.6	*122.8	*120.2	115.9	115.2
N4-C5-C6	123.0	120.6	121.5	121.8	120.5	125.9	122.7
C5-C6-C1	118.5	117.1	116.4	118.2	119.1	118.2	116.3

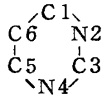

*sign indicates C-NH-C type of bond angles while no sign indicates C=N-C type of bond angles.

for obtain the positions of all the hydrogen atoms, the peaks for the H1 and H3 involved in the hydrogen bond are observed rather clearly. Each of the nitrogen atoms, N2 and N7, obviously possesses a hydrogen atom, while the carboxyl oxygens, O10 and O11, do not. From these results, it may be concluded that the complex consists of a cytosinyl cation and an *N*-benzoylglycyl anion as a result of proton transfer from the carboxyl group to the amidine group; the complex can be well represented by the formula of Fig. 2(b) rather than by that of Fig. 2(a). The NH···O

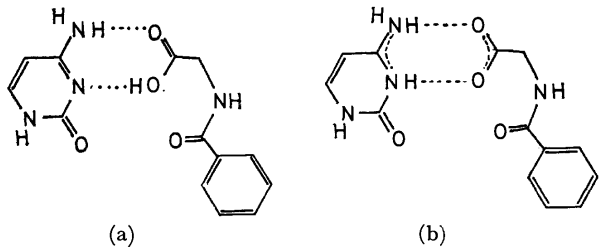

(a) (b)

Fig. 2. Hydrogen bond system between cytosine and *N*-benzoylglycine.

hydrogen bond distances are 2.697 and 2.652 Å, fairly shorter than the normal value,[18] probably because of the enhancement of some ionic force. The intermolecular hydrogen bond between the carboxyl and guanido groups in an arginine crystal[19] is analogous to that in the present complex. The least-squares planes of cytosine, the carboxylic group, and a benzene ring in *N*-benzoylglycine were calculated; the displacements of the atoms from each plane are shown in Table 6. The maximum deviation is 0.04 Å for O8 in the cytosine ring. The dihedral angle between cytosine and the carboxyl group is 3.0°.

As may be seen from Fig. 3, the component molecules have several sites, (A), (B),···(F), which are capable

TABLE 6. LEAST SQUARES PLANES AND DEVIATIONS

Atom	Displacement from the planes
C 1	−0.00Å
N 2	−0.01
C 3	0.02
N 4	−0.02
C 5	0.00
C 6	0.00
N 7	0.00
O 8	0.04
C 9	−0.00
O10	0.00
O11	0.00
C12	0.00
C16	0.02
C17	−0.01
C18	−0.00
C19	0.01
C20	0.00
C21	−0.02

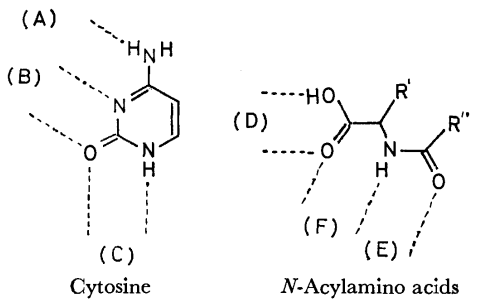

Cytosine *N*-Acylamino acids

Fig. 3. Hydrogen bonding sites in cytosine and *N*-acylamino acids.

of forming an intermolecular hydrogen bond. The favourable condition of the pairing might be affected not only by their characteristic atomic arrangements, but also by their crystalline fields. Therefore, the hydrogen-bonded complexes found in crystal structures might be rather limited. We expect that the hydrogen-bond systems in some of the complexes

18) W. Fuller, *J. Phys. Chem.*, **63**, 1705 (1959).
19) I. L. Karle and J. Karle, *Acta Crystallogr.*, **17**, 835 (1964).
25) G. S. Parry, *ibid.*, **7**, 313 (1954).
26) R. Gerdil, *ibid.*, **14**, 333 (1961).
27) B. D. Sharma and J. F. McConnell, *ibid.*, **19**, 797 (1965).
28) P. J. Wheatley, *ibid.*, **13**, 80 (1960).

Table 7. Short intermolecular distances

N 7–O10	2.652	1	N4 –O15	2.742	4
N 2–O11	2.697	1	C 5–O11	3.601	4
C 5–C16	3.687	2	C 5–O12	3.719	4
C 5–C21	3.664	2	N 5–O 8	3.516	4
C 6–C14	3.766	2	C 9–C18	3.762	5
C 6–O15	3.443	2	C 1–O 8	3.636	6
O 8–C 1	3.636	3	C18–C12	3.568	6
O 8–N 7	2.758	3	N 4–C 6	3.674	7
C12–C18	3.568	3	O15–C 6	3.774	8
C 1–O 8	3.694	4	C20–O 8	3.421	8
N 2–N 2	3.597	4	C21–N 2	3.569	8
N 2–C 3	3.705	4	C21–C 3	3.496	8
N 2–O 8	3.575	4	O22–C 9	3.606	8
N 2–O11	3.473	4	O22–O11	2.884	8
C 3–C 9	3.347	4	O22–C12	3.472	8
C 3–C10	3.681	4	C16–C19	3.528	9
C 3–O11	3.090	4	C17–C19	3.720	9
C 3–O15	3.613	4	C21–C18	3.753	9
N 4–C 9	3.206	4	C21–C19	3.575	9
N 4–O10	3.759	4	O22–O10	2.790	10
N 4–O11	3.190	4	O22–N13	3.637	10
N 4–C12	3.405	4	O22–C14	3.870	10
N 4–C14	3.734	4	O22–C17	3.397	10

1..	x,	y,	z,
2..	$-x$,	$-y$,	$1-z$,
3..	x,	$1+y$,	z,
4..	$-x$,	$1-y$,	$1-z$,
5..	$1-x$,	$-y$,	$2-z$,
6..	x,	$-1+y$,	z,
7..	$-x$,	$1/2+y$,	$1/2-z$,
8..	x,	$1/2-y$,	$1/2+z$,
9..	$1-x$,	$1/2+y$,	$3/2-z$,
10..	x,	$-1/2-y$,	$-1/2+z$.

listed in Table 3 are similar to that in cytosine—*N*-benzoylglycine.

The principal architecture of the present complex crystal is as follows; the complexes are linked to form an infinite column in the direction of the *b*-axis by hydrogen bonds between N7 and O8 in the cytosine molecules, with a distance of 2.758 Å. In this column, water molecules are located between O11 and O10 with distances of 2.789 and 2.884 Å, respectively so as to be hydrogen-bonded along the column. Two of these columns are joined through the hydrogen bonds of N4 with O15 at 2.742 Å. The intermolecular contacts shorter than 3.9 Å are given in Table 7.

Implications concerning Biological Aspects. The details of the interaction between *N*-acylamino acids and nucleotide bases in crystalline complexes can now be presented on the basis of our results. Similar types of molecular interaction may exist *in vivo*, but it is as yet impossible to predict such complex formation in a particular biological process. Here we will only point out some features of the present results which may be of biological significance.

At the terminal position of *t*-RNA molecules, the ususal sequence is CCA. Cytosine and adenine, not uracil nor thymine, are the bases with which *N*-acylamino acid from the complexes. This coincidence seems very attractive in considering the interaction of *t*-RNA and amino acids.

Another point is *N*-acylation, which is necessary for complex formation between amino acids and nucleotide bases. It is widely known that the hydrogen atom of a terminal amino group in many peptides is replaced by formyl or acetyl groups.[20–23] Marcker[24] discovered that methionine-*t*-RNA, which can tranfer a formylated amino acid into polypeptide, is involved in the initiation of protein synthesis in *E. Coli*. Thus, we assume that the binding of *N*-acylamino acid and a nucleotide base, similar to that of the present complex, has occurred in several steps of the protein synthesis.

In conclusion, the complex formation of adenine and cytosine with *N*-acylamino acid occurs generally. The molecular arrangement in the present complexes may be thought of as a candidate in considering possible interactions in biological systems.

We wish to thank Professor Yoshio Sasada of Tokyo Institute of Technology for his valuable discussions and suggestions.

20) E. Margoliash, E. L. Smith, G. Kreil, and H. Tuppy, *Nature*, **192**, 1121 (1961).
21) K. Narita, *Biochem. Biophys. Research Comms.*, **5**, 160 (1961).
22) K. Hofmann and H. Yajima, *J. Amer. Chem. Soc.*, **83**, 2289 (1961).
23) K. Hofmann, H. Yajima, and E. T. Schwartz, *ibid.*, **82**, 3732 (1960).
24) K. A. Marcker and F. Sanger, *J. Mol. Biol.*, **8**, 835 (1964).

The Effects of Higher-boiling Compounds on the Liquid-phase Isomerization of *m*-Xylene over a Silica-Alumina Catalyst under Pressure

Haruo TAKAYA, Naoyuki TODO, Tadasuke HOSOYA, Hideki ŌSHIO,* Mikio YONEOKA,** and Toshio MINEGISHI

National Chemical Laboratory for Industry, Mita, Meguro-ku, Tokyo
**The Research Laboratory, Central Glass Company, Ltd., Imafuku, Kawagoe-shi, Saitama*
***Mitsubishi Gas Chemical Co., Inc., Niigata Research Laboratory, Enoki-cho, Niigata*

(Received January 6, 1972)

The liquid-phase isomerization of *m*-xylene was studied over a silica-alumina catalyst under pressure on the additions of 2% of 8 higher-boiling compounds and 20—50% of benzene to reactant *m*-xylene. The catalyst activity in the isomerization was not greatly affected by hexamethylbenzene, naphthalene, α-methylnaphthalene, diphenyl, or *s*-dibenzyl. On the other hand, the activity was greatly lowered by 1,6-dimethylnaphthalene, diphenylmethane, and anthracene. Moreover, a very rapid exchange reaction occurred between an aromatic ring of diphenylmethane and a reactant xylene molecule, while the content of the isomerization product decreased linearly with an increase in the amount of benzene. From these results, the chemisorption states of xylene were discussed as follows. Most xylene molecules may be deduced to be chemisorbed on acid sites by those benzene rings. On the other hand, the fact that diphenylmethane inhibits the isomerization implies the existence of such a chemisorption state of xylene as a methylbenzylcarbonium ion, which may be an intermediate in the disproportionation reaction of xylene. The acid sites available for the chemisorption of diphenylmethane and for the disproportionation were speculated to be common and to have both acidic characters, protonic and Lewis.

In an earlier paper[1] the present authors reported that a silica-alumina catalyst revealed high activity in the isomerization of *m*-xylene in a liquid-phase reaction under pressure and that no practical decline in activity was observed even after 20 days at a temperature below 380°C. The enhanced activity in the liquid-phase reaction may be ascribed to the cleaning effects of the reactant: the higher-boiling by-products, which are inhibitors, are successively dissolved in the liquid reactant. The dissolution effect suggests the possibility of experiments using higher-boiling compounds in the liquid-phase reaction.

The components of the higher-boiling by-product were studied by the mass spectrometry.[1] However, they could not be identified precisely, since several probable components have the same mass number. This problem may be solved by comparing the effects of pure higher-boiling compounds on the isomerization of *m*-xylene with those of the higher-boiling by-products.

The first purpose of this paper is to study the effects of the pure higher-boiling compounds on the isomerization of *m*-xylene and to discuss the above problem. The second is to examine the pure higher-boiling compounds for the relative intensity of chemisorption on the acid site available for the reactions of xylene and to discuss the chemisorption state of xylene.

Experimental

The equipment used was the same as that described in previous papers.[1,2] The catalytic activity was measured by 4 hr's operations at a feed rate of 24 g/h under a pressure of 300 kg/cm², with using pure *m*-xylene or *m*-xylene solutions containing 2 weight per cent of the higher-boiling compounds. Between these measurements, pure *m*-xylene was fed into the reactor at a rate of 6 g/h in order to desorb the higher-boiling compounds from the catalyst surface or to keep the catalytic activity constant.[1] A temperature as low as 280°C was selected as the reaction temperature, because the change in catalytic activity could be observed sensitively at a low concentration of the isomerization product.

The catalyst used (2.5 g) was powdered Nikki N633L silica-alumina; it was calcined at a temperature of 500°C for 20 hr. The purity of *m*-xylene (produced by Mitsubishi Gas Chemical Co., Inc.) was 99.6%, and it contained 100—130 ppm of water. The other reagents were commercial grade and were used for the experiments without any further purification.

The product was analyzed by gas chromatography at 57°C. The column used for this measurement was 4 m in length, 1 mm in dia., and packed with 5% bentone 34+5% DIDP on diasolid L (100—200 mesh). The higher-boiling compounds were analyzed by means of a Hitachi double-beam mass spectrometer. The mass spectra were obtained at an ionization voltage as low as 15 V in order to allow only the parent peaks of the compounds to appear.

Results

The higher-boiling compounds used were hexamethylbenzene, naphthalene, α-methylnaphthalene, 1,6-dimethylnaphthalene, diphenyl, diphenylmethane, *s*-dibenzyl(1,2-diphenylethane), and anthracene; the results are shown in Figs. 1—5. In these figures, the arrow signs designate the results of 4 hrs' operations using *m*-xylene solutions containing 2 weight per cent of high-boiling compounds. The other points show results when pure *m*-xylene was used as the reactant. The figures show that hexamethylbenzene, naphthalene, α-methylnaphthalene, diphenyl, and *s*-dibenzyl did not greatly affect the activity in the isomerization of *m*-xylene. On the other hand, 1,6-dimethylnaphthalene, diphenylmethane, and anthracene lowered the activity greatly. However, when reactants were changed from the *m*-xylene solutions to pure *m*-xylene, different behavior was observed in the recovery of the activity among

1) H. Takaya, N. Todo, T. Hosoya, T. Minegishi, M. Yoneoka, and H. Oshio, This Bulletin, **44**, 2296 (1971).
2) H. Takaya, N. Todo, T. Hosoya, T. Minegishi, and M. Yoneoka, *Kogyo Kagaku Zasshi*, **73**, 1831 (1970).

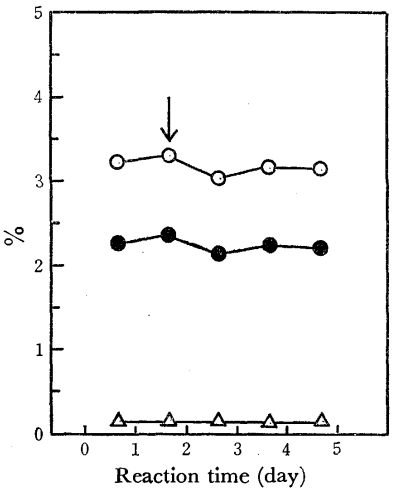

Fig. 1. Effects of hexamethylbenzene on the isomerization of *m*-xylene.
The arrow sign designates the results of four hours operation with using the *m*-xylene containing 2 wt% of hexamethylbenzene.
○: *p*-Xylene. ●: *o*-Xylene. △: Toluene.

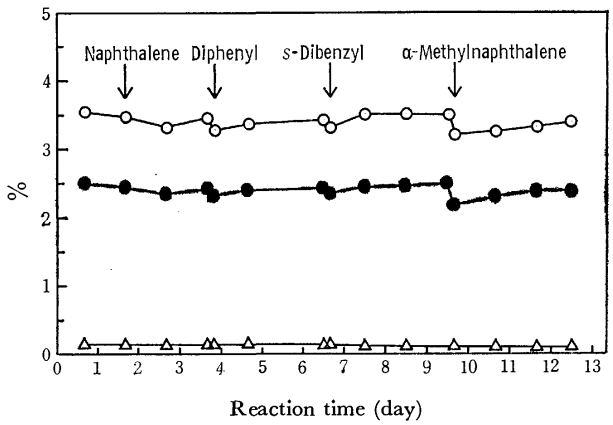

Fig. 2. Effects of naphthalene, diphenyl, *s*-dibenzyl and α-methylnaphthalene on the isomerization of *m*-xylene.
○: *p*-Xylene, ●: *o*-Xylene, △: Toluene.

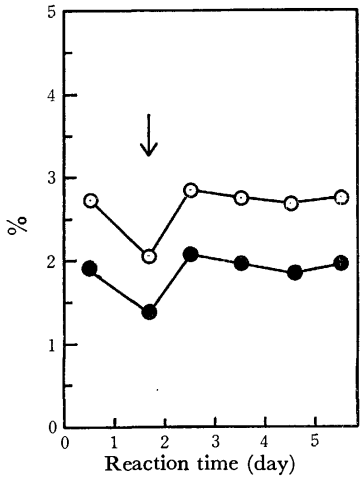

Fig. 3. Effects of 1,6-dimethylnaphthalene on the isomerization of *m*-xylene.
○: *p*-Xylene, ●: *o*-Xylene.

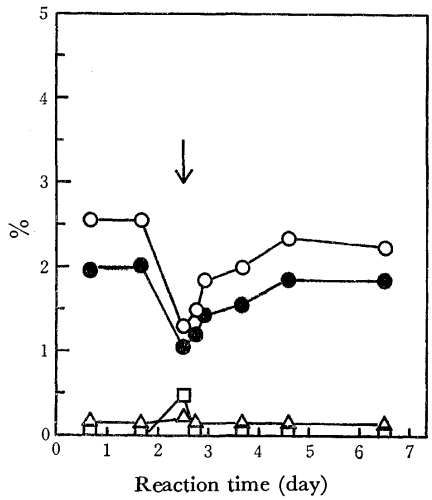

Fig. 4. Effects of diphenylmethane on the isomerization of *m*-xylene.
○: *p*-Xylene, ●: *o*-Xylene, △: Toluene, □: Benzene.

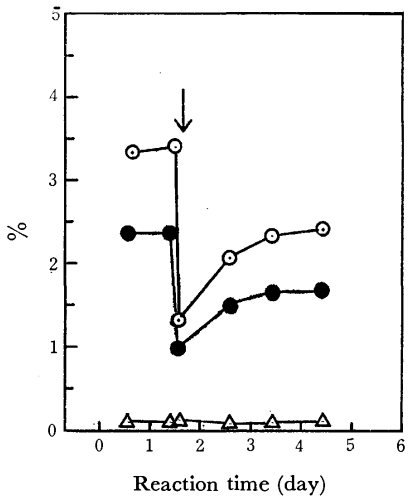

Fig. 5. Effects of anthracene on the isomerization of *m*-xylene
○: *p*-Xylene, ●: *o*-Xylene, △: Toluene.

the three cases: in the case of dimethylnaphthalene, the recovery was 100%; in the case of diphenylmethane, it was 90%, and in the case of anthracene, it was only 60%. It was noted that the addition of diphenylmethane to the *m*-xylene reactant resulted in the production of 0.5% of benzene.

An experiment was carried out using dried *m*-xylene and a dried *m*-xylene solution containing 2 weight per cent of diphenylmethane; we intended to examine the effects of water on the chemisorption of diphenylmethane with reference to the results in Fig. 4. However, when a catalyst was packed in the reactor in a dried box, the catalyst was moistened by *m*-xylene containing a small amount of water in order to obtain a high activity.[3] This reaction was carried out at a temperature of 290°C and at a feed rate of 13 g/h. The *m*-xylene solution was fed into the reactor for

3) H. Takaya, N. Todo, T. Hosoya, H. Oshio, and T. Minegishi, This Bulletin, **45**, 2337 (1972).

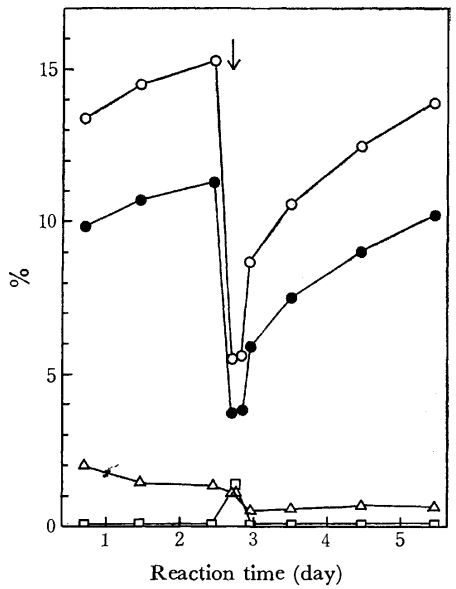

Fig. 6. Effects of diphenylmethane on the isomerization of *m*-xylene. This experiment was carried out with using dried *m*-xylene.
○: *p*-Xylene, ●: *o*-Xylene, △: Toluene, □: Benzene.

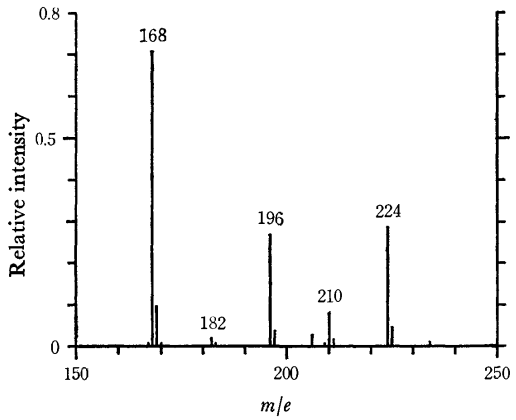

Fig. 7. Mass spectra of the higher-boiling products at the time designated by the arrow sign in Fig. 4.

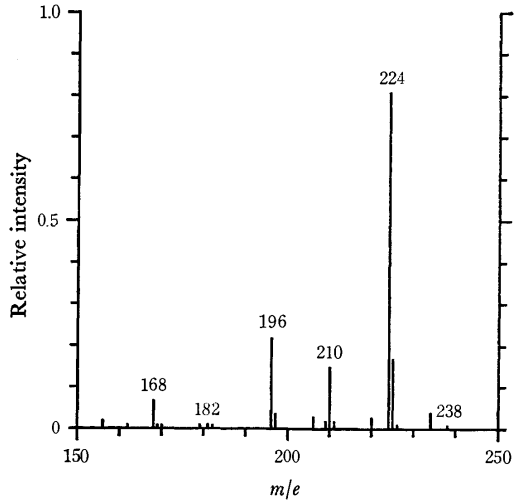

Fig. 8. Mass spectra of the higher-boiling products at the time designated by the arrow sign in Fig. 7.

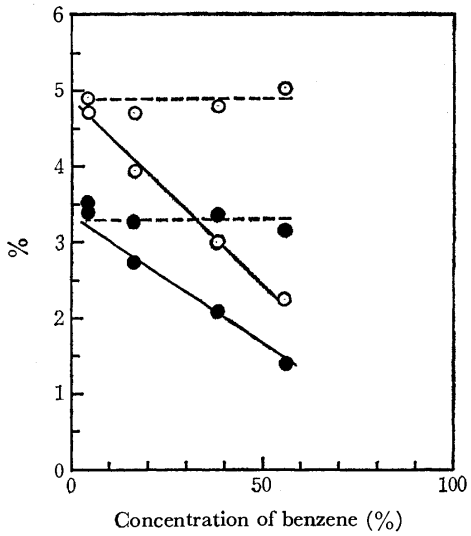

Fig. 9. Effects of benzene on the isomerization of *m*-xylene. —○—: content of *p*-xylene in a product. —●—: content of *o*-xylene in a product. —○—: *p*-xylene content / total xylene content. —●—: *o*-xylene content / total xylene content.

6 hr at the time designated by the arrow sign in Fig. 6. Also, diphenylmethane lowered the activity in the isomerization in this case, and 1.3% of benzene was produced. When the reactant was changed from the solution to pure and dried *m*-xylene, there was a gradual recovery of activity.

Fugures 7 and 8 show the mass spectra of higher-boiling compounds at the times designated by the arrow signs in Figs. 4 and 6 respectively. The compositions of the higher-boiling compounds were obtained from the spectra; they are tabulated in Table 1. The results show that diphenylmethane was converted mainly to di and tetramethyldiphenylmethane.

The influence of benzene on the activity in the isomerization of *m*-xylene was also studied in order to compare the intensity of the chemisorption of benzene on the acid sites available for the reaction with that of xylene. Figure 9 shows a linear decrease in the contents of *p*- and *o*-xylene with an increase in the amount of benzene.

TABLE 1. THE YIELDS OF HIGHER-BOILING COMPOUNDS (wt %)

Mass number	168	182	196	210	224
Number of methyl group	0	1	2	3	4
Sample of Fig. 7[a)]	0.97	0.03	0.43	0.14	0.53
Sample of Fig. 8[b)]	0.07	0.00	0.35	0.27	1.75

a) The concentration of diphenylemthane in the *m*-xylene reactant was 2.22%.
b) The concentration of diphenylmethane in the *m*-xylene reactant was 1.98%.

Discussion

1. The Main Compounds of the Higher-boiling By-product in the Isomerization of m-*Xylene.* As was shown in earlier papers,[1,3] the mass numbers of the main compounds of the higher-boiling by-products were 182, 196, 210, 224, and 238 in the isomerization and the disproportionation of *m*-xylene over a silica-alumina catalyst.

Furthermore, the addition of 2% of the main compounds to the *m*-xylene reactant resulted in a decrease in activity in the isomerization and the production of about 1% of toluene.

Considering only the mass numbers, the main compounds may be polymethyldiphenyl, polymethyldiphenylmethane, or polymethyl-*s*-dibenzyl. However, only diphenylmethane exhibited the behavior shown in Fig. 4, where the activity for the isomerization decreased greatly and about 0.5% of benzene was produced. This was the same behavior as shown by the main compounds in an earlier paper.[1] The production of benzene seemed to correspond to that of toluene on the addition of the main compounds to the *m*-xylene reactant, since the main compounds were polymethyl-ones. On the other hand, the addition of 2% of diphenyl or 2% of dibenzyl to the *m*-xylene reactant did not greatly decrease the catalytic activity and resulted in the production of neither benzene nor toluene. Therefore, it can be concluded that polymethyldiphenylmethanes are the main compounds. This conclusion is consistent with the NMR data in the earlier paper.[1]

2. Effects of Benzene on the Isomerization. As is shown in Fig. 9, the addition of a large amount of benzene to the *m*-xylene reactant resulted in a decrease in the yields of both *p*- and *o*-xylene. However, the ratio of the *p*-xylene yield to the total xylene content as well as that of the *o*-xylene yield to the total xylene content was constant, independent of the benzene concentration, as is shown in Fig. 9. Since the coverage of the active site is 1 under these reaction conditions,[2] this means that the ratio of the number of molecules of benzene adsorbed on the sites available for the isomerization to that of *m*-xylene is equal to the ratio in the reactant. Therefore, the intensity of the adsorptivity of benzene on the sites is equivalent to that of *m*-xylene. Furthermore, this conclusion implies that most molecules of *m*-xylene adsorb on the sites by the benzene rings, not by the methyl groups, since a benzene molecule has no methyl group. This is supported by the fact that the addition of 2% hexamethylbenzene to the *m*-xylene reactant did not greatly affect the activity in the isomerization, as is shown in Fig. 1; the intensity of the adsorptivity of *m*-xylene is approximately equivalent to that of hexamethylbenzene.

3. Chemisorption of Diphenylmethane. It has been well known electronic-spectrally that a triphenylmethylcarbonium ion is formed from triphenylmethane over a silica-alumina.[4-6] The high stability of the ion can be ascribed partly to its character as a resonating structure because of the presence of three phenyl groups. Hence, it may be expected that a stable diphenylmethylcarbonium ion is formed from diphenylmethane on an acid site, since the ion has two phenyl groups, as is shown in Fig. 10. The stable ion may result in a strong chemisorption of diphenylmethane and may be responsible for the relatively larger influence of diphenylmethane on the activity in the isomerization in comparison with the influences of diphenyl or *s*-dibenzyl. In addition, the fact that most of the diphenylmethane added to *m*-xylene was recovered as polymethyldiphenylmethane seems to support the formation of the diphenylmethylcarbonium ion.

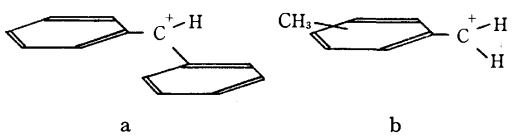

a b

Fig. 10. Possible chemisorption states of diphenylmethane (a) and xylene (b).

Diphenylmethane is considered to be chemisorbed by its methylene group on an acid site. If one of the two phenyl groups in a diphenylmethylcarbonium ion (Fig. 10a) is formally replaced by a hydrogen atom, the ion is converted to a benzylcarbonium ion (Fig. 10b). The benzylcarbonium ion suggests the possibility that xylene chemisorbs on an acid site by means of its methyl group.

4. Exchange Reaction between the Aromatic Ring of Diphenylmethane and Reactant m-*Xylene.* In Table 1, the order of increasing yield is: tetra≥di>trimethyldiphenylmethane, while the yield of monomethyldiphenylmethane is zero. When considering that 0.5—1.3% of benzene was produced in Figs. 4 and 6, this order suggests the occurrence of a rapid exchange reaction between an aromatic ring of diphenylmethane and a reactant *m*-xylene molecule, as is shown in Eqs. (1) and (2). When considering the chemisorption state

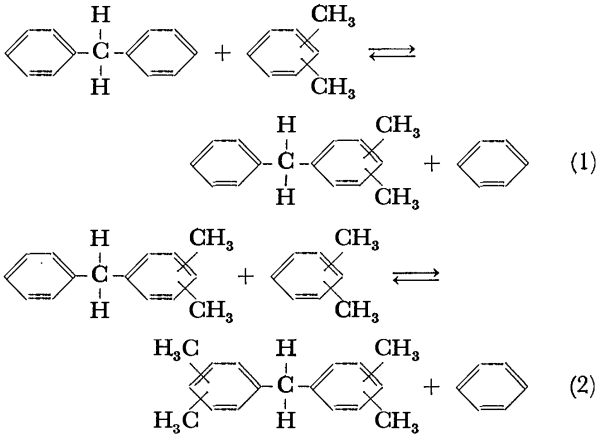

(1)

(2)

of diphenylmethane (Fig. 10a) and the nucleophilic property of aromatic compounds,[7] Fig. 11a is a possible intermediate for the exchange reaction. Hamanaka *et al.*[8] studied the same kind of reaction catalyzed by aluminum chloride at room temperature using methylbenzylbenzene and *p*-xylene, and suggested a benzylcarbonium ion as the intermediate. In the present paper, however, the benzylcarbonium ion can be excluded as the intermediate since the stability of the benzylcarbonium ion is lower than that of the diphenylmethylcarbonium ion. The low stability of the benzylcarbonium ion is confirmed by the fact that most xylene molecules chemisorb on acid sites

4) H. P. Leftin, *J. Phys. Chem.*, **64**, 1714 (1960).
5) R. P. Porter and W. K. Hall, *J. Catal.*, **5**, 366 (1966).
6) A. E. Hirschler and J. O. Hudson, *ibid.*, **3**, 239 (1964).
7) Y. Ogata, "Yuki Han-noron", Maruzen, Tokyo (1962), p. 232.
8) S. Hamanaka, S. Saigan, K. Itoh, and M. Ogawa, *Kogyo Kagaku Zasshi*, **70**, 695 (1967).

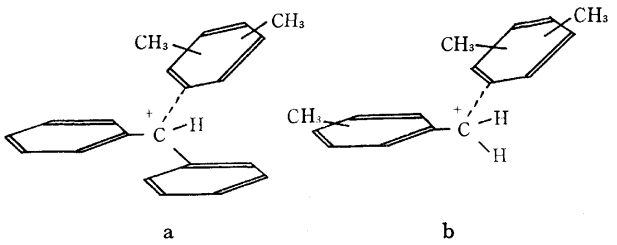

Fig. 11. Possible intermediates for the exchange reaction between an aromatic ring of diphenylmethane and a xylene molecule and for the disproportionation reaction of xylene.
a: for the exchange reaction, b: for the disproportionation reaction.

by means of the benzene rings, not the methyl groups, under the present reaction conditions.

The exchange reaction is similar to the transalkylation reaction which includes the disproportionation of xylene. When an aromatic ring of diphenylmethane is formally replaced by a hydrogen atom in Eq. (1), we obtain Eq. (3), which corresponds to a transmethylation reaction. Figure 11b is a possible intermediate for the transmethylation (or the disproportionation) reaction. This model is consistent with the results reported in an earlier paper.[3]

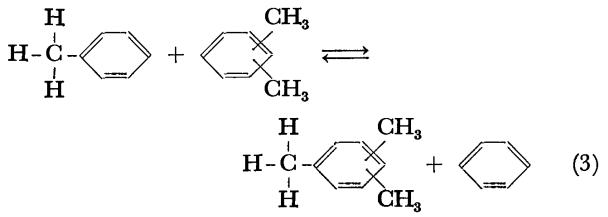

(3)

5. The Acid Site Available for the Chemisorption of Diphenylmethane. On the basis of the discussion in the preceding sections, a common acid site may be available for the formation of a triphenylmethylcarbonium ion, a diphenylmethylcarbonium ion, and a benzylcarbonium ion, and for both the exchange and disproportionation reactions. The reaction of triphenylmethane with a silica-alumina catalyst to form a chemisorbed triphenylmethylcarbonium ion has been interpreted by Leftin and Hall as a hydride abstraction by Lewis-acid sites on the surface.[4] Following this interpretation, the decrease in the catalytic activity for the isomerization on the addition of diphenylmethane to the *m*-xylene reactant indicates that the chemisorption of diphenylmethane on Lewis-acid sites decreases the protonic acidity of the catalyst, since it has been generally accepted that the isomerization is catalyzed by a protonic acid site.[3,9-12] Hence, the acid site available for the chemisorption of diphenylmethane may be considered to have both acidic characters, protonic and Lewis. Figure 12 shows a possible model of such an acid site, which was proposed by Uytterhoeven over H–Y zeolite[13]; (a) is a protonic acid state and (b) is a Lewis acid state. When diphenylmethane is chemisorbed on the b state, the protonic acidity of the site disappears.

It has been reported that the presence of a small amount of water is preferable for the disproportionation of xylene[3] and for carbonium-ion formation from triphenylmethane.[14] On the basis of the above consideration of the acid site, this fact may be interpreted as follows. In a reaction system containing a small amount of water, the chemisorption of water on free Lewis-acid sites may be considered to generate the acid site of Fig. 12, as is shown in Eq. (4). Here, the words "free Lewis-acid sites" mean all the Lewis-acid sites except for the type of Fig. 12b.

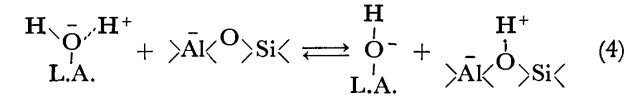

(4)

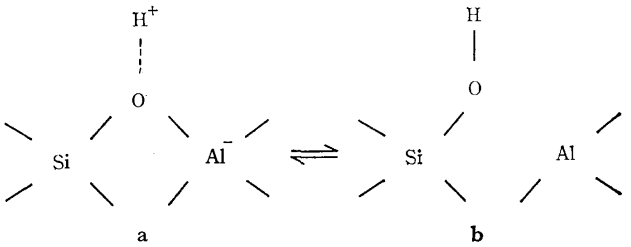

Fig. 12. A model for the acid site which has both acidic characters protonic and Lewis one.
a: a protonic acid state, b: a Lewis acid state.

In view of the fact that only a strong acid such as concentrated sulfuric acid above 85% converts triphenylmethane to the carbonium ion, the strength of the Lewis acid of Fig. 12b has to be stronger than that of a free Lewis acid, since it has been proposed that only the Lewis acid of Fig. 12b is available for the chemisorption of triphenylmethane and for the disproportionation. The consideration that the strength of the binding of an oxygen atom or a hydroxyl group to a Lewis acid increases with an increase in the strength of the Lewis acid supports the above consideration of the acid site of Fig. 12b—that an oxygen atom is still bound to an aluminum atom in the second term in Eq. (4). The aluminum atom is a Lewis acid site in Fig. 12b. Therefore, Eq. (4) indicates the possibility that the adsorption of water on a weak Lewis-acid site may generate a strong Lewis-acid site in a reaction system containing a small amount of water.

There is a different interpretation possible in the case of the chemisorption of diphenylmethane on Lewis-acid sites. It may be considered that the adsorption of water on a Lewis-acid site generates a protonic acid, and that the reverse reaction generates a Lewis one. Hence, the chemisorption of diphenylmethane on a Lewis-acid site results in a decrease in the protonic acidity. However, this interpretation does not seem to be reasonable in view of the results in Fig. 6. In the experiment of Fig. 6, the dried *m*-xylene was used with the intention of preventing a Lewis-acid site from being converted to a protonic acid by the adsorp-

9) V. C. F. Holm and A. Clark, *J. Catal.*, **2**, 16 (1963).
10) H. Matsumoto and Y. Morita, *Bull. Japan Petr. Inst.*, **11**, 40 (1969).
11) S. M. Csicsery and D. A. Hickson, *J. Catal.*, **19**, 386(1970).
12) J. W. Ward, *ibid.*, **17**, 355 (1970).
13) B. Uytterhoeven, L. G. Christener, and W. K. Hall, *J. Phys. Chem.*, **69**, 2117 (1965).
14) F. D. Dollish and W. K. Hall, *ibid.*, **71**, 1005 (1967).

tion of water. Therefore, the adsorption of diphenylmethane on a Lewis-acid site does not affect a protonic one directly. However, the isomerization activity was greatly lowered by diphenylmethane.

Hirshler[6] showed the possibility of the chemisorption of triphenylmethane on a protonic-acid site. He found that triphenylmethane is oxidized by chemisorbed oxygen to triphenylcarbinol, followed by the reaction with a protonic acid to generate the triphenylmethylcarbonium ion, and that 90% or more of the chemisorbed triphenylmethylcarbonium ion was recovered as triphenylcarbinol. On the other hand, Porter[5] reported that it is not necessary to oxidize triphenylmethane to triphenylcarbinol preliminary to carbonium-ion formation. Furthermore, most of the diphenylmethane was recovered as polymethyldiphenylmethane in the present experiment. Therefore, the chemisorption mechanism proposed by Hirschler may be excluded under the reaction conditions of the present paper.

Our and others results do not seem to exclude the possibility of the chemisorption of diphenylmethane on strong protonic-acid sites. However, the interpretation seems to suffer from the defect that the chemisorption state can not be drawn easily. Further investigations will be necessary to solve this problem.

BULLETIN OF THE CHEMICAL SOCIETY OF JAPAN, VOL. 45, 3267—3270 (1972)

Monolayers of Copolymers of Methyl Acrylate and *n*-Butyl Acrylate and Mixed Monolayers of Thier Homopolymers

Seiichiro HIRONAKA,* Takashi KUBOTA, and Kenjiro MEGURO

Faculty of Science, Science University of Tokyo, Kagurazaka, Shinjuku-ku, Tokyo

(Received January 18, 1972)

Poly(methyl acrylate), poly(*n*-butyl acrylate), and their copolymers were prepared by radical polymerization. The monolayers of these polymers and the mixed polymers were studied at the air/water interface. The limiting areas obtained experimentally for various copolymers corresponded well to the theoretical values as calculated from the areas per methyl acrylate and butyl acrylate residues. However, those obtained for their corresponding polymer mixtures were larger than the theoretical limting areas.

Many studies of the relation in surface monolayers between several individual polymers and their mixtures have been reported. Crisp[1] established that the areas and the surface potentials of mixed monolayers of poly(vinyl acetate) and poly(vinyl alcohol) were linear averages of the individual pure monolayers. Ries and his co-workers reported their surface pressure-area measurements of mixtures of stearic acid with poly(vinyl acetate)[2] and poly(vinyl benzoate),[3] both of which acted as ideal surface mixtures. Wu and Huntsberger[4] studied the surface mixtures of polymethacrylate and poly(vinyl acetate) and indicated that most polymers are compatible in the monolayers at the air/water interface, although they are incompatible in the bulk. Isemura *et al.* studied various copolymers of vinyl acetate and vinyl stearate.[5]

However, there have been few studies of the relation of copolymers in surface monolayers and their corresponding polymer mixtures.[1] In the present work, we have investigated the relation between the monolayer properties of various copolymers of methyl acrylate and *n*-butyl acrylate and those of polymer mixtures whose monomer components are nearly the same as those of the copolymers. Then, the relation between the limiting area and the composition ratio of the copolymer and that of the corresponding polymer mixture will be dicussed.

Experimental

Sample Polymers. The methyl actylate and *n*-butyl acrylate were supplied by Toagosei Co., Ltd. The methyl acrylate was purified by reduced-pressure distillation (nitrogen atmosphere) after the removal of the inhibitor by washing it with a 5% sodium hydroxide aqueous solution and distilled water and by subsequent dehydration with silicon dioxide. The *n*-butyl acrylate was purified by reduced-pressure distillation (nitrogen atmosphere) after dehydration with silicon dioxide.

Poly(methyl acrylate), poly(*n*-butyl acrylate), and various copolymers of methyl acrylate and *n*-butyl acrylate were prepared by radical polymerization at 60°C under a nitrogen gas flow. α,α′-Azobisisobutyronitrile was used as the initiator, and benzene as the solvent. The products were purified by repeated precipitation from their acetone solutions into a large excess of methanol. The purified polymers were dried by the refrigeration method, and then the trace solvent was removed *in vacuo* at room temperature.

The average molecular weights of these polymers were

* Present address: Faculty of Engineering, Tokyo Institute of Technology, Ookayama, Meguro-ku, Tokyo.

1) D. J. Crisp, *Research* (London) *Suppl. Surface Chem.*, **17**, 23 (2947).

2) H. E. Ries, Jr. and D. C. Walker, *J. Colloid Sci.*, **16**, 361 (1961).

3) H. E. Ries, Jr. and N. Beredjick, Proc. 4th Intern. Congr. Surface Activity, **2**, 897 (1967), Gordon and Breach Science Publishers, Inc., New York (1967).

4) S. Wu and J. R. Huntsberger, *J. Colloid Interfac. Sci.*, **29**, 138 (1969).

5) T. Isemura, H. Hotta, and T. Miwa, This Bulletin, **26**, 380 (1953).

determined by viscosity measurements. Their average molecular weights were about 6.59, 2.35, 2.89, 3.08, and 2.95×10^5 for poly(methyl acrylate), copolymer A, copolymer B, copolymer C, and poly(*n*-butyl acrylate) respectively.

The composition ratios (mol%) of the copolymers were calculated by means of the following equation:

$$\frac{mX/100+b(100-X)/100}{MX/100+B(100-X)/100}\times 100 = C(\%) \qquad (1)$$

where X is the mole percentage of methyl acrylate in the copolymers; where M and B are the apparent molecular weights of a methyl acrylate and a butyl acrylate residue respectively; where m and b are the weights of carbon in a methyl acrylate and a butyl acrylate residue respectively; and where C (%) is the percentage of carbon as obtained by elemental analysis. Table 1 lists the results of elemental analyses and the composition rarios (mol%) of the three copolymers.

TABLE 1. THE ELEMENTAL ANALYSES AND THE COMPOSITION RATIOS OF COPOLYMERS

	Elemental analysis (%)		Composition ratio (mol%)	
	Carbon	Hydrogen	Methyl acrylate	*n*-Butyl acrylate
Poly (methyl acrylate)	55.84	6.86	100	—
Copolymer A	59.60	8.00	69.7	30.3
Copolymer B	61.00	8.12	56.3	43.7
Copolymer C	63.76	8.78	24.9	75.1
Poly (*n*-butyl acrylate)	65.63	9.14	—	100

Surface-pressure Measurements. A modified Wilhelmy-type film balance[6] was used to measure the surface pressure. The balance was enclosed in the chamber to allow thermostatic control at 20.0 ± 0.2°C. The water in the trough was kept at 20.0 ± 0.2°C by circulating the water from the thermostat bath. The distilled water used as the substrate had a pH of 5.0—6.0 at 20.0 ± 0.2°C. The polymer solutions (0.03 to 0.04 g polymer/100 m*l* benzene) were spread with an "Agla" microsyringe. Thirty minutes were allowed for the solvent to evaporate before compression was started. The rate of compression was 7.5 cm²/min. The surface pressure value was read after the film has first been allowed to reach equilibrium for 5 min. The surface-pressure measurements for all the polymers were repeated several times; the results were reproducible within the range of experimental error (±0.1 Å²/residue in area).

Results and Discussion

The surface pressure-area isotherms obtained for poly(methyl acrylate), poly(*n*-butyl acrylate), and various copolymers of methyl acrylate and *n*-butyl acrylate are shown in Fig. 1. The limiting areas of poly(methyl acrylate) and poly(*n*-butyl acrylate), as determined from the surface pressure-area isotherms shown in Fig. 1, were 21.6 and 29.5 Å²/residue respectively. These values correspond well to those determined by Crisp (21.5 and 29.3 Å²/residue)[7,8] and to our results.[9,10]

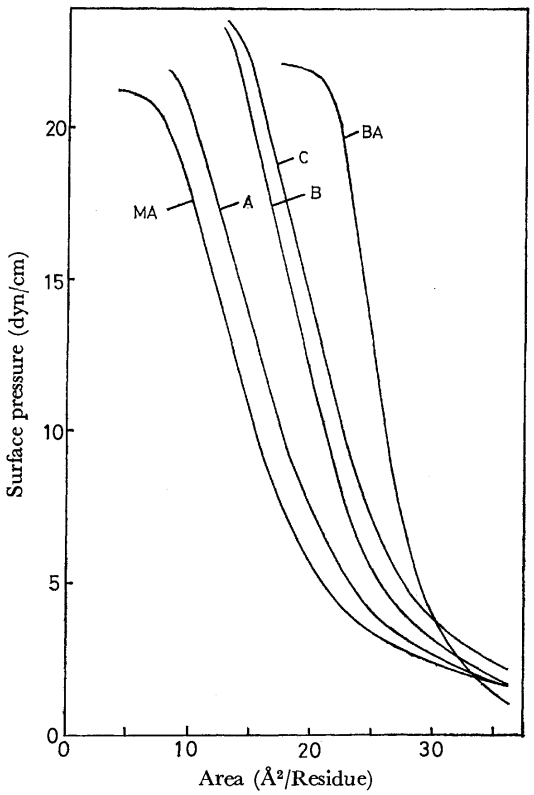

Fig. 1. The surface pressure-area isotherms of copolymers of methyl acrylate and *n*-butyl acrylate on distilled water. MA: poly (methyl acrylate), A: copolymer A, B: copolymer B, C: copolymer C, BA: poly(*n*-butyl acrylate).

With the use of the limiting areas (21.6 Å²/methyl acrylate residue and 29.5 Å²/butyl acrylate residue), the theoretical limiting area (A_t) of the copolymer, assuming the additivity rule between the limiting area and the composition ratio of each polymer component in the copolymer, was calculated by means of the following equation:

$$A_t = 21.6\frac{X}{100} + 29.5\frac{(100-X)}{100} \qquad (2)$$

where X is the mole percentage of methyl acrylate in the copolymer.

The experimental limiting areas of the copolymers and the theoretical limiting areas calculated by means of Eq. (2) *vs.* the composition ratios of methyl acrylate and *n*-butyl acrylate in the copolymers are shown in Fig. 2. It is found that the limiting areas obtained experimentally for various copolymers coincided well with the theoretical ones calculated by means of Eq. (2). The fact that the copolymers did not show such transition points in the surface pressure-area isotherms as were observed in the mixed monolayers suggests that copolymers are very slightly contaminated with traces of the homopolymer. Generally, the monolayers of copolymers do not behave as mixtures of the corresponding homopolymers would, and the introduction of a little comonomer often produces effects far out of proportion to its amount. Isemura

6) D. G. Dervichian, *J. Phys. Radium*, **6**, 221, 429 (1935).
7) D. J. Crisp, *J. Colloid Sci.*, **1**, 49 (1946).
8) D. J. Crisp, *ibid.*, **1**, 161 (1946).
9) S. Hironaka and K. Meguro, *J. Colloid Interfac. Sci.*, **35** (3), 367 (1971).
10) S. Hironaka, T. Kubota, and K. Meguro, This Bulletin, **44**, 2329 (1971).

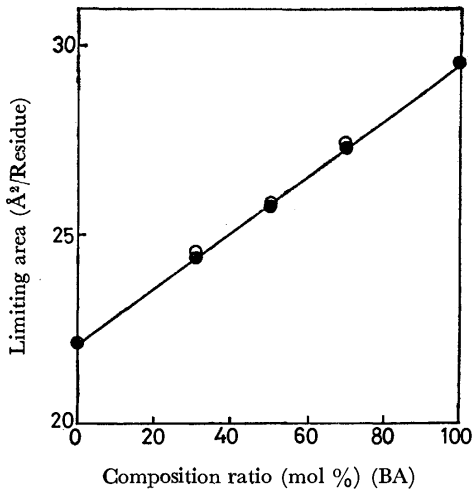

Fig. 2. The limiting areas of copolymers *vs.* their composition ratios. ○: experimental, ●: theoretical, BA: poly(*n*-butyl acrylate).

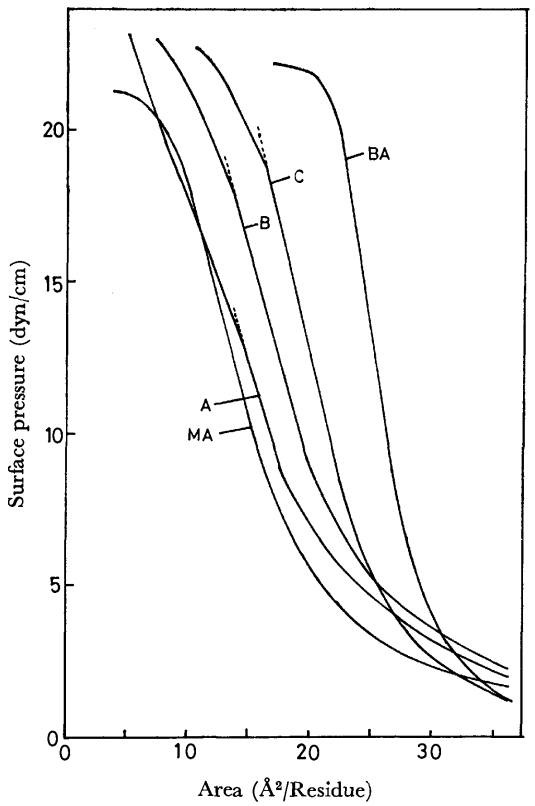

Fig. 3. The surface pressure-area isotherms of mixtures of poly(methyl acrylate) and poly(*n*-butyl acrylate) on distilled water. MA: poly(methyl acrylate), A: mixture A, B: mixture B, C: mixture C, BA: poly(*n*-butyl acrylate).

et al. indicated this for the surface pressure-area isotherms of various copolymers of vinyl acetate and vinyl stearate.[5]

Figure 3 shows the surface pressure-area isotherms for mixtures of poly(methyl acrylate) and poly(*n*-butyl acrylate). The experimental limiting areas obtained for the mixed polymers were larger than those obtained for the copolymers with the same ratios of components and the theoretical ones calculated by Eq. (2). Figure 4 shows the experimental and the

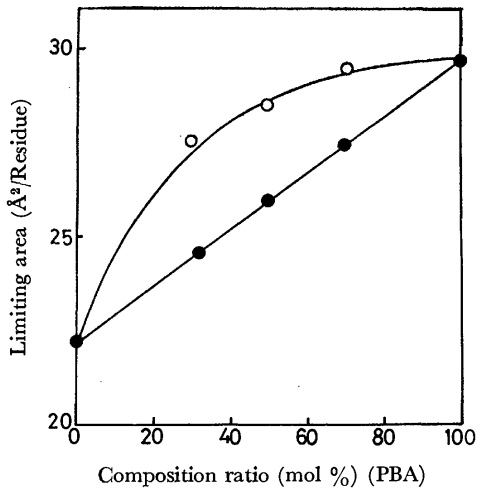

Fig. 4. The limiting areas of mixtures of poly(methyl acrylate) and poly(*n*-butyl acrylate) *vs.* the composition ratio by mixing. ○: experimental, ●: theoretical, PBA: poly(*n*-butyl acrylate).

theoretical limiting areas *vs.* the composition ratios of the mixed polymers. The experimental values deviated largely and positively from the theoretical limiting areas. When the deviation ratio was calculated by means of the following equation:

$$\text{Deviation ratio} = \frac{A_e - A_t}{A_t} \times 100 \qquad (3)$$

the values calculated for mixtures A, B, and C were 12.7, 10.4, and 6.9% respectively. A_e is the experimental limiting area and A_t is the theoretical limiting area, as calculated by Eq. (2). The mixture rich in poly(methyl acrylate) showed the largest positive deviation from the theoretical limiting area. These deviations can be explained by the assumption that the monolayer of poly(methyl acrylate) can expand more than that of poly(*n*-butyl acrylate).

The transition points were observed for the isotherms of each mixed polymer (in Fig. 3). The transition points obtained for mixtures A, B, and C were about 14, 18, and 19 dyn/cm respectively. These values were smaller than the collapse pressures of the individual pure monolayers (20.5 dyn/cm for poly(methyl acrylate) and 22.1 dyn/cm for poly(*n*-butyl acrylate)). The surface pressure at the transition increased with an increase in the amount of poly(*n*-butyl acrylate). Further, the reductions of area occurred after the transition point. The reduction of area after the transition point increased with the amount of poly(*n*-butyl acrylate) present in the mixed polymer. While the mixture rich in poly(*n*-butyl acrylate) had a high transition point and acted like that of poly(*n*-butyl acrylate) below the transition point, the mixture rich in poly(methyl acrylate) behaved at low surface pressures as poly(methyl acrylate) did. The behaviors of these mixed polymers may be affected by the composition. The mixture rich in poly(*n*-butyl acrylate) is mainly subject to poly(*n*-butyl acrylate) and gives the higher transition point, but it also produces the larger reduction of area because of the condensation of poly(*n*-butyl acrylate) at rela-

TABLE 2. THE COMPOSITIONS AND THE LIMITING AREAS OF THE COPOLYMERS AND THEIR CORRESPONDING MIXED POLYMERS

	Components of copolymer (mol%)		Limiting area (Å²/residue)		Deviation ratio (%)
	Methyl acrylate	*n*-Butyl acrylate	Experimental	Theoretical	
Poly(methyl acrylate)	100	—	21.6	21.5 (by Crisp)	
Copolymer A	69.7	30.3	25.0	24.4	2.5
Copolymer B	56.3	43.7	25.8	25.9	−0.4
Copolymer C	24.9	75.1	27.7	27.4	1.1
Poly(*n*-butyl acrylate)	—	100	29.5	29.3 (by Crisp)	
	Components of corresponding polymer mixture (mol%)				
	Poly(methyl acrylate)	Poly(*n*-butyl acrylate)			
Mixture A	69.9	30.1	27.5	(24.4)	12.7
Mixture B	49.4	50.6	28.6	(25.9)	10.4
Mixture C	29.4	70.6	29.3	(27.4)	6.9

tively high pressures.

Finally, the limiting areas of the copolymers were compared with those of mixed polymers in which the compositions were nearly the same as those of the corresponding copolymers. Table 2 shows the compositions and the limiting areas of the copolymers and their corresponding mixed polymers. The limiting areas of the mixed polymers deviated largely and positively from the theoretical limiting areas as calculated by Eq. (2), while those of the copolymers corresponded well to the theoretical ones. This difference suggests that poly(methyl acrylate) in the mixed polymer can expand more than the methyl acrylate component in the copolymer. The additivity holds good in copolymers, but the mixed polymers expand to give larger limiting areas than the theoretical ones.

BULLETIN OF THE CHEMICAL SOCIETY OF JAPAN, VOL. 45, 3270—3276 (1972)

Studies of the Sodium Salts of Homologues of Alkyl Sulfates in Aqueous Solutions in Relation to the Water Structure

Harumi ENDO

Department of Applied Physics, Defense Academy, Yokosuka

(Received January 20, 1972)

The adiabatic compressibility (β) and the partial molar volume at an infinite dilution ($\bar{V}_0$) were obtained for aqueous solutions of the sodium alkylsulfates (SAS) of lower homologues. The sound velocity (U) and the density (ρ) were determined by the use of an ultrasonic interferometer and the float-balance method respectively. The results indicate that the slope at an infinite dilution $(d\beta/dC)_0$ of β *vs.* the concentration (C) diagram is in a linear relation with the carbon number (ϕ) of SAS. A similar relation was obtained between $\bar{V}_0$ and ϕ. We have derived these two relations by a statistical thermodynamical treatment based on the interstitial model of water, consisting of two species, one constituting the framework of an extended ice-1 structure with many cavities, and the other species, non-hydrogen-bonded water, occupying part of these cavities. The occupancy of the cavity with alkyl radical leads to a decrease in the structural compressibility, while the hydration of the ionic parts of the solute leads to a decrease in the compressibility due to the electrostriction. According to the calculations, the theoretical dependency of $(d\beta/dC)_0$ on ϕ is about three times larger than the experimental value. The theoretical dependency of $\bar{V}_0$ on ϕ is nearly in agreement with the experimental value, while the constant-addivite term is different.

It is known that sodium salts of sulfates of higher alkyl, such as *n*-tetradecyl, *n*-dodecyl, and *n*-octyl, are surface-active substances in aqueous solutions. The dissolved state and properties of these salts in an aqueous solution have been studied by various methods. The adiabatic compressibility is a very useful parameter in elucidating the dissolved state and properties of a solution. Shigehara[1-3] has studied the adiabatic com-

1) K. Shigehara, This Bulletin, **38**, 1700 (1965).
2) K. Shigehara, *ibid.*, **39**, 2332 (1966).
3) K. Shigehara, *ibid.*, **39**, 2643 (1966).

pressibility and density of these salts in aqueous solutions. He has found that the slope at an infinite dilution $(d\beta/dC)_0$ of the β *vs.* concentration (C) diagram is in a linear relation:

$$(-d\beta/dC)_0 = (0.776\phi+5.94) \times 10^{-12} \text{ (cm}^2\text{/dyn)/(mol/}l\text{)}$$

with the number of carbon atoms (ϕ) of alkyl chains. A similar relation, $\bar{V}_0=15.9\phi+46$ (cm^3/mol), is obtained between the partial molar volume at an infinite dilution ($\bar{V}_0$) and the number of carbon atoms (ϕ) of sodium alkylsulfate (SAS). He discussed the dissolved state and properties of SAS in aqueous solutions.

In this investigation, we investigated the SAS of lower alkyl homologues (methyl (SMS), ethyl (SES), and butyl (SBS)) in aqueous solutions by means of an ultrasonic interferometer, and found that the systematic dependences of $(d\beta/dC)_0$ and $\bar{V}_0$ are obtained also for lower homologues, the relations in this case being:

$$(-d\beta/dC)_0 = (0.68\phi+5.85) \times 10^{-12} \text{ (cm}^2\text{/dyn)/(mol/}l\text{)}$$

$$\bar{V}_0 = 16\phi + 53 \text{ (cm}^3\text{/mol)}$$

Also, we derived these two relations by a statistical thermodynamical treatment based on the interstitial model[4,5] of the water structure.

Experimental

Materials. The alkylsulfates used are SMS, SES, and SBS. They were prepared from their corresponding alcohols by reactions with chlorosulfonic acid and by further neutralization with sodium hydroxide, and were then purified with alcohol by means of recrystallization. Sodium hydrogen sulfate (SHS) was also used for the purpose of comparison. It was prepared by dissolving an equimolar amount of pure sulfuric acid and sodium sulfate in water, and was obtained as a precipitate.

Apparatus. The apparatus used for the measurement of the sound velocity was a differential ultrasonic interferometer of 1.432 MHz designed by Sasaki and Yasunaga,[6] with an accuracy of ± 3 cm/sec. The measurements were carried out in a thermostat at 30.000 ± 0.003°C. The density of the solution at 30.000°C, controlled to ± 0.001°C, was determined by the float-balance method. The accuracy of the measurements was $\pm 10^{-6}$ (g/cm^3).

The adiabatic compressibility of solutions was calculated from the sound velocity (U) and density (ρ) by the following relation:

$$\beta = 1/(\rho U^2).$$

Determination of Concentration. All the solutions used in the experiment were prepared at a constant temperature of 30°C. The volume of the liquid was measured by means of a measuring flask (250 cc) and a full transfer pipet previously maintained at 30°C. Distilled and degased water was used for the preparation of the solution and for further dilution. A known amount of the solute, measured by means of a chemical balance, was used to obtain a stock solution of 250 cc. When v_0 cc of the stock solution (density ρ_0) is added to v_w cc of water (density ρ_w), we obtain a diluted solution (density ρ) of the volume, V:

$$V = (v_0\rho_0+v_w\rho_w)/\rho.$$

Although V is nearly equal to v_0+v_w for the dilute solutions here investigated, we used the above-mentioned relation as the computed V value; the molarity of the concentration thus determined is better than 0.2%.

Results

Figure 1 shows the density difference ($\Delta\rho$) between the solution and solvent as a function of the concentration (C) for various solutes. The increment of the density difference is proportional to the concentration in all cases.

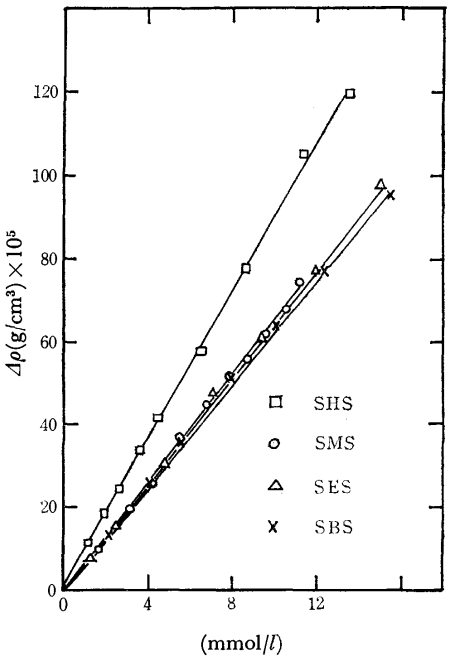

Fig. 1. The difference of density ($\Delta\rho$) between solution and solvent as function of concentration in aqueous solutions at 30°C.

Figure 2 shows the increments in the sound velocity (ΔU) against the concentration for aqueous solutions of SHS, SMS, SES, and SBS, where $\Delta U=U-U_0$ is the difference between the sound velocity for a solution and for the solvent respectively. The increment in sound velocity is proportional to the concentration, except for the case of SHS. The slope $(\partial\Delta U/\partial C)$ of the sound velocity-against-concentration curves increases with an increase in the molecular weight for SAS.

Figure 3 shows the difference in adiabatic compressibility $\Delta\beta(=\beta-\beta_0)$ between a solution and the solvent as a function of the concentration for various salts. Except for the SHS solution, $\Delta\beta$ is proportional to the concentration, the $(|\partial\Delta\beta/\partial C|)$ slope becoming larger with an increase in the molecular weight: -6.6, -7.1, and $-8.5\times(10^{-12})$ (cm^2/dyn)/(mol/l) for SMS, SES, and SBS respectively.

By plotting the value of $(-d\beta/dC)_0$ against the number of carbon atoms (ϕ) for SMS, SES, and SBS, we obtain a linear relation (solid line in Fig. 4). It can be represented by the following empirical relation:

4) O. Nomoto and H. Endo, *ibid.*, **44**, 1519 (1971).
5) A. H. Narten, M. D. Danford, and H. A. Levy, *Discuss. Faraday Soc.*, **43**, 97 (1967).
6) T. Sasaki and T. Yasunaga, *Kagaku to Kogyo*, **7**, 138 (1954).

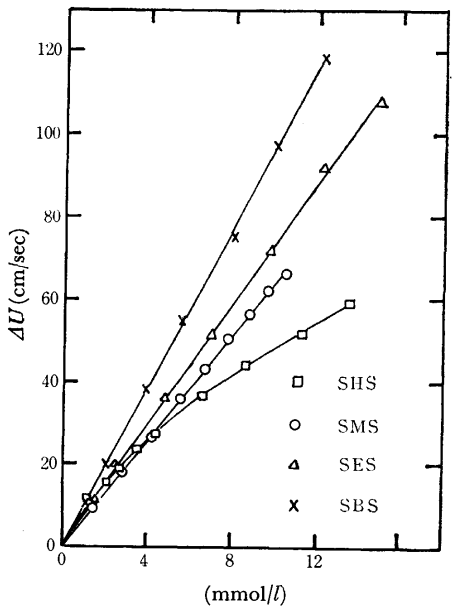

Fig. 2. The difference of sound velocity (ΔU) between solution and solvent as a function of concentration in aqueous solutions at 30°C.

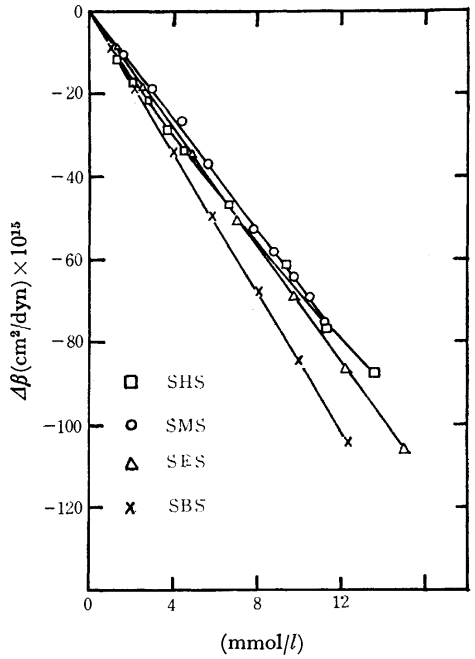

Fig. 3. The difference of adiabatic compressibility ($\Delta\beta$) between solution and solvent as a function of concentration in aqueous solutions at 30°C.

$$(-\mathrm{d}\beta/\mathrm{d}C)_0 = (0.68\phi + 5.85) \times 10^{-12}\ (\mathrm{cm^2/dyn})/(\mathrm{mol}/l) \quad (1)$$

It means that the contribution to $(-\mathrm{d}\beta/\mathrm{d}C)_0$ of each CH_2 (or CH_3) radical in the alkyl chain is constant, being 0.68×10^{-12} per unit of methylene (or methyl) radical. This may indicate that the effect of the destruction of the water structure with a CH_2 (or CH_3) radical, irrespective of the position in the molecule, is always the same.

The values of the partial molar volume ($\bar{V}_0$) at an infinite dilution of the sulfate, obtained from the density of the solution, are plotted as a solid line in Fig. 5.

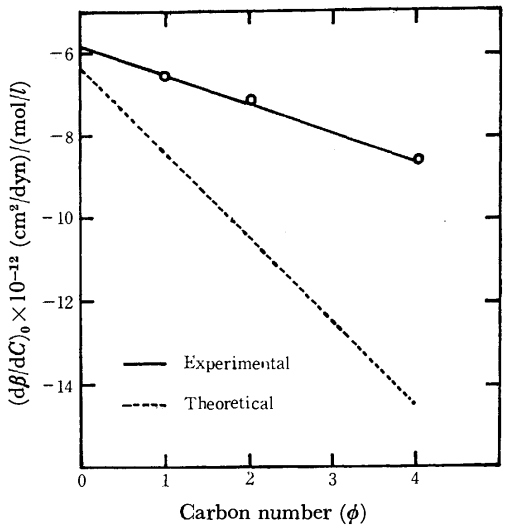

Fig. 4. The slope at infinite dilution $(\mathrm{d}\beta/\mathrm{d}C)_0$ of β against concentration (C) *vs.* carbon number (ϕ) of SAS.

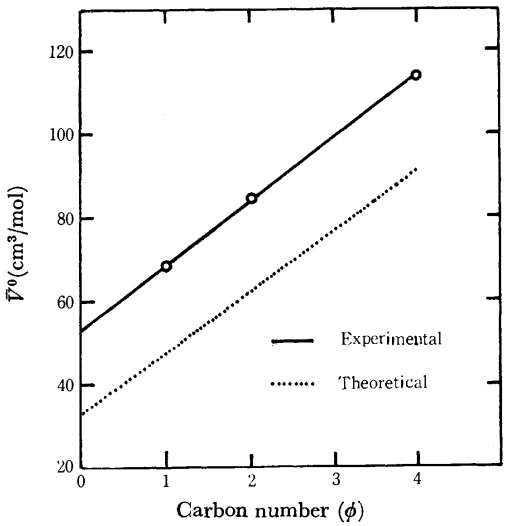

Fig. 5. The partial molar volume at intinite dilution $(\bar{V})_0$ *vs.* carbon number of SAS.

The relation between the partial molar volume and the carbon number in the alkyl chain is also linear and is expressed by the following equation:

$$\bar{V}_0 = 16\phi + 53\ (\mathrm{cm^3/mol}) \quad (2)$$

Theoretical

From their X-ray diffraction studies of liquid water, Narten *et al.*[5] proposed an interstitial model of liquid water, a kind of mixture model. This model consists of two species of water molecules, one constituting the framework of an extended ice-I structure with many cavities, and the other species, non-hydrogen-bonded water, occupying part of these cavities.

Acoustic pressure in water accompanies two sorts of compression: a) the compression of the intermolecular distance, and b) the breakdown of the intermolecular bonds, accompanied by the destruction of the open structure. The former is represented by the instantaneous compressibility, β_∞, while the latter is

the origin of the structural compressibility, β_{st}.

In the case of an aqueous solution, we may expect some changes in the adiabatic compressibility corresponding to changes in water structure under the influence of the solutes. In estimating these changes, we make the following assumptions:

(I) We treat the partial molar volume and the partial molar compressibility extrapolated to "infinite dilution," so that the solute-solvent interaction alone needs to be considered.

(II) When SAS is dissolved in water, we have alkylsulfate anions and sodium cations, almost entirely dissociated. In estimating the influence of the alkylsulfate anion on the partial molar volume and the adiabatic compressibility, we postulate the effect to be composed of two parts, one due to the alkyl chain, $C_\phi H_{2\phi+1}$, and the other, due to OSO_3^-. This is presumably admissible, at least for an infinite dilution.

(III) As regards the effect of the ionic parts (OSO_3^- and Na^+ ions) on $(d\beta/dC)_0$ and $\bar{V}_0$, we use empirical quantities in place of making theoretical treatments. The hydration of the ionic parts of the solute results in a decrease in the volume and compressibility due to the destruction of the water structure by the electrostriction.

(IV) The framework water makes cavities which are large enough to accommodate moderate-sized molecules and various radicals (*cf.* Narten *et al.*,[5,7,8] *etc.*[9-12]); therefore, the solute occupies sites in it as in a quasiclathrate. Since the alkyl chain of the anion is considered to be easily located in the cavity, the carbon-water interaction is very weak, and we assume the framework structure of ice-I not to be deformed or dilated by the occupation of alkyl radicals.

(V) The occupancy of the cavity by a methyl, ethyl, or butyl radical leads to a decease in the structural compressibility, this decrease becoming larger with an increase in the carbon number. When the ethylene radicals successively occupy the cavities, we do not take the C–C bond angle of the alkyl radical into consideration in order to avoid complicated calculations.

(VI) Both the alkyl chain in the cavity sites and the water molecules in the cavity sites have no effective volume. This means that the dimentions of the framework remain the same, whether the cavity is vacant or not. Therefore, the volume of the solution is assumed to be proportional to the number of framework sites.[9] When the cavities are crushed by acoustic pressure, the cavity occupied by the alkyl radical or water molecules leads to a smaller decrease in the cavity volume than does the unoccupied one.

(VII) Each methylene (or methyl) radical occupies one cavity.

(VIII) It is known that the heat of dissolution[13-17] in water of the alkyl homologues series is nearly of a constant increment for each CH_2 group of the alkyl chain. Such a relation may be applicable for SAS. Also, in the SAS aqueous solution, there is a linear relation[18] between ΔC_p (the change in heat capacity at a constant pressure) and the carbon number in SAS molecules.

In considering the molar free energy (G_H) of SAS in an aqueous solution, it is convenient to define the hypothetical state including the term of enthalpy change due to the water-solute interaction at an infinite dilution as the standard state of the Gibbs free energy (G^0_H) of SAS in water. This is the free energy for the hypothetical state in which SAS is imbedded in the cavity at the state of infinite dilution in water, but of the unit mole fraction. Therefore, G^0_H is the standard molar free energy of SAS in the quasiclathrate solution. When the solute (the part of hydrocarbon) is allowed to occupy the cavities to form a quasiclathrate solution, it becomes a "regular solution," *i.e.*, with an ideal entropy of mixing. Accordingly, we can discuss this system by means of the entropy term alone. Also, Frank and Franks[19] have made their treatments of the water-urea-hydrocarbon system based on the entropy terms only.

Now we will derive Eqs. (1) and (2) on the basis of the above assumptions. Let us consider one mole of water containing N molecules (N=Avogadro's number), of which the w fraction is in the network position, while the $(1-w)$ fraction is the non-hydrogen-bonded water situated in the cavities. If z is the number of cavity sites per network site, then the number of total cavity sites becomes Nwz. If f_2 is the occupancy of cavity sites by water molecules, we have:

$$f_2 = \frac{(1-w)}{wz} \tag{3}$$

Here we assume that the cavity sites are independent of each other, whether occupied or not, and, further, that all the sites are occupied with equal probability by non-hydrogen-bonded water. The number of ways in which the non-hydrogen-bonded water can be distributed among the sites are:

$$\Omega_1 = \frac{Nwz!}{(f_2 Nwz)!\{(1-f_2)Nwz\}!} \tag{4}$$

Next we have to distribute the alkyl chain $C_\phi H_{2\phi+1}$ in the remaining cavities. Here, ϕ is the number of carbon atoms constituting the alkyl chain. We will denote the total number of solute molecules by N_H. Then, the ratio of the number of solute molecules to the number of cavity sites is:

7) A. H. Narten and S. Lindenbaum, *J. Chem. Phys.*, **51**, 1108 (1969).
8) A. H. Narten, *J. Phys. Chem.*, **74**, 765 (1970).
9) H. S. Frank and A. S. Quist, *J. Chem. Phys.*, **34**, 604 (1961).
10) D. N. Glew and E. A. Moelwyn-Hughes, *Proc. Roy. Soc. Ser., A*, **211**, 254 (1952).
11) A. G. Mitchell and W. F. K. Wynne-Jones, *Discuss. Faraday Soc.*, **15**, 161 (1953).
12) F. Franks and D. J. G. Ives, *Quart. Rev.*, **20**, 1 (1966).
13) J. M. Corkill, J. F. Goodman, and J. R. Tate, *Trans. Faraday Soc.*, **63**, 773 (1967).
14) J. A. V. Butler, *ibid.*, **33**, 229 (1937).
15) R. Aveyard and R. W. Mitchell, *ibid.*, **64**, 1757 (1968).
16) J. M. Corkill, J. F. Goodman, and J. R. Tate, *ibid.*, **65**, 1742 (1969).
17) F. Franks and B. Watson, *ibid.*, **65**, 2339 (1969).
18) K. Tamaki, Y. Isomura, and Y. Ohara, Preprints for the 26th Meeting of the Chemical Society of Japan, (April 1972), paper 1G19, (p. 508).
19) H. S. Frank and F. Franks, *J. Chem. Phys.*, **48**, 4746 (1968).

$$f_H = \frac{N_H}{Nwz} \tag{5}$$

According to our seventh assumption, each CH_2 (or CH_3) of the alkyl chain occupies one cavity site. Therefore, the number of ways of occupation is diffrent according to the length of the chain.

First, we will consider the case of the methyl radical, *i.e.*, $\phi=1$. In this case, the number of states is:

$$\Omega_{CH_3} = \frac{\{(1-f_2)Nwz\}!}{(f_H Nwz)!\{(1-f_2-f_H)Nwz\}!} \tag{6}$$

In the case of the ethyl radical ($\phi=2$), the CH_2-adjacent to CH_3 must, naturally, occupy the neighboring cavity site. Therefoe, we have, as the number of ways to distribute the second carbon atom (CH_2) in the remaining cavities:

$$\{(\zeta-1)(1-f_2-2f_H)\}^{f_H Nwz} \tag{7}$$

Here, ζ is the cavity-site-nearest-neighbors and $(1-f_2-2f_H)$ is the probability that this is vacant. Similarly, we have, as the number of states for distributing the 3rd carbon atom (CH_2) of the propyl radical:

$$\{(\zeta-1)(1-f_2-3f_H)\}^{f_H Nwz} \tag{8}$$

and as the number of states for distributing the ϕth carbon atom (CH_2) of the $C_\phi H_{2\phi+1}$ radical:

$$\{(\zeta-1)(1-f_2-\phi f_H)\}^{f_H Nwz} \tag{9}$$

Thus, the number of all possible configurations of the alkyl chain in the cavity sites becomes:

$$\Omega_2 = \frac{\{(1-f_2)Nwz\}!}{(f_H Nwz)!\{(1-f_2-f_H)Nwz\}!}[\{(\zeta-1)(1-f_2-2f_H)\}\{(\zeta-1)(1-f_2-3f_H)\}\cdots\{(\zeta-1)(1-f_2-\phi f_H)\}]^{f_H Nwz} \tag{10}$$

The total number of possible configurations for the system containing N_H solute molecules (of $C_\phi H_{2\phi+1}$) and N water molecules, of which the f_2 fraction is in the cavity, is given by $\Omega=\Omega_1\cdot\Omega_2$ or by:

$$\Omega = \frac{(Nwz)!}{(f_2 Nwz)!(f_H Nwz)!\{(1-f_2-f_H)Nwz\}!} \times[\{(\zeta-1)(1-f_2-2f_H)\}\{(\zeta-1)(1-f_2-3f_H)\}\cdots\{(\zeta-1)(1-f_2-\phi f_H)\}]^{f_H Nwz} \tag{11}$$

By employing the approximations of Stirling's formula: $N!\cong\sqrt{2\pi N}\ (N/e)^N\cong(N/e)^N$ and the Boltzmann relationship $S^M=k\ \ln\Omega$. We obtain S^M the entropy of mixing per mole of water. Here $k=\boldsymbol{R}/N$ is the Boltzman constant, and $\boldsymbol{R}$ is the universal gas constant.

$$S^M = \boldsymbol{R}wz[-f_2\ln f_2 - f_H\ln f_H - (1-f_2-f_H)\ln(1-f_2-f_H) + f_H\{(\phi-1)\ln(\zeta-1) + \ln(1-f_2-2f_H) + \ln(1-f_2-3f_H) + \cdots + \ln(1-f_2-\phi f_H)\}] \tag{12}$$

Therefore, we obtain as the molar Gibbs free energy (G):

$$G = wG_N^0 + (1-w)G_I^0 + mG_H^0 - TS^M \tag{13}$$

or:

$$G = G_I^0 + w\Delta G_I^0 + mG_H^0 - TS^M \tag{14}$$

Here, G_N^0, G_I^0, and G_H^0 are the hypothetical standard molar free energies of network molecules, cavity molecules, and SAS molecules respectively. $\Delta G_I^0=G_N^0-G_I^0$, and T and m are the absolute temperature and the N_H/N mole ratio. By differentiating Eq. (14) with respect to w and setting $(\partial G/\partial w)_{P,T,m}=0$, we obtain:

$$\Delta G_I^0 = T\frac{dS^M}{dw} \tag{15}$$

while from Eq. (12) we get:

$$\frac{dS^M}{dw} = \boldsymbol{R}\Big[\ln f_2 - (1+z)\ln(1-f_2-f_H) + \frac{m}{w^2 z}\Big\{\frac{1}{(1-f_2-2f_H)} + \frac{1}{(1-f_2-3f_H)} + \cdots + \frac{1}{(1-f_2-\phi f_H)}\Big\} + \frac{m^2}{w^2 z}\Big\{\frac{2}{(1-f_2-2f_H)} + \frac{3}{(1-f_2-3f_H)} + \cdots + \frac{\phi}{(1-f_2-\phi f_H)}\Big\}\Big] \tag{16}$$

By substituting Eq. (16) into Eq. (15) and by assuming $f_H\ll1$, we obtain approximately:

$$\Delta G_I^0 = \boldsymbol{R}T\Big[\ln f_2 - (1+z)\ln(1-f_2) + \frac{m(1+z)}{wz(1-f_2-f_H)} + \frac{m(\phi-1)}{w^2 z(1-f_2-\phi f_H/2)} + \frac{m^2(\phi-1)(\phi+2)}{2w^2 z(1-f_2-\phi f_H/2)}\Big] \tag{17}$$

Now, we can use the relation $(\partial\Delta G_I^0/\partial p)=V_{fr}-V_I$ to obtain $(\partial w/\partial p)$ from Eq. (17). Here, V_{fr} and V_I mean the molar volumes of the framework water and the cavity water respectively, and we obtain $V_I=0$ using the sixth assumption. Therefore, we obtain from Eq. (17), by differentiating both sides with respect to pressure (p), and after rearrangements the following relation:

$$-\frac{1}{(\partial w/\partial p)} = \frac{\boldsymbol{R}T}{V_{fr}}\Big[\frac{1}{w(1-w)} + \frac{z+1}{w\{w(z+1)-1\}} + \frac{m(m+1)(z+1)}{w^3 z^2(1-f_2-f_H)^2} + \frac{m(z+1)}{w^2 z(1-f_2-f_H)} + \frac{2m(\phi-1)(m\phi+2)}{w^4 z^2(2-2f_2-\phi f_H)^2} + \frac{4m(\phi-1)}{w^3 z(2-2f_2-\phi f_H)} + \frac{m^2(\phi-1)(\phi+2)(m\phi+2)}{w^4 z^2(2-2f_2-\phi f_H)^2} + \frac{2m^2(\phi-1)(\phi+2)}{w^3 z(2-2f_2-\phi f_H)}\Big] \tag{18}$$

From the sixth assumption, the molar volume of the solution, V, is given by the following relation:

$$V = wV_{fr} + mV_{ion}, \tag{19}$$

since the interstitial alkyl chain radical has no effective volume. Therefore, the effective volume of the solution consists of two parts, one the volume of framework water and the other, the molar volume of the ionic parts.

The adiabatic compressibility is thermodynamically given by the following equation: $\beta=-1/V\cdot(\partial V/\partial p)_s$. When we treat the compressibility of aqueous solutions at low concentrations, we assume that the adiabatic compressibility of solutions is nearly equal to the isothermal one, since the ratio of specific heat in water is nearly 1. Therefore, we calculate the compressibility of solutions at the isothermal condition. As the ionic parts have no structural compressibility, we have from Eq. (19) $\beta_{st}=V_{fr}/V\cdot(-\partial w/\partial p)$, where $(-\partial w/\partial p)$ and V are given by Eqs. (18) and (19)

respectively. Here, the constant terms of derivatives are omitted for the simplicity of description. We write Eq. (19) as $-1/(\partial w/\partial p)=(\boldsymbol{RT}/V_{fr})\cdot A$; therefore, we have:

$$\beta_{st}=\frac{V_{fr}}{V}\cdot\left(-\frac{\partial w}{\partial p}\right)=\frac{(V_{fr})^2}{\boldsymbol{RT}}\cdot\frac{1}{VA} \tag{20}$$

We intend to calculate the dependency of β_{st} on the mole ratio, m. We obtain from Eq. (20), by taking logarithm $\log\beta_{st}=\log\{(V_{fr})^2/\boldsymbol{RT}\}-\log V-\log A$:

$$\frac{1}{\beta_{st}}\cdot\frac{d\beta_{st}}{dm}=-\left\{\frac{1}{V}\frac{dV}{dm}+\frac{1}{A}\frac{dA}{dm}\right\} \tag{21}$$

Here, the first term in the parentheses from Eq. (19) as:

$$\frac{1}{V}\left(\frac{dV}{dm}\right)=\frac{V_{fr}}{V}\cdot\left(\frac{dw}{dm}\right)+\frac{\bar{V}_{ion}}{V} \tag{22}$$

By employing Eq. (17), we obtaine (dw/dm) from the equilibrium conditions at the concentration m:

$$(d\Delta G_I^0/dm)=(\partial\Delta G_I^0/\partial w)(dw/dm)+(\partial\Delta G_I^0/\partial m)=0$$

Now, (dw/dm) becomes, at the limit of low concentrations, $\lim_{m\to0}(dw/dm)=(dw/dm)_0$, and, after some calculations, we attain the result:

$$\left(\frac{dw}{dm}\right)_0=\frac{(1-w_0)}{z}\{\phi+w_0(z+1)-1\} \tag{23}$$

where w_0 is the value of w for pure water. Therefore, we obtain from Eqs. (22) and (23) the relation:

$$\frac{1}{V_0}\cdot\left(\frac{dV}{dm}\right)_0=\frac{(1-w_0)}{w_0z}\{\phi+w_0(z+1)-1\}+\frac{(\bar{V}_{ion})_0}{V_0} \tag{24}$$

where $V_0(=w_0V_{fr})$ and $(\bar{V}_{ion})_0$ mean the molar volume of pure water and the molar volume at an infinite dilution of the ionic parts of SAS. The second term in parentheses in Eq. (21) becomes, at the limit of low concentrations:

$$\lim_{m\to0}\left(\frac{1}{A}\frac{dA}{dm}\right)=\frac{1}{A_0}\left(\frac{\partial A}{\partial w}\frac{dw}{dm}+\frac{\partial A}{\partial m}\right)_{m=0}$$

where:

$$A_0=\frac{z}{w_0(1-w_0)\{w_0(z_0+1)-1\}},$$

$$\left(\frac{\partial A}{\partial w}\right)_0=\frac{2w_0-1}{\{w_0(1-w_0)\}^2}-\frac{(z+1)\{2w_0(z+1)-1\}}{[w_0\{w_0(z+1)-1\}]^2},$$

and:

$$\left(\frac{\partial A}{\partial m}\right)_0=\frac{z+1}{w_0\{w_0(z+1)-1\}}+\frac{z+1}{w_0^2z\{w_0(z+1)-1\}}+\frac{(\phi-1)}{[w_0\{w_0(z+1)\}]^2}+\frac{2(\phi-1)}{w_0^2\{w_0(z+1)-1\}}.$$

After some computation, we finally obtain the relaton:

$$\left(-\frac{d\beta_{st}}{dm}\right)_0=\beta_{st}^0\left[\frac{3(1-w_0)}{w_0z}+\frac{(2w_0-1)\{w_0(z+1)-1\}}{w_0z^2}-\frac{(z+1)(1-w_0)^2\{2w_0(z+1)-1\}}{w_0z^2\{w_0(z+1)-1\}}+\frac{(1-w_0)}{w_0z\{w_0(z+1)-1\}}\right]\phi+\frac{(2w_0-1)\{w_0(z+1)-1\}^2}{w_0z^2}-\frac{(z+1)(1-w_0)^2\{2w_0(z+1)-1\}}{w_0z}+\frac{(1-z)(1-w_0)}{w_0z}+\frac{(1+z)(1-w_0)}{z}-\frac{(1-w_0)}{w_0z\{w_0(z+1)-1\}}+\frac{(1-w_0)\{w_0(z+1)-1\}}{w_0z}+\frac{(\bar{V}_{ion})_0}{V_0} \tag{25}$$

where $\beta^0{}_{st}$ is the structural compressibility of pure water. Using the concentration of C mol/l in place of the mole ratio, m, we obtain $(d\beta_{st}/dC)_0=(1/55.5)\,(d\beta_{st}/dm)_0$. Then we can obtain the theoretical relationship for the concentration dependence of the compressibility (extrapolated to infinite dilution) $(-d\beta/dC)_0$ in SAS solutions:

$$(d\beta/dC)_0=(d\beta_{st}/dC)_0+(\Delta\beta_{ion})_0 \tag{26}$$

where $(\Delta\beta_{ion})_0$ is the decrease in the compressibility due to the ionic parts of SAS at an infinite dilution.

On the other hand, the partial molar volume at an infinite dilution being thermodynamically defined as $\bar{V}_0=\lim_{m\to0}\left(\frac{\partial V}{\partial m}\right)_N$ we get from Eq. (19):

$$\bar{V}_0=V_{fr}\left(\frac{dw}{dm}\right)_0+(\bar{V}_{ion})_0 \tag{27}$$

or, by substituting Eq. (23):

$$\bar{V}_0=\frac{V_{fr}(1-w_0)}{z}\cdot\phi+\frac{V_{fr}(1-w_0)\{w_0(z+1)-1\}}{z}+(\bar{V}_{ion})_0 \tag{28}$$

Numerical Computation

We[4] have previously obtained w_0 and z as functions of the temperature using the data[5] of Narten *et al.*; it has been shown that w_0 and z, at 30°C, are 0.808 and 0.295 respectively. The structural compressibility of pure water, β_{st}^0 is 26.7×10^{-12} cm^2/dyn[20] at 30°C.

Generally, the hydration number of ions depends on the methods[21,22] used. The hydration numbers for SO_4^{2-}, as obtained by various methods, range from 4 to 16,[21-23] and those of Na,$^+$ from 1 to 71.[22,23] Here we used the values obtained by the ultrasonic method,[23] *i.e.*, 16 for SO_4^{2-} and 4.7 for Na,$^+$ and assumed the hydration number for the OSO_3^- ion to be 3/4 the value(=12) for SO_4^{2-}. Then, the hydration number for OSO_3^- and Na^+ amounts to 16.7. The decrease in compressibility $(\Delta\beta_{ion})_0$ due to ionic parts becomes -13.4×10^{-12} (cm^2/dyn)/(mol/l). Then, we obtain the theoretical relationship for the concentration dependence of the compressibility (extrapolated to an infinite dilution) $(-d\beta/dC)_0$ as a function of the carbon number, ϕ, of the alkyl group in SAS solutions:

$$(-d\beta/dC)_0=(2.02\phi+6.45)\times10^{-12}\ (\text{cm}^2/\text{dyn})/(\text{mol}/l) \tag{29}$$

The dotted line in Fig. 4 shows this relation.

Now let us consider the partial molar volume. We assume the partial molar volume of $HOSO_3Na$ to be equal to 32.0 cm^3/mol at moderate concentrations,

20) L. Hall, *Phys. Rev.*, **73**, 775 (1948).
21) O. Samoilov, "Ion no Suiwa", (Translation from Russian by W. Uchira) Chijin Shokan, Tokyo, (1967), p. 50.
22) J. F. Hinton and E. S. Amis, *Chem. Rev.*, **71**, 627 (1971).
23) T. Yasunaga, 15th Tyoonpa Kenkyukai Siryo, Denki Tusin Gakai, (1964).

where the solution is considered to contain $HOSO_3^-$ and Na^+ ions. Here, we assume the $(\bar{V}_{ion})_0$ of SAS to be equal to the partial molar volume of SHS. On this assumption, we obtain, as the theoretical relationship between the carbon number, ϕ, in SAS and the partial molar volume at an infinite dilution ($\bar{V}_0$), the following equation:

$$\bar{V}_0 = 14.6\phi + 32.7 \text{ (cm}^3\text{/mol)} \quad (30)$$

The dotted line in Fig. 5 shows this relation.

Disscussion

According to the interstitial model, we can explain the linear chage in the sound velocity and compressibility *vs.* the concentration for the systems of SMS, SES, and SBS. The marked deviation from linearity of these quantities in the SHS solution (*cf.* Figs. 2 and 3) is attributable to the dissociation[24] of the HSO_4^- into H^+ and SO_4^{2-} at low concentrations. At moderate concentrations, SHS behaves as a uni-divalent electrolyte because of its dissociation into $Na,^+$ $H,^+$ and SO_4^{2-}. The $(d\beta/dC)$ in the SHS solution slowly decreases untill the limiting value of about -5.9×10^{-12} $(cm^2/dyn)/(mol/l)$ is reached at *ca.* 15 mmol/*l*; it is considered to act as a uni-univalent electrolyte composed of HSO_4^- and $Na.^+$

The linear dependence of $(d\beta/dC)_0$ on the carbon number ϕ in the alkyl chain can also be explained. The approximate agreement between the constant terms in Eqs. (1) and (29) may indicate that our assumption regarding the hydration number of the ionic parts (OSO_3^- and Na^+) is rather adequate.

The slope of the $(d\beta/dC)_0$ *vs.* ϕ curve, however, indicates that the theoretical dependency on the carbon number is about three times larger than the experimental value. In the theoretical calculation, we used the seventh assumption, that a cavity may be occupied by only one methylene (or methyl) radical. The experimental results may be explained by allowing one cavity to be occupied by up to three radicals. The length of the hydrogen bond in water is 2.76[25]—2.88[5] Å, the diamater of the hexagonal cavity is about 6 Å, and the cavity is wide enough to accommodate up to three methylene radicals, since the length of the C-C bond is about 1.5[26] Å.

As regards the relationship between $\bar{V}_0$ and ϕ, on the other hand, the theoretical dependency on the carbon number is nearly in agreement with the experimental value, while the constant term is different. Also, from the studies of $\bar{V}_0$[27] for the homologue series of alkylamine hydrogen halides and tetraalkylammonium salts, it has been reported that the increment per CH_3 (or CH_2) radical added to the homologue series is $\bar{V}_0$=*ca.* 16.7 m*l*/mol, a value which is nearly in agreement with the present results per carbon atom.

The modification of the theory to admit up to three methylene groups may decrease the slope of the $\bar{V}_0-\phi$ curves. This results that the slope deviates from the experimental results, although the avarage value of $\bar{V}_0$ may approach the experimental value.

An interstitial-solute model similar to that employed here has also been proposed by Glew[28] on the basis of studies of hydrates. Evidence of the occupation of the cavity by the solute is also given by the kinetic study in the solvolysis of *t*-butyl chloride in an alcohol-water system.[29] More direct evidence is afforded by the X-ray diffraction study of aqueous solutions.[7,8]

The author wishes to thank Professor T. Sasaki of Tokyo Metropolitan University for his helpful discussions about and generous support of this research, and also Professor O. Nomoto of the Defense Academy for his valuable suggestions and discussions.

24) P. L. Khre, *Trans. Faraday Soc.*, **58**, 359 (1962).

25) L. Pauling, "The Nature of the Chemical Bond," Cornell University Press, Ithaca, N. Y. (1960) 3rd. ed., (Translation from English by M. Koizumi), p. 420.

26) L. Pauling, *ibid.*, p. 214.

27) R. E. Verrall and B. E. Conway, *J. Phys. Chem.*, **70**, 3961 (1966).

28) D. N. Glew, H. D. Mark, and N. S. Rath in "Hydrogen-Bonded Solvent System," ed. by A. K. Covington and P. Jones, Taylor & Francis, London (1968), p. 195.

29) R. E. Robertson and S. E. Sugamori, *J. Amer. Chem. Soc.*, **91**, 7254 (1969).

Bond Alternation in Tropone as Studied by Gas Electron Diffraction[1)]

Makoto OGASAWARA,* Takao IIJIMA, and Masao KIMURA**
Department of Chemistry, Faculty of Science, Hokkaido University, Sapporo
(Received February 18, 1972)

Assuming a planar conformation with C_{2v} symmetry, and using the estimated mean amplitudes of vibration, the bond alternation in tropone was confirmed. The average C–C and C=C distances were determined by the least-squares method to be 1.454 ± 0.010 and 1.362 ± 0.013 Å respectively; moreover, two probable sets of the structure parameters were obtained. On the basis of conformational arguments regarding the structures of related compounds, the following set of the bond lengths was preferred: C–H, $1.09_8\pm0.01_6$ Å; C_1–O, $1.22_5\pm0.01_2$ Å; C_1–C_2, $1.44_5\pm0.01_2$ Å; C_2–C_3, $1.36_4\pm0.01_2$ Å; C_3–C_4, $1.46_2\pm0.01_2$ Å; and C_4–C_5, $1.34_2\pm0.01_8$ Å.

Since the geometrical configurations of nonbenzenoid aromatic seven-membered ring compounds have been the subject of much interest in conjunction with their aromaticity, a number of X-ray structure analyses have been undertaken regarding tropone derivatives,[2)] tropolone[3)] and its derivatives,[4)] dicyanoheptafulvene[5)] and its derivatives,[6)] and many other related compounds. From the results of these studies, it may be said that the planarity[7)] and bond alternation of the seven-membered rings of compounds, commonly classified as nonbenzenoid aromatics, have been established. As a natural consequence, tropone itself can also be expected to have a planar configuration with alternating bond lengths. This is in accordance with the theoretical consideration that the aromaticity of tropone originates from a significant contribution of a polar structure to the ground state.[8)] Indirect but fairly conclusive experimental evidence for bond alternation was provided, for example, by the presence of the infrared bands assigned to the stretching vibrations of the C–C and C=C bonds.[9,10)] In a previous electron diffraction study, one of the present authors and his coworkers were unable to draw a definite conclusion as to the bond alternation, instead, a regular heptagonal model was assumed.[11)]

Many molecular orbital calculations were carried out[8,12–15)] in order to interpret the ultraviolet absorption spectrum[8,12,16)] and the dipole moment.[17,18)] There still exist two alternative interpretations of the characteristic absorption bands of tropone; one was presented by Hosoya *et al.*[8a)] and the other, by Weltin *et al.*[12)] Because of a lack of accurate structural data, in most of the calculations the bond lengths were assumed at either the values determined by the previous electron-diffraction study or at those estimated from the observed bond lengths for olefins. Hosoya and Nagakura[8b)] and Kunii and Kuroda[15)] estimated the bond lengths on the basis of the resulting bond orders, but they had no experimental data by which to check their results. The former authors then remarked in their paper that a more precise determination of the lengths would provide an effective clue to settle the problem.[8b)] Since it was expected that the current technique of electron diffraction by gases would yield more accurate bond lengths, we decided to reinvestigate this molecule.

After initiating this reinvestigation, we noticed that Bertelli and Andrews, Jr.,[19)] had analysed the dipole

* Present address: Products Development Institute, Teijin Ltd., Iwakuni, Yamaguchi.
** To whom correspondence should be addressed.

1) Presented at the International Symposium on Nonbenzenoid Aromatic Compounds, Sendai, Japan, 1970 (abbreviated by ISNA in this paper).

2) a) D. J. Watkin and T. A. Hamor, *J. Chem. Soc., B*, **1971**, 2167. b) H. Shimanouchi, T. Ashida, Y. Sasada, M. Kakudo, I. Murata, and Y. Kitahara, This Bulletin, **40**, 779 (1967). c) H. Shimanouchi, H. Hata, and Y. Sasada, *Tetrahedron Lett.*, **1968**, 3573; ISNA, Abstract p. 81 (1970). d) T. Hata, H. Shimanouchi, and Y. Sasada, *Tetrahedron Lett.*, **1969**, 753; ISNA, Abstract p. 81 (1970). e) H. Shimanouchi, T. Hata, and Y. Sasada, *ibid.*, p. 81 (1970). f) T. R. R. McDonald, *Acta Crystallogr.*, **8**, 61 (1955).

3) H. Shimanouchi and Y. Sasada, ISNA, Abstract p. 85 (1970).

4) a) J. M. Robertson, *J. Chem. Soc.*, **1951**, 1222. W. M. Macintyre, J. M. Robertson, and R. F. Zahrobsky, *Proc. Roy. Soc. Ser., A*, **289**, 161 (1966). b) Y. Sasada and I. Nitta, *Acta Crystallogr.*, **9**, 205 (1956); R. Shiono, *ibid.*, **14**, 42 (1961). c) Y. Sasada, K. Osaki, and I. Nitta, *ibid.*, **7**, 113 (1954); Y. Sasada and I. Nitta, This Bulletin, **30**, 62 (1957). d) T. A. Hamor and D. J. Watkin, *Chem. Commun.*, **1969**, 440. e) Y. Fukazawa and S. Ito, ISNA, Abstract p. 93 (1970). f) Y. Sasada, This Bulletin, **32**, 171 (1959).

5) H. Shimanouchi, T. Ashida, Y. Sasada, M. Kakudo, I. Murata, and Y. Kitahara, This Bulletin, **39**, 2322 (1966).

6) a) C. Kabuto, Y. Kitahara, H. Shimanouchi, and Y. Sasada, ISNA, Abstract p. 89 (1970). b) C. Kabuto, Y. Kitahara, H. Shimanouchi, and Y. Sasada, *ibid.*, p. 89 (1970).

7) The planarity of the seven-membered rings is not unexceptional. If the 2 and/or 7 positions of a ring (Fig. 3) are substituted by atoms or groups bulkier than the hydrogen atom, the ring may deviate from a plane and take a boat form by steric interactions between the carbonyl oxygen and the substituents.[2e,4e,6a,6b)]

8) a) H. Hosoya, J. Tanaka, and S. Nagakura, *Tetrahedron*, **18**, 859 (1962). b) H. Hosoya and S. Nagakura, *Theor. Chim. Acta* (Berl.), **8**, 319 (1967).

9) Y. Ikegami, This Bulletin, **35**, 967, 972 (1962), and references therein.

10) H. Junge, *Spectrochim. Acta*, **24A**, 1951 (1968), and references therein.

11) K. Kimura, S. Suzuki, M. Kimura, and M. Kubo, *J. Chem. Phys.*, **27**, 320 (1957); This Bulletin, **31**, 1051 (1958).

12) E. Weltin, E. Heilbronner, and H. Labhart, *Helv. Chim. Acta*, **46**, 2041 (1963).

13) A. Julg and B. Bonnet, *Tetrahedron*, **20**, 2243 (1964).

14) K. Inuzuka and Y. Yokota, *J. Chem. Phys.*, **44**, 911 (1966).

15) a) H. Kuroda and T. Kunii, *Theor. Chim. Acta* (Berl.), **7**, 220 (1967). b) T. Kunii and H. Kuroda, *Report of the Computer Center, Univ. of Tokyo*, **1**, 122 (1968).

16) M. Tsuboi, This Bulletin, **25**, 369 (1952).

17) A. D. Giacomo and C. P. Smyth, *J. Amer. Chem. Soc.*, **74**, 4411 (1952).

18) Y. Kurita, S. Seto, T. Nozoe, and M. Kubo, This Bulletin, **26**, 272 (1953).

19) D. J. Bertelli and T. G. Andrews, Jr., *J. Amer. Chem. Soc.*, **91**, 5280 (1969).

moments and NMR spectra of tropone and analogous compounds by the aid of CNDO/2 molecular-orbital calculations for two assumed models, a regular heptagonal ring and a planar ring built from bond lengths suitable for olefins.[20] As a result, they were led to the conclusion that the dipole moment and NMR data are consistent with the planar ring with alternating bond lengths. Furthermore, through several critical discussions of its aromaticity, they stated that tropone resembled a polyenone more closely than an aromatic system and could be best classified as the former. If accurate bond lengths can be determined, they will provide useful information for discussions along this line.

In carrying out the present study, our attention was directed mainly to obtaining experimental evidence for bond alternation and, if possible, bond lengths useful for discussing the properties of tropone. Making some plausible assumptions regarding the molecular symmetry and the parameter values, which are necessary to analyze the diffraction patterns of relatively complex molecules, we obtained two probable sets of structural parameters. Unfortunately, a unique result could not be obtained from the electron diffraction data alone. However, the bond alternation in tropone has unquestionably been verified.

Experimental

The sample of tropone was kindly provided by Professor Yoshio Kitahara of Tohoku University and was used without further purification. The diffraction photographs were taken with an apparatus equipped with an r^3-sector at the camera length of 124.47 mm.[21] The sample vapor was injected into the diffraction chamber by means of a high-temperature nozzle maintained at 108°C. The exposure time was 8 min, with a beam current of 0.15 μA. The wavelength of the beam (an accelerating voltage of about 52.9 kV) was determined by the use of the pattern of carbon disulfide.[22] Three plates were selected from among several plates and were microphotometered.

Data Processing and Structure Determination

The molecular intensity, $qM(q)$, was obtained from the observed total intensities[23] by determining the experimental background by means of the radial distribution curve and its Fourier inverse transformation. In the calculations of the radial distribution curves, the correction factors for non-nuclear scattering were introduced by Bonham and Bartell's method.[24] The other details of data processing have been described elsewhere.[25]

The determination of the molecular parameters was carried out by the least-squares method based upon the molecular intensity.[26] According to our conventional weighting scheme, the data were weighted down from $q=30$ to 21 and from $q=100$ to 130 in order to reduce the influence of uncertainties in the experimental molecular intensities at both small and large scattering angles. In general, accurate determination of interatomic distances are practically impossible for atom pairs which make relatively small contributions to the molecular intensity. Besides, the skeletal heptagonal ring of tropone consists of bonds which are only slightly different in length from one another. In such a case, the mean amplitudes and the differences between the bond lengths are strongly correlated if one wishes to determine all of them from the diffraction pattern by the least-squares method. After various preliminary least-squares treatments, it was found best for our present purpose to use reliable estimates of the mean amplitudes in order to fix some of the strongly correlated parameters and to determine the bond lengths more precisely. The following assumptions were made with respect to the geometrical configuration and mean amplitudes:

(1) Configuration. The molecule has a planar configuration, with C_{2v} symmetry. All the C–H bonds have the same length, and each of them bisects the CCC valence angle. The molecular configuration is, then, defined by the eight interatomic distances, the bonded C–H, C_1–O, C_1–C_2, C_2–C_3, C_3–C_4, C_4–C_5 and non-bonded $C_1\cdots C_3$, $C_1\cdots C_4$ distances (see Fig. 3).

(2) Mean Amplitudes. The mean amplitude used were estimated from the spectroscopic data in the following way. By assuming an appropriate molecular configuration, the Urey-Bradley force constants were determined from the vibrational frequencies observed by Ikegami.[9] The mean amplitudes were then calculated at 373°K, the approximate temperature of the nozzle when the diffraction experiments were carried out. The calculation was limited to in-plane vibrations. The calculated mean amplitudes for the ring and the force constants are shown in Tables 1 and 2 respectively.

Table 1. Mean amplitudes used for the analyses (at $T=373$°K)

Pair	l (Å)	Pair	l (Å)
C_1—O	0.0413	$C_2\cdots C_5$	0.0699
C_1—C_2	0.0470	$C_2\cdots C_6$	0.0707
C_2—C_3	0.0441	$C_3\cdots C_5$	0.0575
C_3—C_4	0.0476	$C_3\cdots C_6$	0.0708
C_4—C_5	0.0432	O$\cdots C_2$	0.0596
$C_1\cdots C_3$	0.0575	O$\cdots C_3$	0.0630
$C_1\cdots C_4$	0.0692	O$\cdots C_4$	0.0713
$C_2\cdots C_7$	0.0596	C—H	0.0771
$C_2\cdots C_4$	0.0588		

20) J. A. Pople and M. Gordon, *J. Amer. Chem. Soc.*, **89**, 4253 (1967).
21) Y. Murata, K. Kuchitsu, and M. Kimura, *Jap. J. Appl. Phys.*, **9**, 591 (1970).
22) C. Kato, S. Konaka, T. Iijima, and M. Kimura, This Bulletin, **42**, 2148 (1969).
23) The primary data for the observed leveled intensities have been filed with the Chemical Society of Japan. (Document No. 7209). A copy may be secured by citing the document number and by remitting, in advance, ¥ 300 for photoprint. Pay by check or money order payable to: Chemical Society of Japan.
24) R. A. Bonham and L. S. Bartell, *J. Chem. Phys.*, **31**, 702 (1959).
25) H. Fujii and M. Kimura, This Bulletin, **43**, 1933 (1970).
26) O. Bastiansen, L. Hedberg, and K. Hedberg, *J. Chem. Phys.*, **27**, 1311 (1957).
27) K. Kuchitsu, This Bulletin, **40**, 498 (1967).

Table 2. Adjusted values of the force constants for tropone (in mdyn/Å)

Bond	K	Angle	H	F
C=O	7.5	OCC	0.32	0.80
C_1–C_2	4.2	CCC[a)]	0.33	0.37
C_2=C_3	6.0	HCC[a)]	0.20	0.48
C_3–C_4	4.2			
C_4=C_5	6.6			
C–H	4.56			

a) The same values were assumed for all CCC and for all HCC force constants.

(3) Asymmetry Constants. The asymmetry constants were fixed at values of 30×10^{-7} and 127×10^{-7} Å^3 for the bonded distacnes in the skeleton and the C–H bond respectively, and were ignored for the non-bonded distances.[27)]

In practical refinements, a strictly constrained least-squares method was not used; rather, unadjusted parameters at each step of calculation were fixed at values evaluated from the r_a distances obtained just before the step, without taking the shrinkage effect into account.[28)]

The observed molecular intensities thus obtained for one arbitrarily selected plate are shown by dots in Fig. 1, while the corresponding radial distribution curve is depicted in Fig. 2, curve a. In the radial distribution curve, there are two complex peaks extending from 1.0 to 1.6 Å, and from 2.0 to 2.7 Å, with maxima at about 1.40 and 2.55 Å respectively. The former corresponds to the bonded atom pairs, and the latter, to the short non-bonded atom pairs. The peaks at about 3.15 and 3.55 Å represent the long non-bonded C:::C and the long non-bonded C:::O and C:::H distances respectively. The still longer distacnes, C:::O and C:::H, contribute to the peak beyond 4.0 Å.

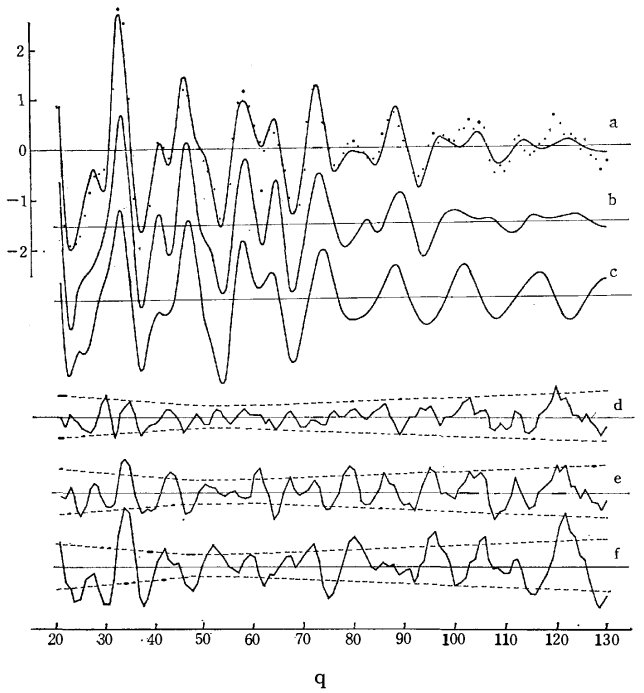

Fig. 1. The molecular intensity and difference curves.
dots: experimental, a: theoretical II, b: theoretical average (see text), c: theoretical non-alternating, d: Exp–a, e: Exp–b, f: Exp–c. The scale of the ordinate is the same for all the curves and is entered only for the experimental one. Broken lines indicate the limit of estimated uncertainties in the experimental intensities.

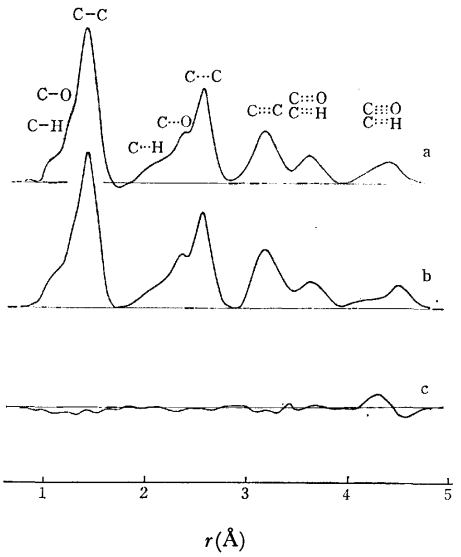

Fig. 2. The radial distribution curves.
a: experimental, b: theoretical II, c: difference a−b.

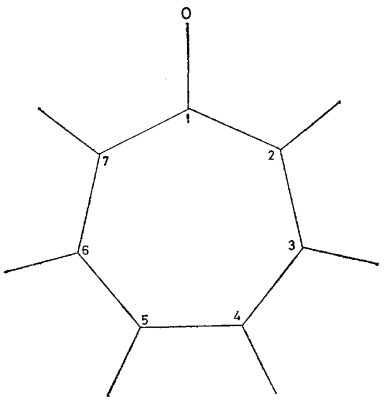

Fig. 3. The numbering of atoms.

Results

Non-equality of Bond Lengths and Average C–C and C=C Bond Lengths. The possibility of a configuration with non-alternating bond lengths was rejected after examining the results of least-squares fittings for various models. When a least-squares fitting was performed, for instance, with respect to the four independent parameters, the C=O, C–C, C···C, and C:::C, by fixing the mean amplitudes at the estimated values in Table 1 and the C–H distance at 1.092 Å, the structure parameters resulting from the data plotted in Fig. 1 were as follows: r_a(C=O), 1.284±0.016;

28) See, *e.g.*, S. J. Cyvin, "Molecular Vibrations and Mean Amplitudes," Universitetsforlaget, Oslo and Elsevier, Amsterdam (1968).

Table 3. Average C–C and C=C, and other interatomic distances determined by the least-squares adjustment

Parameter	r_g	σ	limit of error[a)]
C—C	1.454	0.002	0.010
C=C	1.362	0.003	0.013
C=O	1.231	0.005	0.016
$C_1 \cdots C_3$	2.502	0.009	0.028
$C_1 \cdots C_4$	3.197	0.013	0.035
C—H	1.098	assumed	

a) Described in the succeeding paragraph of the most probable structures.

r_a(C–C), 1.422 ± 0.004; r_a(C···C), 2.507 ± 0.029; r_a(C:::C), 3.109 ± 0.044 Å, and the index of resolution, 0.55 ± 0.03. The theoretical curve based upon these parameters and its differences from the experimental values are shown in Fig. 1c and f respectively. The disparities between the experimental and theoretical curves are far beyond the estimated uncertainties in the observed intensities, shown by broken lines in Fig. 1. The average C–C and C=C bond lengths were then determined by dividing bonds in the ring into two groups, a single bond C_1—C_2, C_3—C_4, *etc*, and a double bond, C_2—C_3, C_4—C_5 *etc*. The results of the least-squares refinement are shown in Table 3. In this table, each structure parameter was given by the average of the results obtained from the three sets of data, while the standard deviation, σ, was estimated by the equation, $\sigma = \langle\sigma\rangle/\sqrt{3}$, where $\langle\sigma\rangle$ is the average of the three standard deviations. The corresponding theoretical intensity curve and its differences from the experimental values are depicted in Fig. 1b and e respectively. The agreement between the theoretical curve and the experimental one was improved to some extent; the sum of square residuals was reduced by a factor of about 2, while the index of resolution increased to 0.82 ± 0.04.

The Most Probable Parameters. Further least-squares refinements were carried out for models with different bond lengths. Since it was difficult to make the refinements converge by allowing the index of resolution and the eight independent distances to vary simultaneously, the index of resolution, the five bonded distances in the skeleton, the C–H distance, and each of the two non-bonded distances were adjusted iteratively so as to make a best-fit theoretical molecular intensity curve. By reference to the average C–C and C=C bond lengths, and also to the reported values for tropone derivatives in the crystalline state, a model with C_1–O=1.23, C_1–C_2=1.48, C_2–C_3=1.37, C_3–C_4=1.43, C_4–C_5=1.34, and C–H=1.10 Å, and others with bond lengths exchanged with respect to either one or both of the C_1–C_2 and C_3–C_4 and the C_2–C_3 and C_4–C_5 pair, were selected initially in order to search for the most probable structure. As a result, we found two sets of parameters which were equally probable and gave the same least-square residuals. Table 4 summarizes the results obtained by the least-squares refinements from the data for three plates. In what follows, these two sets of the parameters will be referred to as I and II.

The two sets of parameter values thus derived explain the experimental molecular intensities equally well, the indices of resolution and the standard deviations being substantially equal in both refinements. The agreement of the theoretical intensity curves for these models with the experimental one was much improved over the previous case, and the sum of the squared residuals was reduced to about one-half the value obtained for the model with the grouped C–C bond lengths. The two theoretical curves based upon the sets I and II differ from each other in some details. However, this cannot be used in discriminating a better model, since the magnitudes of the differences are within the range of random fluctuations, or the limit of uncertainty in the observed intensities. For example, the theoretical intensity curve calculated from the parameters of the set II and its difference curve are shown

Table 4. Results of the least-squares adjustments and their estimated limits of error (distances in Å, angles in degrees)[a)]

Parameter	I			II		
	r_g[b)]	σ[c)]	Limit of error	r_g[b)]	σ[c)]	Limit of error
C—H	1.096	0.005	0.014	1.098	0.006	0.016
C_1—O	1.224	0.004	0.012	1.225	0.004	0.012
C_1—C_2	1.475	0.002	0.012	1.445	0.002	0.012
C_2—C_3	1.362	0.002	0.012	1.364	0.002	0.012
C_3—C_4	1.429	0.002	0.012	1.462	0.002	0.012
C_4—C_5	1.342	0.005	0.016	1.342	0.006	0.018
$C_1 \cdots C_3$	2.560	0.006	0.019	2.590	0.007	0.022
$C_1 \cdots C_4$	3.250	0.009	0.026	3.227	0.009	0.027
Index of resolution	0.92	0.01		0.88	0.01	
$\angle C_7C_1C_2$[d)]	125			122		
$\angle C_1C_2C_3$	127.5			133		
$\angle C_2C_3C_4$	133			126		
$\angle C_3C_4C_5$	127			129.5		

a) Distances in Å, angles in degrees and the indices of resolution are dimensionless.
b) Calculated from the observed r_a distances and the mean amplitudes listed in Table 1.
c) σ does not include the systematic errors.
d) Calculated from the r_g distances for the best-fit structure.

in Fig. 1 a and d respectively. Curve b in Fig. 2 shows the theoretical curve based upon the set II parameters. The agreement with the observed curve is satisfactory except for the peaks in the region beyond 4.0 Å, which are associated with the longest non-bonded distances.

The limits of error quoted in Tables 3 and 4 include the random error, taken as 2.5 times the standard deviation, σ, and the systematic errors. The most significant systematic errors are the error in the scale factor, which was estimated to be 0.15% of the interatomic distance from the results of analysis for the diffraction patterns of the reference material, carbon disulfide, and the errors due to the probable uncertainties in the mean amplitudes and the ignoring of the shrinkage effects. The last two errors were not evaluated numerically, but were estimated roughly as follows.

It is generally known that calculated mean amplitudes are not very sensitive to variations in the force constants of the internal force field if they are only chosen to account a same extent for the observed vibrational frequencies. There is, therefore, little probability that the mean amplitudes for tropone deviate more than 5% from the calculated values listed in Table 1. Five percent of the mean amplitudes in our case amounts to 0.0025 Å for the bonded distances and 0.0030 Å for the short non-bonded distances. These deviations will influence the results, particularly similar distances such as the C_1–C_2 and C_3–C_4, and the C_2–C_3 and C_4–C_5 distances. It was reported by Karle that if the neighboring C–C bonds of benzene differed in length by $2a$ Å, as much as $a/3$ Å smaller mean amplitudes would result.[29] This estimate seems reasonable. If this estimate is applied to the present case, we get, in a very crude approximation, values of the errors due to the uncertainties in the mean amplitudes of 0.008 Å and 0.009 Å for the bonded and short non-bonded distances respectively. For the long non-bonded distances, the error was estimated to be 0.011 Å by assuming simply the uncertainties in their mean amplitudes to be 10%. Since the C–H distance could be determined almost independently of its mean amplitude, an error of this sort was not included.

The shrinkage effects for various molecules have been dealt with by many workers.[28] By examining these results, we assumed the magnitude of shrinkage to be 0.006 Å, a value which is almost the largest value found for ordinary molecules with no extremely low deformaiton frequencies. The uncertainties due to the ignoring of the shrinkage effect in the analyses do not exceed this value. Thus, this amount of uncertainty was included in the limits of error. In considering the limits of error thus estimated, it should be remarked that we can attach no great significance to the differences obtained between the C_1–C_2 and C_3–C_4 distances and between the C_2–C_3 and C_4–C_5 distances by Refinement II.

29) I. L. Karle, *J. Chem. Phys.*, **20**, 65 (1952).
30) H. Kon, This Bulletin, **28**, 275 (1955).
31) H. C. Longuett-Higgins and L. Salem, *Proc. Roy. Soc. Ser. A*, **257**, 445 (1960).
32) T. Nakajima, This Bulletin, **38**, 83 (1965).
33) K. Nishimoto and L. S. Foerster, *Theor. Chim. Acta*, **4**, 155 (1966).
34) L. S. Bartell, E. A. Roth, C. D. Hollowell, K. Kuchitsu, and J. E. Young, Jr., *J. Chem. Phys.*, **42**, 2683 (1965).
35) A. Almeningen, I. M. Anfinsen, and A. Haaland, *Acta Chem. Scand.*, **24**, 43 (1970).
36) K. Kuchitsu, T. Fukuyama, and Y. Morino, *J. Mol. Struct.*, **1**, 463 (1967—1968).
37) M. Traetteberg, *Acta Chem. Scand.*, **20**, 1724 (1966); W. Haugen and M. Traetteberg, "Selected Topics in Structure Chemistry," Universitetsforlaget, Oslo (1967), p. 113.
38) M. Traetteberg, *J. Amer. Chem. Soc.*, **86**, 4265 (1964).

Discussion

Bertelli and Andrews[19] employed, in their CNDO/2 calculations, the standard bond lengths proposed by Pople and Gordon,[20], and after some critical discussion of the aromatic character of tropone they stated that, although there were no direct measurements available, tropone must have bond lengths within the range found for polyolefinic compounds. Roughly speaking, their prediction about the bond lengths coincides with the results of the present study.

Now we have two probable sets of structural parameters. Unfortunately, it is impossible to select a preferred model on the basis of the electron diffraction data alone. Therefore, some other information is needed to decide which structure is more favorable. Hosoya and Nagakura estimated the average C–C and C=C bond lengths to be 1.46 and 1.35 Å respectively, by grouping the data into single and double bonds and by using various empirical relationships among the bond orders, bond length, overlap integrals, and core resonance integrals.[30–32] Kunii and Kuroda[15] estimated the self-consistent bond lengths to be 1.45, 1.37, 1.43, and 1.37 Å for the respective consecutive C–C bonds, and 1.27 Å for the C=O bond by the use of another relationship.[33] The bond lengths given by Hosoya and Nagakura are in perfect agreement with the average distances determined by the present study and are close to the set II structure, while those reported by Kunii and Kuroda agree better with the set I structure except for the C=O distance. As for the C=O distance, the former authors assumed it to be 1.26 Å, while the latter authors estimated it to be 1.27 Å. These values are unacceptably longer than the observed values, 1.22 Å. All of the molecular orbital calculation[8b,15,19] carried out so far lead to very similar bond orders for the C_1–C_2 and C_3–C_4 bonds, resulting in a difference in length of only 0.02 Å or less. If the similarity of the bond orders is a unique solution to be drawn from the molecular-orbital calculations, set I might be ruled out. However, this cannot be stated definitely at present.

It may be instructive to compare the present results with the bond lengths in ethylene,[34] *cis*-2-butene,[35] 1,3-butadiene,[36] 1,3,5,7-cyclooctatetraene (COT),[37] and 1,3,5-cycloheptatriene (CHT).[38] The structures of these molecules are illustrated in Fig. 4. The definitions of the distances shown in Fig. 4 are not identical with one another. However, they will not be affected by more than a few thousandths of one angstrom

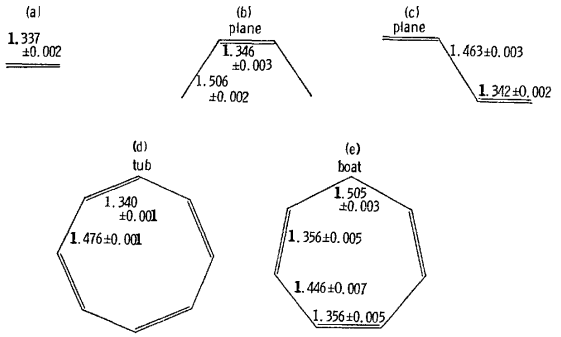

Fig. 4. Bond lengths for compounds related to tropone.
(a): ethylene, r_g, Ref. 34, (b): *cis*-2-butene, r_a, Ref. 35, (c): 1,3-butadiene, r_a^0, Ref. 36, (d): 1,3,5,7-cyclooctatetraene (COT), r_a, Ref. 37, (e): 1,3,5-cycloheptatriene, r_a, Ref. 38. The r_a^0 is the distance r_a extrapolated to the absolute zero temperature.

when they are transformed into distances of the same physical significance. While no significant difference can be found between the C–C bonds of COT and butadiene, the C–C bond length in COT is longer than that in butadiene, and COT has a boat form.[37] The observed bond lengths in CHT except for the C_1–C_2 bond indicate a more conjugate-bond character than those in butadiene. Nevertheless, CHT takes a boat form with C=C–C valence angles of about 120° to relieve the strain in valence angles. Similar phenomena were observed[7] in the X-ray structure analyses of dibenzo[b,f]tropone,[2e] 1-isopropyl-8,8-dicyanoheptafulvene,[6a] and 1,6-dimethyl-8,8-dicyanoheptafulvene,[6a] all of which have $C_2C_3C_4C_5C_6$ frames very close to that in CHT. In such molecules which favor boat forms, however, the C_1–C_2 and C_1–C_7 bonds are usually longer than other single bonds in the same molecule. These facts imply that the conformations of such molecules are determined by a subtle compromise among various factors *e.g.*, π-electron delocalization, steric interaction, and strain in valence angles. When we compare our results with these facts, the set II structure seems to be more likely than the set I structure to have planar structure.

By considering additionally the fact that the vibrational spectra of tropone could be explained by using two kinds of force constants, 4.0 mdyn/Å for the longer bonds and 6.0 and 6.2 mdyn/Å for the shorter bonds, we are inclined to prefer, for the time being, the set II structure, where the bond lengths of the C_1–C_2 and C_3–C_4 bonds are about 1.45 Å, the C_2–C_3 and C_4–C_5 about 1.36 Å, and the C–O about 1.22 Å, and where the planarity is attained by π-electron delocalization.

We wish to thank Professor Y. Kitahara of Tohoku University for providing us with the sample. We are also indebted to Professor K. Ohno of the Department of Chemistry, Hokkaido University, for making it possible for us to use the FACOM 270-20 computer in his laboratory.

BULLETIN OF THE CHEMICAL SOCIETY OF JAPAN, VOL. 45, 3282—3286 (1972)

The Singlet-triplet Absorption Spectra of Heterocyclic Amine *N*-Oxides (I)

Tanekazu KUBOTA, Masumi YAMAKAWA, and Yoshiko MIZUNO

Shionogi Research Laboratory, Shionogi & Co., Ltd., Fukushima-ku, Osaka 553

(Received February 19, 1972)

The singlet-triplet absorption ($T_1 \leftarrow N$) spectra of pyridine *N*-oxide, quinoline *N*-oxide, isoquinoline *N*-oxide, and acridine *N*-oxide have been observed by applying the oxygen-intensification technique. The correlation between the $T_1 \leftarrow N$ absorption bands and the singlet-singlet ($S^* \leftarrow N$) absorption bands of these *N*-oxides has been established and discussed theoretically. The lowest triplet state of the *N*-oxides has been assigned as the π-π^* transition of a ^3L_a (CT) nature. The $T_1 \leftarrow N$ absorption bands obtained show a blue shift in polar solvents. The results have been compared with the case of $S^* \leftarrow N$ transitions and have been reasonably explained by taking into account the contribution from the intramolecular charge transfer.

In the field of the studies of photochemical reactions, heterocyclic amine *N*-oxides constitute one group of substances which are being quite extensively studied at present.[1] Needless to say, the knowledge of excited singlet and triplet states is important for interpreting the mechanism of photochemical reactions. Although the nature of the excited singlet states of heterocyclic amine *N*-oxides has been intensively investigated,[2]

1) a) G. G. Spence, E. C. Taylor, and O. Buchardt, *Chem. Rev.*, **70**, 231 (1970). b) C. Kaneko, *Kagaku No Ryoiki, Zokan*, **93**, 235 (1970), (Review in Japanese). c) I. Tanaka and H. Shizuka, *J. Soc. Org. Syn. Chem.*, Tokyo, **26**, 412 (1968), (Review in Japanese). d) C. Kaneko, S. Yamada, I. Yokoe, and T. Kubota, *Tetrahedron Lett.*, **1970**, 2333 (No. 27). e) F. Bellamy, L. G. R. Barragan, and J. Streith, *Chem. Commun.*, **1971**, 456. f) K. Koyano and H, Suzuki, This Bulletin, **43**, 3582 (1970). g) R. Gleiter, D. Schmidt. and J. Streith, *Helv. Chim. Acta*, **54**, 1645 (1971).

2) a) K. Seibold, G. Wagniere, and H. Labhart, *Helv. Chim, Acta*, **52**, 789 (1969). b) M. Yamakawa, T. Kubota, and H. Akazawa, *Theor. Chim. Acta*, **15**, 244 (1969). c) E. M. Evleth, *ibid.*, **11**, 145 (1968). d) S. Kobinata and S. Nagakura, *ibid.*, **14**, 415 (1969). e) J. D. Bene and H. H. Jaffe, *J. Chem. Phys.*, **49**, 1221 (1968). f) R. M. Hochstrasser and D. A. Wiersma, *ibid.*, **55**, 5339 (1971). g) H. Miyazaki, T. Kubota, and M. Yamakawa, This Bulletin, **45**, 780 (1972). h) J. C. D. Brand and K.-T. Tang, *J. Mol. Spectrosc.*, **39**, 171 (1971).

there have as yet been few studies of their excited triplet states.[3] The main reason for this is some difficulty for measuring the phosphorescence spectra because of their very weak intensity or some instability accompanying a photochemical reaction. In these cases, the observation of the singlet-triplet ($T_1 \leftarrow N$) absorption spectra is very useful in determining the energy level of the lowest triplet state. Several techniques for measuring the $T_1 \leftarrow N$ absorption spectra have already been reported.[4]

In our present case, the technique of high-pressure oxygen perturbation developed by Evans[4a] was the most useful technique for obtaining the $T_1 \leftarrow N$ absorption spectra of the aromatic amine *N*-oxides studied here. In this paper we would like to report on these $T_1 \leftarrow N$ absorption spectra and their interpretations.

Experimental

Absorption Cell. Figure 1 shows the absorption cell employed in this study; it was made of stainless steel and was constructed by referring to the ones used by Evans[4a] and by Robin.[5] A suprasil silica plate 8 mm thick was used as a window. The effective light pass length was ~5.2 cm. This absorption cell was safe for oxygen pressures of ~200 kg/cm^2. The equilibrium state of the sample solution saturated with compressed oxygen gas was easily obtained by shaking the absorption cell moderately. All the spectral measurements were made at room temperature. The sample concentrations are dependent on the solubility and on the degree of the enhancement of the $T_1 \leftarrow N$ absorption with oxygen. In the case of $CHCl_3$ solution, the most suitable concentrations are 0.93, 0.75, and 0.99 mol/*l* for pyridine *N*-oxide (PNO), quinoline *N*-oxide (QNO), and isoquinoline *N*-oxide (IQNO) respectively. However, a saturated solution was used for acridine *N*-oxide (ANO) because of the low solubility. The instrument used for recording the singlet-triplet absorption spectra was a Beckman DK-2A Far-UV spectrometer.

Solvents and Samples. All the solvents used, except for chloroform, were spectro-grade in purity; they were dried sufficiently with calcium chloride, *etc.*,[6] and then rectified carefully. Spectro-grade chloroform containing about 1% ethanol as a stabilizer was used with no further treatment. As to samples, PNO, QNO, IQNO, and ANO were used in this study. The details of the preparation and the purification of these samples have already been reported.[7] Finally, they were again sublimated or distilled before use. In the case of ANO, an alumina column chromatographic method was also used,[8] the *N*-oxide being eluted first with an ether-pentane mixture and later with ether alone. The pure *N*-oxide has been obtained from the ether fraction.

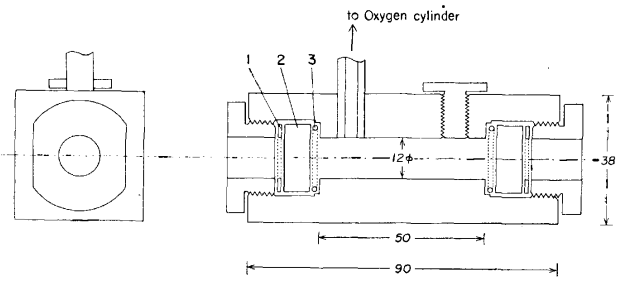

Fig. 1. High pressure cell used for obtaining the singlet-triplet absorption spectra under compressed oxygen perturbation. Dimension is in mm unit. Suprasil silica plate of 8 mm thickness (2) is held between the Teflon O-ring (3) and the Teflon washer (1).

Results and Discussion

$T_1 \leftarrow N$ *Absorption Spectra of PNO, QNO, IQNO, and ANO.* To confirm our experimental technique, we have first examined the $T_1 \leftarrow N$ absorption spectra of naphthalene, *etc.*, under almost the same experimental conditions as those reported by Evans.[4a] The spectra thus obtained reproduced Evans' well. Our experiments can, therefore, be believed to be correct.[9] As a typical example, the oxygen-pressure dependence of the $T_1 \leftarrow N$ absorption spectrum is illustrated in Fig. 2 for a relatively high concentration (~1 mol/*l*) of the PNO chloroform solution. It is now clear that a new absorption band appears in the wavelength region of 370—500 nm and that the intensity of this new band increases in a linear fashion with an increase

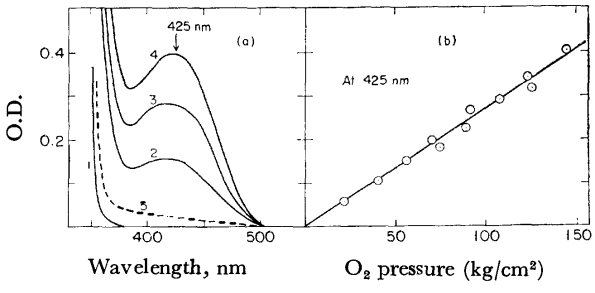

Fig. 2. Oxygen pressure dependence of the $T_1 \leftarrow N$ absorption spectrum of pyridine *N*-oxide in $CHCl_3$ solution (0.93 mol/*l*). (a): The change in the spectrum with no oxygen perturber (curve 1) upon the applied oxygen pressure (kg/cm^2) of 57 (curve 2), 108 (3), and 145 (4). The curve 5 is for the spectrum after removal of the oxygen. The intensity of the curve 5 is a little larger than that of the curve 1. The main reasons would be that the removal of oxygen is incomplete, and thus contact charge transfer spectra caused by weak oxygen complex formation may appear as a tail toward a longer wavelength region. (b): The linear relation of the enhanced $T_1 \leftarrow N$ absorption intensity to the applied oxygen pressure.

3) B. Ziolkowsky and F. Dörr, *Ber. Bunsenges. Phys. Chem.*, **69**, 448 (1965).

4) a) D. F. Evans, *J. Chem. Soc.*, **1957**, 1351, 3885; **1959**, 2753; *Proc. Roy. Soc. Ser A*, **255**, 55 (1960). b) S. P. McGlynn, T. Azumi, and M. Kasha, *J. Chem. Phys.*, **40**, 507 (1964). c) E. V. Donckt and C. Vogels, *Spectrochim. Acta*, **27A**, 2157 (1971).

5) M. B. Robin and N. A. Kuebler, *J. Mol. Spectrosc.*, **33**, 274 (1970).

6) J. A. Riddick and W. B. Bunger, "Organic Solvent," (Third Edition) edited by A. Weissberger, Wiley-Interscience, New York (1970).

7) E. Ochiai, "Aromatic Amine Oxides," Elsevier Publishing Co., Amsterdam (1967), and the other papers cited therein.

8) R. M. Acheson, B. Adcock, G. M. Glover, and L. E. Sutton, *J. Chem. Soc.*, **1960**, 3367.

9) The trial is deemed to have failed in obtaining the $T_1 \leftarrow N$ absorption spectra of the present *N*-oxides in solvents with heavy atoms, such as CH_2Br_2 and CH_2I_2, since the enhancement of the $T_1 \leftarrow N$ absorption intensity in these solvents seems to be small. In addition, there also occurred other kinds of solute-solvent interactions in the case of the present system.

in the oxygen pressure, as may be seen in Fig. 2b. In addition, when the oxygen pressure is reduced to atmospheric pressure, the new absorption band disappears, and the spectrum almost completely returns to that before the introduction of oxygen gas. The reproducibility of this spectral behaviour was quite good. Comparing these expermental results with those found in the literature,[4a,10,11] one can conclude that the above-mentioned new absorption band of PNO is due to the $T_1 \leftarrow N$ transition enhanced by oxygen gas. Quite recently, Bellamy *et al.*[10] carried out the photochemical sensitization reaction of 2-cyanopyridine *N*-oxide, *etc.*, sensitizers which have triplet energy levels of 74 (Xanthone) and 79 kcal/mol (tetrabuthylammonium phenyltetrazolide) being effective. These results are in accord with our experimental results presented above. Furthermore, the contact charge-transfer (CCT) spectra due to the CCT complex formation of PNO with the oxygen molecule may appear as an end-absorption, overlapped with the spectrum of PNO itself, at the shorter-wavelength region than the $T_1 \leftarrow N$ absorption band, since the existence of this kind of CCT spectrum is well known.[11,12]

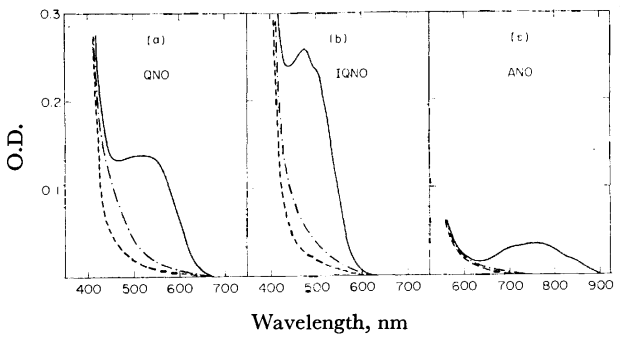

Fig. 3. Singlet-triplet absorption spectra of quinoline *N*-oxide (a), isoquinoline *N*-oxide (b), and acridine *N*-oxide (c) in $CHCl_3$ solution. The concentration (mol/*l*) and the oxygen pressure (kg/cm^2) are in this order: 0.75, 128; 0.99, 100; and the saturated solution, 152; for QNO, IQNO, and ANO, respectively.
----: for initial solution, ——: under high pressure oxygen perturbation, -·-·-: after removing the oxygen gas.

A new absorption band brought about by compressed oxygen gas was also clearly found for QNO, IQNO, and ANO. The spectral behaviour for the oxygen-pressure dependence and the reproducibility of the intensified new band were both very similar to those in the case of PNO discussed above. These absorption bands can, therefore, reasonably be assigned to the $T_1 \leftarrow N$ transition, the spectra being shown in Fig. 3. It should be noticed that the accuracy of the $T_1 \leftarrow N$ absorption spectra of ANO seems to be less than that of the other *N*-oxides, because the solubility of ANO in a $CHCl_3$ solvent, *etc.*, is small; thus, the intensity of the $T_1 \leftarrow N$ transition arising from the oxygen perturbation also becomes small. Nevertheless, the wavelength region and the maximum position of the $T_1 \leftarrow N$ absorption of ANO seem correct.[13] The band positions of the obtained $T_1 \leftarrow N$ spectra, the singlet-singlet π-π^* transition energies in intimate correlation with the $T_1 \leftarrow N$ spectra, and the values of the singlet-triplet separation are all shown in Table 1 for the *N*-oxides studied here. Figure 4 depicts a correlation diagram of all the transitions (see Table 1) pertinent to PNO, QNO, and ANO, the correlation curves of the $S^* \leftarrow N$ transitions having previously been reported by us.[14]

TABLE 1. TRANSITION ENERGIES TO THE T_1, ^1L_b, AND ^1L_a (CT) EXCITED STATES, AND THE T_1—^1L_a (CT) ENERGY SEPARATION (in kK unit)

N-oxide of	$T_1 \leftarrow N$[a]	$^1L_a \leftarrow N$[b]	$^1L_b \leftarrow N$[b]	T_1—^1L_a separation[c]
Pyridine[d]	23.98	35.44	30.7	11.46
Isoquinoline	21.03	32.3	26.5	11.3
Quinoline	18.64	28.6	29.4	10.0
Acridine	13.07	22.1	27.2	9.0

a) Obtained in chloroform.
b) Obtained in *n*-heptane.
c) The $S^* \leftarrow N$ spectra shift considerably to shorter wavelength in $CHCl_3$ (contain ~1% ethanol), in which $T_1 \leftarrow N$ spectra have been recorded, so that the S^*—T_1 separation in $CHCl_3$ should be larger than that listed in this Table.
d) The $T_1 \leftarrow N$ absorption maximum in various solvents is: 23.49 kK (Diethyl oxalate), 23.18 (Benzene), 22.68 (Ether), 23.16 (Ethyl acetate), 23.46 (Dichloromethane), 23.39 (Acetone), 23.87 (Acetonitrile), 24.99 (Ethanol), 25.51 (Methanol), and 25.89 (Water).

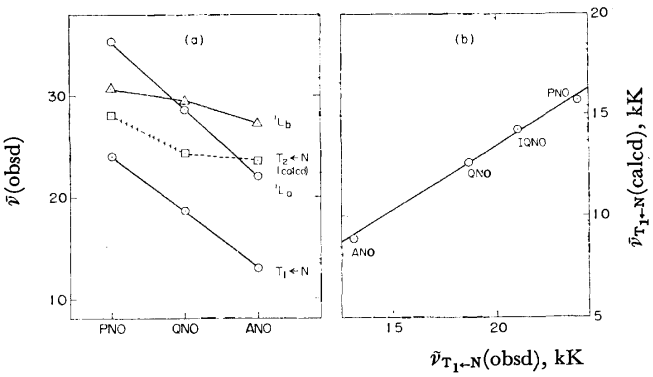

Fig. 4. (a): Correlation curves of the experimentally and the theoretically (only for $T_2 \leftarrow N$ transition) obtained transition energies among the *N*-oxides of pyridine, quinoline, and acridine. (b): Calculated $T_1 \leftarrow N$ transition energies of the *N*-oxides.

Solvent Effect on the $T_1 \leftarrow N$ *Transition of PNO.* It is well known that the singlet-singlet π-π^* bands of aromatic amine *N*-oxides exhibit a dominant blue shift phenomenon in polar solvents, especially in

10) R. A. Raubach and A. V. Guzzo, *J. Phys. Chem.*, **75**, 983 (1971).
11) M. Itoh and R. S. Mulliken, *ibid.*, **73**, 4332 (1969).
12) H. Tsubomura and R. S. Mulliken, *J. Amer. Chem. Soc.*, **82**, 5966 (1960).
13) In the present experiment concerning aromatic *N*-oxides, we have found that, roughly, the degree of the $T_1 \leftarrow N$ absorption enhancement with oxygen decreases in the order of PNO, QNO, and ANO, *i.e.*, in the order of increasing molecular size.
14) M. Yamakawa, T. Kubota, and H. Akazawa, *Theor. Chim. Acta*, **15**, 244 (1969).

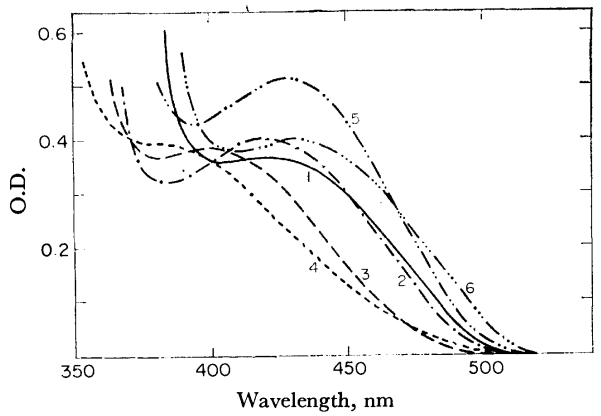

Fig. 5. Enhanced absorption spectra of the $T_1 \leftarrow N$ transition of pyridine *N*-oxide with high pressure oxygen in various solvents.
Solvents; 1: CH_3CN, 2: $CHCl_3$, 3: C_2H_5OH, 4: H_2O, 5: CH_2Cl_2, 6: benzene. All the spectra were drawn so as to give almost the same intensity as that in $CHCl_3$ solution (see Fig. 1) by suitably multiplying the original curves.

protic solvents,[15] where the hydrogen-bonding effect plays an important role.[16] This was attributed to the fact that the solute-solvent interaction, including the hydrogen-bonding effect, is much larger at the ground state than at the π-π^* excited singlet states, because the charge transfer from the oxygen atom of the *N*-oxide group to the ring π electron system is larger at the excited singlet π-π^* states than at the ground state. It is of great interest what kind of solvent shift can be expected for the case of the $T_1 \leftarrow N$ absorption bands. This sort of study was caried out in detail for PNO, the spectra yielded in several solvents being shown in Table 1 and its footnote d), and in Fig. 5. It is clear in Fig. 5 that the $T_1 \leftarrow N$ transition of PNO is quite sensitive to the solvent change and is blue-shifted with an increase in the polarity of the solvents, particularly in protic solvents such as water and ethanol. These are results similar to those observed generally for the singlet π-π^* bands of many *N*-oxides.[15,16] However, note that the degree of the blue shift for the $T_1 \leftarrow N$ transition is smaller than that of the intramolecular CT ($^1A_1$-282 nm) band of PNO. For example, the blue shifts due to the solvent change from CH_3CN (dielectric constant $D=37.5$) to C_2H_5OH (24.55), CH_3OH (32.70), and water (78.38) are 1120, 1360: 1640, 1700: 2020, 3140: (in cm^{-1} units) respectively. Here, in each set the first number should refer to the $T_1 \leftarrow N$ band, and the second, to the above $^1A_1$ CT band. It has been reported that the intramolecular charge transfer from such substituents as OH, and NR_2 to a ring π electron system like benzene and naphthalene is, in general, larger at the singlet excited state than at the lowest triplet state.[17] If the same argument as the above can be applied to the PNO system, since PNO and the phenolate ion are isoelectronic in the π electron system, the aforementioned blue shift of the $T_1 \leftarrow N$ transition, smaller than that of the $^1A_1$ band, seems to be reasonable.[18] Actually, our calculation results obtaind by the PPP method, as well as the CNDO results reported by other authors, all support this kind of consideration, although the difference in CT magnitude between the $^1A_1$ and the $^3A_1$ states of PNO is not very large.[14,19]

Nature of the $T_1 \leftarrow N$ *Transition of PNO, QNO, IQNO, and ANO.* Although it is not easy to discuss the character of the lowest triplet state from the $T_1 \leftarrow N$ transition alone, the nature of the $T_1 \leftarrow N$ absorption spectra will become somewhat clear if we check the singlet-triplet splitting values (see Table 1) and the correlation diagram shown in Fig. 4a, where the energies of the $T_1 \leftarrow N$ and $S^* \leftarrow N$ transitions are plotted in order to make the comparison clear. We can see there that the T_1 energy level is smoothly red-shifted according to the increase in the ring number. This tendency is very similar to that of the ^1L_a (CT) correlation curve among PNO, QNO, and ANO. In addition, the ^1L_a-T_1 energy separation turns out to become smaller with the increase in the ring size, but just the reverse order holds for the energy separation between the ^1L_b and the $T_1 \leftarrow N$ bands. These results are the same as those of the experiments and the theoretical S^*-T_1 energy separations of cata-condensed aromatic hydrocarbon;[20] they lead to the conclusion that the T_1 states of these *N*-oxides correspond to ^3L_a (π-π^*): $^3A_1$ for PNO and ANO, and to $^3A'$ for QNO. The conclusion is also supported by the quite large values of singlet-triplet energy separation listed in Table 1.

In the case of IQNO, systematic discussions based on the correlation diagram can not be applied. Nevertheless, it may be said that the T_1 state has the character of the π-π^* transition because of the fact that there is a good correlation between the observed T_1 energy levels and the calculated values (*vide infra*) for the PNO, QNO, IQNO, and ANO compounds, as may be seen in Fig. 4b.

In order to examine the above-mentioned character of the T_1 states theoretically, we undertook molecular orbital calculations. The calculations were made by the PPP-type SCF-MO-CI method.[14] Special attention was paid to the two-electron repulsion integral, $\gamma_{\mu\nu}$. We used the form given by Beveridge and

15) a) T. Kubota and H. Miyazaki, *Chem. Pharm. Bull.* (Tokyo), **9**, 948 (1961). b) See Chapter 4 of Ref. 7.
16) T. Kubota and M. Yamakawa, This Bulletin, **35**, 555 (1962), and the other papers cited therein.
17) a) K. Kimura and H. Tsubomura, *Mol. Phys.*, **11**, 349 (1966). b) N. Mataga and T. Kubota, "Molecular Interactions and Electronic Spectra," Marcel Dekker, New York (1970), p.364.
18) Here, the following discussion seems appropriate. In the lowest equilibrium triplet state, the electron distribution and the molecular geometry can be expected to be different from those in the singlet excited state. Thus, the solute-solvent interaction potential curve in the triplet state may differ from that in the ground state or in the singlet excited state. Light absorption occurs, according to the Frank-Condon principle, from the ground state. In the present case, therefore, these circumstances would bring about a more exaggerated blue shift than the energy difference of the solute-solvent interaction in the equilibrium state between the lowest triplet and the ground states.
19) C. Leibovici and J. Streith, *Tetrahedron Lett.*, **1971**, 387 (No. 5).
20) S. P. McGlynn, T. Azumi, and M. Kinoshita, "Molecular Spectroscopy of the Triplet States," Prentice-Hall, New Jersey (1969).

Hinze:[21] $\gamma_{\mu\nu}=e^2/[a_{\mu\nu}\cdot\exp(-r_{\mu\nu}^2/2a_{\mu\nu}^2)+r_{\mu\nu}]$; here $a_{\mu\nu}=2e^2/[\gamma_{\mu\mu}+\gamma_{\nu\nu}]$.[22] The calculated results are given in Fig. 4, along with the observed ones. We found that the calculated lowest triplet energy level, T_1, lies quite apart from the other calculated triplet levels T_2, T_3, *etc.* For example, the T_2-T_1 and T_3-T_2 separations (in cm^{-1} unit) are 12296, 1988; 11610, 3408; and 14734, 1045 for PNO, QNO, and ANO respectively. In other words, the change in the character of the T_1 states, which become the ^3L_a species from a consideration of the molecular symmetry, may not occur even if more rigorous calculations are performed.[22] The calculated T_1 state also shifts smoothly to a longer wavelength in the order of PNO, QNO, and ANO, just the observed T_1 states do. Therefore, these calculated results support the previous discussion of the character of T_1 states, although the calculated values themselves are unsatisfactory compared with the observed values because the parametrization seems to be insufficient for a better description of the triplet energy levels of the *N*-oxides. Quite recently, Leibovici and Streith[19] calculated the triplet energy levels of pyridine *N*-oxide using the CNDO-CI method as modified by Bene and Jaffé.[23] They concluded that (i) the lowest triplet state, T_1, is of a π-π^* nature, with its polarization along the molecular axis, and (ii) the charge transfer from the *N*-oxide-group oxygen atom to the pyridine ring π system occurs, to thus reducing the dipole moment at the T_1 state, but the degree is smaller than for the $^1A_1$ CT band. Therefore, the blue shift of the T_1 band can be expected in polar solvents. These theoretical predictions are in accord with our experimental and calculated results discussed hitherto.

Here it should be noticed that, in general, the character of the T_1 state can also be obtained from a study of the phosphorescence spectra if the substances in question phosphoresce. In the case of some heterocyclic amine *N*-oxides, the phosphorescence spectra and their characteristics have been examined by means of the *photographic method.*[3] We repeated these measurements carefully using a Hitachi fluorescence-phosphorescence spectrophotometer, Model MPF-2A, using a red-sensitive photomultiplier for recording the spectra appearing in the longer-wavelength region. However, our experiment on the rigid glass solution at the temperature of liquid nitrogen indicated that, in the present case, the phosphorescence spectra obtained consist of those of heterocyclic amine *N*-oxide and its photochemical reaction product, and that the ratio of these two components is dependent on the solvents and samples. For example, the phosphorescence spectrum of QNO in alcohol reported by Dörr *et al.*[3] may be identified as that of 2-quinolone produced by a photochemical reaction.[24] The true phosphorescence spectra of the *N*-oxides can, then, be estimated by extrapolating the somewhat time-dependent spectra to time zero. Because of these circumstances, the experimental data of the $T_1\leftarrow N$ absorption spectra are very important.

Next, let us pay attention to the intensity of the enhanced $T_1\leftarrow N$ absorption bands. Recent theoretical studies have indicated that the enhancement of $T_1\leftarrow N$ absorption is mainly brought about by the electron-exchange interaction[25] and by the contact charge-transfer interaction[12,26] occurring in the contact-weak complex formed from an electron donor (organic molecules) and an acceptor (a perturber like oxygen). Here, note that these quantum mechanical interactions may lead to the $T_1\leftarrow N$ absorption stealing a part of the strong intensity of the singlet-singlet transitions. The degree of the intensity borrowing is, however, dependent on the molecular orbitals and on the energies of the electron donor and the acceptor. In our experimental results reported here, the $T_1\leftarrow N$ absorption of PNO is most strongly enhanced by the oxygen perturber. However, the oxygen perturbation effect is in the order: PNO>QNO>ANO. This means that the above-mentioned quantum mechanical interactions may decrease with an increase in the π-conjugate system in the present *N*-oxides. The quantitative theoretical treatment of these experimental results is thus quite interesting; it is now proceeding in our laboratory.

21) D. L. Beveridge and J. Hinze, *J. Amer. Chem. Soc.*, **93**, 3107 (1971). See also P. Knowlton and W. R. Carper, *Mol. Phys.*, **11**, 213 (1966); A. Matsuyama and H. Baba, This Bulletin, **44**, 1162 (1971).

22) From the viewpoint of correlation energy, the importance of the parametrization and the approximation was recently discussed for the case of the PPP-type calculation of triplet and singlet transition energies.[21] In the present case, however, the adoption of the Nishimoto-Mataga approximation[14] for $\gamma_{\mu\nu}$, and the calculation according to Zahradnik *et al.* (who suggested simple modifications of the parametrization to fit the experimental triplet energy levels to the calculated ones) both gave the same results for the state symmetry and for the relative correlation among the energy levels, as is stated in the text (see Fig. 4), although the absolute values themselves are different, especially for the NM approximation. R. Zahradnik, I. Tesarova, and J. Pancir, *Collect. Czech. Chem. Commun.*, **36**, 2867 (1971).

23) J. Del Bene and H. H. Jaffé, *J. Chem. Phys.*, **48**, 1807 (1968).

24) T. Yamamuro, I. Tanaka, and N. Hata, This Bulletin, **44**. 667 (1971).

25) a) G. J. Hoytink, *Accounts Chem. Res.*, **2**, 114 (1969). b) G. J. Hoijtink, *Mol. Phys.*, **3**, 67 (1960). c) C. Dijkgraaf and G. J. Hoijtink, *Tetrahedron*, **19**, Suppl. 2, 179 (1963).

26) J. N. Murrell, *Mol. Phys.*, **3**, 319 (1960).

Ultrasonic Study on Dilute Aqueous Solutions of Diamines

Katsutaka SASAKI and Kiyoshi ARAKAWA

Research Institute of Applied Electricity, Hokkaido University, Sapporo

(Received February 21, 1972)

Ultrasonic experiments were carried out on aqueous solutions of diamines (ethylenediamine, 1,3-propanediamine, 1,4-butanediamine, 1,5-pentanediamine, and 1,6-hexanediamine) by means of pulse technique in order to study solute-solvent interactions. Sound velocity and absorption coefficient were determined in the frequency range 15—45 MHz. The magnitude of absorption coefficient for each solution increased rapidly with concentration up to about 0.4 mol%. It is concluded that the initial rapid increase is attributed to the proton transfer in base equilibria. The absorption coefficient at the same molar concentration of each solution increases appreciably with the size of hydrocarbon chain from $-(CH_2)_2-$ to $-(CH_2)_3-$. This is ascribed to the formation of icebergs around hydrocarbon groups.

The influence of solute molecules on the structure of liquid water has been discussed for dilute aqueous solutions,[1-3] and aqueous solutions of alcohols and amines have been extensively investigated.[4-7] However, many problems remain unsolved as yet. Alcohol-water and amine-water interactions have been explained on the basis of the following: polar group-water interaction and hydrocarbon group-water interaction ("hydrophobic interaction").

We have investigated the nature of solute-solvent interactions in various aqueous solutions by means of ultrasonic measurements.[8-10] We have carried out an ultrasonic study on dilute aqueous solutions of diamines with the intention of investigating the polar group-water interaction and hydrocarbon group-water interaction. These compounds are suitable, because of their large solubility in water despite relatively large hydrocarbon groups. This report describes the behavior of ethylenediamine, 1,3-propanediamine, 1,4-butanediamine, 1,5- pentanediamine and 1,6-hexanediamine in water.

Experimental

An ultrasonic pulse technique was used for the measurement of sound velocity and absorption coefficient. The apparatus and procedures of measurements have been described.[11] Sound velocity was measured at a fixed frequency, 5 MHz. The absorption coefficient was measured in the frequency range 15—45 MHz. Temperature range was 10—20°C, the accuracy being within ± 0.1°C. Ethylenediamine and 1,3-propanediamine, obtained from Wako Pure Chem. Ind. Co., Ltd., were used after being refluxed and distilled over sodium metal. The boiling points of ethylenediamine and 1,3-propanediamine were 116 ± 0.3°C and 137 ± 0.3°C, respectively. 1,4-Butanediamine, 1,5-pentanediamine and 1,6-hexanediamine (m.p., 40 ± 0.5°C) were obtained from Aldlich Co., Ltd. and were used without further purification. Viscosity coefficient and density of aqueous solutions of ethylenediamine, 1,3-propanediamine and 1,6-hexanediamine were measured by means of an Ostwald type viscometer and pycnometer at 20°C. The value of pH for each diamine solution was measured by a pH meter (model MH-5A, Toa Electronics Ltd.). The values of pH for ethylenediamine and 1,6-hexanediamine were found to be 11.8 ± 0.1 and 12.2 ± 0.1, respectively.

Results

Sound Velocity and Compressibility. The accuracy of sound velocity data was within ± 1 m/sec. The data obtained for aqueous solutions of 1,3-propanediamine are plotted against concentration in Fig. 1. It was found that the velocity *vs.* concentration curves for the solutions closely resemble each other. Compressibility *vs.* concentration relations calculated from velocity and density data at 20°C are given in Fig. 2, for solutions of ethylenediamine, 1,3-propanediamine and 1,6-hexanediamine. The compressibility data are

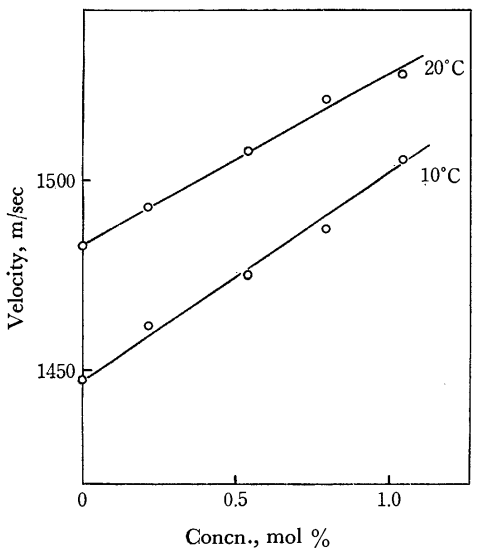

Fig. 1. Ultrasonic velocity for aqueous solutions of 1,3-propanediamine.

1) F. Franks and B. Watson, *Trans. Faraday Soc.*, **65**, 2339 (1969).
2) M. J. Blandamer, N. J. Hidden, M. C. R. Symons, and N. C. Treloar, *ibid.*, **65**, 2663 (1969).
3) F. Franks and D. J. G. Ives, *Quart .Rev.*, (London), **20**, 1 (1966).
4) M. J. Blandamer, N. J. Hidden, and M. C. R. Symons, *Trans. Faraday Soc.*, **66**, 316 (1970).
5) C. J. Burton, *J. Acoust. Soc. Amer.*, **20**, 186 (1948).
6) H. S. Frank and M. W. Evans, *J. Chem. Phys.*, **13**, 507 (1945).
7) J. Kozak, W. S. Knight, and W. Kauzmann, *ibid.*, **48**, 675 (1968).
8) K. Sasaki and K. Arakawa, This Bulletin, **42**, 2485 (1969).
9) K. Arakawa, N. Takenaka, and K. Sasaki, *ibid.*, **43**, 636 (1970).
10) K. Sasaki and K. Arakawa, *ibid.*, **44**, 3223 (1971).
11) K. Arakawa and N. Takenaka, *ibid.*, **39**, 447 (1966).

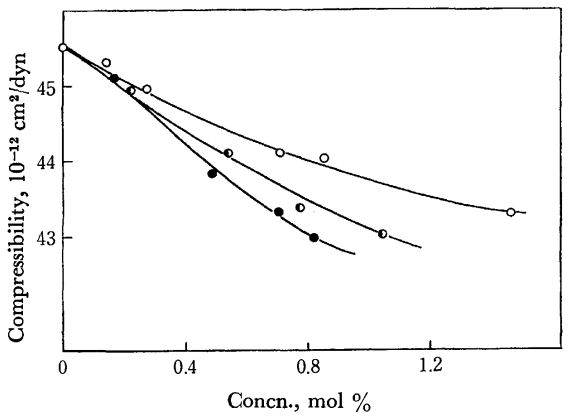

Fig. 2. Compressibility for aqueous solutions of diamines at 20°C.
○: ethylenediamine ◐: 1,3-propanediamine
●: 1,6-hexanediamine

consistent with the results obtained by Hirata and Arakawa,[12] in which the structure of icebergs is found to be more incompressible than ice-like structure in liquid water.

Ultrasonic Absorption. The data of absorption coefficient α were reproducible within $\pm 2\%$. The absorption coefficient *vs.* frequency curves for 1,3-propanediamine solutions are given in Fig. 3. The magnitude of α/f^2 decreases gradually with $\log f$ (f, frequency) for all solutions. α/f^2 *vs.* concentration curves at 35 MHz are given in Fig. 4. The results of α/f^2 *vs.* concentration for ethylenediamine are consistent with the data obtained by Blandamer *et al.*[4] We see that the magnitude of α/f^2 increases rapidly with concentration up to about 0.4 mol%, and increases slightly at higher concentrations.

Viscosity coefficient η was measured in order to obtain the values of classical absorption, which is given by

$$(\alpha/f^2)_{class.} = \frac{8\pi^2\eta}{3\rho V^3} \qquad (1)$$

where ρ is density and V sound velocity. The structural absorption is given by

$$(\alpha/f^2)_{struct.} = (\alpha/f^2)_{obsd.} - (\alpha/f^2)_{class.} \qquad (2)$$

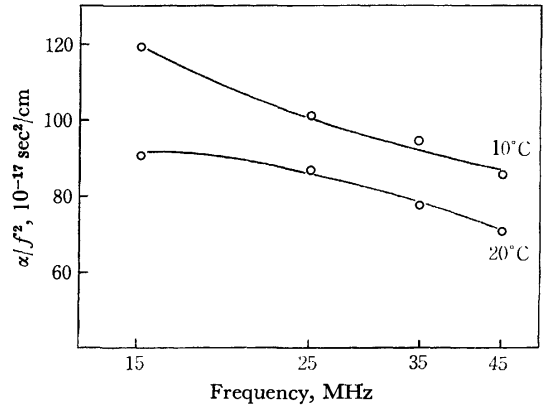

Fig. 3. Ultrasonic absorption for aqueous solutions of 1,3-propanediamine at 0.19 mol % (1 vol %).

12) F. Hirata and K. Arakawa, to be published.

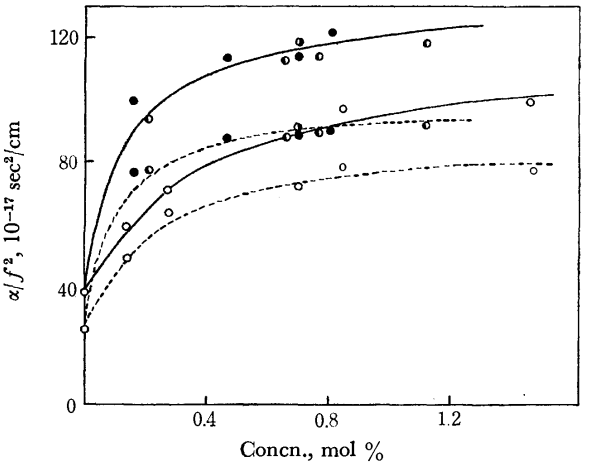

Fig. 4. Concentration dependence of ultrasonic absorption for aqueous solutions of diamines at 35 MHz. (solid line, at 10°C, broken line, at 20°C)
○: ethylenediamine, ◐: 1,3-propanediamine,
◑: 1,4-butanediamine, ●: 1,6-hexanediamine.

The results at 20°C are given in Fig. 5. Since the magnitude of classical absorption is found to increase slowly in this concentration range, the initial rapid increase of α/f^2 is attributed to the increase of $(\alpha/f^2)_{struct.}$

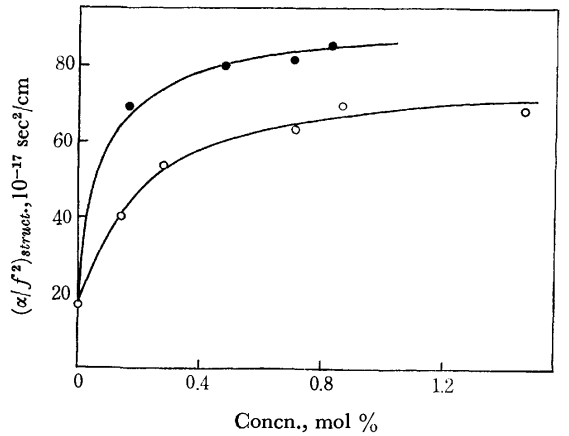

Fig. 5. Concentration dependence of structural absorption for aqueous solutions of diamines at 20°C (35 MHz).
○: ethylenediamine, ●: 1,6-hexanediamine

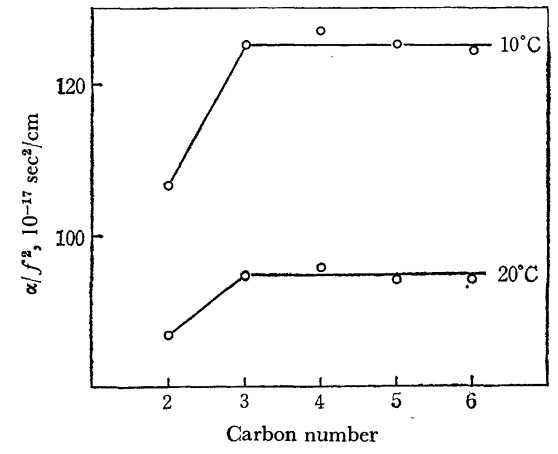

Fig. 6. Ultrasonic absorption for aqueous solutions of diamines as a function of the carbon number in solute molecules. (25 MHz).

The magnitude of α/f^2 in Fig. 6 at the same molar concentration (0.7 mol%) is plotted against the size of hydrocarbon chain of solute molecules. We see that the magnitude of α/f^2 for ethylenediamine is less than that of other higher homologues.

Discussion

Polar Group-Water Interaction. Let us first discuss the initial rapid increase of α/f^2 appearing in all diamine solutions (Fig. 4). It has been pointed out that for dilute aqueous solutions of alcohols, dioxane, urea *etc.*, the value of α/f^2 are nearly equal to those for pure water.[2,9,13] The magnitude of α/f^2 for aqueous solutions of dioxane is nearly the same as that of pure water up to about 4 mol%.[9] On the other hand, for aqueous amine solutions, there is a significant increase in extremely dilute concentration of the order of 1 mol%.[2,4,14] A similar increase of α/f^2 is observed for diamines (Fig. 4). The origin of the initial rapid increase seems to be ascribed to amino groups.

Blandamer *et al.* attributed the ultrasonic absorption caused by the addition of amine molecules to the acid-base equilibria.[14]

$$RNH_2 + H_2O \rightleftarrows RNH_3^+ + OH^- \quad (3)$$

On the other hand, Berfield and Schneider,[15] and Mckellar and Andrea[16] concluded that the hydrogen-bond formation and breaking between amine and water molecules cause the increase of $\alpha/$ [2].

Alei *et al.*[17,18] showed that the proton negative shift by amino groups in aqueous solutions of ethylenediamine as well as the viscosity coefficient reaches maximum at 33 mol% concentration. They proposed that there is a stable dihydrate complex linked with hydrogen-bond in aqueous solutions of ethylenediamine. If the presence of dihydrate complex give rise to the initial excess ultrasonic absorption in dilute aqueous solutions of diamines, the magnitude of α/f^2 should increase linearly with concentration. However, the α/f^2 *vs.* concentration curves become nearly flat above 0.4 mol% after the initial rapid increase (Figs. 4 and 5). Thus we might say that the behavior of α/f^2 in dilute aqueous solutions of diamines does not result from the formation and breaking of hydrogen-bond.

It can be said that in dilute aqueous diamine solutions, the initial rapid increase of absorption and saturation of its magnitude above 0.4 mol% concentration is caused by the proton transfer of base equilibria:

$$NH_2RNH_2 + H_2O \rightleftarrows NH_2RNH_3^+ + OH^- \quad (4a)$$

$$NH_2RNH_3^+ + H_2O \rightleftarrows NH_3^+RNH_3^+ + OH^- \quad (4b)$$

The measured value of pH for each diamine solution is found to correspond to the value of pK in the second dissociation.[19] Thus, it is concluded that the cause of the initial rapid increase of absorption observed for all solutions is the dissociation given by (4b).

Hydrocarbon Group-Water Interaction. We have pointed out the initial rapid increase of α/f^2 as a general property of each diamine solution (Fig. 4). It is seen that the magnitude of α/f^2 above 0.4 mol% becomes nearly flat with concentration (Figs. 4 and 5). We see that the magnitude of α/f^2 increases with the size of hydrocarbon chain of solute molecules from $-(CH_2)_2-$ to $-(CH_2)_3-$ and exhibits a saturation effect in higher homologues (Fig. 6).

We observed[10] that the magnitude of α/f^2 for aqueous solutions of α-amino acids is independent of the size of hydrocarbon chain in solute molecules. Thus, it was concluded that the behavior of neutral α-amino acids in water is essentially similar to each other, and the structure-forming effect due to alkyl groups in amino acid molecules was cancelled out by the strong structure-breaking effect due to the dipolar field by zwitter-ions irrespective of their size.

On the other hand, for aqueous non ionic solutions (alcohols, ethers *etc.*), we see that the formation of icebergs becomes significant around hydrocarbon groups which are larger than methyl groups.[20,21] In liquid water, 1,3-dimethylurea molecules behave as a weak structure breaker but 1,3-diethylurea molecules behave as a structure former.[8]

In diamine solutions, the structure-breaking effect due to ionic dissociation of amino groups is less than that due to dipolar field by zwitter-ions in amino acid solutions. The structure-forming effect by hydrocarbon groups in diamine molecules can not be cancelled out completely by the structure-breaking effect due to ionic dissociation of amino groups. The increase of α/f^2 with the size of hydrocarbon chain from $-(CH_2)_2-$ to $-(CH_2)_3-$ in Fig. 6 can be attributed to the structure-forming effect of hydrocarbon chain in diamine molecules.

Thus, it is concluded that the iceberg formation becomes appreciable above the carbon number 3 in diamine molecules. The structure of icebergs is more incompressible than ice-like structure in liquid water (Fig. 2). This is in line with the idea of Wicke.[22] However, it should be pointed out that the iceberg formation is not dependent linearly on the size of hydrocarbon chain in these molecules, since the magnitude of α/f^2 is saturated above the carbon number of 3.

Concluding Remarks

The following conclusions are obtained from ultrasonic measurements.

1) An initial rapid increase of ultrasonic absorption for the diamine solutions is attributed to the proton

13) M. J. Blandamer, D. E. Clarke, N. J. Hidden, and M. C. R. Symons, *Chem. Comm.*, 342 (1966).
14) M. J. Blandamer, D. E. Clarke, N. J. Hidden, and M. C. R. Symons, *Trans. Faraday Soc.*, **63**, 66 (1967).
15) R. N. Berfield and W. G. Schneider, *J. Chem. Phys.*, **31**, 488 (1959).
16) J. F. Mckellar and J. H. Andrea, *Nature*, **195**, 778 (1962).
17) M. Alei, W. B. Lewis, A. B. Denison, and L. O. Morgan, *J. Chem. Phys.*, **47**, 1062 (1967).
18) M. Alei and A. E. Florin, *J. Phys. Chem.*, **72**, 550 (1968).
19) J. J. Christensen, R. M. Izatt, D. P. Wrathsll, and L. D. Hansen, *J. Chem. Soc., A*, 1212 (1969).
20) D. B. Wetlaufer, S. A. Malik, L. Stoller, and R. I. Coffin, *J. Amer. Chem. Soc.*, **86**, 509 (1964).
21) N. Takenaka and K. Arakawa, The 16th Annual Symposium on Ultrasonic and Chemical Physics, Oct., 1971 Sapporo.
22) E. Wicke, *Angew. Chem. Internat. Edit.*, **5**, 106 (1966).

transfer in base equilibria (the second dissociation).

2) The iceberg formation around hydrocarbon groups in diamine molecules become appreciable at the hydrocarbon chain of $-(CH_2)_3-$ and in higher homologues.

The authors wish to thank Mr. Nobuo Takenaka for his cooperation in this study.

BULLETIN OF THE CHEMICAL SOCIETY OF JAPAN, VOL. 45, 3290—3293 (1972)

Comparison of the Electronic Spectra of Geometric Isomers. II. 1,2-Disubstituted Ethylenes

Takayuki FUENO and Kizashi YAMAGUCHI

Department of Chemistry, Faculty of Engineering Science, Osaka University, Toyonaka, Osaka

(Received February 21, 1972)

The ultraviolet absorption spectra of the *cis* and *trans* isomers of various 1,2-disubstituted ethylenes were measured in isopentane solution. Each isomer showed a single intense band assignable to the lowest π—π^* transition. For the majority of the compounds studied, both energy and oscillator strength of transition are found to be greater for *trans* isomers than for the corresponding *cis* isomers, in accord with the general trend predicted by the Pariser-Parr-Pople calculations. Existence of some anomalous cases which contradict the generalization indicates a limited validity of the usual assumption of virtual orbitals.

Despite abundant data available for the ultraviolet absorption spectra of unsaturated compounds,[1] very few comparative studies have been made on the spectra of *cis* and *trans* isomers of olefins. A study on the π—π^* transitions of *cis*- and *trans*-stilbenes revealed that the *cis* isomer shows absorption peaks in shorter wavelength regions than does the *trans*.[2] Several workers agreed in attributing the higher-energy shift of the lowest transition peak of *cis*-stilbene to its nonplanarity resulting from the *steric repulsion* between the two phenyl groups located *cis* to each other.[3-6]

We recently reported[7] that in both gaseous phase and *n*-hexane the lowest π—π^* transition energy of the majority of terminal-substituted butadienes is more or less greater for isomers bearing the substituent(s) at the *trans* placement(s). Since all these compounds are likely to be planar in structure, the observed trend must be taken as a reflection of a certain *electronic effect* of the fully conjugated chromophores. The LCMO-SCF-CI computations of the Pariser-Parr-Pople (PPP) type[8,9] showed that this electronic effect might be related with the smaller inter-frontier-orbital Coulombic repulsion J_{hl} for the isomers having more of the *trans* ethylenic moieties.

Experimental data which may be tested for the above argument are very scanty for ethylene derivatives. Walsh[10] reported that the lowest π—π^* excitation energies Δ^1E for *trans*- and *cis*-dichloroethylenes in the gaseous phase are 6.36 and 6.53 eV, respectively. Gary and Picket[11] reported that, in the same phase, the values of Δ^1E for the *trans* and *cis* isomers of butene-2 are 6.975 and 7.066 eV, respectively. Both these sets of data show that the excitation energies are smaller for *trans* isomers, in contradiction to the generalization found for the butadiene derivatives. The situation has led us to examine the electronic spectra of 1,2-disubstituted ethylenes more extensively.

We have thus undertaken to measure the ultraviolet absorption spectra of *cis* and *trans* isomers of a variety of 1,2-disubstituted ethylenes.

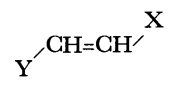

X = CH_3, Cl, OCH_3, CN, or COR

Y = CH_3 (1-substituted propenes)
Y = X (symmetrically 1,2-disubstituted ethylenes)

It has turned out that the generalization also holds for most of the ethylene derivatives here studied. Theoretical treatments of the PPP type rationalize the observed trend. Dichloroethylene and butene-2 have been verified to be exceptions. Most likely, the usual assumption of virtual orbitals is greatly invalidated in such compounds. These results will serve as a guide in the study of the excited electronic structure of olefin isomers.

Experimental

Methyl propenyl ether (**1**),[12] 1,2-dimethoxyethylene (**9**),[13]

1) For instance, H. H. Jaffé, and M. Orchin, "Theory and Applications of Ultraviolet Spectroscopy," Wiley, New York, N. Y. (1962).
2) H. Suzuki, This Bulletin, **33**, 381 (1960).
3) H. Suzuki, *ibid.*, **33**, 379 (1960).
4) H. H. Jaffé and M. Orchin, *J. Chem. Soc.*, 1078 (1960).
5) D. L. Beveridge and H. H. Jaffé, *J. Amer. Chem. Soc.*, **87**, 5340 (1965).
6) H.-H. Perkampus and J. V. Knop, *Theoret. Chim. Acta, (Berl.)*, **6**, 45 (1966).
7) T. Fueno and K. Yamaguchi, *J. Amer. Chem. Soc.*, **94**, 1119 (1972).
8) R. Pariser and R.G. Parr, *J. Chem. Phys.*, **21**, 466, 767 (1953).
9) J. A. Pople, *Trans. Faraday Soc.*, **49**, 1375 (1953).
10) A. D. Walsh, *ibid.*, **41**, 35, 76 (1945).
11) J. T. Gary and L. W. Picket, *J. Chem. Phys.*, **22**, 599 (1954).
12) M. Farina, M. Peraldo, and G. Bressan, *Chim. Ind.* (Milan), **42**, 967 (1960).
13) H. Baganz, K. Praefcke, and J. Rost, *Chem. Ber.*, **96**, 2657 (1963).

and 1,2-dicyanoethylene (**10**)[14] were prepared according to the methods given in the literature. They were separated into geometric isomers by means of preparative gas chromatography. Column packings used were poly(ethylene glycol). Column length (3—5 m) and operating temperature (80—150°C) were so chosen as to best suit the separation. Hydrogen was used as a carrier gas at a flow rate of 25 ml/min.

The *cis* and *trans* isomers of crotononitrile (**2**), crotonic acid (**4**), crotoamine (**5**) and methyl propenyl ketone (**6**) were supplied by Dr. Kobuke, Kyoto University. *trans*-Crotonaldehyde (**3**) and diethyl maleate and fumarate (**11**) were purchased and distilled.

All the geometric isomers were identified from the magnitudes of NMR coupling constants observed between the olefinic hydrogen atoms. Gas chromatography showed that all samples had an isomeric purity exceeding 95%.

The absorption spectra were measured on isopentane solutions. Isopentane was purified by passing through an alumina column of 1.5 m in length and 2 cm in diameter. Sample solutions were prepared by dissolving *ca.* 20 mg of olefin in 10 cc of isopentane. The solutions were further diluted down to *ca.* 10^{-5}M, and were degassed before observation. A quartz cell with a 1 cm path length was used. The spectra were recorded on a Cary Model 15 spectrophotometer at room temperature under an atmosphere of nitrogen gas. The extinction coefficient obtained was not corrected for possible isomeric impurities.

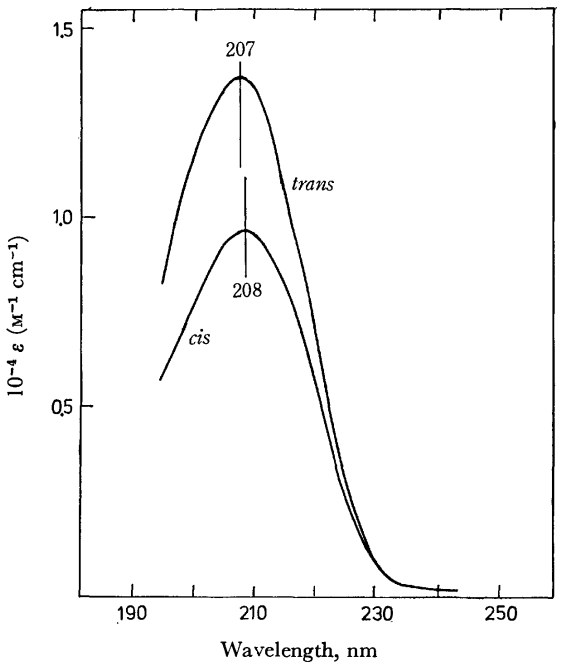

Fig. 1. Absorption spectra of *cis*- and *trans*-crotonic acids in isopentane.

Method of Calculation

The LCAO-MO-CI method of the Pariser-Parr-Pople (PPP) type was used for calculating the energies and oscillator strengths of the π—π^* transitions. The integral parameters used for the present calculations were all the same as those adopted previously.[7]

All the ethylene derivatives were assumed to be coplanar. The bond lengths and angles of the various 1,2-disubstituted ethylenes were taken from the literature.[15]

The spin configurations were constructed using the SCF closed-shell virtual orbitals. The configuration interactions were treated by including lower 10 (at maximum) singly excited configurations. All computations were perfomed on a KDC-II at the Computation Center of Kyoto University.

Results and Discussion

A. Absorption Spectra. Figure 1 shows the absorption spectra of the *cis* and *trans* isomers of crotonic acid (**4**) as an example. They show a strong absorption miximum at 208 and 207 nm, respectively. Although the Franck-Condon maxima are hard to locate, these band maxima may be used for our present purposes.

The spectral data obtained are summarized in Table 1, together with those for butene-2 (**7**)[11] and dichloroethylene (**8**).[10] All the compounds show one intense band with or without vibrational structure in the wavelength region 190—250 nm. No doubt, the observed bands correspond to the lowest π—π^* excitation.

Inspecion of the experimental data given in Table 1 indicates that, except for **2**, **7**, **8**, and **11**, both energy A^1E and oscillator strength f of the lowest π—π^* excitation of a given 1,2-disubstituted ethylene are more or less greater for the *trans* isomer. This tendency has no direct bearing on the relative stabilities of geometric isomers; *cis*-**9** is probably more stable than its *trans* isomer,[16,17] whereas *trans*-**1** is known to be thermochemically more stable than its *cis* isomer by *ca.* 0.9 kcal/mol at ordinary temperature.[17] The exceptions **2**, **7**, **8**, and **11** will be discussed later.

The energy difference between the *cis* and *trans* isomers of **6** is large compared to those for the other carbonyl compounds, **4** and **5**. This is probably due to the concurrent effects of the configurational and conformational differences between the isomers. While α,β-unsaturated carbonyl compounds exist predominantly in the planar *s-trans* conformation, the most stable form of *cis*-**6** is the *s-cis* conformation because of the steric repulsion between the two methyl groups.[18] The *s-trans* conformation of a conjugated framework generally tends to give greater excitation energies than does the *s-cis* counterpart.[19,20]

As regards the oscillator strength, **2** is not anomalous; the *trans* isomer has a greater f value, in harmony with

14) D. T. Mowry and J. N. Butler, "Organic Syntheses," Coll. Vol. 4, 486 (1963).

15) A. D. Mitchell, ed., "Table of Interatomic Distances and Configuration in Molecules and Ions," The Chemical Sosiety, London (1958).

16) T. Okuyama and T. Fueno, *J. Polymer Sci. A-1*, **9**, 629 (1971).

17) T. Okuyama, T. Fueno, and J. Furukawa, *Tetrahedron*, **25**, 5409 (1969).

18) Y. Kobuke, T. Fueno, and J. Furukawa, *J. Amer. Chem. Soc.*, **92**, 6548 (1970).

19) R. G. Parr and R. S. Mulliken, *J. Chem. Phys.*, **18**, 1338 (1950).

20) N. L. Allinger and M. A. Miller, *J. Amer. Chem. Soc.*, **86**, 2811 (1964).

Table 1. Lowest singlet π—π^* transitions of 1,2-disubstituted ethylenes

Serial No	Substituents X	Substituents Y	Geometry[a]	Obsd[b] ΔE, eV	Obsd[b] λ_{max}, nm	Obsd[b] $f(10^{-3}\varepsilon$, $M^{-1}cm^{-1})$	Calcd ΔE, eV	Calcd J_{hl}, eV	Calcd f_x	Calcd f_y
1	OCH_3	CH_3	*cis*	6.41	193		6.798	6.287	0.605	0.017
			trans	6.47	192		6.872	6.251	0.633	0.257
2	CN	CH_3	*cis*	6.17	201	0.135 (5.4)	6.105	5.680	0.804	0.014
			trans	6.14	202	0.344 (13.8)	6.183	5.625	0.819	0.391
3	CHO	CH_3	*cis*				5.646	5.604	0.917	0.0
			trans	5.87	211	0.184 (9.5)	5.698	5.544	0.937	0.200
4	COOH	CH_3	*cis*	5.97	208	0.277 (9.6)	5.819	5.670	0.921	0.0
			trans	5.99	207	0.379 (13.8)	5.859	5.604	0.942	0.201
5	$CONH_2$	CH_3	*cis*	6.12	203		6.031	5.520	0.932	0.004
			trans	6.16	201		6.064	5.492	0.961	0.152
6	$COCH_3$	CH_3	*cis*[c]	5.64	220	0.226 (8.8)	5.589	5.459	0.397	0.356
			cis				5.608	5.500	0.682	0.004
			trans	5.76	215	0.293 (11.5)	5.681	5.419	0.720	0.219
7	CH_3	CH_3	*cis*	7.07[g]		0.59[g]	6.615	5.852	0.804	0.0
			trans	6.98[g]		0.32[g]	6.669	5.809	0.813	0.339
8	Cl	Cl	*cis*	6.53[h]			7.430	6.885	0.711	0.0
			trans	6.36[h]			7.432	6.859	0.715	0.065
9	CH_3O	CH_3O	*cis*[d]				7.395	6.851	1.068	0.000
			cis[e]	6.16	201	0.384 (13.0)	7.322	6.880	0.631	0.022
			trans[d]	6.20	200	0.433 (11.3)	7.344	6.873	0.678	0.084
			trans[f]				7.308	6.903	0.398	0.171
10	CN	CN	*cis*	5.64	220		5.821	5.608	0.881	0.0
			trans	5.65	219		5.900	5.534	0.890	0.448
11	$COOCH_3$	$COOCH_3$	*cis*	6.12	203		5.736	5.702	1.149	0.0
			trans	5.94	209		5.806	5.670	1.178	0.101

a) The molecular conformation, whenever appropriate, is assumed to be *s-trans*, unless otherwise noted.
b) Measured in isopentane, unless otherwise noted.
c) *s-cis* conformation assumed (see text).
d) *s-trans,s-trans*.
e) *s-trans,s-cis*.
f) *s-cis,s-cis*.
g) Gas phase data, Ref. 11. F. H. Watson, Jr. and S. P. McGlynn, *Theoret. Chim. Acta*, (Berl.), **21**, 309 (1971), have also reported gas-phase data: ΔE=6.58 (*cis*) and 6.48 (*trans*) eV and $\varepsilon=12.2\times10^3$ (both *cis* and *trans*).
h) Gas phase data, Ref. 10.

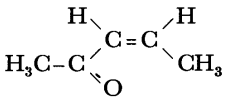

cis-**6** (*s-cis*)

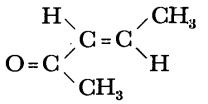

trans-**6** (*s-trans*)

the trend for the majority of "normal" compounds. Butene-2 (**7**), however, is still anomalous.

B. Calculated Excitation Energies. Calculations of the PPP type were performed for all the compounds **1** through **11**. For all isomers of these compounds, the lowest π—π^* excitation was the only intense transition in our wavelength range of interest. In what follows, we will be concerned only with the lowest π—π^* transition. The calculated excitation energies Δ^1E are listed in Table 1.

It may be noticed in Table 1 that the Δ^1E values calculated for *trans* isomers are, without exception, greater than those for the corresponding *cis* isomers. The differences between the calculated values are *ca.* 1% the excitation energies, in rough agreement with those observed for "normal" cases. As our present problem lies in the comparison of geometric isomers, we will not concern ourselves with numerical agreement between the calculated and observed values for individual isomers.

The isomeric difference calculated for **6** is in better agreement with the observed, when the *s-cis* conformation is assumed for the *cis* isomer than when the *s-trans* conformation is assumed. Also, the calculated results for **9** are best correlated with observation, if it is assumed that the *cis* isomer is in the *s-trans,s-cis* conformation while the *trans* isomer is in the *s-trans, s-trans* conformation.

The anomaly encountened in **11** is apparently due to the twisting of the *cis* isomer around its C-C single bonds because of the steric repulsion between the methoxycarbonyl groups. The essential discord between theory and experiment for the cases **2**, **7**, and **8** cannot be interpreted from the conformational consideration. Neither can it be remedied by means of all valence-electron theories. For example, the excitation energies of **2** calculated by the INDO method[21] are 11.137 and 11.163 eV for the *cis* and *trans* isomers, respectively.

21) J. A. Pople, D. L. Beveridge, and P. A. Dobosh, *J. Chem. Phys.*, **47**, 2026 (1967).

By our modified INDO method,[22] they are calculated to be 6.801 and 6.833 eV. Both these calculations give a higher excitation energy for *trans*-**2**, in disagreement with observation. The disagreements in **2**, **7**, and **8** will be discussed in Subsection D.

We previously ascribed the greater excitation energies for *trans* isomers of butadiene derivatives to their smaller Coulomb repulsion J_{hl} between the highest occupied and lowest vacant π orbitals.[7] Exactly the same situation has been confirmed with th Δ^1E values calculated for ethylene derivatives. For the sake of comparison, the calculated values of J_{hl} are included in Table 1. It is our working hypothesis that J_{hl} somehow measures a relief of a molecule from intramolecular electronic repulsion upon excitation, so far as the virtual orbital approximation is not greatly in error. That *cis* isomers have greater values of J_{hl} than the corresponding *trans* isomers is obvious from the relatively small spatial separations between the substituents. Apparently, the hypothesis is invalidated in the cases of **2**, **7**, and **8**.

C. Oscillator Strengths. The oscillator strength f may be calculated from the expression

$$f = 1.085\times10^{-5}\nu(r_x^2+r_y^2) = f_x + f_y \qquad (2)$$

where ν is the frequency of transition (cm^{-1}) and r_s ($s=x$ or y) is the transition moment length (Å) in the specified direction, x or y (Fig. 2). The values of f_x and f_y calculated for isomers of various ethylene derivatives are given in Table 1.

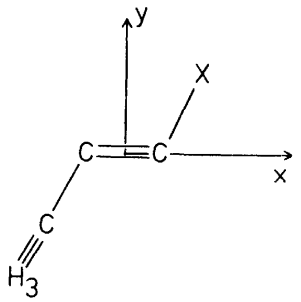

Fig. 2. Coordinate axes chosen for 1-substituted propenes.

It can be seen from Table 1 that there is little difference in the f_x value between the isomers, whereas the f_y value is considerably greater for the *trans* isomers. As a consequence, the sum f_x+f_y for a *trans* isomer is greater than that of the corresponding *cis* isomer, in agreement with observation. However, the unusually large f value reported for *cis*-**7** is hardly justifiable.

D. Ionization Potential. As has already been mentioned, the anomalous spectral features of **2**, **7**, and **8** cannot be attributed to steric strains in the *cis* isomers. A comparison of the ionization potentials of geometric isomers shows this to be the case.

Table 2 gives the observed[23] and calculated (PPP) vertical ionization potentials I_p for the *cis* and *trans* isomers of **1**, **2**, **7**, and **8**. The I_p values observed for *cis* isomers are greater than those for *trans* isomers only by a few hundredths of an electron volt. The isomeric differences calculated by assuming planar structures are found to be in good agreement with the observed. Thus, so far as the ground-state structure is concerned, nothing anomalous is perceptible for those spectroscopically anomalous olefins **2**, **7**, and **8**. If the *cis* isomers were greatly twisted in the ground state, their I_p values relative to the *trans* isomers would be more marked. For the sake of comparison, the relevant data for 1-phenyl-1-propene $C_6H_5CH{=}CHCH_3$ are included in Table 2. The isomeric difference found for this compound is as great as 0.11 eV, which should be attributed to the nonplanarity of the *cis* isomer.[24] All these results lead to the conclusion that stereostructures of the *cis* isomers of **1**, **2**, **7**, and **8** do not differ greatly, irrespective of their excitation characteristics.

Table 2. Vertical ionization potentials of some 1,2-disubstituted ethylenes

Compound	Geometry	I_p, eV Obsd[23]	I_p, eV Cacld (PPP)
1	*cis*	8.47	10.01
	trans	8.43	10.00
2	*cis*	10.21	10.66
	trans	10.20	10.65
7	*cis*	9.12[a]	10.39
	trans	9.12[a]	10.38
8	*cis*	9.83[b]	9.31
	trans	9.81[b]	9.29
1-Phenyl-1-propene	*cis*	8.44	9.78[c]
	trans	8.33	9.67

a) M. J. S. Dewar and S. D. Worley, *J. Chem. Phys.*, **50**, 654 (1969).
b) R. F. Lake and S. H. Thompson, *Proc. Roy. Soc.* (London), **A315**, 323 (1970).
c) The phenyl group is assumed to be rotated out of plane by 30°.[24]

Concluding Remarks

For most of the 1,2-disubstituted ethylenes the energy of the lowest singlet excitation is greater for *trans* isomers than for the corresponding *cis* isomers. Of the various ethylene derivatives studied, butene-2 (**2**), crotononitrile (**7**), dichloroethylene (**8**) were anomalous in the above respect. The oscillator strength is greater for *trans* isomers, with virtually no exceptional case. The generalization can be rationalized by the PPP calculations.

Changes in electronic population upon excitation might be drastic in some ethylene derivatives. In cases where reorganization of the electronic structure upon excitation is considerable, the virtual orbitals would no longer be capable of depicting the Franck-Condon excited states with reasonable accuracy. Anomalous spectral behaviors of the *cis* isomers of **2**, **7**, and **8** could be ascribed to this change. However, the reason for it to occur only in these particualr compounds is still unclarified.

22) K. Yamaguchi and T. Fueno, This Bulletin, **44**, 43 (1971).
23) The authors are indebted to Prof. S. Ikeda and Dr. I. Watanabe, Osaka University, for measurements of the photoelectron spectra for **1**, **2**, and 1-phenyl-1-propene.
24) T. Fueno, K. Yamaguchi, and Y. Naka, This Bulletin, the succeeding article.

Comparison of the Electronic Spectra of Geometric Isomers. III. β-Substituted Styrenes

Takayuki FUENO, Kizashi YAMAGUCHI, and Yuji NAKA*

Department of Chemistry, Faculty of Engineering Science, Osaka University, Toyonaka, Osaka

(Received February 21, 1972)

The ultraviolet absorption spectra of *cis* and *trans* isomers of various β-substituted styrenes have been measured both in the gaseous state and in *n*-hexane solution. The excitation energies observed for *cis* isomers are either smaller or greater than those of the *trans*, depending on the type of β-substituents. The isomeric difference in the energy of the lowest allowed transition was found to be linearly correlated with Taft's steric substituent constants. The electronic states of the various isomeric pairs were calculated by the LCAO-SCF-CI method of the Pariser-Parr-Pople type. The results were found to be entirely in line with the observed spectral features.

We have previously shown that *trans* isomers of terminal-substituted butadienes and ethylenes exhibit ultraviolet absorption at greater energy than do the corresponding *cis* isomers.[1,2] It is known, on the other hand, that *cis*-stilbene has greater excitation energies than its *trans* isomer.[3] Such contradistinctive cases can be characterized by the relative importance of the *electronic* and *steric* effects of substituent groups. Thus, if the entire chromophore of a *cis* isomer is in full π-conjugation, it should show smaller excitation energy as compared with its *trans* isomer.[1,2] The situation is reversed when a *cis* isomer cannot exist in planar form as a result of the steric repulsion between the substituents. The LCAO-SCF-CI theory of the Pariser-Parr-Pople (PPP) type fully rationalizes these interpretations.[1,4]

It is to be expected that β-substituted styrenes lie in between the above two extreme cases. Some compounds of this family would resemble stilbene in their spectral feature while others would be close to the butadiene type in nature, depending on the bulkiness of the β-substituent attached. Examination of this question is the purpose of the present work. The compounds investigated are the following:

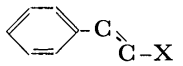

X = CH_3, C_2H_5, COOH, $CONH_2$, $CH{=}CH_2$, CN, OC_2H_5, or F

Spectra of the *cis* and *trans* isomers were measured in the vapor phase and in *n*-hexane solution. Expected results were obtained. The experimental results were justified by the PPP treatments.

Experimental

The β-methyl (1-phenyl-1-propene, **1**),[5] ethyl (1-phenyl-1-butene, **2**),[6] vinyl (1-phenyl-1,3-butadiene, **5**),[7] and ethoxy (styryl ethyl ether, **7**)[8] derivatives of sryrene were prepared according to the methods given in the literature. β-Fluorosryrene (**8**) was synthesized by the method of Bergmann *et al.*[9] All these compounds were then separated into geometric isomers by means of preparative gas chromatography: column packings, poly(ethylene glycol); column length, 3—5 m; operating temperature, 100—170°C; and carrier gas, hydrogen. The *cis* and *trans* isomers of cinnamic acid (**3**), cinnamide (**4**) and cinnamonitrile (**6**) were supplied by Dr. Kobuke, Kyoto University. Isomeric purity of each sample as determined by gas chromatography was no less than 95%.

All the geometric isomers were identified by the magnitudes of the NMR coupling constants observed between the ethylenic hydrogens. In the case of **8**, the HF coupling constants were also useful; $J_{\alpha F}$(Hz) = 45 (*cis*-**8**) and 20 (*trans*-**8**).

The absorption spectra were recorded on a Cary Model 15 spectrophotometer for both gas and solution samples at room temperature. Sample preparation and observation were carried out in the same manner as conducted previously for the butadiene derivatives.[1] Extinction coefficients were determined only for the solution spectra.

Method of Calculation

The LCAO-SCF-CI method of the Pariser-Parr-Pople type[10,11] was used to calculate the energies and oscillator strengths of the π—π* transitions. The necessary atomic parameters were taken from the tables of Hinze and Jaffé[12] and Moore,[13] and listed in a previous article.[1] The one- and two-center repulsion integrals were evaluated according to the Pariser formula[14] and the Nishimoto-Mataga[15] formula, respectively.

The off-diagonal core resonance integrals H_{rs} between

* Present address: Department of Chemical Engineering, Faculty of Engineering, Kyoto University, Yoshida, Kyoto.

1) T. Fueno and K. Yamaguchi, *J. Amer. Chem. Soc.*, **94**, 1119 (1972).
2) T. Fueno and K. Yamaguchi, This Bulletin, the preceding article.
3) H. Suzuki, This Bulletin, **33**, 381 (1960).
4) D. L. Beveridge and H. H. Jaffé, *J. Amer. Chem. Soc.*, **87**, 5340 (1965).
5) R. Adams, "Organic Reactions," Vol. 1, Wiley, New York (1957) p. 251.
6) G. Wittig and G. Harborth, *Ber.*, **77**, 319 (1944).
7) O. Grumitt and F. J. Christoph, *J. Amer. Chem. Soc.*, **73**, 3479 (1951).
8) S. I. Miller, *ibid.*, **78**, 6091 (1956).
9) F. Bergmann, A. Kalmus, and E. Breuer, *ibid.*, **80**, 4540 (1958).
10) R. Pariser and R.G. Parr, *J. Chem. Phys.*, **21**, 466, 467 (1953).
11) J. A. Pople, *Trans. Faraday Soc.*, **49**, 1375 (1953).
12) J. Hinze and H. H. Jaffé, *J. Amer. Chem. Soc.*, **84**, 540 (1962); *J. Phys. Chem.*, **67**, 1501 (1963).
13) C. E. Moore, "Atomic Energy Levels," National Bureau of Standards Circular No. 467, Vol. 1, Washington, D. C. (1949).
14) R. Pariser, *J. Chem. Phys.*, **21**, 568 (1953).
15) K. Nishimoto and N. Mataga, *Z. Phys. Chem.*, (Frankfurt), **12**, 335 (1957).

two neighboring atoms r and s were evaluated according to the Wolfsberg-Helmholtz formula[16]

$$H_{rs}^{0} = -\frac{\kappa}{2}S_{rs}(I_r + I_s) \quad (1)$$

where S_{rs} is the overlap integral between the parallel Slater $p\pi$ atomic orbitals on atoms r and s, and the parameter κ values were empirically determined as to reproduce the state energies observed. The κ values finally adopted were 0.85 for compounds **3**, **5**, and **7**, and 0.9 for the rest.

We assume that molecular geometries of β-substituted styrenes are such as to be constructed schematically by replacing the vinyl group of the parent styrene with a substituted ethenyl group. The bond lengths and angles of both styrene and substituted ethylenes were taken from the literature.[17] The hyperconjugation model was assumed for the methyl group.[1] For nonplanar geometries of *cis* isomers in which the phenyl ring was assumed to be rotated out of plane, the resonance integral for the bond *t*-*u* connecting the benzene ring and the C=C double bond was modified to be

$$H_{tu} = H_{tu}^{0}\cos\theta \quad (2)$$

where θ is the rotation angle. The coordinate axes were chosen as shown in Fig. 1.

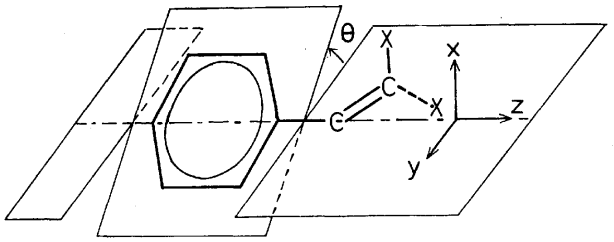

Fig. 1. Coordinate axes and conformation of *cis*-β-substituted styrenes.

The configuration interactions were treated by including lower 10 singly excited configurations. All computations were performed on a KDC-II at the Computation Center of Kyoto University.

Results and Discussion

A. Observed Spectra. Figure 2 shows the absorption spectra of the *cis* and *trans* isomers of β-methylstyrene (**1**), as an example, both in the gaseous state and in *n*-hexane solution. In either phase, the observed spectra have three bands in the wavelength range 200—300 nm. The first band appearing at about 280 nm is very weak, whereas the second (230—260 nm) and the third (~200 nm) are both strong. In the vapor spectra of the geometric isomers, we see that the second absorption peak of the *trans* isomer (λ_{max}= 238 nm) is at a greater wavelength than that of the *cis* isomer (λ_{max}=233 nm). The same is true with the solution spectra. The extinction coefficient was found to be greater for *trans*-**1** (ε=17100) than for its *cis* isomer (ε=12300).

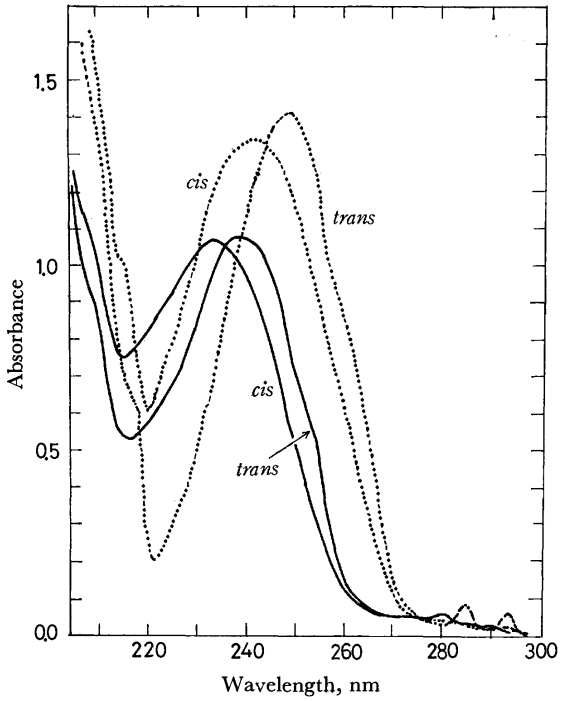

Fig. 2. Absorption spectra of *cis*- and *trans*-β-methylstyrenes (**1**) in the vapor phase (——) and in *n*-hexane solution (·····). Concentration in *n*-hexane: *cis*, 106.0 μM; *trans*, 86.8 μM.

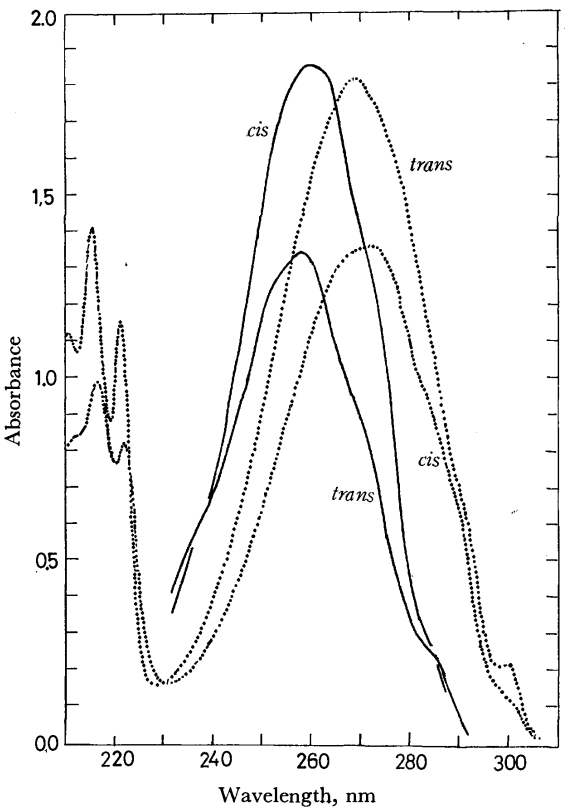

Fig. 3. Absorption spectra of *cis*- and *trans*-cinnamonitriles (**6**) in the vapor phase (——) and in *n*-hexane solution (·····). Concentration in *n*-hexane: *cis*, 78.0 μM; *trans*, 91.0 μM.

The spectral features of the β-ethyl (**2**), the β-carboxy (**3**), β-carbamido (**4**) and β-vinyl (**5**) derivatives were

16) M. Wolfsberg and L. Helmholtz, *J. Chem. Phys.*, **20**, 837 (1952).

17) A. D. Mitchell, ed., "Table of Interatomic Distances and Configuration in Molecules and Ions," The Chemical Society. London (1958).

TABLE 1. SINGLET π-π^* EXCITATIONS OF β-SUBSTITUTED STYRENES

Geometry	Band	Obsd[a] Δ^1E, eV Gas	Obsd[a] Δ^1E, eV Soln	Obsd[a] 10^{-4} ε_{max}, $M^{-1}cm^{-1}$	Obsd[a] f	Calcd[b] Δ^1E, eV	Calcd[b] f_z	Calcd[b] f_y	Calcd[b] f_x	Wt % of the most important spin configurations[c]
						1 CH_3				
cis	1	—	—	—	—	4.878	0.000	0.000	0.000	43.0 (5—7); 42.9 (4—6)
	2	5.33	5.17	1.23	0.35	5.222	0.448	0.175	0.000	98.2 (5—6)
	3	—	—	—	—	6.373	0.000	0.184	0.099	42.6 (5—7); 42.6 (4—6)
						6.592	0.201	0.253	0.012	63.6 (4—7); 13.1 (5—8); 11.0 (3—6)
						6.616	0.000	0.000	0.000	49.0 (5—8); 50.7 (3—6)
trans	1	4.55	4.36	—	—	4.823	0.000	0.000	0	43.6 (5—7); 43.5 (4—6)
	2	5.21	5.01	1.71	0.45	5.124	0.840	0.085	0	98.7 (5—6)
	3	6.26	6.12	2.13	—	6.371	0.013	0.415	0	45.6 (5—7); 45.6 (4—6)
						6.589	0.447	0.176	0	65.4 (4—7); 13.5 (5—8); 13.2 (3—6)
						6.755	0.000	0.000	0	49.8 (5—8); 49.9 (3—6)
						2 C_2H_5				
cis	1	—	—	—	—	4.656	0.000	0.000	0.000	45.4 (3—5); 45.4 (4—6)
	2	5.33	5.15	0.81	0.20	5.355	0.484	0.043	0.000	95.3 (4—5)
	3	—	—	—	—	6.334	0.104	0.226	0.113	37.3 (3—5); 37.3 (4—6); 17.4 (3—6)
						6.472	0.504	0.250	0.037	10.8 (3—5); 10.8 (4—6); 65.6 (3—6)
						6.685	0.000	0.000	0.000	48.6 (4—7); 48.6 (2—5)
trans	1	4.41	4.24	—	—	4.607	0.000	0.000	0	45.8 (3—5); 45.8 (4—6)
	2	5.15	4.98	1.68	0.41	5.219	0.568	0.043	0	96.1 (4—5)
	3	—	—			6.260	0.044	0.414	0	42.7 (3—5); 42.7 (4—6)
						6.459	0.559	0.210	0	75.2 (3—6)
						6.696	0.000	0.000	0	48.6 (4—7); 48.6 (2—5)
						3 COOH				
cis	1	—	—	—	—	4.873	0.003	0.000	0.002	47.4 (5—7); 31.0 (6—8); 14.7 (5—9)
	2		4.70[d]	0.10[d]	—	4.942	0.364	0.248	0.001	97.6 (6—7)
	3		5.80[d]	1.05[d]	—	5.945	0.000	0.045	0.056	51.1 (5—7); 25.4 (6—8); 20.1 (5—9)
						6.291	0.073	0.094	0.000	58.4 (4—7); 40.1 (6—9)
						6.403	0.053	0.168	0.000	21.6 (4—7); 29.8 (6—9); 46.8 (5—8)
trans	1	—	—	—	—	4.736	0.170	0.063	0	41.2 (5—7); 26.7 (6—8); 20.6 (6—7)
	2		4.54[d]	0.2[d]	—	4.682	0.667	0.094	0	78.5 (6—7); 13.9 (5—7)
	3		5.77[d]	1.5[d]	—	6.061	0.000	0.248	0	42.0 (5—7); 45.0 (6—8)
						6.387	0.142	0.139	0	21.7 (4—7); 33.5 (6—9); 41.6 (5—8)
						6.432	0.044	0.064	0	59.1 (4—7); 38.7 (6—9)
						4 $CONH_2$				
cis	1	—	—	—	—	4.958	0.003	0.004	0.001	42.5 (5—7); 35.6 (6—8); 12.6 (5—9)
	2		4.79[d]	—	—	5.146	0.421	0.229	0.001	96.5 (6—7)
	3	—	—	—	—	6.077	0.057	0.153	0.003	85.1 (4—7)
						6.178	0.000	0.067	0.096	52.9 (5—7); 28.9 (6—8); 13.7 (5—9)
						6.412	0.022	0.056	0.000	64.8 (6—9); 30.5 (5—8)
trans	1	—	4.15[d]	—	—	4.794	0.269	0.018	0	32.3 (6—7); 39.1 (5—7); 20.2 (6—8)
	2		4.62[d]	—	—	4.841	0.550	0.131	0	66.5 (6—7); 14.6 (5—7); 14.5 (6—8)
	3	—	—	—	—	6.129	0.008	0.090	0	32.7 (5—7); 34.0 (6—8); 25.9 (4—7)
						6.196	0.018	0.382	0	12.1 (5—7); 11.7 (6—8); 68.1 (4—7)
						6.480	0.119	0.050	0	56.0 (6—9); 41.6 (5—8)
						5 $CH{=}CH_2$				
cis	1	—	—	—	—	4.679	0.000	0.000	0.000	33.7 (4—6); 16.3 (4—8); 16.3 (3—7)
	2	4.94	4.71	—	—	4.871	0.466	0.359	0.000	97.8 (5—6)
	3	—	—	—	—	5.941	0.000	0.000	0.000	50.0 (5—6); 49.4 (5—8)
						6.010	0.002	0.037	0.110	42.6 (4—6); 42.7 (6—7)
						6.098	0.051	0.331	0.015	23.3 (3—6); 23.3 (5—8); 38.1 (4—7)
trans	1	4.13[f]	—	—	—	4.565	0.000	0.000	0	39.6 (4—6); 39.6 (5—7); 10.4 (3—7); 10.4 (4—8)
	2	4.71[f]	4.43[g]	—	—	4.602	0.899	0.197	0	98.9 (5—6)
	3	—	—	—	—	5.979	0.007	0.272	0	44.5 (4—6); 44.6 (5—7)
						6.047	0.000	0.000	0	49.7 (3—6); 49.6 (5—8)
						6.109	0.151	0.329	0	26.7 (3—6); 26.6 (5—8); 35.8 (4—7)

Geometry	Band	Obsd[a] Δ^1E eV Gas	Obsd[a] Δ^1E eV Soln	Obsd[a] 10^{-4} ε_{max}, $M^{-1}cm^{-1}$	Obsd[a] f	Calcd[b] Δ^1E, eV	Calcd[b] f_z	Calcd[b] f_y	Calcd[b] f_x	Calcd[b] Wt % of the most important spin configurations[c]
						6 CN				
cis	1	—	—	—	—	4.764	0.084	0.085	0	22.9 (5—6); 36.3 (4—6); 30.7 (5—7)
	2	4.76	4.55	1.71	0.28	4.689	0.273	0.174	0	75.0 (5—6); 17.7 (4—6)
	3	—	5.72	1.25	—	6.006	0.002	0.190	0	42.3 (4—6); 40.4 (5—7); 10.7 (4—8)
						6.316	0.017	0.000	0	64.9 (5—8); 31.7 (3—6)
						6.485	0.041	0.232	0	30.5 (3—6); 49.0 (4—7)
trans	1	—	4.13	0.13	—	4.778	0.015	0.000	0	48.1 (4—6); 34.9 (5—7); 10.1 (4—8)
	2	4.80	4.61	1.99	0.32	4.841	0.993	0.100	0	97.6 (5—6)
	3	—	5.75	1.56	—	6.211	0.002	0.358	0	47.3 (4—6); 45.9 (5—7)
						6.450	0.230	0.066	0	44.6 (5—8); 47.6 (4—7)
						6.548	0.105	0.035	0	27.8 (5—8); 65.4 (3—6)
						7 OC_2H_5				
cis	1	—	4.21	—	—	4.560	0.002	0.001	0	51.7 (5—7); 38.6 (4—6)
	2	4.93	4.74	1.64	0.40	4.989	0.545	0.070	0	96.3 (5—6)
	3	—	6.15	1.37	—	6.085	0.007	0.329	0	43.5 (5—7); 41.7 (4—6)
						6.383	0.297	0.106	0	64.7 (4—7); 28.8 (3—6)
						6.530	0.153	0.041	0	11.3 (4—7); 54.0 (5—8)
trans	1	—	4.13	—	—	4.569	0.000	0.000	0	63.7 (5—7); 39.7 (4—6)
	2	4.94	4.78	2.30	0.54	5.021	0.624	0.059	0	97.0 (5—6)
	3	—	~6.2	—	—	6.125	0.011	0.365	0	44.5 (5—7); 43.1 (4—6)
						6.385	0.392	0.109	0	70.0 (4—7); 22.5 (3—6)
						6.549	0.092	0.030	0	35.8 (3—6); 54.4 (5—8)
						8 F				
cis	1	—	4.32	—	—	4.837	0.001	0.001	0	51.3 (5—7); 40.5 (4—6)
	2	5.31	5.14	—	—	5.320	0.573	0.060	0	96.2 (5—6)
	3	—	—			6.426	0.014	0.404	0	43.0 (5—7); 43.4 (4—6)
						6.707	0.457	0.157	0	74.4 (4—7); 15.5 (3—6)
						6.936	0.073	0.015	0	42.4 (3—6); 50.8 (5—8)
trans	1	4.43	4.26	—	—	4.845	0.000	0.001	0	50.2 (5—7); 41.5 (4—6)
	2	5.32	5.15	—	—	5.347	0.630	0.053	0	96.8 (5—6)
	3	—	—	—	—	6.458	0.018	0.439	0	43.8 (5—7); 44.7 (4—6)
						6.702	0.515	0.150	0	76.2 (4—7); 12.7 (3—6)
						6.958	0.043	0.012	0	44.5 (3—6); 50.8 (5—8)

a) The extinction coefficients ε_{max} and oscillator strengths f were determined from the spectra in solution. Solvent is *n*-hexane, unless otherwise noted.
b) The rotation angle of the phenyl ring in *cis* isomers (Fig. 1) was assumed to be: 30° for **1** and **2**; 45° for **3**, **4**, and **5**; and 0° for **6**, **7**, and **8**.
c) The symbol (*i*—*j*) indicates the singlet spin configuration resulting from the one-electron transition from the *i*th to the *j*th molecular orbital of the ground-state configuration.
d) In ethanol.
f) R. J. Dolter and C. Curran, *J. Amer. Chem. Soc.*, **82**, 4155 (1960).
g) Ref. 7.

found to be essentially the same as those of **1**. All the data observed for compounds **1** to **5** are summarized in Table 1.

The spectra of cinnamonitrile (**6**) shown in Fig. 3 are in contrast to those of β-methylstyrene. The second ultraviolet absorption of the *trans* isomer (λ_{max}= 269 nm) occurs at a shorter wavelength than that of the *cis* isomer (λ_{max}=272 nm). The tendency is the reverse of that found for **1**.

The β-ethoxy (**7**) and β-fluoro (**8**) derivatives are similar to **6** in their spectral feature (Figs. 4 and 5); the second bands of *cis* isomers are shifted, though only slightly, to longer wavelength relative to the *trans*. The bands show considerable vibrational structure, indicating a planar conformation. The spectral data for **6**, **7**, and **8** are also given in Table 1.

The second excitation energy Δ^1E_2 of the *cis* isomers relative to the *trans* appears to be correlated with the steric repulsion between the *cis* β-substituent and the phenyl group. The isomeric differences

$$\delta\Delta^1E_2 = \Delta^1E_2(cis) - \Delta^1E_2(trans) \quad (3)$$

for the various β-substituted styrenes including stilbene are given in Table 2, together with the steric substituent constants E_s[18] available for the β-substituents. The steric repulsion is the greatest in *cis*-stilbene. The negative values of $\delta\Delta^1E_2$ found for **6**, **7**, and **8** might

18) R. W. Taft, in "Steric Effects in Organic Chemistry," ed., M. S. Newman, Wiley, New York, N. Y. (1956), Chapter 13.

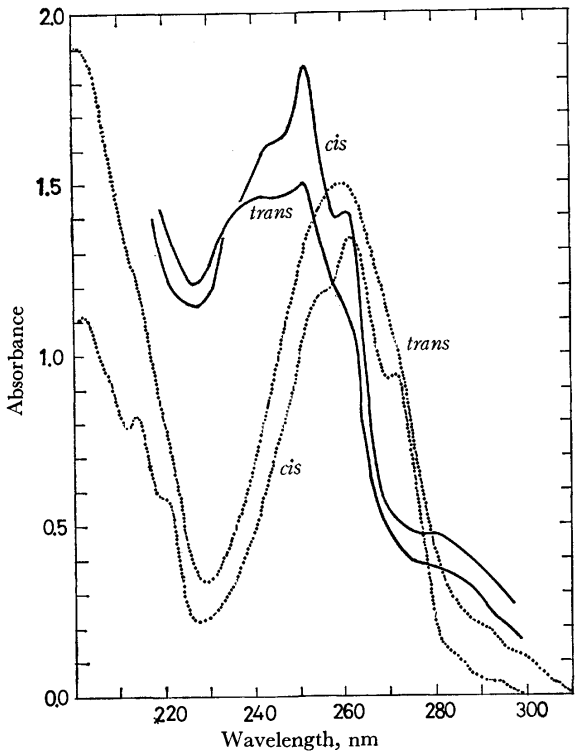

Fig. 4. Absorption spectra of *cis*- and *trans*-β-styryl ethyl ethers (**7**) in the vapor phase (——) and in *n*-hexane solution (·····). Concentration in *n*-hexane: *cis*, 81.1 μM: *trans*, 65.2 μM.

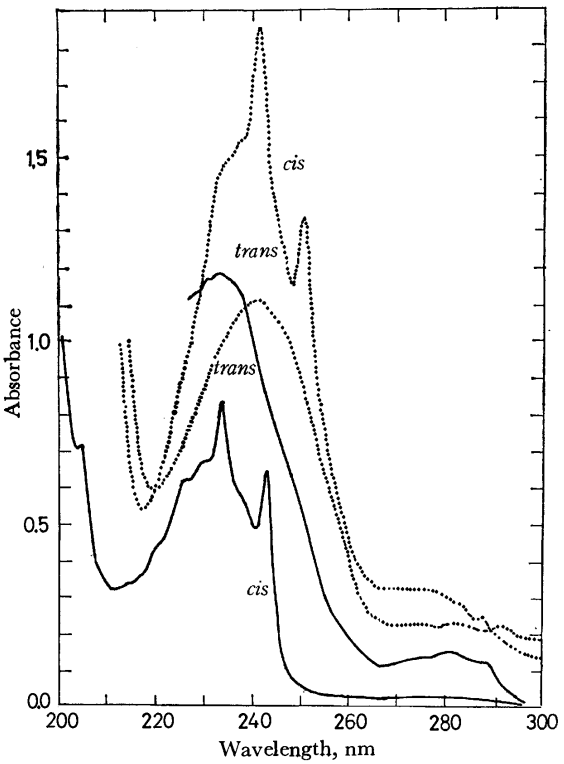

Fig. 5. Absorption spectra of *cis*- and *trans*-β-fluorostyrenes (**8**) in the vapor phase (——) and in *n*-hexane solution (·····).

indicate the electronic effect of *cis* substitutions surpassing their steric contribution.

Plots of $\delta\Delta^1E_2$ against E_s give a good linear relationship (Fig. 6). The solution data are better correlated

TABLE 2. DIFFERENCES BETWEEN THE SECOND EXCITATION ENERGIES OF *cis*- AND *trans*-β-SUBSTITUTED STYRENES

Substituent[a]	$\delta\Delta^1E_2$, eV[b]		E_s[c]
	Gas	Soln	
C_6H_5	—	0.34[d]	−0.90
$CH{=}CH_2$	0.23	0.28	
$CONH_2$	—	0.17	
C_2H_5	0.18	0.17	−0.07
CH_3	0.12	0.16	0.00
COOH	—	0.16	
F	−0.01	-0.00_5	0.49
OC_2H_5	−0.01	−0.04	0.90
CN	−0.04	−0.06	

a) Substituents are listed in decreasing order of $\delta\Delta^1E_2$ in solution.
b) Eq. (3).
c) Steric substituent constants defined from the hydrolysis rates of *o*-substituted benzoic esters (except for C_2H_5, for which the value derived from aliphatic esters has been adopted).[18]
d) The energies corresponding to the Δ^1E_2 are 4.56 (in ethanol) and 4.22 eV (in heptane) for the *cis* and *trans* isomers, respectively.[3]

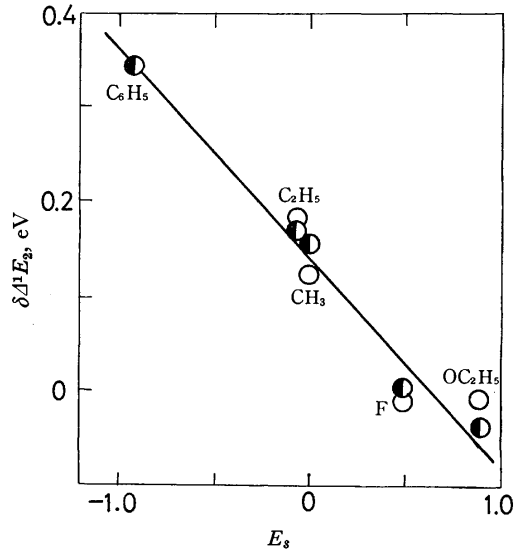

Fig. 6. Linear correlation of $\varepsilon\Delta^1E_2$ with E_s. ○, gas phase; ◐, solution.

with E_s than are the gas-phase data, the regression line being obtained by use of only the former. The linearity in turn permits estimation of the E_s values for substituents for which no such data are available as yet. The estimated values are −0.65, −0.17, 0.00, and 0.90 for the groups $CH{=}CH_2$, $CONH_2$, COOH, and CN, respectively.

B. Electronic States. *cis*- and *trans*-β-methylstyrenes (**1**) were first treated. Figure 7 gives the energy diagram of *trans*-**1** before and after configuration interactions. Each state is characterized as if the molecule were of the C_{2v} symmetry with respect to its pseudo-long axis (z). The transition to the lowest $^1B_2$ state is forbidden, while the second transition to the $^1A_1$ state is allowed. The third ($^1B_2$) and fourth ($^1A_1$) transitions are both allowed and are situated close to each other. The calculated results are consistent

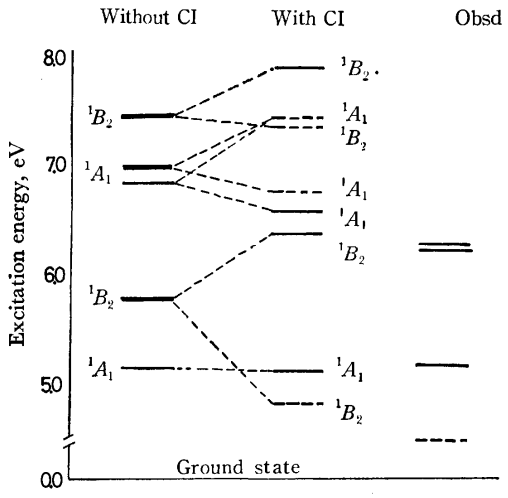

Fig. 7. Energy diagram of *trans*-β-methylstyrene. ——, allowed; ——, forbidden.

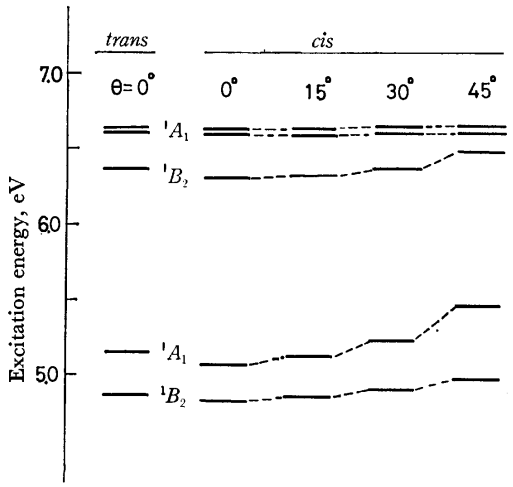

Fig. 8. Dependences of the calculated excitation energies of *cis*-β-methylstyrene on the out-of-plane rotation angle θ of the phenyl ring.

with the observed spectrum.

Fugure 8 illustrates the dependences on θ of the excitation energies calculated for *cis*-**1**. The energies cannot exceed those of the *trans* isomer unless θ is greater than 20°. The angular dependence of energy is the largest for the second excited state. The calculated value of the second excitation energy Δ^1E_2 for *cis*-**1** relative to *trans*-**1** was found to be in best agreement with the observed gas-phase value, when θ was assumed to be 30°.

The excitation energies and oscillator strengths culculated for the *cis* (θ=30°) and *trans* (θ=0°) isomers of **1** are listed in Table 1, together with the weight% of the spin configurations which most importantly contribute to each electronic state. For either isomer the second excited state is well represented by the spin configuration $^1\Phi_{5,6}$ alone, which corresponds to the one-electron transition from the highest occupied (h) to the lowest vacant (l) obrital in the ground configuration. On the other hand, both the first and third excited states are described as superpositions of two configurations, $\Phi_{5,7}$ and $\Phi_{4,6}$, where the orbitals ϕ_4 and ϕ_7 respectively denote the next-highest occupied and next-lowest vacant levels, which are essentially localized in the phenyl ring. Thus, the first and third bands are considered to be analogs of the $^1B_{2u}$ and $^1E_{2u}$ bands of benzene, respectively, whereas the second band ($^1A_1$) is characteristic of the entire chromophore of **1**. It is natural that the Δ^1E_2 value calculated should be the most sensitive to the conformational change of the molecular framework.

Analogous calculations have been performed for all the remaining compounds. The results are summarized in Table 1. For every isomeric compound studied, the second π—π^* excitation is allowed and well represented by a single spin configuration, which corresponds to the electronic promotion from orbital h to l. However, *trans*-**3** and *cis*-**6** are somewhat unusual in this respect. For compounds **1** through **5**, the deformations of the *cis* isomers were necessary to reproduce their increments in Δ^1E_2 value relative to the *trans* isomers. For compounds **6**, **7**, and **8** on the other hand, the planar structure (θ=0°) was found to be plausible even for *cis* isomer.

Numerical agreement between theory and experiment is good for the second band energies but less satisfactory for the first and third bands. Nonetheless, we may be content with the present results in view of the limited accuracy of the virtual orbital approximation.

The oscillator strengths calculated were larger for *trans* isomers than for the corresponding *cis* isomers. The results are in good agreement with those found experimentally. It deserves special mention that the oscillator strengths are larger for *trans* isomers in all the three systems investigated (ethylenes, butadienes, and styrenes). Their values are most reliable in discriminating geometric isomers.

C. Structural Effect on Δ^1E_2. Elucidation of the structural effect on Δ^1E_2 can be achieved most expediently by analyzing the configurational energy $\Delta^1E_2^0$. In the PPP approximation, the energy is given by

$$\Delta^1E_2^0 = \varepsilon_l - \varepsilon_h - J_{hl} + 2K_{hl} \quad (4)$$

where ε_l and ε_h are the energies of the lowest vacant and highest occupied orbitals, respectively, and where J_{hl} and K_{hl} are the inter-frontier-orbital Coulomb and exchange repulsions, respectively.

Variations of these energy terms with structure are diagrammatically shown in Fig. 9, taking β-methylstyrene as an example. It can be seen that the energy gap $\Delta\varepsilon_{hl}$ between the frontier orbitals for the hypothetical planar *cis* isomer (θ=0°) is essentially equal to that for the *trans* isomer. The K_{hl} terms are also nearly equal for both isomers. Clearly, it is the J_{hl} term that would lower the $\Delta^1E_2^0$ for the planar *cis* isomer relative to the *trans*. As θ for the *cis* isomer increases, however, its ε_l increases while ε_l decreases monotonically. The progressive spread of the gap with θ tends to counterbalance the increase in the term (J_{hl}—$2K_{hl}$). The relative magnitudes of $\Delta^1E_2^0$ for the two isomers are thus offset when θ is greater than about 20°. Note that the variation of $\Delta^1E_2^0$ with structure is essentially the same as that of Δ^1E_2 shown in Fig. 8. Incidentally, the considerable lowering in ε_h with θ is compatible with the observation that the vertical

TABLE 3. CONTRIBUTIONS OF VARIOUS ENERGY TERMS TO THE CONFIGURATIONAL ENERGY $\Delta^1E_2^0$ (eV)

No.	X	Geometry	Angle, deg	$\Delta\varepsilon_{hl}$	J_{hl}	K_{hl}	$\Delta^1E_2^0$	Δ^1E_2
1	CH_3	*cis*	30	8.229	4.778	0.899	5.248	5.222
		trans	0	7.992	4.731	0.942	5.145	4.124
2	C_2H_5	*cis*	30	8.367	5.023	1.040	5.420	5.355
		trans	0	8.157	5.208	1.078	5.286	5.219
3	COOH	*cis*	45	7.976	4.597	0.797	4.972	4.942
		trans	0	7.500	4.628	0.877	4.711	4.682
4	$CONH_2$	*cis*	45	8.165	4.754	0.881	5.172	5.146
		trans	0	7.649	4.628	0.911	4.843	4.841
5	$CH=CH_2$	*cis*	45	7.760	4.733	0.920	4.904	4.871
		trans	0	7.335	4.573	0.930	4.622	4.602
6	CN	*cis*	0	7.684	4.666	0.862	4.743	4.689
		trans	0	7.667	4.572	0.887	4.869	4.841
7	OC_2H_5	*cis*	0	7.964	4.957	1.025	5.056	4.989
		trans	0	7.961	4.943	1.032	5.082	5.021
8	F	*cis*	0	8.310	5.000	1.039	5.389	5.320
		trans	0	8.305	4.986	1.044	5.409	5.347

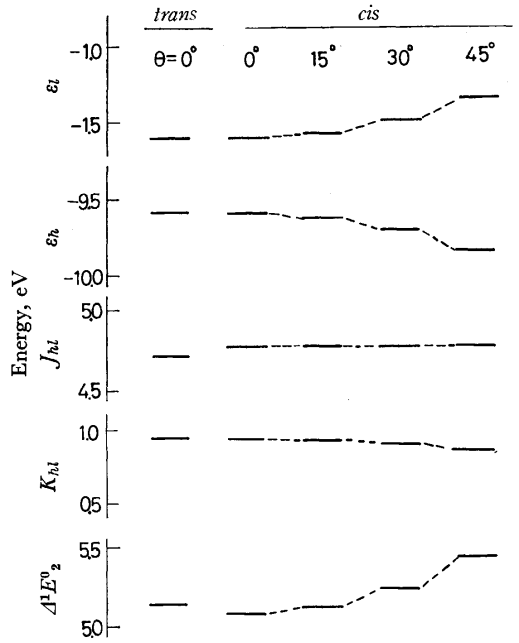

Fig. 9. Concentrations of various energy terms to $\Delta^1E_2^0$ of *cis*- and *trans*-β-methylstyrenes.

ionization potential of *cis*-**1** is greater than that of *trans*-**1** by as much as 0.11 eV.[2]

Exactly the same situation is encountered with all the remaining compounds. In order for the calculated isomeric differences of $\Delta^1E_2^0$ to agree with the observed, rotational angles of $\theta=30°$ (for **1** and **2**) and $\theta=45°$ (for **3**, **4**, and **5**) had to be assumed. For compounds **6**,**7**, and **8**, on the other hand, $\theta=0°$ sufficed to interpret the observed differences. The results of calculations for these conformations are given in Table 3. The relative magnitudes of $\Delta^1E_2^0$ remain much the same as those of Δ^1E_2.

The lower excitation energies for the *cis* isomers of **6**, **7**, and **8** as compared with the *trans* counterparts are noteworthy. We have previously interpreted the lower excitation energies of planar *cis* isomers to imply that they experience greater relief from intramolecular electronic repulsion upon excitation.[1] An alternative interpretation may be possible if the promoted electron is considered to be under the Coulombic field of the rest of the molecule. Withdrawal of an electron from orbital *h* of a molecule would leave an electron hole which is distributed over the molecule with partial positive charges. When the electron withdrawn is placed in orbital *l*, it is subjected to Coulombic attraction ($-J_{hl}$) from the hole. Apparently, the electron-hole attraction is larger for *cis* isomers, for which the molecular framework is relatively compact. We feel that the latter interpretation is of conceptual importance, particularly because it can readily be extended to intermolecular charge-transfer interactions.

Conclusion

The second excitation energy Δ^1E_2 of *cis*-β-substituted styrenes is either smaller or greater than that of the *trans* isomers, depending on the nature of the β-substituents. The relative magnitudes are well correlated with the steric substituent effects. PPP calculations taking account of the out-of-plane rotation of the phenyl group lead to results which are compatible with observation. The greater Δ^1E_2 values for *cis* isomers are attributable to their greater inter-frontier-orbital energy gap due to the steric hindrance between the substituent groups. The smaller values of Δ^1E_2 for presumably planar *cis* isomers can be understood from the concept of intramolecular electron-hole Coulombic attractions.

Behavior of Oxygen Species on the Nickel Oxide Catalyst Surface

Safee CHAUDHRI, Yoshiya KERA, and Kozo HIROTA
Department of Chemistry, Faculty of Science Osaka University, Toyonaka, Osaka
(Received February 25, 1972)

The ^{18}O-oxidation of carbon monoxide was studied on nickel oxide catalysts, and the oxygen exchangeability with the oxide during the reaction was determined. The activities of three oxide samples, obtained under different preparation conditions, were compared. The samples were prepared at 350, 600, and 850°C; they are denoted as NiO-I, NiO-II, and NiO-III respectively. In the case of NiO-I, two kinds of oxygen species, weakly and strongly bound to the surface, were observed. Above 120°C, not only weakly but also strongly bound surface oxygen become reactive; however, the binding energy distribution was quite broad. Similar observations were made in the case of NiO-II, with a similar change above 170°C and with a sharp energy distribution. In contrast, for NiO-III, only a small percentage of the monolayer of the surface oxygen became active and exchangeable below 200°C, but above 250°C about three layers became activated. Models are proposed for the surface state of these oxides on the basis of the behavior of the surface oxygen.

A number of studies have been devoted to the investigation of the oxidation of carbon monoxide over nickel oxide catalysts, but the proposed rate expressions and reaction mechanisms differ from author to author.[1-9] This very fact suggests that the surface structure and properties of the nickel oxide used differ intricately with its biography.

Recently, Uchijima *et al.*[10] successfully measured the amount of "surface excess oxygen" and its oxidation power distribution, and showed that the surface state of nickel oxide varied delicately, depending upon the preparation conditions, especially the sintering temperature of the oxide. Such conclusions were also reported by Dere'n *et al.*[11] However, a main problem still remains whether or not the surface excess oxygen is an effective parameter in the discussion of the mechanism.

In order to examine the behavior of the surface oxygen under the conditions of the working state, the oxidation of carbon monoxide was investigated in the present study by the use of ^{18}O-tracer on nickel oxides, which had been prepared under three different preparation conditions.

Experimental

Material. The NiO catalysts were prepared by the decomposition of $NiCO_3$, followed by sintering. $NiCO_3$ precipitated by mixing an aqueous solution of $Ni(NO_3)_2$ and $(NH_4)_2CO_3$ (both special grade; Wako Pure Chem. Ind. Co.) was completely washed, filtered and dried in a vacuum desiccator containing $CaCl_2$. The preparation conditions, the B.E.T surface area, and colors of the catalysts are summarized in Table I. The B.E.T. surface areas were determined from the adsorption of nitrogen at 77°K.

TABLE 1. PREPARATION CONDITIONS AND SOME CHARACTERISTICS OF THE NiO SAMPLES

Catalyst	Preparation conditions: Temperature (°C)	Preparation conditions: Decomposition time (hr)	Preparation conditions: Sintering time (hr)	BET surface area (m^2/g)	Color
NiO-I	350	3	15	64.0	Black
NiO-II	600	3	15	4.1	Grayish Green
NiO-III	850	3	15	0.9	Green

Carbon monoxide was obtained by the reaction of formic acid and conc. sulfuric acid. Heavy oxygen (4.8 atom% ^{18}O) was obtained by the electrolysis of heavy water containing ^{18}O. Both gases were purified by the usual methods and were found to be mass-spectrometrically pure.

Reaction Apparatus and Procedure. The reaction was carried out in a thermo-cyclic reaction vessel (265 cc), as is shown in Fig. 1. The amount of the catalyst used was 0.5 g in the cases of NiO-I and NiO-II and 2.0 g in the case of NiO-III. After the heat treatment at 300°C in a vacuum (10^{-5} Torr) for 2 hr, 32—36 mmHg of the reaction gas (CO: O_2=2: 1) was introduced into the reaction vessel. The change in the total pressure was measured with a mercury manometer, and the change in the composition

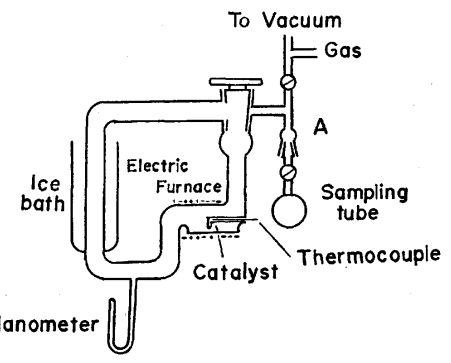

Fig. 1. Thermo-cyclic type reaction vessel.

1) J. Kondo, T. Uchijima, and Y. Yoneda, This Bulletin, **40**, 1040 (1967).
2) G. Parravano, *J. Amer. Chem. Soc.*, **75**, 1448 (1953).
3) E. R. S. Winter, *J. Chem. Soc.*, **1955**, 2726.
4) S. Z. Roginsky and T. S. Tselenskaya, *Zh. Fiz. Khim. SSSR*, **22**, 1360 (1948).
5) N. P. Keier, S. Z. Roginsky, and I. S. Sozonova, *Doklady Akad. Nauk SSSR*, 106 (1956).
6) G. M. Schwab and J. Block, *Z. Phys. Chem. N.F.* **1**, 42 (1954).
7) M. E. Dry and F. S. Stone, *Discuss. Faraday Soc.*, **28**, 192 (1959).
8) J. Coue, P. C. Gravelle, R. E. Ranc, P. Rue, and S. J. Teichner, Proc. Intern. Congr. Catalysis, 3rd, Amsterdam (1964), p. 748.
9) I. Matsuura, H. Kubokawa, and O. Toyama, *Nippon Kagaku Zasshi*, **81**, 1003 (1960).
10) T. Uchijima, M. Takahashi, and Y. Yoneda, *J. Catal.*, **9**, 403 (1967); This Bulletin, **40**, 2767 (1967).
11) J. Dere'n and J. Stoch, *J. Catal.*, **18**, 249 (1970).

of reacting gases and their ^{18}O-concentration, with a mass spectrometer.

The errors of the ^{18}O-concentration were within 0.02—0.1 atom%. The temperature was kept constant within ± 1.0°C.

Results

Carbon Monoxide Oxidation on NiO-I and the Distribution of ^{18}O among the Components during the Reaction. The reaction was carried out in the temperature range from 50° to 350°C, and arrived at equilibrium in all runs except the run at 50°C. The ^{18}O-concentration in unreacted oxygen remained almost the same at its initial value (4.8 atom% ^{18}O), and that in unreacted carbon monoxide gave a constant value equal to the natural abundance or a slight increment during the reaction. On the other hand, the ^{18}O-concentration in the produced CO_2 varied with the time, depending upon the reaction temperature, as is shown in Table 2. From the findings that the ^{18}O-concentrations in oxygen and carbon monoxide remained the same at their initial values, while the $C^{16}O^{18}O$% in carbon dioxide always changed with a value lower than the ^{18}O atom% in oxygen during the reaction, it is clear that oxygen species in the catalyst, NiO-I take part in the catalytic oxidation.

TABLE 2. CHANGE IN $C^{16}O^{18}O$% IN PRODUCED CO_2 DURING THE COURSE OF REACTION ON NiO-I, 0.5 g

Reaction temperature (°C)	Time (min) 2	5	10	15	60
50	—	4.47	4.48	4.58	4.44
80	—	4.71	4.05	4.13	3.82
100	—	3.59	3.71	3.66	3.52
120	—	3.30	3.50	3.60	3.45
150	—	3.33	3.46	3.40	3.38
200	—	3.06	3.25	3.13	3.13
250	—	2.70	2.97	2.82	2.73
300	1.89	—	2.42	2.45	2.46
350	—	2.14	2.04	2.01	1.73

Considering the material balance of ^{18}O during the oxidation, the relation for obtaining the amount of exchangeable or reactive oxygen in the catalyst can be represented by Eq. (1):

$$(\alpha-\beta)n_g = (\beta/2)n_s \quad (1)$$

where the notations are:

α: ^{18}O atom% in gaseous oxygen
β: $C^{16}O^{18}$ O% in carbon dioxide
n_g: number of molecules in the produced carbon dioxide
n_s: number of exchangeable or reactive oxygen atoms in the catalyst.

The left-hand side of Eq. (1) indicates the number of ^{18}O atoms which disappear from the gaseous phase, and the right-hand side, the number of ^{18}O atoms captured by the catalyst, on the assumption of an isotopic equilibrium between the ^{18}O-concentrations in the produced carbon dioxide and that in the catalyst. Then, the number of the exchangeable or reactive oxygen atoms, n_s, is given by Eq. (2):

$$n_s = 2(\alpha-\beta)n_g/\beta \quad (2)$$

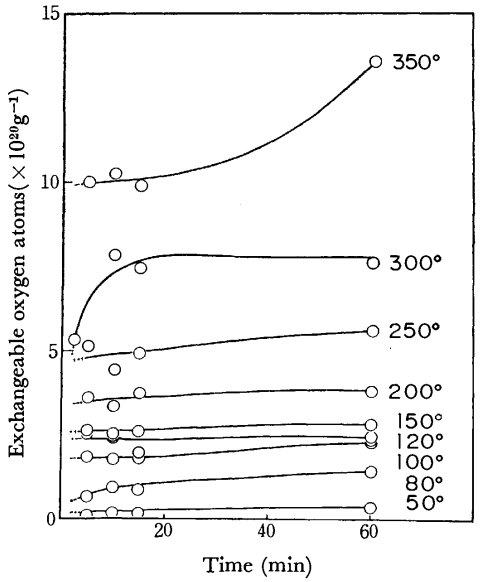

Fig. 2. Temperature dependency of exchangeable oxygen atoms of the surface (n_s) during the oxidation on NiO–I.

The change in n_s with the time, obtained for NiO-I by Eq. (2), are compared in Fig. 2. The figure shows that the n_s remained practically the same after 15 min in all temperatures except at 350°C, though the magnitude depends upon the reaction temperature. This shows that the exchange process of oxygen between carbon dioxide and the catalyst (NiO-I) is very fast. The assumption of the exchange equilibrium, therefore, may be unnecessary at 60 minutes in all runs except that at 350°C.

Carbon Monoxide Oxidation on NiO-II and the Distribution of ^{18}O among the Components during the Reaction. The reaction was carried out in the temperature range from 100° to 400°C, and the reaction equilibrium was practically reached within 10—15 min, except for the run at 100°C. The ^{18}O-concentrations in unreacted O_2 and CO almost remained at their initial values, as in the case of NiO-I. The ^{18}O-concentration in the produced CO_2 changed with the time, as is shown in Table 3.

The numbers of the exchangeable or reactive oxygen atoms, obtained from the Eq. (2), are given in Fig. 3. The n_s in NiO-II is about ten times smaller than that

TABLE 3. CHANGE IN $C^{16}O^{18}O$% IN PRODUCED CO_2 DURING THE COURSE OF REACTION ON NiO-II, 0.5 g

Reaction temperature (°C)	Time (min) 2	5	10	15	60
100	4.60	4.67	4.66	4.65	4.71
150	4.75	4.75	4.70	4.70	4.76
170	4.65	4.62	4.62	—	4.67
190	4.61	4.64	4.63	—	4.67
200	4.70	4.72	4.66	—	4.51
300	4.56	4.59	4.55	4.45	4.27
400	4.09	4.20	4.18	4.20	4.00

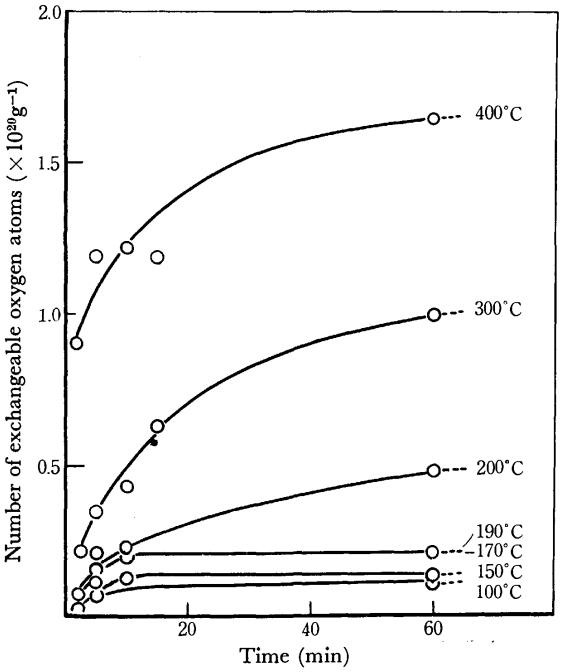

Fig. 3. Temperature dependency of exchangeable oxygen atoms of the surface (n_s) during the oxidation on NiO-II.

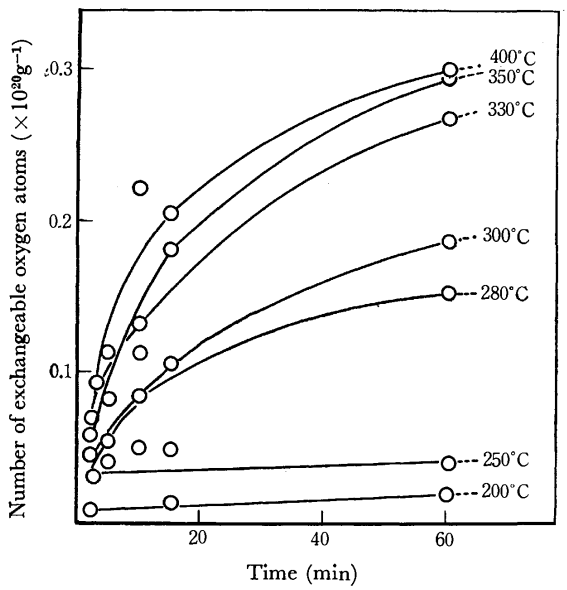

Fig. 4. Temperature dependency of exchangeable oxygen atoms of the surface (n_s) during the oxidation on NiO–III.

in NiO-I; therefore, the errors are estimated to be more or less large. However, it can be observed that the values of n_s remained the same after 10—15 min, at least at temperatures below 190°C. In the case of NiO-II, the exchange equilibrium is not established even after one hour above 200°C, which is lower than in the case of NiO-I.

Carbon monoxide Oxidation on NiO-III and the Distribution of ^{18}O among the Components during the Reaction. The reaction was carried out in the temperature range from 200° to 400°C. The reaction equilibrium was reached within 10—15 minutes in all runs except that at 200°C. The ^{18}O-concentrations in unreacted oxygen and carbon monoxide remained constant at all runs during the course of the reaction, as in the cases of NiO-I and NiO-II. On the other hand, the $C^{16}O^{18}O$% in the CO_2 produced varied with the time, as is shown in Table 4.

The numbers of the exchangeable or reactive oxygen atom, n_s, obtained from Eq. (2), are recorded in Fig. 4. The n_s values show that, in the runs above 280°C, the isotopic equilibrium between CO_2 and the catalyst is still not established even after 60 minutes.

Table 4. Change in $C^{16}O^{18}O$% in produced CO_2 during the course of reaction on NiO-III, 2.0 g

Reaction temperature (°C)	Time (min) 2	5	10	15	60
200	4.4	—	—	4.76	4.71
250	4.55	—	4.66	4.78	4.71
280[a)]	4.67	4.68	4.65	—	4.56
300	4.51	4.68	—	4.69	4.37
330[b)]	4.55	4.66	4.68	4.68	4.57
350	4.52	4.60	4.49	4.37	4.21
400	4.55[c)]	4.55[d)]	4.35	4.41	4.20

a) 1.5 g b) 1.0 g c) 3 min d) 6 min

Discussion

The crystal structure of nickel oxide belongs to that of the NaCl type. If it is assumed, for the sake of convenience, that the exposed surface consists of only the (100) plane, the number of the exchangeable or reactive atoms, n_s, can be easily transformed into the surface fraction of the oxygen atom, θ (n_s). The surface fractions, θ (n_s), obtained on the assumption from the n_s values at 60 min shown in Figs. 2, 3, and 4 are shown in Figs. 5, 6, and 7 respectively.

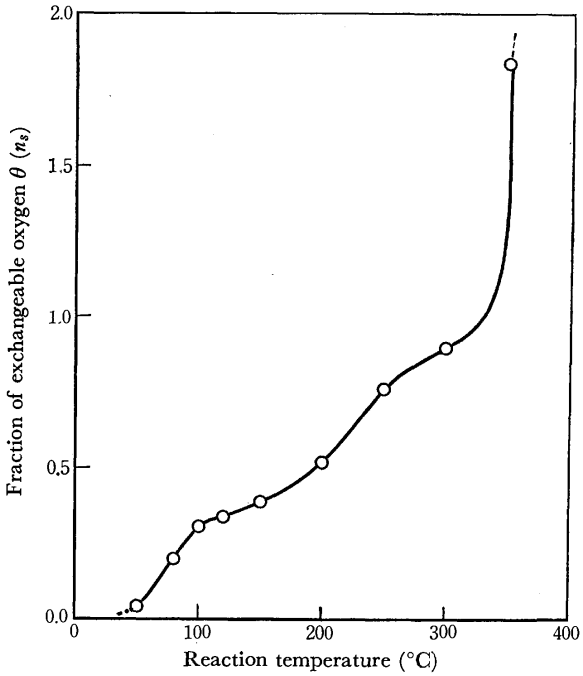

Fig. 5. Fraction of the exchangeable oxygen to the monolayer *versus* reaction temperature on NiO–I.

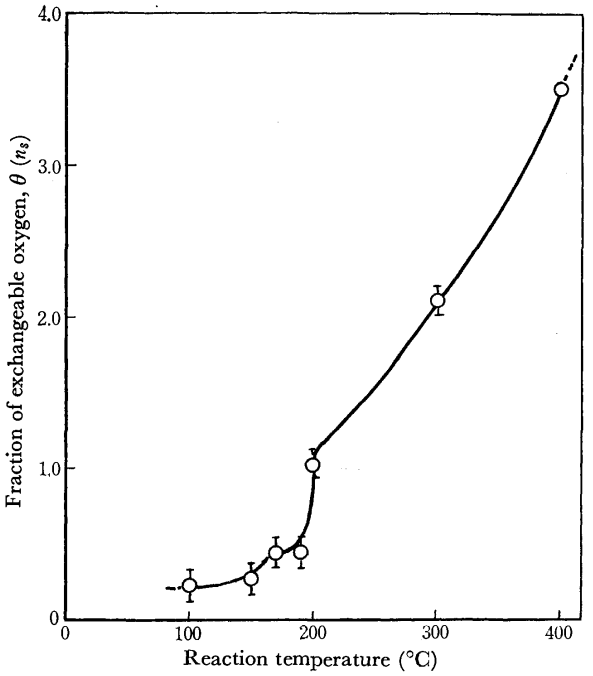

Fig. 6. Fraction of the exchangeable oxygen to the monolayer *versus* reaction temperature on NiO–II.

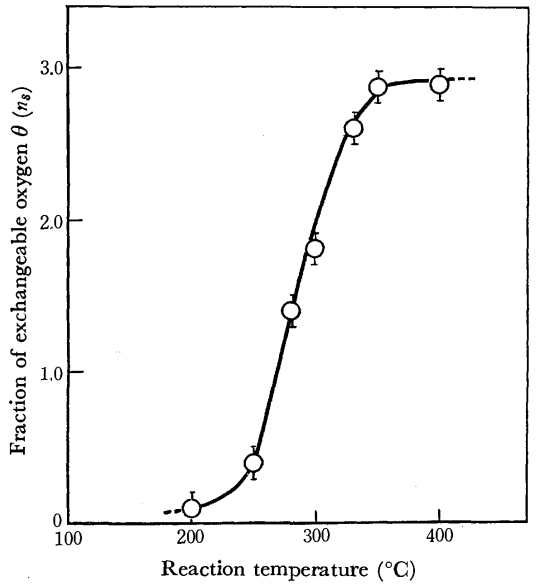

Fig. 7. Fraction of the exchangeable oxygen to the monolayer *versus* reaction temperature on NiO–III.

NiO-I (Fig. 5) shows clear changes in the exchangeability of the oxide at about 120 and 300°C. Oxygen species, which are exchangeable with carbon dioxide or which take part in the reaction below 120°C, correspond to about 30% of the surface, while those in the temperature range between 120 and 300°C correspond to about 60%. By raising the reaction temperatute to above 300°C, the oxygen species in the second layer or below also become exchangeable.

NiO-II (Fig. 6), though the errors are estimated to be more or less large, shows a clear change in the exchangeability at two temperatures, *i.e.*, between 150 and 170°C and between 190 and 200°C. About 40% of the surface is covered with the oxygen species, which can exchange with carbon dioxide or take part in the reaction below 170°C, while about 60% of the remaining surface is covered with the oxygen species, which can participate in the reaction at a temperatute between 170 and 200°C. Since Fig. 6 shows an abrupt change in the exchangeability in the higher-temperature region within a narrower temperature range in comparison with Fig. 5, the surface of NiO-II seems to have less heterogeneity than that of NiO-I.

In the case of NiO-III, the exchangeability increases rapidly and monotonously above 250°C, reaching a constant value at 350° and 400°C, indicating that the amount of the exchangeable or reactive oxygen corresponds practically to the three layers near the surface, that is, the binding state of the oxygen of the first three layers is homogeneous; moreover, the state in the three layers near the surface and that below the layers are clearly different in exchangeability from the above layers.

From the above discussion, the following surface models can be proposed for nickel oxide catalysts:

(i) NiO-I: The surface oxygen is roughly classified in two groups based on the difference in binding energy. About 30% of the surface oxygen is weakly-bound oxygen (W-site), and about 60%, strongly-bound oxygen (S-site). The former becomes reactive even below 120°C, and the latter, in the temperature range between 120 and 300°C, but the distribution of the binding energy is widespread.

(ii) NiO-II: The surface oxygen is composed of about 40% weakly-bound oxygen (W-site) and about 60% strongly-bound oxygen (S-site). The former becomes reactive below 170°C, and the latter, in the temperature range between 170 and 200°C, and the distribution of the binding energy is not so widespread.

(iii) NiO-III: The three layers near the surface are very homogeneous, and the layers below them are clearly different in exchangeability.

Dere'n *et al.*[11] suggested that "excess oxygen," *i.e.*, the ionosorbed oxygens of NiO, are almost entirely concentrated on the surface and are completely removed by evacuation for several minutes at 400°C. According to their suggestion, the surface oxygen which is not in the form of the surface-excess oxygen has become the object of the present research, because in our research the surface-excess oxygen can be removed by pretreatment. From this viewpoint, the results of other authors obtained by kinetic studies, desorption studies of oxygen and carbon dioxide, ^{18}O-exchange studies, and so on will be compared with ours and examined in connection with the above surface model.

Kondo *et al.*[1] observed the desorption of carbon dioxide with the elevation of the temperature on NiO, which seems to have nearly the same properties as NiO-I, because it was prepared by the decomposition and sintering of $NiCO_3$ at 350°C for 24 hr. They found the existence of two types of adsorption sites on the surface; which correspond to the maxima of the desorption curve at 80 (weak adsorption site) and at 300°C (strong adsorption site). Moreover, they measured the rate of the CO-oxidation on the NiO, poisoned by carbon dioxide, and suggested that the strongly-

adsorbed carbon dioxide exists on the site of weakly-bound oxygen of the surface, while, conversely, the weakly-adsrobed carbon dioxide exists on that of strongly-bound oxygen. They concluded that the oxidation rate was controlled by the process on the former site below 110°C and by that on the latter site above this temperature.

The temperature, 120°C, above which the S-site also becomes reactive on NiO-I corresponds fairly well to their transition temperature. However, it is difficult to understand their conclusion that, at lower temperatures, the oxidation rate is controlled by the process on the site of the strong adsroption of carbon dioxide, because the carbon dioxide produced cannot be desorbed from the site at such a temperature, but can be desorbed only at around 300°C. The present results, that the values of $C^{16}O^{18}$ O% increase with the time in the initial stage, suggest that the CO-oxidation is initiated by the extraction of the surface oxygen with carbon monoxide; below 120°C, only the W-site takes part in the oxidation, while above that temperature the W-site and also the S-site in accordance with the reaction temperature take part in the oxidation. Since the ^{18}O-concentration in both carbon monoxide and oxygen gases remained unchanged during the reaction, the stoichiometric change in the reacting gases was observed, and no poisoning effect was indicated, so it is clearly shown by Fig. 8 that Step I or Step II is a very slow process. However, it is not

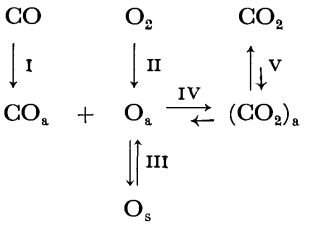

Fig. 8. Schematic representation of carbon-monoxide oxidation

yet clear whether Step I or Step II corresponds to the rate-controlling step below and above the transition temperature.

Kondo *et al.*[1] carried out the same experiment on NiO, which seems to have nearly the same properties as NiO-II; *i.e.*, their oxide was prepared by the decomposition and sintering of $NiCO_3$ at 700°C for 4 hr. The peaks of the CO_2 desorption curve shifted to a higher temperature and the transition temperature of the CO-oxidation became 160°C. Therefore they drew the same conclusion as above. This transition temperature may correspond to the temperature, 170°C, above which the S-site on NiO-II also becomes reactive, but their mechanism has been found to be inconsistent with the present one, as will be discussed below. Parravano[2] investigated the kinetics of carbon-monoxide oxidation on NiO, which seems to have nearly the same properties as NiO-II; *i.e.*, their oxide was prepared by firing $NiCO_3$ at 640°C for 3 hr. He showed that the rate expression between 106 and 174°C was different from that between 205 and 222°C, while the Elovich equation holds in both temperature ranges at the initial stage. He concluded that, at the initial stage, Eq. (3) controlled the reaction rate. At the stationary state of the reaction, Eq. (3) became the rate-determining step in the lower temperature range, while Eq. (4) was that step in the higher:

$$CO + O(s) \longrightarrow CO_2 + (s) \quad (3)$$

$$\frac{1}{2}O_2 + (s) \longrightarrow O(s) \quad (4)$$

The finding for NiO-II that the values of $C^{16}O^{18}$ O% tend to increase rapidly at the initial stage is consistent with Parravano's conclusion that the reaction is initiated by the extraction of surface oxygen with carbon monoxide. Based on the surface model of NiO-II, it can be expected that the oxidation rate in the temperature range between 174 and 205°C, where Parravano did not give any rate expression, is controlled by a different process. Up to 170°C, only the oxygen in the W-site would take part in the reaction, while in the range from 170 to 200°C not only the oxygen on the W-site but also that on the S-site would take part, according to the temperature. Since the ^{18}O-concentrations of O_2 and CO remained the same during the reaction, Step I or Step II in Fig. 8 must be very slow.

Winter[3] investigated the CO-oxidation in the temperature range between 40 and 211°C on $Ni^{18}O$, which was obtained by means of the ^{18}O-exchange between $C^{18}O_2$ and NiO, which seems to have nearly the same properties as NiO-III; *i.e.*, it was prepared by the decomposition of $NiCO_3$ at 870°C for 24 hr. The result indicated that only 2.3% of the surface oxygen takes part in the oxidation. Recently, Gay[12] measured the desorption spectra of adsorbed oxygen on NiO, prepared by the decomposition of $NiCO_3$ at 850°C for 9 hr. He indicated that only a small percentage of surface oxygen became desorbable by the elevation of the temperature to 750°C. The results of both Winter and Gay suggest that only a small percentage of the surface oxygen is active on NiO prepared at the higher temperature. The present results for NiO-III show that the surface oxygen, activated below 200°C in the oxidation, is less than 10%, but otherwise, above 250°C, about three layers of the surface are activated to the same degree. Therefore, it might be expected that the reaction mechanisms in the temperature ranges below 200 and above 250°C are different.

The above discussions were done without considering the surface excess oxygen or ionosorbed oxygen, but the contributions of these species cannot be ruled out, especially at room temperature. Not only CO-oxidation but also interactions among the adsorbed species, O_2, CO, and CO_2, on NiO have been investigated at such low temperatures by several authors.[13–18] For

12) Ian D. Gay, *J. Catal.*, **17**, 245 (1970).

13) S. J. Teichner and J. A. Morrison, *Trans. Faraday Soc.*, **51**, 961 (1955); G. EL Shobaky, P. C. Gravelle, and S. J. Teichner, *J. Catal.*, **14**, 4 (1969).

14) W. E. Garner and F. J. Veal, *J. Chem. Soc.*, **1945**, 1436; W. E. Garner and F. S. Stone, *Proc. Roy. Soc., Ser. A*, **211**, 472 (1952).

15) R. M. Dell and F. S. Stone, *Trans. Faraday Soc.*, **50**, 501 (1954).

16) M. Courtois and S. J. Teichner, *J. Catal.*, **1**, 121 (1962).

instance, Teichner,[13] Garner,[14] and Stone[15] measured the heat of adsorption of CO, O_2, and CO_2, and their heat of reactions on the catalyst. They pointed out the existence of a CO_3-complex, and also suggested that the oxidation reaction could proceed through the path of the formation of the complex on NiO, though they used very different catalysts. Teichner[16] and Eischens[18] have confirmed the existence of the CO_3-complex by measuring the IR spectra of the reacting system. From these results, it can be expected that the site of excess oxygen plays an important role in the formation of the CO_3-complex and in the course of the oxidation reaction at low temperatures.

The authors wish to express their gratitude to Professor Keiji Kuwata for his continued interest in this work and for his valuable suggestions and discussions.

17) K. Klier and M. Jiratova, Intern. Congr. Catalysis, 3rd Amsterdam (1964), p. 47.
18) R. P. Eischens and W. A. Pliskin, *Adv. Catal.*, **9**, 662 (1957); *ibid.*, **10**, 1 (1958).

BULLETIN OF THE CHEMICAL SOCIETY OF JAPAN, VOL. 45, 3306—3308 (1972)

Directly Bonded Carbon-Hydrogen Coupling Constants of *n*-Pentane

Isao ANDO, Atsuo NISHIOKA, and Masao KAMBE

Department of Polymer Engineering, Tokyo Institute of Technology, Ookayama, Meguro-ku, Tokyo

(Received February 28, 1972)

The values of the directly-bonded carbon-hydrogen coupling constants (J_{C-H}) of the methyl and methylene groups in *n*-pentane were calculated by using the CNDO/2 method, taking into account its rotational isomers, and it was found that the calculated values of J_{C-H} agree closely with the observed values.

The groundwork for the theoretical evaluation of spin-spin coupling constants was first laid by Ramsey *et al.*,[1,2] and since then several authors[3-7] have developed the valence-bond or molecular-orbital theory for the spin-spin coupling constants, using the average excitation energy (ΔE), based on Ramsey's theory. Then, on the basis of those theories, the correlation between the observed, directly-bonded carbon-hydrogen spin-spin coupling constant, J_{C-H}, and the degree of hybridization of the carbon atom in various compounds has been studied.[8-18] Recently Maciel *et al.*[19] have also interpreted the observed J_{C-H}'s of a number of compounds using finite pertubation techniques[20] which they have developed. However, in these studies there has been scarcely no study of the J_{C-H} values of molecules which have the various rotational isomers in liquids. In this paper, we will consider the relation between the experimental and the calculated carbon-hydrogen spin-spin coupling constants of the methyl and methylene groups of *n*-pentane, which can take various rotational isomers, and will also study their temperature dependences, using the CNDO/2 (Complete Neglect of Differential Overlap) method[21] as the molecular-orbital method.

Experimental

The carbon-13 NMR spectra of *n*-pentane were measured by means of a Japan Electron Optics Laboratory JEOL PS-100-type spectrometer at 25.15 MHz, at −60 and 22°C, using a 8 mm sample tube and the multiple-scan-average technique. Cyclohexane was used as the external referencee.

Calculation

From the molecular orbital theory[3-5] of nuclear spin-spin coupling constants, it can be shown that, if the Fermi contact term dominates the spin-spin coupling interaction, the magnitude of the coupling constant between directly-bonded nuclei should show a direct dependence on the amount of *s* character in the bond between them as follows:

1) N. F. Ramsey and E, M. Purcell. *Phys. Rev.*, **85**, 143 (1952).
2) N. F. Ramsey, *ibid.*, **91**, 303 (1953).
3) H. M. McConnell, *J. Chem. Phys.*, **24**, 460 (1956).
4) N. Muller and D. E. Prichard, *ibid.*, **31**, 768 ,1471 (1959).
5) J. A. Pople and D. P. Santry, *Mol. Phys.*, **8**, 1 (1963).
6) M. Karplus and D. M. Grant, *Proc. Natl. Acad. Sci. U. S.*, **45**, 1269 (1959).
7) C. Juan and H. S. Gutowsky, *J. Chem. Phys.*, **37**, 2198 (1962).
8) J. N. Shoolery, *ibid.*, **31**, 1427 (1959).
9) J. H. Goldstein and G. S. Reddy, *ibid.*, **36**, 2644 (1962).
10) N. Muller and P. I. Rose, *J. Amer. Chem. Soc.*, **84**, 3973 (1962).
11) K. Frei and H. I. Bernstein, *J. Chem. Phys.*, **48**, 1216 (1963).
12) S. G. Frankiss, *J. Phys. Chem.*, **67**, 752 (1963).
13) K. Frei and H. I. Bernstein, *J. Chem. Phys.*, **48**, 1216 (1963).
14) T. Yonezawa, I. Morishima, M. Fujii, and K. Fukui, This Bulletin, **38**, 1224 (1965).
15) T. Yonezawa, I. Morishima, and M. Fujii, *ibid.*, **39**, 2110 (1966).
16) V. S. Watts and J. H. Goldstein, *Theor. Chim. Acta*, **4**, 265 (1966).
17) T. Yonezawa and I. Morishima, *J. Mol. Spectrosc.*, **27**, 210 (1968).
18) Z. B. Maksic, M. Eckert-Maksic, and M. Randic, *Theor. Chim. Acta.*, **22**, 70 (1971).
19) G. E. Maciel, J. W. McIver, Jr., N. S. Ostlund, and J. A. Pople, *J. Amer. Chem. Soc.*, **92**, 1, 11 (1970).
20) J. A. Pople, J. W. McIver, and N. S. Ostlund, *J. Chem. Phys.*, **49**, 2965 (1968).
21) J. A. Pople and G. A. Segal, *J. Chem. Phys.*, **43**, S 136 (1965).

$$J_{C-H} = \left(\frac{4}{3}\right)^2 h\beta^2\gamma_C\gamma_H(\Delta E)^{-1}(1s_H|\delta|1s_H)(2s_C|\delta|2s_C)P^2_{C-H} \quad (1)$$

where β is the Bohr magneton; γ_X, the nuclear magnetogyric ratio of the X atom; ΔE, the average excitation energy; $(1s_H|\delta|1s_H)$ and $(2s_C|\delta|2s_C)$, the one-electron integrals at the hydrogen and carbon nuclei respectively, and P_{C-H}, the carbon 2*s*-hydrogen 1*s* element of the bond-order matrix. Moreover, when 0.550 and 2.767 a.u.[22] are used as $(1s_H|\delta|1s_H)$ and $(2s_C|\delta|2s_C)$ respectively, Eq. (1) can be simply rewritten as follows:

$$J_{C-H} = 7885(\Delta E)^{-1}P^2_{C-H}\,(\text{Hz}) \quad (2)$$

If the value of ΔE is a constant for each carbon of *n*-pentane, J_{C-H} should be proportional to P^2_{C-H}. Here, the bond orders were calculated using the CNDO/2 method.

Among the nine rotational isomers, *n*-pentane can take seven preferred rotational isomers, the TT, TG, TG′, GT, G′T, GG, and G′G′ forms, but for the GG′ and G′G forms, which are at any rate, negligible because of their steric hindrances. The rotational isomeric states of *trans* (T) and *gauche* (G and G′) are defined as occurring at the rotational angles of 0, 120, and 240° respectively by means of the clockwise rotation around the C–C bond expressed in the Newman projection.

We numbered the carbon atoms in pentane as follows:

$$CH_3(1)\text{-}CH_2(2)\text{-}CH_2(3)\text{-}CH_2(2)\text{-}CH_3(1)$$

The C–C and C–H bond lengths are set as 1.54 Å and 1.10 Å respectively, and both the C–C–C and C–C–H bond angles are set at 109°28′.[23]

The numerical calculations were carried out by means of the HITAC-5020E of the Computer Center of the University of Tokyo.

Results and Discussion

The carbon-13 NMR spectrum of *n*-pentane observed at 22°C is shown in Fig. 1, where a quartet and two triplets are identified as $CH_3(1)$, $CH_2(2)$, and $CH_2(3)$ carbons respectively with a decrease in the field. Then, the directly-bonded carbon-hydrogen coupling constants (J_{C-H}) were obtained; they are shown in Table 1, including those values observed at −60°C. From these results, it was found that the J_{C-H} value of the $CH_3(1)$ is larger than that of the $CH_2(2)$ or $CH_2(3)$, and that the $CH_2(2)$ is slightly larger than the $CH_2(3)$, but no value of J_{C-H} depends upon the temperature.

Next, the calculated values of P^2_{C-H} of seven rotational isomers in *n*-pentane are shown in Table 2, which also gives those values averaged by the populations of these rotational isomers using the following formula:

$$P^2_{C-H_{AV}} = \sum_{i=1}^{7} X_i P^2_{C-H_i} \quad (3)$$

where;

$$X_i = e^{-\Delta E_i/RT} \Big/ \sum_{i=1}^{7} e^{-\Delta E_i/RT} \quad (4)$$

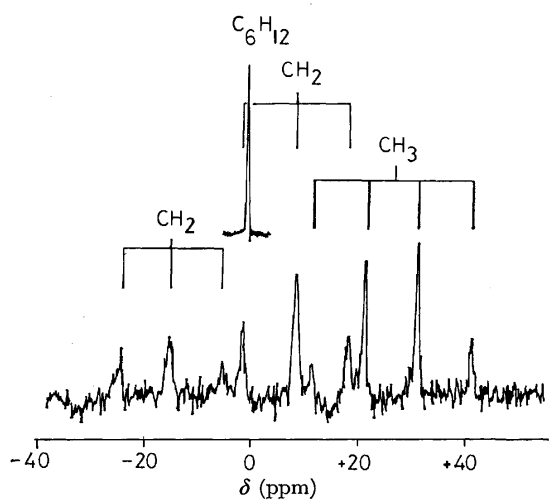

Fig. 1. The carbon-13 NMR spectrum of *n*-pentane in neat liquid at 22°C (128 scans). The reference is cyclohexane signal (proton spin-decoupled).

Table 1. The observed and calculated values of J_{C-H} in *n*-pentane

Temperature	J_{C-H} (Hz)		
	CH_3 (1)	CH_2 (2)	CH_2 (3)
Observed[a]			
−60°C	127.6±0.5	124.6±0.5	122.9±0.5
22°C	127.8±0.5	124.8±0.5	122.6±0.5
Calculated[b]			
ΔE=10 eV			
−60°C	189.5	184.6	182.0
22°C	189.5	184.6	182.1
ΔE=14.8 eV			
−60°C	127.8	124.7	122.9
22°C	127.8	124.7	123.1

a) Averaged using the four data.
b) Calculated using 570 cal/mol as ΔEg.

Table 2. The calculated values of P^2_{C-H} in the preferred isomers and those averaged over the isomers in *n*- pentane

Conformations	P^2_{C-H}		
	$CH_3(1)$	$CH_2(2)$	$CH_2(3)$
TT	0.240	0.232	0.232
TG	0.240	0.231	0.230
TG′	0.240	0.231	0.230
GT	0.240	0.242	0.231
G′T	0.240	0.242	0.231
GG	0.240	0.229	0.228
G′G′	0.240	0.229	0.228
Averaged			
(a)	0.240	0.234_0	0.230_8
(b)	0.240	0.234_1	0.231_0

a) Averaged using 570 cal/mol as ΔE at −60°C.
b) Averaged using 570 cal/mol as ΔE at 22°C.

Here, $P^2_{C-H_i}$ is the square of the carbon 2*s*-hydrogen 1*S* element of the bond-order matrix, X_i, the fraction of the *i*-th isomer: ΔE_i, the energy difference between the TT and the *i*-th isomer; *R*, the gas constant, and

22) N. Muller and D. T. Carr, *J. Phys. Chem.*, **67**, 112 (1963).
23) L. Pauling, "Nature of Chemical Bond," Cornell University Press (1960).

T, the absolute temperature. Then, from Eqs. (2) and (3), the spin-spin coupling constant ($J_{C-H_{Av}}$) averaged by the populations of the rotational isomers is expressed as follows:

$$J_{C-H_{Av}} = \sum_{i=1}^{7} X_i J_{C-H_i}$$

$$= \frac{7885}{\Delta E} \sum X_i P^2_{C-H_i}$$

$$= \frac{7885}{\Delta E} \cdot P^2_{C-H_{Av}} \text{ (Hz)} \quad (5)$$

where J_{C-H_i} is the spin-spin coupling constant of the i-th isomer. We have reported that the observed temperature dependence of the proton chemical shift of n-pentane can be better interpreted by 570 cal/mol as the energy difference (ΔEg) between the *trans* and *gauche* conformations.[24] Thus, 570 cal/mol was used as the ΔEg value of used in our calculations.[25]

The values of $J_{C-H_{Av}}$ calculated using 570 cal/mol as ΔEg are shown in Table 1. Since there is no definite value for the average excitation energy (ΔE) for n-pentane, we at first tried to use 10 eV for ΔE; this value was originally used by Pople[26] in the calculation of the C-13 chemical shift of ethane. The calculations were found to give much larger values than those observed. Then, as the observed values scarcely seem to depend upon the temperature, we determined ΔE using the method of least squares in such a way that the best agreement was between the calculated and observed values of J_{C-H} at -60 and 22°C; we found it to be 14.8 ± 0.06 eV. By substituting this value into Eq. (5), $J_{C-H_{Av}}$ is expresses as:

$$J_{C-H_{Av}} = 533 P^2_{C-H_{Av}} \quad (6)$$

The plots of the observed J_{C-H} value against $P^2_{C-H_{Av}}$ are shown in Fig. 2. It was found that the J_{C-H} values of $CH_3(1)$, $CH_2(2)$, and $CH_2(3)$ are well proportional to those of P^2_{C-H}, calculated using 14.8 eV as ΔE. The solid line is the theoretical one obtained from Eq. (6). The scattering of the observed values from the theoretical line is found to be very small.

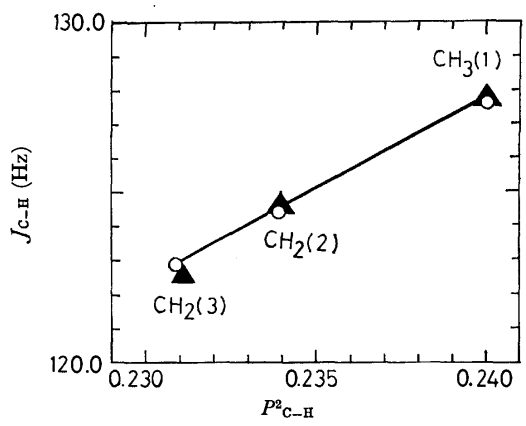

Fig. 2. The plots of the observed J_{C-H} against the $P_{C-H}{}^2$ in n-pentane. The solid line was calculated using Eq. (6). ○: observed at −60°C, ▲: observed at 22°C

As shown in Table 1, the temperature dependence of the values of J_{C-H} is not significant. Also, the calculated values of J_{C-H} depend scarcely at all upon the temperature, because the averaged values of P^2_{C-H} are not so sensitive to the temperature. However, this do not mean that it is not necessary to take the preferred conformations into account in the calculation of J_{C-H}. If the *trans* form is assumed to be the only conformation of n-pentane, the P^2_{C-H} values the $CH_2(2)$ and $CH_2(3)$ groups become equal to each other; therefore, the calculated and observed values of J_{C-H} do not agree with each other (the proportionality between J_{C-H} and P^2_{C-H} does not hold.). Thus, it is necessary to take the rotational isomers into account in order to obtain a better agreement with the observed and calculated results.

As has been described above, the same value, 14.8 eV, was used as ΔE for all the calculations of the J_{C-H} values of the methyl and methylene carbons in the preferred isomers; it was found to explain the experimental values reasonably well. However, there is a possibility that the ΔE values among the preferred isomer and among the carbons in a isomer differ from one another. Thus there remains some question about concluding 14.8 eV to be the ΔE of n-pentane. We will later treat with this problem in association with the carbon-13 chemical shifts of n-pentane.

24) I. Ando and A. Nishioka, Preprint of the 10th Symposium on NMR, 54 (1971), Tokyo.

25) These values were found to be insensitive to the values of ΔEg in the range from 500 to 600 cal/mol.

26) J. A. Pople, *Mol. Phys.*, **7**, 301 (1964).

Far-infrared Spectra of Zinc Halide Complexes with Acetonitrile

Tomoichi KAMO and Masao KIMURA

Department of Chemistry, Faculty of Science Hokkaido University, Sapporo

(Received February 28, 1972)

The infrared spectra of zinc halide complexes with acetonitrile, $ZnX_2 \cdot 2CH_3CN$ (X=Cl, Br, I), in the solid state were recorded in the region from 4000 to 96 cm^{-1}. The Zn–N stretching bands for the chloride and bromide were observed, at 210 and 212 cm^{-1} respectively, as composite bands of the A_1 and B_1 species. For the iodide, the Zn–N stretching band of the B_1 species was observed at 219 cm^{-1}, while the A_1 mode was coupled with the Zn–I stretching mode and was absorbed at 252 and 179 cm^{-1}. The N–Zn–N bending bands were observed at 163, 162, and 153 cm^{-1} and the Zn–N≡C bending bands, at 125, 128, and 132 cm^{-1}, for the chloride, bromide, and iodide respectively. The normal coordinate analysis was carried out by the use of the Urey-Bradley force field, and the Zn–N stretching force constant was obtained as 0.56 mdyn/Å. The force constant is much smaller than the corresponding ones in complexes containing nitrogen donors in the sp^3 and the sp^2 valency states.

It has been known that nitriles react with many metal halides to form σ-complexes by donating the lone-pair electron of the nitrogen atom.[1] The metal-nitrogen bonds in these complexes have generally been considered to be very weak, since the electron-donating ability of the nitrogen atoms in alkyl cyanides is weaker than that in amines or imines.[1] Many investigators have been interested in the strength of these coordinate bonds and have studied the infrared spectra of nitrile complexes with metal halides.[1,2] However, the number of studies in which metal-nitrogen stretching bands are observed is rather limited.

Infrared studies suggesting weak metal-nitrogen bonds have been published of the complexes of acetonitrile with $SnCl_4$,[1,3-5] $ZnCl_2$,[6] and NbX_5 and TaX_5 (X= Cl and Br).[7] In these studies, the metal-nitrogen stretching vibrations, ν_{MN}, have been assigned bands below 225 cm^{-1}.[8] Besides, the spectra of acetonitrile complexes with Pd(II), Pt(II), and Rh(II) halides have been reported to have no band above 200 cm^{-1} which can be assigned unambiguously to ν_{MN}.[9]

In contrast to the studies mentioned above, relatively high frequencies for ν_{MN}, 650—400 cm^{-1}, have been reported for such cyanide complexes as $M(CO)_3 \cdot 3CH_3CN$ (M=Cr, Mo, and W),[10] $BX_3 \cdot CH_3CN$ (X= Cl, Br, and F),[11,12] $AlCl_3ClCN$,[13] and cyanopyridine·$MClO_4$ (M=Cu(I), Ag(I), and Au(I)).[14] However, these high frequencies may be considered to reflect the M–N bonds strengthened by the high electron affinities of the metals characteristic of the IIIb-element halides and the metal carbonyls,[10,11] or by the increased electron-donating ability of the ligand nitrogen due to the contribution of an ionic resonance structure.[14]

Thus, ordinary metal halide-alkyl cyanide complexes appear to have very weak coordinate bonds and to give rise to M–N stretching bands around 200 cm^{-1}. Yet, our information on the coordination of this type cannot be said to be sufficient. Although the spectrum of $ZnCl_2 \cdot 2CH_3CN$ in a CH_3CN solution has already been studied,[6,15] the spectra associated with the skeletal modes have not been analysed completely. In addition, a band at 174 cm^{-1} assigned to the ν_{MN} by Evans and Lo[6] has not been observed in the Raman spectrum by Addison *et al.*[15] In order to get a clear vision of the M–N bonds in nitrile complexes, it was thought necessary to reexamine the far-infrared spectra of $ZnX_2 \cdot 2CH_3CN$.

Experimental

The complexes, $ZnX_2 \cdot 2CH_3CN$ (X=Cl, Br, and I), were prepared in the following manner. A saturated solution of 99% pure zinc halide in dry acetonitrile was prepared in a dry box filled with dry nitrogen gas. After the undissolved portions had then been filtered off, the solvent was evaporated moderately with an aspirator until white crystals appeared. The crystals were then collected and dried over P_2O_5 for two days. The complexes were considerably stable in dry air, but they were readily decomposed by atmospheric water vapour.

Found for the chloride: Cl, 31.79%. Calcd for $ZnCl_2 \cdot 2CH_3CN$: Cl, 32.47%. Found for the bromide: Br, 52.32%. Calcd for $ZnBr_2 \cdot 2CH_3CN$: Br, 52.01%. Found for the iodide: I, 63.16%. Calcd for $ZnI_2 \cdot 2CH_3CN$: I, 63.25%.

The infrared spectra ranging from 4000 to 400 cm^{-1} for liquid acetonitrile and the complexes were observed with KBr plates on a JASCO IR-G infrared spectrophotometer while the spectra in the low-frequency region from 500 to 96 cm^{-1} were observed with polyethylene plates on a Hitachi

1) R. A. Walton, *Quart. Rev.*, **19**, 126 (1965).
2) See, *e.g.*, K. Nakamoto, "Infrared Spectra of Inorganic and Coordination Compounds," John Wiley and Sons, Inc., New York (1963), p. 178.
3) T. L. Brown and M. Kubota, *J. Amer. Chem. Soc.*, **83**, 4175 (1961).
4) I. R. Beattie, G. P. McQuillan, L. Rule, and M. Webster, *J. Chem. Soc.*, **1963**, 1514.
5) M. Farona and J. G. Grasselli, *Inorg. Chem.*, **6**, 1675 (1967).
6) J. C. Evans and G. Y. S. Lo, *Spectrochim. Acta*, **21**, 1033 (1965).
7) G. A. Ozin and R. A. Walton, *J. Chem. Soc., A*, **1970**, 2236.
8) Complexes, such as $NbCl_5 \cdot NCR$ and $TaCl_5 \cdot NCR$ (R= Cl and CH_3), have been studied by J. Maccordick and G. Kaufman, *J. Mol. Struct.*, **6**, 305 (1970). They have assigned the bands near 350 cm^{-1} to the M–N stretching vibrations. Therefore, there still remains a question on these assignments.
9) R. A. Walton, *Spectrochim. Acta*, **21**, 1795 (1965); *Canad. J. Chem.*, **44**, 1480 (1966).
10) M. F. Farona, J. G. Grasselli, and B. L. Ross, *Spectrochim. Acta*, **23A**, 1875 (1967).
11) D. F. Schriver and B. Swanson, *Inorg. Chem.*, **10**, 1354 (1971).
12) B. Swanson and D. F. Shriver, *ibid.*, **9**, 1406 (1970).
13) K. Kawai and I. Kanesaka, *Spectrochim. Acta*, **25A**, 263 (1969).
14) F. Farha and R. T. Iwamoto, *Inorg. Chem.*, **4**, 844 (1965).
15) C. C. Addison, D. W. Amos, and D. Sutton, *J. Chem. Soc., A*, **1968**, 2285; as for free acetonitrile, see also references therein.

TABLE 1. OBSERVED FREQUENCIES FOR THE LIQUID AND COMPLEXED ACETONITRILES (in cm^{-1}) AND THEIR ASSIGNMENTS[a)]

CH_3CN	$ZnCl_2 \cdot 2CH_3CN$	$ZnBr_2 \cdot 2CH_3CN$	$ZnI_2 \cdot 2CH_3CN$	Assignment
	3240 vw	3252 vw	3251 vw	
		3218 vw	3200 vw	
3010 vs	2998 s	2995 s	2980 s	$a\nu$CH
2954 vs	2928 s	2925 s	2922 s	$s\nu$CH
2295 vs	2301 s	2316 s	2307 s	$s\delta CH_3+\nu CC$[b)]
2251 vs	2273 s	2285 s	2274 s	νCN
	2250 s	2251 s	2250 s	νCN[b)]
1440 vs, br	1442 s, br	1414 s, br	1414 s, br	$a\delta CH_3$
	1420 sh			
1375 vs	1376 s	1360 s, br	1356 s, br	$s\delta CH_3$
	1363 m			
1038 vs	1034 m, br	1024 s, br	1024 s, br	ρCH_3
	969 vw			
918 vs	924 m	943 s	940 s	νCC
	913 m			
	794 w	798 vw	786 vw	$2\cdot\delta$CCN
		773 vw	770 vw	$2\cdot\delta$CCN
	398 s	396 s	395 s	δCCN
365 s	389 s	386 s	385 s	δCCN
	380 s	379 s	378 s	δCCN

a) vs, very strong; s, strong; m, medium; w, weak; vw, very weak; ν, stretching; δ, bending; ρ, rocking.
b) Splitted bands due to Fermi resonance. See text.

TABLE 2. OBSERVED FREQUENCIES FOR $ZnX_2 \cdot 2CH_3CN$ IN THE REGION BELOW 350 cm^{-1} AND THEIR ASSIGNMENT

$ZnCl_2 \cdot 2CH_3CN$	$ZnBr_2 \cdot 2CH_3CN$	$ZnI_2 \cdot 2CH_3CN$	Assignment	
333			νZnCl	B_2
265			νZnCl	A_1
	261		νZnBr	A_1, B_2
		252	νZnI, νZnN	A_1
		219	νZnN	B_1
210	212		νZnN	A_1, B_1
		179	νZnN, νZnI	A_1
163	162	153	δNZnN	A_1
125	128	132	δZnNC	B_1, B_2

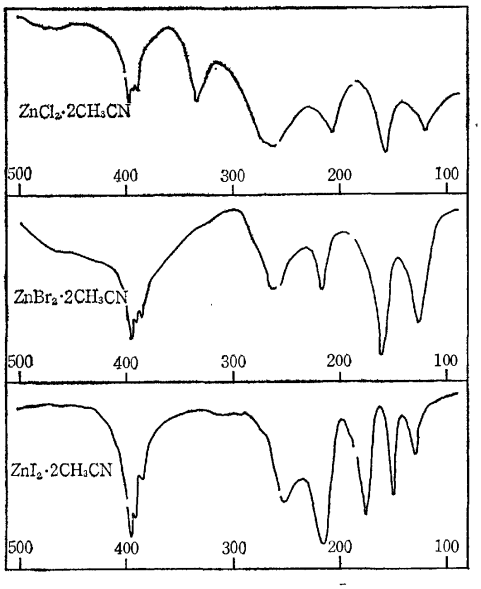

Fig. 1. Observed spectra of the complexes below 500 cm^{-1}.

FIS-21 far-infrared spectrophotometer. The mull method was empolyed for the solid samples. The observed frequencies associated with the ligand acetonitrile and the skeleton about the Zn atom are listed in Tables 1 and 2 respectively, while the spectra below 500 cm^{-1} are reproduced in Fig. 1.

Assignments

By considering the compositions of the samples and by referring to the structures of various zinc complexes previously determined,[16] it was assumed that these complexes have C_{2v} symmetry,[17] as other workers have done.[6,15] The infrared data for the complexes may be divided into intra-ligand and skeletal vibrational modes, which will be discussed separately.

Ligand Vibrations. The spectra of the complexed nitriles are very similar to one another and correspond very well with the spectra for uncomplexed acetonitrile except for the splittings of bands observed in the 2250, 1440, 1370, 920, and 380 cm^{-1} regions. If we consider that these splittings are caused by interaction between the two coordinated nitriles, the assignments of the observed bands to the intra-ligand vibrations can easily be made, as is shown in Table 1, by analogy with those for the free acetonitrile, which have been established

16) L. E. Sutton, "Tables of Interatomic Distances and Configuration in Molecules and Ions," the Chemical Society, London (1965).

17) According to the crystal structure analysis of $ZnCl_2 \cdot 2CH_3CN$ carried out by I. V. Isakov and Z. V. Zvonkova, *Doklady Akad. Nauk U. S. S. R.*, **145**, 801 (1962), this molecule has a distorted tetrahedral structure about the Zn atom with a symmetry very close to C_{2v}. The structure parameters calculated from the given atomic coordinates are as follows: $\angle$N≡C–CH_3 180°, $\angle$Zn–N≡C 111°, $\angle$ClZnCl 131°, $\angle$NZnN 101°, Zn–N 1.95 Å, Zn–Cl 2.18 Å, C–C 1.51 Å, and C≡N 1.12 Å.

by several workers.[15,18,19]

The similarities between the frequencies for the free and complexed acetonitriles suggest that these complexes are formed by a weak σ-bonding through the lone-pair electrons. The band splittings observed over the entire spectra of the complexes, especially the splitting of the C–C≡N bending vibration into three bands, are consistent with the presumed symmetry.

The C–C stretching, ν_{CC}, and the C–C≡N bending frequencies were observed higher by as much as 4—22 cm^{-1} and 23—33 cm^{-1} respectively than those observed for the free ligand. These high frequency shifts may be caused by the coupling of the ligand vibrations with the skeletal mode of the complexes. This interpretation is supported by the normal coordinate analysis, which will be described in a later section. The lowest frequency band in the region of the C≡N stretching vibration, ν_{CN}, for the complexes was observed as low as the C≡N stretching frequency for the free nitrile. Despite the fact that a high frequency shift of ν_{CN} is generally characteristic of coordination through the lone-pair electrons on the nitrogen atoms of nitriles,[1,20] we assigned the lowest frequency band to one of the two expected ν_{CN} bands and the highest frequency band at about 2300 cm^{-1} to a combination band. These assignments are different from the assignments made by Evans and Lo,[6] but they are in accordance with those made by Addison *et al.* except for the assignment of the 2250 cm^{-1} band.[15] This apparently unshifted absorption can be interpreted as being due to the Fermi resonance occurring between the ν_{CN} and the combination band of the symmetric CH_3 deformation, $s\delta_{CH_3}$, and ν_{CC}, as was suggested in the previous studies of the spectra for the free nitrile.[15,18,21] The combination band, *e.g.*, the $1375+918=2293$ cm^{-1} band for the chloride, is located at a higher frequency than the ν_{CN} for the free molecule. When the ν_{CN} is shifted towards a higher frequency upon coordination and approaches more closely to the combination band, the two bands may suffer the effect of the Fermi resonance more strongly. As a result, the combination band may be raised, and the stretching band may be lowered in frequency, more in the complexed state than in the free state.

In addition to the assignment of the ν_{CN} band, the present interpretation is also somewhat different with regard to the splitting bands from those reported by previous workers, who studied the Raman and infrared spectra of a zinc chloride solution in CH_3CN.[6,15] They attributed the observed splitting bands to the fundamental vibrations belonging to the complexed and the free nitrile. However, similar splittings, as observed even in the spectra of the crystalline sample, indicate that the splittings observed in the solution spectra can not simply be ascribed to the vibrations of the sample in different states.

Skeletal Vibrations of Complexes. For the sekleton, L_2ZnX_2, of these complexes, fifteen normal modes of vibration, $4A_1+4A_2+3B_1+4B_2$, can be expected, including the librational modes of the ligands, L. Here, the subscripts 1 and 2 are used with reference to the LZnL plane. Among them, the two normal modes corresponding to methyl torsions, A_2+B_2, will not be observed in infrared spectra. It follows that a total of ten fundamental bands are to be assigned. In view of the similarity in the ligand vibrations, it may be considered that these complexes are in similar electronic states, and that the force constants of the internal potentials have similar magnitudes for all the complexes. Accordingly, each of the vibrational modes associated with the nitrogen atoms can be expected to absorb at nearly the same frequency, independent of the particular halogen atoms, while the other modes involving the halogen atoms absorb at different frequencies from one complex to another. For the chloride and bromide, one can easily identify two groups of bands; the first is a group of the zinc-halogen stretching vibrations, which decrease in frequency as the halogen atoms change from Cl to Br, while the second group consists of three bands, at about 210, 160, and 130 cm^{-1}, which are unaltered in position by the substituents. The observed bands at 333 and 265 cm^{-1} for the chloride undoubtedly belong to the first group and were assigned to the antisymmetric and symmetric Zn–Cl stretching modes, $a\nu_{ZnCl}$ and $s\nu_{ZnCl}$, respectively. The corresponding band for the bromide is that observed at about 260 cm^{-1}, where the two modes seem to overlap. The bands belonging to the second group are related to the coordinated nitrogen atoms. The band at 210 cm^{-1} may be assigned to the Zn–N stretching modes, ν_{ZnN}, which belong to the A_1 and B_1 species. Of the two bands at about 160 and 130 cm^{-1}, the higher was assigned to the N–Zn–N bending mode, δ_{NZnN}, and the lower, to the Zn–N≡C bending mode, δ_{ZnNC}, since the latter mode corresponds to the librational mode of the ligand and is expected to absorb at a lower frequency. There exist three infrared active librational modes of the ligands. Of them, the two modes of the B_1 and B_2 species were considered to overlap at about 130 cm^{-1}, and the A_1 mode, to lie below the observed frequency limit. These assignments were ascertained by the normal coordinate treatment, which will be described later. The present assignment of ν_{ZnN} differs from that made by Evans and Lo. We found no band at 174 cm^{-1}, but observed a band at 163 cm^{-1} (see Fig. 1). This band was then assigned to the δ_{NZnN}, as has been mentioned above.

The identification of bands for the iodide is not so clear as that for the chloride and bromide. However, the spectra of the iodide may be explained as follows. Generally, bands related to the Zn–I stretching modes, ν_{ZnI}, in various zinc iodide complexes are known to be observed at about 220 cm^{-1},[22,23] a frequency nearly equal to those assigned to ν_{ZnN} for the chloride and

18) I. Nakagawa and T. Shimanouchi, *Spectrochim. Acta*, **18**, 514 (1962).

19) G. Graner, *C. R. Acad. Sci. Paris Ser., B*, **269**, 126 (1969).

20) K. F. Purcell and R. S. Drago, *J. Amer. Chem. Soc.*, **88**, 919 (1966).

21) K. Venkateswarhu and R. Thanalkshmir, *Indian J. Pure Appl. Phys.*, **1**, 64 (1963).

22) a) C. Postmus, J. R. Ferraro, and W. Wozniak, *Inorg. Chem.*, **6**, 2030 (1967); b) J. Bradbury, K. P. Forest, R. H. Nuttall, and D. W. Sharp, *Spectrochim. Acta*, **23A**, 2701 (1967).

23) G. B. Deacon, J. H. S. Green, and D. J. Harrison, *ibid.*, **24A**, 1921 (1968).

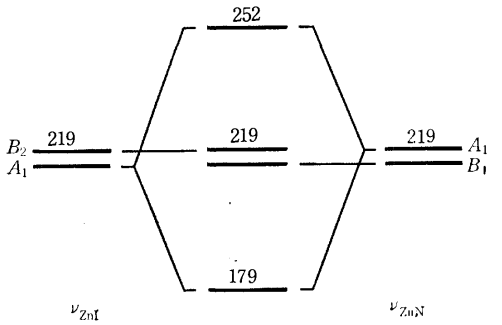

Fig. 2. Schematic illustration of the mode mixing in the 250—150 cm^{-1} region for $ZnI_2 \cdot 2CH_3CN$.

bromide. If this is the case for the present iodide, the ν_{ZnN} and ν_{ZnI} of the A_1 species would couple strongly with each other to result in a comparatively large splitting. Thus, we considered that the ν_{ZnN} and ν_{ZnI} of the A_1 species were split into bands at 252 and 179 cm^{-1}, while the B_1 and B_2 modes remained overlapped at 219 cm^{-1}, as is illustrated in Fig. 2. The band at 153 cm^{-1} for the iodide is slightly lower in position than the corresponding bands for the chloride and bromide, at 163 and 162 cm^{-1} respectively, which were assigned to δ_{NZnN}. This slight lowering in frequency for the iodide is probably due to a coupling of this bending mode with the ν_{ZnI} of the A_1 species. All the bands for $ZnI_2 \cdot 2CH_3CN$ can thus be interpreted successfully by assigning the bands near 210 cm^{-1} to the ν_{ZnN} of the chloride and bromide, and by considering the iodide to have a similar Zn-N coordinate bond. The assignments made for the skeletal modes are shown in Table 2.

Normal Coordinate Analysis

The normal coordinate analyses by the *G-F* matrix method were carried out in order to confirm these assignments and estimate the bond strength between the zinc atom and the ligand. The structure of $ZnCl_2 \cdot 2CH_3CN$ has been reported by Isakov and Zvonkova to have a distorted tetrahedral structure about the Zn atom, with a linear C-C≡N frame and specifically with a Zn-N≡C angle of 111°, a value considerably less than 180°.[17] The nonlinearity of a metal-N≡C system has been reported for the addition compounds of $CuCl_2$ and CH_3CN ($\angle CuNC = 160°$),[24] while the linearity of some metal-N≡C-C systems has been confirmed by X-ray structure analyses for nitrile complexes, such as $SnCl_5 \cdot CH_3CN$[25] and $BX_3 \cdot CH_3CN$.[26] It is probable that the metal-N≡C system is not linear in the crystalline state. However, whether or not such an angle as small as 111° is real in $ZnCl_2 \cdot 2CH_3CN$ will require further investigation. Since all the spectral evidence supports the idea that the C≡N triple bond, advantageous to forming a linear linkage, is virtually retained in the present complexes, in our calculations we did not adopt the results of the crystal structure analysis, but, rather, preferred the following assumed molecular geometry. The structure of a free nitrile as determined by microwave spectroscopy was employed for the ligands.[27] The Zn-N≡C angle was assumed to be 180°, as in previous normal coordinate analyses of nitrile complexes,[6,7,13] and the other valency angles about the Zn atom were assumed to be tetrahedral angles, 109.5°. The Zn-N distance was assumed to be 2.00 Å, and the Zn-X distances, to be 2.30, 2.38, and 2.48 Å for Cl, Br, and I respectively, referring to the literature on several zinc halide complexes.[16]

The complexes are expected to undergo thirty-nine normal modes of vibration, $13A_1+7A_2+11B_1+8B_2$, among which the two torsional vibrations of the methyl groups, A_2+B_2, were not treated because the torsional force constant could be considered to be nearly zero.

A force field of the modified Urey-Bradley type was used:

$$2V = \sum_{ij} K_{ij}(\Delta r_{ij})^2 + \sum_{ij} H_{ij} r_i^0 r_j^0 (\Delta\alpha_{ij})^2 + \sum_{ij} F_{ij}(\Delta q_{ij})^2 + \sum_{ij} F'_{ij} q_{ij}^0 (\Delta q_{ij}) + \kappa(\text{methyl}) + f(\Delta\alpha_{ZnNC} \cdot \Delta\alpha_{NCC})$$

where κ is the force constant for the internal tension of the valence angles of the methyl group and where f is the force constant for the interaction between the Zn-N≡C bending and the C-C≡N bending. The internal tension about the Zn atom was not introduced into the force field, since the bands corresponding to the skeletal deformation modes were not observed. The force constants for the ligand were determined so as to reproduce the observed frequencies for the liquid acetonitrile listed in Table 1, by starting with the force constants of the Urey-Bradley force field determined for free acetonitrile by Nakagawa and Shimanouchi.[18] The force constants thus obtained are shown in Table 3.[28] By transferring them to the complexes, the force constants related to the skeletal modes were then determined by a brute-force method. In the calculations, the force constants, H_{XZnX}, H_{NZnX}, F_{XX}, and F_{NX}, were assumed at plausible values. Since the three complexes have nearly identical coordinate bonds identical force constants associated with the nitrogen atom were chosen for the three complexes, and they were determined so as to reproduce best the observed frequencies belonging to the B_1 species rather than

Table 3. Force constants for liquid acetonitrile (in mdyn/Å)

K_{CC}	4.38	H_{CCH}	0.41	F_{CCH}	0.34
K_{CH}	4.66	H_{HCH}	0.29	F_{HCH}	0.27
K_{CN}	17.35	H_{CCN}	0.19	F_{CCN}	0.00
κ[a]	0.103				

a) κ in mdyn·Å units.

24) R. D. Willett and R. E. Rundle, *J. Chem. Phys.*, **40**, 838 (1964).
25) H. Binas, *Z, Anorg. Chem.*, **352**, 271 (1967).
26) B. Swanson, D. G. Schriver, and J. A. Ibers, *Inorg. Chem.*, **8**, 2183 (1969).
27) C. C. Costain, *J. Chem. Phys.*, **29**, 864 (1958).
28) The normal coordinate analyses using different approximations have also been carried out by other workers.[21,29] The force constants listed in Table 3 were recalculated using the frequencies for liquid acetonitrile observed by us and accordingly, slightly different from those obtained by Nakagawa and Shimanouchi.
29) J. L. Duncan, *Spectrochim. Acta*, **20**, 1197 (1964).

TABLE 4. FORCE CONSTANTS FOR $ZnX_2 \cdot 2CH_3CN$ (in mdyn/Å)[a]

K_{ZnN}		0.56	
H_{NZnN}		0.057	
H_{ZnNC}		0.065	
F_{NN}		0.084	
F_{ZnC}		0.000	
f[b]		0.037	
	X=Cl	X=Br	X=I
K_{ZnX}	1.10	1.10	0.89
H_{XZnX}	(0.075)	(0.035)	(0.035)
H_{NZnX}	(0.023)	(0.023)	(0.024)
F_{XX}	(0.075)	(0.075)	(0.075)
F_{NX}	(0.036)	(0.036)	(0.046)

a) Assumed values were parenthesized.
b) f in mdyn·Å units.

TABLE 5. OBSERVED AND CALCULATED FREQUENCIES FOR $ZnX_2 \cdot 2CH_3CN$ COMPLEXES (in cm^{-1})[a]

Symmetry species	X=Cl		X=Br		X=I	
	obsd	calcd	obsd	calcd	obsd	calcd
A_1	398	394	396	394	395	394
	265	291	247	247	252	230
	210	192	212	177	179	176
	163	174	162	165	153	153
	—	119	—	88	—	73
	—	37	—	37	—	36
B_1	380	383	379	383	378	383
	210	210	212	210	219	215
	125	126	128	125	132	125
	—	61	—	51	—	48
B_2	389	386	386	386	385	386
	333	307	261	256	219	219
	125	144	128	138	132	133
	—	43	—	37	—	34

those belonging to the other species, for the B_1 modes were considered to have no appreciable mode mixings with one another. Among the Zn-X force constants, the K_{ZnI} was determined by using mainly the observed frequencies belonging to the B_2 species in order to see clearly the influence of the mode mixing in the A_1 species. The resulting force constants of the skeleton are listed in Table 4. Table 5 compares the observed and calculated frequencies in the low-frequency region. The non-zero force constant, $f(\Delta\alpha_{ZnNC} \cdot \Delta\alpha_{NCC})$, had to be used in order to obtain calculated C-C≡N bending frequencies in agreement with the observed ones. By introducing this interaction term, the splitting into three bands and the high-frequency shift by about 30 cm^{-1} observed for the δ_{CCN} were accounted for satisfactorily. It must be noted that the calculated Zn-N≡C bending frequencies of the A_1 species were not brought into a frequency region higher than 70 cm^{-1} even if such a cross term was taken into consideration. The spectra in the Zn-I and Zn-N stretching frequency region were previously explained qualitatively in the section of the assignments. This now becomes clearer, as may be seen in Table 5; that is, Table 5 justifies the interpretation that the specific features in the spectra of the iodide are caused by the mode mixings, which were enhanced by the lowering of the Zn-X stretching frequency due mainly to an increase in the mass of the halogen atom. However, since the potential energy distribution for the bands at 252 and 179 cm^{-1} is changed delicately by a slight change in the force constants, the dominant contributor to each band can not be specified definitely. If the Zn-N≡C system is nonlinear, then some force constants necessarily change from the values listed in Table 4. However, it was assured by normal coordinate treatments for bent systems that the K_{ZnN} was substantially unchanged unless the Zn-N≡C angle was extremely small, such as below 150°.

It seems necessary here to comment on the high frequency shifts of the C≡N and C-C stretching frequencies upon coordination. The calculated frequencies for the ν_{CC} were 934 cm^{-1} for the A_1 species and 930 cm^{-1} for the B_2 species. This indicates that a fairly large high-frequency shift occurs in complexing without altering the K_{CC} value. In contrast, the high-frequency shift of the ν_{CN} cannot be explained without assuming an increase in the K_{CN} value, as has been pointed out previously.[1,20] If one wishes a better agreement with the observed frequencies, 2273, 2285, and 2274 cm^{-1} for the chloride, bromide, and iodide respectively, the K_{CN} values must be increased by 0.30, 0.42, and 0.30 mdyn/Å respectively.

Zn-N Force Constant

Table 6 shows the observed frequencies related to the Zn-N stretching mode for several complexes of zinc halides with ligands containing nitrogen as a donor atom. It can be seen in Table 6 that, while the bands for the amine complexes are located at 500—400 cm^{-1}, those for the imine and nitrile complexes lie in a much lower frequency region, 250—200 cm^{-1}. In order to show the strength of the coordinate bonds, Table 7 shows the K_{ZnN} values for $ZnX_2 \cdot 2NH_3$,[30,31] $ZnX_2 \cdot 2CH_3CN$ and $ZnX_2 \cdot 2$ (imidazole),[32] which represent the three types of coordination. The Zn-N force constants for all the complexes listed in Table 6 were not available, and we did not try complete normal coordinate analyses for all these complexes. However, the K_{ZnN}'s in pyridine and thiazole complexes, which have ring systems similar to imidazole, may be considered to have the same order of magnitude as that for the imidazole complexes. The relatively low frequency for the imidazole complex results from the mass effect of the imidazole ring. Thus, the K_{ZnN} values for the nitrile complexes can be said to be much smaller than those for the amine and imine complexes. Ozin

30) K. Krishnan and R. A. Plane, *Inorg. Chem.*, **5**, 852 (1966).
31) T. Kamo, H. Shibuya, and M. Kimura, unpublished work. The force constants for $ZnX_2 \cdot 2NH_3$ were derived by Krishnan and Plane by means of a five-body approximation.[30] The present authors also observed the spectra of $ZnCl_2 \cdot 2NH_3$, calculated the force constants by solving an eleven-body problem, and were led to the same result as that reported by Krishnan and Plane.
32) C. Perchard and A. Novak, *Spectrochim. Acta*, **26A**, 871 (1970).
33) J. A. Weaver, P. Hambright, P. T. Talbert, E. Kang, and A. N. Thorpe, *Inorg. Chem.*, **9**, 268 (1970).

TABLE 6. OBSERVED Zn-N STRETCHING FREQUENCIES OF SOME ZINC HALIDE COMPLEXES WITH *N*-DONORS (in cm^{-1})

	X=Cl	X=Br	X=I
$ZnX_2(NH_3)_2$[a]	432, 429	428, 421	412, 404
$ZnX_2(NH_2CH_2CH_2NH_2)$[b]	480, 468 405	—	—
$ZnX_2(Py)_2$[c]	218	219	222
$ZnX_2(ImH)_2$[a]	259, 244	266, 248	267, 240
$ZnX_2(4\text{-MeT})_2$[b]	239	240, 239	274
$ZnX_2(CH_3CN)_2$[e]	210	212	219

a) ImH: imidazole; Ref. 32.
b) Ref. 30.
c) Py: Pyridine; this molecule was studied by Postmus *et al.*, Ref. 22a, and by Bradbury *et al.*, Ref. 22b. The values listed in Table were quoted from the former atuhors' results.
d) 4-Methyl thiazol; Ref. 33.
e) Present work; for the iodide the frequencies assigned to the B_1 species was entered, see text.

and Walton have found that a value of 0.4 mdyn/Å is best for the metal-nitrogen stretching force constants of the 1:1 complexes of $NbCl_5$ and $TaCl_5$ with acetonitrile.[7] This value is of about the same order as that obtained by us. Pd(II) and Pt(II) halide-acetonitrile complexes must also have a similar force constant in view of their low stretching frequencies as suggested by Walton.[9] On the other hand, much larger force constants, 2.5—3.5 mdyn/Å for $BX_3 \cdot CH_3CN$ molecules and 2.0—3.0 mdyn/Å for $XCN \cdot AlCl_3$, have been reported by Shriver and Swanson[11] and by Kawai and Kanesaka[13] respectively. On surveying these data, it may be noted that the coordinate bonds of ordinary metal halide-alkyl cyanide complexes have force constants of 0.6—0.4 mdyn/Å, giving rise to absorption bands around 200 cm^{-1}, unless some other causes for strengthening the M-N bonds are present. It seems that the strength of the M-N coordinate bond is dependent largely on the valency state or the hybridized state of the nitrogen atom, but is independent of the substituents, and that the order is $sp^3 \geq sp^2 > sp$. Furthermore, the approximate force constants and stretching frequencies of Zn-N coordinate bonds may be predicted from the valency state of the nitrogen atom involved.

TABLE 7. STRETCHING FORCE CONSTANTS, K_{ZnN} FOR THE COMPLEXES WITH *N*-DONORS IN DIFFERENT VALENCY STATES (in mdyn/Å)

	X=Cl	X=Br	X=I
$ZnX_2 \cdot (NH_3)_2$[a]	1.42	1.38	1.28
$ZnX_2 \cdot (ImH)_2$[b]	1.21	1.21	1.21
$ZnX_2 \cdot (CH_3CN)_2$[c]	0.65	0.65	0.65

a) Refs. 30 and 31.
b) Ref. 32.
c) present work.

The authors wish to thank Associate Professor Takao Iijima and Dr. Shun-ichi Ikawa for their helpful advice and discussions. The numerical calculations were performed on a FACOM 230-60 of the Hokkaido University Computing Center and on a FACOM 270-20 in the laboratory of Professor Kimio Ohno, Department of Chemistry, Hokkaido University. The authors' thanks are also due to Professor Ohno.

BULLETIN OF THE CHEMICAL SOCIETY OF JAPAN, VOL. 45, 3314—3320 (1972)

Electrical Conduction in TCNQ Anion Radical Salts

Nobuko SAKAI, Ichimin SHIROTANI, and Shigeru MINOMURA

The Institute for Solid State Physics, The University of Tokyo, Roppongi, Minato-ku, Tokyo, 106

(Received March 7, 1972)

The temperature dependence of the electrical resistivity of single crystals of TCNQ anion radical salts with alkali metal, quinolinium, and triethylammonium cations has been investigated at temperatures between 300 and 540°K. It has been observed in these salts that the activation energy increases in the region of higher temperatures. In the cases of Na- and K(TCNQ) crystals, the reversal of the sign of the thermo-e.m.f. from the *p*-type to the *n*-type has been observed around the temperatures at which the activation energy increases. An interpretation of the experimental results is presented.

The salts based on the anion-radical of 7,7,8,8-tetracyanoquinodimethane (TCNQ) exhibit room-temperature electrical conductivities ranging from 10^2 to about $10^{-5}\ \Omega^{-1}\cdot cm^{-1}$.[1-3] The magnitude of the electrical conductivities depends strongly on the nature of the cation. For example, the salts with metal cations generally show low to intermediate conductivities (10^{-5}—$10^{-2}\ \Omega^{-1}\cdot cm^{-1}$), while the salts with cations of planar aromatic heterocyclic molecules show high conductivities ($\sim 10^2\ \Omega^{-1}\cdot cm^{-1}$). It has been reported that several TCNQ salts with aromatic cations show metallic behavior of temperature-independent conductivities as high as $10^2\ \Omega^{-1}\cdot cm^{-1}$ and temperature-independent paramagnetic susceptibilities which can

1) L. R. Melby, R. J. Harder, W. R. Hertler, W. Mahler, R. E. Benson, and W. E. Mochel, *J. Amer. Chem. Soc.*, **84**, 3374 (1962).

2) J. Siemons, P. E. Bierstedt, and R. G. Kepler, *J. Chem. Phys.*, **39**, 3523 (1963).

3) L. R. Melby, *Can. J. Chem.*, **43**, 1448 (1965).

be interpreted by assuming that the charge carriers are degenerate, as in a metal.[2,4] Recently, it has been found, contrary to the results of Kepler, that the highly conductive salts behave as typical semiconductors; that is, they have an electrical conductivity and a magnetic susceptibility which depend slightly on the temperature, and also absorption edge at about 40 cm^{-1}.[5] The electrical conduction mechanism of these $TCNQ^-$ anion radical salts has subsequently been discussed by several authors.[5-12] On the other hand, only a few studies have been made in connection with the electrical conduction in less conductive simple salts with metal cations.[13,14] The mechanism of electrical conduction in the $TCNQ^-$ anion radical salts seems to be yet unclear in spite of many investigations.

It has been suggested in another paper[15] that the electrical conduction near room temperature in alkali metal cation-TCNQ anion radical simple salts may be due to such extrinsic properties as impurities or defects. This suggestion is based on the scattered values of the activation energy and the pressure coefficient of resistivity from crystal to crystal. In this paper, electrical measurements in the high-temperature region will be reported in more detail.

Experimental

Crystals of alkali metal cation-TCNQ anion radical salts were prepared by the method described in Ref. 15. Crystals of quinolinium$(TCNQ)_2$[Q$(TCNQ)_2$] and triethylammonium$(TCNQ)_2$[TEA$(TCNQ)_2$] which had been synthesized according to the method developed by the du Pont group[1] were provided by Kondow.

The electrical measurement was made along the needle axis in most crystals by the potential-drop method, with two electrode probes in about 10^{-2} Torr. Electrical contacts to the crystal were made with du Pont #4817 silver paste.

A qualitative analysis of the Seebeck effect was carried out in the following manner. Some temperature difference was created during a short time between two junction to the needle crystal, one end of which was fixed vertically on the alumina base connected to a heater. The thermo-e.m.f. appeared transiently in the absence of an applied voltage between the two junctions, the sign of the cold junction being the sign of the Seebeck coefficient.

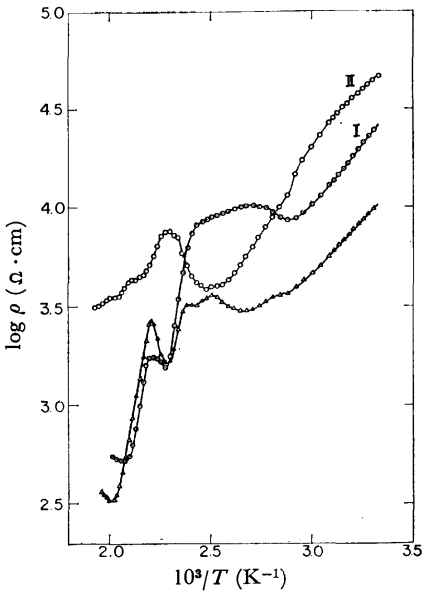

Fig. 1. Electrical resistivity as a function of reciprocal temperature of two Na(TCNQ) crystals. Two thermal cycles for one crystal are shown as Roman numerals I and II.

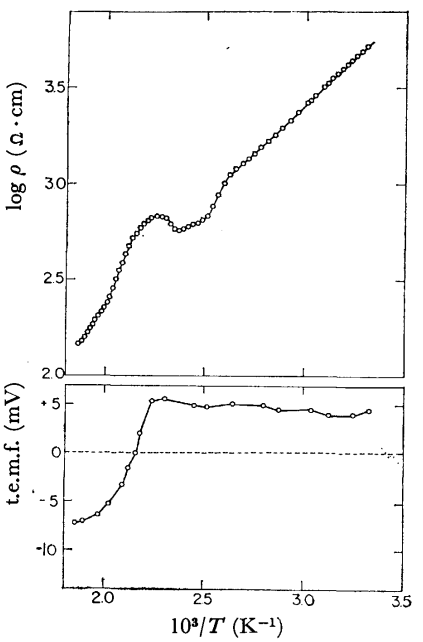

Fig. 2. Electrical resistivity and thermo-e.m.f. as a function of reciprocal temperature of Na(TCNQ).

Results

Figure 1 shows the electrical resistivity as a function of the reciprocal temperature of two Na (TCNQ) crystals. Two thermal cycles for one crystals are shown by the Roman numerals I and II. Figure 2 shows the electrical resistivity and the thermo-e.m.f. as a function of the reciprocal temperature of the Na (TCNQ) crystal measured at the same time. Only the sign of thermo-e.m.f. can be significant because of the qualitative measurement. The positive thermo-e.m.f. corre-

4) R. G. Kepler, *J. Chem. Phys.*, **39**, 3528 (1963).
5) T. Kondow, K. Siratori, and H. Inokuchi, *J. Phys. Soc. Japan*, **23**, 98 (1967).
6) K. Siratori and T. Kondow, *ibid.*, **27**, 301 (1969).
7) I. F. Shchegolev, L. I. Buravov, A. V. Zvarykina, and R. B. Lyubovskii, *ZhETF Pis. Red.*, **8**, 353 (1968) [*JETP Lett.*, **8**, 218 (1968)].
8) L. I. Buravov, D. N. Fedutin, and I. F. Shchegolev, *Zh. Eksp. Teor. Fiz.*, **59**, 1125 (1970) [*Sov. Phys. JETP*, **32**, 612 (1971)].
9) E. Menefee and Y. H. Pao, *J. Chem. Phys.*, **36**, 3472 (1962).
10) O. H. LeBlanc, Jr., *ibid.*, **42**, 4307 (1965).
11) I. Shirotani, T. Kajiwara, H. Inokuchi, and S. Akimoto, This Bulletin, **42**, 366 (1969).
12) J. P. Farges, A. Brau, D. Vasilescu, P. Dupuis, and J. Néel, *Phys. Stat. Sol.*, **37**, 745 (1970).
13) R. M. Vlasova, T. I. Grishaeva, L. D. Rozenshtein, A. I. Sherle, and A. A. Berlin, *Izv. Akad. Nauk SSSR, Ser. Khim.*, No. 3, 659 (1968).
14) R. M. Vlasova, A. I. Gutman, V. V. Kuzina, and A. I. Sherle, *Fiz. Tverd. Tela*, **12**, 3654 (1970) [*Sov. Phys. Solid State*, **12**, 2979 (1971)].
15) N. Sakai, I. Shirotani, and S. Minomura, This Bulletin **45**, 3321 (1972).

sponds to the positive carrier, *p*-type. The behavior of these curves is very complicated. The minimum and the maximum points in the resistivity and an increase in the activation energy were observed in the high-temperature region, above 400°K. The electrical resistivity, ρ, and the activation energy, *E*, obtained from the expression: $\rho=\rho_0\exp(E/kT)$ varied from crystal to crystal. The activation energy of Na (TCNQ) is between 0.23 and 0.32 eV near room temperature and between 0.6 and 1.1 eV in the high-temperature region. The sign of the thermo-e.m.f. is reversed from the *p*-type to the *n*-type above the temperature around which the activation energy increases.

Figures 3 and 4 show similar data for several specimens of K(TCNQ) crystal. The minimum and the maximum points in the resistivity, an increase in the activation energy, and the reversal of the sign of the thermo-e.m.f. from the *p*-type to the *n*-type were observed in the higher-temperature region, passing

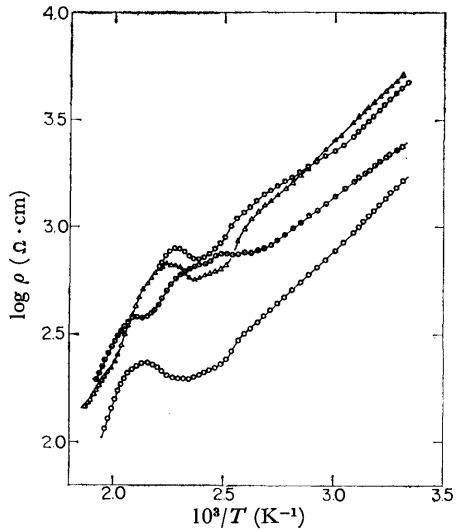

Fig. 3. Electrical resistivity as a function of reciprocal temperature of several K(TCNQ) crystals.

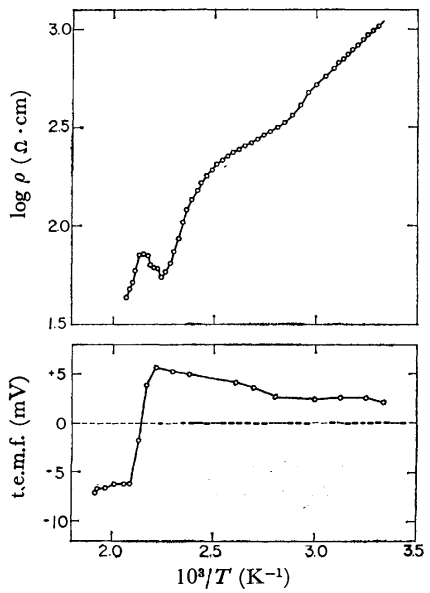

Fig. 4. Electrical resistivity and thermo-e.m.f. as a function of reciprocal temperature of K(TCNQ).

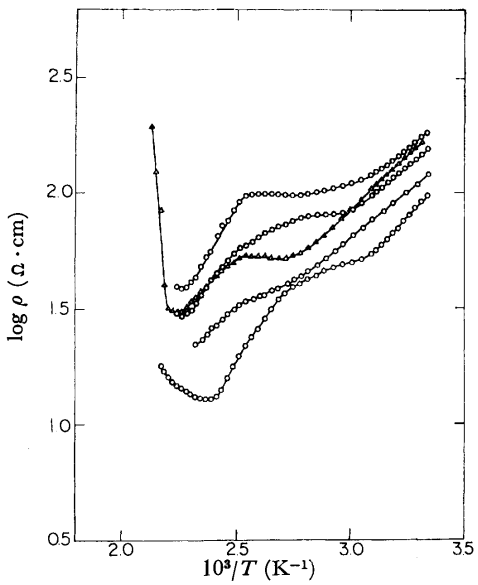

Fig. 5. Electrical resistivity as a function of reciprocal temperature of several dark purple Rb(TCNQ) crystals.

through the phase-transition point similarly to the case of Na(TCNQ). The activation energy of K-(TCNQ) is between 0.15 and 0.45 eV in the lower-temperature region and between 0.4 and 0.6 eV in the high-temperature region. The temperature at which the sign of the thermo-e.m.f. was reversed fell remarkably upon the second thermal cycling in the measurement of the same specimen.

Figure 5 shows the temperature dependence of the resistivity in several specimens of dark purple Rb-(TCNQ) crystals. The activation energy was observed to depend on the temperature, and to increase in the higher-temperature region, similarly to the cases of Na(TCNQ) and K(TCNQ). However, the reversal of the sign of the thermo-e.m.f. was not observed. The sign is positive, *p*-type, over all the temperature range measured. The activation energy of dark purple Rb-(TCNQ) is between 0.16 and 0.22 eV near room temperature and between 0.22 and 0.4 eV in the high-temperature region. The abrupt increase in the resistivity at high temperatures is due to the decomposition of this salt. On the other hand, the dark purple Rb(TCNQ) crystal in the form of a prism obtained from the same batch reveals a temperature dependence of the resistivity different from the above-exhibited results on that in the form of needle, as is shown in Fig. 6. The relation of log ρ *versus* the reciprocal temperature is not linear over the temperature range measured, and it is monotonous, without any discontinuity in activation energy, at high temperatures. The resistivity and the activation energy at room temperature of dark purple Rb(TCNQ) prisms ($\rho_{25}\sim10^4$ Ω·cm and $E\sim0.34$ eV) are larger than those of needles ($\rho_{25}\sim10^2$ Ω·cm and $E\sim0.16$ eV). It has not yet been investigated whether or not the two kinds of dark purple Rb(TCNQ) have an identical crystal structure.

Polymorphism has been shown in Rb(TCNQ) crystals.[16] The reddish-purple Rb(TCNQ) crystal with a crystal structure different from that of the dark purple Rb(TCNQ) crystal shows a larger resistivity

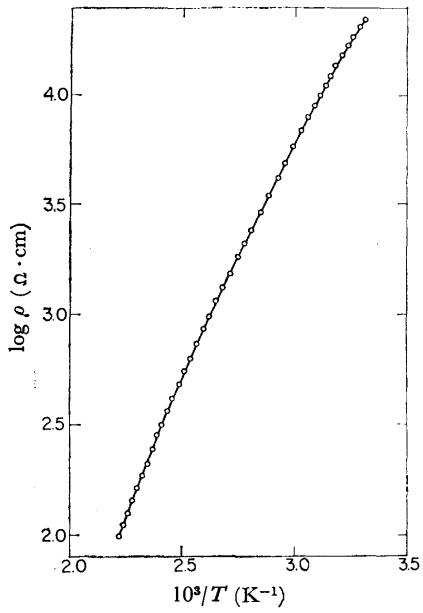

Fig. 6. Temperature depencence of the resistivity for dark purple Rb(TCNQ) with the form of prism.

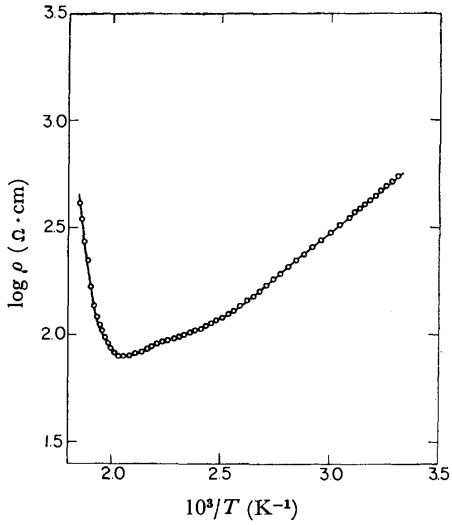

Fig. 7. Temperature dependence of the resistivity for Cs-(TCNQ) crystal.

and activation energy than those of the dark purple Rb(TCNQ) crystal ($\rho_{25}\sim10^5\,\Omega\cdot$cm and $E\sim0.51$ eV). Since most of the reddish-purple Rb(TCNQ) crystals broke down at the phase transition point of 374°K, accurate measurements could not be made in the higher-temperature region. The thermo-e.m.f. shows a positive sign below the phase-transition temperature.

Figure 7 shows the temperature dependence of the resistivity of the Cs(TCNQ) crystal. The outside appearance of this salt resembles that of the dark purple needles Rb(TCNQ). The resistivity changes almost monotonously with the temperature. The abrupt increase in the resistivity at high temperature is due to the decomposition of the compound. The resistivity at room temperature is about $6\times10^2\,\Omega\cdot$cm. The activation energy is about 0.16 eV in the region from room temperature to about 400°K. The sign of

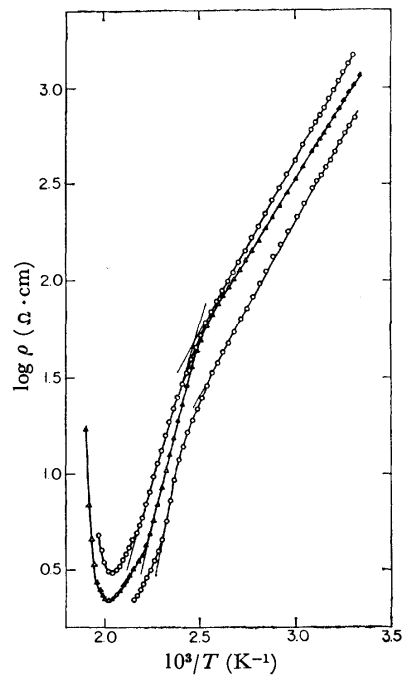

Fig. 8. Electrical resistivity as a function of reciprocal temperature of three $Cs_2(TCNQ)_3$ crystals.

the thermo-e.m.f. is positive over the temperature range measured.

Moreover, the temperature dependence of the resistivity of some salts of the $M^+(TCNQ)_n^-$ type with a value of n higher than one was measured in order to investigate the electrical conduction mechanism in connection with the case of alkali metal cation-TCNQ anion simple salts. Figure 8 shows the resistivity as a function of the reciprocal temperature of three specimens of $Cs_2(TCNQ)_3$ crystals. The discontinuity in the activation energy was observed in the high-temperature region. In one specimen the discontinuity in the activation energy occurred at about 397°K, below and above which the activation energies were 0.32 and 0.78 eV respectively. The sign of the thermo-e.m.f. is negative over the temperature range measured. The abrupt increase in the resistivity at high-tempera-

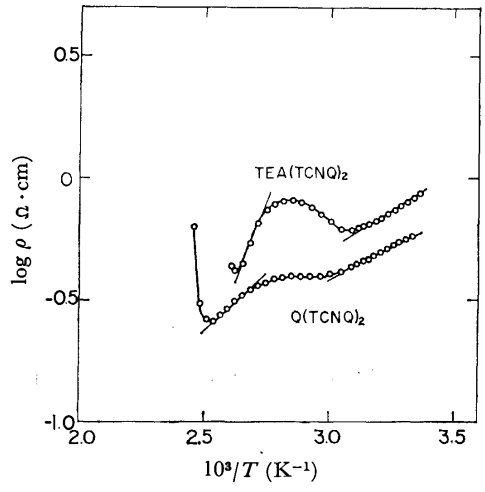

Fig. 9. Electrical resistivity as a function of reciprocal temperature of $Q(TCNQ)_2$ and $TEA(TCNQ)_2$ crystals.

Table 1. Semiconductivity data of several TCNQ anion radical salts

Compound	Present work			Previous work (Ref. 2)	
	Resistivity at 25°C ($\Omega\cdot$cm)	Low temp. activation energy (eV)	High temp. activation energy (eV)	Resistivity at 23°C ($\Omega\cdot$cm)	Activation energy (eV)
Na(TCNQ)	$\sim 1\times 10^{3}$ (//) $\sim 3\times 10^{4}$ ($\perp$)	0.23—0.32	0.6—1.1	1×10^{5} (powder)	0.33
K(TCNQ)	$\sim 5\times 10^{3}$ (//) $\sim 2\times 10^{5}$ ($\perp$)	0.15—0.45	0.4—0.6	1×10^{4} (powder)	0.35
Rb(TCNQ)					
reddish purple	$\sim 3\times 10^{5}$ (//) $\sim 3\times 10^{6}$ ($\perp$)	0.44—0.53			
dark purple	$\sim 1\times 10^{2}$ (//)	0.16—0.22	0.22—0.4		
Cs(TCNQ)	$\sim 6\times 10^{2}$ (//)	$\sim$0.16		3×10^{3} (powder)	0.18
$Cs_2(TCNQ)_3$	$\sim 5\times 10_2$ (//)	0.32—0.35	0.68—0.78	1×10^{3} (//) 2.5×10^{4} 2.5×10^{4}	0.30
TEA $(TCNQ)_2$	1 (//)	0.13	0.56	2.5×10^{-1} (//) 2.5×10 1×10^{3}	0.14
$Q(TCNQ)_2$	1×10^{-1} ($\perp$)	0.10	0.18	1×10^{-2} (//)	0.03

(//): parallel to needle. ($\perp$): perpendicular to needle.

tures is due to the decomposition of the compound.

Figure 9 shows the resistivity as a function of the reciprocal temperature of the $Q(TCNQ)_2$ and TEA-$(TCNQ)_2$ crystals. It was measured perpendicularly to the needle in the single crystal of $Q(TCNQ)_2$. An anomaly in resistivity was also observed in these complex salts. The activation energy near room temperature is about 0.10 eV, and the activation energy in the narrow temperature region from about 370°K to the decomposition temperature of about 395°K is about 0.18 eV, in the case of the $Q(TCNQ)_2$ crystal. The room-temperature resistivity and the activation energy measured here are larger than those generally reported.[1,2,8,25] It should be noted that the temperature dependence of the conductivity is markedly different from those in the direction of the needle reported in Ref. 8 and 25. The room-temperature resistivity and the activation energy of the TEA$(TCNQ)_2$ crystal along the needle axis are about 1.0 $\Omega\cdot$cm and about 0.13 eV respectively. Also in this crystal, the narrow temperature region where the resistivity decreased with an increase in the temperature with the activation energy of about 0.56 eV was observed before the decomposition occured. No qualitative measurement of the thermo-e.m.f. was carried out. At present, the electrical measurement are not sufficient.

The semiconductivity data of several TCNQ anion radical salts are summarized in Table 1, along with data generally reported.

Discussion

The experimental results described above, particularly the observation of the changes in the sign of the thermo-e.m.f. as a function of the temperature and in the activation energy on Na(TCNQ) and K(TCNQ) crystals, suggest that two carrier effects play important roles in the electrical-conduction process in the crystals of the alkali metal cation-TCNQ anion radical simple salts treated in this work. Alkali metal cation-TCNQ anion radical simple salts are considered to be extrinsic semiconductors in the low-temperature region. This has been expected from the scattered values of the activation energy near room temperature and those of the pressure coefficient of resistivity from crystal to crystal.[15] It was observed that some crystals of K(TCNQ) revealed a resistance increasing with an increase in the pressure, while some revealed the reverse. It has also been reported that the pressure coefficients of the ionization energies of impurities in silicon and germanium vary considerably with the kind of impurity.[17] The simplest scheme of energy levels in the *p*-type extrinsic semiconductors contains an acceptor level. Oxygen may act as an acceptor impurity in alkali metal cation-TCNQ simple salts.

The ionic conduction, on the other hand, may be expected to contribute to the electrical conductivity in these salts. That is, alkali cations may be supposed to move in crystals of these TCNQ salts through lattice defects, such as Frenkel or Schottky defects, and vacancies created by the impurity of divalent metal cations substituted for monovalent alkali metal cations, which are well-known in ionic crystals.[18] The ionic conductivity is known to decrease with an increase in the pressure.[19]

The observed conductivities in alkali metal cation-TCNQ anion radical simple salts were off Ohm's law from the low-electric field; for example, they were off about 40 volts/cm in the K(TCNQ) crystal, and at

16) I. Shirotani, H. Kobayashi, N. Sakai, and Y. Saito, to be published.

17) W. Paul and D. M. Warschauer, "Solids under Pressure," McGraw-Hill, New York (1963), p. 220.

18) N. F. Mott and R. W. Gurney, "Electronic Processes in Ionic Crystals," 2nd ed. Oxford Univ. Press., Oxford (1948).

19) S. W. Kurnick, *J. Chem. Phys.*, **20**, 218 (1952).

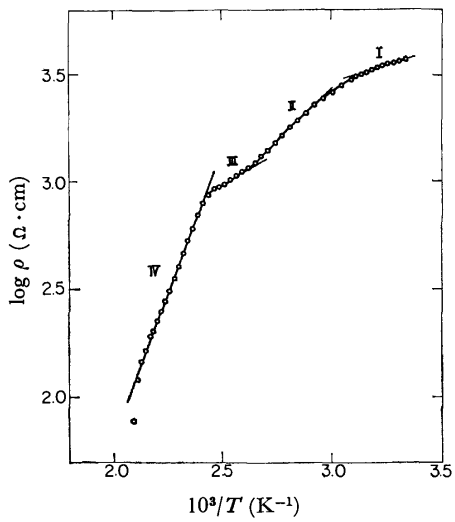

Fig. 10. Temperature dependence of the resistivity for K(TCNQ) crystal containing Ba^{2+} ions of about 0.5 atom%.

higher fields the current increased more than linearly. The negative pressure coefficient of the conductivity, $d\sigma/dP<0$, was observed in some specimens of the K(TCNQ) crystal.[15] These experimental observations seem to show that the contribution of the ionic conduction to the electrical conduction is not negligible. The temperature dependence of the resistvity was measured on the crystal of K(TCNQ) containing Ba^{2+} ions. Since the ionic radius of the Ba^{2+} ion (1.36 Å) is almost equivalent to that of the K^+ ion (1.33 Å), it is expected that the vacancies of the K^+ ion are added in crystal by the substitution of Ba^{2+} ions for the lattice points of K^+ ions. The samples were prepared by the use of a mixture of KI and BaI_2 as the cation source. The electrical resistivity as a function of the reciprocal temperature for the K(TCNQ) crystal containing Ba^{2+} ions of about 0.5 atom% is shown in Fig. 10. As is shown in this crystal, the curves of log ρ *versus* $1/T$ for K(TCNQ) crystals containing Ba^{2+} ions seem to consist of four parts, each with a different activation energy. The activation energy near room temperature, which was about 0.08 eV in the case of the sample shown in Fig. 10, was observed to be dependent on the concentration of Ba^{2+} ions; that is, it decreases with an increase in the concentration of Ba^{2+} ions. The ionic conduction may play some part in the electrical conduction in the narrow temperature region near room temperature in the K(TCNQ) crystal. Though the minimum and the maximum points in the resistivity were not observed in crystals of K(TCNQ) containing Ba^{2+} ions, an increase in the activation energy and a change in the sign of the thermo-e.m.f. were observed in the high-temperature region. The high-temperature region, where the activation energy is larger than in the lower temperature region and where the sings of the carriers are negative, seems to be the intrinsic region of the electrical conduction.

It is reasonable that, in the case of $TCNQ^-$ anion radical salts, the electrical conductivity in the intrinsic region arises from the motion of the odd π electrons among the TCNQ sites. LeBlanc[10] has proposed a model in which the odd electrons are localized and occupy highly-ordered positions so as to minimize their mutual Coulomb repulsions in non-conducting states and conducting states arise from the introduction of defects into the ordered ground-state configuration. According to this model, for the smiple salt an odd electron is removed from one $TCNQ^-$, leaving a $TCNQ^0$, and added to a distant $TCNQ^-$ to give a $TCNQ^{2-}$. The "electron" ($TCNQ^{2-}$) and "hole" ($TCNQ^0$), which are independently mobile, can occupy states in a band with the width Δ. The activation energy for conductivity, E, is given as:

$$2E = C - \Delta$$

where C is an increase in the electrostatic energy by the formation of $TCNQ^0$ and $TCNQ^{2-}$.

The above mechanism may also be applied to the dark purple Rb(TCNQ) crystal, where the $TCNQ^-$ anions pack in a columnar manner with an equivalent interplanar spacing of 3.28 Å at room temperature.[16] In this salt, the absorption band at 6.5 kK, as is shown in Fig. 11, can be assigned to the charge-transfer band between the $TCNQ^-$ anions, which is located in a lower energy region than that of reddish-purple Rb(TCNQ) at 8.6 kK. In the case of the dark purple Rb(TCNQ), the charge-transfer band can be expected to participate in the intrinsic electrical conduction with, for example, the charge-transfer excited state being the conducting state.

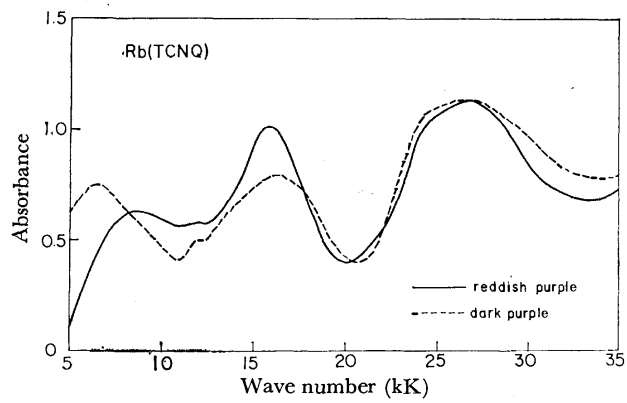

Fig. 11. Electronic absorption spectra of reddish and dark purple Rb(TCNQ).

On the other hand, it has been reported that the TCNQ units in reddish-purple Rb(TCNQ) are stacked in a columnar manner, with alternate interplanar spacings of 3.159 and 3.484 Å at −160°C.[20] It is certain that there is a bimolecular association of TCNQ anion radicals in the column. Although the crystal structures of Na(TCNQ) and K(TCNQ) have not been reported in detail, these salts seem to have a crystal structure similar to that of reddish-purple Rb(TCNQ). It may be considered that the crystalline state of these alkali metal cation-TCNQ anion radical salts is made out of "quasi-molecules" of $(TCNQ)_2^{2-}$, and that the charge-transfer band (Na(TCNQ): 8.6 kK, K(TCNQ): 8.3 kK) is characteristic

20) A. Hoekstra, T. Spoelder, and A. Vos, *Acta Crystallogr.*, *B*, **28**, 14 (1972).

of the intra-quasi-molecular excitation process, in which the electrons are localized in the quasi-molecules. If this is plausible, charge carriers in the intrinsic electrical conduction seem to be produced by the following reaction, in which the electronic state represented is separated by a great distance in the crystal:

$$(TCNQ)_2^{2-} + (TCNQ)_2^{2-} \rightleftharpoons (TCNQ)_2^{-} + (TCNQ)_2^{3-}.$$

The energy for the charge transfer in the above reaction would be larger than the energy of charge-transfer band around 8 kK.

It has been reported that the TCNQ molecules are arranged with repeating units of three molecules and four molecules in $Cs_2(TCNQ)_3$ and $TEA(TCNQ)_2$ respectively, and that an odd π electron is localized at the definite TCNQ molecular site.[21,22] It is expected for $Cs_2(TCNQ)_3$ that the charge transfer will occur between the adjacent pair of $TCNQ^0$ and $TCNQ^-$ and between the adjacent $TCNQ^-$ ions. The absorption bands around 11.7 kK (1.4 eV) and <5 kK (0.6 eV) may be assigned to the charge-transfer band between $TCNQ^-$ ions and to that between $TCNQ^0$ and $TCNQ^-$.[23,24] The activation energy for the electrical conduction of about 0.3 eV below 400°K and that of about 0.7 eV above 400°K seem to be related to the charge-transfer band between $TCNQ^-$ ions and that between $TCNQ^0$ and $TCNQ^-$ respectively. This inference would mean that the discontinuity of activation energy in $Cs_2(TCNQ)_3$ is due to the existence of different conducting states rather than to the existence of an extrinsic electrical conduction arising from impurities or defects. An analogous mechanism may be considered also for other complex TCNQ salts. However, at the present time, the experimental data are not sufficient for us to examine the explanation presented here.

Recently, Farges *et al.* have reported a successful measurement of the Hall effect in single crystals of $TEA(TCNQ)_2$ at room temperature.[12] From the experimental results of the positive Hall constant and Seebeck coefficient along the *a*-axis, and of the negative Seebeck coefficient along the *c*-axis of highest conductivity, it has been reported that two-carrier effects play a role in the conduction process in $TEA(TCNQ)_2$. Furthermore, the small activation energy of 0.065 eV calculated from the expression $\rho = \rho_0 \exp(E/kT)$ has been reported in the case of samples with evaporated silver contacts. This value of the activation energy is much smaller than the generally-reported values and the value obtained in the present work. Farges *et al.* have also described the introduction of impurities which act as acceptros in their samples.

In the present work, the increase in the activation energy was observed in the higher temperature region for single crystals of $TEA(TCNQ)_2$ and $Q(TCNQ)_2$. This also suggests that the high electrical conductivity of these salts is due to the impurity conduction.

Further work is required to make clear the electrical properties in TCNQ anion radical salts. The anisotropy in electrical conductivity and the effect of the pressure on the conductivity in the single crystal of $Q(TCNQ)_2$ will then be investigated in turn.

The authors would like to thank Dr. Tamotsu Kondow for supplying the samples.

21) C. J. Fritchie, Jr. and P. Arthur, Jr., *Acta Crystallogr.*, **21**, 139 (1966).
22) H. Kobayashi, Y. Ohashi, F. Marumo, and Y. Saito, *ibid.*, *B*, **26**, 459 (1970).
23) Y. Iida, This Bulletin, **42**, 637 (1969).
24) S. Hiroma, H. Kuroda, and H. Akamatu, *ibid.*, **44**, 9 (1971).
25) V. Walatka, Jr. and J. H. Perlstein, *Molecular Crystals and Liquid Crystals*, **15**, 269 (1971).

Phase Transition of Alkali Metal Cation-TCNQ Anion Radical Simple Salts

Nobuko SAKAI, Ichimin SHIROTANI, and Shigeru MINOMURA

The Institute for Solid State Physics, The University of Tokyo, Roppongi, Minato-ku, Tokyo, 106

(Received March 7, 1972)

The phase transition at 1 bar has been observed in alkali metal cation-TCNQ anion radical simple salts by means of measurements of the electrical resistivity of their single crystals. The temperature dependence of the resistivity under high hydrostatic pressures has been studied in order to investigate the effect of the pressure on this phase transition. The nature of this phase transition has been discussed. The pressure-induced new phase has also been found in these TCNQ salts at room temperature; thus, more than three phases (α, β, $\gamma\cdots$) are considered to exist in the solid phase of these TCNQ salts.

It has been shown, from the measurement of the volume change under high pressures by Bridgman, that several molecular organic solids exhibit pressure-induced phase transitions.[1] He has described that it appears that polymorphism is an even more common phenomenon among organic than among inorganic compounds in the temperature range of solid CO_2 temperatures up to 200°C and up to about 50 kbar; this can be expected, because it has appeared that the chance that a substance will exhibit polymorphism is roughly greater the lower the melting point, and, in general, the melting points of organic substances are lower than those of inorganics. The molecular interactions in the crystals of organic substances which he had studied are principally van der Waals interactions.

Ion radical salts, which have attracted interest because of their peculiar electrical and magnetic properties, and which have been studied extensively,[2,3] contain complicated molecular interactions, such as the Coulomb forces, the van der Waals forces and the charge-transfer forces. These molecular interactions have different effects on the inter-molecular distances, so that pressure-induced phase transitions, whose mechanism would be different from that in the organic neutral molecular crystals, may be expected to occur in the ion radical salts.

Recently, McConnell and his co-workers[4] have determined the pressure-induced phase transitions in triphenylmethylarsonium$(TCNQ)_2$ (TCNQ: 7,7,8,8-tetracyanoquinodimethane) from the pressure dependence of the exciton magnetic resonance. They have explained the observed P-T phase diagram in terms of a simple theory of non-interacting triplet excitons, contrary to Chesnut's theory,[5] where the phase transition is attributed to attractive exciton-exciton interactions.

In this paper we will report on the effect of pressure on the phase transitions of the crystalline $M^+(TCNQ)^-$ salts (M^+=alkali metal cation) occurring at 1 bar, which have been found by Vegter *et al.*,[6] and the new pressure-induced phase transitions found in these crystals from the pressure dependence of the electrical resistivity at room temperature.

Experimental

Preparation of Single Crystals. Crystals of Na(TCNQ), K(TCNQ), and Rb(TCNQ) were prepared at room temperature by a diffusion process in a solution of commercially-available metal-iodide and TCNQ purified by recrystallization from acetonitrile distilled from phosphorus pentoxide and by sublimation *in vacuo*.[7] An apparatus different from that described by Pott and Kommandeur[8] was used for crystal growing; a test tube of a suitable length within metal-iodide crystals was left standing in a 200 m*l* Erlenmeyer flask within TCNQ crystals; in both of them acetonitrile was poured, and then the flask was covered and allowed to stand two or three weeks at room temperature. Crystals of Cs(TCNQ) were prepared by the metathesis of CsCl with Li(TCNQ) in water using above-mentioned apparatus. The crystals had various sizes; for example, $0.7\times0.3\times0.1$ mm^3—$0.4\times0.3\times0.2$ mm^3 for Na(TCNQ) and $15.0\times1.0\times1.0$ mm^3—$2.0\times0.3\times0.3$ mm^3 for K(TCNQ). Crystals of Li(TCNQ) have not been available large enough for single-crystal measurements in this way. The polycrystalline powder samples of Li(TCNQ) and K(TCNQ) were prepared by mixing boiling acetonitrile solutions of TCNQ and metal iodide.[7]

Electrical Measurements. The electrical resistivity was measured by means of the direct-current method, with two-electrode probes, because of the high resistance of small crystals. Electrical contacts to the crystals were made with silver paste. A high-pressure cylinder with an inside diameter of 30 mm and a piston distance of 80 mm was used. The maximum attainable pressure is 15000 kg/cm^2 in this cylinder. Silicone oil of low viscosity was used as the pressure-transmitting medium. The pressure was measured with a manganin gauge. The high-pressure apparatus and the high-pressure plug, with a sample mounting and a heater, are shown in Fig. 1.

Only one end of the crystal, in the form of a needle, was fixed vertically on the bakelite base with silver paste in order to prevent the crystal from breaking from the difference

1) P. W. Bridgman, *Proc. Amer. Acad. Arts Sci.*, **72**, 227 (1938).
2) F. Gutman, and L. E. Lyons, "Organic Semiconductors," John Wiley & Sons, Inc., New York (1967).
3) D. Fox, M. M. Labes, and A. Weissberger, "Physics and Chemistry of the Organic Solid State," Interscience Publishers, New York (1965).
4) A. W. Merkl, R. C. Hughes, L. J. Berliner, and H. M. McConnell, *J. Chem. Phys.*, **43**, 953 (1965).
5) D. B. Chesnut, *ibid.*, **40**, 405 (1964).
6) J. G. Vegter, T. Hibma, and J. Kommandeur, *Chem. Phys. Lett.*, **3**, 427 (1969).
7) L. R. Melby, R. J. Harder, W. R. Hertler, W. Mahler, R. E. Benson, and W. E. Mochel, *J. Amer. Chem. Soc.*, **84**, 3374 (1962).
8) G. T. Pott and J. Kommandeur, *Mol. Phys.*, **13**, 373 (1967).

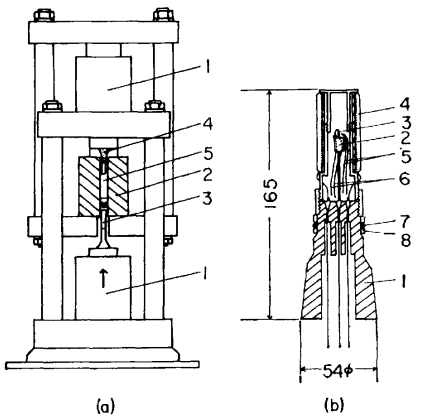

Fig. 1. Schematic diagram of high-pressure apparatus.
a) high pressure cylinder settled on Kennedy type 1000 ton press (1) 1000 ton press (2) high pressure cylinder (3) piston (4) high pressure plug (5) silicone oil
b) high pressure plug with a sample mounting and a heater. (1) hardened steel high pressure plug (2) bakelite base (3) crystal (4) nichrome wire heater around alumina cylinder (5) copper-constantan thermocouple (6) electrical lead (7) O-ring (8) brass ring

in the compressibilities of the crystal and the base when pressure was raised.

The nichrome wire heater around the alumina cylinder, the outside of which was fixed by cement, was used for heating the samples. The temperature was measured by means of a copper-constantan thermocouple placed near the crystal.

Optical Measurements. The measurement of the electronic absorption spectra was carried out using a Cary recording spectrophotometer, Model 14M. The temperature dependence of the absorption spectra was measured on samples rubbed on glass plates using a high-temperature optical cell in about 10^{-2} Torr, the temperature being measured by means of a copper-constantan thermocouple.

Results and Discussion

A. Effect of Pressure on the Phase Transition. The $M^+(TCNQ)^-$ crystals available here for electrical measurements are almost like the twinning crystals. In the case of Rb(TCNQ), two kinds of crystals, whose external appearances are different, were prepared in the same batch by the method described above. One is a reddish-purple needle similar to K(TCNQ), and the other is a dark purple needle similar to Cs(TCNQ) or the prism. The yield of reddish-purple crystals constitutes a small percentage of the total yield of Rb(TCNQ) crystals. The physicochemical properties are remarkably different between the two crystals.[9] For example, the electrical resistivity, ρ, at room temperature is about $10^5\,\Omega\cdot$cm and $10^2\,\Omega\cdot$cm, and the activation energy, E_a, obtained from the expression $\rho=\rho_0\exp(E_a/kT)$ is between 0.41 and 0.53 eV and between 0.16 and 0.19 eV for the reddish-purple Rb(TCNQ) and the dark purple one respectively. The electronic absorption spectra are also different, as has been shown in Fig. 2.

9) Recently, by means of X-ray analysis, the difference of the crystal structure between reddish-purple Rb(TCNQ) and dark purple one was made clear. I. Shirotani, H. Kobayashi, N. Sakai, and Y. Saito, This Bulletin, to be published.

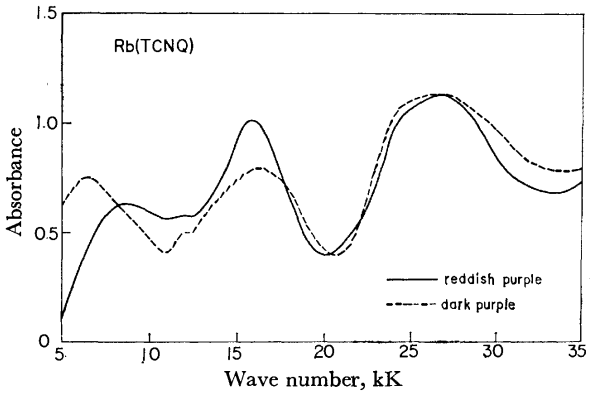

Fig. 2. Electronic absorption spectra of reddish and dark purple Rb(TCNQ).

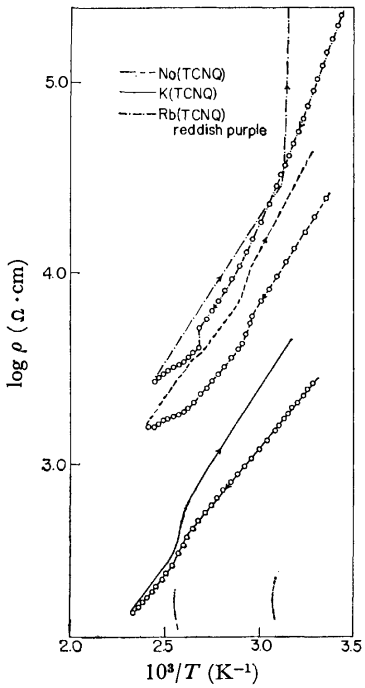

Fig. 3. Electrical resistivity as a function of reciprocal temperature of Na(TCNQ), K(TCNQ), and reddish-purple Rb(TCNQ) in 10^{-2} Torr.

Figure 3 shows the electrical resistivity of $M^+(TCNQ)^-$ crystals as a function of the reciprocal temperature. This measurement was carried out in about 10^{-2} Torr. The presence of the anomalies in resistivity was observed at about 338, 391, and 374°K for Na-, K-, and reddish-purple Rb(TCNQ) respectively. The resistivity, ρ, and the activation energy, E_a, of these $M^+(TCNQ)^-$ crystals varied from crystal to crystal.

The activation energy of Na(TCNQ) is from 0.23 to 0.32 eV below the transition temperature and from 0.16 to 0.22 eV above. The resistivity decreases by a factor of about 0.8 at the transition point. In thermal cycles for the same crystal, the resistivity during cooling is higher than that during the initial heating and the room-temperature resistivity in the second thermal cycle is higher than the initial value by a factor of about 1.2. However, the agreement of the transition temperature among several specimens, among heating

and cooling processes, and among repeated measurements of the same crystal is excellent. The heat of transition of Na(TCNQ) is very small, but it was distinctly observed by the preliminary measurements by means of a differential scanning calorimeter, this is in contrast with the case reported by Vegter *et al.*[6]

The activation energy of K(TCNQ) is from 0.23 to 0.45 eV below the transition point and from 0.15 to 0.31 eV above. In this salt, the resistivity changes slowly over a 5 to 8°K interval before a linear log ρ *versus* $1/T$ relationship in the region of the low activation energy is obtained. The amount of the change in the resistivity at the reverse transition on cooling is larger than that at the transition on heating. The agreement of the transition temperature among the several specimens is within ±6°K.

In the case of reddish-purple Rb(TCNQ), the activation energy is from 0.41 to 0.53 eV below the transition point and from 0.28 to 0.37 eV above. The abrupt decrease in the resistivity by a factor of about 0.6 was observed at the transition, but most of the crystals break down at the transition point, and so it is difficult to obtain accurate measurements of the transport behavior in the high-temperature phase. A large hysteresis in the transition temperature was observed. The transition point is 374±1°K upon heating and 323±4°K upon cooling.

A similar abrupt change in resistivity was observed at about 231 and 254°K for the dark purple Rb(TCNQ) crystals and Cs(TCNQ) crystals respectively. The amount of the change in resistivity at the transition point is very small, and no change in the activation energy was observed above and below the transition point for these salts.

Table 1. Transition temperature and heat of transition for $M^+(TCNQ)^-$ salts

	Transition temperature (°K)		
	Present work	After Vegter *et al.*[a]	Heat of transition[a] ΔH (cal/mol)
Na(TCNQ)	338	348	unobservable
K(TCNQ)	391	395	60
Rb(TCNQ)			
reddish-purple	374	381	1010
dark purple	231	—	—
Cs(TCNQ)	254	210	unobservable

a) Ref. 6)

The transition temperatures observed in the present electrical measurements for various salts are summarized in Table 1, along with the data reported in Ref. 6. The disagreement of the transition temperatures may be due to differences in the methods of measurement or to the differences in the purity of the samples. The scattering values of the activation energy among several specimens seem to be mainly due to the influence of impurities on the electrical conduction.[10]

10) N. Sakai, I. Shirotani, and S. Minomura, *ibid.*, **45**, 3314 (1972).

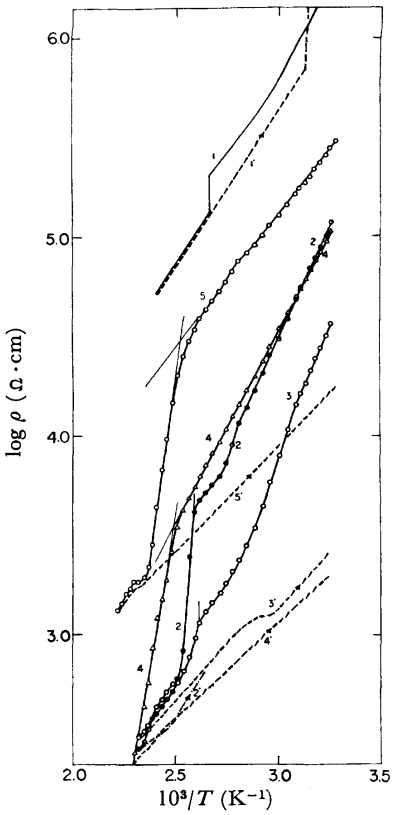

Fig. 4. Electrical resistivity as a function of reciprocal temperature under several constant high pressures of reddish purple Rb(TCNQ).
curve 1: 0 kbar, 2: 2.2 kbar, 3: 4.2 kbar, 4: 8.3 kbar, 5: 10.4 kbar.

The effect of the hydrostatic pressure on the transition temperature was studied in order to obtain information about the nature of the phase transition in $M^+(TCNQ)^-$. Figure 4 shows the resistivity as a function of the reciprocal temperature under several constant high pressures for the reddish-purple Rb(TCNQ) crystal. The transition temperature of 374°K at 1 bar rises with an increase in the pressure. The transition seems to be sluggish under high pressures. The curves of log ρ *versus* $1/T$ under high pressures seem to be complicated because of the appearance of the new pressure-induced phase transition to be described in the next section, B. Although the breakdown of crystals at the transition point occurring at one atmosphere did not occur under high pressures, different crystals were used for each run because of the possibility of the high-temperature phase being quenched at room temperature under high pressures. The activation energy in the low-temperature phase decreased with an increase in the pressure ($dE_a/dP \sim -0.01$ eV/kbar). The pressure dependence of the activation energy in the high-temperature phase was not well known because of the limited temperature region.

Figure 5 shows a phase diagram of the reddish-purple Rb(TCNQ). The slope obtained from the curve is calculated to be:

$$dP/dT = +0.36 \text{ kbar/deg.} \quad (1)$$

The discontinuity in volume at the transition may be calculated from the Clausius-Clapeyron relation for

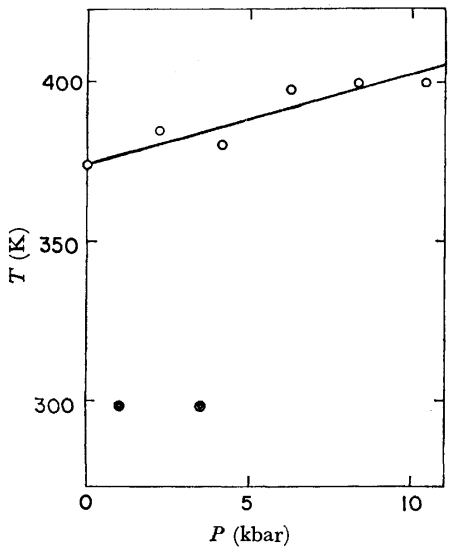

Fig. 5. Phase diagram of reddish-purple Rb(TCNQ). Pressure-induced phase transition points (see the text) are also written in at room temperature.

the first-order transition:

$$dP/dT = \Delta S/\Delta V, \quad (2)$$

where ΔS is the total change in entropy between the two phases. ΔS is evaluated from the latent heat of transition. The ΔS for the reddish-purple Rb(TCNQ) is about 2.65 cal/mol·deg, judging from the data in Table 1; consequently, ΔV is 0.31 cm^3/mol.

The temperature dependence of the resistivity under several constant high pressures was measured also for Na- and K(TCNQ). In these salts, the small amount of change in the resistivity at the transition point became obscurer with an increase in the pressure, and so it was difficult to obtain the pressure coefficients for the transition temperature over a wide region of pressures. The preliminary value of dP/dT for Na(TCNQ) is +0.014 kbar/deg up to about 4 kbar. Data concerning the phase transition for various ion radical salts are summarized in Table 2.

Table 2. Data concerning the phase transition for various ion radical salts

	dP/dT (kbar/deg)	ΔS (cal/mol·deg)	ΔV (cm^3/mol)
Rb(TCNQ)	+0.36	2.65[a]	+0.31
W.B.P.	+0.1[b]	2.19[c]	+0.91[b]
$[(C_6H_5)_3PCH_3]^+$-$(TCNQ)_2^-$	negative	1.72[d]	$\sim$−2
$[(C_6H_5)_3AsCH_3]^+$-$(TCNQ)_2^-$	negative	—	$\sim$−3.51[e]

a) Ref. 6, b) Ref. 11, c) Ref. 12, d) Ref. 13, e) Ref. 4.

The ΔV at the transition of $[(C_6H_5)_3AsCH_3]^+$-$(TCNQ)_2^-$ has been obtained by the following treatment, proposed by McConnell and his co-workers.[4]

The condition for phase equilibrium —that the Gibbs free energies, including the spin-exchange free energy for a strongly-alternating linear array without any exciton-exciton interaction of the two phases, be equal at the transition point— leads to the following equation for the P-T phase separation curve:

$$P = -(\Delta E^0/\Delta V^0) + (kT/\Delta V^0)\ln[(1-\rho_I)/(1-\rho_{II})] \quad (3)$$

where the quantity ρ is the triplet excitation density as defined by the equation of the molar paramagnetic susceptibility as:

$$\chi_p = \rho N_0 g^2\beta^2/3kT, \quad (4)$$

and is related to the energy separation between the thermally-accessible triplet state and the ground state by the following equation:

$$\rho = 3[3+\exp(J/kT)]^{-1}. \quad (5)$$

When Eq. (3) is led, it has been assumed that the two crystal forms have very similar crystal structures, and that the phonon heat capacities of the two phases are equal and are essentially independent of the pressure, and, further, that the thermal coefficients of the volume expansion of both phases are small, nearly equal, and independent of the pressure.

The value of ΔV^0 of $[(C_6H_5)_3AsCH_3]^+(TCNQ)_2^-$ has been determined to be −11.7 Å^3/spin pair from the measurement of P, T, ρ_I, and ρ_{II} at the transition point. The ΔV value of the negative sign indicates a decrease in the crystal volume at the transition to the high-temperature phase, which is the high-pressure phase for $[(C_6H_5)_3AsCH_3]^+(TCNQ)_2^-$.

The total change in entropy between the two phases is composed of electronic terms, lattice terms, and spin-ordering terms:

$$\Delta S = \Delta S_{electronic} + \Delta S_{lattice} + \Delta S_{spin}. \quad (6)$$

The electronic entropy change may be neglected in these ion radical salts because of the small number of carriers. Although, in the case of $[(C_6H_5)_3AsCH_3]^+$-$(TCNQ)_2^-$, the $\Delta S_{lattice}$ has been neglected in the treatment by McConnell and his co-workers, the $\Delta S_{lattice}$ seems to be the main factor in the entropy change in the reddish-purple Rb(TCNQ). The contribution of ΔS_{spin} to ΔS will be several percent in the reddish-purple Rb(TCNQ), as in the cases of Würster's Blue Perchlorate (W.B.P.) and $[(C_6H_5)_3PCH_3]^+$-$(TCNQ)_2^-$. This was estimated from the data of K(TCNQ).[6] For the case of the reddish-purple Rb(TCNQ), the following equation[11] for the phase-separation line may be used instead of Eq. (3):

$$P = -(\Delta E/\Delta V) + T\Delta S_{lattice}/\Delta V + (kT/\Delta V)\ln[(1-\rho_I)/(1-\rho_{II})]. \quad (7)$$

The ΔV values of the positive sign in the reddish-purple Rb(TCNQ) and W.B.P. indicate an increase in the crystal volume at the transition to the high-temperature phase. Recently, the structure determination of the reddish-purple Rb(TCNQ) has been carried out by means of an X-ray diffraction study at a low temperature (−160°C) by Hoekstra, Spoelder, and Vos.[14] The crystal of the reddish-purple Rb-

11) R. C. Hughes, A. W. Merkl, and H. M. McConnell, *J. Chem. Phys.*, **44**, 1720 (1966).
12) H. Chihara, M. Nakamura, and S. Seki, This Bulletin, **38**, 1776 (1965).
13) A. Kosaki, Y. Iida, M. Sorai, H. Suga, and S. Seki, *ibid.*, **43**, 2280 (1970).
14) A. Hoekstra, T. Spoelder, and A. Vos, *Acta Crystallogr., B*, **28**, 14 (1972).

(TCNQ) belongs to the monoclinic symmetry of the $P2_1/c$ space group, with lattice constants of $a=7.187$, $b=12.347$, $c=13.081$ Å, and $\beta=98.88°$ at $-160°C$, and with those of $a=7.30$, $b=12.40$, $c=13.13$ Å, and $\beta=98.8°$ (which are preliminary values) at room temperature, including four molecules in a unit cell.

The room-temperature W.B.P. is orthorhombic, the space group is Pn2n or Pnmn, with a unit cell of dimensions $a=5.98$, $b=10.21$, and $c=10.23$ Å, which includes two molecules in a unit cell; at ~77°K through the phase transition at 186°K, it changes to a monoclinic symmetry with lattice constants of $a=11.70$, $b=20.22$, $c=10.17$ Å, and $\gamma=92.7°$.[15]

According to these crystal data, the rates of the volume change to the molar volume at the transition point are about 0.5% and about 0.17% in W.B.P. and the reddish-purple Rb(TCNQ) respectively. The volume change in Rb(TCNQ) must considerably smaller than that in W.B.P.

Figure 6 shows the temperature dependence of the electronic absorption spectra of the reddish-purple Rb(TCNQ).

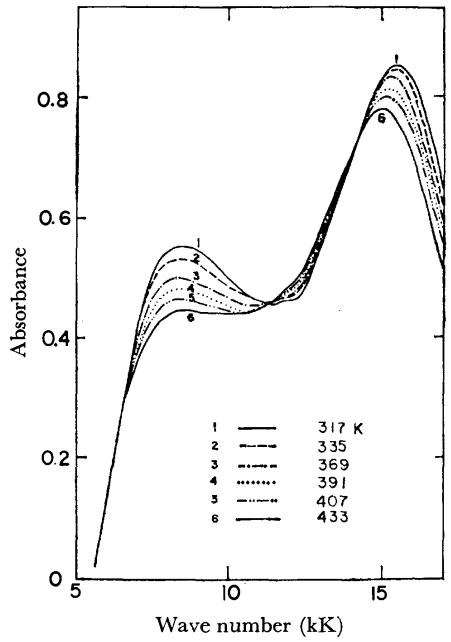

Fig. 6. Temperature dependence of the electronic absorption spectra of reddish-purple Rb(TCNQ).

Figure 7 shows the absorbance of two absorption peaks and the energy of the peak in the higher-energy region as a function of the temperature for the reddish-purple Rb(TCNQ), K(TCNQ), and Na(TCNQ). The absorption spectra of these crystalline TCNQ salts are similar to those of the dimer of the TCNQ anion radical in an aqueous solution.[16–19]

It has been reported that the TCNQ units in the reddish-purple Rb(TCNQ) are stacked in a plane-to-plane manner and that the interplanar spacings of 3.159 and 3.484 Å alternate within a row, and the Rb^+ ions also form rows along the a axis, with alternating distances of 3.483 and 3.726 Å between the ions at $-160°C$.[14] It is certain that there is a bimolecular association of TCNQ anion radicals in the column in the reddish-purple Rb(TCNQ) crystal. The preliminary structure determination of K(TCNQ) by Anderson and Fritchie[20] has shown that the TCNQ anions are stacked plane-to-plane in the column, but it is not certain whether or not there is a bimolecular association of TCNQ anions in the column.

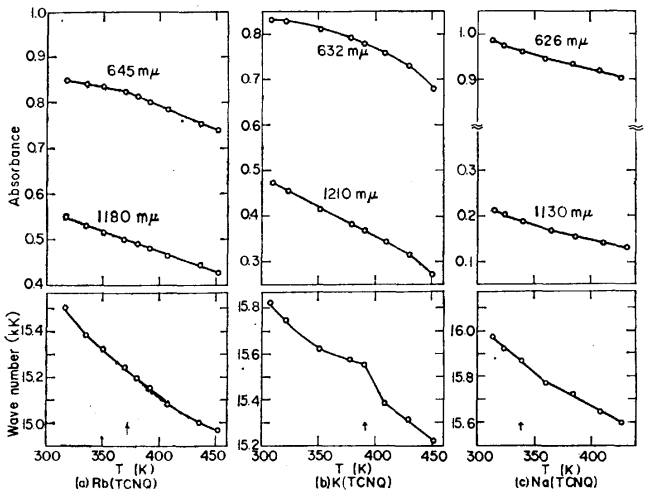

Fig. 7. Absorbance of two absorption peaks and the energy of the peak in the higher energy region as a function of temperature.
(a) reddish-purple Rb(TCNQ) (b) K(TCNQ) (c) Na(TCNQ)

If the phase transition observed in $M^+(TCNQ)^-$ is similar to that at about 190°K in W.B.P., the mechanism of which has been explained by the dimerization scheme, that is, the presence of dimerized Würster's Blue species at low temperatures,[12,15,21,22] it may be expected to occur at the transition point where the absorbance of the charge-transfer absorption band in the near-infrared region changes abruptly, and the peak positions may be expected to shift considerably so that the spectra correspond to those of the TCNQ anion monomer. However, as has been shown in Figs. 6 and 7, the absorbance and the peak energy decrease almost monotonously with an increase in the temperature, and no abrupt change or shift at the transition point was observed except for the small peak shift in K(TCNQ). The spectra seem to be similar to those of the dimer of the TCNQ anion radical above the transition temperature. A little shift of the isosbestic points was observed above and below the transition point.

Although any inequality of interaction between neighboring TCNQ anions in the column would become smaller in the high-temperature phase, the

15) D. D. Thomas, H. Keller, and H. M. McConnell, *J. Chem. Phys.*, **39**, 2321 (1963).
16) R. H. Boyd and W. D. Phillips, *ibid.*, **43**, 2927 (1965).
17) Y. Iida, This Bulletin, **42**, 71 (1969).
18) N. Sakai, I. Shirotani, and S. Minomura, *ibid.*, **43**, 57 (1970).
19) S. Hiroma, H. Kuroda, and H. Akamatu, *ibid.*, **44**, 9 (1971).
20) G. R. Anderson and C. J. Fritchie, Jr., Second National Meeting, Society for Applied Spectroscopy, San Diego, Paper 111 (1963).
21) K. Okumura, *J. Phys. Soc. Jap.*, **18**, 69 (1963).
22) T. Sakata and S. Nagakura, *Mol. Phys.*, **19**, 321 (1970).

bimolecular association of TCNQ anion radicals seems to be preserved in the high temperature phase in the reddish-purple Rb(TCNQ). The phase transition may be principally the result of the change in the manner of packing between the Rb^+ ions and the $TCNQ^-$ column, because the crystals fractured at the transition point in spite of the slight change in the arrangement of TCNQ anions and the small volume change.

On the other hand, only a slight change in the $TCNQ^-$ column would be expected in the case of $M^+(TCNQ)^-$ salts except for the reddish-purple Rb-(TCNQ).

B. New Pressure-induced Phase. In $M^+(TCNQ)^-$ salts anomalies in the pressure dependence of resistivity were found at room temperature; they seem to be attributable to the new pressure-induced phase transition. This is analogous with the fact that a number of inorganic substances show anomalies in the electrical resistivity at their pressure-induced phase transition.[23,24]

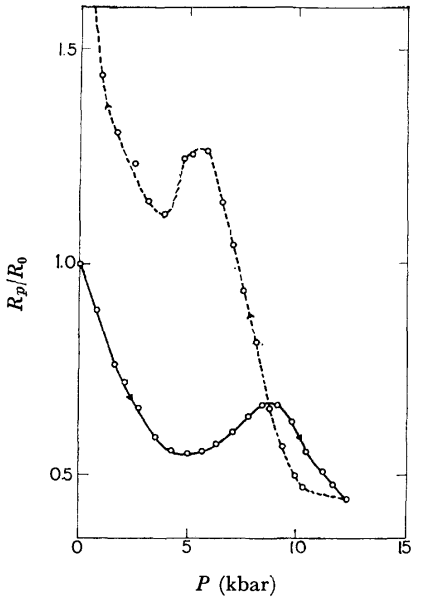

Fig. 8. Relative resistance as a function of pressure at room temperature in the pellet of polycrystalline Li(TCNQ).

Figure 8 shows the relative resistance as a function of the pressure at room temperature in Li(TCNQ). Four high-pressure runs were made on the polycrystalline powder samples pressed into pellets with a pressure of 7 kbar. The main features were identical in all the runs. The resistance decreases up to about 5 kbar, and then it increases, attaining its maximum at about 8.5 kbar and then again decreasing. As the pressure decreases, the minimum and the maximum of resistance shift to about 4 and 5.5 kbar respectively. It is likely that the phase transition occurs around 5 kbar, and that it is complete by about 8 kbar. The phase transition in Li(TCNQ) has not been observed in the temperature range from −150°C to +230°C at one atmosphere.[6] Therefore, the transition found here must be a pressure-induced phase transition.

It has been reported that the resistance decreases monotonously under very high pressures in the range from 28 to 170 kbar.[25] In that pressure region, the pressure dependence of the resistance in the new high pressure phase seems to be shown.

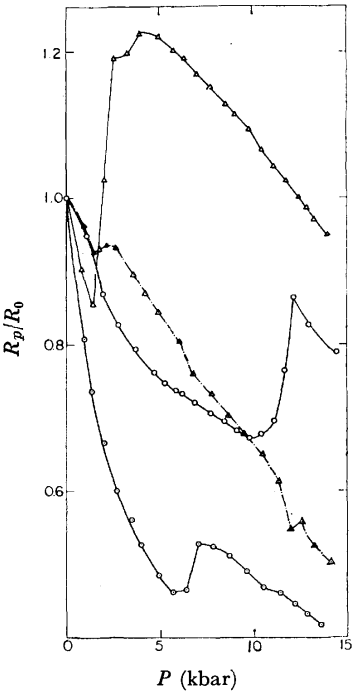

Fig. 9. Relative resistance as a function of pressure at room temperature in several Na(TCNQ) crystals.
-○- and -⊙-: $\rho_a//$, -△- and -◬-: $\rho_b//$.

Figure 9 shows the pressure dependence of the relative resistance at room temperature in several Na(TCNQ) crystals. The crystal axis along which the resistance had been measured was assigned on the basis of a prelimianry X-ray analysis by Konno *et al.*,[26] according to which columns of $TCNQ^-$ ions are parallel to the *a* axis. The anomalies in the resistance were found in all the crystals. However, the pressures at which the anomalies were observed were somewhat different from crystal to crystal. Further, the manner of the anomalies varies; for example, some crystals show a discontinuous rise in resistance, while other crystals show only a change in the slope in the curve of the relative resistance *versus* the pressure around the equal pressure. It is likely that the manner of the anomaly differs with different crystal axes. Probably the phase transitions occur about 1.5, 6, and 10—11 kbar.

Figures 10, 11, and 12 show three typical results in eight measurement runs of the pressure dependence of the resistance in K(TCNQ) crystals. The measurements of the resistance were carried out along the needle axis. K(TCNQ) crystals exhibited a strange behavior in the pressure dependence of the resistance.

23) W. Paul and D. M. Warschauer, "Solids under Pressure," McGraw-Hill, New York (1963).
24) H. G. Drickamer "Solid State Physics," Vol. 17, Academic Press, New York (1965), p. 1.
25) I. Shirotani, T. Kajiwara, H. Inokuchi, and S. Akimoto, This Bulletin, **42**, 366 (1969).
26) M. Konno and Y. Saito, private communication.

That is, in spite of all the crystals having a similar outside appearance, some crystals revealed that the resistance increased with an increase in the pressure, while others revealed the reverse. It was also observed in some crystals that the pressure dependency of the resistance in the course of the first increase in pressure was remarkably different from that in the course of the second increase in pressure after the release of the pressure on the same crystal, as has been shown in Fig. 12. The crystals seemed not to be damaged after the second measurement. The anomalies in the resistance were observed around 2, 5, and 9 kbar.

The pressure dependence of the resistance was measured on polycrystalline powder samples of K(TCNQ)

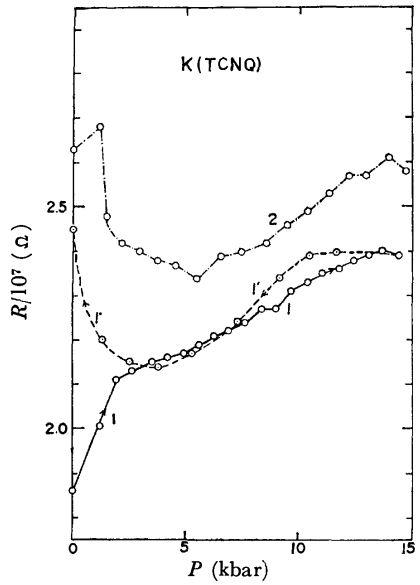

Fig. 10. Resistance as a function of pressure at room temperature in K(TCNQ) crystal A. (1) the first increasing pressure run, (1′) release of pressure run, (2) the second increasing pressure run.

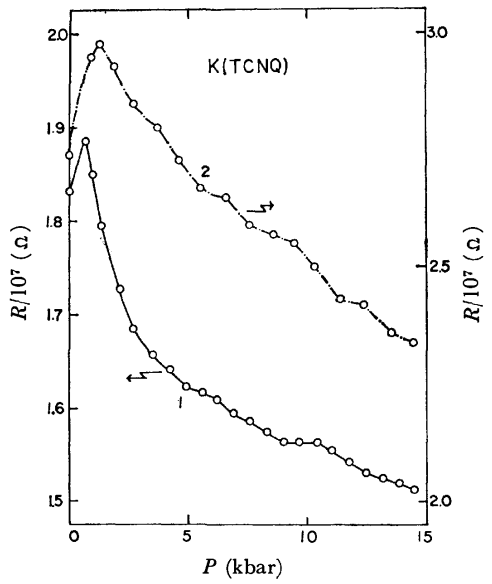

Fig. 11. Resistance as a function of pressure at room temperature in K(TCNQ) crystal B. (1) the first increasing pressure run, (2) the second increasing pressure run.

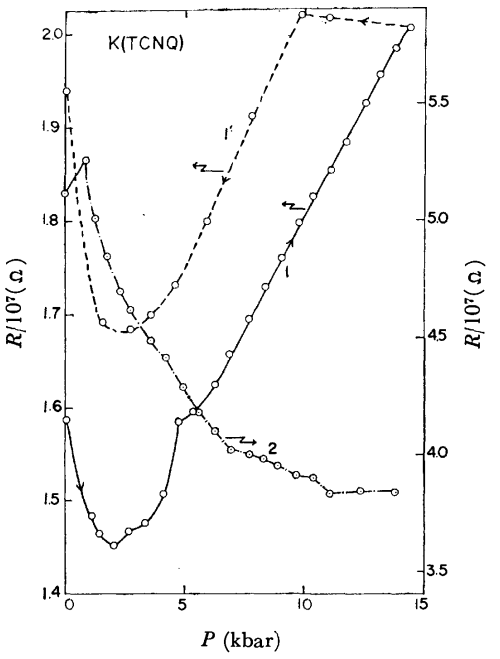

Fig. 12. Resistance as a function of pressure at room temperature in K(TCNQ) crystal C. (1) the first increasing pressure run, (1′) release of pressure run, (2) the second increasing pressure run.

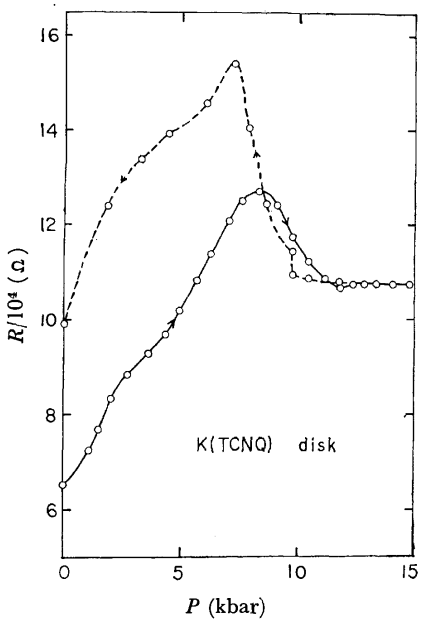

Fig. 13. Resistance as a function of pressure at room temperature in the pellet of polycrystalline K(TCNQ).

pressed into pellets with a pressure of 7 kbar; this was done in order to investigate whether or not the variation in the pressure dependency in crystals was due to the difference in methods of sample preparation; the results are shown in Fig. 13. Four runs were made. The main features were identical in all the runs. The resistance increased up to about 8.2 kbar, and then decreased with an increase in the pressure. The reason for this disagreement in the powder sample and the crystal samples is not clear at present. However, because any imperfection, such as a chemical impurity

or a lattice defect, has an influence on the electrical conduction, it is probable that the slight difference in the imperfection was reflected in the pressure dependence of the resistance. It is possible that each crystal prepared simultaneously by a diffusion process has a different imperfection.

The change in the slope at about 2.2 kbar and the maximum of resistance at about 8.2 kbar in the powder sample seem to correspond to the anomalies around 2 and 5 or 9 kbar respectively observed in the crystal sample. The pressure-induced phase transition must have occurred at those pressures.

Recently, a preliminary experiment was carried out concerning the pressure dependence of the lattice constants of K(TCNQ) by means of X-ray powder diffraction analysis under hydrostatic high pressures.[27] No marked changes in the diffraction pattern were observed up to 4.5 kbar. Therefore, the transformation of the crystal structure at those pressure-induced phase transition points, if any, would be very slight.

The effect of a very high pressure on the resistance of the powder K(TCNQ) has been studied in the pressure region from ~20 to ~500 kbar, and it has been reported that there is a distinct break in the slope of the resistance-pressure curve at 250—300 kbar.[28] However, no explanation for this phenomenon has yet been provided.

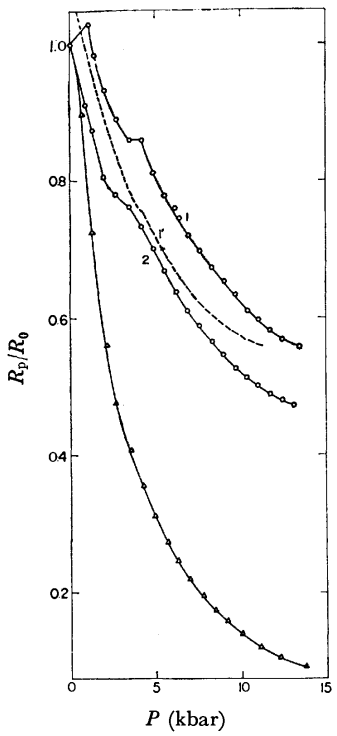

Fig. 14. Relative resistance as a function of pressure at room temperature in Rb(TCNQ).
—○—: reddish-purple crystal (1) the first increasing pressure run, (1′) release of pressure run, (2) the second increasing pressure run, —△—: dark purple crystal.

Figure 14 shows the pressure dependence of the relative resistance in both the reddish- and dark purple Rb(TCNQ) crystals. The anomalies were found at about 1 and 3.5 kbar, at which the new pressure-induced phase transition occurs, in the reddish-purple Rb(TCNQ). These new pressure-induced phase transition points are written in the phase diagram as has been shown earlier in Fig. 5. More than three phases ($\alpha,\beta,\gamma,\cdots$) are considered to exist in the solid phase of Rb(TCNQ); consequently, it is possible that the boundary line shown in Fig. 5 is due to the transition from the new pressure-induced phase to the high-temperature phase in the region of higher pressures. The anomaly at about 1 kbar disappeared in the course of the first release of pressure and the second increase in pressure. In the case of the dark purple Rb(TCNQ), on the other hand, the resistance decreased monotonously with an increase in the pressure, and no anomalies in resistance corresponding to those in the reddish-purple Rb(TCNQ) were observed up to 13.5 kbar. Whether or not the pressure-induced phase transition occurs in the dark purple Rb(TCNQ) is not yet clear.

The effect of pressures up to 7 kbar on the electronic absorption spectra of these $M^+(TCNQ)^-$ salts has been studied.[18] No marked change in the absorption spectra has been observed in the pressure region above and below the transition pressure found here.

For the present, the nature of the new pressure-induced phase transition found in $M^+(TCNQ)^-$ salts is not known. The TCNQ ions are arranged with some periodicity in the column in the $TCNQ^-$ anion radical salts. It would be expected that the phase transition arises from a change in the periodicity in the $TCNQ^-$ column. Even a slight change in the external condition would affect the stabilization of the crystal lattice in the ion radical salts because of the complicated molecular interaction in them. The phenomena of the presence of numerous modifications over a wide region of pressure and temperature would appear to be rather general in the ion-radical salts.

The authors would like to thank Miss Michiko Konno for performing the X-ray diffraction experiment.

27) M. Yokota, private communication.

28) R. B. Aust, G. A. Samara, and H. G. Drickamer, *J. Chem. Phys.*, **41**, 2003 (1964).

The Isomerization of *n*-Butenes over Acidic Ion-exchange Resin

Takayoshi UEMATSU*

Department of Chemical Engineering, Tokyo Institute of Technology, Ohokayama, Meguro-ku, Tokyo

(Received March 13, 1972)

The isomerization of *n*-butenes and the polymerization of propylene were studied in a gas-phase reaction on a sulfonic acid-type resin catalyst. These reactions were considered to proceed *via* the carbonium ion formation on the functional groups, and a strong correlation was found between the activities in these two reactions. The acidity and the acid strength of the resin catalyst were measured by means of amine titration in a nonpolar solvent using Hammett indicators. The value of the acidity obtained at $pK_a=6.8$ seemed to correspond to the number of the ion-exchangeable hydrogen on the functional groups. The effects of poisoning by ion exchange with Na^+, Mg^{2+} or by adsorption of NH_3 were also studied. The decrease in the activity for the isomerization was not proportional to the amount of cations exchanged. The catalytic activities of the protonic hydrogen seemed not to be equal as was suggested by the result of resin catalysts in polar solvents. The possible heterogeneity of the active sites on the resin catalyst was discussed. The six relative rate constants were calculated on the basis of the mutual interconversion among the three isomers of *n*-butene. The apparent energy of activation for the double-bond migration of 1-butene was found to be 17 kcal/mol on the H-form resin, but it was changed by ion exchange with Na^+. The selectivities were characteristic of solid acid catalysts of the protonic type.

Many types of acidic oxide catalysts have been studied in hydrocarbon reactions. However, these catalysts have been found to show a very complicated behavior, reflecting their coexisting various acidic properties of the active sites. The catalyses have been accounted for by the surface-acid sites, which are usually classified into two typical acid types: protonic (Brönsted) acid and non-protonic (Lewis) acid site.[1-3] In some cases, they were extended to oxidative sites to form a cation radical complex on the surface.[4-6] Furthermore, these acid sites have a widespread distribution in terms of acid strength and activity.[7] Thus, a typical solid acid with a single type of acid and homogeneous activity has been expected to be studied.

Attempts have been made to use acidic ion-exchange resins of a conventional gel-type structure in solution[8-10] or in the vapor phase of polar reactants.[11,12] These catalyses have been considered to be similar to those by homogeneous acid catalysts, such as hydrochloric acid or sulfuric acid.[13] An acidic resin of the macroreticular-type was used in the gas-phase reaction.[14] Manassen and his co-worker prepared a sulfonated and a phosphonated polyphenyl resin catalyst which were stable up to 350°C, and observed no special surface effects over them.[15] In the dehydration of alcohol on an acidic resin catalyst, the homogeneous catalytic activities of the functional groups have been reported,[16] while the heterogeneity of the active sites has also been suggested by the different results regarding the poisoning effect by Na^+ and Li^+.[17]

In the present investigation, the catalytic behavior of a sulfonated styrene–divinylbenzene copolymer was studied in terms of olefin reactions, which can give more information about resin catalysts in a gas-phase reaction. The heterogeneity of the resin catalyst will be discussed also.

Experimental

Materials. The sulfonated styrene–divinylbenzene copolymer with a macroreticular structure was prepared from commercial ion-exchange resin Amberlyst-15. The resin was washed with methanol and then with decationized water to remove any extraneous materials. It was converted to the Na-form by treating it with a 1N NaOH solution according to the conventional column method, and was again reversed to H-form (AMH standard) with a 1N HCl solution. After washing with decationized water, it was treated with methanol and dried under reduced pressure. The Na-poisoned catalysts (AMHNa series) were prepared by soaking AMH in a NaOH solution containing the desired quantity of Na^+ ions for 2 weeks at room temperature. They were then washed and dried in a manner similar to that for AMH. The purity of the reactant gases was above 99.8%. They were repeatedly distilled at −196°C prior to use.

Procedures. The ion-exchange capacity of AMH was determined by titration with a NaOH solution. The surface area was measured by the BET method of N_2 adsorption. The isomerization and the polymerization reaction were carried out in a closed circulating system. The catalysts were evacuated first at room temperature and then at 110°C

* Present address: Department of Synthetic Chemistry, Faculty of Engineering, Chiba University, Chiba-city.

1) J. D. Danforth, *J. Phys. Chem.*, **59**, 564 (1955).
2) J. B. Uytterhoven, L. G. Christner, and W. K. Hall, *ibid.*, **69**, 2117 (1965).
3) J. E. Mapes and W. K. Hall, *ibid.*, **58**, 806 (1954).
4) E. P. Parry, *J. Catal.*, **2**, 371 (1963).
5) B. D. Flockert and R. C. Pink, *ibid.*, **4**, 90 (1965).
6) W. K. Hall, *ibid.*, **1**, 53 (1962).
7) J. A. Benesi, *J. Phys. Chem.*, **61**, 970 (1951).
8) G. R. Bodamer and R. Kunin, *Ind. Eng. Chem.*, **43**, 1082 (1951).
9) S. A. Bernhard and L. P. Hammett, *J. Amer. Chem. Soc.*, **75**, 1798 (1953).
10) R. Kunin, E. F. Meitzner, and J. A. Oline, *Ind. Eng. Chem., Prod. Div.*, **1**, 140 (1960).
11) V. J. Frillete, E. B. Mover, and K. Rubin, *J. Catal.*, **3**, 25 (1968).
12) A. A. Yaramian, J. C. Gottifredi, and R. E. Cunningham, *ibid.*, **12**, 257 (1968).
13) L. P. Hammett and V. C. Haskell, *J. Amer. Chem. Soc.*, **71**, 1284 (1949).
14) F. T. Fang, 3rd Intern. Congress on Catalysis, Amsterdam (1964) p. 401.
15) J. Manassen and Sh. Khalif, *J. Catal.*, **7**, 110 (1967).
16) R. L. Kabel and L. N. Johanson, *Amer. Inst. Chem. Engrs. J.*, **8**, 621 (1962).
17) B. C. Gates and L. N. Johanson, *J. Catal.*, **14**, 69 (1969).

for 2 hr. The products were analyzed by means of a gas chromatography, using a propylene carbonate–alumina column at 0°C. The isomerization reaction of 1-butene was also studied in a flow-type reactor, using N_2 as the carrier gas. The catalysts were pretreated in a N_2 stream at 110°C for 2 hr.

Results

Ion-exchange Capacity and BET Surface Area. The titration curve obtained with the powdered AMH is shown in Fig. 1. This result shows behavior characteristic of a strong electrolyte and quite resembles that of the sulfonated polyphenyl resin.[15] The total amount of NaOH added up to the neutral point of pH 7.0 was 3.79 meq/g of dry resin, while 4.03 meq/g was needed up to pH 11.0, above which no more pH change was detected upon the further addition of NaOH. The latter value was in good agreement with the ion-exchange capacity for the evacuated AMH (4.02 meq/g), but was slightly smaller than that of the standard AMH (4.32 meq/g).

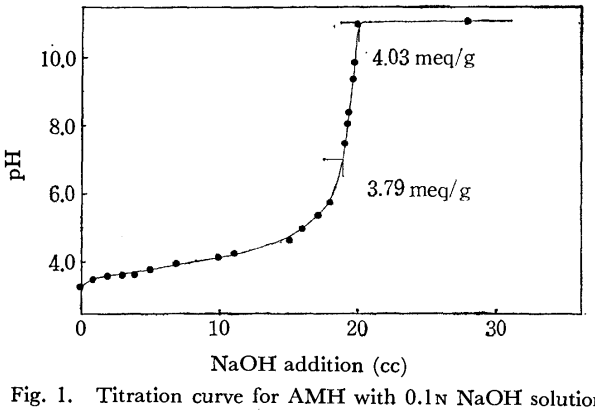

Fig. 1. Titration curve for AMH with 0.1N NaOH solution.

The BET surface areas obtained with the resin catalysts evacuated at 110°C for 2 hr were: 86 m^2/g (AMH), 57 m^2/g (AMHNa05), 74 m^2/g (AMHNa10), 67 m^2/g (AMHNa20), 54 m^2/g (AMHNa40), and 65 m^2/g (AMNa). These results appear not to show any systematic tendency in the effect of cation-exchange on the surface area. The decrease in the surface area of AMH was very small, even after evacuation at temperatures below 140°C. This suggests that the change in the substrate by the ion exchange or the pretreatment of evacuation at 110°C were negligible.

DTA and TGA Observations. The sulfonated styrene–divinylbenzene copolymer catalyst is expected to contain some water in the macro-pores or the channels in the resin matrix. A part of them may be in a hydrated sate to the functional groups. It was found from the DTA and TGA observations that the water of this kind can easily be removed by heating under atmospheric pressure. The total weight losses up to 150°C, above which the DTA and TGA curves showed no more changes, were 34.2 wt-% (AMH) and 22.0 wt-% (AMNa). These results correspond to losses of 4.7 $H_2O/-SO_3H$ and 2.9 $H_2O/-SO_3Na$ respectively, in good agreement with the hydration numbers of the polystyrene sulfonic acid-type resin reported in the literature: 3.9 (to H^+)+0.9 (to $-SO_3^-$) and 1.5 (to Na^+)+0.9 (to $-SO_3^-$).[18] When AMH and AMNa were evacuated at 110°C for 2 hr, the water content decreased remarkably, and the further weight loss by heating up to 140°C was less than 3—5%, and above that temperature desulfonation took place.

Polymerization of Propylene. The polymerization of ethylene was not promoted by AMH, but propylene and *n*-butene were catalyzed under the present experimental conditions below 100°C. The time course of the total pressure decrease could not be explained by Tamele's equation,[19] which is very often applied to the polymerization reaction of propylene over solid acid catalysts. A Langmuir-type rate expression (1) was found to be appicable, as is shown in Fig. 2;

$$r = -\mathrm{d}P/\mathrm{d}t = kP/1 + KP \qquad (1)$$

P: total pressure, t: time, k: rate constant, K: constant of the equilibrium factor, r: rate of the reaction.

The apparent energy of activation for the polymerization on AMH was found to be 10 kcal/mol in the range of temperatures higher than 84°C and 3.5 kcal/mol in the lower range.

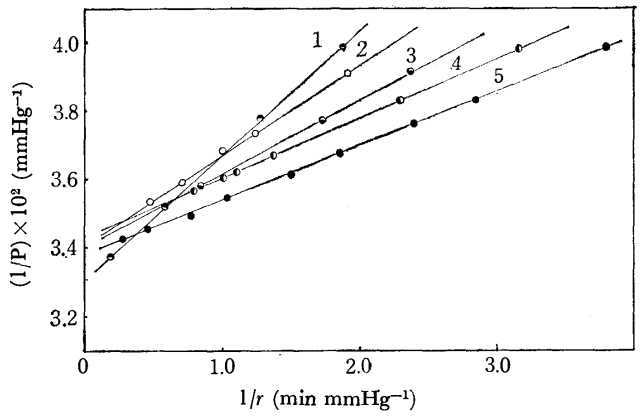

Fig. 2. Langmuir type plot for propylene polymerization over AMH.
1: 100°C 2: 92°C 3: 84°C 4: 72°C 5: 66°C

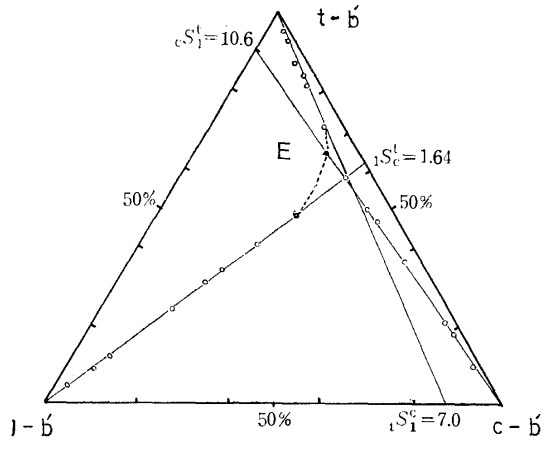

Fig. 3. Ternary system for the *n*-butene isomerization over AMH. Reaction temperature: 70°C. E: equilibrium composition. $_1S_c^t$: the initial selectivity obtained by extrapolation on the reaction curve from 1-butene.

18) E. Glueckauf and G. P. Kitt, *Proc. Roy. Soc., Ser. A*, **228**, 322 (1955).
19) M. W. Tamele, *Discuss. Faraday Soc.*, **8**, 270 (1950).

Isomerization of n-*Butenes.* Under the reaction conditions used for the isomerization of *n*-butenes, the polymerization reaction detected was negligible. Starting from any isomers of *n*-butene, only products from the double-bond migration and the *cis-trans* isomerization were observed. Thus, the reaction system can be approximately expressed by a three-component kinetic system of the Pines type.[20] The change in the relative compositions of the gas-phase products is illustrated by the ternary system as shown in Fig. 3. Starting from each isomer of *n*-butenes, the same equilibrium composition, the point E, was approached after prolonged reaction times, and the curve are nearly linear up to much higher conversions. These facts suggest that the selectivity of the catalyst did not change during the reaction, at least not during the early stage of the conversion. Selectivities expressed by the initial product ratios; ${}_{c}S_{t}^{t}$, ${}_{1}S_{c}^{t}$, ${}_{c}S_{1}^{c}$, were obtained from the tangents of the curves at zero conversion. There were several characteristic features of the behavior, especially in the stereo-selectivities; the double-bond migration of 1-butene showed a strong kinetic preference for the formation of *trans*-2-butene, though the relative ratio of the products, *trans*-2-butene/*cis*-2-butene, was less than that of the thermodynamic equiliblium. In the isomerization of *cis*-2-butene, the relative amounts of the products, *trans*-2-/1-butene, were nearly that of the equilibrium from the very low conversion, while the products from *trans*-2-butene favored the formation of *cis*-2-butene than that of 1-butene.

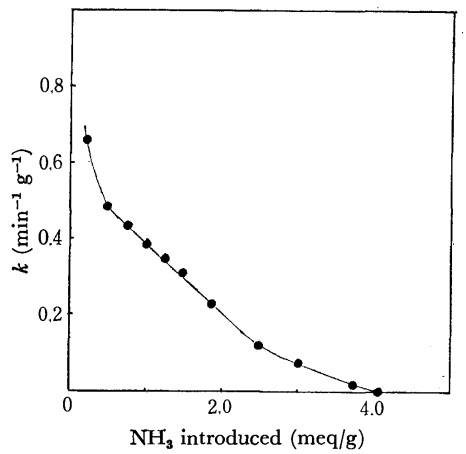

Fig. 4. Poisoning effect by NH_3 on the activity of AMH in flow system. AMH 100 mg. Carrier gas N_2 17.8 cc/min. 1-butene 1.08 cc/min. Temperature 70°C. NH_3 was introduced simultaneously into the carrier gas.

Assuming a mutual interconversion among the three *n*-butenes according to the first-order rate law, the six relative values of the rate constants were calculated from the initial selectivities and the equiliblium constants. They are listed in Table 2, together with the reported values for solid acid catalysts.

Ammonia Titration during the Reaction in the Flow System. The change in the activity by the poisoning of the adsorbed NH_3 was also observed, as is shown in Fig. 4. It can be noticed that, in the poisoning curve, the decrease in the activity was not so abrupt, but was rather proportional to the amount of NH_3 added. The total amount of the NH_3 required to poison the activity completely was 4.03 meq/g. This coincided with the effective ion-exchange capacity measured by Na^+ (4.02 meq/g). The double-bond migration of 1-butene was investigated on a series of partially ion-exchanged resin catalyst, AMHNa or AMHMg. The kinetic parameters are listed in Table 1. This behavior is quite different from that of the simultaneous poisoning by NH_3 adsorption. The selectivity, ${}_{1}S_{c}^{t}$, expressed by the initial ratio of the products, *trans*-2-/*cis*-2-, had a slight tendency to decrease upon cation exchange by Na^+ or Mg^{2+}.

Table 1. Kinetic parameters for 1-butene isomerization over AMHNa series catalysts

Catalyst	$k_1 \times 10^3$ (min^{-1} g^{-1})	${}_{1}S_{c}^{t}$	E (kcal/mol)	log A
AMH	45.6	1.35	17.0	9.8
AMHNa05	26.7	1.19	17.0	9.6
AMHNa10	14.3	1.17	16.0	8.5
AMHNa20	5.5	1.11	14.5	6.9
AMHNa40	1.5	—	—	—
AMNa	0.0	—	—	—

k_1: the first order rate constant for 1-butene double-bond migration at 60°C.
${}_{1}S_{c}^{t}$: selectivity expressed by the initial ratio of the products of the reaction, *trans*-2-butene/*cis*-2-butene.
E: apparent energy of activation.
A: pre-exponential factor.
AMHNa05: partially ion-exchanged catalyst. Added figures mean atom-% of H substituted by Na.

Table 2. Relative value of rate constant for mutual interconversion of the three *n*-butenes over the typical solid-acid

Catayst	Temp. °C	k_{1c}	k_{c1}	k_{ct}	k_{tc}	k_{1t}	k_{t1}
AMH	70	1.0	0.23	2.48	1.16	1.64	0.17
Silica-alumina[a)]	50	1.0	0.21	0.29	0.09	0.91	0.05
Alumina[a)]	50	1.0	0.21	0.91	0.25	0.45	0.03

k_{ij}: the first order rate constant for the reaction, i to j.
a) the deta are taken from Ref. 31.

Discussion

The catalytic activities of the sulfonated resin catalysts can presumably be attributed to the acidic properties of the hydrogens of the sulfonic acid groups. This was easily established by the fact that neither the substrate resin with no functional groups nor the Na-form resin showed any catalytic activities. This was consistent with the observations over the surface of *para*-toluenesulfonic acid and other various substituted benzenesulfonic acid.[21] It has been reported that deuterium adoption was observed in the course of isomerization of *n*-butenes over deuterated sulfonic

20) W. O. Haag and H. Pines, *J. Amer. Chem. Soc.*, **82**, 2488 (1960).

21) T. Uematsu and T. Shiba, 21st Annual Meeting of the Chemical Society of Japan, Osaka (1968).

acid resin catalysts[22] and deuterated *para*-toluenesulfonic acid crystals.[23] Thus, from this point of view, the catalysis over the acidic ion-exchange resin can be considered to be that of a typical type of solid acid catalyst with a protonic character.

The titration curve in Fig. 1 shows that the hydrogens of $-SO_3H$ or AMH were dissociated to some extent to give pH 3.4—3.5 in decationized water. At the neutral point, pH 7.0, some of the exchangeable hydrogens survived. Manassen found that the number of exchangeable acidic groups calculated by the titration method was smaller than that obtained from the chemical analysis.[15] However, these two values do not necessarily correspond to the effective sulfonic acid groups in the working state of the gas-phase catalysis. The coincidence of the number of adsorbed NH_3 with that of the exchangeable hydrogens suggests that almost all the ion-exchangeable hydrogens are effectively active in the isomerization of *n*-butenes, even in the gas phase. The amount of NH_3, 4.03 meq/g, which was required for poisoning the activity correspond to the population of $H^+/3.1$ A^2. This means that the sulfonic groups become close enough for them to interact with each other or with adsorbed species. If there were some hydrated water, the probability of the interaction would increase.

The acid strength of *para*-toluenesulfonic acid and benzenesulfonic acid in an aqueous solution is said to be $pK_a=0.6$.[24] However, the acid strength of the sulfonic acid resin has not been obtained directly. Using Hammett indicators, the acid strength of AMH was observed as strong as $pK_a=-3.0$——-5.6 at the minimum. The acidities measured by means of *n*-butylamine titration in cyclohexane proved to be 3.9 meq/g ($pK_a=6.8$), 2.6 meq/g ($pK_a=1.5$), and 1.0 meq/g ($pK_a=-3.0$). It should be noticed that the value of 3.9 meq/g, which include rather weak acid sites agrees with the total number of ion-exchangeable hydrogen, and that there is an apparent heterogeneity in acid strength among the functional groups on the resin catalyst. In contrast to the phosphonated polyphenyl-type resin,[15] the titration curve for AMH showed no step-by-step ion exchange in a NaOH solution. When the conventional resin catalyst was used in a polar solvent, the heterogeneity of the activity of the functional groups has been considered to have negligibly small effect on the nature of the acid catalysts.[17] In polar solvents, the hydrogens of the sulfonic acid groups on the resin would dissociate into protons and they would be loosely bonded to the counter ion, $-SO_3^-$, much as in a highly concentrated polyelectrolyte solution.[25,26] In the evacuated state, the protonic hydrogens are probably bonded more tightly to the counter groups and thus their activities are more affected by the properties of the substrate. An inhomogeneous structure of the substrate resin is known to be produced in the processes of the polymerization, the crosslinking, and the sulfonation.[25]

On the other hand, the possibility of an induced heterogeneity can not be neglected. Considering the population of the functional groups, which corresponds to one sulfonic group for each phenyl groups, the following interactions can be anticipated: 1) between adjacent sulfonic groups,[25] 2) between adsorbed species and neighboring sulfonic acid groups,[27,28] and 3) between adsorbed species and substrate resin. If these interactions can not be neglected, the catalysis and the poisoning effect will be complicated in a detailed mechanism. The differences between the behavior of the gradual poisoning caused by NH_3 adsorption in the flow system and that caused by Na^+ ion exchange are difficult to explain. However, in the former case, NH_3 molecules may be randomly adsorbed onto the active sites and the front of the poisoned area in the catalyst bed may advance linearly with the addition of NH_3, while in the latter case, the ion exchange proceeds in the static system, where the equilibrium is accomplished progressively from the stronger sites to the weaker sites, so that the activity decreases remarkably on the addition of only a small amount of NaOH. In this case, both the intrinsic and the induced heterogeneities may be responsible for the curvature in the poisoning curve.

The effectiveness of the poisoning per ion by Na^+ and Mg^{2+} are nearly equal irrespective of the different compositions. This fact indicates that the divalent cation, Mg^{2+}, may block only one counter ion, like the monovalent cation Na^+, and that the surface complexes, such as $-SO_3MgCl$ and/or $-SO_3Mg(OH)$, may probably exist on the resin.

A compensation effect seemed to exist between the

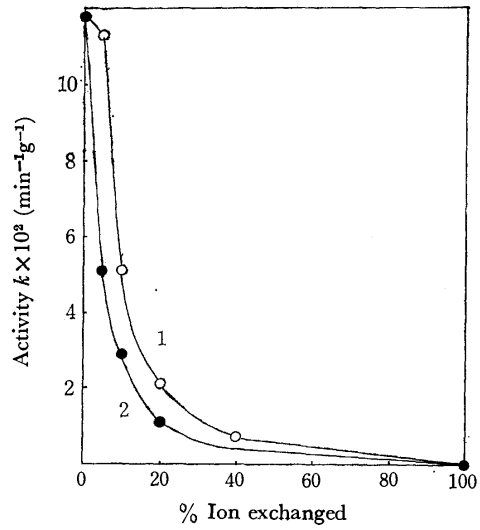

Fig. 5. Effect of partial ion exchange with Na^+ or Mg^{2+} on the activity for 1-butene isomerization. Temperature 70°C. Catalyst 100 mg. Initial pressure 300 mmHg.
1: AMHNa series 2: AMHMg series.

22) S. Tsuchiya and A. Ozaki, *J. Catal.*, **5**, 537 (1966).
23) Y. Kaneda, Y. Sakurai, S. Kondo, T. Ohnishi, E. Hirota, Y. Morino, and K. Tamaru, 4th International Congress on Catalysis Moscow (1968), Prep. 12.
24) S. Ohae and M. Kise, *Chemistry*, **20**, 902 (1965).
25) F. Helfferich, "Ion Exchange", McGraw Hill, New York (1962).
26) F.E. Harrice and S. A. Rice, *J. Chem. Phys.*, **24**, 1258 (1956).
27) G. B. Gates and G. M. Schwab, *J. Catal.* **15**, 430 (1969).
28) G. Zundel, H. Noller, and G. M. Schwab, *Z. Electrochem.*, **66**, 129 (1961).

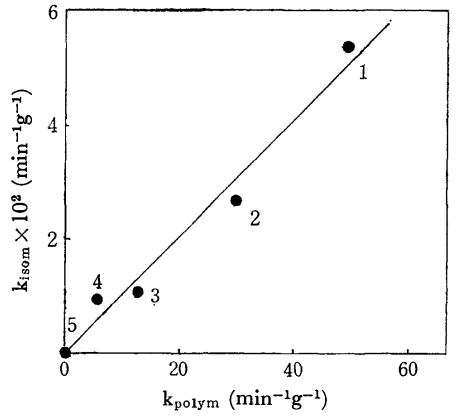

Fig. 6. Correlation of activities between the polymerization of propylene and the isomerization of 1-butene over AMHNa. Temperature 60°C. 1: AMH 2: AMHNa05 3: AMHNa10 4: AMHNa20 5: AMNa.

pre-exponential factors and the apparent energies of activation for the double-bond migration of 1-butene over AMHNa-series catalysts. A similar relation was reported in the decomposition of alcohol over the Dowex-50-Na and -Li series.[17] These facts suggest that the ion exchange provokes the effects on both the enthalpy and the entropy terms of the activated system. The observed change in the selectivities is due to the same causes. The apparent energy of activation for 1-butene isomerization on AMH, 17 kcal/mol, is a little different from the reported value for the 1-butene adsorption forming the carbonium ion on the resin surface, 13.8 kcal/mol.[29]

29) D. Kallo, I. Preszler, and Schay, *Acta Chim. Acad. Sci. Hung.*, **64**, 211 (1970).

The relative values of the first-order rate constants based on the phenomenological ternary system are notably different from the results on the other solid acid catalysts, such as alumina, silica-alumina, and zeolites. The rate constants for *cis-trans* isomerization, k_{ct} and k_{tc}, are relatively large, and the selectivity from 1-butene, k_{1t}/k_{1c}, is more than unity. These findings are different from those for alumina or silica-alumina, as is shown in Table 2. It was found in the previous study that there was an inclination for Lewis-type acid sites to have smaller selectivities for the *trans*-2-butene formation than protonic acid sites on the several solid acid catalysts.[30] The relative values listed are consistent with this view.

The selectivity change during the strong fouling or as a result of poisoning was very samll. The isomerization of *n*-butenes over AMH can probably be explained by the mechanism *via* a common intermediate of the *sec*-butyl carbonium ion, as has already been proposed for similar acid catalysts.[20,31,32] The parallelism found between the catalytic activity for the polymerization of propylene and the double-bond migration can be said to support this idea.

The author wishes to express his thanks to Professor Emeritus Dr. Tadao Shiba for his valuable advice throughout the study.

30) T. Uematsu, *J. Facul. Eng. Chiba Univ.*, **23**, 155 (1972).
31) W. K. Hall and J. W. Hightower, *Kinet. Catal.* **63**, 122 (1967).
32) J. W. Hightower and W. K. Hall, *J. Phys. Chem.*, **71**, 1014 (1967).

BULLETIN OF THE CHEMICAL SOCIETY OF JAPAN, VOL. 45, 3333—3342 (1972)

The Vibrational Assignment and Force Constants of Halogenomethylsilanes and Their Germanium Analogues: $ClCH_2SiH_3$, $ClCH_2SiD_3$, $BrCH_2SiH_3$, $BrCH_2SiD_3$, $ClCH_2GeH_3$, and $ClCH_2GeD_3$

Keiichi OHNO and Hiromu MURATA

Department of Chemistry, Faculty of Science, Hiroshima University, Hiroshima

(Received March 14, 1972)

The infrared spectra of $ClCH_2SiH_3$, $ClCH_2SiD_3$, $BrCH_2SiH_3$, $BrCH_2SiD_3$, $ClCH_2GeH_3$, and $ClCH_2GeD_3$ for both the gaseous and solid states in the 250—4000 cm^{-1} region have been obtained. All the fundamental vibrations except for the skeletal bending and $YH_3(-D_3)$ (Y=Si, Ge) torsional vibrations have been observed and assigned. The normal vibration calculation has been carried out using a modified Urey-Bradley force field. The transferability of the force constants has also been investigated.

In order to get information about the vibrational assignments and the molecular forms of the rotational isomerism from normal vibration calculations, a set of force constants in a modified Urey-Bradley force field for the group of molecules containing silicon or germanium atoms will be obtained.

The force constants of X_nYH_{4-n} (X=Cl, Br; Y=Si, Ge; n=1—4)[1] and $(CH_3)_4Si$[2] in an Urey-Bradley force field have been reported. Vibrational assignments for

1) D. E. Freeman and M. K. Wilson, *Spectrochim. Acta*, **21**, 1825 (1965).

2) N. Ishii and T. Shimanouchi, Annual Meeting of Chemical Society of Japan, Osaka (1965).

TABLE 1. PRINCIPAL MOMENTS OF INERTIA, RAY'S ASYMMETRY PARAMETERS, AND P-R SPACINGS OF PARALLEL BANDS OF HALOGENOMETHYLSILANES AND THEIR GERMANIUM COMPOUNDS

	Principal moments of inertia (amu-Å^2)			κ	P-R (cm^{-1})
	I_a	I_b	I_c		
$Cl^{35}CH_2Si^{28}H_3$	23.27	157.51	171.69	−0.9718	14.7
$Cl^{35}CH_2Si^{28}D_3$	28.86	172.55	186.38	−0.9706	14.3
$Br^{79}CH_2Si^{28}H_3$	25.19	236.21	252.31	−0.9849	11.8
$Br^{79}CH_2Si^{28}D_3$	30.74	258.96	274.68	−0.9847	11.3
$Cl^{35}CH_2Ge^{74}H_3$	24.76	237.84	253.08	−0.9861	11.8
$Cl^{35}CH_2Ge^{74}D_3$	30.59	247.92	262.63	−0.9839	11.6

CH_3YH_3,[3] $CH_3CH_2YH_3$,[4] and $(CH_3)_2SiH_2$[5] (Y=Si, Ge) have also been made.

We will now report the vibrational assignment and force constants of $ClCH_2SiH_3$, $ClCH_2SiD_3$, $BrCH_2SiH_3$, $BrCH_2SiD_3$, $ClCH_2GeH_3$, and $ClCH_2GeD_3$.

These assignments and force constants will be compared with those of the corresponding ethyl halides. These force constants will be transferred to the molecules concerning the rotational isomerism, such as chloromethylmethylsilane.

Experimental

The samples were prepared from tetrahalogenosilanes. The tetrahalogenosilanes were treated by diazomethane, and the resultant halogenomethyltrihalogenosilanes were reduced by $LiAlH_4$ or $LiAlD_4$ in *n*-butyl ether in a vacuum.[6] The crude samples were purified by repeated distillation in a vacuum. The germanium samples were prepared by a similar procedure.

The infrared spectra for the gaseous and solid states were recorded on a Perkin-Elmer model 621 infrared spectrophotometer. 10 cm and 1 m gas cells fitted with KBr or CsI windows were used for the gas measurements. The spectra for the solid states were obtained by condensing the gaseous samples on a CsI window cooled with liquid nitrogen.

Results and Discussion

Band Contours. Chloromethylsilane has been shown by microwave study to have the C_s symmetry and to have a slightly prolate asymmetric top.[7] For $XCH_2YH_3(-D_3)$ (X=Cl, Br; Y=Si, Ge), the principal moments of inertia and Ray's asymmetry parameters given in Table 1 were calculated from the following parameters: C-Cl=1.788 Å, C-Br=1.950 Å, C-Si=1.889 Å, C-Ge=1.945 Å, C-H=1.096 Å, Si-H=1.477 Å, Ge-H=1.529 Å, Y-C-X=109.3°, Y-C-H=109.3°, H-Y-H=110.6°, and H-C-H=107.5°. The bond angles given above have been assumed to be equal to the values for chloromethylsilane. Ray's asymmetry parameters indicate that these molecules may be approximated as a prolate symmetric top. The expected P-R spacing of parallel bands given in Table 1 was calculated by the use of the formulae of Gerhard and Dennison, using $(I_b+I_c)/2$ for I_x.[8] The observed P-R spacing is given in Tables 8—10.

Vibrational Assignments. Halogenomethylsilanes and halogenomethylgermane may have the C_s symmetry. The 18 normal vibrations are reduced to 11 vibrations of the A′ species and 7 of A″, both of which are infrared active. The *a* and *b* internal axes are in the plane of symmetry, while the *c* axis is perpendicular to it. The A′ vibrations may have either *a*-, *b*-, or *ab*-type infrared band contours in the asymmetric top case. The A″ vibrations, on the other hand, have *c*-type infrared band contours. Vibrational assignments of the CH_2 group may be made with reference to the band contours and assignments for CH_2Cl_2,[9] which has magnitudes of rotational constants and asymmetry parameters similar to those for $XCH_2YH_3(-D_3)$. Also, vibrational assignments are made with reference to those of $CH_3YH_3(-D_3)$[3] and $CH_3CH_2YH_3(-D_3)$.[4] The observed frequencies and their assignments are summarized in Tables 2—7. The fundamental vibrations are given in Tables 8—10, together with the intensities, band types, and P-R spacings.

TABLE 2. INFRARED SPECTRA OF CHLOROMETHYLSILANE-d_0

Vapor			Solid		Assignments
cm^{-1}	Type	Int.	cm^{-1}	Int.	
3116		vw			2168+950=3118
2989	C	s	2997	vw	CH_2 antisym. str.
2954, 2948, 2939	AB	s	2943	w	CH_2 sym. str.
2810		vw			
2801b		vw			
2795sh		vw			
2599, 2584	B	vw			1410+1182=2592
2326b		vw			
			2192sh	vs	
2197	C	vs	2186	vs	SiH_3 asym. str. (A′, A″)

3) J. L. Duncan, *Spectrochim. Acta*, **20**, 1807 (1964), J. E. Griffiths, *J. Chem. Phys.*, **38**, 2879 (1963), and E. A. Clark and A. Weber, *ibid.*, **45**, 1759 (1966).

4) K. M. Mackay and R. Watt, *Spectrochim. Acta*, **23A**, 2761 (1967).

5) D. F. Ball, P. L. Goggin, D. C. McKean, and L. A. Woodward, *ibid.*, **16**, 1358 (1960).

6) D. Seyferth and E. G. Rochow, *J. Amer. Chem. Soc.*, **77**, 907 (1955).

7) R. H. Schwendeman and G. D. Jacobs, *J. Chem. Phys.*, **36**, 1251 (1962).

8) S. L. Gerhard and D. M. Dennison, *Phys. Rev.*, **43**, 197 (1933).

9) T. Shimanouchi and I. Suzuki, *J. Mol. Spectrosc.*, **8**, 222 (1962).

TABLE 2. (continued)

Vapor			Solid		Assignments
cm^{-1}	Type	Int.	cm^{-1}	Int.	
2175					
2168	AB	vs	2177	vs	SiH_3 sym. str.
2160					
2040b		vw			1110+925=2035
1978b		vw			
1738b		vw			1182+557=1739
1637b		vw			925+719=1644
1441sh		vw			
			1442	vvw	719×2=1438
1417					
1410	AB	m	1399	ms	CH_2 sci.
1402					
1384sh		vw			
1330	B	w	1327	vw	
1316					
1281	B	w	1269b	vw	719+557=1276
1265					
			1234b	vw	
1189	B	wm	1181	m	CH_2 wag.
1174			1178		
			1152	vw	
1110	C	m	1116	m	CH_2 twist.
1096b		m			
1065		vw	1078	vw	
			1046b	vw	
950sh		s	941	vs	SiH_3 asym. def. (A″)
930	B	vs	926sh	vs	
920			920	vs	SiH_3 asym. def. (A′)
			911sh	vs	SiH_3 sym. def.
			908	vs	
			894	vs	
880		vw			
			870b	vw	
815	C	s	811	s	CH_2 rock.
811sh		s	806sh	m	
773	B	m	756	s	C–Cl str.
756					
			738	vw	
725	B	m	714	ms	C–Si str.
713					
684		vw			
674	C	vw			
662		vw			
			643b	vvw	
			585	vvw	
562					
557	AB	s	552	s	SiH_3 rock. (A′)
548					
522			521	w	
513					
509	C	mw	516	w	SiH_3 rock. (A″)
498					
			276?	vw	Cl–C–Si bend. ?
			264?	vw	

Int.=intensity; s, m, w=strong, medium, weak; v=very; sh=shoulder; b=broad; A, B, C=*a*-type, *b*-type, and *c*-type infrared band contours in the asymmetric top case, respectively.

TABLE 3. INFRARED SPECTRA OF CHLOROMETHYLSILANE-d_3

Vapor			Solid		Assignments
cm^{-1}	Type	Int.	cm^{-1}	Int.	
2993	C	w	2996	w	CH_2 antisym. str.
2958					
2951	AB	m	2948	m	CH_2 sym. str.
2943					
2870b		vw			
2795b		vw			1405×2=2810
2575b		w			1405+1175=2580
2197					
2175	B	w	2186	vw	$ClCH_2SiH_3$
2160					
1728b		w			
			1702	vw	
1603	C	vs	1598sh	vs	SiD_3 asym. str. (A″)
1595		vs	1593	vs	SiD_3 asym. str. (A′)
1584sh		vs			
1575					
1568	AB	vs	1565	s	SiD_3 sym. str.
1560			1559sh	m	
			1525b	vw	765×2=1530, 1113+413=1526
1465		vw			765+700=1465
1413					
1405	AB	m	1393	s	CH_2 sci.
1398					
1365b		vw	1362b	vw	696+676=1372, 682×2=1364
			1324	vvw	
1184					
1175	AB	w	1176	m	CH_2 wag.
1169					
1105	C	w	1113	w	CH_2 twist.
1083b		w			676+409=1085
			1064b	vvw	
			876	vvw	
864sh		w			455+409=864
845		w	851	w	
842		m	835sh	w	
834sh		w	833	w	413×2=826
			823	w	
779	B	s	765	vs	C–Si str.
765	C	s			CH_2 rock.
756sh		m	733	w	
704sh		vs			
700	C	vs	688	vs	SiD_3 asym. def. (A″)
689	B	vs	682	vs	C–Cl str.
676		s	672	vs	SiD_3 asym. def. (A′)
650					
643	A	s	638	s	SiD_3 sym. def.
637					
536	B	w	520	w	
523					
459					
455	AB	s	457	s	SiD_3 rock. (A′)
445					
409	C	m	413	m	SiD_3 rock. (A″)

TABLE 4. INFRARED SPECTRA OF BROMOMETHYLSILANE-d_0

Vapor			Solid		Assignments
cm^{-1}	Type	Int.	cm^{-1}	Int.	
3113		w			
3005sh		m	3004	w	CH_2 antisym. str.
2988sh		m	2967b	vw	2167+797=2964
2964, 2958, 2953	AB	s	2951	w	CH_2 sym. str.
			2931b	vw	
2870		w	2863b	vw	
2787b		vw	2801	vw	
2532, 2521	B	vw			1398+1135=2533
2316b		vw			
2197	C	vs	2181	vs	SiH_3 asym. str. (A′, A″)
2171, 2164, 2158	AB	vs	2167	vs	SiH_3 sym. str.
2092		w	2099	w	
2080		w	2087	vw	1135+944=2079
2033b		vw			
1876b					1135+739=1874
			1490	vw	
1431b		vw	1440b	vw	925+504=1429
			1407b	vw	
1404, 1398, 1392	AB	m	1385	s	CH_2 sci.
1359, 1347	B	vw	1344b	vw	674×2=1348
1314, 1304	AB	vw	1314	vw	804+504=1308
1294b			1298b	vw	797+499=1296
1264, 1259, 1254	AB	w	1250	vw	
			1245	w	
			1168b	vw	674+499=1173
			1155	vw	
1142, 1129	B	m	1131	m	CH_2 wag.
			1112b	w	
1076b		vw			
1060	C	m	1066	s	CH_2 twist.
			1059sh	w	
1016		vw	1024	vw	
			997b	vw	499×2=998
954sh		s			
944	C	s	939	s	SiH_3 asym. def. (A′, A″)
931, 920	B	vs	914sh	vs	SiH_3 sym. def.
			896b	vs	
			884	s	
868		vw	870	w	
			844	vw	
			814	w	
804	C	s	797	s	CH_2 rock.
802	C	s			
795sh		m			
			777	w	
			764	w	
746, 733	B	m	738	m	C–Si str.
693, 681	B	m	674	m	C–Br str.
			635	vw	
			587	vw	
564		vw	557	w	
			518	m	
510, 504, 497	AB	s	499	s	SiH_3 rock. (A′, A″)
			481	w	
			399	vw	

TABLE 5. INFRARED SPECTRA OF BROMOMETHYLSILANE-d_3

Vapor			Solid		Assignments
cm^{-1}	Type	Int.	cm^{-1}	Int.	
3115b		vw			
3114b		vw			
3006	C	w	3006	w	CH_2 antisym. str.
			2999sh	vw	
2966, 2961, 2954	A	m	2959sh	w	
			2954	mw	CH_2 sym. str.
2867b		vw			
2852		vw			
2777, 2766	B	vw			
2528, 2516	B	vw			1393+1133=2526
2263b		vw	2253	vvw	1133×2=2266
2203	C	vw			
2169, 2157	B	vw	2173b	vvw	$BrCH_2SiH_3$
2138		vw			1393+749=2142
1876b		vw			
1809b		vw			1133+678=1811
1710b		w			
1603	C	vs	1591sh	vs	SiD_3 asym. str. (A″)
1596, 1585	B	vs	1587	vs	SiD_3 asym. str. (A′)
1570, 1565, 1558	A	vs	1560, 1588	s	SiD_3 sym. str.
			1539sh	vw	
1501b		w			
			1486sh	vvw	1059+428=1487
1401sh		w			
1399, 1393, 1388	A	m	1380	ms	CH_2 sci.
1360		vw			749+612=1361
1352		vw			678×2=1356
1289		vw	1289b	vvw	678+612=1290

TABLE 5. (continued)

Vapor			Solid		Assignments
cm^{-1}	Type	Int.	cm^{-1}	Int.	
1280		vw			
			1243	vvw	
1196sh		vw			
1181sh		vw			
1170sh		vw			749+426=1175
1139, 1128	B	m	1132, 1129	m	CH_2 wag.
			1104	vvw	
			1074	vvw	647+428=1075
1056	C	w	1059	mw	CH_2 twist.
			1054	vw	
986, 974	B	vvw			
910, 898	B	vvw			
844	C	vw	846	vw	412+426=838
840sh		mw			
834		w	830	vw	
819, 810	B	mw	821	vw	
772sh		m	776sh	vvw	
753	C	vs	747	vs	CH_2 rock.
745	B	vs	740	vs	C–Si str.
			721sh	w	
686, 678	C	vs	677	vs	SiD_3 asym. def. (A″)
666, 657	B	vs	660	vs	SiD_3 asym. def. (A′)
			654, 647	vs	SiD_3 sym. def.
618, 607	B	mw	604	mw	C–Br str.
567sh		vw			
559b		vw			
530		vw	539	vw	
			526sh	vvw	
			482	vw	
			456	vvw	
432, 420	B	s	428	s	SiD_3 rock. (A′)
412sh		m	417	m	SiD_3 rock. (A″)
			353	vw	

TABLE 6. INFRARED SPECTRA OF CHLOROMETHYLGERMANE-d_0

Vapor			Solid		Assignments
cm^{-1}	Type	Int.	cm^{-1}	Int.	
3001sh		w	2987	w	CH_2 antisym. str.
2988sh		m			
2963, 2951	B	m	2955	w	CH_2 sym. str.
2868		mw			
2812		vw			1408×2=2816
2798		vw			
2589, 2578	B	vw			1177+1408=2585
2217b		w			
2115	C	vs	2098	vs	GeH_3 asym. str. (A′, A″)

TABLE 6. (continued)

Vapor			Solid		Assignments
cm^{-1}	Type	Int.	cm^{-1}	Int.	
2092, 2080	B	vs	2091	vs	GeH_3 sym. str.
1909		vw			1116+787=1903
1764, 1752	B	vvw			879×2=1758
1578, 1565	B	vvw			826+743=1569
1464b		vvw			826+641=1467
1416, 1408, 1404	AB	w	1396	m	CH_2 sci.
1391, 1379	B	vw	1382	w	743+641=1384
			1371b	w	879+494=1373
1359, 1353, 1347		vw	1350	w	
1281		vw			787+492=1279, 641×2=1282
1264, 1254, 1244		vw			
1184, 1177, 1172	AB	w	1174	m	CH_2 wag.
			1154	w	decomposed compound?
1142, 1134	B	w	1141	vw	641+492=1133
1116sh		w	1116	m	CH_2 twist.
1077, 1075	B	vvw	1091	vw	
			1079b	vw	
			1043	vw	
994, 983	B	vw	1003b	vw	492×2=984
			934	vw	
888, 879, 875sh	C, AB	s	879	s	GeH_3 asym. def. (A″)
			868	s	GeH_3 asym. def. (A′)
			836sh	w	
834, 826, 822	A	vs	827	s	GeH_3 sym. def.
798b		s	808	s	
787	C	s	778	s	CH_2 rock.
749, 737	B	m	723	m	C–Cl str.
			705sh	vw	
			670	vw	
648, 635	B	m	644	s	C–Ge str.
615		m	619	w	
601, 591	B	w	599	w	
			555	w	
496, 488	B	s	494	s	GeH_3 rock. (A′, A″)
432		vw	444b	vw	

TABLE 7. INFRARED SPECTRA OF CHLOROMETHYLGERMANE-d_3

Vapor			Solid		Assignments
cm^{-1}	Type	Int.	cm^{-1}	Int.	
3004sh	C	w	3008	vw	CH_2 antisym. str.
2989sh		w	2971b	vw	
2968, 2957	B	m	2954	m	CH_2 sym. str.
			2920b	vw	
2868		w	2859b	vw	
2804b		vw			
2589, 2578	B	vw	2561	vw	1408+1178=2586
2115	C				
2092, 2080	B	w	2096	w	$ClCH_2GeH_3$
1606		vw			
1523	C	vs	1513	vs	GeD_3 asym. str. (A″)
1510b		vs			
1504	A				GeD_3 asym. str. (A′)
1498, 1493	B	vs	1498	vs	GeD_3 sym. str.
1414, 1408, 1402	AB	w	1394	m	CH_2 sci.
			1382	vw	754+633=1387
			1370	vw	754+613=1367
1358, 1353, 1347		vw	1349	vw	743+607=1350, 759+591=1350
1185, 1178, 1173	AB	m	1175	m	CH_2 wag.
1142		m	1154	vw	decomposed compound?
1134b		w			759+379=1138, 743+393=1136
1112sh		w	1115	w	CH_2 twist.
1084b		vw	1080	vw	
			1043	vw	
			983	vw	583+397=980
			845	vw	
			796	w	397×2=794
			783	w	397+383=780
			778	w	383×2=766
759	C	s	754	s	CH_2 rock.
749, 737	B	s	725	s	C–Cl str.
			704	w	
638sh		s			C–Ge str.
624	C	s	633	s	GeD_3 asym. def. (A″)
607sh		s	613	s	GeD_3 asym. def. (A′)
			603	s	
596, 586	B	vs	583, 574	vs	GeD_3 sym. def.
			498	w	
			492	vw	
			443	w	
			428	w	
399, 388	B	s	397	s	GeD_3 rock. (A′)
379sh		m	383	m	GeD_3 rock. (A″)

Vibrations of the CH_2 Group. The CH_2 stretching vibrations are expected near 3000 cm^{-1}. In this region, almost all higher bands were of the *c*-type, while the lower bands were of the *ab*- or *b*-type, indicating that the former bands should be assigned to the CH_2 antisymmetric stretching vibration and the latter to this symmetric vibration. These two bands were observed at slightly higher frequencies for molecules with heavier atoms or groups attached to the CH_2 group.

The CH_2 deformation vibrations are expected in the 700—1500 cm^{-1} region. For these molecules, the CH_2 scissors, wagging, twisting, and rocking vibrations were observed as *a*- or *ab*-type bands at about 1400 cm^{-1}, as *ab*- or *b*-type bands at 1100—1200 cm^{-1}, as *c*-type bands at 1050—1120 cm^{-1}, and as *c*-type bands at about 800 cm^{-1}. It is noted that the CH_2 twisting vibrations for $XCH_2YH_3(-D_3)$ are observed clearly as *c*-type bands, similar to those for CH_2X_2(X=Cl, Br),[9] and unlike those for $CH_3CH_2YH_3(-D_3)$[4] and CH_3CH_2X,[10] whose CH_2 twisting vibrations are not well separated from the CH_2 wagging vibrations.

The broad absorptions observed in the gaseous state at 1000—1200 cm^{-1} may be assigned to the vibrations for decomposed compounds, because no corresponding absorptions are observed in the solid state.

Vibrations of the $YH_2(-D_3)$ (Y=Si, Ge) Group. For $CH_3YH_3(-D_3)$, $CH_3CH_2YH_3(-D_3)$, and $XCH_2YH_3(-D_3)$, the corresponding vibrations of $YH_3(-D_3)$ group are expected in the same frequency region and give rise to a similar type of bands in the gaseous state. A very strong *c*-type band assigned to the SiH_3 asymmetric stretching vibrations of both *A′* and *A″* species and an *ab*-type band assigned to the symmetric stretching vibration were observed at 2197 and 2168 cm^{-1} for $ClCH_2SiH_3$, and at 2197 and 2164 cm^{-1} for $BrCH_2SiH_3$, respectively. The separations between the SiH_3 asymmetric and symmetric stretching vibrations for CH_3YH_3 and $CH_3CH_2YH_3$ have been reported to be smaller than 6 cm^{-1}. On the other hand, a larger separation of about 30 cm^{-1} was observed for XCH_2YH_3. However, as no other fundamental vibrations are expected in this region, mixing with the other vibrations cannot be considered. As the YD_3 stretching vibrations were observed in the 1500—1600 cm^{-1} region, mixing with a nearby vibration such as the CH_2 scissors at about 1400 cm^{-1} was expected. The separations for CH_3YD_3 and $CH_3CH_2YD_3$ have been reported to be about 20 cm^{-1}. For XCH_2YD_3, these separations and also a splitting between *A′* and *A″* species of the YD_3 asymmetric stretching vibrations were observed.

The SiH_3 asymmetric deformation of *A′* and *A″* vibrations were assigned to the strong *c*-type band at 950 cm^{-1} for $ClCH_2SiH_3$ and at 944 cm^{-1} for $BrCH_2SiH_3$. This symmetric vibration was assigned to the very strong *b*-type band at 925 cm^{-1} for both $ClCH_2SiH_3$ and $BrCH_2SiH_3$. For $ClCH_2SiD_3$, the strong bands at 700 (*c*-type) and 676 cm^{-1} were assigned to the SiD_3 asymmetric vibrations of the *A″* and the *A′*

10) T. Shimanouchi, Tables of Molecular Vibrational Frequencies, Part I, Bulletin NSRDSNBS 6, p. 40—41, NBS 6, Washington, D. C. (1967) and F. A. Miller and F. E. Kiviat, *Spectrochim. Acta*, **25A**, 1363 (1969).

species respectively. However, this symmetric vibration is considered to mix with the C–Si stretching vibration. Also, for $BrCH_2SiD_3$, the assignments of four bands due to the C–Si, C–Br stretchings, and SiD_3 deformations vibrations with the same symmetry may be complicated, since these vibrations are expected in the same frequency region. These vibrations were assigned on the basis of a normal vibration calculation. For $ClCH_2GeH_3$ and $BrCH_2SiH_3$, both the A' and A'' vibrations of the YH_3 rocking were assigned to the strong *ab*- or *b*-type bands near 500 cm^{-1}. However, for $ClCH_2SiH_3$, a weak *c*-type band assigned to the A'' vibration of the SiH_3 rocking was observed at 509 cm^{-1}. This A' vibration was assigned to the strong *ab*-type band at 557 cm^{-1}. The YD_3 rocking vibrations were observed as strong *b*-type bands (A') at about 400 cm^{-1} and as medium-intensity bands (A'') on the lower frequency side of the former bands.

The vibrational assignments for $ClCH_2GeH_3(-D_3)$ were made similarly; they are given in Tables 6 and 7.

The splittings of the $YH_3(-D_3)$ rocking vibrations ($(\nu_{10}—\nu_{17})$ in Tables 8—10) can be compared for related molecules: 87 cm^{-1} (72 cm^{-1}) for $CH_3CH_2SiH_3(-D_3)$>48 cm^{-1} (46 cm^{-1}) for $ClCH_2SiH_3(-D_3)$> 0 cm^{-1} (14 cm^{-1}) for $BrCH_2SiH_3(-D_3)$ and 29 cm^{-1} (35 cm^{-1}) for $CH_3CH_2GeH_3(-D_3)$>0 cm^{-1} (14 cm^{-1})

Table 8. Fundamental vibrations of chloromethylsilane[a] (cm^{-1})

Vibn. No.	Description	$ClCH_2SiH_3$			$ClCH_2SiD_3$		
A′ 1	CH_2 sym. str.	2948	*ab*[b]	15[c] s[d]	2951	*ab*	15 m
2	$SiH_3(-D_3)$ asym. str.	2197[e]			1595	—	— vs
3	$SiH_3(-D_3)$ sym. str.	2168	*ab*	15 vs	1568	*ab*	15 vs
4	CH_2 sci.	1410	*ab*	15 m	1405	*ab*	15 m
5	CH_2 wag.	1182	*b*	15 wm	1175	*ab*	15 w
6	$SiH_3(-D_3)$ asym. def.	925			676	—	— s
7	$SiH_3(-D_3)$ sym. def.	925	*b*	10 vs	643	*a*	14 s
8	C–Cl str.	764	*b*	17 m	696	*b*	15 vs
9	C–Si str.	719	*b*	12 m	772	*b*	14 s
10	$SiH_3(-D_3)$ rock.	557	*ab*	14 s	455	*b*	14 s
11	Cl–C–Si bend.	—			—		
A″ 12	CH_2 antisym. str.	2989	*c*	— s	2993	*c*	— s
13	$SiH_3(-D_3)$ asym. str.	2197	*c*	— vs	1603	*c*	— vs
14	CH_2 twist.	1110	*c*	— m	1105	*c*	— w
15	$SiH_3(-D_3)$ asym. def.	950	*c*	— s	700	*c*	— vs
16	CH_2 rock.	815	*c*	— s	765	*c*	— s
17	$SiH_3(-D_3)$ rock.	509	*c*	— mw	409	*c*	— m
18	$SiH_3(-D_3)$ torsion	—			—		

a) Frequencies for the gaseous state. Frequencies of the *b*-type bands are average values of P–R branches and those of the *a*-, *ab*-, and *c*-type bands are values of Q branch.
b) *a*, *b*, *c*=*a*-type, *b*-type, and *c*-type infrared band contours in the asymmetric top case, respectively.
c) P–R spacing.
d) s, m, w=strong, medium, weak; v=very.
e) Used twice.

Table 9. Fundamental vibrations of bromomethylsilane[a] (cm^{-1})

Vibn. No.	Description	$BrCH_2SiH_3$			$BrCH_2SiD_3$		
A′ 1	CH_2 sym. str.	2958	*ab*[b]	11[c] s[d]	2961	*a*	12 m
2	$SiH_3(-D_3)$ asym. str.	2197[e]			1590	*b*	11 vs
3	$SiH_3(-D_3)$ sym. str.	2164	*ab*	13 vs	1565	*ab*	12 vs
4	CH_2 sci.	1398	*ab*	12 m	1393	*a*	11 m
5	CH_2 wag.	1135	*b*	13 m	1133	*b*	11 m
6	$SiH_3(-D_3)$ asym. def.	925[e]			661[e]		
7	$SiH_3(-D_3)$ sym. def.	925	*b*	11 vs	661	*b*	9 vs
8	C–Si str.	739	*b*	13 m	749	*b*	8 vs
9	C–Br str.	687	*b*	12 m	612	*b*	11 m
10	$SiH_3(-D_3)$ rock.	504	*ab*	13 s	426	*b*	12 s
11	Br–C–Si bend.	—			—		
A″ 12	CH_2 antisym. str.	3005	—	— m	3006	*c*	— w
13	$SiH_3(-D_3)$ asym. str.	2197	*c*	— vs	1603	*c*	— vs
14	CH_2 twist.	1060	*c*	— m	1056	*c*	— w
15	$SiH_3(-D_3)$ asym. def.	944	*c*	— s	678	*c*	— vs
16	CH_2 rock.	804	*c*	— s	753	*c*	— vs
17	$SiH_3(-D_3)$ rock.	504[e]			412	—	— m
18	$SiH_3(-D_3)$ trosion	—			—		

a, b, c, d, e) See a), b), c), d), and e) of Table 8.

Table 10. Fundamental vibrations of chloromethylgermane[a] (cm^{-1})

Vibn. No.	Description	$ClCH_2GeH_3$			$ClCH_2GeD_3$		
A' 1	CH_2 sym. str.	2957	*b*[b]	12[c] m[d]	2962	*b*	11 m
2	$GeH_3(-D_3)$ asym. str.	2115[e]			1504	—	— vs
3	$GeH_3(-D_3)$ sym. str.	2086	*b*	12 vs	1497	*ab*	11 vs
4	CH_2 sci.	1408	*ab*	12 w	1408	*ab*	12 w
5	CH_2 wag.	1177	*ab*	11 w	1178	*ab*	12 m
6	$GeH_3(-D_3)$ asym. def.	881	*ab*	13 s	607	—	— s
7	$GeH_3(-D_3)$ sym. def.	826	*a*	12 vs	591	—	10 vs
8	C–Cl str.	743	*b*	12 m	743	*b*	12 m
9	C–Ge str.	641	*b*	13 m	638	—	— s
10	$GeH_3(-D_3)$ rock.	492	*b*	8 s	393	*b*	11 s
11	Cl–C–Ge bend.	—			—		
A'' 12	CH_2 antisym. str.	3001	—	— w	3004	*c*	— w
13	$GeH_3(-D_3)$ asym. str.	2115	*c*	— vs	1523	*c*	— vs
14	CH_2 twist.	1116	—	— w	1112	—	— w
15	$GeH_3(-D_3)$ asym. def.	879	*c*	— s	624	*c*	— s
16	CH_2 rock.	787	*c*	— s	759	*c*	— s
17	$GeH_3(-D_3)$ rock.	492[e]			379	—	— m
18	$GeH_3(-D_3)$ torsion	—			—		

a, b, c, d, e) See a), b, c), d), and e) of Table 8.

for $ClCH_2GeH_3(-D_3)$. It is expected that the skeletal bending vibrations go away from the $YH_3(-D_3)$ rocking vibration gradually in this order: C-C-Y<Cl-C-Y< Br-C-Y. The splittings decrease in the same order. Moreover, the ratio $((\nu_{10}-\nu_{17})/\nu_{17}$ in Tables 8—10) for the YH_3 rocking vibration is smaller than that for the YD_3 rocking vibration. This shows that the splittings increase when the frequencies of the $YH_3(-D_3)$ rocking and the skeletal bending vibrations become closely spaced together. It seems that the $YH_3(-D_3)$ rocking vibration is affected by the skeletal bending vibration.

Skeletal Vibrations. The $XCH_2YH_3(-D_3)$ molecules have four skeletal vibrations: the C–Y stretching, C–X stretching, X–C–Y bending, and $YH_3(-D_3)$ torsional vibrations. The latter two vibrations were expected in the region below 300 cm^{-1}, which were not observed in the present study. The C–Y and C–X stretching vibrations have the same symmetry, and their bands are expected to appear in the same spectral region of 600—800 cm^{-1}, mixing with each other. Two strong or medium *b*-type bands were observed in this region. These vibrations were assigned on the basis of a comparison of the infrared spectra of $ClCH_2SiH_3(-D_3)$, $BrCH_2SiH_3(-D_3)$, and $ClCH_2GeH_3(-D_3)$ and the normal vibration calculations.

Overtone and Combination Vibrations. The assignments of some overtone and combination vibrations are given in Tables 2—7. For all of the $XCH_2YH_3(-D_3)$, the CH_2 scissors and CH_2 wagging combination vibrations were observed as *b*-type bands near 2500 cm^{-1}. The unassigned weak absorptions may be due to the combination or overtone vibrations for the X–C–Y bending and the $YH_3(-D_3)$ torsion, or to the difference vibrations for fundamentals.

Normal Vibration Calculation

In order to get information about the vibrational assignments and the molecular forms for the rotational isomerism, a set of force constants of the molecules containing silicon or germanium atoms are investigated. The Urey-Bradley force field may be the most effective force field for this purpose.[11] We have attempted to establish the transferability of the set of force constants for similar molecules.

At first, the force constants for CH_3YH_3 were transferred from those for XYH_3[1] and $(CH_3)_4Si$.[2] The force constants of H(C–Y–H), H(Y-C–H), F(C·Y·H), and F(Y·C·H) were, then, obtained by adjusting the calculated frequencies towards the observed.

Secondly, the force constants for CH_3YH_3 and XCH_2-CH_2X[12] were transferred to those for XCH_2YH_3, where the structural parameters were of the same values used in the calculation of the moments of inertia, but assuming tetrahedral angles. Symmetry coordinates are the usual, commonly-used ones.[3,9]

As no X–C–Y bending vibrations were observed in the present study, the force constants of H(X–C–Y) and F(X·C·Y) could not be determined. For them we used the values for XCH_2CH_2X.

In the simple Urey-Bradley force field, the $YH_3(-D_3)$ rocking, CH_2 rocking, and CH_2 twisting frequencies of the *A''* species strongly suggest the necessity of some modification of the force field. Therefore, *trans* coupling, *t*, and *gauche* coupling, *g*, were added, assuming the *gauche* coupling to be $g=-0.5\,t$.[13] When all the transferred force constants of bending and repulsion were used, the mean errors of the calculated and observed frequencies for these molecules could not be made smaller than 2%. The assumption was made that some bending force constants were variable for each molecule and that the repulsion force constants were transferable.

The set of force constants obtained is listed in Table

11) T. Shimanouchi, *Pure Appl. Chem.*, **7**, 131 (1963).
12) Y. Abe and T. Shimanouchi, Symposium on Molecular Structure, Osaka (1966).
13) T. Shimanouchi, *Nippon Kagaku Zasshi*, **86**, 768 (1965).

TABLE 11. FORCE CONSTANTS OF $ClCH_2SiH_3$, $BrCH_2SiH_3$, AND $ClCH_2GeH_3$

Force const.[a]	Adjusted force constants						
	$ClCH_2SiH_3$	$BrCH_2SiH_3$	$ClCH_2GeH_3$	CH_3SiH_3	CH_3GeH_3	$XSiH_3$[b]	$XGeH_3$[b]
K(C–H)	4.390	4.497	4.439	4.438	4.484	—	—
K(Y–H)	2.638	2.632	2.556	2.586	2.514	2.669	2.602
H(H–Y–C)	0.113	0.133	0.123	0.094	0.119	—	—
H(H–Y–H)	0.170	0.170	0.160	0.180	0.170	0.180	0.170
H(H–C–X)	0.147	0.145	0.140	—	—	—	—
H(H–C–Y)	0.104	0.085	0.130	0.123	0.120	—	—
$\kappa(YH_3)$	0.056	0.034	0.026	0.103	0.059	0.131	0.091
$\kappa(CH_2)$	0.027	0.026	0.011	−0.006	−0.002	—	—
t_1	0.017	−0.019	0.099	—	—	—	—
t_2	0.082	0.097	0.076	0.062	0.092	—	—

	Force constants transferred from XYH_3, CH_3YH_3, and XCH_2CH_2X[c]						
Force const.[a]	$ClCH_2SiH_3$	$BrCH_2SiH_3$	$ClCH_2GeH_3$	Force const.	$ClCH_2SiH_3$	$BrCH_2SiH_3$	$ClCH_2GeH_3$
K(C–Y)	1.991	1.991	1.950	F(H·Y·C)	0.149	0.149	0.077
K(C–X)	1.697	1.346	1.697	F(H·Y·H)	0.041	0.041	0.010
H(H–C–H)	0.349	0.349	0.349	F(H·C·X)	0.558	0.421	0.558
F(H·C·H)	0.200	0.200	0.200	F(H·C·Y)	0.271	0.271	0.240
H(Y–C–X)	0.087	0.102	0.087	Y	0.080	0.080	0.080
F(Y·C·X)	0.747	0.644	0.747				

a) The units are mdyn/Å for stretching, K, bending, H, and repulsion, F, and mdyn·Å for intramolecular tension, κ, internal rotation, Y, *trans* coupling, t (t_1=(YH$_3$, X–C–Y), t_2=(YH$_3$, CH$_2$)), and *gauche* coupling, g. F′ is taken as −0.1F. The value of Y is assumed from the barrier height 2.55 kcal/mol. The g is assumed as −0.5 t. b) Ref. 1. c) Ref. 12.

11, together with those for XYH_3 and CH_3YH_3. As the table shows, it was necessary to vary not only the force constants between XCH_2 and YH_3 groups, H(C–Y–H) and H(Y–C–H), but also the force constants, H(X–C–H) and H(H–Y–H), for each molecule. The latter is a slightly smaller value than those for similar molecules of dihalogenoethane (H(H–C–Cl)=0.175 and H(H–C–Br)=0.160 mdyn/Å), methylsilane, and methylgermane.

The observed and calculated frequencies are given

TABLE 12. OBSERVED AND CALCULATED FREQUENCIES OF CHLOROMETHYLSILANE (cm^{-1})

Vibn. No.	$ClCH_2SiH_3$			$ClCH_2SiD_3$		
	Obs.	Calcd.	Dif.[a]	Obs.	Calcd.	Dif.
A' 1	2948	2974	0.9	2951	2974	0.8
2	2197	2198	0.0	1595	1598	−0.4
3	2168	2195	1.2	1568	1562	−0.4
4	1410	1420	0.7	1405	1420	1.1
5	1182	1172	−0.8	1175	1169	−0.5
6	925	927	0.2	676	663	−2.0
7	925	916	−1.0	643	646	0.5
8	764	745	−2.4	696	710	1.9
9	719	718	−0.1	772	746	−3.4
10	557	560	0.6	455	453	−0.4
11	—	293	—	—	271	—
A'' 12	2989	2967	−0.8	2993	2966	−0.9
13	2197	2200	0.1	1603	1592	−0.7
14	1110	1109	−0.1	1105	1106	0.1
15	950	979	3.1	700	679	−3.0
16	815	795	−2.4	765	786	2.7
17	509	516	1.3	409	406	−0.9
18	—	164	—	—	123	—
Mean error 1.10						

a) (Calcd−Obsd)/Obsd×100 (%).

TABLE 13. OBSERVED AND CALCULATED FREQUENCIES OF BROMOMETHYLSILANE (cm^{-1})

Vibn. No.	$BrCH_2SiH_3$			$BrCH_2SiD_3$		
	Obs.	Calcd.	Dif.[a]	Obs.	Calcd.	Dif.
A' 1	2958	2985	0.9	2961	2985	0.8
2	2197	2195	−0.1	1590	1587	−0.2
3	2164	2192	1.3	1565	1560	−0.3
4	1398	1408	0.7	1393	1408	1.0
5	1135	1129	−0.6	1133	1123	−0.9
6	925	930	0.5	661	667	0.9
7	925	919	−0.6	661	651	−1.6
8	739	717	−2.9	749	740	−1.2
9	687	688	0.2	612	613	0.2
10	504	507	0.6	426	426	0.0
11	—	248	—	—	234	—
A'' 12	3005	2980	−0.8	3006	2980	−0.9
13	2197	2198	0.0	1603	1590	−0.8
14	1060	1061	0.1	1056	1054	−0.2
15	944	965	2.3	678	666	−1.8
16	804	790	−1.8	753	771	2.3
17	504	509	0.9	412	409	−0.7
18	—	162	—	—	122	—
Mean error 0.88						

a) (Calcd−Obsd)/Obsd×100 (%).

Table 14. Observed and calculated frequencies of chloromethylgermane (cm^{-1})

Vibn. No.		$ClCH_2GeH_3$			$ClCH_2GeD_3$		
		Obs.	Calcd.	Dif.[a]	Obs.	Calcd.	Dif.
A'	1	2957	2985	0.9	2962	2985	0.8
	2	2115	2113	−0.1	1504	1508	0.3
	3	2086	2107	1.0	1497	1494	−0.2
	4	1408	1413	0.4	1408	1413	0.4
	5	1177	1174	−0.3	1178	1172	−0.5
	6	881	871	−1.2	607	602	−0.8
	7	826	815	−1.3	591	584	−1.2
	8	743	737	−0.8	743	725	−2.4
	9	641	645	0.7	638	640	0.3
	10	492	492	−0.1	393	400	1.8
	11	—	236	—	—	219	—
A''	12	3001	2978	−0.8	3004	2978	−0.9
	13	2115	2113	−0.1	1523	1508	−1.0
	14	1116	1114	−0.1	1112	1112	0.0
	15	879	900	2.3	624	622	−0.4
	16	787	771	−2.1	759	774	2.0
	17	492	496	0.9	379	376	−0.7
	18	—	161	—	—	124	—
Mean error		0.90					

a) (Calcd−Obsd)/Obsd×100 (%).

in Tables 12—14. The distribution of the potential energy (PED) among the modes shows that the concept of characteristic group frequencies can be applied to all the halogenomethylsilanes and to halogenomethylgermane except for some modes. It may also be seen that the CH_2 rocking, YH_3 rocking, and YH_3 asymmetric deformation modes of the A'' species, and the C-X stretching and YH_3 rocking modes of the A' species, show a considerable amount of mixing for $XCH_2YH_3(-D_3)$ (PED, 5—30%). Especially in $ClCH_2GeH_3(-D_3)$, the Ge-C-Cl bending and $GeH_3(-D_3)$ rocking modes show a mixing of about 20% (PED). It seems that the *trans* coupling, t_1, largely contributed to this, because this value for $ClCH_2GeH_3$ is significantly larger than that for XCH_2SiH_3.

The authors wish to thank Associate Professor Michiro Hayashi of Hiroshima University for his helpful discussions and advice throughout the experiments and Mr. Yasuhiro Takeda and Mr. Kazuki Hamo for their help in the syntheses of the initial samples. The authors also wish to thank Dr. Hiromu Sugeta of Osaka University for the use of his computer programs.

BULLETIN OF THE CHEMICAL SOCIETY OF JAPAN, VOL. 45, 3342—3345 (1972)

Fractionation of Tritiated Water in Potassium Chromium Sulfate Dodecahydrate

Haruhiko TANAKA,* Tsutomu KADO, and Hisao NEGITA

Department of Chemistry, Faculty of Science, Hiroshima University, Higashisenda-machi, Hiroshima

(Received March 21, 1972)

A considerable dilution of tritiated water in the water of crystallization was observed in the crystal-growth process of $KCr(SO_4)_2 \cdot 12H_2O$ from a slightly supersaturated aqueous solution. This was explained in terms of an ionic process in aqueous solution and a surface-diffusion mechanism of crystal growth. It was also found that the tritium content in the hexahydrate was appreciably smaller than that in the liberated water during the course of reaction;

$$KCr(SO_4)_2 \cdot 12H_2O \xrightarrow[in\ vacuo]{40^\circ C} KCr(SO_4)_2 \cdot 6H_2O + 6H_2O.$$

It seems that the stepwise dehydration supports the dehydration mechanism proposed by Garner.

It has been reported that an examination of the fractionation of tritiated water in the crystallization of some hydrated salts from an aqueous solution helps clarifying the crystal-growth mechanism and/or the behavior of water during the course of crystallization.[1] We might expect that examination of the possible fractionation of tritiated water during the course of stepwise dehydration also leads to understanding of the dehydration mechanism. Though various studies have been carried out on the dehydration processes, not much has been done to clarify its mechanism. So far such an elucidation does not seem to have been made in the light of the fractionation of tritiated water.

Recently, the hydration of ions in an aqueous solution has been studied extensively by various methods, the life-time of a hydrated cation being determined.[2] Eigen stated from the relaxation technique that alkali metal ions are very weakly hydrated in aqueous solutions, *i.e.*, the life-time of the hydrated cations is *ca.* 10^{-9} sec.[3]

On the contrary, it is well-known that the water of hydration of a chromium ion is very rigidly held in the sphere, *i.e.*, the life-time of the Cr^{3+} ion is *ca.* 10^5—10^6 sec.[4]

* Present address; Shinonome Branch School, Faculty of Education, Hiroshima University, Shinonome, Hiroshima.

1) H. Tanaka, This Bulletin, **45**, 339 (1972).

2) F. Basalo and R. Johnson, "Coordination Chemistry," W. A. Benjamin, Inc., New York, N. Y. (1964), p. 154.

3) M. Eigen, *Pure Appl. Chem.*, **6**, 97 (1963).

4) J. P. Hunt and R. A. Plane, *J. Amer. Chem. Soc.*, **76**, 5960 (1954).

The crystal growth of a few salts from very slightly supersaturated solutions has been studied extensively by Bennema.[5] He concluded from his study that the crystal growth may occur by means of the surface-diffusion mechanism originally proposed by Burton *et al.*

Hepburn and Phillips reported that the water coordinated to the univalent cation is primarily dissociated *in vacuo* in the case of alum:[6]

$$[M^+(OH_2)_6][M^{3+}(OH_2)_6](SO_4)_2 \longrightarrow M^+[M^{3+}(OH_2)_6](SO_4)_2 + 6H_2O$$

On the contrary, Garner suggested that the exchange of the water coordinated to each cation in alum occurs during the course of stepwise dehydration, the excess water being dissociated to give the hexahydrate.[7] A study from a new view point is desirable for the elucidation of the mechanisms of the crystal growth and dehydration. It seems to be of interest to examine the possible fractionation of tritiated water in alum which would be caused by the crystal growth from a solution and stepwise dehydration.

For this purpose, potassium chromium sulfate dodecahydrate, $KCr(SO_4)_2 \cdot 12H_2O$, was chosen.

Experimental

Commercial potassium chromium sulfate dodecahydrate was purified by recrystallization. Twice-distilled water containing a trace amount of tritiated water (HTO) was used as a solvent. The single crystal of $KCr(SO_4)_2 \cdot 12H_2O$ was grown from a slightly supersaturated tritiated aqueous solution at 20.2°C by evaporating the solvent gradually.

Half of the water of crystallization was removed from the single crystal at 40°C *in vacuo*. Another half of the water was dehydrated completely by heating at 350°C. Water from the dodecahydrate was also recovered by heating at 350°C until no further dehydration was observed. The recovery of water is shown in Fig. 1.

The tritium contents were compared by analyzing the activity of tritium. Measurements were carried out with a liquid scintillation counter, a Packard Model 2002 Tri-Carb Scintillation Spectrometer. As a scintillant we used a solution composed of toluene, ethylene glycol monomethyl ether, 2,5-diphenyloxazole (PPO) and 1,4-bis-2′-(5′-phenyloxazolyl) benzene (POPOP).

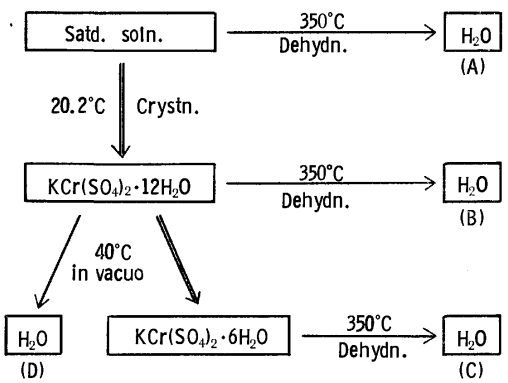

Fig. 1. The scheme for the recovery of water.

Results and Discussion

The separation factor S_1 of HTO for the crystal growth of a hydrated salt from a slightly supersaturated aqueous solution has been defined as $S_1 = N_s/N_l$, where N_s and N_l are the mole fractions of HTO in the solid and liquid phases, respectively.[8] On the contrary, the separation factor S_2 for the dehydration $KCr(SO_4)_2 \cdot 12H_2O \longrightarrow KCr(SO_4)_2 \cdot 6H_2O + 6H_2O$ can be defined as the ratio of the mole fraction of HTO in the hexahydrate to that in the dodecahydrate. The separation factor S_3 can thus be given by the ratio of HTO content in the primarily liberated water to that in the dodecahydrate.

Table 1. Separation factor of HTO in $KCr(SO_4)_2 \cdot 12H_2O$

Comparison of watr	Ratio of cpm[a]	Separation factor
(B)/(A)	(17469±170)/(18191±83)	$S_1 = 0.960 \pm 0.007$
(C)/(B)	(17222± 71)/(17469±170)	$S_2 = 0.986 \pm 0.007$
(D)/(B)	(17895±173)/(17469±170)	$S_3 = 1.024 \pm 0.009$

a) Mean of 5–6 measurements with a counter of 35% efficiency.

Table 1 shows the observed fractionation of tritiated water. (A), (B), (C), and (D) denote the kinds of water shown in Fig. 1. The average net counts per minute (cpm) for 0.1 g of water and the values of the separation factor which are equal to the ratios of cpm are given, each cpm being in proportion to the mole fraction of HTO.

We see from the S_1 value 0.960 that tritiated water is considerably diluted in the dodecahydrate during the course of crystallization from its aqueous solution. It is found from the S_2 value 0.986 that tritiated water is appreciably diluted in the hexahydrate during the course of stepwise dehydration; $KCr(SO_4)_2 \cdot 12H_2O \xrightarrow[in\ vacuo]{40°C} KCr(SO_4)_2 \cdot 6H_2O + 6H_2O$. The dilution in the hexahydrate can also be seen from the S_3 value 1.024.

Tritium Fractionation on the Crystal Growth of $KCr(SO_4)_2 \cdot 12H_2O$. It has been reported that the S_1 value is found to be nearly equal to unity if the crystal grows according to a volume-diffusion mechanism; there is a direct integration of the growth unit from the solution into the kink without any surface diffusion.[9] On the contrary, tritiated water may be diluted in the water of crystallization, if a surface-diffusion mechanism in which the growth unit diffuses over a wide range of the crystal surface before integrating into the kink, controls the crystal growth from a solution.[1]

It has been shown in the crystal growth of potassium aluminum sulfate dodecahydrate $KAl(SO_4)_2 \cdot 12H_2O$ that HTO can be diluted in the water of hydration of

5) P. Bennema, Thesis, The Technical University of Delft (1965); P. Bennema, *J. Cryst. Growth*, **5**, 29 (1969).

6) J. R. I. Hepburn and R. F. Phillips, *J. Chem. Soc.*, **1952**, 2569.

7) W. E. Garner, "Chemistry of the Solid State," Butterworths, London (1955), p. 213.

8) H. Tanaka and H. Negita, This Bulletin, **43**, 3079 (1970).

9) H. Tanaka and H. Negita, *ibid.*, **44**, 2075 (1971).

the K^+ ion in the crystal and the fractionation may not actually take place for the hydration water of the Al^{3+} ion in the crystal.[1] The R_{HTO}/R_{H_2O} ratio has been obtained for the free water on the crystal growth of the hydrated salt *via* surface diffusion:

$$R_{HTO}/R_{H_2O} = (m_{H_2O}/m_{HTO})^{1/2} = 0.949, \quad (1)$$

where R_{HTO}/R_{H_2O} is the ratio of the integration of HTO into the crystal to that of H_2O, and m_{H_2O}/m_{HTO} the mass ratio of H_2O to HTO.

Although the hydration number of an ion in an aqueous solution can not be defined in a strict sense, it may be conveniently taken as the number of water molecules directly coordinated to the central ion, for example, six for the Cr^{3+} ion.[10] The hydration water of the K^+ ion may, as is the case for $KAl(SO_4)_2 \cdot 12H_2O$, be assumed to become free to be integrated into the crystal from a solution, since the life-time of the hydrated cation is extremely short; *ca.* 10^{-9} sec.[3] This seems to be in line with the suggestion of Samoilov that the K^+ ion diffuses in an aqueous solution practically without any hydration water.[11]

It is well-known that the water is strongly bound to the Cr^{3+} ion as compared with the Al^{3+} ion, *i.e.*, the life-time of $Cr(OH_2)_6^{3+}$ and $Al(OH_2)_6^{3+}$ is 10^5—10^6 sec[4] and 1—10 sec,[12] respectively. Thus, the Cr^{3+} ion can be assumed to enter the crystal accompanying the hydration water, since such a behavior may be the case with Al^{3+} ion.[1] As for the sulfate ion, hydration may be negligibly weak in that the ion may be integrated into the crystal practically without accompanying hydration water as is the case for the K^+ ion.

Accordingly, it appears that half of the water in $KCr(SO_4)_2 \cdot 12H_2O$, *i.e.*, the water of crystallization coordinated to the K^+ ion, comes from the free water and another half from the hydration water of the Cr^{3+} ion in the solution. It can be assumed that HTO is diluted in $K(OH_2)_6^+$ of the dodecahydrate according to Eq. (1) and that no practical fractionation takes place in $Cr(OH_2)_6^{3+}$ of the crystal, if we neglect the possible slight enrichment of HTO in the hydration water of the Cr^{3+} ion in the solution.[13]

Although the calculated value of S_1 deviates a little from the observed one, the considerable dilution of HTO in the crystal is explained not by the volume-diffusion but surface-diffusion mechanism and the ionic process.

Validity of the Calculation of S *in Relation to the Data with HDO.* Studies have been carried out on the fractionation of deuterated water (HDO) in the crystallization of hydrated salts from solutions and some important data have been given.[14-16] The data by Barrer and Denny[14] include the S value of HDO less than the lower limiting value of 0.973 which is obtained if the present assumption for the calculation of S of HTO is applied to that of HDO.

Johansson and Holmberg[15] found that HDO is slightly enriched in some hydrated crystals. The enrichment of heavy water in the crystal can not be explained well by the present treatment, *i.e.*, the maximum S value may be estimated to be unity in the case of the volume-diffusion mechanism.[9]

The discrepancy may be due to the following factors: (1) The S value should depend on experimental conditions, especially on the crystallization rate and temperature. (2) Strictly speaking, the fractionation of heavy water in the hydration water is not always negligible in the aqueous solution. (3) The S value might also be influenced by the bond character of the water of crystallization in the crystal.

Factor (1) seems to be the most important at this stage since the well developed single crystal we obtained was grown from a very slightly supersaturated solution under strictly controlled conditions, where the theory of crystal growth can be applied.

Tritium Fractionation on the Dehydration of $KCr(SO_4)_2 \cdot 12H_2O$. Studies have been carried out on the dehydration of hydrated salts *in vacuo*.[17] Numerous examples reveal that an interfacial mechanism is frequently operative during the course of dehydration. It is also assumed generally that water molecules dissociate from the surface of a hydrated crystal to cause a partially dehydrated structure which then leads to a partly amorphous state. A further rearrangement then occurs giving crystalline nuclei of a new phase.

Hepburn and Phillips suggested that (1) the water coordinated to the univalent ion is primarily dissociated *in vacuo* in the case of alum without any exchange of the water with the hydration water of the trivalent ion, and (2) the hexahydrated crystal is then formed in which the structure differs from that of the original dodecahydrate.[6]

It has been suggested that tritiated water is diluted in the hydration water of the K^+ ion in the crystal of the dodecahydrate during the course of crystallization from a solution. Thus, the S_2 and S_3 values can be estimated to be larger and smaller than unity, respectively, if the mechanism proposed by Hepburn and Phillips is the case in the dehydration process.

However, contrary to expectation, the S_2 and S_3 values were found to be 0.986 and 1.024, respectively, implying that the dehydration does not proceed by means of the above mechanism. Thus it can be expected that an alternative mechanism controls the stepwise dehydration of $KCr(SO_4)_2 \cdot 12H_2O$ *in vacuo*.

The dehydration process of $KCr(SO_4)_2 \cdot 12H_2O$ to $KCr(SO_4)_2 \cdot 6H_2O$ is assumed to be followed by three steps.[7] (1) Collapse of the lattice of the dodecahydrate to give an amorphous intermediate and gradual growth of the nuclei of the hexahydrate, (2) diffusion of the dissociated water through the product, and (3) evaporation of the water from the surface of the product. A diagram of the dehydration mechanism is given in Fig. 2. Such a dehydration process implies that the ex-

10) J. F. Hinton and E. S. Amis, *Chem. Rev.*, **71**, 627 (1971).
11) O. Ya. Samoilov, "Structure of Aqueous Electrolyte Solutions and the Hydration of Ions," Consultants Bureau Enterprises, Inc., New York (1965), Chap. 5.
12) D. Fiat and R. E. Connick, *J. Amer. Chem. Soc.*, **90**, 608 (1968).
13) H. Taube, *J. Phys. Chem.*, **58**, 523 (1954).
14) R. M. Barrer and A. F. Denny, *J. Chem. Soc.*, **1964**, 4677.
15) M. Johansson and K. E. Holmberg, *Acta Chem. Scand.*, **23**, 765 (1969).
16) K. Heinzinger, *Z. Naturforsch.*, **A24**, 1502 (1969).
17) For example; W. J. Dunning, *J. Mater. Sci. Res.*, **4**, 132 (1969).

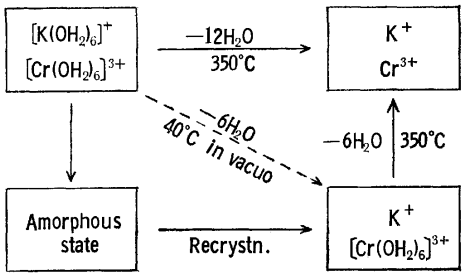

Fig. 2. The mechanism of the stepwise dehydration of $KCr(SO_4)_2 \cdot 12H_2O$. The dotted line refers to the mechanism by Hepburn and Phillips.

change of the hydration water of the Cr^{3+} ion with the other water molecules occurs during the course of dehydration. Such an exchange seems to be supported by the work of Okazaki *et al.*[18]

We believe that Garner's suggestion is appropriate and can be used to account qualitatively for the separation factors, S_2 and S_3. Under the present experimental conditions, the dodecahydrate seems to decompose to give an amorphous intermediate with the adsorbed water molecules on the surface as well as in the interior. The dilution of tritiated water in the hexahydrate may occur in the succeeding rearrangement, since the hydration water of the Cr^{3+} ion is interchangeable with that of the K^+ ion. That is, the hexahydrate may recrystallize from the amorphous state, when the dilution occurs in a similar manner to that in the crystallization of a hydrate from an aqueous solution by means of a surface-diffusion mechanism.

It can be concluded that the dehydration, $KCr(SO_4)_2 \cdot 12H_2O \xrightarrow[in\ vacuo]{40°C} KCr(SO_4)_2 \cdot 6H_2O + 6H_2O$, proceeds by the mechanism of Garner and not by that of Hepburn and Phillips.

The authors express their thanks to Dr. Osamu Yamamoto for his help in measuring the activity of tritium.

18) N. Okazaki, A. Okumura, and K. Nakagawa, This Bulletin, **34**, 983 (1961).

BULLETIN OF THE CHEMICAL SOCIETY OF JAPAN, VOL. 45, 3345—3349 (1972)

The Diffuse Reflection Spectra of 1-Arylazo-2-naphthols Deposited on Various Synthetic Fibers

Yoshio MATSUNAGA and Nobuhiko MIYAJIMA
Department of Chemistry, Faculty of Science, Hokkaido University, Sapporo
(Received March 23, 1972)

The diffuse reflection spectra of sixteen 1-arylazo-2-naphthols deposited on polypropylene, polyacrylonitrile, polyethylene terephthalate, and Nylon-6,6 were recorded in the range from 350 to 700 nm. The spectra indicate the coexistence of the azo and hydrazone tautomers in these systems. By a comparison with the absorption spectra of the compounds dissolved in *n*-hexane, acetonitrile, methyl benzoate, and formamide, it was concluded that the nature of the fibers is the major factor determining the tautomeric equilibria. The effect of moisture on the spectra was found to be rather small except in the cases of the *p*-OH and *p*-MeO derivatives deposited on polyacrylonitrile.

In earlier work, evidence from diffuse reflection spectra was presented for the existence of an azo-hydrazone tautomerism of 1-arylazo-2-naphthols[1] diluted with sodium chloride.[2] The spectra were found, in many cases, to be temperature-dependent. The direction of the change is governed by the kind and position of the substituents; *e.g.*, the change is towards the hydrazone tautomer when the temperature is elevated in the cases of the *p*-Cl and *o*-NO_2 derivatives. Furthermore, the equilibrium was found to move by dilution towards the hydrazone tautomer in all cases. As more and more molecules of the compound are dispersed by dilution, the trend observed was attributed to the stabilization of the hydrazone tautomer by the highly polar surface of the alkali halide. This conclusion has been confirmed by recent measurements of the fluorescence of the same samples.[3] On the other hand, the equilibrium in solution was well established by Burawoy *et al.* about twenty years ago.[4] The relative stability of the hydrazone tautomer was reported to increase in this order of solvents: *n*-hexane<ethanol<chloroform<water. On the basis of these observations, we would expect the tautomeric composition of the azo dyestuff to be much affected by the nature of the substrate on which the compound is deposited.

Our previous work on the diffuse reflection spectra of filter papers dyed with 1-arylazo-2-naphthols revealed that the two tautomeric forms coexist in this state.[5]

1) This designation is used throughout this paper for convenience; it is not intended to define the structure of the compounds.
2) C. Dehari, Y. Matsunaga, and K. Tani, This Bulletin, **43**, 3404 (1970).
3) Y. Matsunaga and M. Shimane, *ibid.*, **45**, 295 (1972).
4) A. Burawoy, A. G. Salem, and A. R. Thompson, *J. Chem. Soc.*, **1952**, 4793.
5) Y. Matsunaga and N. Miyajima, This Bulletin, **44**, 361 (1971).

In addition, the appreciable changes in the hue of the dyed papers caused by moisture could be explained by the deviation from the Kubelka-Munk theory due to the increased regular reflection and, in many cases, by the movement of the equilibrium. In order to demonstrate clearly the effect of substrates on the equilibrium, it would seem to be convenient to employ substrates less hygroscopic than cellulose. Therefore, we selected for this study four synthetic fibers—namely, polypropylene, polyacrylonitrile, polyethylene terephthalate, and Nylon-6,6. To check whether or not the equilibria are essentially determined by the interaction with the substrate, the absorption spectra of 1-arylazo-2-naphthols dissolved in the following solvents were also examined: *n*-hexane, acetonitrile, methyl benzoate, and formamide. These solvents will be considered as model compounds of the synthetic fibers employed.

Experimental

Materials. The samples of 1-arylazo-2-naphthols were the same as those used in our previous work.[5] The derivatives carried one of the following substituents in the *o*-, *m*-, and *p*-positions on the phenyl rings: methyl, chloro, hydroxyl, methoxy, or nitro group.

Fabrics made of polypropylene, polyacrylonitrile, polyethylene terephthalate, and Nylon-6,6 were kindly provided by the Japan Exlan Co. and the Toyo Spinning Co.

Measurements. Fabrics cut into squares, 5 cm×5 cm, were wetted as uniformly as possible with an acetone solution of one of the 1-arylazo-2-naphthols, dropped from a 1 m*l* pipette with graduations. The amount of the compound was then adjusted to about 6 μg per cm^2. The procedure in the diffuse-reflectance measurements was similar to that described in our previous paper.[5] The spectra were plotted using the Kubelka-Munk function, $f(R)=(1-R)^2/2R$, where R is the reflectance. Both the reflection and absorption spectra are presented by taking the maxima arbitrarily as 1.00 in all the figures.

Results and Discussion

1-Phenylazo-2-naphthol (Figs. 1 and 2). The absorption spectra in the four solvents are shown in Fig. 1. For example, the spectrum in *n*-hexane shows two strong bands at about 420 and 460 nm, and a weak one around 500 nm, whereas in formamide the intensity of the first band is relatively reduced and those of the second and third are considerably increased. The band at 420 nm is known to be due to the azo tautomer, and the rest, to the hydrazone tautomer. A comparison of the spectra in Fig. 1 and those recorded in our related works indicates that the concentration of the azo tautomer of 1-phenylazo-2-naphthol decreases in this order of solvents: *n*-hexane (1.890)>acetonitrile (37.5)>ethanol (24.30)>methyl benzoate (6.59)>chloroform (4.806)>formamide (109.5)>50% ethanol. The numbers in parentheses are the dielectric constants of the respective solvents.[6] Burawoy and Thompson noted that the order of solvents obtained by them is approximately in line with the increasing dielectric constant.[7] However, the above-mentioned order, where acetonitrile, methyl benzoate, and formamide were newly added, does not support their suggestion.

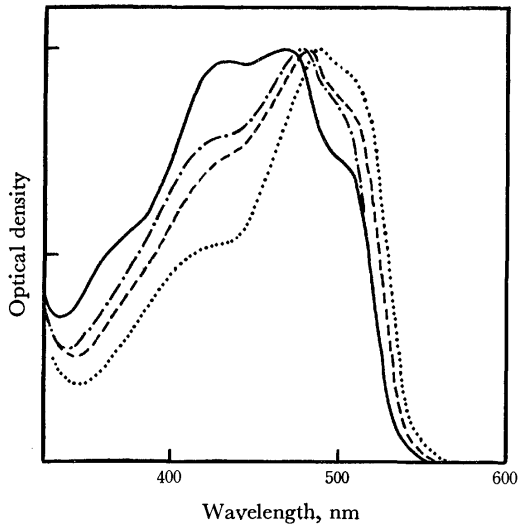

Fig. 1. Absorption spectra of 1-phenylazo-2-naphthol dissolved in *n*-hexane (——), acetonitrile (-·-·), methyl benzoate (----), and formamide (·····).

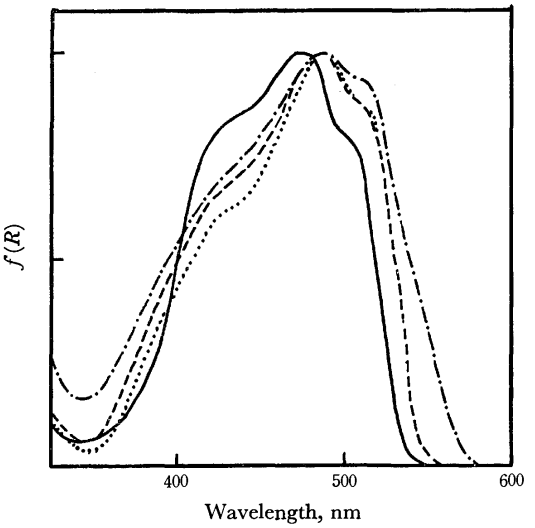

Fig. 2. Reflection spectra of 1-phenylazo-2-naphthol deposited on polypropylene (——), polyacrylonitrile (-·-·), polyethylene terephthalate (----), and Nylon-6,6 (·····).

Figure 2 presents the diffuse reflection spectra of the 1-phenylazo-2-naphthol deposited on the four synthetic fibers. The relative intensity of the 420 nm band due to the azo tautomer decreases in this order of substrates: polypropylene>polyacrylonitrile>polyethylene terephthalate>Nylon-6,6, an order which corresponds well to the order of solvents. Therefore, it seems to be certain that the nature of the fibers is the major factor determining the equilibrium. Unfortunately, the relative intensity of the band appearing around 500 nm and assignable to the hydrazone tautomer is not quite consistent with that of the band at 420 nm. As will be mentioned, the disagreement seems to arise from the anomalous behavior of the compound deposited on polyacrylonitrile.

6) J. A. Riddick and E. E. Toops, Jr., "Organic Solvents," Wiley-Interscience, New York (1955).

7) A. Burawoy and A. R. Thompson, *J. Chem. Soc.*, **1953**, 1443.

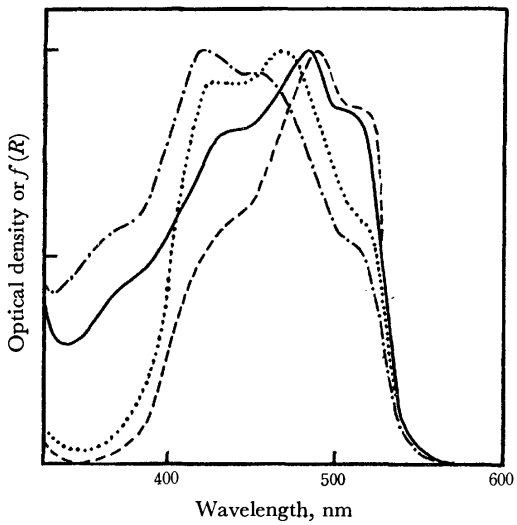

Fig. 3. Absorption spectra of 1-(*o*-tolylazo)-2-naphthol (——) and 1-(*p*-tolylazo)-2-naphthol (-·-·) dissolved in *n*-hexane and reflection spectra of the former compound (——) and the latter (·····) deposited on polypropylene.

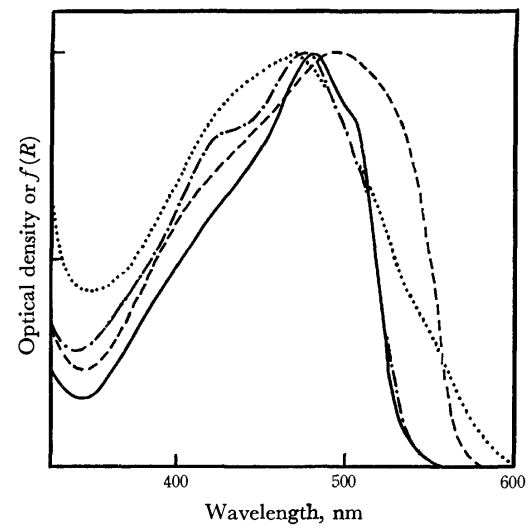

Fig. 4. Absorption spectra of 1-(*o*-chlorophenylazo)-2-naphthol (——) and 1-(*p*-chlorophenylazo)-2-naphthol (-·-·) dissolved in acetonitrile and reflection spectra of the former compound (——) and the latter (·····) deposited on polyacrylonitrile.

1-Tolylazo-2-naphthols (Fig. 3). Burawoy *et al.* reported that the intensity of the absorption band due to the azo tautomer in an ethanolic solution increases in this order of substituents: *o*-Me<*m*-Me~H<*p*-Me.[4] As an example, the absorption spectra of the *o*- and *p*-Me derivatives in *n*-hexane are compared with the reflection spectra of the same compounds deposited on polypropylene in Fig. 3. In accordance with the order of substituents reported by Burawoy *et al.*, the concentration of the azo tautomer in *n*-hexane appears to be higher in the *p*-Me derivative than in the *o*-Me derivative. The same tendency is also found in the reflection spectra. However, it may be noted that the hydrazone tautomer is a little more stabilized by polypropylene than by *n*-hexane. The spectrum of the *p*-Me derivative is the most markedly dependent on not only the solvent, but also on the substrate, among the 1-tolylazo-2-naphthols. The relative intensity of the band due to the azo tautomer around 420 nm was found to decrease in this order: polyacrylonitrile> polypropylene>polyethylene terephthalate>Nylon-6,6. Here again, polyacrylonitrile is not located in the expected position. On the other hand, the intensity of the band due to the hydrazone tautomer at about 520 nm increases in the order to be expected from the nature of the substrates.

1-Chlorophenylazo-2-naphthols (Fig. 4). The relative intensity of the band due to the azo tautomer in solution increases in the following order: *o*-Cl<*m*-Cl< *p*-Cl, as has been reported by Burawoy *et al.*[4] The solution spectra of the last derivative are nearly the same as those of 1-phenylazo-2-naphthol. In the other two cases, the hydrazone tautomers are so favored that their spectra are rather insensitive to the change in solvents. In accordance with this observation, their reflection spectra are not much modified by the substrates. In Fig. 4, the absorption spectra of the *o*- and *p*-Cl derivatives in acetonitrile are compared with the reflection spectra of the compounds deposited on polyacrylonitrile. The structures observed in the former spectra are not detectable in the latter; however, it is not difficult to see that the reflection spectrum bears a similarity to the respective absorption spectrum.

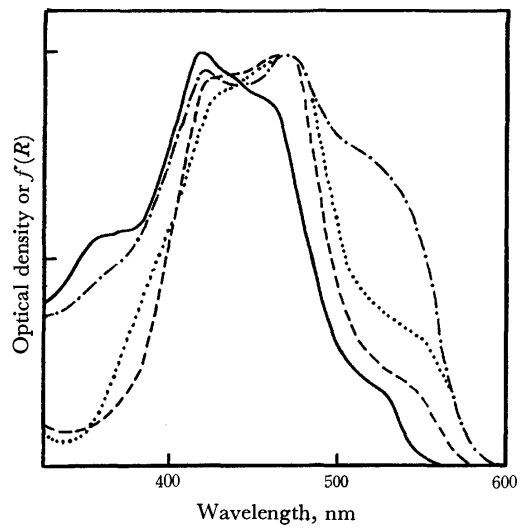

Fig. 5. Absorption spectra of 1-(*p*-hydroxyphenylazo)-2-naphthol dissolved in *n*-hexane (——) and formamide (-·-·) and reflection spectra of the same compound deposited on polypropylene (----) and Nylon-6,6 (·····).

1-Hydroxyphenylazo-2-naphthols (Fig. 5). On the basis of the relative intensity of the band at 420 nm, the concentration of the azo tautomer may be concluded to increase in this order of substituents: *o*-OH< *m*-OH<H<*p*-OH. Consequently, the most pronounced solvent effect on the spectrum can be observed with the *p*-OH derivative. The two extremes of the spectra, that is, those in *n*-hexane and formamide, are shown in Fig. 5. In the former solution, the band at 420 nm, assignable to the azo tautomer, is the strongest. On the other hand, the band due to the hydrazone

tautomer located at 470 nm is much intensified in the latter solution. In addition, it must be noted that the shoulder around 525 nm is appreciably enhanced. The solvent effect on the tautomeric equilibrium is not exactly the same as that found for 1-phenylazo-2-naphthol, suggesting the presence of some specific interaction between the solute and solvents. In the order of solvents for the *p*-OH derivative, methyl benzoate comes before ethanol. As is represented by the spectra of the *p*-OH derivative deposited on polypropylene and Nylon, the effect of substrates on the reflection spectra is much less than that of solvents on the absorption spectra. The tautomeric equilibrium is shifted more towards the hydrazone tautomer compared with that in the model-compound solution. Nevertheless, the spectral change by the substrates is in the expected direction. In the other two derivatives, the effects of the solvents and also of the substrates are generally not appreciable. The only exception is the combination of the *m*-OH derivative and polyacrylonitrile, where a blue shift as much as 25 nm is found.

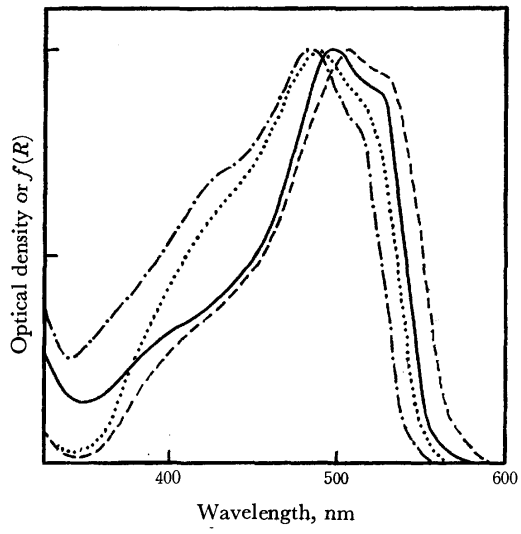

Fig. 6. Absorption spectra of 1-(*o*-anisylazo)-2-naphthol (——) and 1-(*m*-anisylazo)-2-naphthol (-·-·) dissolved in methyl benzoate and reflection spectra of the former compound (——) and the latter (·····) deposited on polyethylene terephthalate.

1-Anisylazo-2-naphthols (Fig. 6). The solution spectra are similar to those of the corresponding hydroxy derivatives. However, the solvent effect on the former spectra is a little more pronounced than that on the latter. In the cases of the *o*- and *m*-MeO derivatives, the order of solvents is modified in the same way as is found with the *p*-OH derivative. In Fig. 6, the absorption spectra of the *o*- and *m*-MeO derivatives in methyl benzoate are compared with the reflection spectra on polyethylene terephthalate. The excellent correspondence between the absorption and reflection spectra supports the hypothesis that the interaction between the compound and the substrate is responsible for the determination of the tautomeric compositions on polyethylene terephthalate. The order of the relative intensities of the band due to the azo tautomer is quite normal in the reflection spectra of the *m*-MeO derivative. However, some anomalies are observed with the other two derivatives deposited on polyacrylonitrile; that is, a red shift of the whole spectrum as much as 30 nm was observed with the *o*-MeO derivative, and an intensification of the bands above 500 nm was noted in both the derivatives.

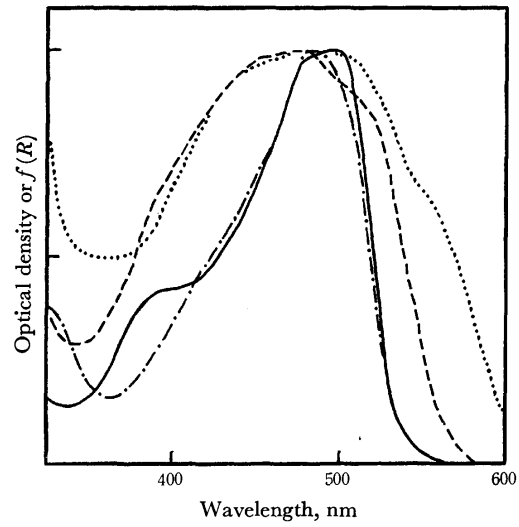

Fig. 7. Absorption spectra of 1-(*o*-nitrophenylazo)-2-naphthol (——) and 1-(*p*-nitrophenylazo)-2-naphthol (-·-·) dissolved in acetonitrile and reflection spectra of the former compound (----) and the latter (·····) deposited on polyacrylonitrile.

1-Nitrophenylazo-2-naphthols (Fig. 7). Except in the case of the *m*-NO_2 derivative, the band to be assigned to the azo tautomer is hardly observable in the solution spectra. As may be expected from this observation, no clear solvent effect is found in these cases. Nonetheless, the reflection spectra of the *o*- and *p*-NO_2 derivatives on polyacrylonitrile were found to be very different from the absorption spectra measured in acetonitrile (see Fig. 7). The reflection spectra are much broader than the absorption spectra and resemble the solid-state spectra reported in our previous works.[2,3] These two compounds appear not to be well dispersed on polyacrylonitrile. As a result, the tautomeric equilibria are shifted to the azo tautomer. It must be added that a similar situation has previously been found in the moistened filter papers dyed with these nitro derivatives.[5]

The moisture regains of the synthetic fibers are known to be as follows: polypropylene, 0%; polyacrylonitrile, 1.3%; polyethylene terephthalate, 0.4%; and Nylon-6,6, 4.5%.[8] In accordance with the low values for polypropylene and polyethylene terephthalate, the reflection spectra do not respond to the addition of moisture. The only exceptions are the *m*-OH and *o*-MeO derivatives deposited on polyethylene terephthalate. In the former case, a blue shift of the absorption maximum by 10 nm is observed. The spectrum of the latter derivative is dominated by the bands located at 505 and 530 nm. The intensity ratio

8) H. Sofue, "Gosei-sen'i (Synthetic Fibers)," Dai-nippon Tosho, Tokyo (1968), p. 167.

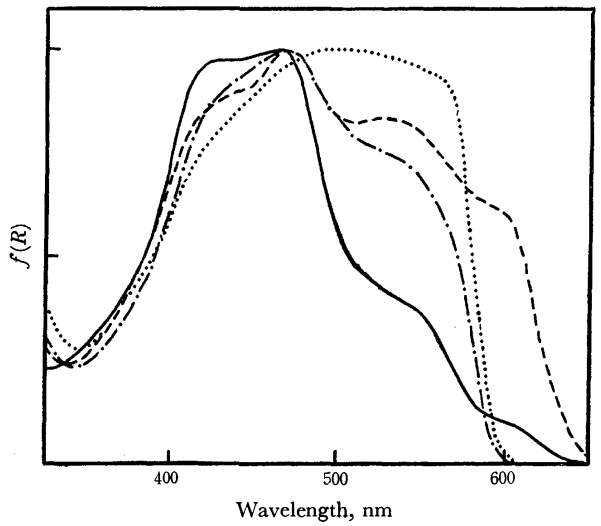

Fig. 8. Reflection spectra of 1-(*p*-hydroxyphenylazo)-2-naphthol deposited on polyacrylonitrile; dried (——) and moistened (– – –), and those of 1-(*p*-anisylazo)-2-naphthol deposited on the same substrate; dried (–·–·) and moistened (·····).

of these two bands is 1.00: 0.95 when dried, but 0.99: 1.00 when moistened, indicating a slight movement of the tautomeric equilibrium towards the hydrazone tautomer on moistening.

The spectra of the *p*-OH and *p*-MeO derivatives deposited on polyacrylonitrile were found to be drastically modified by moistening (see Fig. 8). By a comparison with the spectra recorded in *n*-hexane and formamide (shown in Fig. 5), the change in the spectrum of the *p*-OH derivative can be attributed to the movement of the equilibrium towards the hydrazone tautomer. The spectral change exhibited by the *p*-MeO derivative can also be explained by the movement in the same direction. The latter spectrum after moistening is rather similar to that recorded with a solid sample diluted with sodium chloride.[2] However, the coincidence cannot be considered as an indication that the dye molecules are segregated upon moistening, because the movement is not in the direction to be expected in such a case. In addition, it must be noted that no marked decrease in the absorption intensity due to the segregation is observed here. Therefore, the movement of the tautomeric equilibrium appears to be caused solely by the change in the medium. A less pronounced but definite change in the spectrum was observed with some other derivatives. The results are summarized in Table 1. The intensity ratio of the absorption maximum in the spectrum of a moistened sample to that in the spectrum of the corresponding dried sample is also presented in this table. The latter is the average of the measurements made before moistening and after drying again. The flattening of the spectrum by moisture observed with polyacrylonitrile is found to be rather small if compared with the flattening observed with filter paper.

Table 1. The intensity ratio of the absorption maximum in the spectrum of 1-arylazo-2-naphthol deposited on moistened polyacrylonitrile to that deposited on the dried substrate and the direction of the movement of the equilibrium by moisture; towards the azo tautomer (+) or the hydrazone tautomer (−)

Substituent	Positon		
	ortho	*meta*	*para*
None		0.5 (−)	
Methyl	0.6 (±)	0.9 (−)	0.5 (−)
Chloro	0.9 (±)	1.1 (−)	0.8 (±)
Hydroxy	0.5 (+)	0.7 (±)	0.3 (−)
Methoxy	1.0 (±)	0.8 (−)	0.8 (−)
Nitro	0.8 (±)	0.8 (−)	1.0 (±)

Although the highest moisture regain is shown by Nylon, the effect on the spectra is not very appreciable. The equilibrium was found to move, if at all observable, slightly towards the hydrazone form. As has been mentioned earlier, formamide, the model compound of this substrate, is located next to 50% ethanol in the order of solvents. Therefore, it is not surprising to see that the tautomeric composition in 1-arylazo-2-naphthols deposited on Nylon is not much affected by moisture.

A Computer Simulation of the Oxidation Mechanism. The Liquid-phase Oxidation of Cumene Catalyzed by Triphenylsulfonium Chloride

Katsutoshi OHKUBO and Tohru HASHIMOTO

Department of Synthetic Chemistry, Faculty of Engineering, Kumamoto University, Kurokami, Kumamoto

(Received March 24, 1972)

The mechanism of the liquid-phase oxidation of cumene (RH) catalyzed by triphenylsulfonium chloride was investigated by the computer simulation on the basis of the kinetic analysis. We will discuss particularly the initial short stage of the reaction through the time-conversions of the concentrations of components produced or consumed: R·, RO_2·, ROOH, a complex between the catalyst and O_2 (Cat.-O_2), *etc.* We determined the values of the rate constants appearing in the reaction steps with a good analytic fit to the experimental results, together with the activation energies of all the reaction steps. The following relationships were found between the initial rate of the component formation, r_i (component), and the initial concentration of reactants ($(Cat.)_i$, $(RH)_i$, and $(O_2)_i$):

$$r_i(Cat.\text{-}O_2) \simeq 1.243 \times 10^{-2}(Cat.)_i^{0.970}(RH)_i^{0.0}(O_2)_i^{0.964} \quad mol/l\cdot min$$
$$r_i(R\cdot) \simeq 4.705 \times 10^{-12}(Cat.)_i^{0.648}(RH)_i^{1.886}(O_2)_i^{-0.422} \quad mol/l\cdot min$$
$$r_i(RO_2\cdot) \simeq 5.837 \times 10^{-12}(Cat.)_i^{0.316}(RH)_i^{0.509}(O_2)_i^{0.737} \quad mol/l\cdot min$$
$$r_i(ROOH) \simeq 4.860 \times 10^{-4}(Cat.)_i^{0.436}(RH)_i^{1.842}(O_2)_i^{0.850} \quad mol/l\cdot min$$

It is well known that, in the liquid-phase oxidation of hydrocarbons, some chelate compounds such as copper phthalocyanine[1] participate in the catalytic activation of the ground state, $^3\Sigma_g^-O_2$, as:

$$Cu\text{-}pc + O_2 \longrightarrow Cu\text{-}pc^{\delta+}\cdots O_2^{\delta-} \qquad (1)$$

where Cu-pc denotes copper phthalocyanine. With respect to the catalytic activation of the $^3\Sigma_g^-O_2$, other types of catalysts, such as hemoglobin[2] and sulfonium compounds,[3] can also activate the $^3\Sigma_g^-O_2$:

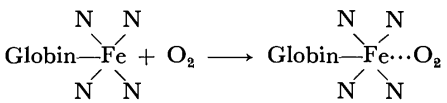

(2)

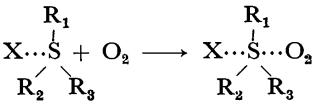

(3)

(R_1, R_2, R_3=alkyl or aryl group)

The complex expressed in Eq. (3) has been previously demonstrated in our kinetic study[4] of the mechanism of cumene oxidation catalyzed by triphenylsulfonium chloride. Such an interaction between sulfonium compounds and the $^3\Sigma_g^-O_2$ has also been confirmed by UV spectroscopic[5] and MO-theoretical studies.[6]

Judging from the fact that a sulfonium catalyst plays an important role in the catalytic activation of the ground state $^3\Sigma_g^-O_2$, the first step can be said to consist of the formation of a complex, Cat.-O_2, as:

$$Cat. + O_2 \underset{k_{t'}}{\overset{k_t}{\rightleftharpoons}} Cat.\text{-}O_2 \qquad (4a)$$

where Cat. denotes a sulfonium compound. Such a complex, Cat.-O_2, then abstracts an active hydrogen from hydrocarbon (RH) to produce an alkyl radical (R·):

$$Cat.\text{-}O_2 + RH \xrightarrow{k_1} R\cdot + Cat. + \cdot O_2H \qquad (4b)$$

This is followed by the usual propagation steps:

$$R\cdot + O_2 \xrightarrow{k_p} RO_2\cdot \qquad (4c)$$

$$RO_2\cdot + RH \xrightarrow{k_2} ROOH + R\cdot \qquad (4d)$$

The termination steps are:

$$2RO_2\cdot \xrightarrow{k_t} \text{inactive products} \qquad (4e)$$

$$Cat. \xrightarrow{k_d} \text{inactive form} \qquad (4f)$$

The deactivation of the catalyst is taken into consideration by Eq. (4f), and the possibility of the radical recombination of other types (R·+R· or R·+RO_2·) is discarded under the present reaction conditions, *i.e.*, an oxygen pressure above 200 mm of mercury.[7] In addition, the decomposition reaction of hydroperoxide is neglected in this paper, because the quantity of O_2 consumed by RH (mol) corresponds to that of hydroperoxide formed (mol) during the initial short stage of the reaction.

The present study has been undertaken in an attempt to elucidate the oxidation mechanism, especially that during the initial short stage of the reaction, by the use of a simulation analysis on a high-speed computer, with attention given to the time-conversions of unstable

1) H. Kropf, *Ann.*, **637**, 73 (1960); H. Kropf and Hd. Hoffmann *Tetrahedron Lett.*, **1967**, 659.

2) L. Pauling and C. D. Coryell, *Proc. Natl. Acad. Sci. U. S.*, **22**, 210 (1936); L. Pauling, *Nature*, **203**, 182 (1964); J. S. Griffith, *Proc. Roy. Soc., Ser. A*, **235**, 23 (1956); J. J. Weiss, *Nature*, **202**, 83 (1964); *ibid.*, **203**, 183 (1964); R. D. Harcourt, *Int. J. Quantum Chem.*, **5**, 479 (1971).

3) K. Fukui, K. Ohkubo, and T. Yamabe, This Bulletin, **42**, 312 (1969); K. Okhubo, T. Yamabe, and K. Fukui, *ibid.*, **42**, 2220 (1969); K. Okhubo and T. Yamabe, *Bull. Jap. Petrol. Inst.*, **12**, 130 (1970).

4) K. Ohkubo, T. Yamabe, and K. Fukui, This Bulletin, **42**. 1800 (1969).

5) K. Ohkubo and T. Yamabe, *J. Org. Chem.*, **36**, 3149 (1971).

6) K. Ohkubo, *Tetrahedron Lett.*, **1971**, 2571, 2897; K. Ohkubo and T. Yamabe, This Bulletin, **44**, 1183 (1971); K. Ohkubo and H. Kanaeda, *Trans. Faraday Soc.*, **68**, 1164 (1972).

7) The effect of the O_2 pressure on the reaction rate does not generally appear above an O_2 pressure of 200 mmHg.

intermediates, oxidants, and reactants; this initial short stage holds the key to the reaction, though chemical and physical studies of the alkyl radical formation are in an early stage of development.

Procedure of Simulation

Normal reaction sequences can be expressed by the following general form:

$$R_1 + R_2 + \cdots + R_n \xrightarrow{k} P_1 + P_2 + \cdots + P_m \quad (5)$$

where R_i are reactants, P_i are products, and k is the rate constant. The reaction increments (or decrements) D are shown, with dt representing a very short time interval, as follows:

$$D = k\prod_{i=1}^{n}(R_i)dt \quad (6)$$

During such a very short time interval, dt, such increments (or decrements) at the reaction time t, D_t, can be expressed by:

$$D_t = \frac{D_{t+dt} + D_{t-dt}}{2} \quad (7)$$

where D_{t+dt} and D_{t-dt} are the reaction increments (or decrements) at the reaction times of $t+dt$ and $t-dt$ respectively ($D_{-dt}=D_0$). The average increments (or decrements), D_{av}, are, then, defined by:

$$D_{av} = \frac{D_t + D_{t+dt}}{2} \quad (8)$$

From Eqs. (7) and (8),

$$D_{av} = 1.5D_t - 0.5D_{t-dt} \quad (9)$$

The concentrations of reactants (R_i) and products (P_i) are, then, changed with D_{av}:

$$(R_i)_t = (R_i)_{t-dt} - D_{av} = (R_i)_{t-dt} - (1.5D_t - 0.5D_{t-dt}) \quad (10a)$$

$$(P_i)_t = (P_i)_{t-dt} + D_{av} = (P_i)_{t-dt} + (1.5D_t - 0.5D_{t-dt}) \quad (10b)$$

This calculation method gives a trapezoidal averaging which is superior to simple decrementing, and this form of calculation is superior to the Runge-Kutta integration.[8] The present simulations on the oxidation mechanism without the ROOH decomposition were carried out in the following way. A series of increments ($D(i)$, $i=1$—7) are defined by the following terms on the basis of the reaction schemes presented previously (see Introduction):

$$D(1) = k_i(O_2)(\text{Cat.})dt \quad (11a)$$

$$D(2) = k_i'(\text{Cat.-}O_2)dt \quad (11b)$$

$$D(3) = k_1(\text{RH})(\text{Cat.-}O_2)dt \quad (11c)$$

$$D(4) = k_p(O_2)(R\cdot)dt \quad (11d)$$

$$D(5) = k_2(\text{RH})(RO_2\cdot)dt \quad (11e)$$

$$D(6) = k_t(RO_2\cdot)^2dt \quad (11f)$$

$$D(7) = k_d(\text{Cat.})dt \quad (11g)$$

For each chemical equation, there is a corresponding differential term:

$$d(\text{Cat.})/dt = k_1(\text{RH})(\text{Cat.-}O_2) + k_1'(\text{Cat.-}O_2) - k_i(O_2)(\text{Cat.}) - k_d(\text{Cat.}) \quad (12a)$$

$$d(\text{Cat.-}O_2)/dt = k_i(O_2)(\text{Cat.}) - k_1(\text{RH})(\text{Cat.-}O_2) - k_i'(\text{Cat.-}O_2) \quad (12b)$$

$$d(R\cdot)/dt = k_1(\text{RH})(\text{Cat.-}O_2) + k_2(\text{RH})(RO_2\cdot) - k_p(O_2)(R\cdot) \quad (12c)$$

$$d(RO_2\cdot)/dt = k_p(O_2)(R\cdot) - k_2(\text{RH})(RO_2\cdot) - k_t(RO_2\cdot)^2 \quad (12d)$$

$$d(\text{ROOH})/dt = k_2(\text{RH})(RO_2\cdot) \quad (12e)$$

$$d(\cdot O_2H)/dt = k_1(\text{RH})(\text{Cat.-}O_2) \quad (12f)$$

$$d(\text{inactive product})/dt = k_t(RO_2\cdot)^2 \quad (12g)$$

$$d(\text{inactive form})/dt = k_d(\text{Cat.}) \quad (12h)$$

From Eqs. (11a—g) and (12a—h), the following relationships can be derived:

$$D(\text{Cat.})_{av} = D(2)_{av} + D(3)_{av} - D(1)_{av} - D(7)_{av} \quad (13a)$$

$$D(\text{Cat.-}O_2)_{av} = D(1)_{av} - D(2)_{av} - D(3)_{av} \quad (13b)$$

$$D(R\cdot)_{av} = D(3)_{av} + D(5)_{av} - D(4)_{av} \quad (13c)$$

$$D(RO_2\cdot)_{av} = D(4)_{av} - D(5)_{av} - D(6)_{av} \quad (13d)$$

$$D(\text{ROOH})_{av} = D(5)_{av} \quad (13e)$$

$$D(\cdot O_2H)_{av} = D(3)_{av} \quad (13f)$$

$$D(\text{inactive product})_{av} = D(6)_{av} \quad (13g)$$

$$D(\text{inactive form})_{av} = D(7)_{av} \quad (13h)$$

The desired concentrations of a component C (reactant, intermediate, or product), $(C)_t$, at the reaction time, t, can be determined by:

$$(C)_t = (C)_i + \int_0^t D(C)_{av}dt \quad (14)$$

where $(C)_i$ and $D(C)_{av}$ are, respectively, the initial concentrations of the components, C, and the over-all increments (or decrements) changing with t. In this paper, the $(C)_t$ values were evaluated every 0.1 sec.

Simulation Results and Discussion

Determination of Rate Constants. Mention should first be made of some characteristic features of the liquid-phase oxidation of cumene (RH) catalyzed by triphenylsulfonium chloride. The oxidation proceeds without any appreciable incubation period; its reaction rate soon reaches its maximum after the start of the reaction (usually up to 600 sec) and then gradually decreases to its stationary state. Moreover, the decomposition of the cumene hydroperoxide (ROOH) accumulated can be neglected for *ca.* 1 hr after the start under the usual reaction conditions.[4] In the previous kinetic study[4] of this cumene oxidation, some values of the rate constants in Eqs. (4a—f) have been determined at 65°C as below:

$$k_i = 2.23\times10^{-2}\ \text{mol}^{-1}\cdot l\cdot\text{sec}^{-1};\quad k_i' = 0.82\times10^{-3}\ \text{sec}^{-1};$$

$$k_1 = 0.794\times10^{-3}\ \text{mol}^{-1}\cdot l\cdot\text{sec}^{-1};\quad k_d = 1.39\times10^{-3}\ \text{sec}^{-1}.$$

With respect to the rate constant of the termination

8) E. Whitaker and A. Robinson, "The Calculation of Observations," Blackie and Son, London (1944), p. 132; H. Margenau and G. H. Murphy, "The Mathematics of Physics and Chemistry," D. van Nostrand, New York (1943), p. 450; R. W. Southwork and S. L. Deleeuw, "Digital Computation and Numerical Methods," McGraw Hill, New York (1965), p. 420.

reaction (Eq. (4e)) Melville and Richards[9] have reported $k_t=3.3\times10^4$ mol$^{-2}\cdot l^2\cdot$sec^{-1} at 65°C in the cumene oxidation. We will here determine the k_p and k_2 values, with a good analytic fit for the simulation analyses. Figure 1 indicates the dependence of the ROOH concentration, (ROOH), upon various k_p and k_2 values (from $k_p(O_2)_i$[10]$=\sim10^6$ to $k_p(O_2)_i=\sim10^2$ with a factor of ten); the time-conversion curves are not directly influenced by the settled k_p values, but are directly changed by k_2 values. Bearing in mind that k_p values usually fall in the range from $\sim10^6$ to $\sim10^7$,[11] the k_p value for the cumene oxidation at 65°C can be set at 1.185×10^7 ($k_p(O_2)_i=5.0\times10^5$).

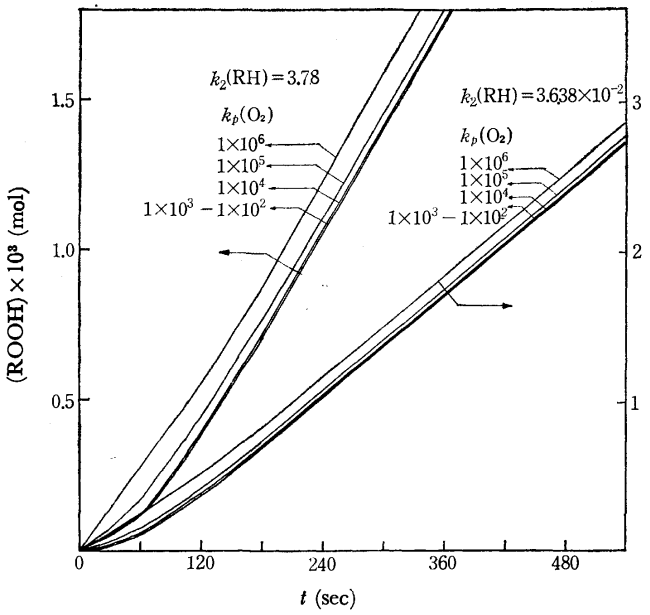

Fig. 1. Variation in time-conversion of (ROOH) with $k_p(O_2)$ and k_2(RH) values.
Initial condition: (Cat.)$_i=3.35\times10^{-4}$mol/l; (RH)$_i$=6.75 mol/l; (O$_2$)$_i=4.22\times10^{-2}$ mol/l.

Next, let us determine the k_2 value, which usually falls in the range of 10^{-1}—10^{-2} as a factor of ten in the autoxidation of cumene, tetralin, or ethyl linoleate at 25—65°C.[14] Figure 2 shows the time-conversion curves of (ROOH) at various k_2 values, together with the experimental curve obtained from cumene (6.75 mol/l) oxidation catalyzed by triphenylsulfonium chloride (3.35×10^{-4} mol/l) at 65°C under atmospheric pressure. As can be seen from Fig. 2, (ROOH) varies in parallel with the k_2(RH) value at a fixed $k_p(O_2)$ value, and the k_2 value of 9.63×10^{-2} mol$^{-1}\cdot l\cdot$sec^{-1} (k_2(RH)$_i$=0.65) can be taken as the most preferable

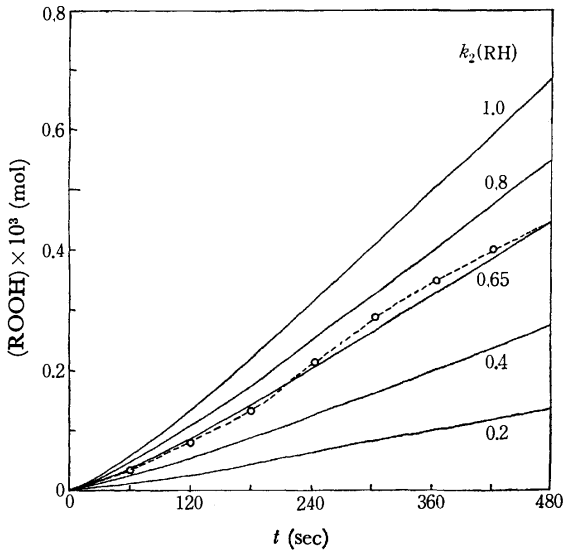

Fig. 2. Variation in time-conversion of (ROOH) with k_2(RH) values. (Dotted curve indicates the experimental result.)
Initial condition: (Cat.)$_i=3.35\times10^{-4}$ mol/l; (RH)$_i$=6.75 mol/l; (O$_2$)$_i=4.22\times10^{-2}$ mol/l.

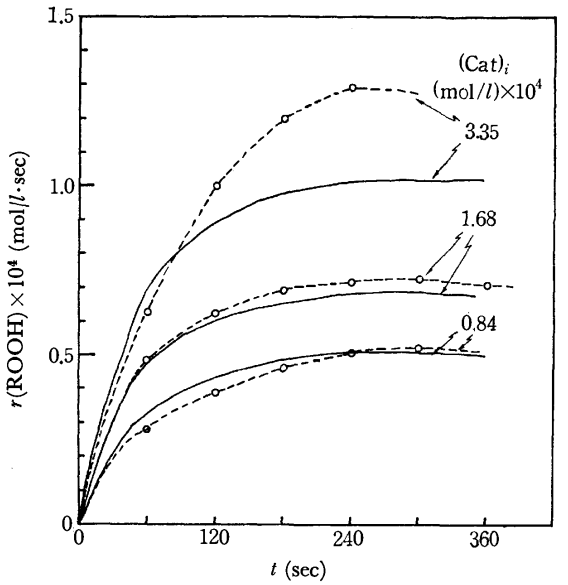

Fig. 3. Variations in time-conversion of ROOH concentration with initial concentration of Cat. (Solid and dotted curves indicate simulation and experimental results respectively.)
Initial condition: (Cat.)$_i$=variable; (RH)$_i$=6.75 mol/l; (O$_2$)$_i=4.22\times10^{-2}$ mol/l.

value with a good analytic fit. Tests of the fitness of k_2 value (9.63×10^{-2} mol$^{-1}\cdot l\cdot$sec^{-1}) for the simulation analyses well made. The results of these tests are shown in Fig. 3, where the variations in the time-conversion of the rate of ROOH formation (r(ROOH)) with (Cat.)$_i$ are illustrated, together with the experimental data.[15] From Fig. 3, $k_2=9.63\times10^{-2}$ mol$^{-1}\cdot l\cdot$sec^{-1} is considered to be fit for the present simulations

9) H. W. Melville and S. Richards, *J. Chem. Soc.*, **1954**, 944,
10) (O$_2$)$_i$ means the initial concentration of O$_2$. Hereafter, the initial concentrations of the components, (C), will be expressed by (C)$_i$; for instance, (RH)$_i$, (Cat.)$_i$, (R·)$_i$, *etc.*
11) For example, k_t(mol$^{-1}\cdot l\cdot$sec^{-1}) at 25°C=6.76×10^7,[12] 1.0×10^7,[13] and 1.0×10^6 [13] for tetralin, ethyl linoleate, and digeranyl respectively.
12) C. H. Banford and M. J. S. Dewar, *Proc. Roy. Soc., Ser. A*, **198**, 252 (1949).
13) L. Bateman, *Quart. Rev.*, **8**, 147 (1954).
14) C. Walling, "Free Radicals in Solution," John Wiley, New York (1957), p. 422.
15) The experimental rate curves can be reproduced with a good analytic fit by $r=k$(RH)$_i^{1.27}$(O$_2$)$_i^{0.68}$(Cat.)$_i$($e^{-at}-e^{-bt}$), where k, a, and b are constants the values of which have been reported in Ref. 4.

of the initial short stage of the oxidation, within the range of observational and calculational errors.[16] Here, the time-conversions of the concentrations of reactants, intermediates, and a product, (Cat.), (Cat.-O_2), ($\cdot O_2H$), (R$\cdot$), ($RO_2\cdot$), and (ROOH), are shown in Fig. 4 for the sake of understanding the reaction system; (Cat.-O_2), ($RO_2\cdot$), and (R$\cdot$) soon arrived at their maxima (t=300 sec) and then gradually lowered to their apparent stationary concentrations. Their distributions were, for instance, at 300 sec, roughly expressed by:

$$(\text{Cat.-O}_2):(\text{R}\cdot):(\text{RO}_2\cdot):(\text{ROOH}) \simeq 1:7\times10^{-8}:5\times10^{-2}:10$$

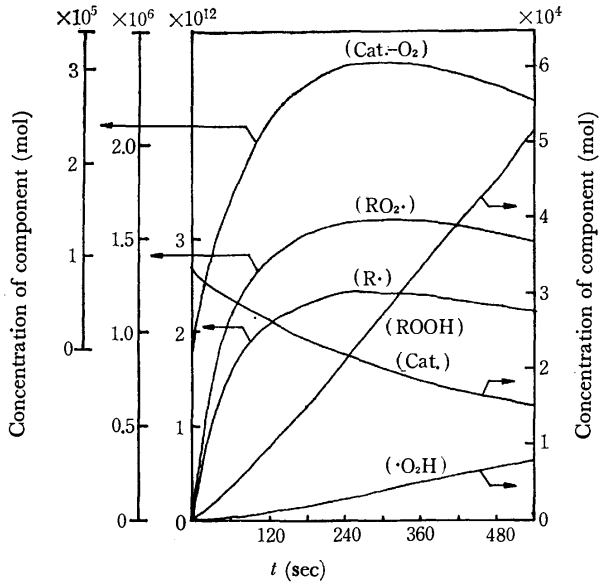

Fig. 4. Time-conversion curves of concentrations of components produced or consumed.
Initial condition: $(\text{Cat.})_i=3.35\times10^{-4}$ mol/l; $(\text{RH})_i=6.75$ mol/l; $(\text{O}_2)_i=4.22\times10^{-2}$ mol/l.

Time Conversion of the Complex, Cat.-O_2. Some remarks should be made before discussing the simulation results. Cat. (*viz.* triphenylsulfonium chloride) interacts with O_2 to form a complex,[5,6] Cat.-O_2, in which the distance between the central S and the center of the O-O bond axis is 2.5—3.0 Å,[6] and in whcih the O-O bond is stretched to a value above 1.30 Å (from 1.2072 Å of the $^3\Sigma_g^-O_2$). In regard to (Cat.-O_2), the simulation results gave at first the time conversions of (Cat.-O_2). The variations in the time conversions of (Cat.-O_2) with $(\text{Cat.})_i$, $(\text{O}_2)_i$, and $(\text{RH})_i$ are shown in Fig. 5. Figure 5 indicates that (Cat.-O_2) possessing the maximum ascends with an increase in $(\text{Cat.})_i$ or $(\text{O}_2)_i$, whilst, interestingly, $(\text{RH})_i$ has little influence on (Cat.-O_2) during the very short stage up to 60 sec. The latter phenomenon may be ascribed to a constant enhancement of the intermolecular interaction between Cat.-O_2 and RH during the above-mentioned period. It is of interest here to pay attention to the dependence of the initial rate of Cat.-O_2 formation, r_i(Cat.-O_2), on $(\text{Cat.})_i$, $(\text{O}_2)_i$, or $(\text{RH})_i$. As shown in Fig. 6, log r_i (Cat.-O_2) *vs.* log $(\text{Cat.})_i$, log $(\text{O}_2)_i$, and/or log$\cdot(\text{RH})_i$ plots gave straight lines and the following relationships can be obtained:

$$r_i(\text{Cat.-O}_2) \propto (\text{Cat.})_i^{0.970} \quad (15a)$$

$$r_i(\text{Cat.-O}_2) \propto (\text{O}_2)_i^{0.964} \quad (15b)$$

$$r_i(\text{Cat.-O}_2) \propto (\text{RH})_i^{0.0} \quad (15c)$$

Eqs. (15a—c) can be rewritten as:

$$r_i(\text{Cat.-O}_2) \simeq 1.243\times10^{-2}(\text{Cat.})_i^{0.970}(\text{O}_2)_i^{0.964}(\text{RH})_i^{0.0} \text{ mol/}l\cdot\text{min} \quad (16)$$

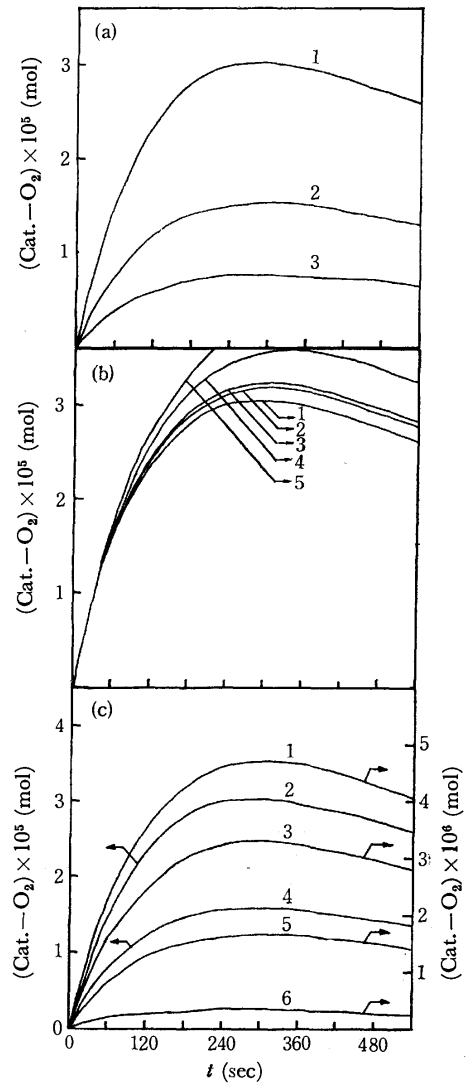

Fig. 5. Variation in time-conversion of (Cat.—O_2) with initial concentrations of Cat., RH, and O_2.
(a) Initial condition
$(\text{RH})_i=6.75$ mol/l; $(\text{O}_2)_i=4.22\times10^{-2}$ mol/l.
$(\text{Cat.})_i$ 1: 3.35×10^{-4} mol/l, 2: 1.68×10^{-4} mol/l, 3: 0.84×10^{-4} mol/l.
(b) Initial condition
$(\text{Cat.})_i=3.35\times10^{-4}$ mol/l, $(\text{O}_2)_i=4.22\times10^{-2}$ mol/l.
$(\text{RH})_i$ 1:6.75 mol/l, 2: 6.31 mol/l, 3: 6.12 mol/l, 4: 5.03 mol/l, 5: 3.80 mol/l.
(c) Initial condition
$(\text{Cat.})_i=3.35\times10^{-4}$ mol/l; $(\text{RH})_i=6.75$ mol/l;
$(\text{O}_2)_i$ 1: 6.03×10^{-3} mol/l, 2: 4.22×10^{-2} mol/l, 3: 4.22×10^{-3} mol/l, 4: 2.11×10^{-2} mol/l, 5: 2.11×10^{-3} mol/l 6: 4.22×10^{-4} mol/l.

16) The experimental data were obtained by the graphic differentiation of the time-conversion curve of (ROOH), this procedure brought about observational errors.

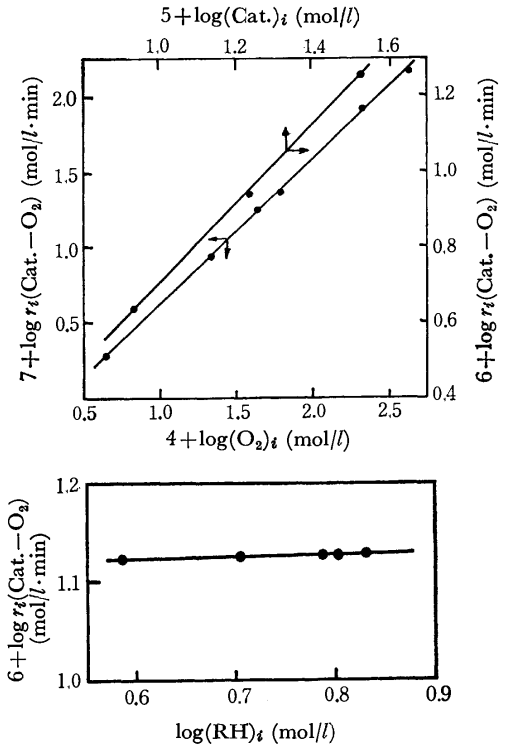

Fig. 6. Plots of log r_i (Cat.—O$_2$)$_i$ *vs.* log(Cat.)$_i$, log(O$_2$)$_i$, and log(RH)$_i$.

Time Conversion of Alkyl Radicals, R·. The process of the R· formation plays an important role in the oxidation reaction, specifically during the initial stage, since the R radical itself acts as a source for the propagating radical chains (Eqs. (4c) and (4d)). Figure 7 indicates the variations in the time conversion of (R·) with (Cat.)$_i$, (O$_2$)$_i$, and (RH)$_i$. As can be seen from Fig. 7, the higher (Cat.)$_i$ and (RH)$_i$ become, the larger becomes the amount of (R·), whilst (O$_2$)$_i$ depresses the R· formation, perhaps because of its predominant consumption of R· through Eq. (4c). The Linear relationships of log r_i (R·) *vs.* log (Cat.)$_i$, log (RH)$_i$, and/or log (O$_2$)$_i$ were rewritten as:

$$r_i(\mathrm{R}\cdot) \propto (\mathrm{Cat.})_i^{0.648} \quad (17a)$$

$$r_i(\mathrm{R}\cdot) \propto (\mathrm{RH})_i^{1.856} \quad (17b)$$

$$r_i(\mathrm{R}\cdot) \propto (\mathrm{O_2})_i^{-0.422} \quad (17c)$$

Eqs. (17a—c) can be rearranged as:

$$r_i(\mathrm{R}\cdot) \simeq 4.705\times10^{-12}(\mathrm{Cat.})_i^{0.648}(\mathrm{RH})_i^{1.886}(\mathrm{O_2})_i^{-0.422} \quad \mathrm{mol}/l\cdot\mathrm{min} \quad (18)$$

Time Conversion of Alkylperoxy Radicals, RO_2·. Considering that (RO_2·) directly controls the rate of ROOH formation through Reaction (4d), the RO_2 radical must also play an impotant role in the oxidation reaction. We will, then, adjust the simulation results as to (RO_2·) similarly to the cases of (Cat.-O$_2$) and (R·). The variations in the time conversion of (RO_2·) with (Cat.)$_i$, (RH)$_i$, and (O$_2$)$_i$, and the plots of log r_i (RO_2·) *vs.* log (Cat.)$_i$, log (RH)$_i$, and log (O$_2$)$_i$ gave the following relationships:

$$r_i(\mathrm{RO_2}\cdot) \propto (\mathrm{Cat.})_i^{0.316} \quad (19a)$$

$$r_i(\mathrm{RO_2}\cdot) \propto (\mathrm{RH})_i^{0.509} \quad (19b)$$

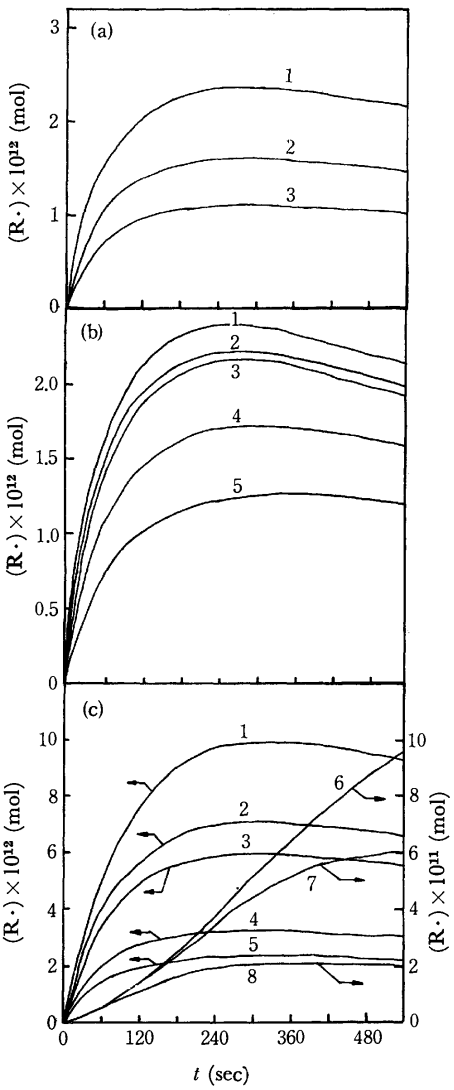

Fig. 7. Variations in time-conversion of (R·) with initial concentrations of Cat., RH, and O$_2$.
(a) Initial condition
(RH)$_i$=6.75 mol/l; (O$_2$)$_i$=4.22×10^{-2} mol/l.
(Cat.)$_i$ 1: 3.35×10^{-4} mol/l, 2: 1.68×10^{-4} mol/l, 3: 0.84×10^{-4} mol/l.
(b) Initial condition
(Cat.)$_i$=3.35×10^{-4} mol/l; (O$_2$)$_i$=4.22×10^{-2} mol/l.
(RH)$_i$ 1: 6.75 mol/l, 2: 6.31 mol/l, 3: 6.12 mol/l, 4: 5.03 mol/l, 5: 3.80 mol/l.
(c) Initial condition
(Cat.)$_i$=3.35×10^{-4} mol/l; (RH)$_i$=6.75 mol/l.
(O$_2$)$_i$ 1: 2.11×10^{-3} mol/l, 2: 4.22×10^{-3} mol/l, 3: 6.03×10^{-3} mol/l, 4: 2.11×10^{-2} mol/l, 5: 4.22×10^{-2} mol/l, 6: 4.22×10^{-6} mol/l, 7: 4.22×10^{-5} mol/l, 8: 4.22×10^{-4} mol/l.

$$r_i(\mathrm{RO_2}\cdot) \propto (\mathrm{O_2})_i^{0.737} \quad (19c)$$

Then,

$$r_i(\mathrm{RO_2}\cdot) \simeq 5.837\times10^{-12}(\mathrm{Cat.})_i^{0.316}(\mathrm{RH})_i^{0.509}(\mathrm{O_2})_i^{0.737} \quad \mathrm{mol}/l\cdot\mathrm{min} \quad (20)$$

Time Conversion of Hydroperoxide, ROOH. In the liquid-phase oxidation of hydrocarbons catalyzed by transition-metal catalysts, it is generally believed that the reaction can proceed after the decomposition of ROOH accumulated during the incubation period (the so-called induction period). The phenomena of ROOH

TABLE 1. ACTIVATION ENERGIES AND RATE CONSTANTS OF REACTION STEPS

Reaction number	Reaction	d_{12} (Å)	$\mu\times10^{23}$ (g)	E (kcal/mol)	Rate constant
(1)	Cat.$+O_2\rightarrow$ Cat.$-O_2$	4.284	4.80	19.93	$9.389\times10^{9}\sqrt{T}\ e^{-19.93/RT}$ mol$^{-1}\cdot l\cdot$sec^{-1}
(2)	Cat.$-O_2\rightarrow$ Cat.$+O_2$	7.36	54.9	21.37	$2.898\times10^{9}\sqrt{T}\ e^{-21.37/RT}$ sec^{-1}
(3)	Cat.$-O_2+$RH$\rightarrow$R$\cdot$+Cat.$+\cdot O_2$H	7.03	14.6	22.46	$1.447\times10^{10}\sqrt{T}\ e^{-22.46/RT}$ mol$^{-1}\cdot l\cdot$sec^{-1}
(4)	R$\cdot+O_2\rightarrow RO_2\cdot$	3.95	4.19	6.38	$8.538\times10^{9}\sqrt{T}\ e^{-6.38/RT}$ mol$^{-1}\cdot l\cdot$sec^{-1}
(5)	$RO_2\cdot+$RH$\rightarrow$ROOH+R$\cdot$	6.88	11.1	19.30	$1.592\times10^{10}\sqrt{T}\ e^{-19.30/RT}$ mol$^{-1}\cdot l\cdot$sec^{-1}
(6)	$RO_2\cdot+RO_2\cdot\rightarrow$ inactive product	7.07	12.55	10.74	$1.582\times10^{10}\sqrt{T}\ e^{-10.74/RT}$ mol$^{-1}\cdot l\cdot$sec^{-1}

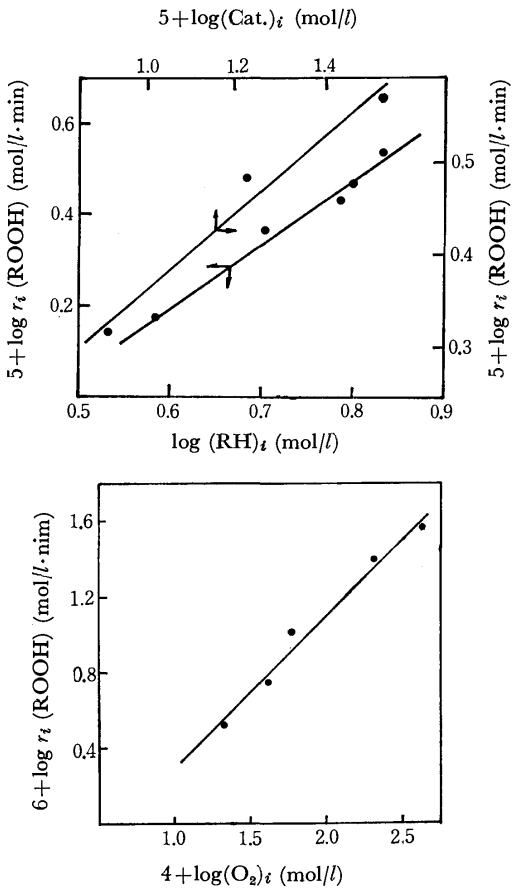

Fig. 8. Plots of log r_i(ROOH) *vs.* log(Cat.)$_i$, log(RH)$_i$, and log(O$_2$)$_i$.

decomposition have been already given in detail,[17-19] but those of ROOH formation during the initial short stage still remain obscure. It is more than of interest —it is necessary— to discuss the dependence of the time conversions of (ROOH) during the above-mentioned period upon the fresh catalyst and the fresh reactants. The plots of log r_i (ROOH) *vs.* log (Cat.)$_i$ and/or log (reactant)$_i$ indicated linear relationships, and we obtained the following equation from the straight lines in Fig. 8:

$$r_i(\mathrm{ROOH}) \simeq 4.860\times10^{-4}(\mathrm{Cat.})_i^{0.436}(\mathrm{RH})_i^{1.842}(\mathrm{O_2})_i^{0.850}\ \mathrm{mol}/l\cdot\mathrm{min} \quad (21)$$

Equation (21) demonstrates that the initial formation of ROOH will be approximately controlled by the square root of (Cat.)$_i$. This implies that we should take into consideration the radical recombination reaction, $RO_2\cdot+RO_2\cdot\longrightarrow$inactive products, even during the initial short stage.

Activation Energies of Reaction Steps. Now, we will estimate the activation energies of the reaction steps (Eqs. (4a—e)) on the basis of the collision theory.[20] The rate constant of the bimolecular reaction, k_{12}, is usually produced by a kinetic theory expression:

$$k_{12}(\mathrm{mol^{-1}}\cdot l\cdot\mathrm{sec^{-1}}) = \pi N d_{12}^2(8kT/\pi\mu)^{1/2}\mathrm{e}^{-E/RT}\times10^{-3} \quad (22)$$

where N, k, d_{12}, and μ stand for the Avogadro number, the Boltzmann constant, the molecular diameter, and the reduced mass respectively. The activation energies evaluated are tabulated in Table 1, together with the rate constants; the formation of Cat.$-O_2$ is an thermic reaction and, suprisingly, the radical recombinations of Eqs. (4c) and (4e) need appreciable activation energies. The latter phenomena must bedue to the reaction of bulky reactants.

In conclusion, more precise discussions of the oxidation mechanism will be undertaken in a succeeding paper on the basis of such favorable methods as the Monte Carlo simulation.

The calculations were carried out on a FACOM 230-60 computer at the Computation Center of Kyushu University.

17) T. Yonezawa, O. Yamamoto, H. Kato, and K. Fukui, *Nippon Kagaku Zasshi*, **87**, 26 (1966).
18) K. Ohkubo and H. Kanaeda, This Bulletin, **45**, 322 (1972).
19) K. Ohkubo, T. Ninomiya, and H. Kanaeda, *Tetrahedron*, **28**, 2969 (1972).
20) In the present reaction system without solvents (the effect of polar oxidation products can be disregarded during the very initial short stage), we can easily establish the Maxwell-Boltzmann distribution, considering that the ascending of collisions in the liquid-phase accompanies the increase in the rates of activation and the deactivation of activated complexes.

Deuteron Magnetic Resonance Studies of Structures and Phase Transitions in the Tantalum-Deuterium System

Keikichi NAKAMURA

National Research Institute for Metals, Nakameguro, Meguro-ku, Tokyo

(Received March 28, 1972)

The deuteron magnetic resonance in the tantalum-deuterium system has been measured as a function of the composition (0.45 to 0.198 D/Ta) and of the temperature (90 to −179°C), and the results has been discussed in relation to the neutron diffraction and the heat capacity data. The most probable arrangement of the deuteriums in the polymorphic varieties has been proposed. For the low temperature form (β_1 form), it has an ordered structure which belongs to the space group $A222$, with the four tantalums at the $4K$ positions and the two deuteriums at the $2a$ positions. Since the deuterium positions are described by a single Z' principal axis direction, which coincides with the c axis, the quadrupole coupling constant is not averaged by the rapid diffusion of the deuteriums. For the intermediate temperature form (β_2 form), a structure constructed with four types of domains has been proposed. In this structure, the space group is the same as that of the β_1 form, and the deuterium positions in the domains are $2a$, $2b$, $2c$, and $2d$ respectively. For the high temperature form (α form), the observed quadrupole coupling constant, which is averaged to zero, can be accounted for if the deuteriums are randomly distributed over all the available tetrahedral sites. However, the calculated configurational entropy based on this assumption is larger than the measured value.

It is a well known phenomenon that many transition metals absorb hydrogen under appropriate conditions.[1] As for the tantalum, the solubility extends to about 44 atomic percent at 200°C and under a 1 atomosphere. However, when the temperature decreases below 60°C, a new phase (β phase) based on the composition Ta_2H is formed.[2,3]

According to the X-ray diffraction study,[2] the high temperature phase (α phase) possesses a body centered cubic structure of elementary tantalum, while the low temperature phase (β phase) is a body centered tetragonal with an axial ratio of $c/a=1.008$. Saba, Wallace, Sandmo, and Craig have measured the heat capacity of Ta_2H[4] from 12 to 555°K and have found three λ points, indicating that the following four forms exist; β_1 below 306°K, β_2 between 306 to 332.5°K, β_3 from 332.5 to 333.5°K, and α above 333.5°K. They have also estimated the configurational entropies. They were zero, 0.7, 3.3, and 4.9 e.u.mol^{-1} for β_1, β_2, β_3, and α respectively. Since there are 12 tetrahedral sites available for each hydrogen atom, they attributed the λ points to the rearrangement of hydrogen among these sites.

The neutron diffraction study by Wallace[5] has shown that the β_1 form is pseudocubic, with $a=2a_0=6.74$ Å, where a_0 is a lattice constant for the β_2 form. He proposed three configurations which satisfied the neutron diffraction intensities for the β_1 form. One of the structures, which he denoted structure A, belongs to the space group $I4$, with half deuteriums located at the general positions of 1/4 1/8 0 and 5/8 0 1/4. To account for the contradiction between the proposed structure and the vanishing residual entropy for the β_1 form, he proposed a structure with a high local order in domains which are not large enough to give rise to superstructure diffractions.

To solve the above contradiction, this problem in the ordered structure of Ta_2D has been discussed in a series of paper.[6-8] Among the three proposed structures, however, the superlattice diffraction reliability factors of the first two structures[6,7] are appreciably worse than that of Wallace's disordered structure. The best agreement with the experimental results was obtained by Petrunin, Somenkov, Shil'shtein, and Chertkov (hereafter abbreviated as PSSC), who took into account the displacement of the Ta atom. This structure is orthorhombic and belongs to the space group $A222$, with $a\approx b\approx\sqrt{2}\,a_0$ and $c\approx a_0$. The four Ta atoms are located at the 4K positions ($-x$ 0 0, 1/2+x 1/2 0, $-x$ 1/2 1/2, 1/2+x 0 1/2), and the two deuterium atoms at the $2a$ positions (1/4 1/4 1/4, 1/4 3/4 3/4). The displacement parameter, x, which was so determined as to minimize the reliability factor, was 0.012, while the minimized reliability factor, for the superlattice diffraction was 0.107.

Among the four proposed structures cited above, the reliability factor for the PSSC ordered model with the displacement of Ta is the smallest, and that for Wallace's model is next. However, one may obtain additional information from the deuteron magnetic resonance. The main purpose of this paper is to obtain additional information on the arrangement of deuteriums in the polymorphic varieties of Ta_2D through studying the deuteron magnetic resonance, which is very sensitive to the position and the translational motion of the deuteriums.

Experimental

Deuterides of tantalum with compositions ranging from

1) G. G. Libowitz, *J. Nucl. Mater.*, **2**, 1 (1960).
2) T. R. Waite, W. E. Wallace, and R. S. Craig, *J. Chem. Phys.*, **24**, 634 (1956).
3) P. Kofstad, W. E. Wallace, and R. S. Craig, *J. Amer. Chem. Soc.*, **81**, 5015 (1959).
4) W. G. Saba, W. E. Wallace, H. Sandmo, and R. S. Craig, *J. Chem. Phys.*, **35**, 2148 (1961).
5) W. E. Wallace, *ibid.*, **35**, 2156 (1961); **41**, 3261 (1964).
6) G. Palenik, *ibid.*, **41**, 3260 (1964).
7) V. A. Somenkov, A. V. Gurskaya, M. C. Zemlyanov, M. E. Kost, N. A. Chernoplekov, and A. A. Chertkov, *Soviet Phys. Solid State*, **10**, 2123 (1969).
8) V. A. Petrunin, V. A. Somenkov, S. Shil'shtein, and A. Chertkov, *Soviet Phys.-Crystallogr.* **15**, 137 (1970).

0.45 to 0.198 D/Ta were prepared by a direct reaction of a known amount of deuterium gas with a known amount of Ta metal powder.

The deuteron magnetic resonance measurements were made using a Varian VF-16 wide line spectrometer operating at 6.53 MHz. The temperatures of the samples from −180 to +90°C were obtained with a Varian variable-temperature accessory.

Results

Deuteron Resonance at Room Temperature. At room temperature, the deuteron resonance of the powdered TaD_n (n=0.45, 0.43, 0.375) consists of two parts; one is at the center of the Larmor frequency, and the other consists of a pair of lines located symmetrically around the Larmor frequency (Fig. 1). The intensity ratio of the central line relative to the two satellite lines increased with a decrease in the deuterium concentration. Since the line width of the satellite lines was broad and the intensity was weak, the satellite lines could not be observed for the samples with deuterium concentrations lower than 0.33/Ta. The integrated intensities of the two components are shown in Fig. 2. The extrapolated intensity of the satellite lines to the lower D/Ta value becomes zero at a D/Ta value between 0.2 to 0.15. If we take into consideration the experimental facts that the solubility of hydrogen in Ta metal is about 20%, and that above this concentration the β Ta_2H phase develops,[2,3] the central line can be assigned to the deuteron resonance of the α Ta, and the satellite lines, to that of the β Ta_2D. The theoretical powder pattern line shape in the presence of quadrupole interaction due to nuclei with I=1 has been calculated.[9,10] We have thus smoothed the theoretical line shape with the Gaussian distribution of various values of the root mean square line width (σ). The results are shown in Fig. 1-(A); a more detailed analysis of the powder pattern for an asymmetric field gradient is shown in the Appendix. From the method described in the Appendix, the quadrupole coupling constant, e^2qQ/h, 33.9 KHz, and the asymmetry parameter, η, 0.15 to 0.25, were obtained.

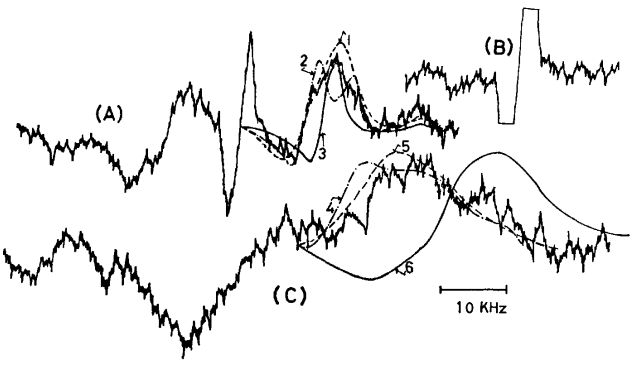

Fig. 1. Observed deuteron resonance signals (derivatives) of $TaD_{0.43}$. (A) R.T. (B) +62°C (C) −179°C. Smoothed curves (1—6) are drawn with various values of asymmetry parameter and σ.

	e^2qQ/h	$\sigma/(3\,e^2q\,Q/4h)$	η
1	33.9 KHz	0.10	0.15
2	33.9 KHz	0.05	0.23
3	33.9 KHz	0.05	0.03
4	33.9 KHz	0.15	0.45
5	33.9 KHz	0.25	0.30
6	67.8 KHz	0.10	0.03

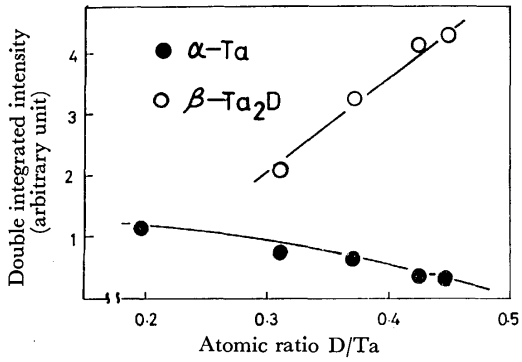

Fig. 2. Concentration dependence of double integrated signal intensity of deuteriums in α Ta and β Ta_2D.

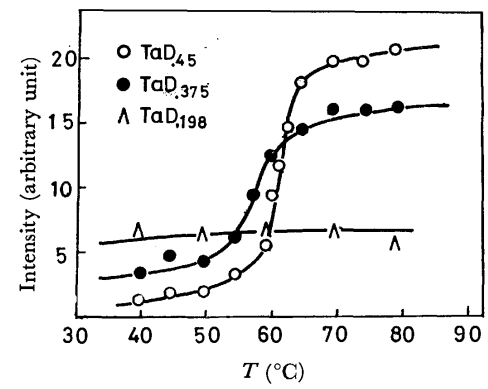

Fig. 3. Temperature dependence of signal intensity of deuteriums in α Ta.

Deuteron Resonance and Phase Transition above Room Temperature. When the TaD_n (n=0.45, 0.43, 0.375) was warmed from room temperature, the deuteron resonance signal intensity of the α Ta began to increase, and that of the β form began to decrease. The signal intensity of the former continued to increase even after that of the β Ta_2D was vanishingly small, but finally it became constant. As shown in Fig. 3, the temperature range where the phase transition proceeded was about 10°C for the $TaD_{0.45}$ sample. The phase transition temperature, which we define as the middle point of the temperature-signal intensity curve, depended on the composition of the sample. As the deuterium concentration decreased, the temperature range of the phase transition became broad and the phase transition temperature became obscure. For the $TaD_{0.198}$ sample, the signal intensity of the α form did not change over the temperature range from +90 to −50°C. For this composition, therefore, most of the deuteriums dissolve in the α Ta metal.

Deuteron Resonance below Room Temperature. As the temperature of the samples decreased, the deuteron signal intensity of the α Ta decreased until it vanished in the temperature range from −30 to −70°C. The

9) M. H. Cohen and F. Reif, "Solid State Physics," Academic Press, New York (1957), Vol. 5, pp. 338—343.
10) T. Chiba, *J. Chem. Phys.*, **36**, 1122 (1959).

temperature at which the signal vanished depended on the sample composition; *i.e.*, it was about $-30°C$ for $n=0.45$ and about $-70°C$ for $n=0.198$. As the temperature decreased, the line width of the β Ta_2D became broad. However, even at $-180°C$, the line shape corresponds to that which has nearly the same quadrupole coupling constant smoothed with a broad Gaussian distribution (Fig. 1-(C)).

Discussion

Deuterium Arrangement in β_1 Ta_2D. To account for the experimental results, it is necessary to calculate the electric field gradient (EFG) at the interstitial deuterium atoms. No precise calculation of EFG at interstitial atoms has yet been made. Bloembergen and Rowland[11] have used a Thomas-Fermi approximation by Mott and Jones[12] and have calculated the EFG at monovalent solvent Cu atoms in Cu–Zn substitutional alloy, where the EFG is produced by the extra positive charge of the divalent solute Zn. A similar treatment has been made by Schreiber and Cott[13] for the calculation of EFG at La in the La–H interstitial system. Coogan and Gutowsky[14] applied this approximation in their calculation of the potential energy for hydrogen diffusion in the Ti–H system. Our problem in the EFG calculation is similar to that of the last case. However, in order to know the arrangement of deuteriums, it is not necessary to know the exact solution of the EFG calculation. What it is desirable to know is the relative sign, the relative magnitude, the principal axis direction, and the asymmetry parameter of the EFG tensor. These parameters, fortunately, are determined only by the array of Ta and deuterium ions and are almost independent of the method of estimation of the conduction electron contribution.[15] In this section, we used Mott's screened potential. By using this, we do not expect to have a completely exact solution of the principal value of the EFG tensor, but can obtain the relative magnitude, the relative sign, the principal axis direction, and the asymmetry parameter of the EFG tensor.

Here we choose a set of orthogonal axes, X', Y', and Z' as the principal axes; the Z' axis lies along the direction of the maximum component, and X' along that of the minimum component. The maximum component, eq, at the i-th deuterium atom may be expressed as;

$$eq = \frac{\partial^2 V}{\partial Z'^2} = \sum_j V''(r_{ij}) \frac{(3\cos^2\theta_{ij} - 1)}{2} \qquad (1)$$

where $V''(r_{ij})$ is the field gradient along the ij direction and is given by;

$$V''(r_{ij}) = \frac{2Z_j e}{r_{ij}^3}(1 + Kr_{ij} + (Kr_{ij}/2)^2)\exp(-Kr_{ij}) \qquad (2)$$

where r_{ij} is the distance between the i-th deuterium and the surrounding j-th ion, θ_{ij} is the angle between the Z' axis and the ij direction, $Z_j e$ is the charge on the j-th ion, and the summation is made over the j-th ions. When the crystal is cubic the EFG at each site is axially symmetric. However, since the low temperature form (β form) is a slightly distorted cubic form, with $c/a = 1+\Delta$, where Δ is a small quantity compared with 1, the EFG is not axially symmetric.

Next, we will calculate the EFG for the deuterium arrangement proposed by Wallace.[5] Structure A, which he assumed to be most reasonable,[16] belongs to the $I4$ space group ($a = 2a_0 = 6.74$ Å) with half deuteriums located at the general positions of 1/4 1/8 0 and 5/8 0 1/4. We denote the 8 positions at 1/4 1/8 0, 7/8 1/4 0, 3/4 7/8 0, 1/8 3/4 0, 5/8 0 1/4, 3/8 0 1/4, 0 3/8 1/4, and 0 5/8 1/4 as TA1, TA2, ·····, TA8, the other 8 positions are, of course, at $+1/2$ 1/2 1/2 translation. Due to r_{ij}^{-3} and $\exp(-Kr_{ij})$ terms in Eq. (2), the EFG due to ions other than the nearest neighbor Ta ions can be disregarded. Then, eq and the asymmetry parameter are;

$$eq = -\frac{2}{5}V''(R_1) - \frac{2}{5}V''(R_2) - \frac{12}{25}\Delta V''(R_2) \qquad (3)$$

$$\eta = 3(1 - V''(R_2)/V''(R_1)) - \frac{6}{5}\Delta < 3(1 - (R_1/R_2)^3) - \frac{6}{5}\Delta \qquad (4)$$

where $R_1 = \sqrt{5}\, a_0/4$ and $R_2 = \sqrt{5}\, a_0\ (1 + 4\Delta/5)/4$ are the deuterium–tantalum distances, and the principal axis directions are;

$Z' \| a$, $Y' \| b$ and $X' \| c$ axes for TA2, TA4, TA5, and TA6

$Z' \| b$, $Y' \| a$ and $X' \| c$ axes for TA1, TA3, TA7, and TA8

From the above considerations, one may draw the following conclusion. When the temperature increases and the jump frequency becomes larger than the quadrupole coupling constant of the deuterium atom, each deuterium atom will experience two sites with different principal axis directions and the quadrupole coupling constant will be averaged. Consequently, the following predictions will be realized; (1) the largest principal component will be $eq(1-\eta)/2 \approx eq/2$; (2) the direction of the largest principal component will become parallel to the c axis, and (3) the asymmetry parameter will become zero. Therefore, the quadrupole coupling constant at a low temperature must be twice that at a high temperature as long as the above situation holds.

The ordered deuterium arrangement proposed by PSSC is shown in Fig. 4. It can easily be seen from the $2a$ positions of the deuteriums and the pseudo-tetragonality of the cell that, in the absence of a displacement of the Ta atoms, the EFG at the deuteriums in this ordered arrangement is axially symmetric with respect to the c axis. However, if we consider the fact that the displacement of Ta atoms at $\pm x$ improves the neutron diffraction reliability factor, the EFG is thought to be distorted from the axial symmetry. The maximum principal component, eq, and the asymmetry parameter, η, calculated from the nearest neighbor

11) N. Bloembergen and J. J. Rowland, *Acta Met.*, **1**, 731 (1953).
12) N. F. Mott and G. H. Jones, "Theory of the Properties of Metals and Alloys," Oxford Univ. Press, New York (1936), p. 86.
13) D. S. Schreiber and R. M. Cott, *Phys. Rev.*, **131**, 1118 (1963).
14) C. K. Coogan and H. S. Gutowsky, *J. Chem. Phys.*, **36**, 110 (1962).
15) M. Pomerantz and T. P. Das, *Phys. Rev.*, **119**, 70 (1960).
16) The other two structures which Wallace denoted as Structure B and C give the same result as Structure A.

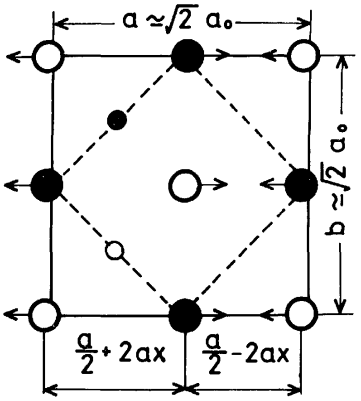

Fig. 4. Projections onto 001 plane of β_1 Ta_2D (PSSC model) Ta's are at $z=0$ (large opened circles) and at $z=1/2$ (large closed circles). D's are at $z=1/4$ (small opened circles) and $z=3/4$ (small closed circles).

four Ta atoms are;

$$eq \approx \left(-\frac{4}{5}+\frac{48}{25}+\frac{96}{25}x\right)V''(R_3) \quad (5)$$

$$\eta \approx 24x \quad (6)$$

where $R_3=\sqrt{5}a_0(1+(8x+\Delta)/5)/4$. Since the deuteriums in this ordered structure are situated in a special position, whose Z' direction is parallel to the c axis, the quadrupole coupling constant is not averaged by the rapid diffusion of the deuteriums; that is, the quadrupole coupling constant at a low temperature must be the same as that at a high temperature. Therefore, in order to determine which of the proposed structures is consistent with the deuteron magnetic resonance results, it is sufficient to know; (1) whether the asymmetry parameter at a high temperature is zero or larger than zero ($\approx 24x$), or (2) whether the quadrupole coupling constant at a low temperature, where the deuterium diffusion is negligible, is twice that at a high temperature.

In the previous section, we have shown that the asymmetry parameter at room temperature lies between 0.15 to 0.25, appreciably larger than zero. In order to examine (2), it is necessary to know the correlation time for deuterium diffusion at −179°C. We obtained the correlation times for hydrogen diffusion at −180°C by an extrapolation method by using the proton magnetic resonance data of the TaH_n interstitial system.[17] These times are 10^{-4} and 1.4×10^{-4} sec for $n=0.66$ and 0.1 respectively. The correlation time for deuterium diffusion is expected to be longer than that for hydrogen diffusion due to the isotope effect. Therefore, we assume that $1/\tau_c \ll e^2qQ/\hbar$. As is shown in Fig. 1, the observed spectrum at −179°C can not be expressed as having twice as large quadrupole coupling constant as that at room temperature. It is better expressed as having approximately the same quadrupole coupling constant as that at room temperature, and it is smoothed with a broad Gaussian distribution. From these considerations, it seems that the ordered arrangement proposed by PSSC is the most probable structure for the β_1 form. The calculated eq, asymmetry parameters and configurational entropies for the other two structures,[6,7] together with the above two, are listed in Table 1.

Deuterium Arrangement in β_2 Ta_2D. According to the neutron diffraction study by Wallace,[5] the unit cell of this form ($a=a_0=3.37$ Å) is the same as the X-ray unit cell, which contains one deuterium and two tantalums. There are 12 tetrahedral sites in a unit cell. According to Wallace's notation, these are T_1, T_2, ⋯, T_6 at 1/2 1/4 0, 1/2 3/4 0, 1/4 1/2 0, 3/4 1/2 0, 0 1/2 1/4 , and 1/2 0 1/4, while the other 6 sites are T'_1, T'_2, ⋯, T'_6 at a +1/2 1/2 1/2 translation. If the crystal is cubic, these 12 sites are structually equivalent. However, since the β_2 is a slightly distorted cubic form, these 12 sites may be divided into S and L groups,[5] S group contains T_5, T_6, T'_5, and T'_6, while L contains the other 8 sites. There are only three arrangements, random distribution in the S sites, in the L sites, and in all the sites. The calculated neutron diffraction intensities for these three arrangements showed an excellent agreement with the experimental results.[5]

The EFG of these 12 sites may be calculated by means of Eqs. (3) and (4) and by substituting $x=0$ in Eqs. (5) and (6). The resulting Z' direction are shown in Table 2. By using consideration similar to that used previously, one may easily reach the following conclusions;

(1) If the deuteriums are distributed over all the tetrahedral sites with equal probability and with a rapid translational motion, the resultant quadrupole coupling constant will be averaged and will become zero (for b. c. c.) or below the level of detection (for b. c. t.)

Table 1. Calculated eq, η and configurational entropies(S_c) for the various proposed β_1 Ta_2D structures

	Space group	Deuterium positions	R[a]	$(eq)_H/(eq)_L$[b]	η[c]	S_c (e.u. mol^{-1})
Wallace[5]	$I4$	$8G$(1/4 1/8 0) $8G$(5/8 0 1/4)	0.17	1/2	c)	2.7
Palenik[6]	$I\bar{4}$	$8G$(0 1/4 1/8)	0.29	1	0	0
Somenkov *et al.*[7]	$Pnnn$	a(1/4 1/4 1/4) b(1/4 3/4 3/4)	0.30	1	0	0
Petrunin *et al.*[8]	$A222$	$2a$ (1/4 1/4 1/4)	0.107	1	$\approx 24x$[d]	0

a) Superlattice diffraction reliability factor.
b) Ratio of eq at a high temperature to that at a low temperature.
c) At a high temperature; $\eta=0$ and, at a low temperature; η is given by Eq. (4).
d) $x=0.012$ at a room temperature, $x=0.017$ at a liquid nitrogen temperature.

17) B. Pederson, T. Krogdahl, and O. E. Stokkeland, *J. Chem. Phys.*, **42**, 72 (1965).

TABLE 2. CALCULATED Z′ AXIS DIRECTION FOR EACH OF THE 12 TETRAHEDRAL SITES OF THE β_2 FORM

Group		Z' axis direction
L	T_1, T_2, T_1', T_2'	$Z'\|\|$ b axis
	T_3, T_4, T_3', T_4'	$Z'\|\|$ a axis
S	T_5, T_6, T_5', T_6'	$Z'\|\|$ c axis

(2) If the deuteriums are distributed over the L sites, the resultant quadrupole coupling constant will be a half of that at a low temperature where the rapid translational motion is absent.

(3) Since the Z' direction of the tetrahedral sites in the S group is parallel to the c axis, the quadrupole coupling constant will not be averaged by the rapid translational motion of the deuteriums. Consequently, the quadrupole coupling constant is approximately the same as that for the ordered β_1 form.

TABLE 3. CALCULATED eq, η AND CONFIGURATIONAL ENTROPIES FOR THE VARIOUS PROPOSED β_2 Ta_2D STRUCTURES

	$eq_{\beta 2}/eq_{\beta 1}$ [a]	η	S_c(e.u. mol^{-1})
L [b]	1/2	0	5.97
S [c]	1	0	4.20
L and S [d]	0	—	6.82

a) $eq_{\beta 1}$ is given by Eq. (5).
b) Random distribution in the L sites.
c) Random distribution in the S sites.
d) Random distribution in all sites.

The calculated eq, the asymmetry parameters, and the configurational entropies for the three proposed structures are shown in Table 3. It should be noted that the observed deuteron resonance line shape exhibits no quadrupole coupling constant change upon the $\beta_1 \rightarrow \beta_2$ phase transition, and that the most probable structure for the β_1 form is the PSSC ordered model. Then, from an inspection of the table, one can see that the distribution in the S sites seems to be the probable structure for the β_2 form. However, the calculated configurational entropy is far larger than the observed value, 0.7 e.u. mol^{-1}. In order to account for the large difference between the calculated and observed entropies, we must take some kinds of local order into consideration.

Local Order in the β_2 Form. The locally ordered structure which we will discuss in this section must satisfy the following three conditions; (1) the deuteron quadrupole coupling constant and asymmetry parameter of the β_2 form must be of the same order as the β_1 form; (2) in spite of the above condition, there must be no superlattice diffraction in the β_2 form, and (3) the configurational entropy of the β_2 form must be only 0.7 e.u. mol^{-1}. From condition (1), we see that the arrangement of Ta atoms around the deuterium atom is the same as that of the β_1 form. This means that the symmetry of the β_2 form must be orthorhombic. From condition (2), we see that the deuteriums must be distributed over all the tetrahedral sites in the S group with a quarter occupancy. This means that the symmetry of the β_2 form must be tetragonal. However, this tetragonality contradicts condition (1), while a quarter occupancy contradicts condition (3).

Let us try to account for the above contradiction. In the A222 space group, without considering the displacement of Ta ($4K$ positions), the $2a$(1/4 1/4 1/4, 1/4 3/4 3/4), $2b$(1/4 1/4 3/4, 1/4 3/4 1/4), $2c$(3/4 1/4 3/4, 3/4 3/4 1/4), and $2d$(3/4 1/4 1/4, 3/4 3/4 3/4) positions are all equivalent. In the ordered structure, the deuteriums are at the $2a$ positions and the Ta are displaced by $\pm x$. However, as the temperature increases, the preservation of the mutual positions of the deuteriums becomes difficult and probability of finding deuteriums in the $2b$, $2c$, and $2d$ positions becomes progressively larger. However, before the deuteriums are found to be statistically distributed over these sites, one may find a locally ordered structure. This consideration yields a concept of a domain structure which is constructed with four types of domains. The deuteriums in the domains are, of course, at the $2a$, $2b$, $2c$, and $2d$ positions. Since the domains are perfectly ordered internally, the configurational entropy is merely the entropy of the mixing of the domains. For one mole of Ta_2D, the number of domains is $N/(2r^3)$, where N is the Avogadro number, where r is a repeat number of a unit lattice per domain, and the number of complexions is $(N/(2r^3))!/((N/(8r^3))!)^4$ and $S_c = R\ln 4/(2r^3)$. The probable value of r, which is determined so that the calculated value coincides with the experimental value of 0.7 e.u. mol^{-1} is 1.4. For such small domains, as Wallace[5] has pointed out, sharp superlattice diffractions do not develop and the diffraction pattern closely resembles that in which deuteriums are randomly distributed over the S sites. Therefore, we can assume that the above domain structure satisfies the three conditions simultaneously and seems to be the most probable structure. An example of the domain structure projected onto 100 plane is shown in Fig. 5.

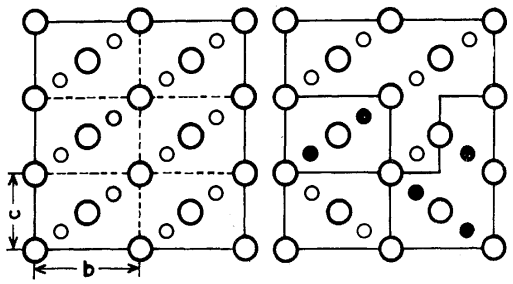

Fig. 5. Projection onto 100 plane of the ordered β_1 (left) and locally ordered β_2 form (right). Only Ta's at $x=0$ (opened large circles) are shown. D's are at $x=1/4$(small opened circles) and $x=3/4$ (small closed circles).

Deuterium Arrangement in α Ta_2D. The quadrupole coupling constant of this form is too small to be detected. This fact can be accounted for if the deuteriums are undergoing a rapid translational motion over all available tetrahedral sites (L and S sites). The configurational entropy calculated from this structure is 6.82 e.u. mol^{-1}. On the other hand, Saba *et al.*[4] have shown that the configurational entropy of this form is 4.9 e.u. mol^{-1}, which does not change even at 573°K. This indicates that the deuteriums are not randomly distributed over all the tetrahedral sites, but are dis-

tributed in a manner which retains some kinds of local order. However, in considering such a locally ordered structure, it should be taken into account that (1) the crystal is cubic and (2) the quadrupole coupling constant is averaged to zero. These conditions require that, in a locally ordered domain, there must be three different equally abundant sites, whose Z' directions are parallel to the a, b, and c axes respecitvely. It is possible to imagine such a domain structure without a loss of crystal symmetry. However, since it is difficult to interpret why such domain structure is energetically stable, we will not discuss further this problem.

Electric Field Gradient Calculation. In the previous section, we have used a simple electrostatic model in which the electric potential from the ions is screened by the conduction electrons around the ions. However, we have left the constant, K, and the electric charge on the ions underemined. In this section, we will discuss these parameters.

It has been shown that when a hydrogen enters the metal, it loses most of its electron cloud to the conduction band or to the metal ions. The ^{139}La magnetic resonance study of La-H[13] system has shown that the EFG at the La ion due to the defect of hydrogen ions can best be calculated by the assumption of a positive charge on the hydrogen ion. However, the relatively large negative proton Knight shift in the Ti-H system[18] has shown that the hydrogen does not lose its electron completely in this system. Schreiber and Graham[19] have suggested, from the zero proton Knight shift in the Ta-H, Nb-H, and V-H systems, the existence of bare protons in these systems. The proton relaxation times of Ta-H[17] and Nb-H[20] systems have shown no contribution of conduction electrons to their relaxation mechanisms. Therefore, the assumption of a positive charge on the interstitial deuterium ions is a good approximation.

In compensation for a positive charge on hydrogen ions, a negatively ionized metal ion model has been presented.[14] However, this assumption is inconsistent in its use of a screened potential and also contradicts the pulsed NMR result[21] that the hydrogen diffusion activation energy is independent of the hydrogen concentration. We assume that the effect of electrons removed from the interstitial hydrogen atoms is merely to change the conduction electron density slightly and that this effect has no influence on the net charge of the Ta ions.

The values of K for Cu, Ag, and Al have been calculated to be 1.72 to 1.81×10^8 cm^{-1}. Due to the r_{ij}^{-3} and $\exp(-Kr_{ij})$ terms in Eq. (2), the summation in Eq. (1) easily converges. The computation has been made over 68 Ta and 29 deuterium ions within the sphere of radius of $R=\sqrt{69}\,a_0/4$. With $a_0=3.37$, $c/a=1.008$, and displacement parameter $x=0.012$, some combinations of K and Z_{Ta} which have been so determined as to the calculated quadrupole coupling constants agree with the observed value, 33.9 KHz, are as follows;

Z_{Ta}	K	η
5	1.75×10^8 cm^{-1}	0.235
4	1.54×10^8 cm^{-1}	0.186
3	1.47×10^8 cm^{-1}	0.128

The dependence of η on Z_{Ta}, of course, comes from the contribution on the Ta ion to the EFG. Since the observed asymmetry parameter lies between 0.25 to 0.15, 4 to 5 charge on the Ta ion seems to be plausible. However, if the deuteriums do not lose their electron cloud completely, a +5 charge on the Ta ion may be more realistic.

The author wishes to express his thanks to Professor Shizuo Fujiwara for his continuing interest and encouragement. Thanks are also given to Drs. Masatoshi Okada and Takeo Yamamoto, who read the manuscript and made some useful comments.

Appendix

Analysis of Powder Pattern for Asymmetric Field Gradient.

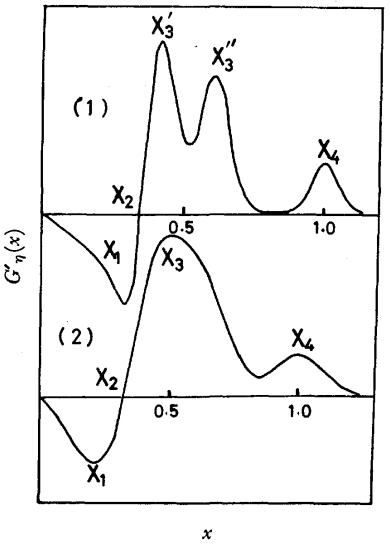

Fig. 6. Calculated powder patterns for $\eta=0.25$.
(1) $\sigma=0.05$ (2) $\sigma=0.1$

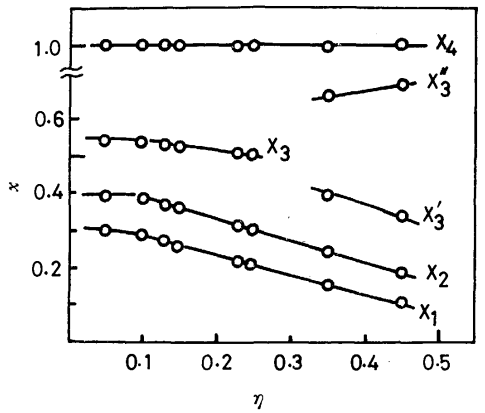

Fig. 7. Plots of x_1, x_2, x_3 (x_3', x_3'') and x_4 against η for $\sigma=0.1$ case.

18) B. Stalinski, C. K. Coogan, and H. S. Gutowsky, *J. Chem. Phys.* **34**. 1191 (1961).
19) D. S. Schreiber and L. D. Graham, *ibid.*, **43**, 2573 (1965).
20) D. Zamir and R. M. Cotts, *Phys. Rev.*, **134**, 666 (1964).
21) C. Korn and D. Zamir, *J. Phys. Chem. Solids*, **31**, 489 (1970).

The first-order powder pattern of one satellite for asymmetric field gradient, $P_\eta(x)$, is defined in Ref. (9) page 342. If the individual lines are assumed to be the form as,

$$f(x) = \exp\left[-(x-x')^2/2\sigma^2\right] \tag{1'}$$

where $x=(\nu-\nu_0)/(3\,e^2qQ/4h)$. The resultant shape function, $G'_\eta(x)$ (derivative), is given

$$G'\eta(x) = \int_{-1}^{1}(x-x')[P(x')+P(-x')]\exp\left[-(x-x')^2/2\sigma^2\right]dx' \tag{2'}$$

Examples for $\eta=0.23$ are shown in Fig. 6. We define x_1, $x_3(x_3', x_3'')$ and x_4 as derivative maxima (minimum) and x_2 as derivative zero. As shown in Fig. 7, x_1 and x_2 are very sensitive to η, x_1 and x_2 may be used to obtain η. Quadrupole coupling constant is most accurately determined by measuring x_4 which is very insensitive to η and σ. When η is large enough or σ is small enough to be able to observe the separation between x_3' and x_3'', η may be very easily obtained by comparing $(x_3''-x_3')/(x_4-x_3'')$ against η as shown in Fig. 8.

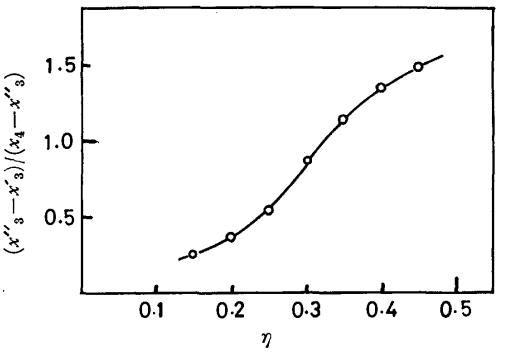

Fig. 8. A plot of $(x_3''-{}_3x')/(x_4-x_3'')$ against η for $\sigma=0.05$ case.

BULLETIN OF THE CHEMICAL SOCIETY OF JAPAN, VOL. 45, 3362—3366 (1972)

Electron Spin Resonance Studies of the Carbon Dioxide Anion Radical Adsorbed on X-Type Zeolites

Kunihisa SOGABE, Akinori HASEGAWA, Yoshio YAMADA,* and Masaji MIURA

Department of Chemistry, Faculty of Science, Hiroshima University, Higashisenda-machi, Hiroshima

(Received April 3, 1972)

The hindered motion and the structure of the CO_2^- radical adsorbed on various zeolites were investigated by means of ESR spectroscopy. The adsorbed CO_2^- radical was obtained by the γ-irradiation of zeolites with carbon dioxide labeled with ^{13}C. The results show that the interaction of the CO_2^- radical with the zeolite surface changes with the electrostatic field on the surface. The motion and the structure of the adsorbed CO_2^- radical are affected by the properties of the zeolite surfaces; the former is also influenced by the extent of exchange of the cation on zeolite, regardless of the time of irradiation, before or after the introduction of carbon dioxide. The formation of the CO_2^- radical on zeolites was interpreted on the basis of such a mechanism that electrons are initially trapped by the surface of zeolite upon the irradiation and then transferred to carbon dioxide molecules. The results also show that the process of the electron transfer depends on the kind of cation.

The application of ESR spectroscopy to adsorbed molecules has been of considerable interest, since it permits detailed studies of their adsorbed state. Several works have been reported on the formation of the CO_2^- radical on an insulator, such as SiO_2 or MgO.[1-4] However, very little information has been obtained on the interaction between the radical and the solid surface.

Sharp and Symons[5] have recently investigated the CO_2^- radicals formed in various formates and shown that the ESR parameters for the CO_2^- radical depend markedly upon the nature of the host lattice. According to their results, the crystal field, which increases as the cation's charge increases or its radius decreases, causes a profound perturbation in the CO_2^- radical. Kasai[6] has studied the crystal-field interaction between an adsorbed paramagnetic species, O_2^-, and Y-type zeolites, and shown that the splitting of energy levels of the O_2^- is exactly twice as large with BaY as with NaY.

In this work, we will attempt to represent the crystal-field interaction in terms of the hindered motion and the structural variation in the CO_2^- radical adsorbed on zeolites.

Experimental

The X-type zeolite was furnished in the sodium form (Linde Lot No. 1380019). Ion-exchanged zeolites were prepared by exchanging the sodium ions with other kinds of

* Present address: National Research Institute for Pollution and Resources, Kawaguchi, Saitama.

1) J. H. Lunsford and J. P. Jayne, *J. Phys. Chem.*, **69**, 2182 (1965).

2) Y. Yamada, A. Hasegawa, and M. Miura, This Bulletin, **42**, 1836 (1969).

3) P. K. Wong and J. E. Willard, *J. Phys. Chem.*, **73**, 2226 (1969).

4) P. O. Kinell, T. Komatsu, A. Lund, T. Shiga, and A. Shimizu, *Acta Chem. Scand.*, **24**, 3265 (1970).

5) J. H. Sharp and M. C. R. Symons, *J. Chem. Soc., A*, **1970**, 3075.

6) P. H. Kasai, *J. Chem. Phys.*, **43**, 3322 (1965).

cations in their chloride solutions by the conventional method.[7] The exchange process was then repeated in order to achieve a high degree of replacement. The exchanged zeolites were washed with distilled water in order to remove the excess chloride ions. Thus, Li-, K-, Mg-, Ca-, and BaX were obtained. The degree of ion-exchange was determined by measuring the amount of the exchanged sodium ions by means of atomic-absorption spectroscopy.

After the exchanged zeolite had been evacuated for 5 hr in a vacuum of 10^{-5} Torr at 500°C, it was slowly cooled to room temperature and transferred into an ESR sample tube. Carbon dioxide containing 59.1 atom% ^{13}C, which had been obtained from Merck Sharp & Dohme of Canada, Ltd., was used in order to observe the ^{13}C hyperfine structure. The carbon dioxide was introduced into the sample tube through a breakable seal at room temperature. After the zeolite had been exposed to the carbon dioxide gas of 20 Torr for 30 min, the physically-adsorbed carbon dioxide was removed by means of a liquid nitrogen trap. The ESR sample tube was sealed off *in vacuo* and then irradiated with ^{60}Co γ-rays (6×10^5 R/hr) for 30 min at 77°K.

The ESR spectra were measured at various temperatures by a spectrometer described elsewhere.[8] In order to study the mechanism of the formation of the adsorbed CO_2^- radical, a pre-irradiation process was also adopted.

Results and Discussion

The percentages of exchanged ions are shown in Table 1. In the case of MgX, only 59.6% of Na^+ was exchanged even when the exchange process was repeated; this seems to be due to the large hydration radius of Mg^{2+}.[9]

Formation and Identification of the CO_2^- Radical. The shapes of the hyperfine structures of ^{13}C in the spectra obtained for the zeolite exchanged by the Li^+ ion and the bivalent cation are very close to that of the $^{13}CO_2^-$ radical adsorbed on silica gel.[2] Each spectrum consists of a central line originating from the $^{12}CO_2^-$ radical and of two additional outer lines due to the $^{13}CO_2^-$ radical. However, no ESR spectrum of the CO_2^- radical adsorbed on NaX or KX was observed under the same experimental conditions as were used for the other zeolites. The CO_2^- radical on NaX or KX was obtained when these zeolites were irradiated for 16 hr at room temperature in the presence of carbon dioxide at 100 Torr. The formation of the radical on the NaX or KX may be interpreted as follows: the irradiation at room temperature enabled electrons to transfer from the surface to adsorbed carbon dioxide. The g-values evaluated from the hyperfine structure of ^{13}C are summarized in Table 1.

Structure of the CO_2^- Radical. Ovenall and Whiffen[10] have observed the ESR spectrum of the CO_2^- radical produced in γ-irradiated sodium formate and determined the structure of the radical by analyses of the g-values and the ^{13}C coupling constants. According to the molecular orbital theory, the unpaired 17th electron occupies the $4a_1$ molecular orbital:[10,11]

$$(4a_1) = c_1C(s) + c_2C(p) + c_3O(P_{z1}+P_{z2}) + c_4O(P_{y1}-P_{y2}) + c_5O(s_1+s_2) \quad (1)$$

Actually, the ^{13}C coupling constants of the $^{13}CO_2^-$ radical are used for the estimation of the atomic orbital coefficient of Eq. (1).

$$A_{iso} = C_1^2A_s, \quad A_{//} - A_{iso} = C_2^2A_p \quad (2)$$

where A_s and A_p are the coupling constants for the electrons in the pure carbon $2s$ and $2p$ orbitals, 1189 and 42.9 G[10,12] respectively, and where C_1^2 and C_2^2 are the spin densities in the carbon $2s$ and $2p$ orbitals respectively, which give information on the hybridization of the orbitals.

The OCO angle of the CO_2^- radical, θ, has been derived in terms of the hybridization:[13]

$$\cos\theta = -\frac{\lambda^2}{\lambda^2+2} \quad (3)$$

where λ^2 is the ratio of hybridization, C_2^2/C_1^2. The anisotropic hyperfine structure of the $^{13}CO_2^-$ radical

Table 1. ESR parameters of CO_2^- radical adsorbed on the zeolites

CO_2^- radical on	g value			A value (gauss)			C_1^2	C_2^2	λ^2	Angle (θ)
	g_x	g_y	g_z	$A_\perp$	$A_{//}$	A_{iso}				
LiX (87.0%)	2.0036	1.9968	2.0036	118	160	132	0.111	0.653	5.88	138°
MgX (59.6% / 42.8%)	2.0033	1.9989	2.0033	154	200	169	0.142	0.723	5.09	135°
CaX (96.4% / 78.5%)	2.0026	1.9977	2.0026	151	199	167	0.140	0.746	5.33	136°
BaX (94.4% / 70.9%)	2.0011	1.9948	2.0011	147	197	164	0.138	0.769	5.57	137°
NaX (—)[a]		$g_0=2.0011$			$A_0=133$					
KX (100%)		$g_0=2.0009$			$A_0=133$					
MgO[1]	2.0029	1.9974	2.0017	184	230	199	0.167	0.723	4.33	134°
SiO_2[a) 2]	2.0024	1.9978	2.0024	190	215	204	0.172	0.256	1.49	116°

a) γ-Irradiation for 16 hr at room temperature in the presence of CO_2.

7) T. I. Barry and L. A. Lay, *J. Phys. Chem. Solids*, **27**, 1872 (1966).
8) A. Hasegawa and M. Miura, This Bulletin, **40**, 2553 (1967).
9) J. W. Ward and H. W. Habgood, *J. Phys. Chem.*, **70**, 1178 (1966).
10) D. W. Ovenall and D. H. Whiffen, *Mol. Phys.*, **4**, 135 (1961).
11) P. W. Atkins, N. Keen, and M. C. R. Symons, *J. Chem. Soc.*, **1962**, 2873.
12) A. Carrington and A. D. Mclachlan, "Introduction to Magnetic Resonance," Harper & Row, New York (1967), p. 138.
13) C. A. Coulson, "Contribution a l'etude de la Structure Moleculaire," Victor Henri Volume Commemoratif, (1948), p. 15.

observed at 77°K was analyzed in order to determine the OCO angle. The values of C_1^2, C_2^2, and λ^2 estimated from the spectra of the CO_2^- radicals adsorbed on the various zeolites are given in Table 1. The results on MgO[1] and SiO_2[2] are also listed in the table. The change in the value of θ, namely, the structural variation in the CO_2^- radical, has been ascribed to the difference in cation radius.[2] The charge of the cation as well as its radius, however, seems to affect the structure of the CO_2^- radical, as can be seen in Table 1.

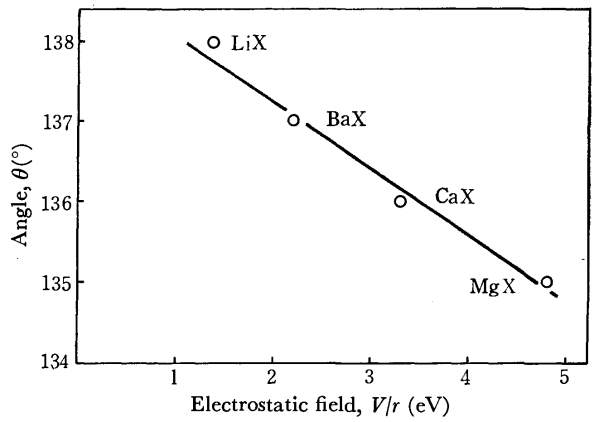

Fig. 1. Relationship between OCO angle of CO_2^- radical and electrostatic field on zeolites.

One aim of the present study is to investigate the interaction between the CO_2^- radical and the zeolite surface through the structural variation in the CO_2^- radical brought about by the change in the kind of cation on zeolite. Rabo *et al.*[14] have calculated the electrostatic fields characteristic of the cations on the zeolite surfaces. In Fig. 1, a good linear relationship can be seen between the electrostatic field on the zeolite surface and the OCO angle of the CO_2^- radical adsorbed on the zeolite. This means that the structure of the adsorbed CO_2^- radical is strongly affected by the electrostatic field; the OCO angle of the CO_2^- radical decreases as the charge of the cation increases or as its radius decreases. These results are consistent with those obtained by ESR studies of the CO_2^- radical trapped in formates.[5] However, the perturbation on the structure of the CO_2^- radical observed in this study is more remarkable than that in formates.

Motion of the CO_2^- Radical. In order to obtain some information on the interaction between the adsorbed CO_2^- radical and the zeolite surface, the motional behavior of the radical was investigated through the observation of the temperature variation in the spectrum of the $^{13}CO_2^-$ radical. It was found that the spectra of the radical on NaX and KX are isotropic even at 77°K, as can be seen in Figs. 2(a) and (b). There is little difference in these spectra, and their ^{13}C hyperfine coupling constants are both equal to 133G. Therefore, the CO_2^- radical on NaX and KX may be free from the cations on the zeolites and may still rotate or vibrate on the surfaces even at this

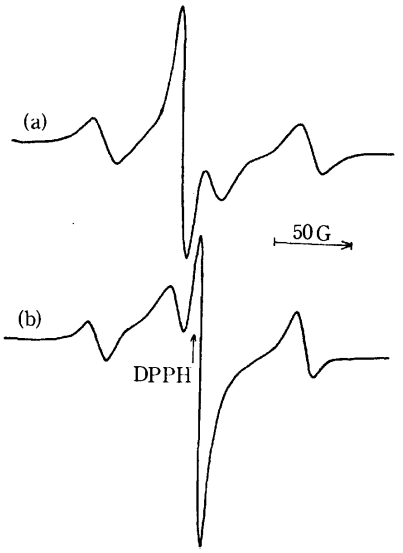

Fig. 2. ESR spectra of CO_2^- radical on (a) NaX and (b) KX at 77°K.

temperature.[15] As may be seen in the figures, a signal having $\Delta H=10$G and $g=2.012$ appeared. The same signal was observed when these zeolites were irradiated at 77°K in the absence of carbon dioxide. This may be ascribed to the hole generated by γ-irradiation, similarly to the cases of NaY reported by Stamires and Turkevich[16] and by Wang and Lunsford.[17] As regards LiX, the CO_2^- radical, as can be seen in Fig. 3, may weakly interact with the surface at 77°K.

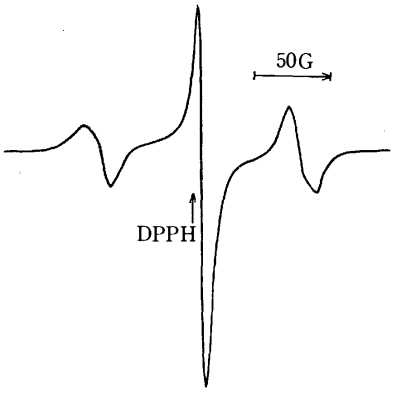

Fig. 3. ESR spectrum of CO_2^- radical on LiX at 77°K.

A distinct difference in the motion appeared on the zeolite exchanged with bivalent cations. The spectrum of the $^{13}CO_2^-$ radical on the MgX (59.6%) shown in Fig. 4 is anisotropic at 77°K. It was found, indeed, that the radical begins to rotate freely at about 200°K. When the sample was cooled down again from 298 to 77°K, the anisotropic spectrum was observed again; the spectral change is completely reversible with respect to the temperature variation. Also, the motion of the

14) J. A. Rabo, C. L. Angell, P. H. Kasai, and V. Schomaker, *Discuss. Faraday Soc.*, **41**, 328 (1966).

15) P. M. Johnson and A. C. Albrecht, *J. Chem. Phys.*, **44**, 1845 (1966).

16) D. N. Stamires and J. Turkevich, *J. Amer. Chem. Soc.*, **86**, 757 (1964).

17) K. W. Wang and J. H. Lunsford, *J. Phys. Chem.*, **73**, 2069 (1969); **74**, 1512 (1970); **75**, 1165 (1971).

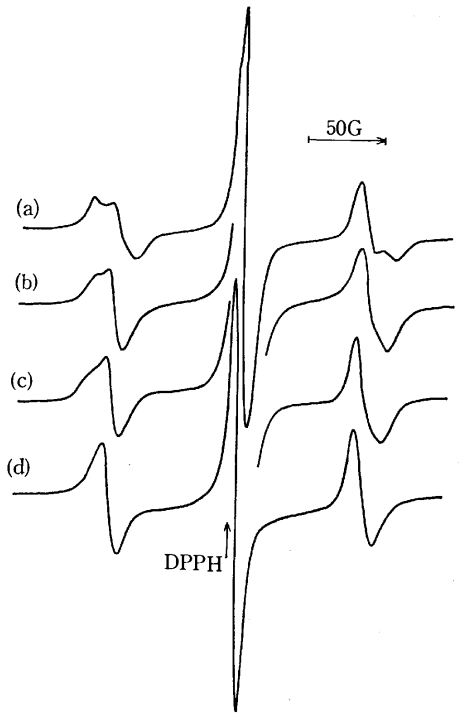

Fig. 4. ESR spectra of CO_2^- radical on MgX at (a) 77°K, (b) 180°K, (c) 190°K, and (d) 200°K.

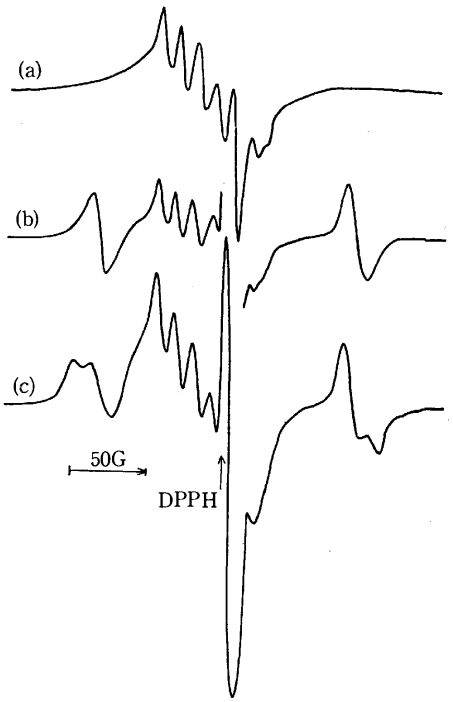

Fig. 5. (a) ESR spectrum of MgX irradiated for 2 hr at 77°K. (b) Spectrum of CO_2^- radical on pre-irradiated MgX at 298°K and (c) that at 77°K.

CO_2^- radical on pre-irradiated MgX was the same as that on post-irradiated MgX, as can be seen in Fig. 5. This indicates that the motional behavior of the CO_2^- radical on the zeolite is independent of the irradiation process.

The CO_2^- radical on the MgX was stable at room temperature for a few days, but bleached at about

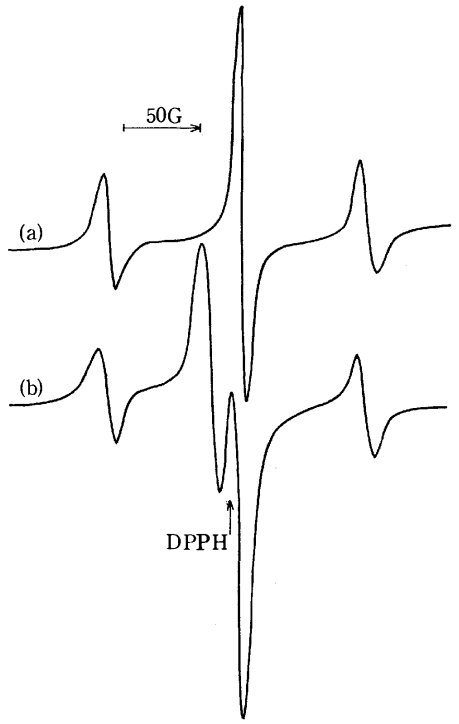

Fig. 6. ESR spectra of CO_2^- radical on MgX (a) at 298°K and (b) after standing for 48 hr at room temperature.

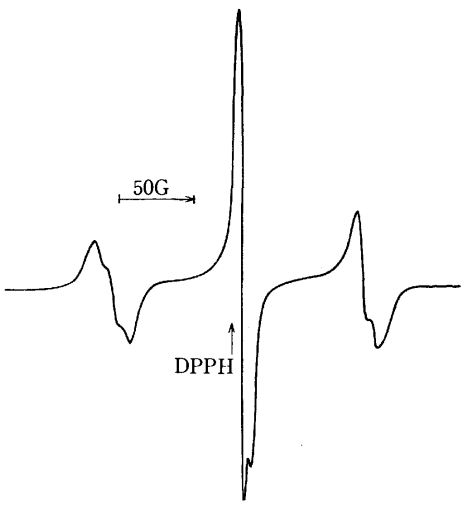

Fig. 7. ESR spectrum of CO_2^- radical on CaX (96.4%) at 77°K.

420°K. However, an additional line ($g=2.012$) appeared after 48 hr at room temperature (Fig. 6(b)); the intensity of this line increased with a decrease in the intensity of the spectrum for the CO_2^- radical while it stood. This additional line may be due to the hole, as in the case of the zeolite irradiated in the absence of carbon dioxide, as has been described above. This increase in the amount of the hole may be accounted for by the electron capture of the CO_2^- radical in the process of the degradation of the radical. The anisotropic spectrum of the $^{13}CO_2^-$ radical on the CaX (96.4%) (Fig. 7) hardly changed between 77 and 420°K. This spectrum was still observed at 77°K even after the sample had been heated to 600°K in

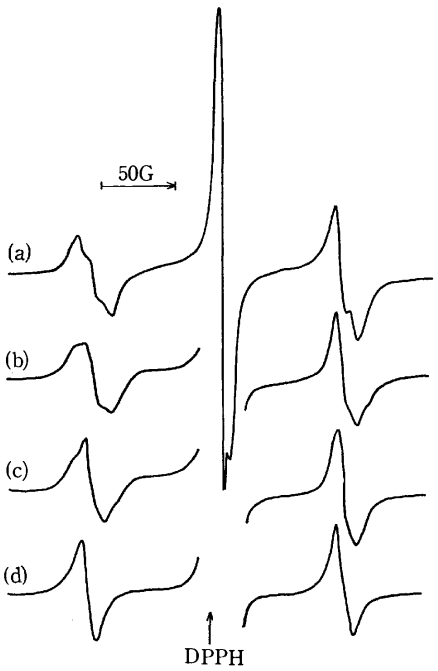

Fig. 8. ESR spectra of CO_2^- radical on CaX (78.5%) at (a) 77°K, (b) 127°K, (c) 150°K, and (d) 163°K.

a furnace. The same result was obtained in the case of BaX. This suggests that the adsorbed CO_2^- radical strongly interacts with the zeolite surfaces and is stabilized on them. Such a stable anisotropic spectrum as obtained on the CaX or BaX could not be observed on the MgX, though the electrostatic field caused by the Mg^{2+} ion is generally expected to be stronger than that caused by the Ca^{2+} or Ba^{2+} ion.[14,18,19] This contradiction may be interpreted in terms of the very low degree of ion exchange on MgX, compared with that on CaX or BaX.

In this view, a series of zeolites differently exchanged by bivalent cations were investigated. For instance, the motional behavior of the radical adsorbed on CaX (78.5%) can be deduced from Figs. 8(a)—(d). The $^{13}CO_2^-$ radical on a zeolite with a lower degree of cation exchange shows almost the same spectrum as that on the zeolite with a higher exchange degree at 77°K, but the temperature at which the radical begins to move or bleach depends remarkably upon the exchange degree, as can be seen in Table 2. That is, an almost complete exchange with a cation such as Ca^{2+} or Ba^{2+} greatly restricts the motion of the radical. All the radicals adsorbed on zeolites of lower degrees of exchange bleach below room temperature. It can be

18) C. L. Angell, *J. Phys. Chem.*, **70**, 2420 (1966).
19) D. Taylor and D. R. Walker, *J. Chem. Soc., A*, **1969**, 2991.

TABLE 2. BEHAVIORS OF CO_2^- RADICAL ADSORBED ON THE ZEOLITES

CO_2^- radical on	Temperature at which the radical begins to		Decay time at R.T.
	rotate, °K	bleach, °K	
LiX (87.0%)	118	258	—
MgX (59.6%)	200	423	a few days
(42.8%)	116	252	—
(59.6%)[a]	202	—	a few days
CaX (96.4%)	420	420	a few months
(78.5%)	163	253	—
BaX (94.4%)	420	420	a few months
(70.9%)	179	271	—

a) Pre-irradiation for 2 hr at 77°K.

deduced from these phenomena that the electrostatic field influences the motion of the CO_2^- radicals more effectively than the perturbation on the structure of the CO_2^- radicals.

The Reaction of Carbon Dioxide with γ-Irradiated Zeolites. Wang and Willard[3] have reported that the addition of carbon dioxide to γ-irradiated silica gel results in the formation of the O_2^- radical, though the CO_2^- radical is formed on the post-irradiated gel, while Yamada *et al.*[2] have found that the latter radical is formed on the pre-irradiated gel. In the present study, the CO_2^- radical was generated on both post- and pre-irradiated zeolites. The results obtained in the case of MgX (59.6%) are shown in Figs. 4 and 5. On the other hand, a hyperfine structure attributed to the interaction of the trapped electron with the aluminum nucleus[16,17] was observed on irradiated MgX in the absence of carbon dioxide, as is shown in Fig. 5(a). However, when the MgX was irradiated in the presence of carbon dioxide, the hyperfine structure due to the ^{27}Al nucleus could not be observed. This can be interpreted as follows: the electrons formed during the irradiation are preferentially captured by the carbon dioxide molecule because this molecule traps electrons more deeply than aluminum does. Thus, the CO_2^- radical may be formed relatively easily on the surface of irradiated zeolite. In the cases of NaX and KX, no CO_2^- radical was observed when they were irradiated at 77°K, but it was generated by irradiation at room temperature. It may be deduced from these observations that the amount of trapped electrons formed during the irradiation is small, or that the ability to transfer the trapped electron to the carbon dioxide molecule is weak, at 77°K. Upon irradiation for 16 hr at room temperature, the amounts of sites sufficient to form the radicals may be obtained. Further work will be needed in order to discuss these sites.

The Mechanism of Decomposition of Hydrogen Peroxide by Iodine in Acid Solutions. The Rates of Associated Reactions

Isao MATSUZAKI,[1] Radmilo SIMIC,[2] and Herman A. LIEBHAFSKY

Department of Chemistry, Texas A & M University, College Station, Texas 77843, U. S. A.

(Received April 4, 1972)

For the purpose of isolating elementary reactions responsible for the decomposition of hydrogen peroxide by iodine and its compounds, the reaction at 50°C of acid solutions containing I_2, I^-, HIO, *etc.* with $[I^-]$ and $[I_2]$ controlled by use of TlI(s) and I_2(s) was studied. The rates of the evolution of oxygen, consumption of hydrogen peroxide and production of H^+ were subjected to measurement and led to a formulation of a complex mechanism consisting of the following reactions: $HIO_2+H_2O_2\longrightarrow HIO+H_2O+O_2$; $H_2OI^++H_2O_2\longrightarrow HIO_2+H^++H_2O$; $HIO+H_2O_2\longrightarrow H^++I^-+H_2O+O_2$; $HIO_2+H^++I^-\longrightarrow 2HIO$; $H_2OI^+\rightleftharpoons HIO+H^+$; $I^-+H^++H_2O_2\longrightarrow HIO+H_2O$; and $I_2+H_2O\rightleftharpoons HIO+H^++I^-$. Absolute or relative rate constants for the first four reactions were evaluated by using equilibrium and rate constants of the others.

A series of preliminary investigations[3–6] has been made at 50°C toward clarifying the mechanism of the decomposition of hydrogen peroxide by iodine and its compounds, the only known completely inorganic oscillating reaction. It has been suggested that the following step might have much to do with the oxygen evolution in the pulses:

Step 10: $HIO + H_2O_2 \longrightarrow H^+ + I^- + H_2O + O_2$[7]

The purpose of the present investigation is to determine the value of the rate constant, which would help us understand to what degree Step 10 contributes to the pulsed oxygen evolution. The step is found to be responsible for most oxygen produced when hydrogen peroxide is oxidized by iodine at 25°C in acid solutions[8] in the virtual absence of iodate ion, which should be present to achieve oscillating decomposition.

Step 10 is difficult to study even in acid solutions because it is always accompanied by other reactions such as

Step 11: $I^- + H^+ + H_2O_2 \longrightarrow HIO + H_2O$

Step 13: $IO^- + H_2O_2 \longrightarrow I^- + H_2O + O_2$

$$I_2 + 5H_2O_2 = 2IO_3^- + 2H^+ + 4H_2O \quad (1)$$

$$3I_2 + 3H_2O = IO_3^- + 5I^- + 6H^+ \quad (2)$$

By using TlI(s) to control the iodide concentration, Liebhafsky[8] accomplished what appeared to be a satisfactory isolation of Step 10 at 25°C in acid solutions saturated with iodine so that oxygen evolution could be measured *as a constant rate* and its rate law deduced. Under these conditions, the overall reaction was assumed to be

$$I_2(s) + 2Tl^+ + H_2O_2 = 2TlI(s) + 2H^+ + O_2 \quad (3)$$

The rate of oxygen evolution at 50°C was studied by the method outlined above. Under certain conditions, the amount of H_2O_2 consumed was considerably greater than that called for by the stoichiometry of (3), and the H^+ produced was considerably less. It accordingly became necessary to investigate the additional reactions. They have been confirmed, and the result will contribute to the eventual understanding of the oscillating decomposition.

Experimental

Materials and Apparatus. Hydrogen peroxide of 30% content without inhibitor from J. T. Baker Chemical Co. and from Mallinckrodt Chemical Works was determined iodometrically before each experiment as follows. After dilution of 0.2 m*l* 30% H_2O_2 to 25 m*l*, 20 m*l* of 2N H_2SO_4, 2 g KI and 3 drops of 3% $(NH_4)_6Mo_7O_{24}$ (to expedite reaction) were successively added. After 3 min, the liberated iodine was titrated with 0.1M $Na_2S_2O_3$, starch indicator being added near the end of the titration.

Perchloric acid of analytical grade (J. T. Baker Chemical Co., 60 or 70% by weight) was used in preparing dilute (0.1N and less) solutions standardized against Na_2CO_3 with bromocresol green as indicator.

Iodine of analytical grade (J. T. Baker Chemical Co.) was pulverized before use.

A stick of highly pure thallium (Fisher Scientific Co.) was shaved as needed for the preparation of thallous perchlorate. The shavings were dissolved in excess strong perchloric acid at 105°C. The precipitated perchlorate was filtered and washed at 5°C with water until the washings were neutral.

Thallous nitrate of analytical grade (K & K Laboratories and Fisher Scientific Co.) was used in the reaction mixtures and also to prepare the slightly soluble thallous iodide by addition of potassium iodide. The precipitate was thoroughly washed with water.

The reaction vessel (Fig. 1), a 125 m*l* Erlenmeyer flask, sharply indented to promote mixing, had a rubber-capped side arm for the addition of reagents and for the withdrawing

1) On leave from Department of Chemistry, Faculty of Science, Hokkaido University, Sapporo, Japan. Present address: Department of Synthetic Chemistry, Faculty of Engineering, Shinshu University, Nagano, Japan.

2) Present address: Hemijska Industrija Pancevo, Pancevo, Yugoslavia.

3) J. H. Woodson and H. A. Liebhafsky, *Nature*, **224**, 690 (1969).

4) J. H. Woodson and H. A. Liebhafsky, *Anal. Chem.*, **41**, 1894 (1969).

5) I. Matsuzaki, J. H. Woodson, and H. A. Liebhafsky, This Bulletin, **43**, 3317 (1970).

6) I. Matsuzaki, R. B. Alexander, and H. A. Liebhafsky, *Anal. Chem.*, **42**, 1690 (1970).

7) Reactions that are probable steps in the oscillating decomposition will be identified by the numbers assigned to them in the tentative complete mechanism formulated here for the very complex overall reaction. Rates of these steps will be represented by V with the appropriate subscript: *e.g.*, V_{10}.

8) H. A. Liebhafsky, *J. Amer. Chem. Soc.*, **54**, 3504 (1932).

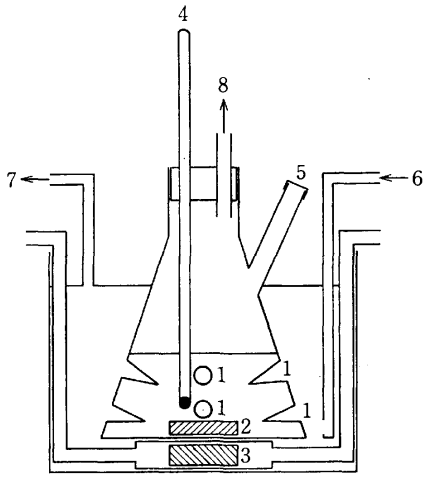

Fig. 1. Apparatus used.
1: Indent, 2: Magnetic stirrer, 3: Air-driven magnet, 4: Thermometer, 5: Rubber cap, 6: Water from thermostat, 7: Water to thermostat, 8: Gas buret.

of samples by means of a syringe. It was connected to a 100 m*l* gas buret for the measurement of evolved oxygen.

Procedure. Water pre-saturated with oxygen, perchloric acid, 0.05 g of TlI(s), thallous perchlorate solution and 2 g of I_2(s) were added successively to the reaction vessel at room temperature to make a liquid volume near 60 m*l*. After thermal equilibrium was reached in the thermostat at 50°C, the prescribed amount of hydrogen peroxide at thermostat temperature was injected from the syringe to start the reaction (t=0). Two minutes later the first sample (1.6 m*l*) was withdrawn. Further samples, the same in volume, were taken at recorded intervals of time. Gas-buret readings were made every 2 or 3 min. From these, rates of oxygen evolution were calculated, correction for the partial pressure of water vapor being made for 25°C, the assumed gas temperature.

The reaction was stopped in the samples as follows. From the 1.6 m*l* of reaction mixture in a 50 m*l* beaker, 1 m*l* was withdrawn with a pipet and discharged into 2 m*l* of carbon tetrachloride and 25 m*l* of water. The mixture was then shaken vigorously to extract iodine. Acid was then determined on one 10 m*l* portion of the aqueous phase by titration with NaOH, and H_2O_2 iodometrically on another by titration with thiosulfate. Blank tests showed that the formation of TlI and of TlI_3, which occurred on the addition of KI prior to titration, did not interfere with the iodine determination. Values of $\Delta[H_2O_2]$ and $\Delta[H^+]$ were calculated for the

TABLE 1. RESULTS OF THREE COMPREHENSIVE EXPERIMENTS AT 50°C

	Exp't No.	1	2	3
Data at time=0[a]	Volume of react. mixt. (m*l*)	58.4	58.4	58.4
	$[I_2]_0\times10^3$ (M)[b]	3.08	3.08	3.08
	$[Tl^+]_0$ (M)[c]	0.225	0.225	0.225
	$[I^-]_0\times10^6$ (M)[d]	1.86	1.86	1.86
	$[H^+]_0$ (M)[e]	0.141	0.413	1.182
	$[H_2O_2]_0$ (M)[e]	0.234	0.484	0.955
	Measured Rates			
	$(dO_2/dt)_0\times10^4$ (mol/*l*/min)	1.02	1.09	1.22
	$(-d[H_2O_2]/dt)_0\times10^4$ (M/min)	1.20	2.19	4.21
	$(d[H^+]/dt)_0\times10^4$ (M/min)	1.20	1.34	0.76
	Rate Quotients			
	$(-dO_2/d[H_2O_2])_0$ (O_2 in mol/*l*)	0.85	0.49	0.29
	$(-d[H^+]/d[H_2O_2])_0$	1.0	0.61	0.18
Data at the end of run	Stoichiometric Data			
	React. time (min)	460	383	268
	Volume of react. mixt. (m*l*)	52.0	55.2	52.0
	ΔO_2 (Total amount of O_2 evolved) $\times10^3$ (mol)	2.085	2.405	2.120
	ΔTlI (TlI formed) $\times10^3$ (mol)	2.74	2.246	−0.15[f]
	$TlIO_3$ formed $\times10^3$ (mol)	0	0	0.046
	Rate Quotient			
	$\Delta TlI/\Delta O_2$	1.31	0.893	−0.071[f]

a) Subscripts 0 in $[H^+]_0$, $(d[H^+]/dt)_0$, *etc.*, specify quantities at time=0.
b) The value of 3.08×10^{-3} M is the solubility of I_2 at 50°C. Two grams of I_2, *i.e.*, 7.9×10^{-3} mol, was added to saturate the reaction mixtures (60 m*l* before the first sampling), so that it may be regarded as saturated with I_2.
c) The value of $[Tl^+]_0$ was obtained by multiplying the amount in mole of $TlClO_4$ added to the reaction mixture (60 m*l*) by 1000/60.
d) The solubility product for TlI is 4.2×10^{-7} M[2] at 50°C as determined by interpolation of the data[9]; this value, on division by $[Tl^+]_0$, gives $[I^-]_0$. Experimentally, in order to ensure the establishment of the dissolution equilibrium of TlI, 0.05 g (=1.5×10^{-4} mol) of TlI was added to each reaction mixture (60 m*l* before the first sampling).
e) The values shown were obtained by extrapolating the concentrations of the withdrawn samples to time=0. They were practically in agreement with those calculated for the amounts of reagents mixed.
f) Lower limit.

9) L. G. Sillen and A. E. Martell, "Stability Constants of Metal-Ion Complexes," Special Publication No. 17, The Chemical Society, Burlington House, London (1964), pp. 339 and 350.

1 ml of reaction mixture by taking the volume ratio 26/10 into account.

At the end of the reaction, information on TlI(s) and $TlIO_3$(s), both sparingly soluble, was obtained from the weighed, filtered residue after removal of I_2(s) by sublimation. Cubic thallous iodide is red at sublimation temperature and changes to a yellow, rhombic form as it is cooled to room temperature. The iodate is white and its presence was confirmed qualitatively by iodine liberation in Experiment 3 (Table 1). No iodate was formed in Experiments 1 and 2 (Table 1).

Results of Comprehensive Experiments. We begin by examining the relative importance of several reactions in this system.

For V_{13}, we have[10]

$$V_{13} \equiv dO_2/dt = -d[H_2O_2]/dt = k_{13}[H_2O_2][IO^-] = k'_{13}[H_2O_2][I_2]/[H^+]^2[I^-] \quad (4)$$

with $k'_{13}=5.62\times10^{-11}$(M²/min) according to Fig. 1, Ref. 10. This corresponds to $(V_{13})_0=1.09\times10^{-6}$, 2.64×10^{-7}, and 6.35×10^{-8}M/min for Experiments 1, 2, and 3, respectively. Comparison with the measured rates in Table 1 shows that V_{13} can be neglected.

For V_{11}, we have[11]

$$V_{11} \equiv -d[H_2O_2]/dt = -d[H^+]/dt = k_{11}[H_2O_2][I^-] + k'_{11}[H_2O_2][I^-][H^+]$$

$$k_{11} = 4.91\times10^9\ e^{-13400/RT}(M^{-1}\cdot min^{-1})$$

$$k'_{11} = 4.58\times10^8\ e^{-10450/RT}(M^{-2}\cdot min^{-1})$$

from which we obtain at 50°C

$$V_{11}(M/min) = (4.18+38.9[H^+])[I^-][H_2O_2] \quad (5)$$

For a comparison with the measured rates in Table 1 as above, we calculate $(V_{11})_0=0.042\times10^{-4}$, 0.182×10^{-4}, and 0.891×10^{-4}M/min for Experiments 1, 2, and 3, respectively. These rates are not negligible relative to the corresponding rates in Table 1.

Formation of I_3^- was neglected in computing $[I^-]_0$ values for Table 1. We have for the tri-iodide equilibrium

$$K_{15} = [I_2][I^-]/[I_3^-] = 2.67\times10^{-3}M$$

the numerical value having been obtained by extrapolating experimental data.[12] For the conditions of Table 1, the equilibrium value of $[I_3^-]$ is 1.28×10^{-7}mol, which is negligible relative to the amount (0.05 g or 1.5×10^{-4}mol) of TlI added and justifies the calculation of $[I^-]_0$ as made.

$TlIO_3$ was formed only in Experiment 3 and in a negligible amount. Reactions (1) and (2) may therefore be disregarded in discussing mechanism.

Schematic Representation of Mechanism: We formulated and tested various mechanisms for their capability of accounting for the results. Of these a plausible one has been found. Because of its complexity the mechanism is shown schematically (Fig. 2). The figure shows only the interaction of the various iodine species. Steps are represented by single arrows; equilibria, by double arrows; H_2O_2, H^+, and H_2O are omitted. The complete equations are

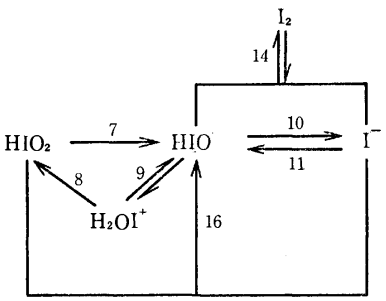

Fig. 2. Schematic representation of the mechanism.

Step 7	$HIO_2 + H_2O_2 \longrightarrow HIO + H_2O + O_2$
Step 8	$H_2OI^+ + H_2O_2 \longrightarrow HIO_2 + H^+ + H_2O$
Equilibrium 9	$H_2OI^+ \overset{K_9}{\rightleftharpoons} HIO + H^+$
Step 10	$HIO + H_2O_2 \longrightarrow H^+ + I^- + H_2O + O_2$
Step 11	$I^- + H^+ + H_2O_2 \longrightarrow HIO + H_2O$
Equilibrium 14	$I_2 + H_2O \overset{K_{14}}{\rightleftharpoons} HIO + H^+ + I^-$
Step 16	$HIO_2 + H^+ + I^- \longrightarrow 2HIO$

The solubility equilibria for I_2(s) and TlI(s) have not been included. Of the intermediate iodine species, HIO and H_2OI^+ exist at equilibrium concentrations; HIO_2 is at a steady-state concentration and is amenable to treatment by the Bodenstein steady-state approximation. The use of this approximation is on a firm basis as the rates in the reaction system are constant.

Analyses of Results According to the Mechanism: The steady-state approximation gives

$$d[HIO_2]/dt = V_8 - V_7 - V_{16} = (k_8/K_9)[HIO][H^+][H_2O_2] - k_7[HIO_2][H_2O_2] - k_{16}[HIO_2][H^+][I^-] = 0 \quad (6)$$

and hence

$$[HIO_2] = (k_8/K_9)[HIO][H^+][H_2O_2]/(k_7[H_2O_2] + k_{16}[H^+][I^-]) \quad (7)$$

The rate of oxygen evolution is

$$dO_2/dt = V_{10} + V_7 = k_{10}[HIO][H_2O_2] + k_7[HIO_2][H_2O_2] \quad (8)$$

By insertion of K_{14} and of $[HIO_2]$, Eq. (8) is transformed into

$$(dO_2/dt)([H^+][I^-]/[I_2][H_2O_2]) = k_{10}K_{14} + (k_8/K_9)K_{14}[H^+]/\{1+(k_{16}/k_7) \times ([I^-][H^+]/[H_2O_2])\} \quad (9)$$

For the sake of brevity the left side of Eq. (9) will be denoted by A, and the right side by A′.

The quantity A is convenient for obtaining k_{10}, k_8/K_9, and k_{16}/k_7 from the experimental results. Let us plot A as a function of $[H^+]$ as abscissa for the experiments in Table 1, in which $[I^-]$ is constant, and denote the intercept on the ordinate axis by A^0. Then, we have by Eq. (9)

$$A^0 = k_{10}K_{14} \quad (10)$$

$$(dA/d[H^+])_{[H^+]=0} = (k_8/K_9)K_{14} \quad (11)$$

The products of constants shown above can be evaluated graphically from the experimentally established variation of A with $[H^+]$. By use[13] of $K_{14}=4.12\times10^{-12}M^2$ and $K_9=6\times10^2$M at 50°C, and of the graphically evaluated results, the following constants were calculated:

$$\left.\begin{aligned} k_{10} &= 2.68\times10^{-8}/4.12\times10^{-12} = 6.5\times10^3(M^{-1}\cdot min^{-1}) \\ k_8/K_9 &= 9.4\times10^{-8}/4.12\times10^{-12} = 2.28\times10^4(M^{-2}\cdot min^{-1}) \\ k_8 &= 2.28\times10^4\times6\times10^2 = 1.37\times10^7(M^{-1}\cdot min^{-1}) \\ k_{16}/k_7 &= 2.14\times10^5(M^{-1}) \end{aligned}\right\} \quad (12)$$

10) H. A. Liebhafsky, *Chem. Rev.*, **17**, No. 1, August, 89 (1935).
11) H. A. Liebhafsky and A. Mohammad, *J. Amer. Chem. Soc.*, **55**, 3977 (1933).
12) A. D. Awtrey and R. E. Connick, *ibid.*, **73**, 1842 (1951).
13) J. D. Burger and H. A. Liebhafsky, unpublished work.

The value of k_{16}/k_7 was calculated from Eq. (9). That the results listed above are satisfactory for all experiments in Table 1 is evident from a comparison of the following values of A and A':

$A \times 10^8$ (mol/l) ··· 3.82(Exp. 1), 5.76(Exp. 2), 9.36(Exp. 3)

$A' \times 10^8$ (mol/l) ··· 3.82(Exp. 1), 5.45(Exp. 2), 10.12(Exp. 3)

The specific rates in Eq. (12) are based on values of dO_2/dt only. A severe test of their reliability is to see whether a mechanism that uses these specific rates can yield the three experimentally determined rate quotients listed in Table 1. For this purpose, the rates V_7, V_8, V_{10}, V_{11}, and V_{16} must be expressed in suitable form.

We begin with

$$V_8 = k_8[H_2OI^+][H_2O_2] = (k_8/K_9)[HIO][H^+][H_2O_2]$$
$$= (k_8/K_9)(K_{14}[I_2]/[H^+][I^-])[H^+][H_2O_2]$$
$$= (k_8/K_9)K_{14}([I_2][H_2O_2]/[I^-]) \quad (13)$$

We then proceed to obtain V_7, V_{10}, and V_{16} by the relations

$$V_{10}/V_8 = k_{10}[HIO][H_2O_2]/(k_8/K_9)[HIO][H^+][H_2O_2]$$
$$= k_{10}/(k_8/K_9)[H^+]$$
$$\therefore \quad V_{10} = \{k_{10}/(k_8/K_9)[H^+]\} \times V_8 \quad (14)$$
$$V_7/V_{16} = k_7[HIO_2][H_2O_2]/k_{16}[HIO_2][H^+][I^-]$$
$$= (k_7/k_{16})([H_2O_2]/[H^+][I^-])$$
$$V_7 + V_{16} = V_8$$

the last of which is derived from the Bodenstein steady-state approximation applied to HIO_2.

By solving the last two equations simultaneously, we find

$$V_{16} = V_8/\{(k_7/k_{16})([H_2O_2]/[H^+][I^-]) + 1\} \quad (15)$$

which leads to V_7 because

$$V_7 = V_8 - V_{16} \quad (16)$$

Expressed in terms of the individual rates, the three rate quotients in Table 1 are

$$-dO_2/d[H_2O_2] = (dO_2/dt)/(-d[H_2O_2]/dt)$$
$$= (V_7 + V_{10})/(V_7 + V_{10} + V_8 + V_{11}) \quad (17)$$
$$-d[H^+]/d[H_2O_2] = (d[H^+]/dt)/(-d[H_2O_2]/dt)$$
$$= \frac{(V_{10} + V_8 - V_{16} - V_{11}) - (V_{11} + 2V_{16} + V_7 - V_{10} - V_8)}{V_7 + V_{10} + V_8 + V_{11}}$$ [14]
$$= (2V_{10} + 2V_8 - 3V_{16} - 2V_{11} - V_7)/(V_7 + V_{10} + V_8 + V_{11}) \quad (18)$$

$$\Delta TlI/\Delta O_2 \doteqdot dTlI/dO_2$$
$$= \{(V_{10} - V_{16} - V_{11}) - (V_{11} + 2V_{16} + V_7 - V_{10} - V_8)\}$$ [15]$$/(V_7 + V_{10})$$
$$= (2V_{10} - 2V_{11} - 3V_{16} - V_7 + V_8)/(V_7 + V_{10}) \quad (19)$$

14) Under the experimental conditions, Equilibrium 14 is maintained, and $[H^+]$, $[Tl^+]$ —and hence $[I^-]$— are virtually constant; consequently so is [HIO]. Therefore, the net rate of HIO production in the reaction system must equal the net rate of HIO consumption in the reverse reaction in Equilibrium 14. This net rate of HIO production is given by the terms in the second parentheses; owing to Equilibrium 9, H_2OI^+ counts as HIO. As one H^+ is consumed for each HIO in the reverse reaction of Equilibrium 14, the terms in the parentheses in question also give the rate of H^+ consumption in this reverse reaction. The terms in the first parentheses give the net rate of H^+ production in all reactions other than the forward reaction of Equilibrium 14.

15) The reasoning here parallels that given in 14) except that I^- (or TlI) and not H^+ is involved.

TABLE 2. COMPARISON OF CALCULATED RATE QUOTIENTS WITH EXPERIMENTAL RATE QUOTIENTS FROM TABLE 1

Exp't No.	1	2	3
$V_7 \times 10^5$ (M/min)	2.92	5.59	9.93
$V_8 \times 10^5$ (M/min)	3.62	7.50	14.80
$V_{10} \times 10^5$ (M/min)	7.35	5.18	3.58
$V_{11} \times 10^5$ (M/min)	0.42	1.82	8.91
$V_{16} \times 10^5$ (M/min)	0.698	1.90	4.87
$(-dO_2/d[H_2O_2])_0$ [a]	0.717 (0.85)	0.536 (0.49)	0.363 (0.29)
$(-d[H^+]/d[H_2O_2])_0$ [a]	1.12 (1.0)	0.519 (0.61)	−0.151 (0.18)
$(dTlI/dO_2)_0$ [b]	1.21 (1.31)	0.272 (0.893)	−1.51 (−0.071)

a) Experimental values from Table 1 in parentheses, the inaccuracies of which are estimated to be less than ±2.5%.

b) Experimental values for $\Delta TlI/\Delta O_2$ from Table 1 in parentheses.

A comparison of experimental and calculated rate quotients is given in Table 2. In light of the complexity of the reaction system and the difficulty of analytical work, we consider the comparison satisfactory.

TABLE 3. DATA FOR SUPPORTING MEASUREMENTS AT 50°C OF OXYGEN EVOLUTION RATE

Exp't No.	4	5	6	7
$[I_2]_0 \times 10^3$ (M)	3.08	3.08	3.08	3.08
$[I^-]_0 \times 10^6$ (M)	1.86	1.12	0.93	1.42
$[H^+]_0$ (M)	0.393	0.112	0.449	0.224
$[H_2O_2]_0$ (M)	1.724	1.722	1.91	2.58
$A \times 10^8$ (mol/l)	5.34	3.40	6.02	5.00
$A' \times 10^8$ (mol/l)	6.07	3.72	6.71	4.72

Supporting Measurements of Oxygen Evolution Rate. To confirm the validity of Eq. (9), and to establish a basis for estimating the reliability of the various specific rates, measurements of the rate of oxygen evolution were carried out at various $[I^-]$ and $[H^+]$. Values of A and A' for these experiments are listed in Table 3. The agreement between each A and the corresponding A' is good enough, in view of the complexity of Eq. (9).

Relation to Previous Work

What began as a simple temperature-coefficient measurement for a reaction previously investigated[8] at 25°C had to be expanded into a complete kinetic investigation because evidence was obtained at 50°C to show that Eq. (3), assumed by Liebhafsky,[8] did not describe what actually took place. An attempt was made to interpret his results at 25°C in terms of the new mechanism. The attempt was partially successful. It gave consistent results and showed in particular that his value of k_{10} must be too high. Because his rate measurements were for calculated *average* (not *initial*) concentrations, they must be repeated if reliable values of the specific rates at 25°C are to be obtained.

The new work has a bearing on the *reduction*[16] of hydrogen peroxide by iodine. One difficulty with this

16) H. A. Liebhafsky, *J. Amer. Chem. Soc.*, **53**, 2074 (1931).

reaction was the need to find some species related to iodine that could *reduce* H_2O_2. HIO seemed to be excluded because it oxidizes H_2O_2 in Step 10. The existence of $H_2I_2O_3$ was consequently postulated. Subsequently Bell and Gelles[17] proved the existence of H_2OI^+, which makes the assumption of Step 8 seem a better way out of the difficulty.

The complexity of the new results shows that the present reaction system is closely related to that in which the oscillating decomposition of peroxide occurs; an important difference is that $[IO_3^-]$ is appreciable in the second system. The new specific rates (k_8, k_{10}, and the ratio k_{16}/k_7) should eventually be useful for describing the oscillating decomposition.

In the previous work, it was assumed that HIO_2 reduces H_2O_2 to form IO_3^-, which contradicts Step 7 if HIO_2 can react with H_2O_2 in only one way. Unfortunately, HIO_2 cannot be isolated under our conditions for a direct test of its reactivity with H_2O_2. The evidence for Step 7 is as strong as indirect evidence of this kind can be.

17) R. P. Bell and E. Gelles, *J. Chem. Soc.*, **1951**, 2734.

Summary

An investigation of the oxidation by iodine of hydrogen peroxide in acid solutions at 50°C has shown the reaction to be more complex than had been expected.

Comprehensive experiments in which $[I^-]$ was controlled by use of TlI(s) gave a mechanism in which the four steps

Step 7 $HIO_2 + H_2O_2 \longrightarrow HIO + H_2O + O_2$

Step 8 $H_2OI^+ + H_2O_2 \longrightarrow HIO_2 + H^+ + H_2O$

Step 10 $HIO + H_2O_2 \longrightarrow H^+ + I^- + O_2 + H_2O$

Step 16 $HIO_2 + H^+ + I^- \longrightarrow 2HIO$

are involved as constituent elementary steps. Numerical values for 50°C: $k_8 = 1.37 \times 10^7 M^{-1} \cdot min^{-1}$; $k_{10} = 6.5 \times 10^3 M^{-1} \cdot min^{-1}$; $k_{16}/k_7 = 2.14 \times 10^5 M^{-1}$. The last two specific rates appear as a ratio because $[HIO_2]$ is unknown.

We are grateful to the Robert A. Welch Foundation for supporting this work.

BULLETIN OF THE CHEMICAL SOCIETY OF JAPAN, VOL. 45, 3371—3375 (1972)

The Estimation of the Surface Properties of Metal Oxides by the Use of TCNQ Adsorption. II. The Electron-donor Property of Silica-Alumina, Silica-Titania, and Alumina-Titania System Surfaces

Hiroshi HOSAKA, Norimichi KAWASHIMA, and Kenjiro MEGURO

Department of Applied Chemistry, Faculty of Science, Science University of Tokyo, Kagurazaka, Shinjuku-ku, Tokyo

(Received April 11, 1972)

The electron-donor property of silica–alumina, silica–titania, and alumina–titania system surfaces was investigated by means of TCNQ adsorption. When TCNQ was adsorbed on the surfaces of the metal oxide systems from its acetonitrile solution, the surfaces of the metal oxides acquired the coloration characteristic of each oxide. The coloration was caused by the formation of TCNQ anion radicals on the metal oxide surfaces. The presence of the TCNQ anion radicals was confirmed by studying the ESR absorption and the electronic spectrum. The silica–alumina, silica–titania, and alumina–titania systems showed lower radical-ion-forming activity (electron-donating power) than the parent oxides-silica, alumina, and titania. The change in the activity with the composition was characteristic of each metal oxide system.

The presence of electron-transfer sites on the surface of certain metal oxides is well known.[1-6] Recently, it has been reported that the formation of TCNQ anion radicals takes place on some metal oxide surfaces, and that the electron-donor property of metal oxides can be estimated by the use of 7,7,8,8-tetracyanoquinodimethane (TCNQ) adsorption.[6]

The present paper will describe the electron-donor property of silica–alumina, silica–titania, and alumina–titania systems as studied by means of TCNQ adsorption.

Experimental

Materials. The samples of the silica–alumina, silica–titania, and alumina–titania systems were prepared by the co-hydrolysis of silicon ethoxide and aluminium butoxide mixtures, silicon ethoxide and titanium butoxide mixtures, and aluminium butoxide and titanium butoxide mixtures, respectively, in different molar ratios. Excess aqueous ethanol was vigorously stirred into the alcoholic solution of alkoxides. Stirring was continued for 10 hr at a temperature near the boiling point. The precipitate was then separated by

1) H. P. Leftin and M. C. Hobson, Jr., *Advan. Catal.*, **14**, 372 (1963).
2) A. Terenin, *ibid.*, **15**, 256 (1964).
3) R. P. Porter and W. K. Hall, *J. Catal.*, **5**, 366 (1966).
4) B. D. Flockhart, J. A. N. Scott, and R. C. Pink, *Trans. Faraday Soc.*, **62**, 730 (1966).
5) B. D. Flockhart, I. R. Leith, and R. C. Pink, *ibid.*, **65**, 542 (1969).
6) H. Hosaka and K. Meguro, This Bulletin, **44**, 2616 (1971).

centrifuging, thoroughly washed with water and methanol, finely ground, and then evacuated at 100°C until the residual pressure was less than 10^{-5} Torr. The complete hydrolysis of these alkoxides was confirmed by studying the infrared spectra. The dried products were calcined for 2 hr at 500°C.

The composition of the metal oxide systems was measured with a Rigaku Denki X-ray vacuum spectrograph by means of X-ray fluorometry. The abbreviations used are as follows: S, silica; A, alumina; T, titania; 4SA, SA, and S4A, silica-aluminas containing 35, 64, and 81% alumina; 4ST, ST, and S4T, silica-titanias containing 21, 55, and 83% titania; 4AT, AT, and A4T, alumina-titanias containing 28, 62, and 83% titania, respectively.

The crystal features as determined by X-ray diffractometry, and the surface areas as determined by studying the nitrogen adsorption of the metal oxides, are set out in Table 1.

TCNQ was synthesized from the condensation product of 1,4-cyclohexanedione and malononitrile.[7] This was purified by repeated recrystallization. The purity was checked by elemental analysis, by the measurement of the melting point, and by spectrophotometry.[6]

Apparatus and Procedure. The metal oxide was placed in a flask which was attached to a high-vacuum line and outgassed at 10^{-5} Torr for 1 hr at 100°C, and then cooled to 25°C *in vacuo* prior to the TCNQ adsorption. A solution of TCNQ in acetonitrile (10 mM) was then poured into the flask through a stop cock. Subsequently, the contents of the flask were transferred into an L-type test tube and then shaken for 2 hr at 25°C. After this shaking, the metal oxide was collected by centrifuging and dried at room temperature *in vacuo*. The dried sample was used for the measurement of the electronic spectrum and was evacuated at 10^{-5} Torr for the ESR measurement.

The ESR spectra were measured by means of a Japan Electrons Optics Laboratory JES-3BS-Xtype ESR spectrometer operating at a cavity resonance frequency of 9400 Hz with 100 kHz modulation. The *g*-value was obtained by comparison with the value for Mn^{2+}. The radical concentration (spin conc.) was estimated by comparing the peak-to-peak height on the first derivative curves with that of an internal-standard Mn^{2+} sample.

The electronic spectra of the samples were measured by means of a diffuse-reflectance spectrophotometer.

Results and Discussion

When TCNQ was adsorbed on the surfaces of the silica-alumina, silica-titania, and alumina-titania from its acetonitrile solution at room temperature, the surfaces of the metal oxides acquired the colorations characteristic of each oxide, as is shown in Table 1. The same colorations were observed when the metal oxides were ground with TCNQ crystal. The colorations of the metal oxide surfaces suggest that new adsorbed species are formed on the surfaces. This suggestion was confirmed by the evidence that the colored metal oxides showed ESR absorptions, indicating the presence of free radical species. The spectra are unresolved (Figs. 1—2; *g*-values, 2.011), which can be explained by the fact that the anisotropy of the hyperfine structure arises from the lack of motional degrees of freedom. The state of the adsorbed species was studied by means of the electronic spectra in addition to the ESR spectra. The electronic spectra of the colored samples are illustrated in Figs. 3—5. The bands appearing below 400 mμ are common to all the metal oxides and may be supposed to correspond to the physically-adsorbed state of neutral TCNQ, which has its absorption band at 395 mμ.[8] In the case of the silica-titania and alumina-titania systems, this assignment does not hold completely because the titania has its characteristic band in the same region. The absorption bands in the visible region observed in the cases of the silica-alumina, silica-titania, and

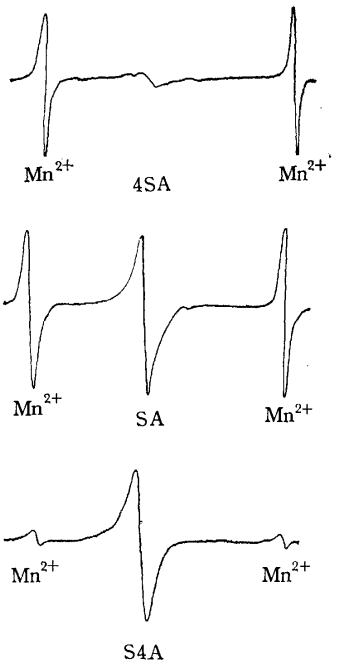

Fig. 1. ESR spectra from TCNQ adsorbed on the silica-alumina systems.

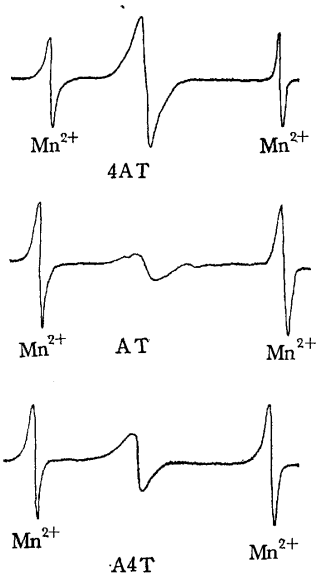

Fig. 2. ESR spectra from TCNQ adsorbed on the alumina-titania systems.

7) D. S. Acker and W. R. Hertler, *J. Amer. Chem. Soc.*, **84**, 3370 (1962).

8) L. R. Melby, R. J. Harder, W. R. Hertler, W. Mahler, R. E. Benson, and W. E. Mochel, *ibid.*, **84**, 3374 (1962).

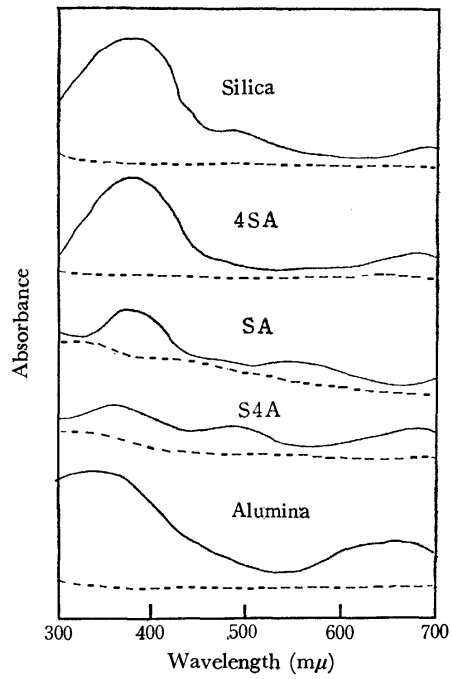

Fig. 3. Electronic spectra from TCNQ adsorbed on the silica-alumina systems. Dotted line, silica-aluminas prior to adsorption.

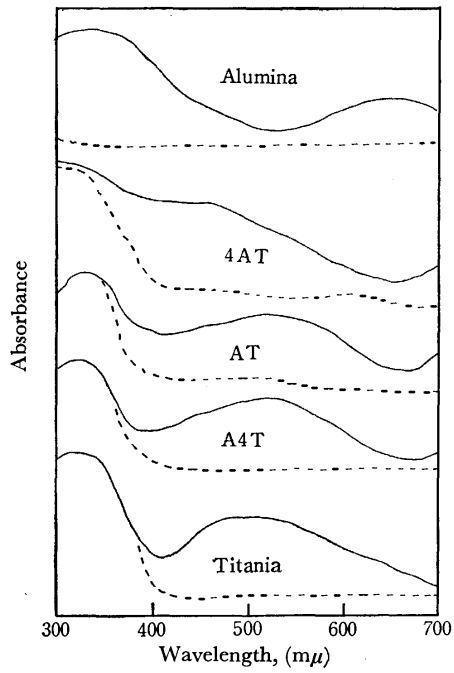

Fig. 5. Electronic spectra from TCNQ adsorbed on the alumina-titania systems. Dotted line, alumina-titanias prior to adsorption.

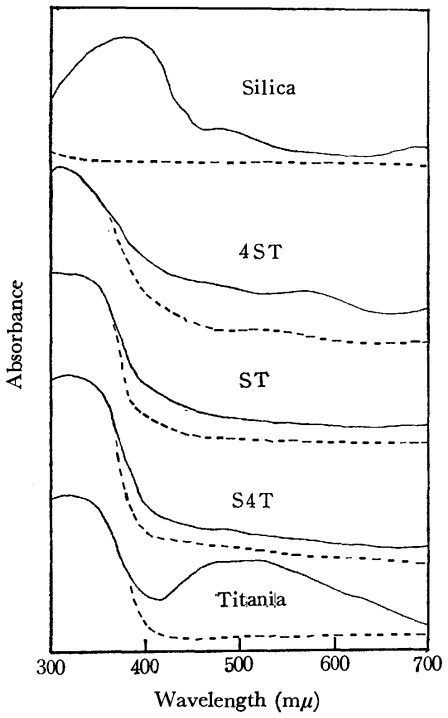

Fig. 4. Electronic spectra from TCNQ adsorbed on the silica-titania systems. Dotted line, silica-titanias prior to adsorption.

alumina-titania systems can be attributed to neither TCNQ nor the metal oxides. The bands near 600 mμ probably stem from the dimer TCNQ anion radical, which absorbs light at 643 mμ.[9] They are very broad and have not been assigned with certainty, but support is given by the characteristic features that neutral TCNQ absorbs only at 395 mμ, that TCNQ has a high electron affinity, and that the TCNQ anion radical derivatives are stable even at room temperature.[10-13]

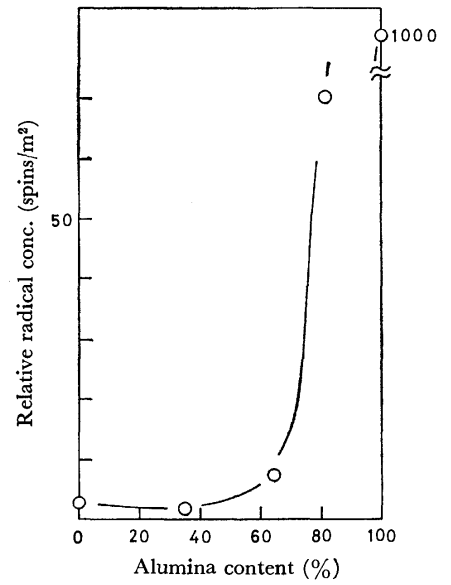

Fig. 6. The change in TCNQ anion radical forming activity of the silica-alumina systems with composition.

9) R. H. Boyd and W. D. Phillips, *J. Chem. Phys.*, **43**, 2927 (1965).

10) D. S. Acker, R. J. Harder, W. R. Hertler, W. Mahler, L. R. Melby, R. E. Benson, and W. E. Mochel, *J. Amer. Chem. Soc.*, **82**, 6408 (1960).

11) R. G. Kepler, P. E. Bierstedt, and R. E. Merrifield, *Phys. Rev. Lett.*, **5**, 503 (1960).

12) D. B. Chesnut, H. Foster, and W. D. Phillips, *J. Chem. Phys.*, **34**, 684 (1961).

13) L. R. Melby, R. J. Harder, W. R. Hertler, W. Mahler, R. E. Benson, and W. E. Mochel, *J. Amer. Chem. Soc.*, **84**, 3374 (1962).

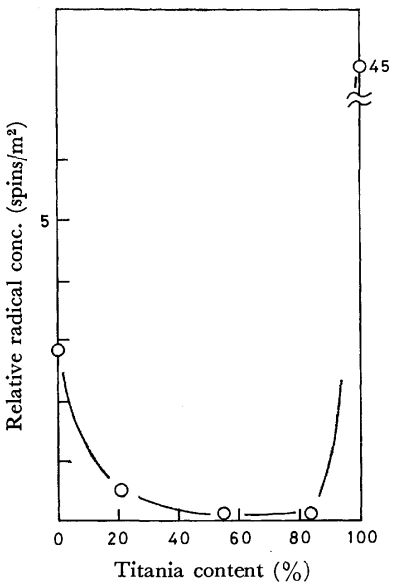

Fig. 7. The change in TCNQ anion radical forming activity of the silica–titania systems with composition.

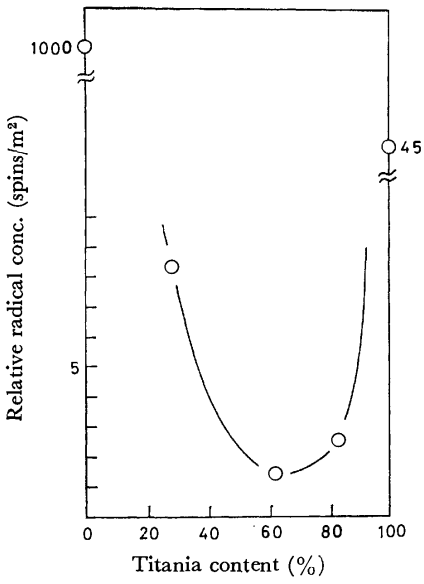

Fig. 8. The change in TCNQ anion radical forming activity of the alumina–titania systems with composition.

In view of the ESR and the electronic spectra, it is confirmed that radical ions are formed from TCNQ on the metal oxide surfaces as a result of electron transfer to TCNQ from the metal oxide surfaces.

The TCNQ anion-radical-forming activity of the metal oxide surfaces is shown in Table 1 and Figs. 6—8. The activity is reflected in the saturation of the color of TCNQ on the metal-oxide surfaces and the increase in absorbance at C-T band. The activity sequence and the color of the samples were found to be: S4A (greenish light grey)>SA (light brown)>4SA (brown tinged white); 4ST (pink)>S4T (brown tinged white)>ST (colorless); 4AT (orange)>A4T (deep pink)>AT (red brown).

The silica–alumina, silica–titania, and alumina–titania systems showed much less activity than the parent oxides-silica, alumina, and titania. The systems exhibit surface properties (surface area, heat of immersion, hydrophilicity, and surface acidity) which would not be qualitatively predicted from a consideration of the independent properties of the parent oxides.[14-16]

Flockhart *et al.*[5] have reported that typical silica–alumina cracking catalysts have negligible reducing (electron donating) power and that silica–aluminas of a higher alumina content possess an appreciable reducing activity, but this may be associated with the presence, in the conglomerate, of a pure alumina phase. It is well known that the -Si-O-Al- structure forms a strong acid site,[17-28] but the formation of an electron-donor site can not be expected. In the present work, all of the silica–alumina systems (4SA, SA, and S4A) showed appreciable radical-forming activity and the activity increased with an increase in the alumina content. However, the silica–alumina systems had much less activity than the alumina. The steep fall in the activity between the silica–alumina system and the alumina suggests that the pure alumina phase is present only a little on the silica–alumina surfaces. The activity increases gradually between 4SA and SA, and then increases steeply between SA and S4A. This suggests the existence of a small part of a pure alumina phase on the surface of S4A. The existence of the pure alumina phase is confirmed by the appearance of the weak band at about 650 mμ in S4A corresponding to the C-T band of TCNQ adsorbed on the alumina.

The surface hydroxyl ion may be one of the electron-donor sites.[5,6] Hall *et al.*[29] reported that the greater part of surface hydroxyls on silica–alumina catalyst consisted of SiOH. SiOH is much more stable than AlOH,[30] and shows little radical-forming activity.[6] The low activity of the silica–alumina systems agreed with Hall's results.

The change in the activity of the silica–alumina systems with the alumina content was approximately inverse to that of the surface acidity.[15]

The silica–titania systems had negligible radical-

14) H. Murayama, K. Kobayashi, M. Koishi, and K. Meguro, *J. Colloid Interfac. Sci.*, **32**, 470 (1970).
15) H. Murayama and K. Meguro, This Bulletin, **43**, 2386 (1970).
16) H. Hosaka and K. Meguro, *ibid.*, **44**, 1252 (1971).
17) C. J. Plank, *J. Colloid Interfac. Sci.*, **2**, 413 (1947).
18) M. Yamaguchi and S. Tsutsumi, *Nippon Kagaku Zasshi*, **69**, 6 (1948).
19) C. L. Thomas, *Ind. Eng. Chem.*, **41**, 2564 (1949).
20) B. S. Greensfelder, H. H. Voge, and G. M. Good, *Ind. Eng. Chem.*, **41**, 2573 (1949).
21) T. H. Millikan, Jr., G. H. Mills, and A. G. Oblad, *Discuss. Faraday Soc.*, **8**, 279 (1950).
22) G. A. Mills and S. G. Hindin, *J. Amer. Chem. Soc.*, **72**, 5549 (1950).
23) R. C. Hansford, *Advan. Catal.*, **4**, 17 (1952).
24) A. G. Oblad, S. G. Hindin, and G. A. Mills, *J. Amer. Chem. Soc.*, **75**, 4096 (1953).
25) J. D. Danforth, *J. Phys. Chem.*, **59**, 564 (1955).
26) R. G. Haldeman and P. H. Emmett, *J. Amer. Chem. Soc.*, **78**, 2917 (1956).
27) J. K. Lee and S. W. Weller, *Anal. Chem.*, **30**, 1057 (1958).
28) M. W. Tamele, *Dicuss. Faraday Soc.*, **8**, 270 (1960).
29) W. K. Hall, H. P. Leftin, F. J. Cheselske, and D. E. O'reilly, *J. Catal.*, **2**, 506 (1963).
30) H. P. Boehm, *Advan. Catal.*, **16**, 179 (1966).

Table 1. Summary of the TCNQ adsorption

Sample	Composition	Crystal features by X-ray diffraction	Surface area (m^2/g)	The color of the metal oxide surface after TCNQ adsorption	The relative radical concentration (radical conc./m^2)
silica		amorphous	600	yellow	2.8
alumina		weak γ-Al_2O_3 lines	263	blue green	1000
titania		weak anatase lines	64	violet	45
4SA	35% Al_2O_3	amorphous	263	brown tinged white	1.3
SA	64% Al_2O_3	amorphous	279	light brown	7.2
S4A	81% Al_2O_3	amorphous	367	greenish light grey	70
4ST	21% TiO_2	amorphous	348	pink	0.5
ST	55% TiO_2	amorphous	343	colorless	0.14
S4T	83% TiO_2	weak anatase lines	239	brown tinged white	0.2
4AT	28% TiO_2	amorphous	331	orange	8.3
AT	62% TiO_2	amorphous	377	red brown	1.4
A4T	83% TiO_2	weak anatase lines	195	deep pink	2.5

forming activity, and the C-T band scarcely appeared at all. This result suggests that the pure titania phase is present only a little on the silica-titania surfaces. It is noteworthy that a weak anatase line in the X-ray diffraction pattern of the S4T suggests the presence, in the conglomerate, of a pure titania phase, but the S4T had negligible radical-forming activity.

The alumina-titania systems showed much less radical-forming activity than the parent oxides-alumina and titania. The TCNQ adsorbed on the alumina-titania systems showed the C-T band at about 500 mμ corresponding to the TCNQ adsorbed on the titania. This observation suggests the presence of a pure titania phase and the absence of a pure alumina phase on the alumina-titania system surfaces. The radical-forming activity decreases steeply between the alumina and 4AT, decreases gradually between 4AT and AT, increases between AT and A4T, and increases markedly between A4T and the titania. The AT has showed the most characteristic surface properties among the alumina-titania systems.[14]

The TCNQ anion radical-forming activity has been proposed as a convenient method for estimating the electron-donor property of metal oxide surfaces.[6] In the present paper, the electron-donor property of silica-alumina, silica-titania, and alumina-titania systems has been revealed and information regarding the surface structure of the mixed-oxide systems has been obtained by means of studying the radical-forming activity and the wavelength of the C-T band.

BULLETIN OF THE CHEMICAL SOCIETY OF JAPAN, VOL. 45, 3375—3379 (1972)

Electrical and Optical Properties of the Iodine Complexes of Phenoxazine, Phenoselenazine, and Benzophenothiazines[1]

Yoshio MATSUNAGA and Yukio SUZUKI*

Department of Chemistry, Faculty of Science, Hokkaido University, Sapporo

(Received April 26, 1972)

The electrical resistivities and Seebeck coefficients of the 2: 3 iodine complexes of phenoxazine, phenoselenazine, and benzophenothiazines were measured as a function of the temperature. They have resistivity values at 20°C ranging from 10 ohm·cm for the phenoxazine complex to 34 ohm·cm for the benzo[*a*]phenothiazine complex. Employing the equation of Johnson and Lark-Horowitz for the Seebeck coefficient of an intrinsic semiconductor, the ratio of the electron-to-hole mobility in the phenoselenazine complex was found to be 1.07 and the electron mobility was estimated as 0.26 cm^2/V sec. By an examination of the vibrational spectra, the expected cation-radical character was confirmed for the complexes of phenoselenazine and benzophenothiazines. The presence of a broad electronic absorption band in the rock-salt region characteristic of low-resistivity organic semiconductors was noted in every case.

The phenothiazine-iodine complex, the formation of which was reported by Pummerer and Gassner as early as 1913,[2] was found to exhibit a relatively low electrical resistivity about a decade ago.[3] Further studies of the electrical resistivity of this complex have

* Present address: Tokyo Shibaura Electric Co., Kawasaki.

1) Presented at the 24th Annual Meeting of the Chemical Society of Japan, Suita, April 1971.

2) R. Pummerer and S. Gassner, *Ber.*, **46**, 2310 (1913).

3) Y. Matsunaga, *Helv. Phys. Acta*, **36**, 800 (1963).

been published by several workers.[4-7] More recently, measurements have been made of the Seebeck coefficient as a function of the temperature by Sano *et al.*[7] In addition, the electrical properties of the iodine complexes of the *N*-methyl and *N*-ethyl derivatives have been compared with those of the above-mentioned complex.[3,7,8] The electronic absorption spectrum in the visible region has been examined by Bhat and Rao, and the diffuse reflection spectrum in both the visible and near-infrared regions, by Matsunaga and Shono.[5,6] The presence of an electronic absorption maximum at 5.5 kK was shown by the latter workers. In the initial report on the resistivity, it was demonstrated that the vibrational spectrum of the phenothiazine-iodine complex is quite different from that of the parent organic compound, but practically the same as that of semiquinoid phenothiazine bromide.[3] On the basis of this observation, which was subsequently confirmed by a more detailed work,[6] it was postulated that every phenothiazine molecule in the solid complex bears an approximately unit-positive charge.

Thus, considerable interest has been shown in the phenothiazine-iodine complex; however, little work has been carried out on the complexes of structurally related compounds. One of the present authors has previously measured the electrical resistivities of the complexes of benzo[*a*]- and benzo[*c*]-phenothiazines.[3] Contrary to the introduction of the *N*-alkyl group, the extra ring does not appreciably affect the resistivity. No attention has been paid to their optical properties. On the other hand, nothing is known about the iodine complexes of phenoxazine and phenoselenazine. Pursuing an inquiry into the effect of the organic component on the electrical and optical properties of the iodine complexes, these four compounds have been taken up in comparison with phenothiazine.

Experimental

Materials. The phenoxazine was prepared by the condensation of *o*-aminophenol in the presence of iodine.[9] The crude product extracted with toluene was recrystallized from ethanol. The reaction between diphenylamine and selenium monochloride was carried out in chloroform, as has been described by Müller *et al.*, instead of the benzene originally used by Cornelius.[10] This compound was recrystallized from ligroin. The selenium monochloride needed for the synthesis of phenoselenazine was made by the addition of concentrated sulfuric acid to a mixture of selenium, selenium dioxide, and concentrated hydrochloric acid, following the procedure of Lenher and Kao.[11] The benzo[*a*]- and benzo[*c*]-phenothiazines were obtained by the reaction of sulfur on α- and β-phenylnaphthylamines respectively, using a small amount of iodine as the catalyst.[12] Both of them were purified by recrystallization from ligroin. The preparation of the semiquinoid bromides was carried out by the oxidation of the organic compounds with bromine, as has been reported for phenothiazine bromide by Kehrmann and Diserens.[13] The iodine complexes were precipitated when the organic component and iodine, separately dissolved in benzene, were mixed.

Measurements. The electrical resistivities and Seebeck coefficients were recorded as a function of the temperature by the methods described in the paper by Kan and Matsunaga.[8] Measurements of the vibrational and electronic spectra were made as have been reported elsewhere.[6]

Results and Discussion

The iodine contents presented in Table 1 indicate that all the complexes consist of two molecules of the organic component and three of iodine. They are all black polycrystalline powder except for the phenoxazine complex, which is in the form of needles with metallic luster.

Table 1. Composition of the iodine complexes

Organic component	Iodine content (%)	
	Calcd for 2:3	Found
Phenoxazine	67.6	67.7
Phenothiazine	65.7	65.6
Phenoselenazine	60.7	60.9
Benzo[*a*]phenothiazine	60.5	61.4
Benzo[*c*]phenothiazine	60.5	61.3

Electrical Properties. The resistivity of the complexes under study shows a temperature dependence which follows the typical semiconductor behavior:

$$\rho = \rho_0 \exp(E/kT) \quad (1)$$

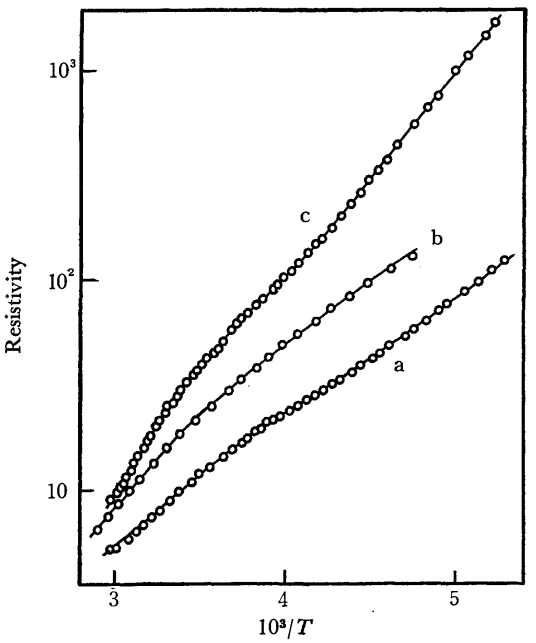

Fig. 1. Electrical resistivities of the iodine complexes of a) phenoxazine, b) phenothiazine, and c) phenoselenazine.

4) F. Gutmann and H. Keyzer, *J. Chem. Phys.*, **46**, 1969 (1967).
5) S. N. Bhat and C. N. R. Rao, *Can. J. Chem.*, **47**, 3899 (1969).
6) Y. Matsunaga and K. Shono, This Bulletin, **43**, 2007 (1970).
7) M. Sano, K. Ohno, and H. Akamatu, *ibid.*, **44**, 3269 (1971).
8) K. Kan and Y. Matsunaga, *ibid.*, **45**, 2096 (1972).
9) P. Müller, N. P. Buu-Hoï, and R. Rips, *J. Org. Chem.*, **24**, 37 (1959).
10) W. Cornelius, *J. Prakt. Chem.*, (2), **88**, 407 (1913).
11) V. Lenher and C. H. Kao, *J. Amer. Chem. Soc.*, **47**, 772 (1925).
12) E. Knoevenagel, *J. Prakt. Chem.*, (2), **89**, 1 (1914).
13) F. Kehrmann and L. Diserens, *Ber.*, **48**, 318 (1915).

Table 2. Electrical properties of the iodine complexes in the higher temperature region

Organic component	ρ at 20°C (ohm cm)	E (eV)	μ_e/μ_h	m_e/m_h	Ref.
Phenoxazine	10	0.14	2.11	1/40	This work
Phenothiazine	20	0.17	—	—	3
Phenothiazine	13	0.19	—	—	6
Phenothiazine	17	0.164	*ca.* 0.7	—	7
Phenothiazine	19	0.19	<1	—	This work
Phenoselenazine	32	0.28	1.07	1/2	This work
Benzo[*a*]phenothiazine	20	0.19	—	—	3
Benzo[*a*]phenothiazine	34	0.16	>1	—	This work
Benzo[*c*]phenothiazine	20	0.20	—	—	3
Benzo[*c*]phenothiazine	18	0.14	>1	—	This work

For example, the logarithm of the resistivity of the complexes of phenoxazine, phenothiazine, and phenoselenazine is plotted against the reciprocal temperature in Fig. 1. The presence of a break near or a little below room temperature is noted in these three cases. The values of the resistivity (ρ) at 20°C and the activation energy (E) in the higher temperature region are summarized in Table 2, where literature values are also included for the sake of comparison. Except for the case of the benzo[*a*]phenothiazine complex, the present results are in fair agreement with the available data. Both the resistivity and activation energy increase in this order of organic components: phenoxazine<phenothiazine<phenoselenazine.

The plot for the benzophenothiazine complexes does not show a break in the temperature range measured. We confirmed the earlier observation that the presence of an extra benzene nucleus —in other words, a more widespread electron delocalization in the organic component— modifies only a little the electrical properties of the iodine complex. This conclusion is in marked contrast with the appreciable effect of the size of an alkyl group on the nitrogen atom of phenothiazine on the electrical resistivity of the iodine complex.[8]

Single crystals of the low-resistivity tetracyanoquinodimethane (TCNQ) anion-radical salts have been known to be highly anisotropic.[14–16] The resistivity value observed along the long-needle axis of crystal of the simple *N*-methylphenazinium salt, 0.007 ohm·cm, is the lowest ever recorded for any organic compound. This value is much lower than the resistivity determined on the polycrystalline compaction of the same salt, 0.5 ohm·cm.[16] Similar results have been reported for the complex *N*-methylquinolinium salt, 0.01 ohm·cm in the long axis direction and 0.5 ohm·cm with a compacted sample. In addition, the activation energy measured with the single crystal is known also to be lower than that obtained with a compaction: <0.01 eV *vs.* 0.07 eV.[15] As was mentioned above, the phenoxazine-iodine complex is obtainable in the form of needles. Therefore, it seemed worthwhile to attempt measurements of the resistivity along the long needle axis of this iodine complex as a function of the temperature. Surprisingly, the resistivity at 20°C was found to be 8 ohm·cm, which must be considered in good agreement with the value observed with a compaction if one takes into consideration the errors involved in the geometrical measurements of small crystals. Moreover, the activation energy estimated by the measurements in the range from −65 to 20°C is 0.14 eV. Here again, the agreement with the value given in Table 2 is excellent.

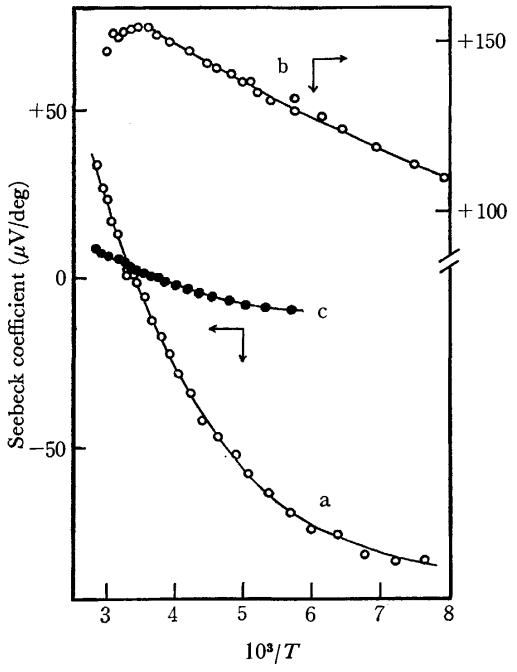

Fig. 2. Seebeck coefficients of the iodine complexes of a) phenoxazine, b) phenothiazine, and c) phenoselenazine.

The temperature dependence of the Seebeck coefficient (Q) is shown in Fig. 2 for the iodine complexes of phenoxazine, phenothiazine, and phenoselenazine. At 20°C, the values are as follows: +5 μV/deg for the oxazine complex, +153 μV/deg for the thiazine complex, and +4 μV/deg for the selenazine complex. Our value for the second complex agrees well with that reported by Sano *et al.*[7] Although a tendency for the better conducting materials to have smaller Seebeck

14) L. R. Melby, R. J. Harder, W. R. Hertler, W. Mahler, R. E. Benson, and W. E. Mochel, *J. Amer. Chem. Soc.*, **84**, 3374 (1962).
15) W. J. Siemons, P. E. Bierstedt, and R. G. Kepler, *J. Chem. Phys.*, **39**, 3523 (1963).
16) L. R. Melby, *Can. J. Chem.*, **43**, 1448 (1965).

coefficients, and *vice versa*, has often been noted,[17] the present complexes do not follow it. The higher-temperature region of the curve is nearly straight in the cases of the first and third complexes. To this region, one may apply the expression for the thermoelectric motive force of an intrinsic semiconductor:[18,19]

$$Q = -\frac{k}{e}\left[\frac{b-1}{b+1}\left(\frac{E_G}{2kT}+2\right)+\frac{3}{4}\ln\frac{m_e}{m_h}\right] \quad (2)$$

where b is the ratio of the electron-to-hole mobility, μ_e/μ_h, E_G is the width of the forbidden band, and m_e and m_h are the effective masses of the electron and the hole respectively. On the assumption that E_G is twice the activation energy given in Table 2, b is evaluated as 2.11 for the oxazine complex and as 1.07 for the selenazine complex. With the values of temperature where the sign of the coefficient changes, the ratio of the effective masses was estimated to be as is shown in the table. The Seebeck coefficients of the benzo[*a*]- and benzo[*c*]-phenothiazine complexes are −47 and −57 μV/deg respectively at 20°C. The curves are nearly parallel to that for the selenazine complex; however, the linear parts are too short to fit Eq. (2).

The conductivity (σ) is given by:

$$\sigma = \frac{1}{\rho} = e\mu_e\left(\frac{b+1}{b}\right)N\exp(-E/kT) \quad (3)$$

On the basis of the density determined from the compactions, N is estimated to be 2.54×10^{22} phenoxazine molecules or 2.50×10^{22} phenoselenazine molecules per cm^3 of the complex. Employing the resistivity and activation energy listed in Table 2, the electron mobility in the selenazine complex is calculated to be 0.26 cm^2/V sec. This value is close to that estimated for the electron in the *N*-methylphenothiazine-iodine complex by the same method,[8] and is of the same order as the only known Hall mobility observed with iodine complexes.[20] On the other hand, the electron mobility estimated for the oxazine complex, 0.004 cm^2/V sec, rules out the application of a band model to this iodine complex. The present organic components are structurally related, and the electrical resistivities of the iodine complexes are of the same order as each other. Nevertheless, the results indicate that the conduction mechanism in the complexes is very sensitive to a minor modification of the component molecule.

An alternative explanation for the behavior shown in Fig. 2 may be proposed on the basis of a hopping model. The Seebeck coefficient for hopping electrons is given by:

$$Q = -\frac{k}{e}\left[(1-2\beta)\frac{E}{kT}+\ln\frac{c_0-c}{c}\right] \quad (4)$$

where c is the charge carrier concentration and where c_0 is the total concentration of accessible sites.[21,22] It may be supposed that the site initially containing the electron requires a fraction, β, of the activation energy. By comparison with the terms in Eq. (2), β is estimated as 0.41 for the oxazine complex and as 0.49 for the selenazine complex; that is, the motional energy is divided into a ratio of about 2:3 between the two sites in the former complex and nearly equally between the two in the latter. The c/c_0 ratios are approximately 0.9 and 0.6 respectively; however, their meaning in the present complexes is still unknown.

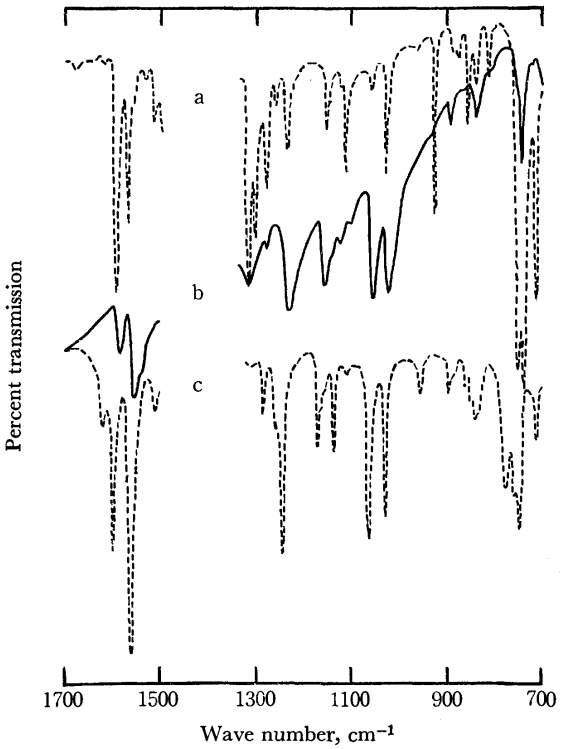

Fig. 3. Vibrational spectra of a) phenoselenazine, b) the iodine complex, and c) the semiquinoid bromide.

Optical Properties. As the phenoxazine complex is difficult to be pulverized, only a spectrum with a very poor resolution could be recorded. Therefore, the vibrational spectra of the other three iodine complexes will be considered in this paper. In Fig. 3 the spectrum of the phenoselenazine-iodine complex in the region from 700 to 1700 cm^{-1} is compared with those of the parent compound and the semiquinoid bromide. Of course, iodine is not active in this spectral region. Each spectrum bears a resemblance to that of the corresponding phenothiazine compound reported earlier.[6] The relative intensity and location of the two bands in the iodine complex appearing in the region from 1550 to 1600 cm^{-1} resemble those of the two in the bromide, but not those in the selenazine itself. Furthermore, the strong bands located at 1025, 1055, and 1235 cm^{-1} can be well compared with the three in the bromide located at 1030, 1060, and 1345 cm^{-1}. Thus, the main feature in the above-mentioned region seems to agree with that of the cation-radical. However, the following differences must be noted. The band to be compared with the one at 1330 cm^{-1} in the iodine complex can be found only in the parent

17) E. A. Perez-Albuerne, H. Johnson, Jr., and D. J. Trevoy, *J. Chem. Phys.*, **55**, 1547 (1971).
18) V. A. Johnson and K. Lark-Horowitz, *Phys. Rev.*, **92**, 226 (1953).
19) J. Tauc, *ibid.*, **95**, 1394 (1954).
20) A. M. Hermann and A. Rembaum, *J. Appl. Phys.*, **37**, 3642 (1966).
21) I. G. Austin and N. F. Mott, *Advan. Phys.*, **18**, 41 (1969).
22) I. Bransky, N. M. Tallan, and A. Z. Hed, *J. Appl. Phys.*, **41**, 1787 (1970).

compound. Neither the selenazine nor the bromide shows the band corresponding to that 1160 cm^{-1} in the iodine complex. It must be added that a strong band appearing at 925 cm^{-1} in the selenazine is not observed in the spectrum of the complex. On the basis of these observations, it is very likely that the positive charge on the selenazine molecule in the complex is fairly large, if not a unit.

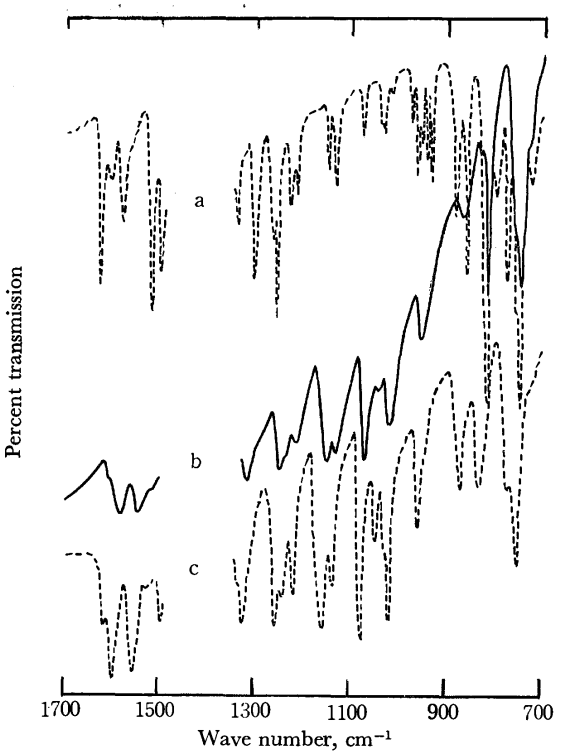

Fig. 4. Vibrational spectra of a) benzo[*c*]phenothiazine, b) the iodine complex, and c) the semiquinoid bromide.

The vibrational spectra of benzo[*c*]phenothiazine, the iodine complex, and the semiquinoid bromide are presented in Fig. 4. The pattern shown by the complex is in essential agreement with that of the bromide, confirming the expected ion-radical character of the iodine complex. The similarity of the iodine complex and the bromide of benzo[*a*]phenothiazine is also found in the vibrational pattern.

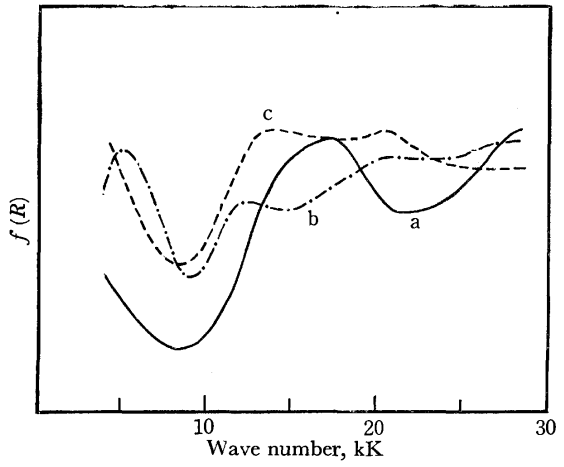

Fig. 5. Diffuse reflection spectra of the iodine complexes of a) phenoxazine, b) phenothiazine, and c) phenoselenazine.

In Fig. 5 the electronic spectra, as measured by the diffuse reflectance method, are shown for the iodine complexes of phenoxazine, phenothiazine, and phenoselenazine. The maximum of the low-energy band in the thiazine complex is found at 5.2 kK, while it was found at 5.5 kK in our previous work.[6] On the other hand, those of the other two complexes are expected to be below 4 kK, the limit of the spectrophotometer employed. This is the reason why a strong back-ground absorption is seen in the vibrational spectrum of the selenazine complex presented in Fig. 3. The appearance of a low-energy absorption band attributable to an electronic transition is common to low-resistivity organic semiconductors, *e.g.*, the TCNQ anion-radical salts and some ionic molecular complexes.[14,17,23–25] However, the location of its maximum is not necessarily correlated with the resistivity, as has been pointed out in our paper on the TCDQ and TBDQ anion-radical salts.[26] In the present complexes, it may be noted that the location of the maximum cannot be correlated with the magnitude of the activation energy (see Table 2).

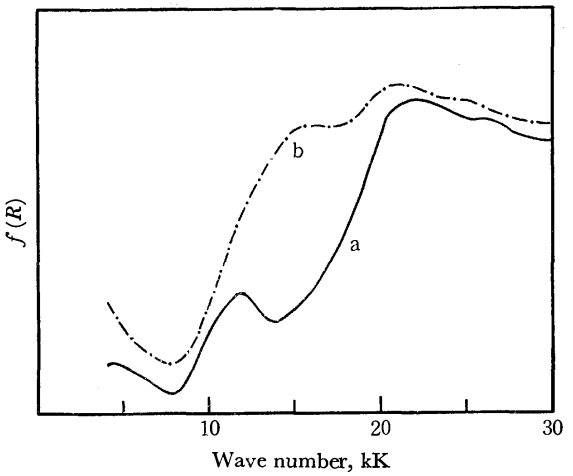

Fig. 6. Diffuse reflection spectra of the iodine complexes of a) benzo[*a*]phenothiazine and b) benzo[*c*]phenothiazine.

The reflection spectra of the benzophenothiazine complexes are given in Fig. 6. In contrast with the complexes in Fig. 5, the low-energy bands are appreciably weaker than those in the visible region. Nevertheless, these two complexes are as conductive as the other three. The maximum is located at 4.4 kK in the case of the benzo[*a*]phenothiazine complex, but below 4 kK in the other. This difference can be noted in the vibrational spectra, too. The recording of the spectrum of the former complex is much easier than that of the latter because of the absence of a strong back-ground absorption, which tends to produce distortions and a lack of resolution in the vibrational spectrum.

The present work was supported by a grant-in-aid from the Ministry of Education, to which the authors' thanks are due.

23) Y. Matsunaga, *J. Chem. Phys.*, **42**, 1982 (1965).
24) Y. Matsunaga, *ibid.*, **42**, 2248 (1965).
25) Y. Matsunaga, *Nippon Kagaku Zasshi*, **89**, 905 (1968).
26) Y. Matsunaga and Y. Narita, This Bulletin, **45**, 408 (1972).

Electron Spin Resonance Study of Amino Acid Radicals Produced by Fenton's Reagent[1]

Hitoshi TANIGUCHI,* Hideyo HASUMI, and Hiroyuki HATANO
Department of Chemistry, Faculty of Science, Kyoto University, Kyoto 606
(Received April 26, 1972)

Free-radical intermediates in the reaction of the hydroxyl radical with amino acids and structurally related compounds such as alcohols, amine, and carboxylic acids have been studied by ESR spectroscopy using a continuous-flow method. The hydroxyl radical is generated by a ferrous ion-hydrogen peroxide system (Fenton's reagent). ESR spectra with fairly good signal-to-noise ratios are obtained for the first time in a Fenton's reagent system from glycine, valine, leucine, glutamic acid, lysine, methionine, tyrosine, ethylamine, acetic acid, propionic acid, *n*-butyric acid, and succinic acid. Structures, *g*-values, and hyperfine coupling constants of these radicals are tabulated. The analysis of ESR spectra shows that the same radical species are produced mainly in a Fenton's reagent system as in a titanous chloride-hydrogen peroxide system. This is consistent with the existence of the hydroxyl radical in both systems. The observed ratio of C_2–H to C_1–H proton hyperfine coupling constants[2] gives information concerning steric conformations, freedom in the internal rotations, and *s*-character of the intermediate radicals.

The hydroxyl radical, generated by a ferrous (Fe^{2+}) ion-hydrogen peroxide (H_2O_2) system (Fenton's reagent),[3] has been found to oxidize a variety of organic substrates.[4,5] A kinetic examination and product analysis have elucidated the various mechanisms of these oxidations of aliphatic[4] and aromatic[5] compounds. Unstable organic radicals produced by Fenton's reagent have been detected successfully by electron spin resonance (ESR) spectroscopy using a continuous-flow method. Much is already known about the unstable radicals from alcohols,[6] aliphatic ethers,[7] alicyclic compounds,[7] and furans.[8] However, little is known about the free radicals obtained by Fenton's reagent from biomolecules other than the amino acids such as α-alanine,[2] β-alanine,[2] serine, aspartic acid, cystine, and cysteine.[9,10]

In the course of investigations on the oxidation of biomolecules, intermediate radicals in the reaction of the hydroxyl radical generated by a titanous (Ti^{3+}) chloride–hydrogen peroxide system with amino acids,[10] amino acid derivatives,[11] nitrogen heterocyclic compounds,[12] and dialkylsulfoxides[13] were reported in previous papers. Our experimental study of the oxidation involving the hydroxyl radical has now been extended in the present work to include also the oxidation by Fenton's reagent.

Since the hydroxyl radical is one of the main products of water radiolysis,[14] a chemical reaction system generating the hydroxyl radical could be used to simulate the effects of ionizing radiation on aqueous organic solutions. Recently, Neta and Fessenden[15] reported an ESR spectrum of $NH_2\dot{C}HCOOH$ radical from aqueous acidic solution of glycine irradiated directly in the ESR cavity with high-energy electrons, and the structure of glycine radical is identical with that obtained in this work. Therefore, a Fenton's reagent system might be a good model system of the radiolysis of aqueous solutions of biomolecules.

Experimental

The experimental arrangements and procedures for the observation of intermediate radicals produced in a Fenton's reagent system were essentially the same as described previously in a Ti^{3+}–H_2O_2 system.[10-13] The ESR spectra of intermediate radicals were recorded on an X-band spectrometer (JEOL, Model JES-ME-3X) at room temperature within 7 to 13 msec after mixing two reactants. The hyperfine (hf) coupling constants and *g*-values were calibrated by comparison with a sample of potassium peroxylamine disulfonate in aqueous sodium carbonate solution (nitrogen hf splitting, 13.0 ± 0.1 G; $g=2.00550\pm0.00005$).[16] Probable errors in hf coupling constants and *g*-values are 0.1 G and 0.0001, respectively.

All materials were obtained commercially and used without further purification. The concentrations of ferrous sulfate ($FeSO_4\cdot7H_2O$) and hydrogen peroxide were 0.005M and 0.1M, respectively. Organic substrates were added to both reactants usually in 0.1 to 1.0M concentration according to their reactivity and solubility. Reactant solutions of cystine and

* To whom the correspondence should be addressed.

1) This work was presented at the 10th Symposium on Electron Spin Resonance under the auspices of the Chemical Society of Japan, Osaka, Japan, October 1971.

2) The designations C_1 and C_2 refer to the position relative to the carbon atom which bears the unpaired electron, while α and β refer to the position relative to that of the carboxyl or hydroxyl group.

3) H. J. H. Fenton, *J. Chem. Soc.*, **65**, 899 (1894).

4) C. Walling and S. Kato, *J. Amer. Chem. Soc.*, **93**, 4275 (1971), and references therein.

5) J. R. L. Smith and R. O. C. Norman, *J. Chem. Soc.*, **1963**, 2897, and references therein.

6) T. Shiga, *J. Phys. Chem.*, **69**, 3805 (1965).

7) T. Shiga, A. Boukhors, and P. Douzou, *ibid.*, **71**, 3559, 4264 (1967).

8) T. Shiga and A. Isomoto, *ibid.*, **73**, 1139 (1969).

9) W. A. Armstrong and W. G. Humphreys, *Can. J. Chem.*, **45**, 2589 (1967).

10) H. Taniguchi, K. Fukui, S. Ohnishi, H. Hatano, H. Hasegawa, and T. Maruyama, *J. Phys. Chem.*, **72**, 1926 (1968).

11) H. Taniguchi, H. Hatano, H. Hasegawa, and T. Maruyama, *ibid.*, **74**, 3063 (1970).

12) H. Taniguchi, *ibid.*, **74**, 3143 (1970).

13) H. Taniguchi, H. Takagi, and H. Hatano, *ibid.*, **76**, 135 (1972).

14) See, for example, B. H. J. Bielski, and A. O. Allen, *Int. J. Radiat. Phys. Chem.*, **1**, 153 (1969).

15) P. Neta and R. W. Fessenden, *J. Phys. Chem.*, **75**, 738 (1971).

16) J. S. Hyde, unpublished result quoted by J. Q. Adams, J. W. Nicksic, and J. R. Thomas in *J. Chem. Phys.*, **45**, 654 (1966).

aspartic acid with comparatively low solubility at room temperature were prepared and flowed through the cavity of ESR spectrometer at 40 to 50°C. Both reactant solutions were acidified to about pH 2 with dilute sulfuric acid and deoxygenated by bubbling nitrogen gas in order to prevent the oxidation of ferrous ion. In the experiment conducted within a pH region of approximate neutrality, the pH of each reactant solution being adjusted with sodium hydroxide, ethylenediaminetetraacetic acid was added to the reactant solution of ferrous sulfate so as to avoid the precipitation of ferric salt.

Results and Discussion

Identification of the Intermediate Radicals. ESR spectra with sufficient signal-to-noise ratios were obtained from glycine, α-alanine, valine, leucine, aspartic acid, glutamic acid, lysine, cystine, methionine, tyrosine, methyl alcohol, ethyl alcohol, isopropyl alcohol, ethylamine, acetic acid, propionic acid, *n*-butyric acid, and succinic acid. The structures of amino acid radicals deduced from the analysis of the spectra, and the

Table 1. Structures, *g*-values, and hyperfine coupling constants of the intermediate radicals in the reaction of Fenton's reagent with amino acids[a]

Substrate	Radical[b]	Ratio	*g*[c]	Coupling constant, *G*[c] C_1–H	C_2–H	N	a_{C_3-H}/a_{C_1-H}
Glycine	$\dot{C}H(NH_2)COOH$		2.0034	11.7	5.4[d]	6.3	
DL-α-Alanine	$\dot{C}H_2$–R		2.0026	22.3	26.2	3.4	1.17
β-Alanine	$\dot{C}H(COOH)CH_2NH_3^+$		(2.0029)	(21.7)	(24.3)	(3.7)	1.12
DL-Serine	$\dot{C}H(OH)$–R		(2.0028)	(17.5)	(8.9)	(7.9)	0.51
L-Valine	$\dot{C}(CH_3)_2$–R	1.6	2.0027		(23.4[e] 7.2	7.2	
	$\dot{C}H_2CH(CH_3)$–R	1	2.0025	21.7	29.9		1.38
L-Leucine	$\dot{C}H_2CH(CH_3)CH_2$–R		2.0026	21.9	21.9		1.00
L-Aspartic acid	$\dot{C}H(COOH)$–R		2.0028	20.6	14.3	3.4	0.69
L-Glutamic acid	$\dot{C}H(COOH)CH_2$–R		2.0032	22.5	20.5		0.91
L-Lysine	$\dot{C}H(CH_2CH_2NH_3^+)CH_2$–R[f]		2.0026	21.9	23.9		1.09
L-Cystine	$\dot{S}CH_2$–R		2.0102		9.4[g]		
L-Cysteine	$\dot{S}CH_2$–R		(2.0108)		(9.5)[g]		
DL-Methionine	$\dot{C}H_2CH_2$–R		2.0026	22.0	24.7		1.12
	$\dot{C}H_3$		2.0025	22.1			
L-Tyrosine	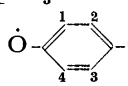		2.0041	6.4[h]	1.6[i]	7.5[j]	

a) See text and Ref. 2 for the notations in columns 1, 5, and 6.
b) R represents $H_3N^+CH(COOH)$–.
c) The values in parentheses were obtained by Armstrong and Humphreys.[9]
d) $a_{N\underline{H}}$. e) $a_{C_1-C\underline{H}_3}$.
f) More than two kinds of radicals exist, but only one can be assigned.
g) $a_{S-C\underline{H}}$. h) $a_{H_1}=a_{H_4}$. i) $a_{H_2}=a_{H_3}$. j) $a_{C\underline{H}_3}$.

Table 2. Structures, *g*-values, and hyperfine coupling constants of the intermediate radicals in the reaction of Fenton's reagent with organic compounds structurally related to amino acids[a]

Substrate	Radical	Ratio	*g*	Coupling constant, *G* C_1–H	C_2–H	N	a_{C_3-H}/a_{C_1-H}
Methyl alcohol	$\dot{C}H_2OH$		2.0032	17.3			
Ethyl alcohol	$\dot{C}H_2CH_2OH$	1.3	2.0027	21.8	27.4		1.26
	$CH_3\dot{C}HOH$	1	2.0032	15.3	22.7		1.48
Isopropyl alcohol	$\dot{C}H_2CH(CH_3)OH$		2.0024	22.1	22.1		1.00
Ethylamine	$\dot{C}H_2CH_2NH_3^+$		2.0026	21.5	26.1	4.6	1.21
Acetic acid	$\dot{C}H_2COOH$		2.0032	21.2			
Propionic acid	$CH_3\dot{C}HCOOH$[b]		2.0033	20.1	24.3		1.21
n-Butyric acid	$CH_3\dot{C}HCH_2COOH$	4.0	2.0028	21.8	(25.3[c] 21.8		(1.16 1.00
	$\dot{C}H_2CH_2CH_2COOH$	1.3	2.0026	21.8	27.0		1.24
	$CH_3CH_2\dot{C}HCOOH$	1	2.0034	20.1	23.7		1.18
Succinic acid	$\dot{C}H(COOH)CH_2COOH$		2.0030	20.5	22.1		1.08

a) See text and Ref. 2 for the notations in columns 5 and 6.
b) See text concerning an unidentified component of propionic acid radicals.
c) $a_{C_1-C\underline{H}_3}$.

estimated g-values and hf coupling constants are summarized in Table 1; g-values and hf coupling data of β-alanine, serine, and cysteine radicals obtained by Armstrong and Humphreys[9] are also shown in parentheses. For comparison, structures, g-values, and hf coupling constants of radicals from organic substrates structurally related to amino acids are tabulated in Table 2. The concentration ratio is also given for the substrates where two or three kinds of radicals were observed, although the ratio might depend upon the kinetic conditions. Radicals from twelve substrates listed in the synopsis section were not previously studied by ESR spectroscopy in a Fenton's reagent system. ESR spectra of the intermediate radicals from glutamic acid and tyrosine are reproduced in Figs. 1 and 2. L-Phenylalanine gave an ESR signal with poor signal-to-noise ratio.

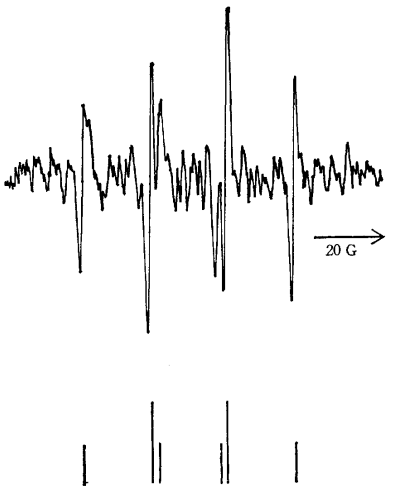

Fig. 1. Electron spin resonance spectrum of the intermediate radical from 0.15M L-glutamic acid with reconstruction. Microwave power, 20 mW; pH, 2.2.

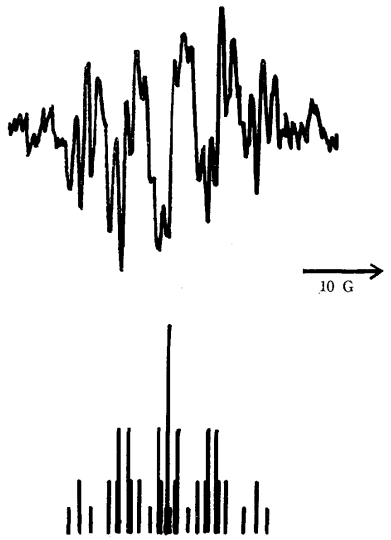

Fig. 2. Electron spin resonance spectrum of the intermediate radical from 0.015M L-tyrosine with reconstruction. Microwave power, 20 mW; pH, 1.7.

Almost all substrates, except aspartic acid, glutamic acid, lysine, and tyrosine which had not been examined in an acidic Ti^{3+}–H_2O_2 system, were found to give the same radical species as those formed in a Ti^{3+}–H_2O_2 system.[9,10,13,17,18] This supports the view that the hydroxyl radical is the active species formed in both Fe^{2+}–H_2O_2 and Ti^{3+}–H_2O_2 systems. However, there were some differences in ESR spectra between the two systems; minor component of α-alanine radicals, $NH_2\dot{C}(CH_3)COOH$,[19] α-hydroxy[2] radical of isopropyl alcohol,[17] methyl radical from acetic acid,[20] and $\dot{C}H_2$-CH_2COOH radical from propionic acid[10] which were observed in a Ti^{3+}–H_2O_2 system, were not recorded in a Fenton's reagent system, while β-hydroxy[2] radical of ethyl alcohol with poor signal-to-noise ratio in a Ti^{3+}–H_2O_2 system and an unidentified component of propionic acid radicals consisting apparently of quartet (splitting, 20.0 G) of triplet (22.7 G) were observed in this Fenton's reagent system.

From ethyl alcohol, Shiga[6] detected only the β-hydroxy radical in a Fenton's reagent system. In contrast, he detected only the α-hydroxy radical from ethyl alcohol oxidized with a Ti^{3+}–H_2O_2 system. He claimed that the active species in Fenton's reagent had different character from that in a Ti^{3+}–H_2O_2 system. We also reexamined intermediate radicals in the reaction of Fenton's reagent with ethyl alcohol, and an ESR spectrum due to two kinds of radicals was observed, in which the hydroxyl radical abstracted a hydrogen atom from different C–H bonds; *i.e.*, from C_α–H and C_β–H bonds.[2] The apparent concentration ratio of α- to β-hydroxy radicals was 1 : 1.3. Consequently, there is no essential difference in reactivities between the Fenton's reagent and a Ti^{3+}–H_2O_2 system, and it is supposed that the active species is the hydroxyl radical in both systems. The relative concentrations of the various organic radicals would depend on the one-electron oxidation of the resulting radicals by both metal ions and hydrogen peroxide as Norman and West[21] stated and recently Czapski *et al.*[22] confirmed; *i.e.*, ferric (Fe^{3+}) ion is a much stronger oxidizing agent than titanic (Ti^{4+}) ion for organic radicals, and the α-hydroxy radical is supposed to be oxidized more readily than the β-hydroxy radical with Fe^{3+} ion. This is applicable to the case of isopropyl alcohol in which an α-hydroxy radical was not observed in a Fenton's reagent system. Walling and Kato[4] developed a new kinetic analysis for the oxidation of ethyl alcohol with Fenton's reagent. They showed also that the hydroxyl radical attacked both α- and β-hydrogens of ethyl alcohol, and the β-hydroxy radical was not oxidized by Fe^{3+} ion but dimerized, while the α-hydroxy radical was oxidized.

The g-values of radicals with C_1–OH and C_1–COOH groups such as methyl alcohol, ethyl alcohol, acetic acid, glutamic acid, propionic acid, n-butyric acid, and

17) W. T. Dixon and R.O.C. Norman, *J. Chem. Soc.*, **1963**, 3119.
18) H. Fischer, K. H. Hellwege, and M. Lehnig, *Ber. Bunsenges. Phys. Chem.*, **72**, 1166 (1968).
19) P. Smith, W. M. Fox, D. J. McGinty, and R. D. Stevens, *Can. J. Chem.*, **48**, 480 (1970).
20) W. T. Dixon, R. O. C. Norman, and A. L. Buley, *J. Chem. Soc.*, **1964**, 3625.
21) R. O. C. Norman and P. R. West, *J. Chem. Soc., B*, **1969**, 389.
22) G. Czapski, A. Samuni, and D. Meisel, *J. Phys. Chem.*, **75**, 3271 (1971).

glycine, and those of radicals from tyrosine, cystine, and cysteine are higher than the g-values of other radicals and in the range of 2.0032—2.0108. This shows that those radicals are π electron radicals in which an unpaired electron is delocalized on oxygen or sulfur atom which has a fairly large spin-orbit coupling constant and lone pairs of electrons.

ESR spectra with good signal-to-noise ratios were obtained from 0.01M cystine and 0.015M tyrosine, whose concentrations were much lower than in the case of the other organic substrates. It is suggested that the reaction mechanism and reactivity of the hydroxyl radical with cystine and tyrosine are different from those with other amino acids. As for tyrosine, the ESR spectrum of the corresponding phenoxy radical was the only one observed as shown in Fig. 2. It was not observed in the absence of ferrous ion. Therefore, tyrosine radical is postulated to be formed in the reaction with the hydroxyl radical and/or ferric ion, either abstracting a hydrogen atom from the hydroxyl group or removing an electron from tyrosine itself. The coupling constants of ring protons in the tyrosine radical are in good agreement with those of p-cresol radical obtained by the oxidation with Ce^{4+} ion.[23] Cystine radical might be formed by the addition of the hydroxyl radical to sulfur atom and consequent cleavage of sulfur-sulfur bond. This is a similar mechanism to the case of methionine radicals. From methionine, ethyl type radical and methyl radical were observed resulting from the cleavage of carbon-sulfur bond, as is the case in a Ti^{3+}–H_2O_2 system.[13]

In the case of lysine, ESR spectrum was obtained at pH 4, which was similar to that observed at pH 2. Since two protonated amino groups deactivate adjacent C-H bonds towards the electrophilic hydroxyl radical,[10] the hydrogen abstraction with the hydroxyl radical is thought to occur mainly at the C_γ–H bond in the side chain.

Hyperfine Coupling Constants. It is well established that the C_1–H coupling constant, a_{C_1-H}, of a π electron radical with a planar configuration of bonding orbitals around the C_1 carbon atom is proportional to the unpaired spin density on the C_1 atom, ρ_{C_1}.[24] The

$$a_{C_1-H} = Q_{C_1-H}\rho_{C_1} \quad (1)$$

C_2–H coupling arises from the hyperconjugative interaction between the unpaired $2p_z$ orbital and the C_2–$H_{3-n}R_n$ group, and the semi-empirical relationship (2) has been used to correlate the C_2–H coupling constant, a_{C_2-H}, with the conformation of free radicals.[25]

$$a_{C_1-H} = \rho_{C_1}(B_0 + B_2\cos^2\theta) \quad (2)$$

The angle θ is the dihedral one between the p-orbital containing the unpaired electron and the C_1–C_2–H plane. In most cases,[26] B_0 is assumed to be negligible relative to B_2.

$$a_{C_1-H} = \rho_{C_1}B_2\cos^2\theta \quad (2)'$$

From the above Eqs. (1) and (2)′, the ratio of C_2–H to C_1–H coupling constants is expressed as Eq. (3).

$$a_{C_2-H}/a_{C_1-H} = B_2\cos^2\theta/Q_{C_1-H} \quad (3)$$

The value of $|B_2/Q_{C_1-H}|$ for an aliphatic π electron radical is estimated experimentally to be 1.20 based on the proton hf coupling constants of the ethyl radical[26] in which the methyl group rotates freely around the C_1–C_2 bond so that $\cos^2\theta = 1/2$. Therefore, the radical with the ratio of a_{C_2-H} to a_{C_1-H} deviating much from 1.20 is supposed to take a restricted conformation in which the internal rotation of the C_2–H bond around the C_1–C_2 axis is hindered much, or is assumed to have some s-character in the orbital of an unpaired electron on C_1 atom.

The ratios of a_{C_2-H} to a_{C_1-H} obtained in the present investigation are shown in column 6 of Tables 1 and 2. Looking at the structures of radicals with ratios more than 1.32 or less than 1.08, we notice that in a group consisting of radicals from aspartic acid (ratio, 0.69), glutamic acid (0.91), n-butyric acid (1.00), isopropyl alcohol (1.00), leucine (1.00), and valine (1.38), the bulky methyl groups, a protonated amino group, and a carboxyl group will severely restrict the internal rotation of C_2–H bond around the C_1–C_2 axis. In the α-hydroxy radical of ethyl alcohol (ratio, 1.48), a large value of the ratio may be ascribed to a somewhat nonplanar configuration around C_1 and the consequent s-character giving small C_1–H coupling constant.[27] For the serine radical (ratio, 0.51), a small value of the ratio might be due to the hindered internal rotation probably because of the formation of an intramolecular hydrogen bond between the hydroxy group and NH_3^+ and/or COOH.

Thus, the ratio of a_{C_2-H} to a_{C_1-H} is expected to become an additional measure concerning steric conformations, freedom in the internal rotations, and planarities of organic radicals.

The authors are very grateful to Prof. E. Suito, Dr. N. Ueda, Dr. T. Kobayashi, Dr. M. Nishino, Dr. J. Yamauchi, and Mr. K. Watanabe of the Institute for Chemical Research, Kyoto University, for their assistance and for the use of their ESR equipment.

23) T. J. Stone and W. A. Waters, *Proc. Chem. Soc.*, **1962**, 253.
24) H. M. McConnell, *J. Chem. Phys.*, **24**, 632, 764 (1956).
25) C. Heller and H. M. McConnell, *ibid.*, **32**, 1535 (1960).
26) R. W. Fessenden and R. H. Schuler, *ibid.*, **39**, 2147 (1963).
27) A. J. Dobbs, B. C. Gilbert, and R. O. C. Norman, *J. Chem. Soc., A*, **1971**, 124.

The Resonance Raman Spectrum of the Poly(vinyl alcohol)-Iodine Complex

Fuyuhiko INAGAKI,* Issei HARADA, Takehiko SHIMANOUCHI, and Mitsuo TASUMI**

Department of Chemistry, Faculty of Science, The University of Tokyo, Bunkyo-ku, Tokyo

***Department of Biophysics and Biochemistry, Faculty of Science, The University of Tokyo, Bunkyo-ku, Tokyo*

(Received May 11, 1972)

The resonance Raman spectra were observed from dilute aqueous solutions of the poly (vinyl alcohol)-iodine complex, using the He–Ne 632.8 nm and Ar^+ ion 488.0 nm lines for excitation. Two kinds of poly (vinyl alcohol) were used; one (A) had the degree of polymerization of 500, and the other, (B) 2000. For both samples, the resonance Raman spectra taken with the 632.8 nm line are similar to that of the starch-iodine complex, the intensity of the Raman band at 155 cm^{-1} being strongly enhanced. This band is assigned to the antisymmetric stretching vibration of the I_3^- ion aligned in the helical poly(viny alcohol) molecule. On the other hand, the intensity of the Raman band at 106 cm^{-1} is enhanced for Sample A when the 488.0 nm line is used for excitation. This band is assigned to the symmetric stretching vibration of the I_3^- ion. Its overtones were observed until the sixth. It is clear that the enhancement of the intensities of the 155 and 106 cm^{-1} bands is closely connected with the absorption bands at 670 and 490 nm respectively.

Much work was done on the resonance Raman effect in the pre-laser period.[1] With the recent development of laser-Raman spectroscopy, renewed interest in the resonance Raman effect has been growing both experimentally and theoretically. It seemed that it would be attractive to apply this effect to the study of the molecular structure of trace amounts of colored substances in solution. As the concentration of a colored substance detectable by the resonance Raman effect is very low (*ca.* 10^{-4} mol/*l*) compared with the ordinary Raman effect or the infrared absorption, this method will find various applications not only in physical chemistry, but also in analytical and biological chemistry.

One of the present authors (MT) has studied the resonance Raman spectra observed from dilute aqueous solutions of the starch-iodine complex.[2] The observed Raman bands have been assigned to the vibrations of the I_3^- ions aligned linearly in the cylindrical cavity inside the helical starch molecule. Since poly(vinyl alcohol) (PVA) is known to form a blue complex with iodine, just as starch does, we have taken up this complex in order to check whether or not it is structurally similar to the starch-iodine complex. The results show that the PVA-iodine complex gives a spectrum similar to that of the starch-iodine complex. Under certain conditions, however, a completely different spectrum is observed for the PVA-iodine complex. The details will be reported in the present paper.

Experimental

Sample. Two kinds of PVA samples were used. One (Sample A) had the average degree of polymerization of 500, and the other (Sample B), 2000. Both samples were purchased from the Wako Chemical Co. and were used without further treatment. The tacticities of these polymers are not precisely known. The other reagents were also obtained commercially. The iodine was purified by sublimation.

Each sample solution of the PVA-iodine complex was prepared as follows: 1 cc of a mixed solution of iodine (0.0029 mol/*l*) and potassium iodide (0.12 mol/*l*) was added to 5 cc of a 0.2 wt% aqueous solution of PVA and then the mixture was diluted to 25 cc with boric acid solutions of various concentrations (0.05—0.30 mol/*l*).[3]

In Table 1, the numbering of the sample solutions is given. The concentration of iodine in each sample was 1.1520×10^{-4} mol/*l* as I_2.

TABLE 1. THE NUMBERING OF SOLUTIONS[a]

PVA	H_3BO_3[b] 0.05	0.10	0.15	0.20	0.25	0.30
DP=500	A-1	A-2	A-3	A-4	A-5	A-6
DP=2000	B-1	B-2	B-3	B-4	B-5	B-6

a) For each solution, the PVA and iodine concentrations are 2.0 wt% and 1.152×10^{-4} mol/*l*, respectively.
b) The concentration of boric acid is expressed in mol/*l*.

Spectral Measurements. The Raman spectra were recorded using a He–Ne laser (632.8 nm) and an Ar^+ ion laser (488.0 nm) for excitation. When the He–Ne laser was used, a spectrometer was employed which consisted of a Spex 1401 double monochromator, a photomultiplier, a phase-sensitive detector, and a recorder.[4] Also, a Raman spectrometer constructed by the Kawaguchi Denki Co. and a JEOL JRS-U1 spectrometer were used, both with an Ar^+ ion laser. The Raman scattering was observed at right angles to the exciting laser beam, which radiates the sample very close to the quartz-cell wall.

Hitachi EPS-3 and 124 spectrophotometers were used to measure the absorption spectrum in the ultraviolet and visible regions.

Results and Discussion

Figure 1 shows an example of the Raman spectrum

* Present address: Department of Biophysics and Biochemistry, Faculty of Science, The University of Tokyo, Bunkyo-ku, Tokyo.

1) J. Behringer, "Raman Spectroscopy," ed. by H.A. Szymanski, Plenum Press, New York, N. Y. (1967).

2) M. Tasumi, *Chem. Lett.*, **1972**, 75.

3) It might be more reasonable to regard the complex as a ternary one consisting of PVA, iodine, and boric acid. However, we keep the tradionally-used name of PVA-iodine complex. Actually, the complex is formed even without boric acid after the mixed solution of PVA and iodine is left for a long time.

4) T. Fujiyama and M. Tasumi, *Bunko Kenkyu* (*J. Spectrosc. Soc. Jap.*), **20**, 28 (1971).

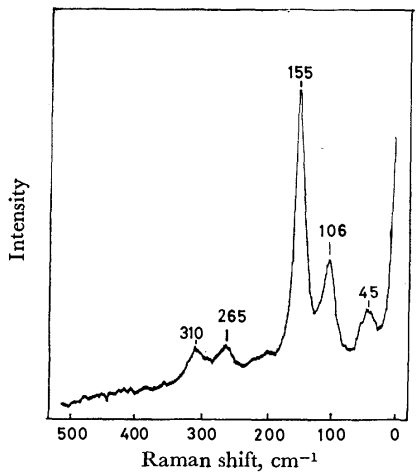

Fig. 1. The Raman spectrum of the solution B-3 taken with the 632.8 nm excitation.

of the PVA-iodine complex obtained with the 632.8 nm line of the He-Ne laser. A close resemblance is found between this and the spectrum reported previously for the starch-iodine complex.[2] It seems reasonable, therefore, to presume that the structure of the PVA-iodine complex is similar to that of the starch iodine complex. In other words, the present result is compatible with the model structure of the PVA-iodine complex proposed by Zwick[5] that a linear polyiodide chain is enclosed by a helical PVA molecule and that the latter, in turn, is surrounded by borates which maintain the PVA helix by forming the -C-O-B-O-C- bridge.

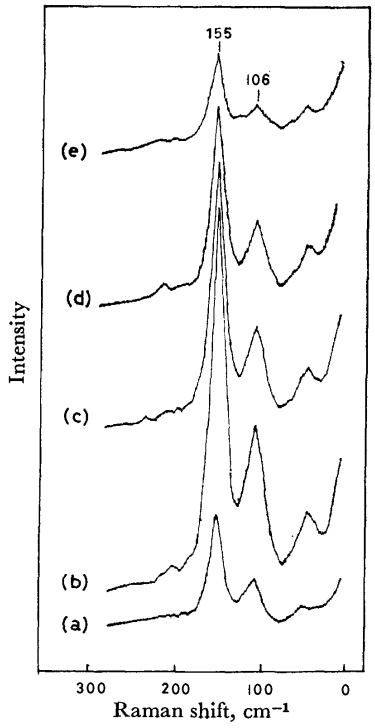

Fig. 2. The Raman spectra of Sample B taken with the 632.8 nm excitation. Iodine concentrations are as I_2:
(a) 2.09×10^{-4} mol/l; (b) 1.05×10^{-4} mol/l;
(c) 0.52×10^{-4} mol/l; (d) 0.26×10^{-4} mol/l;
(e) 0.13×10^{-4} mol/l.

5) M. M. Zwick, *J. Appl. Polym. Sci.*, **9**, 2393 (1965).

By analogy with the starch-iodine case, the three bands at 45, 106, and 155 cm^{-1} in Fig. 1 may be assigned, respectively, to the bending, symmetric stretching, and antisymmetric stretching vibrations of the I_3^- ion. The other two, at 265 and 310 cm^{-1}, may be assigned to a combination tone ($265\approx106+155$) and an overtone ($310\approx155\times2$).

In the following part we will discuss various spectral characteristics observed under different conditions.

(1) Effect of the Concentration on the Raman Intensities. Figure 2 shows the dependence of the Raman intensities on the iodine concentration observed for Sample B. The apparent Raman intensity reaches its maximum at the iodine concentration of 1.0488×10^{-4} mol/l. A similar tendency was also observed in the solution of Sample A.

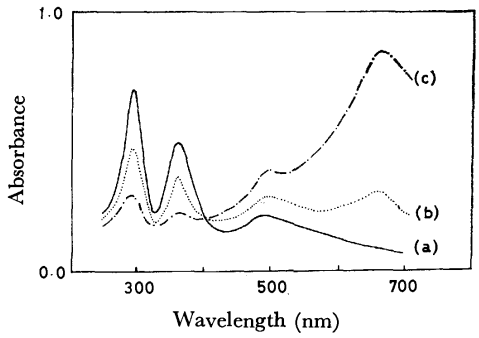

Fig. 3. The absorption spectrum of Sample A in the ultraviolet and visible regions. The solutions used are:
(a), A-1; (b), A-3; (c), A-5.

(2) Correlation between the Absorption and the Raman Spectra. (a) Ultraviolet and Visible Absorption Spectra: The absorption spectrum of Sample A in the ultraviolet and visible regions is shown in Fig. 3. The color of the complex varied from red to blue as the concentration of boric acid was increased. The absorption bands at 290 nm and 350 nm are due to the I_3^- ion. The band at 490 nm is close to the absorption wavelength of the I_2 molecule. However, only a small amount of the I_2 molecule would remain in the solutions treated here because of the presence of excess potassium iodide. As the extinction coefficient of the I_2 molecule is small ($\varepsilon=746$ $l$mol^{-1}cm^{-1}), it is unlikely that the 490 nm band in Fig. 3 arises from I_2. Therefore, this band should be assigned to the PVA(Sample

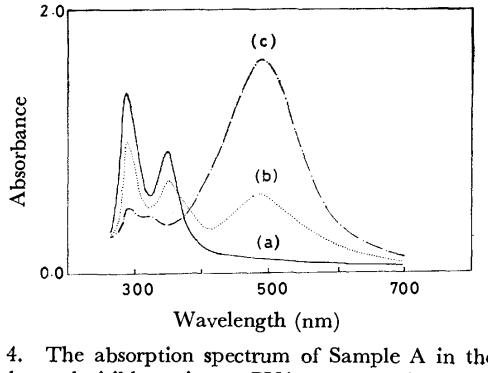

Fig. 4. The absorption spectrum of Sample A in the ultraviolet and visible regions. PVA concentrations are:
(a), 0.04 wt%; (b), 0.2 wt%; (c), 1.0 wt%. No boric acid was added.

A)-iodine complex. This is supported also by the observation that the intensity of this band increases with an increase in the PVA concentration, while, on the other hand, the intensities of the 290 and 350 nm bands of the I_3^- ion decrease, as is shown in Fig. 4. The band at 670 nm appears very strongly when the boric acid concentration is high.

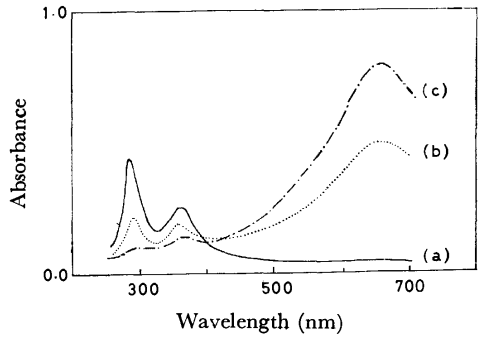

Fig. 5. The absorption spectrum of Sample B in the ultraviolet and visible regions. Boric acid concentrations are: (a), B-1; (b), B-3; (c), B-5.

Figure 5 shows the absorption spectra of the B solution series. The color of the B-1 solution (yellow) was exactly the same as that of the solution of iodine and potassium iodide. This would mean that Sample B does not make a complex with iodine at low boric acid concentrations. At higher boric acid concentrations, Sample B also shows a strong band at 670 nm.

It is noted that the 490 nm band found in the spectra of Sample A is not observed in any of the spectra of Sample B. This difference gives rise to an important effect in the Raman spectra, as will be discussed later.

(b) The Raman Spectra Observed with the 632.8 nm Excitation: The Raman spectra of the A and B solution series are shown in Figs. 6 and 7 respectively; they were obtained with the 632.8 nm line of the He-Ne

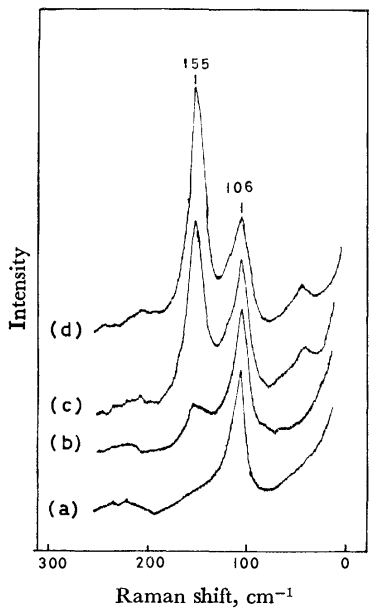

Fig. 6. The Raman spectra of the solution series A taken with the 632.8 nm excitation.
(a), A-1; (b), A-2; (c), A-3; (d), A-5.

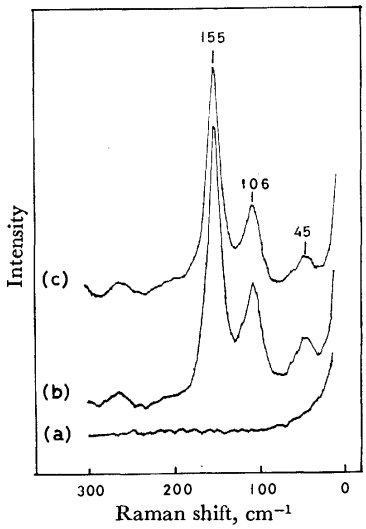

Fig. 7. The Raman spectra of the solution series B taken with the 632.8 nm excitation.
(a), B-1; (b), B-3; (c), B-5.

laser. A marked change may be seen in the spectra of the A solution series. The Raman band at 155 cm^{-1} (the antisymmetric stretching mode) is not observed in the reddish solution A-1. When the color of the complex becomes blue, this band is strongly enhanced. In contrast with this, the intensity of the 106 cm^{-1} band (symmetric stretching mode) remains nearly constant throughout the A solution series, independent of the color of the complex.

No Raman bands are observed for the yellow solution B-1. However, as the color becomes increasingly blue upon the addition of the boric acid, strong Raman bands appear for the B-3, B-4, and B-5 solutions.

(c) The Raman Spectra observed with the 488.0 nm Excitation: Figure 8 shows the spectrum of the A-4 solution obtained with the 488.0 nm line of the Ar^+ ion laser. It can be noted that the Raman band at 106 cm^{-1} is strongly enhanced and that overtones may be observed until the sixth. The Raman line at 155 cm^{-1} is observed only as a weak shoulder. This is in contrast with Fig. 1, in which the band at 155 cm^{-1}

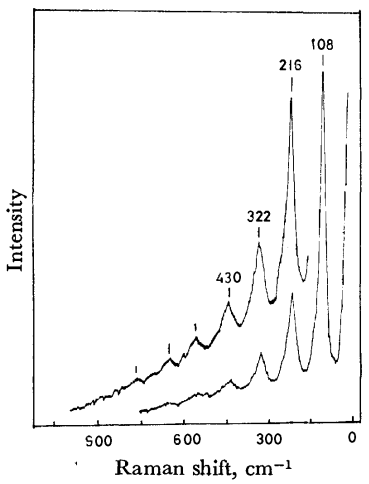

Fig. 8. The Raman spectrum of the solution A-4 with the 488.0 nm line excitation. The solution A-2 gives essentially the same spectrum.

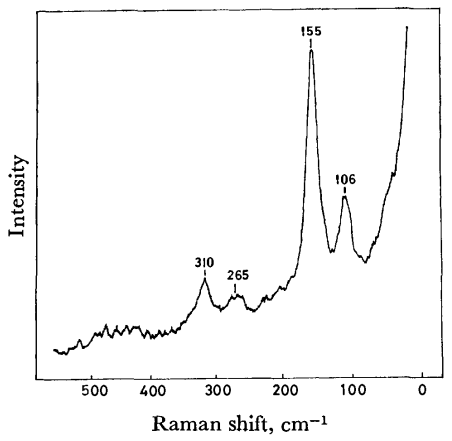

Fig. 9. The Raman spectrum of the solution B-3 taken with the 488.0 nm line excitation.

is much stronger than the band at 106 cm^{-1}.

For Sample B, on the other hand, essentially the same spectra were observed as those obtained with the He-Ne 632.8 nm line (Fig. 9).

The different spectral behavior between Sample A and Sample B with respect to the 488.0 nm excitation seems to be associated with the fact that Sample A has the 490 nm band, which is resonant with the exciting line, whereas Sample B has no such band.

TABLE 2. SUMMARY OF THE RESONANCE EFFECT[a)]

Exciting line	Sample: PVA-iodine A red	A blue	B yellow	B blue	Starch-iodine[b)]	Free I_3^-
632.8 nm	s	s,A	none	s,A	s,A	s
488.0 nm	S	S	none	s,A	s,A	s

a) The capital letters S and A indicate that the intensities of the I_3^- *symmetric* and *antisymmetric* modes are, respectively, enhanced greatly. The small symbol s means that the intensity of the I_3^- *symmetric* stretching is enhanced, but not as greatly as the case indicated by the capital letter.

b) Taken from Ref. 2.

The results obtained above are summarized in Table 2, together with those for the starch-iodine complex and the free I_3^- ion. The Raman spectra of the free I_3^- ion in an aqueous solution are shown in Fig. 10. The measurements were made under much higher I_3^- concentrations than those used in the Raman measurements of the complexes. This indicates that the resonance effect is much weaker for the free I_3^- ion than for I_3^- in the complexes, reflecting the experimental conditions that the exciting wavelengths used are outside the absorption bands of the free I_3^- ion found at 350 and 290 nm (preresonance case).

The following points in Table 2 are most noteworthy: (i) The intensity of the I_3^- antisymmetric stretching mode is strongly enhanced in the complex state under some conditions, whereas it is only weakly observed in the free state. This is undoubtedly due to the presence of the absorption band of the complex at 670 nm (PVA-iodine) or *ca.* 600 nm (starch-iodine).

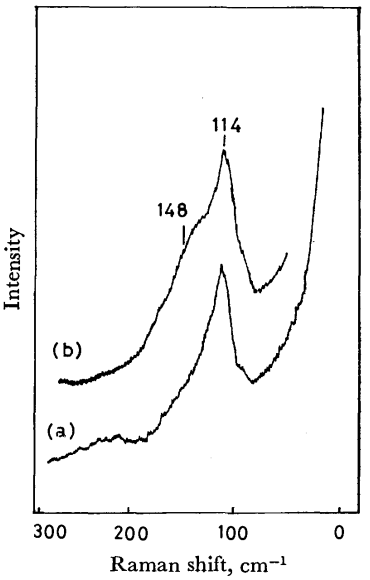

Fig. 10. The Raman spectra of aqueous solutions of potassium iodide.
(a), excited with the 488.0 nm line; (b), excited with the 632.8 nm line.

(ii) The intensity of the I_3^- symmetric stretching mode is enhanced in the free I_3^- spectra. It is strongly enhanced also in the complex-state spectra, instead of the antisymmetric mode, if the exciting wavelength is resonant with the absorption band at 490 nm.

These results clearly show that the alternative enhancement of different Raman bands can be achieved by using the resonance effect. As far as we know, such a clear example of alternative enhancement has not yet been reported. The mechanism which gives rise to the alternative enhancement must be rather complicated. However, we propose a very simple working hypotheses which might be of some value in understanding such a resonance effect: if the direction of a vibrational transition moment of a non-centrosymmetric molecule coincides with that of the electronic transition moment responsible for the resonance effect, the Raman intensity of the relevant vibrations has a chance of being selectively enhanced. As has been discussed in a previous paper,[2)] the transition moment of the 600 nm band of the starch-iodine complex is directed parallel to the linear chain of the I_3^- ion. Therefore, the Raman intensity of the I_3^- antisymmetric stretching mode is enhanced if the 600 nm band is resonant with the exciting wavelength. It seems quite reasonable to expect that the situation is the same for the enhancement of the I_3^- antisymmetric stretching mode of the PVA-iodine complex, though the direction of the transition moment of the 670 nm band of the PVA-iodine complex has not been determined experimentally. On the other hand, the 490 nm band would have its transition moment directed perpendicular to the I_3^- chain, if the working hypothesis described above be true. It is highly probable that the I_3^- ion in the complex deviates slightly from the linear centrosymmetric structure[6)] and, as a result, the transition moment

6) A. G. Maki and R. Forneris, *Spectrochim. Acta.*, **23A**, 867 (1967).

of the I_3^- symmetric stretching mode is directed perpendicularly to the I_3^- chain. In this case, the Raman intensity of this mode may be selectively enhanced by the resonance between the 490 nm band and the 488.0 nm Ar^+ line. However, it should be mentioned that the origin of the 490 nm band is not very clear as yet. It is conceivable that this band is associated with either the tacticity of the polymer or the chain end, since this band is observable only in the spectrum of Sample A. This problem can be clarified only through experiments which utilize well-characterized polymer samples. Also, the validity of that working hypothesis should be tested by choosing suitable molecules, for which not only the molecular structures but also the assignment of the vibrational and electronic spectra are firmly established.

BULLETIN OF THE CHEMICAL SOCIETY OF JAPAN, VOL. 45, 3388—3396 (1972)

The Crystal Structure of the Polymerization Catalyst of Acetaldehyde and Its Derivatives. II.[1] The Crystal and Molecular Structure of the Trimethylamine Oxide Adduct of Dimethylaluminum *N*-Phenylbenzimidate, $[(CH_3)_2Al\cdot O\cdot C(C_6H_5):N(C_6H_5),\ ON(CH_3)_3]$

Yasushi KAI, Noritake YASUOKA, Nobutami KASAI, and Masao KAKUDO*

Department of Applied Chemistry, Faculty of Engineering, Osaka University, Yamadakami, Suita, Osaka, 565

**Institute for Protein Research, Osaka University, Yamadakami, Suita, Osaka, 565*

(Received May 13, 1972)

The molecular structure of a stereospecific (*isotactic*) polymerization catalyst of the acetaldehyde-Lewis base adduct $[Me_2Al\cdot O\cdot CPh:NPh,ONMe_3]$ has been determined from three-dimensional X-ray data collected on a single crystal diffractometer. The crystal belongs to the triclinic system (space group $P\bar{1}$), with two formula units in a cell with dimensions of; $a=8.517\pm0.004$, $b=10.096\pm0.005$, $c=12.256\pm0.005$ Å, $\alpha=104.67\pm0.04$, $\beta=106.97\pm0.04$, and $\gamma=98.10\pm0.04°$. The structure was solved by the symbolic addition method and refined by the block-diagonal, least-squares procedure. The molecule is monomeric, and both amide and $ONMe_3$ groups are connected to the aluminum atom through oxygen atoms. The amide moiety has an imino-ether type structure and two adjacent benzene rings take *trans* configuration about the N–C bond. The co-ordinated $ONMe_3$ group has a structure similar to that of the free molecule.

This work is a part of a series of molecular-structural studies[1–5] of the stereospecific polymerization catalysis of acetaldehyde. In recent years, Tani and his co-workers have found that, among the catalytic systems of the stereospecific polymerization reaction of aldehydes, the reaction products of trialkylaluminums and acid amides show excellent catalytic activities for the *isotactic* polymerization of acetaldehyde and methylmethacrylate.[6–9]

This catalytic system has attractive features which facilitate stereochemical investigations. First, the catalytic system contains few side reactions and gives a very high yield of the stereospecific polymer. Therefore, a rather simple reaction mechanism can be expected. Second, the polymerization reaction is mild, and many interesting complexes can be isolated in a pure crystalline form.

The series of complexes selected for molecular-structural studies in this catalytic system are:

(I) $[Me_2Al\cdot O\cdot CPh:NPh]_2$,[10]

(II) $[Me_2Al\cdot O\cdot CPh:NPh,\ MeCHO]_2$,

(III) $[Me_2Al\cdot O\cdot CPh:NPh,\ MeCHO,\ AlMe_3]$, and

(IV) $[Me_2Al\cdot O\cdot CPh:NPh,\ ONMe_3]$.

The complex I is a highly stereospecific polymerization catalyst of acetaldehyde obtained from an equimolar reaction of trimethylaluminum and benzanilide; its molecular structure has been reported previously.[1,2] The polymerization catalyst-monomer complex II shows the same catalytic activities as I. The co-ordinated aldehyde can be replaced by a free aldehyde present in the solution, but it can not be replaced by other electron donors, such as pyridine or tetrahydrofuran. Using the complex III, a Lewis acid adduct of II, as a catalyst, an *atactic* polymer of acetaldehyde is obtained.

The complex IV is a strong Lewis base adduct of

1) Part I, Y. Kai, N. Yasuoka, N. Kasai, and M. Kakudo, *J. Organometal. Chem.*, **32**, 165 (1971).

2) Y. Kai, N. Yasuoka, N. Kasai, M. Kakudo, H. Yasuda, and H. Tani, *Chem. Commun.*, **1968**, 1332.

3) Y. Kai, N. Yasuoka, N. Kasai, M. Kakudo, H. Yasuda, and H. Tani, *ibid.*, **1969**, 575.

4) Y. Kai, N. Yasuoka, N. Kasai, M. Kakudo, H. Yasuda, and H. Tani, *ibid.*, **1970**, 1243.

5) Y. Kai, N. Yasuoka, N. Kasai, M. Kakudo, H. Yasuda, and H. Tani, *ibid.*, **1971**, 940.

6) H. Tani, T. Araki, and H. Yasuda, *J. Polym. Sci., Part B*, **4**, 727 (1966).

7) H. Tani, T. Araki, and H. Yasuda, *ibid.*, **6**, 389 (1968).

8) H. Tani and H. Yasuda, *ibid.*, **7**, 17 (1969).

9) H. Tani and H. Yasuda, Private communications.

10) Throughout the paper, methyl, ethyl, and phenyl groups will be expressed as Me, Et, and Ph respectively.

the polymerization catalyst; it is obtained from an equimolar mixture of I and $ONMe_3$ in benzene at room temperature:

$$[Me_2Al\cdot O\cdot CPh{:}NPh]_2 \xrightarrow[\text{in benzene at room temperature}]{+ONMe_3} [Me_2Al\cdot O\cdot CPh{:}NPh,\ ONMe_3]$$

I IV

This complex is the most stable one in argon among the four complexes mentioned above. However, it does not show any catalytic activities, and significant differences can be expected between the molecular structures of the polymerization catalyst, $[Me_2Al\cdot O\cdot CPh{:}NPh]_2$ and this complex. The structure determination was undertaken by means of X-ray diffraction. The preliminary results were communicated earlier.[5]

Experimental

The colorless, prismatic crystals were prepared and supplied by Tani and Yasuda of this University. As the crystals decompose immediately in the air, they were sealed in thin-walled glass capillary tubes in argon.

Nickel-filtered Cu$K\alpha$ radiation was used for the preliminary X-ray experiments. Oscillation and Weissenberg photographs showed that the crystal has no crystallographic symmetry, and the space group is $P\bar{1}$ or $P1$.

Both the determination of the unit-cell dimensions and the collection of the intensity data were carried out on a Rigaku on-line controlled, four-circle, single crystal diffractometer. Zirconium-filtered Mo$K\alpha$ radiation was used. The setting angles of each reflection were computed by the Busing-Levy method[11] on an Aicom-C2 computer attached to the diffractometer. The method requires precise values of the centering angles, 2θ, ω, χ, and ϕ, of three linearly-independent reflections of known indices in order for us to determine the orientation of the crystal and the dimensions of the unit cell. The reflections chosen were 500, 030, 007, $0\bar{3}0$, and $00\bar{7}$. During the intensity measurement of each quadrant of the reciprocal lattice, three of the five chosen reflections included in the quadrant were used. The crystal data are listed in Table 1. The accuracies of the cell parameters were estimated from the reproducibilities of the cell parameters as calculated from different sets of reflections. The crystal density was determined by the flotation method in a mixed solution of carbon tetrachloride and *n*-hexane. Intensity measurements were carried out at room temperature by using the ω–2θ scan technique with a β-filter. The scan range, $\Delta(2\theta)$ of each reflection was computed by this equation:

$$\Delta(2\theta) = 2.0° + 0.7° \tan\theta_c.$$

The starting angle of the scan is $(2\theta_c - 1.0°)$, where θ_c is the calculated value of the Bragg angle using the $\lambda(\text{Mo}K\alpha_1)$ (=0.70926 Å), and the scanning speed of the scintillation counter was 4.0°/min. Sheets of nickel foil with graded thicknesses were used as intensity attenuators. Before scanning a reflection, a short, fixed-time (one second) intensity measurement was taken at the $2\theta_c$ position, and an appropriate attenuator was selected and was inserted in order to control the intensity in the optimum range (below 7000 cps in this experiment). The background scattering was measured for five seconds at both ends of the scan range by means of the stationary-crystal stationary-counter technique. The intensities were corrected for the background scattering and for the usual Lorentz and polarization effects. Each structure factor, along with its standard deviation, as estimated by the counting statistics, was calculated and printed out before the measurement of the next reflection. The absorption correction was ignored (μ=1.3 cm^{-1} for Mo$K\alpha$). The intensity of the 300 reflection was chosen as the standard and was measured every 25 reflections. The crystal used had dimensions of about 0.5×0.3×0.3 mm. The collimator was 1.0 mm in diameter. During the intensity measurements, the intensity of the standard reflection gradually decreased. The structure factor magnitudes, therefore, decreased approximately linearly up to $(\sin\theta)/\lambda$=0.458. After this, they showed a sudden decrease. Probably the crystal decomposed completely. Then another crystal of an approximately equal size was chosen and further intensity measurements were carried out up to $(\sin\theta)/\lambda$=0.539. The intensities of about 200 reflections ($(\sin\theta)/\lambda$=0.235) were also remeasured for the second crystal, and the structure factor magnitudes were compared with those obtained from the first crystal. No special anisotropy due to the absorption was found. Then the scalings of the two kinds of data, including the intra- and inter-crystal scaling, were undertaken linearly based on the observed changes in the structure factor magnitudes of the standard reflection. A total of 2399 independent reflections were obtained, among which 2048 were non-zero reflections.

Table 1. Crystal data of $[(CH_3)_2Al\cdot O\cdot C(C_6H_5){:}N(C_6H_5), ON(CH_3)_3]$

Triclinic	$C_{18}H_{25}N_2O_2Al$
a= 8.517 ±0.004Å	M=328.4
b= 10.096 ±0.005Å	Z=2
c= 12.256 ±0.005Å	d_m=1.14 g·cm^{-3}
α=104.67 ±0.04°	d_x=1.149 g·cm^{-3}
β=106.97 ±0.04°	Space group $P\bar{1}$
γ= 98.10 ±0.04°	μ=1.3 cm^{-1} (for Mo$K\alpha$)
V=948.5 Å^3	

Structure Determination and Refinement

The crystal structure was solved by obtaining phases directly from the structure factor magnitudes by means of the symbolic addition procedure.[12] The structure factors reduced previously were placed on an absolute scale by means of a three-dimensional Wilson plot, and the structure factor magnitudes, $|F|$, and the normalized structure factor magnitudes, $|E|$, were computed by means of SIGMA program[13] on a FACOM 230-60 computer at Kyoto University. The distribution of the normalized structure factor magnitudes, $|E|$, and their statistical averages are given in Table 2. On the basis of these statistics, the space group was determined to be $P\bar{1}$, which was confirmed at the later stage of the structure determination. The SIGMA program was also utilized to list the $\sum_2$ relationships for each reflection and to calculate the associated probabilities. The probabilities were determined by

11) W. R. Busing and H. A. Levy, *Acta Crystallogr.*, **22**, 457 (1967).

12) J. Karle and I. L. Karle, *ibid.*, **21**, 849 (1966).

13) T. Ashida, SIGMA, The Universal Crystallographic Computing System (I), edited by T. Sakurai, p. 43, Japanese Crystallographic Association, 1967.

means of the equation:

$$P_+(E_h) = \frac{1}{2} + \frac{1}{2}\tanh(\sigma_3\sigma_2^{-3/2}|E_h|\sum E_k E_{h-k}),$$

and their lower limit was set at 0.97.

Positive signs were assigned to three linearly-independent reflections in order to define the origin of the unit cell. The signs of the five other reflections were then all determined to be + from the $\sum_2$ relationships among the origin-defining reflections. Four additional reflections were chosen, and their phases were designated by the letters *a*, *b*, *c*, and *d* in order to facilitate the symbolic addition procedure. Starting from the phases of these 12 reflections (Table 3), 99 signs out of 103 reflections whose $|E|$ values are greater than 2.0 were determined as functions of *a*, *b*, *c*, and *d* by using the SORT-SIGMA 2 program.[14] Through the application of the $\sum_2$ formula, it was found, from the relationships among the symbols, that $a=c=d$ and $b=+$.

As the + signs were assumed for the three origin-fixing reflections, the − sign was never introduced into these reflections in the course of the application of the $\sum_2$ formula for the space group $P\bar{1}$. It was then necessarily concluded that the signs of *a*, *c*, and *d* are all − ; otherwise, a trivial solution would have resulted. On the basis of these 99 phases, the application of the $\sum_2$ relationship was extended over 303 reflections with $|E|\geqq 1.50$ and the phases of 203 additional reflections were determined. At this stage, one of the 99 phases changed its sign to the correct one.

From the *E*-map (Fig. 1), the locations of all of the 23 nonhydrogen atoms were found easily. On the basis of these atomic locations, block-diagonal least-squares refinement was carried out by means of the HBLS IV program.[15] The atomic scattering factors used in the calculation were taken from those of Hanson and his co-workers.[16] After 5 cycles refinement using the isotropic temperature factors, the *R* index was found to be 0.17 for non-zero reflections. This rather large *R* value was considered to have resulted from the large differences between $|F_o|$ and $|F_c|$ values, especially for small $|F_o|$'s. Therefore, all the $|F_o|$'s smaller than $3\sigma(F_o)$ were excluded from the further refinement. Anisotropic temperature factors were then introduced for all the nonhydrogen atoms and the refinement was continued. After 4 cycles, the *R* value was reduced to 0.097 for 1359 non-zero reflections. From the difference Fourier map computed by means of SFFR program[17] and from the model examination, all of the hydrogen atoms were located. Considering these hydrogen atoms and using a weighting scheme to be described later, the final refinement was undertaken and the *R* index decreased to 0.068 for non-zero reflections. The weighting scheme applied was;

$$|F_o| < F_{\min}: w = F_{wt}$$
$$F_{\min} \leqq |F_o| \leqq F_{\max}: w = 1.0$$
$$F_{\max} < |F_o|: w = F_{\max}/|F_o|$$

where $F_{\max}=20.0$, $F_{\min}=0.0$, and $F_{wt}=0.0$. The weighted *R* index defined as $\{\sum w\cdot(|F_o|-|F_c|)^2/\sum w\cdot(F_o)^2\}^{1/2}$ is 0.082.

TABLE 2. DISTRIBUTION OF THE NORMALIZED STRUCTURE FACTOR MAGNITUDE AND STATISTICAL AVERAGES

	Distribution of $\|E\|$ %		Number of reflections
	Theoretical (Centrosymmetric)	Experimental	
$\|E\|\geqq 3.0$	0.3	0.38	9
$\|E\|\geqq 2.0$	5.0	4.3	103
$\|E\|\geqq 1.0$	32.0	33.0	792
			2399 (total)

	Experimental	Theoretical	
		Centrosymmetric	Noncentrosymmetric
$<\|E^2\|>$	1.000	1.000	1.000
$<\|E\|>$	0.790	0.798	0.886
$<\|E^2-1\|>$	0.946	0.968	0.739

TABLE 3. STARTING SET OF APPLICATION OF $\sum_2$ FORMULA

h	*k*	*l*	$\|E\|$	Phase	
1	$\bar{1}$	2	3.39	+	for origin definition
5	$\bar{5}$	$\bar{5}$	3.48	+	for origin definition
7	2	$\bar{6}$	4.10	+	for origin definition
1	8	$\bar{3}$	2.13	+	
2	7	$\bar{1}$	2.75	+	
5	4	$\bar{10}$	2.19	+	
6	3	$\bar{8}$	2.78	+	
6	$\bar{6}$	$\bar{3}$	2.23	+	
2	$\bar{1}$	6	2.75	*a*	
8	$\bar{2}$	$\bar{6}$	3.18	*b*	
5	3	$\bar{9}$	3.21	*c*	
1	$\bar{2}$	$\bar{1}$	2.33	*d*	

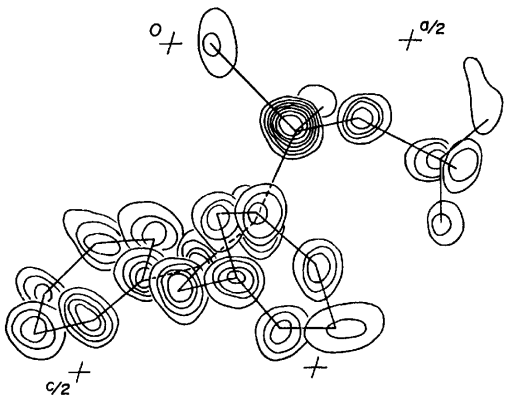

Fig. 1. *E*-map. Contours in an arbitrary scale.

The final atomic co-ordinates of the heavy atoms, along with their estimated standard deviations and the anisotropic temperature factors, are shown in Tables 4 and 5 respectively. The atomic co-ordinates and the

14) N. Yasuoka, SORT-SIGMA2, unpublished program.
15) T. Ashida, HBLS IV, Ref. 13, p. 65.
16) H. P. Hanson, F. Herman, J. D. Lea, and S. S. Skillman, *Acta Crystallogr.*, **17**, 1040 (1964).
17) T. Ashida, SFFR, Ref. 13, p. 74.

Table 4. Atomic co-ordinates of the heavy atoms (in fraction of cell edges) along with their estimated standard deviations (in 10^{-3} Å)

Atom	x	$\sigma(x)$	y	$\sigma(y)$	z	$\sigma(z)$
Al	0.3060	3	−0.2250	3	0.1332	3
O(1)	0.2983	5	−0.1692	5	0.2802	5
O(2)	0.4574	5	−0.0861	6	0.1222	5
N(1)	0.1638	7	−0.0155	6	0.3675	7
N(2)	0.6329	6	−0.0455	7	0.1803	7
C(1)	0.3755	12	−0.4042	10	0.1077	12
C(2)	0.0934	9	−0.2192	11	0.0183	9
C(3)	0.1848	7	−0.1384	8	0.3316	7
C(4)	0.0786	7	−0.2588	7	0.3461	7
C(5)	−0.0156	8	−0.2337	8	0.4208	8
C(6)	−0.1160	9	−0.3460	9	0.4333	10
C(7)	−0.1207	10	−0.4819	9	0.3733	11
C(8)	−0.0236	11	−0.5068	10	0.2998	12
C(9)	0.0753	11	−0.3955	9	0.2867	10
C(10)	0.2654	8	0.1010	7	0.3564	9
C(11)	0.4180	8	0.1738	8	0.4468	9
C(12)	0.5030	8	0.2971	9	0.4403	9
C(13)	0.4441	8	0.3490	9	0.3461	10
C(14)	0.2939	9	0.2738	9	0.2563	10
C(15)	0.2073	8	0.1516	8	0.2613	9
C(16)	0.7134	10	−0.1264	12	0.1033	12
C(17)	0.6806	10	0.1069	10	0.1903	11
C(18)	0.6830	9	−0.0629	12	0.3010	10

Table 5. Anisotropic temperature factors of the heavy atoms expressed in the form of $\exp\{-(\beta_{11}h^2+\beta_{22}k^2+\beta_{33}l^2+\beta_{12}hk+\beta_{13}hl+\beta_{23}kl)\}$

Atom	β_{11}	β_{22}	β_{33}	β_{12}	β_{13}	β_{23}
Al	0.0149	0.0122	0.0087	0.0058	0.0125	0.0063
O(1)	0.0147	0.0151	0.0082	0.0071	0.0127	0.0079
O(2)	0.0139	0.0183	0.0098	0.0066	.00098	0.0137
N(1)	0.0212	0.0122	0.0127	0.0069	0.0195	0.0108
N(2)	0.0128	0.0172	0.0116	0.0049	0.0122	0.0124
C(1)	0.0387	0.0159	0.0185	0.0146	0.0327	0.0126
C(2)	0.0201	0.0255	0.0084	0.0012	0.0086	0.0075
C(3)	0.0132	0.0141	0.0065	0.0062	0.0068	0.0080
C(4)	0.0151	0.0107	0.0067	0.0029	0.0099	0.0045
C(5)	0.0192	0.0134	0.0086	0.0093	0.0154	0.0074
C(6)	0.0219	0.0158	0.0155	0.0085	0.0242	0.0153
C(7)	0.0234	0.0157	0.0180	0.0045	0.0249	0.0150
C(8)	0.0348	0.0133	0.0195	0.0023	0.0337	0.0071
C(9)	0.0346	0.0117	0.0142	0.0044	0.0319	0.0033
C(10)	0.0202	0.0090	0.0117	0.0083	0.0209	0.0083
C(11)	0.0160	0.0149	0.0103	0.0048	0.0093	0.0096
C(12)	0.0166	0.0156	0.0113	0.0001	0.0077	0.0045
C(13)	0.0168	0.0131	0.0163	0.0045	0.0139	0.0125
C(14)	0.0232	0.0138	0.0158	0.0083	0.0184	0.0171
C(15)	0.0174	0.0114	0.0114	0.0034	0.0085	0.0087
C(16)	0.0191	0.0272	0.0195	0.0098	0.0230	−0.0020
C(17)	0.0231	0.0189	0.0154	0.0028	0.0128	0.0130
C(18)	0.0187	0.0319	0.0130	0.0108	0.0062	0.0268

isotropic temperature factors of hydrogen atoms are listed in Table 6. The observed and calculated structure factors are given in Table 7.

Table 6. Atomic co-ordinates (in fraction of cell edges) along with their estimated standard deviations (in 10^{-2}Å) and isotropic temperature factors for the hydrogen atoms (in Å^2)

Atom	x	$\sigma(x)$	y	$\sigma(y)$	z	$\sigma(z)$	B
H(1)	0.460	8	−0.411	8	0.190	8	3.6
H(2)	0.440	8	−0.415	8	0.044	8	3.9
H(3)	0.263	8	−0.496	8	0.072	9	4.3
H(4)	0.001	8	−0.261	8	0.043	8	3.1
H(5)	0.076	8	−0.278	8	−0.072	8	3.9
H(6)	0.087	8	−0.114	8	0.019	8	3.9
H(7)	−0.009	8	−0.125	8	0.471	8	3.1
H(8)	−0.192	8	−0.326	7	0.491	8	3.0
H(9)	−0.199	8	−0.568	8	0.384	8	3.2
H(10)	−0.019	8	−0.614	8	0.255	8	3.9
H(11)	0.155	8	−0.417	8	0.231	8	3.4
H(12)	0.470	8	0.133	8	0.523	8	3.1
H(13)	0.621	8	0.356	8	0.512	8	3.5
H(14)	0.512	7	0.446	7	0.341	8	2.8
H(15)	0.244	8	0.314	8	0.182	8	3.5
H(16)	0.088	8	0.093	7	0.189	8	3.0
H(17)	0.681	8	−0.239	8	0.101	8	3.7
H(18)	0.858	8	−0.098	8	0.128	8	3.5
H(19)	0.658	8	−0.125	8	0.014	8	3.8
H(20)	0.664	8	0.128	8	0.100	8	3.5
H(21)	0.601	8	0.163	8	0.232	8	3.8
H(22)	0.809	8	0.151	8	0.249	8	3.9
H(23)	0.823	8	−0.036	8	0.332	8	3.5
H(24)	0.643	8	0.022	8	0.354	8	4.3
H(25)	0.659	8	−0.169	8	0.317	8	4.0

Results and Discussion

The molecular structure, with the numbering of atoms, as viewed along the b axis is shown in Fig. 2. The interatomic bond distances and angles calculated using the DAPH program[18] are listed in Tables 8 and 9 respectively.

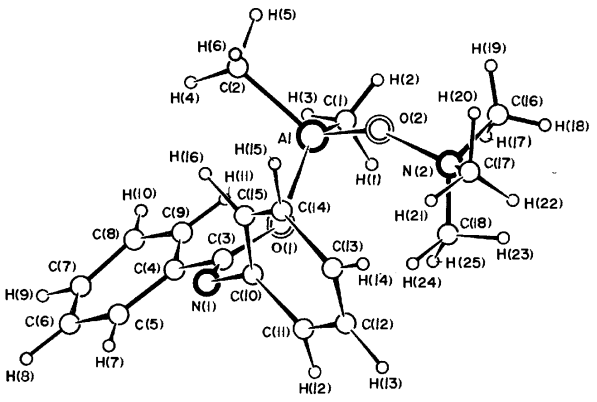

Fig. 2. Molecular structure.

Molecular Structure. The molecule is monomeric. The amide and $ONMe_3$ groups are both connected to the aluminum atom through oxygen atoms. The aluminum atom has a slightly distorted tetrahedral

18) T. Ashida, DAPH, Ref. 13, p. 76.

TABLE 7. THE OBSERVED AND CALCULATED STRUCTURE FACTORS
(each multiplied by the factor of 5.0)

K	FO	FC	K	FO	FC	K	FO	FC	K	FO	FC	K	FO	FC	K	FO	FC	K	FO	FC	K	FO	FC
H=L= 0		-12	H=L= 0		4	3	60	55	0	43	-42	-2	18	-9	-1	210	214	-5	76	76	-1	148	-137	0	79	79	-5	66	-71
5	21	-14	0	174	-175	4	165	-158	1	123	-114	-1	79	82	0	227	212	-4	99	103	0	168	165	1	83	84	-4	26	-25
H=L= 0		-11	1	33	34	5	94	-94	3	80	76	0	125	124	1	142	140	-3	82	-87	1	170	168	2	26	-32	-3	109	115
3	18	-8	2	30	33	6	80	-85	6	31	-25	2	112	-101	2	41	-38	-2	64	-64	3	56	-56	3	59	-61	-2	111	106
4	19	-19	4	81	-77	10	23	-22	7	26	-28	3	78	77	6	54	-59	0	131	128	5	26	-20	4	110	-109	-1	78	71
6	20	21	H=L= 0		5	H=L= 1		-3	H=L= 1		5	4	104	98	7	51	68	2	105	-107	6	72	69	5	35	33	1	44	43
H=L= 0		-10	0	103	-103	-8	32	-25	-9	99	102	5	23	21	8	28	20	3	38	-44	7	28	24	6	44	43	2	143	147
1	49	-50	1	95	-96	-6	56	-59	-8	27	32	6	32	37	H=L= 2		3	4	51	51	H=L= 3		2	8	23	-24	3	50	-52
7	37	32	2	51	-51	-5	45	47	-7	51	-57	7	29	21	-8	62	66	5	31	34	-10	60	-58	H=L= 4		-7	4	89	-93
8	24	22	3	111	107	-4	121	116	-6	64	-64	8	29	28	-7	24	-22	6	31	10	-6	53	-52	-6	28	-26	6	58	56
H=L= 0		-9	4	43	44	-3	87	-85	-4	36	-31	H=L= 2		-5	-6	64	-66	7	38	-36	-5	69	54	-4	74	84	H=L= 4		2
2	57	-52	5	46	-49	-2	80	79	-3	22	30	-7	39	-38	-5	22	20	8	25	28	-4	102	97	-2	47	-50	-9	27	-22
3	43	39	H=L= 0		6	-1	193	197	-2	98	-108	-3	104	-108	-3	47	-50	H=L= 3		-6	-3	51	53	-1	76	-73	-7	39	35
5	42	-46	0	33	32	0	270	261	-1	45	38	-2	165	-160	-2	108	-105	-8	24	4	-2	116	-116	1	96	98	-6	27	-22
6	32	-33	1	33	-44	2	68	66	0	106	96	0	29	28	-1	249	-257	-4	93	96	-1	53	-45	2	100	101	-5	99	-103
8	36	37	3	24	-21	3	48	51	1	56	57	1	43	-42	0	116	112	-3	68	64	0	118	-112	3	28	-30	-4	98	-97
9	31	22	6	28	-30	4	127	131	2	37	-32	2	71	-68	1	37	-36	-2	94	-94	1	24	-23	6	51	47	-3	31	28
H=L= 0		-8	H=L= 0		7	5	19	15	4	43	48	3	65	-61	4	26	26	-1	110	-107	2	27	-26	7	32	25	-2	57	55
1	36	-31	0	101	97	6	82	-85	5	34	24	4	43	42	5	49	47	1	115	117	5	72	75	H=L= 4		-6	0	58	-57
2	39	-42	1	17	-5	7	53	-50	6	33	-32	5	64	62	7	68	-69	3	66	-63	H=L= 3		3	-5	95	-106	1	40	37
3	27	-20	2	71	-70	8	83	85	7	28	-23	H=L= 2		-4	H=L= 2		4	5	32	38	-7	34	40	-4	69	-74	2	59	54
4	57	53	3	40	-41	10	25	21	H=L= 1		6	-8	51	52	-9	64	64	6	43	45	-6	42	-39	-3	31	37	3	43	34
6	83	-81	5	29	25	H=L= 1		-2	-9	53	-52	-6	38	-42	-8	27	32	7	27	-30	-5	163	-161	-2	34	30	6	45	-44
8	51	54	H=L= 0		8	-7	58	-58	-7	51	55	-5	21	21	-6	32	-38	H=L= 3		-5	-3	193	191	-1	105	-98	H=L= 4		3
9	36	34	0	37	37	-6	65	-67	-4	51	45	-4	75	70	-5	62	-59	-8	22	21	-2	52	52	0	96	-97	-10	25	23
H=L= 0		-7	1	47	52	-5	39	-35	-3	85	-81	-3	48	-55	-4	56	58	-6	65	-65	-1	196	-193	1	43	40	-9	25	-26
2	113	-110	H=L= 0		9	-4	27	25	-2	165	-163	-2	75	-84	-3	64	56	-5	32	-31	0	129	-122	2	110	111	-6	28	22
3	52	-54	0	45	40	-2	62	-57	-1	101	-98	-1	80	-79	-2	130	128	-3	103	103	1	21	19	3	52	-56	-4	59	-67
5	49	53	1	26	25	-1	394	-393	0	69	64	0	86	89	-1	25	-24	-2	75	76	3	51	-51	4	68	-65	-2	33	36
7	58	-57	3	32	-29	0	79	-74	1	75	75	1	85	82	0	48	-35	-1	109	104	5	34	32	6	28	21	0	25	20
8	72	-69	H=L= 0		10	1	141	150	3	91	-83	2	40	-38	1	35	33	0	96	-95	7	40	-37	7	21	-29	H=L= 4		4
9	30	-30	1	33	35	2	180	-167	H=L= 1		7	4	27	-30	3	42	-37	1	63	66	H=L= 3		4	H=L= 4		-5	-7	35	-28
H=L= 0		-6	2	47	44	3	50	52	-9	35	27	5	117	120	5	42	46	2	29	-20	-9	42	-41	-7	35	31	-6	54	55
1	165	168	H=L= 0		11	4	238	246	-8	51	49	7	45	-44	7	32	-28	3	211	-206	-7	37	32	-4	107	-115	-5	45	45
2	129	126	1	24	21	5	171	176	-5	34	38	9	40	38	H=L= 2		5	4	76	-81	-6	38	39	-3	54	53	-3	71	-67
3	95	92	2	24	19	7	106	-111	-4	50	52	H=L= 2		-3	-10	62	-57	8	35	-46	-5	23	-25	-2	32	29	2	58	52
4	22	18	H=L= 1		-12	8	28	-21	-3	67	72	-4	110	114	-9	44	-45	H=L= 3		-4	-3	29	-31	0	74	-68	3	65	65
5	27	-27	-1	47	46	9	54	49	-2	24	-21	-3	64	64	-7	37	43	-9	31	-28	-2	124	127	1	48	-46	4	24	24
6	26	21	0	26	29	H=L= 1		-1	-1	101	-105	-2	34	-45	-6	31	-29	-5	68	-71	-1	26	20	2	35	36	5	35	-32
7	92	-96	5	21	-20	-7	49	50	1	68	68	-1	340	-342	-4	88	85	-4	19	12	0	20	-19	3	100	102	H=L= 4		5
8	38	-43	6	27	-31	-5	29	23	2	45	41	0	183	-179	-3	66	57	-3	239	239	1	40	36	5	33	-30	-6	31	-23
H=L= 0		-5	H=L= 1		-11	-3	102	-96	H=L= 1		8	1	168	160	-2	88	-92	-2	163	158	2	36	38	6	32	-39	-3	70	-69
1	109	109	-2	23	7	-2	381	-410	-7	33	28	2	142	-139	0	64	69	-1	53	-60	4	46	-52	H=L= 4		-4	-2	109	-109
2	110	115	3	41	22	-1	38	-41	-6	52	-61	3	42	-46	1	106	103	0	100	92	5	34	-38	-9	30	-23	0	31	-27
4	72	64	4	32	36	0	102	98	-5	72	-71	4	173	157	2	37	-37	1	29	30	6	49	44	-8	21	-22	1	32	-40
5	82	84	H=L= 1		-10	1	66	58	-3	58	61	5	24	18	3	48	-47	2	24	29	H=L= 3		5	-7	35	30	4	34	30
8	34	40	-3	37	-37	2	219	-213	-2	51	60	7	56	-59	6	45	45	3	24	22	-10	26	-24	-6	39	42	5	24	13
9	43	41	1	38	-30	4	57	-55	H=L= 1		9	8	31	19	H=L= 2		6	4	29	-27	-4	21	-16	-5	77	75	H=L= 4		6
H=L= 0		-4	2	31	-32	5	110	109	-9	31	-29	H=L= 2		-2	-10	30	-24	5	44	34	-3	57	57	-4	71	74	-9	26	26
1	174	-174	4	31	30	6	91	81	-7	22	21	-9	20	-10	-9	57	-50	6	36	41	-2	59	-58	-3	99	-102	-8	25	23
2	210	-200	5	32	-11	7	44	40	-6	41	33	-7	51	47	-5	44	-42	7	22	17	0	30	-28	-2	103	-101	-3	31	41
3	87	-82	6	36	-44	8	56	-56	-1	30	-33	-6	58	55	-3	32	32	9	21	12	2	32	39	-1	57	-54	-2	41	42
5	43	43	7	51	-51	9	28	-27	0	76	-80	-5	91	-90	-1	175	-180	H=L= 3		-3	5	33	-41	0	35	37	1	29	-19
6	124	118	H=L= 1		-9	H=L= 1		0	H=L= 1		10	-4	81	77	0	93	-96	-9	40	-42	6	31	-19	1	43	-46	2	45	-44
7	76	77	-4	25	27	-10	28	-25	-8	33	-25	-3	60	66	1	32	33	-8	34	-36	H=L= 3		6	2	109	115	H=L= 4		7
8	82	-87	-2	45	-40	-8	52	53	-6	47	53	-2	281	-273	2	67	66	-7	36	24	-10	39	32	3	99	107	-4	82	86
9	44	-41	0	60	70	-7	34	32	-5	37	39	-1	60	61	4	37	-35	-5	63	-58	-4	50	-52	4	29	-29	-2	37	-30
H=L= 0		-3	1	78	79	-6	34	-41	-1	29	-25	0	202	195	H=L= 2		7	-4	70	-72	-2	97	97	1	29	25	0	29	29
1	236	-239	4	38	45	-4	275	279	0	21	-13	1	165	159	-9	26	23	-3	101	-112	-1	65	73	H=L= 4		-3	H=L= 4		8
2	37	35	5	36	38	-3	24	35	H=L= 1		11	2	56	55	-5	34	-28	-2	126	-141	1	25	-27	-9	22	20	-6	39	-36
4	27	25	6	37	-33	-1	237	-251	-6	22	-11	3	267	-260	-2	58	61	1	47	46	2	27	23	-8	27	-18	-5	29	-29
5	83	-83	7	57	-53	0	54	-49	-3	20	-11	4	213	-211	-1	41	31	2	111	109	H=L= 3		7	-7	45	-46	-3	43	41
6	72	67	9	28	21	1	110	-105	-1	41	44	5	48	-49	0	56	-53	4	46	-46	-9	22	20	-5	27	26	H=L= 4		9
7	93	92	H=L= 1		-8	3	126	-121	1	26	-27	6	83	79	1	57	-56	5	49	-48	-7	38	-33	-4	33	-32	-5	25	-30
8	72	77	-2	33	-33	4	29	-30	H=L= 2		-12	7	33	-26	4	23	-24	6	43	46	-4	38	-47	-3	46	-48	-4	23	-25
9	58	-53	-1	35	-36	5	49	45	2	27	-24	8	54	-58	H=L= 2		8	7	42	49	-3	52	-53	-2	169	166	-3	32	28
H=L= 0		-2	1	65	62	6	67	67	4	52	46	H=L= 2		-1	-4	37	-33	8	22	-19	-2	38	44	0	63	-66	-2	51	46
1	243	-230	3	56	-58	8	40	38	6	32	-28	-9	32	-31	-2	73	73	9	46	-41	-1	59	58	1	27	-30	H=L= 5		-12
2	172	-165	4	36	35	H=L= 1		1	H=L= 2		-11	-6	39	-40	-1	41	43	H=L= 3		-2	2	25	-12	2	100	-97	0	62	61
4	41	35	5	80	82	-7	22	29	-3	33	33	-5	25	22	H=L= 2		9	-9	30	33	3	25	16	4	35	30	1	25	17
6	45	-47	6	112	123	-6	42	38	-2	24	-23	-4	48	-52	-8	39	-44	-6	20	19	4	31	29	5	43	-45	3	38	-43
8	31	29	7	55	65	-5	68	-68	-1	40	-42	-3	157	154	-7	30	-30	-5	23	-13	H=L= 3		8	7	20	-8	4	28	-23
9	68	67	8	33	-35	-3	168	174	4	34	12	-2	254	273	-6	31	31	-4	149	-148	-3	35	-31	H=L= 4		-2	H=L= 5		-11
H=L= 0		-1	H=L= 1		-7	-2	257	253	5	79	72	-1	289	314	0	39	37	-3	86	-92	-2	117	-121	-9	29	35	0	20	-5
1	110	-98	-1	68	-63	-1	232	-228	6	37	35	0	96	-92	1	24	18	-2	55	55	-1	65	-64	-7	35	-35	1	44	44
2	84	-89	0	84	-75	0	375	-364	7	24	-29	1	227	229	H=L= 2		10	-1	68	70	H=L= 3		9	-5	28	29	3	27	-25
3	131	-130	1	110	-110	1	185	187	H=L= 2		-10	2	182	185	-6	41	-37	0	68	-71	-8	26	23	-4	96	98	5	51	51
4	50	51	3	45	-55	2	38	-32	2	31	-17	4	110	-99	-1	24	24	1	38	-39	0	22	-19	-3	85	87	6	27	-18
5	65	-69	4	104	-105	4	47	-43	3	60	-64	5	43	-42	H=L= 3		-11	2	135	126	H=L= 3		10	-1	101	100	H=L= 5		-10
6	210	-209	5	47	44	5	59	-60	7	20	13	7	115	120	-2	22	32	3	63	-61	-3	27	28	0	19	25	-4	24	20
7	24	-22	6	61	67	6	44	47	H=L= 2		-9	9	20	-2	1	32	30	4	58	-56	-2	24	18	1	62	-54	-3	30	28
8	29	-19	9	20	11	8	65	-66	-4	37	37	H=L= 2		0	4	69	-72	5	61	-61	H=L= 4		-13	2	26	-29	-1	47	-50
H=L= 0		0	H=L= 1		-6	H=L= 1		2	-3	49	54	-9	36	-34	H=L= 3		-10	6	27	-22	2	41	40	4	72	73	4	62	65
1	242	255	-7	33	29	-7	32	35	3	58	-56	-8	53	-57	-3	45	-48	7	32	21	H=L= 4		-12	5	77	88	6	23	19
2	113	-121	-3	83	78	-6	64	61	4	68	-70	-7	42	-41	-2	24	21	H=L= 3		-1	1	23	-23	8	22	23	H=L= 5		-9
3	138	-142	-2	67	67	-5	56	-60	6	44	55	-6	23	-16	-1	36	30	-6	48	43	3	30	27	H=L= 6		-1	-5	42	-35
4	21	-21	0	83	-77	-4	121	-119	8	22	-24	-5	59	-55	0	40	49	-5	96	91	4	58	57	-10	25	-20	-2	34	-23
7	24	-26	1	57	52	-3	86	89	H=L= 2		-8	-4	20	-20	2	51	51	-4	73	-75	H=L= 4		-11	-6	29	-27	-1	47	-50
8	48	47	3	25	-28	-1	560	609	-4	69	-64	-3	120	119	3	49	47	-3	23	9	-3	28	-29	-4	52	57	1	29	29
H=L= 0		1	4	21	-15	0	75	64	-3	43	42	-2	36	-28	4	31	-30	-2	19	24	-2	24	-16	-2	58	-65	2	38	34
0	141	-133	5	119	-121	4	43	-41	-2	77	77	-1	269	-278	5	79	-90	-1	39	-35	1	27	-16	-1	136	-139	3	114	-124
1	283	273	6	25	-24	7	33	39	-1	24	22	0	87	-88	6	34	38	0	111	102	2	22	-22	0	50	-53	4	52	-56
2	82	78	7	54	49	H=L= 1		3	0	85	-83	1	201	-202	7	41	41	1	54	-53	4	71	-76	1	26	-23	H=L= 5		-8
3	22	-25	8	47	42	-9	83	-83	1	35	-36	2	45	50	H=L= 3		-9	3	186	187	6	26	21	2	116	-116	-6	23	19
4	68	-63	H=L= 1		-5	-8	47	-45	2	92	95	3	91	90	0	39	-40	5	30	-20	7	30	22	3	22	-27	-5	28	21
5	113	113	-6	46	49	-7	59	-56	3	30	25	4	75	78	1	33	-34	6	60	-60	H=L= 4		-10	4	63	66	-4	24	-23
7	34	-37	-5	27	25	-6	28	26	4	61	-63	8	34	31	3	63	64	H=L= 3		0	-4	42	41	5	92	93	-3	44	41
9	28	22	-4	45	-43	-4	37	32	5	37	-37	H=L= 2		1	4	78	88	-6	21	-26	1	41	-33	7	20	-14	-2	36	26
H=L= 0		2	-3	62	-67	-2	71	-61	6	38	-35	-6	66	67	5	77	90	-4	24	22	2	42	-47	H=L= 4		0	-1	37	-43
0	243	-230	-1	144	132	-1	92	-83	8	34	-40	-5	24	-25	8	30	29	-3	151	-156	4	68	68	-6	74	-74	0	46	-63
1	40	36	0	32	31	0	252	247	9	28	-20	-4	127	-123	H=L= 3		-8	-2	97	-94	7	20	-21	-5	33	-32	2	106	109
2	62	-58	1	117	-114	1	62	63	H=L= 2		-7	-3	33	-32	-5	24	22	0	121	118	H=L= 4		-9	-4	105	104	3	72	87
3	98	89	3	22	-23	2	31	-30	-3	31	-36	-2	98	96	-4	46	-44	1	73	74	-5	41	-36	-3	53	57	4	106	-116
4	38	34	4	39	45	3	125	-116	-2	64	61	-1	45	-30	-3	31	-29	2	67	-70	-4	37	35	-2	57	-58	7	43	39
5	36	33	5	22	-15	5	58	-54	-1	71	72	0	131	-127	-2	27	-25	3	31	-36	0	47	58	-1	95	-98	H=L= 5		-7
6	21	27	6	50	-44	7	73	70	0	108	110	1	147	-148	-1	31	-27	4	82	84	1	39	30	1	113	110	-4	28	-23
7	29	-32	H=L= 1		-4	8	48	43	1	22	-17	3	23	-13	0	51	-54	5	63	62	2	54	-54	2	76	-71	-3	27	-23
8	49	-48	-7	38	-36	H=L= 1		4	2	59	66	4	36	36	1	61	-61	6	75	-84	3	73	-79	3	122	-126	-2	73	82
H=L= 0		3	-5	71	70	-7	67	-66	3	82	75	6	29	-31	2	93	-93	7	32	-81	4	62	61	4	87	-88	0	43	-43
0	112	113	-4	97	-87	-6	48	-50	5	67	-72	H=L= 2		2	3	48	45	8	25	25	6	44	-52	5	47	-50	3	42	56
1	96	98	-3	54	-49	-5	53	56	6	103	-108	-7	20	-12	4	35	32	H=L= 3		1	7	39	-46	H=L= 4		1	4	53	54
2	91	91	-2	28	-26	-4	25	-28	8	42	42	-5	159	159	6	52	-53	-9	21	19	H=L= 4		-8	-10	42	-38	5	22	-18
3	48	-50	-1	40	42	-3	96	-92	H=L= 2		-6	-4	56	56	8	19	7	-5	50	44	-5	23	20	-8	38	37	H=L= 5		-6
5	36	35	0	238	226	-2	40	29	-5	39	39	-3	89	-92	9	21	9	-4	153	154	-4	30	-27	-7	29	20	-6	43	43
6	45	45	2	27	31	-1	96	95	-3	83	-85	-2	277	-283	H=L= 3		-7	-2	72	-76	-1	38	37	-6	45	42	-5	58	-65

Table 7. (continued)

K	FO	FC	K	FO	FC	K	FO	FC	K	FO	FC	K	FO	FC	K	FO	FC	K	FO	FC	K	FO	FC	K	FO	FC
-4	43	-36	-7	41	37	-4	67	-67	H,L=	5	8	2	53	62	3	91	94	H,L=	6	4	-2	43	44	1	40	41	H,L=	8	-5
-2	78	77	-4	32	35	-1	27	-31	-4	22	-21	3	98	-101	5	49	-50	-5	59	-59	0	70	-77	2	29	20	-4	34	-33
-1	51	45	-3	69	65	0	119	-113	-3	28	23	5	19	-14	H,L=	6	-1	-4	59	-65	1	79	-77	H,L=	7	1	-3	54	-56
1	126	-131	-2	24	-22	1	102	-103	H,L=	6	-11	H,L=	6	-5	-8	37	-29	-1	28	-29	3	37	40	-6	43	-41	-1	61	58
2	52	-54	-1	34	31	2	35	30	-2	26	26	-7	26	-24	-6	49	42	H,L=	6	5	H,L=	7	-4	-5	31	-36	0	55	56
H,L=	5	-5	0	26	21	3	66	68	-1	30	-29	-6	26	-33	-4	44	-41	-7	27	26	-7	42	42	-1	31	-38	H,L=	8	-4
-8	28	-25	1	126	133	4	53	57	0	41	-39	-3	58	61	-2	76	70	-3	28	18	-2	52	66	0	26	-32	-5	30	29
-7	27	-22	2	64	70	H,L=	5	2	2	37	34	0	35	35	-1	35	40	0	29	-26	0	44	-49	H,L=	7	2	-3	41	-44
-5	137	149	3	64	-63	-5	64	63	3	25	29	1	70	66	0	57	-62	H,L=	6	6	1	32	-27	-7	35	38	-2	80	-86
-4	43	44	6	27	-23	-4	30	-22	H,L=	6	-10	3	46	47	1	87	-90	-6	35	35	2	92	-89	-6	34	35	H,L=	8	-3
-3	95	-102	H,L=	5	-1	-3	64	-62	-2	22	16	H,L=	6	-4	2	35	-27	-5	23	22	3	29	-30	-5	19	5	-3	26	-28
-2	72	-78	-9	32	-30	1	73	-67	-1	27	23	-7	34	33	4	47	-42	-4	28	-29	H,L=	7	-3	-4	35	-30	-2	32	-30
-1	82	79	-6	45	-44	2	62	-65	4	26	-32	-6	71	-75	5	23	-17	-2	37	36	-7	33	-38	-2	34	27	-1	19	-20
0	23	21	-5	66	-60	H,L=	5	3	5	20	-10	-5	105	-109	H,L=	6	0	H,L=	7	-10	-6	48	49	2	24	16	H,L=	8	-2
2	24	-18	-3	81	82	-9	31	29	H,L=	6	-9	-3	73	73	-6	39	40	-2	22	-16	-5	36	35	H,L=	7	3	-3	28	29
3	70	71	-2	20	-16	-5	34	40	-2	24	22	1	32	33	-5	40	43	-1	45	37	-4	34	30	-7	27	24	0	24	20
H,L=	5	-4	-1	116	-119	-4	61	58	-1	33	-38	2	30	19	-2	84	81	1	24	-25	-2	46	53	-6	42	40	2	67	-66
-6	43	-48	0	25	22	H,L=	5	4	0	51	-47	3	64	-64	-1	70	74	H,L=	7	-9	-1	59	64	-4	24	-17	H,L=	8	-1
-4	27	26	1	64	67	-5	32	32	2	38	42	4	33	-25	0	40	40	0	48	46	0	27	18	-3	23	13	-3	38	39
-3	38	-49	2	113	118	-4	32	38	5	36	-34	5	39	43	2	40	-49	1	25	28	1	51	-53	-2	34	33	1	36	36
-2	73	-72	4	77	-76	0	27	24	H,L=	6	-8	H,L=	6	-3	4	42	36	4	29	35	2	68	69	0	24	-16	2	22	27
-1	78	-77	5	63	-59	H,L=	5	5	-5	34	31	-7	41	39	H,L=	6	1	H,L=	7	-8	3	57	61	H,L=	7	4	H,L=	8	0
0	34	31	6	22	21	-6	50	-43	0	39	-48	-6	73	73	-8	25	-23	-5	25	-21	H,L=	7	-2	-1	27	19	-3	30	29
1	34	42	H,L=	5	0	-5	46	-50	1	49	-47	-5	32	-32	-7	48	-51	-2	20	-16	-7	53	-54	0	27	-17	-2	37	40
2	49	-47	-8	20	-7	-3	69	70	3	92	95	-4	54	-71	-4	43	38	-1	35	42	-6	48	-49	H,L=	7	5	0	43	-42
3	33	-32	-7	34	25	-2	35	37	H,L=	6	-7	-3	23	-17	-2	55	-60	0	48	45	-1	86	86	-4	22	-18	1	36	-30
4	27	28	-6	40	38	0	33	31	-6	23	-27	-2	54	54	-1	29	30	H,L=	7	-7	2	44	-41	-3	25	-22	H,L=	8	1
6	20	-15	-5	32	-23	1	31	26	-5	27	-26	-1	52	-51	0	54	48	-4	22	28	H,L=	7	-1	H,L=	8	-9	-2	39	39
H,L=	5	-3	-4	69	-67	2	30	-28	-1	69	69	0	39	-30	H,L=	6	2	-2	63	-72	-8	19	10	-1	28	-23	H,L=	8	2
-9	22	19	-2	97	96	3	30	-28	1	36	-43	2	69	69	-7	35	-32	-1	57	-65	-7	24	21	H,L=	8	-8	-4	47	-49
-8	30	28	-1	22	13	H,L=	5	6	2	135	-148	5	22	19	-6	46	-43	1	56	62	-5	33	-26	-2	34	32	-3	35	-27
-5	64	-67	0	124	-122	-5	31	-36	4	58	61	6	54	51	-4	59	55	3	26	-29	0	35	37	0	32	-36	-1	38	40
-4	34	35	1	19	-22	-1	27	-21	5	21	-22	H,L=	6	-2	-3	44	42	H,L=	7	-6	2	48	-46	H,L=	8	-7			
-3	46	49	2	70	68	1	32	33	6	47	-49	-5	45	42	1	34	10	-6	31	28	4	33	35	-3	27	28			
-1	19	-20	3	47	23	2	44	41	H,L=	6	-6	-3	29	-32	H,L=	6	3	-3	43	43	H,L=	7	0	-2	24	17			
2	30	-33	6	39	34	H,L=	5	7	-7	26	-19	-2	77	-81	-8	33	23	-1	102	-106	-8	27	21	0	22	-20			
3	100	-97	7	22	19	-5	20	-8	-4	67	68	-1	64	-62	-7	21	18	0	56	-58	-7	22	-22	H,L=	8	-6			
4	47	-50	H,L=	5	1	-4	27	-26	-2	41	-49	0	83	-85	-5	32	-26	1	31	15	-3	46	-48	-4	24	-29			
H,L=	5	-2	-7	47	45	-3	43	-43	0	37	39	1	38	-40	1	51	57	2	132	127	-2	62	-63	-2	82	81			
-8	30	30	-6	52	54	0	35	-32	1	41	43	2	59	64	2	35	36	H,L=	7	-5	0	43	38	-1	66	59			

TABLE 8. INTERATOMIC DISTANCES ALONG WITH THEIR ESTIMATED STANDARD DEVIATIONS

Atoms	Distance (Å)	σ (Å)	Atoms	Distance (Å)	σ (Å)
Al-O(1)	1.770	0.006	O(1)-C(3)	1.330	0.009
Al-O(2)	1.826	0.006	C(3)-C(4)	1.490	0.011
Al-C(1)	1.962	0.012	C(3)-N(1)	1.263	0.011
Al-C(2)	1.962	0.011	N(1)-C(10)	1.419	0.011
O(2)-N(2)	1.402	0.009	N(2)-C(17)	1.499	0.013
N(2)-C(16)	1.474	0.014	N(2)-C(18)	1.477	0.014
C(4)-C(5)	1.383	0.011	C(10)-C(11)	1.391	0.012
C(5)-C(6)	1.390	0.013	C(11)-C(12)	1.382	0.013
C(6)-C(7)	1.372	0.015	C(12)-C(13)	1.378	0.014
C(7)-C(8)	1.393	0.016	C(13)-C(14)	1.380	0.014
C(8)-C(9)	1.379	0.016	C(14)-C(15)	1.371	0.013
C(4)-C(9)	1.379	0.013	C(10)-C(15)	1.378	0.012
C(1)-H(1)	1.08	0.08	C(17)-H(20)	1.15	0.08
C(1)-H(2)	1.07	0.08	C(17)-H(21)	1.10	0.09
C(1)-H(3)	1.13	0.09	C(17)-H(22)	1.08	0.08
C(2)-H(4)	1.00	0.08	C(18)-H(23)	1.11	0.08
C(2)-H(5)	1.07	0.08	C(18)-H(24)	1.09	0.09
C(2)-H(6)	1.07	0.08	C(18)-H(25)	1.14	0.08
C(16)-H(17)	1.13	0.08			
C(16)-H(18)	1.15	0.08			
C(16)-H(19)	1.06	0.08			
C(5)-H(7)	1.10	0.08	C(11)-H(12)	1.11	0.08
C(6)-H(8)	1.09	0.08	C(12)-H(13)	1.09	0.08
C(7)-H(9)	1.08	0.08	C(13)-H(14)	1.09	0.08
C(8)-H(10)	1.09	0.09	C(14)-H(15)	1.09	0.08
C(9)-H(11)	1.09	0.08	C(15)-H(16)	1.10	0.08

geometry. The C(1)-Al-C(2) bond angle (117.3(0.5)°) is equal to that of the polymerization catalyst [$Me_2Al\cdot O\cdot CPh{:}NPh]_2$ (117.6(0.5)°), but it shows a large deviation from the typical tetrahedral bond angle of 109.5°. Such a rather large bond angle of C(methyl)-Al-C(methyl) is often found associated with tetrahedrally co-ordinated aluminum atoms in some organoaluminum compounds.[19-22]

The interatomic bond distances between the aluminum atom and the oxygen of the amide moiety, Al-O(1), is 1.770(6) Å, which is a little shorter than the corresponding distances of the related complexes: 1.805(6) Å in [$Me_2Al\cdot O\cdot CPh{:}NPh]_2$, 2.045(7) Å in [$Me_2Al\cdot O\cdot CPh{:}NPh$,MeCHO]$_2$, and 1.846(7) Å in [$Me_2Al\cdot O\cdot CPh{:}NPh$,MeCHO,$AlMe_3$]. The O(1)-C(3) bond distance of 1.330(9) Å is intermediate between typical single and double bond distances. The C(3)-N(1) distance is 1.263(11) Å. The carbon and nitrogen double bond distance has been given as 1.265 Å by Pauling[23] and as 1.28 Å by Cox and his co-workers.[24] The C-N bond in oximes, >C=N-OH, is generally assumed to be a localized double bond, the distance of which lies between 1.225 and 1.33 Å.[25] From these facts, it can be concluded that the C(3)-N(1) in the present complex is an almost-localized double bond. Five atoms, O(1), C(3), N(1), C(4), and C(10), are co-planar within a deviation of 0.01 Å. The most interesting feature is that, unlike those in [$Me_2Al\cdot O\cdot CPh{:}NPh$, MeCHO]$_2$ and [$Me_2Al\cdot O\cdot CPh{:}NPh$,MeCHO,$AlMe_3$], the two adjacent benzene rings take the more stable, *trans* configuration about the C(3)-N(1) bond, the internal rotation angle being 178.9°. The dihedral angle between the best plane

19) R. G. Vranka and E. L. Amma, *J. Amer. Chem. Soc.*, **89**, 3121 (1967).
20) J. L. Atwood and G. D. Stucky, *ibid.*, **91**, 2538 (1969).
21) V. R. Magnuson and G. D. Stucky, *ibid.*, **91**, 2544 (1969).
22) J. L. Atwood and G. D. Stucky, *ibid.*, **92**, 285 (1970).
23) L. Pauling, "The Nature of the Chemical Bond", Cornell University Press, Ithaca, (1948), p. 164.
24) E. G. Cox and G. A. Jeffrey, *Proc. Roy. Soc., Ser. A*, **207**, 110 (1951).
25) W. C. Hamilton, *Acta Crystallogr.*, **14**, 95 (1961).

TABLE 9. INTERATOMIC ANGLES ALONG WITH THEIR ESTIMATED STANDARD DEVIATIONS

Atoms	Angle(°)	σ(°)	Atoms	Angle(°)	σ(°)
O(1)-Al-C(1)	109.0	0.4	Al-O(2)-N(2)	128.3	0.5
O(1)-Al-C(2)	109.2	0.4	O(2)-N(2)-C(16)	108.8	0.7
O(1)-Al-O(2)	106.7	0.3	O(2)-N(2)-C(17)	105.1	0.7
C(1)-Al-C(2)	117.3	0.5	O(2)-N(2)-C(18)	112.0	0.7
C(1)-Al-O(2)	111.8	0.4	C(16)-N(2)-C(17)	108.8	0.8
C(2)-Al-O(2)	102.2	0.4	C(16)-N(2)-C(18)	111.8	0.8
Al-O(1)-C(3)	137.7	0.5	C(17)-N(2)-C(18)	110.1	0.8
O(1)-C(3)-C(4)	116.3	0.7	C(3)-N(1)-C(10)	120.7	0.7
O(1)-C(3)-N(1)	123.9	0.7			
N(1)-C(3)-C(4)	119.8	0.7			
C(3)-C(4)-C(5)	119.9	0.7	N(1)-C(10)-C(11)	120.4	0.8
C(3)-C(4)-C(9)	120.4	0.7	N(1)-C(10)-C(15)	120.4	0.8
C(9)-C(4)-C(5)	119.7	0.8	C(11)-C(10)-C(15)	118.9	0.8
C(4)-C(5)-C(6)	119.9	0.8	C(10)-C(11)-C(12)	118.8	0.8
C(5)-C(6)-C(7)	120.4	0.9	C(11)-C(12)-C(13)	122.4	0.9
C(6)-C(7)-C(8)	119.5	1.0	C(12)-C(13)-C(14)	117.8	0.9
C(7)-C(8)-C(9)	120.1	1.1	C(13)-C(14)-C(15)	120.7	0.9
C(8)-C(9)-C(4)	120.4	1.0	C(14)-C(15)-C(10)	121.3	0.8
Al-C(1)-H(1)	111	4	Al-C(2)-H(4)	106	5
Al-C(1)-H(2)	111	5	Al-C(2)-H(5)	112	5
Al-C(1)-H(3)	111	4	Al-C(2)-H(6)	112	5
H(1)-C(1)-H(2)	107	6	H(4)-C(2)-H(5)	110	6
H(1)-C(1)-H(3)	108	6	H(4)-C(2)-H(6)	110	6
H(2)-C(1)-H(3)	108	6	H(5)-C(2)-H(6)	107	6
N(2)-C(16)-H(17)	107	4	N(2)-C(17)-H(20)	115	4
N(2)-C(16)-H(18)	120	4	N(2)-C(17)-H(21)	108	4
N(2)-C(16)-H(19)	109	5	N(2)-C(17)-H(22)	110	5
H(17)-C(16)-H(18)	106	6	H(20)-C(17)-H(21)	108	6
H(17)-C(16)-H(19)	106	6	H(20)-C(17)-H(22)	109	6
H(18)-C(16)-H(19)	108	6	H(21)-C(17)-H(22)	107	6
N(2)-C(18)-H(23)	104	4			
N(2)-C(18)-H(24)	104	5			
N(2)-C(18)-H(25)	123	4			
H(23)-C(18)-H(24)	108	6			
H(23)-C(18)-H(25)	100	6			
H(24)-C(18)-H(25)	117	6			
C(4)-C(5)-H(7)	120	4	C(10)-C(11)-H(12)	120	4
C(6)-C(5)-H(7)	120	4	C(12)-C(11)-H(12)	121	4
C(5)-C(6)-H(8)	120	4	C(11)-C(12)-H(13)	119	4
C(7)-C(6)-H(8)	120	4	C(13)-C(12)-H(13)	119	4
C(6)-C(7)-H(9)	120	4	C(12)-C(13)-H(14)	122	4
C(8)-C(7)-H(9)	121	4	C(14)-C(13)-H(14)	120	4
C(7)-C(8)-H(10)	121	5	C(13)-C(14)-H(15)	119	4
C(9)-C(8)-H(10)	119	5	C(15)-C(14)-H(15)	120	4
C(8)-C(9)-H(11)	119	4	C(14)-C(15)-H(16)	120	4
C(4)-C(9)-H(11)	120	4	C(10)-C(15)-H(16)	119	4

of the two benzene rings is 80.5°. The average values of the C-C and C-H distances in benzene rings are 1.381 and 1.09 Å respectively.

The $ONMe_3$ moiety is attached to the aluminum atom by the co-ordination of the oxygen atom. The Al-O(2) bond distance, 1.826(6) Å, takes a reasonable value compared with those found in the related organoaluminum compounds.[1-4] The crystal structure of $[Me_3NO,HCl]$ was determined by Rérat[26] and had since been refined by Caron and his co-workers[27] in the course of the crystal structure analysis of $ONMe_3$.[28] The corresponding bond distances and angles in these complexes are compared with those in the $ONMe_3$ moiety of the present complex (Table 10). The O(2)-N(2) bond distance (1.402(9) Å) is intermediate between those in $[Me_3N^+-O^-]$ and $[Me_3N^+OH\cdot Cl^-]$.

26) P. C. Rérat, *Acta Crystallogr.*, **13**, 63 (1960).
27) A. Caron and J. Donohue, *ibid.*, **15**, 1052 (1962).
28) A. Caron, G. J. Palenik, E. Goldish, and J. Donohue, *ibid.*, **17**, 102 (1964).

Caron and his co-workers considered that the opposite formal charge affects the O–N bond distance in the structure of $ONMe_3$. According to this theory, the negative formal charge on the oxygen atom of the $ONMe_3$ moiety in the present complex may be weakened by the co-ordination to the electron-deficient aluminum atom. The aluminum atom is not so strong a Lewis acid as the proton; however, it may be that the co-ordination of oxygen does not completely cancel the charge on the oxygen atom, as in the case of the proton in [$Me_3N^+OH\cdot Cl^-$]. This can reasonably explain the fact that the O(2)–N(2) distance lies between the corresponding distances in [$Me_3N^+–O^-$] and [Me_3N^+-$OH\cdot Cl^-$]. The average values of the two C–N bond distances are 1.478 ± 0.011 Å in [$Me_3N^+OH\cdot Cl^-$] and 1.477 ± 0.006 Å in [$Me_3N^+–O^-$]. The N(2)–C(16) and N(2)–C(18) bond distances have values equal to those found in the above two compounds. The N(2)–C(17) bond is slightly longer than the other N(2)–C bonds, though the difference is not very significant. The geometry around the N(2) atom is a little distorted tetrahedron. Such a geometry around the nitrogen atom is also found in [$Me_3N^+–O^-$].

Table 10. Comparison of the interatomic distances and angles in the $ONMe_3$ groups

Atoms	[Me_3N^+-OH, Cl^-][a] (Ref. 26)	[$Me_3N^+–O^-$][a] (Ref. 27)	Me_3NO moiety in the present complex	
N–O	1.425 Å (11)	1.388 Å (5)	1.402 Å (9)	
N–C(1)	1.475 (10)	1.470 (8)	1.474 (14)	N(2)–C(16)
	1.480 (11)	1.484 (4)	1.499 (13)	N(2)–C(17)
			1.477 (14)	N(2)–C(18)
O–N–C(1)	103.9° (1.1)	110.4° (0.6)	108.8° (0.7)	O(2)–N(2)–C(16)
O–N–C(2)	109.1 (1.3)	109.6 (0.4)	105.1 (0.7)	O(2)–N(2)–C(17)
C(1)–N–C(2)	111.0 (1.5)	109.2 (0.7)	112.0 (0.7)	O(2)–N(2)–C(18)
C(2)–N–C(2′)	112.3 (1.4)	108.9 (0.4)	108.8 (0.8)	C(16)–N(2)–C(17)
			111.8 (0.8)	C(16)–N(2)–C(18)
			110.1 (0.8)	C(17)–N(2)–C(18)

a) The crystal structure of these compounds has a mirror symmetry and only two carbon atoms of three methyl carbons are independent.

The molecular structures of the polymerization catalyst I and of the present complex IV are compared in Fig. 3 and Table 11. In Fig. 3 both molecules are projected onto the O–C–N plane of the amide moiety, which is present in both compounds. The amide moiety is connected to the electron-deficient aluminum atom by both oxygen and nitrogen atoms in I, but only by oxygen in IV. The nitrogen atom in IV is, therefore, liberated from bonding to the aluminum. The C(3)–N(1) bond distance in IV is a little shorter than that in I. The C(3)–O(1) distance in IV is,

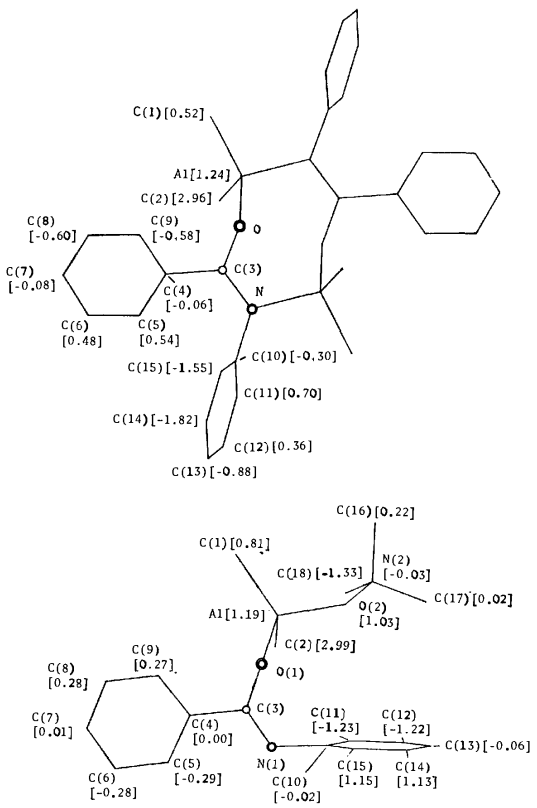

Fig. 3. Comparison of the molecular structure of [$Me_2Al\cdot O\cdot CPh{:}\ NPh]_2$ (*top*) and [$Me_2Al\cdot O\cdot CPh{:}$ NPh, $ONMe_3$] (*bottom*). Both are projected onto the plane of the –O–C–N– skeletons which are contained commonly in both molecules. Deviations from the plane (in Å) are given in brackets.

Table 11. Comparison of the selected interatomic distances and angles and dihedral angles between some planes[a] in the amide moieties of complexes (I) and (IV)

	(I)	(IV)
Al–O(1)	1.805(6) Å	1.770(6) Å
O(1)–C(3)	1.277(10)	1.330(9)
C(3)–N(1)	1.305(11)	1.263(11)
C(3)–C(4)	1.501(12)	1.490(11)
N(1)–C(10)	1.447(12)	1.419(11)
Al–O(1)–C(3)	133.6(0.6)°	137.7(0.5)°
Plane 1–Plane 2	2.9°	0.03°
Plane 1–Plane 3	14.3	1.0
Plane 1–Plane 4	27.6	13.5
Plane 1–Plane 5	75.5	86.2
Plane 2–Plane 3	11.4	1.1
Plane 4–Plane 5	70.3	80.5

a) These planes are consisted of the atoms of;
Plane 1; O(1), C(3), N(1)
Plane 2; N(1), C(3), C(4)
Plane 3; C(3), N(1), C(10)
Plane 4; Least-squares plane of benzene ring (C(4)-C(9))
Plane 5; Least-squares plane of benzene ring (C(10)-C(15))

on the contrary, a little longer than that in I. Such differences in the C–N and C–O bond distances are probably due to the difference in C–N bond character: that is, there a delocalized double bond in I, but an

almost localized double bond in IV. The most remarkable configurational difference in the amide moieties is that the two benzene rings are *cis* in I, but *trans* in IV.

The isolation of the present complex [$Me_2Al\cdot O\cdot CPh$: NPh,$ONMe_3$] in a stable crystalline form and its molecular structure throw some interesting aspects on the chemical reactions of this catalytic system. One is concerned with the reaction from I to IV, the reaction which has been formulated before. When the dimeric complex of I is treated with a strong Lewis base, $ONMe_3$, an nucleophilic attack of the oxygen of $ONMe_3$ on the aluminum occurs. This promotes the cleavage of the Al–N bond, but not that of the Al–O bond. After the bond fission, the benzene ring attached to the nitrogen atom takes the more stable *trans* configuration. This is schematically shown below.

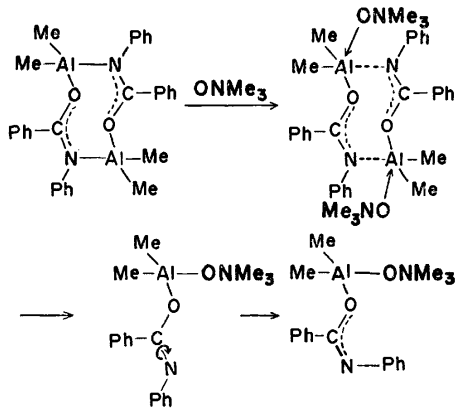

The second is related to the co-ordination scheme in the molecular structure of [$Me_2Al\cdot O\cdot CPh$: NPh]$_2$. The reaction of trialkylaluminum, R^1_3Al, and related compounds with isocyanate, R^2NCO, has been reported;[29,30] the products of this reaction gave *N*-substituted acid amides, R^1CONHR^2, on hydrolysis. Two intermediate compounds have been proposed in this reaction, depending on whether the insertion of isocyanate to an R^1–Al bond occurs by means of the C=N or C=O bond. In the insertion of isocyanate into the Et–Al bond,[31] the reaction products have been proposed to have the eight-membered ring structures of (iii) and (iv), which correspond to the dimeric structures of (i) and (ii) respectively.

Jennings and his co-workers studied the reaction

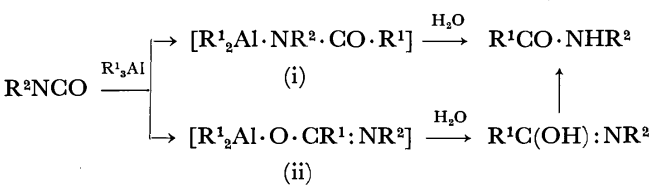

between trialkylaluminum and various *N*-substituted acid amides,[32] and they proposed that the reaction products had eight-membered ring structures like (iii) and (iv). We recently determined the molecular structure of [$Me_2Al\cdot O\cdot CPh$: NPh]$_2$.[1,2] The molecule has a centrosymmetrical eight-membered ring structure, and the bond distances show the molecule to have a hybrid structure of the two canonical forms, (iii) and (iv). On the other hand, the molecular structure of the present complex, [$Me_2Al\cdot O\cdot CPh$: NPh,$ONMe_3$], shows that the Al–O bond is more stable than the Al–N bond towards attack by a strong Lewis base on the aluminum atom. In other words, this result shows that the Al–N bond has much more of a co-ordination-bond character than the Al–O bond. On the basis of this fact, we can assume that the canonical form, (iv), is predominant in the dimeric structure of [$R_2Al\cdot O\cdot CR'$: $NR'']_2$.

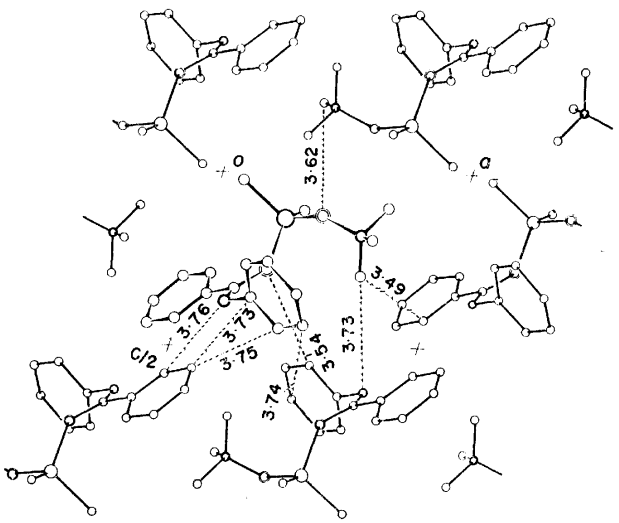

Fig. 4. Crystal structure viewed along the *b* axis.

Crystal Structure. Figure 4 shows the molecular packing projected along the *b* axis. The intermolecular atomic contacts less than 3.8 Å are shown by broken lines. None of them is significantly shorter than the normal van der Waals' contact.

The authors wish to express their deep thanks to Professor Hisaya Tani and Dr. Hajime Yasuda of Osaka University for their kindness in supplying the sample and for their helpful discussions.

29) H. Reinheckel and D. Jahnke, *Chem. Ber.*, **97**, 2661 (1964).
30) H. Reinheckel, D. Jahnke, and G. Kretzschmar, *ibid.*, **99**, 11 (1966).
31) J. R. Horder and M. F. Lappert, *J. Chem. Soc., A*, **1968**, 2004.
32) J. R. Jennings, K. Wade, and B. K. Wyatt, *ibid.*, **1968**, 2535.

The Crystal Structure of the Polymerization Catalyst of Acetaldehyde and Its Derivatives. III. The Crystal and Molecular Structure of the Bis(dimethylaluminum *N*-Phenylbenzimidate-Acetaldehyde) Complex, $[(CH_3)_2Al\cdot O\cdot C(C_6H_5):N(C_6H_5), CH_3CHO]_2$

Yasushi KAI, Noritake YASUOKA, Nobutami KASAI, and Masao KAKUDO*

Department of Applied Chemistry, Faculty of Engineering, Osaka University, Yamadakami, Suita, Osaka, 565

**Institute for Protein Research, Osaka University, Yamadakami, Suita, Osaka, 565*

(Received May 13, 1972)

The molecular structure of a stereospecific (*isotactic*) polymerization catalyst of the acetaldehyde-monomer complex, $[Me_2Al\cdot O\cdot CPh:NPh,MeCHO]_2$, has been determined on the basis of three-dimensional X-ray data collected photographically. The crystal belongs to the orthorhombic system (space group *Pcca*) with four dimer formula units in a cell with the dimensions of: $a=15.83(3)$, $b=12.61(1)$, and $c=17.66(1)$ Å. The structure was established by the heavy-atom method and refined by block-diagonal, least-squares procedure. The molecule is dimeric and has a C_2-2 symmetry. A monomer molecule, acetaldehyde, is inserted in the Al–N bond of the original polymerization catalyst. The oxygen atom bridges both aluminum atoms, Al–O=1.858(6) and 1.985(6) Å. The α-carbon atom of acetaldehyde bonds to the nitrogen atom of the amide moiety, C–N=1.469(12) Å. The aluminum atom is penta-co-ordinated and has a trigonal bipyramidal conformation.

We have been carried out a series of molecular-structural studies of the trimethylaluminum–benzanilide system, a catalytic system of the *isotactic* polymerization of acetaldehyde, by means of X-ray diffraction. Four complexes in the series are assumed to be the key substances for obtaining useful informations about the stereospecific polymerization mechanism of acetaldehyde. They are; (I) the polymerization catalyst, $[Me_2Al\cdot O\cdot CPh:NPh]_2$;[1] (II) the polymerization catalyst-monomer complex, $[Me_2Al\cdot O\cdot CPh:NPh,MeCHO]_2$; (III) the polymerization catalyst-monomer-Lewis acid complex, $[Me_2Al\cdot O\cdot CPh:NPh,MeCHO, AlMe_3]$; and (IV) the polymerization catalyst–Lewis base complex, $[Me_2Al\cdot O\cdot CPh:NPh,ONMe_3]$.

We have already communicated the preliminary results on these four complexes[2-5] and also reported the molecular structures of complexes I[6] and IV[7] in detail. The complex I is dimeric and has a centro-symmetric eight-membered ring, where the amide moieties make bridges between two aluminum atoms by the –O–C–N– skeletons. The complex IV is composed of a monomeric unit of I and a strong Lewis base, $ONMe_3$. The amide moiety in IV takes a stable *trans* configuration, unlike that in I (*cis*).

In this paper we will describe the crystal and molecular structure of the polymerization catalyst–monomer complex, $[Me_2Al\cdot O\cdot CPh:NPh, MeCHO]_2$, which is considered to be essentially the polymerization intermediate of this catalytic system. The main purpose of this work is to clarify the co-ordination state of acetaldehyde to the polymerization catalyst.

Experimental

The crystals of $[Me_2Al\cdot O\cdot CPh:NPh, MeCHO]_2$ were prepared and supplied by Tani and Yasuda of this University. They were far more unstable than the polymerization catalyst, $[Me_2Al\cdot O\cdot CPh:NPh]_2$. Besides being very air-sensitive, they decomposed at temperatures above 20°C. A large number of well-looking crystals were taken from the mother solution; they were sealed in thin-walled glass capillary tubes in argon. During the X-ray experiment, the Weissenberg camera was placed and operated in a cool chamber. As the chamber was temporary, the temperature inside the chamber was controlled only within about 10°C.

Nickel-filtered Cu$K\alpha$ radiation ($\lambda=1.5418$ Å) was used throughout the X-ray experiments. The unit cell dimensions were determined from two zero-level Weissenberg photographs along the *a* and *c* axes. Debye powder lines of tungsten were superposed on the Weissenberg photographs for calibration, and the cell parameters were determined by the least-squares procedure. The space group was determined to be D_{2h}^{8}–*Pcca* (No. 54) on the basis of the extinctions of reflections ($l\neq 2n$ for $0kl$, $l\neq 2n$ for $h0l$, and $h\neq 2n$ for $hk0$). The crystal data are listed in Table 1. These data impose a C_i–$\bar{1}$ or C_2–2 symmetry on the dimeric molecule.

The intensity data were collected by means of multiple-film equi-inclination Weissenberg photographs along the *a* and *c* axes. As the crystal was unstable even in argon at about 10°C, four crystals of a similar size (about 0.4×0.4×1.0 mm) were used (three along the *a* axis and one along the *c* axis). 2053 reflections from $0kl$ through $1l,k,l$, and 515 reflections from

Table 1. Crystal data of $[(CH_3)_2Al\cdot O\cdot C(C_6H_5):N(C_6H_5),CH_3CHO]_2$

Orthorhombic	$C_{34}H_{40}N_2O_4Al_2$ (as a dimer)
$a=15.83(3)$ Å	$M=594.6$
$b=12.61(1)$ Å	$Z=4$
$c=17.66(1)$ Å	$d_m=1.14$ g.cm^{-3}
$V=3525.2$ Å^3	$d_x=1.12$ g.cm^{-3}
	Space group *Pcca*
	$\mu=11.4$ cm^{-1} (for Cu$K\alpha$)

1) Throughout the paper, the methyl and phenyl groups will be expressed as Me and Ph respectively.

2) Y. Kai, N. Yasuoka, N. Kasai, M. Kakudo, H. Yasuda, and H. Tani, *Chem. Commun.*, **1968**, 1332.

3) Y. Kai, N. Yasuoka, N. Kasai, M. Kakudo, H. Yasuda, and H. Tani, *ibid.*, **1969**, 575.

4) Y. Kai, N. Yasuoka, N. Kasai, M. Kakudo, H. Yasuda, and H. Tani, *ibid.*, **1970**, 1243.

5) Y. Kai, N. Yasuoka, N. Kasai, M. Kakudo, H. Yasuda, and H. Tani, *ibid.*, **1971**, 940.

6) Y. Kai, N. Yasuoka, N. Kasai, and M. Kakudo, *J. Organometal. Chem.*, **32**, 165 (1971).

7) Y. Kai, N. Yasuoka, N. Kasai, and M. Kakudo, This Bulletin, **45**, 3388 (1972).

*hk*0 through *hk*2 were collected. Their intensities were estimated visually, and they were corrected for the usual Lorentz and polarization factors and also for the spot-shape effect. The absorption correction was ignored ($\mu=11$ cm^{-1} for Cu$K\alpha$). A total of 2185 independent reflections were obtained, among which 451 reflections were too weak to be measured.

Structure Determination and Refinement

The structure was established by the heavy-atom method. The initial co-ordinates of the aluminum atom were determined from the three-dimensional Patterson maps. The computations of the minimum function and a Fourier synthesis were carried out, both based on the location of the aluminum atom.[8] From these maps, three reasonable atomic locations were found close to the aluminum atom, but none of them could be identified as carbon, nitrogen, or oxygen. The atomic scattering factors of the nitrogen atoms were, therefore, assumed for these atoms in the succeeding Fourier synthesis, and 17 atomic positions out of 21 nonhydrogen atoms could be located. The remaining 4 atomic locations were determined from the successive Fourier synthesis.

Starting from the locations of these nonhydrogen atoms, the block-diagonal least-squares refinement was done, using the HBLS IV program[8] on a FACOM 230-60 computer at Kyoto University. The function minimized was $\sum w(\Delta F)^2$, and at the initial stage w was taken as unity for all reflections. The atomic scattering factors used were taken from those of Hanson and his co-workers.[9] Using the isotropic temperature factors for all the nonhydrogen atoms, the usual R index converged to 0.20 after 3 cycles. The difference Fourier map was computed, and all the hydrogen atoms could be located approximately. The refinement proceeded including these hydrogen atoms and applying the anisotropic temperature factors for nonhydrogen atoms. The weighting scheme described later was also included in the refinement. The R index was improved to 0.15 after 2 cycles. In this refinement, the locations of atoms bearing the hydrogen, especially that of the α-carbon atom in the acetaldehyde moiety, were much improved. The difference Fourier map was again computed based on the new locations of the nonhydrogen atoms, and the positions of hydrogen atoms were determined again. The final refinement was carried out considering the redetermined hydrogen atoms; the final R value is 0.143 for non-zero reflections ($R=0.191$ for all reflections). The weighting scheme applied in the final refinement is: $|F_o|<F_{min}$; $w=F_{wt}$, $F_{min}\leqq|F_o|\leqq F_{max}$; $w=1$, $F_{max}<|F_o|$; $w=(F_{max}/|F_o|)^2$, where $F_{max}=20.0$, $F_{min}=4.0$, and $F_{wt}=0.20$.

The final atomic co-ordinates of the nonhydrogen atoms, along with their estimated standard deviations, and the anisotropic temperature factors are listed in Tables 2 and 3 respectively. The atomic co-ordinates and isotropic temperature factors of the hydrogen atoms are listed in Table 4. Table 5 lists the observed and

8) Most of the programs used in the calculations were taken from "The Universal Crystallographic Computing System (I)," edited by T. Sakurai, Japanese Crystallographic Association (1967), and the other programs were cited in our previous paper.[6,7]

9) H. P. Hanson, F. Herman, J. D. Lea, and S. S. Skillman, *Acta Crystallogr.*, **17**, 1040 (1964).

TABLE 2. ATOMIC CO-ORDINATES OF THE HEAVY ATOMS (IN FRACTION OF CELL EDGES) ALONG WITH THEIR ESTIMATED STANDARD DEVIATIONS (IN 10^{-3} Å)

Atom	x	$\sigma(x)$	y	$\sigma(y)$	z	$\sigma(z)$
Al	0.0844	3	0.1665	3	0.2081	3
O(1)	0.1978	6	0.1818	6	0.2626	6
O(2)	0.0395	5	0.1503	5	0.3046	6
N	0.1538	7	0.1999	7	0.3844	6
C(1)	0.1228	13	0.0463	13	0.1461	13
C(2)	0.0907	11	0.3107	11	0.1667	10
C(3)	0.2109	10	0.2187	8	0.3282	10
C(4)	0.2877	9	0.2789	9	0.3428	9
C(5)	0.3395	8	0.2592	9	0.4052	9
C(6)	0.4175	11	0.3162	12	0.4122	13
C(7)	0.4394	11	0.3971	12	0.3605	12
C(8)	0.3876	11	0.4141	12	0.3004	10
C(9)	0.3143	10	0.3597	11	0.2902	8
C(10)	0.1556	10	0.2625	9	0.4543	9
C(11)	0.1637	11	0.2079	10	0.5247	9
C(12)	0.1658	13	0.2750	13	0.5903	9
C(13)	0.1604	11	0.3841	11	0.5844	10
C(14)	0.1495	12	0.4339	10	0.5173	8
C(15)	0.1458	10	0.3696	9	0.4506	8
C(16)	0.0830	9	0.1265	8	0.3727	10
C(17)	0.1170	13	0.0105	10	0.3703	14

TABLE 3. ANISOTROPIC TEMPERATURE FACTORS OF THE HEAVY ATOMS EXPRESSED IN THE FORM OF $\exp\{-(\beta_{11}h^2+\beta_{22}k^2+\beta_{33}l^2+\beta_{12}hk+\beta_{13}hl+\beta_{23}kl)\}$

Atom	β_{11}	β_{22}	β_{33}	β_{12}	β_{13}	β_{23}
Al	0.0034	0.0062	0.0035	0.0018	−0.0008	−0.0027
O(1)	0.0036	0.0086	0.0041	0.0012	−0.0014	−0.0039
O(2)	0.0019	0.0051	0.0043	0.0006	−0.0013	0.0007
N	0.0030	0.0069	0.0032	−0.0022	−0.0016	0.0008
C(1)	0.0072	0.0137	0.0061	0.0052	−0.0026	−0.0105
C(2)	0.0054	0.0116	0.0038	−0.0012	−0.0013	0.0007
C(3)	0.0041	0.0060	0.0047	0.0046	−0.0035	0.0007
C(4)	0.0035	0.0081	0.0032	0.0017	−0.0021	−0.0044
C(5)	0.0022	0.0087	0.0045	0.0014	0.0004	−0.0028
C(6)	0.0040	0.0116	0.0058	0.0029	−0.0015	−0.0012
C(7)	0.0048	0.0112	0.0057	−0.0041	0.0030	−0.0040
C(8)	0.0050	0.0126	0.0038	−0.0036	0.0018	−0.0003
C(9)	0.0042	0.0113	0.0025	−0.0032	0.0009	0.0001
C(10)	0.0038	0.0071	0.0035	−0.0013	−0.0015	0.0028
C(11)	0.0060	0.0084	0.0039	0.0015	−0.0012	0.0058
C(12)	0.0079	0.0175	0.0016	0.0009	−0.0018	0.0021
C(13)	0.0059	0.0117	0.0036	−0.0008	−0.0012	−0.0024
C(14)	0.0067	0.0108	0.0024	0.0014	−0.0017	0.0006
C(15)	0.0049	0.0089	0.0027	0.0006	0.0001	0.0017
C(16)	0.0035	0.0058	0.0050	−0.0016	−0.0043	0.0024
C(17)	0.0083	0.0055	0.0098	−0.0026	−0.0084	0.0055

Table 4. Atomic co-ordinates (in fraction of cell edges) along with their estimated standard deviations (in 10^{-2} Å) and isotropic temperature factors for the hydrogen atoms (in Å^2)

Atom	x	$\sigma(x)$	y	$\sigma(y)$	z	$\sigma(z)$	B
H(1)	0.081	10	−0.019	10	0.126	9	4.0
H(2)	0.170	10	0.060	10	0.101	10	4.2
H(3)	0.164	10	−0.001	11	0.184	10	4.1
H(4)	0.042	10	0.339	10	0.121	10	4.0
H(5)	0.160	11	0.340	10	0.159	10	3.9
H(6)	0.071	10	0.360	10	0.199	10	3.9
H(7)	0.321	10	0.198	9	0.448	9	3.0
H(8)	0.458	10	0.297	9	0.458	9	3.2
H(9)	0.497	10	0.444	10	0.367	10	3.8
H(10)	0.405	10	0.476	9	0.259	10	3.6
H(11)	0.274	10	0.379	9	0.242	10	3.7
H(12)	0.167	9	0.121	8	0.529	8	2.4
H(13)	0.173	10	0.241	10	0.645	10	3.9
H(14)	0.164	10	0.434	10	0.635	9	3.7
H(15)	0.144	10	0.519	9	0.513	9	3.2
H(16)	0.133	10	0.410	9	0.398	10	3.8
H(17)	0.038	10	0.134	10	0.419	10	3.6
H(18)	0.066	9	−0.039	9	0.356	10	3.3
H(19)	0.173	10	0.020	10	0.340	11	4.6
H(20)	0.130	10	0.018	10	0.434	10	3.7

calculated structure factors.[10]

Results and Discussion

Molecular Structure. The molecular structure viewed along the *b* axis is shown in Fig. 1, along with the numbering of the atoms. The shaded are the seven atoms of the acetaldehyde moiety. The interatomic bond distances and angles are listed in Tables 6 and 7 respectively.

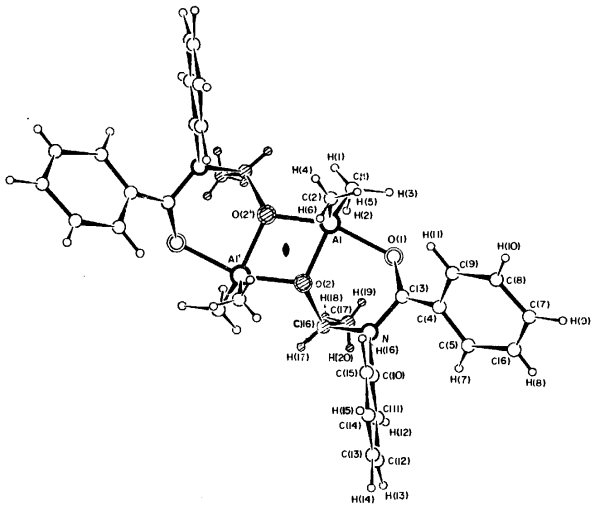

Fig. 1. The molecular structure.

10) Table 5 has been submitted to and is kept as Document No. 7210 by, the office of the Bulletin of the Chemical Society of Japan, 1-5, Kanda-Surugadai, Chiyoda-ku, Tokyo. A copy may be secured by citing the Document number and by remitting, in advance, ¥300 for photo prints. Pay by check or money order payable to: Chemical Society of Japan.

Table 6. Interatomic distances along with their estimated standard deviations

Atoms	Distance (Å)	σ (Å)	Atoms	Distance (Å)	σ (Å)
Al-O(1)	2.045	0.007	C(3)-N	1.364	0.012
Al-O(2)	1.858	0.006	C(3)-C(4)	1.455	0.013
Al-C(1)	1.965	0.013	O(2)-C(16)	1.418	0.011
Al-C(2)	1.962	0.012	C(16)-N	1.469	0.012
Al-O(2′)	1.985	0.006	C(16)-C(17)	1.559	0.017
O(1)-C(3)	1.265	0.012	N-C(10)	1.466	0.012
C(16)-H(17)	1.09	0.11			
C(4)-C(5)	1.396	0.013	C(10)-C(11)	1.426	0.015
C(5)-C(6)	1.434	0.016	C(11)-C(12)	1.436	0.018
C(6)-C(7)	1.412	0.017	C(12)-C(13)	1.382	0.017
C(7)-C(8)	1.359	0.017	C(13)-C(14)	1.353	0.016
C(8)-C(9)	1.359	0.016	C(14)-C(15)	1.431	0.015
C(9)-C(4)	1.443	0.014	C(15)-C(10)	1.361	0.014
C(1)-H(1)	1.16	0.11	C(2)-H(4)	1.11	0.10
C(1)-H(2)	1.16	0.11	C(2)-H(5)	1.11	0.10
C(1)-H(3)	0.91	0.10	C(2)-H(6)	1.11	0.11
C(17)-H(18)	1.06	0.10			
C(17)-H(19)	1.04	0.11			
C(17)-H(20)	1.14	0.10			
C(5)-H(7)	1.11	0.10	C(11)-H(12)	1.09	0.09
C(6)-H(8)	1.05	0.10	C(12)-H(13)	1.07	0.10
C(7)-H(9)	1.09	0.10	C(13)-H(14)	1.09	1.10
C(8)-H(10)	1.10	0.10	C(14)-H(15)	1.08	0.10
C(9)-H(11)	1.09	0.10	C(15)-H(16)	1.09	0.10

As may be seen in Fig. 1, the molecule is dimeric and has a C_2-2 symmetry instead of the C_i-$\bar{1}$ which was found in the catalyst, $[Me_2Al\cdot O\cdot CPh{:}NPh]_2$. The most interesting feature is that the aldehyde molecule is inserted between the aluminum and nitrogen atoms of the catalyst and is connected to the catalyst by two sites, O(2) and C(16). The O(2) co-ordinates to the aluminum (Al), and the C(16) bonds to the nitrogen atom of the amide moiety. These facts show that the relative position of the aldehyde molecule and the catalyst skeleton is uniquely fixed in the solid state. Such a co-ordination might be a main feature, even in the solution.

The oxygen (O(2)) of the aldehyde moiety co-ordinates to the other aluminum atom (Al′) and makes an oxonium ion-type bonding. Three bonds from the O(2) lie on the same plane (within 0.02 Å). The difference between the two Al-O(2) bond distances, (Al-O(2)=1.858(6) Å and Al′-O(2)=1.985(6) Å), is significant. The cryoscopic measurement of the molecular weight suggests that the dimeric molecule dissociates in the dilute solution under the polymerization conditions. For the dissociation, the cleavage of the Al′-O(2) bond is necessary. The rather long distance of Al′-O(2) suggests the possible fission of this bond. This was recently proved to be true by the isolation and structural determination of $[Me_2Al\cdot O\cdot CPh{:}NPh, MeCHO, AlMe_3]$.[4]

The α-carbon atom, C(16) of the aldehyde moiety shows an sp^3 hybridization; all the bond angles around the C(16) are tetrahedral (Table 7), and the bond distances, C(16)-O(2) (1.418(11) Å), C(16)-N (1.469 (12) Å), and C(16)-C(17) (1.559(17) Å), show the

TABLE 7. INTERATOMIC ANGLES ALONG WITH THEIR ESTIMATED STANDARD DEVIATIONS

Atoms	Angle (deg.)	σ (deg.)	Atoms	Angle (deg.)	σ (deg.)
C(1)–Al–O(1)	93.7	0.4	C(3)–N–C(16)	120.8	0.7
C(2)–Al–O(1)	92.5	0.4	C(3)–N–C(10)	120.5	0.7
O(2)–Al–O(1)	85.1	0.3	C(10)–N–C(16)	118.3	0.7
C(1)–Al–O(2′)	99.4	0.4	Al–O(2)–Al′	105.3	0.3
C(2)–Al–O(2′)	95.9	0.4	Al–O(2)–C(16)	128.0	0.5
O(2)–Al–O(2′)	73.3	0.3	C(16)–O(2)–Al′	126.7	0.5
O(2′)–Al–O(1)	158.3	0.3	O(2)–C(16)–C(17)	110.1	0.8
C(1)–Al–O(2)	123.0	0.4	O(2)–C(16)–N	110.9	0.7
C(2)–Al–O(2)	117.5	0.4	N–C(16)–C(17)	109.4	0.8
C(1)–Al–C(2)	119.4	0.5	H(17)–C(16)–O(2)	107	6
Al–O(1)–C(3)	127.6	0.6	H(17)–C(16)–C(17)	109	6
O(1)–C(3)–N	119.6	0.8	H(17)–C(16)–N	110	6
O(1)–C(3)–C(4)	119.4	0.8			
N–C(3)–C(4)	121.0	0.8			
C(3)–C(4)–C(5)	122.6	0.8	N–C(10)–C(11)	118.4	0.8
C(3)–C(4)–C(9)	119.9	0.8	N–C(10)–C(15)	119.5	0.8
C(4)–C(5)–C(6)	119.1	0.9	C(10)–C(11)–C(2)	115	1
C(5)–C(6)–C(7)	121	1	C(11)–C(12)–C(13)	122	1
C(6)–C(7)–C(8)	118	1	C(12)–C(13)–C(14)	122	1
C(7)–C(8)–C(9)	123	1	C(13)–C(14)–C(15)	118	1
C(8)–C(9)–C(4)	121	1	C(14)–C(15)–C(10)	121	1
C(5)–C(4)–C(9)	117.5	0.9	C(11)–C(10)–C(15)	122.1	0.9
H(1)–C(1)–H(2)	107	7	H(4)–C(2)–H(5)	116	7
H(1)–C(1)–H(3)	99	8	H(4)–C(2)–H(6)	90	8
H(2)–C(1)–H(3)	97	8	H(5)–C(2)–H(5)	100	8
Al–C(1)–H(1)	124	5	Al–C(2)–H(4)	120	5
Al–C(1)–H(2)	119	5	Al–C(2)–H(5)	113	5
Al–C(1)–H(3)	105	6	Al–C(2)–H(6)	113	7
			H(18)–C(17)–H(19)	127	8
			H(18)–C(17)–H(20)	115	7
			H(19)–C(17)–H(20)	110	8
			C(16)–C(17)–H(18)	107	5
			C(16)–C(17)–H(19)	102	5
			C(16)–C(17)–H(20)	88	5
H(7)–C(5)–C(4)	120	5	H(12)–C(11)–C(10)	123	5
H(7)–C(5)–C(6)	121	5	H(12)–C(11)–C(12)	122	5
H(8)–C(6)–C(5)	118	6	H(13)–C(12)–C(11)	120	6
H(8)–C(6)–C(7)	121	6	H(13)–C(12)–C(13)	119	6
H(9)–C(7)–C(6)	122	5	H(14)–C(13)–C(12)	121	5
H(9)–C(7)–C(8)	120	5	H(14)–C(13)–C(14)	117	5
H(10)–C(8)–C(7)	119	5	H(15)–C(14)–C(13)	122	5
H(10)–C(8)–C(9)	119	5	H(15)–C(14)–C(15)	120	5
H(11)–C(9)–C(8)	120	5	H(16)–C(15)–C(14)	117	5
H(11)–C(9)–C(4)	119	5	H(16)–C(15)–C(10)	122	5

normal values of the single covalent bond.

The most remarkable features are that the aluminum atom is penta-co-ordinated, and that a distorted trigonal-bipyramid is formed. The geometry around the aluminum atom is shown in Fig. 2. The aluminum atom lies exactly on the C(1)–C(2)–O(2) plane (within 0.01 Å), and the three bond angles around the aluminum in this basal plane show little deviation from 120°, the value expected for the typical trigonal bipyramid. The O(1) atom is just beneath the aluminum atom, and the three bond angles, O(1)–Al–C(1), O(1)–Al–C(2), and O(1)–Al–O(2), show a relatively good coincidence with the expected value of 90°. The interatomic vector, O(1)–Al, makes an angle of 84.6° with the basal plane, while the angle between the O(2′)–Al vector and the basal plane is 73.7°. The latter shows a great deviation from 90°. The distortion of the geometry around the aluminum atom from the trigonal bipyramid may be attributed to the formation of an additional four-membered ring, Al$\begin{matrix}\diagup O(2')\diagdown \\ \diagdown O(2)\diagup\end{matrix}$Al′.

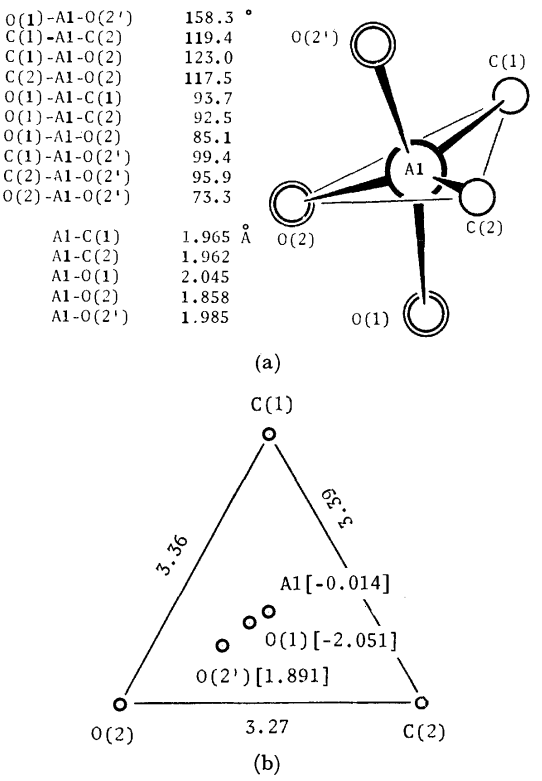

Fig. 2. The co-ordination geometry around the penta-co-ordinated aluminum atom. (a) Bond distances and angles. (b) Projection onto the basal plane (deviation from the plane are given in the brackets in Å unit).

The geometry around the penta-co-ordinated aluminum atom is summarized in Table 8. In [AlH_3, $2NMe_3$],[11] the aluminum atom lies on the crystallographic center of symmetry and two nitrogen and one aluminum atoms lie on a straight line. Because of the disorder, the presence of the six half-hydrogen atoms was assumed on the plane perpendicular to the N–Al–N axis in the hexagonal array. In the infinite-chain molecule with the molecular unit of [Me_2N–CH_2–CH_2–NMe_2]–AlH_3,[12] two aluminum atoms of the asymmetric unit do not lie at any crystallographic special positions. Two nitrogen atoms from two different diamine molecules occupy the apical positions of the trigonal bipyramid, with N–Al–N angles of 178.0° and 176.5°. The three hydrogen atoms around the aluminum atom, which were located by the difference Fourier synthesis, lie on an equatorial plane with an approximate three-fold symmetry. μ-Oxo-di[bis(2-methyl-8-quinolinolato-

11) C. W. Heitsch, C. E. Nordman, and R. W. Parry, *Inorg. Chem.*, **2**, 508 (1963).
12) G. J. Palenik, *Acta Crystallogr.*, **17**, 1573 (1964).

aluminum(III)][13] also contains two penta-co-ordinated, slightly distorted trigonal bipyramidal, aluminum atoms in an asymmetric unit. Three oxygen and one aluminum atoms lie on the equatorial plane, and two nitrogen atoms occupy the apical positions. The average value of the N-Al-N is 163°. On the other hand, in the present complex, two carbon and one oxygen atoms lie on the equatorial plane and two oxygen atoms occupy the apical positions. The O-Al-O angle is 158°; much distortion is seen. In $C_8H_{24}Al_3Br_5O_6Si_4$,[14] each aluminum atom is co-ordinated by four oxygen and one bromine atoms, but the distortion is too large to interpret the geometry as either a trigonal bipyramid or a square pyramid.

Crystal Structure. Figure 3 shows the crystal structure projected along the *b* axis. Intermolecular atomic contacts of less than 3.8 Å are shown by broken lines. They are all considered as normal van der Waals' contacts.

Table 8. Geometry around the penta-co-ordinated aluminum atom

$[AlH_3, 2NMe_3]$[11]		∠N-Al-N=180° *Trigonal bipyramid* Al on $\bar{1}$. 6/2H on the plane perpendicular to N-Al-N axis in the hexagonal array by the disorder
$[AlH_3, Me_2NCH_2CH_2NMe_2]$[12]		∠N-Al-N=178.0°, 176.5° *Trigonal bipyramid* Infinite chain, ····C-C-N-Al-N····
$[Al_2O(C_{10}H_8NO)_4]$[13]		∠N-Al-N=162.2°, 163.5° *Distorted trigonal bipyramid*
$[Me_2Al\cdot O\cdot CPh{:}NPh, MeCHO]_2$[a]		∠O-Al-O=158.3° *Distorted trigonal bipyramid*
$[C_8H_{24}Al_3Br_5O_6Si_4]$[14]		∠O_1-Al-O_3=132° ∠O_2-Al-O_4=158° Difficult to interpret as either trigonal bipyramid or square pyramid

a) Present work

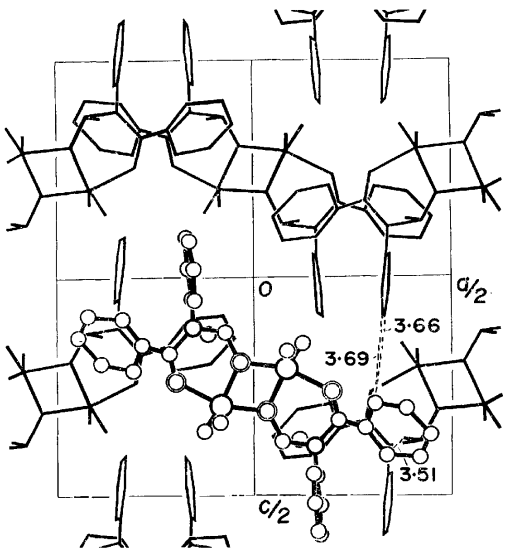

Fig. 3. The crystal structure projected along the *b*-axis.

Some Reactions about the Present Complex. From among the reactions of the trimethylaluminum-benzanilide catalyst system, some important reactions related with the present complex are shown in Fig. 4. In a previous paper,[7] the reaction from complex I to IV was discussed from a molecular-structural point of view. Very recently, Tani and his co-workers discovered that complex IV can also be obtained from complex II (the present complex) and $ONMe_3$ under conditions similar to those above. The complex II is obtained from complex I and MeCHO as has been described before. From these facts, the reaction scheme can be redrawn as is in Fig. 4 by drawing the molecular structures of these complexes.

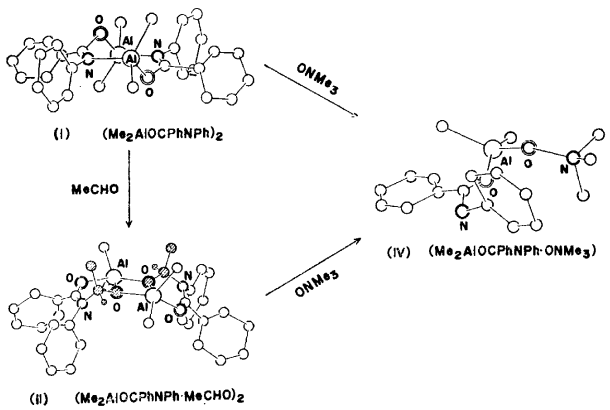

Fig. 4. Reactions related with the present complex (IV).

It is interesting to make some stereochemical consideration of how the polymerization catalyst I reacts with acetaldehyde to form a catalyst-monomer complex II, which is assumed to be essentially the polymerization intermediate. Both of the oxygen atoms of $ONMe_3$ and MeCHO react as the Lewis base, but $ONMe_3$ is much stronger than MeCHO. The most significant difference between these two bases is that $ONMe_3$ is unifunctional, whereas MeCHO is bifunctional; when the oxygen atom of MeCHO acts as a Lewis base, the α-carbon can act like Lewis acid. In Fig. 5, the postulated molecule (ii) may, therefore, not be so stable as (i), which is identical with the complex IV (IV in Fig. 4), even though the amide moiety takes a stable *trans* configuration. The interaction between the electron-deficient α-carbon atom of acetaldehyde and the electron-rich nitrogen atom of the amide moiety can be expected. The subsequent configurational change of the amide moiety from *trans* to *cis* is required to make the interaction possible. This is shown by the postulated molecule (i) in Fig. 6. An additional rotation about the Al-O bond (Fig. 6 (ii)) is necessary to strengthen the interaction. Another rotation about the O-C bond (Fig. 6 (iii)) completes the formation of a half of the complex II (Fig. 6 (iv)). The present complex, (II) is then formed by the association of these two halves.

13) Y. Kushi and Q. Fernando, *J. Amer. Chem. Soc.*, **92**, 91 (1970).
14) M. Bonamico, *Chem. Commun.*, **1966**, 135.

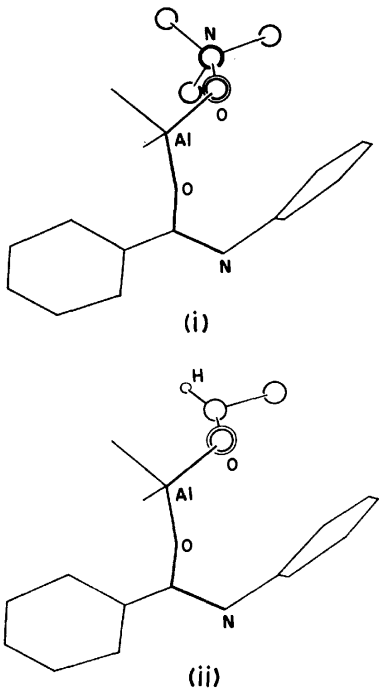

Fig. 5. The comparison of the molecular structure of [Me_2Al·O·CPh: NPh, $ONMe_3$] (i) and a postulated molecule [Me_2Al·O·CPh: NPh, MeCHO] (ii).

The molecular-structural change in the reaction of the complex II with $ONMe_3$ (Fig. 4) can also be discussed in a similar manner, but in the reverse direction. The stronger Lewis base $ONMe_3$ attacks and replaces the aldehyde moiety of a half of the dissociated complex II to form the complex IV.

The α-carbon atom of the acetaldehyde moiety in the complex II is an asymmetric carbon. Since the molecule has a crystallographic C_2-2 symmetry, there are two asymmetric carbon atoms of the same configuration in a molecule. The space group belongs to a centrosymmetric *Pcca*, and there are an equal number of optical isomers in the crystal. The absolute configuration of these asymmetric carbon is, therefore, S–S or R–R. A hypothetical molecule, which has a C_i-$\bar{1}$ symmetry instead of C_2-2, is shown in Fig. 7; the absolute configuration of the asymmetric carbon atoms is S–R or R–S. In the postulated molecule, if the geometry around the aluminum atom is kept significantly unchanged from that of the actual molecule, a rather short contact C(2)···C(17′), 3.3 Å, results between the two methyl groups in a molecule (one attached to the aluminum atom and the other from the aldehyde moiety). Such a steric hindrance probably make it difficult for the molecule of C_i-$\bar{1}$ symmetry to exist or at least makes the molecule unstable.

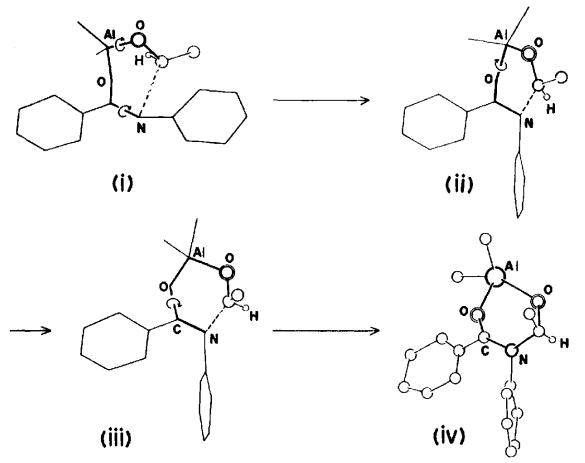

Fig. 6. Schematic representation of a conversion of the postulated molecule, [Me_2Al·O·CPh: NPh, MeCHO] into the real structure, which is a half of the [Me_2Al·O·CPh: NPh, $MeCHO]_2$ molecule.

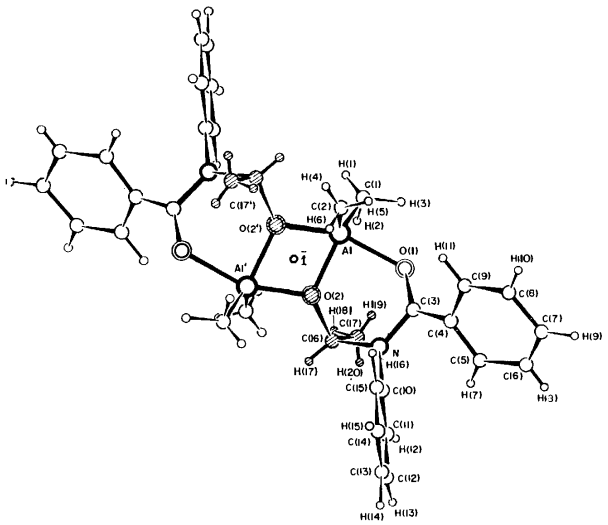

Fig. 7. A hypothetical molecule for [Me_2Al·O·CPh: NPh, $MeCHO]_2$ with C_i-$\bar{1}$ symmetry instead of C_2-2.

The authors wish to express their deep thanks to Professor Hisaya Tani and Dr. Hajime Yasuda of Osaka University for their kindness in supplying samples and for their helpful discussions.

The Crystal Structure of the Polymerization Catalyst of Acetaldehyde and Its Derivatives. IV. The Crystal and Molecular Structure of Dimethylaluminum *N*-Phenylbenzimidate-*O*-(Trimethylaluminum)-Acetaldehyde Complex, $[(CH_3)_2Al\cdot O\cdot C(C_6H_5):N(C_6H_5), CH_3CHO, Al(CH_3)_3]$

Yasushi KAI, Noritake YASUOKA, Nobutami KASAI, and Masao KAKUDO*

Department of Applied Chemistry, Faculty of Engineering, Osaka University, Yamadakami, Suita, Osaka, 565
**Institute for Protein Research, Osaka University, Yamadakami, Suita, Osaka, 565*

(Received May 13, 1972)

The molecular structure of a stereospecific (*isotactic*) polymerization catalyst of the acetaldehyde-monomer-Lewis acid complex, $[Me_2Al\cdot O\cdot CPh: NPh,MeCHO,AlMe_3]$, has been determined from three-dimensional X-ray-diffraction data collected photographically. The crystal belongs to the monoclinic system (space group $P2_1/n$), with four formula units in a cell with dimensions of: $a=13.60(3)$, $b=13.74(2)$, $c=12.40(2)$ Å, $\beta=95.9(2)°$. The structure was solved by the heavy-atom method and was refined by the block-diagonal, least-squares procedure. The trimethylaluminum forms a bond with the electron-rich oxygen atom of acetaldehyde through the electron-deficient aluminum atom. The polymerization mechanism can reasonably be concluded to be the "co-ordinated cationic polymerization".

During the organochemical investigations of the stereospecific polymerization catalysis of aldehydes, Tani and his co-workers prepared many interesting substances and isolated them in the form of crystals.[1-4] The catalytic system of trialkylaluminum-acid amide gave highly stereospecific polyaldehydes almost quantitatively. The reaction with this catalytic system is mild and has few accompanied side reactions. Therefore, the exact structure determinations of the key substances may reveal much important information about the stereospecific polymerization mechanism. Four compounds were chosen as the key substances in the trimethylaluminum-benzanilide catalyst system; (I) the polymerization catalyst $[Me_2Al\cdot O\cdot CPh: NPh]_2$, (II) the catalyst-monomer complex $[Me_2Al\cdot O\cdot CPh: NPh,MeCHO]_2$, (III) the catalyst-monomer-Lewis acid complex $[Me_2Al\cdot O\cdot CPh: NPh,MeCHO,AlMe_3]$, and (IV) the catalyst-Lewis base complex $[Me_2Al\cdot O\cdot CPh: NPh,ONMe_3]$. Among these, the molecular structures of I, II, and IV were already reported in detail.[5-7] The complex III, the last one in this series, which is prepared by the equimolar reaction of II and trimethylaluminum in *n*-hexane at 0°C, acts also as the polymerization catalyst of aldehydes, but gives an *atactic* polymer. In this article we will describe the molecular and crystal structure of III. The preliminary results of the structural analysis were communicated earlier.[8] The polymerization mechanism of acetaldehyde has been investigated from the stereochemical point of view on the basis of the molecular structures of these four key substances, together with the organochemical information.

Experimental

The crystals of $[Me_2Al\cdot O\cdot CPh:NPh, MeCHO, AlMe_3]$ were prepared and supplied by Tani snd Yasuda of this University. The compound is very air-sensitive, and the crystal was sealed in a thin-walled glass capillary tube in argon. Two kinds of crystals with different habits were obtained. One of them grows along the *a* axis, and the other, along the *b* axis. Both are colorless, long, and prismatic. The latter crystal examined always had a twinned structure. Figure 1 shows the twinning in the $h0l$ reciprocal lattice plane. The subscript I or II shows to which component each unit cell belongs. The planes containing the $b^*(=b)$ axis and the reciprocal lattice point rows, $h0\bar{h}_I$ and $h0\bar{h}_{II}$, are the twin planes. If the $h0\bar{h}_I$ is taken as c^*_I and the $h0\bar{h}_{II}$ as c^*_{II}, the space group and the twin plane can be described as $P2_1/c$ and the b^*-c^* plane respectively: the same kind of twinning

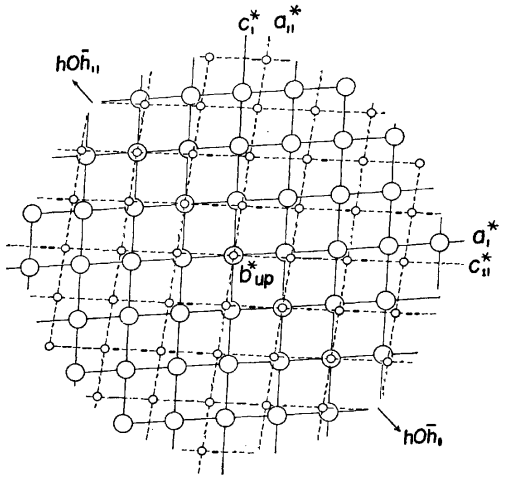

Fig. 1. One reciprocal lattice plane in the twinning crystal of $[Me_2Al\cdot O\cdot CPh: NPh,MeCHO,AlMe_3]$.

1) H. Tani, T. Araki, and H. Yasuda, *J. Polym. Sci., Part B*, **4**, 727 (1966).
2) H. Tani, T. Araki, and H. Yasuda, *ibid.*, **6**, 389 (1968).
3) H. Tani and H. Yasuda, *ibid.*, **7**, 17 (1969).
4) H. Tani and H. Yasuda, Private Communications.
5) Y. Kai, N. Yasuoka, N. Kasai, and M. Kakudo, *J. Organometal. Chem.*, **32**, 165 (1971).
6) Y. Kai, N. Yasuoka, N. Kasai, and M. Kakudo, This Bulletin, **45**, 3397 (1972).
7) Y. Kai, N. Yasuoka, N. Kasai, and M. Kakudo, This Bulletin, **45**, 3388 (1972).
8) Y. Kai, N. Yasuoka, N. Kasai, M. Kakudo, H. Yasuda, and H. Tani, *Chem. Commun.*, **1970**, 1243.

is found in $[Me_2Al\cdot O\cdot CPh: NPh]_2$.[5] The cell dimensions were determined by a least-squares fitting using the theta values obtained from $0kl$ and $h0l$ Weissenberg photographs. The space group was uniquely determined as $P2_1/n$ from the systematic absence of reflections ($h0l$: $h+l\neq 2n$, and $0k0$: $k\neq 2n$). The crystal data are listed in Table 1. The nickel-filtered Cu$K\alpha$ radiation ($\lambda=1.5418$ Å) was used throughout the X-ray experiments. The crystal density was measured by the flotation method in a mixed solution of carbon tetrachloride and *n*-hexane.

TABLE 1. CRYSTAL DATA OF $[(CH_3)_2Al\cdot O\cdot C(C_6H_5): N(C_6H_5), CH_3CHO, Al(CH_3)_3]$

Monoclinic	$C_{20}H_{29}O_2NAl_2$
$a=13.60(3)$ Å	$M=369.4$
$b=13.74(2)$ Å	$Z=4$
$c=12.40(2)$ Å	$d_m=1.07$ g·cm^{-3}
$\beta=95.9(2)°$	$d_x=1.064$ g·cm^{-3}
$V=2304.8$ Å^3	Space group $P2_1/n$
	$\mu=13.0$cm^{-1}(for Cu$K\alpha$)

The intensity data were collected by multiple-film equi-inclination Weissenberg photographs along the *a* axis only. The intensities were measured visually, and were corrected for the usual Lorentz and polarization factors, as well as for the spot-shape effect. Two independent crystals of a similar size (about $1.0\times 0.3\times 0.3$ mm) were used. In the layers from $0kl$ through $9kl$, 2891 independent reflections were observed, among which 2336 were non-zero reflections. The interlayer scales were first set proportional to the exposure times and improved in the course of the least-squares refinements with isotropic temperature factors for nonhydrogen atoms.

Structure Determination and Refinement

The structure was established by the heavy-atom method. From a Patterson map, two independent aluminum atoms were easily located. Two successive Fourier maps gave the locations of all the nonhydrogen atoms. The refinement of the structure was done by the method of block-diagonal least-squares. Computations were carried out using the HBLS IV program[9] on a FACOM 230-60 computer at Kyoto University. The function minimized was $\sum w(\Delta F)^2$, and at the intial stage w was taken as unity for all the reflections. The atomic scattering factors used were taken from those of Hanson and his co-workers.[10] Three cycles of the refinement with isotropic temperature factors for non-hydrogen atoms gave the R index of 0.18. Interlayer scales were improved during this refinement and then fixed. Further refinement was followed with anisotropic temperature factors for heavy atoms, and a weighting scheme to be described later was applied. After 2 cycles, the R index was 0.15. At this stage, a difference Fourier synthesis was computed and all the

9) Most of the programs used in the calculations were taken from "The Universal Crystallographic Computing System (I), edited by T. Sakurai, Japanese Crystallographic Association, 1967," and the other programs were cited in our previous paper.[7]

10) H. P. Hanson, F. Herman, J. D. Lea, and S. S. Skillman, *Acta Crystallogr.*, **17**, 1040 (1964).

TABLE 2. ATOMIC CO-ORDINATES OF THE HEAVY ATOMS (IN FRACTION OF CELL EDGES) ALONG WITH THEIR ESTIMATED STANDARD DEVIATIONS (IN 10^{-3} Å)

Atom	x	$\sigma(x)$	y	$\sigma(y)$	z	$\sigma(z)$
Al(1)	0.4154	3	0.2498	2	0.0494	3
Al(2)	0.2925	3	0.1590	3	0.2485	2
O(1)	0.3687	6	0.2321	6	−0.0940	6
O(2)	0.3017	6	0.2015	5	0.1016	5
N	0.2373	6	0.1400	6	−0.0679	6
C(1)	0.4368	13	0.3877	11	0.0736	12
C(2)	0.5242	12	0.1570	14	0.0667	12
C(3)	0.3066	8	0.1688	8	−0.1290	8
C(4)	0.3198	10	0.1273	9	−0.2385	8
C(5)	0.2438	12	0.1143	11	−0.3129	9
C(6)	0.2620	15	0.0815	14	−0.4159	11
C(7)	0.3504	15	0.0589	14	−0.4451	13
C(8)	0.4305	14	0.0656	15	−0.3703	15
C(9)	0.4141	12	0.1034	12	−0.2632	10
C(10)	0.1785	9	0.0521	8	−0.0895	7
C(11)	0.0820	10	0.0563	9	−0.1206	9
C(12)	0.0298	13	−0.0295	12	−0.1405	12
C(13)	0.0809	12	−0.1176	11	−0.1302	12
C(14)	0.1776	11	−0.1219	10	−0.1001	13
C(15)	0.2272	10	−0.0365	9	−0.0777	10
C(16)	0.2168	9	0.1945	8	0.0311	8
C(17)	0.1693	11	0.2934	10	0.0060	10
C(18)	0.1683	14	0.2156	13	0.2981	11
C(19)	0.4141	15	0.2166	15	0.3195	11
C(20)	0.2901	13	0.0167	11	0.2369	11

TABLE 3. ANISOTROPIC TEMPERATURE FACTORS OF THE HEAVY ATOMS EXPRESSED IN THE FORM OF $\exp\{-(\beta_{11}h^2+\beta_{22}k^2+\beta_{33}l^2+\beta_{12}hk+\beta_{13}hl+\beta_{23}kl)\}$

Atom	β_{11}	β_{22}	β_{33}	β_{12}	β_{13}	β_{23}
Al(1)	0.0042	0.0050	0.0071	−0.0020	−0.0013	0.0006
Al(2)	0.0059	0.0061	0.0056	−0.0033	−0.0011	0.0005
O(1)	0.0050	0.0064	0.0076	−0.0035	0.0010	0.0010
O(2)	0.0047	0.0054	0.0053	−0.0006	−0.0012	−0.0004
N	0.0031	0.0049	0.0058	−0.0003	−0.0005	−0.0005
C(1)	0.0116	0.0062	0.0115	−0.0060	−0.0019	0.0002
C(2)	0.0085	0.0120	0.0097	0.0041	0.0042	−0.0019
C(3)	0.0034	0.0053	0.0061	−0.0018	−0.0018	0.0002
C(4)	0.0056	0.0059	0.0064	−0.0015	0.0031	0.0022
C(5)	0.0114	0.0080	0.0049	−0.0041	−0.0006	0.0005
C(6)	0.0150	0.0104	0.0078	−0.0100	−0.0020	−0.0018
C(7)	0.0120	0.0111	0.0125	−0.0064	0.0108	−0.0059
C(8)	0.0084	0.0119	0.0165	0.0016	0.0137	−0.0036
C(9)	0.0086	0.0098	0.0075	−0.0031	0.0048	−0.0023
C(10)	0.0050	0.0050	0.0052	−0.0013	0.0001	−0.0010
C(11)	0.0048	0.0063	0.0085	−0.0008	−0.0017	−0.0005
C(12)	0.0079	0.0096	0.0106	−0.0036	−0.0029	−0.0007
C(13)	0.0080	0.0065	0.0134	−0.0051	0.0021	−0.0031
C(14)	0.0046	0.0068	0.0161	−0.0018	−0.0004	−0.0012
C(15)	0.0065	0.0047	0.0112	0.0030	−0.0031	−0.0016
C(16)	0.0060	0.0052	0.0053	−0.0002	−0.0026	−0.0023
C(17)	0.0089	0.0062	0.0094	0.0052	−0.0041	−0.0030
C(18)	0.0135	0.0099	0.0076	−0.0044	0.0071	−0.0010
C(19)	0.0136	0.0127	0.0069	−0.0104	−0.0054	0.0044
C(20)	0.0117	0.0063	0.0107	−0.0033	−0.0038	0.0044

Table 4. Atomic co-ordinates (in fraction of cell edges) along with their estimated standard deviations (in 10^{-2}Å) and isotropic temperature factors for the hydrogen atoms (in Å^2)

Atom	x	$\sigma(x)$	y	$\sigma(y)$	z	$\sigma(z)$	B
H(1)	0.460	10	0.421	10	0.001	10	3.6
H(2)	0.378	10	0.419	10	0.088	10	3.6
H(3)	0.502	10	0.400	10	0.139	10	3.8
H(4)	0.554	10	0.168	10	0.150	10	3.5
H(5)	0.572	10	0.168	10	0.012	10	3.6
H(6)	0.495	10	0.087	10	0.061	10	3.7
H(7)	0.168	9	0.132	9	−0.294	9	2.3
H(8)	0.197	9	0.076	10	−0.478	10	3.3
H(9)	0.356	11	0.030	11	−0.522	11	4.7
H(10)	0.505	10	0.045	11	−0.389	11	4.3
H(11)	0.484	10	0.115	11	−0.203	10	4.0
H(12)	0.049	12	0.121	13	−0.129	12	5.8
H(13)	−0.050	12	−0.032	12	−0.166	11	5.1
H(14)	0.035	13	−0.178	14	−0.150	13	6.9
H(15)	0.212	10	−0.190	10	−0.094	10	3.3
H(16)	0.303	11	−0.038	11	−0.054	11	4.5
H(17)	0.159	10	0.154	10	0.067	10	3.6
H(18)	0.138	10	0.325	10	0.069	10	3.6
H(19)	0.222	11	0.349	11	−0.007	11	4.2
H(20)	0.142	10	0.290	10	−0.067	10	3.3
H(21)	0.138	9	0.157	10	0.322	9	3.1
H(22)	0.176	11	0.262	10	0.368	11	3.9
H(23)	0.144	10	0.253	11	0.239	11	4.5
H(24)	0.394	11	0.264	11	0.378	11	4.4
H(25)	0.461	10	0.251	9	0.262	10	3.0
H(26)	0.461	10	0.162	10	0.361	10	3.6
H(27)	0.358	10	−0.009	11	0.220	10	4.0
H(28)	0.240	10	−0.010	10	0.180	10	3.6
H(29)	0.272	11	−0.015	11	0.308	11	4.5

hydrogen atoms were located. By including these hydrogen atoms with the isotropic temperature factors, the refinement was done and the R index was reduced to 0.13 after 2 cycles. The difference Fourier map was again computed to obtain improved hydrogen locations. The final refinement gave an R index of 0.124 for non-zero reflections and one of 0.16 for all the reflections. The weighting scheme applied was; $|F_o|<F_{min}$; $w=F_{wt}$, $F_{min}\leqq|F_o|\leqq F_{max}$; $w=1.0$, and $F_{max}<|F_o|$; $w=(F_{max}/|F_o|)^2$, where F_{min}, F_{max}, and F_{wt} were, each changed during the refinements to balance the $\sum w(\Delta F)^2$ over the whole range of $|F_o|$ and $(\sin\theta)/\lambda$. Those values applied at the final refinement were $F_{min}=2.57$, $F_{max}=12.85$, and $F_{wt}=0.15$ respectively.

The final atomic co-ordinates of the heavy atoms, and their estimated standard deviations and the anisotropic temperature factors, are listed in Tables 2 and 3 respectively. The atomic co-ordinates and the isotropic temperature factors of the hydrogen atoms are listed in Table 4. The observed and calculated structure factors are given in Table 5.[11]

11) Table 5 has been submitted to, and is kept as Document No. 7211 by, the office of the Chemical Society of Japan, 1-5 Kanda Surugadai, Chiyoda-ku, Tokyo. A copy may be secured by citing the Document number and by remitting, in advance, ¥ 300 for photo prints. Pay by check or money order payable to: Chemical Society of Japan.

Results and Discussion

Molecular Structure. Figure 2 shows the molecular structure projected along the *a* axis. The seven atoms of the acetaldehyde moiety are shown as hatched circles. The bond distances and angles were calculated using the DAPH program;[9] they are listed in Tables 6 and 7 respectively.

The trimethylaluminum connects with [$Me_2Al\cdot O\cdot CPh{:}NPh$,MeCHO], one half of the polymerization catalyst-monomer complex, by co-ordination between

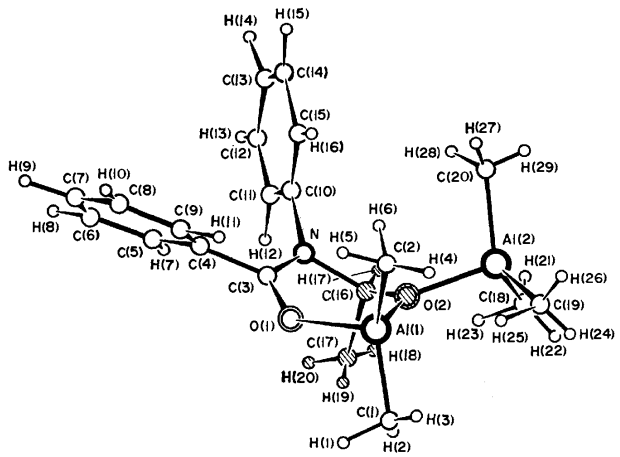

Fig. 2. The molecular structure.

Table 6. Interatomic distances along with their estimated standard deviations

Atoms	Distance (Å)	σ (Å)	Atoms	Distance (Å)	σ (Å)
Al(1)-C(1)	1.936	0.013	Al(2)-C(18)	2.012	0.014
Al(1)-C(2)	1.948	0.014	Al(2)-C(19)	1.960	0.015
Al(1)-O(1)	1.842	0.007	Al(2)-C(20)	1.960	0.013
Al(1)-O(2)	1.860	0.006	Al(2)-O(2)	1.928	0.006
O(1)-C(3)	1.259	0.010	O(2)-C(16)	1.378	0.011
C(3)-N	1.329	0.011	C(16)-C(17)	1.523	0.015
C(3)-C(4)	1.500	0.013	C(16)-N	1.489	0.011
N-C(10)	1.458	0.011	C(16)-H(17)	1.09	0.10
C(4)-C(5)	1.325	0.015	C(10)-C(11)	1.331	0.013
C(5)-C(6)	1.401	0.019	C(11)-C(12)	1.385	0.016
C(6)-C(7)	1.328	0.021	C(12)-C(13)	1.395	0.018
C(7)-C(8)	1.359	0.021	C(13)-C(14)	1.331	0.018
C(8)-C(9)	1.464	0.019	C(14)-C(15)	1.369	0.017
C(9)-C(4)	1.388	0.015	C(15)-C(10)	1.386	0.014
C(1)-H(1)	1.08	0.10	C(18)-H(21)	0.97	0.10
C(1)-H(2)	0.94	0.10	C(18)-H(22)	1.08	0.11
C(1)-H(3)	1.15	0.10	C(18)-H(23)	0.93	0.11
C(2)-H(4)	1.08	0.10	C(19)-H(24)	1.03	0.11
C(2)-H(5)	1.01	0.11	C(19)-H(25)	1.11	0.10
C(2)-H(6)	1.04	0.10	C(19)-H(26)	1.08	0.10
C(17)-H(18)	1.02	0.10	C(20)-H(27)	1.04	0.11
C(17)-H(19)	1.06	0.11	C(20)-H(28)	1.00	0.10
C(17)-H(20)	0.94	0.10	C(20)-H(29)	1.03	0.11
C(5)-H(7)	1.11	0.09	C(11)-H(12)	1.00	0.13
C(6)-H(8)	1.11	0.10	C(12)-H(13)	1.11	0.12
C(7)-H(9)	1.04	0.11	C(13)-H(14)	1.05	0.14
C(8)-H(10)	1.10	0.11	C(14)-H(15)	1.05	0.10
C(9)-H(11)	1.15	0.11	C(15)-H(16)	1.04	0.11

TABLE 7. INTERATOMIC ANGLES ALONG WITH THEIR ESTIMATED STANDARD DEVIATIONS

Atoms	Angle (deg.)	σ (deg.)	Atoms	Angle (deg.)	σ (deg.)
C(1)-Al(1)-C(2)	121.6	0.6	O(2)-Al(2)-C(18)	108.0	0.5
C(1)-Al(1)-O(1)	108.1	0.5	O(2)-Al(2)-C(19)	99.8	0.5
C(1)-Al(1)-O(2)	114.4	0.4	O(2)-Al(2)-C(20)	103.6	0.4
C(2)-Al(1)-O(1)	101.7	0.5	C(18)-Al(2)-C(19)	113.7	0.6
C(2)-Al(1)-O(2)	112.2	0.5	C(18)-Al(2)-C(20)	113.6	0.6
O(1)-Al(1)-O(2)	94.1	0.3	C(19)-Al(2)-C(20)	116.3	0.6
Al(1)-O(1)-C(3)	125.3	0.6	Al(1)-O(2)-Al(2)	125.0	0.3
O(1)-C(3)-N	119.9	0.8	Al(1)-O(2)-C(16)	118.5	0.5
O(1)-C(3)-C(4)	115.9	0.8	Al(2)-O(2)-C(16)	116.6	0.5
N-C(3)-C(4)	124.1	0.7	O(2)-C(16)-N	110.0	0.7
C(3)-N-C(16)	121.7	0.7	O(2)-C(16)-H(17)	111	5
C(3)-N-C(10)	123.3	0.7	O(2)-C(16)-C(17)	112.2	0.8
C(16)-N-C(10)	115.0	0.7	N-C(16)-H(17)	106	5
			C(17)-C(16)-H(17)	104	5
			N-C(16)-C(17)	113.0	0.8
C(3)-C(4)-C(5)	121.6	0.9	N-C(10)-C(11)	121.5	0.8
C(3)-C(4)-C(9)	119.2	0.9	N-C(10)-C(15)	117.4	0.8
C(5)-C(4)-C(9)	119	1	C(11)-C(10)-C(15)	121.1	0.9
C(4)-C(5)-C(6)	119	1	C(10)-C(11)-C(12)	119	1
C(5)-C(6)-C(7)	125	1	C(11)-C(12)-C(13)	119	1
C(6)-C(7)-C(8)	119	1	C(12)-C(13)-C(14)	122	1
C(7)-C(8)-C(9)	117	1	C(13)-C(14)-C(15)	118	1
C(8)-C(9)-C(4)	121	1	C(14)-C(15)-C(10)	121	1
Al(1)-C(1)-H(1)	110	5	Al(2)-C(18)-H(21)	100	6
Al(1)-C(1)-H(2)	111	6	Al(2)-C(18)-H(22)	118	6
Al(1)-C(1)-H(3)	110	5	Al(2)-C(18)-H(23)	102	7
H(1)-C(1)-H(2)	107	8	H(21)-C(18)-H(22)	105	8
H(1)-C(1)-H(3)	105	8	H(21)-C(18)-H(23)	125	9
H(2)-C(1)-H(3)	114	8	H(22)-C(18)-H(23)	108	9
Al(1)-C(2)-H(4)	103	5	Al(2)-C(19)-H(24)	107	6
Al(1)-C(2)-H(5)	112	6	Al(2)-C(19)-H(25)	114	5
Al(1)-C(2)-H(6)	109	6	Al(2)-C(19)-H(26)	111	5
H(4)-C(2)-H(5)	115	8	H(24)-C(19)-H(26)	114	8
H(4)-C(2)-H(6)	107	8	H(24)-C(19)-H(26)	107	8
H(5)-C(2)-H(6)	111	8	H(25)-C(19)-H(26)	105	7
C(16)-C(17)-H(18)	115	6	Al(2)-C(20)-H(27)	110	6
C(16)-C(17)-H(19)	113	6	Al(2)-C(20)-H(28)	115	6
C(16)-C(17)-H(20)	106	6	Al(2)-C(20)-H(29)	111	6
H(18)-C(17)-H(19)	99	8	H(27)-C(20)-H(28)	107	8
H(18)-C(17)-H(20)	126	8	H(27)-C(20)-H(29)	109	9
H(19)-C(17)-H(20)	96	8	H(28)-C(20)-H(29)	104	9
C(4)-C(5)-H(7)	120	5	C(10)-C(11)-H(12)	119	7
C(6)-C(5)-H(7)	121	5	C(12)-C(11)-H(12)	122	7
C(5)-C(6)-H(8)	117	5	C(11)-C(12)-H(13)	124	6
C(7)-C(6)-H(8)	118	5	C(13)-C(12)-H(13)	117	6
C(6)-C(7)-H(9)	119	6	C(12)-C(13)-H(14)	113	8
C(8)-C(7)-H(9)	121	6	C(14)-C(13)-H(14)	125	8
C(7)-C(8)-H(10)	122	6	C(13)-C(14)-H(15)	118	6
C(9)-C(8)-H(10)	121	6	C(15)-C(14)-H(15)	123	6
C(8)-C(9)-H(11)	116	5	C(14)-C(15)-H(16)	120	6
C(4)-C(9)-H(11)	123	5	C(10)-C(15)-H(16)	120	6

the electron-deficient aluminum atom and the electron-rich oxygen atom of the acetaldehyde moiety. In the molecular structure of [dioxane, $(AlMe_3)_2$], a similar co-ordination of $AlMe_3$ to the oxygen atom is found.[12] The Al(2)-O(2) distance of 1.928(6) Å is shorter than the corresponding distance of 2.02(2) Å in [dioxane, $(AlMe_3)_2$]. The geometry of the Al(2) atom is a slightly distorted tetrahedron. The average value of the O(2)-Al(2)-C(methyl) angles of 103.8(0.5)° is a little smaller than that of C(methyl)-Al(2)-C(methyl), 114.5(0.6)°. The average bond distance between Al(2) and three methyl carbons is 1.977(14) Å. The Al(1) atom has a much more distorted tetrahedral geometry than Al(2). The maximum and minimum bond angles around the Al(1) atom are 121.6(0.6)° of C(1)-Al(1)-C(2) and 94.1(0.3)° of O(1)-Al(1)-O(2) respectively.

12) J. L. Atwood and G. D. Stucky, *J. Amer. Chem. Soc.*, **89**, 5362 (1967).

TABLE 8. THE COMPARISON OF THE SELECTED INTERATOMIC DISTANCES AND ANGLES IN [$Me_2Al\cdot O\cdot CPh{:}NPh$,MeCHO, $AlMe_3$] (III) WITH THE CORRESPONDING VALUES IN [$Me_2Al\cdot O\cdot CPh{:}NPh$, MeCHO]$_2$ (II)

Atoms	(III)	(II)
Al(1)-O(1)	1.842(7) Å	2.045(7) Å
Al(1)-O(2)	1.860(6)	1.858(6)
O(1)-C(3)	1.259(10)	1.265(12)
C(3)-N	1.329(11)	1.364(12)
N-C(16)	1.489(11)	1.469(12)
C(16)-O(2)	1.378(11)	1.418(11)
C(3)-C(4)	1.500(13)	1.455(13)
N-C(10)	1.458(11)	1.466(12)
C(16)-C(17)	1.523(15)	1.559(17)
O(1)-Al(1)-O(2)	94.1(0.3)°	85.1(0.3)°
Al(1)-O(1)-C(3)	125.3(0.6)	127.6(0.6)
O(1)-C(3)-N	119.9(0.8)	119.6(0.8)
C(3)-N-C(16)	121.7(0.7)	120.8(0.7)
N-C(16)-O(2)	110.0(0.7)	110.9(0.7)
C(16)-O(2)-Al(1)	118.5(0.5)	128.0(0.5)

The molecular structure of this compound, except for the trimethylaluminum moiety, is very similar to that of one-half of the polymerization catalyst-monomer complex II. Table 8 compares the selected interatomic bond distances and angles in the present complex, [$Me_2Al\cdot O\cdot CPh:NPh$,MeCHO,$AlMe_3$] (III), with those of the corresponding parts in [$Me_2Al\cdot O\cdot CPh:NPh$,MeCHO]$_2$ (II). In Fig. 3 are compared the molecular structures of II and III projected onto the O-C-N plane of the amide moiety, which is present in both complexes. The numbers in brackets show the deviations of each atom from the O-C-N plane (in Å units).

The Al(1)-O(1) distance in II is much longer than that in III. This may be due to the difference in the co-ordination geometries of aluminum atoms. In the complex II the aluminum atom is penta-co-ordinated, it has a trigonal-bipyramidal geometry, and the oxygen atom of the amide moiety, O(1), occupies the apical position. The Al(1)-O(2) bond distances, on the contrary, show a good agreement in these two compounds. The C-O bond distance in the co-ordinated aldehyde moiety in III, C(16)-O(2)=1.378(11) Å, is a little shorter than the normal C-O single bond distance, though not significantly so. The C(16)-C(17) (1.523 (15) Å) and N-C(16) (1.489(11) Å) distances agree well with the respective expected single-bond distances.

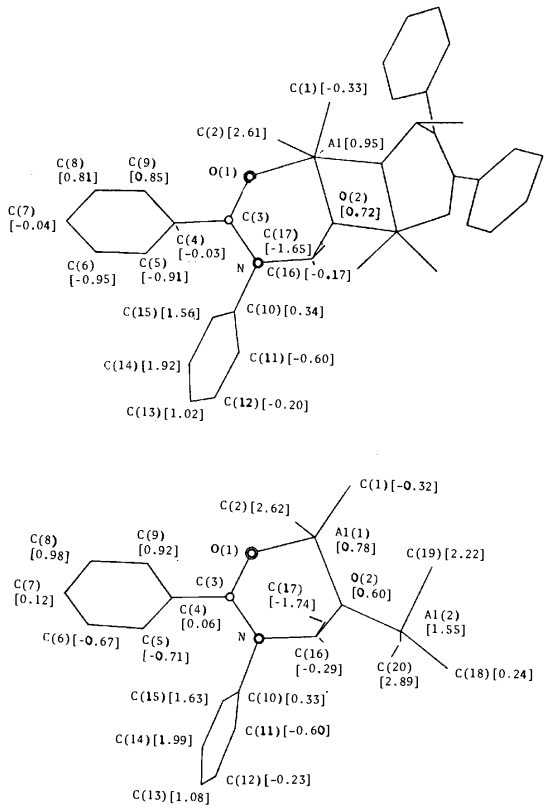

Fig. 3. Comparison of the molecular structure of [$Me_2Al \cdot O \cdot CPh:NPh$,MeCHO]$_2$ (*top*) and [$Me_2Al \cdot O \cdot CPh:NPh$, MeCHO,$AlMe_3$] (*bottom*). Both are projected onto the plane of the -O-C-N- skeletons which are contained commonly in both molecules. Deviations from the plane (in Å) are given in brackets.

The two adjacent benzene rings in the amide moiety in III have a *cis* configuration, and the internal rotation angle around the C(3)–N bond is 12.7°. The dihedral angle between the best planes of these rings is 67.4°.

Crystal Structure. Figure 4 shows the molecular packing in the unit cell. The intermolecular atomic contacts shorter than 3.8 Å are shown by the broken lines. These are the usual van der Waals' contact distances.

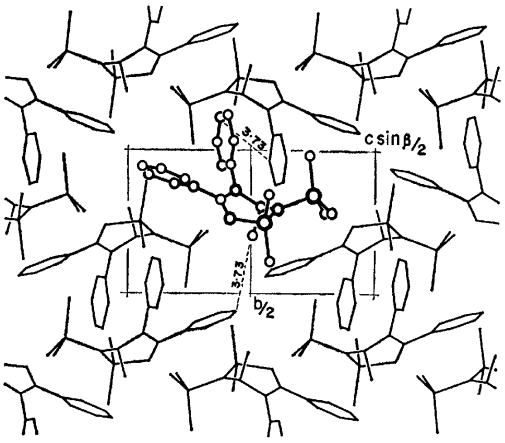

Fig. 4. Crystal structure viewed along the *a* axis.

Polymerization Mechanism in This Catalytic System

In the catalytic system of the highly stereospecific polymerization of acetaldehyde, we have previously undertaken the X-ray structure analysis of the following four key substances in an attempt to clarify the reaction mechanism. They are;

(I) [$Me_2Al \cdot O \cdot CPh:NPh]_2$

(II) [$Me_2Al \cdot O \cdot CPh:NPh$, $MeCHO]_2$

(III) [$Me_2Al \cdot O \cdot CPh:NPh$, MeCHO, $AlMe_3$]

(IV) [$Me_2Al \cdot O \cdot CPh:NPh$, $ONMe_3$]

The molecular geometries of these four complexes and the organochemical backgrounds have already been reported.[1-8] Figure 5 shows the molecular structures of these complexes viewed along arbitrary orientations, for an easy understanding of them (the numbers from I to IV correspond to the above complexes).

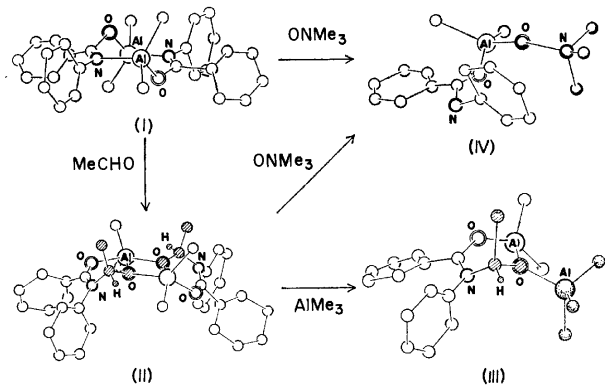

Fig. 5. Moleculer structures and their reactions of four key substances in the catalytic system of trimethylaluminum-benzanilide.

The dimeric catalyst I takes an imino-ether-type structure: a centro-symmetrical eight-membered ring is composed of the -O-C-N- bridges of amide moieties between two aluminum atoms. The complex IV is monomeric and *catalytically inactive.* The Al-O-C-N moiety takes the same configuration as the monomeric unit of the catalyst I, except that two benzene rings adopt a *trans* configuration.

The catalyst-monomer complex II has a dimeric structure related by the two-fold axis. The aldehyde moiety is maintained by the catalyst at the sites of both oxygen and α-carbon atoms. The oxygen atom co-ordinates to the two aluminum atoms, and the α-carbon atom bonds to the nitrogen of the amide moiety. However, the Al-O-C-N moiety takes a different configuration from that in I or IV. In the structure of III, the configuration of the monomeric unit of II is exactly maintained. The typical Lewis acid, $AlMe_3$, attacks and co-ordinates to the aldehyde oxygen atom, but not to the amide oxygen. This suggests that the aldehyde oxygen atom is more active than the amide oxygen in response to the attack of the electrophilic reagent.

Besides the above-mentioned molecular geometries, much chemical evidence has been accumulated.[1-4]

They are: (a) both catalysts, I and II, lose their activities when they are absolutely dried; a small amount of water behaves as the co-catalyst in this system, and both the yield of polymer and the stereospecificity of the polymerization reach their maxima at the optimum water concentration (1/30 mole per mole of the catalyst I, *i.e.*, *ca.* 1×10^{-4} mol% of the aldehyde); and (b) the polymerization is hindered by the existence of the strong electron donor. These two facts show that the polymerization system belongs to the cationic type; we will call the present polymerization the "co-ordinated cationic polymerization". Other important evidences are: (c) the aldehyde moiety of II can be easily replaced by a free aldehyde present in the solution; and (d) the water which is a co-catalyst in this system does not affect the exchange reaction of aldehyde.

In the reaction from I to II, we can postulate the following steps: (1) the fission of the Al–N bond in I induced by the co-ordination of the acetaldehyde to the aluminum atom by its oxygen, as in the co-ordination of $ONMe_3$ in IV; (2) the formation of an imino-ether-type intermediate, in which two benzene rings take a stable *trans* configuration; (3) bond formation between the nitrogen atom (in amide) and α-carbon (in aldehyde), followed by the configurational change of benzene rings from *trans* to *cis*, and (4) dimeric association. The association reaction is placed last because the cryoscopic measurement of the molecular weight of II shows the compound is likely to be monomeric in such a dilute solution as in the present polymerization conditions; this may be supposed on the basis of the long Al–O (aldehyde oxygen) distance of 1.985(6) Å. The formation of the monomeric complex III also supports the dissociation of the II in the dilute solution. The configurational change from (1) to (4) was examined by using a molecular model reported elsewhere.[7]

From the knowledge of the molecular structures given by the chemical evidence, a plausible mechanism of *isotactic* polymerization is proposed; it is shown in Fig. 6 (Schemes V to VII).

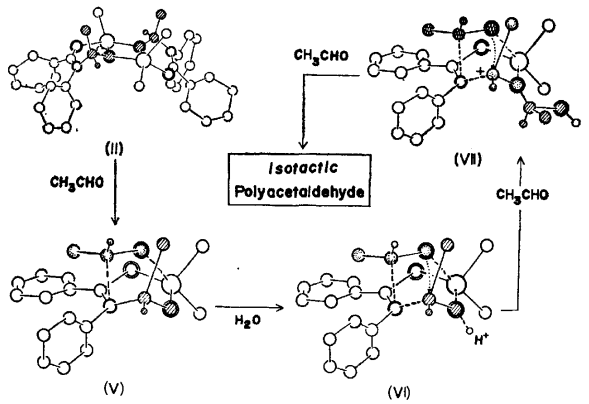

Fig. 6. Proposed mechanism for stereospecific polymerization of acetaldehyde.

The scheme V is constructed as an intermediate complex both for the aldehyde exchange reaction and for the initiation of the polymerization reaction. The broken lines show the postulated weak bonds caused by the co-ordination of the aldehyde. Model examination shows that the steric hindrance gives little possibility of taking a co-ordination other than that drawn in the scheme V. This fact probably contributes to the stereospecificity of the polymerization. In the exchange reaction, the aldehyde moiety in the catalyst is replaced by the weakly co-ordinated second aldehyde and there is no further change.

In the polymerization initiation, the formation of a chemical bond takes place between these two aldehyde molecules. This case is shown in scheme VI. First, a proton (probably from the water, the co-catalyst) attacks the oxygen atom of the initially-co-ordinated aldehyde, as the trimethylaluminum attacks the corresponding aldehyde oxygen in II. Then the cationic character of the proton transfers to the oxygen to form an oxonium cation, which weakens the co-ordination bond between the oxygen and aluminum atoms. After that, the cationic character moves to the α-carbon atom and generates a carbonium cation, which increases the affinity to the oxygen atom of the secondary co-ordinated aldehyde and at the same time weakens the bonding to the nitrogen atom. The secondary co-ordinated aldehyde now adds to the initially-co-ordinated one, and the aldehyde dimer thus formed replaces the initially co-ordinated aldehyde. The replacement is accompanied by the stimulation of the co-ordination of a new, third aldehyde. This is shown in scheme VII. The new aldehyde adds to the dimer, and the newly-formed trimer replaces the dimer in its co-ordination. The succession of these reactions produces the linear *isotactic* polymer of acetaldehyde.

As has been reported, the polymerization of acetaldehyde by the catalysis of complex III gives an *atactic* polymer. This fact can be explained by the dissociation of trimethylaluminum from III. The trimethylaluminum itself also acts as a polymerization catalyst and gives an *atactic* polyaldehyde under the conditions of the polymerization reaction by the complex III.[4] The polymerization reaction by the I or II catalyst is very mild compared with the reaction by the trimethylaluminum itself. Therefore, if the complex III is placed under the polymerization conditions, the dissociation of trimethylaluminum from this complex occurs. The dissociated trimethylaluminum acts predominantly as a polymerization catalyst and gives an *atactic* polymer.

The authors wish to express their deep thanks to Professor Hisaya Tani and Dr. Hajime Yasuda of Osaka University for their kindness in supplying the samples and for many their helpful discussion.

Measurements of Acid-strength Distribution beyond $H_0=-8.2$ of Sillca-Alumina Catalysts by UV-Spectrophotometric *n*-Butylamine Titration Method[1)]

Jun-ichiro TAKE, Tetsuo TSURUYA,[2)] Tetsuo SATO,[3)] and Yukio YONEDA

Department of Synthetic Chemistry, Faculty of Engineering, The University of Tokyo, Hongo, Bunkyo-ku, Tokyo

(Received May 29, 1972)

A new UV-spectrophotometric *n*-butylamine titration method was proposed for measuring acid-strength distribution of acid sites on solid acid catalysts. The method can provide information on acid-strength distribution of acid sites beyond $H_0=-8.2$, which can not be obtained by the conventional visual *n*-butylamine titration method. Acid-strength distributions were measured for a series of silica-alimina catalysts differing in sodium content, using 4-benzeneazodiphenylamine ($pK_a=1.5$), *trans*-benzalacetophenone ($pK_a=-5.6$), 4-nitrotoluene ($pK_a=-10.5$), and 2,4-dinitrotoluene ($pK_a=-12.8$) as indicators. The results revealed that about one-half of the acid sites on an unpoisoned silica-alumina catalyst lay in the H_0 region from -10.5 to -12.8, and the strongest ones in the H_0 region beyond -12.8. The strong acid sites were eliminated with the modification of acid-strength distribution as the catalyst was poisoned with sodium ions. UV spectra of the above indicators in adsorbed state were discussed.

Various methods have been developed for the measurement of acid-strength distributions of solid surfaces. The method frequently referred to as the Benesi or *n*-butylamine titration method[4,5)] has been widely employed. In this method, solids suspended in a nonpolar solvent such as benzene are titrated with *n*-butylamine and a series of visible H_0 indicators, the end-point being determined by the naked eye. Benesi[5)] revealed, using this method, that most of the acid sites on silica-alumina lay in the region $H_0 \leq -8.2$. Information on acid-strength distributions in this region is indispensable for the study of solid acid catalysis. No such information, however, can be provided by the conventional *n*-butylamine titration method, since anthraquinone is the least basic ($pK_a=-8.2$) of well-known visible H_0 indicators. Available H_0 indicators having a pK_a lower than -8.2 change color in the ultraviolet region, and thus UV-spectrophotometric titration becomes essential. Moreover, such titration is superior to the conventional method by the naked eye in determining the end-point.

From the viewpoint of homogeneity of acid sites in acid strength, Kobayashi[6)] has recently analyzed the data on silica-alumina that were obtained by UV-spectrophotometric titration using visible dimethyl yellow ($pK_a=3.3$) or methyl red ($pK_a=4.8$) as an indicator. Durshel and Sommers[7)] showed ultraviolet and visible absorption spectra of several visible H_0 indicators in adsorbed state in order to examine their suitability for the conventional titration of surface acidity.

We have applied UV-spectrophotometry to the conventional method using 4-benzeneazodiphenylamine, the use of which was recommended by Drushel and Sommers.[7)] The method was then extended to titration using other indicators, especially 4-nitrotoluene ($pK_a=-10.5$) and 2,4-dinitrotoluene ($pK_a=-12.8$), both of which respond to very strong acid sites with color change in the ultraviolet region. The use of these indicators furnished new information on acid-strength distributions in the H_0 region beyond -8.2 of acid sites on silica-alumina catalysts.

Experimental

Materials. The silica-alumina catalysts listed in Table 1 were taken from batches used in previous studies,[8)] and were calcined at 550°C for 8 hr in atmosphere. Silica gel (WAKOGEL Q-12 for chromatography) was also used. The indicators, 4-benzeneazodiphenylamine (BADA), *trans*-benzalacetophenone (BAP), 4-nitrotoluene (NT), and 2,4-dinitrotoluene (DNT), were of EP or GR grade and were dissolved in decaline after repeated recrystallization. Their pK_a values are 1.5 for BADA, -5.6 for BAP, -10.5 for NT, and -12.8 for DNT.[9)] A 0.1 N decaline solution of *n*-butylamine, purified by distillation, was used as a titrant. Decaline used as a nonpolar solvent was passed through two chromatographic columns containing freshly activated silica gel and alumina[10)] in order to remove water, aromatics and other impurities. The water content was reduced to below 10 ppm.

Titration Procedure. The catalyst sample was activated at 450°C overnight in a vacuum. After ten to twenty 20 m*l* conical flasks with ground glass stoppers had been weighed, roughly one gram of the sample was placed in each in a dry box replaced with dried nitrogen. The tightly stoppered flasks were reweighed, and about 10 m*l* of decaline was then added to each in the dry box. A solution of *n*-butylamine was introduced into the sample slurries so that they differed in amine content. After vigorous shaking, the tightly stoppered sample slurries were placed in a desiccator at 30°C for two days for equilibration, and then an indicator was added to each. They were put to stand in the desiccator for additional three or four days for reaction of the indicator. The result-

1) Presented at the 18th Annual Meeting of the Chemical Society of Japan, Osaka, April 1965.

2) Present address: Central Research Laboratory, Showa Dneko Co. Ltd., Tamagawa, Ota-ku, Tokyo.

3) Present address: Central Technical Research Laboratory, Nippon Oil Co. Ltd., Yokohama, Kanagawa.

4) O. Johnson, *J. Phys. Chem.*, **59**, 827 (1955).

5) H. A. Benesi, *ibid.*, **61**, 970 (1957).

6) J. Kobayashi, *Nippon Kagaku Zasshi*, **84**, 25 (1963).

7) H. V. Drushel and A. L. Sommers, *Anal. Chem.*, **38**, 1723 (1966).

8) I. Mochida and Y. Yoneda, *J. Catal.*, **7**, 393 (1967); H. Matsumoto, J. Take, and Y. Yoneda, *ibid.*, **11**, 211 (1968).

9) M. A. Paul and F. A. Long, *Chem. Rev.*, **57**, 1 (1957).

10) J. Take, N. Kikuchi, and Y. Yoneda, *J. Catal.*, **21**, 164 (1971).

TABLE 1. CATALYSTS

No	Symbol	Surface area[a] (m^2/g)	Remarks
1	SA-1	540	Silica-alumina, 13%Al_2O_3, Nippon Cat, a cracking catalyst of the Shokubai Kasei Co.
2	SA-1-Na-1	450	0.048 meq Na/g, by impregnation of SA-1 with NaOH aq. soln.
3	SA-1-Na-2	480	0.087 meq Na/g, by impregnation of SA-1 with NaOH aq. soln.
4	SA-1-Na-3	480	0.168 meq Na/g, by impregnation of SA-1 with NaOH aq. soln.
5	SA-Na-HCl	...	0.119 meq Na/g, by treatment of SA-Na (another lot of silica-alumina impregnated with NaOH) with HCl
6	SA-Na-HAcO	...	0.200 meq Na/g, by treatment of SA-Na with HAcO

a) Measured by the BET method with N_2.

ing sample slurry was transferred to a conventional 10 mm absorption cell with a 9 mm quartz spacer to provide a light-path length of 1 mm.

No indicators were detected in the supernatant layer of decaline. The following amounts of indicators were used: 0.3 for BADA, 1 for BAP, and 1.5 to 2.0 for NT and DNT, in μmol/g-catalyst.

Evaluation of Molar Absorptivities. Ultraviolet and visible absorption spectra were recorded against reference cell containing fresh sample slurries (not treated with amine) on Hitachi Recording Spectrophotometer (Model EPS-2). The molar absorptivity ε of an adsorbed indicator was evaluated by the equation

$$\varepsilon = \frac{Av}{mwl}, \qquad (1)$$

where A is absorbance, v the volume of a sample slurry in an absorption cell (liter), m the amount of an adsorbed indicator (mol/g-catalyst), w the amount of a sample in an absorption cell (g), determined after decaline has been removed by evaporation, l the light-path length (cm).

Results and Discussion

The relevant UV absorption spectra of the indicators are summarized in Table 2.

4-Benzeneazodiphenylamine (BADA). A decaline solution of BADA (yellow) shows absorption at 390 mμ. This is slightly red-shifted (415 mμ) in a polar solvent such as ethanol because of the interaction between indicator and solvent. An absorption band at 535 mμ (purple) in acidified aqueous solution is evidently due to the conjugate acid of BADA. Adsorption of BADA on every fresh silica-alumina catalyst gave a band at 550 mμ alone, in good agreement with the spectrum obtained by Drushel and Sommers,[7] showing that all the adsorbed molecules were in the conjugate-acid form. As the level of neutralization of the surface was raised, the band decreased in intensity with the development of an absorption band near 450 mμ due to the physically adsorbed neutral indicator, and finally only the band near 450 mμ remained. The slight red-shift to 450 mμ from 440 mμ for silica gel seems to be due to a stronger physical adsorption of the indicator. The presence of an isosbestic point was also observed in a series of spectra, each being determined for a catalyst at a different level of neutralization, indicating that none other than the simple acid-base reaction took place on the solid surface.[11] The above behavior is very similar to that observed in a series of aqueous sulfuric acid solutions, each having a different acidity.

TABLE 2. ABSORPTION SPECTRA OF INDICATORS[a]

Indicator	In solution		On solid surface		
	Acidic	Neutral	Fresh SA-1	Neutralized SA-1	Silica gel
BADA	535	415	550	450	440
BAP	320 (w) 400—430 (s)	315	320 (sh) ~400	320	315
NT	380	310	300 (w,sh) 340 (s) ~500 (w)	300	295
DNT	280 (m) 340 (s)	260	260 (s) 320 (sh) ~500 (w)	260	255

a) λ in mμ; (s), strong; (m);, medium (w), weak; (sh), shoulder.

Changes in the level of neutralization of solid surfaces may therefore be followed quantitatively by observing the concentration of BADA adsorbed either in tht conjugate-acid form c_A or in the neutral form c_P. Spectrophotometric determination of the concentration requires data on the following molar absorptivities: (1) ε, the molar absorptivity at a selected wavelength of the adsorbed indicator, generally containing both the conjugate-acid species and the neutral one, (2) ε_A and ε_P, the molar absorptivity at the same wavelength of the pure species adsorbed in the conjugate-acid form and that in the neutral form, respectively. These are connected with c_A or c_P by the equation

$$\frac{c_A}{c_0} = \frac{\varepsilon-\varepsilon_P}{\varepsilon_A-\varepsilon_P} \text{ or } \frac{c_P}{c_0} = \frac{\varepsilon-\varepsilon_A}{\varepsilon_P-\varepsilon_A} \qquad (2)$$

only when $c_A+c_P=c_0$, where c_0 is the total concentration of the adsorbed indicator and can be determined from the amount of addition. Since the relation, $c_A+c_P=c_0$, holds evidently for adsorbed BADA, a titration curve can be obtained by plotting the color change ratio $x_A=c_A/c_0$ or $x_P=c_P/c_0$ of BADA against

11) H. H. Jaffe and M. Orchin, "Theory and Applications of Ultraviolet Spectroscopy," John Wiley and Sons, New York (1962), p. 563.

Table 3. Molar absorptivities of adsorbed BADA at 550 mμ

Amount of *n*-butylamine[a]	Catalysts									
	SA-1			SA-1-Na-1			SA-1-Na-2	SA-1-Na-3	SA-Na-HCl	SA-Na-HAcO
	$\varepsilon\times10^{-4}$[b]		n[c]	$\varepsilon\times10^{-4}$[b]		n[c]	$\varepsilon\times10^{-4}$	$\varepsilon\times10^{-4}$	$\varepsilon\times10^{-4}$	$\varepsilon\times10^{-4}$
0	4.20	(6.7%)	9	4.04	(0.4%)	2	3.85	4.46	4.49	4.31
0.05	...	...	..	3.63	(3.0%)	2	3.60	3.52	4.47	4.38
0.10	4.08	(12.4%)	3	2.20	(16.8%)	2	3.25	2.78	3.74	3.65
0.15	3.67	(13.7%)	3	2.48	(13.7%)	2	3.30	1.69	3.06	3.28
0.20	3.12	(5.6%)	3	0.92	(58.7%)	2	0.44	0.31	0.72	1.48
0.25	1.49	...	1	...	...	..	...	0.18	0.14	0.37
0.30	0.69	(18.9%)	3	0.07	(19.2%)	2	0.15	0.02	...	...
0.35	...	...	..	...	...	..	...	...	0.10	0.18
0.40	0.26	(19.2%)	2	0.12	(94.3%)	2	0.12	0.01	...	...
0.50	0.04	...	1	...	...	..	...	...	...	...

a) meq/g catalyst. b) Quantity in parentheses is the relative standard deviation.
c) Number of separate spectral measurements.

the amount of *n*-butylamine added.

The ε values at 550 mμ are given in Table 3, each being for a different level of neutralization of each silica-alumina catalyst. The reproducibility of the ε values is considerably good when it is taken into account that a specimen for spectral measurement is in slurry form.

We see that each fresh catalyst provides the same ε value within experimental error, and also that a few fresh catalysts including SA-1 remain practically unchanged even upon addition of the 0.05 or 0.1 meq/g-catalyst of *n*-butylamine. Thus the ε value for each fresh catalyst can be taken as the ε_A value of the indicator. This is also in line with the fact that a band appears only at 550 mμ on each fresh catalyst. The average ε_A value, $(4.3\pm0.4)\times10^4$, is in accordance with that (3.8×10^4) determined from a linear relationship between the absorbance at 550 mμ of adsorbed BADA and its amount with a thin wafer of SA-1.[12] It is lower than that in an aqueous sulfuric acid solution, 5.88×10^4 at the maximum peak position of 535 mμ, by a factor of about 1.4. A similar observation was reported for dimethyl yellow and methyl red adsorbed on silica-alumina catalyst by Kobayashi.[13] Molar absorptivity ε for each catalyst sufficiently neutralized corresponds to ε_P. It can be neglected since its value is very small compared with the ε_A value.

Titration curves are shown in Fig. 1. In the calculation of the color change ratio, ε for each fresh catalyst was taken as ε_A for the corresponding one. The color change of an indicator is visually observed when the surface concentrations of the neutral and the conjugate-acid species become equal. The point of color change or the end-point therefore corresponds to the intersection of a titration curve with a horizontal line at $x_A=0.5$.

According to Benesi,[5] acid strength of solid surfaces can be expressed with the Hammett and Deyrup H_0 function

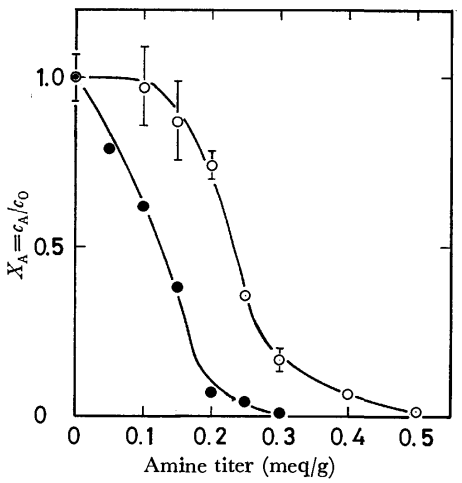

Fig. 1. Titration curves with BADA for SA-1(○) and SA-1-Na-3 (●).

$$H_0 = -\log(a_{H^+}f_B/f_{BH^+}) = pK_a + \log(c_B/c_{BH^+}). \quad (3)$$

The value of abscissa of the intersection therefore gives the amount of acid sites having an H_0 equal to or lower (stronger) than the pK_a of the indicator used. The amount of acid sites so determined for each silica-alumina catalyst is shown in Table 4. The acid content ($H_0\leq1.5$) of SA-1 decreases to about two-thirds of its original value on treatment with aqueous sodium hydroxide solution, but those for the set of the SA-1-Na and SA-Na catalysts scarcely differ from each other.

Table 4. Acid contents[a]

Catalyst	Indicators			
	BADA $pK_a=1.5$	BAP $pK_a=-5.6$	NT $pK_a=-10.5$	DNT $pK_a=-12.8$
SA-1	0.23	0.18	0.13	0.02
SA-1-Na-1	0.16	0.12	0.03	0
SA-1-Na-2	0.15_5	0.10_5	0.01_5	0
SA-1-Na-3	0.12_5	0.08	0	0
SA-Na-HCl	0.15	0.10	0	0
SA-Na-HAcO	0.18	0.07	0	0

a) In meq/g catalyst.

12) J. Take, H. Kawai, and Y. Yoneda, presented at the 25th Symposium on Catalysis of the Catalysis Society of Japan, Fukuoka, Oct. 1969.
13) J. Kobayashi, *Nippon Kagaku Zasshi*, **82**, 288 (1961).

TABLE 5. MOLAR ABSORPTIVITIES[a] FOR SA-1 AT DIFFERENT LEVELS OF NEUTRALIZATION

Amount of *n*-butylamine[b]	Indicators								
	BAP			NT			DNT		
	$\varepsilon \times 10^{-3}$		n[c]	$\varepsilon \times 10^{-3}$		n[c]	$\varepsilon \times 10^{-3}$		n[c]
0	11.8	(18.7%)	10	10.2	(19.6%)	13	5.09	(20.4%)	14
0.025	...	...	..	10.9	(25.7%)	3	...	...	..
0.05	11.2	(18.7%)	4	7.57	(31.4%)	4	2.90	(18.3%)	3
0.10	10.2	(19.5%)	4	7.19	(18.5%)	5	2.75	(9.5%)	3
0.15	8.07	(37.1%)	4	5.97	(31.0%)	5	1.87	(47.1%)	3
0.20	4.77	(79.2%)	4	4.65	(58.3%)	4	1.36	(25.7%)	3
0.25	...	...	..	2.98	(87.0%)	2	...	...	..
0.30	0.86	(105%)	4	3.93	(59.3%)	4	0.29	(114%)	2
0.40	0.06	(66.7%)	2	2.09	(70.8%)	6	0.79	(65.8%)	3

a) Quantity in parentheses is the relative standard deviation. b) In meq/g catalyst.
c) Number of separate spectral measurements.

TABLE 6. MOLAR ABSORPTIVITIES[a] FOR FRESH CATALYSTS

Catalyst	Indicators								
	BAP			NT			DNT		
	$\varepsilon \times 10^{-3}$		n[b]	$\varepsilon \times 10^{-3}$		n[b]	$\varepsilon \times 10^{-3}$		n[b]
SA-1	11.8	(18.7%)	10	10.2	(19.6%)	13	5.09	(20.4%)	14
SA-1-Na-1	12.9	(29.5%)	2	7.08	(8.3%)	3	4.39	(7.7%)	2
SA-1-Na-2	10.4	...	1	5.85	...	1	...	...	..
SA-1-Na-3	10.0	...	1	3.88	...	1	1.52	...	1
SA-Na-HCl	12.2	...	1	4.83	...	1	3.13	...	1
SA-Na-HAcO	8.04	...	1	1.91	...	1	1.45	...	1

a) Quantity in parentheses is the relative deviation. b) Number of separate spectral measurements.

Thus UV-spectrophotometric titration is useful for measuring an acid-strength distribution of acid sites on catalyst surfaces.

trans-*Benzalacetophenone (BAP).* A protonated BAP molecule in a concentrated sulfuric acid solution exhibits a strong band at 400—430 mμ depending upon acidity of the solution and a weak one near 320 mμ, as shown by Noyce and Jorgenson.[14] The former decreases in intensity with the development of the latter as acidity of the solution is reduced, and finally disappears.

The spectrum of BAP adsorbed on fresh SA-1, where a strong band near 400 mμ and a weak one near 320 mμ (shoulder) appear, shows that the conjugate-acid species is formed on the fresh surface of SA-1. Recent workers[7] observed that BAP adsorbed on silica-alumina gave a strong band at 390 mμ and a weak one at 310 mμ. They attributed the former mainly to the strongly adsorbed neutral species, presumably, on the basis of the difference between the wavelength of absorption on the silica-alumina (390 mμ) and that in concentrated sulfuric acid solution (430 mμ). Our assignment is also based on the fact that the intensity of the strong band near 400 mμ decreases as *n*-butylamine is added. The spectra in the ultraviolet region below 340 mμ varied in a somewhat complicated manner upon titration. No isosbestic point was observed. This suggests that some reactions besides the simple acid-base reaction take place in the system under investigation. When the complicated behavior of the spectra is ignored, an increase in the extent of neutralization of solid surfaces may be followed by observing a decrease in the intensity of the band near 400 mμ, as was the case in the titration using BADA.

The ε values at 400 mμ are summarized for different levels of neutralization of SA-1 in Table 5, and their variations with fresh catalysts in Table 6. They decrease with increasing amount of *n*-butylamine. Reproducibility is fair but not so good as that for adsorbed BADA. The value for fresh SA-1 does not change upon addition of the 0.05 meq/g-catalyst of *n*-butylamine (Table 5). This is also the case for SA-1-Na-1. The ε values for the fresh catalysts other than SA-Na-HAcO do not differ within experimental error (Table 6). These findings support the conclusion that the ε_A value of BAP corresponds to the ε value for each fresh catalyst except for SA-Na-HAcO. All the ε values for catalysts sufficiently neutralized, on which only the physically adsorbed neutral species is probably present, are very small compared with the ε_A value. Accordingly, in the calculation of the color change ratio, the ε_P was neglected for all the catalysts, and ε for each fresh catalyst was taken as ε_A for the corresponding one, except for SA-Na-HAcO. For the latter, the average ε value for other fresh catalysts, $(11.5 \pm 1.2) \times 10^3$, was taken as the ε_A value. The value is lower than that in an aqueous sulfuric acid solution of $H_0 = -7.3$ by a factor of about 3.4. The decrease in absorption intensity exceeds that observed for BADA.

14) D. S. Noyce and M. J. Jorgensen, *J. Amer. Chem. Soc.*, **84**, 4312 (1962).

Further study has revealed that this remarkable decrease in absorption intensity resulted from contamination with the *cis*-isomer produced by light-induced *trans-cis* isomerization of BAP either in adsorbed state or in solvent, and that the ε_A value of the *trans*-isomer adsorbed on SA-1 corresponded to about 56% of that in a sulfuric acid solution of $H_0=-7.3$.[15] Since the *cis*-isomer is almost as basic as the *trans*-isomer,[14] the use of the spectral data obtained without consideration for contamination with the *cis*-isomer are not likely to lead to a serious error.

A typical titration curve is shown in Fig. 2. Such a curve furnishes the amount of acid sites having an H_0 equal to or lower than -5.6 (Table 4). The acid contents ($H_0 \leq -5.6$) decrease with an increase in sodium content.

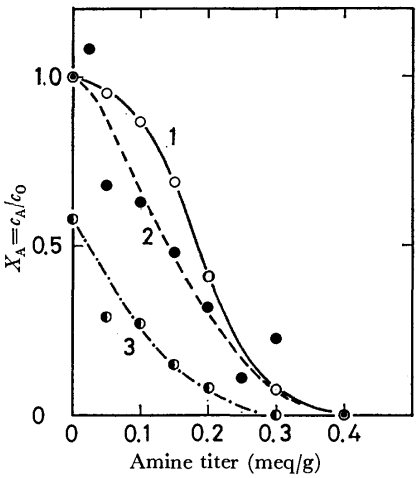

Fig. 2. Titration curves with (1) BAP, (2) NT, and (3) DNT for SA-1.

4-Nitrotoluene (NT). In dilute oleum protonated NT molecules show strong absorption only at 380 mμ. On successive dilution, the band decreases in intensity with the development of a band at 310 mμ due to the solvated neutral molecules, and finally disappears. In the spectrum of NT adsorbed on fresh SA-1, three bands appear near 300, 340, and 500 mμ. In most cases, the band near 300 mμ behaved in a complicated manner upon successive titration: that is, its absorption intensity decreased in an early stage and subsequently increased. On silica gel and silica-alumina catalysts sufficiently neutralized, NT gives only a band at 300 mμ. Thus it is apparent that the physically adsorbed molecules show absorption near 300 mμ, but it is difficult to conclude that the band is due only to the physically adsorbed molecules because of its complicated behavior during the course of titration. On the other hand, the strong band near 340 mμ, with a similar wavelength of absorption to that in acidic solutions, decreased in intensity without exception upon successive titration. This indicates that the band near 340 mμ is due to the species adsorbed in the conjugate-acid form. The very weak band near 500 mμ, which disappears on addition of excess *n*-butylamine, can be attributed to the anion radical of NT.

The absorbance of the band near 340 mμ was determined at 357 mμ, slightly longer than the wavelength of absorption maximum, in order to reduce the contribution from the band around 300 mμ (see Table 5 and 6). The ε value for fresh SA-1 appears to decrease slightly on addition of the 0.05 meq/g-catalyst of *n*-butylamine even when experimental error is considered (Table 5). The ε values for the fresh catalysts vary with catalyst (Table 6), showing that the fresh silica-alumina catalysts differ in their ability to adsorb NT molecules in the conjugate-acid form. Both facts imply that a new criterion is required for the determination of the ε_A value of the indicator.

Neither non-empirical nor empirical methods have been established for the estimation of the molar absorptivity of a certain species in adsorbed state from that in solution. With BADA and BAP, the molar absorptivity of the adsorbed conjugate-acid species has proved to fall to about 70% and to about 56% of that in acidic solution, respectively. If these correlations hold for NT, ε_A will be estimated to be 10.7×10^3 (60%) to 12.5×10^3 (70%) for the adsorbed conjugate-acid species of NT. These values are equal to the ε value observed for fresh SA-1 within experimental error. The assumption may be reasonable in view of the fact that the ε value for fresh SA-1 is substantially constant even on addition of the 0.025 meq/g-catalyst of *n*-butylamine (Table 5). The ε value for fresh SA-1 was therefore taken as the ε_A value for all the silica-alumina catalysts. As the ε_P value for each catalyst, the ε value for the corresponding one neutralized sufficiently with the 0.35—0.4 meq/g-catalyst of *n*-butylamine was taken, since it was not negligible as compared with the ε_A value.

In the calculation of the color change ratio, the complicated behavior of the band near 300 mμ was ignored as in the case of BAP (see Fig. 2 and Table 4). The acid contents ($H_0 \leq -10.5$) decrease with ε for fresh catalyst. The difference of acidity between SA-1-Na-3, SA-Na-HCl, and SA-Na-HAcO may become apparent by using an indicator slightly more basic than NT.

2,4-Dinitrotoluene (DNT). The spectral data in solutions were taken from literature.[16] Protonated DNT absorbs strongly at 340 mμ and moderately near 280 mμ. A band due to strongly solvated neutral DNT appears near 260 mμ. In the spectrum of DNT adsorbed on fresh SA-1, three bands appear: a strong one near 260 mμ, and weak ones near 320 (shoulder) and 500 mμ. On silica gel and SA-1 poisoned sufficiently with *n*-butylamine, DNT shows absorption only near 260 mμ. The intensity of the band near 320 mμ decreased upon successive titration, indicating that it was due to the adsorbed conjugate-acid species, while the band 260 mμ behaved in a similar manner to one near 300 mμ of adsorbed NT. Thus no isosbestic point was observed. The very weak band near 500 mμ can be attributed to the anion radical of DNT.

The absorbance of the band near 320 mμ was deter-

15) Presented at the 19th Annual Meeting of the Chemical Society of Japan, Yokohama, April 1966.

16) J. C. D. Brand, W. C. Horing, and M. B. Thornley, *J. Chem. Soc.*, **1952**, 1374.

mined at 340 mμ in order to reduce the contribution from the band near 260 mμ (see Tables 5 and 6). We see from these tables that an assumption is required for the calculation of the color change ratio of DNT as in the case of NT. The ε_A value for each catalyst was estimated to be 8.2×10^3, which corresponded to 60% of the value in oleum (1.37×10^4),[16] according to the criterion used for NT. The ε value for each catalyst sufficiently neutralized was taken as the ε_P value for the corresponding one (see Fig. 2 and Table 4).

Acid-strength Distribution. The acid strength distributions of acid sites on all of the silica-alumina catalysts are shown in Table 7. They are obtained from Table 4 as the difference of acid contents with two adjacent indicators.

TABLE 7. ACID-STRENGTH DISTRIBUTION[a),17]

Catalyst	H_0			
	1.5 to −5.6	−5.6 to −10.5	−10.5 to −12.8	≤−12.8
SA-1	0.05	0.05	0.11	0.02
SA-1-Na-1	0.04	0.09	0.03	0
SA-1-Na-2	0.05	0.09	0.01_5	0
SA-1-Na-3	0.04_5	0.08	0	0
SA-Na-HCl	0.05	0.10	0	0
SA-Na-HAcO	0.11	0.07	0	0

a) In meq/g catalyst.

The original unpoisoned silica-alumina catalyst SA-1 has the largest amount of strong acid sites ($-12.8< H_0\leq-10.5$) along with relatively small amounts of the strongest ones ($H_0\leq-12.8$), moderately strong ones ($-10.5<H_0\leq-5.6$), and weak ones ($-5.6<H_0\leq1.5$). This is qualitatively in line with the results of Benesi,[5] who found that the strength of most acid sites on synthetic silica-alumina lies beyond an H_0 of −8.2. Apparently strong acid sites ($H_0\leq-10.5$) on SA-1 are eliminated as it is poisoned with sodium ions. The effect of alkali-treatment on surface acidity, however, is not a mere disappearance of acid sites but a modification of acid-strength distribution where strong acid sites are eliminated and replaced in some manner with sites of lower acid strength. A similar effect was found for more severely alkali-poisoned silica-alumina by Hirschler[18] using H_R indicators.

Anion Radicals. Reducing ability of alumina and silica-alumina catalysts has recently been demonstrated with tetracyanoethylene[19] and various aromatic nitrocompounds.[20] For example, the latter compounds formed stable anion radicals on these catalysts, giving a three-line ESR spectrum insensitive to molecular oxygen. Adsorption of NT and DNT on fresh SA-1 gave ESR spectra (g value=2.004) similar to that of the adsorbed trinitrobenzene anion radical[20] and insensitive to molecular oxygen. This indicates that stable NT anion radical is formed on the catalyst surface. There seems to be no publication on UV spectra of NT anion radical. Comparison of the UV and ESR data on two different kinds of "free radicals" produced from NT in strongly basic solution[21] with another publication on ESR data[22] shows that one absorption at 538 mμ may be due to the anion radical (the other, 517 mμ). In the light of this and the fact that the surface of alumina became reddish-purple when it adsorbed trinitrobenzene,[20] the very weak bands near 500 mμ for NT and DNT (Table 2) can be attributed to their anion radicals. Accordingly, the wavelength employed for analysis of adsorbed NT or DNT is free from the band due to its anion radical. The concentration of reducing sites on the surface of SA-1 with alumina content of 13% is estimated to be 1×10^{-5} meq/g-catalyst from literature,[20] corresponding to about 1% of that of NT or DNT added. It is therefore concluded that the material balance, $c_A+c_P=c_0$, for each indicator is hardly affected by ignoring the formation of its anion radical. This is also given at least qualitative support by the fact that a reduction of absorptivity observed for the adsorbed conjugate-acid species of NT is not unusual.

The authors thank Dr. Y. Saito and Dr. H. Arai for their helpful discussions.

17) Numerical data before revision was presented by one of the authors (Y.Y.) at the plenary lecture of the 4th International Congress on Catalysis, Moscow, 1968.

18) A. E. Hirschler, *J. Catal.*, **2**, 428 (1963).
19) B. D. Flockhart, I. R. Leith, and R. C. Pink, *Trans. Faraday Soc.*, **65**, 542 (1969).
20) B. D. Flockhart, I. R. Leith, and R. C. Pink, *ibid.*, **66**, 469 (1970).
21) J. M. Millar and H. Pobiner, *Anal. Chem.*, **36**, 238 (1964).
22) G. A. Russell and E. G. Janzen, *J. Amer. Chem. Soc.*, **89**, 300 (1967).

Topological Index and Thermodynamic Properties. I. Empirical Rules on the Boiling Point of Saturated Hydrocarbons

Haruo HOSOYA, Keiko KAWASAKI,* and Kimiko MIZUTANI**
Department of Chemistry, Ochanomizu University, Bunkyo-ku, Tokyo
(Received June 10, 1972)

Empirical relations are proposed for the boiling point (bp) and the topological index (Z_G) of a saturated hydrocarbon as

$bp = a \log Z_G + b$

or $bp = (a \log Z_G + c)/\sqrt{N} + b$,

where N is the number of the carbon atoms. A number of compounds with or without ring(s) are plotted for these relations. Correlation is generally better for cyclic compounds than for chain compounds. Sterically hindered paraffins deviate appreciably. Several empirical rules on the isomeric lowering of the boiling point of saturated hydrocarbons are presented and most of them are shown to be consistent with the above relations. Several empirical formulae for the boiling point of normal paraffins are compared and discussed.

Topological index Z_G has been defined for a non-directed graph G, or the carbon atom sekeleton of a saturated hydrocarbon.[1-3] In relation to the mathematical treatment on Z_G many interesting properties were found. A graphical method for enumerating the coefficients of the characteristic or secular polynomial of the Hückel molecular orbital was proposed.[4] It was also pointed out that Z_G is correlated well with several of the thermodynamic quantities of molecules such as the boiling point.[1]

In this paper relations between the topological index and the boiling point of saturated hydrocarbons are analyzed in detail and several empirical rules on the boiling point are presented and discussed.

Topological Index

The definition and enumerating method of the topological index are summarized below.[1-4]

A non-adjacent number $p(G,k)$ for graph G is the number of ways in which such k bonds are so chosen from G that no two of them are connected, $p(G,0)$ being unity and $p(G,1)$ the number of bonds.

The topological index Z_G for G is defined as the sum of $p(G,k)$'s,

$$Z_G = \sum_{k=0}^{m} p(G, k). \quad (1)$$

For example Z_G's for the two graphs I and II are obtained as follows:[5]

$$Z_I = 1 + 6 + 8 + 2 = 17$$
$$Z_{II} = 1 + 6 + 5 = 12.$$

For larger graphs Z_G can be obtained using either

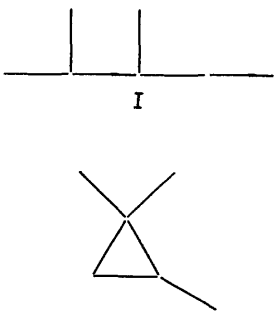

Chart 1

of the two composition principles, CPI and CPII. With the notations adopted in Fig. 1 we have

$$\text{CPI: } Z_G = Z_L Z_M + Z_A Z_B Z_C Z_D Z_E Z_F \quad (2)$$

$$\text{CPII: } Z_G = Z_A Z_B Z_C Z_M + Z_D Z_E Z_F Z_L - Z_A Z_B Z_C Z_D Z_E Z_F \quad (3)$$

Application of CPI and CPII, respectively, to graphs I and II is illustrated in Fig. 2.

Tables of the $p(G,k)$ numbers and Z_G values for smaller tree graphs and non-tree graphs are respectively given in Refs. 2 and 3.

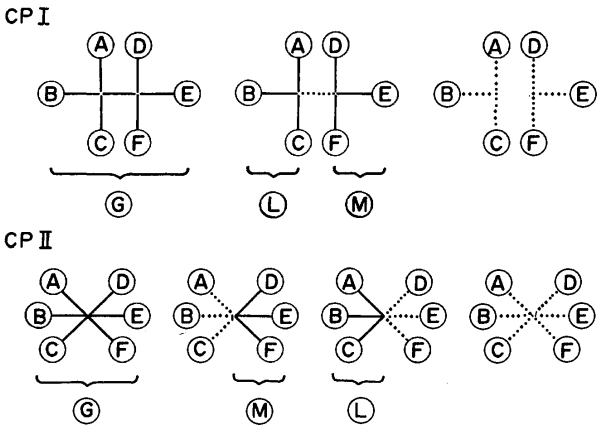

Fig. 1. Illustration for the two composition principles. A, B,···F, L, and M are subgraphs of graph G. Cutting of a bond is represented by a dotted line.

* Present address: Department of Industrial Chemistry, Tokyo University of Agriculture and Technology, Koganei-shi, Tokyo.

** Present address: Department of Chemistry, College of Science and Engineering, Aoyama Gakuin University, Megurisawa, Setagaya-ku, Tokyo.

1) H. Hosoya, This Bulletin, **44**, 2332 (1971).

2) K. Mizutani, K. Kawasaki, and H. Hosoya, *Natural Science Report of Ochanomizu Univ.*, **22**, 39 (1971).

3) K. Kawasaki, K. Mizutani, and H. Hosoya, *ibid.*, **22**, 181 (1971).

4) H. Hosoya, *Theor. Chim. Acta*, **25**, 215 (1972).

5) I and II are, respectively, the carbon atom skeletons of 2,3-dimethylpentane and 1,1,2-trimethylcyclopropane.

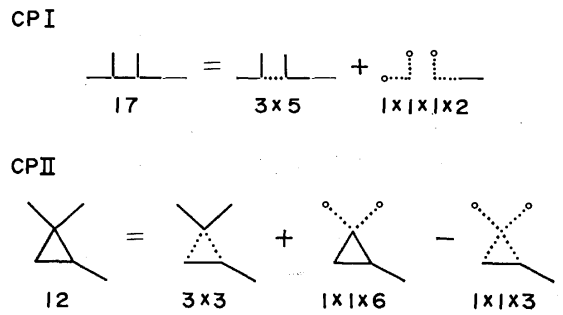

Fig. 2. Application of the composition principles I and II, respectively, to graphs I and II.

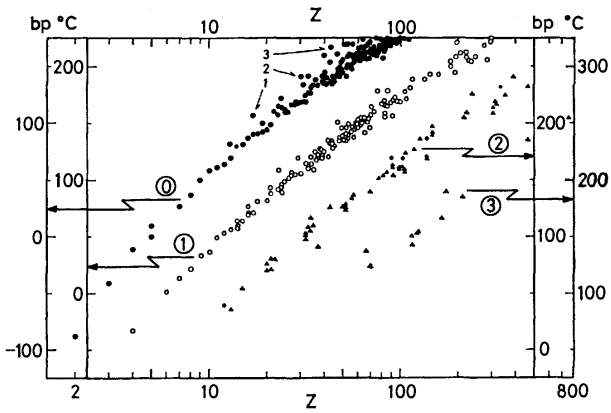

Fig. 3. Boiling point-topological index plot of chain, monocyclic, bicyclic, and tricyclic saturated hydrocarbons. The point for methane is omitted ($bp=-161.5$°C, $Z=1$). Note the shift in the ordinate. The numbers in circles represent the numbers of rings. The small numbers 1, 2, and 3 are referred to the text.

General Aspects of Correlation

Figure 3 gives plots of the boiling points against $\log Z_G$ for chain, monocyclic, bicyclic, and tricyclic saturated hydrocarbons. The boiling point data were taken from the API report[6] and supplemented by the Beilstein Handbuch.[7] There exist serveral geometrical isomers which can not be discriminated by the topological index, *e.g.*, 1,*cis*- and 1,*trans*-2-dimethylcyclopropanes. An averaged value is plotted for a group of such isomers.

Although there are observed several scattered points,[8] the boiling point for a series of compounds with similar structures rises roughly linear to $\log Z_G$, namely,

$$bp = a \log Z_G + b. \quad (4)$$

For all the groups of compounds studied, the slope a is almost the same and the value b decreases with an increase in the number of rings. In other words, if two saturated hydrocarbons with the same Z_G value but with different numbers of rings are compared, the more the rings the lower the boiling point.

Strictly speaking, the slope a slowly decreases with $\log Z_G$ and the plots can be straightened up by taking $\log(Z_G-3)$ as the abscissa. However, it must be emphasized here that, contrary to the attempts by many authors,[10-13] our standpoint is not to find out the best-fit empirical formula but to understand the topological aspects of the boiling point with as few parameters as possible. Further, it may be noted that several thermodynamic quantities such as critical temperature, heat of vaporization, absolute entropy, vapor pressures at various temperatures are also correlated with the topology of a molecule,[14] and that the boiling point is chosen here as the most typical of them.

Let us see the relation (4) in more detail. The plot bp—$\log Z_G$ for the chain isomers C_7H_{16} and the plot

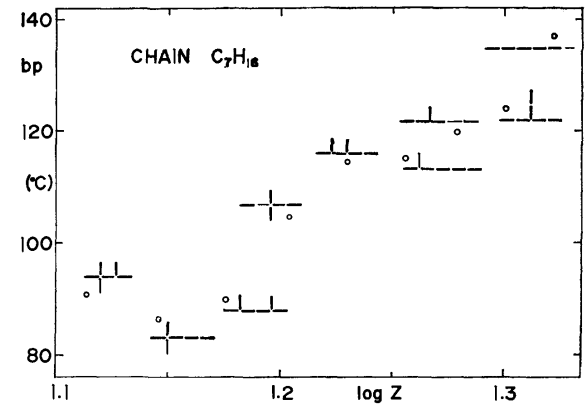

Fig. 4. Boiling point-topological index plot of the chain C_7H_{16} isomers.

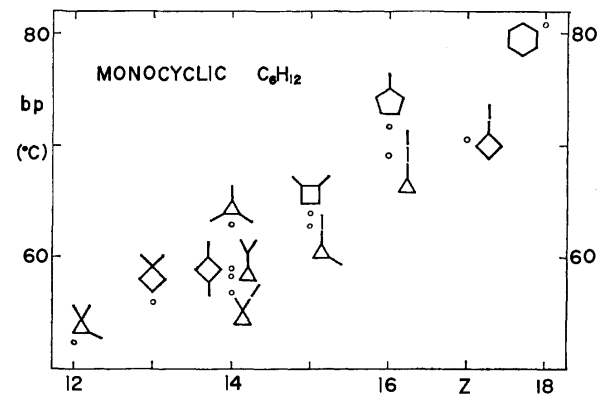

Fig. 5. Boiling point-topological index plot of the monocyclic C_6H_{12} isomer.

6) American Petroleum Institute Research Project 44, "Selected Values of Properties of Hydrocarbons and Related Compounds", Thermodynamics Research Center, Texas A & M Univ. (1971).

7) Deutschen Chemisches Gesellschaft, "Beilstein Handbuch der organischen Chemie".

8) The points for the following compounds deviate appreciably from other members of the series and are omitted from Fig. 3. They are 1,2,3-trimethyl-4-isopropylcyclopentane ($Z=125$, $bp=157$—158°C),[7] 1-methyl-2,3-diisopropylcyclopentane ($Z=194$, $bp=150$—152°C),[7] 1,1,3,3-tetramethyl-2,4-diethylcyclobutane ($Z=161$, $bp=124$—125°C)[7], and 1,4-dimethylbicyclo[2.1.1]hexane ($Z=37$, $bp=91$°C).[9] It is possible that these data are wrong.

9) A. Cairncross and E. P. Blanchard, Jr., *J. Amer. Chem. Soc.*, **88**, 496 (1966).

10) H. Wiener, *ibid.*, **69**, 17 (1947); *J. Phys. Chem.*, **52**, 425 (1948).

11) J. R. Platt, *J. Phys. Chem.*, **56**, 328 (1952).

12) W. J. Taylor, J. M. Pignocco, and F. D. Rossini, *J. Res. Natl. Bur. Stand.*, **34**, 413 (1945); K. Li, R. L. Arnett, M. B. Epstein, R. B. Ries, L. P. Bitler, J. M. Lynch, and F. D. Rossini, *J. Phys. Chem.*, **60**, 1400 (1956); J. B. Greenshields and F. D. Rossini, *ibid.*, **62**, 271 (1958).

13) K. Altenburg, *Brenstoff-Chem.*, **47**, 100, 331 (1966).

14) H. Hosoya, unpublished.

bp—Z_G for the monocyclic isomers C_6H_{12} are shown, respectively, in Figs. 4 and 5. The boiling points are fairly well correlated with Z_G or log Z_G both for chain and cyclic compounds. This is the case for other lower members of hydrocarbons. However, as molecules become larger the plots for chain compounds are getting scattered as seen in Fig. 3. Most points deviating appreciably are those of sterically crowded compounds such as 2,2,3,3-tetramethylbutane (marked with 1 in Fig. 3), 2,2,3,3-tetramethylpentane (2) and 2,2,3,3,4-pentamethylpentane (3).

On the other hand, for higher members of cyclic compounds the correlation is as good as the smaller molecules. Surprisingly, the plots for the known family of cyclenes ($C_{10}H_{16}$ and $C_{11}H_{18}$) with three fused rings are lined up as seen in Fig. 6. Thus let us consider the problem separately for chain and cyclic compounds.

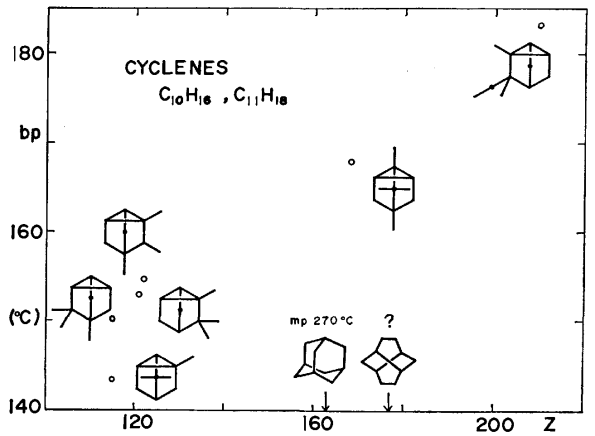

Fig. 6. Boiling point-topological index plot of the cyclene isomers $C_{10}H_{16}$ and $C_{11}H_{18}$.

Chain Paraffins

Since the effect of the branching of the topological index is analyzed elsewhere,[1] discussion will be given here of phenomenological point of view.

Empirical Formula. During an attempt in straightening up of the relation (4) for normal paraffins it was found that the plot of $\sqrt{N}(bp-a)$ of branched chain paraffins with N carbon atoms against log Z_G gives an interesting pattern as shown in Fig. 7. The points for normal paraffins lie perfectly on a line passing the origin, while isomeric paraffins lie on "branches" stemming from the points of the corresponding normal paraffins. The slopes of the branches seem to be almost the same. Although many points still deviate in this plot, the points for a series of compounds with similar structures such as 2-methyl isomers are found to lie on a line parallel to that of the normal paraffins. Thus we get

$$bp = (a \log Z_G + c)/\sqrt{N} + b. \quad (5)$$

The values of a and b are constant for a series of compounds either with the same N or with similar structures and are given in Table 1. Accuracy of Eq. (5) for normal paraffins will be compared in Appendix with a variety of hitherto proposed empirical formulae.

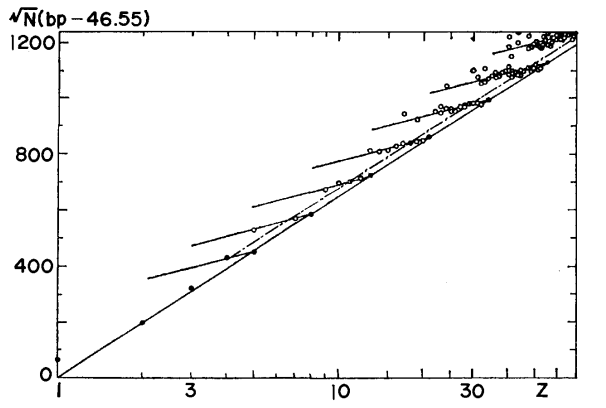

Fig. 7. Plots of $\sqrt{N}(bp-46.55)$ against log Z for chain saturated hydrocarbons. Boiling points are in °K.
●: normal paraffins, ◑: 2-methyl isomers and ○: other isomers.

Table 1. The values of the constants in the boiling point-topological index relation[a)]

Category	a	b	c
Normal paraffins	650.3	46.55	0
Compounds with similar structures[b)]	650.3	46.55	Dependent on the type
Compounds with the same N[c)]	310.0	46.55	Dependent on N

a) The boiling point (in °K) can be obtained from the relation $bp=(a \log Z_G+c)/\sqrt{N}+b$.
b) Obtained from the least squares calculation for the compounds with N from 2 to 10.
c) Obtained from the least squares calculation for the heptane isomers by omitting 3-ethylpentane and 2,2,3-trimethylbutane. N is the number of the carbon atoms.

Empirical Rules. From Eq. (5) the boiling point lowering (Δbp) of an isomer is expected to be

$$\Delta bp = bp(\text{normal}) - bp(\text{isomer}) \quad (6)$$

$$= a \log (Z_{\text{normal}}/Z_{\text{isomer}})/\sqrt{N}. \quad (7)$$

In Tables 2 and 3 observed and calculated values are compared for six different series of paraffin isomers.

Table 2. Observed and calculated boiling point lowering of paraffins by introducing a tertiary carbon atom

N	Series A			Series B			Series C		
	Z_G	Δbp[a)] (°C)		Z_G	Δbp (°C)		Z_G	Δbp (°C)	
		obsd	calcd		obsd	calcd		obsd	calcd
4	4	11.2	15.0						
5	7	8.2	8.1						
6	11	8.4	9.2	12	5.4	4.4			
7	18	8.3	7.9	19	6.5	5.1			
8	29	8.1	7.6	31	6.8	4.4	30	8.0	5.9
9	47	7.6	7.1	50	6.6	4.3	49	8.4	5.2
10	76	7.1	6.7	81	6.3	4.0	79	8.4	5.1
11	123	6.7	6.4	131	5.9	3.9	128	8.0	4.8
12	199	6.3	6.2	212	5.5	3.6	207	7.3	4.7

a) $\Delta bp(\text{obsd})=bp\,(\text{normal})-bp(\text{isomer})$. $\Delta bp(\text{calcd})=310 \log(Z_{\text{normal}}/Z_{\text{isomer}})/\sqrt{N}$.

Table 3. Observed and calculated boiling point lowering of paraffins by introducing a quarternary carbon atom[a)]

N	Series D			Series E			Series F		
	Z_G	Δbp (°C)		Z_G	Δbp (°C)		Z_G	Δbp (°C)	
		obsd	calcd		obsd	calcd		obsd	calcd
5	5	9.5	28.4						
6	9	19.0	20.3						
7	14	19.2	20.7	16	12.3	13.7			
8	23	18.9	18.7	25	13.7	14.7			
9	37	18.1	17.9	41	13.8	13.2	39	15.6	15.5
10	60	17.2	16.9	66	12.9	12.8	64	16.6	14.1
11	97	16.3	16.1	107	13.9	12.1	103	17.9	13.7
12	157	15.5	15.4	173	13.3	11.6	167	17.3	13.0
	—C(—)(—)—...			—C(—)(—)—...			—C(—)(—)—...		

a) See the footnote of Table 2.

In some series of compounds the values for the lowest members deviate appreciably as is reasonably expected and may be omitted from the consideration. We get several empirical rules on the boiling points of chain paraffins. The topological index is shown to be in parallel with the boiling point change through Eq. (5).

Rule 1) Of all the isomeric paraffins the normal compound has the highest boiling point.

Rule 2) A monomethyl substitution lowers the boiling point by about 7 ± 1°C. (See Series A, B, and C in Table 2).

Rule 3) A *geminal*-dimethyl substitution lowers the boiling point by about 2 ± 1°C more than the double of a monomethyl substitution. (Compare pairs of Series A and D, B and E, and C and F in Tables 2 and 3).

Rule 4) The magnitude of the boiling point lowering by a monomethyl or *geminal*-dimethyl substitution alternates as the site of the substitution runs from the terminal towards insides. (See Series A, B,···F).

No exception has long been observed for Rule 1). It is proved in Ref. 1 as Theorem 4 that the topological index of the normal compound is the largest of all the isomeric structures.

Rule 4) deserves to be noted. As evident from Table 2, 2-methyl and 4-methyl substitutions lower the boiling point by about the same amount, which is larger than the contribution by a 3-methyl substitution. This is also the case for *geminal*-dimethyl substitutions. In both cases the boiling point lowering by further inner substitutions converges rapidly to a limit. This behavior reminds one of the zig-zag change of melting points of chain compounds with the increase of the chain length. That the topological index has just the same property can be shown as follows.

Let the topological index of a normal paraffin with N carbon atoms (n-N-ane) be $Z_{\bar{N}}$. For a 2-methyl substituted isomer (2-Me-(N-1)-ane) the topological index $Z_{2\text{-Me}}$ is expressed as

$$Z_{2\text{-Me}} = Z_{\bar{N-1}} + Z_{\bar{N-3}}$$

by using the composition principle. (Eq. (15) of Ref. 1) For larger N's the value $Z_{\bar{N}}$ increases asymptotically as $\alpha^{N+1}/\sqrt{5}$,[15)] with $\alpha=(1+\sqrt{5})/2$. Thus the ratio

Table 4. Observed and calculated boiling point lowerings of paraffins by a 2-methyl substitution

N	Series G			Series H			Series J		
	Z_G	$\Delta\Delta bp$[a)] (°C)		Z_G	$\Delta\Delta bp$ (°C)		Z_G	$\Delta\Delta bp$ (°C)	
		obsd	calcd		obsd	calcd		obsd	calcd
6	10	2.3[b)]	5.2						
7	15	9.6	9.3	17	2.1[b)]	5.7	13	−1.7[b)]	3.8
8	25	8.5	7.1	26	9.5	8.4	19	7.6	9.1
9	40	8.0	7.3	43	8.2	6.8	32	8.6	6.5
10	65	7.1	6.7	69	7.4	6.8	51	8.0	6.9
11	105	6.2	6.5	112	7.0	6.4	83	7.0	6.3
12	170	6.0	6.2	181	6.0	6.1	134	6.0	6.2
Isomer	—C(—)(—)—C_{N-6}—C(—)(—)—			—C(—)(—)—C_{N-7}—C(—)(—)— —			—C(—)(—)—C_{N-7}—C(—)(—)—		
Reference	— —C_{N-5}—C(—)(—)—			— —C_{N-6}—C(—)(—)— —			— —C_{N-6}—C(—)(—)—		

a) $\Delta\Delta bp$(obsd) = bp(ref.) − bp(isomer), $\Delta\Delta bp$(calcd)310 $\log(Z_{ref}/Z_{isomer})/\sqrt{N}$.
b) Deviating from the additivity.

15) $Z_N=(\alpha^{N+1}-\beta^{N+1})/\sqrt{5}$, where $\alpha=(1+\sqrt{5})/2$ and $\beta=(1-\sqrt{5})/2$.[1)]

TABLE 5. OBSERVED AND CALCULATED BOILING POINT LOWERINGS OF PARAFFINS BY A 2,2-DIMETHYL SUBSTITUTION

N	Series K			Series L			Series M		
	Z_G	$\Delta\Delta bp$[a] (°C)		Z_G	$\Delta\Delta bp$ (°C)		Z_G	$\Delta\Delta bp$ (°C)	
		obsd	calcd		obsd	calcd		obsd	calcd
7	13	9.2[b]	16.6						
8	19	18.4	20.1	31	9.0[b]	16.3	17	0.3[b]	14.4
9	32	19.2	17.3	50	17.7	18.7	24	10.4[b]	19.4
10	51	18.1	17.0	81	17.0	16.5	41	19.4	16.2
11	83	16.2	16.0	131	16.0	16.1	65	17.0	16.3
12	134	15.0	15.4	212	15.0	15.3	106	16.0	15.3
Isomer	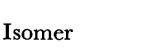			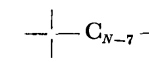					
Reference	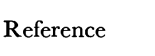			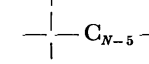					

a) $\Delta\Delta bp$(obsd)=bp(ref.)−bp(isomer), $\Delta\Delta bp$(calcd)=310 $\log(Z_{ref}/Z_{isomer})/\sqrt{N}$.
b) Deviating from the additivity.

TABLE 6. OBSERVED AND CALCULATED BOILING POINT LOWERINGS OF DECANE ISOMERS BY MONOMETHYL SUBSTITUTIONS[a]

Reference	2-Methyl	3-Methyl	4-Methyl
	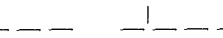 7.1 (6.7)	6.3 (4.0)	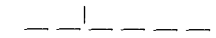 8.4 (5.1)
	7.1 (6.7)	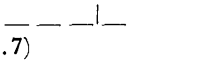 6.6 (4.1)	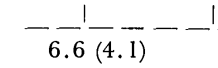 8.5 (4.7)
	7.4 (6.8)	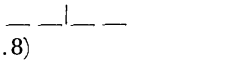 7.0 (3.9)	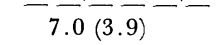 8.4 (5.6)
	8.0 (6.9)	6.1 (3.7)	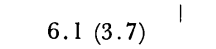 8.6 (6.1)
	8.4 (6.2)	5.5 (4.8)	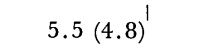 −0.7 (2.7)

a) Numerals in parentheses are calculated from Eq. (7).

$Z_{\bar{N}}/Z_{2\text{-Me}}$ converges to a limit $(5+3\sqrt{5})/10=1.171$ with increasing N's. Similarly we get

$Z_{\bar{N}}/Z_{3\text{-Me}} \to 1.099$, $Z_{\bar{N}}/Z_{4\text{-Me}} \to 1.125$,
$Z_{\bar{N}}/Z_{5\text{-Me}} \to 1.115$ and finally
$\lim_{m\to\infty} (Z_{\bar{N}}/Z_{m\text{-Me}}) \to \sqrt{5}/2 = 1.118$.

In order to check the additivity of the lowering of the boiling point by branching, the lowering of the boiling point, $\Delta\Delta bp$, of disubstituted paraffins with respect to a reference mono-substituted compound was studied. Some of the results are shown in Tables 4—6.

Let us consider the octane isomers as an example. The boiling point of 2,5-dimethylhexane is lower than that of 2-methylheptane by 8.5°C (Series G in Table 4), which is very close to the value 8.1°C (Series A) of the lowering of the latter with respect to *n*-octane. These values are estimated from the topological index through Eq. (5) or (7) to be 7.6 and 7.1°C, respectively. Both for the observed and calculated values, good agreement is observed between Δbp's of Series A and $\Delta\Delta bp$'s of Series G. The $\Delta\Delta bp$ values for Series H and J represent other examples of the boiling point lowering by 2-methyl substitution. Rule 2) seems to be obeyed for Series G, H, and J. However, the boiling point lowerings of 2,3-dimethylated butane, pentane, and hexane are as small as about 2°C with respect to 2-methylpentane, 3-methylhexane, and 4-methylheptane (not shown), respectively. Sterically hindered substitution seems to raise the boiling point appreciably.

Series K, L, and M in Table 5 give the boiling point lowering by *geminal*-dimethyl substitutions. In Table 6 observed and calculated boiling point lowerings (Δbp and $\Delta\Delta bp$) of 2-, 3-, and 4-methyl subsitutions for dodecane isomers are demonstrated. Thus we get

Rule 5) If two substituents are well separated from each other, the lowering of the boiling point is additive.

Rule 6) Too much crowded substitution does not lower the boiling point effectively.

If one admits the relation (5), all these empirical rules except for Rule 6) can be predicted. Qualitatively the same conclusions can be obtained from the simpler relation (4). It has been known that the boiling point is well correlated with the absolute entropy of a molecule in gaseous state and we have found that the absolute entropy of saturated hydrocarbons are linearly dependent on log Z_G fairly well.[14] Thus it can be said that the topological index is a good index for the topological properties of molecules and is useful for rough estimation of some thermodynamic quantities. By the term "topological properties" we mean such quantities that may be related with the entropy or the number of the degree of freedom for

Table 7. Isomers of the smallest topological index and those with the lowest boiling points

N	Smallest Z	Lowest bp 1	Lowest bp 2
5			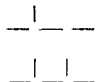
6			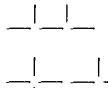
7	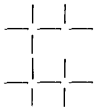	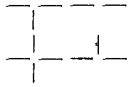	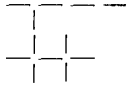
8		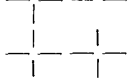	
9	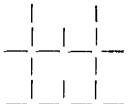		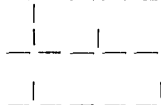
10	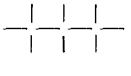	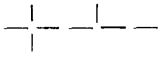	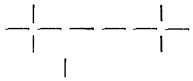
11	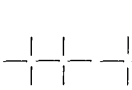	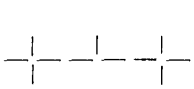	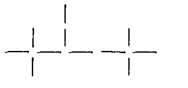
12			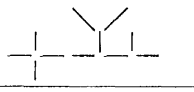

internal rotations of a molecule.

Steric effect seems to be one of the most important factors that could improve the empirical relations (4) and (5). This point has already been discussed by Platt[9] that the polarity number or the number of "steric pairs" p[16] proposed by Wiener[10] is the best parameter for evaluating this effect. Thus the isomer with the lowest boiling point is not necessarily the one with the smallest topological index. This is seen in Table 7.

Cyclic Paraffins

Figure 5 for the plot of all the possible isomers of monocyclic C_6H_{12} hydrocarbons is instructive to realize the effect of branching on the boiling point of cyclic compounds. Plots of other series, though not complete, show similar trend and we get

Rule 7) Among all the isomers of monocyclic saturated hydrocarbons (C_NH_{2N}) the isomer with no branch (cyclo-N-ane) has the highest boiling point.

Rule 8) For polycyclic saturated hydrocarbons isomers without branches have generally higher boiling points than those with branches.

Rule 9) For cyclic compounds with the same ring skeleton, the longer the longest branch the higher the boiling point.

Rule 10) For cyclic compounds with the same ring skeleton, the more the quarternary carbon atoms, the lower the boiling point.

Rule 7) is analogous to Rule 1), that is, the normal paraffin has the highest boiling point among the isomers of chain saturated hydrocarbons. The remaining Rules 8)—10) are consistent with the general aspects of the topological index.[3] As an application of these Rules let us consider some interesting topics.

We can predict that among the possible twenty bornane isomers, *i.e.*, trimethylbicyclo[2.2.1]heptanes, 2,3,7-trimethyl derivative III and 1,3,3-trimethyl derivative V, respectively, give the highest (*ca.* 170°C) and lowest (*ca.* 150°C) boiling points, while bornane, 2,7,7-trimethyl isomer IV boils at 160°C.

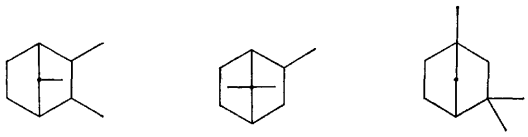

III $Z=116$ IV $Z=102$ V $Z=88$

It is also predicted that among the possible isomers of $C_{10}H_{16}$ cyclenes, the isomers VI and VII respectively give the highest (*ca.* 160°C) and lowest (*ca.* 145°C) boiling points (See Fig. 7).

VI $Z=138$ VII $Z=106$

Adamantane is known to be volatile but to melt at as high as 270°C. The topological index is calculated as 163 and the boiling point is estimated as below as 165°C from the interpolation of the plots of tricyclic compounds (Fig. 7). A paradoxical result is also obtained for twistane with $Z=177$. So we must say that for highly fused ring compounds the topological index alone cannot account for the boiling point.

Appendix

Comparison of Several Empirical Relations of the Boiling Points of Normal Paraffins. Empirical formulae of the boiling points of the lower members of normal paraffins have been proposed by many authors. Typical of them are as follows:

Table 8. Comparison of the empirical formulae for the boiling point of normal paraffins[a)]

N	Exp. bp (°K)	Error=calcd−obsd (°K)					
		(8)	(9)	(10)	(11)	(12)	(13)
1	111.7	17.9	15.3	−12.2	7.5	7.1	65.2
2	184.5	0.2	−0.7	−6.8	−2.4	−3.0	0.4
3	231.1	0.5	0.3	−0.4	0.3	−0.2	−5.5
4	272.7	−0.1	−0.2	0.7	0.3	0.0	1.1
5	309.2	−0.1	−0.1	0.8	0.2	0.1	−0.1
6	341.9	−0.1	0.0	0.6	−0.1	0.2	0.4
7	371.6	−0.1	0.1	0.3	−0.4	0.1	−0.3
8	398.8	0.0	0.1	0.0	−0.6	0.1	−0.2
9	424.0	−0.1	0.0	−0.3	−0.9	−0.1	−0.3
10	447.3	−0.1	−0.2	−0.4	−1.0	−0.1	0.0
20	617.0	0.9	−4.8	−0.9	2.0	0.1	16.8
40	798.2	13.5	−18.3	−30.2	20.3	−0.2	93.4
80	951.2	68.4	−26.9	−167.7	75.9	−0.2	300.7
100	988.2	100.3	−25.1	−237.2	104.3	−0.3	408.2

a) The number in parentheses indicates the equation number in text.

$$bp = 745.42 \log (N+4.4) - 416.31 \quad (8)^{17)}$$

$$bp = 1209.59 - 1162.9/(1+0.074189N^{0.85}) \quad (9)^{18)}$$

$$bp = \{(21720N-11820)/(1+0.000283N^2)\}^{1/2} \quad (10)^{19)}$$

$$bp = 127.55N^{2/3}/(1+0.07033N^{2/3}) \quad (11)^{20)}$$

$$\log (1078-bp) = 3.0319 - 0.04999N^{2/3} \quad (12)^{21)}$$

16) The number p is defined as the number of pairs of carbon atoms which are separated by three carbon-carbon bonds.

17) G. Egloff, J. Sherman, and R. B. Dull, *J. Phys. Chem.*, **44**, 730 (1940).

18) J. R. Platt, *J. Chem. Phys.*, **15**, 419 (1947).

19) Y. Varshni, *J. Ind. Chem. Soc.*, **28**, 535 (1951).

20) K. Nakanishi, M. Kurata, and M. Tamura, *J. Chem. Eng. Data*, **5**, 210 (1960).

21) A. Kreglewski and B. J. Zwolinski, *J. Phys. Chem.*, **65**, 1050 1961).

Boiling points are in °K and N is the number of carbon atoms. Expressions with many parameters or of complicated forms are not chosen here.[12,13)] Now let us add our Eq. (5).

$$bp = 650.3 \log Z_{\bar{N}}/\sqrt{N} + 46.55 \quad (13)$$

By using the asymptotical form of $Z_{\bar{N}}$ we get

$$bp = 135.90\sqrt{N} + 46.55 - 91.37/\sqrt{N}. \quad (14)$$

for larger N.

Although the forms of these formulae are quite different from each other they give fairly good values for paraffins with N from 2 to 10 as shown in Table 8. Since all these relations were obtained so as to fit the lower members of the series most of them including our relations (13) and (14) are in poor agreement with experiments for higher members of the series up to $N=100$. However, the relation (12) gives surprisingly good results.

Conditions Favorable for the Formation of γ-FeOOH by Aerial Oxidation in an Acidic Suspension of Iron Metal Powder

Masao KIYAMA, Toshikazu AKITA, Shigeki SHIMIZU,*
Yoshiro OKUDA,* and Toshio TAKADA
Institute for Chemical Research, Kyoto University, Kyoto
(Received December 2, 1971)

Dilute solutions of ferrous sulfate, sulfuric acid, hydrochloric acid, nitric acid and acetic acid in which iron powders are dispersed have been oxidized at below 80°C by blowing air into them. The resulting precipitates have been examined by means of X-ray diffraction, chemical analysis and optical and electron microscopy. When the iron powder is well dispersed, γ-FeOOH is formed with or without α-FeOOH, α-Fe_2O_3, or Fe_3O_4. The mode of formation depends on such factors as particle size, amount of iron powder, kind of anion present and temperature. Particle size greatly influences the formation of γ-FeOOH in the sulfate system, but not in the other systems.

Clarification of conditions for the formation of ferric oxyhydrate (FeOOH) would be significant with respect to the theory of mechanism of corrosion of iron. Ferric oxyhydrate has four modifications: α-, β-, γ-, and δ-forms. The first three are nonferromagnetic[1-3] and the last is ferromagnetic.[4,5] By dehydration of γ-FeOOH, which is isomorphous with boehmite γ-AlOOH, ferromagnetic ferric oxide γ-Fe_2O_3 is formed.[6,7] This drew the attention of many chemists who investigated conditions favorable for its formation. γ-FeOOH can be obtained by slow oxidation of a suspension of ferrous compound precipitated by adding alkali to excess ferrous salt solution under certain conditions.[8-10] By oxidation γ-FeOOH is always formed *via* a dark green compound called green rust I or II. Presence of the green rust has been considered to be indispensable for the formation of γ-FeOOH. However, we have found that γ-FeOOH can also be formed directly from aqueous solutions of ferrous salt ($FeBr_2$ or a mixture of $FeCl_2$ and excess NaI solutions).[11] In order to clarify the mechanism of formation of γ-FeOOH more systematical experiments are needed.

In the present paper experimental conditions favorable for the formation of γ-FeOOH in acidic suspensions of iron powder are given.

Experimental

Materials. Chemical reagents of analytical grade were used. Crushed electrolytic iron powders of 270, 240, 140, 117, 104, 74, 61, and 43μ in particle size were prepared by use of 50, 60, 100, 120, 150, 200, 250, and 325 mesh sieves, respectively. Air for stirring and oxidizing the solution containing iron powder was passed through washing vessels containing KOH solution to remove dust and organic elements.

Apparatus. An ordinary reaction vessel was found to be unsuitable, since with such a vessel the rate of precipitate formation is very low because of aggregation of the iron particles. For the sake of uniform stirring and oxidation we used a hard glass vessel 7 cm in internal diameter and 80 cm in height as shown in Fig. 1. The vessel is composed of a cylindrical tube A, a perforated plate B 0.1 cm in thickness with small holes of 0.1 cm in diameter arranged at equal distances of about 0.8 cm, and a gas holder C. The vessel is closed with a rubber D into which are inserted a temperature regulator E, a thermometer F, a quartz tube containing nichrome heater G and a water condenser H. The temperature regulator consists of a spiral bimetal dipped in oil in a glass tube.

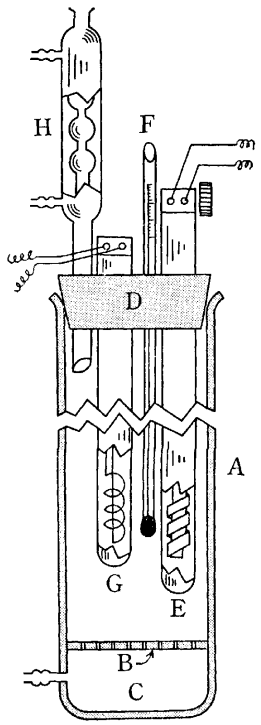

Fig. 1. Schema of reaction vessel
A: Cylindrical tube, B: Perforated plate, C: Gas holder, D: Rubber stopper, E: Thermoregulator, F: Thermometer, G: Heater, H: Condenser.

* Present address: Toda Industrial Co., Ltd. Yokogawa Shin-machi, Hiroshima.

1) W. H. Albrecht, *Ber.*, **62**, 1475 (1929).
2) T. Takada, M. Kiyama, Y. Bando, T. Nakamura, M. Shiga, T. Shinjo, N. Yamamoto, Y. Endoh, and H. Takaki, *J. Phys. Soc. Jap.*, **19**, 1744 (1964).
3) I. Dezsi, L. Keszthelyi, D. Kulgawczuk, B. McInar, and N. A. Eissa, *Phys. Stat. Sol.*, **22**, 617 (1967).
4) M. H. Francombe and H. P. Rooksby, *Clay Min. Bull.*, **4**, (21) 1 (1959).
5) S. Okamoto, *J. Amer. Ceram, Soc.*, **51**, 594 (1968).
6) L. A. Welo and O. Baudisch, *Phil. Mag.*, **17**, 753 (1934).
7) J. Bohm, *Z. Krist.*, **68**, 567 (1928).
8) G. Schikorr, *Z. Anorg. Allgem. Chem.*, **191**, 322 (1930).
9) W. Feitknecht, *Z. Electrochem.*, **63**, 34 (1959).
10) J. D. Bernal, E. R. Dusgupta, and A. L. MacKay, *Clay Min. Bull.*, **4**, (21) 15 (1959).
11) M. Kiyama and T. Takada, This Bulletin, **45**, 1923 (1972)

Procedure. Compressed air was bubbled into the vessel from the bottom through the perforated plate at a rate of 100 *l*/hr by operating a cock. One liter of each acidic solution was poured into the vessel from the top, but it was scarcely observed to fall into the gas holder. The iron powder was poured into the solution and the air flow rate was increased to a certain degree. The solution in which the iron powder was dispersed was quickly heated by the nichrome heater and kept at a certain temperature. After being separated from the remaining iron particles by decantation, the precipitate was filtered, washed with water, and then dried at about 105°C. pH measurements were carried out with a Horiba electrode pH meter.

Identification. The sample thus prepared were examined by means of chemical analysis and X-ray diffraction using Fe*Kα* radiation, and observed under optical and electron microscopes. The content of γ-FeOOH (*R*) was determined from the equation $R=I_\gamma/I_\gamma+I_\alpha$, where I_γ and I_α are the relative intensities of the X-ray diffraction lines of γ-EeOOH (*d*(020)6.32 Å) and α-FeOOH (*d*(110) 4.21 Å), respectively.

Results and Discussion

Precipitation in Sulfate Suspensions. Experiments were carried out by use of the iron powder with size distributions: 140—104=1.0, 104—74=8.4, 74—61=10.4, 61—43=15.8, below 43μ=64.4 wt%. Air was blown at the rate of 650 *l*/hr for 10 hr into 0.5M-$FeSO_4$ and 0.2M-$FeSO_4$ solutions containing 20 g (0.36 mol) of the iron powder. These suspensions were kept at 70°C. 0.2M-H_2SO_4 solution containing 31 g (0.56 mol) of the iron powder was also subjected to the same treatment. These sulfate suspensions changed gradually from grayish black to brownish yellow, as the reaction proceeded. In order to know the relation between the pH of the suspensions and the remaining iron particles, a part of each suspension (about 50 m*l*) was taken out for examination during the course of oxidation. The pH values are plotted against time in the logarithmic scale in Fig. 2. The pH value increased to about 7 by addition of the iron powder to the solution, and then decreased to about 4. It remained at about 4 while the iron powder was present in the solution. When the iron powder disappeared completely, the pH dropped to below 3. It is believed that precipitation takes place when the iron powder is dissolved and the ferrous ions are oxidized as follows.

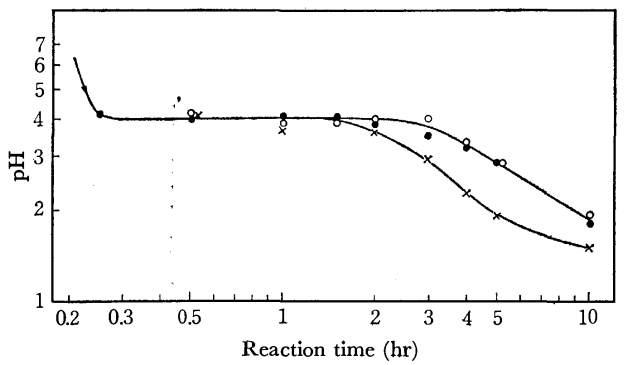

Fig. 2. pH of suspension at various time intervals: × =0.5M-$FeSO_4$, ○=0.2M-$FeSO_4$, ●=0.2M-H_2SO_4 as the starting solution.

$$2Fe(metal) + 4H^+ = 2Fe^{2+} + 2H_2(gas)$$

$$2Fe^{2+} + 3H_2O + \frac{1}{2}O_2 = 2FeOOH + 4H^+$$

When the iron powder is uniformly dispersed, the ferrous ions consumed by oxidation to form a precipitate are replenished by neutralization between the acid formed and the iron powder. This might be the reason that the pH remained at about 4. The solubility products of iron hydroxides are: $(Fe^{2+})(OH)^2=10^{-14}$ and $(Fe^{3+})(OH)^3=10^{-36}$. In these suspensions, no ferrous precipitate can exist but ferric ions which are to be precipitated.

The samples thus obtained (Found: Fe_2O_3 87.5—88.6 wt%, Calcd for $Fe_2O_3\cdot H_2O$, Fe_2O_3 89.9 wt%) were mixtures of α-FeOOH and γ-FeOOH. Their γ-FeOOH content R progressively increased to about 0.3 in the samples prepared from 0.5M-$FeSO_4$ (sample A), 0.2M-$FeSO_4$ (B) and 0.2M-H_2SO_4 (C) which were the starting solutions. Optical micrographs of these samples show that acicular particles are present with granular ones (Fig. 3). Their shapes and sizes depend

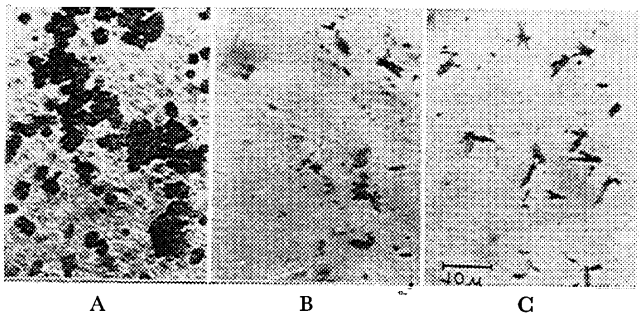

Fig. 3. Optical microscope photographs of FeOOH particles: A=0.5M-$FeSO_4$, B=0.2M-$FeSO_4$, C=0.2M-H_2SO_4 used as the starting solution.

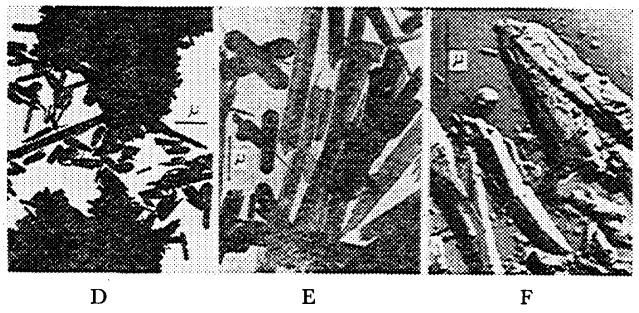

Fig. 4. Electron micrographs of typical shapes of particles prepared from the sulfate suspension.

on the concentration of ferrous ions in the starting solution. Electron micrographs of typical particles are given in Fig. 4 (D) and (E) and that of twin particles observed by carbon replica method in Fig. 4 (F). Very elongated and big bur-like particles can be seen together with X-, Y-, and tablet-shaped ones. According to electron microdiffraction, the very elongated particles were γ-FeOOH and the other ones α-FeOOH. The X- and Y- shaped ones as well as the big bur-like ones did not overlap one another. The former had a re-entrant angle of about 60°.

In order to find the favorable conditions for the formation of γ-FeOOH, experiments were carried out by use of the same iron powder. Oxidation was continued for 6 hr under various conditions, such as the flow rate of air blown, concentration of sulfuric acid, amount of the iron powder added and reaction temperature.

Table 1. Iron compounds formed by oxidation of iron powder ($<140\,\mu$) present in sulfuric acid solutions under various conditions

Reaction conditions				
Composition (mol/l)		Temp. (°C)	Flow rate (l/hr)	Iron compounds[a]
SO_4^{2-}	Fe			
0.20	0.57	70	100	α-H
0.20	0.57	70	350	α-H$\gg\gamma$-H
0.20	0.57	70	500	α-H$>\gamma$-H
0.20	0.57	70	650	α-H$\approx\gamma$-H
0.20	0.57	80	650	α-H
0.20	0.57	70	650	α-H$\approx\gamma$-H
0.20	0.57	60	650	α-H$\approx\gamma$-H
0.20	0.57	50	650	α-H$>\gamma$-H
0.16	0.57	70	650	α-H$\approx\gamma$-H
0.07	0.57	70	650	α-H$>\gamma$-H
0.00	0.57	70	650	α-H$\approx Fe_3O_4$
0.20	0.92	70	650	α-H
0.20	1.62	70	650	α-H
0.20	3.27	70	650	α-H

a) Abbreviations: α-H=α-FeOOH, γ-H=γ-FeOOH.

The results are summarized in Table 1. With the increase of air flow rate the iron powder becomes more uniformly dispersed, the formation of γ-FeOOH being accelerated. In water the rate of precipitation was very slow and the oxidation product contained not γ-FeOOH but a mixture of α-FeOOH and Fe_3O_4 (or γ-Fe_2O_3). The formation of γ-FeOOH depends strongly on the amount of iron powder, γ-FeOOH being always formed together with α-FeOOH.

In order to examine the effects of particle size and amount of iron powder experiments were carried out as follows. Four iron powders with different particle sizes (270—240 μ, 140—117 μ, 74—61 μ, and below 43 μ) were used and different amounts of each iron powder were added to 0.2M-H_2SO_4 solutions. The suspensions were oxidized for 8 hr at 65°C by blowing air into them at 1000 l/hr.

The γ-FeOOH contents R for different iron particle sizes are plotted against the amount of iron powder in Fig. 5. After 8 hr, the solutions to which 80 g (1.43 mol/l) and 200 g (3.58 mol/l) of the iron powder with 117—140 μ in particle size and 20 g or more of the iron powder with 240—270 μ had been added, had a pH of about 4 and still retained the iron powder. For a given amount of iron powder the larger the particle size, the higher the R, the maximum of R on each curve depending on particle size. This indicates that the particle size of iron powder is more effective for γ-FeOOH formation than its total surface area which is the product of its amount and particle size at the initial stage of oxidation.

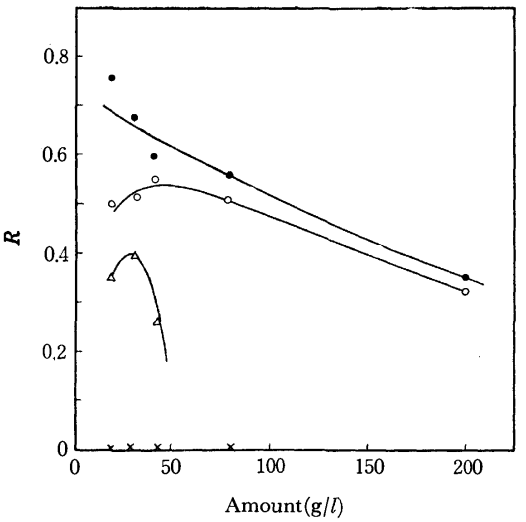

Fig. 5. Effects of the size and amount of the iron powder on the γ-FeOOH content R.
●: 270—240 μ, ○: 140—117 μ, △: 74—61 μ, ×: —43 μ

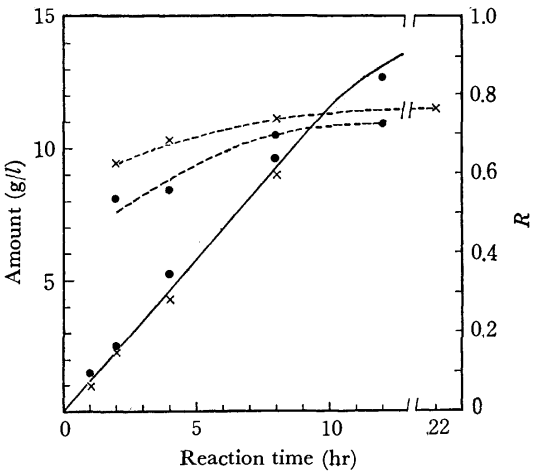

Fig. 6. Amount of precipitates formed and R(γ-FeOOH content) at various periods. Iron powder with particle size of 240—270 μ, 20 g=×, 40 g=●. ——: Amount, ----: R

In order to increase R, the following experiments were carried out. 0.35 mol (20 g) and 0.70 mol of iron powder (240—270 μ) were added to 0.2M-H_2SO_4 solution. The suspensions were oxidized at 65°C for different periods by blowing air into them at a rate of 1500 l/hr. The amount of precipitate formed and R are plotted against time in Fig. 6. Neither depends strongly on the amount of iron powder added and R hardly varies with time.

Precipitation in Other Suspensions. Since a single phase of γ-FeOOH was hardly formed in the sulfate suspensions, experiments were carried out with hydrochloric, nitric and acetic acids in order to examine the effect of anions on the formation of γ-FeOOH.

33 g (0.675 mol/l) of iron powder (104—140 μ) was added to each of the solutions 0.25M-HCl, CH_3COOH and HNO_3. The suspensions were oxidized at 40, 55, 70, and 80°C for 8 hr by blowing air at the rate 1000 l/hr. When the iron powder was added to the acetic acid solution, foaming occurred so heavily that at first

Table 2. Iron compounds formed by oxidation of iron powder (140—104 μ) in chloride, nitrate and acetate solutions (0.25 M in acid) at various temperatures

Temp. (°C)	Chloride	Nitrate	Acetate
40	γ-H>α-H	α-H>γ-H>Sp	α-H
55	γ-H>α-H	γ-H>α-H>Sp	γ-H>α-H
70	γ-H≫α-H	α-H≈Sp>γ-H ≈α-O	γ-H≫α-H
80	γ-H>α-H ≈α-O	α-H≈α-O>γ-H ≈Sp	α-O>γ-H

α-H=α-FeOOH, γ-H=γ-FeOOH, α-O=α-Fe_2O_3, Sp=Fe_3O_4 or γ-Fe_2O_3.

air had to be jetted from the top of the vessel into the suspension to subdue the farm. No iron particles remained in the chloride suspensions oxidized at 70 and 80°C, and the acetate suspensions oxidized at 55, 70, and 80°C. The pH of the chloride suspensions remained at about 4 while iron particles were present, whereas the pH of the acetate suspensions was about 4 regardless of the presence of iron particles. In the nitrate suspensions oxidized at temperatures between 40 and 80°C, iron particles were present. The remaining iron particles in the nitrate suspensions oxidized at 70 and 80°C were coated with black material (probably Fe_3O_4), the rate of precipitation being slow. The kinds of precipitates obtained from each suspension at various temperatures are given in Table 2. γ-FeOOH is formed below 70°C together with α-FeOOH in the chloride and acetate suspensions. α-Fe_2O_3 begins to be formed at 70°C in the nitrate suspension and is formed with other precipitates in all the suspensions at 80°C.

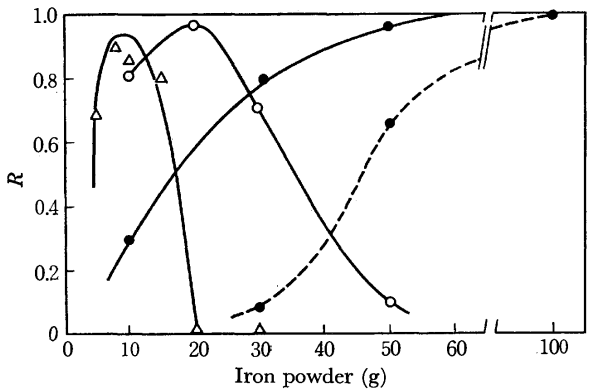

Fig. 7. Effects of the particle size and amount of iron powders added to acetate solution (0.5 *l*) on *R*: △=<43 μ, ●=117—140 μ, ○=240—270 μ.
Solid curves: at 70°C, air flow rate 1500 *l*/hr,
Dotted curve: at 55°C, 1000 *l*/hr.

In order to examine the effect of the air flow rate on *R* at temperatures where α-Fe_2O_3 is hardly formed, the same suspensions were oxidized for 8 hr at different air flow rates between 500 and 1500 *l*/hr at 70°C for the chloride and acetate and at 55°C for the nitrate. The *R* value for acetate increased with the increase of air flow rate. It reached 1.0 at the rate of 1500 *l*/hr. The *R* values for the other suspensions did not depend strongly on the air flow rate. It was about 0.8 for the chloride and 0.4 for the nitrate.

The effects of the particle size and the amount of iron powder on *R* were examined. Three kinds of iron powders with different particle sizes (<43, 117—140 and 240—270 μ) were added to acidic solutions containing 0.25M-acid, their amounts being between 10 and 200 g (0.358 and 3.58 mol/*l*), and each suspension was oxidized at 70°C for 6 hr by blowing air into it at 1500 *l*/hr. Of the three suspensions the total volume of the acetate suspension decreased to 1/2 liter, since foaming became heavier with the increase of surface area of the iron powder. With the acetate suspension, *R* depends on both the amount and particle size of the iron powder (Fig. 7). It increases with the increase or decrease in the amount of iron powder, depending on the particle size, *viz.*, it depends on the total surface area of the iron powder present at the initial stage. The surface area favorable for the formation of γ-FeOOH changes with reaction condition as can be seen by the dotted curve in Fig. 7 (reaction temperature: 55°C, air flow rate: 1000 *l*/hr, the other conditions the same as above). When the suspensions containing more than 30 g (0.54 mol/*l*) of iron powder with particle size of below 43 μ was oxidized at 70°C, fine particles of Fe_3O_4 (about 0.1 μ) were formed.

Table 3. Conditions favorable for the formation of γ-FeOOH from 0.25N-acid solutions containing iron powder
(air flow rate=1500 *l*/hr, time=6 hr)

	Acid	Iron powder		Temp. (°C)	γ-FeOOH content *R*
		size (μ)	amount (mol/*l*)		
No. 1	CH_3COOH	104—140	1.75	70	1.00
No. 2	HCl	104—140	1.75	70	0.97
No. 3	HNO_3	74—61	2.53	55	1.00

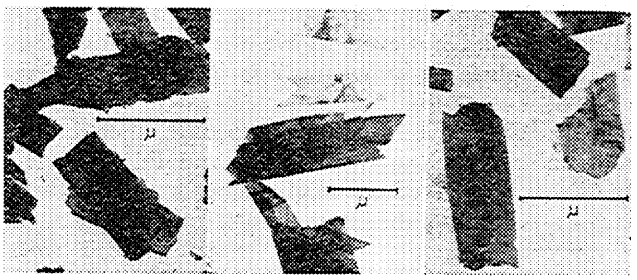

(No. 1) (No. 2) (No. 3)

Fig. 8. Electron micrographs of γ-FeOOH particles formed in acetate (No. 1), chloride (No. 2) and nitrate suspensions (No. 3) as in Table 3.

The effects of particle size and amount of iron powder on *R* for chloride and nitrate were less marked than for acetate suspension. γ-FeOOH was obtained in the chloride and nitrate suspensions under proper conditions, iron particles remaining. Fine particles of Fe_3O_4 (about 0.1 μ) were also formed in the surface layer of iron particles in nitrate suspension containing more than 30 g of the iron powder (<43 μ) and in chloride suspension containing more than 60 g of iron powder (<43 μ). The conditions favorable for the formation of γ-FeOOH are summarized in Table 3

and electron micrographs of the γ-FeOOH particles separated from the remaining iron particles are shown in Fig. 8. The γ-FeOOH particles evidently differ from the very elongated ones prepared from sulfate.

The presence of green rust has been considered to be indispensable for γ-FeOOH formation, and it has been suggested that γ-FeOOH is formed by its surface oxidation. However, the shape of γ-FeOOH particles (acicular) prepared *via* the green rust does not resemble that of the particles of green rust (hexagonal plate-like). γ-FeOOH can also be formed by oxidizing ferrous salt solutions or suspensions of iron powder not *via* the green rust. It is thus proposed that γ-FeOOH may be formed not by surface oxidation of the green rust but by oxidation of hydroxo iron (II) complex formed by dissolution of either the green rust or iron powder.

BULLETIN OF THE CHEMICAL SOCIETY OF JAPAN, VOL. 45, 3426—3429 (1972)

The Preparation and Some Reactions of Platinum(II) and Palladium(II) Complexes of Vinyl Ethers[1)]

Yasuo WAKATSUKI,* Shun-ichi NOZAKURA, and Shunsuke MURAHASHI
Faculty of Science, Osaka University, Toyonaka, Osaka

(Received December 18, 1971)

Stable complexes with the general formula $[Cl_2ML]_2$ (M=Pt, Pd; L=vinyl ethers, propenyl ethers, 1,2-dimethoxyethylene) have been prepared. The IR spectra of $[Cl_2Pt(trans\text{-}CH_3CH{=}CHOCH_3)]_2$ showed a change which was attributed to the *trans—cis* isomerization of the coordinated olefin. A similar *cis—trans* isomerization was also suggested for the other propenyl ether and 1,2-dimethoxyethylene complexes. The palladium complex of vinyl *t*-butyl ether was found to react with aqueous NaOH in a way similar to the Wacker process.

Although many transition metal–olefin complexes are known, few reports have appeared concerning complexes of olefins with strong electron-releasing substituents such as vinyl ethers; indeed, it has only been known that Fe(0) forms a very unstable complex with vinyl ethyl ether.[2)] Such olefins will form unstable complexes with low valent transition metals because they have a strong σ-donating ability, but a poor π-accepting ability. In Pt(II) and Pd(II) complexes of ethylene, the contribution of the back donation has been emphasized, as in the case of the Zeise salt.[3)] A detailed study of IR spectra has, however, shown that σ-donation from the olefin plays an important role in these complexes, while back-donation from the metal is of little importance.[4)] Vinyl ethers can be expected, therefore, to form stable complexes with Pt(II) and Pd(II). Also, coordinated vinyl ethers might show an unusual behavior as a result of the interaction of lone-pair electrons of the oxygen atom with the metal. In this work, Pt(II) and Pd(II) complexes of vinyl ethers and their derivatives will be prepared, and the properties of the novel complexes will be studied by means of IR spectroscopy.

Results and Discussion

The analytical data and some physical properties of the novel complexes obtained by the following reactions are listed in Tables 1 and 2.

$$[Cl_2PtC_2H_4]_2 + 2\text{olefin} \longrightarrow [Cl_2P\text{tolefin}]_2 + 2C_2H_4$$

$$2Cl_2Pd(PhCN)_2 + 2\text{olefin} \longrightarrow [Cl_2Pd\text{olefin}]_2 + 4PhCN$$

As expected, all the complexes are moderately stable in air at room temperature except for the vinyl trimethylsilyl ether complex, which is moisture-sensitive.[5)] They can be stored at −20°C for months.

The last columns in Tables 1 and 2 show the configuration of the coordinated olefin, as determined by IR spectroscopy.

Figure 1 shows the IR spectra of the platinum complex of propenyl methyl ether. The spectrum of the freshly-prepared complex of *trans*-propenyl methyl ether (I) is shown at the top (a). When the solid sample, I, was allowed to stand under argon at 70°C for 48 hr, the spectrum changed to (b), indicating that the change takes place even in a solid state, while the sample I dissolved in toluene at 70°C for several hours showed the spectrum at the bottom (c). The spectrum (c) was also obtained when the complex (II) was prepared from the *cis*-isomer. The dotted line in Fig. 1-(c) shows the spectrum of the palladium analog (III); it was virtually identical with that of the platinum complex. As will be described later, the decomposition of the sample III with pyridine yielded almost pure *cis*-propenyl methyl ether. These facts indicate that the sample I was a mixture of *cis*- and *trans*-olefin complexes,

* Present address: The Institute of Physical and Chemical Research, Wako-shi, Saitama.

1) Presented at the Annual Meeting of the Chemical Society of Japan, April, 1970 (Tokyo).

2) E. K. Gustorf, M. C. Henry, and C. Di Pietro, *Z. Naturforsch. B*, **21** 42 (1966).

3) J. Chatt and L. A. Duncanson, *J. Chem. Soc.*, **1953**, 2939.

4) K. Nakamoto, *Kagaku no Ryoiki Zokan*, **84**, 21 (1968).

5) Y. Wakatsuki, S. Nozakura, and S. Murahashi, This Bulletin, **42**, 273 (1969).

Table 1. Analytical data and some physical properties of $[ClPt_2olefin]_2$

Olefin used	Yield, %	Analysis, % (Calcd)	Decomp. temp., °C	IR ν(C=C) cm^{-1}	Configuration of coordinated olefin
CH_2=CHOCH$_3$	80	C, 11.23 (11.11) H, 1.91 (1.87) Pt, 59.27 (60.20)	123—124	1518	
CH_2=CHOCH$(CH_3)_2$	68	C, 17.29 (17.05) H, 2.88 (2.86) Pt, 55.02 (55.40)	90—100	1521	
CH_2=CHOC$(CH_3)_3$	83	C, 19.75 (19.68) H, 3.37 (3.30) Pt, 52.80 (53.28)	80—90	1515	
CH_2=CHOCH$_2$CH$_2$Cl	48	C, 12.87 (12.90) H, 1.96 (1.89) Pt, 51.88 (52.36)	100—110	1516	
CH_2=CHOCH$_2$CF$_3$	72	C, 12.01 (12.19) H, 1.33 (1.28) Pt, 50.59 (49.50)	122—125	1510	
CH_2=CHOSi$(CH_3)_3$		C, 15.77 (15.71) H, 2.86 (3.16) Cl, 19.13 (18.55) Pt, 51.27 (51.04)	120—122	1510	
cis-CH_3CH=CHOCH$_3$	95	C, 14.84 (14.21) H, 2.38 (2.39) Pt, 57.21 (57.70)	137—140	1520	*cis*
trans-CH_3CH=CHOCH$_3$	16	C, 14.82 (14.21) H, 2.41 (2.39) Cl, 20.70 (20.97) Pt, 57.21 (57.70)	145—148	1533 1520	*cis-trans* mixture
cis-CH_3CH=CHOSiMe$_3$	71	C, 18.70 (18.19) H, 3.55 (3.56)	118—121	1507	*cis*
trans-CH_3CH=CHOSiMe$_3$	65	C, 18.02 (18.19) H, 3.42 (3.56) Cl, 18.68 (17.90)	121—123	(1507) [a]	*cis*
cis-CH_3OCH=CHOCH$_3$	82	C, 13.81 (13.20) H, 2.29 (2.21) Cl, 19.83 (19.48) Pt, 53.04 (53.58)	140—145	1562 1535	*cis-trans* mixture
trans-CH_3OCH=CHOCH$_3$		C, 13.91 (13.20) H, 2.28 (2.21) Cl, 20.17 (19.48) Pt, 53.01 (53.58)	143—145	1535	*trans*
cis-C_6H_5CH=CHCH$_3$	77	C, 28.40 (28.14) H, 2.57 (2.62) Pt, 50.14 (50.78)	135—140	1512	*cis*
trans-C_6H_5CH=CHCH$_3$	76		120—130	1523	*trans*

a) Isomerization had been finished before IR spectrum was taken.

Table 2. Analytical data and some physical properties of $[Cl_2Pdolefin]_2$

Olefin used	Yield, %	Analysis, % (Calcd)	Decomp. temp., °C	IR ν(C=C) cm^{-1}	Configuration of coordinated olefin
CH_2=CHOCH$_3$	76	C, 14.67 (15.31) H, 2.48 (2.57) Cl, 30.29 (30.13)	60—70	1538	
CH_2=CHOCH$(CH_3)_2$	57	C, 23.33 (22.80) H, 3.83 (3.83)	63—71	1527	
CH_2=CHOC$(CH_3)_3$	47	C, 26.19 (25.97) H, 4.41 (4.36)	64—67	1520	
cis-CH_3CH=CHOCH$_3$		C, 19.50 (19.26) H, 3.18 (3.23)	65—75	1531	*cis*
trans-CH_3CH=CHOCH$_3$	50		70—78	(1531) [a]	*cis*
cis-CH_3OCH=CHOCH$_3$	74		120—130	(1543) [a]	*trans*
trans-CH_3OCH=CHOCH$_3$	54	C, 19.08 (18.10) H, 3.13 (3.04)		1543	*trans*

a) Isomerization had been finished before IR spectra were taken.

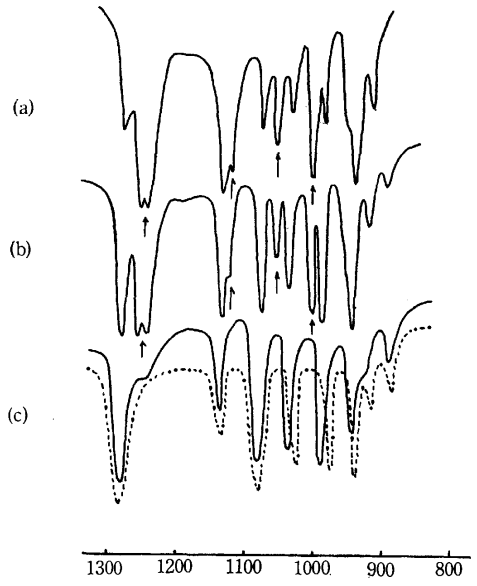

Fig. 1. IR spectra of $[Cl_2Pt(CH_3CH{=}CHOCH_3)]_2$ (Nujol mull)
(a) Complex prepared from *trans*-$CH_3CH{=}CHOCH_3$ (sample I).
(b) Sample I isomerized in a solid state.
(c) Sample I isomerized in a solution.
Complex prepared from *cis*-$CH_3CH{=}CHOCH_3$ (sample II). ------Pd analog (sample III)

whereas the sample II was a pure *cis*-olefin complex and coordinated propenyl methyl ether was isomerized from *trans* to *cis*.

In the case of the 1,2-dimethoxyethylene coordinated to platinum, a similar isomerization in a solid state was followed by studying the IR spectra; however, the isomerization was from *cis* to *trans* in this case.

The platinum complex of propenyl trimethylsilyl ether and palladium complexes of propenyl methyl ether and 1,2-dimethoxyethylene all showed one kind of IR spectrum independent of the olefin isomers used. The configuration of the coodinated olefins in these complexes was determined by comparing the IR spectra with those of platinum complexes.

To compare these olefins with those having no oxygen atoms among their substituents, platinum complexes of *cis*- and *trans*-2-butene and *cis*- and *trans*-β-methylstyrene were prepared; however, they did not show any isomerization. The results with the 2-butene complex are in agreement with those reported by Jonassen and Kirsch.[6] The fact that coordinated propenyl ethers and 1,2-dimethoxyethylene isomerized readily under the conditions under which coordinated 2-butene and β-methylstyrene did not isomerize at all suggests that the contribution of the oxygen atom in the vinyl ether derivatives is essential for the isomerization. The most probable explanation may be some kind of interaction of the oxygen atom with the metal, thus stabilizing the transition state.

cis-Propenyl methyl ether coordinated to palladium or platinum was displaced with pyridine, and the propenyl methyl ether thus liberated was analyzed by glc. Propenyl methyl ether of the *cis*/*trans* ratio of 45 : 1 was liberated from the palladium complex, but the ratio was 3.1 : 1 when it was displaced from the platinum complex, indicating that a considerable amount of the *trans*-isomer was formed in the course of the displacement reaction. Orchin and his co-workers suggested that the displacement of coordinated ethylene by pyridine may proceed by a prior $\pi \rightarrow \sigma$ rearrangement:[7]

$$\begin{matrix} CH_2 & Cl \\ \| & | \\ CH_2 & Pt\text{–}NC_5H_5 \end{matrix} \overset{C_5H_5N}{\rightleftharpoons} C_5H_5N\rightarrow CH_2\text{–}CH_2\text{–}\underset{\displaystyle Cl}{\overset{\displaystyle Cl}{\underset{|}{\overset{|}{Pt}}}}\leftarrow NC_5H_5$$

An analogous σ-bonded intermediate may account for the observation that the *trans*-isomer is formed during the *cis*-propenyl ether displacement by pyridine:

$$Pt\cdots\begin{matrix} CH & CH_3 \\ \| & \\ CH & OCH_3 \end{matrix} \xrightarrow{C_5H_5N} C_5H_5N\rightarrow Pt\text{–}\underset{\displaystyle CH_3}{CH}\text{–}\underset{\displaystyle OCH_3}{CH}\leftarrow NC_5H_5$$

$$\Updownarrow$$

$$C_5H_5N\rightarrow Pt\text{–}\underset{\displaystyle CH_3}{CH}\text{–}\underset{\displaystyle OCH_3}{CH}\leftarrow NC_5H_5 \longrightarrow C_5H_5NPt + \underset{\displaystyle CH_3}{\overset{\displaystyle OCH_3}{CH{=}CH}}$$

If the olefin molecule, which is about to leave the metal, spends enough time in the σ-complex state to allow rotation around the C–C bond, the *cis*/*trans* ratio of the liberated olefin will be controlled by the conformations of the σ-complex as well as by relative rate of its decomposition.

The palladium complex of vinyl *t*-butyl ether was treated with an aqueous hydrogen fluoride and with an aqueous sodium hydroxide. The complex was recovered unchanged from a suspension in 45% aqueous hydrogen fluoride; this is in contrast to the fact that free vinyl ethers are readily hydrolyzed into aldehyde and alcohol in an acid. On the other hand, the complex reacted vigorously with a 45% aqueous sodium hydroxide to yield palladium metal and a quantitative amount of the acetate ion; furthermore, about 84% of the theoretical amount of *t*-butyl alcohol was detected by glc. By analogy with the Wacker process, the reaction may be described as follows:

$$\frac{1}{2}[Cl_2Pd(CH_2{=}CHOCMe_3)]_2 \xrightarrow{OH^-} CH_3COOCMe_3 + Pd^0 + HCl + Cl^-$$

$$CH_3COOCMe_3 \xrightarrow{OH^-} CH_3COO^- + Me_3COH$$

Experimental

Solvents. The toluene and petroleum ether (bp 30—50°C) were purified by the ordinary method and were dried by refluxing over sodium for several days. They were freshly distilled before use.

Olefins. The vinyl methyl ether, vinyl 2-chloroethyl

6) H. B. Jonassen and W. B. Kirsch, *J. Amer. Chem. Soc.*, **79**, 1279 (1957).

7) P. D. Kaplan, S. Schmist, and M. Orchin, *ibid.*, **90**, 4175 (1968).

ether, vinyl 2,2,2-trifluoroethyl ether, and 2-butene were commercial reagents. The other olefins were prepared by the known methods.[9-12] The *cis*- and *trans*-isomers of propenyl ethers were separated by fractional distillation and were confirmed by studying their NMR coupling constants. The *cis*- and *trans*-isomers of 1,2-dimethoxyethylene were separated by fractional distillation and were identified by dipole-moment measurements in benzene (*cis*, 2.00D; *trans*, 1.83D).

[Cl_2Ptolefin]$_2$. This complex was prepared simply by the addition of an olefin to a suspension of $[Cl_2PtC_2H_4]_2$ in toluene. The complexes of vinyl 2,2,2-trifluoroethyl ether, 1,2-dimethoxyethylene, and β-methylstyrene were prepared at room temperature, but the reactions of the other olefins were carried out at low temperatures in order to prevent side reactions. The preparation of the propenyl methyl ether complex will be described as an example; about a 100 mg portion of $[Cl_2PtC_2H_4]_2$ was suspended in 10 m*l* of toluene under a nitrogen atmosphere, and then the suspension was cooled in a dry ice–methanol bath. About 0.2 m*l* of propenyl methyl ether was added, and the mixture was stirred for about 1 hr. The heterogeneous mixture gradually turned homogeneous as the reaction proceeded. The toluene and the excess of propenyl methyl ether were evaporated at −35°C under reduced pressure. The resulting yellow powder of the complex was recrystallized, if necessary, from hot toluene–petroleum ether.

[Cl_2Pdolefin]$_2$. This complex was prepared by the reaction of $Cl_2Pd(PhCN)_2$ and an olefin according to Kharasch's method.[13] The reaction was carried out in toluene at room temperature. The preparation of 1,2-dimethoxyethylene complex was as follows: about a 200 mg portion of $Cl_2Pd(PhCN)_2$ was dissolved in 20 m*l* of toluene under a nitrogen atmosphere, after which the undissolved material was removed by filtration. To this filtrate, 0.05 m*l* of 1,2-dimethoxyethylene was added, and then the solution was continuously stirred. The precipitation of the desired complex occurred within 1 hr. The supernatant solution was removed by decantation, and the precipitate was washed with toluene several times.

Decomposition of the Complexes with Pyridine. The platinum and palladium complexes of propenyl methyl ether were decomposed with pyridine, thus liberating the original olefin without forming any by-product. For example, to 200 mg of $[Cl_2Pt$ *cis*-$CH_3CH{=}CHOCH_3]_2$ we added 1 m*l* of toluene containing a calculated amount of pyridine. The complex dissolved immediately, and there precipitated within 1 hr white crystals which appeared to be $[Pt\ Py_4]Cl_2$. The supernatant solution was analyzed by glc (tricresyl phosphate, 1.5 m, 40°C).

8) W. H. Watanabe and L. E. Conlon, *ibid.*, **79**, 2828 (1957).
9) A. N. Nesmeyanov, L. F. Lustenko, and V. A. Brattsev, *Dokl. Akad. Nauk SSSR*, **128**, 551 (1959). S. I. Sadykh-Zade and A. D. Petrov, *Khim. i. Prakt. Primenenie Kremneorg. Soedinenii*, **1958**, 212.
10) M. Farina, *Chim. e. Ind.*, **42**, 967 (1960).
11) H. Baganz, K. Praefcke, and J. Rost, *Chem. Ber.*, **96**, 2657 (1963).
12) C. M. Foltz and B. Witkop, *J. Amer. Chem. Soc.*, **79**, 201 (1957).
13) M. S. Kharasch, R. C. Seyler, and F. R. Mayo, *ibid.*, **60**, 882 (1938).

BULLETIN OF THE CHEMICAL SOCIETY OF JAPAN, VOL. 45, 3429—3433 (1972)

Determination of the Formation Constants of Actinoid and Lanthanoid Lactate Complexes by Means of Electrophoresis

Masanobu SAKANOUE and Mitsuo NAKATANI

Radiochemical Laboratory, Faculty of Science, Kanazawa University, Kanazawa

(Received February 14, 1972)

Determination of the complex formation constant of actinides (Am, Cm) and lanthanides (Pm, Eu, Lu) with lactic acid was carried out by means of the electrophoretic method. "Cellogel", a gelatinized cellulose acetate was used as the supporting medium for electrophoresis at 10°C. Electrolyte solutions of various pH at an ionic strength of 1.5 were prepared from 0.5M lactic acid solution for electrophoresis at various pH values. The migration zones of α- and β-emitter were determined by α track on cellulose nitrate and autoradiographic image on X-ray film, respectively. The mobility of each nuclide at different pH was analyzed to obtain the formation constants of lactate complex of each element with reference to dissociation equilibrium. The β_1 values thus obtained were consistent with those obtained by other methods. The method was found to be especially useful for determining the complex formation constants of *trans*-uranium elements with only tracer amounts of these elements.

Electrophoresis has been used not only for the separation of various ions, but also for the study of coordination compounds or ion pairs in certain solution systems. Since it is possible to get information on the presence of the functional groups in a given solution system from the relationship[1-4] $U=aZ/\sqrt{M}$ (U: the zone mobility of the migrating substances, Z: their charge, M: the molecular weight), studies[5-10] have

1) V. Jokl, *J. Chromatog.*, **13**, 454 (1964).
2) W. Preetz and E. Blasius, *Z. Anorg. Allg. Chem.*, **332**, 140 (1964).
3) E. Blasius and W. Preetz, *ibid.*, **335**, 16 (1965).
4) Y. Kiso, M. Kobayashi, Y. Kitaoka, K. Kawamoto, and J. Takada, *J. Chromatog.*, **36**, 215 (1968).
5) A. V. Stenanov and T. P. Makaroba, *Radiokhimiya*, **7**, 664 (1965).
6) A. V. Stenanov and T. P. Makaroba, *ibid.*, **7**, 670 (1965).
7) A. V. Stenanov and V. P. Shvedov, *Zhur. Neorgan. Khim.*, **10**, 1000 (1965).
8) I. A. Lebedev, A. M. Maksomova, A. B. Stepanov, and A. B. Shalinets, *Radiokhimiya*, **9**, 707 (1967).
9) I. A. Labedev and A. B. Shalinets, *ibid.*, **10**, 233 (1968).
10) E. Ohyoshi, A. Ohyoshi, and M. Shinagawa, *Radiochim. Acta*, **13**, 10 (1970).

been carried out on the determination of formation constants of complex compounds. The method is suitable and effective for radioactive elements, especially *trans*-uranium elements, since their radioactivities can be easily measured by various methods including autoradiography even in tracer amounts of these elements.

Basic factors concerning electromigration mobility have been studied and the formation constants of some actinide and lanthanide element complexes with lactic acid have been estimated radiochemically, the results of which are reported in this paper.

Theoretical Consideration

In order to estimate the formation constants from electrophoretic mobility data, the following theoretical consideration can be made. Since the trivalent metal ions of lanthanide and actinide elements do not form polynuclear complexes,[11] the consecutive equilibria of mononuclear complexes ML, ML_1, $\cdots ML_N$ and the corresponding equilibrium constants are given by the following equations.

$$\left.\begin{aligned} &M^{3+} + L = ML^{2+};\ K_1 = \frac{[ML]}{[M][L]} \\ &ML^{2+} + L = ML_2^{+};\ K_2 = \frac{[ML_2]}{[ML][L]} \\ &ML_{N-1}^{3-(N-1)} + L = (ML_N)^{3-N};\ K_N = \frac{[ML_N]}{[ML_{N-1}][L]} \end{aligned}\right\} \quad (1)$$

In the method of Bjerrum to arrive at the values of K_N, the stability or formation constant, the underlying principle is the unambiguous relationship between the average number $\bar{n}$ of anionic ligands bound to a metal ion in an equilibrium mixture and the total anion concentration.

$\bar{n}$ can be expressed as

$$\bar{n} = \frac{[ML] + 2[ML_2] + \cdots + N[ML_N]}{[M] + [ML] + [ML_2] + \cdots + [ML_N]} \quad (2)$$

The concentrations of complexes in this equation can be substituted by the expression derived from Eq. (1). Eliminating [M] in both the numerator and denominator, we have

$$\bar{n} = \frac{(K_1[L]) + 2(K_1K_2[L]^2) + \cdots + N(K_1K_2\cdots K_N[L]^N)}{1 + (K_1[L]) + (K_1K_2[L]) + \cdots + (K_1K_2\cdots K_N[L]^N)} \quad (3)$$

Introducing the complex product defined by

$$\beta_n = \frac{[ML_N]}{[M][L]^n} = \prod_{i=1}^{N} K_i \quad (4)$$

Eq. (3) can be written in a more concise form:

$$\bar{n} = \frac{\sum_{n=1}^{N} n\beta_n[L]^n}{1 + \sum_{n=1}^{N} \beta_n[L]^n} \quad (5)$$

If the average charge of a complex of trivalent metal ion with n of anion ligands is represented by $\bar{Z}$, the zone mobility U_c is expressed by

$$U_c = a\frac{\bar{Z}}{\sqrt{M}} = \frac{a}{\sqrt{M}}(3-\bar{n}) = U_k - a\frac{\bar{n}}{\sqrt{M}} \quad (6)$$

where the mobility of non-coordinated trivalent metal ions is given by $U_k = a\ 3/\sqrt{M}$.

Substituting $\bar{n}$ of Eq. (5) into Eq. (6), we get

$$\begin{aligned} U_c &= U_k - \frac{a}{\sqrt{M}} \cdot \frac{\sum_{n=1}^{N} n\beta_n[L]^n}{1 + \sum_{n=1}^{N} \beta_n[L]^n} \\ &= \frac{U_k + \sum_{n=1}^{N} \left(U_k - a\frac{n}{\sqrt{M}}\right)\beta_n[L]^n}{1 + \sum_{n=1}^{N} \beta_n[L]^n} \\ &= \frac{U_k + \sum_{n=1}^{N} U_n\beta_n[L]^n}{1 + \sum_{n=1}^{N} \beta_n[L]^n} \end{aligned} \quad (7)$$

where U_n is the mobility of a complex of trivalent metal ion coordinated with n univalent anion ligands (n: integer) and can be represented by the following equation from the relation $U_k = a\ 3/\sqrt{M}$.

$$U_n = a\frac{(3-n)}{\sqrt{M}} = a\frac{3}{\sqrt{M}} - a\frac{n}{\sqrt{M}} = U_k - \frac{n}{\sqrt{M}} \quad (8)$$

In Eq. (7), the values of U_k, U_n, and β_n are constant under the same experimental conditions, whereas U_c varies with [L].

To determine β_n from U_c and U_n, mobility U_c should be obtained for different organic ligand concentrations. As the functional groups of the organic acid accept or donate protons, the dissociation constant of the equilibrium ($H_nL \rightleftarrows H_{n-1}L + H^+$) is determined by the pH value. The ligand concentration $[H_{n-1}L]$ is then obtained as a function of the pH values. Thus solutions with different ligand concentrations can be prepared from those with identical concentrations of the organic acid by changing pH value. The relationship between the dissociation degree α of univalent organic acid and pH value is given by

$$\alpha = \frac{1}{1 + 10^{-(pH - pK)}} \quad (9)$$

where pK is $-\log K_d$, K_d being the dissociation constant of the organic acid. The ligand concentration can be determined by multiplying the dissociation degree by the normality of the organic acid. The formation constant β_n can then be determined from the relationship between the experimental mobility U_c and the defined pH value.

In Eq. (7), $\sum_{n=2}^{N} \beta_n[L]^n$ can be neglected at low ligand concentrations because it is much smaller than $\beta_1[L]$. Thus, at low ligand concentrations, β_1 can be calculated by

$$U_c = \frac{U_k + U_1\beta_1[L]}{1 + \beta_1[L]} \quad (10)$$

from which we get

$$\beta_1 = \frac{U_k - U_c}{U_c - U_1} \cdot \frac{1}{[L]} \quad (11)$$

Therefore

11) K. Buchtela, "Isotopenpraxis" 3, Jahrgang. Heft 12 (1967).

$$\log \frac{U_k - U_c}{U_c - U_1} = \log \beta_1 - p[\mathrm{L}] \quad (12)$$

Thus the plot of $\log (U_k - U_c)/(U_c - U_1)$ *vs.* $p[\mathrm{L}]$ should give a straight line with slope 1. The intercept of this line with the abscissa is $\log \beta_1$.

The β_2 value can be calculated from the following equations.

$$U_c = \frac{U_k + U_1\beta_1[\mathrm{L}] + U_2\beta_2[\mathrm{L}]^2}{1 + \beta_1[\mathrm{L}] + \beta_2[\mathrm{L}]^2} \quad (13)$$

$$\beta_1 = \frac{\beta_1[\mathrm{L}](U_1 - U_c) + (U_k - U_c)}{[\mathrm{L}]^2(U_c - U_2)} \quad (14)$$

Experimental

Materials and Apparatus. The supporting medium is "Cellogel," the gelatinized cellulose acetate provided from Chemetron-Milano, Italy. It was found by preliminary electrophoretic studies[12] of ^{147}Pm and ^{177}Lu on various supporting materials, that, except for "Cellogel," metal ions were liable to be adsorbed on filter papers usually used for electrophoresis. The "Cellogel" strips preserved in 40% methanol solution were rinsed and stored in distilled water for a few days to remove methanol.

Electrophoresis was carried out by mean of the apparatus provided by Mamino Industry Co. The supporting medium was placed in carbon tetrachloride bath cooled by circulating water of constant temperature (10±0.1°C) in order to avoid heat caused by electric current. The background electrolyte solution was 0.5M lactic acid and its ionic strength was adjusted to 1.5 with potassium chloride, since mobility is affected by ionic strength (Fig. 1) through the change of either resistance or complex formation constants.

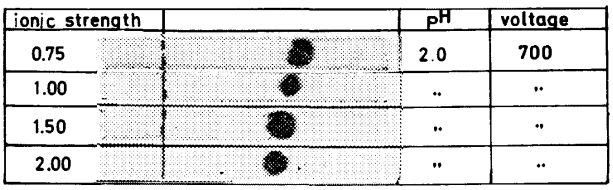

Fig. 1. Autoradiograms of promethium at different ionic strength.

The radioisotopes used were ^{147}Pm, ^{152}Eu, ^{177}Lu, ^{241}Am, and ^{242}Cm. ^{152}Eu and ^{177}Lu having high specific activity were prepared by neutron irradiation of europium and lutetium target in KUR reactor. ^{242}Cm was obtained in carrier-free state after the radiochemical separation of neutron irradiated ^{241}Am target.[13]

The reagents used were all extra pure ones supplied from Wako Pure Chem Ind. Ltd. The stock solutions (1—3N HCl solution) of radioactive nuclides were evaporated to dryness dissolved into electrolyte solutions of various pH and allowed to stand for one day.

The electrolyte solutions were prepared as follows. Lactic acid solution (about 1N) was prepared and its concentration was determined by titration with 0.1N sodium hydroxide. Solutions of NaOH(2N) and $HClO_4$(2N) were prepared and each was mixed with 1N lactic acid in the volume ratio 1:1. This gave two solutions; 0.5M lactic acid—1N NaOH, 0.5M lactic acid—1N $HClO_4$. They were mixed together in various ratios to obtain solution of desired pH.

Procedure. The "Cellogel" strips were dipped at first in the solutions of the background electrolyte (pH 3, 7, and 10) and then in the solutions with various pH used for migration. The excess electrolyte on the "Cellogel" strips was removed with filter paper and then about 1—2 μl of the radioactive sample solution was placed at the starting point marked on the strip. The diameter of the sample spot was about 3 mm. After the "Cellogel" strip had been placed in the migration chamber, a constant voltage was applied between the two electrodes.

After the migration, the "Cellogel" strip was dried in air and fixed to a thick paper. The migration zones of the β-emitter were determined by autoradiograph with X-ray films (Fuji medical X-ray Film), and that of α-emitters by the α-track method[14] with a cellulose nitrate film. The cellulose nitrate film was etched with a 6N sodium hydroxide solution at 60°C for 10 minutes to reveal the α tracks, and was then observed with a microscope.

Results and Discussion

The autoradiogram of ^{147}Pm and the α-track electrophoregram of ^{241}Am are shown in Figs. 2 and 3, respectively.

The relationship between the mobility of ^{147}Pm and the pH value of the electrolyte solution (lactic acid) is shown in Fig. 4. The mobility decreases remarkably with increasing pH in the pH range 0—4, and is almost independent of the pH in the range 5—8. The mobility also decreases above pH 8.

The dissociation of lactic acid at different pH values is shown in Fig. 5 according to the data $pK=3.6$ for lactic acid by means of Eq. (9). It can be seen that the ligand concentration changes remarkably in the pH region 2—5, and is almost constant above pH 6.

The first drop in mobility in the pH range 0—4 (Fig. 4) depends on the decrease of the average charge

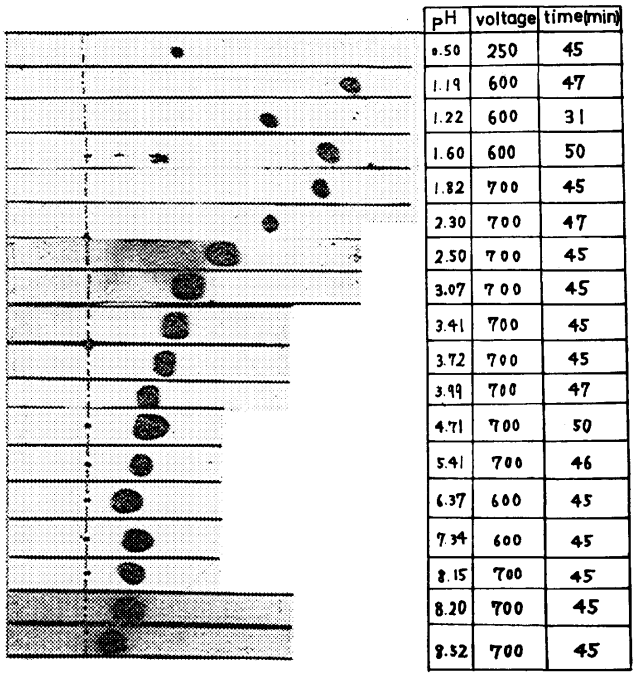

Fig. 2. Autoradiograms of promethium at different pH value.

12) M. Nakatani, M. S. Thesis, Kanazawa University, (1971).
13) M. Sakanoue and M. Nakatani, *Radioisotopes*, **20**, 9 (1971).
14) M. Sakanoue, *Kagaku no Ryoiki*, **24** (2), 124 (1970).

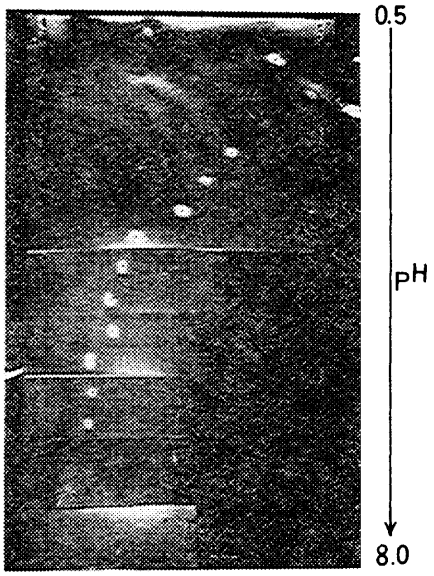

Fig. 3. Cellulose nitrate α-track after the migration of Am in different pH value (voltage and migration times are indicated in Fig. 2).

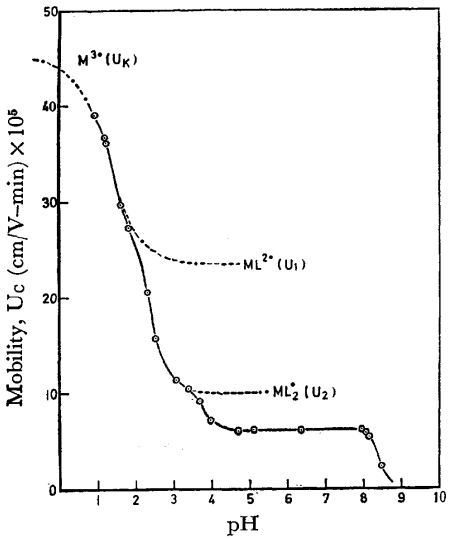

Fig. 4. Mobility — pH curve of ^{147}Pm.

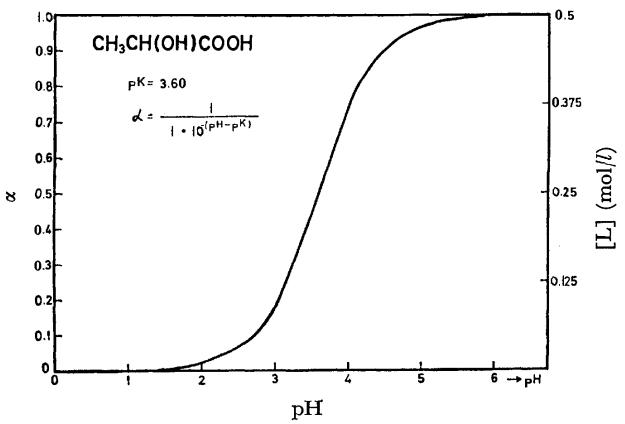

Fig. 5. Dependence of lactic acid dissociation on pH.

of the complex due to the increase of the number of anionic ligands coordinated to promethium. The constancy of mobility in the pH range 5—8 can be understood to be due to the constancy of ligand concentration of lactic acid in this pH region. The decrease of mobility above pH 8 might be due to the formation of complexes with both hydroxy and lactate ions as ligands, since the concentration of hydroxy ion is rather high. This, together with the existence of a plateau at the pH range 4—8 suggests that the effect of hydroxy ion is negligible over the pH range 0—4.

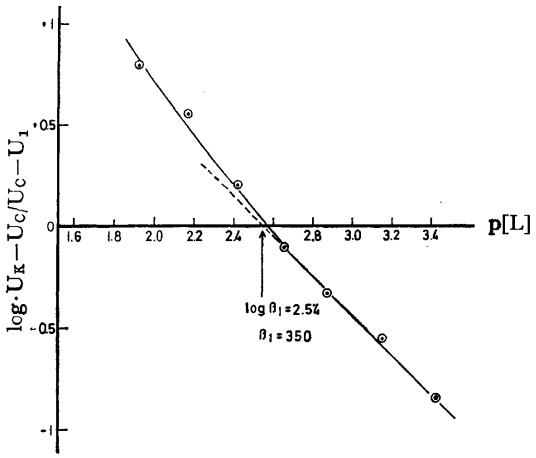

Fig. 6. The analysis for β_1 value from electrophoretic data of promethium in the lactate solution.

By estimating the value of U_k and U_1 from the mobility-pH curves (Fig. 4), we obtain the graphical plot of Eq. (12) for promethium (Fig. 6). The slope of this straight line is 1 in the range of large p[L] value, *i.e.*, of small [L] values due to small values of pH. However, in the range of small p[L] value, the gradient

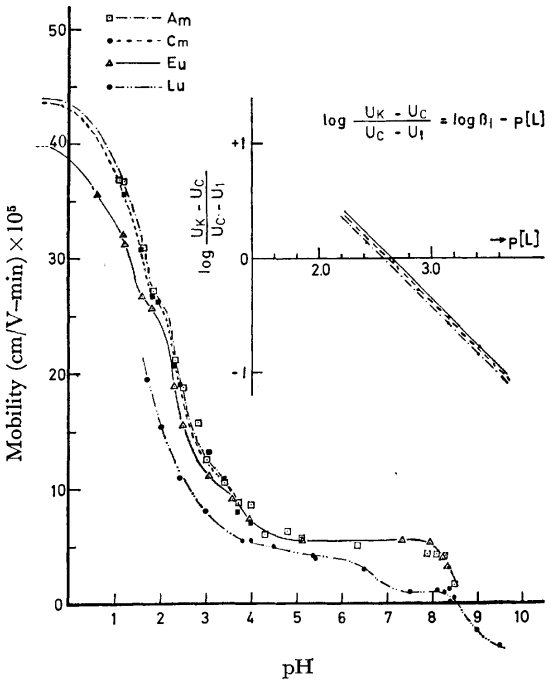

Fig. 7. Mobility — pH curves of Eu, Lu, Am, and Cm lactates and the analysis for β_1 values.

is slightly larger than 1. The reason might be that $\beta_2[L]^2$ is not negligible any more in this case, because of the formation of PmL_2 complexes. As shown in Fig. 6, the value for β_1 should be read from the intercept at the point $p[L]=2.54$, giving the value 350.

The mobility-pH curves for Eu, Lu, Am, and Cm are shown in Fig. 7. They are similar to those for promethium and can be analyzed in the same manner as before.

At any pH, the smaller the mobility, the larger the tendency of complex formation. Therefore, it is shown qualitatively that the formation constants increase in the order Am<Cm<Eu<Lu.

The difference in the formation constants of Am and Cm is very small. The maximum number of coordinated lactate ions may be estimated to be about 2.4 for Lu, but about 2.5 for Eu, Am, and Cm under the conditions employed.

The plots of $\log (U_k-U_c)/(U_c-U_1)$ *vs.* $p[L]$ are also shown (upper right, Fig. 7). The gradients are approximately 1 for all these elements. The curve for Lu is not given since no data are available for the low pH range.

The logarithms of β_1, β_2, and β_3 values are summarized in Table 1 with the previous data. The stability constants β_1 of the lactate complexes of the rare earth elements have been found to decrease with increasing ionic strength.[15,16] The β_1 values we obtained agree fairly well with those obtained by the different methods if the effect of ionic strength on β_1 values is considered. Each $\log \beta_1$ value we obtained may include an error of about 1% (absolute value) as in other works.[8,9] However, under the same conditions, a comparison of $\log \beta_1$ can be made more strictly for Am, Cm, and Eu (Fig. 7). The β_2 values determined are slightly samller than those previously reported, though a larger error (about 10% of $\log \beta_2$ value) may be included in the estimation of β_2.

Table 1. Logarithms of stability constants of Pm, Eu, Am, and Cm lactates

Element	Method	Temp. (C°)	Ionic strengh	$\log \beta_1$	$\log \beta_2$	$\log \beta_3$	Ref.
Pm	(a)	10	1.5	2.54	4.24		this work
Eu	(b)	25	2.0	2.53	4.60		(15)
	(a)	10	1.5	2.62	4.22		this work
Am	(c)	20	0.5			5.71	(17)
	(d)	20	0.5			5.73	(17)
	(d)	—	0.5	2.77	4.64		(18)
	(a)	10	1.5	2.57	4.21		this work
Cm	(c)	20	0.5			5.76	(17)
	(d)	20	0.5			5.78	(17)
	(d)	—	0.5	2.79	4.55		(18)
	(a)	10	1.5	2.59	4.29		this work

Method: (a) electrophoresis, (b) potentiometric titration, (c) distribution measurement, (d) ion exchange.

The electrophoretic method requires only small amounts of samples to determine stability constants. Since the difference in β_1 values of each element becomes small at high ionic strength, it is recommended that separation of elements should be carried out at low ionic strength, as the separation factor of two elements is proportional to the ratio of their stability constants.

15) G. R. Choppin and J. A. Chopoorian, *J. Inorg. Nucl. Chem.*, **22**, 97 (1961).
16) M. A. Gouveia and R. Guedes, *ibid*, **28**, 1684 (1966).
17) V. A. Ermakov and J. Stray, *Radiokhimiya*, **9**, 196 (1967).
18) I. A. Lebedev and G. N. Yakovlev, *ibid.*, **3**, 455 (1961).

Potentiometric Titration of Iron(III) with Hydrazine Sulphate at Room Temperature

G. Gopala Rao, P. V. Krishna Rao, and G. Bala Bhaskara Rao
Department of Chemistry, Andhra University, Waltair, India
(Received May 13, 1971)

Conditions have now been developed for a direct potentiometric titration of iron(III) with hydrazine sulphate at room temperature. Osmium tetroxide markedly catalyses the reaction in medium of 2.0—3.0 pH. Under the conditions prescribed four moles of iron(III) are reduced per every mole of hydrazine oxidised. Application of the new method to the assay of iron(III) in an alloy is also considered.

Hydrazine sulphate, $N_2H_4 \cdot H_2SO_4$ is now readily available at the purity required of a primary standard. It is non-hygroscopic and has a long shelf life. Aqueous hydrazine sulphate solutions are reported to be stable even for a long period of two months.[1] In view of these considerations it has been proposed as a primary standard in acid-base titrimetry[2] and in redox titrimetry.[3] The use of the hydrazine sulphate as a reducing agent has been reviewed by Berka, Vulterin, and Zyka.[4] A survey of the literature shows that the reagent has not been used till now for the detremination of iron(III). Many years ago Kirk and Browne[5] propounded an interesting hypothesis that one electron oxidising agents react with hydrazine to give nitrogen and ammonia according to the equation:

$$N_2H_4 - e \longrightarrow \frac{1}{2}N_2 + NH_3 \qquad (1)$$

and with two electron oxidising agents giving only nitrogen according to the overall equation

$$N_2H_4 - 4e \longrightarrow N_2 + 4H^+ \qquad (2)$$

The stoichiometry of four equivalents of oxidising agent per mole of hydrazine required by Eq. (2) is found to be followed by reactions of hydrazine with iodine, bromine, iodine monochloride and thallic chloride. With one electron oxidising agents like iron(III), manganese(III), and cerium(IV) the number of equivalents of oxidising agent per mole of hydrazine was never found to be one as required by Eq. (1) but was found to be lying between 1 and 2. For the reaction with cerium(IV) in sulphuric acid medium Benrath and Ruland,[6] and Gopala Rao, Subramanyam, and Krishna Rao[7] obtained values of 1.221 and 1.224 respectively for the value of the equivalents of cerium-(IV) reacted with one mole of hydrazine at 80—90°C. The latter workers showed that a direct titration of hydrazine in 1N sulphuric acid medium can be made at 50° with a potentiometric end-point in the presence of manganous sulphate as a catalyst. It was observed that manganese(II) not only affected a considerable acceleration of the reaction but also brought down the stoichiometry of the reaction from 1.224 to 1.016. The value of 1.016 is closer to 1.0 as required by the hypothesis of Kirk and Browne and this improvement in stoichiometry could be understood in terms of the hypothesis because manganese(II) acts as a catalyst through a one-electron mechanism by its oscillation between the +2 and the +3 oxidation states. A more striking change in the stoichiometry was observed by Gopala Rao and Krishna Rao[8] in their titration of hydrazine hydrochloride in hydrochloric acid medium with cerium(IV) nitrate at room temperature in the presence of potassium bromide as a mediator. In this case there is a swing in the stoichiometry of the reaction in the other direction, changing from 1.224 to 4.0. The reaction of hydrazine with cerium(IV) in the presence of potassium bromide undoubtedly occurs through bromine as per Eq. (2) above. Having thus achieved the change of type in the case of hydrazine-cerium(IV) reaction from a mixed type to an accurately stoichiometric 2-electron type with the use of bromide as a mediator or from a mixed type to a very nearly 1-electron type with the use of manganese(II) as a catalyst, we undertook an investigation to see if the iron(III)-hydrazine reaction can also be made to conform to an accurate integral stoichiometry of any one type. Studying the reaction of iron(III) with hydrazine in sulphuric acid medium at 80—90° under varying conditions of acidity and ratio of the reactants but always keeping iron(III) in excess, Cuy[9] found that the stoichiometry varied in the limits 1.32—1.92. A few representative results are listed in Table 1.

It would thus appear that iron(III) functions both as a one-electron type and a two-electron type oxidising

Table 1. Stoichiometry of the iron (III) hydrazine reaction

Acidity	Initial Fe(III) / N_2H_4	Stoichiometry no. of moles of iron(III) consumed per mole of N_2H_4
2N	66	1.32
2.6N	200	1.45
0.12N	66	1.74
0.11N	200	1.92

1) E. C. Gilbert, *J. Amer. Chem. Soc.*, **51**, 2744 (1929). *Proc. Indian. Acad. Sci.*, **35**, 165 (1925).
2) Mellon and Morris, *cf*: "The Chemistry of hydrazine," by L. F. Audrieth, and B. A. Ogg, John Wiley (1951), p. 171.
3) Jannasch and Jahn, *Ber.*, **38**, 1576 (1905).
4) A. Berka, J. Vulterin, and J. Zyka, *Chemist-Analyst*, **52**(2), 56 (1963).
5) Kirk and Browne, *J. Amer. Chem. Soc.*, **50**, 337 (1928).
6) A. Benrath and K. Ruland, *Z. Anorg. Allg. Chem.*, **114**, 226 (1920).
7) G. Gopala Rao, I. Subrahmanyam, and P. V. Krishna Rao, *Z. Anal. Chem.*, **177**, 36 (1960).
8) G. Gopala Rao and P. V. Krishna Rao, *Talanta*, **11**, 1489 (1964).
9) E. J. Cuy, *J. Amer. Chem. Soc.*, **46**, 1810 (1924).

agent for hydrazine, with regard to the type classification of Kirk and Browne. This classification has been adopted by many kineticists[10-12] in their studies of the hydrazine-iron(III) reaction. A close look at the results of Cuy shows that the two-electron type of oxidation increasingly manifests itself with decreasing acidity and with increasing proportion of iron(III). This may be understood in terms of hydrolysis of iron(III) and its dimerisation. Remy[13] states that the exchange of OH^- group for ClO_4^- in aqueous iron(III) perchlorate solution is associated with a simultaneous condensation process of the type

$$2Fe(ClO_4)_3 + H_2O \rightleftharpoons [(ClO_4)_2Fe\text{-}O\text{-}Fe(ClO_4)_2] + 2HClO_4$$

Millburn and Vosburgh,[14] from a spectrophotometric study of 0.01—0.001M iron(III) perchlorate solutions, suggested the dimerisation of the first hydrolysis product by the following scheme.

$$Fe^{3+} + H_2O \longrightarrow [Fe(OH)]^{2+} + H^+$$

$$2Fe(OH)^{2+} \longrightarrow [Fe(OH)_2Fe]^{4+}$$

Whatever may be the formula of the dimeric species, it will be noted that the dimeric species functions as a two-electron oxidiser. Even at the low acidity of 0.11N sulphuric acid, there is still a good deal of one electron type of oxidation of hydrazine because the maximum stoichiometry obtained was only 1.92 and not 4. Moreover the rate of oxidation of hydrazine by iron(III) in this acidity range is not fast enough at room temperature or even at 80 or 90° to facilitate a direct titration. We have now made the interesting observation that the use of osmium tetroxide in trace amounts profoundly accelerates the reaction besides regulating the reaction type to accurately conform to a stoichiometry of 4.0. The details of a potentiometric titration of iron(III) with hydrazine sulphate are presented below. A visual titration was not found possible using the redox indicators, methylene blue, thionine, and variamine blue.

Experimental

Reagents. *Hydrazine Sulphate Solution*: A 0.1M stock solution was prepared from AR, BDH hydrazine sulphate, $N_2H_4\text{-}H_2SO_4$, which was dried at 150°C for one hour. The weight purity agreed within ±0.2% with the purity determined by the bromate method of Kurtenacker and Wagner[15] as modified by Kolthoff.[16] This stock solution was suitably diluted with distilled water when required.

Iron(III) Solution: A 0.1M solution is prepared from AR, BDH ferric ammonium sulphate in 0.2N sulphuric acid. The solution was standardised by photochemical reduction with oxalic acid and subsequent titration with sodium vanadate following the method of Gopala Rao and Madhusudana Rao,[17] and also by the standard procedure of reduction in the Jone's reductor and titration of the reduced solution with standard dichromate solution.

Osmium Tetroxide Solution: A 0.2% solution of osmium tetroxide was prepared in 0.1N sulphuric acid from a sample supplied by M/s. Johnson Mathey, England.

All other chemicals employed in this investigation are of analytical reagent grade. The pH of the titration mixtures was adjusted with a 10% solution of sodium bicarbonate with the aid of strips of indicator-paper supplied by M/s. British Drug House (India) Ltd.

Apparatus. The potentiometric titration assembly employed in this investigation comprises of a Junior potentiometer, a Taut suspension galvonometer (both supplied by M/s. W. G. Pye & Co., England), a bright platinum rod as indicator electrode, and a saturated calomel electrode as a reference electrode. Contact between test potential and the reference electrode has been established by means of a porous plate-end salt bridge filled with a saturated solution of potassium sulphate. The titration vessel consists of a 150 ml Pyrex beaker fitted with a five-holed rubber stopper. The holes accomodate respectively a salt bridge, an indicator electrode, the nozzle of a microburette, and the inlet and outlet tubes for nitrogen.

Our preliminary experiments have shown (i) that the reduction of iron(III) with hydrazine sulphate in an acid solution is extremely slow at room temperature (ii) the speed of reduction increases with decreasing acidity of the medium (iii) even in a medium of pH 2.0—3.0 the reaction is too slow for a potentiometric titration to be carried out at room temperature. (iv) At higher temperatures the iron-(III) solution undergoes rapid hydrolysis in this pH range and precipitates as the hydroxide. However we made the interesting observation that when traces of osmium tetroxide are added to the reaction mixture, the reaction is markedly accelerated at room temperature in this pH range and this catalysed reaction can be utilised for a direct potentiometric titration of iron(III) with hydrazine sulphate.

Effect of Varying the pH *of the Medium.* The influence of pH on the shape of the *E-V* curve is shown in Fig. 1. When the pH of the iron(III) solution is 1.0 the potentials attain stable values in about two min in the early stages of the titration, but a wait of 10—12 min is required near the equivalence point. Moreover, at this pH, the potential break at the equivalence point was not quite satisfactory being about 15 mV for 0.04 ml of the titrant. At pH 2.5—3.0, the potentials attain stable values within one minute in the early stages of the titration, in about 2—3 min near the equivalence point and in about 5 min at the equivalence point. The potential break at the equivalence is about 60—70 mV per 0.04 ml of 0.025M hydrazine sulphate. In titrations with a 0.1M solution of hydrazine sulphate, the break in potential at the equivalence point is about 90 mV per 0.04 ml of the titrant.

Effect of Oxygen of the Air. Titrations conducted in presence of atmospheric oxygen gave results which agree with those conducted in an inert atmosphere. This shows that nitrogen evolved in the reaction is sufficient to act as a blanket against the interference of the oxygen of the air.

Stoichiometry. Under the conditions prescribed, it has been found that four moles of iron(III) are reduced per mole of hydrazine oxidised, in accordance with the equation

10) W. C. E. Higginson, D. Sutton, and P. Wright, *J. Chem. Soc.*, **1953**, 1380.
11) J. W. Cahn and R. Powell, *J. Amer. Chem. Soc.*, **76**, 2568 (1964).
12) D. R. Rosseinsky, *J. Chem. Soc.*, **1957**, 4685.
13) H. Remy, "Treatise on Inorganic Chemistry," p. 282. Vol. 2, Elsevier Publishing Company, London, (1956).
14) R. M. Millburn and W. C. Vosburg, *J. Amer. Chem. Soc.*, **77**, 1352 (1956).
15) A. Kurtenacker and J. Wagner, *Z. Anorg. Allg. Chem.*, **120**, 261 (1922).
16) I. M. Kolthoff, *J. Amer. Chem. Soc.*, **46**, 2009 (1924).
17) G. Gopala Rao and V. Madhusudana Rao, *Current Sci.*, **13**, 317 (1944); *Proc. Nat. Inst. Sci., India*, **12**, 217 (1946).

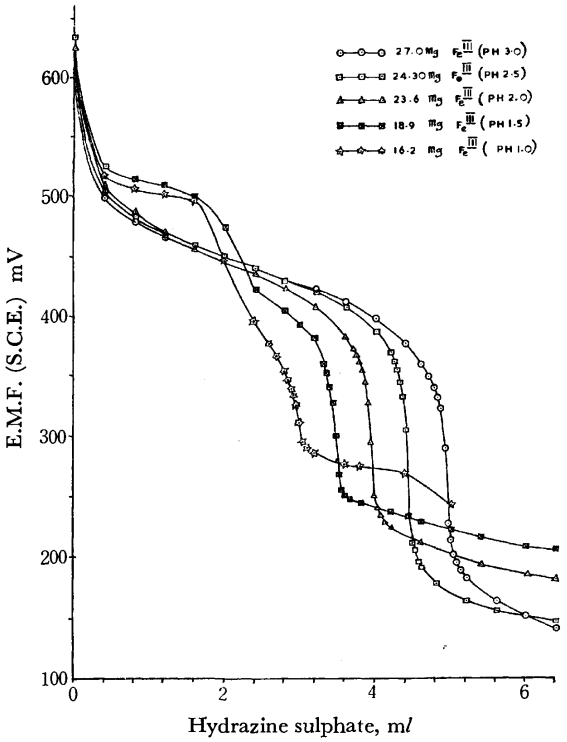

Fig. 1. Effect of pH on the potential break at the equivalence point in the titration of iron(III) with 0.025M hydrazine sulphate.

$$N_2H_5^+ + 4Fe^{3+} \longrightarrow N_2 + 4Fe^{2+} + 5H^+.$$

Effect of Varying Osmium Tetroxide Concentration. Our experiments with varying amounts of osmium tetroxide have shown that a minimum of 0.2 m*l* of a 0.2% solution of the catalyst is needed for a satisfactory potentiometric titration while quantities beyond 0.5 m*l* result in slightly higher titers.

Recommended Procedure. The pH of an aliquot of the iron(III) solution taken in a titration vessel is carefully adjusted with the aid of strips of pH indicator paper to lie between 2.5 and 3.0 using a 10% solution of sodium bicarbonate. Then 0.2 m*l* of a 0.2% solution of osmium tetroxide is added, the mixture diluted to 50 m*l* and then titrated with a 0.025—0.1M hydrazine solution to a potentiometric endpoint using the titration assembly described above. The potential values were recorded with a wait of one minute after the addition of each drop of the titrant in the initial stages of the titration, and after a wait of 2 min near the equivalence point. During the titration a drop or two of bicarbonate solution is added from time to time to neutralise the acid formed in the reaction. The potential reading at the equivalence point is noted after a wait of 5 min. After the equivalence point the potentials again attain stable values within a minute after the addition of the titrant. Some representative results of titrations carried out according to the new procedure are recorded in Table 2.

Table 2. Recovery of iron(III) by potentiometric titration with hydrazine sulphate

Amount of iron(III), mmol	
Taken	Found
0.0634	0.0636
0.1105	0.1096
0.3120	0.3125
0.4199	0.4200
0.9287	0.9265
1.3950	1.3910
2.0410	2.0530

Titrations of dilute solutions of iron(III) with hydrazine sulfate are not possible when the over all concentration of iron(III) is below 10^{-2} mol/*l*. Reverse titrations of hydrazine sulphate with iron(III) are not feasible under the pH and catalyst conditions stated above. It was observed that when osmium tetroxide was added to the hydrazine sulphate solution, it was reduced to a black colloidal mass which was not reoxidised by the iron(III) solution dropped from the burette.

Interferences. Vanadium(V) and chromium(VI) interfere by simultaneously reacting with hydrazine sulphate under the experimental conditions. Molybdenum(VI) interferes at higher concentrations (when Mo(VI)/Fe(III) is 20) by formation of an insoluble white precipitate, presumably iron(III) molybdate. Molybdenum(VI) also interferes at low concentrations (1.85×10^{-2} mg/50 m*l*) through formation of molybdenum blue presumably by reduction of molybdenum(VI) by the iron(II) formed in the reaction. In the presence of titanium(IV) the titration of iron(III) is not possible, probably due to hydrolysis of titanium(IV) at the prescribed pH and deposition of the hydrolysed product on the platinum electrode.

Uranium(VI), vanadium(IV), copper(II), nickel(II), cobalt(II), chromium(III), and manganese(II) do not interfere. Sulphate and perchlorate also do not interfere. Chloride interferes at a final concentration greater than 35 mg/50 m*l* by lowering the potential break. In the presence of complexing anions like phosphate, fluoride, salicylate, and thiocyanate the titration of iron(III) is not possible.

Application of the New Procedure for the Determination of Iron(III) in Alloys

Analysis of an Alloy. An accurately weighed sample (*ca.* 1.0 g) of the alloy (soft iron nail) is treated with 25 m*l* of 1:1 (vol/vol) nitrogen free sulphuric acid in a 250 m*l* beaker covered with a watch glass and heated on a hot plate till it completely dissolves. The resulting solution which contained a few black floating particles (carbon) is filtered after dilution with water through a Whatman No. 42 filter paper into a 500 m*l* Pyrex beaker and treated dropwise with 0.1N solution of potassium permanganate until a very pale pink colour of $KMnO_4$ persists. The excess of permanganate is destroyed by adding one or two drops of a 10% (vol/vol) hydrogen peroxide solution. The resulting solution is gently heated to boiling on a hot plate to destroy the excess hydrogen peroxide. It is then cooled to room temperature, quantitatively transferred to a 500 m*l* volumetric flask and made up to the mark.

Table 3. Assay of iron(III) in an iron nail

Wt. of the sample analysed, g	Iron(III) found, g		
	Present method, g	Jone's reduction method, g	Photochemical reduction method, g
1.3058	1.3020	1.3031	1.3017
1.1810	1.1776	1.1780	1.1767
0.9894	0.9876	0.9877	0.9877

Aliquots of this solution are titrated with 0.025M hydrazine sulphate solution to a potentiometric end-point according to the recommended procedure. The results are compared with those obtained by titration with a standard solution of potassium dichromate after reduction in a Jone's reductor, and also with those obtained by the photochemical reduction method of Gopala Rao *et al.*[17] The data in Table 3 show that the results obtained by the new procedure are in excellent agreement with those obtained by the standard procedures.

BULLETIN OF THE CHEMICAL SOCIETY OF JAPAN, VOL. 45, 3437—3439 (1972)

Titrimetric Determination of Iron(II), Molybdenum(V), and Thallium(I) with Potassium Chlorate Using Redox Indicators

G. Gopala Rao and C. Radhakrishnamurty*
Department, of Chemistry Andhra University, Waltair, India

(Received May 17, 1971)

Accurate and convenient procedures have now been devised for the titrimetric determination of iron(II), molybdenum(V), and thallium(I) with potassium chlorate using visual indicators. These procedures are more advantageous than the procedures involving bromate. Further, chlorate is to be preferred as it is more inexpensive than bromate or iodate. Potassium chlorate is now obtainable at the purity required of a primary standard at a nominal cost. The chlorate titration procedure for iron(II) works satisfactorily even in the presence of organic materials such as oxalic acid, tartaric acid, and citric acid, so that it can be used for the determination of ferrous iron in pharmaceutical preparations or of ferric iron after reduction. It has been observed by us that oxygen of the air interferes in the titration of iron(II) in 6—7M hydrochloric acid medium using naphthol blue black or methyl orange as a redox indicator but not in the titration of iron(II) in sulphuric acid medium using ferroin as an indicator. An inert atmosphere is not necessary for the titration of molybdenum(V) and thallium(I) in hydrochloric acid medium.

Although potassium chlorate is available at the purity required of a primary standard, it has not been very much used as a titrimetric reagent. Potassium chlorate may function in acid solution either as a five electron oxidant giving chlorine or as a six electron oxidant giving chloride as the end product. The calculated redox potentials for these two reactions are 1.47 and 1.45 V respectively, comparable to those of cerium(IV) sulphate and potassium permanganate. Inspite of these high redox potentials potassium chlorate is comparatively inert in dilute acid solution. Its comparative chemical inertness is explicable from kinetic considerations. The rates of reactions of potassium chlorate even with substances of very low redox potentials like tin(II) and titanium(III) are very slow. Recent studies on the kinetics of reactions involving chlorate have shown that the reaction rates increase with increasing hydrogen ion concentration. Since resonance stabilisation is large for oxyanions, it is necessary to overcome this stability in order that a chemical reaction takes place. On the addition of hydrogen ions at high concentration the oxyanions are converted into less stable forms which can easily react with other chemical species. Taking advantage of the kinetic results we have been able to establish conditions under which potassium chlorate can be used as an oxidimetric reagent for the direct titration of iron(II), molybdenum(V), and thallium(I) at room temperature using suitable redox indicators.

* Department of Chemical Engineering, Andhra University, Waltair, India.

Experimental

Preparation of Solutions. A 0.1N solution of potassium chlorate is prepared from "Pro Analysi" reagent supplied by E. Merck and its purity is checked by the method prescribed by Vogel.[1] The assayed purity agreed with the weight purity.

A 0.1N solution of iron(II) was prepared from Analar reagent grade Mohr's salt supplied by British Drug Houses. The final concentration of sulphuric acid in the solution is 1.0N. The solution is standardised against potassium dichromate.

A 0.1N solution of molybdenum(V) was prepared from Analar reagent grade ammonium molybdate which was reduced in 3M hydrochloric acid in a mercury reductor according to the instructions of Furman and Murray[2] and standardised against standard cerium(IV) sulphate by the procedure of Gopala Rao and Suryanarayana.[3]

A 0.1N thallium(I) sulphate solution was prepared from Analar reagent grade thallous sulphate and standardised against potassium dichromate according to the procedure of Erdey, Vigh, and Buzas.[4]

All other chemicals used in the investigation are of chemically pure grade.

1) A. I. Vogel, "A Text book of Quantitative Inorganic Analysis," Longmans Green and Co. Ltd., London (1964) 3rd ed., p. 313.
2) N. H. Furman and W. M. Murray, *J. Amer. Chem. Soc.*, **58**, 1689 (1936).
3) G. Gopala Rao and M. Suryanarayana, *Z. Anal. Chem.*, **169**, 161 (1959).
4) L. Erdey, K. Vigh, and I. Buzas, *Acta Chim. Acad. Sci. Hung.*, **26**, 85, 93 (1961).

Visual Titration of Iron(II) with Potassium Chlorate. From preliminary studies it was observed that ferroin is rapidly oxidised only in a medium containing sulphuric acid and phosphoric acid at final concentrations of 8—9 and 2M respectively. The oxidised indicator is, however, reduced rapidly by iron(II) under all conditions of acidity. In 9 and 10M sulphuric acid alone titrations cannot be conducted because ferroin decomposes as the end-point is approached. Phosphoric acid not only stabilises the indicator but also catalyses the oxidation of indicator by chlorate. In view of these considerations the following procedure is recommended for the titrimetric determination of iron(II) with potassium chlorate.

Recommended Procedures for the Titration of Iron(II).

Procedure 1: A known volume of 12M sulphuric acid is taken in a 150 m*l* pyrex titration cell and enough distilled water added to give an overall acidity of 8—9M when diluted to 50 m*l*. The mixture is cooled to the room temperature and then an aliquot of iron(II) solution is added followed by 5 m*l* of 85% syrupy phosphoric acid. Stirring the mixture well, add 0.1 m*l* of 0.01M ferroin and titrate with 0.1N solution of potassium chlorate. The titration is to be made dropwise towards the end, giving a wait of 10 seconds between successive additions. At the end-point the colour change is from red to pale blue. The indicator correction is 0.07 m*l* of 0.1N chlorate solution to be deducted from the titer. The average relative error of determination of iron(II) is ±0.2%.

Procedure 2: The addition of 1—2 m*l* of 0.1N of vanadium(IV) sulphate in place of phosphoric acid also catalyses the reaction at overall acidity of 7—8M sulphuric acid using 0.1 m*l* ferroin as an indicator. The average relative error of determination of iron(II) is ±0.2%.

Procedure 3: Titrations of iron(II) with potassium chlorate have been found possible in 6—7M hydrochloric acid medium in an inert atmosphere, using 0.1 m*l* of 0.2% naphthol blue black or 0.1 m*l* of 0.1% methyl orange as a redox indicator. The colour changes at the end-point are from green to yellow with naphthol blue black and red to yellow with methyl orange. The indicator correction amounts to 0.06 m*l* of 0.1N potassium chlorate per 0.1 m*l* of any of the two indicator solutions, to be deducted from the experimental titre. For titrations of iron(II) in 6—7M hydrochloric acid medium an inert atmosphere is necessary, because iron(II) will be oxidised by oxygen of the air due to lowering of the iron(III)/iron(II) potential in hydrochloric acid medium.

Interferences: Five hundred milligram of oxalic acid, 75 mg of tartaric acid, 525 mg of citric acid, 41 mg of cobalt(II), 53 mg of nickel(II), 13 mg of chromium(III), and 15 mg of vanadium(IV) do not interfere in a volume of 50 m*l*. Glucose interferes. Representative results are presented in Tables 1 and 2.

Table 1. Titration of iron(II) with potassium chlorate

Indicator	Amount of iron(II) in mmol	
	Taken	Found
Ferroin	0.3960	0.3950
8—9 M H_2SO_4	0.4384	0.4390
+	0.5245	0.5234
2 M H_3PO_4	0.7091	0.7111
Ferroin	0.2567	0.2572
7—8 M H_2SO_4	0.5200	0.5190
+	0.6200	0.6182
1—2 m*l* of 0.1 M vanadium(IV)	0.7316	0.7335

Table 2. Titration of iron(II) with potassium chlorate

Indicator	Amount of iron(II) in mmol	
	Taken	Found
Naphthol blue black	0.3570	0.3651
6—7 M HCl	0.4039	0.4048
	0.4529	0.4536
	0.6806	0.6794
Methyl orange	0.3468	0.3476
6—7M HCl	0.4487	0.4478
	0.5665	0.5670
	0.7018	0.7037

Visual Titration of Molybdenum(V). Satisfactory visual titrations of molybdenum(V) with potassium chlorate can be made in 5—7M hydrochloric acid medium with the addition of 1 m*l* of 0.01M iron(III) as a catalyst per 50 m*l* using 0.1 m*l* of 0.1% methyl orange or methyl red as an indicator. While using 0.1 m*l* of 0.2% napthol blue black as an indicator it is necessary to add 3 m*l* of the iron(III) solution as a catalyst. The titration is carried out rapidly in the beginning and slowly towards the equivalence point allowing 20—25 sec, after each addition of a drop of the reagent; with methyl orange or methyl red the end-point is denoted by the disappearance of red colour. In the case of naphthol blue black the colour change is from bluish green to yellow. The indicator correction with 0.1N chlorate solution is 0.06 m*l* per 0.1 m*l* of any of these indicator solutions. These indicators do not work in sulphuric acid medium. The average relative error of determination is ±0.2%. Our observations showed that an inert atmosphere is not necessary for the titration of molybdenum(V).

Interferences: Twenty six milligram of chromium(III) and 44 mg of vanadium(IV) do not interfere.

Some typical results are given in Table 3.

Table 3. Titration of molybdenum(V) with potassium chlorate

Indicator	Amount of molybdenum(V) in mmol	
	Taken	Found
Methyl orange	0.2357	0.2352
5—7M HCl	0.3593	0.3600
+	0.4428	0.4424
1 m*l* of 0.01M iron(III)	0.5036	0.5024
Methyl red	0.2332	0.2327
5—7M HCl	0.4715	0.4706
+	0.5977	0.5966
1 m*l* of 0.01 M iron(III)	0.6585	0.6600
Naphthol blue black	0.2642	0.2636
5—7M HCl	0.3807	0.3814
+	0.4592	0.4584
3 m*l* of 0.01M iron(III)	0.5452	0.5439

Visual Titration of Thallium(I). Accurate visual titrations of thallium(I) are possible with potassium chlorate in 6—8M hydrochloric acid using 0.1 m*l* of 0.1% methyl orange or methyl red or neutral red or phenosafranine and 0.1 m*l* of 0.2% naphthol blue black as indicators. The titration with potassium chlorate is made rapidly in the beginning and dropwise towards the end giving a wait of 20—25 sec between drops. The indicator corrections are 0.1 m*l* in the

Table 4. Titration of thallium(I) with potassium chlorate

Indicator	Amount of thallium(I) in mmol	
	Taken	Found
Methyl orange	0.2168	0.2174
6—8M HCl	0.2423	0.2430
	0.4354	0.4346
	0.4782	0.4770
Methyl red	0.2104	0.2108
6—8M HCl	0.2265	0.2272
	0.3443	0.3433
	0.4948	0.4940
Neutral red	0.2533	0.2528
6—8M HCl	0.3663	0.3675
	0.4055	0.4045
	0.4827	0.4840
Phenosafranine	0.2435	0.2440
6—8M HCl	0.2622	0.2626
	0.3376	0.3366
	0.4386	0.4373
Naphthol blue black	0.2022	0.2026
6—8M HCl	0.3175	0.3185
	0.3632	0.3621
	0.3936	0.3944

case of methyl orange and methyl red, 0.06 m*l* in the case of phenosafranine and neutral red and 0.04 m*l* in the case of naphthol blue black. The average relative error of determination is found to be $\pm 0.25\%$. Methyl red and methyl orange turn from red to yellow, naphthol blue black turns from blue to light pink at the end-point. Phenosafranine changes color from blue violet to colorless through pink, while neutral red gives a transition of violet to colorless through pink. It has been observed by us that titrations of thallium(I) gave identical results both in air and an inert atmosphere. This shows that thallium(I) is not oxidised by oxygen inspite of the lowering of the thallium(III)/thallium(I) potential.

Some typical results are given in Table 4.

Discussion

The procedure now developed for the determination of iron(II) with potassium chlorate is much more simple and convenient than the procedure with potassium bromate. Moreover potassium chlorate is more inexpensive than potassium bromate. Kolthoff and Belcher[5] state that in the titration of ferrous iron with bromate using methyl red or methyl orange as an indicator, the colour of the indicator disappears long before the equivalence point is reached, due to the slowness of the reaction between iron(II) and bromate. Smith and Bliss[6] recommended the addition of a copper salt as a catalyst. However, as the copper also catalyses the atmospheric oxidation of the ferrous iron, arsenate is proposed to be added. They also recommended the addition of phosphoric acid to lower the oxidation potential of the system.

It is noteworthy that in the potassium chlorate method now developed for the determination of iron(II), various organic materials such as oxalic acid, tartaric acid, and citric acid do not show any interference; whereas the permanganate and dichromate methods cannot be used in their presence. The chlorate method, therefore, holds out great promise for the determination of iron(II) in pharmaceutical preparations.

The titration method for thallium(I) now developed by us is also more advantageous than the bromate procedure as the latter requires heating to 50—60°C.

5) I.M. Kolthoff and R. Belcher, "Volumetric Analysis," Vol. III, Interscience Publishers, Inc., New York, (1957), p. 521.

6) G.F. Smith and H.H. Bliss, *J. Amer. Chem. Soc.*, **53**, 4291 (1931).

Substituent Effects on Suspected Phenonium Ion Reactions

Charles A. KINGSBURY and D. C. BEST
Department of Chemistry, University of Nebraska, Lincoln, Nebraska 68508, U.S.A.

(Received May 15, 1971)

The stereochemistry of the various conversions in the 1,2-diphenyl-1-propyl system was measured as a function of aromatic substituent. For β-anisyl groups the reaction occurred with retention of configuration. For compounds with indifferent electron donating aryl groups, the conversions were stereoselective forming mostly *threo* product. For β-*p*-nitrophenyl groups the stereochemical course of the reaction was "racemization." The latter reactions were associated with the presence of open ions. In certain reactions, acetate products were formed in low yield with retention of configuration, irrespective of substituent. The kinetics of ethanolysis were consistent with (partial) bridged ion formation for the *threo* isomers and with extensive open ion formation for the *erythro* species.

The problem of the intermediacy of a phenonium ion species has occupied the attention of chemists for a considerable period.[1,2] In a sense, the question of whether or not a phenonium ion can exist has been answered by the direct spectral observation of Olah, Pittman, Namenworth, and Comisarow,[3] and in a related system, by Winstein and Baird.[4] The question remains whether the type of ion thus observed is similar to a solvolysis reaction intermediate.

The nature of the solvolysis intermediate has been inferred from stereochemical[5] and in other cases from kinetic data.[6] The inferences from stereochemical data are in actuality concerned with the relative rates of processes that give retention of configuration, (*e.g.* C→D→E of Scheme 1) and processes that give other stereochemical results (*e.g.* C′→D′→E′). These processes are sensitive not only to the nature of the intermediate (or intermediates) but also to the energy levels of the various possible transition states leading to products.[1c] Thus, product of a certain stereochemistry (*e.g.* E′) may not reflect the nature of the most stable intermediate (*e.g.* C), but merely the lowest energy pathway for conversion to products.

On the other hand, inferences from kinetic data depend on the relative energy levels A and B, and do not directly involve the intermediate C. The hope is that the energy level of B will parallel that of the first-formed intermediate C or C′. This expectation is perhaps reasonable if anchimeric assistance is present, that is where the β-aryl group pushes off the leaving group. Brown and co-workers[6,7] have advanced the existence of a large rate enhancement (over a standard compound) as the criterion for the presence of a phenonium ion intermediate. This criterion is not met in the solvolysis of 3-phenyl-2-butyl compounds, although certain β-anisyl substrates appear to fulfill this criterion.[6,7] However, in non-nucleophilic solvents such as trifluoroacetic acid, Nordlander and Deadman[8] have shown that ordinary β-phenyl substrates are indeed characterized by large rate enhancements. On the other hand, Lancelot and Schleyer believe that even a small rate enhancement may reflect the intermediacy of a bridged ion.[9]

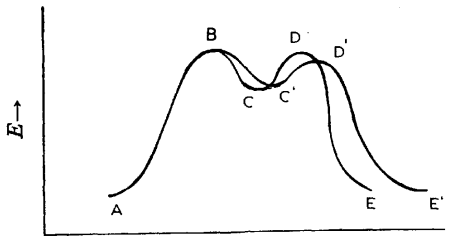

Scheme 1.

The compounds of interest to this study are shown in Scheme 2. In these studies various of the groups Z were interposed. The question of interest is whether any evidence for participation by a β-aryl group can be detected, if the cationic center is stabilized by the effect of an α-aryl group. In a bicyclic system, Brown and co-workers have suggested that additional stabilization of a quite stable tertiary cation by participation would be unnecessary.[10] Winstein has questioned this conclusion.[11] The elegant tracer studies of Collins and Benjamin were discouraging in this regard, as there was no evidence for the existence of a bridged ion of the σ variety in the 1,2,2-triphenylethyl cation.[12] This work also showed that one must be cognizant of the fact that one of the prime pieces of evidence for participation, namely retention stereochemistry, may arise by other means. In this work, steric interference with the inversion pathway by a β-aryl group was

1) (a) H. Tanida, *Accounts Chem. Res.*, **1**, 239 (1968). (b) B. Capon, *Quart. Rev.* (London), **12**, 173 (1958). (c) B. Capon, M. Perkins, and C. Rees, "Organic Reaction Mechanisms, 1966," Interscience Publishers, New York, N. Y., (1965).

2) J. L. Coke, F. McFarlane, M. Mourning, and M. Jones, *J. Amer. Chem. Soc.*, **91**, 1154 (1969) and references cited therein.

3) G. Olah, C. Pittman, E. Namenworth, and M. Comisarow, *ibid.*, **88**, 5571 (1966); **89**, 711 (1967).

4) R. Baird, and S. Winstein, *ibid.*, **85**, 567 (1963); see also M. Brookhart, F. Anet, D. J. Cram, and S. Winstein, *ibid.*, **88**, 5659 (1966).

5) D. J. Cram, *ibid.*, **86**, 3767 (1964). This work presents the case for the phenonium ion.

6) H. C. Brown, K. Morgan, and F. Chloupek, *ibid.*, **87**, 2137 (1965). This work presents the opposing case.

7) H. C. Brown and C. Kim, *ibid.*, **90**, 2082 (1968); *ibid.*, **91**, 4289 (1969).

8) J. E. Nordlander and W. Deadman, *ibid.*, **90**, 1590 (1968).

9) C. J. Lancelot and P. Schleyer, *ibid.*, **91**, 4294 (1969).

10) H. C. Brown, F. Chloupek, and M.-H. Rei, *ibid.*, **86**, 1246 (1964).

11) S. Winstein, *ibid.*, **87**, 381 (1965).

12) C. V. Collins and B. M. Benjamin, "Advances in Physical-Organic Chemistry," Vol. 2, Academic Press, London, England, 1964, p. 1, and references cited therein. See also W. B. Smith and M. Schowalter, *J. Amer. Chem. Soc.*, **86**, 4136 (1964).

Table 1. Activation parameters and first order rate constants for the solvolysis of **1**, in 80% aqueous[a] ethanol

	k, sec^{-1} ($\times 10^4$)							ΔH^*	ΔS^*
Temp.	34.9°C	45.0°C	55.0°C	62.5°C	70.0°C	75.0°C	k_{rel}[b]	(kcal)[c]	(e.u.)[d]
Threo **1**									
a *p*-CH_3O	4.06±0.04	10.5±0.4	25.6±0.4	52.4±0.9			390	18[e]	−15
b *o*-CH_3O	6.50±0.01	18.6±0.1	52±4				780	20	− 8
c H			2.05±0.12	4.19±0.01	8.34±0.2	11.8±0.05	31	21	−11
d *p*-NO_2			0.194±0.007	0.416±0.004	0.88±0.04	1.39±0.01	2.9	22	−14
Erythro **1**									
a *p*-CH_3O			0.926±0.013	2.01±0.07	4.34±0.01	7.11±0.04	14	22	− 9
c H			0.313±0.004	0.69±0.013	1.41±0.03	2.24±0.01	4.7	22[e]	−14
d *p*-Cl			0.159±0.006	0.362±0.001	0.805±0.068	1.20±0.07	2.4	22[e]	−12
e *p*-NO_2			0.0664±0.0003	0.167±0.006	0.352±0.007	0.541±0.004	1	21[e]	−19

a) Actual composition 79.6% by weight.
b) At 55°C.
c) The activation enthalpies are considered good to ±1 kcal.
d) The activation entropies are considered good to 4 ±e.u.
e) Taken from the most linear portion of a curved Arrhenius plot.

postulated.[13] On the other hand, the early work of Cram and Elhafez[14] on the 1,2-diphenyl-1-propyl system was interpreted in terms of β-aryl participation, although the nature of the intermediates perhaps needs to be recast in more modern terms.[14,15] In still other work, retention has been observed in solvolyses forming several types of α-aryl cations, in which no possibility of participation exists.[16-19] The leaving group may lead in the attacking solvent fragment producing retention, but, generally speaking, the mechanism of these processes requires further elaboration.

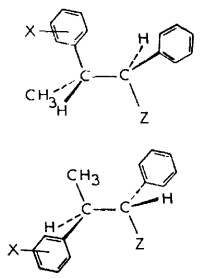

Z	X
1 Br	**a** *p*-CH_3O
2 OH	**b** *o*-CH_3O
3 OCH_3	**c** H
4 OAc	**d** *p*-Cl
5 Cl	**e** *p*-NO_2

Scheme 2.

The solvolysis data are listed in Table 1. These data will be discussed in terms of the mechanism shown in Scheme 3, which is similar to that originally proposed by Cram and Elhafez.[14] The greater reactivity of the *threo* compounds could be explained by the greater stability of the bridged intermediate **6** than the analogous intermediate, **8**, which results from *erythro* **1**. The latter intermediate would be destabilized

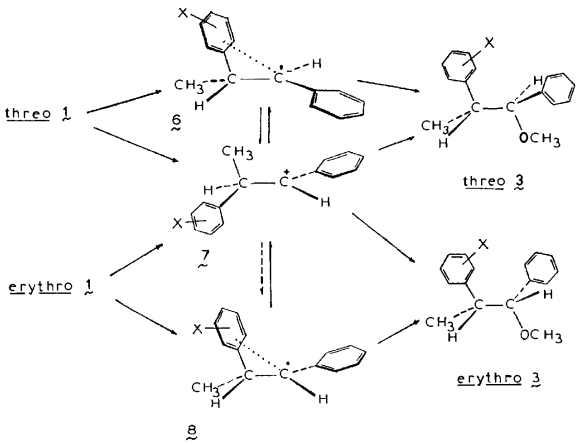

Scheme 3.

by an unfavorable phenyl-methyl interaction. However, Cram and Elhafez also showed that the *threo* **1c** is more reactive than *erythro* **1c** in S_N2 reactions.[14,20] Thus, a sizable *threo*/*erythro* rate ratio would be expected for both β-aryl participation (k_Δ) and direct solvent attack (k_s).[2,9] Of more significance is the fact that a large *threo*/*erythro* ratio is observed for the *p*-methoxy compounds (*ca.* 28). Participation, if any, should be facilitated by this substituent.[9] Conversely, the *threo*/*erythro* ratio is minimum for the *p*-nitro compounds (2.9), which, most likely, form open ions.[21] The rate differences between *erythro* and *threo* isomers cannot be ascribed to differences in ground state energies. Equilibration of either pure *threo* or pure *erythro* **1c** produced 52±5% *erythro* and 48±5% *threo* **1c**, indicative of very similar stabilities.[20]

The absolute rates of reaction are also largest for the *p*-methoxy compounds and minimum for the *p*-nitro compounds. For the *threo* isomers, a linear ρ—σ^+ dependence is observed, in which ρ is −1.3. This value is rather low compared to certain model compounds which solvolyze by anchimerically assisted

13) B. Murr and C. Santiago, *J. Amer. Chem. Soc.*, **88**, 1127 (1966).
14) D. J. Cram and F. Abd Elhafez, *ibid.*, **76**, 30 (1954); *ibid.*, **75**, 339 (1953); **74**, 5828 (1952); **74**, 5825 (1952).
15) H. C. Brown, R. Bernheimer, C. Kim, and S. Schepelle, *ibid.*, **89**, 370 (1967).
16) H. L. Goering and S. Change, *Tetrahedron Lett.*, **1965**, 3107.
17) P. A. Levene, and A. Rothen, *Science*, **87**, 510 (1938).
18) K. M. Okamoto, M. Hayashi, and H. Shingu, This Bulletin, **39**, 408 (1966).
19) See however, W. Doering, and H. Zeiss, *J. Amer. Chem. Soc.*, **75**, 4733 (1953).
20) D. J. Cram, C. DePuy, and F. Greene, *ibid.*, **78**, 790 (1956).
21) D. J. Cram and J. Thompson, *ibid.*, **89**, 6762 (1967).

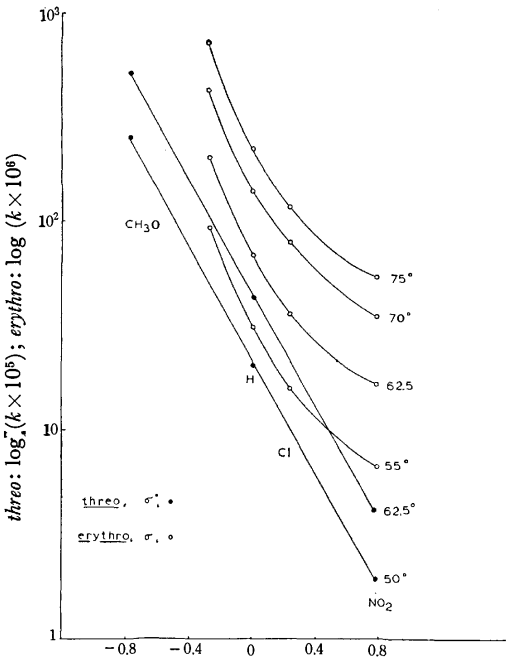

Fig. 1. Plots of log k *vs.* Hammett σ parameters for the *erythro* isomers, and Okamoto-Brown σ^+ parameters for the *threo* isomers.

paths (ρ near -3).[9,22,23]

For the *erythro* isomers, curved ρ—σ plots are observed (Fig. 1), which, in other cases, have been ascribed to a change in mechanism from the k_s route to the k_Δ route as the electron donating character of the substituent progressively improves.[9] However, for the *p*-nitro and *p*-chloro compounds, the ΔS^* values are generally higher than the value given by Winstein as indicative of nucleophilic assistance to ionization by solvent (-18 e.u.).[24] The cation, which is stabilized by the α-aryl group, requires less solvent stabilization.

TABLE 2. PER CENT *threo* OF AN *erythro*/*threo* MIXTURE IN THE REACTION **1**→**3** AT 56±3°C IN 90% AQUEOUS METHANOL

			% *Threo* **3**[e]
Thero	**1 a**	*p*-CH_3O	(89)[a]
	1 b	*o*-CH_3O	*ca.* 100[b]
	1 c	H	73
	1 e	*p*-NO_2[c]	43
Erythro	**1 a**	*p*-CH_3O	35
	1 c	H	76[d]
	1 d	*p*-Cl	62
	1 e	*p*-NO_2	55

a) Total *threo* product (80% ether **3** plus 20% alcohol **2**).
b) No *erythro* product was observable.
c) Uncorrected for *ca.* 10% *erythro* inpurity.
d) At 75°C, 68% *threo* **3c** was observed.
e) The overall yield is 80±5% ethers **3** and 20% alcohols **2**.

Table 3 lists the bromide **1** to methyl ether **3**, and the bromide to acetate **4** conversions catalyzed by silver acetate. These conversions contrast the effects of acetic acid and the more nucleophilic solvent, methanol. Compared to the data in Table 2, a greater tendency for inversion is noted for these silver catalyzed reactions in methanol, particularly for electron withdrawing substituents. The effect of temperature for these conversions is quite pronounced. For example, *erythro* **1c** gave 86% *threo* methyl ether **3c** at room temperature, and 78% at 55°C. On the other hand, *erythro* **1a** gave 33% *threo* **3a** at 3°C, 40% at 34°C, and 54% at 55°C. Thus, the stereochemistry changed from retention to slight inversion.[17]

The loss of stereoselectivity[17] with increasing temperature is interpreted in terms of the greater importance of the open ion **7** (and possibly also of **6**). In acetic acid the **8**→**7**⇌**6** equilibration sequence also has a greater chance of becoming established, due to lower solvent nucleophilicity, and indeed *erythro* **1a** forms predominately *threo* products.

The product ratios in ethanol were difficult to establish by NMR due to overlapping of peaks. The stereochemistry of the solvolysis in 90% aqueous methanol was therefore determined, and the results are recorded in Table 2. The stereochemistry in methanol and in ethanol was qualitatively similar, however. The data shown in Table 2 were somewhat temperature dependent with lower stereoselectivity observed at higher temperatures.

The data in Tables 1 and 2 indicate a fairly good correlation between solvolysis rate and stereochemistry. For the anisyl compounds, which solvolyze the most rapidly, a high degree of retention is observed for the *threo* isomers, and somewhat less retention is observed for the *erythro* compound. In the latter case, formation of the open ion **7** is quite important due to steric strains present in the bridged ion **8**. We agree with Brown that π bridged intermediates,[15,24b] such as **6** and **8**, deserve serious consideration due to the absence of strong rate accelerations and the absence of high stereospecificity.

For the *p*-nitro compounds, which are unreactive, a slight overall inversion of configuration is noted, but the product ratios are close to the equilibrium *threo*/*erythro* ratio. The *erythro* unsubstituted and *p*-chloro compounds give predominately *threo* products. The bridged ion **8** (which would yield *erythro* product) is unimportant because the weak stabilizing character of the β-aryl group is not able to overcome steric repulsions. The predominate pathway is thought to be the formation of the open ion **7**, which forms products of mixed stereochemistry. Internal rotation may also occur in **7**, with concurrent formation of **6**, which yields *threo* products.

22) R. Heck and S. Winstein, *J. Amer. Chem. Soc.*, **79**, 3432 (1957).
23) See also V. J. Shiner, Jr., W. Buddenbaum, B. Murr, and G. Lamaty, *ibid.*, **90**, 418 (1968).
24) (a) E. F. Jenny and S. Winstein, *Helv. Chim. Acta*, **41**, 897 (1958). (b) S. Winstein, C. Lindegren, H. Marshall, and L. Ingraham, *ibid.*, **75**, 147 (1953). (c) See also R. Heppolette, and R. F. Robinson, *Can. J. Chem.*, **44**, 677 (1966).
25) The activation entropies seem more variable than originally found by Winstein and co-workers, although the k_Δ route uniformly gives higher ΔS^* values than the k_s route. See Ref. 9 and M. G. Jones, and J. L. Coke, *ibid.*, **91**, 4285 (1969).
26) G. Frisone and E. Thornton, *ibid.*, **90**, 1211 (1968) and references cited therein.

Table 3. Overall yield and stereochemical purity of silver acetate catalyzed conversions 1→3 and 1→4 in methanol and acetic acid at 34±4°C

	X		Methanol solvent: % Ether 3 (% *Threo* 3)[a]	Methanol solvent: % Acetate 4 (% *Threo* 4)[a]	Acetic acid solvent (% *Threo* acetate 4)[a]
Thero	**1a**	*p*-CH_3O	92 (91)	8 (>90)	(92)
	1c	H	91 (52)	9 (>90)	(74)
	1e	*p*-NO_2	89 (36)	11 (74)	(52)
Erythro	**1a**	*p*-CH_3O	92 (40)	8 (10)	(62)
	1c	H	91 (86)	9 (43)	(70)
	1d	*p*-Cl	87 (84)	13 (30)	(63)
	1e	*p*-NO_2	93 (70)	7 (30)	(48)

a) % *Threo* of an *erythro/threo* mixture.

In methanol, small amounts of acetates **4** are also formed in addition to the ethers **3**. Although the stereochemistry of **4** is difficult to measure accurately by NMR, predominate retention stereochemistry is evident. The acetates **4** formed from reactions in methanol may result from a four-center type of mechanism.[18]

In order to show the generality of the stereochemical changes, the conversions of the alcohols **2** to the chlorides **5** were studied. The reaction mixture was 4:1 acetic acid and concentrated hydrochloric acid. The products were not stable under the reaction conditions. Epimerization and olefin formation were evident upon long reaction times. The data listed in Table 4 were determined by trial and error variation of reaction times, in an attempt to achieve minimum olefin formation and maximum stereoselectivity. The stereochemistry of the chlorides is rather similar to that of the acetates in Table 3 and the ethers in Table 2. No conclusion is drawn from the acetate data in Table 4 due to the possibilities for Fischer esterification of the parent alcohol.

In conclusion, the stereochemical results are a function of the intrinsic characteristics of the molecules, and not functions of the reaction conditions except for certain minor variations as discussed above. We feel there is definite evidence for participation by β-anisyl groups (rapid solvolysis and generally retention stereochemistry). Participation by the β-phenyl group may be of importance through an ion such as **6**, but no evidence exists for the presence of the less stable ion **8**. While it is true that the α-aryl group reduces the demand for β-aryl participation, the necessity for solvent stabilization is also reduced, which gives the phenonium ion more of a chance.

The possibility exists that the predominate *threo* products, which occur from substrates **c** and **d**, result from a simple lower energy pathway from the open ion. However, the trend of the stereochemical data, as substituent progressively becomes more electron donating, is precisely what one would expect on the basis of reaction through a π-phenonium ion. These substituents should not affect the reaction pathways available to an open ion. As discussed in the Introduction, one cannot state that the bridged ion is more stable than the open ion, since relative product yields reflect the relative energies of the intermediate ions and the relative transition state energies leading to products. A second alternate explanation of the data, involving steric interference of groups at the β-carbon upon attack upon one of the two faces of the open ion, would predict predominately *erythro* product,[14] which is not observed. This work and related studies emphasize the importance of *both* open ions and bridged ions in a single reaction sequence,[2,9,14] rather than *either* an open ion[6] *or* a bridged ion mechanism.[5]

Table 4. Overall yield and stereochemical purity of the 2→4 and 2→5 conversion in acetic acid–con. HCl, 4:1 at 26±3°C

	X		%Chloride 5 (% *Threo* 5)[c]	%Acetate 4 (% *Threo* 4)[c]
Threo	**2a**	*p*-CH_3O	94 (>90)	6 (>80)
	2b	*o*-CH_3O	95 (94)	5[a]
	2c	H	87 (68)	9 (37)
Erythro	**2a**	*p*-CH_3O	87 (67)	13 (25)
	2b	*o*-CH_3O	80 (66)	20[b]
	2c	H	89 (66)	11 (27)
	2d	*p*-Cl	67 (48)	33 (11)

a) The product was mostly *threo* **4** but an accurate determination was not possible.

b) Mostly *erythro* **4** but an accurate determination was not possible.

c) % *Threo* product of an *erythro/threo* mixture.

Experimental

The substrates **2** (except **2e**) were prepared by aryl Grignard addition to the appropriate 2-arylpropanals. The latter were usually prepared from the glycidic ester.[23] The following procedure is typical.[27] To 1-(4-chlorophenyl)-1-ethanone (77 g, 0.5 mol) and ethyl chloroacetate (56 g, 0.5 mol) plus 120 m*l* benzene in a 2 *l* three-necked flask, 0.5 mol of potassium *t*-butoxide was added in increments as a solid, and the mixture vigorously stirred for 24 hr. The resulting red solution was poured over ice and extracted with benzene. The organic layers were dried ($MgSO_4$), and the solvent evaporated. The glycidic ester was distilled, the fraction boiling at 121°C/0.75 mmHg was collected. This material was treated with sodium ethoxide (5.8 g sodium in *ca.* 100 m*l* ethanol) and after 2 hr the flask was cooled to 0°C and 8 m*l* of water was added. The sodium salt derived from the glycidic ester

27) A. I. Vogel, "Practical Organic Chemistry," 3rd Edition, Longmans, Green and Co., Ltd., London (1956), p. 907.

separated and was collected by filtration. The mother liquor yielded a second crop when cooled and diluted with ether, total 37 g. This salt was treated with dilute hydrochloric acid (28 m*l* conc. acid plus 150 m*l* water). The mixture was stirred for 2 hr and heated to *ca.* 80°C for 2 hr. The mixture was poured over ice and extracted with ether. The ether layer was washed with water, dil. sodium bicarbonate solution, dried over magnesium sulfate, and distilled; the fraction boiling from 78—80°C/10.7 mmHg was collected, 12.7 g.

The above aldehyde (17.3 g, 0.132 mol) was added dropwise to a solution of phenyl magnesium bromide prepared from 6.5 g magnesium plus 27.4 m*l* bromobenzene. The mixture was poured into ice/ammonium chloride. Hydrochloric acid was added until the aqueous layer was slightly acidic. The ether extract was washed with water, dil. sodium bicarbonate, and distilled, the fraction boiling from 148—150°C/0.7 mmHg (15.7 g) was taken (mixed *erythro* and mostly *threo* diastereomers **2d**).

To 3.14 g (0.0177 mol) of the above alcohol in 70 m*l* pyridine was added 3.5 g *p*-nitrobenzoyl chloride. This mixture was heated on a steam bath for 15 min and stirred for 0.5 hr. The mixture was poured onto ice, and extracted twice with 10% hydrochloric acid, water, twice with dil. sodium hydroxide, and twice with water. The ether layer was dried and evaporated yielding crystals, which were recrystallized from ethanol–water and from pentane–carbon tetrachloride. These were the *threo* **2d** *p*-nitrobenzoate mp 111.6—111.8°C. The *erythro* isomer was elusive in this case but could be prepared by oxidizing the alcohol to the ketone and reducing the ketone with lithium aluminum tri-*t*-butoxy hydride. In general the diastereomerically pure alcohols **2** were prepared by hydrolyzing the purified *p*-nitrobenzoates. Substrates **2c** however were prepared by the method of Cram and Elhafez.[14]

Mixed diastereomers **2e** were prepared from 2-(4-nitrophenyl)-1-phenyl-1-ethanone by the following reactions.[28] To 0.5 g (0.00207 mol) of the above ketone in 50 m*l* dry acetone, 5 g potassium carbonate and 5 m*l* iodomethane were added with rapid stirring. The resulting purple reaction mixture was refluxed 2 hr and poured into ice and extracted with ether. The ether layer was washed with water, dried and the solvent evaporated yielding an oil, whose NMR spectrum indicated predominantly 2-(4-nitrophenyl)-1-phenyl-1-propanone. The material from several runs (9.5 g 0.037 mol) was dissolved in anhydrous tetrahydrofuran and added dropwise to a suspension of 10.0 g (0.0394 mol) of lithium aluminum tri-*t*-butoxy hydride with rapid stirring. After stirring 2 hr the mixture was refluxed 4 hr cooled, treated with saturated potassium carbonate solution and poured onto ice. The mixture was extracted with ether, and the organic layer washed with water, dried solvent evaporated and the product chromatographed on silica gel. The benzene eluant was evaporated to yield yellow crystals, mp 102.8—103.1°C, *erythro* **2e**.

The bromides **1** were prepared from the alcohols by treatment with HBr. The following procedure is illustrative. To *erythro* **2c** (1.0 g, 0.0047 mol) dissolved in 20 m*l* CCl_4, cooled to 0°C, 50 m*l* of chilled conc. HBr and 39 g LiBr were added to the rapidly stirred mixture and the resulting mixture was stirred 4 hr and then allowed to come to room temperature.

The organic phase was separated, and the diluted aqueous phase was extracted with CH_2Cl_2. The combined organic layers were washed several times with distilled water, and then dried ($MgSO_4$). The filtered solution was concentrated by rotary evaporation. The resulting oil was *ca.* 80% *threo* **1c** and 20% *erythro* **1c**. Crystallization was induced by cooling. The isomers were separated by repeated recrystallization making use of the fact that the *erythro* isomer was not soluble in ethanol (for other compounds, **1a**, **b**, **d**, pentane was used). Of the 1.29 g (94% of theoretical) crude product usually about 0.2 g pure *erythro* **1c**, mp 157—159°C, and 0.6 g *threo* **1c**, mp 57—59°C, could be isolated in a pure state.

Threo **2a** (X=*p*-CH_3O), bp 150°C (0.1 mmHg); PNB (*p*-nitrobenzoate), mp 92.8—93.8°C; NMR (CCl_4) δ 1.17 (d, 3, C<u>H</u>$_3$), 2.45 (s, 1, O<u>H</u>), 2.87 (m, 1, C<u>H</u>-CH_3), 3.54 (s, 3, C<u>H</u>$_3$O), 4.48 (d, 1, J=6 Hz, C<u>H</u>-OH), and *ca.* 6.8 (m, 9. Ar).

PNB, Found: C, 70.50; H, 5.52%. Calcd for $C_{23}H_{21}NO_5$: C, 70.57; H, 5.42%.

Threo **2b** (X=*o*-CH_3O), bp 140—144°C (0.05 mmHg); PNB, mp 99.5—100.5°C; NMR (CCl_4) δ 1.11 (d, 3, C<u>H</u>$_3$), 2.65 (s, 1, O<u>H</u>), 2.8 (m, 1, C<u>H</u>-CH_3), 3.5 (s, 3, C<u>H</u>$_3$O), 4.66 (d, 1, J=5 Hz, C<u>H</u>-OH), and 6.5—7.2 (m, 9, Ar).

Found: C, 70.26; H, 5.84%. Calcd for $C_{23}H_{21}NO_5$: C, 70.57; H, 5.42%.

Threo **2c**, (X=H), bp 154—156°C (1.7 mmHg); PNB, mp 143—144°C (lit,[14] 143—144°C); NMR ($CDCl_3$) δ 1.22 (d, 3, J=7 Hz, C<u>H</u>$_3$), 1.82 (s, 1, O<u>H</u>), 2.95 (m, 1, C<u>H</u>-CH_3), 4.6 (d, 1, J=6 Hz C<u>H</u>-OH), and 7.15 (s, 10, Ar).

Threo **2d** (X=*p*-Cl), bp 148—150°C (0.7 mmHg); PNB, mp 111—112°C; NMR (CCl_4) δ 1.18 (d, 3, C<u>H</u>$_3$), 2.35 (s, 1, O<u>H</u>), 2.87 (m, 1, C<u>H</u>-CH_3), 4.75 (d, 1, J=6 Hz, C<u>H</u>-CH_3), and *ca.* 6.8 (m, 9, Ar).

PNB, Found: C, 66.53; H, 4.52%. Calcd for $C_{22}H_{18}ClNO_4$: C, 66.75; H, 4.57%.

Erythro **2a** (X=*p*-CH_3O), mp 86—87°C; NMR ($CDCl_3$) δ 1.05 (d, 3, C<u>H</u>$_3$), 1.95 (s, 1, O<u>H</u>), 2.97 (m, 1, C<u>H</u>-CH_3), 4.58 (d, 1, J=8.4 Hz, C<u>H</u>-OH), 7.04 (d of d, 4, CH_3O-$C_6\underline{H}_4$), and 7.3 (s, 5, $C_6\underline{H}_5$).

Found: C, 79.34; H, 7.60%. Calcd for $C_{10}H_{18}O_2$: C, 79.12; H, 7.50%.

Erythro **2b**, (X=*o*-CH_3O), oil; PNB, oil; 3,5-DNB, oil; NMR (CCl_4) δ 0.98 (d, 3, C<u>H</u>$_3$), 2.3 (s, 1, O<u>H</u>), 3.51 (m, 1, C<u>H</u>-CH_3), 3.58 (s, 3, OC<u>H</u>$_3$), 4.6 (d, 1, J=7.7 Hz, C<u>H</u>-OH), and 6.5—7.2 (m, 9, Ar).

Erythro **2c** (X=H), bp 118—123°C (1.5 mmHg), mp 52—53°C (lit,[14] mp 51—52°C); NMR (CCl_4) δ 1.06 (d, 3, C<u>H</u>$_3$), 1.60 (s, 1, O<u>H</u>), 2.95 (m, 1, C<u>H</u>-CH_3), 4.5 (d, 1, J=8.4 Hz, C<u>H</u>-OH), and 7.12 (s, 10, Ar).

Erythro **2d** (X=*p*-Cl), mp 87—88°C; NMR ($CDCl_3$) δ 1.06 (d, 3, C<u>H</u>$_3$), 1.93 (s, 1, O<u>H</u>), 3.0 (m, 1, C<u>H</u>-CH_3), 4.61 (d, 1, J=8.2 Hz, C<u>H</u>-OH), 7.28 (s, 5, $C_6\underline{H}_5$), and 7.05—7.38 (d of d, 4, Cl-$C_6\underline{H}_4$).

Found: C, 73.12; H, 6.07%. Calcd for $C_{15}H_{15}OCl$: C, 73.02; H, 6.13%.

Erythro **2e** (X=*p*-NO_2), mp 102.8—103.8°C; NMR ($CDCl_3$) δ 1.16 (d, 3, C<u>H</u>$_3$), 1.88 (s, 1, O<u>H</u>), 3.16 (m, 1, C<u>H</u>-CH_3), 4.74 (d, 1, J=7.8Hg, C<u>H</u>-OH), 7.28 (s, 5, $C_6\underline{H}_5$), 7.36 (d, 2, Ar), and 8.13 (d, 2, Ar).

Found: C, 70.00; H, 5.84%. Calcd for $C_{15}H_{15}NO_3$: C, 70.02; H, 5.87%.

Threo **1a** (X=*p*-CH_3O), oil; NMR (CCl_4) δ 1.51 (d, 3, C<u>H</u>$_3$O),3.3 (doublet of quartets, 1, C<u>H</u>-CH_3), 3.45 (s, 3, C<u>H</u>$_3$O), 4.95 (d, 1, J=9.2 Hz, C<u>H</u>-Br), 6.52 (d, 2, $C_6\underline{H}_4$-OCH_3), 8.82 (d, 2, $C_6\underline{H}_4$-OCH_3), and 6.8—7.3 (m, 5, $C_6\underline{H}_5$). Mass spectrum: molecular ion 304, 306; base peak 135.

Threo **1b** (X=*o*-CH_3O), mp 86—87°C; NMR ($CDCl_3$) δ 1.52 (d, 3, C<u>H</u>$_3$), 3.66 (s, 3, C<u>H</u>$_3$O), 3.83 (doublet of quartets, 1, C<u>H</u>-CH_3), 5.33 (d, 1, J=8.6 Hz, C<u>H</u>-Br), and 6.5—7.4

28) G. Badcock, G. Cavill, A. Robertson, and W. Whailey, *J. Chem. Soc.*, **1950**, 2961.

(m, 9, Ar).

Found: C, 62.76; H, 5.70%. Calcd for $C_{16}H_{17}BrO$: C, 62.91; H, 5.61%.

Threo **1c** (X=H), mp 57—59°C(lit,[14] mp 60—61°C); NMR ($CDCl_3$) δ 1.60 (d, 3, $C\underline{H}_3$), 3.43 (doublet of quartets, 1, $C\underline{H}$-CH_3), 5.06 (d, 1, J=9.5, $C\underline{H}$-Br), 7.02 (s, 5, Ar), and 7.11 (s, 5, Ar).

Threo **1e** (X=*p*-NO_2), mp 70—71°C; NMR ($CDCl_3$) δ 1.60 (d, 3, $C\underline{H}_3$), 3.58 (doublet of quartets, 1, $C\underline{H}$-CH_3), 5.08 (d, 1, J=9.0 Hz, $C\underline{H}$-Br), 7.15 (s, 5, Ar), 7.17 (d, 2, $C_6\underline{H}_4NO_2$), and 8.0 (d, 2, $C_6\underline{H}_4NO_2$).

Found: C, 56.04; H, 4.27%. Calcd for $C_{15}H_{14}BrNO_2$: C, 56.45; H, 4.11%.

Erythro **1a** (X=*p*-CH_3O), mp 132—133°C, NMR ($CDCl_3$) δ 1.13 (d, 3, $C\underline{H}_3$), 3.43 (doublet of quartets, 1, $C\underline{H}$-CH_3), 3.78 (s, 3, $C\underline{H}_3O$), 5.00 (d, 1, J=9.2 Hz, $C\underline{H}$-Br), 6.84 (d, 2, $C_6\underline{H}_4$-OCH_3), 7.15 (d, 2, $C_6\underline{H}_4OCH_3$), 7.30 (s, 5, $C_6\underline{H}_5$).

Found: C, 62.83; H, 5.49%. Calcd for $C_{16}H_{17}BrO$: C, 62.96; H, 5.61%.

Erythro **1c** (X=H), mp 157—159°C, (lit,[14] mp 159—160°C); NMR ($CDCl_3$) δ 1.14 (d, 3, $C\underline{H}_3$), 3.49 (doublet of quartets, 1, $C\underline{H}$-CH_3), 5.07 (d, 1, J=9.7 Hz, $C\underline{H}$-Br), 7.30 (s, 5, Ar), and 7.35 (s, 5, Ar).

Erythro **1d** (X=*p*-Cl), mp 115—116°C; NMR ($CDCl_3$) δ 1.10 (d, 3, $C\underline{H}_3$), 3.45 (doublet of quartets, 1, $C\underline{H}$-CH_3), 4.98 (d, 1, J=9.6 Hz, $C\underline{H}$-Br), 7.20 (d, 2, $C_6\underline{H}_4Cl$), 7.30 (d, 2, $C_6\underline{H}_4Cl$), and 7.30 (s, 5, Ar).

Found: C, 58.18; H, 4.41%. Calcd for $C_{15}H_{14}ClBr$: C, 58.18; H, 4.56%.

Erythro **1e** (X=*p*-NO_2), mp 139—140°C; NMR ($CDCl_3$) δ 1.16 (d, 3, $C\underline{H}_3$), 3.62 (doublet of quartets, 1, $C\underline{H}$-CH_3), 5.03 (d, 1, J=9.7 Hz, $C\underline{H}$-Br), 7.35 (s, 5, Ar), 7.40 (d, 2, $C_6\underline{H}_4NO$), and 8.20 (d, 2, $C_6\underline{H}_4NO_2$).

Found: C, 56.30; H, 4.11%. Calcd for $C_{15}H_{14}BrNO_2$: C, 56.45; H, 4.11%.

Product Runs. A typical run is given (silver acetate catalyzed reaction of *threo* **2e** in methanol, Table 2). Approximately 150 mg of substrate was dissolved in 30 m*l* absolute methanol, and 150 mg silver acetate was added. The mixture was stirred at *ca.* 35°C for 6 hr. The mixture was filtered, and the liquid added to a separatory funnel containing ether and water. The aqueous layer was extracted with ether several times. The combined organic layers were extracted with water twice, and dried ($MgSO_4$). The solvent was removed by rotary evaporation and the product analyzed by NMR (Fig. 2).

Product Analyses. *Erythro* and *threo*-1,2-diphenyl-1-propyl bromides, chlorides, methyl ethers, and acetates were prepared which showed the literature physical constants in each case. Since the NMR resonances were only slightly affected by aromatic substituent, the above compounds sufficed as models for all compounds. The NMR analyses were possible because the methyl resonances of the *threo* isomers uniformly fell in the region δ 1.2—1.5, whereas the resonances of the *erythro* isomers fell upfield (δ 1.0—1.2).

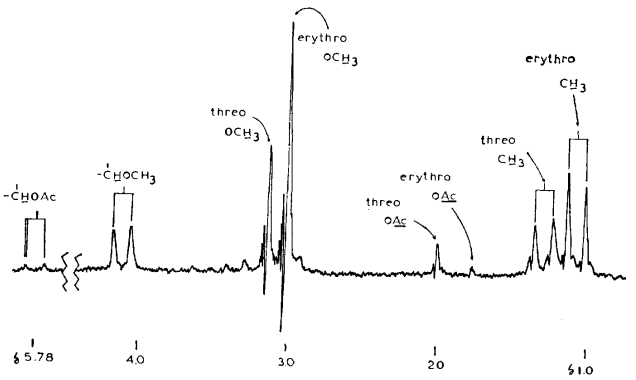

Fig. 2. Silver acetate catalyzed reaction product (**1e**→**3e**, **4e**).

The percentage of each isomer was determined from an average of 3—5 integrations. The methyl ethers also showed separate resonances for the *erythro* and *threo* isomers, an integration over the CH_3O peaks was always in good agreement with integration over the methyl resonances. The various conversions were very clean, with no apparent rearrangement, and little or no olefin formation (olefin formation was only apparent in the alcohol to chloride conversions, Table 4). The possible rearrangement products 2-methoxy-1,2-diphenylpropane and 3,3-diphenyl-2-propanol were synthesized. The distinctive resonances of these materials were never observed. Similarly *erythro*-1,2-diphenyl-1-deuterio-1-propanol was subjected to the **2**→**5** conversion. No deuterium scrambling was evident. Only in the case of the *o*-methoxy were small peaks observed, not associated with the normal products.

Kinetics. The rates of reaction were followed conductometrically. By making up known standards, it was proved that conductance was linear with hydrogen bromide concentration. Two cells were used, one with platinized electrodes, the other with plain platinum electrodes. These gave the same rates at low temperature although some divergence occurred at the higher temperatures. At the lower temperatures, due to the difference in surface area of the two cells, it is unlikely that the platinum surface was catalyzing the reaction. At higher temperatures the lower rates found with the plain cell were considered the most reliable. From sixteen to fifty-five points were taken. The rate plots were always linear over three and usually over four to five half-lives, with little scatter evident except in the latest stages of the reaction. The rates were determined graphically. The data given in Table 1 are the average of two to four runs. In one case **1c**, four-fold variation of concentration of the substrate produced very similar rate constants indicative of true first-order kinetics. Substrate concentration normally was *ca.* 10^{-4} to 10^{-5}M. The solvent (ρ=0.8403 at 25°C; 79.6% ethanol by weight) was prepared by mixing weighed amounts of redistilled ethanol with redistilled water. Activation parameters were obtained from least squares analysis of log rate *vs.* inverse temperature plots.

The Determination of Sulfide- and Sulfate-Sulfur in Igneous Rocks with Tin(II)-Strong Phosphoric Acid and Strong Phosphoric Acid[1)]

Shigeru NAGASHIMA, Minoru YOSHIDA, and Takejiro OZAWA

Department of Chemistry, Faculty of Science, Tokyo Institute of Technology, Ookayama, Meguro-ku, Tokyo

(Received March 15, 1972)

A method for the determination of minute amounts of sulfide- and sulfate-sulfur in igneous rocks was investigated. A rock sample is easily dissolved by heating with tin(II)-strong phosphoric acid or strong phosphoric acid. When the rock sample is dissolved with tin(II)-strong phosphoric acid, total-sulfur is evolved as hydrogen sulfide. With strong phosphoric acid, sulfide-sulfur is evolved as hydrogen sulfide, but sulfate-sulfur is not. The hydrogen sufide evolved is fixed as zinc sulfide, and then determined by the photometric method, using mercuric thiocyanate and ferric iron. The conditions for separating sulfide- and sulfate-sulfur in rocks were examined by using samples which had been prepared by mixing rock or silica (each of them, $<0.001\%$ S) with sulfides or sulfates. The application of the method to some igneous rock samples gave results with a coefficient of variation of about 5% for sulfur contents of 0.01—0.02%. The sulfur in samples with more than 0.001% can be determined by using about 0.1 g of samples. The sulfide- and sulfate-sulfur in two standard rock samples were also determined: W-1 (Total-S, 0.012%; Sulfide-S, 0.005%; Sulfate-S, 0.007%) and G-1 (Total-S, 0.004%, Sulfide-S, $<0.001\%$; Sulfate-S, 0.004%).

It has been said that sulfur in igneous rocks exists in the forms of sulfides and sulfates. The proportion of sulfide- and sulfate-sulfur, and their amounts, would reflect the conditions of igneous rocks at the time of formation. In 1960, Ricke[2)] determined the sulfide- and sulfate-sulfur content of rocks by two titrimetric methods. Recently, Schneider[3)] separated the sulfide- and sulfate-sulfur in basalts, and measured the isotope composition of each sulfur. However, their methods have some defects. In these methods, rock sample is treated with hydrochloric acid in the separation of sulfide- and sulfate-sulfur. The decomposition of rocks, however, requires a very long time (more than about 6 hr). Moreover, the rock sample is not perfectly dissolved with hydrochloric acid, and all the sulfide-sulfur in the sample may not be determined. Moreover, they did not check that sulfate-sulfur was not determined in the determination of sulfide-sulfur.

One of the present authors (T. O.) and others[4)] have previously reported a sensitive method for the determination of total-sulfur in igneous rocks. The method consists of decomposing a rock sample by heating it with tin(II)-strong phosphoric acid,[5)] releasing the sulfur as hydrogen sulfide, and finally determining it by the photometric method, using mercuric thiocyanate and ferric iron.[6)] A rock sample is easily dissolved with tin(II)-strong phosphoric acid or strong phosphoric acid. The present authors were aware that when the sample is dissolved with strong phosphoric acid without tin(II), sulfide-sulfur is evolved as hydrogen sulfide, while sulfate-sulfur is not.

It is not clearly known what forms of sulfur exist in usual igneous rocks, for the sulfur content is generally very low. However, many investigators[7-10)] have microscopically detected sulfides in igneous rocks with relatively high contents of sulfur, *e.g.* pyrite, pyrrhotite, chalcopyrite, pentlandite, bornite, cubanite, covellite, and digenite. Schneider[3)] forecast the sulfate-sulfur in basalts as follows: (a) as sulfate minerals, *e.g.* barite, anhydrite, nosean, and haüyne; (b) in the crystal lattice of silicates and apatite; (c) in fluid inclusions.

On the other hand, we expected pyrite, pyrrhotite, chalcopyrite, barium sulfate and calcium sulfate as typical sulfur compounds in igneous rocks. In order to examine the conditions for separating sulfide- and sulfate-sulfur, samples were prepared by mixing rock or silica with these sulfides or sulfates.

Experimental

Apparatus. The apparatus used in this study (Fig. 1 and 2) was mostly the same as that described by Arikawa *et al.*[4)]

The nitrogen flow rate was measured by a Kusano flowmeter KG-1 type.

A Hirama photoelectric-spectrophotometer type 6, and 10 mm cells were used to measure the absorbance.

Reagents. All the chemicals used were of an analytical reagent quality. Redistilled water was used for the reagent preparation and throughout the procedure.

Strong Phosphoric Acid: This reagent was prepared by heating 1000 g of orthophosphoric acid ($d=1.7$) in a round bottomed silica flask (Fig. 1) up to 250°C on a mantle heater.

Tin(II)-Strong Phosphoric Acid: This reagent was prepared by heating 78 g of stannous chloride dihydrate and the above obtained strong phosphoric acid in the round-bottomed silica flask up to 280°C on the mantle heater.

1) A part of this report was presented at the 20th Annual Meeting of the Japan Society for Analytical Chemistry, Tokyo, Oct., 1971.

2) W. Ricke, *Geochim. Cosmochim. Acta*, **21**, 35 (1960).

3) A. Schneider, *Contr. Mineral. Petrol.*, **25**, 95 (1970).

4) Y. Arikawa, T. Ozawa, and I. Iwasaki, *Bunseki Kagaku*, **21**, 920 (1972).

5) T. Kiba and I. Kishi, This Bulletin, **30**, 44 (1957); T. Kiba, I. Akaza, and N. Sugishita, *ibid.*, **30**, 972 (1957).

6) S. Utsumi, *Nippon Kagaku Zasshi*, **74**, 301 (1953); *ibid.*, **74**, 608 (1953).

7) W. H. Newhouse, *Bull. Geol. Soc. Amer.*, **47**, 1 (1936).

8) P. Ramdohr, *Abh. Preuss. Akad. Wiss.*, **2**, 1 (1940).

9) L. R. Wager, E. A. Vincent, and A. A. Smales, *Econ. Geol.*, **52**, 855 (1957).

10) G. A. Desborough, A. T. Anderson, and T. L. Wright, *ibid.*, **63**, 636 (1968).

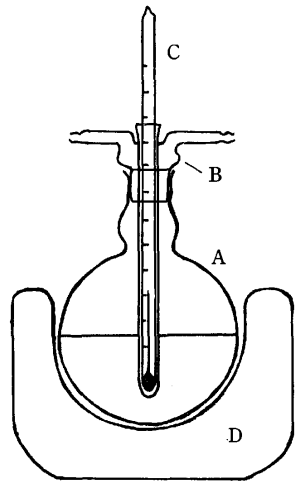

Fig. 1. Apparatus for the preparation of strong phosphoric acid and tin(II)-strong phosphoric acid.
A: Round-bottomed silica flask (1 *l*), B: Gas-delivery silica cap with thermometer-protecting tube, C: Thermometer (360°C), D: Mantle heater.

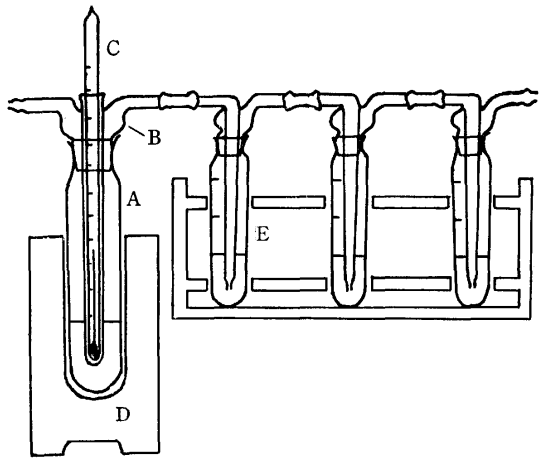

Fig. 2. Apparatus for the determination of total- and sulfide-sulfur.
A: Silica test tube (inner-diameter: 3.5 cm, length: 17 cm), B: The same as B in Fig. 1, C: Thermometer (360°C), D: Electric furnace, E: Absorption tube: centrifuge tube (15 m*l*) fitted with gas-delivery cap.

Standard Sodium Sulfate: Dissolve 4.43 g of dried sodium sulfate in water and dilute to exactly 1 *l*. The solution is standardized by the gravimetric method of the determination of sulfate as barium sulfate. It contains 1 mg of sulfur per m*l*. Prepare the working solution by diluting this solution adequately.

Saturated Barium Hydroxide Solution:

Zink Sulfate Solution (3%): Dissolve 5.3 g of zinc sulfate heptahydrate in water and dilute to 100 m*l*.

Sodium Hydroxide Solution (1M):

Acetic Acid Solution (1M):

Mercuric Thiocyanate Solution: Solid mercuric thiocyanate was prepared as has been described by Utsumi.[11] Dissolve 0.5 g of mercuric thiocyanate in 100 m*l* of methyl alcohol.

Ferric Nitrate-Perchloric Acid Solution: Dissolve 28.3 g of ferric nitrate in 100 m*l* of a 4M perchloric acid solution.

Sodium Carbonate Solution (1%):

Carbon Tetrachloride: *Nitrogen Gas*: Nitrogen from a commercial cylinder is purified with an alkaline pyrogallol solution, and then dried with solid calcium chloride.

Preparation of Mixed Samples. The mixed samples (Table 1) were prepared by the following procedure. For example, in the case of mixing rock with pyrite, 1 g of a finely-powdered rock and 0.03 g of pyrite were thoroughly mixed in an agate mortar with a pestle for one hour. They were mixed again with 2 m*l* of carbon tetrachloride for one hour. Next, 0.1 g of the mixed sample and 1 g of rock were mixed in the same manner. The procedure was repeated by using 0.1 g of this mixed sample and 1 g of rock. The other mixed samples were also prepared by the same procedure. These samples contained about 15 μg of sulfur per 100 mg. In the present study, basalt from Aokigahara, Mt. Fuji, Yamanashi Prefecture, silica (99.99%) from the Ko-Jundo-Kagaku Institute (their total-sulfur contents were less than 0.001%), pyrite from Udo Mine, Shimane Prefecture, pyrrhotite from Yanahara Mine, Okayama Prefecture, and chalcopyrite from Miyatamata Mine, Akita Prefecture, were used. The barium sulfate and the calcium sulfate were prepared from a barium chloride solution, a calcium chloride solution, and sulfuric acid.

Procedure and Calibration Curve. *Procedure (1) (the Determination of Total-Sulfur)*: In a silica test tube, place about 0.1 g of a finely-powdered rock sample and 15 m*l* of tin(II)-strong phosphoric acid. Mix them with a silica rod (length: about 18 cm). During the heating, keep this rod in the test tube. Into three absorption tubes, add 0.5 m*l* of a zinc sulfate solution (3%), 3 drops of a 1M sodium acetate solution, and about 4.5 m*l* of water respectively. Connect all the parts of the apparatus, as is shown in Fig. 2. Introducing nitrogen gas (flow rate, 50—180 m*l*/min), heat the silica test tube by an electric furnace (800W). When it reaches 280°C,[12] keep it at 280±3°C for 30 min by using a slide auto-transformer. Disconnect the absorption tubes from the apparatus, and rinse the inside of the first absorption tube's cap into the tube with a small quantity of water. To it add one drop of phenolphthalein as an indicator, and then 0.1M sodium hydroxide solution dropwise until the color changes. By this procedure, micro amounts of zinc sulfide coprecipitate with zinc hydroxide. After centrifugation, discard the supernatant liquid. Into the absorption tube, transfer the solution in the second absorption tube. Run the same procedure again, and then repeat it for the solution in the third absorption tube. In order to wash the precipitate, add 3 m*l* of a sodium carbonate solution (1%) and about 7 m*l* of water, shake vigorously, centrifuge, and discard the supernatant liquid. To the precipitate, add 0.5 m*l* of a 1M acetic acid solution, 1 m*l* of a mercuric thiocyanate solution, and 2 m*l* of a ferric nitrate-perchloric acid solution, in this order. After diluting to exactly 10 m*l* with water, in order to collect the mercuric sulfide, add 0.5 m*l* of carbon tetrachloride, shake vigorously, and centrifuge. Measure the absorbance of the supernatant liquid at 460 mμ, using water as the reference.

Procedure (2) (the Determination of Sulfide-Sulfur): Using the apparatus shown in Fig. 2, place about 0.1 g of a finely-powdered rock sample containing less than about 10 mg of ferrous iron as ferrous oxide and 15 m*l* of strong phosphoric acid. The subsequent procedure is the same as that described in (1).

Calibration Curve: The calibration curve (Fig. 3) was obtained by using a standard sodium sulfate solution (0—30 μg as S) and 2 drops of a saturated barium hydroxide solution,

11) S. Utsumi, *Nippon Kagaku Zasshi*, **73**, 835 (1952).

12) The time necessary to reach 280°C is about 20 min after the start of heating.

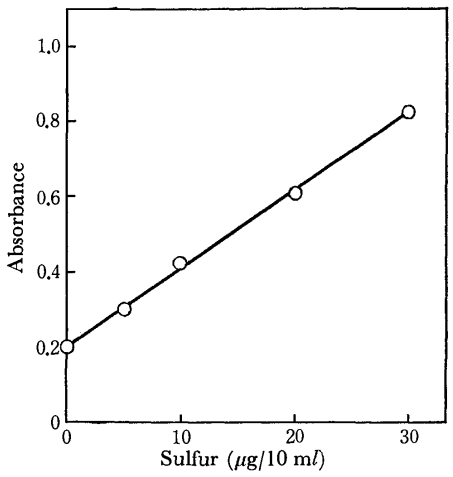

Fig. 3. Calibration curve.

which had been evaporated to dryness in a silica test tube; the sulfur was subsequently determined by Procedure (1).

Results and Discussion

The total-sulfur in igneous rocks was determined by the method of Arikawa *et al.*[4] With a slight modification of the method, several tests were carried out.

The Effect of the Heating Time on Procedure (1). The recovery of sulfur was examined by varying the heating time (5—40 min) using the standard sodium sulfate solution (30 μg as S). The heating time of 30 min was decided on the basis of the results (Fig. 4).

The Effect of the Nitrogen Flow Rate on Procedure (1).

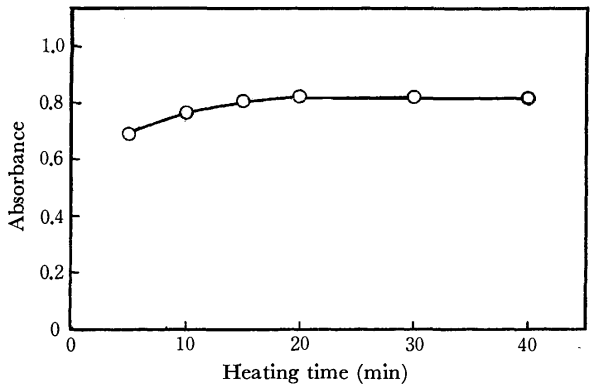

Fig. 4. Effect of the heating time on Procedure (1).

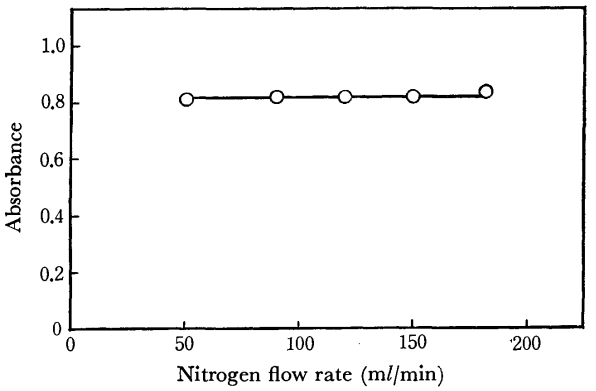

Fig. 5. Effect of the nitrogen flow rate on Procedure (1).

TABLE 1. DETERMINATION OF TOTAL-SULFUR IN THE MIXED SAMPLES BY PROCEDURE (1)

Sample	S (μg) added	found	difference	Relative deviation (%)
Rock+FeS_2	15.7	15.3	−0.4	2.5
	17.5	17.2	−0.3	1.7
	19.2	19.3	+0.1	0.5
Rock+FeS	17.6	17.6	0	0
	20.7	20.9	+0.2	1.0
Rock+$CuFeS_2$	17.3	17.1	−0.2	1.2
	20.0	20.0	0	0
SiO_2+FeS_2	10.2	9.8	−0.4	3.9
	24.3	25.0	+0.7	2.9
Rock+$BaSO_4$	19.7	18.9	−0.8	4.1
	21.4	22.1	+0.7	3.3
	26.9	27.2	+0.3	1.1
Rock+$CaSO_4$	9.7	10.0	+0.3	3.1
	19.4	19.0	−0.4	2.1
SiO_2+$BaSO_4$	14.5	14.1	−0.4	2.8
	29.0	29.5	+0.5	1.7

Rock: Basalt (Mt. Fuji, S: ≪0.001%)

The recovery of sulfur was tested by varying the nitrogen flow rate (50—180 ml/min) using the standard sodium sulfate solution (30 μg as S). The results (Fig. 5) indicate that the nitrogen flow rate in this range has no effect on the recovery of sulfur.

Determination of Total- and Sulfide-Sulfur in Mixed Samples. The mixed samples previously described were analyzed by Procedure (1). As Table 1 shows, the results give values with a relative deviation of less than 5%. The total-sulfur in the forms of both sulfides and sulfates can be determined by Procedure (1). Therefore, if only the sulfide-sulfur in igneous rocks can be determined, the sulfate-sulfur content can be obtained from the difference between the total- and the sulfide-sulfur.

The condition of determining only the sulfide-sulfur with strong phosphoric acid was examined by using the mixed samples. At first, the mixed sample of rock-pyrite and that of rock-barium sulfate (each of them including about 15 μg of S) were used. The

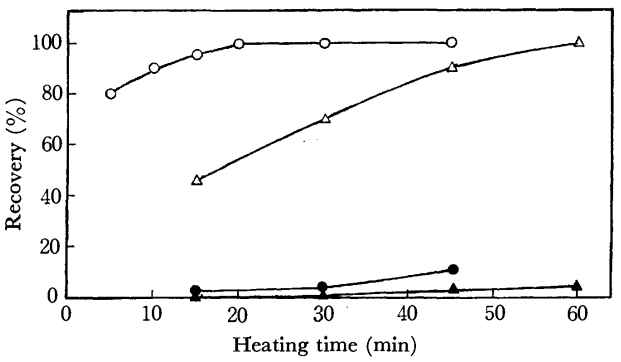

Fig. 6. Determination of sulfide-sulfur with strong phosphoric acid (1).
○ Rock+FeS_2 } at 280°C
● Rock+$BaSO_4$ }
△ Rock+FeS_2 } at 260°C
▲ Rock+$BaSO_4$ }
These samples contain about 15 μg as S.

temperature (260 and 280°C) and the heating time (5—60 min) were varied. The results are given in Fig. 6. At 280°C, the sulfur in the mixed sample of rock-pyrite is completely recovered in 30 min At the same temperature, the sulfur in the mixed sample of rock-barium sulfate is partly evolved as hydrogen sulfide. Within 30 min, the amount of sulfur is almost negligible (<5%), but in 45 min it grows appreciable (>10%). The sulfate-sulfur sppears to be reduced by the ferrous iron in the rock. This problem will be discussed later. At 260°C, the results of the heating time of 60 min seem to be the same as those of the heating time of 30 min at 280°C. However, the use of 260°C requires a longer time than does that of 280°C. Therefore, the heating time of 30 min at 280°C has been investigated further.

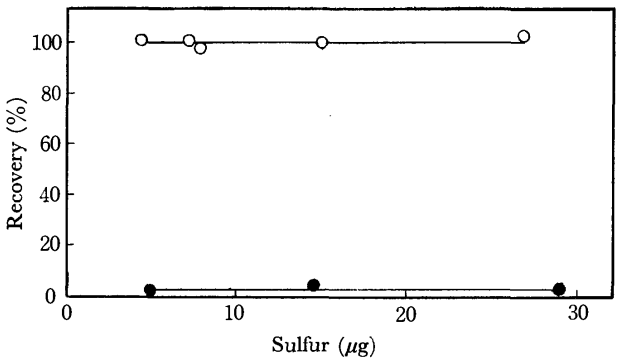

Fig. 7. Determination of sulfide-sulfur with strongs phosphoric acid (2).
○ Rock+FeS_2 } at 280°C
● Rock+$BaSO_4$ }
Heating time: 30 min

Under this conditions and using Procedure (2), recovery was tested using various amounts of the mixed sample of rock-pyrite and that of rock-barium sulfate. According to the results (Fig. 7), the sulfur in the mixed sample of rock-pyrite is completely recovered, and the evolution of sulfur in the mixed sample of rock-barium sulfate is almost negligible (<5%).

The results of the recovery tests by means of Procedure (2) and using various kinds of mixed samples are summarized in Table 2. They indicate that the separation of the sulfide- and the sulfate-sulfur is possible.

The Effect of Ferrous Iron on Procedure (2). As has already been mentioned, it has been thought that, in Procedure (2), the sulfate-sulfur is partly reduced by the ferrous iron in the rock. This point was checked by using the standard sodium sulfate solution (15 μg as S) and various amounts of iron oxide. As the ferrous oxide, wüstite (Found: FeO, 98%) was used; it had been synthesized as described by Darken and Gurry.[13] The ferric oxide was prepared from a ferric chloride solution and aqueous ammonia. The sulfur contents of these oxides were less than 0.001%. The results (Fig. 8) indicate that sulfate-sulfur is partly reduced in the presence of ferrous oxide. The evolution of sulfur is almost negligible (<5%) with less than about 10 mg of ferrous oxide. It is independent of the amount of ferric oxide in the range of 0—30 mg. Therefore, in analysis by Procedure (2), a rock sample which contains less than about 10mg of ferrous iron as ferrous oxide should be placed in a silica test tube.

13) L. S. Darken and R. W. Gurry, *J. Amer. Chem. Soc.*, **67**, 1398 (1945).

Table 2. Determination of sulfide-sulfur in the mixed samples by procedure (2).

Sample	S added (μg) as sulfide	as sulfate	S found (μg)
Rock+FeS+$BaSO_4$	16.9	9.5	16.7
	23.0	19.3	22.0
Rock+FeS_2	14.9		15.0
	26.0		26.7
Rock+FeS	17.4		16.7
	23.0		22.0
Rock+$CuFeS_2$	17.5		18.0
	20.0		19.1
SiO_2+FeS_2	12.6		11.6
	30.0		29.3
Rock+$BaSO_4$		14.5	<1
		29.0	<1
Rock+$CaSO_4$		16.0	<1
		24.0	<1
SiO_2+$BaSO_4$		14.2	<1
		30.0	<1
Rock+FeS_2+$BaSO_4$	12.1	9.7	12.8
SiO_2+FeS_2+$BaSO_4$	18.9	14.5	17.8

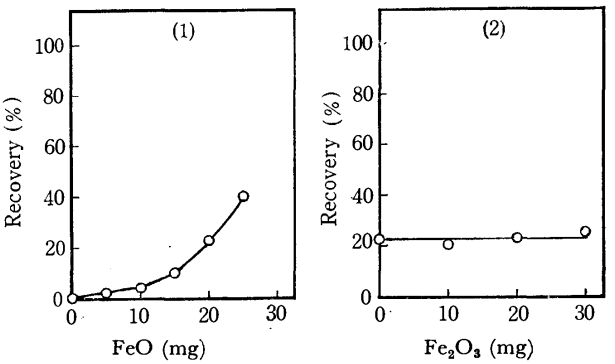

Fig. 8. Effect of iron on Procedure (2).
Procedure (2) was done by taking standard sodium sulfate solution (15 μg as S) and various amounts of iron oxide in the silica test tube.
(1) Fe_2O_3 not added (2) FeO: 20 mg

The Determination of Sulfide- and Sulfate-Sulfur in Rock Samples. In order to confirm the reproducibility of the method, various igneous rock samples were analyzed by Procedures (1) and (2). These results (Table 3) show the coefficient of variation to be about 5% for sulfur contents of 0.01—0.02%.

The method was also checked by adding known amounts of sulfide- and sulfate-sulfur to the sample No. 3. The results (Table 4) are in good agreement with the values in Table 3.

The Analysis of Standard Rocks. The sulfide- and sulfate-sulfur in two standard rock samples, G-1 and W-1, prepared by the U. S. Geological Survey, were also determined by Procedures (1) and (2) (Table 5). The data reported previously for the two rock samples

TABLE 3. DETERMINATION OF SULFUR IN IGNEOUS ROCKS

Sample No. 1: Andesite; Lave of 1946, Sakura-jima, Kagoshima Pref.

	Total-S				Sulfide-S			Sulfate-S
	Sample taken (g)	S found (μg)	S (%)		Sample taken (g)	S found (μg)	S (%)	S (%)
1	0.0563	10.0	0.018	1	0.0652	13.2	0.020	−0.002
2	0.1120	21.3	0.019	2	0.0875	17.0	0.019	0
3	0.1188	23.6	0.020	3	0.1028	18.5	0.018	0.002
4	0.1325	26.2	0.020	4	0.1243	23.6	0.019	0.001
5	0.1472	27.0	0.018	5	0.1446	26.7	0.018	0
			0.019_0	Mean			0.018_8	<0.001
			0.0010	Standard deviation			0.0008	—
			5.3	Coefficient of variation			4.3	—

Sample No. 2: Alkali rhyolite; Madara-jima, Saga Pref.

	Total-S				Sulfide-S			Sulfate-S
	Sample taken (g)	S found (μg)	S (%)		Sample taken (g)	S found (μg)	S (%)	S (%)
1	0.0546	5.0	0.009	1	0.0567	<1	<0.001	0.009
2	0.0887	8.7	0.010	2	0.0935	1.1	0.001	0.009
3	0.1048	10.5	0.010	3	0.1155	<1	<0.001	0.010
4	0.1243	12.1	0.010	4	0.1252	1.2	0.001	0.009
5	0.1514	14.7	0.010	5	0.1430	<1	<0.001	0.010
			0.009_8	Mean			<0.001	0.009_4
			0.0004	Standard deviation			—	0.0005
			4.1	Coefficient of variation			—	5.3

Sample No. 3: Trachyte; Nishino-shima, Oki, Shimane Pref.

	Total-S				Sulfide-S			Sulfate-S
	Sample taken (g)	S found (μg)	S (%)		Sample taken (g)	S found (μg)	S (%)	S (%)
1	0.0524	8.7	0.017	1	0.0473	3.5	0.007	0.010
2	0.0838	13.1	0.016	2	0.0810	5.1	0.006	0.010
3	0.1041	18.7	0.018	3	0.1022	6.2	0.006	0.012
4	0.1323	22.5	0.017	4	0.1221	8.4	0.007	0.010
5	0.1548	25.4	0.016	5	0.1511	12.2	0.008	0.008
			0.016_8	Mean			0.006_8	0.010_0
			0.0008	Standard deviation			0.0008	0.0014
			4.8	Coefficient of variation			11.8	14.0

TABLE 4. ADDITION TESTS

	Total-S					Sulfide-S					Sulfate-S
Sample taken (g)	S (μg) added	S (μg) found	S (μg) added − found	S (%)		Sample taken (g)	S (μg) added	S (μg) found	S (μg) added − found	S (%)	S (%)
0.1034	6.8 (as FeS_2)	22.9	16.1	0.016		0.0973	6.1 (as FeS_2)	13.8	7.7	0.008	0.008
0.1047	5.6 (as FeS)	21.9	16.3	0.016		0.1044	6.0 (as FeS)	13.3	7.3	0.007	0.009
0.1009	9.7 (as $BaSO_4$)	26.5	16.8	0.017		0.0988	9.7 (as $BaSO_4$)	7.9	—	0.008	0.009

Sample: Sample No. 3.

(shown in Table 5) indicate a very wide scatter. According to the present analysis, for the total-sulfur our value of W-1 is in good agreement with the values of Ricke[2] and Frost *et al.*,[14] but our value of G-1 is lower than both of theirs, being nearer to the value of Frost *et al.* than to Ricke's. For the sulfide-sulfur, our values of W-1 and G-1 are significantly lower than those of Ricke.

Table 5. Analysis of standard rocks

Sample	S (%)			
	Total-S	Sulfide-S	Sulfate-S	
W-1	0.012	0.005	0.007	a)
	0.0135	0.0130	0.0005	ref. 2)
	0.0124			ref. 14)
	0.0003			ref. 15)
G-1	0.004	<0.001	0.004	a)
	0.0175	0.0060	0.0115	ref. 2)
	0.0074			ref. 14)
	0.0003			ref. 15)

a) The present data.

Conclusion

By the use of the present method, the determination of sulfide- and sulfate-sulfur in igneous rocks is possible with tin(II)-strong phosphoric acid and strong phosphoric acid. The method is excellent in that a rock sample can be easily dissolved by heating for a relatively brief time (30 min), and the sulfide- and sulfate-sulfur in rocks can be determined by using the above two reagents respectively in the same procedure. The application of this method to some igneous rock samples gave results with a coefficient of variation of about 5% for sulfur contents of 0.01—0.02%. The sulfur in samples with more than 0.001% can be determined by using about 0.1 g of samples. The time necessary to analyze one sample is about two hours.

The authors wish to thank Professor Iwazi Iwasaki of Toho University and Dr. Yoshiko Arikawa of Japan Women's University, for their hearty encouragement and suggestions during this study. Thanks are also due to Professor Takashi Katsura and Mr. Kenzo Kitayama of the Tokyo Institute of Technology, and Mr. Hiroshi Haramura of Tokyo University, for many discussions and for their kind supply of the standard rock samples, G-1 and W-1, and wüstite.

14) I. C. Frost and J. A. Thomas, as Private communication (1964) quoted in *Geochim. Cosmochim. Acta*, **29**, 1263 (1965).
15) R. Brown and W. A. Wolstenholme, *Nature*, **201**, 598 (1964).

BULLETIN OF THE CHEMICAL SOCIETY OF JAPAN, VOL. 45, 3451—3455 (1972)

Isomerism of the Metal Complexes Containing Multidentate Ligands. II. The Cobalt(III), Cobalt(II), and Nickel(II) Complexes of *N,N,N',N'*-Tetrakis(2-aminoethyl)ethylenediamine and -1,2-propanediamine and Their Absolute Configurations

Yuzo Yoshikawa, Ekyo Fujii, and Kazuo Yamasaki
Department of Chemistry, Faculty of Science, Nagoya University, Chikusa-ku, Nagoya

(Received May 1, 1972)

The cobalt(III), cobalt(II), and nickel(II) complexes of *N,N,N',N'*-tetrakis(2-aminoethyl)ethylenedianime and -1,2-propanediamine were prepared, and the cobalt(III) complex of the former ligand was resolved by fractional crystallization and column chromatography on SE-Sephadex. The absolute configurations of the cobalt(III) complexes were assigned on the basis of the stereospecificity of the latter ligand; they were later confirmed by the X-ray analysis. The electronic absorption, circular dichroism, and optical rotatory dispersion spectra of the complexes prepared were also measured.

The cobalt(III) complex of *N,N,N',N'*-tetrakis(2-aminoethyl)-ethylenediamine (abbreviated as penten) was first prepared by Emmenegger and Schwarzenbach;[1] it has been characterized by infrared and electronic spectral measurements and by stability studies in an aqueous solution. The absolute configuration of the complex was assigned from its rotatory dispersion[1] and its circular dichroism spectrum.[2] We have prepared nickel(II) and cobalt(II) complexes of penten in addition to the cobalt(III) complexes, and assigned the absolute configuration of the latter using the stereospecificity of *N,N,N',N'*-tetrakis(2-aminoethyl)-1,2-propanediamine (abbreviated as R-mepenten) and its cobalt(III) complex.

The absolute configuration thus tentatively assigned (Fig. 1) was enantiomeric to that of Emmenegger and Schwarzenbach,[1] and to that of Mason and Norman,[2]

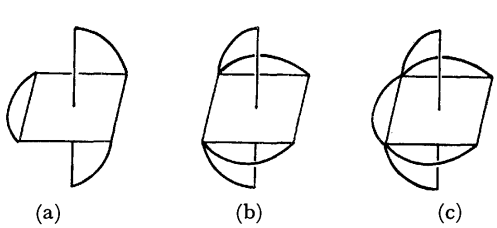

Fig. 1. Absolute configurations of (a): $(-)_{589}$-$[Co(en)_3]^{3+}$, (b): $(-)_{589}$-*u-facial*-$[Co(dien)_2]^{3+}$, and (c): $(-)_{589}$-$[Co(penten)]^{3+}$. The configurations are denoted by Δ, $\Delta\Delta\Delta$, and $\Delta\Lambda\Delta$ respectively. By summing the contribution from each skew chelate pair, the net contribution of the latter two will become Δ.

1) E. P. Emmenegger and G. Schwarzenbach, *Helv. Chim. Acta*, **49**, 625 (1966).
2) S. F. Mason and B. J. Norman, *Chem. Commun.*, **1965**, 73.

but the same as that of Gollogly and Hawkins.[3] The absolute configuration assigned by us was confirmed by the X-ray analysis of Saito *et al.*[4] Since only a brief preliminary report[5] has been published on these nickel and cobalt complexes of penten and R-mepenten, a detailed report will be published here.

Experimental

1. Ligands. The penten and laevorotatory R-mepenten were specially prepared by the Seikenkagaku Co., the latter being synthesized from R-propylenediamine. They were then further purified by vacuum distillation. Penten, bp 159—163°C (0.08—0.10 mmHg); R-mepenten, bp 147—153°C (0.10 mmHg).

2. Preparation of the Complexes. *2.1.* *[Co(penten)]Br_3·$2H_2O$*: *Method A*: One gram of penten and 2 g of finely ground $[CoBr(NH_3)_5]Br_2$ were mixed in a 100 m*l* round-bottomed flask; the flask was then gently heated over a flame until the color of the mixture became reddish-brown, ammonia having been evolved during the reaction. After the mixture had then been cooled to room temperature, a 2 m*l* portions of water was added and the unreacted $[CoBr(NH_3)_5]Br_2$ was filtered off. By adding ethanol to the filtrate, a red syrup was obtained; this syrup yielded red hexagonal crystals after repeated recrystallizations from water. Found: Co, 10.03; N, 14.14; C, 21.39; H, 5.44; Br, 42.56; H_2O, 6.39%. Calcd for $CoC_{10}H_{28}N_6Br_3\cdot 2H_2O$: Co, 10.39; N, 14.82; C, 21.18; H, 5.69; Br, 42.28; H_2O, 6.35%.

Method B: Two and half grams of $[CoBr(NH_3)_5]Br_2$, 1.3 g of penten, and 0.2 g of active charcoal were mixed with 30 m*l* of water, and the mixture was stirred for 11 hrs. After filtering off the charcoal, the filtrate was concentrated and the red syrup thus obtained was purified as Method A.

2.2. *$(-)_{589}$-[Co^{III}(R-mepenten)]$I_3\cdot H_2O$*: This complex was prepared in the same way as Method B. A hygroscopic reddish-brown powder obtained by adding ethanol to the reaction mixture was dissolved in water, and to this solution an aqueous solution of potassium hexacyanocobaltate(III) was added. The reddich-brown crystals of $(-)_{589}$-[Co(R-mepenten)][$Co(CN)_6$]·$3H_2O$ thus precipitated were purified by recrystallization. These crystals were suspended in water together with the ion-exchange resin (Dowex 1-X8, 20—50 mesh) in the bromide form, and the mixture was stirred for several hours. The filtrate was evaporated, and by the subsequent addition of potassium iodide, red crystals of $(-)_{589}$-[Co(R-mepenten)]$I_3\cdot H_2O$ were obtained. Found: Co, 8.62; N, 12.23; C, 19.07; H, 4.48; I, 53.86; H_2O, 2.38%. Calcd for $CoC_{11}H_{30}N_6I_3\cdot H_2O$: Co, 8.37; N, 11.94; C, 18.77; H, 4.58; I, 54.07; H_2O, 2.56%.

The molar rotation of this complex iodide is $[M]_{545}=-5150°$, $[M]_{485}=+9980°$. The complex iodide was converted to the chloride by passing it through a column of Dowex 1-X8 in the chloride form. The molar rotation of the chloride is $[M]_{546}=-5200°$, and $[M]_{485}=+10220°$.

2.3. *[Ni(penten)]$(ClO_4)_2$*: Two grams of nickel(II) perchlorate hexahydrate dissolved in 1 m*l* of water, and 1 g of penten dissolved in 1 m*l* of water were mixed; when the mixture was left standing, a reddish-violet syrup separated out. After the repeated recrystallization of this syrup from hot water, violet crystals were obtained. Found: Ni, 12.18; N, 17.09; C, 24.77; H, 5.85%. Calcd for $NiC_{10}H_{28}N_6O_8Cl_2$: Ni, 11.98; N, 17.15; C, 24.51; H, 5.76%.

2.4. *$(+)_{589}$-[Ni(R-mepenten)]$(ClO_4)_2\cdot 1/2H_2O$*: Five grams of nickel(II) perchlorate hexahydrate and 4 g of R-mepenten were dissolved in 20 m*l* of water. On evaporating the solution, violet crystals were obtained, and they were purified by recrystallization from water. Found: Ni, 11.57; N, 16.14; H_2O, 1.78%. Calcd for $NiC_{11}H_{30}N_6O_8Cl_2\cdot 1/2H_2O$: Ni, 11.44; N, 16.38; H_2O, 1.76%. The molar rotation is $[M]_{494}=+520°$.

2.5. *$[Co^{II}(penten)]^{2+}$ and $(+)_{589}$-$[Co^{II}$(R-mepenten)]$^{2+}$ Ions*: These complexes were not isolated in solid states, but were prepared only in aqueous solutions under nitrogen, since they were oxidized in air. About 74 mg of R-mepenten was dissolved in a small amount of water. Nitrogen was bubbled through this solution and also the solution of the equivalent amount of cobalt(II) chloride, and then both solutions were mixed in a vessel filled with nitrogen and connected to a quartz cell 1 cm thick for the spectral measurements. All the measurements were carried out in nitrogen to prevent oxidation.

The concentration of the complex was determined by chelatometric titration using a 0.01M EDTA solution after decomposing the complex with a mixture of perchloric and sulfuric acids. The complex ion $[Co^{II}(penten)]^{2+}$ was prepared in a manner similar to that described above.

3. Resolution of the Cobalt(III) Penten Complex. *Method A*: As the resolving agent, $(-)_{589}$-$K_3[Co(C_2O_4)]_3$ was used. When 1 g of [Co(penten)]$Br_3\cdot 2H_2O$ dissolved in 8 m*l* of water and 0.5 g of the resolving agent dissolved in 4 m*l* of water were mixed, a sparingly soluble diastereoisomer of $(+)_{589}$-[Co(penten)]$^{3+}$ was precipitated. To this diastereoisomer suspended in water, barium iodide was added. After removing barium trisoxalatocobaltate(III) by filtration, the filtrate was evaporated; $(+)_{589}$-[Co(penten)]$I_3\cdot H_2O$ was thus obtained. Found: Co, 8.39; N, 12.04; C, 17.49; H, 4.19; I, 54.99; H_2O, 2.56%. Calcd for $CoC_{10}H_{28}N_6I_3\cdot H_2O$: Co, 8.54; N, 12.18; C, 17.41; H, 4.38; I, 55.17; H_2O, 2.61%.

The enantiomer, $(-)_{589}$-iodide, was obtained from the mother liquor as the dihydrate. The molar rotation is $[M]_{542}=+5700°$ and $[M]_{481}=-9810°$ for the $(+)_{589}$-iodide, and $[M]_{542}=-5640°$ and $[M]_{481}=+9660°$ for the $(-)_{589}$-iodide.

Method B: A column chromatographic method on SE-Sephadex was used to resolve the complex; the details have been described previously.[6] Both enantiomers were completely separated on the column by the use of 0.3M sodium antimony $(+)_{589}$-tartrate as the eluent. First the $(-)_{589}$-isomer and then the $(+)_{589}$-isomer were eluted. Each effluent was diluted four to five times, and then again adsorbed on a P-cellulose column.

After washing the column with a large amount of 0.01N HCl, each enantiomer was eluted with 0.5N HCl. The enantiomers were further purified through the hexacyanocobaltate(III), which was reconverted to the chloride by passing it through a column of Dowex 1-X8 in the chloride form. The molar rotation for the $(+)_{589}$-chloride is $[M]_{542}=$

3) J. R. Gollogly and C. J. Hawkins, *Chem. Commun.*, **1966**, 873; *Aust. J. Chem.*, **20**, 2395 (1967).

4) A. Muto, F. Marumo, and Y. Saito, *Inorg. Nucl. Chem. Lett.*, **5**, 85 (1969); *Acta Crystallogr.*, **B26**, 226 (1970). The determination of the absolute configuration by X-rays was carried out for $(+)_{589}$-[Co(penten)][$Co(CN)_6$]$2H_2O$. The absolute configuration of the $(-)_{589}$-[Co(R-mepenten]$^{3+}$ ion was reported by Saito *et al.* (Proc. XII ICCC, Sydney, 1969, p. 90).

5) Y. Yoshikawa, E. Fujii, and K. Yamasaki, *Proc. Japan Acad.*, **43**, 495 (1967).

6) Y. Yoshikawa and K. Yamasaki, *Inorg. Nucl. Chem. Lett.*, **6**, 523 (1970); This Bulletin, **45**, 179 (1972). The absolute configuration of *u-facial*-$[Co(dien)_2]^{3+}$ assigned in these reports was later confirmed by the X-ray crystal analysis of Y. Saito *et al.* (Paper read at the annual meeting of the Chemical Society of Japan, April, 1972).

Table 1. Absorption and circular dichroism spectra

Complex	Absorption spectra		CD spectra	
	$\nu_{max}(cm^{-1})$	ε_{max}	$\nu_{max}(cm^{-1})$	$\Delta\varepsilon_{max}$
$(+)_{589}$-$[Co(penten)]Cl_3\cdot H_2O$	20500	214	19600	+3.64
			22300	−0.49
	29200	166	29900	+1.06
	43700	19890	43900	−10.8
			50800	+4.6
$(-)_{589}$-$[Co(penten)]Cl_3\cdot H_2O$	20500	214	19600	−3.61
			22300	+0.49
	29200	163	29900	−1.04
	43700	19440	43900	+10.9
			50800	−4.5
$(-)_{589}$-$[Co(R\text{-}mepenten)]Cl_3\cdot 2H_2O$	20500	215	19570	−3.31
			22000	+0.79
	29200	170	29900	−1.05
	43500	19150	43700	+9.1
			50300	−4.6
$[Ni(penten)](ClO_4)_2$	10600	20.9		
	18500	12.3		
	27800	15.8		
$(+)_{589}$-$[Ni(R\text{-}mepenten)](ClO_4)_2\cdot 1/2H_2O$	11000	16.6	9700[a]	−0.130[a]
			11500[a]	−0.132[a]
	18600	10.0	18800	−0.140
	28200	12.9	27600	−0.067
$[Co(penten)]^{2+}$	10700	4.5		
	17500	3.5		
	19900	8.5 sh		
	20800	10.5		
	21600	10.5		
$(+)_{589}$-$[Co(R\text{-}mepenten)]^{2+}$	11000	3.7	10700	−0.112
	14200	5.1		
	17600	12.3	16700	−0.136
			17400	−0.118 sh
	19800	19.1 sh	19700	−0.092
	20900	22.9		
	21600	21.9	21800	−0.085

sh: shoulder

a) These values were obtained for the more soluble chloride.

+5920° and $[M]_{481}=-10280°$, while that for the $(-)_{589}$-chloride is $[M]_{542}=-5910°$ and $[M]_{481}=+10280°$. The active isomers resolved by Method A were further subjected to the chromatographic resolution, but no further increase in rotation occurred, indicating the complete resolution by the crystallization of the diastereoisomers.

4. Measurements. The electronic absorption(AB), and optical rotatory dispersion(ORD) spectra of aqueous solutions of the complexes were measured at 25°C by the use of a JASCO ORD/UV-5 recording spectrometer, using quartz cells 1 and 10 mm thick. The circular dichroism(CD) spectrum in the region 190—700 nm was measured with the same apparatus, and that in the region 700—1200 nm with a Shimadzu QV-50 spectrophotometer equipped with a CD attachment.

Results and Discussion

1. Co(III) Complexes. Table 1 lists the data of the AB and CD spectra of the complexes studied, and in Fig. 2 the AB, CD, and ORD spectra of $(-)_{589}$-$[Co(penten)]^{3+}$ and the CD spectrum of $(-)_{589}$-$[Co(R\text{-}mepenten)]^{3+}$ are shown. These two complexes, which have the same absolute configuration, as determined by the X-ray crystal analysis,[4] show almost the same AB and CD spectra.

Among the CoN_6-type complexes, $[Co(en)_3]^{3+}$ was most extensively studied for the AB, CD, and absolute configuration. It has been found that the sign of CD band at about 20000 cm^{-1}, which corresponds to the $^1A_1\rightarrow{}^1E_a$ transition of the first *d-d* absorption band in the D_3 symmetry, depends on the chirality around the central cobalt atom; that is, the Δ configuration[7] shows a minus sign and the Λ configuration, a plus sign.

When three complexes, $[Co(en)_3]^{3+}$,[8] *u-facial*-$[Co(dien)_2]^{3+}$,[6] and $[Co(penten)]^{3+}$,[4] whose absolute configurations have been determined by X-ray crystal analysis, are compared (Fig. 1), the complexes with the Δ configuration always show the same minus sign

7) *IUPAC Information Bull.*, No. 33, 68 (1968); *Inorg. Chem.*, **7**, 1 (1970).

8) Y. Saito, K. Nakatsu, M. Shiro, and H. Kuroya, *Acta Crystallogr.*, **8**, 729 (1955); This Bulletin, **30**, 158, 795 (1957).

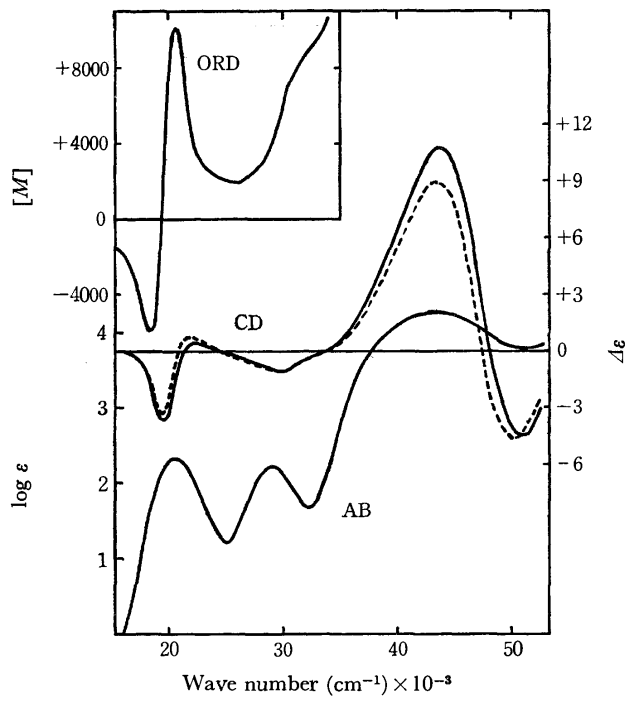

Fig. 2. The AB, CD, and ORD spectra of $(-)_{589}$-[Co(penten)]$Cl_3 \cdot H_2O$ (——) and the CD spectrum of $(-)_{589}$-[Co(R-mepenten)]$Cl_3 \cdot 2H_2O$ (----).

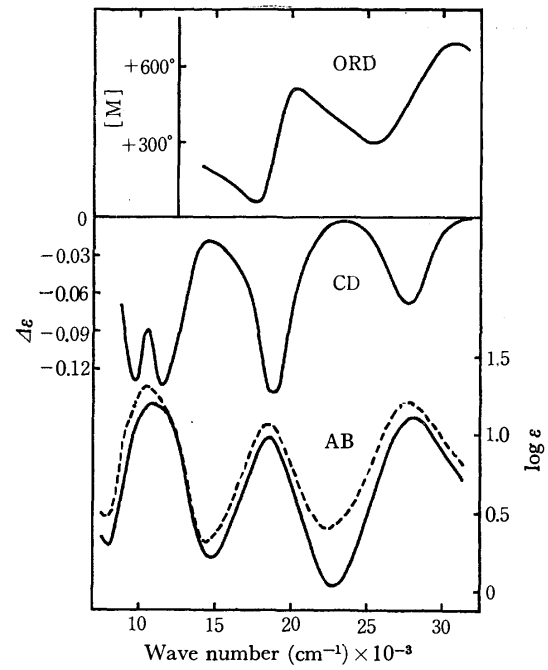

Fig. 3. The AB, CD, and ORD spectra of $(+)_{589}$- [Ni(R-mepenten)]$(ClO_4)_2$ (——) and the AB spectrum of [Ni-(penten)]$(ClO_4)_2$ (----).

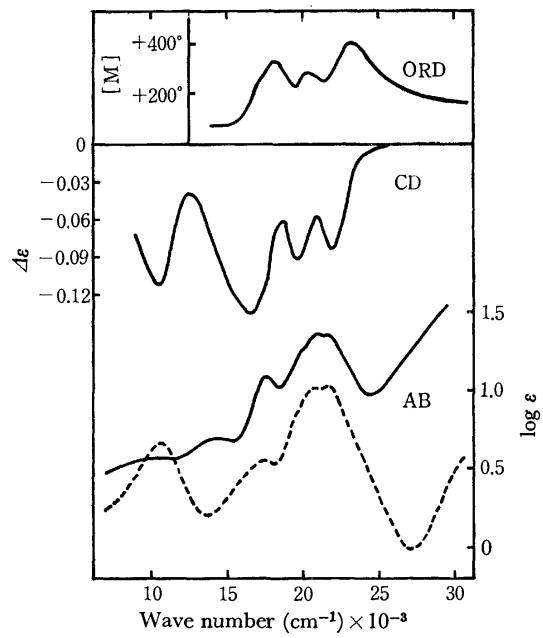

Fig. 4. The AB, CD, and ORD spectra of $(+)_{589}$-[Co(R-mepenten)]$^{2+}$ (——) and the AB spectrum of [Co(penten)]$^{2+}$ (----).

of the CD band at about 20000 cm^{-1}. Thus, for these complexes a close relationship exists between the absolute configuration and the sign of the CD band, and the absolute configuration tentatively assigned from the sign of the CD band is found to agree with those determined by the use of X-rays. In these three cases, the configurations derived from the octant rule[9] and the ring-pairing method[10] agree with those determined by the X-ray crystal analysis.

2. Co(II) Complexes. In Fig. 4, the AB, CD, and ORD spectra of $(+)_{589}$-[Co(R-mepenten)]$^{2+}$ and the AB spectrum of [Co(penten)]$^{2+}$ ions are shown. The first AB band of the former complex splits into two at 11000 and 14200 cm^{-1}; these bands may be assigned to the transition, $^4T_{1g}(^4F) \rightarrow {}^4T_{2g}(^4F)$ split in the lower symmetry. The signs of the CD bands are all minus.

3. Ni(II) Complexes. In Fig. 3, the AB, CD, and ORD spectra of $(+)_{589}$-[Ni(R-mepenten)]$(ClO_4)_2$ and the AB spectrum of [Ni(penten)]$(ClO_4)_2$ are shown. Three absorption bands of the former complex at 11000, 18600, and 28200 cm^{-1} are assigned to the transitions, $^3A_{2g}(^3F) \rightarrow {}^3T_{2g}(^3F)$, $^3A_{2g}(^3F) \rightarrow {}^3T_{1g}(^3F)$, and $^3A_{2g}(^3F) \rightarrow {}^3T_{1g}(^3P)$ respectively in the octahedral field. The signs of the CD bands are all minus.

4. Absolute Configuration of the Co(II) and Ni(II) Complexes. When R-mepenten coordinates to a metal in a six coordination, its methyl group takes an equatorial position, and the absolute configuration of the complex thus formed is stereospecifically determined. The configuration thus determined was confirmed by X-ray analysis of [Co(R-mepenten)]$^{3+}$. On the basis of the stereospecificity of R-mepenten thus confirmed it seems reasonable to assume that the cobalt(II) and nickel(II) complexes of R-mepenten have the same absolute configuration as the cobalt(III) complex of the same ligand.

The transitions of the first *d-d* absorption band of the octahedral cobalt(III), cobalt(II), and nickel(II) complexes are all magnetically allowed. Although the complexes of R-mepenten are not strictly octahedral, the sign of the CD band corresponding to the first

9) C. J. Hawkins and E. Larsen, *Acta Chem. Scand.*, **19**, 185 (1965).

10) J. I. Legg and B. E. Douglas, *J. Amer. Chem. Soc.*, **88**, 2967 (1966).

absorption band is minus for $(+)_{589}$-[Co(R-mepenten)]$^{2+}$ and for [Ni(R-mepenten)]$^{2+}$, that of $(-)_{589}$-[Co(R-mepenten)]$^{3+}$, corresponding to the $^1A_1 \rightarrow {}^1E_a$ transition, is also minus, indicating a close relationship between these signs and their absolute configurations.

In addition to the cobalt(III), cobalt(II), and nickel(II) complexes, we have tried to prepare the copper complexes of penten and R-mepenten from copper(II) perchlorate and the ligands. For both ligands, complexes with the approximately 1 : 1 composition were obtained as blue powders, but it was not possible to isolate them in chromatographically pure states and to characterize them.

We wish to thank Professor Y. Shimura of Osaka University and Dr. T. Yasui for permission to use their laboratory's Shimadzu spectrophotometer and its CD attachment.

BULLETIN OF THE CHEMICAL SOCIETY OF JAPAN, VOL. 45, 3455—3457 (1972)

The Synthesis of 2,3-Dimethoxy-5-methyl-*p*-benzoquinone

Kikumasa SATO, Seiichi INOUE, and Haruhito SATO

Department of Applied Chemistry, Faculty of Engineering, Yokohama National University, Ooka, Minami-ku, Yokohama, 233

(Received December 28, 1971)

2,3-Dimethoxy-5-methylbenzoquinone, the key intermediate of the synthesis of coenzyme Q, was synthesized *via* two new routes. The methylation of 5-nitrovanillin gave 5-nitroveratraldehyde, which was then catalytically reduced to afford 5-aminohomoveratrol. The oxidation of 5-aminohomoveratrol gave 2,3-dimethoxy-5-methylbenzoquinone. 2,3,4-Trimethoxyphenol was obtained by the decarboxylation of 3,4,5-trimethoxysalicylic acid. This was converted *via* Mannich reaction to 2,3,4-trimethoxy-6-methylphenol, which was then easily oxidized to 2,3-dimethoxy-5-methylbenzoquinone.

Coenzyme Q_n (n=1—12) (**1**),[1] the 2,3-dimethoxy-5-methylbenzoquinone containing the unsaturated isoprenoid substituent in the 6-position, was first discovered in rat liver and heart muscle as coenzyme Q_{10} in 1958 by Morton *et al.*,[2] who used the designation "ubiquinone (50)."

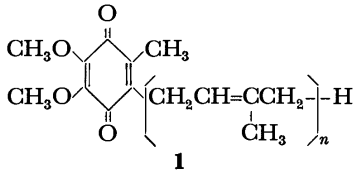

1

A subsequent search for other examples of this new class of isoprenoid benzoquinones revealed their widespread distribution in many kinds of animal tissue and bacteria.

Coenzyme Q has also been synthesized by the condensation of 2,3-dimethoxy-5-methylhydroquinone with polyprenyl alcohol (**2** or **3**), followed by the oxidation of the condensation product[3,4].

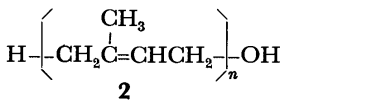

2

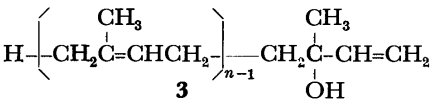

3

Several investigators have studied the synthesis of 2,3-dimethoxy-5-methylbenzoquinone (**4**) from vanillin[5–9] and gallic acid.[10–12] The present paper will describe convenient methods for the preparation of **4**.

From 5-Nitrovanillin. Anslow *et al.*[5] synthesized **4** from vanillin in five steps. If the reduction of both formyl and nitro groups of nitrovanillin is achieved in the same stage, all the reaction steps are much shortened.

Anhydrous potassium salt of 5-nitrovanillin (**5**),[13]

1) For a review, see a) R. A. Morton, *Nature*, **182**, 1764 (1958); b) K. Folkers, C. H. Shunk, B. O. Linn, N. R. Trenner, D. E. Wolf, C. H. Hoffman, and A. C. Page, "Ciba Foundation Symposium on Quinones in Electron Transport," Churchill, London (1961), p. 100; c) K. Sato, T. Matsuura, and S. Inoue, *Yuki Gosei Kagaku Kyokai Shi*, **27**, 138 (1969).

2) G. N. Festenstein, F. W. Heaton, J. S. Lowe, and R. A. Morton, *Biochem. J.*, **59**, 558 (1955); J. C. Cain and R. A. Morton, *ibid.*, **60**, 274 (1955); F. W. Heaton, J. S. Lowe, and R. A. Morton, *J. Chem. Soc.*, **1956**, 4094.

3) U. Gloor, O. Isler, R. A. Morton, R. Ruegg, and O. Wiss, *Helv. Chim. Acta*, **41**, 2357 (1958).

4) C. H. Shunk, B. O. Linn, E. L. Wong, P. E. Wittreich, F. M. Robinson, and K. Folkers, *J. Amer. Chem. Soc.*, **80**, 4753 (1958).

5) W. K. Anslow, J. N. Ashley, and H. Raistrick, *J. Chem. Soc.*, **1938**, 439.

6) M. Shimizu and K. Koshi, *Chem. Pharm. Bull.* (Tokyo), **11**, 404 (1963).

7) M. Matsui and Y. Mori, Jap. 1963—17322, 17323, 21362, 22574 (1963).

8) L. Bláha and J. Weichet, *Coll. Czech. Chem. Commun.*, **30**, 2068 (1965).

9) L. M. Weinstock, R. Tull, B. Handelsmen, and E. F. Schoenewaldt, *J. Chem. Eng. Data*, **12**, 154 (1967).

10) O. Isler, R. Ruegg, A. Rangemann, P. Schundel, G. Ryser, and J. Wursch, "Ciba Foundation Symposium on Quinones in Electron Transport" (*cf.* Ref. 1b), p. 82.

11) F. Hoffmann-La Roche Co., Brit. 889704 (1962); *Chem. Abstr.*, **57**, 4596 (1962).

12) E. A. Obol'nikova, O. I. Volkova, and G. I. Samokhvalov, *Zh. Obshch. Khim.*, **38**, 459 (1968).

13) K. H. Slotta and G. Szyszka, *Ber.*, **68**, 184 (1935).

obtainable from vanillin, and dimethyl sulfate in refluxing xylene afforded 5-nitroveratraldehyde (**6**) in a moderate yield. 5-Nitrocreosol has been reported to be easily methylated to 5-nitrohomoveratrol.[5] The presence of a formyl substituent in **5**, on the contrary, seems to diminish the reactivity of the O-methylation.

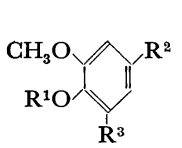

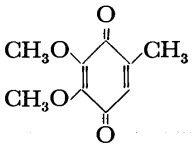

4

5, $R^1=H$, $R^2=CHO$, $R^3=NO_2$
6, $R^1=CH_3$, $R^2=CHO$, $R^3=NO_2$
7, $R^1=CH_3$, $R^2=CH_2OH$, $R^3=NH_2$
8, $R^1=CH_3$, $R^2=CH_3$, $R^3=NH_2$

The catalytic hydrogenation of **6** then gave 5-amino-3,4-dimethoxybenzyl alcohol (**7**), which could not be further reduced under the same reaction conditions because of the poisonous effects of the amino group on the catalyst. Therefore, the alcohol (**7**) was hydrogenated over palladium/charcoal in the form of its hydrochloride to afford **8**, which has been transformed to the quinone (**4**) by Anslow *et al.*[5]

From 3,4,5-Trimethoxysalicylic Acid. In 1956 Mayer and Fikentscher[14] found that 2-bromo-3,4,5-trimethoxybenzoic acid (**9**) underwent a relatively facile hydrolysis with the aid of cupric ions in an aqueous alkaline medium to give 3,4,5-trimethoxysalicylic acid (**10**). This acid (**10**) was then decarboxylated by heating in *N,N*-dimethylaniline to afford 2,3,4-trimethoxyphenol (**11**).

The transformation of **11** to 6-methyl-2,3,4-trimethoxyphenol (**13**) was successfully achieved by means of the Mannich reaction. When the phenol (**11**) was treated with dimethylamine and formaldehyde, the Mannich base, 6-(*N,N*-dimethylamino)methyl-2,3,4-trimethoxyphenol (**12a**), was obtained in a quantitative yield. The structure of this compound was apparent from its PMR spectrum, which had a singlet for the aminomethylene at δ 3.42, and another singlet at δ 2.26 for the aminomethyl groups, in the ratio of 1 : 3. The phenolic proton peak appeared far downfield at δ 8.90 because of hydrogen bonding with the amino-nitrogen. That the dimethylaminomethyl group was introduced at the *ortho* position to the hydroxy was also confirmed by the infrared spectrum, in which the O–H stretching absorption band was broadened and shifted to *ca.* 3000 cm^{-1} as a result of the chelation with the nitrogen atom. This Mannich base was then subjected to hydrogenolysis in the presence of copper chromite to give **13** in a moderate yield.

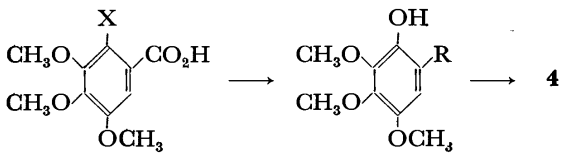

9, X=Br
10, X=OH

11, R=H
12a, $R=CH_2N(CH_3)_2$
b, $R=CH_2SCN(CH_3)_2$ (‖ S)
13, $R=CH_3$

On the other hand, recently Byck and Dawson[15] used a modified Mannich reaction in preparing 6-methylcatechol derivatives, where the methyl group was derived by the hydrogenolysis of the *N,N*-dimethyldithiocarbamoylmethyl group. When this procedure was applied to the present study, 6-(*N,N*-dimethyldithiocarbamoyl)methyl-2,3,4-trimethoxyphenol (**12b**), which had been obtained from **11**, gave **13** upon hydrogenolysis with Raney nickel W-7.

Finally, the phenol (**13**) was oxidized with potassium bichromate and hydrochloric acid to afford the desired quinone (**4**) quantitatively; this quinone was identica in all respects with an authentic material.

The former method of the synthesis of **4** has shorter reaction steps, but suffers from a low overall yield. On the other hand, the latter one consists of easily practicable reactions and **4** is obtained in a moderate overall yield.

Experimental

All the melting points and boiling points are uncorrected. The infrared (IR) spectra were recorded on a Hitachi EPI-S2 spectrophotometer as neat liquids or KBr pellets. The PMR spectra were obtained on a JEOL Model C-60 spectrometer in a carbon tetrachloride solution, with tetramethylsilane as the internal standard.

5-Nitroveratraldehyde (6). 5-Nitrovanillin (**5**)[13] was heated with an equivalent of 1N potassium hydroxide, and the resultant clear solution was allowed to cool. The precipitated material was collected and then dried at 110°C under reduced pressure. A mixture of well-dried 5-nitrovanillin potassium salt (6 g, 25.5 mmol), dimethyl sulfate (3.6 m*l*, 38.3 mmol), and xylene (60 m*l*) was stirred at 125°C for 8 hr. After the reaction mixture had then been cooled to room temperature, an aqueous 5% potassium hydroxide solution was added and the mixture was filtered. The ethereal extract of the filtrate was dried over anhydrous sodium sulfate and concentrated to afford crude 5-nitroveratraldehyde, which was then recrystallized from aqueous ethanol; mp 88—89°C (lit, mp 90—91°C).[13] Yield, 3.1 g (57%).

5-Amino-3,4-dimethoxybenzyl Alcohol (7). 5-Nitroveratraldehyde (**6**) (8 g, 37.8 mmol) was reduced in ethanol (45 m*l*) in the presence of 5% Pd/C (2 g) under a pressure of 100 atm of hydrogen at room temperature. The catalyst was then removed by filtration, and the solvent was distilled off. The distillation of the residual oil gave a pale brown liquid, bp 135°C/0.4 mmHg, which, on standing, gradually crystallized to colorless crystals. Yield, 4.35 g (63%); mp 64—65°C (from benzene—ligroin). IR: 3500, 3400, 1630, 1600, 1510, 1140, 1060, 840 cm^{-1}.

Found: C, 58.74; H, 7.51%. Calcd for $C_9H_{13}O_3N$: C, 59.00; H, 7.15%.

5-Aminohomoveratrol (8). A solution of 5-amino-3,4-dimethoxybenzyl alcohol (**7**) (28 g, 0.153 mol) in methanol (250 m*l*) and concentrated hydrochloric acid (16 m*l*) was shaken with 5% Pd/C (8 g) under an atomospheric pressure of hydrogen. When the absorption of hydrogen ceased, a second crop of the catalyst (3 g) was added, after which the mixture was shaken further until hydrogen was no more absorbed. After the catalyst and solvent had then been removed, the

14) W. Mayer and R. Fikentscher, *Chem. Ber*, **89**, 511 (1956).

15) J. S. Byck and C. R. Dawson, *J. Org. Chem.*, **33**, 2451 (1968).

residue was dissolved in dilute aqueous potassium hydroxide (200 ml) and extracted with ether. The ethereal extract was dried over potassium hydroxide; the subsequent evaporation of the solvent and distillation afforded **8**; bp 90—95°C/0.3 mmHg. Yield, 8.2 g (32%). *N*-Acetyl derivative, mp 89°C (lit, mp 89°C).[16]

2,3,4-Trimethoxyphenol (11). 3,4,5-Trimethoxysalicylic acid (**10**)[14] monohydrate (20 g) was dissolved in dimethylaniline (60 ml) and heated under reflux with vigorous stirring. After the evolution of carbon dioxide had ceased, and aqueous sodium hydroxide solution was added to the reaction mixture and dimethylaniline was separated from the aqueous layer. The aqueous alkaline layer, after several extractions with ether, was carefully acidified with hydrochloric acid and extracted with ether. The ethereal extract was then dried and distilled to afford **11** (6.0 g, 46%); bp 141°C/15 mmHg; mp 40—40.5°C (methylene chloride). IR: 3400, 1480, 1090 cm^{-1}. PMR: δ 3,67. 3.78, 3.81 (CH_3O), 5.65 (OH), and 6.45 ppm (aromatic H).

Found: C, 58.88; H, 6.73%. Calcd for $C_9H_{12}O_4$: C, 58.69; H, 6.57%.

6-(N,N-Dimethylamino)methyl-2,3,4-trimethoxyphenol (12a). To a solution of **11** (5.08 g, 27.6 mmol) in ethanol (20 ml), cooled in an ice-water bath, we added 40% aq. dimethylamine (3.26 g, 29 mmol) and then, drop by drop, 37% formalin (2.32 g, 28.6 mmol). The mixture was allowed to stand overnight and then heated under a gentle reflux for 2 hr. The solvents were evaporated under reduced pressure, leaving an oily material (6.2 g, 93% yield) which was shown not to contain any detectable contaminants *via* PMR spectroscopy and thin-layer chromatography on silica gel; n_D^{20} 1.5287. IR: 3000 (broad), 1480, 1127, and 1087 cm^{-1}. PMR: δ 2.26 (NCH_3), 3.42 (CH_2), 3.62, 3.68, 3.73 (OCH_3), 6.00 (aromatic H), and 8.90 ppm (OH).

Found: C, 59.31; H, 7.97%. Calcd for $C_{12}H_{19}O_4N$: C, 59.73; H, 7.94%.

6-(N,N-Dimethyldithiocarbamoyl)methyl-2,3,4-trimethoxyphenol (12b). To a solution of **11** (3.68 g, 20 mmol) in ethanol (20 ml), were added carbon disulfide (1.68 g, 22.1 mmol), 37% formalin (1.68 g, 20.7 mmol), and 40% aq. dimethylamine (2.36 g, 21.0 mmol), successively in this order. After being allowed to stand overnight, the mixture was heated under reflux for 2 hr and then concentrated *in vacuo* to give a crystalline mass which was subsequently purified by column chromatography on silica gel; 4.75 g (75%); mp 86.5—87°C (MeOH). IR: 3350 (OH), 1495, 1468, and 1075 cm^{-1}. PMR: δ 3.45 (NCH_3), 3.77, 3.80, 3.92 (OCH_3), 4.47 (CH_2), 5.53 (OH), and 6.73 (aromatic H).

Found: C, 49.01; H, 6.12%. Calcd for $C_{13}H_{19}O_4NS_2$: C, 49.18; H, 6.03%.

6-Methyl-2,3,4-trimethoxyphenol (13). *(a)* A solution of 6.2 g of the Mannich base (**12a**) in 200 ml of dry dioxane was put into an autoclave and hydrogenated at 160°C for 4 hr in the presence of Cu-CrO (6.0 g), with an initial hydrogen pressure of 140 kg/cm^2. The filtreed solution was then concentrated *in vacuo*. The residual oil was dissolved in 3N HCl (26 ml), saturated with sodium sulfate, and extracted three times with ether. The extract was dried over calcium chloride and distilled to afford **13** (2.5 g, 45.6%); bp 96—97°C/0.35 mmHg; mp 25.6—26.7°C. IR: 3440 (OH), 1470, 1123, and 1080 cm^{-1}. PMR: δ 2.13 (CH_3), 3.72, 3.77, 3.87 (CH_3O), and 6.32 ppm (aromatic H).

Found: C, 60.45; H, 7.44%. Calcd for $C_{10}H_{14}O_4$: C, 60.59; H, 7.12%.

(b) A solution of **12b** (obtained from 3.68 g of **11**) in dry dioxane (120 ml) was refluxed for 16 hr with Raney nickel W-7, prepared from 36.8 g of a nickel aluminum alloy. The filtered solution was diluted with ether (100 ml) and acidified with dilute hydrochloric acid. Two layers were separated, and the aqueous layer was extracted with ether. The combined organic layer was dried over magnesium sulfate and distilled to give **13** (1,5 g. 38% based on the phenol **11**); bp 140°C/14 mmHg. The IR and PMR spectra and the retention time on glpc were all identical with those of the sample of *(a)*.

2,3-Dimethoxy-5-methylbenzoquinone (4). *(a)* Aminohomoveratrol (**8**) was oxidized with sodium bichromate in dilute sulfuric acid, essentially according to the method of Anslow. The quinone (**4**) was thus obtained in 29% yield; mp 58—59°C (lit, mp 59°C).[5]

(b) To a solution of **13** (0.198 g, 1 mmol) in 5% sodium hydroxide (1 ml), were added a solution of potassium bichromate (0.147 g, 2 mmol) in water (10 ml) and then 1N hydrochloric acid (4 ml). The mixture was stirred for several minutes before it was extracted with ether. The extracts were dried and freed of any solvent to afford **4** (0.18 g, quantitative yield); mp and mixed mp 57—58°C.

The authors wish to express their gratitude to Mr. Takehiko Goshi for his capable technical assistance in these experiments.

16) L. Bláha and J. Weichet, Czech. 110938 (1964); *Chem. Abstr.*, **62**, 1601 (1965).

The Stereochemistry and the Circular Dichroism of Several Pinane Derivatives[1]

Toshifumi HIRATA

Department of Chemistry, Faculty of Science, Hiroshima University, Higashisenda-machi, Hiroshima

(Received November 4, 1971)

The optical rotatory dispersion and the circular dichroism curves were measured for some bicyclo[3.1.1]-heptane derivatives. The applicability of the octant rule to a bicyclo[3.1.1]heptane system was discussed in connection with its preferred conformation; the conformation was determined on the basis of nuclear magnetic resonance spectrum measurements.

Some questions[3-7] have arisen as to the application of the octant rule to the optical rotatory dispersion (ORD) and the circular dichroism (CD) measurements of a pinane system. A combination of the examination of molecular models and physico-chemical study has suggested[8-10] that the preferred conformation of pinane derivatives differ from the chair conformation of an unstrained cyclohexane ring because of the strain caused by the cyclobutane ring. From this point of view, the author now wishes to study the applicability of the octant rule to a bicyclo[3.1.1]heptane system, as well as the preferred conformation of several pinane derivatives.

Results and Discussion

The Preferred Conformation. The preferred conformations of several pinane derivatives were determined on the basis of the anisotropic effect[11-13] of the carbonyl group in the NMR spectrum by comparing the chemical shifts of the sample with those of the corresponding carbonyl-free compound. The conformers, **1a** and **1b**, are proposed as the preferred conformations for (−)-10β-pinan-3-one (**1**). A large upfield shift may be predicted for the C-9 methyl group of **1a**, whereas a downfield one may be predicted for that of **1b**, as is shown in Fig. 1. The signal of the C-9 methyl resonance shows the upfield shift of 0.12 ppm, when the chemical shift of the ketone (**1**) is substracted from that of 10β-pinane (**2**). This fact indicates that **1a** is

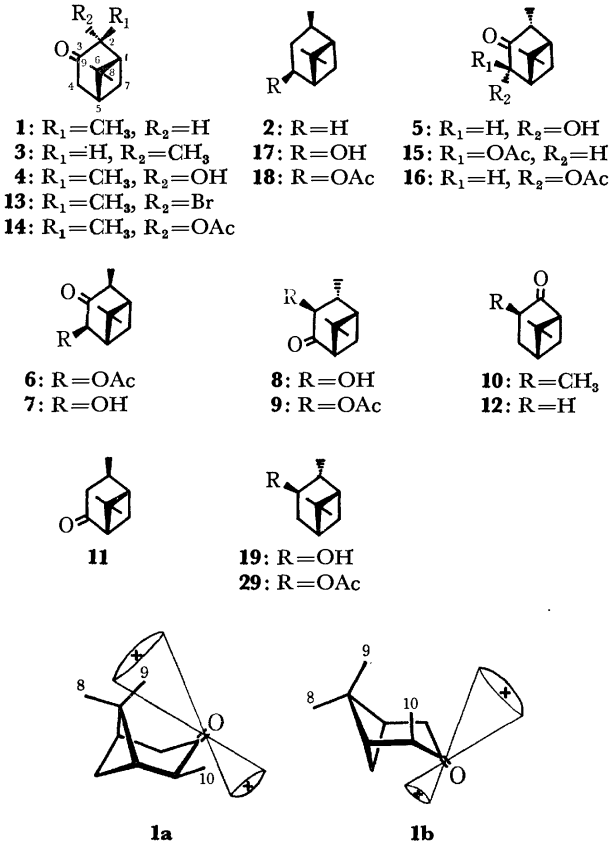

Fig. 1. Possible preferred conformations and predicted anisotropic effect of the carbonyl group for the ketone (**1**).

the preferred conformation of the ketone (**1**). Similarly, the anisotropic effect of the C-9 methyl resonance (Table 1) indicates that the preferred conformations of 10α-pinan-3-one (**3**), 2α-hydroxy-10β-pinan-3-one (**4**), 4α-hydroxy-10α-pinan-3-one (**5**), 4β-acetoxy-10β-pinan-4-one (**8**), 3β-acetoxy-10α-pinan-4-one (**9**), 3β-methylnopinone (**10**), 10β-pinan-4-one (**11**), and nopinone (**12**) are **3a**—**12a** respectively, as is shown in Figs. 2 and 3.

The proposed preferred conformations were further examined by studying the solvent effect[14-16] of the NMR spectrum. As a general rule, Δ values are positive for protons lying at the back of a reference plane and negative for protons lying in front of the

1) This paper forms Part XX[2] in the Hiroshima University series on "Stereochemical Studies of Monoterpene Compounds." A part of this work has been read at the 23rd Anuual Meeting of the Chemical Society of Japan, Tokyo, April, 1970.

2) Part XIX, T. Hirata, This Bulletin, **45**, 3169 (1972).

3) M. P. Hartshorn and A. F. A. Wallis, *Tetrahedron*, **21**, 273 (1965).

4) T. Suga, T. Shishibori, T. Hirata, and T. Matsuura, This Bulletin, **41**, 1180 (1968).

5) R. G. Carlson, J. K. Pierce, T. Suga, T. Hirata, T. Shishibori, and T. Matsuura, *Tetrahedron Lett.*, **1968**, 5941.

6) J. M. Coxon, R. P. Garland, and M. P. Hartshorn, *Aust. J. Chem.*, **23**, 1069 (1970).

7) A. I. Scott and A. D. Wrixon, *Tetrahedron*, **26**, 3695 (1970).

8) N. Nakagawa, S. Saito, A. Suzuki, and M. Itoh, *Tetrahedron Lett.*, **1967**, 1003.

9) A. J. Baretta, C. W. Jefford, and B. Waegell, *Bull. Soc. Chim. Fr.*, **1970**, 3899, 3985.

10) Y. Bessière-Chrétien and C. Grison, *ibid.*, **1971**, 1454.

11) J. A. Pople, *Proc. Roy. Soc., Ser. A*, **1957**, 239, 541, 550.

12) J. M. Lehn and A. Vystrcil, *Tetrahedron*, **19**, 1733 (1963).

13) G. J. Karabatsos, G. C. Sonnichsen, N. Hsi, and D. J. Fenoglis, *J. Amer. Chem. Soc.*, **89**, 5067 (1967).

14) D. H. Williams and N. S. Bhacca, *Tetrahedron*, **21**, 2021 (1965).

15) G. Agami and J.-L. Pierre, *Bull. Soc. Chim. Fr.*, **1969**, 1963.

16) D. H. Williams, *Tetrahedron Lett.*, **1965**, 2305.

Table 1. Anisotropic effects of the carbonyl group for methyl group

Compd.	$\Delta\delta$ reference[a]-ketone (ppm)		
	C-8	C-9	C-10
1	−0.13	+0.12	−0.15
3	−0.15	−0.08	−0.18
4	−0.11	+0.07	−0.05
5	−0.15	−0.22	−0.12
6	−0.10	+0.18	−0.16
7	−0.10	+0.30	−0.13
8	−0.17	+0.16	−0.24
9	−0.17	+0.09	−0.18
10	−0.17	+0.07	—
11	−0.16	−0.01	−0.16
12	−0.16	−0.01	—

a) The reported value[8,10,17,18] for methyl signals of 10β-pinane, 10α-pinane, 2α-hydroxy-10β-pinane, 4α-hydroxy-10α-pinane, 3β-methylapopinane, and apopinane, was used as a reference value for the corresponding carbonyl compounds.

Table 2. Solvent effects of NMR spectra for methyl groups

Compd.	$\Delta\delta$ CCl_4–C_6H_6 (ppm)			$\Delta\delta$ CCl_4–C_5H_5N (ppm)		
	C-8	C-9	C-10	C-8	C-9	C-10
1	+0.27	+0.22	0.00	+0.17	+0.15	−0.02
3	+0.29	+0.32	+0.01	+0.17	+0.20	−0.01
4	+0.28	+0.28	−0.04	+0.11	+0.08	−0.25
5	+0.29	+0.34	+0.05	+0.11	+0.17	−0.07
6	+0.34	+0.06	+0.07	+0.14	−0.01	0.00
7	+0.29	+0.02	+0.06	+0.10	−0.20	−0.07
10	+0.34	+0.14	−0.03	+0.19	+0.08	−0.03
13	+0.47	+0.42	+0.05	+0.22	+0.18	−0.03
14	+0.35	+0.31	−0.19	+0.17	+0.12	−0.19
15	+0.35	+0.13	+0.26	+0.19	+0.05	+0.09

plane. The reference plane was supposed to go through the carbonyl carbon at right angles with the carbon-oxygen bond of the carbonyl group for a benzene-induced effect, and also through the α-position to the carbonyl group for a pyridine-induced effect. The C-10 methyl protons of ketones, **1**, **3**, **4**, **5**, **7**, **10**, and **13**, suffer only a small shift when the solvent is changed from carbon tetrachloride to benzene, and a downfield shift when a change of the solvent from carbon tetrachloride to pyridine (Table 2). These facts show that the C-10 methyl group of these compounds is equatorial. However, the preferred conformations of 4β-acetoxy-10β-pinan-3-one (**6**), 2α-acetoxy-10β-pinan-3-one (**14**), and 4β-acetoxy-10α-pinan-3-one (**15**) were not determined by means of the solvent effect only because of the disturbance caused by the acetoxyl group. The IR spectra of hydroxyketones, **5**, **7**, and **8**, showed, respectively, an intramolecularly hydrogen-bonded hydroxyl band at 3536, 3540, and 3514 cm^{-1}, assigned to the equatorial hydroxyl group. Although the preferred conformation of the acetate (**14**) was not assigned by these methods, the conformer (**14a**) may be proposed as the preferred conformation, because of the decrease in the steric hindrance of the C-10 methyl group and the stabilization by the dipole-moment of the acetoxyl and the carbonyl groups. In addition, since **4a** and **13a** are the preferred conformations for compounds **4** and **13**, respectively, similar to the compound (**14**), the conformer **14a** seems to be appropriate. On the other hand, conformations keeping the coplanarity of the C-1—C-5 atoms have been considered[6] to hold for pinane derivatives. The coplanar conformation can, however, be rejected on the grounds of the fact that the intramolecular hydrogen bonding is formed in the ketones, **5**, **7**, and **8**. No reason to consider the coplanar conformation for the other ketones has been given by the physico-chemical data.

The Application of the Octant Rule. In order to examine the applicability of the octant rule to a pinanone system, the present author prepared some pinane derivatives belonging to two groups as follows: (A) pinan-2- or 4-one, with the carbonyl group adjacent to the four-membered ring, and (B) pinan-3-one, with the carbonyl group at the symmetric position to the ring.

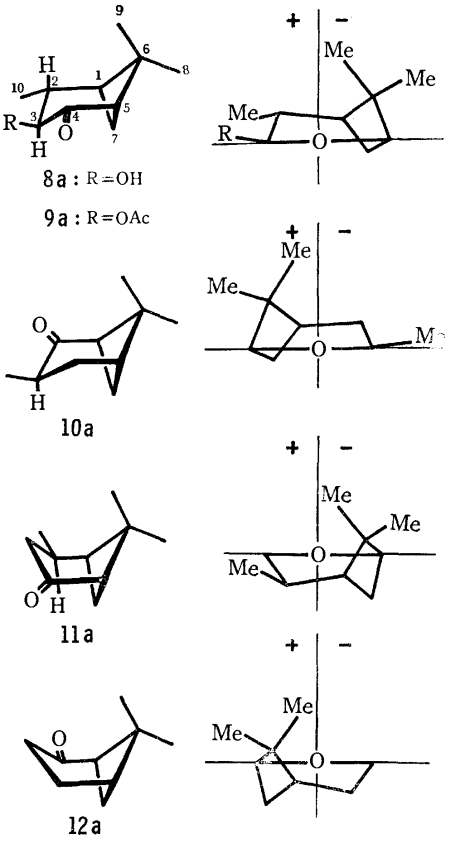

Fig. 2. Preferred conformations and octant projection diagrams for ketones (**8**), (**9**), (**10**), (**11**), and (**12**).

The compounds of the A group are the ketones, **8**, **9**, **10**, **11**, and **12**. Octant projection diagrams for the preferred conformation of these ketones are shown in Fig. 2. The diagrams indicate a large contribution of the C-6 *gem*-dimethyl group to the optical activity. The predicted Cotton effect is negative for **8a**, **9a**, and **11a**, but positive for **10a** and **12a**. Even if the preferred conformation of these compounds is coplanar, the same sign of a Cotton effect can be predicted.

17) A. F. Regan, *Tetrahedron*, **25**, 3801 (1969).
18) J. M. Coxon, E. Dansted, M. P. Hartshorn, and K. E. Richards, *Tetrahedron Lett.*, **1969**, 1149.

The ORD and the CD curves in both polar and nonpolar solvents showed a large, negative Cotton effect for **8**, **9**, and **11**, and a large, positive one for **10** and **12**. In addition, the same sign of a Cotton effect was observed for various-temperature CD curves in the EPA solvent[19] and in decalin. It was thus established that a Cotton effect for compounds of the A group is in good agreement with the predicted one obtained by applying the octant rule of the cyclohexanone pattern.

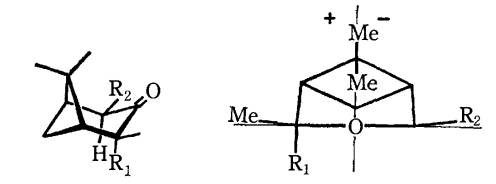

1a: R_1,R_2=H
4a: R_1=OH, R_2=H
6a: R_1=H, R_2=OAc

7a: R_1=H,R_2=OH
13a: R_1=Br, R_2=H
14a: R_1=OAc, R_2=H

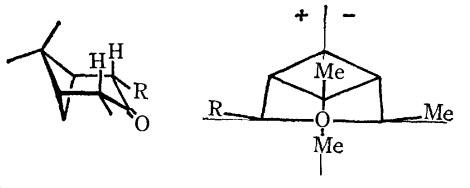

3a: R=H
5a: R=OH

Fig. 3. Preferred conformations and octant projection diagrams for ketones (**1**), (**3**), (**4**), (**5**), (**6**), (**7**), (**13**), and (**14**).

On the other hand, the direct application of the octant rule to the ketones of the B group presented complicated problems. Octant projection diagrams of the conformers, **1a**, **3a**, **4a**, **5a**, **6a**, **7a**, **13a**, and **14a**, are shown in Fig. 3. The predicted Cotton effect is positive for **1a**, but negative for **3a**, **4a**, **13a**, and **14a**. A Cotton effect for **5a**, **6a**, and **7a** cannot be predicted, since the contribution of the hydroxyl and the acetoxyl groups to the optical rotation can not be compared

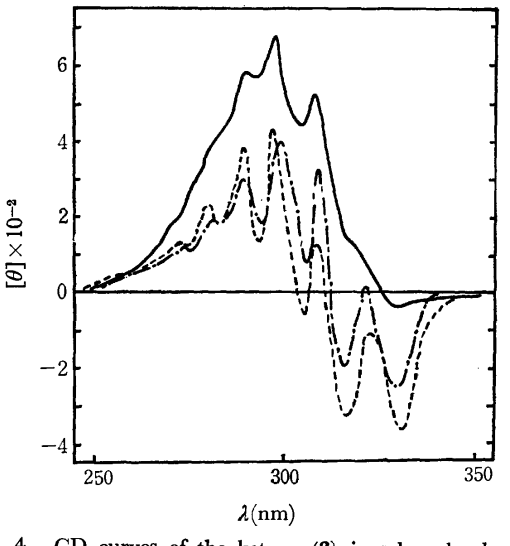

Fig. 4. CD curves of the ketone (**3**) in selected solvents at 25°C: ——, in MeOH; – – –, in isooctane; ——, in CCl_4.

19) The EPA solvent is composed of ether–isopentane–ethanol in the ratio 5: 5: 2 by volume.

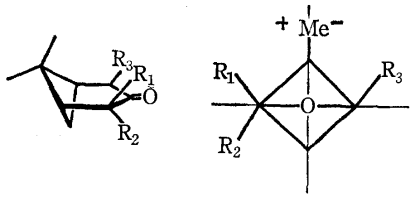

1b: R_1=CH_3; R_2,R_3=H
3b: R_1, R_3=H; R_2=CH_3
4b: R_1=CH_3, R_2=OH, R_3=H
6b: R_1=CH_3, R_2=H, R_3=OAc
13b: R_1=CH_3, R_2=Br, R_3=H
14b: R_1=CH_3, R_2=OAc, R_3=H

Fig. 5. Octant projection diagram for the coplanar conformer of ketones (**1**), (**3**), (**4**), (**6**), (**13**), and (**14**).

with that of the methyl group. The compound **1** showed a negative Cotton effect, while compounds **4** and **14** showed a positive one. The observed Cotton effect of these samples was not identical with the prediction. The bromoketone (**13**), however, showed a negative Cotton effect which coincides with the prediction. The ketone **3** in the nonpolar solvent exhibited a positive Cotton effect at a shorter wavelength and a weak negative effect at a longer one. However, the negative effect diminished in the polar solvent (Fig. 4). The CD curve of the ketone **3** at lower temperatures (Fig. 7) showed an increase in the positive strength of the shorter wavelength band and a decrease in the negative strength of the longer one; it is temperature-dependent. This double-humped Cotton effect may result from a solvation, because the $n\rightarrow\pi^*$ absorption of a solvated ketone generally appears at a shorter wavelength than that of an unsolvated one. In addition, octant projection diagrams for the coplanar conformations, (**1b**), (**3b**), (**4b**), (**6b**), (**13b**), and (**14b**), may be possible for the ketones **1**, **3**, **4**, **6**, **13**, and **14** respectively, as is shown in Fig. 5. The predicted Cotton effect was positive for **1b** and negative for **3b**, while the signs for **4b**, **6b**, and **14b** could not be predicted, because the rotational strength of the hydroxyl and the acetoxyl groups could not be estimated. A negative Cotton effect, however, was predicted for **13b**, since the bromine atom contributes to a larger extent to the optical rotational strength than the methyl group does. The ketone **15** may be at the equilibrium among the conformers **15a**⇌**15b**⇌**15c**, but the preferred conformation was not implied even by any physico-chemical data. However, all these con-

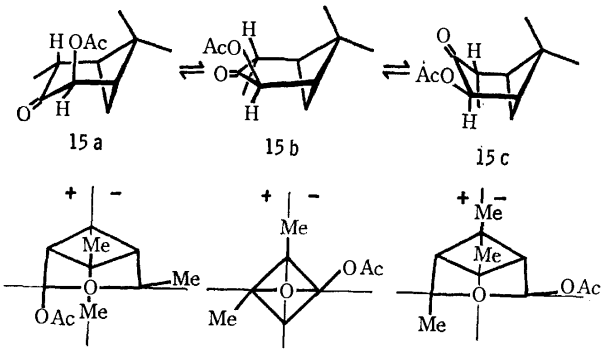

15a 15b 15c

Fig. 6. Possible preferred conformations and octant projection diagrams for the ketone (**15**).

Table 3. Methyl proton signals of the pinane derivatives

Compd.	CCl_4			C_6H_6			C_5H_5N		
	C-8	C-9	C-10	C-8	C-9	C-10	C-8	C-9	C-10
1	1.33	0.90	1.16	1.06	0.68	1.16	1.16	0.75	1.18
3	1.35	0.92	1.05	1.06	0.60	1.04	1.18	0.72	1.06
4	1.35	0.88	1.29	1.07	0.60	1.33	1.24	0.88	1.54
5	1.37	1.00	1.06	1.08	0.66	0.99	1.26	0.83	1.13
6	1.33	0.93	1.21	0.99	0.87	1.13	1.19	0.94	1.21
7	1.32	0.86	1.20	1.03	0.84	1.14	1.22	1.06	1.27
8	1.37	0.74	1.23	0.97	0.62	1.05	1.21	0.83	1.26
9	1.38	0.81	1.15	0.92	0.68	0.92	1.18	0.79	1.08
10	1.34	0.71	1.11	1.00	0.57	1.14	1.15	0.63	1.14
11	1.36	1.02	1.17	1.03	0.80	0.89	1.17	0.88	0.98
12	1.34	0.86	—	1.02	0.65	—	1.14	0.72	—
13	1.41	0.91	1.93	0.94	0.49	1.88	1.19	0.73	1.96
14	1.37	0.86	1.49	1.02	0.55	1.68	1.20	0.74	1.68
15	1.35	0.95	1.14	1.00	0.82	0.88	1.16	0.90	1.05

These data are represented by the δ value in ppm.

formers are capable of predicting a negative Cotton effect, as is shown in Fig. 6. The ORD and CD curves of the compound **15** exhibited a positive Cotton effect; it is not identical with the prediction.

It was also observed that the amplitudes ([θ] *ca.* 300—2000 in methanol) of the CD curves for the B group are considerably small in comparison with those of the A group ([θ] *ca.* 3000—8000). This may be explained as follows: the symmetric skeleton of the compounds of the B group to their carbonyl group necessarily shows a relatively small contribution to the optical rotatory strength, whereas the *gem*-dimethyl bridge occupying unsymmetrically the compounds of the A group shows a large one. These facts suggest that the CD curves of the compounds of the B group are influenced easily by other factors, such as the temperature, the solvation, and the strain of the skeleton. Thus, these observations indicate the necessity of prudent care in the application of the octant rule to the pinan-3-one system.

Experimental

The NMR spectra were taken with a Varian Associates, HA-100 spectrometer, and a Hitachi Perkin-Elmer, R-20, High-resolution spectrometer on solutions in concentrations of 10 per cent, using tetramethylsilane as the internal standard. The signals of the C-8, C-9, and C-10 methyl protons of pinane derivatives are shown in Table 3. The ORD and the CD curves were measured on a Japan Spectroscopic Co., ORD/UV-5, Spectropolarimeter, equipped with a circular dichroism attachment, at 25°C. The variable-temperature CD curves were obtained by the use of the same spectrometer, using a low- and high-temperature cell. The IR spectra in the hydroxyl-stretching region were measured with a Perkin-Elmer, 621, Grating Infrared Spectrometer in a 0.002M carbon tetrachloride solution at a spectral slit-width of less than 2 cm^{-1} at 25°C, using a salt absorption cell 20 mm in length.

(−)-10β-Pinane-3-one (1). Following the procedure previously reported,[20] 20 g of (+)-isopinocamphenol (mp 55—57°C, $[\alpha]_D^{25}$ +31.6°) prepared from (−)-α-pinene ($[\alpha]_D^{25}$ −39.9°) through hydrobarotion[21] was oxidized with sodium dichromate to give 17.8 g of 10β-pinane-3-one (**1**): $[\alpha]_D^{25}$ −9.77° (neat) (lit,[21] $[\alpha]_D^{25}$ +10.3°, from (−)-isopinocamphenol); UV (MeOH) 291 nm (ε 17.6), (isooctane) 295 nm (ε 16.6); ORD (*c* 1.1, MeOH) $[\phi]_{400}$ −100, $[\phi]_{319}$ −889, $[\phi]_{276}$ +1200, $[\phi]_{248}$ +960, $[\phi]_{230}$ +1360, (*c* 0.25, isooctane) $[\phi]_{400}$ +30, $[\phi]_{320}$ −617, $[\phi]_{313}$ −440, $[\phi]_{309}$ −617, $[\phi]_{302}$ −65, $[\phi]_{298}$ −216, $[\phi]_{292}$ +277, $[\phi]_{288}$ +205, $[\phi]_{277}$ +617, $[\phi]_{245}$ +404, $[\phi]_{220}$ +645; CD (*c* 1.1, MeOH) $[\theta]_{338}$ 0, $[\theta]_{294}$ −1670, $[\theta]_{247}$ 0, (*c* 0.25, isooctane) $[\theta]_{331}$ 0, $[\theta]_{315}$ −365, $[\theta]_{305}$ −760, $[\theta]_{296}$ −832, $[\theta]_{285}$ −649, $[\theta]_{249}$ 0; variable temp. CD (*c* 0.21, EPA) $[\theta]^{-192°}_{341}$ 0, $[\theta]_{335}$ −105, $[\theta]_{330}$ +176, $[\theta]_{324}$ −491, $[\theta]_{318}$ −175, $[\theta]_{311}$ −1630, $[\theta]_{307}$ −1020, $[\theta]_{301}$ −2380, $[\theta]_{296}$ −1400, $[\theta]_{292}$ −2140, $[\theta]_{286}$ −1160, $[\theta]_{284}$ −1230, $[\theta]_{255}$ 0, $[\theta]^{+25°}_{337}$ 0, $[\theta]_{330}$ +175, $[\theta]_{302}$ −834, $[\theta]_{299}$ −790, $[\theta]_{295}$ −1010, $[\theta]_{256}$ 0,

(−)-10α-Pinan-3-one (3). Following the method in the literature,[21] 0.50 g of (−)-10β-pinan-3-one (**1**) was added to an ethanol solution of sodium ethoxide, which had been prepared by dissolving 0.12 g of metallic sodium in 25 m*l* of absolute ethanol; then the mixture was let to stand for 24 hr at room temperature. The usual treatment of the mixture gave 0.35 g of the ketone (**3**): $[\alpha]_D^{25}$ −18.6° (*c* 1.99, EtOH) (lit,[22] α_J −15°); UV (MeOH) 295 nm (ε 20.0), (isooctane) 318 nm (ε 13.5), 306 (18.0), 296 (18.0); ORD (*c* 0.29, MeOH) $[\phi]_{400}$ −45, $[\phi]_{321}$ +255, $[\phi]_{317}$ +230, $[\phi]_{310}$ +351, $[\phi]_{304}$ +105, $[\phi]_{302}$ +121, $[\phi]_{269}$ −845, $[\phi]_{257}$ −860, $[\phi]_{245}$ −1000, (*c* 0.31, isooctane) $[\phi]_{400}$ −37, $[\phi]_{334}$ −425, $[\phi]_{327}$ +88, $[\phi]_{320}$ −120, $[\phi]_{312}$ +450, $[\phi]_{307}$ −50, $[\phi]_{301}$ +375, $[\phi]_{296}$ −188, $[\phi]_{291}$ +75, $[\phi]_{287}$ −300, $[\phi]_{282}$ −188, $[\phi]_{220}$ −800; CD (*c* 0.29, MeOH), (*c* 0.31, isooctane), and (*c* 0.55, CCl_4) (Fig. 4); variable temp. CD (*c* 0.26, EPA) and (*c* 0.28, decalin) (Fig. 7).

(+)-2α-Hydroxy-10β-pinan-3-one (4). Following the procedure previously reported,[23] (−)-α-pinene ($[\alpha]_D^{25}$ −39.9°) was oxidized with potassium permanganate in 90% aqueous acetone for 8.5 hr at −5°C to obtain the hydroxyketone (**4**) in a 24% yield: mp 34—35°C (lit,[24] mp 34.5—35.3°C), $[\alpha]_D^{25}$ +23.3° (*c* 4.64, EtOH) (lit,[23] $[\alpha]_D^{25}$ −18.56° (*c* 14.44, EtOH) from (+)-α-pinene); UV (MeOH) 308 nm (ε 28.0), (isooctane)

20) H. C. Brown and C. P. Garg, *J. Amer. Chem. Soc.*, **83**, 2952 (1961).

21) G. Zweifel and H. C. Brown, *ibid.*, **86**, 393 (1964).

22) A. Kergomard, *Bull. Soc. Chim. Fr.*, **1958**, 394.

23) T. Kuwata, *J. Amer. Chem. Soc.*, **59**, 2509 (1937).

24) H. Schmidt, *Chem. Ber.*, **93**, 2485 (1960).

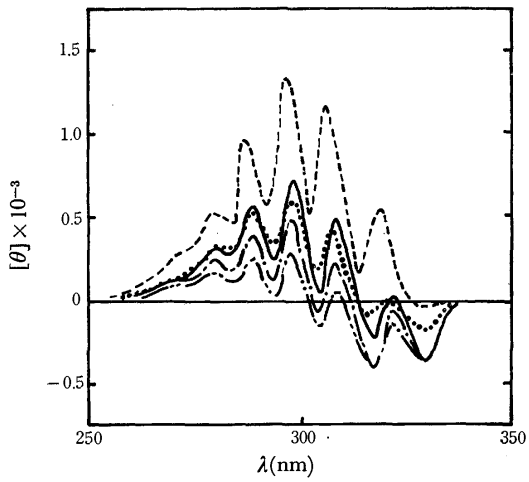

Fig. 7. CD curves of the ketone (**3**) in selected solvents at various temperatures: ——, – – –, and — — —, at −74, +25, and +138°C in decalin, —— and ·····, at −138 and +25°C in EPA, respectively.

309 nm (ε 24.6); ORD (*c* 0.61, MeOH) $[\phi]_{400}$ +220, $[\phi]_{337}$ +1680, $[\phi]_{333}$ +1300, $[\phi]_{326}$ +1530, $[\phi]_{316}$ +237, $[\phi]_{304}$ −1010, $[\phi]_{296}$ −1740, $[\phi]_{288}$ −1940, (*c* 0.61, isooctane) $[\phi]_{400}$ +387, $[\phi]_{338}$ +2460, $[\phi]_{332}$ +1520, $[\phi]_{325}$ +2370, $[\phi]_{319}$ +83, $[\phi]_{314}$ +690, $[\phi]_{308}$ −1350, $[\phi]_{304}$ −1100, $[\phi]_{297}$ −2180, $[\phi]_{294}$ −2040, $[\phi]_{290}$ −2320, $[\phi]_{230}$ −900; CD (*c* 0.61, MeOH) $[\theta]_{347}$ 0, $[\theta]_{322}$ +2360, $[\theta]_{313}$ +2740, $[\theta]_{303}$ +2290, $[\theta]_{260}$ 0, (*c* 0.61, isooctane) $[\theta]_{346}$ 0, $[\theta]_{335}$ +1920, $[\theta]_{322}$ +3550, $[\theta]_{310}$ +3780, $[\theta]_{301}$ +3010, $[\theta]_{260}$ 0; variable. temp. CD (*c* 0.68, EPA) and (*c* 0.70, decalin) (Fig. 8).

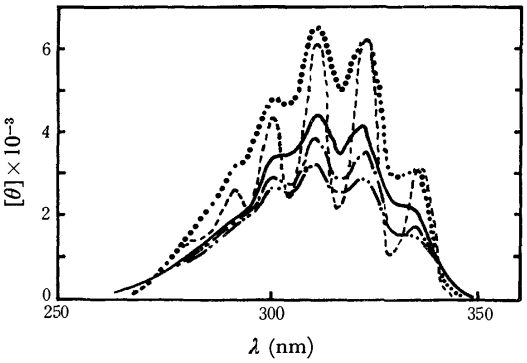

Fig. 8. CD curves of the hydroxyketone (**4**) in selected solvents at various temperatures: ——, – – –, and — — —, at −74, +25, and +138°C in decalin; ---- and ·····, at −138 and +25°C in EPA, respectively.

*Acetates (**6**), (**14**), (**15**), and (**16**). (See Ref. 25 for the details of this reaction)* A mixture of (+)-hydroxyketone (**4**) (22.0 g) and acetic anhydride (35.0 g) was refluxed for 6 hr at 160°C. The reaction mixture was then extracted with ether to obtain an oily product (22.9 g), which was composed of (+)-4β-acetoxy-10β-pinan-3-one (**6**) (17% yield), (+)-2α-acetoxy-10β-pinan-3-one (**14**) (14%), (−)-4β-acetoxy-10α-pinan-3-one (*15*) (20%), and (−)-4α-acetocy-10α-pinan-3-one (**16**) (39%).

*a) (+)-4β-Acetoxy-10β-pinan-3-one (**6**)*: mp 100.5—101.0 °C $[\alpha]_D^{25}$ +66.1° (*c* 6.0, EtOH); UV (MeOH) 292 nm (ε 27.7), (isooctane) 297 nm (ε 24.2); ORD (*c* 1.3, MeOH) $[\phi]_{400}$ +48, $[\phi]_{323}$ +232, $[\phi]_{275}$ −175, $[\phi]_{230}$ −38, (*c* 1.1, isooctane) $[\phi]_{400}$ +29, $[\phi]_{326}$ +151, $[\phi]_{280}$ −99, $[\phi]_{240}$ −30; CD (*c* 1.3, MeOH) $[\theta]_{337}$ 0, $[\theta]_{301}$ +262, $[\theta]_{250}$ 0, (*c* 1.1, isooctane) $[\theta]_{340}$ 0, $[\theta]_{305}$ +147, $[\theta]_{260}$ 0.

*b) (+)-2α-Acetoxy-10β-pinan-3-one (**14**)*: mp 38—40°C, $[\alpha]_D^{25}$ +23.1° (*c* 0.26, MeOH); UV (MeOH) 300 nm (ε 29.5), (isooctane) 301 nm (ε 23.0); ORD (*c* 0.26, MeOH) $[\phi]_{400}$ +163, $[\phi]_{339}$ +1470, $[\phi]_{328}$ +1840, $[\phi]_{317}$ +990, $[\phi]_{280}$ −2970 $[\phi]_{255}$ −2640, $[\phi]_{240}$ −3010, (*c* 0.19, isooctane) $[\phi]_{400}$ +164, $[\phi]_{344}$ +1470, $[\phi]_{336}$ +1140, $[\phi]_{331}$ +1720, $[\phi]_{322}$ +326, $[\phi]_{319}$ +622, $[\phi]_{309}$ −1080, $[\phi]_{307}$ −982, $[\phi]_{298}$ −2180, $[\phi]_{296}$ −2110, $[\phi]_{289}$ −2540, $[\phi]_{284}$ −2470, $[\phi]_{280}$ −2570, $[\phi]_{257}$ −2210, $[\phi]_{245}$ −2470; CD (*c* 0.26, MeOH) $[\theta]_{340}$ 0, $[\theta]_{317}$ +1120, $[\theta]_{311}$ +1710, $[\theta]_{302}$ +1650, $[\theta]_{260}$ 0, (*c* 0.19, isooctane) $[\theta]_{349}$ 0, $[\theta]_{337}$ +820, $[\theta]_{333}$ +800, $[\theta]_{324}$ +2030, $[\theta]_{319}$ +1770, $[\theta]_{312}$ +2550, $[\theta]_{306}$ +2030, $[\theta]_{302}$ +2200, $[\theta]_{292}$ +1560, $[\theta]_{260}$ 0.

*c) (−)-4β-Acetoxy-10α-pinan-3-one (**15**)*; $[\alpha]_D^{25}$ −8.5° (*c* 0.37, MeOH); UV (MeOH) 302 nm (ε 27.1), (isooctane) 304 nm (ε 25.4); ORD (*c* 0.37, MeOH) $[\phi]_{400}$ +67.0, $[\phi]_{339}$ +905, $[\phi]_{328}$ +1070, $[\phi]_{279}$ −2180, $[\phi]_{262}$ −2110, $[\phi]_{234}$ −3150, (*c* 0.15, isooctane) $[\phi]_{400}$ +42, $[\phi]_{345}$ +807, $[\phi]_{337}$ +721, $[\phi]_{332}$ +975, $[\phi]_{323}$ +297, $[\phi]_{319}$ +339, $[\phi]_{308}$ −636, $[\phi]_{298}$ −1400, $[\phi]_{272}$ −1780, $[\phi]_{262}$ −1700, $[\phi]_{228}$ −3140; CD (0.37, MeOH) $[\theta]_{347}$ 0, $[\theta]_{309}$ +1790, $[\theta]_{243}$ 0, (*c* 0.15, isooctane) $[\theta]_{351}$ 0, $[\theta]_{338}$ +443, $[\theta]_{325}$ +1100, $[\theta]_{320}$ +1070, $[\theta]_{313}$ +1440, $[\theta]_{307}$ +1230, $[\theta]_{303}$ +1280, $[\theta]_{240}$ 0.

*d) (−)-4α-Acetoxy-10α-pinan-3-one (**16**)*: $[\alpha]_D^{25}$ −78.1° (*c* 0.49, MeOH); UV (MeOH) 298 nm (ε 30.2), (isooctane) 294 nm (ε 28.4), 302 (27.1); ORD (*c* 0.49, MeOH) $[\phi]_{400}$ −596, $[\phi]_{340}$ −2680, $[\phi]_{329}$ −3020, $[\phi]_{282}$ +3150, $[\phi]_{230}$ +1450, (*c* 0.32, isooctane) $[\phi]_{400}$ −463, $[\phi]_{343}$ −2580, $[\phi]_{338}$ −2450, $[\phi]_{330}$ −2970, $[\phi]_{320}$ −1390, $[\phi]_{308}$ +859, $[\phi]_{298}$ +2640, $[\phi]_{285}$ +3370, $[\phi]_{215}$ +1720; CD (*c* 0.49, MeOH) $[\theta]_{350}$ 0, $[\theta]_{309}$ −4440, $[\theta]_{250}$ 0, (*c* 0.32, isooctane) $[\theta]_{348}$ 0, $[\theta]_{323}$ −3400, $[\theta]_{313}$ −4540, $[\theta]_{303}$ −4190, $[\theta]_{294}$ −3230, $[\theta]_{254}$ 0.

*(−)-4α-Hydroxy-10α-pinan-3-one (**5**) and (−)-3β-Hydroxy-10α-pinan-4-one (**8**).*[25] The acetate (**16**) was hydrolyzed by methanolic potassium hydroxide at room temperature overnight to give hydroxyketones (**5**) and (**8**) (67% and 33% yields respectively).

*a) (−)-4α-Hydroxy-10α-pinan-3-one (**5**)*: $[\alpha]_D^{25}$ −52.8° (*c* 0.55, MeOH); IR (CCl_4) 3536 cm^{-1} (intramol. bonded OH); UV (MeOH) 285 nm (ε 29.7), (isooctane) 283 nm (ε 35.3); ORD (*c* 0.55, MeOH) $[\phi]_{400}$ −337, $[\phi]_{340}$ −1470, $[\phi]_{330}$ −1500, $[\phi]_{281}$ +1620, $[\phi]_{247}$ +1220, $[\phi]_{225}$ +1590, (*c* 0.71, isooctane) $[\phi]_{400}$ −294, $[\phi]_{325}$ −1850, $[\phi]_{273}$+2530, $[\phi]_{245}$ +2320, $[\phi]_{220}$ +5470; CD (*c* 0.55, MeOH) $[\theta]_{346}$ 0, $[\theta]_{309}$ −2220, $[\theta]_{250}$ 0, (*c* 0.71, isooctane) $[\theta]_{346}$ 0, $[\theta]_{298}$ −3080, $[\theta]_{240}$ 0.

*b) (−)-3β-Hydroxy-10α-pinan-4-one (**8**)*: mp 44—45°C, $[\alpha]_D^{25}$ −147.7° (*c* 0.27, MeOH); IR (CCl_4) 3514 cm^{-1}(intermol. bonded OH); UV (MeOH) 282 nm (ε 36.9), (isooctane) 284 nm (ε 37.9); ORD (*c* 0.27, MeOH) $[\phi]_{400}$ −689, $[\phi]_{302}$ −5570, $[\phi]_{264}$ +5200, $[\phi]_{220}$ +751, (*c* 0.17, isooctane) $[\phi]_{400}$ −778, $[\phi]_{299}$ −6610, $[\phi]_{258}$ +7100, $[\phi]_{227}$ +4670, $[\phi]_{215}$ +6610; CD (*c* 0.27, MeOH) $[\theta]_{321}$ 0, $[\theta]_{282}$ −8020, $[\theta]_{245}$ 0, (*c* 0.17, isooctane) $[\theta]_{315}$ 0, $[\theta]_{281}$ −9860, $[\theta]_{224}$ 0.

*(+)-4β-Hydroxy-10β-pinan-3-one (**7**).* The hydrolysis of the acetate (**6**) (420 mg) with methanolic sodium hydroxide gave the hydroxyketone (**7**) (292 mg): mp 67—68°C, $[\alpha]_D^{25}$ +33.5° (*c* 0.25, MeOH); IR (CCl_4) 3540 cm^{-1} (intramol. bonded OH); UV (MeOH) 288 nm (ε 29.8), (isooctane) 283 nm (ε 31.5); ORD (*c* 0.25, MeOH) $[\phi]_{400}$ +332, $[\phi]_{322}$ +1660, $[\phi]_{279}$ −1990, $[\phi]_{253}$ −1590, $[\phi]_{225}$ −3380, (*c* 0.22, isooctane) $[\phi]_{400}$ +375, $[\phi]_{317}$ +2480, $[\phi]_{273}$ −3300, $[\phi]_{248}$ −2100, $[\phi]_{225}$ −6000; CD (*c* 0.25, MeOH) $[\theta]_{344}$ 0, $[\theta]_{301}$ +1880, $[\theta]_{250}$ 0, (*c* 0.22, isooctane) $[\theta]_{331}$ 0, $[\theta]_{296}$ +2770,

25) T. Hirata, This Bulletin, **45**, 599 (1972).

$[\theta]_{247}$ 0.

(−)-3β-Acetoxy-10α-pinan-4-one (9). The acetylation of the hydroxyketone (**8**) (100 mg) with acetic anhydride in pyridine gave the acetate (**9**) (95 mg): mp 38—39°C; $[\alpha]_D^{25}$ −135.2° (*c* 0.49, MeOH); UV (MeOH); 284 nm (ε 54.9), (isooctane) 290 nm (ε 63.0); ORD (*c* 0.14, MeOH) $[\phi]_{400}$ −1200, $[\phi]_{303}$ −7410, $[\phi]_{263}$ +5560, $[\phi]_{230}$ +1390, (*c* 0.20, isooctane) $[\phi]_{400}$ −685, $[\phi]_{308}$ −5000, $[\phi]_{267}$ +4660, $[\phi]_{230}$ +2330; CD (*c* 0.14, MeOH) $[\theta]_{322}$ 0, $[\theta]_{285}$ −6830, $[\theta]_{237}$ 0, (*c* 0.20, isooctane) $[\theta]_{326}$ 0, $[\theta]_{290}$ −4870, $[\theta]_{245}$ 0.

(+)-3β-Methylnopinone (10). To a stirred solution of potassium hydroxide (7.0 g) in methanol (20 m*l*), was added a sample of (−)-10β-pinan-2α,3α-diol monotosylate (6.2 g) which had been prepared in our previous work.[26] The solution was heated to 65°C for 3 hr had then kept further at room temperature overnight. The reaction mixture was extracted with ether to give an oily product (2.5 g), which was subsequently subjected to chromatography on a silica-gel column to isolate the ketone (**10**) in an 8.5% yield: $[\alpha]_D^{25}$ +59.7° (neat); UV (MeOH) 275 nm (ε 30.1); ORD (*c* 0.64, MeOH) $[\phi]_{400}$ +380, $[\phi]_{301}$ +3550, $[\phi]_{265}$ −3380, $[\phi]_{230}$ −1080, (*c* 0.77, isooctane) $[\phi]_{400}$ +157, $[\phi]_{304}$ +1490, $[\phi]_{268}$ −1530, $[\phi]_{230}$ −315; CD (*c* 0.64, MeOH) $[\theta]_{317}$ 0, $[\theta]_{285}$ +2740, $[\theta]_{240}$ 0, (*c* 0.77, isooctane) $[\theta]_{322}$ 0, $[\theta]_{290}$ +1240, $[\theta]_{238}$ 0; variable temp. CD (*c* 0.61, EPA) $[\theta]_{323}^{-192°}$ 0, $[\theta]_{289}$ +2940, $[\theta]_{248}$ 0, $[\theta]_{320}^{+25°}$ 0, $[\theta]_{283}$ +2410, $[\theta]_{250}$ 0, (*c* 0.59, decalin) $[\theta]_{317}^{-74°}$ 0, $[\theta]_{287}$ +2580, $[\theta]_{254}$ 0, $[\theta]_{316}^{+25°}$ 0, $[\theta]_{288}$ +1630, $[\theta]_{254}$ 0, $[\theta]_{317}^{+137°}$ 0, $[\theta]_{288}$ +1920, $[\theta]_{253}$ 0.

(−)-10β-Pinan-4-one (11). *a) Preparation of (−)-verbenone*: To a stirred sample of 100 g of (−)-α-pinene ($[\alpha]_D^{25}$ −39.9°), was added a *t*-butyl chromate solution, which had been prepared from chromiun trioxide (220.5 g), *t*-butyl alcohol (330 g), benzene (500 m*l*), glacial acetic acid (150 g), and acetic anhydride (150 g) following the method in the literature.[27] The mixture was stirred for 12 hr at room temperature in an atmosphere of nitrogen, and then it was treated with water and oxalic acid as usual.[27] The reaction product extracted with benzene was subjected to distillation and then to column chromatography to isolate (−)-verbenone (39.4 g); bp 80—84°C/9 mmHg, $[\alpha]_D^{25}$ −208.6° (neat).

b) Preparation of Ketone 11: (−)-verbenone (1.3 g) in ethanol was hydrogenated in the presence of palladium hydroxide on calcium carbonate, under an atmospheric pressure, to yield an oily product (1.2 g). The product was rectified by distillation under a reduced pressure to give the ketone (**11**) (1.0 g): bp 59—61°C/11 mmHg, $[\alpha]_D^{25}$ −47.8° (neat), d_D^{25} 0.9693, n_D^{25} 1.4751; UV (MeOH) 274 nm (ε 34.5), (isooctane) 285 nm (ε 20.2); ORD (*c* 0.15, MeOH) $[\phi]_{400}$ −250, $[\phi]_{305}$ −2620, $[\phi]_{266}$ +2720, $[\phi]_{235}$ +1250, (*c* 0.17, isooctane) $[\phi]_{400}$ −250, $[\phi]_{317}$ −1670, $[\phi]_{314}$ −1450, $[\phi]_{307}$ −1800, $[\phi]_{270}$ +1800, $[\phi]_{230}$ +710; CD (*c* 0.15, MeOH) $[\theta]_{320}$ 0, $[\theta]_{285}$ −3550, $[\theta]_{230}$ 0, (*c* 0.35, isooctane) $[\theta]_{324}$ 0, $[\theta]_{294}$ −2380, $[\theta]_{250}$ 0; variable temp. CD (*c* 0.20, EPA) and (*c* 0.27, decalin) (Fig. 9); the semicarbazone derivative, mp 222—223°C.

(+)-Nopinone (12). Into a solution of 5.0 g of (−)-β-pinene ($[\alpha]_D^{25}$ −21.8°) in 30 m*l* of dichloromethane, was passed ozonized oxygen at −60°C. The solution was subjected to steam distillation, and then extraction with chloroform to give 2.8 g of an oily product. The distillation of the product gave 14.5 g of (+)-nopinone (**12**): bp 76.5—77.5°C /7 mmHg, $[\alpha]_D^{25}$ +18.9° (neat), d_D^{25} 0.9786, n_D^{25} 1.4761; IR (liq.) 1713 cm^{-1} (C=O); UV (MeOH) 273 nm (ε 30.2),

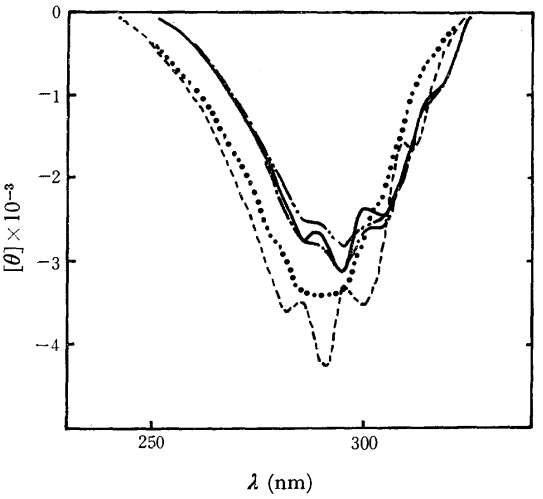

Fig. 9. CD curves of the ketone (**11**) in selected solvents at various temperatures: ——, —·—, and —··—, at −74, +20, and +138°C in decalin; ----- and ·····, at −192 and +25°C in EPA, respectively.

(isooctane) 286 nm (ε 18.9); ORD (*c* 1.3, MeOH) $[\phi]_{400}$ +150, $[\phi]_{301}$ +3440, $[\phi]_{262}$ −4140, $[\phi]_{220}$ −1800, (*c* 0.30, isooctane) $[\phi]_{400}$ +125, $[\phi]_{316}$ +1680, $[\phi]_{312}$ +1600, $[\phi]_{306}$ +1850, $[\phi]_{265}$ −2230, $[\phi]_{230}$ −1010; CD (*c* 1.3, MeOH) $[\theta]_{304}$ 0, $[\theta]_{283}$ +4390, $[\theta]_{235}$ 0, (*c* 30, isooctane) $[\theta]_{354}$ 0, $[\theta]_{292}$ +2220, $[\theta]_{284}$ 2150, $[\theta]_{233}$ 0; variable temp. CD (*c* 0.41, EPA) $[\theta]_{323}^{-192°}$ 0, $[\theta]_{289}$ −4500, $[\theta]_{238}$ 0, $[\theta]_{322}^{0°}$ 0, $[\theta]_{283}$ −4090, $[\theta]_{322}$ 0, (*c* 0.36, decalin) $[\theta]_{320}^{-74°}$ 0, $[\theta]_{292}$ +3150, $[\theta]_{288}$ +3000, $[\theta]_{285}$ +3300, $[\theta]_{250}$ 0, $[\theta]_{320}^{+25°}$ 0, $[\theta]_{290}$ +2710, $[\theta]_{250}$ 0, $[\theta]_{320}^{+140°}$ 0, $[\theta]_{321}$ +2560, $[\theta]_{250}$ 0.

(−)-2α-Bromo-10β-pinan-3-one (13).[28] *a) Preparation of 3-Acetoxy-pin-2-ene*: Following the method in the reference,[3] the treatment of (−)-10β-pinan-3-one (**1**) with acetic anhydride in the presence of perchloric acid afforded (−)-3-acetoxy-pin-2-ene in a 76% yield: $[\alpha]_D^{25}$ −35.0° (*c* 0.29, MeOH) (lit,[3] $[\alpha]_D^{25}$ +36° (*c* 1.00), derived from (+)-10β-pinan-3-one).

b) Preparation of Bromoketone 13: Bromine (0.94 g) dissolved in carbon tetrachloride (4 m*l*) was added to a stirred suspension of (−)-3-acetoxy-pin-2-ene (1.08 g) and anhydrous sodium carbonate (1.00 g) in carbon tetrachloride (5 m*l*) over a 5 min period at 0°C. After stirring for a further 5 min, the ether extract gave 1.13 g of an oily product, which was composed of 84% of the bromoketone (**13**): $[\alpha]_D^{25}$ −101.8° (*c* 1.18, MeOH); IR (liq.) 1722 cm^{-1} (C=O); UV (MeOH) 313 nm (ε 135.3); ORD (*c* 1.18, MeOH) $[\phi]_{400}$ −638, $[\phi]_{335}$ −1620, $[\phi]_{305}$ −1080, $[\phi]_{250}$ −3430, $[\phi]_{230}$ −1720, (*c* 0.24, isooctane) $[\phi]_{400}$ −692, $[\phi]_{349}$ −1800, $[\phi]_{302}$ −143, $[\phi]_{250}$ −2240, $[\phi]_{230}$ −1190; CD (*c* 1.18, MeOH) $[\theta]_{365}$ 0, $[\theta]_{317}$ −1000, $[\theta]_{293}$ −227, $[\theta]_{258}$ −1000, (*c* 0.24, isooctane) $[\theta]_{364}$ 0, $[\theta]_{318}$ −1700, $[\theta]_{285}$ −315.

(−)-4β-Hydroxy-10β-pinane (17) and Its Acetate (18). A solution of 1.0 g of (−)-10β-pinan-4-one (**11**) in 20 m*l* of ether was stirred into a suspension of 0.3 g of lithium aluminum hydride in 50 m*l* of ether. The mixture was then refluxed for 2 hr. The reaction mixture, after having been treated in the usual manner, afforded 1.0 g of **17**. The subsequent acetylation of **17** (100 mg) with acetic anhydride in pyridine gave the acetate (**18**) (95 mg).

a) 4β-Hydroxy-10β-pinane (17): Mp 72—73°C, $[\alpha]_D^{25}$ −5.1° (*c* 4.0, benzene); NMR (CCl_4) δ 1.22 (s, C_8-3H), 1.16, (s, C_9-3H), 1.07 (d, J=7.0 Hz, C_{10}-3H), and 4.22 ppm (m,

26) T. Hirata and T. Suga, *J. Org. Chem.*, **36**, 412 (1971).
27) T. Matsuura and K. Fujita, *J. Sci. Hiroshima Univ. Ser. A-II*, **16**, 173 (1952).
28) T. Hirata and T. Suga, This Bulletin, **44**, 2833 (1971).

C_4-H).

b) 4β-Acetoxy-10β-pinane (18): IR (liq.) 1745 cm^{-1} ($OCOCH_3$); NMR (CCl_4) δ 1.23 (s, C_8-3H), 1.11 (s, C_9-3H), 1.05 (d, J=7.0 Hz, C_{10}-3H), 1.91 (s, $OCOCH_3$), and 5.08 ppm (m, C_4-H).

(−)-3β-Hydroxy-10α-pinane (19) and Its Acetate (20). Into a stirred suspension of 120 mg of lithium aluminum hydride in 15 m*l* of ether, was added a solution of 950 mg of (−)-10α-pinan-3-one (**3**) in 15 m*l* of ether, and then the mixture was stirred for 1 hr at room temperature. After a usual treatment, the ether extract gave 590 mg of a crystalline product, which was subsequently chromatographed on a silica-gel column with a mixture of *n*-hexane and ethyl acetate to yield 50 mg of (+)-3α-hydroxy-10α-pinane (mp 26—27°C, $[\alpha]_D^{25}$ +15.8° (*c* 0.20, MeOH)) and 400 mg of (−)-3β-hydroxy-10α-pinane (**19**). The acetylation of **19** (100 mg) with acetic anhydride in pyridine gave the acetate (**20**) (92 mg)

a) 3β-Hydroxy-10α-pinane (19): Mp 66—67°C (lit,[29] mp 67°C), $[\alpha]_D^{25}$ −59.0° (*c* 0.40, MeOH); NMR (CCl_4) δ 1.21 (s, C_8-3H), 0.77 (s, C_9-3H), 0.93 (d, J=7.0 Hz, C_{10}-3H), and 3.99 ppm (t, J=6.5 Hz, C_3-H); 3,5-dinitrobenzoate, mp 118—119°C (lit,[30] mp 118—119°C).

b) 3β-Acetoxy-10α-pinane (20): IR (liq.) 1744 cm^{-1} ($OCOCH_3$); NMR (CCl_4) δ 1.21 (s, C_8-3H), 0.90 (s, C_9-3H), 0.97 (d, J=7.0 Hz, C_{10}-3H), 1.99 (s, $OCOCH_3$), and 4.66 ppm (m, C_3-H).

The author wishes to express his hearty gratitude to Dr. Takayuki Suga of Hiroshima University for his guidance and encouragement, and to Dr. E. von Rudloff for measuring the NMR spectra by a Varian Associates, HA-100, Spectrometer.

29) H. Schmidt, *Ber.*, **77**, 544 (1944).

30) T. Takemoto, G. Kusano, and H. Hikino, *Yakugaku Zasshi*, **86**, 1162 (1966).

BULLETIN OF THE CHEMICAL SOCIETY OF JAPAN, VOL. 45, 3464—3472 (1972)

Elektrochemische Untersuchungen über den Litheffekt

Tsuneo SUGA

Forschungslaboratorium der Konishiroku Photoindustrie AG., Sakura-machi, Hino, Tokio, 191

(Eingegangen am 18. April 1972)

Es wurde der Mechanismus des Litheffektes diskutiert. Um dieses Problem zu behandeln, wäre es nützlich, daß man sich den Litheffekt in Verbindung mit Lithemulsion und Lithentwickler überlegt. Nach Yule[1] beschleunigen die bei der Entwicklung entstandenen Oxydationsprodukte des Hydrochinons die Lithentwicklung. In der vorliegenden Arbeit wurde die Rolle der Oxydationsprodukte weiter vom Standpunkt der Oxydation aus elektrochemisch untersucht. Die Oxydationsprodukte beschleunigen die Entwicklung der stärker belichteten Körner durch die Herabsetzung des Ladungsbarriereeffektes und hemmen die Entwicklung der schwächer belichteten Körner durch die Oxydationsfähigkeit. Wenn diese beiden Faktoren miteinander ins Gleichgewicht gebracht werden, könnte man einen guten Litheffekt erhalten. Nach dieser Ansicht konnte man die Ursache für den guten Litheffekt einer Lithemulsion gut erklären.[2]

Der Lithentwickler, der oft als „Ansteckungsentwickler" bezeichnet wird, ist ein Hydrochinonentwickler, dessen Gehalt an Sulfit stark herabgesetzt ist. Wenn ein Lithfilm in diesem Entwickler behandelt wird, erhält man den Litheffekt, der eine ultraharte Gradation und eine steile Bildschärfe kennzeichnet.

Obwohl der Lithentwickler bis heute in der Reproduktionstechnik häufig verwendet worden ist, erschienen wenige Arbeiten darüber. Yule hat 1945 den Mechanismus der Lithentwicklung mitgeteilt und dieser Mechanismus ist bis heute von vielen Forschern wie Baines,[3] Vanreusel,[4] Wood,[5] Umberger,[6] Zwicky[7], und Frank[8] unterstützt worden. Nach der Meinung von Yule[1] beschleunigen die Oxydationsprodukte des Hydrochinons die Entwicklung der belichteten Körner. Wegen der niedrigen Konzentration von Sulfit bleiben die Oxydationsprodukte als Semichion oder Chinon, ohne sich durch Versetzen mit Sulfit zu Hydrochinonsulfonsäure zu verwandeln. Kürzlich ist die Entwicklungsaktivität des Semichinons bei der Lithentwicklung wieder von Eggers[9] und Zwicky[10] betont worden. Lu Valle[11,12] und Goldberg[12] diskutierten die Entwicklungsaktivität des Hydroxyhydrochinons. In alkalischer Lösung ist Chinon nicht beständig und geht durch die sogenannte Hydratationenolisation in Hydroxyhydrochinon über. James[13] zeigte die superadditive Aktivität der Reaktionsprodukte von Aminogruppen der Gelatine mit Chinon und deutete die oxydative Wirkung des entstehenden Chinons an. Auf Grund unserer Meinungen ist die

1) J. A. C. Yule, *J. Franklin Inst.*, **239**, 221 (1945).
2) T. Suga, *Int. Cong. Photogr. Sci. Moscow*, CD-76 (1970).
3) H. Baines, *Process Engraver Monthly*, **61**, 331 (1954).
4) G. Vanreusel und R. Verbrugghe, *Int. Kong. Reprogr. Köln*, s. 91 (1963).
5) H. W. Wood, *J. Photogr. Sci.*, **12**, 5 (1964).
6) J. Q. Umberger, *Photogr. Sci. Eng.*, **10**, 8 (1966).
7) H. Zwicky, *Photogr. Korresp.*, **102**, 11 (1966).
8) K. Frank, *Int. Cong. Photogr. Sci. Tokyo*, Sec. 3 (1967).
9) J. Eggers, *Photogr. Sci. Eng.*, **15**, 128 (1971).
10) H. Zwicky, *Photogr. Korresp.*, **107**, 151 (1971).
11) J. E. Lu Valle, *Photogr. Eng.*, **5**, 73 (1958).
12) J. E. Lu Valle und G. M. Goldberg, *J. Photogr. Sci.*, **6**, 176 (1958).
13) T. H. James, *Photogr. Sci. Eng.*, **12**, 67 (1968).

oxydative Wirkung des Chinons von großer Wichtigkeit. In einer neueren Arbeit hat Zwicky[10] aber keinen Oxydationseffekt bei der Lithentwicklung vertreten.

Da es nötig ist, daß der Litheffekt mit Lithemulsion und Lithentwickler in Zusammenhang steht, ist es ratsam, auf Grund der photographischen Eigenschaften von Emulsion über den Mechanismus der Lithentwicklung zu diskutieren. Soweit wir bisher festgestellt haben, erschienen aber solche Arbeiten selten. In der Zusammenfassung unserer Arbeiten[2,14-20] ist eine weitere Überlegung für den Litheffekt durch Einführen des Begriffes „Oxydation" wie folgt erlangt worden.

Experimentelles

Entwicklung und Sensitometrie. Die hinter einem Graukeil in einem Sensitometer vom Typ Konishiroku KS-7 belichteten Filmstreifen wurden im Entwickler bei 20°C behandelt. Der verwendete Lithentwickler[14,18] war ein normaler formaldehydbisulfithaltiger Hydrochinonentwickler. Dem Versuchsziel entsprechend wurde Natriumsulfit zugesetzt. Nach der Schwärzungsmessung trug man den Logarithmus der relativen Belichtungswerte (log rel. E) auf die Abszisse und die Schwärzungswerte (S) auf die Ordinate auf, um die sogenannte Schwärzungskurve zu erhalten. Die Bestimmung der Empfindlichkeit wurde aus der notwendigen Lichtmenge für eine Schwärzung von 1,0 durchgeführt.

Lithfilm. Der orthochromatische Lithfilm von Konishiroku Photoindustrie AG.

Emulsion. Benutzte Emulsionen wurden durch Doppeleinlauf hergestellt.[15] Als Lithemulsion diente eine Chlorbromsilberemulsion, deren Gehalt an AgBr 30 Mol % war. Die mit Inertgelatine hergestellten Emulsionen wurden mit verschiedenen Sensibilisatoren nachgereift. Die Zusatzmengen der Sensibilisatoren pro 1 Mol AgX waren $3{,}4\times10^{-5}$ Mol $Na_2S_2O_3$ für Schwefelsensibilisierung, 1×10^{-5} Mol $HAuCl_4$ für Goldsensibilisierung, und $3{,}4\times10^{-5}$ Mol $Na_2S_2O_3$ plus 1×10^{-5} Mol $HAuCl_4$ für Schwefelgoldsensibilisierung. Die nachgereiften Emulsionen wurden auf Unterlage gegossen und getrocknet.

Bleicher. Das Bleichen des latenten Bildes und des Makrosilbers wurde in 0,12%iger Chinonlösung bei 20°C durchgeführt.[18] Ihr pH-Wert wurde durch Metaborat kontrolliert.

Redoxpuffer. Das Redoxpotential des latenten Bildes wurde nach der Reinders'schen Methode gemessen. Als Redoxpuffer[18] wurden Fe^{3+}/Fe^{2+}-Lösungen [0,25 Mol $FeSO_4$-$(NH_4)_2SO_4 6H_2O/l$ plus 0,25 Mol $Fe_2(SO_4)_3(NH_4)_2SO_4 24H_2O$ /*l*] benutzt, deren Potential mit Natriumzitrat eingestellt war. Die Messung des Redoxpotentials wurde gegen eine gesättigte Kalomelelektrode durchgeführt. Alle Potentialzahlenwerte in dieser Arbeit sind aber auf die Normalwasserstoffelektrode bezogen.

Versuchsergebnisse

1. Litheffekt. Ein guter Litheffekt für die 2,5 Min. lithentwickelte schwefelsensibilisierte AgCl/Br-Emulsion ist in Abb. 1a dargestellt. Er ging aber in Anwesenheit des Sulfites verloren, so daß die Schwärzungskurve eine wesentlich weiche Gradation mit einer vorgerückten Schwelle hatte.

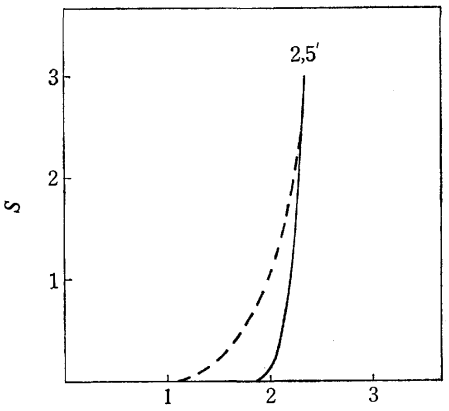

Abb. 1. (a) Schwärzungskurven der AgCl/Br-Lithemulsion, entwickelt in 2,5 Min.
—— Lithentwickler
—— Lithentwickler + 60 g Na_2SO_3/l

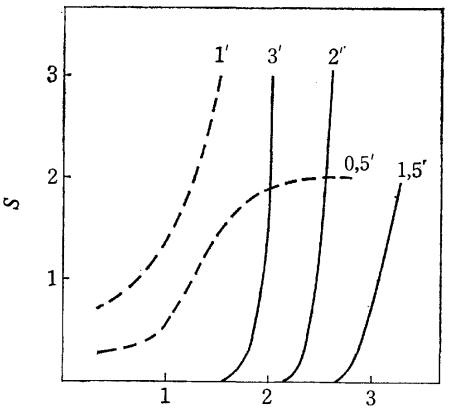

(b) Zeitlicher Entwicklungsablauf der Lithemulsion.
—— Lithentwickler
---- Lithentwickler ohne Bromid
Die Zahlen an den Kurven geben die Entwicklungszeit in Minuten.

In Abb. 1b[14] rückten die Schwärzungskurven mit der fortschreitenden Lithentwicklungszeit vor, indem sie den Litheffekt zeigten. Ohne Bromid war der Litheffekt auch bei kürzerer Entwicklungszeit ganz verloren.

Substanzen,[2] die mit Ag^+-Ionen schwerlösliche Salze bilden, wurden in einer Hydrochinon-Alkali-Lösung zugesetzt. Wie aus Tabelle 1 ersichtlich ist, sind Br^--

Tabelle 1. Einfluß von Zusätzen (0, 0168 Mol/*l*) auf den Litheffekt

Originallösung (1*l*)	Zusatz	Litheffekt
60 g $HCHONaHSO_3$	KBr	groß
18 g Hydrochinon	NaBr	groß
	KSCN	klein
42 g Na_2CO_3	NaCl	ohne
	Na_3PO_4	ohne

14) T. Suga, *Nippon Shashin Gakkai Kaishi*, **32**, 87 (1969).
15) T. Suga, *ibid.*, **32**, 138 (1969).
16) T. Suga, *ibid.*, **32**, 216 (1969).
17) T. Suga, T. Shibata, und K. Nakamura, *ibid.*, **32**, 263 (1970).
18) T. Suga, *Bull. Soc. Sci. Photogr. Jap.*, **19**, 32 (1969).
19) T. Suga, *Nippon Insatsu Gakkai Ronbunshu*, **7**, 111 (1964).
20) T. Suga und Y. Kuroda, *ibid.*, **10**, 80 (1968).

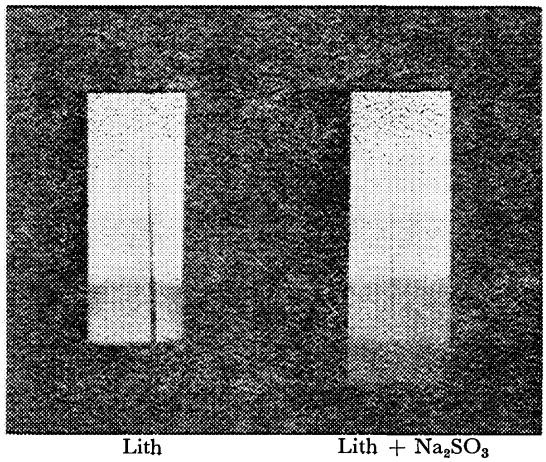

Abb. 2. Bildausbreitung der mit 0,1%iger $AgNO_3$-Lösung gezogenen Linien.
links: Lithentwickler
rechts: Lithentwickler + 60 g Na_2SO_3/l

Ionen für den Litheffekt sehr wichtig. SCN^--Ionen geben einen kleinen Litheffekt und die anderen Ionen scheinen eine geringe Rolle für den Litheffekt zu spielen.

2. *Bildausbreitung in der Lithentwicklung.*[16] Auf zwei mit Graukeil belichteten Filmschichten wurden Linien mit Feder und 0,1% iger $AgNO_3$-Lösung gezogen. Nach dem Trocknen wurden die eine mit dem Lithentwickler und die andere mit dem sulfithaltigen Entwickler 2,5 Min. behandelt. Bei der Lithentwicklung konnte man in Abb. 2 eine auffällige Bildausbreitung wahrnehmen. Mit der Schwärzungszunahme des Hintergrundes wurde die Linienbreite vergrößert, während keine Ausbreitung im Beisein des Sulfites stattfand.

Sobald eine AgCl-Emulsion unter geschmolzten Umständen dem Entwickler zugefügt wurde, schwärzte sie sich. Eine Minute nach der Emulsionszufügung wurden die belichteten Filmstreifen in den Entwickler getaucht. 1 Liter Entwickler enthielten 0,03 Mol AgCl und 9 g Gelatine. Zum Kontrolle-Entwickler wurden nur 9 g Gelatine addiert. Die zur Versuche gebrauchten Entwickler waren folgende. 1) Lithentwickler 2) Lithentwickler plus 120 g Na_2SO_3/l 3) Lithentwickler ohne KBr. In Abb. 3 ist der Verlauf der Empfindlichkeit als Funktion der Entwicklungszeit in drei Entwicklern dargestellt. Durch Zusatz von AgCl-Emulsion wurde eine nennenswerte Empfindlichkeitssteigerung im Fall des Lithentwicklers, fast keine im Fall der Anwesenheit von 120 g Sulfit/l erwiesen. Bei der Entwicklung ohne Bromid wirkte die Emulsionszufügung umgekehrt ein. Wie in Abb. 3 gezeigt, setzte sich die Empfindlichkeit herab.

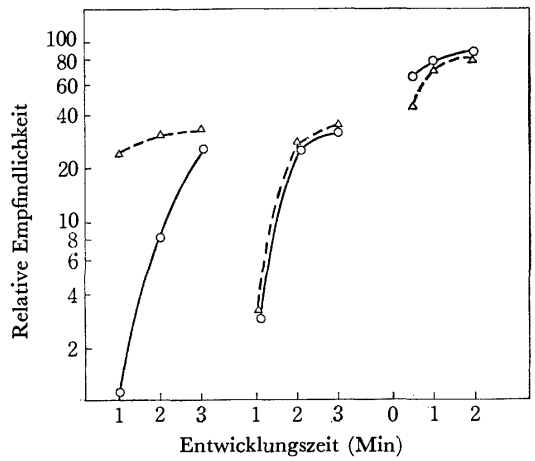

Abb. 3. Einfluß der AgCl-Emulsion zugefügten Entwickler (----) auf den Empfindlichkeitsverlauf im Vergleich zum Kontrolle-Entwickler (——).
links: Lithentwickler
mitten: Lithentwickler mit 120 g Na_2SO_3/l
rechts: Lithentwickler ohne KBr

3. *Oxydierbarkeit des Chinons.* Chinon wirkt oxydativ ein. Hier wurde die oxydative Wirkung desselben auf das Makrosilber[14] und das Mikrosilber des latenten Bildes[15,18] untersucht. Die entwickeltes Silberteilchen enthaltenen Filmstreifen wurden in Chinonlösungen (pH 3,6) getaucht. Nach Fixieren wurden die Schwärzungswerte gemessen. Das Silberteilchen in Filmstreifen wurde durch Chinon nicht oxydiert. Bei der Anwesenheit von Cl^--, SCN^--, und Br^--Ionen wurde Schwärzungsabnahme in dieser Reihenfolge

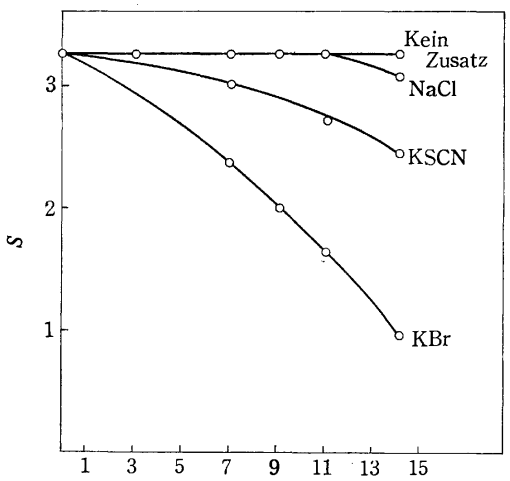

Abb. 4. Abhängigkeit der Zusätze (0.0168 Mol/l) von der Oxydation des Makrosilbers mit Chinonlösung (pH 3,6).

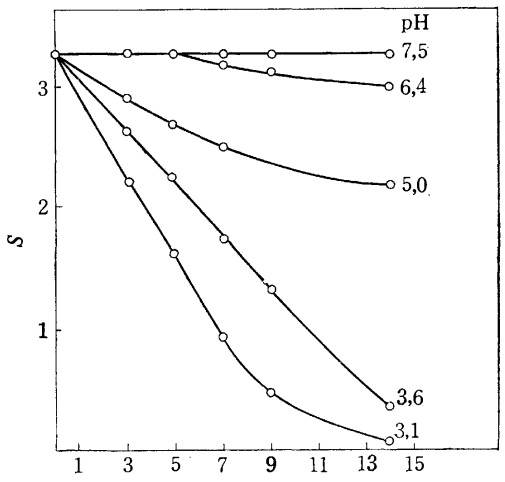

Abb. 5. Einfluß des pH-Wertes von Chinonlösungen auf die Oxydation des Makrosilbers.

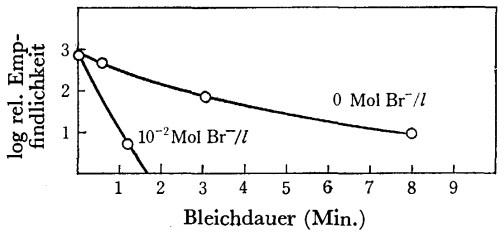

Abb. 6. Oxydierbarkeit des latenten Bildes der Lithemulsion als Funktion der Chinonbleichdauer.

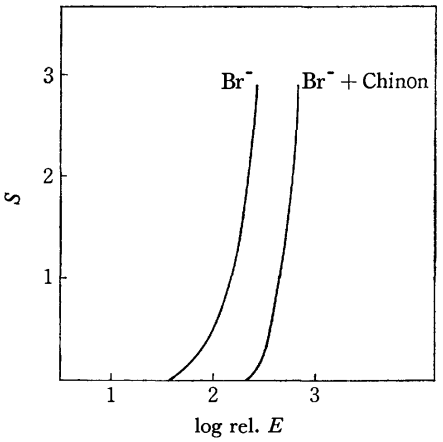

Abb. 7. Einfluß der Vorbehandlung in Chinonlösung (pH 3,6) auf den Typ der Schwärzungskurve von Lithemulsion.
30 Sek. vorbehandelt in Br⁻-Lösung (0,1 g KBr/*l*), dann 3 Min. lithentwicklt.
30 Sek. vorbehandelt in Chinon-Lösung (0,1 g KBr/*l* + 0,4 g Chinon/*l*), dann 3 Min. lithentwickelt.

größer. (Abb. 4) Der Einfluß des pH-Wertes von Chinonlösung auf die Oxydation des Silbers wurde in Abb. 5 dargestellt. Je niedriger der pH-Wert war, desto größer wurde die Schwärzungsabnahme.

Wenn man die belichteten Filmstreifen vor der Lithentwicklung in Chinonlösung behandelte, besonders im Beisein der Br⁻-Ionen, fand die Oxydation der latenten Bildkeime statt. (Abb. 6) Aus Schwärzungskurven in Abb. 7 kann man ersehen, daß eine größere Desensibilisierung und eine steilere Gradation durch Vorbehandlung mit Chinon-Br⁻-Bad im Vergleich mit Br⁻-Bad erzielt wurden. Durch Vorbehandlung in Chinonlösungen, deren pH-Werte variiert waren, konnte man, wie in Abb. 8 gezeigt, die Empfindlichkeitsabnahme unter pH-Wert von 7, die Empfindlichkeitssteigerung über pH-Wert von 7 beobachten.

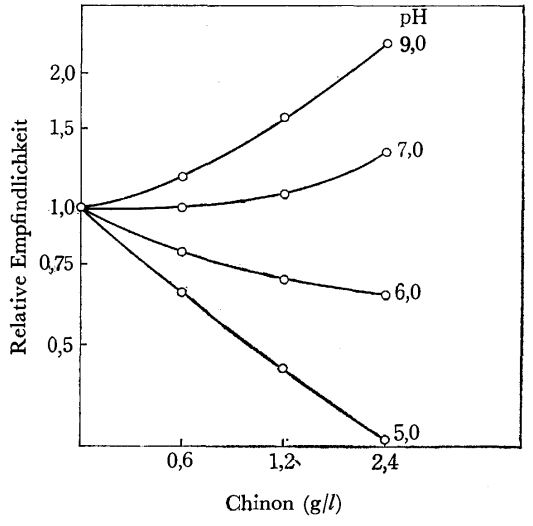

Abb. 8. Einfluß des pH-Wertes und Chinonkonzentration von Vorbehandlungsbad auf die Empfindlichkeit der Emulsion.

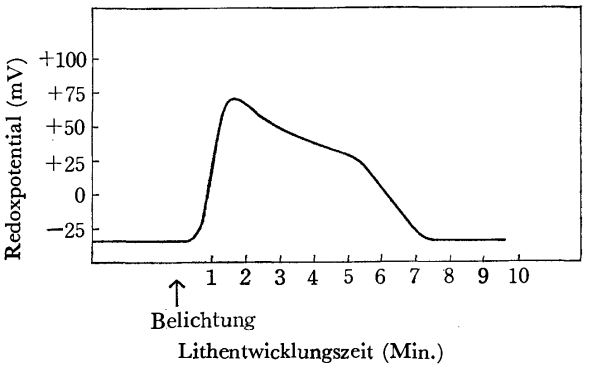

Abb. 9. Redoxpotentialänderung an der Unterseite der Emulsionschichten während der Lithentwicklung.

4. Redoxpotentialänderung während der Entwicklung. Die Redoxpotentialänderung in der Emulsionschicht wurde in Abhängigkeit von der Entwicklungszeit geprüft.[18] Die mit Thiosulfat gereifte Emulsion wurde auf die Oberfläche der Platinelektrode aufgetragen und bis zum Erstarren gekühlt. Die beschichtete Pt-Elektrode wurde im Lithentwickler getaucht, dann mit einer Birne bestrahlt. Die Potentialänderung wurde gegen eine gesättigte Kalomelelektrode gemessen. (Abb. 9) Bei einigen Versuchen lagen die Redoxpotentialsverschiebungen zwischen 80 und 100 mV. Die Redoxpotentialänderung an der Oberfläche des entwickelnden Lithfilms und dieselbe im Entwickler an der von der Emulsionsoberfläche den Abstand von 1 mm entfernten Stelle werden in Tabelle 2 beschrieben. Bei der Lithentwicklung war die Potentialänderung an der Oberfläche so groß wie die in der Emulsionschicht. Man konnte aber keine Potentialänderung im Lithentwickler, auch an der dem Film nahen Stelle finden. Sulfit verschob die Potentialänderung nach kleineren Werten, und diese kleine Potentialänderung wurde auch im Entwickler an der Filmschicht nahen Stelle deutlich bemerkt.

Tabelle 2. Redoxpotentialänderung im Entwickler auf und über den entwickelnden Lithemulsionschichten

Entwickler	auf der Emulsionschicht	1 mm über der Emulsionschicht
Lithentwickler	130 mV	0 mV
Lithentwickler + 60 g Na_2SO_3/*l*	40 mV	35 mV

5. Redoxpotential des latenten Bildes.[18] Die belichteten Filmstreifen wurde in Fe^{3+}/Fe^{2+}-Redoxlösungen 6 Stunden gebadet. Die zur Ausbildung eines stationären Zustandes benötigte Dauer waren 6 Stunden, wie sie auch Hillson[21] im Fall der AgCl-Emulsion gezeigt hat. Die Streifen wurden nachher mit 1% iger ÄDTE-

21) P. J. Hillson, *J. Photogr. Sci.*, **6**, 97 (1958).

Tabelle 3. Redoxpotential des latenten Bildes von verschiedenen Emulsionen

Sensibilisator	Cl^--Konzentration in Redoxlösung (Mol/*l*)	das Redoxpotential des latenten Bildes (mV)	
		AgCl/Br-Em.	AgCl-Em.
ohne Zusatz	0	240	320
	10^{-2}	180	200
$Na_2S_2O_3$	0	240	320
	10^{-2}	180	200
$HAuCl_4$	0	310	
	10^{-2}	240	
$Na_2S_2O_3+HAuCl_4$	0	320	
	10^{-2}	250	

Lösung zur Maskierung der Eisenionen gewaschen und dann entwickelt. Aus den Versuchsergebnissen wurde das kritische Potential, bei dem die Oxydation des latenten Bildes beginnt, im Vergleich mit Nullprobe in Tabelle 3 ermittelt.

6. Saumeffekt in der Lithentwicklung. An scharfen Grenzen zweier Bildfläche verschiedener Schwärzung tritt der Saumeffekt auf, der die Schwärzung am Rand der schwächer belichteten Fläche durch Diffusion von entwicklungshemmenden Reaktionsprodukten erniedrigt. Hier wurde der Saumeffekt des Lithfilms untersucht. Man belichtete den zuerst im Streulicht gelegenen Lithfilm wieder mit einer scharfen Kante. Der Schwärzungsverlauf beim Übergang von hohen zu niedrigen Schwärzungswerten wurde mit Hilfe des Mikrodensitometers durch unsere frühere Methode[20] in Abb. 10 registriert. Die Streulichtmengen wurden

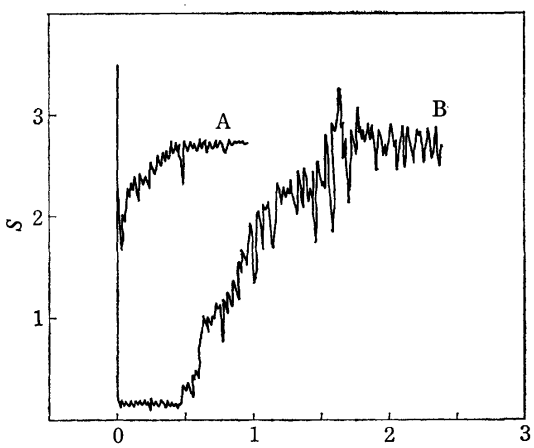

Abstand von der Grenze einer Kante (mm)

Abb. 10. Saumeffekt einer Lithemulsion an der scharfen Grenze zweier Flächen verschiedener Schwärzung.
Kurve A: stärker belichtet, 1,25 Min. entwickelt.
Kurve B: schwächer belichtet, 2,5 Min. entwickelt.

so kontrolliert, daß die Schwärzung Werten von 2,7 erreicht. Daher waren die Lichtmengen für Kurve A höher als für Kurve B. Der Saumeffekt für Kurve B (2,5 Min. entwickelt) war groß, während derselbe für Kurve A (1,25 Min. entwicklt) klein war. Durch Zusatz des Sulfites wurde der Saumeffekt stark verabsetzt.

7. Oxydierbarkeit, Entwickelbarkeit und Litheffekt der verschiedenen Emulsionen. Die Oxydierbarkeit des latenten Bildes der schwefelsensibilisierten AgCl-, AgCl/Br-, und AgBr-Emulsion[15] und der schwefel-, gold- und goldschwefel-sensibilisierten AgCl/Br-Emulsion[18] ist in Abb. 11 gegeben. Man behandelte die belichteten

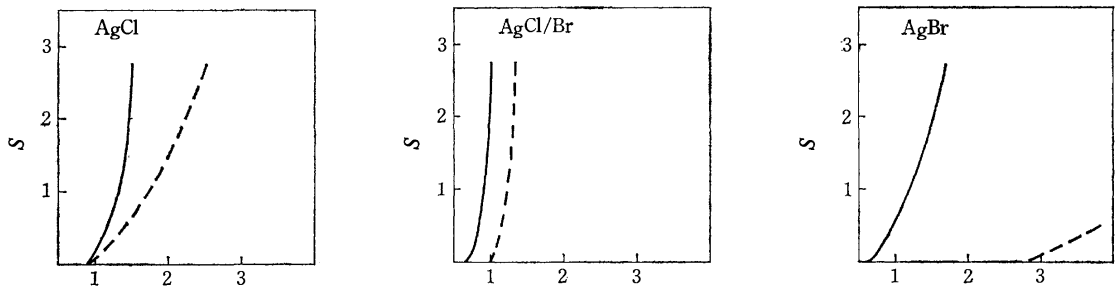

(a) Schwefelsensibilisierte AgCl-, AgCl/Br- und AgBr-Emulsion, 30 Sek. vorbehandelt mit Chinon (pH 5) dann lithentwickelt.

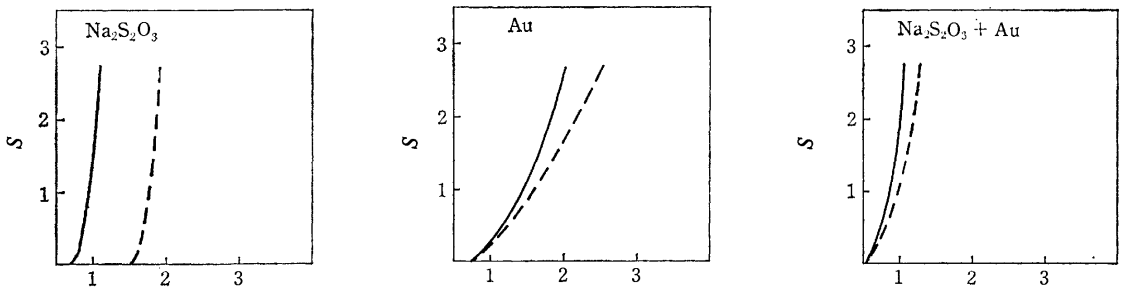

(b) AgCl/Br-Emulsion, die mit $Na_2S_2O_3$, $HAuCl_4$ und ($Na_2S_2O_3$ + $HAuCl_4$) gereift, 3 Min. vorbehandelt mit Chinon (pH 5), dann lithentwickelt.

Abb. 11. Oxydierbarkeit des latenten Bildes mit Chinonlösung (----) im Vergleich zu Originalkurven (——).

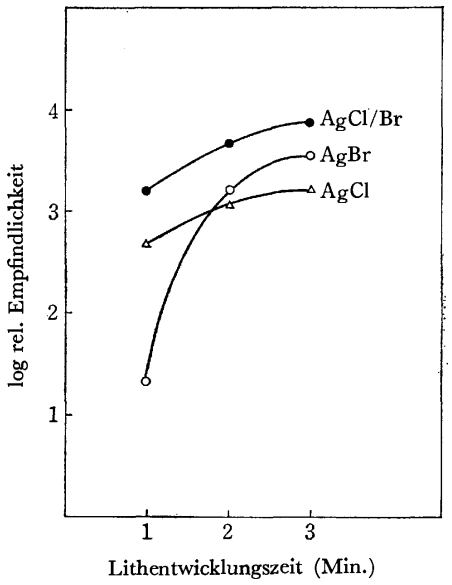

(a) Schwefelsensibilisierte AgCl-, AgCl/Br- und AgBr-Emulsion.

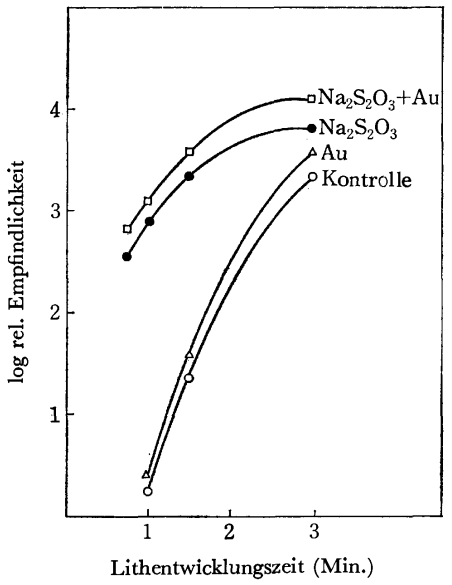

(b) AgCl/Br-Emulsionen, die mit $Na_2S_2O_3$, $HAuCl_4$ und ($Na_2S_2O_3$ + $HAuCl_4$) gereift wurden.

Abb. 12. Verlauf der Empfindlichkeit verschiedener Emulsionen als Funktion der Lithentwicklungszeit.

Filmstreifen vor der Entwicklung mit Chinonlösung, die 0,1 g KBr und 0,4 g Chinon pro Liter bei pH 5 behielt. Als Kontrolle diente KBr-Bad ohne Chinon. Unter den versuchten Emulsionen verschoben sich die Schwärzungskurven der AgCl/Br-Emulsion, besonders der schwefelsensibilisierten, durch Chinon parallel zu der Originalkurve. Die Gradation blieb trotz des Bleichens ungefähr konstant. Dies zeigt, daß die latenten Bildkeime dieser Emulsionen im Gebiet der schwächeren Belichtungen durch Chinon und Br^--Ionen leicht oxydiert sind, dagegen dieselben der anderen Emulsionen etwas schwieriger oxydiert sind.

Der Verlauf der Empfindlichkeitszunahme der oben genannten Emulsionen[15,17] in Abhängigkeit von der Entwicklungszeit ist in Abb. 12 gegeben. Unter diesen Emulsionen hatten die schwefelgereifte AgCl-, die schwefelgereifte AgCl/Br- und die goldschwefelgereifte AgCl/Br-Emulsion hohe Entwickelbarkeit an stärker belichteten Körnern durch Hydrochinon. Die gleiche Tendenz wie die in Abb. 12 gezeigt, wurde auch vom sulfithaltigen Hydrochinonentwickler erhalten.

Die schwefelsensibilisierte AgCl/Br-Emulsion zeigte einen guten Litheffekt, während man bei der AgCl-Emulsion etwas verringerten, bei der AgBr-Emulsion fast keinen Litheffekt fand.

Diskussion

Hydrochinon wird bei der Lithentwicklung ohne Sulfit über die radikalische Zwischenstufe des Semichinons in das Chinon verwandelt. Aus Hydrochinon und Chinon läßt sich Semichinon bilden. In der Lithentwicklung entstehen als erste Stufe die Oxydationsprodukte des Hydrochinons wie Semichinon und Chinon. Wegen der niedrigen Konzentration des Sulfites sammeln sich diese in der Gelatineschicht. In alkalischer Lösung geht Chinon durch Disproportionierung in Hydrochinon und Hydroxyhydrochinon über.[11,12] Nach Meinungen von Eigen und Matthies[22] liegt die Reaktionsgeschwindigkeitskonstante der Hydroxychinonbildung aus Chinon in alkalischer Lösung viel niedriger als die Bildungsgeschwindigkeit des Semichinons aus Hydrochinon und Chinon. Daher könnten die enolisierten Hydratationsprodukte des Chinons bei der Lithentwicklung eine kleine Rolle spielen. Nach Yule[1] verursachen die Oxydationsprodukte des Hydrochinons die Ansteckungsentwicklung, indem sie die Entwicklung benachbarter wenig belichteten Körner beschleunigen. Die Resultate in Abbildungen 2 und 3 beweisen die beschleunigende Wirkung der Oxydationsprodukte. Die Bildausbreitung in Abb. 2, mit anderen Worten, die ansteckende Schwärzungszunahme läßt sich wahrscheinlich von den Oxydationsprodukten ableiten. In der Gegenwart von Sulfit, welches diese Oxydationsprodukte unter Bildung von Hydrochinonsulfonsäure beiseite bringt, kann man wohl die auffallende Bildausbreitung in Abb. 2 und das Entwicklungsbeschleunigen in Abb. 3 nicht mehr beobachten. Das dem Entwickler zugefügte Chinon zeigte keine so große Beschleunigung wie die AgCl-Emulsion. Daher wirkt wahrscheinlich der naszierende Zustand der Oxydationsprodukte stärker ein. Dagegen wirkten die durch AgCl-Emulsion[16] entstandenen Oxydationsprodukte bei der Lithentwicklung ohne Bromid weniger beschleunigend als hemmend ein. Dies wird wohl von der James'schen Ladungsbarrieretheorie[23] wie folgt erklärt. Die sich um die Körner bildende Ladungsbarriere von Br^--Ionen überwindet das Herantreten der negativ geladenen Hydrochinonionen zu den Körnern, so daß sich die Entwicklungsgeschwindigkeit verringert. Nach Brauer und Staude[24] wird Chinon an belichtete Körner adsorbiert, das seinerseits imstande ist, zwei Moleküle Hydrochinon pro ein Molekül Chinon zu adsorbieren. Die Rolle der Oxydationsprodukte

22) M. Eigen und P. Matthies, *Chem. Ber.*, **94**, 3309 (1969).
23) T. H. James, *J. Phy. Chem.*, **43**, 701 (1939).
24) E. Brauer und H. Staude, *Z. Elektrochem.*, **58**, 129 (1954).

als der Entwicklungsbeschleuniger ist wohl dadurch erklärt, daß sie den durch die Ladungsbarriere hervorgerufenen Effekt verringern, um die Elektronenübertragung vom herantretenden Hydrochinon auf den Entwicklungskeim zu erleichtern. Hydrochinon ist vermutlich das stärkere Reduktionsmittel als Semichinon, so daß die Entwicklung ohne Bromid durch die entstandenen Oxydationsprodukte wie Abb. 3 gehemmt wird.

Die bisherigen Vorstellungen über die Lithentwicklung sind zwar passend für die Erklärung der oben angegebenen Resultate, aber können nicht genug beweisen, warum der Litheffekt bei der Entwicklung ohne Bromid nicht gewahr wurde. Dies zeigt, daß man weiterer Vorstellungen über die Lithentwicklung bedarf. Hierbei kann es als angemessen betrachtet werden, die Oxydation durch Chinon und deren Einfluß auf die Lithentwicklung zu bemerken.

Das Silberpotential ist wie Gleichung (1) beschrieben, wobei das Normalpotential des Silbers E°_{Ag} den Wert von 808 mV hat.

$$E_{Ag} = E^{0}_{Ag} + (RT/F) \ln [Ag^{+}] \quad (1)$$

Die in dieser Arbeit benutzte Chinonlösung hatte bei pH-Wert von 3,6 das Redoxpotential 526 mV. Unter diesen Bedingungen kann das Makrosilber durch Chinonlösung nicht oxydiert werden. Zusätze von NaCl, KSCN, und KBr zur Chinonlösung setzen den E_{Ag}-Wert herunter. Man rechnet die Silberpotentiale gemäß der Gleichung (1) mit Löslichkeitsprodukt in der oben angegebenen Reihenfolge als 333 mV, 208 mV, und 184 mV. Alle diese Werte zeigen eine elektrochemische Möglichkeit, das Makrosilber zu oxydieren, was in Abb. 4 verwirklicht ist. Das Redoxpotential der Chinonlösung beschreibt man gemäß der Gleichung (2).

$$E_{Q} = E^{0}_{Q} + (RT/2F) \ln ([Q][H^{+}]^{2}/[HQ]) \quad (2)$$

wo das Normalpotential E°_{Q} den Wert von 696 mV hat, und [ ] die Aktivität jeder Substanzen bedeutet. Die Potentialdifferenz zwischen E_{Ag} und E_{Q} ist eine treibende Kraft der Oxydation des Silbers. Die Ergebnisse in Abb. 4 entsprechen der Größe der Potentialdifferenz. Wie in Abb. 6 gezeigt, wurde dagegen das Mikrosilber des latenten Bildes durch Chinon oxydiert. Als Gründe kann man hier zwei Vorstellungen bezeichnen.

1. Nach der Thomson-Ostwald'schen Formel hat das Mikrosilber des latenten Bildes die größere Löslichkeit im Vergleich zum massiven Silber.

2. Die aus Silberhalogenidkristalle aufgelösten Halogenionen verschieben das Silberpotential des latenten Bildes zur negativeren Werten.

Beim Versuch der Abb. 4 konnte man eine erhebliche Schwärzungserniedrigung des Makrosilbers auch durch die mit AgCl gesättigte Chinonlösung nicht beobachten. Daher könnte der erste Grund eine Hauptrolle spielen.

Vorbehandlung mit der bromidhaltigen Chinonlösung gab die erhebliche Desensibilisierung, besonders am Fuß der Schwärzungskurve. (Abb. 7) Gleichung (2) beschreibt, daß die Oxydationskraft der Chinonlösung mit steigender Konzentration des Chinons und der H^{+}-Ionen stärker wird. Mit diesen Verhältnissen kann man die Abhängigkeit des pH-Wertes und der Chinonkonzentration auf das Bleichen des Silbers erklären. (Abb. 5 und 8) Bei den Vorbehandlungen mit Chinon im pH-Bereich über 7 wurde das Empfindlichkeitssteigen beobachtet. Beim höheren pH-Bereich wird sich die Oxydationskraft des Chinons verringern und geht Chinon ins Reduktionsmittel über, so daß dieses Mittel das latente Bild wahrscheinlich verstärkt. Dieses Resultat stimmt mit dem von Zwicky[10] überein, in dem der mit Lithentwickler vorbehandelte Lithfilm bei der nachfolgenden Entwicklung mit der phenidonhaltigen Hydrochinonlösung eine höhere Schwärzung zeigte. Daraus kommt ein Schluß, daß kein Oxydationseffekt bei der Lithentwicklung erfolgt. Es könnte aber schwer sein, die Oxydationskraft bei der Lithentwicklung nur mit der nachfolgenden anderen Entwicklung sichtbar nachzuweisen.

Das Redoxpotential der Hydrochinonlösungen wird, wie in Abb. 9 gezeigt, durch die Entstehung der Oxydationsprodukte und der H^{+}-Ionen, durch die Konzentrationsabnahme des Hydrochinons, nach positiveren Werten verschoben. Die Potentialänderungen der auf Pt-Elektrode beschichteten nassen Lithemulsion lagen während der Lithentwicklung zwischen 80 mV und 100 mV. Als man die Pt-Elektrode auf dem entwickelnden Lithfilm kontakt setzte, zeigten die Potentialverschiebungen noch größere Werte. Dies wird wohl auf den Unterschied der Quellung der zwei Emulsionschichten zurückgeführt. Die Potentialsteigerung konnte man in der Lithentwicklerlösung an der Stelle gar nicht finden, die nur 1 mm von der entwickelnden Emulsionschicht entfernt ist. Wie aus Tabelle 2 ersehen ist, setzte Sulfit die Potentialänderung auf der Emulsionschicht stark herab, während man in diesem Fall die gleiche Potentialänderung im Entwickler über der Schicht bemerkte. Das kommt wahrscheinlich auf die Oxydationsprodukte an, die, bei Anwesenheit des Sulfites leicht, bei Abwesenheit desselben schwer, aus der Schicht herausdiffundieren. Nach Meinungen von Frieser und Eger[25] können die Oxydationsprodukte im Fall des Bisulfitgehaltes auf weniger als 2 g pro Liter nicht leicht aus der Schicht herausdiffundieren und mit der Gelatine der Schicht zur Vernetzung reagieren.

Das gemessene Redoxpotential des latenten Bildes ist ein kritisches Potential, bei dem die Entwicklungsgeschwindigkeit Null ist und dann die Oxydation beginnt. Nach den Vorstellungen von Reinders,[26] Hillson[21], und Frei[27] ist das kritische Potential mit dem makroskopischen Silber-Gleichgewichtspotential nicht identisch, vielmehr liegt es um 100 mV bis 200 mV negativer. Matejec, Moisar[28] und Schmidt[29] zeigten, daß das Redoxpotential des latenten Bildes demselben des Makrosilbers nahe liegt. Nach Matejec und Moisar[28] treten Störungen in Messungen durch Fe^{3+}/Fe^{2+}-Lösungen auf, wird das Redoxpotential der verwendeten Fe^{3+}/Fe^{2+}-Lösungen durch Zugabe des Zitrates variiert, und verschieben die mit Silberhalogenid nicht

25) H. Frieser und H. Eger, *Photogr. Korresp.*, **104**, 61 (1968).
26) W. Reinders, *J. Phys. Chem.*, **38**, 783 (1934).
27) E. A. Frei, *Photogr. Korresp.*, **105**, 5 (1969).
28) R. Matejec und E. Moisar, *Photogr. Korresp.*, **100**, 39 (1964).
29) I. Schmidt, *Z. Wiss. Photogr., Photophys. Photochem.*, **60**, 1 (1967).

gesättigten Lösungen die gemessenen Werte zu negativeren Werten. Unserer Messung nach war die Verschiebung des Silberpotentials der mit AgCl gesättigten Lösung durch Zusatz von 1,5 bis 4,0 Mol Zitrat/l um 57 mV und in Gegenwart von 10^{-2} Mol NaCl/l nur um 7 mV. Mit diesen Werten wurde das gemessene Potential korrigiert. Das gemessene Redoxpotential der AgCl-Emulsion war 320 mV. Deshalb sind die korrigierte Werte 377 mV bei 0 Mol Cl^-/l, und 207 mV bei 10^{-2} Mol Cl^-/l. Diese Werte liegen um 136 mV bei 0 Mol Cl^-/l, um 137 mV bei 10^{-2} Mol Cl^-/l negativer als das aus der Thermodynamik berechnete Potential des Makrosilbers. Das Redoxpotential der AgCl/Br-Emulsion lag negativer als das der AgCl-Emulsion. Bei der Anwesenheit von Br^--Ionen würde es noch negativer liegen. Die exakte Messung ist schwer wegen der Konvertierung von AgCl durch Br^--Ionen. Das makroskopische Silberpotential bei 0,025 Mol Br^-/l liegt rechnerisch bei 172 mV. Unter Annahme der Erniedrigung um 140 mV im Fall des latenten Bildes würde der oxydative Abbau des latenten Bildes von AgCl/Br-Emulsion in der Nähe des Wertes von 30 mV beginnen. Eine merkliche Redoxpotentialsteigerung konnte man in der entwickelnden Schicht finden. Schließlich lag das Redoxpotential in der Schicht während der Lithentwicklung bei 60 mV oder über 60 mV. Auf Grund thermodynamischer Überlegungen könnte man unter diesen Bedingungen eine Oxydation der latenten Bildkeime durch die bei der Lithentwicklung entstandenen Oxydationsprodukte erwarten. Das Redoxpotential des latenten Bildes ist ein in reversiblen Systemen gemessenes Gleichgewichtspotential. Die chemische Entwicklung und der Abbau des latenten Bildes sind irreversibel, dabei spielt nicht der Gleichgewichtszustand, sondern die Reaktionsgeschwindigkeit eine große Rolle. Daher ist es fraglich, ob man nur durch Messung des Redoxpotentials die Eigenschaften der Entwicklung erfassen kann. Man könnte aber dadurch eine Möglichkeit der Oxydation des latenten Bildes in der Lithentwicklung diskutieren. Bei der Oxydation des latenten Bildes sind einige Fälle vorstellbar, d.h. der ganze Abbau, der partielle Abbau und die Entwicklungshemmung ohne Abbau des latenten Bildes. Den ersten Fall könnte man sich nicht vorstellen. Der ganze Abbau würde eine Empfindlichkeitssteigerung nach längerer Entwicklungszeit nicht hervorbringen. Eine Oxydation in der Lithentwicklung sollte man im zweiten oder im dritten Fall erwarten, obgleich sich diese zwei Fälle deutlich voneinander unterscheiden. Unseren Beobachtungen nach[19] wurde der an der Lithentwicklung teilnehmende Bildkeim viel leichter oxydiert als der an der üblichen Entwicklung teilnehmende. Ein kleiner partieller Abbau im zweiten Fall, der bei der Lithentwicklung nur eine geringe Empfindlichkeitsabnahme verursachen kann, würde keinen bemerklichen Effekt bei der üblichen Entwicklung erweisen. Der dritte Fall hängt an von der Verringerung der Werte zwischen den Potentialen des latenten Bildes und des umliegenden Entwicklers. Mit anderen Worten dürfte man erklären, daß die Oxydationsprodukte des Hydrochinons in der Lithentwicklung mit Hilfe von Br^- und H^+-Ionen oxydativ einwirken. Eine Ursache des Saumeffektes bei der Lithentwicklung wird auch wohl auf die oxydative Wirkung der aus der Stelle hoher Schwärzung diffundierenden Oxydationsprodukte zurückgeführt. Daher verringert Sulfit den Saumeffekt bei der Lithentwicklung durch Beseitigung der Oxydationsprodukte. In Abb. 10 ist gezeigt, daß der Saumeffekt von dem 2,5 Min. entwickelten Bild viel größer als der von dem 1,25 Min. ist. Daraus kann man annehmen, daß die oxydative Wirkung stärker auf die schwächer belichteten als auf die stärker belichteten ist. Nach Yule wird die Schwärzung durch Streulicht herabgesetzt, wenn man den Film zusammen mit Rasterpünkten entwickelt. Nach unserem Versuch war dieser Effekt desto stärker, je der Raum des Rasterpunktes größer war. Diese Resultate sind auch mit der oxydativen Wirkung diffundierender Oxydationsprodukte zu erklären.

Die Schärfe am Rand des Rasterpunktes hängt vermutlich in großem Maße von den diffundierenden Oxydationsprodukte ab. Bei der Entwicklung der mit Graukeil belichteten Schicht spielen die Wirkungen diffundierender Oxydationsprodukte auf den Fuß der Schwärzungskurve vermutlich keine große Rolle. Dies könnte der Grund sein, warum die Erzielung einer steilen Gradation im makroskopischen Bereich und eines scharfen Punktes im mikroskopischen Bereich nicht immer direkt miteinander gekoppelt sind.

Die latenten Bildkeime der Emulsion, die einen guten Litheffekt zeigt, sind in der schwächer belichteten Stelle leicht, in der stärker belichteten schwer oxydiert, wie es in Abb. 11, in Tabellen 4 und 5 gezeigt ist. Man sollte hier beobachten, daß das Verhalten des latenten Bildes einer Lithemulsion an der schwächer belichteten Stelle und der stärker belichteten merklich verschieden ist. Der Unterschied der beiden Schwärzungskurven in Abb. 1a ist der oxydativen Wirkung zuzuschreiben. Der Lithentwickler ohne Bromid zeigte auch in kürzerer Entwicklungszeit keinen Litheffekt. Eine wichtige Rolle der Br^--Ionen in der Lithentwicklung liegt wahrscheinlich darin, daß sich das Redoxpotential des latenten Bildes erniedrigt, um von den Oxydationsprodukten oxydativ beeinflußt werden zu können. Die anderen außer Br^--Ionen in Tabelle 1 können das Redoxpotential des latenten Bildes nicht genug erniedrigen, so daß man einen guten Litheffekt nicht erhalten kann. Im Beisein der SCN^--Ionen konnte man einen kleinen Litheffekt erhalten. Eine Erklärung dafür ist, daß die Erniedrigung des Redoxpotentials durch SCN^--Ionen kleiner als durch Br^--Ionen ist.

Der Mechanismus der Lithentwicklung ist zwar noch heute nicht genug klar,[30] aber aus obigen Tatsachen kommt eine erweiterte Ansicht wie folgt zum Schluß.

In der ersten Stufe wird der Ablauf der Entwicklung gehemmt, da die Oxydationsprodukte des Hydrochinons mit Hilfe von Br^-- und H^+-Ionen auf die latenten Bildkeime oxydativ einwirken. Dies entspricht der sehr niedrigen Schwärzung, die man bei kürzerer Lithentwicklungszeit kaum beobachten kann. Diese

30) H. Frieser, G. Haase, und E. Klein, „Die Grundlagen der photographischen Prozesse mit Silberhalogeniden," Bd. 2, herausgegeben von Akademische Verlagsgesellschaft, Frankfurt am Main (1968), S. 884.

oxydative Einwirkung geht aber in der Lösung mit Sulfit weg. Die oxydative Hemmung ist vor allem stark an der schwächer belichteten Stelle. Das latente Bild an der stärker belichteten Stelle widerstrebt der Oxydation und wird weiter entwickelt. Die entstandenen Oxydationsprodukte diffundieren einigen Abstand zu den umliegenden Körnern, teils um die Entwicklung der stärker belichteten Körner durch die Herabsetzung des Ladungsbarriereeffektes zu beschleunigen, teils um dieselbe der schwächer belichteten Körner durch den oxydativen Abbau des latenten Bildes oder durch die Hemmung der Entwicklung niederzuhalten.

Der Litheffekt ist abhängig von der Entwickelbarkeit der stärker belichteten Bildkeime und von der Oxydierbarkeit der schwächer belichteten. Wenn diese beiden Faktoren miteinander ins Gleichgewicht gebracht werden, könnte man einen guten Litheffekt erhalten. Mit anderen Worten, beruht der Litheffekt auf der Entwickelbarkeit der stärker belichteten Bildkeime durch Hydrochinon und der Oxydierbarkeit der schwächer belichteten durch Chinon. Der Litheffekt, die Entwickelbarkeit durch Hydrochinon und die Oxydierbarkeit durch Chinon, wie sie in Abbildungen 11 und 12 dargestellt, sind in Tabellen 4 und 5 wieder zusammengefaßt. Die AgCl/Br-Emulsion von drei Silberhalogenidemulsionen und die schwefelsensibilisierte Emulsion von drei chemisch sensibilisierten AgCl/Br-Emulsionen beweisen einen guten Litheffekt. Die Ursache dafür ist so erklärt, daß ihre latenten Bildkeime in der stärker belichteten Stelle durch Hydrochinon schnell entwickelt werden und dieselben in der schwächer belichteten Stelle durch Chinon leicht oxydiert werden. Der Litheffekt der AgBr-Emulsion ist schlecht, da die Entwicklbarkeit und die Oxydierbarkeit von AgBr-Emulsion miteinander nicht im Gleichgewicht sind. Wenn die latenten Bildkeime der AgCl-Emulsion noch etwas leichter oxydiert werden könnten, würde sie einen besseren Litheffekt beweisen.

TABELLE 4. ERKLÄRUNG DES LITHEFFEKTES VON DREI SILBERHALOGENIDEMULSIONEN

Litheffekt	$AgCl/Br > AgCl \gg AgBr$
Entwickelbarkeit	$AgCl \fallingdotseq AgCl/Br \gg AgBr$
Oxydierbarkeit	$AgBr \gg AgCl/Br > AgCl$

TABELLE 5. ERKLÄRUNG DES LITHEFFEKTES VON DREI CHEMISCH SENSIBILISIERTEN AgCl/Br-EMULSIONEN

Litheffekt	$S > S+Au \gg Au$
Entwickelbarkeit	$S+Au \fallingdotseq S \gg Au$
Oxydierbarkeit	$S \gg Au > S+Au$

Herrn Prof. Dr. K. Honda an der Universität Tokio möchte ich für die wertvolle Diskussion herzlich danken.

NOTES

BULLETIN OF THE CHEMICAL SOCIETY OF JAPAN, VOL. 45, 3473—3474 (1972)

A Study of Catalysis by Uranium Oxide and Its Mixed Catalysts. III.[1] A Comparison of the Uranium Oxide Catalyst with Vanadium Oxide, Molybdenum Oxide and Tungsten Oxide Catalysts for the Catalytic Oxidation of Carbon Monoxide

Fumio Nozaki and Keiichi Ohki

Department of Industrial Chemistry, Faculty of Engineering, Chiba University, Yayoi-cho, Chiba

(Received March 17, 1972)

The catalytic oxidation of carbon monoxide over various metal oxides has been studied by several workers discussing the order of oxidation activity.[2] However, there have been very few reports about the uranium oxide catalyst. The present authors have reported previously about the supported uranium oxide catalysts.[3] The purpose of this paper is to make a survey of the oxidation activity of U_3O_8, V_2O_5, MoO_3, and WO_3 catalysts, and to discuss the causative relationship between the catalytic activity and the thermodynamic properties of the oxides, such as the heat of formation or the heat of oxide-interconversion.

Experimental

Catalyst Samples. All of the catalysts were obtained by the usual method of preparation. U_3O_8 was prepared by the thermal decomposition of ammonium diuranate, $(NH_4)_2U_2O_7$, obtained from uranyl nitrate by precipitation with NH_4OH. The sample calcined at 450°C for 3 hr in an air stream was green-black in color and 20.8 m^2/g in B.E.T. surface area. The V_2O_5 catalyst was prepared from NH_4VO_3 by calcination. The sample calcined at 500°C for 3 hr in an air stream was tan-orange and 5.2 m^2/g in surface area. The MoO_3 catalyst was obtained by the calcination of the precipitate prepared from $(NH_4)_6Mo_7O_{24}$ and HNO_3. The sample calcined at 500°C for 2 hr in an air stream was white and 3.0 m^2/g in surface area. The WO_3 catalyst was obtained by the calcination of the precipitate prepared from $(NH_4)_{10}W_{12}O_{41}$ and HNO_3. After it had been calcined at 500°C for 2 hr, the sample was yellow and 12.1 m^2/g in surface area.

Catalytic Oxidation of Carbon Monoxide. The flow-type apparatus and the procedure for the rate measurements were the same as those previously reported.[3] All of the experiments were carried out under the following identical conditions: total flow rate of feed gas=100 ml (20°C)/min, feed ratio of $CO:O_2:N_2=3:3:4$, total pressure=1 atm. The amount of catalyst packed in the reactor was controlled in the range from 0.2 to 1.2 g according to the catalyst specimen in order to prevent the conversion of carbon monoxide from exceeding 20%. Under these experimental conditions, the observed conversion of carbon monoxide was proportional to the amount of catalyst used. The equation used in the calculation of the reaction rate was:

$$r = \frac{1}{S}\frac{y_0 x}{(W/F)} \quad (1)$$

where r: reaction rate per unit of surface area of the catalyst (mol/m^2 hr), y_0: CO mol fraction at the inlet of the catalyst bed (=0.3), S: surface area of the catalyst (m^2/g), W: amount of catalyst (g), F: total flow rate of feed gas (=0.268 mol/hr).

Results and Discussion

The conversion data as a function of the reaction temperature are shown in Fig. 1. We calculated the reaction rates by using Eq. (1) and plotted log (r) as a function of $1/T$ in Fig. 2. From Figs. 1 and 2, it is found that U_3O_8 is exceedingly high in oxidative activity and that the order of catalytic activity is as follows: $U_3O_8>V_2O_5>MoO_3>WO_3$. We estimated the reaction rates from Fig. 2 at a reaction temperature of 500°C and have illustrated the rate data as a function of the heat of formation, $(-\Delta H°_f)$[4] or of the heat of oxide-interconversion, $(\Delta H°_{MO_{x-1}} - \Delta H°_{MO_x})$[5]

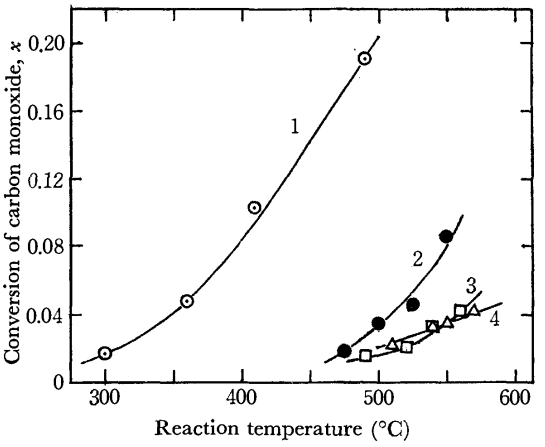

Fig. 1. Conversion of carbon monoxide as a function of reaction temperature.
1: —⊙— U_3O_8 (W=0.252 g)
2: —●— V_2O_5 (W=0.804 g)
3: —□— MoO_3 (W=1.202 g)
4: —△— WO_3 (W=0.623 g)

1) Part II of this series; F. Nozaki and H. Okada, *Nippon Kagaku Kaishi*, **1972**, 842.

2) a) S. Makishima, Y. Yoneda, and Y. Saito, *Shokubai (Catalyst)*, **2**, 168 (1960). b) M. Tarama, S. Teranishi, and A. Yasui, *Nippon Kagaku Zasshi*, **81**, 1034 (1960). c) T. Seiyama, A. Suematsu, and W. Sakai, *ibid.*, **82**, 292 (1961).

3) F. Nozaki, M. Kobayashi, and S. Yoshida, *Nippon Kagaku Kaishi*, **1972**, 26.

4) This is the heat of formation per metal atom (kcal/metal atom). The data of $-\Delta H°_f$ are quoted from "Shokubai Kogaku Koza", Vol. 2 (ed. by Catalysis Soc. of Japan), p. 141 and "Chemistry of Uranium" (by Katz and Rabinowitch), p. 295.

5) The value of $(\Delta H°_{MO_{x-1}} - \Delta H°_{MO_x})$ corresponds to the heat of reaction of the following deoxygenation: $MO_x \rightarrow MO_{x-1} + 1/2\ O_2$, where MO_{x-1} means the next lower oxidized state of metal oxide, MO_x. In the present case, the chemical formulas of MO_{x-1} are U_3O_7, V_2O_4, MoO_2, and WO_2 respectively. The data of the heat of reaction are quoted from the books noted in Ref. 4).

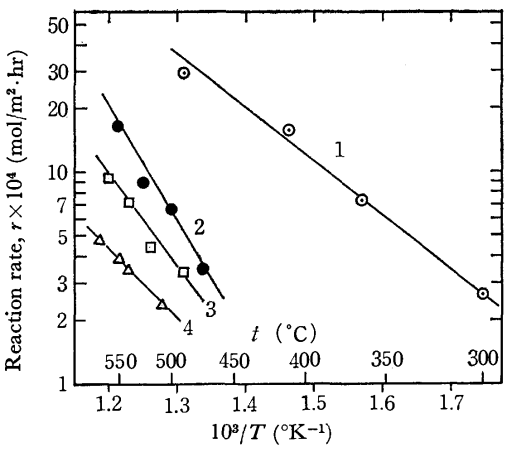

Fig. 2. Arrhenius plot.
1: U_3O_8 (apparent activation energy, E_a=14 kcal/mol)
2: V_2O_5 (E_a=25 kcal/mol) 3: MoO_3 (E_a=22 kcal/mol)
4: WO_3 (E_a=16 kcal/mol)

in Fig. 3. In order to characterize the U_3O_8 catalyst, the available data or estimated values[6] of $r_{500°C}$ in the cases of NiO, ZnO, Cr_2O_3, and TiO_2 are also illustrated in Fig. 3 by quoting data from published papers.[7-9]

As is shown in Fig. 3, the correlation between $r_{500°C}$ and $-\Delta H°_f$ has a tendency to move towards a low activity with the increase in $-\Delta H°_f$; however, the activity of U_3O_8 is much higher, as would be expected from $-\Delta H°_f$, and is situated between the ZnO (or NiO) and Cr_2O_3 (or V_2O_5) catalysts. It should be emphasized in this study that U_3O_8 is considerably high in oxidative activity for an *n*-type semiconducting oxide catalyst. Within the limits of the catalyst species investigated in this study, the correlation between

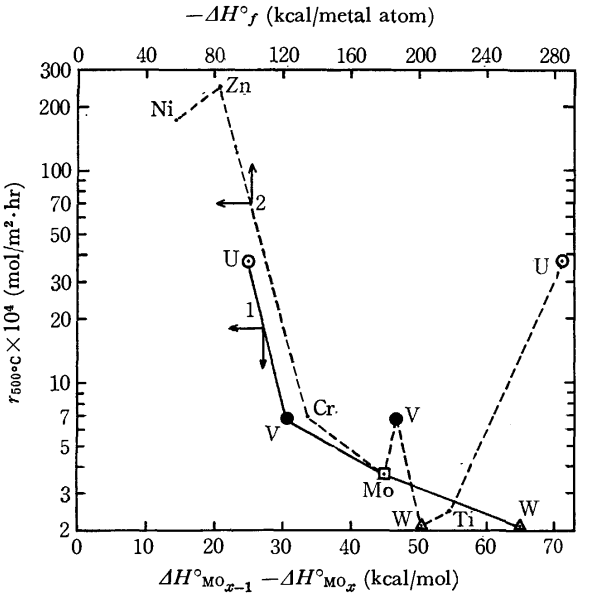

Fig. 3. Correlation between catalytic activity and thermodynamic property of catalyst oxides.
1: (solid line) reaction rate at 500°C *vs.* ($\Delta H°_{MO_{x-1}} - \Delta H°_{MO_x}$)
2: (dotted line) reaction rate at 500°C *vs.* $-\Delta H°_f$

$r_{500°C}$ and ($\Delta H°_{MO_{x-1}} - \Delta H°_{MO_x}$) is regular and shows a predictable variation with a change in ($\Delta H°_{MO_{x-1}} - \Delta H°_{MO_x}$). A probable explanation of why U_3O_8 is active in spite of the large heat of formation can be given on the basis of the fact that U_3O_8 is readily reduced with CO and reoxidized with O_2 because of the small heat of oxide-interconversion.[3] This finding suggests that all of the oxygen atoms in U_3O_8 are not on an equal footing and that some of the specified oxygen atoms showing a high reactivity are involved, as Tarama *et al.*[10] have already pointed out with regard to the V_2O_5 catalyst. We will attempt to obtain more detailed information on this aspect after we have investigated the physico-chemical structure of the uranium oxide catalyst.

6) The values of $r_{500°C}$ were computed or estimated from the rate equations or from the Arrhenius plots of the rate data for identical experimental conditions with this work.

7) I. Matsuura, Y. Kubokawa, and O. Toyama, *Nippon Kagaku Zasshi*, **81**, 997, 1003 (1960).

8) M. Tarama, S. Teranishi, and K. Hattori, *ibid.*, **63**, 714 (1960).

9) Y. Onishi, This Bulletin, **44**, 1460 (1971).

10) M. Tarama, S. Teranishi, S. Yoshida, and N. Tamura, "The Proc. 3rd Inter. Congress on Catalysis", North-Holland Pub. Co. (1965), p. 282.

BULLETIN OF THE CHEMICAL SOCIETY OF JAPAN, VOL. 45, 3475—3476 (1972)

An MO-theoretical Account of the Catalytic Property of Transition-metal Carbides and Nitrides in Dehydrogenation Reactions

Katsutoshi OHKUBO, Hidetoshi SHIMADA, and Masahide OKADA

Department of Synthetic Chemistry, Faculty of Engineering, Kumamoto University, Kurokami, Kumamoto

(Received April 10, 1972)

Refractory compounds of transition-metal carbides and nitrides have been pronounced to be catalysts possessing high catalytic activity in the dehydrogenation of ethylbenzene,[1] cyclohexane,[2] *etc.*, while those of transition-metal borides have proved to be quite inactive.[2] The catalytic properties of refractory compounds, however, have not yet been strictly established on a molecular level. The present study was undertaken in an attempt to correlate the electronic states of transition-metal carbides and nitrides and their catalytic properties in the dehydrogenation reactions, using the all-valence-shell-electron extended Hückel MO (EHMO) method[3] involving metal *d*-orbitals. The FCC NaCl-type carbides and nitrides (named MC and MN respectively) of TiC, VC, ZrC, NbC, HfC, TaC, TiN, VN, CrN, ZrN, NbN, and HfN have been studied; a simple model of their solid states for the EHMO calculations is presented in Fig. 1 and in Table 1.

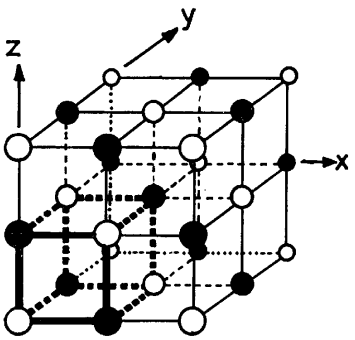

○: metal
●: carbon or nitrogen

Fig. 1. Calculated model (enclosed by thick solid- and dotted-lines) of FCC NaCl-type transition metal carbides and nitrides.

TABLE 1. BOND DISTANCES[a] OF M–C AND M–N

MC	M–C (Å)	MN	M–N (Å)
TiC	2.1658	TiN	2.12
VC	2.091	VN	2.065
ZrC	2.349	ZrN	2.28
NbC	2.235	NbN	2.19
HfC	2.314	HfN	2.26
TaC	2.227	CrN	2.08

a) Taken from H. F. Mark, J. J. McKetta, Jr., and D. F. Othmer, "Encyclopedia of Chemical Technology," 2nd, Ed., Vol. 4, (1964), p. 13.

First, let us discuss the correlation between the atomic charges of M in MC or MN and the rate constants,[1] *k*, reflecting the catalytic activity in the dehydrogenation of ethylbenzene at 560 and 600°C. As Fig. 2 indicates, the MC series tested showed the formal charges of M in the range of *ca.* +0.3—3.5 and gave a maximum indicative of their catalytic activities near the tri-valent charge of M (transition metal).

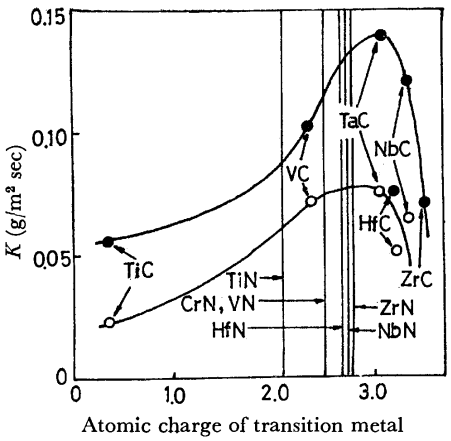

Fig. 2. Correlation between the catalytic activities of transition metal carbides and nitrides and the atomic charges of their metals.
○: 560°C; ●: 600°C

Next, a more precise discussion will be undertaken. The transition-metal carbides and nitrides are characterized by the lowest unoccupied (LU), triply-degenerate d_{xz}, d_{yz}, and d_{xy} metal-orbitals, and also by the LU+1, doubly-degenerate $d_{x^2-y^2}$ and d_{z^2} metal-orbitals. The net orbital populations of the *s* and *p* orbitals of metal and carbon (or nitrogen) atoms at the highest occupied (HO) or the LU level are neglegibly small. This implies that the *s* and *p* orbitals cannot participate directly in the electron donor-acceptor process between the catalyst and such reactants as ethylbenzene. Table 2 lists the orbital populations of the d_{xz}, d_{yz}, and d_{xy} orbitals on the metal at the triply-degenerate levels (denoted as $1/2N_{xz}$, $1/2N_{yz}$, and $1/2N_{xy}$ respectively)

1) G. V. Samsonov, T. G. Bulankova, P. A. Khodak, E. M. Preshedromirskaya, V. S. Sinel'nikova, and V. M. Sleplosov, *Kinet. Katal.*, **10**, 1057 (1967).

2) A. A. Balandin, Editor, "Scientific Selection of Catalysts," (translated from the Russian), Israel Program for Scientific Translations, Jerusalem (1968), p. 263.

3) R. Hoffmann, *J. Chem. Phys.*, **39**, 1397 (1963); *ibid.*, **40**, 2474 (1964): the ionization energies (eV unit) of the outer *s*, *p*, and *d* shells for Coulomb integrals of transition metals were taken from Moor's table (C. E. Moor, "Atomic Energy Levels," Natl. Bur. Std. Circ., No. 467 (1958), Vols. 1, 2, and 3) as follows: 10.33, 6.38, and 11.84 for Ti; 8.0, 6.0, and 10.0 for V; 8.0, 7.0, and 9.0 for Cr; 7.14, 4.78, and 7.14 for Zr; 7.58, 4.99, and 7.58 for Nb; 7.87, 5.87, and 7.87 for Hf; 8.14, 5.15, and 8.14 for Ta.

Table 2. Electronic states of transition metal carbides and nitrides

MC or MN	Bond population of M–C or M–N	Net orbital populations at degenerate levels	
		$1/2N_{xz}=1/2N_{yz}=1/2N_{xy}$	$1/2N_{x^2-y^2}=1/2N_{z^2}$
TiC	0.438	0.1421	0.0355
VC	0.438	0.2324	0.0252
ZrC	0.241	0.1449	0.0322
NbC	0.296	0.2397	0.0153
HfC	0.363	0.1351	0.0461
TaC	0.364	0.2389	0.0157
TiN	0.287	0.2432	0.0084
VN	0.217	0.2447	0.0075
ZrN	0.106	0.2453	0.0073
NbN	0.133	0.2455	0.0065
HfN	0.173	0.2444	0.0008
CrN	0.235	0.2109	0.0575

and of the $d_{x^2-y^2}$ and d_{z^2} orbitals at the doubly-degenerate levels (denoted as $1/2N_{x^2-y^2}$ and $1/2N_{z^2}$ respectively), together with the bond populations of the M–C and M–N. Bearing in mind the connection between the catalytic activity and the degree of incompleteness of the *d*-electron subshells in the dehydrogenation reactions,[4] the correlation between the activity and the values of $1/2N_{xz}$ (or $1/2N_{yz}$) and/or $1/2N_{xy}$ seems significant.[5] As can be seen from Fig. 3, there is a linear dependence between the *k* values and the above-mentioned populations of MC (M=Ti, V, Nb, Hf, and Ta); it can be concluded that the transition-metal carbides thus catalyze the dehydrogenation of ethylbenzene as an electron acceptor.

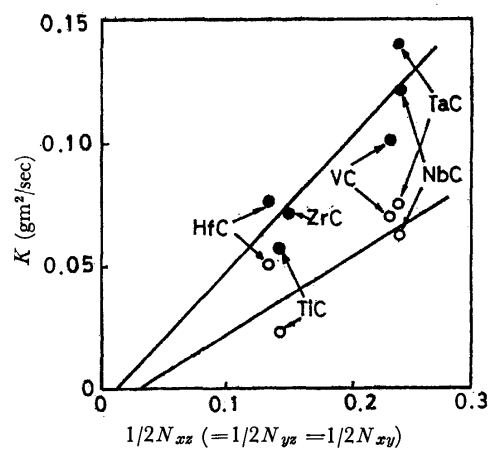

Fig. 3. Correlation between the catalytic activities of transition metal carbides and nitrides and the values of $1/2N_{xz}$ (or $1/2N_{yz}$) and /or $1/2N_{xy}$.
○: 560°C; ●: 600°C

Finally, it is worthy of emphasis, on the basis of the above consideration, that the transition-metal nitrides are not less active than the carbides thereof and that the catalytic activity follows the order: NbN≳ZrN> VN≳HfN≳CrN.

We wish to express our appreciation to the Data Processing Center of Kyushu University for the generous permission to use the FACOM 230-60 computer.

4) S. Z. Roignskii, *Zh. Fiz. Khim.*, **5**, 249 (1935).

5) An increase in the formal charge of M, which is almost directly related to the sum of net orbital populations of the d_{x^2}, d_{yz}, d_{xy}, $d_{x^2-y^2}$, and d_{z^2} orbitals at triply- and doubly-degenerate levels, does not always give a high catalytic activity (see Fig. 1); the relatively large values of $^1/_2N_{x^2-y^2}$ and/or $^1/_2N_{z^2}$ of such nitrides as ZrN and HfN diminish the values of $^1/_2N_{xz}$ (or $^1/_2N_{yz}$) and/or $^1/_2N_{xy}$ in spite of their large formal charges of M (+3.494 and +3.157 for Zr and Hf respectively). The net orbital populations of the d_{xz}, d_{yz}, and d_{xy} orbitals at the LU degenerate levels seem more significant than the formal charge of transition metal.

BULLETIN OF THE CHEMICAL SOCIETY OF JAPAN, VOL. 45, 3476—3478 (1972)

Colloidal Structure of Aluminum Soaps Dispersed in Organic Media

Yuhei Uzu and Michihiro Hattori

Chemical Institute, Faculty of Science, Shinshu University, Asahi, Matsumoto, Nagano

(Received April 19, 1972)

In connection with the structure of gels formed by metal soaps in organic media, aluminum soaps exhibit many interesting properties. Till now, the colloidal structures of many metal soaps have been widely studied by a variety of techniques. In particular, a perfect image of the soap fibers constituting the dispersed phase can be obtained by means of the electron microscope, provided that a portion of the liquid which masks the fibers is eliminated in a suitable manner.

Especially in the case of 12-hydroxystearic acid and its uni- and bivalent metal soaps, it is recoginized that the soap fibers are twisted in the form of aggregates.[1,2] However, no data on the trivalent metal soaps of 12 hydroxystearic acid have yet been shown, to say nothing of such a twisting structure. Its main causes seem to be its susceptibility to thermal decomposition and the difficulty of obtaining pure soaps.

To elucidate the mechanism of occurrence of such a twisting, various explanations have been proposed in the literature.[3,4,5] Above all, it seems reasonable to assume that the twisting is related to the conformation of the soap molecules, as has been suggested by

1) J. W. Wilson, NLGI *Spokesman*, **27**, 373 (1964).
2) T. Tachibana, K. Kayama, and H. Takeno, This Bulletin, **45**, 415 (1972).
3) H. Wilman, *Proc. Phys. Soc.*, **64**, 329 (1951).
4) A. L. McClellan, *J. Chem. Phys.*, **32**, 1271 (1960).
5) G. Rooney and R. J. Bird, *Nature*, **190**, 337 (1961).

Tachibana.[2] The present work shows that similar twisted fibers were found in the aggregates of aluminum 12-hydroxystearate dispersed in such solvents as *n*-hexadecane and white mineral oil.

Aluminum 12-hydroxystearate was prepared by an aqueous metathesis similar to the manner described for the preparation of aluminum stearate.[6] The fatty acids of the commercial products used in this work were purified by repeated recrystallization from ethanol or acetone until those of over 99% purity were obtained, as established by gas-chromatographic analysis. The acids in aqueous ethanol were treated with a slight excess of a potassium hydroxide solution at 50—60°C to yield potassium soaps. The potassium soaps were, then, heated to dissolve them in water, and a hot solution of aluminum chloride at about 90°C was added slowly until the precipitation was complete. The aluminum soaps thus obtained were filtered and thoroughly washed with distilled water and acetone to remove the residue contained in the soaps. Finally, they were dried over P_2O_5 *in vacuo* at 60°C.

The infrared absorption spectra for aluminum stearate and aluminum 12-hydroxystearate were almost identical. Moreover, a comparison of the spectra of the corresponding fatty acids with those of these aluminum soaps showed that the major distinction was the complete absence of the band at 1695 cm^{-1} due to the presence of free fatty acid in the latter, which contains little or no extractable fatty acid. In addition, the thermal analysis confirmed the absence of the transition peak of the free fatty acid. The soaps have a strong band at 983 cm^{-1}, one which is possibly due to an Al–O– covalent and coordinate type of band, as has been reported of aluminum stearate.[6] Also, two absorption bands are displayed at about 1450 and 1590 cm^{-1} which are due to the symmetric and assymmetric stretching vibrations respectively of the carboxylate group. The splitting of the latter band expected in the hydrated forms did not appear. Besides, the elementary analysis indicated that the str./Al and 12 hydroxystr./Al ratio of these soaps were about 2.0 and 1.8 respectively. On the basis of these data, the aluminum 12-hydroxystearate prepared is considered to be a mixture which consists of a disoap plus a small quantity of a monosoap.

A series of studies of the colloidal structures of these soaps has made parallel to one of the gelling properties of these soaps for various organic media. Considerable care was taken in the preparation of the specimen for examination by means of the electron microscope in order to prevent the deformation of the soap thickner structure. In order to make a specimen for electron microscopy, a small amount of the gel or gel-like precipitates was spread in a thin layer on the electron microscope's specimen grids covered with a thin film of carbon, which are then placed on a filter paper. After deoiling by wetting the paper slowly with *n*-hexane, the specimens were chromium-shadowed and examined in the electron microscope.[7] Figures 1 and 2 depict typical electron micrographs of fibers of aluminum 12-hydroxystearate dispersed in *n*-hexadecane and highly-refined mineral oil at 110°C. Further, the similar twisted shapes were obtained in such other organic media as amyl acetate, octyl acetate, and decyl alcohol.

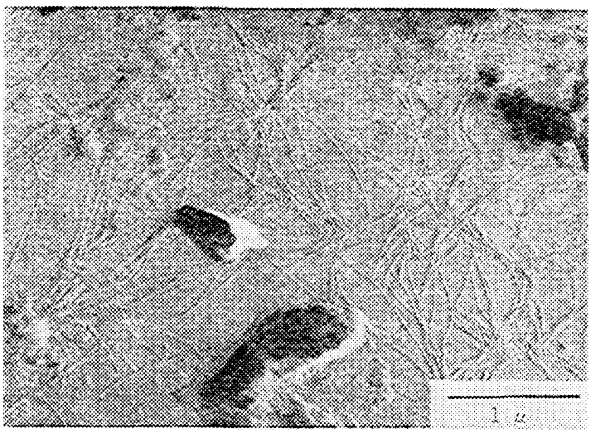

Fig. 1. Electron micrograph of twisted fiber of almuinum 12-hydroxystearate dispersed in *n*-hexadecane at 110°C.

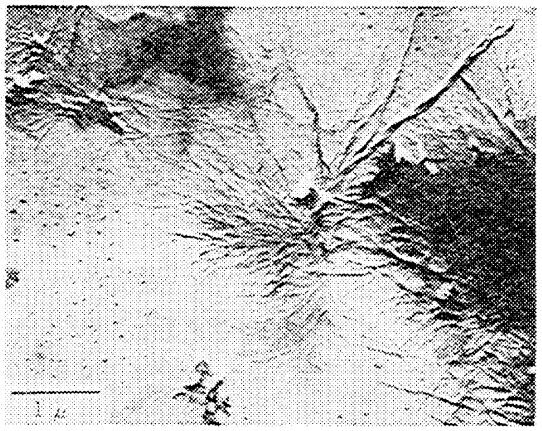

Fig. 2. Electron micrograph of aluminum 12-hydroxystearate dispersed in mineral oil at 110°C.

Out of a fear of decomposition and a release of their free acid with a rise in the temperature, the IR spectra were examined and thermal analysis was carried out

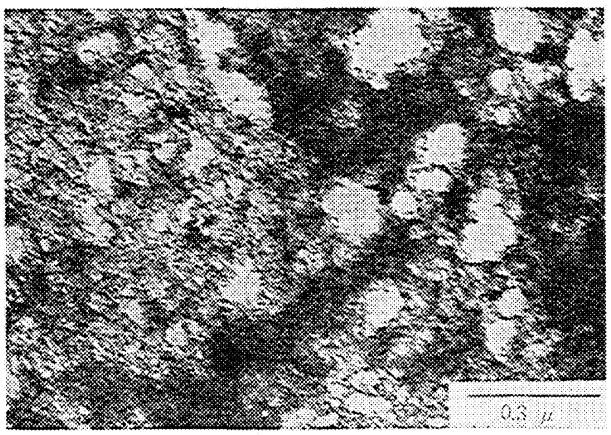

Fig. 3. Electron micrograph of aluminum stearate dispersed in mineral oil at 110°C.

6) G. H. Smith, H. H. Pomeroy, C. G. McGee, and K. J. Mysels, *J. Amer. Chem. Soc.*, **70**, 1053 (1949).

7) F. W. Anderson, R. C. Nelson, and F. F. Farley, NLGI *Spokesman*, **31**, 252 (1967).

for specimens which has been treated thermally at 90 and 110°C. There was no evidence of the release of free fatty acid as a result of the decomposition. Accordingly, it is considered probable that the twisting structure is ascribable to that of aluminum 12-hydroxystearate.

Figure 3 shows a dense honey-combed structure formed in the aggregates of aluminum stearate. It seems to indicate that such a network structure of aluminum stearate is not so easy to break as in other metal soaps in the deoiling process. This supports the view that it is due to the polymerization of aluminum stearate, as has been reported elsewhere.[8] Furthermore, this idea may be associated, in some manner, with the abnormal low long spacing value of 40.9 Å derived from the X-ray diffraction patterns of aluminum stearate. On the other hand, the large value of 47.8 Å of the aluminum 12-hydroxystearate closely approximates the long spacing values of bivalent soaps.[9] It is suggested that these remarkable differences of the long spacing value, together with the electron-microscopic work, may be interpreted as additional evidence supporting the difference in the degree of gelatization.

8) A. E. Legar, R. L. Haines, C. E. Hubley, J. C. Hyde, and H. Sheffer, *Can. J. Chem.*, **35**, 799 (1957).

9) R. Matsuura, *Nippon Kagaku Zasshi*, **36**, 560 (1965).

BULLETIN OF THE CHEMICAL SOCIETY OF JAPAN, VOL. 45, 3478—3479 (1972)

Charge-transfer and Proton-transfer in the Formation of Molecular Complexes. III.[1] 2,4-Dinitrophenol Complexes with Various Anilines

Nobuaki INOUE and Yoshio MATSUNAGA

Department of Chemistry, Faculty of Science, Hokkaido University, Sapporo

(Received April 22, 1972)

When picric acid is combined with a number of the derivatives of aniline, the acid-base interaction generally predominates in both the solid and molten states. However, we found earlier that the complexes with the following four anilines can be essentially of the charge-transfer type above the melting points: *o*-chloroaniline, *m*-nitroaniline, 3-nitro-4-methylaniline, and *N,N*-dimethylamino-*p*-benzaldehyde.[2] Their pK_a values are rather low, in the range between 1.6 and 3.0.

2,4-Dinitrophenol is weaker than picric acid as a proton-donor; that is, the pK_a value of the former phenol is higher, at least by 3, than that of the latter. If the range of pK_a values of anilines, in which the phenomenon of complex isomerization by melting is observable, is essentially determined by the balance between the pK_a value of a polynitrophenol and those of anilines, one would expect the range observable with 2,4-dinitrophenol to be shifted higher by approximately the above-mentioned amount than that found with picric acid. Hertel's observation that this dinitrophenol forms a yellow complex with *o*-anisidine (pK_a= 4.52) and a red one with *p*-bromoaniline (pK_a=3.86) seems not to be inconsistent with this anticipation.[3]

We attempted to prepare molecular complexes of 2,4-dinitrophenol with about thirty derivatives of anilines. The complexes dissolve well into most organic solvents. Chloroform was often found to be suited for the isolation. The solid complexes were obtained, with the nineteen anilines arranged in the order of decreasing pK_a value as is shown in Table 1.[4] Ten anilines from *p*-anisidine to *m*-anisidine, the pK_a values of which are above 4.20, were found to form yellow-colored complexes with 2,4-dinitrophenol. The presence of a NH_3^+ pattern in their vibrational spectra indicates that they are salts formed by means of proton-transfer from the phenol to the anilines. All of them turn orange or red upon melting. The isomerization was confirmed by measuring the vibrational and electronic spectra above the melting points. For example, Fig. 1 presents the vibrational spectra in the region from 2000 to 4000 cm^{-1} of the *p*- and *m*-anisidine complexes in the solid and molten states. By a comparison with the spectra of the corresponding anilinium chloride, two broad bands appearing at about 2600 and 2900 cm^{-1} in the spectra of the solid complexes were assigned to the NH_3^+ group. This pattern has been well known to be typical of picrates of primary amines.[5] Upon melting, the above-mentioned broad bands disappear and several sharp bands are observed in the region from 2850 to 3450 cm^{-1} (see Curves b and d). The bands at 2840, 2950, 3350, and 3450 cm^{-1} arise from the aniline, and those at 3100 and 3250 cm^{-1}, from the phenol. The two located at 3350 and 3450 cm^{-1} can be assigned to the NH_2 group. These solid complexes exhibit electronic absorptions only below 500 nm; however, the appearance of an absorption band in the

1) Part II. Y. Matsunaga and G. Saito, This Bulletin, **45**, 963 (1972).
2) G. Saito and Y. Matsunaga, *ibid.*, **44**, 3328 (1971).
3) E. Hertel, *Ann.*, **451**, 179 (1926).
4) D. D. Perrin, "Dissociation Constants of Organic Bases in Aqueous Solution", Butterworths, London (1965), pp. 58—91.
5) R. P. Mariella, M. J. Gruber, and J. W. Elder, *J. Org. Chem.*, **26**, 3217 (1961).

Table 1. 2,4-Dinitrophenol complexes with various anilines

Aniline	pK_a	Color below mp	mp	Color above mp
p-Anisidine	5.34	Bright yellow	117 —118	Red
p-Phenetidine	5.20	Dark yellow	110	Red
p-Toluidine	5.09	Yellow	111 —112	Red
2,4-Dimethylaniline	4.90	Yellow	89 — 90	Red
m-Toluidine	4.68	Yellow	92 — 93	Red
Aniline	4.59	Yellow	78 — 80[a]	Red
o-Anisidine	4.52	Yellow	85 — 86	Red
o-Phenetidine	4.43	Golden yellow	76 — 77	Red
o-Toluidine	4.39	Yellow	54.5— 55	Orange
m-Anisidine	4.20	Yellow	73 — 74	Red
p-Chloroaniline	3.99	Red	57.5— 58.5	Red
p-Bromoaniline	3.86	Red	70[b]	Red
3-Nitro-4-methylaniline	2.96	Orange	73	Orange
o-Chloroaniline	2.71	Orange	51	Orange
o-Iodoaniline	2.60	Orange	55	Orange
o-Bromoaniline	2.55	Orange	54	Orange
m-Nitroaniline	2.46	Yellow	79	Yellow
N,*N*-Dimethylamino-*p*-benzaldehyde	1.62	Red	87 — 88	Red
p-Nitroaniline	0.99	Yellow	96.5	Yellow

a) 78—79°C by Hertel, Ref. 3. b) Reported by Hertel, Ref. 3.

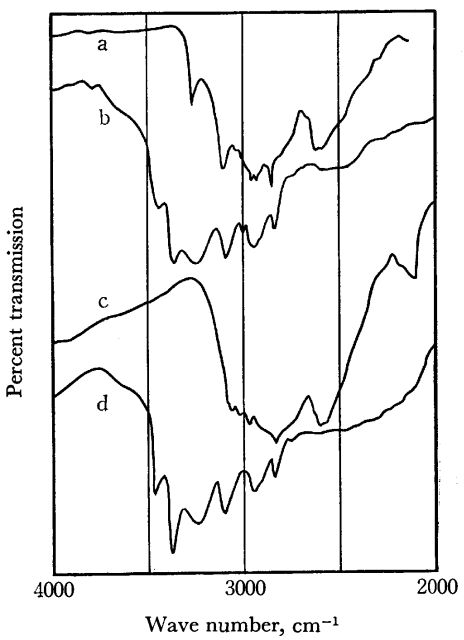

Fig. 1. Vibrational spectra, a) the *p*-anisidine-2,4-dinitrophenol at room temperature, b) the same above the melting point, c) the *m*-anisidine-2,4-dinitrophenol at room temperature, and d) the same above the melting point.

region from 500 to 600 nm was noted in the melts. The corresponding *m*-dinitrobenzene complex could be isolated only with unsubstituted aniline. The similarity in spectrum between the molten 2,4-dinitrophenol complex and the *m*-dinitrobenzene complex suggests that the band appearing upon melting is due to the intermolecular charge-transfer interaction. No change in color was observed upon the melting of the rest of the solid complexes. Their vibrational spectra indicate the absence of proton-transfer either in the solid state or in the molten state. These nine complexes may be supposed to be of the charge-transfer type.

The lower limit of the pK_a range where the phenomenon of complex isomerization by melting is observable appears to be very close to the pK_a of 2,4-dinitrophenol, 4.09.[6] The results given in Table 1 show that a complex is of the proton-transfer type when the pK_a value of aniline is higher than this and that a complex is of the charge-transfer type when the pK_a value of aniline is lower. It must be added that such a coincidence is not necessarily seen with other phenols. On the basis of the vibrational spectrum, the *p*-nitroaniline-picric acid complex was found to be of the charge-transfer type. Although the pK_a values reported for picric acid are rather scattered, ranging from 0.22 to 0.708,[6] *p*-nitroaniline has a pK_a value higher than they.

On the other hand, the upper limit of the pK_a range could not be established with the present phenol. Possibly, it is located higher than the upper limit observed with picric acid, the 2.96 of 3-nitro-4-methylaniline, by approximately the difference between the pK_a values of these two phenols.

6) G. Kortüm, W. Vogel, and K. Andrussow, "Dissociation Constants of Organic Acids in Aqueous Solution", Butterworths, London (1961), pp. 452, 453.

BULLETIN OF THE CHEMICAL SOCIETY OF JAPAN, VOL. 45, 3480—3482 (1972)

Molecular Vibrations and Force Fields of Alkyl Sulfides. V. Infrared Spectra of Methyl Isopropyl Sulfide

Masaru OHSAKU, Yuji SHIRO,* and Hiromu MURATA

Department of Chemistry, Faculty of Science, Hiroshima University, Higashisenda-machi, Hiroshima
**Shinonome Branch School, Faculty of Education, Hiroshima University, Shinonome-3-chome, Hiroshima*

(Received May 4, 1972)

A vibrational treatment of methyl isopropyl sulfide was made by McCullough *et al.*,[1] who suggested the existence of two rotational isomers, C_1 (G) and C_S (T), on the basis of their vibrational data; they claimed that the C_1 form is stable in the solid state. Lately, Scott and El-Sabban[2] carried out a normal coordinate treatment of this sulfide using a valence force field, and concluded that only the C_1 conformation exists, while the C_S conformation must have too high energy to exist even in the liquid state. In this paper, in order to overcome the above-mentioned disagreement among the conformational analyses of methyl isopropyl sulfide, and in order to obtain complete infrared data, we newly recorded the infrared spectra in the gaseous, liquid, and solid states; we have then tentatively assigned the observed bands.

Results and Discussion

The obtained infrared data of methyl isopropyl sulfide are summarized in Table 1. In the C–H stretching, the CH_3 degenerate deformation, and the CH_3 symmetrical deformation, the spectra obtained are well-resolved. In the 1500—1400 cm^{-1} region the CH_3 degenerate deformation, in the 1400—1300 cm^{-1} region, the CH_3 symmetrical deformation, and in the 1300—800 cm^{-1} region, the C–H in-plane and out-of-plane bending, CH_3 rocking, and C–C stretching bands are expected. In the last region, there are some bands which disappear in the crystalline state. Most of the bands which disappear in the crystalline state may be due to the less stable conformation. Here, the existence of the rotational isomers can be suggested for this sulfide. The existence of the rotational isomers, however, is more clearly shown in the C–S stretching and skeletal deformation regions. Methyl isopropyl sulfide has two C–S stretching vibrational freedoms for one comformation. In the liquid state, four bands appear; two bands remain in the solid state. In the skeletal deformation region, 500—200 cm^{-1}, about five bands, including two torsional bands, are expected for one conformation. In this region, eleven bands appear

Table 1. Infrared frequencies (cm^{-1}) and assignments of methyl isopropyl sulfide[a]

Gaseous Room Temp.	Liquid Room Temp.	CS_2 soln. Room Temp.	Solid		Assignment[b]
			Unannealed	Annealed	
2985 sh, vs 2978 sh, vs				2985 m	ν_{C-H}
2974 vvs	2974 vs		2972 s	2973 s	ν_{C-H}
2963 sh, vs	2963 vs		2963 vs	2957 vs	ν_{C-H}
2933 vs	2930 sh, m		2925 sh, w	2931 sh, w	ν_{C-H}
2925 vs	2921 s		2915 s	2920 vs	ν_{C-H}
2905 s				2906 sh, m	ν_{C-H}
2885 s 2880 s	2895 sh, m		2885 m	2890 m	ν_{C-H}
2875 s	2867 m		2866 m	2865 s	ν_{C-H}
2855 m				2855 sh, w	
~2840 sh, w	2837 w		2830 vw	2829 vw	
1470 s	1469 sh, w		1468 sh, w	1469 s	$\delta^{d}_{CH_3}$
1460 vs	1462 vs		1462 s	1462 w	$\delta^{d}_{CH_3}$
1452 vs	1454 vs		1453 s 1448 sh, w	1452 s	$\delta^{d}_{CH_3}$
1445 vs	1445 vs		1443 s	1447 s	$\delta^{d}_{CH_3}$
1435 vs	1435 vs		1434 s	1432 s	$\delta^{d}_{CH_3}$
1428 sh, m	1428 vs		1421 s	1425 s	$\delta^{d}_{CH_3}$
1420 sh, w	1420 sh, w			1420 sh, w	
1397 sh, w 1394 sh, w 1387 s	1383 s	1380 s	1383 sh, m 1380 m	1382 sh, m 1380 s	$\delta^{s}_{CH_3}$

1) J. P. McCullough, H. L. Finke, J. F. Messerly, R. E. Pennington, I. A. Hossenlopp, and G. Waddington, *J. Amer. Chem. Soc.*, **77**, 6119 (1955).

2) D. W. Scott and M. Z. El-Sabban, *J. Mol. Spectrosc.*, **30**, 317 (1969).

Table 1 (Continued)

Gaseous Room Temp.	Liquid Room Temp.	CS_2 soln. Room Temp.	Solid		Assignment[b]
			Unannealed	Annealed	
1378 s 1368 s	1366 s	1365 s	1367 m 1364 s	1372 s 1363 s	$\delta^s_{CH_3}$
1329 w 1323 w	1321 w	1319 w	1328 w	1328 vw	
1316 w 1308 w	1313 w	1312 w	1316 w	1318 m	$\delta^s_{CH_3}$
1285 sh, vw	~1280 sh, vw	~1280 sh, vw	1282 sh, w	—	
1276 sh, w	1275 sh, m	1275 sh, m	1275 w	1276 m	
1270 sh, w	1268 sh, m	1268 sh, m	—	—	
1265 sh, w	1263 m	1263 s	—	—	
1256 vs 1249 vs 1242 vs	1244 vs	1243 vs	1245 vs	1245 vs	
1230 sh, vw	1229 sh, vw	1227 sh, vw	—	—	
1167 s 1162 s 1155 s	1159 s	1157 s	1159 s 1155 sh, s	1161 sh, s 1158 s	
1115 vw	1113 w	1114 w	1113 w	1113 vw	
1108 vvw	1108 sh, vw	1108 sh, vw	—	—	
1075 sh, m 1068 m	1064 s	1063 s	1060 s	1059 s	
1060 m 1054 sh, m	1059 s	1057 s	1057 sh, w	—	
~1025 vvw	1038 sh, vvw	1038 sh, vvw	—	—	
1015 vvvw	1015 vvw	1015 vvw	—	—	
	~990 vvw	~990 vvw	992 vw	994 vw	
	~985 sh, vw	~985 sh, vw	—	—	
975 sh, w	980 sh, vw	980 sh, vw	—	—	
970 sh, w	970 sh, w	970 sh, w	969 sh, s	—	
965 m	965 sh, m	965 sh, m	966 s	966 s	
958 sh, m 955 m	957 s	955 s	959 m	—	
952 sh, m	952 sh, m	951 sh, m	952 m	952 w	
940 sh, w	941 sh, vw	940 sh, vw	944 sh, vw	945 m	
925 vw	927 w	927 w	927 w	932 m	
920 vw	920 sh, vw	920 sh, vw	921 sh, vvw	—	
	918 sh, vvw	917 sh, vvw	918 sh, vvw	—	
885 w, br	884 w	884 w	884 w	884 m	
725 vw	725 w	725 w	727 w	727 m	ν_{C-S}
690 vw	690 vvvw	690 vvvw	—	—	
647 w 638 w 630 w	637 m	637 m	637 m	638 m	ν_{C-S}
610 vw	610 w	610 w	—	—	ν_{C-S}
	537 vvw, br		—	—	
	456 vvvw		—	—	
	427 vw		426 w	429 w	δ_{skel}
	420 sh, vw		419 sh, vw	—	
	349 vw		353 vw	~355 vw	δ_{skel}
	334 vw		337 sh, vw	338 vw	δ_{skel}
	327 vw		329 vvw	—	
	323 sh, vvw		325 sh, vvw	—	
	276 vvw		—	—	
	255 vvw		—	—	
	234 vvvw		~235 vvw	~235 vvw	δ_{skel}
	217 vvw		217 vvw	217 vvw	δ_{skel}

s, strong; m, medium; w, weak; v, very; sh, shoulder; br, broad.

a) Above 3000 cm^{-1} and 2800—1500 cm^{-1} regions are omitted.

b) ν, stretching; δ^d, degenerate deformation; δ^s, symmetrical deformation; δ_{skel}, skeletal deformation (including torsions).

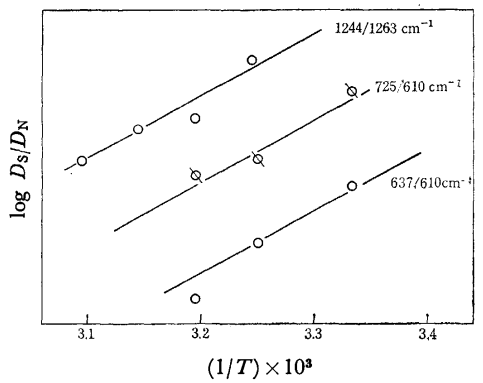

Fig. 1. Plots of log D_S/D_N *vs.* $1/T\times10^3$ of the three liquid-band pairs of methyl isopropyl suifide. D_S: Stable form, D_N: Less stable form.

in the liquid state and five bands remain in the annealed state. Thus, in the liquid or gaseous spectra in the C–S stretching and skeletal deformation regions, there are bands which correspond to two forms. In the annealed state, this sulfide may exist in one form.

In order to confirm the existence of the rotational isomers, we attempted to make an experiment on the solvent effects. We took up the bands at 637 and 610 cm^{-1} and used cyclohexane and acetone as the solvents. In this species, however, it seems that the difference in the dipole moment between the two conformations, C_S and C_1, is not very much. In the observed spectra, we cannot see any clear difference. We have, then, tried to determine the temperature dependence of the liquid bands at temperatures of 27—50°C. Figure 1 shows the plots of log D_S/D_N *vs.* $1/T\times10^3$ of the three liquid-band pairs. In Fig. 1, D_S means the stable forms and D_N means the less stable forms. The origin of log D_S/D_N is different in each case. The pairs of bands at 1244/1263, 725/610, and at 637/610 cm^{-1} show nearly the same temperature dependence. From these slopes, we can see the enthalpy difference between two rotational isomers; the order of ΔH is evaluated to be *ca.* 1—1.5 kcal/mol. We cannot, however, determine an exact value, since our obtained data are not sufficient.

From the obtained infrared data, therefore, we can postulate for this sulfide that: a) two conformations coexist in the liquid and gaseous states (energy difference $\Delta H\fallingdotseq1$—1.5 kcal/mol), and b) one form exists in the crystalline state.

Experimental

The methyl isopropyl sulfide was prepared by the method of McAllan *et al.*,[3] bp 84—85°C/760 mmHg (reported bp[3] 84.8°C/760 mmHg). The purity of this sulfide was checked by means of gas chromatography. The methods of infrared recording and instrument used were described previously.[4]

3) D. T. McAllan, T. V. Cullum, R. A. Dean, and F. A. Fidler, *J. Amer. Chem. Soc.*, **73**, 3627 (1951).

4) M. Ohsaku, Y. Shiro, and H. Murata, This Bulletin, **45**, 954 (1972).

BULLETIN OF THE CHEMICAL SOCIETY OF JAPAN, VOL. 45, 3482—3484 (1972)

Reaction Rates in the Monomer-Dimer Equilibrium of TCNQ Anion Radicals as Studied by the Temperature-Jump Method

Akihiko YAMAGISHI, Yôichi IIDA, and Masatoshi FUJIMOTO
Department of Chemistry, Faculty of Science, Hokkaido University, Sapporo
(Received May 13, 1972)

In spite of electrostatic repulsion, various ion-radical molecules are known to dimerize in solution. There have been a number of investigations concerning the equilibrium constants and the heats of dimerization in the reversible monomer-dimer equilibria of ion radicals.[1-5] Up to now, however, no attempt has been made to measure the reaction rate constants for such systems.

Boyd and Phillips found a reversible monomer-dimer equilibrium of the 7,7,8,8-tetracyanoquinodimethane (TCNQ) anion radicals in an aqueous solution. The equilibrium constant for dimerization at 25°C and the heat of dimerization were determined to be $2.5\times10^{3}\text{M}^{-1}$ and -10.4 kcal/mol·dimer respectively.[2] In the present paper, the temperature-jump technique was applied to this equilibrium in order to investigate the kinetics of the formation and dissociation of the TCNQ anion radical dimers. The intermolecular interaction between the ion radicals in solution will be discussed on the basis of these experimental results.

Experimental

The kinetic measurements were performed on a temperature-jump apparatus, Messanlagen Studiengesellschaft. A Teflon cell was constructed so that the measurements could be made under deaerated conditions. The temperature rise was attained by Joule heating. For this cell, the time constant of the abrupt temperature rise was estimated by using

1) K. Uemura, S. Nakayama, Y. Seo, K. Suzuki, and Y. Ooshika, This Bulletin, **39**, 1348 (1966).
2) R. H. Boyd and W. D. Phillips, *J. Chem. Phys.*, **43**, 2927 (1965).
3) K. Kimura, H. Yamada, and H. Tsubomura, *ibid.*, **48**, 440 (1968).
4) N. Sakai, I. Shirotani, and S. Minomura, This Bulletin, **44**, 675 (1971).
5) T. Yamazaki and K. Kimura, *ibid.*, **44**, 298 (1971).

the acid hydrolysis of *p*-nitrophenol, in which the rate constant is of the order of 10^{10} M^{-1} sec^{-1}.[6] In its aqueous solution with an ionic strength of 0.23, the time constant required for a 90% rise of about 2°C was found to be 4 μsec at a 30 kV discharge. An aqueous solution of Li^+ $TCNQ^-$ containing 0.2M $LiClO_4$ as a supporting electrolyte was prepared *in vacuo* and was then admitted into the cell without any exposure to air. The measurements were made after nitrogen gas (1 atm) had been introduced into the cell.

Results and Discussion

First, the monomer-dimer equilibrium of theTCNQ anion radicals in 0.2M aqueous $LiClO_4$ solution, as expressed by Eq. (1), was examined by measuring the absorption spectrum and its concentration dependence:

$$2TCNQ^- \rightleftharpoons (TCNQ^-)_2. \quad (1)$$

The concentrations of the monomer, [$TCNQ^-$], and the dimer, [$(TCNQ^-)_2$], in the equilibrium state were determined by using the values for their molar extinction coefficients at 660 and 740 nm respectively in a pure aqueous solution reported by Boyd and Phillips.[2] The equilibrium constant:

$$K = \frac{[(TCNQ^-)_2]}{[TCNQ^-]^2} \quad (2)$$

was thus estimated to be 1.2×10^4M^{-1} at 14°C in a 0.2M $LiClO_4$ aqueous solution. This value was found to be rather larger than that of 4.9×10^3M^{-1} at 14°C in a pure aqueous solution reported by Boyd and Phillips.[2] This means that the ionic atmosphere of the solvent favors the dimer form in the equilibrium of Eq. (1).

For the equilibrium of Eq. (1) in a 0.2M $LiClO_4$ aqueous solution at 14°C, the temperature-jump relaxation measurements were made by observing the time dependence of the optical absorption and its concentration dependence. When the temperature was abruptly raised, we found a decrease in the absorbance in the region of 450—540 nm, where the dimer of the TCNQ anion radicals mostly absorbs.[2] The observed decrease in the absorbance is, then, attributable to the decrease in the dimer concentration in Eq. (1); that is, the equilibrium expressed by Eq. (1) is shifted to the left when the temperature is raised. For example, the solution of [$TCNQ^-$]$=5.7\times10^{-5}$M at 20°C is given in Fig. 1. Figure 2 shows experimental plots of the reciprocal value of the observed relaxation time, τ^{-1}, *versus* the concentration of [$TCNQ^-$] for various solutions.

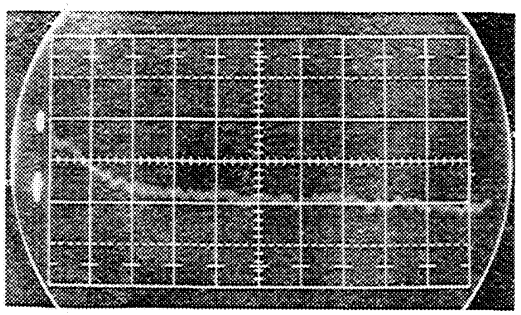

Fig. 1. The decrease of the absorbance observed by the temperature-jump method in the monomer-dimer equilibrium of Eq. (1) at 20°C; λ=525 nm, 5 μsec/division, [$TCNQ^-$]$=5.7\times10^{-5}$M.

In the monomer-dimer equilibrium of Eq. (1) let the rate constants for the dimerization and the dissociation be $\vec{k}$ and $\overleftarrow{k}$ respectively. In this case, we have the following relation:

$$\tau^{-1} = 4\vec{k}[TCNQ^-] + \overleftarrow{k}. \quad (3)$$

If we put the average τ value in the experimental results into this equation, we obtain the following values for $\vec{k}$ and $\overleftarrow{k}$:

$$\vec{k} = 3.5\times10^8 \text{ M}^{-1} \text{ sec}^{-1}, \quad (4)$$

$$\overleftarrow{k} = 9\times10^4 \text{ sec}^{-1}. \quad (5)$$

We can relate these values to the monomer-dimer equilibrium constant as $K=\vec{k}/\overleftarrow{k}$. The K value thus estimated, 4×10^3M^{-1}, is consistent with that previously estimated from the static measurement of the absorption spectra. The τ value, however, may be almost independent of [$TCNQ^-$], because the observed τ values in Fig. 2 include some uncertainty. In this case, the

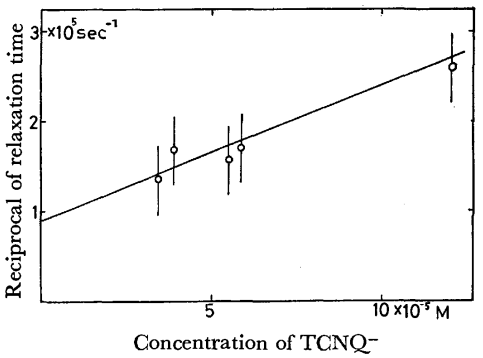

Fig. 2. The dependence of a relaxation time τ^{-1} on [$TCNQ^-$] in the monomer-dimer equilibrium of Eq. (1) at 15°C.

observed τ values practically coincide with the cell constant of the apparatus, and the $\vec{k}$ and $\overleftarrow{k}$ values may be larger than those for Eqs. (4) and (5) respectively. Although more accurate measurements are desirable for the determination of the τ values, we can consider, at present, that the values in Eqs. (4) and (5) give the lower limits of the intrinsic $\vec{k}$ and $\overleftarrow{k}$ values respectively.

On the other hand, if the reaction rate for the dimerization of the TCNQ anion radicals in an aqueous solution can be described by a diffusion-controlled process for charged particles, the theoretical reaction rate at the temperature, T, can be represented by:[7]

$$\vec{k}(\text{calc}) = \frac{4\pi q^2 N D(N/1000)}{\varepsilon R T[\exp(q^2 N/\varepsilon R T\sigma) - 1]} \quad (6)$$

where q is the charge of a particle; N, Avogadro's number; D, the diffusion coefficient of a particle; ε, the dielectric constant of a medium, and R, the gas constant. σ represents the diameter of a particle, which is assumed to be a sphere. Putting the reasonable values of $D=1.8\times10^{-5}$ cm^2 sec^{-1} and $\sigma=4.0\times$

6) M. Eigen and K. Kustin, *J. Amer. Chem. Soc.*, **82**, 5952 (1960).

7) A. A. Frost and R. G. Pearson, "Kinetics and Mechanism," John Wiley and Sons, New York (1961), p. 271.

10^{-8} cm into Eq. (6), we obtain, at 15°C:

$$\vec{k}(\text{calc}) = 1.8 \times 10^{9}\ \text{M}^{-1}\ \text{sec}^{-1}. \quad (7)$$

The observed $\vec{k}$ value in Eq. (4) was found to agree with the $\vec{k}$(calc) value. Therefore, the reaction rate for the dimerization of the TCNQ anion radicals in an aqueous solution can be understood in terms of the diffusion-controlled process.

BULLETIN OF THE CHEMICAL SOCIETY OF JAPAN, VOL. 45, 3484—3485 (1972)

On the Phase Transition of *N*-Methylchloroacetamide

Hideaki CHIHARA, Tokutsuka KIICHI,* and Nobuo NAKAMURA

Department of Chemistry, Faculty of Science, Osaka University, Toyonaka, Osaka 560

(Received July 13, 1972)

N-Methylchloroacetamide is one of model compounds of peptide. The infrared and dielectric studies were carried out on the molecular conformation in solution in 1956.[1] Recently Miyazawa has found a phase transition at 38°C by his infrared measurements.[2] He considered that this phase transition is accompanied with the change in the molecular conformation from one of the '*gauche*' type in the low temperature phase (Phase II) to the '*trans*' type in the high temperature phase (Phase I). Later it was found by an X-ray structural study[3] that there are two different kinds of molecules in a monoclinic unit cell of $P2_1/n$ in Phase II: The molecules of one kind assume a planar structure but the others are non-planar. Each kind of molecules assumes '*cis*'-conformation instead of *gauche* form as suggested by previous workers. The N-H···O type hydrogen-bond network exists between the same kind of molecules and extends along the crystalline *c*-axis. The present Note describes the results of the differential thermal analysis (DTA), dielectric measurements, and ^{35}Cl nuclear quadrupole resonance (NQR) studies in an attempt to obtain detailed information with respect to the phase transition.

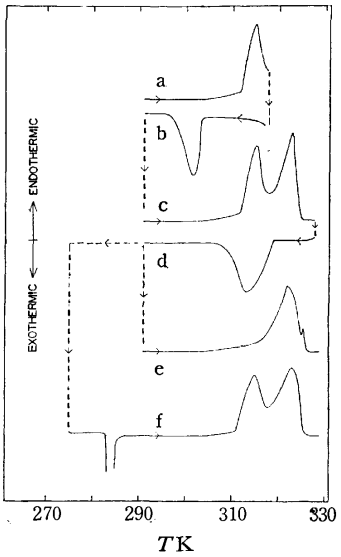

Fig. 1. Differential thermal analysis curves.

The specimen was prepared according to the literature[4] and purified by sublimation under reduced pressure. (mp 45.8±0.2°C; literature value 46°C[1]). Figure 1 shows the DTA curves of the samples having different thermal history. It was found that (1) the specimen which has never been melted or has been stored at room temperature for a long time after melting and freezing undergoes a typical first-order phase transition at 311.6 K which is reversible with a thermal hysteresis effect (curves a, b, and c in Fig. 1), (2) when the specimen is cooled from the melt no phase transition occurs both in cooling and heating directions (curves d and e). The solid phase (Phase III) obtained by cooling the liquid is probably the same as Phase I because their mp and shape and magnitude of the thermal anomaly coincide with each other, (3) Phase

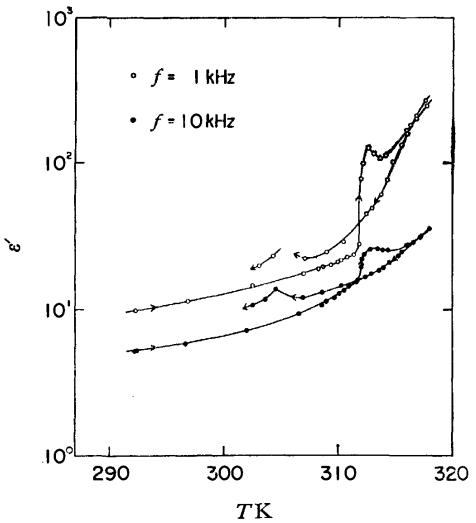

Fig. 2. Dielectric constant ε′ at 1 kHz (○) and 10 kHz (●).

* Present address: *Ashigara Laboratories, Fuji Photo Film Co. Ltd., Ashigara, Kanagawa-ken.*

1) S. Mizushima, T. Shimanouchi, I. Ichishima, T. Miyazawa, I. Nakagawa, and T. Araki, *J. Amer. Chem. Soc.*, **78**, 2038 (1956).

2) T. Miyazawa, This Bulletin, **42**, 3021 (1969).

3) Y. Koyama, T. Shimanouchi, and Y. Iitaka, *Acta Crystallogr.*, **B 27**, 940 (1971).

4) W. A. Jacobs and M. Heidelberger, *J. Biol. Chem.*, **21**, 145 (1915).

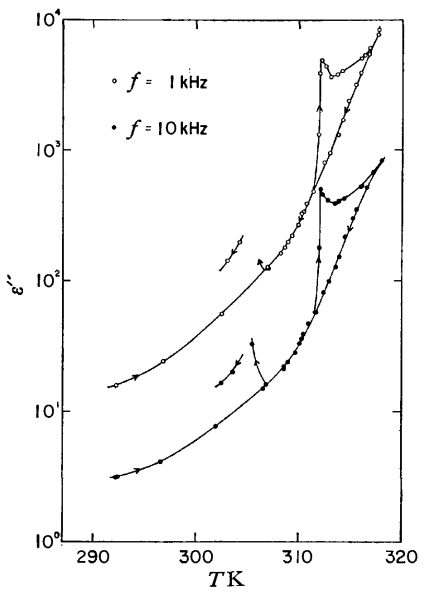

Fig. 3. Dielectric loss factor ε'' at 1 kHz (○) and 10 kHz (●).

III can exist at room temperature as a metastable phase for a few days but it transforms gradually to Phase II at room temperature, and (4) a sharp transformation of Phase III to Phase II occurs at about 283 K when Phase III is heated from a low temperature with an exothermic phenomenon as shown in the curve f in Fig. 1.

Two ^{35}Cl NQR lines were observed only in Phase II. The resonance frequencies are $\nu_1=34.658\pm0.003$ and $\nu_2=34.783\pm0.001$ MHz at 24.2 K, which decreased monotonously and merged into a single line above 304 K ($\nu_1=\nu_2=33.381$ MHz at 310.2 K). The ^{35}Cl spin-lattice relaxation time T_1 changes slightly from 30 ms at 170 K to 7 ms at 309 K. This fact shows that the internal rotation of molecules is not seen until the transition point T_c is reached. Because the resonance lines are not observable in Phase I, it is considered to be a disordered phase probably with respect to the molecular conformation.

On the other hand, dielectric constant and the loss factor ($\varepsilon'=9.72$, $\varepsilon''=15.9$ at 292 K, $f=1$ kHz) increase gradually with increasing temperature and discontinuous jump occurs at T_c as shown in Figs. 2 and 3.

From ε'' we calculated the DC conductivity σ according to the equation $\sigma=(1/2)\varepsilon''f$. The values of σ (in 10^{-8} ohm^{-1}cm^{-1}) were 0.79 (292 K), 9.4 (309 K), 77 (312 K), and 264 (316 K).

The very high conductivity in Phase I may be interpreted in terms of the proton transfer mediated by the internal rotation of $-CONHCH_3$ group about the C–C bonds as follows:

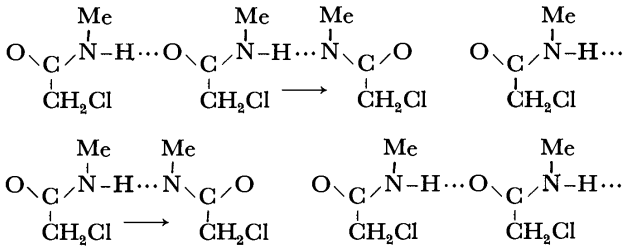

This mechanism is similar to that proposed for the conduction in imidazole crystal.[5]

5) J. T. Daycock, G. P. Jones, J. R. N. Evans, and J. M. Thomas, *Nature*, **218**, 672 (1968).

BULLETIN OF THE CHEMICAL SOCIETY OF JAPAN, VOL. 45, 3485—3487 (1972)

Syntheses of 1,ω-Bis(5-ethyl-8-hydroxy-7-quinolyl)-alkanes and Their Copper(II) Complexes

Kiyoshi TOBINAGA,[1] Masakuni MUKAINO,[2] Takahiko INAZU,* and Tamotsu YOSHINO

Department of Chemistry, Faculty of Science, Kyushu University, Hakozaki, Higashi-ku, Fukuoka

(Received February 7, 1972)

It is of interest to synthesize compounds in which two molecules of 8-quinolinol are connected by a polymethylene bridge in their 7-positions, and also to examine their complexes as formed with metal ions, because the structure of the complex is expected to be one of three types: mono-, di-, or poly-nuclear metal complexes—that is, A, B, and C in Fig. 1, depending on the chain length of the polymethylene bridge.

The synthetic routes are shown in Scheme 1. The III_n compounds (n=6, 8, and 10) were synthesized by the Friedel-Crafts acylation of 5-ethyl-8-quinolinol[3] with polymethylenedicarbonyl chlorides of different chain lengths. In order to cause the acylation exclusively at the 7-position, the 5-position of 8-quinolinol was blocked by an ethyl group. The IV_n compounds were obtained by the Huang-Minlon modification of the Wolff-Kischner reduction of the corresponding III_n compounds. The copper(II) complexes were obtained by the addition of an ethanolic solution of copper(II) acetate monohydrate to a solution of the corresponding IV_n compounds in ethanol (n=6 and 10) or dioxane (n=8).

* To whom all correspondence should be addressed.

1) Present address: Mitsubishi Monsanto Chemical Co. Ltd., 1 Tohocho, Yokkaichi, Mie.

2) Present address: Okamoto, Kasuga, Fukuoka.

3) K. W. Rosenmund and G. Kerst, *Arch. Pharm.*, **279**, 154 (1941).

Table 1.

Comp[a]	Cryst. form[b]	Cryst. Solv.[b]	Mp (°C)	Analyses, % Found C	H	N	Cu	Calcd C	H	N	Cu	Yield %
III_6	py. n	CH_2Cl_2	219.0—219.5	73.62	6.37	5.94		73.66	6.18	6.14		69
III_8	w. n	THF	184.6—185.2	74.26	6.63	5.61		74.35	6.66	5.78		69.4
III_{10}	py. c	C_2H_5OH	136.0—136.5	75.14	7.21	5.35		74.97	7.08	5.46		70
IV_6	w. n	C_6H_6	174.0—174.6	77.82	7.09	6.81		77.97	7.05	7.00		69
IV_8	w. c	$CHCl_3$	158.0—158.4	79.18	8.02	5.92		78.91	7.95	6.14		35.4
IV_{10}	w. c	C_2H_5OH	103.8—104.5	79.52	8.23	5.51		79.30	8.32	5.78		66
IV_6-Cu[c]	rb. l			68.09	6.47	5.26	12.38	68.61	6.17	5.26	12.96	63
IV_8-Cu	or. p			69.69	6.67	5.16	12.04	69.54	6.61	5.40	12.26	43.2
IV_{10}-Cu	or. p			69.96	7.00	5.06	12.09	69.85	6.96	5.09	11.54	60.3

a) Percentages were calculated according to the formula. III_6: $C_{28}H_{28}N_2O_4$, III_8: $C_{30}H_{32}N_2O_4$, III_{10}: $C_{32}H_{36}N_2O_4$, IV_{16}: $C_{28}H_{32}N_2O_2$, IV_8: $C_{30}H_{36}N_2O_2$, IV_{10}: $C_{32}H_{40}N_2O_2$,, IV_6-Cu: $C_{28}H_{30}N_2O_2Cu$, IV_8-Cu: $C_{30}H_{34}N_2O_2Cu$, IV_{10}-Cu: $C_{32}H_{38}N_2O_2Cu$.

b) c; crystals. l,; leaflets. n; needles. or: ;orange. p; powder. py; pale yellow. rb; reddish brown. THF; tetrahydrofuran. w; white.

c) Anal; mol wt, 985 in $CHCl_3$. Calcd for $C_{56}H_{60}N_4O_4Cu_2$ as B in Fig. 1; mol wt, 980.18.

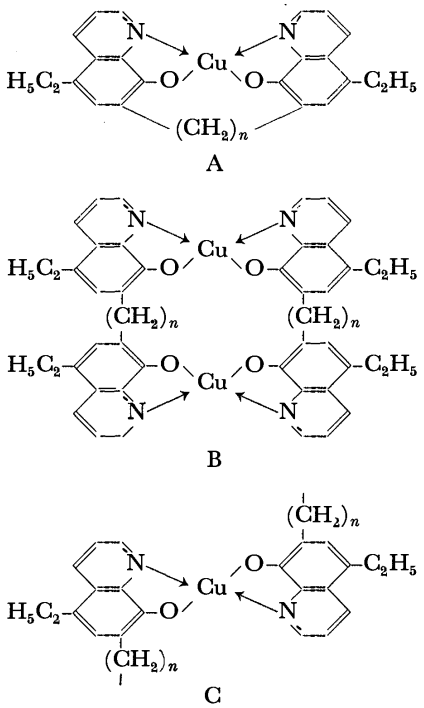

Fig. 1

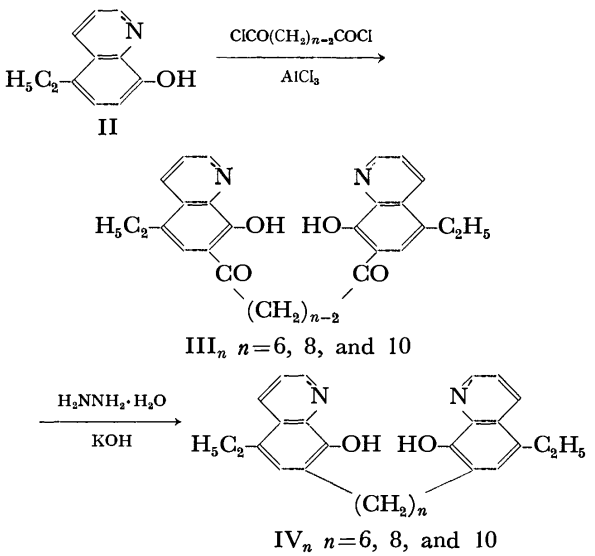

Scheme 1.

The physical properties and analytical data are shown in Table 1. The results of the molecular-weight determination indicate that the benzene-soluble copper(II) complex of the IV_6 compound is dimeric. For the copper(II) complexes of the IV_8 and IV_{10} compounds, the molecular weight could not be determined owing to the extremely low solubility in the solvents suitable for molecular weight determination. Bis(5-ethyl-8-quinolinolato)copper(II) is considered to have a *trans*-planar configuration, as does the well-known bis(8-quinolinolato)copper(II),[4] and to have an absorption maximum at 693 mμ in chloroform, as is shown in Table 2. The copper(II) complexes of the IV_8 and IV_{10} compounds also showed an absorption maximum at a similar position. Therefore, these complexes are inferred to have probably a polymeric, *trans*-planar structure either C in Fig. 1 or a similar structure. In the case of the copper(II) complex of the IV_6 compound, however, the absorption maximum is slightly different from those of the complexes of 5-ethyl-8-quinolinol as well as those of the IV_8 and IV_{10} compounds. From

Table 2. Absorption maxima of copper(II) complexes of II, IV_6, IV_8, and IV_{10} in chloroform

	λ_{max}	ε_{max}
II-Cu	693	52
IV_6-Cu	715	46
IV_8-Cu	690	a)
IV_{10}-Cu	690	a)

a) Accurate measurements of extinction coefficients could not be obtained in chloroform, owing to extremely low solubility of the compounds in this solvents.

4) R. C. Hoy and R. H. Morris, *Acta Crystallogr.*, **22**, 476 (1967).

the fact that the absorption maximum differed from those of the *trans*-structure and the fact that the molecular weight coincided with that of the dimer, as has been described above, the benzene-soluble copper(II) complex of the IV_6 compound may be concluded probably to have such a dinuclear *cis*- or near-*cis*-structure as B in Fig. 1.

Experimental

The melting points are uncorrected. The infrared spectra were obtained on a Hitachi EPI-S2 spectrophotometer in a KBr disk. The electronic spectra were measured in chloroform on a Hitachi EPI-3T spectrophotometer. The molecular weight was determined on a Hitachi Perkin-Elmer molecular-weight-determination apparatus, using benzene as the solvent.

1,6-Bis(5-ethyl-8-hydroxy-7-quinolyl)hexane-1,6-dione. III_6. To a stirred solution of 5-ethyl-8-quinolinol[3] (5 g) in tetrachloroethane (140 m*l*), adipyl chloride (2 g) was added. The then separated yellow precipitate was dissolved during the portion-by-portion addition of anhydrous aluminum chloride (15.5 g). The resulting yellow solution was kept at about 70°C for 15 hr to separate a green precipitate. After being cooled, the mixture was poured onto ice to precipitate hydrochloride of the III_6 compound, which was collected, washed with benzene, and boiled with water to change it into the corresponding free base. The base was then crystallized to give pale yellow needles by extraction with methylene chloride using a Soxhlet extractor. $\nu_{C=O}$, 1628 cm^{-1}.

1,8-Bis(5-ethyl-8-hydroxy-7-quinolyl)octane-1,8-dione. III_8. A mixture of 15 g of 5-ethyl-8-quinolinol, 9 g of suberyl chloride, 33 g of anhydrous aluminum chloride, and 150 m*l* of tetrachloroethane was heated at 65—68°C for 15 hr. The reaction mixture was poured onto crushed ice. The tetrachloroethane was removed by steam distillation. A precipitate of III_8 hydrochloride was filtered and suspended in water. The free base, III_8, was obtained by the neutralization of III_8 hydrochloride with sodium hydroxide. $\nu_{C=O}$, 1658 cm^{-1}.

1,10-Bis(5-ethyl-8-hydroxy-7-quinolyl)decane-1,10-dione. III_{10}. A mixture of 10 g of 5-ethyl-8-quinolinol, 6.8 g of sebacyl chloride, 31.5 g of anhydrous aluminum chloride, and 120 m*l* of tetrachloroethane was heated at 65—70°C for 20 hr. After the subsequent removal of the tetrachloroethane by steam distillation, a separated precipitate of the III_{10} hydrochloride was filtered and then suspended in water. The free base, III_{10}, was obtained by the neutralization of the III_{10} hydrochloride with sodium hydroxide. $\nu_{C=O}$, 1662 cm^{-1}.

1,6-Bis(5-ethyl-8-hydroxy-7-quinolyl)hexane. IV_6. A mixture of the III_6 compound (2 g), hydrazine hydrate (20 m*l*), and potassium hydroxide (15 g) in triethylene glycol (75 m*l*) was heated at 200—220°C for 1 hr until gas evolution ceased. The resulting red solution was poured into water and neutralized with hydrochloric acid to give a yellow precipitate, which was then collected and dried. The crude product was dissolved in benzene and chromatographed on silica gel to afford colorless needles.

1,8-Bis(5-ethyl-8-hydroxy-7-quinolyl)octane. IV_8. A mixture of 1 g of the III_8 diketone, 15 m*l* of hydrazine hydrate, 10 g of potassium hydroxide, and 60 m*l* of diethylene glycol was heated at 200—230°C for 1.5 hr. After being cooled, the reaction mixture was poured into water and then neutralized with hydrochloric acid to give a precipitate. The precipitate was collected by filtration and dried. The crude product was dissolved in chloroform and chromatographed on silica gel to afford colorless crystals.

1,10-Bis(5-ethyl-8-hydroxy-7-quinolyl)decane. IV_{10}. A mixture of 1 g of the III_{10} diketone, 13 m*l* of hydrazine hydrate, 10 g of potassium hydroxide, and 80 m*l* of triethylene glycol was heated at 220°C for 1.5 hr. The crude product was dissolved in benzene and chromatographed on silica gel to afford colorless needles.

Copper(II) Complex of the Compound IV_6. $B(n=6)$. A solution of copper(II) acetate monohydrate (100.8 mg) in ethanol (100 m*l*) was vigorously stirred, drop by drop over a 20 min period, into a warm solution of the IV_6 compound (214 mg) in ethanol (150 m*l*) to give reddish-brown leaflets. About 1 mg of the complex is soluble in 1 m*l* of benzene.

Copper(II) Complex of the Compound IV_8. $B(n=8)$. A solution of 20.1 mg of copper(II) acetate monohydrate in 15 m*l* of ethanol was added to a solution of 45.8 mg of IV_8 in 30 m*l* of dioxane. The solution turned dark yellow, and after it had stand overnight the orange precipitate was separated. It was insoluble in benzene and chloroform.

Copper(II) Complex of the Compound IV_{10}. $B(n=10)$. A solution of 100.7 mg of copper(II) acetate monohydrate in 100 m*l* of ethanol was added, drop by drop to a solution of 21.7 mg of VI_{10} in 150 m*l* of ethanol. The mixture turned yellow and the orange precipitate was separated. It was very slightly soluble in chloroform and soluble in pyridine, but the pyridine solution gave no precipitate when concentrated and cooled.

BULLETIN OF THE CHEMICAL SOCIETY OF JAPAN, VOL. 45, 3488—3490 (1972)

An ESR Study of the 1:2 Complexes of Copper(II) with Optically-active and Racemic α-Amino Acids

Hiroshi Yokoi, Mitsuru Sai, and Taro Isobe

Chemical Research Institute of Non-aqueous Solutions, Tohoku University, Katahira, Sendai

(Received February 10, 1972)

Any of the crystal structures of the metal complexes of amino acids are unpredictably unique because of their characteristic hydrogen-bonding behavior.[1,2] Various properties of the complexes in crystal have been studied by the IR,[3-6] visible absorption,[6,7] and ESR[8] methods. Special attention has been given to stereospecific effects in complexes of metals with optically-active ligands.[9] The purpose of this paper is briefly to communicate the ESR results of the 1:2 complexes of copper(II) with various optically-active and racemic α-amino acids in various states.

Experimental

Materials. The copper(II) complexes employed here are listed in Table 1, together with their abbreviations. They all were prepared according to the usual methods,[6,10] using commercial G.R.-grade α-amino acids, and were recrystallized from water. $[Cu(L\text{-}Ala)_2]$ and $[Cu(L\text{-}Val)_2]$ were prepared by heating the corresponding hydrates *in vacuo* at about 160°C. All the complexes were identified by elemental analysis.

Measurements. The X-band and K-band ESR spectra of the complexes were measured in a polycrystalline state at room temperature and in a frozen solution at the temperature of liquid nitrogen with a Hitachi ESR spectrometer, Model MES-4001. The sample solutions contained the complexes in concentrations of 10^{-3}—10^{-2}M, where an equivolume mixture of water and methanol was used as the solvent. The visible absorption spectra of the complexes in a polycrystalline state were measured by the so-called opal glass method with a Cary model 14 spectrometer.[11]

Table 1. Experimental data

Ligand	Copper (II) complex[a]	Polycrystals[b] g_1	g_2	g_3	λ_{max}[d] (nm)	Frozen solution[c] $g_{//}$[e]	$g_\perp$[f]	$\lvert A_{//}\rvert$[g] $\times 10^4$ (cm^{-1})	λ_{max}[h] (nm)
L-Alanine	$[Cu(L\text{-}Ala)_2]$	2.059	2.107	2.198	590	2.264	2.056	178.3	620
DL-Alanine	$[Cu(DL\text{-}Ala)_2]\cdot H_2O$	2.053	2.122	2.180	580	2.264	2.056	178.5	620
	$[Cu(DL\text{-}Ala)_2]$	2.054	2.100	2.202	580				
L-Valine	$[Cu(L\text{-}Val)_2]\cdot H_2O$	2.059		2.243	617	2.269	2.055	171.9	615
	$[Cu(L\text{-}Val)_2]$	2.054		2.237	622				
DL-Valine	$[Cu(DL\text{-}Val)_2]$	2.056	2.105	2.202	603	2.268	2.056	174.9	615
L-Serine	$[Cu(L\text{-}Ser)_2]$	2.056	2.157		603	2.266	2.057	176.2	623
DL-Serine	$[Cu(DL\text{-}Ser)_2]$	2.058	2.111	2.208	615	2.264	2.056	179.4	623
L-Proline	$[Cu(L\text{-}Pro)_2]\cdot 2H_2O$	2.059	2.158		610	2.261	2.058	188.0	610
DL-Proline	$[Cu(DL\text{-}Pro)_2]\cdot 2H_2O$	2.065[i]		2.190[i]	605	2.266	2.056	178.7	610

a) The abbreviations of L-Ala *etc.* represent the anions of ligands.
b) The numbers written between neighboring g columns express the g values in both of the column.
c) The $g_{//}$ and $A_{//}$ values were determined from the X-band ESR spectra measured in aqueous-methanolic (an equivolume mixture) solution at 77°K.
d) ±4 nm.
e) ±0.001.
f) The $g_\perp$ values were determined from the K-band ESR spectra, as an example in Fig. 2 shows.
g) ±0.5.
h) measured in aqueous solution at room temperature.
i) The g values were tentatively determined from the positions shown by arrows in Fig. 1 (10).

1) H. C. Freeman, "The Biochemistry of Copper," ed. by J. Peisach, P. Aisen, and W. E. Blumberg, Academic Press, New York (1966), p. 77.
2) W. E. Hatfield and R. Whyman, "Transition Metal Chemistry," ed. by R. L. Carlin, Vol. 5, Marcel Dekker, New York (1969), p. 95.
3) K. Nakamoto, "Infrared Spectra of Inorganic and Coordination Compounds," John Wiley & Sons, New York (1963), p. 201, and the references therein.
4) A. W. Herlinger, S. L. Wenhold, and T. V. Long, II, *J. Amer. Chem. Soc.*, **92**, 6474 (1970), and the references therein.
5) A. W. Herlinger and T. V. Long, II, *ibid.*, **92**, 6481 (1970).
6) D. P. Graddon and L. Munday, *J. Inorg. Nucl. Chem.*, **23**, 231 (1961).
7) G. Dijkgraaf, *Theoret. Chim. Acta*, **2**, 422 (1964); T. Yasui and Y. Shimura, This Bulletin, **39**, 604 (1966).
8) H. Yokoi, M. Sai, T. Isobe, and S. Ohsawa, This Bulletin, **45**, 2189 (1972).
9) R. D. Gillard, H. M. Irving, R. M. Parkins, N. C. Payne, and L. D. Pettit, *J. Chem. Soc., A*, **1966**, 1159; R. D. Gillard, R, Mason, N. C. Payne, and G. B. Robertson, *ibid.*, **1969**, 1864; R. D. Gillard and S. H. Laurie, *ibid.*, **1970**, 59.
10) E. Abderhalden and E. Schnitzler, *Z. Physiol. Chem.*, **163**, 94 (1927).
11) K. Shibata, "Jikken Kagaku Koza," Vol. 11, ed. by *Chem. Soc. Japan*, Maruzen, Tokyo (1965), p. 192.

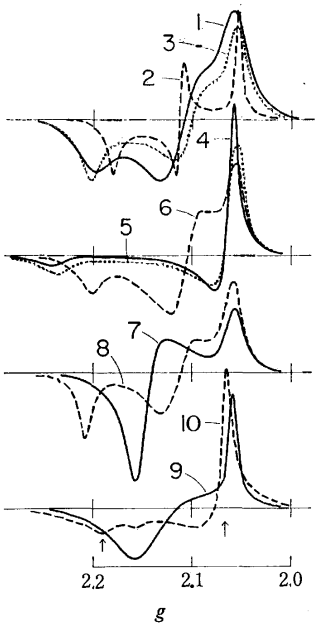

Fig. 1. Powder K-band ESR spectra at room temperature.
(1): $[Cu(L\text{-}Ala)_2]$, (2): $[Cu(DL\text{-}Ala)_2]\cdot H_2O$, (3): $[Cu(DL\text{-}Ala)_2]$, (4): $[Cu(L\text{-}Val)_2]\cdot H_2O$, (5): $[Cu(L\text{-}Val)_2]$, (6): $[Cu(DL\text{-}Val)_2]$, (7): $[Cu(L\text{-}Ser)_2]$, (8): $[Cu(DL\text{-}Ser)_2]$, (9): $[Cu(L\text{-}Pro)_2]\cdot 2H_2O$, (10): $[Cu(DL\text{-}Pro)_2]\cdot 2H_2O$.

Results and Discussion

Powder ESR Spectra. All the powder K-band ESR spectra are shown in Fig. 1; they were analyzed by the use of the approximation of Kneubühl.[12] The results are listed in Table 1, together with the visible absorption data. It has been suggested that there may be no such strong spin-exchange interactions as affect the g values in most crystals of the *trans* 1:2 complexes of copper (II) with amino acids.[8,13]

The ESR line shape of $[Cu(DL\text{-}Ala)_2]\cdot H_2O$ was quite different from that of $[Cu(L\text{-}Ala)_2]$. The dehydration of $[Cu(DL\text{-}Ala)_2]\cdot H_2O$ caused a drastic change in the ESR spectrum; the resulting spectrum resembled that of $[Cu(L\text{-}Ala)_2]$. This fact indicates that the water molecule of $[Cu(DL\text{-}Ala)_2]\cdot H_2O$ in a crystal is influential in determining the copper(II)-ion environment. The ESR line shapes of $[Cu(DL\text{-}Val)_2]$ and $[Cu(DL\text{-}Ser)_2]$ were also similar to that of $[Cu(L\text{-}Ala)_2]$. Their optically-active isomers, however. were quite different in line shape from $[Cu(L\text{-}Ala)_2]$, The spectra of both $[Cu(L\text{-}Val)_2]$ and its hydrate, whose g values were almost the same, indicate an elongated-tetragonal copper(II)-ion environment; therefore, the water molecule of this hydrate is of little importance to the copper(II)-ion environment. On the other hand, $[Cu(L\text{-}Ser)_2]$ showed a so-called reverse ESR spectrum ($g_{//}<g_{\perp}$) as well as $[Cu(L\text{-}Pro)_2]\cdot 2H_2O$. $[Cu(L\text{-}Ser)_2]$ is known to adopt a *cis*-configuration,[14] and it has been inferred from IR measurements that $[Cu(L\text{-}Pro)_2]\cdot 2H_2O$ also adopts a *cis*-geometry.[5] The crystal of $[Cu(L\text{-}Ser)_2]$ is quite different from those of the other *trans* complexes in the packing of crystallographically non-equivalent molecular pairs,[1,8,14] and it seems likely that the reverse ESR spectrum is caused by a spin-exchange interaction which is effective on the crystal structure of the *cis* complex. In a word, all the above-mentioned experimental facts clearly indicate that a sensitive detection and investigation of the stereospecificity in a metal complex in a crystylline solid can be carried out by the ESR method.

Solution ESR Spectra. All the ESR line shapes observed for the complexes in a frozen aqueous-methanolic solution were quite similar to each other; this fact is in striking contrast with the results in a crystalline solid. The K-band ESR line shapes indicate especially clearly that the copper(II) ions are present in a tetragonal field, as the example shown in Fig. 2 shows. This behavior of the complexes in solution may be regarded as a general property of the planar copper (II) complexes.[15]

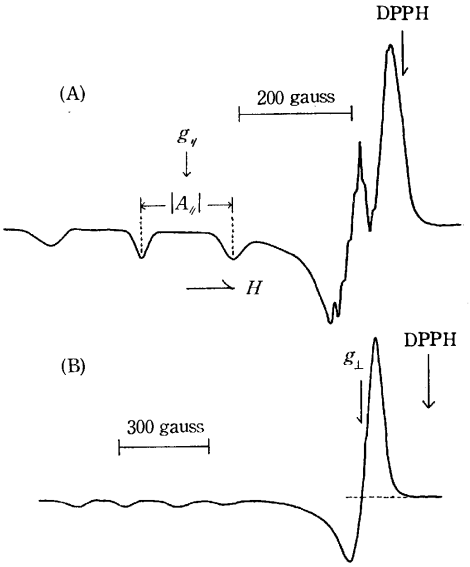

Fig. 2. The ESR spectra of $[Cu(L\text{-}Val)_2]\cdot H_2O$ in aqueous-methanolic solution at 77°K.
(A): X-band, (B): K-band.

Each of the data of $g_{//}$ and $|A_{//}|$ in Table 1 was obtained as the average of 5—8 experiments. These data clearly indicate that there is a small but significant difference in the copper(II)-ion environment between the optical isomers in frozen solutions. Interestingly, the ORD experiments for analogous samples in aqueous solutions showed that the conformation of the chelate ring influences the apical coordination of water molecules.[16] In this work, however, the observed difference between the isomers is too small to reveal what structural difference there is practically. A racemic copper(II) complex in solution is distributed among the three isomers, $[Cu(L\text{-}A)_2]$, $[Cu(D\text{-}A)_2]$, and $[Cu(L\text{-}A)(D\text{-}A)]$,

12) F. K. Kneubühl, *J. Chem. Phys.*, **33**, 1074 (1960).
13) H. Yokoi and T. Isobe, *Chem. Lett.*, **1972**, 95.
14) D. van der Helm and W. A. Franks, *Acta Crystallogr.*, **B25**, 451 (1969).
15) H. Yokoi, M. Otagiri, and T. Isobe, This Bulletin, **44**. 2395 (1971); *ibid.*, to be published.
16) K. M. Wellman, T. G. Mecca, W. Mungall, and C. R. Hare, *J. Amer. Chem. Soc.*, **89**, 3646 (1967); *ibid.*, **89**, 3647 (1967); *ibid.*, **90**, 805 (1968).

in the statistically-expected concentration ratio of 1 : 1 : 2,[17] where A represents an α-amino acid anion. This fact indicates that the essential difference in any parameter between [Cu(L-A)$_2$] and [Cu(L-A)(D-A)] is larger than the observed one.

17) R. D. Gillard, H. M. Irving, and L. Pettit, *J. Chem. Soc.*, *A*, **1968**, 673; S. Bruckenstein and L. D. Pettit, *J. Amer. Chem. Soc.*, **88**, 4790 (1966).

BULLETIN OF THE CHEMICAL SOCIETY OF JAPAN, VOL. 45, 3490—3492 (1972)

O-Alkylation of Phenols by Esters

Taketoshi KITO, Norimichi YANAI, and Ichiro HIRAO

Laboratory of Industrial Chemistry, Department of Chemical Engineering, Kyushu Institute of Technology, Tobata-ku, Kita-kyushu

(Received March 10, 1972)

We have reported that methyl *p*-hydroxybenzoate adds to acrylonitirle and methyl acrylate in the presence of triton B or metal sodium to give compounds with cyanoethyl and methoxycarbonylethyl groups respectively.[1] In these reactions, good results were obtained below 150°C. However, when methyl methacrylate was used in place of acrylonitrile or methyl acrylate, no product was obtained under the conditions employed in the above reactions. Therefore, we carried out the reaction of potassium salt of methyl *p*-hydroxybenzoate with methyl methacrylate at 200°C, and the resulting mixture was analyzed by gas chromatography. As a result, the mixture was found to contain methyl *p*-anisiate and a dimer of methyl methacrylate. The latter is methyl 2-methyl-5-methoxycarbonyl-5-hexenoate [CH_2=C($COOCH_3$)$CH_2CH_2CH(CH_3)COOCH_3$], whose structure was confirmed by instrumental analysis. This reaction is interesting as an *O*-alkylation of phenols.

This reaction was then also applied to other phenols, and good results were obtained there. Moreover, alkyl esters of acrylic acid and acetic acid were also found to be effective alkylating agents. The present paper will deal with the *O*-alkylation of phenols by esters.

Experimental

The NMR spectra were obtained on a Japan Electron Optics Laboratory spectrometer (JNM C-60HL), with TMS used as the internal standard. The mass spectra were obtained on a Hitachi mass spectrometer (RMU-6L), using an electron-accelerating voltage of 70eV. The IR spectrum was measured with a Japan Spectroscopic spectrometer (IRA-2). The gas chromatography was performed with a Yanagimoto apparatus (G80T).

Reaction of Potassium Salt of Methyl p-*Hydroxybenzoate with Methyl Methacrylate.* In a 300 m*l* autoclave, with an electro-magnetic stirrer, we placed 0.07 mol of potassium salt of methyl *p*-hydroxybenzoate and 0.7 mol (70.0 g) of methyl methacrylate containing 0.1 wt% of hydroquinone. After the air had been replaced by nitrogen, the mixture was heated to the prescribed temperature (it took about 30 min) and kept there for 5 hr. After cooling, the insoluble product was filtered off and the filtrate was washed with an aqueous alkaline solution and water. The mixture was found by gas chromatography to contain two main components (I and II).

The another reactions were carried out under the same conditions.

The components, I and II, were separated by gas chromatography and were analyzed by NMR, MS, IR, and elementary analysis. The results were as follows. Component I: NMR ($CHCl_3$); τ 2.98 (a part of the AB system, 2H, J=9.0 Hz), 3.07 (a part of the AB system, 2H, J=9.0 Hz), 6.07 (s, 3H), and 6.12 (s, 3H). Mass; *m/e* 168 (1.2%), 167 (9.9), 166 (M^+, 93.7), 136 (27.0), 135 (100), 107 (37.1), 92 (45.2), 77 (65.5), 64 (31.5), 63 (28.0), 50 (15.5), and 15 (12.6). Found: C, 65.18; H, 6.35%. Calcd for $C_9H_{10}O_3$: C, 65.05; H, 6.07%. Component II: NMR (neat); τ 3.92 (d, 1H, J=1.4 Hz), 4.45 (d, 1H, J=1.4 Hz), 6.29 (s, 3H), 6.38 (s, 3H), 7.5—7.9 (m, 3H), 8.1—8.5 (m, 2H), and 8.87 (d, 3H, J=7.3 Hz). Mass; *m/e* 200 (M^+, 1.0%), 141 (33.9), 140 (55.3), 126 (63.0), 125 (37.6), 109 (44.7), 88 (100), 81 (94.2), 59 (52.4), 57 (36.9), 56 (33.2), 53 (32.5), 41 (57.3), 39 (38.6), and 15 (57.6). IR (cm^{-1}); 1727 (s, broad), 1633 (m), and 945 (m). Found: C, 59.83; H, 8.15%. Calcd for $C_{10}H_{16}O_4$: C, 59.98; H, 8.05% On the basis of these data, these components, I and II, were identified as methyl *p*-anisiate and CH_2=C($COOCH_3$)-$CH_2CH_2CH(CH_3)COOCH_3$ respectively.

Determination of Products. All the products were determined by gas chromatography, using dimethylaniline or nitrobenzene as the internal standard. The conditions were as follows: column, PEG 20M or Apiezone Grease L 2.25 m; temp. 200°C; He, 10 m*l*/min. Authentic samples of *O*-methyl products (anisole derivatives), if necessary, were prepared from phenols and dimethyl sulfate in aqueous alkali. Phenyl butyl ether was prepared by Williamson ether synthesis.

Results and Discussion

The reaction of alkali phenoxides with methyl methacrylate was carried out at 150, 200, and 250°C for 5 hr. In the gas chromatograms of those reaction mixtures, no products with retention times longer than that of methyl methacrylate were found, or if any were found, they were all minor products except for the *O*-methyl product and the dimer. Therefore, the resulting *O*-methyl product and dimer were determined by gas chromatography. The results are summarized in Table 1.

1) The 24th Annual Meeting of the Chemical Society of Japan, Osaka, 1971.

Table 1. *O*-Methylation of phenols by methyl methacrylate

R-C_6H_4-OM R	M	MMA[a]/RC_6H_4OM (mol/mol)	Temp[b] (°C)	*O*-Methyl Product, Yield (%)[c]	Dimer Yield (%)[d]
H	K	10	150	16.9	0.2
H	K	10	200	73.2	3.6
H	K	10/3	200	73.6	0.8
H	Na	10	150	8.9	0.2
H	Na	10	200	44.6	3.6
H	Na	10	250	59.6	12.9
H	Na	10/3	250	50.9	11.6
o-CH_3	K	10	200	29.4	5.1
m-CH_3	K	10	200	74.8	3.1
p-CH_3	K	10	200	84.5	6.8
p-CH_3	Na	10	200	69.4	1.8
o-Cl	K	10	200	13.9	2.7
p-Cl	K	10	200	48.9	3.7
p-$COOCH_3$	K	10	150	0.1	0.2
p-$COOCH_3$	K	10	200	11.9[e]	0.8[e]
p-$COOCH_3$	K	10	250	74.8	1.2
H	H	10	250	0.0	8.5
—	—	—	200	—	3.2[f]

a) MMA: Methyl methacrylate, 0.1 wt% of hydroquinone is contained.
b) Reaction time; 5 hr.
c) Yields are based on phenols used.
d) Yields are based on MMA used.
e) NMR, MS, and IR data are present in the experimental section.
f) MMA was heated in the absence of phenoxides.

Similar reactions were carried out in methyl acetate and acrylate in place of methyl methacrylate. *O*-methyl products were also obtained from both reactions, but an appreciable amount of polymer was formed in the latter and this complicated the post-treatment of the reaction mixture. The yields from both reactions were lower than those from the reactions in methyl methacrylate under comparable conditions, but the yield of the *O*-methyl product was not appreciably affected by the reaction temperature.

From the reactions of potassium phenoxide with ethyl methacrylate, acrylate, and acetate at 200°C for 5 hr, phenetole was obtained. Similarly, from the reaction of potassium phenoxide with butyl methacrylate and acetate, phenyl butyl ether was obtained. These results are listed in Table 2.

Patai and his co-worker reported that 2-alkoxynaphthalene was formed in the reaction of 2-naphthol (0.04 mol) with the ester (0.08 mol), in which methyl methacrylate, methyl acetate, ethyl acetate, and ethyl butyrate were included, in the presence of concentrated sulfuric acid (0.1 m*l*) at the reflux temperature.[2] The yield of 2-methoxynaphtalene from methyl acetate was 20—25%, that from methyl methacrylate was 45—50%, that of 2-ethoxynaphthalene from ethyl acetate was 40—45%, and that from ethyl butyrate, 20—25%. These results suggest that the alkylation was caused by the alkyl hydrogen sulfate formed from the ester and sulfuric acid.

Table 2. *O*-Alkylation of phenols by esters

R-C_6H_4-OM R	M	Ester[a]	Temp.[b] (°C)	*O*-Alkyl Product Alkyl	Yield(%)[c]
H	K	AcOMe	200	CH_3	41.1
H	K	AcOMe	250	CH_3	54.6
H	Na	AcOMe	200	CH_3	54.8
m-CH_3	K	AcOMe	250	CH_3	73.6
p-Cl	K	AcOMe	250	CH_3	50.0
H	K	AcOEt	200	C_2H_5	49.4
H	K	AcOEt	250	C_2H_5	46.4
H	Na	AcOEt	200	C_2H_5	49.4
H	Na	AcOEt	250	C_2H_5	49.0
H	K	AcOBu	250	*n*-C_4H_9	52.8
H	Na	AcOBu	250	*n*-C_4H_9	22.0
H	K	MA	200	CH_3	41.6
H	K	EA	200	C_2H_5	17.9
H	K	MMA	200	CH_3	73.2
H	K	EMA	200	C_2H_5[d]	46.4
H	K	BMA	200	*n*-C_4H_9	29.9

a) Ester/RC_6H_4OM(mol/mol) = 10; MA,EA,EMA, and BMA are methyl acrylate, ethyl acrylate, ethyl methacrylate, and butyl methacrylate, respectively. These esters contain 0.1 wt% of hydroquinone.
b) Reaction time; 5 hr.
c) Yields are based on phenols used.
d) The structure was confirmed by NMR and IR.

Pierce and his co-worker reported that anisole was formed in the reaction of sodium phenoxide with methyl trichloroacetate at room temperature in carbon tetrachloride, although the reaction of sodium phenoxide with ethyl trifluoroacetate gave no phenetole, but only phenyl trifluoroacetate.[3]

The reaction process treated in this paper may be expressed as in Eq. (1), where R_1 is isopropenyl, ethenyl or methyl, where R_2 is methyl, ethyl, or butyl, where

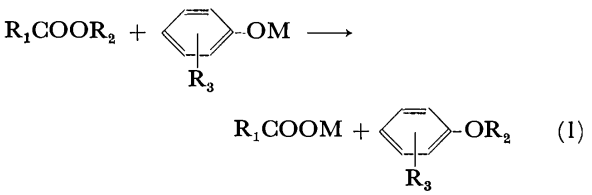

(1)

R_3 is a substituent on a phenyl nucleus, and where M is sodium or potassium. If the oxygen atom of phenol attacks the carbonyl carbon atom of the ester, the resulting product would be the phenyl ester; this is the reaction of sodium phenoxide with ethyl trifluoroacetate reported by Pierce and his co-worker.[3] However, in the present reactions, the oxygen atom of phenoxides must attack the alkyl carbon atom adjacent to the ether linkage and the alkyl-oxygen cleavage must occur. This mechanism is supported by the formation of phenetole and phenyl butyl ether described above. The reactions will be favored, thus, by a greater charge separation between oxygen and alkali atoms of alkali phenoxides. Therefore, the potassium salts must give better results than the sodium salts. On the contrary, the reaction will not be favored by an electron-attracting group, such as chloro and

2) S. Patai and M. Bentov, *J. Amer. Chem. Soc.*, **74**, 6118 (1952).
3) A. C. Pierce and M. M. Joullié, *J. Org. Chem.*, **27**, 3968 (1962).

methoxycarbonyl groups, as an *ortho* substituent. Higher alkyl esters, such as butyl and ethyl esters, will also reduce the yield of the *O*-alkyl product. The results listed in Tables 1 and 2 are almost all consistent with the above idea.

The reaction with methyl methacrylate proceeded in two directions, the one being an *O*-methylating reaction, and the other, a dimerization of methyl methacrylate. The latter reaction has been reported by Albisetti and his co-workers; they determined the structure of the resulting dimer by a chemical technique.[4] The yield of the dimer was not affected by the molar ratio of methyl methacrylate: phenoxides (Table 1), suggesting that the two reactions—that is, an *O*-alkylation and a dimerization of methacrylate (methyl, ethyl, or butyl ester)—proceed independently of one other.

Thanks are due to Mr. Takatomo Funamoto for his assistance in the experimental work.

4) C. J. Albisetti, D. C. England, M. J. Hogsed, and R. M. Joyce, *J. Amer. Chem. Soc.*, **78**, 472 (1956).

BULLETIN OF THE CHEMICAL SOCIETY OF JAPAN, VOL. 45, 3492—3493 (1972)

Studies of Organosulfur Compounds. VII. The Preparation and Reaction of Some Crystalline Piperidinium Salts of Aliphatic Dithio Acid

Shinzi KATO and Masateru MIZUTA
Faculty of Engineering, Gifu University, Kagamihara, Gifu

(Received March 21, 1972)

Although the syntheses of aliphatic dithio acid derivatives have been carried out, no isolation of the salts (almost entirely metal salts), which are very important as intermediates in the preparation of derivatives, have been reported as yet. In the course of the studies of the reactions bis(thioaroyl)disulfides with amines, it was found that the crystals of amine salts of aromatic dithio acid were very stable[1] and could easily be obtained from the corresponding aromatic dithio acids and various secondary or tertiary amines.[2] In this paper, we wish to report the successful preparation of some crystalline piperidinium salts of aliphatic dithio acid.

Results and Discussion

The reaction of dithiopropionic acid in ethyl acetate with an equimolar amount of piperidine gave piperidinium salts (IIa) of dithiopropionic acid in a 67% yield as glistering yellow crystals. The structure of IIa was identified by elemental analysis and by studying the IR and UV spectra. In the IR spectrum, strong broad absorption bands due to amine salts were observed in the range of 3000—2500 cm^{-1}, while the UV spectrum showed its maximum band at 455 mμ (ε 39). Furthermore, the structure of IIa was supported by the quantitative formation of the methylester through the action of methyl iodide. An analogous treatment of dithioisobutyric, dithiopentanoic, dithiohexanoic, and dithiocyclohexanecarboxylic acid with the piperidine gave the corresponding piperidinium salts (IIb—e) in good yields. The results are summarized in Table 1.

All the piperidinium salts obtained, except for that of dithiopropionic acid, were fairly stable in solid states at room temperature, and did not change when left standing for 3 days, but the salts gradually decomposed over 50°C, with the evolution of hydrogen sulfide. On the other hand, the salts of dithiopropionic acid

Table 1. Physical properties and elemental analyses of the amine salts of aliphatic dithio acid

Comp	R of $RCS_2^-\overset{+}{N}H_2\langle$	Mp (°C)	Yield %	IR, KBr $\nu_{C=S}$ cm^{-1}	λ_{max}^{EtOH} (ε)		Color[a]	Formula	Found (Calcd), % C	H	S	N
IIa	C_2H_5	113—114	67	950 925	339 (17300)	455 (31)	Y	$C_8H_{17}NS_2$	50.83 (50.26)	8.63 (8.67)	33.33 (33.51)	7.10 (7.33)
IIb	*i*-C_3H_7	133—134	82	850	339 (16500)	455 (39)	Y	$C_9H_{19}NS_2$	52.83 (52.68)	9.18 (9.27)	31.12 (31.22)	6.91 (6.83)
IIc	*n*-C_4H_9	62—63	72	970	339 (17500)	455 (30)	OY	$C_{10}H_{12}NS_2$	54.88 (54.79)	9.63 (9.59)	29.83 (29.22)	6.28 (6.39)
IId	*n*-C_5H_{11}	92—93	84	1000	399 (17300)	455 (31)	OY	$C_{11}H_{23}NS_2$	56.98 (56.65)	9.91 (9.87)	28.09 (27.46)	6.22 (6.01)
IIe	*cyclo*-C_6H_{11}	131—132	79	990	339 (17700)	455 (39)	OY	$C_{12}H_{25}NS_2$	58.00 (58.53)	9.88 (9.76)	26.01 (26.02)	5.77 (5.69)

a) Y: Yellow, OY: Orange Yellow

1) S. Kato and M. Mizuta, *Int. J. Sulfur Chem.*, in press.

2) S. Kato, T. Mitani, and M. Mizuta, unpublished data.

Table 2. Alkylation of the amine Salts (II)

R of $RCS_2^-\overset{+}{N}H_2\langle$	RX	Solvent	Temp °C	Time hr	Products	Bp °C/mmHg	Yield %
C_2H_5	CH_3I	CH_2Cl_2	rt	3	$C_2H_5CS_2CH_3$	51/13	98
C_2H_5	C_2H_5I	CH_2Cl_2	rt	3	$C_2H_5CS_2C_2H_5$	65/13	97
i-C_3H_7	CH_3I	CH_2Cl_2	rt	4	i-$C_3H_7CS_2CH_3$[a]	70/ 8	97
n-C_4H_9	CH_3I	CH_2Cl_2	rt	5	n-$C_4H_9CS_2CH_3$[b]	84/ 9	96
C_6H_{11}	CH_3I	CH_2Cl_2	rt	5	$C_6H_{11}CS_2CH_3$	77/ 1	98

a) Found: C, 44.92; H, 7.22; S, 48.10%; (Calcd for $C_5H_{10}S_2$: C, 44.80; H, 7.12; S, 47.80%. b) Found: C, 48.76; H, 8.29; S, 43.36% (Calcd for $C_6H_{12}S_2$: C, 48.60; H, 8.12; S, 43.31%.

were unstable, and after one week even at 0°C completely changed from solid to oily material, with the evolution of hydrogen sulfide.

The salts were only slightly soluble in ether, benzene, and acetonitrile, but were easily soluble in dichloromethane, chloroform, acetone, and ethanol. The salts readily reacted with alkyl bromides or iodides in dichloromethane to give the corresponding alkyl esters in almost quantitative yields, but the reactions with t-butyl bromide or alkyl chlorides with no electron withdrawing group on their α-position did not occur, even under more severe conditions (Table 2).

Spectral Data. *a) IR Spectra*: Mecke and Spiesecke[3] assigned $\nu_{C=S}$ to 1216 cm^{-1} for dithioacetic acid. However, there has been only one recent report on the subject; in it Lindner and Kunze[4] assigned $\nu_{C=S}$ for 1242 cm^{-1} for silver and lead trifluorodithioacetates. We reported that $\nu_{C=S}$ for the amine salts of aromatic dithio acids was observed near 1000 cm^{-1}.[2] In the amine salts, very intensive absorption bands seemingly due to $\nu_{C=S}$ of the dithiocarboxylate group were observed in the 1000—925 cm^{-1} range without any exceptions (Table 1). This results fits with those of the amine salts of aromatic dithio acids, and also with the assignment given for metal salts of dialkyldithiocarbamates (near 982 cm^{-1})[5] and xanthates (1040 and 1080 cm^{-1}),[6] and for trialkylphosphonidithioformulate ($R_3P^+CSS^-$, near 1050 cm^{-1}).[7]

b) UV Spectra: Table 1 lists the absorption maxima (λ max) in mμ and the molecular extinction coefficients (ε) at each maximum. As is shown in Table 1, the amine salts (II) showed two characteristic maximum band, 339 (ε 16000—18000) and 455 mμ (ε 30—40), without any exceptions, indicating that the former bands are due to $\pi\rightarrow\pi^*$, and the latter, due to $n\rightarrow\pi^*$.

Attempts at the isolation of the amine salts of dithioacetic and dithio-2-methyl-isobutyric acids, and the crystallization of secondary or tertiary amine salts other than the piperidinium salts were unsuccessful.

Experimental[8]

Materials. Aliphatic dithio acids were prepared in dry THF by the method of Houben.[9]

Some typical procedures are shown, and the detailed data are summarized in Table 1.

Piperidinium Salts (IIb) of Dithioisobutyric Acid. A solution of 1.7 g (0.02 mol) of piperidine in ethyl acetate (2 m*l*) was added to ethyl acetate (10 m*l*) containing 4.1 g (0.02 mol) of dithioisobutyric acid at 5°C and allowed to stand for overnight below −20°C. The precipitates were filtered and recrystallized from dichloromethane-n-hexane to give 3.9 g of IIb as plate crystals.

Reaction of the Piperidinium Salts (IIa) of Dithiopropionic Acid with Methyl Iodide. A solution of IIa (0.03 mol) and methyl iodide (0.04 mol) in dichloromethane (10 m*l*) was stirred at room temperature for 1 hr. After evaporating the solvent and the excess of methyl iodide, a small portion of petroleum ether (bp below 40°C) was added to the residue and insoluble parts (piperidinium iodide) were filtered off. Vacuum distillation of the filtrate gave 3.4 g (94%) of methyl dithiopropionate: bp 46—47°C/10—11 mmHg; IR (neat): $\nu_{C=S}$ 1190 cm^{-1}. The boiling point, and the IR spectrum were identical with those of an authentic sample prepared by the method of Houben and Shultze.[9]

The authors wish to thank Professor Yoshio Hirabayashi and Mr. Hideharu Ishihara of Gifu University for discussion.

3) R. Mecke and H. Spiesecke, *Chem. Ber.*, **89**, 1110 (1956).

4) E. Linder and U. Kunze, *Z. Anorg. Allg. Chem.*, **383**, 255 (1971).

5) J. Chatt, L. A. Duncanson, and L. M. Venanzi, *Suomen Kemistilehti*, **29** *B*, 75 (1956) See Ref. 7).

6) L. H. Little, G. W. Poling, and J. Leja, *Can. J. Chem.*, **39**, 745 (1961).

7) K. A. Jensen and P. H. Nielsen, *Acta Chem Scand.*, **17**, 547 (1963).

8) All melting points are uncorrected. The IR spectra were measured on a JASCO grating infrared spectrophotometer IR-G. The UV spectra were measured on a Hitachi 124 spectrophotometer.

9) J. Houben and K. M. L. Schultze, *Ber.*, **43**, 2481 (1910).

BULLETIN OF THE CHEMICAL SOCIETY OF JAPAN, VOL. 45, 3494—3495 (1972)

Dimorphic Forms of 2-Amino-4-(*N*-methylanilino)-6-isopropenyl-*s*-triazine

Yasuo YUKI, Tadao TAIKA, and Masamitsu NAGANO

Department of Fiber and Polymer, Nagoya Institute of Technology, Gokiso, Showa-ku, Nagoya

(Received April 11, 1972)

2-Amino-4-(*N*-methylanilino)-6-isopropenyl-*s*-triazine (AMIT) was prepared by the reaction of N^1-methyl-N^1-phenylbiguanide with methyl methacrylate, as has previously reported.[1] In this paper, it has been found that AMIT has dimorphic forms. In the case of the recrystallization of AMIT from methanol, two different crystals were obtained. The sample immediately crystallized was named AMIT-β, while that slowly crystallized was named AMIT-α. AMIT-β melted at 104°C and immediately solidified into a crystal that melted at 118°C. AMIT-α melted at 118°C. When the acetone solution of AMIT-α was poured into water, AMIT-β was precipitated. AMIT-α was also obtained by the crystallization of AMIT-β or an AMIT-α and β mixture from benzene. AMIT-α and β were easily changeable by crystallization by different procedures.

TABLE 1. ELEMENTARY ANALYSES AND NMR DATA OF AMIT

Sample	Elementary analyses C%	H%	N%	NMR data (DMSO-d_6, 35°C) (ppm)
AMIT-α	64.60	6.06	29.84	H_a, CH_3 H_a, 5.40(q)
AMIT-β	64.81	6.19	29.67	C=C H_b, 6.22(d)
Calcd for $C_{13}H_{15}N_5$	64.71	6.27	29.02	H_b, CH_3, 2.00(s) N-CH_3, 3.45(s) NH_2, 6.79(s) C_6H_5, 7.32(s)

The results of the elementary analyses and the NMR data of AMIT-α and β are shown in Table 1. The elementary analytical results were identical with the calculated value of AMIT. The NMR data in DMSO-d_6 were also identical with each other. The ultraviolet spectra of AMIT-α and β in ethanol, water, or cyclohexane were identical. From the above results, it was found that AMIT-α and β were the same compound.

The existence of two crystal forms has been confirmed by the entirely different X-ray powder diagrams for AMIT-α and β. Some absorptions of the infrared spectra of AMIT-α and β were different when the infrared spectra was measured in the crystal state in potassium bromide disks. The differences were shown in the absorptions of amino groups and isopropenyl groups. The N-H stretching absorptions were at 3325 (small), 3290, and 3190 cm^{-1} for AMIT-α, but they were at 3450, 3280, 3180 cm^{-1} for AMIT-β. The NH_2 bending absorptions of AMIT-α were at 1642 and 640 cm^{-1}, while that of AMIT-β were at 1620 and 655 cm^{-1}. The bending absorption of the isopropenyl group was at 940 cm^{-1} for AMIT-α and at 918 cm^{-1} for AMIT-β. The absorptions of the phenyl (760 and 695 cm^{-1}) and *s*-triazinyl (825 cm^{-1}) groups were identical with each other. From the above results, it was assumed that there was a different interaction between the proton of the amino group and the π electrons of the isopropenyl group of AMIT in crystals.

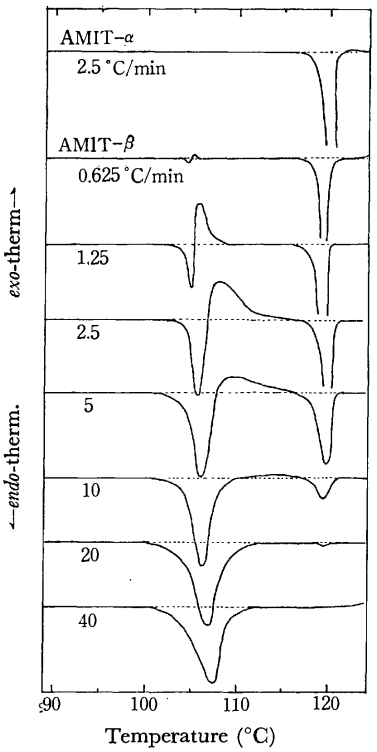

Fig. 1. DSC curves of AMIT-α and AMIT-β.

TABLE 2. ΔH OF AMIT-α AND β

Sample	Heating rate (°C/min)	ΔH_β	ΔH_{cr}	ΔH_α (kcal/mol)	$\Delta H_\beta'$
AMIT-α	2.6	—	—	6.6	—
AMIT-β	0.625	0.1	0.1	6.8	6.8
	1.25	2.8	2.5	6.9	7.2
	2.5	4.3	4.2	5.7	5.8
	5	6.0	2.6	3.4	6.8
	10	6.5	0.3	0.7	6.9
	20	6.4	—	0.1	6.5
	40	6.7	—	—	6.7

The thermal behavior of samples was examined by the technique of a differential scanning calorimeter (DSC). The results are shown in Fig. 1. AMIT-α showed only an endothermic peak at 118°C by fusion, and the heat of fusion of AMIT-α was 6.6 kcal/mol. On the other hand, AMIT-β showed two endothermic peaks, at 104 and 118°C, by fusion, and one exothermic peak between the two endothermic peaks. This exotherm was caused by crystallization. The heat of

1) Y. Yuki, T. Kakurai, and T. Noguchi, This Bulletin, **43**, 2123 (1970).

fusion at 104°C (ΔH_β), the heat of fusion at 118°C (ΔH_α) and the heat of crystallization (ΔH_{cr}) of AMIT-β are summed up in Table 2. These heats depended on the heating rate. ΔH_β was increased as the heating rate became faster. On the other hand, ΔH_α decreased as the heating rate became faster. ΔH_α was 6.8 kcal/mol at a heating rate of 0.625°C/min. This value was almost equal to the ΔH of AMIT-α. This is thought to be because the heat of fusion of AMIT-β is compensated for by the heat of crystallization. The theoretical heat of fusion of AMIT-β ($\Delta H_\beta'$) was obtained from Eq. (1):

$$\Delta H_\beta' = \Delta H_\beta + \Delta H_\alpha - \Delta H_{cr} \quad (1)$$

The values of $\Delta H_\beta'$ are also described in Table 2, and the mean value of $\Delta H_\beta'$ was 6.8 kcal/mol.

The infrared spectra of the sample that was heated at 115°C was identical with that of AMIT-α. From the above results, AMIT-β can be said to be the thermodynamically unstable crystal form compared with AMIT-α, and it can be seen that AMIT-β crystallizes after melting at 104°C into the stable form, AMIT-α.

BULLETIN OF THE CHEMICAL SOCIETY OF JAPAN, VOL. 45, 3495—3496 (1972)

The Determination of the Enantiomeric Purity of Methyl *p*-Tolyl Sulfoxide by Means of an NMR Shift Reagent

Hitosi NOZAKI, Kimiaki YOSHINO, Koichiro OSHIMA, Yasusi YAMAMOTO

Department of Industrial Chemistry, Kyoto University, Yoshida, Sakyo-ku, Kyoto, 606

(Received April 17, 1972)

The NMR method for determining the enantiomeric excess of amines and alcohols employs a chiral complex of europium, tris[3-(*tert*-butylhydroxymethylene)-*d*-camphorato]europium(III) (**1**).[1] The NMR shift of oxiranes and sulfoxides has also been recorded.[2-4] We have independently been engaged in the same subject of research and wish to record the NMR shifts of optically-resolved sulfoxides as well as the analytical practice, neither of which has yet been described. A modified method of preparing **1** is also described.

Figure 1a shows a spectrum of a carbon tetrachloride solution of (±)-methyl *p*-tolyl sulfoxide (**2**) and **1** (3.0: 1.0 mol ratio). The separation of the enantiotopic methyl singlets was 0.14 ppm. A mixture of the optically-pure (+)-(R)-methyl *p*-tolyl sulfoxide (**2**) ($[\alpha]_D$ +145.5°, *c* 0.40, acetone) and **1** (3.5: 1.0 mol ratio) exhibited the NMR spectrum shown in Fig. 1b, only one S-methyl singlet being observed. The NMR spectrum of partially-resolved sulfoxide **2** ($[\alpha]_D$ +47.9°, *c* 1.06, acetone, 33% calculated optical purity) in the presence of **1** is given in Fig. 1c. Obviously, the S-methyl protons of (R)-**2** resonate at a higher field than their counterparts in (S)-**2**. The overlapping methyl peak areas in Fig. 1c were separated by means of the Brace method.[5] Each peak was cut out and weighed. The values gave an enantiomeric ratio of 1.0/2.0 or a 33% enantiomeric excess. The absolute rotation of methyl *p*-tolyl sulfoxide was calculated to be

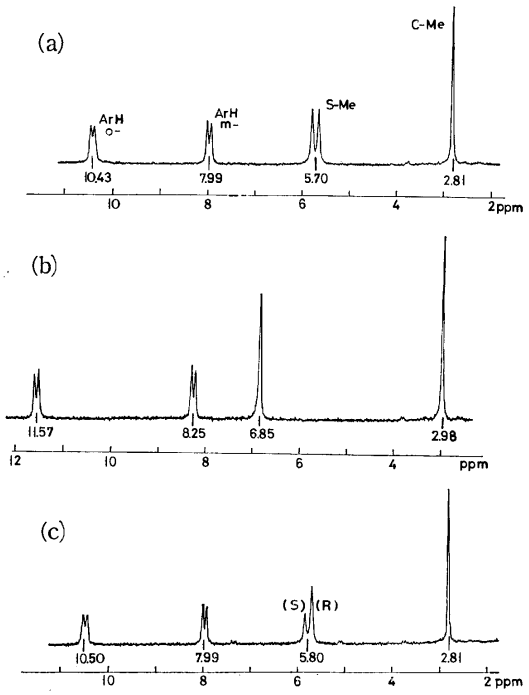

Fig. 1. Spectra of (a) (±)-methyl *p*-tolyl sulfoxide (**2**) (0.091 mmol) in CCl_4 (0.4 m*l*) containing the shift reagent, **1** (0.030 mmol), (b) (+)-(R)-**2** (0.91 mmol), CCl_4 (0.4 m*l*), **1** (0.026 mmol), and (c) partially resolved sulfoxide, **2** (1.04 mmol), CCl_4 (0.5 m*l*), **1** (0.032 mmol).

144° (lit. 145.5° [6a]).

The NMR method is naturally applicable to further sulfoxides. The S-methyl singlet of methyl phenyl sulfoxide resonating at the higher field in a carbon tetrachloride solution has been shown to arise from

1) G. M. Whitesides and D. W. Lewis, *J. Amer. Chem. Soc.*, **92**, 6979 (1970).

2) H. L. Goering, J. N. Eikenberry, and G. S. Koermer, *ibid.*, **93**, 5913 (1971).

3) G. M. Whitesides and D. W. Lewis, *ibid.*, **93**, 5914 (1971).

4) R. R. Fraser, M. A. Petit, and J. K. Saunders, *Chem. Commun.*, **1970**, 1450.

5) R. L. Pecsok, "Principles and Practices of Gas Chromatography," Chapman & Hall, London, 1959; Private communication from R. O. Brace at Beckman Instrument, Fullerton, California.

6) a) K. Mislow, M. M. Green, P. Laur, J. T. Mellilo, T. Simmons, and A. L. Jernay, Jr., *J. Amer. Chem. Soc.*, **87**, 1958 (1965); b) K. K. Andersen, *J. Org. Chem.*, **29**, 1953 (1964).

the isomer of the R-configuration. In a chloroform solution, however, this method proved unsuccessful, as no difference between the methyl protons of enantiomers was observed. The attempted application of the present method to the methyl ester of a *p*-tolylsulfinic acid failed because of the samll separation of the enantiomeric signals.

Experimental

The NMR spectra were obtained on a 100 MHz instrument (Varian HA-100), using TMS as the internal standard. The optically-active sulfoxides were prepared from (−)-menthyl arylsulfinate and methylmagnesium iodide by the known method.[6] The optically-active complex **1** was obtained from *tert*-butylhydroxymethylene-*d*-camphor and europium(III) nitrate in the presence of sodium hydroxide.[1,7] The diketone was prepared from camphor and pivaloyl chloride by the following modified method.

A mixture of camphor (24 g, 0.16 mol) and sodium hydride (3.8 g, 0.16 mol) in hexamethylphosphoric triamide (150 m*l*) under N_2 was stirred at 70°C for 5 hr to give a dark brown carbanion solution. This solution was diluted with THF (30 m*l*), and then a solution of pivaloyl chloride (8.8 g, 0.08 mol) in THF (10 m*l*) was added under ice-cooling. The reaction mixture was then stirred at room temperature for 12 hr, poured into water (500 m*l*), acidified with 10% hydrochloric acid (50 m*l*), and extracted with benzene. The product was purified by chromatography on a silica-gel column, followed by distillation; bp 130°C/2 mmHg. The 3-*t*-butylhydroxymethylene-*d*-camphor thus obtained (11%) formed white crystals; mp 65—67°C. We could find no suitable recrystallization solvent. The IR, NMR, the mass spectrum, and the analyses supported the structure.

The financial support from the Ministry of Education, the Japanese Government, and from the Toray Science Foundation is acknowledged with pleasure.

7) K. J. Eisentraut and R. E. Sievers, *J. Amer. Chem. Soc.*, **87**, 5254 (1965).

BULLETIN OF THE CHEMICAL SOCIETY OF JAPAN, VOL. 45, 3496—3498 (1972)

Synthetic Studies of Carbohydrate Derivatives with Photochemical Reaction. III.[1] Solvent Effects on the Photocycloaddition of Acetone to 3,4,6-Tri-*O*-acetyl-D-glucal

Kazuo MATSUURA, Younosuke ARAKI, and Yoshiharu ISHIDO

Department of Chemistry, Tokyo Institute of Technology, O-okayama, Meguro-ku, Tokyo

(Received April 26, 1972)

In a previous paper,[2] the present authors reported the photochemical reaction of mercaptans or 1,3-dioxolane with enoses in the presence of acetone (**1**) as a photosensitizer. In the present paper, we wish to report the photocycloaddition of **1** to 3,4,6-tri-*O*-acetyl-D-glucal (**2**); this resulted in the formation of an oxetane derivative, *i.e.*, 5,6,8-tri-*O*-acetyl-2,4;3,7-dianhydro-1-deoxy-2-*C*-methyl-D-*glycero*-D-*ido*-octitol (**3**), and there were interesting solvent effects on the reaction. According to a recent paper,[3] incidentally, the photocycloaddition of **1** to **2** without the utilization of any solvent gave **3** in a 33% yield; this yield was calculated on the basis of the amount of **2** consumed (recovery yield=47%), and the structure of **3** was deduced by deriving **3** into some derivatives.

Results and Discussion

The irradiation of **2** in **1**—2-propanol (100: 1) with an ultraviolet lamp under nitrogen at room temperature for 100 hr gave **3** in a good yield. The structure of **3**, especially with respect to the stereochemistry in the mutual fusion of its pyranose and oxetane rings at C-3 and C-4 of **3**, was examined as follows.

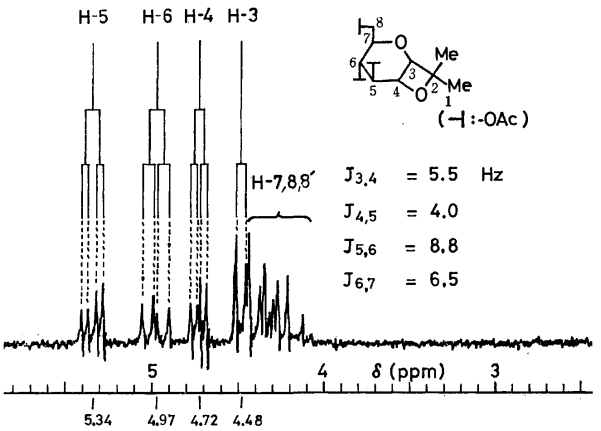

Fig. 1. 100 MHz NMR spectrum of 5,6,8-tri-*O*-acetyl-2,4; 3,7-dianhydro-1-deoxy-2-*C*-methyl-D-*glycero*-D-*ido*-octitol (**3**) in $CDCl_3$ with TMS as the internal standard. (δ 2.5—5.8 ppm)

i) The NMR spectrum of **3**, whose signals were assigned by the double-resonance technique, shows (*cf.* Fig. 1) that the H-3 and H-4 signals give a doublet at δ 4.48 ($J_{3,4}$=5.5 Hz) and a quartet at 4.72 ppm ($J_{4,5}$=4.0 Hz), respectively. Consequently, the facts lead to the conclusion that the carbonyl oxygen of **1** links to C-2, and the carbonyl carbon to C-1 of the

1) K. Matsuura, S. Maeda, Y. Araki, and Y. Ishido, This Bulletin, **44**, 292 (1971).

2) K. Matsuura, S. Maeda, Y. Araki, Y. Ishido, and A. Murai, *Tetrahedron Lett.*, **1970**, 2869.

3) Khong-Seng Ong and R. L. Whistler, *J. Org. Chem.*, **37**, 572 (1972).

pyranose ring of **2**.[4] The coupling constants of H-6—H-7 (6.5 Hz) and H-5—H-6 (8.8 Hz) indicate that H-6 and H-7 are not in a true diaxial *trans* correlation; hence, the pyranose ring of **3** can be considered to be strained to some extent.

ii) The addition of piperylene as a quencher to the system resulted in no formation of **3**, and the reaction was confirmed to involve the addition of the n—π^* triplet acetone to **2**. It is well known[5] that the carbonyl oxygen in the n—π^* triplet state is electron-deficient. Thus, the attack of the carbonyl oxygen should take place at the more electron-sufficient C-2 of **2**, and the resultant radical at C-1 should be stabilized by the resonance with the pyranose ring oxygen. Moreover, the general mode of the oxetane ring formation in the photochemistry is considered to involve the biradical intermediate.[6] On the basis of the above considerations, the mechanism of this reaction may be formulated as below. The selective formation of **3**

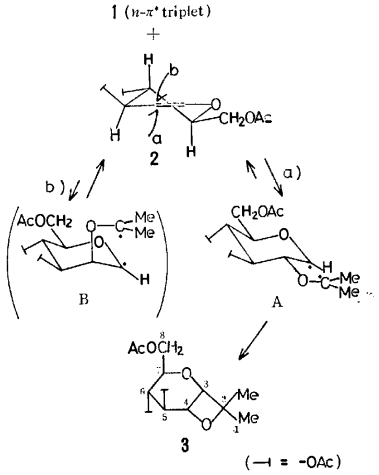

with the chirality of *S* at C-4 may be explained by comparing the stereochemical stability between the biradical intermediates, A and B. This conclusion agrees with that reported by Ong and Whistler.[3]

Subsequently, the solvent effects on this reaction were examined; the results are summarized in Table 1. Interestingly, the addition of solvents (about 1%) to **1** promoted the formation of **3**, whereas the addition of 100 times of a solvent to **1** brought about no formation of **3** and a quantitative recovery of **2**; this is in contrast with the addition of 2-propanol, which resulted in the formation of two new products detected gas-chromatographically with retention volumes of 2.5 and 2.6 (observed as a shoulder on the preceding peak), and the recovery of **2** in a 5% yield.[7]

Table 1. The examination of sovent effects on the photocycloaddition reacion[a]

Solvent added[b]	Yield of the Octitol (**3**), %[c]
2-Propanol	99
2-Propanol-Piperylene[d]	0
Ethanol	70
Diethyl Ether	46
Tetrahydrofuran	30
1,4-Dioxane	87
Cyclohexane	25
Benzene	26
Toluene	52
Pyridine	24

a) All the reactions were carried out by the use of **2** (35 mg), acetone (10 m*l*) under nitrogen at room temperature by the irradiation with an ultraviolet lamp (450 W) for 32 hr.
b) Zero point one m*l* of the solvents were added, respectively, and, on the other hand, the addition of a large excess amount of them other than 2-propanol resulted in no reaction.
c) All the yields were calculated from glc. *cf.* Without any solvent, the reaction gave the product in 17% yield.[3]
d) The addition of piperylene (0.5 and 0.1 m*l*, respectively) resulted in quntitative recoveries of **2**.

Similar phenomena were found in the same reactions of the other enoses; those investigations are now in progress in our laboratory.

Experimental

The solvents applied in the experiments were purified in the usual manner before use. Irradiations were carried out with a high-pressure mercury lamp (450W) of Ushio Electric, Inc., in a Pyrex-glass test tube at the distance of about 5 cm. The TLC was carried out by the use of Wakogel B-5 and the solvent system of benzene–methanol (9: 1 v/v) for the development. The NMR spectra were taken with Varian XL-100 in $CDCl_3$ by the use of tetramethylsilane (TMS) as the internal standard, while a mixture of $CDCl_3$-CD_3CN (1: 1) was used for the improvement of the resolution of the spectrum. The glc was done with a Hitachi K-53 apparatus; column: 1% of SE-30 on Chromosolb W(60—80 mesh), carrier gas: N_2 under 1.5 atm, oven temperature: 200°C, and injection temperature: 300°C. MS was taken with a Hitachi RMU-6E apparatus.

*Irradiation of 3,4,6-Tri-*O*-acetyl-*D*-glucal (2) with Acetone (1).* A solution of **2** (1.00 g) in a mixture of **1** (10 m*l*) and 2-propanol (0.1 m*l*) was irradiated under a nitrogen atmosphere at room temperature for 100 hr, and then the volatiles were evaporated *in vacuo*. The residue was subsequently chromatographed on a silica gel column by the use of benzene–acetone (19: 1 v/v) as an eluting solvent system; this gave a chromatographically-pure syrup of **3** (330 mg, 27% yield[9]). $[\alpha]_D^{25}$ +49.5° (*c* 1.0 Me_2CO) $[\alpha]_D^{25}$ +54.1° (*c* 1.0, $CHCl_3$)[3]. NMR ($CDCl_3$) δ 4.48 (H-3, d, $J_{3,4}$=5.5 Hz), 4.72 (H-4, q, $J_{4,5}$=4.0 Hz), 5.34 (H-5, q, $J_{5,6}$=8.8 Hz), 4.97 (H-6, q, $J_{6,7}$=6.5 Hz), 4.4—4.1 (H-7,8,8′, m), 1.43 and 1.45 ($2CH_3$), and 2.06, 2.08, and 2.11 ppm ($3CH_3CO$), and NMR ($CDCl_3$-CD_3CN=1: 1) δ 4.47 (H-3), 4.69 (H-4), 5.30 (H-5), 4.93 (H-6), 4.45—4.10 (H-7,8,8′), 1.40 and 1.43 ($2CH_3$), and

4) *cf.* H. Sakurai, K. Shima, and S. Toki, *Nippon Kagaku Zasshi*, **89**, 537 (1968).
5) A. Padwa, *Tetrahedron Lett.*, **1964**, 3465.
6) D. R. Arnold, "Advances in Photochemistry," Vol. 6, Interscience Publishers, New York, (1968), p. 301.
7) More detailed investigation is necessary to make a decisive discussion on the solvent effect in this reaction. In addition, the reaction in water gave 4,6-di-*O*-acetyl-*psudo*-D-glucal[8] (39% yield), and that in tetrachloromethane the adduct of **2** with the solvent, respectively. No formation of **3** was observed in both cases.
8) E. Fischer. *Ber.*, **47**, 196 (1914).
9) Prior to the column chromatography, the yield of **2** and **3** were calculated from glc as 13 (recovery) and 71% yield, respectively.

2.04, 2.07, and 2.07 ppm ($3CH_3CO$). IR: no absorption of OH group was observed. glc: retention volume=2.4 (**2**: 1.00). Found: C, 54.52; H, 6.66%. Calcd for $C_{15}H_{22}O_8$: C, 54.54; H, 6.71%. MS: $m/e=329[(M-1)^+]$.

The authors wish to thank Dr. M. Kainosho, Central Research Lab., Ajinomoto Co., Inc., for the assignment of the NMR spectrum.

BULLETIN OF THE CHEMICAL SOCIETY OF JAPAN, VOL. 45, 3498—3499 (1972)

The Stereochemistry of Hydrogenation with Tris(triphenylphosphine)chlororhodium

Yasuhisa SENDA,* Sekio MITSUI, Hiroshi SUGIYAMA,** and Shuichi SETO**

Department of Applied Science, Tohoku University, Sendai

***Chemical Research Institute of Non-Aqueous Solutions, Tohoku University, Sendai*

(Received May 17, 1972)

Wilkinson and his co-workers have shown that tris(triphenylphosphine)chlororhodium is an efficient catalyst for the hydrogenation of alkenes and alkynes.[1] The stereochemistry of the addition of hydrogen to the olefinic bond has been investigated only by Wilkinson and his co-workers[1] and by Birch and Walker.[2] Wilkinson and his co-workers confirmed, by a study of the IR spectrum, that the deuteration of maleic acid proceeded to give mainly *meso*-1,2-dideuterosuccinic acid; this means that the hydrogenation occurs with the *cis* addition of hydrogen to the double bond. Birch and Walker found that the deuteration of 22-dihydroergosteryl acetate occurred in a *cis* fashion.

In order to obtain further evidence on the stereochemistry of the addition of hydrogen, several olefinic compounds were deuterated and the steric configuration of the products were examined by the NMR procedure. The following olefins were used as substrates; *trans*-benzalacetophenone, *trans*-benzalpinacolone, methyl *trans*-cinnamate, *trans*-crotononitrile, and *trans*-cinnamonitrile. Deuteration was performed in benzene at an ordinary pressure and temperature. The products were separated from the complex catalyst by alumina chromatography and were subjected to NMR.

The NMR spectrum of methyl β-phenylpropionate-d_2, the reduction product from methyl *trans*-cinnamate, showed that its ethylene moiety resonated at δ: 2.55 and 2.93 as a broad doublet. The vicinal coupling constant, J_{HH}, was approximately 6.5 Hz. In order to confirm the coupling constant, the double resonance of the deuterium atom was performed. The spectrum of -CHD-CHD- obtained was a sharp AB-type doublet whose coupling constant was 5.46 Hz. The spectra were shown in Fig. 1. In the NMR spectrum of phenylpropionitrile-d_2 from *trans*-cinnamonitrile, the signal of the ethylene moiety appeared at δ: 2.33 and 2.71; in shape it was a broad doublet, and their vicinal coupling constant was 6.60 Hz.

TABLE 1. CHEMICAL SHIFT AND COUPLING CONSTANT OF DEUTERATION PRODUCTS WITH $RhCl(PPh_3)_3$

trans-Olefin	d_2-Product	-CHD-CHD- δ (ppm)	-CHD-CHD- J (Hz)
Methyl Cinnamate	Methyl β-Phenylpropionate	2.55 2.93	5.46
Benzalacetophenone	Diphenylpropanone	3.04 3.17	4.86
Benzalpinacolone	Dimethylphenylpentanone	2.67 2.79	5.11
Cinnamonitrile	Phenylpropionitrile	2.33 2.71	6.60
Crotononitrile	Butyronitrile	1.57 2.24	6.56

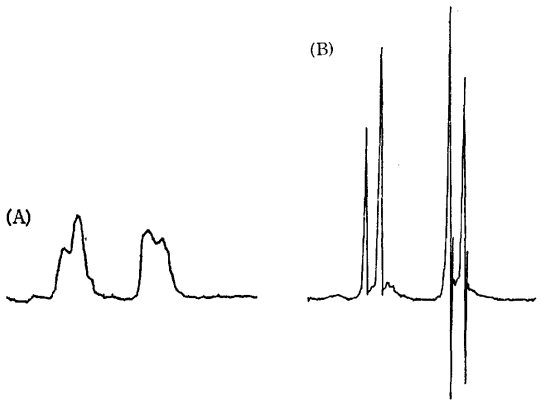

(A) Undecoupled Spectrum (B) Deuterium Decoupled Spectrum

Fig. 1. The NMR spectra of ethylene part of methyl β-phenylpropionate-d_2.

In spite of our expectation that the spectra of the ethylene parts of diphenylpropanone-d_2, the reduction product from *trans*-benzalacetophenone, and of dimethylphenylpentanone-d_2, from *trans*-benzalpinacolone, being an AB-type signal, the former compound showed the signal at around δ: 3.00, and the latter, at around 2.75 as a multiplet. In order to examine these spectra in detail, the double resonance of the deuterium atoms of these compounds was performed. As a consequence,

1) J. A. Osborn, F. H. Jardine, J. F. Young, and G. Wilkinson, *J. Chem. Soc., A*, **1966**, 1711; F. H. Jardine, J. A. Osborn, and G. Wilkinson, *ibid., A*, **1967**, 1574.

2) A. J. Birch and K. A. M. Walker, *Tetrahedron Lett.*, **1966**, 4939.

we obtained the coupling constants of these AB-type signals as 4.86 Hz in diphenylpropanone-d_2 and 5.11 Hz in dimethylphenylpentanone-d_2 accompanying the unidentified peaks.

The deuterium decoupling of the complicated spectra of butyronitrile-d_2 obtained from *trans*-crotononitrile showed signals which were a sharp doublet at δ: 2.24 and an A_3B-type octet at 1.57. The coupling constant of the signal at δ: 2.24, which corresponds to the methine proton, α to the cyano group, was 6.56 Hz. The spectra are shown in Fig. 2.

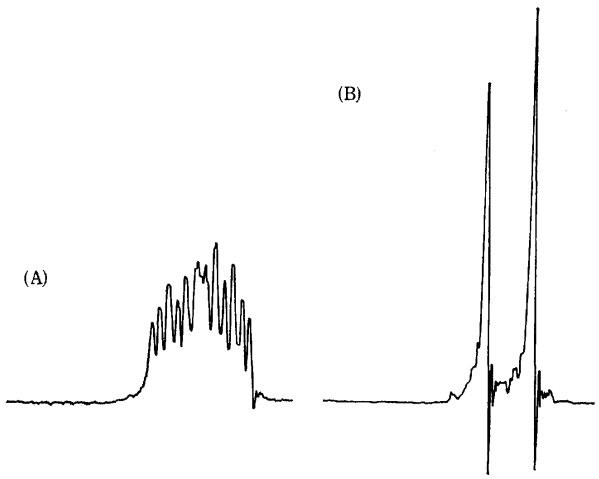

(A) Undecoupled spectrum (B) Deuterium decoupled spectrum

Fig. 2. The NMR spectra of methylene proton α to the cyano group of butyronitrile

The NMR spectra of methyl β-phenylpropionate-d_2 and phenylpropionitrile-d_2 were also measured at low and high temperatures. When the temperature was decreased to -55, -70, -80, and -90°C, the spectra showed no significant change in the shape of the signals as the coupling constant of the protons of the ethylene moiety. On the other hand, when the spectra of methyl β-phenylpropionate-d_2 were measured at a high temperature, those signals became broad at 100°C, but again became sharp at 150°C. In this case, no significant change in the coupling constant of the methylene protons of the ethylene moiety was observed.

Jackmann reported[3] that the vicinal coupling constants of the *erythro* and the *threo* isomers of *p*-methoxycinnamic acid dibromides were found to be 11.6 and 9.9 Hz respectively. He also reported that in a typical case it could perhaps be assumed that the J_{AB} in the *erythro* isomer is essentially in the range above 10 Hz, while that in the *threo* isomer is essentially in the range below 5 Hz.

Whitesides and his co-workers[4] confirmed, from a measurement study of dimethylbutane derivatives, that J_{trans} is normally 10—14 Hz and that J_{gauche} is 4—6 Hz.

When the spectra of methyl β-phenylpropionate-d_2 were measured at several points of the temperature, the width of the signal of the ethylene protons showed a temperature dependence at high temperatures. The signal became broader at 100°C than at room temperature. A further increase of the temperature made the signal sharp. This fact shows that the compounds used in the present study seem to take a fixed conformation at room temperature. As the temperature is elevated, a restricted rotation around the carbon-carbon single bond may occur; a high rate of interconversion is inferred at 150°C.

These results show that all of the diastereoisomers of open-chain compounds which were obtained in the present study by deuteration with tris(triphenylphosphine)chlororhodium may be assumed to be *threo* isomers. Therefore, deuteration occurs to the olefinic double bond in a *cis* fashion, supporting the results of Wilkinson and his co-workers and of Birch and Walker.

Experimental

Materials. The methyl *trans*-cinnamate was prepared from commercial *trans*-cinnamic acid by esterification. The *trans*-benzalacetophenone was prepared by the Claisen-Schmidt condensation of benzaldehyde and acetophenone with a 1.7 mol solution of sodium hydroxide in aqueous ethanol.[5] The *trans*-benzalpinacolone was obtained from benzaldehyde and pinacolone as the above unsaturated ketone.[6] The *trans*-crotononitrile was separated from commercial isomeric mixture by preparative gas chromatography. The *trans*-cinnamonitrile was prepared by the dehydration of cinnamaldoxime in boiling acetic anhydride.[7] All the olefinic compounds agreed in physical constants with the samples earlier prepared and were checked by studying their NMR and IR spectra.

Hydrogenation. In a typical experiment, a 80 mg portion of tris(triphenylphosphine)chlororhodium in 5.0 m*l* of benzene was presaturated with deuterium for 2 hr, and then the substrate (0.01 mol) in 5.0 m*l* of benzene was added, through a side-arm entry port, to the reaction flask. After the reaction flask had been stirred for 24 hr, the complex catalyst was removed by alumina-column chromatography and the solvent was distilled off.

NMR Spectra. The NMR spectra were measured with a JNM-C-60HL apparatus at 60 MHz and a JNM-PS-100 apparatus at 100 MHz. Simultaneous decoupling was accomplished at 14.349152 MHz using JNM-PS-100. The samples were examined at approximately 20% (w/v) in CCl_4. TMS was used as the internal standard. The low-temperature NMR was measured at approximately 5% (w/v) in CS_2 while at high temperatures the samples were in a neat condition.

3) L. M. Jackmann and S. Sternhell, "Applications of Nuclear Magnetic Resonance Spectroscopy in Organic Chemistry," 2nd ed., Pergamon Press, Oxford, London (1969), p. 291.

4) G. M. Whitesides, J. P. Sevenair, and R. W. Goetz, *J. Amer. Chem. Soc.*, **89**, 1135 (1967).

5) E. P. Kohler and H. M. Chadwell, "Org. Syntheses," Coll. Vol. I, (1941) p. 71.

6) G. A. Hill and G. M. Braumann, *ibid.*, Coll. Vol. I, (1941) p. 74.

7) E. Pozner, *Ann. Chem.*, **389**, 117 (1912).

BULLETIN OF THE CHEMICAL SOCIETY OF JAPAN, VOL. 45, 3500—3501 (1972)

The Photochemical and Thermal Reaction of Ethyl Azidoformate with Cyclohexanone Ethylene Acetal

Tamejiro HIYAMA, Shinsaku FUJITA, and Hitosi NOZAKI
Department of Industrial Chemistry, Kyoto University, Yoshida, Kyoto

(Received May 19, 1972)

Ethoxycarbonylnitrene reacts regioselectively with cyclic ethers to afford α-C–H insertion products.[1] Radical species and/or oxygen-imine intermediates have been proposed[1,2] as the explanation of the selectivity. In order to obtain further information on this problem, we have examined the reactions of ethoxycarbonylnitrene with cyclohexanone ethylene acetal (I) which has four kinds of methylene groups.

Ethyl azidoformate in I was decomposed photochemically or thermally; the products shown in Scheme 1 were then collected by distillation and preparative gas chromatography (GC). Since the separation of II by preparative GC was not satisfactory, the isomer was isolated by the selective acid hydrolysis of the crude products and by subsequent preparative GC. The regioisomers, III, IV, and V, were identified by comparing them with authentic samples prepared by the acetalization of the corresponding amino ketone. *N*-Ethoxycarbonyl-2-aminocyclohexanone (VI) was obtained by the DMSO-oxidation of 7-ethoxycarbonyl-7-azanorcarane.[3] *N*-Ethoxycarbonyl-3-,[4] and 4-aminocyclohexanone (VIII and X) were prepared by the hydrogenation of ethyl 3- and 4-hydroxycarbanilate, followed by chromic oxidation.

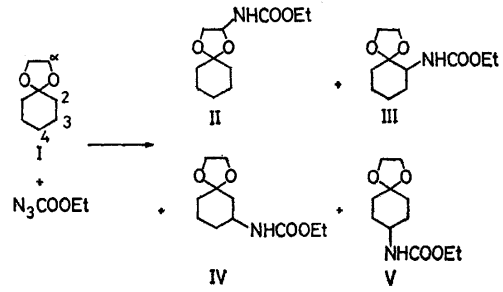

Scheme 1

The reaction conditions and product distributions are summarized in Table 1. The direct photolysis[5] gave a fair amount of V. This may be ascribed to the transition state XIc, arising from the boat-form conformation of an oxygen-imine XI, or simply to the singlet nitrene. Meanwhile, the formation of III and IV can be understood in terms of the intermediacy of the oxygen-imine reaction *via* the two transition states of XIa and XIb. The yield of II increased both in the dilution experiment and, more especially, in the acetophenone-sensitized photolysis. This suggests that a triplet nitrene or a triplet azide attacks the α-methylene of the acetal in a radical sense, producing II *via* a hydrogen abstraction-recombination mechanism. The thermolytic decomposition gave a comparable yield of II, which was, however, absent among the products in the dilution experiment. This may be explained similarly as in the reaction of cyanogen azide with ether.[6] Thus, the acetal oxygen may attack the azide group bimolecularly to form an oxygen-imine intermediate (XI), which may subsequently produce the α-insertion product (II). The dilution

TABLE 1. PHOTOLYSIS AND THERMOLYSIS OF ETHYL AZIDOFORMATE IN I

Condition	Additive	Yield (%)[a] II	III	IV	V
hν[b]	——	8.6 (0.17)	24 (0.48)	17 (0.34)	25 (1.0)
	CH_2BrCH_2Br[c]	1.8 (0.95)	1.3 (0.70)	0.46 (0.84)	0.96 (1.0)
	PhCOMe[d]	11.8 (1.4)	3.9 (0.45)	2.7 (0.32)	4.3 (1.0)
Δ[e]	——	9.0 (0.60)	3.2 (0.21)	7.0 (0.45)	7.7 (1.0)
	CH_2BrCH_2Br[c]	trace (0)	5.7 (1.2)	2.3 (0.48)	2.4 (1.0)

a) Determined by GC (Dowfax 9N9 on Neopak 1A, 10%, 3 mm×2 m, 190°C), with diethyl phthalate as the internal standard. The relative reactivities per methylene are given in parentheses.
b) A solution of ethyl azidoformate (1 mmol) in I (10 m*l*) was placed in a quartz tube and irradiated with a 200 W high-pressure mercury lamp for 40 hr.
c) Dibromoethane (3 m*l*) was added. The products were accompanied by other unidentified by-products.
d) Acetophenone (1 mmol) was added, and the irradiation was effected through a 9% aqueous solution of cupric sulfate (>300 nm) for 50 hr.
e) A mixture of ethyl azidoformate (0.87 mmol) and I (5 m*l*) was heated at 130°C for 3 hr.

1) H. Nozaki, S. Fujita, T. Takaya, and R. Noyori, *Tetrahedron*, **23**, 45 (1967).
2) T. Shingaki, M. Inagaki, N. Torimoto, and M. Takebayashi, *Chem. Lett.*, **1972**, 297.
3) S. Fujita, T. Hiyama, and H. Nozaki, *Tetrahedron*, **26**, 4347 (1970).
4) T. Hiyama, H. Taguchi, S. Fujita, and H. Nozaki, This Bulletin, **45**, 1863 (1972).
5) The direct photolysis of ethyl azidoformate has been reported to generate singlet ethoxycarbonylnitrene mainly, a) D. W. Cornell, R. S. Berry, and W. Lwowski, *J. Amer. Chem. Soc.*, **87**, 3626 (1965). b) W. Lwowski and T. W. Mattingly, Jr., *ibid.*, **87**, 1947 (1965).
6) "Nitrenes," ed. by W. Lwowski, John Wiley & Sons, New York (1970), p. 342.

Table 2. Physical properties of the new compounds

Compound	Mp (°C)[a] [bp (°C/mmHg)]	IR (cm^{-1})[b]	NMR (δ)[c]
II[g]	80—81	3325, 1690, 1550	1.0—1.8 (m+t, 13H), 3.5—4.4 (m+q, 4H), 5.1—5.8 (m, 2H)
III[h]	60—61	3325, 1686, 1540	0.9—2.1 (m+t, 11H), 3.4—4.3 (m+q, 7H), 4.4—4.9 (br d, 1H)
IV[i]	[110—120/0.15]	3325, 1698, 1524[d]	0.9—2.1 (m+11H), 3.6—4.2 (s+q+m, 7H), 5.1—5.5 (br d, 1H)
V[j]	95—96[e]	3350, 1700, 1530	1.1—2.2 (m+t, 11H), 3.3—3.8 (m, 1H), 3.87 (s, 4H), 4.05 (q, 2H), 4.6—5.1 (br d, 1H)
VIII[k]	[140/2][f]	3325, 1705, 1690, 1530[d]	1.0—3.0 (m+t, 11H), 3.4—4.2 (m+q, 3H), 5.8—6.2 (br d, 1H)
X[l]	85—86	3340, 1710, 1685, 1545	0.9—2.6 (m+t, 11H), 3.5—4.4 (m+q, 3H), 4.9—5.6 (br s, 1H)

a) From *n*-hexane. b) KBr. c) Carbon tetrachloride solution. d) Neat. e) From benzene-*n*-hexane.
f) Bath temperature.
g) MS: *m/e* (relative abundance) 229 (M^+, 4), 186 (5), 141 (15), 131 (100), 114 (63), 112 (32), 69 (30), 59 (28), 55 (94). Found: C; 57.4, H; 8.3, N; 6.1%. Calcd for $C_{11}H_{19}NO_4$: C; 57.6, H; 8.4, H; 6.1%.
h) MS: *m/e* (relative abundance) 229 (M^+, 10), 186 (4), 141 (9), 113 (7), 99 (100), 86 (19). Found: C; 57.3, H; 8.4, N; 6.2%. Calcd for $C_{11}H_{19}NO_4$: C; 57.6 H; 8.4, N; 6.1%.
i) MS: *m/e* (relative abundance) 229 (M^+ 10), 186 (83), 141 (100), 129 (21), 113 (26), 99 (60), 86 (87). Found: C; 57.5, H; 8.5, N; 6.0%. Calcd for $C_{11}H_{19}NO_4$: C; 57.6, H; 8.4, N; 6.1%.
j) MS: *m/e* (relative abundance) 229 (M^+, 4), 142 (24), 100 (17), 99 (100), 86 (43), 55 (15). Found: C; 57.5, H; 8.4, N; 6.2%. Calcd for $C_{11}H_{19}NO_4$: C; 57.6, H; 8.4, N; 6.1%.
k) MS: *m/e* (relative abundance) 185 (M^+, 9), 156 (57), 128 (79), 115 (52), 114 (46), 96 (84), 56 (98), 43 (100). Found: C; 58.1, H; 8.0, N; 7.8%. Calcd for $C_9H_{15}NO_3$: C; 58.4, H; 8.2, N; 7.6%.
l) MS: *m/e* (relative abundance) 185 (M^+, 2), 156 (3), 128 (36), 96 (100), 90 (92), 84 (32), 56 (69). Found: C; 58.3, H; 8.4, N; 7.6%. Calcd for $C_9H_{15}NO_3$: C; 58.4, H; 8.2, N; 7.6%.

with dibromoethane disfavors the formation of the oxygen-imine (XI) and, consequently, that of II.

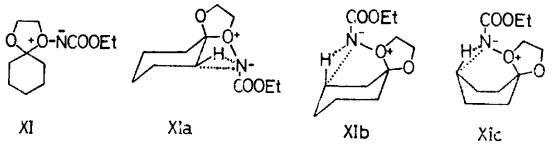

XI XIa XIb XIc

Experimental

Table 2 lists the physical properties of the new compounds.

Photolysis of Ethyl Azidoormate in I. Ethyl azidoformate (2.60 g, 22.6 mmol) and cyclohexanone ethylene acetal (44 m*l*) were irradiated for 20 hr. The recovery of the excess acetal, followed by distillation at 122—143°C/0.18 mmHg, gave a mixture of II, III, IV, and V (0.99 g). The isolation of IV and V was effected by preparative GC (Silicone SE 30, 30%, 6 mm×1 m, 150°C.)

Isolation of II. A mixture (3.6 g) of the products obtained as has been described above was dissolved in ether (150 m*l*), and the solution was shaken with 10% hydrochloric acid (140 m*l*) for 5 min, washed with water, neutralized with aqueous sodium bicarbonate, and dried over anhydrous sodium sulfate. Concentration and distillation then yielded crude II (0.69 g). The hydrolysis was repeated, and the pure sample was obtained by preparative GC.

Thermolysis of Ethyl Azidoformate in I. A mixture of ethyl azidoformate (1.05 g, 9.1 mmol) and I (5 m*l*) was added, drop by drop (over 40 min), to I (15 m*l*) at 120°C under a nitrogen atmosphere, and thereafter heating was continued for 3 hr. Concentration and distillation gave a mixture of II, III, IV, and V (1.16 g). The separation of each component was effected as has been described above.

N-Ethoxycarbonyl-3-aminocyclohexanone (VIII). Ethyl 3-hydroxycarbanilate (10.7 g, 59 mmol), Raney nickel (W-2) (3 g), and ethanol (150 m*l*) were heated at 175—190°C in an autoclave under a hydrogen atmosphere (110 kg/cm^2) for 2 days. The subsequent filtration of the catalyst and evaporation of the solvent yielded VII as a viscous oil (9.8 g, 89%). IR (neat): 3300, 1690, 1540 cm^{-1}. MS: *m/e* 187 (M^+).

A mixture of sodium dichromate dihydrate (6.0 g), concentrated sulfuric acid (5 m*l*), and water (30 m*l*) was added, drop by drop, to a solution of VII (9.8 g) in ether (50 m*l*) at 0°C, and subsequently 20% sulfuric acid (5 m*l*) was added. After stirring for 2 hr, the ether layer was separated, washed with water, and dried (sodium sulfate). Concentration and distillation gave VIII[4] (3.13 g, 32%).

The hydrogenation of ethyl 4-hydroxycarbanilate was performed as has been described above to afford IX in a quantitative yield. IR (Nujol): 3330, 1695, 1540 cm^{-1}. The chromic oxidation of IX, followed by distillation, gave X (27% yield).

Acetalization of VI. A mixture of VI (0.24 g), ethylene glycol (2.0 m*l*), boron trifluoride etherate (0.5 m*l*), and dichloromethane (5 m*l*) was stirred at room temperature for a day. The mixture was then poured into water (100 m*l*), extracted with ether, washed with aqueous sodium bicarbonate, and dried over anhydrous sodium sulfate. Concentration and preparative layer chromatography on silica gel (benzene) gave III (0.113 g, 38%).

The acetalization of VIII and X afforded IV and V in 25 and 44% yields respectively.

Financial support from the Ministry of Education, the Japanese Government, is acknowledged with pleasure.

BULLETIN OF THE CHEMICAL SOCIETY OF JAPAN, VOL. 45, 3502—3504 (1972)

The Stereochemistry of (+)-Occidentalol. Further Support for the Revised Structure

Takayuki SUGA, Kiyoshi IMAMURA, Tsuyoshi SHISHIBORI, and Ernst von RUDLOFF*

Department of Chemistry, Faculty of Science, Hiroshima University, Higashisenda-machi, Hiroshima, Japan

**Prairie Regional Laboratory, National Research Council, Saskatoon, Saskatchewan, Canada*

(Received June 3, 1972)

(+)-Occidentalol, an eudalene-type sesquiterpene alcohol isolated from the heartwood of *Thuja occidentalis* L., has been shown[1] to possess *cis* ring-fusion[2] and a 1,3-diene system. The optical rotatory dispersion

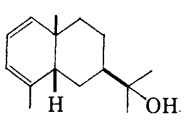

1

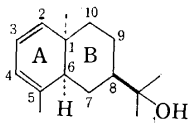

2

(ORD) study[3,4] of its related compounds has led to the acceptance of structure **1** of two structures **1** and **2** possible for (+)-occidentalol. However, recently the structure has been revised to **2** on the basis of nuclear magnetic resonance (NMR) spin-decoupling[5] and synthesis[6] of the antipode of (+)-occidentalol from α-santonin. We now wish to present additional evidence supporting absolute configuration (**2**), and to describe the conformational study of (+)-occidentalol and its dehydration products (**5**) and (**6**) by circular dichroism (CD) measurements at various temperatures.

Results and Discussion

Further Support for the Absolute Configuration of (+)-Occidentalol. According to Mislow's suggestion,[3]

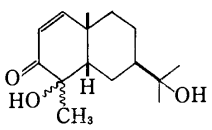

3

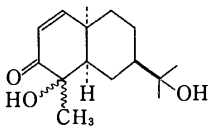

4

the structure possible for (+)-5-hydroxy-8-(1-hydroxy-1-methylethyl)-1,5-dimethylbicyclo-[4.4.0]-2-decen-4-one[7] derived from (+)-occidentalol may be **3** or **4**, each of which can take two possible conformations **3a** and **3b**, and **4a** and **4b**. The infrared spectrum of the α'-hydroxy-α,β-unsaturated ketone in the hydroxyl-stretching region indicated four absorption bands at 3635 (ε 34), 3622 (ε 66), 3592 (ε 80), and 3490 cm^{-1} (ε 6) in 0.0042M carbon tetrachloride solution. The two high-frequency bands can be attributed to free hydroxyl stretching due to the hydroxyisopropyl group and the hydroxyl group at C-5. The third band was assigned to the OH···π intramolecularly-interacted hydroxyl group and the fourth to the OH···O interacted hydroxyl group adjacent to the carbonyl group.[8] Since the A-ring of the four conformers has been postulated to exist in the most stable half chair conformation,[9] the hydroxyl group at C-5 should be in the axial orientation and will easily form the OH···π hydrogen bond. Accordingly, in the conformational equilibrium between **3a** and **3b** and between **4a** and **4b**, conformers **3a** and **4a** may be expected to predominate because they suffer the less 1,3-diaxial interaction.

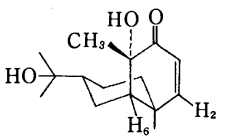

3a

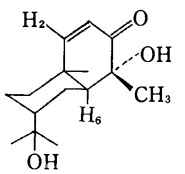

3b

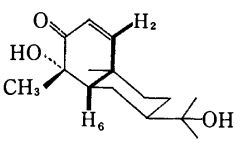

4a

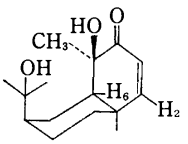

4b

Long range coupling of the W or the M type[10] between H-2 and H-6 may be expected for **4a**, since the H-2, C-2, C-1, C-6, and H-6 portion of this conformer is in a coplanar zigzag spatial arrangement; this is not the case for the conformer (**3a**). The NMR spectrum (60 MHz) of compound **4** showed the characteristic resonance pattern for olefinic protons of H-2 and H-3 at 6.59 and 5.95 ppm respectively. Upon irradiation of the signal due to H-6 at 1.82 ppm, the spin-coupling pattern due to H-2 at 6.59 ppm (dd, $J_{2,3}$=10.5 Hz and $J_{2,6}$=2.0 Hz) was transformed to a doublet ($J_{2,3}$=10.5 Hz). This observation of the long range coupling ($J_{2,6}$=2.0 Hz) indicates that the compound (**4**) exists in the preferred conformation (**4a**).

1) T. Nakatsuka and Y. Hirose, *Bull. Agr. Chem. Soc. Japan*, **20**, 215 (1956); Y. Hirose and T. Nakatsuka, *ibid.*, **23**, 140 (1959).

2) E. von Rudloff and H. Erdtman, *Tetrahedron*, **18**, 1315 (1962).

3) K. Mislow and A. Moscowitz, *Tetrahedron Lett.*, **1963**, 699

4) H. Ziffer, T. J. Batterham, U. Weiss, and E. von Rudloff, *Tetrahedron*, **20**, 67 (1964).

5) A. G. Hortmann and J. B. De Roos, *J. Org. Chem.*, **34**, 736 (1969).

6) M. Ando, K. Nanaumi, T. Nakagawa, T. Asao, and K. Takase, *Tetrahedron Lett.*, **1970**, 3891.

7) T. Suga, K. Imamura, and E. von Rudloff, *J. Chem. Soc., Perkin Trans. I*, **1972**, 962.

8) T. Suga, T. Shishibori, and T. Matsuura, *ibid.*, **1972**, 171.

9) E. Toromanoff, "Topics in Stereochemistry," Vol. 2, ed. by N. L. Allinger and E. L. Eliel, Interscience Publishers, New York (1967), p. 157.

10) T. Nozoe, Y. S. Cheng, and T. Toda, *Tetrahedron Lett.*, **1966**, 3663.

Table 1. The percentage change of molecular ellipticity of compounds **2**, **5**, and **6** in the MI solvent and decalin

Compds.	MI solvent[a]			Decalin		
	$[\theta](\lambda_{max})\times10^{-4}$ at 25°C (T_2)	$[\theta]$ $(\lambda_{max})\times10^{-4}$ at -180 ± 2°C (T_1)	$I^{T_2}_{T_1}$	$[\theta]$ $(\lambda_{max})\times10^{-4}$ at 143 ± 1°C (T_2)	$[\theta]$ $(\lambda_{max})\times10^{-4}$ at 25°C (T_2)	$I^{T_2}_{T_1}$
2	6.10	6.65	− 8.3	6.21	6.61	− 6.1
5	5.16	6.19	−16.6	4.53	5.60	−19.1
6	7.49	8.81	−15.0	6.32	7.76	−18.6

a) The MI solvent is composed of methylcyclohexane–isopentane in the ratio 1:3 by volume.

This further supports the revised absolute configuration of (+)-occidentalol (**2**).

The Conformation of (+)-Occidentalol (2) and Its Dehydration Products (5) and (6). (+)-Occidentalol (**2**) may take two possible preferred conformations (**2a**)

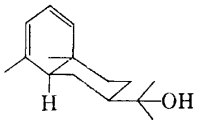

2a

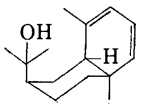

2b

and (**2b**). The diene system of the conformer (**2a**) is skewed in the sense of a right-handed helix, whereas the system of **2b** in the sense of a left-handed helix. The helicity rule[11] predicts a positive Cotton effect for the conformer (**2a**) and a negative one for the conformer (**2b**). The CD curve of **2** exhibited a positive Cotton effect at 25°C, keeping the sign with the same rotational strength as above in a range of +140 to −180°C. The percentage change of molecular ellipticity[12] expressed as $I^{T_2}_{T_1}=([\theta](T_2)-[\theta](T_1))\times100\%/[\theta](T_1)$ is small, being almost within the deviation (6.1%) (Table 1). The result indicates the predominance of the conformer (**2a**). Furthermore, the population of the conformer (**2a**) is deduced to be more than 99% at room temperature,[13] because the difference between the conformational energies of **2a** and **2b** is more than 3.85 kcal/mol, as estimated by summation of the conformational energies of the methyl (1.70 kcal/mol)[14] and the isopropyl (2.15 kcal/mol)[14] groups.

Additional evidence in favor of the stability of the conformer (**2a**) was obtained by means of the NMR spectrum of the three olefinic protons H-2 (5.21 ppm), H-3 (5.74 ppm), and H-4 (5.49 ppm), and the H-6 proton (1.65 ppm), at various temperatures. The spectrum showed the same spin-coupling pattern[5] at +50, −10, and even −60°C in deuterochloroform.

The dehydration products, (**5**) and (**6**), of occidentalol can exist in two interconvertible conformations (**5a**) and

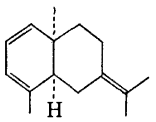

5

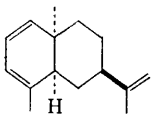

6

(**5b**), and (**6a**) and (**6b**), respectively, where the A-ring of the conformers (**5a**) and (**6a**) has a skewed diene system in the sense of a right-handed helix, whereas the diene system of the conformers (**5b**) and (**6b**) is skewed in a left-handed helix. The temperature-dependence of the CD curve of these compounds (Table 1) showed the presence of the conformational equilibrium between **5a** and **5b** and between **6a** and **6b**, since the

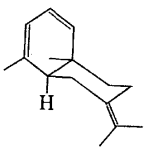

5a

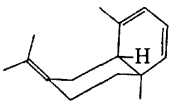

5b

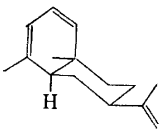

6a

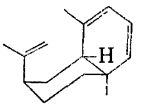

6b

percentage change of the molecular ellipticity for these compounds are about two times as large as that of **2**. The increase in the positive rotational strength with a lowering of the temperature indicated the predominance of the conformers (**5a**) and (**6a**).

Experimental

(+)-Occidentalol (2). The same sample of (+)-occidentalol as described in the previous report[2] was used.

Dehydration of (+)-Occidentalol (2). 8-Isopropylidene-1,5-dimethylbicyclo[4.4.0]-2,4-decadiene (5): To the solution of 0.3 g of (+)-occidentalol in 6 ml of pyridine was added dropwise phosphorus oxychloride (0.6 ml), and the mixture was left to stand at 5—10°C for 5 hrs and then treated in the usual way. The oily product (0.23 g) obtained was separated into two fractions by column-chromatography on silica-gel (Merck Kieselgel G, less than 0.08 mm) impregnated with 20% (w/w) silver nitrate. The first fraction gave the dehydration product (**5**) as a viscous oil: $[\alpha]_D^{25}$ +698° (*c* 0.034, EtOH); λ_{max} (EtOH) 269 nm (ε 4720); δ ($CDCl_3$) 0.82 (s, 3H, methyl), 1.63 (s, 6H, two vinylic methyls), 1.76 (s, 3H, vinylic methyl), 5.32 (d, J=9.0 Hz, 1H, vinyl), 5.55 (b, 1H, vinyl), and 5.85 ppm (dd, J=9.0 and 5.0 Hz, 1H, vinyl).

11) A. Moscowitz, E. Charney, U. Weiss, and H. Ziffer, *J. Amer. Chem. Soc.*, **83**, 4661 (1961).

12) G. Snatzke, D. M. Piatak, and E. Caspi, *Tetrahedron*, **24**, 2899 (1968).

13) E. L. Eliel, N. L. Allinger, S. J. Angyal, and G. A. Morrison, "Conformational Analysis," Interscience Publishers, New York (1965), p. 36.

14) J. A. Hirsch, "Topics in Stereochemistry," Vol. 1, ed. by N. L. Allinger and E. L. Eliel, Interscience Publishers, New York (1967), p. 199.

8-Isopropenyl-1,5-dimethylbicyclo[4.4.0]-2,4-decadiene (6): The second fraction gave the dehydration product (**6**) as a viscous oil: $[\alpha]_D^{25}$ +674° (*c* 0.036, EtOH); ν_{max} (liq. film) 3100, 1645, 1586, 892, and 735 (vinyl) cm^{-1}; λ_{max} (EtOH) 265 nm (ε 4920); δ ($CDCl_3$) 0.84 (s, 3H, methyl), 1.63 (d, J=1.0 Hz, 3H, vinylic methyl), 1.74 (d, J=1.0 Hz, vinylic methyl), 4.63 (s, 2H, vinyl), 5.25 (d, J=9.0 Hz, 1H, vinyl), 5.55 (b, 1H, vinyl), and 5.80 ppm (dd, J=9.0 and 5.0 Hz, 1H, vinyl).

BULLETIN OF THE CHEMICAL SOCIETY OF JAPAN, VOL. 45, 3504—3505 (1972)

Reactions of Benzenediazonium-2-carboxylate with Arylimino- and Acylmethylenetriphenylphosphoranes

Takayuki KAWASHIMA and Naoki INAMOTO

Department of Chemistry, Faculty of Science, The University of Tokyo, Hongo, Bunkyo-ku, Tokyo 113

(Received July 18, 1972)

There is no report on the reaction of benzenediazonium-2-carboxylate (I) with arylimino- (II) or acylmethylenetriphenylphosphoranes (III).

The reactions of I with II gave 3-aryl-3,4-dihydrobenzo[*e*][1,2,3]triazin-4-ones (IV), *N*-arylbenzamides (V), *N*,*N*′-diarylureas (VI) and triphenylphosphine oxide (VII) in dichloromethane at room temperature, their yields being dependent upon aryl group of II (Table 1).

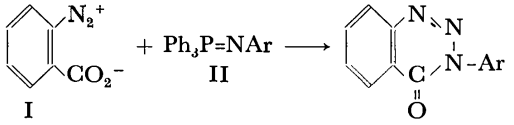

I + Ph_3P=NAr (II) → IV + PhCONHAr (V) + $(ArNH)_2CO$ (VI) + Ph_3PO (VII)

a: Ar=Ph
b: Ar=*p*-MeC_6H_4
c: Ar=*p*-ClC_6H_4

Table 1. Reactions of benzenediazonium-2-carboxylate (I) with aryliminotriphenylphosphoranes (II)[a)]

II	Ar	IV(%)	V(%)	VI(%)	VII(%)
a	Ph	13.4	9.6	—	81.5
b	*p*-MeC_6H_4	20.0	—	4.4	90.0
c	*p*-ClC_6H_4	—	20.2	3.8	91.1

a) Yields were calculated on the basis of the amount of II used.

The products were identified by the comparison of the melting points and IR spectra with those of authentic samples and on the basis of the MS spectra.

The formation of IV is explicable by the attack of the diazonium group of I to the imino nitrogen atom of II, followed by the elimination of VII. Separate experiments indicated that benzanilide (Va) was not produced from IVa but produced quantitatively by the reaction of IIa with benzoic acid,[1)] which is produced by the decomposition of I,[2)] under the same condition. Urea (VI) is considered to be formed by the reaction of II with carbon dioxide, which was produced by decomposition of I, followed by the hydrolysis of isocyanate or carbodiimide thus produced during the isolation.

Variation in the yields of IV, V, and VI is attributable to a competition of the reaction between I and II with the decomposition of I to benzoic acid and carbon dioxide. For example, the absence of IVc in the case of IIc is attributable to a low nucleophilicity of the imino nitrogen in IIc because of the presence of electron-attractive *p*-chlorine atom.

Next, the reactions of I with acylmethylenetriphenylphosphoranes (III) were carried out in dichloromethane at room temperature. The products were phosphonium betaines (VIII) instead of expected IX.

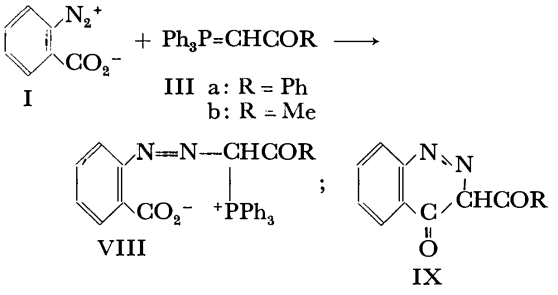

I + Ph_3P=CHCOR (III a: R = Ph, b: R = Me) → VIII ; IX

The structure of VIII was determined by the elemental analyses, the IR, ^{1}H-, and ^{31}P-NMR spectra. The ^{31}P-NMR spectra (δ −4.5 (in $CHCl_3$) and −3.8 (in $C_2H_4Cl_2$) from 85% phosphoric acid as external standard for VIIIa and VIIIb, respectively) support the structure of alkylidenephosphorane or phosphonium salt.[3)] The IR spectra showed the absence of carboxyl group and the presence of carboxylate group (I: 1630 and 1360; VIIIa: 1595 and 1360; VIIIb: 1625 and 1360 cm^{-1}). From these data, another possible structures were ruled out.

Thermal decomposition of VIII gave VII and tarry material containing carboxyl group, instead of IX.

A reason why IX is not formed is attributable to a lack of nucleophilicity of α-carbon atom in VIII.

N-Benzoylimino- and α-benzoylbenzylidenetriphenylphosphoranes did not react with I under the same condition.

1) L. Horner and A. Gross, *Ann. Chem.*, **591**, 117 (1955).
2) *E.g.*, G.P. Chiusoli and C. Venturello, *Chem. Commun.*, **1969**, 771.
3) M. Yoshifuji, *Yuki Gosei Kagaku Kyokaishi*, **28**, 177 (1970).

Experimental

Materials. The following compounds were prepared by the methods described in literatures: benzenediazonium-2-carboxylate (I);[4] phenylimino- (IIa),[5] mp 128—131°C; *p*-tolylimino- (IIb),[6] mp 133—136°C; *p*-chlorophenylimino- (IIc),[6] mp 116—118°C; benzoylmethylene- (IIIa),[7] mp 181—183°C; and acetylmethylenetriphenylphosphoranes (IIIb),[8] mp 203—205°C.

Reactions of I. *a) With Phenyliminotriphenylphosphorane (IIa)*: To an excess amount of I in dichloromethane was added 4.47 g (12.7 mmol) of IIa in dichloromethane under nitrogen and the mixture was stirred at 10°C overnight. After filtration of unchanged I and removal of the solvent *in vacuo*, the residue was chromatographed on alumina to afford 0.38 g (13.4%) of IVa (with benzene–chloroform), mp 149—150°C (from benzene) (lit,[9] 150—151°C), $\nu_{C=O}$ 1660 cm^{-1}, *m/e* 223 (M^+), 2.87 g (81.5%) of triphenylphosphine oxide (VII) (with chloroform), 0.24 g (9.6%) of benzanilide (with chloroform–ether), mp 159—160°C (from methanol), and 1.274 g of red tarry material (with ethanol).

b) With p-*Tolyliminotriphenylphosphorane (IIb)*: A similar reaction using 3.66 g (10 mmol) of IIb for 5 hr gave 0.47 g (20%) of IVb, mp 142—143°C (from benzene) (lit,[10] 143°C), $\nu_{C=O}$ 1680 cm^{-1}, *m/e* 237 (M^+), 2.50 g (90%) of VII and 0.21 g (4.4%) of VIb, mp 250°C (from ethanol) (lit,[11] 256°C).

c) With p-*Chlorophenyliminotriphenylphosphorane (IIc)*: The reaction was carried out using 4.23 g (10.9 mmol) of IIc. The reaction was slow and the presence of unchanged IIc was observed even after stirring overnight. Similar treatment gave 0.51 g (20.2%) of *N*-*p*-chlorophenylbenzamide, mp 192—193°C (from benzene) (lit,[12] 187—187.5°C), 2.76 g (91.1%) of VII and 0.23 g (3.8%) of VIc, mp 300°C from ethanol) (lit,[13] 310°C).

d) With Benzoylmethylenetriphenylphosphorane (IIIa): A similar reaction was carried out using 1.3 g (3.4 mmol) of IIIa at 0°C until the presence of unchanged IIIa was not observed by tlc. After filtration of unchanged I, the solvent was removed *in vacuo* to afford 1.1 g (61.2%) of brown crystals, mp 196—197°C (decomp.) (from ethyl acetate); IR (KBr disk): 1690, 1595, 1360, and 1105 cm^{-1}; $\lambda_{max}^{CH_2Cl_2}$: 262 (ε 23,000) and 409 nm (32,000); ^{1}H-NMR ($CDCl_3$): δ 7.3—8.2 (m); ^{31}P-NMR ($CHCl_3$): δ −4.5; *m/e*: 277 (10%), 262 (39), 184 (11), 183 (37), 108 (26), 105 (100), 77 (59), and 51 (11).

Found: C, 74.84; H, 4.71; N, 5.29%. Calcd for $C_{33}H_{25}N_2O_3P$: C, 74.99, H, 4.77; N, 5.30%.

e) With Acetylmethylenetriphenylphosphorane (IIIb): Reaction of 9.3 g (29.2 mmol) of IIIb with excess amount of I finished after 15 min at 0°C. Similar treatment gave 13.0 g (95.5%) of yellow crystals, mp 192—194°C (decomp.) (from ethyl acetate); IR (KBr disk): 1695, 1625, 1360, and 1110 cm^{-1}; $\lambda_{max}^{CH_2Cl_2}$: 258 (ε 18,000) and 398 nm (25,000); ^{1}H-NMR ($CDCl_3$): δ 2.61 (3H, s, $COCH_3$) and 7.0—7.8 (20H, m, Ph, and $-CH\langle$); ^{31}P-NMR ($C_2H_4Cl_2$): δ −3.8; *m/e*: 277 (10%), 263 (14), 262 (84), 261 (20), 185 (10), 184 (27). 183 (100), 152 (16), 133 (20), 108 (70), 107 (27), 77 (45), 52 (43), 51 (45), and 43 (39).

Found: C, 72.05; H, 4.83; N, 6.02%. Calcd for $C_{28}H_{23}N_2O_3P$: C, 72.10; H, 4.97; N, 6.01%.

4) F. M. Logullo, A. H. Seitz, and L. Friedman, "Organic Synthesis," Vol. 48, p. 12 (1968).
5) H. Staudinger and J. Meyer, *Helv. Chim. Acta*, **2**, 635 (1919).
6) L. Horner and H. Oediger, *Ann. Chem.*, **627**, 142 (1959).
7) F. Ramirez and S. Derschowitz, *J. Org. Chem.*, **22**, 41 (1957).
8) G. Aksnes, *Acta Chem. Scand.*, **15**, 692 (1961).
9) A. Pictet and A. Gonset, *Chem. Zentr.*, **1897**, 413.
10) P. Grammaticakis, *C. R. Acad. Sci., Paris*, **243**, 2094 (1956); *Chem. Abstr.*, **51**, 8765c (1957).
11) A. E. Dixon, *J. Chem. Soc.*, **79**, 102 (1901).
12) E. E. Slosson, *J. Amer. Chem. Soc.*, **29**, 306 (1903).
13) F. D. Chattaway and K. J. P. Orton, *Ber.*, **34**, 1073 (1901).

SHORT COMMUNICATION

Reduction of Carbonyl Compounds with Various Hydrosilane-Rhodium(I) Complex Combinations

Iwao OJIMA, Tetsuo KOGURE, Mitsuru NIHONYANAGI, and Yoichiro NAGAI*

Sagami Chemical Research Center, Onuma, Sagamihara, 229

**Department of Chemistry, Gunma University, Kiryu, Gunma, 376*

(Received September 5, 1972)

It has been known that the hydrosilation of carbonyl compounds can be effected by various catalytic systems such as metal halides *e.g.* $ZnCl_2$[1] and H_2PtCl_6,[2] and UV light.[3] Among them, metal or metal halide catalyst systems have been used within the limit of monohydrosilanes, mainly due to the fact that the disproportionation of polyhydrosilane is also catalyzed by these substances.[4] Gilman and Wittenberg[5] found that diphenylsilane adds to benzophenone at temperature of 220—270°C, but the reaction conditions are too drastic to allow the use of a wide variety of carbonyl compounds in solution. We found that tris(triphenylphosphine)chlororhodium (**1**) is an extremely effective catalyst for the hydrosilation of carbonyl compounds in comparison with other knwon catalysts. Now we wish to report the effective hydrosilation of carbonyl compounds, which is equivalent to hydrogenation after hydrolysis, using a variety of hydrosilane-rhodium(I) complex **1** combinations. The hydrosilation with monohydrosilanes was found to take place under very mild conditions to give the expected products. Further, the rate of the reaction was found to increase when dihydro- and trihydrosilanes were employed, and the disproportionation of these hydrosilanes were virturally negligible.

A typical procedure is described for the hydrosilation of cyclohexanone by diphenylsilane: To a mixture of 0.98 g (10 mmol) of cyclohexanone and 1.84 g (10 mmol) of diphenylsilane, 9.5 mg (0.1 mol%) of $(Ph_3P)_3RhCl$ (**1**) was added, and the mixture was stirred at ice-cold temperature, and the hydrosilation was completed within 10 min. *n*-Hexane (50 m*l*) was added to the reaction mixture, the resulting precipitate filtered off, the solvent was evaporated, and the residual solution was distilled under reduced pressure, and 2.78 g (98%) of cyclohexyloxydiphenylsilane (**2 g**) was obtained. The silylether **2 g** thus obtained was smoothly hydrolyzed by MeOH–KOH–H_2O solution to afford cyclohexanol quantitatively. Results of the hydrosilation using various hydrosilanes, ketones and aldehydes are summarised in Table 1.

The hydrosilation of α,β-unsaturated ketones and aldehydes also proceeded smoothly under mild conditions to give the adducts in fairly high yield. In these cases, the reaction proceeded in a manner of 1,4-addition, and afforded silylenolethers **3**, which were easily hydrolyzed to saturated ketones or aldehydes by acetone–MeOH–H_2O–K_2CO_3 quantitatively. These findings clearly indicate that the reaction using hydrosilane-rhodium(I) complex combinations with α,β-unsaturated carbonyl compounds may open a new route to selective hydrogenation of the carbon-carbon double bond in α,β-unsaturated carbonyl compounds, and also open an important route to the preparation of silylenolethers, which are much interested as a synthetic intermediate. Results are listed in Table 2.

Though a hydrosilane has been known as a reducing agent for certain ketones, the scope of those reactions is limited to a very narrow area as quoted before. However, many carbonyl systems became able to be reduced by hydrosilane-rhodium(I) complex combinations taking advantage of easily hydrolyzable character of silylethers. Application of this reducing method to other systems and the mechanism of the reaction are now under active investigation. We believe that this reducing method has a wide potential utility as hydroboration.

Table 1. Silylethers (**2**) obtained by the hydrosilation of ketones and aldehydes using hydrosilane-rhodium (I) complex combinations[a]

$[(R^1R^2CHO)_nSiR_{4-n}]$

	R^1	R^2	n	Silyl group	Conditions	Yield (%)
a	Ph	H	1	$PhMe_2Si$–	r. t., 5 min	94
b	Me	Me	1	Ph_3Si–	reflux, 120min	98
c	Ph	Me	1	Et_2HSi–	r. t., 5 min	95
d	Ph	Ph	1	Et_2HSi–	r. t., 5 min	95
e	*n*-Pr	H	1	PhMeHSi–	r. t., 5 min	98
f	Ph	Ph	1	Ph_2HSi–	80°, 30 min	93
g	$-(CH_2)_5-$		1	Ph_2HSi–	0°, 10 min	98
h	$-(CH_2)_5-$		2	PhHSi=	0°, 10 min	98
i	$-(CH_2)_5-$		3	PhSi≡	70°, 6 hr	98

a) Amount of **1** used was 0.1—1.0 mol%.

Table 2. Silylenolethers (**3**) obtained by the hydrosilation of α,β-unsaturated ketones and aldehydes[a]

$[(R^1R^2CHCH{=}CR^3{-}O)_nSiR_{4-n}]$

	R^1	R^2	R^3	n	Silyl gronp	Conditions	Yield (%)
a	Ph	H	H	1	Et_3Si–	60°, 15 min	96
b	Me	Me	Me	1	$PhMe_2Si$–	50°, 30 min	98
c	Me	H	H	1	Ph_3Si–	60°, 30 min	97
d	Ph	H	Me	1	Et_2HSi–	50°, 10 min	85
e	Ph	H	H	2	PhHSi=	10°, 5 min	99

a) Amount of **1** used was 0.1—0.5 mol%.

1) R. Calas, E. Frainnet, and J. Bonastre, *C. R. Acad. Sci. Paris*, **251**, 2987 (1960).

2) S. I. Sadykh-Zade and A. D. Petrov, *Zh. Obshch. Khim.*, **29**, 3194 (1959).

3) R. Calas and N. Duffaut, *C. R. Acad. Sci. Paris*, **245**, 906 (1957): C. Eaborn, "Organosilicon Compounds" Butterworth, London, (1960), p. 213.

4) H. Gilman and D.H. Miles, *J. Org. Chem.*, **23**, 326 (1958).

5) H. Gilman and D. Wittenberg, *ibid.*, **23**, 501 (1958).

A Deuteron Magnetic Resonance Study of the Motion of Ligands in $[Co(ND_3)_5(D_2O)](ClO_4)_3$

Takeshi Ito

Department of Chemistry, Faculty of Engineering, Yokohama National University, Minami-ku, Yakohama

(Received February 18, 1972)

The deuteron magnetic resonance of single crystals of aquopentamminecobalt(III) perchlorate was measured at various temperatures. The observed quadrupole coupling shows that $[Co(ND_3)_5(D_2O)]^{3+}$ ions execute a rapid isotropic reorientation at high temperatures (above 320°K), while only a C_3 axis reorientation of the ligand ND_3 groups is present at low temperatures (below 290°K). No anisotropic uniaxial reorientation was observed about the C_4 axis parallel to the Co–(D_2O) direction. At temperatures between 310°K and 320°K, the spectrum of a fast exchange limit was observed, together with the spectrum of a slow exchange limit. This anomaly may be explained by the classical rotation of the D_2O ligand.

When clusters of atomic groups rotate in crystals, there are several possibilities with regard to the symmetry of the crystal and the cluster. If both the symmetry of the crystal and that of the cluster are cubic, the reorientational motion of such a cluster may be isotropic because there is no preferential axis of reorientation. On the other hand, in the case of the crystal whose symmetry is lower than cubic, the possibility of some anisotropy in such a motion exists because of the effect of the crystal field even if the cluster has cubic symmetry. In fact, reorientational motion about a single C_3 or C_4 axis is observed in a suitable temperature range for a few compounds.[1-3] In the case of a cluster symmetry lower than cubic, such as *trans*-MA_4X_2 and MA_5X-type complex ions, the M–X bond is the preferential axis for reorientational motions because the motions about all the C_3 axes or C_4 axes except the M–X bond cause an exchange of the A ligand for a different ligand, X, and the motion is usually anisotropic. By proton magnetic resonance studies of cobalt ammine complexes, motional narrowing has been observed in several pentammine and tetrammine complexes at temperatures lower than room temperature, but the second moment of these complexes at room temperature are twice or more as large as those of hexammine complexes.[4-6] This presumably suggests that only the anisotropic uniaxial motion about a C_4 axis parallel to the Co-X bond direction is excited.

In the present work, the deuteron magnetic resonance of single crystals of aquopentamminecobalt(III) perchlorate is studied as one of the singular cases mentioned above. About this crystal it has been reported that the symmetry of the crystal is cubic, while that of the $[Co(NH_3)_5(H_2O)]^{3+}$ ion is lower than cubic, and that the cluster ions are statistically oriented in three possible orientations in the crystal.[7,8] Therefore, it is very interesting to know whether the motion of this tetragonal cluster ion is anisotropic or not in the cubic crystal field.

Experimental

The sample was prepared by the standard method.[9] Deuteration was performed by the repeated isotope exchange of $[Co(NH_3)_5(H_2O)](ClO_4)_3$ with D_2O. The single crystals were obtained by the slow cooling of a saturated solution of $[Co(ND_3)_5(D_2O)](ClO_4)_3$ in D_2O. The crystals exhibit {111} faces. The typical sample used was about $10\times10\times10$ mm^3. The measurements were carried out at 10 MHz using a Robinson-type oscillator detector with field sweep and field modulation (230 cps). The field calibration was performed by means of a D_2O signal at various frequencies, as measured by means of an electronic counter. Temperature control was accomplished by using an electric heater wound outside the probe.

Results and Discussion

The observed spectrum at room temperature consists of three pairs of lines (hereafter, these will be denoted

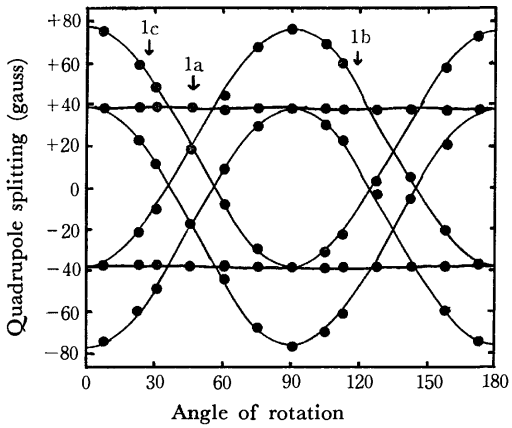

Fig. 1. Rotation pattern of deuteron magnetic resonance of $[Co(ND_3)_5(D_2O)](ClO_4)_3$ at room temperature, for the rotation about one of the crystal axes. θ is the angle between the applied external magnetic field H_0 and the crystal axis.

1) R. E. Rechards, *Trans. Faraday Soc.*, **57**, 210 (1961).
2) D. J. Genin and D. E. O'Reilly, *J. Chem. Phys.*, **50**, 2842 (1969).
3) T. Ito and T. Chiba, This Bulletin, **42**, 108 (1969).
4) S. Hayashi, *Kogyo Kagaku Zasshi*, **68**, 1449 (1965).
5) S. S. Dharmatti, V. Saraswati, and R. Vijayaraghavan, *Proc. Colloque Ampere*, **13**, 133 (1960).
6) G. R. Murray, Jr. and J. S. Waugh, *J. Chem. Phys.*, **29**, 207 (1958).
7) Y. Okaya, N. Stemple, S. Hoshino, and R. Pepinsky, *Bull. Amer. Phys. Soc.*, **3**, 59 (1958).
8) H. Hartmann and H. Sillescu, *Theoret. Chim. Acta*, **2**, 371 (1964).
9) K. Yamazaki, "Zikken Kagaku Koza" Vol. 11, Maruzen Tokyo (1958), P. 20.

as lines 1a, 1b, and 1c). The rotation pattern of this spectrum is shown in Fig. 1. In most of the metal ammine complexes, the $ND_3(NH_3)$ ligand makes a rapid C_3-axis reorientation even at 77°K. In this case, the averaged electric field gradient at deuterons in ND_3 is in the direction of the Co-N bond. Therefore, assuming the axially symmetric field gradient about the Co-N bonds, we obtain the deuteron quadrupole coupling constant of $e^2qQ/h=67.1$ kHz. This value seems reasonable when compared with the deuteron quadrupole coupling constant, which is about 180 kHz for the rigid ND_4^+[10,11] and which is estimated to be about 60 kHz by averaging the C_3-axis reorientation of ND_3. The spectrum at 77°K is almost identical except that the splittings are about two percent greater than those at room temperature. This may be due to the difference between the amplitudes of torsional vibrations at 77°K and those at room temperature. No D_2O signal was observed over the temperature range from 77°K to room temperature. The intensity of the D_2O signal should be one- and two-fifteenth as large as that of the ND_3 signal for stationary and rapid 180°-flipping D_2O respectively. Possibly, the failure to detect the D_2O signal is due to the lack of sensitivity in the apparatus.

The features of the absorption lines at temperatures higher than room temperature are more interesting. The intensity of the absorption lines, 1a, 1b, and 1c, gradually decreases with an increase in the temperature. A new absorption line (line 2) at the Larmor frequency appeared at high temperatures, as is shown in Fig. 2. The line broadening and reappearing must be due to the reorientation of the $[Co(ND_3)_5(D_2O)]^{3+}$ ion. Since the quadrupole splitting of the high-temperature line is almost zero, it is evident that this reorientational motion is not uniaxial but isotropic. However, as can clearly be seen in Fig. 2, both the low-temperature lines (1a, 1b) and the high-temperature line (2) are simultaneously observed at some temperatures. Such an anomalous phenomenon of the coexistence of spectra of a slow exchange limit and of a fast exchange limit can be explained by only the theory of simple motional averaging. In tracing the motional broadening of deuteron resonance lines, there is commonly a range of temperature where the spectrum is completely washed out and unobservable between the two limitting ranges. Therefore, the 1 and 2 lines must be due to the different origins. To explain these facts, we should examine the following three possibilities:

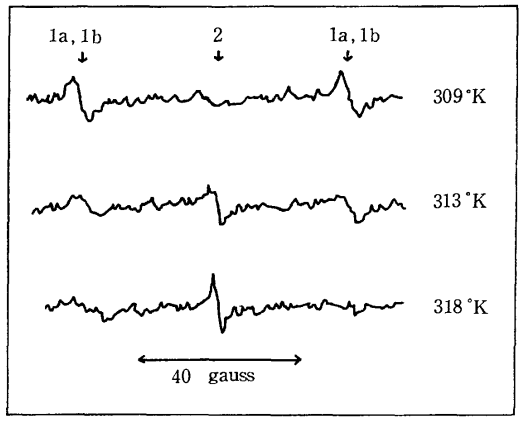

Fig. 2. Line broadening at 309°K, 313°K and 318°K. The magnetic field is applied parallel to the crystal axis.

(A) Although there is only one equivalent site in this crystal, the crystal fields acting on the individual complex cations may be slighly different from each other because the complex cations are randomly oriented in the crystal.[7,8] As a result, the rates of the reorientation of complex cations may not all be the same. Therefore, the 1 and 2 lines may be signals from the cations with a slower rate of reorientation and with a faster rate of reorientation respectively.

(B) In this crystal, the order-disorder phase transition was reported at 314°K.[7] If the rate of reorientation is slow in the ordered phase and fast in the disordered phase, the 1 and 2 lines may originate from the complex cations in the ordered phase and the disordered phase respectively, because both phases usually coexist near the transition temperature.

(C) In contrast with (A) and (B), the 1 and 2 lines may be due to the same type of complex cations, not different types. In this case, the 1 and 2 lines may be considered to originate from ND_3 and D_2O respectively.

Of course, the propriety of these interpretations should be examined by taking the experimental results of the proton second moment, the spin-lattice relaxation time in the laboratory frame (T_1), and that in the rotating frame ($T_{1\rho}$) into consideration. For this compound, the second moment decreases smoothly as the temperature increases in the range from 290°K to 340°K. The spin-lattice relaxation times, T_1 and $T_{1\rho}$, have no discontinuity over the temperature range studied. $T_{1\rho}$ has a sharp minimum at 333°K.[12]

In the case of Model (A), either a very broad linewidth transition of a proton resonance or a shallow minimum in a spin-lattice-relaxation-time-*versus*-temperature curve should appear, because various correlation times of reorientation can be expected. However, the experimental results are contradictory. Therefore, this model may be inadequate. In the case of Model (B), the correlation time of reorientation should exhibit a discontinuity at the temperature of phase transition. In fact, the broadening of the 1 lines and the narrowing of the 2 line occur more quickly at temperatures near the transition point. Therefore, it is certain that the phase transition is accompanied by a discontinuity in the correlation time of reorientation. However, if the signals due to the stationary and rotating ions are observed in the ordered and disordered phase respectively, the difference between the correlation times in the two phases must be considerably large. As a result, the spin-lattice relaxation time should have a clear discontinuity at the transition temperature. However, the experimental results do not exhibit such a discontinuity.

10) P. Pyykko and J. -L. calais, *Kondens. Marterie*, **5**, 1 (1966).
11) D. E. O'Reilly and T. Tsang, *J. Chem. Phys.*, **46**, 1291 (1967).
12) T. Ito and T. Chiba, *Nippon Kagaku Zasshi*, **90**, 466 (1969).

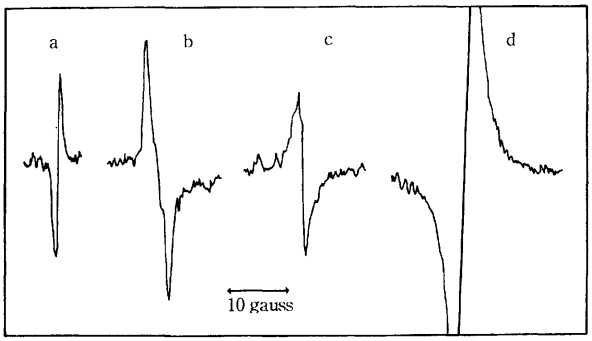

Fig. 3. Deuteron magnetic resonance spectra of $[Co(ND_3)_5(D_2O)](ClO_4)_3$ at 365°K. (a): $\theta=0°$, with small modulation; (b): $\theta=0°$, with large modulation; (c): $\theta=45°$, with small modulation; (d): $\theta=45°$, with large modulation. θ is the angle between the external magnetic field H_0 and the crystal axis.

Moreover, in order to test the possibility of Model(B), the following experiment was made at a temperature sufficiently above the transition point (365°K), as is shown in Fig. 3. If the external magnetic field, H_0, is applied parallel to the crystal axis (θ=0°), a sharp line is observed when the modulation width is small (Fig. 3a), and the peak intensity of this line scarcely changes with an increase in the modulation width (Fig. 3b). On the other hand, if H_0 is applied parallel to the bisector of the crystal axes (θ=45°), a somewhat broad line is observed when the modulation width is small (Fig. 3c). The peak intensity of this line is markedly increased with an increase in the modulation width (Fig. 3d). This suggests that the absorption line consists of a sharp and a broad component at this temperature, and that the latter component is too broad to be observed when H_0 is applied parallel to the crystal axis. Since only one phase should exist at this temperature, Model (B) may be inadequate to explain these experimental results, in which case only Model (C) is possible.

The line widths due to the motion, $\Delta\nu_M$, at the limit of slow and rapid exchange rates have been derived from the general formula as follows:[13,14]

slow exchange limit: $$\Delta\nu_M = \frac{1}{4\pi\tau_c} \quad \text{(inside lines 1a, 1b)} \tag{1}$$

and $$\Delta\nu_M = \frac{1}{2\pi\tau_c} \quad \text{(outside line 1c)} \tag{2}$$

rapid exchange limit: $$\Delta\nu_M = \frac{4}{9}(\nu_1^2 + \nu_2^2 + \nu_3^2)\,\tau_c, \tag{3}$$

where τ_c is the correlation time of this motion and where ν_i is the frequency difference at the site i from the center of gravity of the spectra (*i. e.*, $\nu_1+\nu_2+\nu_3=0$). As a result, the width of the motional averaged line is strongly dependent on the initial splitting. That is, the lines with a small splitting are averaged more effectively than the lines with a large splitting by motion. In the present case, if the motion of the D_2O ligand is a usual 180°-flip reorientation, the deuteron quadrupole splitting of D_2O is larger than that of the ND_3 under a rapid C_3-axis reorientation. However, if the motion of the D_2O ligand is a classical rotation about the Co–O bond axis and if its rate is sufficiently fast at this temperature, the averaged deuteron quadrupole splitting is very small because the bond angle of D_2O is close to the tetrahedral angle. Assuming that the bond angle of D_2O is 105°[15] and that the quadrupole coupling constant of stationary coordinated D_2O is 240 kHz,[14] we obtain the quadrupole coupling constant of D_2O averaged by such motion as 13.4 kHz. Therefore, the following explanation is possible: the 1 and 2 lines are the stationary signals of ND_3 and the motional averaged signal of the D_2O ligand respectively. Here we use the words "stationary" and "motional averaged" with respect to the motion of the whole complex cation. The stationary D_2O signal may not be observed because of its weakness, and the averaged ND_3 signal may be the broad component of the high-temperature spectrum. On the basis of this model, the correlation times of the motion of the complex ion are calculated from the line width due to the motion, $\Delta\nu_M$, which is itself estimated from the observed signal intensity by an apporoximate procedure.[16] The results thus obtained are shown in Fig. 4, together with those obtained from the proton second moment and the spin-lattice relaxation time in the rotating frame ($T_{1\rho}$). Although a considerable difference is observed between the correlation times derived from the deuteron resonance and those from the second moment or $T_{1\rho}$, the qualitative features of line broadening and reappearing may be explained by Model (C). This discrepancy may be due to the effect of the overmodulation. In the procedure of Chiba and Kakiuchi[16] the signal is as-

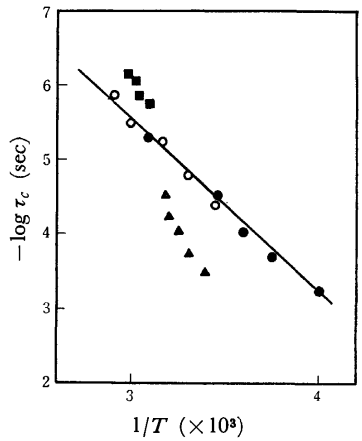

Fig. 4. Correlation times of the motion of aquopentammine-cobalt(III) ion calculated from the deuteron resonance, from the proton second moments and from the proton spin-lattice relaxation times in the rotating frame, $T_{1\rho}$. ○ from proton second moments; ● from proton $T_{1\rho}$; ▲ from deuteron resonance of ND_3; ■ from deuteron resonance of D_2O.

13) A. Abragam, "The Principles of Nuclear Magnetism" Oxford Clarendon Press, Oxford (1961), Ch. 10.
14) T. Chiba and G. Soda, This bulletin, **41**, 1524 (1968).
15) G. Harzberg "Molecular Spectra and Molecular Structure II" D. Van Nostrand Company Inc. Princeton, New Jersey (1945), p. 489.
16) T. Chiba and Y. Kakiuchi, This Bulletin, **41**, 828 (1968).

sumed to be a first derivative; that is, the modulation width is assumed to be infinitely small. In the present experiment, however, a fairly large modulation was used, especially for the motional broadening lines, since the intensities of the lines are weak. As a result, the decrease in intensity due to the line broadening is smaller than that estimated by the procedure of Chiba and Kakiuchi.[16] Therefore, the correlation times derived from the motional narrowing lines of D_2O (■ in Fig. 4) may be smaller, and the motional broadening lines of ND_3 (▲ in Fig. 4) may be larger, than the respective true value. Using Eq. (3) and τ_c derived from the second moment and $T_{1\rho}$, we obtained the line width due to the motion as 3.93 kHz and 0.99 kHz in the cases of $\theta=0°$ and 45° respectively, for the signals of ND_3 at 365°K. These results do not contradict the experimental finding that the broad component of the absorption lines at 365°K is not observed in the case of $\theta=0°$, while it is observed in the case of $\theta=45°$, since the observable limit of line width due to the motion is estimated to be about 3 kHz.

For the crystal treated here, no anisotropy was found in the motion of the cluster, and the motion of the D_2O ligand may be similar to the reorientation of the ND_3 about a C_3 axis rather than the usual 180°-flip one. This suggests that the D_2O and ND_3 ligands are essentially undistinguishable in this crystal. This conclusion seems reasonable in view of the fact that the symmetry of the crystal is cubic in contrast with the lower symmetry of the cluster.

The author would like to thank Professor Takehiko Chiba of Nihon University and Professor Jiro Higuchi of Yokohama National University for their valuable comments and criticism on the manuscript. Also, he wishes to thank Professor Chiba for the use of his facilities.

BULLETIN OF THE CHEMICAL SOCIETY OF JAPAN, VOL. 45, 3510—3514 (1972)

A Consideration of Orbital Interaction in the Reaction of $^1\Delta_g$ Molecular Oxygen with Ethylene Derivatives

Satoshi INAGAKI, Shinichi YAMABE, Hiroshi FUJIMOTO, and Kenichi FUKUI

Faculty of Engineering, Kyoto University, Kyoto

(Received March 27, 1972)

The stereochemical path of the reaction between the $^1\Delta_g$ oxygen molecule and ethylene was examined in terms of orbital interaction. The results here obtained suggest that a path *via* the perepoxide intermediate or *via* a perepoxide-like transition state should be carefully examined in discussing not only the steric path to dioxetane, but also the mechanism of hydroperoxide formation.

Extensive studies[1] of the reactions of the $^1\Delta_g$ oxygen molecule with olefinic bonds have revealed the existence of cycloaddition products (both $2+2$[2] and $4+2$ cycloadducts[3-5]), allylic hydroperoxides,[4,6] and fragmentation products — that is, carbonyl compounds. The fact that a single species, the singlet oxygen, gives both $2+2$[2a] and $4+2$[1] cycloadducts, with the configuration of olefin retained, provides us with an interesting problem to be examined from the viewpoint of molecular orbital symmetry. In addition, there are now heated controversies[1] regarding the mechanism of the reactions between the singlet oxygen and ethylene derivatives, especially concerning the existence of the perepoxide intermediate or the perepoxide-like transition state. Here, the following questions come to mind. Is the 1,2-cycloadduct, namely, dioxetane, formed as a primary product or as a rearranged compound of an initially-formed intermediate, perepoxide? Furthermore, does a concerted "ene" reaction occur in fact, or does an allylic hydroperoxide have any precursor? If any, what is the precursor?

In order to obtain some information about the detailed reaction path, Kearns,[1,7] using correlation diagrams, recently examined three different models for the concerted addition of the singlet oxygen to ethylene, IA, IIA, and IIIA, and suggested that IA and IIA are generally allowed, while IIIA is allowed only for the olefins with particularly low π ionization potentials. These results, obtained from the correlation diagrams, are not necessarily satisfactory in our attempt to ascertain the stereochemistry of the reaction paths, for there remains the important problem of whether dioxetane, previously detected,[2] is a primary product or a rearranged product of perepoxide. Hence, another discussion from a different standpoint, that of particular orbital interaction,[8] is worth being presented.

Choice of Models

In discussing the mechanisms of both dioxetane and allyic hydroperoxide formations, perepoxide has been

1) D. R. Kearns, *Chem. Rev.*, **71**, 395 (1971).

2) a) P. D. Bartlett and A. P. Schaap, *J. Amer. Chem. Soc.*, **92**, 3223 (1970); b) S. Mazur and C. S. Foote, *ibid.*, **92**, 3225 (1970).

3) K. Gollnick and G. O. Schenck, "1,4-Cycloaddition Reactions", J. Hamer, Ed., Academic Press, New York, 1967, p. 255.

4) T. Matsuura, *Yūki Gōsei Kyōkai Shi*, **26**, 217 (1969).

5) Furthermore, a $6+2$ cycloadduct is proposed as the intermediate of the reaction of the singlet oxygen with cycloheptatriene. See, A. S, Kende and Y. -C. Chu, *Tetrahedron Lett.*, **1970**, 4937.

6) C. S. Foote, *Accounts Chem. Res.*, **1**, 104 (1969).

7) D. R. Kearns, *J. Amer. Chem. Soc.*, **91**, 6554 (1969).

8) K. Fukui, *Accounts Chem. Res.*, **4**, 57 (1969) and the references cited therein.

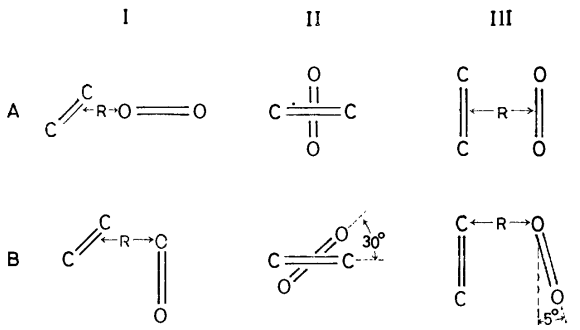

recommended as a feasible intermediate,[1] but this recommendation still remains without any theoretical are experimental conclusive evidence for or against it. As typical models of perepoxide, IA and IB are chosen in this study. In IA, one oxygen is placed in the plane determined by the carbons of ethylene and the other oxygen, while one oxygen is located vertically away from the coplane in IB. IB is our originally-chosen model.

On the other hand, some concerted processes, namely, the $2\pi_s+2\pi_a$ and $2\pi_s+2\pi_s$ cycloadditions represented by the models IIA and IIIA respectively, have naturally been proposed[1] in analogy to ethylene dimerization.[9] It should be noted that the frontier orbitals to interact with each other are orthogonal; therefore, the overlapping between them is zero in IIA. Hence, the IIB model in which the plane containing the C_2 axis and O-O bond axis and the one containing the C_2 axis and the C-C bond axis intersect with the 30° angle, was examined in order to evaluate the actual effectiveness of IIA.

The last model, IIIB, will be used to examine the possibility of an unsymmetrical ionic or biradical-like transition state. The deformation from the symmetrical structure was introduced by rotating the O-O bond in the plane by an arbitrary angle (5°).

Consideration of the Particular Orbital Interaction

From numerous instances of actual chemical reactions, it is now well-established that a majority of chemical reactions take place at the position, and in the direction, where the overlapping between the highest occupied (HO) molecular orbital (MO) and the lowest unoccupied (LU) MO is most favored.[8] Accordingly, it is first necessary to look into the nodal properties of the frontier orbitals of $^1\Delta_g$ oxygen in order to determine the most probable reaction path in terms of particular orbital interaction.

The electronic configuration of $^1\Delta_g$ molecular oxygen is $(1\sigma_g)^2(1\sigma_u)^2(2\sigma_g)^2(2\sigma_u)^2(1\pi_u)^4(3\sigma_g)^2(1\pi_{gyz})^2(1\pi_{gzx})^0$ taking the O-O axis along the Z-axis. The MO's π_{gyz} and π_{gzx} have two nodal planes, one involving the O-O axis and the other perpendicular to this axis (Fig. 1). It follows that the singlet oxygen has the HOMO and the LUMO of the same symmetry property, extending in two planes perpendicular to each other.

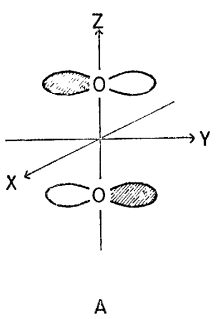

Fig. 1. The nodal property and the direction of the extension of the HOMO (A) and the LUMO (B) of $^1\Delta_g$ molecular oxygen.

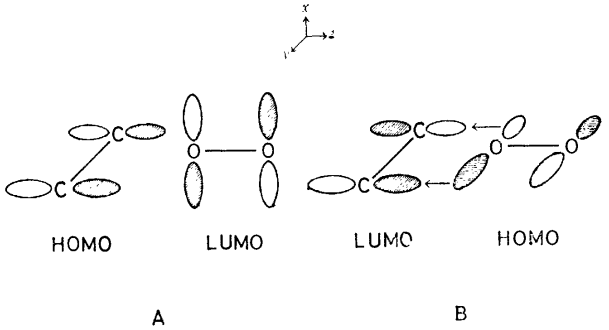

Fig. 2. The modes of HOMO-LUMO interactions between $^1\Delta_g$ molecular oxygen and ethylene in the model IA;
(A) intreraction between the HOMO of ethylene and the LUMO of $^1\Delta_g$ molecular oxygen;
(B) interaction between the LUMO of the former and the HOMO of the latter.

The IA model will first be considered here in terms of orbital interaction, which has been examined by means of a correlation diagram and which has been shown to represent an allowed process from the viewpoint of the conservation of orbital symmetry.[1] Suppose that the molecular plane and the C-C bond axis of ethylene are fixed parallel to the XY-plane and the Y-axis respectively, and $^1\Delta_g$ molecular oxygen is on the Z-axis (Fig. 2). Then, it can readily be found from the requirement of orbital symmetry that the HOMO of ethylene and the LUMO of the oxygen do not overlap at all, irrespective of any rotation of oxygen about the Z-axis (Fig. 2A). On the other hand, the LUMO of ethylene can overlap with the HOMO of the singlet oxygen because they have the same symmetry property with respect to reflection in the ZX-plane (Fig. 2B). This mode of orbital interaction may, however, be less important, since it means a charge-transfer from oxygen to ethylene; this mode of electron delocalization contradicts the generally-accepted electronegativity order. Accordingly, the model IA is not expected to represent the most favorable reaction path.

In the model IB, both modes of frontier orbital interactions which imply the charge-transfer from ethylene to oxygen, and the reverse, are favorable. The HOMO of ethylene can effectively interact with the terminus of the LUMO of the singlet oxygen (Fig. 3A), while the HOMO of oxygen, with its maxi-

9) R. B. Woodward and R. Hoffmann, *Angew, Chem., Int. Ed. Engl.*, **8**, 781 (1969).

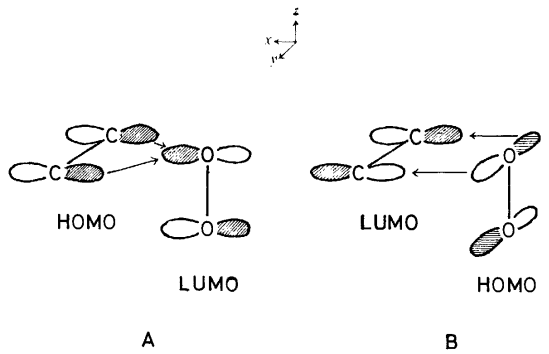

Fig. 3. The modes of HOMO-LUMO interactions between $^1\Delta_g$ molecular oxygen and ethylene in the model IB;
(A) interaction between the HOMO of ethylene and the LUMO of $^1\Delta_g$ molecular oxygen;
(B) interaction between the LUMO of the former and the HOMO of the latter.

mum extension in the direction parallel to the C–C bond, can also interact with the LUMO of ethylene (Fig. 3B), because these interacting MO's have the same symmetry with respect to the bisecting plane of the combined system (ZX-plane). Accordingly, the model IB may be supposed to be the most promising candidate for the actual reacting system.

A concerted mechanism can be alternative interpretation of the formation of 1,2-cycloadduct dioxetane. The characteristic of such a reaction path is that the way of approach of oxygen to ethylene maintains a certain symmetry, at lowest, the C_2 element. In these cases, there are two typical modes of frontier orbital interaction. One of them is a suprafacial-antarafacial interaction between the HOMO of the ethylenic π orbital and the LUMO of the singlet oxygen $1\pi_{gzx}$, as is illustrated in Fig. 4A (ethylene approaches oxygen along the Y-axis, with the π orbital in the XY-plane). This interaction mode, which corresponds to the IIA or IIB model, would not be so favored by the geometry as to eventuate in the stabilizing of the transition state. The other significant interaction is a suprafacial-suprafacial interaction between the LUMO of ethylene and the HOMO of the singlet oxygen (Fig. 4B, model IIIA). This mode of interaction is geometrically most feasible, but again it results in an unfavorable charge-transfer from the singlet oxygen to ethylene.

The last model, IIIA, cannot be discussed here by taking only the orbital symmetry into consideration, for this model does not have any particular symmetry. Accordingly, the estimation of the IIIB model will be made by the MO calculation to be described in the following section.

As a result, $^1\Delta_g$ molecular oxygen is expected to approach a double bond of olefins, most probably forming trigonal ring composed of two carbons and an oxygen atom, and tailed by the other oxygen, which drops out of the plane of the ring.

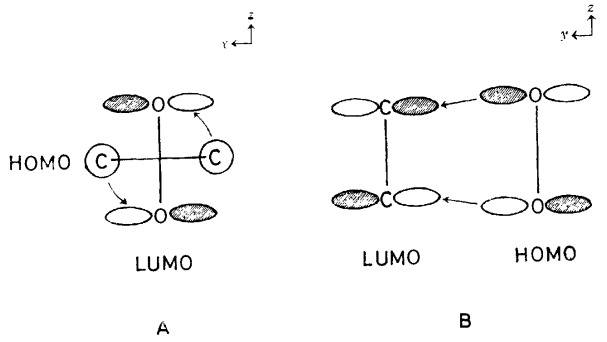

Fig. 4. The modes of HOMO-LUMO interactions between $^1\Delta_g$ molecular oxygen and ethylene in the model IIA and IIIA; (A) the interaction between the HOMO of ethylene (suprafacial) and the LUMO of the singlet oxygen (antarafacial) and (B) that between the LUMO of the former (suprafacial) and the HOMO of the latter (suprafacial).

Calculation

The chemical interaction at the early stage of a reaction was discussed by dividing the interaction energy, ΔW, into Coulomb (E_Q), exchange (E_K), delocalization (D), and polarization (Π) terms by the use of the configuration-interaction method (Eq. (1)):[10]

$$\Delta W = E_Q + E_K - D - \Pi. \quad (1)$$

E_Q is the quantity which reflects the charge distribution of the two independent reactants. E_K has a positive value with regard to the reactions between two closed-shell molecules, serving as a repulsive term. D is the stabilization energy due to the mixing-in of the charge-transferred states, in which one electron of an occupied MO of one molecule is transferred into an unoccupied MO of the other molecule. The last term, Π, contributes to the stabilization resulting from the involvement of the local excited states within one molecule under the influence of the approach of the other. The most preferable reaction path may be defined as the one which makes ΔW the smallest.

In Table 1, the results of the calculation are given with regard to some assumed models of the reaction of the singlet oxygen with ethylene derivatives. By comparing the terms in Table 1, we can see, first, that E_Q is zero, for the singlet oxygen has no net charge on both nuclei and Π is also small. The superiority or the inferiority of an assumed reaction path to others is determined essentially by the terms E_K and D. That is, the reaction may favorably proceed through a geometry capable of enlarging the D term and of depressing the E_K term. Accordingly, IA and IB can be expected to be more favorable than others. It is, however, noteworthy that the model IIIB has a re-

Table 1. Interaction energies between $^1\Delta_g$ oxygen molecule and ethylene, shown in eV.

	IA	IB	IIA	IIB	IIIA	IIIB
E_Q	0.000	0.000	0.000	0.000	0.000	0.000
E_K	0.110	0.158	0.186	0.213	0.221	0.182
D	0.058	0.082	0.019	0.033	0.041	0.033
Π	0.002	0.001	0.000	0.000	0.000	0.000
ΔW	0.051	0.075	0.167	0.181	0.180	0.148

10) K. Fukui and H. Fujimoto, This Bulletin, **41**, 1989 (1968).

TABLE 2. THE ABSOLUTE VALUES OF INTERMOLECULAR OVERLAP INTEGRALS

Model IB

Oxygen	Ethylene					
	σ_2	σ_3	σ_4	σ_5	π	π^*
$2\sigma_g$	0	0.005	0.004	0	0.017	0
$2\sigma_u$	0	0.006	0.001	0	0.007	0
$1\pi_u$	0	0.005	0.002	0	0.020	0
$1\pi_u$	0.006	0	0	0.002	0	0.007
$3\sigma_g$	0	0.002	0.001	0	0.002	0
$1\pi_g$	0.001	0	0	0.002	0	0.003
$1\pi_g$	0	0.006	0.001	0	0.008	0
$3\sigma_u$	0	0.002	0.000	0	0.001	0

Model IIIA

Oxygen	Ethylene					
	σ_2	σ_3	σ_4	σ_5	π	π^*
$2\sigma_g$	0	0	0.005	0	0.020	0
$2\sigma_u$	0.010	0	0	0	0	0.012
$1\pi_u$	0	0.006	0	0	0	0
$1\pi_u$	0	0	0.003	0	0.025	0
$3\sigma_g$	0.000	0	0.004	0	0.003	0
$1\pi_g$	0.010	0	0	0	0	0.014
$1\pi_g$	0	0	0	0.003	0	0
$3\sigma_u$	0.002	0	0	0	0	0.001

latively low ΔW, implying a tendency toward a biradical-like character of the reactions.

In order to examine E_K and D in detail, it is worthwhile to look into the overlap integrals between the MO's of oxygen and ethylene (given in Table 2), since both the energy terms, E_K and D, are overlap-dependent quantities. Roughly speaking, E_K is parallel to the overlap integrals between the occupied MO's of oxygen and the occupied MO's of ethylene, while D increases as the magnitueds of the overlap integrals increase between the occupied MO's and the unoccupied MO's of the two species. With this as well as the orbital symmetry in mind, we will compare the values of the overlaps, especially with regard to two different models, IB and IIIA.

Among the overlaps, some larger values are found, in which the HOMO, denoted by π, of ethylene, participates. This π orbital, having a large extension in the direction of the singlet oxygen, can overlap with the MO's of the oxygen with a suitable symmetry property, that is, σ_g and π_u in the model IIIA, and all the MO's in the model IB except for $1\pi_u$ and $1\pi_g$ having an extension of the lobes perpendicular to the π orbital of ethylene. The overlap integrals between the π MO of ethylene and $2\sigma_u$, $1\pi_u$, and $3\sigma_g$ of the singlet oxygen in the model IIIA are larger than the corresponding ones in the model IB. This presumably results from the difference in the geometry of the assumed models. In the model IIIA, the relevant orbital lobes extend face to face with each other, while, in the model IB, only a terminus of singlet oxygen can be effectively involved in the orbital overlapping. It follows that, though the π of ethylene can overlap with more MO's of the singlet oxygen in IB than in IIIA, the absolute values are smaller. In addition, since, in the model IIIA, there are considerably large overlap integrals between σ_2 of ethylene and the σ_u and π_g of the singlet oxygen, as well as the accumulating contributions of the other modes of exchange interaction, a larger value of E_K results in IIIA compared with that in the IB model. The sum of the squares of the overlap integrals between the occupied MO's of ethylene and the occupied MO's of the singlet oxygen was calculated to be 1.31×10^{-3} in the model IB and 1.84×10^{-3} in the model IIIA. Therefore, the preference of the model IB to the model IIIA is partly attributable to the smaller occupied-occupied MO interactions, resulting in the smaller exchange energy E_K.

Table 2 gives other valuable information about the orbital interaction between the occupied MO's of one molecule and the unoccupied MO's of the other, that interaction contributing to the stabilization of the system through the delocalization energy, D. That the overlap integral is zero between the LUMO $1\pi_g$ of the singlet oxygen and the HOMO π of ethylene in the IIIA model indicates numerically that this orbital interaction is symmetry-forbidden, as has been described in the previous section of considering orbital interaction. On the other hand, the orbital interaction between the LUMO of ethylene and the HOMO of oxygen is symmetry-allowed. In the model IB, both the HOMO-LUMO interactions are allowed. Although the overlap integral between ethylene π^* and oxygen π_g is a larger value, 0.014, in the model IIIA as compared with the others, this charge-transfer state is located too high ($\sim$9.4 eV) above the initial state. Therefore, this interaction does not contribute very effectively to the stabilization of the reacting system, since the delocalization energy is in inverse proportion to the energy difference. On the contrary, the interaction between the HOMO of ethylene and the LUMO of oxygen is favorable because of the smaller energy difference between this charge-transfer state and the initial state (2.6 eV). As a result, in spite of the smaller value of the overlap integral in the model IB (0.008), this HOMO-LUMO interaction, in which ethylene acts as an electron-donor and the oxygen serves as an electron-acceptor, yields a larger stabilization in the model IB than the HOMO-LUMO interaction in the model IIIA as mentioned above. Thus, the examination of the exchange and delocalization energies in terms of MO overlap integrals reveals the reason for the superiority or inferiority of one assumed reaction path to another.

The HOMO-LUMO interaction reflected by the D term is now found to be most favored in the geometry of the model IB among all the models examined here. On the contrary, the smaller value of E_K for the model IA than for IB reserves the possibility of the preference of IA. Any attempt to reach a conclusive statement about the preference of IA or of IB is futile, since it depends on the subtle balance between D and E_K terms. The most favorable geometry of the transition state can probably be expected

TABLE 3. TOTAL ENERGY EVALUATED BY CNDO METHOD

	IA	IB	IIA	IIB	IIIA	IIIB
R=2Å	−1451.874	−1451.897	−1450.977	−1450.939	−1450.912	−1451.237
R=3Å	−1452.769	−1452·760	−1452.748	−1452.749	−1452.748	−1452.755
Difference	0.895	0.863	1.771	1.810	1.836	1.518

to assume a nuclear configuration intermediate between IA and IB.

A CNDO[11] calculation was carried out with respect to the six models (IA, IB, IIA, IIB, IIIA, and IIIB) in order to affirm the conclusion drawn from the consideration and the calculation of orbital interaction. As the numerical values in Table 3 show, the nuclear configurations represented by the models IA and IB have lower total energies than the other, corresponding models.[12] In addition, these two models are less destabilized than the others as the two reactants approach further from R=3Å to R=2Å, as is shown in Table 3.[12] This result is in conformity with the prediction of the previous calculation of intermolecular interactions.

Conclusion

The speculative consideration of particular orbital interaction between the frontier orbitals supplies us with some information concerning the modes of interaction between $^1\Delta_g$ molecular oxygen and ethylene derivatives. The finding that the nuclear configuration represented by the model I is energetically favorable for the early-stage interaction between $^1\Delta_g$ molecular oxygen and ethylene is interesting since the way of the approach of a diatomic molecule with the HOMO and the LUMO of the same symmetry to ethylene has now been examined for the first time.

Our present study seems to suggest the presence of a perepoxide intermediate (which may or may not be stable) on the route to the corresponding dioxetane,[14] which is then readily subjected to decomposition into carbonyl compounds.[16] It is also probable that a perepoxide intermediate may be rearranged to allylic hydroperoxide.[17] Alternatively, it is likely that the allylic hydroperoxides are formed through a perepoxide-like transition state.

It may be true that there is some room for reviewing the choices of the models, especially in connection with the intermolecular distances and the changes in the nuclear configurations with the progress of the reaction to be compared, but the essential features of the reactions of $^1\Delta_g$ molecular oxygen with ethylene derivatives, which are derived here from our considerations and from the calculation of the orbital interaction, could not be very much changed by choosing the assumed models. With all the features here revealed, we can say with some certainty that a suprafacial-antarafacial interaction, as in the case of thermal dimerization of ethylene derivatives, is directly inapplicable to the reaction path to dioxetane formation, and that a path *via* a perepoxide intermediate or a perepoxide-like transition state should be carefully examined in discussing not only the steric path to dioxetane, but also the mechanism of hydroperoxide formation.

11) J. A. Pople and D. L. Beveridge, "Approximate Molecular Oribital Theory", McGraw-Hill Book Co., New York, 1970.

12) The extended Hückel MO method[13] gives the same prediction.

13) R. Hoffmann, *J. Chem. Phys.*, **39**, 1397 (1963).

14) The intermediate of the photosensitized oxidation of indene to the exclusive formation of homophthaldehyde in methylene chloride,[15] was trapped by menthanol and was reduced to *vicinal*-hydroxy-methoxy-2,3-dihydroindene.[15] This result suggests the intermediacy of dioxetane[15] or that of perepoxide. However, it should be noted that the possibilities of the photochemical reaction between the olefin and methanol and the reaction between $^1\Delta_g O_2$ and methanol cannot be ruled out here.

15) W. Fenical, D. R. Kearns, and P. Radlick, *J. Amer. Chem. Soc.*, **91**, 3396 (1969).

16) K. R. Kopecky and C. Mumford, *Can. J. Chem.*, **47**, 709 (1969).

17) Fenical *et al.*[18] proposed allylic hydroperoxides arise from perepoxide on the basis of the experimental results that the photooxydation of 1,2-dimethylcyclohexene yielding normal allylic hydroperepoxide affords *vicinal*-hydroxy-azido-derivative in the presence of azide ion. However, this proposal was recently pointed out to be irrelevant because of direct involvement of azide in azidohydroperoxide formation.[19]

18) W. Fenical, D. R. Kearns, and P. Radlick, *J. Amer. Chem. Soc.*, **91**, 7771 (1969).

19) C. S. Foote, T. T. Fujimoto, and Y. C. Chang, *Tetrahedron Lett.*, **1972**, 45; N. Hasty, P. B. Merkel, P. Radlick, and D. R. Kearns, *ibid.*, **1972**, 49.

Electron Spin Resonance during Photolysis of *p*-Benzoquinone and Its Derivatives in Ethanol

Hiroshi YOSHIDA, Koichiro HAYASHI, and Tetsuo WARASHINA*

Faculty of Engineering, Hokkaido University, Sapporo

**Research Reactor Institute, Kyoto University, Kumatori-cho, Osaka*

(Received April 22, 1972)

Electron spin resonance measurements were carried out at room temperature during photolysis of solutions containing *p*-benzoquinone, 2-methyl-*p*-benzoquinone, 2,5-dimethyl-*p*-benzoquinone and 1,4-naphthoquinone in ethanol. From all quinones, the semiquinone radicals and semiquinone anions are found to form simultaneously. When the solution is made acidic, the semiquinone anion transforms into the semiquinone radical, so that the spectrum of the latter is easily determined. For benzoquinone, the semiquinone radical is formed efficiently by light of $\lambda \approx 300$ nm, and has a life of about 0.05 sec. The semiquinone anion is formed by light of $\lambda \approx 460$ nm and is rather long-lived (about 0.5 sec). These results suggest that the semiquinone anion may be formed mostly by photodissociation of charge-transfer complex between benzoquinone and alcohols. Observed proton hyperfine coupling constants were subjected to the molecular orbital treatment. The coupling constants in all the semiquinone anions examined are well interpreted by McLachlan's approximate SCF-MO method and Colpa-Bolton's relation with $Q=27$ G and $K=12.8$ G. However, good agreement is not attained between the observed coupling constants and the calculated ones for the semiquinone radicals.

Semiquinone anions and semiquinone radicals are well known to be involved in both reduction and oxidation processes between quinones and hydroquinones. Since Venkataraman and Fraenkel's pioneering work of detecting electron spin resonance (ESR) spectra of semiquinone anions by oxidizing hydroquinone and durohydroquinone in alkaline solution with oxygen,[1] ESR studies have been extensively made on semiquinone anions formed by oxidizing hydroquiones,[2,3] and by reducing quinones with glucose or sodium dithionite,[3] or electrochemically[4,5] in alkaline solutions. Semiquinone anion was also observed by photolysing duroquinone in the presence of excess alkoxide ion in the solution.[6]

Observed hyperfine structure due to protons in semiquinone anions were first examined with reference to the spin densities calculated from the simple Hückel molecular orbital treatment combined with the McConnell relation.[7] Their observed values agreed rather well with the theoretically expected ones, except for methyl-substituted benzosemiquinone anions.[3,8] The hyperfine coupling constants were found to be affected, more or less depending on the position of proton, by solvent,[4] which was interpreted as due to the complexing between the oxygen atoms in the semiquinone anion and the solvent molecules, using the approximate SCF-MO method developed by McLachlan[9] to estimate the spin densities with the Coulomb integral of oxygen atoms and the resonance integral of C–O bond as adjustable parameters.[5,10] Later, this solvent effect was elucidated from the hyperfine structure due to ^{13}C nuclei.[11,12]

By means of flash photolysis, Bridge and Porter first observed semiquinone anions and radicals as intermediate entities formed in the solutions of many quinones.[13] Photolysis was found to be a convenient and useful way to form semiquinone radicals for ESR studies. Gough and Symons detected ESR spectra of *p*-benzosemiquinone[14] and durosemiquinone radicals[6,15] and described the dependence of their hyperfine structure upon the nature of the solvent by the valence-bond treatment. They reported that the semiquinone radicals or anions were observable depending on pH of the solutions. Recently, Wilson[16] examined the hyperfine structure of his spectrum of *p*-benzosemiquinone radical in photolyzed dimethoxyethane solution in reference with the McLachlan's SCF-MO calculation of spin densities and excess charges and Colpa and Bolton's relation[17] instead of the McConnell's.

The present authors studied the kinetical behavior of free radicals formed during photolysis of benzophenone solution in alcohols by using a flow-technique combined with ESR.[18] Here, this study is extended to solutions of *p*-benzoquinone and its derivatives in alcohols, mainly ethanol, and it is found that both semiquinone radicals and anions are formed simultaneously in neutral solution. The mechanism of

1) B. Venkataraman and G. K. Fraenkel, *J. Amer. Chem. Soc.*, **77**, 2707 (1955); *J. Chem. Phys.*, **23**, 588 (1955).
2) B. Venkataraman, B. G. Segel, and G. K. Fraenkel, *J. Chem. Phys.*, **30**, 1006 (1959).
3) G. Vincow, G. K. Fraenkel, *ibid.*, **34**, 1333 (1961).
4) E. W. Stone and A. H. Maki, *ibid.*, **36**, 1944 (1962).
5) R. Dehl and G. K. Fraenkel, *ibid.*, **39**, 1793 (1963).
6) T. E. Gough and M. C. R. Symons, *Trans Faraday Soc.*, **62**, 269 (1966).
7) H. M. McConnell, *J. Chem. Phys.*, **24**, 764 (1956); H. M. McConnell and D. B. Chesnutt, *ibid.*, **28**, 107 (1958).
8) R. W. Brandon and E. A. C. Lucken, *J. Chem. Soc.* **1961**, 4273.
9) A. D. McLachlan, *Mol. Phys.*, **3**, 233 (1960).
10) J. Gendell, J. H. Freed, and G. K. Fraenkel, *J. Chem. Phys.*, **37**, 2832 (1962).
11) E. W. Stone and A. H. Maki, *J. Amer Chem. Soc.* **87**, 454 (1965).
12) M. R. Das and G. K. Fraenkel, *J. Chem. Phys.*, **42**, 1350 (1965).
13) N. K. Bridge and G. Porter, *Proc. Roy. Soc., Ser. A*, **244**, 259, 276 (1958).
14) T. E. Gough, *Trans Faraday Soc.*, **62**, 2321 (1966).
15) T. A. Claxton, T. E. Gough, and M. C. R. Symons, *ibid.*, **62**, 279 (1966).
16) R. Wilson, *J. Chem. Soc., B*, **1968**, 1581.
17) J. P. Colpa and J. R. Bolton, *Mol. Phys.*, **6**, 273 (1963).
18) H. Yoshida and T. Warashina, This Bulletin, **44**, 2950 (1971).

their formation is examined in detail for *p*-benzoquinone. The observed hyperfine structure due to protons is discussed for all quinones examined in terms of the McLachlan's MO treatment and the Colpa and Bolton's relation.

Experimental

The apparatus used has been described in detail previously.[18] ESR measurements were carried out with a conventional X-band spectrometer (Varian, E-3) during photolysis with a super-high pressure mercury arc (Philips, SP 500) of solutions from which dissolved oxygen was removed by bubling helium gas beforehand. The effective volume of a quartz flat cell was $7 \times 0.2 \times 32$ mm.

All chemicals were analytical grade and used as received without further purification, except where otherwise stated.

Results and Discussion

Formation and Decay of p-*Benzosemiquinone Anions and Radicals.* When the solution of *p*-benzoquinone in ethanol is photolyzed, the ESR signal as shown in Fig. 1a is observed. Apparently, the signal is composed of an quintet spectrum and that of triple double-triplet. The former is attributed to *p*-benzosemiquinone anion with four equivalent protons, while the latter is due to *p*-benzosemiquinone radical (monoprotonated benzosemiquinone). If the solution is made acidic by adding a small amount of acetic acid, almost all of the semiquinone anion transforms into the semiquinone radicals as expected from the observation in the flash photolysis study,[13] through the protonation reaction,

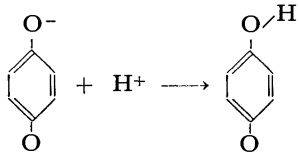

(1)

though a weak spectrum of the semiquinone anion is still observable (see Fig. 1b). The observed concentration of the semiquinones is of the order of 10^{-6} M. The half-life is found, by shutting off and flashing the photolyzing light rapidly, to be a few hundreds milliseconds for the semiquinone anion and less than one hundred milliseconds (the response time of the spectrometer) for the semiquinone radicals in the absence of acetic acid.

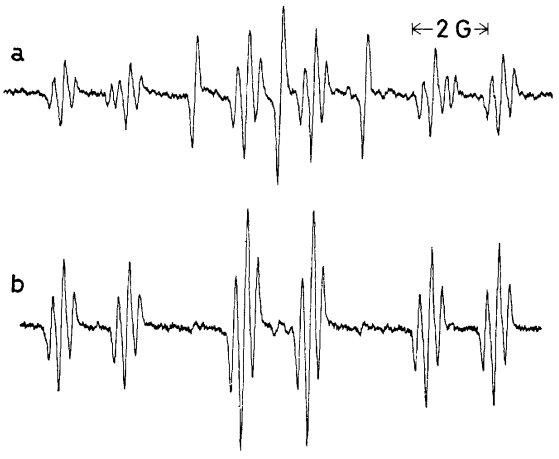

Fig. 1. ESR spectra observed during photolysis of *p*-benzoquinone solution in ethanol (5.5 mM). (a) Spectra due to benzosemiquinone radical (triple double-triplets) and due to benzosemiquinone anion (quintet) formed in neutral solution. (b) Spectrum due to benzosemiquinone radical in acidic solution containing 30 mM of acetic acid.

The temperature dependence of the yield was examined for both anion and radical at a fixed flow rate of solution, and the results are shown in Fig. 2 for methanol and in Fig. 3 for ethanol as solvent. The yield of anion decreases with increasing temperature, while that of radical remains almost unchanged. The dependence of yield upon the resident time of solution in the cell (the effective volume of the cell/the flow rate) is examined for the solution in methanol, as shown in Fig. 4. As the solution is heated during photolysis, its temperature varys depending on the flow rate. In Fig. 4, the observed values are plotted after correcting the temperature effect by using the relationship between the yield and the temperature shown in Fig. 2. The observed yield of anion increases remarkably with increasing the resident time of solution, reaching at a plateau value. This suggests that the life time of

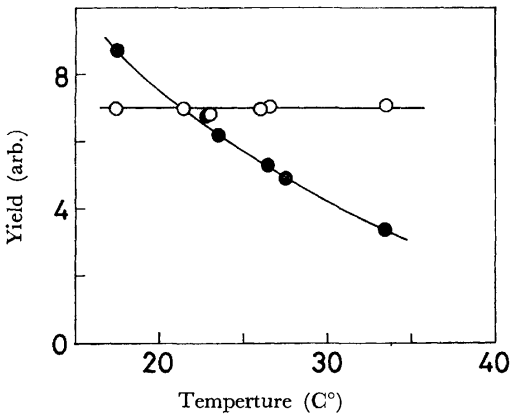

Fig. 2. Observed yield of benzosemiquinone radical (○) and benzosemiquinone anion (●) formed during photolysis of *p*-benzoquinone solution in methanol (5.5 mM) as a function of temperature. Resident time of flowing solution in the cell: 1.1 sec.

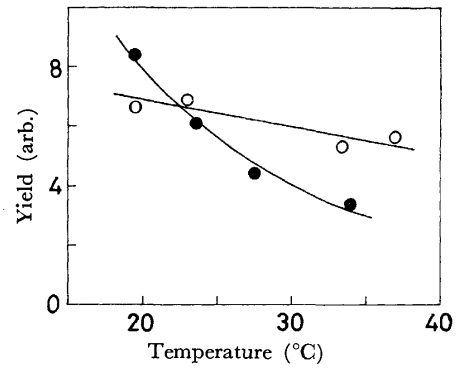

Fig. 3. Observed yield of benzosemiquinone radical (○) and benzosemiquinone anion (●) formed during photolysis of *p*-benzoquinone solution in ethanol (5.5 mM) as a function of temperature. Resident time of flowing solution in the cell: 1.5 sec.

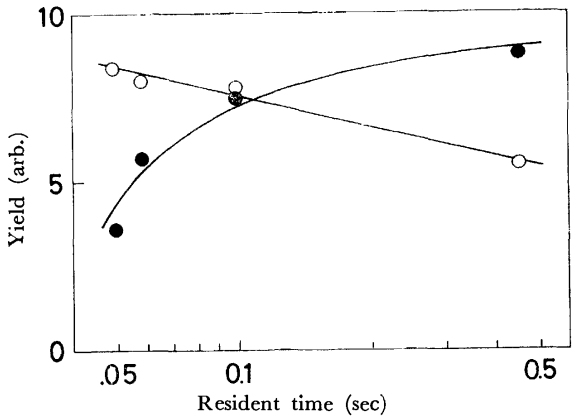

Fig. 4. Dependence of the yield of benzosemiquinone radical (○) and benzosemiquinone anion (●) formed during photolysis of *p*-benzoquinone solution in ethanol (5.5 mM) upon resident time of flowing solution in the cell. Observed values were plotted after the correction of temperature effect.

the anion is rather long (~0.5 sec) and that a fraction of the anions flow out of the cell before their chemical decay. On the other hand, the radical yield decreases with increasing resident time, and the reason is not known at the moment. This trend indicates, at least, that the radical formed disappears in the cell and that its life time is less than 0.05 sec. The above observation of the yields may indicate that the fate of anion, from its formation till disappearance, is independent of the radical in neutral solutions.

In order to elucidate the above argument, the effect of wavelength of the light on the formation of anion and radical was examined by inserting a cut-off filter in the light path. The results are shown in Fig. 5, where the abscissa indicates the wavelength of 50% transmission of filters used and the plots at 270 nm represent the observed yield for the photolysis without filter. The free radical is formed efficiently with light of $\lambda<300$ nm, whereas the anion is formed with light of $\lambda\approx460$ nm. The initial faint decrease in the yield of anion at $\lambda=270-310$ nm may be interpreted by the process,

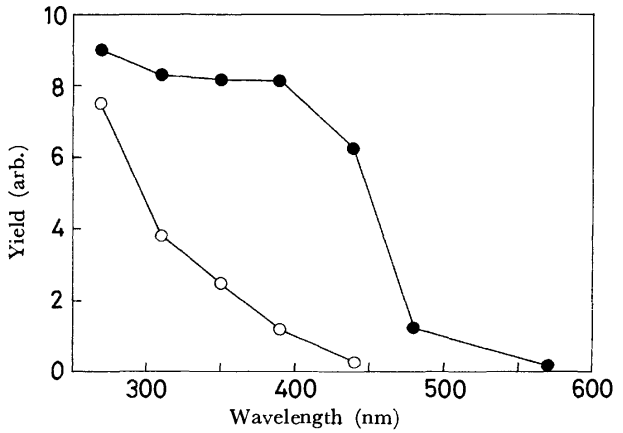

Fig. 5. Dependence of the yield of benzosemiquinone radical (○) and benzosemiquinone anion (●) formed during photolysis of *p*-benzoquinone solution in ethanol (5.5 mM) upon the wavelength of light.

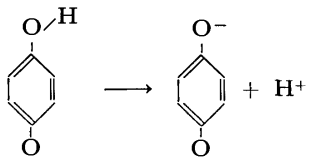

(2)

However, the anion forms mostly for the wavelength appreciably longer than that for the formation of the radical.

The previous results of the flash photolysis study indicated that the primary process in the photolysis of duroquinone was the hydrogen abstraction of the singlet excited quinone to form semiquinone radical. However, in ethanol solution, formation of the semiquinone anion other than in process (2) was also suggested to occur.[13] In the present ESR study, the semiquinone anion is found not to form through the semiquinone radical, by using a selective wavelength of photolyzing light.

If electron transfer occurs directly from the solvent to *p*-benzoquinone under the light of $\lambda\approx460$ nm, the charge transfer interaction between *p*-benzoquinone and the solvent is necessarily involved so that the photo-excited electron donor and acceptor complex dissociates into ions. The efficiency of semiquinone anion formation did not change, though the ethanol was purified by distilling with concentrated sulfuric acid, refluxing with silver nitrate and sodium hydroxide and distilling again. Using dichloromethane as a solvent, the semiquinone radical is observed but the semiquinone anion is not. According to these results, the photo-excited quinone-alcohol complex probably dissociates to form the semiquinone anion, though the possibility cannot be excluded at this moment that some impurities in ethanol play an important role in the formation of the semiquinone anion.

An alternative interpretation is that the *p*-benzohydroquinone formed by disproportionation of the semiquinone radical[13] photo-dissociates to form the semiquinone anion. As a matter of fact, when the solution of *p*-benzohydroquinone in ethanol is photolyzed, an intense ESR spectrum of *p*-benzosemiquinone anion is observed, while the spectrum of semiquinone radical is so weak that it may be ignored. In this case, the question still remains as to why the hydroquinone dissociates to form the anion rather than to form the radical.

For all quinones examined, 2-methylbenzoquinone, 2,5-dimethylbenzoquinone and 1,5-naphthoquinone, corresponding semiquinone anions are observed in addition to semiquinone radicals.

Observed Hyperfine Coupling Constants. Proton hyperfine coupling constants in *p*-benzosemiquinone anion have been reported by several workers[1,2,19] in protic solvent, and the reported values are all very close to 2.368 determined by Venkataraman *et al.*[2] As it is independent of temperature in the range examined (18—36°C), this value was taken as a reference to determine hyperfine coupling constants in other semiquinones studied in the present investigation.

19) D. C. Reitz, F. Dravnieks, and J. E. Wetz, *J. Chem. Phys.*, **33**, 1880 (1960).

Table 1. Observed proton hyperfine coupling constants of *p*-benzosemiquinone radical

Solvent	Temperature	Hyperfine coupling constant (G)		
		2 Ring protons	2 Ring protons	Hydroxy proton
Ethanol	19°C	0.29	5.09	1.86
	26°C	0.31	5.11	1.84
	36°C	0.34	5.21	1.81
Dichloromethane	34°C	0.85	5.64	1.40

Observed hyperfine coupling constants for the benzosemiquinone radical are summarized in Table 1. Their values in ethanol are compared with the values reported by Gough.[14] They are found to be a little dependent on temperature; the coupling constants of ring protons increase with increasing temperature, whereas that of the hydroxy proton decreases. Such a trend agrees with what was observed by Wilson[16] for the radical in dimethoxyethane as solvent.

Figure 6a and 6b show the ESR signals observed from neutral and acidic solution of 2-methylbenzosemiquinone in ethanol, respectively. Evidently, 2-methylbenzosemiquinone anion and some free radical are formed simultaneously in neutral solution, as in solution of *p*-benzoquinone. Venkataraman *et al.* reported hyperfine coupling constants of 2.462, 2.537 and 1.764 G for the ring protons and 2.045 G for the methyl protons, for 2-methylbenzosemiquinone anion.[2] Although the signal in Fig. 6a is complex because of overlapping spectra, almost all hyperfine lines of the anion spectrum are seen at the position expected from the reported coupling constants. Separation between the outer most line (indicated by arrows) is measured to be 12.9 G, which agrees very well with 12.898 G, the sum of all hyperfine separation.

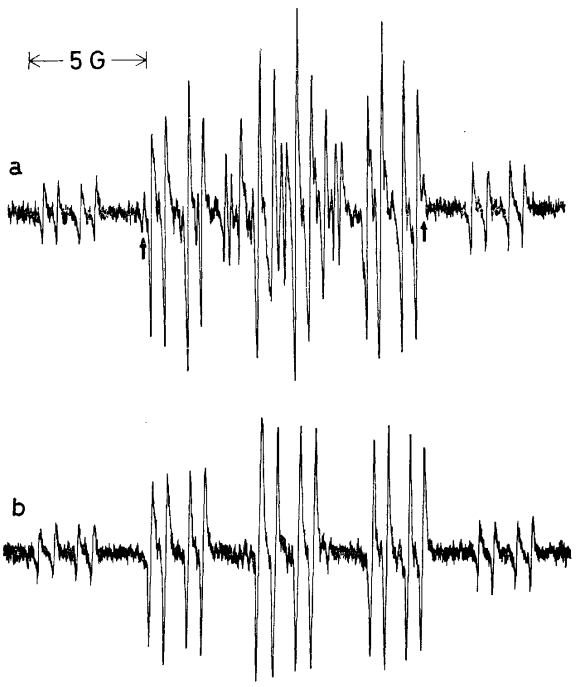

Fig. 6. ESR spectra observed during photolysis of 2-methyl-*p*-benzoquinone solution in ethanol (4.9 mM) (a) in the absence and (b) in the presence of 30 mM of acetic acid.

If the solution is made acidic, the signal becomes much simpler and only a spectrum of the quintet of double-doublet is observed. It may be ascribed to a neutral free radical. However, the number of protons involved is six, which indicates that the spectrum is not due to the semiquinone radical (monoprotonated 2-methylbenzosemiquinone). Although this interpretation has not yet been made, the observed hyperfine coupling constants are 5.00 (4 protons), 1.72 and 0.71 G at 24°C.

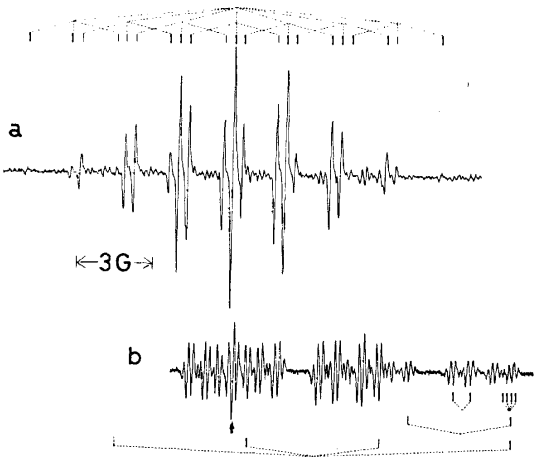

Fig. 7. ESR spectra observed during photolysis of 2,5-dimethyl-*p*-benzoquinone solution in ethanol (4.4 mM) (a) in the absence and (b) in the presence of 30 mM of acetic acid.

The ESR signal observed from the neutral solution of 2,5-dimethylbenzoquinone is shown in Fig. 7a. In addition to a very weak spectrum, the spectrum of septet of triplet (indicated by sticks) is observed and reasonably attributed to 2,5-dimethylbenzosemiquinone anion. The observed hyperfine coupling constant of 1.83 G due to the ring protons and that of 2.25 G due to the methyl protons are in good agreement with the values reported previously.[2] Figure 7b shows the spectrum observed from the acidic solution, which has hyperfine structure due to three unequivalent protons (4.32, 1.70 and 0.71 G) and two kinds of methyl protons (5.18 and 0.20 G at 18°C) attributable to the 2,5-dimethylbenzosemiquinone. The weak background spectrum in Fig. 7a looks like the spectrum due to the semiquinone radical. Therefore, both the semiquinone radical and anion are also formed simultaneously in the neutral solution of 2,5-dimethylbenzoquinone.

ESR signals observed from 1,4-naphthoquinone show a rather complex feature, because they are sometimes recorded as emission lines depending on the measuring conditions and will be reported in detail elsewhere.[20] In this case, the 1,4-naphthosemiquinone radical and anion are also formed simultaneously in neutral solution, but their spectra are separable by referring to the spectrum from the acidic solution.

20) H. Yoshida, J. Sohma, and T. Warashina, to be published.

TABLE 2. PROTON HYPERFINE COUPLING CONSTANT OBSERVED AND CALCULATED FROM MOLECULAR ORBITAL TREATMENT

Semiquinone Anion	Position	Calculated		Observed	
		Spin density	Excess charge	a_H	$\|a_H\|$
	1	0.11026	0.16202		
	2	0.08806	−0.01697	−2.3586	2.368
	0	0.21361	−0.62808		
	1	0.12913	0.14981		
	2	0.12305	−0.04014	−3.2592	3.25
	7	0.02386	0.01275	−0.6482	0.64
	8	0.01822	0.04537	−0.5025	0.51
	9	0.02695	−0.02712		
	0	0.17878	−0.64066		
	1	0.11281	0.15870		
	2	0.09859	−0.00924		
	3	0.07289	−0.04003	−1.9341	1.83
	0	0.20752	−0.63146		
	1	0.11309	0.16310		
	2	0.09331	−0.00824		
	3	0.07466	−0.03805	−1.9796	1.764[2]
	4	0.10994	0.15784		
	5	0.09372	−0.01830	−2.5086	2.537[2]
	6	0.08615	−0.01886	−2.3052	2.462[2]
	0	0.21582	−0.62582		
	0′	0.20549	−0.63345		

Wertz and Vivo[21], and Adams *et al.*[22] reported poor resolved spectra of the nephthosemiquinone anion, and later Venkataraman *et al.* suceeded in observing its spectrum with well resolved hyperfine structure.[2] The present observation (see Table 2) is in good agreement with those previously reported. The observed hyperfine coupling constants for the naphthosemiquinone radical are 6.80, 1.63 (2 protons), 1.50, 0.34 and 0.17 G (2 protons) at 34°C.

Molecular Orbital Calculation. The observed spectra of semiquinone anions and semiquinone radicals indicate well resolved hyperfine structure and, therefore, may be compared to molecular orbital calculations. Vincow and Fraenkel examined the observed hyperfine coupling constants of semiquinone anions with reference to the simple Hückel MO calculations and obtained a good agreement between the observed coupling constants and expected ones.[3] However, Brandon and Lucken claimed that the agreement was obtained not only for a unique pair but also for several pairs of parameters, the Coulomb integral of the oxygen atom and the resonance integral of the carbon-oxygen bond, in the frame of the simple Hückel MO calculations.[23] In the present investigation, McLachlan's approximate SCF-MO method[9] with a value of 1.2 for λ was used to calculate spin densities, ρ_i, and excess charge densities, ε_i. Colpa and Bolton[17] suggested the dependence of isotropic hyperfine coupling constants in hydrocarbon radical anions and cations upon the excess charge density, and postulated the relation, $a_i^H=(Q+K\varepsilon_i)\rho_i$. According to the observed spectra of radical ions of anthracene, Bolton and Fraenkel suggested −27 and −12.8 G for Q and K,[24,25] which were used in the present investigation. Calculations were made with FACOM 230—60 computer of Hokkaido University Computing Center.

For *p*-benzosemiquinone and 1,4-naphthosemiquinone anions, computations were carried out with adjustable parameters γ_{CO} and δ_O ($\alpha_O=\alpha+\delta_O\beta$ and $\beta_{CO}=\gamma_{CO}\beta$ where α and β are the Coulomb and resonance integral for carbon atoms and carbon-carbon bond) for the carbonyl group. In the range of 0.3—3.0 and 0.3—2.0 for δ_O and γ_{CO} (with the interval of 0.05 units), respectively, the best agreement is obtained between the observed hyperfine coupling constants and calculated ones with the values of $\delta_O=1.2$ and $\gamma_O=1.3$, as shown in Table 2.

Gendell *et al.*[10] obtained the best agreement with $\delta_O=1.6$, $\gamma_{CO}=1.55$ and $\lambda=1.2$, using the simple McConell relation, $a_i^H=-23.7\rho_i$. Therefore, it is indicated that the smaller parameters are more suitable for the Colpa-Bolton's relationship than for McConell's. Das and Fraenkel examined the proton and ^{14}C splittings of *p*-benzosemiquinone and anthrasemiquinone anions with the McLachlan's method of calculating spin densities and the simple McConell's relationship, and found that unique pair of δ_O and γ_{CO} did not interpret well the hyperfine splittings of these semiquinone anions simultaneously.[12] The present results suggest that a unique pair of parameters may interpret the hyperfine splittings of *p*-benzosemiquinone derivatives.

For the methyl substituted benzosemiquinone anions, a conjugative model C-C′-H_3 was considered, and the previously used parameters,[26] $\delta_{H_3}=-0.5$, $\delta_{C'}=-0.1$,

21) J. E. Wertz and J. L. Vivo, *J. Chem. Phys.*, **24**, 479 (1956).
22) M. Adams, M. S. Bois Jr., and R. H. Sands, *ibid.*, **28**, 774 (1958).
23) R. W. Brandon and E. A. C. Lucken, *J. Chem. Soc.*, **1961**, 4273.
24) J. R. Bolton and G. K. Fraenkel, *J. Chem. Phys.*, **40**, 3307 (1964).
25) L. C. Snyder and T. Amos, *ibid.*, **42**, 3670 (1965).
26) R. Wilson, *Can. J. Chem.* **44**, 551 (1966).

$\gamma_{C'-H_3}=2.5$ and $\gamma_{C'-C}=0.9$, were used. The calculated coupling constants of the ring protons agree rather well with the observed ones for dimethyl-*p*-benzosemiquinone and methyl-*p*-benzosemiquinone anions.

For semiquinone radicals, the agreement between experimental results and the molecular orbital calculations has not been attained satisfactorily. Any combinations of the parameters for hydroxy group ($\delta_O=$ 0.3—3.0 and $\gamma_{CO}=0.3$—1.7) do not account for the observed proton hyperfine coupling constants in the *p*-benzosemiquinone radical and those in the naphthosemiquinone radical simultaneously, if the parameters for the carbonyl group are fixed to the values determined above for the semiquinone anions. The replacement of one of the carbonyl groups in the semiquinone anions with a hydroxy group may cause the decrease in the electronic charge on the other carbonyl group, which requires a set of parameters for the carbonyl group in the semiquinone radicals different from that in the semiquinone anions. This may be one of the possible reasons why the satisfactory resutls have not been obtained in the MO calculations for the semiquinone radicals.

Conclusion

Photolyzing the solutions of *p*-benzoquinone, 1,4-naphthoquinone, 2-methyl-*p*-benzoquinone and 2,5-dimethyl-*p*-benzoquinone in alcohol at room temperature, the short-lived semiquinone anions and radicals were observed simultaneously by ESR measurements, combined with a flow technique. Although a fraction of the semiquinone radicals possibly transforms into the semiquinone anion, the latter is mostly formed directly from the solute.

The proton hyperfine coupling constants were determined for the semiquinone anions and radicals except for those from 2-methyl-*p*-benzoquinone. For the semiquinone anions, the observed coupling constants agree well with those computed from the McLachlan's approximate SCF-MO method and the Colpa-Bolton's relationship between the coupling constants and the spin densities and excess charge densities.

The authors express their sincere thanks to Prof. T. Higashimura for giving the opportunity to use the experimental facilities.

BULLETIN OF THE CHEMICAL SOCIETY OF JAPAN, VOL. 45, 3520—3526 (1972)

Positive Charge Distribution of Secondary Alkylamines and Its Correlation with the Bond-Scission Probability Appearing in Their Mass Spectra[1]

Masao YAMAMOTO, Iwao FUJITA,* Michiyasu ITOH,*,[2] and Kozo HIROTA*,[3]

Department of Chemistry, Faculty of Science, Nara Women's University, Nara

** Department of Chemistry, Faculty of Science, Osaka University, Toyonaka, Osaka*

(Received April 24, 1972)

With respect to the correlation between scission probabilities and positive charge distributions on the skeletal bonds of amines appearing in their mass spectra, further research is reported on four secondary amines (diethylamine, dipropylamine, dibutylamine and methylbutylamine). In each secondary alkylamine the fragment ions formed by the scission of α–CC bond are the most abundant experimentally, *i. e.*, the scission probability of α–CC bond is the largest in monoamines as well. Agreement between experiments and LCBO-MO calculations on four secondary alkylamines is found to be satisfactory as in the case of propylamine, using the same semi-empirical parameters as those of monoamines in the calculation. It is shown that from detailed calculations of diethylamine by CNDO method the scission of α–CC bond is also easy due to concentration of the positive charge at the bond, theoretically in accordance with the semi-empirical calculation. Change of mass spectra *vs.* ionizing voltage is explained on a generalized scheme, which combines two existing theories of fragmentation (QET and MOT).

We have shown that the molecular orbital theory (MOT) for mass spectra can explain quantitatively the skeletal fragmentation of compounds such as normal[4] and cyclic alkanes,[5] ketones,[6] amines,[7] ethers,[8] esters[9] and aminoacid esters.[10] In MOT it is assumed that relative scission probability of each skeletal bond of of the electron-bombarded molecule is proportional to the positive charge distribution of the highest occupied molecular orbital (HO-MO) at the corresponding bond of its molecular ion, where the positive charge distribution means the distribution of the positive hole formed by losing an electron from the HO-MO of the neutral molecule. Thereby, knowledge of the con-

1) Report XXVI on molecular orbital theory for mass spectra.

2) Present Address: Hitachi Central Research Laboratory, Kokubunji, Tokyo.

3) Present Address: Osaka Laboratory of Japan Atomic Energy Research Institute, Neyagawa, Osaka.

4) K. Fueki and K. Hirota, *Nippon Kagaku Zasshi*, **80**, 1202 (1959).

5) K. Hirota and Y. Niwa, *J. Phys. Chem.*, **72**, 5 (1968); M. Yamamoto and K. Hirota, *Shitsuryo Bunseki, (Mass Spectroscopy)*, **17**, 563 (1969).

6) M. Hatada and K. Hirota, This Bulletin, **38**, 599 (1965).

7) (a) M. Itoh, M. Yamamoto, and K. Hirota, *Nippon Kagaku Zasshi*, **89**, 443 (1968); (b) M. Yamamoto, M. Itoh, I. Fujita, and K. Hirota, *ibid.*, **89**, 752 (1968).

8) K. Hirota and J. Takezaki, This Bulletin, **41**, 76 (1968).

9) T. Isoya, T. Nagumo, and K. Hirota, *Z. Phys. Chem. N. F.*, **61**, 1 (1968).

10) M. Saito, M. Yamamoto, and K. Hirota, *Nippon Kagaku Zasshi*, **90**, 663 (1969).

stants characteristic to each functional group is required for calculation of the HO-MO, except for normal and cyclic alkanes.

As far as the mass spectra of the normal and cyclic alkanes are concerned, the above assumption seems to be acceptable.[11] Several comments have been given on the use of the assumption for predicting the mass spectra of the compounds containing heteroatoms. Lorquet et al.[12] criticized the use of calculated results of alkylamines based on the LCBO-MO approximation in our attempt to extend the research to normal alkylamines, *i. e.*, although the positive charge densities at the CN bond and lone pair are 16% and 71% of the total, respectively, only that at the CC bond is taken in discussing the scission probability. In the LCBO-MO approximation, however, the positive charge distribution of the lone pair is included implicitly in that of the CN bond, so that net charge distribution at the CN bond might occupy only a small fraction of the total and be even smaller than that of the α-CC bond adjacent to it. We therefore adopted in our previous work on ethylamine and propylamine[13] the CNDO (the complete neglect of differential overlap) method of LCAO-MO-SCF proposed by Pople *et al.*[14] The results were found to be favorable.

In our research[6] on propyl-, butyl-, amyl-, hexyl- and heptylamine, calculation was carried out by the LCBO-MO method, and two parameters concerned with amino group were determined empirically from the observed values of propylamine and butylamine. The parameters were found transferable also in the calculation of alkyldiamines from C_4 to C_7[7b] and aminoacid esters.[10]

We report herewith that a good agreement can be found for four secondary alkylamines between the calculated values obtained by the LCBO-MO method and the observed from mass spectra by use of the two parameters of the primary amines, and also diethylamine by use of the calculated positive charge obtained by the CNDO method.

Calculations

LCBO-MO Method. According to the assumption, the scission probability of the skeletal bonds is proportional to the positive charge densities of the HO-MO of the molecular ion. In actual calculation, the charge densities are assumed to be equal to the electron densities of the corresponding neutral molecule, calculated by the LCBO-MO method. The MO belonging to the skeletal bond Φ is given by

$$\Phi = \sum_{i=1}^{n} c_i \phi_i, \qquad (1)$$

where ϕ_i is the bond-orbital of the i-th skeletal bond. The summation is carried out on all the bond adopting the united atom approximation.[15]

The secular equation of a molecule is

$$|e_{ij} - \delta_{ij}E| = 0, \qquad (2)$$

where e_{ij} denotes the matrix element and E the energy of the molecular orbital. All the interactions except for those adjacent group bonds are assumed to be zero. The required parameters in the calculation are the Coulomb integrals of CN and α-CC bond and resonance integral of CN bond as follows.

$$\alpha_{C-N} = \alpha_0 + 0.5\beta_0,\ \alpha_{C-CN} = \alpha_0 - 2.0\beta_0,\ \beta_{C-N} = \beta_0 \qquad (3)$$

where α_0 and β_0 are the Coulomb integral and the resonance integral of normal alkane, respectively. The parameters in Eq. (3) were determined from the experimental values of propylamine and butylamine.[7a]

CNDO Method. The CNDO method is a semi-empirical LCAO-MO-SCF method calculating molecular orbitals and is known to be applicable to π electrons and lone pair electrons as well as σ electrons. Nine possible conformations of diethylamine and three of methylethylamine were calculated. Atomic distances of both amines were adopted as follows: C-C, 1.540 Å; C-N, 1.474Å; C-H, 1.085Å; N-H, 1.012Å.

Table 1. Matrix elements $U_{\mu\mu}$ (in electron volts)

	H	C	N
s orbital	−7.176	−14.051	−19.316
p orbital	—	−5.572	−7.275

$U_{\mu\mu} = (\mu|-\frac{1}{2}\nabla^2 - Z_A/r_{1A}|\mu)$

All the bond angles were taken to be 109°28′. Atomic integrals necessary in the calculation were the same as in the paper of Pople and Segal[14] (Table 1). In the calculation of electron densities, $2s$, $2p_x$, $2p_y$, $2p_z$, orbitals of nitrogen and carbon atoms were adopted as the basis set of orbitals, which were transformed into sp^3-hybrid orbitals after the calculation.

Experimental

The mass spectra were measured on a high resolution type apparatus (Hitachi RMU-7HR), its resolution being *ca.* 5000, and on an ordinary one (Hitachi RMU-5B) installed at Osaka University. Ionization voltage (V_i) was varied in several steps from 10 to 80 volts, the repeller voltage being fixed at 3 volts. The gas-reservoir temperature was maintained at about the boiling point of each sample during the course of measurement. The compounds studied were diethylamine, dipropylamine, dibutylamine and methylbutylamine.

Results

Mass Spectra of Secondary Amines. The mass spectra of four secondary amines at V_i=80 and 20 volts and abundance ratios of the ions in the main peaks from the high resolution measurement are shown in Tables 2 and 3, respectively.

11) R. D. Finney and G. G. Hall, *Intern. J. Mass Spectrom. Ion Phys.*, **4**, 489 (1970).
12) J. C. Lorquet, A. J. Lorquet, and J. C. Leclerc, *Advan. Mass Spectrom.*, **4**, 569 (1968).
13) K. Hirota, I. Fujita, M. Yamamoto, and Y. Niwa, *J. Phys. Chem.*, **74**, 410 (1970).
14) (a) J. A. Pople, D. P. Santry, and G. A. Segal, *J. Chem. Phys.*, **43**, S129 (1965); (b) J. A. Pople and G. A. Segal, *ibid.*, **43**, S136 (1965); (c) J. A. Pople and G. A. Segal, *ibid.*, **44**, 3289 (1966).
15) G. R. Lester, *Advan. Mass Spectrom.*, **1**, 287 (1959).

TABLE 2. MASS SPECTRA OF *sec*-AMINES

m/e	$(C_2H_5)_2NH$		$(C_3H_7)_2NH$		$(C_4H_9)_2NH$		$CH_3NHC_4H_9$	
	80V	20V	80V	20V	80V	20V	80V	20V
15	1.9		6.8		5.2		5.2	
27	10.5		27.0	1.4	25.8		10.8	
28	13.5	1.8	19.6	1.8	18.9	0.3	12.7	
29	11.5	4.7	11.2	0.5	33.9	2.9	8.2	1.1
30	59.5	46.7	85.7	57.4	58.5	31.7	12.3	6.4
39			11.8		11.7		5.1	
41	3.2		21.1	4.1	24.0	4.3	6.7	1.1
42	8.5	1.8	9.0	1.2	8.2	0.7	6.6	0.9
43	2.5	0.2	31.7	13.2	10.8	1.6	4.8	1.4
44	27.1	18.4	14.0	12.6	65.6	60.9	100.0	100.0
56	3.2	1.3	4.0	0.8	6.4	0.9	2.6	0.7
57	0.9	0.2	0.5	0.2	17.5	7.3	3.2	1.4
58	100.0	100.0	6.2	4.5	1.6	0.9	7.1	5.9
70			3.4	1.2	1.8	0.4	0.9	0.3
72	16.7	16.7	100.0	100.0	6.9	5.9	2.9	2.4
73	31.1[a]	33.9	5.0	5.0				
84					1.7	0.9		
86			0.3	0.3	100.0	100.0	8.1	7.7
87					5.9	6.0	8.4	10.9
100			2.2	2.1	0.6	0.6		
101			13.8	14.8				
128					1.6	1.4		
129					12.1	13.9		

a) Underlined values denote parent peaks.

TABLE 3. THE ABUNDANCE RATIOS OF IONS BY HIGH RESOLUTION MEASUREMENT (%)

m/e	Ion	$(C_2H_5)_2NH$		$(C_3H_7)_2NH$		$(C_4H_9)_2NH$		$CH_3NHC_4H_9$	
		80V	20V	80V	20V	80V	20V	80V	20V
27	$(CNH)^+$	3		2	11	2	37	6	46
	$(C_2H_3)^+$	97		98	89	98	63	94	54
28	$(CNH_3)^+$	90	91	89	66	82	53	87	72
	$(C_2H_4)^+$	10	9	11	34	18	47	13	28
29	$(CNH_3)^+$	11	6	37	21	10	2	19	8
	$(C_2H_5)^+$	89	94	63	79	90	98	81	92
41	$(C_2NH_3)^+$			7		7		27	12
	$(C_3H_5)^+$			93	100	93	100	73	88
42	$(C_2NH_4)^+$			79	69	100	100	100	100
	$(C_3H_6)^+$			21	31				
43	$(C_2NH_5)^+$			17	4	81	78	86	86
	$(C_3H_7)^+$			83	96	19	22	14	14

The largest peak of each amine arose from the ion formed by the scission of α-CC bond as in primary amines, *i. e.*, diethylamine, *m/e* 58 $(C_2H_5NHCH_2)^+$; dipropylamine, *m/e* 72 $(C_3H_7NHCH_2)^+$; dibutylamine, *m/e* 86 $(C_4H_9NHCH_2)^+$; methylbutylamine, *m/e* 44 $(CH_3NHCH_2)^+$.

From the high resolution mass spectra (Table 3), ions of *m/e* 43 of dipropylamine are found to consist of $(C_2NH_5)^+$ (20%) and $(C_3H_7)^+$ (80%), while in dibutylamine and methylbutylamine the ratios of both ions in *m/e* 43 are the reverse. The differences are caused by the processes giving $(C_3H_7)^+$ such that scission at the CN bond occurs in dipropylamine while at the α-CC bond in the latter two amines.

The peaks derived from the metastable ions and the fragmentation processes are shown in Table 4. The metastable peaks were fairly large (Fig. 1). In primary amines they could not be observed. We see from Table 4 that the ions of *m/e* 30 and *m/e* 44 are assigned to be those formed by secondary scission (except for *m/e* 44 of methylbutylamine). In the case of dipropylamine, after the ion of *m/e* 72 was first formed by the

Table 4. Meta-stable peaks of *sec*-amines and their fragmentation processes

Amine	Fragmentation process	Obsd. m^*	Calcd. m^*
$(C_2H_5)_2NH$	$(CH_2NHC_2H_5)^+$ m/e 58 → $(CNH_4)^+$ m/e 30	15.5	15.5_2
	?	22.8	
$(C_3H_7)_2NH$	$(CH_2NHC_3H_7)^+$ m/e 72 → $(CNH_4)^+$ m/e 30	12.5	12.5_0
	$(CH_2NHC_3H_7)^+$ m/e 72 → $(C_2NH_6)^+$ m/e 44	26.9	26.8_8
$(C_4H_9)_2NH$	$(CH_2NHC_4H_9)^+$ m/e 86 → $(CNH_4)^+$ m/e 30	10.5	10.4_6
	$(NHC_4H_9)^+$ m/e 72 → $(CNH_4)^+$ m/e 30	12.5	12.5_0
	$(CH_2NHC_4H_9)^+$ m/e 86 → $(C_2NH_6)^+$ m/e 44	22.5	22.5_1
$CH_3NHC_4H_9$	$(NHC_4H_9)^+$ m/e 72 → $(CNH_4)^+$ m/e 30	12.5	12.5_0
	$(CH_3NHC_4H_9)^+$ m/e 87 → $(C_2NH_6)^+$ m/e 44	22.3	22.2_5

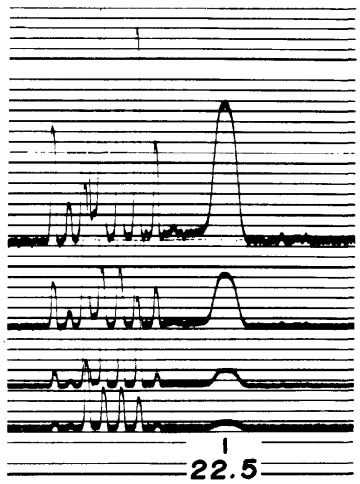

Fig. 1. Metastable peak of dibutylamine.

scission of α-CC bond, the scission at the residual α-CC bond produced the m/e 44 and the successive scission at CN bond produced the m/e 30. Both ions were the rearrangement ions. They did not decrease practically by lowering the ionizing voltage. Thus the phenomenon differs from the case of primary amines.

Scission Probabilities. The observed scission probabilities were evaluated by using ordinary mass spectra and the individual high resolution mass spectra for the necessary ions. As an example, in the case of dipropylamine, it was considered that since the ions of m/e 30 and m/e 44 were formed by the secondary scission of the m/e 72, the ion formed by the scission at the α-CC bond was the sum of the ions of m/e 72, m/e 30 and m/e 44. In the case of methylbutylamine, it was also possible that the ion of m/e 30 was formed by the scission at the CN bond of butyl group. The m/e 30 ion through process A is produced by the primary scission at the CN bond of butyl group (Bond 1) and that through process B is produced by the secondary scission of m/e 72 ion (Bond 1′ and 2).

$$CH_3\overset{1'}{-}NH\overset{1}{-}CH_2\overset{2}{-}CH_2\overset{3}{-}CH_2\overset{4}{-}CH_3$$

$$\nearrow\ (CNH_4)^+\ m/e\ 30 \qquad (A)$$

$$\searrow\ (NHCH_2CH_2CH_3)^+\ m/e\ 72 \rightarrow (CNH_4)^+\ m/e\ 30 \qquad (B)$$

Since the origin of these ions cannot be distinguished experimentally yet, the amount of the ion through process A and that through process B were estimated to be half, assuming that these two processes were brought about in a simillar proportion. The observed values thus estimated are shown in Table 5 in comparison with those calculated by the LCBO-MO method.

Table 5. Scission probabilies of the skeletal bonds (%)

Amine		Bond Number[a] 1	2	3	4(4+1′)
$(C_2H_5)_2NH$	Exp. 80V	26.7	73.3		
	20V	14.3	85.7		
	Calcd.	20.0	80.0		
$(C_3H_7)_2NH$	Exp. 80V	14.7	83.5	1.8	
	20V	10.7	89.1	0.2	
	Calcd.	14.4	74.9	9.7	
$(C_4H_9)_2NH$	Exp. 80V	18.9	65.1	14.6	1.4
	20V	13.9	84.3	1.8	0.0
	Calcd.	13.5	73.2	11.9	1.5
$CH_3NHC_4H_9$	Exp. 80V	14.6	64.9	15.4	5.1
	20V	5.7	84.8	7.3	2.2
	Calcd.	8.7	75.6	13.2	2.6

a) Bond Number

$$C\overset{3}{-}C\overset{2}{-}C\overset{1}{-}N\overset{1}{-}C\overset{2}{-}C\overset{3}{-}C$$
$$C\overset{1'}{-}N\overset{1}{-}C\overset{2}{-}C\overset{3}{-}C\overset{4}{-}C$$

The calculated values by the CNDO method are given in Table 6. The subscripts for each carbon atom are the same as those in Fig. 2. The positive charge distributions of the HO-MO of each conformation are shown in %, where the mean value was evaluated on the assumption that the contribution was equal. About 40% of the positive charge is located at the lone pair orbitals. From the table, the positive charge distributions of the HO-MO at the skeletal bonds were calculated by summing up those of the atomic orbitals which constituted the skeletal bonds and normalizing these values. The positive charge distributions concerned with the skeletal bonds are indicated in Fig. 3. The positive charge distribution of the α-CC bond contains about 60% of the total charge, and the expected tendency of easy scission at the α-CC bond is realized experimentally.

TABLE 6. CHARGE DISTRIBUTION OF THE HO ORBITALS OF DIETHYLAMINE

Atomic Orbitals			C–N *trans*			C–N *gauche* I			C–N *gauche* II			Mean value
Numbering		Relating bond	I	II	III	I	II	III	I	II	III	
N	1	Lone pair	53.9	53.2	53.5	53.5	53.3	0.0	53.2	53.3	0.0	41.5
	2	CN (I)	0.9	1.1	0.9	1.1	1.2	1.2	0.7	0.8	1.2	1.0
	3	CN (II)	0.9	0.7	1.1	0.9	0.8	1.0	1.1	1.2	1.2	1.0
	4	NH	0.9	1.0	0.8	0.8	0.9	0.0	1.0	0.9	0.0	0.7
C_I	5	CN	1.7	1.9	1.7	2.1	2.1	0.5	1.4	1.6	0.5	1.5
	6	α-CC	0.4	0.7	4.4	0.4	0.6	0.1	0.5	4.4	0.1	1.3
	7	CH	3.4	0.2	0.7	3.6	0.2	1.0	0.5	0.7	1.0	1.3
	8	CH	0.4	3.4	0.2	0.3	3.6	0.2	3.4	0.3	0.1	1.3
C_{II}	9	α-CC	0.9	1.6	8.2	0.9	1.4	0.2	1.0	8.3	0.1	2.5
	10	CH	0.0	0.1	0.4	0.4	0.5	22.5	0.0	0.0	22.5	5.2
	11	CH	0.0	0.0	0.8	0.1	0.0	0.7	0.4	0.6	0.8	0.4
	12	CH	0.4	0.6	0.0	0.0	0.1	0.0	0.0	0.4	0.1	0.2
C_{III}	13	CN	1.7	1.4	2.1	1.7	1.6	0.6	1.9	2.1	0.5	1.5
	14	α-CC	0.4	0.5	0.4	4.4	4.4	0.1	0.7	0.6	0.1	1.3
	15	CH	3.4	3.4	3.6	0.2	0.3	1.0	0.2	0.2	1.0	1.5
	16	CH	0.4	0.5	0.3	0.7	0.7	1.0	3.4	3.6	0.1	1.1
C_{IV}	17	α-CC	0.9	1.0	0.9	8.2	8.3	0.1	1.6	1.4	0.1	2.5
	18	CH	0.0	0.0	0.1	0.4	0.4	0.8	0.1	0.1	0.8	0.3
	19	CH	0.0	0.0	0.0	0.8	0.7	22.2	0.5	0.5	22.5	5.2
	20	CH	0.4	0.4	0.4	0.0	0.0	0.1	0.0	0.0	0.1	0.2
H	21	CH	0.1	0.3	0.5	1.2	1.3	15.4	0.1	0.0	15.6	3.8
	22	CH	0.1	0.0	0.6	0.2	0.0	3.3	1.1	0.5	0.1	0.7
	23	CH	1.2	1.4	0.0	0.2	0.0	0.1	0.1	0.8	3.4	0.8
	24	CH	9.7	0.8	1.7	9·9	0.9	4.1	1.7	1.7	3.9	3.8
	25	CH	1.6	9.6	0.6	1.5	9.8	1.0	9.8	0.8	0.6	3.9
	26	NH	3.1	3.3	2.8	2.8	3.0	0.0	0.3	3.0	0.0	2.0
	27	CH	9.7	9.8	9.9	0.6	0.8	0.6	0.8	0.9	3.9	4.1
	28	CH	1.6	1.7	1.5	1.7	1.7	3.8	9.6	9.8	0.6	3.6
	29	CH	0.1	0.1	0.2	0.8	0.8	3.4	0.3	0.2	3.4	1.0
	30	CH	0.1	0.1	0.1	0.6	0.5	15.6	1.4	1.3	0.1	2.2
	31	CH	1.2	1.1	1.2	0.0	0.0	0.1	0.0	0.0	15.6	2.1

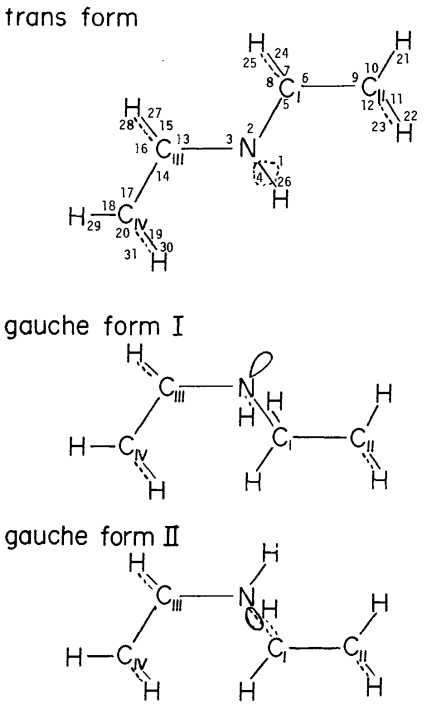

Fig. 2. Numbering of atomic orbitals of diethylamine used in CNDO-calculation.

trans form

I C 16.7 C 33.3 N 33.3 C 16.7 C

II C 16.9 C 23.6 N 33.7 C 25.8 C

III C 6.6 C 16.2 N 13.2 C 64.0 C

gauche form I

I C 64.0 C 13.2 N 16.2 C 6.6 C

II C 62.2 C 11.8 N 16.2 C 9.8 C

III C 5.3 C 42.1 N 44.8 C 7.9 C

gauche form II

I C 25.8 C 33.7 N 23.6 C 16.9 C

II C 9.8 C 16.2 N 11.8 C 62.2 C

III C 5.3 C 44.7 N 44.7 C 5.3 C

mean value

C 60.3 C 39.7 N —— C —— C

mean value of I in each form

C 55.8 C 44.2 N —— C —— C

Fig. 3. Positive charge distribution of the HO orbital on the skeletal bond (%).

Discussion

The Quasi-Equilibrium Theory (QET)[16] and the molecular orbital theory (MOT) for mass spectra deal with an explanation of the production processes of the ions appearing in mass spectra. According to QET, the ions are produced by the thermal unimolecular decomposition of molecular ions in high vibrational excited states by the electron bombardment. According to MOT, they are produced by the autoionization from molecules in the superexcited states by the electron bombardment. As shown by the investigations of Platzman[17] and Hatano *et al.*[18], the ion production from the superexcited state is predominant at the bombarding voltage V_i higher by several volts or above than the ionization potential, while the radical production from the superexcited state is predominant at V_i near the ionization potential. Thus, at lower V_i the ions are produced mostly by the unimolecular decomposition explaned by QET, but at higher V_i they are produced *via* the superexcited state explained by MOT in addition to that by QET.

A comparison of the 30V and 80V-mass spectra shows that the fraction of fragment ion peaks losing many hydrogen atoms such as $(C_2H_3)^+$ and $(C_3H_3)^+$ is large in the 80V-mass spectrum, but there is little in the main peaks of both spectra. From the comparison of 30V and 80V-mass spectra, it is indicated that bombarded molecules absorb energy of about 30 eV, while the difference between 20V and 80V-mass spectra is very large as shown in Table 2, the mass spectra changing markedly for making 30eV the border. This is in line with the result in radiation chemistry whose mean total energy accepted by the molecules bombarded with high energy radiation is about 30 eV. As V_i approaches the ionization potential, the selective scission of the bonds obeying the scheme of QET becomes more predominant, making that of MOT less on the contrary. At higher V_i the scission obeying the schemes of MOT and QET takes place simultaneously, but it might be explained mainly by MOT, its interpretation agreeing with the mass spectra of amines. It can thus be concluded that at V_i near the ionization potential most of the ions are produced by the scheme of QET; the higher V_i, the larger the contribution of the scheme of MOT to production of the ions.

The scission probability calculated by the LCBO-MO method and the experimental results (V_i=80V and 20V) in Table 5 are compared in Fig. 4. The parameters used in the calculation by LCBO-MO method were determined empirically from the mass spectra of propylamine and butylamine. Agreement between calculation and experiment is satisfactory. These findings indicate that the parameters can be transferred to secondary amines. Their transferability is also given in the explanation of aminoacid esters.[10] The present results of diethylamine obtained by the

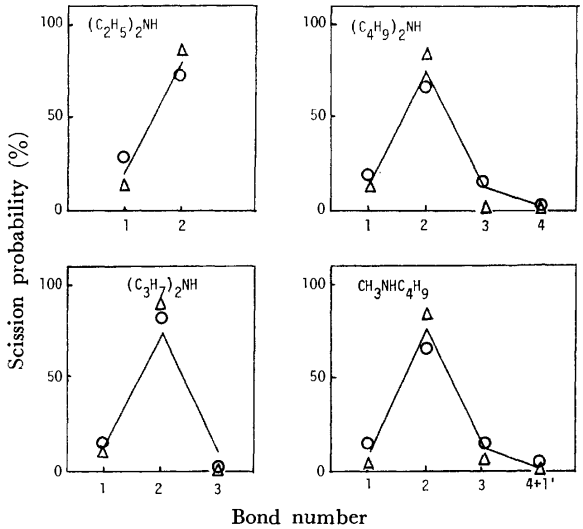

Fig. 4. Scission probability of the skeletal bonds of secondary amines.
○: V_i=80 V., △: V_i=20 V., —: Calcd.

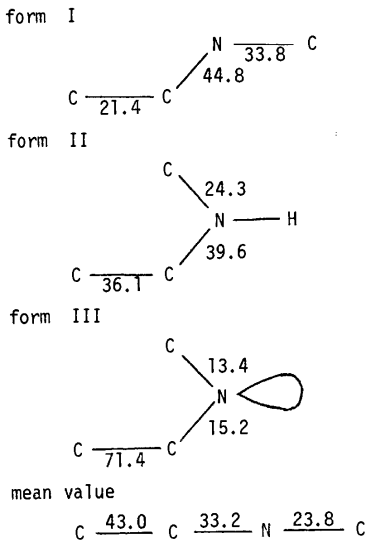

Fig. 5. Positive charge distribution of the HO orbital on the skeletal bond (%).

calculation of the CNDO method offers a good support to the semi-empirical result. Moreover, in the CNDO-calculation of methylethylamine their mean charge density concerning the skeletal bonds is the largest at the α-CC bond (Fig. 5).

Agreement between calculation and experiment is better at higher V_i than at lower V_i in the cases of secondary amines, and the degree of agreement is superior to the case of propylamine. The fragment ions produced by QET and by MOT are observed simultaneouly in mass spectra. The alkanes produce many fragment ions at higher V_i, especially the ions of small carbon numbers such as $(C_2H_4)^+$, $(C_2H_5)^+$, $(C_3H_5)^+$, $(C_3H_7)^+$ which occupy most of the fragment ions. They might be considered to be secondary fragment ions produced by QET. On the other hand, changes of mass spectra against the variation of bombarded voltages are relatively small in these amines. This

16) H. M. Rosenstock, M. B. Wallenstein, A. L. Wahrhaftig, and H. Eyring, *Proc. Natl. Acad. Sci. U. S.*, **38**, 667 (1952).
17) R. L. Platzman, *Voltex*, **23**, 372 (1962).
18) Y. Hatano, S. Shida, and S. Sato, This Bulletin, **41**, 1120 (1968); Y. Hatano, *ibid.*, **41**, 1126 (1968).

suggests that the secondary scission originating successively from the first scission might be very few.

With respect to the production of fragment ions of lower hydrocarbons at the skeletal scission, Stevenson concluded that the fragment with the higher carbon number of the two fragments produced from the molecular ion becomes an ion, while the other becomes a radical.[19] Saito et al.[20] indicated that good correlations existed between the amount of the fragmentions and the positive charge in them for the higher hydrocarbons. Most of the peaks appearing in the mass spectra of amines are originated from the ions containing N-atoms such as *m/e* 30 $(CNH_4)^+$, *m/e* 44 $(C_2NH_6)^+$, *m/e* 86 $(C_3NH_{12})^+$. Positive charges of each group containing those of CH bond, NH bond and lone pair obtained by CNDO-calculations, are given in Fig. 6. When the α-CC bond is broken the positive charge of the fragments containing N-atom occupies 80% in propylamine and 87% in diethylamine. From the experimental results total amount of the fragment ions containing N-atom formed by the scission of α-CC bond occupies 92% in propylamine and 99% in diethylamine. Though the correlation of positive charge *vs.* amount of ions with amines is not so good as with hydrocarbons, it is suggested that the fragment having more charge of the two fragments is liable to become an ion.

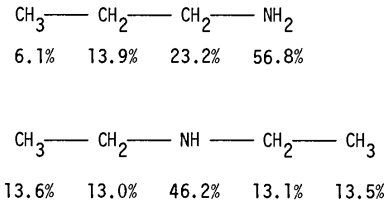

Fig. 6. Charge density of each group calculated by CNDO method.

19) D. P. Stevenson, *Discuss. Faraday Soc.*, **10**, 35 (1961).
20) M. Saito, I. Fujita, and K. Hirota, *J. Phys. Chem.*, **74**, 3147 (1970).

BULLETIN OF THE CHEMICAL SOCIETY OF JAPAN, VOL. 45, 3526—3530 (1972)

Zero-point Average Structure of a Molecule Containing Two Symmetric Internal Rotors. Acetone

Takao Iijima

Department of Chemistry, Faculty of Science, Hokkaido University, Sapporo

(Received May 18, 1972)

The theory of vibrational correction to the observed moments of inertia of a molecule which contains an internal rotor has been extended to the case of two symmetric internal rotors, and applied to the analysis of the structure of acetone. The zero-point average structure has been determined by using the moments of inertia obtained by microwave spectroscopy and the bond distances from gas electron diffraction. The zero-point average parameters have been determined as follows: C–C 1.517±0.003 Å; C=O 1.210±0.004 Å; C–H 1.091±0.003 Å; ∠HCH 108° 30′±30′; ∠CCC 116° 0′±15′. The isotope effects in the structure parameters have also been observed in terms of the increase caused by deuteration to be δ(DCD) +10′±12′; δ(CCC) −17′±2′. The tilt angle of the methyl top was determined to be 2° 0′±30′.

Large amplitude intramolecular motions give rise to additional complexity in the method of vibrational correction to the rotational constants. This was discussed in some detail in a previous paper, where the theory for a molecule with internal torsion was presented.[1] However, the scope was restricted to the molecule containing only one internal top. In view of ever increasing interest in the accurate structure parameters of many simple molecules which have two internal rotors, the method has been extended to the two-top case, and the zero-point average structure of acetone has been determined. The present study is to replace the previous one on the average structure of acetone,[2] where the torsional motion was treated as a vibrational one.

The treatment is based on a specified condition that the molecule has at least one symmetry plane by which the two tops are exchanged with each other. The restriction is compensated by the simplicity of numerical procedure and the applicability to many two-top molecules.

1) T. Iijima and S. Tsuchiya, *J. Mol. Spectrosc.*, **44**, 88 (1972).
2) T. Iijima, This Bulletin, **43**, 1049 (1970).

Theory for the One-top Case[1]

First, a brief survey of the theory for the one-top case seems to be necessary. The essential part of the procedure for vibrational correction is to calculate the effective values of the rotational constants $\sigma_{\alpha\beta}$ which are supposed to differ from the rigid values due to vibrational motions. The theoretical expression for the vibrational correction is therefore characterized by matrices l and n which specify the relations between the normal coordinate Q_s, torsional velocity $\dot{\gamma}$, Cartesian displacement $\boldsymbol{\rho}_i$ and velocity vector $\mathbf{v}_i$ of each atom in the molecule. The relations are

$$\sqrt{m_i}\,\boldsymbol{\rho}_i = \sum_s l_{is} Q_s \tag{1}$$

$$\sqrt{m_i}\,\mathbf{v}_i = \sum_s l_{is}\dot{Q}_s + \sum_s \dot{\gamma} n_{is} Q_s \tag{2}$$

where m_i is the mass of the i-th atom. The components of $\boldsymbol{\rho}_i$ and $\mathbf{v}_i$ are given as projected onto the frame-fixed coordinate axes, the matrix element n_{is} vanishing for the atoms belonging to the frame.

The four dimensional moments of inertia tensor, for three angular velocities of overall rotation and an additional one of the torsional motion, are calculated in terms of l and n for an instantaneous situation where only the s-th normal coordinate Q_s has a non-zero value. It may be denoted by $I(Q_s)$. A slightly modified inertia tensor I' is set up as

$$I'(Q_s)_{\alpha\beta} = I(Q_s)_{\alpha\beta} - \sum_{s'} \zeta^{(\alpha)}_{ss'}\zeta^{(\beta)}_{ss'}Q_s^2 \tag{3}$$

in order to make conversion of the velocity representation of the kinetic energy into the momentum representation.[3] The zeroth and first order term of the rotational constants can be obtained by taking the inverse of I'. The averaging over the ground vibrational state and appropriate repetition of the process over all normal coordinates are performed according to the equations

$$\sigma_{\alpha\beta} = \sigma^{(0)}_{\alpha\beta} + \sigma^{(1)}_{\alpha\beta} + \sigma^{(2)}_{\alpha\beta} \tag{4}$$

$$\sigma^{(0)}_{\alpha\beta} + \sigma^{(1)}_{\alpha\beta} = \sum_s \frac{1}{2}\{\mu_{\alpha\beta}(D_s) + \mu_{\alpha\beta}(-D_s)\} \tag{5}$$

$$\sigma^{(2)}_{\alpha\beta} = -\sum_{ss'}\frac{D_s^2}{2}\cdot\frac{(\omega_s-\omega_{s'})^2}{\omega_{s'}(\omega_s+\omega_{s'})} \times \sum_{\alpha'\beta'}\zeta^{(\alpha')}_{ss'}\zeta^{(\beta')}_{ss'}\mu^0_{\alpha\alpha'}\mu^0_{\beta\beta'} \tag{6}$$
$$(a, \beta, \alpha', \beta' = x, y, z, \gamma)$$

where D_s is the root mean square value of Q_s and μ is the inverse of I'.

The elements of I and ζ for the principal axis components are given by ordinary expressions, and the γ-components are given by the following.[1]

$$I_{\tau\tau} = J_{\tau\tau} + \sum_i (n_{is}\cdot n_{is})Q_s^2 + 2\boldsymbol{\lambda}\cdot\sum_i(\Lambda_{is}\times n_{is})Q_s^2 \tag{7}$$

$$I_{\tau\alpha} = \lambda_\alpha J_{\tau\tau} + \sum_i (l_{is}\times n_{is})_\alpha Q_s^2 - (\boldsymbol{\lambda}\times L_{R's})_\alpha Q_s \tag{8}$$
$$(\alpha = x, y, z)$$

$$\zeta^{(\tau)}_{ss'} = \boldsymbol{\lambda}\cdot\sum_i(\Lambda_{is}\times l_{is'}) + \sum_i n_{is}\cdot l_{is'} \tag{9}$$

where all notations follow Ref. 1, and the subscript i runs over the atoms belonging to the top. $J_{\tau\tau}$ is the geometrical moment of inertia of the top around its axis where the vibrational displacement of each atom due to Q_s is taken into account; $L_{R's}$ is the L matrix which relates the symmetry coordinate of the infinitesimal rotation of the top to the Q_s and Λ_{is} is the l-matrix relative to the center of gravity of the top.

Extension of the Method to the Two-top Case

The angular velocity vector ω for a two-top molecule consists of five components, three for the overall rotation and two for the torsinal motions. Accordingly the tensors of moments of inertia and rotational constants are (5×5) dimensional ones. The $\zeta_{ss'}$ also has five components.

Eq. (1) is still valid for the relation between the frame-fixed Cartesian displacement $\boldsymbol{\rho}_i$ and Q_s, and so is the time derivative Eq. (2). It is obvious that the $\mathbf{v}_i$ for an atom of top 1 is independent of the torsional velocity of top 2, and *vice versa*. It is thus concluded that the elements of I-tensor and ζ are given by exactly the same expressions as Eqs. (7), (8) and (9), if the numbering of atoms i covers top 1 for the $\gamma_1\alpha$-components and top 2 for the $\gamma_2\alpha$-components. The $\gamma_1\gamma_2$-term of I does not appear.

The (4×4) part of the (5×5) I-tensor can therefore be obtained by making full use of the routine procedure for the one-top case, where one of the two tops, *e. g.* top 2, is included in the frame group, both γ_2 and $\dot{\gamma}_2$ being put equal to zero. The remaining $\gamma_2\alpha$-components can be obtained by simple symmetry consideration.

Top 1 is transferred to top 2 by symmetry operation σ_h. If atom i_1 of top 1 is transferred to atom i_2 of top 2 by σ_h, every component of $l_{i2,s}$ projected onto the principal axes x, y, and z is equivalent either to that of $l_{i1,s}$ or $-l_{i1,s}$ depending on the symmetry of the s-th normal coordinate. Consistency between the direction of torsinal motion for positive γ and the direction of the unit vector λ should be maintained within each top in such a manner that clockwise rotation around λ facing towards its direction is the motion corresponding to positive γ. However, arbitrary choice is allowed for the symmetry property of one of them in relation to the transference between the two tops. In the present treatment, λ is taken to be symmetric to σ_h. Then γ becomes anti-symmetric with respect to σ_h. By choosing the yz-plane to be the plane of symmetry and the x-axis perpendicular to it, the symmetry property of l_{is} and that of n_{is} *etc.* are easily obtained as summarized in Table 1. The entry $-$, for example, in column (x) for l_{is} means that $l^{(x)}_{i2,s}$ is equal to $-l^{(x)}_{i1,s}$, and so on.

Table 1. Symmetry properties of l_{is}, Λ_{is}, n_{is} and $L_{R's}$

	l_{is} and Λ_{is}			n_{is} and $L_{R's}$		
	(x)	(y)	(z)	(x)	(y)	(z)
$s\subset A'$	$-$	$+$	$+$	$+$	$-$	$-$
$s\subset A''$	$+$	$-$	$-$	$-$	$+$	$+$

By means of Eqs. (7), (8) and Table 1, the $\gamma_2\alpha$-components of I-tensor can be related to those of $\gamma_1\alpha$-components, simply as

$$I(Q_s)_{\tau 2,x} = -I(Q_s)_{\tau 1,x} \tag{10}$$

$$I(Q_s)_{\tau 2,\alpha} = I(Q_s)_{\tau 1,\alpha} \quad \text{for } \alpha = y \text{ and } z, \tag{11}$$

and

$$I(Q_s)_{\tau 2,\tau 2} = I(Q_s)_{\tau 1,\tau 1} \tag{12}$$

if Q_s belongs to the symmetry species A' which is symmetric with respect to σ_h. If Q_s belongs to A'', the Q_s on the right-hand side of the above equations should be replaced by $-Q_s$. Changing the sign of Q_s is relevant to the term linear in Q_s and also to $J_{\tau\tau}$ and λ_α which implicitly contain terms linearly dependent on Q_s.

3) E. B. Wilson, Jr. and J. B. Howard, *J. Chem. Phys.*, **4**, 260 (1936).

Similarly, $\zeta_{ss'}^{(\gamma 2)}$ is given by

$$\zeta_{ss'}^{(\gamma 2)} = \zeta_{ss'}^{(\gamma 1)}, \text{ if } s \subset A', s' \subset A'' \text{ and } \textit{vice versa} \quad (13)$$

and

$$\zeta_{ss'}^{(\gamma 2)} = -\zeta_{ss'}^{(\gamma 1)}, \text{ if } s \subset A', s' \subset A' \text{ or } s \subset A'', s' \subset A'' \quad (14)$$

The second term of Eq. (3) and $\sigma_{\alpha\beta}^{(2)}$ of Eq. (6) are thus easily calculated in terms of $\zeta_{ss'}^{(\gamma 1)}$ and the above symmetry rule.

The symmetry property of $\zeta_{ss'}^{(\gamma)}$, combined with the non-vanishing conditions (Table 2) leads to the symmetry properties of the second term of Eq. (3) and that of $\sigma_{\alpha\beta}^{(2)}$ of Eq. (6). The result is simply that the sign should be changed only for the x-components and otherwise equivalent to the corresponding $\gamma_1\alpha$-terms. The $\gamma_1\gamma_2$-term of I' is not necessarily zero in contrast to that of I.

Table 2. Non-vanishing conditions for $\zeta_{ss'}^{(\alpha)}$

(x)		(y)		(z)		(γ)	
s	s'	s	s'	s	s'	s	s'
A'	A'	A'	A''	A'	A''	A' or A''	A' or A''
or							
A''	A''		*vice versa*				

The whole symmetry consideration may be stated in a more compact way as follows. The γ_2-components of I' and $\sigma_{\alpha\beta}^{(2)}$ tensors are obtained by applying a symmetry operation σ_h to the γ_1-components. The symmetry operation σ_h implies change of the sign of Q_s, if Q_s, is anti-symmetric to σ_h and change of the sign of γx-components. Naturally the new cross terms, $\gamma_1\gamma_2$-elements, can not be covered by this symmetry operation.

Zero-point Average Structure of Acetone

Zero-point Moments of Inertia and Angle between the two Top-axes. The formulation was applied to the determination of the zero-point average structure of acetone which has two internal rotors. The microwave spectra of this molecule and those of isotopic species were investigated by Nelson and Pierce.[4] The spectra of the d_6-species were observed by Swalen and Costain.[5]

The vibrational correction was calculated by assuming an appropriate set of structure parameters and by use of the force constants determined by Cossee and Schachtschneider.[6] The observed moments of inertia, the corrections for the vibrational effect and the zero-point values are listed in Table 3 for the normal and the d_6-species. The microwave data of $(^{13}CH_3)_2CO$ and $(CH_3)_2C^{18}O$ were also used. The vibrational corrections for these species were almost equivalent to those of the normal species.

The direction cosines of the top-axes λ_a and λ_b were determined from the parameters α and β reported by Nelson and Pierce.[4] The effective values of λ_a and

Table 3. Effective and zero-point moments of inertia of acetone. (in amu Å^2 units)

		I^{eff} a)	ΔI	$I^{(z)}$
$(CH_3)_2CO$	a	49.730	0.096	49.826
	b	59.370	0.106	59.476
	c	102.956	0.029	102.985
	γ	(3.226) b)	−0.067	3.159
$(CD_3)_2CO$	a	59.690	0.106	59.796
	b	78.748	0.119	78.867
	c	126.028	0.027	126.055
	γ	(6.398) b)	−0.094	6.304

a) Determined by Nelson and Pierce.[4]
b) Estimated from $I_\gamma^{(z)}$.

λ_b were obtained by the relation

$$\frac{\beta}{\alpha} = \frac{\lambda_b I_a}{\lambda_a I_b} \quad (15)$$

which is derived from the definitions of α and β, and the constraint $\lambda_a^2+\lambda_b^2=1.0530$ for the normal species and 1.0352 for the d_6-species. The ratio β/α was used as an experimental value, since it is independent of I_τ, the effective moment of inertia of methyl top around its axis, and might be free from possible systematic errors introduced in the course of the barrier height analysis.

The effective values were then converted into the zero-point values by corrections which were evaluated by the model calculation for the vibrational effect. The zero-point value of the angle between the two top-axes $2\theta_z$ was then evaluated to be $120.0\pm0.4°$ for both normal and d_6-species. The two values of $2\theta_z$ obtained from λ_a and λ_b were in excellent agreement with each other within 0.1°.

Adjustment of Structure Parameters. The r_z-parameters were determined from the $I^{(z)}$ values and C–C and C=O r_z-distances obtained by means of electron diffraction[2,7,8] in a way quite parallel to that for acetaldehyde.[1] The isotope effect on the C–H and C–D distances was evaluated by $\langle \Delta z \rangle_0$ or the mean displacement projected along the equilibrium bond direction, by use of the calculated values of the parallel and perpendicular mean amplitudes[9] and the Morse anharmonicity parameter a. Two values were assumed for a, 2.0 Å^{-1} and 2.6 Å^{-1}, which are supposed to be the possible extremes of the a value for a C–H bond.[10] The difference between r_z values for the C–H bond was 0.001 Å and 0.002 Å for the two extremes.

4) R. Nelson and L. Pierce, *J. Mol. Spectrosc.*, **18**, 344 (1965).
5) J. D. Swalen and C. C. Costain, *J. Chem. Phys.*, **31**, 1562 (1959).
6) P. Cossee and J. H. Schachtschneider, *ibid.*, **44**, 97 (1966).
7) C. Kato, S. Konaka, T. Iijima, and M. Kimura, This Bulletin, **42**, 2148 (1969).
8) The centrifugal stretchings of C–C and C–O distances were assumed to be 0.0002 Å in the previous study. Resently Dr. Hilderbrandt calculated them rigorously and obtained 0.0006 Å and 0.0002 Å for C–C and C–O, respectively. (Private communication *via* Professor R. A. Bonham.) There is no important change in the r_z(ED) values even with these exact numbers.
9) Dr. S. J. Cyvin kindly informed the author of his calculated values of the mean amplitudes of the normal species. His results are in excellent agreement with the author's. It should be noted, however, that the mean amplitudes should not include the contribution from the torsional motions in the present scheme of analysis.
10) K. Kuchitsu, *J. Chem. Phys.*, **49**, 4456 (1968).

The mean value 0.0015Å was then assumed to be the difference r_z(C-H)$-r_z$(C-D) in the following analysis.

A large shortening of r_z from the equilibrium bond length, obtained as a result of the calculation in the preceding paper,[2] originated from a large perpendicular amplitude due to the torsional motion of the methyl tops. In the present treatment, however, the torsional motion is separated out of the vibrational motions and the r_z(C-H) becomes the average value on the vibrational ground state not including the torsional motion. The methyl tops undergo the torsional motion while performing vibrational harmonic motions about the structure expressed in terms of the zero-point structure parameters.

The adjusted structure parameters were r_z(C=O), r_z(C-C), r_z(C-H). α_z(CCC) and α_z(HCH). In addition to these, α_z(CCC) and α_z(DCD) of the d_6-species were included as independent parameters. The $2\theta_z$ values were fixed to the value obtained in the preceding section. The trial values of r_z(C=O) and r_z(C-C) were varied within the error limits of electron diffraction values. For each set of these two parameters, the remaining parameters were so adjusted that the calculated moments of inertia might best fit the observed zero-point values.

In a scheme where the diffraction values are utilized as much as in the present treatment, the contribution from the isotopically substituted species, especially the ^{13}C and ^{18}O species, to the structure parameters is rather small and the final result would have been substantially the same if the parameters had been adjusted by use of the normal species only. This was pointed out by Kuchitsu *et al.*[11] Inclusion of the deuterated species would produce no more than additional ambiguity if the possible isotope effects in the structure parameters were assumed to be estimated values, unless the estimates are somehow known accurately enough. In the present treatment the isotope effects in the α_z(CCC) and α_z(DCD) were regarded as adjustable, or in other words, unknown parameters. As a result, the spectroscopic moments of the deuterated species had a role not only of affording additional information on the overall structure parameters but also of giving experimental evidence of the isotope effects on the less known parameters such as bond angles. The assumption that there is no appreciable isotope effect in the C-C and C=O distances seems to be reasonable.

Although the addition of two more independent parameters for the deuterated species seems to reduce the usefulness of the d_6-data as supplementary information, it actually turns out that the d_6-data are still very useful in alleviating strong mutual correlation existing between the structure parameters of the molecule.

The best fit values of the parameters are listed in Table 4 together with the ranges indicating the uncertainties, which were estimated by criteria discussed in Ref. 1. The corresponding r_g-values are also shown in Table 4. The allowable amounts of deviations of the parameters are not independent of, but related to, each other by the mutual correlation. Since it is difficult to show the correlation scheme in the Table, the listed values simply indicate the widest possible deviations which could be allowed by an appropriate combination of the values of the parameters. The zero-point moments of inertia calculated by use of these best fit values of the parameters are in agreement with the observed values within 0.01 amu. Å^2 for all of the twelve $I^{(z)}$ of the four species. The consistency between spectroscopic and diffraction data is almost perfect.

Table 4. Structure parameters of acetone[a] (in Å units)

	r_z and α_z		
C-C	1.517 (3)	∠HCH	108°30′ (30′)
C=O	1.210 (4)	δ(DCD)[b]	+10′ (12′)
C-H	1.091 (3)	∠CCC	116° 0′ (15′)
δ(C-D)[b]	−0.0015 (assumed)	δ(CCC)[b]	−17′ (2′)
$2\theta_z$	120°0′ (24′)	tilt	2° 0′ (30′)
	r_g[c]	r_e and α_e	
C-C	1.520	C-H	1.083
C=O	1.213	∠CCC	114°57′
C-H	1.103	∠HCH	109° 8′

a) Limits of error are shown in parentheses, the number being attached to the last digit. b) δ(C-D)$=r_z$(C-D)$-r_z$(C-H); δ(DCD)$=\angle$DCD$-\angle$HCH; δ(CCC)$=\angle$CCC(d_6)$-\angle$CCC. c) Cf. the diffraction results, r_g; C-C 1.517 (5) and C=O 1.211 (4) Å.[7]

Isotope Effects in Deuterated Species. We see from Table 4 that appreciable isotope effects due to deuterium substitution were observed in the zero-point average values of CCC and HCH angles. The CCC angle of the d_6-species is less than that of the normal species by 17′. A similar amount 18′ was obtained and discussed in a previous paper,[2] where it was interpreted to be caused by anharmonicity in the symmetric rocking motion of the two methyl tops. The same argument holds in the present case, although there seems to be no sound reason to exclude intramethyl HCH bending from the possible source of anharmonicity, because there has also been an isotope effect observed in the DCD angle.

However, the fact that the DCD angle is not smaller but larger than HCH by 10′ strongly suggests that a repulsive force between the two methyl tops might be the major source of anharmonicity. Such a force would push the two tops so that the three hydrogens are bent closer to each other, and the zero-point vibration would suffer such anharmonicity as to make it harder for the methyl tripod to open than to close. This is the type of anharmonicity which lead to a larger DCD angle than HCH, and be predominant in the cubic term of the symmetric rocking mode.

The same manipulation as was applied to the CCC angle[2] was also applied to the HCH angle, and the $\langle\Delta\alpha\rangle_0$ value of HCH was evaluated to be −38′ assuming that the anharmonicity is mainly due to the methyl rocking.

The direction of tilt is also consistent with the presence of repulsive interaction between the two tops.

11) K. Kuchitsu, T. Fukuyama and Y. Morino, *J. Mol. Structure*, **4**, 41 (1969).

However, according to the microwave studies by Pierce and co-workers on several molecules, the existence of tilted methyl tops is closely related to the presence of an unsaturated carbon atom adjacent to the methyl top.[12] The tilt in acetone is probably caused by superposed effect of both repulsive interaction and the electronic state of the central carbon. More exact pinning down of the origin of the tilting is still left to future investigations.

Approximate equilibrium values of the structure parameters can be estimated from the zero-point average values and $\langle \Delta z \rangle_0$ and $\langle \Delta \alpha \rangle_0$. The estimated values for C–H, $\angle$CCC and $\angle$HCH are shown also in Table 4. r_e(C–H) 1.08_3 Å is fairly reasonable as compared with some reported values of C–H, *viz.*, 1.08_7 Å of CH_3CHO[1] and 1.085 Å of CH_4.[13] As for the equilibrium values of the bond angles, no data are available for comparison. It is interesting, however, to note that the equilibrium angle of HCH in the methyl top seems to be very close to that of acetaldehyde 108°42′, while the zero-point average values are apart from each other because of the opposite direction of the effect of anharmonicity.

Determination of the barrier height by use of the effective value of the moment of inertia of the methyl top and the non-unity constraint of $\lambda^2_a + \lambda^2_b$ would be interesting, if it were possible to follow the sophisticated procedure of the barrier height analysis by Nelson and Pierce.

The author wishes to thank Professor Masao Kimura for his encouragement, and Dr. Shigehiro Konaka for his helpful comments. Numerical computations were performed on a FACOM 230—60 of the Hokkaido University Computing Center and also on a FACOM 270—20 at the laboratory of Professor Kimio Ohno, to whom the author's thanks are also due.

12) See reference 4 and the references cited therein.

13) L. S. Bartell, K. Kuchitsu and R. J. deNeui, *J. Chem. Phys.*, **35**, 1211 (1961).

BULLETIN OF THE CHEMICAL SOCIETY OF JAPAN, VOL. 45, 3530—3534 (1972)

Nuclear Quadrupole Resonance Study of Chloral Hydrate

Hideaki CHIHARA and Nobuo NAKAMURA

Department of Chemistry, Faculty of Science, Osaka University, Toyonaka, 560

(Received June 5, 1972)

Three nuclear quadrupole resonance lines were observed in chloral hydrate at temperatures 20—300K, the frequencies being 38.2863±0.0004 MHz(ν_1), 39.5415±0.0002(ν_2), and 39.6252±0.0002(ν_3) at 20.3K. Their temperature dependence was measured below 77K, showing monotonous decrease with increasing temperature. The difference in frequency between ν_1 and ν_2(or ν_3) is probably due to a crystal field effect rather than OH···Cl hydrogen bonding as has been suggested. The spin-lattice relaxation time for all the lines, determined by pulse techniques, coincides with each other and tends to decrease rapidly above 250K. The decrease was interpreted as arising from hindered internal rotation of the CCl_3 group with the activation energy of 8.8 kcal mol^{-1}.

It is known that O-H···Cl type hydrogen bond exists in a few crystalline solids.[1] Chloral hydrate has been considered to have this type of hydrogen bond. Existence of the hydrogen bond was first predicted by Kondo and Nitta on the basis of their X-ray crystal structure analysis.[2] Allen found that one of the three ^{35}Cl nuclear quadrupole resonance (NQR) lines was much lower in frequency than the other two and interpreted the low frequency in terms of a hydrogen bond between an O-H group and the chlorine atom.[3] The crystal structure of chloral hydrate was later redetermined by Ogawa by an X-ray method and the possibility of a bifurcated hydrogen bond of the type O–H$\langle^{Cl}_{O}$ was suggested on the basis of the short intermolecular O-Cl and O-O distances.[4]

The structural data of Ogawa was further refined and all the hydrogen atoms were located with a neutron diffraction method by Brown.[5] The hydrogen atoms of the two crystallographically non-equivalent hydroxyl groups were found between two oxygen atoms of different molecules, O–H···O type hydrogen bonds being rather long in the crystallographic *ac*-plane.

Recently a question was raised by Biedenkapp and Weiss[6] as to whether or not the large NQR frequency shift is due really to the hydrogen bonding to chlorine. They examined the temperature range 77—323K and found that only a small change occurs in the ^{35}Cl NQR spectra upon deuteration; the observation led them to conclude that the "crystal field effects" rather than the OH···Cl hydrogen bond could account for the spectra.

The purpose of the present paper is to examine the existence and nature of the possible O–H···Cl hydrogen

1) G. C. Pimentel and A. L. McClellan, "The Hydrogen Bond" Freeman (1960).
2) S. Kondo and I. Nitta, *X-rays*, **6**, 53 (1950).
3) H. C. Allen, Jr., *J. Amer. Chem. Soc.*, **74**, 6074 (1952).
4) K. Ogawa, This Bulletin, **36**, 610 (1963).
5) G. M. Brown, private communication to Prof. K. Ogawa.
6) D. Biedenkapp and H. Weiss, *Z. Naturforsch.*, **22a**, 1124 (1967).

bonding in chloral hydrate by means of the single crystal NQR method.

Experimental

Chloral hydrate (Merck) was recrystallized from chloroform solution by evaporation at 25°C. A single crystal (approximately $1\times1\times0.7$ cm^3) was grown also in the chloroform solution.

The ^{35}Cl NQR frequencies were measured at temperatures 20—80K by using a Dean-type super-regenerative spectrometer on a powdered specimen. Single crystal Zeeman effect experiment was carried out at liquid nitrogen temperature. The spin-lattice relaxation times were measured by the 180°—90° method[7] at 77—300K using a pulsed spectrometer. Details of the experimental methods were described elsewhere.[8]

Results and Discussion

Description of Crystal Structure. Chloral hydrate crystallizes in a monoclinic system with the space group $P2_1/c$ and contains four molecules in a unit cell. Figure 1 shows the crystal structure which was determined by Brown.[5] There are two relatively long O–H···O hydrogen bonds (H···O=1.908 and 1.933 Å). There is a somewhat short H···Cl distance of 2.643 Å between the hydrogen H_1 and the chlorine Cl_1 to be compared with the sum of the van der Waals radii of H and Cl atoms (3.0 Å).

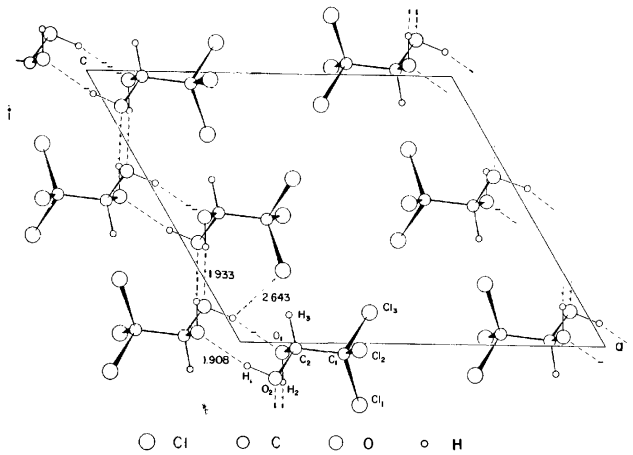

Fig. 1. Crystal structure of chloral hydrate projected along the crystalline *b* axis. (Ref. 5)

Figure 2 shows the position of the zero-splitting loci for four of the six independent C–Cl bond directions in a laboratory coordinate system. The direction of principal *Z*-axis and the asymmetry parameter η of the electric field gradient of ^{35}Cl in each C–Cl bond were calculated by using a NEAC-2200 computer from the observed zero-splitting loci by means of the relation[9]

$$\sin^2\theta = 2/(3-\eta\cos 2\varphi),$$

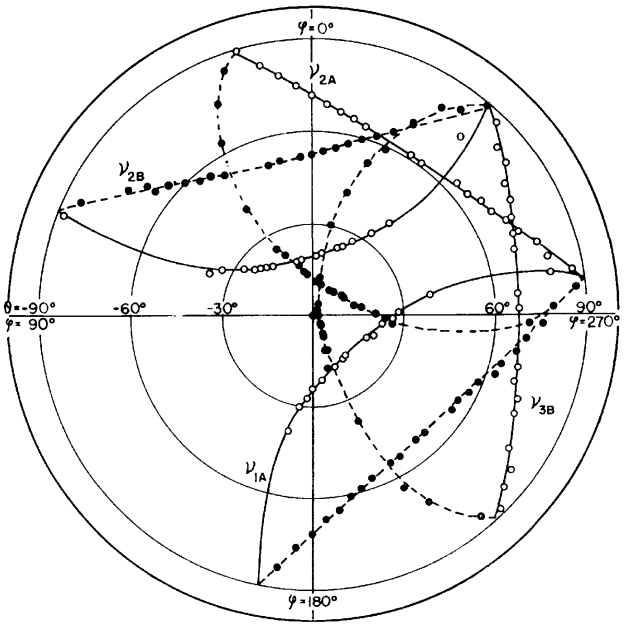

Fig. 2. Zero-splitting loci of four C–Cl bonds at 77K.
—○— locus projection from above the plane of paper,
--●-- locus projection from below the plane of paper.

where θ and φ are respectively the polar and azimuthal angles of the Zeeman field direction that gives zero splitting in the coordinate system fixed to the principal EFG tensor axes. The number of data collected was 40 for Cl_{1A}, 40 for Cl_{2A}, 43 for Cl_{2B} and 46 for Cl_{3B}. The results are given in Table 1, with the direction cosines of the other two unobserved cones[10] (Cl_{1B} and Cl_{3A}), which were calculated by utilizing the fact that there is a glide plane perpendicular to the crystalline *b*-axis. From an examination of the relative directions of the six C–Cl bonds (assumed to coincide with the *Z*-axes of EFG) we can unambiguously assign each NQR frequency to a particular chlorine atom in Fig. 1, *viz.*, ν_1, ν_2, and ν_3 correspond to Cl_1, Cl_3 and Cl_2, respectively. It is noticeable that ν_1, which is anomalously lower than the other two, corresponds to the Cl_1 atom which has a close hydrogen neighbor.

Interactions between Chlorine Cl_1 and Other Atoms. We now attempt to find the possible interactions that make the ν_1 frequency lower than ν_2 or ν_3. The geometry of the CCl_3 group as determined by diffraction methods is quite normal in that every C–Cl distance (1.760 to 1.765 Å) is typical of a single bond length and that the angles between the three C–Cl bonds are close to the tetrahedral angle (see Table 2). Thus there seems to be no interaction of intramolecular origin through σ bonds that will be responsible for the difference between ν_1 and ν_2 (or ν_3). The fact that the asymmetry parameters for the three chlorines are small and about the same in magnitude also supports such a view.

Of the intermolecular interactions, the hydrogen

7) D. E. Woessner and H. S. Gutowsky, *J. Chem. Phys.*, **39**, 440 (1963).

8) T. Kiichi, N. Nakamura, and H. Chihara, *J. Magn. Reson.*, **6**, 516 (1972).

9) C. Dean, *Phys. Rev.*, **96**, 1053 (1954).

10) These lines could not be observed because of unfavorabel orientations of the EFG *Z*-axes with respect to the orientation of the rf-coil.

TABLE 1. NUCLEAR QUADRUPOLE RESONANCE FREQUENCIES, QUADRUPOLE COUPLING CONSTANTS, ASYMMETRY PARAMETERS AND THE DIRECTION COSINES OF PRINCIPAL Z-AXIS OF ELECTRIC FIELD GRADIENT TENSORS IN A LABORATORY FIXED COORDINATE SYSTEM (77K). THE STANDARD DEVIATIONS ARE SHOWN IN PARENTHESES

Resonance line	Frequency (MHz)	e^2Qq/h (MHz)	η	Direction cosines		
				X_L	Y_L	Z_L
ν_{1A}	38.1894	76.373	0.022(0.010)	−7002(22)	−6429(23)	3105(69)
ν_{2A}	39.4330	78.858	0.025(0.008)	7548(17)	−4913(23)	−4346(39)
ν_{3A}	39.5189			3426	4781	8088*
ν_{1B}	38.1894			−5826	−1410	8005*
ν_{2B}	39.4330	78.837	0.048(0.013)	9273(14)	2443(47)	2836(63)
ν_{3B}	39.5189	79.021	0.035(0.013)	0267(36)	8452(14)	5337(23)

TABLE 2. RELATIVE ORIENTATIONS OF PRINCIPAL Z-AXIS OF ELECTRIC FIELD GRADIENT TENSORS. THE RELATIVE ORIENTATIONS OF C-Cl BONDS CALCULATED BY USING THE NEUTRON DIFFRACTION DATA (Ref. 5) ARE GIVEN IN PARENTHESES

	$\nu_{1A}(Cl_1)$	$\nu_{2A}(Cl_3)$	$\nu_{3A}(Cl_2)$	$\nu_{1B}(Cl_1')$	$\nu_{2B}(Cl_3')$
$\nu_{2A}(Cl_3)$	110.3 (109.5)				
$\nu_{3A}(Cl_2)$	107.2 (109.2)	109.1 (109.2)			
$\nu_{1B}(Cl_1')$	41.7 (41.6)	135.9	67.6		
$\nu_{2B}(Cl_3')$	135.9	62.8 (62.2)	48.4	110.3 (109.5)	
$\nu_{3B}(Cl_2')$	69.0	48.1	145.6 (147.5)	108.9 (109.2)	109.4 (109.2)

bonding between O_2-H_1 and Cl_1 is an obvious possibility which could account for the NQR frequency of Cl_1. Two models of hydrogen bond, electrostatic and charge-transfer, will now be studied in turn.

In an electrostatic model, we consider that a net positive charge δ is produced on the proton H_1 as a result of the formation of the hydrogen bond O_2-H$\cdots$ O_1 and this charge interacts with the effective negative charge on Cl_1. The additional electrostatic interaction makes the system more stable. This model corresponds to the bifurcated hydrogen bond O-H$\langle^{Cl}_{O}$ suggested by Ogawa[4]. An excess EFG Δq should be produced by the charge δ, at the position of the Cl_1 nucleus. This is given by

$$\Delta q = \delta\left(\frac{3\cos^2\theta-1}{r^3}\right)(1-R),$$

where θ is the angle between the C-Cl_1 axis and the Cl$\cdots$H direction, r the Cl$\cdots$H distance and R the shielding or antishielding coefficient of covalently bonded chlorine atom. If we put $\delta=+0.1e$,[11] $\theta=122.5°$, and $r=2.64$ Å, R is required to be as large as 10^3 in order to explain $\Delta\nu=1.3$ MHz. This is mainly because the angle θ is close to the magic angle (54°44′ or 125°16′), and therefore the electrostatic part of the hydrogen bond alone, if any, is not sufficient to account for $\Delta\nu$.

According to a simple charge-transfer theory of hydrogen bond[12] a fraction of $3p$ electrons in a Cl lone pair orbital has to be transferred to a vacant antibonding orbital of the O-H group.[13] In this case the EFG tensor components can be analyzed by using the p-electron population numbers U_x, U_y, and U_z on the Cl atom.[14] Here U_z is the population number in the C-Cl bonding orbital, U_x and U_y are those in the lone pair orbitals in the absence of charge transfer. If U_x is assumed to change to U_x' by the charge transfer interaction, the decrease in EFG Δq is given by

$$\Delta q = \frac{1}{2}(U_x-U_x')q_{at}$$

or, in terms of the frequency shift $\Delta\nu$,

$$\Delta\nu = \frac{1}{2}(U_x-U_x')\nu_{at}, \quad \nu_{at} = \frac{1}{2}e^2Qq_{at}$$

where q_{at} is the EFG in the atomic chlorine. The change in η is approximately given by

$$\Delta\eta \doteqdot \frac{3}{2}\frac{\nu_{at}}{\nu}(U_x'-U_x).$$

$\Delta\eta$ can be either positive or negative according to the sign of (U_x-U_y) in the molecule without the charge transfer.

We can estimate the quantity U_x-U_y and then η by assuming that $\Delta\nu$ is produced only by charge transfer: On substitution of $\Delta\nu=+1.29$ MHz and

11) C. A. Coulson and O. Danielsson, *Arkiv Fysik*, **8**, 245 (1954).
12) R. S. Mulliken, *J. Amer. Chem. Soc.* **74**, 811 (1952).
13) The overlap integral between the hydrogen 1s and chlorine 3p lone pair orbital amounts to 0.07 if the Slater-type atomic orbitals are used.
14) T. P. Das and E. L. Hahn, "Nuclear Quadrupole Resonance Spectroscopy," Academic Press, New York (1958): H. Chihara and N. Nakamura, This Bulletin, **44**, 2676 (1971).

$\nu_{at}=+54.87$ MHz, we obtain $U_x-U_x'=0.046$ and $\Delta\eta=-0.096$. While the value of U_x-U_x' is not of an unacceptable magnitude, the difference in the experimental asymmetry parameter on different chlorine atoms is trivial as shown in Table 1.

The charge-transfer model does not satisfactorily account for observation.

We are now left with what is generally called a crystal field effect. From the crystal structure as depicted in Fig. 1, we find that both the Cl_2 and Cl_3 atoms have Cl···Cl intermolecular contacts whereas the Cl_1 atom has as close neighbors two oxygen atoms of the same molecule and two oxygen atoms of the neighboring molecules. In particular, the intramolecular Cl···O distances are short (3.06 and 3.09 Å) and the orientation of hydroxyl groups is such that the polarization of oxygen $2p$ lone-pair orbitals would affect the EFG at the Cl_1 site to some extent. The fact that the temperature coefficient of the three NQR lines are similar to each other (Fig. 3) also suggests that the intermolecular (including non-bonded intramolecular) interactions in which the chlorine atoms participate are of long range.

Molecular Motion. The temperature dependence of the NQR frequencies below 80K is shown in Fig. 3. NQR frequencies at 79K were in agreement with published results.[3,6] The resonance frequencies at 20.3K are ν_1, 38.2863±0.0004; ν_2 39.5415±0.0002; and ν_3, 39.6252±0.0002 MHz. These values are rather larger than those for the frequencies at 0K predicted by Biedenkapp and Weiss.[6] It is apparent that ν_1 shows no anomalous temperature dependence as is usually expected in the solid where intermolecular charge transfer exists.[15,16] This has already been discussed by Biedenkapp and Weiss on the experimental data above 77K. The normal behavior of ν_1 above 20K supports the view that the resonance frequency shift originates mainly from the polarization of lone pair orbitals of oxygen.

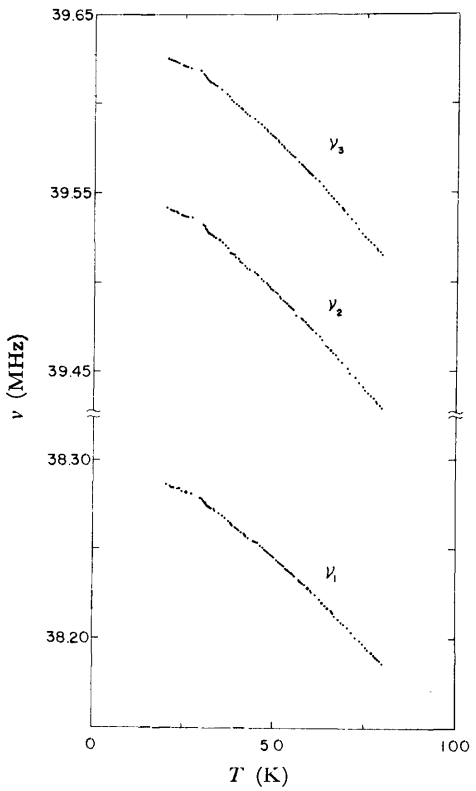

Fig. 3. Temperature dependence of ^{35}Cl nuclear quadrupole resonance frequencies.

The result of measurements of the spin-lattice relaxation time T_1 is shown in Fig. 4. Values of T_1 of ν_1, ν_2 and ν_3 coincide with each other within experimental error over the entire temperature range examined.

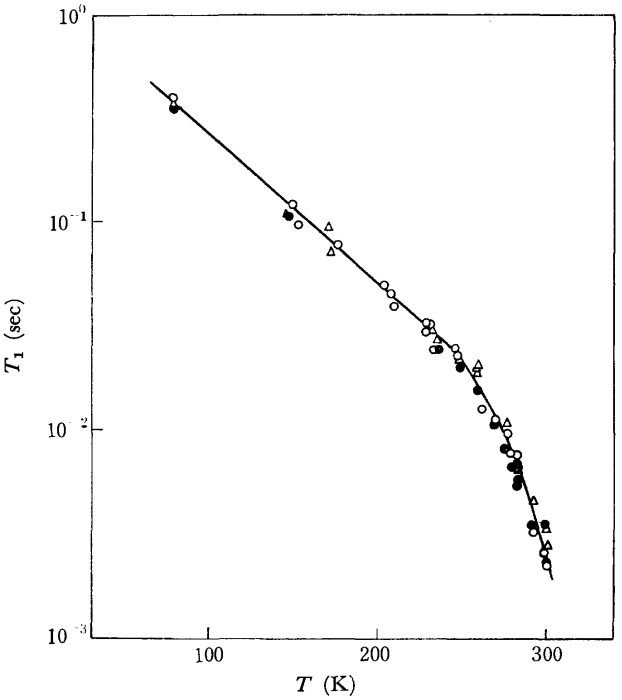

Fig. 4. Nuclear quadrupole spin-lattice relaxation time.
○: ν_1, ●: ν_2, △: ν_3

This suggests that there exists no excess electric quadrupolar or magnetic dipolar interaction between Cl_1 and its environment.

The T_1 value decreases rapidly above 250K. This phenomenon is interpreted as due to the excitation of the internal rotation of the CCl_3 group about the molecular C-C axis. The plot of $\ln 1/T_1$ against $1/T$ gives a straight line; thus, the relation $1/T_1=Ae^{-E_a/RT}$ holds. The slope of the line gives the activation energy $E_a=8.8+0.8$ kcal/mol.[17] This value is much larger than 4 kcal/mol for CCl_3COOH.[19] It may be reasonable to consider that the high potential barrier in chloral hydrate is attributed to large

15) H. Chihara, N. Nakamura, and H. Okuma, *J. Phys. Soc. Jap.* **24**, 306 (1968).
16) H. Okuma, N. Nakamura, and H. Chihara, *ibid.*, **24**, 453 (1968).
17) Recently the T_1 measurement was carried out by Ainbinder *et al.*[18] Their rigorous analysis gives $V_0=11.4$ kcal/mol which is considerably larger than ours.
18) N. E. Ainbinder, B. F. Amirkhanov, I. V. Izmest'ev, A. N. Osipenko and G. B. Soifer, *Soviet Physics-Solid State*, **13**, 344 (1971).
19) M. Buyle-Bodin, *Ann. Phys.* (Paris), **10**, 533 (1955).

intramolecular steric hindrance due to short Cl···O distances. Such intramolecular origin as potential height has also been reported in the case of *p*-CCl_3-C_6H_4Cl.[8]

The authors are grateful to Professor Kazuhide Ogawa for his interest and valuable discussions. They are also indebted to Dr. Hideo Ōkuma for his assistance in NQR frequency measurement.

BULLETIN OF THE CHEMICAL SOCIETY OF JAPAN, VOL. 45, 3534—3541 (1972)

Photolysis of Nitromethane in Gas Phase at 313 nm

Koichi HONDA,* Hitoshi MIKUNI, and Makoto TAKAHASI

Department of Pure and Applied Sciences, College of Gerneal Education, The University of Tokyo, Komaba, Meguro-ku, Tokyo

(Received June 8, 1972)

Photolysis of nitromethane in gas phase at 313.0 nm was studied at 55°C. Methyl nitrite, formaldehyde, nitrosomethane and NO were obtained as main products, their quantum yields being determined to be $\phi_{CH_3ONO}=0.22$, $\phi_{HCHO}=0.20$, $\phi_{CH_3NO}=0.06$ and $\phi_{NO}=0.10$. The dependence of the quantum yields on the pressure of quenching gases such as ethylene, *cis*-2-butene, CO_2 and NO were investigated. The quantum yields of products except formaldehyde decrease with increase in pressure of ethylene or *cis*-2-butene. The sensitized isomerization of 2-butene was also observed. The quantum yield of triplet nitromethane was determined by the Cundall method and compared with that by product analysis. Both give the identical value 0.6. Since ϕ_{HCHO} is not affected by any quencher, it is concluded that formaldehyde is formed directly from singlet excited nitromethane.

Numerous investigations have been carried out on the decomposition of nitromethane. They have revealed that the main primary process is the rupture of C–N bond as shown by (I) under various conditions, *i.e.*, continuous photolysis,[1-6] flash photolysis.[7-9] radiolysis,[4,10,11] and pyrolysis.[12]

$$CH_3NO_2 \rightarrow CH_3 + NO_2 \quad (I)$$

In the case of pyrolysis, the main reaction subsequent to (I) is hydrogen atom abstraction by methyl radical from nitromethane, but in the case of photolysis, the recombination reaction between methyl radical and nitrogen dioxide is dominant, because hydrogen atom abstraction requires an activation energy of more than several kcal/mol. Thus, the final products in photolysis differ markedly from those in pyrolysis in spite of the same primary process. The diversity of the decomposition products of the compound suggests the complexity of secondary successive reactions.

The fact that reaction (I) is the main primary process of photolysis of nitromethane was shown by several authors. McGarvey and McGrath,[8] and Napier and Norrish[9] observed the strong absorption spectrum of methyl radical immediately after flashing nitromethane. Bielski and Timmons[6] detected the ESR spectra of methyl radical and of nitrogen dioxide during photolysis of nitromethane at 77°K. However, Christie *et al.*[3] suggested that a molecular elimination process (II), first proposed by Hirschlaff and Norrish,[1] was involved in the primary processes of photolysis of nitromethane from the fact that the yield of formaldehyde was unaffected by the addition of nitric oxide.

$$CH_3NO_2 \rightarrow CH_2O + HNO \quad (II)$$

Moreover, Cundall *et al.*[4] suggested that in the liquid phase photolysis of nitromethane at 253.7 nm an oxygen atom elimination process (III) might be involved in the primary processes, as in the case of aromatic nitrocompounds, because so much formation of nitrosomethane cannot be explained by a cage reaction between methyl radical and nitrogen dioxide.

$$CH_3NO_2 \rightarrow CH_3NO + O \quad (III)$$

There seems to be little doubt that the decomposition proceeds at least partly from an initial dissociation into methyl radical and nitrogen dioxide, as shown in (I), but a contribution of (II) and/or (III) also appears to be possible according to the results of the above workers.

Rebbert and Slagg[2] suggested that two excited states would be related to photo-decomposition of

* Present Address: The National Chemical Laboratory For Industry, 7th Division, 85 Shinshuku, Hiratsuka Kanagawa.

1) E. Hirschlaff and R. G. W. Norrish, *J. Chem. Soc.*, **1936**, 1580.
2) R. E. Rebbert and N. Slagg, *Bull. Soc. Chim. Belges*, **71**, 709 (1962).
3) M. I. Christie, C. Gilbert, and M. A. Voisey, *J. Chem. Soc.*, **1964**, 3137.
4) R. B. Cundall, A. W. Locke, and G. C. Street, "The Chemistry of Ionization and Excitation" G. R. A. Johnson and G. Scholes, Ed., Taylor * Francis Ltd., London (1967), pp. 131—140.
5) H. W. Brown and G. C. Pimentel, *J. Chem. Phys.*, **29**, 883 (1958).
6) B. H. J. Bielski, and R. B. Timmons, *J. Phys. Chem.*, **68**, 347 (1964).
7) F. W. Dalby, *Can. J. Phys.*, **36**, 1336 (1958).
8) J. J. McGarvey and W. D. McGrath, *Trans. Faraday Soc.*, **60**, 2196 (1964).
9) I. M. Napier and R. G. W. Norrish, *Proc. Roy. Soc., Ser. A*, **299**, 317 (1967).
10) S. Paszyc, *Photochem. Photobiol.*, **4**, 841 (1965)
11) J. L. Corey and R. F. Firestone, *J. Phys. Chem.*, **74**, 1425 (1970).
12) a) C. G. Crawforth and D. J. Waddington, *Trans. Faraday Soc.*, **65**, 1334 (1969). b) C. G. Crawforthe and D. J. Waddington, *J. Phys. Chem.*, **74**, 1425 (1970).

liquid nitromethane, in order to explain the fact that the quantum yield of methyl nitrite was larger at 253.7 nm than at 313.0 nm.

Cundall *et al.*[4] pointed out that the two excited states might be a triplet π–π^* and triplet n–π^* state respectively from the reduction of the quantum yield of methyl nitrite in the presence of oxygen and wavelength effect in the photolysis of liquid nitromethane. However, it is still open to question whether the decomposition process really occurs from the triplet state and if so, how much the quantum yield of the triplet state is.

We have thus attempted to obtain more information on the following problems in the photolysis of nitromethane in gas phase, when the n–π^* band is irradiated.

(i) The possibility of processes other than (I).

(ii) The triplet quantum yield of nitromethane by applying the so called "Cundall method."[3]

Experimental

Materials. Commercial nitromethane (Tokyo-Kasei and Wako-Junyaku) was purified by distilling with rejection of large amounts of initial and final fractions, after dissolved nitrogen dioxide was removed by refluxing for several hours with flushing nitrogen. The pure material was stored in a 500 ml flask *in vacuo* after being dried by anhydrous sodium sulfate and distilled into high vacuum apparatus as required. All the gases were of high purity and obtained from Takachiho Kagaku. *cis*-2-Butene contained 0.44% *trans*-isomer as an impurity, but was used without further purification. Ethylene still contained 0.03% methane and 0.08% ethane after bulb-to-bulb distillation. Nitric oxide was used every time after fresh distillation to avoid contamination of nitrogen dioxide. Carbon dioxide was used without further purifications.

Apparatus and Method. The light source was an Ushio 250 D super high pressure mercury arc lamp with a Pyrex filter to eliminate light shorter than about 300 nm and with a quartz lens, diameter 5 cm and focas length 5 cm to make the incident light parallel.

Under these conditions, the light effectively absorbed by nitromethane was mainly in the 313.0 nm region. This region is the tail part of the n–π^* band, and the contamination of the effect of the π–π^* band adjacent to the n–π^* band is considered to be eliminated. As the molar extinction coefficient of the region is very small ($\varepsilon<4$), strong light intensity is necessary to perform experiments during the relatively short irradiation time. We did not elaborate further optical arrangements to monochromatize the incident light.

The reaction cell was a quartz cylinder with a small cold finger tip, 5 cm in diameter and 20 cm in length with a volume of 410 m*l*. The cell part was held in an electric furnace with quartz window and a stirring fan to keep constant temperature within ± 1°C during the course of an experiment. It was separated from other parts by a greaseless valve.

The vacuum system was the conventional one, being set up completely mercury free to avoid the reaction of nitrogen dioxide with mercury. Sample gas was introduced into a constant volume vessel (410 m*l*). The pressure was measured by a calibrated Bourdon gauge, and the gas in the vessel was trapped into the cold finger of reaction cell with a liquid nitrogen bath. When a mixture of nitromethane with other gas was required, these procedures were repeated for each gas. The mixture prepared was kept at a reaction temperature for complete mixing at least one hour before irradiation. The usual experiments were carried out at 28 Torr (at 25°C) of nitromethane and at reaction temperature 55°C.

Actinometry. Rebbert and Slagg[2] showed that the quantum yield of ethylene formed from nitroethane is 0.074 in gaseous photolysis at 313.0 nm. Since the absorption spectrum of nitromethane was almost the same as that of nitroethane,[14] the quantum yields of products of nitromethane were easily determined. The amount of incident light in the reaction cell is determined to be 1.7×10^{17} photon/sec.

Analysis. The products were collected in a series of traps; the first was a U type tube, the second and the third were removable tubes each containing completely degassed water (about 2 m*l*) and a detachable large volume bulb (about 3 *l*). The analytical procedure was as follows.

(i) The first trap was cooled by a liquid nitrogen bath, and non-condensable gases (H_2, N_2, CO, CH_4 and most of NO) were collected in a large bulb by diffusion after the occluded gases in frozen materials were removed with freeze-melt cycles. The bulb was then detached and jointed to a Toepler pump-gas buret system. The gases were analysed by gas-chromatography (molecular sieve 5 A column, 1 m, room temp., He carrier), but the amount of NO was estimated by subtracting the moles of the other products from the total amount of noncondensable gases, because NO could not be analysed by gas-chromatography with good reproducibility. The analytical error of NO was thus larger than that of other non-condensable gases. In a very small conversion experiment, the first trap was cooled by ethyl bromide slush bath (—120°C) and gases (H_2, N_2, CO, CH_4, NO, N_2O, and C_2H_6) noncondensable at —120°C were analysed by mass-spectrometry.

(ii) The valve to the second trap cooled by a liquid nitrogen bath was opened, and the water soluble products (mainly formaldehyde and methyl nitrite) and nitromethane were dissolved in water. The aqueous solutions prepared were diluted to a constant volume and were used for quantitative analysis of formaldehyde and methyl nitrite. When both could not be measured simultaneously, they were measured separately by repeating the experiment twice.

(iii) Nitrosomethane was known to dimerize almost completely when condensed; it deposited as a white powder on the wall of the first trap together with formaldehyde polymer after procedure (ii). The materials were then vaporized by warming up to about 100°C with an electric oil bath and were condensed into the third trap cooled by a liquid nitrogen bath and dissolved into water. The analytical methods were the same as those for the second trap. The total quantity of formaldehyde was determined as the sum obtained in procedures (ii) and (iii).

The analytical methods of methyl nitrite, formaldehyde and nitrosomethane: Parker's method[15] (quantitative formation of diazo-dye by the reaction of α-naphthylamine with the nitrite ions produced by hydrolysis of methyl nitrite), Bricker's method[16] (dye formation by the reaction

13) W. A. Noyes and I. Unger, "Advances in Photochemistry" **4**, p. 64, John Wiley & Sons, Inc. (1966).

14) J. G. Calvert and J. N. Pitts, "Photochemistry" John Wiley & Sons, Inc., p. 454 (1966).

15) C. A. Parker, *Analyst*, **74**, 112 (1949).

16) a) C. E. Bricker and H. R. Johnson, *Ind. Eng. Chem.*, **17**, 400 (1945). b) C. E. Bricker and W. A. Vail, *Anal. Chem.*, **22**, 720 (1950).

of chromotropic acid with formaldehyde in the presence of concd sulfuric acid) and UV-spectroscopy of *cis*-nitrosomethane dimer[17] (λ_{max}; 265 mn, ε_{max}; 1.0×10^4). It was confirmed that these methods were not affected by nitromethane and added gases except nitric oxide. If nitric oxide is present, Briker's method cannot be applied, but the amount of formaldehyde in the first trap is a solid polymer. The total amount of formaldehyde in the presence of nitric oxide was then estimated assuming the ratio of total amount to partial amount in the first trap is the same as the ratio in the absence of nitric oxide. Moreover, since Parker's method is also affected remarkably by dissolved nitric oxide, the analysis of methyl nitrite was carried out after the nitric oxide dissolved in the second trap solution was expelled completely by flushing with nitrogen for several hours.

The original impurity content as well as the isomerization product content of *cis*-2-butene were determined by gas chromatographic analysis (active alumina with 2% squalane column, 2 m, 100°C, N_2 carrier, FID).

Miner products not analysed were checked also by gas chromatography (DOP, 2 m, 100°C, He carrier, TCD).

Analytical methods described above were modified in some cases.

Results

(I) Quantum Yields of Products at Small Conversions. In the gas phase photolysis of nitromethane (55°C, 28 Torr at 25°C), the products of quantum yields more than 0.05 at small conversions were methyl nitrite, formaldehyde, nitric oxide, nitrosomethane and nitrous oxide, their amounts decreasing in this order. When irradiation was prolonged, CO joined the main products (up to $\phi_{CO}=0.13$ at 90 min. irradiation) and the quantum yields of main products (methyl nitrite, formaldehyde and nitric oxide) decreased with the irradiation time (up to $\phi_{CH_3ONO}=0.07$, $\phi_{CH_2O}=0.10$ at 90 min. irradiation).

Minor products analysed quantitatively were methane, hydrogen, carbon monoxide and nitrogen. Other minor products detected in gas-chromatograph were ethane, methanol, water, methyl nitrate and carbon dioxide. Nitrogen dioxide was not detected in the final products (at least at small conversions) by mass spectroscopic analysis. This agreed with the results of earlier workers,[2,4] although the possibility of loss during the course of pumping gaseous products with a Toepler-pump was not completely excluded, since nitrogen dioxide is very reactive with mercury.

As shown in Fig. 1, formaldehyde is the main product even at such a small conversion as 0.3% (at 1 min irradiation), differing from the result of Rebbert and Slagg.[2] Process (III), if it exists at all, would not be so important at least under the experimental condition, since the quantum yield of nitrosomethane is so small.

The quantum yields of products larger than 0.05 are summarized in Table 1.

The quantum yields of minor products determined by mass spectroscopy at small conversions (1 min. and 2 min. irradiations) were $\phi_{H_2}=0.02$; $\phi_{CH_4}=0.02$; $\phi_{N_2+CO}=0.05$, and except CO, they decreased to one tenth, when irradiated longer than 15 min.

17) a) H. T. J. Chilton, B. G. Gowenlock, and J. Trotman, *Chem. and Ind.* (london), **1955**, 538. b) B. G. Gowenlock and J. Trotman, *J. Chem. Soc.*, **1956** 1670.

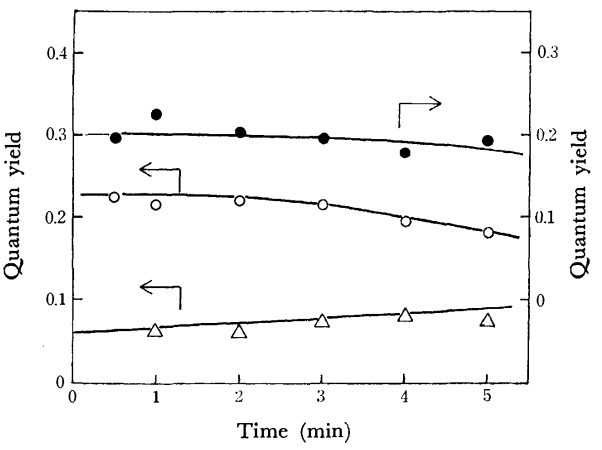

Fig. 1. The quantum yields of methyl nitrite, formaldehyde and nitrosomethane against irradiation time within 5 min. ○; methyl nitrite, ●; formaldehyde, △; nitrosomethane

TABLE 1. SUMMARY OF THE QUANTUM YIELDS OF MAJOR PRODUCTS

($\phi>0.05$)

Product	Quantum yield
CH_3ONO	0.22[a]
CH_2O	0.20[a]
CH_3NO	0.06[a]
NO	0.10[b]
N_2O	0.05[b]

a) Obtained by extrapolating the irradiation time to zero in Fig. 1.
b) Obtained from mass spectral results from 1 and 2 min. irradiation products.

(II) Effects of Added Gases. The variations of quantum yield of methyl nitrite, formaldehyde and nitric oxide with the pressures of added gases, *i.e.*, ethylene, *cis*-2-butene, NO or CO_2 are shown in Fig. 2a, 2b, 2c and 2d.

The quantum yield of formaldehyde is almost independent of the added gases, ethylene or *cis*-2-butene, while those of methyl nitrite and nitric oxide decrease with increase in the pressure of olefins (Fig. 2a and 2b). In other words, the formation of methyl nitrite and nitric oxide are suppressed by the presence of olefins, but that of formaldehyde is little affected. In the case of addition of *cis*-2-butene, isomerization of *cis*-2-butene to *trans*-isomer occurred simultaneously.

Minor products also decreased with increasing pressures of olefins, and at pressures above several tens of Torr, methane and hydrogen were below detectable limit. To know whether the decrease of the quantum yield of methyl nitrite might be due to the scavenging action of methyl radicals by the olefins, the amount of methyl radicals produced in the excess of ethylene was estimated from the yield of hydrocarbons (CH_4, C_2H_6, C_3H_6, C_3H_8, C_4H_{10}). It was found that the quantum yield of methyl radical is at most 0.01, if excess ethylene exists.

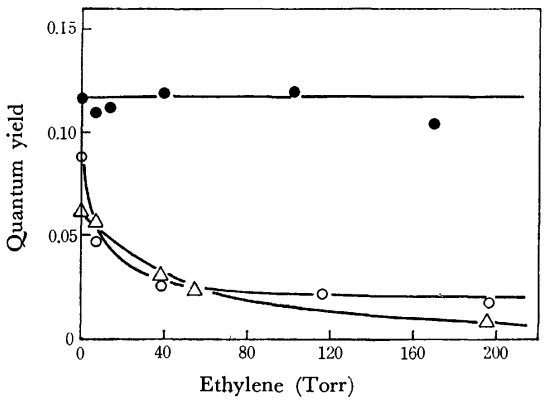

Fig. 2a. The quantum yields of methyl nitrite, formaldehyde and nitric oxide against the press. of ethylene. Irradiation time; 60 min.
○; methyl nitrite, ●; formaldehyde, △; nitric oxide

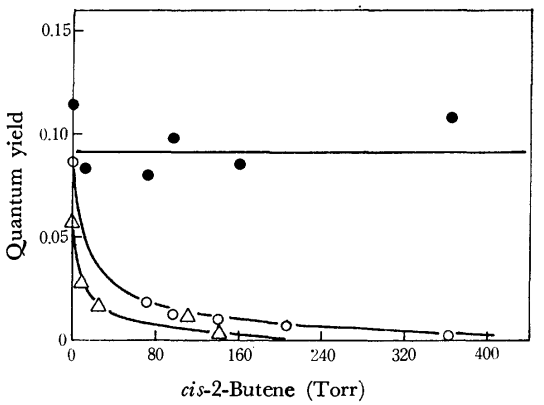

Fig. 2b. The quantum yields of methyl nitrite, formaldehyde and nitric oxide against the press. of *cis*-2-butene. Irradiation time; 60 min.
○; methyl nitrite, ●; formaldehyde, △; nitric oxide

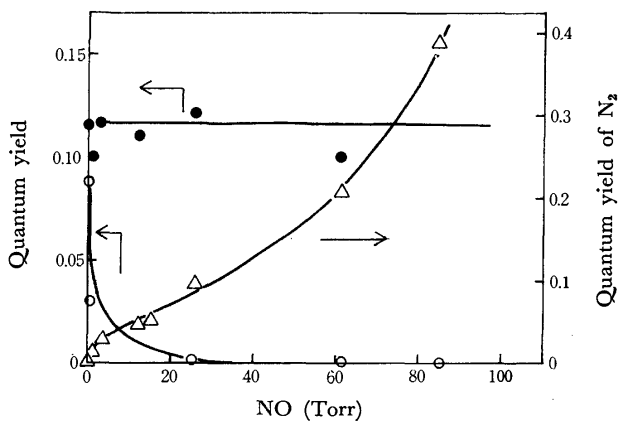

Fig. 2c. The quantum yields of methyl nitrite, formaldehyde and nitrogen against the press. of nitric oxide. Irradiation time; 60 min.
○; methyl nitrite, ●; formaldehyde, △; nitrogen

The quantum yield of methyl nitrite decreased sharply in the presence of nitric oxide and became almost zero above 25 Torr of nitric oxide (Fig. 2c). In this case, methane was not detectable at all and on the contrary, nitrogen increased remarkably with nitric oxide pressure.

As established by many workers, nitrogen formation

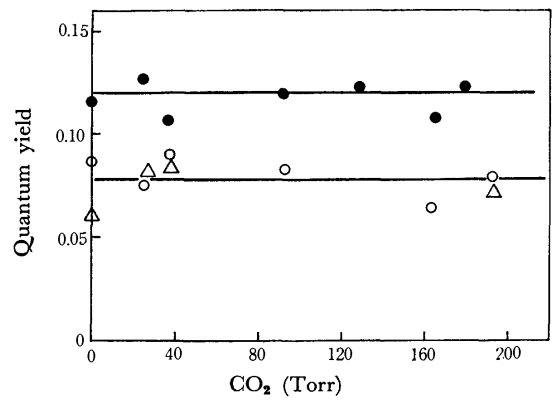

Fig. 2d. The quantum yields of methyl nitrite, formaldehyde and nitric oxide against the press. of CO_2. Irradiation time; 60 min.
○; methyl nitrite, ●; formaldehyde, △; nitric oxide

from nitric oxide is caused by disproportionation ($4NO \rightarrow N_2+2NO_2$) under the catalytic action of methyl radical. The sharp increase of nitrogen and the failure of methane formation therefore supports the view that process (I) to form methyl radical is involved in the primary processes of nitromethane photo-decomposition.

That the yield of formaldehyde was not affected by the addition of nitric oxide suggests that almost all the formaldehyde should be formed by the molecular elimination process like (II).[3]

The effect of added CO_2 was not noticeable either in the main products formation as shown in Fig. 2d or in minor products formation. Hence, the vibrationally excited states quenchable by added CO_2 is not supposed to be involved in the photo-decomposition of nitromethane.

(III) Effect of Reaction Temperature. In order to know the temperature effect of the primary processes of nitromethane photolysis, the quantum yields of methyl nitrite and formaldehyde were measured in the temperature range 25—200°C. The results shown in Fig. 3 indicate that methyl nitrite formation was

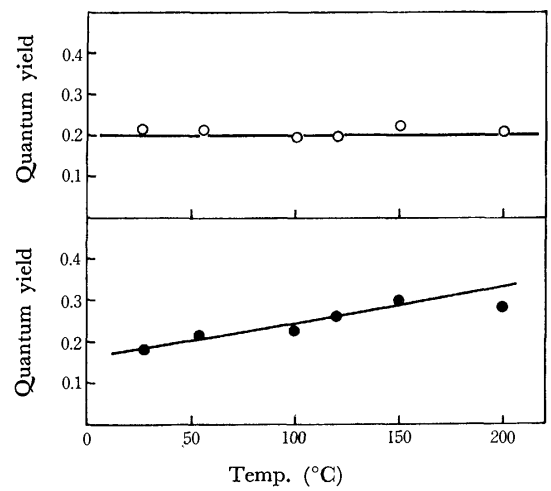

Fig. 3. Temperature dependence of the quantum yields of methyl nitrite, and formaldehyde. Irradiation time 1 min.
○; methyl nitrite, ●; formaldehyde

nearly temperature independent, whereas formaldehyde formation increased with increasing temperature. The increase of formaldehyde with reaction temperature cannot be ascribed to the pyrolytic formation of formaldehyde by the degradation of $\cdot CH_2NO_2$ radicals. If this is the case, the consumption of methyl radical by the abstraction reaction with nitromethane would be expected with increase of reaction temperature, resulting in a decrease of methyl nitrite with temperature. The activation energy of formaldehyde formation was estimated to be 0.7 kcal/mol.

Discussion

(I) Reaction Mechanism. The effect of added gases in the photolysis of nitromethane was shown to be as follows.

(i) Addition of *cis*-2-butene caused a decrease of the quantum yield of methyl nitrite and nitric oxide. A part of *cis*-2-butene was simultaneously isomerized to *trans* form, whereas it little affected formaldehyde formation. This implies that the processes to yield methyl nitrite and nitric oxide proceed through a triplet state of nitromethane, but not those for formaldehyde formation, since the isomerization of *cis*-2-butene is thought to take place through triplet 2-butene formed by the photosensitization of a triplet nitromethane.

(ii) Ethylene acts in the same way as *cis*-2-butene, although less effectively, suggesting that ethylene also can quench the triplet state of nitromethane. Thus the lowest triplet energy of nitromethane is supposed to be greater than that of ethylene (about 78 kcal/mol).

(iii) The rate of methyl nitrite and methane formation decreased to zero while nitrogen formation increased remarkably on addition of nitric oxide, showing that the main primary process is the C–N bond fission (I), and methyl radical formed is scavenged by nitric oxide to give nitrosomethane, which reacts further with nitric oxide to produce nitrogen.

Since nitric oxide does not affect the rate of formaldehyde formation, formaldehyde is not formed by a radical reaction but by a molecular elimination reaction like process (II).

The above results suggest that process (I) takes place from the lowest triplet state of nitromethane, $T_{n-\pi^*}$, and process (II) takes place from such a very short lived state as not quenched by added gases, probably the lowest excited singlet state $S_{n-\pi^*}$.

The proposed reaction mechanism is as follows, where elementary reactions supposed to be important at a small conversion are underlined. Rate constants determined recently by several authors are shown in Table 2.

$$N \xrightarrow{h\nu} N_S$$

(1) $N_S(+M) \rightarrow N + (M)$

(2) $N_S \rightarrow N + h\nu_f$ (actually not observed)

(3) $N_S \rightarrow N_T$

Table 2. Summary of rate constants used in our calculations[a)]

Rate const	l/mol, sec
k_{9a}	4.1×10^{9} [18,19,b)]
k_{9b}	7.9×10^{9} [18,19,b)]
k_{9c}	$\ll k_{9a}, k_{9b}$ [19,c)]
k_{10a}	1.8×10^{8} [20)]
k_{10b}	2.4×10^{9} [18)]
k_{10c}	1.0×10^{8} [18,19)]
k_{10d}	2.3×10^{7} [20)]
k_{10e}	3.0×10^{10} [20)]
k_{10f}	1.2×10^{10} [c)20,d)]
k_{10g}	$4.8—14.4\times10^{6}$ [20)]

a) Rate const of (9a), (9b) and (10c) are based on the data at 90°C, and the others at 25°C. However, they can be all applied to the present case at 55°C, since activation energies of the reactions are nearly zero.
b) Calculated values from the ratio of k_{9a}, k_{9b} and k_{10c} to k_{10b} determined by Phillips and Shaw, and the value of k_{10b} obtained by Basco *et al.*
c) Reaction (9c) is not important in gaseous reactions, since CH_3O-NO bond undergoes rupture easily.
d) A tentative value determined by McGraw *et al.*

(4) $N_S \rightarrow CH_2O + HNO$

(5) $N_T \rightarrow CH_3\cdot + NO_2$

(6) $N_T(+M) \rightarrow N + (M)$

(7) $N_T \rightarrow N + h\nu_p$ (actually not observed)

(8) $N_T + Q \rightarrow N + Q_T$

(9a) $CH_3\cdot + NO_2 \rightarrow CH_3NO_2$

(9b) $CH_3\cdot + NO_2 \rightarrow CH_3O\cdot + NO$

(9c) $CH_3\cdot + NO_2 \rightarrow CH_3ONO$

(10a) $CH_3O\cdot + NO \rightarrow CH_3ONO$

(10b) $CH_3\cdot + NO \rightarrow CH_3NO$

(10c) $CH_3O\cdot + NO_2 \rightarrow CH_3ONO_2$

(10d) $CH_3O\cdot + NO \rightarrow CH_2O + HNO$

(10e) $CH_3O\cdot + HNO \rightarrow CH_3OH + NO$

(10f) $CH_3O\cdot + CH_3O\cdot \rightarrow CH_3OH + CH_2O$

(10g) $HNO + HNO \rightarrow H_2O + N_2O$

(10h) $CH_3\cdot + CH_3O\cdot \rightarrow CH_4 + CH_2O$

where N_S denotes the lowest excited singlet stage, N_T the lowest triplet state, N the ground state nitromethane and Q the triplet quenchers, respectively.

On the basis of the proposed reaction scheme, we can estimate the quantum yield of reaction (5), ϕ_5, to be 0.6 from the sum of quantum yields of the products at small conversions (Table 1) with the help of rate constants (k_{9a} and k_{9b}) reported by Philips and Show,[19] *viz.*, the quantum yield of reaction (9b), ϕ_{9b}, sum of ϕ_{CH_3ONO}, ϕ_{CH_3NO} and ϕ_{NO} is no less than 0.4, because these products are formed only from the sub-

18) N. Basco, D. J. L. James, and R. D. Suart, *Int. J. Chem. Kinet.*, II, 215 (1970).
19) L. Phillips and R. Shaw, Symp. Combust, 10th, Univ. Cambridge, England, 1964, pp. 453—461 (1965).
20) G. E. McGraw and H. S. Johnston, *Int. J. Chem. Kinet.*, I, 89 (1969).

sequent reactions of (9b), keeping in mind that reaction (9c) is negligible; the quantum yield of reaction (9a), ϕ_{9a}, is estimated to be about 0.2 on the basis of the ratio of the rate constants obtained by Phillips and Shaw;[19] Thus, ϕ_5 is estimated to be about 0.6.

The primary quantum yield of reaction (4), ϕ_4, the observed quantum yield of formaldehyde at small conversions, is about 0.2. The contribution of (10d), (10f) and (10h) is considered to be small for the production of formaldehyde.

The mechanism of CO formation might be complex; CO seems to be formed by the secondary photolysis of methyl nitrite and formaldehyde and/or by oxidation reaction of oxygen atom formed by the photolysis of nitrogen dioxide since CO formation is appreciable only on being irradiated for a long time.

Hydrogen may be formed also by the secondary photolysis of formaldehyde. Formation of small amounts of methanol, water, nitrous oxide and methyl nitrate is explained by the reactions (10e), (10f), (10g) and (10c).

In the case of nitric oxide addition, reaction (5) is followed by the chain reactions described below as established by several researchers.[3,9,21,22]

(10b) $CH_3\cdot + NO \rightarrow CH_3NO$

(11) $CH_3NO + 2NO \rightleftharpoons CH_3\text{-}\underset{\underset{NO}{|}}{N}\text{-}O\text{-}NO \rightarrow CH_3N_2NO_3$

(12a) $CH_3N_2NO_3 \rightarrow CH_3\cdot + NO_3 + N_2$

(12b) $CH_3N_2NO_3 \rightarrow CH_3NO_3 + N_2$

(13) $NO_3 + NO \rightarrow 2NO_2$

(14) $CH_3NO \rightarrow CH_2{=}NOH$

(15) $2CH_3NO \rightarrow (CH_3NO)_2$

(16) $CH_3NO + NO_2 \rightarrow CH_3NO_2 + NO$

Although reaction (9a) and reactions subsequent to (9b) might act as chain termination reactions to some extent, (14), (15) and (16) may become dominant as pressure of nitric oxide is increased, since we cannot detect methyl nitrite if nitric oxide is present in more than several Torr.

Formation of a trace of nitrogen without addition of nitric oxide may be interpreted also in terms of the above reactions. Since it was confirmed that HNO radical and methoxy radical have no ability to act as a chain carrier in the above disproportionation reactions of nitric oxide,[3] the anomalous increase of nitrogen in the presence of nitric oxide should be caused by (10b) and the successive reactions.

We confirmed that the plot of the quantum yield of nitrogen against the second power of nitric oxide pressure satisfied the linear relationship above several Torr of the pressure (not shown in the figure). This suggests that (12) is the rate determining step of these nitrogen formation reactions.

(II) Sensitized Isomerization of cis-2-*Butene by Nitromethane and Photostationary State.* It is generally accepted that the quantum yield of triplet state can be determined by the "Cundall method."[13] However, in order to apply this method, it should be confirmed that the isomerization does not occur through radical mechanism (Schenck mechanismm).[23]

Main radicals formed by the decomposition of nitromethane are methyl, methoxy, nitrogen dioxide, nitric oxide and HNO radical. Cundall and Davies[24,25] confirmed in their study of the photolysis of acetone and acetaldehyde that methyl radical does not cause the isomerization of 2-butenes. It is known that nitrogen dioxide and nitric oxide act as a catalyst of the thermal isomerization of 2-butenes and they reduce the activation energy from 63 kcal/mol to 12 kcal/mol[26] and 26 kcal/mol[27] respectively. However, under our experimental conditions (50°C), isomerization by either species must be negligible, because the calculated rate of isomerization is at least ten times slower than our experimental result. HNO radical may react with *cis*-2-butene in the same way as formyl radical to form secondary butyl radical and nitric oxide, but the secondary butyl radical is expected to decompose into methyl radical and propylene but not to reproduce 2-butenes. Although there seems to be no data on reactions of methoxy radical with olefins, our experimental results where the quantum yield of *trans*-2-butene increased with increasing *cis*-2-butene pressure in spite of the decrease of the quantum yield of methyl nitrite suggest that isomerization by methoxy radicals is less probable.

Another possibility may be isomerization through butenyl radical which may be formed by the abstraction of hydrogen atom from 2-butene by some radical. However, this is also less likely under our experimental conditions, since it requires activation energy of more than several kcal.

If the possibilities of isomerization through radical mechanism can be neglected, sensitized-isomerization by triplet nitromethane should be considered. For photosensitized isomerization to be possible, triplet energy of sensitizer should be larger or at least not much less than that of 2-butene. So far neither phosphorescence[28] nor S–T absorption spectrum has been observed, and we cannot predict from spectroscopic data whether the sensitized isomerization of 2-butene by nitromethane is possible or not. However, when we see that sensitized isomerization actually takes place, we can presume that the triplet level of nitromethane lies above that of 2-butene (76 kcal)[29] or ethylene (78 kcal).[29]

We shall discuss the sensitized isomerization of 2-

21) a) W. Frost and O. K. Rice, *Can. J. Chem.*, **41**, 562 (1963). b) O. P. Strauss and H. G. Gunning, *ibid.*, **41**, 1207 (1963).
22) J. R. Gilbert, R. M. Lambert and J. W. Linnett, *Trans. Faraday Soc.*, **66**, 2837 (1970).
23) N. J. Turro, *Photochem. Photobiol.*, **9**, 555 (1969).
24) R. B. Cundall and A. S. Davies, *Proc. Roy. Soc. Ser. A*, **290**, 563 (1966).
25) R. B. Cundall and A. S. Davies, *Trans. Faraday Soc.*, **62**, 2793 (1966).
26) J. L. Sprung, H. Akimoto, and J. N. Pitts, Jr., *J. Amer. Chem. Soc.*, **93**, 4358 (1971).
27) R. B. Cundall, "Progress in Reaction Kinetics" Pergamon Press (1964). Vol. 2, 182.
28) Dr. Kuboyama, The National Chemical Laboratory For Industry, kindly attmepted to measure the phosphorescence of nitromethane, but it could not be observed at least in the sensitivity range of the instrument.

butene by nitromethane more in detail. Completely in the same way as Cundall et al.[30] and Lee *et al.*,[31] the following reaction scheme is assumed for sensitized isomerization.

$$\begin{aligned}
&(8a) && N_T + B_{cis} \rightarrow N + B_{T\,cis}\\
&(8b) && N_T + B_{trans} \rightarrow N + B_{T\,trans}\\
&(17a) && B_{T\,cis} \rightarrow B_{T\,trans}\\
&(17b) && B_{T\,trans} \rightarrow B_{T\,cis}\\
&(18a) && B_{T\,trans} \rightarrow B_{trans}\\
&(18b) && B_{T\,cis} \rightarrow B_{cis}
\end{aligned}$$

where N_T denote triplet nitromethane, B_{cis} and B_{trans} *cis* and *trans*-2-butene, $B_{T\,cis}$ and $B_{T\,trans}$ triplet of 2-butene in *cis* and *trans* form respectively. The following rate expressions are derived in the usual way, under steady state conditions. The initial rate of isomerization of *cis*-2-butene to *trans* form, $R_{c\rightarrow t}$, under a fixed pressure of nitromethane and light intensity and in the absence of *trans*-2-butene, is given below.

$$R_{c\rightarrow t} = \left(\frac{I_a}{k_1+k_2[M]+k_3+k_4}\right) \times \left(\frac{k_{17a}k_{18a}}{k_{17a}k_{18a}+k_{17b}k_{18b}+k_{18a}k_{18b}}\right) \times \left(\frac{k_{8a}[B_{cis}]}{k_5+k_6[N]+k_7+k_{8a}[B_{cis}]}\right) \quad (1)$$

An analogous equation can be derived for reversed isomerization, and the ratio $R_{c\rightarrow t}/R_{t\rightarrow c}$ is expressed simply as follows.

$$R_{c\rightarrow t}/R_{t\rightarrow c} = k_{17a}k_{18a}/k_{17b}k_{18b} \quad (2)$$

In addition, in the photostationary state (abbreviated as pss), the ratio $([B_{trans}]/[B_{cis}])_{pss}$ can be expressed as follows.

$$([B_{trans}]/[B_{cis}])_{pss} = \frac{k_{8a}k_{17a}k_{18a}}{k_{8b}k_{17b}k_{18b}} = \frac{k_{8a}R_{c\rightarrow t}}{k_{8b}R_{t\rightarrow c}} \quad (3)$$

In the benzene-sensitized isomerization of 2-butene, Cundall *et al.*[30] reported the value of 1.37 for $R_{c\rightarrow t}/R_{t\rightarrow c}$, but later Lee et al.[31] obtained the value of 1.02. At the same time, for the value of $([B_{trans}]/[B_{cis}])_{pss}$, Cundall and his co-workers gave the value of 1.37, assuming that k_{8a}/k_{8b} is unity (no difference between *cis*- and *trans*-2-butene) on the basis of their observation that several efficient quenchers have identical quenching cross sections for triplet benzene but this observation seems to be supported neither by Tanaka *et al.*[32] nor Lee's group. In order to determine the exact value of $([B_{trans}]/[B_{cis}])_{pss}$, it is preferable to carry out the isomerization experiment starting from a mixture of *cis*- and *trans*-2-butene whose initial composition is already near the stationary state. Lee *et al.*[31] obtained the value of 0.92 by this method. Applying this technique to nitromethane-sensitized isomerization, we obtained the value of 0.90, irradiating a sample containing 28 Torr of nitromethane and 8.7 Torr of a mixture of *cis*- and *trans*-2-butene in an equal amount (Table 3). For the sake of comparison, the pss ratios for several sensitizers are given in Table 5. It is interesting that the organic sensitizers investigated so far give the value of around 0.9 for the pss ratio except Cundall's value for benzene. Larger quenching cross section of *trans*-2-butene to these organic sensitizers may be interpreted either in terms of the small difference in triplet energy of *cis*- and *trans*-2-butene or the difference in the ease of collision complex formation between the sensitizer and the quencher, but no well-established explanation has been given yet.

Table 3. Variation of *trans/cis* with irradiation time[a)]

Time (hr)	0	0.5	1.0	1.5	2.0	2.5	3.0	3.5	4.0
trans/cis	1.01	0.99	0.98	0.96	0.94	0.92	0.90	0.90	0.90

a) Nitromethane press.; 28 Torr, *trans*-, *cis*- mixture press.; 8.7 Torr, photolysis temp.: 55°C.

(III) Quantum Yield of Triplet Nitromethane by the Cundall Method and by Product Analysis. We determined the quantum yield of triplet nitromethane according to the ordinary procedure of the Cundall method. A good linear relationship is obtained between $1/\phi_{Bc\rightarrow t}$ and $1/[B_{cis}]$ (Fig. 4) where $\phi_{Bc\rightarrow t}$ is the quantum yield of *trans*-2-butene from *cis*-form in the absence of *trans* form, *viz.*, $\phi_{Bc\rightarrow t}=R_{c\rightarrow t}/I_a$.

The linear relationship is consistent with the following equation which is derived from equation (1).

$$1/R_{c\rightarrow t} = \frac{k_1+k_2[M]+k_3+k_4}{k_3I_a} \times \left(\frac{k_{17a}k_{18a}+k_{17b}k_{18b}+k_{18a}k_{18b}}{k_{17a}k_{18a}}\right) \times \left(\frac{k_5+k_6[N]+k_7}{k_{8a}[B_{cis}]}+1\right) \quad (4)$$

As shown in Fig. 4, the reciprocal of intercept gives the value of 0.3 which corresponds to $\phi_{c\rightarrow t}$ at an infinitely high pressure of *cis*-butene. Although we did not measure the ratio $R_{c\rightarrow t}/R_{t\rightarrow c}$ for nitromethane, we may assume that it is approximately unity as Haninger determined for benzene-sensitization, if we assume that

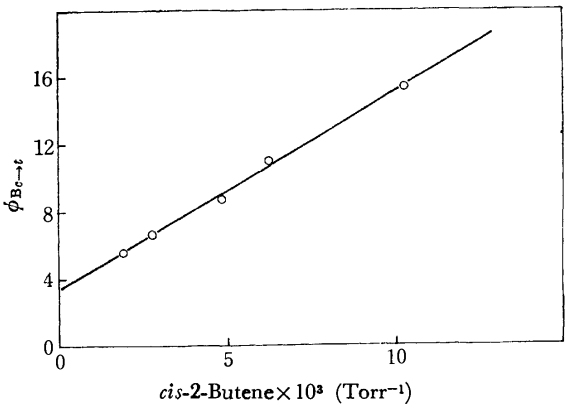

Fig. 4. Reciprocal-reciprocal plot of the quantum yields of triplet 2-butene and the press. of *cis*-2-butene.

29) M. W. Schmidt and E. K. C. Lee, *J. Amer. Chem. Soc.*, **92**, 3579 (1970).
30) R. B. Cundall, F. J. Fletcher, and D. G. Milne, *Trans. Faraday Soc.*, **60**, 1146 (1964).
31) E. K. C. Lee, H. O. Denschlar, and G. A. Haninger, *J. Chem. Phys.*, **48**, 4547 (1968).
32) M. Tanaka, T. Terao, and S. Sato, This Bulletin, **38**, 1645 (1965).

the ratio is independent of the triplet energy of sensitizer. In addition, we may assume that k_{17a} and k_{17b} are much larger than k_{18a} and k_{18b}, although Haninger pointed out there is some doubt as to this assumption. Thus, we obtain the following relationship.

$$\phi_3 = \phi_{N_T} = \phi^{\infty}_{B_T} = (\phi^{\infty}_{B_{c\to t}} + \phi^{\infty}_{B_{t\to c}}) = \phi_{B_{c\to t}}(R_{c\to t}+R_{t\to c})/R_{c\to t} \doteqdot 2R_{c\to t}/I_a = 2\phi_{B_{c\to t}} = 0.6 \quad (5)$$

Using the obtained values ϕ_3 and ϕ_4, we can estimate the value of ϕ_1 to be 0.2 as the difference $(1-\phi_3-\phi_4)$, neglecting the fluorescence process.

We showed that the quantum yield ϕ_5 is 0.6 which is calculated from the product analysis. Therefore, ϕ_{NT} obtained by the Cundall method is consistent with ϕ_5 obtained by product analysis, indicating that the non-radiative process (6) and radiative process (7) are not important, even though they exist. The quantum yields of reactions (1)—(7) are summarized in Table 4. Equation (4) can be made simpler as follows.

Table 4. Summary of the quantum yields of reactions (1)—(5)

ϕ_1	0.2
(ϕ_2	0)
$\phi_3(\phi_T)$	0.6
ϕ_4	0.2
ϕ_5	0.6
(ϕ_6	0)
(ϕ_7	0)

$$1/\phi_{B_T} = \left(\frac{k_1+k_3+k_4}{k_3}\right)\left(\frac{k_5}{k_{8a}[B_{cis}]}+1\right) \quad (6)$$

From the ratio of slope to intercept in Fig. 4, the ratio of rate constant for the dissociation to that for energy transfer, k_5/k_{8a}, is calculated to be 1.7×10^{-2} mol/l at 55°C. Since nitro compounds resemble carbonyl compounds in the behaviors of their absorption and phosphorescence spectra of n-π^* transition and 2-butene isomerization, it may be interesting to compare triplet quantum yield ϕ_T, and the rate constants k_5 and k_{8a}, as given in Table 4. We could not measure k_{8a} directly, unlike the case of carbonyl compounds, so that we can only compare the ratio k_5/k_{8a}, but if we could assume tentatively that k_{8a} of nitromethane is equal to that of acetaldehyde, k_5 would be 3.4×10^6 sec^{-1}.

We investigated the change of quantum yield of methyl nitrite with the increase in the pressure of

Table 5. Summary of photostationary state ratio

Sensitizer	E_T (kcal/mol)	$([B_{trans}]/[B_{cis}])_{pss}$
Hg($^3P_1$)	112.7	1.0[33]
Benzene	84.4	1.37[30]
Benzene	84.4	0.92[31,32]
Acetone	79—82	0.94[34]
Nitromethane	80	0.90

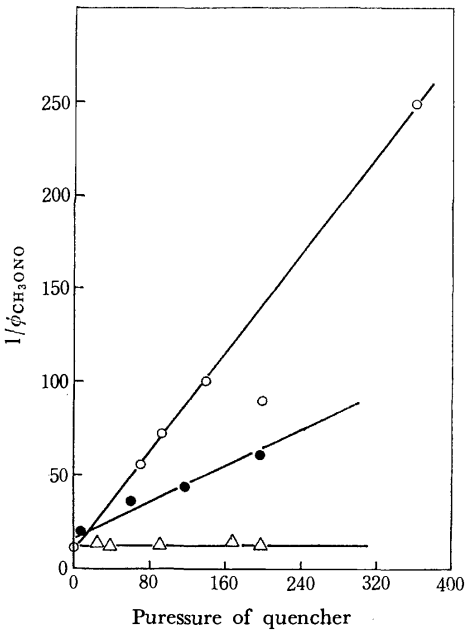

Fig. 5. Stern-Volmer plots of the quantum yield of methyl nitrite against the press. of quenchers.
○; *cis*-2-butene, ●; ethylene, △; CO_2

cis-2-butene. The Stern-Volmer plot of $1/\phi_{CH_3ONO}$ against ethylene and *cis*-2-butene gives a good linear relationship (Fig. 5). The result is consistent with the following equation derived on the basis of the reaction mechanism we proposed.

$$\frac{1}{\phi_{CH_3ONO}} = \frac{1}{\phi_T}\left(\frac{k_{9a}+k_{9b}}{k_{9b}}\right)\left(1+\frac{k_8[Q]}{k_5}\right) \quad (7)$$

The ratio k_5/k_8 is again calculated from the slope with the values of ϕ_T, and $(k_{9a}+k_{9b})/k_{9b}$, giving the value 2.0×10^{-2} mol/l for *cis*-2-butene and 5.8×10^{-2} mol/l for ethylene, respectively. The value for *cis*-2-butene is about 20% larger than that derived by the Cundall method from isomerization data. When the assumption and experimental errors are taken into account, both values may be in good agreement.

Table 6

	ϕ_T	k_5/k_{8a} (mol/l)	k_5 (sec^{-1})	k_8 (l/mol, sec)	$\frac{k_8\ (cis\text{-2-butene})}{k_8\ (CH_2=CH_2)}$
Nitromethane	0.6	1.7×10^{-2}	3.4×10^6	2×10^8	2.9
Acetone[24]	1.0	6×10^{-2}—6×10^{-4}	1.25×10^6	2×10^7—2×10^9 a)	6.2
Acetaldehyde[25]	0.4	3—6×10^{-3}	6.2×10^5	1—2×10^8	

a) Depending on the amount of excess vibrational energy of triplet sensitizer ($2.5\times10^{10}\exp(-6400/\boldsymbol{RT})$ sec^{-1}).

33) R. J. Cvetanovic and L. C. Doyle, *J. Chem. Phys.*, **37**, 543 (1962).

34) R. E. Rebbert and P. Ausloos, *J. Amer. Chem. Soc.*, **87**, 5569 (1965).

The Resonance Raman Effect of Azobenzene and *p*-Aminoazobenzene

Shiro KOIDE, Yasuo UDAGAWA, Naohiko MIKAMI, Koji KAYA, and Mitsuo ITO
Department of Chemistry, Faculty of Science, Tohoku University, Sendai
(Received July 12, 1972)

The resonance Raman spectra of azobenzene and *p*-aminoazobenzene were measured precisely at various excitation wavelengths. It was found that the π–π^* excited state played a dominant role in the Raman intensities but not the n–π^* excited state and that there was no correlation between the Raman intensity and the absorption coefficient at excitation wavelength.

Resonance Raman effect (RRE) is observed[1,2] when the frequency of Raman exciting light falls in the electronic absorption. One of the characteristic aspects of RRE is enormous enhancement of Raman intensity. In general, aromatic molecule has more than two absorptions in the visible and ultra-violet regions. Thus, it is interesting to see what difference occurs in the intensity enhancement when the excitations are made at different wavelengths which coincide with the absorptions of different electronic transitions of the molecule.

Azobenzene is suitable for such an experiment. It has two different electronic absorption bands centered at 450 and 320 nm (Fig. 1), which are assigned to n-π^* and π–π^* transitions, respectively[3,4]. Moreover, two different lasers whose lasing wavelengths fall in the above absorptions are now available.

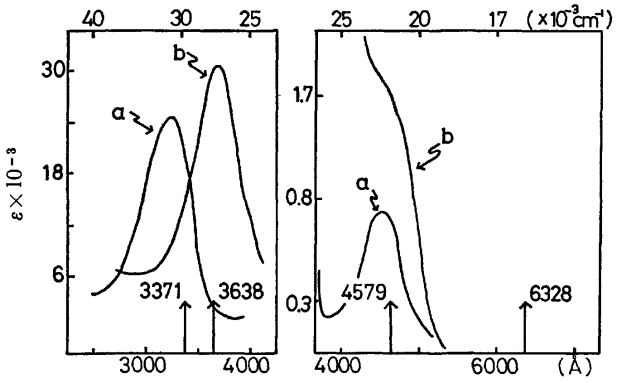

Fig. 1. The electronic absorption spectra of azobenzene and *p*-aminoazobenzene in the visible and ultraviolet regions.
a: Azobenzene in carbon tetrachloride.
b: *p*-Aminoazobenzene in carbon tetrachloride.

The Raman spectra of azobenzene and its derivatives excited by visible Hg lines have been reported by Brandmuller and Hacker,[5] who observed the intensity enchancement of several Raman lines in resonant condition with the n-π^* excited state.

We have studied the wavelength dependence of the Raman intensities of azobenzene and *p*-aminoazobenzene with various kinds of lasers covering from visible to near ultraviolet regions. It was concluded from the results that the excited electronic states corresponding to π–π^* absorptions were primarily important in RRE.

Experimental

Experimental details for taking Raman spectra have been described.[6] The exciting light sources used were a 6328 Å He–Ne laser, a 4579 Å Ar ion laser and a 3371 Å nitrogen pulsed laser. The 3638 Å lasing line of the Ar ion laser was also used.

The sample solution was prepared by dissolving the stock solution of benzene containing known amounts of the sample in an appropriate solvent (carbon tetrachloride or chloroform). Depending on the excitation wavelengths used, the concentration of the solution was so adjusted as to obtain the maximum efficiency. The concentrations appropriate to 6328, 4579, 3638 and 3371 Å excitations are about 10^{-1}, 10^{-4}, 10^{-4} and 10^{-5} mol/*l*, respectively. The intensities of the Raman lines of the sample were determined relative to the 992 cm^{-1} Raman line of benzene which was used as an internal standard for intensity.

The observed intensities of the individual Raman lines should be corrected for absorption of the sample to obtain the original intensities. The correction was made by $I=I_{obs}\times 10^{\varepsilon cx}$, where I is the original Raman intensity, I_{obs} is the intensity observed after passing the sample solution of concentration c and path length x, and ε is the absorption coefficient at the wavelength of the Raman line concerned. x represents the distance between the incident laser beam and the wall of the sample cell through which the Raman scattering is observed. Since c and x were determined from the experimental conditions and ε was also known by the electronic absorption measurement, the original intensity I was determined from I_{obs}. Corrections for the wavelength dependence of the detection system as well as for polarization character of the monochromator were also carried out.

Results and Discussion

The intensities of several main Raman lines of the sample relative to the intensity of the 992 cm^{-1} line of benzene were evaluated from the integrated areas of the individual Raman line of the recorded spectral chart and the corrections described above were made to the observed intensities. The corrected relative intensities normalized for the intensities at 6328 Å excitation are given in Table 1 for various excitation wavelengths. Errors in the values are also listed. The

1) J. Behringer, "Raman Spectroscopy", ed. by H. Szymanski, Plenum Press, New York, (1967) Ch. 6.
2) M. C. Hutley and D. J. Jacobs, *Chem. Phys. Lett.* **6**, 269 (1970).
3) H. H. Jaffe, S. J. Yeh, and R. W. Garner, *J. Mol. Spectrosc.*, **2**, 120 (1958).
2) D. L. Beveridge and H. H. Jaffe, *J. Amer. Chem. Soc.*, **88**, 1948 (1966).
5) a) J. Brandmuller and H. Hacker, *Z. Physik.*, **184**, 14 (1965). b) H. Hacker, *Spectrochim. Acta*, **21**, 1989 (1965).
6) K. Kaya, N. Mikami, Y. Udagawa, and M. Ito, *Chem. Phys. Lett.*, **13**, 221 (1972).

TABLE 1. THE WAVELENGTH DEPENDENCES OF RAMAN INTENSITIES[a)]

Excitation wavelength		6328Å	4579Å	3638Å	3371Å
Azobenzene	1140 cm^{-1}	1	4	30	60
	1182 cm^{-1}	1	6	—[b)]	80
	1440 cm^{-1}	1	4	60	90
p-Amino-azobenzene	1139 cm^{-1}	1	10	100	100
	1184 cm^{-1}	1	9	—[b)]	200
	1422 cm^{-1}	1	20	200	300

a) The corrected relative Raman intensities of azobenzene and *p*-aminoazobenzene are normalized for the intensities at 6328Å excitation. Experimental errors at 4579 Å, 3638Å and 3371Å are ±20%, ±30% and ±30%, respectively.

b) The Raman line around 1180 cm^{-1} at 3638Å excitation is far weaker than the other Raman lines, so that it is not possible to obtain the quantitative value.

errors are due to the low signal to noise ratio and the relatively small magnitude of the signals. In spite of the large errors, the following discussions are possible through repeated measurements. The Raman line of 1440 cm^{-1} of azobenzene as well as the 1422 cm^{-1} line of *p*-aminoazobenzene has been assigned as due mainly to the N=N stretching vibration.[7-9] The vibrational modes of the other Raman lines around 1140 and 1180 cm^{-1} are not well established.

As seen in Table 1, the N=N stretching vibration undergoes more or less stronger enhancement than the other two Raman lines under rigorous resonant conditions (3638 and 3371 Å excitation). This indicates the close connection between the nature of the enhanced vibration and the electronic absorption band (the intramolecular charge transfer from benzene to the N=N group). It is concluded from the measurements at the two excitation wavelengths (3638 and 3371 Å) falling in the same π-π^* transition band that there is no correlation between the enhanced degree of the Raman line and the absorption coefficient at the excitation wavelength. This is clearly seen in the case of azobenzene. The degrees of enhancement differ at most twice in spite of the enormous distinction of the absorption coefficients at the two wavelengths (the molar absorption coefficients are 4.6×10^2 at 3638 Å and 2.0×10^4 at 3371 Å, respectively).

Mortensen[10] reported that the enhanced degree of Raman line was proportional to the square of the absorption coefficient at the excitation wavelength. Kiefer and Bernstein[11] asserted linear proportionality between these two quantities. Our result does not fit with either of these and further consideration is required.

For the RRE in the n-π^* absorption region by 4579 Å excitation, the relative intensities at the 4579 Å excitation (Table 1) do not seem to be as large as expected from the rigorous resonant condition. They seem to be of an order of magnitude anticipated from the preresonance effect contributed from the higher excited state. In order to see this, the wavelength dependences of the relative intensities of the Raman lines of azobenzene were calculated by means of the equation given by Albrecht and Hutley.[12] Assuming only the π-π^* excited state of azobenzene corresponding to the 320 nm absorption to be responsible to the preresonance effect, the relative intensities[13] at 4579 Å excitation were calculated to be about four times the intensity at 6328 Å, in which the wavelength dependence of the reference Raman line of benzene was taken into account by postulating the excited state corresponding to the 180 nm band of benzene as an active intermediate state.[12] The calculated value is of about the same order of magnitude as the observed values given in Table 1. The fairly large observed intensities at 4579 Å excitation for *p*-aminoazobenzene can also be explained by the closer preresonant condition achieved by the shift of the π-π^* absorption toward longer wavelength (the maximum peak of the π-π^* absorption of *p*-aminoazobenzene is located at 370 nm).

Thus it may be concluded qualitatively that the π-π^* excited states of azobenzene and *p*-aminoazobenzene play a dominant role in the Raman intensities but not n-π^* excited state.

7) R. Kubler, W. Luttke and S. Weckherlin, *Z. Elektrochem.*, **64**, 650 (1960).

8) F. X. Powell, E. R. Lippincott and D. Steele, *Spectrochim. Acta.* **17**, 880 (1961).

9) H. W. Schrotter, "Raman Spectroscopy", Plemum Press, New York-London, (1970) Vol. 2, ed. by H. Szymanski, Ch. 3.

10) O. S. Mortensen, *J. Mol. Spectrosc.*, **39**, 48 (1971).

11) W. Kiefer and H. J. Bernstein, *Mol. Phys.* to be published.

12) A. C. Albrecht and M. C. Hutly, *J. Chem. Phys.*, **55**, 4438 (1971).

13) In this case, we considered to totally symmetric vibrational modes and $F_A{}^2$ term. (See Eq. (5′) in Ref. 12)

Characterization of the Geometrical Isomers of the Carbonato(or oxalato)-aminoacidatodiammine Complexes of Cobalt(III)[1]

Kiyoshi NAKAI, Shuji KANAZAWA, and Muraji SHIBATA

Department of Chemistry, Faculty of Science, Kanazawa University, Kanazawa

(Received April 12, 1972)

Three geometrical isomers of the $[CoCO_3(aa)(NH_3)_2]$-type complex (aa stands for the α-alaninate, β-alaninate or valinate ion)—the *mer*(*cis*-diammine)-, *mer*(*trans*-diammine)- and *fac*-isomers—have been prepared. Three similar isomers of the $[Co\ ox(gly)(NH_3)_2]$ and $[Co\ ox(\beta\text{-ala})(NH_3)_2]$ complexes have been obtained by reactions of the corresponding carbonato complexes with an oxalate. In addition, the corresponding three isomers of a related $[Co(gly)(NH_3)_2(OH_2)_2]^{2+}$ complex have been prepared. The isomers thus obtained have been characterized by their absorption, PMR, and IR spectra. Of the *mer*(*trans*) isomers of the present complexes, those of the carbonato-α-alaninato and carbonatovalinato complexes revealed clear shoulders in their second absorption bands. Through the present study, some relationships between the appearance of such a shoulder in the *mer*(*trans*-diammine) isomer and the ring size of chelates have been deduced.

In a previous paper,[2] we reported that three possible geometrical isomers of the $[CoCO_3(gly)(NH_3)_2]$ complex could be isolated from a reaction mixture of the *cis*-$[Co(CO_3)_2(NH_3)_2]^-$ complex with glycine, and that an isomer characterized as the *mer(trans)* form showed an interesting absorption spectrum with a clear shoulder in the second absorption band. Here, *mer(trans)* represents the isomer which has two NH_3 groups in the *trans* positions and three N (or O) atoms in the *cis-trans* positions (Fig. 1).

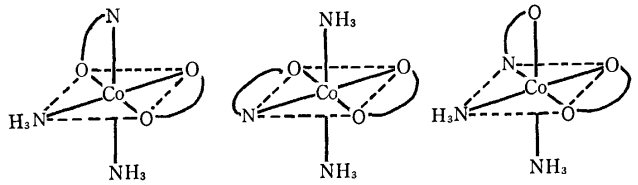

Fig. 1. Possible geometrical isomers.

The present work was first undertaken in order to obtain complexes by using α-alanine, valine, and β-alanine instead of the glycine used in the previous work. Then the work was proceeded in obtaining the related glycinatodiammine and β-alaninatodiammine complexes containing oxalate ion in place of the carbonate ion. In each preparation three geometrical isomers of a desired complex were obtained. In addition, three isomers of the $[Co(gly)(NH_3)_2(OH_2)_2]^{2+}$ complex were obtained through the acid hydrolysis of each isomer of the corresponding carbonato complex.

As to the *mer(trans)* isomers, the absorption spectra of the carbonato-α-alaninato and carbonatovalinato complexes showed a shoulder such as that observed for the previous glycinato complex, while the spectra for the carbonato-β-alaninato, oxalatoglycinato, and oxalato-β-alaninato complexes revealed no shoulder. On the other hand, a shoulder was observed on the shorter-wave-length-side of the first band for the oxalato-β-alaninato and diaquoglycinato complexes.

1) Presented at the 26th Annual Meeting of the Chemical Society of Japan, April 3rd, 1972, Hiratsuka.

2) S. Kanazawa and M. Shibata, This Bulletin, **48**, 2424 (1971).

Experimental

Preparation. The procedure for the preparation of the $[CoCO_3(aa)(NH_3)_2]$-type complexes (where aa stands for the α-alaninate, β-alaninate, or valinate ion) was essentially the same as that for the glycinato complex previously reported.[2] In that preparation of the glycinato complex, the *mer(trans)* isomer was precipitated during the reaction between the *cis*-$[Co(CO_3)_2(NH_3)_2]^-$ and glycine, while no precipitate was obtained in the present preparation. The reacted solution, therefore, was directly chromatographed in order to separate geometrical isomers of a desired complex.

The formation ratio among the three isomers for the carbonato complexes, *mer(cis)* : *mer(trans)* : *fac*, was determined spectrophotometrically with the fractions obtained in chromatographic separation. The results obtained were: 4.4 : 1.0 : 1.5 for the α-alaninato complex, 5.1 : 1.0 : 1.4 for the valinato complex, and 6.0 : 1.0 : 0.6 for the β-alaninato complex.

The $[Co\ ox(gly)(NH_3)_2]$ complex was prepared as follows. To a suspension of the *mer(trans)*-$[CoCO_3(gly)(NH_3)_2]$ complex (1.5 g, 0.005 mol) in water (20 ml), we added 60% perchloric acid (ca. 1 ml) under an iced condition; the mixture was then stirred for about 30 min under the same conditions in order to complete the acid hydrolysis. Then, potassium oxalate (2 g, 0.01 mol) was added to the solution, and it was neutralized with an aqueous solution of potassium hydroxide, whereby potassium perchlorate was precipitated. After the removal of the precipitates by filtration, the filtrate was stirred for 30 minutes at room temperature. The resulting solution was then chromatographed in the same manner as the carbonato complexes. During the addition of water to a column of Dowex 50W-X8 (Na-form), three bands were separated. After each band had been collected in a fraction, the fraction was concentrated and kept in a refrigerator. Very fine crystals were obtained from each concentrate.

The oxalato-β-alaninato complex could be obtained by a similar preparation, using the carbonato-β-alaninato complex as the starting material.

When an isomer of the carbonatoglycinato complex was treated with a saturated solution of oxalic acid, very fine crystals were deposited. This compound was the corresponding isomer of the $[Co(gly)(NH_3)_2(OH_2)_2]^{2+}$ complex.

The results of the elemental analyses for the complexes obtained in the present work are given in Table 1.

Measurements. The absorption, infrared (IR), and

Table 1. The analytical data of the present complexes

Compound	C(%)		H(%)		N(%)	
	Found	Calcd	Found	Calcd	Found	Calcd
mer(*cis*)-$[CoCO_3(\alpha\text{-ala})(NH_3)_2]\cdot H_2O$	18.09	18.54	5.28	5.45	16.09	16.22
mer(*trans*)-$[CoCO_3(\alpha\text{-ala})(NH_3)_2]$	20.36	19.93	5.00	5.00	16.83	17.43
fac-$[CoCO_3(\alpha\text{-ala})(NH_3)_2]$	19.73	19.93	4.94	5.00	17.16	17.43
mer(*cis*)-$[CoCO_3(val)(NH_3)_2]$	26.69	26.77	6.03	6.11	15.46	15.61
mer(*trans*)-$[CoCO_3(val)(NH_3)_2]\cdot 0.5H_2O$	25.85	25.90	5.71	6.17	17.16	17.43
fac-$[CoCO_3(val)(NH_3)_2]$	26.62	26.77	5.91	6.11	15.48	15.61
mer(*cis*)-$[CoCO_3(\beta\text{-ala})(NH_3)_2]$	19.51	19.93	5.15	5.00	17.21	17.43
mer(*trans*)-$[CoCO_3(\beta\text{-ala})(NH_3)_2]\cdot 0.5H_2O$	19.33	19.21	4.96	5.24	17.07	16.80
fac-$[CoCO_3(\beta\text{-ala})NH_3)_2]$	19.67	19.93	5.09	5.00	17.84	17.43
mer(*cis*)-$[Co\ ox(gly)(NH_3)_2]\cdot 2H_2O$	16.63	16.50	4.51	4.86	14.35	14.44
mer(*trans*)-$[Co\ ox(gly)(NH_3)_2]$	18.84	18.83	4.05	3.96	16.55	16.48
fac-$[Co\ ox(gly)(NH_3)_2]\cdot H_2O$	17.93	17.59	4.65	4.44	15.07	15.39
mer(*cis*)-$[Co\ ox(\beta\text{-ala})(NH_3)_2]$	22.86	22.40	4.55	4.14	15.30	15.68
mer(*trans*)-$[Co\ ox(\beta\text{-ala})(NH_3)_2]\cdot 1.5H_2O$	20.67	20.34	5.20	5.13	13.99	14.24
fac$[Co\ ox(\beta\text{-ala})(NH_3)_2]\cdot 1.5H_2O$	20.57	20.34	5.00	5.13	14.26	14.24
mer(*cis*)-$[Co(gly)(NH_3)_2(OH_2)_2]\cdot C_2O_4$	16.77	16.50	4.66	4.87	14.94	14.44
mer(*trans*)-$[Co(gly)(NH_3)_2(OH_2)_2]\cdot C_2O_4\cdot 0.5H_2C_2O_4$	17.72	17.86	4.68	4.51	12.22	12.50
fac-$[Co(gly)(NH_3)_2(OH_2)_2]\cdot C_2O_4\cdot 0.5H_2C_2O_4$	17.90	17.86	4.53	4.51	12.15	12.50

proton magnetic resonance (PMR) spectra were measured with the same instruments as were used in a previous work.[2] Since it had been reported in the previous paper that the geometrical configuration of an isomer of the carbonato complex was retained in the process of acid hydrolysis, the PMR spectra were measured in a mixture of D_2O and D_2SO_4 (1 : 1 v/v), using sodium 3-(trimethylsilyl)-propanesulfonate as the internal or external reference.

Results and Discussion

Characterization of Isomers. The absorption spectra of the three isomers for each complex are shown in Figs. 2—7, while the numerical data are listed in Table 2, in which the data for the known $[CoCO_3(gly)(NH_3)_2]$ complex are also included for the sake of comparison.

In the cases of α-alaninato and valinato complexes, the isomers obtained from the first fractions in

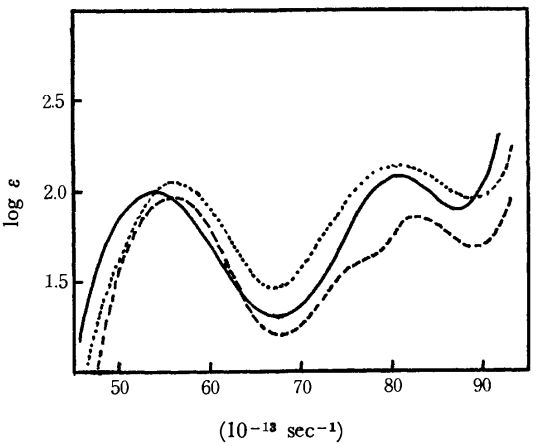

Fig. 3. Absorption spectra of the three isomers of the $[Co(CO_3)(val)(NH_3)_2]$ in $KHCO_3$ aq.
—— *mer*(*cis*), ---- *mer*(*trans*), ···· *fac*

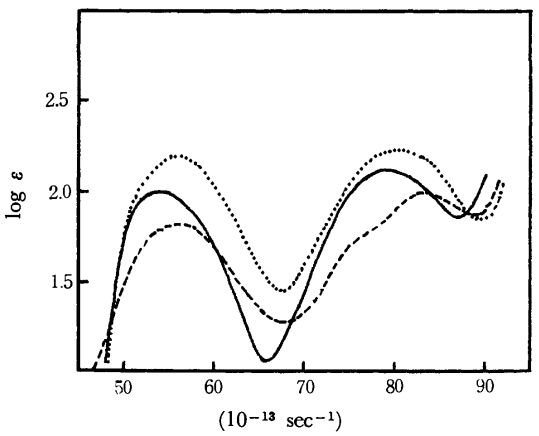

Fig. 2. Absorption spectra of the three isomers of the $[Co(CO_3)(\alpha\text{-ala})(NH_3)_2]$ in $KHCO_3$ aq.
—— *mer*(*cis*), ---- *mer*(*trans*), ···· *fac*

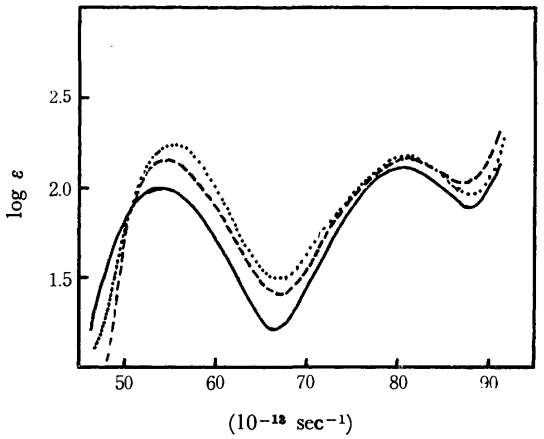

Fig. 4. Absorption spectra of the three isomers of the $[Co(CO_3)(\beta\text{-ala})(NH_3)_2]$ in $KHCO_3$ aq.
—— *mer*(*cis*), ---- *mer*(*trans*), ···· *fac*

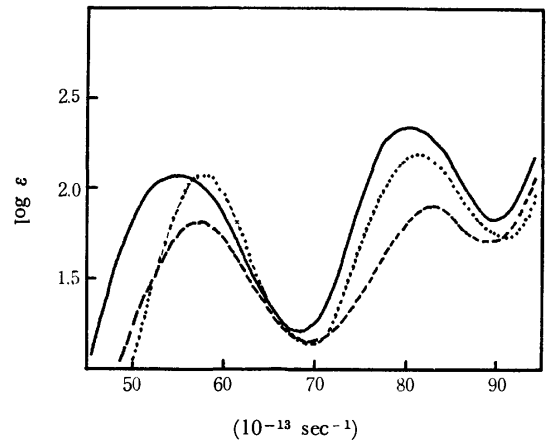

Fig. 5. Absorption spectra of the three isomers of the $[Co(ox)(gly)(NH_3)_2]$ in ca. 10% $HClO_4$.
—— *mer(cis)*, ---- *mer(trans)*, ···· *fac*

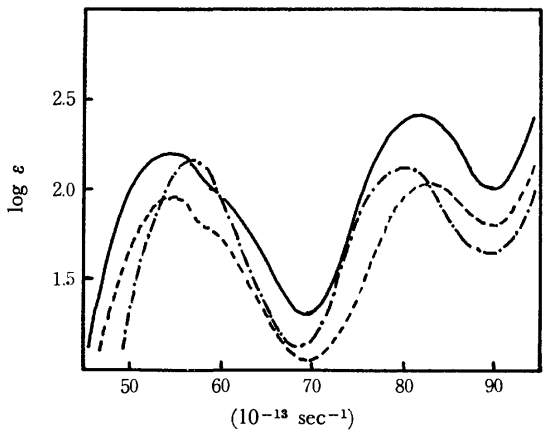

Fig. 6. Absorption spectra of the three isomers of the $[Co(ox)(\beta\text{-ala})(NH_3)_2]$ in *ca.* 10% $HClO_4$.
—— *mer(cis)*, ---- *mer(trans)*, -·-·- *fac*

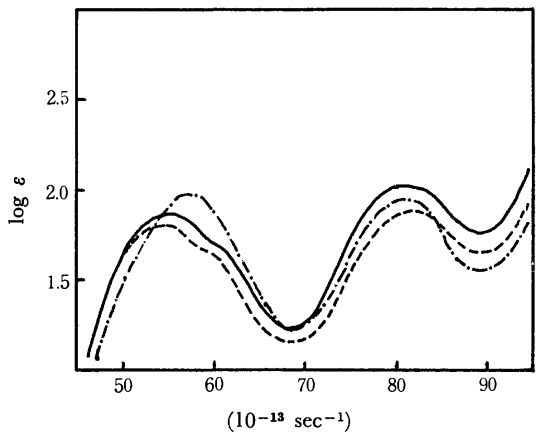

Fig. 7. Absorption spectra of the three isomers of the $[Co(gly)(NH_3)_2(OH_2)_2]^{2+}$ in *ca.* 10% $HClO_4$.
—— *mer(cis)*, ---- *mer(trans)*, -·-·- *fac*

their chromatographic separations exhibit absorption spectra very similar to that for the *mer(cis)* isomer of the glycinato complex. The same situation holds between the isomers of the third fractions of the present complexes and the *fac* isomer of the glycinato complex. Each spectrum for the isomers of the second fractions

TABLE 2. THE SPECTRAL DATA OF THE PRESENT COMPLEXES

Compound	ν_1[a] (log ε)	Half width (ν_1)	ν_2[a] (log ε)
mer(cis) Isomers			
$[CoCO_3(\alpha\text{-ala})(NH_3)_2]$	54.5 (1.97)	17.7	79.3 (2.11)
$[CoCO_3(val)(NH_3)_2]$	54.0 (1.97)	13.6	80.3 (2.08)
$[CoCO_3(gly)(NH_3)_2]$	54.2 (2.13)	12.5	79.5 (2.25)
$[CoCO_3(\beta\text{-ala})(NH_3)_2]$	54.0 (1.99)	11.7	80.0 (2.10)
$[Co\ ox(gly)(NH_3)_2]$	54.8 (2.06)	12.0	80.0 (2.34)
$[Co\ ox(\beta\text{-ala})(NH_3)_2]$	54.5 (2.18)	12.8	81.0 (2.39)
	ca. 60 sh		
$[Co(gly)(NH_3)_2(OH_2)_2]^{2+}$	55.8 (1.85)	13.0	80.8 (2.02)
	ca. 60 sh		
mer(trans)-Isomers			
$[CoCO_3(\alpha\text{-ala})(NH_3)_2]$	56.5 (2.00)	11.0	72.5 sh
			82.0 (2.04)
$[CoCO_3(val)(NH_3)_2]$	56.3 (1.90)	11.8	72.0 sh
			82.0 (1.80)
$[CoCO_3(gly)(NH_3)_2]$	56.0 (1.93)	11.2	72.0 sh
			81.8 (1.85)
$[CoCO_3(\beta\text{-ala})(NH_3)_2]$	54.8 (2.11)	11.0	80.5 (2.15)
$[Co\ ox(gly)(NH_3)_2]$	56.5 (1.78)	13.4	82.0 (1.88)
$[Co\ ox(\beta\text{-ala})(NH_3)_2]$	53.8 (1.94)	10.4	81.5 (2.04)
	ca. 60 sh		
$[Co(gly)(NH_3)_2(OH_2)_2]^{2+}$	54.0 (1.79)	13.3	82.8 (1.83)
	ca. 59 sh		
fac-Isomers			
$[CoCO_3(\alpha\text{-ala})(NH_3)_2]$	56.2 (2.15)	11.2	81.2 (2.20)
$[CoCO_3(val)(NH_3)_2]$	56.2 (2.04)	11.0	80.8 (2.13)
$[CoCO_3(gly)NH_3)_2]$	56.2 (2.16)	10.0	80.1 (2.22)
$[CoCO_3(\beta\text{-ala})(NH_3)_2]$	55.8 (2.17)	10.2	80.0 (2.18)
$[Co\ ox(gly)(NH_3)_2]$	57.0 (2.06)	9.5	81.0 (2.21)
$[Co\ ox(\beta\text{-ala})(NH_3)_2]$	57.0 (2.13)	9.4	80.0 (2.12)
$[Co(gly)(NH_3)_2(OH_2)_2]^{2+}$	57.5 (1.96)	12.0	81.0 (1.93)

a) $\times 10^{13}\ sec^{-1}$

clearly shows a shoulder in the second absorption band, similar to the spectrum for the *mer(trans)* isomer of the glycinato complex. However, the intensity of the second band of the α-alaninato complex is rather larger than that of the first band, contrary to the cases of the corresponding isomers of the glycinato and valinato complexes (Figs. 2 and 3). From these similarities in absorption spectra, *mer(cis)*, *mer(trans)*, and *fac* structures (Fig. 1) could be assigned to the isomers isolated, according to the order of elution.

For the carbonato-β-alaninato complex, the *mer* and *fac* assignments to the isomers can easily be done from the shapes of the first absorption bands, but *cis* and *trans* assignments for the two *mer*-isomers are difficult because their spectra resemble each other very much (Fig. 4). However, from the order of elution, it may be assumed that the *mer(cis)* isomer is the compound obtained from the first fraction. Further confirmation is provided by PMR spectral studies to be described later.

As to the oxalatoglycinatodiammine complex, the isomer obtained from the second fraction shows its first and second absorption maxima at considerably shorter wavelengths compared with the isomer obtained from the first fraction (Fig. 5). Apart from the

disappearance of a shoulder, this hypsochromic shift of the absorption bands in the former isomer corresponds well to that in the *mer(trans)* isomers of the carbonato-α-aminoacidato complexes. Thus, the *mer* isomer of the second fraction may be regarded as the *mer(trans)* isomer.

As to the oxalato-β-alaninato complex, the two *mer* isomers show similar spectra; it is impossible to determine their geometrical configurations by means of the electronic spectra (Fig. 6). Therefore, the confirmation is based on the PMR spectral data.

In the previous paper, it was reported that the configuration of each isomer of the carbonatoglycinato complex was retained during acid hydrolysis. The electronic spectrum of each isomer of the aquo complex isolated as an oxalate in the present work is consistent with the previous observation (Fig. 7).[2)]

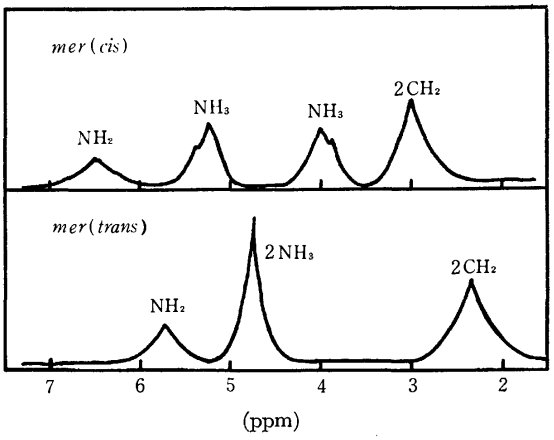

Fig. 8. PMR spectra of the *mer*-isomers of the $[Co(CO_3)(\beta\text{-ala})(NH_3)_2]$ in D_2O/D_2SO_4.

The PMR spectra of the two *mer* isomers of the carbonato-β-alaninato complex are shown in Fig. 8. The isomer tentatively identified as the *cis* isomer, based on the order of elution, shows four peaks, at 6.5, 5.3, 4.0, and 3.0 ppm, with an integrated ratio of ca. 2 : 3 : 3 : 4. As is indicated in the figure, this ratio corresponds to the NH_2 group of the chelated β-alaninate, the two NH_3 groups in different environments, and the two CH_2 groups of the β-alaninate undistinguishable from each other. On the other hand, the isomer assigned tentatively to the *trans* isomer shows three peaks, at 5.7, 4.8, and 2.7 ppm, with a ratio of ca. 2 : 6 : 4. This ratio corresponds to the NH_2 group, the two NH_3 groups in equivalent environments, and the two CH_2 groups respectively. From these results, the previous assignments are now ascertained.

The PMR spectra of the two *mer*-isomers of the oxalatoglycinato complex are shown in Fig. 9. The spectrum of the isomer assumed to be *cis* exhibits four peaks; the one observed at 5.7 ppm is due to the NH_2 group of the chelated glycinate, while the other three peaks, close together between 3.5 and 4.5 ppm, are due to the complexed NH_3 groups and the CH_2 group of the glycinate. The integrated ratio of these peaks is estimated to be ca. 2 : 3 : 2 : 3, ranging from lower to higher fields. Provided that the two peaks at 4.3

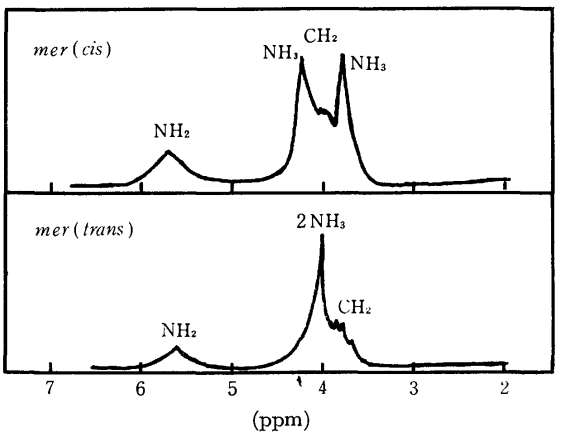

Fig. 9. PMR spectra of the *mer*-isomers of the $[Co(ox)(gly)(NH_3)_2]$ in D_2O/D_2SO_4.

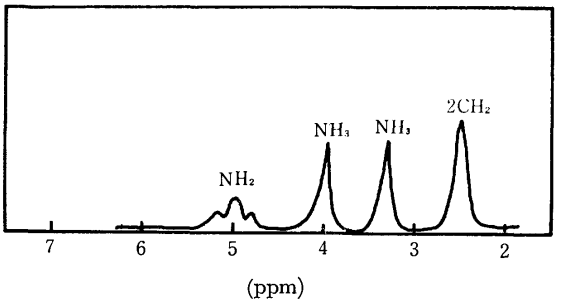

Fig. 10. PMR spectrum of the *mer(cis)*-$[Co(ox)(\beta\text{-ala})(NH_3)_2]$.

and 3.8 ppm are due to the NH_3 groups in different environments, the above ratio corresponds to the proton numbers concerned. Thus, the PMR results also support the assignment of the *cis* configuration to this isomer. On the other hand, the spectrum of the other *mer* isomer exhibits three peaks, at 5.6, 4.0, and 3.8 ppm, with a ratio of ca. 2 : 6 : 2. Since the middle peak, with the highest value, is attributable to the two NH_3 groups in equivalent situations, the *mer(trans)* configuration is assigned to this isomer.

The PMR spectrum of the *mer*-isomer of the oxalato-β-alaninato complex obtained from the first fraction is shown in Fig. 10. The isomer exhibits four peaks, at 5.2, 4.0, 3.3, and 2.5 ppm, with a ratio of ca. 2 : 3 : 3 : 4. This result suggests that the two coordinated NH_3 groups are in different environments and that, therefore, this isomer may be assigned the *mer(cis)* configuration. Though the PMR spectrum of the other *mer*-isomer was not measured, it is certain from the above-mentioned analogue of the configurational determination that this isomer has the *mer(trans)* configuration.

The PMR spectrum of each isomer for the present diaquo complex is essentially the same as that in the previous work.[2)]

The evidence for the chelation of a carbonate ion in the β-alaninato complex was supported by the IR spectral data—that is, by the observation of the bands near 1600 (ν_s(C=O)), 1270 (ν_s(C-O)+δ(O-C=O)), 1030 (ν_s(C-O)), and 760 cm^{-1} (in-plane def. of

CO_3^{2-}).[3] The evidence for the chelation of an oxalate ion in the oxalato complexes was also supported by the observation of characteristic bands at 1710 and 1680 (ν_{as}(C=O)), 900 (ν_s(C–O)+δ(O–C=O)), 1400 (ν_s(C–O)+ν(C–C)), and 1260 cm^{-1} (ν_s(C–O)+δ(O–C=O)).[3] In the IR spectra of the aquo-complex, the existence of an oxalate ion as the counterion was also supported by the absorption near 1700 cm^{-1}; the band of oxalic acid of crystallization is also observed in this region.

Mer(trans) *Isomers.* As has been mentioned in the foregoing discussion, the absorption spectra of the *mer(trans)* isomers for the α-alaninato and valinato complexes, like that for the glycinato complex, show shoulders in their second absorption bands. A similar shoulder in the second absorption band has been found in a few complexes: Jørgensen[4] cited the spectra for the [Co edta(OH)]$^{2-}$ and [Cr edta(OH)]$^{2-}$ species. Furlani *et al.*[5] stated that such effects upon the second absorption band for the [Cr edta(OH)]$^{2-}$ species could be due to a lower symmetry caused by a distortion of the octahedron. Emmenegger and Schwarzenbach[6] reported a similar splitting in the spectrum of the [Co penten(OH)]$^{2+}$ complex (penten=*N,N,N',N'-tetrakis*(α-aminoethyl)ethylenediamine). Recently, Igi *et al.*[7] have reported that the second absorption bands for the [Co(guH)(en)$_2$]$^{3+}$ and [Co(gu)(en)$_2$]$^{2+}$ complexes (guH stands for a guanylurea) split into two components.

It should be noticed that even though the second absorption band exhibits a remarkable splitting for the present *mer(trans)* isomer, the first absorption band shows nothing remarkable. In addition, it is a noteworthy fact that the half-width of the first band for the *mer(trans)* isomer of a carbonato-α-aminoacidato complex is less than that for the *mer(cis)* isomer of the same complex (Table 1).

For the *mer(trans)* isomer of the carbonato-β-alaninato complex, both the first and second absorption maxima are at considerably lower wavelengths than those for the same isomer of a carbonato-α-aminoacidato complex. Moreover, no shoulder is found in the second band region for this isomer of the β-alaninato complex.

When the absorption spectral data are compared between the *mer(trans)* isomers of the carbonatoglycinato and oxalatoglycinato complexes, their maxima are at almost the same positions, though the carbonato ligand lies in a lower position in the spectrochemical series than the oxalato ligand, and no shoulder is observed for the isomer of the oxalato complex. When the same comparison is made between the *mer(cis)* and *mer(trans)* isomers of the oxalato complex, a considerable hypsochromic shift is observed in the latter isomer. This feature is the same as in the case of the corresponding carbonato complex.

As to the absorption spectrum of the *mer(trans)* isomer of the oxalato-β-alaninato complex, both the first and second bands are observed at rather longer wavelengths than those of the corresponding oxalatoglycinato complex, and a shoulder appears in the shorter wavelength-side of the first absorption band. Comparing this spectrum with that of the *mer(cis)* isomer, both the first and second bands are observed at almost the same positions.

From an X-ray study of the $[CoCO_3(NH_3)_4]^+$ complex,[8] it has been pointed out that the bond lengths between the complexed NH_3 groups lying at the *trans* positions to the carbonate chelate and the central cobalt are longer than those between the other NH_3 groups lying at the *cis* positions, and that the ∠NCoN with N atoms of the NH_3 groups in the *trans* positions is larger than the other N–Co–N angles. Thus, we can now expect that the two NH_3 groups lying at the *trans* positions to the carbonate chelate behave as weaker ligands than the NH_3 groups at the *cis* positions. Moreover, such an effect will more strongly appear when a rigid five-membered chelate ring is in a co-plane with the carbonate chelate ring. Thus, it can be expected in regard to the present carbonato-α-aminoacidato complex, that the α-aminoacidate chelate lying on a co-plane with the carbonate chelate behaves as a somewhat weaker ligand than the same chelate forming a spiral with the carbonate chelate. The remarkable differences in absorption spectrum between a *mer(trans)* and the corresponding *mer(cis)* isomer may be related to the different effects of the carbonate chelates upon the α-aminoacidate chelates. The absorption spectrum of the *mer(cis)* isomer of a carbonato-α-amino acidato complex can be understood with the aid of a ligand field theory, such as in Yamatera's prediction,[9] but the spectrum of the *mer(trans)* isomer of the same complex can not be interpreted at present.

As a result of the present work, we can say the following thing: 1) An octahedral cobalt(III) complex consisting of a five-membered α-aminoacidate ring, two ammonia groups in *trans* positions, and a four-membered carbonate ring reveals a shoulder which is considered to be one component of the split second absorption band, while, when the five-membered aminoacidate ring is replaced by a six-membered one, or when the four-membered carbonate ring is replaced by a five-membered oxalate ring, no such shoulder appears. 2) The half-width of the first absorption band of the *mer(trans)* is less than that of the *mer(cis)* isomer for a carbonato-α-aminoacidato complex. 3) A *mer(trans)* isomer containing a five-membered aminoacidate and a carbonate or an oxalate chelate ring shows its first and second absorption maxima at shorter wavelengths than the *mer(cis)* isomer of the same complex.

3) K. Nakamoto, "Infrared Spectra of Inorganic Coordination Compounds," John Wiley and Sons Inc., New York (1966).
4) C. K. Jørgensen, *Acta. Chem. Scand.*, **9**, 1362 (1955).
5) C. Furlani, G. Morpurgo, and G. Sartori, *Z. Anorg. Allg. Chem.*, **363**, 1 (1960).
6) F. P. Emmenegger and G. Schwarzenbach, *Helv. Chim. Acta*, **99**, 625 (1966).
7) K. Igi, T. Yasui, J. Hidaka, and Y. Shimura, This Bulletin **44**, 426 (1971).
8) G. A. Barclay and B. F. Haskins, *J. Chem. Soc.*, **1962**, 586.
9) H. Yamatera, This Bulletin, **31**, 95 (1958).

Determination of the Stability Constants of the Bis(selenocyanato)mercury(II) and Tris(selenocyanato)mercurate(II) Complexes by a Polarographic Method

Teisuke MURAYAMA and Akio TAKAYANAGI

Department of Industrial Chemistry, Faculty of Engineering, Shizuoka University, Hamamatsu

(Received May 1, 1972)

Selenocyanate ions give an anodic polarographic wave with a half-wave potential of 0.033 V (*vs.* SCE) at 25°C and 0.044 V at 35°C for a 1 mM solution. The electrode process is: $Hg \rightleftarrows Hg^{2+} + 2e$, $Hg^{2+} + 2SeCN^- \rightleftarrows Hg(SeCN)_2$, $Hg^{2+} + 3SeCN^- \rightleftarrows Hg(SeCN)_3^-$. By means of an equation which gives the relation between the anodic current and electrode potential, stability constants of the bis(selenocyanato)mercury(II) and tris(selenocyanato)-mercurate(II) complexes (β_2 and β_3, respectively) were calculated from the polarograms. Values of log β_2 and log β_3 at ionic strength 0.3 are, respectively, 21.4_3 and 25.6_6 at 25°C, and 20.4_4 and 24.4_8 at 35°C.

We reported in previous papers on the determination of stability constants of mercuric cyanide, the tri- and tetra-cyanomercurate(II) ions, and the tris(thiosulfato)mercurate(II) ion by a polarographic method.[1,2] This paper describes the determination of stability constants of the bis(selenocyanato)mercury(II) and tris(selenocyanato)mercurate(II) complexes by the same method. The constant of the tris complex was given by Toropova,[3] but that of the bis complex does not seem to have been reported.

Experimental

Commercial potassium selenocyanate (Koso Kagaku-Yakuhin) was used without purification. The concentration of the potassium selenocyanate stock solution was determined by argentometric titration.[4]

The stock solution of mercuric chloride was prepared by dissolving a weighed amount of the reagent of guaranteed grade.

The supporting electrolyte was 0.3 M potassium nitrate. For the amperometric titration of mercuric chloride, 0.002% Triton X-100 was added as a maximum suppressor.

All solutions were prepared with redistilled water.

The dropping mercury electrode had the following characteristics (in 0.3 M potassium nitrate solution at zero applied potential *vs.* SCE and at 25°C): the rate of flow of mercury (m), 1.978 mg/sec; the drop time (τ), 4.13 sec; $m^{2/3}\tau^{1/6} = 2.00$.

The cell and the salt bridge were described previously.[2] To prevent interaction between the oxidation product and the mercury accumulated on the bottom of the cell, it was necessary to start measurements of the anodic wave as soon as the dropping mercury electrode was introduced into test solutions which had been degassed with nitrogen. The measurements were made at 25.0 and 35.0±0.1°C. All potentials were corrected for the internal resistance (*iR* drop) across the cell.

Polarograms were measured by a Yanagimoto PA-102 polarograph operated manually. The bridge of the polarograph was calibrated by a precise potentiometer.

Results and Discussion

Fig. 1 shows anodic waves of the selenocyanate ion. The half-wave potential is 0.033 V *vs.* SCE at 25°C and 0.044 V at 35°C when the concentration of selenocyanate ions is 1 mM. The limiting current measured at a potential of 0.300 V *vs.* SCE is directly proportional to the concentration of selenocyanate ions, as shown in Fig. 2. The temperature coefficient of the limiting current is 1.2%.

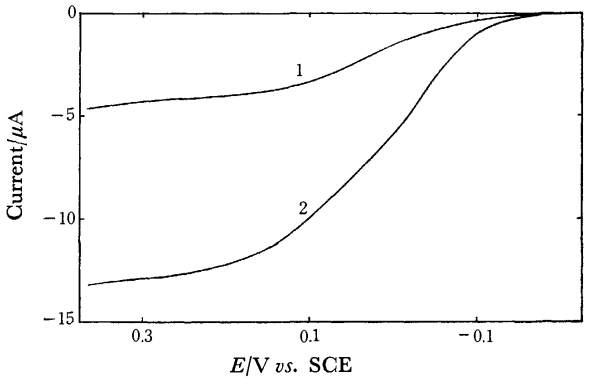

Fig. 1. Polarograms of the selenocyanate ion at 25°C. Corrected for the residual current. Supporting electrolyte, 0.3 M potassium nitrate. Concentration of potassium selenocyanate: 1; 1.142 mM, 2; 3.42_6 mM.

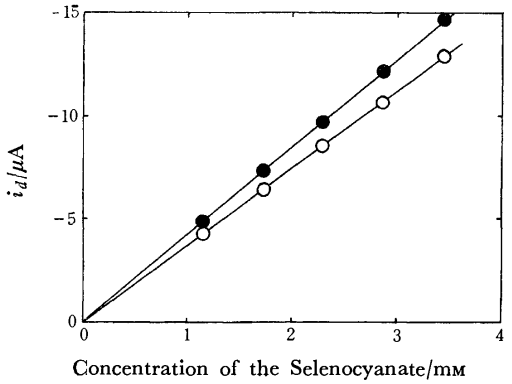

Fig. 2. Dependence of the diffusion current on the concentration of the selenocyanate. Temperature: ○; 25°C, ●; 35°C.

By analogy with other anodic processes in which mercuric complexes are produced,[1,2,5] the overall electrode process of the selenocyanate ion may be

1) T. Murayama, *Sci. Rep. Tohoku Univ., Series I*, **45**, 84 (1961).

2) T. Murayama, T. Sawaki, and S. Sakuraba, This Bulletin, **43**, 2820 (1970).

3) V. F. Toropova, *Zhur. Neorg. Kihm.*, **1**, 243 (1956); *Chem. Abst.*, **51**, 4192i (1957).

4) I. M. Kolthoff and V. A. Stenger, "Volumetric Analysis," Vol. II, Interscience Publishers, New York, N. Y. (1947), p. 280.

5) N. Tanaka, K. Ebata, and T. Murayama, This Bulletin, **35**, 124 (1962).

considered to be composed of an electron transfer step

$$Hg = Hg^{2+} + 2e \quad (1)$$

and complex formation reactions:

$$Hg^{2+} + 2SeCN^- = Hg(SeCN)_2 \quad (2)$$

$$Hg^{2+} + 3SeCN^- = Hg(SeCN)_3^- \quad (3)$$

Reactions (1), (2), and (3) are assumed to be reversible. The formation of $Hg(SeCN)_4^{2-}$ and higher complexes are not considered here, because the polarographic behavior of the anodic wave is fully explained with reactions (1), (2), and (3) as shown in the following.

The potential E of the dropping mercury electrode is given by

$$E = E^0 + \frac{2.303RT}{2F}\log\frac{2\gamma_1\kappa_4}{\beta_2\kappa_2} + \frac{2.303RT}{2F}\log\frac{10^{-3}y}{(1+rx)x^2} + \frac{6.909RT}{2F} \quad (4)$$

where E^0 is the standard potential of mercuric-mercury electrode, R the gas constant, T the absolute temperature, F the Faraday constant, γ_1 the activity coefficient of the mercuric ion, β_2 the stability constant of the bis(selenocyanato)mercury(II) complex, κ_2 the Ilkovič constant for the same complex, κ_4 the Ilkovič constant for the selenocyanate ion, x the concentration of selenocyanate ions at the surface of the dropping mercury electrode, and

$$r = \frac{\beta_3\kappa_3}{\beta_2\kappa_2} \quad (5)$$

$$y = \frac{i}{2\kappa_4} \quad (6)$$

Here β_3 and κ_3 are, respectively, the stability and Ilkovic constants of the tris(selenocyanato)mercurate-(II) ion, and i is the anodic current. The value of x is calculated by

$$x = \frac{r(x_0-3y)-1+\sqrt{r^2(x_0-3y)^2+2r(x_0-y)+1}}{2r} \quad (7)$$

where $x_0 = i_d/\kappa_4$.[2] The value of κ_4 is 3.75 μA/mM at 25°C and 4.22 μA/mM at 35°C.

If the correct value of r is used, the logarithmic plot construced according to Eq. (4) should produce a straight line with a reciprocal slope equal to 2.303 $RT/(2F)$. By the method of trial and error the best value of r was determined to be 1.7×10^4 at 25°C, and 1.1×10^4 at 35°C. Figure 3 shows the logarithmic plot constructed from polarograms observed at 25°C. Table 1 shows the reciprocal slope of the plot constructed with these values of r and the potential e_0 where $\log 10^{-3}y(1+rx)^{-1}x^{-2}$ becomes zero. Fair agreement among the values in the respective columns is considered as evidence in support of the assumption that reactions (1), (2), and (3) are responsible for the anodic wave and that $Hg(SeCN)_4^{2-}$ and higher complexes do not participate.

Values of β_2 and β_3 can be calculated from r and e_0, if E^0, γ_1, κ_2, and κ_3 are known. The standard electrode potential E^0 at 25°C was given as 0.8500 V *vs.* SHE (=0.6056 V *vs.* SCE) by Hietanen and Sillén.[6]

6) S. Hietanen and L. G. Sillén, *Arkiv Kemi*, **10**, 103 (1956).

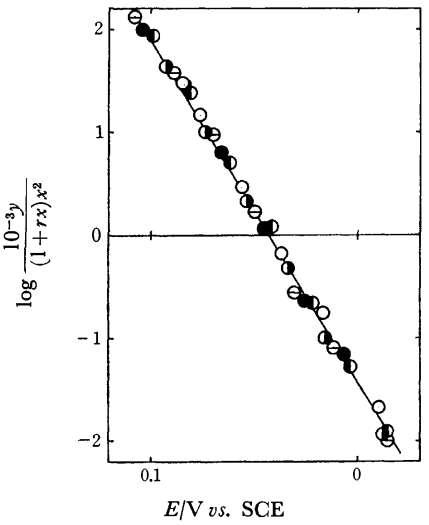

Fig. 3. Relation of $\log 10^{-3}y(1+rx)^{-1}x^{-2}$ *vs.* E at 25°C. $r=1.7\times10^4$. Concentration of the selenocyanate: ○; 1.142 mM, ●; 1.713 mM, ◑; 2.28_4 mM, ◐; 2.85_5 mM, ⊖; 3.42_6 mM.

TABLE 1. RECIPROCAL SLOPES OF LOGARITHMIC PLOTS CONSTRUCTED ACCORDING TO Eq. (4)

Concentration of the selenocyanate mM	Reciprocal slope mV	e_0[a] *vs.* SCE V
Temperature, 25°C; r=1.7×10⁴		
1.142	30	0.041
1.713	30	0.042
2.28_4	30	0.044
2.85_5	30	0.041
3.42_6	29	0.044
	average	0.042
Temperature, 35°C; r=1.1×10⁴		
1.142	31	0.050
1.713	31	0.051
2.28_4	31	0.050
2.85_5	30	0.053
3.42_6	30	0.051
	average	0.051

a) The potential where $\log 10^{-3}y(1+rx)^{-1}x^{-2}$ becomes zero.

The value at 35°C was calculated to be 0.6040 V *vs.* SCE from this and the entropy change of reaction (1) at 25°C.[7]

The activity coefficient of the mercuric ion was estimated through the Debye and Hückel equation without the extended term.[8]

$$\log\gamma_i = -\frac{Az_i^2(2I)^{1/2}}{1+Ba_i(2I)^{1/2}} \quad (8)$$

7) W. M. Latimer, "Oxidation Potentials," Prentice-Hall, New York, N. Y. (1952), p. 30 and p. 176.

8) G. N. Lewis, M. Randall, K. S. Pitzer, and L. Brewer, "Thermodynamics," McGraw-Hill Book Co., New York, N. Y. (1961), p. 344.

In this equation γ_i, z_i, and a_i are the activity coefficient, the charge number, and the ionic size parameter, respectively, of the ion i, I is the ionic strength of the solution, and A and B are constants at a given temperature.[9] The value of a_i was assumed to be 5 Å for the mercuric ion.[10] The value of γ_1 was calculated to be 0.261 at 25°C and 0.255 at 35°C.

For the determination of κ_2 and κ_3, 25 m*l* of 0.260 mM mercuric chloride was titrated amperometrically with 11.42 mM potassium selenocyanate at a potential of −0.50 V *vs.* SCE. Figure 4 shows the titration curves. At first an approximate value of β_2 was estimated to be $10^{21.8}$ from Eq. (4) by introduction of the average value of e_0 at 25°C and of an approximate relation $\kappa_2=2\kappa_4$. From this and stability constants of chloro complexes of mercury(II),[11] it was concluded that the formation of the bis(selenocyanato)mercury(II) complex is quantitative if the total concentration of the selenocyanate is below 0.52 mM. The same holds at 35°C. Hence, 99% of the total mercury in the solution exists as bis(selenocyanato)mercury(II) when 1.13 m*l* of 11.42 mM potassium selenocyanate solution is added. From the diffusion current observed in the solution of this composition, the value of κ_2 was calculated to be 8.38 μA/mM at 25°C and 9.85 μA/mM at 35°C. Further addition of the selenocyanate causes little change in the diffusion current. This indicates that κ_3 is nearly equal to κ_2. In the following the ratio κ_3/κ_2 is assumed to be equal to unity. (At 35°C the ratio is not exactly equal to unity, but the discrepancy does not alter the result).

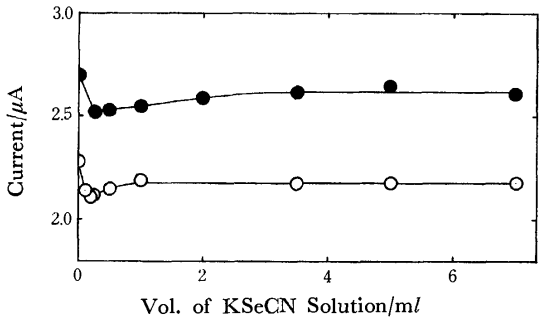

Fig. 4. Titration of 25 m*l* of 0.260 mM mercuric chloride with 11.42 mM potassium selenocyanate. Titrated at $E=-0.50$ V *vs.* SCE. Temperature: ○; 25°C, ●; 35°C.

By introduction of e_0 and other values given in the above into Eq. (4), the exact value of log β_2 was calculated to be 21.4_3 at 25°C and 20.4_4 at 35°C. From r, log β_2, and the relation $\kappa_3/\kappa_2=1$, the value of log β_3 was found to be 25.6_6 at 25°C and 24.4_8 at 35°C. Toropova gave 26.40 for log β_3 at 25°C.[3] Her value is greater than the value given in this study by about 0.7, the reason being not clear at present.

9) G. Kortüm and J. O'M. Bockris, "Textbook of Electrochemistry," Vol. II, Elsevier Publishing Co., Amsterdam (1951), p. 645.

10) J. Kielland, *J. Amer. Chem. Soc.*, **59**, 1675 (1937).

11) B. Lindgren, A. Jonsson, and L. G. Sillén, *Acta Chem. Scand.*, **1**, 475 (1947); *Chem. Abst.*, **42**, 2161 g (1948). Stability constants at 35°C were calculated from values at 25°C and enthalpy data given in the following: P. K. Gallagher and E. L. King, *J. Amer. Chem. Soc.*, **82**, 3510 (1960).

BULLETIN OF THE CHEMICAL SOCEITY OF JAPAN, VOL. 45, 3551—3555 (1972)

Mass Spectrometry of 1-Phenylazo-2-naphthols

Kousuke KOBAYASHI, Kenji KURIHARA, and Kazutoyo HIROSE
Dai-Nippon Ink Institute of Chemical Research, Kamikizaki, Urawa-shi, Saitama

(Received January 14, 1972)

In order to examine the azo-hydrazone tautomerism of substituted 1-phenylazo-2-naphthols and to estimate the effect of substituents on the equilibrium, mono-substituted 1-phenylazo-2-naphthols were synthesized and the spectra were compared with those of the respective acetylated derivatives and β-naphthoquinone-methylphenylhydrazone as references of the azo and hydrazone forms respectively. The spectra of acetylated derivatives show the same pattern as those of the original samples except for the molecular ion and ion at *m/e*: 43. Moreover, β-naphthoquinone-methylphenylhydrazone displays a different fragmentation process, the cleavage of the N–N bond. In conclusion, the substituted 1-phenylazo-2-naphthols exist in the gaseous state as only the azo form; this is different from the results in the liquid and solid states. The fragmentation processes, in which the reactions of $M^+ \rightarrow (m/e: 171)^+ \rightarrow (m/e: 143)^+ \rightarrow (m/e: 115)^+$ mainly occur, are clarified on the basis of these results. The effect of substituents on the reaction rate of the formation of ions at *m/e*: 171 from molecular ions is examined. The correlation with the Hammett σ constants is $\rho = 0.078$ for meta substituents, and the plots for para substituents lie under the line, which means that the reaction rate for para substituents is slow. This is explained on the basis of the resonance effect.

Many studies have been carried out in an attempt elucidate the structure of 1-phenylazo-2-naphthols (PAN), which may exist as a true azo form (I) or as a hydrazone form (II).[1)]

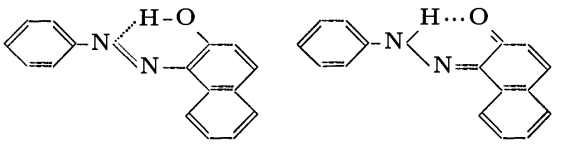

(I) (II)

1) H. Zollinger, "Azo and Diazo Chemistry," Interscience, New York (1961), p. 322.

Over thirty years ago, Hendricks and his co-workers[2] and Kuhn[3] discussed how they exist as a resonance hybride or a tautomeric mixture. Later Burawoy and his co-workers, based on the electronic spectra in various solvents, clearly demonstrated that they exist in solution as tautomeric equilibria.[4] Further evidence for the presence of tautomerism in both solid and solution of PAN has been provided by many techniques, such as measurements of the electronic spectra,[5-8] the infrared spectra,[9] the chemical shift of ^{14}N in NMR,[10] the diamagnetic susceptibility,[11] and the fluorescence.[12] Recently Bansho and his co-workers[7] studied these phenomena quantitatively, and concluded that 50—70% of the molecules exist as the hydrazone form whatever the state, a solid in KBr disk or a solution in a polar (ethanol) or non-polar solvent (cyclohexane), by a comparison of the extinctions in the regions of 410—420 mμ and 480—500 mμ. They also pointed out that there is no linear relation between the percentage of the hydrazone form and the Hammett σ constants.

Unfortunately, the tautomeric equilibria of PAN in the gaseous state have not been studied. Recently, it has become apparent that no keto-enol tautomerism takes place after electron bombardment in a mass spectrometer.[13] Thus, we tried to elucidate the tautomeric equilibria in the gaseous state and the effect of substituents by using a mass spectrometer.

Experimental

Measurement of the Mass Spectra. The spectra were obtained by the use of a JMS-01SG double-focusing mass spectrometer (Japan Electron Optics Laboratory Co., Ltd.). Using 75 eV electrons at a regulated emission current of 200 μA, all the experiments were made by the electrical detection method under low resolution conditions, several samples were also examined by the photo-plate detection method under high resolution conitions (*ca.* 20000) in order to confirm the elemental compositions. Samples were introduced through the direct sample inlet system under the condition of an ion-source temperature of 200—210°C and a sample-vaporizing temperature of 50—110°C (selected for each sample). The metastable ion was detected by the accelerating-voltage-scan method.[14] The pattern coefficients were measured at the maximum of the beam current by using a rapid scan to avoid any change in the ion beam.

Samples. The samples used were 15 PAN (Table 1), 7 PAN acetates (Table 2), and β-naphthoquinonemethylphenylhydrazone (NQH). The PAN were synthesized by the usual coupling reaction between β-naphthol and substituted anilines, were purified three times by recrystallization, and were confirmed by studying the melting point and the mass spectrum. The PAN acetates were synthesized by the usual acetylation of PAN using pyridine and acetic anhydride. They were also purified and confirmed in the same manner. NQH was synthesized by a reaction of β-

Table 1. PAN and their pattern coefficients[a]

Sample No.	Substituents	Melting point °C	Relative Intensities						
			$M^{+\cdot}$	$(M-1)^+$	*m/e* : 171	*m/e* : 143	*m/e* : 115	Ph-X$^+$	Sp$^+$ (*m/e*)[b]
PAN- 1	H	134	82.8	11.1	24.7	100	59.4	42.7	13.3 (51)
2	*o*-NO_2	206	41.8	0.1	27.6	100	47.2	—	21.8 (276)
3	*m*-NO_2	193	65.6	7.2	25.2	100	59.8	—	—
4	*p*-NO_2	246	100	5.4	21.7	99.9	53.2	6.3	—
5	*o*-Cl	166	71.4	5.8	25.3	100	60.2	16.8	14.0 (75)
6	*m*-Cl	159	69.0	6.5	27.2	100	63.7	14.3	14.4 (75)
7	*p*-Cl	161	91.7	9.2	24.6	100	70.6	26.5	18.4 (75)
8	*o*-CH_3	131	86.2	12.3	18.3	100	71.5	70.8	31.2 (65)
9	*m*-CH_3	139	95.7	12.7	27.8	100	46.9	42.1	17.5 (65)
10	*p*-CH_3	134	100	12.7	16.4	70.3	53.4	80.8	33.9 (65)
11	*o*-OCH_3	181	100	1.0	18.8	75.8	39.4	—	16.9 (77)
12	*m*-OCH_3	144	83.8	7.2	25.6	100	38.7	20.5	17.6 (77)
13	*p*-OCH_3	140	100	8.4	9.3	43.7	30.1	50.3	45.4 (77)
14	*p*-$COCH_3$	145	74.7	6.6	20.4	100	42.5	12.4	15.7 (43)
15	3,4-di-CH_3	183	100	9.5	16.2	82.2	39.7	63.1	21.4 (77)

a) The observed values are the mean of quintuples of the measurement.
b) Sp$^+$ means other characteristic ion and the value in parentheses exhibits *m/e* value of the ion.

2) S. B. Hendricks, O. R. Wulf, C. E. Hilbert, and U. Liddel, *J. Amer. Chem. Soc.*, **58**, 1991 (1936).
3) R. Kuhn and F. Bar, *Ann.*, **516**, 143 (1935).
4) A. Burawoy, A. G. Salem, and A. R. Thompson, *J. Chem. Soc.*, **1952**, 4793.
5) E. Fisher and Y. F. Frei, *ibid.*, **1959**, 3159.
6) D. Hadzi, *ibid.*, **1956**, 2143.
7) I. Saito, Y. Bansho, and A. Katsuta, *Kogyo Kagaku Zasshi*, **70**, 1715 (1967).
8) C. Dehari, Y. Matsunaga, and K. Tani, This Bulletin, **43**, 3404 (1970).
9) K. J. Morgan, *J. Chem. Soc.*, **1961**, 2151.
10) A. H. Berri, P. Hampson, S. W. Longworth, and A. Mathias, *ibid*, (B), **1968**, 1308.
11) Y. Matsunaga, This Bulletin, **30**, 429 (1957).
12) H. Rau and B. Bunsengeo, *Phys. Chem.*, **72**, 637 (1968).
13) a) H. Budzikiewicz, C. Djerassi, and D. H. Williams, "Mass Spectrometry of Organic Compounds," Holden-Day, Inc., (1967), p. 158. b) H. Nakata and A. Tatematsu, This Bulletin, **42**, 1678 (1969).
14) E. Watanabe, T. Aoyama, and M. Shino, *Shitsuryo Bunseki (Mass Spectroscopy)*, **17**, 603 (1969).

Table 2. Acetylated derivatives of PAN and their pattern coefficients[a)]

Sample No.	Substituents	Melting point °C	Relative Intensities							
			$M^{+\cdot}$	$(M-42)^+$	$(M-43)^+$	m/e : 171	m/e : 143	m/e : 115	Ph-X$^+$	m/e : 43
PAN-Ac-1	H	115	42.6	100	15.0	30.8	89.1	29.2	40.3	25.2
2	*m*-NO	161	14.7	85.0	9.4	29.8	100	40.2	4.5	35.4
3	*p*-NO_2	190	20.6	100	11.2	23.4	88.2	32.8	6.1	29.4
4	*p*-Cl	132	34.0	100	12.6	27.6	93.0	28.3	23.2	21.4
5	*p*-OCH_3	—[b)]	44.1	100	13.2	11.5	49.4	20.0	64.8	27.2
6	*p*-$COCH_3$	127	36.0	100	12.8	28.2	89.1	26.7	12.3	45.0
7	3,4-di-CH_3	101	53.1	100	15.9	20.3	62.5	24.4	56.4	25.9

a) The observed values are the mean of quintuples of the measurement.
b) This can not be measured because of its tar-like property.

naphthoquinone and methylphenylhydrazinesulfate,[15] and was purified by crystallizing it three times from benzene-ligroin. The sample thus obtained consisted of long, flat, amethyst-colored crystals and melted at 118°C.

Results and Discussion

Mass Spectra of PAN. The characteristic ions observed in the spectra of PAN are $M^{+\cdot}$, $(M-1)^+$, $(m/e : 171)^+$, $(m/e : 143)^+$, $(m/e : 115)^+$, a substituted phenyl ion, and a further decomposed ion of the substituted phenyl ion, as is shown in Table 1. The main reaction is $M^{+\cdot} \rightarrow (m/e : 171)^+ \rightarrow (m/e : 143)^+ \rightarrow (m/e : 115)^+$, which is confirmed by the measurement of the metastable ions. The reaction is similar to that of azobenzenes.[16] It is, however, very dangerous to decide that PAN exist in the gaseous state as the azo form, since there is some possibility that the hydrazone form would react in the same manner.

Recently, some organic compounds which possess keto-enol tautomerism have been studied by means of mass spectrometer.[13,17] As has been mentioned above, no movement of tautomeric equilibria was observed after electron impact. This means that the mass spectra reflect the state of tautomeric equilibria in the gaseous state. Using this phenomenon, Zamir and his co-workers discussed the effect of the inlet temperature on the keto-enol equilibria of the acetylacetone.[18]

It is, at any rate, necessary to determine the state of tautomeric equilibria in order to make the fragmentation process clear.

Azo-hydrazone Tautomerism. It was revealed that the (M-42) ion radical, observed in the mass spectra of acetylated derivatives of compounds which possess keto-enol tautomeric equilibria, corresponds to the enol form of original compounds.[19,20] The acetylated derivatives of PAN were synthesized and measured by means of the mass spectrometer. The spectra obtained were then compared with those of the original PAN (See Figs. 1, 2, and 3). The spectra of PAN and their acetates resemble each other except for a few differences in intensity. That the relative intensities of $(M\text{-}42)^+$ to $(m/e : 171)^+$ and/or $(m/e :$

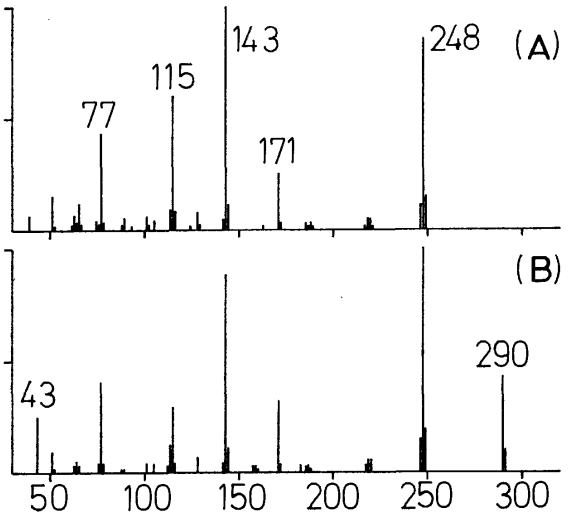

Fig. 1. Mass spectra of 1-phenylazo-2-naphthol (A) and 1-phenylazo-2-naphthol acetate (B).

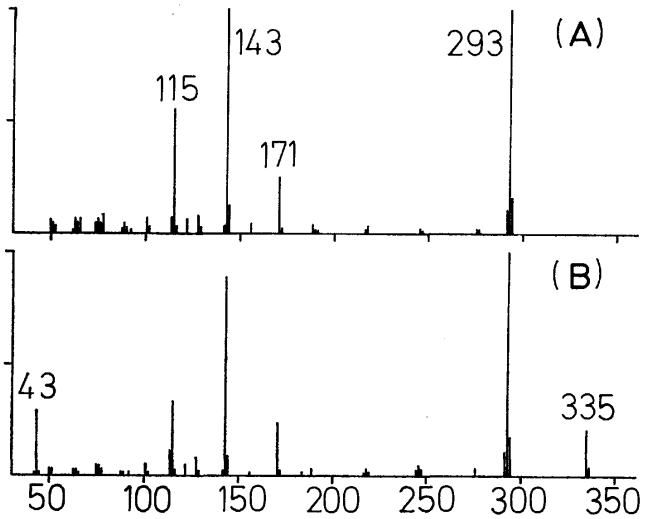

Fig. 2. Mass spectra of 1-(*p*-nitrophenylazo)-2-naphthol (A) and 1-(*p*-nitrophenylazo)-2-naphthol acetate (B).

15) W. MacPherson, *Amer. Chem. J.*, **22**, 364 (1899).
16) J. H. Bowie and G. E. Lewis, *J. Chem. Soc., B*, Part 1, **1967** 621.
17) J. K. McLeod, J. B. Thompson, and C. Djerassi, *Tetrahedron*, **23**, 2095 (1967).
18) L. Zamir, B. S. Jensen, and E. Larsen, *Org. Mass Spectrom.*, **2**, 49 (1969).
19) K. Heyns and D. Muller, *Tetrahedron Lett.*, **1966**, 6061.
20) D. G. B. Boocock and E. S. Waight, *J. Chem. Soc., B*, **1968** 258.

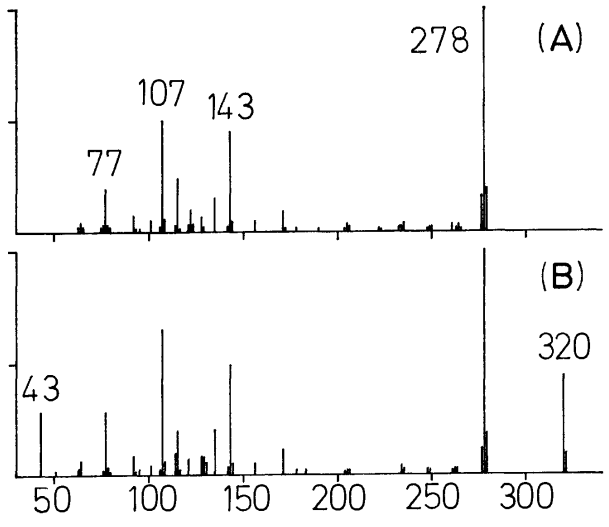

Fig. 3. Mass spectra of 1-(*p*-methoxyphenylazo)-2-naphthol (A) and 1-(*p*-methoxyphenylazo)-2-naphthol acetate (B).

$143)^+$ in the spectra of acetylated derivatives are somewhat larger than those of M^+ to $(m/e : 171)^+$ and/or $(m/e : 143)^+$ in the spectra of original ones, can be reasonably explained by the energy loss at a de-ketene reaction. Actually, the spectra of PAN electron-bombarded at 50 eV are more similar even in intensity to those of acetylated derivatives electron-bombarded at 75 eV. An examination of the metastable ions generated in the first field-free region showed that the fragmentation processes were all same except for $(M\text{-}43)^+$. Also, the metastable ions generated in the second field-free region were found to be equal in shape and in relative abundance to the precursor ions; this means that the structure of the precursor ions in the spectra of both PAN and their acetates are the same.[21] These facts also support the theory that PAN exist in the gaseous state as the azo form, but they are insufficient to clarify the tautomeric equilibria, because the fragmentation processes of the hydrazone form remain undissolved. As it is impossible to measure the mass spectrum of PAN in the hydrazone form, we synthesized *β*-naphthoquinone-methylphenylhydrazone (NQH) as a model compound for the hydrazone form and measured its mass spectrum, which is shown in Fig. 4. The fragmentation process,

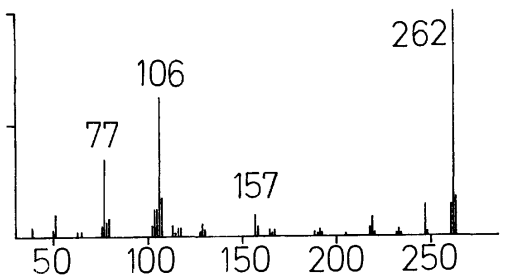

Fig. 4. Mass spectrum of *β*-naphthoquinonemethylphenylhydrazone.

21) T. W. Shannon and F. W. McLafferty, *J. Amer. Chem. Soc.*, **88**, 5021 (1966).

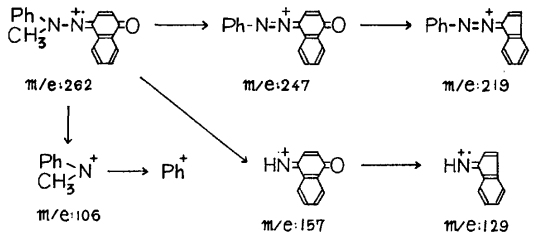

Scheme 1

as determined by the measurements of the precise mass and the metastable ions, is shown in Scheme 1. The main reaction can be understood as a cleavage of $M^{+\cdot}$ to $(m/e : 106)^+$, which corresponds to an ion designated as $(X\text{-}Ph\text{-}NH)^+$ in the spectra of PAN. The reaction of $M^{+\cdot} \rightarrow (m/e : 247)^+ \rightarrow (m/e : 219)^+$ in the spectrum of NQH corresponds to that of $M^{+\cdot} \rightarrow (M-1)^+ \rightarrow (M-1-28)^+$ in the spectra of PAN. These observations do not always support the existence of the hydrazone form in PAN, because there is some possibility that the azo form reacts in the same manner. That $(M\text{-}CH_3)^+$ is observed, while $(M\text{-}Ph)^+$ is not, means that the hydrazone form of PAN will produce $(M-1)^+$ rather than $(M\text{-}Ph)^+$. This also supports the theory that PAN exists as the azo form. The ion radical at $m/e : 157$ in the spectrum of NQH would be produced by the cleavage of the N-N bond with hydrogen transfer from CH_3, so the reaction does not give any information about the tautomerism of PAN. The fact that the $(X\text{-}Ph\text{-}NH)^+$ ion, which should come from the hydrazone form, is not observed supports the idea that PAN exist in the gaseous state as the azo form. In the spectrum o f PAN-13 (p-OCH_3), an ion at $m/e : 122$ corresponding to $(X\text{-}Ph\text{-}NH)^+$ was observed as a 9% intensity of the base peak. This fact indicates some coexistence of the hydrazone form.

It can be concluded, for the foregoing reasons, that PAN exist in the gaseous state at the measured temperature as the azo form, except for the para methoxy derivative, in which a little hydrazone form coexists.

Fragmentation Process of PAN. The fragmentation process of PAN-1 is determined on the basis of the azo form by measurements of the precise mass and the metastable ions (see Scheme 2). The other PAN

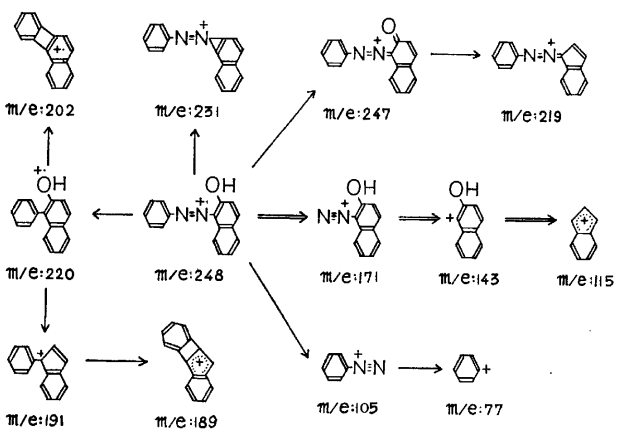

Scheme 2

are explained by the same process. The scission of both sides of the azo group is a main reaction which resembles that of azobenzenes.[16] The cleavage of $M^{+\cdot}$ to $(m/e : 171)^+$ is more liable to occur than that to $(m/e : 105)^+$, for the naphthol ring is a stronger electron donor than the phenyl ring.[22] The $(Ph-X)^+$ ion becomes stronger with an increase in the electron-donating power of the substituents (see Table 1).

The common ions with intensities of less than several percent are $(M-1)^+$, $(M-17)^+$, $(M-28)^+$, $(M-29)^+$, $(m/e : 218)^+$, and $(m/e : 189)^+$. The $(M-28)^+$ contains reaction products of the elimination of a nitrogen molecule and a carbonyl group.

When a substituent is attached to the ortho position, characteristic reactions have been observed by the mass spectrometer; this has been called the "ortho effect".[23] In the spectra of PAN, the ortho nitro group shows typical effect compared with the meta and para positions-i.e., the very weak $(M-1)^+$, strong $(M-17)^+$, and strong $(M-47)^+$ corresponding to $(M-OH-NO)^+$. As for the methoxy group, the ortho derivative shows the weak $(M-1)^+$, strong $(M-15)^+$, strong $(M-31)^+$, weak $(m/e : 107)^+$, and strong $(m/e : 77)^+$ relative to the meta and para derivatives. The last two cases can be explained in terms of the low-energy barrier of a reaction as follows:

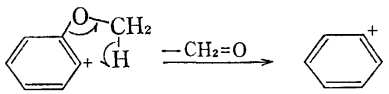

m/e : 107 m/e : 77

In the case of chloro and methyl groups, the typical ortho effect was not observed.

Effects of Substituents on the Rate of Reaction from $M^{+\cdot}$ to Ion at m/e : 171. Bursey and his co-workers[24-26] have examined the kinetic approach to the reaction of acetophenones and benzophenones in a mass spectrometer. They have stated that electron-impact fragmentations may be related to ground-states processes, since the relative abundances of acetyl $(m/e : 43)$ and benzoyl $(m/e : 105)$ cations in various spectra are quantitatively related to the Hammett σ constants. Bowie and his co-worker observed the same correlations for the $(Ph-N=N)^+$ ion in the monosubstituted azobenzenes ($\rho=1.05$).[16] In our experiments, the effect of substituents on the reaction from M^+ to $(m/e : 171)^+$ were examined. The results obtained are shown in Fig. 5, where Z and Z_0 indicate the relative intensities of $(m/e : 171)^+$ to $M^{+\cdot}$ in the spectra of PAN and PAN-1 respectively. The same treatment of the reaction from $(M-42)^+$ to $(m/e : 171)^+$ was done upon the acetylated derivatives; the log (Z/Z_0) thus obtained was consistent with that of the original samples within the range of experimental error. In Fig. 5 the meta substituents correlate with each other by means

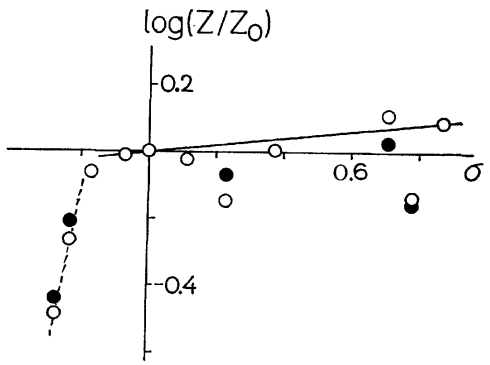

Fig. 5. Correlation of the intensities of ion at m/e: 171 with Hammett σ.
○: PAN, ●: PAN acetates

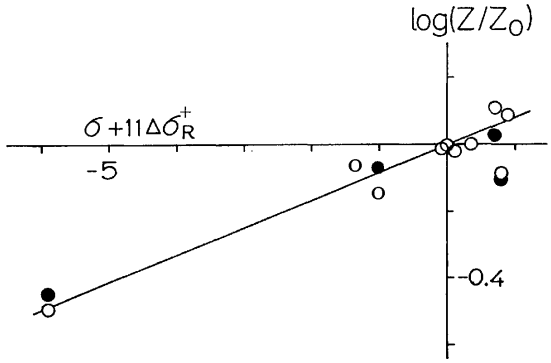

Fig. 6. Improved correlation of the intensities of ion at m/e: 171 with Hammett σ by using Yukawa-Tsuno equation.
○: PAN, ●: PAN acetates

of Hammett σ constants, but some deviations are observed with regard to the para substituents. Such poor correlations have so far been observed.[27] In order to solve this problem, Johnstone and his co-worker have proposed a concept of the participation of excited-state reactions, where good Hammett correlations are found for para but not meta substituents.[28] In our case, however, the results may indicate that the reaction proceeds through a ground state rather than through an excited state, since good Hammett correlations are found for meta but not para substituents. Moreover, the correlations are improved by an application of the Yukawa-Tsuno equation[29] except for the para nitro derivative, as is shown in Fig. 6; the vafues obtained are $\sigma=0.08$ and $r=11$ (r is a parameter of the relative strength of the resonance effect.). The small ρ-value, which is very different from that of azobenzenes, is probably dependent on a relaxation effect of the hydrogen bond.

The authors express their thanks to Mr. M. Sawai of Teikoku Hormone MFG. Co., Ltd. for generous support of this work and to Prof. T. Takeuchi of Nagoya University for his constant interest and encouragement.

22) Y. Okamoto and H. C. Brown, *ibid.*, **79**, 1903 (1957).
23) H. Budzikiewicz, C. Djerassi, and D. H. Williams, Ref. 13-a, p. 197, 297 etc.
24) M. M. Bursey and F. W. McLafferty, *J. Amer. Chem. Soc.*, **88**, 529 (1966).
25) M. M. Bursey and F. W. McLafferty, *ibid.*, **88**, 4484 (1966).
26) M. M. Bursey and F. W. McLafferty, *ibid*, **89**, 1 (1967).
27) F. W. McLafferty and T. Wachs, *ibid.*, **89**, 5043 (1967).
28) R. A. W. Johnstone and D. W. Payling, *Chem. Commun.*, **1968**, 601.
29) Y. Yukawa and Y. Tsuno, This Bulletin, **32**, 971 (1959).

The Stereoselective Reactivities of DL-Amino Acid *N*-Carboxyanhydrides for (−)-Menthol

Tadao HAYAKAWA, Hiroyuki YAMAMOTO, Yukiko MURAKAMI, Yoshihiro YOBIKO, and Shunji MITANI

Institute of High Polymer Research, Faculty of Textile Science and Technology, Shinshu University, Ueda

(Received January 31, 1972)

The stereoselective reactivities of some neutral DL-amino acid *N*-carboxyanhydrides for (−)-menthol were studied by varying the concentration of hydrogen chloride as a catalyst and the reaction temperature. From the results of gas-liquid-chromatographic analyses, the esterification rates of D-amino acids were shown to be higher than those of L-amino acids in all cases. The highest ratio of the esterification rate, V_D/V_L, is 2.37. The recovered unreacted amino acids were always enriched in the L-form. The stereoselective reactivities were influenced by the catalyst concentration and not influenced by the reaction temperature.

In the previous papers, (−)-menthyl esters of α-amino acids have been synthesized from amino acids and (−)-menthol by the use of the azeotropic distillation method[1] and the amino acid *N*-carboxyanhydride (NCA) method.[2] In these reactions, D-form amino acid (−)-menthyl esters gave better yields than L-form esters. This suggests that the reactions proceed through different esterification rates of the two enantiomers.

In the present study, the stereoselective reactivity of amino acid enantiomers for (−)-menthol and the optical purity of the recovered unreacted amino acids were studied. The experimental conditions were as follows. Racemic amino acid NCAs of alanine, valine, and phenylalanine were reacted with one half a molar equivalent of (−)-menthol in dioxane, while the hydrogen chloride concentration and the reaction temperature were varied. After the unreacted NCA has then been hydrolyzed and removed, the amino acid (−)-menthyl esters were acetylated. The amounts of two diastereomers were determined from the gas-liquid-chromatographic (glc) analyses[3] by correcting them with the calibration curves made by authentic amino acid (−)-menthyl esters. From the results obtained under several experimental conditions, the stereoselective reactivities can be said to be influenced by the concentration of hydrogen chloride as a catalyst and not to be influenced by the reaction temperature. We consider that, at high catalyst concentrations, the NCA ring changes to the acid chloride, which easily accepts the steric effect of (−)-menthol.

Experimental

Preparation of Amino Acid (−)-Menthyl Ester Hydrochlorides. The (−)-menthyl ester hydrochlorides of L- and D-alanine, L- and D-valine, and L- and D-phenylalanine were synthesized by azeotropic distillation using *p*-toluenesulfonic acid, as has been described previously.[1]

Acylation of Amino Acid (−)-Menthyl Ester Hydrochlorides. Acetylation: To a solution of L- and D-amino acid (−)-menthyl ester hydrochloride in 10 m*l* of ethyl acetate, a 2 molar equivalent of a 1 N sodium carbonate solution and a 1.5 molar equivalent of acetic anhydride were added at 0°C. After stirring for 1 hr at 0°C and then for 2 hr at room temperature, the organic layer was washed successively with water, a 0.5 N sodium bicarbonate solution, water, 0.5 N hydrochloric acid, and water; dried over sodium sulfate, and evaporated to dryness *in vacuo*. The product was treated with *n*-hexane, filtered, and dried; the yield was, on the average, 90—95%.

Benzoylation: To a solution of L- and D-amino acid (−)-menthyl ester hydrochloride in 5 m*l* of ethanol containing a 2 molar equivalent of sodium ethoxide, a 1.2 molar equivalent of benzoyl chloride was added at 10°C. After stirring for 3 hr, the solution was evaporated to dryness *in vacuo*. The product was extracted with ethyl acetate, and the organic layer was successively washed with water, a 0.5 N sodium bicarbonate solution, water, 0.5 N hydrochloric acid, and water; dried over sodium sulfate, and evaporated to dryness *in vacuo*. The residue was treated with *n*-hexane, filtered, and dried; the yield was, on the average, 80—88%.

Retention Times of Standard Samples. The retention times of standard samples, as determined by glc, are shown in Table 1. As is shown in Table 1, the acetyl derivatives were well and rapidly separated. We carried out all the glc analyses using acetyl amino acid (−)-menthyl esters.

Table 1. Gas chromatographic separation of acyl-α-amino acid menthyl esters

Amino acid menthyl ester	Column temp. (°C)	Retention time of diastereomers (min)		t_D/t_L
		t_D[a]	t_L[b]	
Acetyl Ala	175	27	24	1.13
Benzoyl Ala	220	38	33.5	1.13
Acetyl Val	220	15	13	1.15
Benzoyl Val	220	31	27.5	1.13
Acetyl Phe	220	39.5	37	1.07
Benzoyl Phe	220	21.5	19.5	1.10

a) Retention time of acyl-D-amino acid-(−)-menthyl ester.
b) Retention time of acyl-L-amino acid-(−)-menthyl ester.

DL-Amino Acid NCA's. The NCA's were synthesized by the phosgene method.[4] All the NCA's were recrystallized from ethyl acetate and *n*-hexane.

N-Acetyl Amino Acid (−)-Menthyl Esters. To a solution of (−)-menthol (0.01 mol) in 100 m*l* of dioxane containing 1N, 2N, 4N, and 5.8N (saturated) hydrogen chloride as catalysts, DL-amino acid NCA (0.02 mol) was added, then the mixture was reacted with stirring at 10, 20, and 30°C. At regular time intervals, 10-m*l* portions of the reaction mixture were taken out, and then 10 m*l* of water was added to it. The unreacted NCA was hydrolyzed by heating in a boiling-

1) K. Harada and T. Hayakawa, This Bulletin, **37**, 191 (1964).
2) T. Hayakawa and K. Harada, *ibid.*, **38**, 1354 (1965).
3) B. Halpern and J. W. Westley, *Chem. Commun.*, **1965**, 421.

water bath for 2 min. The dioxane was removed *in vacuo*. The aqueous layer was made alkaline by the addition of a sodium bicarbonate solution. The amino acid (−)-menthyl ester was extracted with 25 m*l* of ethyl acetate. This organic layer was acetylated with acetic anhydride and sodium carbonate in the same way as above. The acetyl amino acid (−)-menthyl ester in ethyl acetate was directly analyzed by glc.

The Test of the Stereoselective Hydrolysis. In order to check the stereoselective hydrolysis of the amino acid menthyl esters in a hydrochloric acid solution in the above experiments, the following experiments were designed. To a solution of DL-alanine menthyl ester (0.0002 mol) in 1.0 m*l* of dioxane, 1.0-m*l* portions of 1N, 2N, 4N, and 6N hydrochloric acid were added separately. Then the mixture was heated in the boiling-water bath for 2 min. After the reaction mixture has been treated in the same way as above, the recovery of the L- and D-alanine menthyl esters was determined by glc. The results are shown in Table 2.

Table 2. Recovery of amino acid menthyl esters by hydrolysis

HCl concn. (N)	Recovery, %	
	L-Alanine deriv.	D-Alanine deriv.
1	100.0	100.0
2	98.8	100.0
4	92.4	94.1
6	88.7	90.6

As is shown in Table 2, the hydrolysis of the ester was little affected by heating in 1N and 2N hydrochloric acid. In higher concentrations of hydrochloric acid, the stereoselective hydrolysis was observed slightly in two diastereomers. The recovery ratio of the two diastereomers (D/L) was 1.02 in 6N hydrochloric acid. This ratio suggests that the stereoselective hydrolysis has little influence on the stereoselective reactivity of DL-NCA for (−)-menthol.

Recovery of Unreacted Amino Acid. Amino acid NCA (0.002 mol) and a one-half molar equivalent of (−)-menthol (0.001 mol) in 10 m*l* of 4N HCl/dioxane were reacted at 20°C for 12 hr. After the same treatment as has been described above, the aqueous layer was made alkaline by sodium bicarbonate. The amino acid (−)-menthyl ester was extracted with ethyl acetate. To this basic aqueous solution, 2,4-dinitrofluorobenzene (DNFB, 0.0018 mol) was added, and the mixture was stirred at 40°C until a clear solution was obtained. The unreacted DNFB was extracted with ether. The aqueous layer was acidified to Congo Red with 6N hydrochloric acid and extracted with 50 m*l* of ether. The ethereal layer was washed with water, dried over sodium sulfate, and then passed through a cellite column treated with a pH-6.5 phosphate buffer[5] to purify it. The organic solvent was evaporated to dryness *in vacuo*, and the residue was redissolved in 1N sodium hydroxide. From the absorbance of the ultraviolet absorption at nearly 360 mμ of this solution, the yields of DNP-amino acids were calculated. The yields and $[\alpha]_D$ are shown in Table 3. From the $[\alpha]_D$ values of the DNP-amino acids shown in Table 3, each amino acid is L-form rich. This suggests that the (−)-menthyl esterification of DL-amino acid prefers the D-form to the L-form.

Table 3. Recovery of unreacted α-amino acid

DNP-Amino acid	Recovery[a] %	$[\alpha]_D$ 1N NaOH	Confign.	Optical purity,[b] %
Ala	41.0	+8.6°	L	5.9
Val	26.1	+4.2°	L	3.9
Phe	49.1	−3.8°	L	4.1

a) Recoveries were calculated from starting DL-amino acid NCA. b) Defined as ($[\alpha]_D$ obsd/$[\alpha]_D$ lit)×100. DNP-L-Ala, $[\alpha]_D$ +143.9° (1N NaOH); DNP-L-Val, $[\alpha]_D$ +109.2° (1N NaOH); DNP-L-Phe, $[\alpha]_D$ −93.6° (1N NaOH).

Method. Glc analyses were carried out on a Hitachi K 53 gas chromatograph with a flame ionization detector, using a 1 m×3 mm glass column (60/80 mesh 20% poly-neopenthyl glycol succinate on chromosorb W AW DMCS) and with a nitrogen flow rate of 30 m*l*/min.

Results and Discussion

The Reaction Rates and Their Ratios of the Esterification of Two Enantiomers. The yields of the diastereomers obtained by the reaction of DL-alanine NCA and (−)-menthol at 20°C using 4 N HCl/dioxane are shown in Fig. 1 as a function of the time. This suggests that the esterification rate of D-amino acid, V_D, is larger than that of L-amino acids, V_L. At their initial stages, a linear relationship exists between the yields of the amino acid (−)-menthyl esters and the reaction time. At a prolonged reaction time, though the increments of both yields per unit of time decreased, constant (V_D/V_L) ratios were observed. The dependences on the temperature and the concentration of the hydrogen chloride catalyst for stereoselective reactivity of each amino acid NCA are shown in Table 4. From these results, the ratios of the reactivity of the diastereomers were calculated. As is shown in Table 4, V_D and V_L increase with an increase in the temperature and in the concentration of a catalyst under each set of conditions. In all cases, V_D is larger than V_L. This suggests that the ratio of stereoselective reactivity, V_D/V_L, is not influenced by the reaction temperature, but is influenced by the concentration, of a catalyst.

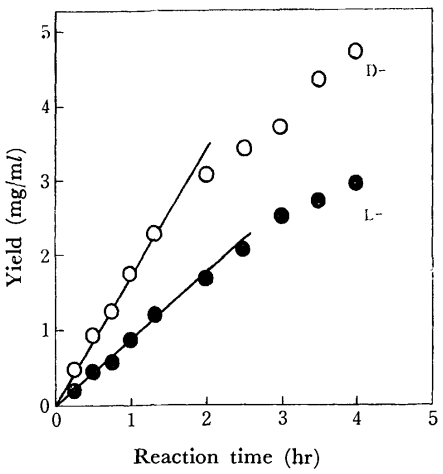

Fig. 1. The relationship between the reaction time and the yield of D- and L-alanine (−)-menthyl esters.
○: D-alanine (−)-menthyl ester,
●: L-alanine (−)-menthyl ester.

4) A. C. Farthing, *J. Chem. Soc.*, **1950**, 3213.

5) A. J. Woiwod, *J. Gen. Microbiol.*, **3**, 312 (1949).

TABLE 4. REACTION RATES AND RATIOS OF DL-AMINO ACID NCAS FOR (−)-MENTHOL

DL-Amino acid NCA	HCl concn. (N)	Reaction rates and ratios								
		At 10°C			At 20°C			At 30°C		
		V_D[a]	V_L[b]	V_D/V_L	V_D	V_L	V_D/V_L	V_D	V_L	V_D/V_L
Ala	1	0.051	0.046	1.10	0.058	0.052	1.12	0.071	0.062	1.15
	2	0.21	0.15	1.40	0.44	0.32	1.38	1.09	0.79	1.38
	4	0.34	0.17	2.00	1.70	0.88	1.93	1.82	0.96	1.90
	5.8	0.77	0.36	2.14						
Val	1	0.0032	0.0029	1.10	0.0066	0.0057	1.16	0.0097	0.0083	1.17
	2	0.0083	0.0065	1.28	0.020	0.016	1.25	0.10	0.075	1.33
	4	0.070	0.037	1.89	0.13	0.068	1.87	0.21	0.11	1.91
	5.8	0.20	0.084	2.37						
Phe	1	0.022	0.021	1.05	0.041	0.038	1.09	0.078	0.072	1.08
	2	0.045	0.035	1.29	0.059	0.045	1.31	0.098	0.075	1.31
	4	0.39	0.28	1.39	0.53	0.38	1.39	0.62	0.45	1.38
	5.8	0.55	0.32	1.72						

a) Reaction rate of D-amino acid NCA (mg/m*l*·hr).
b) Reaction rate of L-amino acid NCA (mg/m*l*·hr).

Moreover, the maximum ratios of stereoselectivity were observed when the reaction was carried out using saturated hydrogen chloride as a catalyst in three amino acids. As is shown in Table 3, the recovered unreacted amino acids are always L-form rich.

Reaction Mechanism. It was found that the stereoselective reactivity of DL-amino acid NCA for (−)-menthol is not influenced by the reaction temperature in the range from 10 to 30°C, but is influenced by the catalyst concentration of hydrogen chloride. This suggests that the reaction may proceed by the route of scheme 1 or 2.

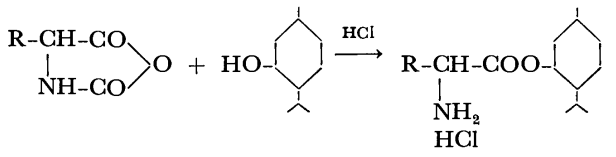

(1)

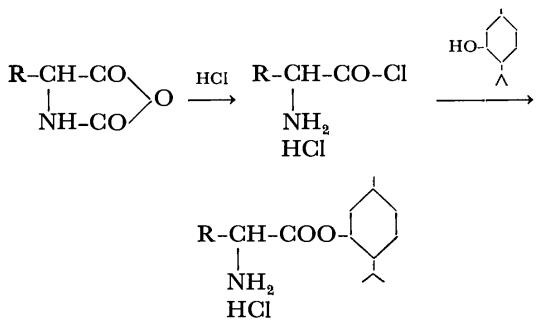

(2)

At low hydrogen chloride concentrations, the reaction may proceed mainly by the route of scheme 1 and the stereoselective reactivity is small. On the other hand, at high hydrogen chloride concentrations, the reaction may proceed by the route of scheme 2 and large stereoselectivities are obtained.

TABLE 5. REACTION RATES AND RATIOS FOR (−)-MENTHOL AFTER REACTED WITH DL-VALINE NCA AND HYDROGEN CHLORIDE

Reaction time (hr)	V_D[a]	V_L[b]	V_D/V_L
0	0.025	0.021	1.19
1	0.035	0.027	1.30
2	0.041	0.029	1.41
3	0.044	0.030	1.47

Solvent: 2N HCl/dioxane, Temp: 20°C
a) Reaction rate of D-amino acid NCA (mg/m*l*·hr).
b) Reaction rate of L-amino acid NCA (mg/m*l*·hr).

In order for the reaction to proceed *via* the route of scheme 2 exclusively, DL-valine NCA was reacted with 2 N HCl/dioxane for 1, 2, and 3 hr at 20°C, and then (−)-menthol was added to the solution. This mixture was allowed to react for 2.5 hr. The valine (−)-menthyl ester thus obtained was analyzed by glc in order to determine the yield of each diastereomer by the method described above. The results are shown in Table 5. As is shown in Table 5, the higher stereoselectivity was observed when the NCA and hydrogen chloride were kept for a long time before the addition of (−)-menthol. Therefore, it is considered that, at high hydrogen chloride concentrations, the NCA changes to the acid chloride, which is more susceptible to the steric effect of (−)-menthol. Such a difference may cause the higher stereoselective reactivity.

The authors wish to express their thanks to Dr. K. Harada of the University of Miami for his helpful discussions and encouragement.

The Thermal Reaction of 3-Benzoylguaiazulene and Methyl Guaiazulene-3-carboxylate

Shinji KUROKAWA, Mamoru HASHIMOTO,* and Shûichi HAYASHI

Department of Chemistry, Faculty of Education, Saga University, Honjo-machi, Saga

Department of Chemistry, Faculty of Science, Hiroshima University, Higashisenda-machi, Hiroshima

(Received January 31, 1972)

3-Benzoylguaiazulene (I) and methyl guaiazulene-3-carboxylate (XI) were heated at 250—260°C. From 3-benzoylguaiazulene we obtained, besides S-guaiazulene (II), three new azulenoids, which were established to be 2-benzoylguaiazulene (III), 1-benzoyl-7-isopropyl-3,4-dimethylazulene (IVa) and 2-benzylguaiazulene (V). On the other hand, the products yielded from methyl guaiazulene-3-carboxylate, together with S-guaiazulene, were elucidated to be methyl 7-isopropyl-3,4-dimethylazulene-1-carboxylate (XII) and methyl guaiazulene-2-carboxylate (XIII). In addition to the loss and the migration of the acyl group, the exchange of acyl and methyl groups in the five-membered ring took place in both acylguaiazulenes, as well as in the case of 3-acetylguaiazulene reported earlier. Moreover, the reduction of the acyl group was also observed in 3-benzoylguaiazulene.

In an earlier paper[1] dealing with the thermal reaction of 3-acetylguaiazulene at 200°C, it was shown that S-guaiazulene (II) and 2-acetylguaiazulene (VI) were formed by the loss or the migration of the acetyl group. In the same reaction, 1-acetyl-7-isopropyl-3,4-dimethylazulene (XIV) was also found to be formed by the exchange of acetyl and methyl groups in the five-membered ring of the azulene nucleus.[2] The present investigation was undertaken to see if this kind of reaction could occur in another acylguaiazulene having an acyl group such as benzoyl or methoxycarbonyl.

Results and Discussion

The Thermal Reaction of 3-Benzoylguaiazulene (I). When 3-benzoylguaiazulene (I) was heated at 250—260°C for 2 hr, three new compounds were obtained in addition to the S-guaiazulene (II) formed by the loss of the benzoyl group.

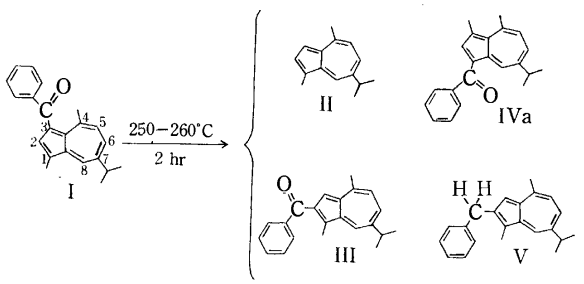

Chart 1.

a) 2-Benzoylguaiazulene (III). The green crystalline substance (mp 87.5—88.5°C) which was isolated as the major product in this reaction had the same molecular formula, $C_{22}H_{22}O$, as the I used as the starting material. The existence of a benzoyl group in this compound was known from the appearance of the $\nu_{C=O}$ band at 1633 cm^{-1} in its IR spectrum and from the presence of the notable ions at *m/e* 197 and 105 respectively, ascribed to $(M-C_6H_5CO)^+$ and $C_6H_5^+$ in the mass spectrum.

In the NMR spectrum of the compound taken in a deuterochloroform solution (*cf.* Experimental section) we observed, besides five aromatic proton signals ascribed to the benzoyl group, signals due to one isopropyl-, two aromatic methyl-, and four aromatic ring-protons corresponding to the guaiazulene moiety. These chemical shifts and coupling constants ($J_{5,6}$= 10.1 Hz, $J_{6,8}$=1.5 Hz) were quite close to those of 3-benzoylguaiazulene. Thus, the compound may be thought to be an isomer which differs from 3-benzoylguaiazulene in the position of the benzoyl group.

On the other hand, the NMR spectrum taken in a trifluoroacetic acid solution lacked the H_2 signal which was observed in the spectrum of I (7.50 ppm). This agreed well with the fact that the Me_1 and C_3-methylene signals[3] appeared as a triplet and a quartet (2.45 and 4.59 ppm, J=2.0 Hz) respectively because of the absence of the H_2 proton. The compound may, therefore, be concluded to hold the benzoyl group at the 2-position.

In order to confirm the above deductions, we attempted to synthesize 2-benzoylguaiazulene (III) starting from 2-acetylguaiazulene (VI), whose structure had previously been established.[1] As the first step, we attempted to prepare the carbinol (X) by the reaction of VI and a Grignard reagent derived from bromobenzene. The product, however, consisted of two kinds of blue oil. On the basis of the NMR data (*cf.* Experimental section), these compounds were elucidated to be 2-(1-phenylethenyl)guaiazulene (VII) and 2-(1-phenylethyl)guaiazulene (VIII), which would be formed from carbinol (X) through dehydration or hydrogenation, respectively. Successively, the olefin

* Present address: Department of Industrial Chemistry, Kyushu Technical University, Sensui-machi, Tobata-ku, Kitakyushu.

1) S. Kurokawa, This Bulletin, **43**, 509 (1970).

2) S. Kurokawa, *Tetrahedron Lett.*, **1969**, 3567.

3) For instance, the protonation occurs in 2-benzoylguaiazulene as follows. All the compounds in this paper except the 1-benzoyl compound (IVa) take this type of conjugate acid form, in which protonation occurs at the 3-position:

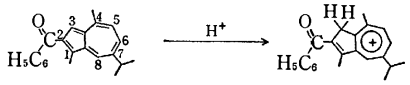

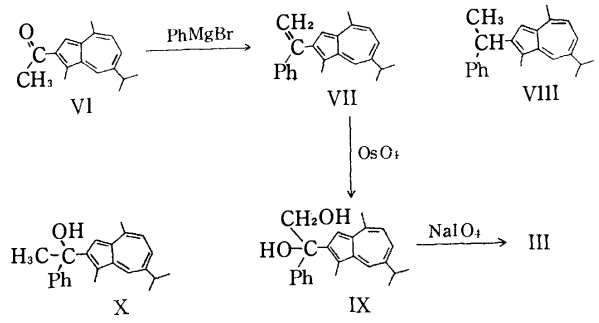

Chart 2.

(VII) was oxidized with osmium tetroxide[4] to give glycol (IX), which was then further oxidized with periodate to afford III. The green crystalline substance obtained in the thermal reaction of I was identical with the synthesized product; thus, it was concluded to be 2-benzoylguaiazulene (III).

b) 1-Benzoyl-7-isopropyl-3,4-dimethylazulene (IVa). A purple oil with a molecular formula of $C_{22}H_{22}O$ was isolated from a benzene-eluted fraction in the elution chromatography of the reaction products. This compound exhibited a $\nu_{C=O}$ band at 1606 cm^{-1} in the IR spectrum and gave 2,4-dinitrophenylhydrazone (mp 249—251°C). Moreover, the *m/e* 105 ion, the base peak in the mass spectrum, was attributed to $C_6H_5CO^+$. Thus, it is certain that the compound also contains a benzoyl group.

Furthermore, all the signals observed in the NMR spectrum (Fig. 1A) corresponded well to those in the spectra of the starting material (I) and 2-benzoylguaiazulene (III). This compound may, therefore, be thought to be an isomer which differs from I and III only in the positions of the substituents.

The two doublet signals of 9.78 (d, 1H, J=2.1 Hz) and 7.17 ppm (d, 1H, J=10.5 Hz) seen in the aromatic-proton region of the NMR spectrum can reasonably be assigned to H_8 and H_5 respectively, for their coupling constants and coupling pattern agree very closely with those of S-guaiazulene (II) and I. The H_6 proton, though unrecognizable due to the overlap of the benzene-ring protons, must exist, because no other proton can be a coupling partner of the above two protons. Consequently, the seven-membered ring of this compound has the same 4,7-disubstitution as that of the starting material.

Among these signals, the signal of the H_8 proton (9.78 ppm) moves downfield by 1.73 ppm relative to that of S-guaiazulene. Such a remarkable shift is characteristic of the acylazulenes with an acyl group at the peri position (1-position) [*cf.* 1-acetylazulene; 9.89 ppm.[5] 1-acetyl-7-isopropyl-3,4-dimethylazulene; 10.28 ppm[2]]. Thus, the compound has the benzoyl group at the 1-position.

The methyl doublet of 2.79 ppm with J=1.0 Hz (Me_3) observed in the NMR spectrum taken in a trifluoroacetic acid solution (Fig. 1B) may be attributed to the methyl protons of the five-membered ring spin-coupled with an adjacent olefinic proton

4) J. B. Brown, H. B. Henbest, and E. R. H. Jones, *J. Chem. Soc.*, **1952**, 3172.

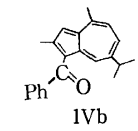

Chart 3.

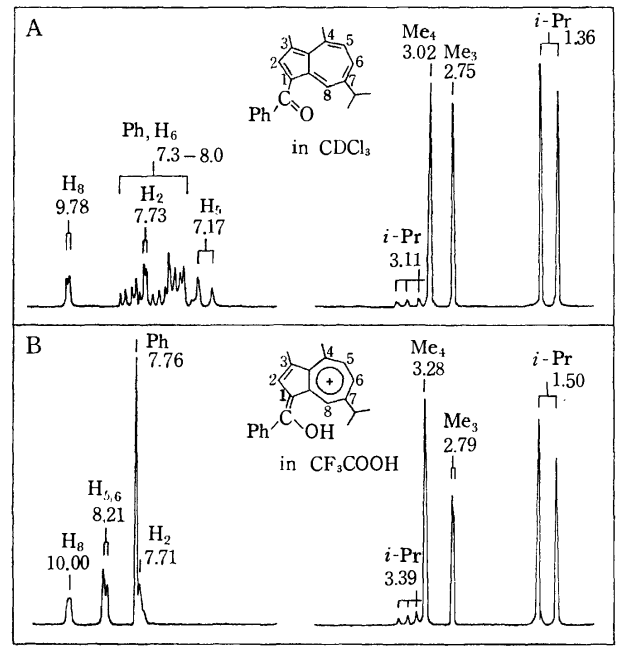

δ, ppm

Fig. 1. NMR spectra of 1-benzoyl-7-isopropyl-3,4-dimethylazulene (A) and its conjugate acid (B).

(7.71 ppm; H_2). One of the methyl groups should, therefore, be located at either the 2- or 3-position. From the above data, the two formulae of IVa and IVb become possible for this compound.[6] However, the compound represented by IVb has already been reported by Treibs *et al.* to be the benzoylation product of Se-guaiazulene,[7] and it is evidently different from the present compound. The present compound must, therefore, be 1-benzoyl-7-isopropyl-3,4-dimethylazulene (IVa).

c) 2-Benzylguaiazulene (V). A blue oily substance, which had a molecular formula of $C_{22}H_{24}$ and which gave a dark brown picrate (mp 106—108°C), was separated by the *n*-hexane-silica-gel elution chromatography of the reaction products.

In the NMR spectrum of the compound taken in a deuterochloroform solution (*cf.* Experimental section) we observed a sharp singlet (4.29 ppm, 2H) assigned to the protons of a methylene group, in addition to the

5) D. Meuche, D. Dreyer, K. Hafner and E. Heilbronner, *Helv. Chim. Acta.* **50**, 1178 (1967).

6) Strictly speaking, the following formulae are also possible for this compound. The examination on these formulae is, however, abbreviated in this paper for they, accompanying the changes in the seven-membered ring, have already been discussed in a preceding paper (Ref. 2):

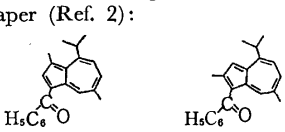

7) W. Treibs, Ch. Vollard, and M. Reimann, *Ann.*, **648**, 164.

signals due to a benzene ring and a guaiazulene moiety. Thus, the compound may be thought to have a benzyl group formed through the reduction of the benzoyl group in the starting material (I).

When a visible absorption maximum (592 nm) of the compound is analyzed according to the Plattner rule,[8] three positions, 2, 6, and 8, are possible for the benzyl group. Of these positions, the 2-position is selected, since the signal attributable to H_2 is not observed in the NMR spectrum of the compound taken in a trifluoroacetic acid solution (*cf.* Experimental section); this is in accordance with the appearance of the C_3-methylene and Me_1 signals as a quartet and a triplet respectively (3.89 and 2.52 ppm respectively; $J=1.8$ Hz).

Based on the above knowledge, this compound was synthesized through the Huang-Minlon reduction of 2-benzoylguaiazulene (III), whose structure had been established before (*cf.* a); thus, it was determined to be 2-benzylguaiazulene (V).

The Thermal Reaction of Methyl Guaiazulene-3-carboxylate (XI). The heating of the methyl ester (XI) at 250°C for 1 hr produced two kinds of ester compounds besides S-guaiazulene.

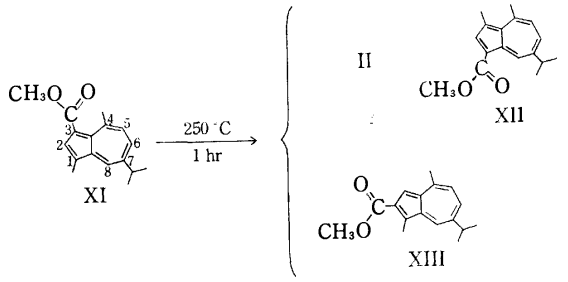

Chart 4.

a) Methyl 7-Isopropyl-3,4-dimethylazulene-1-carboxylate (XII). A purple oily substance, the major product of the reaction, had a molecular formula of $C_{17}H_{20}O_2$, the same as XI. This compound showed a $\nu_{C=O}$ band at 1688 cm^{-1} in its IR spectrum, and it exhibited a sharp methyl singlet (3.91 ppm) in its NMR spectrum (Fig. 2A) which was assigned to a methoxy group. Moreover, the *m/e* 225 peak seen in the mass spectrum was attributed to the $(M-OCH_3)^+$ ion. Thus, the compound is a methyl ester similar to the starting material. A doublet signal of an aromatic-ring proton (9.78 ppm, 1H, $J=2.0$ Hz), observed at the lowest field in the NMR spectrum (Fig. 2A), was ascribed to the H_8 proton by comparison with the spectra of other azulenes. The chemical shift of this proton was, however, of an extremely downfield nature, which is the characteristic of the acylazulenes having an acyl group at the peri position [*cf.* 1-benzoyl compound (IVa)]. Accordingly, the compound may be thought to hold a methoxycarbonyl group at the 1-position.

Furthermore, the NMR spectrum of a conjugate acid (Fig. 2B) showed a methyl singal (1.62 ppm, d, $J=7.2$ Hz; Me_3) and a methine signal (4.48 ppm, double quartet, $J=7.2$ and 1.8 Hz; H_3), spin-coupled to one another. On the other hand, as only the 3-position is known to be possible for the protonation in an azulene nucleus,[3] the above methyl group apparently exists at the 3-position.

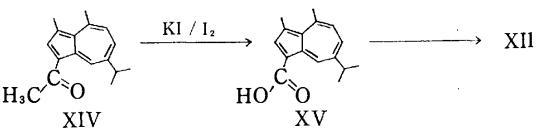

Chart 5.

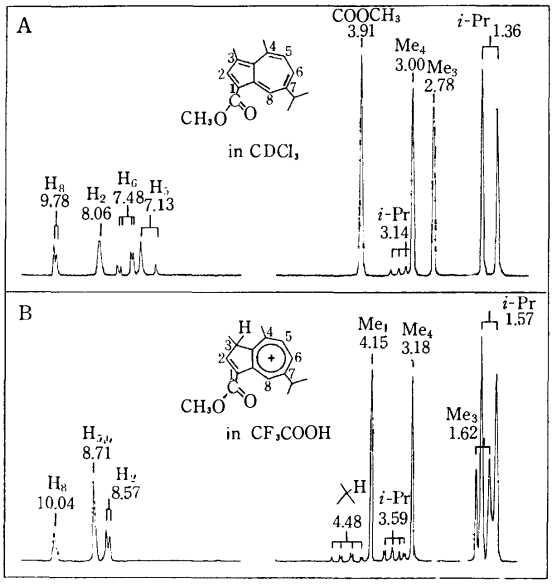

δ, ppm

Fig. 2. NMR spectra of methyl 7-isopropyl-3,4-dimethylazulene-1-carboxylate (A) and its conjugate acid (B).

These data suggest that the compound has the structure of methyl 7-isopropyl-3,4-dimethylazulene-1-carboxylate (XII). On the basis of this deduction, the structure was established as follows: 1-Acetyl-7-isopropyl-3,4-dimethylazulene (XIV), elucidated earlier,[2] was oxidized with hypoiodite to give the carboxylic acid (XV), which was then treated with diazomethane to afford the same methyl ester (XII) as was obtained from XI.

b) Methyl Guaiazulene-2-carboxylate (XIII). Trace amounts of a blue oil isolated from the reaction products were found to be XIII by comparison with an authentic specimen.[1]

Sequence of the Reaction. Table 1 lists the yields (%) of the reaction products formed from the three

Table 1. The yield (%) of the thermal isomerization products

Products	Acyl groups		
	CH_3CO[1,2]	C_6H_5CO	CH_3OCO
S-Guaiazulene	1.4	1.8	0.8
2-Acylguaiazulene	16.4	11.3	0.08
1-Acyl-7-isopropyl-3,4-dimethylazulene	7.0	5.7	5.3
2-Benzylguaiazulene	—	2.5	—

8) J. F. Tilney-Basset and W. A. Waters, *J. Chem. Soc.*, **1959**, 3123. *cf.* E. Heilbronner, "Non-Benzenoid Aromatic Compounds," ed. by D. Ginsburg, Interscience, New York (1959), p. 171.

3-acylguaiazulenes studied thus for.

As is obvious from Table 1, all of the 3-acylguaiazulenes gave reaction products of the common type, *viz.*, those formed through the loss of the acyl group, through the migration of the same group from the 3- to the 2-position, and through the exchange between acyl- and methyl-groups in the five-membered ring of the azulene nucleus. However, some discrepancy among the reactions due to the differences in the acyl substituents is also observed: the main reaction in ketone is the migration of the acyl group, while that in the methyl ester is the exchange of acyl- and methyl-groups in the five-membered moiety, and the reduction of acyl group is noted only in the benzoyl compound. How these differences in the reactivity occur is not apparent at present, but we are continuing to make our best efforts to solve this problem in our laboratory.

Experimental

All the melting points in this paper are uncorrected. The UV and visible absorption spectra were taken in a cyclohexane solution. The IR spectra were obtained using liquid films or KBr disks, and the mass spectra (MS), at 70 eV. The NMR spectra were measured at 60 MHz, and the chemical shifts are given by ppm, using TMS as the internal standard. The thin-layer chromatography (tlc) was conducted by the use of silica gel-G (Merck).

3-Benzoylguaiazulene (I). This compound was synthesized by the reaction of S-guaiazulene (II) and benzoyl chloride in the presence of an aluminium chloride catalyst.[9] The recrystallization of the product from *n*-hexane-ethanol (1 : 1) gave green prisms [mp 122.8—123.2°C (mp 121.5°C,[9] mp 120—121°C[10])], which showed a single brown spot (R_f, 0.20) in tlc using benzene. IR: 1606 cm^{-1} (C=O) [1637 cm^{-1} in nujol mull[10]]. UV: nm (log ε), 244.5 (4.51), 280sh (4.30), 290 (4.42), 309 (4.08), 323.5 (4.10), 401 (3.91) [249, 289, 314, and 319 nm respectively[10]]. Visible absorption spectrum: nm (ε), 586 (443), 639sh (329) [583 nm[10]]. NMR ($CDCl_3$): 2.55 (s, 3H; Me_1), 7.55 (S, 1H; H_2), 2.71 (s, 3H; Me_4), 7.12 (d, 1H, J=11.0 Hz; H_5), 1.37/3.09 (d, 6H/m, 1H, J=6.0 Hz; i-Pr), 8.20 (d, 1H, J=1.8 Hz; H_8), 7.3—8.0 (m, 6H; Ph, H_6). NMR (CF_3COOH)[3]: 2.51 (q, 3H; Me_1), 7.50 (m, 1H; H_2), 6.44 (m, 1H; H_3), 2.96 (s, 3H; Me_4), 8.78 (s, 2H; $H_{5,6}$), 1.62/3.61 (d, 6H/m, 1H, J=6.8 Hz; *i*-Pr), 8.84 (s, 1H; H_8), 7.7—8.5 (m, 5H; Ph). MS: *m/e* 302 (M, $C_{22}H_{22}O$; 1.7%), *m/e* 287 (M-CH_3; 46.5%), *m/e* 105 (C_6H_5CO; 25.8%), *m/e* 77 (C_6H_5; 90%).

Thermal Reaction of 3-Benzoylguaiazulene (I). 3-Benzoylguaiazulene (2.00 g) was heated at 250—260°C in a sealed tube for 2 hr. The reaction mixture, after being dissolved in a small amount of benzene, was eluted through a silica-gel column with benzene, and separated into the following four fractions, depending upon the color:[11]

Fr. 1 blue oil (654.9 mg)··· {S-guaiazulene (II) (35.3 mg) / 2-benzylguaiazulene (V) (50.0 mg)}

Fr. 2 green oil (338.6 mg)···2-benzoylguaiazulene (III) (225.9 mg)

Fr. 3 purple oil (340.1 mg)···1-benzoyl-7-isopropyl-3,4-dimethylazulene (IVa) (113.4 mg)

Fr. 4 brown oil (715.2 mg)···3-benzoylguaiazulene (I) (recovered)

2-Benzylguaiazulene (V). The blue oil of Fr. 1 showed two blue spots (R_f, 0.36 and 0.16) in tlc with *n*-hexane. By means of *n*-hexane-silica-gel elution chromatography, it was separated into two components, corresponding to the two spots in tlc. The oil of R_f, 0.36 was identical with the authentic specimen of II in tlc. V was obtained as a blue oil with an R_f of 0.16, and it gave a dark brown picrate upon treatment by the usual method. After being recrystallized from ethanol, it showed a mp of 106—108°C. UV: nm (log ε), 247.6 (4.38), 291 (4.75), 297 (4.80), 309 (4.23), 341 (3.65), 355 (3.76), 382 (3.26), 390sh (2.74). Visible absorption spectrum: nm (ε), 550sh (313), 592 (422), 632sh (368). NMR ($CDCl_3$): 2.53 (s, 3H; Me_1), 4.29 (s, 2H; CH_2), 7.20 (s, 5H; Ph), 2.75 (s, 3H; Me_4), 1.34/2.95 (d, 6H/m, 1H, J=6.8 Hz; *i*-Pr), 8.16 (d, 1H, J=1.8 Hz; H_8), 6.8—7.7 (m, 3H; $H_{3,5,6}$). NMR (CF_3COOH)[3]: 2.52 (t, 3H, J=1.8 Hz; Me_1), 4.20 (s, 2H; CH_2), 7.34 (s, 5H; Ph), 3.89 (q, 2H, J=1.8 Hz; $2H_3$), 2.92 (s, 3H; Me_4), 8.47 (s, 2H; $H_{5,6}$), 1.55/3.53 (d, 6H/m, 1H, J=6.8 Hz; i-Pr), 8.67 (s, 1H; H_8). MS: *m/e* 288 (M, $C_{22}H_{24}$; 14.3%), *m/e* 273 (M-CH_3; 11.4%), *m/e* 197 (M-$C_6H_5CH_2$; 11.2%), *m/e* 91 (C_7H_7; base peak).

Huang-Minlon Reduction of 2-Benzoylguaiazulene (III). By reference to the procedure of Treibs,[12] a solution of III (104.9 mg) and 100% hydrazine hydrate (0.2 m*l*) in triethylene glycol (2 m*l*) was heated under reflux for 1 hr. To this hot solution, powdered potassium hydroxide (100 mg) was slowly added; the mixture was then gradually brought to room temperature, during which time a vigorous evolution of nitrogen gas was observed and the color of the mixture changed from green to blue. A blue-colored fraction was collected by distilling, under reduced pressure, a mixture of triethylene glycol diluted with water, and the colored material was extracted repeatedly with benzene to give a blue oil (70.7 mg). By means of successive petroleum ether-silica-gel elution chromatography, 2-benzylguaiazulene (V) was separated as a blue oil (36.8 mg) which showed a single spot (R_f, 0.16) in tlc with *n*-hexane.

2-Benzoylguaiazulene (III). The green oil of Fr. 2 was purified by repeated benzene-silica-gel elution chromatography to afford green crystals which showed, after recrystallization from ethanol, a mp of 87.5—88.5°C. It exhibited a single spot (R_f, 0.42) in tlc with benzene. IR: 1633 cm^{-1} (C=O). UV: nm (log ε), 252.5 (4.45), 302 (4.73), 307.5sh (4.67), 345 (3.82), 356 (3.81). Visible absorption spectrum: nm (ε), 645 (598), 736sh (258). NMR ($CDCl_3$): 2.69 (s, 3H; Me_1), 2.74 (s, 3H; Me_4), 6.94 (d, 1H, J=10.1 Hz; H_5), 1.35/3.04 (d, 6H/m, 1H, J=6.4 Hz; *i*-Pr), 8.27 (d, 1H, J=1.5 Hz; H_8), 7.2—8.0 (m, 7H; Ph, $H_{3,6}$). NMR (CF_3COOH)[3]: 2.45 (t, 3H, J=2.0 Hz; Me_1), 4.59 (q, 2H, J=2.0 Hz; $2H_3$), 3.18 (s, 3H; Me_4), 8.91 (s, 2H; $H_{5,6}$), 1.63/3.54 (d, 6H/m, 1H, J=7.0Hz; *i*-Pr), 9.03 (s, 1H; H_8), 7.6—8.2 (m, 5H; Ph). MS: *m/e* 302 (M, $C_{22}H_{22}O$; base peak), *m/e* 287 (M-CH_3; 69.1%), *m/e* 259 (M-C_3H_7; 8.4%), *m/e* 197 (M-C_6H_5CO; 19.1%), *m/e* 105 (C_6H_5CO; 76.2%), *m/e* 77 (C_6H_5; 83.8%).

Found: C, 87.05; H, 6.82. Calcd for $C_{22}H_{22}O$: C, 87.37; H, 7.33%.

The Grignard Reaction of 2-Acetylguaiazulene (VI) with Bromobenzene. To an ethereal solution of a Grignard reagent prepared from bromobenzene (8.4 g) in the usual manner,

9) W. Treibs, *Chem. Ber.*, **90**, 761 (1957).

10) D. H. Reid, W. H. Stafford, and W. L. Staffored, *J. Chem. Soc.*, **1958**, 1118.

11) Next to the dotted lines are shown the compounds obtained from each fraction after it had been further purified by means of elution chromatography or recrystallization.

12) W. Treibs, H.-J. Neupert, and J. Hiebsch, *Chem. Ber.*, **92**, 141 (1959).

under water cooling, another solution of VI (1.9 g) in ether (20 ml) was added, drop by drop, over a 10-min period. After the mixture had then been allowed to stand at room temperature for 7 hr, the excess reagent was decomposed with methanol (25 ml) and subsequently with a dilute aqueous solution of ammonium hydroxide. From the ether layer, a green resinous material was obtained; it was separated into two components by the use of petroleum ether-silica-gel elution chromatography. The olefin (VII) was obtained from the quickly-eluted fraction as a blue oil (169.0 mg) which showed a single spot (R_f, 0.68) in tlc with petroleum ether. NMR ($CDCl_3$): 2.37 (s, 3H; Me_1), 5.74/5.35 (d, 1H/d, 1H, J=2.0 Hz; $=CH_2$), 7.16 (s, 5H; Ph), 2.72 (s, 3H; Me_4), 6.84 (d, 1H, J=10.5 Hz; H_5), 1.28/3.02 (d, 6H/m, 1H, J=7.2 Hz; *i*-Pr), 8.04 (d, 1H, J=1.8 Hz; H_8), 7.0—7.4 m, 2H; $H_{3,6}$).

From the slowly-eluted fraction, the reduced product (VIII) was obtained as a blue oil (269.3 mg), which exhibited a single spot (R_f, 0.58) in tlc with petroleum ether. NMR ($CDCl_3$): 2.40 (s, 3H; Me_1), 1.74/4.45 (d, 3H/q, 1H, J=7.5 Hz; $-CH-CH_3$), 7.05 (s, 5H; Ph), 2.76 (s, 3H; Me_4), 6.80 (d, 1H, J=10.5 Hz; H_5), 1.30/2.98 (d, 6H/m, 1H, J=6.8 Hz; *i*-Pr), 7.97 (d, 1H, J=2.0 Hz; H_8), 7.0—7.3 (m, 2H; $H_{3,6}$).

The Oxidation of 2-(1-Phenylethenyl)guaiazulene (VII) with Osmium Tetroxide. The olefin (VII) (169.0 mg) thus obtained was dissolved in a mixed solvent of pyridine (0.14 ml) and ether (5 ml), and then the solution was added, under dry ice-ethanol cooling (*ca.* −53°C), to a solution of osmium tetroxide (136 mg) in ether (15 ml). The mixture, when cooled for a further hour and then left to stand for a few hrs at room temperature, yielded green crystals; these crystals were separated by filtration and combined with those resulting from the filtrate by letting them stand a further hour at room temperature. The combined crystals were taken up into chloroform (20 ml), and the solution was shaken for 10 min with an aqueous solution (20 ml) containing mannitol (2.1 g) and potassium hydroxide (0.2 g). The subsequent removal of the solvent yielded rough glycol (IX) as a dark green oil (293.2 mg).

Periodate Oxidation of 1-Phenyl-1-(2-guaiazulenyl)ethanediol-1,2 (IX). The rough glycol (IX) dissolved, without further purification, in methanol (29 ml) was oxidized with a 0.05M aqueous solution of sodium metaperiodate by stirring the mixture at room temperature for 40 min under a nitrogen atmosphere. The reaction mixture was then poured into a saturated aqueous solution of sodium chloride, and the precipitate was extracted with ether to give a green mass (372.9 mg). This mass was chromatographed on silica gel with benzene, and then separated into blue crystals (1.9 mg, II) and green crystals (3.1 mg) of 2-benzoylguaiazulene (III).

1-Benzoyl-7-isopropyl-3,4-dimethylazulene (IVa). The purple oil of Fr 3 was further purified with benzene - silica-gel-elution chromatography to give IVa as a purple oil which showed a single spot (R_f, 0.24) in tlc with benzene. IR: 1606 cm^{-1} (C=O). UV: nm (log ε), 250 (4.43), 292 (4.34), 316 (4.38), 393 (4.01), 408sh (3.94). Visible absorption spectrum: nm (ε), 532sh (648), 565 (722), 600sh (576).

The 2,4-dinitrophenylhydrazone of this compound was obtained by using a mixed solvent of ethanol and phosphoric acid[13] as a reddish-brown powder. After being recrystallized with a mixed solvent of ethanol and ethyl acetate, it showed a mp of 249—251°C.

Found: C, 68.97; H, 5.56; N, 11.56%. Calcd for $C_{28}H_{26}N_4O_4$: C, 69.69; H, 5.43; N, 11.61%.

Methyl Guaiazulene-3-carboxylate (XI). This compound was synthesized by treating II with phosgene, followed by the treatment of acid chloride with methanol.[14] It was obtained as a purple oil which showed a single spot (R_f, 0.33) in tlc with benzene. IR: 1699 cm^{-1} (C=O). UV: nm (log ε), 228.5 (4.72), 238 (4.47), 239.5 (4.47), 243.5 (4.57), 249 (4.65), 255 (4.61), 261 (4.37), 264sh (4.00), 267.5 (4.00), 273sh (4.17), 280sh (4.40), 292sh (4.60), 298.5 (4.61), 314sh (4.39), 382 (3.86). Visible absorption spectrum: nm (ε), 544sh (462), 575 (552), 617sh (454) [572 nm[15]]. NMR ($CDCl_3$): 2.55 (s, 3H; Me_1), 7.94 (s, 1H; H_2), 3.87 (s, 3H; MeO), 2.91 (s, 3H; Me_4), 7.19 (d, 1H, J=10.8 Hz; H_5), 7.50 (dd, 1H, J=10.8 and 1.8 Hz; H_6), 1.34/3.07 (d, 6H/m, 1H, J=5.8 Hz; *i*-Pr), 8.23 (d, 1H, J=1.8 Hz; H_8). NMR (CF_3COOH)[3]: 2.46 (t, 3H, J=1.8 Hz; Me_1), 7.37 (m, 1H; H_2), 3.91 (s, 3H; MeO), 5.16 (m, 1H; H_3), 3.01 (s, 3H; Me_4), 1.56/3.44 (d, 6H/m, 1H, J=6.6 Hz; *i*-Pr), 8.68 (s, 3H; $H_{5,6,8}$). MS: *m/e* 256 (M, $C_{17}H_{20}O_2$; base peak), *m/e* 241 (M-CH_3; 25.5%), *m/e* 225 (M-OCH_3; 31.8%).

Thermal Reaction of Methyl Guaiazulene-3-carboxylate (XI). XI (1.66 g) was heated in a sealed tube at 250°C for 1 hr. The reaction mixture was chromatographed on silica gel with benzene, and then separated into the following fractions:

Fr. 1 S-guaiazulene (II) (13.2 mg)
Fr. 2 methyl guaiazulene-2-carboxylate (XIII) (1.3 mg)[1]
Fr. 3 methyl 7-isopropyl-3,4-dimethylazulene-1-carboxylate (XII) (87.3 mg)
Fr. 4 methyl guaiazulene-3-carboxylate (XI) (1.22 g) (recovered)

Methyl 7-Isopropyl-3,4-dimethylazulene-1-carboxylate (XII). In order to prevent contamination by a non-azulenic component or an acidic material, the purple oil of Fr. 3 (30.2 mg) was dissolved in a mixed solvent of benzene (1 ml) and petroleum ether (100 ml), after which the solution was extracted twice with 85% phosphoric acid (50 ml). An orange-colored phosphoric acid layer was washed repeatedly with petroleum ether and diluted with ice-water, and purple oil thus isolated was taken up into petroleum ether. After the removal of the solvent, XII was obtained as a purple oil (29.9 mg) which exhibited a single spot (R_f, 0.34) in tlc with benzene. IR: 1688 cm^{-1} (C=O). UV: nm (log ε), 228.5sh (4.23), 234sh (4.34), 240.5sh (4.47), 243.5 (4.56), 249 (4.63), 254.5 (4.54), 261 (4.22), 264 (3.71), 267.5 (3.69), 299.5 (4.68), 306.5 (4.66), 312 (4.51), 350 (3.73), 367 (3.93), 385 (4.08). Visible absorption spectrum: nm (ε), 532sh (540), 571 (720), 615.5 (594). MS: *m/e* 256 (M, $C_{17}H_{20}O_2$; base peak), *m/e* 241 (M-CH_3; 70.2%), *m/e* 225 (M-OCH_3; 23.6%).

Found: C, 78.96; H, 7.72%. Calcd for $C_{17}H_{20}O_2$: C, 79.65; H, 7.86%.

Hypoiodate Oxidation of 1-Acetyl-7-isopropyl-3,4-dimethylazulene (XIV). A solution of XIV (169.0 mg) in dioxane (22 ml) was mixed with a 10% aqueous solution of sodium hydroxide (23 ml) with stirring at 80°C. To this mixture, kept at 80°C, we added, drop by drop over a 20-min period, another aqueous solution (8.2 ml) of iodine (820 mg) and potassium iodide (1.64 g). After the mixture had been stirred for a further 10 min, the excess iodine was reduced by adding a few drops of a saturated sodium hydrogen sulfite

13) G. D. Johnson, *J. Amer. Chem. Soc.*, **73**, 5888 (1951).

14) W. Treibs, H.-J. Neupert and J. Hiebsch, *Chem. Ber.*, **92**, 1216 (1959).

15) W. Treibs, *ibid.*, **92**, 2152 (1959).

solution, the mixture was cooled to room temperature, and the reddish-brown iodoform thus precipitated was filtered off. The filtrate was diluted with water (30 ml), the solution was washed repeatedly with chloroform and acidified with 2N hydrochloric acid, and a crude acidic material was taken up into ether. A rough carboxylic acid (XV) was thus obtained as a brown oil (82.7 mg).

Preparation of Methyl Ester of 7-Isopropyl-3,4-dimethylazulene-1-carboxylic Acid (XV). To a solution of crude carboxylic acid (XV) (82.7 mg) in ether, we added an ethereal solution of diazomethane prepared from nitrosomethylurethane (4 g); the solution was then kept at room temperature for 8 hr. The reaction mixture was, after being treated in the usual manner, submitted to benzene - silica-gel elution chromatography to afford methyl 7-isopropyl-3,4-dimethylazulene-1-carboxylate (XII) as a purple oil (8.1 mg).

BULLETIN OF THE CHEMICAL SOCIETY OF JAPAN, VOL. 45, 3564—3566 (1972)

The Synthesis of 3′-Phosphate and 2′,3′-Cyclic Phosphate of 2-Amino-4-hydroxy-6-(1′,2′,3′-trihydroxypropyl)pteridine

Katsura SUGIURA, Haruhiro YAMASHITA, and Miki GOTO

Department of Chemistry, Gakushuin University, Toshima-ku, Tokyo

(Received February 9, 1972)

2-Amino-4-hydroxy-6-(D-*erythro*-1′,2′,3′-trihydroxypropyl)pteridine 3′-phosphate and 2′,3′-cyclic phosphate, important intermediates of pteridine biosynthesis, were prepared by simple methods. D-*erythro*-, L-*erythro*-, D-*threo*-, and L-*threo*-isomers of 2-amino-4-hydroxy-6-(1′,2′,3′-trihydroxypropyl)pteridine, prepared by the method of Viscontini, were phosphorylated with a mixture of phosphorus pentoxide and phosphoric acid. The products were separated by chromatography on a DEAE-cellulose column. The main phosphorylated compounds were 3′-phosphates; small amounts of 2′,3′-diphosphates were also produced. On treatment with DCC, the 3′-phosphate gave 2′,3′-cyclic phosphate.

In 1961, Goto and Forrest isolated a new phosphorylated pteridine from *E. coli*; the structure of 2-amino-4-hydroxy-6-(1′,2′,3′-trihydroxypropyl)pteridine-3′-phosphate was proposed for this compound.[1] The pteridine was synthesized in a very low yield by the condensation of 2,4,5-triamino-6-hydroxypyrimidine with D-ribose-5-phosphate[1,2] and by the reaction of 2-amino-4-hydroxy-6-(D-*erythro*-1′,2′,3′-trihydroxypropyl)pteridine (neopterin) with 2-cyanoethyl phosphate, followed by mild alkaline hydrolysis.[3] The biological function of this compound (neopterin-3′-phosphate) was proved to be that of a key compound in the biosynthesis of folic acid and the biopterin group of co-factors.[4-6] The occurrence of L-*threo*-neopterin (monapterin), and possibly its 2′,3′-cyclic phosphate, in nature has been reported.[7-9] Recently, the enzymic transformation of D-*erythro*-neopterin to D-*threo*-neopterin has been demonstrated.[10]

For the study of the biosynthesis of pteridines, we have synthesized the 3′-phosphates of D-*erythro*-, L-*erythro*-, D-*threo*-, and L-*threo*-neopterins by simplified methods; we used the phosphorylation procedure usually applied to nucleosides.[11] The neopterins were prepared by the method of Viscontini *et al.*[12] and were phosphorylated with a mixture of phosphorus pentoxide and phosphoric acid. The products were separated by chromatography on a DEAE-cellulose column. The main phosphorylated compounds were 3′-phosphates (I); small amounts of 2′,3′-diphosphates were also produced. Furthermore, the 2′,3′-cyclic phosphate of D-*erythro*-neopterin was synthesized by the action of DCC on D-*erythro*-neopterin-3′-phosphate.[13] The cyclic phosphate of D- or L-*erythro*-neopterin was recently isolated from *Photobacterium phosphoreum* (Suzuki and Goto, unpublished).

The biochemical function of the pteridines thus synthesized will be discussed elsewhere.

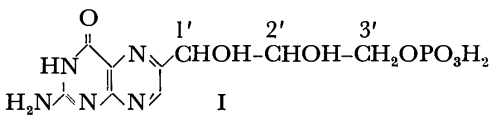

I

Expeirmental

2-Amino-4-hydroxy-6-(1′,2′,3′-trihydroxypropyl)pteridine.[14] D-*erythro*-, L-*erythro*-, D-*threo*-, and L-*threo*-neopterins were prepared as has been described by Viscontini *et al.*[12] D-Arabinose phenylhydrazone (8.9 g, 34.8 mmol) and 2,4,5-triamino-6-hydroxypyrimidine dihydrochloride (6.8 g, 31.8 mmol) in 50% methanol (1600 ml, a few drops of 2-thio-

1) M. Goto and H. S. Forrest, *Biochem. Biophys. Res. Commun.*, **6**, 180 (1961).
2) R. Tschesche and G. Sturm, *Chem. Ber.*, **98**, 851 (1965).
3) M. Goto, M. Ohno, H. S. Forrest, and J. M. Lagowski, *Arch. Biochem. Biophys.*, **110**, 444 (1965).
4) J. B. Mathis and G. M. Brown, *J. Biol. Chem.*, **245**, 3015 (1970).
5) K. Sugiura and M. Goto, *Biochem. Biophys. Res. Commun.* **28**, 687 (1967).
6) K. Sugiura and M. Goto, *J. Biochem.*, **64**, 657 (1968).
7) M. Viscontini, M. Pouteau-Thouvenot, R. Bühler-Moor, and M. Schroedder, *Helv. Chim. Acta.*, **47**, 1948 (1964).
8) K. Iwai, M. Kobayashi, and H. Fujisawa, "Chemistry and Biology of Pteridines," ed. by K. Iwai, M. Akino, M. Goto and Y. Iwanami, International Academic Printing Co., Tokyo (1970), p. 199.
9) G. Guroff and C. A. Rhoads, *J. Biol. Chem.*, **244**, 142 (1969); T. Urushibara, H. S. Forrest, D. S. Hoare, and R. N. Patel, *Biochem. J.*, **125**, 141 (1971).
10) G. M. Brown, "Chemistry and Biology of Pteridines," ed. by K. Iwai, M. Akino, M. Goto, and Y. Iwanami, International Academic Printing Co., Tokyo (1970), p. 243.
11) A. M. Michelson, *J. Chem. Soc.*, **1958**, 1957.
12) M. Viscontini, R. Provenzale, S. Ohlgart, and J. Mallevialle, *Helv. Chim. Acta*, **53**, 1202 (1970).
13) M. Smith, J. G. Moffatt, and H. G. Khorana, *J. Amer. Chem. Soc.*, **80**, 6204 (1958).
14) Abbreviated as neopterin in this paper; neopterin is actually a D-*erythro* form of the compound.

ethanol were added) were refluxed for 3.5 hr under nitrogen. The reaction mixture was then concentrated to dryness *in vacuo*, the residue was dissolved in water (1600 m*l*), and the solution was neutralized with a 5% sodium bicarbonate solution. After aeration for 18 hr, the solution was acidified with acetic acid to pH 3—4 and acetone (30 m*l*) was added. The precipitate was collected by centrifugation and washed, in succession, with ice water, ethanol, acetone, and ether. The crude product was then dissolved in ammonia (pH 8.0) and purified by a conventional chromatographic method using a Dowex 1X8 column ($HCOO^-$, 7.5×24.0 cm) and a 0.03M ammonium formate buffer; the pH of the developer was changed continuously from 8 to 7. The reaction mixture was then separated into three fluorescent bands. The eluate of the second band was concentrated to 1 *l*, and the solution was kept in a refrigerator to give 3.0 g (37%) of D-*erythro*-neopterin. Recrystallization from water gave 1.1 g of needles.

Similarly, L-*erythro*-, D-*threo*-, and L-*threo*-neopterins were prepared by the condensation of 2,4,5-triamino-6-hydroxypyrimidine with L-arabinose-, D-xylose-, and L-xylose-phenylhydrazones respectively. The analyses, yields, and optical rotations of the products are summarized in Table 1.

Phosphorylation. D-*erythro*-Neopterin (1 mmol), 85% phosphoric acid (6 g) and phosphorus pentoxide (4 g) were mixed at 0°C, after which the mixture was stirred at 40—45°C for 1 hr. Water (60 m*l*) was added and heated for 30 min at 95—100°C. The compounds were adsorbed on charcoal (5 g); the charcoal was then washed well with water and eluted with a solution containing 50% ethanol and 4% ammonia (1 : 1). The eluted solution was concentrated to a small bulk at below 40°C; then it was put on the top of a DEAE-cellulose column (3.0×15.0 cm), which was then washed successively with 0.001N hydrochloric acid, 0.003N hydrochloric acid-0.01M lithium chloride, and 0.003N hydrochloric acid-0.1 M lithium chloride. Neopterin was eluted

Table 1. Synthesis of neopterin-analysis, yield and $[\alpha]_D$

Compound	Analysis			Yield (%)	$[\alpha]_D$ [a] (c=0.3 in 0.1N HCl)
Found:	C%	H%	N%		
D-*erythro*-Neopterin	42.60	4.25	27.66	37	+47.8±2.5° (27.5°C)
L-*erythro*-Neopterin	42.99	4.37	27.66	42	−33±3° (24.5°C)
D-*threo*-Neopterin	43.12	4.00	27.07	33	−112±2 (24.5°C)
L-*threo*-Neopterin	42.32	4.33	27.91	67	+85±2° (24.5°C)
Calcd for $C_9H_{11}N_5O_4$	42.69	4.38	27.67		

a) For Ref. see lit. 12, 15, 16, 17.

Table 2. Phosphorylation of neopterin—yield (in TOD[a])

Neopterin		Phosphorylated compound		
		neopterin 0.001 N HCl	3'-phosphate 0.003N HCl—0.01 M LiCl	2',3'-phosphate 0.003 N HCl—0.1 M LiCl
D-*erythro*	7480	2000	1880	157
L-*erythro*	7480	2300	2310	666
D-*threo*	7480	3200	2370	500
L-*threo*	7480	1680	2400	540

a) TOD: Optical density (365 nm) of the product in 1 m*l* of 0.1—0.2 N NaOH.

Table 3. Analysis of neopterin-phosphates

Compound	Analysis			
	C%	H%	N%	P%
Found:				
D-*erythro*-Neopterin-3'-phosphate	30.64	4.09	22.19	8.47
L-*erythro*-Neopterin-3'-phosphate	30.03	3.96	21.65	7.90
D-*threo*-Neopterin-3'-phosphate	31.11	4.06	22.71	7.55
L-*threo*-Neopterin-3'-phosphate	—	—	—	—
Calcd for $C_9H_{11}O_7N_5P^- \cdot NH_4^+ \cdot H_2O$	29.35	4.62	22.83	8.42
Found:				
D-*erythro*-Neopterin-2',3'-diphosphate	20.35	4.51	19.83	11.7
Calcd for $C_9H_{11}O_{10}N_5P_2^{2-} \cdot 2NH_4^+ \cdot 4H_2O$	20.81	5.20	18.88	11.9

15) K. J. M. Andreus, W. E. Barber, and B. P. Tong, *J. Chem. Soc., C*, **1969**, 928.
16) H. Rembold and L. Buschmann, *Chem. Ber.*, **96**, 1406 (1963).
17) M. Viscontini and R. Provenzale, *Helv. Chim. Acta*, **51**, 1500 (1968).

by the first solvent, the 3′-phosphate, by the second, and the 2′,3′-diphosphate, by the third solvent. Each eluted fraction was treated with charcoal as has been described above, and the crude material thus obtained was recrystallized from 50% ethanol. The product was obtained as ammonium salt. Likewise, the phosphorylation was carried out for L-*erythro*-, D-*threo*-, and L-*threo*-neopterin. The yields are given by total optical density (TOD), and the analytical values of the products are summarized in Tables 2 and 3.

Neopterin-3′-phosphate. On treatment with potassium metaperiodate in a 0.1 M potassium carbonate solution for 24 hr, this compound gave 2-amino-4-hydroxypteridine-6-carboxylic acid quantitatively. The phosphate (*ca.* 0.3 mg), magnesium acetate (0.005 mM), and alkaline phosphatase (10 units, from calf mucosa) in a 0.1 M tris-buffer (pH 9.5) were incubated at 37°C for 30 min; it was then hydrolyzed to neopterin theoretically. The phosphate was identical with the neopterin-3′-phosphate prepared by the condensation of 2,4,5-triamino-6-hydroxypyrimidine and D-ribose-5-phosphate; the comparison was carried out by chromatographic and electrophoretic methods.

Neopterin-2′,3′-diphosphate. On treatment with potassium periodate in a 0.1 M potassium carbonate solution for 24 hr at room temperature, neopterin-2′,3′-diphosphate remained unchanged. On treatment with alkaline phosphates, this compound gave neopterin quantitatively. This evidence indicates that the conversion of the 2′-phosphate to the 3′-phosphate occurred during the incubation process.

D-erythro-*Neopterin-2′,3′-cyclic phosphate.* Free D-*erythro*-neopterin-3′-phosphate was obtained by passing the ammonium salt (74 mg, 0.2 mM) through a Dowex 50 (H^+) column (developer: water). The effluent was evaporated to dryness *in vacuo* at below 30°C. The residue was dissolved in a mixture of triethylamine (0.03 m*l*, 0.2 mM) and water (2 m*l*). Methanol (15 m*l*) and DCC (1.03 g, 5 mM) were added, and the whole was refluxed for 30 min and evaporated to dryness. The residue was dissolved in a mixture of water (100 m*l*) and ether (50 m*l*) by shaking, and the insoluble portion was removed by filtration. The aqueous layer was evaporated to dryness *in vacuo*. The crude material thus obtained was purified further by chromatography using cellulose columns (5.0×25.0 cm) and the following developers: A, 2-propanol, 1% ammonia (2 : 1), and B, water. Recrystallization from a little water gave the faint yellow cyclic phosphate (yield, 44 mg).

Found: C, 33.30; H, 3.38; N, 20.02; P, 8.92%. Calcd for $C_9H_{10}O_6N_5P \cdot H_2O$: C, 32.43; H, 3.60; N, 21.02; P, 9.31%.

The sample was dried at 70—80°C and 0.01 mmHg for 12 hr over P_2O_5 for analysis. On treatment with 0.1 N hydrochloric acid at 95—100°C for 15 min, the cyclic phosphate gave only D-*erythro*-neopterin-3′-phosphate; this was identified by determining the optical rotation of the hydrolysis product (alkaline phosphatase). On treatment with a large excess of potassium metaperiodate in a 1 M sodium carbonate solution at room temperature for 12 hr, it remained unchanged.

The R_f-values of the pteridines are given in Table 4.

TABLE 4. PAPER CHROMATOGRAPHY AND ELECTROPHORESIS OF PTERIDINES

Compounds	R_f in Solvents[a]					
	A	B	C	D	E	F
2-Amino-4-hydroxypteridine (pterin)	0.67	0.54	0.37	0.29	0.45	0 mm
Pterin-6-COOH	0.44	0.21	0.05	0.11	0.44	−16
D-*erythro*-Neopterin	0.69	0.41	0.21	0.10	0.61	0
L-*erythro*-Neopterin	0.69	0.41	0.21	0.10	0.61	—
D-*threo*-Neopterin	0.65	0.38	0.18	0.10	0.59	—
L-*threo*-Neopterin	0.65	0.38	0.18	0.10	0.59	—
D-*erythro*-Neopterin-3′-phosphate	0.42	0.07	0.03	0.02	0.77	−15
L-*erythro*-Neopterin-3′-phosphate	0.42	0.07	0.03	0.02	0.77	—
D-*threo*-Neopterin-3′-phosphate	0.42	0.07	0.01	0.02	0.77	—
L-*threo*-Neopterin-3′-phosphate	0.42	0.07	0.01	0.02	0.77	—
D-*erythro*-Neopterin-2′,3′-diphosphate	0.29	~0	0.01	~0	0.89	−28
D-*erythro*-Neopterin-2′,3′-cyclic phosphate	0.67	0.35	0.07	0.02	0.74	−17

a) Solvents: A, 2-propanol, 2% ammonium acetate (1 : 1); B, 2-propanol, 1% ammonia (2 : 1); C, 2-propanol, 5% boric acid (4 : 1); D, 1-butanol, acetic acid, water (4 : 1 : 1); E, 3% ammonium chloride F, distance to anode in electrophoresis; buffer: 0.05 M acetic acid-sodium acetate (pH 4.25); 30 min and 500 volt/25 cm.

Photolyses of Ethoxalyl Azide in Alcohols and in Hydrocarbons Reactions of Ethoxalylnitrene

Tadao SHINGAKI, Masao INAGAKI, Matsuji TAKEBAYASHI,* and Walter LWOWSKI**

Institute of Chemistry, College of General Education, Osaka University, Toyonaka, Osaka

*** Research Center, New Mexico State University, Las Cruces, New Mexico 88001, U. S. A.*

(Received February 29, 1972)

The photolysis of ethoxalyl azide gives ethoxalylnitrene and ethoxycarbonyl isocyanate. The nitrene adds to C=C double bonds and is inserted into O-H and C-H bonds. At high ethanol concentrations, where the singlet nitrene predominates, the O-H insertion product is formed dominantly. At low ethanol concentrations, where much of the nitrene changes to the triplet state, the hydrogen-abstraction product is preferred. The reactivity of the nitrene toward the C-H bonds of 2-methylbutane is more selective than that of ethoxycarbonylnitrene.

In a preliminary communication,[1] we reported that thermolysis of ethoxalyl azide in alcohols gave ethoxycarbonylurethanes *via* ethoxycarbonyl isocyanate, the Curtius rearrangement product, whereas the photolysis of the azide in alcohols or hydrocarbons yielded *N*-alkoxy- or *N*-alkyl-ethoxalamides, whose formation could be explained by the assumption of ethoxalylnitrene as an intermediate. This paper will deal cheifly with the reactions of ethoxalylnitrene with alcohols and hydrocarbons, and with the reactivities of the nitrene toward C-H bonds of hydrocarbons studied in further detail.

Results and Discussion

All experiments on the photolysis of ethoxalyl azide were carried out in dichloromethane, since the neat azide was explosive.

Photolysis of Ethoxalyl Azide in Alcohols and in Hydrocarbons. Ethoxalyl azide (I) was decomposed by the light (mainly 2537 Å) of a low-pressure mercury arc in a mixture of dichloromethane with alcohols at —78°C in an atmosphere of nitrogen. The reaction gave ethoxalamide (IV) and *N*-alkoxyethoxalamides (V), accompanied by *N*-alkoxycarbonylurethanes (III) and the dehydrogenation products of the alcohols employed.

Similarly, the photolysis of I with hydrocarbons yielded *N*-alkyl- or *N*-cycloalkyl-ethoxalamides (VI) and ethoxalamide (IV), in addition to ethoxycarbonyl isocyanate (II). The yields of the products are listed in Table 1.

As is shown in Table 1, the yields of isocyanate (II) were almost the same in all cases, while those of the amides (IV and V, IV and VI) varied with the substrate employed. The results suggest that the mechanism for the formation of isocyanate is different from that for the formation of amides; the rearrangement of I into II seems to proceed *via* a concerted mechanism, whose transition state is expressed by I', as has been

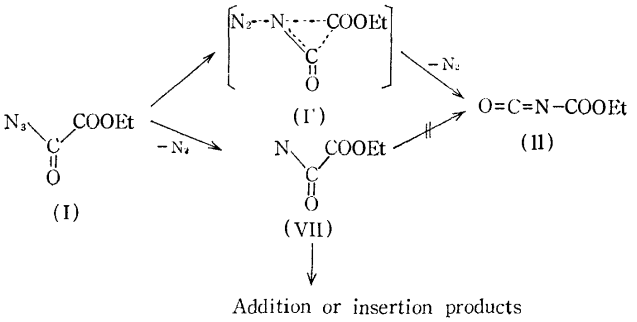

Scheme 1.

TABLE 1. PHOTOLYSIS OF ETHOXALYL AZIDE IN DICHLOROMETHANE

Substrate	Product (%)[a]			
	OCN-COOEt (II)	H_2NCO-COOEt (IV)	RONHCO-COOEt[b] (V)	R'NHCO-COOEt[c] (VI)
None	47	2.8	—	—
Ethanol	45[d]	9.8	26	—
2-Propanol	45[d]	16.0	22	—
Cyclohexane	41	3.7	—	16
Cyclopentane	45	3.7	—	17
Cyclohexene	43	5.3	—	e)
Benzene	48	3.8	—	11
2-Methylbutane	47	9.3	—	21[f]

a) The yields are calculated based on the amount of azide. b) R indicates an alkyl group. c) R' indicates a hydrocarbon rest. d) Determined as urethanes. e) *N*-Ethoxalylcyclohexanonimine (20%). f) Total yields of different types of C-H insertion products.

* Present address; Department of Chemistry, Faculty of Science and Technology, Kinki University, 321 Kowakae, Higashi-osaka, Osaka. To whom correspondence should be addressed.

1) T. Shingaki, M. Inagaki, M. Takebayashi, R. Lebkücher, and W. Lwowski, This Bulletin, **43**, 1912 (1970).

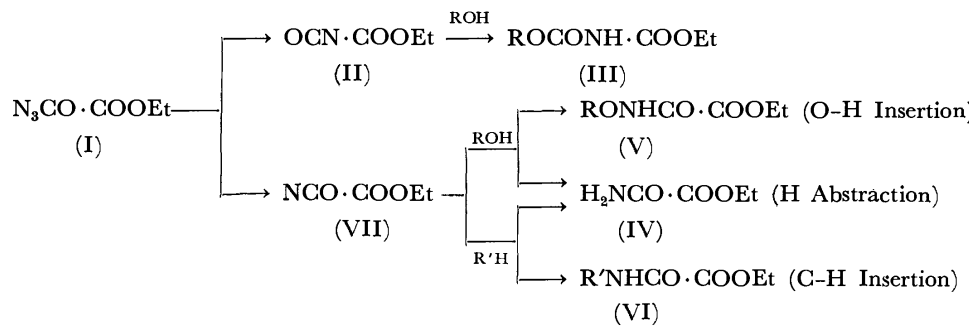

R: C_2H_5, $(CH_3)_2CH$
R': Alkyl, cycloalkyl, C_6H_5

Scheme 2.

pointed out in the Curtius rearrangement of pivaloyl azide[2,3] (Scheme 1).

On the contrary, the formation of IV, V, and VI can be explained by assuming the intermediacy of a carbonylnitrene, ethoxalylnitrene (VII), in a manner similar to that of the photolyses of ethyl azidoformate[4] and pivaloyl azide[3] in hydrocarbons (Scheme 2).

In the reaction with alcohols, no insertion products of ethoxalylnitrene into C-H bonds of alcohols were recognized in the reaction products (Table 1). This shows that ethoxalylnitrene is inserted preferentially into O-H bonds rather than C-H bonds, suggesting the electrophilic character of the nitrene, in analogy with ethoxycarbonylnitrene[5,6] and benzoylnitrene[7].

In the reaction with hydrocarbons, however, products (VI) from the insertion of ethoxalylnitrene into different types of C-H bonds were formed, excepting the case of cyclohexene (Table 1). The decomposition of I in cyclohexene gave a 20% yield of *N*-ethoxalylcyclohexanonimine (VIII) in place of insertion products. The product (VIII) may be formed by the addition of ethoxalylnitrene to the double bond of cyclohexene, followed by isomerization during gas chromatography at a column temperature.

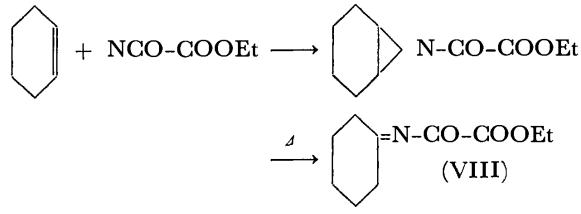

Dilution Effect. If it is assumed that the nitrene is formed in the singlet state and that part of the nitrene then changes into triplet nitrene before reacting with substrates, the lower the substrate concentration, the greater should be the quantity of triplet nitrene, leading to an increase in the formation of hydrogen-abstraction product (IV). This expectation led us to investigate the effect of the ethanol concentration on the distribution of ethoxamide (IV) and *N*-ethoxyethoxalamide (Va) in the product mixture. Table 2 shows the results of the photolyses of ethoxalyl azide in ethanol-dichloromethane mixtures, employing a 4 : 10 molar ratio of azide to ethanol. The ratio of the yield of IV to that of Va increased with the decrease in the ethanol concentration in dichloromethane. A similar tendency has been observed in the photolyses of ethyl azidoformate in isoprene-dichoromethane mixtures[8] and of pivaloyl azide in cyclopentane-neopentane (solvent) mixtures.[2]

TABLE 2. DISTRIBUTION OF IV AND Va IN THE PHOTOLYSIS OF ETHOXALYL AZIDE AT VARIOUS ETHANOL CONCENTRATION

Mole % of ethanol in CH_2Cl_2	Yield of IV[a] (%)	Yield of Va[a] (%)	Ratio of IV:Va
64	9.8	26	0.38
15	7.6	8.1	0.94
12	7.8	6.4	1.2
10	13	4.0	3.3
7.9	14	3.8	3.7
5.4	13	3.5	3.7
4.1	14	3.3	4.2
0	2.8	—	

a) The yields are calculated based on the amount of azide.

The results indicate that the singlet ethoxalylnitrene is inserted into the O-H bond of ethanol to give Va, while the triplet nitrene abstracts hydrogen atoms from ethanol to afford IV.

Reactivities of Ethoxalylnitrene toward the C-H Bonds in 2-Methylbutane. When ethoxalyl azide was photolyzed in a dichloromethane solution of 2-methylbutane, four isomeric insertion products (VIa—VId) were formed in a total yield of 21%.

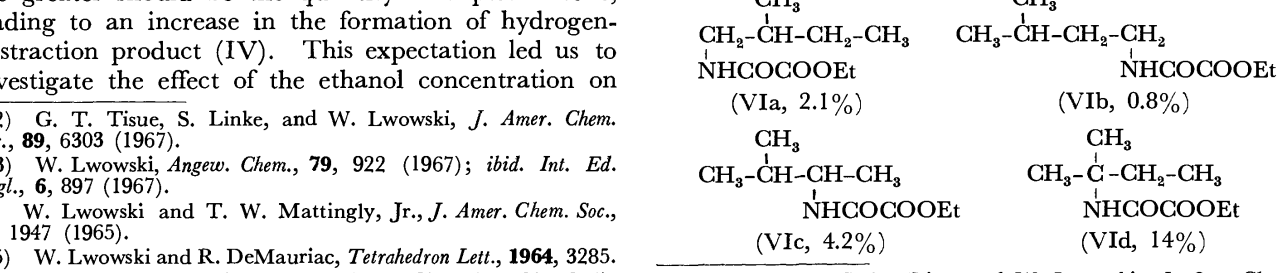

2) G. T. Tisue, S. Linke, and W. Lwowski, *J. Amer. Chem. Soc.*, **89**, 6303 (1967).
3) W. Lwowski, *Angew. Chem.*, **79**, 922 (1967); *ibid. Int. Ed. Engl.*, **6**, 897 (1967).
4) W. Lwowski and T. W. Mattingly, Jr., *J. Amer. Chem. Soc.*, **87**, 1947 (1965).
5) W. Lwowski and R. DeMauriac, *Tetrahedron Lett.*, **1964**, 3285.
6) R. Kreher and G. H. Bockhorn, *Angew. Chem.*, **76**, 681 (1964).
7) L. Horner and A. Christmann, *Chem. Ber.*, **96**, 388 (1963).
8) A. Mishra, S. N. Rice, and W. Lwowski, *J. Org. Chem.*, **33**, 481 (1968).

The division of their yields by the number of hydrogen atoms of each type available gives the relative reactivities of the various sites on 2-methylbutane. The two different sites of primary C-H bonds had nearly the same reactivity, within the limits of the accuracy of our measurements. The reactivities of ethoxalylnitrene toward primary (1°), secondary (2°), and tertiary (3°) C-H bonds of 2-methylbutane are summarized in Table 3, those of ethoxycarbonylnitrene[9] and pivaloylnitrene[2] toward the same C-H bonds are also cited there for the sake of comparison.

Table 3. Reactivities of ethoxalylnitrene and other carbonylnitrenes toward the C-H bonds in 2-methylbutane

Carbonylnitrene (from photolysis of azide)	Type of C-H bond		
	1°	2°	3°
N-CO-COOEt	1	6.6(±11%)[a]	43(±14%)
N-CO-OEt	1	9 (±10%)	34(±5%)
N-CO-C(CH_3)$_3$	1	8.6(±10%)	160(±25%)

a) The relative errors appear in parentheses.

The results indicate that the reactivity of ethoxalylnitrene is more selective than that of ethoxycarbonylnitrene, because of the larger resonance stabilization of the former.

Experimental

The IR spectra were recorded on a Hitachi EP-S spectrophotometer, and the NMR spectra were taken on a Hitachi R-20 instrument, using tetramethylsilane as the internal standard. Gas chromatography (vpc) was done on Yanagimoto GCG-3DH and GCG-5DH units, employing the following adsorbents: A, 10% Dioctyl phthalate on Neopak 1A (40~60 mesh); B, 15% Polyethylene glycol succinate on Neopak 1A (40~60 mesh). Quantitative analyses by vpc were carried out by calibrating the detector response for the compound in question by injecting known volumes of standard solutions and aliquots of the reaction mixture. Tests for the decomposition of samples during vpc analysis were made by collecting all the effluent in a dry ice-methanol trap, and by reinjecting. If no new vpc peaks appeared and no significant change was observed in the relative size and height of the peaks, decomposition was regarded as being absent.

Materials. Ethoxlyl azide (I) has been described in the literature[10], but the preparation of I from sodium azide and ethoxalyl chloride is much superior to the method reported in Ref. 10. Ethoxalyl chloride (29 g, 0.2 mol) dissolved in 60 g of dichloromethane was dropped, over a period of 0.5 hr, into a vigorously stirred solution of sodium azide (16 g, 0.24 mol) in 90 ml of water at −5~0°C. After the mixture had been stirred at 0°C for another 3 hr, the layers were separated, the aqueous layer was extracted with 20 ml of cold dichloromethane, and the combined dichloromethane solution was washed twice with a 10% sodium carbonate solution and water as soon as possible. The dichloromethane solution was dried repeatedly over anhydrous sodium sulfate at the dry ice-methanol temperature until a clear solution was obtained. Since free ethoxalyl azide, like other carbonyl azides of a low molecular weight, was predicted to be explosive at room temperature, the formation of ethoxalyl azide in the solution was confirmed by the reaction with ethanol at 35°C to give *N*-ethoxycarbonylurethane (IIIa), the yield of azide was observed to be 50—60% by the measurement of nitrogen evolved during the reaction. The dichloromethane solution of azide may be preserved for a couple of days at the dry ice-methanol temperature.

The alcohols and hydrocarbons, except for cyclohexene, were purified according to published directions[11]. Cyclohexene was prepared from cyclohexanol[12] and was then purified. The purities of the substrates and solvents were sufficiently proved by vpc.

Photolysis of I in Alcohols. About 50 g of a dichloromethane solution of I (about 0.04 mol), prepared by the reaction of 9.6 g (0.07 mol) of ethoxalyl chloride with 5.3 g (0.08 mol) of sodium azide, was placed in an irradiation vessel immersed in a dry ice-methanol mixture, and then 1.0 mol of an alcohol was added to the solution with stirring. After being flushed with dry nitrogen, the mixture was irradiated. When the evolution of nitrogen was over, the solvent was removed at room temperature under a 1-mmHg pressure, and the residue was distilled at 30—150°C under a 1×10^{-2}-mmHg pressure. The distillate was analyzed by vpc using the A adsorbent, the structures of the products were determined by means of elemental analyses and by measurements of IR and NMR spectra.

In the photolysis of I (6 g, 0.042 mol) in ethanol, *N*-ethoxycarbonylurethane (IIIa), ethoxalamide (IV), and *N*-ethoxyethoxalamide (Va) were obtained in yields of 3.0 g (45%), 0.48 g (9.8%), and 1.8 g (26%) respectively. In the photolysis of I (5.6 g, 0.039 mol) in 2-propanol, *N*-isopropoxycarbonylurethane (IIIb), IV, and *N*-isopropoxyethoxalamide (Vb) were isolated in yields of 3.1 g (45%), 0.73 g (16%), and 1.5 g (22%) respectively. These products showed the following physical properties.

N-Ethoxycarbonylurethane (IIIa): mp: 49—50°C. IR (KBr, cm^{-1}): 3220 (NH); 1750 (C=O); 1210 (C-O). NMR (CCl_4, τ): 1.83 (NH, bs); 5.79 (C-CH_2, 4H, q); 8.70 (CH_3, 6H, t). Found: C, 44.71; H, 6.88; N, 8.69%. Calcd for $C_6H_{11}O_4N$: C, 44.90; H, 7.13; N, 8.60%.

N-Isopropoxycarbonylurethane (IIIb): IR (CCl_4, cm^{-1}): 3250 (NH); 1770, 1727 (C=O); 1380, 1360 (Me_2CH); 1215, 1200 (C-O).

NMR (CCl_4, τ): $(CH_3)_2CH$-OCO-NH-COO-CH_2-CH_3

8.73 (d) 5.06 (h) 1.98 (bs) 5.84 (q) 8.70 (t)

Found: C, 47.56; H, 7.29; N, 7.78%. Calcd for $C_7H_{13}O_4N$: C, 47.99; H, 7.48; N, 8.00%.

Ethoxalamide (IV): mp: 114°C. IR (KBr, cm^{-1}): 3350, 3200 (NH); 1735, 1685 (C=O); 1215 (C-O). NMR ($CDCl_3$, τ): 3.10 (NH_2, bs); 5.62 (O-CH_2, q); 8.60 (CH_3, t). Found: C, 41.31; H, 6.12; N, 11.91%. Calcd for $C_4H_7O_3N$: C, 41.99; H, 6.03; N, 11.96%.

N-Ethoxyethoxalamide (Va): IR (CCl_4, cm^{-1}): 3300 (NH); 1750, 1720 (C=O); 1215 (C-O).

9) W. Lwowski and T. J. Maricich, *J. Amer. Chem. Soc.*, **86**, 3164 (1964); cf. *ibid.*, **87**, 3630 (1965); M. F. Sloan, T. J. Prosser, N. R. Newburg, and D. S. Breslow, *Tetrahedron Lett.*, **1964**, 2445; D. S. Breslow, T. J. Prosser, A. F. Marcantonio, and C. A. Genge, *J. Amer. Chem. Soc.*, **89**, 2384 (1967).

10) T. Curtius and K. Hochschowender, *J. Prakt. Chem.*, (2) **91**, 415 (1915).

11) A. Weissberger and W. S. Pooskauer, "Organic Solvents," in "Technique of Organic Chemistry", Vol. VII, Interscience Publishers, Inc., New York, N. Y. (1935).

12) C. S. Marvel and A. B. Adams, "Organic Syntheses", Coll. Vol. I, (1956) p. 183.

NMR (CCl_4, τ): CH_3-CH_2-ONH-COCOO-CH_2-CH_3
8.70 6.05 0.15 5.80 8.65
(t) (q) (bs) (q) (t)

Found: C, 44.31; H, 6.72; N, 8.65%. Calcd for $C_6H_{11}O_4N$: C, 44.71; H, 6.88; N, 8.69%.

N-Isopropoxyethoxalamide (Vb): IR (CCl_4, cm^{-1}): 3200 (NH); 1770, 1750 (C=O); 1380, 1360 (Me_2CH); 1220 (C-O). NMR (CCl_4, τ): $(CH_3)_2$CH-ONH-COCOO-CH_2-CH_3
8.74 5.80 0.30 5.74 8.62
(d) (h) (bs) (q) (t)

Found: C, 47.48; H, 7.45; N, 8.07%. Calcd for $C_7H_{13}O_4N$: C, 47.99; H, 7.48; N, 8.00%.

Photolysis of I in Cyclic Hydrocarbons. To about 50 g of a dichloromethane solution of I (about 0.04 mol), prepared from ethoxalyl chloride (9.6 g, 0.07 mol) with sodium azide (5.3 g, 0.08 mol), we added a mixture of a cyclic hydrocarbon (ten times the molar quantity of the I employed) and about 60 g of dichloromethane (the total amount of dichloromethane was adjusted to thirty times the molar quantity of the I), and then the photolysis was carried out as has previously been described. The isocyanate (II) thus produced was trapped at room temperature under a 1-mmHg pressure in a vessel, cooled by dry ice-methanol, and refluxed for two hr with an adequate amount of ethanol in order to convert it into *N*-ethoxycarbonylurethane (IIIa). The yield of II was estimated from that of IIIa, since the conversion of II into IIIa proceeded quantitatively.

The other products contained in the distillation residue were collected at 30—200°C under a 1×10^{-2}-mmHg pressure and were analyzed by vpc using the B adsorbent and the corresponding urethanes as standard materials.

In the photolysis (I: 5.4 g, 0.0378 mol) in cyclohexane, *N*-cyclohexylethoxalamide (VI-1), IV, and II were obtained in yields of 1.2 g (16%), 0.17 g (3.7%), and 2.5 g (41%) respectively. In the photolysis (I: 5.7 g, 0.04 mol) in cyclopentane, *N*-cyclopentylethoxalamide (VI-2), IV, and II were obtained in yields of 1.3 g (17%); 0.17 g (3.7%), and 2.9 g (45%) respectively. In the photolysis (I: 6.0 g, 0.042 mol) in benzene, *N*-phenylethoxalamide (VI-3), IV, and II were isolated in yields of 0.9 g (11%), 0.19 g (3.8%), and 3.3 g (48%) respectively. In the photolysis (I: 6.4 g, 0.045 mol) in cyclohexene, however, 1.8 g (20 %) of *N*-ethoxalylcyclohexanonimine (VIII) was obtained, accompanied by 0.28 g (5.3%) of IV, 2.2 g (43%) of II, and 3 g of an unidentified tarry substance.

The physical properties of VI-1, VI-2, VI-3, and VIII are shown below.

N-Cyclohexylethoxalamide (VI-1): mp: 145°C. IR (KBr, cm^{-1}): 3300 (NH); 1735, 1655 (C=O); 1205 (C-O). NMR (CCl_4, τ): 2.81 (NH, bs); 5.80 (C-CH_2, q); 6.33 (N-CH, m); 8.65 (CH_3, t). Found: C, 60.01; H, 8.37; N, 7.01%. Calcd for $C_{10}H_{17}O_3N$: C, 60.28; H, 8.60; N, 7.03%.

N-Cyclopentylethoxalamide (VI-2): IR (CCl_4, cm^{-1}): 3250 (NH); 1730, 1675 (C=O); 1210 (C-O). NMR (CCl_4, τ): 2.65 (NH, bs); 5.3—6.0 (N-CH, m); 5.74 (O-CH_2, q); 7.7—8.8 (ring CH_2, 8H, m); 8.63 (CH_3, t). Found: C, 58.20; H, 8.20; N, 7.60%. Calcd for $C_9H_{15}O_3N$: C, 58.36; H, 8.10; N, 7.56%.

N-Phenylethoxalamide (VI-3): mp: 66°C. IR (KBr, cm^{-1}): 3325 (NH); 3100, 1595 (arom. CH); 1710, 1695 (C=O). NMR (CCl_4, τ): 0.74 (NH, bs); 2.2—2.4, 2.55—3.0 (ring CH, 5H, m); 5.76 (O-CH_2, q); 8.72 (CH_3, t). Found: C, 62.02; H, 5.68; N, 7.22%. Calcd for $C_{10}H_{11}O_3N$: C, 62.16; H, 5.74; N, 7.25%.

N-Ethoxalylcyclohexanonimine (VIII): IR (CCl_4, cm^{-1}): 1745, 1700 (C=O); 1670 (C=N); 1200 (C-O). No bands of NH and olefinic CH were observed. NMR (CCl_4, τ): 5.68 (O-CH_2, q); 8.60 (CH_3, t); 7.9—8.8 (ring CH_2, 10H, m). No signals expected at the aziridine[4] and oxazoline[13] rings were recognized. Found: C, 60.61; H, 7.78; N, 7.21%. Calcd for $C_{10}H_{15}O_3N$: C, 60.89; H,

Table 4. Yields of ethoxalamides in reaction of ethoxalylnitrene with 2-methylbutane

Azide, mol	Product, g (mol %)				Relative ratio of product		
	VIa (1°)	VIb (1°)	VIc (2°)	VId (3°)	1°	2°	3°
0.145	0.61 (2.3)	0.23 (0.9)	1.11 (4.1)	3.67 (13.5)	1	5.8	38
0.125	0.51 (2.2)	0.16 (0.7)	0.94 (4.0)	3.04 (13.0)	1	6.2	40
0.135	0.53 (2.1)	0.23 (0.9)	1.11 (4.4)	3.46 (13.7)	1	6.6	41
0.141	0.52 (2.0)	0.18 (0.7)	1.13 (4.3)	3.56 (13.5)	1	7.2	45
0.117	0.42 (1.9)	0.18 (0.8)	0.96 (4.4)	3.26 (14.9)	1	7.3	50
mean	(2.1±9%)	(0.8±12%)	(4.2±5%)	(13.7±9%)	1	6.6 (±11%)	43 (±14%)

Table 5. IR of VIa—VId (CCl_4, cm^{-1})

	VIa	VIb	VIc	VId
N-H	3405 1510	3415 1520	3300 1530	3255 1520
C-H	2950	2935	2950	2950
C=O	1712	1710	1735 1690	1725 1695
C-N	1290 1270	1295 1275	1295 1275	1305 1287
C-O	1208 1160	1208 1160	1208 1163	1203 1165

13) W. Lwowski and T. J. Maricich, *J. Amer. Chem. Soc.*, **87**, 3630 (1965); cf. M. A. Weinberger and R. Greenhalgh, *Can. J. Chem.*, **41**, 1938 (1963).

Table 6. NMR of VIa—VId (in CCl_4, τ)

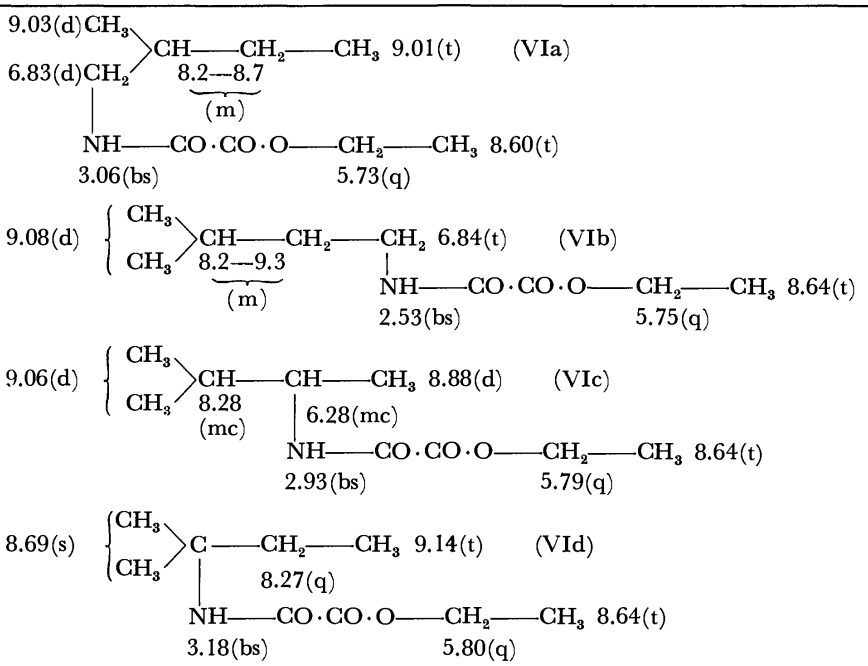

Table 7. Analytical data of VIa—VId

		C	H	N
Found (%):	VIa	57.51	9.10	7.62
	VIb	57.29	9.10	7.52
	VIc	57.48	9.17	7.49
	VId	57.65	9.20	7.60
Calcd (%) for $C_9H_{17}O_3N$:		57.73	9.15	7.48

7.67; N, 7.10%.

Dilution Effect. Dilution experiments were carried out, keeping the molar ratio of azide to ethanol at 4 : 10 (0.084 : 0.20 mol) and using dichloromethane as the diluent. For the quantitative determination of the products, the crude reaction mixture was injected into the vpc apparatus.

Photolysis of I in 2-Methylbutane (Reactivities of Ethoxalylnitrene toward C–H Bonds). A solution of 2-methylbutane (72 g, 1.0 mol) in 85 g of dichloromethane was added to 115 g of a dichloromethane solution of I (about 0.12 mol) on cooling, after which the mixture was irradiated as has been described. The reaction products were fractionated into two portions, as has been described in the case of cyclic hydrocarbons. The one fraction obtained under a 1-mmHg pressure gave 9.1 g (47%) of II. The other fraction, obtained under a 1×10^{-2}-mmHg pressure, was analyzed by vpc on a column containing the B adsorbent at 160°C, using *N*-cyclohexylethoxalamide as the standard material.

Four isomeric ethoxalamides, VIa—VId, were obtained in a total yield of 21%, besides 1.3 g (9.3%) of IV. The yields of the four isomers were determined by assuming that the detector response is nearly the same for VIa—VId, and were taken as the bases for the calculation of the relative reactivities in Table 3. The results are arranged on Table 4, while the physical and analytical data of VIa—VId are shown in Tables 5, 6, and 7.

Studies of Dithiobiurets. III. The Preparation and Properties of 3,5-Disubstituted 3*H*-1,2,4-Dithiazoles

Isao IWATAKI

Chemical Research Laboratory, Nippon Soda Co., Ltd., Kozu, Odawara

(Received March 2, 1972)

3,5-Disubstituted 3*H*-1,2,4-dithiazoles were prepared by the oxidation of dithiobiurets, *S*-benzylisodithiobiurets, and alkyl trithioallophanates, and then 3-acyl or carbamoylimino derivatives were obtained by the direct acylation or carbamoylation of the dithiazole salts. From the spectral data of these compounds, it is concluded that the carbonyl group affects the pseudoaromatic character of the dithiazole ring system.

We previously reported that 2-acetylimino-5-dimethylamino-3*H*-1,2,4-dithiazole hydrothiocyanate was obtained by the thermal decomposition of 1,1-dimethyl-5-acetyldithiobiuret.[1] The free base which was prepared by the neutralization with potassium carbonate did not show any carbonyl absorption in the infrared spectrum in spite of the existence of the acetyl group, while its hydrochloride or sulfate showed a strong carbonyl absorption band at 1690 cm^{-1}.

In this investigation, we prepared many related compounds and obtained new information concerning their pseudoaromatic chartacteristics from their spectral properties. Indeed, 3-acylimino or carbamoylimino dithiazole derivatives showed the same behavior as 2-acetylimino-5-dimethylamino-3*H*-1,2,4-dithiazole, except in a few cases.

Dithiazole derivatives, prepared by the oxidation of dithiobiurets, are well known as thiurets. Their structure had been studied by mean of IR, UV, X-ray, *etc.*, and their pseudoaromatic ring system has been confirmed by many workers. Unsubstituted thiuret, prepared by the oxidation of dithiobiuret with hydrogen peroxide in hydrochloric acid, was first formulated as having a hydrochloride of diiminodithiazole structure I,[2] but this compound formed salt with only one equivalent of acid; therefore, Jensen, Baccaro and Buchardt[3] considered that the basic ion was the diaminodithiazolyl ion, II. Furthermore, they described that 1,2,4-dithiazole derivatives showed an strong infrared band at 1510—1540 cm^{-1} which is due to the aromatic ring system.

Foss and Tjomsland[4] obtained data denying the I structure by X-ray methods, but they suggested that the conjugation does not extend over the S–S bond, unlike the cases of 3-alkyl or phenyl-1,2-dithiolium salts.[5]

Hordvik and Sundsfjord[6] concluded, from their structural investigations of the hydrobromide and the hydrochloride, that the relative weight of the resonance form containing the S–S double bond should be smaller in the 3,5-diamino-1,2-dithiolium ion than in the unsubstituted 1,2-dithiolium ion. Prinzbach and Futterer[7] described, with regard to the ion structure of 1,2 and 1,3-dithiolium salts, that the positive charge is largely locarized on the exocyclic nitrogen atom; they concluded this from the chemical shift of the proton at the 4 position in the nmr spectra. That is, the chemical shifts for H-4 in the cases of the 3,5-diamino VI and dimorpholino VIII derivatives appear in a high field (6.52 and 6.46 ppm) in comparison with the substituted 1,2-dithiolium salts (8—9 ppm). Thus, it is clear that the 3,5-diamino-1,2,4-dithiazole salts are of the III structure because they have the same properties as 3,5-diaminodithiolium salts. This fact has already been confirmed by Jensen, Baccaro, and Buchardt.[3] On the other hand, a preliminary result of a X-ray structural determination of 3,5-diacetamino-1,2-dithiolium iodide[8] indicates that a partial bonding between sulfur and oxygen leads to a shortening of the S–S bond; consequently, the stability of the dithiolium cation increases upon acetylation.

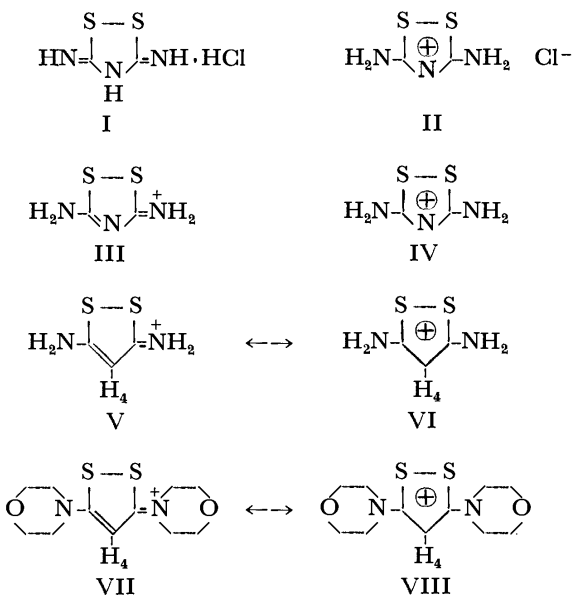

Results and Discussion

Preparation of the Starting 3H-1,2,4-Dithiazole Salts. 1-Mono or disubstituted 2,4-dithiobiurets, which were the starting materials of this study, were prepared by known methods. The first of these is by the fusion of

1) I. Iwataki and A. Ueda, This Bulletin, in press.
2) P. W. Preisler and M. M. Bateman, *J. Amer. Chem. Soc.*, **69**, 2632 (1947).
3) K. A. Jensen, H. R. Baccaro, and O. Buchardt, *Acta Chem. Scand.*, **17**, 163 (1963).
4) O. Foss and O. Tjomsland, *ibid.*, **12**, 1799 (1958).
5) A. Hordvik and H. M. Kjoge, *ibid.*, **19**, 935 (1965).
6) A. Hordvik and L. Sundsfjord, *ibid.*, **19**, 753 (1965).
7) H. Prinzbach and E. Futterer, Advances in Heterocyclic Chemistry, **7**, 39 (1966), Academic Press, New York, N. Y.
8) A. Hordvik and H. M. Kjoge, *Acta Chem. Scand.*, **19**, 523 (1965).

arylamines with perthiocyanic acid.[9] The second method is that of Dixit[10] whereby perthiocyanic acid is treated with aliphatic amines in water. He described that 1-alkyl-2,4-dithiobiurets were obtained in good yields at an ordinary temperature, but most of the 1,1-disubstituted derivatives could not be obtained by this method. The third method is the action of amines on methyl trithioallophanate. Bousquet obtained 1-aryl-2,4-dithiobiurets by the reaction of potassium trithioallophanate with anilines.[11] Aliphatic amines reacted with it, but no pure product could be obtained. On the other hand, methyl trithioallophanate which has been prepared from the potassium salt with dimethyl sulfate reacted with dialkylamines at an ordinary temperature to give 1,1-dialkyl-2,4-dithiobiurets. 1,1,5-Trisubstituted-2,4-dithiobiurets were also obtained from dialkylthiocarbamoylisothiocyanates.[12] The dithiobiurets thus prepared were oxidized with chlorine in an alcohol or chloroform solution to give the corresponding 3*H*-1,2,4-dithiazole hydrochlorides in good yields.

5-Alkylamino-*3*-imino or *5*-alkylamino-*3*-alkylimino dithiazole salts were prepared by Dixit's method[13] by means of the oxidative debenzylation of S-benzylisodithiobiurets which had previously been obtained by the reaction of S-benzylisothioureas and alkylisothiocyanates without going through dithiobiurets. Generally, free bases of 5-substituted amino-3-iminodithiazole salts are unstable and decompose to substituted cyanothioureas under alkaline conditions, even at low temperatures,[14] but 3-alkylimino derivatives are stable and can be isolated as free bases.[13]

Acylation of the Imino Group. Salts of the dithiazole derivatives react with acid anhydride in acetone or benzene at ordinary temperatures in the presence of 2 mole equivalents of tertiary amines to give the corresponding 3-acylimino derivatives. Higher fatty acid anhydrides, such as capric or palmitic anhydride, are less reactive and require heating. Acid halides also react with the salts, but the yields are always very low. In these cases, the acylation will occur on sulfur atoms and results in ring opening and decomposition. Acetic and propionic anhydrides react with them without tertiary amines, and keeping only at room temperature gives the corresponding acetylated or propionylated derivatives in good yields. 3-Acyliminodithiazoles are thermally unstable under alkaline conditions. When the reaction is carried out at a higher temperature, the primary product is formed first, but it is decomposed later by excess tertiary amine.

*Preparation of 3-acylimino-5-alkylthio-3*H*-1,2,4-dithiazoles.* Hydroiodides of 5-alkylthio derivatives were prepared by the method of Allen and Shelton from alkyl trithioallophanates.[15] The subsequent treatment of these salts with acid anhydrides, as described above, afforded the corresponding acylated compounds.

Spectral Properties. The dithiazole derivatives which were prepared by the above methods showed characteristic behavior in the infrared spectra. The frequencies of the carbonyl and C=N stretching bands of the related compounds are shown in Table 1. Most of the free bases of the 3-acylimino or carbamoylimino derivatives do not show carbonyl absorption in the region normally expected for amide groups, but a pair of absorptions appears at 1550—1600 cm^{-1}. These two bands have equal intensities, and one of them may be assigned to the C=N stretching band. All the 3-acylimino derivatives form salts with mineral acids, and the infrared spectra of the corresponding salts show an carbonyl absorption in the ordinary region, like mesoionic compounds (cf. Table 2).

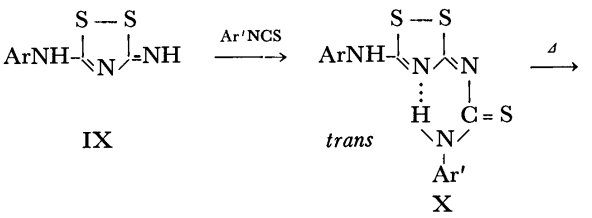

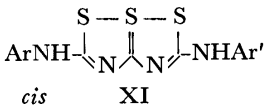

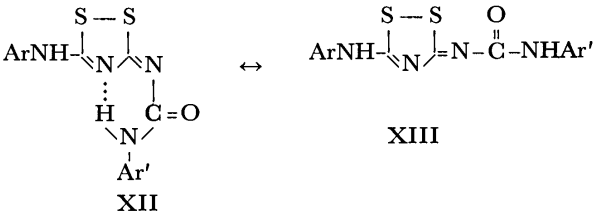

Behringer and Weber[16] obtained a trans form of 5-anilino-3-(N-phenyl)thiocarbamoylimino-3H-1,2,4-dithiazole X when IX was treated with phenylisothiocyanate, then it was converted to the *cis* form XI by heating. They confirmed those structures by studying the UV spectra. On the other hand, they also prepared carbamoyl derivatives; in those cases, they presumed that the carbamoyl groups were present in the tautomeric form, as is shown (XII and XIII). However, 5-dimethylamino-3-carbamoylimino derivatives showed an infrared absorption band of the carbonyl group in a region similar to that of the corresponding acyl derivatives, unlike the cases of 5-alkylamino or anilino-3-carbamoylimino derivatives. The difference between 5-dimethylamino and 5-monoalkyl or arylamino derivatives was further confirmed by studying the UV spectra. The UV spectra of the related compounds are shown in Table 3 and Fig. 1—3. Fig. 1 shows the spectra of the starting dithiazole

9) E. Fromm, *Ann.*, **275**, 20 (1893), A. E. S. Fairfull and D. A. Peak, *J. Chem. Soc.*, **1955**, 796.
10) S. N. Dixit, *J. Indian Chem. Soc.*, **38**, 44 (1961).
11) E. W. Bousquet and H. G. Guy, U. S. 2410862 (1946).
12) L. A. Spurlock and P. E. Newallis, *J. Org. Chem.*, **33** 2073 (1968). J. Goerdeler and H. Ludke, *Ber.*, **103**, 3393 (1970).
13) S. N. Dixit and V. K. Verma, *Indian J. Chem.*, **1** 487 (1963), S. N. Dixit, *J. Indian Chem. Soc.*, **39**, 407 (1962), C. P. Joshua and V. K. Verma, *ibid.*, **38**, 988 (1961), S. N. Dixit, *ibid.*, **40**, 153 (1963).
14) V. L. Nirenburg and I. Ya. Postouskii, *Zhur. Obshchei Khim.*, **28**, 198 (1958).
15) R. E. Allen, R. S. Shelton, and M. G. Van Campen, *J. Amer. Chem. Soc.*, **76**, 1158 (1954).
16) H. Behringer and D. Weber, *Chem. Ber.*, **97**, 2567 (1964).

Table 1. Infrared spectra of 3,5-disubstituted 3*H*-1,2,4-dithiazoles

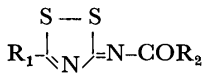

S. No.	R_1	R_2	C=O	C=N	Kind of salts and Mp (°C)		C=O	C=N or NH (cm^{-1})
(1)		CH_3	1600	1570	HCl	215[a)]	1690	1600
(2)		C_2H_5	1600	1560	HSCN	183—184[a)]	1685	1610
(3)		*n*-C_3H_7	1590	1570	HSCN	152—153	1690	1600
(4)		*n*-C_5H_{11}	1600	1570	HCl	92— 94	1690	1610
(5)		*n*-C_9H_{19}	1590	1560	HCl	115—117	1690	1610
(6)		CH=CH-CH_3	1590	1540	HCl	166—169[a)]	1670	1605
(7)		C_6H_5	1580	1530	HCl	148—149	1655	1605
(8)		CH_3	1570	1540	HSCN	159—160	1685	1580
(9)		CH_3	1560	1540	HSCN	157—159	1680	1590
(10)		CH_3	1560	1550	HCl	196—197[a)]	1695	1600
(11)		CH_3	1570	1540	HSCN	160—162[a)]	1660	1600
(12)		CH_3	1590	1585	HCl	194—195[a)]	1690	1620
(13)		CH_3	1690 1590	1585	HCl	180—181	1690 1680	1590
(14)		CH_3	1670 1590	1575	HCl	142—145[a)]	1680 1670	1600
(15)	SCH_3	CH_3	1570	1560	HSCN	143—144[a)]	1690	(1520)
(16)	SC_2H_5	CH_3	1580	1570	HSCN	112—113[a)]	1700 1680	(1510)
(17)	$SCH_2C_6H_5$	CH_3	1560	1555	HSCN	132—135[a)]	1680	(1510)
(18)		$NHCH_3$	1610	1590	HCl	230[a)]	1680 1670	1600
(19)		NHC_6H_5	1590	1550	HCl	212—214[a)]	1705	1705
(20)	NHC_6H_5	$NHCH_3$	1720	1610	HSCN	171—172[a)]	1680 1660	1600
(21)	NHC_6H_5	NHC_6H_5	1690	1630	HCl	202—203[a)]	1700	1630

a) Decomp.

Table 2. Infrared spectra of mesoionic compounds

S. No.	Compounds	C=O	Kind of salts	C=O	Ref.
(1)	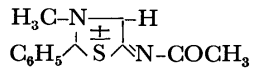	1560	HCl	1660	17)
(2)	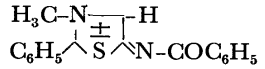	1580 1560	HCl	1750 1650	17)
(3)	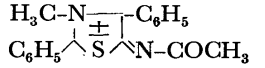	1550	HCl	1660	17)
(4)	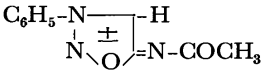	1640	HCl	1720	18)
(5)	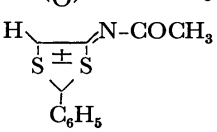		HCl	1670	19)

TABLE 3. UV SPECTRA OF 3,5-DISUBSTITUTED 3*H*-1,2,4-DITHIAZOLES

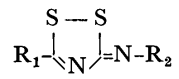

S. No.	R_1	R_2	λ_{max}^{EtOH} mμ (log ε)		$\lambda_{max}^{EtOH+HCl}$ mμ (log ε)		
(1)	$N(CH_3)_2$	$COCH_3$	297.7	(4.25)	312.6	(3.90)	272.1 (4.00)
(2)	$N(CH_3)_2$	COC_2H_5	297.8	(4.32)	311.9	(3.89)	273.1 (4.22)
(3)	$N(CH_3)_2$	CO-*n*-C_3H_7	299.1	(4.32)	313.4	(3.90)	273.9 (4.23)
(4)	$N(CH_3)_2$	CO-*n*-C_5H_{11}	298.7	(4.31)	313.1	(3.86)	273.0 (4.21)
(5)	$N(CH_3)_2$	COC_6H_5	319.5 253.6	(4.19) (4.20)	319.5	(4.12)	284.2 (4.51) 254.3 (4.37)
(6)	$N(C_6H_5)CH_3$	$COCH_3$	299.5	(4.31)	321.2	(3.87)	277.4 (4.23)
(7)	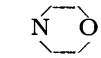	$COCH_3$	301.2	(4.33)	319.8	(4.12)	275.2 (4.30)
(8)		$COCH_3$	300.1	(4.37)	314.2	(4.02)	273.5 (4.25)
(9)	$N(C_6H_5)H$	$COCH_3$	314.7 244.0[a]	(4.22) (4.16)	345.9	(4.03)	281.9 (4.16)
(10)	SCH_3	$COCH_3$	340.1[a] 307.2	(3.91) (4.20)	332.3	(3.99)	301.8 (4.18)
(11)	$N(CH_3)_2$	$COOC_2H_5$	285.7	(4.37)	301.2	(3.91)	265.6 (4.31)
(12)	$N(CH_3)_2$	*t*-C_4H_9	290.0[a] 258.0	(4.16) (4.39)	294.0[a]	(4.19)	266.0 (4.46)
(13)	$N(CH_3)_2$	C_6H_5	299.9[a] 257.9	(3.95) (4.36)	318.4[a]	(4.17)	285.7 (4.33)

a) shoulder

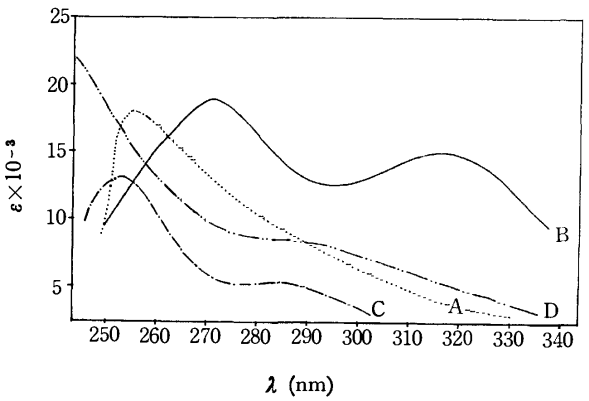

Fig. 1. UV spectra of 5-alkylamino or anilino-3-imino-3H-1,2,4-dithiazole salts.
A ····· 5-dimethylamino-3-imino-, hydrochloride.
B ——— 5-anilino-3-imino-, hydrochloride.
C —·—· 5-methylamino-3-imino-, hydrobromide.
D —··— 5-anilino-3-imino-.

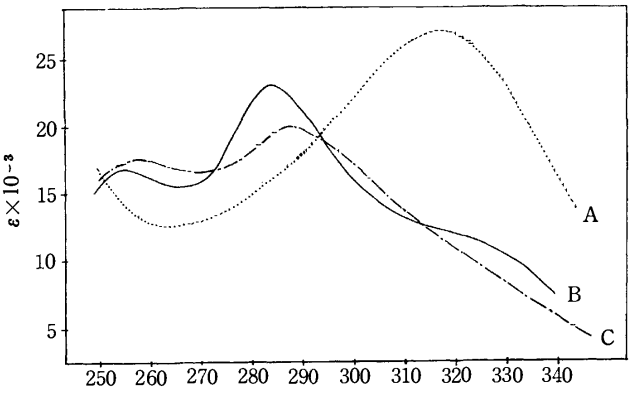

Fig. 2. UV spectra of 5-anilino or dimethylamino-3-(N-phenyl)carbamoylimino or benzoylimino-3*H*-1,2,4-dithiazoles.
A ····· 5-anilino-3-(*N*-phenyl)carbamoylimino-.
B ——— 5-dimethylamino-3-benzoylimino-.
C —·—· 5-dimethylamino-3-(*N*-phenyl)carbamoylimino-.

salts. The spectrum of 5-dimethylamino-3-(N-phenyl)carbamoylimino derivative is very similar to the corresponding 3-benzoylimino derivative and differs a little from the spectrum of the 5-anilino-3-(N-phenyl)carbamoylimino derivative. From this fact, it is obvious that the carbamoyl group of the 5-dimethylamino compound has the same conformation as the corresponding acyl derivatives and is located at the *cis* position, because the interaction between S and O can occur only at the *cis* form. Actually, all the acylimino derivatives will be in the *cis* form, because the intramolecular hydrogen bonding can not arise in the acyl series. The spectra of 3-(*N*-methyl)-carbamoylimino-5-substituted amino dithiazoles are shown in Fig. 3. The 5-monoalkylamino and 5-anilino derivatives gave similar spectra. They contain two amino protons, namely, *a* and *b*; the *a* proton is able to shift to the imino nitrogen at the 3 position by resonance, as is shown in XV, and then XV isomerizes to the trans structure, such as XVI or XVII.

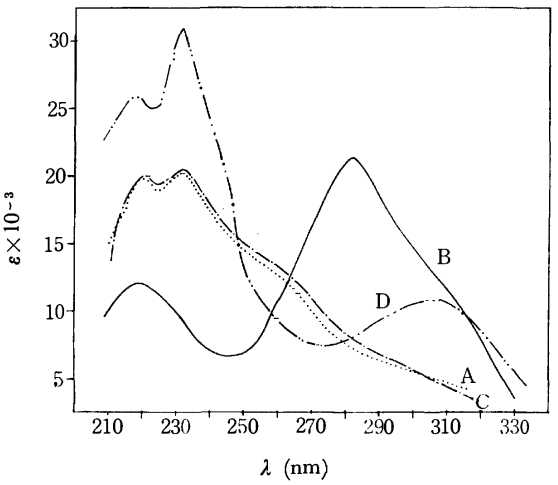

Fig. 3. UV spectra of 3-(*N*-methyl)carbamoylimino-3*H*-1,2,4-dithiazole derivatives.
A ····· 5-methylamino-.
B ———— 5-dimethylamino-.
C —·—· 5-ethylamino-.
D —··— 5-anilino-.

The presence of the *b* proton facilitates the formation of the stable *trans* conformation by intramolecular hydrogen bonding. On the other hand, as the 5-dimethylamino derivative does not contain the *a* proton, the resonance between XIV and XV does not occur and the *cis* compound is formed as in the cases of the acylation.

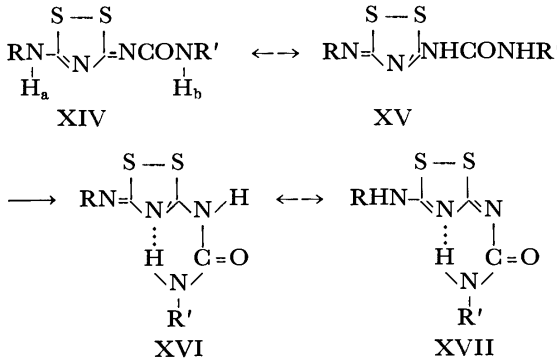

All the acylimino derivatives showed an absorption at about 290 mμ similar to the *N*-acyl sydnonimines,[19] and their salts showed a charge separation between the dithiazole ring and the exocyclic acylimido group.

A carbonyl group which combines with the 3-imino group facilitates the formation of a dithiazolyl cation, as is shown by XVIII and XIX; as a result, the dithiazole ring may be stable, like other heteroaromatic compounds.

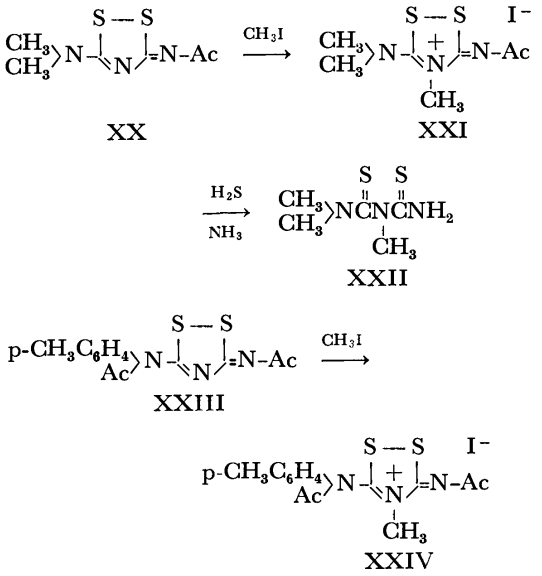

5-Alkyl or arylamino-3-acyliminodithiazoles were easily reacted with methyl iodide to give the methiodides in good yields. In these cases, the methylation occurred at the 4 position because, by the treatment of an alcoholic solution of a dithiazole with alkaline sulfide, it is smoothly reduced to a 3-methylated dithiobiuret. For instance, XX reacted with methyl iodide to form XXI, when kept at only room temperature, and was then reduced to XXII with hydrogen sulfide and ammonia in a hot ethanolic solution. Diacetyl derivatives such as XXIII also reacted with methyl iodide to give the corresponding methiodide XXIV. The methiodides thus obtained showed an infrared absorption band of the carbonyl group at 1670 cm^{-1}, and they decomposed upon treatment with alkali, even with sodium bicarbonate. These results suggest that the positive charge may be localized on the nitrogen atom at the 4 position and that the dithiazole ring may be unstable.

Experimental

The melting points are uncorrected. The ultraviolet spectra were recorded on a Shimadzu model MPS-50L apparatus. The infrared spectra were recorded on a JASCO model IR-G spectrophotometer in Nujol mull.

Formation of 1-Substituted 2,4-Dithiobiuret from Amines and Methyl Trithioallophanate. To a suspended solution of methyl trithioallophanate (0.1 mol) in 50 m*l* of ethanol, the amine (0.2 mol) was added at an ordinary temperature. When the reaction mixture was warmed with stirring, the methyltrithioallophanate gradually went into the solution. The resulting solution was stirred for 1 hr at 30—40°C and poured into 300 m*l* of 1 N-hydrochloric acid. The precipitate was then filtered off and recrystallized from ethanol. In this manner, the following dithiobiurets were prepared.

Di-*n*-propyl, di-*i*-propyl and di-*n*-butyl amines all failed to react with methyl trithioallophanate.

Formation of 3,5-Disubstituted 3H-*1,2,4-Dithiazoles, Oxidation of 1,1-Disubstituted 2,4-Dithiobiurets.* 2,4-Dithiobiurets were easily oxidized to the related dithiazole salts with many oxidizing reagents, for example, iodine, bromine, hydrogen peroxide, ferric chloride and sodium hypochlorite in an acidic medium.

17) T. Shiba and H. Kato, This Bulletin, **44**, 1864 (1971).
18) H. V. Daeniker and J. Druey, *Helv. Chim. Acta*, **45**, 2426 (1962).
19) M. Ohta and M. Sugiyama, This Bulletin, **36**, 1437 (1963).

Table 4. Formation of *l*-substituted 2,4-dithiobiurets

Dithiobiuret prepared	Yield %	Mp °C	Mol. formula	Nitrogen, % Found	Nitrogen, % Reqd	Sulfur, % Found	Sulfur, % Reqd
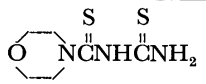	65	138[a)]	$C_6H_{11}N_3OS_2$	20.27	20.49	31.45	31.22
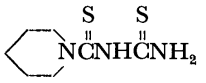	57	138—139	$C_7H_{13}N_3S_2$	20.57	20.69	31.64	31.53
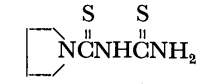	89	188[a)]	$C_6H_{11}N_3S_2$	22.35	22.22	33.71	33.86
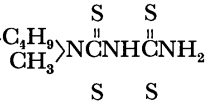	48	69— 72	$C_7H_{15}N_3S_2$	20.61	20.49	31.32	31.22
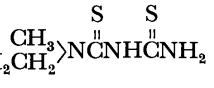	43	137—138*	$C_5H_{11}N_3OS_2$	21.49	21.72	33.34	33.16

a) Decomp.

A small quantity (0.1 mol) of the dithiobiuret was dissolved in 50 m*l* of chloroform or ethanol, and an excess of chlorine gas was passed through the solution with stirring at an ordinary temperature. The hydrochloride thus precipitated was filtered and washed with acetone. It was almost pure and could be used in the next reaction without recrystallization. All of the 1,1-disubstituted 2,4-dithiobiurets were oxidized in a similar manner.

*Oxidation of 1-Alkyl-4*S*-benzyliso-2,4-dithiobiurets.* 5-Methylamino, 5-isopropylamino, and 5-*n*-butylamino-3*H*-1,2,4-dithiazole hydrobromides were prepared by Dixit's method.[13)]

The isodithiobiuret (0.1 mol) was dissolved in 50 m*l* of chloroform, and then bromine (0.11 mol) was stirred in 40°C. The precipitate was filtered and washed with acetone. The yield was 80—90%: 5-methylamino-3-imino-3*H*-1,2,4-dithiazole hydrobromide, mp 232—233°C (decomp.) (Ref. 13, mp 228°C), 5-isopropylamino-3-imino-, mp 215—218°C (decomp), 5-*n*-butylamino-3-imino-, mp 189—193°C (decomp.).

Formation of 1,1,5-Trisubstituted 2,4-Dithiobiurets. Freshly-prepared dimethylthiocarbamoyl isothiocyanate[12)] (0.1 mol) was dissolved in 50 m*l* of acetone, and then the amine (0.1 mol) was added at an ordinary temperature. The solution was stirred for 1 hr, the solvent was removed *in vacuo*, and the crystalline residue was recrystallized from ethanol. The yield was almost quantitative. In this manner, the following new dithiobiurets were prepared:
1,1-dimethyl-5-*t*-butyl-2,4-dithiobiuret, mp 102—103°C. Found: C, 43.84; H, 7.76; N, 19.18; S, 29.22%. Required for $C_8H_{17}N_3S_2$: C, 43.55; H, 7.76; N, 18.84; S, 28.88%.
1,1-dimethyl-5-phenyl-, mp 83—84°C. Found: C, 50.21; H, 5.44; N, 17.57; S, 26.78%. Required for $C_{10}H_{13}N_3S_2$; C, 50.08; H, 5.81; N, 17.37; S, 26.88%.

*Formation of 1,1-Dimethyl-5-t-butylimino-*3H*-1,2,4-dithiazole.* 1,1-Dimethyl-5-*t*-butyl-2,4-dithiobiuret (11 g, 0.05 mol) was dissolved in 50 m*l* of ethanol, and then bromine (8 g) was added at 0°C. The precipitate was filtered and dissolved in 300 m*l* of water; subsequent neutralization with potassium carbonate gave 10 g (91%) of the dithiazole. The substance was recrystallized from ethanol as pale yellow prisms. Mp 76—77°C. Found: C, 43.94; H, 6.61; N, 19.10; S, 29.54%. Required for $C_8H_{15}N_3S_2$: C, 44.24; H, 6.91; N, 19.35; S, 29.49%.

1,1-Dimethyl-5-phenylimino-3*H*-1,2,4-dithiazole was prepared by the same procedure. Mp 89—90°C. Found: C, 50.33; H, 4.58; N, 17.81; S, 26.86%. Required for $C_{10}H_{11}N_3S_2$: C, 50.63; H, 4.64; N, 17.72; S, 27.00%.

*Formation of 5-Alkylthio-3-imino-*3H*-1,2,4-dithiazole Hydroiodide.* Alkyl trithioallophanate were oxidized by the known method.[15)] The yield was always quantitative, and the following hydroiodides were thus prepared: 5-methylthio-3-imino-3H-1,2,4-dithiazole hydroiodide, mp 161—163°C (Ref. mp 157°C), 5-ethylthio-, mp 143—144°C (Ref. mp 143—145°C), 5-benzylthio-, mp 133—134°C. Found: C, 29.61; H, 2.34; N, 7.53; S, 26.38; I, 34.55%. Required for $C_9H_9IN_2S_3$: C, 29.32; H, 2.45; N, 7.61; S, 26.09; I, 34.51%.

*Acylation of 5-Substituted Amino or Alkylthio-3-imino-*3H*-1,2,4-dithiazole Salts.* *(A) With Tertiary Amine*: The dithiazole salt (0.05 mol) and the required acid anhydride (0.1 mol) were mixed in 50 m*l* of acetone, and then triethylamine (0.1 mol) was stirred in at room temperature. The exothermic reaction was observed, and the temperature was raised to 30—40°C. The mixture was stirred for 1 hr at this temperature, and then poured into water and made alkaline with potassium carbonate. The resulting precipitate was filtered off, washed with water, and recrystallized from methanol or ethanol.

(B) Without Tertiary Amine: The dithiazole salt (0.05 mol) and the acid anhydride (0.2 mol) were heated at 50—60°C for 1 hr with stirring; the mixture was then poured into water, and the precipitate was filtered off, washed with water, and recrystallized from methanol or ethanol.

(C) With Acyl Halides Instead of Acid Anhydrides: Into a mixture of the dithiazole salt (0.05 mol) and the acyl halide (0.05 mol) in 50 m*l* of acetone, pyridine (0.05 mol) was stirred at room temperature, that temperature was maintend for 20 min. The mixture was then poured into water, and the precipitate was collected and then recrystallized from alcohol, acetone, *n*-hexane, *etc.* The results are summarized in Table 5.

*Formation of 5-Anilino-3-acetylimino-*3H*-1,2,4-dithiazole.* A mixture of 5-anilino-3-imino-3*H*-1,2,4-dithiazole (1.1 g) and 1-acetylimidazole (0.6 g) in 10 m*l* of tetrahydrofuran was allowed to stand for 1 week at room temperature. The solution was then poured into water, and the precipitate was collected. Recrystallization from alcohol gave 1 g of yellow needles, melting at 191—192°C with decomposition. Found: C, 47.92; H, 3.51; N, 16.64; S, 25.72%. Re-

quired for $C_{10}H_9N_3OS_2$: C, 47.81; H, 3.59; N, 16.73; S, 25.50%. This substance was converted to a diacetyl derivative with acetic anhydride and pyridine. The melting points and infrared spectra were identical.

*Formation of 3-Acetylimino-5-dimethylamino-4-methyl-*3H-*1,2,4-dithiazolium Iodide, XX.* 3-Acetylimino-5-dimethylamino-3H-1,2,4-dithiazole (3 g) and methyl iodide (10 m*l*) were refluxed in acetone (20 m*l*) for 1 hr and then allowed to stand at room temperature for 2 days. The resulting precipitate was filtered off, washed with acetone, and recrystallized from ethanol, affording the methiodide (4.2 g, 85%) as pale yellow needles. Mp 208—209°C with decomposition. Found: C, 24.36; H, 3.52; I, 36.73; N, 12.32; S, 18.89%. Required for $C_7H_{12}IN_3OS_2$: C, 24.35; H, 3.48; I, 36.81; N, 12.17; S, 18.55%. IR: 1670 cm^{-1} (C=O).

3-Acetylimino-4-methyl-5-(*N-p*-tolyl)acetamido-3*H*-1,2,4-dithiazolium iodide XXIII was prepared by the same procedure as a yellow powder. The yield was 65%. Mp 190—191°C with decomposition. Found: C, 35.91; H, 3.10; I, 28.95; N, 9.42; S, 14.85%. Required for $C_{13}H_{14}IN_3O_2S_2$: C, 35.86; H, 3.22; I, 29.20; N, 9.66; S, 14.71%. IR: 1690, 1680 cm^{-1} (C-O).

*Reduction of 3-Acetylimino-5-dimethylamino-4-methyl-*3H-*1,2,4-dithiazolium Iodide, XXII.* Into a suspended solution of the methiodide (2.8 g) in 10 m*l* of ethanol and 20 m*l* of 28%-aqueous ammonia, hydrogen sulfide was passed for 1 hr

TABLE 5. 5-SUBSTITUTED AMINO OR ALKYLTHIO-3-ACYLIMINO-3*H*-1,2,4-DITHIAZOLES PREPARED

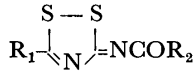

S. No.	R_1	R_2	Method	Yield %	Mp °C		Anal. C	H	N	S
(1)	$N(CH_3)_2$	C_2H_5	B	82	89— 90	Found	38.73	5.36	19.44	29.73
						Calcd	38.71	5.07	19.35	29.49
(2)	$N(CH_3)_2$	n-C_3H_7	B	65	85— 84	Found	41.87	5.35	18.06	28.00
						Calcd	41.55	5.62	18.18	27.70
(3)	$N(CH_3)_2$	n-C_5H_{11}	A	64	69— 70	Found	46.18	6.74	16.20	24.98
						Calcd	46.33	6.56	16.22	24.71
(4)	$N(CH_3)_2$	n-C_9H_{19}	A	31	73— 74	Found	53.29	8.11	12.98	20.18
						Calcd	53.33	7.94	13.33	20.32
(5)	$N(CH_3)_2$	n-$C_{15}H_{31}$	A	23	83— 84	Found	60.15	9.34	10.63	15.87
						Calcd	60.15	9.27	10.52	16.04
(6)	$N(CH_3)_2$	C_3H_5	A	16	141—142	Found	41.87	4.79	18.40	27.90
						Calcd	41.92	4.80	18.34	27.95
(7)	$N(CH_3)_2$	C_6H_5	A	75	209—210	Found	50.22	4.13	16.02	24.14
						Calcd	49.81	4.15	15.85	24.15
(8)	$N(CH_3)_2$	C_6H_4-p-Cl	C	16	204—205	Found	44.16	3.28	13.97	21.13
						Calcd	44.07	3.34	14.02	21.37
(9)	$N(CH_3)_2$	CH_2Cl	A	86	151—152	Found	30.16	3.52	17.40	27.35
						Calcd	30.32	3.37	17.68	26.95
(10)	$N(CH_3)_2$	CF_3	A	11	146—147	Found	28.02	2.65	16.60	24.99
						Calcd	28.02	2.33	16.34	24.90
(11)	$N(CH_3)_2$	OC_2H_5	C	34	129—130	Found	36.16	4.97	17.70	27.62
						Calcd	36.05	4.72	18.03	27.47
(12)	$N(CH_3)C_6H_5$	CH_3	A	83	145—146	Found	49.94	4.07	15.88	23.97
						Calcd	49.81	4.15	15.85	24.15
(13)		CH_3	A	71	161—162	Found	39.36	4.34	16.97	25.99
						Calcd	39.18	4.44	17.14	26.12
(14)		CH_3	A	74	101—102	Found	44.34	5.47	17.25	26.05
						Calcd	44.34	5.34	17.28	26.33
(15)		CH_3	A	88	169—170	Found	41.69	4.78	18.29	27.66
						Calcd	41.92	4.80	18.34	27.95
(16)	$N(CH_3)COCH_3$	CH_3	A	38	158—159[a]	Found	36.37	3.86	18.03	27.63
						Calcd	36.36	3.90	18.18	27.71
(17)	$N(i$-$C_3H_7)H$	CH_3[b]	A	55	167—168	Found	38.69	5.15	19.32	29.33
						Calcd	38.71	5.07	19.36	29.49
(18)	$N(n$-$C_4H_9)COCH_3$	CH_3	A	45	163—164	Found	43.97	5.41	15.14	23.56
						Calcd	43.96	5.49	15.38	23.44
(19)	$N(C_6H_4$-p-$CH_3)COCH_3$	CH_3	A	74	178—179	Found	50.72	4.19	13.71	20.92
						Calcd	50.81	4.23	13.68	20.85
(20)	SCH_3	CH_3	A	71	111—112[a]	Found	32.48	3.51	12.91	43.57
						Calcd	32.73	3.64	12.73	43.64
(21)	SC_2H_5	CH_3	A	64	173—174[a]	Found	28.98	2.65	13.49	46.91
						Calcd	29.13	2.91	13.59	46.60
(22)	$SCH_2C_6H_5$	CH_3	A	53	128—129	Found	46.74	3.92	9.78	34.04
						Calcd	46.81	3.55	9.93	34.04

a) Decomp. b) Diacetyl compound could not be obtained.

at 40°C. The methiodide was then gradually fed into the solution, which thereby turned yellow. The solution was then cooled and acidified with concentrated hydrochloric acid. The white solid was filtered off, washed with water, and recrystallized from ethanol. Thus, 1,1,3-trimethyl-2,4-dithiobiuret (0.65 g) was obtained, while from the mother liquor, 1,1,3-trimethyl-5-acetyl-2,4-dithiobiuret (0.09 g) was obtained. The latter compound was obtained by the acetylation of the dithiobiuret. Their IR, tlc, and mp were identical. 1,1,3-trimethyl-2,4-dithiobiuret: mp 100—102°C. Found: C, 33.60; H, 6.11; N, 23.39; S, 36.48%. Required for $C_5H_{11}N_3S_2$: C, 33.90; H, 6.21; N, 23.73; S, 36.16%. 1,1,3-triemethyl-5-acetyl-2,4-dithiobiuret: mp 161—162°C. IR: 1720 cm^{-1} (C=O).

Formation of 5-*Methylamino*-3-*(N-methyl)carbamoylimino*-3H-1,2,4-*dithiazole.* To a suspended solution of 3-imino-5-methylamino-3H-1,2,4-dithiazole hydrobromide (2.3 g) and methyl isocyanate (0.6 g) in 20 m*l* of tetrahydrofuran, triethylamine (1 g) was added at room temperature. The solution was stirred for 1 hr, and poured into water, and then the precipitate was filtered off. Recrystallization from dimethylformamide gave 1 g of white crystals, melting at 229—230°C. Found: C, 29.38; H, 3.99; N, 27.23; S, 31.49%. Required for $C_5H_8N_4OS_2$: C, 29.41; H, 3.92; N, 27.45; S, 31.37%. IR: 1670 cm^{-1} (C=O). The following new 3-(*N*-substituted)carbamoyliminodithiazoles were prepared by the same method. 5-Ethylamino-3-(*N*-methyl)carbamoylimino-: mp 223—224°C. Found: C, 29.81; H, 4.62; N, 25.38; S, 29.39%. Required for $C_6H_{10}N_4OS_2$: C, 33.03; H, 4.59; N, 25.69; S, 29.36%. IR: 1680 cm^{-1} (C=O). 5-Anilino-3-(*N*-methyl)carbamoylimino-: mp 162—163°C with decomposition. Found: C, 45.23; H, 3.85; N, 20.91; S, 24.02%. Required for $C_{19}H_{10}N_4OS_2$: C, 45.11; H, 3.76; N, 21.05; S, 24.06%. 5-Dimethylamino-3-(*N*-methyl)carbamoylimino-: mp 218°C with decomposition. Found: C, 33.15; H, 4.92; N, 25.68; S, 29.57%. Required for $C_6H_{10}N_4OS_2$: C, 33.03; H, 4.59; N, 25.69; S, 29.36%. 5-Dimethylamino-3-(*N*-phenyl)carbamoylimino-: mp 183.5°C with decomposition. Found: C, 46.88; H, 4.57; N, 20.05; S, 22.46%. Required for $C_{11}H_{12}N_4OS_2$: C, 47.17; H, 4.29; N, 20.00; S, 22.86%.

The author is grateful to Dr. Kanji Taniguchi and Mr. Reiji Sakimoto, the Head of our Organic Chemistry Research Laboratory for their permission and advice to carry out these studies.

BULLETIN OF THE CHEMICAL SOCIETY OF JAPAN, VOL. 45, 3579—3583 (1972)

Solvent Effects under High Pressures. IV.[1] A Procedure for the Estimation of Solvation in the Transition State

Yasuhiko KONDO, Masaru OHNISHI, and Niichiro TOKURA

Department of Applied Chemistry, Faculty of Engineering, Osaka University, Suita, Osaka

(Received March 3, 1972)

The rate constants and activation parameters were measured for the reaction of pyridine with benzyl bromide in various solvents. The rate constants were better correlated to the activation volumes than to the activation entropies. The linear free-energy relationships were observed in the plots of the log k values of some Menschutkin reactions *vs.* the log k values of the present reaction in various solvents. Corresponding to their good correlations between the values of log k and of their pressure derivatives for the present reaction, the values of $(z \cdot \Delta P)$, which are the slopes of the plots of $\Delta V_0^{\neq}$ *vs.* KV^0, increased with the increase in the slopes of the above linear free-energy relationships. The activation volumes in various solvents are linearly correlated to their pressure derivatives. An equation which predicts the relationship has been derived. Using this equation, the solvation number in the activated complex and the average pressure within its cosphere have been estimated to be *ca.* 4 and 910 (kg. cm^{-2}) respectively. Based on these results, discussions have been given on the solvation in the transition state for the present reaction.

In the works of this series,[1,2] the Menschutkin reaction of triethylamine with ethyl iodide has been chosen as the standard system in order to investigate the mechanisms of the solute-solvent interaction in the transition state. As the work continued, we needed a system sensitive to the change in the medium. As an example of such a system, the reaction of pyridine with benzyl bromide was chosen.

On the other hand, this system has long been referred to as the standard example of conforming to the Kirkwood theory.[3,4] However, contributions from the specific interaction between a solute and solvents have been suggested to play a significant role in the solvent effect in typical Menschutkin reactions.[5-7]

Therefore, the detailed analysis of the present system will throw some light on the origin of these interactions.

In this paper, the activation parameters of the reaction will be analyzed by empirical procedures, and then we will discuss the pressure dependence of

1) Part III; Y. Kondo and N. Tokura, This Bulletin, **42**, 1660 (1969).
2) Y. Kondo, M. Uchida, and N. Tokura, *ibid.*, **41**, 992 (1968).
3) S. Glasstone *et al.*, "The Theory of Rate Processes," McGraw-Hill Book Company, New York (1941).
4) K. B. Wiberg, "Physical Organic Chemistry," John Wiley & Sons, New York (1964).
5) H. Hartmann and A. P. Schmidt, *Z. Phys. Chem.*, (Frankfurt), **62**, 312 (1968).
6) H. Hartmann and A. P. Schmidt, *ibid.*, **66**, 183 (1969).
7) Y. Kondo and N. Tokura, This Bulletin, **40**, 1433 (1967).

the activation volumes.

Experimental

Materials. Pyridine, a special-grade reagent, was refluxed over potassium hydroxide for a few days and then distilled. The middle fraction was stored over barium oxide and redistilled before use. Benzyl bromide, another special-grade reagent, was dried over anhydrous potassium carbonate and distilled twice under reduced pressure. The other solvents were commercial reagent-grade reagents and were purified by procedures described elsewhere.[8-11]

Kinetic Procedure. Separate solutions of pyridine and the bromide in a solvent were prepared by weight (usually the concentrations of the reagents were *ca.* 0.01—0.05 M in the reaction mixture). The solutions were mixed in polyethylene ampoules. These ampoules were sealed quickly, shaken vigorously, and immersed into a glass test tube containing mercury which was maintained at the reaction temperature. The test tube was then immersed into the oil of the pressure vessel in a thermostat bath. After a given period, the reaction mixture was partitioned between light petroleum and water. The aqueous layer was potentiometrically titrated with a silver nitrate solution.

Usually reactions were carried out at six fixed pressures (1, 300, 600, 900, 1,200, and 1,500 kg cm^{-2}) and at four fixed temperatures (20.0, 30.0, 40.0, and 50.0°C).

The Rate Law in Alcohols. In methanol and 2-propanol, a spontaneous solvolysis has been observed for the bromide. Therefore, the total rate law can be written as follows:

$$\frac{dx}{dt} = k_2(a-x)(b-x) + k_1(a-x) \quad (1)$$

where a, b, x stand for the initial mole fractions of benzyl bromide and of pyridine, and the mole fraction of the bromide ion at the time, t; respectively.

The second-order rate constants (k_2) for the Menschutkin reaction were calculated by means of Eq. (1) after the corrections of the first-order solvolysis rate (k_1), which was measured independently under the same reaction conditions.

Results

All the reaction rates followed second-order kinetics except in alcohols, where both the first order- and second order-rate constants were calculated by the procedure mentioned above. All the second order-rate constants, k_x, are expressed in a mole fraction unit (sec^{-1}), which is related to the rate constants in a molar unit, k_M ($l \cdot mol^{-1} \cdot sec^{-1}$), by the equation: $k_x = k_M V_s^{-1}$, where V_s stands for the molar volume of the solvent (in l) at the reaction temperature. For most of the reaction conditions, the measurements were repeated more than twice. The rate constants thus obtained under hydrostatic pressures were first scrutinized by the procedure developed by the present authors,[2] and then the pressure-dependence parameters were calculated by the least-squares method based on the following equations:

$$\ln k = A + BP + CP^2 \quad (2)$$

$$\Delta V_0^{\neq} = -RTB \quad (3)$$

$$(\partial \Delta V^{\neq}/\partial P)_0 = -2RTC \quad (4)$$

The least-squares calculations were also performed for the temperature-dependence parameters on the basis of the following equations:

$$\ln (k_x/T) = A'/T + B' \quad (5)$$

$$\Delta H^{\neq} = -RA' \quad (6)$$

$$\Delta S^{\neq} = R(B' - \ln k_b/h) \quad (7)$$

where k_b and h stand for the Boltzmann and the Plank constants.

These calculations were done using a NEAC 2200—500 computer. The results thus obtained are collected in Table 1.

The estimated errors are as follows: k_x; ±1.7%, $\Delta V_0^{\neq}$; ±1.3 (cm^3·mol^{-1}), $(\partial \Delta V^{\neq}/\partial P)_0$; ±0.002 (cm^5·mol^{-1}·kg^{-1}), $\Delta H^{\neq}$; ±0.2 (kcal·mol^{-1}), $\Delta S^{\neq}$;

TABLE 1. RATE CONSTANTS AND ACTIVATION PARAMETERS (30°C)

No.	Solvents	$k_x \times 10^5$	$-\Delta V_0^{\neq}$	$(\partial \Delta V^{\neq}/\partial P)_0$	$\Delta H^{\neq}$	$\Delta S^{\neq}$
1	Toluene	4.85	39.1	0.0154	13.4	34.2
2	Benzene	10.996	35.3	0.0193	—	—
3	Chlorobenzene	50.0	29.1	0.0077	12.1	33.9
4	Bromobenzene	60.4	24.9	0.0031	—	—
5	Nitrobenzene	601.	23.7	0.0120	11.8	29.9
6	Acetone	297.	34.9	0.0115	11.7	31.4
7	Tetrahydrofuran	28.8	32.3	0.0118	12.4	33.7
8	Dichloroethane	129.	25.4	0.0000	—	—
9	2-Propanol	147.	20.4	0.0057	—	—
10	Methanol	629.	27.2	0.0134	16.5	14.3
11	Acetonitrile	2140.	29.2	0.0105	11.4	28.8
12	Cyclohexanone	177.	—	—	12.2	31.1
	Solvolysis of Benzyl Bromide					
	Methanol	0.337	22.8	0.0064	20.3	16.8
	2-Propanol	0.0275	19.4	0.0064	—	—

Dimensions, k_x; (sec^{-1}), $-\Delta V_0^{\neq}$; (cm^3·mol^{-1}), $(\partial \Delta V^{\neq}/\partial P)_0$; (cm^5·mol^{-1}·kg^{-1}), $\Delta H^{\neq}$; (kcal·mol^{-1}), $\Delta S^{\neq}$; (e.u.)

8) Y. Kondo, T. Matsui and N. Tokura, This Bulletin, **42**, 1037 (1969).
9) T. Matsui and N. Tokura, *ibid.*, **44**, 756 (1971).
10) J. F. Coetzee, G. P. Cunningham, D. K. McGuire, and G. R. Padmanabhan, *Anal. Chem.*, **34**, 1139 (1962).
11) "Technique of Organic Chemistry, VII. Organic Solvents," ed. by A. Weissberger, Interscience, New York (1955).

±0.4 (e. u.).

Discussion

Empirical Analysis of Activation Parameters. Figure 1 shows the relation between these parameters and the solvent characteristics.

An interesting feature of the plot is that the activation volumes are fairly well correlated to the rate constants, except for a few solvents, the molar volumes of which are fairly smaller than those of the correlative solvents; *i.e.*, for the former solvents they are *ca.* 40—75 ml·mol^{-1}, and for the latter, 100—110 ml·mol^{-1}. However, the sign of the slope suggests, if we use the theory of the absolute reaction rates[3] as a base, that the reaction systems are under a negative pressure. This unreasonable conclusion indicates that the solvent characteristics manifest themselves on the rate constant through the form of an enthalpy and of an entropy, but not directly in the form of a volume.

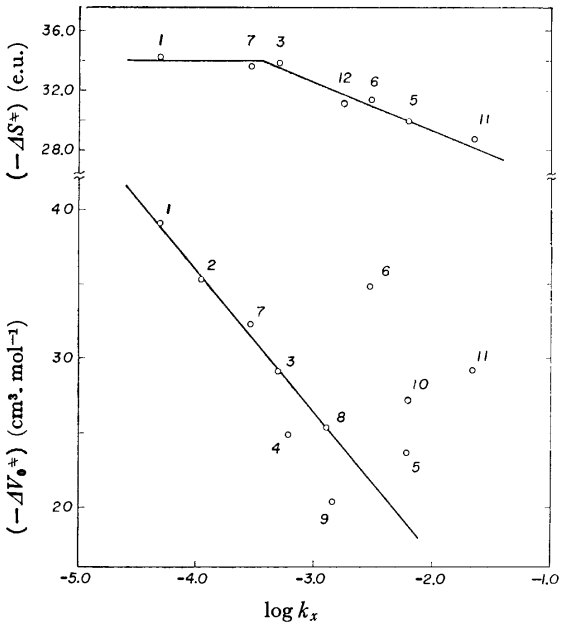

Fig. 1. Plots of activation parameters *vs.* rate constants for the reaction of pyridine and benzyl bromide at 30°C.
The numbers refer to the Table 1.

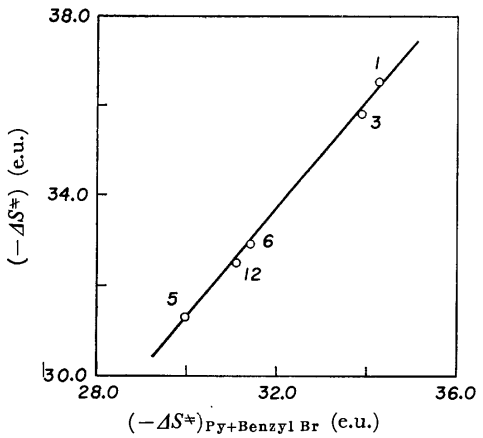

Fig. 2. The activation entropies of the two types of the Menschutkin reactions.
ordinate; the reaction of ω-bromoacetophenone with α-picoline[14]
abscissa; the present system
The numbers refer to the Table 1.

As far as the activation entropy is concerned, there seem to be two series of solvents, each grouped around a line; it follows that there exist two negative isokinetic temperatures with regard to the solvent variations. The accuracy of our measurements may be discerned by the nearly complete correlation with a slope greater than unity (Fig. 2). As will be described in the next discussion, the activation volumes of the present reaction show the largest sensitivity to environmental changes. Therefore, the above observation on the activation entropies is in contrast to the behavior of the activation volumes.

Up till now, as for the Menschutkin reaction four systems have been reported in connection with the systematic studies of the solvent effects on their reaction rates under high pressure.[2,12–15] These results are plotted against those of the present system in Fig. 3. It should be noted that over a fairly wide range of rate constants there are very good correlations among them.

The slope of the plot serves as a measure of the sensitivity of the relevant system to the environmental change.

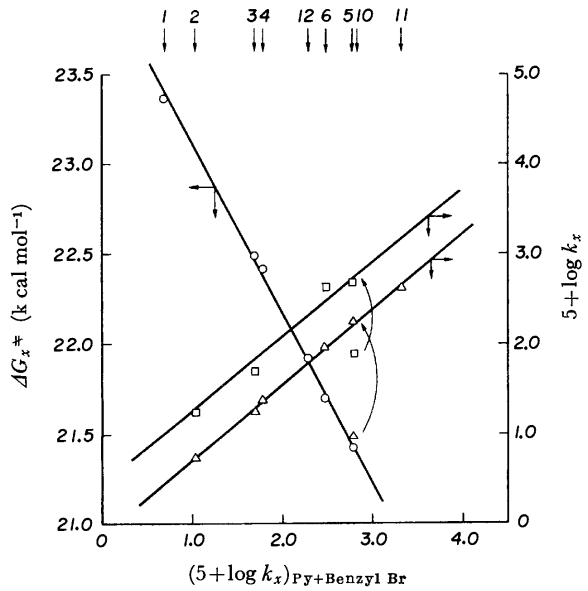

Fig. 3. The linear free energy relationships for the Menschutkin reactions in various solvents.
ordinate, ○; ω-Bromoacetophenone+α-Picoline[14]
△; MeI+Pyridine[13]
□; EtI+Et$_3$N by the present authors
abscissa; the present system
The numbers refer to the Table 1.

12) M. G. Gonikberg and B. S. EL'yanov, *Dokl. Akad. Nauk SSSR*, **138**, 1103 (1961).
13) H. Hartmann, H. Kelm, and G. Rink, *Z. Phys. Chem.*, (Frankfurt), **44**, 335 (1965).
14) H. Heydtmann, A. P. Schmidt, and H. Hartmann, *Ber. Bunsenges. Phys. Chem.*, **70**, 444 (1966).
15) H. Hartmann, H. D. Brauer, H. Kelm, and G. Rink, *Z. Phys. Chem.*, (Frankfurt), **61**, 53 (1968).

TABLE 2. COMPARISONS OF TWO TYPES OF SLOPES

	$\Delta\log k/(\Delta\log k)_{\text{Benzyl Br+Py}}$	$(z\cdot\Delta P)$[kg·cm^{-2}]
Benzyl bromide + Pyridine	1.0	3.45×10^3
Ethyl iodide + Triethylamine	0.84	2.6×10^3
Methyl iodide + Pyridine	0.82	2.6×10^3
ω-Bromoacetophenone + α-Picoline	0.68	1.9×10^3

In our previous papers, the activation volume has been reported to have a linear relation with the product of the compressibility and the molar volume of the solvent, KV^0. According to our model, the slope of the plot should give the value of $(z\cdot\Delta P)$, which is supposed to act as a measure of sensitivity to the solvent variation, as may partly be inferred from the observations in Fig. 1. These two types of slopes, *i.e.*, the slopes of the plots of Figs. 3 and 4, are collected in Table 2 (the listed values of $(z\cdot\Delta P)$ indicate the least-squared values as calculated by means of Eq. (12)).

Based on the values of Table 2, it would be possible to classify the systems into three groups—(pyridine+benzyl bromide), (Et_3N+EtI and pyridine+MeI), and (α-picoline+ω-bromoacetophenone). The sensitivity difference between the first two groups may be ascribed to the nature of the benzyl bromide, since the C–Br bond of the bromide is expected to be more labile than that of the aliphatic halides, and, as a result, all the reacting systems, *i.e.*, both the reactants and the activated complex, will be more sensitive to the environmental change. On the contrary, the difference between the last two groups may be understood by taking into account the steric hindrance due to both α-methyl and carbonyl groups to solvation at the cationic center.

Another interesting feature shown by Fig. 3 is that the rate constants in methanol show a marked deviation from the correlating lines. This deviation should be ascribed to the extra acceleration of the pyridine-benzyl bromide system by methanol compared to that of the aliphatic alkyl iodide systems, as can partly be anticipated from the fact that the benzyl bromide solvolyses fairly easily in methanol compared to the other halides shown in Table 2.

In another respect, this effect may be responsible for the discrepancy pointed out by Heydtmann and Buttner[16] that, for benzyl bromide, the rate constants in ethanol-benzene mixtures satisfy the Kirkwood relationship, whereas for the reaction of methyl iodide with pyridine in the same mixture, they do not.

Glew and Moelwyn-Hughes studied the base-catalyzed and uncatalyzed hydrolyses of methyl halides in water and found that the activation energies for the latter process are greater by *ca.* 3.5 (kcal·mol^{-1}) than those of the former.[17,18] The situation is quite similar to the present case. However, the absolute magnitudes of the activation parameters are not particularly helpful in leading to a conclusion as to the type of mechanism.

A linear relation between $\Delta S^{\neq}$ and $\Delta V^{\neq}$ has been observed by Laidler *et al.* for miscellaneous reactions in aqueous solvent,[19,20] and has been supposed to be evidence for the electrostriction theory. For the present case and the other quaternization reactions, no simple relations between the two quantities could be observed. This fact is not unexpected from the figures described above.

As can partly be inferred from the above discussion, these facts suggest that the major factors which give rise to perturbations on the activation entropy are not necessarily the same as those influencing the activation volumes, especially for the Menschutkin reaction.

Activation Volumes and Its Pressure Dependence. In a previous publication,[2] an equation which is helpful for correlating the activation volume with the solvent characteristics has been developed. In discussing the pressure dependence of the activation volumes, a slight modification is necessary.

Based on a concept similar to that used in the previous publication,[2] the total volume, V_t, of a solution composed of N moles of the pure solvents and n moles of the solute at a certain pressure, P, would be given by:

$$V_t = (N-nz)V_p^0 + nV_s + nzV' \tag{8}$$

where V_p^0, V_s, V', and z are the molar volumes of a pure solvent, of a pure solute and of a solvated solvent, and the solvation number of the solute, respectively.

In this case, the partial molar volume of the solute, V_s^0, is given by:

$$\overline{V}_s^0 = (\partial V_t/\partial n)_N = V_s + z(V'-V_p^0) \tag{9}$$

As for the Menschutkin reaction, it has been suggested that the polarity of the activated complex is considerably larger than those of the reactants,[3,14] and that the change in the activation volume by solvents is mainly controlled by the interaction between the activated complex and solvent molecules.[14]

On the basis of these facts, the activation volume at an external pressure P, $\Delta V_p^{\neq}$, would be given by this equation, applying Eq. (9) only to an activated complex:[1]

$$\Delta V_p^{\neq} = (\overline{V}_{\neq}^0-(\overline{V}_a^0+\overline{V}_b^0)) = (V_{\neq}-(\overline{V}_a^0+\overline{V}_b^0)) + z(V'-V_p^0) \tag{10}$$

Using the definition of the compressibility of the solvent, the activation volume at zero external pressure, $\Delta V_0^{\neq}$, is expressed as follows:

$$K = -\frac{1}{V}(\partial V/\partial P)_T \tag{11}$$

$$\Delta V_0^{\neq} = (V^{\neq}-(\overline{V}_a^0+\overline{V}_b^0)) - (z\cdot\Delta P)KV^0 \tag{12}$$

where V^0 and ΔP stand for the molar volume of a pure solvent and the difference between the average pressure in the cosphere of the activated complex and

16) H. Heydtmann and D. Buttner, *ibid.*, **63**, 39 (1969).
17) E. A. Moelwyn-Hughes, *Proc. Roy. Soc. Ser. A*, **164**, 295 (1938).
18) D. N. Glew and E. A. Moelwyn-Hughes, *ibid.*, **211**, 254 (1952).
19) D. Chen and K. J. Laidler, *Trans. Faraday Soc.*, **54**, 1026 (1958).
20) K. J. Laidler and R. Martin, *Int. J. Chem. Kinet.*, **1**, 113 (1969).

the atmosphere.

As for the pressure dependence of $\Delta V^{\neq}$, by the differentiation of Eq. (10) with respect to a pressure:

$$(\partial \Delta V^{\neq}/\partial P) = (\partial/\partial P)\{V_{\neq} - (\overline{V}_a{}^0 + \overline{V}_b{}^0) + zV'\} - z(\partial V_p{}^0/\partial P) \quad (13)$$

Since, for the discussions of the solvent dependence of the activation volume and its pressure derivative, the first term of Eq. (13) would be taken as a constant, the pressure derivative of the activation volume at zero external pressure, $(\partial \Delta V^{\neq}/\partial P)_0$, is given by:

$$(\partial \Delta V^{\neq}/\partial P)_0 = \text{const.} + zKV^0 \quad (14)$$

By the cancellation of the KV^0 term from Eqs. (12) and (14):

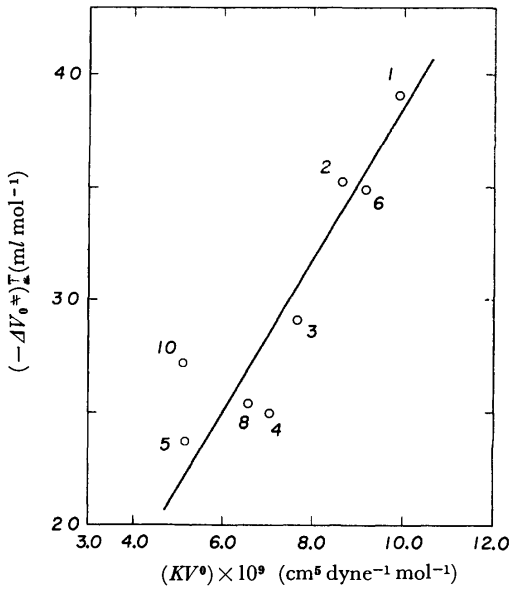

Fig. 4. Plots of $(-\Delta V_0^{\neq})$ *vs.* KV^0 for the reaction of pyridine and benzyl bromide at 30°C.
The numbers refer to the Table 1.

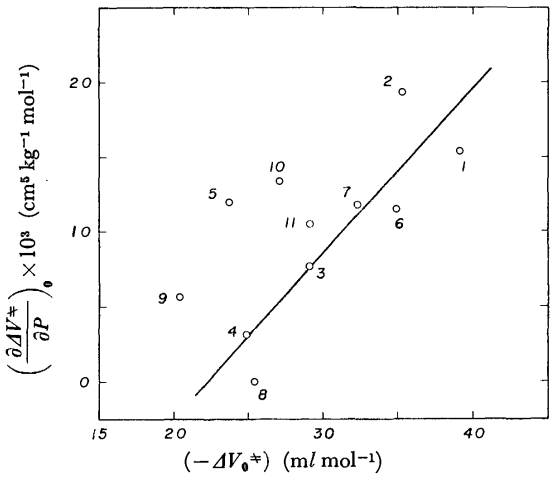

Fig. 5. Plots of $(\partial \Delta V^{\neq}/\partial P)_0$ *vs.* $(-\Delta V_0^{\neq})$ for the reaction of the pyridine and benzyl bromide at 30°C.
The numbers refer to the Table 1.

$$(\partial \Delta V^{\neq}/\partial P)_0 = \text{const.} + (1/\Delta P)(-\Delta V_0^{\neq}) \quad (15)$$

Two types of plots, *i.e.*, Eqs. (12) and (15), are shown in Figs. 4 and 5. In Fig. 5, the regression line is drawn with the exception of three solvents-*i.e.*, nitrobenzene methanol, and 2-propanol, which show larger deviations than would be expected from the experimental errors.

From these slopes, the solvation number of the activated complex is estimated to be *ca.* 4 (*i.e.*, $(z\cdot\Delta P)/\Delta P = (3.8\times 10^3)/(9.1\times 10^2) \fallingdotseq 4$), and the average pressure within the cosphere of the activated complex, to be 9.1×10^2 (kg·cm^{-2}).

Although it is difficult to estimate the uncertainties to be associated with those values, at least three factors should be taken into account in doing so.

First, the fundamental ideas on the reaction systems are based on the discrete model, which might give only a qualitative description of the reaction system. Further, the linear assumptions used in deriving these equations would be the second factor restricting the conclusions reached. Finally, for evaluating the solvation number in the transition state, it is necessary to calculate the second derivatives of the rate constant with respect to the pressure.

Linear relations have been found between ΔV^0 and $(\partial \Delta V^0/\partial P)$ for the dissociation of weak acids in water.[21,22] These slopes correspond to *ca.* 4.7×10^3 (kg·cm^{-2}). Similar values have been estimated for the ionization in water by a different procedure.[23]

According to our model, these values indicate the effective pressures in the vicinity of the ion. A comparison of the two slopes is quite interesting, leading to the view that the charge development in the transition state of the Menschutkin reaction is about one-fifth of the ionization reaction.

As has been described above, the reference works were carried out in aqueous solvents,[19-23] while the present works were done in non-aqueous solvents. Many recent works have clearly shown the marked differences in solvent characteristics between aqueous and non-aqueous solvents. Some uncertainties might be introduced into the above conclusion as a result of having avoided the factor in our model.[24]

Although qualitative, the above estimation of the charge development in the transition state is not unexpected, for the transition state has been suggested to be not so highly ionic as quaternary ammonium halides.[25] The incomplete charge development in the transition state might be responsible for the lack of linear relationships between $\Delta S^{\neq}$ and $\Delta V_0^{\neq}$ for the present reaction.

21) D. A. Lown, H. R. Thirsh, and Lord Wynne-Jones, *Trans. Faraday Soc.*, **64**, 2073 (1968).
22) D. A. Lown, H. R. Thirsh, and Lord Wynne-Jones, *ibid.*, **66**, 51 (1970).
23) L. G. Hepler, *J. Phys. Chem.*, **69**, 965 (1965).
24) The authors wish to express their gratitude to the referee for his helpful discussions.
25) K. E. Weale, "Chemical Reactions at High Pressures," E. & F. N. Spon., London (1967).

Oxidative Dimerization of Pyrrole Derivatives. III. Studies on the 3-Carbonyl Substituted Pyrryl Radicals.[1,2]

Kuniyuki TOMITA and Norio YOSHIDA

Central Research Laboratories, Sankyo Co., Ltd., Shinagawa-ku, Tokyo

(Received March 15, 1972)

The thermochromic properties of the dimers in solution, obtained by oxidation of 3-carbonyl substituted pyrroles, was determined as being due to the reversible dissociation into pyrryl radicals. The structure and character of the pyrryl radicals are discussed on the basis of substituent effect on thermochromism and ESR studies.

In previous papers,[3),4)] we reported the oxidative dimerization of some pyrroles and the structures of the resulting dimers. This paper describes the radical mechanism for the thermochromic properteis of some dimers and discusses the structures and characters of the pyrryl radicals.

Results and Discussion

Thermochromism in Solution. When a colorless benzene solution of dimer I, bis[3-ethoxycarbonyl-4,5-bis(*p*-methoxyphenyl)-2-methylpyrryl], is heated, a slightly reddish purple color (λ_{max} 555 mμ) and ESR signal are observed at about 60°C, the intensities being enhanced with the rise in temperature. On cooling, the colour disappears reversibly with diminution of the ESR signal intensity. This indicates that the thermochromic property is caused by reversible radical dissociation of the dimer.

It is well-known that the dissociation of such dimers is enhanced by the resonance stabilization of the radicals formed. We examined the properties of other dimers, II–XI, to clarify the substituent effects on the stabilizing ability of the resulting pyrryl radicals. The results are listed in Table 1.

The difference in behavior between dimer I and III makes it clear that a carbonyl substituents in the 3-position is essential for thermochromism. This suggests that the carbonyl groups have a potential radical stabilizing ability presumably due to resonance and the carbonyl function should lie in the same plane as the pyrryls.[5)]

Table 1 also shows that the 3-carbonyl substituted dimers dissociate only when they have a radical stabilizing *p*-anisyl group at 5-position, the 4-substituents being less important. Therefore, it seems that these radicals have a similar steric structure to the original dimers,[3)] in which the phenyl ring at 4-position is bent out of the pyrryl radical plane differing from that at 5-position. The hyperfine splitting of the ESR spectra also supports this view.

The substituent effects are in line with those observed in the dimerization reaction and the rate of interconversion of the dimers,[4)] supporting the intermediacy of identical radical species in these reactions.

ESR Spectra of the Pyrryl Radicals. Figure 1a

TABLE 1. THERMOCHROMIC PROPERTY OF VARIOUS DIMERS IN BENZENE SOLUTION

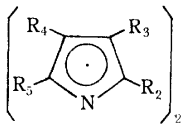

	R_2	R_3	R_4	R_5	Thermochromism
I	CH_3	$CO_2C_2H_5$	*p*-$CH_3OC_6H_4$	*p*-$CH_3OC_6H_4$	+
II	CH_3	$COCH_3$	*p*-$CH_3OC_6H_4$	*p*-$CH_3OC_6H_4$	+
III	CH_3	H	*p*-$CH_3OC_6H_4$	*p*-$CH_3OC_6H_4$	−
IV	C_2H_5	$CO_2C_2H_5$	*p*-$CH_3OC_6H_4$	*p*-$CH_3OC_6H_4$	+
V	CH_3	$CO_2CH_2C_6H_5$	CH_3	*p*-$CH_3OC_6H_4$	+
VI	CH_3	$CO_2C_2H_5$	C_6H_5	*p*-$CH_3OC_6H_4$	+
VII	CH_3	$COCH_3$	C_6H_5	*p*-$CH_3OC_6H_4$	+
VIII	CH_3	$CO_2C_2H_5$	*p*-$CH_3OC_6H_4$	C_6H_5	−
IX	CH_3	$COCH_3$	*p*-$CH_3OC_6H_4$	C_6H_5	−
X	CH_3	$CO_2C_2H_5$	C_6H_5	C_6H_5	−
XI	CH_3	$COCH_3$	C_6H_5	C_6H_5	−

+; Thermochromism shown. −; Thermochromism not shown.
Neither irradiation nor grinding of the dimers caused visible change in color.

1) Part II of this series: Ref. 4.
2) Presented at the 24th Meeting of the Chemical Society of Japan, Tokyo, October 13, 1971.
3) K. Tomita and N. Yoshida, *Tetrahedron Lett.*, **1971**, 1169.
4) K. Tomita and N. Yoshida, This Bulletin, **45**, 3160 (1972).
5) An analogous radical stabilizability of carbonyl groups, including their steric requirement, was reported in the case of pyridinyl radicals. M. Ito and S. Nagakura, This Bulletin, **39**, 369 (1966).

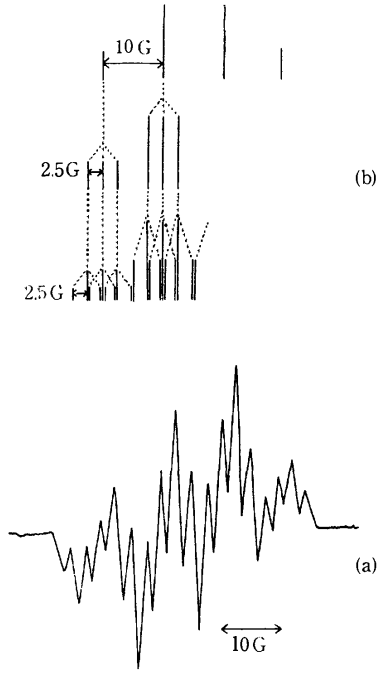

Fig. 1. ESR spectrum from I in degassed toluene at 110°C. (a) Observed spectrum. (b) Stick diagram.

shows the ESR spectra observed for a solution of I in toluene at 110°C. At large amplitude of magnetic modulation, the spectrum showed broad quintet lines (1 : 3 : 3 : 1, a=10G). The ESR spectrum from dimer IV (2-ethyl) exhibited triplet lines (1 : 2 : 1, a=10G) and further subsplittings in each component of the triplet just like those observed in I. It is clear, therefore, that the largest splitting (10G) is caused by the α-protons of the 2-alkyl substituents.

On the other hand, the absence of any interaction of the unpaired electron with protons of the 3-ester group was confirmed by the fact that the radical from dimer II(3-acetyl) gave the same spectrum as that from I. Little participation of the 4-phenyl ring protons was also suggested by the observation of identical spectra from dimer VI(4-phenyl) and I.[6]

The subsplittings should therefore be caused by the nitrogen and the protons(ortho) of the 5-phenyl ring. The isotope labelled dimer XII(^{15}N labelled I) and XIII (I deuterated at an ortho proton of 5-phenyl ring) were prepared and ESR spectra of the corresponding radicals were recorded, as shown in Figs. 2 and 3.

From a comparison of the spectra shown in Figs. 1a, 2 and 3, hyperfine splitting of the pyrryl radical from I could be assigned as follows[7]: a_H=10G(2-alkyl protons); a_H=2.5G (ortho protons of 5-phenyl ring): a_{14N}=2.5G(a_{15N}=3.3G), as illustrated in Fig. 1b.

The ESR data suggest the occurrence of the large spin densities at 2, 5 and 1(N) positions and consequently a high probability of dimerization of the radicals at these positions, which is consistent with the preferential formation of 2,2′- and 5,5′-dimers.[3),4)] The lack of N,N′ bonding can be attributed to steric hindrance which makes recombination of the radical difficult or weakens the bond of the dimer, if formed at all. It is uncertain why no unsymmetrical dimer, 2,5′, was formed. One possible explanation is that the dimerization proceeds by symmetry-controlled secondary orbital interactions.[8)] Thus, the highest overlap of the molecular orbitals could become possible in the assumed transition state leading to the symmetrical dimers, as illustrated in the following scheme.[9)]

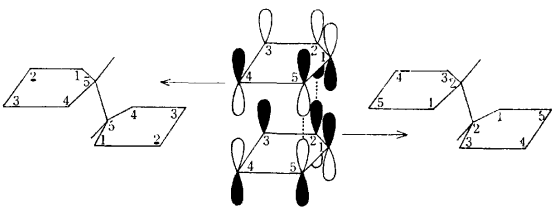

Experimental

Melting points are uncorrected. The IR spectra were determined by means of Nujol mulls with a Hitachi EPI-S2 spectrophotometer. The NMR spectra were obtained using a Varian A-60 NMR spectrometer, using tetramethylsilane as the internal standard at 32°C. The mass spectra were

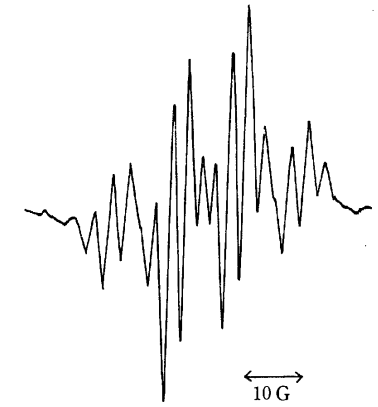

Fig. 2. ESR spectrum from XII in degassed toluene at 110°C.

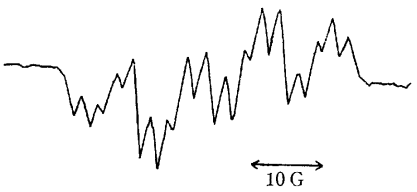

Fig. 3. ESR spectrum from XIII in degassed toluene at 110°C.

6) This also shows that the 4-phenyl ring is twisted from the plane of the pyrryl radical and supports the given steric structure.

7) Partial disagreement in intensities with the theoretical spectrum may be attributed to the difficulty in finding optimum conditions for ESR measurement of these pyrryl radicals.

8) R. Hoffman and R. B. Woodward, *J. Amer. Chem. Soc.*, **87**, 4388 (1965).

9) The diagram of the orbital occupied with an odd electron was obtained from HMO calculation. The calculated spin density of the radical is appreciably in accord with that predicted from ESR results.

obtained using a JEOL-JMS-OIS mass spectrometer. The ESR measurements were carried out in *ca.* 10% deaerated solution with a Hitachi MES 4001 type X-band spectrometer, with MES 4701 Thermocontroller, and the splitting constants were measured relative to aqueous solution of Fremy's salt. Visible spectra were obtained using a Cary-14, with Coolnics Circulator CTE-IA.

*Bis[4,5-bis(*p*-methoxyphenyl)-2-methylpyrryl] (III).* By a similar procedure as described for the preparation of I, II, IV—XI,[3),4)] III was obtained quantitatively from 4,5-bis(*p*-methoxyphenyl)-2-methylpyrrole as colorless powder, which was recrystallized from acetone to give colorless prisms, mp 142—145°C(decomp.). Found: C, 78.26; H, 6.25; N, 4.78%. Calcd for $C_{38}H_{36}O_4N_2$: C, 78.06; H, 6.21; N, 4.79. Mass spectrum: M^+ 584.

*Bis[3-ethoxycarbonyl-4,5-bis(*p*-methoxyphenyl)-2-methylpyrryl-^{15}N] (XII).* *a)*: After $^{15}NH_3$ gas, generated from $^{15}NH_4Cl$(1.0 g) and 15% aqueous NaOH(10 m*l*), was introduced into acetic acid(50 m*l*), 1.3 g of anisoin and 1.0 g of ethyl acetoacetate were added and the mixture was refluxed for 2 hr. The reaction mixture was poured into ice water and the resulting precipitate was separated by filtration, washed with water and dried *in vacuo* to give 1.65 g of ethyl 4,5-bis(*p*-methoxyphenyl)-2-methylpyrrole-3-carboxylate-^{15}N, mp 131—134°C(benzene-petroleum ether). IR(cm^{-1}): ν_{NH} 3370, $\nu_{C=O}$ 1675. Mass spectrum: M^+ 366.

b): Oxidation of pyrrole-^{15}N afforded dimer XII, quantitatively. mp 138—140°C(decomp.). IR(cm^{-1}): $\nu_{C=O}$ 1725. Mass spectrum: M^+ 730.

*Bis[4,5-bis(*o*-deuterio-*p*-methoxyphenyl)-3-ethoxycarbonyl-2-methyl-pyrryl] (XIII).* *a)*: A mixture of 6.4 g of *o*-bromo-*p*-methoxybenzaldehyde,[10)] 2.5 g of 10% palladium on carbon, 4.0 g of sodium acetate and 100 m*l* of methanol was shaken with deuterium under atmospheric pressure at room temperature until uptake ceased (about 20 min). After the mixture was filtered and concentrated below 50°C under reduced pressure, the residue was extracted with ether and the solution was washed with water and dried. After evaporation of ether, the resulting oil was distilled (at 250°C, bath temp.) to give 3.7 g of anisaldehyde-2-*d*. Mass spectrum: M^+ 137. NMR spectrum (ppm in CCl_4): 3.90 (3H, singlet), 6.90—7.87 (3H, multiplet), 9.87(1H, singlet).

b): Anisaldehyde-2-*d* gave anisoin-2,2'-d_2 by the usual benzoin condensation method. Mp 104—107°C. Mass spectrum: M^+ 274.

c): Reaction of 0.25 g of anisoin-2,2'-d_2 and 0.4 g of ethyl acetoacetate in the presence of 1.0 g of ammonium acetate in 20 m*l* of acetic acid afforded 0.20 g of ethyl 4,5-bis(*o*-deuterio-*p*-methoxyphenyl)-2-methylpyrrole-3-carboxylate, mp 131—133°C, by a similar procedure as described for the preparation of pyrrole-^{15}N. NMR spectrum (ppm in $CDCl_3$): 6.70—7.40(6H, multiplet). Mass spectrum: M^+ 367.

d): Oxidation of pyrrole-d_2 gave dimer XIII quantitatively. Mp 136—138°C(decomp.). IR(cm^{-1}): $\nu_{C=O}$ 1725. Mass spectrum: M^+ 732.

The authors would like to thank Dr. Genshun Sunagawa, the director of these laboratories, for his encouragement and Drs. K. Murayama and T. Toda for the ESR spectra measurement and helpful discussions.

10) H. H. Hodgson and T. A. Jenkinson, *J. Chem. Soc.*, **1927**, 3041.

BULLETIN OF THE CHEMICAL SOCIETY OF JAPAN, VOL. 45, 3586—3590 (1972)

Sulfilimine. XVII. Syntheses and Reactions of *N*-Carbamoylsulfilimines

Shigeru OAE, Toshiaki MASUDA, Kenji TSUJIHARA, and Naomichi FURUKAWA

Department of Applied Chemistry, Faculty of Engineering, Osaka City University, Sumiyoshi-ku, Osaka

(Received March 18, 1972)

The physical and chemical properties of several new sulfilimines, *N*-carbamoylsulfilimines, and their syntheses were studied. The sulfilimines were prepared by the action of *N*-chlorourea on appropriate sulfides in acetonitrile, and their IR and NMR spectra were obtained. Thermolysis, hydrolysis and reactions with thiophenol and sodium nitrite were carried out and the results were discussed.

Sulfilimines with the general structural formula R'RS→NR'' were first prepared by Nicolet and Willard[1] in 1921. Recently, Whitfield *et al.*[2] reported the syntheses of a new class of sulfilimines, dimethyl and diethyl *N*-ethoxycarbonylsulfilimines from the corresponding sulfides and *N*-chloroethyl carbamate.

We have found that *N*-chlorourea[3] also reacts with sulfides giving the corresponding sulfilimines, *N*-carbamoylsulfilimines. Their syntheses and reactions are reported.

1) B. H. Nicolet and J. Willard, *Science*, **53**, 217 (1921).
2) G. F. Whitfield, H. S. Beilan, D. Saika, and D. Swern, *Tetrahedron Lett.*, **1970**, 3534.
3) R. A. Wiesboeck, *J. Org. Chem.*, **30**, 3161 (1965).

Results and Discussion

Syntheses and Spectroscopic Data. Syntheses of *N*-carbamoylsulfilimines are shown in Scheme 1.

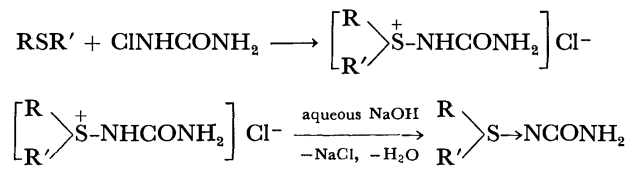

[R: aryl, R': alkyl]

Scheme 1.

Alkyl aryl sulfides were treated with *N*-chlorourea in acetonitrile to afford the corresponding *N*-carbamoyliminosulfonium chlorides. They were treated directly with an aqueous alkaline solution without being isolated. *N*-carbamoylsulfilimines were obtained as white solids in 40—70% yield, after the aqueous alkaline solution had been extracted with chloroform. No diaryl sulfilimines were obtained under the same conditions. The sulfilimines were recrystallized from chloroform, acetone-alcohol or benzene-alcohol. The products and their yields are shown in Table 1.

Table 1. Products and yields

$$\left[\begin{matrix}R\\R'\end{matrix}\!\!>\!S\rightarrow NCONH_2\right]$$

R	R′	Mp, °C	Yield, %
Ph	Me	175—6	64
p-MeC_6H_4	Me	168—9	55
p-ClC_6H_4	Me	150—1	42
p-$MeOC_6H_4$	Me	160—1	42
Ph	Et	173—4	68
Ph	*n*-Pr	122—3	50
p-MeC_6H_4	*n*-Pr	119—20	59
Ph	*i*-Pr	122—3	67
Ph	*n*-Bu	101—2	66

Kucsman *et al.*[4] and Whitfield *et al.*[2] reported that the C=O and S=N IR absorption bands of *N*-dihaloacetyl- or *N*-ethoxycarbonylsulfilimine appear at 1620—1640 cm^{-1} (C-O), and 810—820 cm^{-1}(S-N), respectively. They proposed that the structure of the compound can best be represented by betaine form (II). However, the strong C=O stretching absorption band of *N*-carbamoylsulfilimines appears at 1640—1685 cm^{-1} and is similar to that of urea, but the S-N band is at 960—1040 cm^{-1}. Thus, the major contributing form of the *N*-carbamoylsulfilimines is not always form (II) but either form (I) or (II) depending on the kind of sulfilimine.

The methyl protons of the NMR spectra of the methyl phenyl *N*-carbamoylsulfilimine appear as a singlet at δ 2.97 ppm, and the chemical shift appears about 0.3 ppm and 0.1 ppm downfield from those of the corresponding sulfoxide and dimethyl *N*-ethoxycarbonylsulfilimine,[2] respectively. Thus, the S(IV) atom in the methyl phenyl *N*-carbamoylsulfilimine is considered to have a more positive charge than that of the corresponding sulfoxide or dimethyl *N*-ethoxycarbonylsulfilimine, and the shift is analogous to that of the methyl protons of methyl phenyl *N*-*p*-tolylsulfonylsulfilimine.

Thus the canonical form (I) appears to be the major contributor to the *N*-carbamoylsulfilimine structure.

Reactions. We have carried out extensive studies on the reactions of sulfilimines, particularly *N*-sulfonylsulfilimines.[5-10] In order to compare the chemical behaviors of *N*-carbamoylsulfilimine with those of the *N*-sulfonyl derivative, we treated the new sulfilimine under similar reaction conditions as those of the *N*-*p*-tolylsulfonyl derivative.

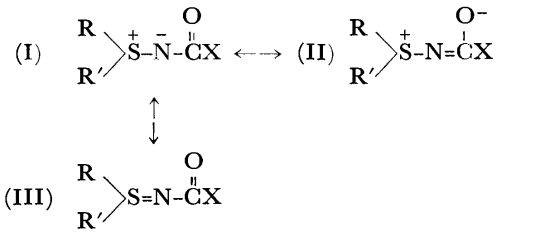

[X: $CHCl_2$, $CHBr_2$, OEt, NH_2]

Scheme 2.

1) Thermolysis: *N*-*p*-Tolylsulfonylsulfilimines with β-proton have recently been found to give olefins in high yields.[6] When ethyl phenyl *N*-carbamoylsulfilimine was heated in benzene, sulfenamide and ethylene were similarly found to be obtained in good yields.

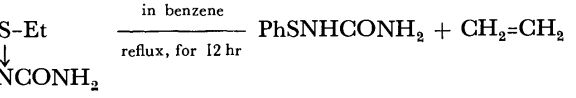

Scheme 3.

The mechanism of the reaction is not clear but the reaction is considered to proceed *via* an Ei mechanism involving a five membered cyclic transition state as in the case of *N*-*p*-tolylsulfonylsulfilimines.[6),10] When thermolysis was carried out in methanol solution, the sulfide, α-methoxy sulfide and urea were obtained as shown in Scheme 4.

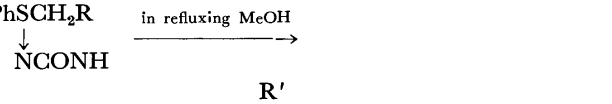

		(A)	(B)	(C)
		A	B	C
R′	H	75%	14%	~100%
	Me	73%	17%	~100%

Scheme 4.

The reaction with this type of sulfilimine is unique since the *N*-*p*-tolylsulfonyl derivatives do not react under the same conditions. An analogous reaction was observed when alkoxysulfonium salt[11] or *N*-*p*-tolylsulfonylsulfilimine[12] was treated with a base such as alkoxide or hydroxide in alcohol solution. As in the case of the sulfonium salt or *N*-*p*-tolylsulfonylsul-

4) A. Kucsman, I. Kapovits, and F. Ruff, *Tetrahedron*, **22**, 1843 (1966).

5) K. Tsujihara, N. Furukawa, and S. Oae, This Bulletin, **43**, 2153 (1970).

6) S. Oae, K. Tsujihara, and N. Furukawa, *Tetrahedron Lett.*, **1970**, 2663.

7) K. Tsujihara, T. Aida, N. Furukawa, and S. Oae, *ibid.*, **1970**, 3415.

8) A. Nakanishi and S. Oae, *Chem. and Ind.*, **1971**, 960.

9) S. Oae, T. Aida, K. Tsujihara, and N. Furukawa, *Tetrahedron Lett.*, **1971**, 1145.

10) K. Tsujihara, K. Harada, N. Furukawa, and S. Oae, *Tetrahedron*, **27**, 6101 (1971).

11) C. R. Johnson and W. G. Phillips, *J. Amer. Chem. Soc.*, **91**, 682 (1969).

12) H. Kobayashi, N. Furukawa, T. Aida, K. Tsujihara, and S. Oae, *Tetrahedron Lett.*, **1971**, 3109.

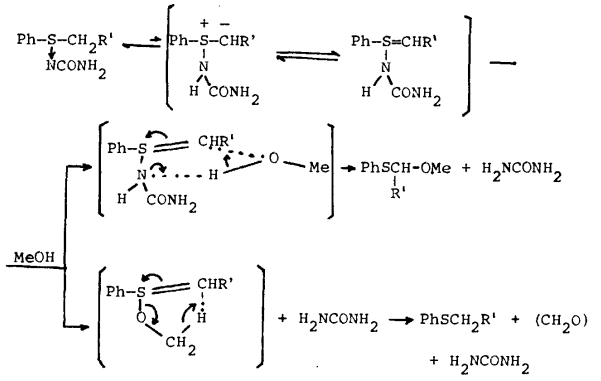

Scheme 5.

filimine, the reaction seems to proceed through the initial proton transfer from C atom to N atom to form an intermediate which upon addition of methanol affords the α-alkoxy sulfide and the sulfide.

2) Hydrolysis: Treatment of methyl phenyl *N*-carbamoylsulfilimine with 5% aqueous alkaline solution, water or 5% aqueous hydrogen chloride solution at 55°C for 8 hr gave phenyl methyl sulfoxide.

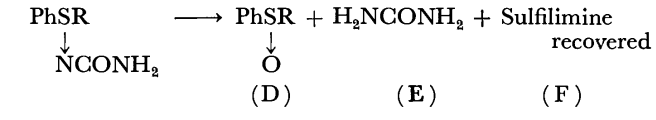

R	Reaction conditions	D	E	F
Me	5% KOH-H_2O	98%	not detd.	0%
	H_2O	99%	not detd.	0%
	5% HCl-H_2O	56%	not detd.	37%
Et	5% KOH-H_2O	98%	not detd.	0%

Scheme 6.

Thus, methyl phenyl *N*-carbamoylsulfilimine easily hydrolyzes in water as well as in aqueous alkaline solution. However, it hydrolyzed slowly in aqueous hydrogen chloride solution since the attack of hydroxide anion on the S(IV) atom is considered to lead to the hydrolysis product. A similar treatment of ethyl phenyl *N*-carbamoylsulfilimine with 5% aqueous alkaline solution at 60°C for 6 hr gave ethyl phenyl sulfoxide.

3) Reaction with Thiophenol: When the *N*-carbamoylsulfilimine was treated with thiophenol, it was easily reduced at room temperature within a few minutes to the corresponding sulfide (Scheme 7). Besides the sulfide, both urea and diphenyl disulfide were obtained quantitatively. For the reduction of one equivalent mole of sulfilimine two equivalent moles of thiophenol were required stoichiometrically.

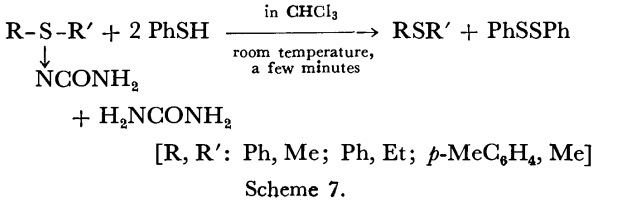

Scheme 7.

This reaction is analogous to that of sulfoxide or *N*-*p*-tolylsulfonylsulfilimine with thiophenol or *O,O*-dialkyl dithiophosphoric acid.[8] Thus the mechanism is considered to involve the initial nucleophilic attack by thiophenolate ion on S(IV) atom forming the sulfonium salt as an intermediate.

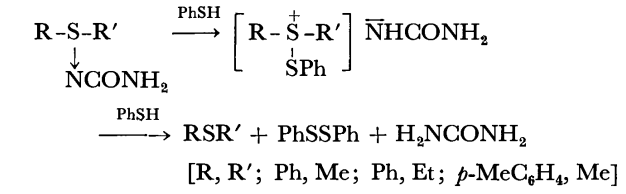

Scheme 8.

4) Reaction with Sodium Nitrite: It was reported by Appel and Buechner[13] that treatment of dialkyl sulfilimine with carbon dioxide gives the compound $R_2SNH \cdot CO_2$.

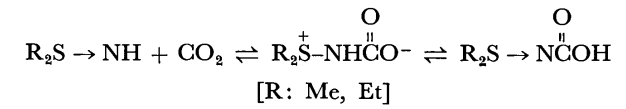

Scheme 9.

We therefore carried out the diazo-decomposition of *N*-carbamoylsulfilimine in the hope of obtaining the alkyl aryl sulfilimine. However, treatment of *N*-carbamoylsulfilimine hydrochloride with sodium nitrite at 0°C in water led to the evolution of N_2 and CO_2 gases, and the product obtained was found to be only the sulfoxide, no free sulfilimine derivative being obtained.

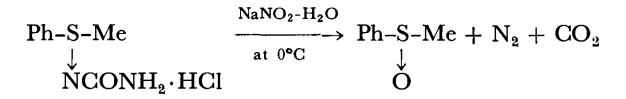

Scheme 10.

Although free sulfilimine (IV) was not actually isolated, its formation as an intermediate during the diazo-decomposition of *N*-carbamoylsulfilimine might be expected, since decarboxylation was observed as by Appel *et al.* The mechanism is considered as shown in Scheme 11.

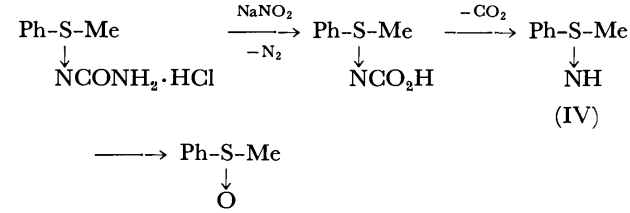

Scheme 11.

Experimental

Materials. All the solvents, *i.e.*, benzene, methanol and chloroform were purified by standard procedures.[14] The others used were of chemical grade. Aqueous hydrogen chloride, sodium nitrite and sodium hydroxide were of special

13) R. Appel and W. Buechner, *Chem. Ber.*, **95**, 849 (1962).
14) A. Weissberger, E. S. Proskauer, J. A. Riddick, and E. E. Toops, Jr., "Organic Solvents", Interscience Publishers, New York (1955).

grade. Thiophenol, sulfide, sulfoxide and disulfide were prepared by the usual procedures.

N-Chlorourea.[3] A suspension of 0.25 mol (15 g) of pulverized urea in 100 ml of acetonitrile was cooled to 0°C and chlorinated with Cl_2 gas with rapid stirring. Moisture was excluded by means of dry nitrogen gas.

Introduction of Cl_2 gas was stopped as soon as 0.1 mole (7.1 g) of chlorine was absorbed. The resulting clear, colorless solution was stirred for 30 min.

Synthesis of N-*carbamoylsulfilimine.* A solution of about

TABLE 2. IR SPECTRA OF *N*-CARBAMOYLSULFILIMINE[a]

$$\begin{matrix} R \\ R' \end{matrix}\!\!>\!S\rightarrow NCONH_2$$

R	R′	NH (cm^{-1})	C=O (cm^{-1})	S-N (cm^{-1})	Anal, %, Found (Calcd) C	H	N
Ph	Me	3340, 3170	1655	968	52.80(52.72)	5.44(5.54)	15.20(15.35)
p-MeC_6H_4	Me	3320, 3170	1640	960	54.53(55.08)	6.14(6.16)	14.43(14.26)
p-ClC_6H_4	Me	3350, 3180	1658	980	43.65(44.35)	4.21(4.20)	12.86(12.96)
p-$MeOC_6H_4$	Me	3350, 3180	1660	975	50.61(50.92)	5.75(5.70)	13.50(13.19)
Ph	Et	3340, 3180	1650	1028	55.42(55.07)	6.11(6.16)	13.93(14.26)
Ph	*n*-Pr	3360, 3190	1662	1021	56.61(57.11)	6.86(6.70)	13.44(13.31)
Ph	*i*-Pr	3350, 3200	1649	1039	57.17(57.11)	6.67(6.70)	13.47(13.31)
Me	*n*-Pr	3320, 3180	1680	1038	59.00(58.89)	7.02(7.18)	12.21(12.48)
Ph	*n*-Bu	3320, 3190	1685	1035	59.04(58.89)	7.24(7.18)	12.51(12.48)
Ph, Me>S→NTs[5]				930			
Ph, Me>S→NCOCHCl$_2$[4]			1638, 1625	821, 808			
Me, Me>S→NCO$_2$Et[2]			1620				

a) All IR spectra were taken as KBr disks with a 215 Hitachi grating infrared spectrophotometer.

TABLE 3. NMR SPECTRA OF *N*-CARBAMOYLSULFILIMINE[a]

$$\begin{matrix} R \\ R' \end{matrix}\!\!>\!S\rightarrow NCONH_2$$

R	R′	Ar-H	$CH_3C_6H_4$	$CH_3OC_6H_4$	$=SCH_3$	$-NCONH_2$
Ph	Me	7.91(m)			2.97(s)	4.94(s)
p-MeC_6H_4	Me	7.82(q)	2.58(s)		2.95(s)	4.97(s)
p-ClC_6H_4	Me	8.03(q)			3.05(s)	4.97(s)
p-$MeOC_6H_4$	Me	7.56(q)		4.08(s)	2.98(s)	5.08(s)

R	R′	Ar-H	$CH_3C_6H_4$	$=S-CH_2$ or $=S-CH$	$=S-CH_2CH_2$ or $=S-CH_2(CH_2)_2$	$-CH_3$ or $=(CH_3)_2$	$-NCONH_2$
Ph	Et	7.77(m)		3.07(q)		2.27(t)	5.02(s)
Ph	*n*-Pr	7.95(m)		3.18(m)	1.86(m)	1.14(t)	5.44(s)
Me	*n*-Pr	7.66(q)	2.48(s)	3.10(m)	1.76(m)	1.10(t)	5.10(s)
Ph	*i*-Pr	7.73(m)		3.32(m)		1.27(d), 1.36(d)	5.08(s)
Ph	*n*-Bu	7.97(m)		3.15(m)	1.20—2.10(m)	1.10(t)	5.37(s)

	Ar-H	$=SCH_3$
Ph, Me>S→NTs	7.63(m)	2.83(s)
Me, Me>S→NCO$_2$Et[2]		2.73(s)
Ph, Me>S→O	7.52(m)	2.73(s)

a) The chemical shifts (ppm) were measured with a Hitachi Perkin-Elmer R-20 High Resolution NMR Spectrometer (60 MHz) using TMS as an internal standard (δ=0.00) in $CDCl_3$. The multiplicity of the signal is given by s=singlet, d=doublet, t=triplet, q=quartet and m=unresolved multiplet.

0.08 mol of sulfides in 50 ml of acetonitrile was dropped with stirring into the above mentioned *N*-chlorourea solution maintained at 15—20°C by external cooling. After the addition, the temperature was raised to 60—70°C for 1 hr. A 10% aqueous solution of sodium hydroxide was added dropwise for about 30 min until the solution became alkaline. *N*-Carbamoylsulfilimine was then extracted with chloroform from alkaline solution. The compound was recrystallized as white solid from chloroform, acetone-alcohol or benzene-alcohol. Yield, 40—70%. IR and NMR spectra of *N*-carbamoylsulfilimine are summarized in Tables 2 and 3.

Thermolysis of Ethyl Phenyl N-*Carbamoylsulfilimine in Benzene.* About 0.004 mol (0.88 g) of ethyl phenyl *N*-carbamoyl-sulfilimine was heated in refluxing benzene (10 ml) for 10 hr under nitrogen stream. Ethylene was produced in 60% yield by this reaction and was converted into 1,2-dibromoethylene. This was confimed by comparing its glc behavior with that of the authentic compound. Benzene was removed from the residue and *N*-phenylthiourea, mp 163°C, was isolated in 95% yield. IR spectra: (ν_{N-H} 3440, 3200, $\nu_{C=O}$ 1677), NMR spectra: (δ 7.43, 5-Ar-H (multiplet), δ 8.19, 1-H (singlet), δ 6.54, 2-H (singlet)). The NMR spectra were measured with TMS internal standards (δ=0.00) as a reference peak in DMSO-d_6.

Found: C, 49.20; H, 16.35: N, 16.42%. Calcd. for $PhSNHCONH_2$: C, 49.99; H, 16.68; N, 16.65%.

Thermolysis of Methyl Phenyl N-*Carbamoylsulfilimine in Methanol.* About 0.005 mol (0.88 g) of methyl phenyl *N*-carbamoyl-sulfilimine was heated in refluxing methanol (10 ml) for 10 hr. The products obtained were separated by column chromatography and identified by comparing their IR and NMR spectra with those of the authentic compounds. Yields of sulfide, α-methoxy sulfide and urea were 0.44 g (75%), 0.12 g (14%) and about 0.30 g (100%), respectively.

Thermolysis of Ethyl Phenyl N-*Carbamoylsulfilimine in Methanol.* About 0.004 mol (0.88 g) of ethyl phenyl *N*-carbamoyl-sulfilimine was heated in refluxing methanol (10 ml) for 6 hr as well as methyl *p*-tolyl *N*-carbamoylsulfilimine. The products were determined by comparing their IR and NMR spectra with those of the authentic compounds. Yields of sulfide, α-methoxy sulfide and urea were 0.43 g (73%), 0.13 g (17%) and about 0.30 g (100%), respectively.

Hydrolysis of Methyl Phenyl and Ethyl Phenyl N-*Carbamoylsulfilimine.* Methyl phenyl *N*-carbamoylsulfilimine 0.002 mol (0.363 g) was heated at 55°C for 8 hr in 5 ml of 5% aqueous potassium hydroxide solution, water or 5% aqueous hydrogen chloride solution. The reaction solution was then acidified with a 10% aqueous hydrogen chloride solution and reactants were extracted with chloroform. The solution was then made alkaline by a 10% aqueous sodium hydroxide solution and the reactants were again extracted with chloroform. The products were identified by comparing their IR, NMR spectra with those of the authentic samples. Yield of sulfoxide was 0.24 g (98%), 0.25 g (99%) and 0.14 g (56%), respectively. Yields of the sulfilimine recovered were 0%, 0% and 37%, respectively.

Ethyl phenyl *N*-carbamoylsulfilimine (0.002 mol) was hydrolyzed by the same method, to the corresponding sulfoxide (98% yield) at 60°C for 6 hr in 5 ml of 5% aqueous potassium hydroxide solution. The product was identified by comparing its IR, NMR spectra with those of the authentic compound.

Reaction of N-*Carbamoylsulfilimine with Thiophenol.* A 10% solution of thiophenol in chloroform was dropped with stirring into a solution of about 0.005 mol of *N*-carbamoylsulfilimines (methyl phenyl, methyl *p*-tolyl or ethyl phenyl *N*-carbamoylsulfilimine) in 10 ml of chloroform at room temperature. After the addition, the solution was maintained at room temperature for a few minutes. Thiophenol (0.01 mol) was required to complete the reaction. The products, sulfide, disulfide and urea were separated by column chromatography and were identified by comparing their IR, NMR spectra with those of the authentic compounds.

Reaction of Methyl Phenyl N-*Carbamoylsulfilimine with Sodium Nitrite.* Two drops of a 35% aqueous hydrogen chloride solution was added to a solution of about 0.002 mol (0.37 g) of methyl phenyl *N*-carbamoylsulfilimine in 3 ml of water. Into this was dropped a solution of about 0.003 mol (0.20 g) of sodium nitrite in 2 ml of water, the temperature being maintained at 0°C with an ice bath. The solution was stirred overnight at 0°C, and the products were then extracted with chloroform. Methyl phenyl sulfoxide was obtained in 28% yield (0.08 g) and identified by comparing its IR and and NMR spectra with those of the authentic compound. Methyl phenyl *N*-carbamoylsulfilimine was recovered in 63% yield.

Studies of Acyl and Thioacyl Isocyanates. X.[1] The Cycloaddition Reaction of Benzoyl and Thiobenzoyl Isocyanates with Benzaldazines

Otohiko TSUGE and Shuji KANEMASA

Research Institute of Industrial Science, Kyushu University, Hakozaki, Higashi-ku, Fukuoka, 812

(Received March 11, 1972)

Although benzoyl isocyanates do not react with benzaldazines at room temperature, the criss-cross cycloadducts are formed if the reaction is carried out in refluxing xylene. On the other hand, thiobenzoyl isocyanate behaves quite differently toward the same azines. It reacts easily with azines at room temperature to afford to mono- or the bis(4+2) cycloadducts depending on the nature of the substituent in the azines. We found that the mono (4+2) cycloadduct can be thermally dissociated into its components. Neither benzoyl isocyanate nor thiobenzoyl isocyanate react with aromatic ketazines.

Azines having the conjugated system C=N-N=C exhibit a curious behavior toward cycloaddition reactions. Benzaldazines react with cyanic acid,[2] thiocyanic acid,[2,3] isocyanates,[3] maleic anhydride[4,5] and methyl acrylate[6] to form the corresponding criss-cross cycloadducts. On the other hand, the reaction of propionaldazine with methyl acrylate affords a Diels-Alder type adduct;[6] in this case the aldazine behaves as a diene (Scheme 1).

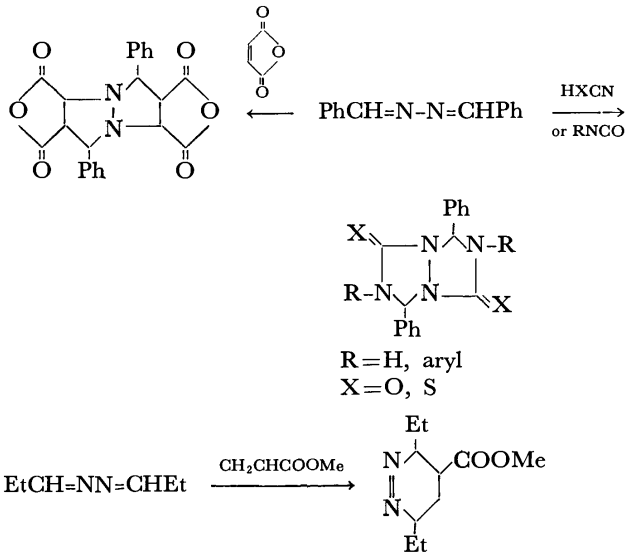

Scheme 1

Benzoyl (I) and thiobenzoyl isocyanates (II) react with the C=N bonds of anils[7,8] and carbodiimides[9] to give the (4+2) and/or (2+2) cycloadducts. Accordingly, in the reaction of acyl isocyanate with azines, we might expect the formation of a criss-cross cycloadduct or Diels-Alder adduct, besides mono- or bis(4+2) or (2+2) cycloadduct of C=N bonds of azines. However, no study has been reported on the addition of acyl isocyanate to azines. As part of the investigation of the chemistry of I and II with compounds having a C=N bond, their reaction with aromatic azines was studied.

Results and Discussion

Reaction of Benzoyl Isocyanates with Benzaldazines. Although no reaction of benzoyl isocyanate (Ia) with benzaldazine (IIIa) took place at room temperature, Ia reacted with IIIa in refluxing xylene to afford a 2 : 1 adduct IVa in 58% yield. The IR spectrum of IVa showed bands ascribable to $\nu_{C=O}$ at 1760 and 1680 cm^{-1}. The NMR spectrum in deuteriochloroform ($CDCl_3$) exhibited a singlet (2H) assignable to two equivalent methine protons at δ 7.20 ppm, besides signals of aromatic protons. The mass spectrum showed the parent peak (M^+) at *m/e* 502, together with major peaks at *m/e* 397 (M^+—PhCO), 355 (M^+—PhCONCO), 278 (355$^+$—Ph), 250 (278$^+$—CO), 208 ([Ph–CH=N-N=CH-Ph]$^+$), 147 ([PhCONCO]$^+$) and 105 ([PhCO]$^+$).

Hydrolysis of IVa with hydrochloric acid afforded hydrazodicarbonamide (V) and benzaldehyde. The structure of V was confirmed by spectral data and elemental analysis as well as by comparison with an authentic sample prepared from urea and hydrazine hydrate;[10] benzaldehyde was identified as its 2,4-dinitrophenylhydrazone (Scheme 2). It is thus deduced that the most reasonable structure for IVa of the possible 2 : 1 cycloadducts, including bis (2+2), (4+2) and mixed cycloadducts, is the criss-cross cycloadduct.

Benzoylation of the criss-cross cycloadduct VI[2] prepared from IIIa and cyanic acid, with benzoyl chloride in pyridine afforded perhydro-2,6-dibenzoyl-1,5-diphenyltriazolo[1,2-a]triazole-3,7-dione (IVa), as shown in Scheme 2.

Similar reactions of benzoyl isocyanates (Ia-Id) with benzaldazines (IIIa—IIIe) gave the corresponding criss-cross cycloadducts IV. The yields, physical properties and results of elemental analyses of IV are summarized in Table 1.

We see that the yield of IV is affected by the nature of the substituents R^1 and R^2. The stronger the

1) Part IX of this series: O. Tsuge and S. Kanemasa, This Bulletin, **45**, 2877 (1972).
2) J. R. Bailey and N. H. Moore, *J. Amer. Chem. Soc.*, **39**, 279 (1917).
3) J. R. Bailey and A. T. McPherson, *ibid.*, **39**, 1322 (1917).
4) T. Wagner-Jauregg, *Ber.*, **63**, 3213 (1930).
5) J. van Alphen, *Rec. Trav. Chim.*, **61**, 892 (1942).
6) M. Häring and T. Wagner-Jauregg, *Helv. Chim. Acta*, **40**, 852 (1957).
7) O. Tsuge, M. Tashiro, R. Mizuguchi, and S. Kanemasa, *Chem. Pharm. Bull.* (Tokyo), **14**, 1055 (1966).
8) O. Tsuge and S. Kanemasa, This Bulletin, **45**, 2877 1972.
9) O. Tsuge and K. Sakai, This Bulletin, **45**, 1534 (1972).
10) T. Curtius and K. Heidenreich, *Ber.*, **27**, 55 (1894).

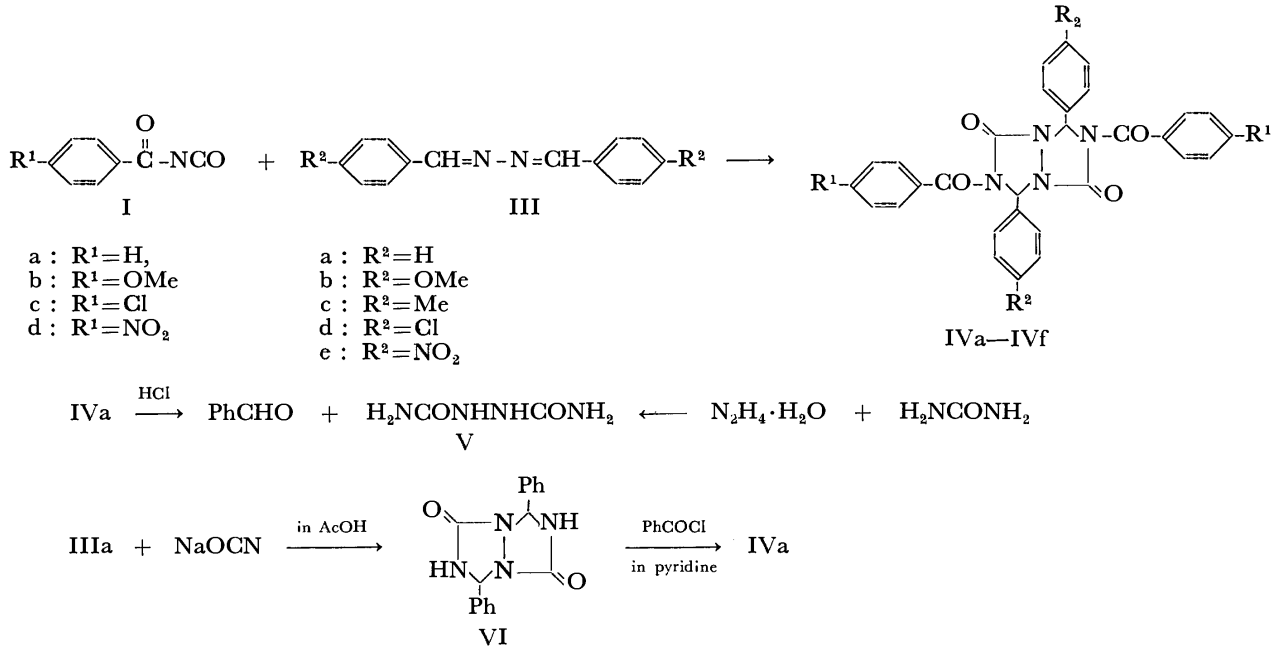

Scheme 2

Table 1. Perhydro-2,6-diaroyl-1,5-diaryltriazolo[1,2-a]triazole-3,7-diones IV[a)]

IV	R¹	R²	Reaction time,[b)] hr	Yield, %	Mp, °C	IR, cm^{-1} $\nu_{C=O}$	NMR ($CDCl_3$) >CH δ ppm	Microanalysis, % Found C	Found H	Found N	Calcd N	Calcd N	Calcd N
a	H	H	23	58	130.5—131 (decomp.)	1760, 1680	7.20	71.68	4.59	11.03	71.78	4.41	11.15
b	H	OMe	20	82	202—203	1760, 1690	7.11	68.52	4.75	9.95	68.32	4.66	9.96
c	H	Me	24	72	193—193.5	1760, 1680	7.15	72.51	5.04	10.74	72.44	4.94	10.56
d	H	Cl	48	34	200.5—201	1770, 1680	7.19	63.29	3.37	9.43	63.10	3.54	9.81
e	Cl	H	24	62	224—225	1770, 1690	7.21	63.43	3.47	9.69	63.10	3.54	9.81
f	NO_2	H	26	92	240—241 (decomp.)	1770, 1690	7.13	61.15	3.52	13.96	60.81	3.40	14.19

a) All the compounds are colorless prisms. b) Reaction temperature: 140°C. Reaction of Ia with IIIe (24 hr) and of Ib with IIIa (48 hr) did not take place.

electron-donating nature of substituent R^2 in III, the higher the yield of IV, while the effect of substituent R^1 in I on the yield is the reverse: although Ia and Ib did not react with IIIe and IIIa, respectively, the reactions of Ia with IIIb and of Id with IIIa gave excellent yields of IV. On the other hand, I did not react with aromatic ketazines such as acetophenone and benzophenone azines under similar conditions.

Reaction of Thiobenzoyl Isocyanate with Benzaldazines. In contrast with benzoyl isocyanates (I), thiobenzoyl isocyanate (II) reacted easily with benzaldazine (IIIa) at room temperature to afford a quantitative yield of the 1 : 1 adduct VIIa. The IR spectrum of VIIa showed no bands assignable to ν_{NH}, but displayed bands of $\nu_{C=O}$ and $\nu_{C=N}$ at 1680, 1660 and 1650 cm^{-1} respectively; it is very similar to that of the (4+2) cycloadduct[8)] of II to benzylidenaniline. In the NMR spectrum ($CDCl_3$) singlets appeared at δ 6.42 (1H, >C**H**) and 9.48 ppm (1H, -C**H**=N-), besides signals of aromatic protons.

Thus, VIIa was deduced to be 3-benzylidenamino-2,6-diphenyl-2*H*-1,3,5-thiadiazin-4(3*H*)-one, whose structure corresponds to the (4+2) cycloadduct of II to one C=N bond of IIIa.

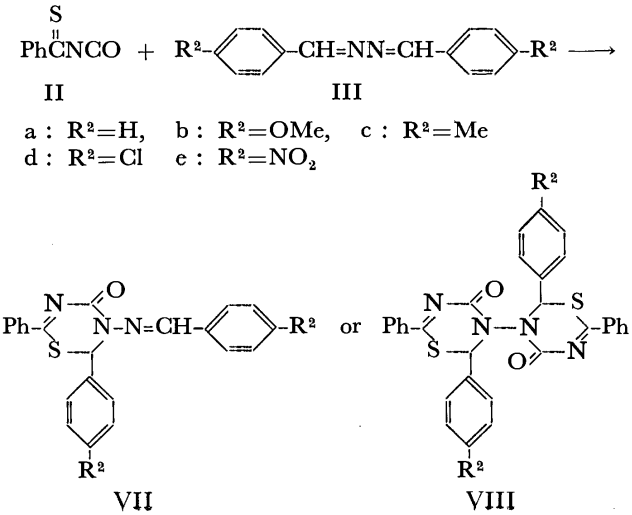

Table 2. Mono- and bis-2*H*-1,3,5-thiadiazin-4(3*H*)-ones VII and VIII.[a]

	R^2	Mp, °C	Yield, %	IR, cm^{-1}		Microanalysis, %					
						Found			Calcd		
				$\nu_{C=O}$	$\nu_{C=N}$	C	H	N	C	H	N
VIIa	H	148—149 (decomp.)	100	1680 1660	1650	71.05	4.45	11.24	71.15	4.61	11.32
VIIIb-1	OMe	181 (decomp.)	50	1690 1670	1645	64.96	4.11	9.08	64.64	4.41	9.42
VIIIb-2	OMe	141—142	39	1700 1670	1650	65.13	4.26	9.22	64.64	4.41	9.42
VIIIc	Me	201 (decomp.)	62	1690 1675	1650	68.28	4.68	9.72	68.32	4.66	9.96
VIId[b]	Cl	165—168 (decomp.)	80	1670	1655	60.31	3.11	9.27	60.00	3.41	9.55

a) All the compounds are colorless needles. b) NMR δ ppm: 6.41 (1H, singlet, $\rangle$C**H**), 9.52 (1H, singlet, -C**H**=N-) in $CDCl_3$; 7.07 (1H, singlet, $\rangle$C**H**), 8.75 (1H, singlet, -C**H**=N-) in CF_3COOH.

In similar reactions of II with azines IIIb—IIId, a 1 : 1 or a 2 : 1 adduct was formed, depending on the nature of substituent R^2 in III. When R^2 is electron-donating such as methoxy or methyl, the 2 : 1 adduct VIII was obtained, while the 1 : 1 adduct VIId was only formed if R^2 is electron-withdrawing such as chlorine. However, the reaction with IIIe having nitro groups did not take place even under forced conditions. The results are summarized in Table 2.

The structures of 1 : 1 adduct VIId, and of 2 : 1 adducts VIIIb and VIIIc were confirmed to be those of the corresponding mono(4+2) and bis(4+2) cycloadducts of II to one and both C=N bonds in III on the basis of spectral studies. In spite of having a second C=N bond to which to add, II did not react further with the 1 : 1 adduct VII under more forced conditions (at 50°C for 5 min and then at room temperature for 3 hr); instead the unchanged 1 : 1 adduct was recovered almost quantitatively.

The NMR spectrum of VIIIc indicated that its configuration is symmetrical; singlets attributable to two equivalent methyl and methine protons appeared at δ 2.25 and 6.22 ppm in $CDCl_3$, and at δ 2.35 and 6.79 ppm in trifluoroacetic acid (CF_3–COOH), respectively.

On the other hand, two stereoisomers VIIIb-1 and VIIIb-2 were obtained in the reaction with IIIb. Their NMR spectra could not be measured in the same solvent, because VIIIb-1 is insoluble in $CDCl_3$ and VIIIb-2 decomposed in CF_3COOH. The NMR spectrum of VIIIb-1 in CF_3COOH showed two singlets at δ 3.89 (6H, O**C**$\mathbf{H}_3$) and 6.81 ppm (2H, $\rangle$C**H**), while four singnlets appeared at δ 3.77, 3.81 (each 3H, O**C**$\mathbf{H}_3$) and 5.35, 6.59 ppm (each 1H, $\rangle$C**H**) in the NMR spectrum of VIIIb-2 ($CDCl_3$). This indicates that the configuration of VIIIb-1 is symmetrical, while that of VIIIb-2 is asymmetrical.

Dreiding models of VIII show that the free rotation of N^3–$N^{3'}$ bond is hindered by the steric interaction between the 2- or 2′-aryl group and 4′- or 4-carbonyl group. Thus, two isomers resulting from the configurations of 2- and 2′-aryl groups are possible for symmetrical 2 : 1 adduct VIIIb-1 or VIIIc: one (VIII-A) in which both 2- and 2′-aryl groups are quasi-axial,

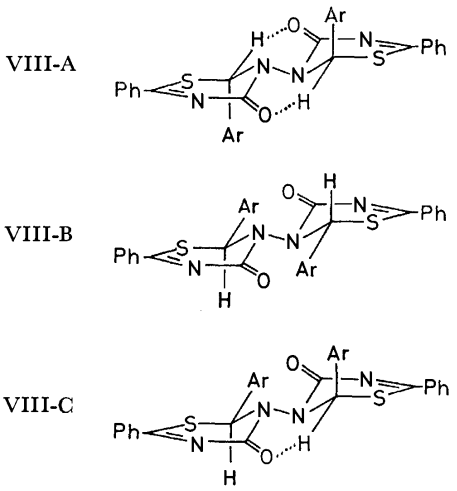

Fig. 1.

and the other (VIII-B) in which they are quasi-equatorial. However, it is conceivable that VIII-A is more favorable since there is a significant repulsion between 2- or 2′-aryl group and 4′- or 4-carbonyl group in VIII-B (Fig. 1).

On the other hand, the configuration VIII-C in which 2- and 2′-aryl groups are quasi-equatorial and quasi-axial, respectively, is only possible for asymmetrical 2 : 1 adduct VIIIb-2. In this case, there is a steric interaction between 2-aryl group and 4′-carbonyl group, and the rotation of N^3–$N^{3'}$ bond should occur to attain minimum steric hindrance.

The singlet of methine protons of VIIIc is shifted to a lower field by about 0.6 ppm, in changing from $CDCl_3$ to CF_3COOH. If the value of the shift is applied to the methine protons of VIIIb-1, a singlet should appear at δ ca. 6.2 ppm in $CDCl_3$. Consequently, the singlets at 5.35 and 6.59 ppm in VIIIb-2 could be assigned to the 2-quasi-axial and 2′-quasi-equatorial hydrogens, respectively. The shift of equatorial hydrogens to a lower field can be explained in terms of hydrogen bonding with the carbonyl group in the adjacent ring as shown in Fig. 1. Isolation of the 2 : 1 adduct of type VIIIb-2 was unsuccessful, probably owing to its instability.

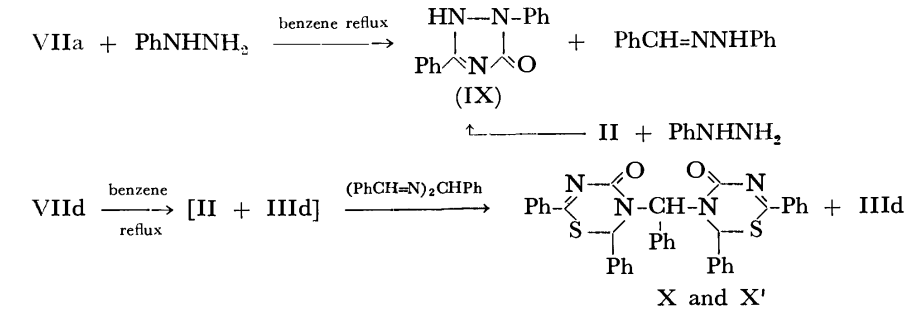

Scheme 3.

It is of interest to note that II behaves quite differently from I toward benzaldazines, although just as in the case of I, no reaction took place with aromatic ketazines.

Thermal Dissociation of Mono(4+2) Cycloadducts VII. The 1 : 1 adducts VII decomposed at their melting points and changed to reddish violet substances. When a solution of VII in dry benzene was heated to reflux, it gradually turned red. Upon cooling, the red color disappeared, the solution becoming colorless. This suggests that VII could be thermally dissociated into its components, since the benzene solution of II is reddish violet. We established thermal dissociation by the following experiments.

Phenylhydrazine reacted with VIIa in refluxing benzene to give 2,3-dihydro-2,5-diphenyl-1,2,4-triazol-3(1*H*)-one (IX) and the phenylhydrazone of benzaldehyde,[11] although hardly any reaction took place at room temperature. The structure of IX was confirmed by comparison with an authentic sample prepared from II and phenylhydrazine.[12] When VIId was treated with hydrobenzamide in refluxing benzene, two isomeric bis(4+2) cycloadducts X and X'[8] of II to hydrobenzamide and *p*-chlorobenzaldazine IIId were obtained (Scheme 3).

Experimental

All melting points are uncorrected. The IR spectra were measured as KBr pellets on a JASCO IR-S spectrophotometer; the NMR spectra were determined at 60 MHz on a Hitachi R-20 NMR spectrometer with TMS as an internal reference. The mass spectra were obtained on a Hitachi RMS-4 mass spectrometer with a direct inlet and an ionization energy of 70 eV. Elemental analyses were carried out by Miss M. Akita.

Materials. Benzoyl isocyanates (Ia–Id) were prepared by the method reported previously.[13] Thiobenzoyl isocyanate (II):[12] a solution of 1.0 g of 2-phenylthiazoline-2,4-dione[14] in 10 m*l* of xylene was heated at 120°C, producing a reddish violet solution of II. This is referred as the standard solution of II. Benzaldazines were prepared from the corresponding aldehydes and hydrazine hydrate in acetic acid. Benzaldazine (IIIa), mp 93°C (lit,[15] mp 93°C); *p*-methoxy- (IIIb), mp 169—170°C (lit,[16] mp 170—172°C); *p*-methyl- (IIIc), mp 153°C (lit,[17] mp 153°C); *p*-chloro- (IIId), mp 207—208°C (lit,[16] mp 208°C); *p*-nitrobenzaldazine (IIIe), mp 296—297°C (lit,[18] mp 297—298°C).

Reaction of Benzoyl Isocyanates (I) with Benzaldazines (III). The procedure is illustrated by a reaction of benzoyl isocyanate (Ia) with benzaldazine (IIIa).

A solution of 2.0 g of Ia and 1.4 g of IIIa in 15 m*l* of dry xylene was refluxed in an atmosphere of nitrogen for 23 hr, and the reaction mixture was allowed to stand at room temperature for 2 days, during which time crystals deposited. Filtration gave 1.18 g of colorless crystals. The filtrate was evaporated *in vacuo* to leave resinous materials, which solidified on trituration with petroleum ether to yield 0.78 g of crystals. Recrystallization of the combined crystals (1.96 g (58%)) from petroleum ether (bp 45—65°C) gave perhydro-2,6-dibenzoyl-1,5-diphenyltriazolo[1,2-b]triazole-3,7-dione (IVa), mp 130.5—131°C (decomp.), as colorless prisms.

Similarly, the reaction of benzoyl isocyanates (Ia—Id) with benzaldazines (IIIa—IIIe) gave the corresponding criss-cross cycloadduct IV. However, Ia and Ib did not react with IIIe and IIIa, respectively. The reaction conditions and yields, physical porperties and results of elemental analyses are summarized in Table 1.

Hydrolysis of Criss-cross Cycloadduct IVa. A suspension of 0.4 g of IVa in 20 m*l* of concentrated hydrochloric acid was stirred at 100°C for 3 hr. After cooling, it was filtered to recover 0.17 g (40%) of unreacted IVa. Evaporation of the filtrate *in vacuo* left a residue, which was washed with a small amount of water and then recrystallized from water to afford 55 mg (58%) of hydrazodicarbonamide (V), mp 255.5°C (decomp.) (lit,[10] mp 244—245°C (decomp.)), as colorless prisms. The compound was identical with an authentic sample prepared from hydrazine hydrate and urea.[10]

Found: C, 20.10; H, 4.90; N, 47.71%. Calcd for $C_2H_6N_4O_2$: C, 20.34; H, 5.12; N, 47.44%.

From the washings, benzaldehyde was identified to be its 2,4-dinitrophenylhydrazone.

Preparation of IVa. To a stirred solution of 4.5 g of IIIa in 30 m*l* of acetic acid was added 5.25 g of sodium cyanate at room temperature over a period of 15 min. After the reaction mixture had been stirred for 30 min at the same temperature, it was then poured into 100 m*l* of water. Filtration gave 4.8 g (76%) of perhydro-1,5-diphenyltriazolo-[1,2-a]triazole-3,7-dione (VI), mp 235°C (decomp.) (lit,[2]

11) The formation of the hydrazone indicates that benzaldazine IIIa generated by dissociation was hydrolyzed to benzaldehyde.

12) O. Tsuge, S. Kanemasa, and M. Tashiro, *Tetrahedron*, **24**, 5205 (1968).

13) O. Tsuge and R. Mizuguchi, *Kogyo Kagaku Zasshi*, **69**, 939 (1966).

14) J. Goerdeler and H. Schenk, *Chem. Ber.*, **98**, 2954 (1965).

15) H. H. Hatt, "Organic Syntheses", Coll. Vol. II, p. 395 (1943).

16) N. C. Barany, E. A. Braude, and M. Pianka, *J. Chem. Soc.*, **1949**, 1898.

17) L. B. Howard and G. E. Hilbert, *J. Amer. Chem. Soc.*, **54**, 3628 (1932).

18) E. R. Blout and R. M. Gostein, *ibid.*, **67**, 13 (1945).

mp 234°C (decomp.)), as pale yellow prisms. A mixture of 0.5 m*l* of benzoyl chloride and 0.5 g of VI in 10 m*l* of pyridine was stirred at room temperature for 18 hr. It was then poured into water to precipitate a colorless solid, which on recrystallization from petroleum ether (bp 45—65°C) afforded 0.85 g (99.5%) of IVa, mp 130.5—131°C (decomp.).

Reaction of Thiobenzoyl Isocyanate (II) with p-*Methoxybenzaldazine (IIIb).* The standard solution of II was stirred with 0.7 g of IIIb at 50°C for 30 min. Filtration gave 0.78 g (50%) of bis(4+2) cycloadduct VIIIb-1. The analytical sample was prepared by recrystallization from xylene.

The filtrate was evaporated *in vacuo* to leave isomeric bis(4+2) cycloadduct VIIIb-2, which was recrystallized from benzene-petroleum ether (bp 45—65°C).

Similarly, the reaction of II with IIIa, IIIc and IIId gave the corresponding mono(4+2) cycloadducts VIIa, VIId and bis(4+2) cycloadduct VIIIc, respectively, while II did not react with IIIe. The yields, physical properties and results of elemental analyses of VII and VIII are given in Table 2.

Reaction of VIIa with Phenylhydrazine. A solution of 0.1 g of VIIa and 5 drops of phenylhydrazine in 10 m*l* of dry benzene was refluxed for 30 min, during which time 40 mg (63%) of 2,3-dihydro-2,5-diphenyl-1,2,4-triazol-3(1*H*)-one (IX), mp 230—231°C, precipitated. Compound IX was identical with an authentic sample, mp 230–231°C,[12] prepared from II and phenylhydrazine. The filtrate was concentrated *in valuo* to give 0.11 g (95%) of phenylhydrazone of benzaldehyde, identical with an authentic sample.

Reaction of VIId with Hydrobenzamide. A solution of 0.2 g of VIId and 0.1 g of hydrobenzamide in 15 m*l* of dry benzene was refluxed for 1 hr. The crystalline precipitate was filtered and washed with hot benzene to leave 80 mg (30%) of bis(4+2) cycloadduct X, mp 208—209°C (decomp.).[8] The filtrate was evaporated *in vacuo* to give a mixture of 40 mg of azine IIId and 80 mg (30%) of isomeric bis(4+2) cycloadduct X', mp 186°C,[8] which were separated by extraction with carbon tetrachloride. Evaporation of benzene washings afforded 50 mg of azine IIId; the total yield of azine IIId is 90 mg (72%).

This work was partially supported by a grant from the Ministry of Education. The authors would like to express their thanks to Professor J.-P. Anselme, University of Massachusetts, Boston, for reading the manuscript.

BULLETIN OF THE CHEMICAL SOCIETY OF JAPAN, VOL. 45, 3595—3598 (1972)

Studies on Nitro Carboxylic Acids. II. Synthesis of α,β-Unsaturated β-Nitro Carboxylic Esters[1]

Chung-gi SHIN, Yasuchika YONEZAWA, Hirotoshi NARUKAWA, Katsumi NANJO, and Juji YOSHIMURA*

Laboratory of Organic Chemistry, Faculty of Technology, Kanagawa University, Rokkakubashi, Kanagawa-ku, Yokohama

** Laboratory of Chemistry for Natural Products, Faculty of Science, Tokyo Institute of Technology, Ookayama, Meguro-ku, Tokyo*

(Received March 28, 1972)

Synthetic studies on ethyl α,β-unsaturated β-nitrocarboxylates (IV) through two routes are described. Ethyl α-hydroxy-β-nitrocarboxylates (II) obtained by the reactions of ethyl α,β-unsaturated carboxylates with fuming nitric acid or by those of nitroparafins with ethyl glyoxylate, were treated with acetic anhydride to afford ethyl α-acetoxy-β-nitrocarboxylates (III), which were subsequently converted into IV by treatment with bases used as catalysts. On the other hand, IV was also obtained from ethyl α-chloro-β-nitrocarboxylates derived from the reactions of ethyl α,β-unsaturated carboxylates with nitryl or nitrosyl chloride. The structural assignments of IV were made on the basis of elementary analysis, infrared spectra and its conversion into the corresponding α-methoxy derivatives.

General methods for the syntheses of ethyl α,β-unsaturated α-nitrocarboxylates (I) are found in literature. They can be classified into two methods; (a) by elimination of the corresponding β-hydroxycarboxylates obtained from appropriate aldehydes and ethyl nitroacetate, *via* the acetoxy derivatives,[2-5] and (b) by nitration of ethyl α,β-unsaturated carboxylates with nitric acid or dinitrogen trioxide.[6-9]

However, there are no reports on the general synthesis ethyl α,β-unsaturated β-nitrocarboxylates (IV) except for that of β-nitroacrylic acids by the elimination of α-halo-β-nitropropionic acids.[10-12]

1) Part I of this series: C. Shin, M. Masaki, and M. Ohta, This Bulletin, **43**, 3219 (1970). A part of the present work was presented at the 24th Annual Meeting of the Chemical Society of Japan, Osaka, April, 1971.

2) A. Dornow and H. Menzel, *Ann. Chem.*, **588**, 40 (1958).

3) K. M. Rodionov and V. M. Belikov, *Dokl. Akad. Nauk. SSSR.*, **93**, 829 (1953); *Chem. Abstr.*, **49**, 1550 (1955).

4) I. S. Ivanova, Yu. V. Konnova, and S. S. Novikov, *Izv. Akad. Nauk, SSSR., Otd. Khim, Nauk*, **1962**, 1677; *Chem. Abstr.*, **58**, 4419 (1962).

5) S. Umezawa and S. Zen, This Bulletin, **36**, 1143 (1963).

6) L. Bouveault and A. Wahl, *C. R. Acad. Sci. Paris*, **131**, 687, 1212 (1900).

7) L. Bouveault and A. Wahl, *Bull. Soc. Chim. Fr.*, **25**, 801, 913 (1901).

8) S. Tatsuoka, M. Murakami, and T. Tamura, *Yakugaku Zasshi*, **70**, 230 (1950).

9) K. Yamagishi and Y. Ishibiki, *Nippon Kagaku Zasshi*, **81**, 971 (1960).

10) a) H. Shechter, F. Conrad, A. L. Daulton, and R. B. Kaplan, *J. Amer. Chem. Soc.*, **74**, 3052 (1952); b) S. S. Novikov, G. A. Shvekhgeheimer, and N. F. Pyatakov, *Izv. Akad. Nauk, SSSR., Otd. Khim. Nauk*, **1961**, 914; *Chem. Abstr.*, **55**, 22121 (1961).

11) K. A. Ogloblin and V. P. Semenov, *Zh, Org. Khim.*, **1** (**8**), 1361 (1965); *Chem. Abstr.*, **64**, 588 (1966).

12) A. Hassner, *J. Org. Chem.*, **34**, 2628 (1969).

In a previous paper,[1] one of the authors (C. S.) reported on the direct synthesis of I and ethyl α-hydroxy-β-nitrocarboxylates (II) by treatment of ethyl α,β-unsaturated carboxylates with fuming nitric acid.

In this paper, we report detailed studies on the preparation of IV through two synthetic routes.

Results

Synthesis of IV from Nitroparaffins and Ethyl Glyoxylate. Condensation of appropriate nitroparaffins and ethyl glyoxylate[13] obtained by lead tetraacetate oxidation of ethyl tartrate in benzene gave II in about 50% yield (Table 1). The absorption patterns and boiling points of these nitro alcohols (II) are identical with those II prepared from the olefinic esters and fuming nitric acid.[1]

Acetylation of II with acetic anhydride under reflux for 1.5 hr afforded ethyl α-acetoxy-β-nitrocarboxylates (III) in good yields (Table 2). When III was treated with a small amount of inorganic or organic bases as catalysts in the absence of solvent by shaking for 15 minutes at 80—120°C, the expected ethyl α,β-unsaturated β-nitrocarboxylates (IV) were obtained (Table 3).

Formation of ethyl α-nitroolefin carboxylates (I) by elimination of β-acetoxy group from ethyl β-acetoxy-α-nitrocarboxylates was carried out by using sodium carbonate as a catalyst in benzene.[5] However, in the case of elimination of α-acetoxy group from III, it was found that sodium hydrogen carbonate without solvent was superior to sodium carbonate in benzene.

Synthesis of IV from Ethyl α,β-Unsaturated Carboxylates. When olefinic esters were treated with nitryl chloride in ether below 0°C for 5 hr, ethyl α-chloro-β-nitrocarboxylates (V) were obtained as the main products, together with ethyl α,β-dichlorocarboxylates (VI), a small amount of higher-boiling product and polymerized reddish residue. The higher-boiling product was identified as ethyl α-nitrito-β-nitrocarboxylates (VII) from the fact that it showed an infrared absorption band of an intense nitrito group in the 1620—1630 cm^{-1} region and that it was converted into II by boiling in water.[9] Nitration by nitrosyl chloride under similar conditions also gave the same products (V and VI), but the formation of VII and the residue was found to be less than in the case of nitryl chloride. Other products such as ethyl α,β-dinitrito- and β-nitrito-α-nitrocarboxylates could not be detected. The elimination reaction of V with triethylamine afforded IV in about 50% yield.

In order to confirm its structure, compound IV was converted into the corresponding α-methoxy deriva-

TABLE 1. ETHYL α-HYDROXY-β-NITROCARBOXYLATES (II)

Compound	R	Yield (%)	Bp. °C/mmHg (Mp. °C)
IIa	CH_3	52.1	108—112/3[a]
IIb	C_2H_5	51.5	122—125/4
IIc	n-C_3H_7	53.8	127—129/4.5
IId	i-C_3H_7	28.2	125—127/4
IIe	C_6H_5	65.0	(81—82)[b]

a) Found: C, 40.29; H, 6.29; N, 7.88%. Calcd for $C_6H_{11}NO_5$: C, 40.68; H, 6.26; N, 7.91%. b) Found: C, 54.98; H, 5.61; N, 5.89%. Calcd for $C_{11}H_{13}NO_5$: C, 55.23; H, 5.48; N, 5.86%. Colorless needles from benzene-petroleum ether.

TABLE 2. ETHYL α-ACETOXY-β-NITROCARBOXYLATES (III)

Compound	Yield (%)	Bp °C/mmHg	Formula	Found, %			Calcd, %			IR Spectrum cm^{-1}, in KBr disk
				C	H	N	C	H	N	
IIIa	80.2	99—102/2	$C_8H_{13}NO_6$	43.71	6.07	6.37	43.83	5.98	6.39	1750, 1555, 1370
IIIb	88.4	110—115/2	$C_9H_{15}NO_6$	46.62	6.19	5.93	46.35	6.48	6.01	1760, 1560, 1375
IIIc	95.0	120—123/4	$C_{10}H_{17}NO_6$	48.69	6.83	6.38	48.81	6.93	5.67	1760, 1560, 1370
IIId	72.0	100—104/3	$C_{10}H_{17}NO_6$	48.58	6.75	6.05	48.81	6.93	5.67	1755, 1570, 1370

TABLE 3. ELIMINATION OF α-ACETOXY-4-METHYL-3-NITROVALERATE (IIId)

Catalyst (7×10^{-4} mol)[a]	Reaction conditions: Temp (°C)	Reaction conditions: Time (min)	Yield of IVd (%)
—	110—120	15	0
Na_2CO_3	110—120	15	49
Na_2CO_3	60[b]	20	5
$NaHCO_3$	110—120	15	82
CH_3COONa	110—120	15	71
$(C_2H_5)_3N$	80—90	15	71
Pyridine	110—120	15	50
Piperidine	110—120	15	26
$C_6H_5NHCH_3$	110—120	15	8
$C_6H_5N(CH_3)_2$	110—120	15	28

a) 10^{-1} mol of IIId was used. b) In dry benzene (20 ml).

13) Y. Hamamura, M. Otsuka, and M. Suzumoto, *Nippon Nogei Kagaku Kaishi*, **22**, 24 (1948).

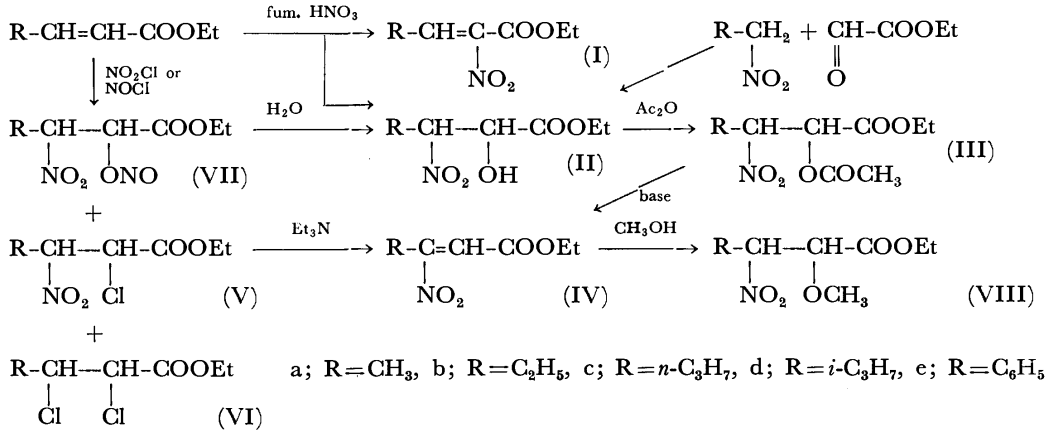

Scheme 1.

tives. When IV was treated with methanol in the presence of sodium methoxide below −10°C, the expected ethyl α-methoxy-β-nitrocarboxylates (VIII) were obtained. The disappearance of carbon-carbon double bond absorption in the 1640—1680 cm^{-1} region of the infrared spectrum of IV indicates the formation of VIII.

Experimental

All boiling and melting points are uncorrected. The IR spectra were recorded with a Hitachi EPI-G2 Spectrometer.

Reaction of Nitroparaffin with Ethyl Glyoxylate Derived from Ethyl Tartrate and Lead Tetraacetate. Lead tetraacetate (0.048 mol) was added portionwise with stirring to a cooled solution of ethyl tartrate (0.048 mol) in dry benzene (50 m*l*). After stirring for 1.5 hr at room temperature, separated crystals were filtered off and washed well with dry benzene. The filtrate and the washings were combined (about 100 m*l*). Appropriate nitroparaffin (0.098 mol) and 6% ethanolic solution of sodium ethoxide (from 2.4 g of sodium in ethanol (40 m*l*)) were added to the combined solution, with vigorous stirring. The weak alkaline solution was allowed to stand overnight with stirring at room temperature. After concentration of the solution, the residual oil was added to a mixture of benzene (100 m*l*) and water (50 m*l*). The solution was then acidified with 3 N hydrochloric acid. After removal of the precipitated crystals, the solution was washed with water twice (each 30 m*l*), and then dried over anhydrous magnesium sulfate and evaporated. Distillation of the residual oil afforded ethyl β-hydroxy-α-nitrocarboxylates (II), which were confirmed to be the same as the specimens prepared from ethyl α,β-unsaturated carboxylates and fuming nitric acid from their boiling points and IR spectra. The results are summarized in Table 1.

Acetylation of Ethyl α-Hydroxy-β-nitrocarboxylates (II) with Acetic Anhydride. A mixture of II (0.05 mol) in acetic anhydride (0.1 mol) was refluxed for 1.5 hr. Subsequent distillation of the reaction product under reduced pressure afforded an almost colorless oil, which was identified as ethyl α-acetoxy-β-nitrocarboxylates (III). However, ethyl 2-acetoxy-3-nitro-3-phenylpropionate (IIIe) could not be isolated in pure state and directly converted into ethyl 3-nitro-3-phenyl-2-propenoate (IVe) during the course of distillation. The results are summarized in Table 3.

Reaction of α,β-Unsaturated Carboxylic Esters with Nitryl Chloride (Procedure A). Nitryl chloride (0.48 mol) was added drop by drop, with vigorous stirring, to a solution of ethyl α,β-unsaturated carboxylates (0.32 mol) in dry benzene (60 m*l*) cooled below 0°C with an ice-salt bath. After being stirred for 5 hr at 0°C, the reaction mixture was

Table 4. Ethyl α-chloro-β-nitrocarboxylates (V)

Compound	Yield (%) A[a]	Yield (%) B[b]	Bp °C/mmHg	Formula	Found, % C	Found, % H	Found, % N	Calcd, % C	Calcd, % H	Calcd, % N	IR Spectrum cm^{-1}, in KBr disk
Va	42.0	27.0	77—85/3	$C_6H_{10}NO_4Cl$	37.21	5.22	6.98	36.83	5.12	7.16	1750, 1560, 1385
Vb	38.6	30.0	103—112/10	$C_7H_{12}NO_4Cl$	40.71	5.82	6.55	40.09	5.73	6.68	1740, 1550, 1365
Vc	34.5	24.5	116—125/7	$C_8H_{14}NO_4Cl$	42.98	6.08	5.92	42.95	6.26	6.26	1740, 1550, 1360
Vd	28.4	23.5	91—104/2	$C_8H_{14}NO_4Cl$	43.46	6.09	5.82	42.95	6.26	6.26	1740, 1555, 1370

a) Procedure A. b) Procedure B.

Table 5. Ethyl α-β-dichlorocarboxylates (VI)

Compound	Yield (%) A[a]	Yield (%) B[b]	Bp °C/mmHg	Formula	Found, % C	Found, % H	Calcd, % C	Calcd, % H	IR Spectrum cm^{-1}, in KBr disk
VIa	18.7	25.1	35—37/3	$C_6H_{10}O_2Cl_2$	39.21	5.31	39.91	5.40	1750
VIb	26.1	24.8	57—60/7	$C_7H_{12}O_2Cl_2$	42.02	6.21	42.21	6.03	1750
VIc	24.2	19.9	55—60/2	$C_8H_{14}O_2Cl_2$	45.38	6.44	45.07	6.57	1750
VId	17.3	20.2	85—88/10	$C_8H_{14}O_2Cl_2$	44.80	6.82	45.07	6.57	1750

a) Procedure A. b) Procedure B.

allowed to attain room temperature and to stand for 3 days. The benzene solution was washed successively with ice water (60 ml), 5% aqueous solution of sodium carbonate and finally twice with water. The solution was dried over anhydrous sodium sulfate and then evaporated. Distillation of the residual oil afforded three fractions, two of which were identified as ethyl α-chloro-β-nitrocarboxylates (V) and ethyl α,β-dichlorocarboxylates (VI). The highest boiling fraction was identified as ethyl α-nitrito-β-nitrocarboxylates (VII), though it could not be obtained in a pure state. The results are summarized in Tables 4 and 5.

Reaction of α,β-Unsaturated Carboxylic Esters with Nitrosyl Chloride (Procedure B). Nitrosyl chloride (0.5 mol) was added in a stream to a solution of ethyl α,β-unsaturated carboxylates (0.3 mol) in dry benzene (100 ml) cooled below 0°C with an ice-salt bath. After being stirred for 3 hr at 0°C, the reaction mixture was allowed to attain room temperature and to stand for 5 days. The benzene solution was washed with 5% aqueous solution of sodium carbonate and with water, and then dried over anhydrous sodium sulfate and evaporated. Distillation of the residual oil afforded V and VI. The results are summarized in Tables 4 and 5.

Conversion of Ethyl 4-Methyl-2-nitrito-3-nitrovalerate (VIIId) into Ethyl 2-Hydroxy-4-methyl-3-nitrovalerate (IId). A mixture of the crude VIId (5 g, bp 128—160°C/2 mmHg) in water (20 ml) was refluxed for 5.5 hr, and the resulting yellow solution was extracted three times with ether. The ethereal solution was washed with water, and dried over magnesium sulfate. After the evaporation of ether, the residue was distilled to give an almost colorless oil (IId; 1.5 g, 34.0%), bp 125—127°C/4 mmHg.

Analogous treatment of ethyl 2-nitrito-3-nitrobutyrate (VIIa; 7 g, bp 130—160°C/3 mmHg) with boiling water afforded the corresponding hydroxy compound (IIa; 2.6 g, 60.1%), bp 108—112°C/5 mmHg.

Elimination Reaction of Ethyl α-Chloro-β-nitrocarboxylates(V) with Triethylamine (Procedure C). Dry triethylamine (0.05 mol) was added drop by drop, with shaking, to a solution of V (0.05 mol) in dry benzene (30 ml) at room temperature. After stirring for 1 hr, water (30 ml) was added to the reaction solution and then the mixture was extracted three times with benzene. The combined benzene extracts were washed with water and then dried over anhydrous sodium sulfate. After concentrating the benzene extract, distillation of the residual oil afforded a yellow oil which was identified as ethyl α,β-unsaturated β-nitrocarboxylates (IV). The results are summarized in Table 6.

Elimination Reaction of Ethyl α-Acetoxy-β-nitrocarboxylates (III) with Sodium Acetate in the Absence of Solvent (Procedure D). Compound III (0.043 mol) was heated in the presence of sodium acetate (0.06 g) with shaking for 15 min at 110—120°C and subsequent distillation of the reaction product under reduced pressure afforded IV together with a small quantity of acetic acid. The results are summarized in Table 6.

Elimination Reaction of Ethyl 2-Acetoxy-4-methyl-3-nitrovalerate (IIId) with Several Bases. Compound IIId (0.1 mol) was heated in the presence of various bases (7×10^{-4} mol) with shaking for 5—15 min at 80—120°C. Subsequent distillation of the reaction product under reduced pressure afforded ethyl 4-methyl-2-nitro-2-valerate (IVd) together with a small quantity of acetic acid. The results are summarized in Table 3.

Methoxylation of Ethyl α,β-Unsaturated β-Nitrocarboxylates (IV) with Methanol. A solution of IV (0.07 mol) in methanol (80 ml) was added, with vigorous stirring, to a 5% methanolic solution of sodium methoxide (from 3.5 g of sodium in methanol (70 ml)) cooled below −10°C. The temperature of the reaction mixture rose up to about 15°C, at which stirring was continued for 1 hr. A small amount of of crushed dry ice was then added portionwise. The cooled mixture was poured into water (500 ml), and the resulting solution was acidified with glacial acetic acid, whereby an oily product separated out. The product was extracted several times with ether. The combined ethereal extracts were washed with water, dried over anhydrous magnesium sulfate and evaporated. Distillation of the residual oil afforded ethyl α-methoxy-β-nitrocarboxylates (X) as an almost colorless oil. The results are summarized in Table 7.

TABLE 6. ETHYL α,β-UNSATURATED β-NITROCARBOXYLATES (IV)

Compound	Yield (%) C[a]	Yield (%) D[b]	Bp. °C/mmHg	Formula	Found, % C	Found, % H	Found, % N	Calcd, % C	Calcd, % H	Calcd, % N	IR Spectrum cm^{-1}, in KBr disk
IVa	50.2	78.9	65—70/3	$C_6H_9NO_4$	45.37	5.43	7.50	45.28	5.70	8.80	1730, 1680, 1540, 1335
IVb	52.1	80.3	65—69/2.5	$C_7H_{11}NO_4$	48.56	6.17	7.96	48.55	6.40	8.09	1730, 1670, 1540, 1340
IVc	52.8	78.7	69—72/1.5	$C_8H_{13}NO_4$	51.38	6.95	7.26	51.33	7.00	7.48	1740, 1670, 1540, 1340
IVd	54.8	71.5	79—81/2	$C_8H_{13}NO_4$	51.31	7.17	7.62	51.33	7.00	7.48	1730, 1660, 1530, 1360
IVe		61.5[c]	120—123/0.4[d]	$C_{11}H_{11}NO_4$	59.96	4.98	6.63	59.72	5.01	6.33	1725, 1640, 1540, 1360

a) Procedure C. b) Procedure D. c) Evaluated from IIe. d) Mp 69—70°C; recrystallized from petroleum ether-benzene to give colorless needles.

TABLE 7. ETHYL α-METHOXY-β-NITROCARBOXYLATES (VIII)

Compound	Yield (%)	Bp °C/mmHg	Formula	Found, % C	Found, % H	Found, % N	Calcd, % C	Calcd, % H	Calcd, % N	IR Spectrum cm^{-1}, in KBr disk
VIIIa	65.6	72—75/1	$C_7H_{13}NO_5$	43.66	7.02	7.43	43.97	6.85	7.33	1745, 1550, 1365, 1120
VIIIb	55.7	80—83/3	$C_8H_{15}NO_5$	47.11	7.25	6.59	46.82	7.37	6.83	1750, 1555, 1375, 1120
VIIIc	60.5	95—98/3	$C_9H_{17}NO_5$	49.27	7.68	6.61	49.30	7.82	6.39	1760, 1560, 1370, 1120
VIIId	63.9	94—99/3	$C_9H_{17}NO_5$	48.97	7.72	6.18	49.30	7.82	6.39	1760, 1560, 1375, 1120

A Theoretical Aspect on the Mechanism of Thermal Dimerization of Cyclooctatetraene[1]

Hiizu IWAMURA and Kazuhiko MORIO

Department of Chemistry, Faculty of Science, The University of Tokyo, Bunkyo-ku, Tokyo

(Received March 31, 1972)

Thermal isomerization of cyclooctatetraene to semibullvalene **6** has been studied theoretically by the MINDO methods. The reaction is predicted to be exothermic by comparison of the calculated heats of formation and to be allowed as a concerted cyclization by constructing a complete MO correlatiom diagram. These findings together with the knowledge of thermal interconversion of cyclooctatetraene and bicyclo[4.2.0]octa-2,4,7-triene **5** suggest a tentative mechanism for thermal dimerization of cyclooctatetraene in which dimers **2**, **3**, and **4** are formed by coupling of the two isomers **5** and **6** of cyclooctatetraene.

It has been shown by Reppe *et al.*,[2] Jones,[3] and Schröder[4] that cyclooctatetraene forms several dimers on heating under various reaction conditions. A mixture of isomers **1**, mp 53°C, and **2**, mp 76°C, for example, is obtained by heating neat cyclooctatetraene at 100° in a sealed tube. Refluxing in *o*-dichlorobenzene and *N,N*-diethylaniline as the diluents results in formation of dimers **3**, mp 41.5°C, and **4**, mp 18.5°C, respectively. In spite of their fascinating structures and utility as the excellent intermediates for synthetic works highlighted by preparation of bullvalene,[5] little study has been done on the mechansim of formation of these dimers **1**~**4**.

We notice by simple inspection of the molecular framework of these dimers that structural units of bicyclo[4.2.0]-octa-2,4,7-triene **5** and semibullvalene **6** are incorporated in **2**, **3** and **4** as shown in Chart 1, and are led to propose a hypothesis that these dimers could be formed by coupling of **5** and **6** which in turn might be produced by thermal valence isomerization of cyclooctatetraene. While thermal interconversion of cyclooctatetraene and **5** has been unambiguously established,[6] the thermal conversion of the former to **6** has been the subject of considerable controversy. Thus **6** can be formed by the acetone sensitized photolysis of cyclooctatetraene.[7] In the case of 1,3,5,7-tetramethylcyclooctatetraene, it is a pyrolytic condition of heating at 250°C for 15 hr rather than irradiation under various conditions which gives the corresponding semibullvalene.[7] Criegee and Askani reported efficient conversion at elevated temperature of octamethylcyclooctatetraene to the semibullvalene.[8]

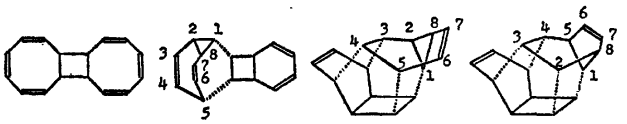

1 **2** **3** **4**

Chart 1. Molecular framework of dimers **1**~**4** of cyclooctatetraene.

With all the findings mentioned above which are suggestive of a possible thermal transformation of cyclooctatetraene to **6**, experimental efforts to detect the latter in the gaseous and condensed phase pyrolysates of the former have proved to be totally unsuccessful. The products are usually styrene and dihydropentalene as well as benzene and acetylene.[9,10] Formal application of the orbital symmetry rule is also controversial; the same 1,3 ; 2,6 concerted multicyclization of cyclooctatetraene has been predicted as an allowed process in the ground state by a group of authors[11] while others reasoned the allowedness in the excited state.[12]

With no operational test available, we began theoretical approach to the problem and present here the analyses of the electronic structure of the molecular reorganization reaction represented by the equation;

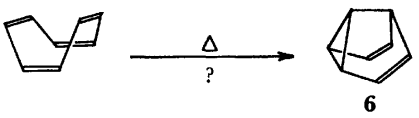

6 (1)

Methods of Theoretical Calculation

The theoretical methods employed here are to construct a quantitative molecular orbitals correlation diagram between cyclooctatetraene and semibullvalene **6**, and to see if the occupied MO levels are correlated between the two species. Since the experimental data concerning the geometry of **6** are not available, the theoretical geometry has to be sought by minimizing the molecular energy with respect to all the bond lengths and angles in the molecule. Out of several versions of the semi-empirical SCF MO theories, the MINDO/2

1) Part IV of Studies of Reaction Mechanisms by All-valence-electron Semiempirical SCF MO Theories. For Part III, see H. Iwamura, K. Morio, and T. L. Kunii, This Bulletin, **45**, 841 (1972).

2) W. Reppe, O. Schlichting, K. Klager, and T. Toepel, *Ann.*, **560**, 1 (1948).

3) W. O. Jones, *J. Chem. Soc.*, **1953**, 2036; *Chem. Ind.* (London), **1955**, 16.

4) G. Schröder, *Chem. Ber.*, **97**, 3131 (1964); *Angew. Chem.*, **78**, 117 (1966).

5) G. Schröder, *ibid.*, **75**, 91, 722 (1963); W. von E. Doering and W. R. Roth, *ibid.*, **75**, 27 (1963); W. von E. Doering and W. R. Roth, *Chem. Ber.*, **97**, 3140 (1964).

6) R. Huisgen and F. Mietzsch, *Angew. Chem.*, **76**, 36 (1964); E. Vogel, H. Kiefer, and W. R. Roth, *ibid.*, **76**, 432 (1964).

7) H. E. Zimmerman and H. Iwamura, *J. Amer. Chem. Soc.* **90**, 4763 (1968); **92**, 2015 (1970).

8) R. Criegee and R. Askani, *Angew. Chem.*, **80**, 531 (1968).

9) M. Jones, Jr. and L. O. Schwab, *J. Amer. Chem. Soc.*, **90**, 6549 (1968).

10) H. E. Zimmerman and H. Iwamura, unpublished work.

11) R. B. Woodward and R. Hoffmann, "The Conservation of Orbital Symmetry," Academic Press, Inc., New York, N. Y. (1970) p. 81.

12) K. Fukui, *Accounts Chem. Res.*, **4**, 57 (1971); R. C. Dougherty, *J. Amer. Chem. Soc.*, **93**, 7187 (1971).

method[13] proposed by Dewar *et al.* is considered to reproduce the best geometry; the geometry which gave the minimum value of total energy by the MINDO/2 method was taken as the equilibrium geometry of the actual molecule. For the sake of consistency of comparison, the optimized geometry of cyclooctatetraene was also employed in the present study.

Correlation between the MO's of the species in either side of Eq. (1) is not straightforward because cyclooctatetraene and **6** lack any common symmetry element. It is, however, rendered possible to find the MO correlation by imposing in the reaction coordinate close to the end product the intermediate which corresponds to the transition state structure for the degenerate Cope rearrangement of **6**.[1] The C_2 symmetry operation is kept for the first half of the reaction, and the C_s symmetry element holds throughout the last half of the reaction coordinate (see Chart 2). Since the activation energy for the Cope rearrangement is known to be exceptionally low,[14] the above specification of the reaction as passing through this intermediate does not necessarily mean the restriction of the course of the reaction to a stepwise reaction; the intermediate and **6** are energetically too close to be separated on the entire potential energy surface interrelating the $(CH)_8$ isomers.

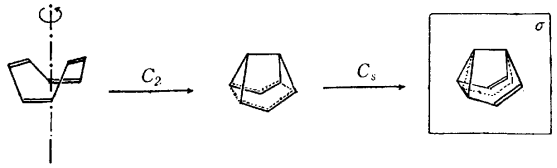

Chart 2. Symmetry elements along the reaction coordinates.

Estimation of heats of formation of cyclooctatetraene and **6** is considered to be illuminative as a measure of the exothermicity of the forward reaction of Eq. (1). The MINDO/2 approximation is reputed to underestimate heats of formation of the cyclopropane ring by about 10 kcal/mol.[13] In this respect, it is worthwhile to recourse to the original version (MINDO/1) of the approximation which, although artificially parametrized, gives best results of the theoretical heats of formation with the use of the standard bond lengths; even a seriously strained cyclobutene deviates only by 3.4 kcal/mol from the experimental value.[15] Therefore more reliable estimation of heats of formation of cyclooctatetraene and **6** was made by the MINDO/1 calculations in which the optimal lengths reached by the MINDO/2 approximations were replaced by the standard bond lengths of Baird and Dewar.[15] Heats of formation are by definition given by total bonding energies minus heats of formation of the free atoms in the molecule in the standard state. The total bonding energies are in turn calculated by subtracting the sum of isolated atom energies from the total valence shell energies.

Partitioning of the total valence shell energy (E) of a molecule into the terms due to one-center (E_A) and two-center (E_{AB}) was performed at the level of MINDO approximations analogously to the method elaborated by Gordon in the CNDO/2.[16]

$$E = \sum_{A} E_A + \sum_{A<B}\sum E_{AB} \tag{2}$$

The one-center terms can be expressed in terms of standard integrals as

$$E_A = \sum_{\mu}^{A}\left[P_{\mu\mu}U_{\mu\mu} + \frac{1}{2}P_{\mu\mu}^2\langle\mu\mu|\mu\mu\rangle\right] + \sum_{\nu\neq\mu}^{A}\sum^{A}\left\{P_{\mu\mu}P_{\nu\nu}\left[\langle\mu\mu|\nu\nu\rangle - \frac{1}{2}\langle\mu\nu|\mu\nu\rangle\right] + P_{\mu\nu}^2\left[\frac{3}{2}\langle\mu\nu|\mu\nu\rangle - \frac{1}{2}\langle\mu\mu|\nu\nu\rangle\right]\right\} \tag{3}$$

Full expression for the bi-centric terms (E_{AB}) are

$$E_{AB} = E_{AB}^{R} + E_{AB}^{X} + E_{AB}^{E} \tag{4}$$

where:

$$E_{AB}^{R} = 2\sum_{\mu}^{A}\sum_{\nu}^{B}P_{\mu\nu}\beta_{\mu\nu} \tag{5}$$

$$E_{AB}^{X} = -\frac{1}{2}\sum_{\mu}^{A}\sum_{\nu}^{B}P_{\mu\nu}^2\gamma_{AB} \tag{6}$$

$$E_{AB}^{E} = (P_AP_B - P_AZ_B - P_BZ_A)\gamma_{AB} + Z_AZ_BR_{AB}^{-1} \tag{7}$$

and E_{AB}^{R}, E_{AB}^{X}, and E_{AB}^{E} represent the resonance, exchange and electrostatic energies, respectively.

Results and Discussion

In Fig. 1 is summarized the MO correlation diagram obtained by application of symmetry operation and the noncrossing rule to the final MO's. We notice that the occupied MO levels are satisfactorily correlated between the starting cyclooctatetraene and product **6**.

The second clear-cut criterion obtained in the present study which supports the thermal route of Eq. (1) is, as shown in Table 1, that the heats of formation of cyclooctatetraene is higher than that of **6** by 13.4 kcal/mol; the forward reaction is predicted to be exothermic.

Turning now to the consideration of the driving force of the exothermic reaction, we note that the MO numbers 1, 8 and 20 of cyclooctatetraene are mostly responsible for lowering the electronic energy as the reaction proceeds. Nature of these levels is not obvious at a glance over the eigen vectors of the all-valence-electron SCF MO method, since separation of the σ and π character of a given MO is not clear. In this respect, it is instructive to go back to the correlation diagram constructed on the π-orbital approximation. Starting from cyclooctatetraene in which the occupied levels are made of four ethylene groups weakly overlapped through σ-bonds, we end up, as illustrated in Fig. 2, with two σ- and two π-orbitals of **6** with the aid of the bonding levels of two interacting allylic orbitals of the intermediate. In reality all

13) M. J. S. Dewar and E. Haselbach, *J. Amer. Chem. Soc.*, **92**, 590 (1970); N. Bodor, M. J. S. Dewar, A. Harget, and E. Haselbach, *ibid.*, **92**, 3854 (1970).

14) H. E. Zimmerman and G. L. Grunewald, *ibid.*, **88**, 183 (1966); H. E. Zimmerman, R. W. Binkley, R. S. Givens, G. L. Grunewald, and M. A. Sherwin, *ibid.*, **91**, 3316 (1969).

15) N. C. Baird and M. J. S. Dewar, *J. Chem. Phys.*, **50**, 1262 (1969); N. C. Baird, M. J. S. Dewar, and R. Sustman, *ibid.*, **50**, 1275 (1969).

16) M. S. Gordon, *J. Amer. Chem. Soc.*, **91**, 3122 (1969).

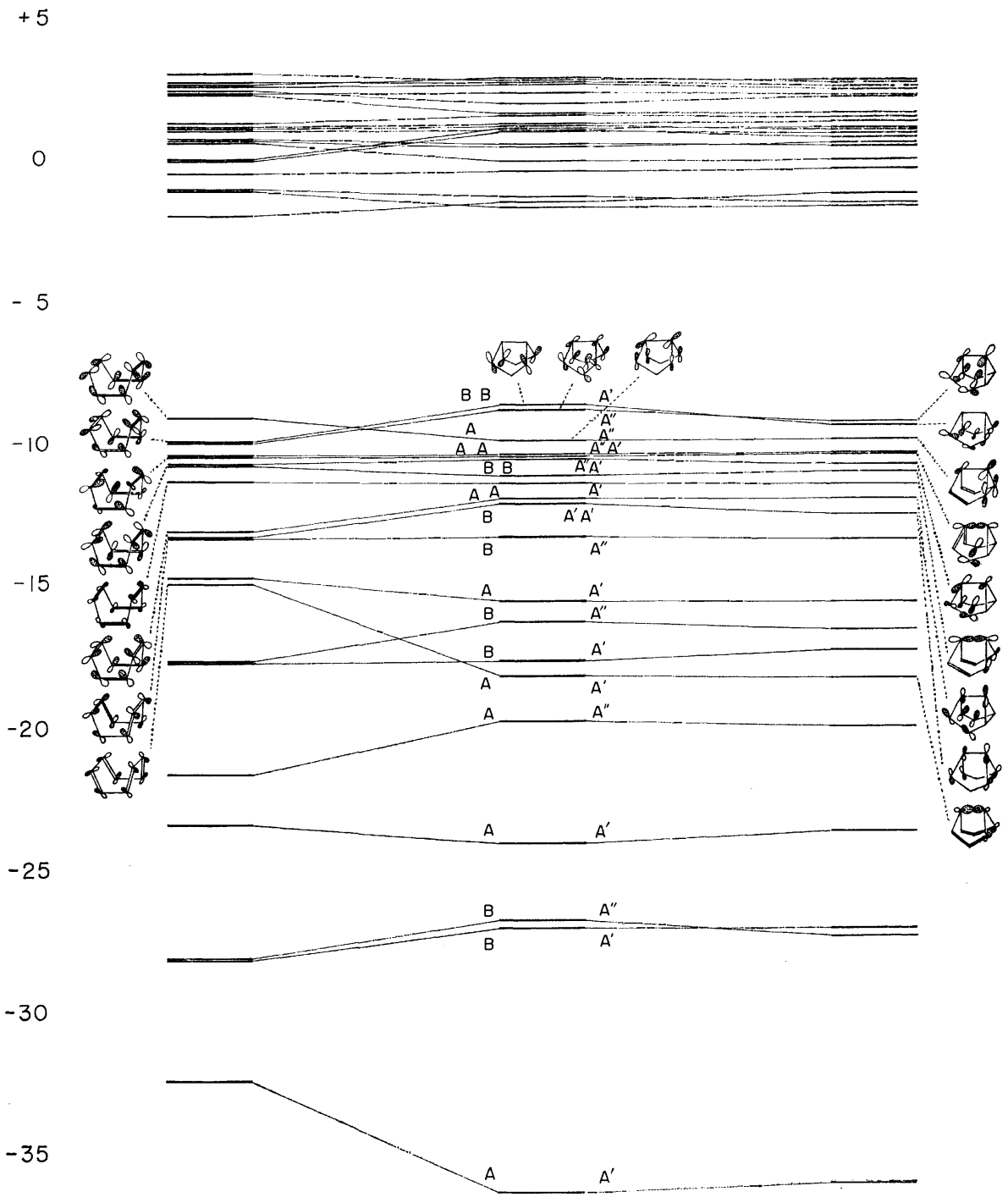

Fig. 1. Correlation diagram of the MINDO MO's for the isomerization of cyclooctatetraene to semibullvalene. (In some pairs of degenerate MO's of cyclooctatetraene, slight deviation from D_{2d} symmetry was imposed in the Figs. 1 and 2 to show the fate of the MO's during the course of the reaction.)

TABLE 1. HEATS OF FORMATION AND DISSECTED VALUES OF TOTAL VALENCE SHELL ENERGIES

	Heats of formation (kcal/mol)		Total valence shell energies			
			$\sum_A E_A$ (eV)	$\sum_{A<B} E_{AB}$ (eV)		
	MINDO/2	MINDO/1		Resonance	Exchange	Electrostatic
Cyclooctatetraene	56.7	66.4	−921.9	−153.4	−75.0	−0.13
Intermediate[a)]	45.4	53.6	−922.3	−155.1	−73.3	−0.15
6	27.1	53.0	−922.9	−154.0	−73.9	−0.21

a) Transition state structure of the Cope rearrangement of **6**.

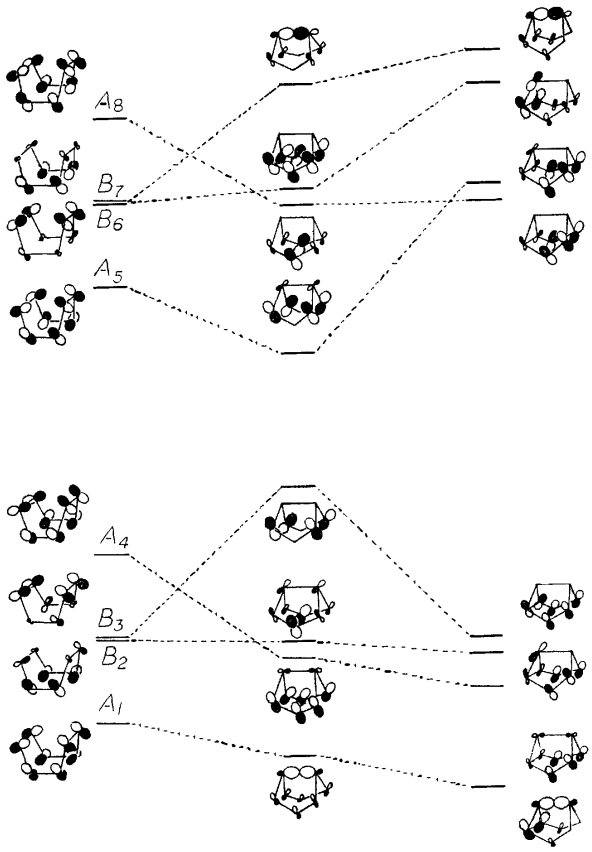

Fig. 2. Approximate correlation diagram of the π MO's of cyclooctatetraene for its isomerization to semibullvalene.

these levels split further on coupling with a combination of σ-orbitals of the same symmetry. As a result, none of the MO's in Fig. 1 can be exactly equivalent to any one MO in Fig. 2. Closer inspection of the MO coefficents reveals, however, that the 8th and 20th MO's of cyclooctatetraene in Fig. 1 are most reasonably approximated by the A_4 orbital in Fig. 2.[17] The behavior of the two MO's of cyclooctatetraene during the course of the reaction indicates that 1,3 ; 2,6 interaction of the π-orbitals of cyclooctatetraene is of bonding in nature. The reaction may figuratively be regarded as an intramolecular Diels-Alder ($2_\pi + 4_\pi$) reaction between the C-1, C-2 ene unit and the diene C-3~C-6. Instead of suprafacial overlap between the front lobes of C-2 and C-3, and C-1 and C-6 which leads to **5**, the opposite lobes of the p-orbitals on C-1 and C-2 are involved to form the new σ-bonds of **6** with the bottom lobe of C-3 and the top p-lobe of C-6, respectively (Chart 3).

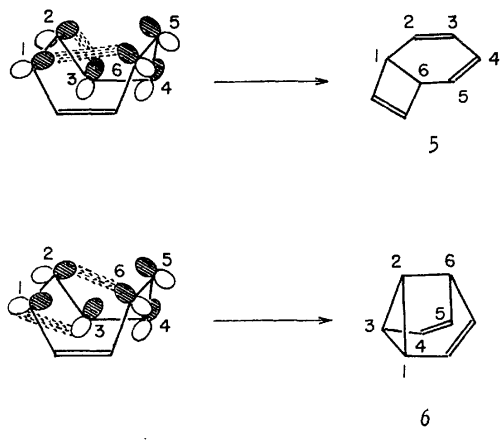

Chart 3. Two modes of thermally allowed closure.

Another aspect of the origin of the driving force for the reaction of Eq. (1) can be found in Table 1. In terms of resonance energy, the transition state structure of the Cope rearrangement of **6** is most favored (−155.16 eV) by the aromaticity of the Hückel type array of the 6π electrons. Cyclooctatetraene (−153.40 eV) is presumably destabilized to some extent by its anti-aromaticity due to cyclic array of 8π electrons. It is also interesting to note that contribution of the non-bonded interaction to the bi-centric resonance energy in cyclooctatetraene is −0.0074, −0.0038, and +0.3485 eV for the atomic pair of C_1~C_6, C_2~C_6, and C_1~C_3, respectively; a nagative value for E_{AB} implies bonding between atoms A and B while a positive value implies an anti-bonding interaction. It is also apparent in Table 1 that the one center terms are largely responsible for the total energy difference between cyclooctatetraene and **6**. The main contribution comes from the terms for C_2, $C_4(C_8)$, and C_5-(C_7) of **6**, and the effect appears to be associated with an increase in electron density and consequently one-center core binding energy of these carbon atoms. Of special importance is the high p_y electron density at C_2 of **6** which characterizes the electronic structure of this molecule (the y axis is taken parallel to the C_1—C_3 bond. The numbering system is given for **6** in Chart 3 only to clarify the original positions of atoms in the precursor, and does not conform to the IUPAC rules).

It is now conclusive on the theoretical bases that the reaction of Eq. (1) is an allowed process as a concerted cyclization in the ground state. Prediction to the contrary in Ref. 12 is found to be due to wrong drawing of the orbitals in which ring closure should lead to unrealistic semibullvalene with the cyclopropane ring fused trans (Chart 4).

Chart 4. Double cyclization of cyclooctatetraene according to the drawings in Ref. 12.

So far is rationalization of the thermally allowed conversion of cyclooctatetraene to semibullvalene. We are now halfway to give full theoretical account for the hypothesis that dimers **2**~**4** could be formed by way of coupling between **5** and **6**. In Chart 5 are shown one of the conceivable modes in which the coupling takes place. By application of the mnemonics of

17) The highest occupied orbital A_4 in Fig. 2, for example, appears to split into the MO's 20, 13, and 8 in Fig. 1 by mixing with a combination of σ orbitals in the ethylenic double bonds which has A symmetry for C_2 operation.

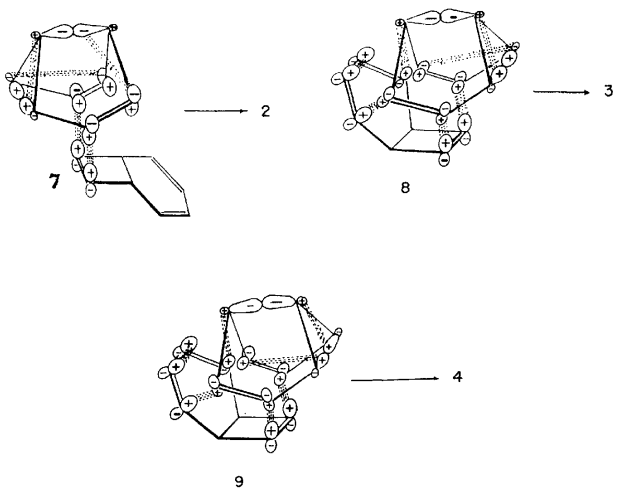

Chart 5. Mechanism I of the dimer formation of cyclooctatetraene from **5** and **6**.

Zimmerman for determining the allowedness or forbiddenness of symmetry controlled reactions, **7** is described as containing a cyclic array of ten atomic orbitals in which there are zero or even numbers of sign inversion resulting from plus-minus overlaps.[7,18] The type of the system is classified as Hückel and the process is predicted to be symmetry allowed in a ground state reaction. In the terminology of Woodward and Hoffmann,[11] the process can be described as $[{}_{\pi}2_s+{}_{\pi}2_a+{}_{\sigma}2_a+{}_{\sigma}2_a+{}_{\pi}2_a]$ processes. In **8** and **9** there are 14 AO's overlapping next to each other to form a cyclic array of orbitals. Irrespective of the choices of the sign of the basis set AO's, the total number of sign inversion resulting from plus-minus overlaps is zero or even. The Hückel system is again predicted to be allowed. Thus the modes of closure given in Chart 5 are proposed as a tentative mechanism for thermal dimerization of cyclooctatetraene.

In view of the multi-center interaction between **5** and **6** in the transition states **7**~**9** the proposed mechanism should require a large negative entropy of activation. Although no quantitative study has yet been carried out, the fact that the dimers are formed only in condensed phases and that in neat or moderately concentrated solution is in accord with the expectation.[2-4] When the entropy requirement of mechanism I is seriously taken as a disadvantage, an alternative mechanism of the intermediacy of **10** followed by intramolecular closure to give **1**~**4** may be considered as another candidate (Chart 6). The first step is a typical Diels-Alder reaction— the $[{}_{\pi}4_s+{}_{\pi}2_s]$ cycloaddition. The routes to **3** and **4** include internal closure of the cyclooctatriene moiety to the dihydrosemibullvalene. The theoretical argument developed in the first half of the present paper can similarly be applied to predict the allowedness of this part of the reactions.[7] Thus mechanisms I and II differ only in the chronology of the ring closure and can not be differentiated from the standpoint of orbital symmetry control of electrocyclic reactions.

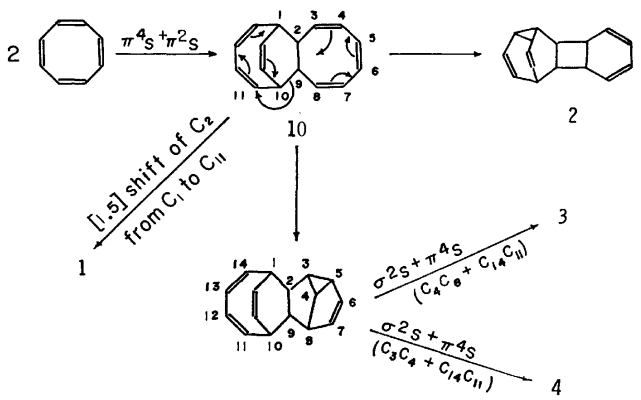

Chart 6. Mechanism II of the dimer formation of cyclooctatetraene.[19]

18) H. E. Zimmerman, *J. Amer. Chem. Soc.*, **88**, 1564 (1966); *ibid.*, **88**, 1566 (1966); *Science*, **153**, 837 (1966); *Accounts Chem. Res.*, **4**, 272 (1971).

19) Dimers **1** and **2** formed at relatively low temperatures are not precursors of **3** and **4**. Prolonged heating of **2** has been shown to give a tetramer instead of an isomeric dimer.[4]

Synthetic Reactions by Complex Catalysts XXVIII. Reaction of β-Propiolactone with Alkyl Halide Caused by Cu_2O-Isonitrile Complex

Takeo SAEGUSA, Ichiki MURASE, Michio NAKAI, and Yoshihiko ITO

Department of Synthetic Chemistry, Faculty of Engineering, Kyoto University, Kyoto

(Received April 24, 1972)

Oligomerization of β-propiolactone (BPL) caused by the Cu_2O-isonitrile complex in the presence of alkyl halide was studied, and an oligomeric mixture of acrylate derivatives **3** ($n=1$, 2 and 3 in Eq. (3)) was isolated in fairly high yields. The complex catalyst showed a distinguished catalytic activity for the oligomerization of BPL. The reaction mechanism involving an intermediate of organocopper(I) isonitrile **4**, which is converted into copper(I) acrylate isonitrile complex **5** was presented.

In our continuing studies on the reactions caused by the Cu_2O-isonitrile complex, it has been established[1,2] that the Cu_2O-isonitrile complex abstracts hydrogen atom from the so-called active methylene compound to produce organocopper(I) isonitrile complex **1** which plays a key role as an intermediate in the respective reaction.

$$\begin{matrix}X\\Z\end{matrix}\!\!>\!CH_2 + Cu_2O + n\text{RNC} \rightarrow \begin{matrix}X\\Z\end{matrix}\!\!>\!CHCu(\text{RNC})_n \quad (1)$$

1

In the present study, β-propiolactone (BPL) was employed as an active hydrogen compound, which was subjected to the reaction with the Cu_2O-isonitrile complex in the presence of alkyl halide. It was found that the Cu_2O-isonitrile complex readily caused oligomerization of BPL, in which oligomers having an acrylic carbon-carbon double bond as the terminal group were selectively produced. It might be of interest to compare with the usual base-catalyzed oligomerization of BPL.[3] For the present oligomerization, a scheme involving an intermediate of organocopper(I) isonitrile complex **2** is presented.

$$\begin{matrix}CH_2\text{—}CH_2\\ |\quad\ |\\ O\text{——}C{=}O\end{matrix} \xrightarrow{Cu_2O,\ m\text{RNC}} \begin{matrix}Cu(\text{RNC})_m\\ |\\ CH_2\text{—}CH\\ |\quad\ |\\ O\text{——}C{=}O\end{matrix} \quad (2)$$

2

Results and Discussion

BPL was heated at 80°C with Cu_2O-*t*-butyl isocyanide as a catalyst in the presence of alkyl halide to produce an oligomer mixture of acrylate derivatives **3** ($n=1,2$ and 3 in Eq. (3)) in fairly high yields. Each product was isolated by glpc and was identified by NMR and IR spectra as well as elemental analysis. No higher oligomer ($n\geq 4$ of **3**) was detected by glpc analysis.

$$n\begin{matrix}CH_2\text{—}CH_2\\ |\quad\ |\\ O\text{——}C{=}O\end{matrix} + \text{RX} \xrightarrow{Cu_2O\cdot R'NC} CH_2{=}CHCOO(CH_2CH_2COO)_{n-1}\text{-R} \quad (3)$$

3

Some representative reactions are summarized in Table 1.

The reaction of BPL with primary and secondary alkyl halides caused by the Cu_2O-isonitrile system gave the corresponding ester **3**. However, the reaction

TABLE 1. REACTION OF β-PROPIOLACTONE WITH ALKYL HALIDE CAUSED BY THE Cu_2O-*t*-BUTYL ISOCYANIDE[a]

$$n\begin{matrix}CH_2\text{—}CH_2\\ |\quad\ |\\ O\text{——}C{=}O\end{matrix} + \text{RX} \xrightarrow{Cu_2O\ t\text{-BuNC}} CH_2{=}CHCOO(CH_2CH_2COO)_{n-1}\text{-R}$$

Alkyl halide	Product yield (%)[b]		
	$n=1$	$n=2$	$n=3$
$CH_3O_2CCH_2Cl$	35	26	2
n-BuI	30	27	11
n-BuCl	42	6	1
sec-BuBr	9	29	11
$PhCH_2Br$	15	5	—
$ClCH_2CN$	20	—	—

a) Reaction condition: BPL 20 mmol, alkyl halide 20 mmol, Cu_2O 10 mmol, *t*-BuNC 30 mmol, benzene 5 m*l*, at 80°C, 7 hr. b) Yield is based upon BPL.

TABLE 2. REACTION OF β-PROPIOLACTONE WITH *n*-BUTYL BROMIDE[a]

$$n\begin{matrix}CH_2\text{—}CH_2\\ |\quad\ |\\ O\text{——}C{=}O\end{matrix} + n\text{-BuBr} \xrightarrow{Cat.} CH_2{=}CHCOO(CH_2CH_2COO)_{n-1}\text{-}n\text{-Bu}$$

	Catalyst system			Product yield (%)[b]		
	Cu_2O (mmol)	*t*-BuNC (mmol)	Pyridine (mmol)	$n=1$	$n=2$	$n=3$
1	10	30	—	21	39	9
2	10	—	30	6	26	9
3	10	—	—	0	0	0
4	—	30	—	0	0	0

a) Reaction condition: BPL 20 mmol, *n*-BuBr 20 mmol, benzene 5 m*l* at 80°C, 7 hr. b) Yield is based upon BPL.

1) T. Saegusa, Y. Ito, and S. Tomita, This Bulletin, **45**, 496 (1972).

2) T. Saegusa, Y. Ito, and S. Tomita, *J. Amer. Chem. Soc.*, **93**, 5656 (1971).

3) Y. Yamashita, Y. Ishikawa, T. Tsuda, and S. Miura, *Kogyo Kagaku Zasshi*, **66**, 104 (1963).

with *t*-butyl bromide was unsuccessful, since it underwent elimination virtually exclusively under the present reaction conditions, producing isobutene. The reaction with aromatic halide gave no ester derivative.

The Cu_2O-pyridine system also gave rise to oligomerization, although it was somewhat less effective than the Cu_2O-isonitrile system, as seen in Table 2. The presence of Cu_2O was essential. Without Cu_2O, isonitrile alone caused no reaction under the present conditions.

The activities of some copper and silver compounds were examined (Table 3). Cu_2O and Ag_2O in combination with isonitrile showed distinguished results.

Table 3. Effect of some copper and silver compounds on oligomerization of BPL with *n*-butyl bromide[a]

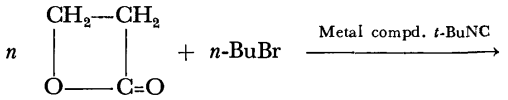

$CH_2=CHCOO(CH_2CH_2COO)_{n-1}$-*n*-Bu

Metal compd.	Product yield (%)[b]		
	$n=1$	$n=2$	$n=3$
Cu_2O	21	39	9
CuO	3	3	Trace
Cu	Trace	3	Trace
CuBr	2	6	Trace
Ag_2O	10	60	18

a) Reaction conditions: BPL 5 mmol, *n*-BuBr 5 mmol, *t*-BuNC 7.5 mmol, metal compound 2.5 mmol, benzene 2.5 m*l*, at 80°C, 7 hr. b) Yield is based upon BPL.

The following scheme explains several experimental findings.

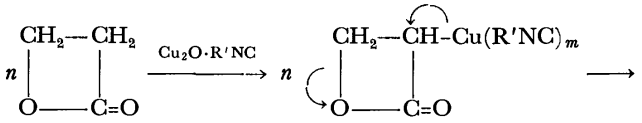

4

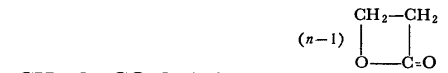

5

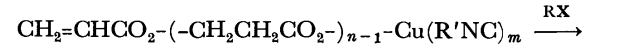

6

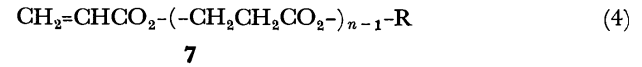

(4)

7

First, the α-hydrogen of BPL is abstracted by the Cu_2O-isonitrile system to form an organocopper(I) isonitrile complex **4**, which is converted into copper(I) acrylate isonitrile complex **5** through the ring-opening of **4**. The nucleophilic attack of **5** to the second molecule of BPL and the subsequent propagation of the BPL ring-opening will lead to the formation of the oligomeric copper(I) carboxylate **6**. Copper(I) salt complexes of acrylate and oligomeric carboxylates react with alkyl halide to produce the corresponding esters.

Several findings support the above scheme of the reactions. The nucleophilic attack of copper(I) carboxylate isonitrile complex to BPL was verified by an experiment in which BPL was treated with a complex of copper(I) phenylacetate *t*-butyl isocyanide **8** at 80°C in the presence of *n*-butyl bromide. The products were as follows.

8

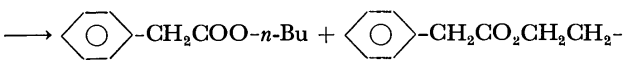

9 27% **10**

COO-*n*-Bu + $CH_2=CHCOO(CH_2CH_2COO)_{n-1}$-*n*-Bu (5)

63% 5% ($n=1$ and 2)

Butyl phenylacetate **9** is formed by the direct reaction of **8** with butyl bromide, and **10** is produced by the sequence of reactions of ring-opening of BPL and esterification. The esterification of carboxylic acid with alkyl halide caused by the Cu_2O-isonitrile system has recently been found[4] and may have various applications.

When BPL was treated with the Cu_2O-isonitrile complex in the absence of alkyl halide, a mixture of oligomeric acids ($n=1$, 2 and 3 of **11**) was obtained after work-up with acidic water.

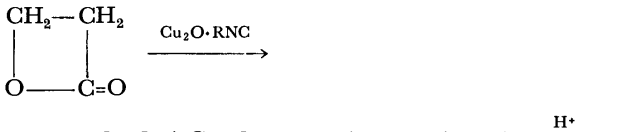

12

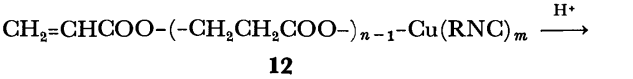

(6)

11

A mixture of the oligomeric copper(I) carboxylate **12** obtained in Eq. (6) was treated with ethyl bromide to give an oligomer mixture of acrylate derivatives, in which the oligomer distribution was roughly the same as that in the Cu_2O-isonitrile induced oligomerization of BPL in the presence of ethyl bromide.

Experimental

Reagents. Commercial analytical Cu salts and Ag salts were dried under N_2 before use. *t*-Butyl isocyanide was prepared according to Ugi's procedure.[5] Commercial BPL was purified by distillation under nitrogen after being dried over molecular sieves 3A. Commercial alkyl and aryl halides were purified by distillation under nitrogen. Commercial phenylacetic acid of extra pure grade was used.

Oligomerization of BPL caused by Cu_2O-t-Butyl Isocyanide in the Presence of n-*Butyl Bromide.* A mixture of 1.43 g (10 mmol) of Cu_2O, 2.50 g (30 mmol) of *t*-BuNC, 1.45 g

4) T. Saegusa and I. Murase, *Synth. Commun.*, **2**, 1 (1972).
5) I. Ugi, *Angew. Chem.*, **77**, 492 (1965).

Table 4. Characterization of products
$CH_2=CHCOO(CH_2CH_2COO)_{n-1}R$

R	n	Mass (m/e)	Formula	Anal. Calcd % C	Calcd % H	Found % C	Found % H	IR (neat) cm^{-1}	NMR, τ ($CDCl_3$)
n-C_4H_9-	n=2	127(P-C_4H_9O) 55($CH_2=CHCO$)	$C_{10}H_{16}O_4$	59.98	8.05	59.76	8.37	1740, 1730 (C=O) 1640, 1620, 1410 (C=C) 1180 (C-O)	3.6—4.2 (3H, m, **CH_2=CH**-) 5.5 (2H, t, =CHCO$_2$**CH_2**) 7.25 (2H, t, **CH_2CO_2**-)
	n=3	199(P-C_4H_9O) 127 55($CH_2=CHCO$)	$C_{13}H_{20}O_6$	57.34	7.40	57.55	7.44	1740 (C=O) 1640, 1620, 1410 (C=C) 1170 (C-O)	3.6—4.3 (3H, m, **CH_2=CH**-) 5.55 (4H, t, -COO**CH_2CH_2**-CO) 7.3 (4H, t, **CH_2**CO-)
sec-C_4H_9-	n=1		$C_7H_{12}O_2$	65.59	9.44	65.66	9.36	1740 (C=O) 1640, 1620 (C=O)	3.6—4.3 (3H, m, **CH_2=CH**-)
	n=2	127(P-C_4H_9O)	$C_{10}H_{16}O_4$	59.98	8.05	60.28	8.23	1735, (C=O) 1640, 1620, 1410 (C=C) 1180 (C-O)	3.6—4.3 (3H, m, **CH_2=CH**-) 5.55 (2H, t, =CH-COO**CH_2**) 7.3 (2H, t, **CH_2CO_2**-)
	n=3	199(P-C_4H_9O) 127 55 ($CH_2=CHCO$)	$C_{13}H_{20}O_6$	57.34	7.40	57.02	7.31	1740 (C=O) 1640, 1620, 1420 (C=C) 1180 (C-O)	3.7—4.3 (3H, m, **CH_2=CH**-) 5.7 (4H, t, COO**CH_2**-**CH_2**-CO) 7.45 (4H, t, **CH_2**CO)
C_2H_5-	n=2	127(P-C_2H_5O)	$C_8H_{12}O_4$	55.80	7.03	55.97	7.02	1740 (C=O) 1640, 1620, 1410 (C=C) 1180 (C-O)	3.6—4.3 (3H, m, **CH_2=CH**-) 5.6 (2H, t, =CHCO$_2$**CH_2**) 7.4 (2H, t, **CH_2**CO)
	n=3	127 55($CH_2=CHCO$)	$C_{11}H_{16}O_6$	54.09	6.60	(53.96	6.54)	1740 (C=O) 1640, 1620, 1410 (C=C) 1180 (C-O)	3.6—4.3 (3H, **CH_2=CH**-) 5.6 (4H, t, COO**CH_2CH_2**CO) 7.4 (4H, t, **CH_2CO_2**)
CH_3OCOCH_2	n=1	144 (P) 114(P-CH_3O) 55($CH_2=CH\cdot CO$)	$C_6H_8O_4$	50.00	5.60	49.93	5.73	1740, 1770 (C=O) 1640, 1620, 1410 (C=C) 1160 (C-O)	3.5—4.2 (3H, m, **CH_2=CH**-) 5.3 (2H, s, CO_2**CH_2**CO_2) 6.2 (3H, s, COO**CH_3**)
	n=2	127 55($CH_2=CH\cdot CO$)	$C_9H_{12}O_6$	50.00	5.60	49.72	5.65	1730, 1750 (C=O) 1640, 1620, 1410 (C=C) 1160 (C-O	3.5—4.2 (3H, m, **CH_2=CH**-) 5.3 (2H, s, CO_2**CH_2**CO_2) 5.5 (2H, t, COO**CH_2**CH_2CO) 6.2 (3H, s, CO_2**CH_3**) 7.1 (2H, t, **CH_2**CO)
	n=3	199, 127 55($CH_2=CH\cdot CO$)						1740 (C=O) 1640, 1620, 1410 (C=C) 1160 (C-O)	
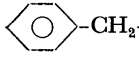 -CH_2-	n=1	162 (P) 55 ($CH_2=CHCO$)	$C_{10}H_{10}O_2$	74.05	6.22	74.29	6.50	3025, 1500 (ArH) 1730 (C=O) 1640, 1620 (C=C) 1180 (C-O)	2.6 (5H, s, ArH) 3.6—4.2 (3H, m, **CH_2=CH**-) 4.8 (2H, s, **CH_2**Ar)
NCCH_2-	n=1	111 (P)	$C_5H_5NO_2$	54.05	4.54	54.30	4.60	2250 (CN) 1740 (C=O) 1640, 1410 (C=C) 1170 (C-O)	3.5—4.1 (3H, m, **CH_2=CH**-) 5.2 (2H, s, O**CH_2**CN)

(20 mmol) of BPL and 2.74 g (20 mmol) of *n*-BuBr in 5 m*l* of benzene was heated under nitrogen with stirring at 80°C for 7 hr. 20 m*l* of petroleum ether was then added and undissolved Cu_2O and precipitated complex were separated by filtration. The filtrate was subjected to distillation, collecting a fraction of 80°C/760 mmHg—110°C/6 mmHg. Each product was purified by means of preparative glpc. Structures of the products were determined by IR and NMR spectra and elemental analysis. The results are summarized in Table 4.

In the case of the other alkyl halides, the reactions were carried out by a similar procedure to that of the reaction with *n*-BuBr under the conditions shown in Tables 1, 2, and 3. The identification data of products are summarized in Table 4.

Reaction of BPL with Copper(I) Phenylacetate t-*Butyl Isocyanide Complex (**8**) in the Presence of* n-*Butyl Bromide.* A mixture of 1.43 g (10 mmol) of Cu_2O, 2.72 g (20 mmol) of phenylacetic acid, and 2.08 g (25 mmol) of *t*-butyl isocyanide in 15 m*l* of benzene was heated at 80°C for 3 hr. Formation of water was observed during the course of the reaction. The reaction mixture was subjected to filtration under nitrogen, and the filtrate was evaporated to remove benzene and water. Cu(I) phenylacetate-*t*-butyl isocyanide complex remained and was dried at 80°C in a vacuum (2 mmHg) for 3 hr. Cu(I) phenylacetate-*t*-butyl isocyanide complex was used for the following reaction without further purification. To this Cu(I) carboxylate *t*-butyl isocyanide complex was added 15 m*l* of benzene and 1.45 g (20 mmol) of BPL and the mixture was heated at 80°C for 3 hr under nitrogen. 20 mmol of *n*-butyl bromide was then added, and the reaction mixture was heated at 80°C for 6 hr. After 20 m*l* of *n*-pentane was added, precipitated CuBr-isonitrile complex was separated. The organic layer was subjected to distillation. *n*-Butyl phenylacetate (**9**) and **10** were obtained in yields of 27% and 63%, respectively. **9**: Found: C, 74.82; H, 8.14%. Calcd for $C_{12}H_{16}O_2$: C, 74.97; H, 8.39%. NMR ($CDCl_3$): τ 2.70 (5H), 6.40 (2H), **10**: Found: C, 68.33; H, 7.65%. Calcd for $C_{15}H_{20}O_4$: C, 68.16; H, 7.63%. NMR ($CDCl_3$): τ 2.71 (5H), 5.69 (2H), 6.39 (2H), 7.38 (2H).

Only small amounts (less than 5%) of acrylate derivatives were identified by comparison of the glpc retention time and the IR spectrum with that of the authentic sample.

*Reaction of Oligomeric Copper(I) Carboxylate (**12**) with Ethyl Bromide.* A mixture of 2.15 g (15 mmol) of Cu_2O, 3.85 g (45 mmol) of *t*-butyl isocyanide and 2.18 g (30 mmol) of BPL in 7.5 m*l* of benzene was heated at 80°C for 5 hr. After the reaction mixture was cooled to room temperature, 4.32 g (40 mmol) of ethyl bromide was added, and the mixture was stirred for 2 hr at room temperature. *n*-Pentane was then added and CuBr-isonitrile complex was separated. The organic layer was subjected to distillation, and the products were purified by preparative glpc. $CH_2=CHCOO(CH_2CH_2COO)_{n-1}C_2H_5$ ($n=1$ (10%), $n=2$ (21%), $n=3$ (16%)) was obtained in a total yield of 47%.

When BPL (30 mmol), ethyl bromide (40 mmol), *t*-butyl isocyanide (45 mmol) and Cu_2O (15 mmol) were all mixed together and the mixture was heated at 80°C for 7 hr, almost the same result as above was obtained. The product yields were as follows. $CH_2=CHCOO(CH_2CH_2COO)_{n-1}C_2H_5$: $n=1$ (10%), $n=2$ (17%), $n=3$ (8%); Total yield was 35%. Data for the identification of these products are summarized in Table 4.

BULLETIN OF THE CHEMICAL SOCIETY OF JAPAN, VOL. 45, 3607—3611 (1972)

Preparations and Reactions of *N*-Benzoyl- and *N*-Ethoxycarbonylcarbodiimides

Oyo MITSUNOBU, Masazumi TOMARI, Hiroo MORIMOTO, Toshio SATO, and Michio SUDO

Department of Chemistry, College of Science and Engineering, Aoyama Gakuin University, Chitosedai, Setagaya-ku, Tokyo

(Received April 27, 1972)

The reaction of *N*-benzoyl-*N'*-*t*-butylthiourea with either diethyl azodicarboxylate or azodibenzoyl resulted in the formation of benzoyl-*t*-butylcarbodiimide in 84% and 48% yields, respectively. Dehydrosulfurization of various thioureas was also effected with mercuribenzamide. Benzoyl- or ethoxycarbonylcarbodiimides were obtained in over 80% yields. The reaction of benzoyl-*t*-butylcarbodiimide with one equivalent each of *N*-benzoylglycine and glycine ethyl ester led to the formation of N^1-benzoyl-N^2-*t*-butyl-N^3-(ethoxycarbonyl)methylguanidine in a good yield, no *N*-benzoylglycylglycine ethyl ester being isolated. When benzoyl-*t*-butylcarbodiimide was allowed to react with benzoic acid, dibenzimide and *t*-butyl isocyanate were formed. Similarly, *N*-ethoxycarbonylbenzamide and *N*-benzoylglycine(*N'*-ethoxycarbonyl)amide were prepared in good yields.

Carbodiimides have been used as versatile reagents in organic synthesis. For the preparation of peptides and nucleotides, dicyclohexylcarbodiimide (DCC) has been extensively used.[1] The reactivity of DCC, however, decreases in the presence of strong bases.[2] Thus, it is desirable to prepare more reactive carbodiimides such as *N*-acylcarbodiimides. α,β-Unsaturated carbonyl compounds undergo base catalyzed addition (Michael reaction)[3] and *N*-acylcarbodiimides are expected to show a similar reaction.

Some *N*-acyl-, *N*-ethoxycarbonyl- and *N*-sulfonylcarbodiimides have been synthesized but with low

1) a) H. G. Khorana, *Chem. Rev.*, **53**, 145 (1953): b) F. Kurzer and K. Douraghi-Zadeh, *ibid.*, **67**, 107 (1967): c) J. P. Greenstein and M. Winitz, "Chemistry of the Amino Acids," John Wiley & Sons, Inc., (1961): d) P. T. Gilham and H. G. Khorana, *J. Amer. Chem. Soc.*, **80**, 6212 (1958): e) K. L. Agarwal, A. Yamazaki, and H. G. Khorana, *ibid.*, **93**, 2754 (1971).

2) a) H. Schaller and H. G. Khorana, *ibid.*, **85** 3828 (1963). b) T. M. Jacob and H. G. Khorana, *ibid.*, **86**, 1630 (1964). c) R. Lohrmann and H. G. Khorana, *ibid.*, **86**, 4188 (1964). d) R. K. Ralph, W. J. Connors, H. Schaller, and H. G. Khorana, *ibid.*, **85**, 1983 (1963).

3) E. D. Bermann, D. Ginsburg, and R. Pappo, "Organic Reactions," Vol. 10, John Wiley & Sons, Inc, (1959), p 179.

yields.[4] In this report we present convenient methods for the preparation of *N*-benzoyl- and *N*-ethoxycarbonylcarbodiimides and some reactions of the carbodiimides.

Preparation of N-*Benzoylcarbodiimides by Means of either Diethyl Azodicarboxylate or Azodibenzoyl and Triphenylphosphine.* The reaction of *N*, *N'*-disubstituted thioureas (I) with diethyl azodicarboxylate (IIa) followed by treatment with triphenylphosphine resulted in the formation of the corresponding disubstituted carbodiimides in good yields.[5] Since the reaction proceeds in a neutral medium without any formation of reactive compounds such as water or strong acids, the process might be applied to preparation of more reactive carbodiimides.

When *N*-benzoyl-*N'*-*t*-butylthiourea (Ie) was allowed to react with an equimolar amount of IIa in tetrahydrofuran(THF) at room temperature, orange red of IIa faded in 3 days. After treatment with triphenylphosphine, benzoyl-*t*-butylcarbodiimide (IIIe), diethyl hydrazodicarboxylate and triphenylphosphine sulfide were obtained in 84%, 79%, and 71% yields, respectively.

We might assume that the reactivity of azo compounds depends on electron affinity of the nitrogen-nitrogen double bond. Thus, azodibenzoyl (IIb) was used in place of IIa in the above reaction.

The reaction of Ia, Ib, or Id with IIb in THF at room temperature led to the formation of the corresponding carbodiimide (IIIa, IIIb, or IIId) and *N,N'*-dibenzoylhydrazine in nearly quantitative yields. Thin layer chromatography (tlc) of the reaction mixture revealed the presence of sulfur. Unlike the reaction of I with IIa,[5] no 1 : 1 adduct of I with IIb could be isolated. When *N*-benzoyl-*N'*-*t*-butylthiourea (Ie) was treated with an equimolar amount of IIb at room temperature, the orange red of IIb disappeared within 4 hr and IIIe was isolated in a 47% yield. In order to facilitate the purification of the carbodiimide, an equimolar amount of triphenylphosphine was added before working up. An attempt to isolate benzoylcyclohexylcarbodiimide (IIIf) by distillation, however, was unsuccessful, presumably due to limited stability against moisture. Thus, the reaction mixture resulting from the reaction of *N*-benzoyl-*N'*-cyclohexylthiourea (If) with IIb was treated with water and *N*-benzoyl-

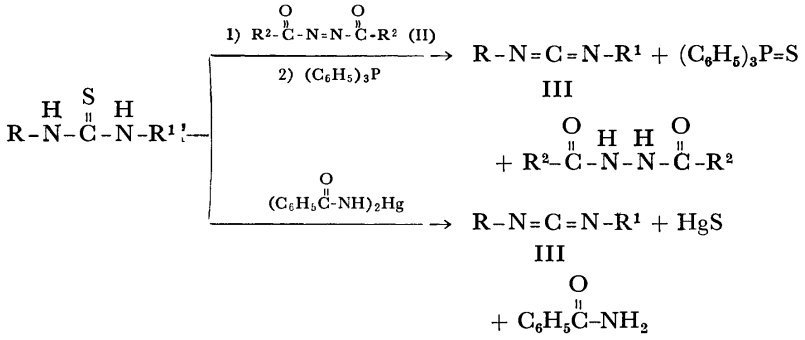

I, III a : $R=R^1=C_6H_5-$ d : $R=R^1=$*cyclo*-$C_6H_{11}-$ g : $R=C_2H_5OCO-$, $R^1=t$-C_4H_9-
b : $R=R^1=p$-$CH_3OC_6H_4-$ e : $R=C_6H_5CO-$, $R^1=t$-C_4H_9 h : $R=C_2H_5OCO-$, $R^1=$*cyclo*-$C_6H_{11}-$
c : $R=R^1=p$-$CH_3C_6H_4-$ f : $R=C_6H_5CO-$, $R^1=$*cyclo*-$C_6H_{11}-$
II a : $R^2=C_2H_5O-$ b : $R^2=C_6H_5-$

TABLE 1. PREPARATION OF *N*-BENZOYL- AND *N*-CARBOETHOXYCARBODIIMIDES FROM THIOUREAS

Method[a]	R-N=C=N-R' R	R'	Yield %	Bp°C (mmHg)	IR (ν cm^{-1}) -N=C=N-	C=O
A	C_6H_5CO-	t-C_4H_9-	48	72—74(0.08)	2150	1660
A'			84	110(0.55)		
B			88	98(0.2)		
A	C_6H_5CO-	*cyclo*-$C_6H_{11}-$	46[b]		2150	1687
B			82[b]			
B	C_2H_5OCO-	t-C_4H_9-	88	57—58(0.35)	2150	1730
B	C_2H_5OCO-	*cyclo*-$C_6H_{11}-$	86	83—86(0.01)	2150	1725

a) A; Reaction with azodibenzoyl and triphenylphosphine. A'; Reaction with diethyl azodicarboxylate and triphenylphosphine. B; Reaction with mercuribenzamide.
b) Yield of *N'*-benzoyl-*N'*-cyclohexylurea obtained by treatment of the reaction mixture with water.

4) a) H. Ulrich and A. A. R. Sayigh, *Angew. Chem.*, **76**, 781 (1964): b) H. Ulrich, B. Tucker, and A. A. R. Sayigh, *Tetrahedron*, **22**, 1565 (1966): c) R. Neidlein and E. Heukelbach, *Tetrahedron Lett.*, **1965**, 149: d) R. Neidlein and E. Heukelbach, *Arch. Pharm.*, **299**, 709 (1966), *Chem. Abstr.*, **66**, 37600j (1967): e) Larbwerke Hoechst A. -G., Ger. 1240519; *Chem. Abstr.*, **67**, 73181c (1967): f) Chemische Fabrik von Heyden A. -G., Neth. Appl., 6610608; *Chem. Abstr.*, **67**, 90554u (1967): g) J. Goerdeler, H. Lohmann, R. Losch, and S. Raddatz, *Tetrahdron Lett.*, **1971**, 2765.

5) a) O. Mitsunobu, K. Kato, and F. Kakese, *ibid.*, **1969**, 2473: b) O. Mitsunobu, K. Kato, and M. Tomari, *Tetrahedron*, **26**, 5731 (1970).

N'-cyclohexylurea was obtained in a 46% yield.

Preparation of Disubstituted Carbodiimides by Means of Mercuribenzamide. The above reaction is coupled to a redox system, *i. e.*, the hydrogen atoms in thiourea are abstracted by azo compounds and the sulfur atom in it is eliminated by the formation of triphenylphosphine sulfide. Other reagents capable of abstracting hydrogen and sulfur atoms may therefore be used for the preparation of carbodiimides. Mercuribenzamide (IV) was chosen for this purpose.

Mercuribenzamide was allowed to react with an equimolar amount of Ia, Ic, or Id in benzene at room temperature for 2 hr. After removal of mercuric sulfide, IIIa, IIIc, or IIId was obtained in nearly quantitative yields.

Similarly, some *N*-benzoyl- and *N*-ethoxycarbonylcarbodiimides (IIIe—h) were prepared in over 80% yields. The results are summarized in Table 1.

Reaction of N-*Benzoyl*-N'-t-*butylcarbodiimide and* N-*Ethoxycarbonyl*-N'-t-*butylcarbodiimide.* A special merit asociated with the use of DCC in the preparation of peptides is ease in manipulation. However, under certain conditions, *O*-acylisoureas initially formed from DCC and *N*-protected amino acids exhibit a marked propensity to undergo ready rearrangement of the acyl group giving *N*-acylureas.[1c]

The reaction of IIIe with an *N*-protected amino acid may also lead to the formation of corresponding *O*-acylisourea, in which the electron density of the nitrogen atom having a benzoyl group is reduced and another nitrogen atom is crowded by *t*-butyl group. Thus we might expect that the rearrangement to an *N*-acylurea *via* acyl transfer is prevented.

The reaction of IIIe with one equivalent each of *N*-benzoylglycine and glycine ethyl ester in dichloromethane at room temperature unexpectedly resulted in the formation of N^1-benzoyl-N^2-*t*-butyl-N^3-ethoxycarbonylmethylguanidine (V) in a 76% yield, 77% of *N*-benzoylglycine being recovered. *N*-Benzoyl-*N'*-*t*-butylurea was obtained in an 18% yield, but no *N*-benzoylglycylglycine ethyl ester was isolated. Similarly, V was prepared in a 71% yield when the reaction was carried out in THF.

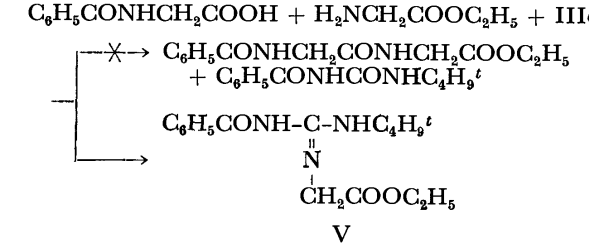

In general, DCC reacts with the carboxyl function of amino acids even when both amine and carboxylic acid reactants exist. Thus, the reactivity of IIIe is quite different from that of DCC and closely resembles that of isocyanates.

The reaction of IIIe with benzoic acid was attempted in order to test its reaction with carboxylic acid. Benzoic acid was allowed to react with an equimolar amount of IIIe in dichloromethane at room temperature

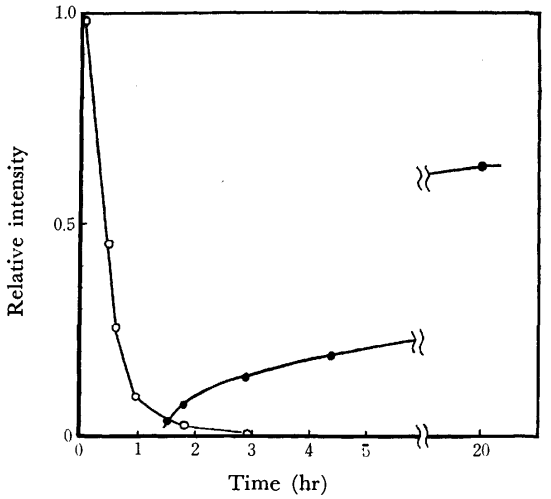

Fig. 1. Relative intensity of absorptions at 2150 and 2250 cm^{-1}.
—○— : Absorption at 2150 cm^{-1}
—●— : Absorption at 2250 cm^{-1}

and the reaction was followed by IR spectrum. The absorption at 2150 cm^{-1} attributed to the -N=C=N- bond virtually disappeared in 2 hr, and a new absorption at 2250 cm^{-1} appeared in 1.5 hr. Intensity of the new absorption became constant after 20 hr and dibenzimide was isolated in a 72% yield from the reaction mixture (Fig. 1). When IIIe was allowed to react with benzoic acid for 20 hr followed by treatment with aniline, *N*-phenyl-*N'*-*t*-butylurea was obtained in an 87% yield. This unexpected result may be explained as follows: *O*-benzoyl-isourea (VI) formed from IIIe and benzoic acid is converted into *N*-dibenzoyl-*N'*-*t*-butylurea (VIII). VIII subsequently is decomposed to dibenzimide and *t*-butyl isocyanate by intramolecular hydrogen transfer. The possibility of initial formation of an imidoyl benzoate (VII) prior to VIII could not be ruled out.

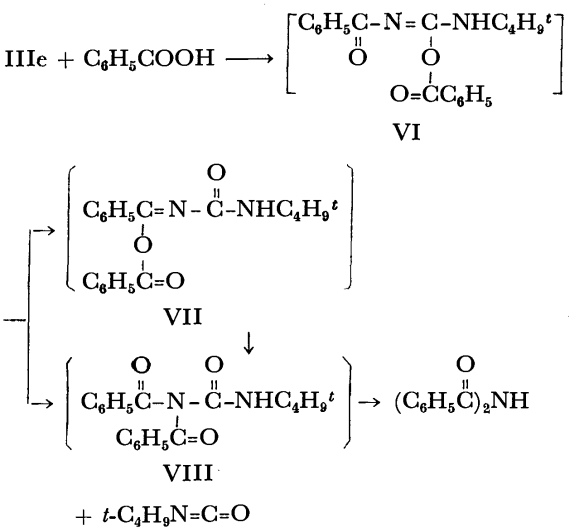

That the transfer of the benzoyl group took place rapidly was proved by the following experiment. When IIIe was treated with benzoic acid for 2 hr at room temperature and then aniline was added, benzanilide was obtained only in a 33% yield along with *N*-benzoyl-

N'-t-butylurea, *N*-phenyl-*N'-t*-butylurea, and benzamide.

When the reaction of IIIe with benzoic acid was carried out in the presence of a catalytic amount of triethylamine and the reaction was followed by IR spectrum as above, it took over 5 hr for the carbodiimide to disappear. On the other hand, a new absorption at 2250 cm^{-1} appeared in 30 min.

Similarly, the reaction of ethoxycarbonyl-*t*-butylcarbodiimide (IIIg) with an equimolar amount of benzoic acid or *N*-benzoylglycine resulted in the formation of *N*-ethoxycarbonylbenzamide and *N*-benzoylglycine(*N'*-ethoxycarbonyl)amide in fairly good yields.

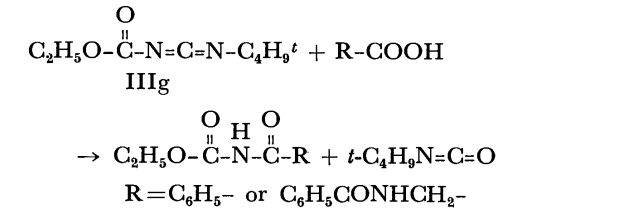

$C_2H_5O-\overset{O}{\overset{\|}{C}}-N=C=N-C_4H_9^t$ + R-COOH

IIIg

$\rightarrow C_2H_5O-\overset{O}{\overset{\|}{C}}-\overset{H}{N}-\overset{O}{\overset{\|}{C}}-R + t\text{-}C_4H_9N=C=O$

$R = C_6H_5-$ or $C_6H_5CONHCH_2-$

Experimental

The IR spectra were measured on a Nippon Bunko IR-G spectrophotometer. The NMR spectra were obtained on a Hitachi Perkin-Elmer R-20 high resolution spectrometer at 60 MHz, using tetramethylsilane as an internal standard. Thin layer chromatography (tlc) was carried out on Merck PF_{254} or Wako Gel B-5.

Reagents. Diethyl azodicarboxylate,[6] azodibenzoyl,[7] and mercuribenzamide[8] were prepared by the usual procedures. *N*-Benzoyl- and *N*-ethoxycarbonyl thioureas were prepared from an amine and either benzoyl or ethoxycarbonyl thioisocyanate. The solvents were purified by ordinary procedures.

Preparation of Benzoyl-t-butylcarbodiimide by the Reaction of N-Benzoyl-N'-t-butylthiourea with an Azo Compound and Triphenylphosphine. a) Using Diethyl Azodicarboxylate. A solution of diethyl azodicarboxylate (1.74 g, 10 mmol) in THF (3 m*l*) was added dropwise to a solution of *N*-benzoyl-*N'-t*-butylthiourea (2.36 g, 10 mmol) in THF (10 m*l*) with stirring at room temperature. After the solution was kept standing at room temperature for 2 days, triphenylphosphine (2.62 g, 10 mmol) in THF (6 m*l*) was added, The solution was stirred for 1 hr and concentrated *in vacuo*. The residue was extracted with petroleum ether (30—60°C) to separate soluble material from the remainder. The extract was concentrated and distilled to give benzoyl-*t*-butylcarbodiimide, bp 110°C/0.55 mmHg, 1.65 g (84%), IR (neat): 2150 (-N=C=N-) and 1660 cm^{-1} (>C=O). NMR (CCl_4): δ 1.40 (s, 9H, $-C(CH_3)_3$), 7.30 and 7.90 (m, 3H and 2H, aromatic protons). The material, insoluble in petroleum ether, was applied to a column (2.5×25 cm) of alumina in benzene. The column was eluted first with benzene and then with methanol. Triphenyl phosphine sulfide (71%) was obtained from the benzene fraction and diethyl hydrazodicarboxylate (79%) was obtained from the methanol fraction.

b) Using Azodibenzoyl. A solution of azodibenzoyl (1.19 g, 5 mmol) in benzene (35 m*l*) was added dropwise to a solution of *N*-benzoyl-*N'-t*-butylthiourea (1.18 g, 5 mmol) in benzene with stirring at room temperature. After the mixture was stirred for 5 hr, dibenzoylhydrazine (mp 245—248°C, 1.12 g, 93%) was filtered off. Triphenylphosphine (1.31 g, 5 mmol) in benzene (10 m*l*) was then added to the filtrate and a white precipitate formed was removed by filtration. The filtrate was concentrated *in vacuo* and the residue was extracted with petroleum ether (30—60°C) to separate soluble material from the remainder. The extract was concentrated and distilled to give IIIe, bp 71—74°C/0.08 mmHg, 482 mg (48%). The material, insoluble in petroleum ether, was triphenylphosphine sulfide, mp 155—162°C, 1.14 g (78%).

Reaction of N-Benzoyl-N'-cyclohexylthiourea with Azodibenzoyl. A solution of IIb (238 mg, 1 mmol) in benzene (1 m*l*) was added dropwise to a solution of **If** (262 mg, 1 mmol) in benzene (2 m*l*) with stirring at room temperature. After the mixture was stirred for 4 hr, dibenzoylhydrazine (mp 244—245°C, 195 mg, 81%) was removed by filtration. The IR spectrum of the filtrate showed strong absorption at 2150 cm^{-1} (-N=C=N-). The filtrate was treated with water (1 m*l*), the product being separated by preparative tlc (dichloromethane, benzene-THF (1 : 1), and benzene) to give sulfur (20 mg, 63%) and *N*-benzoyl-*N'*-cyclohexylurea, mp 161—162°C, 57 mg (46%). IR (KBr): 3250 (>N-H), 1690 (>C=O), and 1600 cm^{-1} (C_6H_5-). NMR (CCl_4): δ 1.8 (m, 11H, *cyclo*-$C_6H_{11}-$), 3.75 (broad s, 1H, >N-H), 7.5 and 8.15 (m, 3H and 2H, aromatic protons), and 9.0 (1H, >N-H).

Preparation of N-Benzoyl- and N-Ethoxycarbonylcarbodiimides from Thioureas and Mercuribenzamide. Equimolar amounts (20 mmol) of *N*-benzoyl- or *N*-ethoxycarbonylthiourea (I) and IV were suspended in benzene (100 m*l*) and the mixture was stirred for 3 hr at room temperature. After mercuric sulfide was removed by filtration, the filtrate was evaporated and the residue was extracted with petroleum ether. The corresponding carbodiimide was obtained by distillation from the extracts. The results are summarized in Table 1.

Reaction of N-Benzoyl-N'-t-butylcarbodiimide with N-Benzoylglycine and Glycine Ethyl Ester. A suspension of *N*-benzoylglycine (179 mg, 1 mmol) and IIIe (202 mg, 1 mmol) in dichloromethane (6 m*l*) was stirred for 20 min at room temperature. A solution of glycine ethyl ester (103 mg, 1 mmol) in dichloromethane was then added dropwise in 20 min to the suspension. After the mixture was kept standing overnight, *N*-benzoylglycine was separated by filtration, mp 187—191°C, 137 mg (77%). The filtrate was applied to silica gel plates which were developed in chloroform. The main band was further separated by tlc (ether) giving *N*-benzoyl-*N'-t*-butylurea, 40 mg, 18%, mp 144—145°C (from ethanol): Found: C, 65.46; H, 7.34%. Calcd for $C_{12}H_{16}N_2O_2$: C, 65.43; H, 7.32%. NMR (CCl_4): δ 1.5 (s, 9H, $-C(CH_3)_3$), 7.4—8.15 (m, 5H, aromatic protons), 9.1 (1H, >N-H), and 10.9 (1H, >N-H), and N^1-benzoyl-N^2-*t*-butyl-N^3-carboethoxymethylguanidine (232 mg, 76%, mp 96—98°C (from petroleum ether). Found: C, 62.98; H, 7.59; N, 13.74%. Calcd for $C_{16}H_{23}N_3O_3$: C, 62.93; H, 7.59; N, 13.76%. IR (KBr): 1750 cm^{-1} (>C=O). NMR (CCl_4): δ 1.25 (t, 3H, $-O-\overset{|}{C}-CH_3$), 1.5 (s, 9H, $-C(CH_3)_3$), 2.5 (1H, >N-H), 4.25 (m, 4H, $>NCH_2CO_2CH_2\overset{|}{C}-$), 7.4 and 8.15 (m, 5H, aromatic protons), and 10.4 (1H, >N-H).

When the reaction was carried out in THF, the guanidine was obtained in a 71% (215 mg) yield.

Reaction of N-Benzoyl-N'-t-butylcarbodiimide with Aniline. A solution of aniline (93 mg, 1 mmol) in dichloromethane (1.5 m*l*) was added dropwise to a solution of IIIe (202 mg, 1 mmol) in dichloromethane (1.5 m*l*) with stirring at room temperature. After about 1 hr, the tlc of the solution re-

6) N. Rabjohn, "Organic Syntheses," Coll. Vol. III, p 375 (1955).
7) H. Bock and J. Kroner, *Chem. Ber.*, **99**, 2039 (1966).
8) J. W. Williams, W. T. Rainey, Jr., and R. S. Leopold, *J. Amer. Chem. Soc.*, **64**, 1738 (1942).

vealed a new spot while no starting materials remained. The solution was kept standing overnight and the solvent was removed under reduced pressure giving N^1-benzoyl-N^2-*t*-butyl-N^3-phenylguanidine, mp 100—101°C, 286 mg (97%). The guanidine was recrystallized from petroleum ether, mp 102°C. NMR (CCl_4): δ 1.5 (s, 9H, $-C(CH_3)_3$), 4.8 (1H, >N-H), 7.25 and 8.15 (m, 10H, aromatic protones), and 12.4 (1H, >N-H).

*Reaction of Benzoyl-*t*-butylcarbodiimide with Benzoic Acid. a) Measurement of IR Spectrum of the Reaction Mixture.* A solution of IIIe (202 mg, 1 mmol) and benzoic acid (122 mg, 1 mmol) in dichloromethane (3 m*l*) was placed in 0.05 cm matched cell (NaCl) and the reaction was followed by means of IR spectrum at room temperature. Figure 1 shows relative intensity of absorption at 2150 and 2250 cm^{-1}.

b) Treatment of the Reaction Mixture with Aniline. A solution of IIIe (202 mg, 1 mmol) and benzoic acid (122 mg, 1 mmol) in dichloromethane (4.5 m*l*) was stirred at room temperature for 2 hr. Aniline (93 mg, 1 mmol) in dichloromethane (3 m*l*) was then added and the solution was stirred for additional 5 hr. After the solution was kept standing overnight, the products were isolated by preparative tlc (1,2-dichloroethane–ether (30 : 1) and 1,2-dichloroethane–ether (15 : 1)) giving benzanilide (mp 163—164°C, 64 mg, 33%), *N*-benzoyl-*N'*-*t*-butylurea (mp 140—142°C), *N*-phenyl-*N'*-*t*-butylurea (mp 164—165°C) and benzamide.

In a separate experiment in which the mixture obtained as above was stirred for 20 hr, followed by treatment with aniline (93 mg, 1 mmol) in dichloromethane (3 m*l*), benzanilide (mp 162—163°C, 44 mg, 22%), benzamide (mp 127—128°C, 23 mg, 19%) and *N*-phenyl-*N'*-*t*-butylurea (mp 166—168°C, 167 mg, 87%) were obtained.

c) Treatment of the Reaction Mixture with Water. A mixture obtained as above was stirred for 20 hr at room temperature followed by addition of water (0.1 m*l*). After the solution was kept standing overnight, dibenzimide was obtained by preparative tlc using dichloromethane–ether (10 : 1) in a 72% yield, mp 150—151°C (from ethanol–water, 1 : 1). Satisfactory analytical and spectra data were obtained.

Reaction of N-*Ethoxycarbonyl*-N'-t-*butylcarbodiimide with Benzoic Acid.* A solution of IIIg (85 mg, 0.5 mmol) and benzoic acid (61 mg, 0.5 mmol) in THF (1.5 m*l*) was refluxed for 3.5 hr and kept standing overnight. After removal of the solvent under reduced pressure, a quantitative amount of *N*-ethoxycarbonylbenzamide (mp 108—109°C) was obtained which was recrystallized from ethanol, mp 113°C. The product was shown to be identical with the authentic sample by comparison of IR spectra.

*Reaction of Ethoxycarbonyl-*t*-butylcarbodiimide with* N-*Benzoylglycine.* A solution of IIIg (85 mg, 0.5 mmol) and *N*-benzoyl glycine (89 mg, 0.5 mmol) in THF (8 m*l*) was refluxed for 3 hr. After the solution was kept standing overnight at room temperature, the solvent was removed under reduced pressure. The residue was applied to silica gel plates developed in 1,2-dichloroethane–ether (5 : 1). *N*-Benzoylglycine(*N'*-ethoxycarbonyl)amide was thus isolated in a 73% (91 mg) yield, mp 152—154°C. Recrystallization from ethanol gave an analytical sample which gave satisfactory analytical and IR data.

BULLETIN OF THE CHEMICAL SOCIETY OF JAPAN, VOL. 45, 3611—3614 (1972)

Studies on Amino-hexoses. XV. Synthesis of Deoxy-*N*-acetyl-muramic Acid

Hitoshi ARITA, Kiyofumi FUKUKAWA, and Yoshio MATSUSHIMA

Department of Chemistry, Osaka University College of Science, Toyonaka

(Received February 9, 1972)

Benzyl 2-acetamido-6-*O*-acetyl-4-chloro-2,4-dideoxy-3-*O*-[D-1-(methyl carboxylate)ethyl]-α-D-galactopyranoside and benzyl 2-acetamido-4,6-dichloro-2,4,6-trideoxy-3-*O*-[D-1-(methyl carboxylate)ethyl]-α-D-galactopyranoside were prepared by the reaction of sulfuryl chloride on *N*-acetyl-muramic acid derivatives. 2-Acetamido-2,4-dideoxy-3-*O*-(D-1-carboxyethyl)-D-xylohexo-pyranose (*N*-acetyl-4-deoxy-muramic acid) and 2-acetamido-2,4,6-trideoxy-3-*O*-(D-1-carboxyethyl)-D-xylohexo-pyranose (*N*-acetyl-4,6-dideoxy-muramic acid) were prepared by the reduction of these chlorodeoxy derivatives with tri-*n*-butyltin hydride.

N-Acetyl-muramic acid (Formula 1), now known to be a constituent of the cell walls of both gram-positive and gram-negative bacteria, was isolated at first as a nucleotide derivative that plays the role of precursor in cell wall biosynthesis.[1] Lindberg and Agback prepared some analogues of muramic acid with variations of the lactic side chain for the purpose of inspecting antibacterial activity.[2] Diana synthesized 6-deoxy analogues of muramic acid for the same purpose.[3] As is well-known, *N*-acetyl-muramic acid is glycosidically bound at C-4 with *N*-acetyl-D-glucomine in the bacterial cell wall mucopeptides, and the

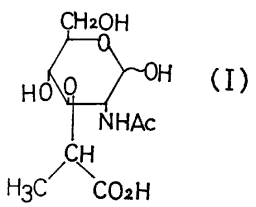

(I)

Formula 1

hydroxyl group at C-4 of muramic acid seems to be indispensable for cell wall biosynthesis. We attempted to prepare 4-deoxy- and 4,6-dideoxy-*N*-acetyl-muramic acid on the basis of the stereospecific synthesis of muramic acid reported by Matsushima and Park.[4] Introduction of chlorodeoxy group at C-4 or C-6 of

1) J. T. Park, *J. Biol. Chem.*, **194**, 885 (1952).

2) B. Lindberg and H. Agbach, *Acta Chem. Scand.*, **18**, 185 (1964).

3) G. D. Diana, *J. Org. Chem.*, **35**, 1910 (1970).

4) Y. Matsushima and J. T. Park, *ibid.*, **27**, 3581 (1962).

N-acetyl-muramic acid was performed by the reaction with sulfuryl chloride in pyridine.[8] The chlorodeoxy sugars were successfully reduced by tri-*n*-butyltin hydride and α-α'-azobisisobutyronitrile as an initiator of the radical reaction.

Results and Discussion

The route of the synthesis is shown in the Scheme 1. Intermediate **1** was prepared according to the method of Flowers and Jeanloz.[5] Partial acetylation giving 6-*O*-acetyl compound of **1** was successful, its structure being confirmed by NMR spectrometry. Two methyl signals appeared in the region δ 2.0—2.1, one being assigned as *N*-acetyl (δ 2.03) and the other as 6-*O*-acetyl (δ 2.0). No signal for 4-*O*-acetyl was observed. Complete selectivity of acetylation between C-6 and C-4 may be due to the influence of a lactyl side chain at C-3. We found no such selectivity between primary and secondary hydroxyl groups under the same reaction conditions.[6,7] Treatment of **1** and **2a** with sulfuryl chloride resulted in chlorodeoxy compounds **4a** and **3b**. The chloro groups were introduced most probably through the intermediates **3a** and **2b**. The configuration of the chloro group at C-4 of both **4a** and **3b** was inferred to be galacto-type on the basis of the data presented by Jennings and Jones.[8] Reduction of **4a** with tri-*n*-butyltin hydride proceeded without producing any by-product under mild conditions, but reduction of **3b** required refluxing overnight to complete the reaction. As in the case of reduction of chlorodeoxy neutral sugars, no reaction occurred without co-existence of a small amount of α,α'-azobis-isobutyronitrile.[7] Compounds **5a** and **4b** were deacetylated with sodium hydroxide and debenzylated by catalytic reduction with palladium on charcoal. The structures of the synthetic substances were confirmed by NMR spectrometry. The NMR assignment of compound **5a** is as follows (Fig. 1). Irradiation at δ 1.40 caused the quartet of $CH_3\underline{CH}$-$COOCH_3$ at δ 4.10 to collapse to a singlet. Conversely, irradiation at δ 4.10 caused the doublet at δ 1.40 to collapse to a singlet. Irradiation of H-2 at δ 3.60 caused the doublet of H-1 at δ 5.38 to collapse to a singlet. Integration suggested that H-4e existed in the region δ 1.8-2.3 overlapping the signal of the *N*-acetyl group. Similarly H-4a existed in the region δ 1.2—1.8 overlapping the signal of $\underline{CH_3}$-$CHCOOCH_3$. Furthermore, integration suggested that H-3 and H-5 existed in the region δ 3.7—4.1 overlapping CH_3-$CHCOO\underline{CH_3}$. The spectrum of compound **4b** is shown in Figs. 2 and 3. Irradiation at δ 1.37 caused the quartet of $CH_3\underline{CH}COOCH_3$ at δ 4.10 to collapse to a singlet. Irradiation of H-5 at δ 3.98 caused the doublet of CH_3-5 at δ 1.16 to collapse to a singlet. Irradiation of H-2 at δ 3.65 also caused the doublet of H-1 at δ 5.30 to collapse to a singlet. Integration suggested that H-3 existed in the region δ 3.7—4.1, which overlapped the signal of $CH_3CHCOO\underline{CH_3}$.

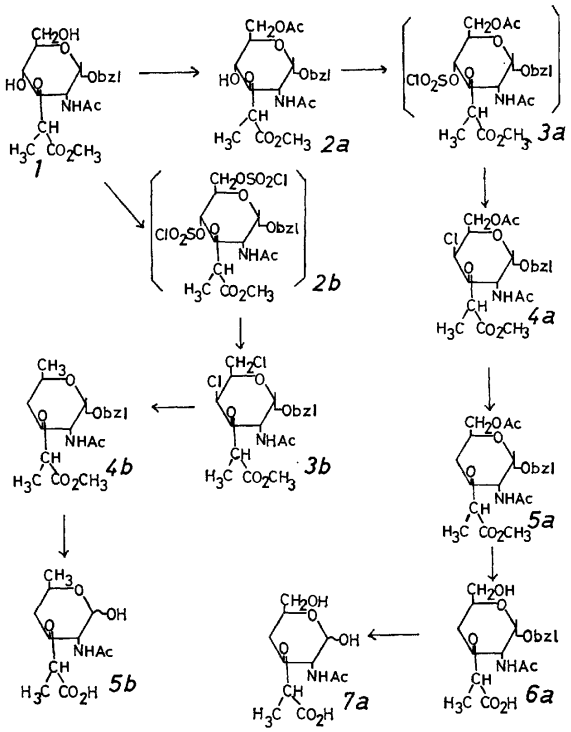

Scheme 1.

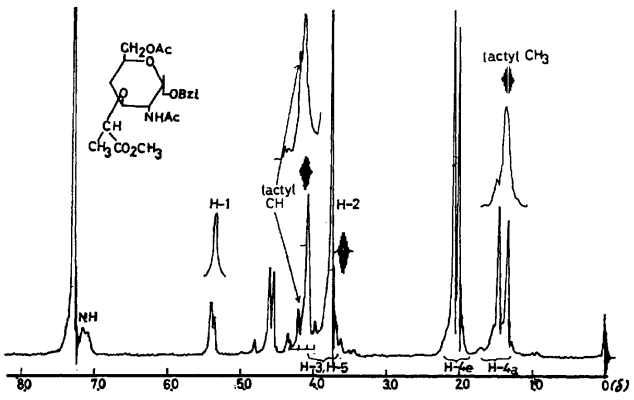

Fig. 1. The NMR spectrum of **5a** in $CDCl_3$.

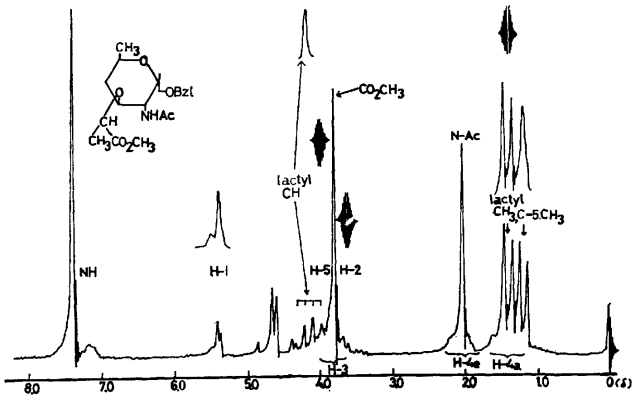

Fig. 2. The NMR spectrum of **4b** in $CDCl_3$.

5) H. M. Flowers and R. W. Jeanloz, *J. Org. Chem.*, **28**, 2983 (1963).

6) H. Arita and Y. Matsushima, *J. Biochem.*, **70**, 795 (1971).

7) H. Arita, N. Ueda, and Y. Matsushima, This Bulletin, **45**, 567 (1972).

8) H. J. Jennings and J. K. N. Jones, *Can. J. Chem.*, **40**, 1408 (1962).

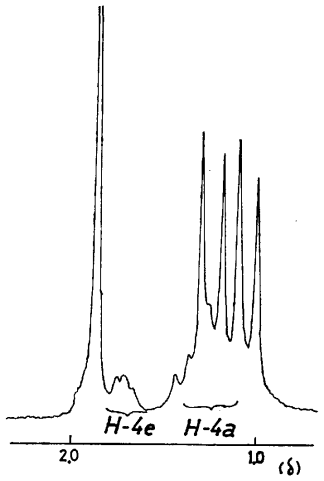

Fig. 3. The NMR spectrum of **4b** in $CDCl_3$+Benzene-d_6.

Integration also suggested that H-4e, H-4a existed in the region δ 1.8—2.3 and δ1.1—1.7 overlapping the signals of C-5 CH_3 and $\underline{CH_3}CHCOOCH_3$, respectively. The assignment of H-4e was confirmed by the addition of benzene-d_6 to the solution of **4b** in $CDCl_3$ (Fig. 3). The signal of H-4e appeared in a higher field.

Experimental

General Methods. All the melting points were uncorrected. Nuclear magnetic resonance spectra were recorded using the specimens dissolved in chloroform-*d* with tetramethylsilane as an internal standard. A Varian T-60 spectrometer was employed. Thin layer chromatagraphy (tlc) was performed with silica gel G (Merck). The spots were detected by spraying with 5% sulfuric acid in methanol and heating at 150°C. Tri-*n*-butyltin hydride was prepared by thermal decomposition of tri-*n*-butyltin formate according to the method of Okawara and Ohara.[9]

*Benzyl 2-Acetamido-2-deoxy-3-O-[D-1-(methyl carboxylate)ethyl]-α-D-glucopyranoside (**1**).* Compound (**1**) was prepared from benzyl 2-acetamido-4,6-*O*-benzylidene-3-*O*-[D-1-methyl carboxylate ethyl]-2-deoxy-α-D-glucopyranoside by treatment in a 80% aqueous acetic acid at 60°C for 2 hr.[5] $[\alpha]_D^{46}$+127° (*c* 1.08, in chloroform)

*Benzyl 2-Acetamido-6-O-acetyl-2-deoxy-3-[D-1-(methyl carboxylate)ethyl]-α-D-glucopyranoside(**2a**).* Compound **1** (13 g) was dissolved in a mixture of anhydrous chloroform (50 m*l*) and pyridine (50 m*l*), and the solution was cooled in a dry ice-acetone bath. Acetic anhydride (3.75 m*l*) was added dropwise to the solution, and the reaction solution was kept at −20°C for 40 hr. A few drops of water was added to destroy residual acetic anhydride and the solution was dried up *in vacuo*. The residual syrup was extracted with chloroform and the extract was washed with water several times. The chloroform layer was dried up *in vacuo* to give a slightly colored syrup (13.5 g), which showed a single spot on tlc with the solvent system *n*-BuOH-EtOH-H_2O (3 : 1 : 1). $[\alpha]_D^{20}$+91.2° (*c* 1.25, in chloroform) NMR (in $CDCl_3$); δ 1.4 (3H d; *J* 7 Hz $\underline{CH_3}CHCOOCH_3$) 2.10 (3H s, OAc) 2.04 (3H s, NAc) 2.34 (1H s, OH) 3.74 (3H s, $-CO_2CH_3$) 5.33 (1H d, *J* 3 Hz H-1) 7.6 (1H d, *J* 5 Hz NH)

*Benzyl 2-Acetamido-6-O-acetyl-4-chloro-2,4-dideoxy-3-O-[D-1-(methylcarboxylate) ethyl]-α-D-galactopyranoside(**4a**).* Compound **2a** (13 g) was dissolved in anhydrous pyridine (30 m*l*) and the solution was cooled in an ice-water bath. Sulfuryl chloride (2.9 m*l*) was added dropwise, and the solution was kept in a refrigerator overnight and then kept at room temperature for 3 hr. The reddish reaction solution was extracted with chloroform and the extract was washed with water several times. Evaporation *in vacuo* gave a syrup which was co-distilled with toluene until residual pyridine was completely removed. Rapid crystallization occurred, and recrystallization with 2-propanol gave colorless needles (8.4 g) which melted at 139—140°C and had $[\alpha]_D^{20}$+182° (*c* 1.0 in chloroform) Found: C, 55.10; H, 6.20; N, 3.12; Cl, 7.59%. Calcd for $C_{21}H_{28}O_8NCl$: C, 55.07; H, 6.16; N, 3.06; Cl, 7.74%. NMR (in $CDCl_3$) δ 1.42 (3H d, *J* 7 Hz $\underline{CH_3}CHCOOCH_3$) 2.0 (3H s, OAc) 2.03 (3H, s, NAc) 3.72 (3H s, $COOCH_3$) 4.0 (1H unresolved. H-2) 4.03 (1H q, *J* 7 Hz $\underline{CH_3}CHCOOCH_3$) 5.43 (1H d, *J* 3 Hz H-1) 7.1 (1H d, *J* 5 Hz NH)

*Benzyl 2-Acetamido-6-O-acetyl-2,4-dideoxy-3-O-[D-1-(methyl carboxylate) ethyl]-α-D-xylohexopyranoside(**5a**).* Six grams of **4a** was dissolved in anhydrous toluene under nitrogen atmosphere. Tri-*n*-butyltin hydride (5 m*l*) and α,α′-azobisisobutyronitrile (10 mg) were added to the solution. The mixture was heated at 80°C under stirring for 2 hr. Evaporation *in vacuo* gave a syrup, which was chromatographed on silica gel column with ethyl acetate-toluene (1 : 1) as an eluant. A colorless syrup (4.5 g) was obtained, which failed to crystallize. The syrup was re-chromatographed on a silica gel column with the same solvent. $[\alpha]_D^{20}$+154° (*c* 1.57 in chloroform) Found: C, 58.71; H, 6.72; N, 3.29%. Calcd for $C_{21}H_{29}O_8N$: C, 59.56; H, 6.90; N, 3.31%. NMR (in $CDCl_3$) δ 1.4 (3H d, *J* 7 Hz $\underline{CH_3}CHCOOCH_3$) *ca.* 1.5 (1H H-4a) *ca.* 2.2 (1H H-4e) 2.01 (3H s, OAc) 2.04 (3H s, NAc) *ca.* 3.6 (1H unresolved H-2) 3.74 (3H s, CO_2CH_3) 4.10 (1H q, *J* 7 Hz $\underline{HC}(CH_3)COOCH_3$) 5.38 (1H d, *J* 3 Hz H-1) 7.1 (1H d, 5 Hz NH)

*2-Acetamido-2,4-dideoxy-3-O-(D-1-carboxyethyl)-D-xylohexopyranose (**7a**).* Two grams of **5a** was dissolved in a mixture of methanol (25 m*l*) and 2N aqueous sodium hydroxide (2 m*l*), and the solution was kept at room temperature for 40 hr. It showed no color reaction of ester,[10] and was neutralized with glacial acetic acid. Reduction with hydrogen over 10% palladium on charcoal was carried out at room temperature. The reduction was complete within 24 hr. Palladium charcoal were filtered off, and the filtrate was passed through a column of Dowex-50X8 (H^+) to remove sodium ion and then dried up *in vacuo* to a colorless syrup (1.2 g), which failed to crystallize. The syrup was further purified on a Bio-gel P-2 column (3.0×200 cm) with 0.02 M acetic acid as an eluant. $[\alpha]_D^{20}$+71° (*c* 1.22 in water) Found: C, 47.32; H, 6.85; N, 4.78%. Calcd for $C_{11}H_{19}O_7N$: C, 47.65; H, 6.91; N, 5.05%. NMR (in D_2O) δ 1.4 (3H d, *J* 7 Hz $\underline{CH_3}COOCH_3$) *ca.* 1.68 (1H H-4a) 2.05 (3H s, NAc) *ca.* 2.3 (1H H-4e) 5.34 (1H d, *J* 3 Hz H-1).

*Benzyl 2-Acetamido-4,6-dichloro-2,4,6-trideoxy-3-O-[D-1-(methyl carboxylate)ethyl]-α-D-galactopyranoside(**3b**).* Four grams of **1** was dissolved in anhydrous pyridine (40 m*l*) and the solution was cooled in an ice-water bath. Sulfuryl chloride (2.0 m*l*) was then added to the solution, which was kept in a refrigerator overnight and then kept at room temperature for 3 hr. The reaction solution was extracted with chloroform and the extract was washed several times with water.

9) R. Okawara and M. Ohara, *J. Organometal. Chem.*, **3**, 484 (1965).

10) N. Abdel-Akher and F. Smith, *J. Amer. Chem. Soc.*, **73**, 5869 (1951).

The chloroform extract was evaporated *in vacuo* to a syrup, which was extracted with toluene–ligroin (3 : 1) several times on a boiling water bath. The extracts were collected and dried up *in vacuo*. Crystals appearing in methanol were recrystallized with the same solvent to give colorless needles (2.5 g) melting at 131—135°C and had $[\alpha]_D^{20}+103°$ (*c* 1.0, in chloroform). Found, C, 52.52, H, 5.69; N, 3.26; Cl, 15.94%. Calcd for $C_{19}H_{25}O_6NCl_2$: C, 52.54; H, 5.80; N, 3.23; Cl, 16.33%.

*Benzyl 2-Acetamido-2,4,6-trideoxy-3-O-[D-1-(methyl carboxylate)ethyl]-α-D-xylohexopyranoside(**4b**).* Two grams of **3b** was dissolved in anhydrous toluene (50 m*l*) under nitrogen atmosphere and tri-*n*-butyltin hydride (3 m*l*) and α,α'-azobisisobutyronitrile (*ca.* 10 mg) were added. The solution was refluxed for 24 hr. The slightly yellow solution was passed through silica gel column with a solvent mixture of ethylacetate and toluene (1 : 1) as an eluant. The syrup obtained was pure as judged by tlc (ethylacetate–toluene 1 : 1), its Beilstein test being negative. $[\alpha]_D^{20}+177°$ (*c* 1.0, in chloroform) Found: C, 63.01; H, 7.38; N, 3.81%. Calcd for $C_{19}H_{27}O_6N$: C, 62.45; H, 7.45; N, 3.83%.

NMR (in $CDCl_3$) δ 1.16 (3H d, *J* 7 Hz CH_3-5) 1.37 (3H d, *J* 7 Hz $\underline{CH_3}CHCOOCH_3$) *ca.* 1.5 (1H H-4a) 2.0 (3H s, NAc) *ca.* 2.1 (1H H-4e) *ca.* 3.65 (1H H-2) 3.73 (3H s, CO_2-CH_3) 4.1 (1H q, *J* 7 Hz $CH_3CHCOOCH_3$) 3.98 (1H q, *J* 7 Hz H-5) 5.31 (1H d, *J* 3 Hz H-1) 7.15 (1H d, *J* 5 Hz NH).

*2-Acetamido-2,4,6-trideoxy-3-O-(D-1-carboxyethyl)-D-glucopyranose (**5b**).* Compound **4b** (800 mg) was dissolved in 10 m*l* of methanol, and 2 N aqueous sodium hydroxide (1 m*l*) was added. The solution was kept at room temperature for 40 hr and then neutralized with glacial acetic acid. Evaporation *in vacuo* gave a syrup which was dissolved in 2-propanol (50 m*l*) and reduced with hydrogen over palladium charcoal at room temperature. The reaction was complete after 24 hr. The charcoal was filtered off and the filtrate dried up *in vacuo*. The residual syrup was dissolved in 3 m*l* of water and the solution was passed through a column of Dowex-50X8 (H^+) to remove sodium ion. Although the product showed a single spot on tlc (BuOH–EtOH–water 3 : 1 : 1), it failed to crystallize. $[\alpha]_D^{20}+63°$ (*c* 1.7, in water) Found: C, 49.75; H, 7.32; N, 5.24%. Calcd for $C_{11}H_{19}O_6N$: C, 50.56; H, 7.33; N, 5.36%.

BULLETIN OF THE CHEMICAL SOCIETY OF JAPAN, VOL. 45, 3614—3619 (1972)

Studies on Amino-hexoses. XVI. Synthesis of Deoxy-analogues of *N*-Acetyl-D-glucosamine

Hitoshi ARITA, Kiyofumi FUKUKAWA, and Yoshio MATSUSHIMA

Department of Chemistry, Osaka University College of Science, Toyonaka

(Received May 10, 1972)

For deoxy analogues of *N*-acetyl-D-glucosamine and three deoxy-analogues of phenyl *N*-acetyl-β-D-glucosaminide were synthesized by means of chlorination with sulfuryl chloride and reduction of the chlorides with tri-*n*-butyltin hydride. The free sugars thus obtained failed to crystallize except for 6-deoxy and 4,6-dideoxy compounds. Phenyl glycosides were mostly crystalline. The yield of chlorination and reduction was generally high.

As is well-known, many bacteria contain in their cell walls a polysaccharide composed of alternate *N*-acetyl-D-glucosamine and *N*-acetyl-muramic acid residues.[1] It is a substrate for the bacteriolytic enzymes of various origins among which hen egg white lysozyme is known to bind at its active site the substrate, some of the constituent monosaccharide units of which form hydrogen bondings with appropriate portions of the peptide bonds of the enzyme.[2] For a study of the mode of binding between the enzyme and the substrate, it may be interesting to use deoxy-analogues of the substrate as an inhibitor or a model substrate where the definite position of the saccharide is incapable of forming hydrogen bonding. Deoxy-analogues of *N*-acetyl-D-glucosamine are not known except for 6-deoxy-*N*-acetyl-D-glucosamine which was synthesized by Morel[3] and isolated later by Smith[4] from a bacterial polysaccharide. In the following the syntheses of 3-, 4-, 6-deoxy-, and 4,6-dideoxy-*N*-acetyl-D-glucosamine and phenyl glycosides of the former three compounds are described.

Results and Discussion

The routes of the synthesis are shown in Scheme 1 and 2. Partial acetylation of compound II gave compound III in a good yield, and its structure was confirmed by NMR spectrometry. The NMR spectra showed that one OH group (δ 2.87) and three acetyl groups(δ 1.9—2.2) existed. Threatment of II and III with sulfuryl chloride gave the respective chlorodeoxy derivatives. Jennings and Jones reported that 3-chlorodeoxy derivative could not be prepared by the reaction of sulfuryl chloride with alkyl 4,6-*O*-benzylidene-α-glucoside on account of 1,3-diaxial interaction between C-1 axial alkyl group and chloride ion attacking C-3 from an axial direction.[5] The rule held also for the derivatives of *N*-acetyl-glucosaminide, although it had neiboring *trans* acetamide group. Thus, benzyl 2-acetamido-2-deoxy-β-D-glu-

1) M. R. Salton, "The Bacterial Cell Wall," Elsevier Publishing Co., New York, N. Y. (1964).

2) C. C. F. Blake, L. N. Johnson, G. A. Mair, A. C. T. North, D. C. Phillips, and V. R. Sarma, *Proc. Roy. Soc. Ser. B*, **167**, 378 (1967).

3) C. J. Morel, *Helv. Chim. Acta*, **41**, 1501 (1958).

4) E. J. Smith, *J. Biol. Chem.*, **243**, 5139 (1968).

5) H. J. Jennings and J. K. N. Jones, *Can. J. Chem.*, **43**, 2372 (1965).

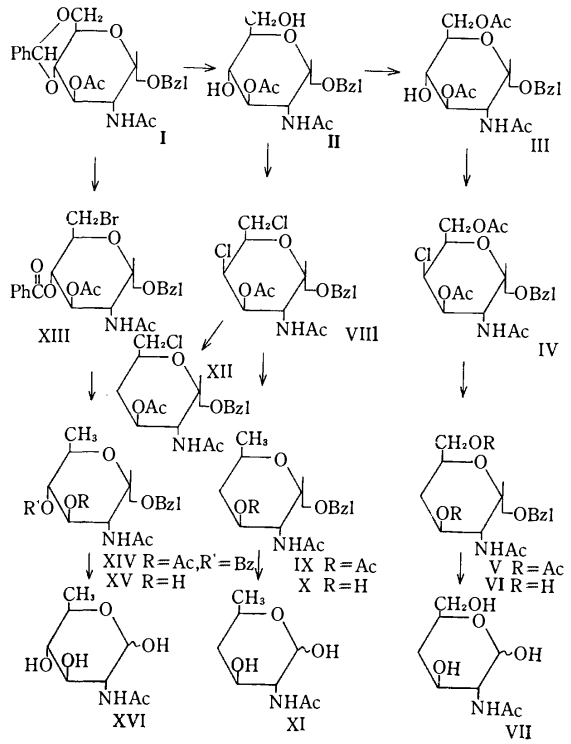

Scheme 1.

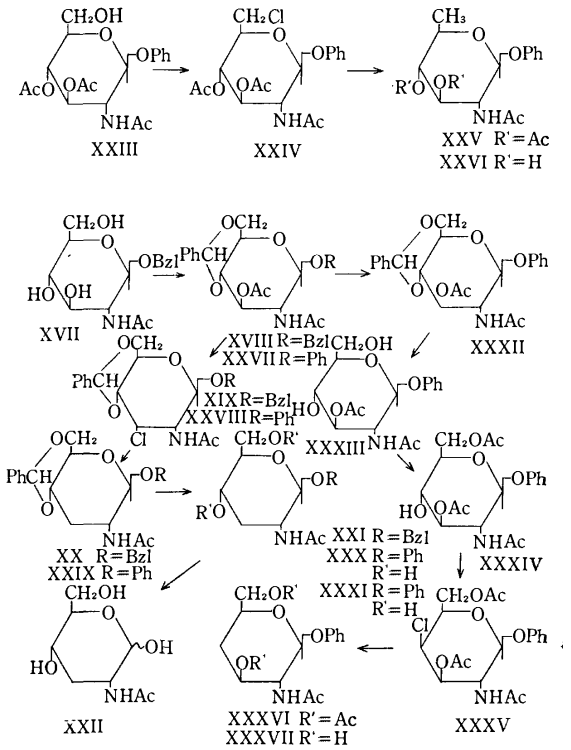

Scheme 2.

copyranoside(XVII) reacted with sulfuryl chloride to give the chlorodeoxy derivative, but benzyl 2-acetamido-2-deoxy-α-D-glucopyranoside did not give the expected product. Hannesian was successful in obtaining 6-bromo-6-deoxy derivative by the cleavage of 4,6-*O*-benzylidene group with *N*-bromosuccinimide (NBS).[6] This reaction was applied for obtaining XIII from I. Reduction of the deoxyhaloderivatives was successfully performed with tri-*n*-butyltin hydride and α,α'-azobisisobutyronitrile(AIBN). Selectivity between primary and secondary halides of the reduction with tri-*n*-butyltin hydride was observed previously.[7] VIII was then selectively reduced at C-4 under appropriate reaction conditions. NMR spectrometry of XII showed that primary halogen was hardly reduced. The structures of the reduced substances were confirmed by NMR spectrometry (Figs. 1 and 2).

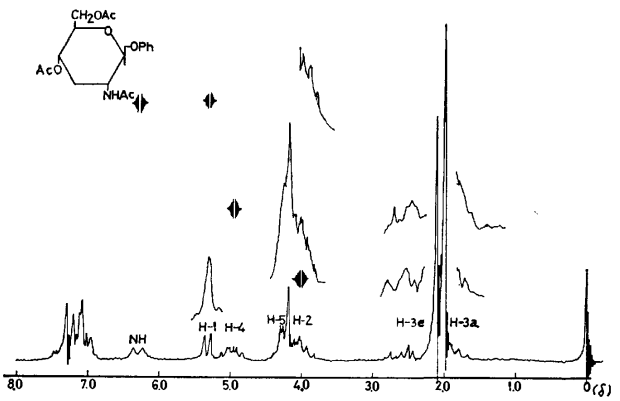

Fig. 1. The NMR spectrum of XXXI in $CDCl_3$.

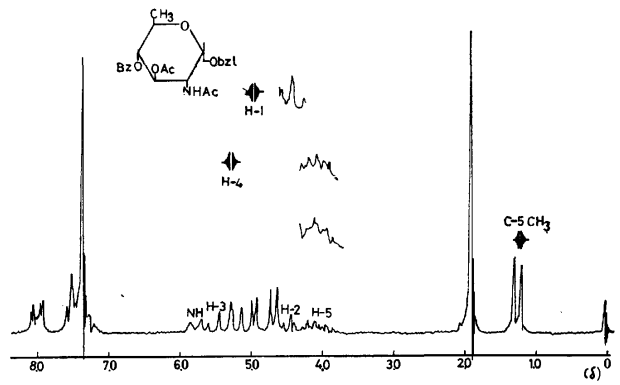

Fig. 2. The NMR spectrum of XIV in $CDCl_3$.

NMR spectra of XIV was assigned as follows. Irradiation at δ 1.20(C-5 CH_3) caused the octet of H-5 at δ 4.10 to collapse to a doublet. Irradiation at δ 5.20(H-4) caused it to collapse to a quartet. Irradiation at δ 4.86(H-1) simplified the region δ 4.35—4.5, which was expected to be H-2 proton signal. NMR spectra of XXXI were assigned as follows. Irradiation at δ 5.0(H-4) simplified the region δ 4.2—4.4 and δ 1.7—2.8. The former was assigned as a H-5 proton signal and the latter as H-3a, H-3e from the irradiation and decoupling data. Irradiation at δ 6.35(NH) and δ 5.35(H-1) simplified the region δ 3.8—4.2, which was expected to be H-2 proton singal. Irradiation at δ 4.10(H-2) caused the doublet of H-1 at δ 5.35 to collapse to a singlet.

6) S. Hannessian, *Carbohyd. Res.*, **2**, 86 (1966).

7) H. Arita, N. Ueda, and Y. Matsushima, This Bulletin, **45**, 567 (1972).

Experimental

General Methods. All the melting points were uncorrected. Nuclear magnetic resonance spectra were recorded with a Varian T-60 spectrometer. The specimens were dissolved in chloroform-d with tetramethylsilane as an internal standard. Thin layer chromatography (tlc) was carried out with Silica gel G(Merck). The spots were detected by spraying with 5% sulfuric acid in methanol and heating. As detection of the 3-deoxy derivatives of *N*-acetyl-D-glucosamine could not be made by this method, they were detected on a plate treated with fluorescein(DC-Fertigplatten Kieselgel F 254). Silica gel column chromatography was carried out with silicic acid (100 mesh, Mallinckrodt) with a solvent system toluene-ethyl acetate(1 : 1) as an eluant. Tri-*n*-butyltin hydride was prepared by the thermal decomposition of tri-*n*-butyltin formate.[8]

Benzyl 2-Acetamido-3-O-acetyl-4,6-O-benzylidene-2-deoxy-α-D-glucopyranoside(I) Benzyl 2-acetamido-4,6-*O*-benzylidene-2-deoxy-α-D-glucopyranoside(20 g)[9] was dissolved in a mixture of pyridine(150 m*l*) and acetic anhydride(20 m*l*). The solution was kept at room temperature overnight. The solvent was evaporated *in vacuo*, and the residual pyridine was removed by co-distillation with dry toluene. Crystallization took place in ethanol, and recrystallization in the same solvent gave colorless needles(18.5 g), mp 215—216°C. Found: C, 65.35; H, 6.08; N, 3.24%. Calcd for $C_{24}H_{27}O_7N$: C, 65.29; H, 6.16; N, 3.17%.

Benzyl 2-Acetamido-3-O-acetyl-2-deoxy-α-D-glucopyranoside(II). Compound I (16.0 g) was dissolved in 80% aqueous acetic acid (600 m*l*) and the solution was kept at 65—70°C for 2 hr. Evaporation of the solvent *in vacuo* gave a syrup. The residual solvent in the syrup was co-distilled several times with dry toluene. The crystals appeared in toluene (9.0 g), mp 113—116°C. Found: C, 57.79; H, 6.51; N, 3.96%. Calcd for $C_{17}H_{23}O_7N$: C, 57.78; H, 6.56; N, 3.93%.

Benzyl 2-Acetamido-3,6-di-O-acetyl-2-deoxy-α-D-glucopyranoside (III) Compound II (15.0 g) was dissolved in a mixture of pyridine(30 m*l*) and chloroform(50 m*l*). The solution was cooled in a dry ice-acetone bath, and acetic anhydride (2.7 m*l*) was added to the solution. The reaction was continued at −20°C for 48 hr. Evaporation *in vacuo* gave a syrup which was subsequently passed through a column of silica gel. The fractions which contained compound III were collected and dried *in vacuo* to give a syrupy product (9.8 g). $[\alpha]_D^{20}$+80° (*c* 1.0, chloroform) Found: C, 59.12; H, 6.42; N, 3.43%. Calcd for $C_{19}H_{25}O_8N$: C, 57.71; H, 6.37; N, 3.54%. NMR (in $CDCl_3$) δ2.87(1H, s, OH) 4.92 (1H, d, *J* 3Hz H-1) 5.85 (1H d, *J* 8Hz NH) 2.12 (3H s, NAc) 1.98(3H s, 3-O-Ac) 2.08(3H s, 6-O-Ac)

Benzyl 2-Acetamido-3,6-di-O-acetyl-4-chloro-2,4-dideoxy-α-D-galactopyranoside(IV). Compound III (9.4 g) was dissolved in pyridine (50 m*l*) and the solution was cooled in an ice-water bath. Sulfuryl chloride(2.4 m*l*) was then added to the solution, and the mixture was kept in a refrigerator overnight and then kept at room temperature for 3 hr. Excess solvent was removed by evaporation *in vacuo*, and the residue was extracted with chloroform and the extract was washed with water several times. The chloroform layer was collected and dried *in vacuo* to a syrup which crystallized in toluene. Recrystallization in the same solvent gave colorless crystals(5.5 g); mp 132—133°C, $[\alpha]_D^{20}$+159° (*c* 1.03, chloroform). Found: C, 55.32; H, 5.85; N, 3.38; Cl, 8.76%. Calcd for $C_{19}H_{24}O_7NCl$: C, 55.14; H, 5.85; N, 3.38; Cl, 8.57%.

Benzyl 2-Acetamido-3,6-di-O-acetyl-2,4-dideoxy-α-D-xylohexopyranoside(V) Compound IV (2.5 g) was dissolved in dry toluene(30 m*l*) under nitrogen atmosphere. To this solution were added tri-*n*-butyltin hydride(3.0 m*l*) and AIBN (*ca.* 30 mg). The reaction was continued for 2 hr at 80—90°C under stirring. The solution was dried *in vacuo* to give a syrup, which was passed through a column of silica gel with a solvent system (toluene-ethyl acetate 1 : 1) as an eluant. The product was crystallized in ethanol. Recrystallization in the same solvent gave needles(1.9 g); mp 105—107°C, $[\alpha]_D^{20}$+101° (*c* 0.87, chloroform). Found: C, 59.80; H, 6.59; N, 3.63%. Calcd for $C_{15}H_{21}O_5N$: C, 60.14; H, 6.64; N, 3.63%. NMR (in $CDCl_3$) δ4.93 (1H d, *J* 3 Hz H-1) 5.70 (1H d, NH) 1.4—2.1(H-4a,e) 2.05 (3H s, NAc) 1.95 (3H s, 6-OAc) 1.84(3H s, 3-OAc).

Benzyl 2-Acetamido-2,4-dideoxy-α-D-xylohexopyranoside (VI). Compound V(1.23 g) was deacetylated with 0.1 M sodium methoxide in methanol, and the solution was treated with Dowex 50×8 (H^+) to remove sodium ion. Evaporation of methanol *in vacuo* gave crystals, which were recrystallized in ethanol giving 700 mg of a colorless specimen. Mp 170.5—171°C. Found: C, 60.87; H, 7.16; N, 4.68%. Calcd for $C_{15}H_{21}O_5N$: C, 61.00; H, 7.17; N, 4.74%.

2-Acetamido-2,4-dideoxy-D-xylohexopyranose (VII). Compound VI (650 mg) was dissolved in ethanol (50 m*l*) and 10% palladium on charcoal (2.0 g) was added to the solution. Hydrogen was passed through the solution for three days at room temperature. The charcoal was filtered off, and the filtrate was dried *in vacuo* to give 300 mg of a syrup which did not crystallize. $[\alpha]_D^{20}$+78° (*c* 1.58, water). Found: C, 46.71; H, 7.43; N, 6.57%. Calcd for $C_8H_{15}O_5N$: C, 46.82; H, 7.37; N, 6.83%.

Benzyl 2-Acetamido-3-O-acetyl-4,6-dichloro-2,4,6-trideoxy-α-D-galactopyranoside (VIII). Compound II (4.0 g) was dissolved in pyridine (30 m*l*) and the solution was cooled in an ice-water bath. Sulfuryl chloride(2.3 m*l*) was then added dropwise to the solution. The reaction solution was kept in a refrigerator overnight and then kept at room temperature for 3 hr. Excess pyridine was removed by evaporation. The residue was extracted with chloroform and the extract washed with water several times. The chloroform layer was dried *in vacuo*. The residue was extracted with boiling toluene several times, and the extracts were dried *in vacuo*. Recrystallization in ethanol gave colorless needles(2.8 g); mp 158—160°C, $[\alpha]_D^{20}$+128° (*c* 1.0, chloroform). Found: C, 52.49; H, 5.44; N, 3.61; Cl, 18.13%. Calcd for $C_{17}H_{21}O_5NCl_2$: C, 52.32; H, 5.42; N, 3.59; Cl, 18.17%. NMR (in $CDCl_3$) δ4.93 (1H, d, *J* 3 Hz H-1)) 5.70 (1H d, NH) 2.05 (3H s, NAc) 1.87 (3H s, 3-O-Ac)

Benzyl 2-Acetamido-3-O-acetyl-2,4,6-trideoxy-α-D-xylohexopyranoside (IX). Compound VIII (1.8 g) was dissolved in dry toluene (30 m*l*) under nitrogen atmosphere. To this solution was added tri-*n*-butyltin hydride (2.0 m*l*) and AIBN (*ca.* 20 mg). The reaction mixture was refluxed for 24 hr. The solution was then dried *in vacuo*. The residual sirup was dissolved in ligroin (10 m*l*) and the solution was kept in a refrigerator overnight. Crystals were obtained and washed with cold ligroin and recrystallized in the same solvent giving 1.5 g of the specimen. Mp 122—123°C, $[\alpha]_D^{20}$+106° (*c* 1.15, chloroform). Found: C, 62.18; H, 7.06; N, 4.29%. Calcd for $C_{17}H_{23}O_5N$: C, 63.53; H, 7.21; N, 4.36%. NMR (in $CDCl_3$) δ4.93 (1H d, *J* 3 Hz H-1) 1.75—2.2 (1H H-4e) 1.3—1.6 (1H H-4a) 3.7—4.1 (1H m, H-5) 5.83 (1H d, NH) 2.0 (3H s, NAc) 1.9 (3H 3-O-Ac) 1.28 (3H d, *J* 6 Hz CH_3-5).

8) R. Okawara and M. Ohara, *J. Organometal. Chem.*, **3**, 484 (1965).

9) R. Kuhn, H. H. Baer, and A. Seeliger, *Ann.*, **611**, 236 (1958).

Benzyl 2-Acetamido-2,4,6-trideoxy-D-xylohexopyranoside (X). Compound IX (500 mg) was deacetylated with *ca.* 0.1 M sodium methoxide in methanol by the same manner as described for VI. Recrystallization in ethanol gave colorless crystals; mp 183—185°C, $[\alpha]_D^{20}+107°$ (*c* 1.03, methanol). Found: C, 63.96; H, 7.56; N, 4.98%. Calcd for $C_{15}H_{24}O_4N$: C, 64.49; H, 7.58; N, 5.01%.

2-Acetamido-2,4,6-trideoxy-xylohexopyranose (XI). Compound X (300 mg) in 2-propanol (50 ml) was reduced with hydrogen over 10% palladium on charcoal (1.5 g) at room temperature. The reaction was complete within 20 hr and charcoal was filtered off, the filtrate being dried *in vacuo*. Crystallization took place in ethanol-ethyl acetate, and recrystallization in the same solvent gave colorless needles; mp 147—150°C, $[\alpha]_D^{20}+88°$ (*c* 0.43, water). Found: C, 47.17; H, 8.07; N, 6.82%. Calcd for $C_8H_{15}O_4N\cdot H_2O$: C, 46.37; H, 8.27; N, 6.76%.

Benzyl 2-Acetamido-3-O-acetyl-6-chloro-2,4,6-trideoxy-α-D-xylohexopyranoside (XII). Compound VIII (1.3 g) was dissolved in dry toluene (30 ml) under nitrogen atmosphere, and to the solution were added tri-*n*-butyltin hydride (1 ml) and AIBN. The reaction was continued for 1 hr at 80—90°C under stirring. Evaporation *in vacuo* gave a product which was washed with cold ligroin several times. Recrystallization in ethanol gave colorless needles (800 mg); mp 121—126°C, $[\alpha]_D^{20}+136°$ (*c* 1.0, chloroform). Found: C, 58.27; H, 6.32; N, 4.04; Cl, 8.83%. Calcd for $C_{17}H_{22}O_5NCl$: C, 57.55; H, 6.25; N, 3.95; Cl, 9.71%.

Benzyl 2-Acetamido-3-O-acetyl-4-O-benzoyl-6-bromo-2,6-dideoxy-α-D-glucopyranoside (XIII). Compound I (5.0 g) was dissolved in a mixture of carbon tetrachloride (100 ml) and tetrachloroethane (40 ml). To this solution were added NBS (2.25 g) and barium carbonate (10 g). The reaction mixture was refluxed for 1.5 hr. Insoluble substances were filtered off, the brown filtrate was extracted with chloroform and the extract washed with water several times. The solvent was evaporated *in vacuo* to a syrup. The product was found in tlc to be contaminated with the starting material (compound I). The syrup was thus treated with 80% aqueous acetic acid at 70°C for 2 hr to remove benzylidene group from the remaining compound I. Evaporation *in vacuo* gave a syrup, which was subsequently placed on a silica gel column and eluated with a solvent system (ethyl-acetate–toluene 1 : 1). The product (1.4 g) did not crystallize, although it was shown on tlc to be highly pure. $[\alpha]_D^{20}+27°$ (*c* 0.99, chloroform). Found: C, 55.77; H, 5.26; Br, 13.71%. Calcd for $C_{24}H_{26}O_7NBr$: C, 55.41; H, 5.04; Br, 15.36%.

Benzyl 2-Acetamido-3-O-acetyl-4-O-benzoyl-2,6-dideoxy-α-D-glucopyranoside (XIV). Compound XIII (800 mg) was dissolved in dry toluene under nitrogen atmosphere, and to this solution were added tri-*n*-butyltin hydride (1 ml) and AIBN (*ca.* 20 mg). The reaction mixture was refluxed overnight, and the solution was dried in vacuo. The residual syrup was dissolved in ligroin (5 ml) and the solution was kept in a refrigerator overnight. Crystals were obtained and were washed with cold ligroin several times. Purity of the crystals did not improve by recrystallization, and they were subjected to silica gel column chromatography. Colorless crystals were obtained (440 mg); mp 144—146°C, $[\alpha]_D^{20}+57°$ (*c* 0.90, chloroform). Found: C, 65.49; H, 6.23; N, 3.23%. Calcd for $C_{24}H_{27}O_7N$: C, 65.29; H, 6.16; N, 3.17%. NMR (in $CDCl_3$) δ 4.86 (1H d, *J* 3 Hz H-1) 4.3—4.5 (1H unresolved H-2) 5.4 (1H unresolved H-3) 5.3 (H-4) 4.1 (H-5) 1.20 (3H d, *J* 6 Hz CH_3-5) 1.88 (3H s, NAc) 1.88 (3H s, 3-OAc) 5.78 (1H d, NH)

2-Acetamido-2,6-dideoxy-glucopyranose (XVI). Compound XIV (400 mg) was treated with *ca.* 0.1 M sodium methoxide in methanol, and the solution was neutralized with acetic acid. Ten percent palladium on charcoal (1.0 g) was added to this solution, and hydrogen was led in for 24 hr at room temperature. The charcoal was filtered off, and the filtrate was passed through a column of Dowex 50X 8 (H^+). The eluant was dried *in vacuo*, and the residue crystallized immediately; mp 207—210°C, $[\alpha]_D^{20}+26.4°$ (*c* 1.0, water). Found: C, 47.01; H, 7.42; N, 6.76%. Calcd for $C_8H_{15}O_5N$: C, 46.82; H, 7.37; N, 6.83%. NMR (in D_2O) δ5.05 (1H d, *J* 3 Hz H-1) 1.25 (3H d, *J* 6 Hz CH_3-5) 2.0 (3H s, NAc)

Benzyl 2-Acetamido-2-Deoxy-β-D-glucopyranoside (XVII).[10] Pentaacetyl glucosamine (20.0 g) was dissolved in glacial acetic acid saturated with HBr (100 ml) and the solution was kept at room temperature overnight under stirring. The solution was extracted with chloroform and the extract was washed with water and aqueous sodium bicarbonate several times.[11] The chloroform layer was dried over sodium sulfate. To this solution was added benzyl alcohol (15 ml), Drierite (20 g) and silver carbonate (15 g), and the mixture was kept at room temperature in the dark under vigorous stirring. The insoluble substances were filtered off, and the filtrate was dried *in vacuo* to a syrup. Crystallization took place in ethanol. Recrystallization in the same solvent gave colorless needles (12.5 g); mp 162—164°C, $[\alpha]_D^{20}-54°$ (*c* 1.23, chloroform). The specimen was subsequently deacetylated with *ca.* 0.1 M sodium methoxide in methanol. Recrystallization in 2-propanol gave colorless needles (6.5 g); mp 191—192°C $[\alpha]_D^{20}-29°$ (*c* 0.93, water). Found: C, 57.83; H, 6.80; N, 4.52%. Calcd for $C_{15}H_{21}O_6N$: C, 57.86; H, 6.80; N, 4.50%.

Benzyl 2-Acetamido-4,6-O-benzylidene-2-deoxy-β-D-glucopyranoside (XVIII). Compound XVII (6.5 g) was mixed with benzaldehyde (50 ml). To this was added zinc chloride (6.5 g), and the mixture was shaken at room temperature overnight. The homogeneous solution thus obtained was poured into ice-water and the precipitates were washed with water and ligroin several times. Recrystallization in ethanol gave a crystalline product (6.7 g) which decomposed over 200°C. Found: C, 63.13; H, 6.64; N, 3.59%. Calcd for $C_{22}H_{25}O_6N$: C, 66.15; H, 6.31; N, 3.51%. Though the specimen was crystalline, its benzylidene residue gradually split for some unknown reason even in the solid state. As a result the analytical value of carbon was far less than the theoretical one.

Benzyl 2-Acetamido-3-chloro-4,6-O-benzylidene-2,3-dideoxy-β-D-allopyranoside (XIX). Compound XVIII (6.0 g) was dissolved in pyridine (150 ml) and the solution was cooled in an ice-water bath. Sulfuryl chloride (1.6 ml) was added to the solution, and the reaction mixture was kept in a refrigerator for 2 hr and then at room temperature overnight. Excess pyridine was removed by evaporation. The residue was extracted with chloroform and the extract was washed with water several times. The chloroform layer was dried *in vacuo* to a syrup, which was immediately crystallized in ethanol. Recrystallization in the same solvent gave colorless crystals (2.0 g); mp 205°C (decomp.), $[\alpha]_D^{20}-87°$ (*c* 0.87, chloroform). Found: C, 63.38; H, 5.85; N, 3.39; Cl, 8.17%. Calcd for $C_{22}H_{24}O_5NCl$: C, 63.23; H, 5.79; N, 3.35; Cl, 8.48%.

Benzyl 2-Acetamido-4,6-O-benzylidene-2,3-dideoxy-β-D-ribo-hexopyranoside (XX). Compound XIX (700 mg) was dissolved in dry toluene under nitrogen atmosphere. To this solution were added tri-*n*-butyltin hydride (1.0 ml) and

10) R. Kuhn and W. Kirschenlohr, *Chem. Ber.*, **86**, 1331 (1953).
11) Y. Inouye, K. Onodera, S. Kitaoka, and H. Ochiai, *J. Amer. Chem. Soc.*, **79**, 4218 (1957).

AIBN (*ca.* 20 mg). The reaction was complete within 15 min, and the product obtained immediately as white needles was collected and washed with ligroin several times. Recrystallization in methanol gave colorless needles (620 mg); mp 246°C (decomp.) Found: C, 68.73; H, 6.59; N, 3.72%. Calcd for $C_{22}H_{25}O_5N$: C, 68.91; H, 6.57; N, 3.65%.

2-Acetamido-2,3-dideoxy-ribohexopyranose (XXII). Compound XX (50 mg) was dissolved in 80% aqueous acetic acid (300 ml) and the solution was kept at 65—70°C for 2 hr. The clear solution was evaporated *in vacuo* to a syrup, which was dissolved in cold water (5 ml). Insoluble substances were filtered off. To the filtrate was added 10% palladium on charcoal (1.5 g) and hydrogen was passed into the solution at room temperature. The reduction was complete within 24 hr, and charcoal was removed. The filtrate was dried *in vacuo* to a syrup, which did not crystallize. $[\alpha]_D^{20}$ −6.5° (*c* 2.15, H_2O). Found: C, 45.36; H, 7.32; N, 6.73; Calcd for $C_8H_{15}O_5N$: C, 46.82; H, 7.37; N, 6.83.

Phenyl 2-Acetamido-3,4-di-O-acetyl-2-deoxy-β-D-glucopyranoside (XXIII). Compound XXIII was prepared from phenyl 2-acetamido-6-*O*-trityl-3,4-di-*O*-acetyl-2-deoxy-β-D-glucopyranoside according to the method of Mega *et al.*[12] Mp 228—229°C $[\alpha]_D$ −10.8° (*c* 0.5, chloroform).

Phenyl 2-Acetamido-3,4-di-O-acetyl-6-chloro-2,6-dideoxy-β-D-glucopyranoside (XXIV). Compound XXIII (2.0 g) was dissolved in pyridine (20 ml) and the solution was cooled in an ice-water bath. To this solution was added sulfuryl chloride (0.56 ml) and the reaction mixture was kept in a refrigerator overnight and then at room temperature for 3 hr. Excess pyridine was removed by evaporation *in vacuo*, and the residue was extracted with chloroform and the extract washed with water several times. Chloroform layer was dried *in vacuo* to a syrup. The syrup crystallized in ethanol, and recrystallization in the same solvent gave colorless needles; (800 mg); mp 190°C (decomp.), $[\alpha]_D^{20}$ −15° (*c* 0.93, chloroform). Found: C, 53.55; H, 5.55; N, 3.53; Cl, 8.71%. Calcd for $C_{18}H_{22}O_7NCl$: C, 54.07; H, 5.55; N, 3.50; Cl, 8.87%.

Phenyl 2-Acetamido-3,4-di-O-acetyl-2,6-dideoxy-β-D-glucopyranoside (XXV). Compound XXIV (750 mg) was dissolved in dry toluene (50 ml). To this were added tri-*n*-butyltin hydride (0.8 ml) and AIBN (*ca.* 20 mg). The reaction was continued overnight at 80—90°C with stirring. The solvent was evaporated *in vacuo* to a syrup, which crystallized immediately. Recrystallization in ethanol gave a colorless product (700 mg); mp 200°C (decomp.), $[\alpha]_D^{20}$ +48° (*c* 1.03, chloroform). Found: C, 58.08; H, 6.23; N, 3.68%. Calcd for $C_{18}H_{23}O_7N$: C, 59.18; H, 6.33; N, 3.83%.

Phenyl 2-Acetamido-2,6-dideoxy-β-D-glucopyranoside (XXVI). Compound XXV (510 mg) was deacetylated with sodium methoxide by the same method as described for VI. Recrystallization in 2-propanol gave colorless needles (1.34 mg); mp 210°C (decomp.), $[\alpha]_D^{20}$ −16° (*c* 0.7, methanol). Found: C, 58.31; H, 6.53; N, 4.96%. Calcd for $C_{14}H_{19}O_5N$: C, 58.77; H, 6.81; N, 4.98%.

Phenyl 2-Acetamido-4,6-O-benzylidene-2-deoxy-β-D-glucopyranoside (XXVII).[13] Phenyl 2-acetamido-2-deoxy-β-D-glucopyranoside (5.0 g)[14] was reacted with benzaldehyde (30 ml) and zinc chloride (5.0 g) at room temperature overnight. The solution was poured into ice-water and the precipitates were washed with water and ligroin several times. Recrystallization in ethanol gave colorless needles (5.5 g) which decomposed at 250°C. Found: C, 65.32; H, 6.00; N, 3.61%. Calcd for $C_{21}H_{23}O_6N$: C, 65.44; H, 6.02; N, 3.63%.

Phenyl 2-Acetamido-3-chloro-4,6-O-benzylidene-2,3-dideoxy-β-D-allopyranoside (XXVIII). Compound XXVII (4.0 g) was dissolved in pyridine (150 ml). To this solution was added sulfuryl chloride (1.0 ml) under cooling in an ice-water bath. The reaction solution was kept in a refrigerator overnight and then at room temperature for 10 hr. The solvent was removed by evaporation *in vacuo* and the residue was extracted with chloroform and the extract washed with water several times. The chloroform layer was separated and dried *in vacuo*, and the residue was crystallized in methanol–water (4 : 1). Recrystallization in the same solvent mixture gave colorless needles (1.2 g); mp 184°C (decomp.), $[\alpha]_D^{20}$ −24° (*c* 1.0, chloroform). Found: C, 62.20; H, 5.50; N, 3.49; Cl, 8.85. Calcd for $C_{21}H_{22}O_5NCl$: C, 62.45; H, 5.49; N, 3.47; Cl, 8.87.

Phenyl 2-Acetamido-4,6-O-benzylidene-2,3-dideoxy-β-D-ribohexopyranoside (XXIX). Compound XXVIII (516 mg) was dissolved in dry toluene (100 ml). To the solution were added tri-*n*-butyltin hydride (0.5 ml) and AIBN (*ca.* 20 mg) at 90°C under stirring. The reaction was complete within 10 min. White precipitates were obtained and were filtered off and washed with ligroin several times. Recrystallization in methanol gave colorless needles (476 mg); mp 250°C. Found: C, 67.46; H, 6.24; N, 3.75%. Calcd for $C_{21}H_{23}O_5N$: C, 68.28; H, 6.28; N, 3.79%.

Phenyl 2-Acetamido-2,3-dideoxy-β-D-ribohexopyranoside (XXX). Compound XXIX (470 mg) was dissolved in 80% aqueous acetic acid (300 ml) and the solution was kept at 65—70°C for 2 hr. The solution was evaporated *in vacuo*, and the residual syrup was dissolved in water (5 ml). Insoluble substances were removed by filtration, and the filtrate was dried *in vacuo*. Crystallization took place in 2-propanol. Recrystallization in the same solvent gave colorless needles (170 mg); mp 178—180°C, $[\alpha]_D^{20}$ −33° (*c* 0.8, methanol). Found: C, 59.06; H, 6.80; N, 4.91%. Calcd for $C_{14}H_{19}O_5N$: C, 59.77; H, 6.81; N, 4.98%.

Phenyl 2-Acetamido-4,6-di-O-acetyl-2,3-dideoxy-β-D-ribohexopyranoside (XXXI). Compound XXX (50 mg) was dissolved in a mixture of pyridine (5.0 ml) and acetic anhydride (2.5 ml), and the solution was kept at room temperature overnight. Evaporation *in vacuo* gave a syrup, and the contaminating reagents were co-distilled with toluene. Crystallization took place in ethanol. Recrystallization in the same solvent gave colorless needles (43 mg); mp 138—139°C. Found: C, 58.62; H, 6.33; N, 3.89%. Calcd for $C_{18}H_{23}O_7N$: C, 59.18; H, 6.33; N, 3.83%. NMR (in $CDCl_3$) δ5.32 (1H d, *J* 7 Hz H-1) 4.00 (1H unresolved H-2) 2.50 (1H unresolved H-3e) 1.80 (1H unresolved H-3a) 4.95 (1H octet H-4) 2.15 (3H s, NAc) 2.00 (6H s, OAc) 6.25 (1H d, NH).

Phenyl 2-Acetamido-3-O-acetyl-4,6-O-benzylidene-2-deoxy-β-D-glucopyranoside (XXXII). Compound XXVII (5.0 g) was acetylated with acetic anhydride (10 ml) in pyridine (200 ml). Recrystallization in ethanol gave colorless needles (5.0 g). Found: C, 63.91; H, 5.71; N, 3.27%. Calcd for $C_{23}H_{25}O_7N$: C, 64.62; H, 5.90; N, 3.28%.

Phenyl 2-Acetamido-3-O-acetyl-2-deoxy-β-D-glucopyranoside (XXXIII). Compound XXXII (5.0 g) was dissolved in hot glacial acetic acid (500 ml). To this solution was added water (100 ml) dropwise under shaking in a water bath kept at 65°C. The reaction was continued for 2 hr at 65—70°C. Evaporation of the solvent *in vacuo* gave crystals which were washed with ether several times. Recrystallization in ether gave white powder (3.5 g). Found: C, 56.53; H, 6.21; N, 4.10%. Calcd for $C_{16}H_{21}O_7N$: C,

12) T. Mega, T. Ikenaka, and Y. Matsushima, *J. Biochem.*, **71**, 107 (1972).
13) D. H. Leaback and P. G. Walker, *J. Chem. Soc.*, **1957**, 4754.
14) K. Yamamoto, M. Fujinaga, and Y. Matsushima, This Bulletin, **36**, 1275 (1963).

56.63; H, 6.24; N, 4.13%.

Phenyl 2-Acetamido-3,6-di-O-acetyl-2-deoxy-β-D-glucopyranoside (XXXIV). Compound XXXIII (3.0 g) was dissolved in a mixture of pyridine (20 ml) and chloroform (10 ml), and the solution was cooled in a dry ice-acetone bath. Acetic anhydride (0.93 ml) was then added to the solution, and the reaction mixture was kept at −20°C for 48 hr. The solvent was evaporated *in vacuo*, and the residual syrup was crystallized in 2-propanol. Recrystallization in the same solvent gave colorless crystals (2.2 g); mp 180—185°C, $[\alpha]_D^{20}$ −22° (*c* 1.2, chloroform). Found: C, 56.59; H, 6.30; N, 3.62%. Calcd for $C_{18}H_{23}O_8N$: C, 56.68; H, 6.08; N, 3.67%.

Phenyl 2-Acetamido-3,6-di-O-acetyl-4-chloro-2,4-dideoxy-β-D-galactopyranoside (XXXV). Compound XXXIV (1.5 g) was dissolved in pyridine (20 ml). To this solution was added sulfuryl chloride (0.45 ml). The reaction solution was kept in a refrigerator overnight and then at room temperature for 3 hr. Excess pyridine was removed by evaporation *in vacuo*, and the residue was extracted with chloroform and the extract was washed with water several times. Chloroform was evaporated *in vacuo*. Crystals appeared in 2-propanol, and recrystallization in the same solvent gave colorless needles (1.1 g); mp 216°C (decomp.), $[\alpha]_D^{20}$ +21° (*c* 1.25, chloroform). Found: C, 54.05; H, 5.53; N, 3.54; Cl, 9.22. Calcd for $C_{18}H_{22}O_7NCl$: C, 54.07; H, 5.54; N, 3.50; Cl, 8.87.

Phenyl 2-Acetamido-3,6-di-O-acetyl-2,4-dideoxy-β-D-xylohexopyranoside (XXXVI). Compound XXXV (500 mg) was dissolved in toluene (20 ml) and reacted with tri-*n*-butyltin hydride (0.5 ml) in the presence of AIBN (*ca.* 20 mg) at 80—90°C for 2 hr. Crystals were obtained on evaporation of the solvent *in vacuo*. Recrystallization in 2-propanol gave colorless needles (300 mg); mp 168.5—170°C, $[\alpha]_D^{20}$ −47° (*c* 0.57, chloroform). Found: C, 59.07; H, 6.29; N, 3.92%. Calcd for $C_{18}H_{23}O_7N$: C, 59.17; H, 6.34; N, 3.83%.

Phenyl 2-Acetamido-2,4-dideoxy-β-D-xylohexopyranoside (XXXVII). Compound XXXVI (200 mg) was deacetylated with sodium methoxide in methanol. Recrystallization in water gave colorless needles (80 mg); mp 201—203°C, $[\alpha]_D^{18}$ −6.5° (*c* 0.65, water). Found: C, 59.71; H, 6.78; N, 4.92%. Calcd for $C_{14}H_{19}O_5N$: C, 59.77; H, 6.81; N, 4.98%.

BULLETIN OF THE CHEMICAL SOCIETY OF JAPAN, VOL. 45, 3619—3624 (1972)

Studies on Aminosugars. XXXI. Synthesis of 3,4-Dideoxy-3-enosides and the Corresponding 3,4-Dideoxysugars[1)]

Sumio UMEZAWA, Yasushi OKAZAKI, and Tsutomu TSUCHIYA

Department of Applied Chemistry, Faculty of Engineering, Keio University, Hiyoshi-cho, Kohoku-ku, Yokohama

(Received May 11, 1972)

As model experiments to prepare unsaturated and deoxy variants of complex aminoglycosidic antibiotics, methyl 3,4-dideoxy-α-D-*erythro*-hexopyranoside (**8**) and methyl 2,6-diamino-2,3,4,6-tetradeoxy-α-D-*erythro*-hexopyranoside (**15**) have been synthesized through the corresponding 3,4-unsaturated glycosides (**6**, **12**), which were prepared from the corresponding 3,4-di-*O*-mesyl derivatives (**5**, **11**) by treatment with sodium iodide and zinc dust in high yields. These are rare examples of 3,4-dideoxy and 3,4-unsaturated sugars.

Unsaturated sugars are drawing attention in recent years from biological point of view. However, 3,4-unsaturated sugars were rarely reported. Recently, we described the synthesis of 3′,4′-dideoxykanamycin B[2)] which is active against drug-resistant bacteria, by utilizing a 3,4-unsaturated intermediate. The present synthesis was undertaken as a fundamental experiment to see if a practical method could be worked out for converting aminoglycosidic antibiotics into their unsaturated and dehydroxylated derivatives.

Cyclic sugars having one double bond and no substituents on the unsaturated carbons can be classified into four groups, namely, 1,2- (glycals), 2,3-, 3,4- (in pyranoses) and 5,6-double bonded (in furanoses) sugars. Among them, glycals are most popular and 2,3-dideoxy-2-enoses are prepared mostly by the double bond migration of glycals. Terminal 5-enoses are also prepared fairly easily from mother sugars by applying the methods adopted to open-chain sugars. In order to introduce 2,3-unsaturation into cyclic sugars 2,3-epoxide,[3)] 2,3-episulfide,[4)] 2,3-epimine,[5)] 2,3-iodotosylates,[6)] azidotosylate,[7)] 2,3-iodoacetates,[8)] 2,3-iodohydrin,[9)] 2,3-carbonate,[10)] 2,3-thionocarbonate,[11)] 2,3-disulfonates[11)] and compounds having a deoxy group at 2 or 3 position[12)] are utilized as an intermediate.

1) A part of this paper was read by S. Umezawa at New Natural Product Syntheses, the 23rd International Congress of Pure and Applied Chemistry at Boston, U. S. A., July 28, 1971. Short communication: S. Umezawa, T. Tsuchiya, and Y. Okazaki, This Bulletin, **44**, 3494 (1971).

2) H. Umezawa, S. Umezawa, T. Tsuchiya, and Y. Okazaki, *J. Antibiot.* (Tokyo), **24**, 485 (1971).

3) D. Horton and W. N. Turner, *Tetrahedron Lett.*, **1964**, 2531.

4) J. E. Christensen and L. Goodman, *J. Amer. Chem. Soc.*, **83**, 3827 (1961).

5) R. D. Guthrie and D. King, *Carbohyd. Res.*, **3**, 128 (1966).

6) F. H. Newth, *J. Chem. Soc.*, **1956**, 471; R. U. Lemieux, E. Fraga, and K. A. Watanabe, *Can. J. Chem.*, **46**, 61 (1968).

7) R. D. Guthrie, R. D. Well, and G. J. Williams, *Carbohyd. Res.*, **10**, 172 (1969).

8) A. Rosenthal and J. N. C. Whyte, *Can. J. Chem.*, **46**, 2245 (1968).

9) S. Hanessian and N. R. Plessas, *J. Org. Chem.*, **34**, 2163 (1969).

10) A. Klemer and G. Mersmann, *Carbohyd. Res.*, **12**, 219 (1970).

11) E. Albano, D. Horton, and T. Tsuchiya, *ibid*, **2**, 349 (1966).

12) H. R. Bolliger and D. A. Prins, *Helv. Chim. Acta*, **29**, 1061 (1946); R. J. Ferrier, *J. Chem. Soc.*, **1964**, 5443.

As for the examples of 3,4-unsaturated sugars, Bock and Pedersen[13] prepared a 3,4-dideoxy-3-enopyranoside by reduction of the corresponding 3,4-dideoxy-3-eno-2-keto precursor which was prepared by double bond migration of a glycal. Ferrier and Vethaviyaser[14] prepared 3,4-dideoxy-3-enopyranosides by 1,3-azido or 1,3-thiocyano migration of the corresponding 2,3-unsaturated precursors. Hains[15] prepared benzyl 2-*O*-benzyl-3,4-dideoxy-3-eno-α-D-*glycero*-pentoside from benzyl 2-*O*-benzyl-β-L-arabinopyranoside 3,4-thionocarbonate by utilizing Corey-Winter method.[16] In this paper, we wish to describe the syntheses of the 2,6-di-*O*-benzoyl derivative (**6**) of methyl 3,4-dideoxy-α-D-*erythro*-hex-3-enopyranoside, methyl 2,6-diamino-2,3,4,6-tetradeoxy-α-D-*erythro*-hex-3-enopyranoside (**13**) and their hydrogenation products, namely, methyl 3,4-dideoxy-α-D-*erythro*-hexopyranoside (**8**) and methyl 2,6-diamino-2,3,4,6-tetradeoxy-α-D-*erythro*-hexopyranoside (**15**).

We intended to prepare some unsaturated and deoxy derivatives of 2,6-diamino-2,6-dideoxy-D-glycose because an appreciable number of useful antibiotics (kanamycin B,[17] neomycin B, C, vistamycin, butyrosin A, B *etc.*) contain the sugar as one of their constituents. Since the deoxy derivatives of aminosugars are rarely known, we initiated the synthesis of an unsaturated derivative of methyl α-D-galactopyranoside (**1**) as a model experiment, taking into consideration the presence of 3,4-*cis*-diol group in it.

Methyl 3,4-*O*-isopropylidene-α-D-galactopyranoside (**2**) prepared from **1** in a high yield was benzoylated and the isopropylidene group of the di-*O*-benzoyl derivative (**3**) was removed by 75% acetic acid to yield methyl 2,6-di-*O*-benzoyl-α-D-galactopyranoside (**4**) quantitatively.

Tipson-Cohen method,[18] which utilized vicinal disulfonic ester groups for making an unsaturated bond was then applied to this product, because the method had been proved to be applicable to cyclic sugars having *trans*-diequatorial sulfonyloxy groups by Horton *et al.*[11] Mesylation of **4**, giving a di-*O*-mesyl derivative (**5**) was followed by treatment with sodium iodide and zinc dust at 130—150°C for 1.5 hr in DMF to give a 3,4-unsaturated derivative, namely, methyl 2,6-di-*O*-benzoyl-3,4-dideoxy-α-D-*erythro*-hex-3-enopyranoside (**6**) in a yield of 93%, syrup, $[\alpha]_D^{22}$ −17.3° (*c* 1, chloroform). The high yield is noteworthy in contrast with that (~50%) from[11] methyl 4,6-*O*-benzylidene-2,3-di-*O*-sulfonyl-α-D-glucopyranosides, and may suggest that the initial nucleophilic attack of iodide ion might occur at C-4 of **5** much more easily[19] than that at C-3 or C-2 of the above-mentioned sugar

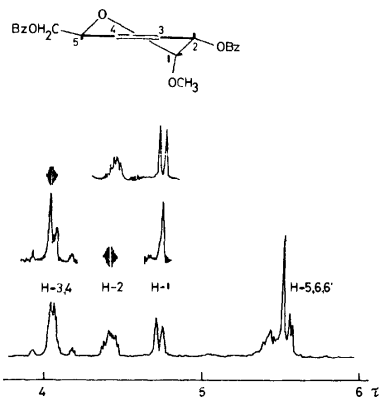

Fig. 1. The NMR spectrum of **6** in $CDCl_3$ at 100 MHz.

derivatives, though details of the mechanism of the reaction remain equivocal. The structure of **6**, was confirmed by the NMR spectrum (Fig. 1); Irradiation of a multiplet at τ 4.42 caused the H-1 doublet (τ 4.73, J~4 Hz) to collapse to a singlet, and consequently it was assigned to H-2. At the same time, 2-proton deformed AB quartet centered at τ 4.06 was assigned to double bond protons at C-3 and 4; the τ-value and the signal pattern ($J_{3,4}$~11 Hz) agreed with the structure. Irradiation of H-3,4 caused H-2 multiplet to collapse to a quartet ($J_{1,2}$ 4 Hz and ~2.5 Hz), the latter coupling being assigned to $J_{2,5}$. The magnitude of this homoallylic coupling[20] showed that H-2 and 5 stand nearly axially to the plane including the C_2–C_3=C_4–C_5 bond and the result shows that **6** is a derivative having 3,4-unsaturated α-D-*erythro* structure in the half-chair conformation. The conformation is reasonable also in view of anomeric effect.

Compound **6** was hydrogenated in an usual manner to give a 3,4-dideoxy derivative (**7**).[21] In its NMR spectrum, a 4-proton multiplet appeared at τ 7.6—8.5, indicating the presence of a ethylene protons. Removal of the protecting groups from **7** gave methyl 3,4-dideoxy-α-D-*erythro*-hexopyranoside (**8**), $[\alpha]_D^{22}$+126° (*c* 1.1, water)

Next, an analogous sequence of reactions were applied to methyl 2,6-dideoxy-2,6-dimethoxycarbonylamino-α-D-glucopyranoside (**10**) which was prepared by methanolysis of tetra-*N*-methoxycarbonylneamine (**9**), and the di-*O*-mesyl derivative (**11**) of **10** was treated likewise as described in the preparation of **6**. Treatment of **11** with sodium iodide and zinc dust in DMF at 98°C for 3 hr gave the 3,4-unsaturated derivative (**12**), $[\alpha]_D^{20}$−35° (*c* 0.7, methanol), in a yield of 90%. Since **11** has vicinally situated *trans*-diequatorial sulfonic ester groups, this reaction will be the first example that *trans*-diequatorial sulfonic ester groups went to unsaturation smoothly in a high yield. The smooth reaction will in part be attributable to the presence of a C-4 sulfonyloxy group, which is suscep-

13) K. Bock and C. Pedersen, *Tetrahedron Lett.*, **1969**, 2983.
14) R. J. Ferrier and N. Vethaviyaser, *J. Chem. Soc., C*, **1971**, 1907.
15) A. H. Haines, *Carbohyd. Res.*, **1**, 214 (1965).
16) E. J. Corey and R. A. E. Winter, *J. Amer. Chem. Soc.*, **85**, 2677 (1963).
17) H. Umezawa, M. Ueda, K. Maeda, K. Yagishita, S. Kondo, Y. Okami, R. Utahara, Y. Osato, K. Nitta, and T. Takeuchi, *J. Antibiot.* (Tokyo), *Ser. A*, **10**, 188 (1957); T. Ito, M. Nishio, and H. Ogawa, *ibid*, **17**, 189 (1964).
18) R. S. Tipson and A. Cohen, *Carbohyd. Res.*, **1**, 338 (1965).
19) A. C. Richardson, *ibid.*, **10**, 395 (1969).
20) L. M. Jackman and S. Sternhell, "Application of NMR spectroscopy in organic chemistry," 2nd edition, Pergamon Press (1969), p. 325.
21) This compound (**7**) has recently been synthesized by a different way: K. Bock and C. Pedersen, *Acta Chem. Scand.*, **25**, 1021 (1971).

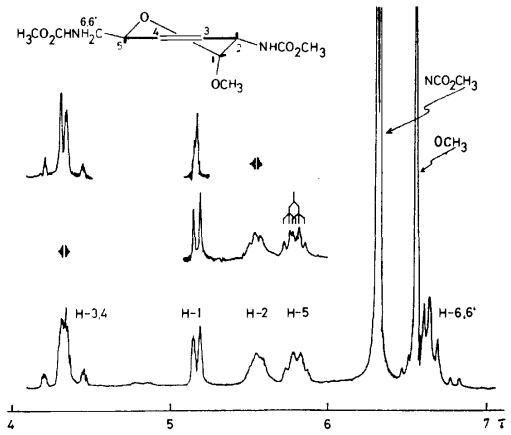

Fig. 2. The NMR spectrum of **12** in $CDCl_3$–D_2O at 100 MHz.

tible to an attack by a nucleophilic reagent, but neighboring group assistance by methoxycarbonylamino groups at C-2 and 6 should also be considered. The structure of **12** was confirmed by its NMR spectrum (Fig. 2) and double irradiation experiments (see Experimental). The coupling constants $J_{1,2}$ 4.2 Hz, $J_{3,4}$ 11 Hz, $J_{2,5}$~4 Hz (homoallylic), $J_{5,6}$ 5.3 Hz and $J_{5,6'}$ 4 Hz were confirmed. Small couplings ($J<1$ Hz) were also observed between H-3,4 and H-1, between H-3,4 and H-2, and between H-3,4 and H-5. These values indicated that **12** is in a half-chair conformation as depicted in Fig. 2.

Removal of the protecting groups from **12** gave the desired 3,4-unsaturated glycoside (**13**) as needles of monosulfate hemihydrate, $[\alpha]_D^{22}+26°$ (*c* 1, water). The NMR experiments of **13** (Fig. 3) again showed the coupling constants, $J_{1,2}$ 4.2 Hz, $J_{3,4}$ 11 Hz, $J_{2,5}$ 3.5 Hz, $J_{5,6}$ 6 Hz and $J_{5,6'}$ 4 Hz, being consistent with the half-chair conformation.

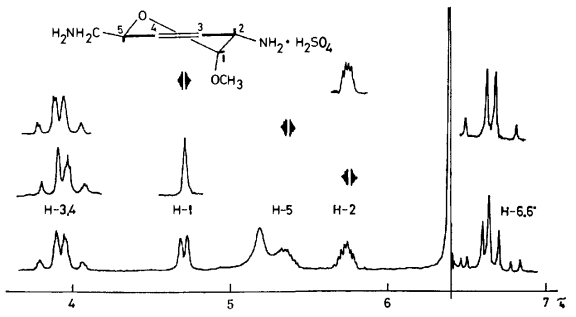

Fig. 3. The NMR spectrum of **13** in D_2O at 100 MHz.

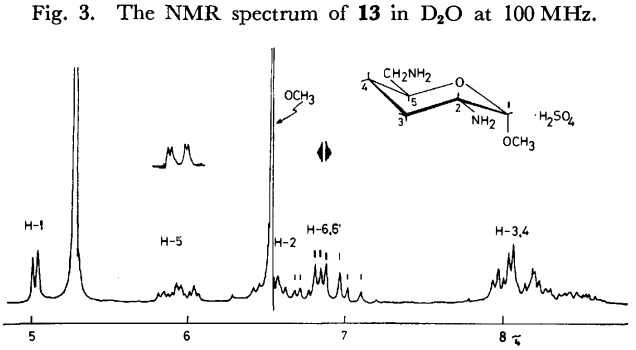

Fig. 4. The NMR spectrum of **15** in D_2O at 100 MHz.

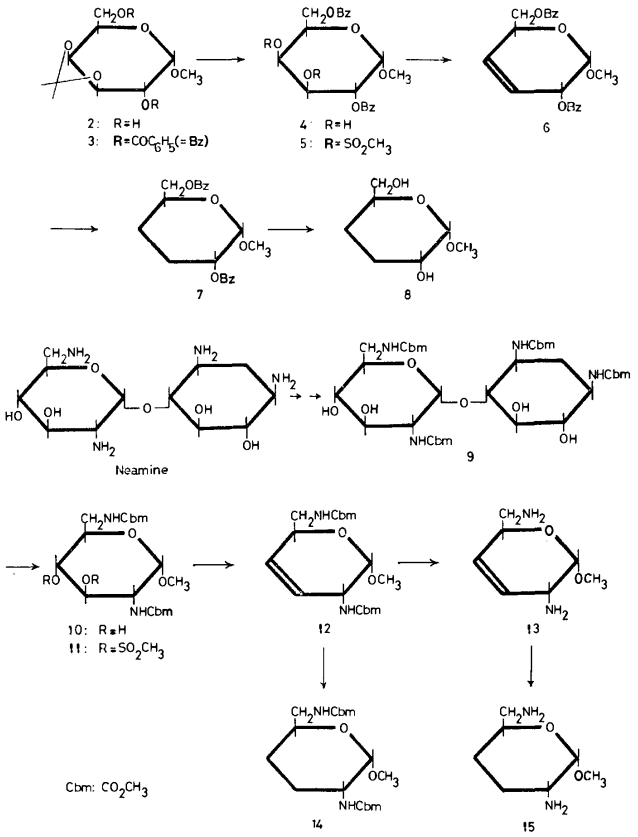

Chart 1.

Hydrogenation of **12** gave a tetradeoxy derivative (**14**), $[\alpha]_D^{19}+126°$ (*c* 0.7, methanol). Removal of the protecting groups then gave the 3,4-saturated glycoside (**15**) as needles of monosulfate hydrate, $[\alpha]_D^{22}+128°$ (*c* 1, water). The NMR spectrum was shown in Fig. 4.

Experimental

The NMR spectra were measured with a Varian A-60D or a Varian HA-100(at 100 MHz) spectrometer. Tetramethylsilane (for the solution of deuteriochloroform) and sodium 4,4-dimethyl-4-silapentane-1-sulfonate (for the solution of deuterium oxide) were used as the internal standards. Thin layer chromatography (tlc) was carried out on microscope slides coated with silica gel, and the spots were visualized with sulfuric acid.

Methyl α-D-Galactopyranoside (1). A suspension of D-galactose (5 g) in 4% hydrogen chloride in methanol (200 m*l*) was refluxed for 7 hr. Tlc (chloroform–methanol 5 : 2) of the reaction mixture showed that the starting material (R_f 0.30) disappeared and methyl α-D-galactofuranoside (R_f 0.63) and methyl α and β-D-galactopyranosides (R_f 0.47) appeared. Basic lead carbonate (30 g) was added and, after vigorous stirring, the suspension was centrifuged. The supernatant layer was evaporated to give a syrup (6 g). The syrup (22 g) was passed through a short column of Dowex 1×2 (OH form, 80 m*l*) with aid of water and the fraction containing galactopyranosides were evaporated. The resultant syrup (18.5 g) was dissolved in water and ethanol (12 m*l*) was added to cause crystallization of **1**, 7.15 g, mp ~97°C (not sharp), $[\alpha]_D^{20}+180°$ (*c* 1, water) (lit,[22] 111—

22) D. F. Mowery, Jr. and G. R. Ferrante, *J. Amer. Chem. Soc.*, **76**, 4103 (1954).

115°C, $[\alpha]_D^{20}+178°$). From the mother liquor another crop (2.73 g) was obtained. Total yield was 46%.

Found: C, 39.85; H, 7.90%. Calcd for $C_7H_{14}O_6 \cdot H_2O$· C, 39.62; H, 7.60%.

Methyl 3,4-O-Isopropylidene-α-D-galactopyranoside (2). Compound **1** was treated likewise as described by Buchanan and Saunders[23] and the crude product was extracted with ethyl acetate instead of acetone.[23] The solution was evaporated to give a syrup, which was chromatographed on a column of silica gel with ethyl acetate. From the earlier eluate, **2** was obtained in a yield of 64% (lit,[23] 47%), mp 103—105°C, $[\alpha]_D^{20}+163°$ (*c* 1.8, water) (lit,[23] 103—104°C, $[\alpha]_D^{22}+161°$ in chloroform). From the late eluate the 4,6-*O*-isopropylidene derivative was obtained in a yield of 17%.

Methyl 2,6-Di-O-benzoyl-3,4-O-isopropylidene-α-D-galactopyranoside (3). To a solution of **2** (3.0 g) in dry pyridine (60 m*l*), benzoyl chloride (4.5 m*l*) was added and the solution was allowed to stand for 30 min. After addition of water (0.8 m*l*), the solution was concentrated to approximately 10 m*l*, and to the concentrate, chloroform (200 m*l*) was added. After stirring, the organic layer was washed successively with potassium hydrogen sulfate solution, sodium hydrogen carbonate solution and water, dried over sodium sulfate and evaporated to give a syrup, 5.5 g (97%), $[\alpha]_D^{21}+134°$ (*c* 2.3, methanol); IR: 1725, 1260, 1110, 1070; 1043, 1023, 1010 (w), 995, 958 (w), 915, 865, 840, 800, 773 (w), 708 (s) cm^{-1}.

Found: 65.02; H, 6.11%. Calcd for $C_{24}H_{26}O_8$: C, 65.14; H, 5.92%.

NMR (in $CDCl_3$): τ 8.62 and 8.41 (both 3H singlets, isopropylidene), 6.60 (3H s, OCH_3), 5.2—5.7 (5H m), 4.92 (1H d, J 3.5 Hz, H-1), 4.75 (1H q, J 3.5 and 7.3 Hz, H-2), 2.3—2.7 (6H) and 1.75—2.0 (4H)(each multiplet, typical for benzoyl protons); $J_{1,2}$ 3.5 Hz, $J_{2,3}$ 7.3 Hz.

Methyl 2,6-Di-O-benzoyl-α-D-galactopyranoside (4). A solution of **3** (1.19 g) in 75% aqueous acetic acid (10 m*l*) was heated at 90°C for 15 min. The solution was evaporated and coevaporated with toluene to give a syrup. The syrup was dissolved in ethyl acetate and the solution was washed with sodium hydrogen carbonate solution and water, dried over sodium sulfate and evaporated to give a syrup, 1.05 g (97%), which crystallized on seeding. Recrystallization was carried out from methyl ethyl ketone-petroleum ether, mp 125—127°C, $[\alpha]_D^{22}+107°$ (*c* 1, chloroform); IR (KBr): 1720, 1275, 1115, 1095; 1040, 1023, 1010 (w), 995 (w), 970, 935 (w), 915, 890, 840 (w), 800, 780, 707 (s) cm^{-1}.

Found: C, 62.92; H, 5.65%. Calcd for $C_{21}H_{22}O_8$: C, 62.68; H, 5.51%.

Methyl 2,6-Di-O-benzoyl-3,4-di-O-mesyl-α-D-galactopyranoside (5). A solution of **4** (3.09 g) and methanesulfonyl chloride (2.7 g) in pyridine (78 m*l*) was allowed to stand at room temperature overnight. On tlc with benzene-ethyl acetate (10 : 1), **4**, (R_f 0.04) and initially appeared mono-*O*-mesyl derivative (R_f 0.15) disappeared and **5** (R_f 0.40) appeared as the final product. Water (0.8 m*l*) was added and the solution was evaporated to give a syrup, which was dissolved in chloroform. The solution was washed with sodium hydrogen carbonate solution and with water, dried over sodium sulfate and evaporated to give a thick syrup, 4.21 g (98%), $[\alpha]_D^{25}+136°$ (*c* 1.3, chloroform); IR (KBr): 1725, 1360 (ν_{as} SO_2), 1270, 1175, (ν_s SO_2), 1110; 1025, 965, 930 (sh), 915 (s), 850 (s), 805, 777, 760, 710 (s).

Found: C, 49.41; H, 4.84; S, 11.43%. Calcd for $C_{23}H_{26}O_{12}S_2$: C, 49.45; H, 4.69; S, 11.48%.

NMR (in $CDCl_3$): τ 6.93 and 6.76 (both 3H singlets, SO_2CH_3), 6.57 (3H s, OCH_3), 5.2—5.75 (3H m), 4.67—4.80 (1H m), 4.55 (3H, singlet-like pattern, width at half-height was 3.5 Hz); 2.3—2.7 (6H) and 1.7—1.95 (4H) (benzoyl protons).

Methyl 2,6-Di-O-benzoyl-3,4-dideoxy-α-D-erythro-hex-3-enopyranoside (6). To a solution of **5** (2.07 g) in dry DMF (40 m*l*, dried over CaH_2), dry sodium iodide (10 g) and zinc dust (4 g) were added and the mixture was heated in an oil bath (130—150°C) with vigorous stirring for 1.5 hr. Hot chloroform was added and the mixture was filtered while hot and the solution was evaporated *in vacuo* with subsequent coevaporation with toluene. The residue obtained was extracted with chloroform and the solution was washed successively with water, sodium thiosulfate solution and with water again, dried over sodium sulfate and evaporated to give a syrup, 1.27 g (93%). On tlc with benzene-ethyl acetate (10 : 1), the syrup showed a single spot (R_f 0.66). The syrup was distilled under vacuum (0.0005 mm) on an oil bath (180—190°C) to give a liquid, $[\alpha]_D^{22}-17.3°$ (*c* 1, chloroform); IR: 1725; no peaks in 1610—1700; 1265, 1100, 707 cm^{-1}.

Found: C, 68.36; H, 5.72%. Calcd for $C_{21}H_{20}O_6$: C, 68.47; H, 5.47%.

NMR (in $CDCl_3$ at 100 MHz)(Fig. 1): τ 6.25 (3H s, OCH_3), 5.35—5.6 (3H m, H-5,6,6'), 4.73 (1H d with small splittings, J~4 Hz, H-1), 4.42 (1H m, H-2); 4.06 (2H multiplet, which is a deformed AB quartet (J_{AB}~11 Hz), H-3,4); 2.35—2.70 (6H m.) and 1.85—2.0 (4H m) (benzoyl protons).

Methyl 2,6-Di-O-benzoyl-3,4-dideoxy-α-D-erythro-hexopyranoside (7). A solution of **6** (1.36 g) in methanol (5 m*l*) was hydrogenated with palladium black and hydrogen under pressure (50 lbs/sq. inch) at room temperature for 5 hr. The reaction mixture was filtered and the solution was evaporated to give syrup, 1.22 g (88%), which crystallized on standing. This was recrystallized from ethanol, mp 70—71°C, $[\alpha]_D^{22}+56.7°$ (*c* 1, chloroform); IR (KBr): 1720, 1715, 1270, 1095; 1038, 1025, 1010, 995, 955, 900, 875, 860, 705 (s), 680 cm^{-1}.

Found: C, 68.34; H, 6.13%. Calcd for $C_{21}H_{22}O_6$: C, 68.09; H, 5.99%.

NMR (in $CDCl_3$): τ 7.6—8.6 (4H m, H-3,3', 4,4'), 6.54 (3H s, OCH_3), 5.5—6.0 (3H m, H-5,6,6'), 4.7—5.1 (2H m, H-1 and 2), 2.3—2.7 (6H) and 1.75—2.05 (4H) (benzoyl protons).

Methyl 3,4-Dideoxy-α-D-erythro-hexopyranoside (8). To a solution of **7** (4.73 g) in methanol (40 m*l*), 3 M sodium methoxide in methanol (1.4 m*l*) was added and the solution was allowed to stand for 10 min. After addition of a small amount of Amberlite IR-120 (H^+ form), the solution was filtered and evaporated to give a syrup. The aqueous solution (500 m*l*) of the syrup was shaken with a small amount of ether and the aqueous layer separated was evaporated to give a syrup, 1.84 g (89%), $[\alpha]_D^{22}+126°$ (*c* 1.1, water); IR (KBr): 1450, 1050 (s), 985 (sh), 963, 925, 900, 845, 785 (w) cm^{-1}.

NMR (in D_2O): τ 7.9—8.6 (4H m, H-3,3',4,4'), 6.53 (3H s, OCH_3), 6.05—6.5 (4H m., H-2,5,6,6'), 5.29 (1H d, $J_{1,2}$ 3.5 Hz, H-1).

Methyl 2,6-Dideoxy-2,6-dimethoxycarbonylamino-α-D-glucopyranoside (10). To a mixture of neamine tetrahydrochloride[24] (1.02 g) and basic lead carbonate (7 g) in aqueous acetone (1 : 1, 20 m*l*), methoxycarbonyl chloride (1.01 g) was added dropwise with stirring at room temperature, and stirring was continued for 3 hr. Tlc (ethyl acetate-methanol 5 : 1) of

23) J. G. Buchanan and R. M. Saunders, *J. Chem. Soc.*, **1964**, 1796.

24) K. Tatsuta, E. Kitazawa, and S. Umezawa, This Bulletin, **40**, 2371 (1967).

the reaction mixture showed that neamine (R_f 0) disappeared and the tetra-*N*-methoxycarbonyl derivative (**9**, R_f 0.45) appeared. The reaction mixture was filtered, and the mass separated was washed with hot water several times. Filtrate and the washings were combined and concentrated to a small volume. Dowex 1×2 (OH form) resin (1.5 m*l*) was added and the mixture was shaken for a while whereupon some precipitates were liberated. The mixture was filtered and the solution was evaporated and then coevaporated with benzene to give a solid (1.07 g)[25], which still contained some inorganic salts. The crude **9** (4 g) obtained above was suspended in 8% hydrogen chloride in methanol (80 m*l*) and the mixture was refluxed for 40 hr. Tlc (ethyl acetate–ethanol 8 : 1) of the resulting solution showed three spots of R_f 0.56 (**10**), 0.40 (β-anomer of **10** ?) and 0.09 (probably *N,N'*-dimethoxycarbonyl-2-deoxystreptamine; the color appeared on strong heating after spraying sulfuric acid; when the crude isolated product was treated with hot basic solution, the product liberated 2-deoxystreptamine). The pale-brown solution was neutralized with anhydrous sodium carbonate (13.5 g) under stirring and the inorganic salts precipitated were removed by centrifuging. The supernatant layer was evaporated and coevaporated with toluene and the residue obtained was extracted with *p*-dioxane (30 m*l*×3). The solution, which contained **10** and a small amount of 2-deoxystreptamine derivative described above but was free from inorganic salts, was evaporated. The methanol solution (10 m*l*) of the residue (2.3 g) was charged on a short column of alumina (50 g, Woelm acidic) and developed with ethyl acetate–methanol (1 : 1). The eluate containing **10** was evaporated to give a solid (1.54 g), which was proved to contain only a slight amount of the 2-deoxystreptamine derivative. The solid was then recrystallized from methanol to give **10** (0.79 g). The mother liquor, after evaporation, was chromatographed with methanol on a column of Dowex 1×2 (OH form, 100 m*l*), pretreated with methanol. Compound **10**, the 2-deoxystreptamine derivative (R_f 0.09) and a by-product (R_f 0.40) were eluted in this order. The fraction containing **10** was evaporated to give a solid (0.37 g). Total yield of **10** was 1.16 g (52%). The combined product was finally recrystallized from a hot mixture of methanol–acetone (1 : 4), mp 175—177°C, $[\alpha]_D^{21}$ +108° (*c* 0.7, water); IR (KBr): 1690 (s, broad), 1550, 1440, 1290, 1275, 1060; 978, 947, 925 (w), 900 (w), 835 (w), 785, 770 (w), 760 (w), 710 cm^{-1}.

Found: C, 42.60; H, 6.76; N, 8.88%. Calcd for $C_{11}H_{20}N_2O_8$: C, 42.86; H, 6.54; N, 9.09%.

NMR (in D_2O): τ 6.63 (3H s, OCH_3), 6.31 (6H s, $NHCO_2C\underline{H}_3$), 6.2—7.2 (6H), 5.23 (1H d, $J_{1,2}$ 2.3 Hz, H-1).

The fraction containing the product of R_f 0.40 was evaporated to give a solid (125 mg), $[\alpha]_D^{21}$ −9.8° (*c* 0.7, water).

*Methyl 2,6-Dideoxy-3,4-di-*O*-mesyl-2,6-dimethoxycarbonylamino-α-*D*-glucopyranoside (**11**).* To a solution of **10** (615 mg) in pyridine (12 m*l*), methanesulfonyl chloride (600 mg) was added and the solution was allowed to stand overnight. Tlc (benzene–ethyl acetate 1 : 3) showed that **10** (R_f 0.14) and a monomesyl derivative (R_f 0.47), which appeared in an early stage, disappeared, and **11** (R_f 0.59) appeared as the final product. Similar treatment of the solution with that described in the preparation of **5** gave a solid, 840 mg (92%), which was recrystallized from ethanol, mp 193—195 °C, $[\alpha]_D^{23}$ +94° (*c* 1.5, chloroform); IR (KBr): 1710 (sharp), 1545, 1355 (ν_{as} SO_2), 1277, 1175 (ν_s SO_2); 1055, 1030, 975, 965, 930, 908, 852, 842, 820, 777, 755, 722 cm^{-1}.

25) This experiment was performed by Yasushi Takagi of our laboratory.

Found: C, 33.84; H, 5.03; N, 6.04; S, 13.99%, Calcd for $C_{13}H_{24}N_2O_{12}S_2$: C, 33.62; H, 5.21; N, 6.03; S, 13.81%.

NMR (in $CDCl_3$): τ 6.90 and 6.77 (both 3H singlets, SO_2CH_3), 6.59 (3H s, OCH_3), 6.29 (6H s, $NHCO_2C\underline{H}_3$), 5.36 and 5.06 (both 1H triplets, J 9 Hz, H-3 and 4), 5.22 (1H d, $J_{1,2}$ 3.2 Hz, H-1); $J_{2,3}=J_{3,4}=J_{4,5}$ 9 Hz.

*Methyl 2,3,4,6-Tetradeoxy-2,6-dimethoxycarbonylamino-α-*D*-erythro-hex-3-enopyranoside (**12**).* To a solution of **11** (503 mg) in dry DMF (10 m*l*), dry sodium iodide (5.5 g) and zinc dust (2.5 g) were added and the mixture was heated in an oil bath (98±1°C) for 3 hr with vigorous stirring. On tlc with benzene–ethyl acetate (1 : 2), **11** (R_f 0.39) disappeared and a product (R_f 0.52) appeared. Hot chloroform (60 m*l*) was added and the reaction mixture was filtered. The solution was washed successively with water (60 m*l*), saturated sodium thiosulfate solution (30 m*l*) and with water (60 m*l*×2), dried over sodium sulfate and evaporated to give a syrup, 268 mg (90%), which crystallized on standing and recrystallized from ethanol, mp 157—159°C, $[\alpha]_D^{20}$ −35° (*c* 0.7, methanol); IR (KBr): 1695, 1540, 1250, 1105, 1055, 1008; 955 (w), 942, 915, 843, 803, 784, 733, 700 cm^{-1}.

Found: C, 48.20; H, 6.43; N, 10.02%. Calcd for $C_{11}H_{18}N_2O_6$: C, 48.17; H, 6.61; N, 10.21%.

NMR: To a solution of **12** in deuteriochloroform, deuterium oxide was added and, after storage for one day, the solution was measured at 100 MHz (Fig. 2): τ 6.69 (1H q, *J* 5.3 and 14 Hz, H-6), 6.59 (1H q, *J* 4 and 14 Hz, H-6'), 5.80 (1H incomplete quartet, H-5), 5.55 (1H m, H-2), 5.17 (1H d, H-1), 4.17—4.48 (2H m, H-3,4).

Irradiation at τ 4.32 (H-3,4) caused the H-5 multiplet to become double triplets (*J* 4, 4 and 5.3 Hz), the H-2 multiplet to become an incomplete triplet (*J*∼4 Hz) and H-1 doublet to become a sharp doublet (*J* 4.2 Hz). Irradiation at τ 5.55 (H-2) caused the H-1 doublet to collapse to a singlet and H-3,4 multiplet to collapse to an AB quartet (J_{AB} 11 Hz); as for the AB quartet, the pair in the lower field became more sharpened than that in the higher field. Irradiation at τ 5.80 (H-5) caused the H-6,6' octet to collapse to an AB quartet (*J* 4 Hz).

*Methyl 2,6-Diamino-2,3,4,6-tetradeoxy-α-*D*-erythro-hex-3-enopyranoside (**13**).* To a solution of **12** (179 mg) in aqueous methanol (5 : 1, 3 m*l*), barium hydroxide octahydrate (600 mg) was added and the mixture was refluxed for 4 hr. On tlc with *n*-butanol–pyridine–water–acetic acid (6 : 4 : 3 : 1), the reaction mixture showed two spots of R_f 0.25 and 0.69 (very weak). Carbon dioxide was introduced and the resulting precipitates were removed by centrifuging. The supernatant layer was evaporated to give a residue, which was neutralized with 1 N sulfuric acid and after treatment with charcoal, the mixture (pH∼3) was concentrated to approximately 0.5 m*l*. Addition of acetone gave needles, 146 mg (85% as **13** sulfate hemihydrate), mp: gradually decomposed over than 180°C, $[\alpha]_D^{22}$ +26° (*c* 1, water).

Found: C, 31.96; H, 6.63; N, 9.94; S, 11.84%. Calcd for $C_7H_{14}N_2O_2\cdot H_2SO_4\cdot 1/2H_2O$: C, 31.69; H, 6.46; N, 10.56; S, 12.09%.

NMR (in D_2O at 100 MHz)(Fig. 3): τ 6.69 (1H q, *J* 6 and 14 Hz, H-6), 6.61 (1H q, *J* 4 and 14 Hz, H-6'), 5.74 (1H m, H-2), 5.35 (1H m, H-5), 4.70 (1H d, *J* 4.2 Hz, H-1), 3.92 (2H m, H-3,4).

Irradiation of H-1 caused the H-2 multiplet to collapse to a quartet (*J*∼1.5 and 3.5 Hz).

*Methyl 2,3,4,6-Tetradeoxy-2,6-dimethoxycarbonylamino-α-*D*-erythro-hexopyranoside (**14**).* A solution of **12** (416 mg) in aqueous methanol (1 : 4, 5 m*l*) was hydrogenated with palladium black and hydrogen under pressure (50 lbs/sq. inch) at 35°C overnight. On tlc with benzene–ethyl acetate (1 : 2),

both the starting material (**12**) and the product (**14**) gave the same R_f-value (0.52), however, they were distinguished each other by their coloration with anisaldehyde-sulfuric acid[26]: **12** colored orange initially and then turned brown after 1 hr and **14** colored blueviolet to yellow (after 1 hr). The mixture was filtered and evaporated to give a thick syrup, 400 mg (95%), $[\alpha]_D^{19}+126°$ (*c* 0.7, methanol); IR (KBr): 1700, 1540, 1275, 1260; 1050, 1027, 1020, 980, 948, 915, 890 (w), 784, 715 (w) cm^{-1}.

Found: C, 48.10; H, 7.42; N, 10.21%, Calcd for $C_{11}H_{20}N_2O_6$: C, 47.82; H, 7.30; N, 10.14%.

NMR (in $CDCl_3$): τ 8.0—8.6 (4H m, H-3,3',4,4'), 6.62 (3H s, OCH_3),6.31 (6H s, $NHCO_2C\underline{H}_3$), 5.35 (1H d, $J_{1,2}$ 3.5 Hz, H-1).

*Methyl 2,6-Diamino-2,3,4,6-tetradeoxy-α-*D*-erythro-hexopyranoside (**15**).* To a solution of **14** (414 mg) in aqueous methanol (5 : 1, 6 m*l*), barium hydroxide octahydrate (1.2 g) was added and the mixture was refluxed under stirring for 3 hr. Carbon dioxide was introduced and the mixture was treated as described in the preparation of **13** to give **15**, needles, 288 mg (94% as sulfate monohydrate). Mp: gradually decomposed over than 180°C (slightly changed at ~135°C), $[\alpha]_D^{22}+128°$ (*c* 1, water).

Found: C, 30.45; H, 7.04; N, 9.85; S, 11.62%. Calcd for $C_7H_{16}N_2O_2\cdot H_2SO_4\cdot H_2O$: C, 30.43: H, 7.30; N, 10.14; S, 11.60%.

NMR (in D_2O at 100 MHz)(Fig. 4): τ 7.9—8.7 (4H m, H-3,3',4,4'); 6.96 (1H q, *J* 8.7 and 13.5 Hz, H-6) and 6.80 (1H q, *J* 3.5 and 13.5 Hz, H-6'); these signals formed the AB part of an ABX system; 6.53 (3H s, OCH_3), 6.52 (1H m, H-2), 5.94 (1H m, H-5), 5.03 (1H d, *J* 3.3 Hz, H-1).

Irradiation at τ 6.52 (H-2) caused the H-1 doublet to collapse to a singlet and the multiplet at τ 7.9—8.7 to change. Irradiation at τ 6.87 caused the H-5 multiplet to collapse to a quartet (*J* 2 and 10.5 Hz); $J_{1,2}$ 3.3 Hz, $J_{4ax,5}$ 10.5 Hz, $J_{4eq,5}$ 2 Hz, $J_{5,6}$ 8.7 Hz, $J_{5,6'}$ 3.5 Hz, $J_{6,6'}$ 13.5 Hz.

The authors wish to thank Dr. Hiroshi Naganawa of the Institute of Microbial Chemistry for carrying out decouplings in the NMR spectra and to Mr. Saburo Nakada for the elemental analysis.

26) E. Stahl and U. Kaltenbach, *J. Chromatogr.*, **5**, 351 (1961).

BULLETIN OF THE CHEMICAL SOCIETY OF JAPAN, VOL. 45, 3624—3628 (1972)

Studies on Aminosugars. XXXII. Synthesis of 3′, 4′-Dideoxykanamycin B[1]

Sumio UMEZAWA,* Hamao UMEZAWA,** Yasushi OKAZAKI,* and Tsutomu TSUCHIYA*

* *Department of Applied Chemistry, Faculty of Engineering, Keio University, Hiyoshi-cho, Kohoku-ku, Yokohama*

** *Institute of Microbial Chemistry, Shinagawa-ku, Tokyo*

(Received May 11, 1972)

Penta-*N*-ethoxycarbonylkanamycin B (**1**) prepared from kanamycin B was treated with 2,2-dimethoxypropane in DMF to give a 3′,4′;4″,6″-di-*O*-isopropylidene derivative (**3**). Subsequent benzoylation afforded a 2″-*O*-benzoyl derivative (**4**), Removal of the isopropylidene groups from **4** followed by controlled isopropylidenation afforded the corresponding 4″,6″-*O*-isopropylidene derivative (**5**), which was then transformed to a 3′,4′-di-*O*-mesyl derivative (**6**). Treatment of **6** with sodium iodide and zinc dust in DMF gave the desired 3′,4′-unsaturated derivative (**7**). Hydrogenation and removal of the protecting groups gave the title compound. The 3′,4′-dideoxykanamycin B expectedly showed remarkable activity against kanamycin-resistant bacteria as well as sensitive strains.

As described in the preceding papers, the 3′-deoxykanamycin[2] exhibited antibiotic activity in the same strength as the parent antibiotic and, moreover, it showed strong inhibition against resistant bacteria such as *E. coli* carrying R factor, resistant *Staphylococci* and *Pseudomonas*, whereas 3′-*O*-methylkanamycin[3] is inactive. On the other hand, we have found that 3,4-unsaturation of glycopyranosides smoothly proceeded by treatment of their 3,4-di-*O*-mesyl derivatives with iodide and zinc dust in dimethylformamide (DMF) as described in the foregoing paper.[4] The interest in this particular method of dehydroxylation is first that unsaturation occurs at C-3,4 position of an aminosugar and, fortunately, the yield of the reaction is excellent. Secondly, the reaction opens the possibility for us to synthesize a 3′,4′-dideoxy derivatives of kanamycin and allied antibiotics, though the structures of such antibiotics are much more complex. We were interested in the 3′,4′-dehydroxylation of kanamycin B because the antibiotic contains 2,6-diamino-2,6-dideoxy-D-glucose on which experience of 3,4-dehydroxylation has been gained.[4] Thus, the synthesis of 3′,4′-dideoxykanamycin B was undertaken.

The amino groups of kanamycin B were protected by ethoxycarbonyl chloride in aqueous acetone in the presence of sodium carbonate to give penta-*N*-ethoxycarbonylkanamycin B (**1**). The reason for the use of ethoxycarbonyl groups instead of benzyloxycarbonyl

1) A part of this paper was read by S. Umezawa at Symposium of New Natural Product Syntheses, 23rd International Congress of Pure and Applied Chemistry at Boston, U. S. A., July 28, 1971. Short communication: H. Umezawa, S. Umezawa, T. Tsuchiya, and Y. Okazaki, *J. Antibiot.* (Tokyo), **24**, 485 (1971).

2) S. Umezawa, T. Tsuchiya, R. Muto, Y. Nishimura, and H. Umezawa, *ibid* **24**, 274 (1971); S. Umezawa, Y. Nishimura, H. Hineno, K. Watanabe, S. Koike, T. Tsuchiya, and H. Umezawa, This Bulletin, **45**, 2847 (1972).

3) H. Umezawa, T. Tsuchiya, R. Muto, and S. Umezawa, *ibid.*, **45**, 2842 (1972).

4) S. Umezawa, T. Tsuchiya, and Y. Okazaki, *ibid.*, **44**, 3494 (1971); *ibid.*, **45**, 3619 (1972).

or acyl (acetyl or benzoyl) groups are that the benzyloxycarbonyl group seemed to have no special advantage over the ethoxycarbonyl group in the present synthesis and that the acyl protection of the amino groups in kanamycins renders the kanamycin-derivatives scarcely soluble in usual organic solvents. The product (**1**) was acetonated with 2,2-dimethoxypropane in DMF in the presence of *p*-toluenesulfonic acid giving 4″,6″-mono-*O*-isopropylidene derivative (**2**) in a yield of 95%. Its NMR spectrum in dimethyl sulfoxide-d_6 showed that the isopropylidene methyls resonated separately at τ 8.60 and 8.72, indicating[3] that the isopropylidene group was attached to C-4 and 6 of the 3-amino-3-deoxy-D-glucose moiety of the derivative (**2**). Compound **2** was again treated with 2,2-dimethoxypropane to give 3′,4′;4″6″-di-*O*-isopropylidene derivative (**3**), $[\alpha]_D^{20}+87°$ (*c* 1, DMF) in approximately 30% yield. Since the *N*-protected 4,5;4″,6″-di-*O*-isopropylidene derivative[3] of 6-*O*-(3-amino-3-deoxy-α-D-glucopyranosyl)-2-deoxystreptamine was obtained from the corresponding precursor in a yield of 84%, the above low yield may be ascribable to the molecular complexity of the kanamycin derivative (**2**). However, when dimethoxycyclohexane was used instead of dimethoxypropane and the reaction was performed under diminished pressure,[5] **1** gave the corresponding di-*O*-cyclohexylidene derivative in a high yield (90%), on which details will be published elswhere. Benzoylation of **3** gave 2″-*O*-benzoyl derivative (**4**), $[\alpha]_D^{21}+114°$ (*c* 1, DMF). Increase in optical rotation ($[\alpha]_D+87°$(in **3**)⟶$+114°$ (in **4**)) showed that the benzoylation occurred at the hydroxyl group on C-2″ but not on C-5 where is optically least sensitive and is sterically hindered. The inactivity of the hydroxyl group at C-5 to acylation was also encountered in the synthesis of kanamycin-6″-uronic acid.[6] Removal of the isopropylidene groups of **4** followed by controlled isopropylidenation gave the 2″-*O*-benzoyl-4″,6″-*O*-isopropylidene derivative (**5**) in a 73% yield. The positions selectively isopropylidenated were confirmed by its NMR spectrum.

Mesylation of **5** with mesyl chloride in pyridine gave the 3′,4′-di-*O*-mesyl derivative (**6**). 3′,4′-Unsaturation of **6** was performed by treatment[7] with sodium iodide and zinc dust in DMF as described in the previous paper.[4] 2″-*O*-Benzoyl-3′,4′-dideoxy-3′-eno-penta-*N*-ethoxycarbonyl-4″,6″-*O*-isopropylidenekanamycin B (**7**), $[\alpha]_D^{21}+36°$ (*c* 4, DMF), was obtained in a yield of 38%. Since methyl 2,6-di-*O*-benzoyl-3,4-dideoxy-α-D-*erythro*-hex-3-enopyranoside[4] (93%), methyl 2,3,4,6-tetradeoxy-2,6-dimethoxycarbonylamino-α-D-*erythro*-hex-3-enopyranoside[4] (90%) and 5,6-*O*-cyclohexylidene-3′,4′-dideoxy-3′-eno-tetra-*N*-methoxycarbonylneamine[8] (70%) were obtained from the corresponding precursors in high yields, the comparatively low

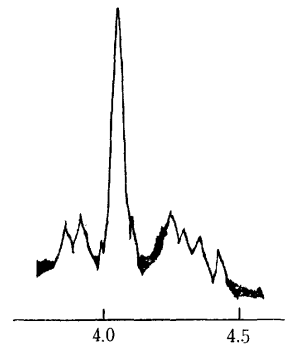

Fig. 1. The NMR spectrum of **7** in pyridine-d_5 at 60 MHz.

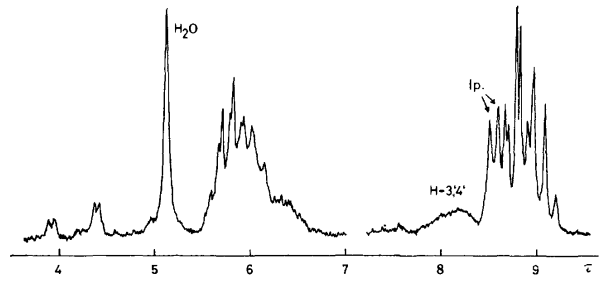

Fig. 2. The NMR Spectrum of **8** in pyridine-d_5 at 60 MHz.

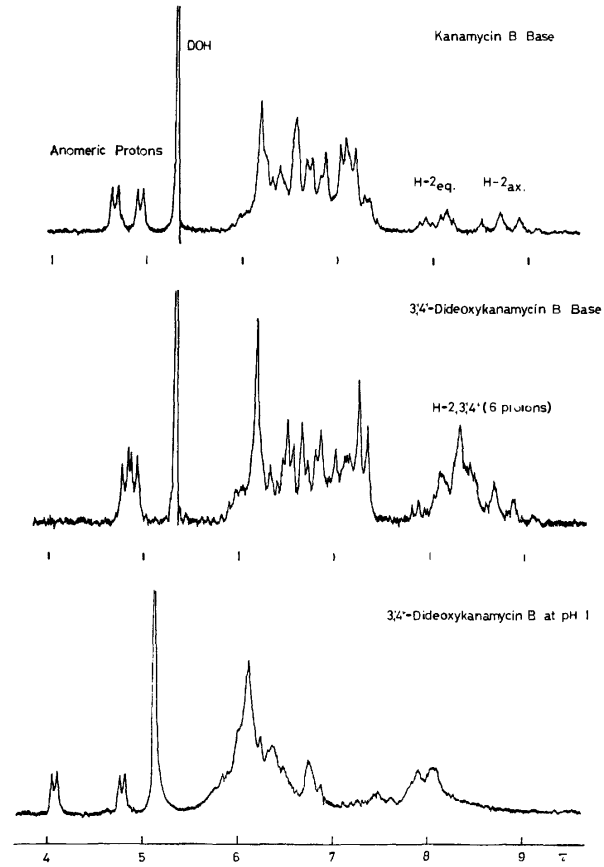

Fig. 3. The NMR spectra of kanamycin B base, 3′,4′-dideoxykanamycin B base and 3′,4′-dideoxykanamycin B at pH 1 (acidified with sulfuric acid) in D_2O at 60 MHz.

5) F. H. Bissett, M. E. Evans, and E. W. Parrish, *Carbohyd. Res.*, **5**, 184 (1967).
6) T. Kobayashi, T. Tsuchiya, K. Tatsuta, and S. Umezawa, *J. Antibiot.* (Tokyo), **23**, 226 (1970).
7) R. S. Tipson and A. Cohen, *Carbohyd. Res.*, **1**, 338 (1965).
8) S. Umezawa, T. Tsuchiya and T. Jikihara and H. Umezawa, *J. Antibiot.* (Tokyo), **24**, 711 (1971).

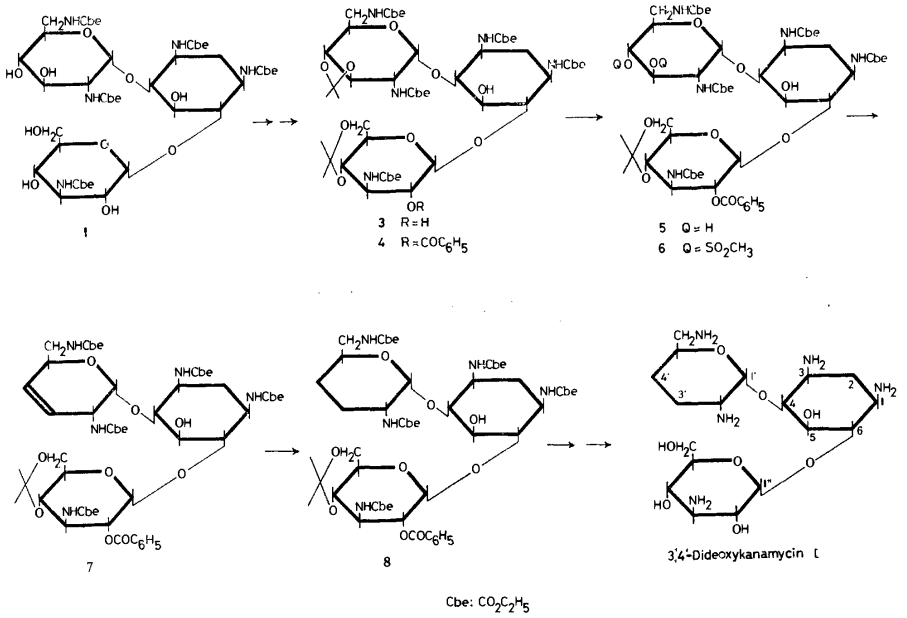

Chart 1.

yield of **7** may be due to some unfavorable influence of the free hydroxyl group of C-5 in **6**. 3',4'-Unsaturation of **7** was confirmed by its NMR spectrum (Fig. 1): a two proton singlet appeared at τ 4.04 characteristic to 3,4-alkene protons.[8] The low optical rotation (+36°) of **7** also required the above structure. As the hydrogenated product (**8**) described below had $[\alpha]_D$+93.5° (in DMF), the difference in molecular rotation between **7** and **8** is calculated to be (36—93.5°)×954 (MW of **7**)≃−55000°. The value, which will be the net contribution of the 3,4-unsaturation bond to the rotation of the α-D-*erythro*-hexopyranoside, is in good accord with that of structurally related compound **12** and **14** described in the preceding paper,[4] although methanol was used as the medium: (−35—126°)×274 (MW of **12**)≃−45000°.

Compound **7** was then catalytically hydrogenated to a dideoxy derivative (**8**), $[\alpha]_D^{22}$+93.5° (*c* 0.4 DMF). In the NMR spectrum (Fig. 2), a broadened signal corresponding to ethylene protons appeared (τ 7.8—8.5). Hydrolysis of **8** with aqueous acetic acid gave a deacetonation product (**9**), which, on removal of the other protecting groups with barium hydroxide, gave 3',4'-dideoxykanamycin B. The elemental analysis, the NMR spectrum (Fig. 3) and the result of hydrolysis of the product with 6 N hydrochloric acid confirmed the structure of the product as expected. It is worth describing that, in the NMR spectra, one of the doublets (J 3.5 Hz) of anomeric protons of 3',4'-dideoxykanamycin B base markedly shifts to down field (τ 4.80→4.08) on addition of sulfuric acid. The similar effect is also observed in the case of kanamycin B base (τ 4.66→4.12).

The semisynthetic 3',4'-dideoxykanamycin B exhibited the desired antibacterial spectrum. Microbiological studies[1] showed that resistant bacteria including various strains of *E. coli* carrying R factor, resistant *Staphylococci* isolated from patients, and *Pseudomonas aeruginisa* are remarkably sensitive to the antibiotic derivative.

Experimental

General. The general methods used were the same as those given in a previous paper.[4] Paper chromatography was performed on Toyo Roshi paper No. 50 with *n*-butanol-pyridine-water-acetic acid (6 : 4 : 3 : 1) and the spots were detected with 0.5% ninhydrin in pyridine and heating to 110°C. Frequently used solvent systems for TLC were as follows: benzene-methanol (4 : 1) (Solvent A) and chloroform-ethanol (12 : 1) (Solvent B).

*Penta-*N-*ethoxycarbonylkanamycin B (**1**).* To a mixture of kanamycin B base (1.0 g) and anhydrous sodium carbonate (0.9 g) in aqueous acetone (1 : 1, 20 m*l*), ethoxycarbonyl chloride (1.16 g) was added dropwise and the mixture was agitated for 1 hr at room temperature and then allowed to stand overnight. After the resulting slurry was neutralized with 1 N hydrochloric acid, the mixture was filtered, and the solid was washed with water, dried (1.46 g, 84%), and recrystallized from aqueous methanol (2 : 3), mp 304—306°C, $[\alpha]_D^{22}$+93.5° (*c* 0.3, DMF); R_f 0.34 (TLC with Solvent A); IR (KBr): 1700 (sh), 1690 (s), 1540 (s); 1040 (s), 975 (sh), 932 (w), 875 (m), 778 cm^{-1}. NMR (in dimethyl sulfoxide-d_6): τ 8.85 and 8.82 (each triplet, 15H in total, J 6.7 Hz, $NHCO_2CH_2\underline{CH_3}$).

Found: C, 47.03; H, 6.89; N, 8.32%. Calcd for $C_{33}H_{57}N_5O_{20}$: C, 46.97; H, 6.81; N, 8.30%.

*Penta-*N-*ethoxycarbonyl-4″,6″-*O-*isopropylidenekanamycin B (**2**).* To a mixture of **1** (1.05 g, 1.19 mmol) and anhydrous *p*-toluenesulfonic acid (29 mg, dried at 80°C *in vacuo*) in dry DMF (20 m*l* dried over CaH_2), 2,2-dimethoxypropane (0.43 g, 4.1 mmol) was added and the mixture was allowed to stand at 37°C for 1.5 hr. The starting material (R_f 0.29 on tlc with Solvent A) disappeared and the product (**2**, R_f 0.47) appeared with a slight amount of diisopropylidene product (**3**, R_f 0.76). A small amount of Amberlite IRA 400 (OH form) was added, and after filtration, the solution was concentrated *in vacuo* to a syrup, which was poured into water. The resulting solid was filtered and washed thoroughly with benzene, 1.05 g (95%). The solid was dissolved in dioxane and reprecipitated by the addition of water, mp>300°C,

$[\alpha]_D^{22}$+84° (*c* 0.5, DMF); IR (KBr): 1700 (s, broad), 1675 (sh), 1540; 1040 (broad), 945 (w), 907 (vw), 877, (w), 850 (w), 780 cm^{-1}.

Found: C, 48.62; H, 7.10; N, 8.02%. Calcd for $C_{36}H_{61}N_5O_{20}$: C, 48.92; H, 6.96; N, 7.92%.

NMR (in dimethyl sulfoxide-d_6): τ 8.84 (15H t, *J* 6.7 Hz, $NHCO_2CH_2C\underline{H}_3$), 8.72 and 8.60 (both 3H sinlgets, isopropylidene), 6.00 (10H q, *J* 6.7 Hz, $NHCO_2C\underline{H}_2CH_3$).

Penta-N-*ethoxycarbonyl-3′,4′;4″,6″-di*-O-*isopropylidenekanamycin B* (**3**). To a solution of **2** (13.7 g) and anhydrous *p*-toluenesulfonic acid (0.35 g) in dry DMF (70 m*l*), 2,2-dimethoxypropane (18.8 g) was added and the solution was heated at 65°C for 30 min. After concentration to approximately 60 m*l*, another 2,2-dimethoxypropane (35 g) and anhydrous *p*-toluenesulfonic acid (0.15 g) were added and the solution was again heated at 65°C for 30 min. After triethylamine (6 m*l*) was added, the solution was poured into a mixture of benzene (500 m*l*) and water (600 m*l*) with stirring. Resulting precipitates, which were suspended between aqueous and organic layers, were filtered, washed with benzene and dried to give a solid (6.5 g). This was proved to be the starting material unchanged (**2**, R_f 0.12 on tlc with Solvent B) and was again used in another run. The organic layer and the benzene washings were allowed to stand overnight, and some precipitates appeared were removed by filtration. The solution was evaporated to give solid (**3**), having an R_f 0.32 on tlc with Solvent B. The solid was dissolved in dioxane and reprecipitated by the addition of water, yielding 4.2 g (25.3%) of **3**, mp 236—237°C, $[\alpha]_D^{20}$ +87° (*c* 1, DMF); IR (KBr): 1735, 1705 (s), 1535; 1040, 1025, 985 (sh), 947 (w), 880 (w), 850 (w), 780 cm^{-1}.

Found: C, 50.54; H, 7.30; N, 7.59%. Calcd for $C_{39}H_{65}N_5O_{20}$: C, 50.70; H, 7.09; N, 7.58%.

NMR (in pyridine-d_5): τ 8.86 (15H t, *J* 6.7 Hz, $NHCO_2CH_2C\underline{H}_3$), 8.60 (12H a slightly broadened singlet, isopropylidene), 5.4—6.5 (27H multiplet, skeleton protons and $NHCO_2C\underline{H}_2$ CH_3).

2″-O-*Benzoyl-penta*-N-*ethoxycarbonyl-3′,4′;4″,6″-di*-O-*isopropylidenekanamycin B* (**4**). To a solution of **3** (3.24 g) in pyridine (48 m*l*), benzoyl chloride (1.68 g) was added and the solution was allowed to stand for 1 hr. After addition of water (0.4 m*l*), the solution was evaporated to give a syrup, which was dissolved in chloroform (200 mg). The solution was washed with sodium hydrogencarbonate solution and with water, dried over sodium sulfate and concentrated to approximately 20 m*l*. Addition of *n*-hexane (140 m*l*) to the solution gave a solid, 3.35 g (96%), mp 205—209°C, $[\alpha]_D^{21}$ +114° (*c* 1, DMF); IR (KBr): 1735—1700, 1535; 1030, 985 (sh), 950 (w), 877 (sh), 865 (w), 850 (w), 780, 715 cm^{-1}.

Found: C, 54.01; H, 7.11; N, 6.66%. Calcd for $C_{46}H_{69}N_5O_{21}$: C, 53.74; H, 6.77; N, 6.81%.

2″-O-*Benzoyl-penta*-N-*ethoxycarbonyl-4″,6″*-O-*isopropylidenekanamycin B* (**5**). A solution of **4** (282 mg) in aqueous acetic acid (1 : 3, 4 m*l*) was heated at 95°C for 1 hr. A deacetonated product (R_f 0.06 on tlc with Solvent B) appeared. The solution was coevaporated with toluene to give a solid, which was washed with water and dried (258 mg, 99%). To a solution of the deacetonated product (935 mg) in dry DMF (6 m*l*), 2,2-dimethoxypropane (230 m*l*) and anhydrous *p*-toluenesulfonic acid (20 mg) were added and the solution was allowed to stand at 30°C for 1 hr. On tlc with Solvent, B, a spot (R_f 0.36) appeared together with two minor spots of R_f 0.49 (**4**) and R_f 0.06. Another portion of 2,2-dimethoxypropane (96 mg) was added and the solution was allowed to stand for 1 hr at room temperature, the deacetonated substance (R_f 0.06) disappearing. Triethylamine (0.2 m*l*) was added and solution was poured into cold water (100 m*l*). The resulting precipitates were filtered, washed with water and dried. The solid, after washing with benzene, was dissolved in dioxane and reprecipitated by the addition of water, 722 mg (73% based on **4**), mp 305—307°C, $[\alpha]_D^{21}$ +105° (*c* 1, DMF); IR (KBr): 1735—1690, 1540; 1035, 985 (sh), 950 (w), 877 (w), 865 (w), 850 (w), 782, 713 cm^{-1}.

Found: C, 52.52; H, 6.67; N, 7.31%. Calcd for $C_{43}H_{65}N_5O_{21}$: C, 52.27; H, 6.63; N, 7.09%.

NMR (in dimethyl sulfoxide-d_6): τ 9.10, 8.86 and 8.83 (6H, 3H and 6H triplet, respectively, *J* 6.7 Hz, $NHCO_2CH_2C\underline{H}_3$), 8.70 and 8.56 (both 3H singlets, isopropylidene), 2.0—2.6 (5H multiplet, typical for benzoyl protons).

2″-O-*Benzoyl-penta*-N-*ethoxycarbonyl-4″,6″*-O-*isopropylidene-3′,4′-di*-O-*mesylkanamycin B* (**6**). To a solution of **5** (1.18 g) in pyridine (15 m*l*), methanesulfonyl chloride (0.56 g) was added and the solution was allowed to stand at room temperature for 1.5 hr. On tlc with chloroform–ethanol (12 : 1), a spot (R_f 0.30, mono-*O*-mesyl derivative) which appeared in an early stage of the reaction disappeared and a spot (R_f 0.35) appeared. After addition of water (0.1 m*l*), the solution was concentrated *in vacuo* to one-third volume and poured into water. Resulting precipitates were filtered, washed with water and dried yielding 1.32 g (96%), mp 198°C, $[\alpha]_D^{22}$ +107° (*c* 1.5, DMF); IR (KBr): 1735, 1720, 1700, 1540, 1350 (broad), 1175 (νSO_2); 1035, 965, 930 (sh), 877 (w), 865 (w), 850, 827, 782, 757 (w), 712 cm^{-1}.

Found: C, 47.36; H, 6.06; N, 5.38; S, 5.57%. Calcd for $C_{45}H_{69}N_5O_{25}S_2$: C, 47.24; H, 6.08; N, 6.12; S, 5.60%.

NMR (in pyridine-d_5): τ 8.95, 8.91 and 8.78 (3H, 6H and 6H triplet, respectively, *J* 6.7 Hz, $NHCO_2CH_2C\underline{H}_3$), 8.66 and 8.55 (both 3H singlets, isopropylidene).

2″-O-*Benzoyl-3′,4′-dideoxy-3′-eno-penta*-N-*ethoxycarbonyl-4″,6″*-O-*isopropylidenekanamycin B* (**7**). To a solution of **6** (100 mg) in dry DMF (2 m*l*), dry sodium iodide (1.1 g) and zinc dust (500 mg) were added and the mixture was heated in an oil bath (95±1°C) for 1 hr under vigorous stirring. A hot mixture of chloroform (10 m*l*) and water (10 m*l*) were added and, after stirring for a while, the mixture was filtered and the solid separated was washed with a mixture of chloroform–methanol (1 : 1, 2 m*l*×2). The filtrate and the washings were combined and the organic layer was washed successively with water, sodium thiosulfate solution and with water again, dried over sodium sulfate and evaporated to give a solid (94 mg). On tlc with benzene–ethyl acetate (1 : 3), the solid showed four spots of R_f 0.53 (**6**), 0.43 (**7**), 0.32 and 0.22 (major). The undesirable products (R_f 0.53, 0.32 and 0.22) were successfully removed from the solid by extraction with ethyl acetate several times. The residue (32 mg, 38%) was dissolved in a mixture of methanol (0.1 m*l*) and chloroform (0.2 m*l*) and to the solution, ethyl acetate (0.7 m*l*) was added. **7** gradually crystallized, mp 282—284°C, $[\alpha]_D^{21}$ +36° (*c* 4, DMF); IR (KBr): 1735, 1700 (s, sharp), 1540; 1040, 1030, 987, 950 (w), 925 (vw), 867 (w), 850 (w), 783, 745 (w), 714 cm^{-1}.

Found: C, 54.00; H, 6.71; N, 7.52%. Calcd for $C_{43}H_{63}N_5O_{19}$: C, 54.14; H, 6.66; N, 7.34%.

NMR (in pyridine-d_5): τ 8.97, 8.85, 8.81 and 8.78 (6H, 3H, 3H and 3H triplet, respectively, *J* 6.7 Hz, $NHCO_2CH_2C\underline{H}_3$), 8.56 and 8.51 (both 3H singlets, isopropylidene), 4.04 (2H s, H-3′,4′).

The major product (R_f 0.22) was proved not to be a deacetonation product of **7**; the structure is now under study.

2″-O-*Benzoyl-3′,4′-dideoxy-penta*-N-*ethoxycarbonyl-4″,6″*-O-*isopropylidenekanamycin B* (**8**). To a solution of **7** (115 mg) in a mixture of dioxane (4.5 m*l*), methanol (2.5 m*l*) and water (2.5 m*l*), platinum oxide (40 mg, preactivated with hydrogen) was added and the mixture was hydrogenated under

pressure (50 lbs/sq. inch) for 5 hr. The solution was filtered and the filtrate was evaporated to give a colorless solid (110 mg, 96%), which was dissolved in dioxane, and recrystallized by the addition of water, mp 271—272°C, $[\alpha]_D^{22}$ +93.5° (*c* 0.4, DMF).

Found: C, 54.15; H, 6.75; N, 7.64%. Calcd for $C_{43}H_{65}N_5O_{19}$: C, 54.02; H, 6.85; N, 7.33%.

NMR (in pyridine-d_5): τ 9.08, 8.97, 8.83 and 8.79 (3H, 3H, 3H and 6H triplet, respectively, *J* 6.7 Hz, $NHCO_2CH_2\text{-}C\underline{H}_3$), 8.60 and 8.51 (both 3H singlets, isopropylidene), 7.8—8.5 (~4H unresolved broadened signals, CH_2CH_2 at C-3′ and 4′), 5.5—6.5 (~24H m, skeleton protons and $NHCO_2C\underline{H}_2CH_3$), 4.42 and 3.93 (each 1H d, *J* 3 Hz, H-1′, 1″).

*2″-O-Benzoyl-3′,4′-dideoxy-penta-N-ethoxycarbonylkanamycin B (**9**).* A solution of **8** (98 mg) in a mixture of water (0.5 m*l*) and acetic acid (0.8 m*l*) was heated in a boiling water bath for 5 min and the solution was allowed to stand at room temperature to give crystalline **9**. The mixture was stored in a refrigerator for several hours and the crystals were filtered, washed with cold water and dried to yield 73 mg (78%), mp 247—249°C, $[\alpha]_D^{24}$ +89° (*c* 2.7, DMF); IR (KBr): 1735 (sharp), 1700 (sharp), 1540; 1035, 1015 (sh), 990, 945 (w), 905 (w), 880 (w), 782, 720 cm^{-1}.

Found: C, 52.41; H, 6.54; N, 7.92%. Calcd for $C_{40}H_{61}N_5O_{19}$: C 52.45; H, 6.71; N, 7.65%.

*3′,4′-Dideoxykanamycin B (**10**).* A mixture of **9** (30 mg) and barium hydroxide octahydrate (250 mg) in aqueous dioxane (1 and 0.8 m*l*) was heated in a boiling water bath for 4.5 hr. Carbon dioxide was introduced, and the resulting suspension was heated for a while and centrifuged. The supernatant layer and the washings combined were evaporated to give a residue, which on paper chromatogram showed two spots of $R_{f\,\text{kanamycin B}}$ 1.3 (major, **10**) and 2 (minor); on tlc with the same solvent system, the residue also showed two spots of R_f 0.13 (major) and 0.26. The residue was charged on a column of Amberlite IRC-50 (NH_4 form) and, after washing with water, developed with 0.1—0.5 N ammonia with gradual increase of concentration. The minor substance (R_f 0.26 on tlc) was eluted with 0.3 N ammonia and the major with 0.5 N ammonia. The latter fraction was evaporated to give a solid, 9.6 mg (65%), $[\alpha]_D^{20}$ +132° (*c* 0.65, water).

Found: C, 48.05; H, 8.49; N, 15.54%. Calcd for $C_{18}H_{37}N_5O_8$: C, 47.88; H, 8.26; N, 15.51%.

Hydrolysis of 3′,4′-Dideoxykanamycin B. A solution of 3′,4′-dideoxykanamycin B in **6** N hydrochloric acid was heated at 95°C for 2 hr. Paper chromatogram of the resulting solution showed three spots of $R_{f\,\text{deoxystreptamine}}$ 1 (2-deoxystreptamine), 3 (3-amino-3-deoxy-D-glucose) and 2. The latest was assigned to be the spot of 2,6-diamino-2,3,4,6-tetradeoxyerythrose, which was obtained from the hydrolysis of methyl 2,6-diamino-2,3,4,6-tetradeoxy-α-D-erythropyranoside.[4]

The authors wish to thank Mr. Saburo Nakada for the elemental analysis.

BULLETIN OF THE CHEMICAL SOCIETY OF JAPAN, VOL. 45, 3628—3633 (1972)

Crystal and Molecular Structure of ω-Amino Acids, ω-Aminosulfonic Acids and Their Derivatives. I. The Crystal and Molecular Structure of γ-Guanidinobutyric Acid Hydrochloride and Hydrobromide

Tomie MAEDA, Takaji FUJIWARA, and Ken-ichi TOMITA

Faculty of Pharmaceutical Sciences, Osaka University, Toneyama, Toyonaka, Osaka

(Received May 12, 1972)

The crystals of γ-guanidinobutyric acid (GGBA) hydrochloride and hydrobromide, $C_5H_{12}O_2N_3Cl$ and $C_5H_{12}O_2N_3Br$, are both triclinic, space group $P\bar{1}$, with two molecules in a unit cell with the following dimensions; hydrochloride: $a=7.41$, $b=9.12$, $c=7.25$ Å, $\alpha=101.5°$, $\beta=112.4°$, $\gamma=65.2°$; hydrobromide: $a=7.94$, $b=9.36$, $c=7.78$ Å, $\alpha=103.2°$, $\beta=115.5°$, $\gamma=61.5°$. The X-ray structure analysis was carried out by the application of heavy atom method and refined by three dimensional least-squares method. Since GGBA hydrochloride and hydrobromide are isomorphous, the structure analysis was started by using of X-ray data of the hydrobromide to determine the rough atomic coordinates of its molecule, and the data of hydrochloride were used for the further refinement. The positions of the involved twelve hydrogen atoms were located by a three dimensional difference Fourier analysis. GGBA cation, $^{+}NH_2(NH_2)CNH(CH_2)_3COOH$, and Cl^- ion were almost perfectly on the $(20\bar{1})$ plane and formed a pararell sheet structure with six hydrogen bonds. The possible resonance structures were also discussed.

γ-Guanidinobutyric acid (GGBA) is one of the amino acids related to γ-aminobutyric acid (GABA), which was first discovered in mammalian brain by Roberts and Frenkel[1] and others,[2-3] and was also found in *Crustacea* as a depressive transmitter by Elliott *et al.*,[4,5] or in cerebral cortex of mammalian brain as an anti-convulsive substance by Hayashi and Nagai.[6] Since then, the significance of GABA has been widely studied from the physiological and biological standpoints. On the other hand, GGBA has been found in

1) E. Roberts and S. Frenkel, *J. Biol. Chem.*, **187**, 55 (1950).
2) J. Awapara, A. J. Landau, R. Everet, and B. Seale, *ibid.*, **187**, 35 (1950).
3) S. Udenfriend, *ibid.*, **187**, 65 (1950).
4) A. Bazemore, K. A. C. Elliott, and E. Florey, *Nature*, **178**, 1052 (1956).
5) K. A. C. Elliott and E. Florey, *J. Neurochem.*, **1**, 181 (1956).
6) T. Hayashi and K. Nagaki, Abstr. XX Inst. Physiol. Congr. 410 (1956).

brain as a complex of GABA with basic amino acid,[7,8] and it acts as a depressive substance in peripheral nervous system of *Crustacea*,[9] as a stimulant in mammalian brain,[10,11] and as a convulsive substance in cerebrum of rabbit.[12]

The crystal and molecular structure of GGBA, therefore, is of most interest in order to elucidate the correlation between its structural specificity and pharmacological action of GABA, GGBA and other related ω-amino acids. Preliminary structural feature of these compounds has been discussed,[13] and this paper deals with the precise structure analysis of GGBA hydrochloride and hydrobromide.

Experimental

GGBA was synthesized from GABA and methyl-isothiourea sulfate, confirmed by Sakaguchi's and ninhydrin reactions, and recrystallized from aqueous solution at room temperature.

The crystals of GGBA were dissolved in concentrated solution of hydrochloric acid or hydrobromic acid and the crystals of GGBA hydrochloride or hydrobromide were obtained after staying for about three days. They are both colorless needles and the marked cleavage plane is parallel to $(20\bar{1})$. Intensity data were collected by the multiplefilm method of the equi-inclination Weissenberg photographs with Ni-filtered Cu-$K\alpha$ radiation and estimated by visual comparison with a calibrated scale. Lorentz-polarization and spot-shape correction were applied, but no correction for absorption.

Weissenberg photographs around the *a*- and *b*- axes demonstrated that almost all the crystals of hydrochloride and hydrobromide were twins consisting of two components, in which *a**- and *b**- axes have the opposite directions for each component in the reciprocal lattice.

The two-dimensional intensity data for (*h*0*l*) and (0*kl*) reflections of hydrobromide were collected, in which almost all the reflections of each component were separable except a few overlapped reflections. A single crystal of hydrochloride was incidentally obtained and the three-dimensional intensity data around the *a*- and *b*- axes were collected and totally 1435 independent reflections were used for the refinement.

Unit cell parameters of GGBA hydrochloride and hydrobromide were determined by Weissenberg and precession photographs and the space group $P\bar{1}$ was confirmed by statistical method. Densities were measured by floatation method with benzene and carbon tetrachloride mixture. Crystallographic data so obtained are listed in Table 1.

Structure Determination

GGBA hydrochloride and hydrobromide seem to be isomorphous, as shown in Table 1. The Patterson projections on (010) and (100) planes of hydrochloride and hydrobromide are similar and, therefore, the molecular structure and packing in the crystal lattice should be similar in both crystals.

Table 1. Crystal data

γ-Guanidinobutyric acid

Hydrobromide $C_5H_{12}O_2N_3Br$ (M.w=226.13)

Hydrochloride $C_5H_{12}O_2N_3Cl$ (M.w=181.73)

Cell constant	Hydrobromide	Hydrochloride
a (Å)	7.94±0.03	7.41±0.04
b (Å)	9.36±0.01	9.12±0.02
c (Å)	7.78±0.02	7.25±0.03
α (°)	103.2±0.2	101.5±0.3
β (°)	115.5±0.3	112.4±0.5
γ (°)	61.5±0.3	65.2±0.3
Space group	$P\bar{1}$	$P\bar{1}$
Crystal system	Triclinic	Triclinic
Z	2	2
V (Å^3)	459.08	410.80
D_o (g·cm^{-3})	1.664	1.429
D_c (g·cm^{-3})	1.654	1.433

The structure determination was carried out by the usual heavy atom method. To determine the coordinates of heavy atoms, bromine and chlorine, in the unit cell, the Patterson projections along the *a*- and *b*-axes were calculated. The coordinates of light atoms except hydrogen atoms in GGBA hydrobromide could be determined from the Fourier projections on (010) and (100) planes of GGBA hydrobromide with the phase based on the coordinate of heavy atom.

In the following stage, the three-dimensional full data of hydrochloride were used. Since GGBA molecule itself has pseudo center of symmetry at the midpoint of C_β–C_γ bond and the both end groups of the molecule occupied by oxygen or nitrogen atoms have similar scattering power for X-ray, it is difficult to distinguish which end group is carboxyl or guanidyl group.

In Fig. 1, model (1) shows the Fourier map calculated with one chlorine and ten carbon atoms on the supposition that GGBA molecule is constituted by carbon atom alone, and model (2) and (3) give both Fourier maps calculated from two models in which the former has guanidyl group as the left terminal group and the latter as the right terminal group of GGBA molecular chain. From these Fourier maps, overall feature of peak heights in (1) is similar to that in (2) and the peak corresponding to N(3) in (2) has reasonable height but the peak in (3) is too high to assume it as a carbon atom. Therefore, Fourier map by the model (2) was thought to show the most probable electron density distribution of this compound, and it was also confirmed by the following least-squares refinement.

Table 2 lists up the isotropic temperature factors for each atoms, the scale factors for F_o, k, and R-index, $R=\Sigma||F_o|-|F_c||/\Sigma|F_o|$, for two models, (2) and (3), after five cycles of block-diagonal least-squares refinement. In this table, several features will be

7) J. J. Pisano, D. Abraham, and S. Udenfriend, *Arch. Biochem. Biophys.*, **100**, 323 (1963).
8) F. Irreverre, R. L. Evans, A. R. Hayden, and R. Silber, *Nature*, **180**, 704 (1957).
9) C. Edwards and S. W. Kuffer, *J. Neurochem.*, **4**, 19 (1959).
10) H. Takahashi, B. Arai, and C. Koshino, *Jap. J. Physiol.*, **11**, 403 (1961).
11) D. P. Purpura, M. Girado, and H. Grundfest, *Science*, **127**, 1179 (1958).
12) D. Jinnai, A. Sawai, and A. Mori, *Nature*, **212**, 617 (1966).
13) K. Tomita, *Tetrahedron Lett.*, **1971**, 2587.

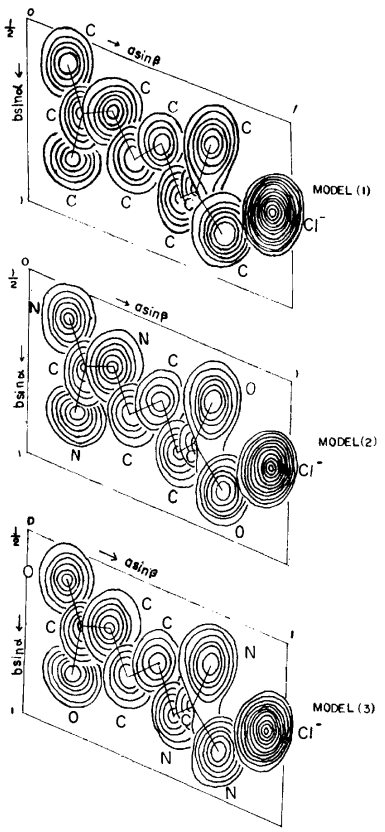

Fig. 1. The electron density maps for three models, viewed down along the c-axis.

TABLE 2. THE ISOTROPIC TEMPERATURE FACTORS ($Å^{-2}$)

Model (2)		Model (3)	
Cl^-	3.13	Cl^-	3.15
N(1)	3.22	O(1)	5.34
N(2)	3.00	O(2)	5.09
C(1)	2.72	C(1)	2.31
N(3)	2.72	C(2)	1.33
C(2)	3.77	C(3)	3.38
C(3)	3.46	C(4)	3.59
C(4)	3.72	N(1)	4.88
C(5)	3.72	C(5)	3.02
O(1)	3.53	N(2)	1.87
O(2)	4.24	N(3)	2.75
$R=0.299$		$R=0.324$	
$k=0.961$		$k=0.974$	

noted. For example, in comparison of N(1) in model (2) with O(1) in model(3), the temperature factor of O(1) is found to be larger than that of N(1). Considering that all atoms of GGBA molecule are covalently bonded with each other, it seems reasonable that the temperature factors of all atoms might be nearly equal as found in model (2) in Table 2. Therefore, if the resultant scale factor, k, is equal for two models and the model(2) is correct, the temperature factor of the oxygen atom assigned improperly in model(3) might become larger and that of nitrogen atom should be much smaller for the minimizing of the difference between $|F_o|$ and $|F_c|$.

The block-diagonal least-squares refinement was then carried out on the structure corresponding to the model (2). After five cycles of refinement with isotropic temperature factors to all the non-hydrogen atoms, the R-index value reduced to 0.254. Further five cycles of refinement with anisotropic temperature factor to chlorine atom and isotropic temperature factors to other ten atoms dropped the R-index to 0.195.

At this stage, a difference Fourier synthesis was computed in order to find the hydrogen atoms and all twelve hydrogen atoms could be located. After several cycles of refinement with anisotropic temperature factors to all non-hydrogen atoms, the R-index dropped to 0.153. One more refinement with all the twenty-three atoms including hydrogen atoms with isotropic temperature factors was performed to reduce the R-factor to 0.143 (0.129 except $F_o=0$). The agreement between the observed and calculated struc-

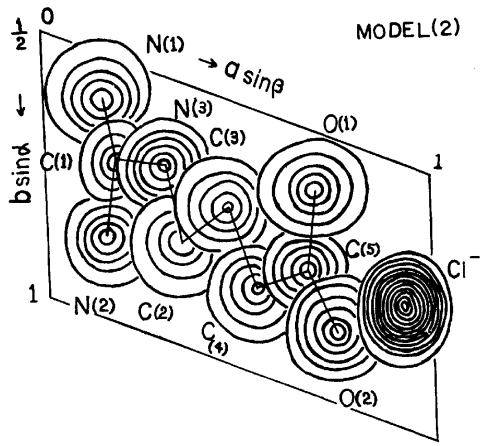

Fig. 2. A view of sections of final electron density map along the c-axis. Contours are at intervals of $2\,eÅ^{-3}$, starting with the contour of $1\,eÅ^{-3}$.

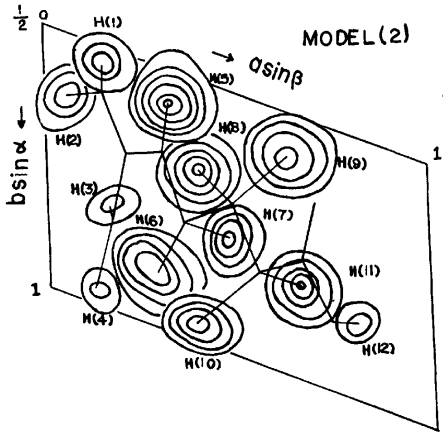

Fig. 3. A view of sections of a difference map for the location of hydrogen atoms along the c-axis. Contours are at intervals of $0.2\,eÅ^{-3}$, starting with the contour of $0.1\,eÅ^{-3}$.

Table 3. Final fractional coordinates and their standard deviations (in Å) of GGBA hydrochloride

	x	$\sigma(x)$	y	$\sigma(y)$	z	$\sigma(z)$
Cl^-	0.9370	0.003	0.7677	0.003	1.8913	0.002
N(1)	0.1428	0.010	0.5894	0.008	0.3033	0.007
N(2)	0.1739	0.011	0.8349	0.007	0.3635	0.007
C(1)	0.2078	0.011	0.6963	0.009	0.4314	0.007
N(3)	0.3049	0.010	0.6679	0.008	0.6227	0.007
C(2)	0.3781	0.013	0.7835	0.009	0.7746	0.007
C(3)	0.4862	0.012	0.7049	0.010	0.9762	0.008
C(4)	0.5608	0.013	0.8288	0.009	1.1345	0.008
C(5)	0.6658	0.011	0.7654	0.009	1.3420	0.008
O(1)	0.6845	0.010	0.6410	0.007	1.3844	0.006
O(2)	0.7394	0.009	0.8666	0.007	1.4747	0.005

Final anisotropic temperature factors and their standard deviations ($\times 10^4$). The anisotropic temperature factors are in the form of $\exp\{-(B_{11}h^2+B_{22}k^2+B_{33}l^2+B_{12}hk+B_{13}hl+B_{23}kl)\}$

	B_{11}	σB_{11}	B_{22}	σB_{22}	B_{33}	σB_{33}	B_{12}	σB_{12}	B_{13}	σB_{13}	B_{23}	σB_{23}
Cl^-	280	7	170	4	43	3	−173	9	10	8	49	6
N(1)	276	25	80	11	67	13	−135	28	46	29	−13	19
N(2)	370	30	48	10	95	15	−137	29	80	34	6	19
C(1)	219	26	81	12	25	13	16	29	41	29	63	20
N(3)	280	25	90	11	44	12	−129	29	−4	28	4	19
C(2)	359	34	79	13	14	13	−131	35	9	34	17	20
C(3)	304	32	86	13	30	14	−144	34	−8	33	31	21
C(4)	358	34	72	13	23	13	−122	34	19	34	2	20
C(5)	238	28	75	13	48	15	−24	31	56	32	25	21
O(1)	450	29	91	10	70	12	−229	28	0	29	53	17
O(2)	409	26	83	9	32	10	−200	26	31	26	−9	15

Table 4. The atomic coordinates for the hydrogen atoms of GGBA hydrochloride

Atom	Bonded to	x	y	z
H(1)	N(1)	0.198	0.502	0.399
H(2)	N(1)	0.067	0.631	0.175
H(3)	N(2)	0.090	0.842	0.204
H(4)	N(2)	0.203	0.938	0.420
H(5)	N(3)	0.308	0.554	0.626
H(6)	C(2)	0.228	0.901	0.773
H(7)	C(2)	0.483	0.815	0.725
H(8)	C(3)	0.381	0.676	1.016
H(9)	C(3)	0.627	0.592	0.974
H(10)	C(4)	0.420	0.943	1.130
H(11)	C(4)	0.672	0.858	1.100
H(12)	O(2)	0.810	0.839	1.601

ture amplitudes is reasonable.[14]

The final electron density map and the difference map indicating the locations of the twelve hydrogen atoms are shown in Figs. 2 and 3, respectively. The final atomic coordinates and anisotropic temperature factors are listed in Table 3, and the coordinates for hydrogen atoms are given in Table 4.

All the numerical computations were carried out on the NEAC 2203, the NEAC 2200—500 computers of this University, and the HITAC 5020E of the Computer Centre, University of Tokyo. The programs used for the correction of X-ray data, three-dimensional Patterson and Fourier syntheses and difference Fourier synthesis are written by one of the authors (T.F) and that for the block-diagonal least-squares refinement of the structure is written by Dr. Tamaichi Ashida.

Results and Discussion

The bond lengths and angles are shown in Fig. 4 (a) and (b), and also listed in Table 5 with their esti-

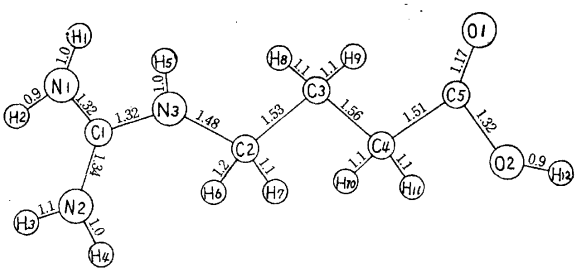

Fig. 4. (a) Bond distances (in Å) of GGBA hydrochloride.

14) A complete list of the observed and calculated structure factors has been submitted to, and is kept as Document No. 7212 at the office of the Bulletin of the Chemical Society of Japan, 1-5 Kanda-Surugadai, Chiyodaku, Tokyo. A copy may be secured by citing the Document number. Pay by check or money order payable to: The Chemical Society of Japan.

TABLE 5. BOND DISTANCES AND ANGLES OF GGBA HYDROCHLORIDE

N(1)-C(1)	1.318±0.015 (Å)	N(1)-C(1)-N(2)	118.7±1.0 (°)
N(2)-C(1)	1.338±0.015	N(2)-C(1)-N(3)	120.3±1.0
N(3)-C(1)	1.317±0.014	N(1)-C(1)-N(3)	120.9±1.0
C(2)-N(3)	1.477±0.016		
C(2)-C(3)	1.528±0.017	C(1)-N(3)-C(2)	123.7±1.0
C(3)-C(4)	1.557±0.016	N(3)-C(2)-C(3)	107.8±1.0
C(4)-C(5)	1.510±0.017	C(2)-C(3)-C(4)	107.1±1.0
C(5)-O(1)	1.173±0.015	C(3)-C(4)-C(5)	111.8±1.0
C(5)-O(2)	1.320±0.014		
		C(4)-C(5)-O(2)	111.9±1.0
		O(2)-C(5)-O(1)	122.7±1.1
		C(4)-C(5)-O(1)	125.5±1.1

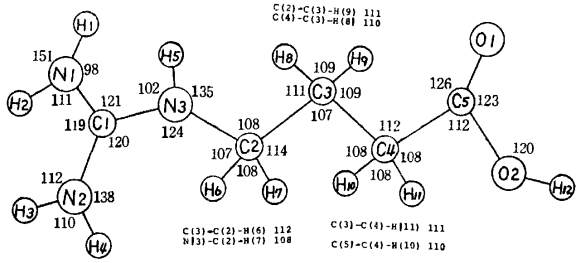

Fig. 4. (b) Bond angles (in degree) of GGBA hydrochloride.

mated standard deviations.

In guanidyl group, the average of three C–N bond lengths; 1.32, 1.32 and 1.34 Å, is 1.33 Å. These values are very similar to those reported so far in other compounds[15-19] with guanidyl group. However, these C–N bond distances are halfway between the normal C–N single bond length (1.47 Å) and the pure double bond distance (1.24 Å) proposed by Shomaker *et al.*[20]

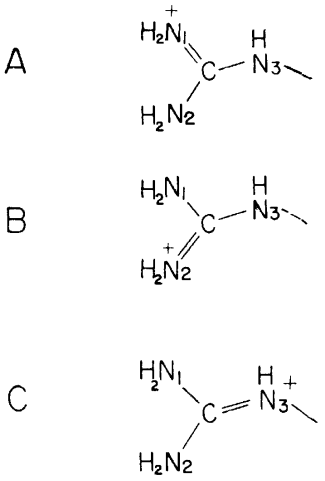

Fig. 5. Resonance of the guanidyl group in GGBA molecule.

Therefore, three C–N bonds of GGBA molecule have somewhat double bond character and the calculation by Pauling's method[21] indicated that the double bond characters of C(1)–N(1), C(1)–N(2) and C(1)–N(3) bonds are about 35%, 29% and 36% respectively. The major three resonance structures, A, B and C of the guanidyl group in GGBA cation, are shown in Fig. 5.

Three N–C–N angles, 119°, 120° and 121°, are not different with each other within the standard deviation. Similar bond angles are reported in guanidium chloride[17] and L-arginine dihydrate.[19]

The guanidyl group is attached to the carbon chain by a normal C–N bond of 1.48 Å. The average of the three C–C bond lengths is 1.53 Å and the C(3)–C(4)–C(5) angle of 112° is significantly larger than the other two angles, 107° and 108°.

The skeletal conformation of GGBA molecule is the 'trans-zigzag' form which is also found in GABA hydrochloride.[22]

In carboxyl group, C(5)–O(1) and C(5)–O(2) bond lengths are 1.17 and 1.32 Å respectively, and the three angles around the C(5) atom are 123°, 125° and 112° respectively. These values are not particularly different from those reported for α-amino acids so far investigated. However, C(5)–O(1) bond length is significantly shorter than C(5)–O(2) bond distance, and the angle of C(4)–C(5)–O(2) is smaller than that of C(4)–C(5)–O(1). Therefore, a hydrogen atom attaches to O(2) atom, which is confirmed by the difference Fourier synthesis, and GGBA hydrochloride is of the form, $^{+}NH_2(NH_2)CNH(CH_2)_3COOH \cdot Cl^{-}$, and GGBA molecule has probably zwitter-ion structure in free state. A similar conclusion is also reported in GABA hydrochloride[22] and L-leucine hydrobromide.[23]

The molecule of GGBA hydrochloride is almost perfectly planar and lies nearly on the (20$\bar{1}$) plane as shown in Fig. 6. The deviations of individual atoms from a least-squares plane are listed in Table 6. Six hydrogen atoms attached to nitrogen and oxygen

15) J. Drenth, W. Drenth, A. Vos and E. H. Wiebenga, *Acta Crystallogr.*, **6**, 424 (1953).
16) C. N. Morimoto and E. C. Lingafelter, *ibid.*, **B26**, 335 (1970).
17) D. J. Haas, D. R. Harris and H. H. Mills, *ibid.*, **19**, 676 (1965).
18) J. H. Bryden, L. A. Burkardt, E. W. Hughes and J. Donohue, *ibid.*, **9**, 573 (1956).
19) I. L. Karle and J. Karle, *ibid.*, **17**, 835 (1964).
20) V. Shomaker and D. P. Stevenson, *J. Amer. Chem. Soc.*, **63**, 37 (1941).
21) L. Pauling, "The Nature of the Chemical Bond," 3rd ed., Ithaca, Cornell University Press (1960).
22) K. Tomita, *Jap. J. Brain Physiol.*, **61**, 1 (1966).
23) E. Subramanian, *Acta Crystallogr.*, **22**, 910 (1967).

Table 6. The equation of a least-squares plane and deviations of the individual atoms from this plane

$0.89028X-0.43109Y-0.14687Z+0.17068=0,$

Cl^-	−0.03 (Å)	C(3)	+0.04 (Å)
N(1)	+0.01	C(4)	−0.02
N(2)	−0.02	C(5)	+0.00
C(1)	+0.00	O(1)	+0.00
N(3)	+0.01	O(2)	+0.03
C(2)	−0.02		

Table 7. The hydrogen bond distances

N(1)−H···O(1)	2.934±0.016 (Å)
N(2)−H···O(2)	2.970±0.014
N(3)−H···O(1)	2.775±0.017
N(1)−H···Cl^-	3.206±0.010
N(2)−H···Cl^-	3.266±0.009
O(2)−H···Cl^-	2.947±0.012

atoms lie also on the plane, but the other six hydrogen atoms attaching to the carbon atoms are situated above and below this plane.

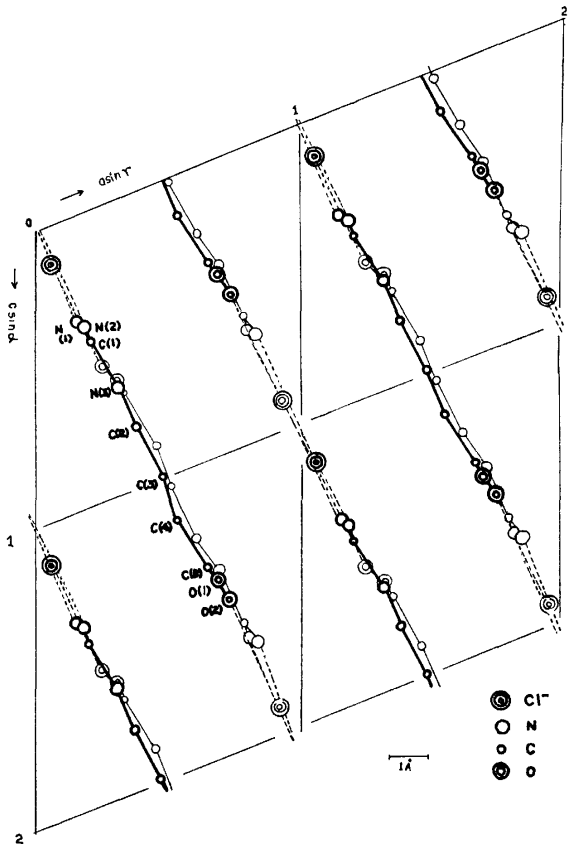

Fig. 6. A drawing of the structure of GGBA hydrochloride viewed down along the *b*-axis. The dashed lines indicate the hydrogen bonding.

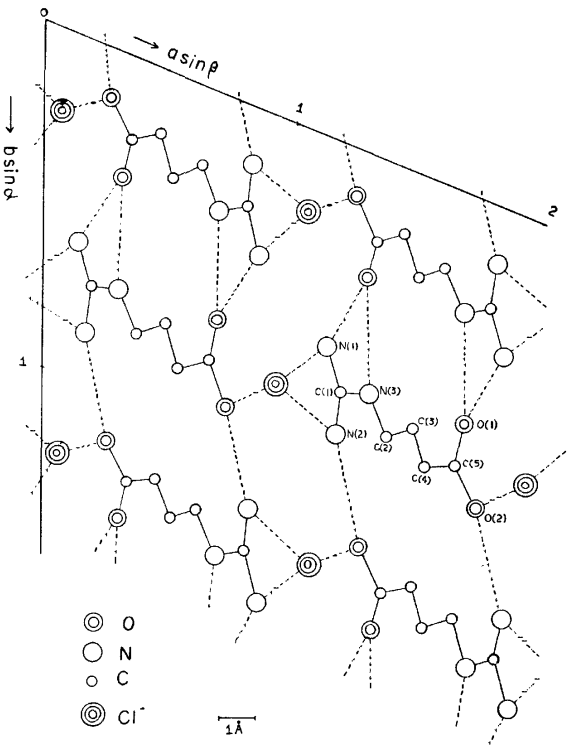

Fig. 7. A drawing of the structure of GGBA hydrochloride viewed down along the *c*-axis. The dashed lines indicate the hydrogen bonding.

The structure as viewed down the *c*-axis is shown in Fig. 7 and the hydrogen bond lengths are listed in Table 7. In guanidyl group, five hydrogen atoms attached to nitrogen atoms are used to form three N-H···O hydrogen bonds, 2.78 Å, 2.93 Å and 2.97 Å, and two N-H···Cl^- hydrogen bonds, 3.21 Å and 3.27 Å. One hydrogen atom attached to O(2) forms O-H···Cl^- hydrogen bond, 2.95 Å in length. Similar hydrogen bond lengths are reported in L-arginine dihydrate[19], L-tryptophan hydrochloride[24] and L-cystine hydrochloride.[25] All hydrogen bonds hold molecules together to form parallel sheets along $(20\bar{1})$ plane and no interaction except van der Waals force acts between the adjacent molecular planes as shown in Fig. 6 which is viewed down along the *b*-axis. This result explains the existence of the marked cleavage on $(20\bar{1})$ plane in the crystal.

This investigation was partly supported by the research grant from the Ministry of Education, Japan. We wish to express our sincere thanks for this support.

24) T. Takigawa, T. Ashida, Y. Sasada, and M. Kakudo, This Bulletin, **39**, 2369 (1966).

25) L. K. Steinrauf, J. Peterson, and L. H. Jensen, *J. Amer. Chem. Soc.*, **80**, 3835 (1958).

Crystal and Molecular Structure of ω-Amino Acids, ω-Amino Sulfonic Acids and Their Derivatives. II. The Crystal and Molecular Structure of α-Form of 3-Aminopropane Sulfonic Acid, Homotaurine

Sumiko UEOKA,* Takaji FUJIWARA, and Ken-ichi TOMITA

Faculty of Pharmaceutical Sciences, Osaka University, Toneyama, Toyonaka, Osaka

(Received May 12, 1972)

From ethanol aqueous solution, two forms of crystals of 3-aminopropane sulfonic acid (homotaurine) have been obtained in different crystal systems. The α-form is orthorhombic, space group $Pmn2_1$, with two molecules in a unit cell of the dimensions; $a=7.059$, $b=5.492$ and $c=7.428$ Å. The X-ray structure analysis was carried out by the application of usual heavy atom method and refined by three dimensional least-squares procedure. The final R-value is 0.059. In the crystalline state, homotaurine molecule has the zwitterionic structure, $NH_3^+-CH_2-CH_2-CH_2-SO_3^-$, with *trans-zigzag* skeletal configuration, and non-hydrogen atoms except two oxygen atoms lie exactly on a mirror plane. Each molecule in the crystal is connected by three dimensional network of three NH···O hydrogen bonds.

As described in previous papers,[1-3] we have been interested in the relationship between molecular conformation and physiological action of ω-amino acids and ω-amino sulfonic acids. 3-Aminopropane sulfonic acid, homotaurine, is a structural analogue of γ-aminobutyric acid (GABA), and it has one more methylene group than taurine, 2-aminoethane sulfonic acid. As a specific inhibitor of impulse transmission in the central nervous system, the pharmacological properties and possible physiological role of GABA have been recently reviewed in detail,[4] and it has been reported that homotaurine has more potent inhibitory effect than those of taurine[4-7] and also has a hypotensive and a cardiotonic effect.[8-10] As the detailed structure of taurine was reported by Okaya,[11] we describe here the crystal and molecular structure of homotaurine, comparing its molecular conformation with that of taurine.

Experimental

The powder sample of homotaurine was kindly supplied by Prof. S. Tsunoo, School of Medicine, Showa University, Tokyo. Dissolving this sample into hot ethanol aqueous solution, it was kept cool for crystallization. We have obtained two crystallographically different crystals, α- and β-form; the former is crystallized by cooling slowly and the latter by rapid cooling. The structure analysis of β-form is now in progress and as a part of our investigation on the molecular conformation of ω-amino sulfonic acid, the report will be published in near future. Therefore, we wish to discuss here just the detailed crystal and molecular structure of the α-form.

The cell dimensions were obtained on a Rigaku Denki four circles diffractometer with Mo-$K\alpha$ radiation, and they were given in Table 1. According to the systematic absences of reflections ($h0l$; $h+l=2n+1$, $h00$; $h=2n+1$, $00l$; $l=2n+1$), the orthorhombic space groups, $P2_122_1$, $Pmnm$ and $Pmn2_1$, are all possible. In consequence of the density measurement by floatation in carbon tetrachloride and ethylene bromide mixture, the number of molecule in a unit cell is two. On the other hand, homotaurine molecule itself has no two-fold symmetry. Therefore, the space group of the crystal is determined to be $Pmn2_1$.

TABLE 1. CRYSTAL DATA OF 3-AMINOPROPANE-SULFONIC ACID (HOMOTAURINE)

Crystal system:	orthorhombic
Cell constants:	$a=7.059\pm0.005$ Å
	$b=5.492\pm0.006$ Å
	$c=7.428\pm0.004$ Å
Space group:	$Pmn2_1$
Density (obsd):	$D_o=1.610\pm0.002$ g/cm³
(calcd):	$D_c=1.605$ g/cm³

The prismatic crystal was cut down to be approximately $0.2\times0.2\times0.2$ mm for intensity measurement. The intensity data were collected on the Rigaku Denki computer controlled automatic four-circles diffractometer. The $\omega/2\theta$ scan technique using Zr-filtered Mo-$K\alpha$ radiation was employed. A total of 1143 independent reflections in the range of $\sin\theta/\lambda=0.95$ Å^{-1} were collected and these observed structure factors were converted into absolute values by a program for Wilson's statistics.

Structure Determination

As expected from the fact that the space group of the α-form is $Pmn2_1$ and the unit cell contains two molecules, homotaurine molecule should be located on a mirror plane.

The coordinate of sulfur atom was determined by vector relation on three Harker sections of the sharpened Patterson synthesis with coefficient of $|F_o|^2_{\text{mod.}}=$

* Present address: Osaka Branch, National Institute of Hygienic Sciences, Hoenzaka-cho, Higashi-ku, Osaka.

1) K. Tomita, *Tetrahedron Lett.*, **1971**, 2587.
2) K. Tomita, T. Fujiwara, and H. Higashi, *Jap. J. Brain Physiol.*, **111**, 4127 (1971).
3) T. Maeda, T. Fujiwara, and K. Tomita, This Bulletin, **45**, 3628 (1972).
4) D. R. Curtis and J. C. Watkins, *Pharmacol. Rev.*, **17**, 347 (1965).
5) D. R. Curtis and J. C. Watkins, *Nature*, **191**, 1010 (1961).
6) J. M. Crawford, *Biochem. Pharmacol.*, **12**, 1443 (1963).
7) J. M. Crawford and D. R. Curtis, *Brit. J. Pharmacol.*, **23**, 313 (1964).
8) S. Tsunoo, K. Horisaka, H. Tanabe, T. Chida, S. Nakajima, and Z. Fukai, *J. Showa Med. Assoc.*, **30**, 521 (1971).
9) S. Tsunoo, K. Horisaka, H. Tanabe, T. Chida, S. Nakajima, Z. Fukai, and S. Nakayama, *ibid.*, **30**, 721 (1971).
10) T. Furukawa, H. Kawasaki, N. Ono, K. Kushiku, and B. Nuki, *Folia Pharmacol. Japan.*, **67**, 131 (1971).
11) Y. Okaya, *Acta Crystallogr.*, **21**, 726 (1966).

Table 2(a). The final fractional coordinates and their standard deviations (in Å)

	x/a	y/b	z/c	$\sigma(x)$	$\sigma(y)$	$\sigma(z)$
S	0.0	0.1178	0.2000	0.0	0.001	0.001
O (1)	0.0	−0.1260	0.1269	0.0	0.003	0.004
O (2)	0.1713	0.2549	0.1515	0.002	0.002	0.002
O (3)	−0.1713	0.2549	0.1515	0.002	0.002	0.002
N	0.0	0.5523	0.8187	0.0	0.003	0.004
C (1)	0.0	0.0908	0.4362	0.0	0.004	0.004
C (2)	0.0	0.3386	0.5291	0.0	0.004	0.004
C (3)	0.0	0.3092	0.7310	0.0	0.004	0.003
H (1)	0.142	−0.025	0.471	0.04	0.05	0.04
H (2)	−0.142	−0.025	0.471	0.04	0.05	0.04
H (3)	0.145	0.438	0.479	0.04	0.04	0.04
H (4)	−0.145	0.438	0.479	0.04	0.04	0.04
H (5)	0.147	0.221	0.784	0.04	0.04	0.04
H (6)	−0.147	0.221	0.784	0.04	0.04	0.04
H (7)	0.139	0.625	0.802	0.05	0.05	0.05
H (8)	−0.139	0.625	0.802	0.05	0.05	0.05
H (9)	0.0	0.568	0.947	0.0	0.08	0.09

Table 2(b). The final temperature factors and their standard deviations ($\times 10^4$)
The anisotropic temperature factors are in the form of $\exp[-(\beta_{11}h^2+\beta_{22}k^2+\beta_{33}l^2+\beta_{12}hk+\beta_{13}hl+\beta_{23}kl)]$

	β_{11}	σ	β_{22}	σ	β_{33}	σ	β_{12}	σ	β_{13}	σ	β_{23}	σ
S	78	1	139	2	52	1	0	0	0	0	−40	3
O (1)	235	9	166	9	114	6	0	0	0	0	−112	13
O (2)	106	3	309	8	89	3	−127	9	42	6	−33	8
O (3)	106	3	309	8	89	3	127	9	−42	6	−33	8
N	114	5	203	10	65	4	0	0	0	0	−60	12
C (1)	147	7	137	9	57	4	0	0	0	0	15	10
C (2)	128	6	159	9	56	4	0	0	0	0	−27	11
C (3)	191	9	196	11	49	5	0	0	0	0	−12	11
	β (isotropic)	σ										
H (1)	1.8	0.9										
H (2)	1.8	0.9										
H (3)	2.2	1.1										
H (4)	2.2	1.1										
H (5)	2.3	1.1										
H (6)	2.3	1.1										
H (7)	3.3	1.3										
H (8)	3.3	1.3										
H (9)	3.7	2.0										

$|F_o|^2 \exp[2\beta(\sin\theta/\lambda)^2]$. All positions of the non-hydrogen atoms were easily determined by a Fourier synthesis with phases based on the sulfur atom. After successive Fourier refinements, the discrepancy factor, $R=\Sigma||F_o|-|F_c||/\Sigma|F_o|$, decreased to 0.20.

Further refinement was carried out by the block-diagonal least-squares method. After five cycles of refinement with isotropic temperature factors ($R=$ 0.12) and further five cycles with anisotropic temperature factors for all non-hydrogen atoms ($R=0.066$), a difference Fourier synthesis was calculated to determine the locations of hydrogen atoms. Six hydrogen atoms bound to carbon atoms and two hydrogen atoms connected on the nitrogen atom were satisfactorily located with reasonable peak heights. However, peak height for the last one which was thought to be bound to the nitrogen atom was about half of others. There was also no peak to be assigned as a hydrogen atom near the sulfonic oxygen atoms on the difference map. Further five cycles least-squares refinement of positional parameters with anisotropic temperature factors for non-hydrogen atoms and isotropic for hydrogen atoms reduced the R factor to 0.059 (0.054 for $F_o \neq 0$).

The final atomic coordinates and temperature factors together with their estimated standard deviations are given in Table 2. The observed and calculated structure factors are listed in Table 3.

All the numerical calculations were carried out on a NEAC 2200—500 in the computing center of this University, a FACOM 230—60 in the data processing center at the Kyoto University and a HITAC 5020E in the computing center at University of Tokyo, using the programs written by Dr. Tamaichi Ashida and by

TABLE 3. THE OBSERVED AND THE FINAL CALCULATED STRUCTURE FACTORS

H	FO	FC	H	FO	FC	H	FO	FC	H	FO	FC	H	FO	FC	H	FO	FC	H	FO	FC	H	FO	FC	H	FO	FC	H	FO	FC
K,L= 0 0			4	40	42	5	49	49	7	22	24	K,L= 7 3			6	28	28	8	26	26	5	23	22	2	118	118	0	102	108	0	27	23
2	559	581	5*	0	0	6	18	17	8	21	22	0	61	62	7	50	51	9	22	22	6	9	13	4	103	101	1	13	19	1	36	38
4	321	318	6	23	28	7	31	31	9	17	14	1	29	28	8	4	8	K,L= 7 5			7	14	15	6	50	53	2	63	64	2	44	46
6	311	317	K,L= 10 0			8*	0	11	K,L= 8 2			2	48	45	9	31	31	0	71	73	8	9	*9	8	56	57	3	16	14	3	33	34
8	118	114	0	16	6	K,L= 9 1			0	52	53	3	21	20	10	12	7	1	28	29	K,L= 8 6			10	39	37	4	51	57	4	37	38
10	78	75	1	7	13	0	12	14	1	12	6	4	43	40	K,L= 7 4			2	71	75	0	22	23	K,L= 1 8			5	11	10	5	25	26
12	53	56	2	8	10	1	22	23	2	38	37	5	15	16	0	22	22	3	26	26	1	13	14	0	65	61	6	65	66	6	16	10
K,L= 1 0			3	20	13	2	10	6	3	12	8	6	35	39	1	54	54	4	59	61	2	15	21	1	52	51	7	16	13	7	22	21
0	155	153	K,L= 0 1			3	24	23	4	30	33	7	10	17	2	21	19	5	17	19	3	13	10	2	60	56	8	30	27	8	20	21
1	388	398	1	266	271	4	2	7	5*	0	6	8	15	19	3	43	41	6	41	42	4	15	19	3	89	91	9	5	5	K,L= 2 11		
2	142	146	3	62	48	5	20	18	6	35	33	9*	0	6	4	18	12	7	20	17	5	19	9	4	50	48	K,L= 4 9			0	45	46
3	21	15	5	169	164	6	16	10	7	12	2	K,L= 8 3			5	42	41	8	29	31	6	15	16	5	38	39	0	16	14	1*	0	13
4	117	110	7	89	85	K,L= 10 1			8	21	14	0	13	20	6	8	14	K,L= 8 5			K,L= 9 6			6	43	41	1	75	77	2	43	43
5	178	176	9	29	25	0	13	9	K,L= 9 2			1	41	42	7	28	27	0	11	13	0	17	19	7	17	24	2	18	16	3	16	15
6	76	66	11	39	42	1*	0	9	0	24	23	2	23	20	8	8	9	1	26	25	1	16	17	8	29	29	3	43	44	4	36	36
7	103	99	13	21	18	2	15	9	1	10	11	3	34	33	9	17	16	2	8	11	2	15	17	9	35	33	4	18	16	5	5	13
8	42	45	K,L= 1 1			3	14	11	2	26	23	4	22	19	K,L= 8 4			3	23	22	3	9	14	10	11	17	5	60	59	6	31	31
9	26	24	0	270	269	K,L= 0 2			3	11	4	5	28	31	0	41	44	4*	0	9	K,L= 0 7			K,L= 2 8			6	7	7	7	14	6
10	30	32	1	400	418	0	458	480	4	22	21	6	15	11	1	27	27	5	22	20	1	44	32	0	77	73	7	40	41	K,L= 3 11		
11	40	44	2	212	195	2	186	147	5	6	10	7	23	21	2	30	33	6	13	8	3	85	84	1	148	146	8	8	4	0	28	33
12	17	15	3	271	274	4	146	129	6	11	14	8	8	7	3	22	23	7	11	14	5	37	36	2	36	32	K,L= 5 9			1	38	35
13	18	18	4	105	89	6	179	167	K,L= 10 2			K,L= 9 3			4	32	30	K,L= 9 5			7	28	27	3	124	124	0	49	46	2	13	10
K,L= 2 0			5	169	167	8	58	51	0*	0	6	0	16	19	5	22	19	0	7	11	9	39	41	4	26	21	1	52	54	3	33	31
0	159	152	6	114	109	10	44	42	1	17	16	1	30	34	6	25	28	1	15	19	11	21	16	5	96	98	2	36	33	4	9	14
1	107	116	7	100	100	12	33	35	2*	0	8	2	20	17	7	16	13	2	4	8	K,L= 1 7			6	41	42	3	53	53	5	21	25
2	143	130	8	37	30	K,L= 1 2			3	13	16	3	31	32	K,L= 9 4			3	19	17	0	100	91	7	70	72	4	28	26	6	22	24
3	115	116	9	64	65	0	182	195	K,L= 0 3			4	11	14	0	14	18	4*	0	7	1	84	80	8	11	13	5	42	42	7	16	21
4	72	63	10	29	26	1	184	188	1	485	496	5	25	26	1*	0	2	K,L= 0 6			2	88	86	9	47	44	6	32	28	K,L= 4 11		
5	99	100	11	41	37	2	166	166	3	125	115	6	10	11	2	18	17	0	130	122	3	74	71	10	9	4	7	18	26	0	19	18
6	46	43	12	28	28	3	110	103	5	217	224	K,L= 10 3			3*	0	6	2	102	111	4	74	72	K,L= 3 8			8	19	14	1	35	33
7	70	69	13	19	18	4	125	119	7	132	132	0	15	20	4	15	15	4	103	105	5	62	61	0	68	65	K,L= 6 9			2	22	19
8	38	37	K,L= 2 1			5	114	115	9	56	54	1	4	2	5	8	2	6	75	75	6	48	46	1	78	81	0	45	47	3	13	13
9	58	59	0	127	130	6	76	72	11	55	54	2	17	18	K,L= 10 4			8	52	56	7	45	47	2	59	58	1	26	22	4	19	16
10	10	12	1	53	50	7	61	63	13	25	24	K,L= 0 4			0	16	15	10	40	40	8	35	36	3	53	51	2	49	47	5	28	27
11	38	37	2	132	142	8	49	48	K,L= 1 3			0	254	248	K,L= 0 5			12	21	20	9	31	31	4	49	48	3	32	28	6	10	9
12*	0	6	3	172	168	9	14	15	0	264	259	2	146	133	1	163	154	K,L= 1 6			10	25	24	5	53	58	4	41	42	K,L= 5 11		
13	16	17	4	138	132	10	33	34	1	81	85	4	120	115	3	122	121	0	48	50	11	24	19	6	42	43	5	15	13	0	39	38
K,L= 3 0			5	30	34	11	30	33	2	108	87	6	122	116	5	115	115	1	124	122	K,L= 2 7			7	42	40	6	25	28	1	27	29
0	85	89	6	95	88	12	16	18	3	80	82	8	63	60	7	69	71	2	47	46	0	126	122	8	28	30	K,L= 7 9			2	26	26
1	11	8	7	12	3	13*	0	13	4	79	70	10	42	42	9	53	55	3	163	167	1	47	48	9	14	15	0	13	14	3	27	29
2	96	96	8	64	65	K,L= 2 2			5	63	63	12	24	26	11	40	36	4	42	41	2	115	111	10	18	16	1	1	9	4	18	21
3	164	163	9	31	32	0	274	262	6	112	111	K,L= 1 4			K,L= 1 5			5	83	80	3	28	27	K,L= 4 8			2	22	23	5	21	23
4	91	90	10	45	50	1	200	188	7	42	43	0	227	226	0	158	150	6	39	40	4	89	90	0	68	72	3	10	8	K,L= 6 11		
5	29	21	11	9	9	2	74	48	8	34	33	1	205	201	1	80	78	7	50	52	5	36	37	1	21	22	4	15	19	0	20	24
6	48	45	12	26	24	3	127	115	9	30	32	2	194	194	2	82	76	8	32	31	6	67	70	2	45	45	5*	0	5	1	13	8
7	42	39	13	14	0	4	49	32	10	33	30	3	191	195	3	73	73	9	49	51	7	20	15	3	23	26	K,L= 8 9			2	21	24
8	27	30	K,L= 3 1			5	92	97	11	14	19	4	148	148	4	70	66	10	25	19	8	44	47	4	37	39	0	14	18	3	12	12
9	59	59	0	175	169	6	81	77	12	28	26	5	123	121	5	64	64	11	22	22	9	2	10	5	18	19	1	20	17	K,L= 0 12		
10	27	29	1	189	184	7	67	71	13*	0	10	6	107	105	6	77	73	12	11	13	10	28	27	6	49	48	K,L= 0 10			0	31	35
11	15	12	2	209	203	8	18	19	K,L= 2 3			7	70	71	7	50	50	K,L= 2 6			11	11	11	7	9	10	0	69	71	2	50	53
12	0	11	3	154	157	9	50	52	0	144	149	8	71	70	8	28	30	0	35	37	K,L= 3 7			8	27	24	2	91	95	4	41	42
K,L= 4 0			4	143	140	10	5	7	1	27	22	9	51	50	9	32	33	1	85	87	0	108	107	9	15	10	4	76	74	6	23	22
0	126	125	5	103	107	11	33	33	2	141	138	10	51	45	10	19	24	2	62	64	1	44	44	K,L= 5 8			6	40	40	K,L= 1 12		
1	142	143	6	68	66	12	15	13	3	141	137	11	36	31	11	20	20	3	76	74	2	86	81	0	47	49	8	45	44	0	46	49
2	227	232	7	56	56	13	20	16	4	124	119	12	28	24	12	16	17	4	43	42	3	35	36	1	46	47	K,L= 1 10			1	26	27
3	109	112	8	80	81	K,L= 3 2			5	16	19	K,L= 2 4			K,L= 2 5			5	63	60	5	63	63	2	50	50	0	41	41	2	48	46
4	169	170	9	42	44	0	106	106	6	87	84	0	97	95	0	264	264	6	20	19	5	31	34	3	29	33	1	26	25	3	49	46
5	79	77	10	40	41	1	28	21	7	13	9	1	156	156	1	127	127	7	43	46	6	62	64	4	42	47	2	40	38	4	37	38
6	70	70	11	24	25	2	94	96	8	58	59	2	80	78	2	232	228	8	25	24	7	28	29	5	29	33	3	55	54	5	19	18
7	62	62	12	9	15	3	132	127	9	35	33	3	143	147	3	56	60	9	30	30	8	35	36	6	35	31	4	33	32	6	31	30
8	85	86	K,L= 4 1			4	81	86	10	44	43	4	50	48	4	176	174	10	6	9	9	19	18	7	24	24	5	11	13	K,L= 2 12		
9	30	28	0	32	29	5	21	18	11	10	5	5	116	113	5	73	76	11	16	18	10	8	19	8	22	22	6	28	27	0	22	17
10	44	44	1	142	138	6	52	55	12	19	22	6	39	37	6	132	129	K,L= 3 6			K,L= 4 7			K,L= 6 8			7	16	17	1	34	35
11	14	14	2	35	38	7	29	29	K,L= 3 3			7	75	76	7	44	45	8	44	43	0	22	18	0	26	24	8	20	19	2	8	7
12	12	15	3	203	201	8	35	38	0	131	132	8	22	25	8	85	84	1	107	108	1	63	63	1	44	45	9	21	23	3	28	31
K,L= 5 0			4	38	41	9	45	48	1	107	102	9	56	54	9	16	16	2	42	42	2	21	20	2	38	36	K,L= 2 10			4*	0	4
0	166	164	5	88	84	10	30	30	2	121	120	10	13	8	10	49	48	3	70	65	3	44	45	3	44	44	0	39	40	5	28	25
1	57	52	6	14	9	11	14	10	3	100	99	11	32	32	11	20	18	4	40	40	4	11	10	4	29	29	1	69	69	6	14	9
2	152	152	7	68	68	12*	0	13	4	91	89	12	12	8	12	28	27	5	71	74	5	50	52	5	33	34	2*	0	1	K,L= 3 12		
3	111	111	8	14	5	K,L= 4 2			5	73	72	K,L= 3 4			K,L= 3 5			6	20	24	6	5	9	6	13	12	3	56	58	0	18	19
4	115	113	9	61	64	0	71	63	6	57	57	0	97	93	0	146	147	7	50	52	7	41	40	7	17	20	4	11	7	1	47	49
5	43	38	10	13	11	1	38	38	7	38	39	1	160	159	1	111	106	8	18	17	8	8	6	K,L= 7 8			5	44	48	2	19	17
6	90	91	11	19	20	2	161	157	8	56	56	2	89	89	2	109	103	9	19	24	9	22	21	0*	0	11	6	27	24	3	26	28
7	37	38	12*	0	1	3	35	32	9	32	32	3	172	167	3	90	89	10	14	14	10	11	8	1	48	45	7	34	38	4	14	12
8	61	60	K,L= 5 1			4	116	114	10	29	27	4	79	79	4	84	81	11	25	22	K,L= 5 7			2	9	12	8*	0	2	5	39	38
9	43	43	0	44	48	5	23	21	11	16	19	5	97	98	5	78	74	K,L= 4 6			0	57	60	3	49	47	9	22	23	K,L= 4 12		
10	22	27	1	92	93	6	43	41	12*	0	14	6	48	46	6	76	76	0	83	83	1	33	30	4	18	13	K,L= 3 10			0	52	57
11	13	10	2	32	23	7	15	17	K,L= 4 3			7	75	76	7	56	56	1	21	21	2	29	29	5	29	31	0	44	44	1	8	11
K,L= 6 0			3	71	70	8	63	64	0	65	68	8	27	31	8	38	43	2	65	63	3	33	33	6	17	8	1	41	42	2	42	40
0	42	47	4	16	16	9	12	9	1	114	114	9	35	37	9	35	34	3	27	23	4	24	26	K,L= 8 8			2	40	39	3*	0	8
1	60	57	5	55	58	10	32	32	2	57	63	10	22	25	10	20	22	4	53	53	5	23	26	0	1	10	3	16	13	4	33	36
2	15	3	6	15	15	11	13	5	3	166	167	11	23	25	11	21	20	5	14	17	6	38	36	1	15	9	4	30	31	K,L= 5 12		
3	44	43	7	48	54	12	11	11	4	37	40	12	17	10	K,L= 4 5			6	57	58	7	22	19	2	21	15	5	26	34	0	28	27
4	11	8	8	23	22	K,L= 5 2			5	75	75	K,L= 4 4			0	26	27	7	10	9	8	5	10	3	12	7	6	30	28	1	12	16
5	39	39	9	25	26	0	96	94	6	38	38	0	98	96	1	75	73	8	33	36	9	19	16	4	15	13	7	23	23	2	29	26
6	28	29	10*	0	9	1	37	36	7	63	63	1	35	37	2	28	26	9	7	8	K,L= 6 7			K,L= 0 9			8	18	19	K,L= 0 13		
7	40	41	11	11	16	2	84	82	8	25	26	2	128	129	3	90	88	10	17	21	0	66	67	1	73	74	K,L= 4 10			1	62	62
8	8	0	K,L= 6 1			3	68	67	9	52	56	3	43	46	4	21	23	K,L= 5 6			1	6	10	3	110	114	0	61	61	3	68	64
9	21	19	0	66	65	4	57	59	10*	0	7	4	103	102	5	52	55	0	50	53	2	64	65	5	60	56	1	44	43	5	42	40
10*	0	5	1	48	45	5	24	24	11	21	20	5	31	30	6	10	16	1	70	70	3	28	22	7	42	41	2	37	34	K,L= 1 13		
K,L= 7 0			2	63	60	6	53	55	12	13	10	6	66	66	7	47	47	2	56	54	4	57	55	9	47	44	3	39	37	0	20	23
0	41	37	3	13	11	7	19	22	K,L= 5 3			7	18	13	8	14	11	3	62	64	5	12	8	K,L= 1 9			4	31	32	1	26	25
1	51	51	4	48	48	8	37	38	0	64	59	8	56	59	9	34	35	4	47	51	6	41	39	0	71	70	5	29	30	2	29	33
2	29	32	5	34	36	9	27	28	1	81	83	9	12	13	10	3	11	5	46	47	7	9	5	1	80	82	6	41	39	3	24	22
3	28	26	6	48	48	10	13	16	2	87	86	10	30	32	11	22	19	6	32	35	8	25	27	2	102	105	7	16	21	4	22	24
4	20	20	7	20	19	11*	0	6	3	64	68	11	10	7	K,L= 5 5			7	36	35	K,L= 7 7			3	69	71	K,L= 5 10			5	20	18
5	43	43	8	37	36	K,L= 6 2			4	68	68	K,L= 5 4			0	55	52	8	20	25	0	36	34	4	85	86	0	38	37	K,L= 2 13		
6	21	21	9	10	2	0	24	25	5	49	54	0	96	96	1	48	48	9	21	24	1	20	16	5	56	57	1	31	32	0	38	37
7	29	29	10	20	17	1	75	71	6	34	36	1	50	54	2	52	52	10	18	20	2	39	37	6	39	38	2	32	33	1	9	11
8	5	14	K,L= 7 1			2	32	30	7	47	48	2	92	92	3	46	48	K,L= 6 6			3	17	16	7	42	43	3	10	14	2	36	36
9	12	13	0	69	68	3	63	61	8	40	43	3	30	28	4	39	40	0	23	22	4	29	31	8	43	45	4	31	29	3	12	13
K,L= 8 0			1	44	44	4	19	22	9	25	25	4	73	76	5	37	39	1	67	68	5	12	13	9	27	27	5	23	26	4	29	31
0	43	41	2	45	43	5	48	50	10	23	21	5	36	36	6	32	31	2	23	24	6	23	20	10	24	26	6	21	20	K,L= 3 13		
1	29	30	3	31	33	6	15	18	11	15	16	6	58	60	7	32	32	3	66	66	7*	0	9	K,L= 2 9			K,L= 6 10			0	24	26
2	29	26	4	40	40	7	44	45	K,L= 6 3			7	18	21	8	27	26	4	13	15	K,L= 8 7			0	68	70	0	7	6	1	23	20
3	31	30	5	23	26	8	17	14	0	48	49	8	41	41	9	23	22	5	48	50	0*	0	7	1	24	24	1	29	25	2	20	18
4	25	23	6	45	44	9	21	24	1	25	23	9	10	12	10	15	12	6	17	11	1	21	24	2	62	63	2	15	18	3	18	18
5	23	23	7	24	24	10*	0	7	2	49	47	10	25	24	K,L= 6 5			7	31	32	2*	0	5	3	29	32	3	25	26	K,L= 4 13		
6	25	26	8	15	18	K,L= 7 2			3*	0	10	11	12	9	0	58	59	8	14	11	3	28	25	4	51	51	4	12	13	0	27	24
7*	0	11	9	12	9	0	58	57	4	37	39	K,L= 6 4			1	51	52	9	24	23	4*	0	3	5	10	20	5	29	20	K,L= 0 14		
8	7	10	K,L= 8 1			1	42	43	5	19	20	0	45	47	2	59	59	K,L= 7 6			5	22	18	6	40	43	K,L= 0 11			0*	0	10
K,L= 9 0			0	30	30	2	53	53	6	34	34	1	97	98	3	62	64	0	26	20	K,L= 9 7			7	7	5	1	48	51	K,L= 1 14		
0	49	49	1	70	67	3	36	35	7	11	9	2	21	19	4	50	49	1	31	29	0	14	16	8	30	30	3	75	73	0	30	32
1	7	4	2	29	28	4	39	40	8	18	25	3	87	87	5	36	34	2	17	19	1	13	14	9	16	13	5	35	36			
2	46	47	3	50	48	5	35	35	9	9	4	4	19	19	6	36	36	3	29	27	K,L= 0 8			10	10	16	7	29	27			
3	12	9	4	27	24	6	29	33	10	10	14	5	65	68	7	25	25	4	20	14	0	79	76	K,L= 3 9			K,L= 1 11					

the authors.

Results and Discussion

The bond distances and angles are shown in Fig. 1 (a) and (b).

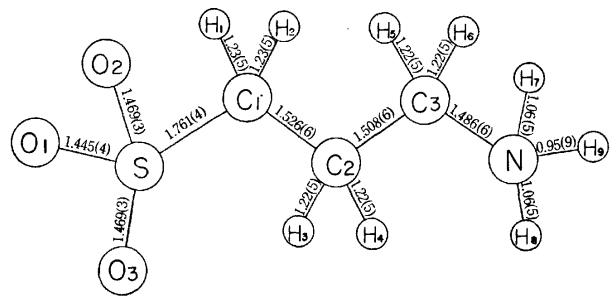

(a)

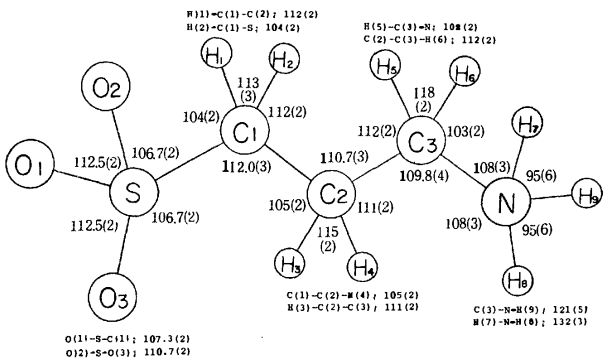

(b)

Fig. 1. (a) Bond distances and their standard deviations in parentheses (in Å).
(b) Bond angles and their standard deviations in parentheses (in degree).

In crystal of the α-form, homotaurine molecule has the zwitterionic structure NH_3^+–CH_2–CH_2–CH_2–SO_3^-, and the seven atoms, O(1), S, C(1), C(2), C(3), N and H(9), in a molecule are exactly on a mirror plane and these atoms preserve the planar *trans-zigzag* configuration, while the same zwitterionic molecule of taurine has the *gauche* configuration around the central methylene linkage. A hydrogen atom, H(9), the location of which is still obscure, should be on the mirror plane and has to be *trans* configuration to C(2) atom with respect to C(3)–N bond, participating in NH···O hydrogen bond formation with the adjacent molecule on the same mirror plane.

It is still unknown about the general feature of molecular conformation of ω-amino sulfonic acid, but such *trans-zigzag* configuration in the homotaurine molecule is also found in GABA hydrochloride[12] and γ-guanidinobutyric acid (GGBA) hydrochloride and hydrobromide,[3] which are particularly interesting substances for the investigation on the relation between their molecular conformations and their characteristic physiological actions.

The configuration of the sulfonic group is considerably interesting. O(2) and O(3) oxygen atoms in a molecule are related by the mirror plane symmetry, and have exactly equal S–O distances of 1.469 Å, whereas O(1) atom exhibits a smaller separation of 1.445 Å. Considering the fact cited above and the longer O(1)···HN hydrogen bond distance of 2.892 Å, O(1) atom might be loosely interacted with an amino group, and it may reflect the ambiguity of H(9) position. Larger C(1)–S–O bond angle was found in the shorter S–O bonds, and it was also observed in taurine.

The C(1)–S distance of 1.761 Å is very similar to that of taurine molecule.[11] Taurine is a structural analogue of homotaurine, and as shown in Table 4 one significant deviation is found in bond angle C–C–N, 109.8° in homotaurine and 112.6° in taurine, while the corresponding angle in ω-amino acids is 111.2° in GABA[13] and 108.4° in β-alanine.[14]

The intramolecular distances between sulfonic group and amino group of ω-amino sulfonic acid are shown in Table 5. Considering the fact that taurine is less active than homotaurine on depression of cortical responses.[4-7] the conformational difference between these compounds might be substantial in these physiological significances. Another interesting feature to be noted here is that NH_3^+–$\underset{|}{CH}$–CH_2–SO_3^- configuration of taurine is same as that of L-cysteic acid,[15] which is active on excitation of cortical responses,[5] and furthermore homocysteic acid which possesses NH_3^+–$\underset{|}{CH}$–CH_2–CH_2–SO_3^- group as homotaurine, has much stronger excitatory action than cysteic acid. The configuration of homocysteic acid might be same as that of homotaurine.

Table 4. A comparison of bond distances and angles between homotaurine and taurine

	Taurine[11] NH_3^+-CH_2-CH_2-SO_3^-	Homotaurine NH_3^+-CH_2-CH_2-CH_2-SO_3^-
∠OSO	110.9°, 113.0°, 113.7°	110.7°, 112.5°, 112.5°
∠CSO	105.8°, 105.8°, 106.9°	106.7°, 106.7°, 107.3°
∠SCC	112.9°	112.0°
∠CCC	—	110.7°
∠CCN	112.6°	109.8°
S-O	1.44_8, 1.46_1, 1.46_5 Å	1.44_5, 1.46_9, 1.46_9 Å
S-C	1.78_0 Å	1.76_1 Å
C-C	1.52_0 Å	1.50_8, 1.52_6 Å
C-N	1.48_4 Å	1.48_6 Å

Table 5. Intramolecular distances between sulfonic and amino group of ω-amino sulfonic acid

	N-O(1)(Å)	N-O(2)(Å)	N-O(3)(Å)
Taurine[11]	4.54	3.82	2.93
L-Cysteic acid[15]	4.41	4.11	2.84
Homotaurine	6.38	5.36	5.36

12) K. Tomita, *Jap. J. Brain Physiol.*, **61**, 1 (1965).

13) H. Higashi, T. Fujiwara and K. Tomita, to be published.

14) P. Jose, L. M. Pant and A. B. Biswas, *Acta Crystallogr.*, **17**, 24 (1964).

15) H. Konishi, T. Ashida, and M. Kakudo, This Bulletin, **41**, 2305 (1968).

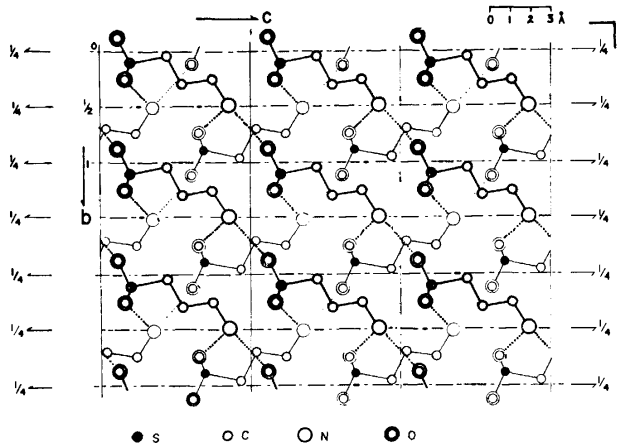

Fig. 2. (a) The crystal structure of homotaurine viewed down along the *a*-axis.

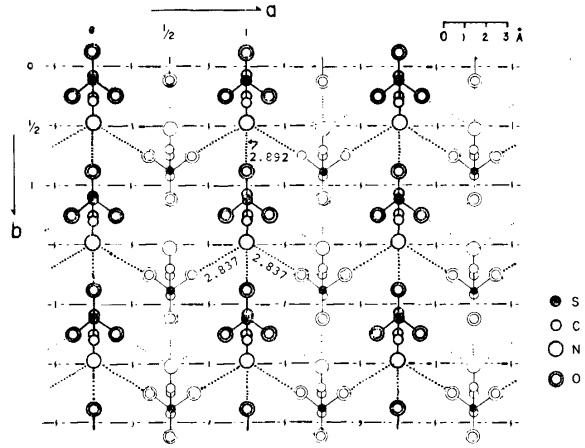

Fig. 2. (b) The crystal structure of homotaurine viewed down along the *c*-axis.

Figure 2 (a) and 2 (b) show the packing of molecules in crystal lattice projected along the *a*- and *c*-axis respectively, where the dotted lines indicate the hydrogen bonds. Homotaurine molecules are jointed to each other with three NH···O hydrogen bonds (2.837, 2.837 and 2.892 Å) to form three dimensional network structure, whereas in taurine structure, there are three NH···O intermolecular hydrogen bonds of 2.793, 2.893, and 2.939 Å, and one intramolecular hydrogen bonding of 2.926 Å. The intermolecular contacts between adjacent molecules are kept by normal van der Waals distances, of which the shortest one between N and C(2) atoms related by two-fold screw axis is 3.906 Å.

This work was partly supported by the research grant from the Ministry of Education, Japan, and we wish to express our sincere thanks for this support.

BULLETIN OF THE CHEMICAL SOCIETY OF JAPAN, VOL. 45, 3638—3645 (1972)

Linear Conjugated Systems Bearing Aromatic Terminal Groups. X.[1] Syntheses and Electronic Spectra of α,ω-Di-1-naphthyl- and α,ω-Di-2-naphthylpolyenes

Akio YASUHARA, Shuzo AKIYAMA, and Masazumi NAKAGAWA

Department of Chemistry, Faculty of Science, Osaka University, Toyonaka, Osaka, 560

(Received May 12, 1972)

Syntheses of di-1-naphthyl- and di-2-naphthylpolyenes (I_n, $n=1$—4,6 and I_n', $n=1$—6) have been carried out by the Wittig reaction. Naphthaldehydes (III and III'), 3-naphthyl-2-propenals (V and V'), 5-naphthyl-2,4-pentadienals (VI and VI') and muconic aldehyde were used as carbonyl components. Naphthylmethyltriphenylphosphonium halides (IV and IV'), 3-naphthyl-2-propenyltriphenylphosphonium bromides (XI and XI') and 5-(2-naphthyl)-2,4-pentadienyltriphenylphosphonium bromide (XII') were synthesized and converted into the corresponding phosphoranes by reaction with phenyllithium. The reaction of carbonyl moiety with phosphorane by a proper combination afforded dinaphthylpolyenes (I_n and I_n'). The electronic spectra of di-1-naphthylpolyenes (I_n) showed broad and structureless absorption curves. In contrast, the absorption curves of di-2-naphthylpolyenes (I_n') exhibited a distinct vibrational fine structure. It was found that the bathochromic shift of the longest-wavelength peak (λ_{max}) along with the increase of the number of double bond (n) can be expressed by the following empirical formula:

$$\lambda_{max}=45.4n^{0.7}+302 \text{ (nm in tetrahydrofuran)}$$

The electronic spectra of α,ω-di-1-anthrylpolyenes[1] suggest that the aromatic terminal groups exert an appreciable effect on the electronic excitation of polyene chromophore. However, the spectral regularity of dianthrylpolyenes could not be discussed in detail owing to the broad and structureless bands in the longest-wavelength region. Preparation of other di-

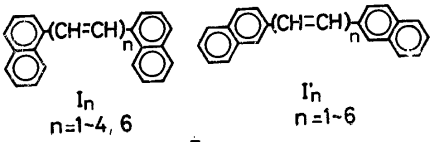

I_n n=1~4, 6 I_n' n=1~6

1) Part IX of this series: Y. Takeuchi, S. Akiyama, and M. Nakagawa, This Bulletin, **45**, 3183 (1972).

arylpolyenes was desirable to get further information on the role of aromatic terminal groups in spectral regularity. This paper deals with the syntheses and electronic spectral properties of di-1-naphthyl- and di-2-naphthylpolyenes (I_n and I_n'), and the spectral regularity of the latter.

Syntheses. Syntheses of di-1-naphthyl- and di-2-naphthylpolyenes (I_n and I_n') have been carried out according to the reaction sequence outlined in the Scheme. 1-Chloromethyl-[2] and 2-bromomethylnaphthalenes were converted into the corresponding naphthylmethyltriphenylphosphonium halides (IV and IV'). 3-(1-Naphthyl)-2-propenal (V) was prepared by the Meyer-Schuster rearrangement of 1-naphthylethynylcarbinol.[3] 2-Naphthaldehyde (III') prepared from 2-hydroxymethylnaphthalene was converted into 3-(2-naphthyl)-2-propenal (V') by a modified J. F. Arens and van Dorp method,[4] since the Meyer-Schuster rearrangement of 2-naphthylethynylcarbinol gave less satisfactory results. Naphthyl-2-propen-1-ols

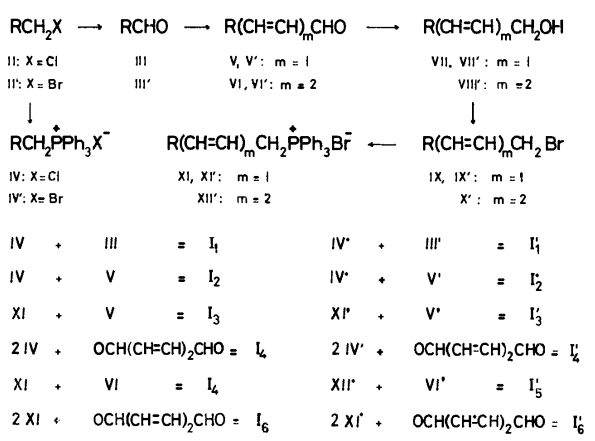

Scheme. Syntheses of dinaphthylpolyenes (I_n and I_n'). R means a 1- or 2-naphthyl group, and the prime on the Roman figure indicates that R is 2-naphthyl group.

(VII and VII') obtained by the reduction of naphthyl-2-propenals (V and V') by means of sodium borohydride were converted into unstable allylic bromides (IX and IX'). IX and IX' afforded naphthylpropenyltriphenylphosphonium bromides (XI and XI') on treatment with triphenylphosphine. The reaction of Grignard derivative of methoxybutenyne[5] with 1- or 2-naphthaldehyde (III or III') followed by reduction with lithium aluminum hydride and treatment with acid yielded 5-(1-naphthyl)- or 5-(2-naphthyl)-2,4-pentadienal (VI or VI'). 5-(2-Naphthyl)-2,4-pentadien-1-ol (VIII') was prepared by the reduction of 2-naphthylpentadienal (VI') with sodium borohydride. 5-(2-Naphthyl)-pentadienyltriphenylphosphonium bromide (XII') was obtained from 2-naphthylpentadienol (VIII) *via* bromide (X').

The Wittig reaction between the aldehyde component (III, III', V, V', VI, and VI') and the phosphorane moiety obtained from phosphonium halide (IV, IV', XI, XI', and XII') according to the combination shown in the Scheme gave α,ω-dinaphthylpolyenes (I_{1-4}, I'_{1-3} and I'_5). The reaction of muconic aldehyde with phosphoranes derived from IV, IV', XI, and XI' afforded dinaphthyloctatetraenes (I_4 and I'_4) and dinaphthyldodecahexaenes (I_6 and I'_6), respectively. The 2-naphthyl series gave a lower yield than the 1-naphthyl series in the Wittig reaction (Table 1). Di-1-naphthylpolyenes (I_{1-4} and I_6) were found to be stable against heat and light and showed definite melting points. Di-2-naphthylpolyenes (I'_{1-6}) exhibited much higher melting points than those of 1-naphthyl analogues. Some of them decomposed on attempted melting point determination. Di-1-naphthylpolyenes (I_n) were found more soluble than di-2-naphthylpolyenes (I_n') in organic solvents. Decrease of solubility due to increase in the length of polyene chain was observed in both series. The color of crystals, melting points and the wave number of IR absorption in the region of C–H out-of-plane defor-

Table 1. Physical properties and yields of dinaphthylpolyenes (I_n and I_n')

n	Di-1-naphthylpolyenes (I_n)				Di-2-naphthylpolyenes (I_n')			
	Color of crystals	Mp(°C)	δ(cm⁻¹)	Yield(%)	Color of crystals	Mp(°C)	δ(cm⁻¹)	Yield(%)
1	pale yellow	160—162	952[a], 970 / 975	34	pale yellow	258—259	956	74
2	pale yellow	173—173.5	978	71	pale yellow	271—273	997, 967 / 953	32
3	yellow	217—219	1000	82	yellow	251—262 (decomp.)	1002, / 963	36
4	orange yellow	225	1005	*ca.* 100	yellow	266—267	1005, / 982	92
5	—		—	—	orange yellow	268—269 (decomp.)	1007, 984, 964	33
6	orange	240—242	1010	*ca.* 100	orange	265—273 (decomp.)	1000, / 963	35

a) The wave numbers of the strongest absorptions are underlined.

2) O. Grumitt and A. Buck, "Organic Syntheses," Coll. Vol. III, p. 195 (1955).
3) I. Iwai and Y. Okajima, *Yakugaku Zasshi*, **79**, 1284 (1959).
4) O. Isler, M. Montavon, R. Rüegg, and P. Zeller, *Helv. Chim. Acta*, **39**, 259 (1956).
5) Cf., D. Marshall and M. C. Whiting, *J. Chem. Soc.*, **1956**, 4082.

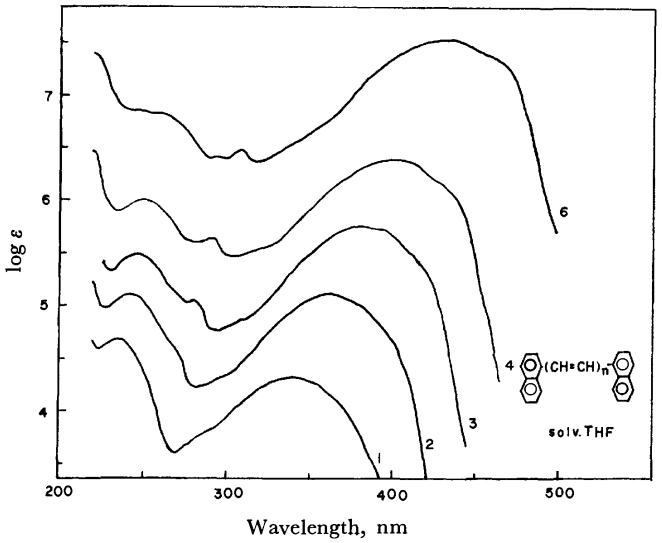

Fig. 1. Absorption curves of di-1-naphthylpolyenes (I_n). Each curve, except for the lowest one, has been displaced upward by a 0.5 log ε unit increment from one immediately below it. The curve of I_6 was displaced upward by a 1.0 log ε unit increment from that of I_4.

TABLE 2. ELECTRONIC SPECTRAL DATA OF I_n

n	λ_{max} (ε) in nm in tetrahydrofuran				
1	237 (47,100)	341 (20,300)			
2	242.3 (39,400)	270* (12,000)	362.5 (38,000)		
3	247.5 (30,700)	281.5 (11,400)	381 (52,900)		
4	252.5 (30,900)	280 (12,800)	292 (13,800)	406.5 (52,900)	
6	247.5 (18,500)	260 (20,700)	296.5 (10,100)	299 (11,200)	436.5 (107,700)

An asterisk indicates shoulder.

mation (δ) of *trans*-double bond are given in Table 1.

Electronic Spectra. The absorption curves and numerical data of electronic spectra of both series of dinaphthylpolyenes (I_n and I_n') are shown in Figs. 1 and 2 and Tables 2 and 3. Di-1-naphthylpolyenes (I_n) show broad and structureless intense bands in the long-wavelength region indicating the presence of steric interference between hydrogen atoms of ethylenic bonds and those of *peri*- and *o*-positions of naphthalene nuclei. The intense absorption bands in the

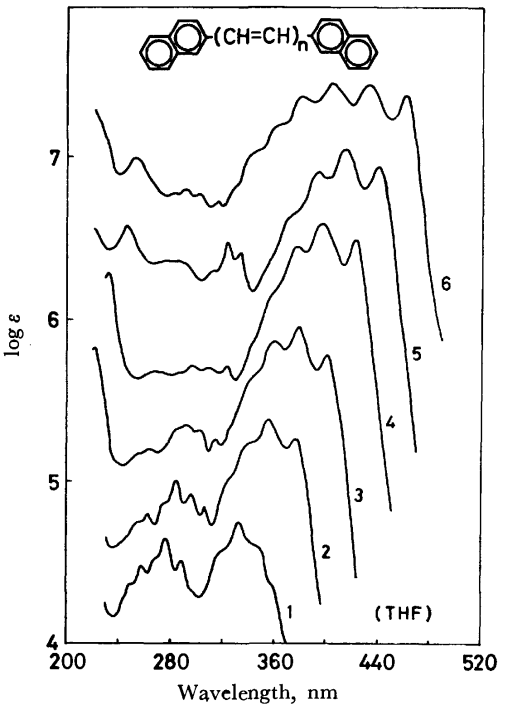

Fig. 2. Absorption curves of di-2-naphthylpolyenes (I_n'). Each curve, except for the lowest one, has been displaced upward by a 0.5 log ε unit increment from one immediately below it.

TABLE 3. ELECTRONIC SPECTRAL DATA OF I_n'

n	λ_{max} (ε) in nm in tetrahydrofuran									
1	249 (23,200)	257.5 (30,000)	267.7 (33,100)	276 (44,600)	287.5 (33,100)	297* (20,900)	320* (37,700)	333 (51,900)	347* (39,400)	357* (23,170)
2	240* (13,500)	253 (17,600)	261.7 (19,400)	275 (24,000)	284.5 (31,600)	295 (26,700)	305.8 (22,000)	342 (55,600)	356 (76,200)	377 (59,300)
3	222 (66,700)	256 (14,500)	262 (15,500)	265 (15,700)	284.5 (20,700)	291 (22,000)	301.5 (20,300)	315 (18,400)	343[a] (43,500)	360 (69,900)
	379 (88,700)	401 (86,200)								
4	232 (62,700)	268 (15,000)	286 (14,700)	296.5 (16,600)	308.5 (16,600)	323.5 (16,500)	379 (86,100)	399 (123,000)	423 (104,000)	
5	245.5 (37,500)	273 (23,200)	283 (23,200)	292* (21,600)	312 (20,400)	324.5 (30,000)	333.5 (25,200)	373* (43,700)	393 (79,900)	415 (110,700)
	441 (88,000)									
6	251.5 (30,200)	265* (23,000)	280.5 (10,000)	290 (23,000)	301.5 (20,900)	314.5 (19,300)	340[a] (35,300)	347 (36,900)	362* (46,900)	382 (71,700)
	404 (88,400)	433 (86,800)	462 (71,700)							

An asterisk indicates shoulder.

long-wavelength region in the electronic spectra of di-2-naphthylpolyenes (I_n') show a well-defined vibrational fine structure (Fig. 2). The long-wavelength band can be considered to arise from an interaction of ^1L_a band of naphthalene with polyene chromophore. The shoulder at longest-wavelength (357 nm) observed in the spectrum of di-2-naphthylethylene (I_1') seems to be related to the ^1L_b band of naphthalene nucleus. In the higher members (I'_{2-6}), the band related to ^1L_b seems to be submerged under intense ^1L_a bands. The spacings between the longest-wavelength subbands (λ_I) and the next longest-wavelength subbands (λ_{II}) are found to be 1400—1500 cm^{-1} except for di-2-naphthylethylene (I'_1) (Table 4).

Table 4. Spacing of vibrational fine structure of I'_n (cm^{-1})

n	1	2	3	4	5	6
	1210	1560	1450	1420	1420	1440

Regularity of the electronic spectra of di-1-naphthylpolyenes (I_n) could not be discussed owing to the broad and structureless features of the longest-wavelength bands. On the other hand, well-developed sub-peaks in the spectra of I_n' made it possible to determine the exact location of maxima at long-wavelength region. We consider the longest-wavelength bands of diarylpolyenes to shift linearly with the x-th power of the number of double bond (n), and the wavelength of maxima (λ_I and λ_{II}) might be expressed by the empirical formula

$$\lambda = A_n{}^x + B$$

just as in the case of diarylpoly-ynes. The plots of λ_I and λ_{II} *versus* $n^{0.7}$ gave good straight lines (Fig. 3).

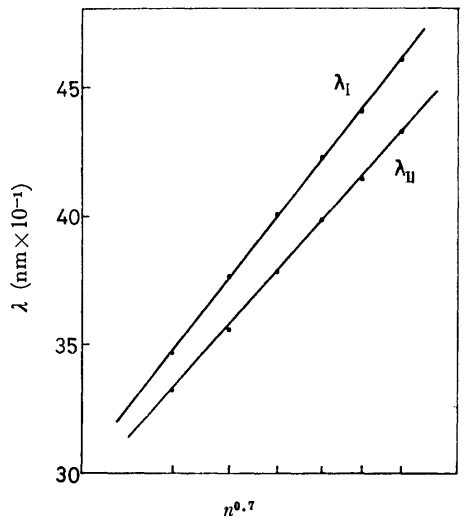

Fig. 3. Plot of λ_{max} *vs.* $n^{0.7}$ for di-2-naphthylpolyenes (I_n').
λ_I: longest-wavelength maxima
λ_{II}: second-longest-wavelength maxima

6) K. Nakasuji, S. Akiyama, K. Akashi, and M. Nakagawa, This Bulletin, **43**, 3567 (1970).
7) M. Nakagawa, S. Akiyama, K. Nakasuji, and K. Nishimoto, *Tetrahedron*, **27**, 5401 (1971).

The linear relationships can be expressed by the following empirical formulas:

$\lambda_I = 45.4\ n^{0.7} + 302$ (nm in tetrahydrofuran)
$\lambda_{II} = 40.0\ n^{0.7} + 292$ (nm in tetrahydrofuran)

The calculated values show excellent agreement with the observed values (Table 5). The spectral regularity

Table 5. Observed and calculated λ_I and λ_{II} of I_n'

	n	1	2	3	4	4	6
λ_I	Calcd	347	377	401	423	441	462
	Obsd	347	375.5	400	422	442	461
	$\Delta\lambda$	0	1.5	1	1	−1	1
λ_{II}	Calcd	333	356	379	399	415	433
	Obsd	332	357	378	398	416	432
	$\Delta\lambda$	1	−1	1	1	−1	1

of 2,2'-dinaphthylpoly-ynes, acetylenic analogues of I_n', could be expressed by the empirical formula, $\lambda = 15.5\ n^{1.3} + 319$ (nm in tetrahydrofuran).[6,7] It should be noted that the B-values of both series are found to be nearly the same. However, the coefficient A of di-2-naphthylpolyenes (I_n') is much larger than that of 2,2'-dinaphthylpoly-yens.

Experimental

All the melting points are uncorrected. The electronic spectra were measured with a Hitachi EPS-3T spectrophotometer at room temperature employing a well-matched pair of 1-cm quartz cells, otherwise stated. The IR spectra were obtained on a Hitachi EPI-2 infrared spectrophotometer by the KBr-disk method. Evaporation of solvent was performed under reduced pressure.

1-Naphthylmethyltriphenylphosphonium Chloride (IV). A solution of 1-chloromethylnaphthalene[2] (II, 12.3 g, 0.07 mol) and triphenylphosphine (20.2 g, 0.077 mol) in xylene (100 m*l*) was refluxed to yield a colorless precipitate. The precipitate was filtered and washed with benzene, yielding colorless crystalline powder (33.1 g, quantitative). The material was recrystallized from ethanol to afford IV as colorless plates, mp 292—301°C (decomp.).

Found: C, 79.62; H, 5.38; Cl, 8.15%. Calcd for $C_{29}H_{24}PCl$: C, 79.35; H, 5.51; Cl, 8.08%.

3-(1-Naphthyl)-2-propen-1-ol (VII). A solution of sodium borohydride (1.5 g, 0.04 mol) and 3-(1-naphthyl)-2-propenal (V, 4.0 g, 0.022 mol) prepared by the Meyer-Schuster rearrangement of 1-(1-naphthyl)-2-propyn-1-ol,[3] in 2-propanol (200 m*l*) was refluxed for 2 hr. The residue obtained by concentration of the reaction mixture was treated with dilute hydrochloric acid and extracted with ether. After washing and drying, the extract was evaporated to yield crude VII (3.08 g, 76.2%) as a brown liquid. The crude alcohol (VII) was subjected to the following reaction.

3-(1-Naphthyl)-2-propenyl Bromide (IX). To a solution of the crude alcohol (VII, 3.08 g, 0.017 mol) in chloroform (50 m*l*) containing 10 drops of pyridine was added a solution of phosphorus tribromide (2.16 g, 0.008 mol) in chloroform (20 m*l*) over a 30-min period. After stirring for 20 hr, cracked ice was added to the chilled reaction mixture and then the mixture was poured onto ice-water. The aqueous layer was extracted with chloroform. The extract was successively washed with water, a saturated sodium hydrogencarbonate solution and water, and dried. The residue obtained by evaporation of the extract was dissolved in carbon

tetrachloride and filtered. The crystals deposited on concentration of the filtrate were washed with the same solvent to afford IX as brownish yellow crystals, mp 56—59°C, 4.09 g (quantitative).

3-(1-Naphthyl)-2-propenyltriphenylphosphonium Bromide (XI). A solution of bromide (IX, 4.09 g, 0.021 mol) and triphenylphosphine (5.56 g, 0.021 mol) in toluene (70 ml) was refluxed for 17 hr. Pale yellow solid deposited was collected by filtration and washed with toluene. The crude material 8.21 g, 98.1%) was recrystallized twice from ethanol to give pure phosphonium bromide (XI), mp 238—240°C,

Found: C, 73.28; H, 5.25; Br, 15.29%. Calcd for $C_{31}H_{26}PBr$: C, 73.09; H, 5.14; Br, 15.68%.

5-(1-Naphthyl)-2,4-pentadienal (VI). To a stirred solution of 4-methoxy-3-buten-1-yne (1.58 g, 0.019 mol) in tetrahydrofuran (10 ml) maintained at 38—40°C was added over a 30-min period a solution of ethylmagnesium bromide in the same solvent (20 ml) [prepared from ethyl bromide, 2.8 g (0.026 mol) and magnesium, 0.31 g (0.013 g-atom)] under nitrogen atmosphere. After stirring for further 30 min at room temperature, the mixture was chilled in an ice-salt bath and a solution of 1-naphthaldehyde (III, 1.0 g, 0.0064 mol) in tetrahydrofuran (20 ml) was added over a 25-min period. Stirring was continued overnight. A saturated solution of ammonium chloride (50 ml) was added to the reaction mixture under cooling with an ice-salt bath. The aqueous layer was extracted with ether. The combined organic layer was dried and evaporated to give a red liquid. Crude 1-(1-naphthyl)-5-methoxy-4-penten-2-yn-1-ol thus obtained was dissolved in ether (20 ml). The ethereal solution was added over a 40-min period to a stirred solution of lithium aluminum hydride (0.72 g, 0.019 mol) in ether (20 ml) under cooling in an ice-salt bath. After further stirring for 6.5 hr at room temperature, a mixture of ethyl acetate (5 ml) and ether (6 ml) and then ethyl acetate (3.5 ml), water (3 ml) and 4 N sulfuric acid (27 ml) were added successively to the ice-cooled reaction mixture. After being stirred overnight at room temperature, the aqueous layer was extracted with ether. The combined ethereal solution was washed successively with a solution of sodium hydrogencarbonate and water, and dried. Crude 1-naphthylpentadienal (VI, 1.108 g) was obtained as brownish liquid on evaporation of the solvent. This material was subjected to chromatography on silica gel and used in the subsequent reaction.

2-Hydroxymethylnaphthalene. To a refluxing solution of lithium aluminum hydride (6.50 g, 0.171 mol) in ether (200 ml) was added a solution of methyl 2-naphthoate (32.8 g, 0.171 mol) in ether (200 ml) and tetrahydrofuran (50 ml) over a period of 30 min. After the mixture had been stirred for 3 hr under reflux, methanol (60 ml) was added under cooling in an ice-bath and stirring was continued overnight. A saturated solution of ammonium chloride containing hydrochloric acid was added to the reaction mixture. The aqueous layer was extracted with ether. The combined organic layer was washed successively with aqueous sodium carbonate solution and water, and dried. Colorless crystals (27.1 g, 97.1%) obtained by evaporating the solvent were recrystalized from ethanol to give pure 2-hydroxymethylnaphthalene, mp 80—82°C (lit,[8] mp 80—80.5°C).

2-Naphthaldehyde (III'). A solution of 2-hydroxymethylnaphthalene (15.8 g, 0.10 mol) in pyridine (40 ml) was added to an ice-cooled suspension of chromium trioxide-pyridine complex in pyridine [prepared from chromium trioxide, (31.5 g, 0.30 mol) and pyridine (350 ml)] and kept at the same temperature for 1 hr. The reaction mixture was then allowed to stand at room temperature for 2 hr, and poured onto water and extracted with ether (1.5 l). The extract was washed successively with 10% hydrochloric acid, water, 10% aqueous sodium carbonate solution and water, and dried. Colorless crystals (14.8 g, 94.9%) obtained by evaporation of the solvent were recrystallized from carbon tetrachloride and then from ethanol, yielding pure III', mp 60—61°C (lit,[9] 59—60°C).

2-Bromomethylnaphthalene (II'). To an ice-cooled and stirred solution of 2-hydroxymethylnaphthalene (5.0 g, 0.032 mol) in chloroform (70 ml) containing 1 ml of pyridine was added dropwise a solution of phosphorus tribromide (9.6 g, 0.035 mol) in chloroform (15 ml). After stirring for 1 hr at room temperature, crushed ice was added to the reaction mixture under ice-cooling and the mixture was then poured onto ice-water. The aqueous layer was extracted with chloroform. The combined chloroform layer was washed successively with sodium hydrogencarbonate solution and water, and dried. Evaporation of the solvent afforded colorless crystals, 6.1 g (87.1%) which were recrystallized from ethanol to give pure II', mp 53—55°C (lit, 48°C[10], 53—56°C[11]).

2-Naphthylmethyltriphenylphosphonium Bromide (IV'). A solution of triphenylphosphine (6.71 g, 0.0256 mol) in benzene (100 ml) was added to a solution of 2-bromomethylnaphthalene (II', 5.60 g, 0.0253 mol) in benzene (100 ml). After the mixture had been stirred under reflux for 4.5 hr, the solid deposited was collected and washed with benzene, yielding colorless crystals, 11.4 g (93.4%). Recrystallization of the crystals from ethanol yielded pure IV', mp 251—252°C lit,[12] mp 248—251°C (decomp.)).

3-(2-Naphthyl)-2-propenal (V'). *(a) By the Meyer-Schuster Rearrangement*: To an ice-cooled and stirred solution of ethynylmagnesium bromide in tetrahydrofuran (70 ml) [prepared from ethyl bromide, 7.0 g (0.064 mol), magnesium, 1.2 g (0.05 g-atom) and excess acetylene][13] was added a solution of 2-naphthaldehyde (III', 5.0 g, 0.032 mol) in the same solvent (10 ml). The mixture was stirred overnight under cooling in an ice-bath. The reaction mixture was poured onto a saturated solution of ammonium chloride (150 ml). The aqueous layer was extracted with ether (200 ml). The combined organic layer was dried and evaporated. The residue was dissolved in benzene and passed through a short column of alumina (10 g). 1-(2-Naphthyl)-2-propyn-1-ol was obtained as pale yellow crystals (6.1 g) on concentration of the filtrate. The crude carbinol was dissolved in a mixture of dioxane (150 ml), water (25 ml) and concentrated sulfuric acid (3 ml) and the mixture was refluxed for 30 hr. The mixture was then poured onto water (280 ml) and extracted with benzene (300 ml). The extract was washed successively with 10% aqueous solution of sodium hydrogencarbonate (50 ml) and water (100 ml) and dried. Brown crystals obtained by evaporation of the solvent were dissolved in ether-benzene and the solution was stirred with a saturated solution of sodium hydrogensulfite for 3 hr to give sulfite adduct of V'. The adduct deposited was collected and decomposed with a dilute sodium hydroxide solu-

8) E. Bamberger and O. Boekmann, *Ber.*, **20**, 1115 (1887).

9) E. B. Hershberg and J. Cason, "Organic Syntheses," Coll. Vol. III, p. 627 (1955).

10) P. Mamalis, J. Green, and D. McHale, *J. Chem. Soc.*, **1960**, 229.

11) O. A. Pintado, *Rec. Fac. Cienc. Quim. Univ. Nacl. La Plata*, **29**, 53 (1955—56), *Chem. Abstr.*, **53**, 264[a] (1959).

12) J. P. Geert and R. H. Martin, *Bull. Soc. Chim. Belges*, **69**, 563 (1960).

13) E. R. H. Jones, L. Skatteböl, and M. C. Whiting, *J. Chem. Soc.*, **1956**, 4765.

tion. 2-Naphthylpropenal (V′) liberated was taken up in benzene. After washing and drying, the benzene solution was evaporated. The residue redissolved in benzene (50 ml) was passed through a thin layer of alumina (4 g). Evaporation of the filtrate gave pure V′ as pale yellow crystals, mp 119—122°C, 1.26 g (21.6%).

(b) By the Modified Arens and van Dorp Method: To a stirred solution of lithium amide [from lithium (2.1 g, 0.303 g-atom)] in liquid ammonia (160 ml) was added over a 20-min period a solution of 2-chlorovinyl ethyl ether (16.52 g, 0.16 mol) in tetrahydrofuran (15 ml) under cooling in a dry ice-ethanol bath, and the mixture was stirred for further 1.5 hr at −60°C. To a solution of lithium ethoxyacetylide thus prepared was added a solution of 2-naphthaldehyde (III′, 5.95 g, 0.038 mol) in tetrahydrofuran (50 ml) over a period of 30 min. After the mixture had been stirred overnight at −40—30°C, ammonium chloride (18 g) was added to the mixture under cooling in a dry ice-ethanol bath. Stirring was continued for 15 min at −60°C. Ammonia was then allowed to evaporate. The residue was mixed with a saturated ammonium chloride solution (200 ml) and the organic layer was separated. The aqueous layer was extracted with ether (500 ml). The combined organic layer was dried and evaporated to yield a red liquid. A benzene solution of the red liquid was passed through a short column of alumina (5 g). The reddish liquid obtained by evaporation of the filtrate was dissolved in ether (30 ml). The ethereal solution was added to an ice-cooled solution of lithium aluminum hydride (2.01 g, 0.053 mol) in ether (70 ml) and stirring was continued overnight at room temperature. Ethyl acetate (10 ml) and 6 N sulfuric acid (100 ml) were then added dropwise in the ice-cooled reaction mixture and stirring was continued for 7 hr at room temperature. The organic layer was separated and the aqueous layer was extracted with ether and then with benzene. After washing and drying, the combined organic layer gave orange yellow crystals on evaporation of the solvent. The filtrate obtained by percolation of a benzene solution of the crude crystals through a column of alumina (15 g) was concentrated to yield 2-naphthylpropenal (V′, 4.5 g, 64.8%) which was recrystallized from ethanol to yield pure V′, pale yellow crystals, mp 122—124°C (lit, mp 118—119°C[14]; mp 125°C[15]).

3-(2-Naphthyl)-2-propen-1-ol (VII′). To a solution of 2-naphthylpropenal (V′, 1.91 g, 0.0105 mol) in tetrahydrofuran (50 ml) was added sodium borohydride (0.48 g, 0.0127 mol) and the mixture was refluxed for 1 hr under stirring. The reaction mixture was concentrated, treated with dilute hydrochloric acid and extracted with benzene. After washing and drying, the extract was evaporated to yield yellow crystals, 1.83 g (94.8%) which were recrystallized from carbon tetrachloride, thus affording pure VII′, mp 103—105°C.

Found: C, 84.43; H, 6.44%. Calcd for $C_{13}H_{12}O$: C, 84.75; H, 6.57%.

3-(2-Naphthyl)-2-propenyl Bromide (IX′). To an ice-cooled solution of 2-naphthylpropenol (VII′, 0.96 g, 0.0052 mol) in chloroform (30 ml) containing pyridine (1 ml) was added dropwise a solution of phosphorus tribromide (1.42 g, 0.0052 mol) in chloroform (10 ml). The mixture was stirred for 1 hr at 10°C. Cracked ice was then added to the reaction mixture under ice-cooling. After most of the organic solvent has been removed, the mixture was poured onto water and extracted with benzene. The extract, after washing and drying, was concentrated to afford IX′ as colorless crystals, 0.9 g (70%). This material was used without further purification in the following reaction.

3-(2-Naphthyl)-2-propenyltriphenylphosphonium Bromide (XI′). A solution of 2-naphthylpropenyl bromide (IX′, 0.9 g, 0.0036 mol) and triphenylphosphine (0.91 g, 0.0037 mol) in benzene (50 ml) was stirred for 48 hr at room temperature. Colorless crystals deposited (1.478 g, 80.0%) were recrystallized from aqueous ethanol to give colorless plates, mp 235—236°C. An analytical specimen was prepared on drying the crystals at 130°C for 6 hr *in vacuo*.

Found: C, 73.50; H, 5.31; Br, 15.54%. Calcd for $C_{31}H_{26}BrP$: C, 73.09; H, 5.14; Br, 15.69%.

5-(2-Naphthyl)-2,4-pentadienal (VI′). To a solution of ethylmagnesium bromide (0.04 mol) in tetrahydrofuran (40 ml) was added a solution of 4-methoxy-3-buten-1-yne (4.45 g, 0.054 mol) in the same solvent (30 ml) under nitrogen atmosphere at 40°C. After the evolution of ethane subsided, 2-naphthaldehyde (III′, 5.0 g, 0.032 mol) in tetrahydrofuran (30 ml) was added dropwise to the ice-cooled reaction mixture. After stirring overnight, the reaction mixture was poured onto an ice-cooled saturated solution of ammonium chloride (150 ml). The aqueous layer was extracted with ether. The extract was combined with the organic layer and dried. The residue obtained by evaporation of the solvent was dissolved in benzene and passed through a short column of alumina. Evaporation of the filtrate gave a reddish liquid which was dissolved in ether (50 ml). The ethereal solution was added dropwise to an ice-cooled and stirred solution of lithium aluminum hydride (1.53 g, 0.0404 mol) in ether (100 ml) and the mixture was stirred for 2 hr at 18°C. To this were added ethyl acetate (20 ml, 0.20 mol) and, after 30 min, 9 N sulfuric acid (90 ml). After being stirred overnight, the aqueous layer was extracted with benzene. The combined organic layer was worked up according to the usual manner and evaporated to give yellowish brown crystals, 3.64 g (54.6%). The crystals were recrystallized from carbon tetrachloride to yield pure 2-naphthylpentadienal (VI′), mp 135—137°C.

Found: C, 86.11; H, 5.78%. Calcd for $C_{15}H_{12}O$: C, 86.51; H, 5.81%.

5-(2-Naphthyl)-2,4-pentadien-1-ol (VIII′). To a suspension of finely powdered sodium borohydride (0.36 g, 0.0096 mol) in a mixture of tetrahydrofuran (90 ml) and ethanol (10 ml) was added a solution of 2-naphthylpentadienal (VI′, 2.0 g, 0.0096 mol) in tetrahydrofuran (30 ml). After the mixture had been refluxed for 1 hr, stirring was continued for 1 hr at room temperature. The reaction mixture was concentrated to one-third its original volume and mixed with dilute hydrochloric acid. The aqueous layer was extracted with benzene. After washing and drying, the combined organic layer was evaporated to give VIII′ as yellow crystals, 1.98 g (98.1%). Slightly crude VIII′ was used in the following reaction without further purification.

5-(2-Naphthyl)-2,4-pentadienyl Bromide (X′). To an ice-cooled and stirred mixture of 2-naphthylpentadienol (VIII′, 1.98 g, 0.0094 mol), tetrahydrofuran (40 ml) and pyridine (2 ml) was added dropwise a solution of phosphorus tribromide (2.55 g, 0.0094 mol) in tetrahydrofuran (10 ml). After stirring for 1.5 hr at room temperature, cracked ice was added to the reaction mixture under ice-cooling. The aqueous layer obtained by evaporation of the organic solvent was extracted with benzene. After the usual washing and drying, the extract was concentrated to afford X′ as yellow crystals, 1.57 g (61.0%). This material was subjected directly to the following reaction.

5-(2-Naphthyl)-2,4-pentadienyltriphenylphosphonium Bromide (XII′). A solution of X′ (1.57 g, 0.00575 mol) and triphenylphosphine (2.10 g, 0.00802 mol) in benzene (60 ml)

14) S. Israelashvili, Y. Gottlieb, M. Imber, and A. Habas, *J. Org. Chem.*, **16**, 1519 (1951).

15) C. Jutz, *Chem. Ber.*, **91**, 1867 (1958).

was refluxed to yield colorless crystalline precipitate. The precipitate was filtered and washed with benzene to give yellow fine crystals, 2.255 g (73.3%). The crystals were recrystallized three times from ethanol, yielding pure phosphonium bromide (XII'), mp 217.7—219.1°C (decomp.).

Found: C, 73.51; H, 5.30; Br, 15.15%. Calcd for $C_{33}H_{28}PBr$: C, 74.02; H, 5.27; Br, 14.92%.

1,2-Di(1-naphthyl)ethylene (I_1). To a stirred suspension of 1-naphthylmethyltriphenylphosphonium chloride (IV, 8.8 g, 0.020 mol) in benzene (65 m*l*) was added an ethereal solution of phenyllithium (0.98 N, 20.5 m*l*, 0.020 mol) under nitrogem atmosphere. After the resulting deep red solution had been stirred for 30 min, a solution of 1-naphthaldehyde (III, 3.4 g, 0.020 mol) in benzene (10 m*l*) was added and the mixture was stirred for 111 hr at room temperature. Yellowish red precipitate deposited was collected and washed with benzene. Ethanol was added to a hot solution of the precipitate in benzene to give a pale yellow precipitate (1.5 g, 34%). The material was recrystallized three times from ethanol and dissolved in benzene. The benzene solution was passed through a short column of alumina (10 g). The crystals obtained on concentrating the filtrate were recrystallized from cyclohexane to give pure I_1 as pale yellow crystals, mp 160—162°C (lit,[16] 161°C).

Found: C, 94.55; H, 5.79%. Calcd for $C_{22}H_{16}$: C, 94.25; H, 5.75%.

1,4-Di(1-naphthyl)-1,3-butadiene (I_2). To a stirred solution of 1-naphthylmethylidenetriphenylphsophorane prepared from 1-naphthylmethyltriphenylphsophonium chloride (IV, 1.38 g, 0.0032 mol) in benzene (20 m*l*) and an ethereal solution of phenyllithium (5 m*l*, 0.0032 mol) was added under nitrogen atmosphere a solution of 3-(1-naphthyl)propenal (V, 0.568 g, 0.0031 mol) in benzene (10 m*l*). Stirring was continued for 20 hr to cause deposition of a yellow precipitate. The precipitate was washed with toluene and digested with the same solvent. The extract was concentrated to yield bright yellow needles, 0.678 g (71.1%). A benzene solution of the crystals was treated with active charcoal and the filtrate was passed through a thin layer of alumina. The crystals obtained from the filtrate were recrystallized three times from acetic acid to afford pure I_2 as yellow crystals, mp 173—173.5°C (lit,[14] mp 170°C).

Found: C, 94.37; H, 5.98%. Calcd for $C_{24}H_{18}$: C, 94.08; H, 5.92%.

1,6-Di(1-naphthyl)-1,3,5-hexatriene (I_3). A solution of 3-(1-naphthyl)-2-propen-1-ylidenetriphenylphosphorane was prepared by the reaction of phosphonium bromide (XI, 3.08 g, 0.006 mol) in benzene (40 m*l*) with an ethereal solution of phenyllithium (7.72 m*l*, 0.006 mol) under nitrogen atmosphere. After the resulting deep red solution had been stirred for 30 min, a solution of 3-(1-naphthyl)propenal (V, 1.0 g, 0.0055 mol) in benzene (20 m*l*) was added over a 20-min period under cooling. Stirring was continued for 15 hr. The yellow precipitate formed was digested with hot toluene. Concentration of the extract gave yellow crystals, 1.503 g (82.4%) which were dissolved in benzene and passed twice through a thin layer of alumina. The crystals obtained from the filtrate were recrystallized three times from benzene to afford pure I_3, mp 217—219°C.

Found: C, 93.93; H, 6.33%. Calcd for $C_{26}H_{20}$: C, 93.94; H, 6.06%.

1,8-Di(1-naphthyl)-1,3,5,7-octatetraene (I_4). *(a) From 1-Naphthylmethyltriphenylphosphonium Chloride and Muconaldehyde.* A mixture of 1-naphthylmethyltriphenylphosphonium chloride (IV, 1.317 g, 0.003 mol) in benzene (40 m*l*) and an ethereal solution of phenyllithium (5.8 m*l*, 0.003 mol) was stirred for 40 min under nitrogen atmosphere. To the resulting deep red solution of phosphorane was added rapidly a solution of muconaldehyde (0.110 g, 0.001 mol) in benzene (10 m*l*). After stirring overnight a crystalline precipitate was formed. This was filtered and the filtrate was concentrated to yield a second crop. The combined precipitate was digested with hot benzene. The extract was filtered and the filtrate gave yellow crystals (0.360 g, quantitative) on concentration. After the crystals had been recrystallized three times from benzene, a benzene solution of the crystals was percolated through a short column of alumina. Pure I_4, mp 225.7—225.8°C was obtained from the filtrate.

Found: C, 93.84; H, 6.13%. Calcd for $C_{28}H_{22}$: C, 93.81; H, 6.19%.

(b) From 5-(1-Naphthyl)-2,4-pentadienal (VI). To a stirred suspension of 3-(1-naphthyl)-2-propen-1-yltriphenylphosphonium bromide (XI, 1.28 g, 0.0025 mol) in benzene (20 m*l*) was added over a 10-min period an ethereal solution of phenyllithium (10 m*l*, 0.0025 mol) under nitrogen atmosphere to give a deep red solution of phosphorane. After 35 min, a solution of slightly crude 5-(1-naphthyl)-2,4-pentadienal (VI, 0.455 g, 0.0022 mol) in benzene (10 m*l*) was added over a period of 15 min to the solution of phosphorane. After stirring for 24 hr, the orange red precipitate formed was filtered and washed with benzene. The precipitate was digested with hot benzene and toluene and the combined extract was concentrated to half its original volume and treated with alumina (2 g). The concentrated solution was passed through a short column of alumina (5 g). Yellow crystals (0.505 g, 64.5%) obtained by concentration of the filtrate were recrystallized from toluene to give pure I_4, 222.4—225.1°C.

Found: C, 93.88; H, 6.38%. Calcd for $C_{28}H_{22}$: C, 93.81; H, 6.19%.

1,12-Di(1-naphthyl)-1,3,5,7,9,11-dodecahexaene (I_6). A solution of 3-(1-naphthyl)-2-propenylidenetriphenylphosphorane was prepared from 3-(1-naphthyl)propenyltriphenylphosphonium bromide (XI, 1.528 g, 0.003 mol) in benzene (40 m*l*) and an ethereal solution of phenyllithium (5.8 m*l*, 0.003 mol) under nitrogen atmosphere. To this was added repidly a solution of muconaldehyde (0.11 g, 0.001 mol) in benzene (10 m*l*) and the mixture was stirred for 48 hr at room temperature. Crystalline solid deposited was collected by filtration and the filtrate was evaporated to give second crop of crystalline solid. The combined material was extracted with hot benzene (total 500 m*l*). Brown crystals (0.563 g, quantitative) obtained by evaporation of the extract were recrystallized from toluene. Crude I_6 thus obtained was dissolved in hot toluene and passed through a thin layer of alumina (1.5 g). The crystals obtained by concentration of the filtrate were recrystallized twice from the same solvent, yielding pure I_6 as orange crystals, mp 240—242°C.

Found: C, 93.44; H, 6.32%. Calcd for $C_{32}H_{26}$: C, 93.62; H, 6.38%.

1,2-Di(2-naphthyl)ethylene (I_1'). To a stirred suspension of 2-naphthylmethyltriphenylphosphonium bromide (IV', 2.321 g, 0.0048 mol) in benzene (40 m*l*) was added an ethereal solution of phenyllithium (0.635 N, 7.5 m*l*, 0.0048 mol). After stirring for 1 hr, a solution of 2-naphthaldehyde (III', 0.726 g, 0.0047 mol) in benzene (15 m*l*) was added dropwise to the deep red solution of phosphorane and the mixture was stirred overnight. Crystalline solid deposited was digested with hot benzene and the hot extract was percolated through a short column of alumina. The crystals obtained from the filtrate were recrystallized from benzene

16) J. H. Wood, J. A. Bacon, A. W. Meibohm, W. H. Throckmorton, and G. P. Turner, *J. Amer. Chem. Soc.*, **63**, 1334 (1941).

to afford pure I_1' as pale yellow crystals, 0.968 g (74.3%), mp 258—259°C (lit, 257—258°C,[12] 255°C[16]).

1,4-Di(2-naphthyl)-1,3-butadiene (I_2'). A solution of 2-naphthylmethylidenetriphenylphosphorane was prepared by the reaction of phosphonium bromide (IV′, 1.049 g, 0.00217 mol) in benzene (40 m*l*) with an ethereal solution of phenyllithium (0.53 N, 4.05 m*l*, 0.00215 mol) under nitrogen atmosphere. To this was added a solution of 3-(2-naphthyl)-propenal (V′, 0.383 g, 0.0021 mol) in benzene (15 m*l*) and the mixture was stirred overnight. The residue obtained by evaporation of the solvent was digested with hot toluene. Crude crystals deposited on concentration of the filtrate were recrystallized from toluene, and the crystals were dissolved in the same solvent. The toluene solution was refluxed for several min with alumina (2 g) and filtered. The crystals deposited on cooling the filtrate were recrystallized from toluene, yielding pure I_2' as pale yellow needles, 0.208 g (32.3%), mp 271—273°C (lit,[14]: 268°C).

Found: C, 94.32; H, 5.90%. Calcd for $C_{24}H_{18}$: C, 94.08; H, 5.92%.

1,6-Di(2-naphthyl)-1,3,5-hexatriene (I_3'). To a stirred suspension of 3-(2-naphthyl)-2-propenyltriphenylphosphonium bromide (XI′, 0.764 g, 0.0015 mol) in benzene (50 m*l*) was added under nitrogen atmosphere an ethereal solution of phenyllithium (0.336 N, 4.5 m*l*, 0.0015 mol). After stirring for 30 min, 3-(2-naphthyl)propenal (V′, 0.182 g, 0.0010 mol) in benzene (20 m*l*) was added to the resulting deep red solution of phosphorane and the mixture was stirred overnight. The precipitate formed was digested with hot benzene and toluene. The combined extract was passed through a short column of alumina. The crystals obtained by evaporation of the filtrate were recrystallized from toluene to yield pure I_3' as yellow crystals, 0.121 g, (36.4%), mp 251—262°C (decomp.).

Found: C, 93.82; H, 5.99%. Calcd for $C_{26}H_{20}$: C, 93.94; H, 6.06%.

1,8-Di(2-naphthyl)-1,3,5,7-octatetraene (I_4'). To a stirred solution of 2-naphthylidenetriphenylphosphorane prepared from phosphonium bromide (IV′, 1.450 g, 0.003 mol) and phenyllithium (0.003 mol) according to the procedure for the preparation of I_1' and I_2' was added a solution of muconaldehyde (0.110 g, 0.001 mol) in benzene (12 m*l*) and the mixture was stirred overnight. Yellow crystalline solid deposited was digested with hot benzene. The filtrate obtained by percolation of the extract through a short column of alumina (5 g) was evaporated to yield yellow crystals. Recrystallization of the crystals from toluene afforded pure I_4' as yellow crystals, 0.330 g, (92.1%), mp 266—267°C.

Found: C, 93.47; H, 6.11%. Calcd for $C_{28}H_{22}$: C, 93.81; H, 6.19%.

1,10-Di(2-naphthyl)-1,3,5,7,9-decapentaene (I_5'). An ethereal solution of phenyllithium (0.277 N, 9.0 m*l*, 0.0025 mol) was added under nitrogen atmosphere to a stirred suspension of 5-(2-naphthyl)-2,4-pentadienyltriphenylphosphonium bromide (XII′, 1.338 g, 0.0025 mol) in benzene (40 m*l*) to give a deep red solution of phosphorane. To this was added after stirring for 30 min a solution of 5-(2-naphthyl)-2,4-pentadienal (VI′, 0.416 g, 0.0020 mol) in benzene (60 m*l*). After the mixture had been stirred overnight, the solid deposited was digested with hot benzene and toluene. The filtrate obtained by percolation of the combined extract through a thin layer of alumina (5 g) was concentrated to yield crystals. The crystals were recrystallized from toluene to give pure I_5' as yellowish orange needles, 0.252 g (32.8%), mp 268—269°C (decomp.).

Found: C, 93.66; H, 6.38%. Calcd for $C_{30}H_{24}$: C, 93.71; H, 6.29%.

1,12-Di(2-naphthyl)-1,3,5,7,9,11-dodecahexaene (I_6'). A solution of 3-(2-naphthyl)-2-propenylidenetriphenylphosphorane was prepared under nitrogen atmosphere from 3-(2-naphthyl)-2-propenyltriphenylphosphonium bromide (XI′, 1.273 g, 0.0025 mol) in benzene (50 m*l*) and an ethereal solution of phenyllithium (0.336 N, 7.45 m*l*, 0.0025 mol). To the resulting deep red solution was added a solution of muconic aldehyde (0.110 g, 0.001 mol) in benzene (20 m*l*). After the mixture had been stirred overnight at room temperature, the precipitate formed was digested with hot benzene and toluene. The extract was passed through a short column alumina. The crystals obtained by concentration of the filtrate were recrystallized from toluene to afford pure I_6' as orange crystals, 0.142 g (34.5%), mp 265—273°C decomp.), rate of temperature increase: 10°C/min).

Found: C, 93.64; H, 6.25%. Calcd for $C_{32}H_{26}$: C, 93.62; H, 6.38%.

Optically Active Triptycenes. II.[1] Synthesis of Optically Active 7-Substituted 2,5-Dimethoxytriptycenes

Fumio OGURA, Yoshiteru SAKATA, and Masazumi NAKAGAWA

Department of Chemistry, Faculty of Science, Osaka University, Toyonaka, Osaka, 560

(Received May 16, 1972)

A series of optically active 7-substituted 2,5-dimethoxytriptycenes has been prepared from (+)-2,5-diacetoxy-7-carboxytriptycene (I) as suitable model compounds for a study of the relationship between their structure and optical rotatory properties. The single crystal of 2,5-dimethoxy-7-dimethylaminotriptycene hydrobromide (VII) thus prepared was subjected to X-ray crystallographic analysis and proved to have 1*R*, 6*S* absolute configuration. Consequently, it became clear that all compounds of this series have the same 1*R*, 6*S* configuration. They showed without exception positive optical rotation in visible wavelength region.

Triptycene is a highly symmetrical cage compound and has a definite and rigid molecular structure confirmed by reactivities,[2] various spectroscopic properties,[3] electric dipole moments,[4] and X-ray crystallographic analysis.[5,6]

Triptycene derivatives bearing different substituent groups in two of the three benzene rings can be resolved into optical antipodes. We reported on the synthesis and optical resolution of 2,5-diacetoxy-7-carboxytriptycene (I).[1] The optically active triptycene may be regarded as one of the most appropriate substances for studying the relation between structure and rotatory properties for the following reasons.

1. The difinite and rigid molecular structure should exclude the influence of complicated effects arising from the flexibility of the molecule.
2. The structural transformation necessary for the investigation can be accomplished without causing recemization and Walden inversion.
3. Theoretical approach to the analysis of the ORD and CD properties might be possible by utilizing the results of investigations on the electronic spectra of benzenoid chromophore.

We wish to report on the preparation of a series of 7-substituted 2,5-dimethoxytriptycenes with identical absolute configuration starting from (+)-2,5-diacetoxy-7-carboxytriptycene (I).[1] The general scheme of the transformation is summarized in Fig. 1. Hydrolysis of I by means of aqueous acetic acid containing hydrogen bromide afforded 2,5-dihydroxy-7-carboxytriptycene (II). Methylation of II with dimethyl sulfate in acetone in the presence of anhydrous potassium carbonate resulted in the formation of 2,5-dimethoxy-7-methoxycarbonyltriptycene (III).[7] 2,5-Dimethoxy-7-carboxytriptycene (IV) was obtained by hydrolysis of III in aqueous acetic acid containing sulfuric acid.[8]

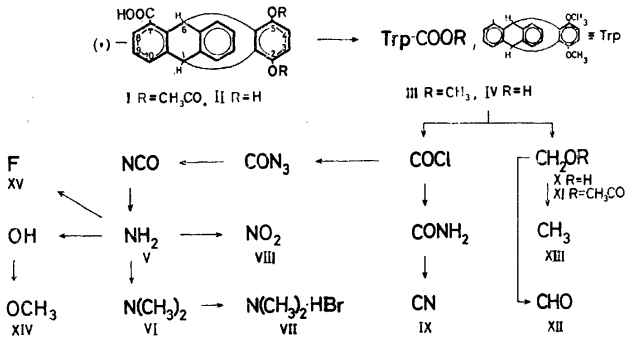

Fig. 1. General scheme of preparation of optically active triptycenes.

Treatment of IV in tetrahydrofuran with thionyl chloride yielded acid chloride, which was subjected to the Curtius reaction *via* acid azide and isocyanate to give 2,5-dimethoxy-7-aminotriptycene (V).

Methylation of V with trimethyl phosphate yielded 2,5-dimethoxy-7-dimethylaminotriptycene (VI).[9]

Amine (V) was oxidized to 2,5-dimethoxy-7-nitrotriptycene (VIII) by peracetic acid in chloroform.[10]

The above-mentioned acid chloride was treated with ammonia in tetrahydrofuran to yield acid amide. Dehydration of the amide by thionyl chloride in dimethylformamide afforded 2,5-dimethoxy-7-cyanotriptycene (IX).

Reduction of the ester (III) with lithium aluminum hydride in tetrahydrofuran gave 2,5-dimethoxy-7-hydroxymethyltriptycene (X), which was converted into 2,5-dimethoxy-7-acetoxymethyltriptycene (XI) on treatment with acetic anhydride.

Oxidation of carbinol (X) with chromium trioxide-pyridine complex in pyridine yielded 2,5-dimethoxy-7-formyltriptycene (XII).[11]

1) Part I of this series, A. Sonoda, F. Ogura, and M. Nakagawa, This Bulletin, **35**, 853 (1962).

2) P. D. Bartlett, M. J. Ryan, and S. G. Cohen, *J. Amer. Chem. Soc.*, **64**, 2649 (1942); P. D. Bartlett and E. S. Lewis, *ibid.*, **72**, 1005 (1950); P. D. Bartlett and F. D. Greene, *ibid.*, **76**, 1088 (1954); G. Wittig and W. Tochtermann, *Ann.* **660**, 23 (1962).

3) W. Theilacker, A. Albrecht, and H. Uffmann, *Chem. Ber.*, **98**, 428 (1965): M. I. Bruce, *Chem. Commun.*, **1968**, 593; L. H. Schwartz, *J. Org. Chem.*, **33**, 3977 (1968).

4) F. Ogura, Y. Toshiyasu, K. Kimura, R. Fujishiro, and M. Nakagawa, This Bulletin, **37**, 757 (1964).

5) N. Sakabe, K. Sakabe, K. Ozeki-Minakata, C. Katayama, and J. Tanaka. Presented at The Ninth International Congress of Crystallography, Kyoto (1972). *Acta Crystallogr.*, in press.

6) K. J. Palmer and D. H. Templeton, *ibid.*, **B24**, 1048 (1968).

7) The phenolic hydroxyl group in II could not be methylated even by an excess of diazomethane, probably owing to their low acidity.

8) Hydrogen bromide could not be used as partial demethylation occurred.

9) J. H. Billman, A. Radike, and B. W. Mundy, *J. Amer. Chem. Soc.*, **64**, 2977 (1942); D. G. Thomas, J. H. Billman, and C. E. Davis, *ibid.*, **68**, 895 (1946).

10) W. D. Emmons, *J. Amer. Chem. Soc.*, **79**, 5528 (1958); *idem*, *ibid.*, **76**, 3470 (1954).

11) J. H. Holum, *J. Org. Chem.*, **26**, 4814 (1961).

Chloromethyl derivative obtained by the reaction of X with thionyl chloride was reduced to 2,5-dimethoxy-7-methyltriptycene (XIII) with lithium aluminum hydride in refluxing tetrahydrofuran.[12]

Amine (V) was diazotized with sodium nitrite in acetic acid. Diazonium compound thus obtained was hydrolyzed in dilute boiling sulfuric acid to afford phenol derivative.[13] The crude phenol was methylated with dimethyl sulfate in acetone in the presence of anhydrous potassium carbonate to yield methyl ether (XIV).

Fluoro derivative (XV) was obtained from amine (V) by the Schiemann reaction.

All the new compounds described above gave satisfactory data of elemental analyses and their structures were confirmed by means of IR, UV, and NMR spectra.

X-Ray crystallographic analysis performed on the single crystal of (+)-2,5-dimethoxy-7-dimethylaminotriptycene hydrobromide (VII) demonstrated that the absolute configuration of VII was 1*R*,6*S* as shown in Fig. 2.[5] Consequently, all the compounds shown in Fig. 1 were proved to have the same 1*R*,6*S* configuration. All the compounds of this series showed dextro optical rotation regardless of the change of nature of substituent group at 7-position.

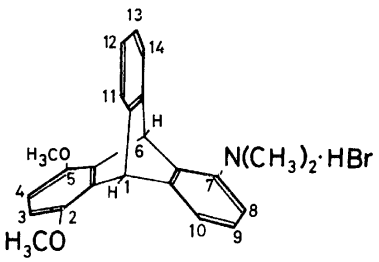

Fig. 2. The absolute configuration of (+)-2,5-dimethoxy-7-dimethylaminotriptycene hydrobromide.

Experimental

All the melting points were not corrected. The experimental procedures refer to the optically active substances, and purified anhydrous solvents were used throughout the experiments unless otherwise stated. Ligroin boiling at 60—80°C was used. The IR spectra were measured with a Hitachi EPI-2 and a JASCO DS-301 spectrophotometer. The NMR spectra in deuteriochloroform solution were obtained with a Varian A-60 spectrometer using TMS as an internal standard. Chemical shifts are recorded in δ unit. The electronic spectra were obtained with a Hitachi EPS-3T and a Zeiss PMQIIM4QIIId spectrometer. The optical rotations were measured with a Rudolf Model 200S-80 and a Yanagimoto ORD-185 spectropolarimeter. The circular dichroism spectra were measured with a Roussel-Jouan dichrograph B, II-CD-185 and JASCO J-20 spectropolarimeter with CD attachments. The inflections and shoulders are indicated with an asterisk. The optical rotations were measured at 20°C throughout the present research unless otherwise stated. Ethanol (99%) containing 0.1 N aqueous hydrochloric acid (2 m*l* of the hydrochloric acid was made up to 20 m*l* solution with the ethanol) was used as a solvent of measurement and abbreviated as 99% EtOH-HCl.

2,5-Dihydroxy-7-carboxytriptycene (II). To a hot solution of (+)-2,5-diacetoxy-7-carboxytriptycene (I, 1.436 g) was added hydrobromic acid (47%, 3.3 m*l*). The mixture was refluxed for 6 hr and allowed to cool to room temperature to precipitate fairly pure II (light brown leaflets, sintered at *ca.* 220°C and melted at *ca.* 300°C, 0.999 g, 94.5%) which could be used directly for the preparation of derivatives. Recrystallization of this material from acetic acid-water gave pure II, mp 332—335°C (decomp.). Elemental analyses of this substance gave no satisfactory results presumably owing to its nature of incomplete combustibility. IR (Nujol mull): 3700—2500 (ν_{O-H}, -COOH, -OH), 1689 (ν_{C-O}, -COOH) cm^{-1}. UV: $\lambda_{max}^{99\%EtOH}$ (ε) 261 (4160) 269 (4200), 294 (8330) nm. ORD: $[M]_{5791}^{18°C}$+189.4°, $[M]_{5461}^{18°C}$+215.9°, $[M]_{4358}^{18°C}$+412.2°, $[M]_{4047}^{18°C}$+535.5°, $[M]_{3650}^{18°C}$+849.0° (*c*, 0.4356, dioxane).

Hydrolysis of *dl*-I was carried out under somewhat different conditions. Racemic I (20 g) was dissolved in hot acetic acid (20 m*l*). A mixture of water (30 m*l*) and hydrobromic acid (47%, 4 m*l*) was added to the solution and refluxed for 7 hr. Racemic II was obtained as faint pink plates (1.3 g, 84.5%) on cooling the reaction mixture, mp 325°C (decomp.). Racemate exhibited a slightly different IR spectrum.

2,5-Dimethoxy-7-methoxycarbonyltriptycene (III). A mixture of II (0.60 g), dimethyl sulfate (1.1 g), anhydrous potassium carbonate (3.0 g), and acetone (40 m*l*) was refluxed for 8 hr under stirring. After cooling, the reaction mixture was poured onto water (*ca.* 300 m*l*) and extracted 3 times with benzene. The crude crystalline product obtained from the extract was dissolved in benzene and purified by passing through a short column of alumina (25 g). Colorless crystals (0.6 g) were obtained on evaporating the first 500 m*l* fraction. Recrystallization from a small amount of benzene gave pure III, mp 261.5—262.5°C (racemate, mp 227—228.5°C). IR (KBr-disk): 2830 (ν_{C-H}, $-OCH_3$), 1715 ($\nu_{C=O}$, $-COOCH_3$) cm^{-1}. NMR: 3.83 (6H, s, $-OCH_3$), 4.02 (3H, s, $-COOCH_3$), 5.95 (1H, s, C_1-H), 6.56 (2H, aromatic at C_{3-4}), 6.97—7.71 (8H, m, aromatic at C_{8-14} and C_6-H).[14] UV: $\lambda_{max}^{99\%EtOH}$ (ε) 294 (8220), 270 (3450), 262 (2790), 208 (63600), 195 (52500) nm. $\lambda_{max}^{dioxane}$ (ε) 295 (8200), 270 (3230), 262 (2500) nm. ORD: $[M]_{5791}^{25°C}$+91.6°, $[M]_{5461}^{25°C}$+104.6°, $[M]_{4358}^{25°C}$+195.9°, $[M]_{4047}^{25°C}$+248.8°, $[M]_{3650}^{25°C}$+386.2° (*c*, 0.7475, dioxane). CD: $\lambda_{max}^{99\%EtOH}$ ($\Delta\varepsilon$) 302 (+1.35), 279 (+0.43), 268.5 (−3.83), 262 (−2.87), 249 (+1.82), 244 (−1.25), 232 (+5.14), 219 (−10.42), 207 (+37.64) nm. $\lambda_{max}^{dioxane}$ ($\Delta\varepsilon$) 303 (+1.61), 280 (+0.57), 267 (−3.06), 262 (−2.66) nm.

Found: C, 77.19; H, 5.48%. Calcd for $C_{24}H_{20}O_4$: C, 77.40; H, 5.41%.

2,5-Dimethoxy-7-carboxytriptycene (IV). Methyl ester (III, 0.30 g) in acetic acid (20 m*l*) was mixed with 6 N sulsulfuric acid (5 m*l*) and the mixture was refluxed for 12 hr. Crystals obtained on cooling the reaction mixture were recrystallized from acetic acid to give pure IV, mp 320—321°C (racemate, mp 305—306°C (decomp.)). IR (KBr disk): 3400—2200 (ν_{O-H}, -COOH), 2835 (ν_{C-H}, $-OCH_3$), 1683 ($\nu_{C=O}$, -COOH) cm^{-1}. UV: $\lambda_{max}^{99\%EtOH}$ (ε) 293 (6800),

12) Racemic XIII was obtained by lithium aluminum hydride reduction of tosylate of *rac*-X which was prepared by the reaction of sodium salt of *rac*-X with tosyl chloride (see Experimental).

13) Diazotization of amine (V) with nitrosyl sulfate in sulfuric acid resulted in the formation of a nitrosophenol derivative.

14) The signal of the bridgehead proton bonded to C_6 was shifted to down-field by the effect of anisotropy of the methoxycarbonyl group.

268.5 (3340), 261 (2780), 209 (59300) nm. $\lambda_{max}^{dioxane}$ (ε) 295 (8330), 270 (3660), 263 (2910), 220 (38300) nm. ORD: $[M]_{5893}$+144.2°, $[M]_{5461}$+167.3°, $[M]_{4358}$+301.4°, $[M]_{4047}$+398.0°, $[M]_{3650}$+588.4° (*c*, 0.0497, dioxane). CD: $\lambda_{max}^{dioxane}$ ($\Delta\varepsilon$) 303.5 (+1.28), 279 (+0.49), 267.5 (−2.50), 263 (−2.23), 250 (+0.93) nm.

Found: C, 77.22; H, 5.19%. Calcd for $C_{23}H_{18}O_4$: C, 77.08; H, 5.06%.

2,5-Dimethoxy-7-aminotriptycene (V). Carboxylic acid (IV, 0.410 g) was dissolved in tetrahydrofuran (25 m*l*) and treated with thionyl chloride (2 m*l*) under reflux for 3 hr. The solvent was removed under reduced pressure to give colorless crystals. The acid chloride obtained was fairly pure and could be used directly in the following reaction [IR (Nujol mull): 1755 ($\nu_{C=O}$, −COCl) cm^{-1}]. A solution of sodium azide (0.140 g) in water (3 m*l*) was added to an ice-cooled solution of the acid chloride (0.458 g) in tetrahydrofuran (35 m*l*). The reaction mixture was stirred for 2 hr and poured onto 300 m*l* of cold water. Colorless precipitate was collected by filtration and washed with water and dried. The acid azide is fairly stable and can be handled safely at room temperature, though spontaneous rearrangement to isocyanate occurred in part even under room temperature [IR (Nujol mull): 2150 ($\nu_{N=N=N}$, $-CON_3$), 1695 ($\nu_{C=O}$, $-CON_3$) cm^{-1}. Weak absorption band at 2270 cm^{-1} indicated the presence of a minor amount of isocyanate]. The well-dried acid azide (0.429 g) was spread over the bottom of a 300 m*l* Erlenmeyer flask and heated slowly up to 130°C and maintained at this temperature for 3 hr yielding light brown crystalline powder (0.385 g) with evolution of nitrogen [IR (Nujol mull): 2270 ($\nu_{N=C=O}$) cm^{-1}]. A mixture of the isocyanate (0.249 g), 99% ethanol (40 m*l*) and water (10 m*l*) was refluxed for 8 hr. Crystals deposited were collected by filtration and washed with 50% ethanol and water, successively, to give V as faintly pink leaflets (0.191 g). The filtrate and washings were combined and poured water(300 m*l*) and extracted 4 times with benzene. The combined extracts were washed with water and dried (sodium sulfate). Evaporation of the solvent afforded further 0.036 g of the amine (total yield 93% based on IV). Colorless pure crystals of V [mp 259—261°C (decomp.) in a sealed tube] were obtained by repeated sublimation under reduced pressure (bath temp. 200—220°C/3 mmHg). IR (KBr disk): 3495, 3470 (ν_{N-H}, $-NH_2$), 1623 (δ_{N-H}, $-NH_2$), 2845 (ν_{C-H}, $-OCH_3$) cm^{-1}. UV: $\lambda_{max}^{99\%EtOH}$ (ε) 296 (5540), 275 (3630), 269 (3840), 260 (3200), 217 (53500), 195 (50800) nm. $\lambda_{max}^{dioxane}$ (ε) 302 (6500), 275 (4040), 269.6 (4100), 219.5 (52600) nm. $\lambda_{max}^{99\%EtOH\cdot HCl}$ (ε) 296 (4090), 277.5 (3820), 271 (2750), 262.5 (2560), 212 (61700), 194 (55400) nm. CD: $\lambda_{max}^{99\%EtOH}$ ($\Delta\varepsilon$) 303 (+6.37), 270 (−9.11), 244 (−7.50), 225 (+26.5), 204 (−6.38), 197 (−7.46) nm. $\lambda_{max}^{dioxane}$ ($\Delta\varepsilon$) 303 (+6.77), 268 (−9.83), 245 (−5.53), 225 (+27.7) nm. $\lambda_{max}^{99\%EtOH\text{-}HCl}$ ($\Delta\varepsilon$) 297 (+1.77), 277.5 (+4.30), 273.5 (−0.70), 262 (−9.08), 239 (+2.86), 219 (−5.14) nm. ORD: $[M]_{5893}$ +62.44°, $[M]_{5461}$+66.60°, $[M]_{4358}$+149.9°, $[M]_{4047}$+233.1°, $[M]_{3650}$+562.0° (*c*, 0.3165, dioxane).

Found: C, 79.84; H, 5.84%. Calcd for $C_{22}H_{19}O_2N$: C, 80.22; H, 5.81%.

Racemate was recrystallized from methanol and showed no tendency to sublime, mp 267—268°C.

2,5-Dimethoxy-7-dimethylaminotriptycene (VI). The amine (V, 0.080 g) was mixed with trimethyl phosphate (0.60 g) and heated to reflux for 3 hr. After cooling, a mixture of water (1.3 m*l*) and sodium hydroxide (1.7 g) was added to the reaction mixture and refluxed for 30 min. Colorless crystals deposited were collected by filtration and washed with water. Sublimation under reduced pressure (bath temp. 220—230°C/3 mmHg) afforded pure VI, mp 246—248°C. IR (KBr disk): 2970 (ν_{C-H}, $-N-CH_3$), 2840 (ν_{C-H}, $-OCH_3$) cm^{-1}. UV: $\lambda_{max}^{99\%EtOH}$ (ε) 294 (4770), 275* (4510), 268* (5900), 261* (6760), 230* (*ca.* 25000, broad), 211 (45100), 195 (55500) nm. $\lambda_{max}^{dioxane}$ (ε) 295 (4820), 275* (4970), 268* (6560), 256* (8000, broad), 230* (24700, broad), 216 (41300) nm. $\lambda_{max}^{99\%EtOH\text{-}HCl}$ (ε) 297.5 (4300), 279 (4730), 272.5 (3520), 263 (3320), 255 (2920), 208 (60200), 197 (54200) nm. CD: $\lambda_{max}^{99\%EtOH}$ ($\Delta\varepsilon$) 304 (+1.82), 275.5 (−4.72), 271 (−5.17), 261.5 (+1.40), 244 (−9.65), 228 (+27.9), 214 (−17.8), 204 (+3.80), 199 (−6.33) nm. $\lambda_{max}^{dioxane}$ ($\Delta\varepsilon$) 298 (+2.60), 272.5 (−6.11), 260.5 (+3.20), 243 (−10.0), 228 (+31.8) nm. $\lambda_{max}^{99\%EtOH\cdot HCl}$ ($\Delta\varepsilon$) 297 (+1.26), 279 (+2.45), 273.5 (−1.03), 264.5 (−8.61), 247 (+5.47), 213 (−9.45) nm. ORD: $[M]_{4047}$ +5.40°, $[M]_{3650}$+34.10° (*c*, 0.2788, dioxane).

Found: C, 80.45; H, 6.57%. Calcd for $C_{24}H_{23}O_2N$: C, 80.64; H, 6.49%.

2,5-Dimethoxy-7-dimethylaminotriptycene Hydrobromide (VII). The dimethylamine (VI, 0.038 g) dissolved in 99% ethanol (22 m*l*) was mixed with 47% aqueous hydrobromic acid (3 m*l*) and water (3 m*l*). Clear and homogeneous solution obtained on warming and filtration was placed in a loosely stoppered ground joint vessel and kept in the dark. Beautiful rhomboidal single crystals of VII developed gradually on storing the solution over a period of two or three months. Sometimes VII crystallized in needles. In such cases the solution had to be warmed to dissolve the needles and filtered again to get rhomboidal crystals. The crystals began to sublime at *ca.* 240°C and partly melted at the same time. It crystallized again in needles and perfectly decomposed to red oil at 250°C, IR (KBr disk): 2845 (ν_{C-H}, $-OCH_3$), 2785 (ν_{C-H}, $-N-CH_3$), 2700—2000 (ν_{N-H}, $-\overset{+}{N}H(CH_3)_2$) cm^{-1}. UV: $\lambda_{max}^{99\%EtOH}$ (ε) 297 (4490), 278.5 (4320), 269.5 (4460), 262 (4870), 255* (5100), 210 (55900), 196.5 (68700) nm. CD: $\lambda_{max}^{99\%EtOH}$ ($\Delta\varepsilon$) 299.5 (+1.52), 279.5 (+0.88), 273.5 (−2.33), 264 (−5.84), 256 (−1.17), 248.5 (−0.53), 230 (+9.21), 214.5 (−14.3) nm.

Found: C, 65.70; H, 5.48; Br, 18.33%. Calcd for $C_{24}H_{24}O_2NBr$: C, 65.75; H, 5.52; Br, 18.23%.

2,5-Dimethoxy-7-nitrotriptycene (VIII). Ninety percent hydrogen peroxide (0.083 m*l*) and a small drop of concentrated sulfuric acid were added to ice-cooled chloroform (0.36 m*l*). Acetic anhydride (0.4 g) was then added to the mixture. The cooling bath was removed and the mixture was stirred for 15 min. After further addition of chloroform (0.24 m*l*) the mixture was heated to reflux under stirring. The heating bath was removed and a solution of V (0.196 g) in chloroform (20 m*l*) was added dropwise to the hot oxidizing mixture. Deposition of pale yellow crystals from the yellow reaction mixture was observed. The reaction mixture was refluxed under stirring. The resulting brown reaction mixture was poured onto water (100 m*l*) and extracted 3 times with chloroform. The combined extracts were washed successively with 10% aqueous potassium hydroxide, 10% aqueous hydrochloric acid and water, and dried (sodium sulfate). Brown yellow solid (0.203 g) obtained on evaporating the solvent under reduced pressure was dissolved in benzene and passed through a short column alumina (15 g). Yellow crystals (0.135 g) were obtained on concentrating the first 300 m*l* fraction eluted. The crude material was recrystallized 3 times from a mixture of ethyl acetate and ethanol, and then sublimed under reduced pressure (bath temp. 250°C/3 mmHg) to afford faintly yellow crystals. This material did not melt up to 300°C. IR (KBr disk): 2840 (ν_{C-H}, $-OCH_3$), 1525 ($\nu_{N-O\ asym}$, $-NO_2$), 1350

($\nu_{N-O\ sym}$, $-NO_2$) cm^{-1}. NMR: 3.83 (6H, s, $-OCH_3$) 5.98 (1H, s, bridgehead proton at C_1), 6.55 (2H, s, aromatic at C_{3-4}), 6.97—7.70 (8H, m, aromatic st C_{8-14} and C_6-H). The signal of bridgehead proton at C_6 is shifted to down-field owing to the anisotropic effect of the nitro group. UV: $\lambda_{max}^{99\%EtOH}$ (ε) 330* (2700, broad), 294.5 (7030), 273 (6670), 267 (6940), 261 (6730), 207 (62200), 194 (48500) nm. $\lambda_{max}^{dioxane}$ (ε) 330* (2770, broad), 296 (6780), 273.5 (6810), 267 (7120), 262 (7060), 220 (27700) nm. CD: $\lambda_{max}^{dioxane}$ ($\Delta\varepsilon$) 350 (+1.45), 301.5 (+3.78), 265 (−7.90), 238 (+3.52), 225 (+5.42), 209 (+28.48), 195 (−12.03) nm. $\lambda_{max}^{dioxane}$ ($\Delta\varepsilon$) 350 (+0.69), 302 (+3.28), 264 (−6.76), 236 (+4.14) nm. ORD: $[M]_{4358}$+117.3°, $[M]_{4047}$+207.7°, $[M]_{3730}$+334.7° (peak), $[M]_{3650}$+260.0° (*c*, 0.006785, EtOH). $[M]_{4358}$+51.9°, $[M]_{4047}$+111.0°, $[M]_{3770}$+161.0° (peak), $[M]_{3650}$+110.0° (*c*, 0.00706, dioxane).

Found: C, 73.87; H, 4.80%. Calcd for $C_{22}H_{17}O_4N$: C, 73.53; H, 4.77%.

Careful combustion of a mixture of VIII (2.019 mg) and sucrose (1.295 mg) gave the above results.

Racemate was recrystallized from benzene-ligroin, mp 270—274°C (decomp.). It showed no tendency to sublime.

2,5-Dimetoxy-7-cyanotriptycene (IX). Acid chloride (0.680 g) obtained by the reaction of IV with thionyl chloride according to the above procedure was dissolved in tetrahydrofuran (40 m*l*). Aqueous ammonia (28%, 5 m*l*) was added to the solution and the resulting clear two-layer mixture was allowed to stand overnight at room temperature. Colorless crystals of amide (0.353 g) deposited were filtered and washed with tetrahydrofuran. The combined filtrate and washings were concentrated under reduced pressure, yielding a second crop of the amide (0.257 g). The combined crystals were recrystallized from methyl acetate-methanol to yield pure amide, mp 305—320°C (decomp.). IR (Nujol mull): 3400, 3300, 3250, 3140 (ν_{N-H}, $-CONH_2$), 1680 ($\nu_{C=O}$, $-CONH_2$) cm^{-1}.

The amide (0.454 g) was dissolved in warm dimethylformamide (15 m*l*) and mixed with thionyl chloride (9 m*l*). Immediate development of red color and generation of heat were observed. As soon as the mixture was heated on a water-bath (80—90°C), deposition of a considerable amount of colorless solid was observed. Most of the solid again dissolved in the solution in a period of 10 min with evolution of sulfur dioxide and hydrogen chloride. The reaction mixture was kept at 80—90°C for 20 hr and then chilled in an ice-bath. Crystals of sulfur (0.125 g) deposited were removed by filtration and washed with dimethylformamide. The combined filtrate and washings were poured into water (300 m*l*). Red brown oil separated under evolution of gas was extracted 3 times with ether and once with benzene. The combined extracts were washed with water and dried over sodium sulfate. Yellow solid (0.554 g) obtained on evaporating the solvent under reduced pressure was dissolved in benzene and passed through a short column of alumina (25 g). IX was obtained as colorless crystals (0.270 g) on drying up the first 500 m*l* fraction eluted. It crystallized in fine needles from 99% ethanol. IX sublimed on heating *ca.* 200°C, mp 263—265°C. IR (KBr disk): 2840 (ν_{C-H}, $-OCH_3$), 2225 ($\nu_{C\equiv N}$) cm^{-1}. UV: $\lambda_{max}^{99\%EtOH}$ (ε) 296.5 (8880), 268.5 (3180), 262 (2190), 206 (73000), 194* (46500) nm. $\lambda_{max}^{dioxane}$ (ε) 297 (9200), 268.5 (3190), 261 (2180), 215.5 (45900) nm. ORD: $[M]_{5893}$+71.4°, $[M]_{5461}$+95.6°, $[M]_{4358}$+178.8°, $[M]_{4047}$+248.1°, $[M]_{3650}$+432.3° (*c*, 0.1264, dioxane). CD: $\lambda_{max}^{99\%EtOH}$ ($\Delta\varepsilon$) 305 (+1.86), 279 (+0.60), 268.5 (−2.55), 261.5 (−1.53), 246 (+1.45), 235.5 (−1.24), 221 (−5.62), 206 (+11.81) nm. $\lambda_{max}^{dioxane}$ ($\Delta\varepsilon$) 303 (+2.18), 293 (+1.20), 268 (−2.66), 260* (−1.7) nm.

Found: C, 81.19; H, 5.07%. Calcd for $C_{23}H_{17}O_2N$: C, 81.39; H, 5.05%.

2,5-Dimethoxy-7-hydroxymethyltriptycene (X). A solution of III (0.438 g) in tetrahydrofuran (10 m*l*) was added dropwise to a stirred suspension of lithium aluminum hydride (0.438 g) in the same solvent (10 m*l*). After stirring for 6 hr at room temperature, ethyl acetate, wet ether, water, and 6 N sulfuric acid were added successively to the reaction mixture under ice-cooling. The acidified mixture was poured onto water (200 m*l*) and extracted with ether. The combined extracts were washed with a saturated aqueous solution of sodium chloride and dried (sodium sulfate). Colorless crystals obtained on evaporating the solvent under reduced pressure were recrystallized from 99% ethanol to yield pure X, mp 224°C. IR (KBr disk): 3600—3100 (ν_{O-H}), 2840 (ν_{C-H}, $-OCH_3$) cm^{-1}. UV: $\lambda_{max}^{99\%EtOH}$ (ε) 293.5 (3910), 280.5 (4100), 264.5 (2640), 216 (66900), 194 (57200) nm. $\lambda_{max}^{dioxane}$ (ε) 294 (4280), 280 (4200), 264 (2620), 219 (59800) nm. ORD: $[M]_{5893}$+93.2°, $[M]_{5461}$+118.0°, $[M]_{4358}$+247.6°, $[M]_{4047}$+313.4°, $[M]_{3650}$+507.5° (*c*, 0.5285, dioxane). CD: $\lambda_{max}^{99\%EtOH}$ ($\Delta\varepsilon$) 297 (+0.60), 279.5 (+2.31), 263 (−5.44), 238 (−2.97), 224 (+5.95), 205 (+17.1) nm. $\lambda_{max}^{dioxane}$ ($\Delta\varepsilon$) 295 (+0.96), 279 (+2.24), 263.5 (−3.99) nm.

Found: C, 80.47; H, 5.77%. Calcd for $C_{23}H_{20}O_3$: C, 80.21; H, 5.85%.

Racemate was recrystallized from methanol, mp 235—236°C.

2,5-Dimethoxy-7-acetoxymethyltriptycene (XI). A mixture of carbinol (X, 0.100 g) and acetic anhydride (3 m*l*) was heated on a boiling water-bath for 6 hr. The excess of anhydride was decomposed by water to yield crude yellow crystals. The crystals were recrystallized twice from 99% ethanol, yielding XI, mp 177—178°C. IR (KBr disk): 2840 (ν_{C-H}, $-OCH_3$), 1740 ($\nu_{C=O}$, $CH_3CO_2CH_2-$) cm^{-1}. UV: $\lambda_{max}^{dioxane}$ (ε) 294.5 (3940), 281 (4470), 264 (2650), 221.5 (37400) nm. ORD: $[M]_{5893}$+64.0°, $[M]_{5461}$+72.8°, $[M]_{4358}$+128.1°, $[M]_{4047}$+168.5°, $[M]_{3650}$+281.0° (*c*, 0.6215, dioxane). CD: $\lambda_{max}^{dioxane}$ ($\Delta\varepsilon$) 295 (+1.56), 281 (+1.89), 263.5 (−5.18) nm. $\lambda_{max}^{99\%EtOH}$ ($\Delta\varepsilon$) 297 (+0.60), 279.5 (+2.31), 263 (−5.44), 238 (−2.97), 223 (+5.95), 205 (+17.1) nm.

Found: C, 77.45; H, 5.72%. Calcd for $C_{25}H_{22}O_4$: C, 77.70; H, 5.74%.

2,5-Dimethoxy-7-formyltriptycene (XII). To a slurry of pyridine-chromium trioxide complex prepared from pyridine (4 m*l*) and chromium trioxide (0.2 g) was added a solution of X (0.202 g) in pyridine (4 m*l*) under ice-cooling. After 30 min ice-bath was removed and the reaction mixture was stirred for 5 hr at room temperature. After being put to stand overnight in a refrigerator, the mixture was poured onto cold water and extracted with ether. The combined extracts were worked up in the usual way,[15] yielding colorless crystals (0.165 g, 82.2%). This material was recrystallized from 99% ethanol to result in pure XII, mp 258—259°C. IR (KBr disk): 2830 (ν_{C-H}, $-OCH_3$), 2720 (ν_{C-H}, $-CHO$), 1694 ($\nu_{C=O}$, $-CHO$) cm^{-1}. NMR: 3.81 (6H, s, $-OCH_3$), 5.96 (1H, s, bridgehead proton at C_1), 6.53 (2H, s, aromatic at C_{3-4}), 7.13—7.70 (8H, m, bridgehead proton at C_6 and aromatic at C_{8-14}), 10.51 (1H, s, $-CHO$). The down-field shift of the signal of bridgehead proton at C_6 can be attributed to the anisotropic effect of the formyl group. UV: $\lambda_{max}^{99\%EtOH}$ (ε) 317* (3780), 302 (6430), 272* (4210), 258* (11600), 252* (12900), 230—236* (15300), 212.5 (56300), 194 (53800) nm. $\lambda_{max}^{dioxane}$ (ε) 315* (4440), 302 (7130), 272.5 (3120), 261* (11200), 252* (15400), 237* (19800), 215 (56300) nm.

15) A small amount of IV (0.012 g, 5.7%) was obtained from 10% aqueous potassium carbonate washings on acidification.

ORD: $[M]_{5893}$+70.2°, $[M]_{5461}$+71.4°, $[M]_{4358}$+154.9°, $[M]_{4047}$+210.1°, $[M]_{3750}$+405.0° (peak), $[M]_{3650}$+354.0°, $[M]_{3600}$+400.9° (peak), (*c*, 0.295, dioxane). CD: $\lambda_{max}^{99\%EtOH}$ ($\Delta\varepsilon$) 354 (+0.13), 334 (−0.23), 324 (−0.29), 297 (+1.78), 280* (+0.80), 271* (−1.78), 263* (−3.83), 256* (−4.97), 250 (−5.33), 238 (+6.02), 223 (−4.24), 211 (+27.7) nm. $\lambda_{max}^{dioxane}$ ($\Delta\varepsilon$) 295 (+1.49), 280* (+0.94), 272* (−2.60), 263* (−3.70), 248 (−5.82), 232.5 (+5.75) nm.

Found: C, 80.64; H, 5.36%. Calcd for $C_{23}H_{18}O_3$: C, 80.68; H, 5.30%.

Racemate was recrystallized from *n*-propyl alcohol and purified on sublimation at *ca.* 220°C, mp 246—248°C.

2,5-Dimethoxy-7-methyltriptycene (XIII). A solution of carbinol (X, 0.195 g) in benzene (25 m*l*) was mixed with thionyl chloride (2 m*l*). The mixture was stirred for 4 hr at room temperature and then refluxed for 30 min. Light brown solid [mp 160—180°C (decomp.)] obtained by evaporating the solvent and volatile material under reduced pressure gave no absorption of hydroxyl group in its IR spectrum. Owing to the unstable nature of the halide, the crude material was used directly in the following reaction. A solution of the crude chloride (0.213 g) in tetrahydrofuran (25 m*l*) was added dropwise to a mixture of lithium aluminum hydride (0.4 g) in the same solvent (20 m*l*) which had been stirred previously for 30 min at room temperature. After the mixture had been refluxed under stirring for 4 hr, it was cooled on an ice-bath and treated with methyl acetate, water and 6 N sulfuric acid, successively. The acidified mixture was poured onto water (200 m*l*) and extracted with ether. The combined extracts were washed with 5% aqueous sodium hydroxide and water, successively, and dried (sodium sulfate). Colorless solid obtained on evaporating the solvent under reduced pressure was dissolved in benzene and passed through a short column of alumina (20 g). Colorless crystals were obtained from the first fraction (300 m*l*). The crystals were recrystallized from methanol–methyl acetate to afford pure XIII, mp 207—209°C. IR (KBr disk): 2845 (ν_{C-H}, $-OCH_3$) cm^{-1}. NMR: 2.52 (3H, s, $-CH_3$), 3.81 (6H, s, $-OCH_3$), 5.58 (1H, s, bridgehead proton at C_6), 6.18 (1H, s, bridgehead proton at C_1) 6.51 (2H, s, aromatic at C_{3-4}) 6.81—7.52 (7H, m, aromatic at C_{8-14}). UV: $\lambda_{max}^{96\%EtOH}$ (ε) 293.5 (3780), 279 (3170), 276* (2770), 272 (2370), 264 (2360), 258* (1820), 216 (67500), 195.5 (53000) nm. $\lambda_{max}^{dioxane}$ (ε) 294 (4130), 279 (3110), 273* (2310), 264 (2330) 219.5 (49800) nm. ORD: $[M]_{5893}$+99.4°, $[M]_{4358}$+136.6°, $[M]_{4047}$+161.5°, $[M]_{3650}$+335.4° (*c*, 0.02115, dioxane). CD: $\lambda_{max}^{99\%EtOH}$ ($\Delta\varepsilon$) 301 (+0.91), 290 (+1.17), 278.5 (+2.76), 274 (−0.20), 263 (−4.48), 240.5 (−2.44), 228 (+1.47), 221 (−2.23), 215 (+5.83), 206 (−13.0). $\lambda_{max}^{dioxane}$ ($\Delta\varepsilon$) 300* (+0.90), 279 (+2.24), 263 (−3.54).

Found: C, 84.08; H, 6.05%. Calcd for $C_{23}H_{20}O_2$: C, 84.12; H, 6.14%.

The racemate was prepared as follows. Racemate of X (1.310 g) dissolved in a mixture of ether (50 m*l*) and tetrahydrofuran (25 m*l*) was mixed with a sodium hydride suspension (content 50%, 0.229 g). The mixture was refluxed for 2 hr under vigorous agitation and allowed to stand overnight at room temperature. An additional sodium hydride suspension (0.236 g) was added and the mixture was refluxed for further 2 hr under vigorous agitation. *p*-Toluenesulfonyl chloride (0.728 g) in tetrahydrofuran (15 m*l*) was added under ice-cooling and the mixture was stirred for 48 hr. The mixture was filtered under careful protection from moisture. The filtrate was concentrated under reduced pressure to give crude tosylate as a solid.[16] The presence of unreacted X was clearly indicated by its IR spectrum. As the purification by recrystallization or by chromatography on alumina was not feasible owing to its unstable nature, the crude tosylate was subjected directly to the following reaction. A solution of the crude tosylate in tetrahydrofuran was added to a mixture of lithium aluminum hydride (0.250 g) in the same solvent (15 m*l*) which had been stirred for 30 min at room temperature. The mixture was refluxed for 7 hr. After being put to stand overnight at room temperature, methyl acetate, water, and 6 N sulfuric acid were successively added to the reaction mixture. The mixture was poured onto a saturated aqueous sodium chloride solution and extracted with ether. The combined ethereal extracts were washed with water and dried (sodium sulfate). Colorless solid obtained on evaporating the solvent was dissolved in benzene and passed through a short column of alumina (25 g). From the first fraction (300 m*l*), colorless crystals contaminated with mineral oil were obtained. It was digested with boiling ligroin for a short period and recrystallized from methanol–methyl acetate (2 : 3), mp 228—230°C.

Found: C, 83.90; H, 6.08%. Calcd for $C_{23}H_{20}O_2$: C, 84.12; H, 6.14%.

2,5,7-Trimethoxytriptycene (XIV). The amine (V, 6.953 g) was dissolved in acetic acid (307 m*l*) on warming and the resulting clear pink solution was cooled to 12—14°C. Sodium nitrite (1.468 g) in water (41.6 m*l*) was added dropwise to the solution under stirring in a period of 1.5 hr. To the resulting red brown solution was added acetic acid (100 m*l*) and stirring was continued for further 30 min at 12—14°C. Strongly cooled red brown solution of the diazonium compound was added dropwise to refluxing 6 N sulfuric acid (918 m*l*) to yield phenolic derivative. The resulting light brown solution containing brown precipitate was extracted 3 times with benzene. The combined extracts were washed with water and dried over sodium sulfate. Crude phenol derivative (6.440 g, 92.4%) was obtained as light brown solid on evaporating the solvent. A solution of the phenol (100.0 mg) in acetone (15 m*l*) was refluxed with dimethyl sulfate (0.1 g) in the presence of anhydrous potassium carbonate (1 g) for 2 hr. After being put to stand overnight at room temperature, the reaction mixture was poured onto cold water (150 m*l*) and extracted 3 times with benzene. The combined extracts were washed with water and dried over sodium sulfate. Light brown solid obtained on evaporating the solvent was dissolved in benzene and passed through a short column of alumina (30 g) and eluted with the same solvent. Light yellow crystals obtained from the first eluate (300 m*l*) were dissolved in carbon tetrachloride and passed again through a short column of alumina (30 g). Colorless crystals obtained in a quantitative yield on evaporating the first eluate (300 m*l*) were recrystallized twice from a mixture of methanol and methyl acetate to give pure XIV, mp 273—275°C. IR (KBr disk): 2840 (ν_{C-H}, $-OCH_3$), 1265 (ν_{C-O}, Ar–O–CH_3) cm^{-1}. UV: $\lambda_{max}^{99\%EtOH}$ (ε) 293 (4360), 276 (3440), 267.5 (3750), 216 (63900), 195 (46400) nm. ORD: $[M]_{5893}$+22.4°, $[M]_{5461}$+32.6°, $[M]_{4358}$+65.2°, $[M]_{4047}$+94.6°, $[M]_{3650}$+180.8° (*c*, 0.2695, dioxane). CD: $\lambda_{max}^{99\%EtOH}$ ($\Delta\varepsilon$) 290 (+2.11), 279 (+1.87), 269 (+0.87), 241.5 (−9.91), 218.5 (+17.38), 212 (+21.36), 199 (−14.80) nm.

Found: C, 80.29; H, 5.92%. Calcd for $C_{23}H_{20}O_3$: C 80.21; H, 5.85%.

2,5-Dimethoxy-7-fluorotriptycene (XV). To a red brown solution of diazonium compound, prepared from V (0.187 g) according to the procedure used in the case of XIV, was

16) Tosylate of *d*-X could not be obtained by the reaction of *d*-X with *p*-toluenesulfonyl chloride in the presence of pyridine. In this case an unidentified solid bearing carbonyl group was obtained.

added a solution of sodium fluoroborate (0.1 g) in water (2 m*l*). The resulting reaction mixture was poured into a nearly saturated aqueous solution of sodium fluoroborate (15 g in 30 m*l* of water) to obtain the diazonium fluoroborate as red brown precipitate. The precipitate was collected by filtration and washed throughly with a small amount of cold water and dried exhaustively under reduced pressure. The dried fluoroborate (0.201 g) was spread over the bottom of a 300 m*l* Erlenmeyer flask and heated slowly up to 150 °C. The temperature of the flask was maintained at 150—160°C for 1.5 hr. The fluoroborate decomposed under evolution of nitrogen, yielding purple red crystalline powder. The reaction mixture was mixed with water (150 m*l*) and extracted with benzene. The combined extracts were washed with water and dried over sodium sulfate. The crude fluoro derivative obtained on evaporating the solvent was dissolved in benzene and passed through a short column of alumina (30 g). Concentration of the first benzene eluate (300 m*l*) gave the fluoro derivative as faintly yellow crystals (0.0816 g, 43.3%). The crystals were further purified by passing through a short column of alumina using carbon tetrachloride as a solvent. Colorless crystals (0.076 g) obtained from the first eluate (300 m*l*) were recrystallized twice from methanol give pure XV, mp 253.5—256.5°C (racemate, mp 248—249.5°C). UV: $\lambda_{max}^{99\%EtOH}$ (ε) 294 (4290), 276 (2570), 269 (1980), 261 (2010), 212.5 (70900), 195 (51800) nm. ORD: $[M]_{5893}+16.6°$, $[M]_{5461}+23.3°$; $[M]_{4358}+56.5°$, $[M]_{4047}+70.5°$, $[M]_{3650}+126.3°$ (*c*, 0.250, dioxane). CD: $\lambda_{max}^{99\%EtOH}$ ($\Delta\varepsilon$) 290 (+0.68), 276 (+3.50), (+0.84), 260 (−2.65), 228 (+1.60), 215.5 (−8.11), 202 (+9.05) nm.

Found: C, 79.46; H, 5.16%. Calcd for $C_{22}H_{17}O_2F$: C, 79.50; H, 5.16%.

BULLETIN OF THE CHEMICAL SOCIETY OF JAPAN, VOL. 45, 3651—3653 (1972)

Reaction of Organoaluminum Coordination Compound with Carbon Dioxide

Shohei INOUE and Yoshiharu YOKOO

Department of Synthetic Chemistry, Faculty of Engineering, The University of Tokyo, Hongo, Bunkyo-ku, Tokyo

(Received May 16, 1972)

The reaction of trialkylaluminum with carbon dioxide was suppressed by the presence of *N,N,N',N'*-tetramethylethylenediamine, 2,2'-dipyridyl, *N*-methylimidazole (MIm), and diethyl ether. On the other hand, the insertion reaction of carbon dioxide into the Al–N bond of diethylaluminum diethylamide was accelerated by the presence of MIm, *N*-methylbenzimidazole, and pyridine. The complexing agents are considered to play two different roles, *i. e.*, affecting the nucleophilicity of Al–C or Al–N bond and the ability of aluminum atom to accomodate carbon dioxide.

We have studied the reaction of organozinc coordination compound with secondary amines,[1,2] acidic hydrocarbons,[3] and carbon dioxide.[4] In these reactions, the complexes of dialkylzinc with *N,N,N',N'*-tetramethylethylenediamine (TMEDA), 2,2'-dipyridyl (Dipy), and *N*-methylimidazole (MIm) exhibit much enhanced reactivity when compared with dialkylzinc itself. The remarkable effect of MIm in the reaction with carbon dioxide was discussed in relation to the action of carbonic anhydrase, a zinc enzyme.[4]

Differently from dialkylzinc, trialkylaluminum is known to react readily with carbon dioxide at ordinary temperature and pressure.[5] In the present paper is reported the effect of the complex formation of organoaluminum compound with the above-mentioned complexing agents in the reaction toward carbon dioxide.

Results and Discussions

Reaction of Trialkylaluminum and Carbon Dioxide. The reaction of triisobutylaluminum with an atmos-

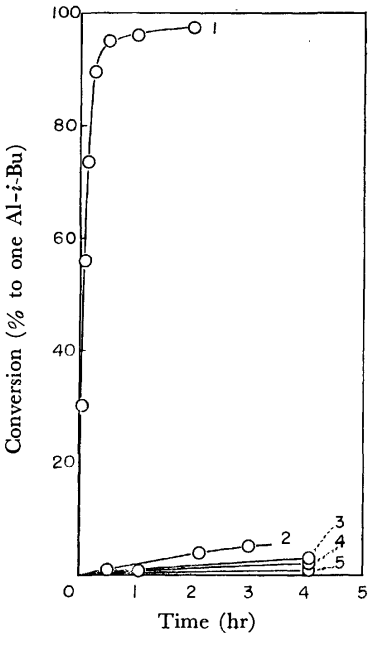

Fig. 1. Reaction of triisobutylaluminum and carbon dioxide, in toluene at 0°C.
$[i\text{-Bu}_3\text{Al}]_0$, 0.5 M; CO_2, 1 atm; complexing agent (molar ratio to Al):
1: none, 2: Dipy(1), 3: MIm(1), 4: TMEDA(1), 5: diethyl ether.

1) S. Inoue and T. Yamada, *J. Organometal. Chem.*, **25**, 1 (1970).
2) S. Inoue and Y. Imanaka, *ibid.*, **35**, 1 (1972).
3) S. Inoue and K. Furukawa, *ibid.*, **37**, 25 (1972).
4) S. Inoue and Y. Yokoo, *ibid.*, **39**, 11 (1972).
5) K. Ziegler, F. Krupp, K. Weyer, and W. Larbig, *Ann. Chem.*, **629**, 251 (1960); H. Lehmkuhl, *Angew. Chem.*, **76**, 817 (1964).

pheric pressure of carbon dioxide was examined at 0°C in toluene. As seen in Fig. 1, one of the isobutylaluminum linkages reacted rapidly and quantitatively with carbon dioxide, as determined by the absorption of carbon dioxide as well as by the formation of isovaleric acid. In the presence of an equimolar amount to triisobutylaluminum of TMEDA, Dipy, and MIm, the reaction was much suppressed, in contrast to the case of dialkylzinc. Even diethyl ether, which shows no effect on the reactivity of dialkylzinc, behaved similarly to TMEDA, etc. in the reaction of triisobutylaluminum.

When the reaction of triethylaluminum with carbon dioxide was carried out at 20°C, the absorption of carbon dioxide stopped at a quantity corresponding to 66% conversion of one ethyl-aluminum bond, and as the reaction products triethylcarbinol was detected together with propionic acid, indicating the fact that reaction (1) is accompanied by reactions (2) and (3).[5]

$$R_3Al + CO_2 \rightarrow RCOOAlR_2 \quad (1)$$

$$RCOOAlR_2 + R_3Al \rightarrow R_2CO + R_2AlOAlR_2 \quad (2)$$

$$R_2CO + R_3Al \rightarrow R_3COAlR_2 \quad (3)$$

In this case also, the absorption of carbon dioxide was much supperssed by the presence of TMEDA, MIm, diethyl ether; Dipy showed less suppressing effect.

Reaction of Diethylaluminum Diethylamide and Carbon Dioxide. As shown in Fig. 2, diethylaluminum diethylamide exhibited very low reactivity towards carbon dioxide even at 60°C. In the presence of some complexing agents, however, the absorption of carbon dioxide was accelerated, in contrast to the case of trialkylaluminum. In the infrared spectrum of the reaction mixture of diethylaluminum diethylamide-MIm (1 : 2) system with carbon dioxide, strong and broad IR bands were observed around 1490—1580 cm^{-1}, while diethylaluminum propionate shows corresponding band at 1550—1630 cm^{-1}. Upon acid hydrolysis of the reaction mixture, no propionic acid was detected. These facts indicate the formation of aluminum carbamate group, *i. e.*, the insertion of carbon dioxide to Al-N, but not to Al-C bond.

$$Et_2N\text{-}AlEt_2 + CO_2 \xrightarrow{\text{Complexing Agent}} Et_2N\text{-}COO\text{-}AlEt_2 \quad (4)$$

As seen in Fig. 2, aromatic monodentate complexing agents such as MIm, *N*-methylbenzimidazole, and pyridine were effective. Dipy exhibited only slight accelerating effect. The effect of MIm was very remarkable and the reaction took place readily even at 20°C. Furthermore, Al-N bond of diethylaluminum diethylamide reacted quantitatively with carbon dioxide even in the presence of a half mole ratio of MIm to the aluminum compound, indicating that MIm was effective as a catalyst (curve No. 9 of Fig. 2).

Factors affecting the reactivity. Triethylaluminum is dimeric with Al-C bridges[6] while triisobutylaluminum is monomeric, and triethylaluminum is known to form complexes such as $Et_3Al\cdot Dipy$ (1 : 1),[7] $Et_3Al\cdot TMEDA$ (2 : 1),[7] and $Et_3Al\cdot O(C_2H_5)_2$ (1 : 1). Triisobutylaluminum probably forms similar complexes. Then the decrease in the reactivity of trialkylaluminum towards carbon dioxide in the presence of the complexing agents may be ascribed to low reactivity of such complexes. Although the nucleophilicity of C-Al linkage will be increased by the coordination with Lewis base, the coordination of the reacting carbon dioxide to the aluminum atom is considered to be hindered by the complex formation of trialkylaluminum. The reactivity is thus much lowered.

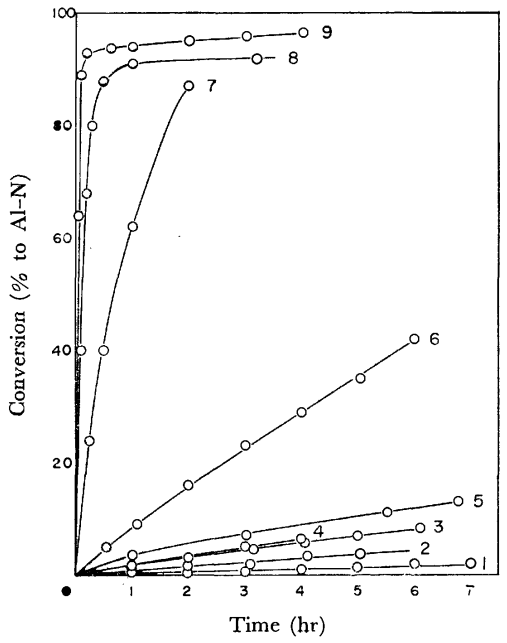

Fig. 2. Reaction of diethylaluminum diethylamide and carbon dioxide, in *p*-xylene at 60°C.
$[Et_2AlNEt_2]_0$, 0.5 M; CO_2, 1 atm; complexing agent (molar ratio to Al): 1: none, 2: tetrahydrofuran(2), 3: Dipy(1), 4: triethylamine(2), 5: TMEDA(1), 6: pyridine(2), 7: *N*-methylbenzimidazole(2), 8: MIm(2), 9: MIm(0.5).

In this respect, apparently reverse effect of the complexing agents on the reactivity of diethylaluminum diethylamide is interesting. Diethylaluminum diethylamide exists in a dimeric form with Al-N bridges.[8] In the presence of some of the complexing agents, it will probably become monomeric by the complex formation. In this monomeric complex the nucleophilicity of Al-N bond, freed from the bridge, is further enhanced by the coordination with Lewis base. But, as in the case of trialkylaluminum, the coordination of the reacting carbon dioxide to the aluminum atom is considered unfavorable in the complex. However, the nuclophilicity of Al-N is much higher than Al-C bond, as exemplified by the fact that the reaction of diethylaluminum diethylamide with carbon dioxide took place at Al-N but not at Al-C linkage. Therefore, the nucleophilicity of Al-N bond is considered so much enhanced by the complex formation that the coordination of the reacting carbon dioxide is not important

6) K. S. Pitzer and H. S. Gutowsky, *J. Amer. Chem. Soc.*, **68**, 2204 (1946).

7) W. Brüser, K. H. Thiele, and H. K. Müller, *Z. Chem.* **2**, 342 (1962); G. E. Coates and K. Wade, "Organometallic Compounds," Vol. 1, Methuen, London (1967), p. 295.

8) W. P. Neumann, *Ann. Chem.*, **667**, 1 (1963).

for the reactivity of diethylaluminum diethylamide in the presence of the complexing agent.

Thus, by the present study we may conclude that the complexing agents studied here play two different roles, *i. e.*, affecting the nucleophilicity of Al–C or Al–N bond and affecting the ability of Al atom to accommodate carbon dioxide. It should be noted here that the observed reactivity is also dependent on the stability of the complex, *i. e.*, the effective concentration of the complex.

The reverse effect of the complexing agents on the reactivity of trialkylaluminum and of dialkylzinc[4] might be understood by different contribution of the above-mentioned factors in the Al and the Zn compounds. The contribution of *d*-orbitals (filled in Zn, but not in Al) might also be considered, but no conclusion may be made from the results so far obtained.

Experimental

Materials. Triethylaluminum was purified by distillation in a nitrogen atmosphere, bp 97°C/10 mmHg. Triisobutylaluminum was also purified by distillation, bp 86°C/10 mmHg. Diethylaluminum diethylamide[8] was prepared by refluxing a *p*-xylene solution (200 m*l*) containing triethylaluminum (0.2 mol) and diethylamine (0.2 mol) for 6 hr. After the removal of *p*-xylene under reduced pressure, the product was obtained by distillation, bp 125°C/0.5 mmHg.

Carbon dioxide was purified by passing through a series of columns packed with cupric sulfate, potassium bicarbonate, reduced copper, phosphorus pentoxide, actived cupric oxide.

TMEDA was refluxed over calcium hydride and distilled, bp 121°C. Dipy was recrystallized from *n*-hexane, mp 69—70°C. MIm was prepared from imidazole, sodium and methyl iodide in liquid ammonia,[9] bp 115°C/54 mmHg. *N*-methylbenzimidazole was prepared from benzimidazole (obtained by the reaction of *o*-phenylenediamine and formic acid[10]) by the same method as MIm, mp 60°C. Pyridine and triethylamine were purified by distillation over barium oxide.

Benzene, toluene, *p*-xylene, diethyl ether, and tetrahydrofuran were purified by usual methods, refluxed over methallic sodium, and distilled.

Procedure. A mercury-sealed gas burette was connected with a 50 m*l* reaction flask by a three-way stopcock, the system was substituted by carbon dioxide, complexing agent and solvent was added, and the solution was saturated by carbon dioxide, The organoaluminum compound was added, and the absorption of carbon dioxide was followed by keeping the gas burette at the atmospheric pressure. The volume absorbed was corrected for temperature, atmospheric pressure and the partial pressure of the solvent. In order to determine carboxylic acid as the product, a definite amount of the reaction mixture was taken out, added by conc. hydrochloric acid, and subjected to gas chromatography using *p*-cymene as internal standard.

The authors wish to express their thanks to Professor Teiji Tsuruta for his valuable discussion.

9) A. M. Roe, *J. Chem. Soc.*, **1963**, 2195.
10) E. C. Wagner and W. H. Millett, "Organic Syntheses", Coll. Vol. II, p. 65 (1955).

BULLETIN OF THE CHEMICAL SOCIETY OF JAPAN, VOL. 45, 3653—3657 (1972)

Studies of Organosulfur Compounds. VI. The Preparation of Carbamoyl Esters of Aromatic Dithio Acids and Their Spectral Properties

Shinzi KATO, Tsuyoshi MITANI, and Masateru MIZUTA
Faculty of Engineering, Gifu University, Kagamihara, Gifu

(Received March 22, 1972)

It was found that aromatic dithio acids readily reacted with aryl isocyanate at room temperature to give the corresponding mixed thioanhydrides with the general formula of (ArCS·S·CONHAr) in excellent yields as stable crystals. The mixed thioanhydrides reacted with primary amines at room temperature to give the corresponding thioamides and asymmetric ureas, while the reaction with secondary amines gave the corresponging amine salts and asymmetric ureas in good yields. The spectral properties of the mixed thioanhydrides were discussed.

Although a few studies of the preparation of the mixed anhydrides (I[1], II[1e], *etc.*) and asymmetric thioanhydrides (III)[2] have been reported, there has been no report on the preparation of the mixed thioanhydrides of Structure (IV) except for the unsuccessful attempt by Houben and Schultze[3] to prepare

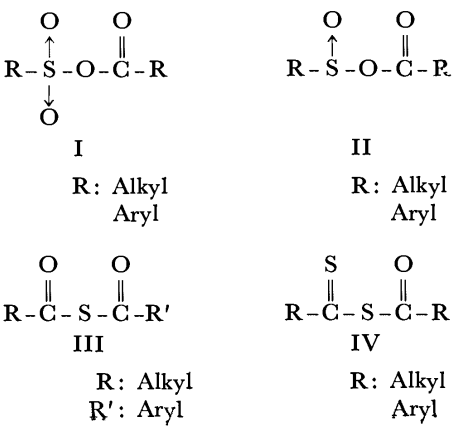

1) a) A. Fahlberg, *Ber.*, **22**, 758 (1889). b) A. Baroni, *Atti Accad. Naz. Lincei*, **17**, 1081 (1933). c) C. G. Overberger and E. Sarlo, *J. Amer. Chem. Soc.*, **85**, 2446 (1963). d) G. A. Olah and S. J. Kuhn, *J. Org. Chem.*, **27**, 2667 (1962). e) H. Böhme and K. H. Meyer-Dulheuer, *Ann.*, **688**, 78 (1965). f) M. H. Karger and Y. Mazur, *J. Amer. Chem. Soc.*, **90**, 3878 (1968). M. H. Karger and Y. Mazur, *J. Org. Chem.*, **36**, 528 (1971).

2) Q. Minagoia, *Gazz. Chem. Ital.*, **55**, 713 (1925).

3) J. Houben and K. M. L. Schultze, *Ber.*, **43**, 2481 (1910).

the anhydrides (IV, Ar; C_6H_5, R'; C_6H_5, CH_3) of dithio and carboxylic acid from magnesium halogenide salts of aromatic dithio acids and acid chlorides or anhydrides. Dithio acids in general are stronger acids[4] than the corresponding carboxylic acid or thio acid, and it is expected that dithio acids react with heterocumulenes (isocyanates, ketenes, *etc.*) to give the corresponding mixed thioanhydrides. In a previous work,[5] it was found that bis(thioacyl)disulfide was readily reacted with secondary amines to give their amine salts in good yields, and the use of the amine salts for the purification of aromatic dithio acids was more effective than that of the metal salts. In this paper, we will describe the preparation of the mixed thioanhydride with the general formula of VII from aromatic dithio acids and aryl isocyanates (Eq. (1)) and an investigation of some aspect of their chemistry.

$$\underset{\text{V}}{\text{ArCS}_2\text{H}} + \underset{\text{VI}}{p\text{-XC}_6\text{H}_4\text{NCO}} \rightarrow \underset{\text{VII}}{\text{ArCS-CNHC}_6\text{H}_4\text{-X-}p} \quad (1)$$

Ar: Aromatic X: Substituents

Results and Discussion

When *p*-methyldithiobenzoic acid in an ethyl acetate–ether (1 : 1) mixture was treated with an equimolar amount of phenyl isocyanate, phenylcarbamoyl *p*-methyldithiobenzoate (VIIg) was easily obtained in an 86% yield as reddish yellow crystals. The structure VIIg was identified by means of elemental analysis and by studying the spectral data. In the IR spectrum, very intensive absorption bands at 1708 cm^{-1} due to carbonyl stretching and at 1540 cm^{-1} due to amide II band stretching were observed. The NMR spectrum showed peaks at τ 7.70 (CH_3, s, 3H), 2.00—2.90 (aromatic, 9H), and −2.31 (NH, s, 1H). On the other hand, the absorption band at 499 mμ (ε 113) due to the $n \rightarrow \pi^*$ transition of the thiocarbonyl group was observed in the visible region. By an analogous treatment of other aromatic dithio acids with *para*-substituted phenyl isocyanates, the corresponding mixed thioanhydrides (VII) were prepared in good yields. The results are summarized in Table 1.

The mixed thioanhydrides (VII) thus obtained, except for VIIu, VIIv, and VIIw, were fairly stable crystals, and did not change in atmosphere for over two months. However, the heating of VII over their melting points decomposed VII to give the corresponding isocyanates, together with dark brown, intractable oil. Similar formations of the isocyanates on the heating of alkyl thiocarbamates have been described in German Patents.[6,7] On the other hand, the carbamoyl α-dithionaphthoates (VIIu, VIIv, and VIIw), except for VIIx which contains a *p*-nitro substituted carbamoyl group, were dark brown oil and gradually decomposed on standing in the atmosphere or in a solution (ethyl acetate or dichloromethane) at room temperature to give bis(α-thionaphthoyl)disulfide and the corresponding ureas in almost quantitative yields. These formations can be explained by the following scheme 1:[8]

$$\text{VIIu-w} \xrightarrow{rt} [\alpha\text{-}C_{10}H_7CS_2H] + [p\text{-X-}C_6H_4NCO]$$

$$\downarrow O_2 \qquad \downarrow H_2O$$

$$\alpha\text{-}(\text{-}C_{10}H_7CS_2)_2 \qquad (p\text{-X-}C_6H_4NH)_2CO$$

Scheme 1.

One of the interesting points about in the mixed thioanhydrides is their reaction with nucleophilic reagents because of their multi-reaction center, shown with the arrows a, b, and c, in Fig. 1. When the mixed

$$\overset{a}{\uparrow}\ \overset{b}{\uparrow}\ \overset{c}{\uparrow}$$
$$\text{-C(=S)-S-C(=O)-NH-}$$

Fig. 1.

thioanhydride was treated with a two-molar amount of *p*-toluidine in dichloromethane at room temperature, *N*-*p*-tolylthiobenzamide (VIII) and phenyl-*p*-tolylurea (IX) were obtained in 94 and 95% yields, and also hydrogen sulfide evolved (Eq. (2)). Unlike *p*-toluidine, a similar treatment of VIIi with piperidine afforded piperidinium dithiobenzoate (X)[9] and the asymmetric urea (XI) in quantitative yields, and no evolution of hydrogen sulfide was observed (Eq. 3).

$$\underset{\text{VIIi}}{C_6H_5C(=S)\text{-}S\text{-}C(=O)\text{-}NHC_6H_5} + 2p\text{-}CH_3C_6H_4NH_2 \xrightarrow[CH_2Cl_2]{rt} H_2S$$

$$+ \underset{\text{VIII}}{C_6H_5C(=S)NHC_6H_4CH_3\text{-}p} + \underset{\text{IX}}{p\text{-}CH_3C_6H_4NHC(=O)NHC_6H_5} \quad (2)$$

$$\text{VIIi} + 2\text{HN}\langle\rangle \xrightarrow[CH_2Cl_2]{rt}$$

$$\underset{\text{X}}{C_6H_5CS^-\ {}^+NH_2\langle\rangle} + \underset{\text{XI}}{\langle\rangle N\text{-}C(=O)NHC_6H_5} \quad (3)$$

Furthermore, the competitive reactions of an equimolar mixture of VIIi and dithiobenzoic acid with an equimolar amount of *p*-toluidine or piperidine in the same

4) M. J. Jansen, "The Chemistry of Carboxylic Acids and Esters" ed. by S. Patai, Interscience-Publisher, New York (1969), p. 717.

5) S. Kato and M. Mizuta, *Int. J. Sulfur Chem. A*, **2** (No.4), 27 (1972).

6) H. Pelster, E. Muelbauer, and D. Delfs, Ger. 1176127 (1964).

7) H. Pelster, E. Muchlbauer, and D. Delfs, Ger. 1171421 (1964).

8) α-Dithiohaphthoic acid was readily oxidized with oxygen to give bis(α-thiohaphthoyl)disulfide in a quantitative yield: J. Houben, *Ber.*, **39**, 3219 (1906).

9) An analogous formation of the amine salts from bis(thioaroyl) disulfide and secondary amines was observed: S. Kato and M. Mizuta, This Bulletin, **45**, 3492 (1972).

TABLE 1. PHYSICAL PROPERTIES AND ELEMENTAL ANALYSIS OF ARYLCARBAMOYL DITHIOAROYLATES

Compd	ArCS·S·OC-NHC$_6$H$_4$-X-*p* Ar	X	Yield %	Mp °C	IR (cm^{-1}), KBr νC=O	δN-H[a]	νC=S	UV, mμ, CH_2Cl_2 λ_{max} (ε)			Formula	Found (Calcd), % C	H	Br	Cl	N	S
VIIa	*p*-$CH_3OC_6H_4$	CH_3O	94	103—104	1680	1540	1234	249 (4.36)	365 (4.27)	473 (2.09)	$C_{16}H_{15}NO_3S_2$	57.55 (57.65)	4.48 (4.50)			4.19 (4.20)	19.88 (19.21)
b		CH_3	88	120—121	1707	1540	1245		365 (4.17)	484 (2.06)	$C_{16}H_{15}NO_2S_2$	60.93 (60.56)	4.62 (4.73)			3.38 (4.42)	20.68 (20.19)
c		H	92	94— 95	1700	1545	1230	288	365 (4.22)	486 (2.03)	$C_{15}H_{13}NO_2S_2$	60.21 (59.41)	4.22 (4.29)			4.76 (4.62)	20.55 (21.12)
d		NO_2	89	129—130	1715	1552	1258		294 (4.25)	477 (2.07)	$C_{15}H_{13}N_2O_4S_2$	52.03 (51.57)	3.68 (3.72)			8.03 (8.02)	18.63 (18.34)
e	*p*-$CH_3C_6H_4$	CH_3O	74	95.0—96.5	1690	1534	1236	245 (4.31)	327 (4.18)	486 (2.05)	$C_{16}H_{15}NO_2S_2$	61.11 (60.57)	4.77 (4.73)			4.44 (4.42)	20.55 (20.19)
f		CH_3	91	122—123	1700	1530	1240		320 (4.19)	497 (2.06)	$C_{16}H_{15}NOS_2$	63.70 (63.79)	4.87 (4.87)			4.66 (4.65)	21.28 (21.26)
g		H	86	92.0—93.8	1708	1540	1252		323 (4.21)	498 (2.05)	$C_{15}H_{13}NOS_2$	62.09 (62.72)	4.51 (4.53)			4.90 (4.88)	22.36 (22.30)
h		NO_2	90	110.5—112.0	1695	1549	1250		330 (4.38)	488 (2.07)	$C_{15}H_{13}N_2O_3S_2$	54.88 (54.22)	3.99 (3.92)			8.51 (8.43)	19.23 (19.28)
i	C_6H_5	CH_3O	83	84.0—85.0	1688	1542	1250	246 (4.21)	311 (4.20)	490 (2.05)	$C_{15}H_{13}NO_2S_2$	59.32 (59.41)	4.33 (4.29)			4.58 (4.62)	21.65 (21.12)
j		CH_3	32	oil	1710	1525	1240				$C_{15}H_{13}NOS_2$	63.00 (62.72)	4.49 (4.53)			4.83 (4.88)	22.46 (22.30)
k		H	90	63.5—65.5	1697	1546	1250		324 (4.19)	506 (2.05)	$C_{14}H_{11}NOS_2$	62.03 (61.54)	4.12 (4.03)			5.26 (5.13)	23.48 (23.44)
l		NO_2	90	109.0—109.5	1696	1556	1256		314 (4.41)	485 (2.05)	$C_{14}H_{11}N_2O_3S_2$	52.88 (52.83)	3.49 (3.46)			8.92 (8.81)	20.54 (20.13)
m	*p*-ClC_6H_4	CH_3O	83	82.0—83.0	1690	1540	1245	245 (4.16)	319 (4.24)	478 (2.09)	$C_{15}H_{12}ClNO_2S_2$	53.00 (53.33)	3.55 (3.56)		11.02 (10.52)	4.21 (4.15)	18.83 (18.96)
n		CH_3	46	oil	1735	1555	1245				$C_{15}H_{12}ClNOS_2$	56.09 (55.99)	3.68 (3.73)		11.33 (11.04)	4.36 (4.35)	19.32 (19.91)
o		H	90	71.0—72.0	1693	1527	1250		330 (4.22)	493 (2.11)	$C_{14}H_{10}ClNOS_2$	54.48 (54.63)	3.23 (3.25)		12.05 (11.54)	4.44 (4.55)	21.05 (20.81)
p		NO_2	88	106—108	1714	1552	1256		323 (4.35)	4.85 (2.08)	$C_{14}H_{10}ClN_2O_3S_2$	47.34 (47.66)	2.69 (2.84)		9.93 (10.07)	7.88 (7.94)	18.44 (18.16)
q	*p*-BrC_6H_4	CH_3O	75	109—110	1685	1528	1240	245 (4.11)	316 (4.32)	500 (2.06)	$C_{15}H_{12}BrNO_2S_2$	47.28 (47.12)	3.21 (3.14)	20.65 (20.94)		3.68 (3.66)	17.02 (16.75)
r		CH_3	28	93— 94	1685	1528	1240		325 (4.30)	501 (2.09)	$C_{15}H_{12}BrNOS_2$	50.00 (49.18)	3.22 (3.28)	20.99 (21.86)		3.88 (3.83)	17.77 (17.49)
s		H	67	90— 91	1700	1538	1245		322 (4.12)	494 (2.02)	$C_{14}H_{10}BrNOS_2$	48.79 (48.72)	2.82 (2.84)	22.76 (22.73)		3.87 (3.98)	18.18 (18.18)
t		NO_2	88	132—133	1708	1546	1252		328 (4.34)	488 (2.06)	$C_{14}H_{10}N_2O_3S_2$	42.44 (42.42)	2.65 (2.53)	20.12 (20.20)		3.45 (3.54)	16.58 (16.16)
u	α-$C_{10}H_7$	CH_3O	39	oil	1690	1545	1242				$C_{19}H_{15}NO_2S_2$	65.43 (64.59)	4.16 (4.25)			3.94 (3.97)	18.63 (18.13)
v		CH_3	42	oil	1710	1520	1245				$C_{19}H_{15}NOS_2$	68.01 (67.66)	4.38 (4.45)			4.07 (4.15)	19.94 (19.99)
w		H	44	oil	1700	1520	1245				$C_{18}H_{13}NOS_2$	66.66 (66.87)	4.01 (4.02)			4.32 (4.33)	19.32 (19.81)
x		NO_2	91	129—130	1695	1510	1255		323 (4.32)	504 (2.03)	$C_{18}H_{13}N_2O_3S_2$	58.37 (58.70)	3.55 (3.53)			3.81 (3.80)	17.41 (17.39)

conditions gave the asymmetric ureas (IX or XI) in yields of over 60%. These results indicate the possibility of the nucleophilic attack of amines on the carbonyl carbon of the mixed thioanhydrides and the formation of the corresponding dithio acid (XII) as an intermediate (Scheme 2).

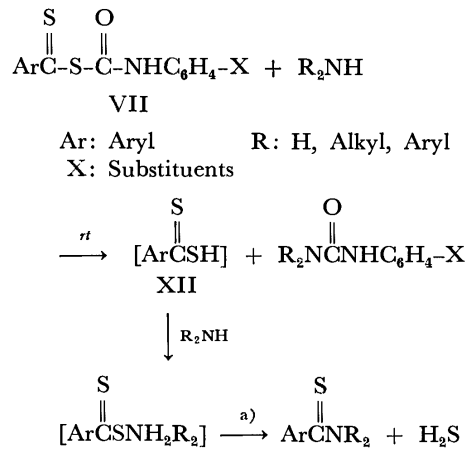

a) in the case of primary amines.

Scheme 2.

Spectral Data. *a) IR Spectra*: The IR spectra of all these anhydrides, without any exception, surprisingly showed no N–H stretching absorption band in the expected range (3100—3400 cm^{-1}); instead, we observed new absorption bands near 2900 cm^{-1} considered to be due to the N–H stretching band. Such an unusual shift in νN–H suggests a structure (XIII) containing an intramolecular hydrogen bond between sulfur and hydrogen. The NMR spectrum (NH near -2.30τ) further supported the XIII structure.

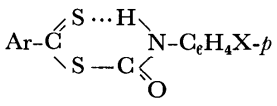

XIII

Ar: Aryl X: Substituents

The location of C=S group frequencies in organosulfur compounds has been a matter of considerable discussion. Bak *et al.*[10] reported that the two frequencies (ν C=S and C–S) obtained by a simplified force-constant calculation must be looked for in the vicinity of 1200 cm^{-1} (C=S) and 700 cm^{-1} (C–S), and the locations of the C=S in a series of twenty-one carboxymethyl dithio esters were observed between 1190 and 1225 cm^{-1}. Lately, Bellamy and Rogasch[11] have confirmed those results using solvent effects, and also suggested in a recent review[12] that ν C=S lies between 1225 and 1190 cm^{-1} in the dithio esters. The arylcarbamoyl dithio esters obtained, almost without exceptions, showed two fairly intensive absorption bands at near 1250 and 1050 cm^{-1}. However, it is difficult to assign the lower-frequency band to the C=S because that of amine salts of aromatic dithio acids was observed between 990 and 1020 cm^{-1}. Therefore, it seemed reasonable that the intensive absorption bands at near 1250 cm^{-1} are due to the C=S stretching bands in arylcarbamoyl dithioesters (VII). This also fits well with the assignment given by Bak *et al.*[10] and Bellamy.[11]

b) UV and Visible Spectra: Table 1 lists the absorption maxima in mμ and the molecular extinction coefficients at each maximum. As is shown in Table 1, all the mixed anhydrides (VII), showed two characteristic maximum absorption bands near 300 mμ (ε 15000—25000) and 500 mμ (ε 100—130). It may be considered that the former absorption bands are due to $\pi\rightarrow\pi^*$, and the latter, to the $n\rightarrow\pi^*$ transition of the thiocarbonyl group. The location of $n\rightarrow\pi^*$ fits well with the assignment given by Fabian *et al.*[13] for the methyl esters of aromatic dithio acids.

Experimental[14]

Materials. The aromatic dithio acids were prepared by the method described in a previous report[5], using THF as the solvent. Phenyl isocyanate was of a commercial grade and was distilled before use. The other aryl isocyanates were prepared, following the directions of the literature,[15] from the corresponding amines and phosgen; *p*-methoxyphenyl isocyanate, bp 105—106°C/8 mmHg *p*-tolyl isocyanate, bp 52—53°C/5 mmHg; *p*-nitrophenyl isocyanate: mp 55—57°C. The *p*-toluidine and piperidine were of a commercial grade and were purified by distillation or recrystallization before use. The solvents were dried and distilled.

Reactions were carried out under nitrogen. Some typical procedures will be described below, while the detailed data are summarized in Table 1.

Reaction of p-*Methyldithiobenzoic Acid with Phenyl Isocyanate.* An equimolar amount of phenyl isocyanate was added to a solution of *p*-methyldithiobenzoic acid (1.68 g, 0.01 mol) in 10-m*l* of ether-ethyl acetate (1 : 1), and the mixture was stirred for 30 min, at room temperature. The evaporation of the solvent from the reaction mixture below 20°C *in vacuo*, the recrystallization of the residue from ethyl acetate–petroleum ether (bp below 50°C, 1 : 3) gave 2.45 g of phenylcarbamoyl *p*-methyldithiobenzoate (VIIg).

Thermolysis of Phenylcarbamoyl Dithiobenzoate (VIIk). Phenylcarbamoyl dithiobenzoate (VIIk), 5.30 g, 0.02 mol) in a glass ampoule under nitrogen was heated for 30 min at 120°C. The distillation of the decomposition mixture gave 1.5 g (63%, based on the VIIk used) of phenyl isocyanate.

Decomposition of Phenylcarbamoyl α-Dithionaphthoate (VIIv) on Standing in an Atmosphere. A solution of 1.6 g (0.005 mol) of VIIv in ethyl acetate (20 m*l*) was allowed to stand in the atmosphere at room temperature. After 7 days, the color of the solution completely changed from dark brown to pink, and the precipitates appeared. After the removal of the solvent, the fractional crystallization of the residue from di-

10) B. Bak, L. Hansen-Nygaard, and C. Pedersen, *Acta Chem. Scand.*, **12**, 1451 (1958).

11) L. J. Bellamy and P. E. Rogasch, *J. Chem. Soc.*, **1960**, 2218.

12) L. J. Bellamy, "Advances in Infrared Group Frequencies" Methuem & Co. Ltd., London (1968), p. 213.

13) J. Fabian, St. Scheithauer, and R. Mayer, *J. Prakt. Chem.*, **311**, 45 (1969).

14) All melting points were not corrected. The IR spectra were measured on a JASCO Grating Infrared Spectrophotometer IR-G. The UV spectra were recorded on Hitachi 124 Spectrophotometer. The NMR spectra were taken on a JEOL H-60 apparatus.

15) R. J. Slocombe, E. E. Hardy, T. H. Saunder, and R. L. Jenkins, *J. Amer. Chem. Soc.*, **72**, 1888 (1950).

chloromethane-ether gave 0.82 g (80%) of bis(α-thionaphthoyl)disulfide (mp 169—170°C[16]) and 0.55 g (91%) of diphenylurea (mp 60—70°C), which were identified by a comparision of their melting points and IR spectrum with those of an authentic sample.

Reaction of Phenylcarbamoyl Dithiobenzoate (VIIk) with p-Toluidine or Piperidine. *a*): *p*-Toluidine (1.07 g, 0.01 mol) was added to a solution of 1.36 g (0.005 mol) of VIIk in dichloromethane (10 m*l*) and stirred for 8 hr at room temperature. After the vacuum evaporation of the solvent from the reaction mixture, the residue was extracted with a small portion of ether. After the evaporation of the ether from the extracts, the recrystallization of the residue gave 1.2 g of *N*-*p*-tolylthiobenzamide (mp 126—127°C). On the other hand, the recrystallization of the ether-insoluble parts from dichloromethane gave 1.05 g of phenyl-*p*-tolylurea (mp (196—197°C). The thiobenzamide and the urea were identified by a comparision of the melting points and IR spectrum with those of authentic samples.[17]

b): The reaction of VIIk (0.05 mol) and piperidine (0.01 mol) under the same conditions as in a) gave 1.08 g (86%) of piperidinium dithiobenzoate (mp 112—114°C) and 0.97 g (96%) of phenylpiperidylurea (mp 165—166°C). The melting points and the IR spectra of the amine salts and the urea coincided exactly with those of authentic samples.

c) Competitive Reaction: A similar treatment of a mixture of dithiobenzoic acid (0.01 mol) and VIIk (0.01 mol) in dichloromethane (15 m*l*) with 0.01 mol of *p*-toluidine gave 1.43 g (63%, based on the *p*-toluidine used) of *N*-*p*-tolylphenylurea and 0.59 g (26%, based on the *p*-toluidine used) of *N*-*p*-tolylthiobenzamide.

d): A similar treatment of a mixture of dithiobenzoic acid (0.01 mol) and VIIk (0.01 mol) in dichloromethane (15 m*l*) with piperidine (0.01 mol) gave 1.47 g (72%, based on the piperidine used) of phenylpiperidylurea and 0.37 g (13%, based on the piperidine used) of piperidinium dithiobenzoate.

The authors wish to thank Professor Yoshio Hirabayashi and Mr. Hideharu Ishihara for their discussions.

16) For bis(α-thionaphthoyl)disulfide: J. Houben, *Ber.*, **39**, 3219 (1906).

17) a) For *p*-tolylthiobenzamide: S. Kato, and M. Mizuta, This Bulletin, submitted for. b) *p*-Tolylphenylurea was prepared from phenyl isocyanate and *p*-toluidine.

18) a) For piperidinium dithiobenzoate: see Ref. 5. b) Phenylpiperidylurea was prepared from phenyl isocyanate and piperidine.

BULLETIN OF THE CHEMICAL SOCIETY OF JAPAN, VOL. 45, 3657—3660 (1972)

Studies of Acenaphthene Derivatives. XXVI.[1] The Thermal Cycloaddition of 2-Diazoacenaphthenone to Isocyanates

Otohiko Tsuge,[2] Ichiro Shinaki, and Masahiro Koga

Research Institute of Industrial Science, Kyushu University, Hakozaki, Higashi-ku, Fukuoka, 812

(Received May 19, 1972)

Although 2-diazoacenaphthenone did not react with phenyl isocyanate or phenyl isothiocyanate on prolonged reflux in toluene, it reacted with strongly electrophilic benzoyl and *p*-chlorobenzoyl isocyanates and thiobenzoyl isocyanate to give the corresponding spiro[acenaphthenone-2,5′-oxazolin-4′-one] and the spiro-thiazolin-4′-one in good yields. On the other hand, the reaction of the α-diazoketone with benzoyl isothiocyanate gave 8-benzoylacenaphtho[1,2-*d*]isoxazolin-9-thione, which on catalytic hydrogenolysis over PtO_2 gave the dihydro compound corresponding to reductive cleavage of N–O bond of the isoxazoline ring. Furthermore, the reaction of the α-diazoketone with benzenesulfonyl isocyanate gave two stereoisomeric bis-spiro-azetidinones. The mechanisms of these reactions are proposed.

In an earlier publication,[3] it was reported that the reaction of 2-diazoacenaphthenone (**1**) with olefins gave diastereoisomeric spiro-cyclopropanes under mild conditions. In contrast, acetylenes yielded spiro-3*H*-pyrazoles. The reaction of α-diazoketones has been extensively studied by Ried and his co-workers,[4] and it has been shown that the reactions of α-diazoketones with multiple bonds form 1,3-[5] or 1,5-cycloaddition products under rather mild conditions (Scheme 1). For example, the reaction of α-diazoketones with isothiocyanate[6] or thiophosgene[7] gave thiazoles. Recently, in order to prepare medium-sized heterocycles,

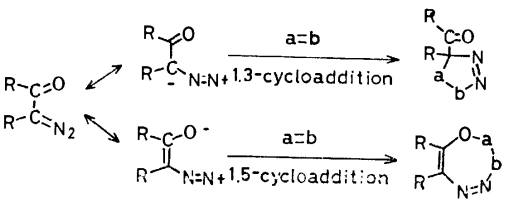

Scheme 1.

1) Part XXV of this series: O. Tsuge and I. Shinkai, *Organic Preparations and Procedures (OPP) International*, in press (1972).

2) Author to whom correspondence should be directed.

3) O. Tsuge, I. Shinkai, and M. Koga, *J. Org. Chem.*, **36**, 745 (1971).

4) W. Ried and H. Lohwasser, *Ann.*, **683**, 118 (1965); for a review, see G. Pfundt and G. O. Schenck, "1,4-Cycloaddition Reactions," ed. by J. Hamer, Academic Press, New York and London (1967), p. 405.

5) For the 1,3-dipolar cycloaddition reaction of ketocarbenes generated from the thermolysis or photolysis of α-diazoketones, see R. Huisgen, G. Binsch, H. Konig, and H. J. Strum, *Angew. Chem.*, **73**, 368 (1961).

6) W. Ried and B. M. Beck, *Ann.*, **673**, 128 (1964).

7) W. Ried and B. M. Beck, *ibid.*, **673**, 124 (1964).

the addition of 1,5-dipoles such as vinyldiazomethane,[8] vinylazide,[9] and other similar compounds,[10] has been investigated. However, the 1,5-dipoles cyclized intramolecularly to yield stable five-membered heterocycles rather than 1,5-cycloadducts.

Only the reaction of *o*-quinonediazide with ketenes[11] and ketenimines[12] resulted in 1,5-cycloaddition to yield the oxadiazepines. It would be expected that **1** might add to heterocumulene such as isocyanate to give the (2+5) cycloadduct, oxatriazepine. Since little information about the thermal cycloaddition reaction of **1** with isocyanates is available, we have investigated the reaction of **1** with several isocyanates under mild conditions, and now report our findings in this area.

Results and Discussion

It was previously reported[3] that thermolysis of α-diazoketone **1** did not take place in boiling toluene and the ketocarbene from **1** is not formed under such conditions. It has now been found that **1** did not react with phenyl isocyanate or isothiocyanate on prolonged reflux in toluene; **1** was recovered quantitatively. However, when a toluene solution of **1** and benzoyl isocyanate (**2a**) was refluxed for 30 hr, a 38.5% yield of **3a** was obtained as colorless needles, in addition to recovered **1**. The results of microanalysis and mass spectrum of **3a** fitted the molecular formula $C_{20}H_{11}NO_3$, which would arise from the elimination of nitrogen from a 1 : 1 adduct of **1** and **2a**. The IR spectrum of **3a** showed bands ascribable to carbonyl groups at 1762 and 1729 cm^{-1}. On the basis of the above observations, it may be deduced that **3a** is 2′-phenyl-spiro[acenaphthenone-2,5′-oxazolin-4′-one].

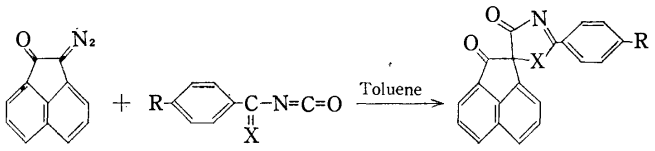

1 **2** **3**

a: R=H, X=O; b: R=Cl, X=O; c: R=H, X=S

Under similar conditions, *p*-chlorobenzoyl (**2b**) and thiobenzoyl isocyanate (**2c**) gave the corresponding spiro-oxazolin-4′-one (**3b**) and spiro-thiazolin-4′-one (**3c**). The mass spectra of **3a**—**3c** were also compatible with the proposed structures.

It has been reported[13] that the C=N bond of isocyanate reacts easily with 1,3-dipoles, whereas the C–S bond of isothiocyanate is attacked predominantly. In order to compare with the reactivity of acyl isocyanates, the reaction of **1** with benzoyl isothiocyanate (**4**) was investigated.

When a toluene solution of **1** and **4** was refluxed for 10 hr, a 31% yield of a product **5** was obtained as yellow needles. The microanalysis and mass spectral data were in agreement with the molecular formula $C_{20}H_{11}NO_2S$ (M^+ m/e 329). Its IV spectrum exhibited a single carbonyl absorption at 1632 cm^{-1}. The thiocarbonyl test[14] was positive.

The hydrogenolysis of **5** over PtO_2 in dioxane at room temperature afforded a dihydro compound **6** as yellow needles. The IR spectrum of **6** showed the band ascribable to amide I absorption at 1645 cm^{-1}, and the NMR spectrum in carbon tetrachloride exhibited signals at δ 10.18 (1H, singlet, OH) and 14.15 ppm (1H, singlet, NH) besides aromatic protons. Treatment of the compound **6** with acetic anhydride afforded the *O*-acetylated derivative **7** as golden yellow needles.

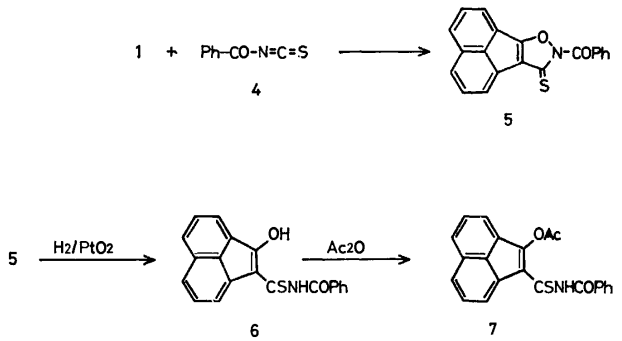

Scheme 2.

On the basis of these observations, **5** and **6** were assigned as 8-benzoyl-acenaphtho[1,2-*d*]-Δ^4-isoxazolin-9-thione and 2-benzoylthiocarbamoyl-1-acenaphthylenol, respectively (Scheme 2).

Confirmatory evidence for the structure of **5** was provided by the mass spectrum; the spectrum of **5** showed no peak at *m/e* 226 which would arise by the elimination of benzonitrile from parent peak (M^+ *m/e* 329), while the fragment peaks (M^+— ArCN) appeared in the spectra of **3a**—**3c**.

These results show clearly that a ketocarbene intermediate was not involved. We view these reactions as depicted in Scheme 3. α-Diazoketone **1** would react with **2** to form intermediate **A** (X=Y=O or X=S, Y=O) which would cyclize to the triazoline, followed by the elimination of nitrogen and cyclization to **3**.

In contrast, the negative charge in the intermediate **A** (X=O, Y=S) formed from the reaction with **4** would be located on the sulfur atom, since diazomethane,[6] ketocarbenes[15] and epoxides[16] react predominantly

8) I. Tabushi, K. Takagi, M. Okano, and R. Oda, *Tetrahedron*, **23**, 2621 (1967).
9) H. Reimlinger, *Chem. Ber.*, **103**, 1900 (1970).
10) H. Reimlinger, J. J. M. Vandewalle, G. S. D. King, W. R. F. Linger, and R. Merenyi, *ibid.*, **103**, 1918 (1970).
11) W. Ried and R. Dietrich, *Ann.*, **666**, 113 (1963); W. Ried and K. Wagner, *ibid.*, **681**, 45 (1965); W. Ried and R. Kraemer, *ibid.*, **681**, 52 (1965).
12) W. Ried and P. Junker, *ibid.*, **713**, 119 (1968).
13) E. Pfeil and K. Milzner, *Angew. Chem. Int. Ed. Engl.*, **5**, 667 (1966).
14) F. Feigl, "Spot Test in Organic Analysis," Elsevier Publishing Co., New York, N. Y. (1966), p. 84.
15) R. Huisgen, G. Binsch and H. König, *Chem. Ber.*, **97**, 2868 (1964).
16) K. Hartmann, *ibid.*, **98**, 1782 (1965).

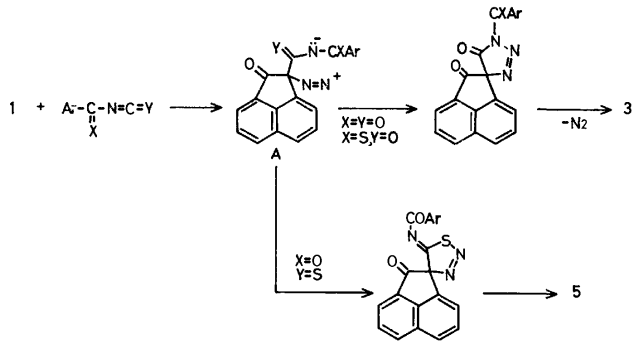

Scheme 3.

with the C=S bond of phenyl isothiocyanate. It would thus seem reasonable to assume that the betaine **A** would cyclize to the exo-double bonded thiadiazoline, followed by the elimination of nitrogen and ring closure to **5**.[17]

Since the sulfonyl group does not enter into conjugative effects,[18] products analogous to **3** would thus not be expected from the reaction of **1** with benzenesulfonyl isocyanate (**8**). The reaction of **1** with **8** in benzene at room temperature for 72 hr yielded two products **9** and **10** in 16 and 28.2% yields, respectively. Microanalyses of both **9** and **10** agreed with the molecular formula ($C_{31}H_{17}NO_5S$) derived from a 2 : 1 adduct of **1** and **8** with the elimination of nitrogen. The IR spectra of both **9** and **10** showed carbonyl bands at about 1800 cm^{-1}, which are assignable to carbonyl group in four-membered rings.[19] Thermal decomposition of both **9** and **10** at 230°C gave biacenedione in 77.6 and 31% yields, respectively.

From a consideration of the high carbonyl frequency and the result of the thermal decomposition to biacenedione, **9** and **10** may be considered as stereoisomeric

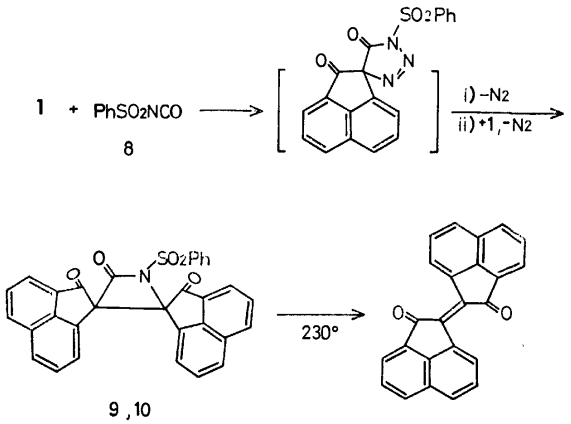

Scheme 4.

bis-spiro-azetidinone. However, their configurations have not been clarified (Scheme 4).

Recently, it has been reported that sulfonyl isocyanate reacted with diazofluorene to give bis-spiro-azetidinone which was converted thermally to bis-fluorenylidene.[20] We also reported that biacenedione was obtained by thermal decomposition of *N*-phenyl-bis-spiro-pyrrolidine formed from the 1,3-dipolar cycloaddition of 2-benzylidenacenaphthenone to azomethine oxide.[2]

On the basis of these results, it can be concluded that **1** does not react as a 1,5-dipole but rather as a 1,3-dipole incycloaddition to isocyanate, followed by cyclization to spiro-heterocycles.

Experimental

All melting points are uncorrected. The IR spectra were measured as KBr pellets and the NMR spectra were determined at 60 MHz with Hitachi R-20 NMR spectrometer using TMS as an internal reference. The mass spectra were obtained on a Hitachi RMS-4 mass spectrometer using a direct inlet and an ionization energy of 70 eV.

Materials. 2-Diazoacenaphthenone (**1**) was prepared by the reported method[22] and purified by chromatography (alumina), mp 93—94°C (lit,[22] mp 94°C); benzoyl (**2a**),[23] *p*-chlorobenzoyl (**2b**),[23] thiobenzoyl (**2c**),[24] benzenesulfonyl isocyanate (**8**),[25] and benzoyl isothiocyanate (**4**)[26] were prepared by the methods described in the literatures respectively.

*Reaction of **1** with Isocyanates (2).* The general procedure used is illustrated with the reaction of **1** with **2a**.

A solution of 780 mg (4.0 mmol) of **1** and 730 mg (5.0 mmol) of **2a** in 30 m*l* of toluene was refluxed for 30 hr, the reaction mixture was then cooled and filtered to give crystals, which on recrystallization from benzene-petroleum benzine (bp 42—60°C) afforded 360 mg (38.5%) of 2′-phenyl-spiro [acenaphthenone-2,5′-oxazolin-4′-one] (**3a**), mp 246—247°C, as colorless needles.

Found: C, 76.48; H, 3.61; N, 4.52%. Calcd for $C_{20}H_{11}NO_3$: C, 76.67; H, 3.54; N, 4.47%. IR cm^{-1}: $\nu_{C=O}$ 1729, 1762.

Mass spectrum *m/e* (rel. intensity): 313 (M^+, 54.5), 210 (M^+—PhCN, 37.8), 182 (210$^+$—CO, 75.5) 154 (182$^+$—CO, 100), 126 (154$^+$—CO, 63.6).

The toluene filtrate was concentrated *in vacuo* and the residue was purified by chromatography on alumina to yield 480 mg (61.5%) of unreacted **1**.

Similarly, the reaction of **1** with **2b** and **2c** for 30 and 12 hr respectively afforded the corresponding spiro-oxazolin-4′-one **3b** and spiro-thiazolin-4′-one **3c**.

3b: mp 269—271°C, colorless prisms (benzene). Yield, 59%.

Found: C, 69.17; H, 2.71; N, 4.04%. Calcd for $C_{20}H_{10}NO_3Cl$: C, 69.06; H, 2.88; N, 4.03%. IR cm^{-1}: $\nu_{C=O}$ 1730, 1766.

17) This reaction seems to be the same type as the decomposition of 4-acyltriazolones to form isoxazolines (K. H. Oehring, *Monatsch. Chem.*, **89**, 588 (1958)).

18) For the conjugation of anions to sulfonyl group, see D. J. Cram, "Fundamentals of Carbanion Chemistry," Academic Press, New York, N. Y. (1965), p. 71.

19) L. L. Muller and J. Hamer, "1,2-Cycloaddition Reactions," ed. by G. A. Olah, Interscience Publishers, New York, N. Y. (1967), p. 195.

20) G. Lohaus, *Tetrahedron Lett.*, **1970**, 130.

21) O. Tsuge and I. Shinkai, *ibid.*, **1970**, 3847.

22) M. P. Cava, R. L. Litle, and D. R. Napier, *J. Amer. Chem. Soc.*, **80**, 2257 (1958).

23) A. J. Speziale and R. L. Smith, *J. Org. Chem.*, **28**, 1805 (1963).

24) J. Goerdeler and H. Schenk, *Chem. Ber.*, **98**, 2954 (1965).

25) O. C. Billeter, *Ber.*, **37**, 690 (1904).

26) T. B. Johnson and L. H. Chernoff, *J. Amer. Chem. Soc.*, **34**, 164 (1912).

Mass spectrum *m/e* (rel. intensity): 349 (33.2), 347 (100) (M^+), 210 (M^+—Cl- 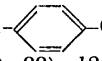 -CN, 57.5), 182 (210$^+$—CO, 44), 154 (210$^+$—CO, 88), 126 (154$^+$—CO, 36.4).

3c: mp 239—240°C, pale yellow prisms (benzene). Yield, 28%.

Found: C, 73.24; H, 3.29; N, 4.41%. Calcd for $C_{20}H_{11}NO_2S$: C, 72.94; H, 3.37; N, 4.25%. IR cm^{-1}: $\nu_{C=O}$ 1710, 1736.

Mass spectrum *m/e* (rel. intensity): 329 (M^+, 14), 226 (M^+—PhCN, 55), 198 (226$^+$—CO, 75), 170 (198$^+$—CO, 100), 126 (170$^+$—CS, 25.6).

In a similar fashion, 8-benzoylacenaphthol[1,2-*d*]-Δ^4-isoxazoline-9-thione (**5**), mp 215—217°C, was obtained in a 31% yield as yellow needles (from ligroin (bp 80—110°C)); a 33% yield of **1** was recovered.

Found: C, 73.14; H, 3.24; N, 4.15%. Calcd for $C_{20}H_{11}NO_2S$: C, 72.94; H, 3.37; N, 4.25%. IR cm^{-1}: $\nu_{C=O}$ 1632.

Mass spectrum *m/e* (rel. intensity): 329 (M^+. 100), 288 (8), 210 (288$^+$—CS, 4.4), 192 (6.6), 120 (5.2), 105 ($PhCO^+$, 66).

Catalytic Hydrogenation of ***5***. Hydrogenation of 200 mg of 5 in 30 m*l* of dioxane with 100 mg of PtO_2 resulted in smooth absorption of one equivalent of hydrogen in about 5 hr at room temperature. The reaction mixture was filtered and the catalyst was washed with 5 m*l* of dioxane. Concentration of the filtrate *in vacuo* left a residue which on trituration with petroleum benzine (20 m*l*) gave 160 mg of yellow crystals. The crystals were recrystallized from acetonitrile to give 2-benzoylthiocarbamoyl-1-acenaphthylenol (**6**), mp 155—157°C, as yellow needles.

Found: C, 72.57; H, 3.81; N, 4.21%. Calcd for $C_{20}H_{13}NO_2S$: C, 72.50; H, 3.96; N, 4.23%. IR cm^{-1}: $\nu_{C=O}$ 1645.

NMR (in CCl_4) δ ppm: 7.4—8.3 (11**H**, multiplet, aromatic protons), 10.18, (1H, singlet, O**H**), 14.15 (1H, singlet, N**H**).

Mass spectrum *m/e*: 331 (M^+).

A solution of **6** in methanol containing trace amounts of pyridine was treated with acetic anhydride at room temperature for 10 min to give a quantitative yield of yellow crystals, which on recrystallization from benzene–petroleum benzine yielded *O*-acetyl derivative **7**, mp 152—153°C decomp.), as golden yellow needles.

Found: C, 70.76; H, 3.80; N, 3.91%. Calcd for $C_{22}H_{15}NO_3S$: C, 70.77; H, 4.05; N, 3.75%. IR cm^{-1}: $\nu_{C=O}$ 1693, 1715.

NMR (in $CDCl_3$) δ ppm: 2.63 (3H, singlet, $COCH_3$), 7.39—8.3 (11**H**, multiplet, aromatic protons), 13.36 (1H, singlet, N**H**).

Mass spectrum *m/e*: 373 (M^+).

Reaction of ***1*** *with* ***8***. A solution of 1.55 g (8.0 mmol) of **1** and 1.83 g (10.0 mmol) of **8** in 50 m*l* of benzene was stirred for 72 hr at room temperature. The precipitated crystals were fractionally recrystallized several times from benzene to afford 190 mg (15%) of biacenedione, mp 294°C, identical with an authentic sample prepared from acenaphthenequinone and acenaphthenone, and 330 mg (16%) of bis-spiro-azetidinone **9**, mp 228—230°C (decomp.), as colorless prisms.

Found: C, 72.34; H, 3.71; N, 2.71%. Calcd for $C_{31}H_{17}NO_5S$: C, 72.23; H, 3.30; N, 2.72%. IR cm^{-1}: $\nu_{C=O}$ 1807, 1746, 1720.

The benzene filtrate was concentrated *in vacuo*; recrystallization of the residue from benzene–petroleum benzine gave 580 mg (28.2%) of isomeric bis-spiro-azetidinone **10**, mp 213—216°C (decomp.), as pale yellow needles.

Found: C, 72.09; H, 3.86; N, 2.54%. Calcd for $C_{31}H_{17}NO_5S$: C, 72.23; H, 3.30; N, 2.72%. IR cm^{-1}: $\nu_{C=O}$ 1806, 1738, 1710.

Thermal Decomposition of ***9***. Forty miligrams of **9** were heated at 230°C for 5 min without solvent. After cooling, the resulting semicrystalline residue was chromatographed on alumina. Elution with chloroform afforded 20 mg (77.6%) of biacenedione, mp 294°C. Similarly, thermolysis of **10** at 230°C gave a 31% yield of biacenedione.

BULLETIN OF THE CHEMICAL SOCIETY OF JAPAN, VOL. 45, 3660—3667 (1972)

Inositol Derivatives. V. Selective Benzoylation of 1,2-*O*-Cyclohexylidene-*myo*-inositol and Preparation of New *O*-*p*-Tolylsulfonyl-*myo*-inositols

Tetsuo SUAMI, Seiichiro OGAWA, Kumiko OHASHI, and Shuichi OKI

Department of Applied Chemistry, Faculty of Engineering, Keio University, Hiyoshi, Yokohama

(Received May 30, 1972)

The reaction of 1,2-*O*-cyclohexylidene-*myo*-inositol (**1a**) with 1.5 equiv. of benzoyl chloride below 0°C gave 3-*O*-benzoate (**2a**) predominantly in 40% yield, together with easily separable 3,6-di-*O*-benzoate (**3a**) in 2.5% yield. Selective sulfonylation of **2a** gave three new *O*-*p*-tolylsulfonyl-*myo*-inositols (the 4,6- (**8a**), 4,5- (**9a**), and 4,5,6-*p*-toluenesulfonates (**10**)). From **3a**, two *O*-*p*-tolylsulfonyl derivatives (5- (**15a**) and 4,5-*p*-toluenesulfonates (**16**)) were obtained. The relative reactivities, toward benzoylation, of the hydroxyl groups of **1a** were shown to be almost similar to those observed in tosylation. The *p*-tolylsulfonyloxy function on C-5 of **10** was found to be readily displaced preferentially by chloride ion.

As the continuation to a program[1] to elucidate relative reactivities of hydroxyl groups of cyclitols toward esterification, a selective benzoylation of 1,2-*O*-cyclohexylidene-*myo*-inositol (**1a**)[2] was studied. We wish to report on the preparation of two benzoates by selective benzoylation of **1a**, from which four new *p*-toluenesulfonates of *myo*-inositol were obtained by

1) T. Suami, S. Ogawa, T. Tanaka, and T. Otake, This Bulletin, **44**, 835 (1971); T. Suami, S. Ogawa, and S. Oki, *ibid.*, **44**, 2820, 2824 (1971).

2) S. J. Angyal, M. E. Tate, and S. D. Gero, *J. Chem. Soc.*, **1961**, 4116.

sulfonylation. Preferential replacement of the *p*-tolylsulfonyloxy function with chlorine atom in dry pyridine in the presence of pyridine hydrochloride was observed at elevated temperature.

The reaction of **1a** with 1.5 equiv. of benzoyl chloride in dry pyridine at −5—0°C for 3 days gave, in 40% yield, the 3-*O*-benzoate (**2a**) as the sole crystalline monobenzoate together with a considerable proportion of a mixture of the di- and tri-benzoates, from which the 3,6-di-*O*-benzoate (**3a**) was readily isolated in 2.5% yield by fractional crystallization. Acetylation of **2a** and **3a** in the usual way afforded the acetates (**2b**) and (**3b**), and mesylation gave the tri-*O*-mesyl derivative (**2c**) and di-*O*-mesyl derivative (**3c**), respectively.

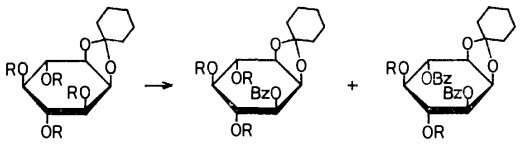

The structures of **2a** and **3a** were established by the following evidences. In analogy to the tosylation of **1a**,[1] the hydroxyl group at C-3 was also expected to be the most active toward benzoylation. Removal of the cyclohexylidene group from **2a** with boiling 80% aqueous acetic acid, followed by acetylation, gave 1-*O*-benzoyl-*myo*-inositol pentaacetate (**4**), which was proved to be identical with the compound derived from 1,4,5,6-tetra-*O*-acetyl-3-*O*-benzoyl-*myo*-inositol (**5**).[3] The proposed structure of **2a** was thus confirmed.

The reaction of **2a** with 3 equiv. of benzoyl chloride at 30°C was monitored by thin layer chromatography (tlc). After 2 days, the result was almost the same as that obtained in the reaction of **1a** with 4 equiv. of benzoyl chloride. Thus, it was clear that **3a** was formed from **2a** by further benzoylation and that an ester group was located at C-3.

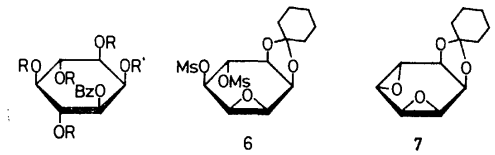

When **3c** was treated with a slight excess of sodium methoxide in a mixture of chloroform and methanol, 1,2: 5,6-dianhydro-3,4-*O*-cyclohexylidene-*allo*-inositol (**7**)[4] was obtained. Since **7** can be formed from either 3,6- or 4,5-disulfonate, the structure of **3a** could be assigned to 3,6-dibenzoate. By similar treatment with sodium methoxide, **2c** afforded 2,3-anhydro-4,5-*O*-cyclohexylidene-1,6-di-*O*-methylsulfonyl-*epi*-inositol (**6**), whose proton magnetic resonance (PMR) spectrum in dimethyl sulfoxide-d_6 (DMSO-d_6) was consistent with the proposed structure, namely, the signal due to H-2 and H-3 appeared as a broad singlet at τ 6.29, and H-6 double doublet and H-1 doublet at τ 5.34 and 4.69, respectively. The up-field shift of H-6 signal might be interpreted by assuming the shielding effect above a plane of the epoxide ring in a skew conformation.[5] It is of interest to note that, in the PMR spectrum of the corresponding di-*p*-toluenesulfonate,[4] the complex multiplet (τ 6.45) due to H-2 and H-3, and H-5 triplet (τ 5.90) were only upshifted by *ca.* 0.20 ppm, as compared with those of **6**, due to the shielding effect of tosyloxy aromatic rings.

Compound **2a** may be a versatile intermediate in the synthesis of a number of inositol derivatives of biological interest. Selective sulfonylation of **2a** was carried out in order to synthesize new *O*-*p*-tolylsulfonyl-*myo*-inositols. The reaction of **2a** with 7 equiv. of *p*-toluenesulfonyl chloride in dry pyridine at room temperature (20—25°C) was monitored by tlc. After 4 days, formation of two di- and one tri-*p*-toluenesulfonates was shown by tlc. The crude mixture was then fractionated by crystallization to give 4,6-di- (**8a**) and 4,5,6-tri-*p*-toluenesulfonates (**10**) in 22 and 5% isolated yields, respectively. The oily 4,5-diester (**9a**) could be characterized by being converted into crystalline acetate (**9b**) (20% yield).

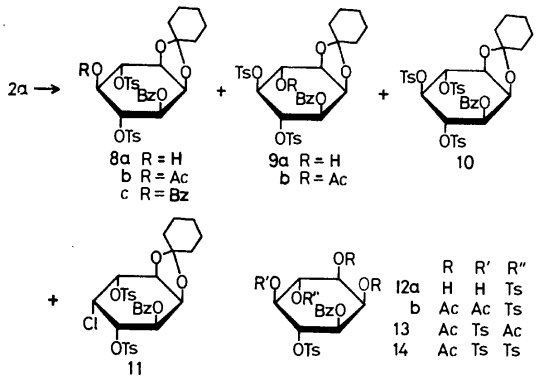

When the same reaction was carried out at 30°C for 3 days, compounds **8a**, **9b** and **10** were isolated in 30, 7, and 12% yields, respectively. Thus in view of the relative yields of the *p*-toluenesulfonates, it might be deduced that **9a** reacts with the acylating agent more rapidly than **8a** to yield **10** smoothly.

On the other hand, when the same reaction was carried out at 80—85°C, formation of an unidentified faster-moving product was observed. After 12 hr, fractionation of the crude reaction mixture by crystallization gave an unknown compound (**11**) in 9% yield, together with a mixture of **8a** and **10** (*ca.* 20%), **9b** (8%), and **10** (30%).

The acetate (**8b**) and benzoate (**8c**) were prepared in the usual way from **8a**. Removal of cyclohexylidene group from **8a** gave 1-*O*-benzoyl-4,6-di-*O*-*p*-tolylsulfonyl-*myo*-inositol (**12a**), which was converted into the triacetate (**12b**). Similarly, 1,2,6-tri-*O*-acetyl-3-

3) T. Suami, F. W. Lichtenthaler, and S. Ogawa, This Bulletin, **39**, 170 (1966).

4) T. Suami, S. Ogawa, S. Oki, and K. Ohashi, *ibid.*, **45**, 2597 (1972).

5) L. M. Jackman and S. Sternhell, "Application of Nuclear Magnetic Resonance Spectroscopy in Organic Chemistry," Pergamon Press (1969), p. 99.

Table 1. PMR data[a)]

Compound	R	R'	R''	R'''	H-1 ($J_{1,2}$)	H-2 ($J_{2,3}$)	H-3 ($J_{3,4}$)	H-4 ($J_{4,5}$)	H-5 ($J_{5,6}$)	H-6 ($J_{1,6}$)	OTs	OAc
1b[b)]	Ac	Ac	Ac	Ac	5.74 t (5.5)	5.43 dd (3.8)	4.77 dd (9.9)	4.43 dd (8.3)	4.96 t (8.9)	4.67 dd (6.6)		7.88 7.92 7.98 7.99
1c	Bz	Bz	Bz	Bz	5.38 t (5.5)	5.08 dd (3.5)	4.34 dd (10.5)	3.71 dd (7.5)	—	— (6.5)		
2b	Bz	Ac	Ac	Ac	5.64 t (5.5)	5.26 dd (3.5)	4.53 dd (9.5)	4.26 dd (8.0)	4.84 t (8.0)	4.54 dd (6.5)		7.89 7.95 8.03
3b	Bz	Ac	Ac	Bz	5.50 t (6.0)	5.20 dd (3.5)	4.43 dd (9.5)	4.13 dd (7.5)	4.64 t (8.5)	4.38 dd (6.0)		8.02 8.07
8a	Bz	Ts	H	Ts	5.71 t (5.5)	5.40 dd (3.5)	4.55 dd (9.0)	4.84 dd (9.0)	6.12[c)] t (8.0)	5.10 dd (5.5)	7.52 7.79	
8b	Bz	Ts	Ac	Ts	5.73 t (6.0)	5.39 dd (3.0)	—	—	—	— (6.0)	7.55 7.75	8.04
8c	Bz	Ts	Bz	Ts	—	—	4.10[d)] d (8.0)	4.63 t (9.0)	4.17 t (10.0)	4.91 dd (6.5)	7.69 7.90	
9b	Bz	Ts	Ts	Ac	5.66 t (6.0)	5.40 dd (3.5)	4.36 dd (8.0)	4.69 dd (6.0)	5.05 dd (8.0)	4.55 dd (6.0)	7.54 7.73	7.96
10	Bz	Ts	Ts	Ts	—	—	—	—	—	—	7.55[e)] 7.71	
15b	Bz	Ac	Ts	Bz	5.59 dd (5.5)	5.27 dd (3.0)	4.49 dd (10.0)	4.05 dd (9.0)	5.00 dd (9.0)	4.30 dd (7.0)	7.79	8.03
16	Bz	Ts	Ts	Bz	5.59 t (6.0)	5.31 dd (3.5)	4.37 dd (9.0)	4.57 dd (9.0)	5.02 dd (9.0)	4.30 dd (6.0)	7.69 7.73	
18	Ts	Ts	Ts	Ts	—	—	—	—	—	—	7.55[f)]	
21[g)]	Ts	Bz	Bz	Ts	5.63 t (5.5)	5.35 dd (3.5)	4.93 dd (9.0)	4.07 t (9.0)	4.54 t (9.0)	4.85 dd (6.0)	7.75[e)]	
22	Ts	Bz	Ts	Bz	5.61 t (5.5)	5.36 dd (3.5)	4.89 dd (10.0)	4.04 dd (9.0)	4.99 t (9.0)	4.31 dd (6.0)	7.75 7.94	
23	Ts	Ts	Bz	Bz	5.58 t (6.0)	5.31 dd (3.0)	—	—	—	— (6.0)	7.54 7.81	
24	Ts	Bz	Bz	Bz	5.48 t (5.0)	5.25 dd (3.5)	4.76 dd (10.0)	3.90 t (9.0)	4.40 t (9.0)	4.18 dd (6.0)	7.78	

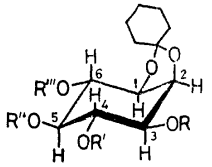

a) Measured at 60 MHz in $CDCl_3$, unless otherwise stated. Chemical shifts are given in τ-values. Abbreviations: d (doublet); t (triplet); dd (double doublet). First order coupling constant (Hz) are expressed. For convenience, all the compounds listed are named as derivatives of 1,2-*O*-cyclohexylidene-*myo*-inositol. b) Measured at 100 MHz. c) The signal appeared on deuteration. d) Broad doublet. e) Singlet for two methyl protons. f) Broad singlet for four methyl protons. g) Preparation of **21**, **22**, **23**, and **24** is given in Experimental.

O-benzoyl-4,5-di- (**13**) and 1,2-di-*O*-acetyl-3-*O*-benzoyl-4,5,6-tri-*O*-*p*-tolylsulfonyl-*myo*-inositol (**14**) were prepared from **9b** and **10**, respectively.

Determination of the positions of the *p*-tolylsulfonyloxy groups was accomplished by means of PMR spectroscopy. In the PMR spectrum of **8a** in $CDCl_3$ (Table 1), two double doublets due to H-4 and H-6 appeared at τ 4.84 and 5.10, respectively, while H-5 triplet was observed at τ 6.12 upon addition of deuterium oxide, indicating the location of two sulfonyloxy groups at C-4 and C-6. The PMR spectrum of **9b** (Table 1) revealed the double doublet at τ 4.55, which could be assigned to H-6 signal, showing that the acetoxy group was attached at C-6.

Treatment of **9b** with excess methanolic sodium methoxide afforded **7**, excluding the 5,6-disulfonate structure of **9b**. Both the proposed structures of **8a** and **9b** were thus assigned unequivocally.

Selective sulfonylation of **3a** was conducted. The reaction of **3a** with 3 equiv. of *p*-toluenesulfonyl chloride at room temperature was monitored by tlc. After 3 days, **3a** disappeared and two mono- and one di-

p-toluenesulfonates were formed. Fractionation of the crude mixture by crystallization gave the 5-*O*- (**15a**) and 4,5-di-*O*-*p*-tolylsulfonyl derivatives (**16**) in 12 and 20% isolated yields, respectively. The faster-moving disulfonate, presumably 4-*O*-*p*-toluenesulfonate, could not be obtained in a crystalline form. However, judging from tlc, two monosulfonates seem to have been formed nearly in the same proportion.

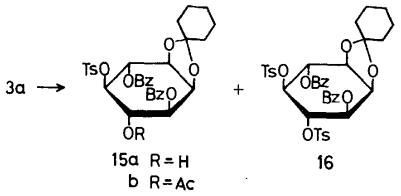

In the PMR spectrum of the acetate (**15b**) derived from **15a**, the triplet due to H-5 appeared at higher-field (τ 5.00) as compared with H-4 double doublet (τ 4.05), indicating that the sulfonyloxy group was located at C-5.

Structural elucidation of **11** was carried out in the following way. Removal of cyclohexylidene group from **11** gave the dihydroxyl derivative (**17a**), which was transformed into the diacetate (**17b**). It was shown by elemental analyses of **11**, **17a** and **17b** that one of the tosyloxy functions of **10** was replaced by a chlorine atom. In the PMR spectrum of **11** (Fig. 1), two double doublets appeared at τ 4.73 and 4.23, having J=3.0 and 10.0 Hz, and J=4.0 and 10.0 Hz, respectively. From the coupling constants and their shapes they were clearly coupled to each other. Therefore, the former should be ascribed to the signal of the proton attached to the carbon atom bearing the tosyloxy group and the latter to that of 3-proton since it must be at the lowest field. Thus H-2, H-3, H-4, and H-5 were shown to be in equatorial, axial, axial, and equatorial arrangement, respectively. Consequently, the presence of the chlorine atom at C-5, its configuration being inverted, might only account for the above spectral data. The structure of **11** was tentatively assigned to 3-*O*-benzoyl-5-chloro-1,2-*O*-cyclohexylidene-5-deoxy-4,6-di-*O*-*p*-tolylsulfonyl-*neo*-inositol.

Mechanistically, a direct S_N2 attack of chloride ion

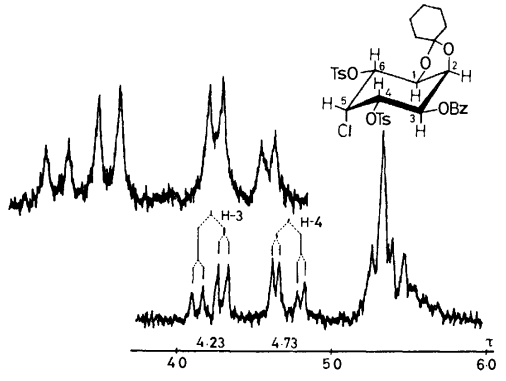

Fig. 1. Partial PMR spectrum of 3-*O*-benzoyl-5-chloro-1,2-*O*-cyclohexylidene-5-deoxy-4,6-di-*O*-*p*-tolylsulfonyl-*neo*-inositol (**11**) in $CDCl_3$ at 60 MHz. An amplified (magnification, 2) spectrum is shown above.

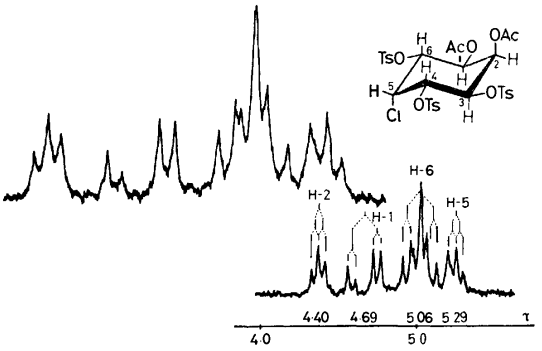

Fig. 2. Partial PMR spectrum of 1,2-di-*O*-acetyl-5-chloro-5-deoxy-3,4,6-tri-*O*-*p*-tolylsulfonyl-*neo*-inositol (**20b**) in $CDCl_3$ at 60 MHz. An amplified (magnification, 2) spectrum is shown above.

generated from pyridine hydrochloride formed might be postulated to occur at C-5 of **10**. This was supported by the following results: treatment of **10** with excess pyridine hydrochloride in dry pyridine at 90—95°C gave **11**, although in a poor yield (3.5%), but **11** could not be formed by a similar treatment of **8a**. As an analogous example, Hess and Stenzel[6] reported a facile replacement of C-6 and C-4 tosyloxy functions of methyl α-D-glucoside by treatment in dry pyridine with 6 equiv. of *p*-toluenesulfonyl chloride at 85°C.

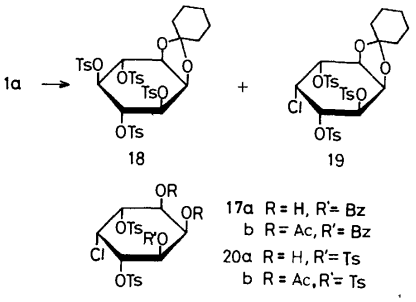

In order to examine the proposed reaction mechanism, **1a** was subjected to similar reaction conditions yielding **11**. The expected chlorodeoxy compound (**19**) was obtained in 10% yield, together with the tetra-*O*-*p*-toluenesulfonate (**18**) (isolated yield 30%). Removal of the cyclohexylidene group from **19** gave the dihydroxyl derivative (**20a**), which was converted into diacetate (**20b**). Assuming that the displacement reaction occurred at C-5 of **18**, **19** might be formulated as 5-chloro-1,2-*O*-cyclohexylidene-5-deoxy-3,4,6-tri-*O*-*p*-tolylsulfonyl-*neo*-inositol. In the PMR spectrum of **20b** (Fig. 2), two narrow triplets appeared at τ 5.28 and 4.39, having J=2.5 and J=3.0 Hz, respectively, which were attributed to the signals of two equatorial protons (H-5 and H-2). The H-1 and H-6 signals appeared as double doublets at τ 4.69 and 5.05, having J=2.5 and 10.0, and J=3.0 and 10.0 Hz, respectively, indicating that the chlorine atom was situated axially orientated at C-5. The proposed structure was thus confirmed.

Consequently, it was demonstrated that C-5 *p*-tolylsulfonyloxy function of *p*-toluenesulfonic esters

6) K. Hess and H. Stenzel, *Ber.*, **68**, 981 (1935).

of 1,2-*O*-cyclohexylidene-*myo*-inositol was most readily replaced by chloride ion among four functions. The result is of interest in contrast to its lower reactivity toward esterification.

PMR spectra——The PMR spectra of the benzoates and sulfonates together with those of some related compounds are given in Table 1. The signals due to H-1 and H-2 could be readily assigned because they occurred up-field and were sufficiently separated from those of the protons on the remaining carbon atoms. Comparing the chemical shifts of the ring protons for **1c** with those for **1b**, the deshielding effect was observed in **1c** due to the benzoyl carbonyl group at C-3; namely, the signals for H-4, H-5, and H-6 were shifted down-field by 0.17, 0.12, and 0.13 ppm, respectively. In **3b**, H-4 and H-5 signals showed considerable down-field shifts (0.30 and 0.32 ppm) due to two ester groups at C-3 and C-6.

Interesting shielding effects on methyl signals of *p*-tolylsulfonyloxy groups were observed. The methyl protons of all the *p*-toluenesulfonates of *myo*-inositol derivatives so far reported[1] resonate in the range τ 7.54—7.59. For instance, the methyl signals of four *p*-tolylsulfonyl groups of **18** appeared at τ 7.55 as a slightly broadened singlet, whereas the introduction of benzoyl groups at vicinal positions to the *p*-tolylsulfonyloxy groups was found to cause intense up-field shifts for the methyl signals of the latter. That is, when the equatorial *p*-tolylsulfonyl group is flanked by an equatorial benzoyloxy group, the methyl signal upshifts by 0.14—0.24 ppm, and, when flanked by two, by 0.35—0.39 ppm.

It is well established that protons situated in the space above or below a benzene ring are subjected to shielding effects. The effects observed show that the benzoyloxy group adopts a conformation in which the aromatic ring is in a position at right angles to the plane of the ring of the ester group restricted of free rotation. The above effect may be applied adequately for the structural assignment of **8a** and **9b**. Thus, one of the signals of the tosyloxy methyl groups was shifted up-field by 0.20 and 0.19 ppm, respectively, showing that they were situated adjacent to the benzoyloxy group at C-3.

Experimental

Melting points were determined on a Mitamura Riken micro hot stage and are uncorrected. PMR spectra were measured on a Varian Associates A-60D (60 MHz) spectrometer at a concentration of *ca.* 10% deuteriochloroform or dimethyl sulfoxide-d_6 with tetramethylsilane as an internal standard. Chemical shifts are expressed in τ-values and signals are denoted by s (singlet), t (triplet), dd (double doublet), and m (complex multiplet). Values given for coupling constants are of first-order. Tlc was performed with silica gel (Wakogel B-10, Wako pure chemical industries Ltd.) using toluene–methyl ethyl ketone (4 : 1 or 3 : 1 volume) as the the solvent system. The compounds were detected by exposing the plate to iodine vapor or by heating after spraying 50% sulfuric acid. All solutions were concentrated by a rotary evaporator at 40—50°C under reduced pressure. All the compounds described in this paper are racemic.

3,4,5,6-Tetra-O-*benzoyl-1,2*-O-*cyclohexylidene*-myo-*inositol* (**1c**). To a solution of 1,2-*O*-cyclohexylidene-*myo*-inositol (**1a**)[2] (1.00 g) in dry pyridine (15 m*l*) was added 6 equiv. of benzoyl chloride (2.04 m*l*) under ice cooling and the mixture was kept in a refrigerator for 3 days. The solution was then poured into ice and water, and the precipitates were collected; yield 2.34 g, mp 227—241°C. By tlc, the crude crystals were shown to be contaminated with several minor components. Recrystallization from chloroform–ethanol gave colorless crystals (0.64 g, 25%) of **1c**, mp 241—243°C.

Found: C, 70.51; H, 5.05%. Calcd for $C_{40}H_{36}O_{10}$: C, 70.99; H, 5.36%.

3-O-*Benzoyl-1,2*-O-*cyclohexylidene*-myo-*inositol* (**2a**) *and 3,6-di*-O-*benzoyl-1,2*-O-*cyclohexylidene*-myo-*inositol* (**3a**). a) To a solution of **1a** (13.0 g) in dry pyridine (200 m*l*) was added, under cooling (−5—0°C), 1.5 equiv. of benzoyl chloride (8.7 m*l*) dropwise for 10 min. After being kept in a refrigerator overnight, the mixture was poured into ice and water (1 *l*). The resulting white precipitates were collected and washed thoroughly with water. The crude product (2.1 g) was recrystallized twice from methyl ethyl ketone to give colorless needles (0.58 g, 2.5%) of **3a**, mp 234—237°C. Tlc of the mother liquor indicated at least five spots: **3a**, three dibenzoates, and one tribenzoate.

Found: C, 66.85; H, 6.02%. Calcd for $C_{26}H_{28}O_8$: C, 66.65; H, 6.02%.

Evaporation of the water layer gave white crystals (5.60 g), which were recrystallized from methanol to give colorless needles (4.66 g, 39.5%) of **2a**, mp 203—205°C. From the mother liquor, an additional crop of **2a** (0.82 g) was obtained, which contained a small amount of **3a**, mp 199—205°C. Recrystallization from methanol afforded an analytical sample, mp 203.5—205°C.

Found: C, 62.87; H, 6.72%. Calcd for $C_{19}H_{24}O_7$: C, 62.62; H, 6.64%.

b) Compound **1a** (1.30 g) was treated with 1.0 equiv. of benzoyl chloride (0.58 m*l*) in dry pyridine (20 m*l*) overnight in a refrigerator, and an additional portion of benzoyl chloride (0.58 m*l*) was then added to the mixture. After being kept in a refrigerator overnight, the reaction mixture was processed as described above to give **3a** (102 mg, 4.4%), mp 234—237°C, and **2a** (569 mg, 31%), mp 200—203°C.

4,5,6-Tri-O-*acetyl-3*-O-*benzoyl-1,2*-O-*cyclohexylidene*-myo-*inositol* (**2b**). Compound **2a** (305 mg) was acetylated with acetic anhydride (4 m*l*) and pyridine (4 m*l*) overnight at room temperature. The reaction mixture was then poured into water and the crude crystals (402 mg, mp 175—177°C) were collected by suction, and then recrystallized from ethanol to afford colorless needles (344 mg, 85%) of **2b**, mp 176—178°C.

Found: C, 61.79; H, 6.27%. Calcd for $C_{25}H_{30}O_{10}$: C, 61.21; H, 6.17%.

3-O-*Benzoyl-1,2*-O-*cyclohexylidene-4,5,6-tri*-O-*methylsulfonyl*-myo-*inositol* (**2c**). To a solution of **2a** (202 mg) in dry pyridine (5 m*l*) was added methanesulfonyl chloride (0.21 m*l*, 5 equiv.) at 0°C. After being kept in a refrigerator for 2 days, the reaction mixture was poured into ice and water, and the resulting crystals (307 mg) were recrystallized from ethanol to give thin needles (239 mg, 72%) of **2c**, mp 208—210°C. An analytical sample was obtained by recrystallization from chloroform–ethanol, mp 208.5—211°C.

Found: C, 44.39; H, 5.05; S, 16.23%. Calcd for $C_{22}H_{30}O_{13}S_3$: C, 44.15; H, 5.05; S, 16.07%.

4,5-Di-O-*acetyl-3,6-di*-O-*benzoyl-1,2*-O-*cyclohexylidene*-myo-*inositol* (**3b**). Compound **3a** (195 mg) was acetylated in the same way as for **2b** to give a crude product (221 mg, mp 189—191°C), which was recrystallized from chloroform–ethanol to afford colorless rods (190 mg, 83%) of **3b**, mp 189—

192°C. Recrystallization from the same solvent gave an analytical sample, mp 192—193°C.

Found: C, 65.35; H, 6.16%. Calcd for $C_{30}H_{32}O_{10}$: C, 65.21; H, 5.84%.

*3,6-Di-O-benzoyl-1,2-O-cyclohexylidene-4,5-methylsulfonyl-myo-inositol (**3c**).* Compound **3a** (199 mg) was treated with methanesulfonyl chloride (0.17 ml, 5 equiv.) in dry pyridine (5 ml) in a similar way as for **2c** to give crude mesylate, which was recrystallized from chloroform–ethanol to give pure needles (181 mg, 68%) of **3c**, mp 244.5—245°C.

Found: C, 54.08; H, 5.45; S, 10.23%. Calcd for $C_{28}H_{32}O_{12}S_2$: C, 53.82; H, 5.17; S, 10.27%.

*1-O-Benzoyl-myo-inositol pentaacetate (**4**).* a) Compound **2a** (205 mg) was treated with boiling 80% aqueous acetic acid (10 ml) for 2 hr. The mixture was then evaporated to dryness, and the crystalline residue was acetylated with acetic anhydride and pyridine in the usual way to give a crude product (238 mg, mp 171—175°C), which was recrystallized from ethanol to afford colorless prisms (176 mg, 63%) of **4**, mp 176—180°C. An analytical sample was obtained by recrystallization from ethanol, mp 178—179°C.

Found: C, 56.27; H, 5.46%. Calcd for $C_{23}H_{26}O_{12}$: C, 55.87; H, 5.30%.

b) 1,4,5,6-Tetra-*O*-acetyl-3-*O*-benzoyl-*myo*-inositol (**5**)[3] (1.0 g) was acetylated, in the same way as for **2b**, to give crude crystals (1.02 g, mp 170—173°C), which were recrystallized from ethanol to afford pure crystals (886 mg, 81%) of **4**, mp 176—178.5°C. It was identical with the compound obtained in (a).

*2,3-Anhydro-4,5-O-cyclohexylidene-1,6-di-O-methylsulfonyl-epi-inositol (**6**).* To a solution of **2c** (82 mg) in a mixture of methanol (2 ml) and 2-methoxyethanol (2 ml) was added methanolic sodium methoxide (0.28 ml, equiv.) at room temperature. After 30 min, the mixture was evaporated to dryness and the residue was extracted with hot ethyl acetate. Evaporation of the extracts gave a crystalline residue which was triturated with petroleum ether and collected by suction: yield 34 mg (78%), mp 205—207°C. Recrystallization from 2-methoxyethanol afforded an analytical sample of **6**, mp 205.5—207°C.

Found: C, 42.66; H, 5.76; S, 16.43%. Calcd for $C_{14}H_{22}O_9S_2$: C, 42.20; H, 5.57; S, 16.10%.

*1,2 : 5,6-Dianhydro-3,4-O-cyclohexylidene-allo-inositol (**7**).* a) To a solution of **3c** (285 mg) in chloroform (7 ml) was added 1 equiv. of methanolic sodium methoxide (0.465 ml) and the mixture was kept in a refrigerator for 2 days. Tlc indicated one major spot together with two minor ones. The solution was then evaporated to dryness and the residue was extracted several times with hot ethyl acetate. The extracts were evaporated to give a crystalline residue, which was recrystallized from chloroform–ethanol to give colorless plates (39 mg, 38%) of **7**, mp 141—142°C. It was shown to be identical with an authentic sample.[4]

b) Compound **9b** (158 mg) was treated with 5 equiv. of methanolic sodium methoxide in a similar way to that described above to give crystals (40 mg, 87%) of **7**, mp 138—142°C.

p-*Toluenesulfonylation of **2a**. Preparation of 3-O-benzoyl-1,2-O-cyclohexylidene-4,6-di-O-p-tolylsulfonyl-myo-inositol (**8a**), 3-O-benzoyl-1,2-O-cyclohexylidene-4,5,6-tri-O-p-tolylsulfonyl-myo-inositol (**10**), and 6-O-acetyl-3-O-benzoyl-1,2-O-cyclohexylidene-4,5-di-O-p-tolylsulfonyl-myo-inositol (**9b**).* a) To a solution of **2a** (3.00 g) in dry pyridine (45 ml) was added 7 equiv. of *p*-toluenesulfonyl chloride (11.0 g) and the mixture was kept at room temperature for 4 days (20—25°C). The mixture was then poured into water (200 ml) and the resulting oily product was collected by decantation. It was dissolved in chloroform (100 ml) and washed successively with 10% aqueous sodium carbonate, N hydrochloric acid and water. After drying over anhydrous sodium sulfate, the solution was evaporated to give an oily product, which was crystallized from chloroform–ethanol to afford crystals (2.6 g). Tlc showed two major spots (**8a** and **10**). Fractional crystallization from the same solvent gave practically pure rods (1.66 g, 30%) of **8a**, mp 184—187°C, and needles (0.51 g, 7.6%) of **10**, mp 163—167°C. Analytical pure samples were obtained by recrystallization twice from the same solvent: **8a** (1.20 g, 21.6%), mp 186—188°C; **10** (0.30 g, 4.5%), mp 169—172°C.

8a: Found: C, 59.01; H, 5.32; S, 9.30%. Calcd for $C_{33}H_{36}O_{11}S_2$: C, 58.91; H, 5.39; S, 9.53%.

10: Found: C, 57.97; H, 5.17; S, 11.23%. Calcd for $C_{40}H_{42}O_{13}S_3$: C, 58.09; H, 5.12; S, 11.63%.

The mother liquor of the crude mixture was evaporated and dried by co-distillation with toluene to give a glassy product (2.11 g). A 970 mg-portion of the product was acetylated with acetic anhydride and pyridine in the usual way to give crude crystals, which were recrystallized from ethanol–toluene, affording needles (0.54 g, 19.8%) of **9b**, mp 181—184°C. Recrystallization from chloroform–ethanol gave an analytical sample, mp 182—184.5°C.

Found: C, 58.67; H, 5.33; S, 8.58%. Calcd for $C_{35}H_{41}O_{12}S_2$: C, 58.55; H, 5.76; S, 8.93%.

A 958 mg-portion of the glassy product was treated with boiling 80% aqueous acetic acid for 2 hr and the reaction mixture was evaporated to dryness, and the residue was crystallized from ethanol to give crystals (413 mg), whose tlc indicated the presence of two components. Recrystallization from ethanol–methyl ethyl ketone gave chromatographically pure crystals (55.9 mg), mp 227—228.5°C. An attempt to elucidate its structure failed. The mother liquor was evaporated to dryness and the residue was acetylated in the usual way to afford crude crystals which were recrystallized from chloroform–ethanol to give crystals (257 mg, 12%) of **13**, mp 202—205°C. This compound was identified with the compound derived from **9b**.

b) Compound **2a** (2.98 g) was treated with 7 equiv. of *p*-toluenesulfonyl chloride (11.0 g) at room temperature for 5 days. The reaction mixture was treated in a similar way to that described in (a) to give crude crystalline mixture (3.5 g) of **8a** and **10**. Fractional crystallization from chloroform–ethanol gave **8a** (0.58 g, 12.5%) and **10** (1.17 g, 17.3%) purely. The mother liquor of the crude crystals was evaporated, and, similarly, acetylated to give **9b** (1.15 g, 23%).

c) Compound **2a** (10.0 g) was treated with 7 equiv. of *p*-toluenesulfonyl chloride (36.7 g) at 30°C for 3 days. The reaction mixture was processed as described above to give crude crystalline mixture (14.9 g), from which **8a** (5.53 g, 29.8%) and **10** (2.67 g, 11.7%) were obtained by fractional crystallization. Compound **9b** (1.38 g, 7.0%) was obtained by acetylation from mother liquor.

p-*Toluenesulfonylation of **2a** at Elevated Temperature. Preparation of 3-O-benzoyl-5-chloro-1,2-O-cyclohexylidene-5-deoxy-4,6-di-O-p-tolylsulfonyl-neo-inositol (**11**).* a) Compound **2a** (2.95 g) was treated with 7 equiv. of *p*-toluenesulfonyl chloride at room temperature for 4 days and the reaction mixture was kept at 80—85°C for 12 hr. The mixture was poured into water and the resulting crystals (6.46 g) were collected by suction. Tlc indicated the presence of a faster-moving component together with **8a** and **10**. The mixture was fractionated by recrystallization from chloroform–ethanol to give pure crystals (1.98 g, 29.8%) of **10**, and cubic crystals (0.46 g, 9.4%) of **11**, mp 180—181°C. PMR ($CDCl_3$): τ 7.53,

7.67 (3, s, OTs C-CH_3).

Found: C, 57.56; H, 5.00%. Calcd for $C_{33}H_{35}O_{10}S_2Cl$: C, 57.34; H, 5.10%.

A crystalline mixture of **8a** and **10** (1.5 g), and **8a** (0.38 g, 8%) were isolated from the mother liquor.

b) Compound **2a** (3.03 g) was treated with 7 equiv. of *p*-toluenesulfonyl chloride at room temperature as described in (a) and the mixture was heated for 45 hr at 90—95°C. Fractional crystallization of the crude product afforded **10** (1.83 g, 31.7%), and **11** (1.03 g, 15.2%) purely.

5-O-Acetyl-3-O-benzoyl-1,2-O-cyclohexylidene-4,6-di-O-p-tolylsulfonyl-myo-*inositol* (***8b***). Compound **8a** (102 mg) was acetylated as in the preparation of **2b** to give an oily product, which was crystallized from chloroform–ethanol to afford crystals (69.4 mg, 65.2%) of **8b**, mp 124—126°C.

Found: C, 58.36; H, 5.42; S, 8.58%. Calcd for $C_{35}H_{38}O_{12}S_2$: C, 58.55; H, 5.76; S, 8.93%.

3,5-Di-O-benzoyl-1,2-O-cyclohexylidene-4,6-di-O-p-tolylsulfonyl-myo-*inositol* (***8c***). To a solution of **8a** (605 mg) in dry pyridine (11 m*l*) was added 6 equiv. of benzoyl chloride (0.63 m*l*) and the mixture was kept for 5 days at 80°C. The mixture was then poured into water and the resulting crystals (672 mg) were recrystallized from chloroform–ethanol to give colorless needles (583 mg, 84%) of **8c**, mp 195.5—198.5°C. Recrystallization from the same solvent afforded an analytical sample, mp 197—199°C.

Found: C, 61.45; H, 4.88; S, 8.57%. Calcd for $C_{40}H_{40}O_{12}S_2$: C, 61.83; H, 5.19; S, 8.26%.

1-O-Benzoyl-4,6-di-O-tolylsulfonyl-myo-*inositol* (***12a***). A mixture of **8a** (1.00 g) and 80% aqueous acetic acid (50 m*l*) was refluxed for 80 min. After being kept standing at room temperature overnight, the resulting precipitates were collected by suction: yield 0.625 g (71.0%), mp 221.5—223°C. An analytical sample was obtained by recrystallization from 2-methoxyethanol, mp 225—228°C.

Found: C, 54.53; H, 4.70; S, 10.53%. Calcd for $C_{27}H_{28}O_{11}S_2$: C, 54.72; H, 4.76; S, 10.53%.

1,2,5-Tri-O-acetyl-3-O-benzoyl-4,6-di-O-p-tolylsulfonyl-myo-*inositol* (***12b***). A mixture of **8a** (1.00 g) and 80% aqueous acetic acid (50 m*l*) was refluxed for 80 min, and then evaporated to dryness. The residue was acetylated with acetic anhydride (5 m*l*) and pyridine (5 m*l*) at 85°C for 40 min to give an oily product, which was crystallized from methanol, affording colorless plates (0.86 g, 86%) of **12b**, mp 197.5—198.5°C. An analytical sample was obtained by recrystallization from chloroform–ethanol, mp 189.5—200°C. PMR ($CDCl_3$): τ 7.55, 7.74 (3, s, OTs C-CH_3), 7.74, 8.06, 8.10 (3, s, OAc).

Found: C, 55.15; H, 4.71; S, 8.72%. Calcd for $C_{33}H_{34}O_{14}S_2$: C, 55.14; H, 4.74; S, 8.92%.

1,2,6-Tri-O-acetyl-3-O-benzoyl-4,5-di-O-p-tolylsulfonyl-myo-*inositol* (***13***). A mixture of **9b** (145 mg) and 80% aqueous acetic acid (10 m*l*) was refluxed for 3.5 hr and then evaporated to dryness. Tlc showed that **9b** disappeared and at least two major components were contained in the crude mixture. The residue was acetylated in the usual way to give an oily product which was crystallized from ethanol, affording colorless needles (22.3 mg, 15%) of **13**, mp 202.5—205°C. Recrystallization from chloroform–ethanol gave an analytical sample, mp 206—209°C. PMR ($CDCl_3$): τ 7.56, 7.83 (3, s, OTs C-CH_3), 7.85, 8.01, 8.02 (3, s, OAc).

Found: C, 55.13; H, 4.46; S, 8.65%. Calcd for $C_{33}H_{34}O_{14}S_2$: C, 55.14; H, 4.74; S, 8.92%.

1,2-Di-O-acetyl-3-O-benzoyl-4,5,6-tri-O-p-tolylsulfonyl-myo-*inositol* (***14***). A mixture of **10** (500 mg) and 80% aqueous acetic acid (25 m*l*) was refluxed for 2 hr and then evaporated to dryness. Tlc showed two spots together with a trace of **14**. The residue was digested with ethanol–pyridine to give a crude mixture (292 mg), mp 125—145°C. A 100 mg-portion of the mixture was acetylated with acetic anhydride (1 m*l*) and pyridine (1 m*l*) at 85°C for 1 hr and the solution was evaporated to dryness. Crystallization from chloroform–ethanol gave crystals (102 mg, 59%) of **14**, mp 174—177.5°C. An analytical sample recrystallized showed the same melting point. PMR ($CDCl_3$): τ 7.56 (6, s, 2OTs C-CH_3), 7.77 (3, s, OTs C-CH_3), 7.85, 8.16 (3, s, OAc).

Found: C, 54.81; H, 4.55; S, 11.46%. Calcd for $C_{38}H_{38}O_{15}S_3$: C, 54.93; H, 4.61; S, 11.58%.

p-*Toluenesulfonylation of* ***3a***. *Preparation of 3,6-di-O-benzoyl-1,2-O-cyclohexylidene-5-O-p-tolylsulfonyl*-myo-*inositol* (***15a***) *and 3,6-di-O-benzoyl-1,2-O-cyclohexylidene-4,5-di-O-p-tolylsulfonyl*-myo-*inositol* (***16***). a) To a solution of **3a** (1.00 g) in dry pyridine (12 m*l*) was added, under ice cooling, 7 equiv. of *p*-toluenesulfonyl chloride (2.85 g) and the reaction mixture was allowed to stand at room temperature for 3 days. The mixture was then poured into water and the resulting crystals were collected. The crude mixture weighed 1.10 g, its tlc showing three components. Recrystallization of the crude mixture from chloroform gave thin needles (378 mg, mp 201—203°C) of **16**. An analytically pure sample of **16** was obtained by recrystallization from chloroform–ethanol: plates (335 mg, 20.2%), mp 203—205°C. From the mother liquor of crude **16**, by crystallization from chloroform, practically pure crystals (238 mg) of **15a**, and a mixture of **15a** and **16** (181 mg) were obtained. Further recrystallization from chloroform–ethanol afforded prisms (162 mg, 12%) of **15a**, mp 196—198°C.

15a: Found: C, 63.13; H, 5.39; S, 5.46%. Calcd for $C_{33}H_{34}O_{10}S$: C, 63.65; H, 5.50; S, 5.15%.

16: Found: C, 61.83; H, 5.27; S, 8.35%. Calcd for $C_{40}H_{40}O_{12}S_2$: C, 61.83; H, 5.19; H, 8.26%.

b) Compound **3a** (1.00 g) was treated with 3 equiv. of *p*-toluenesulfonyl chloride (1.22 g) in dry pyridine (10 m*l*) at room temperature for 2 days. The reaction mixture was processed as in (a) to give crude crystals which were recrystallized from chloroform–ethanol, giving pure crystals (413 mg, 31%) mp 196.5—198.5°C. By tlc, it was shown to be contaminated with a trace of **16**.

A 50 mg-portion of the compound was acetylated as in the preparation of **14** to give crystals (50 mg, 94%) of the acetate (**15b**) mp 194—197°C. Recrystallization from chloroform–ethanol afforded an analytical sample, mp 197.5—199.5°C.

Found: C, 62.84; H, 5.25; S, 5.41%. Calcd for $C_{35}H_{36}O_{11}S$: C, 63.24; H, 5.46; S, 4.82%.

1-O-Benzoyl-5-chloro-5-deoxy-4,6-di-O-p-tolylsulfonyl-neo-*inositol* (***17a***). A mixture of **11** (0.50 g) and 80% aqueous acetic acid (25 ml) was refluxed for 100 min, and the mixture was evaporated to dryness to give a crystalline residue. It was recrystallized from ethanol to give colorless rods (351 mg, 80%) of **17a**, mp 186—188°C. Recrystallization from ethanol afforded an analytical sample with the same melting point.

Found: C, 53.12; H, 4.44%. Calcd for $C_{27}H_{27}O_{10}S_2Cl$: C, 53.07; H, 4.45%.

1,2-Di-O-acetyl-3-O-benzoyl-5-chloro-5-deoxy-4,6-di-O-p-tolylsulfonyl-neo-*inositol* (***17b***). Compound **17a** (190 mg) was acetylated as in the preparation of **12b** to give crystals (223 mg, 100%) of **17b**, mp 197—203°C. Recrystallization from chloroform–ethanol gave an analytical sample, mp 198—200°C. PMR ($CDCl_3$): τ 5.20 (1, t, H-5, J=3.0 Hz), 7.51, 7.64 (3, s, OTs C-CH_3), 7.88, 8.14 (3, s, OAc).

Found: C, 53.21; H, 4.33%. Calcd for $C_{31}H_{31}O_{12}S_2Cl$: C, 53.54; H, 4.50%.

Reaction of ***10*** *with Pyridine Hydrochloride.* A mixture

of **10** (1.04 g) and pyridine hydrochloride (1.20 g) was heated in a sealed tube at 105—110°C for 45 hr. The brown mixture was then poured into water and the resulting oily product was extracted with chloroform. The extract was washed successively with 10% aqueous sodium carbonate, N hydrochloric acid and water, and dried over anhydrous sodium sulfate. Evaporation of the solution gave an oily product which was crystallized from ethanol to afford a mixture of **10** and **11** (100 mg), and **11** (34.5 mg, 3.9%), mp 182—183°C.

Compound **8a** was subjected to the same reaction condition as described above, but, no formation of **11** could be observed.

p-*Toluenesulfonylation of* ***1a*** *at Elevated Temperature. Preparation of 1,2-O-Cyclohexylidene-3,4,5,6-tetra-*O-p-*tolylsulfonyl-*myo-*inositol (****18****) and 5-Chloro-1,2-O-cyclohexylidene-5-deoxy-3,4,6-tri-*O-p-*tolylsulfonyl-*neo-*inosotol (****19****).* To a solution of **1a** (10.0 g) in dry pyridine (100 m*l*) was added *p*-toluenesulfonyl chloride (51 g, 7 equiv.), and the mixture was kept at room temperature for 2 days and then at 90—95°C for 10 hr. The mixture was then poured into ice and water and the resulting oily product crystallized gradually. The precipitates were dissolved in chloroform (100 m*l*) and the solution was washed successively with 10% aqueous sodium carbonate, N hydrochloric acid and water, and dried over anhydrous sodium sulfate. Removal of the solvent gave an oily product which was crystallized from chloroform–ethanol to give crystals (3.9 g, 12%) of **19**, mp 175—179°C. Recrystallization from the same solvent afforded an analytical sample, mp 182—183.5°C. PMR ($CDCl_3$): τ 7.54 (9, s, OTs C-CH_3).

Found: C, 53.68; H, 5.30%. Calcd for $C_{33}H_{37}O_{11}S_3Cl$: C, 53.45; H, 5.00%.

From the mother liquor of **19**, **18** (9.4 g, 28%) was obtained by crystallization from ethanol and methyl ethyl ketone. Recrystallization from the same solvent gave an analytical sample, mp 127.5—130.5°C.

Found: C, 55.22; H, 5.20; S, 14.66%. Calcd for $C_{40}H_{44}O_{14}S_4$: C, 54.78; H, 5.06; S, 14.62%.

*2-Chloro-2-deoxy-1,3,4-tri-*O-p-*tolylsulfonyl-*neo-*inositol* (***20a***). A mixture of **19** (535 mg) and 80% aqueous acetic acid (20 m*l*) was refluxed for 2 hr and then evaporated to dryness. The residue was recrystallized from ethanol to give crystals (462 mg, 96%) of **20a**, mp 187—188°C. Recrystallization from ethanol–methyl ethyl ketone gave an analytical sample mp 187—189°C.

Found: C, 49.32; H, 4.39%. Calcd for $C_{27}H_{29}O_{11}S_3Cl$: C, 49.04; H, 4.42%.

*1,2-Di-*O-*acetyl-5-chloro-5-deoxy-3,4,6-tri-*O-p-*tolylsulfonyl-*neo-*inositol* (***20b***). Crude **20a** obtained from **19** (0.53 g) by the above procedure was acetylated with acetic anhydride (5 m*l*) and pyridine (10 m*l*) overnight at room temperature. Evaporation of excess reagent gave an oily product which was crystallized from ethanol to afford needles (0.52 g, 100%) of **20b**, mp 149—152°C. Recrystallization from ethanol–methyl ethyl ketone gave plates or needles (0.17 g, 35%), mp 175—176°C (after sintering at 150°C. PMR ($CDCl_3$): τ 7.53 (6, s, OTs C-CH_3), 7.57 (3, s, OTs C-CH_3), 7.88, 8.14 (3, s, OAc).

Found: C, 50.24; H, 4.57%. Calcd for $C_{31}H_{33}O_{13}S_3Cl$: C, 50.05; H, 4.44%.

*4,5-Di-*O-*benzoyl-1,2-*O-*cyclohexylidene-3,6-di-*O-p-*tolylsulfonyl-*myo-*inositol* (***21***). To a solution of 1,2-*O*-cyclohexylidene-3,6-di-*O*-*p*-tolylsulfonyl-*myo*-inositol[1] (200 mg) in dry pyridine (2 m*l*) was added benzoyl chloride (0.16 m*l*, 4 equiv.) under ice cooling and the solution was allowed to stand in a refrigerator overnight. The mixture was then poured into water and the resulting crystals (289 mg) were recrystallized from chloroform–ethanol to give pure needles (266 mg, 97%) of **21**, mp 217—218°C.

Found: C, 62.02; H, 5.08; S, 8.28%. Calcd for $C_{40}H_{40}O_{12}S_2$: C, 61.83; H, 5.19; S, 8.26%.

*4,6-Di-*O-*benzoyl-1,2-*O-*cyclohexylidene-3,5-di-*O-p-*tolylsulfonyl-*myo-*inositol* (***22***). 1,2-*O*-Cyclohexylidene-3,5-di-*O*-*p*-tolylsulfonyl-*myo*-inositol[1] (203 mg) was similarly treated with benzoyl chloride (0.20 m*l*, 5 equiv.) to give needles (228 mg, 82%) of **22**, mp 212—214°C. Recrystallization from chloroform–ethanol gave an analytical sample, mp 216—216.5°C.

Found: C, 62.12; H, 5.07; S, 8.03%. Calcd for $C_{40}H_{40}O_{12}S_2$: C, 61.83; H, 5.19; S, 8.26%.

*5,6-Di-*O-*benzoyl-1,2-*O-*cyclohexylidene-3,4-di-*O-p-*tolylsulfonyl-*myo-*inositol* (***23***). 1,2-*O*-Cyclohexylidene-3,4-di-*O*-*p*-tolylsulfonyl-*myo*-inositol[1] (200 mg) was treated with benzoyl chloride (0.16 m*l*, 4 equiv.) in the same way described for **21** to give needles (218 mg, 81%) of **23**, mp 152—154°C. An analytical sample was obtained by recrystallization from chloroform–ethanol, mp 153—154°C.

Found: C, 62.18; H, 5.12; S, 8.35%. Calcd for $C_{40}H_{40}O_{12}S_2$: C, 61.83; H, 5.19; S, 8.26%.

*4,5,6-Tri-*O-*benzoyl-1,2-*O-*cyclohexylidene-3-*O-p-*tolylsulfonyl-*myo-*inositol* (***24***). 1,2-*O*-Cyclohexylidene-3-*O*-*p*-tolylsulfonyl-*myo*-inositol[1] (1.00 g) was treated with benzoyl chloride (1.13 m*l*, 4 equiv.) in a refrigerator for 3 days. The reaction mixture was treated in the same way as for **21** to give crystals (1.61 g, 92%) of **24**, mp 198—200°C. Recrystallization from chloroform–ethanol gave an analytical sample with the same melting point.

Found: C, 66.82; H, 5.52; S, 3.96%. Calcd for $C_{40}H_{38}O_{11}S$: C, 66.11; H, 5.27; S, 4.41%.

The authors are grateful to Professor Sumio Umezawa for his kind advice, and to Mr. Saburo Nakada for carrying out the elementary analyses. Financial support from the Ministry of Education for this work is gratefully acknowledged.

Chemical Studies on Tuberactinomycin. IV.[1] The Chemical Structure of γ-Hydroxy-β-lysine, A New Amino Acid Isolated from Tuberactinomycin A and N[2]

Tateaki WAKAMIYA, Tetsuo SHIBA, and Takeo KANEKO*

Department of Chemistry, Faculty of Science, Osaka University, Toyonaka, Osaka

(Received July 5, 1972)

γ-Hydroxy-β-lysine is a new basic amino acid isolated from the hydrolyzates of antitubercular peptides, tuberactinomycin A and N as one of the composite amino acids. The chemical structure and stereochemistry of the amino acid were established on the basis of chemical reactions and physical measurements, *i.e.*, IR, NMR, and ORD. One stereoisomer obtained in hydrochloric acid hydrolysis was determined as *threo*-γ-hydroxy-L-β-lysine (Ia), while the other one obtained in concentrated sulfuric acid hydrolysis as an *erythro* isomer (Ib).

Tuberactinomycin is a family of peptide antibiotics effective against tubercular bacilli.[3] Tuberactinomycin A and B were isolated from the broth filtrate of *Streptomyces griseoverticillatus* var. *tuberacticus*[4] and a mutant of the original microorganism produced tuberactinomycin N and O.[5]

Tuberactinomycin A is composed of following five amino acids, *i. e.*, L-serine, L-α,β-diaminopropionic acid, 3-ureidodehydroalanine,[6] L-tuberactidine,[7] and a new basic amino acid (I) with the molecular ratio of 2 : 1 : 1 : 1 : 1, while tuberactinomycin N contains capreomycidine[8] instead of tuberactidine and the other amino acids are common to those of tuberactinomycin A.[9]

Acid hydrolyzate of tuberactinomycin A or N was separated by ion-exchange column chromatography, using pyridine–formic acid buffer as an eluent. Serine, α,β-diaminopropionic acid, tuberactidine[10] (capreomycidine, in the case of tuberactinomycin N) and finally a new amino acid Ia were eluted from the column in this order. However, 3-ureidodehydroalanine was not obtained because of ease of decomposition to NH_3 and CO_2 during acid hydrolysis.

From the final fraction, the new basic amino acid was secured as hydrochloride. It had a molecular formula of $C_6H_{14}O_2N_2Cl_2$ (IIa·2HCl) and showed γ-lactone absorption at 1780 cm^{-1} in IR spectrum. A spot of IIa on thin-layer chromatogram was not identical with the original one in the eluate. This indicated that Ia is a basic γ-hydroxy amino acid and was converted to the γ-lactone IIa in the course of isolation procedure after column chromatography.

Taking advantage of the easy formation of γ-lactone from Ia as mentioned above and of insolubility of its derivatives, we attempted the direct and sole isolation of this amino acid from the tuberactinomycin hydrolyzate as acyl derivatives of the lactone. Thus, the acid hydrolyzate of tuberactinomycin A was benzyloxycarbonylated. The oily product formed even in alkaline medium was extracted and then purified by silica gel column chromatography. In this way the expected benzyloxycarbonyl lactone derivative $C_{22}H_{24}O_6N_2$ (IIIa) was obtained. This compound was identical with the benzyloxycarbonyl derivative of IIa. The compound IIIa thus obtained was debenzyloxycarbonylated with 30% hydrogen bromide in glacial acetic acid and the lactone IIa was prepared as dihydrobromide without difficulty.

For the purpose of structural determination of the amino acid Ia, the lactone IIa was saponified to prepare a hydroxy acid which was then reduced with hydriodic acid and red phosphorus. When the product was 2,4-dinitrophenylated, a small amount of di-DNP-β-lysine[11] was obtained together with di-DNP-IIa. Secondly, when the saponified product was oxidized with periodic acid followed by potassium permanganate treatment, β-alanine was detected by thin-layer chromatography as a single product of positive ninhydrin reaction. From these results, the structure of the new basic amino acid Ia could be assigned to γ-hydroxy-β-lysine unequivocally as shown in Scheme 1.

Furthermore, this structure was confirmed by NMR spectrum of dibenzyloxycarbonyl derivative IIIa in $CDCl_3$ as follows; α-CH_2 (d,d at δ 2.36 and 2.82 ppm), β-CH and γ-CH (overlapped at 4.50 ppm), δ-CH_2 (q at 1.80 ppm), ε-CH_2 (q at 3.30 ppm, changed to a triplet in addition of D_2O), β-NH and ε-NH (d at 6.2 ppm and t at 5.4 ppm, both disappeared in addition of D_2O).[12]

When tuberactinomycin A or N was 2,4-dinitrophenylated and then hydrolyzed, no other DNP amino acids than di-DNP-γ-hydroxy-β-lysine lactone (IVa) were detected. Therefore, γ-hydroxy-β-lysine is a sole N-terminal amino acid in the molecules of tuberac-

* Present address: Shiseido Laboratory, Nippa-cho, Kohoku-ku, Yokohama.

1) Part III: T. Noda, T. Take, A. Nagata, T. Wakamiya, and T. Shiba, *J. Antibiot.* (Tokyo), **25**, 427 (1972).

2) Presented at the 13th Symposium of The Chemistry of Natural Products, Sapporo, Japan, September, 1969; p. 17.

3) M. Toyohara, *Kekkaku*, **43**, 245 (1968).

4) A. Nagata, T. Ando, R. Izumi, H. Sakakibara, T. Take, K. Hayano, and J. Abe, *J. Antibiot.* (Tokyo), **21**, 681 (1968).

5) R. Izumi, T. Noda, T. Ando, T. Take, and A. Nagata, *ibid.*, **25**, 201 (1972).

6) B. W. Bycroft, D. Cameron, L. R. Croft, A. Hassanali-Walji, A. W. Johnson, and T. Webb, *Tetrahedron Lett.*, **1968**, 5901.

7) T. Wakamiya, T. Shiba, T. Kaneko, H. Sakakibara, T. Take, and J. Abe, *ibid.*, **1970**, 3497.

8) E. B. Herr, Jr., Antimicrobial Agents Chemotherapy 1962, 201 (1963).

9) H. Yoshioka, T. Aoki, H. Goko, K. Nakatsu, T. Noda, H. Sakakibara, T. Take, A. Nagata, J. Abe, T. Wakamiya, T. Shiba, and T. Kaneko. *Tetrahedron Lett.*, **1971**, 2043.

10) It was obtained as a mixture with viomycidine.

11) DNP stands for 2,4-dinitrophenyl.

12) The terms of d, t, and q show doublet, triplet, and quartet respectively.

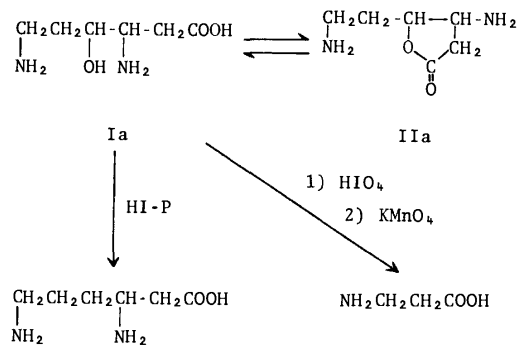

Scheme 1.

tinomycin A and N. The DNP derivative IVa showed the absorption band characteristic to γ-lactone at 1780 cm^{-1} likely as that of the lactone IIa. The lactone IVa was saponified with 1 N NaOH to prepare the corresponding hydroxy acid Va. Reversely, Va was easily converted to IVa by acid treatment.

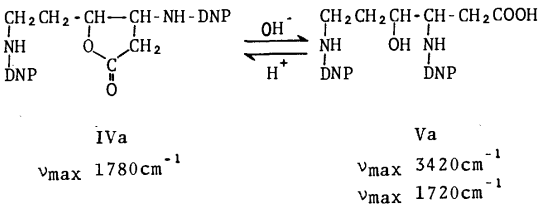

Interestingly, we have obtained a diastereoisomer of the amino acid Ia mentioned above as its lactone derivatives, when tuberactinomycin A was treated with concentrated sulfuric acid with the intention of carrying out N,O-migration reaction. It was benzyloxycarbonylated or 2,4-dinitrophenylated to prepare the corresponding derivatives, IIIb and IVb respectively, both of them showing the γ-lactone absorption in IR spectrum. Though these compounds IIIb and IVb were certainly the derivatives of γ-hydroxy-β-lysine lactone, they were not identical with IIIa and IVa obtained above in respects of IR spectrum, thin-layer chromatogram and melting point. Moreover, debenzyloxycarbonylated products IIa and IIb dihydrobromide prepared respectively from IIIa and IIIb evidently differed each other in thin-layer chromatogram, paper electrophoresis, $[\alpha]_D$, IR, NMR spectra and so on. Thus it was concluded that IIIb and IVb should be the diastereoisomers of IIIa and IVa respectively.

Concerning the stereochemistry of the amino acid I, it was first attempted to determine the configuration of β-carbon atom by the reduction of γ-hydroxyl group to drive to β-lysine. When γ-hydroxy-β-lysine I itself was used for the reduction, always the lactone was obtained as a main product indicating that the lactone formation proceeded much faster than the reduction. Therefore, dibenzyloxycarbonyl-γ-hydroxy-β-lysine amide VIa and VIb prepared by ammonolysis of IIIa and IIIb were used for this purpose. VIa and VIb were reduced with hydriodic acid and red phosphorus, and then 2,4-dinitrophenylated respectively. From the products of dinitrophenylation, di-DNP-β-lysine was separated and purified by preparative thin-layer chromatography and found to be completely identical with the authentic di-DNP-L-β-lysine (VII) in its ORD spectrum in both cases. In this respect, both isomers of γ-hydroxy-β-lysine must belong to L-series at β-carbon atom configurations.

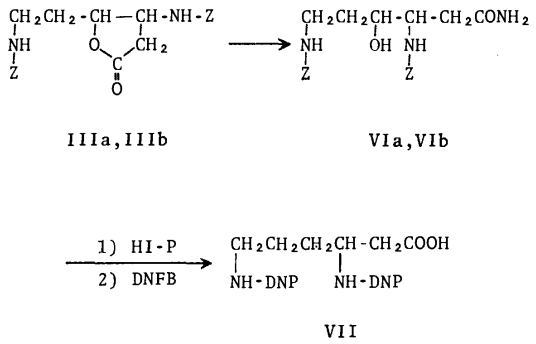

On the other hand, the configurations of γ-carbon atoms of Ia and Ib were assigned by extended application of Hudson's lactone rule[13] as in the case of γ-hydroxylysine.[14] Thus, the lactone IIa and IIb were saponified with silver acetate to the corresponding hydroxy acids Ia and Ib respectively. Although these acids could not be isolated in pure states, mutarotations of them were measured in acidic solutions. From the facts that the rotation of Ia showed the positive shift in the course of time, while that of Ib indicated negative shift (Fig. 1), the configuration of γ-carbon atom was determined as D_g in Ia and L_g in Ib. In these cases, D_g should correspond to *R* and L_g to *S* configuration.

Consequently, it was concluded that Ia must be assigned to *threo*-γ-hydroxy-L-β-lysine and Ib to *erythro*-γ-hydroxy-L-β-lysine. This conclusion was supported by the following investigations. First, in the NMR spectra of IIa and IIb as shown in Fig. 2 and 3, coupl-

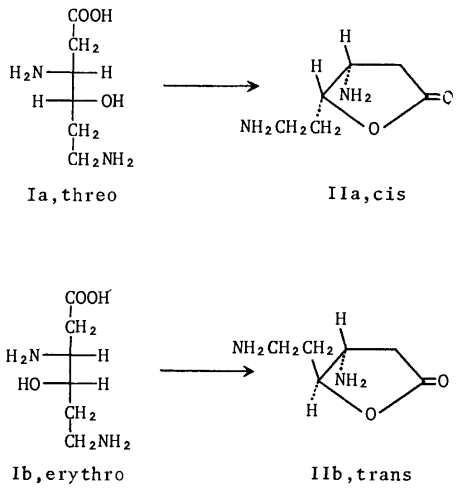

13) B. Witkop, *Experientia*, **12**, 372 (1956). Hudson's lactone rule says that γ- or δ-sugar lactones in which the carbon atom carrying the hydroxyl group contributed to the lactone linkage is related to D-glyceraldehyde show positive value of $[\alpha]_D$ (lactone) − $[\alpha]_D$ (acid) and those to L-glyceraldehyde give negative one.

14) N. Izumiya, Y. Fujita, F. Irreverre, and B. Witkop, *Biochemistry*, **4**, 2501 (1965).

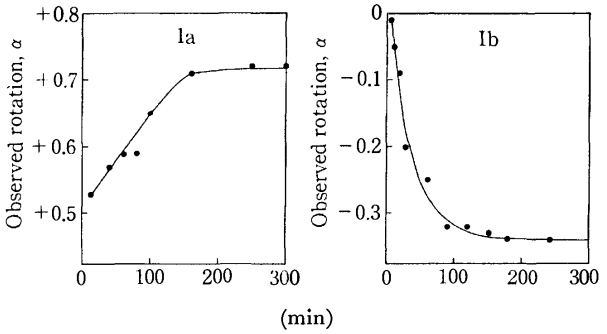

Fig. 1. Mutarotations of Ia and Ib.

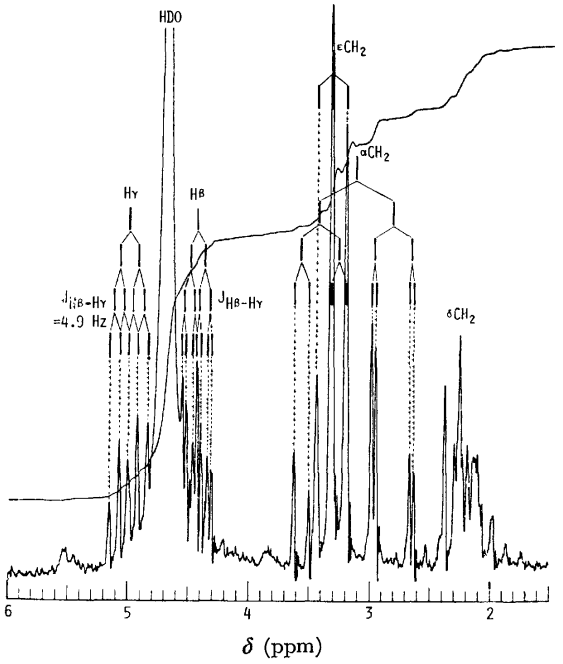

Fig. 2. NMR spectrum of IIa in D_2O.

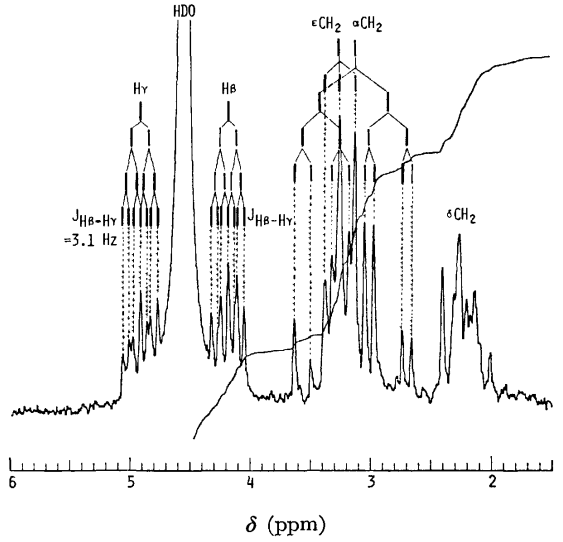

Fig. 3. NMR spectrum of IIb in D_2O.

ing constants between β and γ protons, of 4.9 Hz in the former and 3.1 Hz in the latter, indicated that vicinal protons in the lacton ring of IIa has a *cis* configuration and that of IIb a *trans* configuration, since dihedral angle consisting of vicinal protons in the five-membered lactone ring is near to 0° in *cis* form and to 120° in *trans* form, and therefore the coupling constant of *cis* configuration must be larger than that of of *trans* configuration. This assignment is consistent with the expectation that *threo*-γ-hydroxy-L-β-lysine forms *cis* γ-lactone ring and *erythro*-γ-hydroxy-L-β-lysine forms *trans* γ-lactone ring.

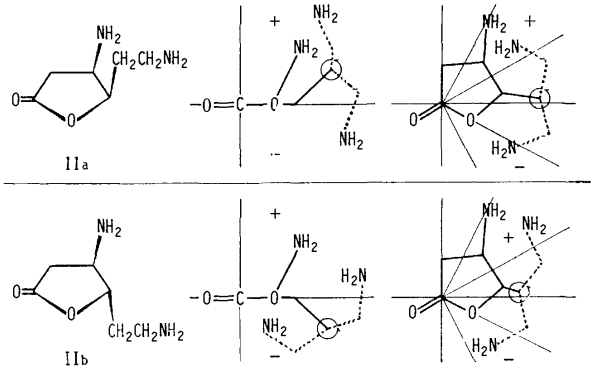

Fig. 4. Estimate of Cotton effects of IIa and IIb.

The above conclusion concerning the configurations of asymmetric carbon atoms in γ-hydroxy-β-lysine was also supported by ORD curve on the basis of Klyne's lactone sector rule.[15] According to this rule, it is expected that the ORD curves of *threo*- and *erythro*-γ-hydroxy-β-lysine lactone will show the positive Cotton effects as illustrated in Fig. 4, if they have β-L-configurations. There may exist negative contribution due to free rotations at δ-carbon atoms, which is, however, overcome by positive contribution as a whole. In fact, both ORD curves of IIa and IIb, in the range of 350 nm to 210 nm, showed positive plain curves indicating presences of positive Cotton effects at lower wavelength than 210 nm.

Recently, we carried out the synthetic work for this amino acid. Synthetic *erythro*-γ-hydroxy-DL-β-lysine in a form of lactone dihydrobromide was identical with that of *erythro* form of the natural amino acid.[16] Therefore, the conclusion of our study on chemical structure and stereochemistry of the new basic amino acid isolated from the antibiotics tuberactinomycin A and N was confirmed unequivocally.

Finally a problem remains, whether *threo* or *erythro* form of this amino acid is original one in the molecule of tuberactinomycin A or N and which is the artificial one converted during the acid treatment. At present, this subject is not yet clarified and must be left to a future investigation.

Experimental

All melting points are uncorrected. The infrared spectrum was obtained in nujol mull with a Nihon Bunko IR-S spectro-

15) W. Klyne, P. M. Scopes and A. Williams, *J. Chem. Soc.*, **1965**, 7211, 7299.

16) T. Wakamiya, T. Teshima, and T. Shiba, Presented at the 26th Annual Meeting of the Chemical Society of Japan, Hiratsuka, April, 1972; p. 1275.

photometer. The NMR spectrum was obtained with a Hitachi NMR R-20 spectrometer and Nihon Denshi C-60 spectrometer. Tetramethylsilane (TMS) was used as an internal reference in deuterochloroform solution, and sodium 2,2-dimethyl-2-silapentane-5-sulfonate (DSS) as an external reference in the case of deuterium oxide solution. The chemical shifts are expressed as ppm from TMS or DSS. The ORD curve was obtained with a Yanagimoto ORD-185 spectropolarimeter in 1N hydrochloric acid and in methanol. The specific rotation was obtained with a Perkin-Elmer 141 polarimeter in water and in dimethylformamide. Thin-layer chromatography was carried out by the ascending method on silica gel G and preparative thin-layer chromatography on silica gel H.

Isolation of threo-*γ-Hydroxy*-L-*β-lysine Lactone (IIa) Dihydrochloride.* A solution of 20 g of tuberactinomycin A hydrochloride in 180 m*l* of 6N hydrochloric acid was heated at 100°C in a sealed tube or under reflux for 24 hr. Hydrochloric acid was evaporated *in vacuo* and the residue was dissolved in water. The evaporation was repeated three times. The solution of the residue thus obtained in a small amount of water was applied on a column (2.5×65 cm) of Dowex 50W×2 ion-exchange resin which was previously equilibriated with a buffer solution of 0.2 M pyridine and formic acid (pH 3.1). In the elution using 5.5 *l* of the same buffer solution (pH 3.1), serine, α, β-diaminopropionic acid and a mixture of tuberactidine and viomycidine were eluted successively. When the buffer solution was changed to a mixture of 2 M pyridine and formic acid (pH 5.2), γ-hydroxy-β-lysine was eluted. Fractions containing γ-hydroxy-β-lysine were collected and evaporated *in vacuo*. The residue was dissolved in hydrochloric acid and evaporated again. Crystalline residue was dissolved in ethanol and allowed to stand in refrigerator. Colorless prisms obtained were recrystallized from water-ethanol, mp 250—252°C (decomp.), $[\alpha]_D^{25}+65°$ (*c* 0.5, H_2O).

Found: C, 33.04; H, 6.54; N, 12.85; Cl, 32.65%. Calcd for $C_6H_{14}O_2N_2Cl_2$: C, 33.19; H, 6.50; N, 12.90; Cl, 32.66%.

N^{β},N^{ϵ}-*Dibenzyloxycarbonyl*-threo-*γ-hydroxy*-L-*β-lysine Lactone (IIIa).* Hydrolysis of each 10 g of tuberactinomycin A or N hydrochloride was carried out under the similar condition to that mentioned above and hydrolyzate was evaporated *in vacuo*. Residue was dissolved in 100 m*l* of water and neutralized with sodium carbonate on cooling. The neutralized hydrolyzate was benzyloxycarbonylated by the usual method using 50 g of benzyloxycarbonylchloride and 100 m*l* of 2N sodium hydroxide. Oily substance formed before acidification was extracted with ethyl acetate and the extract was washed with aqueous sodium carbonate solution and then water thoroughly. The organic layer was dried over anhydrous sodium sulfate and then evaporated *in vacuo*. Oily residue obtained was purified by silica gel (Merck, 0.05—0.20 mm mesh) column chromatography. Chloroform (500 m*l*) and then chloroform-methanol (100 : 1, 1500 m*l*; 100 : 1.5, 200 m*l*) were passed through the column. Benzyl carbamate was eluted first, followed by the desired N^{β},N^{ϵ}-dibenzyloxycarbonyl-*threo*-γ-hydroxy-L-β-lysine lactone (IIIa). Recrystallization of 2.5 g of crude IIIa from ethyl acetate gave colorless needles, yield 2.1 g, mp 149.5°C, $[\alpha]_D^{20}+48.0°$ (*c* 0.4, DMF).

Found: C, 64.02; H, 5.73; N, 6.84%. Calcd for $C_{22}H_{24}O_6N_2$: C, 64.06; H, 5.87; N, 6.79%.

Finally, when a mixture of chloroform-methanol (100 : 4, 1200 m*l*) was used as an elution solvent, N^{α},N^{β}-dibenzyloxycarbonyl-L-α,β-diaminopropionamide was eluted.

Reduction of γ-Hydroxy-β-lysine to β-Lysine. In 2 m*l* of 1N sodium hydroxide, 50 mg of IIa dihydrochloride was dissolved, and allowed to stand at room temperature. After 2 hr, the reaction mixture was neutralized with 1N hydrochloric acid and concentrated *in vacuo*. The residue was dissolved in 5 m*l* of hydriodic acid, and 50 mg of red phosphorus was added. After heating for 3 hr under reflux at 135°C, the solution was evaporated *in vacuo*. The residue was dissolved in water and evaporation was repeated several times. To the solution of the residue in water was added silver oxide and the suspension was stirred for a half hour. Insoluble materials were filtered off and the filtrate was acidified with 1N hydrochloric acid. After filtration of silver chloride, the filtrate was neutralized with aqueous sodium hydrogencarbonate. To this solution was added 100 mg of 2,4-dinitrofluorobenzene in 5 m*l* of acetone and the pH of the solution was controlled always in alkaline side by further additions of sodium carbonate. After stirring at room temperature for 5 hr, it was acidified with diluted hydrochloric acid and the reaction mixture was extracted with ethyl acetate. Di-DNP-β-lysine was detected in the extract on thin-layer chromatogram using developing solvents of chloroform-methanol-acetic acid (95 : 5 : 1) and benzene-pyridine-acetic acid (40 : 10 : 1).

Periodic Acid Oxidation of γ-Hydroxy-β-lysine. To a solution of 50 mg of IIa dihydrochloride in 5 m*l* of 0.5N sodium hydroxide, 50 mg of crystalline periodic acid were added. After allowing to stand at room temperature for 2 hr, diluted potassium permanganate solution was added dropwise to the reaction mixture until the color of the solution remained. In the reaction mixture, β-alanine was detected by thin-layer chromatography. The reaction mixture was subjected to 2,4-dinitrophenylation. Thus, formation of DNP-β-alanine was confirmed also by thin-layer chromatography.

N^{β},N^{ϵ}-*Di-2,4-dinitrophenyl*-threo-*γ-hydroxy*-L-*β-lysine Lactone (IVa).* To a solution of 15 g of tuberactinomycin A hydrochloride in 400 m*l* of water, 15 g of 2,4-dinitrofluorobenzene in 400 m*l* of acetone was added. A mixture was stirred for 20 hr magnetically. It was evaporated *in vacuo* to remove acetone. Precipitate was filtered and washed with water, ethanol, and ether successively. DNP-Tuberactinomycin A obtained was reprecipitated from dimethylformamide-ether, yield 10.2 g. When 7.0 g of DNP-peptide prepared as above was suspended in 350 m*l* of 6N hydrochloric acid and heated under reflux for 24 hr, dark green insoluble material formed. It was filtered and recrystallized from dimethylformamide-ether to give 2.2 g of yellowish needles of N^{β},N^{ϵ}-di-DNP-*threo*-γ-hydroxy-L-β-lysine lactone (IVa), mp 245—246°C (decomp.), $[\alpha]_D^{22}-63.9°$ (*c* 0.5, DMF).

Found: C, 45.47; H, 3.50; N, 17.66%. Calcd for $C_{18}H_{16}O_{10}N_6$: C, 45.38; H, 3.39; N, 17.64%.

N^{β},N^{ϵ}-*Di-2,4-dinitrophenyl*-threo-*γ-hydroxy*-L-*β-lysine (Va).* A suspension of 600 mg of IVa in 6 m*l* of 1N sodium hydroxide was warmed at 90°C. After IVa was dissolved, the reaction mixture was immediately cooled and neutralized with 6 m*l* of 1N hydrochloric acid. Oily product formed was extracted with ethyl acetate and washed with water. Organic layer was dried over anhydrous sodium sulfate. It was concentrated *in vacuo* to give a crystalline residue which was then recrystallized from methanol, yield 0.4 g, mp 161—162°C (sint.) and 245°C (decomp.).

Found: C, 43.76; H, 3.86; N, 16.93%. Calcd for $C_{18}H_{18}O_{11}N_6$: C, 43.73; H, 3.67; N, 17.00%.

N^{β},N^{ϵ}-*Dibenzyloxycarbonyl*-erythro-*γ-hydroxy*-L-*β-lysine Lactone (IIIb).* A solution of 5.0 g of tuberactinomycin A hydrochloride in 140 m*l* of concentrated sulfuric acid was allowed to stand for five weeks in a sealed tube. The solution was poured into acetone on cooling with a freezing mixture.

A gel precipitated was filtered off, washed with acetone and ether, and then dried *in vacuo*. Dried precipitate was dissolved in 6N hydrochloric acid and allowed to stand at room temperature. After 18 hr, the acidic solution was neutralized with sodium hydrogencarbonate on cooling and benzyloxycarbonylation was carried out by the usual way. Oily product was extracted with ethyl acetate and washed with saturated aqueous sodium chloride solution. Organic layer was dried and concentrated *in vacuo*. Oily residue obtained was washed with petroleum ether and then made to powder by trituration with ether. The powder was extracted with ether using Soxhlet's extractor. Combined filtrate and extract were evaporated and residual oil was dissolved in ether. Crystals formed on addition of petroleum ether were filtered off and recrystallized from ethyl acetate and petroleum ether to afford 0.5 g of colorless needles, mp 96.5—97.5°C, $[\alpha]_D^{20}-9.0°$C (*c* 0.4, DMF).

Found: C, 64.07; H, 5.87; N, 6.81%. Calcd for $C_{22}H_{24}O_6N_2$: C, 64.06; H, 5.87; N, 6.79%.

N^{β},N^{ε}-*Di-2,4-dinitrophenyl*-erythro-*γ-hydroxy*-L-*β-lysine Lactone (IVb)*. Tuberactinomycin A was treated with concentrated sulfuric acid as described above and 500 mg of the product obtained was treated with 35 ml of 6N hydrochloric acid at room temperature for 20 hr. After the acid solution had been neutralized with sodium hydrogencarbonate, it was 2,4-dinitrophenylated by the usual manner. The reaction mixture was evaporated *in vacuo* to remove acetone and then insoluble materials were filtered off. The filtrate was extracted with ethyl acetate and washed with aqueous sodium hydrogencarbonate and water. Organic layer was dried and concentrated *in vacuo*. Crystalline residue was recrystallized from acetone and ether, yield 70 mg, mp 145°C (decomp. after sint.), $[\alpha]_D^{22}-177.8°$ (*c* 0.5, DMF).

Found: C, 45.39; H, 3.58; N, 17.77%. Calcd for $C_{18}H_{16}O_{10}N_6$: C, 45.38; H, 3.39; N, 17.64%.

N^{β},N^{ε}-*Dibenzyloxycarbonyl*-threo-*γ-hydroxy*-L-*β-lysine Amide (VIa)*. A solution of 500 mg of IIIa in methanol was saturated with ammonia. After allowing to stand at room temperature for a few days in a pressure bottle, methanol was evaporated under reduced pressure. Residual crystals were recrystallized from methanol to give colorless needles, yield 410 mg, mp 209°C, $[\alpha]_D^{20}+13.0°$ (*c* 0.4, DMF).

Found: C, 61.28; H, 6.34; N, 9.79%. Calcd for $C_{22}H_{27}O_6N_3$: C, 61.52; H, 6.34; N, 9.79%.

N^{β},N^{ε}-*Dibenzyloxycarbonyl*-erythro-*γ-hydroxy*-L-*β-lysine Amide (VIb)*. Colorless needles of VIb were prepared from 170 mg of IIIb as shown in VIa, yield 140 mg, mp 209—210°C, $[\alpha]_D^{20}-3.5°$ (*c* 0.4, DMF).

Found: C, 61.18; H, 6.24; N, 9.78%. Calcd for $C_{22}H_{27}O_6N_3$: C, 61.52; H, 6.34; N, 9.79%.

Reduction of VIa and VIb with Hydriodic Acid and Red Phosphorus. To a solution of 50 mg of VIa or VIb in 2 ml of 57% hydriodic acid, 80 mg of red phosphorus was added. After heating at 100°C for 20 hr in a sealed tube, excess red phosphorus was filtered off and the filtrate was evaporated *in vacuo*. The residue was dissolved in water. Hydriodic acid was decomposed with hydrogen peroxide. Iodine was filtered off and the filtrate was extracted with ethyl acetate. An aqueous layer was treated with 5% Pd-C to decompose excess hydrogen peroxide. After concentration, it was subjected to 2,4-dinitrophenylation. The product was purified by preparative thin-layer chromatography using developing solvent of chloroform-methanol-acetic acid (95 : 5 : 3). Di-DNP-*β*-lysine obtained was identified with an authentic sample by thin-layer chromatography. It was applied to the measurement of ORD curve.

Debenzyloxycarbonylation of IIIa to IIa dihydrobromide. A solution of 1 g of IIIa in 5 g of 30% hydrogen bromide in glacial acetic acid was kept at room temperature for 1 hr. When ether was added, IIa was precipitated as hydrobromide, yield 740 mg. Recrystallization from 94% ethanol gave prisms, mp 235—6°C (decomp.), $[\alpha]_D^{20}+48°$ (*c* 0.5, H_2O).

Found: C, 23.88; H, 4.53; N, 8.84; Br, 51.80%. Calcd for $C_6H_{12}O_2N_2\cdot 2HBr$: C, 23.54; H, 4.61; N, 9.16; Br, 52.23%.

Debenzyloxycarbonylation of IIIb to IIb Dihydrobromide. Removal of benzyloxycarbonyl group from 280 mg of IIIb was carried out as mentioned in the reaction of IIIa to IIa, to obtain IIb hydrobromide, yield 100 mg, mp 222—223°C (decomp.), $[\alpha]_D^{20}-18.0°$ (*c* 0.5, H_2O).

Found: C, 23.92; H, 4.62; N, 8.95; Br, 51.98%. Calcd for $C_6H_{12}O_2N_2\cdot 2HBr$: C, 23.54; H, 4.61; N, 9.16; Br, 52.23%.

Preparation of Hydroxy Acid Ia and Ib. To a solution of 200 mg of the lactone IIa or IIb hydrobromide in 5 ml of water, 1.0 g of silver acetate was added. Suspended solution was heated at 90°C with stirring for 2 hr. Silver bromide formed and excess silver acetate were filtered off. Filtrate was acidified to pH 3.5 with 1N hydrochloric acid. Precipitated silver chloride was filtered off and the filtrate was concentrated below the temperature of 30°C *in vacuo*. The hydroxy acids, Ia and Ib were obtained as oily products. These were applied to the measurement of mutarotation directly.

The authors wish to express their appreciations to Toyo Jozo Co. Ltd., for the supply of the samples of tuberactinomycins.

The Structural Elucidation of Sesquiterpene Lactones from *Petasites japonicus* Maxim[1]

Keizo NAYA, Mitsuo HAYASHI, Ichiro TAKAGI, Seisuke NAKAMURA, and Masakazu KOBAYASHI

Department of Chemistry, Faculty of Science, Kwansei Gakuin University, Uegahara, Nishinomiya, Hyogo

(Received February 25, 1972)

The structures and absolute configurations of five new sesquiterpenic lactones—fukinolide (**1**), dihydrofukinolide (**2**), homofukinolide (**3**), S-fukinolide (**4**), and fukinanolide (**5**)—isolated from the flower stalks of *Petasites japonicus* Maxim. have been established by a combination of spectroscopic and chemical methods, and by correlation with the known fukinone (**25**).

In a preliminary communication,[2] we reported the isolation and the structural proofs of three new lactones,[3] fukinolide (**1**), S-fukinolide (**4**), and fukinanolide (**5**), obtained from the flower stalks of wild butterburs, *Petasites japonicus* Maxim. ("Fuki" in Japanese). Our subsequent work has led to the isolation of two new sesquiterpenic lactones, named dihydrofukinolide (**2**)[4] and homofukinolide (**3**),[4] from the wild plant. The present paper will describe the isolation and structural determination of these five lactones. All of them belong to the class of novel skeletal sesquiterpenoids of the fukinane (**6**) type,[5,6] and all are shown to be ester derivatives of fukinolidol (**8**), which is the common sesquiterpenic moiety of these lactones.

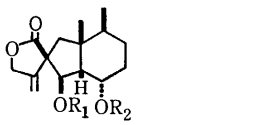

1 R_1=Ac, R_2= 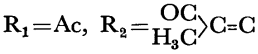 (ang)

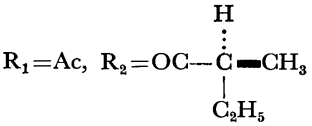

2 R_1=Ac, R_2=

3 R_1=R_2=ang.

4 R_1=Ac, R_2= 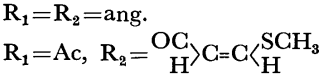

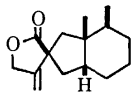

5

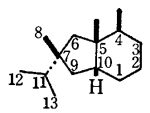

6

Fig. 1. Formulas **1**—**6**.

*Structure of Fukinolide (**1**).* Fukinolide (**1**) ($C_{22}H_{30}O_6$, mp 101.5—102.0°C, $[\alpha]_D^{22}$ −126°) is the most abundant constituent of the flower stalks of the wild strain. In the UV spectrum, **1** showed only an end absorption (ε, 11300 at 215 mμ). The functional groups of **1** were inferred from the IR(KBr) absorption bands to be as follows (Fig. 2): 1775 (γ-lactone), 1737, 1706, 1693, 1263, 1230 (esters), 3090, 1666, 1643, 917 cm^{-1} (double bonds).

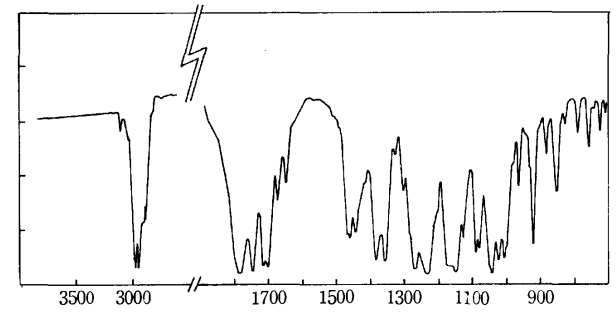

Fig. 2. IR spectra of fukinolide **1** and fukinolidol **8**.

The mild hydrolysis of fukinolide (**1**) with dilute hydrochloric acid gave deacetylfukinolide (**7**) ($C_{20}H_{28}O_5$, mp 167.0—167.5°C), which was then reconverted to **1** by acetylation with acetic anhydride-pyridine. The treatment of **1** with 2 N alcoholic potassium hydroxide afforded angelic acid,[7,8] and a doil, named fukinolidol (**8**) ($C_{15}H_{22}O_4$, mp 176.5—177.5°C). Thus, fukinolide (**1**) proved to be an acetate-angelate of fukinolidol (**8**).

The presence of a γ-lactone group in **1** was presumed from the reaction behavior of alkaline hydrolysis to **8**, as well as from its IR band at 1775 cm^{-1} (Fig. 2).

1) This work was supported in part by a grant from the Ministry of Education of Japan.

2) K. Naya, I. Takagi, M. Hayashi, S. Nakamura, M. Kobayashi, and S. Katsumura, *Chem. Ind.* (London), **1968**, 318.

3) K. Naya, I. Takagi, M. Hayashi, S. Nakamura, and M. Kobayashi, 11th Symposium on the Chemistry of Natural Products, Symposium Papers (1967), p. 88.

4) M. Hayashi, S. Nakamura, I. Takagi, and K. Naya, Annual Meeting of the Chemical Society of Japan (1968), Abstract of Paper, Vol. 3, p. 2152.

5) The numbering system is based on that of the presumed biogenetic precursor possessing eremophilane skeleton.

6) For the preparation of fukinane see: K. Naya and M. Kobayashi, This Bulletin, **44**, 258 (1971).

7) W. Herz and M. V. Laksmikantham, *Tetrahedron*, **21**, 1711 (1965).

8) A. Stoll, R. Morf. A. Rheiner, and J. Renz, *Experientia*, **12**, 360 (1956).

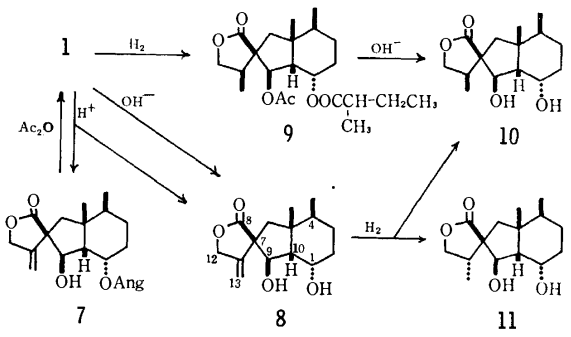

Fig. 3. Formulas **7**—**11**.

One of the two ethylenic double bonds clearly belongs to the angelyl group, as above, while the other seems to be an end-methylene group, judging from the IR bands at 3090, 1666, and 917 cm^{-1}. On hydrogenation with a platinum catalyst in acetic acid, **1** gave the tetrahydro derivative (**9**), which then afforded only dihydrofukinolidol (**10**) ($C_{15}H_{24}O_4$, mp 190.0—191.0 °C) on alkaline hydrolysis, while the similar hydrogenation of fukinolidol (**8**) gave dihydrofukinolidol (**10**) and its epimer, epidihydrofukinolidol (**11**) ($C_{15}H_{24}O_4$, mp 148.0—149.0°C). The IR spectra of **10** and **11** showed no band for an end-methylene group. It can readily be supposed that the above isomeric nature are caused by the hydrogenation of end-methylene groups by different steric environments depending on the existence of ester groups between fukinolide (**1**) and fukinolidol (**8**). The details of the stereochemistry will be described below.

The structure of fukinolidol (**8**) was established from the following evidence.

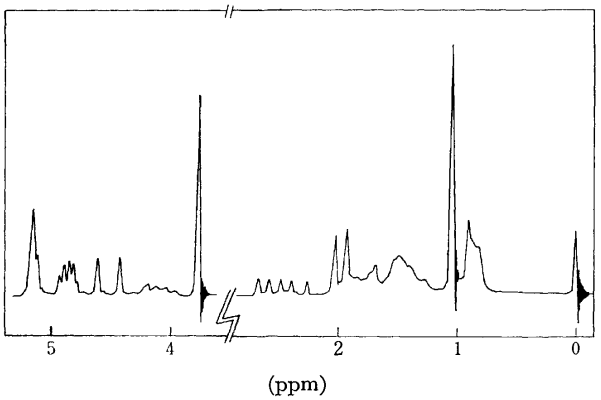

Fig. 4. NMR spectrum of fukinolidol **8**.

Spiro-lactone Group. Fukinolide (**1**) and fukinolidol (**8**) showed essentially similar NMR spectra,[9] except for the signals due to angelate and acetate groups in **1** (Fig. 4). The NMR spectra of **1** and **8** showed the presence of a $-O-CH_2-C=CH_2$ grouping with allyl coupling signals: *i. e.*, 5.20 (d, J=2.0 Hz, $-C=CH_2$) and 4.67 (t, J=1.5 Hz, $-O-CH_2-$) in **1**, and 5.12 (t, J=2.0 Hz, $-C=CH_2$) and 4.81 (m, $-O-CH_2-$) in **8**.

9) The NMR chart of fukinolide **1** was inserted in Ref. 2; NMR spectra in this paper were taken on a JEOL C-60 spectrometer with TMS as an internal reference. The values are reported in ppm.

The reduction of fukinolide (**1**) or fukinolidol diacetate (**12**) ($C_{19}H_{26}O_6$, mp 224.5—226.0°C) with lithium aluminum hydride afforded the same product, a tetrol (**13**) ($C_{15}H_{26}O_4$, mp 106.0—107.0°C), whose IR spectrum showed no C=O band, but the presence of an end-methylene group at 1649 and 906 cm^{-1}. The NMR spectrum of **13** exhibited the signals at 4.23 (slightly split s, 2H) and 5.28 (d, J=5.0 Hz, 2H) due to $HO-CH_2-$ and $-C=CH_2$ respectively, and newly-appeared signals at 3.84 and 3.51 (ABq, J=11.0 Hz, 2H) assignable to the $HO-CH_2-$ group, which was probably derived from the lithium aluminum hydride reduction of the lactone C=O group of **1** or **12**.

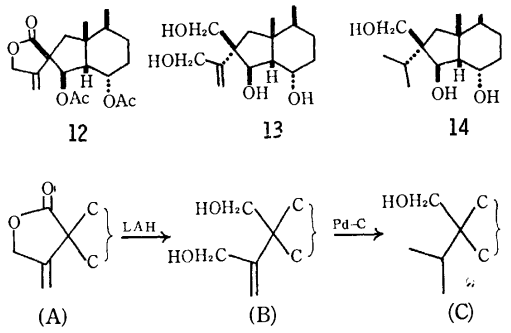

Fig. 5. Formulas **12**—**14**, Partial structure A, B and C.

The above data led to the conclusion that a partial structure (A) was present in **1**. The allylic hydroxyl group in the partial formula (B) was confirmed by the following chemical method.

On the hydrogenation of tetrol (**13**) with palladium charcoal in ethanol, the allylic hydroxyl group was eliminated by hydrogenolysis to yield a triol (**14**) ($C_{15}H_{28}O_3$, mp 88.5—89.5°C). The NMR spectrum of **14** showed signals at 0.97 and 1.07 (each d, J=6.5 Hz) due to a newly-introduced isopropyl group, as in the partial structure (C).

Carbon-ring System and 1,3-Diol Relationship. The NMR spectrum to fukinolidol (**8**) showed signals at 0.86 (d, J=5.0 Hz), 1.04 (s) assignable to a secondary methyl and a tertiary methyl respectively. Accordingly, considering the presence of a spiro-lactone group, two methyls, and the lack of saturation of fukinolidol (**8**) ($C_{15}H_{22}O_4$), the remaining nine carbon atoms seems to consist of a bicyclononane, most probably

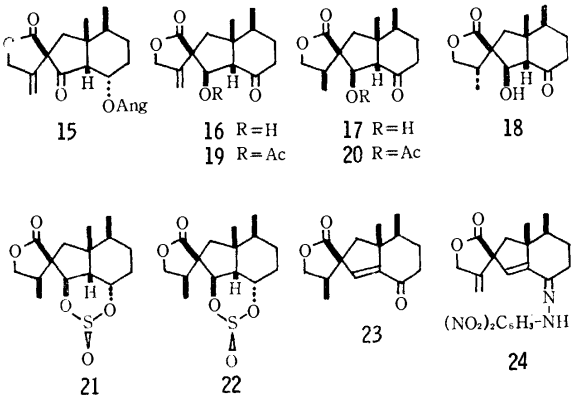

Fig. 6. Formulas **15**—**24**.

a 5-6 fused ring system. This assumption was verified chemically as follows.

The oxidation of deacetylfukinolide (**7**) with Jones' reagent gave a ketone (**15**) ($C_{20}H_{26}O_5$, mp 96.0—97.0°C), whose IR spectrum showed C=O bands for γ-lactone (1770 cm^{-1}), 5-membered ring ketone (1751 cm^{-1}), and α,β-unsaturated ester (1715, 1646, 1239 cm^{-1}). Similarly, Jones' oxidations of fukinolidol (**8**), dihydrofukinolidol (**10**), and epidihydrofukinolidol (**11**) gave three ketols, **16** ($C_{15}H_{20}O_4$, mp 141.5—142.0°C), **17** ($C_{15}H_{22}O_4$, mp 184.0—186.0°C), and **18** ($C_{15}H_{22}O_4$, mp 137.0—138.0°C) respectively, whose IR spectra showed bands at 3490 and 3365 (H-bonded OH), 1773 and 1755 (γ-lactone), and 1702sh and 1680 cm^{-1} (H-bonded 6-membered ring ketone) in **16**, at 3350 (H-bonded OH), 1767 (γ-lactone), and 1680 cm^{-1} (H-bonded 6-membered ring ketone) in **17**, and at 3470sh and 3405 (H-bonded OH), 1755 (γ-lactone), and 1680 cm^{-1} (H-bonded 6-membered ring ketone) in **18**. The IR spectra of both **16**-acetate (**19**) and **17**-acetate (**20**) showed C=O bands at *ca.* 1700 cm^{-1} attributable to 6-membered ring ketones, but no OH bands. Thus, the two hydroxyl functions of the above ketol derivatives are apparently located on the 5- and 6-membered ring respectively. Furthermore, the 1,3-relationship of the diols in fukinolidol (**8**) and dihydrofudkinoliol (**10**) was defined as will be described below.

The treatment of dihydrofukinolidol (**10**) with thionyl chloride-pyridine gave a mixture of two isomeric cyclic sulfites,[10] $C_{15}H_{22}O_5S$, which were separated by column chromatography to afford **21** (mp 190.5—191.5°C) and **22** (mp 187.5—188.5°C). These isomers were assigned to the **21** and **22** formulas from an examination of both the physical and chemical properties previously reported.[11] On the other hand, the treatment of the ketol **17** with phosphorus oxychloride-pyridine readily provided a dehydration product (**23**) ($C_{15}H_{20}O_3$, mp 103.0—103.5°C), whose IR, UV, and NMR spectra showed the presence of an α,β-unsaturated ketone; IR(KBr): 1681, 1629 cm^{-1}, λ_{max}^{EtOH} 250 mμ (ε, 7100), δ^{CDCl_3}: 6.07 (s) due to C-CH=C-CO. An alcoholic solution of the 2,4-dinitrophenylhydrazone of the **16** ketol was refluxed in the presence of a few drops of 85% phosphoric acid to give a dehydration product, **24** (mp 209.5—210.0°C), which showed the presence of a C-CH=C-C=N- grouping by the following data: λ_{max}^{EtOH} 373 mμ (ε, 31600),[12] δ^{CDCl_3}: 5.80 (s). The ease of dehydration suggests strongly that the **16** and **17** compounds both possess β-hydroxyketone groups. In the NMR spectra of **23** and **24**, the sharp singlets at both 6.07 and 5.80 indicate that the adjacent carbon atom of the ethylenic double bond bears no proton.

From the above results, all the two hydroxyl groups in fukinolidol (**8**), dihydrofukinolidol (**10**), and epidihydrofukinolidol (**11**) were confirmed to be in a 1,3-relationship. Subsequently, the outlines of H_a, H_b, and H_c in the 1,3-diol system, and the further expanded grouping $-CH_a(OH)-CH_b-CH_c(OH)-CH_2-$ in fukinolidol (**8**) could be drawn from the NMR data in Table 1.

Table 1. Chemical shifts (ppm as δ-values) of protons in 1,3-diol systems

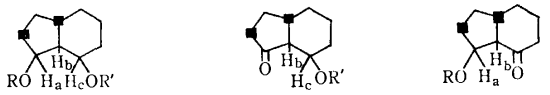

D E F

■: bears no proton.

Compounds	H_a	H_b	H_c
Fukinolide **1**	5.79 d	2.82 dd	5.15 m
D: R=Ac R'=angelyl	J=10.5	J=5.0, 10.5	W ½=13.5
Deacetylfukinolide **7**	4.58 d	2.60 dd	5.20 m
D: R=H R'=angelyl	J=10.5	J=5.0, 10.5	W ½=13.5
Fukinolidol **8**	4.49 d	2.55 dd	4.08 m
D: R=R'=H	J=11.0	J=5.5, 11.0	W ½=13.5
Ketone **15**		3.02 d	5.05 m
E: R'=angelyl		J=5.0	
Ketone **16**	4.38 d	2.86 d	
F: R=H	J=11.0	J=11.0	
Ketone **17**	4.36 d	2.90 d	
F: R=H	J=11.0	J=11.0	

In addition, the NMR spectra of fukinolide (**1**) and fukinolidol (**8**) showed a pair of signals at 2.26 and 1.93 (ABq, J=14 Hz, 2H) and at 2.14 and 1.84 (ABq, J=14.5 Hz, 2H) respectively, indicating the presence of an isolated methylene group. If fukinolide (**1**) is genetically derived from eremophilane derivatives as those of the main constituents isolated from the *Petasites* species,[13,14] the summary of the above evidence leads to the carbon-ring system of fukinolidol (**8**) and also implies its stereochemistry; *i. e.*, two methyls on the carbon-ring system should be situated at at C-4 and C-5 with β-configurations, and the 5-6 ring juncture should be a *cis*-fused ring system, as in Formulas **1** and **8**. Accordingly, the H_a, H_b, and H_c in **8** may be assignable to the α-, β-, and β-configurations respectively, as is shown in Formula **8** on the basis of the coupling constants, J_{ab}=11.0 Hz, and J_{bc}=5.0 Hz, in the NMR spectra of the **15**, **16**, and **17** ketones

10) For the isomeric cyclic sulfites of 1,3-diol: *e. g.* see: A. T. Rowland, T.B. Adams, H. W. Atland, W. S. Creasy, S. A., Dressner and T. M. Dyott, *Tetrahedron Lett.*, **1970**, 4405; E. L. Eliel and N. L. Allinger, "Topics in Stereochemistry," Vol. 4, Willey-Interscience, New York (1967), p. 48.

11) K. Naya, I. Takagi, and T. Kasai, This Bulletin, **44**, 3204 (1971).

12) E. S. Stern and C. J. Timmons, "Electronic Absorption Spectroscopy in Organic Chemistry," Edward Arnold, London (1970), p. 200.

13) K. Naya, I. Takagi, Y. Kawaguchi, Y. Asada, Y. Hirose, and N. Shinoda, *Tetrahedron*, **24**, 5871 (1968).

14) K. Naya and I. Takagi, *Tetrahedron Lett.*, **1968**, 629; A. Aebi, T. Waaler, and J. Buchi, *Pharm. Weekblad*, **93**, 397 (1958); C. Djerassi, M. Mauli, and L. H. Zalkow, *J. Amer. Chem. Soc.*, **81**, 3429 (1959); L. Novotný, J. Jizba, V. Herout, F. Sorm, L. H. Zalkow, S. Hu, and C. Djerassi, *Tetrahedron*, **19**, 1101 (1963); L. H. Zalkow, F. X. Markley, and C. Djerassi, *J. Amer. Chem. Soc.*, **82**, 6354 (1960); L. H. Zalkow, A. M. Shaligram, S. Hu, and C. Djerassi, *Tetrahedron*, **22**, 337 (1966).

(Table 1). Therefore, the configurations of the two hydroxyl groups in fukinolidol (**8**) can be assigned to the 1α(eq) and 9β orientations respectively. Further evidence of the stable 1α(eq) orientation was provided by the reduction of the ketol acetate (**20**) with sodium] borohydride, giving dihydrofukinolidol (**10**). The chemical shifts of the C-15 methyls in the NMR spectra of fukinolidol (**8**) ($CDCl_3$, 1.04; pyridine, 0.97) and dihydrofukinolidol (**10**) ($CDCl_3$, 1.03; benzene, 0.99) showed the anisotropic effect of of the spiro-lactone carbonyl group, suggesting that the lactone and 15β-methyl are located on the same side of the *cis*-fused 5-6 carbon-ring system. The ORD curves of the three ketones, **15**, **16**, and **17**, are in good agreement with the above stereochemistry (**15**: +Cotton; **16** and **17**: −Cotton effects).[15]

Thus, the above results lead to the stereoformulas of **8** and **1** for fukinolidol and fukinolide respectively.

The final evidence for the structure and stereochemistry of fukinolidol (**8**) was provided by the following chemical method for correlation to the known eremophilane derivative, fukinone (**25**),[13] *via* fukinan-8-ol (**26**).

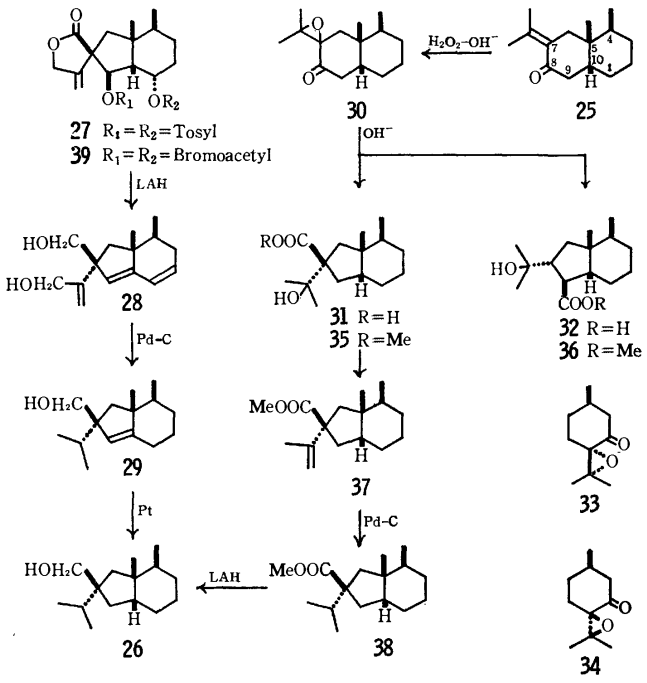

Fig. 7. Formulas **25**—**39**.

The treatment of fukinolidol ditosylate (**27**) (mp 179.5—180.0°C dec) with lithium aluminum hydride gave a diol, **28** ($C_{15}H_{22}O_2$, mp 119.5—120.0°C), whose spectra indicate the presence of a conjugated diene; λ_{max}^{EtOH} 237 mμ (ε, 18700); δ^{CDCl_3}: 6.21 (d, J=9.5 Hz, C-1 H), 5.75 (dt, J=9.5, 2.0 Hz, C-2 H) and 5.50 (s, C-9 H). The subsequent hydrogenation of **28** with palladium charcoal in ethanol afforded a product, **29**, by the hydrogenolysis of the allylic hydroxyl group, as has been described before. The IR and NMR spectra of **29** still showed the existence of an ethylenic bond; IR (film): 1662 cm^{-1}; δ^{CCl_4}: 4.95 (s, C-9 H). Subsequent hydrogenation with a platinum catalyst in acetic acid gave a saturated monol, fukinan-8-ol (**26**) ($C_{15}H_{28}O$, mp 38.0—39.0°C).

On the other hand, fukinan-8-ol (**26**) was prepared from the eremophilane-type, known fukinone (**25**), which is supposed to be a precursor for the genesis of fukinolide (**1**) and its homologues.

The treatment of a mixture of fukinone epoxides (**30**)[16] with an aqueous sodium hydroxide–ethanol solution gave mainly a mixture of a spiro-acid (**31**) and a nonspiro-acid (**32**), similar to the products of the Favorskii rearrangements of the two pulegone epoxides **33** and **34**.[17] The spiro-acid (**31**) was isolated as its ester, **35** ($C_{16}H_{28}O_3$, mp 63.5—64.5°C) by column chromatography. The stereochemistry of the spiro-acid can be properly described by Formula **31** in accordance with the known mechanism demonstrated for the rearrangement of the pulegone epoxides, **33** and **34**.[17] The spiro-ester (**35**) was dehydrated with phosphorus oxychloride-pyridine to afford an unsaturated ester (**37**); subsequent hydrogenation with 10% palladium charcoal in ethanol gave an oil (**38**). The reduction of the saturated alcohol (**38**) with lithium aluminum hydride gave a monol ($C_{15}H_{28}O$, mp 38.0—39.0°C), which was identical in all respects

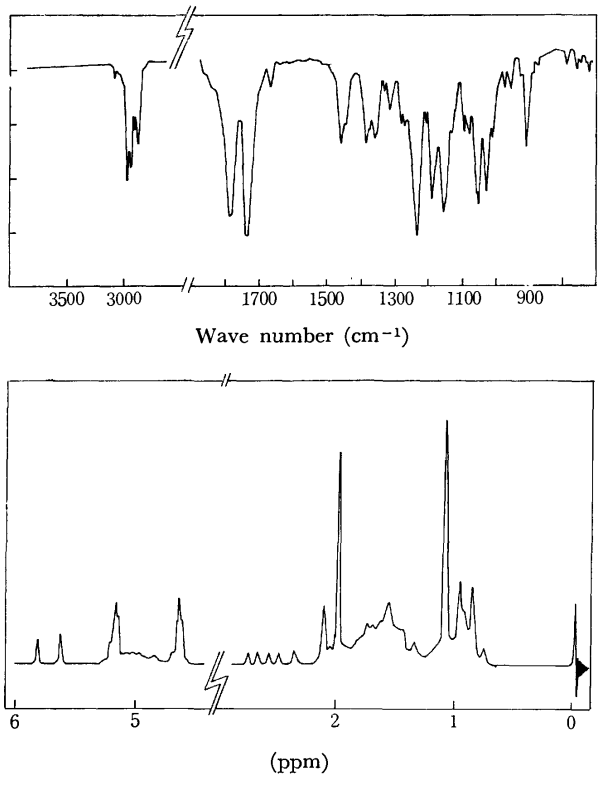

Fig. 8. IR and NMR spectra of dihydrofukinolide (**2**).

15) G. V. Baddeley, T. G. Halsall, and E. R. H. Jones, *J. Chem. Soc.*, **1960**, 1715; C. Djerassi, R. Riniker, and B. Riniker, *J. Amer. Chem. Soc.*, **78**, 6362 (1956); C. Djerassi, W. Closson, and E. Lippman, *ibid.*, **78**, 3163 (1956).

16) Recently α- and β-epoxides of fukinone have been separated and examined their stereospecific natures for Favorskii rearrangement. The details will be published soon.

17) G. W. K. Cavill and C. D. Hall, *Tetrahedron*, **23**, 1119 (1967); W. Reusch and P. Mattison, *ibid.*, **23**, 1953 (1967); S. A. A. Achmad and G. W. K. Cavill, *Aust. J. Chem.*, **16**, 858 (1963).

with the fukinan-8-ol (**26**) prepared from fukinolide (**1**).

At this stage, the structures and absolute configurations of fukinolidol and fukinolide can be represented as in Formulas **8** and **1**. In conjunction with this study, an X-ray analysis[18] has been performed with fukinolidol dibromoacetate (**39**); this also secured the molecular structure of fukinolidol (**8**).

Structure of Dihydrofukinolide (2). Dihydrofukinolide (**2**) ($C_{22}H_{32}O_6$, mp 125.0—126.0°C, $[\alpha]_D^{22}$ −105.5°) was named on the basis of having two hydrogens more than fukinolide (**1**) ($C_{22}H_{30}O_6$). Its IR and NMR spectra resemble those of fukinolide (**1**) except for the absorptions and signals attributable to the angelyl group[7] in **1**. Dihydrofukinolide (**2**) was deduced to be an ester of fukinolidol (**8**) from its IR spectrum; IR(KBr): 1788 (γ-lactone), 1734, 1236 (saturated ester), 3085, 1667, 909 cm^{-1} (end-methylene). In fact, the **2** compound afforded fukinolidol (**8**), acetic acid, and *d*-(S)-α-methylbutyric acid (**40**)[19] upon alkaline hydrolysis. These acids were identified as *p*-phenylphenacyl esters by comparison with authentic sample (tlc, mixed-melting-point determination, and IR spectra). Therefore, dihydrofukinolide (**2**) proved to be the acetate and *d*-(S)-α-methylbutyrate of fukinolidol (**8**).

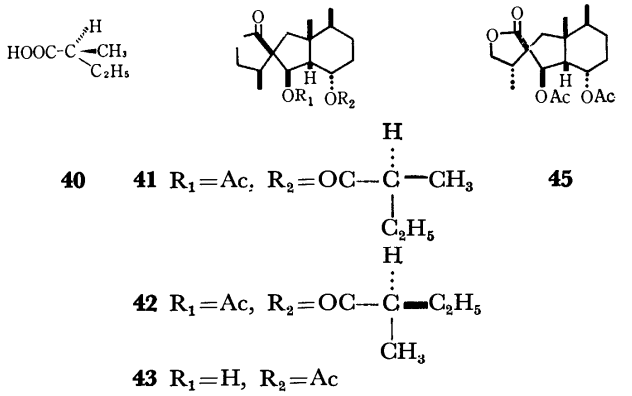

Fig. 9. Formulas **40**—**45**.

The final evidence for the structure of dihydrofukinolide (**2**) was obtained by the correlation with fukinolide (**1**) through its hydrogenated derivatives as follows.

The reduction of fukinolide (**1**) with a platinum catalyst in acetic acid afforded a mixture of two diastereomers, **41** and **42** ($C_{22}H_{34}O_6$), each of which was separated by repeated recrystallization with aqueous methanol, **41**, colorless needles, mp 112.0—113.0°C, $[\alpha]_D^{22}$ −52.25°; **42**, colorless prisms, mp 121.5—122.5°C, $[\alpha]_D^{22}$ −67.5°. The lower-melting isomer, **41**, was identical with tetrahydrofukinolide (mp 116.5—117.0°C, $[\alpha]_D^{22}$ −51.0°), which was obtained exclusively by the hydrogenation of dihydrofukinolide (**2**) with palladium charcoal in ethanol. On the other hand, the higher-melting isomer, **42**, showed a depression of the mixed-melting-point on admixture with tetrahydrofukinolide (**41**) prepared from dihydrofukinolide (**2**), and a different IR spectrum from that of **41**. The above diastereomers are only concerned with an asymmetric center derived from the hydrogenation of the angelyl moiety of fukinolide (**1**). This fact indicates that the addition of hydrogens to the end-methylene group of **1** proceeds preferentially from one side of the lactone ring, namely, from the opposite, less-hindered side to the attaching site of ester groups. The epimeric mixture of **41** and **42**, therefore, upon alkaline hydrolysis afforded only dihydrofukinolidol (**10**). On the other hand, the hydrogenation of fukinolidol (**8**) with palladium charcoal in ethanol gave two diastereomers connected with the configuration of C-13 methyl, $C_{15}H_{24}O_4$—namely, dihydrofukinolidol (**10**) (mp 190.0—191.0°C, $[\alpha]_D^{22}$ −14.5°) and epidihydrofukinolidol (**11**) (mp 148.0—149.0°C, $[\alpha]_D^{22}$ −69.5°), as has been described above. The above results apparently demonstrate that the the absence of ester groups facilitates the addition of hydrogens to the end-methylene group from both sides

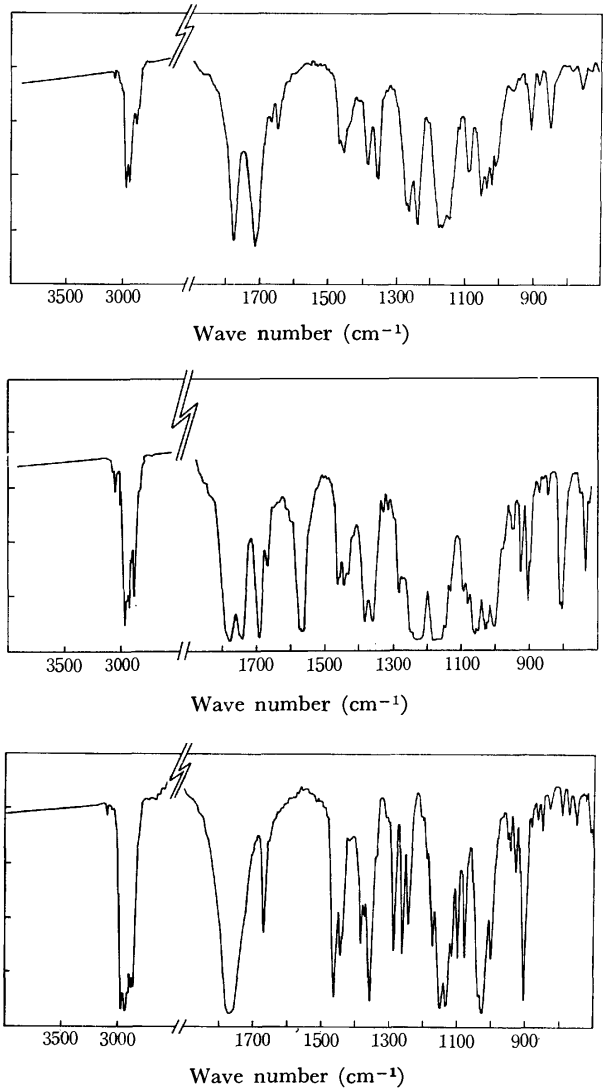

Fig. 10. IR spectra of homofukinolide **3**, S-fukinolide **4**, and fukinanolide **5**.

18) C. Katayama, A. Furusaki, I. Nitta, M. Hayashi, and K. Naya, This Bulletin, **43**, 1976 (1970).

19) A. Yagi and T. Kawasaki, *Yakugaku Zasshi*, **82**, 210 (1962).

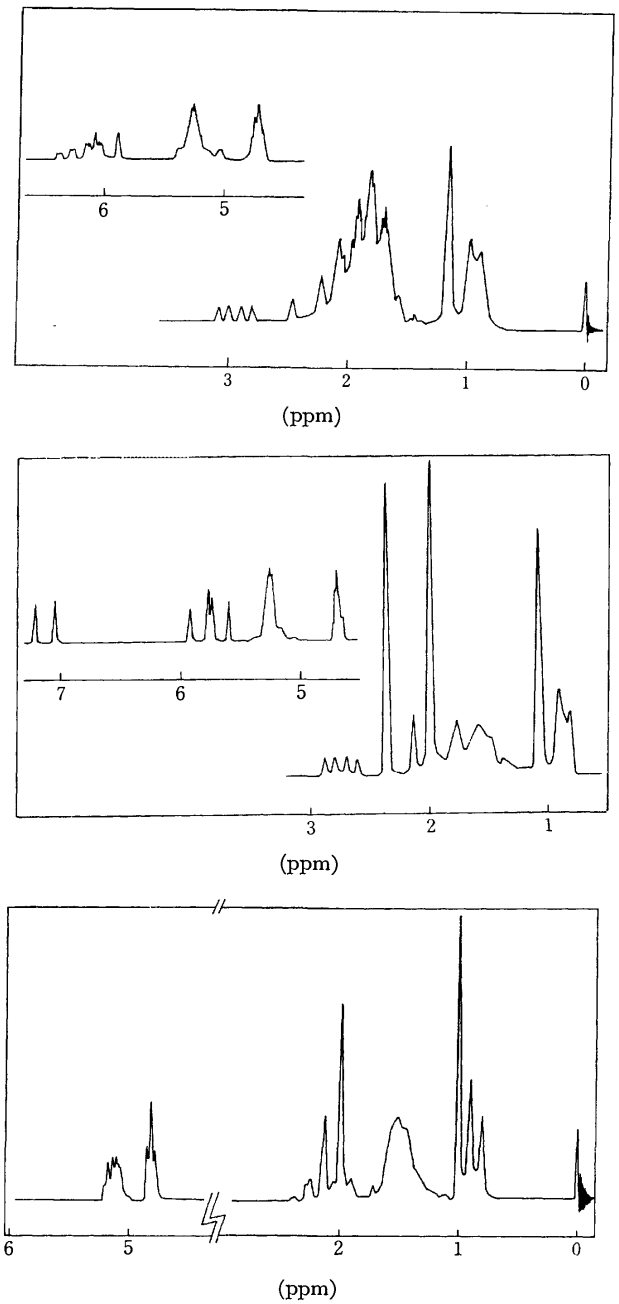

Fig. 11. NMR spectra of homofukinolide **3**, S-fukinolide **4**, and fukinanolide **5**.

of the lactone ring. Thus, the epimer can be represented by Formula **11** in connection with Fomula **10**, with 13β-methyl for dihydrofukinolidol. This configurational postulation at the C-13 methyl group was also supported by the following chemical behavior in response to the steric hindrance caused by 13β-methyl: the acetylation of dihydrofukinolidol (**10**) containing 13β-methyl with acetic anhydride-pyridine gave a mixture of monoacetate (**43**) ($C_{17}H_{26}O_5$, mp 194.0—196.0°C) and diacetate (**44**) ($C_{19}H_{28}O_6$, mp 246.0—248.0°C, $[\alpha]_D^{22}$ −42.5°), while the acetylation of epidihydrofukinolidol (**11**) containing 13α-methyl under conditions similar to the above readily afforded only the diacetate (**45**) (mp 214.0—215.0°C, $[\alpha]_D^{22}$ −50.5°) quantitatively.

Homofukinolide (3). The spectroscopic absorption of homofukinolide (**3**) ($C_{25}H_{34}O_6$, mp 184.0—186.0°C, $[\alpha]_D^{22}$ −127°) were also similar to those of fukinolide (**1**). The NMR spectrum of **3** showed the signals at 6.13 attributable to two vinyl protons, and four vinyl methyl signals between 1.70—1.95 due to the two angelyl groups. The intensity of the UV maximum, ε, 23500 at 215 mμ supported the above assignment.[20] Homofukinolide (**3**) was hydrolysed with alcoholic potassium hydroxide to give fukinolidol (**8**) (mp 177.0—178.0°C) and angelic acid.[8] Those results led to the conclusion that homofukinolide (**3**) is the diangelate of fukinolidol (**8**).

S-Fukinolide (4). Compound **4** ($C_{21}H_{28}O_6S$, mp 200.0—201.0°C, $[\alpha]_D^{22}$ −161°) shows spectroscopic absorptions closely similar to those of fukinolide (**1**), except for the IR band at 1568 cm^{-1} and the NMR signals at 7.00 (d, J=9.5 Hz, 1H), 5.60 (d, J=9.5 Hz, 1H), 2.38 (s, 3H) instead of 5.96 (q, J=7.0 Hz, 1H), 1.80 (d, J=7.0 Hz, 3H) and 1.78 (s, 3H) due to the angelate group in **1**. Further, besides the above spectra, the UV spectra (λ_{max}^{EtOH} 287.5 mμ (ε, 15700)) suggest that Compound **4** may include an isolated disubstituted ethylenic acid residue containing a β-*S*-alkyl group. The hydrolysis of **4** with alcoholic potassium hydroxide gave fukinolidol (**8**) and *cis*-β-methylthioacrylic acid (**46**) ($C_4H_6O_2S$, mp 119.0—120.0°C).[8,21] Thus, S-fukinolide can be represented by Formula **4**.

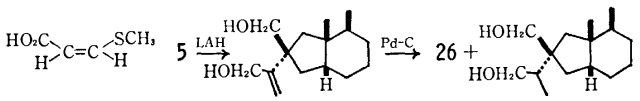

46 **47** **48**

Fig. 12. Formulas **46**—**48**.

Fukinanolide (5). Fukinanolide (**5**) ($C_{15}H_{22}O_2$, mp 80.5—80.6°C, $[\alpha]_D^{22}$ +17.0°) showed IR bands indicating the presence of a γ-lactone (1770 cm^{-1}) and an end-methylene group (1665, 898 cm^{-1}). From a comparison of the NMR spectra of **5** and fukinolidol (**8**), this compound was readily inferred to possess the **5** structure.

The above conclusion was ascertained by the chemical method as follows.

The reduction of **5** with lithium aluminum hydride gave a diol, **47** ($C_{15}H_{26}O_2$, mp 81.5—82.0°C). Compound **47** was hydrogenated with 10% palladium charcoal to afford a monol ($C_{15}H_{28}O$) and another diol, **48** ($C_{15}H_{28}O_2$, mp 121.0—122.0°C). The monol is identical in all respects with fukinan-8-ol (**26**), as is to be expected.

Therefore, the structure and absolute configuration of fukinanolide can be represented by Formula **5**.

Fukinolide (**1**), *S*-fukinolide (**4**), and fukinanolide (**5**) have also been isolated from the flower stalks of *Petasites japonicus* subsp. *giganteus* Kitam. and named bakkenolide-B, -D, and -A respectively by Kitahara

20) A. T. Nielsen, *J. Org. Chem.*, **22**, 1539 (1957).
21) L. Novotný, V. Herout and F. Sorm, *Collect. Czech. Chem. Commun.*, **2**, 2182 (1964).

and his colleagues. They have independently reached the same conclusions.[22]

Experimental

All the melting and boiling points are uncorrected. The IR spectra were recorded with a JASCO DS-402G spectrophotometer, and the UV spectra were obtained with a Cary Model 14 spectrophotometer. The optical rotations were measured with a Hitachi EPU-2A spectrophotometer, and the ORD curves were taken with a JASCO spectrophotometer, Model ORD-5. The mass spectra were measured with a Hitachi RMU-6 mass spectrometer. The analytical and preparative glc were performed with a Shimadzu GC-1C apparatus on a stainless steel column ($\phi=3$ mm). The tlc were run on silica gel (Merck Kieselgel G). The microanalyses were carried out in the microanalytical section of the Shionogi Research Laboratory, Shionogi and Co., Ltd.

*Isolation of Fukinolide (**1**), Dihydrofukinolide (**2**), Homofukinolide (**3**), S-Fukinolide (**4**), and Fukinanolide (**5**).* The dried flower stalks of *P. japonicus* Maxim. collected near the northern margin of Lake Biwa, at the foot of Mt. Ibuki, in Shiga Prefecture, and at Mt. Shirouma in Nagano Prefacture, were extracted in the cold with methanol for 20 days. The solvent was then removed under reduced pressure, and the residue was dissolved in benzene. The solution was washed with a saturated sodium hydrogen carbonate aqueous solution and then with water, dried over anhydrous sodium sulfate, and evaporated *in vacuo*, thus leaving a dark oil (95 g). This oil was repeatedly chromatographed on silica gel, and elution with benzene, benzene–ethyl acetate (50 : 1), or light petroleum–ethyl ether (50 : 1) gave fukinanolide (**5**) (tlc: R_f, 0.77, benzene–ethyl acetate, 15 : 1), homofukinolide (**3**) (R_f, 0.64), dihydrofukinolide (**2**) (R_f, 0.47), fukinolide (**1**) (25 g; R_f, 0.45), and S-fukinolide (**4**) (3 g; R_f, 0.34).

*Fukinolide (**1**)*: mp 101.5—102.0°C, colorless prisms (from light petroleum), $[\alpha]_D^{22}$ −126.0° (*c*, 1.0, MeOH), −117.5° (*c*, 1.0, $CHCl_3$); MS: *m/e* 390 M^+; IR (KBr): 1775 (γ-lactone), 1737, 1706, 1693, 1263, 1230 (ester), 3090, 1666, 1643, 917 cm^{-1} (double bond), (CCl_4): 1788 (γ-lactone), 1744, 1716, 1235 (ester), 3080, 1667, 1645, 900 cm^{-1} (double bond); NMR($CDCl_3$): 5.96 (q, $J=7.0$ Hz, =CH- in angelate), 5.79 (d, $J=10.5$ Hz, 9-CH), 5.20 (d, $J=2.0$ Hz, 13-CH_2), ca 5.15 (m, 1-CH), 4.67 (t, $J=1.5$ Hz, 12-CH_2), 2.82 (dd, $J=5.0$, 10.5 Hz, 10-CH), 2.26, 1.93 (ABq, $J=14.0$ Hz, 6-CH_2), 1.93 (s, AcO), 1.80 (d, $J=7.0$ Hz, β-CH_3 in angelate), 1.78 (s, α-CH_3 in angelate), 1.13 (s, 15-CH_3), 0.90 (d, $J=7.0$ Hz, 14-CH_3).

Found: C, 67.62; H, 7.83%. Calcd for $C_{22}H_{30}O_6$: C, 67.67; H, 7.74%.

*Dihydrofukinolide (**2**)*: mp 125.0—126.0°C, colorless prisms (from light petroleum), $[\alpha]_D^{22}$ −105.5° (*c*, 1.0, MeOH); IR-(KBr): 1788 (γ-lactone), 1734, 1236 (ester), 3085, 1667, 909 cm^{-1} (double bond); UV: λ_{max}^{EtOH} end absorption; NMR-($CDCl_3$): 5.80 (d, $J=11.5$ Hz, 9-CH), 5.20 (t, $J=1.0$ Hz, 13-CH_2), 5.09 (m, 1-CH), 4.69 (t, $J=2.0$ Hz, 12-CH_2), 2.66 (dd, $J=5.5$, 11.5 Hz, 10-CH), 2.30, 1.71 (ABq, $J=14.0$ Hz, 6-CH_2), 2.07 (s, AcO), 1.12 (s, 15-CH_3), 1.07 (d, $J=6.5$ Hz, 3H), 0.94 (d, $J=6.5$ Hz, 14-CH_3), ca 0.90 (m, 3H); (C_6H_6): 5.87 (d, $J=11.0$ Hz, 9-CH), 5.18 (m, 1-CH), 4.90 (t, $J=0.5$ Hz, 13-CH), 4.70 (t, $J=0.5$ Hz, 13-CH), 4.32 (m, 12-CH_2), 2.84 (dd, $J=5.5$, 11.0 Hz, 10-CH), 2.19, 1.66 (ABq, $J=14.0$ Hz, 6-CH_2), 1.83 (s, AcO), 1.05 (d, $J=6.5$ Hz, 3H), 0.91 (d, $J=6.5$ Hz, 14-CH_3), 0.84 (s, 15-CH_3), 0.62 (m, 3H).

Found: C, 67.20; H, 8.26%. Calcd for $C_{22}H_{32}O_6$: C, 67.32; H, 8.22%.

*Homofukinolide (**3**)*: mp 184.0—186.0°C, colorless needles (from light petroleum), $[\alpha]_D^{22}$ −127.0° (*c*, 1.0, $CHCl_3$); IR-(KBr): 1773 (γ-lactone), 1723sh, 1708, 1233 (ester), 3080, 1668, 1648, 905, 850 cm^{-1} (double bond); (CCl_4): 1785 (γ-lactone), 1717, 1235 (ester), 3080, 1670sh, 1645, 902, 845 cm^{-1} (double bond); UV: λ_{max}^{EtOH} 215 mμ (ε, 23500); NMR($CDCl_3$): 6.13 (q, $J=8.0$ Hz, 2H, β-CH in angelate), 5.90 (d, $J=11.5$ Hz, 9-CH), 5.20 (d, $J=2.5$ Hz, 13-CH_2), 5.16 (m, 1-CH), 4.65 (t, $J=2.0$ Hz, 12-CH_2), 2.92 (dd, $J=4.5$, 11.5 Hz, 10-CH), 2.35, 1.97 (ABq, $J=14.0$ Hz, 6-CH_2), 1.95—1.70 (4×CH_3), 1.18 (s, 15-CH_3), 0.96 (d, $J=5.5$ Hz, 14-CH_3).

Found: C, 69.68; H, 8.05%. Calcd for $C_{25}H_{34}O_6$: C, 69.74; H, 7.96%.

*S-Fukinolide (**4**)*: mp 200.0—201.0°C, colorless needles (from light petroleum), $[\alpha]_D^{22}$ −161.0° (*c*, 1.0, $CHCl_3$); IR-(KBr): 1778 (γ-lactone), 1743, 1693, 1234 (ester), 3090, 1668, 1568, 903, 803 cm^{-1} (double bond); UV: λ_{max}^{EtOH} 287.5 mμ (ε, 15700); NMR($CDCl_3$): 7.00 (d, $J=9.5$ Hz, β-CH in an acid residue), 5.73 (d, $J=11.0$ Hz, 9-CH), 5.60 (d, $J=9.5$ Hz, α-CH in an acid residue), 5.16 (d, $J=2.0$ Hz, 13-CH_2), 5.15 (m, 1-CH), 4.64 (t, $J=2.0$ Hz, 12-CH_2), 2.77 (dd, $J=4.5$, 11.0 Hz, 10-CH), 2.38 (s, S-CH_3), 2.28, 1.91 (ABq, $J=14.0$ Hz, 6-CH_2), 2.01 (s, AcO), 1.12 (s, 15-CH_3), 0.90 (d, $J=5.5$ Hz, 14-CH_3).

Found: C, 62.09; H, 6.99; S, 8.04%. Calcd for $C_{21}H_{28}O_6S$: C, 61.74; H, 6.91; S, 7.83%.

*Fukinanolide (**5**)*: mp 80.5—80.6°C, colorless leaflets (from light petroleum), $[\alpha]_D^{22}$ +17.0° (*c*, 1.0, MeOH); IR-(KBr): 1770 (γ-lactone), 1665, 898 cm^{-1} (end-methylene); NMR($CDCl_3$): 5.11 (dd, $J=2.0$, 2.0 Hz, 13-CH), 5.02 (dd, $J=2.0$, 2.0 Hz, 13-CH), 4.75 (ABq, $J=2.0$ Hz, 12-CH_2), 1.00 (s, 15-CH_3), 0.87 (d, $J=6.0$ Hz, 14-CH_3).

Found: C, 76.94; H, 9.53%. Calcd for $C_{15}H_{22}O_2$: C, 76.88; H, 9.46%.

*Acid Hydrolysis of Fukinolide (**1**).* A mixture of fukinolide (**1**) (1.0 g) in ethanol (10 m*l*) and a 6N hydrogen chloride solution (10 m*l*) was refluxed for 2.5 hr. The reaction mixture was then poured into water and extracted with ether. The ethereal extract was washed with a saturated sodium hydrogen carbonate solution and water, dried over anhydrous sodium sulfate, and evaporated to dryness. The residue (850 mg) was chromatographed on silica gel (25 g); subsequent elution with benzene–ethyl acetate (50 : 1) gave the crude deacetylfukinolide (**7**) (540 mg), which was then recrystallized from light petroleum as colorless needles, mp 167.0—167.5°C, $[\alpha]_D^{22}$ −144.0° (*c*, 1.0, MeOH); IR(KBr): 3530, 3440, 1752, 1709, 1695, 1669, 1642, 1233, 895 cm^{-1}; NMR ($CDCl_3$): 6.18 (q, $J=7.0$ Hz, β-CH in angelate), 5.17 (t, $J=2.0$ Hz, 13-CH_2), *ca.* 5.20 (m, 1-CH, partly superimposed with 13-methylene), 4.86 (m, 12-CH_2), 4.58 (d, $J=10.5$ Hz, 9-CH), 2.75 (OH), 2.60 (dd, $J=5.0$, 10.5 Hz, 10-CH), 2.25, 1.94 (ABq, $J=14.0$ Hz, 6-CH_2), 1.94 (d, $J=7.0$ Hz, β-CH_3 in angelate), 1.85 (s, α-CH_3 in angelate), 1.11 (s, 15-CH_3), 0.90 (d, $J=5.5$ Hz, 14-CH_3).

Found: C, 68.68; H, 8.11%. Calcd for $C_{20}H_{28}O_5$: C, 68.94; H, 8.10%.

Further elution with benzene–ethyl acetate (5 : 1) gave fukinolidol (**8**) (75 mg), which was recrystallized from ethyl acetate–light petroleum as colorless prisms; mp 174.0—176.0 °C, $[\alpha]_D^{22}$ −79.0° (*c*, 1.0, MeOH).

22) N. Abe, R. Onoda, K. Shirahata, T. Kato, M. C. Woods, and Y. Kitahara, *Tetrahedron Lett.*, **1968**, 369; 11th Symposium on the Chemistry of Natural Products, Symposium Paper (1967), p. 96; N. Abe, R. Onoda, K. Shirahata, T. Kato, M. C. Woods, Y. Kitahara, K. Ro, and T. Kurihara, *Tetrahedron Lett.*, **1968**, 1993.

Found: C, 67.81; H, 8.53%. Calcd for $C_{15}H_{22}O_4$: C, 67.64; H, 8.33%. This is identical with the specimen of fukinolidol (**8**) obtained by the alkaline hydrolysis of fukinolide (**1**), as determined by a mixed-melting-point determination and a comparison of the IR spectra.

*Regeneration of Fukinolide (**1**).* Deacetylfukinolide (**7**) (50 mg) was acetylated in the usual manner with acetic anhydride-pyridine. The product (47 mg) was recrystallized from light petroleum as colorless prisms; mp 101.5—102.0°C, $[\alpha]_D^{22}$ −137.0° (*c*, 1.0, MeOH).

Found: C, 67.94; H, 7.88%. Calcd for $C_{22}H_{30}O_6$: C, 67.67; H, 7.74%. This was found to be identical with an authentic sample of natural fukinolide (**1**) by a mixed-melting-point determination and by a comparison of the IR spectra.

*Alkaline Hydrolysis of Fukinolide (**1**).* Fukinolide (**1**) (3 g) was dissolved in 2N potassium hydroxide-menthanol (20 m*l*), and the mixture was allowed to stand at room temperature for 3 days. After the removal of the solvent and acidification with 2N sulfuric acid, the reaction mixture was extracted with ethyl acetate. The extract was washed with a saturated sodium hydrogen carbonate solution and water, and dried over anhydrous sodium sulfate. The subsequent evaporation of the solvent gave fukinolidol (**8**) (1.54 g) (mp 176.5—177.5°C) as colorless prisms (from ethyl acetate-light petroleum). $[\alpha]_D^{22}$ −75.5° (*c*, 1.0, MeOH); IR(KBr): 3440 (OH), 1755 (γ-lactone), 3100, 1675, 910 cm^{-1} (double bond); NMR($CDCl_3$): 5.12 (t, *J*=2.0 Hz, 13-CH_2), 4.81 (m, 12-CH_2), 4.49 (d, *J*=11.0 Hz, 9-CH), 4.08 (m, 1-CH), 3.77 (2×OH), 2.55 (dd, *J*=5.5, 11.0 Hz, 10-CH), 2.14, 1.84 (ABq, *J*=14.5 Hz, 6-CH_2), 1.04 (s, 15-CH_3), 0.86 (d, *J*=5.0 Hz, 14-CH_3); (pyridine): 5.60 (s, 2H), 5.08 (d, *J*=3.0 Hz, 2H), 4.84 (m, 2H), 4.67 (d, *J*=11.0 Hz, 1H), ca 4.15 (m, 1H), 2.80 (dd, *J*=6.0, 11.0 Hz, 1H), 2.17, 1.81 (ABq, *J*=14.5 Hz, 2H), 0.97 (s, 3H), 0.77 (d, *J*=6.0 Hz, 3H).

Found: C, 67.42; H, 8.42%. Calcd for $C_{15}H_{22}O_4$: C, 67.64; H, 8.33%.

The above sodium hydrogen carbonate solution was acidified with 2N sulfuric acid and extracted with ether. The extract was washed with water and dried. The solvent was removed to give a residue (600 mg). The residue (200 mg) was then transformed to the *p*-phenylphenacyl ester in the usual manner, using *p*-phenylphenacyl bromide (356 mg). The product was chromatographed on silica gel (10 g); subsequent elution with light petroleum-ether (50 : 1) gave *p*-phenylphenacyl angelate (104 mg) (mp 89.5—90.5°C) as leaflets (from ethanol).

Found: C, 77.52; H, 6.19%. Calcd for $C_{19}H_{18}O_3$: C, 77.53; H, 6.16%.

The *p*-bromophenacyl ester of angelic acid was obtained in a similar manner (mp 64.0—66.0°C) as leaflets (from ethanol).

Found: C, 52.32; H, 4.34%. Calcd for $C_{13}H_{13}O_3Br$: C, 52.54; H, 4.41%.

*Acetylation of Fukinolidol (**8**).* Fukinolidol (**8**) (100 mg) was dissolved in acetic anhydride (1 m*l*) and pyridine (0.5 m*l*), and the mixture was left at room temperature for 48 hr. The reaction mixture was then worked up in the usual manner to give, quantitatively, crude diacetate (**12**) as an amorphous solid which was crystallized from ethanol as prisms; mp 224.5—226.0°C, $[\alpha]_D^{22}$ −120.0° (*c*, 1.0, $CHCl_3$); IR(KBr): 3080, 1773, 1746, 1741, 1668, 1241, 1231, 913 cm^{-1}; NMR($CDCl_3$): 5.78 (d, *J*=11.0 Hz, 9-CH), 5.20 (m, 13-CH_2), 5.00 (m, 1-CH), 4.68 (t, *J*=2.0 Hz, 12-CH_2), 2.71 (dd, *J*=5.0, 11.0 Hz, 10-CH), 2.27, 1.93 (ABq, *J*=14.0 Hz, 6-CH_2), 2.06 (s, AcO), 1.94 (s, AcO), 1.11 (s, 15-CH_3), 0.90 (d, *J*=5.5 Hz, 14-CH_3).

Found: C, 65.06; H, 7.50%. Calcd for $C_{19}H_{26}O_6$: C, 65.12; H, 7.48%.

*Dihydrofukinolidol (**10**).* A solution of fukinolide (**1**) (10.7 g) in acetic acid (30 m*l*) was hydrogenated with Adams' catalyst (626 mg) at room temperature. Hydrogen uptake (2 mol) ceased after 3 hr. After the filtration of the catalyst, the solvent was removed *in vacuo* to give crude tetrahydrofukinolide (**9**), which was used for the next step without any further purification. A solution of the above product in 2N potassium hydroxide-methanol was allowed to stand at room temperature for 2 days. The solvent was then removed, and the residue was diluted with water, and extracted with ether to take off the neutral part. The aqueous layer was acidified with 5N sulfuric acid and extracted with ethyl acetate. The extract was washed with a saturated sodium hydrogen carbonate solution and water, and then dried. The solvent was removed to give dihydrofukinolidol (**10**) (5.6 g); mp 190.0—191.0°C, colorless prisms (from ethyl acetate-light petroleum), $[\alpha]_D^{22}$ −14.5° (*c*, 1.0, MeOH); IR(KBr): 3525, 3445, 1766 cm^{-1}; NMR($CDCl_3$): 4.60 (d, *J*=11.0 Hz, 9-CH), 4.23 (t, *J*=8.5 Hz, 12-CH), 4.12 (m, 1-CH), 3.92 (dd, *J*=8.5, 10.0 Hz, 12-CH), 3.19 (s, 2×OH), 2.55 (dd, *J*=5.5, 11.0 Hz, 10-CH), 2.01, 1.49 (ABq, *J*=14.0 Hz, 6-CH_2), 1.13 (d, *J*=7.0 Hz, 13-CH_3), 1.03 (s, 15-CH_3), 0.80 (d, *J*=4.5 Hz, 14-CH_3); (C_6H_6): 4.54 (d, *J*=11.0 Hz, 1H), ca 4.0 (m, 1H), 3.92 (m, 2H), 3.78 (s, 2H), 2.79 (dd, *J*=5.5, 11.0 Hz, 1H), 1.97, 1.23 (ABq, *J*=14.0 Hz, 2H), 0.99 (s, 3H), 0.79 (d, *J*=7.0 Hz, 3H), 0.61 (d, *J*=5.0 Hz, 3H).

Found: C, 67.12; H, 9.20%. Calcd for $C_{15}H_{24}O_4$: C, 67.13; H, 9.02%.

*Reduction of Fukinolide (**1**) with Lithium Aluminum Hydride.* A solution of fukinolide (**1**) (600 mg) in dry ether (20 m*l*) was stirred, drop by drop, into a suspension of lithium aluminum hydride (280 mg) in dry ether (30 m*l*), and then the mixture was refluxed for 5 hr. The excess reagent was destroyed by the careful addition of ethyl acetate and water, followed by treatment with a saturated sodium sulfate solution. The organic layer was separated, and the aqueous layer was extracted with ether. The combined extracts were washed with water, and dried. The solvent was removed to leave an oily residue (543 mg), which was then chromatographed on silica gel (8 g). Elution with ethyl acetate-benzene (3 : 2) gave a tetrol (**13**) (300 mg); mp 106.0—107.0°C, $[\alpha]_D^{22}$ −14.0° (*c*, 1.0, MeOH); IR(KBr): 3390, 3275, 1649, 906 cm^{-1}; NMR($CDCl_3$): 5.28 (d, *J*=5.0 Hz, 13-CH_2), 4.86 (d, *J*=11.0 Hz, 9-CH), 4.23 (slightly split s, 12-CH_2), 4.00 (m, 1-CH), 3.84, 3.51 (ABq, *J*=11.0 Hz, 8-CH_2), 3.56 (s, 4×OH), 2.20 (dd, *J*=5.5, 11.0 Hz, 10-CH), 2.00, 1.34 (ABq, *J*=14.0 Hz, 6-CH_2), 0.91 (s, 15-CH_3), 0.76 (d, *J*=4.0 Hz, 14-CH_3); (pyridine): 0.87 (s, 15-CH_3), 0.67 (d, *J*=5.0 Hz, 14-CH_3).

Found: C, 66.96; H, 9.74%. Calcd for $C_{15}H_{26}O_4$: C, 66.63; H, 9.69%.

Tetrol-acetate. Tetrol (**13**) (65 mg) was acetylated with acetic anhydride (0.3 m*l*) and pyridine (0.2 m*l*) at room temperature for 40 hr. Working up in the usual manner gave the tetraacetate (95 mg) as a viscous oil; IR(film): 3090, 1742, 1642, 1245, 907 cm^{-1}; NMR($CDCl_3$): 6.10 (d, *J*=10.5 Hz, 9-CH), 5.38 (d, *J*=8.0 Hz, 13-CH_2), 5.05 (m, 1-CH), 4.10 (slightly split s, 12-CH_2), 4.20, 3.95 (ABq, *J*=11.5 Hz, 8-CH_2), 2.08 (s, 1×AcO), 2.03 (s, 2×AcO), 1.96 (s, 1×AcO), 1.00 (s, 15-CH_3), 0.80 (d, *J*=5.0 Hz, 14-CH_3).

*Reduction of Fukinolidol Diacetate (**11**) with Lithium Aluminum Hydride.* A solution of fukinolidol diacetate (**11**) (380 mg) in dry ether (45 m*l*) and dry benzene (5 m*l*) was stirred into a suspension of lithium aluminum hydride (310 mg) in dry ether (10 m*l*). After refluxing for 7 hr, working up as above afforded a crude tetrol (**13**) (84 mg). This was chro-

matographed on silica gel (5 g) and eluted with ethyl acetate-benzene (3 : 2). Mp 106.0—107.0°C, colorless leaflets (from ethyl acetate-light petroleum).

Found: C, 66.62; H, 9.51%. Calcd for $C_{15}H_{26}O_4$: C, 66.63; H, 9.69%.

This substance is identical with the tetrol (**13**) described above.

*Hydrogenation of Tetrol (**13**).* A solution of tetrol (**13**) (690 mg) in ethanol (5 m*l*) was shaken with hydrogen at room temperature in the presence of 10% palladium charcoal (68 mg) for 4 hr, until the hydrogen-uptake (1.37 mol) had ceased. After the subsequent filtration of the catalyst, the solvent was removed *in vacuo* to leave an oily residue (700 mg). The crude product was chromatographed on silica gel (20 g); elution with benzene-ethyl acetate (15 : 1) then gave triol (**14**); mp 88.5—89.5°C, colorless needles (from cyclohexane); $[\alpha]_D^{22}$ −5.5° (*c*, 1.0, MeOH); IR(KBr): 3430, 3330, 1386, 1370, 1088, 1047 cm^{-1}; NMR($CDCl_3$): 4.58 (d, J=11.0 Hz, 9-CH), 4.10 (m, 1-CH), 3.80, 3.54 (ABq, J=11.5 Hz, 8-CH_2), 3.30 (s, 3×OH), 2.78 (dd, J=5.5, 11.0 Hz, 10-CH), 1.88, 1.47 (ABq, J=10.5 Hz, 6-CH_2), 1.07 (d, J=6.5 Hz, 12- or 13-CH_3), 0.97 (d, J=6.5 Hz, 12- or 13-CH_3), 0.90 (s, 15-CH_3), 0.77 (d, J=5.0 Hz, 14-CH_3).

Found: C, 70.91; H, 11.25%. Calcd for $C_{15}H_{28}O_3$: C, 70.27; H, 11.01%.

*Oxidation of Deacetylfukinolide (**7**).* Jones' reagent (1.9 m*l*) was added to a solution of deacetylfukinolide (**7**) (1.0 g) in acetone (15 m*l*) under ice-salt cooling at −8— −12°C over a period of 3 hr with stirring. After stirring for a further 4 hr under the same conditions, the mixture was concentrated *in vacuo* and extracted with ether. The extract was washed with water and dried. The solvent was then removed to give a crude product (880 mg), which was subsequently crystallized from light petroleum to yield the pure ketone (**15**) (320 mg) as colorless needles; mp 96.0—97.0°C, $[\alpha]_D^{22}$ −110° (*c*, 1.0, MeOH), ORD (*c*, 0.1, MeOH): $[\alpha]_{589}$ −90°, $[\alpha]_{380}$ −220°, $[\alpha]_{342}$ 0°, $[\alpha]_{323}$ +1340°, $[\alpha]_{312}$ 0°; (*c*, 0 01, MeOH): $[\alpha]_{268}$ −5800°, $[\alpha]_{262}$ −5600°, $[\alpha]_{226}$ −12400°; IR(KBr): 3095, 1770, 1751, 1715, 1672, 1646, 1239, 902 cm^{-1}; NMR($CDCl_3$): 6.08 (q, J=7.0 Hz, β-CH in angelate), 5.22 (d, J=2.5 Hz, 13-CH), *ca.* 5.05 (m, 1-CH), 5.00 (d, J=2.5 Hz, 12-CH_2), 4.86 (d, J=2.5 Hz, 13-CH), 3.02 (d, J=5.0 Hz, 10-CH), 2.46, 2.17 (ABq, J=14.0 Hz, 6-CH_2), 1.96 (d, J=7.0 Hz, β-CH_3 in angelate), 1.90 (s, α-CH_3 in angelate), 1.23 (s, 15-CH_3), 0.98 (d, J=2.0 Hz, 14-CH_3).

Found: C, 69.47; H, 7.38%. Calcd for $C_{20}H_{26}O_5$: C, 69.34; H, 7.57%.

*Oxidation of Fukinolidol (**8**).* A solution of chromium trioxide (235 mg) in water (0.55 m*l*) and concentrated sulfuric acid (0.16 m*l*) was stirred, drop by drop over a 1-hr period, into a solution of fukinolidol (**8**) (560 mg) in acetone (3.5 m*l*) under a nitrogen atmosphere at 5°C. After stirring for a further 30 min, the reaction mixture was worked up as has been described above to yield a crude product (376 mg). Recrystallization from ethyl acetate-light petroleum gave monoketone (**16**) as colorless leaflets; mp 141.5—142.0°C, $[\alpha]_D^{22}$ −232° (*c*, 1.0, MeOH); ORD (*c*, 0.10, MeOH): $[\alpha]_{598}$ −170°, $[\alpha]_{315}$ −5000°, $[\alpha]_{296}$0°, $[\alpha]_{276}$+3670°, $[\alpha]_{250}$0°; (*c*, 0.005, MeOH): $[\alpha]_{228}$−8220°, $[\alpha]_{219}$0°; IR(KBr): 3490, 3365, 3085, 1773, 1755, 1680, 1675sh, 1666sh, 1190, 1162, 1096, 920, 913 cm^{-1}; NMR($CDCl_3$): 5.20 (t, J=2.0 Hz, 13-CH_2), 4.78 (m, 12-CH_2), 4.38 (d, J=11.0 Hz, 9-CH), *ca.* 3.5 (broad signal, OH), 2.86 (d, J=11.0 Hz, 10-CH), 1.00 (s, 15-CH_3), 0.97 (d, J=5.5 Hz, 14-CH_3).

Found: C, 68.20; H, 7.65%. Calcd for $C_{15}H_{20}O_4$: C, 68.16; H, 7.63%.

*Acetate (**19**).* The above monoketone (**16**) (50 mg) was acetylated with acetic anhydride (0.2 m*l*) and pyridine (0.2 m*l*) at room temperature for 50 hr. Working up in the usual manner gave an oil (42 mg), which was then chromatographed on silica gel (5 g); subsequent elution with benzene afforded the acetate (**19**) (24 mg), mp 132.5—133.0 °C, $[\alpha]_D^{24}$ −210° (*c*, 1.0, $CHCl_3$); IR(KBr): 1770, 1744, 1698, 918 cm^{-1}; NMR($CDCl_3$): 5.50 (d, J=11.0 Hz, 9-CH), 5.28 (d, J=2.7 Hz, 13-CH_2), 4.72 (t, J=3.0 Hz, 12-CH_2), 3.01 (d, J=11.0 Hz, 10-CH), 1.98 (s, AcO), 1.05 (s, 15-CH_3), 0.98 (d, J=6.0 Hz, 14-CH_3).

Found: C, 66.75; H, 7.31%. Calcd for $C_{17}H_{22}O_5$: C, 66.65; H, 7.24%.

*2,4-Dinitrophenylhydrazone of Monoketone (**16**).* The 2,4-dinitrophenylhydrazone was prepared by Brady's method and crystallized from aqueous ethanol as yellow needles; mp 220.0—221.0°C.

Found: C, 56.63; H, 5.45; N, 12.50%. Calcd for $C_{21}H_{24}O_7N_4$: C, 56.75; H, 5.44; N, 12.61%.

Dehydration of Monoketone 2,4-Dinitrophenylhydrazone. The above 2,4-dinitrophenylhydrazone (20 mg) in ethanol was refluxed with 85% phosphoric acid (3 drops) for 10 hr. The reaction mixture was concentrated *in vacuo*, poured into water, and extracted with ether. The extract was washed with a saturated sodium hydrogen carbonate solution and water, and dried. The subsequent evaporation of the solvent gave a crude product which was chromatographed on silica gel (3 g). Elution with benzene gave a dehydration product (**24**) (13 mg), which was then crystallized from ethanol as orange-red needles; mp 209.5—210.0°C; IR(KBr): 3090, 1775, 1673 cm^{-1}; NMR($CDCl_3$): 11.18 (m, 1H), 9.11 (d, J=2.5 Hz, 1H), 8.30 (dd, J=2.5, 9.5 Hz, 1H), 8.01 (d, J=9.5 Hz, 1H), 5.80 (s, 9-CH), 5.14 (m, 13-CH_2), 4.89 (t, J=2.0 Hz, 12-CH_2), 2.52, 1.95 (ABq, J=14.0 Hz, 6-CH_2), 1.28 (s, 15-CH_3), 0.97 (d, J=6.0 Hz, 14-CH_3).

Found: C, 59.02; H, 5.20%. Calcd for $C_{21}H_{22}O_6N_4$: C, 59.15; H, 5.20%.

*Oxidation of Dihydrofukinolidol (**10**).* A solution of chromium trioxide (1.44 g) in acetone (21 m*l*), water (3.3 m*l*) and concentrated sulfuric acid (1 m*l*) was stirred, drop by drop over 70 min under a nitrogen atmosphere at 3—5°C, into a solution of dihydrofukinolidol (**10**) (2.91 g) in acetone (35 m*l*). After stirring for a further 20 min, the excess reagent was decomposed with methanol (3 m*l*), diluted with water, and extracted with ether. The extract was washed with a 5% potassium hydroxide solution and then water, and dried. The removal of the solvent gave a crude product as a solid (2.4 g). The product was chromatographed on silica gel (80 g); subsequent elution with benzene-ethyl acetate (9 : 1) gave dihydromonoketone (**17**) (1.8 g); mp 184.0—186.0°C, colorless prisms (from acetone-light petroleum), $[\alpha]_D^{22}$ −79.0°(*c*, 1.0, MeOH); ORD (*c*, 0.1, MeOH): $[\alpha]_{589}$ −60°, $[\alpha]_{315}$ −2100°, $[\alpha]_{297}$0°, $[\alpha]_{275}$+2100°, $[\alpha]_{236}$+690°, $[\alpha]_{220}$+2100°; IR(KBr): 3350, 1767, 1680 cm^{-1}, (CCl_4): 3540, 1765, 1690 cm^{-1}; NMR($CDCl_3$): 4.36 (d, J=11.0 Hz, 9-CH), 4.33 (t, J=8.5 Hz, 12-CH), 4.02 (dd, J=8.5, 10.0 Hz, 12-CH), 2.90 (d, J=11.0 Hz, 10-CH), 2.80 (OH), 1.97, 1.61 (ABq, J=14.0 Hz, 6-CH_2), 1.21 (s, 15-CH_3), 1.15 (d, J=6.5 Hz, 13-CH_3), 0.93 (d, J=5.5 Hz, 14-CH_3).

Found: C, 67.71; H, 8.41%. Calcd for $C_{15}H_{22}O_4$: C, 67.64; H, 8.33%.

*Acetate (**20**).* Dihydromonoketone (**17**) (140 mg) in pyridine (0.4 m*l*) was treated with acetic anhydride (0.5 m*l*) at room temperature for 32 hr. Working up in the usual manner yielded the acetate (**20**) (120 mg); mp 158.5—159.5°C, colorless needles (from ethyl acetate-light petroleum), $[\alpha]_D^{22}$ −93° (*c*, 1.0, MeOH); IR(KBr): 1764, 1738, 1696 cm^{-1}; NMR($CDCl_3$): 5.67 (d, J=11.0 Hz, 9-CH), 4.38

(t, J=8.5 Hz, 12-CH), 3.73 (dd, J=8.5, 10.5 Hz, 12-CH), 2.94 (d, J=11.0 Hz, 10-CH), 1.98 (s, AcO), 1.16 (d, J=6.0 Hz, 13-CH_3), 1.07 (s, 15-CH_3), 0.97 (d, J=6.0 Hz, 14-CH_3).

Found: C, 65.93; H, 7.88%. Calcd for $C_{17}H_{24}O_5$: C, 66.21; H, 7.85%.

*Reduction of Dihydromonoketone Acetate (**20**) with Sodium Borohydride.* The acetate (**20**) (370 mg) in methanol (3 ml) was treated with sodium borohydride (200 mg) in methanol (7 ml) at room temperature for 19 hr. The reaction mixture was then diluted with water (3 ml) and allowed to stand at room temperature for 24 hr. Working up in the usual manner gave a solid (320 mg), which was subsequently crystallized from ethyl acetate; mp 190.0—191.0°C, colorless prisms, $[\alpha]_D^{22}$ −14.0° (*c*, 1.0, MeOH).

Found: C, 67.33; H, 9.01%. Calcd for $C_{15}H_{24}O_4$: C, 67.13; H, 9.02%.

The above substance was found to be identical in all respects with the dihydrofukinolidol (**10**) obtained from tetrahydrofukinolide (**9**) by mixed-melting-point determination and a comparison of the IR spectra.

*Oxidation of Epidihydrofukinolidol (**11**).* Jones' reagent (2.2 ml) was stirred, over a 45-min period at −15°C under a nitrogen atmosphere, into a solution of epidihydrofukinolidol (**11**) (1.0 g) in acetone (15 ml). After stirring for a further 30 min under the same conditions, the reaction mixture was treated with a little methanol and concentrated *in vacuo*. Extraction with chloroform gave ketone (**18**) (850 mg), which was then crystallized from ethyl acetate–light petroleum; mp 137.0—138.0°C, colorless needles, $[\alpha]_D^{22}$ −125° (*c*, 1.0, MeOH); ORD (*c*, 0.108, MeOH): $[\alpha]_{589}$ −140°, $[\alpha]_{400}$ −440°, $[\alpha]_{350}$ −880°, $[\alpha]_{311}$ −2580°, $[\alpha]_{293}$0°, $[\alpha]_{274}$+1680°, $[\alpha]_{232}$+690°, $[\alpha]_{220}$+790°; IR(KBr): 3470sh, 3405, 1755, 1714, 1689sh, 1680 cm^{-1}; NMR($CDCl_3$): 4.53 (dd, J=7.0, 8.5 Hz, 12-CH), 4.34 (dd, J=6.0, 11.0 Hz, 9-CH), 3.80 (dd, J=7.0, 9.5 Hz, 12-CH), 3.31 (d, J=6.0 Hz, OH), 2.87 (d, J=11.0 Hz, 10-CH), 1.99, 1.70 (ABq, J=14.0 Hz, 6-CH_2), 1.13 (s, 15-CH_3), 1.11 (d, J=7.0 Hz, 13-CH_3), 0.95 (d, J=6.0 Hz, 14-CH_3).

Found: C, 67.81; H, 8.46%. Calcd for $C_{15}H_{22}O_4$: C, 67.64; H, 8.33%.

*Dehydration of Dihydromonoketone (**17**).* The ketone (**17**) (120 mg) in pyridine (1.0 ml) was treated with phophorus oxychloride (0.4 ml) at room temperature for 30 hr. The reaction mixture was poured onto ice and extracted with ether. The extract was washed successively with dilute hydrochloric acid, a saturated sodium hydrogen carbonate solution and water, and dried. The removal of the solvent gave a crude product (90 mg) which was chromatographed on silica gel (5 g). Elution with benzene–ethyl acetate (50 : 1) afforded the dehydration product, **23** (80 mg); mp 103.0—103.5°C, colorless needles (from light petroleum); $[\alpha]_D^{22}$ −36° (*c*, 1.0, MeOH); ORD (*c*, 0.09, MeOH): $[\alpha]_{589}$ −70°, $[\alpha]_{360}$ −920°, $[\alpha]_{335}$0°, $[\alpha]_{310}$+1220°, $[\alpha]_{282}$0°; (*c*, 0.009, MeOH): $[\alpha]_{262}$ −1330°, $[\alpha]_{254}$0°, $[\alpha]_{232}$+20440°; IR(KBr): 1776, 1681, 1629 cm^{-1}; λ_{max}^{EtOH} 250 mμ (ε, 7100); NMR($CDCl_3$): 6.07 (s, 9-CH), 4.45 (dd, J=8.5, 9.5 Hz, 12-CH), 3.93 (t, J=9.5 Hz, 12-CH), 2.38, 1.79 (ABq, J=14.0 Hz, 6-CH_2), 1.24 (s, 15-CH_3), 1.00 (d, J=7.0 Hz, 13- and 14-CH_3).

Found: C, 72.54; H, 8.23%. Calcd for $C_{15}H_{20}O_3$: C, 72.55; H, 8.12%.

*Tosylation of Fukinolidol (**8**).* Fukinolidol (**8**) (2 g) was treated with *p*-toluenesulfonyl chloride (6.3 g) in pyridine (10 ml) and left for 72 hr at room temperature. The reaction mixture was diluted with water to deposit a solid. The collected precipitates (4.3 g) were chromatographed on silica gel (50 g); subsequent elution with benzene–ethyl acetate (30 : 1) gave ditosylate (**27**) (3.5 g); mp 179.5—180.0°C decomp., colorless prisms (from ethyl acetate–light petroleum); IR(KBr): 3060, 1774, 1673, 1600, 1498, 1179, 923 cm^{-1}.

Found: C, 60.65; H, 5.91; S, 11.19%. Calcd for $C_{29}H_{34}O_8S_2$: C, 60.60; H, 5.94; S, 11.16%.

*Reduction of Ditosylate (**27**) with Lithium Aluminum Hydride.* Ditosylate (**27**) (4.05 g) in dry tetrahydrofuran (30 ml) was added, drop by drop over a 2-hr period under refluxing, to a suspension of lithium aluminum hydride (3.0 g) in dry tetrahydrofuran (20 ml). After refluxing for 20 hr, the excess reagent was decomposed with tetrahydrofuran–water (1 : 1, 14 ml) and diluted with water (30 ml), and then 6N sulfuric acid (40 ml) was added. This mixture was extracted with ether to give an oily product (1.64 g). The chromatography of the product on silica gel (60 g) and elution with benzene–ethyl acetate (50 : 1) gave a fraction (422 mg) as the main product on tlc; this product was crystallized from light petroleum to afford diol (**28**); mp 119.5—120.0°C, colorless needles; IR(KBr): 3290, 1642, 1068, 1037, 1028, 901, 882 cm^{-1}; λ_{max}^{EtOH} 237 mμ (ε, 18700); NMR($CDCl_3$): 6.21 (d, J=9.5 Hz, 1-CH), 5.75 (dt, J=9.5, 2.0 Hz, 2-CH), 5.50 (s, 9-CH), 5.11 (d, J=9.0 Hz, 13-CH_2), 4.15 (s, 12-CH_2), 3.73 (s, 8-CH_2), 2.85 (2×OH), 2.02, 1.68 (ABq, J=11.0 Hz, 6-CH_2), 1.00 (s, 15-CH_3), 0.91 (d, J=6.0 Hz, 14-CH_3).

Found: C, 76.82; H, 9.52%. Calcd for $C_{15}H_{22}O_2$: C, 76.88; H, 9.46%.

*Hydrogenation of Diol (**28**).* A solution of diol (**28**) (631 mg) in ethanol was hydrogenated over 10% palladium charcoal (303 mg) at room temperature until the hydrogen-uptake had ceased (2.08 mol). After working up as usual, the chromatography of the crude product (509 mg) on silica gel (10 g) and elution with benzene–ethyl acetate (50 : 1) gave a fraction, an unsaturated monol (**29**) (110 mg) which showed the existence of an ethylenic linkage in the IR and NMR spectra; IR(film): 3330, 1662, 1380, 1365, 1038 cm^{-1}; NMR(CCl_4): 4.95 (s, 9-CH), 3.38 (s, 8-CH_2), 2.85 (s, OH), 0.93 (d, J=6.0 Hz, 12- and 13-CH_3), 0.88 (s, 15-CH_3), 0.82 (d, J=6.0 Hz, 14-CH_3).

The above sample in acetic acid (5.0 ml) was further hydrogenated with Adams' catalyst (20 mg) by the standard method. Working up as usual gave a monol, fukinan-8-ol (**26**), which was then purified by preparative glc (PEG 6000, 2.6 m; column temperature, 180°C; H_2, flow-rate, 150 ml/min), mp 38.0—39.0°C, $[\alpha]_D^{22}$+15.6° (*c*, 1.6, MeOH); IR(KBr): 3300, 1387, 1375, 1049, 1041, 1023 cm^{-1}; NMR(CCl_4): 3.37 (s, 8-CH_2), 2.71 (OH), 0.89 (d, J=6.0 Hz, 12- and 13-CH_3), 0.84 (s, 15-CH_3), 0.75 (d, J=6.5 Hz, 14-CH_3).

Found: C, 80.23; H, 12.66%. Calcd for $C_{15}H_{28}O$: C, 80.29; H, 12.58%.

*Favorskii Rearrangement of Fukinone Epoxide (**30**).* A solution of fukinone (**25**) (9.92 g) in methanol (300 ml) was treated with a mixture of 30% hydrogen peroxide (70 ml) and 2N sodium hydroxide–methanol (70 ml) at room temperature. After the removal of the solvent under reduced pressure, the mixture was diluted with water and extracted with ether to give a colorless oil, **30** (10.03 g); IR(film): 1722 cm^{-1}.

The above epoxide (**30**) in ethanol (42 ml) was refluxed with a 4N sodium hydroxide solution (34 ml) under a nitrogen atmosphere for 11 hr. The reddish-brown solution was then concentrated *in vacuo* and extracted with ether to remove the neutral part. The aqueous layer was acidified under ice-cooling with dilute sulfuric acid and then extracted with ether. The product was separated into neutral and acidic parts. The acidic part was treated with diazomethane-etherate overnight at room temperature, and then the reac-

tion mixture was evaporated to leave a yellow oil (8.12 g). Chromatography of the oil on silica gel (240 g) and elution with benzene-ethyl acetate (100 : 1) gave a spiro-ester, **35** (2.26 g, tlc: R_f, 0.37, benzene-ethyl acetate, 20 : 1); mp 63.5—64.5°C, colorless needles (from *n*-pentane), $[\alpha]_D^{22}$ +23.5° (*c*, 1.0, MeOH); IR(KBr): 3480, 1725, 1705, 1195, 1150 cm^{-1}; NMR(CCl_4): 3.68 (s, CH_3O-CO), 3.07 (s, OH), 1.13 (slightly split s, 12- and 13-CH_3), 0.88 (s, 15-CH_3), 0.77 (d, J=6.5 Hz, 14-CH_3).

Found: C, 80.23; H, 12.66%. Calcd for $C_{16}H_{28}O_3$: C, 80.29; H, 12.58%.

Further elution with the same solvent afforded a nonspiro-ester, **36**[16] (3.78 g, tlc: R_f, 0.18, benzene-ethyl acetate, 20 : 1), mp 52.0—54.0°C, colorless needles (from aqueous methanol), $[\alpha]_D^{22}$ +14.0° (*c*, 1.0, MeOH); IR(KBr): 3560, 3250, 1735, 1725, 1190 cm^{-1}.

*Dehydration of the **35** Ester.* A solution of the **35** ester (2.26 g) in dry pyridine (7 m*l*) was treated with phosphorus oxychloride (7.7 m*l*) under cooling and then left at room temperature for 46 hr. The mixture was subsequently poured onto ice and extracted with ether. After working up as usual, the product was chromatographed on silica gel (38 g); elution with light petroleum gave an unsaturated ester **37** (1.776 g); bp 87.0—95.0°C (bath temperature)/1 mmHg; IR(film): 1720, 1630 cm^{-1}; NMR(CCl_4): 4.77 (d, J=6.0 Hz, 12-CH_2), 3.59 (s, CH_3O-CO), 1.68 (s, 13-CH_3), 0.90 (s, 15-CH_3), 0.78 (d, J=6.0 Hz, 14-CH_3).

Found: C, 76.71; H, 10.57%. Calcd for $C_{16}H_{26}O_2$: C, 76.75; H, 10.47%.

*Hydrogenation of the Unsaturated Ester (**37**).* The above ester in ethanol (13 m*l*) was hydrogenated with 10% palladium charcoal (70 mg) at room temperature and atmospheric pressure to afford a saturated ester **38** as an oil; bp 66.0—86.0°C (bath temperature)/1 mmHg; $[\alpha]_D^{22}$ +23.8° (*c*, 1.51, MeOH); IR(film): 1720, 1235, 1180, 1141 cm^{-1}. The pure sample was obtained by glc (PEG 6000, 2.8 m; column temperature, 150°C; H_2-flow rate, 67 m*l*/min, retention time 10.7 min).

Found: C, 76.57; H, 11.16%. Calcd for $C_{16}H_{28}O_2$: C, 76.14; H, 11.18%.

*Reduction of the Saturated Ester (**38**) with Lithium Aluminum Hydride to Fukinan-8-ol (**26**).* The above ester (**38**) (1.7 g) in dry ether (15 m*l*) was stirred, drop by drop over a 50 min period at room temperature, to a suspension of lithium aluminum hydride (800 mg) in dry ether (20 m*l*), and then the mixture was refluxed for 2 hr. Working up as usual gave a colorless oil (1.51 g) which was subsequently purified by preparative glc (PEG 6000, 2.6 m; column temperature, 180°C; H_2-flow rate, 150 m*l*/min), mp 38.0—39.0°C, $[\alpha]_D^{22}$ +18.5° (*c*, 1.6, MeOH); MS: *m/e* 206 (M^+—18), 193 (base peak). This sample was identical in all respects with the fukinan-8-ol (**26**) prepared from fukinolide (**1**) and fukinanolide (**5**).

*Alkaline Hydrolysis of Dihydrofukinolide (**2**).* Dihydrofukinolide (**2**) (800 mg) was dissolved in 2 N potassium hydroxide-methanol (30 m*l*), and then the mixture was left for 90 hr at room temperature. After removal of the solvent and acidification with 2 N sulfuric acid, the reaction mixture was extracted with chloroform, and the extract washed with a saturated sodium hydrogen carbonate solution and then water. The dried extract was evaporated *in vacuo* to give fukinolidol (**8**) (340 mg); colorless prisms (from ethyl acetate), mp 177.0—178.0°C; $[\alpha]_D^{22}$ −83.0° (*c*, 1.0, MeOH).

Found: C, 67.74; H, 8.33%. Calcd for $C_{15}H_{22}O_4$: C, 67.64; H, 8.33%. This sample was identified with the authentic sample of fukinolidol (**8**) obtained from fukinolide (**1**) by a comparison of their IR spectra and by a mixed-melting-point determination.

The sodium hydrogen carbonate solution was acidified with dilute sulfuric acid and extracted with ether. The acidic extract was transformed to the *p*-phenylphenacyl esters in the usual way and gave a product. This was chromatographed on silica gel; subsequent elution with light petroleum-ether (50 : 1) afforded the *p*-phenylphenacyl ester of *d*-(S)-α-methylbutyric acid (**40**);[19] colorless needles, mp 71.0—72.0°C (from ethanol), $[\alpha]_D^{22}$ +16.5° (*c*, 1.0, $CHCl_3$); IR(KBr): 1746, 1694, 1605, 1244, 1183, 1158 cm^{-1}.

Found: C, 77.01; H, 6.84%. Calcd for $C_{19}H_{20}O_3$: C, 77.00; H, 6.80%.

*Hydrogenation of Dihydrofukinolide (**2**).* Dihydrofukinolide (**2**) (100 mg) was dissolved in ethanol (6 m*l*) and hydrogenated with 10% palladium charcoal (20 mg) at room temperature. After hydrogen-uptake (2 mol), the filtrate was evaporated *in vacuo* to furnish tetrahydrofukinolide (**41**) (95 mg); mp 116.5—117.0°C, colorless needles (from aqueous methanol); $[\alpha]_D^{22}$ −51.0° (*c*, 1.0, MeOH); IR(CCl_4): 1785 (γ-lactone), 1741, 1721sh, 1244 cm^{-1} (ester), (KBr): 1783 (γ-lactone), 1735, 1236 cm^{-1} (ester).

Found: C, 67.25; H, 8.65%. Calcd for $C_{22}H_{34}O_6$: C, 66.98; H, 8.69%. This sample was found to be identical with the lower-melting isomer (**41**) of tetrahydrofukinolide (**9**) obtained by the hydrogenation of fukinolide (**1**) by a mixed-melting-point determination and by a comparison of the IR spectra.

*Hydrogenation of Fukinolide (**1**).* Fukinolide (**1**) (200 mg) was hydrogenated with platinum oxide (20 mg) in acetic acid (10 m*l*) at room temperature. Hydrogen-uptake (25 m*l*, 2 mol) ceased after 45 min. The catalyst was then filtered off, and the solvent was evaporated *in vacuo* to afford a crystalline mass. The product was recrystallized from light petroleum to deposit a mixture of two crystals, each of which was separated mechanically and recrystallized from aqueous methanol.

One isomer (**41**) (50 mg) was in the form of colorless needles; mp 112.0—113.0°C, $[\alpha]_D^{24}$ −52.25° (*c*, 0.95, MeOH); IR(CCl_4): 1785 (γ-lactone), 1741, 1244 cm^{-1} (ester); (KBr): 1783 (γ-lactone), 1735, 1236 cm^{-1} (ester); NMR($CDCl_3$): 5.99 (d, J=11.5 Hz, 9-CH), 5.05 (m, 1-CH), 4.25 (t, J=8.5 Hz, 12-CH), 3.51 (dd, J=8.5, 10.5 Hz, 12-CH), 2.68 (dd, J=5.0, 11.5 Hz, 10-CH), 2.04 (s, AcO), 2.18, 1.62 (ABq, J=14.0 Hz, 6-CH_2), 1.23 (d, J=7.5 Hz, 13-CH_3), 1.10 (s, 15-CH_3), 1.08 (d, J=7.0 Hz, α-CH_3 in α-methylbutyrate), 0.88 (t, J=7.0 Hz, β-CH_3 in α-methylbutyrate), 0.85 (d, J=6.5 Hz, 14-CH_3).

Found: C, 66.89; H, 8.72%. Calcd for $C_{22}H_{34}O_6$: C, 66.98; H, 8.69%.

The other isomer (**42**) (70 mg) was in the form of colorless prisms; mp 121.5—122.5°C, $[\alpha]_D^{24}$ −67.5° (*c*, 1.0, MeOH); IR(CCl_4): 1785, 1741, 1244 cm^{-1}; (KBr): 1779, 1751, 1732, 1242 cm^{-1}.

Found: C, 66.79; H, 8.78%. Calcd for $C_{22}H_{34}O_6$: C, 66.98; H, 8.69%.

*Fukinolidol Dibromoacetate (**39**).* A mixture of dry benzene (25 m*l*), bromoacetyl bromide (2 m*l*), and fukinolidol (**8**) (500 mg) was refluxed for 5 hr. After working up as usual, the crude product (700 mg) was chromatographed on silica gel (11 g). Elution with benzene–ethyl acetate (80 : 1) gave dibromoacetate (**39**) (270 mg), which was then crystallized from ethyl acetate–light petroleum as colorless needles; mp 156.5—158.0°C, $[\alpha]_D^{22}$ −77.5° (*c*, 1.0, $CHCl_3$); IR(KBr): 1767, 1748, 1742sh, 1666, 1272, 910, 688, 604, 553, 530 cm^{-1}; NMR($CDCl_3$): 5.82 (d, J=11.0 Hz, 9-CH), 5.25 (t, J=2.0 Hz, 13-CH_2), *ca.* 5.1 (m, 1-CH), 4.75 (t, J=2.0 Hz, 12-CH_2), 3.87 (s, CH_2 in bromoacetate), 3.70

(s, CH_2 in bromoacetate), 2.82 (dd, J=5.0, 11.0 Hz, 10-CH), 2.32, 1.95 (ABq, J=14.0 Hz, 6-CH_2), 1.12 (s, 15-CH_3), 0.91 (d, J=5.0 Hz, 14-CH_3).

Found: C, 44.80; H, 4.77; Br, 31.25%. Calcd for $C_{19}H_{24}O_6Br_2$: C, 44.90; H, 4.75; Br, 31.45%.

Hydrogenation of Fukinolidol (8). Fukinolidol (**8**) (2.0 g) in ethanol (20 ml) was hydrogenated at room temperature and atmospheric pressure in the presence of 10% palladium charcoal (200 mg). After the absorption of hydrogen (195 ml), the catalyst was filtered and the solvent was evaporated *in vacuo*. The product was chromatographed over silica gel (50 g); subsequent elution with benzene–ethyl acetate (5 : 1) afforded dihydrofukinolidol (**10**) (1.20 g), which was then crystallized from ethyl acetate as colorless prisms; mp 190.0—191.0°C, $[\alpha]_D^{22}$ −14.5° (*c*, 1.0, MeOH). This was identical with the dihydrofukinolidol (**10**) obtained by the alkaline hydrolysis of tetrahydrofukinolide (**9**) (mixed-melting-point determination and a comparison of their IR spectra).

Further elution with the same solvent gave epidihydrofukinolidol (**11**) (600 mg), which was crystallized from ethyl acetate as colorless prisms; mp 148.0—149.0°C, $[\alpha]_D^{22}$ −69.5° (*c*, 1.0, MeOH); IR(KBr): 3365, 3330, 1758 cm^{-1}; NMR-($CDCl_3$): 4.52 (dd, J=7.0, 8.5 Hz, 12-CH), 4.47 (d, J= 10.5 Hz, 9-CH), 4.05 (OH), *ca.* 3.95 (m, 1-CH), 3.81 (dd, J=2.5, 8.5 Hz, 12-CH), 3.65 (OH), *ca.* 2.50 (m, 1H), 2.32 (dd, J=5.0, 10.5 Hz, 10-CH), 1.83 (s, 6-CH_2), 1.06 (d, J=6.0 Hz, 13-CH_3), 0.98 (s, 15-CH_3), 0.81 (d, J=3.5 Hz, 14-CH_3).

Found: C, 67.06; H, 9.03%. Calcd for $C_{15}H_{24}O_4$: C, 67.13; H, 9.02%.

Acetylation of Dihydrofukinolidol (10). Dihydrofukinolidol (**10**) (100 mg) was treated with acetic anhydride (0.5 ml) and pyridine (0.3 ml) at room temperature for 48 hr. The reaction mixture was then worked up in the usual manner. The crude product (130 mg) was chromatographed on silica gel (5 g); subsequent elution with benzene–ethyl acetate (80 : 1) gave diacetate (**44**) (70 mg), mp 246.0—248.0°C, colorless prisms (from ethyl acetate), $[\alpha]_D^{22}$ −42.5° (*c*, 1.0, $CHCl_3$); IR(KBr): 1769, 1738sh, 1733, 1241sh, 1233 cm^{-1}; NMR ($CDCl_3$): 5.95 (d, J=11.5 Hz, 9-CH), 5.00 (m, 1-CH), 4.24 (t, J=8.0 Hz, 12-CH), 3.50 (dd, J=8.0, 11.0 Hz, 12-CH), 2.68 (dd, J=5.5, 11.5 Hz, 10-CH), 2.15, 1.59 (ABq, J=14.0 Hz, 6-CH_2), 2.03 (s, AcO), 1.92 (s, AcO), 1.20 (d, J=7.0 Hz, 13-CH_3), 1.07 (s, 15-CH_3), 0.83 (d, J=4.5 Hz, 14-CH_3).

Found: C, 64.59; H, 8.04%. Calcd for $C_{19}H_{28}O_6$: C, 64.75; H, 8.01%. This was identical with the diacetate prepared by the hydrogenation of fukinolidol diacetate (**12**).

Further elution with the same solvent gave monoacetate (**43**) (30 mg); mp 194.0—196.0°C, colorless prisms (from ethyl acetate–light petroleum); IR(KBr): 3445, 1760, 1715sh, 1702, 1265 cm^{-1}.

Found: C, 66.00; H, 8.64%. Calcd for $C_{17}H_{26}O_5$: C, 65.78; H, 8.44%.

Acetylation of Epidihydrofukinolidol (11). Epidihydrofukinolidol (**11**) (150 mg) was acetylated under conditions similar to those above to furnish, quantitatively, diacetate (**45**) (190mg). The product was crystallized from ethyl acetate as colorless prisms; mp 214.0—215.0°C, $[\alpha]_D^{22}$ −50.5° (*c*, 1.0, $CHCl_3$); IR(KBr): 1768, 1731, 1235 cm^{-1}; NMR-($CDCl_3$): 5.75 (d, J=10.5 Hz, 9-CH), 5.02 (m, 1-CH), 4.27 (dd, J=6.5, 9.0 Hz, 12-CH), 3.82 (dd, J=2.5, 9.0 Hz, 12-CH), 2.50 (dd, J=5.5, 10.5 Hz, 10-CH), 2.04 (s, AcO), 1.98 (s, 6-CH_2), 1.92 (s, AcO), 1.06 (d, J=7.0 Hz, 13-CH_3), 1.05 (s, 15-CH_3), 0.88 (d, J=3.0 Hz, 14-CH_3).

Found: C, 65.00; H, 7.93%. Calcd for $C_{19}H_{28}O_6$: C, 64.75; H, 8.01%.

Hydrogenation of Fukinolidol Diacetate (12). Fukinolidol diacetate (**12**) (193 mg) in acetic acid (2 ml) was hydrogenated in the presence of platinum oxide (24.8 mg) at room temperature and atmospheric pressure. Working up in the usual manner afforded the dihydro compound (**44**); mp 246.0—248.0°C, colorless needles (from ethyl acetate–light petroleum).

Found: C, 64.48; H, 8.01%. Calcd for $C_{19}H_{28}O_6$: C, 64.75; H, 8.01%. This was identical with the dihydrofukinolidol diacetate (**44**) obtained by the acetylation of dihydrofukinolidol (**10**).

Hydrolysis of Homofukinolide (3). Homofukinolide (**3**) (0.4 g) was dissolved in 2 N alcoholic potassium hydroxide (20 ml), and then the mixture was left for 70 hr at room temperature. After the removal of the solvent and acidification with dilute sulfuric acid, the reaction mixture was extracted with chloroform. The extract was washed with a saturated sodium hydrogen carbonate solution and water, and dried. The subsequent evaporation of the solvent gave fukinolidol (**8**) (180 mg) as colorless prisms (from ethyl acetate); mp 177.0—180.0°C, $[\alpha]_D^{22}$ −79.5° (*c*, 1.0, MeOH).

Found: C, 67.78; H, 8.37%. Calcd for $C_{15}H_{22}O_4$: C, 67.64; H, 8.33%. This was identical with the sample of fukinolidol (**8**) obtained by the hydrolysis of fukinolide (**1**).

Acidification of the sodium hydrogen carbonate solution with dilute sulfuric acid and extraction with ether gave a crude acidic part (150 mg), which was then transformed into the *p*-phenylphenacyl ester in the usual manner. The product (450 mg) was chromatographed over silica gel (10 g) and eluted with light peroleum–ether (50 : 1) to afford *p*-phenylphenacyl angelate (130 mg) as colorless leaflets (from ethanol); mp 89.0—90.0°C.

Found: C, 77.54; H, 6.29%. Calcd for $C_{19}H_{18}O_3$: C, 77.53; H, 6.16%. This was identical with the authentic sample of *p*-phenylphenacyl angelate.

Hydrolysis of S-Fukinolide (4). S-Fukinolide (**4**) (300 mg) was dissolved in 2 N methanolic potassium hydroxide (10 ml), and then the mixture was left overnight at room temperature. The solvent was removed *in vacuo*, and the residue was acidified with dilute sulfuric acid and extracted with ether. The extract was washed with a saturated sodium hydrogen carbonate solution and water, and dried. The subsequent evaporation of the solvent gave a product (110 mg) which was crystallized from ethyl acetate as colorless prisms; mp 176.0—178.0°C, $[\alpha]_D^{22}$ −78.5° (*c*, 1.0, MeOH), −75.0° (*c*, 1.0, $CHCl_3$).

Found: C, 67.84; H, 8.42%. Calcd for $C_{15}H_{22}O_4$: C, 67.64; H, 8.33%. This was identical with the fukinolidol (**8**) obtained by the alkaline hydrolysis of fukinolide (**1**) according to a mixed-melting-point determination and a comparison of their IR spectra.

The sodium hydrogen carbonate solution was concentrated *in vacuo*, acidified with dilute sulfuric acid, and extracted with ether. The extract was washed with water and dried. After the removal of the solvent, the residue (100 mg) was crystallized from ethanol–cyclohexane to give an acid (**46**) as colorless prisms; mp 119.0—120.0°C, NMR($CDCl_3$): 11.10 (s, COOH), 7.20 (d, J=10.0 Hz, β-CH=), 5.85 (d, J=10.0 Hz, α-CH=), 2.39 (s, S-CH_3).

Found: C, 40.54; H, 5.19%. Calcd for $C_4H_6O_2S$: C, 40.66; H, 5.12%.

The above acid was transformed into the *p*-phenylphenacyl ester, which was then crystallized from ethanol as colorless needles; mp 132.5—133.5°C.

Found: C, 69.19; H, 5.20; S, 10.46%. Calcd for $C_{18}H_{16}O_3S$: C, 69.20; H, 5.16; S, 10.26%. The acid (**46**) was identified as *cis*-β-methylthioacrylic acid from the above

data.

*Reduction of Fukinanolide (**5**) with Lithium Aluminum Hydride.* A solution of fukinanolide (**5**) (662 mg) in dry ether (20 m*l*) was added, drop by drop, to a suspension of lithium aluminum hydride (264 mg) in dry ether (35 m*l*) at room temperature over a 1-hr period, and then the mixture was refluxed for 4hr. Working up as usual gave a crude diol (**47**) (657 mg), which was then crystallized from light petroleum; mp 81.5—82.0°C, colorless leaflets, $[\alpha]_D^{22}+22.0°$ (*c*, 1.0, MeOH); IR(KBr): 3280, 1638, 1063, 1040, 903 cm^{-1}.

Found: C, 75.61; H, 11.08%. Calcd for $C_{15}H_{26}O_2$: C, 75.84; H, 11.00%.

*Hydrogenation of Diol (**47**).* The diol (**47**) (410 mg) was hydrogenated with 10% palladium charcoal (70 mg) in ethanol (15 m*l*) at room temperature and atmospheric pressure. Working up in the usual manner gave a crude product (400 mg) which was subsequently chromatographed on silica gel (10 g). Elution with benzene afforded fukinan-8-ol (**26**) (78 mg); this was followed by purification on glc (PEG 6000, 2.6 m; column temperature, 180°C; H_2-flow rate, 150 m*l*/min; retention time, 29.5 min), mp 38.0—39.0°C, $[\alpha]_D^{22}+18.0°$ (*c*, 1.01, MeOH).

Found: C, 80.04; H, 12.52%. Calcd for $C_{15}H_{28}O$: C, 80.29; H, 12.58%. This was identical with the fukinan-8-ol (**26**) obtained from fukinone epoxide (**30**) and fukinolidol (**8**) as shown by a comparison of their IR spectra and by a mixed-melting-point determination.

Further elution with ethyl acetate afforded diol (**48**) (290 mg), which was subsequently crystallized from light petroleum; mp 121.0—122.0°C, colorless needles, $[\alpha]_D^{22}+11.7°$ (*c*, 0.94, MeOH); MS: *m/e* 240 M^+: IR(KBr): 3230, 1250, 1135, 1100, 1070, 1045 cm^{-1}.

The authors wish to thank Professor Yoshio Kitahara for his generous gift of lactone **5**, the staff of the Shionogi Research Laboratory, Shionogi and Co., Ltd., for the microanalysis, and the Institute of Food Chemistry for the measurement of the MS and NMR spectra.

BULLETIN OF THE CHEMICAL SOCIETY OF JAPAN, VOL. 45, 3685—3692 (1972)

The Allylic Rearrangement. II.[1] Reactions of 5,5,5-Trichloro-3-penten-2-one with Nucleophiles[2]

Akira TAKEDA, Sadao TSUBOI, Takashi MORIWAKE, and Eiji HIRATA

Department of Synthetic Chemistry, School of Engineering, Okayama University, Tsushima, Okayama

(Received April 11, 1972)

Reactions of 5,5,5-trichloro-3-penten-2-one (**1**) with a number of nucleophiles have been carried out. It was found that the Grignard reagents (**5**) primarily attacked the carbonyl carbon of **1** yielding the corresponding tertiary alcohols (**7**). The reaction sequence of ethylmagnesium bromide (**5a**) is given as an example. The reaction of **5a** with **1** gave 6,6,6-trichloro-3-methyl-4-hexen-3-ol (**7a**) as the major constituent of the primary product. The hexenol **7a** readily underwent the allylic rearrangement by heating at distilling temperature (88—90°C/6 mmHg) to afford 4,6,6-trichloro-3-methyl-5-hexen-3-ol (**8a**), which was in turn converted into 6,6-dichloro-3-methyl-3,4-epoxy-5-hexene (**9a**) by treatment with sodium methoxide. The stereoselective synthesis of *dl-erythro*-4,6,6-trichloro-3-methyl-5-hexen-3-ol (**8a**-I) was achieved by using 3,5,5-trichloro-4-penten-2-one (**3**) as the starting material in place of **1**. *dl-trans*-6,6-Dichloro-3-methyl-3,4-epoxy-5-hexene (**9a**-I) was derived by the cyclization of **8a**-I with a base. The stereochemistry of **8a** and **9a** was discussed on the basis of NMR data. Nucleophiles such as methanol, hydrogen chloride, anilines, thiophenol, sodium acetate, sodium phenolate, and diethyl sodiomalonate gave the products of the conjugate addition (**15**). Ethyl sodioacetoacetate gave 2-chloro-3-acetonyl-4-ethoxycarbonyl-5-methylfuran (**17**).

As a class of compounds with polyfunctionality 3,3,3-trichloro-1-propenyl ketones have attracted the attention of several authors.[3a] Nevertheless, only a little is known of their chemical properties, and their behavior toward nucleophiles still remains uninvestigated. We have recently reported on the allylic rearrangement of 5,5,5-trichloro-3-penten-2-one (**1**) and phenyl 3,3,3-trichloro-1-propenyl ketone (**2**), and also some reactions of the rearranged products (**3**, and **4**) as an α-chloroketone.[1] To extend our knowledge of its chemical properties we carried out reactions of compound **1** with a number of nucleophiles such as ethylmagnesium bromide (**5a**), methylmagnesium iodide (**5b**), phenylmagnesium bromide (**5c**), diethyl sodiomalonate, ethyl sodioacetoacetate, methanol, and anilines. This paper will describe and discuss the results of these reactions.

$$CCl_3\text{-}CH{=}CH\text{-}\underset{\underset{O}{\|}}{C}\text{-}R \quad \rightleftarrows \quad Cl_2C{=}CH\text{-}\underset{\underset{Cl}{|}}{CH}\text{-}\underset{\underset{O}{\|}}{C}\text{-}R$$

1, R=CH_3 **3**, R=CH_3

2, R=C_6H_5 **4**, R=C_6H_5

It was found that the Grignard reagent (**5**) primarily attacked the carbonyl carbon of **1** yielding the corresponding tertiary alcohols (**7**). The reaction sequence of ethylmagnesium bromide (**5a**) is given in Scheme 1 as an example. When **5a** reacted with **1** at a lower temperature (−10——30°C), *trans*-6,6,6-trichloro-3-methyl-4-hexen-3-ol (**7a**) was formed as

1) The first paper of this series: A. Takeda and S. Tsuboi, *J. Org. Chem.*, **35**, 2690 (1970).

2) Presented in part at the 20th Anniversary Local Meeting of Chugoku-Shikoku Branch, the Chemical Society of Japan, October 7, 1970 (Hiroshima).

3) a) H. Gault and G. Mennicken, *C. R. Acad. Sci. Paris*, **229**, 1239 (1949). b) I. Salkind, *J. Russ. Phys. Chem. Soc.*, **30**, 906 (1898).

the sole primary product in a 53% yield together with a trace of 6,6-dichloro-3-methyl-3,4-epoxy-5-hexene (**9a**).[4] It is reasonable to consider that the highly electron-withdrawing group of trichloromethyl retards the transfer of the ethylenic electrons to the carbonyl carbon, thus preserving its reactivity to afford the 1,2-adduct rather than the 1,4-adduct, since the reaction of Grignard reagents with alkylideneacetone tends to result in the predominant formation of the 1,4-adducts.[5] Kohler[6] also reported that the 1,4-adduct, *i. e.* phenyl 3,3,3-trichloro-2-phenylpropyl ketone (**15j**) was the only product in the reaction of the ketone **2** with phenylmagnesium bromide (**5c**), but we confirmed that both the ketone **15j** and the 1,2-adduct, *i.e.* 4,4,4-trichloro-1,1-diphenyl-2-buten-1-ol (**7e**), were formed in a ratio of 3 : 4 in the same reaction.

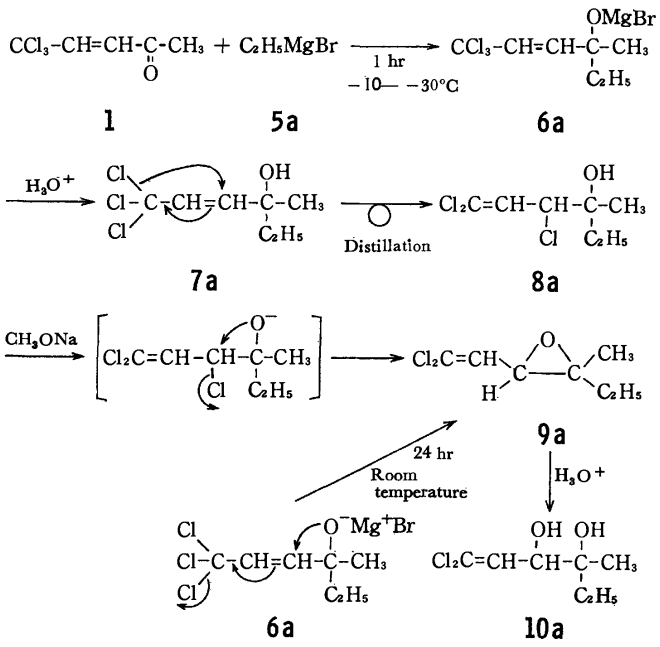

Scheme 1.

The chlorine atom of the hexenol **7a** is so labile on heating that it readily undergoes the allylic rearrangement to afford 4,6,6-trichloro-3-methyl-5-hexen-3-ol (**8a**) at distilling temperature (88—90°C/6 mmHg). The hexenol **8a** exists in two diastereomeric forms, *i.e. dl-erythro* (**8a**-I) and *dl-threo* (**8a**-II), which correspond to the peaks with the retention times[7] of 13.5 min (**8a**-I) and 14.5 min (**8a**-II) on glpc but were indistinguishable by means of either tlc[8] or by IR

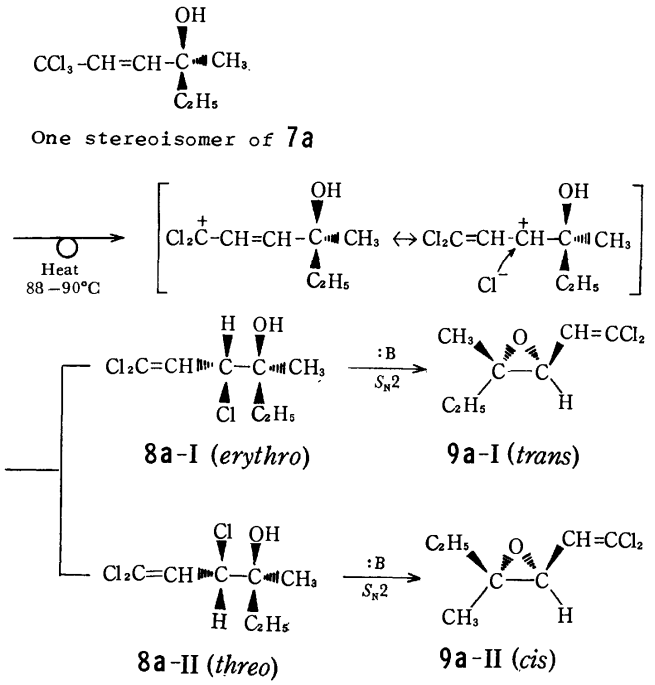

Scheme 2.

spectrum. The planar structure of the intermediate carbonium ion enabled the chlorine atom of **7a** to migrate to its allylic position, from both sides of the plane with equal chances, yielding a mixture of nearly equal amounts of the diastereomers, **8a**-I and **8a**-II. The hexenol **8a** was further transformed into the epoxide **9a** in a 33% yield by treatment with a base in dry ether, which also consisted of two diastereomeric epoxides, **9a**-I and **9a**-II. The steric course of these reactions is illustrated in Scheme 2.

The stereoselective synthesis of **8a**-I was achieved by using the ketone **3** as the starting material in place of **1**. It is presumed from Cram's rule[9] that the reagent **5a** can attack the carbonyl carbon of the ketone **3** more readily from the opposite side of the 2,2-dichlorovinyl group as shown in Scheme 3. In fact the reaction of **5a** with **3** afforded only the hexenol **8a**-I in a 73% yield, which was then converted into *trans*-6,6-dichloro-3-methyl-3,4-epoxy-5-hexene (**9a**-I) in a 88% yield. The *trans* structure of **9a**-I was supported by NMR data, the signal due to the methyl protons appearing at a higher field (δ, s, 1.24 ppm) in **9a**-I than the

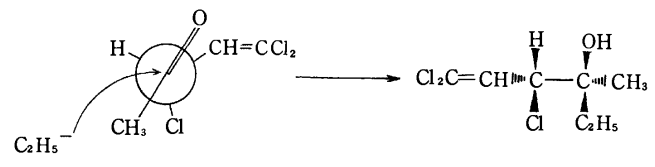

Scheme 3.

4) On March 30, 1971, we received a copy of the doctoral dissertation of Mr. François de Champs submitted to the Faculty of Science, the University of Paris, on October 31, 1970, entitled "Etude de la transposition allylique et de quelques proprietes de cetones α,β-ethyleniques γ,γ,γ-trichlorees". Champs obtained similar results. He suggested the possible formation of an epoxide in a small quantity.

5) E. R. Alexander and G. R. Coraor, *J. Amer. Chem. Soc.*, **73**, 2721 (1951).

6) E. P. Kohler, *Am. Chem. J.*, **38**, 511 (1907); *Chem. Abstr.*, **2**, 824 (1908).

7) Column, 10% Apiezon Grease L on Chromosorb W, 3 mm×1 m; column temp., 120°C; carrier gas, N_2 (0.5 kg/cm², 42 ml/min); detector, FID.

8) Conditions of preparative tlc: support, silica gel G (E. Merck AG, Darmstadt), 0.8 mm; developer, *n*-hexane–acetone–chloroform (5 : 2 : 1, v/v); eluent, acetone.

9) D. J. Cram and F. A. Abd Elhafez, *J. Amer. Chem. Soc.*, **74**, 5828 (1952); D. J. Cram and K. R. Kopecky, *ibid.*, **81**, 2748 (1959); J. H. Stocker, P. Sidisunthorn, B. M. Benjamin, and C. J. Collins, *ibid.*, **82**, 3913 (1960).

methyl protons of the diastereomeric epoxide **9a**-II (δ, s, 1.30 ppm).[10] A similar differential shielding effect of the 2,2-dichlorovinyl group was also observed in 5,5-dichloro-2-methyl-2,3-epoxy-4-pentene (**9b**), which exhibited the signal due to the *cis* methyl protons at δ 1.28 ppm and the signal due to the *trans* methyl protons at δ 1.34 ppm. The prolonged reaction of **1** with **5a**, being conducted at room temperature, caused the cyclization of the intermediate **6a** to afford the epoxide **9a** in a 25% yield. It is assumed that the cyclization occurred in a concerted manner in which the oxyanion of **6a** attacks the carbon atom allylic to the chlorine of the trichloromethyl group as shown in Scheme 1. The treatment of the epoxide **9a** (**9a**-I/**9a**-II = *ca.* 1 : 1) with a 20% H_2SO_4 gave an epimeric mixture of 6,6-dichloro-3-methyl-5-hexene-3,4-diol (**10a**) in a 52% yield. The same treatment of the *trans* isomer (**9a**-I) gave *dl-erythro*-6,6-dichloro-3-methyl-5-hexene-3,4-diol (**10a**-I).

When the reagent **5a** was used in much excess in the Grignard reaction, 6-chloro-3-methyl-5-octene-3,4-diol (**12**) was obtained in addition to the compounds **8a** and **9a**. Small amounts of the by-products such as 5,5-dichloro-4-penten-2-one (**13**) and 6,6-dichloro-3-methyl-5-hexen-3-ol (**14**) were also isolated. The possible ways in which compounds **12**, **13**, and **14** were produced are shown in Schemes 4 and 5.[11] The pentenone **13** was prepared in a 29% yield in an alternative synthesis from **1** and magnesium.

The yields, properties, spectral data, and analyses of the tertiary alcohols **7**, the rearranged alcohols **8**, and the epoxides **9** obtained in analogous ways are listed in Tables 1, 2, and 3 respectively.

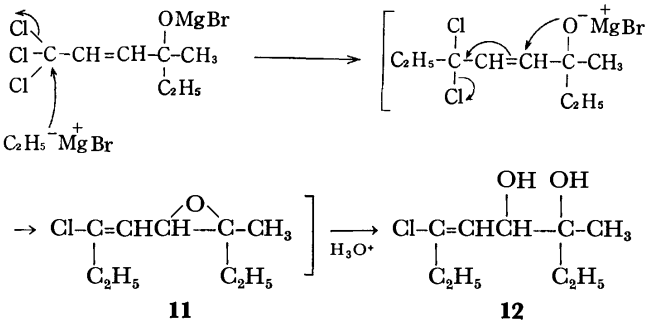

Scheme 4.

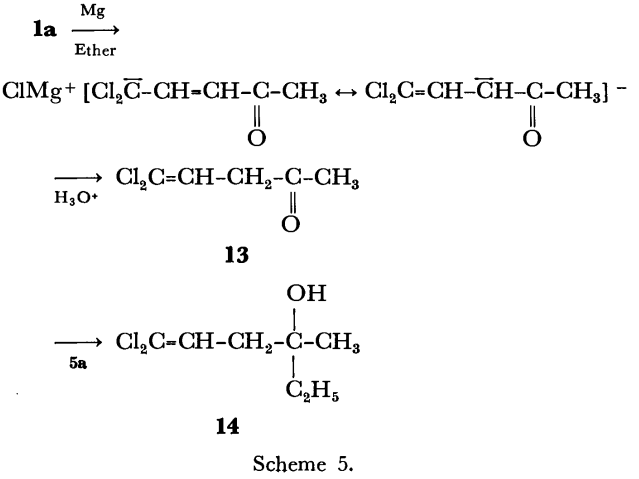

Scheme 5.

Nucleophiles such as methanol,[12a] hydrogen chloride, aniline, thiophenol gave the products of conju-

TABLE 1. CCl_3-CH=CH-C(OH)(R_1)-R_2 **7**

Compd.	R_1	R_2	Procedure: Ketones	Procedure: Grignard Reagent	Yield %	Anal (Calcd), % C	Anal (Calcd), % H	IR (cm^{-1}, liquid)	NMR δ ppm
7c	CH_3	C_6H_5	**1**	**5c**	58	52.64 (52.94	4.17 4.45)	3500 (OH) 1625 (C=C)	1.64 (s, 3H, $-CH_3$) 2.56 (s, 1H, -OH) 6.42 (2d, 2H, -CH=CH-) 7.30 (broad s, $-C_6H_5$)[a]
7d	C_6H_5	C_2H_5	**2**	**5a**	45[c]	51.32 (51.55	4.75 4.69)	3550 (OH) 1625 (C=C) 1605 and 1590 (benzene ring)	0.87 (t, 3H, J=7.5 Hz, $-CH_2\underline{CH_3}$) 1.92 (q, 2H, J=7.5 Hz, $-\underline{CH_2}CH_3$) 2.10 (s, 1H, -OH) 6.43 (s, 2H, -CH=CH-) 7.31 (broad s, 5H, $-C_6H_5$)[a]
7e	C_6H_5	C_6H_5	**2**	**5c**	57[c]	58.90 (58.66	3.93 4.00)	3510 (OH) 1625 (C=C) 1605 and 1586 (benzene ring)	2.50 (s, 1H, -OH) 6.50 and 6.90 (2d, 2H, -CH=CH-) 7.31—8.00 (m, 10, 2-C_6H_5)[b]

a) Measured in CCl_4. b) Measured in $CDCl_3$. c) In addition to 1,2-adducts, 1,4-adducts were also obtained (see Experimental).

10) The substituents in heterocyclopropanes tend to cause methyl protons *cis* to them to appear at higher fields than those *trans* to them. *Cf.* L. M. Jackman and S. Sternhell, "Application of Nuclear Magnetic Resonance Spectroscopy in Organic Chemistry, 2nd Edition," Pergamon Press Ltd., London W. 1 (1969), p. 229.

11) Excess magnesium, which was present unreacted in the Grignard reagent, probably reacted with **1** to give pentenone **13**.

12) a) Champs (*loc. cit.*) described the formation of compounds **15a** (mp 25.5°C) and **15b** (bp 108—110°C/15 mmHg) as due to conjugate addition to **1** of methanol and hydrogen chloride, respectively. b) Champs detected the formation of 5,5,5-trichloro-4-diethylamino-2-pentanone in a 40% yield on NMR spectra.

TABLE 2. $CCl_2=CH-\underset{Cl}{\underset{|}{CH}}-\overset{R_2}{\overset{|}{\underset{OH}{\underset{|}{C}}}}-R_1$ **8**

Compd.	R_1	R_2	Procedure: Ketones	Procedure: Grignard Reagent	Yield %	Bp (mmHg) °C	Anal (Calcd), % C	Anal (Calcd), % H	IR (cm^{-1}, liquid)	NMR δ ppm
8b	CH_3	CH_3	**1**	**5b**	43	65—70 (4)	35.65	4.51	3420 (OH)	1.25 (s, 3H, *cis*-CH_3)
							(35.42	4.46)	1612 (C=C)	1.33 (s, 3H, *trans*-CH_3)
									755 (C-Cl)	4.57 (d, 1H, J=10.1 Hz, >CHCl)
										6.11 (d, 1H, J=10.1 Hz, Cl_2C=CH-)[a]
8c	CH_3	C_6H_5	**1**	**5c**	73	126—128 (3)[c]	49.82	4.30	3600—3500 (OH)	1.72 (s, 3H, -CH_3)
							(49.75	4.18)		2.34 (s, 1H, -OH)
									1623 (C=C)	4.93 (d, 1H, J=11 Hz, >CHCl)
										6.03 (d, 1H, J=11 Hz, =CH-)[b]
8d	C_6H_5	C_2H_5	**2**	**5a**	45	128—131 (0.22)[d]	51.48	4.88	3600 (OH)	0.69 (t, 3H, J=7.5 Hz, -$CH_2\underline{CH_3}$)
							(51.55	4.69)	1622 (C=C)	1.96 (q, 2H, J=7.5 Hz, -$\underline{CH_2}CH_3$)
										2.12 (s, 1H, -OH)
										4.92 (d, 1H, J=9.5 Hz, >CHCl)
										5.94 (d, 1H, J=9.5 Hz, Cl_2C=CH-)
										7.31 (broad s, 5H, -C_6H_5)[a]

a) Measured in CCl_4. b) Measured in $CDCl_3$. c) NMR spectrum indicates that this fraction consists of **7c** (27%) and **8c** (73%). d) Tlc analysis[17] of this fraction showed two spots at R_f values of 0.80 and 0.67 in the ratio 1 : 1. The 0.80 R_f component was separated by preparative tlc[18] and identified as phenyl 2-trichloromethylbutyl ketone (**15i**) by comparison of its IR spectrum with that of the authentitic sample. The 0.67 R_f component was separated by preparative tlc.[18] NMR spectrum showed it to be a mixture of **7d** and **8d** (3 : 5).

TABLE 3. $CCl_2=CH-\underset{\diagdown R_1}{\overset{\diagup O \diagdown}{CH-C}}\overset{R_2}{}$ **9**

Compd.	R_1	R_2	Yield %	Bp (mmHg) °C	Anal (Calcd), % C	Anal (Calcd), % H	IR (cm^{-1}, liquid)	NMR (CCl_4) δ ppm
9b	CH_3	CH_3	36	60—61 (13)	43.02	4.63	3040	1.28 (s, 3H, -CH_3, *cis* to Cl_2C=CH-)
					(43.15	4.83)	1618 (C=C)	1.34 (s, 3H, -CH_3, *trans* to Cl_2C=CH-)
							670 (C-Cl)	3.32 (d, 1H, J=7.2 Hz, >CHCl)
								5.70 (d, 1H, J=7.2 Hz, Cl_2C=CH-)
9c	CH_3	C_6H_5	69	110 (3)	58.01	4.65	3070	1.61 and 1.63 (2s, 3H, *cis* and *trans* -CH_3)
					(57.67	4.40)	1620 (C=C)	3.40 (d, 1H, J=7.0 Hz, $\underset{H}{>}C\overset{O}{\diagup\diagdown}C<$)
							1251 ($>C\overset{O}{\diagup\diagdown}C<$)	5.81 (d, 1H, J=7.0 Hz, =CH-)
								7.25 (s, 5H, -C_6H_5)

gate addition (**15**). Neither acetic acid nor phenol reacted with **1**, but a 90 wt% aqueous acetic acid caused hydration of **1** to give chloralacetone.[3b] On the contrary, both acetate and phenolate anions were found to be sufficiently nucleophilic to produce the compounds **15g** and **15h** when their conjugate acids were used as solvents. Diethyl sodiomalonate and **1** in dry ether afforded 5,5,5-trichloro-4-diethoxycarbonylmethyl-2-pentanone (**15f**) in a 70% yield indicating that the conjugate addition of the carbanion of sodiomalonate had occurred. These compounds, with the exception of **15h**, exhibited no IR absorption bands in the region of 1600—1700 cm^{-1}. On treatment of **1** with diethylamine in ether a resinous material was obtained with deposition of a large amount of diethylammonium chloride.[12b]

The reaction of **1** with ethyl sodioacetoacetate **16** gave exclusively a crystalline solid melting at 62°C in a 18% yield to which the structure 2-chloro-3-acetonyl-4-ethoxycarbonyl-5-methylfuran (**17**) was assigned on the basis of elemental analysis and spectral data. No other distillable products were obtained. Formation of the furan compound can be best interpreted by setting up a mechanism where the ambident anion of **16** attacks β and γ carbons of **1** as shown in Scheme 6, although no intermediate compounds have

been isolated as yet.

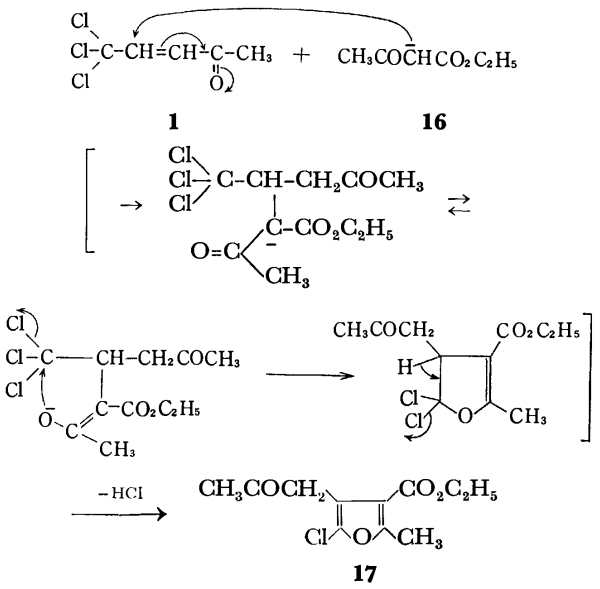

Scheme 6.

Experimental

The melting points and boiling points are uncorrected. Elemental analyses were carried out by Mr. Eiichiro Amano. Analytical determinations by glpc were performed on a Hitachi K-53 model gas chromatograph (3 mm o.d. × 1 m, 10% Apiezon Grease L on Chromosorb W), and the preparative isolations by glpc were performed on a Yanagimoto GCG-550T model gas chromatograph (3 mm o.d. × 2.25 m, 10% Apiezon Grease L on Chromosorb W). The mass spectra were obtained with a Hitachi RMS-4 model mass spectrometer. We are indebted to Mr. Hiroshi Ooyama, Hokko Chemical Industry Co., Ltd., and Mr. Heizan Kawamoto and Miss Hiromi Ootani for the NMR measurements. The microanalyses and spectral measurements were performed on the samples collected by glpc or tlc.

Ketones **1** and **3** were prepared by the methods reported previously.[1] Tertiary alcohols, **7c**, **7d**, and **7e**, listed in Table 1, were prepared in the same way as in the preparation of **7a**. Rearranged tertiary alcohols **8b**, **8c**, and **8d** were prepared by Procedure B. Epoxides **9b** and **9c** were obtained from **8b** and **8c** in the same ways as **9a**.

*trans-6,6,6-Trichloro-3-methyl-4-hexen-3-ol (**7a**).* Ethylmagnesium bromide (**5a**) was prepared from 5.5 g (0.05 mol) of ethyl bromide and 1.4 g (0.055 g atom) of magnesium in 20 m*l* of dry ether. The unreacted magnesium metal was recovered by decantation. To a solution of 7.5 g (0.04 mol) of **1** in 25 m*l* of dry ether was added dropwise the ethereal solution of **5a** with stirring at −30°C. The reaction mixture was stirred for additional 2 hr at −20—−10°C, and then acidified with 10% HCl. The ethereal layer was washed with water and dried over Na_2SO_4. Removal of the solvent gave 6.4 g (74% yield) of the residual oil containing **7a** as the major product. Tlc analysis[13] showed two spots at the R_f values 0.73 and 0.84, in a ratio of 9 : 1. Pure sample of **7a** with the R_f value of 0.73 was obtained by preparative tlc[14]: IR (cm^{-1}, liquid) 3425 (OH), 2980, 1620 (C=C), 735 (C–Cl); NMR (CCl_4) δ 0.91 (t, 3H, J=7.2 Hz, $-CH_2\underline{CH_3}$), 1.30 (s, 3H, $>C(OH)\underline{CH_3}$), 1.58 (q, 2H, J=7.2 Hz, $-\underline{CH_2}CH_3$), 2.02 (s, 1H, –OH), 6.08 and 6.38 (dd, 2H, J=14.5 Hz, *trans* $-\underline{CH}=\underline{CH}-$).

dl-erythro-*4,6,6-Trichloro-5-hexen-3-ol (**8a-I**).* The Grignard reagent **5a** was prepared from 4.9 g (0.045 mol) of ethyl bromide, 1.1 g (0.045 g atom) of magnesium in 30 m*l* of dry ether. The ethereal solution of **5a** was added dropwise to a solution of **3** (6 g, 0.032 mol) in 24 m*l* of dry ether with stirring at −30°C. The stirring was continued for additional 1 hr at −30——20°C. The reaction mixture was then acidified with 10% HCl. The ethreal layer was washed with water, dried over Na_2SO_4. The removal of the solvent gave 5.3 g (76%) of the crude product. Tlc analysis of this product showed two spots with the R_f values 0.61 and 0.72, in a ratio of the spot areas 20 : 1, corresponding to the R_f values of **8a** (R_f=0.61) and **3** (R_f=0.72).[15a] The analytical sample of **8a-1** was obtained by preparative tlc:[15b] IR (cm^{-1}, liquid) 3475 (OH), 3040, 2980, 1720, 1620 (C=C), 740 (C–Cl); NMR (CCl_4) δ 0.93 (t, 3H, J=7.2 Hz, $-CH_2\underline{CH_3}$), 1.27 (s, 3H, $>C(OH)-\underline{CH_3}$), 1.61 q, 2H, J=7.2 Hz, $-\underline{CH_2}CH_3$), 2.50 (s, 1H, –OH), 4.57 (d, 1H, J=9.0 Hz, $=CH-\underline{CH}Cl-$), 6.1 (d, 1H, J=9.0 Hz, $Cl_2C=\underline{CH}-$). Glpc analysis[7] of the purified sample indicated that it consisted of two components with the retention times, 13.5 min (**8a-II**, 1 part) and 14.6 min (**8a-I**, 9 parts).

Found: C, 38.58; H, 5.26%. Calcd for $C_7H_{11}Cl_3O$: C, 38.65; H, 5.10%.

*The Epimeric Mixture of 4,6,6-Trichloro-5-hexen-3-ol (**8a**).* *Procedure A*: Distillation of hexenol **7a** (5.4 g, 0.025 mol) afforded the crude product of **8a** (4.4 g, 81%), bp 88—90°C/6 mmHg; IR (cm^{-1}, liquid) 3475 (OH), 3040, 2980, 1720, 1620 (C=C), 920, 740 (C–Cl); NMR (CCl_4) δ 0.95 (t, 3H, J=7.2 Hz, $-CH_2\underline{CH_3}$), 1.14 (s, $>\underline{C}(OH)-\underline{CH_3}$, *threo*) and 1.27 (s, $>\underline{C}(OH)-\underline{CH_3}$, *erythro*) (epimeric mixture, 3H), 1.55 (q, 2H, J=7.2 Hz, $-\underline{CH_2}CH_3$), 1.95 (s, 1H, –OH), 4.59 (d, 1H, J=9.0 Hz, $=CH\underline{CH}Cl-$), 6.1 (d, 1H, J=9.0 Hz, $Cl_2C=CH-$). Glpc analysis[7] of this product showed three peaks. The components, retention times (min), and integrated percentages are as follows: 1, 4.7, 2%; 2, 13.5, 55%; 3, 14.6, 43%. Component 1 was identified as **9a** by comparison of its retention time with the authentic sample described in the next section.

Procedure B: The reaction of **5a** with **1** was carried out in the same way as the preparation of the hexenol **7a** using 15 g (0.08 mol) of **1** as the starting material. Distillation of the crude product gave 13.1 g of a clean oil, bp 78—100°C/4 mmHg. Glpc analysis[7] indicated that this fraction contained three components, which were fractionated by preparative glpc and identified by comparison of the IR spectra with those of the authentic samples; peaks (nos), compounds (nos), retention times (min), and the integrated peak areas are: 1, **9a**, 4.7, 14%; 2, **8a-II**, 13.5, 50%; 3, **8a-I**, 14.6, 36%.

Procedure C: The reaction of **5a** with **1** was conducted in a similar manner to Procedure B at room temperature for 24 hr, using 15 g (0.08 mol) of **1** as the starting material.

13) Conditions of tlc: support, silica gel GF_{254} (E. Merk AG, Darmstadt), 0.1 mm; developer, benzene-methanol (9 : 1 v/v); spray reagent, H_2SO_4–$KMnO_4$ (7 : 3 w/w). The spot of **1** on tlc appeared at R_f 0.84.

14) Conditions of preparative tlc: support, silica gel GF_{254} (E. Merk AG, Darmstadt), 1 mm; developer, benzene-methanol (9 : 1 v/v); eluent, acetone.

15) a) Conditions of tlc: support, silica gel GF_{254} (E. Merk AG, Darmstadt), 0.3 mm; developer, *n*-hexane-acetone-chloroform (5 : 1 : 1 v/v). b) The same support (1 mm) and the same developer as above were used. Eluent, acetone.

The ethereal extract of the crude product was distilled *in vacuo*. The results of the glpc analysis of each fractions are as follows:

Fractions (bp, °C/mmHg)	Weight (g)	Compounds detected by glpc[7] (retention times, min)			
		9a (4.7)	unknown (12.2)	**8a**-II (13.5)	**8a**-I (14.6)
I (59—69/12)	2.4	81	1	9	9
II (69—84/5)	3.3	45	20	21	14
III (84—90/5)	1.7	3.5	18	48	30
IV (>90/5)	1.0	—	—	—	—

The last fraction turned white crystals in a cooler. One recrystallization from petroleum ether (bp 45—55°C) gave 0.9 g of white crystals, to which the structure 6,6-dichloro-3-methyl-5-hexene-3,4-diol (**10**) was assigned: mp 81°C; IR (cm^{-1}, nujol) 3300 (OH), 1620 (C=C), 910, 800—650 (C–Cl); NMR ($CDCl_3$) δ 0.9 (t, 3H, J=6.8 Hz, $-CH_2\underline{CH_3}$), 1.20 (s, 3H, $>\overset{OH}{\underset{|}{C}}-\underline{CH_3}$), 1.43 (broad q, 2H, J=6.8 Hz, $-\underline{CH_2}-CH_3$), 2.01 (s, 2H, 2OH), 4.16 (d, 1H, J=9 Hz, $>\underline{CH}OH$), 6.02 (d, 1H, J=9 Hz, $Cl_2C=\underline{CH}-$).

Found: C, 42.40; H, 5.99%. Calcd for $C_7H_{12}Cl_2O_2$: C, 42.23; H, 6.08%.

Procedure D: The reaction of **5a** with **1** was carried out in a similar manner to Procedure C except that excess ethylmagnesium bromide (equivalent to 0.16 mol) was used on 18.7 g (0.1 mol) of **1**. The ethereal extract of the crude product was worked up as usual. The fraction distilling at 44—112°C/5 mmHg was collected and analyzed by glpc.[7] Peaks (nos), retention times (min), and the integrated peak areas are: 1, 2.9, 13%; 2, 4.7, 11%; 3, 7.9, 9%; 4, 10.1, 2%; 5, 12, 5%; 6, 13.5, 27%; 7, 14.6, 21%; 8, 16, 10%. Components 1, 2, 6, and 7 were identified as compounds **13**, **9a**, **8a**-II, and **8a**-I, by comparison of the IR spectra and retention times with those of the authentic samples. Components 3 and 8 were collected by preparative glpc and analyzed. The structure 6,6-dichloro-3-methyl-5-hexen-3-ol (**14**) was assigned to component 3 on the basis of the IR spectrum and analysis: IR (cm^{-1}, liquid) 3450 (OH), 2980, 1612 (C=C), 918, 700 (C–Cl).

Found: C, 46.41; H, 6.75%. Calcd for $C_7H_{12}Cl_2O$: C, 45.92; H, 6.61%.

The structure 6-chloro-3-methyl-5-octene-3,4-diol (**12**), was assigned to component 8: IR (cm^{-1}, liquid) 3400 (OH), 2980, 1615 (C=C), 1460, 904 (=C–H).

Found: C, 55.99; H, 8.59%. Calcd for $C_9H_{17}ClO_2$: C, 56.01; H, 8.89%.

*The Epimeric Mixture of 6,6-Dichloro-3-methyl-3,4-epoxy-5-hexene (**9a**).* Sodium methoxide (1.2 g, 0.022 mol) was added in several portions to a solution of 2.2 g (0.01 mol) of **8a** in 20 ml of dry ether at 0°C. The mixture was stirred at 0°C for 1 hr and then allowed to cool to room temperature. The mixture was poured into 20 ml of water and neutralized with dilute HCl. The ethereal layer was washed with water and dried over Na_2SO_4. After evaporation of the solvent the residual oil was distilled to yield 0.6 g (33%) of **9a**: bp 50—51°C/4 mmHg; IR (cm^{-1}, liquid) 3040 (=C–H and H–C(O)–C<), 2960—70, 1617 (C=C), 1250 (>C(O)–C<), 905, 865, 835, 812, 803, 690—660 (C–Cl); NMR (CCl_4) δ 0.97 (t, J=7.2 Hz, $-CH_2\underline{CH_3}$) and 1.0 (t, J=7.2 Hz, $-CH_2\underline{CH_3}$) (epimeric mixture, 3H), 1.24 (s, $>\overset{O}{\underset{\diagdown\diagup}{C}}-\underline{C}-\underline{CH_3}$, *cis* to $Cl_2C=CH-$) and 1.30 (s, $>\overset{O}{\underset{\diagdown\diagup}{C}}-\underline{C}-\underline{CH_3}$, *trans* to $Cl_2C=CH-$) (epimeric mixture, 3H), 1.35—1.90 (m, 2H, $-\underline{CH_2}CH_3$), 3.28 (d, 1H, J=7.5 Hz, H–C(O)–C<), 5.69 (d, 1H, J=7.5 Hz, $Cl_2C=\underline{CH}-$). Glpc analysis[7] of this product showed two very close peaks (the ratio of peak areas, 1 : 1) at the retention times (min), 4.5 and 4.7.

Found: C, 46.39; H, 5.88%. Calcd for $C_7H_{10}Cl_2O$: C, 46.44; H, 5.57%.

dl-*trans-6,6-Dichloro-3-methyl-3,4-epoxy-5-hexene (**9a**-I).* From 1 g (0.005 mol) of hexenol **8a**-I, treated with sodium methoxide in the same way as in the cyclization of the epimeric mixture (**8a**), 0.6 g (66%) of the glpc[7] pure product (**9a**-I) with the retention time (min) of 4.5 was obtained, oil: bp 62—64°C/6 mmHg; NMR (CCl_4) δ 0.97 (t, 3H, J=7.2 Hz, $-CH_2\underline{CH_3}$), 1.24 (s, 3H, $-\overset{O}{\underset{\diagdown\diagup}{C}}-\underline{C}-CH_3$, *cis* to $Cl_2C=\underline{CH}-$), 1.35—1.80 (broad q, 2H, J=7.2 Hz, $-\underline{CH_2}CH_3$, *trans* to $Cl_2C=\underline{CH}-$), 3.28 (d, 1H, J=7.5 Hz, $\underline{H}-\overset{O}{\underset{\diagdown\diagup}{C}}-\underline{C}-$), 5.69 (d, 1H, J=7.5 Hz, $Cl_2C=\underline{CH}-$). The IR spectrum of the purified sample (liquid) was identical with that of the epimeric mixture **9a**.

*The Epimeric Mixture of 6,6-Dichloro-3-methyl-5-hexene-3,4-diol (**10a**).* A mixture of 0.88 g (0.005 mol) of **9a** (**9a**-I/**9a**-II = *ca.* 1 : 1) and 50 ml of 20% H_2SO_4 was heated with stirring for 1 hr at 50°C. The ethereal extract of the reaction mixture was washed with water, and dried over Na_2SO_4. Removal of the solvent gave 0.5 g (52%) of white crystals (**10a**): mp 69—75°C (two recrystallizations from *n*-hexane); IR (cm^{-1}, nujol) 3300 (OH), 1620 (C=C), 910, 800—650 (C–Cl); NMR ($CDCl_3$) δ 0.94 (t, 3H, J=6.8 Hz, $-CH_2\underline{CH_3}$), 1.10 (s, 1.2H, $-CH_3$) and 1.20 (s, 1.8H, $-CH_3$) (epimeric mixture, 3H), 1.43 (broad q, 2H, J=6.8 Hz, $-\underline{CH_2}-CH_3$), 2.32 (s, 2H, 2-OH), 4.26 (d, 1H, J=9 Hz, $>\underline{CH}OH$), 8.02 (d, 1H, J=9 Hz, $Cl_2C=\underline{CH}-$).

dl-*erythro-6,6-Dichloro-3-methyl-5-hexene-3,4-diol (**10a**-I).* Hydrolysis of **9a**-I (0.57 g, 0.003 mol) carried out as above, afforded 0.34 g (55%) of white crystals exhibiting only one spot in tlc (R_f=0.17):[16] mp 75—82°C (two recrystallizations from *n*-hexane); IR (cm^{-1}, liquid) 3300 (OH), 1620 (C=C), 910, 800—650 (C–Cl); NMR ($CDCl_3$) δ 0.94 (t, 3H, J=6.8 Hz, $-CH_2\underline{CH_3}$), 1.20 (s, 3H, $-CH_3$), 1.43 (broad q, 2H, $-\underline{CH_2}CH_3$), 2.15 (s, 2H, 2OH), 4.26 (d, 1H, J=9 Hz, $>\underline{CH}-OH$), 6.02 (d, 1H, J=9 Hz, =CH–).

*5,5-Dichloro-4-penten-2-one (**13**).* A solution of 9.4 g (0.05 mol) of **1** in 30 ml of dry ether was added dropwise to 1.2 g (0.05 g atom) of magnesium at room temperature under the atmosphere of nitrogen. After being stirred for 2 hr, the mixture was acidified with 10% HCl. The ethereal layer was washed with water, dried over Na_2SO_4, and the solvent was then evaporated. The residual oil was distilled to give 2.2 g (29%) of **13**, oil: bp 51—55°C/5 mmHg; IR (cm^{-1}, liquid) 3050 (=C–H), 1720 (C=O), 1625 (C=C), 910; NMR (CCl_4) δ 2.20 (s, 3H, $-COCH_3$), 3.24 (d, 2H, J=6.75 Hz, $=CH-\underline{CH_2}-$), 6.03 (t, 1H, $=\underline{CH}-CH_2-$); mass spectrum (80 eV) *m/e* (relative intensity) 152 (31), 133 (14), 125 (35), 109 (53), 89 (42), 73 (44), 61 (38), 53 (34), 49 (39), 43 (100).

Found: C, 39,13; H, 3.89%. Calcd for $C_5H_6Cl_2O$: C, 39.25; H, 3.95%.

*Reaction of Ketone **2** with Grignard reagents **5a**, and **5c**.* Working up in the same ways as for **7a**, the reaction of ketone **2** (5 g, 0.02 mol) with **5a** (0.02 mol) gave 5.0 g of a

16) Conditions of tlc: support, Silica gel GF_{254} (E. Merk AG, Darmstadt), 0.2 mm; developer, *n*-hexane–acetone–chloroform (5 : 2 : 1 v/v); spray reagent, H_2SO_4-$KMnO_4$ (7 : 3 w/w).

light yellow oil. Tlc analysis[17] of this oil showed two spots at the R_f values 0.80 and 0.67, in the ratio 1 : 1. Pure sample of phenyl 2-trichloromethylbutyl ketone (**15i**) with the R_f value of 0.80 was separated by preparative tlc,[18] yield 45%; IR (cm^{-1}, liquid) 1692 (C=O), 1603 and 1586 (benzene ring); NMR (CCl_4) δ 0.98 (t, 3H, J=7.5 Hz, $-CH_2-C\underline{H}_3$). 2.0 (m, 2H, $-C\underline{H}_2CH_3$), 3.25 (m, 2H, $-C\underline{H}_2COC_6H_5$), 3.58 (m, 1H, $CCl_3C\underline{H}\langle$), 7.2—8.1 (m, 5H, $-C_6H_5$); mass spectrum (70 eV) (relative intensity) 278 (9, M^+, 3Cl), 206 (19), 120 (80), 105 (100), 77 (74).

Found: C, 51.37; H, 4.69%. Calcd for $C_{12}H_{13}Cl_3O$: C, 51.55; H, 4.69%.

The compound **7d** with the R_f value of 0.67 was similarly separated.

Ketone **2** *(5 g, 0.02 mol) and equimolar amount of* **5c**, worked up in the same ways as for **7a**, gave a mixture of light yellow needles (2.1 g) and a light brown oil (4.9 g). The crystals were separated by filtration and identified as compound **15j**: 125—126°C (from benzene); IR (cm^{-1}, liquid) 1680 (C=O), 1600 (benzene ring); NMR (CCl_4) δ 3.91 (d, 2H, J=6 Hz, $-CH_2CO$), 4.60 (t, 1H, J=6 Hz, $CCl_3C\underline{H}\langle$), 7.2—8.05 (m, 10H, $2C_6H_5$).

Found: C, 59.00; H, 4.12%. Calcd for $C_{16}H_{13}Cl_3O$: C, 58.66; H, 4.00%.

Tlc analysis[17] of the oily filtrate showed four spots at the R_f values 0.31, 0.52, 0.61, and 0.73, in the ratio 1 : 12 : 2 : 1. The spot of **15j** appeared at R_f 0.61. The component with the R_f value of 0.52 was separated by preparative tlc[18] and identified as **7e**.

*5,5,5-Trichloro-4-methoxy-2-pentanone (**15a**).* A solution of 5 g (0.027 mol) of **1** in 80 m*l* of dry methanol was refluxed for 9 hr. Excess methanol was removed *in vacuo*, and the residue, on distillation, gave 3.5 g (60%) of **15a**: bp 78°C/3 mmHg; IR (cm^{-1}, liquid) 1720 (ketone C=O); NMR (CCl_4) δ 2.19 (s, 3H, $-COCH_3$), 2.76 (dd, 1H, J=7.0 and 17.5 Hz, $-C\underline{H}_2COCH_3$), 3.10 (dd, 1H, J=3.7 and 17.5 Hz, $-C\underline{H}_2COCH_3$), 3.68 (s, 3H, $-OCH_3$), 4.24 (dd, 1H, J= 3.7 and 7.0 Hz, $\rangle C\underline{H}OCH_3$).

Found: C, 32.83; H, 4.07%. Calcd for $C_6H_9Cl_3O_2$: C, 32.83; H, 4.14%.

*4,5,5,5-Tetrachloro-2-pentanone (**15b**).* To a solution of 5 g (0.027 mol) of **1** in 30 m*l* of dry ether was passed dry hydrogen chloride gas at 0°C for 24 hr. The solvent was removed *in vacuo*, and the residue, on distillation, gave 5.9 g (98%) of **15b**: bp 87°C/3.5 mmHg; IR (cm^{-1}, liquid) 1720 (ketone C=O) and 790—770 (C–Cl); NMR ($CDCl_3$) δ 2.25 (s, 3H, $-CH_3$), 3.14 (dd, 1H, J=17.4 and 7.9 Hz, $-C\underline{H}_2-CO-$), 3.49 (dd, 1H, J=17.4 and 3.8 Hz, $-C\underline{H}_2CO-$), 4.97 (dd, 1H, J=7.9 and 3.8 Hz, $\rangle C\underline{H}Cl-$).

Found: C, 27.10; H, 2.91%. Calcd for $C_5H_6Cl_4O$: C, 26.82; H, 2.70%.

*5,5,5-Trichloro-4-anilino-2-pentanone (**15c**).* Fifteen grams (0.08 mol) of **1** and 7.4 g (0.08 mol) of aniline were dissolved in 10 m*l* of ether. The mixture was allowed to stand at room temperature for 10 hr, and then at 0°C—−5°C for 24 hr. The resulting solid was recrystallized from ether to afford 21.7 g (98%) of **15c**: mp 45°C; IR (cm^{-1}, nujol) 3320 (NH), 1703 (C=O), 1596 (benzene C=C), 768 and 750 (C–Cl).

Found: C, 47.40; H, 4.35; N, 4.90%. Calcd for $C_{11}H_{12}Cl_3NO$: C, 47.09; H, 4.31; N, 4.99%.

*5,5,5-Trichloro-4-(p-chloroanilino)-2-pentanone (**15d**).* A mixed solution of 15 g (0.08 mol) of **1** and 10.2 g (0.08 mol) of *p*-chloroaniline in 30 m*l* of ether similarly gave 22.8 g of a crude product, which was recrystallized from benzene to afford 21.6 g (90%) of **15d**: mp 115°C; IR (cm^{-1}, nujol) 3230 (NH), 1702 (C=O), 1590 (benzene C=C), 798 and 767 (C–Cl); NMR ($CDCl_3$) δ 2.2 (s, 3H, $-CH_3$), 2.85 (dd, 1H, J=16 and 8.0 Hz, $-C\underline{H}_2COCH_3$), 3.33 (dd, 1H, J=16 and 3.5 Hz, $-C\underline{H}_2COCH_3$), 4.87 (dd, 1H, $\rangle C\underline{H}CH_2COCH_3$), 6.65—7.22 (m, A_2B_2 with strong doublet centered at 6.93, 4H, aromatic).

Found: C, 41.92; H, 3.49; N, 4.13%. Calcd for $C_{11}H_{12}Cl_4NO$: C, 41.94; H, 3.52; N, 4.45%.

*5,5,5-Trichloro-4-phenylmercapto-2-pentanone (**15e**).* To a stirred solution of 10 g (0.053 mol) of **1** in 30 m*l* of benzene was added a solution of 6 g (0.053 mol) of thiophenol in 30 m*l* of benzene at 50°C. After the mixture was stirred at 50°C for 5 hr, the solvent was removed, and the residual solid was recrystallized from petroleum ether (bp 40—55°C) to afford 15 g (95%) of **15e**: mp 58°C; IR (cm^{-1}, nujol) 1720 (C=O), 1580 (benzene C=C), and 780—730 (C–Cl).

Found: C, 44.37; H, 3.56%. Calcd for $C_{11}H_{11}Cl_3OS$: C, 44.39; H, 3.73%.

*5,5,5-Trichloro-4-diethoxycarbonylmethyl-2-pentanone (**15f**).* To a stirred solution of 8.6 g (0.053 mol) of diethyl malonate in 80 m*l* of dry ether, 3.6 g (0.053 mol) of sodium ethoxide was added in several portions, and a solution of 10 g (0.053 mol) of **1** in 10 m*l* of dry ether was added dropwise at 0—5°C. The reaction mixture was stirred at 0°C for 1 hr, finally at room temperature for 1 hr, and then was made weakly acidic with dilute HCl (pH *ca.* 5). The ethereal extract of the organic layer was washed with water and dried over Na_2SO_4. Removal of the solvent left a yellow liquid which, on distillation, gave 13 g (70%) of **15f**: bp 155—157°C/5 mmHg; IR (cm^{-1}, liquid) 1745 and 1730 (C=O), and 790—760 (C–Cl).

Found: C, 41.74; H, 5.20%. Calcd for $C_{12}H_{17}Cl_3O_5$: C, 41.46; H, 4.93%.

*5,5,5-Trichloro-4-acetoxy-2-pentanone (**15g**).* A mixed solution of 1.5 g (0.018 mol) of sodium acetate and 3.4 g (0.018 mol) of **1** in 20 m*l* of acetic acid was refluxed for 30 min. It was diluted with 100 m*l* of water and then extracted with ether. The ethereal extract was washed with water and dried over Na_2SO_4. After recovery of the starting meterial at 94—96°C/20 mmHg, 0.4 g (9%) of the liquid distilling at a higher temperature was collected. Glpc analysis[7] showed it to contain 79% **15g**: IR (cm^{-1}, liquid) 2950, 1760 (acetoxy C=O), 1718 (ketone C=O), 770 (C–Cl).

Found: C, 33.72; H, 3.51%. Calcd for $C_7H_9Cl_3O_3$: C, 33.97; H, 3.66.

*5,5,5-Trichloro-4-phenoxy-2-pentanone (**15h**).* A mixed solution of 3.1 g (0.027 mol) of sodium phenoxide and 5 g (0.027 mol) of **1** in 45 m*l* of phenol was heated with stirring at 100°C for 4 hr. The reaction mixture was poured into a large amount of water and the organic layer was extracted with chloroform. The extract was washed with water and dried over Na_2SO_4. After recovery of chloroform and the starting materials, the fraction distilling at 123—125°C/3 mmHg was collected (1.4 g). Glpc analysis[19] showed it to contain 80% **15h** which was separated by preparative glpc: IR (cm^{-1}, liquid) 3050, 1723 (C=O), 1625 and 1593 (benzene ring), 770, 760, 700; NMR (CCl_4) δ 2.08 (s, 3H, $-COC\underline{H}_3$), 3.05 (m, 2H, $-C\underline{H}_2COCH_3$), 5.36 (dd, 1H, J=

17) Conditions of tlc: support, Silica gel GF_{254} (E. Merk AG, Darmstadt), 0.2 mm; developer, *n*-hexane-acetone (3 : 1 v/v); spray reagent, H_2SO_4–$KMnO_4$ (7 : 3 w/w).

18) Conditions of tlc: support, Silica gel GF_{254} (E. Merk AG, Darmstadt), 1 mm; developer, *n*-hexane-acetone (3 : 1 v/v); eluent, acetone.

19) Observed on a 1 m 10% Silicone SE-30 on Diasolid L. Column temp., 180°C; carrier gas, N_2 (0.7 kg/cm^2, 60 m*l*/min); detector, FID.

6 and 4.8 Hz, $>C\underline{H}CH_2-$), 6.85—7.35 (m, 5H, C_6H_5O-); mass spectrum (70 eV) *m/e* (relative intensity) 280 (4, M^+, 3Cl), 163 (15), 105 (70), 94 (98), 87 (35), 65 (37), 51 (51), 43 (100), 39 (47).

Found: C, 47.20; H, 4.15%. Calcd for $C_{11}H_{11}Cl_3O_2$: C, 46.92; H, 3.94%.

*2-Chloro-3-acetonyl-4-ethoxycarbonyl-5-methylfuran (**17**).* Sodium (2.3 g, 0.1 g atom) was dissolved in 80 m*l* of absolute ethanol with moderate cooling. To the resulting solution was added 13 g (0.1 mol) of ethyl acetoacetate at room temperature with stirring. A solution of 18.7 g (0.1 mol) of **1** in 20 m*l* of absolute ethanol was then added dropwise at 0°C with stirring. After stirring was continued for additional 2 hr at room temperature, 200 m*l* of water was added with cooling. After being acidified with 10% HCl, the mixture was extracted with ether. The ethereal solution was washed with water, dried over Na_2SO_4 and evaporated. The residual oil was distilled at 100—125°C/0.05 mmHg to give 4.4 g (18% yield) of **17**: mp 62°C (*n*-hexane); IR (cm^{-1}, nujol) 1715 (C=O), 1610 and 1577 (furan C=C), 785 (C–Cl); NMR (CCl_4) δ 1.33 (t, 3H, $-CH_2C\underline{H}_3$), 2.12 (s, 3H, $-CO-C\underline{H}_3$), 2.55 (s, 3H, furan $-CH_3$), 3.61 (s, 2H, $-C\underline{H}_2CO-$), 4.29 (q, 2H, $-C\underline{H}_2CH_3$); mass spectrum (80 eV) *m/e* (relative intensity) 246 (4.3), 244 (13), 204 (11), 203 (33), 202 (33), 201 (83), 175 (17), 173 (47), 156 (46), 43 (100).

Found: C, 54.30; H, 5.39%. Calcd for $C_{11}H_{13}ClO_4$: C, 54.00; H, 5.35%.

BULLETIN OF THE CHEMICAL SOCIETY OF JAPAN, VOL. 45, 3692—3698 (1972)

The Acid-catalyzed Degradation of Methyl 2,3,4,5-Tetra-*O*-acetyl-α-L-xylo-2-hexulopyranosonate. A Model for the Degradation of L-xylo-Hexulosonic Acid[1]

Kazuaki GOSHIMA, Norihide MAEZONO, and Kanji TOKUYAMA

Shionogi Research Laboratory, Shionogi & Co., Ltd., Fukushima-ku, Osaka, 553

(Received April 15, 1972)

The degradation reaction of L-xylo-hexulosonic acid (**1**) was studied, using methyl 2,3,4,5-tetra-*O*-acetyl-L-xylo-2-hexulopyranosonate (**11**) as a model compound. The degradation of **11** proceeded *via* two pathways, **11**→α,β-unsaturated ketone compound→a furan compound (path a) and **11**→a dihydropyrone compound→further decomposed products (not furans) (path b). The major pathway was path a in benzene and path b in water. The results supported the idea that the acid-catalyzed degradation of L-ascorbic acid (**2**) to furans would not proceed *via* **1**, but directly.

In spite of the long-standing interest in the degradation of L-ascorbic acid (**2**) in acidic solutions, the mechanism for the degradation under anaerobic conditions is still not well understood.[2-6] The reaction may be summarized in two major pathways. One involves the pathway of **2**→L-xylo-hexulosonic acid (**1**)→2-furaldehyde (**3**); the other involves the alternative one of **1**→**2**→**3**. The latter one seemed to have been established by kinetic studies,[5,6] whose validities were confirmed over wide ranges of acid concentration by our reinvestigation.[7] The former pathway, however, has recently received renewed attention because of the isolation of a new intermediate.[4] In this paper, we will attempt to study the behavior of **1** in acidic media when the conversion of **1** into **2** is inhibited. For this purpose, methyl 2,3,4,5-tetra-*O*-acetyl-α-L-xylo-hexulopyranosonate (**11**) was prepared as a starting material. If the pathway of **2**→**1**→**3** is probable, **11** can be converted into furan compounds.

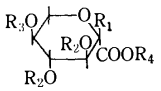

1: R_1=OH, R_2=R_3=R_4=H
4: R_1=OH, R_2=R_3=H, R_4=Me
5: R_1=OH, R_2=R_3=Ac, R_4=Me
6: R_1=OAc, R_2=Ac, R_3=H, R_4=Me
7: R_1=Br, R_2=R_3=Ac, R_4=Me
11: R_1=OAc, R_2=R_3=Ac, R_4=Me

33 **34**

Chart 1.

The acetylation of methyl L-xylo-hexulosonate (**4**)[8] gave a triacetate (**5**), which was converted into the desired **11** by further acetylation. The pyranose

1) Sorboses. Part 21. For Part 20, see Ref. 7. A part of this paper was reported in preliminary forms: K. Goshima and K. Tokuyama, *Tetrahedron Lett.*, **1969**, 2383; K. Goshima, N. Maezono, and K. Tokuyama, *Carbohyd. Res.*, **17**, 245 (1971).

2) S. Kamiya, *Nippon Nogei Kagaku Kaishi*, **33**, 398, 402 (1959); **34**, 13 (1960).

3) A. Cier, C. Nofre, and B. Drevon, *Bull. Soc. Chim. Fr.*, **1959**, 74.

4) T. Kurata and Y. Sakurai, *Agr. Biol. Chem.*, **31**, 179 (1967).

5) P. P. Regna and B. P. Caldwell, *J. Amer. Chem. Soc.*, **66**, 246 (1944).

6) R. Yamamoto and E. Yamamoto, *Yakuzaigaku*, **25**, 42 (1965).

7) K. Tokuyama, K. Goshima, N. Maezono, and T. Maeda, *Tetrahedron Lett.*, **1971**, 2503.

8) T. Reichstein and A. Gruessner, *Helv. Chim. Acta*, **17**, 311 (1934).

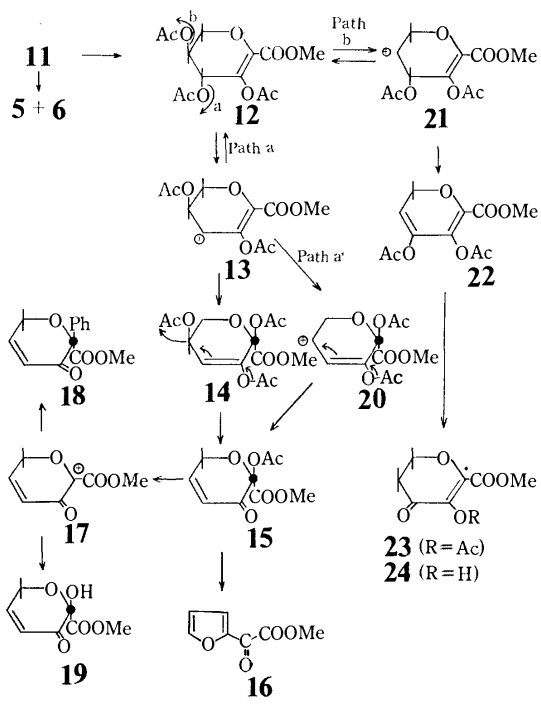

Chart 2.

structure of **11** was confirmed by the large coupling constants among ring-protons in the NMR spectrum.[9]

The heating of **11** in acetic acid–water (1 : 9, v/v) on a boiling-water bath gave no furan compounds. After 7 hr, four products, **5** and three unknown ones, were isolated by preparative thin-layer chromatography, along with the recovery of **11** to some extent. The elemental analysis of unknown products suggested them to be partially hydrolyzed derivatives of **11**; that is, one seemed to be the triacetate of **4** (**6**) and the others, to be diacetates. With **6**, the signals in the NMR spectrum were quite similar to those of **11**, but the multiplet due to H_5 shifted upfield. Therefore, the structure was determined to be methyl 2,3,4-tri-*O*-acetyl-L-xylo-hexulopyranosonate. The structures of diacetates were not determined, but the fact that the acetylation of them gave **11** suggested that they were hydrolyzed products of **11**. The results apparently showed that, in aqueous media, the degradation of **11** proceeded much slower than its hydrolysis; the studies under anhydrous conditions were clearly called for.

When **11** in dry benzene was treated with boron trifluoride-etherate, the reaction smoothly proceeded at a reflux temperature. The preparative thin-layer chromatography of the product gave three compounds **15**, **16**, and **18**, though trace amounts of other components were not isolated in pure states. The UV and IR spectra of **15** and **18** revealed bands indicative of α,β-unsaturated ketone and ester groups. The NMR spectra for ring-protons appeared as an ABXY system, which were similar to those previously reported for 1-*O*-acetyl-2-*O*-methyl-4,5-dideoxy-2,3-hexodiulopyranos-4,5-ene (**34**).[10] The spectra also suggested the presence of one acetoxyl group in **15** and one phenyl group in **18**. Therefore, **15** and **18** were identified as methyl 2-*O*-acetyl-4,5-dideoxy- and methyl 2-*C*-phenyl-2,4,5-trideoxy-2,3-hexodiulopyranosonate-4,5-ene respectively. Both compounds were racemates from optical rotations. The mass spectrum of **16** was identical with that of **3** except for the molecular ion peak (M^+)[11] and the IR spectrum showed the presence of ketone and ester groups. The structure of **16** was thus determined to be 2-methoxalylfuran. This structure was also supported by the NMR and UV spectra.

As **15** corresponded to the intermediates in the degradation of hexoses,[12] the degradation of **11** must proceed *via* the pathway of **11**→**15**→**16**. This idea was supported by the fact that the treatment of **15** in benzene containing boron trifluoride-etherate or in acetic acid–water gave **16**. As a small amount of **18** was also detected in the reaction of **15**, **18** must be formed *via* the pathway of **15**⇄**17**→**18**. The use of 1,2-dimethoxyethane as a solvent instead of benzene inhibited the formation of **18** and retarded the degradation rate. No further degradation of **18** was observed under the reaction conditions employed.

To elucidate the earlier stages of the degradation reaction in benzene, the reaction was performed under milder conditions. When **11** was treated at 60°C, the formation of **15** and a new compound was initially observed. The structure of the new compound was identified as the racemate of methyl 3,4,5-tri-*O*-acetyl-2-deoxy-L-threo-hexulopyranosonate-2,3-ene (**12**) by a comparison of its NMR and IR spectra with those of an authentic sample of **12**. The sample was prepared by a procedure similar to the preparation of 1,3,4,5-tetra-*O*-acetyl-2-deoxy-L-threo-hexulopyranos-2,3-ene (**33**)[10] to be described below. The aceto-bromination[13] of **4** gave a 2-bromo compound (**7**), while the dehydrobromination of **7** with mercuric cyanide in toluene yielded **12**, whose structure was confirmed by spectral data. Signals due to the ring protons of **12** appeared in an ABXY system quite similar to that of **33** in the NMR spectrum[10] and the characteristic band due to a double bond appeared in the IR. As the transformation of **33** to **34** under acidic conditions had already been established, the major pathway of the degradation of **11** was proposed to be **11**→**12**→**15**→**16**.

If the suggested pathway is reliable, the reaction rate (k_2) of **12**→**15** should be larger than that (k_1) of **11**→**12**, since the yield of **12** was very poor. Expectedly, the k_2/k_1 ratio given from the kinetic measurement of both reactions by following the decreases in the respective starting materials polarimetrically was about 15; consequently, it supported the pathway.

The fact that **11** was first isomerized to **12** prompted

9) T. Maeda, K. Tori, S. Satoh, and K. Tokuyama, This Bulletin, **41**, 2495 (1968); **42**, 2635 (1969).

10) M. Katsuhara, S. Wakahara, and K. Tokuyama, *ibid.*, **41**, 1208 (1968).

11) K. Heyns, R. Stute, and H. Scharmann, *Tetrahedron*, **22**, 2223 (1966).

12) E. F. L. J. Anet, *Adv. Carbohydrate Chem.*, **19**, 181, (1964).

13) R. U. Lemieux, "Methods in Carbohydrate Chemistry," Vol. 2, ed. by R. L. Whistler and M. L. Wolfrom, Academic Press, New York (1963), p. 221.

us to study the reaction of **12** as a starting material. First of all, reactions in benzene were examined. The treatment of **12** in boiling benzene containing boron trifluoride-etherate showed a tlc similar to that of the reaction of **11** under similar conditions. From the product, three major products, **15**, **18**, and **16**, and two minor ones were isolated. When the reaction was allowed to continue for longer periods of times, the amounts of **16** and **18** increased at the expense of **15**. This result also supported the existence of the above pathway of **12**→**15**→**16**.

The two minor products were identified, by a comparison of the tlc, as the minor components detected in the above-described reaction of **11** in benzene. One of them was also obtained by the mild hydrolysis of **15** and showed the characteristic bands due to hydroxyl and ester groups in the IR spectrum. Therefore, it was determined to be methyl 4,5-dideoxy-2,3-hexodiulopyranosonate-4,5-ene (**19**), which satisfied the NMR spectrum, too. As the mild hydrolysis of **15** yielded **19**, **19** must be formed by the hydrolysis of **15** during the reaction and/or preparative thin-layer chromatography.

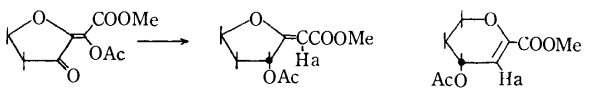

8 **10** **9**

Chart 3.

The other minor product showed the characteristic bands due to three kinds of carbonyl groups and a conjugate double bond in the IR spectrum. The NMR spectrum showed two 3-proton singlets due to one carbomethoxy and one acetoxyl and two 2-proton triplets, which constitute an A_2X_2 system. These spectral data suggested that this compound was a six-membered ring compound (**23**) or a five-membered ring one (**8**). The reduction of the compound with sodium borohydride in pyridine, followed by acetylation, gave a monoacetate. The combined data of spectral and elemental analyses, which showed the presence of one acetoxyl, one carbomethoxy and a double bond, suggested that the monoacetate was **9** or **10**. The signal due to Ha (see Chart 3) appeared as a doublet (J=5 Hz). As the Ha signal of **9** should appear as a doublet, and that of **10** as a singlet, the monoacetate was determined to be **9**; consequently, the parent compound must be **23**. The spectral data of analogus compounds also supported this conclusion.[14,15] The formation of **23** was very interesting. Although kojic acid and maltol are formed *via* enolone intermediates,[16] **23** was not derived from an enolone compound, **15**, and was not converted into furan derivatives on further acid treatments.

Chart 2 shows a summarized pathway of the reaction of **11**, which involves an initial 4→2 migration[10,17] of the acetoxyl group at C_4 of **12** (**11**→**12**→**13**→**14**→**15**→**16**, path a) and an initial elmination of the acetoxyl group at C_5 of **12** (**11**→**12**→**21**→**22**→**23**, path b). The racemization of **12** during the reaction supported the presence of the equilibrium among **12**, **13**, and **21**. In path a, the possibility of the 5→2 migration of the acetoxyl group (**11**→**12**→**13**→**20**→**15**→**16**, path a') could not be excluded, judging from the facts described below.

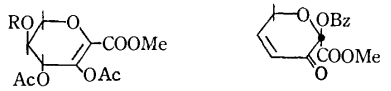

25: R=H
26: R=Bz

27

Chart 4.

The partial deacetylation of **12** under milder conditions, followed by benzoylation, gave 5-benzoate (**26**). The fact that the H_5 signal of a partially-deacetylated compound (**25**) appeared more in upfield than that of **12** supported the structures of **25** and **26**. The reaction of **26** under conditions similar to the above reaction afforded **15**, **16**, **18**, and **27**. The new product, **27**, was identified as the benzoyl analog of **15** by spectral and elemental analyses, and its formation suggested the existence of the 5→2 migration (path a').

It was difficult to study the degradation of **11** in aqueous media, since the hydrolysis of **11** was more rapid than the degradation. On the other hand, as **12** was established to be the initial intermediate in benzene, the reaction of **12** in acetic acid-water was carried out.

When **12** in water containing 10% acetic acid was heated on a boiling-water bath for 6 hr, multispots were detected in the tlc. From the chloroform extract of the product, three major components, **23**, **24**, and **25**, were isolated. Proof of the structure of the unknown compound, **24**, was provided by acetylation, which gave **23**. Among many minor components, **3** and **16** were successfully isolated. The water layer was evaporated to dryness. When the residue was dissolved in pyridine, the pyridine salt of oxalic acid was precipitated. After the removal of the salt by filtration, the pyridine solution was acetylated with acetic anhydride. The tlc of the product also showed many spots, from which relatively major component, **23**, and two unknown compounds, were isolated in pure states. The compound **23** isolated must naturally exist as **24** in the reaction medium. The NMR spectrum of the one of the unknown compounds showed one 3-proton singlet due to acetoxyl, one 1-proton singlet at a lower field and two 2-proton triplets, which constitute an A_2X_2 system. Therefore, its structure was identified as **32**. This structure was also supported by the UV and IR spectra. The other compound showed the characteristic band due to a carbonyl group in the IR spectrum, but no absorption

14) S. Gelin and R. Gelin, *Bull. Chim. Soc. Fr.*, **1969**, 1383.
15) K. Nakanishi, M. Nagao, and K. Okada, *Yakugaku Zasshi*, **88**, 1944 (1968).
16) F. W. Lichtenthaler and P. Heidel, *Angew. Chem. Int. Ed. Engl.*, **8**, 978 (1969).
17) R. J. Ferrier and N. Parasad, *J. Chem. Soc., C*, **1969**, 570.

maximum in the UV. The NMR spectrum showed two 3-proton singlet due to acetoxyl groups, one 2-proton singlet, and two 2-proton triplets of A_2X_2 system. Its structure was thus determined to be the acetate of 3-deoxy-tetroulose (**30**).

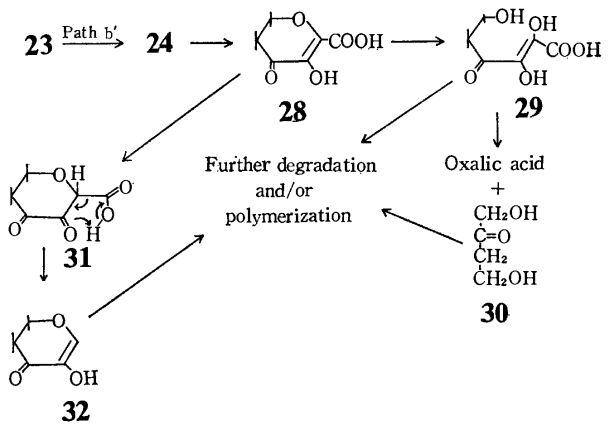

Chart 5.

Only a limited amount of 2-furaldehyde (**3**) was obtained from the degradation of **12** in water, contrary to that in benzene. The degradation in water must proceed mostly *via* path b (Chart 2), followed *via* path b′ (Chart 5). Some minor products were isolated, but their structures could not be determined. They must be further decomposed and/or polymerized products of the various intermediates shown in Chart 5. The possibility of path b′ was experimentally established; the treatment of **23** in acetic acid–water afforded oxalic acid, **30**, and **32**.

It is surprising that the pathway forming furans is not a major one in an aqueous solution. This fact suggested that **1** is not a probable intermediate in the acid-catalyzed degradation of **2**, as the kinetic data have previously presented.[5-7]

Experimental

All the melting points were recorded on a Kofler block and are uncorrected. The NMR spectra were taken in chloroform-*d* with a Varian A-60-A spectrometer using tetramethylsilane as the internal standard. The chemical shifts and coupling constants are expressed in τ unit and Hz respectively. The multiplicities of the signals are abbreviated as follows: s=singlet, d=doublet, t=triplet, q=quartet, and m=multiplet. The UV spectra were observed in 95% ethanol unless otherwise stated, and they are shown in nm. The IR spectra are expressed in cm^{-1}. The optical rotations were determined in a 10-cm microtube in chloroform containing 1% of ethanol, and the concentrations were recorded in percentages. Preparative thin-layer chromatography (ptc) and tlc were performed on a silica-gel plate. The solvent-systems (v/v) used were acetone and benzene (7 : 15, solvent A_1, and 1 : 4, solvent A_2), acetone and chloroform (1 : 9, solvent B), acetone and petroleum ether (1 : 3, solvent C), ether and benzene (7 : 15, solvent D_1, 1 : 3, solvent D_2, and 1 : 7, solvent D_3), ether and petroleum ether (4 : 1, solvent E_1, 7 : 3, solvent E_2, 3 : 2, solvent E_3, 1 : 1, solvent E_4, 2 : 3, solvent E_5, and 1 : 2, solvent E_6), and ether and chloroform (3 : 35, solvent F). The separated materials were developed with iodine vapor and the developed zones were extracted with acetone. Fraction 1 showed the fastest-moving components.

The evaporation of solvents used was carried out under reduced pressure.

*Methyl 3,4,5-Tri-O-acetyl-L-xylo-hexulopyranosonate (**5**).* To a solution of methyl L-xylo-hexulosonate (**4**)[8] (15 g) in pyridine (150 ml), we added, drop by drop, acetic anhydride (15 g) at −50°C. After stirring at the same temperature for 4 hr, the solution was evaporated to dryness. The residue was washed with petroleum ether and then recrystalized from ether, and then from a mixture of ethyl acetate and petroleum ether. The yield was 5.6 g, mp 109.6—112°C. $[\alpha]_D^{25.0}$ −27°(0.995). Found: C, 46.84; H, 5.47%; mol wt, 338. Calcd for $C_{13}H_{18}O_{10}$: C, 46.71; H, 5.43%; mol wt, 334.27.

*Methyl 2,3,4,5-Tetra-O-acetyl-α-L-xylo-hexulopyranosonate (**11**).* *(1) Synthesis*: A mixture of **5** (0.4 g), acetic anhydride (6 ml), and sodium acetate (0.4 g) was stirred at 70°C for 4 hr. The mixture was poured onto ice water, neutralized with sodium bicarbonate, and then extracted with chloroform. The chloroform solution was washed with water, and the chloroform was evaporated. The recrystallization of the residue from ether gave colorless columns; (0.32 g), mp 118—119°C. $[\alpha]_D^{25}$ −73.9° (0.973). NMR H_3, 4.48[d], ($J_{3,4}$ 10), H_4, 4.45[q] ($J_{4,5}$ 9.0), H_5, 4.89[m] ($J_{5,6}$, 6.0, $J_{5,6'}$, 10.5), H_6, 5.88[m] ($J_{6,6'}$, 11.5) $H_{6'}$, 6.46[m]. Found: C, 47.92; H, 5.37%; mol wt, 380. Calcd for $C_{15}H_{20}O_{11}$: C, 47.89; H, 5.36%; mol wt, 376.31.

(2) Reaction with Acetic Acid-water: A solution of **11** (2.0 g) in acetic acid–water (1 : 9, v/v) was heated for 7 hr on a boiling-water bath and then evaporated to dryness. The residual syrup was fractionated by ptc (solvent A_1). From Fraction 1, **11** (102 mg) was recovered. From Fractions 2, 3, and 4, **5** (53 mg), methyl 2,3,4-tri-*O*-acetyl-α-L-xylo-hexulopyranosonate (**6**) (328 mg) and a diacetate of **4** (92 mg) were obtained respectively. From Fraction 5 (the slowest-moving component), another diacetate of **4** (342 mg) was isolated. The acetylation of both the diacetates in a procedure similar to **5** gave **11**. **6**: mp 198—200°C. $[\alpha]_D^{25.0}$ −72.7° (1.019). NMR($CDCl_3$): H_5, 6.1[m]. Found: C, 46.95; H, 5.43%. Calcd for $C_{13}H_{18}O_{10}$: C, 46.71; H, 5.43%. Fraction 4 (a diacetate of **4**); Found: C, 45.02; H, 5.48%. Calcd for $C_{11}H_{16}O_9$: C, 45.21; H, 5.52%. Fraction 5 (a diacetate of **4**); Found: C, 45.22; H, 5.66%. Calcd for $C_{11}H_{16}O_9$: C, 45.21; H, 5.52%.

(3) Reaction in Benzene Containing Boron Trifluoride-etherate: (a) A solution of **11** (0.5 g) in dry benzene (5 ml) containing boron trifluoride-etherate (0.25 ml) was refluxed for 3 hr and then evaporated to dryness. The residual syrup was fractionated to two components by ptc (solvent D_1). The further ptc (solvent E_5) of the fast-moving component gave faster-moving 2-methoxalyfuran (**16**) (40 mg) and slower-moving **18** (4.5 mg). The purification of the slow-moving component by ptc (solvent D_1), followed by recrystallization from methanol, afforded **15** (41 mg). **15**: mp 95—96°C. $[\alpha]_{D.436}^{25.2}$ 0°. UV 226 (ε 9.8×10^3), 335 (ε 7.3×10). IR(KBr) 1762, 1700, 1629 (C=C, C=O). NMR H_4, 3.75[m] ($J_{4,5}$ 10.5, $J_{4,6}=J_{4,6'}$, 2), H_5, 2.88[m] ($J_{5,6}=J_{5,6'}$, 3), $H_{6,6'}$, 5.37[m]. Found: C, 50.65; H, 4.57%. Calcd for $C_9H_{10}O_6$: C, 50.47; H, 4.71%. **16**: mp 42—42.5°C (recryst. from ether and petroleum ether). UV 233 (ε 2.2×10^3), 291.5 (ε 1.2×10^4). IR(KBr) 1740, 1667 (C=C), 1557, 885 (furan).[18] NMR H_3, H_5, 2.2—2.35[m], H_4, 3.37[m] ($J_{3,5}$ 3.5, $J_{3,4}$ 1.5). Found: C, 54.59; H, 3.97%. Calcd for $C_7H_6O_4$: C, 54.55; H, 3.92%. **18**: syrup. $[\alpha]_D^{25.1}$ +2.0° (1.001). UV 296 (ε

18) A. R. Katritzky and L. M. Logowsky, *J. Chem. Soc.*, **1959**, 657.

3.5×10^2). IR(film) 1745, 1685, 1627 (C=O, C=C), 1548 (phenyl). NMR H_4, 3.78^m ($J_{4,5}$ 10.5, $J_{4,6}=J_{4,6'}$ 2.0), H_5, 3.03 ($J_{5,6}=J_{5,6'}$ 3.0) $H_{6,6'}$, 5.35^m, 5.60^m ($J_{6,6'}$ 19.5). Phenyl group (5H), 2.45—2.73^m. Found: C, 67.29; H, 5.45%; mol wt 243. Calcd for $C_{13}H_{12}O_4$: C, 67.23; H, 5.21%; mol wt 232.

(b) A solution of **11** (1.0 g) in dry benzene (10 ml) containing boron trifluoride-etherate (0.05 ml) was kept at 60°C for 10 hr, and then the solvent was removed. The residual syrup was fractionated by ptc (solvent E_1). Fractions 1, 2, 3 (a syrup, 101 mg), and **4** (a crystalline syrup, 692 mg) were obtained, but Fractions 1 and 2 could not be examined because of very limited amounts. The recrystallization of Fraction 3 gave **12** (5 mg), which was identified by a comparison of its IR and NMR spectra with those of an authentic sample (see below). However, the value of optical rotation was very small. [$[\alpha]^{25.0}$ 8° (1.00)]. The preparative thin-layer chromatography of Fraction 4 (solvent E_1) afforded **11** (529 mg) and **15** (40 mg).

Reaction of ***15****.* *(1) In the presence of Boron Trifluoride-etherate*: (a) A solution of **15** (20 mg) in dry benzene (0.5 ml) containing boron trifluoride-etherate (0.025 ml) was refluxed for 30 min and then evaporated to dryness. Preparative thin-layer chromatography (solvent E_1) of the residual syrup gave **16** (9 mg) and **18** (3 mg). (b) A solution of **15** (100 mg) in 1,2-dimethoxyethane (1 ml) containing boron trifluoride-etherate (0.05 ml) was stirred at 80°C for 20 hr and then evaporated to dryness. From the residue, a large part of the starting material was recovered, and **16** (36 mg) was isolated by ptc (solvent E_2).

(2) In Acetic Acid-water: A mixture of **15** (450 mg), acetic acid (0.5 ml) and water (4.5 ml) was heated on a boiling-water bath for 2 hr and then extracted with chloroform. The chloroform layer was evaporated to dryness and fractionated by ptc (solvent E_4). Forty-one miligrams of **16** and 7 mg of **15** were obtained. The water layer was also evaporated to dryness. The treatment of the residue with diazomethane, followed by purification by ptc (solvent E_4), gave **16** (26 mg).

(3) Hydrolysis: A solution of **15** (260 mg) in a mixture of methanol (2 ml), chloroform (2 ml) and one drop of hydrochloric acid was left to stand for 2 days at room temperature, and then the solvent was removed. The purification of the residue by ptc (solvent A_2) gave **19** (61 mg).

*Methyl 2-Deoxy-2-bromo-3,4,5-tri-*O*-acetyl-*L*-xylo-hexulopyranosonate* (***7***).* Acetic anhydride (260 ml) was cooled in an ice and water mixture, and then 60% perchloric acid (1.6 ml) was added, drop by drop. The solution was warmed to room temperature and **4** (64.5 g) was added to the stirred mixture at such a rate, over an about 30-min period, that the reaction temperature was kept between 30 and 40°C. The solution was then stirred at 0°C for 6 hr. Red phosphorus (19.4 g) was added slowly, and then bromine (116 g) was added at such a rate as to keep the reaction temperature below 20°C. Water (26 ml) was added, drop by drop, the continuously stirred and cooled mixture over an about 30-min period to pervent the temperature from rising above 20°C. The reaction mixture was kept for 10 hr at room temperature. Chloroform (60 ml) was added, and the mixture was filtered. The chloroform layer was washed with water, a saturated sodium bicarbonate solution and then water, subsequently it was dried, and the chloroform was removed. The recrystallization of the residue from ether gave needles of **7** (51 g), mp 107—109°C. $[\alpha]_D^{24.0}$ −134.8°(0.994). Found: C, 39.46; H, 4.35; Br, 20.41%; mol wt 400. Calcd for $C_{13}H_{17}O_9Br$: C, 39.28; H, 4.29; Br, 19.89%; mol wt 397.19.

*Methyl 3,4,5-Tri-*O*-acetyl-2-deoxy-*L*-threo-hexulopyranosonate-2,3-ene* (***12***).* *(1) Synthesis*: To a suspension of mercuric cyanide (13.7 g) in dry toluene (300 ml), a dry toluene solution (100 ml) of **7** (21 g) was added. Traces of water were removed by azeotropic distillation with toluene. After it had been refluxed for 10.5 hr with stirring, the reaction mixture was filtered and the filtrate was evaporated. The residue was extracted with chloroform (500 ml) and the chloroform was washed with a 30% potassium iodide solution and then water and dried. The subsequent removal of the chloroform gave a brown syrup. The repeated recrystallization of the syrup from ether gave needles of **12** (8 g), mp 109—111°C. $[\alpha]_D^{21.0}$ +236.9° (0.966). UV 243 (ε 7.6×10^3). IR(KBr) 1780—1720, 1655 (C=O, C=C). NMR H_4, 4.58^m, 5.02^m, H_6 5.60^m, $H_{6'}$ 5.97^m. Found: C, 49.41; H, 5.14%; mol wt 315. Calcd for $C_{13}H_{16}O_9$: C, 49.37; H, 5.10%; mol wt 316.26.

(2) Reaction in Benzene Containing Boron Trifluoride-etherate: A solution of **12** (1.0 g) in dry benzene (10 ml) containing boron trifluoride-etherate (0.5 ml) was refluxed with stirring, and then the solvent was removed. The residue was fractionated by ptc (solvent D_1). Fractions 1, 2, 3, 4, and 5 corresponded to **16**, **18**, **23**, **15**, and **19** respectively. The yields in mg are shown below:

Product	Reaction time			
	1 hr	3 hr	5 hr	13 hr[a]
15	194	157	27	56
18	31	32	41	—
16	22	47	131	115
23	54	46	22	32
19	trace	trace	trace	trace

a) As a solvent, 1,2-dimethoxyethane was used instead of benzene.

19: mp 48.49°C. $[\alpha]_D^{21.5}$ 0° (1.275). UV 226 (ε 9.9×10^3). IR(KBr) 3450 (OH), 1775, 1688, 1623 (C=O, C=C). NMR H_4, 3.75^m ($J_{4,5}$ 10.5, $J_{4,6}=J_{4,6'}$ 2), H_5 2.85^m ($J_{5,6}=J_{5,6'}$ 3), $J_{6,6'}$ 5.55^m, 5.25 ($J_{6,6'}=19$). Found: C, 48.96; H, 4.66%. Calcd for $C_7H_8O_5$: C, 48.84; H, 4.68%. **23**: mp 149—150°C (recryst. from methanol). UV 285 (ε 8.1×10^3), IR(nujol) 1765, 1739, 1689, 1620 (C=O, C=C). NMR $H_{5,5'}$, 5.22^t ($J_{5,6}$ 7), $H_{6,6'}$, 5.22^t. Found: C, 50.71; H, 4.77%; mol wt 218. Calcd for $C_9H_{10}O_6$: C, 50.47; H, 4.71%; mol wt 214.17.

(3) Reaction in Acetic Acid-Water: A solution of **12** (18 g) in acetic acid (18 ml) and water (162 ml) was heated on a boiling-water bath for 6 hr, and then, after cooling, extracted with chloroform (50 ml×4). The aqueous layer was evaporated to dryness. A syrup (5.9 g) was thus obtained (syrup C). The chloroform layer was washed with a 5% sodium carbonate solution (60 ml×2) and water, and dried, and then the chloroform was removed. An yellow syrup, (2.7 g) was thus obtained (syrup A). The sodium carbonate solution was made acid to pH 2 with hydrochloric acid, and extracted with chloroform, and then the chloroform was removed. Another syrup (520 mg) was thus obtained (syrup B). Syrup A was fractionated by ptc as follows:

The syrup B was purified by ptc (solvent B). Fifty-five milligrams of **24** were obtained.

The syrup C (2.0 g) was dissolved in dry pyridine (10 ml), and the pyridine salt of oxalic acid thus precipitated (424 mg) was collected by filtration. To the filtrate, we added acetic anhydride (10 ml). The solution was kept at room temperature for 2 days and then evaporated to dryness. The residue (2.4 g) was fractionated by ptc as follows:

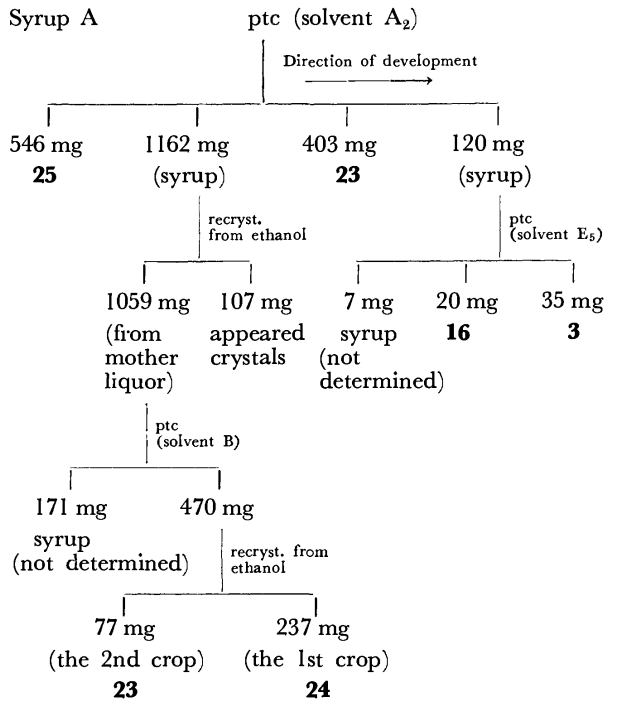

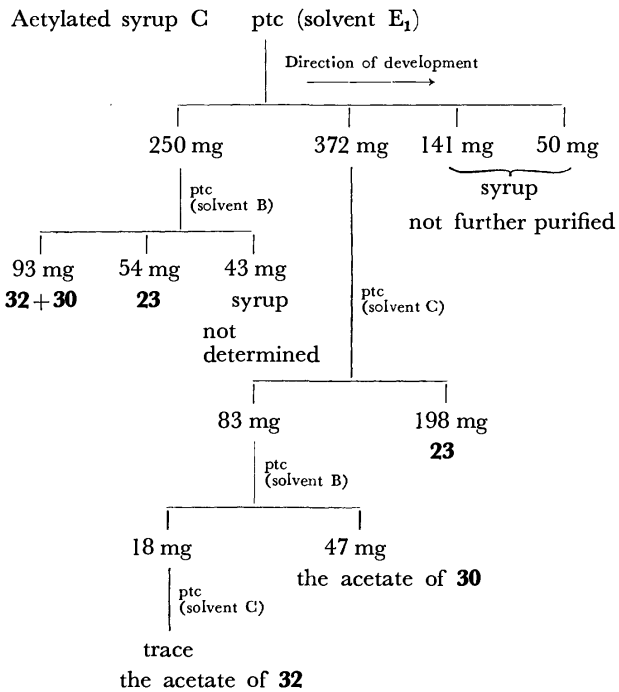

24: mp 78—79°C. UV 325 (ε 8.3×10^3). Found: C, 48.65; H, 4.65%; mol wt 182. Calcd for $C_7H_8O_5$: C, 48.84; H, 4.68%; mol wt 172.13. **32** (acetate): syrup. UV(MeOH) 267 (ε 7.9×10^3). IR(film) 1760, 1670, 1620 (C=O, C=C). NMR H_1 2.62^s, $H_{4,4'}$ 7.31^q, $H_{5,5'}$ 5.47, CH_3COO 7.81^s (Satisfactory elementary analysis was not obtained). **30** (acetate): syrup. IR(film) 745 (OAc). NMR H_1 5.32^s, $H_{3,4}$ 7.25^t, 5.65^t, CH_3COO 7.85^s, 8.00. Found: C, 51.14; H, 6.35%. Calcd for $C_8H_{12}O_5$: C, 51.66; H, 6.43%.

Reduction of ***23***. To a solution of **23** (3.0 g) in pyridine (70 m*l*) we added finely powdered sodium borohydride (0.8 g) at 0°C under cooling. The solution was allowed to stand for 3 days in a refrigerator, made acidic with acetic acid and then evaporated to dryness. The residue was added to a mixture of acetic anhydride (75 m*l*) and pyridine (75 m*l*), left to stand in a refrigerator for 4 hr, and then evaporated to dryness. The residue was purified by ptc (R_f 0.75, solvent D_2), followed by ptc (R_f 0.31, solvent E_6). Eighty-one grams of **9** were thus obtained as a syrup. UV 240 (7.4×10^3). IR(KBr) 1740, 1640 (C=O, C=C). NMR ACO 7.95^s, COOMe 6.19, H_3 (Ha) 3.89^d ($J_{3,4}$ 5.0), H_4 4.75^m, $H_{5,5'}$ 7.43—8.17^m, $H_{6,6'}$ 5.46—6.14^m. Found: C, 53.40; H, 6.10%; mol wt 210. Calcd for $C_9H_{12}O_5$: C, 53.99; H, 6.04%; mol wt 200.12.

Reaction of ***23*** *in Acetic Acid–Water.* (1) A mixture of **23** (500 mg), acetic acid (0.5 m*l*), and water (4.5 m*l*) was heated on a boiling-water bath. After 3 hr, the reaction mixture was worked up in a manner similar to the one described above. The acetate of **30** (31 mg) was obtained.

(2) A mixture of **23** (2.5 g), acetic acid (2.5 ml) and water was heated on a boiling-water bath for 6 hr, and then worked up in a manner similar to the one described above. The pyridine salt of oxalic acid (10 mg), the acetate of **30** (15 mg), **24** (248 mg), and a mixture of the acetates of **30** and **32** (28 mg) were obtained.

*Methyl 3,4-Di-*O*-acetyl-*L*-*threo*-hexulopyranosonate-2,3-ene (****25****).* To a solution of **12** (4.0 g) in a mixture of dioxane (10 m*l*) and methanol (400 m*l*), we added a solution of potassium carbonate (2.0 g) in water (10 m*l*) below 5°C. After stirring for 30 min, the solution was neutralized by Amberlite IR 120 and then evaporated to dryness. The purification of the residue by ptc (solvent A_2) gave **25** (syrup, 0.68 g). $[\alpha]_D^{22}+222.1°$ (0.592). UV 247.5 (ε 1.47×10^4). IR(CCl_4) 3500 (OH). 1780, 1750, 1675 (C=O, C=C). NMR H_4 5.65^m, H_5 5.9—6.2^m. Found: C, 47.88; H, 5.35%; mol wt 295. Calcd for $C_{11}H_{14}O_8$: C, 48.14; H, 5.15%; mol wt, 274.32.

*Methyl 3,4-Di-*O*-acetyl-5-*O*-benzoyl-*L*-threo-hexulopyranosonate-2,3-ene (****26****).* *(1) Synthesis*: To a solution of **24** (1.0 g) in pyridine (10 ml), we added freshly distilled benzoyl chloride (1.0 g) under cooling, and then the mixture was left to stand overnight in a refrigerator. The solution was poured into water and extracted with chloroform. The chloroform was washed with 5% hydrochloric acid, a 5% sodium carbonate solution and then water, and dried, and the solvent was removed. The residual syrup was purified by ptc (solvent D_3). One gram of **26** was thus obtained, mp 120—121.5°C. $[\alpha]_D^{25.6}+256.7°$ (0.379). UV 233.5 (ε 2.0×10^4), 282 (ε 9.4×10^2). IR(KBr) 1777, 1743, 1727, (C=O, C=C). 1600 (phenyl). NMR H_4 4.41^m, H_5 4.75^m ($J_{4,5}$ 2.5), H_6 5.42^m ($J_{5,6}$ 3.0, $J_{4,6}$ 1.5), $H_{6'}$ 5.86^m ($J_{5,6}=J_{4,6}$ 1.5). Found: C, 57.29; H, 4.92%. Calcd for $C_{18}H_{18}O_9$: C, 57.14; H, 4.80%.

(2) Reaction in Benzene Containing Boron Trifluoride-etherate: A solution of **26** (750 mg) in dry benzene (7.5 m*l*) containing boron trifluoride-etherate (0.4 m*l*) was refluxed for 1 hr and then evaporated to dryness. The residue was fractionated into two fractions by ptc (solvent D_3). The slow-moving compound (270 mg) was **15**. The fast-moving fraction was further fractionated to two fractions and benzoic acid by ptc (solvent F). The fast-moving fraction (18 mg) contained **16** and **18**, and the slow-moving one, **27**. **27**: syrup. $[\alpha]_D^{25.6}$ 0.° UV 232.5 (ε 2.1×10^4), 276 (ε 1.2×10^3). IR (CCl_4) 1778, 1747, 1626 (C=O, C=C). Found: C, 60.99; H, 4.55%. Calcd for $C_{14}H_{12}O_6$: C, 60.87; H, 4.38%.

*Methyl 2-*O*-Benzoyl-4,5-dideoxy-2,3-hexodiulopyranosonate-4,5-ene (****27****).* To a solution of **19** (0.1 g) in pyridine (1 ml) we added benzoyl chloride (0.1 g), and then the mixture was left overnight in a refrigerator. The solution was poured into water and extracted with chloroform. The chloroform

was washed with 5% hydrochloric acid, a 5% sodium carbonate solution and then water; subsequently it was dried, and the solvent was removed. The residue was purified by ptc (solvent E_3), Pure **27** (0.1 g) was thus obtained.

*The Decrease Rates of **11** and **12**.* Kinetic measurements were made polarimetrically. About 0.025 mol of **11** (or **12**) was dissolved in an appropriate volume of benzene in a 250-m*l* volumetric flask at 50°C. Boron trifluoride-etherate (1 m*l*) was added to the solution, and the flask was filled exactly to the mark with benzene at 50°C. Samples (2 m*l*) was quickly transfered to a 5-m*l* volumetric flask containing triethylamine (0.1 m*l*); the flask was filled exactly with methanol at 25° for an optical rotation determination at 578 nm. The decreases in optical activities obeyed first-order kinetics. k_1 (decrease of **11**): 2.9×10^{-5} sec^{-1}; k_2 (decrease of **12**): 4.4×10^{-4} sec^{-1}.

BULLETIN OF THE CHEMICAL SOCIETY OF JAPAN, VOL. 45, 3698—3702 (1972)

Reduction of 7-Methylenebicyclo[3.3.1]nonan-3-one and Related Compounds: Structural Investigation of the Products

Koichi KIMOTO, Takeshi IMAGAWA, and Mituyosi KAWANISI

Department of Industrial Chemistry, Faculty of Engineering, Kyoto University, Yoshida, Sakyo-ku, Kyoto 606

(Received April 24, 1972)

Hydrogenation of 7-methylenebicyclo[3.3.1]nonan-3-one (**1**) over platinum oxide in acetic acid yielded 7α-methylbicyclo[3.3.1]nonan-3α-ol (**2**) as the sole product. Hydrogenation of (**1**) in ethyl acetate afforded 7α-methylbicyclo[3.3.1]nonan-3-one (**3**) as a reduced product and 7-methylbicyclo[3.3.1]non-6-en-3-one (**4**) as an isomerized product. Hydrogenation of **1** over palladium on carbon gave no reduced product but **4** in 100% conversion. Hydrogenation of 7-methylenebicyclo[3.3.1]nonan-3α-ol (**7**) and -3β-ol (**8**) over platinum oxide in acetic acid gave **2** and 7α-methylbicyclo[3.3.1]nonan-3β-ol (**5**), respectively. From studies based on NMR spectroscopy with use of a shift-reagent, it is concluded that the major conformer of **2** and **5** is of chair-boat form. By the equilibration experiment between **2** and **5** using aluminum isopropoxide in isopropyl alcohol at 110°C, the ΔG° value was found to be −2.2 kcal/mol.

In the bicyclo[3.3.1]nonane system, the preferred conformation is believed to possess a double chair form so long as the substitutents at C-3 and/or C-7 have β-configuration. Crystallographic investigation[1] has indicated that the preferred conformation of the bicyclo[3.3.1]nonane skeleton is of a double chair form in spite of the considerable interactions between the α-hydrogen atoms at C-3 and C-7. If this system takes predominantly such a preferred conformation, two interesting phenomena can be expected, a transannular reaction involving C-3 and C-7 and a steric effect toward the reagents. Examples of these phenomena have been given by many workers.[2] We have also reported on some novel transannular reactions.[3]

However, when a bulky substituent at C-3 has α-configuration, the substituted cyclohexane ring has been reported to exist in a boat conformation.[4-10] It has been reported that the symmetrically 3α,7α-disubstituted bicyclo[3.3.1]nonanes exist as an equilibrium mixture or in a double boat conformation owing to the bulkiness of the substituent.[11] The report prompted us to publish our study on the conformation of the compound unsymmetrically disubstituted at C-3 and C-7 both in α-configuration.

Catalytic hydrogenation of 7-methylenebicyclo[3.3.1]-nonan-3-one[12] (**1**) in acetic acid over platinum oxide gave exclusively 7α-methylbicyclo[3.3.1]nonan-3α-ol (**2**). However, hydrogenation in ethyl acetate gave 7α-methylbicyclo[3.3.1]nonan-3-one (**3**) and an isomerized product, 7-methylbicyclo[3.3.1]non-6-en-3-one (**4**). All the reductions gave stereospecifically α-substituted products. The geometry of the reduction product (**2**), in which both the hydroxyl and methyl groups have α-configuration, and that of the epimeric alcohol (**5**) were studied by NMR spectroscopy, analy-

1) M. Dobler and J. D. Dunitz, *Helv. Chim. Acta*, **47**, 695 (1964); W. A. C. Brown, J. Martin, and G. A. Sim, *J. Chem. Soc.*, **1965**, 1844; W. A. C. Brown, G. Eglington, J. Martin, W. Parker, and G. A. Sim., *Proc. Chem. Soc.*, **1964** 57; I. Laszlo, *Rec. Trav. Chim. Pays-Bas*, **84**, 251 (1965).

2) For pertinent references see G. D. Buchanan, "Topics in Carbocyclic Chemistry," Vol 1, Ed. by D. Lloyd, Ed., Logos Press, London (1963), p. 236; R. C. Bingham and P. v. R. Schleyer, "Topics in Current Chemistry 18, Chemistry of Adamantane," Springer-Verlag, Berlin (1971); A. C, Cope, M. M. Martin, and M. A. Mc-Kervey, *Quart. Rev.*, (London), **20**, 119 (1966).

3) a) T. Mori, K. Kimoto, M. Kawanisi, and H. Nozaki, *Tetrahedron Lett.*, **1969**, 3653, b) T. Mori, K. H. Yang, K. Kimoto, and H. Nozaki, *ibid.*, **1970**, 2419, c) M. Kawanisi and H. Kato, *ibid.*, **1970**, 721, d) K. Kimoto and M. Kawanisi, *Chem. Ind.* (London), **1971**, 1174.

4) W. D. K. Macrosson, J. Martin, and W. Parker, *Tetrahedron Lett.*, **1965** 2589.

5) a) C.-Y. Chen and R. J. W. Le Fèvre, *J. Chem. Soc. B*, **1966**, 539; b) C.-Y. Chen and R. J. W. Le Fèvre, *Tetrahedron Lett.*, **1965**, 737.

6) E. N. Marvel and R. S. Knutson, *J. Org. Chem.*, **35**, 388 (1970).

7) M. Fisch, S. Smallcombe, J. C. Gramain, M. A. McKervey, and J. E. Anderson, *ibid.*, **35**, 1886 (1970).

8) M. A. Eakin, J. Martin, and W. Parker, *Chem. Commun.*, **1968**, 298.

9) R. A. Appleton, D. H. G. C. Egan, J. M. Evans, S. H. Graham, and J. R. Dixon, *J. Chem. Soc. C*, **1968**, 1110.

10) J. M. McEuen, R. P. Nelson, and R. G. Lawton, *J. Org. Chem.*, **35**, 690 (1970).

11) D. A. Peters, J. D. Remijnse, A. van der Wiele, and R. van Bekkum, *Tetrahedron Lett.*, **1971**, 3065.

12) A. R. Gagneux and R. Meier, *ibid.*, **1969**, 1365.

sis of the patterns of the carbinyl protons, and with a shift-reagent developed for expansion of the chemical shift to analyze the signals.[13] The preferred conformations of **2** and **5** were concluded to be of boat-chair form. Equilibration between **2** and **5** with aluminum isopropoxide in isopropyl alcohol at 110°C gave a mixture consisting of 94.6% of **5**. The $\Delta G°$ value was calculated to be −2.18 kcal/mol. This could be considered as the gross energy difference between the two 1,3-diaxial hydroxyl-methylene interactions of the distorted cyclohexanol ring in **2** and the two 1,3-diaxial methylene-hydrogen interactions of the chair form in **5** providing that the methylcyclohexane ring takes a boat form.

Results and Discussion

We have reported two new transannular reactions of **1**; photoreduction[3b] leading to 7-methyl-3-noradamantanol (**6**) and diimide reduction[3d] giving the same compound in high yield. Our observations suggest that **1** might exist predominantly in a double chair form. In such a case, catalytic hydrogenation may be expected to occur exclusively from the less hindered β-face of the substrate (**1**). Actually, when hydrogenation of **1** over platinum oxide was conducted in acetic acid, 7α-methylbicyclo[3.3.1]nonan-3α-ol (**2**) was obtained quantitatively and stereospecifically. The compound was also obtained as a sole product by the hydrogenation of 7-methylene-bicyclo[3.3.1]nonan-3α-ol (**7**)[8] under the same conditions, whereas the same hydrogenation of 7-methylenebicyclo[3.3.1]nonan-3β-ol (**8**)[8] afforded 7α-methylbicyclo[3.3.1]nonan-3β-ol (**5**). Configuration-α of the methyl group in **2** and **5** was established by the oxidation of either **2** and **5** to give the same compound, 7α-methylbicyclo[3.3.1]nonan-3-one (**3**), the structure of which was confirmed by the fact that the compound (**3**) differs from the known 7β-methylbicyclo[3.3.1]nonan-3-one (**9**)[14] in all respects. The configurational assignments of the hydroxyl groups were not only obvious from the reaction schemes, but were also confirmed by the observation that lithium aluminum hydride reduction of **3** gave a mixture of **2** and **5** in the ratio 4 : 1, since the reagent preferably attacks from the sterically less hindered β-face.[15]

Hydrogenation of **1** over platinum oxide in ethyl acetate gave 7α-methyl ketone (**3**) as the reduced product together with **4** resulting from the migration of the double bond. When this reaction was allowed to proceed to completion, **4** was converted slowly but exclusively into **3**. When the amount of the catalyst was reduced (0.01 mol ratio), **3** and **4** were obtained in the ratio 3 : 2. The structure of **4** was assigned on the basis of IR, NMR, and elemental analysis. The reaction was followed by glc, which shows that at 50% hydrogenation, **4** was already formed together with **3**, and when the reaction was allowed to proceed further the amount of **3** increased at the expense of **4**. Pure sample of **4** afforded **3** when allowed to react for an extended period under the same conditions. This shows unamibiguously that hydrogenation and isomerization compete in the reaction of **1** under neutral conditions. When **1** was refluxed in ethanol under an atmosphere of nitrogen for 24 hrs, an isomeric mixture (**1** : **4**=2 : 1) was obtained. Attempted hydrogenation of **1** over palladium on carbon in ethanol failed and resulted in the complete isomerization into **4**.

Several workers[4-7] concluded from analysis of the NMR patterns corresponding to the carbinyl proton in the bicyclo[3.3.1]nonan-3-ols (**10**, **11**, **13**), that in the β-ols the major conformer is of a double chair form but in the α-ols the cyclohexanol ring exists in a boat form as a more stable conformer. In the same way, the conformation of the cyclohexanol rings of the two epimers (**2** and **5**) were studied by analysis of the patterns of the carbinyl protons by the first order approximation. The coupling constants obtained are shown in Table 1 with the values of the analogous compounds. The values for the β-ol (**5**); $J_{3,2\beta}$=11.4 and $J_{3,2\alpha}$=5.3 Hz indicate that the cyclohexanol ring exists in a normal chair form with an equatorial hydroxyl group as compared with the other β-ols. The values obtained for α-ol (**2**), $J_{3,2\beta}$=6.1 and $J_{3,2\alpha}$=1.1 Hz, differing from the other α-ols in the boat form, indicate that the cyclohexanol ring takes a chair ar-

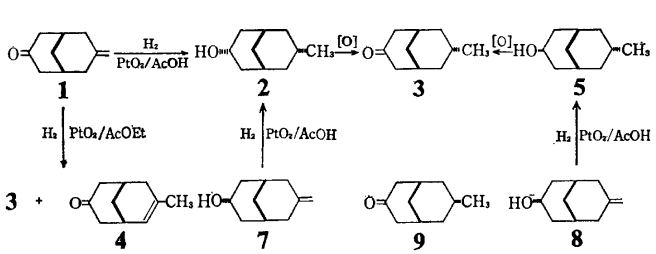

Scheme 1.

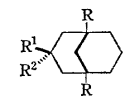

10a R=R¹=H, R²=OH
10b R=R²=H, R¹=OH
11a R=CH_3, R¹=H, R²=OH
11b R=CH_3, R¹=OH, R²=H
12a R=R¹=H, R²=$COOCH_3$
12b R=R²=H, R_1=$COOCH_3$

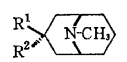

13a R¹=H, R²=OH
13b R¹=OH, R¹=H

14a R=COOH
14b R=$COOCH_3$
14c R=$C(CH_3)_2OH$

Formula 1.

13) For extensive literature survey see W. D. Horock, Jr., J. R. Sipe, III, and J. R. Luber, *J. Amer. Chem. Soc.*, **93**, 5258 (1971).
14) M. A. Eakin, J. Martin, W. Parker, C. Egan, and S. H. Graham, *Chem. Commun.*, **1969**, 737.
15) J. P. Schaefer, J. C. Lark, C. A. Flegal, and L. M. Honig, *J. Org. Chem.*, **32**, 1372 (1967).

Table 1. Coupling constans of H_3-H_2 in the bicyclo[3.3.1]nonane systems

Compound	Substituent (s)	$J_{3,2\beta}$	$J_{3,2\alpha}$	Supposed Conformation	Reference
2	α	6.1	1.1	chair	this work
5	β	11.4	5.3	chair	this work
10a	α	6.2	10.0	boat	7
11a	α	6.6	9.0	boat	4
11b	β	11.4	6.6	chair	4
13a	α	4	11	boat	5
13b	β	9.8	6.9	chair	5
14a	α,α	7.1[a]	7.1[a]	boat-chair	11
14b	α,α	7.1[a]	7.1[a]	boat-chair	11
14c	α,α	6.0	12.0	boat-boat	11

a) Time-averaged values for the boat-chair equilibrium.

rangement with an axial hydroxyl group. It was reported[16] that in ring A of steroids where the ring is known to be in a regular chair form, the vicinal coupling constants are $J_{3,2\beta}\cong 10$ and $J_{3,2\alpha}=5.5\pm1.0$ Hz for the axial carbinyl proton and $J_{3,2\beta}=J_{3,2\alpha}=2.0$—3.2 Hz for the equatorial carbinyl proton. If we take the above steroid system as a model, the chair form of the cyclohexanol ring of **2** might be supposed to undergo a considerable distortion[17] or make some contribution of the boat form to the conformational equilibrium, since flattening would increase one dihedral angle (between $H_{(3)}$ and $H_{(2)}$) and decrease the other from their initial values of 60°, which would lead to a somewhat smaller value for $J_{3,2\alpha}$ and a slightly larger value for $J_{3,2\beta}$.

The deduction that the cyclohexanol rings in **2** as well as **5** take chair conformations seems curious from the fact that the boat form is preferred in all α-ols (**10a**, **11a**, **13a**). To obtain information on the conformation, the NMR spectra of **2** and **5** were studied with NMR shift-reagent, $Eu(DPM)_3$, which complexes with a lone pair to induce shift mainly dependent on Eu–H distances.[13]

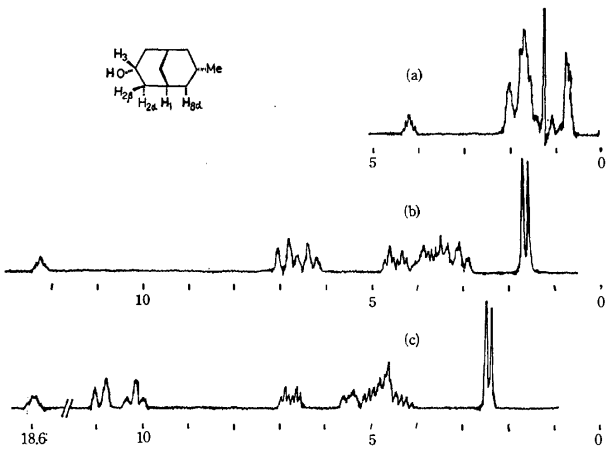

Fig. 1. 60 MHz NMR spectra of **2** in $CDCl_3$ containing $Eu(DPM)_3$ (a) 0, (b) 0.3 and (c) 0.5 in mole ratio.

NMR spectra of **2** before and after addition of 0.3 and 0.5 molar ratio of $Eu(DPM)_3$ are shown in Fig. 1. In spectrum 1(b), the one-proton signal at the lowest field (δ 12.3) is assignable to the carbinyl proton from chemical shift. On irradiation at this signal position, the doublet of triplets (2H) centered at δ 4.60 collapsed into a two-line multiplet, indicating that the signal is assignable to $H_{(2\beta)}$. However, the assignment of β-configuration mainly rested in the generality[18] that the extent of deshielding to the protons located vicinally to a hydroxyl group appears to be dependent upon the magnitude of the dihedral angle between the hydroxyl group and the proton under consideration when $Eu(DPM)_3$ was used as the shift-reagent. The two-line multiplet (2H) centered at δ 6.96 is assigned to $H_{(2\alpha)}$ from the spacing of 15 Hz which is included also in the signal of $H_{(2\beta)}$ and from the mutual decoupling experiments (although imperfect) with the $H_{(2\beta)}$. From these signals in the spectra 1(b) and 1(c), the following coupling constants were obtained; $J_{3,2\beta}=6.0$, $J_{3,2\alpha}<1.5$, $J_{2\alpha,2\beta}=15$, $J_{1,2\beta}=4.5$ Hz. They are reasonably coincident with those obtained earlier. The three-line multiplet (2H) centered at δ 6.44 (Fig. 1 (b)) is assigned to $H_{(8\alpha)}$ because the signal collapsed into a two-line multiplet upon irradiation at the point where maximum coalescence of the three-proton

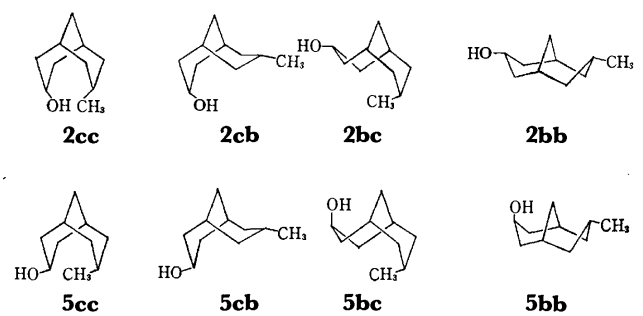

Formula 2.

16) L. M. Jackman and S. Sternhell, "Application of Nuclear Magnetic Resonance Spectroscopy in Organic Chemistry," 2nd Ed., Pergamon Press, Oxford (1969), p. 283.

17) As a rough approximation the deviation ($\Delta\Phi$) from the normal value (60°) was calculated as 22.5°, using the relationship $J=J_0\cos^2\Phi-C$(Ref. 16, p. 281) provided that $J=3.0$ Hz at $\Phi=60°$(taking the value for the equatorial carbinyl proton as a model (see text)), $J=6.1$ Hz at $\Phi=60°-\Delta\Phi$, and $J=1.1$ Hz at $\Phi=60°+\Delta\Phi$ were adopted.

18) P. V. Demarco, T. K. Elzey, R. B. Lewis, and E. Wenkert, *J. Amer. Chem. Soc.*, **92**, 5737, 5739 (1970).

doublet (δ 1.70) of the methyl protons could be obtained. It should be noted that the signal due to $H_{(8\alpha)}$ is more shifted than that of $H_{(2\beta)}$ indicating that $H_{(8\alpha)}$ proton is situated in the proximity of the hydroxyl group; this requires the cyclohexanol ring to be in the chair form and the methylcyclohexane ring in the boat form (2cb). The observation that the methyl protons are shifted much less than the other protons at both concentrations of $Eu(DPM)_3$ (1(b) and 1(c) in Fig. 1) suggests that the methyl group is located farthest from the hydroxyl group; this requires the methyl cyclohexane ring to be in a boat conformation since the cyclohexanol ring exists in a chair form.

NMR spectra of the epimeric alcohol (**5**) before and after addition of $Eu(DPM)_3$ in molar ratios 0.3 and 0.5 are shown in Fig. 2; the decoupling experiments and the assignments were made on spectrum 2(c).

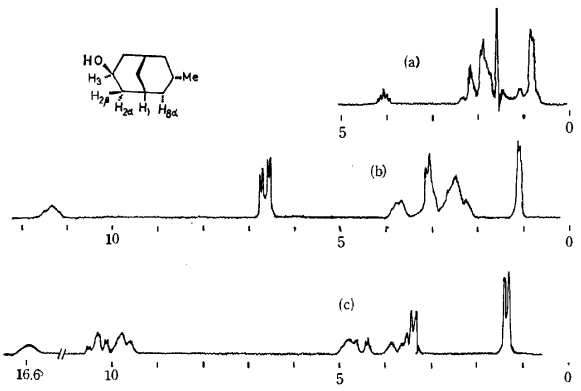

Fig. 2. 60 MHz NMR spectra of **5** in $CDCl_3$ containing $Eu(DPM)_3$ (a) 0, (b) 0.3 and (c) 0.5 in mole ratio.

From the change in pattern induced by the irradiation at the one-proton signal at δ 16.60 due to the carbinyl proton ($H_{(3)}$), the signals (each 2H) centered at δ 10.35 and 9.76 are assigned to $H_{(2\alpha)}$ and $H_{(2\beta)}$. Judging from these signals especially on the irradiation at the $H_{(1)}$ signal (the assignment is mentioned later), the following values are obtained; $J_{3,2\beta}=11$, $J_{3,2\alpha}=ca.$ 5, $J_{2\alpha,2\beta}=14$, $J_{1,2\beta}=3$ Hz. They indicate that the cyclohexanol ring is in a normal chair conformation with an equatorial hydroxyl group. In contrast to the case of **2**, the infiuence of the shift-reagent on the $H_{(8\alpha)}$ (tentatively assigned to the signal at δ 4.55) is much smaller. The smallest effect of the shift-reagent on the methyl protons implies that the methylcyclohexane ring takes a boat form since the cyclohexanol ring exists in the chair form.

Another assignable proton in **2** and **5** is the bridgehead proton ($H_{(1)}$) judging from the featureless broadening due to the six vicinal protons and from the decoupling experiments irradiated at the $H_{(2\beta)}$ signals. The signals have a half-height width of 18.1 Hz (δ5.5) in spectrum 1(c) for **2** and 18.5 Hz (δ4.8) in 2(c) for **5**.

The deduction that in **2** and **5** the methylcyclohexane ring exists in a boat conformation might be supported by the following fact. In the IR spectra of the bicyclo[3.3.1]nonane systems which exist predominantly in a double chair conformation, the stretching and bending bands are known to appear in the abnormally higher-frequency region (near 2990 and 1490 cm^{-1}, respectively.)[19] Both **2** and **5** show no such absorption. This indicates the relief of strain due to the double chair form.

In consequence, the actual preferred conformer for **2** is the boat-chair form (**2cb**) with a considerable flattening of the cyclohexanol ring or with a slight contribution of the double boat form (**2bb**) to the equilibrium.[20] In the case of **5** the boat-chair form (**5cb**) is predominantly preferred.

Two 1,3-diaxial methyl-methylene interactions may be estimated roughly to be 2×3.7 kcal/mol and two 1,3-diaxial hydroxyl-methylene interactions to be $2\times$ 2.4 kcal/mol.[21] This is why the methylcyclohexane ring (**2cb**), and not the cyclohexanol ring (**2bc**), takes the boat conformation in order to avoid the repulsion in the double chair form (**2cc**). A similar deduction is derived for **5** since the two 1,3-diaxial hydrogen-methylene interactions are estimated to be 2×0.85 kcal/mol.

The ΔG° values for the equilibration between **10a** and **10b**,[6] and **12a** and **12b**[9] have been reported to be -2.5 and -2.7 kcal/mol, respectively. Since the β-isomer exists predominantly in the double chair form and the α-isomer in the chair-boat form and the substituents in both cases have equatorial arrangement, the ΔG° values can be ascribed to the energy difference of the structural change between the double chair and chair-boat forms. It is thus interesting that in **2** the double boat conformation **2bb** is not preferred over **2cb** although the former does not possess the two 1,3-diaxial methylene-hydroxyl interactions which are present in the latter.

The ΔG° value for the equilibration between **2** and **5** was found to be -2.18 kcal/mol by the equilibration starting from either **2** or **5** with aluminum isopropoxide in isopropyl alcohol at 110°C. Since the cyclohexanol rings in **2** and **5** exist in the chair form, contrary to reported cases, this value can be supposed to be the free energy difference dependent on the axial-equatorial nature of the hydroxyl group. Since two 1,3-diaxial hydroxyl-methylene interactions may be estimated to be 2×2.4 kcal/mol or somewhat smaller and two hydrogen-methylene interactions as 2×0.85 kcal/mol,[21] the energy difference would be about 3.1 kcal/mol. Agreement with the experimental value is considered to be reasonably satisfactory.

Experimental

All the melting and boiling points are uncorrected. IR spectra were recorded on a Shimadzu IR-27C spectrometer, and NMR spectra were obtained with a JEOL C-60H spectrometer in $CDCl_3$ and CCl_4 solutions using tetramethyl-

19) G. Eglinton, J. Martin, and W. Parker, *J. Chem. Soc.*, **1965**, 1243.

20) Attempts to obtain NMR spectra of the fixed conformations of **2** and **5** at lower temperature were unsuccessful due to the crystallization of the substrates in carbon disulfide as well as Freon 11 solution at -50°C.

21) E. L. Eliel, N. L. Allinger, S. J. Angyal, and G. A. Morrison, "Conformational Analysis," Interscience, New York (1965), p. 50.

silane as an internal standard. Mass spectra were recorded with a Hitachi RMS-4 mass spectrometer with a nominal ionizing energy of 70 eV and a source temperature of 150°C. Glc analyses and separation were carried out on a Shimadzu GC-4APT using a 3 mm×3 m column with 15% polyethylene glycol on Chromosorb W (60/80 mesh) operating at 150°C with helium flow rate 40 ml/min. Microanalyses were carried out by Mrs. K. Fujimoto.

7-Methylenebicyclo[3.3.1]nonan-3-one (**1**),[12] 7-methylenebicyclo[3.3.1]nonan-3α-ol (**7**)[14] and -3β-ol[14] were prepared according to the published methods. Tris(dipivalomethanato)europoium(III), Eu(DPM)$_3$, was prepared in a similar manner to the method of Eisentraut[22]; mp 189.5—190°C (lit,[23] mp 190—191°C).

Hydrogenation of ***1*** *over Platinum Oxide in Acetic Acid.* A solution of **1** (300 mg) in acetic acid (20 ml) was hydrogenated over platinum oxide (70 mg) for 20 hr. The catalyst was removed by filtration and the filtrate was neutralized with aqueous sodium bicarbonate solution and extracted with ether. The extract was dried (Na_2SO_4) and evaporated. The residue was purified by sublimation to give 293 mg (95%) of **2**, mp 101—102°C. Found: C, 77.70; H, 11.99%. Calcd for $C_{10}H_{18}O$: C, 77.86; H, 11.76%. IR (KBr): 3252, 2903, 1455, 1368, 1119 cm^{-1}; IR (CCl_4): 2908, 1461 cm^{-1}. NMR ($CDCl_3$): δ 0.85 (d, CH_3), 1.34 (s, OH), 4.15 (m, $H_{(3)}$). MS: *m/e* 154 (M^+).

Hydrogenation of ***7*** *over Platinum Oxide in Acetic Acid.* Platinum oxide (8 mg) in 3 ml of acetic acid was added to a solution of **7** (50 mg) in 3 ml of acetic acid, and the mixture was stirred under an atmosphere of hydrogen for 24 hr. After the same work-up as described above, 46 mg (92%) of **2** was obtained.

Hydrogenation of ***8*** *over Platinum Oxide in Acetic Acid.* A sample of **8** (45 mg) in acetic acid (6 ml) was hydrogenated for 16 hr over 10 mg of platinum oxide. After the usual work-up, sublimation of the residue *in vacuo* afforded 43 mg (95%) of **5**. Found: C, 77.97; H, 11.92%. Calcd for $C_{10}H_{18}O$: C, 77.86; H, 11.76%. IR (KBr): 3274, 2923, 1462, 1375, 1059 cm^{-1}; IR (CCl_4): 2925, 1466 cm^{-1}. NMR($CDCl_3$): δ 0.84 (d, CH_3), 1.59 (s, OH), 3.97 (m, $H_{(3)}$). MS: *m/e* 154 (M^+).

Oxidation of ***2*** *and* ***5*** *into* ***3***. To a solution of a complex prepared from chromic trioxide (600 mg) and pyridine (950 mg) in 20 ml of dichloromethane was added 100 mg of **2** in 3 ml of dichloromethane. The mixture was treated as described by Ratcliffe.[24] After the usual work-up, sublimation gave the ketone (**3**), mp 42.5—43.5°C in 90% yield. The same treatment of **5** also afforded **3** in almost the same yield. Found: C, 78.87; H, 10.77%. Calcd for $C_{10}H_{16}O$: C, 78.89; H, 10.59%. IR(KBr): 1704, 1379, 1354, 1087 cm^{-1}. MS: *m/e* 152 (M^+).

Hydrogenation of ***1*** *over Platinum Oxide in Ethyl Acetate.* A solution of **1** (100 mg) in 11 ml of ethyl acetate was hydrogenated for 2 days over 20 mg of platinum oxide. Removal of the catalyst and evaporation of the solvent gave a mixture of **3** and **4** in the ratio 4.5 : 1. Prolonged reaction (4 days) gave **3** exclusively. Hydrogenation of **1** (4.9 g) over a small amount of platinum oxide (100 mg) for 4 days gave a mixture of **3** and **4** in the ratio 3 : 2. Isolation of **3** and **4** was carried out by preparative glc, followed by sublimation and distillation, respectively. **3** was also isolated from the mixture by recrystallization three times from methanol at −65°C, mp 42.5—43.5°C. Ketone (**3**) was identical with the one obtained above by oxidation of **2** and **5** (spectroscopic data and mixed mp).

The analytical sample of **4**, bp 106—107°C/11 mmHg, showed single peak in glc analysis. Found: C, 79.69; H, 9.35%. Calcd for $C_{10}H_{14}O$: C, 79.69; H, 9.35%. IR (liquid): 3010, 1713, 1376, 1358 cm^{-1}. NMR(CCl_4): δ 1.64 (s, CH_3), 5.41 (d, =C–H). MS: *m/e* 150 (M^+).

Isomerization of ***1***. A solution of **1** (100 mg) in 8 ml of ethanol was stirred overnight over 20 mg of 5% palladium on charcoal under hydrogen atmosphere. Removal of the catalyst and evaporation of the solvent gave **4** in 100% conversion. A solution of **1** (100 mg) in 5 ml of ethanol was refluxed under vigorous stirring for 24 hr over 20 mg of platinum oxide under nitrogen atmosphere. After removal of the catalyst and evaporation of the solvent the residue was found to consist of 33% of **4** and 67% of **1** by glc analysis. A similar treatment over palladium on charcoal instead of platinum oxide gave no isomerization product and led to the recovery of the starting material.

Hydrogenation of ***4***. A solution of 60 mg of **4** in 5 ml of ethyl acetate was hydrogenated for 80 hr over 10 mg of platinum oxide. The usual work-up quantitatively gave **3** as the sole product.

Lithium Aluminum Hydride Reduction of ***3***. A solution of **3** (98 mg) in 6 ml of ether was added dropwise to a slurry of 32 mg of lithium aluminum hydride in 10 ml of ether under stirring. The reaction mixture was refluxed for 6 hr and then dilute hydrochloric acid was added to destroy the excess hydride. The ethereal layer was dried (Na_2SO_4) and evaporated. The residue was found to consist of **2** and **5** in the ratio 4 : 1 by glc analysis.

Equilibration. Reagents and solvents for equilibration were prepared according to the method described by Eliel.[25] The reaction was carried out in sealed tubes because of sublimation of the substrates.

Equilibration was performed on each 10 mg sample of the alcohols in a mixture of 12 mg of aluminum isopropoxide, 2 ml of acetone and 0.5 ml of isopropyl alcohol at 110°C. The reaction was quenched by pouring the mixture into 1 ml of 0.7 N hydrochloric acid and extracted with petroleum ether (bp 40—60°C). The extracts were dried (Na_2SO_4) and used for glc analysis which showed the equilibrium was established after 20 days. The results are summarized in Table 2.

TABLE 2. EQUILIBRATION BETWEEN **2** AND **5**

Run	Starting substrate	Time (days)	Composition **2** : **5**
1	2	7	9.1 : 90.9
2	2	20	5.4 : 94.6
3	5	7	2.0 : 98.0
4	5	23	5.3 : 94.7

We wish to thank Prof. H. Nozaki for his helpful discussions and encouragement.

22) K. J. Eisentraut and R. E. Sievers, *J. Amer. Chem. Soc.*, **87**, 5254 (1965).
23) J. Selbin, N. Ahmad, and N. Bhacca, *Inorg. Chem.*, **10**, 1383 (1971).
24) R. Ratcliffe and R. Rodehorst, *J. Org. Chem.*, **35**, 4000 (1970).
25) E. L. Eliel and S. H. Schroeter, *J. Amer. Chem. Soc.*, **87**, 5031 (1965).

Studies on Oxosulfonium Salts. I. Preparation and Physical Properties.[1]

Michio KOBAYASHI, Kenji KAMIYAMA, Hiroshi MINATO, Yukio OISHI, Yoko TAKADA, and Yoshitaka HATTORI

Department of Chemistry, Tokyo Metropolitan University, Fukazawa, Setagaya-ku, Tokyo

(Received June, 1 1972)

Methods for preparation and physical properties of oxosulfonium salts have been discussed. Optically active ethylmethylphenyloxosulfonium salts have been prepared and their absolute configurations have been determined.

Very little has been reported on the oxosulfonium salts (I) except trimethyloxosulfonium iodide (II), which can easily be prepared by heating dimethyl sulfoxide and methyl iodide[2,3] and are used as a source of dimethyloxosulfonium ylid (III).

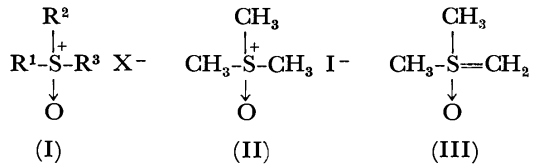

(I) (II) (III)

It seems of interest to investigate the methods for synthesizing oxosulfonium salts containing various substituents, especially the optically active salts containing three different substituents. The results of the investigation carried out in our laboratories will be described in this paper.

Results and Discussion

(I) Methods for Syntheses of Oxosulfonium Salts. As methods for synthesizing oxosulfonium salts, the following two approaches have been examined.

1) Oxidation of Sulfonium Salts: In the literature[4,5] oxidations of sulfonium salts to the corresponding oxosulfonium salts by use of hydrogen peroxide were described, but the products were not isolated as pure substances. In an attempt to examine this route as a possible method for synthesis of oxosulfonium salts, several sulfonium salts were treated with 30% H_2O_2, 87% H_2O_2-CF_3CO_2H, $PhCO_3H$-MeCN, NaOBr, HNO_3, Cl_2-CH_3CO_2H and PhIO under varied conditions, but no oxosulfonium salts were found. These results indicate that oxidation of sulfonium salts is not likely to be a general method for synthesizing oxosulfonium salts.

2) Alkylation or Arylation of Sulfoxides: In contrast with the very easy *S*-methylation of dimethyl sulfoxide, alkylation (alkyl groups larger than methyl) of dimethyl sulfoxide or methylation of dialkyl sulfoxides is very difficult. It was stated in the literature[6] that alkylations did not take place, but the reason why oxosulfonium salts were not formed was not discussed and what happened instead was not described.

When *n*-alkyl bromides or chlorides and sulfoxides were heated at 100°C for several days, no reaction took place. When a mixture of dialkyl sulfoxides or aryl sulfoxides and methyl iodide was refluxed for one day, almost no reaction took place. However, when mercury(II) iodide was added the reaction was greatly accelerated, but an NMR study indicated that the first step is the *O*-alkylation instead of the *S*-alkylation; the oxosulfonium salt must arise by subsequent rearrangement of the *O*-alkylated product or reaction of the unchanged sulfoxide with the *O*-alkylated product. At the same time a great amount of the corresponding sulfonium salt was always formed, and iodine and dimethyl ether were found as by-products. A typical example is shown below.

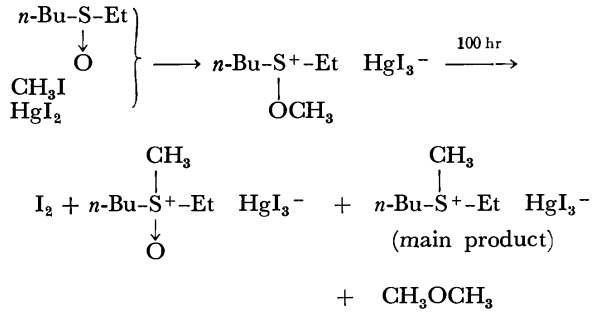

A plausible mechanism for the formation of the sulfonium salt is expressed as follows.

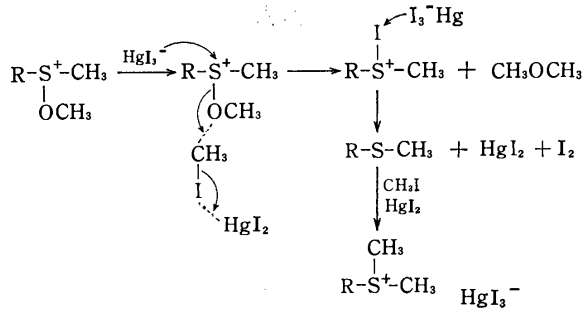

Since the solubilities of sulfonium salts and oxosulfonium salts are similar, their separation is difficult. However, repeated recrystallizations (more than a dozen times) from tetrahydrofuran-ether or alcohol can separate the two salts. Sulfonium salts are always the main product, and the yields of oxosulfonium salts are very low.

In the reaction between *p*-substituted phenyl methyl sulfoxides and methyl iodide-mercury iodide, considerable substituent effect was observed; the reaction was very slow with the sulfoxides containing electron-withdrawing substituents. With the *p*-bromophenyl

1) Organic Sulfur Compounds. Part XXXVII.
2) R. Kuhn and H. Trischmann, *Ann*, **611**, 117 (1958).
3) E. J. Corey and M. Chaykovsky, *J. Amer. Chem. Soc.*, **87**, 1957 (1965).
4) H. Distler and F. Fucks, *Tenside*, **6**, 65 (1969).
5) D. R. P. 1258865
6) R. T. Major and H. -J. Hess, *J. Org. Chem.*, **23**, 1563 (1958).

methyl sulfoxide, formation of the oxosulfonium salt was detected after 100 hr of refluxing. With the *p*-nitrophenyl methyl sulfoxide it was detected after 300 hr of refluxing, and the maximum yield after longer refluxing was below 1%.

When such powerful alkylating agent as trimethyl- or triethyloxonium tetrafluoroborate was used, only *O*-alkylation took place.[7]

Although sulfoxides generally do not react with aryl halides, heating a mixture of dimethyl sulfoxide and an anhydrous aryldiazonium salt results in the formation of an aryldimethyloxosulfonium salt,[8] but the main reaction was *O*-arylation and the maximum yield of oxosulfonium salts was 20%. Since substituted benzenediazonium salts are generally more stable than the non-substituted salt, higher temperature was used for their decomposition and the yields were lower (for the *p*-nitro salt, the yield was about 1%).

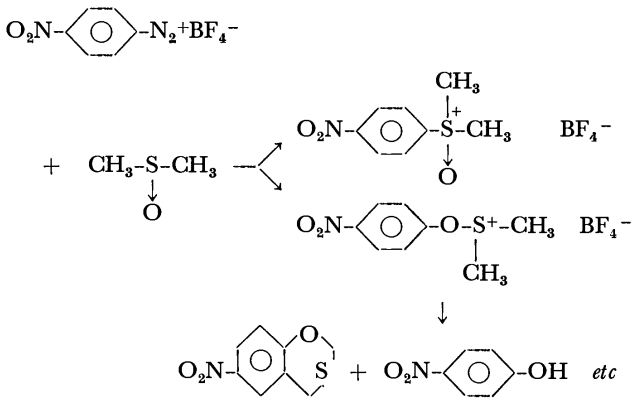

In the literature, it was described that the reaction among dimethyl sulfoxide, phenol and dicyclohexylcarbodiimide yields the *O*-phenylated dimethyl sulfoxide, which changes into 1,3-oxathian.[9]

(II) Physical Properties. 1) *Solubilities*: Oxosulfonium salts are soluble in acetone, acetonitrile, tetrahydrofuran, trifluoroacetic acid, hot methanol or hot ethanol, and insoluble in benzene, ether, chloroform, or carbon tetrachloride.

2) *Infrared Spectra*: Oxosulfonium salts show a strong absorption ($\varepsilon\sim300$) at 1220—1240 cm^{-1} due to their S–O stretching. The wave number of this absorption is approximately equal to the average of the wave numbers of the symmetric and asymmetric stretching of the S–O bond of the sulfones (1220 cm^{-1}) or that of the sulfoximines (1220—1240 cm^{-1}). This suggests that the double bond character of the S–O bond of oxosulfonium salts is similar to those of sulfones and sulfoximines, and much stronger than that of sulfoxides (1050 cm^{-1}).

The ν_{S-O} of *p*-substituted dimethyl phenyl oxosulfonium salts changes with the substituents, and a Hammett relationship was found to hold between $\Delta\nu$ and σ^+ values, as shown in Table 1.

TABLE 1. ν_{S-O} OF *p*-X-C_6H_4-$\overset{+}{S}(Me)_2$ HgI_3^- (O)

X	ν_{S-O} (in MeCN)
CH_3O	1238
CH_3	1240
H	1242
Br	1243
NO_2	1245

3) *NMR Spectra*: Oxosulfonium salts show the S^+—CH_3 signals at δ 4—4.5 and the S^+—CH_2—signals at δ 5. Since the corresponding methyl and methylene signals of sulfonium salts are observed at higher magnetic fields (by 0.5 ppm), these signals can be used for detection and quantitative determination of oxosulfonium and sulfonium salts. Changes of the methyl signals of *p*-substituted dimethylphenyloxosulfonium salts are shown in Table 2. A Hammett relationship was found to hold between $\Delta\nu$ and σ^+ values.

TABLE 2. NMR METHYL SIGNALS OF *p*-X-$C_6H_4\overset{+}{S}(Me)_2$ HgI_3^- AND *p*-X-$C_6H_4\overset{+}{S}(Me)_3$ HgI_3^- (O)

(in acetone-d_6)

X	Oxosulfonium Salts	Sulfonium Salts
CH_3O	δ 4.35	δ 3.50
CH_3	4.40	3.51
H	4.43	3.57
Br	4.47	3.59

(III) Reactions. 1) *Alkylation by Use of Oxosulfonium Salts*: Oxosulfonium salts can alkylate reactive anions. The reaction of dimethylphenyloxosulfonium ion with sodium *p*-toluenesulfinate gave methyl *p*-tolyl sulfone exclusively, and no methyl *p*-toluenesulfinate was found. When dimethylphenyloxosulfonium ion was heated with sodium iodide in acetone, the oxosulfonium ion was readily demethylated and converted to methyl phenyl sulfoxide.

The results of a detailed investigation on these S_N2 type reactions with nucleophiles will be described in a separate paper.

2) *Oxidation by Use of Oxosulfonium Salts*: Since an oxosulfonium ion contains an extra oxygen compared with a sulfonium ion, it may be expected to act as an oxidizing agent under some conditions. However, when a mixture of an oxosulfonium salt and benzyl alcohol, cyclohexanol, or *sec*-butyl alcohol was heated at 120—140°C, no oxidation to carbonyl compounds was observed. Neither hydroiodic acid nor zinc and hydrochloric acid reacted with oxosulfonium salts at room temperature. These findings indicate again that the S–O bond of an oxosulfonium salt is as strong as that of sulfones.

7) C. R. Johnson and W. G. Phillips, *J. Amer. Chem. Soc.*, **91**, 682 (1967).

8) M. Kobayashi, H. Minato, E. Yamada, and N. Kobori, This Bulletin, **43**, 215 (1970).

9) M. G. Burdon and G. Moffatt, *J. Amer. Chem. Soc.*, **88**, 5855 (1966).

10) M. Kobayashi, K. Kamiyama, H. Minato, Y. Oishi, Y. Takada, and Y. Hattori, *Chem. Commun.*, **1971**, 1577.

(IV) Optical Resolution.[10] Trimethyloxosulfonium ion was shown to possess a tetrahedral structure,[11] and the oxosulfonium ions containing three different substituents must be resolvable to a pair of enantiomers.

Ethylmethylphenyloxosulfonium mercuritriiodide (IV) was converted to its *d*-camphor-10-sulfonate (V), which was separated to *d-d* crystals (mp 142—143.5°C) and *l-d* crystals (mp 125—126°C) by repeated recrystallizations from acetone.

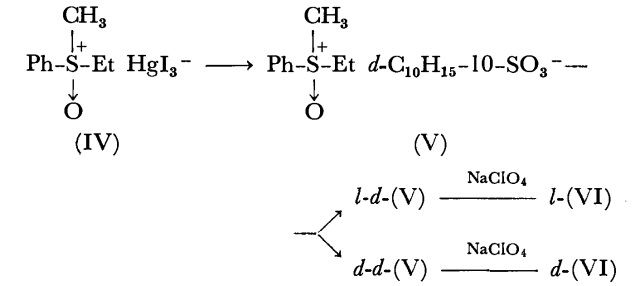

A solution of the *d-d*(V) or *l-d*(V) in acetone–water (1 : 1) was then passed through an anion-exchange resin which had been treated with aqueous sodium perchlorate solution. Recrystallization from ethanol yielded the *d*-perchlorate (VI) (mp 79.0—79.5°C, $[\alpha]_D^{32}+14.5°$, *c* 5.52, acetone) and the *l*-perchlorate (mp 79.0—79.5°C, $[\alpha]_D^{30}-14.3°$, *c* 4.61, acetone).

The absolute configuration of the *d*- and *l*-perchlorate (VI) were determined by conversion into the corresponding sulfoxides. From the *d*-perchlorate, the *d*-sulfoxide was obtained. Since Mislow and his co-workers have established that *d*-alkyl aryl sulfoxides possess the R-configuration,[12] the *d*-sulfoxide obtained here must also possess the R-configuration.

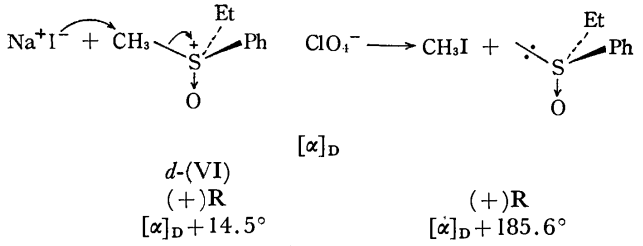

Since demethylation of the ethylmethylphenyloxosulfonium ion proceeds by S_N2 attack of iodide ion on the methyl group, not the sulfur atom, the stereochemistry of the sulfur atom must be retained during this demethylation. Therefore, the *d*-ethylmethylphenyloxosulfonium ion must also have the R-configuration.

These findings establish the following assignments for absolute configuration of the oxosulfonium ions.

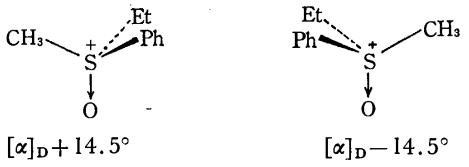

11) I. C. Zimmermann, M. Barlow, and J. D. McCullough, *Acta Crystallogr.*, **16**, 883 (1963).

12) K. Mislow, M. M. Green, P. Laur, J. T. Melillo, T. Simmons, and A. L. Ternary, *J. Amer. Chem. Soc.*, **87**, 1958 (1965).

Experimental

Materials. Ethyl phenyl sulfoxide was synthesized by oxidation of the corresponding sulfide with 30% H_2O_2 in acetone at 25—30°C for one week.[13] Bp 102—110°C/5 mmHg, IR, ν_{S-O} 1040 cm^{-1}.

Synthesis of Ethylmethylphenyloxosulfonium Mercuritriiodide (IV). After a mixture of mercury(II) iodide (11.0 g, 24.2 mmol) and methyl iodide (15 m*l*) was stirred in a 50 m*l* flask for 0.5 hr, ethyl phenyl sulfoxide (10.0 g, 64.6 mmol) was added. After nitrogen was bubbled through the mixture for 45 min, the mixture was refluxed under nitrogen for 65 hr. Then the excess methyl iodide was evaporated and the unchanged sulfoxide was removed with ether. When the reddish brown oil obtained was washed with ether several times, crude crystals were obtained, which gave yellow plates upon recrystallizations from methanol. Yield, 8.7 g (17.7%); mp 94—95°C; IR, 1240, 1210, 750 cm^{-1}; NMR, δ 1.54 (t, 3H), 4.37 (s, 3H), 4.58 (q, 2H), 8.10 (m, 5H).

In this reaction, a considerable amount of ethylmethylphenylsulfonium mercuritriiodide is formed. When the amount of methyl iodide relative to the amount of the sulfoxide is smaller, the yield of the sulfonium salt is greater. The reaction conditions described above are the optimum ones on the basis of the results of many experiments. When mercury(II) iodide was not added, no reaction takes place.

Optical Resolution. After *d*-10-camphorsulfonic acid (14.0 g, 60.0 mmol) and silver oxide (16.8 g) were let to react in acetonitrile (50 m*l*) for 7 hr, the excess silver oxide was filtered. To this acetonitrile solution of silver 10-camphorsulfonate, a solution of (IV) (45 g) in acetonitrile (60 m*l*) was added drop by drop at room temperature, and the AgI and HgI_2 were filtered. After the acetonitrile was removed under reduced pressure, water (100 m*l*) was added to the residue and the insoluble materials were filtered off. Complete removal of water from the aqueous layer by use of a vacuum pump gave colorless crystals of (V); Yield, 18.6 g (80.8%); $[\alpha]_D^{33}+25.6°$ (c 8.32, EtOH); IR, 1730, 1210, 1190, 1170 cm^{-1}; Anal. Calcd. for $C_{19}H_{28}O_5S_2$: C, 56.97; H, 7.05; Found: C, 56.64; H, 6.80%.

When fractional recrystallization of (V) (18.6 g) from acetone was repeated for 7 times, crystals of *d-d*-(V) were obtained; 3.1 g (33%); mp. 142—143.5°C; $[\alpha]_D^{33}+39.7°$ (c 2.90, EtOH). After the mother liquor was concentrated and the crystals initially formed were removed, the filtrate was further concentrated. When the crystals thus obtained were fractionally recrystallized six times, crystals of *l-d*-(V) were obtained; 1.07 g (12%); mp. 125—126°C; $[\alpha]_D^{32}+11.6°$ (c 4.66, EtOH).

Preparation of Ethylmethylphenyloxosulfonium Perchlorate (VI). After about 2 *l* of an aqueous sodium perchlorate solution was passed through a column of ion-exchange resin (Amberlite IRA 400), *d-d*-(V) (2.7 g) dissolved in a small amount of aqueous acetone was added to the column. Then a 1 : 1 mixture (by volume) of water and acetone was passed through the column. Evaporation of the eluate (about 1 *l*) under reduced pressure gave crystals, which were recrystallized from EtOH–ether; 1.52 g (84%); $[\alpha]_D^{32}+14.5°$ (*c* 5.52, acetone); mp. 79.0—79.5°C; IR, 1240, 1210, 1100 cm^{-1}; Anal. Calcd. for $C_9H_{13}O_5SCl$; C, 40.23; H, 4.88; Found: C, 40.21; H, 4.75%.

From *l-d*-(V) (1.07 g), *l*-(VI) was obtained in a similar manner; 0.63 g (87.2%); $[\alpha]_D^{30}-14.3°$ (c 4.61, acetone); mp. 79.0—79.5°C.

13) R. L. Shriner, H. C. Struck and J. Jorison, *ibid.*, **52**, 2066 (1930).

Reaction between Optically Active (VI) and Sodium Iodide. A mixture of *d*-(VI) (0.276 g, 1.09 mmol) and NaI (0.327 g, 2.18 mmol) in 5 m*l* of acetone was refluxed for 1 hr. Water was added to the mixture, and the sulfoxide was extracted with ether. When the ethereal extracts were dried over anhydrous magnesium sulfate and the ether was removed under reduced pressure, ethyl phenyl sulfoxide was obtained; 86.7 mg (51.3%); $[\alpha]_D^{33}+164.9°$ (*c* 1.7, acetone). When this sulfoxide was purified by column chromatography (Florisil), pure sulfoxide was obtained; $[\alpha]_D^{26}+185.6°$ (c 0.71, acetone); NMR, δ 1.14 (t, 3H), 2.70 (q, 2H), 7.49 (m, 5H). In a similar manner, *l*-(VI) (0.230 g, 0.86 mmol) gave *l*-sulfoxide; $[\alpha]_D^{35}-173.4°$ (c 0.89, acetone).

BULLETIN OF THE CHEMICAL SOCIETY OF JAPAN, VOL. 45, 3706—3710 (1972)

Asymmetric Hydrogenation of the C=N Bond. A Study of the Controlling Factors on the Stereoselectivity

Takao YOSHIDA and Kaoru HARADA*

Department of Chemistry, Faculty of Science, Osaka University, Toyonaka, Osaka
**Institute for Molecular and Cellular Evolution, University of Miami, Coral Gables, Florida, U. S. A.*

(Received June 24, 1972)

Asymmetric catalytic hydrogenation of Schiff bases, *i. e.*, *N*-(methylbenzylidene)-α-methylbenzylamine and *N*-(ethylbenzylidene)-α-ethylbenzylamine, using 10% palladium hydroxide on charcoal was studied to elucidate the steric course of the reaction. Effects of temperature, solvent, pressure, the amount of the catalyst, and ratio of the *syn* and *anti* isomers on the asymmetric hydrogenation were investigated. Temperature, solvent, the amount of the catalyst were found to be factors which controlled the stereoselectivity of the reaction. The hydrogenation of *N*-(methylbenzylidene)-α-methylbenzylamine always gave a higher asymmetric yield than that of *N*-(ethylbenzylidene)-α-ethylbenzylamine. Lowering the reaction temperature, lowering the polarity of the solvent, and decreasing the amount of the catalyst gave higher stereoselectivities in the hydrogenation reactions.

Studies of the hydrogenolytic asymmetric transamination of Schiff bases between keto acids or their esters and optically active amines have been reported.[1] For the possible steric course of this type of asymmetric hydrogenation, a chelation hypothesis was postulated to explain the experimental results. Solvent and temperature effects were studied to support this hypothesis.[1d,e,f]

Prelog and Scherrer studied the asymmetric hydrogenation of optically active esters of β-methylcinnamic acid.[2] They discussed the relation between the conformations of substrates and the configurations of products. They applied the Prelog rule for the homogeneous reactions to explain the steric course of the heterogeneous hydrogenation. Since there are many other experimental results which can not be explained using the Prelog rule, the mechanism of the hydrogenation reaction was investigated. In order to investigate the reaction mechanism we carried out systematic studies of the asymmetric synthesis in which many parameters of the reaction were examined.

Overberger and his co-workers reported that the asymmetric hydrogenation of (*S*)(−)-*N*-(methylbenzylidene)-α-methylbenzylamine gave a product consisting of 88% (*S,S*) isomer and 12% (*S,R*) isomer.[3] They explained the observed result as follows. "There is a very facile equilibrium between the *syn* and *anti* forms and the *syn* isomer, being a higher energy state, is more easily reduced". However, there is no firm experimental basis for this explanation.

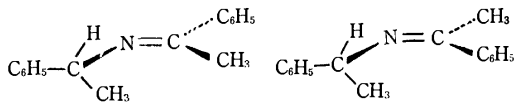

Fig. 1.

In this work *N*-(methylbenzylidene)-α-methylbenzylamine and *N*-(ethylbenzylidene)-α-ethylbenzylamine (I) were used as substrates. Effects of temperature, solvent, pressure, amount of the catalyst, and ratio of the *syn* and *anti* isomers of the substrate on the asymmetric hydrogenation of these substances were investigated.

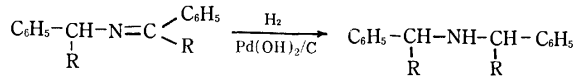

I R = CH_3, C_2H_5

Fig. A.

Results and Discussion

Hydrogenation reactions were carried out using 10% palladium hydroxide on charcoal as a catalyst.

1) a) R. G. Hiskey and R. C. Northrop, *J. Amer. Chem. Soc.*, **83**, 4798 (1961): b) K. Matsumoto and K. Harada, *J. Org. Chem.*, **31**, 1956 (1966): c) K. Harada and K. Matsumoto, *ibid.*, **32**, 1794 (1967): d) K. Harada and K. Matsumoto, *ibid.*, **33**, 4467 (1968): e) K. Harada and T. Yoshida This Bulletin, **43**, 921 (1970): f) K. Harada and T. Yoshida, *Chem. Commun.* **1970**, 1071.

2) V. Prelog and H. Scherrer, *Helv. Chim. Acta*, **42**, 2227 (1959).

3) C. G. Overberger, N. P. Marullo, and R. G. Hiskey, *J. Amer. Chem. Soc.*, **83**, 1374 (1961).

Ratios of two diastereoisomers in the products were determined by gas chromatographic separation using a column packed with 1.5% neopentylglycol succinate on chromosorb-W.

Temperature Effect. Temperature showed marked effect on the hydrogenation reaction. This effect is shown in Table 1 and Fig. 2 in which the percentage of DL isomers is plotted against temperature. As the reaction temperature decreased, the stereoselectivity of the reaction increased from 68% at 50°C to 89% at −20°C when R was CH_3 in I, and from 61% at 50°C to 81% at −20°C when R was C_2H_5 in I. The table shown below indicates the time required for the absorption of the equimolar amount of hydrogen. The rate of the hydrogenation reaction slowed down as the reaction temperature decreased from 30°C to −20°C, but at high temperatures the rate slowed down slightly.

React. temp. (°C)	50	40	30	20	10	0	−10	−20
React. time required (min)	14	10	8	8	10	10	22	60

Solvent Effect. Solvent effects are summarized in Table 2 and Fig. 3.

Pressure Effect. Pressure did not show any significant effect as shown in Table 3. Only a 5% increase in stereoselectivity was observed when the pressure was changed from 1 to 10 atm.

Effect of Amount of Catalyst. The amount of the catalyst was also found to be the one of the factors that controlled stereoselectivity. As the amount of the catalyst decreased, the DL-isomer ratio was increased as shown in Table 4.

Effect of syn-anti *Ratio of Substrate.* It was found that the ratio of the *syn* and *anti* forms of substrates was changed after redistillation. The *syn* and *anti* forms reached an equilibrium if they were allowed to stand for a few days at room temperature. In this experiment the substrates which had different ratios of *syn* and *anti* forms were hydrogenated in methanol and benzene. As shown in Table 5, the ratios of the products were not affected by the *syn* and *anti* ratios of the substrates.

In Table 6 the isomer ratio of the product during the reaction is shown. From the fact that the amine produced did not affect the stereoselectivity of the hydrogenation of the substrate secondarily during the reaction, it appears that the hydrogenated substrate desorbed rapidly from the active surface of the catalyst and exchanged with the unreacted substrate.

TABLE 1. TEMPERATURE EFFECT[a]

Substrate	C_6H_5–C(=N–CH(C_6H_5)–CH_3)–CH_3 (*S*)(−)		C_6H_5–C(=N–CH(C_6H_5)–C_2H_5)–C_2H_5 (±)
Reaction Temp. (°C)	Ratio of (*S*,*S*) to (*S*,*R*)		Ratio of (±) to *meso*
+50	68 : 32[b]	(61 : 39)[c]	61 : 39[b]
+40	70 : 30	(67 : 33)	62 : 38
+30	74 : 26	(46 : 54)	68 : 32
+20	77 : 23	(75 : 25)	70 : 30
+10	81 : 19	(76 : 24)	72 : 28
0	86 : 14	(56 : 44)	75 : 25
−10	87 : 13	(81 : 19)	80 : 20
−20	89 : 11	(88 : 12)	81 : 19

a) Hydrogenation was carried out in methanol under atmospheric pressure.
b) Ratios were determined by the gas chromatographic separation of two diastereoisomers.
c) Ratios were determined by measuring optical rotations of distilled products.

We propose the following reaction mechanism for the hydrogenation of this type of substrate. The substrate is isomerized rapidly by the catalyst bringing about an equilibration of the *syn* and *anti* isomers. Each isomer is then hydrogenated at a different rate from the least hindered side. This mechanism is supported by the fact that the ratio of the *syn* and *anti* isomers of the substrate does not affect the stereoselectivity of the hydrogenation. The conformation of the substrate on the catalyst which was proposed by

TABLE 2. SOLVENT EFFECT[a]

Substrate		C_6H_5–C(=N–CH(C_6H_5)–CH_3)–CH_3 (±)	C_6H_5–C(=N–CH(C_6H_5)–CH_3)–CH_3 (±)	C_6H_5–C(=N–CH(C_6H_5)–C_2H_5)–C_2H_5 (±)
Reaction temp. (°C)		10	20	20
Solvent (ε)		Ratio of (±) to *meso*[b]	Ratio of (±) to *meso*[b]	Ratio of (±) to *meso*[b]
Methanol	(32.6)	81 : 19	77 : 23	70 : 30
Ethanol	(24.3)	83 : 17	80 : 20	71 : 29
Propanol	(18.3)	84 : 16	82 : 18	72 : 28
n-Amylalcohol	(13.9)	——	83 : 17	76 : 24
Tetrahydrofuran	(7.6)	——	85 : 15	77 : 23
Ethyl acetate	(6.0)	89 : 11	86 : 14	77 : 23
Benzene	(2.3)	85 : 15	——	——
Dioxane	(2.2)	——	85 : 15	70 : 30

a) Hydrogenation was carried out under atmospheric pressure.
b) Ratios were determined by the gas chromatographic separation of two diastereoisomers.

Table 3. Pressure effect[a]

Substrate (S)(−) C_6H_5-C(=N-CH(C_6H_5)-CH_3)-CH_3	
Pressure applied (atm)	Ratio of (*S*,*S*) to (*S*,*R*)[b]
10	80 : 20
8	79 : 21
6	79 : 21
4	74 : 26
2	75 : 25
1	75 : 25

a) Hydrogenation was carried out in methanol at 25°C.
b) Ratios were determined by the gas chromatographic separation of two diastereoisomers.

Table 4. Effect of amount of catalyst[a]

Substrate (200 mg) (S)(−) C_6H_5-C(=N-CH(C_6H_5)-CH_3)-CH_3	
Catalyst (mg)	Ratio of (*S*,*S*) to (*S*,*R*)[b]
200	73 : 27
100	73 : 27
50	76 : 24
30	80 : 20
10	85 : 15

a) Hydrogenation was carried out in methanol at 25°C and under atmospheric pressure.
b) Ratios were determined by the gas chromatographic separation of two diastereoisomers.

Table 5. Effect of *Syn-Anti* ratio of substrate[a]

Substrate (±) C_6H_5-C(=N-CH(C_6H_5)-C_2H_5)-C_2H_5		
Solvent	Ratio of *syn* to *anti* of substrate	Ratio of (±) to *meso* of Product
Methanol	40 : 60[b]	73 : 27[c]
Methanol	52 : 48	73 : 27
Benzene	39 : 61	75 : 25
Benzene	57 : 43	73 : 27

a) Hydrogenation was carried out at 14°C under atmospheric pressure.
b) Ratios were determined by the NMR spectra.
c) Ratios were determined by the gas chromatographic separation of two diastereoisomers.

Overberger *et al.*, as shown in Fig. 1, cannot explain the experimental results obtained in this study. In other words the relatively high stereoselectivity would not be expected from the difference in the bulkiness of the hydrogen and methyl groups. If this is the case the stereoselectivity would increase when the methyl group is replaced by the ethyl group.

On the other hand, if we consider that the most populated conformation is the one in which hydrogen is located on the same plane of C_6H_5-C=N, and the

Table 6. Isomer ratio of product during reaction[a]

Substrate (S)(−) C_6H_5-C(=N-CH(C_6H_5)-CH_3)-CH_3	
% of Reaction completed[b]	Ratio of (*S*,*S*) to (*S*,*R*)[c]
100	80 : 20
80	81 : 19
57	82 : 18
46	82 : 18
20	82 : 18

a) Hydrogenation was carried out in methanol at 10°C and under atmospheric pressure.
b) The percentages were calculated from the gas chromatographic data.
c) The ratios determined by the gas chromatographic separation of two diastereoisomers.

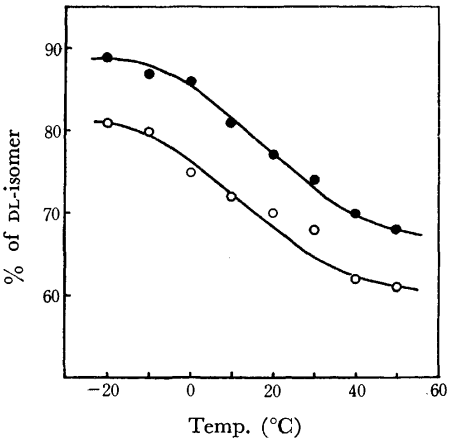

Fig. 2.
—●— C_6H_5-CH(NH-CH(C_6H_5)-CH_3)-CH_3 —○— C_6H_5-CH(NH-CH(C_6H_5)-C_2H_5)-C_2H_5

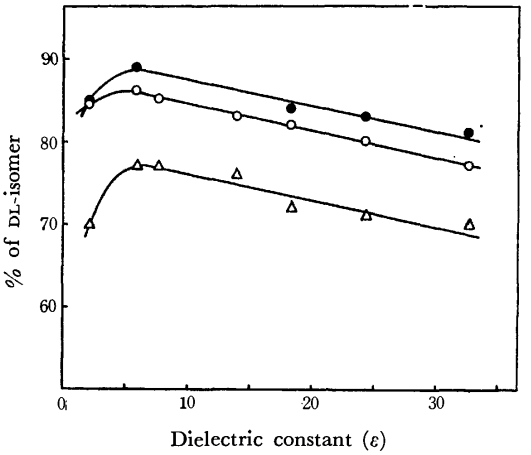

Fig. 3.
—●— (10°C) —○— (20°C) C_6H_5-CH(NH-CH(C_6H_5)-CH_3)-CH_3 —△— (20°C) C_6H_5-CH(NH-CH(C_6H_5)-C_2H_5)-C_2H_5

anti isomer (II), being a lower energy state, is readily hydrogenated from the least hindered side, that is, from the side of methyl and ethyl group, the difference in bulkiness of methyl (or ethyl) and phenyl group could induce the relatively high stereoselectivity. And also the lowering of stereoselectivity by replacing the methyl with the ethyl group is reasonable when this conformation is considered. This conformation is shown in Fig. 4.

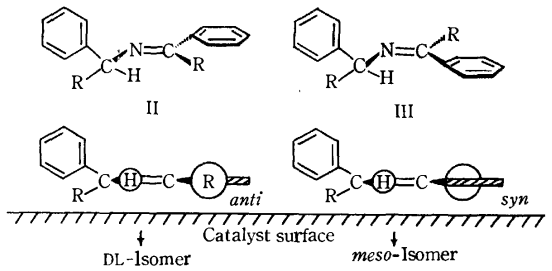

Fig. 4.

Recently the asymmetric reduction of Schiff bases, $R(CH_3)C{=}N{-}CH(CH_3){-}C_6H_5$ (R=Et, *i*-Pr, *t*-Bu), using $LiAlH_4$ and B_2H_6, and also the catalytic reduction using palladium hydroxide on charcoal were reported by Charles *et al.*[4] They discussed the steric course of the reaction and concluded that the conformation of the substrate at the transition state would be the one represented in Fig. 5. Interestingly their proposed substrate conformation on the catalyst is the same as we proposed.

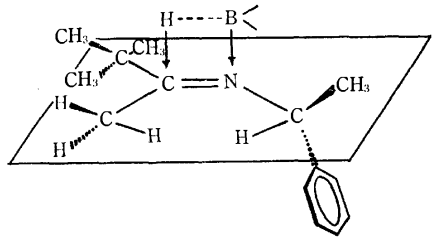

Fig. 5.

The temperature effect could be explained as follows. At low temperature the hydrogenation of the *anti* isomer (II), which is more stable in the preffered conformation, takes place much faster than that of the *syn* isomer (III), thereby resulting in high stereoselectivity. As the temperature increases, the difference of the hydrogenation rate for both isomers becomes smaller resulting in lower stereoselectivity.

The solvent effect could be explained as follows. When a polar solvent was used, the interaction between the solvent and the substrate is stronger and it causes the adsorptive strength of the substrate to be weaker. Therefore it is reasonable that the stereoselectivity of the reaction is lowered in polar solvents. However an increase in the stereoselectivity was not found in the less polar solvents, benzene and dioxane. The strong interaction between the solvent and the catalyst could possibly explain this result.

4) J. P. Charles, H. Christol, and G. Solladie, *Bull. Soc. Chim. Fr.*, **1970**, 4439.

The small effect of pressure is expected for this type of substrate, because the π-electrons of the C=N bond would conjugate with the π-electrons of the phenyl group. The π-benzyl group would then be adsorbed on the surface of the catalyst resulting in fast *cis*-addition of hydrogen.

The effect of the amount of the catalyst could also be rationalized by the competitive adsorption of the substrate. When the amount of catalyst is small, the more reactive *anti* isomer could be adsorbed faster than the *syn* isomer resulting in higher stereoselectivity.

In earlier work we found that solvents and temperatures could affect the stereoselectivity of the asymmetric hydrogenolytic transamination.[1e,f] For the reaction mechanism, it was proposed that two predominant conformations on the catalyst surface were possible, and under certain conditions, one conformation would prevail over the other. Since *N*-(methylbenzylidene)-α-methylbenzylamine and *N*-(ethylbenzylidene)-α-ethylbenzylamine have only one polar group to be hydrogenated, effects of temperatures and solvents could be expected to be smaller than that observed in earlier work.[1e,f] In fact, experimental results showed that these effects were smaller.

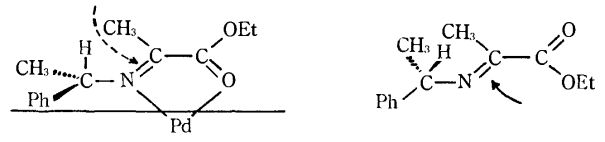

Fig. 6.

We conclude that the factors, which control the stereoselectivity of the asymmetric hydrogenation reaction, are mainly the structure of the molecule, temperature, solvent, and the amount of the catalyst.

Experimental

All melting points are uncorrected. IR and NMR were measured respectively by use of a Jasco IR-S and Varian A-60, T-60.

N-(Methylbenzylidene)-α-methylbenzylamine. This compound was prepared as described by Overberger.[3] bp 104—106°C/0.1 mmHg; (*S*)(−)-isomer, $[\alpha]_D^{25}$ −98.4° (*c* 5.59, benzene).

(S,S)(−)-α,α'-Dimethyldibenzylamine. The same procedure[3] was used to prepare this optically active amine. bp 110°C/1 mmHg $[\alpha]_D^{25}$ −197.3° (*c* 3.65, benzene). The hydrochloride did not melt at temperatures up to 300°C as described in literature. $[\alpha]_D^{25}$ −72.1° (*c* 2.94, ethanol).

N-(Ethylbenzylidene)-α-ethylbenzylamine. This compound was prepared in a similar manner, by using toluene as a solvent with a reaction time of 48 hr. Yield 74%, bp 123—124°C/2 mmHg.

Found: C, 85.57; H, 8.48; N, 5.43%. Calcd for $C_{18}H_{21}N$: C, 86.01; H, 8.42; N, 5.57%.

The optically active (*S*)(−)-isomer showed $[\alpha]_D^{25}$ −41.2° (*c* 4.31, benzene).

(S,S)(−)-α,α'-Diethylbenzylamine. (*S*)(−)-*N*-(Ethylbenzylidene)-α-ethylbenzylamine (3.6 g. 0.014 mol) in ethyl acetate (60 ml) was hydrogenated at room temperature under atmospheric pressure using 10% palladium hydroxide on charcoal as a catalyst. After one molar amount of

hydrogen was taken up, the catalyst was filtered off. The solvent was removed and the residual oil was distilled *in vacuo*. Yield, 2.7 g (74%), bp 115—118°C/1 mmHg.

Found: C, 84.94; H, 9.13; N, 5.63%. Calcd for $C_{18}H_{23}N$: C, 85.32; H, 9.15; N, 5.53%.

Amine obtained (2.7 g, 0.011 mol) was treated with 50 m*l* of 0.5 N hydrochloric acid to crystallize the hydrochloride. The hydrochloride (2.7 g) was collected and recrystallized from water three times. The pure (*S,S*)(−)-α,α′-diethyldibenzylamine hydrochloride melted at 210.5—211.5°C, $[\alpha]_D^{25}$−66.0 (*c* 1.91, ethanol).

Found: C, 74.55; H, 8.48; N, 4.85; Cl, 12.11%. Calcd for $C_{18}H_{24}NCl$: C, 74.59; H, 8.35; N, 4.83; Cl, 12.23%.

Optically pure (*S,S*)(−)-α,α′-diethyldibenzylamine was recovered from this hydrochloride by decomposition with aqueous sodium hydroxide. $[\alpha]_D^{25}$−203.1° (*c* 2.91, benzene).

Hydrogenation of Schiff Bases. Hydrogenation was carried out in a three-necked round bottom flask provided with a thermometer. Stirring was conducted with using a magnetic stirrer. In every reaction, the 10% palladium hydroxide on charcoal was all from the same lot that was prepared by a method described in the literature.[1)]

Temperature Effect. Schiff base (0.004 mol) in methanol (25 m*l*) was hydrogenated using 200 mg of 10% palladium hydroxide on charcoal under atmospheric pressure. Temperature was controlled by cooling the reaction flask in dry ice–methanol bath or by heating in a water bath. The experimental error of temperature was ±1°C in any reaction. The results obtained are listed in Table 1. The diastereoisomeric ratio of the reaction product was determined by gas chromatography directly instead of measuring the optical rotation of the distilled product to avoid possible fractionation during distillation. In fact the values obtained by the latter method did not correspond to the ones obtained by the gas chromatographic method.

Solvent Effect. Schiff bases (0.004 mol) in various solvents (25 m*l*) were hydrogenated using 200 mg of 10% palladium hydroxide on charcoal at 10° and 20° under atmospheric pressure. The results are listed in Table 2.

Pressure Effect. (*S*)(−)-*N*-(methylbenzylidene)-α-methylbenzylamine (0.002 mole) in methanol (25 m*l*) was hydrogenated using 100 mg of 10% palladium hydroxide on charcoal at 25° in a high pressure durable glass tube using a magnetic stirrer for agitation. The pressure was maintained by connecting the hydrogen cylinder at a fixed pressure to the reaction tube. The decrease of the pressure during reaction by consumption of hydrogen was negligible. The results are listed in Table 3.

Effect of Amount of Catalyst. (*S*)(−)-*N*-(methylbenzylidene)-α-methylbenzylamine (0.001 mol) in methanol (12 m*l*) was hydrogenated using 200, 100, 50, 30, and 10 mg of 10% palladium hydroxide on charcoal respectively at 25°C under atmospheric pressure. The results are listed in Table 4.

Effect of syn-anti *Ratio of Substrate.* (±)-*N*-(Ethylbenzylidene)-α-ethylbenzylamine (0.001 mol) in methanol or benzene (12 m*l*) was hydrogenated using 50 mg of 10% palladium hydroxide on charcoal at 14°C under atmospheric pressure. The ratio of *syn* to *anti* isomers of the substrate was calculated from the NMR spectrum in which the integral of the peaks at δ 4.05 (*syn*) and 4.53 (*anti*) ppm for a methine proton was used. The results are listed in Table 5.

Isomer Ratio of the Product during the Reaction. (*S*)(−)-*N*-(methylbenzylidene)-α-methylbenzylamine (0.004 mol) in methanol was hydrogenated using 200 mg of 10% palladium hydroxide on charcoal at 10°C under atmospheric pressure. The reactions were interrupted when the hydrogen consumption equaled 20, 40, 60, 80, and 100% of the theoretical amounts. The real percentages of the reaction completed were determined by the gas chromatographic method. The results are listed in Table 6.

Gas Chromatographic Separation of Diastereoisomers. The separation of (*S,S*)(−)-or (±)-α,α′-dimethyldibenzylamine from *meso* isomer, and (±)-α,α′-diethyldibenzylamine from *meso* isomer was carried out with the use of Shimadzu GC-3AF. Column length; 3 m, liquid phase; Neopentylglycol succinate 1.5% on Chromosorb-W, Column temperature; 155°C, Retention time; (*S,S*)(−)-and (±)-α,α′-dimethyldibenzylamine- 8.5 min, *meso*-α,α′-dimethyldibenzylamine-9.5 min, (*S,S*)(−)-and (±)-α,α′-diethyldibenzylamine- 8.7 min, *meso*-α,α′-diethyldibenzylamine-9.8 min, *N*-(methylbenzylidene)-α-methylbenzylamine-14.5 min, *N*-(ethylbenzylidene)-α-ethylbenzylamine-11.5 min.

The authors wish to express their thanks to Professor T. Shiba of the Department of Chemistry, Osaka University, for his valuable discussions and suggestions.

BULLETIN OF THE CHEMICAL SOCIETY OF JAPAN, VOL. 45, 3710—3714 (1972)

High Modulus Carbon Fibers from Pitch Materials[1)]

Sugio ŌTANI, Shoji WATANABE, Hosaku OGINO, Kazuo IIJIMA, and Teruyo KOITABASHI

Faculty of Technology, Gunma University, Kiryu, Gunma

(Received July 15, 1971)

Preparation of high modulus carbon fibers from pitch materials was attempted by two methods, stretch-graphitization and the use of a special pitch material composed of highly oriented constituent molecules. It was shown that carbon fiber of high tensile strength and of high modulus can be prepared by stretch-graphitization, and high modulus carbon fiber by heat treatment without stress from the pitch of tetrabenzophenazine. The property of precursor was found to have an important effect on the structure of the fiber.

Studies on the preparation and structure of high modulus carbon fibers have shown that they exhibit a high degree of preferred orientation of the constituent layer planes[2,3)] and heat treatment under stress

1) This work was presented at the Meeting of the Chemical Society of Japan held in Tokyo, April 2 (1971) Preprint No. 5248, p. 1018.

2) J. W. Johnson and W. Watt, *Nature*, **215**, 385 (1968).

3) A. Fourdeux, R. Perret, and W. Ruland, International Conference on Carbon Fiber, their Composites and Applications, London, Preprint No. 9 (1971).

is essential for successful preparation.[4,5] Most of these investigations have dealt with PAN(polyacrylonitrile) or rayon precursors. Until 1968, pitch precursor had not been thought to be very suitable material for high modulus carbon fiber.[6] Since then some works[7–11] were reported on the preparation of high modulus carbon fiber from pitch precursor by stretch-graphitization. The results, however, were not so satisfactory as those for rayon or PAN precursors. We found that two kinds of pitch based carbon fibers of which mechanical properties are almost equal to PAN based high modulus or high strength carbon fibers could be prepared by stretch-graphitization using a larger stress and a higher temperature than in the preliminary works.[7–9]

During the course of investigation on carbonization of synthetic aromatic compounds, it was found that tetrabenzo(a,c,h,j)phenazine was converted by heating into a pitch-like material which had a high degree of preferred orientation of the constituent molecules. By use of this material, carbon fiber having a high degree of preferred orientation of constituent layer planes was prepared without stretch-graphitization.

This paper describes improved results obtained by stretch-graphitization method and the evaluation of new method.

Experimental

Carbon Fibers Prepared by Heat Treatment under Stress. Original carbon fibers was two kinds of commercial pitch based carbon fibers with the different purches time. Both fibers with diameters 8—12 μ, named (M) and (S) respectively, were prepared at 1000°C by the Kureha process.[12] No distinct difference was observed in their mechanical properties, X-ray diffraction profiles or densities.

Preparation. Improvement of the design of the furnace gave rise to successful application of higher temperature and greater stress than those in previous work.[7–9] The bundles (2000—3000 deniers) of the original carbon fibers were suspended along the central axis of graphite tube heater. A load (0.5—1.0 g per denier) was attached to the end of the bundle. The bundles were then heated in nitrogen atmosphere from room temperature up to 2800°C at a rate of 270±20°C per minute and then immediately cooled. There was a gradient of temperature along the fiber axis in the tube heater and the homogeneous region at maximum temperature was about 4 cm in length. A change in length of the carbon fibers was clearly observed at temperatures above 1800°C. The amount of change increased with the increase of applied stress.

Mechanical Properties. The preferred orientation of the basal planes in the fibers remarkably increased by the plastic deformation during the course of heating under stress. The diameter of the resulting fibers was 4—7 μ. Their tensile strength was closely related with their orientation parameters as shown in Fig. 1. The orientation parameters are represented by the definition of Brydges and Badami.[13] Mechanical properties were measured with a Tensilon using a cross-head speed of 2 mm/min and 2 cm guage length. The average values were calculated from 30—50 runs. The values of typical PAN based carbon fibers, Royal Aircraft Establishment(RAE) carbon fiber Type I (high modulus type) and Type II (high strength type), measured under the same conditions, are also plotted as control. We see that both pitch based carbon fibers have the same trend as regards relationship between tensile strength and orientation parameter. However, samples from the carbon fiber (M) generally have a higher Young's modulus at a given tensile strength than other samples (Fig. 2).

The carbon fiber with the highest modulus (G-1) has one of about 49×10^2 ton/cm^2. That with the highest tensile strength (G-2) and prepared from carbon fiber (S) has a strength of about 29 ton/cm^2. G-1 might be said to be a high modulus carbon fiber and G-2 a high strength carbon fiber. Other properties of G-1 and G-2 are listed in Table 1.

Carbon Fiber from Highly Oriented Pitch Materials. It is well-known[14,15] that a number of anisotropic spherules are formed in amorphous molten pitch materials by heating at 350—400°C. They grow with rising temperature and/or extending heating period. The mesophase anisotropic spherules are composed of highly oriented polycyclic aromatic plane molecules. Thus the pitch materials heated at 400—500°C generally consist of anisotropic spherules

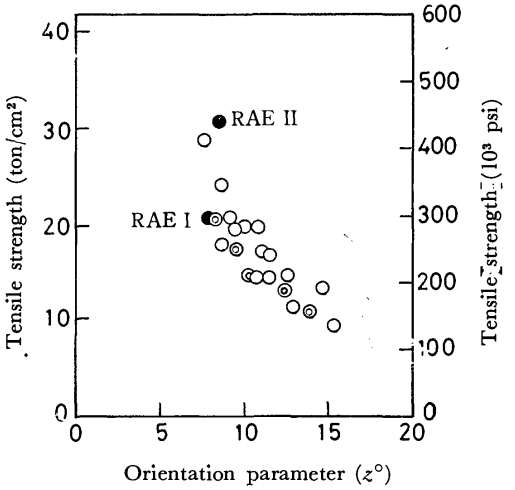

Fig. 1. Tensile strength of the fibers as a function of the orientation parameter.
○ Samples from carbon fiber (S)
◎ Samples from carbon fiber (M)
RAE I: RAE carbon fiber Type I (as control)
RAE II: RAE carbon fiber Type II (as control)

4) J. W. Johnson, J. R. Marjoran, and P. G. Rose, *Nature*, **221**, 357 (1969).
5) R. Bacon and W. A. Schalamon, Eighth Conference on Carbon, Abstract, Paper No. 58; *Carbon*, **6**, 199 (1968).
6) S. Otani, A. Yokoyama, and A. Nukui. A. C. S. 156th National Meeting, Atlatic City, N. J. (Sept. 1968), Preprint p. 1385. Applied Polymer Symposia No. 9, 325 (1969).
7) S. Otani, Y. Kokubo, and T. Koitabashi, 22th Meeting on Carbon Materials, Tokyo, (Dec. 1969), Preprint p. 5.
8) S. Otani, Y. Kokubo, and T. Koitabashi, This Bulletin, **43**, 3291 (1970).
9) S. Otani and S. Watanabe, 9th Conference on Carbon at Boston, (June, 1969), Summary of Paper, 29.
10) H. Hawthorne, C. Baker, R. H. Bentall, and K. R. Linger, *Nature*, **227**, 946 (1970).
11) H. Hawthorne, International Conference on Carbon Fibers, their Composites and Application, at London, (1971), Preprint Paper No. 13.
12) T. Araki and S. Gomi, Applied Polymer Symposia, No. 9, 331 (1969).
13) W. T. Brydges, D. V. Badami, J. C. Joiner, and G. A. Jones, Appllied Polymer Symposia No. 9, 255 (1969).
14) J. D. Brooks and G. H. Taylor, *Carbon*, **3**, 185 (1965).
15) H. Honda, H. Kimura, Y. Sanada, S. Sugawara, and T. Furuta, *ibid.*, **8** 181 (1970).

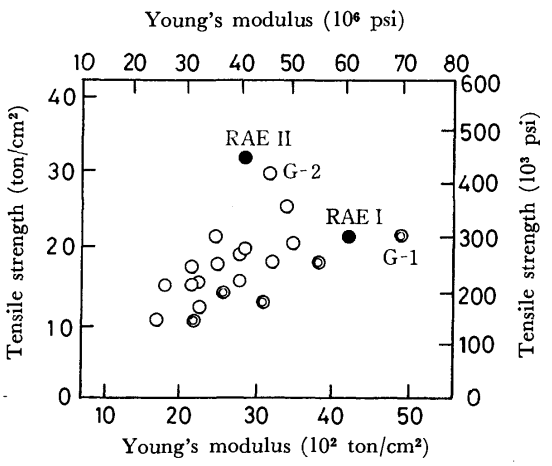

Fig. 2. Mechanical properties of the stretch-graphitized carbon fibers.
○: Samples from carbon fiber (S)
◎: Samples from carbon fiber (M)
RAE I: RAE carbon fiber Type I (as control)
RAE II: RAE carbon fiber Type II (as control)

and amorphous parts.

Tetrabenzo(a,c,h,j)phenazine ($C_{28}H_{16}N_2$) was converted into a pitch-like material by heating, which was optically anisotropic over the whole body (PZ pitch). It can thus be regarded as a typical highly oriented pitch material.

Preparation of Tetrabenzo(a,c,h,j)phenazine. Tetrabenzo-(a,c,h,j)phenazine was synthesized from diaminophenanthrene chlorohydrate and phenanthraquinone according to Schmidt and Söll.[16] The crystal purified by recrystallization from nitrobenzene solution is denoted by PZ-1. Since recrystallization was rather cumbersome, an attempt was made to omit final purification treatment by use of both raw materials purified before synthesis. The crystal thus prepared is denoted by PZ-2, which is essentially the same as PZ-1 except for the presence of about 1% of oxygen, appearance of a very weak absorption band around 1700 cm^{-1} in infrared spectrum and a low melting point of 462°C.

Conversion of Pitch Material from PZ Crystals. PZ-1 was fused into a yellowish brown liquid at 480°C and was converted gradually into a pitch-like material above 550°C and into a coke at 600°C. When PZ-1 was heated in a glass tube under nitrogen, the yields of the coke at 600°C and of PZ recrystallized through vapor phase in the cold part of the tube were respectively 65 and 33 wt%, gaseous product being about only 1 wt%. The spinnable pitch material was formed from PZ-1 by heating at 580°C for 60 min.

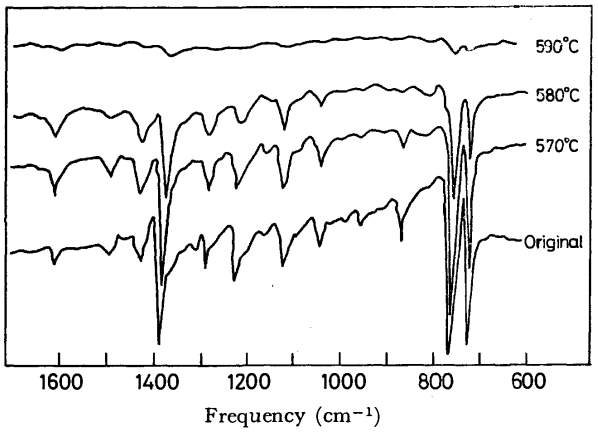

Fig. 3. Changes of IR spectra of PZ by heating under nitrogen.

Change of the infrared spectrum of PZ-1 by heating is shown in Fig. 3. We see that all bands, especially the two bands at 720 and 755 cm^{-1}, decreased remarkably at 580°C, a weak band appearing at 810 cm^{-1}.

Only the content of hydrogen decreased with temperature rise, from 34.8 to 32 atom% of sample treated at 580°C and 31.6 atom% treated at 600°C. Loss of a hydrogen up to 580°C and 600°C corresponds to 3—3.5 atoms of hydrogen per molecule. The content of nitrogen below 600°C remains almost the same as that of the original. Remarkable changes of X-ray diffraction profile were also observed at 580°C (Fig. 4). Below this temperature, the crystal structure of the original PZ is not greatly damaged, and 002 diffraction line appears at 580°C and grows with rising temperature.

The results of microscopic observation with crossed Nicols are shown in Fig. 5. The needle-like crystalline material

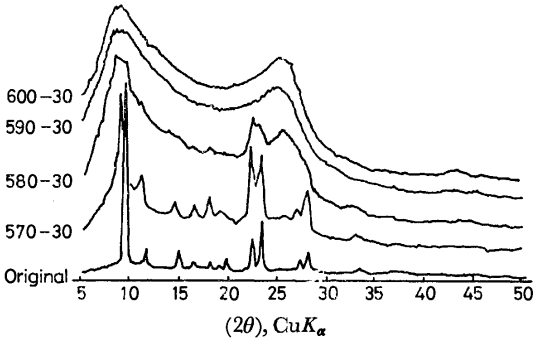

Fig. 4. Changes of X-ray diffraction profile with raising temperature. (Numbers show temperature (°C)—period (min)

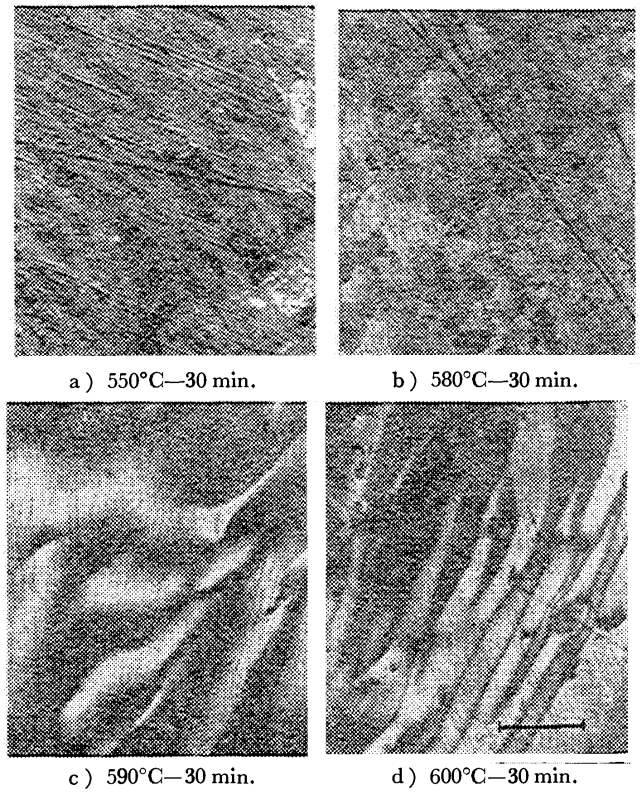

a) 550°C—30 min. b) 580°C—30 min.
c) 590°C—30 min. d) 600°C—30 min.

Fig. 5. Microscopic photograph with crossed nicols (Scale is 50 μ)

16) J. Schmidt and J. Söll, *Ber.*, **40**, 2456 (1907).

(Fig. 5-a) appears to be converted into the oriented mesophase at 580°C (Fig. 5-c).

It has been found that pure PZ is converted into an anisotropic pitch-like material with a loss of about three hydrogen atoms per molecule. Since there are four overcrowed positions caused by four hydrogen atoms as shown in Fig. 6, the first step of dehydrogenation probably occurs at these positions and the plane dimer may be formed. Thus, it seems reasonable to consider that the pitch-like material formed at 580°C is mainly composed of a mixture of the monomer and the dimer, and the anisotropic structure caused by the interaction between these plane molecules.

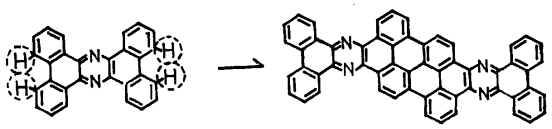

Fig. 6. Formation of dimer from PZ monomer.

PZ-2 crystal which contains some impurity gave the spinnable pitch-like material at lower heating temperature than that in the case of pure PZ-1 crystal. PZ-2 crystal was converted gradually into a black molten substance above 500°C. Spinnable pitch-like material was formed by heating under nitrogen at 530°C for 110 min. Various changes caused by heating in this case occurred during the process which was essentially the same as that for PZ-1.

Graphitizability of PZ Pitch. In order to determine the graphitizability of PZ pitch, the coke obtained was crushed and then heated under nitrogen at various temperatures below 2800°C. The coke made from PZ-1 pitch is a graphitizing carbon with interlayer distance d_{002} 3.361Å and crystallite thickness $Lc_{(002)}$ 850Å after 2800°C-treatment. PZ-2 pitch gave almost the same results as those of PZ-1 pitch.

Preparation of Carbon Fiber from PZ Pitch. The procedure was essentially the same as that previously reported.[12,17] In the case of PZ-2 pitch, the spinning temperature was 410—440°C and the spinning speed 300—400 m/min. It was better material than PZ-1 pitch from the viewpoint of spinnability and ability of conversion into an infusible fiber by oxidation. However, even in the case of PZ-2 pitch, its spinnability was not very satisfactory. The diameter of carbon fibers finally obtained was thus around 20 μ. This value is considerably greater than that of carbon fibers from petroleum asphalt, PVC pitch, and other pitch materials.[8,12,17] There was no difference between PZ-1 and PZ-2 pitch in the fundamental structure of the resulting carbon fibers. However, in mechanical properties, the carbon fiber from PZ-2 was better to some extent.

Carbonization was carried out under nitrogen up to the desired temperature below 2800°C. Heating rate was 5°C/min up to 1000°C and was 50°C/min above 1000°C. Throughout the process after spinning, heat treatment was carried out without mechanical stress.

Changes in Property with Heat Treatment. Changes in bulk density, electric resistivity and degree of preferred orientation of the basal planes are plotted in Fig. 7, and changes in crystal thickness(Lc), crystal size(La) and interlayer distance (d_{002}) in Fig. 8. It is noteworthy that the value of preferred orientation parameter is small. Even in the stage before heat treatment, it was only 23° and decreased to 6° with the rise in temperature. Since heat treatment was carried out with no stress, it is evident that the

17) S. Otani, *Carbon*, **3**, 31 (1965).

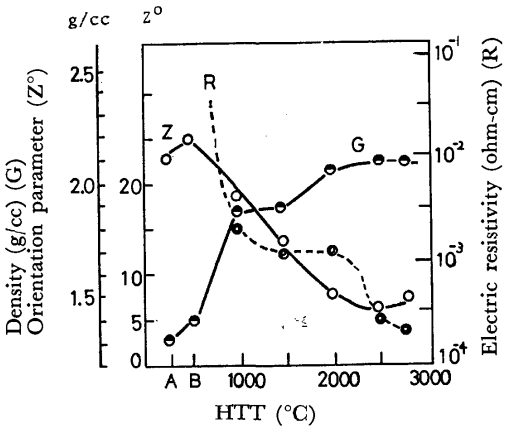

Fig. 7. Variations of the properties of PZ pitch fiber with raising temperature.
A: stage of pitch fiber
B: oxidized fiber

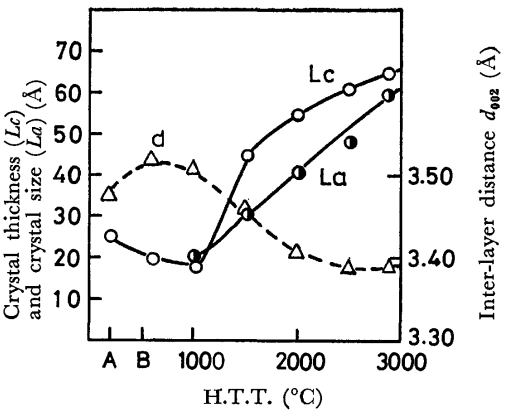

Fig. 8. Variations of the X-ray diffraction parameters of PZ pitch fiber with raising heat-treatment temperature.
A: stage of pitch fiber
B: oxidized fiber

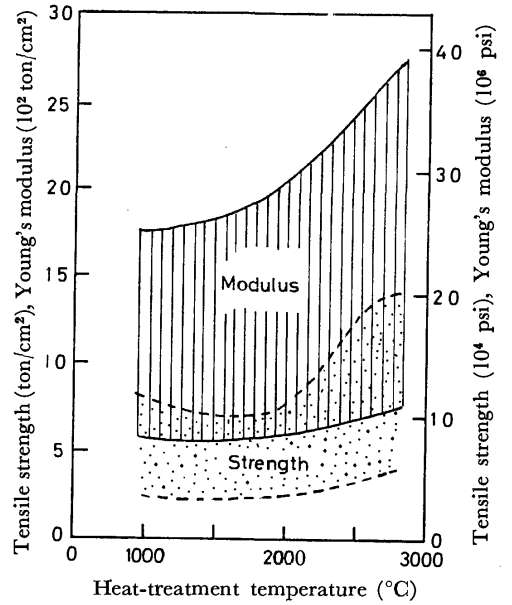

Fig. 9. Variations of mechanical properties of PZ pitch based carbon fiber with raising heat-treatment temperature.

Table 1. Characteristics of typical pitch-based carbon fibers

Characteristic	Pitch-based carbon fibers			PAN based carbon fiber
	Stretch-graphitized,		Non-stretch-graphitized PZ based fiber heated at 2800°C	RAE Type I
	G-1	G-2		
Orientation parameter (Z°)	9	8	6	8
Immersion density	1.85	1.75	2.08	2.01
Electrical resistance (ohm-cm)	5×10^{-4}	1×10^{-3}	4×10^{-4}	3×10^{-4}
Inter-layer distance (Å)	3.40	3.55	3.39	3.39
Crystal thickness (Å)	60	40	60	60
Young's modulus ($\times10^6$ psi)	70	45	20 (40)[a]	60
Tensile strength ($\times10^3$ psi)	300	420	120 (180)[a]	300

a) Maximum value.

the progress of orientation is due to the nature of the original pitch material.

The mechanical properties, tensile strength and Young's modulus are shown in Fig. 9. The maximum Young's modulus reaches about 280×10^8 g/cm^2(40×10^6 psi), but the maximum tensile strength is only 13×10^6 g/cm^2(180×10^3 psi). We see that Young's modulus increases with the rise in heat treatment temperature, the tensile strength having a minimum at around 2000°C.

Discussion

X-Ray diffraction parameters and the properties of the three typical carbon fibers are given in Table 1. PZ-pitch based carbon fiber heated at 2800°C and PAN based high modulus one are identical in their characteristics except for mechanical properties. Stretch-graphitized carbon fibers G-1 and G-2 are characterized by their low densities. From the data of interlayer distance, crystal thickness and electric resistance, it seems that the crystal growth in G-2 is restricted to some extent as compared with other fibers.

The mechanical properties of the pitch based carbon fibers were remarkably improved by means of stretch-graphitization using higher temperature and greater stress. From the data in Fig. 2, it is seen that two kinds of carbon fibers, high modulus and high strength, were prepared from pitch based carbon fibers by this method. Since the two carbon fiber M and S were heat treated under almost the same conditions, it seems reasonable that their formation is attributed mainly to the nature of the original carbon fibers. However, no distinct difference between the two original fibers was observed in their mechanical properties and structure. This seems to result from the lack of an effective method to detect the difference.

PZ pitch is less spinnable, and PZ pitch fiber has less ability to be converted into infusible fiber by oxidation as compared with PVC pitch and petroleum pitch.[17,18] PZ pitch based carbon fibers we obtained were somewhat rough, their diameter being around 20 μ. However, it has been found (Table 1) that the elemental nature, except for mechanical properties, of PZ pitch based carbon fiber is almost the same as that of PAN based high modulus fiber prepared by stretch-graphitization. Since PZ pitch based carbon fiber can be prepared without any stretching through the whole heating process, stretch-graphitization is not always necessary for preparing highly oriented carbon fiber, and thus the precursor nature has an essential effect on the structure of the fiber. Since Young's modulus of PZ pitch based fiber reaches 280×10^8 g/cm^2 (40×10^6 psi) in maximum value and 140×10^8 g/cm^2 (20×10^6 psi) in average value, one might say that PZ pitch based carbon fiber belongs to a high modulus, at least a middle modulus, carbon fiber. However, mechanical properties of the PZ pitch based carbon fibers are generally lower than those expected from their fundamental structure. It was shown that both Young's modulus and tensile strength were closely related to the diameter, increasing with decrease of the diameter.[17,18] When the diameter becomes smaller than 10 μ, the mechanical properties are remarkably improved. Thus, the lower mechanical properties of PZ based fiber is expected to improve remarkably, if the PZ based fiber having smaller diameter than 10 μ is prepared. For this purpose, it should be noted that PZ-2 pitch containing some amount of impurities was more spinnable and was more easily converted into the infusible fiber than PZ-1 pitch.

Little attention has been paid to finding a new procedure which does not require stretch-graphitization. The authors think there is a fair prospect that high modulus carbon fibers can be prepared by use of a graphitization process without stretching from pitch composed of highly oriented constituent molecules.

The authors are indebted to Dr. E. Ōta for supply of the PZ crystal and for helpful discussions.

18) S. Otani, K. Yamada, T. Koitabashi, and A. Yokoyama, *Carbon*, **4**, 425 (1966).

NOTES

BULLETIN OF THE CHEMICAL SOCIETY OF JAPAN, VOL. 45, 3715—3716 (1972)

An SCF-MO-INDO Study of Isotropic and Anisotropic Hyperfine Coupling Constants for Sigma Radicals

Tetsuo MORIKAWA and Osamu KIKUCHI

Department of Chemistry, Tokyo Kyoiku University, Otsuka, Bunkyo-ku, Tokyo

(Received November 25, 1971)

A knowledge of theoretically calculated hyperfine coupling constants (hfc) for a radical is helpful in interpreting its electronic structure and explaining the magnitudes and signs of the observed values. In the calculation of the isotropic hfc, the spin-polarization effect should be included.[1] The one-center dipolar interaction integrals mainly contribute to anisotropic hfc.[2] With these two factors taken into consideration, an improved SCF-MO function has been constructed and the isotropic and anisotropic hfc have been calculated.

The ground electron-configuration (Ψ_g) for a radical was obtained in terms of the approximate open-shell MO's of Longuet-Higgins and Pople using INDO approximation.[3] There are four types of one-electron-excited electron-configurations which are eigen functions (doublet) of S_z and S^2. When SCF-MO's are used, however, only one of them (Ψ_{ik}(II))[4] interacts with Ψ_g and the wave function Ψ_g can be improved by use of the first order perturbation: $\Psi=\Psi_g+\sum\lambda_{ik}\Psi_{ik}$ (II). The i, j components (i, $j=X$, Y, Z) of the anisotropic hfc, A^N_{ij}, and the isotropic hfc, a^N, for a nucleus N are:

$$A^N_{ij}=g\beta\hbar\gamma_N tr(\rho P),\ P_{rs}=\langle\chi_r|r_N{}^{-5}(3r_{Ni}r_{Nj}-r_N{}^2\delta_{ij})|\chi_s\rangle, \quad (1)$$

$$a^N=(8\pi/3)g\beta\hbar\gamma_N tr(\rho Q),\ Q_{rs}=\langle\chi_r|\delta(r_N)|\chi_s\rangle, \quad (2)$$

$$\rho_{rs}=C_{rm}C_{sm}+\sum_{i,k}(C_{ri}C_{sk}+C_{si}C_{rk})(mi|mk)/\Delta E_{ik}, \quad (3)$$

where C_{ri} are the LCAO coefficients ($\phi_i=\sum\chi_r C_{ri}$), ΔE_{ik} the energy differences between Ψ_{ik}(II) and Ψ_g, ρ_{rs} an element of the AO spin density matrix, and the other notations have their usual meaning. The second term in ρ_{rs} is what appears by spin-polarizarion. If AO's χ_r and χ_s belong to different atoms, dipolar interaction integrals P_{rs} are evaluated over the Slater type AO's[2] and one-center P_{rs} over the SCF-AO's expanded by Löwdin.[5] Q_{rs} are also evaluated over the Löwdin's SCF-AO's, only if both χ_r and χ_s are centered on the atom N.

The hfc of HCO, CO_2^-, CH_2=CH, HCN^-, and CH≡C were calculated. The results for HCO, a typical σ-radical, are described in some detail. The electronic structure of this radical has been reported.[3]

Table 1. Contribution of electron-configurations to hfc (MHz) of ^{1}HCO in the principal axes

Configuration	a	A_{xx}	A_{xy}	A_{yy}	A_{zz}
Ψ_g	243	23.2	−3.3	−6.3	−16.9
$1\sigma\rightarrow6\sigma$	1	−0.1	0.2	0.0	0.1
$2\sigma\rightarrow6\sigma$	31	−3.3	2.1	1.3	2.0
$2\sigma\rightarrow7\sigma$	5	−1.0	−0.4	0.6	0.4
$3\sigma\rightarrow6\sigma$	9	−1.1	0.9	0.4	0.7
$3\sigma\rightarrow7\sigma$	2	−0.4	0.1	0.3	0.2
$1\pi\rightarrow2\pi$	0	0.6	−0.1	−0.6	0.0
$4\sigma\rightarrow7\sigma$	−3	0.8	0.5	−0.5	−0.4
Sum of $i\rightarrow k$	45	−4.6	3.3	1.5	3.1
Total	288	18.7	0.0	−4.8	−13.9

Table 2. Contribution of each atom to the anisotropic hfc (MHz) of H^{13}CO in the principal axes

Atom		A_{xx}	A_{xy}	A_{yy}	A_{zz}
C	$2p_x{}^2$	−4.3	0	2.2	2.2
	$2p_y{}^2$	−27.4	0	54.8	−27.4
	$2p_z{}^2$	−1.5	0	−1.5	2.9
	Others	0	−0.1	0	0
	Total of C	−33.2	−0.1	55.5	−22.3
H		3.1	2.9	−0.8	−2.3
O		4.6	−2.8	−1.3	−3.3
	H+O	7.7	0.1	−2.1	−5.6
Total		−25.5	0	53.4	−28.0

The contribution of each electron-configuration to hfc for the proton is shown in Table 1. We see that the most important contribution is C-H $\sigma\rightarrow\sigma^*$ ($2\sigma\rightarrow6\sigma$). Spin-polarization should be included in the calculation of anisotropic hfc as for the isotropic hfc.

Each atom of HCO contributes to hfc of ^{13}C (Table 2). Holmberg[6] resolved the experimentally observed hfc (MHz) of ^{13}C into two axial parts: (A_{xx}, A_{yy}, A_{zz})=(−48, 72, −24)=(−40, 80, −40)$_{2py}$+(−8, −8, 16)$_{2pz}$. The second term shows the contribution of the carbon $2p_z$ orbital normal to the molecular plane. Table 2 suggests that the effect of neighbouring atoms is larger than that of C($2p_z$), and that the observed values can be resolved into those of $2p_x$ and $2p_y$. Direction cosines obtained show that the principal axis y of ^{1}H, ^{13}C, and ^{17}O rotate by 75°, 33°, and 16° from the C-O bond, respectively. The results for HCO are compared with available experimental data in Table 3. Satisfactory agreement was found for both

1) T. Yonezawa, T. Kawamura, and H. Kato, This Bulletin, **43**, 74 (1970).
2) T. Morikawa, O. Kikuchi, and K. Someno, *Theoret. chim. Acta*, **24**, 393 (1972).
3) T. Morikawa, O. Kikuchi, K. Someno, *ibid.*, **22**, 224 (1971).
4) O. Kikuchi and K. Someno, This Bulletin, **40**, 2972 (1967).
5) P.-O. Löwdin, *Phys. Rev.*, **90**, 120 (1953).
6) R. W. Holmberg, *J. Chem. Phys.*, **51**, 3255 (1969).

Table 3. Calculated results for σ-radicals (MHz)
(Data in the parentheses are experimental.)

Radical	Nucleus	a	A_{xx}	A_{yy}	A_{zz}	Ref.
HCO	^{1}H	288	19	−5	−14	
		(354)	(25)	(−8)	(−17)	6
		(381)	(15)	(−2)	(−14)	7
	^{13}C	550	−25	53	−28	
		(365)	(−48)	(72)	(−24)	6
		(378)	(−39)	(50)	(−12)	7
	^{17}O	−22	47	−100	54	
		(—)	(—)	(—)	(—)	
CO_2^-	^{13}C	610	−21	54	−33	
		(467)	(−47)	(79)	(−33)	8
	^{17}O	−29	38	−75	38	
		(−90)	(25)	(−53)	(28)	8
HCN^-	^{1}H	356	19	−8	−11	
		(384)	(—)	(—)	(—)	9
	^{13}C	550	−21	35	−14	
		(207)	(—)	(—)	(—)	9
	^{14}N	10	43	−20	−23	
		(18)	(—)	(—)	(—)	9
Vinyl	$^{1}H_{\alpha}$	56	36	−9	−27	
		(45)	(38)	(−11)	(−27)	10, 11
	$^{1}H_{trans}$	251	8	−6	−2	
		(190)	(—)	(—)	(—)	10
	$^{1}H_{cis}$	118	10	−5	−5	
		(95)	(—)	(—)	(—)	10
	$^{13}C_{\alpha}$	388	−58	110	−51	
		(301)	(—)	(—)	(—)	12
	$^{13}C_{\beta}$	−27	13	−4	−9	
		(−24)	(—)	(—)	(—)	12
Ethynyl	^{1}H	151	4	−2	−2	
		(45)	(—)	(—)	(—)	10
	$^{13}C_{\alpha}$	978	87	−44	−44	
		(—)	(—)	(—)	(—)	
	$^{13}C_{\beta}$	54	27	−13	−13	
		(—)	(—)	(—)	(—)	

the isotropic and the anisotropic hfc. The present results are slightly better than the previous ones,[2] *e. g.*, for the anisotropic hfc (MHz) of ^{13}C, from (−17, 47, −30) to (−25, 53, −28). The isotropic and anisotropic hfc of other σ-radicals calculated by the present method, some of which are given in Table 3, are useful for the analysis of complicated ESR spectra in solid solution.

7) E. L. Cochran, F. J. Adrian, and V. A. Bowers, *J. Chem. Phys.*, **44**, 4626 (1966).
8) S. Schlik, B. L. Silver, and Z. Luz, *ibid.*, **54**, 867 (1971).
9) K. D. J. Root, M. C. R. Symons, and B. C. Weatherly, *Mol. Phys.*, **11**, 161 (1966).
10) E. L. Cochran, F. J. Adrian, and V. A. Bowers, *ibid.*, **40**, 213 (1964).
11) M. Iwasaki and B. Eda, *ibid.*, **52**, 3837 (1970).
12) R. W. Fessenden, *J. Phys. Chem.*, **71**, 74 (1967).

BULLETIN OF THE CHEMICAL SOCIETY OF JAPAN, VOL. 45, 3717—3718 (1972)

Binuclear Structure of Copper(II) 2-Pyridinolate Complex

Shuji EMORI, Isamu OKANO, and Yoneichiro MUTO

Department of Chemistry, Faculty of Science and Engineering, Saga Univesity, Honjo-machi, Saga, 840

(Received June 1, 1972)

Copper(II) acetate monohydrate has a typical isolated binuclear structure.[1] The temperature dependence of its magnetic susceptibility was clearly interpreted by a simple singlet-triplet equilibrium.[2,3] However, there has been controversy over the coupling mechanism in the crystal; direct interaction by a metal-metal δ-bond or superexchange interaction *via* the acetate bridges. Dubicki and Martin[4] pointed out that the δ-bond in the crystals of copper(II) acetate monohydrate is virtually nonbonding and that the configuration of the binuclear clusters is maintained by four bridging acetate groups. Their view has been supported by the following experimental results. The Cu–Cu separation, 3.02 Å in dichlorobis(6-hydroxypurine)copper(II) monohydrate[5] is much greater than 2.66 Å in copper(II) acetate monohydrate, although their exchange integrals are nearly equal.[6] The exchange integral -305 cm^{-1} of $(CH_3)_4NCu(CH_3COO)_2(NCS)$ is much higher than -485 cm^{-1} of of $(CH_3)_4NCu(HCOO)_2(NCS)$, although their Cu–Cu distances are nearly equal.[7] Thus we see that the cause of the formation of binuclear clusters of the type of copper(II) acetate monohydrate is the relative position of two active sites in the bidentate ligand and the direction of lone pairs of the active sites. We have attempted a synthesis of the copper(II) complex with 2-pyridinol whose ligand has the same site-structure and directionality as acetic acid.

Copper(II) 2-pyridinolate mono(2-pyridinol) was prepared by adding freshly prepared copper(II) hydroxide to a solution of excess 2-pyridinol. The reactants were agitated vigorously for 15 min to ensure maximum contact between the reactants. From the resulting suspension, crystals of $Cu(pyO)_2\cdot pyOH$ (py denotes 2-pyridyl radical) were formed in a week. The remaining non-reacted copper(II) hydroxide was removed by decantation and the crystals of pyridinolate were washed by ethanol and dried over silica gel in a desiccator. The salt was also prepared by adding dropwise a solution of sodium hydroxide to a mixture of copper(II) chloride and 2-pyridinol solution. Crystals of $Cu(pyO)_2\cdot pyOH$ were obtained overnight from the dark green suspension. No difference was observed between the two samples in analytical and magnetic data. Found: C, 51.10; N, 11.86; H, 3.74; Cu, 18.29%. Calcd for $CuC_{15}N_3O_3H_{13}$: C, 51.95; N, 12.12; H, 3.78; Cu, 18.32%.

The molar magnetic susceptibility of the complex was determined to be 565 μemu/mol (18°C) by the Gouy method, the magnetic field strength amounting to about 8000 Oe. Corrections were made for diamagnetic contributions (in μemu/mol) from 2-pyridinol (-54) and copper(II) ion (-11).[8] The value for the ligand was calculated from Pascal's constants.[9] Bleaney and Bowers[2] proposed a theoretical equation for the susceptibility χ of copper(II) compounds having a binuclear structure.

$$\chi = \frac{Ng^2\beta^2}{3kT}\left(1+\frac{1}{3}e^{2J/kT}\right)^{-1} + N\alpha$$

where J is the exchange integral and $N\alpha$ the temperature independent paramagnetism assumed to be equal to 60 μemu/mol,[3] the other quantities having their usual meanings. The observed susceptibility of the compound agrees well with the theoretical curve (Fig. 1), indicating the existence of dimer molecule in crystals. We realized that the structure of bidentate ligand is a factor in the formation of the dimeric structure of the type of copper(II) acetate mono-

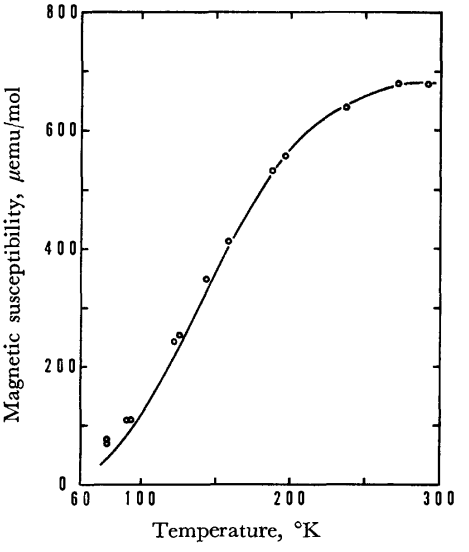

Fig. 1. Magnetic susceptibility of copper(II) 2-pyridinolate mono(2-pyridinol). The solid curve represents the Bleaney-Bowers equation.

1) J. N. van Niekerk and F. R. L. Schoening, *Acta Crystallogr.*, **6**, 227 (1953).
2) B. Bleaney and K. D. Bowers, *Proc. Roy. Soc. Ser. A*, **214**, 451 (1952).
3) B. N. Figgis and R. L. Martin, *J. Chem. Soc.*, **1956**, 3837.
4) L. Dubicki and R. L. Martin, *Inorg. Chem.*, **5**, 2203 (1966).
5) E. Sletten, *Acta Crystallogr.*, **B26**, 1609 (1970).
6) T. Asakawa, M. Inoue, K. Hara, and M. Kubo, This Bulletin, **45**, 1054 (1972).
7) D. M. L. Goodgame, N. J. Hill, D. F. Marsham, A. C. Skapski, M. L. Smart, and P. G. H. Troughton, *Chem. Commun.*, **1969**, 629.
8) P. W. Selwood, "Magnetochemistry," 2nd Ed., Interscience Publishers Inc., New York, N. Y. (1956).
9) G. Foëx, "Constantes Sélectionées, Diamagnétisme et Paramagnétisme," Masson, Paris (1957).

hydrate. This indicates that the spin interactions between copper atoms occur by superexchange *via* pyridinol groups. The exchange integral and g-value of $Cu(pyO)_2 \cdot pyOH$ are evaluated as $J/k = -245°K$, $g = 2.10$. The magnitude of superexchange interaction depends to a great extent on the electronic structure of bridging ligands. This was proved by the fact that magnetic interaction operates more strongly in bis(6-aminopurinato)copper(II) tetrahydrate.[6] Our result where the antiferromagnetic interaction operates more strongly in the complex of $Cu(pyO)_2 \cdot pyOH$ than in $Cu(CH_3COO)_2 \cdot H_2O$ can be explained by considering that 2-pyridinol promotes the migration of positive holes to a greater extent than acetate groups.

BULLETIN OF THE CHEMICAL SOCIETY OF JAPAN, VOL. 45, 3718—3719 (1972)

Decarboxylation of Sodium β-Phenylglycidate under Conditions of Kolbe Electrolysis

Akira TAKEDA, Tosio MORIWAKE, Sigeru TORII,* and Takehiko TAKAKI*

Department of Synthetic Chemistry, School of Engineering, Okayama University, Okayama

** Department of Industrial Chemistry, School of Engineering, Okayama University, Okayama*

(Received May 16, 1972)

The anodic decarboxylation of glycidic acids has recently been reported by Waters and Witkop.[1] They found that the anodic oxidation of aromatic glycidate such as piperonal glycidate gave a low yield of neutral material consisting of numerous compounds which were not further investigated. As an extension of our previous work on the anodic reaction of aldehyde,[2),3)] ketone,[3)] cinnamic acid,[4)] 5-alkyl-2-furoic acids,[5)] and cyclopropanecarboxylic acids,[6)] we studied the anodic decarboxylation of aromatic glycidic acids in protic media and obtained some information on the primary and secondary products in the reaction.

The anodic reaction of sodium β-phenylglycidate (**1**) in a mixed solvent of acetic acid–methanol–water using smooth platinum electrodes gave a neutral mixture in 51—63% yields based on **1**. When the neutral mixture was extracted with an aqueous Girard P reagent, it was separated into active carbonyl component (26% in weight) and non-active carbonyl component (74%), which were further analyzed by glpc. The ratios of peak areas (%) of the constitutents in the active carbonyl and non-active carbonyl components are summaried in Table I. Compounds such as benzaldehyde (**2**), acetophenone (**3**), methyl benzoate (**4**), benzyl acetate (**5**), and 1-phenethyl alcohol (**6**) were detected as principal products by glpc.

The electrochemical reaction of benzaldehyde in an aqueous acetic acid–potassium hydroxide solution has been shown[2)] to afford compounds **3**, **4**, and benzyl alcohol (**7**) as principal products and 1-phenethyl alcohol (**8**), *p*-tolualdehyde (**8**), *p*-methylacetophenone (**9**), propiophenone (**10**), and methyl toluates as minor components. A similar electrochemical reaction of acetophenone gave a small amount of neutral mixture which contained **10** as a major constituent (see Experimental). Although the pathway in which these prin-

TABLE 1. COMPOSITION OF THE ACTIVE AND NON-ACTIVE CARBONYL COMPONENTS OBTAINED IN THE ELECTROLYSIS OF SODIUM β-PHENYLGLYCIDATE (**1**)

Carbonyl component	Constituent	Relative ratio of peak area[a)] (%)
Active toward Girard's reagent (100%)	Benzaldehyde	59.7
	Acetophenone	21.3
	p-Tolualdehyde	2.5
	o-Methylacetophenone	0.6
	Propiophenone	0.6
	p-Methylacetophenone	1.7
	Phenacyl acetate	1.0
	Others	12.5
Non-active toward Girard's reagent (100%)	Methyl benzyl ether	0.5
	Phenyl acetate	0.9
	——	0.6
	——	1.6
	Methyl benzoate	14.2
	Benzyl alcohol	2.8
	Benzyl acetate	30.8
	Methyl phenylacetate	4.4
	Methyl *o*-toluate	2.2
	1-Phenethyl alcohol	8.4
	2-Phenethyl alcohol	1.7
	——	3.1
	Methyl *p*-toluate	3.4
	2-Phenethyl acetate	0.8
	p-Methylbenzyl acetate	trace
	Others (fifteen minor peaks)	24.6

a) Gas chromatography with a 45 m, 10% SE-30 coated Hitachi Golay column (Z-45) operating at 100°C; carrier gas N_2 (0.5 kg/cm²).

1) J. A. Waters and B. Witkop, *J. Org. Chem.*, **36**, 3233 (1971).
2) A. Takeda, S. Torii, and H. Oka, *Tetrahedron Lett.*, **1968**, 1781.
3) A. Takeda, S. Wada, S. Torii, and Y. Matsui, This Bulletin, **42**, 1047 (1969).
4) A. Takeda, S. Torii, and H. Oka, *Mem. Sch. Eng., Okayama Univ.*, **3**, 107 (1968).
5) S. Torii, H. Tanaka, H. Ogo, and S. Yamasita, This Bulletin, **44**, 1079 (1971); S. Torii, H. Tanaka, and T. Okamoto, *ibid.*, **45**, 2783 (1972).
6) A. Takeda, S. Wada, and Y. Murakami, *ibid.*, **44**, 2730 (1971).

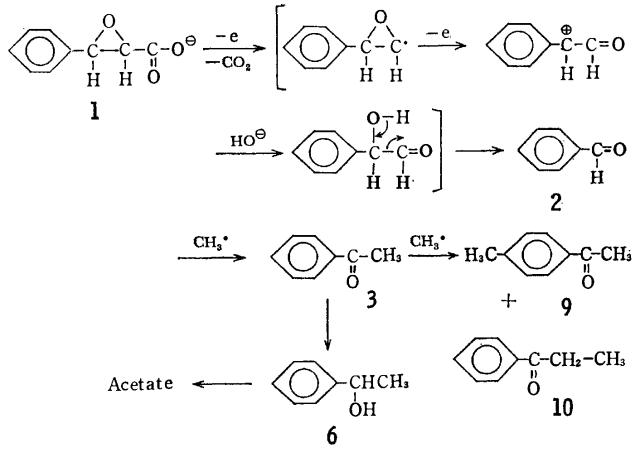

cipal products of the anodic reaction of **1** were formed is not certain at present, it seems that the mechanism proposed by Waters[1] for the electrochemical decarboxylation of α-methyl-α,β-epoxycyclohexylideneacetate and the related compounds can be applied to the formation of **2**. It can be suggested that benzaldehyde produced primarily underwent secondary reactions such as anodic methylation[2,3] to give **3**, and electrochemical reduction to give **7**. Compounds **8** and **9** may be interpreted as the products of ring methylation.[7] The anodic decarboxylation of sodium β-methyl-β-phenylglycidate (**11**) in an aqueous media afforded **3** as a predominant product when the reaction was carried out for a shorter period.

Experimental

All the boiling points are uncorrected. The products were analyzed by vapor-phase chromatography using a Hitachi F6-D instrument, Golay column (Z-45) coated with silicone oil (10%, SE-30). Electrolyses were carried out in the apparatus described previously.[2-4] The cell was immersed in a water-bath cooled with circulating cold water. The electrodes were two platinum foils (1.5×2.0 cm²) about 2 mm apart and the current direction was changed every 30 sec by means of a commutator.

Analytical grade acetic acid, methanol, acetophenone, and potassium hydroxide were used. Sodium β-phenylglycidate and sodium β-methyl-β-phenylglycidate were prepared by saponification of the corresponding ethyl esters[8] with sodium ethoxide. The following reference compounds were of commercial grade: benzaldehyde, benzyl alcohol, 1- and 2-phenethyl alcohols, benzoic acid, methyl benzyl ether, propiophenone, phenyl acetate, methyl *o*-toluate, methyl benzoate, *p*-tolualdehyde, *m*- and *p*-methylacetophenones, and methyl phenylacetate. The following acetates were prepared from the appropriate hydroxy compounds: benzyl acetate, bp 93°C/10 mmHg,[9] 2-phenethyl acetate, bp 118°C/13 mmHg,[10] *p*-methylbenzyl acetate, bp 95°C/13 mmHg,[11] phenacyl acetate, bp 150—164°C/2 mmHg,[12] *p*-acetoxyacetophenone, bp 165—170°C/19 mmHg.[13] Methyl *p*-toluate was prepared by treating *p*-toluic acid with diazomethane, bp 102—105°C/10 mmHg.[14] *o*-Methylacetophenone was also prepared: bp 110°C/14 mmHg.[15]

*Anodic Reaction of Sodium β-Phenylglycidate (**1**).* A mixture of **1** (18.6 g, 0.1 mol) with acetic acid (100 m*l*), methanol (50 m*l*), water (70 m*l*) and potassium hydroxide (4 g, 0.07 mol) was electrolyzed for 54 hr at 31—35°C with terminal voltage 10—13 V and a current of 0.8—0.9 A/cm². During the electrolysis a 40 m*l* portion of acetic acid was added every 8 hr. The reaction mixture was diluted with 300 m*l* of water and extracted with ether. The extract was washed with aqueous sodium chloride and sodium hydrogen carbonate, and was concentrated *in vacuo* to afford 9.5 g (51%) of neutral oil. 0.2 g of acidic product was obtained from the aqueous layer. After 5 g of the neutral mixture was treated with an excess (10 g) of Girard P reagent in ethanol at reflux temperature, 2.3 g of an oil consisting of non-active carbonyl components was recovered by extraction with ether. From the residual solution, 0.8 g of active carbonyl component was recovered by acid hydrolysis. The composition of the active carbonyl and the non-active carbonyl components analyzed by glpc is given in Table 1.

*Anodic Decarboxylation of Sodium β-Methyl-β-phenylglycidate (**11**).* A solution of 30 g (0.15 mol) of **11** in 150 m*l* of water was electrolyzed for 8 hr at 30—35°C with terminal voltage 11—12 V and a current of 0.9—1.0 A/cm². The reaction mixture was extracted with ether, washed with water and dried (Na_2SO_4). After evaporation of the solvent, 2.8 g of an oil was obtained which was chromatographed on silica gel and eluted with benzene (200 m*l*), ether (500 m*l*), and methanol (250 m*l*). From the fractions eluted by ether and methanol, 2.2 g of an oil was isolated. The IR spectrum of this oil was identical with that of an authentic sample of **3** and gave 2,4-DNP which was identified as that of **3** by mixed mp 235—237°C, IR spectrum, and microanalyses.

*Anodic Methylation of Acetophenone (**3**).* A mixture of **3** (12.1 g, 0.1 mol) with acetic acid (53 m*l*), methanol (67 m*l*), water (110 m*l*) and potassium hydroxide (4.0 g) was electrolyzed for 53 hr at 23—33° with terminal voltage 11—13 V and a current of 0.8—0.9 A/cm². During the course of electrolysis 30 m*l* of acetic acid was added every 7 hr. The reaction mixture was washed as usual and dried. After distilling off unreacted **3** with a Widmer column, 2.2 g of neutral oil was obtained from the reaction mixture. The glpc analysis of the mixture is given in Table 2.

Table 2. Composition of the products obtained in the anodic methylation of acetophenone

Constituent	Peak Area[a]
Acetophenone	13.6
o-Methylacetophenone	10.6
Propiophenone	31.4
m-Methylacetophenone	7.3
p-Methylacetophenone	12.2
——	6.6
——	2.4
p-Acetoxyacetophenone	3.6
Phenacyl acetate	3.2
Others	9.1

a) Gas chromatographic peak area (%) with a 45 m, 10% SE-30 coated Hitachi Golay colum (Z-45) operating at 140°C; carrier gas N_2(0.5 kg/cm²).

7) F. D. Mango and W. A. Bonner, *J. Org. Chem.*, **29**, 1367 (1964).
8) W. S. Johnson, J. S. Belew, L. T. Chinn, and R. H. Hund, *J. Amer. Chem. Soc.*, **75**, 4995 (1953); L. Claisen, *Ber.*, **38**, 693 (1905).
9) M. Gomberg and C. C. Buchler, *J. Amer. Chem. Soc.*, **42**, 2064 (1920).
10) R. Huisgen, *Ann. Chem.*, **573**, 163 (1951).
11) C. K. Ingold and E. Rothstein, *J. Chem. Soc.*, **1928**, 1279.
12) J. B. Rather and E. E. Reid, *J. Amer. Chem. Soc.*, **43**, 630 (1921).
13) P. D. Gardner, *ibid.*, **77**, 4674 (1955).
14) J. Kendal and J. E. Booge, *ibid.*, **38**, 1723 (1916).
15) K. V. Auwers, A. Boennecke, F. Krollpfeiffer, and G. Peters, *Ann. Chem.*, **408**, 212 (1915).

SHORT COMMUNICATIONS

A New Method for the Determination of the Volume Magnetic Susceptibility by NMR

Koichi HATADA, Yoshio TERAWAKI, and Hiroshi OKUDA

Department of Chemistry, Faculty of Engineering Science, Osaka University, Toyonaka, Osaka

(Received September 7, 1972)

The determination of the volume magnetic susceptibility (χ_v) by NMR have been done by several workers using a special sample tube.[1-3] In the present work we have developed a new NMR method for determining the χ_v by the use of precision coaxial tubing (Wilmad Glass Co., inside diameters: inner tube, 1.3 mm; outer tube, 4.2 mm) and an NMR shift reagent.

The measurements were carried out on a JNM-4H-100 Spectrometer (100 MHz) at 22.5±0.2°C using an internal locking system. All the organic chemicals were obtained commercially, and they were purified and dried by the usual method. A solution of the shift reagent, $Eu(fod)_3$, in CCl_4 containing hexamethyldisiloxane (HMDS) was placed in the central capillary of the coaxial cell, and the sample of interest in the surrounding annulus. After optimizing the performance of the spectrometer and minimizing the intensity of the spinning sideband, the spectrum was measured using the HMDS signal from the inner tube as a lock signal. The signal of the sample in the outer tube is accompanied with fairly strong sidebands, as is illustrated in Fig. 1. The spacing of the bands is twice the spinning rate. The intensities of these sidebands increased with decreases in the spinning rate and in the χ_v of the sample in the surrounding annulus and with an increase in the concentration of $Eu(fod)_3$ in the central capillary. The peak height intensity of the first pair of sidebands(I) increased linearly with an increase in the reciprocal of the spinning rate (Fig. 2). When the intensities at a certain spinning rate

Fig. 1. NMR Spectrum of benzene in precision coaxial tubing.
Inner tube: 18.3(wt/vol%) solution of $Eu(fod)_3$ in CCl_4 and HMDS (1 : 1 vol/vol).
Outer tube: benzene.
Spinning rate: 23.2 Hz.

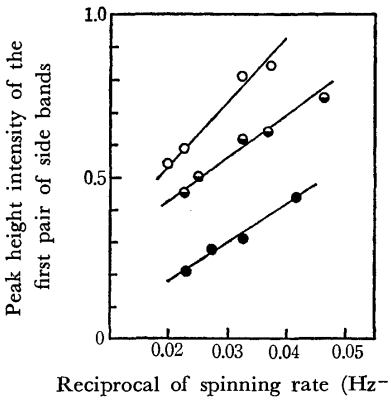

Fig. 2. The intensities of the first pair of sidebands at various spinning rates.
○: Bromoform, ◒: Chloroform, ●: Acetone

are deduced from the results shown in Fig. 2 and plotted against the known values of χ_v[4] for acetone, chloroform, and bromoform, a good linear relation is obtained. The relation at the spinning rate of 30 Hz is as follows:

$$I = -890000\,\chi_V - 0.068 \quad (1)$$

Using Eq. (1), the χ_v values of organic compounds can be determined. Some of our results ($-\chi_v \times 10^6$) are: acetonitrile, 0.540; *o*-xylene, 0.661; ethylbenzene, 0.639; benzene, 0.611. These values agree well with those recorded in the literature[4] (0.534, 0.644, 0.634, and 0.611 respectively). Similar results were obtained by placing a solution of $Pr(fod)_3$ or of cupric nitrate in the central capillary. However, on the Varian 220 MHz spectrometer, in which the direction of magnetic field was along the axis of sample spinning, such strong sidebands as are shown in Fig. 1 were not observed and the measurement of χ_v by this method could not be done.

1) J. R. Zimmerman and M. R. Foster, *J. Phys Chem.*, **61**, 282 (1957).
2) H. J. Bernstein and K. Frei, *J. Chem. Phys.*, **37**, 1891 (1962).
3) K. Hatada, Y. Terawaki, and H. Okuda, This Bulletin, **42**, 1781 (1969).
4) J. W. Emsley, J. Feeney, and L. H. Sutcliffe, "High Resolution Nuclear Magnetic Resonance Spectroscopy," Pergamon Press (1965), p. 605.

Novel Polymetallic Cobalt and Zinc Complexes formed with an Arsenic Sulphide Ligand. The X-Ray Structure Determination of Racemic Hexa-μ-dithiocacodylato-tetrazincsulphide $[SZn_4\{AsS_2(CH_3)_2\}_6]$

D. JOHNSTONE, J. E. FERGUSSON,* and Ward T. ROBINSON
Department of Chemistry, University of Canterbury, Christchurch, New Zealand
(Received October 31, 1972)

The reaction of the compound[1,2]

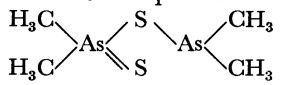

with $M(ClO_4)_2 \cdot 6H_2O$ (M=Co, Zn) in ethanol or acetone solution yields isomorphous hexagonal crystals, space group $P6_3$, unit cell dimensions (M=Co) $a=32.262$, $c=10.303$ Å, $D_m=2.05$ and stoichiometry (chemical and atomic absorption analyses) consistent with the formula $M_4As_6S_{13}C_{12}H_{36}$. Mixtures of the pure cobalt and zinc reactant or product molecules cause formation of isomorphous crystals with mixed metal stoichiometry. Recrystallization of the hexagonal crystals from dichloromethane solution yields isomorphous monoclinic crystals, space group $P2_1/n$, unit cell dimensions (M=Zn) $a=30.55$, $b=18.50$, $c=32.63$ Å; $\beta=95.7°$, $D_m=2.00$ and different stoichiometry. The title compound and its cobalt isomorph are minor recrystallization products.

The infrared spectra of all these compounds are strikingly similar in the range 1300—200 cm^{-1}, and similar to the spectra of dithiocacodylate complexes recently reported.[3] The NMR spectra of the zinc compounds confirm the expected retention by arsenic of the methyl groups coordinated to it in the free ligand.

Solution molecular weight determinations and numerous physical measurements indicate large polynuclear transition metal structures abound. For example one crystalline product containing zinc has hexagonal unit cell dimensions $a=15.42$, $c=34.65$ Å.

Electronic spectral measurements on the cobalt hexagonal crystals indicate a tetrahedral environment around the cobalt ions. The magnetic moment over the temperature range 193—93K drops from 3.49 to 2.16 BM per cobalt suggesting spin coupling between the metal ions in the polynuclear structure. The coupling is retained in solution, but can be reduced by forming mixed solutions with the isomorphous zinc complex. A compound with the composition $[Co\{AsS_2(CH_3)_2\}_2]$ is also reported to show spin coupling.[4]

The title compound was selected for initial X-ray analysis because it was ideally suited to locally available computing techniques.

Crystal Data. $Zn_4As_6S_{13}C_{12}H_{36}$, $M=1308.3$, Monoclinic, $a=11.586(8)$, $b=33.08(2)$, $c=11.996(8)$ Å, $\beta=117.39(1)°$, $U=4082$ Å^3, $D_m=2.12$ (by floatation), $Z=4$, $D_c=2.13$, $F(000)=2536$, Mo$K\alpha$ radiation, $\lambda=0.7107$ Å, μ(Mo$K\alpha$)=81.21 cm^{-1}. Space group $P2_1/c$. 4520 independent intensity data ($0<\theta\leqq21°$) were collected on a Hilger and Watts 4-circle automatic diffractometer. After correction for LP and absorption effects, 2637 intensities exceeded 3 times their estimated standard deviations. The structure was solved by the symbolic addition procedure then refined using these data and full-matrix least-squares methods until $R=0.058$.

The structure consists of well separated neutral molecules one of which is shown in the figure. All non-hydrogen atoms are in approximately tetrahedral coordination environments and bond lengths lie in the ranges normally expected for the atoms concerned. The structure has topological similarity to basic beryllium acetate. In each structure a central non-metallic atom (S,O) is bonded to four metal atoms (Zn, Be) located at the corners of a tetrahedron. The six edges of this tetrahedron are bridged by polyatomic anionic ligands ($\{AsS_2(CH_3)_2\}^-$, $(CH_3CO_2)^-$). However the high symmetry (T-23) exhibited by basic beryllium acetate, and related oxy- compounds, is not developed in this sulphide which has only ana pproximate C_3 axis of symmetry.[5] Figure 1 shows that the three six-membered SZnSAsSZn rings, which include the S and Zn atoms on the C_3 axis, have approximate chair conformations while the three which do not include the axial Zn atom have twist boat conformations. Models show no interactions precluding the existence of a molecule with the higher (T-23) symmetry and all twist boat ring conformations. This stereochemistry may be expected in some of the more complicated crystal modifications. Chirality of individual molecules has been demonstrated from the X-ray structural evidence, as well as studies of optical rotation.

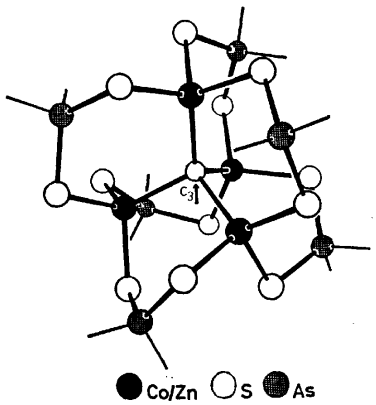

Fig. 1. Structure of $[SZn_4\{AsS_2(CH_3)_2\}_6]$
(Three top rings are chairs, three bottom rings are boats.)

We thank Drs. M. D. Brice, G. A. Rodley, and Professor C. J. Wilkins for helpful advice and the New Zealand University Grants Committee for financial support.

1) R. W. Bunsen, *Ann. Chem.*, **46**, 2 (1843).
2) N. Cameron and J. Trotter, *J. Chem. Soc.*, **1964**, 497.
3) A. T. Casey, N. S. Ham, D. J. Mackey, and R. L. Martin, *Aust. J. Chem.*, **23**, 1117 (1970).
4) A. T. Casey, D. J. Mackey, and R. L. Martin, *ibid.*, **24**, 1587 (1971).
5) A. J. Burn and G. W. Smith, *Chem. Commun.*, **1965**, 394.

Stereoselective Reduction of Ketones with Hydrosilane-Rhodium(I) Complex Combinations

Iwao OJIMA, Mitsuru NIHONYANAGI, and Yoichiro NAGAI*

Sagami Chemical Research Center, Onuma, Sagamihara 229

** Department of Chemistry, Gunma University, Kiryu, Gunma 376*

(Received September 5, 1972)

Aluminum hydrides,[1] aluminum alkoxides,[1,2] tin hydrides[3] and hydroboranes[5] can reduce ketones to alcohols stereoselectively and each reducing agent displays the respective characteristics of stereoselectivity. It is rather surprising that, in spite of the known capability of silicon hydrides to reduce ketones,[6] no attention has been so far drawn to stereochemistry in the reductions with these hydrides. Now, we wish to report here our preliminary results of the reduction of terpene ketones by hydrosilane-rhodium(I) complex combinations[4] which finds several marked differences in stereochemical selectivity from other reducing systems.

The reaction was carried out by stirring an equivalent mixture of a ketone and a hydrosilane at 0—80 °C in the presence of a catalytic amount of $(Ph_3P)_3$-RhCl. Alcohols were obtained by hydrolysis of the resulting silylethers. Yields of alcohols were nearly quantitative in all cases. Results of the hydrosilane reduction of camphor and menthone, representative terpene ketones, are listed in the Table. Included also in the Table are the reported selectivities achieved by other known reducing agents.

TABLE. STEREOSELECTIVITIES IN THE REDUCTION OF TERPENE KETONES BY HYDROSILANE-RHODIUM(I) COMPLEX COMBINATIONS (% less stable alcohol)

Reducing agent	Camphor	Menthone
$PhSiH_3$	90[a]	90[a]
Et_2SiH_2	91[a]	83[a]
$PhMeSiH_2$	75[a]	86[a]
Ph_2SiH_2	73[a]	85[a]
Et_3SiH	30[b]	64[c]
$PhMe_2SiH$	—[d]	0[c]
$LiAlH_4$	91[e]	29[f]
$Al(OPr\text{-}i)_3$		70[g]
$NaBH_4$		51[g]
B_2H_6	52[e]	
Disiamylborane	65[e]	
Dicyclohexylborane	93[e]	
Diisopinocamphenylborane	100[e]	
Ph_2SnH_2		52[g]

a) The reaction was performed without solvent using 0.1 mol% $(Ph_3P)_3RhCl$. b) 1.0 mol% $(Ph_3P)_3RhCl$ was used and *n*-hexane was employed as a solvent. c) 1.0 mol% $(Ph_3P)_3RhCl$ was used without solvent. d) Camphor was recovered without any hydrosilation. e) See Ref. 5a. f) A. K. Macbeth and J. S. Shannon, *J. Chem. Soc.*, **1952**, 2852. g) See Ref. 3.

As shown in the Table, the bulkiness of silanes exerts large influence on the stereochemical course of the reduction and a bulky hydrosilane favors the production of the more stable alcohols. This trend is quite unusual since it has been shown by Brown and Varma that, in the reduction of monocyclic and bicyclic ketones, the more bulky hydroborane produces the larger percentage of less stable of the two possible alcohols.[5a] The peculiarity found in the hydrosilane reduction catalyzed by rhodium(I) complex suggests that the transition state for the reaction cannot be accommodated with a simple four-centered type.[7] However, a possible explanation for the observed trend can be advanced by taking into account the intermediacy of the organorhodium complex III as shown below, the formation of which is quite reasonable[10] in view of the well-documented "soft-hard conception".[9] As the steric course would be governed only by the size of the silyl moiety,[10] it can be said that the bulkier the substituents on silicon, the more pronounced may be the formation of the complex IIIa which is a precursor of the more stable alcohol. A further work on the mechanism of the rhodium(I) complex catalyzed reductions is now under investigation.

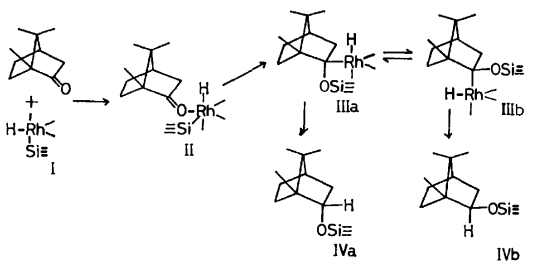

1) For example, E. L. Eliel, and D. Nasipuri, *J. Org. Chem.*, **30**, 3809 (1965); W. Hückel, M. Maier, E. Jordan, and W. Seeger, *Ann. Chem.*, **616**, 46 (1958) and references therein.

2) J. C. Richer, *J. Org. Chem.*, **30**, 324 (1965); E. L. Eliel and Y. Senda, *Tetrahedron*, **26**, 2411 (1970); E. C. Ashby, J. P. Sevenair, and F. R. Dobbs, *J. Org. Chem.*, **36**, 197 (1971).

3) H. G. Kuivila, *Synthesis*, **1970**, 499; H. G. Kuivila and O. F. Beumel, Jr., *J. Amer. Chem. Soc.*, **83**, 1246 (1961).

4) I. Ojima, T. Kogure, M. Nihonyanagi, and Y. Nagai, This Bulletin, **45**, 3232 (1972).

5) a) H. C. Brown and V. Varma, *ibid.*, **88**, 2871 (1966); b) D. C. Wigfield and D. J. Phelps, *Chem. Commun.*, **1970**, 1152.

6) C. Eaborn, "Organosilicon Compounds," Butterworth, London (1960), p. 213.

7) For example, H. O. House, and J. E. Oliver, *J. Org. Chem.*, **33**, 929 (1968); H. C. Brown and H. R. Deck, *J. Amer. Chem. Soc.*, **87**, 5620 (1965).

8) The conversion of the complex II to III will be favored on the basis of the following two points; i) as the Rh^I complex I is a soft acid, the Rh^I-C bond may be stronger than the Rh^I-O bond. ii) the Si-O bond newly formed in the complex III is very strong.

9) R. G. Pearson, *J. Amer. Chem. Soc.*, **85**, 3533 (1963).

10) The only variable steric factor is the size of silyl group, and therefore the bulky silyloxy group may occupy the less hindered site when the silyloxy group becomes larger than the rhodium moiety which is kept constant in the complex III.

A Convenient Method for the Hydrolysis of Vinyl Sulfides to Ketones

Teruaki MUKAIYAMA, Kunimasa KAMIO, Susumu KOBAYASHI, and Hisashi TAKEI

Laboratory of Organic Chemistry, Tokyo Institute of Technology, Ookayama, Meguro-ku, Tokyo

(Received October 14, 1972)

In this communication, a convenient method for the hydrolysis of vinyl sulfides to ketones by the use of $TiCl_4$ is reported. In the previous paper,[1] it was shown that $AgClO_4$ is effective for the hydrolysis of thioketals or thioacetals. However, it was found that the $AgClO_4$-promoted hydrolysis of vinyl sulfide gave the hydrolyzed product in a low yield. Hydrolysis of vinyl sulfides has been generally performed under rather drastic acidic conditions[2] except the Hg(II)-promoted hydrolysis[3] reported by Corey *et al.*

Based on the consideration that there are two possible ways of activation of vinyl sulfides towards hydrolysis, namely the activation of carbon-carbon double bond and carbon-sulfur bond, we examined the hydrolysis using various metal salts which might have strong affinity toward either double bond or sulfur atom. Finally, it was established that vinyl sulfides were easily hydrolyzed in the presence of 2 molar amounts of $TiCl_4$. For example, when α-ethylthiostilbene, **1**, was added to 2 molar amounts of $TiCl_4$ in acetonitrile at room temperature, the color of the solution changed from yellow to deep red. After stirring for about 20 min, 4 molar amounts of water was added and the reaction mixture was stirred at room temperature for an additional 4 hr. Then usual work-up afforded desoxybenzoin, **2**, in 78% yield and 21% of **1** was recovered. Further, it was found that,

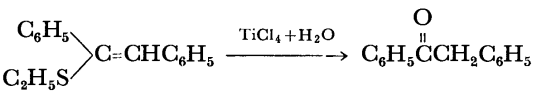

1 **2**

when 2 molar amounts of $Pb_2O(OH)_2$ was added in the above reaction in order to remove ethanethiol formed at the same time, the increase of the yield was achieved and **2** was obtained in 92% yield and 8% of **1** was recovered. On the other hand, in the case of phenyl vinyl sulfide, there was no remarkable effect in the yield by the addition of $Pb_2O(OH)_2$.

In a similar manner, various vinyl sulfides were hydrolyzed to the corresponding ketones in high yields. For example, β-aryl substituted vinyl sulfide[4], **3**, was hydrolyzed quantitatively to 3-phenyl-2-butanone by the use of $TiCl_4$ in acetic acid. The results are shown in Table 1.

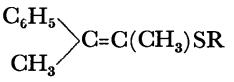

3 $R = C_2H_5$ or C_6H_5

In conclusion, it is noted that vinyl sulfides are easily hydrolyzed to the corresponding ketones in high yields without accompanying by-product under mild conditions by the action of $TiCl_4$. Further works are now in progress and will be reported at a later date.

TABLE 1. $R^1R^2C{=}CR^3(SR^4) \xrightarrow{2TiCl_4 + 4H_2O + n\ Pb_2O(OH)_2} R^1R^2CHCR^3$ (O)

Vinyl sulfide				Solvent	n	Time (hr)	Isolated yield (%) [recovered vinyl sulfide(%)]
R^1	R^2	R^3	R_4				
C_6H_5	H	C_6H_5	C_2H_5	C_6H_6	2	4	94
				CH_3CN	0	4	78[21]
				CH_3CN	2	4	92[8]
				CH_3CO_2H	0	4	97
C_6H_5	n-C_4H_9	C_6H_5	C_2H_5	C_6H_6	2.2	12	91[a]
				CH_3CO_2H	0	4	quant
CH_3	H	C_6H_5	C_6H_5	CH_3CN	0	6	88
				CH_3CO_2H	0	6	90
				CH_2Cl_2	0	6	95
C_6H_5	H	C_6H_5	C_6H_5	CH_3CO_2H	0	7	96
C_6H_5	n-C_4H_9	C_6H_5	C_6H_5	CH_2Cl_2	0	14	62[b]
C_6H_5	CH_3	CH_3	C_2H_5	CH_3CO_2H	0	4	quant
C_6H_5	CH_3	CH_3	C_6H_5	CH_3CO_2H	0	7	97

a) 2.2 molar amounts of $TiCl_4$ was used. b) 5 molar amounts of H_2O was added.

1) T. Mukaiyama, S. Kobayashi, K. Kamio, and H. Takei, *Chem. Lett.*, **1972**, 273.

2) J. H. S. Weiland and J. F. Arens, *Rec. Trav. Chim. Pays-Bas*, **79**, 1293 (1960). B. S. Kupin and A. A. PeTrov, *Zh. Org. Khim.*, **3**, 975 (1967). T. Mukaiyama, S. Fukuyama, and T. Kumamoto, *Tetrahedron Lett.*, **1968**, 3787.

3) E. J. Corey and J. I. Shulman, *J. Org. Chem.*, **35**, 777 (1970).

4) E. J. Corey and J. I. Shulman reported[3] that the Hg(II)-promoted hydrolysis of β-aryl substituted vinyl sulfide required an elevated temperature.

A Convenient Method for Hydrolysis of 1,3-Dithiane Derivatives Using Cupric Chloride

Koichi NARASAKA, Takeshi SAKASHITA, and Teruaki MUKAIYAMA

Laboratory of Organic Chemistry, Tokyo Institute of Technology, Ookayama, Meguro-ku, Tokyo

(Received October 19, 1972)

A variety of methods for generation of carbonyl compounds from 1,3-dithiane derivatives has been developed, however, none of these methods is general.[1] Therefore, in connection with the studies on the activation of carbon-sulfur bond with cupric chloride[2], we investigated the hydrolysis of 1,3-dithiane derivatives with cupric chloride.

The mixture of 5 mmol of 2-methyl-2-phenethyl-1,3-dithiane (**1**), 10 mmol of cupric chloride and 20 mmol of cupric oxide in 50 m*l* of aqueous 99% acetone[3] was refluxed for 1 hr. A precipitate was filtered off and the filtrate was condensed under reduced pressure. Ether was added to the residue and the resulting precipitate was filtered off. The filtrate, which was homogeneous by tlc and vpc, was distilled and benzylacetone (**2**) was obtained in 93% yield. When the reaction was carried out at room temperature for 2 hr, **2** was isolated in 83% yield.

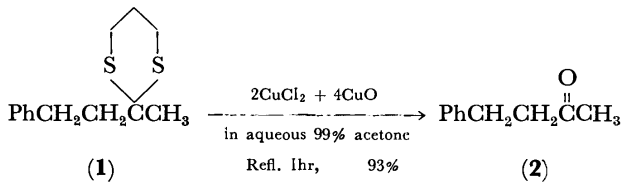

(**1**) (**2**)

The hydrolysis of several other 1,3-dithiane derivatives was examined by the same procedure to test the generality of this method.

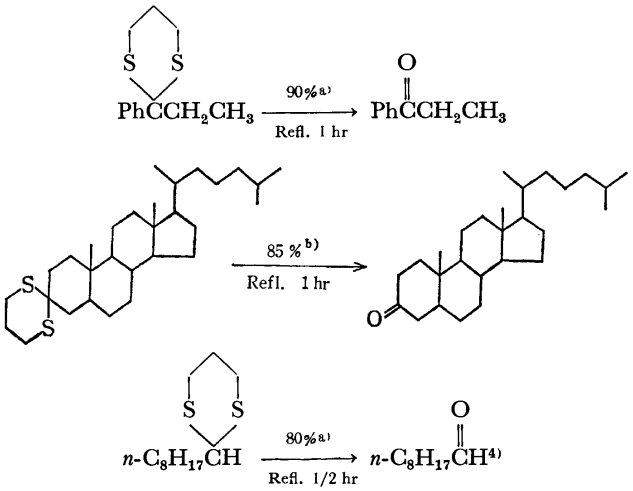

a) Yield of pure carbonyl compound isolated by distillation.
b) Yield of recrystallized product.

From the results shown in the above equations, it was confirmed that this method is applicable to hydrolysis of a wide variety of 1,3-dithiane derivatives and the corresponding carbonyl compounds were isolated in good yields by the simple procedure.

In addition, it was found that 2-*n*-octyl-1,3-dithiane is readily hydrolyzed with cupric chloride to the corresponding aldehyde in higher yield as compared with the cases of the hydrolyses of 2-monoalkyl-1,3-dithianes, such as 2-benzyl-1,3-dithiane and 2-*n*-hexyl-1,3-dithiane with mercuric chloride[1e,f], *n*-hexyl-1,3-dithiane with boron trifluoride–mercuric oxide[1f] and 2-*n*-octyl-1,3-dithiane with silver perchlorate.[5]

In conclusion, it is noted that this method affords a convenient method for hydrolysis of 1,3-dithiane derivatives, a useful synthetic intermediates, to carbonyl compounds. The further application is now in progress.

1) a) K. Kuhn and F. A. Neugebauer, *Chem. Ber.*, **94**, 2629 (1961): b) D. Seebach, *Synthesis*, **1**, 17 (1969): c) M. L. Wolform, *J. Amer. Chem. Soc.*, **51**, 2188 (1929): d) E. J. Corey and D. Crouse, *J. Org. Chem.*, **33**, 298 (1968): e) E. J. Corey and B. W. Erickson, *ibid.*, **36**, 3553 (1971): f) E. Vedejs and P. L. Fuchs, *ibid.*, **36**, 366 (1971): g) W. Huurdeman and H. Wynberg, *Synthetic Commun.*, **2**, 7 (1972): h) T. Mukaiyama, S. Kobayashi, K. Kamio and H. Takei, *Chem. Lett.*, **1972**, 237.

2) T. Mukaiyama, K. Narasaka, and H, Hokonoki, *J. Amer. Chem. Soc.*, **91**, 4315 (1969); T. Mukaiyama, K. Maekawa and K. Narasaka, *Tetrahedron Lett.*, **1970**, 4669.

3) The reaction proceeds in various aqueous organic solvents (acetone, acetonitrile, methanol, and tetrahydrofuran), but it was noted that benzylacetone is obtained in the best yield in the case of aqueous 99% acetone.

4) In this case, the reaction was carried out under an argon atmosphere for 30 min.

5) T. Mukaiyama, S. Kobayashi, and K. Kamio, Unpublished work.